Talanta, Vol. 40, No. 1, pp. 1–7, 1993
Printed in Great Britain

0039-9140/93 $6.00 + 0.00
Pergamon Press Ltd

THEORY OF INTRALABORATORY VALIDATION OF ACCURACY OF AN ANALYTICAL TECHNIQUE BY STANDARD REFERENCE MATERIALS

I. KUSELMAN

National Physical Laboratory of Israel, Danziger A Building, Hebrew University, Jerusalem 91904, Israel

(*Received* 9 *January* 1992. *Revised* 6 *May* 1992. *Accepted* 6 *May* 1992)

Summary—The theory is presented for intralaboratory accuracy validation of a sample analysis technique, employing standard reference materials. The validation criteria and the corresponding probabilities of erroneous conclusions concerning accuracy are given.

The most problematic part of metrological certification of a sample analysis technique is its accuracy validation, *i.e.*, evaluation of accuracy of the analysis results received by this technique.* Interlaboratory experiment is a common method for accuracy validation,[1–11] requiring, however, significant organization efforts, expenses and time.[12] In the absence of standard reference materials (SRM's) adequate for the object being analysed this expenditure might be unavoidable. On the other hand, the use of SRM's allows validation of the accuracy by means of an intralaboratory experiment, employing the SRM values as the result of convolution of data of previous interlaboratory experiments, carried out in the course of certification of the reference material. An intralaboratory experiment consists of the SRM analysis according to a technique being certified, carried out K times in a single laboratory. Accuracy of the analysis results is characterized by the bias[13] of their mathematical expectation C_r from the true value of the determined mass fraction of the element δ_{tr}, *i.e.*, by the magnitude $C_r - \delta_{tr}$. Thus, it is possible to calculate, using the K results of the analysis, the sample average $\bar{C}_r$, which, at the normal distribution of the analysis results, constitutes a sample estimate of C_r and allows us to obtain the respective estimate of the bias magnitude $\bar{C}_r - \delta_{tr}$. The sample estimate S_r of the standard deviation σ_r of the analysis results from their mathematical expectation C_r allows the construction of the confidence interval for $C_r - \delta_{tr}$. This, in turn, permits us to infer whether the accuracy has been satisfactory or not, provided the requirements on $C_r - \delta_{tr}$ have been specified in terms of σ_r fractions. This method has been introduced in ferrous metallurgy.[14,15]

In these and later works the certified values C_{cert} have been used for the true component contents' in SRM's, *i.e.*, δ_{tr} and C_{cert} have been taken as identical ones. At the same time, it is known that the greater the uncertainty in the determination of the true value of the component mass fraction in a SRM, the greater the standard deviation σ_{cert} of C_{cert}.[12] Nearly the same is true about the uncertainty of the analysis results, as far as the magnitude σ_r is concerned. Thus there is also uncertainty in the accuracy validation of the analytical technique using SRM's.[1,2]

The present paper considers the relation of the interlaboratory experiment data on the reference material (RM) certification to the intralaboratory experiment results used for validation of the technique accuracy under conditions of the above-mentioned uncertainty, when distributions only are known and the certified value in the SRM is not being accepted as a true one. The criteria for intralaboratory validation of a technique accuracy has been formulated and the confidence indexes of such validation have been calculated.

The relation between RM certification data and results of experiment for validation of the technique accuracy

Since the technique which is being studied could not be used in RM certification, the data of RM certification and results of experiment for validation of the technique accuracy are to

*The techniques considered here do not include sampling.

be considered as independent random events. Due to this independence, the correspondence of these data to the experimental results can be characterized by the total area P under their density function curves. The value P allows the determination of the degree of proximity of the results, obtained by the studied technique, to the results, obtained by the techniques used in RM certification. Taking into account that the accuracy of the techniques, used in the RM certification, has been proved previously, the correspondence will imply the acceptability of the studied technique as satisfying the accuracy requirements. The above-mentioned problem is similar to several known problems of mathematical statistics, such as determination of the degree of connection between the observed and expected frequencies. Unfortunately, the common tools employed in this context—the so-called connection coefficients[16] are quite cumbersome and their physical meaning is less elucid compared to the magnitude P introduced below.

Let, for the sake of simplicity, both distributions be normal with parameters C_{cert}, σ_{cert} and C_r, σ_r as shown in Fig. 1(a). The area to be determined (probability) P has been shaded. To calculate the latter, let us find first the mass fraction of element C_1 and C_2, corresponding to the density function curves crossings. As both density functions are equal at these values

$$f_{cert} = \frac{1}{\sqrt{2\pi}\sigma_{cert}} e^{-\frac{(C-C_{cert})^2}{2\sigma_{cert}^2}} = \frac{1}{\sqrt{2\pi}\sigma_r} e^{-\frac{(C-C_r)^2}{2\sigma_r^2}} = f_r, \quad (1)$$

which yields the quadratic equation

$$(\sigma_{cert}^2 - \sigma_r^2)C^2 - 2(\sigma_{cert}^2 C_r - \sigma_r^2 C_{cert})C + \left(\sigma_{cert}^2 C_r^2 - \sigma_r^2 C_{cert}^2 - 2\sigma_{cert}^2\sigma_r^2 \ln\frac{\sigma_{cert}}{\sigma_r}\right) = 0, \quad (2)$$

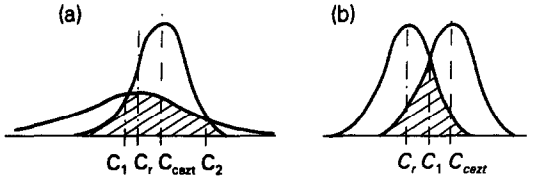

Fig. 1. Density functions of the RM certification data and experiment results for the validation of the technique accuracy: (a) at different σ_r and σ_{cert}; (b) at $\sigma_r = \sigma_{cert}$.

whose roots are the required values C_1 and C_2:

$$C_{1,2} = \frac{(\sigma_{cert}^2 C_r - \sigma_r^2 C_{cert}) \pm \sigma_{cert}\sigma_r\sqrt{\rho}}{\sigma_{cert}^2 - \sigma_r^2}, \quad (3)$$

where

$$\rho = (C_{cert} - C_r)^2 + 2(\sigma_r^2 - \sigma_{cert}^2)\ln\frac{\sigma_r}{\sigma_{cert}}. \quad (4)$$

Then the probability is

$$P = \int_{-\infty}^{C_1} f_{cert}\,dc + \int_{C1}^{C2} f_r\,dC + \int_{C_2}^{\infty} f_{cert}\,dc = \phi\left(\frac{C_1 - C_{cert}}{\sigma_{cert}}\right) + \phi\left(\frac{C_2 - C_r}{\sigma_r}\right) - \phi\left(\frac{C_1 - C_r}{\sigma_r}\right) - \phi\left(\frac{C_2 - C_{cert}}{\sigma_{cert}}\right) + 1; \quad (5)$$

where ϕ stands for normalized normal distribution.

Substituting C_1 and C_2 given by equation (3) into equation (5) we obtain, after some transformations

$$P = \phi\left[\frac{\sigma_{cert}(C_{cert} - C_r) - \sigma_r\sqrt{\rho}}{\sigma_r^2 - \sigma_{cert}^2}\right] + \phi\left[\frac{\sigma_r(C_{cert} - C_r) + \sigma_{cert}\sqrt{\rho}}{\sigma_r^2 - \sigma_{cert}^2}\right] - \phi\left[\frac{\sigma_r(C_{cert} - C_r) - \sigma_{cert}\sqrt{\rho}}{\sigma_r^2 - \sigma_{cert}^2}\right) - \phi\left[\frac{\sigma_{cert}(C_{cert} - C_r) + \sigma_r\sqrt{\rho}}{\sigma_r^2 - \sigma_{cert}^2}\right] + 1. \quad (6)$$

If $\sigma_{cert} = \sigma_r = \sigma$, there is only one point of intersection of the curves of the density function [Fig. 1(b)], the second point being shifted to infinity. In this connection, for $\sigma_{cert} = \sigma_r = \sigma$, it follows from (2) that $C_1 = (C_{cert} + C_r)/2$, and also:

$$P = 2\left[1 - \phi\left(\frac{|C_{cert} - C_r|}{2\sigma}\right)\right]. \quad (7)$$

In particular, since $\phi(0) = 0.5$, for $C_{cert} = C_r$, $P = 1$. This is the only case when we can definitely say that the accuracy of the studied technique is satisfactory: the distributions coincide. At any other choice of distribution parameters, $P < 1$. For example, if $C_r = 3.20$, $\sigma_r = 0.04$, $C_{cert} = 3.25$, $\sigma_{cert} = 0.03$, the value $P = 0.46$. For more complicated distributions, the problem under consideration may be solved numerically, if the analytical methods are not available.

At the first sight, the received relationships seem to contradict to the "common sense" of accuracy validation, according to which the smaller the certification error of the SRM employed the better.[12] On the other hand, it has been concluded here that for the situation to be optimal, the certification errors and the SRM analysis errors according to the technique which is being studied, should be equal. The meaning of this becomes clear if one takes into account both uncertainty components in the validation of technique accuracy, *i.e.*, if instead of identifying the true element content in SRM with C_{cert}, one remembers that each of the certification data may be equal to the true one, but with a different probability. In the same manner, $\bar{C}_r$ is not the only value received in the experiment, the others must also be taken into account, although their probability is lower than that of $\bar{C}_r$.

In particular, for $C_{cert} = C_r$ and $\sigma_r > \sigma_{cert}$, it is impossible to conclude definitely about the accuracy of the technique, as opposed to the case when all distribution parameters are equal.

Thus, in formulating "yes–no" type sample criteria for accuracy validation of a technique the correctness of the neglection of the SRM certification error as well as the correctness of the null hypothesis concerning the bias insignificance have to be established in each case. For example, let us consider the null hypothesis

$$H_0: |C_r - C_{cert}| \leqslant 0.3\sqrt{\sigma_r^2 + \sigma_{cert}^2}, \qquad (8)$$

meaning that the systematic errors in the results of measurement performed are insignificant* as compared with the total of random errors of the analytical technique and the RM certification. Let us denote $\sigma_{cert}/\sigma_r = \gamma$. Equations (6) and (7) show that such a null hypothesis at $\gamma = 0.4$ corresponds to $P \geqslant 0.56$, at $\gamma = 0.7 - P \geqslant 0.77$, and at $\gamma = 1.0$ to $P \geqslant 0.83$.

In comparison, a similar hypothesis

$$H_0: |C_r - C_{cert}| \leqslant 0.3(\sigma_r + \sigma_{cert}) \qquad (9)$$

at $\gamma = 0.4$ corresponds to $P \geqslant 0.54$, at $\gamma = 0.7$ to $P \geqslant 0.63$, and at $\gamma = 1.0$ to $P \geqslant 0.76$, *etc.* Apparently, the hypothesis (8) is preferable as implying higher probability P for the same γ value. The increase of the numerical coefficient in the right hand side of equations (8) and (9) yields a decrease of probability P, whereas for $|C_r - C_{cert}| > 2(\sigma_r + \sigma_{cert})$ the distributions "diverge" that is $P \to 0$. In this case it is unbelievable that technique under consideration would be accurate. Almost the same is done for $|C_r - C_{cert}| > 2\sqrt{\sigma_r^2 + \sigma_{cert}^2}$, which suggests that the tradiational two sigma criterion, based on the hypothesis

$$H_0: |C_r - C_{cert}| \leqslant U_{1-\alpha/2}\sqrt{\sigma_r^2 + \sigma_{cert}^2}, \qquad (10)$$

at $\alpha = 0.05$ is unacceptable (here U—quantile of normal distribution). The same applies to the t-criterion using quantile of Student's distribution instead $U_{1-\alpha/2}$ in equation (10) when population standard deviations σ_r and σ_{cert} are unknown, but their sample values S_r and S_{cert} are known.

It is necessary to keep in mind that the probability P as such is not an indicator of accuracy. For example, $P \to 0$ also if $\sigma_{cert} \to 0$ ($\gamma \to 0$) which only means that, unlike the reproduced values, the certified one is practically non-random. In this relation, the experimental results for the accuracy validation of a technique do not match the RM certification data. In such a case (for $\gamma < 0.3$), it is possible to neglect the uncertainty of the true element content in SRM. We should also take into consideration that the information about the distributions of both certified and experimental values are limited by small sample sizes of experimental data. Therefore, the discussed magnitude P can adequately characterize the technique only as long as the hypothesis concerning the certified and experimental value distributions fit the reality.[17]

The practical importance of the above presentation lies in the fact that the P calculation may guide a search for a suitable null hypothesis for the construction of a sample criterion directed at the accuracy evaluation of a technique, through the results of an experiment of relatively small size.

Confidence of accuracy validation

Naturally, when it is necessary to validate the accuracy of an analytical technique through the results of an experiment limited by time and expense, the confidence of this validation is being questioned.

The confidence is characterized by the probabilities of not rejecting the hypothesis about technique's accuracy when it is true, and rejecting it when it is untrue.[18] It is known that these probabilities depend on how the hypotheses have been formulated as well as the criterion for their examination.

*The ratio 1/3 (~0.3) used in equation (8) is commonly accepted in metrology as a condition for insignificance.[12,15]

Let the null hypothesis H_0 consist of the assumption that the systematic errors of the technique are negligible compared to the sum of random errors of the SRM analysis results (experiment results) and the RM certification errors. It corresponds to the formula (8), where standard deviation σ_{cert} approximately equal to half the semiwidth of confidence interval for C_{cert}, given in the SRM certificate.

Alternative hypothesis H_1 assumes that systematic errors are significant, *e.g.*,

$$H_{11}: |C_r - C_{cert}| = 0.8\sqrt{\sigma_r^2 + \sigma_{cert}^2}, \quad (11)$$

$$H_{12}: |C_r - C_{cert}| = 0.9\sqrt{\sigma_r^2 + \sigma_{cert}^2} \quad (12)$$

etc.

With the results of K analysis of SRM at our disposal, it is possible to view the accuracy of a technique as satisfactory, if

$$|\bar{C}_r - C_{cert}| + t_{1-\alpha/2} S_r/\sqrt{K} \leqslant 0.3\sqrt{\sigma_r^2 + \sigma_{cert}^2}, \quad (13)$$

where the left hand side of this expression represents the upper bound of the confidence interval for $|C_r - C_{cert}|$; $1-\alpha/2$ is the probability that the bias $|C_r - C_{cert}|$ does not exceed the upper bound of its confidence interval; S_r, sample value of standard deviation of the SRM analysis results (sample estimate of σ_r for the number of degrees of freedom $K-1$, calculated from the same K results of analysis as the sample average $\bar{C}_r$). Substituting the ratio $\sigma_{cert}/\sigma_r = \gamma$ into expression (13), we obtain, after some simple transformations:

$$\frac{|\bar{C}_r - C_{cert}|}{S_r} \leqslant 0.3\frac{\sigma_r}{S_r}\sqrt{1+\gamma^2} - \frac{t_{1-\alpha/2}}{\sqrt{K}}. \quad (14)$$

Let us introduce in equation (14) instead of S_r/σ_r the magnitude $\sqrt{\chi^2_{\alpha/2}/(K-1)}$, where χ^2-quantile of chi-square distribution for the number of degrees of freedom $K-1$. Then we obtain the following accuracy criterion

$$\frac{|\bar{C}_r - C_{cert}|}{S_r} \leqslant 0.3\sqrt{\frac{(K-1)(1+\gamma^2)}{\chi^2_{\alpha/2}}} - \frac{t_{1-\alpha/2}}{\sqrt{K}}. \quad (15)$$

Table 1 gives the numerical values for the right hand side of the criterion at $\alpha = 0.05$. These tabulated values are the bias norms of the average analysis result from the value indicated in SRM (in S_r units).

For example, in silicon determination in samples of SRM No. 1721-79 (USSR) of tinless bronzes by the extractive photometric method according to the standard:[19] $C_{cert} = 0.100$, $\sigma_{cert} = 0.005$, $\gamma = 1.0$. If $\bar{C}_r$ will be derived from $K = 30$ analysis results, then the accuracy may be viewed as satisfactory, when $|\bar{C}_r - 0.100|/S_r \leqslant 0.20$, *i.e.*, $|\bar{C}_r - 0.100| \leqslant 0.20 S_r$.

Table 1. Bias norms of average analysis result from the value indicated in SRM (in S_r units) by null hypothesis (8)

	K			
γ	20	30	40	50
0.4	0.01	0.06	0.10	0.12
0.7	0.07	0.12	0.16	0.17
1.0	0.15	0.20	0.23	0.24

Table 1 shows that for small size experiments the requirements on $\bar{C}_r$ are more strict since for the small size experiment $\bar{C}_r$ may deviate further from the population C_r as compared to the large size experiment.

The criterion obtained does not allow rejection of hypothesis H_0 with probability $1-\alpha/2$, when it is true. The probability to reject H_0, when it is untrue, *i.e.*, when the alternative hypotheses H_1 are correct (criterion power)[20] is:

$$P_a = \phi\left(\frac{t_{\alpha/2} + \lambda}{\sqrt{1 + \frac{t^2_{1-\alpha/2}}{2(K-1)}}}\right), \quad (16)$$

$$\lambda = \frac{|C_r - C_{cert}| - 0.3\sigma_r\sqrt{1+\gamma^2}}{\sigma_r/\sqrt{K}} \quad (17)$$

The magnitude λ is being calculated by substituting into equation (17) instead of the expression $|C_r - C_{cert}|$ its value, corresponding to an alternative hypothesis. For example, for the hypothesis (11) this is $0.8\sqrt{\sigma_r^2 + \sigma_{cert}^2}$. Thus for H_{11} given by (11) and (17) we have $\lambda = 0.5\sqrt{(1+\gamma^2)K}$ and at H_{12} $\lambda = 0.6\sqrt{(1+\gamma^2)K}$. Figure 2 shows the results of P_a calculation for $\alpha = 0.05$.

In the accuracy validation procedure the probabilities of errors of the first and second type relate in a simple manner to the calculated confidence characteristics: the probability of an error of the first type (to reject the H_0 hypothesis when it is correct) equals $\alpha/2$; the probability of an error of the second type β (not to reject the H_0 when it is not correct) equals $1 - P_a$ (see Fig. 2).

When $\gamma \leqslant 0.3$ and it is possible to neglect the RM certification error, as compared with the random errors of analysis, a special case follows from the criterion (15).[21] In this case the null hypothesis consists of the statement that the

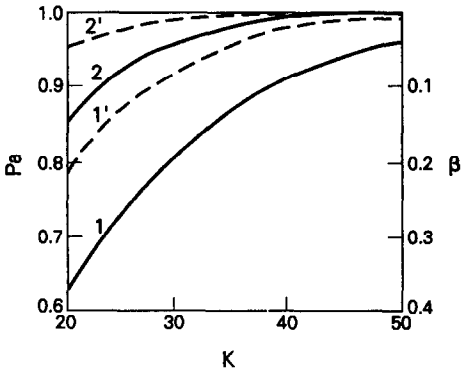

Fig. 2. Operational characteristics of criterion (15), *i.e.*, power P_a and probability of the error of second type β versus experiment size (K) with probability of the error of first type $\alpha/2 = 0.025$. Solid curves correspond to alternative hypothesis H_{11}, dotted lines $-H_{12}$: 1 and 1'—at $\gamma = 0.4$; 2 and 2'—at $\gamma = 1.0$.

accuracy of the analytical technique is satisfactory when the systematic errors of the analysis results are insignificant as compared to the random errors.

At the first sight, it seems that the requirements obtained for the accuracy of the analytical techniques are excessively strict in comparison to those used, for example, in verification of routine measuring instruments by standard ones.[22] However, the relation between the analytical technique and the SRM is basically different from that between the routine and standard measuring instruments, since the technique considered may be used further for certification of another (new) RM.

So far as different null hypotheses lead to different criteria and, accordingly, to different confidences of accuracy validation of the analytical technique, the experiment for accuracy validation can be executed only after a detailed discussion of the programme for the technique certification. Such a discussion should exclude incorrect problem formulations[11] and specify the limitations on applicability of the technique concerned. The characteristics of the used SRM's should be taken into account, in particular, in connection with possible composition variations in the samples analysed, compared with the SRM composition.

Accuracy criterion for techniques of routine analysis

Let us consider a technique which is not meant for the RM certification or similar purposes, but is only meant for the routine analysis of samples whose composition is compatible with the available SRM composition. Then by analogy with the routine measuring instruments according to Ref. 22, we shall consider the accuracy of the analysis results as satisfactory when their systematic errors exceed the standard deviation σ_{cert} by a magnitude which is insignificant in comparison with random errors of the analysis. In this case the null hypothesis has the following form:

$$H_0: |C_r - C_{cert}| \leqslant \sqrt{(0.3\sigma_r)^2 + \sigma_{cert}^2} \quad (18)$$

In the course of a SRM analysis according to such a technique, the probability P to consider the obtained results of the analysis as belonging to the population of SRM is: $P \geqslant 0.53$ for $\gamma \geqslant 0.4$ (Fig. 1 shows it as a shaded area). Respectively, the right hand side of equation (18) reaches in this case the value of $1.25\sigma_{cert}$.

In comparison, the authors of Ref. 22 recommend the errors of the routine measuring instruments, erroneously accepted as fit ones, to exceed the allowed values no more than 1.35 times, and the probability to accept an actually defective instrument as fit to be no more than 0.5.

Alternative hypotheses H_1 assume that systematic errors of the analytical technique exceed significantly the RM certification errors, *i.e.*,

$$H_{11}: |C_r - C_{cert}| = 2.0\sqrt{(0.3\sigma_r)^2 + \sigma_{cert}^2}, \quad (19)$$

$$H_{12}: |C_r - C_{cert}| = 2.1\sqrt{(0.3\sigma_r)^2 + \sigma_{cert}^2} \quad (20)$$

etc.

Considering, as in the previous case, the upper bound of the confidence intervals for $|C_r - C_{cert}|$ on the basis of a sample from K results of the SRM analysis, we get

$$|\bar{C}_r - C_{cert}| + t_{1-\alpha/2} S_r/\sqrt{K} \leqslant \sqrt{(0.3\sigma_r)^2 + \sigma_{cert}^2}. \quad (21)$$

From here, after some transformations we obtain the criterion

$$\frac{|\bar{C}_r - C_{cert}|}{S_r} \leqslant \sqrt{\frac{(K-1)(0.09+\gamma^2)}{\chi^2_{\alpha/2}}} - \frac{t_{1-\alpha/2}}{\sqrt{K}}. \quad (22)$$

Table 2 gives the numerical values of the right hand side of this criterion at $\alpha = 0.05$. They are significantly "softer" than those given in Table 1. In particular for the given example of silicon in tinless bronzes, it is necessary that $|\bar{C}_r - 0.100| \leqslant 1.03 S_r$.

Table 2. Bias norms of average analysis result from the value indicated in SRM (in S_r units) by null hypothesis (18)

	K			
γ	20	30	40	50
0.4	0.26	0.30	0.32	0.34
0.7	0.64	0.65	0.66	0.67
1.0	1.06	1.03	1.02	1.02

According to the formula (22), the criterion like the previous one, allows us with probability $1-\alpha/2$ not to reject the hypothesis H_0 [equation (18)], when it is correct. The criterion power can be calculated according to formula (16), where

$$\lambda = \frac{|C_r - C_{cert}| - \sigma_r\sqrt{0.09+\gamma^2}}{\sigma_r/\sqrt{K}}. \quad (23)$$

According to formulae (19) and (20), respectively, for H_{11} $\lambda = \sqrt{(0.09+\gamma^2)K}$ and for H_{12} $\lambda = 1.1\sqrt{(0.09+\gamma^2)K}$. Figure 3 shows the results of P_a and β calculated at $\alpha = 0.05$ for the considered hypothesis. It is clear, that with increasing γ the criterion power (22) increases faster than the criterion power (15), and at $\gamma = 1.0$ they both approach unity. This is so because when γ increases, criterion (22) reveals greater values of systematic errors [the right hand side of expression (18) increases more rapidly than the right hand side of (8) when γ is increased]. Thus, accuracy validation of analytical techniques for routine control of a sample composition may be performed under less stringent requirements than those applied for RM's certification and other arbitration purposes.

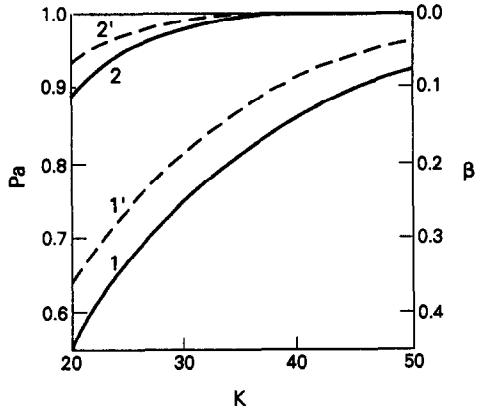

Fig. 3. Operational characteristics of criterion (22), *i.e.*, power P_a and probability of the error of second type β versus experiment size (K) with probability of the error of first type $\alpha/2 = 0.025$. Solid curves correspond to alternative hypothesis H_{11}, dotted lines $-H_{12}$: 1 and 1'—at $\gamma = 0.4$; 2 and 2'—at $\gamma = 0.7$.

When $\sigma_{cert} \ll \sigma_r$, criteria (15) and (22) reduce to a simpler one introduced previously.[21]

CONCLUSIONS

It has been shown that intralaboratory accuracy validation of an analytical technique by SRM's may be carried out by means of testing a statistical hypotheses about the relation between the systematic and random errors of analytical results under conditions of uncertainty due to errors of SRM's used.

In order to compare the systematic errors of a certificated technique with the random errors of another ("standard") technique, as it is practised in ferrous[23] and non-ferrous[18,21,24,25] metallurgy, it is sufficient to introduce the value σ_r for this "standard" technique into hypotheses (8) and (18).

In cases when distribution of the analysis results differs from the normal one, and it is impossible to determine and remove the causes for this difference, similar criteria can be formulated by the nonparametric statistics methods.[25,26]

The considerations presented have been used successfully for metrological certification of numerous analytical techniques, applied in secondary non-ferrous metallurgy.[27,28]

Acknowledgements—The author thanks Prof. E. Schoenberger, Prof. I. Rubinshtein, Dr. V. Glezer and Dr. O. Lev for helpful discussions.

REFERENCES

1. R. Sutarno and H. F. Steger, *Talanta*, 1985, **32**, 439.
2. *Idem, ibid.*, 1985, **32**, 1088.
3. B. Lister, *Anal. Chim. Acta*, 1986, **186**, 325.
4. H. H. Hughes and P. W. Hurley, *Analyst*, 1987, **112**, 1445.
5. D. R. Williams, *J. Assoc. Off. Anal. Chem.*, 1986, **69**, 432.
6. O. Cozzoli, E. Fedeli, *Essenze Deriv. Agrum.*, 1987, **57**, 295.
7. M. Grasserbauer, W. Pfannhauser, W. Wegscheider, *Oesterr. Chem. Z.*, 1987, **88**, 130.
8. I. Lengyel, *ICP Inf. Newslett.*, 1987, **5**, 305.
9. L. Leisztner, G. Veress, E. Pungor, *Magy. Kem. Foly.*, 1987, **93**, 149.
10. K. Doerffel, H. Zwanziger, *Z. Anal. Chem.*, 1987, **328**, 1.
11. A. B. Shaevich, *Zavod. Lab.*, 1987, **53**, 4.
12. A. B. Shaevich, *Standard Reference Materials for Analytical Purposes*, Khimiya, Moscow, 1987.
13. R. A. Nadkarni, *Anal. Chem.*, 1991, **63**, 675A.
14. Yu. L. Pliner and E. A. Svechnikova, *Zavod. Lab.*, 1978, **44**, 1073.
15. Yu. L. Pliner, E. A. Svechnikova and V. M. Ogurtsov, *Quality Control of Chemical Analysis in Metallurgy*, Metallurgiya, Moscow, 1979.

16. A. Afifi and S. Aijzen, *Statistical Analysis. Point of View with Computer Applications*, Mir, Moscow, 1982.
17. I. Kuselman and M. S. Podol'skij, *Zavod. Lab.*, 1988, **54**, 1.
18. I. Kuselman, *Metrologiya*, 1989, **4**, 57.
19. GOST 15027.6-77 (ST SAV 1539-79). Bronzes Tinless. Methods for Silicon Determination, Izd. Standartov, Moscow, 1983.
20. L. Hald, *Mathematical Statistics with Technical Applications*, Inostr. Literatura, Moscow, 1956.
21. I. Kuselman and L. G. Scrabina, *Zavod. Lab.*, 1987, **53**, 55.
22. National System of Assurance of Uniformity of Measurements. Confidence and Requirements to Verification Techniques of Measuring Instruments. Procedural Rules. MI 187–86, MI 188–86, Izd. Standartov, Moscow, 1987.
23. Yu. L. Pliner and I. M. Kuz'min. Metrological Problems of Analytical Control of Metal Product Quality, Metallurgiya, Moscow, 1989.
24. I. Kuselman and L. G. Scri'abina, *Tsv. Metallurgiya*, 1988, **4**, 34.
25. *Idem*, *Metrologiya*, 1983, **3**, 59.
26. B. Ia. Yufa., *Zh. Anal. Khim.*, 1989, **44**, 2148.
27. I. Kuselman, *Zavod. Lab.*, 1990, **56**, 1.
28. *Idem*, *Izmer. Tekh.*, 1991, **2**, 56.

GLOSSARY

RM	Reference material
SRM	Standard reference material
Sample (chem.)	A finite portion of material for analysis
Sample (stat.)	A finite number of possible results of analysis
C_r	Mathematical expectation of analysis results
$\bar{C}_r$	Sample average of analysis results
K	Number of analysis results (size of the statistical sample)
σ_r	Standard deviation of analysis results from C_r
S_r	Sample estimate of σ_r
δ_{tr}	True value of the mass fraction of the element in the sample
C_{cert}	Certified value of the mass fraction of the element in the RM
σ_{cert}	Standard deviation of the C_{cert}
P	Probability equals the total area under two curves of density function
C_1, C_2	The mass fractions of the element, at which the density function curves cross
f_{cert}, f_r	Respectively, density functions of RM certification data and experiment results for accuracy validation of a technique
π	Constant ($=3.14\ldots$)
ϕ	Function of normalized normal distribution
ρ	See formula (4)
H_0	Null hypotheses
$H_1 (H_{11}$ *etc.*)	Alternative hypotheses
U, t, χ^2	Respectively, quantiles of normal, Student's and chi-square distributions
γ	σ_{cert}/σ_r;
α, β	Probabilities of errors
P_a	Power of criterion for accuracy validation
λ	See formula (17)

Talanta, Vol. 40, No. 1, pp. 9–15, 1993
Printed in Great Britain.

0039-9140/93 $6.00 + 0.00

DETERMINATION OF TRACES OF RARE EARTH ELEMENTS IN GEOLOGICAL SAMPLES

EVA BAUER-WOLF, WOLFHARD WEGSCHEIDER, SONJA POSCH and GÜNTER KNAPP
Institute for Analytical Chemistry, Micro- and Radiochemistry, Graz University of Technology, Technikerstraße 4, A-8010-Graz, Austria

HANS KOLMER
Institute for Engineering Geology and Applied Mineralogy

FRANZ PANHOLZER
Institute for Inorganic Chemical Technology

(*Received* 25 *November* 1991. *Revised* 7 *May* 1992. *Accepted* 6 *May* 1992)

Summary—A procedure for the determination of traces of rare earth elements by inductively coupled plasma–optical emission spectrometry (ICP–OES) and X-ray fluorescence spectrometry (XRF) is presented. The samples are decomposed either by fusion with lithium tetraborate or by acid attack in a microwave oven. Separation of the rare earth elements from accompanying elements is achieved by anion exchange. For the determination by ICP–OES the samples are injected in hydrochloric acid solution, for the determination by XRF the rare earth element traces are co-precipitated with rhodizonate and tannin and measured as a thin film on a membrane filter. All preconcentration steps have been optimized and tested using radiotracers. Furthermore the rare earth element contents of some international standard reference rocks have been determined; the results are compared to the certified values and other values given in the literature. The procedure is applied to a series of petrographically identical metabasites with different degrees of metamorphism to show the mobility of those ions under metamorphic conditions.

In spite of their similar chemical behaviour the rare earth elements may be fractionated during mineralogical and petrological processes. This fractionation arises from different types and volumes of coordination polyhedra that can be formed and is also due to the fact that some of the elements, especially cerium and europium, occur in oxidation states other than +III, the main oxidation state of the group. The type and degree of fractionation can therefore be an indicator of the genesis of a rock and give hints for processes like partial melting, fractional crystallization or mixing of magmas as far as igneous rocks are concerned.[1]

For many years most of the rare earth element determinations in geological samples have been carried out by neutron activation analysis.[2,3] This method offers low detection limits and can sometimes be applied without sample preparation but the need for a suitable reactor and long cooling times prior to the determination are disadvantageous. Some other techniques usually applied to the determination of rare earth element traces are inductively coupled plasma optical emission spectrometry (ICP–OES),[4–6] stable isotope dilution–mass spectrometry[7] and to a minor extent X-ray fluorescence spectrometry (XRF).[8,9] For each of these techniques at least a group separation of the rare earth elements from accompanying elements is required.

The aim of this work was to develop a procedure that allows the determination of rare earth element traces by XRF and ICP–OES. Important characteristics of the new preconcentration procedure are high reliability, corrections for too low recoveries are not necessary, and reproducibility. The elution volumes for preconcentration by anion exchange are smaller than those of comparable cation exchange procedures.[10]

EXPERIMENTAL

Reagents and reference materials

For decomposition by fusion Spectromelt A 10 (lithium tetraborate, Merck) is used. Decomposition by microwave heating is done

using HF (40%), HNO_3 (68%) and HCl (33%); in the separation procedure HCl, HNO_3, acetic acid (100%) and propanol-2 are used. The ion exchange steps are carried out on strongly basic anion exchange resin Dowex 1 × 8, 100–200 mesh. For the mixed solvent anion exchange the resin is in the nitrate form, for the separation of iron it is used in the chloride form. The pH for the co-precipitation is adjusted by addition of sodium hydroxide. Sodium rhodizonate and tannin are dissolved in water to give solutions of 2.5 and 2.0 mg/ml, respectively. The precipitate is collected on Millipore membrane filters HVLP 01300. All reagents except tannin and rhodizonate are of analytical grade. Stock solutions of the rare earth elements are prepared from the oxides (99.99%, Johnson Matthey). The procedure has been optimized using the following radiotracers: ^{139}Ce, ^{152}Eu, ^{153}Gd, ^{169}Yb and ^{59}Fe.

The procedure has been tested by analyzing samples of the following standard reference rocks: NIM-G granite, NIM-S syenite, NIM-L lujavrite, NIM-N norite (National Institute of Metallurgy, South Africa), USGS AGV-1 andesite (US Geological Survey).

Apparatus

Decomposition by fusion is done in platinum crucibles in a muffle furnace. For the decomposition assisted by microwave heating a microwave system with pressure resistant vessels and an optical pressure control (Anton Paar, Graz) is used. The beaker and the pressure containment are schematically shown in Fig. 1.

The filtrations are carried out in a previously described vessel[12] that permits the simultaneous filtration of five solutions under nitrogen pressure. For the anion exchange procedure a peristaltic pump Ismatec ip-12 is used.

A γ-spectrometer (E & G Ortec) has been used to determine the count rates for the radiotracer experiments.

X-ray spectrometry. For nearly all measurements a wavelength dispersive spectrometer Philips PW 1410 with a gold tube operated at 60 kV and 40 mA and a flow counter is used. This system is equipped with an automation unit (Dapple Inc., Sunnyvale) to drive the goniometer, set the discriminator and acquire the data. Further measurements are done using a wavelength dispersive spectrometer Philips PW 1140 with tandem operation of flow counter and scintillation counter and a tungsten tube. At an earlier stage some measurements with an energy dispersive spectrometer Philips EDAX Exam VI with zirconium secondary target and a Si(Li)-detector have been done.

For the determination by ICP–OES a sequential spectrometer Perkin Elmer Plasma II (range 170–440 nm) with a cross flow nebulizer is used.

Sample preparation

A schematic overview of the procedure is given in Fig. 2. Each step of this sample preparation scheme has been optimized using

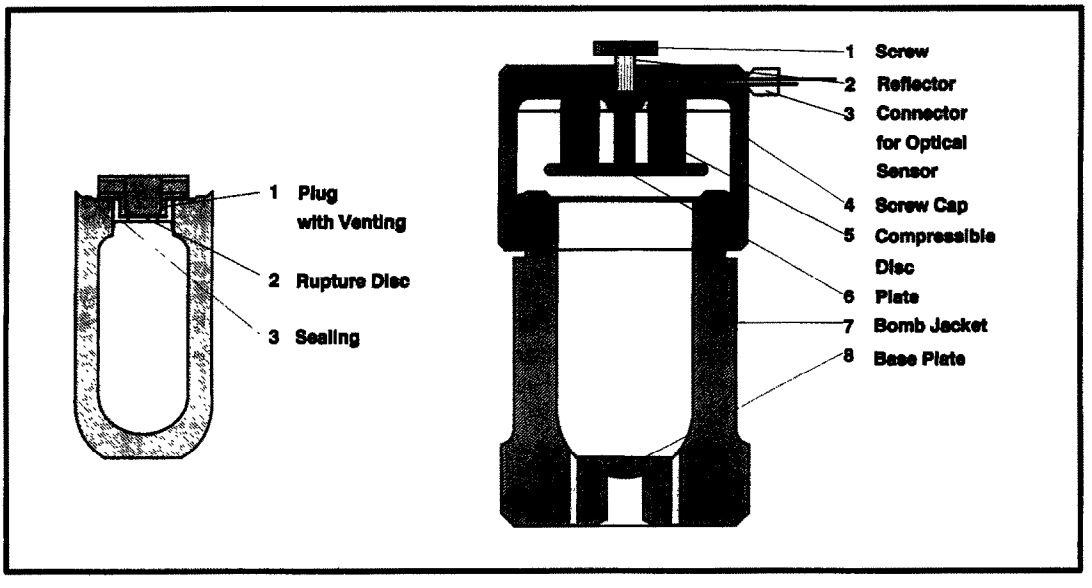

Fig. 1. Pressure resistant beaker and pressure containment.

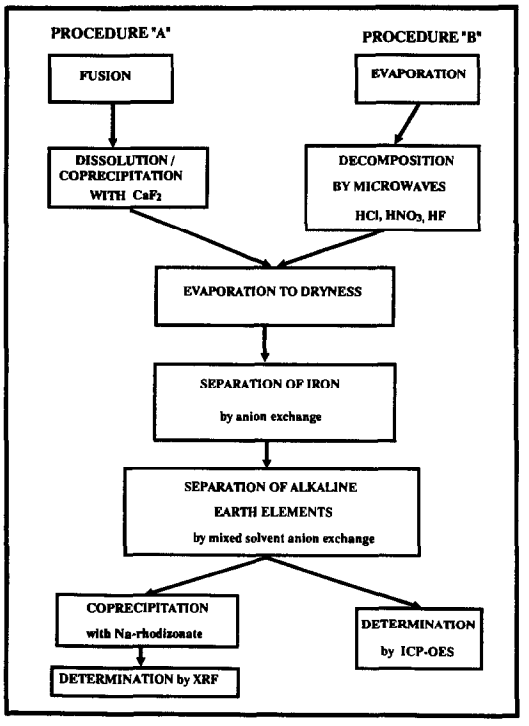

Fig. 2. Analytical procedure.

radiotracers for some of the rare earth elements, those results will be given below.

Decomposition

During our work we tested two decomposition procedures; samples were decomposed by fusion or by microwave heating in a pressure resistant vessel.

For the decomposition by fusion the samples are mixed with the five-fold mass of lithium tetraborate in platinum crucibles, which are put into a muffle furnace and kept at a temperature of 1000° for one hour. The melt is dissolved in HF and HNO_3. To volatilize silicium and part of the boron in the form of their fluorides around 30 ml of HF—added in five portions—and 10 ml of HNO_3 are used. Under these conditions the alkaline earth elements form fluoride precipitates, the rare earth elements are coprecipitated and a first separation can be achieved by centrifugation. Elements that tend to form fluoride complexes like zirconium and titanium can be separated at that stage.

For decomposition by microwave heating the samples (approximately 0.25 g) are weighed into the beaker and taken to dryness with 2 ml of HF once to avoid deposits of silica near the plug during the decomposition. Then HNO_3 (1.5 ml), HCl (0.5 ml) and HF (0.5 ml) are added, the beaker is closed, put into the pressure containment and put into the oven. The samples are decomposed at a pressure of approximately 30 bar for 10 min (setting #8 of 10 in the microwave oven). After cooling down the samples are transferred to teflon beakers and treated according to the preconcentration scheme.

If the samples are decomposed by fusion with lithium tetraborate prior to preconcentration, the procedure is referred to as procedure A in the following text, if the samples are decomposed by microwave heating, then they are referred to as procedure B.

Preconcentration

The volumes given in the following sections corresponds to procedure B and samples of 0.25 g.

To remove fluoride the samples are taken to dryness with hydrochloric acid (3 ml) and nitric acid (3 ml) several times and the residue is taken up in 10 ml of 5*M* hydrochloric acid. From this solution iron is removed in the form of its chloride complexes on anion exchange columns (10 mm in diameter, height: 6 mm; washings: 20 ml of 5*M* hydrochloric acid. The solution containing the rare earth elements is taken to dryness, the residue is taken up in approximately 4 ml of 5.8*M* nitric acid.

The removal of alkaline earth elements and other accompanying elements is achieved by mixed solvent anion exchange[11] from acetic acid/nitric acid (90 + 10, v/v) media. The rare earth ions are retained on anion exchange columns while the alkaline earth ions pass through. The columns are washed with 40 ml of 5.8*M* nitric acid propanol-2 (10 + 90 v/v) to remove residual alkaline earth elements, then the rare earth elements are eluted with 15 ml of 5*M* hydrochloric acid.

After heating for the removal of alcohol and cooling down again the solution is transferred to a standard flask.

To produce a sample well suited for X-ray fluorescence measurements the rare earth elements are finally coprecipitated with rhodizonate and tannin at pH 13 (pH adjusted by addition of sodium hydroxide). The precipitate is collected on membrane filters which are mounted on Spectrocups for the measurement.

Determination by X-ray fluorescence spectrometry

$L\alpha_1$-lines are measured for all the rare earth elements with the exception of praseodymium

Table 1. Detection limits for the determination by wavelength dispersive XRF

Element	Detection limit (μg)
La	0.8
Ce	0.7
Pr	0.6
Nd	0.6
Sm	0.6
Eu	0.3
Gd	0.3
Tb	0.2
Dy	0.2
Ho	0.2
Er	0.2
Tm	0.2
Yb	0.2
Lu	0.2

Conditions: PW 1410, Autube, 60 kV, 40 mA, fine collimator, flow counter, vacuum.

Table 2. Detection limits for the determination by ICP–OES (μg/ml)
Procedure A

Element	Wavelength (nm)	Blank	5*M* HCl
La	398.852	0.016	0.011
Ce	413.380	0.028	0.027
Ce	413.765	0.033	0.030
Ce	418.660	0.029	0.028
Pr	422.535	0.046	0.042
Nd	394.151	0.168	0.045
Nd	430.358	0.030	0.029
Sm	428.079	0.081	0.080
Eu	412.967	0.003	0.003
Gd	335.047	0.012	0.011
Tb	350.917	0.013	0.013
Dy	353.602	0.014	0.014
Ho	381.073	0.017	0.016
Er	390.631	0.012	0.009
Tm	313.126	0.033	0.033
Yb	328.937	0.0005	0.0005
Lu	261.542	0.0006	0.0006

Experimental conditions: Power 1200 W, plasma flow 15 l./min, neublizer flow 1 l./min, photomultiplier voltage 600 V, sampling time 50 msec.
The blank solution contains some Li-tetraborate.

($L\beta_1$). For iron, manganese and nickel, where some blank values occurred, the Kα-lines are measured. A calibration set consisting of 20 different compositions in the expected concentration range was prepared from stock solutions according to an experimental design by precipitation with rhodizonate. Overlap coefficients were derived from those samples, furthermore absorption corrections in the Delta-I mode were applied to samples with high concentrations of La, Ce and Nd. The detection limits (3 s) are listed in Table 1.

Determination by ICP–OES

First, single element standard solutions have been used to detect line interferences. The different concentration ranges of the rare earth elements in rock samples have been taken into account. The lines chosen for the determination and the corresponding limits of detection (3 s) are listed in Table 2. The values were estimated from data for a blank solution from pure lithium tetraborate treated according to procedure A. The values for 5*M* hydrochloric acid are given there, too. For gadolinium the spectral line has to be changed to 358.496 nm when the samples are prepared according to scheme B, because titanium and zirconium are not removed and lead to a line interference of Ti at 335.047 nm.

RESULTS AND DISCUSSION

As the rare earth elements can often be enriched in minerals that are hardly attacked by acids at normal pressure (*e.g.*, zircon) the complete decomposition of the samples is most important. We used two procedures, fusion with tetraborate of acid attack at 30 bars in a microwave oven. Both methods have been successfully applied to zircon bearing granitic standard reference materials but there are still some differences that must be taken into account: there is no limitation of the sample mass if the sample is fused with lithium tetraborate but a large amount of "salt" is imported to the sample. Therefore solution volumes and time consumption in the following preconcentration steps are higher compared to the samples decomposed by microwave heating. On the other hand the decomposition by microwave heating is limited to sample masses of up to 0.3–0.4 g leading to detection problems if the rare earth element content of the samples is low. To reduce the problem due to the high salt content after decomposition by fusion coprecipitation with calcium fluoride has been introduced to the procedure. This coprecipitation is incomplete up to calcium concentrations of 0.7%, the recoveries for higher calcium contents (that means 1% Ca in the test samples) have been determined in tracer experiments and are listed in Table 3, column 1.

The group separation of the rare earth elements is achieved by mixed solvent anion exchange. Although the recoveries for propanol-2 (recovery: 96.8% for 90% organic phase in a batch experiment) are higher, acetic

Table 3. Recoveries for each preconcentration step

Tracer	R1	R2	R3	R4	R5
Ce	99.6 ± 0.8	100.2 ± 1.6	97.6 ± 0.8	101.1 ± 1.5	97.8 ± 3.8
Eu	99.3 ± 0.5	99.6 ± 2.8	97.8 ± 2.0	99.8 ± 2.4	98.3 ± 2.0
Gd	100.4 ± 0.4	101.4 ± 2.0	99.6 ± 0.6	102.4 ± 2.7	98.0 ± 2.0
Yb	98.7 ± 0.6	97.8 ± 3.8	—	101.1 ± 1.7	97.2 ± 3.8
Fe	—	18.3 ± 3.2	—	—	—
Number	24	10	10	10	5

Definitions: R1: Coprecipitation of rare earth elements with calcium fluoride. R2: Preconcentration by mixed solvent anion exchange from propanol-2/HNO_3. R3: Preconcentration by mixed solvent anion exchange (acetic acid/HNO_3, washings: propanol-2/HNO_3; the recovery for Yb is missing because the activity of our standard was already too low when we started these experiments. R4: Separation of iron. R5: Coprecipitation with sodium rhodizonate and tannin. —: no data. Number: Number of experiments.

acid (recovery 87.6% under similar conditions) was chosen for the preconcentration procedure because the residues of the former preconcentration steps are more readily dissolved in this solution. In the washings propanol-2 was used as organic phase. Table 3, column 3 shows the recoveries for some of the rare earth elements for this preconcentration step.

Iron could not be removed quantitatively by mixed solvent anion exchange, therefore a second ion exchange step has been introduced. Figure 3 shows the elution profile for Eu (fractions 1–20, 5*M* hydrochloric acid) and Fe (fractions 21–27, 0.6*M* nitric acid), the recoveries for the rare earth elements are given in Table 3, column 4.

It is advantageous to present samples in the solid form if small concentrations are to be determined by XRF. In addition, the geometry has to be kept constant. Therefore a coprecipitation of the rare earth element traces with an organic complexing agent was taken into consideration. Best results were achieved with sodium rhodizonate and tannin at pH 13; the recoveries that have been determined from tracer experiments are given in Table 3, column 5. For samples containing more than approximately 100 μg rare earth elements in total an absorption correction was applied.

Finally, procedure A has been tested with rock samples spiked with radiotracers to estimate an overall recovery which is given in Table 4. The variances given there are much smaller than the sum of the variances of the single preconcentration steps. One reason is that the measured standard deviation always includes the counting statistics, in addition the activities used for spiking the rock samples have been higher than those used for the other experiments. To test the decomposition and preconcentration procedure as well as the model used for calculating the rare earth element concentrations from X-ray intensities the rare earth element contents of some international standard reference rocks have been determined. Some of the results are listed in Tables 5–8. In general the agreement between certified and measured concentrations appears to be satisfactory although there are some difficulties to take into account the influence of manganese on dysprosium when calculating the concentrations from X-ray intensities (*e.g.*, for NIM-G, Table 5).

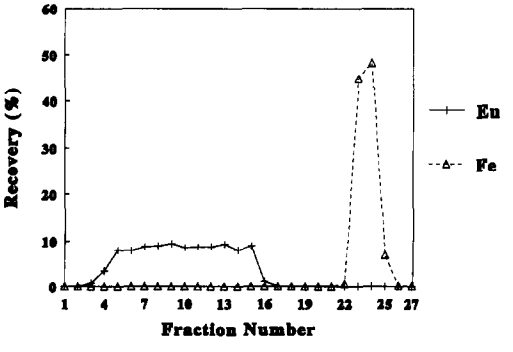

Fig. 3. Separation of iron. Fractions 1–20:1 ml hydrochloric acid 5*M*. Fractions 21–27:5 ml HNO3 0.6 mol/l.

Table 4. Recoveries for the complete procedure

Element	Recovery (%)	Standard deviation (%)
Ce	97.8	2.9
Eu	95.1	1.7
Gd	96.2	3.9

Number of experiments: 5.

Table 5. Data for standard reference materials: NIM-G, granite The concentrations are given in μg/g

Element	Concentrations given by NIM (from ref. 16)	Procedure A XRF	Procedure A ICP–OES	Procedure B ICP–OES
La	109*	104 ± 4	110 ± 2	108 ± 2
Ce	195*	182 ± 9	190 ± 4	183 ± 2
Pr		20 ± 3	22 ± 1	21 ± 1
Nd	72*	69 ± 6	74 ± 3	65 ± 3
Sm	15.8*	16.0 ± 3	13.4 ± 0.8	13 ± 1
Eu	0.35*	0.3 ± 0.2	0.34 ± 0.03	0.37 ± 0.06
Gd	14	15 ± 2	13.5 ± 0.9	12.4 ± 0.3
Tb	3.0*	2.8 ± 0.4	2.6 ± 0.2	2.1 ± 0.4
Dy	17	11 ± 2	18.4 ± 0.8	15.6 ± 0.6
Ho		3.6 ± 0.5	3.2 ± 0.1	3.3 ± 0.2
Er		13.0 ± 0.5	12.5 ± 0.7	10.5 ± 0.2
Tm	2	1.6 ± 0.4	1.6 ± 0.2	1.6 ± 0.2
Yb	14.2*	10.4 ± 2	12.7 ± 1.3	11.2 ± 0.4
Lu	2	1.6 ± 0.3	1.9 ± 0.2	1.62 ± 0.04
		N = 3	N = 4	N = 5

Definition: *Certified value. NIM National Institute for Metallurgy (South Africa).

Application

The analytical procedure presented within the previous sections is applied to rock samples from the complex of the Saualpe in Carinthia (Austria). The metabasites of this crystalline massif show different degrees of metamorphism (from weakly metamorphic spilites to amphibole-eclogite).[14,15] Those rocks are well suited for studies of the mobility of ions under metamorphic conditions. Some results presented in the literature indicate conservative metamorphosis but other results point to a progressive "homogenization". The determination of the rare earth element concentrations is supposed to give valuable further information.

Our first results indicate that there is no single "rare earth element pattern" characterizing all the samples we analyzed but there are some groups of samples with similar rare earth element contents. Figure 4 shows the rare earth element pattern for two different samples to give an example; as usual in geochemistry they are presented as chondrite normalized plots, but we abstain at this place from any geochemical interpretation.

By way of concluding it can be stated that both methodological variants described in

Table 6. Data for standard reference materials: NIM-S, syenite. The concentrations are given in μg/g, the presented values are means of three samples

Element	Concentrations given by NIM (from ref. 16)	Procedure A XRF	Procedure A ICP–OES
La	5	5.8 ± 0.4	5.5 ± 0.3
Ce	11.9*	12.0 ± 2	9.5 ± 0.9
Pr		1.5 ± 0.3	1.7 ± 0.3
Nd	6	5.4 ± 0.2	6.3 ± 1
Sm	1	1.4 ± 0.2	1.5 ± 0.1
Eu	0.30*	0.5 ± 0.2	0.24 ± 0.00
Gd		0.9 ± 0.3	0.87 ± 0.1
Tb		<0.2	<0.19
Dy	0.4	0.4 ± 0.1	0.37 ± 0.03
Ho		<0.2	<0.25
Er		<0.2	0.12 ± 0.02
Tm		<0.2	<0.5
Yb	0.07	<0.2	0.12 ± 0.01
Lu		<0.2	0.01†

*Certified value.
†Just slightly above detection limit.

Table 7. Data for standard reference materials: NIM-N, norite. The concentrations are given in μg/g

Element	Concentrations given by NIM (from ref. 16)	Procedure A XRF	Procedure A ICP–OES
La	3	2.4 ± 1	3.9 ± 0.1
Ce	6	7.3 ± 3	5.0 ± 0.7
Pr		0.7 ± 0.3	0.7 ± 0.1
Nd	3	2.0 ± 0.6	3.1 ± 0.3
Sm	0.8	0.8 ± 0.2	<1.2
Eu	0.63*	0.5 ± 0.2	0.52 ± 0.15
Gd		0.6 ± 0.2	0.98 ± 0.1
Tb		<0.2	<0.19
Dy		1.3 ± 0.2	1.12 ± 0.2
Ho		<0.2	<0.25
Er		0.5 ± 0.2	0.71 ± 0.08
Tm		<0.2	<0.5
Yb	0.7	0.6 ± 0.2	0.71 ± 0.06
Lu	0.2	0.3 ± 0.1	0.17 ± 0.05

Number of samples: XRF: 3. ICP–OES: 4. *Certified value.

Table 8. Data for standard reference materials sample preparation: procedure B. Concentrations are given in μg/g

	NIM-L lujavrite		AGV-1 andesite	
Element	ICP–OES	From ref. 13	ICP–OES	From ref. 13
La	288 ± 8	250	40 ± 4	38
Ce	257 ± 7	240	61 ± 4	67
Pr	16.8 ± 0.7		8 ± 1	7.6
Nd	45 ± 1	48	33 ± 1	33
Sm	3.1 ± 0.2	5	4.9 ± 0.6	5.9
Eu	1.00 ± 0.08	1.2	1.4 ± 0.1	1.64
Gd	4.4 ± 0.5		5.6 ± 0.7	5.0
Tb	<0.5		0.46*	
Dy	2.6 ± 0.3		3.1 ± 0.4	3.6
Ho	<0.7		1.0 ± 0.1	0.67
Er	2.23 ± 0.04		1.6 ± 0.1	1.7
Tm	<1.3		<0.9	
Yb	2.7 ± 0.1	3	1.6 ± 0.2	1.72
Lu	0.53 ± 0.06	0.4	0.25 ± 0.02	0.27

*Just slightly above the detection limit.
Number of samples: The presented concentrations are the means of three samples.

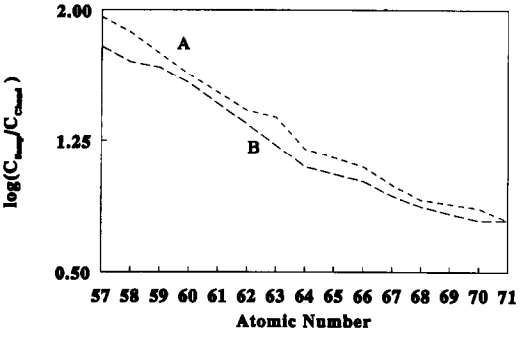

Fig. 4. Chondrite-normalized rare earth element concentrations for two samples from the Saualpe. A, sample A; B, sample B.

this work are feasible. Although the X-ray fluorescence procedure has proved reliable, the additional precipitation step and the higher detection limit at least on the currently used X-ray spectrometer have made this variant somewhat less desirable compared to ICP–OES measurements.

Acknowledgements—This work has been supported in part by projects P 5200 and P 7115 from the Fonds zur Förderung der wissenschaftlichen Forschung, Vienna.

REFERENCES

1. P. Henderson, *General Geochemical Properties and Abundances of the Rare Earth Elements*, in *Rare Earth Element Geochemistry*, P. Henderson (ed.), Developments in Geochemistry **2**, 1, Elsevier, Amsterdam, 1984.
2. P. Voldet, *Trends in Anal. Chem.* 1982, **1**, 262.
3. J. E. Whitley, *Proc. Analyt. Div. Chem. Soc.*, 1982, 120.
4. K. E. Jarvis and I. Jarvis, *Geostand. Newslett.*, 1988, **12**, 1.
5. K. Govindaraju and G. Mevelle, *J. Anal. Atom. Spectrom.*, 1987, **2**, 615.
6. J. G. Crock and F. Lichte, *Anal. Chem.*, 1982, **54**, 1329.
7. P. J. Hooker, R. K. O'Nions and R. J. Pankhurst, *Chem. Geol.*, 1975, **16**, 189.
8. Hou Qing-Lie, T. C. Hughes, Maunu Honkka and P. Hannaker, *Talanta*, 1985, **32**, 495.
9. I. Roelandts, *Anal. Chem.*, 1981, **53**, 676.
10. J. Erzinger, in, *Instrumentelle Multielementanalyse*, B. Sansoni (ed.), VCH, Weinheim, 1985.
11. J. Korkisch, *Modern Methods for the Separation of Rarer Metal Ions*, Pergamon Press, 1969.
12. S. E. Raptis, W. Wegscheider, G. Knapp and G. Tölg, *Anal. Chem.*, 1980, **52**, 1292.
13. K. Govindaraju, *Geostand. Newslett.*, 1989, **13**, 1.
14. C. K. W. Lodemann, *N. Jb. Miner. Abh.*, 1973, **118**, 134.
15. *Idem, ibid.*, 1970, **112**, 188.
16. R. G. Hansen and E. J. Ring, *Geostand. Newslett.*, 1985, **9**, 233.

Talanta, Vol. 40, No. 1, pp. 17–20, 1993
Printed in Great Britain.

0039-9140/93 $6.00 + 0.00

SPECTROFLUORIMETRIC DETERMINATION OF ZINC IN FOODS WITH 8-(*p*-TOLUENESULPHONAMIDO)QUINOLINE IN MICELLAR MEDIUM

M. FALCON, J. GUITERAS, A. IZQUIERDO and M. D. PRAT
Departament de Química Analítica, Universitat de Barcelona, Avda. Diagonal 647, Barcelona 08028, Spain

(*Received* 10 *February* 1992. *Revised* 11 *May* 1992. *Accepted* 11 *May* 1992)

Summary—A new method for the spectrofluorimetric determination of zinc with 8-(*p*-toluenesulphonamido)quinoline in a Brij-35 micellar medium has been developed. This method allows the determination of 8–550 ng/ml Zn(II) and is relatively free from interferences. It has been applied to food samples with satisfactory results.

The use of 8-(*p*-toluenesulphonamido)quinoline [Fig. 1(a)] as a reagent for the spectrofluorimetric determination of Zn(II) and Cd(II) was first described in 1959 by Bozhevol'nov *et al.*[1] in a paper stating that 0.1 μg of Zn(II) could be detected in 5 ml of solution at pH 8.0–8.3, and that this sensitivity could be increased to 0.01 μg/ml after extraction of the complex into $CHCl_3$. Later papers confirmed these data and also indicated that Al(III) had little interference.[2,3] In 1962, Shcherbov and Kolmogorova[4] used this reagent to determine zinc in iron ores, with an absolute error of 15–25%. The use of 8-(*p*-toluenesulphonamido)quinoline as a spectrofluorimetric reagent was also reported by Bozhevol'nov and co-workers,[5–7] which gave a 2:1 stoichiometry for the TSQ:Zn complex [Fig. 1(b)].

The use of surfactant agents can increase the stability and solubility of many organic compounds and metal complexes in water and, when these are fluorescent, a marked increase in fluorescence intensity can frequently be observed. For this reason the use of surfactant agents can improve many existing spectrofluorimetric methods by increasing their sensitivity and/or eliminating the need for extraction procedures or the use of mixed hydroorganic solvents.[8–12]

In this paper, the influence of several surfactant agents (anionic, cationic and non-ionic) on the fluorescence of the complex of Zn(II) with 8-(*p*-toluenesulphonamido)quinoline has been studied and a new method for the spectrofluorimetric determination of zinc is proposed. This method has the advantage of a better detection limit than flame AAS and has been successfully used for the determination of zinc in natural samples.

EXPERIMENTAL

Apparatus

Perkin–Elmer MPF-66 fluorescence spectrophotometer with 150 W Xenon lamp and 10-mm silica cells. Excitation and emission slits were both set at either 2 nm or 4 nm, depending on the concentration of Zn(II). All spectra and intensities were corrected against Rodamine B.

Perkin Elmer 1100B atomic absorption spectrometer.

Radiometer pHM64 pHMeter with Orion 8102 SC combination electrode. It was standardized against aqueous buffer solutions at pH 4.008 and pH 6.863 at 25°C (DIN 19266).

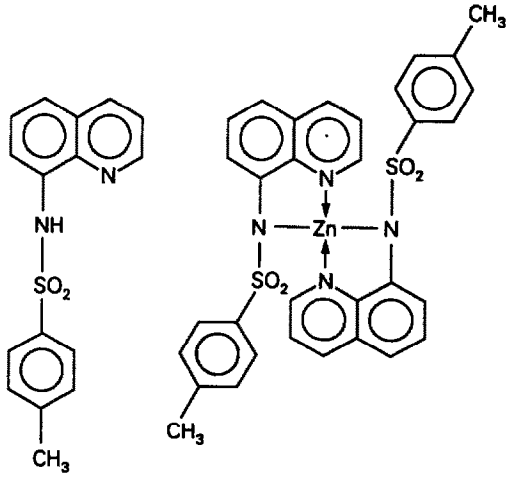

Fig. 1. Structures of (a) TSQ (b) TSQ–Zn complex.

All glassware was previously soaked in 10% nitric acid for 24 hours and rinsed with doubly distilled water (Culligan Ultrapure).

Reagents

8-(*p*-toluenesulphonamido)quinoline (TSQ) was synthesized following the method of Billman and Chernin,[13] by reaction of 8-aminoquinoline with *p*-toluenesulphonylchloride in pyridine. The product was recrystallized from ethanol as white needles. The melting point (153–154°) was in good agreement with literature values. Elementary analysis also agreed with theoretical values. (Calculated for $C_{16}H_{14}N_2O_2S$: C:64.41%; H:4.73%; N:9.39%; S:10.75%. Found: C:64.45%; H:4.68%; N:9.41%; S:10.80%.).

TSQ stock solution ($8.5 \times 10^{-3}M$) in ethanol was used.

Buffer solutions were prepared with R.A.-grade succinic acid–NaOH, Na_2HPO_4–KH_2PO_4, tris(hydroxymethyl)amminomethane–HCl and glycine. After the optimum pH range was selected, all further work was carried out in a $0.4M$ tris–HCl buffer.

Zinc stock solution, approximately 1 g/l., was prepared by dissolving about 4 g of $Zn(NO_3)_2.4H_2O$ (Merck, p.a.) in 1 l. of water and was standardized against EDTA.

Surfactant solutions. Stock solutions of the following surfactant agents were prepared: sodium dodecylsulphate (SDS) (Merck, $0.61M$, 75 cmc), polyoxyethylenedodecylether (Brij-35) (Scharlau, $1.8 \times 10^{-2}M$, 200 cmc), and hexadecyltrimethylammonium bromide (HTAB) (Merck, $9.2 \times 10^{-2}M$, 100 cmc).

Organic solvents (ethanol, dimethylketone and dioxane) were Merck p.a. and were used without further purification.

Doubly distilled water (Culligan Ultrapure GS) of 18.3 MΩ/cm resistivity was used in all cases.

General procedure

Into 25-ml standard flasks add 2 ml of buffer solution, the required volume of zinc solution, 2.5 ml of surfactant solution, 0.5 ml of $8 \times 10^{-3}M$ TSQ in ethanol and dilute to volume with distilled water.

RESULTS AND DISCUSSION

Effect of surfactants

In Fig. 2 the emission spectra of the Zn–TSQ complex in the presence of different surfactant agents (SDS, Brij-35 and HTAB) are represented. For comparison purposes, the spectra of the same complex in ethanol–water, dimethylketone–water and dioxane–water mixtures are also represented. Fluorescence intensities are higher in solutions containing non-ionic (Brij-35) or anionic (SDS) surfactants than in those containing cationic surfactants (HTAB) or the mixed hydroorganic solutions. Wavelengths for the excitation and emission maxima are similar in all tested media.

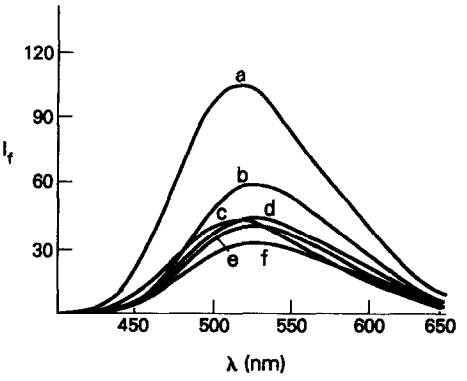

Fig. 2. Emission spectra of the Zn–TSQ complex in (a) 20 × cmc Brij-35 (b) 20 × cmc Sodium dodecylsulphate (c) 20 × cmc HTAB (d) 30% (v/v) ethanol/water (e) 30% (v/v) dimethylketone/water (f) 30% (v/v) dioxane/water.

The highest emission intensities are obtained in the presence of non-ionic surfactants, and for this reason all further research has been carried out in a Brij-35 micellar medium.

Effect of pH

In Fig. 3 the fluorescence intensity of the Zn–TSQ complex *vs.* pH in a Brij-35 micellar medium is plotted. Intensity does not depend on pH in the range 7.0–8.7.

Effect of surfactant concentration

For solutions containing less than 100 ng/ml Zn(II), the intensity is independent of surfactant

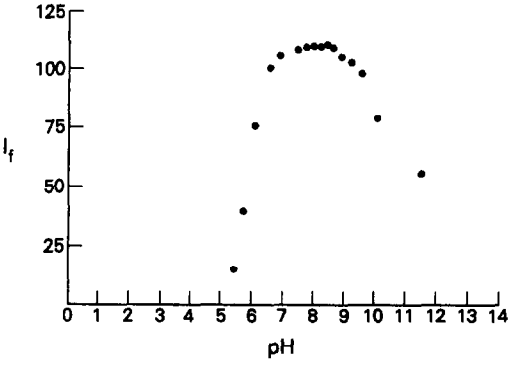

Fig. 3. Effect of pH on the fluorescence intensity of the Zn–TSQ complex in a Brij-35 micellar medium.

concentration when this is higher than $9.0 \times 10^{-5}M$ (about the critical micellar concentration). However, surfactant concentration should be higher than this value if zinc concentration is relatively high, to prevent precipitation of the Zn–TSQ complex, which has a low solubility in water. In further experiments Brij-35 concentration has been $1.8 \times 10^{-3}M$ (20-fold cmc).

Effect of reagent concentration

Fluorescence intensity increases with increasing TSQ concentration until the TSQ/Zn molar ratio reaches a value of 20. Higher TSQ concentrations have no significant influence.

Effect of ethanol concentration

The influence of ethanol on the fluorescence intensity of the Zn–TSQ complex has been investigated because TSQ is used in ethanolic solution. Fluorescence intensity decreases slightly when ethanol concentration is increased from 0.4% v/v (minimum possible concentration, corresponding to 0.1 ml of ethanolic TSQ solution) to 12%. In further experiments, ethanol concentration has been 2% v/v.

Stability of the complex

Fluorescence intensity reaches a maximum in a few seconds and remains constant for over two hours.

Order of mixing

The order in which reagent, surfactant, metal ion and buffer solutions are mixed has no influence on fluorescence intensity. However, in some cases a precipitate may appear. It dissolves readily when the surfactant is added, but in order to avoid this the recommended order of mixing is as follows: buffer, zinc, surfactant and reagent solutions.

Optimum working conditions

The conditions for the determination of zinc with TSQ in Brij-35 micellar medium are as follows:

excitation wavelength: 367.2 nm
emission wavelength: 515.4 nm
pH: 7.0–8.7
[TSQ] > $2.3 \times 10^{-5}M$
[Brij-35] > $1.8 \times 10^{-3}M$ (20 cmc).

Analytical characteristics

Calibration graphs are linear in the range 8–200 ng/ml Zn (excitation and emission slits set at 4 nm, [TSQ] = $3.8 \times 10^{-5}M$, $r = 0.9999$) and 70–550 ng/ml Zn (excitation and emission slits set at 2 nm, [TSQ] = $2.1 \times 10^{-4}M$, $r = 0.9991$). These two ranges have been selected because a low TSQ concentration has the advantage of a lower reagent background blank, but it is necessary to increase reagent concentration at greater zinc concentrations in order to keep the required TSQ/Zn molar ratio.

The detection limit, calculated from $3s$ (where s is the standard deviation of the blank) ($n = 15$) is 3 ng/ml Zn. Quantification limit, calculated from $10s$ ($n = 15$) is 8.0 ng/ml Zn. The precision of the method has been determined at two different zinc concentrations. Relative standard deviations are 2.4% for 25 ng/ml Zn and 1.9% for 150 ng/ml Zn.

Interferences

The effect of several ions on the fluorescence intensity of the Zn–TSQ complex has been investigated. An ion is considered to be an interference if its presence produces greater than a 5% change in fluorescence intensity. The investigated ions and the maximum concentration at which they do not interfere are listed in Table 1. It should be mentioned that Al(III) and Fe(III) have little influence and can be tolerated in relatively high concentrations.

Table 1. Concentration ratio of foreign ions that produce a greater than 5% change in the fluorescence intensity of Zn–TSQ complex

$[Zn^{2+}] = 74$ ng/ml Interfering ion	[Brij-35] = 20 × cmc pH = 8.5 [Interfering ion]/[Zn^{2+}]
Na^+	>20,000
K^+	>20,000
Ca^{2+}	>1,000
Ba^{2+}	>1,000
NH_4^+	>1,000
B^{3+}	1,000
Li^+	900
Al^{3+}	200
Mg^{2+}	150
Pb^{2+}, Be^{2+}	100
Mn^{2+}	80
Fe^{3+}, Ga^{3+}	50
Hg^{2+}	20
Fe^{2+}	15
Cu^{2+}	5 (100)*
Co^{2+}, Ni^{2+}	4
Cd^{2+}	0.2 (2.5)†
ClO_4^-	>20,000
Cl^-	>20,000
PO_4^{3-}	10,000
Br^-	1,000
I^-	1,000

*In a solution containing $Na_2S_2O_3$.
†In a solution containing $Na_2P_2O_7$.

Table 2.

	Spectrofluorimetric method, μg/g	AAS, μg/g	Certified value, μg/g
Powdered milk (commercial brand)	43.4 ± 1.0*	42.9 ± 1.2*	—
Powdered milk (NBS SRM-1549)	47.3 ± 1.1*	—	46.2 ± 2.2
Tinned clams	10.9 ± 0.6*	11.0 ± 1.2*	—

*Mean of six independent determinations.

APPLICATION

The proposed method has been used for the determination of zinc in two different samples of powdered milk (one of them of a commercial brand, the other a NBS standard) and in commercial tinned clams. In the commercial samples, results have been confirmed by atomic absorption spectroscopy. In all cases the method of standard addition was employed.

Procedure

The required amount of sample (0.5 g of powdered milk or 2–3 g of drained, tritured clams) was mineralized in a Kjeldahl flask with a H_2SO_4–HNO_3 mixture. Most of the acid was then neutralized with sodium hydroxide, the solution was transferred to a 100-ml calibrated flask and diluted to volume with water.

For spectrofluorimetric determinations, 10-ml aliquots of this sample solution were added into five 25-ml calibrated flasks, which contained 2.5 ml of pH 8.2 tris–HCl buffer solution, 2.5 ml of 200 cmc Brij-35 solution, 0.5 ml of $4 \times 10^{-3}M$ TSQ solution, 2.5 ml of $0.5M$ sodium thiosulphate solution, 1.0 ml of $10^{-3}M$ $Na_2P_2O_7$ solution and different volumes of standard zinc solution, and diluted to volume. Fluorescence intensities were measured against blanks via the same procedure.

For AAS, 10-ml aliquots of the sample solution were added into five 25-ml calibrated flasks, which contained different volumes of standard zinc solution, and diluted to volume. Absorbances were measured against blanks run through the same procedure.

Results are shown in Table 2. In all cases there is a very good agreement between values obtained by the spectrofluorimetric method and either certified NBS values or those found by AAS, with the additional advantage that the spectrofluorimetric method has a detection limit of 3 ng/ml and a quantification limit of 8 ng/ml, which are much better than the limit for Zn by flame AAS.

REFERENCES

1. E. A. Bozhevol'nov, V. M. Dziomko and G. V. Serebriakova, U.S.S.R. 120,029, May 1959; *Chem. Abstr.*, 1960, **54**, 20676a.
2. E. A. Bozhevol'nov and G. V. Serebryakova, Sb. Statei, Vses. Nauchn.-Issled. Inst. Khim. Reaktivov i Osobo Chistykh Khim. Veshchestv 1961, **24**, 36; *Chem. Abstr.*, 1962, **57**, 24b.
3. E. A. Bozhevol'nov and G. V. Serebryakova, *Acta Chim. Acad. Sci. Hung.*, 1962, **32**, 199; *Chem. Abstr.*, 1963, **58**, 5026d.
4. D. P. Shcherbov and V. V. Kolmogorova, *Metody Analyza Khim. Reaktivov i Preparatov, Gos. Kom. Sov. Min. SSSr po Khim.*, 1962, **4**, 120; *Chem. Abstr.*, 1964, **61**, 2480d.
5. E. A. Bozhevol'nov and G. V. Serebryakova, *ibid.*, 1962, **4**, 120; *Chem. Abstr.*, 1964, **61**, 690c.
6. G. V. Serebryakova and E. A. Bozhevol'nov, *Metody Analyza Khim. Reaktivov i Preparatov*, 1965, **11**, 89; *Chem. Abstr.*, 1966, **65**, 1381a.
7. G. V. Serebryakova, I. A. Krasavin, E. A. Bozhevol'nov and V. M. Dziomko, *Tr. Vses. Nauchn.-Issled. Inst. Khim. Reaktivov i Osobo Chist. Khim. Veshchestv.* 1964, **26**, 97; *Chem. Abstr.*, 1967, **66**, 72198f.
8. E. Pelizzetti and E. Pramauro, *Anal. Chim. Acta*, 1985, **169**, 1.
9. L. J. Cline Love, J. G. Habarta and J. G. Dorsey, *Anal. Chem.*, 1984, **56**, 1132A.
10. E. Pramauro and E. Pelizzetti, *Trends in Anal. Chem.*, 1988, **7**, 260.
11. W. L. Hinze, in *Solution Chemistry of Surfactants*, K. L. Mittal (ed.), Vol. 1, p. 79. Plenum Press, New York, 1979.
12. K. Soroka, R. S. Vithanage, D. A. Phillips, B. Walker and P. K. Dasgupta, *Anal. Chem.*, 1987, **59**, 629.
13. H. Billman and R. Chernin, *ibid.*, 1962, **34**, 408.

Talanta, Vol. 40, No. 1, pp. 21–36, 1993
Printed in Great Britain.

0039-9140/93 $6.00 + 0.00

SOLID INTERFACES AS ANALYTICAL PROBLEM SOLVERS IN FLOW INJECTION ANALYSIS

M. D. LUQUE DE CASTRO and M. T. TENA
Department of Analytical Chemistry, Faculty of Sciences, University of Córdoba, E-14004 Córdoba, Spain

(*Received* 14 *February* 1992. *Revised* 24 *April* 1992. *Accepted* 14 *May* 1992)

Summary—An overview of the advantages gained by using solid interfaces in flow injection analysis is presented. The enhancing effect on such basic analytical features as selectivity and sensitivity, diminished sample and reagent consumption, ease of automation of the preliminary steps of the analytical process and of implementation of multideterminations arising from the use of solid interfaces are discussed and illustrated by selected examples.

The new problems of social concern with which analytical chemistry is confronted call for solutions relying on complex, expensive technologies.[1] Flow injection analysis (FIA) is one exception to this general rule as it is based on straightforward systems characterized by their flexibility to accommodate the specific demands of each situation or problem.[2,3] The wide variety of FI methodologies developed in the last decade make FIA a firmly established analytical tool. However the high potential of this technique remains unknown to many analytical chemists who are therefore missing an advantageous alternative to other automatic and manual methods for a number of purposes.

The aim of this paper is to illustrate the potential of solid interfaces as parts of FI systems through selected examples. The different nature of these interfaces and the versatility of FIA offer a host of opportunities to improve such analytical features as sensitivity, selectivity and sample and reagent consumption.

Solid phases included or formed in FI manifolds can be of very different nature, which in turn determines their function, performance and advantages derived from their use.

Thus, the role of the solid phase can be played by the sample itself if it is inserted into the system in a solid state. Alternatively, the solid phase can be formed along the flow system as a result of a chemical reaction (*e.g.*, precipitation), or on a solid surface by an electrochemical reaction (stripping techniques). Also, the solid phase can be a reactant that interacts with the analyte, its reaction product or undesirable components of the sample, as is the case with absorbent or ion-exchange material, immobilized catalysts or solid reagents.

The material presented in this paper is organized according to the analytical parameter or aspect that is improved as a result of using a solid interface. Thus, solid interfaces have been classified according to whether they provide enhancement of sensitivity; increased selectivity; decreased sample and reagent consumption; or allow one to automate the preliminary steps of the analytical process; develop multidetermination methods; indirect determinations, and other methods.

Increasing sensitivity by using solid interfaces

The sensitivity of FI methods is usually lower than that of their manual and air-segmented counterparts as a result of measurements in an FI manifold being performed under non-steady state conditions and also owing to dispersion. The fact that the derivatizing reaction does not develop to completion results in decreased sensitivity to an extent dependent on the point of the kinetic curve at which measurements are performed. The dispersion of the sample plug, whether into the carrier stream or through mixing with streams of reagents, masking agents, *etc.*, detracts from the sensitivity. Nevertheless, the sensitivity of an FI method can be increased in two main ways[4] by using solid interfaces, namely: 1) by on-line preconcentration or *in situ* concentration, 2) by decreasing dilution using solid reagents. Micellar media and amplification reactions also provide increased sensitivity in this respect.

Preconcentration. The use of a preconcentration step is one of the more effective ways of increasing sensitivity. This operation can be performed in an FI system by: (a) coupling it on-line to a conventional separation unit such as a minicolumn packed with a suitable adsorbent or ion-exchange material, or a liquid–liquid extraction unit; (b) by implementing a precipitation reaction in the flowing injected plug and collecting the solid phase formed *in situ* by means of a suitable filter; and (c) by forming a solid phase in the detection cell or electrode surface, as in stripping techniques implemented in FI systems.[5]

(a) Minicolumns used for preconcentration involve a chemical reaction between the analyte and the solid column packing if the active material is an ion exchanger rather than an adsorbent.[6] The minicolumn can be placed [Fig. 1(A)] in the loop of the injection valve or between the injection and detections systems.

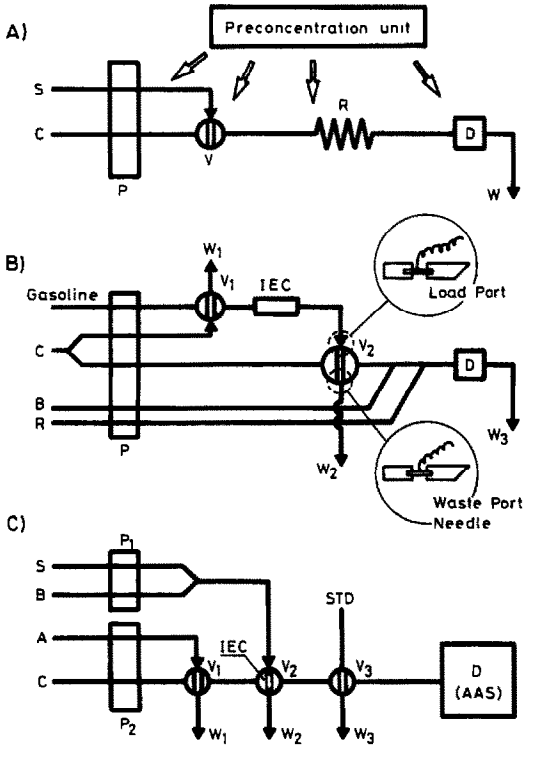

Fig. 1. A) Possible locations of separation units for preconcentration. B) Arrangement for the measurement of mercaptans in gasoline (the insets show the conductivity probes connected to V_2). C) Manifold for preconcentration/determination of lead with timed sample loading (V_2) and injection of reagent and standard solutions (V_1 and V_3, respectively) with saving purposes. S denotes sample, A eluent, C carrier, P pump, V valve, D detector, W waste, B buffer, R reagent, IEC ion-exchange column, STD standard and AAS atomic absorption spectrometer.

Occasionally, it is also inserted into the sample stream prior to the injection point. Also, placement of the solid material in the flow-cell of a non-destructive optical detector provides a peculiar *in situ* concentration mode involving integrated reaction and detection[7,8] or retention and detection.[9] The performance and efficiency of minicolumns used for preconcentration can be boosted in various ways. Thus, performance can be improved by loading the column in the opposite direction to elution, thus avoiding the shortcomings derived from the increased compactness of the packed material and from the appearance of parasitic signals due to the sample matrix, which can be sent directly to waste. Higher efficiency can be achieved by using conical rather than cylindrical columns, which must be arranged in the FI manifold in such a way that sample loading takes place from the narrower to the broader end. Also, the retained analytes must be eluted in the opposite direction in order to minimize dispersion in the column,[10] which can be accomplished by using time-based injection techniques.[11]

C_{18} bonded silica beads and, to a lesser extent, alumina and silica, are the most commonly used solid adsorptive materials for packing minicolumns. Sorbent extraction in flow injection system with AAS detection has been proposed by Růžička and Arndal for preconcentrating copper and lead by complexation with several chelating agents.[12] A typical example of preconcentration by using a conical column packed with C_{18} is the method reported by Fang *et al.*, in which lead is preconcentrated as a diethyldithiocarbamate chelate before determination by graphite furnace atomic absorption spectrometry which a 26-fold increase in peak area for 60-sec preconcentration compared with direct introduction of 50 μl of sample,[10] activated alumina has been used for adsorption of oxyanions[13] and Mo[14] prior to their determination by ICP/AES.

Solid exchange materials used as packings for preconcentration minicolumns can be commercially available ion-exchange resins or ion exchangers prepared in the laboratory from an adsorbent material (*e.g.*,C_{18}, silica gel, controlled-pore glass) that is activated and bonded to a chelating molecule. The concentration step usually precedes introduction of the sample into an atomic detector for individual or multideterminations by AES and ICP techniques. Such is the case with the determination of twenty elements by ICP/AES proposed by Wang and

Barnes,[15] who assessed the performance of two resins. Implementing the separation step prior to molecular spectroscopic detection is usually intended either for preconcentration or for interference removal (*e.g.*, in the photometric method for determination of sulphate after separation by a strong anion-exchange resin minicolumn located in the loop of the injection valve). By using adequate preconcentration times and a less sensitive method (displacement of the methylthymol blue/barium complex by the analyte) Karlsson *et al.* accomplished a determination range between 25 and 1000 ng/ml.[16] The decrease in the sampling frequency resulting from the preconcentration step can be overcome by using a system of two columns that function alternately for retention and elution. Wu and Qi achieved a sampling frequency of 30 hr and a detection limit of 3 ng/ml in the photometric determination of uranium in geological samples.[17] An unconventional method was developed by Lei *et al.* for the determination of mercaptans in gasolines based on preconcentration of the analytes on ion-exchangers and elution with an immiscible eluent[18] in the manifold shown in Fig. 1(B). The gasoline sample was circulated through an electropneumatically actuated rotary valve, V_1 (sample loop 60 μl), and a microcolumn packed with a strong anion-exchanger, and then through the load port of valve V_2 to waste. Valve V_2 is the same as V_1 but has a 15-μl loop volume. The loading loop and waste port of this valve accommodate a stainless-steel hypodermic needle inserted as shown in Fig. 1(B). The conductivity between these two metal probes is monitored; when the loop is filled with a conductive aqueous eluent rather than gasoline carrier, the electrical resistance drops and valve V_2 is automatically switched to its injection position.

8-Hydroxyquinoline has been the most frequently immobilized chelating agent used for preconcentration purposes. It is usually supported on silica and placed in the transport zone[19,20] or in the loop of the injection valve.[21] Occasionally, it has also been immobilized on controlled-pore glass[22] and on Fractogel.[23] Preconcentration of lead was assayed by using various FI manifolds and chelating agents for the determination of this element by FAAS. Detection limits down to 1.4 ng/ml Pb were obtained by using an FI manifold with three serially arranged injection valves such as that shown in Fig. 1(C), in which timed sample loading and matrix removal without the matrix reaching the nebulizer were achieved with a single valve. Reagent consumption and the calibration time were reduced by using two additional valves to introduce the eluting and standard solutions.[24] Inert columns such as SBSRs (single beads string reactors[2,3]) also exert a sensitivity enhancing effect by avoiding dilution.

(b) Such an old technique as precipitation has not been incorporated into flow systems other than FIA. *In situ* formation of a solid phase in a flow injection manifold and retention on an appropriate filter provides high preconcentration factors, in both direct and indirect methods for individual species or multideterminations.[25]

The filter used can be stainless-steel and located prior to an atomic absorption detector (*e.g.*, in the direct determination of lead, where a preconcentration factor of 700 was achieved by precipitating the metal with ammonia[26]), non-metallic (*e.g.*, a disposable cellulose acetate membrane—that was also used for the direct AAS determination of copper by precipitation as hydroxide, and of calcium as oxalate.[27]) A special filter (Tygon tubing 7 cm long, 2.8 mm bore, filled with 1.9-mm diameter Pyrex glass beads) was used for the indirect determination of chloride and carbonate ions by AAS after preconcentration by precipitation as silver and calcium salts, respectively.[28] A reagent injection manifold in which the dissolving and washing solutions were introduced through an injection valve was used. Detection limits of 3×10^{-7} and $5 \times 10^{-7} M$ were achieved for Cl^- and CO_3^{2-}, respectively, by using thiosulphate and hydrochloric acid as dissolution agents.

A procedure for co-precipitation of lead in the presence of high concentrations of iron and its subsequent determination by FAAS was reported by Fang *et al.*[29] Lead was co-precipitated quantitatively with an iron(II) complex and collected in a knotted reactor made of Microline tubing without using a filter. The precipitate was dissolved in isobutyl methyl ketone and introduced directly into the nebulizer-burner of an AA detector. A preconcentration factor of 20 was obtained for a co-precipitation time of 30 sec and a sampling frequency of 90 hr. The results obtained in the determination of lead in reference materials (blood and bovine liver) showed the procedure to be suitable for biological materials.

(c) Stripping techniques[30] are among the most frequently used enhancers of the key

analytical parameters, namely sensitivity and selectivity. Stripping techniques (whether voltammetric or potentiometric) and FIA have a synergistic effect,[5] particularly for preconcentrations; in fact, detection limits as low as a few pg/ml have been accomplished by using differential pulse voltammetry for the determination of lead in blood with no sample deoxygenation.[31,32] Also, potentiometric stripping has provided excellent determination methods for lead and cadmium in whole blood by using carbon fibre electrodes,[33] and in acid digest of biological samples without further treatment.[34] A special chemical stripping and potentiometric hybrid method was developed by Nakayama *et al.* for the determination of iodine species in seawater by using a continuous flow system in which the iodide was electrochemically oxidized to iodine and quantitatively concentrated onto a carbon wool electrode in a preconcentration cell. After interfering ions were removed, the iodine was eluted with a reductant and subsequently measured at a polished Ag_3SI electrode in the detection cell. Iodate was determined on reduction to iodide.[35] The new mode of performing stripping voltammetry proposed by Wang (batch injection stripping[36]) is a very promising alternative in this field.

Preconcentration as well as an efficient control of the accuracy were provided with a dual detection system based on potentiometric stripping and atomic absorption spectrometry.[37,38]

Increasing sensitivity by decreasing dilution. Flow injection system provides various means of introducing or bringing reagents and catalysts into contact with the sample in the manifold. Solid interfaces consisting of solid reactors, such as redox, enzymatic, passive and pressurized membrane releasers, decreasing dilution.

(a) The earliest solid reactors used in FIA were redox in nature (*e.g.*, those employed in the photometric determination of nitrate by its reduction to nitrite prior to its reaction with the classical Griess reagents). The dilution arising from the use of an additional reductant was thus avoided.[39] Configurations including internally coupled injection valves and a solid reactor in the loop of the injection valve allowed nitrogen speciation.[40] Also, organic species have been oxidized by using solid reactors, as in the determination of paracetamol with potassium hexacyanoferrate(III) previously immobilized on an anion-exchange column for the oxidation of the analyte prior to its photometric determination based on its reaction with an imine reagent.[41] Other reagents have been assayed, whether immobilized and packed in microcolumns or as derivatizing agents. Mottola developed interesting strategies to optimizing their performance.[42] The reagent itself can also be packed in the microcolumn as in peroxyoxalate solid reactors, thereby avoiding mixing problems and facilitating instrumental development.[43] The features of chemiluminescence monitoring make it preferable to immobilize the reagent in the flow-cell in order to accomplish integration of reaction and detection.

(b) Reagent-releaser membranes. Dasgupta *et al.* have used both passive membranes (ion-exchange membranes that release ammonia or sodium hydroxide) for conditioning the reaction medium, as well as pressurized membranes that are crossed by the derivatizing reagent or catalyst. Such is the case with the fluorometric determination of aqueous sulphite, sulphide and methanethiol after reaction with *N*-acridinylmaleimide (introduced through a pressurized membrane) in an ammonia medium (introduced through a passive membrane),[44] and that of peroxides based on the *p*-hydroxyphenyl acetate/peroxide/peroxidase system, in which a pressurized porous PTFE membrane reactor introduces the enzymes and the pH of the flow stream is altered by inserting NH_3 through a non-porous cation-exchange membrane reactor.[45]

(c) Enzymes immobilized on suitable supports have been widely used in on-line couplings to FI manifolds, both for determining substrates[46,47] and for facilitating monitoring in the determination of the activities of other enzymes.[48] Although the most commonly used support for immobilization of these catalysts is controlled-pore glass and to a lesser extent gels,[46] magnetic particles have also been used for this purpose.[49] Also catalysts have been entrapped in tubular microporous membranes.[50] The efficiency of the catalytic effect involved depends on the number of molecules of catalyst that were immobilized (or entrapped) and on the ability of the analyte to reach the active sites. Two,[51] three,[52] four[53] and up to five[54] enzyme reactors have been used in serial arrangements to develop FI methods.

In addition to the decreased dilution achieved by using immobilized catalysts other solid interfaces included in FI manifolds can be used for different purposes. One case in point is the determination of serum-galactose, which calls

for on-line dialysis, activator, ion-exchange and enzyme reactors.[52] Immobilization on the walls of a cell placed in an ordinary photometer or fluorimeter enables reaction-rate measurements with decreased dilution.[55] A further increase in sensitivity can be achieved by coupling an amplification reaction for determining very small amounts of substrates. Thus, a substrate recyling system was developed by Hansen *et al.*[56] by incorporating a small column reaction containing co-immobilized enzymes into the FI manifold in order to implement the degradation step and ensuing detection of a suitable reaction product to be individually optimized for assays of lactate or pyruvate in the micromolar range with an amplification factor of 40 for each of the substrates.

(d) Micellar media make special solid interfaces that are used in FIA to increase sensitivity in different ways. Among major roles of micellar media are increasing the solubility of reagents and acting as concentration sites in order to shift the derivatizing reaction equilibrium.[57–59] But micellar media can also increase selectivity by acting as ideal interfaces in reaction between water-soluble reagents and non-aqueous samples, thus allowing the development of liquid–liquid extraction processes without phase separation.[60,61] A novel chemiluminescence system was reported for the flow injection determination of phenylpyruvic acid (PPA) in which the presence of both ordered surfactant molecular assemblies and a metal ion catalyst was essential to the phosphorescence of benzaldehyde (emitter) produced by aerobic oxidation of PPA in alkaline solution. Dioctadecyldimethylammonium chloride bilayer aggregates and cobalt allowed PPA to be selectively determined down to $1 \times 10^{-7}M$. The bilayer aggregates were found to contribute favourably both to the production of key intermediates and to efficient phosphorescence emission.[62]

Increasing selectivity by using solid interfaces

Flow injection methods usually surpass their manual and segmented-flow counterparts in selectivity as a result of measurements being made under non-steady state conditions which avoids interferences from species reacting more slowly than the analyte.[63] In addition to the characteristic fixed-time kinetic measurements of FIA, selectivity can be enhanced by using solid interfaces for, 1) interference removal; 2) reaction-rate measurements based on immobilized enzymes; 3) and coupling of FI manifolds to powerful separation techniques such as HPLC.

Interference removal. One of the most typical ways of increasing selectivity is by interference removal, which can be accomplished in FI manifolds by coupling/forming solid interfaces such as ion-exchange or sorbent columns, membranes or precipitation processes.

(a) Separation on an ion-exchange or sorbent column involves retention of the analyte or the interferents. Thus, the interferences from cations in the chemiluminescence determination of bromide was overcome by using a strong cation-exchange column.[64] Also, ammonia, the only interferent with the determination of biuret in fertilizers, was removed by using a Dowex ion-exchange column located prior to or after the injection valve.[65] When a reagent injection manifold is used[66] or for the removal of reagents interferences when the normal FI mode is used, the matrix interference removal column must always be inserted into the main stream, as it must for the removal of reagents interferences when the normal FI mode is used.[52,67] Absorbents such as C_{18} bonded silica beads have been used for retention of the sample matrix in the determination of bitterness in virgin olive oils by using a solid minicolumn located in the loop of the injection valve in order to avoid passage of the matrix through the detector in the eluting/washing step.[68] On the other hand, the amperometric determination of copper in complex matrices such as serum with high albumin content was carried out by using a chelating column to retain heavy metals while allowing albumin to run to waste.[69]

Enhanced selectivity was accomplished together with interference removal by using masking agents such as triethanolamine, thiourea, fluoride and cyanide in the preconcentration of lead by using 8-hydroxyquinoline immobilized on silica,[70] and by on-line coupling of another separation technique such as hydride generation.[71]

(b) Membranes have been widely used in FI manifolds as they allow selective passage of a great variety of substances (gases and low molecular weight, ionic, polar and non-polar compounds, *etc.*) depending on their nature. The low yield of these separation processes is a result of equilibrium not being reached in the very short contact time between sample and membrane. This sensitivity loss has been overcome in different ways (Fig. 2), namely: by using ultrasounds on the separation unit[72]; by halting the

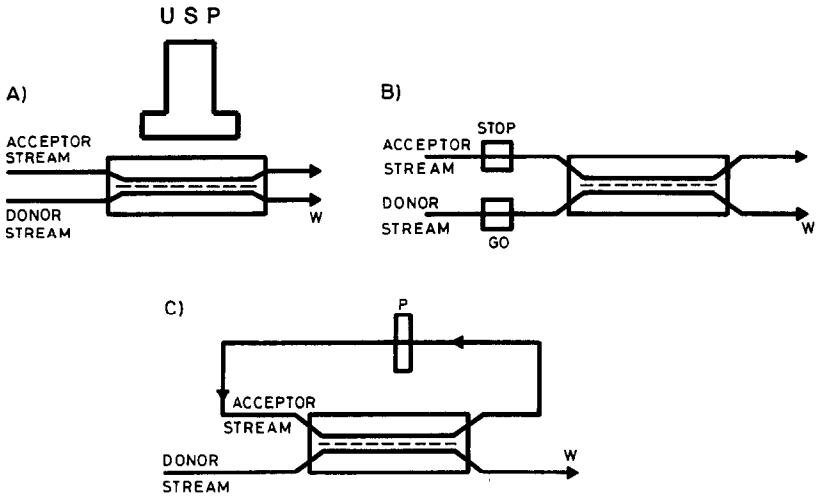

Fig. 2. Different ways of increasing sensitivity in membrane/separation processes. A) By use of an ultrasonic source acting on the separation unit. B) By halting the flow of the acceptor stream. C) By using a closed-loop system to recirculate the acceptor stream. USP denotes ultrasonic probe. The rest as in Fig. 1.

flow of the acceptor stream, whether by using valve,[73] or a time-based mode[74]; and by using a closed loop through which the acceptor stream is recirculated for the analyte to build up.[75]

Dialysis is a very useful means of avoiding interferences from proteins and other macromolecules occurring in biological samples, as was shown in the potentiometric determination of chloride in milk by using a selective electrode for this analyte. The interference from casein was thus overcome and a stable baseline was obtained.[76] The determination of this analyte in serum calls for both interference removal and dilution, which was accomplished by using a dialysis membrane whose yield was accommodated within the linear range of the determination method by employing an adequate ratio of acceptor to donor stream.[77] A dialysis step was also required to isolate low molecular-weight substances from samples obtained in a cellular permeation process in order to monitor the intracellular enzyme activity.[78] A particular method for extraction-preconcentration of phenol compounds from kerosene and naphtha was based on separation through a silicone membrane into a basic acceptor stream which contained 4-aminoantipyrine.[79] The sensitivity of the method was also manipulated by modifying the size of the extraction cell and the preconcentration time. Ionomer membranes enhance the selectivity of electrode-based biosensors, thereby improving the quality of FI measurements, as shown by Rosario *et al.*[80] in the determination of urea in blood serum and *L*-glutamine in hybridoma bioreactor media. A coil of cation-exchange tubing was used as a direct replacement for the injection loop of a conventional sample injector enabling Donnan dialysis to be performed under static conditions while allowing enriched samples to be injected into an FAA spectrometer.[81] On-line coupling of a dialyzer to another solid interface for separation or derivatization purposes results in improved features, as in the determination of galactose by use of up to three enzyme reactors and two separation minicolumns after the dialyzer in order to ensure a selective determination of this analyte in serum.[52]

Membranes allowing gas-diffusion to take place across them have also been widely used in FI manifolds for the determination of either species occurring as gases in the samples (e.g., O_3, ClO_2),[82–84] or others that can be converted into gases by an acid–base reaction[85–93] or by heating.[93,94] A method that is 1500 times more selective towards chlorine dioxide than it is towards chlorine on a mole basis, and with a detection limit of 5 ng/ml, was developed by combining gas-diffusion and chemiluminescence detection.[84] The method avoided the interference from iron and manganese compounds, as well as those of other oxychlorinated compounds such as chloride ion and chlorate ion. Species that are readily converted into gases (*e.g.*, cyanide and ammonium ions) have been determined in complex matrices by using an FI manifold including a gas-diffusion cell.[85–89] A method for the determination of cyanide based

on gas-permeation and reaction with a highly selective reagent has been recently proposed by Kubán.[95] It featured a detection limit of 3 ng/ml and most interferences, including those of SCN were eliminated by discrimination of mass transport through a non-porous silicone-rubber membrane. Urea has also been determined after enzymatic conversion into ammonia and diffusion of the generated gas as in the conductimetric determination involving a reactor packed with naturally immobilized urease in the donor stream and mixed bead ion-exchange minicolumn in the acceptor stream for final purification of demineralized water prior to the separation unit in order to facilitate monitoring of conductivity changes involved.[67]

Microporous membranes provide excellent results in the separation of hydrides generated prior to their introduction into an atomic detector, whether AAS[96] or ICP/AES.[95] Tubular designs are more efficient in this respect, and allow fast, quantitative release of the gas phase.[96,97] Also gas-diffusion separation and detection have been integrated. A porous gold layer, deposited on one side of a porous Teflon membrane, serves as an amperometric electrode which consumes volatile species transported from the flowing solution through the membrane. Thus, nitrite ion has been determined without interference from nonvolatile electroactive species by reaction to produce nitric oxide and iodine.[98]

Pervaporation, *i.e.*, integrated evaporation and gas-diffusion, can be used to enhance selectivity dramatically, as shown in the determination of ethanol and diacetyl in fermentation monitoring.[93] A simple modification of the membrane (*e.g.*, with silicone) allows the linear range for the determination of ethanol to be expanded to 0.0006–60% v/v.[94]

On-line coupling of an FI manifold to a continuous liquid–liquid extractor including a membrane separator has been used for the selective determination of both organic and inorganic species.[99,100] This solid interface offers major advantages over separators based on density differences (*i.e.*, smaller inner volume, possibility of using high flow-rates, no density differences between the aqueous and organic phase required, and a higher efficiency). One example of the enhanced selectivity inherent in liquid–liquid extraction is the method for the determination of lithium in biological fluids by using cryptand 211, which features a linear range for the analyte of 70 ng/ml to 2.1 μg/ml and tolerates up to 1000 μg/ml sodium ion.[101] A higher selectivity can be achieved by coupling the liquid–liquid extraction process to another separation technique such as chromatography. The discriminating effect of GC allows the separation/determination of phenol compounds prior to simultaneous on-line derivatization–extraction into n-hexane of the esters formed with acetic anhydride.[102]

Inert hydrophobic membranes[103,104] as well as thin layers of organic solvent immobilized on microporous inert supports (liquid supported membranes)[105,106] have been used for sample clean up and preconcentration in FI systems even coupled to a gas chromatograph as an alternative to liquid–liquid extraction. Amines in urine and phenols, chlorinated aromatic compounds and pesticides are examples of nonpolar compounds extracted by means of these devices, the advantages of which have been recently reviewed by Jönsson and Mathiasson.[107]

(c) Precipitation allows the selective determination of calcium at the μg/ml level in the presence of over 1000 μg/ml aluminium thereby avoiding its interference with the AAS determination of this alkaline earth by use of an air–acetylene flame.[28]

(d) Reaction-rate methods based on the use of immobilized enzymes combine the selectivity of the enzymatic processes with the advantages of reaction-rate monitoring, viz. avoidance of interferences from the matrix signal and from species that react faster or slower than the analyte. There are three main alternatives to performing these measurements which involve three different. FI approaches, namely: stopped-flow,[2,3] iterative change of the flow direction,[108] and open-closed configurations.[109]

Enzymes immobilized on the walls of a photometric or fluorometric flow-cell enable reaction-rate measurements by halting the flow as the sample plug reaches the flow-cell. Pairs of signal-time data can be acquired during the stop interval, and related to the concentration of the analyte. Iterative passage of the sample plug through an ordinary photometer or fluorimeter can be accomplished either by changing the flow direction[108] or by using an open-closed system.[109] In both cases, an enzyme reactor can be included in the FI manifold so the sample can be circulated through it between two consecutive passages through the detector, thereby providing additional development of the enzyme reaction.[110]

Both selectivity and sensitivity can be improved through biochemical reactions, whether by using immobilized catalysts (*e.g.*, enzymes, as described in section A) or reagents. Immunoassay makes a very powerful means of enhancing the selectivity of FI methods.[111] The FIA-ELISA coupling allows on-line monitoring of biological macromolecules. The operational principle is based on the competitive binding of an antibody and a native antigen in the sample to an enzyme-labelled antigen that is added in a preset amount. The antibodies are immobilized onto a solid support and placed in a small column inserted in the flow system. After one assay cycle, the system is rinsed and the column is re-used for the next assay. The total time for one assay cycle is 6–10 min.[112] Fluorometric on-line monitoring of monoclonal antibodies in the course of a hybridoma cell fermentation has also been accomplished by using immunoreactors containing membranes for magnetic particles as the solid phase for the bound antibodies.[113]

Multideterminations based on FI systems involving solid interfaces

The development of multiparameter methods is one of the current goals of FIA as they may make this technique competitive with other automatic alternatives, whether continuous or batch.[1] Multideterminations in FI/solid interface systems are made possible either by the presence of the solid interface itself, by the features of the detector (*e.g.*, MS, ICP), by alterations to the detection zone [integration of reaction(retention) and detection], or by more than one of the previous choices (stripping techniques, use of derivative synchronous fluorescence in integrated reaction-detection systems). Solid interfaces used for discrimination purposes in FIA include the following:

Precipitation. Precipitation of the analytes with further selective dissolution, as in the indirect sequential determination of chloride and iodide by AAS after precipitation with silver ion, retention of the precipitated salt on a filter and dissolution of chloride and iodide by sequential injection of ammonia and cyanide solutions.[114]

Membranes. Membranes accommodated in liquid–liquid extractors, dialysers and gas-diffusers have been used for multidetermination purposes. Membranes for separation of immiscible phases have been used in the simultaneous determination of diphenydramine and 8-chlorotheophylline in dramamine tablets.[115] A porous membrane was used to isolate the cyclohexane phase and a paper membrane was employed to separate the aqueous buffer phase after solvent extraction via a segmented flow. At pH 10, diphenydramine was quantitatively extracted into the cyclohexane phase while 8-chlorotheophylline remained in the buffer phase. Assays were performed at the rate of two per minute and with r.s.d. values of 1%. Speciation of calcium in milk (as total and free calcium) was accomplished by using a dialysis membrane which allows the photometric determination of free calcium in the acceptor stream and that of total calcium on an undialysed sample by AAS.[116] Inclusion of a further dialyser arranged in series with the previous one allows the potentiometric determination of chloride in milk in addition to calcium speciation. Three parallel detectors are required in this case.[117] Also, two serially arranged dialysers were used for the simultaneous determination of sodium and potassium by flame emission spectrometry and of chloride by spectrophotometry.[118]

The use of diffusion membranes for simultaneous determinations occasionally involves passing only one analyte through the membrane, as in the simultaneous determination of hydroxylamine and cyanide, where cyanide is amperometrically determined in the acceptor stream, while hydroxylamine remains in the donor stream and is oxidized by iodine, which is then determined photometrically.[119] However, sometimes both species are allowed to cross the porous membrane in order to be simultaneously determined in the acceptor stream by using two serial detectors, as in the determination of CO_2 and SO_2 with a potentiometric detector responsive to both analytes and a photometric detector for SO_2 alone (*p*-rosaniline-formaldehyde method).[120] If a single detector is used, discrimination between analytes can be achieved sequentially by changing the pH of the acceptor stream, as in the determination of cyanide and thiocyanate, which react with pyridine/barbituric acid at pH 6.0, whereas only cyanide reacts at pH 8.1.[121]

Microcolumns. Microcolumns packed with solid materials have been used to develop a number of multidetermination methods.

(a) Ion-exchange resins can selectively retain one analyte, thereby enabling discrimination, as in the resolution of V(V)–Ti(IV) mixtures by use of a modified injection valve to introduce two

samples sequentially into the reagent stream. One of the samples is passed through a cation exchanger minicolumn and the other through an empty column before reaching the detector. The former allows vanadium alone to be measured, and the latter vanadium plus titanium.[122]

(b) Redox columns, particularly those of cadmium and copperized cadmium have been employed for nitrogen speciation as nitrite and nitrate on the basis of the Griess reaction. The complexity of FI manifolds used for this purpose has increased with time. Thus, Anderson[123] reported a fairly simple design in which, after injection, the sample was split and driven through two parallel configurations, one of which included a redox column, and then through a photometric detector. A more recent reversed FI system uses a valve to switch the cadmium column in and out of line so that nitrate plus nitrite or nitrite alone can be determined.[124] A configuration with internally coupled valves and a reductant column located in the loop of the secondary valve provided plugs with two distinct reaction zones, one of which was passed through the redox column while the other was not.[33] A similar manifold using an MnO_2 solid reactor instead was used for the determination of hydrogen peroxide and organic peroxides.[125]

(c) Immobilized catalysts, usually enzymes, have also been employed to determine one or more of the analytes in multideterminations.

Thus, two types of configurations were used for the simultaneous determination of two species, of which one required an enzymatic reaction: one of the manifolds included two injection valves coupled in parallel [Fig. 3(A)] or in series [Fig. 3(B)] in such a way that only one of the injected plugs passed through the enzymatic reactor. This was the basis of the simultaneous fluorometric determination of urea and ammonium with the *o*-phthalaldehyde/2-mercaptoethanol system and a reactor containing immobilized urease.[126] The FI manifold to be

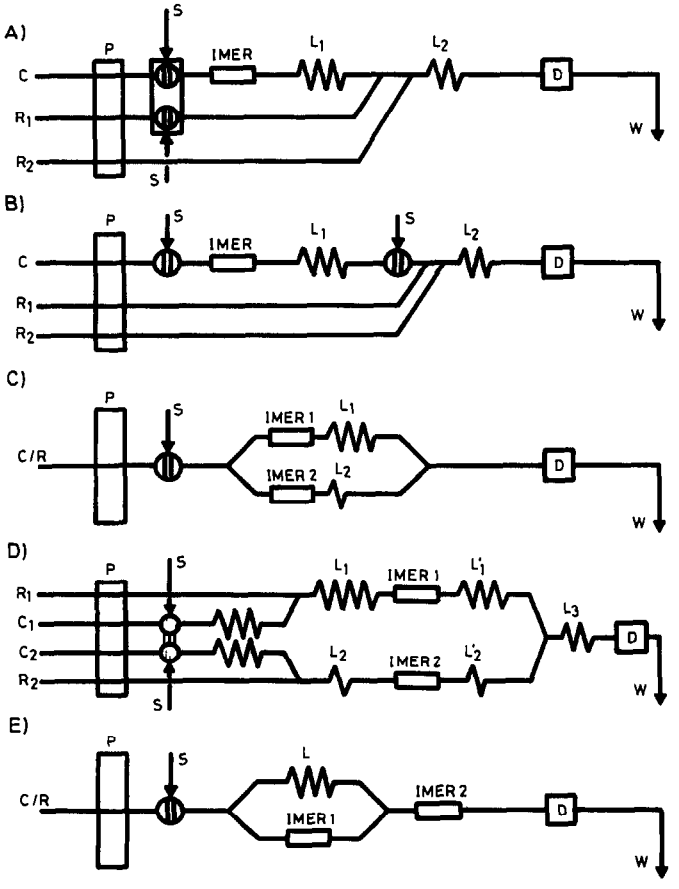

Fig. 3. Approaches to multideterminations based on immobilized reactors. A) and B) Only one of the determinations is based on enzyme reactions. C) and D) A different enzyme is required for each analyte. E) One analyte requires two enzymatic steps and the other only one, but common with the former. IMER denotes enzyme reactor, L an open reactor, the rest as in Fig. 1.

used when both analytes require an enzymatic derivatizing reaction is determined by whether or not one of the biocatalysts is common to both analytes. Thus, two solid interfaces were used for derivatization in the simultaneous determination of L(+) and L(−) lactic acid, which require different enzymes, so an FI manifold with splitting and confluence points [Fig. 3(C)] and two channels including an enzymatic reactor each was used.[127] By performing two-fold injections the splitting point can be dispensed with, as in the determination of ethanol and acetaldehyde in wines by using alcohol and aldehyde dehydrogenases and monitoring the formation of the reduced form of the coenzyme photometrically. Despite the rather different concentrations at which these analytes occur in wines, they required only a single dilution of the sample and appropriate choice of the injected volumes and length ratios of the $IMER_1$–$IMER_2$, and L_1–L_2 reactors [Fig. 3(D)].[128] On the other hand, the simultaneous determination of species which call for a common reagent and another specific to each, such as sucrose and glucose, can be developed in a manifold such as that shown in Fig. 3(E)].[129]

Multideterminations involving separations by using two solid interfaces have been effected with, as in the photometric method for the determination of sodium and potassium by separation on a silica column and liquid–liquid extraction into benzo-18-crown-6 and tetrabromophenylphthalein ethyl ester.[130]

Two different solid interfaces were used for separation–discrimination and derivatization, respectively, in the determination of bile acids in serum by use of an enzymatic derivatizing reaction after chromatographic separation. The overall manifold allows the determination of total or individual analytes depending on whether or not the sample is injected via the FIA or the HPLC valve. Thus, the FIA plug does not pass through the chromatographic column, but only through the enzymatic reactor, while the HPLC plug calls for individual determination.[131] When the HPLC instrument is coupled to an open-closed FI manifold[109] including the enzymatic reactor, reaction-rate measurements can be performed in addition to separation and enzymatic derivatization. Such is the case with the overall determination of the activity of creatine kinase and its different isoenzymes.[132]

Three solid interfaces were used in the sequential determination of NH_3, NO_2 and NO_3 in the manifold shown in Fig. 4. Ammonia was determined by merging the injected sample with an alkaline solution (NaOH/EDTA) and passing the resulting mixture through a diffusion cell. Released ammonia was collected by a flowing stream of deionized water that was subsequently passed through a conductance flow cell. The nitrate and nitrite concentrations were determined after reduction to ammonia in an alkaline medium by using a column filled with metal zinc. The ammonia thus produced was then measured as described above. Speciation was accomplished by adding sulphanilic acid to remove nitrite from the sample and determine the ammonia without using the column.[133]

Unconventional detectors. Some multideterminations rely both on intrinsic features of unconventional detectors and on the use of solid interfaces in the FI manifold which play a major role in the overall process. Such is the case with the on-line monitoring of acetic acid, acetoin and ethanol by membrane introduction tandem mass spectrometry proposed by Hayward *et al.*,[134] in which the analyte is directly inserted by a membrane probe that introduces aqueous solutions past a membrane place in the ion source of a mass spectometer,[134] or in an ion-exchanger coupled to an ICP/AES instrument for the preconcentration and simultaneous determination of metals.[15]

Modified flow-cells located in conventional or unconventional detectors. These arrangements have been used to integrate reaction (retention) and detection of analytes in mixtures. Any of the components of an analytical reaction

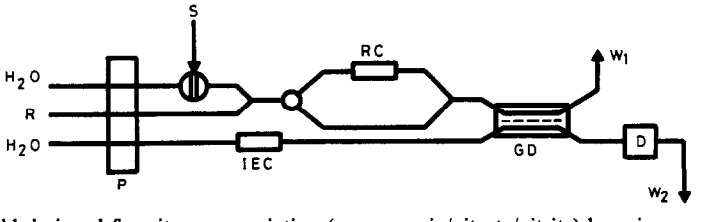

Fig. 4. Manifold designed for nitrogen speciation (as ammonia/nitrate/nitrite) by using a redox column and conductimetric detection. RC denotes redox column and GD gas-diffuser. For more details, see text.

(analytes, reagents, catalysts and products) can be permanently or temporarily retained on a support that is used to pack the flow-cell.[7-9] The rate difference of the derivatizing reactions of two analytes retained on the C_{18} packing of the flow-cell of an ordinary spectrophotometer was the basis for a simultaneous determination of phosphate and silicate. A kinetic optosensing method was developed in which the rate difference in the reduction of the heteropoly complexes allowed the simultaneous determination of phosphate in the ng/ml range, and that of silicate at the μg/ml levels.[135] By placing a flow-cell packed with C_{18} support in a diode array spectrophotometer (DAS), the retained analytes can be simultaneously monitored at various wavelengths provided their absorption spectra are fairly different, as is the case with the simultaneous triple determination of aromatic amines based on differences in their spectral features.[136] The same type of cell and support, but placed in a spectrofluorimeter, were used for the determination of pyridoxal, pyridoxal-5-phosphate and pyridoxic acid based on derivative synchronous fluorometric measurements.[137]

Saving sample and reagent consumption by using solid interfaces in FIA: miniaturization

Miniaturization. Miniaturization is one of the main trends in today's analytical chemistry in response to social demands for assays involving increasingly smaller amounts of sample (particularly in the clinical field) and expensive reagents that must be used sparingly (especially in routine analyses). Flow injection analysis is in itself a miniaturized technique that can be further improved in this respect. Integrated microconduits[138] make the most promising approaches to miniaturization. Their performance can be boosted by incorporating ion-exchange minicolumns and enzyme reactors[139] in the transport system, or by integrating reaction(retention) and detection. Flow-through sensors for penicillin[140] and urea[141] microconduits have thus been developed. They consist of penicilinase or urease that is cross-linked with bovine albumin into a cellulose pad, and an acid–base indicator dye covalently bound to the surface of the cellulose, the sensor pad being placed at the endface of fibre optic bundles. Another, more sophisticated approach to the determination of urea involved a flow-cell combining gas-diffusion and optosensing; the separating barrier between the donor and accepting stream is a sandwich of a hydrophobic gas-permeable membrane and a hydrophylic membrane between which a gel of covalently immobilized urease is contained. The urea content in the sample is quantified by the colour change of an acid–base indicator contained in the acceptor stream.[142]

Another advantage of miniaturization is the possibility of performing *in vivo* monitoring. A rapid, specific measurement of the lactic acid content of extracellular fluid can be accomplished by direct combination of intracerebral dialysis and flow injection analysis with enzymatic fluorescence detection.[143]

Integration of reaction (retention) and detection. The integration of these two aspects is the central philosophy of one other of the most exciting trends in analytical chemistry: (bio)chemical sensors. Some (bio)chemical sensors were already commented on earlier (*e.g.*, in dealing with immobilization in the flow-cell in section A, and with analyte/product immobilization for simultaneous determinations in section C. There are other interesting examples in the FIA literature that testify to the suitability of these approaches. One such example is the immobilization of a reagent on a support packed in a flow-cell (luminol on CPG or silica for peroxide determinations[144]) and the attachment of antigens (IgG) to a membrane mounted in a flow-cell of 5-μl dead volume.[145] In this case, the analyte, in the form of mouse antibovine IgG, was injected into the flowing stream followed by a goat anti-mouse IgG horseradish peroxidase (HRP) conjugate. The HRP was used to catalyse the enhanced luminol reaction, which produced chemiluminescence that was detected directly within the immunoreactor. Other interesting biosensors for determination of ATP with bioluminescence detection,[146] that of ammonia with gas-diffusion/optosensing system,[147] and for enzyme activity monitoring[148] have been reported. Also, a solid-surface room-temperature optosensor was developed for the determination of aluminium in clinical chemistry.[149]

Automation of the preliminary steps of the analytical process by use of solid interfaces

One of the chief targets of automation is the preliminary steps of the analytical process, which involve a variety of tedious operations that are the source of major error in the overall process.[1] Several attempts have been made at developing FI methods in which solid samples are directly introduced into the manifold, thus

avoiding the dissolution step by leaching the solid sample with a suitable agent and the aid of auxiliary external energy such as ultrasounds, electrical current or heat.

Selective electrolytic dissolution. Selective electrolytic dissolution of some minor components in stainless-steels has been achieved by applying an adequate current intensity, whether for further simultaneous determination by ICP/AES[150] or for a single determination by using FAAS[151] or a conventional spectrophotometer after a derivatizing complex-formation reactions.[152]

Ultrasonic energy. This allows lixiviation of solid samples placed in a special cell through which the leaching solution is recirculated while the cell is subjected to ultrasonic cavitation. The photometric determination of boron in soils[153] and that of iron in plant material[154] testify to the high potential of this approach.

The determination of total organic halogen in solid substances was addressed by sample combustion/FI conductimetry with on-line preconcentration.[155] The sample was subjected to high-temperature combustion in an oxygen stream. Halogen-containing decomposition products were preconcentrated from the gas stream by absorption in a capillary denuder tube coated with an aqueous solution of hydrazine monohydrohalide salt, whereas carbon-sulphur- and nitrogen-containing combustion products were removed by the carrier gas. The hydrohalic acid formed in the liquid film was then eluted by a stream of the adsorbent circulated through an electrolytic conductivity microdetector.

Indirect determinations involving solid interfaces

On-line couplings of continuous separation techniques such as ion-exchange, liquid–liquid extraction and precipitation to atomic absorption spectrometric detection results in the above-described advantages, and also in the possibility of implementing indirect determinations and thus extend the scope of application of these detectors to organic and non-metal inorganic species. These determinations may involve dissolution of the retained precipitate,[156] or ion-exchange processes.

Precipitation. Chloride and oxalate were determined by continuous precipitation/filtration/dissolution in the ranges 3–100 μg/ml and 5–90 μg/ml, respectively.[157] The precipitate was formed by injecting the anion (analyte) into a carrier containing a cation (reagent) and was retained on a stainless-steel filter. In the determination of local anaesthetics (lidocaine, tetracaine and procaine) at the μg/ml level[158] and of sulphonamides in pharmaceutical preparations,[159] the precipitate was formed by injecting cobalt, copper or silver ion into a carrier containing the sample and was subsequently retained on a filter. The difference between the signals obtained by injecting the cation into a blank carrier and by using the sample as carrier was related to the concentration of the drug.

Ion-exchange processes. These also provide a means of performing indirect determinations. Thus, a Chelex-100 resin packed column was used to determine EDTA by FAAS. In a first step, a copper(II) solution was injected to regenerate the column. The excess copper ion not retained on the column was washed with an ammonia solution carrier. In the second step, an injected EDTA sample displaced an equivalent amount of copper(II) from the chelating column which was subsequently determined by FAAS.[160] Petersson *et al.* reported an FI method that combines precipitation and ion-exchange for the indirect determination of sulphide by FAS. Sulphide was precipitated by cadmium(II) and the precipitate was allowed to pass unhindered through the FI system for AAS detection, while excess cadmium was removed by the ion-exchange column and later eluted.[161] Also, the overall concentration of anionic surfactants was determined indirectly by AAS measurement of the copper(II) present in an organic layer after formation of a detergent/1,10-phenanthroline/copper(II) ion-pair and extraction into methyl isobutyl ketone.[162]

Other problems solved by using solid interfaces in FI systems

In addition to the above-described advantages, solid interfaces provide a valuable means of circumventing some shortcoming and improving the features of given methods. Thus, by *in situ* formation of unstable reagents in FI systems using solid redox reactors, derivatizing reaction can be improved by avoiding heat losses (thermochemical reactions) by allowing sequential development of multi-step derviatizing reactions, or enabling simultaneous measurements on matrix and sample, among others.

Generation of unstable reagents. Shortcomings involved in the use of unstable reagents in batch systems (*e.g.*, frequent standardization, storage difficulties, time consumption) are avoided by

in situ generation in the flow manifold as the time interval between production and use is quite short and reproducible.[163] Strong reductants such as chromium(II),[164–166] vanadium(II)[165–167] and molybdenum(III)[168] can be generated in-line from stable Cr(III), V(IV) and Mo(VI), respectively, by using a Jones reductor column.

Minimization of heat losses. A packed bed reactor was used instead of the ordinary narrow-bore in the thermochemical determination of iodine based on its catalytic effect on the reaction between Ce(IV) and As(III) in order to minimize heat losses. As a rule, thin tubes have a much larger surface area across which heat can leak than do packed beds of an equivalent volume.[169]

Simultaneous samples and matrix measurements. Two conductance cells and an enzyme reactor placed between them provide a simple means of performing simultaneous sample and matrix measurements. Figure 5(A) shows the FI manifold used for the determination of urea based on its urease-catalysed hydrolysis and conductimetric monitoring of the sample both before and after passage through the enzyme reactor.[170]

Sequential development of different steps. Figure 5(B) makes an excellent example of the different steps involved in the pre-treatment and derivatizing reaction for complex samples. This manifold, which was used for the determination of galactose in serum samples, allows sequential development of the following items: a dialysis process for removing macromolecules, passage of the dialysate through a Bond-Elut-NH_2Cu column for interference removal and through a catalase reactor for withdrawal of hydrogen peroxide (not only that from the sample, but also that yielded in reactions taking place in the Cu reactor). On passing through the galactosidase reactor, galactose produces hydrogen peroxide that is monitored through the colour formed in an oxidative coupling reaction in the peroxidase reactor. A column packed with arylamine-activated porous glass inserted in the reagent stream adsorbs the impurities.[52]

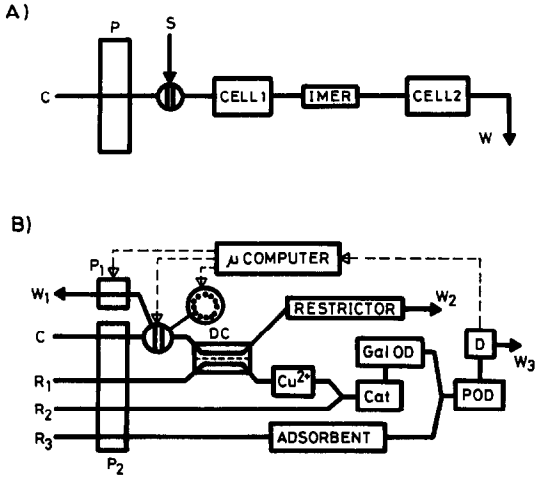

Fig. 5. A) Simultaneous sample and matrix measurements. B) Sequential development of the different steps of a conditioning/derivatizing reaction. For details see text.

CONCLUSIONS

As shown above, solid interfaces endow flow injection analysis with an even higher potential that can be exploited for a wide variety of purposes only limited by the user's ingenuity.

Future developments in the use of solid interfaces in FIA will presumably be concerned with:

(a) The introduction of solid samples into FI manifolds in order to avoid or reduce the preliminary steps of the analytical process,

(b) the miniaturization of experimental setups so as to decrease sample and reagent consumption, and

(c) the development of new types of (bio)chemical sensors for on-line and in-line measurements in the industrial and clinical field.

These three general trends of today's analytical chemistry are particularly outstanding in flow injection analysis, for which the use of solid interfaces is an irreplaceable means of implementing approaches that open up new prospects for solving past, present and future problems.

Acknowledgement—Dirección General de Investigación Científica y Técnica, DGITCyT, is thanked for financial support (Grant No. PB90-0925).

REFERENCES

1. M. Valcárcel and M. D. Luque de Castro, *Automatic Methods of Analysis*, Elsevier, Amsterdam, 1988.
2. *Idem, Flow Injection Analysis: Principles and Applications*, Ellis Horwood, Chichester, 1987.
3. J. Růžička and E H. Hansen, *Flow Injection Analysis* 2nd Ed., J. Wiley, New York, 1988.
4. M. Valcárcel and M. D. Luque de Castro, *Microchem. J.*, 1992, **45**, 189.
5. M. D. Luque de Castro and A. Izquierdo, *Electroanal.*, 1991, **3**, 457.
6. M. D. Luque de Castro, *Trends Anal. Chem.*, 1992, **11**, 149.
7. M. Valcárcel and M. D. Luque de Castro, *Analyst*, 1990, **115**, 699.
8. M. D. Luque de Castro and M. Valcárcel, *Lab. Robotics Autom.*, 1991, **3**, 199.

9. *Ibid., Trends Anal. Chem.*, 1991, **10**, 114.
10. Z. Fang, M. Sperling and B. Welz, *J. Anal. Atom. Spectrom.*, 1990, **5**, 639.
11. M. Sperling, X. Xuefeng and B. Welz, *ibid.*, 1991, **6**, 295.
12. J. Ruzicka and A. Arndal, *Anal. Chim. Acta*, 1989, **216**, 243.
13. I. G. Cook, C. W. McLeod and P. J. Worsfold, *Anal. Proc.*, 1986, **23**, 5.
14. N. Furuta, K. R. Brushwyler and G. M. Hieftje, *Spectrochim. Acta*, 1989, **44B**, 349.
15. X. Wang and R. M. Barnes, *J. Anal. Atom. Spectrom.*, 1989, **4**, 509.
16. M. Karlsson, J. A. Persson and J. Möller, *Anal. Chim. Acta*, 1991, **244**, 109.
17. X. Wu and W. Qi, *ibid.*, 1988, **214**, 279.
18. W. Lei, P. K. Dasgupta, J. L. López and D. C. Olson, *Anal. Chem.*, 1989, **61**, 496.
19. M. A. Marshall and H. A. Mottola, *ibid.*, 1985, **57**, 729.
20. O. R. Purohit and S. Devi, *Anal. Chim. Acta*, 1992, **259**, 53.
21. T. Yamane, K. Watanabe and H. A. Mottola, *ibid.*, 1988, **207**, 331.
22. F. Malamas, M. Bengtsson and G. Johansson, *ibid.*, 1984, **160**, 1.
23. V. A. Elrod, K. S. Johnson and K. H. Coale, *Anal. Chem.*, 1991, **63**, 893.
24. S. R. Bisouth, J. F. Tyson and P. B. Stockwell, *Anal. Chim. Acta*, 1988, **214**, 329.
25. M. Valcárcel and M. Gallego, *Trends Anal. Chem.*, 1989, **8**, 34.
26. P. Martínez-Jiménez, M. Gallego and M. Valcárcel, *Analyst*, 1987, **112**, 1233.
27. E. Debrah, C. E. Adeeyinwo, S. R. Bysouth and J. F. Tyson, *ibid.*, 1990, **115**, 1543.
28. F. T. Esmadi, M. A. Kharoaf and A. S. Attiyat, *Talanta*, 1990, **37**, 1123.
29. Z. Fang, M. Sperling and B. Welz, *J. Anal. Atom. Spectrom.*, 1991, **6**, 301.
30. J. Wang, *Stripping Analysis: Principles Instrumentation, Applications*, VCH Publishers, New York, 1985.
31. J. Wang and H. D. Dewald, *Anal. Chem.*, 1984, **56**, 156.
32. J. A. Wise and W. R. Heineman, *Anal. Chim. Acta*, 1985, **172**, 1.
33. L. Almestrand, D. Jagner and L. Renman, *ibid.*, 1987, **193**, 71.
34. W. Frenzel and P. Brätter, *ibid.*, 1986, **179**, 389.
35. E. Nakayama, T. Kimoto and S. Okazaki, *Anal. Chem.*, 1985, **57**, 1160.
36. J. Wang, J. Lu and L. Chen, *Anal. Chim. Acta*, 1992, **259**, 123.
37. G. Schulze, M. Koschany and O. Elsholz, *ibid.*, 1987, **196**, 153.
38. G. Schulze, O. Elsholz and W. Frenzel, *Z. Anal. Chem.*, 1985, **320**, 650.
39. J. F. van Staden, A. E. Joubert and H. R. Vliet, *ibid.*, 1986, **325**, 150.
40. B. Bermúdez, A. Ríos, M. D. Luque de Castro and M. Valcárcel, *Talanta*, 1988, **35**, 810.
41. J. Martínez Calatayud and S. Sagrado Vives, *J. Pharm. Biomed. Anal.*, 1989, **10**, 1165.
42. H. A. Mottola, *Quim. Anal.*, 1989, **8**, 119.
43. P. van Zoonen, D. A. Kamminga, C. Gooijer, N. H. Velthorst and R. W. Frei, *Anal. Chim. Acta*, 1985, **167**, 249.
44. P. K. Dasgupta and H. C. Yang, *Anal. Chem.*, 1986, **58**, 2839.
45. H. Hwang and P. K. Dasgupta, *ibid.*, 1986, **58**, 1521.
46. J. Ruz, Lázaro and M. D. Luque de Castro, *J. Autom. Chem.*, 1988, **10**, 15.
47. E. H. Hansen, *Anal. Chim. Acta*, 1989, **216**, 257.
48. J. M. Fernández-Romero and M. D. Luque de Castro, *Chim. Oggi*, 1988, November, 17.
49. R. Kindervater, W. Künnecke and R. D. Schmid, *Anal. Chim. Acta*, 1990, **234**, 113.
50. H. Hwang and P. K. Dasgupta, *Anal. Chem.*, 1987, **59**, 1356.
51. I. Ogbomo, R. Kittsteiner-Eberle, U. Englbrecht, U. Prinzing, J. Danzer and H. L. Schmidt, *Anal. Chim. Acta*, 1991, **249**, 137.
52. B. Olsson, H. Lundbäck and G. Johansson, *ibid.*, 1985, **167**, 123.
53. K. Zaitsu, K. Jamagishi and Y. Ohkura, *Chem. Pharm. Bull*, 1988, **36**, 4488.
54. Y. Hayashi, K. Zasitsu and Y. Ohkura, *Anal. Chim. Acta*, 1986, **186**, 131.
55. P. Linares, M. D. Luque de Castro and M. Valcárcel, *ibid.*, 1990, **230**, 199.
56. E. H. Hansen, A. Arndal and L. Nogaard, *Anal. Lett.*, 1990, **23**, 225.
57. M. Yamada and S. Suzuki, *ibid.*, 1984, **17**, 251.
58. *Idem, Anal. Chim. Acta*, 1987, **193**, 337.
59. J. Hayashi, M. Yamada and T. Hobo, *ibid.*, 1992, **259**, 67.
60. M. H. Memon and P. J. Worsfold, *ibid.*, 1986, **183**, 179.
61. *Idem, ibid.*, 1987, **201**, 345.
62. M. Kishida, Y. Makita, T. Suzuki, M. Yamada and T. Hobo, *Anal. Chem.*, 1991. **63**, 2301.
63. M. Valcárcel and A. Ríos, *Analusis*, 1990, **18**, 469.
64. I. M. A. Shakir and A. T. Faizullah, *Analyst*, 1989, **114**, 951.
65. J. Szpunar-Lobinska and M. Trojanowicz, *ibid.*, 1990, **115**, 319.
66. M. E. León-González, M. HJ. Santos-Delgado and L. M. Polo-Diez, *ibid.*, 1990, **115**, 609.
67. L. C. de Faria, C. Pasquini and G. de Oliveira Neto, *ibid.*, 1991, **116**, 357.
68. J. A. García-Mesa, M. D. Luque de Castro and M. Valcárcel, *Anal. Chim. Acta*, 1991, in the press.
69. M. Noufi, Ch. Yarnitzky and M. Ariel, *ibid.*, 1990, **228**, 117.
70. S. R. Bysouth, J. F. Tyson and P. B. Stockwell, *Analyst*, 1990, **115**, 571.
71. S. G. Offley, N. J. Seare, J. F. Tyson and H. A. B. Kibble, *Anal. Proc.*, 1991, **28**, 18.
72. R. Nakata, T. Kawamura, H. Sakashita and A. Nitta, *Anal. Chim. Acta*, 1988, **208**, 81.
73. H. Gunasingham, K. P. Ang, P. Y. T. Teo, C. B. Tan and B. T. Tay, *ibid.*, 1989, **221**, 205.
74. R. Appelqvist and E. H. Hansen, *ibid.*, 1990, **235**, 265.
75. E. B. Milosavljevic, L. Solujic, J. L. Hendrix and J. H. Nelson, *Anal. Chem.*, 1988, **60**, 2791.
76. J. F. van Staden, *Anal. Lett.*, 1986, **19**, 1407.
77. E. H. Hansen and J. Ruzicka, *Anal. Chim. Acta*, 1976, **87**, 353.
78. G. Blankenstein and M. R. Kusa, *ibid.*, 1991, **248**, 371.
79. E. Rodríguez, J. L. Pérez Pavón, J. Ruzicka, G. D. Christian and D. C. Olson, *ibid.*, 1992, **259**, 37.

80. S. A. Rosario, G. S. Cha and M. E. Meyerhoff, *Anal. Chem*, 1990, **62**, 2418.
81. J. A. Koropchak and L. Allen, *ibid.*, 1989, **61**, 1410.
82. M. R. Straka, G. Gordon and G. E. Pacey, *ibid.*, 1985, **57**, 1799.
83. D. A. Hollowell, J. R. Gord, G. Gordon and G. E. Pacey, *ibid.*, 1986, **58**, 1524.
84. J. R. Gord, G. Gordon and G. E. Pacey, *ibid.*, 1988, **60**, 2.
85. Z. Zhu and Z. Fang, *Anal. Chim. Acta*, 1987, **198**, 25.
86. G. Svensson and T. Anfält, *Clin. Chim. Acta*, 1982, **119**, 7.
87. S. Alegret, J. Alonso, J. Bartrolí and E. Martínez-Fábregas, *Analyst*, 1989, **114**, 1443.
88. T. L. Spinks and G. E. Pacey, *Anal. Chim. Acta*, 1990, **237**, 503.
89. M. Garn, M. Gisin, Ch. Thommen and P. Cevey, *Biotechnol. Bioengineering*, 1989, **34**, 423.
90. W. R. van der Linden, *Anal. Chim. Acta*, 1983, **151**, 359.
91. G. Schulze, C. Y. Liu, M. Brodowski, O. Elsholz, W. Frenzel and J. Möller, *ibid.*, 1988, **214**, 121.
92. W. Frenzel, *Z. Anal. Chem.*, 1990, **336**, 21.
93. U. Prinzing, I. Ogbomo, C. Lehn and H. L. Schmidt, *Sensors & Actuators*, 1990, **B1**, 542.
94. W. Künnecke and R. D. Schmid, *J. Biotechnol.*, 1990, **14**, 127.
95. V. Kuban, *Anal. Chim. Acta*, 1992, **259**, 45.
96. M. Yasuda, K. Takada, T. Kumamaru, M. Yasuda, S. Yokoyama and Y. Yamamoto, *Anal. Chem.*, 1987, **59**, 2446.
97. F. Nakata, H. Sunahara, H. Fujimoto, M. Yamamoto and T. Kumamaru, *J. Anal. Atom. Spectrom*, 1988, **3**, 579.
98. A. Trojanek and S. Bruckenstein, *Anal. Chem.*, 1986, **58**, 866.
99. M. D. Luque de Castro, *J. Autom. Chem.*, 1986, **8**, 56.
100. B. Karlberg, *Anal. Chim. Acta*, 1988, **214**, 29.
101. G. E. Pacey, Y. P. Wu and K. Sasaki, *Anal. Biochem.*, 1987, **160**, 243.
102. E. Ballesteros, M. Gallego and M. Valcárcel, *Anal. Chem.*, 1990, **62**, 1587.
103. R. G. Melcher, *Anal. Chim. Acta*, 1988, **214**, 299.
104. R. G. Melcher and P. L. Morabito, *Anal. Chem.*, 1990, **62**, 2183.
105. G. Audunsson, *ibid.*, 1986, **58**, 2714.
106. G. Audunsson, *Anal. Chem.*, 1988, **60**, 1340.
107. J. A. Jönsson and L. Mathiasson, *Trends Anal. Chem.*, 1992, **3**, 106.
108. A. Ríos, M. D. Luque de Castro and M. Valcárcel, *Anal. Chem.*, 1988, **60**, 1540.
109. *Idem*, *ibid.*, 1985, **57**, 1803.
110. J. M. Fernández-Romero, M. D. Luque de Castro and M. Valcárcel, *Anal. Chim. Acta*, in the press.
111. R. D. Schmid and W. Künnecke, *J. Biotechnol.*, 1990, **14**, 3.
112. M. Nilson, H. Hakanson and B. Mattiasson, *Anal. Chim. Acta*, 1991, **249**, 163.
113. W. Stöcklein and R. D. Schmid, *ibid.*, 1990, **234**, 83.
114. P. Martínez-Jiménez, M. Gallego and M. Valcárcel, *Anal. Chem.*, 1987, **59**, 69.
115. L. Fossey and F. F. Cantwell, *ibid.*, 1983, **55**, 1882.
116. J. F. van Staden, *Analyst*, 1990, **115**, 605.
117. J. F. van Staden and A. van Rensburg, *J. Anal. Chem.*, 1990, **337**, 393.
118. J. F. van Staden, *Talanta*, 1991, **38**, 1033.
119. D. Utley, *Analyst*, 1990, **115**, 1239.
120. P. Linares, M. D. Luque de Castro and M. Valcárcel, *Anal. Chim. Acta*, 1989, **225**, 443.
121. A. Tanaka, K. Mashiba and T. Deguchi, *ibid.*, 1988, **214**, 259.
122. A. M. Almuaibed and A. Townshend, *J. Anal. Chem.*, 1989, **335**, 905.
123. L. Anderson, *Anal. Chim. Acta*, 1979, **110**, 123.
124. K. S. Johnson and R. L. Petty, *Limmol. Oceanogr.*, 1983, **28**, 1260.
125. P. K. Dasgupta and H. Hwang, *Anal. Chem.*, 1985, **57**, 1009.
126. A. Izquierdo, P. Linares, M. D. Luque de Castro and M. Valcárcel, *J. Anal. Chem.*, 1990, **336**, 490.
127. T. Yao and T. Wasa, *Anal. Chim. Acta*, 1985, **175**, 301.
128. F. Lázaro, M. D. Luque de Castro and M. Valcárcel, *Anal. Chem.*, 1987, **59**, 1859.
129. M. Masoom and A. Townshend, *Anal. Chim. Acta*, 1985, **171**, 185.
130. S. Motomizu and M. Onoda, *ibid.*, 1988, **214**, 289.
131. A. Membiela, F. Lázaro, M. D. Luque de Castro and M. Valcárcel, *ibid.*, 1991, **249**, 461.
132. M. D. Luque de Castro and J. M. Fernández-Romero, *ibid.*, in the press.
133. L. C. de Faria and C. Pasquini, *ibid.*, 1991, **245**, 183.
134. M. J. Hayward, T. Kotiaho, A. K. Lister, R. G. Cooks, G. D. Austin, R. Narayan and G. T. Tsao, *Anal. Chem.*, 1990, **62**, 1798.
135. N. Lacy, G. D. Christian and J. Růžička, *ibid.*, 1990, **62**, 1482.
136. B. Fernández-Band, F. Lázaro, M. D. Luque de Castro and M. Valcárcel, *Anal. Chim. Acta*, 1990, **229**, 177.
137. D. Chen, M. D. Luque de Castro and M. Valcárcel, *ibid.*, 1992, **261**, 269.
138. J. Ruzicka, *Anal. Chem.*, 1983, **55**, 1040A.
139. B. A. Petersson, E. H. Hansen and J. Růžička, *Anal. Lett.*, 1986, **19**, 649.
140. T. D. Yerian, G. D. Christian and J. Růžička, *Anal. Chem.*, 1988, **60**, 1250.
141. *Idem*, *Anal. Chim. Acta*, 1988, **204**, 7.
142. B. A. Petersson, H. B. Andersen and E. H. Hansen, *Anal. Lett.*, 1987, **20**, 1977.
143. W. G. Kuhr and J. Korf, *Anal. Chim. Acta*, 1988, **205**, 53.
144. K. Hool and T. A. Nieman, *Anal. Chem.*, 1987, **59**, 869.
145. H. Liu, J. C. Yu, D. S. Bindra, R. S. Givens and G. S. Wilson, *ibid.*, 1991, **63**, 666.
146. P. J. Worsfold and A. Nabi, *Anal. Chim. Acta*, 1986, **179**, 307.
147. J. Růžička and G. D. Christian, *ibid.*, 1990, **234**, 31.
148. K. A. Defillipo and M. L. Grayeski, *ibid.*, 1991, **249**, 155.
149. R. Pereiro García, Y. M. Liu, M. E. Diaz García and A. Sanz-Medel, *Anal. Chem.*, 1991, **63**, 1759.
150. I. G. Souza, H. Bergamin F°, F. J. Krug, J. A. Nóbrega, P. V. Oliveira, B. F. Reis and M. F. Giné, *Anal. Chim. Acta*, 1991, **241**, 211.
151. D. Yuan, Z. Wang, P. Yang and B. Huang, *ibid.*, 1991, **243**, 65.
152. H. Bergamin F°, F. J. Krug, B. F. Reis, J. A. Nóbrega, M. Mesquita and I. G. Souza, *ibid.*, 1988, **214**, 397.

153. D. Chen, F. Lázaro, M. D. Luque de Castro and M. Valcárcel, *ibid.*, 1989, **226**, 221.
154. F. Lázaro, M. D. Luque de Castro and M. Valcárcel, *ibid.*, 1991, **242**, 283.
155. I. Gács and K. Payer, *ibid.*, 1990, **241**, 71.
156. P. Martínez-Jiménez, M. Gallego and M. Valcárcel, *Anal. Chem.*, 1987, **57**, 69.
157. R. Montero, M. Gallego and M. Valcárcel, *Anal. Chim. Acta*, 1988, **215**, 241.
158. *Idem, J. Anal. Atom. Spectrom.*, 1988, **3**, 725.
159. E. B. Milosavkçljevic, L. Solojic, J. L. Hendrix and J. H. Nelson, *Analyst*, 1989, **114**, 805.
160. B. A. Petersson, Z. Fang, J. Růžička and E. H. Hansen, *Anal. Chim. Acta*, 1986, **184**, 165.
161. M. Gallego, M. Silva and M. Valcárcel, *Anal. Chem.*, 1986, **58**, 2265.
162. G. den Boef, *Anal. Chim. Acta*, 1989, **216**, 289.
163. R. C. Shothorst and G. den Boef, *ibid.*, 1983, **153**, 133.
164. *Idem, ibid.*, 1985, **175**, 305.
165. R. C. Schothorst, J. M. Reijn, H. Poppe and G. den Boef, *Anal. Chim. Acta*, 1983, **145**, 197.
166. R. C. Shothorst, J. J. F. van Veen and G. den Boef, *ibid.*, 1984, **161**, 27.
167. W. T. Kok, D. T. Thuy, T. V. Nghi and G. den Boef, *ibid.*, 1987, **200**, 533.
168. J. M. Elvecrog and P. W. Carr, *ibid.*, 1980, **121**, 135.
169. D. Taylor and T. A. Nieman, *ibid.*, 1986, **186**, 91.
170. *Idem, ibid.*, 1986, **186**, 91.

Talanta, Vol. 40, No. 1, pp. 37–42, 1993
Printed in Great Britain.

0039-9140/93 $6.00 + 0.00

DETERMINATION OF SULFUR SPECIES BY CATHODIC SQUARE WAVE STRIPPING VOLTAMMETRY; COMPOUNDS RELEVANT TO NATURAL SULFUR MINERALIZATION

R. VON WANDRUSZKA* and X. YUAN
Department of Chemistry, University of Idaho, Moscow, ID 83843, U.S.A.

M. J. MORRA
Division of Soil Science, University of Idaho, Moscow, ID 83843, U.S.A.

(*Received* 17 *March* 1992. *Revised* 7 *May* 1992. *Accepted* 13 *May* 1992)

Summary—The feasibility of rapid analysis of a number of environmentally important sulfur compounds by cathodic square wave stripping voltammetry at a mercury electrode has been investigated. For cysteine/cystine a relatively anodic peak was identified, which is ascribed to the stripping of a mercurous species. The dependence of the peak currents on pH was found to be different for cysteine and cystine. Methionine and thioproline gave similar stripping peaks to those for cysteine. It is proposed that they arise from species deposited by oxidative hydrolysis. A complex ion is proposed to cause the stripping peak of thiosulfate and tetrathionate, while polysulfides give both a HgS stripping peak and a non-adsorptive reduction peak. Limits of detection are in the 10^{-8}–$10^{-9}M$ range.

A number of analytical techniques have been used to investigate the mineralization processes of *L*-cysteine, $HSCH_2CH(NH_2)COOH$, [CySH], and *L*-cystine, $HOOC(NH_2)CHCH_2S$-$SCH_2CH_2CH(NH_2)COOH$, [CySSCy], in soils and other matrices.[1–8] A general shortcoming of the various determinations is the analytical speed, which is often too slow to resolve the rapid chemical changes that occur during the incubation of the compounds with soil, especially in the early stages. Square wave voltammetry provides a fairly comprehensive analysis in a matter of seconds, without sample pretreatment. Its high sensitivity and wide range of application for S-compounds allow the use of small sample sizes, minimizing the disturbance of the system.

Many of the major sulfur containing anions other than sulfate react with the mercury electrode according to the reactions in Table 1.[9,10] The anodic reactions of sulfide, sulfite, and thiosulfate have been much studied, and in general their $E_{1/2}$ values depend on the pH and the composition of the supporting electrolyte. Some compounds give double voltammetric waves, of which the first (least negative $E_{1/2}$) is usually the best defined. Recently, adsorptive stripping voltammetry has been developed to determine organic S-compounds at the mercury electrode.[10–16] Florence[10] explained the adsorption in terms of the formation of a mercury-thiol complex. Forsman[14] observed that in the presence of copper ion, the stripping current of cysteine and cystine is enhanced due to the adsorption of their Cu(I) complexes. In this investigation, a number of species relevant to natural mineralization has been determined. The present study focuses on the mechanism of the electrode reactions involved.

EXPERIMENTAL

Instrumentation and procedure

Voltammetric measurements were taken with a Sargent-Welch 7001 voltammetric analyzer. The working electrode was a Metrohm 335 hanging mercury drop electrode (HMDE), with an electrode surface of 1.4 mm^2. A platinum wire auxiliary electrode and a saturated calomel reference electrode were used to complete the cell, which was closed, deaerated, and blanketed with oxygen-free nitrogen. The assembly was connected to a Sargent-Welch Model-VES electrode stand. For mechanistic studies, 60-sec anodic accumulation times and stirred solutions

*Author for correspondence.

Table 1. Reactions of S-species at the mercury electrode

1.	$2\,S_2O_3^{2-} + Hg = Hg(S_2O_3)_2^{2-} + 2e^-$	$E_{1/2} = -0.12$ V
2.	$2\,SO_3^{2-} + Hg = Hg(SO_3)_2^{2-} + 2e^-$	$E_{1/2} = -0.60$ V
3.	$SH^- + Hg = HgS + H^+ + 2e^-$	$E_{1/2} = -0.68$ V
4.	$S_x^{2-} + Hg = HgS + (x-1)S + 2e$	$E_{1/2} = -0.68$ V
5.	$S_x^{2-} + 2(x-1)e^- + xH_2O = xOH^- + xSH$	$E_{1/2} = -0.68$ V
6.	$2\,CySH + Hg = (CyS)_2Hg + 2H^+ + 2e^-$	$E_{1/2} = -0.52$ V
7.	$CySSCy + Hg = (CyS)_2Hg$	$E_{1/2} = -0.52$ V

were used, unless stated otherwise. Each determination was carried out on a fresh mercury drop. Square wave voltammograms were run at a frequency of 150 Hz, with 5-mV step size and 5-mV pulse amplitude. Cyclic voltammetry was conducted in the staircase mode, with a step width of 5 msec and a scan rate of 100 mV/sec.

Chemicals

The sulfur containing organic and inorganic compounds used in the experiments: *L*-cysteine, *L*-cystine, thioproline (4-thiazolidinecarboxylic acid), DL-methionine, *L*-cysteic acid (cysteine sulfonic acid), cysteamine, sodium sulfate, sodium thiosulfate, sodium sulfite, sodium sulfide, sodium tetrathionate, sodium dithionite, and sodium meta-disulfite were of reagent grade, supplied by Sigma, Baker, and Aldrich. The purity of organic reagents was checked by thin-layer chromatography, using silica gel plates and 1:1 ethanol:water eluent. All stock solutions were prepared in deaerated demineralized water, treated with a Millipore purification system to 18 MΩ cm resistivity. The buffer solutions used were $0.01M$ $NaB_2O_7 + 0.01M$ Na_2HPO_4 (pH 8.5), $0.1M$ $KH_2PO_4 + 0.017M$ NaOH (pH 6.2), and $0.01M$ NaOAc + $0.01M$ HOAc (pH 4.5). They were purged with oxygen-free nitrogen to remove dissolved oxygen, before being used for the determination of easily oxidized S-compounds.

RESULTS AND DISCUSSION

Cysteine and cystine

It is generally agreed that the anodic voltammetric behavior of cysteine is a result of the reaction:

$$Hg + 2CySH \rightarrow Hg(CyS)_2 + 2H^+ + 2e^- \quad [1]$$

It has been observed, however, that the reduction of mercury cysteinate sometimes results in two waves, separated by 0.1 V, usually at relatively high cysteine concentrations.[10,17-19] Miller[19] attributes the double wave to the presence of both $Hg_2^I(CyS)_2$ and $Hg^{II}(CyS)_2$ deposited on the surface, the more positive peak being due to the Hg(I) compound. Stankovich[17] explains the split as a result of "compacting" of the mercury cysteinate film, while Florence[10] ascribes it to a surface impurity. In the present study, cathodic square wave voltammetry (CSWV) was found to produce a narrow, well defined peak at −0.55 V (SCE) for low concentrations (nM level) of both cysteine and cystine. The wave is split somewhat unpredictably, with a separation of 0.05–0.1 V, but the peak areas are complimentary (Fig. 1). The split may be due to the formation of an adsorbed Cu(I)-cysteinate complex,[14,15] the Cu(I) arising from a copper impurity and producing the more positive peak. The possible influence of other

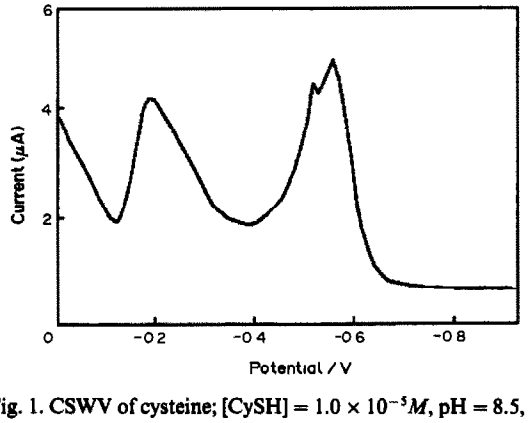

Fig. 1. CSWV of cysteine; [CySH] = $1.0 \times 10^{-5}M$, pH = 8.5, accumulation at for one minute 0.0 V.

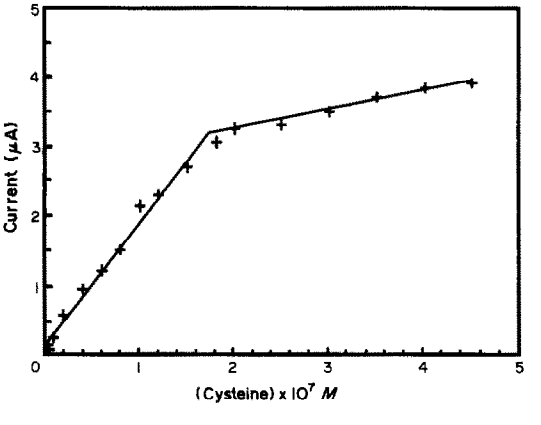

Fig. 2. Calibration curve for cysteine using current peak at −0.5 V; conditions as in Fig. 1.

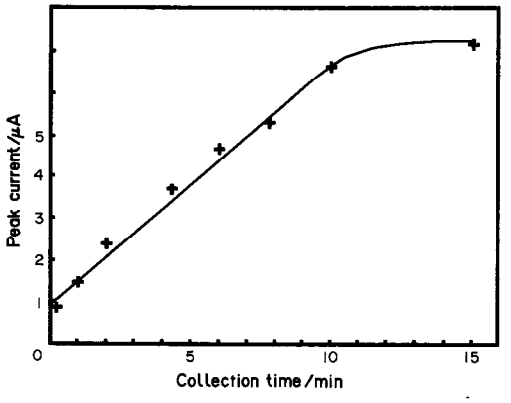

Fig. 3. Plot of combined cysteine stripping peak heights (−0.15 V and −0.55 V) *vs.* collection time; [CySH] = $1.0 \times 10^{-7}M$; pH = 8.5; deposition potential 0.0 V.

adventitious metal ions requires further investigation. The CSWV peak current at −0.55 V was found to be proportional to the cysteine concentration up to $5 \times 10^{-7}M$ with measurement possible down to $5 \times 10^{-9}M$ (Fig. 2) when a −0.2 V deposition potential was used. This is an improvement over results obtained with differential pulse cathodic stripping voltammetry.[10] When a 0.0 V deposition potential, or open circuit conditions are used, the calibration curve loses its linearity at concentrations greater than $5 \times 10^{-8}M$.

Besides the peak at −0.55 V, a broad wave around −0.15 V was found for both cysteine and cystine (Fig. 1). The peak height increases with concentration in the range 8×10^{-8} to $1 \times 10^{-6}M$, but this variation is not linear, since the peak heights at −0.15 V and at −0.55 V were found to be complementary. Their sum varies linearly with concentration, as well as with deposition time up to about 10 min (Fig. 3). The loss of linearity at longer times may be due to eventual surface saturation. The cyclic voltammogram (taken after 60 sec deposition at 0.0 V; Fig. 4) shows only an anodic peak, corresponding to the −0.55 V cathodic peak.

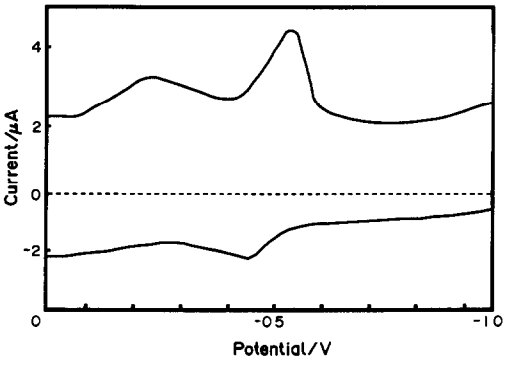

Fig. 4. Cyclic voltammogram of cysteine; [CySH] = $1.0 \times 10^{-5}M$.

In view of these observations it may be proposed that both $Hg_2^{I}(CyS)_2$ and $Hg^{II}(CyS)_2$ are formed, and that the former can be stripped over a fairly wide potential range around −0.15 V. Cysteine is therefore present in two adsorbed forms, resulting in the complementary nature of the two stripping peaks. Once stripped, the mercurous species does not reform at the electrode in the reverse (anodic) sweep of the cyclic voltammogram. This seeming irreversibility, indicated by the absence of the anodic peak at −0.15 V, may be due to a disproportionate reoxidation of the stripped species to the mercuric complex during the reverse sweep.

To provide further evidence for the origin of the peak at −0.15 V, cathodic scans were taken from a deposition potential of +0.20 V, at a relatively high cysteine concentration of $1.0 \times 10^{-6}M$. The only peak observed was the one at −0.55 V, corresponding to $Hg^{II}(CyS)_2$. This is consistent with the proposed process, since Hg_2^{2+}—and hence the mercurous complex —cannot exist at such an anodic potential.

The solubility product of $Hg_2^{I}(CyS)_2$ can be estimated from the peak potential, E_p, of the complex and the dissociation constant of the amino acid:[10]

$$E_p = E^\circ(Hg_2^{2+}/Hg) + 0.060(0.5 \log K_{sp} + \log K_a - \mathrm{pH} - \log[\mathrm{CySH}]) \quad (2)$$

With a buffer solution of pH 8.5, [CySH] = 1.0×10^{-7}, $E_p = -0.15$ V (SCE), $E^\circ(Hg_2^{2+}/Hg) = 0.556$ V, and $pK_a = 8.36$ (thiol group), pK_{sp} for $Hg_2^{I}(CyS)_2$ is 29.2. In view of the much smaller solubility of $Hg^{II}(CyS)_2$ ($pK_{sp} = 56.7$), the loss of linearity of the calibration curve can be explained. When the cysteine concentration is low ($< 5 \times 10^{-8}M$), only $Hg^{II}(CyS)_2$ is produced, because of the larger solubility of $Hg_2^{I}(CyS)_2$, which shifts its decomposition potential in an anodic direction [equation (2)], precluding the formation of the complex at a deposition potential of 0.0 V. At higher cysteine concentrations both species can be formed, and a deposition potential of −0.2 V (more cathodic than the first stripping peak) is necessary to avoid formation of $Hg_2^{I}(CyS)_2$. The occurrence of $Hg_2^{I}(CyS)_2$ is therefore limited to potentials that lie roughly between 0.2 V and −0.2 V. Cystine behaves similarly.

Equation (2) indicates that a lowering of the pH should cause an anodic shift of the cathodic

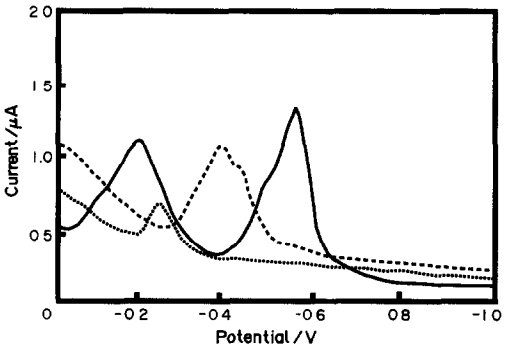

Fig. 5. Effect of pH on CSWV of cysteine. —— pH = 8.5; – – – pH = 6.2; · · · pH = 4.5.

Table 2. CSWV of S-compounds. pH 8.5 buffer, 1 min deposition time, scan range 0.0 to −1.2 V *vs.* SCE

Compound ($5 \times 10^{-7}M$)	Peak potential E_1	E_2*	E_3†
Cysteine	−0.55	−0.15	−0.50
Cystine	−0.55	−0.15	−0.48
Cysteamine	−0.53	−0.09	−0.65
Methionine	−0.47	−0.05	−0.62
Thioproline	−0.53	−0.09	−0.48
Carbon disulfide	−0.70		
Thiosulfate	−0.2 to −0.35		
Tetrathionate	−0.2 to −0.27		
Polysulfides	−0.67		

*Peak appears at relatively high concentration.
†Peak may be split.

stripping peak for the cysteine–mercury complex. This is borne out by the data presented in Fig. 5. A lowering of the pH also causes a decrease in peak heights due to proton competition [a shift to the left in the amino acid dissociation, equation (1)]. At pH 8.5 the sensitivities of the peaks are nearly the same for cysteine and cystine. However, the sensitivity for cysteine is much greater than that for cystine at pH 6.2 and 4.5, *i.e.*, cystine is more strongly affected by pH change. At a total amino acid concentration of $5 \times 10^{-7}M$ and a pH of 6.2, the peak for cysteine reduces to about 80% of its size at pH 8.5, but the cystine peak reduces to about 20% under similar conditions. At pH 4.5 the peak corresponding to the cystine reaction disappears, while the one for cysteine remains (Fig. 5). The different effect of pH on cysteine and cystine could provide a way to distinguish the two compounds by CSWV.

The peak due to the mercurous cysteine complex, $Hg^{I}_2(CyS)_2$, also disappears at pH 4.5. This may be due to increased solubility of the complex at lower pH values, or to the anodic shift of E_p, that moves it beneath the large mercury oxidation wave at 0.2–0.3 V.

Other sulfur compounds

The cathodic square wave stripping peaks of a number of compounds important for sulfur cycling in soil are listed in Table 2. Thioproline and methionine give voltammograms that are similar to those of cysteine/cystine, with only slight shifts in the three peaks. In view of the fact that these compounds give strong stripping peaks that are proportional to the bulk concentration, and that thin layer chromatography shows the absence of detectable cysteine/cystine impurities, it must be concluded that the similarity of the stripping peaks of cysteine, cystine, methionine, and thioproline indicates that the anodically adsorbed species of these four compounds are alike. This calls for an adsorption mechanism involving the methylated sulfhydryl group. In order to lead to similar stripping behavior, this interaction probably also involves oxidative compound formation, as shown in cysteine in Table 1. It may be suggested that the following anodic accumulation reactions take place with methionine and thioproline, respectively:

$$2HOOC(NH_2)CHCH_2CH_2SCH_3 + Hg + 2H_2O \rightarrow (HOOC(NH_2)CHCH_2CH_2S)_2Hg + 2CH_3OH + 2H^+ + 2e^-$$

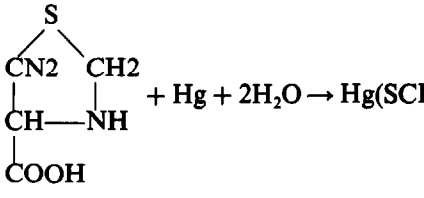

The stripping of these compounds produces the observed cathodic peaks. The stripping behavior of cysteamine, $HSCH_2CH_2NH_2$ is also similar to that of cysteine, which is expected in view of its chemical similarity.

Cathodic stripping voltammetry of inorganic sulfide has been extensively studied.[12,20–23] In the present work, a sharp stripping peak was

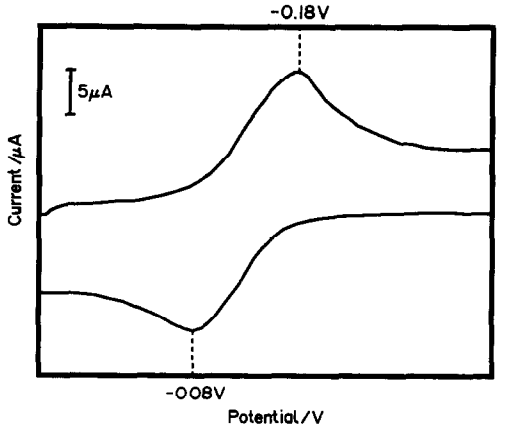

Fig. 6. Cyclic voltammogram of thiosulfate ($5.0 \times 10^{-5}M$).

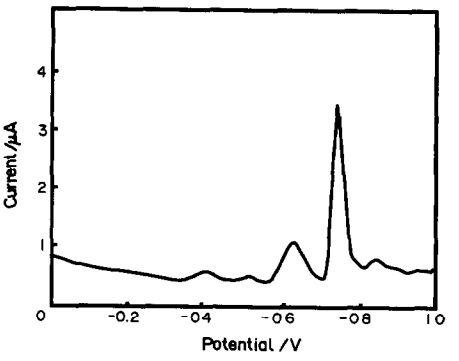

Fig. 7. CSWV of polysulfide ($1.0 \times 10^{-6}M$).

observed at −0.72 V by CSWV. An accumulation potential of 0.0 V was applied for 60 sec prior to stripping, and analytical results were similar to those obtained by other workers.[21]

The anodic electrode reaction of thiosulfate has been used for analytical purposes for many years.[9,24,25] Wienhold and Sohr[26] have described a catalytic hydrogen wave, useful for the determination of thiosulfate in the concentration range 5×10^{-8}–$5 \times 10^{-5}M$. No information is available in the literature on the determination of thiosulfate by cathodic scan voltammetry. In the present investigation, a reductive stripping peak was found at −0.18 V, which is linearly related to the thiosulfate concentration over the range 8×10^{-9} to $5 \times 10^{-7}M$. The peak height and potential are virtually unaffected by pH in the range 2.5–9.2 and by deposition time. The latter indicates that the electrode process is not an adsorptive one. The cyclic voltammogram shows both cathodic and anodic peaks (Fig. 6).

A mechanism for the production of the thiosulfate peak by CSWV may be proposed, which is the reverse of the anodic mechanism described by Renard *et al.*[25] These authors suggest that the anodic peak is due to the following reactions:

$$Hg \rightarrow Hg^{2+} + 2e^- \quad [3]$$

$$Hg^{2+} + 2\ S_2O_3^{2-} \rightarrow [Hg(S_2O_3)_2]^{2-} \quad [4]$$

The $E_{1/2}$ value for this process (Table 1) is −0.12 V, and it will therefore occur significantly in the early parts of the cathodic scan starting in 0.0 V. A surface equilibrium of the ionic species is quickly established, and extended accumulation does not substantially alter its concentration near the electrode, as it is subject to diffusion. During the cathodic scan, the reverse of reactions 3 and 4 takes place, leading to the observed current peak. The cathodic process has a limit of detection of $8 \times 10^{-9}M$, which is almost 4 orders of magnitude lower than the reported value for the anodic process. This may be partially due to the inherent response of the fast square wave scan, and partially to a relatively high surface concentration of $[Hg(S_2O_3)_2]^{2-}$, enhanced by some degree of electrostatically induced adsorption of the ion.

Polysulfides, synthesized as described by Rosen and Tegman,[27] gave cathodic square wave voltammograms that were very similar to those of sulfide, showing a large HgS stripping peak at −0.72 V (Fig. 7). In addition, some smaller peaks are shown, that probably arise from other adsorbed sulfide species. However, the peak at −0.62 V is independent of accumulation time and may be due to the reaction:

$$S_2^{2-} + 2e^- + 2H_2O \rightarrow 2SH^- + 2OH^- \quad [5]$$

Reaction (5) involves no anodically adsorbed species and depends on bulk concentrations only.

Tetrathionate gives cathodic scan peaks that are similar to those observed for thiosulfate, and probably arise through a similar mechanism. Sulfite gives no peaks in CSWV.

CONCLUSION

CSWV of environmentally important sulfur compounds is a sensitive and widely applicable analytical technique that provides the speed of analysis needed for natural samples that are subject to rapid chemical changes. A series of applications to the mineralization study in natural samples will be communicated in a subsequent publication. A number of the analytically useful current peaks observed require mechanistic interpretation, and anodic compound formation is proposed in most instances.

Acknowledgements—This work was supported by a grant from the University of Idaho Research Council.

REFERENCES

1. K. Minami and S. Fukushi, *Soil Sci. Plant Nutr.*, 1981, **27**, 105.
2. M. J. Morra and W. A. Dick, *Soil Sci. Am. J.*, 1985, **49**, 882.
3. *Idem*, *ibid.*, 1989, **53**, 440.
4. *Idem*, *Appl. Environ. Microbiol.*, 1991, **57**, 1413.
5. R. J. Swaby and R. Fedel, *Soil Biol. Biochem.*, 1973, **5**, 773.
6. K. Minami and S. Fukushi, *Soil Sci. Plant Nutr.*, 1981, **27**, 339.
7. W. L. Banwart and J. M. Bremer, *Soil Biol. Biochem.*, 1975, **7**, 359.
8. H. Kumagai, Y. J. Choi, S. Sejima and H. Yamada, *Agri. Biol. Chem.*, 1975, **39**, 387.
9. G. W. Luther, A. E. Giblin and R. Varsolona, *Limnol. Oceanogr.*, 1985, **30**, 727.
10. T. M. Florence, *J. Electroanal. Chem.*, 1979, **97**, 219.
11. F. G. Banica, *Talanta*, 1985, **32**, 1145.
12. M. Youssefi and R. L. Birke, *Anal. Chem.*, 1977, **49**, 1380.
13. P. A. Grier and R. W. Andrews, *Anal. Chim. Acta*, 1981, **124**, 333.
14. U. Forsman, *J. Electroanal. Chem.*, 1981, **122**, 215.
15. *Idem*, *ibid.*, 1983, **152**, 241.
16. C. M. G. Van den Berg, B. C. Househam and J. P. Riley, *J. Electroanal. Chem.*, 1988, **239**, 137.
17. M. T. Stankovich and A. J. Bard, *ibid.*, 1977, **75**, 487.
18. C. A. Mairesse-Ducarmois, G. J. Patriarche and J. L. Vandenbalk, *Anal. Chim. Acta*, 1974, **71**, 165.
19. I. R. Miller and J. Teva, *J. Electroanal. Chem.*, 1972, **36**, 157.
20. T. Miwa, Y. Fujii and T. Mizuike, *Anal. Chim. Acta*, 1972, **60**, 475.
21. H. Gerge and P. Jeroschewski, *Z. Anal. Chem.*, 1965, **207**, 110.
22. W. Davison, *Limnol. Oceanogr.*, 1977, **22**, 746.
23. W. Davison and C. D. Gabbutt, *J. Electroanal. Chem.*, 1979, **99**, 311.
24. S. Zhandov, *Sulfur*, in *Encyclop. Electrochem. Elem.*, Vol. 4, p. 273. Marcel Dekker, New York, 1979.
25. J. J. Renard, G. Kubes and H. I. Bolker, *Anal. Chem.*, 1975, **47**, 1347.
26. K. Wienhold and H. Sohr, *Z. Chem.*, 1980, **20**, 265.
27. E. Rosen and R. Tegman, *Acta Chem. Scand.*, 1971, **25**, 3329.

Talanta, Vol. 40, No. 1, pp. 43–51, 1993
Printed in Great Britain.

0039-9140/93 $6.00 + 0.00

APPLYING THE PHENOL RED COLORIMETRIC METHOD FOR BROMIDE ANALYSIS TO REDUCING WATERS

DAVID R. JONES
CSIRO Division of Coal and Energy Technology, P.O. Box 136, North Ryde, N.S.W. 2113, Australia

(*Received* 26 *March* 1992. *Accepted* 12 *May* 1992)

Summary—Chemical species present in reducing waters have the potential to produce severe negative interferences by consuming the chloramine T (CT) which is used as the oxidising agent in the phenol red-based colorimetric method for trace bromide analysis. Mn^{2+} and Fe^{2+} were found not to interfere at concentrations up to 200μM. However, hydroxylamine (NH_2OH), which can be present in both ground- and surface-waters, exerts a strong negative interference. A method involving pre-treatment with permanganate and hydrogen peroxide has been developed for the destruction of NH_2OH prior to adding the colour reagents. The procedure is not only compatible with the chemistry of the colorimetric method, but is also robust and technically easy to implement.

The reaction of hypobromite with phenol red to produce bromophenol blue affords a very sensitive method for the determination of bromide in solution.[1] Previous work by the author has been directed towards optimizing this method for the analysis of bromide in aerobic surface waters.[2,3]

However, there are many cases in which naturally or anthropogenically produced waters of low redox potential may need to be analysed for bromide. The Chloramine T (CT) used in the colorimetric method for the oxidation of Br^- to reactive OBr^- can be consumed by competitive reactions with the reduced chemical species that are present under such circumstances. Significant depletion of CT by this route would result in a negative interference in the formation of bromophenol blue.

Iron and manganese oxides dissolve under mildly reducing conditions to produce Mn^{2+} and Fe^{2+}. The electrochemical half cell potentials for reactions involving these ions indicate they should be oxidized by CT.[4,5] Elevated levels of Mn^{2+} and Fe^{2+} are typically found in groundwaters and in surface water draining areas such as marshes where decay processes have lowered the redox potential. The reduced nitrogen compound hydroxylamine (NH_2OH) is an intermediate both in nitrification reactions and in the reduction of oxidized nitrogen to ammonia.[6,7] This compound is therefore likely to be found in mildly reducing waters. Concentrations up to 100μM have been measured in water draining marshlands in Ethiopia.[7] It has also been detected, at much lower concentrations, in coastal marine systems.[8] Anthropogenic sources of hydroxylamine include boiler water to which it is added as a corrosion inhibitor.

Previous work by the author has shown that hydroxylamine produces a severe negative interference in the bromide method since it reacts stoichiometrically with CT, with a rate constant that is comparable with the oxidation of bromide.[2] Although both Mn^{2+} and Fe^{2+} have the potential to interfere with the method, little work has been published on quantifying the extent of such interferences.[9,10]

There were two major objectives for the work reported in this paper. Firstly, to establish the extent to which hydroxylamine, Mn^{2+} and Fe^{2+} interfere with the colorimetric method for bromide analysis. Secondly, to develop a robust and technically practical method to overcome the identified interferences. The essential criterion for such a method was that it must be compatible with the chemistry of the CT–phenol red procedure.

EXPERIMENTAL

Reagents

All chemicals used were of analytical reagent grade or better. The Chloramine T (sodium *N*-chloro-4-toluenesulphonamide), CT, was recrystallised from hot water and freeze dried

prior to use.[11] Stock solutions of hydrogen peroxide were prepared by dilution of 100 volume hydrogen peroxide, and standardized by titration with potassium permanganate. The stock solutions of hydroxylammonium chloride (NH_3OHCl), potassium permanganate, hydrogen peroxide, CT, and sodium thiosulphate used for this work were stored in amber glass bottles at 4° between experiments to minimise degradation. Fresh working solutions of the $KMnO_4$, H_2O_2, and CT were prepared daily by dilution. The preparation of the reagent solutions (acetate buffer, phenol red, and CT) required for the colorimetric bromide method has been reported previously.[1,2]

All experiments were carried out in 20-ml capacity screw-cap polyethylene scintillation vials. These vials had been precleaned by sequential soaking with detergent and dilute nitric acid. They were rinsed three times with distilled, demineralized water and oven dried prior to use.

Effect of Fe^{2+}, Mn^{2+}, NH_2OH and H_2O_2 on colour development

A separate series of vials was prepared for each of the four test species. For each series 0.5 ml of acetate buffer (final pH on dilution = 4.6) and 0.5 ml of a $5 \times 10^{-3}M$ potassium bromide stock solution (to produce a final concentration of $25\mu M$ Br^- in a volume of 10 ml) was added to each vial. Increasing volumes of working solutions of Fe^{2+}, Mn^{2+}, NH_2OH, or H_2O_2, as appropriate, plus the required volume of distilled water to make up a 10-ml total volume, were then added to each successive vial in the series so that a range of concentrations from 0 to $200\mu M$ was spanned. The bromide colorimetric procedure was then applied to each of the test series, and the extent of bromophenol blue formation measured at 590 nm.[2]

Reaction of Fe^{2+} with CT

The rate of this reaction was studied by measuring the residual concentration of Fe^{2+}. The reaction was initiated by adding CT to a solution of iron(II) sulphate in pH 4.6 acetate buffer such that the initial concentrations of CT and Fe^{2+} were 40 and $100\mu M$, respectively. Aliquots of solution were withdrawn at 30-sec intervals, and quenched by the addition of $100\mu M$ NH_2OH. A solution of 2,2′-bipyridyl was added after 2 min to form the extremely stable and intensely red coloured Fe^{2+}-bipyridyl complex.[12] The colour produced was measured at 470 nm, and the concentration of Fe^{2+} determined by comparison with a standard curve.

The NH_2OH was added to destroy residual CT, whilst preserving the redox speciation of the iron. Although NH_2OH will reduce Fe^{3+} to Fe^{2+}, a preliminary control experiment showed that, under the conditions of this experiment, the rate of this process was sufficiently slow that it would not complicate interpretation of the results from the above experiment.

Screening of reagents to decompose hydroxylamine

To vials containing $25\mu M$ potassium bromide and $100\mu M$ NH_2OH buffered at pH 4.6 were added stoichiometric excesses of $NaClO_3$, $Fe_2(SO_4)_3$, $KMnO_4$, K_2CrO_4, or H_2O_2. After 20 min the bromide colorimetric reagents were added. The developed colour was measured at 590 nm after a further 20 min.

Stoichiometry of the MnO_4^-/NH_2OH reaction

The optimum MnO_4^- to NH_2OH ratio was found by measuring the extent of colour formation following the addition of the phenol red and CT reagents to solutions containing fixed concentrations of Br^- and NH_2OH that had been treated with different amounts of MnO_4^-. The MnO_4^- to NH_2OH ratios studied ranged from 0 to 0.67.

The required volume of potassium permanganate stock solution plus sufficient distilled water to make up 1 ml was rapidly mixed with 10 ml of a premixed solution containing $25\mu M$ Br^-, $110\mu M$ NH_2OH, and 0.5 ml of acetate buffer concentrate. The initial concentration of NH_2OH in the total volume of 11 ml was therefore $100\mu M$. The phenol red and CT reagents were added after 20 min since spectrophotometric kinetic experiments showed that the reaction between the MnO_4^- and NH_2OH was complete within 10 min in the temperature range 20–25°. A second experiment was carried out in order to measure the extent of MnO_2 production as a function of the amount of MnO_4^- added. In this case the procedure was terminated after 20 min when the absorbance of the solution was measured at 425 nm. This wavelength, although not corresponding to the maximum in absorbance for the colloidal suspension of MnO_2, was found to be the least susceptible to overlap from chromophores of the other reagents used in this investigation.

The first experiment detailed above was repeated with the addition of $250\mu M$ hydrogen

peroxide prior to the colorimetric reagents. The H_2O_2 was added to decompose the excess MnO_4^- that would otherwise negatively interfere with the subsequent colour development. Kinetic experiments showed that the reaction with hydrogen peroxide was complete in less than 5 min. A time of 10 min was therefore allowed for this step.

Reaction between Mn^{2+} and MnO_4^-

The reaction between these two species was monitored at both 425 and 542 nm. The former wavelength provides a measure of the production of MnO_2 (see above) whilst the latter corresponds to the absorbance maximum of MnO_4^-. Appropriate volumes of dilute solutions of $MnCl_2$ and $KMnO_4$ were rapidly mixed to obtain the required initial concentrations of reactants.

Measurement of NO_2^- production

The NO_2^- produced in the reaction between NH_2OH and MnO_4^- was measured by using a colorimetric diazotization procedure.[13] Trial experiments showed that the pH for the NO_2^- method must be below 2 to ensure full colour development. This necessitated preparing the sulphanilamide reagent in a 36% (v/v) solution (36 ml of concentrated acid in 100 ml total volume) of hydrochloric acid in order to overcome the buffering capacity of the acetate buffer solution in which the reaction between NH_2OH and MnO_4^- was carried out.

It was also found that the presence of MnO_2 (generated when the MnO_4^- to NH_2OH ratio exceeded 0.5) resulted in a severe negative interference. This was overcome by reducing the MnO_2 to Mn^{2+} with 130μM hydrogen peroxide prior to adding the nitrite reagents. A standard curve prepared in the presence of 130μM hydrogen peroxide was used to convert absorbance values to concentrations.

Evaluation of the method

All of the experiments described above were done in a reaction medium based on distilled water. However, in evaluating the robustness and precision of the coupled NH_2OH decomposition-bromide colorimetric procedure a synthetic medium of initial ionic composition likely to be more typical of a real sample was used. This contained 3mM NaCl, 1mM $NaHCO_3$, 1.5mM $MgCl_2$, and 0.3mM $MgSO_4$.

Four standard curves (0, 5, 10, 15, 20, 30μM Br^-) were prepared using 0, 20, 50 or 100μM NH_2OH. Each point on each of the standard curves was run in triplicate. The generic procedure used is detailed below:

(1) Prepare a vial containing the required volume of 500μM potassium bromide standard, the required volume of 2000μM NH_3OHCl standard, and sufficient synthetic ionic medium to make up a total of 10 ml.

(2) Add 0.5 ml of acetate buffer, and mix.

(3) Add 0.5 ml of a 2mM potassium permanganate solution, and mix. Then stand for 20 min.

(4) Add 0.5 ml of a 6mM hydrogen peroxide solution, and mix. React for 10 min.

(5) Add 0.5 ml of phenol red solution.

(6) Add 0.5 ml of CT and **immediately** mix well. React for 20 min.

(7) Add 0.1 ml of sodium thiosulphate reagent, and mix. Stand for at least 10 min before measuring the absorbance of the solution at 590 nm.

RESULTS AND DISCUSSION

An initial set of experiments was carried out to determine the ability of hydroxylamine, Mn^{2+} and Fe^{2+} to interfere with colour development. The colorimetric procedure developed by the author was applied to solutions containing 25μM Br^- and varying concentrations of the three test solutes (Table 1).[2] The hydroxylamine (NH_2OH) would be predominantly in its protonated hydroxylammonium form (NH_3OH^+, $pK_a = 5.98$) at the prevailing pH of 4.6.[14] The results in Table 1 show that NH_2OH is by far the most potent inhibitor of bromophenol blue formation. Fe^{2+} exhibits a slight interference at 200μM, whilst Mn^{2+} has no significant effect up to 200μM. This result was surprising since electrochemical potentials indicate that Fe^{2+} and Mn^{2+} should be readily oxidized by CT.[4] The reaction between Fe^{2+} and CT was therefore investigated in more detail to determine

Table 1. Effect of inhibitor concentration on colour development

Concentration of inhibitor, μM	Percent colour development at 590 nm		
	NH_2OH	Fe^{2+}	Mn^{2+}
0	100	100	100
20	61	100	—
40	0	101	101
80	0	101	—
100	0	100	103
200	—*	95	103

*This concentration of potential inhibitor was not used.

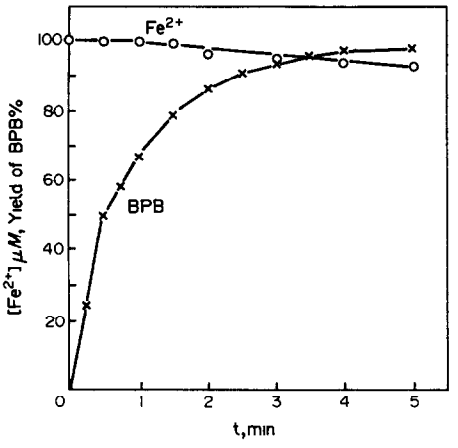

Fig. 1. Kinetics of oxidation of Fe^{2+} by CT (O——O) compared with kinetics of bromophenol blue (BPB) formation (×——×) in the bromide method. The generation of BPB is expressed as a percentage of the maximum absorbance at 590 nm attained by applying the colorimetric method to a 25μM Br^- standard solution.

why the above results differed from the outcome predicted by thermochemical considerations.

Reactivity of Fe^{2+}

The data from the experiment to measure the rate of reaction between Fe^{2+} and CT are plotted in Fig. 1. They show that the rate of this reaction is at least an order of magnitude slower than the series of reactions leading to the formation of bromophenol blue. In this case the extent of interference is limited by kinetic rather than thermodynamic constraints. It is probable that the reaction with Mn^{2+} is similarly rate limiting.

Removal of interference by hydroxylamine

The starting point for this investigation was the selection of reagents that could oxidize NH_2OH. There are several possible oxidation products of this compound that could be formed.[15] However, published work indicates that N_2, N_2O, NO_2^- and NO_3^- (nitrogen oxidation states of 0, +1, +3, and +5, respectively) are the most likely ones in this case.[16–18] The half cell reactions for each of these potential products are shown in equations (1) to (4). The half cell potentials were obtained directly from the literature or were derived from published thermodynamic data.[4,19] It should be noted that a number of sequential fundamental steps could be involved in the multiple electron transfer half cell reactions described by equations (1) to (4).

$$N_2 + 4H^+ + 2H_2O + 2e^- \rightarrow 2NH_3OH^+ \qquad E^0 = -1.87\ V \quad (1)$$

$$N_2O(aq) + 6H^+ + H_2O + 4e^- \rightarrow 2NH_3OH^+ \qquad E^0 = -0.03\ V \quad (2)$$

$$NO_2^- + 6H^+ + 4e^- \rightarrow NH_3OH^+ + H_2O \qquad E^0 = 0.66\ V \quad (3)$$

$$NO_3^- + 8H^+ + 6e^- \rightarrow NH_3OH^+ + 2H_2O \qquad E^0 = 0.72\ V \quad (4)$$

Based on purely thermodynamic considerations, there are a number of common inorganic oxidizing agents that could oxidize the hydroxylamine. Organic reagents were not considered to be suitable since they could potentially compete with phenol red as substrates for reaction with hypobromite in the subsequent production of bromophenol blue.[2,20]

Potential inorganic oxidizing agents were tested for their ability to decompose hydroxylamine to a non-interfering form. The species studied were MnO_4^-, Fe^{3+}, H_2O_2, $HCrO_4^-$ and ClO_3^-. Solutions containing stoichiometric ratios of hydroxylamine and the test reagents were prepared, and the interference by hydroxylamine measured after 20 min and 3 hr. The criterion for success was that the reaction should be complete within 20 min at pH 4.6 in the temperature range 20–25°. These boundary conditions were selected for both chemical compatibility (with the colorimetric method) and technical (an acceptable time) reasons. Of the reagents tested only permanganate passed this initial screening test.

Permanganate was then subjected to a much more rigorous evaluation. The optimum conditions for reaction needed to be determined, and its compatibility with the colorimetric method rigorously evaluated.

The mechanism of the NH_2OH-MnO_4^- reaction

There are a number of potential products [equations (1) to (4)] of the MnO_4^- oxidation of NH_2OH and each of these will have its own stoichiometric requirements. Since there are two possible half reactions involving the MnO_4^-, this makes a total of eight possible overall reactions that initially needed to be considered. These reactions, together with their respective NH_2OH: MnO_4^- ratios are listed in Table 2. Since the oxidation of NO_2^- to NO_3^- occurs readily only under strongly acidic conditions,[21]

Table 2. Potential reactions between NH_2OH and MnO_4^-*

	Reaction	NH_3OH^+/MnO_4^-
(A)	$4MnO_4^- + 10NH_3OH^+ + 2H^+ \rightarrow 4Mn^{2+} + 5N_2O + 2H_2O$	2.5
(B)	$4MnO_4^- + 5NH_3OH^+ + 2H^+ \rightarrow 4Mn^{2+} + 5NO_2^- + 11H_2O$	1.25
(C)	$MnO_4^- + 5NH_3OH^+ \rightarrow Mn^{2+} + 2.5N_2 + 9H_2O + 2H^+$	5
(D)	$6MnO_4^- + 5NH_3OH^+ + 8H^+ \rightarrow 6Mn^{2+} + 5NO_3^- + 14H_2O$	0.83
(E)	$4MnO_4^- + 6NH_3OH^+ \rightarrow 4MnO_2 + 3N_2O + 11H_2O + 2H^+$	1.5
(F)	$4MnO_4^- + 3NH_3OH^+ \rightarrow 4MnO_2 + 3NO_3^- + 5H_2O + 2H^+$	0.75
(G)	$MnO_4^- + 3NH_3OH^+ \rightarrow MnO_2 + 1.5N_2 + 5H_2O + 2H^+$	3
(H)	$2MnO_4^- + NH_3OH^+ \rightarrow 2MnO_2 + NO_3^- + 2H_2O$	0.5

*At pH 4.6 the NH_2OH will be in its protonated form.

it was considered that the overall reactions represented by equations D and H (which undoubtedly would involve NO_2^- as an intermediate) were not likely to be of relevance to this work. This was confirmed by measuring the rate of reaction between MnO_4^- and NO_2^- at pH 4.6. The half time was found to be of the order of several hours.

The effect of the MnO_4^- to NH_2OH ratio was determined by measuring the extent of colour development in a series of solutions containing fixed concentrations of NH_2OH and bromide, and increasing levels of MnO_4^- (Fig. 2). The initial rise in the percentage of colour (bromophenol blue) formed indicates that the interference from NH_2OH is being removed. However, a maximum of only 80% colour development is attained at $40\mu M$ MnO_4^-. Above $60\mu M$ MnO_4^- there is a steep decline in colour yield.

During the 20 min reaction period following the addition of the MnO_4^- to the reaction vials

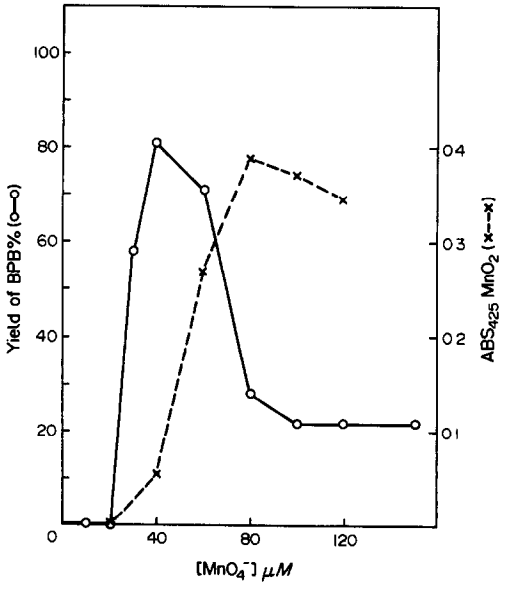

Fig. 2. Production of BPB (O——O) and MnO_2 (×---×) as a function of $[MnO_4^-]$; $[Br]_0 = 25\mu M$, $[NH_2OH]_0 = 100\mu M$, pH = 4.6.

(and prior to the addition of PR and CT) it was noted that a marked brown coloration (presumably due to colloidal manganese oxide, MnO_2) developed in the vials containing greater than $40\mu M$ added MnO_4^-. A surrogate measure of the amount of MnO_2 produced was provided by measuring the absorbance of the solutions at 425 nm after 20 min. These data have been plotted in Fig. 2 for comparison with the bromophenol blue colour development profile.

The above result suggested that manganese oxide, or a residual excess of MnO_4^- was inhibiting colour development. Two control experiments were carried out to test the effects of these species. In the first experiment, the colorimetric reagents were added to a bromide standard solution containing a pre-formed colloidal suspension of manganese oxide. This suspension was produced by stoichiometric reaction between Mn^{2+} and MnO_4^- according to equation (5).[21] Complete development of colour occurred in this case.

$$2MnO_4^- + 3Mn^{2+} + 2H_2O \rightarrow 5MnO_2 + 4H^+ \quad (5)$$

In contrast, the addition of MnO_4^- resulted in a substantial diminution of colour. More detailed testing showed that the MnO_4^- destroyed the bromophenol blue after it was formed (Fig. 3). [The solid line in Fig. 3(b) shows the effect of adding MnO_4^- after colour development was complete, whilst the broken line shows the effect of added MnO_4^- on a standard solution of bromophenol blue.]

The data in Fig. 2 provide a firm foundation for deciding which of the possible reactions listed in Table 2 make a significant contribution. Reactions D and H have already been eliminated from consideration for the reasons given above. Reactions C and G are inconsistent with the stoichiometry revealed in Fig. 2 (maximum BPB production occurs for a NH_2OH to MnO_4^- ratio close to 2.5). The reactions described by equations E and F are also unlikely, both for stoichiometric reasons and for the fact that no

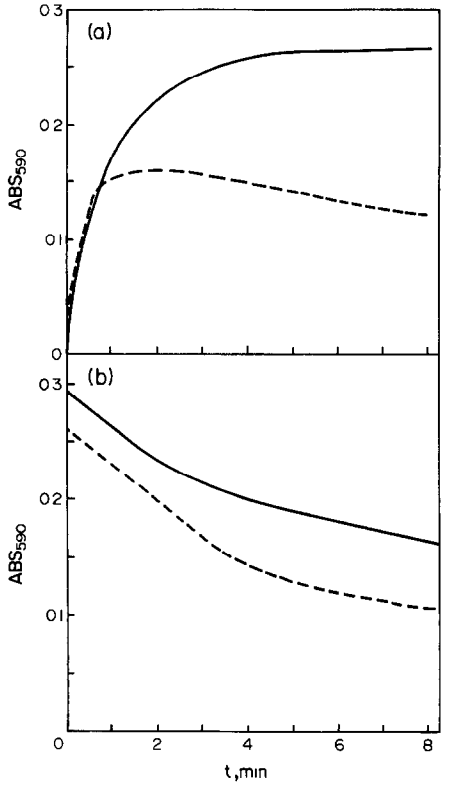

Fig. 3. (a) Kinetics of BPB formation in a 25μM Br^- standard solution in the presence (– – –) and absence (——) of 100μM MnO_4^- (b) Decay of BPB absorbance following the addition of 60μM MnO_4^- to a 25μM Br^- solution in which the colour had initially been fully developed (——); reduction of colour in a solution of reagent grade BPB dye after 60μM MnO_4^- was added (– – –).

MnO_2 is produced until the NH_2OH has been largely destroyed. As a result of this process of elimination, one is left with equations A and B. The results in Fig. 2 are consistent with the stoichiometry of equation A. However, only 80% of the expected colour development in the bromide method occurs at this equivalence point, where there should be no residual NH_2OH or excess MnO_4^- (inhibitors).

The possible products of the oxidation of the NH_2OH in this system are NO_2^- and N_2O (equations A and B, respectively). If the concentration of one of these species is measured directly, the yield of the other product can be obtained by difference. In this case the amount of NO_2^- produced was measured.[13] The results in Fig. 4 show that NO_2^- is a minor, albeit significant, product with a peak solution concentration of 14μM at 40μM MnO_4^-.

This is a very important finding since NO_2^- is the one oxidation product of NH_2OH that will rapidly react with, and consume CT.

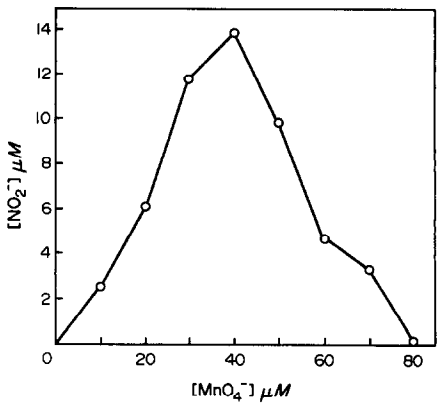

Fig. 4. Production of NO_2^- as a function of $[MnO_4^-]$; $[NH_2OH] = 100\mu M$.

The less than 100% colour yield of bromophenol blue at 40μM MnO_4^- is therefore explained by the production of a small amount of NO_2^-. This problem with residual NO_2^- can be overcome by increasing the concentration of MnO_4^- to 80μM. However, as seen in Fig. 2, the excess MnO_4^- causes serious problems.

The remaining unanswered question is the origin of the colloidal manganese oxide produced in appreciable amounts at MnO_4^- concentrations greater than 40μM. The distribution of the initial products of the reaction between MnO_4^- and NH_2OH can be calculated for each concentration of MnO_4^- by using the yield of NO_2^- (Fig. 4), coupled with the stoichiometries specified by equations A and B in Table 2. This method for calculating the initial distribution of products is a valid one since kinetic measurements show that the MnO_4^- is consumed before MnO_2 is produced (Fig. 5). For 60μM MnO_4^- the absorbance measured at 542 nm (the MnO_4^- chromophore) does not decay to zero owing to

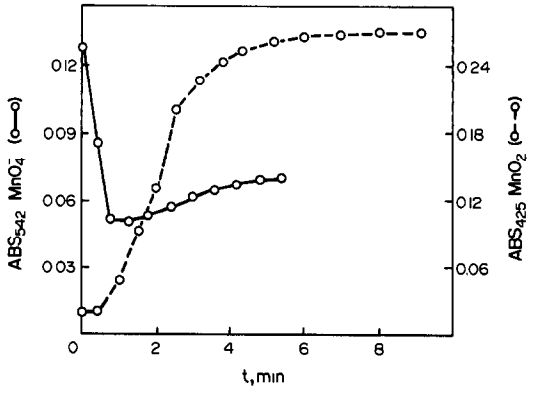

Fig. 5. Reaction between 100μM NH_2OH and 60μM MnO_4^-; decay of MnO_4^- (O——O) and production of MnO_2 (O– – –O).

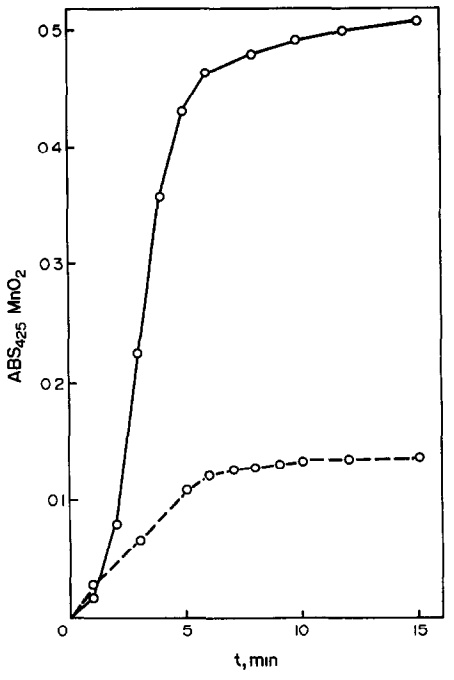

Fig. 6. Production of MnO_2 from the reaction between MnO_4^- and Mn^{2+}. The initial reactant concentrations corresponded to those calculated in Table 4 for the primary distribution of products arising from initial MnO_4^- concentrations of 50μM (O---O) and 80μM (O——O).

spectral overlap from the broad absorbance band of colloidal MnO_2 that develops after 1 min.

The initial calculated concentration balances for the reaction products are shown in Table 3. These results show there will be an excess of MnO_4^- for initial MnO_4^- concentrations greater than 40μM. It has already been mentioned above that Mn^{2+} and MnO_4^- can react at pH 4.6 to produce MnO_2 [equation (5)]. The results of kinetic experiments (Fig. 6) using Mn^{2+} and MnO_4^- concentrations corresponding to $[MnO_4^-]_0$ concentrations of 50 and 80μM in Table 3 showed that the profile of MnO_2 production in Fig. 2 could be accounted for by this reaction. This also explains why the yield of MnO_2 plateaus above $[MnO_4^-] = 80\mu M$. The concentration of Mn^{2+} reaches a constant value, and hence imposes an upper limit on the amount of MnO_2 that can be produced by its reaction with MnO_4^- [equation (5)].

Destruction of residual MnO_4^-

The above investigation showed that residual MnO_4^- must be decomposed before the bromide colorimetric reagents are added. Hydrogen peroxide was initially chosen for this purpose since not only do mildly acidic solutions of this reagent reduce MnO_4^- to Mn^{2+} [equation (6)] but it has also been shown that the Mn^{2+} product of this reaction would not adversely affect the bromide method.

$$2MnO_4^- + 5H_2O_2 + 6H^+ \rightarrow 2Mn^{2+} + 8H_2O + 5O_2 \quad (6)$$

The effect of hydrogen peroxide itself on the colorimetric method was evaluated by measuring the extent of colour production in solutions containing hydrogen peroxide. It was found that colour yield was not decreased by concentrations of hydrogen peroxide as high as 300μM. Trial experiments that involved the mixing of a slight stoichiometric excess of hydrogen peroxide with pH 4.6 solutions containing 80μM MnO_4^- or suspensions of manganese oxides (generated by reaction between 100μM solutions of MnO_4^- and NH_2OH) showed that reduction to Mn^{2+} was complete in less than 10 min (T = 20–25°).

The experiment shown in Fig. 2 was repeated with a hydrogen peroxide reduction step between the initial MnO_4^- treatment and the addition of the colorimetric reagents (Fig. 7). The results from Fig. 2 are included for comparison. The yield of bromophenol blue is seen to be 100% (relative to a bromide standard solution) for MnO_4^- concentrations greater than 70μM ($[NH_2OH]_0 = 100\mu M$).

Although a maximum of 100μM NH_2OH was used in the above optimization experiments, higher concentrations could be readily

Table 3. Calculated initial product distribution for reaction between NH_2OH and MnO_4^- ($[NH_2OH]_0 = 100\mu M$)

$[MnO_4^-]$, μM Initial	$[MnO_4^-]$, μM Residual	Mn^{2+}, μM Produced	NH_2OH, μM Residual	NO_2^-, μM Produced
40	0	40	14	14
50	6	44	0	10
60	18	42	0	5
70	29	41	0	3
80	40	40	0	0

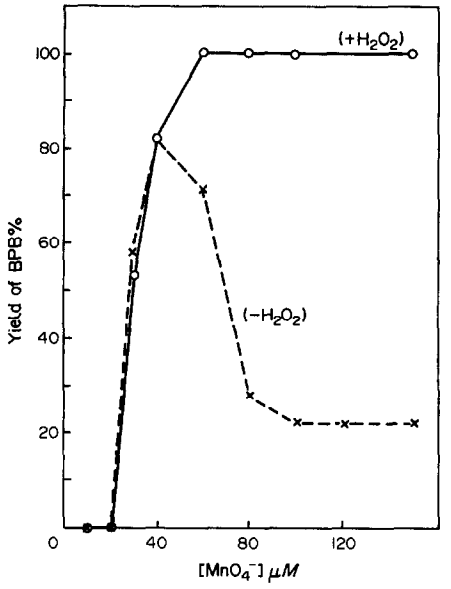

Fig. 7. Effect of 250μM H_2O_2 in removing the negative interference due to residual MnO_4^- as a function of the initial concentration of MnO_4^- (O——O), $[NH_2OH] = 100\mu M$. The yield of colour obtained in the absence of the H_2O_2 (data from Fig. 2) is shown for comparison (×---×).

accommodated by proportional scaling of the amounts of MnO_4^- and hydrogen peroxide.

Implementation and testing of the method

The robustness of the method was evaluated by producing a series of standard curves in the presence of 0, 20, 50, and 100μM NH_2OH. Each measurement was made in triplicate. It should be noted that, in contrast to the mechanistic investigations described above, a reaction medium containing Na^+, Mg^{2+}, Cl^-, and SO_4^{2-} ions was used to simulate the ionic composition likely to be found in real freshwater samples. The blank-corrected absorbances for the standard curves corresponding to each concentration of NH_2OH are listed in Table 4. The coefficient of variation between replicate absorbance values was always better than 3% for bromide concentrations spanning the range 5–30μM.

Table 4. Bromide standard curves as a function of $[NH_2OH]$*

Br^-, μM	Br^-, mg/l	NH_2OH, μM 0	20	50	100
0	0	0	0	0	0
5	0.4	0.029	0.028	0.030	0.027
10	0.8	0.070	0.070	0.071	0.070
15	1.2	0.118	0.118	—	—
20	1.6	0.169	0.168	0.171	0.169
30	2.4	0.277	0.284	0.287	0.281

*Absorbance measured at 590 nm. Standard deviation for triplicate determinations was less than 3% for $[Br^-] = 5$ to 30 μM.

The data in Table 4 show that the colorimetric method incorporating the NH_2OH decomposition step is capable of yielding excellent results. However, a potential problem could arise if the MnO_4^- is consumed in competing side reactions with other dissolved species, at a rate which is comparable with its reaction with NH_2OH. It has already been noted above that Fe^{2+} could be present at significant concentrations in water that contains NH_2OH. Whilst Fe^{2+} does not cause problems with the colorimetric method itself (see above), it does react quite rapidly with MnO_4^- at pH 4.6. The potential for Fe^{2+} to interfere with the decomposition of NH_2OH by MnO_4^- was evaluated by measuring the response of the integrated MnO_4^--colorimetric method to increasing concentrations of Fe^{2+}. The results showed that a maximum of 300μM Fe^{2+} could be tolerated in the presence of 100μM NH_2OH. Higher levels would require an additional amount of MnO_4^- to be added. For this reason it is recommended that the approximate concentration of Fe^{2+} be measured in samples collected from reducing environments.

Acknowledgements—The technical and experimental assistance provided by Stephen Persi throughout the course of this work is gratefully acknowledged. The author thanks Robert Jung for helpful discussions about the colorimetric determination of nitrite.

REFERENCES

1. American Public Health Association, American Water Works Association, Water Pollution Control Federation, Standard Methods for the Examination of Water and Wastewater, 16th ed, pp. 278–279. American Public Health Association: Washington D.C., 1985.
2. D. R. Jones, *Talanta*, 1989, **36**, 1243.
3. D. R. Jones, submitted to *Anal. Chim. Acta*.
4. CRC Handbook of Physics and Chemistry, Robert C. Weast (ed.), 55th Ed., CRC Press, Ohio, 1975.
5. T. Yoshida and M. Alexander, *Can. J. Microbiol.*, 1964, **10**, 923.
6. D. M. Yordy and K. L. Ruoff, in C. C. Delwiche, *Denitrification, Nitrification and Atmospheric Nitrous Oxide*, pp. 171–190. Wiley, New York, 1981.
7. L. R. Pitwell, *Mikrochim. Acta*, 1975 **II**, 425.
8. J. H. Butler, J. E. Pequegnat, L. I. Gordon and R. D. Jones, *Estuar. Coast. Shelf Sci.*, 1988, **27**, 181.
9. C. L. Basel, J. D. Defreese and D. O. Whittemore, *Anal. Chem.*, 1982, **54**, 2090.
10. F. W. Sollo, T. E. Larson and F. F. McGurk, *Environ. Sci. Technol.*, 1971, **5**, 240.
11. Vogel-Practical Organic Chemistry, 3rd Ed., p. 823. Longman, London, 1956.

12. S. I. Heaney and W. Davison, *Limnol. Oceanogr.*, 1977, **22**, 753.
13. F. Koroleff, in K. Grasshoff, M. Ehrhardt and K. Kremling, *Methods of Seawater Analysis*, 2nd Ed., pp. 141–142. Verlag Chemie, Weinheim, 1983.
14. H. Erlenmeyer, C. Flierl and H. Sigel, *J. Am. Chem. Soc.*, 1969, **91**, 1065.
15. F. A. Cotton and G. Wilkinson, *Advanced Inorganic Chemistry*, 5th Ed., pp. 312–328. Wiley-Interscience, New York, 1988.
16. V. K. Jindal, M. C. Agrawal and S. P. Musran, *J. Chem. Soc. (A)*, 1970, 2060.
17. M. N. Hughes and H. G. Nicklin, *ibid.*, 1971, 164.
18. J. H. Butler and Gordon, *Mar. Chem.*, 1986, **19**, 229.
19. D. D. Wagman, W. H. Evans, V. B. Parker, I. Halow, S. M. Bailey and R. H. Schumm, *Selected Values of Chemical Thermodynamic Properties-Tables for the First Thirty-Four Elements*, NBS Technical Note 270-3, pp. 61–67, U.S. Gov. Printing Office, 1968.
20. D. R. Jones and R. F. Jung, *Water Res.*, 1990, **24**, 125.
21. A. I. Vogel, *A Textbook of Quantitative Inorganic Analysis*, 3rd Ed., pp. 279, Longmans, London, 1961.

Talanta, Vol. 40, No. 1, pp. 53–74, 1993
Printed in Great Britain.

0039-9140/93 $6.00 + 0.00

LIGHT EMITTING DIODE BASED FLOW-THROUGH OPTICAL ABSORPTION DETECTORS

PURNENDU K. DASGUPTA,* HARVEY S. BELLAMY, HANGHUI LIU, JORGE L. LOPEZ, ELLIS L. LOREE,† KAVIN MORRIS, KAJ PETERSEN‡ and KALAM A. MIR

Department of Chemistry and Biochemistry, Texas Tech University, Lubbock, Texas 79409-1061, U.S.A.

(*Received* 9 *December* 1991. *Revised* 27 *January* 1992. *Accepted* 27 *January* 1992)

Summary—Simple inexpensive high performance optical absorption detectors are possible using light emitting diodes (LEDs) as light sources. The designs presented in the literature are reviewed. Designs used by the investigators are described in detail with respect to construction, electronic design, performance and cost; these have not previously been described in the literature. Characteristics of commercially available LEDs are tabulated. At the simple end, a single beam, dc driven, transmittance output detector can be constructed within the body of a LED. At the high performance end, fully referenced, computer interfaced detectors are described that are pulsed at high speeds to attain measurement standard deviations in the range of 2–3 × 10^{-6} absorbance.

Light-emitting diodes (LEDs) are small, inexpensive, power-efficient light sources that are widely used as indicator lamps. These electroluminescent devices first became commercially available in the late 1960's. Today, it would be difficult to find an electronic instrument that does not sport an LED. Of special interest to the analytical chemist is that LEDs cover much of the visible and some near infrared (NIR) wavelengths of interest (470–1300 nm; 630–1550 nm for laser diodes) with acceptable monochromaticity for most applications. Further, without abuse, the expected lifetimes for LEDs are orders of magnitude greater than incandescent or discharge sources; mean time between failure for operation at 25° is typically 5 × 10^4 hr or approximately 6 yrs[1] of continuous service for typical LEDs; for some infrared LEDs, expected lifetimes are more than 10^6 hrs.[2] The short term spatial and intensity stability of a typical LED is respectively 30–200 and 50 times better than a He–Ne laser.[3] With a battery operated power source, the intensity noise is stated to be about 2 × 10^{-3}% of the total amplitude (throughout the present paper noise levels cited are the peak to peak values). If this were the only noise source in a complete detector, absolute noise levels of the order of 9 × 10^{-6} in absorbance and a detection limit (LOD) of 3 × 10^{-5} absorbance (based on a S/N = 3 criterion) would be possible; this can be favorably compared with noise specifications of present day state-of-the-art commercial flow-through absorption detectors (1 × 10^{-5} absorbance with a rise time of 1.0 sec).

*Author for correspondence.
†Present address: Department of Electrical Engineering, Texas Tech University, Lubbock, TX 79490.
‡Perkin-Elmer AB, Birkerød Kongevej 137 F, 3460 Birkerød, Denmark.

LED based optical absorption detectors

LED-based photometers were first proposed by Barnes in 1970 (as stated by Flaschka *et al.*[4]) and the concept of an LED-phototransistor (PT) photometer with a 30-cm pathlength flow-through cell was realized in 1973.[4] Three years later, Anfält *et al.*[5] described a dual beam LED-based photometric titration probe for the measurement of total alkalinity in seawater. The LED was powered by a symmetrical square wave and both reference and principal detector photodiode (PD) outputs were processed by synchronized demodulators tuned to the LED chopping frequency, thus providing immunity against ambient light. However, such measures are largely unnecessary in flow-through photodetectors which are easily protected from ambient light by their design. The first practical LED-based flow-through photodetector of this type was described by Betteridge *et al.*[6] This was a single beam instrument utilizing an ∪-geometry and a path-length of 3 cm with a reported LOD (S/N = 2) corresponding to 6 × 10^{-4} absorbance for a 1-cm cells, from which a noise level of 9 × 10^{-4} absorbance can be calculated. The development of this detector was of particular help to the facile practice of flow injection analysis (FIA).[7] Several papers have

since appeared that utilize this basic detector design; particularly notable are the applications reported by Johnson *et al.*[8,9] who report on the seaworthiness of such instruments for continuous shipboard analysis of seawater, including submerged applications. For a nitrate/nitrite determination system,[8] noise levels of 8×10^{-4} absorbance were reported (2-cm cell). A variation of this cell design was reported by Trozanowicz *et al.*[10] to permit facile replacement of the LED and the photodetector. Since the original work,[6] a different design was reported by Betteridge *et al.*;[7,11–13] the LED and the PT were located on the radially opposite sides of a transparent tubular flow conduit (0.3–2.0 mm dia), thus facilitating construction. Sufficient data are not available to judge if any meaningful changes in S/N performance resulted over the previous design. Schmidt and Scott[14] reported the design and construction of a Z-geometry flow cell of 4-mm pathlength as an LED-based dedicated detector for metal ion chromatography utilizing postcolumn reaction with 4-(2-pyridylazo)resorcinol. A PD was used as the detecting transducer in this single beam design and the signal processing circuitry included a simple but effective second-order Butterworth filter (50% cut-off at 10 Hz) to reduce noise. From the reported data on the LOD of the various metals, their known molar absorptivities, injected and observed peak volumes, we estimate that the absorbance noise level of this detector was about 5×10^{-4}. This was a particularly small aperture microvolume detector (0.74 mm bore, 1.7 μl) and this performance in a post column reaction system, where mixing noise is always a factor, is noteworthy.

Since this time, several papers have reported the utilization of LED-based absorbance detectors but few details appear in regard to either design or performance characteristics. Imasaka *et al.*[15] appear to hold the record on the lowest noise performance, albeit this was based on static measurements. With an ultrabright 814 nm emitter operated from batteries and producing an optical output of 36 mW, it was reportedly possible to attain a noise level of 7.5×10^{-7} absorbance using a dual beam arrangement, conversion of the PD outputs using voltage→frequency converter and an integration time of 50 sec. More recently, Worsfold *et al.*[16–20] have championed the use of LED-based photometric detectors in field monitors for various water quality parameters and have also provided an overview of their use in flow injection analysis.[21] The detector design involves two individual LEDs and radial beam path flow cells; the two individual PD outputs were fed into a differential amplifier. The dual cell arrangement was used to compensate for turbidity in unfiltered river water samples and performed acceptably in that regard. However, it is not strictly a double beam arrangement as stated;[16] it was not intended for compensating source fluctuations. A computer-addressable single beam photometer with multiple LED sources and a **-geometry flow cell is reportedly commercially available;[22] no performance details have been given. Fluorometric applications of LEDs as excitation sources have also been described.[23,24]

In this laboratory, LED-based optical absorbance detectors have been used for several years now, with many different cell designs. We have used them with and without coupling to optical fibers, in referenced and unreferenced source configurations, with transmittance or absorbance as the primary output, in stand-alone or computer-controlled configuration, in dc and in pulsed mode. They have been configured as part of both laboratory and field-deployable instruments. The use of such detectors was mentioned in several publications[25–30] but no details were cited. A detailed consideration of their design, both in the form where the ultimate in performance is not necessary and also where the latter is desirable, is presented here.

Sources

Light emitting diodes and laser diodes. Several excellent volumes are available for more detailed information on LEDs and laser diodes (LDs).[31–35] Briefly, when charge carriers are injected across a forward-biased p–n junction, the current is largely due to hole-electron recombination in the transition region and in the neutral regions near the junction. In indirect band gap semiconductors like Si or Ge, the energy is released as heat. In a semiconductor permitting direct recombination, a considerable amount of the energy is released as light, the effect being known as injection electroluminescence. The wavelength of the light emitted is related to the band gap of the semiconductor. Some common semiconductor materials are listed below with the corresponding photon wavelengths in nm given in parenthesis: ZnS (345), SiC (434), ZnSe (460), AlP (507), CdS (513), GaP (550), AlAs (575) CdSe (718), GaAs (868), Si (1120), Ge

(1850), PbSe (4600) and InSb (6900). Virtually all can be configured into some type of photodetector where they respond to light of wavelength equal to or less than that corresponding to the bandgap. Only some semiconductors show practical injection electroluminescence. The energy distribution of the emitted photons corresponds approximately to a skewed normal distribution, the typical peak wavelength being somewhat higher than the wavelength corresponding to the cited band gap energy. However, the photon wavelength can be varied by making compound semiconductors. Thus, while GaAs emits in the NIR and GaP in the green, various amounts of As can be introduced into GaP. The resulting material is often written as $GaAs_{1-x}P_x$ (or simply GaAsP) and the resulting light can range from green to far red, depending on the degree of As content. From one production batch to another, the composition can vary sufficiently for the peak wavelength to change by 5–10 nm (typically the uncertainty is 1% of the stated wavelength in nm) for the same device designation; this should be borne in mind before a search is mounted to find an emitter that precisely matches some wavelength. Moreover, the exact peak wavelength depends on the junction temperature; at a fixed ambient temperature the junction temperature is a function of the drive current. Leidecker and Powers[36] report that for a common "660 nm" LED, the peak wavelength changed linearly from 663 nm to 671 nm as the case temperature was varied from 20 to 75°.

Commercially available LEDs. Most commercial LEDs are made from GaAs or GaP substrates. An epitaxial layer is grown thereon to form the light emitting p–n junction. Common red LEDs are based on an GaAsP epitaxial layer grown on GaAs. GaAsP epitaxi are grown on GaP to produce high efficiency yellow and red LEDs. GaP epitaxi are grown on GaP to produce green LEDs. More recently, Al is being doped into the epitaxial layer to produce a double heterojunction AlGaAs structure that produces a very intense red light at modest currents. Blue LEDs, with peak emission at 490 nm were originally introduced in late 1984 by Panasonic Industrial Co. and were based on GaN. These multijunction devices required a forward bias of 7.5 V. The present generation of blue LEDs are based on SiC and are more power-efficient but the optical output is still small compared to longer wavelength emitters. very recently high output GaN LEDs have been reintroduced, these emit in the green-blue (482 nm). Infrared LEDs in the 880–950 nm region are based on GaAs or AlGaAs and those in the 1200–1300 nm region are based on AlInGaAsP. Very high output orange LEDs based on the AlInGaP structure have been realized and are expected to be commercially available soon.[37]

Most LEDs are made starting with slicing the base crystals into thin wafers. The epitaxial layer is then grown. The wafers are next scribed and broken into individual LED chips, typically 0.25 mm square. The crystal base is the cathode and the epitaxi side is the anode. The chips are then attached to a lead frame. The cathode is usually shaped like a cup to reflect the emitted light forward and the chip is connected to it by conductive silver epoxy. The anode is then wire bonded (typically 25 μm in diameter gold wire, ending in a ball) to the top of the chip and the whole is packaged in epoxy. Tie-bars that hold cathode and anode leads together during the above operations are finally sheared, resulting in the familiar device of Fig. 1.

Performance characteristics of available LEDs. The use of a bright, narrowly focused source is preferred for all detector applications to obtain the best S/N. Table 1 lists several commercially available LEDs with their characteristics; based on our experience, they are particularly well suited for detector applications. With a few exceptions (such as a device that can provide an optical output of 100 mW and can handle peak currents up to 10 amperes) we have considered here only LEDs in the most common size (T 1–3/4, 5 mm). It should be noted that the values cited are typical values, considerable variations may be encountered for the optical power output of individual LEDs. For example, in a lot of 1000 LEDs supplied to us by a

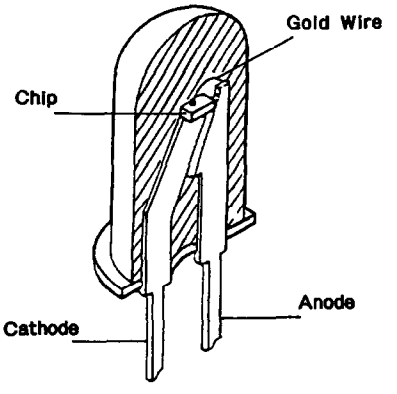

Fig. 1. Cutaway view of a typical T-1-3/4 epoxy bodied LED.

Table 1. Characteristics of some commercially available LEDs well suited for detector applications[a]

Device type	Peak wavelength, *nm*	Manufacturer	Device designation	Intensity/ Power (at rated current, *mA*)	Half-intensity wavelength bounds, *nm*	Maximum continuous current, *mA*	Maximum pulse current, *mA*[c]
SiC	470	L[d]	L200CWB5	20 mcd (20)	435–510	50	300
GaN	482, 435	L	L200CWGB6	75 mcd (20)	418–510	30	N/A[h]
GaP	555	S[e]	HBG5566X	150 mcd (20)	538–568	50	100
GaP	560	S	HPG5566X	200 mcd (20)	552–582	50	100
GaP	565	H[f]	HLMP3950	120 mcd (20)	548–576	30	90
GaP	570	S	HPY5566X	300 mcd (20)	556–587	50	100
GaAsP/GaP	580	S	HAY5566X	150 mcd (20)	569–601	50	100
GaAsP/GaP	583	H	HLMP3850	140 mcd (20)	565–601	20	60
GaAsP/GaP	585	L	L200CY5A	66 mcd (20)	572–607	20	80
AlInGaP	590	H	HLMACLOO[g]	1300 mcd (20)	584–598	30	100
GaAsP/GaP	605	S	HAA5566X	250 mcd (20)	591–622	50	100
GaAsP/GaP	610	L	L200CO4D	45 mcd (20)	602–632	20	N/A
AlInGaP	630	H	HLMADGOO[g]	650 mcd (20)	620–637	30	100
GaAsP/GaP	635	H	HLMP3750	125 mcd (20)	616–658	30	90
AlGaAs/GaAs	645	H	HLMP4101	1000 mcd (20)	637–658	30	300
AlGaAs	650	H	HLMP8104[i]	4000 mcd (20)	637–659	50	300
GaAsP	655	H	HLMP3050	2.5 mcd (20)	643–667	50	1000
AlGaAs	660	S	H-3000	3000 mcd (20)	646–671	50	300
AlGaAs	660	L	L200CWR5K	4100 mcd (25)	645–670	50	300
GaP	700	S	SPR5501	6 mcd (70)	658–706	30	100
AlGaAs	818	O[j]	OD-820W[k]	6 mW (100)	793–847	100	3000
AlGaAs	840[l]	M[m]	ME1504	1.5 mW (50)	812–857	75	120
AlGaAs	850	S	DN305	80 mW/sr (50)	825–875	100	1000
AlGaAs	880	L	L200CWIR880	2 mW/cm^2 (20)	858–907	50	3000
AlGaAs	880	S	CN305	30 mW/sr (50)	840–920	100	1000
AlGaAs	880	O	OD-100[n]	100 mW (500)	872–974	50	10000
GaAs	925	S	BN301	7 mW/sr (20)	835–915	500	1000
GaAs	940	L	L200CWIR940	10 mW (200)	929–978	100	3000
GaAs	950	S	AN305	25 mW/sr (50)	922–972	100	1000
InGaAsP	1300	M	ME7021[o]	1 mW (100)	1230–1370	120	N/A

[a]At 25°.
[b]Specified for visible LEDs in lumens per unit solid angle (lm/sr = Candela) and for NIR LEDs in mW/sr or in terms of aperture incidence power mW/cm^2, or total power, mW. Note that intensity specifications depend on the focusing ability of the device; when much of the dome is removed and a fiber is coupled to it, the total power output specification is the more relevant parameter.
[c]The specified value is generally allowable only at very low duty cycles, manufacterer's data sheets should be consulted for exact conditions.
[d]LEDTRONICS Inc., Torrance, CA.
[e]Stanley Electric Co. Inc., Tokyo, Japan.
[f]Hewlett-Packard, San Jose, CA.
[g]These devices will be available in bulk quantities in 1993, design samples are available now.
[h]Data not available.
[i]An even higher output (15000 mcd) device is available in a larger package (T-4, 13.3 mm), HLMP-8150.
[j]Opto Diode Corp., Newbury Park, CA.
[k]5.3 mm TO-46 metal case.
[l]Can range from 780 to 880 nm depending on production lot; 5.5 mm dia. metal case.
[m]Mitsubishi Electric Co., Tokyo, Japan.
[n]9.1 mm TO-39 metal case.
[o]5.4 mm dia. metal case.

manufacturer, the brightest 10% averaged 4x greater luminous intensity than the dimmest 10%. We have recorded the emission spectra of some LEDs and have generally found them to correspond closely to manufacturer's data, within the 1% tolerance limit previously stated. With the exception of the GaN emitter, in no case were distinct doublets as reported by Worsfold *et al.*[17,21] observed. Cited peak wavelengths are somewhat dependent on the operating temperature as well as the total output. Some NIR LEDs are known to show a negative wavelength shift in the location of the peak maximum with increasing output power, the direction of shift is reversed at still higher powers.[2] Operating LEDs at excessive currents

(short of catastrophic failure) for prolonged periods can permanently reduce the luminous output *and* change the peak wavelength. One astute observation has been made: "... like traffic lights, all turn yellow before they go".[38]

Laser diodes. Laser diodes are 2–2.5 orders of magnitude more expensive than their LED counterparts. Nevertheless, on an absolute scale, this cost is modest for many applications. Based on several different layered structures (GaAs, AlGaAs, InGaAsP), LDs presently span a wavelength of 630–1550 nm with continuous power levels ranging from a few mW to several watts. Experimental ZnSe LDs, emitting in the blue–green, have been made.[39] Many LDs operate with a multimode pattern that involves emission over a large wavelength range (as much as 80–90 nm) with emission bands equally spaced, 1 to several nm apart. The intensity, spacing and the location of the principal emission band change with the temperature and the operating power; often, single mode emission results at higher powers. The half bandwidth of an LD emission band can range from 1–10 nm depending on the device. The use of LDs in analytical chemistry has been reviewed.[40] If used in a conventional mode to perform absorption measurements, they offer no significant advantage over LEDs. Still, it is possible to operate with LDs in the laser intracavity absorption spectroscopic mode where the sample is placed in an optical feedback path between the LD and a mirror; absorbance noise levels of 1×10^{-5} are reportedly routinely attained with very simple apparatus.[41,42] Practical applications, ruggedness, and immunity from mechanical perturbations are still to be unequivocally demonstrated and further discussion of the use of LDs is best deferred until such time.

Use of optical fibers in constructing a detector cell. Some of the cell designs reported here use optical fibers for light transmission. Relative to directly locating the LED and the photodetector(s) within the cell, such an arrangement unavoidably involves some light loss. However, the cell itself can be made very small and located in a region remote from any electronic components. Longer wavelength high optical output LEDs, used for optical communication purposes, are often available with attached fiber pigtails. But the fiber core diameter is rarely larger than 250 μm; this is generally too small for typical detector applications. Several manufacturers (*e.g.*, Sanyo Inc., Stanley Electric, Telefunken AG) also market specially molded LEDs with optical fiber connectors. In our experience, the best permanent fiber connection to a 5-mm LED is made by cutting off most of the dome material, getting down to within 0.5 mm of the chip using fine sand paper and finally polishing the surface by rubbing it on smooth paper. If a plastic optical fiber is used, its end can be polished in the same manner or by using a wet polishing stone. With both components held in place (the fiber being positioned to cover the chip), the two are glued together using UV-cure optical adhesive (Norland Optical Products, New Brunswick, NJ) and then epoxy is applied around the fiber to make the connection more secure. Fibers can be coupled to the sensing chip of a photodetector in the same manner. Figure 2 shows the relative amounts of light reaching a photodetector under different coupling conditions, at identical LED drive currents.

Detectors—photodiodes or phototransistors?

Both photodiodes and phototransistors can be used as detectors. The difference is that the latter typically provide 1.5–2 orders of magnitude greater current output albeit the response is slower.[43] This does not necessarily mean that the use of phototransistors results in better S/N. If the detector cell and the connecting cables are appropriately shielded, extraneous noise can be minimized. Even with blue LEDs, the photocurrent from a detector photodiode is in the several nA range and can be directly handled by present-day log-ratio amplifier chips (*vide infra*). Under such circumstances, we have observed that phototransistors are typically more noisy than photodiodes. But if a single beam arrangement is used with a low output source and if the photodetector in the cell is coupled to an external low-cost photocurrent→voltage converter, a phototransistor may be worthy of consideration. Phototransistors, and especially the even higher gain photodarlingtons, are generally not desirable for high speed pulsed detector applications because of their slower response speed. Excellent descriptions of the different strategies of monitoring photodiode outputs with operational amplifiers are available.[44,45]

Major suppliers of photodetectors include EG&G Optoelectronics, Hamamatsu Corp., United Detector Technologies, among others. For the detector applications at hand, very inexpensive small silicon photodiodes (active area 3×3 mm, polymer encapsulated) commonly available from surplus houses (*e.g.*, type S2007,

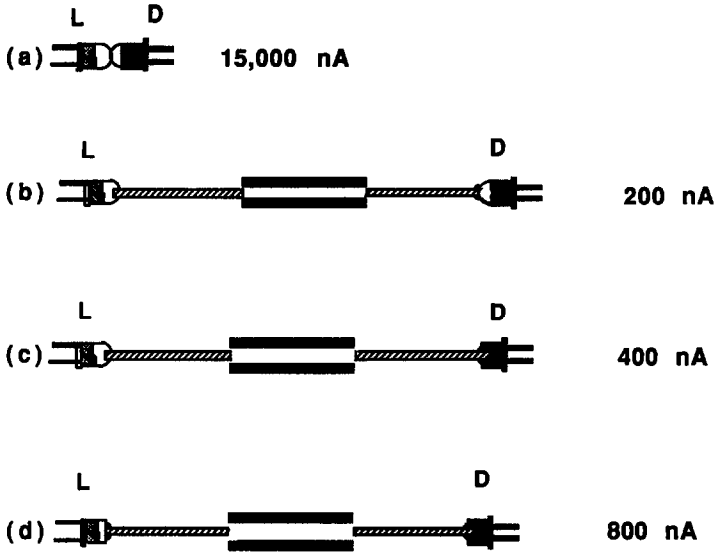

Fig. 2. Light throughput with different test configurations, 560 nm LED, 50 mA drive current. (a) LED (L) and lens end photodiode (D) coupled face to face; (b) 1.5 mm fiber optic coupled to drilled hole in L, intervening cell is air filled glass tube (1.6 mm i.d. × 10 mm), 1.5 mm fiber optic coupled to lens end of D; (c) as in *b* except fiber coupled directly to chip on D: and (d) as in *c* except fiber coupled to L after dome removal.

Electronic Goldmine, Phoenix, AZ) produce results that are indistinguishable from their more expensive counterparts. Because of a greater illuminated area, the total photocurrent obtained is larger than the small profile photodiodes. But the signal gain with increasing active area of the detector is also associated with increasing noise; a detector with an active area much larger than the transmitted beam cross section is undesirable. The relative response profiles of a few detector types, of importance to the present discussion are shown in Fig. 3 as a function of the wavelength of light. NIR detectors that do not respond to visible light are also commonly available. This makes it possible to have simple DC dual wavelength detectors using a bifurcated optical fiber (*e.g.*, from Dolan Jenner Industries, Woburn, MA). This is schematically shown in Fig. 4(a); independent electronics can serve each source-detector combination. As shown, each emitter can be individually referenced. Alternatively the simpler design of Fig. 4(b) can be used with any pair of LEDs. An appropriate electronic strategy is used to alternately turn on each LED (*ca.* 100 Hz) through a clock and a flip-flop circuit, take the log ratio of the reference and the signal detectors and provide individual outputs via appropriately enabled sample/hold (S/H) amplifiers (Fig. 5). To achieve good S/N in this type of design, it is vital to reduce external noise and the (log) amplifier circuitry is preferably located within the same metal housing as the flow cell itself. The cell body is used as the common ground. This approach is easily extended to a multiplicity of LEDs. If the capability to set each of the final outputs individually to zero is desired, a final offset stage not shown in Fig. 5 is, in general, necessary after each S/H amplifier.

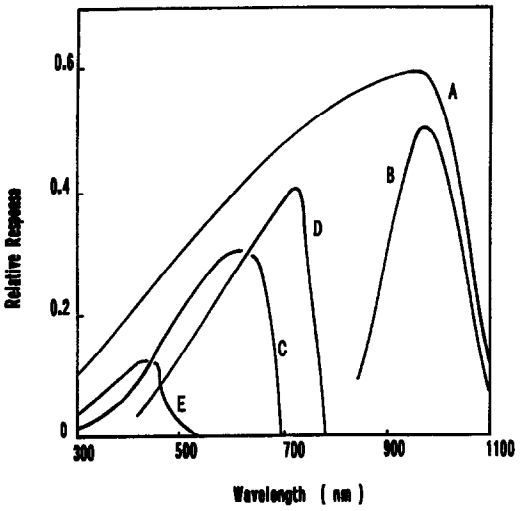

Fig. 3. Typical response profiles of solid state photodetectors as a function of wavelength. (A) Silicon, *e.g.*, type S2386; (B) silicon, with visible light cutoff, *e.g.*, type S2506; (C) GaAsP, standard, *e.g.*, type G1115; (D) GaAsP, extended red sensitivity, *e.g.*, type G1735; and (E) GaP, *e.g.*, type G1961; device numbers refer to products from the Hamamatsu Corp. The ordinate scale is approximately equal to photocurrent in amperes per watt of incident power.

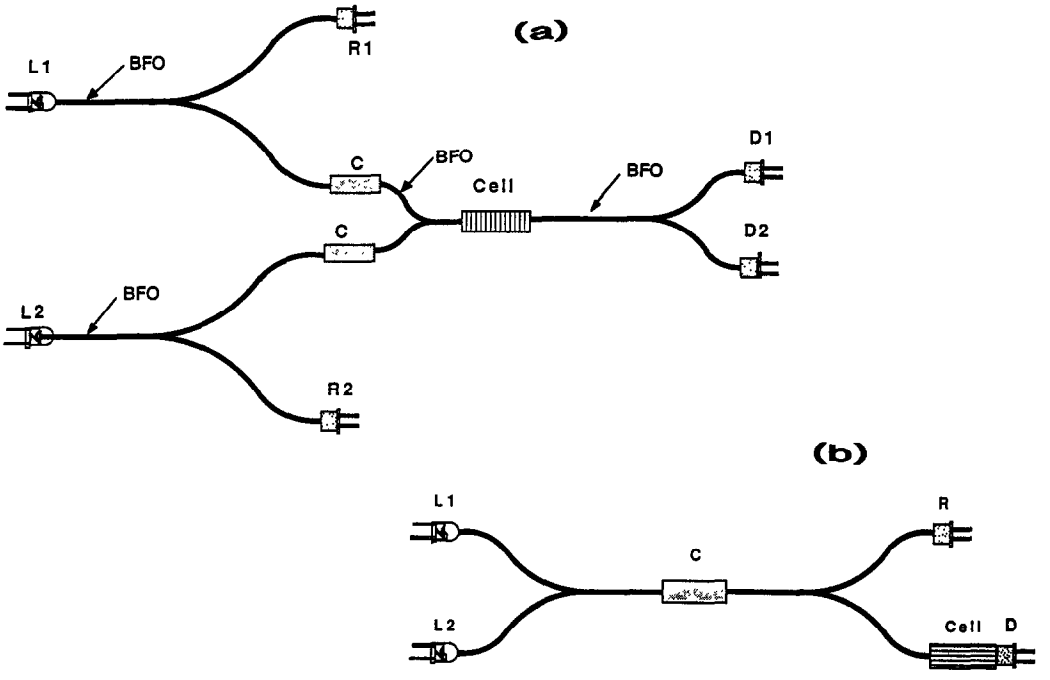

Fig. 4. (a) Dual wavelength photodetector using wavelength selective detectors. L1: visible LED; L2: infrared LED; BFO: bifurcated fiber optic; C: coupler; R1, R2: reference detectors responding to L1 and L2 respectively; D1, D2: signal detectors responding to L1 and L2, respectively. (b) Dual wavelength photodetector using single reference and signal detectors and the time-multiplexing circuitry in Fig. 5 to provide individual outputs.

The offset capability provided to the S/H amplifiers themselves is not adequate for this task.

In this connection, it is interesting that like any other p–n junction, LEDs respond to light, *i.e.*, they are photodiodes as well. This bidirectional transducer behavior (see Table 2) can be used to construct dual wavelength detectors of adjacent wavelengths, with an LED mounted on each side of the cell and functioning alternately as a source and a detector. However, such an approach should be regarded more as a curiosity than a practical method; LEDs are photodiodes, but pretty poor ones!

Cell design

Poppe[46] has provided an outline on the basic characterization and design of liquid phase flow-through detector systems and in a subsequent paper[47] has specially considered miniaturization of such detectors. Stone and Tyson[48] have shown that the design of flow cells can significantly affect the peak profile observed in FIA. Stewart[49,50] has specially considered the optics of flow cells used in liquid chromatography (LC). Optical acceptance of a flow cell is inversely related to the optical path length, by as much as the fourth power of the latter. Most typical present-day flow cells for conventional LC are designed with pathlengths of 4–8 mm. By appropriately imaging the source at the exit window and using a tapered cell construction, Stewart[49] showed that it is possible to reduce refractive index (RI) effects greatly. The RI effect was reduced to the limit where it was solely due to the change in reflectivity at the interface of two media with different RI. The original detector of Betteridge *et al.*[6] was sufficiently sensitive to changes in RI to function as an RI detector. The role of the flow cell in influencing the apparent effect from changing RI has recently received more attention.[51] The full importance of the flow cell is rarely appreciated, however. Figure 6(A) shows the detector response when 50% methanol is injected into a water carrier in a FIA system (shown in inset)

Table 2. Photocurrents (nA) with LEDS as detectors*

Emitter LED	Detector LED 555 nm	570 nm	605 nm	660 nm
555 nm	1.2	3.6	3.0	2.4
570 nm	2.5	9.0	22	52
605 nm	0.02	0.2	6.4	105
660 nm	0.01	0.02	0.27	200

*All are Stanley 5566x series LEDs (see Table 1), emitter drive current 50 mA, emitter and detector separated by 1 cm, intervening medium is air.

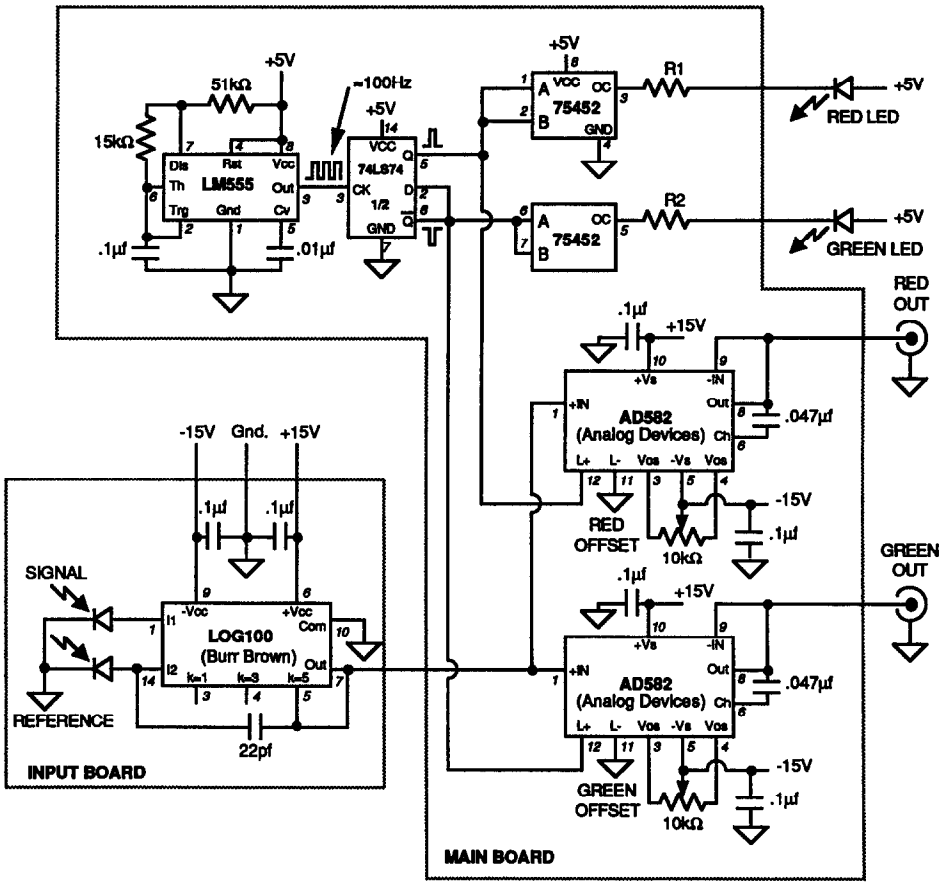

Fig. 5. Schematic for performing dual wavelength absorbance measurement with a time-shared reference and signal detector. R1 and R2 are chosen to obtain the desired value of the current pulse; 33 ohms provide a pulse of *ca.* 100 mA for most LEDs. The input board is integrated with the flow cell. This concept can be extended to use a greater number of LED sources.

using an 8-μl and a 40-μl volume black wall flow cell installed in a Perkin–Elmer 559 spectrophotometer. The reflectivity of the wall also entirely changes the qualitative behavior of the artifact signal. Figure 6(B) shows the appearance of the signal upon 50% methanol injection when a flow cell with integral LED-photodiode detectors (1.5 × 10 mm path) is used; in one case the exterior of the glass tube constituting the flow path has been painted black, in the other case it has been silvered to increase reflectivity. Note that in one case a peak appears before a dip and in the other case the peak follows the dip.

Radial path flow cells. The simplest flow-cell construction undoubtedly involves using the radial dimension of a tube as the optical path. The original design of Betteridge *et al.*[11–13] has already been cited; a filter photometric detector in which the detector body can slide along a glass tube was also described earlier.[52] Presently, this type of radial optical path detection strategy is obligatorily used in capillary electrophoresis and capillary LC where dispersion induced by connections to external detectors cannot be tolerated. For conventional bore LC, tubes of 1–1.5 mm bore are the largest that can be used as radial path detectors without causing major dispersion; this often causes a larger sacrifice in detection sensitivity (due to the small optical path length) than can be tolerated. The sensitivity requirements are often less stringent in FIA or similar analytical systems and this type of cell may be ideally suited for such applications. This is particularly true if the emitter used is of low optical output (*e.g.*, a blue LED) because the S/N in an absorbance detector based on such a source quickly becomes limited by the decreasing amount of light reaching the light detector with increasing path length. Strategies and considerations of designing small bore radial optical path detectors using optical fibers have been recently outlined.[53,54] The radial path design we favor for FIA applications is shown

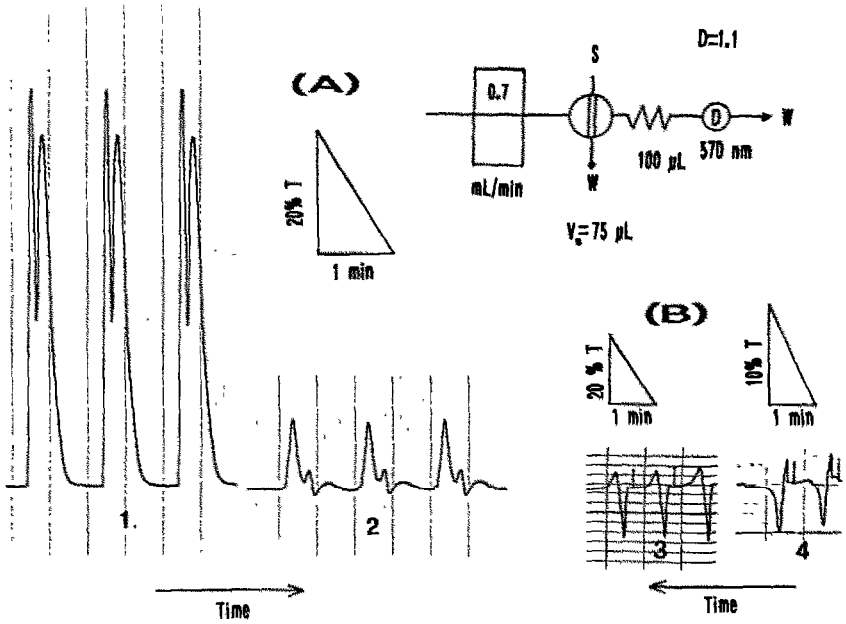

Fig. 6. Detector output upon injection of 50% methanol into a water carrier using the flow injection manifold depicted in the inset. (A) Detector: Perkin–Elmer 559A dual monochromator spectrophotometer equipped with black walled cells of volume (1) 8 μl and (2) 40 μl; (B) detector: LED based, 8 mm path length, 16.5 μl volume, (3) black walls and (4) reflective walls. In all cases light is incident on the window next to the fluid entrance point.

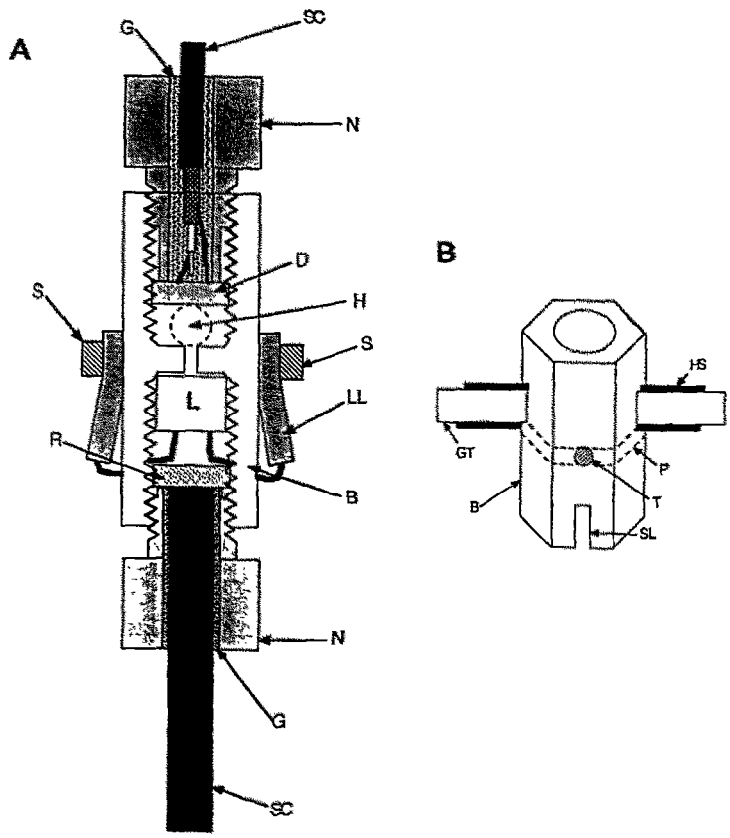

Fig. 7. Radial path detector. (A) Cross sectional view. N: male fitting; B: 1/4-28 threaded union with center partition; L: flat faced LED; LL: LED leads soldered to miniature lugs held in place by screws S; R,D: reference and signal photodiodes; SC: shielded cable to photodiode: G: opaque glue. (B) Front view of the union B. SL: slot cut on opposing sides to fold over LED leads; P: location of center partition; T: 0–80 threads for screw S; GT: glass tube; HS: opaque heat shrink tubing.

in Fig. 7. Opaque 1/4-28 threaded polymeric unions with a center partition containing a small connecting hole are inexpensively available (*e.g.*, from Dionex Corp., Sunnyvale, CA and Upchurch Scientific, Oak Harbor, WA). An appropriately centered hole is drilled through the wall of the fitting immediately adjacent to the partition, to snugly fit the glass tube used as the flow conduit. The LED (dome removed, flat faced) is then put on the other side of the partition with the leads extending through slits cut on the sides of the union, as shown. The LED termini and connecting leads are held firmly in place by 0–80 threaded miniature screws. The reference PD is immediately behind the LED and receives light reflected off the front plane. It is held in place by a threaded male fitting, with (shielded) leads exiting through the 1/8 in. bore of the fitting; the bore is then filled with opaque adhesive. If a single beam arrangement is used (no reference), the LED can be held in place directly by the male fitting with its leads exiting through the bore of the fitting; it is not necessary to make slits in the union. The hole in the partition may be drilled out to the extent desired to define the optical aperture (preferably $\leq$ tube radius). The glass tube and polymeric inlet/outlet tubes connected to it (inserted within it) are affixed in place with opaque heat-shrunk polyolefin tubing. The detector PD is cemented to the end of a threaded male plug, with a hole drilled in it for the connecting leads.

The optical path using the radial dimension of a tube actually involves a multiplicity of path lengths.[52–54] For the purist, this problem is solved and the response linearity over a large range is improved by replacing the circular tube with one of square (or rectangular) cross section. Such tubes are available (both in glass and silica) from many sources (*e.g.*, Wilmad Glass Co., Buena, NJ; Vitro Dynamics Inc., Rockaway, NJ). The great virtue of the straight flow path design with the optical probe traversing it at a right angle is that when it is deployed in a vertical configuration, stray bubbles are never trapped in the cell.[55]

Z-path flow cells. The biggest shortcoming of the radial path design is the limited optical path lengths that can be attained without excessive dispersion. The small bore Z-geometry flow cell is widely used in commercial detectors and represents a good combination of reasonable optical path length, low volume, low dispersion and fast washout profile (minimum unswept volume). Some commercial cells also utilize a bore that is tapered, rather than uniform, to minimize artifact signals from RI changes.[49] Making such a cell requires skilled machining; the design is also patent-protected. Figure 8(a) shows a design that is fabricated very simply. The choice of the material is largely governed by the intended application. If the application is compatible with acrylic polymers (used for many inexpensive polymeric optical fibers,

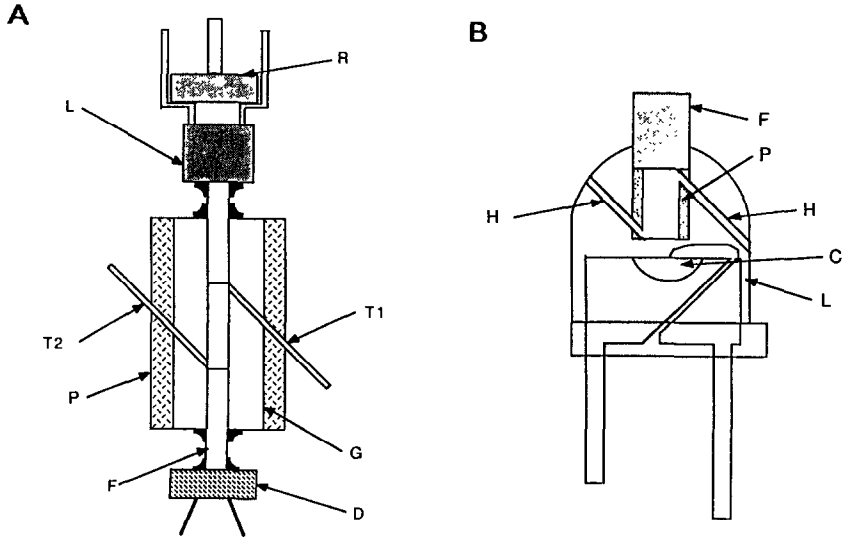

Fig. 8. Two simple flow cell designs. (A) Z-configuration flow cell with direct connection to fiber optic. L: LED; R: reference PD; F: fiber optic; G: flow conduit; T1, T2: flow in/out tubes; P: PVC pump tubing (used when conduit G is of glass); D: detector photodiode. (B) Flow cell built within the body of an LED. C: emitting chip; H: entrance/exit apertures; P: opaque PEEK sleeve; F: fiber optic leading to signal photodiode; a reference photodiode can be placed under the LED.

e.g., ESKA fibers from Edmund Scientific, Barrington, NJ), 1.0 or 1.5 mm dia. optical fibers (F) can be placed 6–10 mm apart at the termini of the main flow conduit (G), their spacing defining the optical path length. The conduit G itself is a 15–20 mm segment of a 6.3-mm diameter rod, drilled out to accommodate snugly the optical fibers. The conduit can be of any polymer that accepts an adhesive and is compatible with the application. Inlet/outlet holes are drilled at a $\sim 45°$ angle and inlet/outlet tubes (stainless steel hypodermic needle tubing, Small Parts Inc., Miami, FL or small o.d. PEEK tubing, Upchurch Scientific) are cemented in place with epoxy adhesive, without protrusion in the main flow conduit. The fiber optic ends, already connected to an LED (L) or PD (D) by a short length, are then inserted to the measured depth and cemented in place. If the application involves solvent media that are compatible with epoxy resin and any reactants or products formed do not absorb strongly thereon, many LEDs are available already terminated in a 2-mm diameter cylindrical protrusion ("chimney shaped") and can be directly used, with the corresponding end of the conduit G being drilled to accept the LED terminus. If a reference detector (R) is used, it is cemented on the bottom of the LED, using optical adhesive. For additional strength and protection from ambient light, the whole assembly can now be encased in an opaque material. Black silicone sealant is particularly useful for this purpose since it is removed easily if necessary.

For some applications, polymeric optical fibers are simply not suitable. Essentially the same design can be attained with a 1-mm i.d. glass tube as the flow conduit and 1-mm single strand silica optical fibers (available, *e.g.*, from Ensign–Bickford Optics Co., Avon, CT). To maintain good S/N with the limited optical aperture, the pathlength should not be greater than 6 mm. The difficult part about using a glass conduit is to provide the inlet/outlet apertures. Even for a skilled machinist using diamond-tipped bits, it is difficult to drill holes in small bore thin wall glass tubes. But it is possible to create a slanted cut into the wall of a glass tube with a thin motorized cutting wheel (as with a DREMEL Moto-Tool®, available in most hardware and hobby stores) without much difficulty. Once the apertures have been made, the glass tube is coated with a thin layer of epoxy adhesive. While the adhesive is still tacky, the coated tube is slipped inside a plasticized poly(vinyl chloride) tubing P (commonly used with peristaltic pumps, a great variety of such tubing, of varying i.d. are available from Elkay Products, Shrewsbury, MA). Connecting inlet/outlet tubing are then put in and cemented in place after first puncturing the protective tubing P at the appropriate locations with a hypodermic needle.

Flow cells within an LED. If the application is compatible with epoxy, very simple detectors are possible where the flow cell is built wholly within the body of the original LED, as shown in Fig. 8(b). With 5-mm LEDs, a maximum path length of 3 mm is possible, larger pathlengths are possible with a 13-mm (T-4) size LED. A hole of desired size, typically 1.5 mm, is drilled from the top of the LED to within 1 (preferably 0.5) mm of the chip C. Careful manual drilling under a low magnification microscope is recommended. The bottom of the hole is then made flat with an appropriate bottoming tool. Angled entrance and exit holes (H) of desired diameters are now drilled. However, the bottom surface is still rough and light transmission through this surface will be very poor if it is used in this state. Polishing compounds cannot be used since it is not possible to remove them from the surface. Rather, it is best to use some slow curing transparent epoxy and coat the drilled rough surface with it, using the bottom of a suitably sized drill bit for even distribution. When the adhesive cures, an even and transparent surface is left. An optical fiber F is then cemented in at the distal end and terminates in the detector PD. Again, if desired, a reference PD can be placed at the bottom of L. Beyond a compact design, this configuration results in some interesting properties. When the bottom of the flow path is very close to the chip, the flowing fluid actually helps to cool the chip; the light output is measurably higher when the chip is cooled (*vide infra*) by the flowing fluid. (Conceivably, this may be used as the basis of a flow transducer, albeit such use is likely to be complicated by variations in the ambient and the fluid temperature and heat capacity of the fluid.) The response of such a detector is not linear over a large range of absorbance; stray light is conducted to the detector fiber through the body of the LED. The linear range can be extended by drilling the initial flow path to accommodate a small segment of an opaque PEEK tube P (1.0 mm i.d./1.5 mm o.d.) as an optical isolation sleeve.

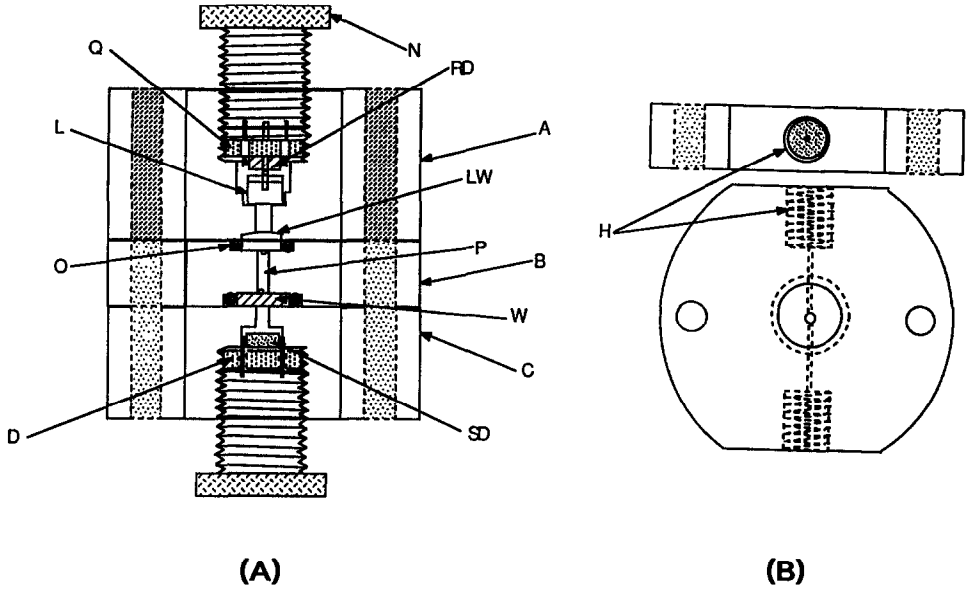

Fig. 9. Demountable cell shown in horizontal cross section in (A) and the top view and vertical cross section of the middle section B appears in (B). A, C: aluminum end-blocks; B: central polymer block housing the flow cell; N: knurled male nuts; Q: socket; RD, SD: reference and signal PD; L: LED; LW: lens window; W: flat window; P: flow-path; O: O-rings; D: opaque disc; H: threaded apertures for fluid inlet/outlet.

Demountable flow cells. The above designs call for little machining but sacrifice versatility. Two robust designs in which the various components of the cell are readily changed are shown in Figs. 9 and 10 respectively. The flow cell of Fig. 9 is shown in horizontal cross section in (A). It is composed of two aluminum parts (A and C) sandwiching a central part B made from an inert plastic. (Most of our cells were made from translucent Kel-F®. While this material is very inert and machines well, all exposed surfaces need to be covered up by an opaque tape to prevent intrusion of light. We have also used glass filled Ryton®; this is highly opaque and reasonably inert but requires carbide faced tools for machining. More recent experience shows that PEEK may be the best choice; opaque Kel-F is also available.) The three parts are held together by two 8–32 screws (not shown in the figure) placed at opposite corners; one endplate contains recessed holes and the other contains a threaded aperture with through holes in block B to complete the assembly. A top view of block B and a vertical cross-section is shown in (B). Threaded (1/4–28) Inlet/outlet apertures (H) are provided in B. These terminate in 0.5-mm bore passages that open on the optical windows LW and W. It is important to note that the termini of the entrance/exit passages break out partially into the surface facing the windows, if these termini are completely contained within the flow path, the cell will be more prone to occasional bubbles being trapped in the cell. The optical path P is 1.5 × 6 mm. A circular recess, 1.6 mm deep and 9 mm in diameter, is machined on each face of block B. These recesses hold the window W and lens L, each surrounded by a No. 009 O-ring O. The latter are thick enough to protrude slightly out of the recess and when the three blocks are assembled, a seal is formed by compression. If machining is not sufficiently precise to accomplish this, circular gaskets can be punched out of folded-over Teflon tape and used between the optical windows and the

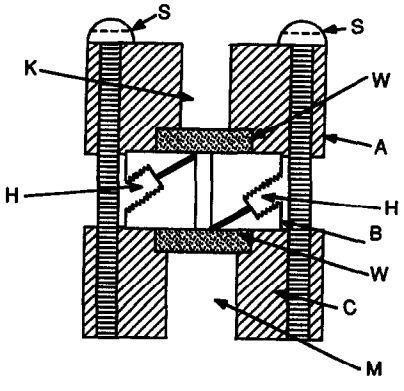

Fig. 10. Fiber optic based demountable cell. H: 1-72 threaded aperture communicating to the 1.0 × 6 mm illuminated flow path; S: Machine screws (4), holding blocks A, B and C together; K, M: aperture for optical fibers; W: flat optical windows.

aluminum faceplates. Window W is a 6.3-mm diameter 1.5-mm thick optically flat glass disc and LW is a 6-mm diameter, 9-mm focal length piano convex lens (center thickness 1.75 mm), both inexpensively available from Edmund Scientific. The use of the lens instead of a flat window (cost difference *ca.* $5) is not essential but results in at least 25% better light throughput through the cell. Blocks A and B are similar and both contain 1/2–20 threaded holes, terminating in 3 mm diameter apertures. Hollow knurled aluminum male fittings N are machined to fit into these threads. On the detector side, disc D, *ca.* 1.5 mm thick, machined from nonconductive opaque plastics like phenolic resins, sits atop of N and appropriate small holes are drilled in D to allow passage of the leads of the signal detector SD (3 × 3 mm silicon PD, Electronic Goldmine) that end in a shielded cable S and a BNC connector. On the source side, below N sits an 8-pin socket Q (ECG 407, only 4 pins are used) and reference detector RD (same as SD) straddles two opposite holes. The leads of the LED L (dome removed, face polished) are carefully bent and excess lengths cut off such that it will fit tightly over R and into the two unused holes in Q. At the bottom of Q (the pin end), unused pins are removed and the cathode ends of RD and L are combined into a single lead (constituting a common ground in a shielded cable; the center conductor carries the anode signal from RD, the whole terminating in a coaxial connector). The anode lead from L is connected to a current limiting resistor that will limit the current to *ca.* 80% of the maximum value continuously allowable for the LED when connected to the positive power supply of the signal processing electronics (typically +12 or +15 V) and thus terminates in a lead going to the power supply. Such a detector allows rapid change of the emitter and thus the wavelength.

Demountable flow cells with optical fibers. There are certain advantages if signal communications to the flow cell are solely by optical fibers, in particular regarding noise caused by the environment around the detector. The design in Fig. 9 is easily modified to accept optical fibers, especially jacketed fiber bundles terminating in polished, metal-colleted ends. Simpler and substantially smaller designs are possible, however. Figure 10 shows such a design, composed of three individual blocks, machined from PEEK. The central block B is 6.3 mm in diameter and 6 mm long, containing a 1-mm bore central flow path. Angled holes H terminating in 0.5-mm apertures provide liquid inlet/outlet paths and are provided with 1–72 threads and a flat seat. PEEK chromatography tubing, 1.5 mm in o.d. are threaded on the exterior with a 1–72 die and can then be screwed into holes H to form leakproof connections that will withstand considerable pressure.[56] The top block A contains a 0.135 inch diameter drilled aperture K to house snugly a 0.130 inch o.d. jacketed, 0.08 inch core plastic optical fiber, held in place by a set screw not shown in the drawing (perpendicular to the plane of the paper). The polished end of the fiber butts directly against the cell window W (same as that in Fig. 9) and the latter is housed within an appropriately sized recess machined into block A. The depth of the recess is marginally less than the thickness of W; the compression on the window itself provides the necessary sealing. The bottom block C is similar to A except that hole M is larger (*ca.* 0.190 inch) to accommodate one leg of a standard bifurcated fiber optic bundle (Dolan-Jenner type E624, terminal o.d. 0.187 inch) held in place with a set screw not shown in the drawing. The common arm goes to an LED. The fiber end and the LED are essentially of the same diameter, they are put face to face in an aluminum sleeve and held in place by set screws. The second bifurcated leg goes to the reference photodetector, typically placed directly on the detector electronics board and the fiber optic end put thereon with appropriate protection from adventitious light. The fiber from A also returns to the detector electronics board, to communicate with the signal photodetector on the electronics board. The three blocks are held together by four 2–56 × 3/4 inch screws between blocks A and C, two of the screws (S) are shown in Fig. 10.

Unreferenced vs. referenced detectors. Transmittance or absorbance output?

For most analytical applications, absorbance is the parameter directly related to the analyte concentration and is therefore of the most immediate interest. That the choice of a transmittance output is considered at all is because the output of the detector phototransducer is typically linearly related to the intensity of light falling on it, *i.e.*, it is linear with transmittance. The simplest designs (which includes virtually all of the LED-based detectors described in the literature thus far), contain an unreferenced LED source and the photodetector output signal is typically processed by some amplifying

and noise filtering circuitry and provided with a variable offset capability. The final output signal remains linearly related to the transmittance. It is possible to convert the transmittance signal into absorbance via the logarithmic transfer function of a device, *e.g.*, a transistor[43] or better, a dedicated logarithmic amplifier (*e.g.*, AD755N, Analog Devices, Norwood, MA). However, in our judgment, the additional effort is better spent by providing a reference detector to the LED source and a log ratio amplifier (LRA) integrated circuit (IC) that then directly provides an absorbance output (*vide infra*). At the very least, before log conversion circuitry is added to an unreferenced detector (which are really best suited for the less demanding applications), it should be recognized (especially in defense of the many previous designs that have utilized transmittance outputs) that at low absorbance levels (≤ 0.3), essentially a linear relationship exists between transmittance and absorbance. This is graphically illustrated in Fig. 11.

Of course, if the output of an (unreferenced) detector is acquired by a computer, all transformations can be made in the software. One caveat is necessary, if the effective resolution of the data acquisition process is not high enough, this may become the determining factor governing noise as well as the accuracy of any subsequent mathematical transformations.

The major shortcoming of an unreferenced detector is its temporal drift at high sensitivities. Although an LED is a substantially more stable source than any incandescent lamp, the luminescence efficiency does still depend on temperature. Consequently, even if constant current sources are used to drive it, ambient temperature fluctuations lead to changes in the junction temperature that translate to variations in light

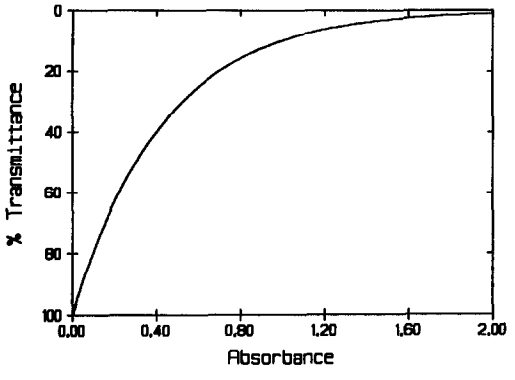

Fig. 11. The relationship between absorbance and Transmittance is linear at low absorbance values.

output. There is little or no difference in short-term noise between single-beam and referenced designs but a vast difference exists in long term drifts. The differences in initial stabilization time are also substantial. In our opinion, the additional energy and investment required to fabricate a referenced detector compared to an unreferenced detector is minor and it is difficult to justify continued fabrication of unreferenced detectors. When a referenced source design is used, it is most convenient to use a log-ratio amplifier IC as previously mentioned. Such a device can directly accept the signal and reference photocurrent inputs (from 1 nA to 1 mA) and provide an output linearly related to log i_s/i_r with user selectable gain per decade (*i.e.*, volts per absorbance unit), with very large offset capabilities to set the initial zero. These ICs are not inexpensive ($60–160) but their performance and convenience make it well worth the investment. These include for example, AD757N (Analog Devices) and its less expensive counterparts 4127KG, 4127JG, LOG100JP, etc. (Burr-Brown Corp.). For most LED-based detector applications, there is no significant performance difference among these devices. Few additional components are necessary with these devices; necessary circuits are very simple and are detailed in the literature from the manufacturer. Experimentally we find that a plot of log i_s *vs.* log i_r has a slope of 1.00 ± 0.01 (tested over 5 orders of magnitude for all of the above amplifiers, the manufacturers claim "less than 1% deviation of linearity over six orders of magnitude"). One additional note of caution is in order, our experience indicates that the last device, the least expensive among the choices above, is best used with an additional final buffer amplifier stage to avoid spurious noise caused by feedback.

Radiant output from LEDs. Effect of temperature and device type

The optical output of an LED is temperature dependent; the efficiency of injection electroluminescence increases with decreasing junction temperature. This is shown in Fig. 12 for a 560-nm LED (HPG5566X). The light output was measured by coupling a fiber optic to the LED and connecting a photo diode at the other end. Relative to the standard mold, removing most of the encapsulating epoxy from the standard LED ("modified LED") improves coupling to the fiber. When the device is surrounded with dry ice, the junction is cooled and the

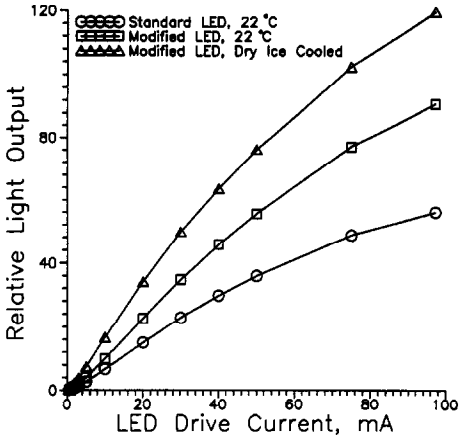

Fig. 12. Temperature dependence of LED light output. Modified LED connotes removal of most of the dome plastic material and coupling of the fiber optic to the polished, flat faced LED.

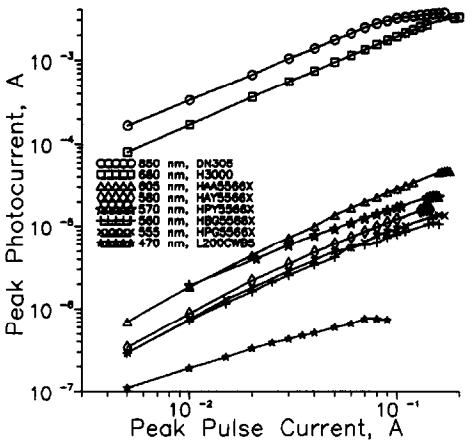

Fig. 13. Light output of various LEDs as a function of drive current, 100 μsec pulses, 1% duty cycle,.

optical output increases by 30–200%, depending on the drive current level. Based on these data, if we assume a nominal figure of 100% increase in light output for a temperature change of 100°, the temperature coefficient of the light output is *ca.* 0.7%/°C. An absorbance change of 10^{-3} is equal to a change in the light level of 0.23%; it should be obvious why referenced beam designs are vital to a practical detector that does not drift excessively.

The optical output is greatly dependent on the nature of the LEDs. In Table 1, a deliberate effort has been made to choose the brightest LEDs available in their class, because higher light levels reaching the detector typically translates into a better signal to noise ratio. The light output of several high brightness LEDs was measured using 50-μsec wide constant current pulses with a 1% duty cycle, supplied by the pulsed emitter photodetector electronics (*vide infra*), the light output measurement being made after the initial 10 μsec of the pulse (to avoid jitter) by a fast photodiode. The light output is presented in terms of detector photocurrent in Fig. 13. The sensitivity of the detector increases with increasing wavelength in the range studied, the sensitivity at 850 nm being about twice that at 470 nm. This difference is, however, insignificant relative to the orders of magnitude differences observed in photocurrent output. The longer wavelength LEDs can handle much greater currents before they saturate and it is remarkable that at high drive currents they elicit photocurrents exceeding 1 mA in a coupled photodiode. It is interesting that the LEDs shown in Fig. 13 clearly fall in three groups of output intensities that are characteristic of the substrates, with the AlGaAs pair at the top and SiC at the bottom and the GaP (or GaAsP/GaP) group in the middle.

Performance, DC excitation

Representative examples are given below for the performance of some of the flow cell designs/electronic arrangements. The flow cell of Fig. 8(a) operated with a typical midwavelength LED (HAA5566X @30 mA, 605 nm) in the single beam mode (transmittance output) with a constant current source and a high quality commercial current→voltage converter (Keithley model 427) exhibited a noise level of 7×10^{-5} absorbance (0.3 sec rise time, water flowing through the cell under gravity, no pulsations). This S/N performance was degraded by a factor of 2–3 with a low offset error FET-input operational amplifier based current→voltage converter. More importantly, the output drift rate of this configuration was high, often higher than 10^{-3} absorbance/hr. A plot of the logarithm of the output signal was linearly correlated with the concentration of indigotrisulfonate over two orders of magnitude, with a linear correlation coefficient of 0.9998 and an uncertainty of slope of 0.42%.

When the same LED was used as the light source in a referenced beam design in the cell of Fig. 10, output drift improved substantially, to $\leq 10^{-4}$ absorbance/hr and a noise level of 7×10^{-5} absorbance was observed. (LOG100JP log-ratio amplifier with an output buffer was used and only modest capacitive damping was utilized, permitting 10→90% and 90→10% respective rise and fall times of 420 and 190 msec.)

With a lower output LED, both the noise and the drift increased, *e.g.*, to 10^{-4} absorbance and 3×10^{-4} absorbance/hr respectively with a 470 nm (L200CWB5) source. However, this performance is respectable considering this is the lowest output emitter in Table 1. Linearity of response for the above detectors was tested with indigotrisulfonate and acidic dichromate solutions respectively for the two above detectors, in a FIA configuration with each analyte spanning a two orders of magnitude range in concentration. Typical chart outputs indicating attainable S/N are shown in Fig. 14. It is interesting to note that the nature of the noise changes considerably between the two detectors, this is caused by a loss of effective bandwidth of the LRA at low input currents as with the 470 nm source. In a duplicate series of tests, the respective linear coefficients of determination (r^2) for the peak height *vs.* injected concentration data were respectively 0.9998 and 1.0000 with y-intercepts statistically indistinguishable from zero. The uncertainty of the linear slope was 0.91 and 1.00% for the 605 nm detector data and 0.40 and 0.42% for the 470 nm detector calibration. This performance is better than many commercial detectors using a continuum source and a monochromator where stray light degrades linearity. Similar experiments conducted with the cell design of Fig. 9 and an AD757N LRA produced essentially the same results with regard to linearity. In this case, a rise time of 0.5 sec was used and a marginal improvement in the noise level of the 605 nm detector was observed, to 5×10^{-5} absorbance. It should be noted that this appears to be the performance limit of this basic design approach, it is not further improved with longer wavelength higher power emitters. It has also been our experience that the best results are not necessarily obtained by driving the emitters at their maximum rated current to obtain the maximum amount of light possible. No referencing scheme is perfect and excessive heat generated degrades the relative stability of the LED output and S/N performance actually deteriorates.

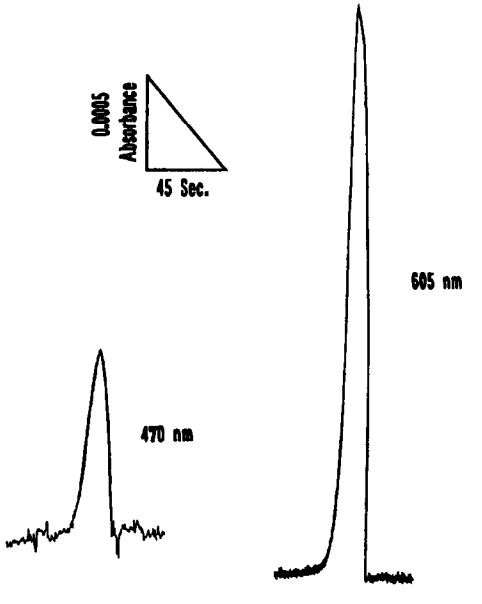

Fig. 14. Typical FIA chart output from detector of Figure 10 operated in the referenced beam absorbance output configuration.

It may therefore appear that the performance difference between low output and high output sources is not very great after all. This is true, but only if considerable trouble is taken to shield the detector and the electronics from external noise, *e.g.*, by using heavy gauge metallic enclosures, *etc.* The detectors with higher output sources are simply much more immune to extrinsic noise and the limiting level of performance, *e.g.*, that cited above, can be reached without extraordinary shielding needs. A consideration of the absolute current levels involved with the lowest output LED should be illustrative of the need for good shielding. Figure 13 indicates that the 470 nm LED L200CWB5, when driven at 50 mA, produces about 200 nA in a PD coupled head on to it. When installed in a flow cell, the reference PD on the back of the LED generates about 20 nA and the signal PD, separated from the source by several mm and a small aperture, generates a current only marginally greater than this. An absorbance change of 10^{-4} is equal to an induced noise current of < 5 pA under these conditions!

The results observed with the radial path flow cell (AD757N LRA) of Fig. 7 conforms to the criterion of $< 1\%$ deviation from linearity (with the 470 nm LED and acidic dichromate as test solution) over a 1.7 order of magnitude range of concentration. The exact design of this detector strictly involves a multiplicity of pathlengths because the optical aperture is not infinitesimally small compared to the tube diameter. The simplicity of the design makes it nevertheless an attractive candidate where detector induced dispersion is to be avoided. For the other designs, it should be noted that the intrinsic linearity of response (electronic linearity) is much greater, as previously mentioned, than the two orders of magnitude cited above. The half bandwidths

of LED sources are obviously not negligible (Table 1), the concentration-absorbance linearity observed in any given situation is more dependent on the degree of match between the emission band of the LED and the absorption band of the LED than any other factor. The broadly centered absorption band of the dye methylene blue at 666 nm matches closely the 660 nm emission band of an AlGaAs LED, with such a source the observed absorbance showed excellent linearity with the concentration of methylene blue over a 3.5-order of magnitude range of concentrations ($r^2 = 0.9997$, uncertainty of linear slope 0.6%, flow cell of Fig. 9, AD757N LRA).

Pulsed detector operation

Especially for low output LEDs it is possible to enhance performance by increasing the output in a transient fashion, *i.e.*, by pulsing it for brief periods at high current. A modest degree of sophistication is necessary to accomplish this; a suitable schematic is shown in Fig. 15. A programmable crystal oscillator (U7) provides the time base and synchronization for all operations. The width of the emitter pulse is governed by U9A while U11, its associated circuitry and a driver transistor hold the current pulse constant at some desired adjustable value. The signal and reference photodiode outputs are processed respectively by input amplifiers U1 and U3; these signals are sampled and held by U2 and U4, respectively. The sampling is delayed from the initiation of the emitter pulse to avoid problems associated with jitter and allow emitter stabilization; this delay is selected by U8A and the duration of the sample period is set by U8B. The outputs of U2 and U4 are processed by the log-ratio amplifier U5 and the final output is provided through the buffer and offset amplifier U6. This arrangement permits attainment of noise levels of $2\text{–}3 \times 10^{-5}$ absorbance with a rise time less than 0.3 sec for all the LEDs other than the 470 nm; for the latter, a noise level of 5×10^{-5} absorbance is attainable under the same conditions. The linearity performance is the same as that with the DC detectors described in the foregoing section.

Automated zeroing of detector output

For all detectors described above, the output is offset (or adjusted to zero) by a manually operated potentiometer. The schematic in Fig. 16 allows one to zero the output with 12-bit precision by a reset button (or by a logic signal from a remote source) and is particularly convenient when the determination system shows a systematic drift; auto-zeroing can be carried out every time the injection valve is switched. Approximate component cost is $100; essentially identical commercial units are offered for $1200 (*e.g.*, from Systec Inc., Minneapolis, MN). Of course, the use of such a device is not limited to the present detector applications.

Computer interfaced operation of pulsed detectors. Performance

The ultimate in flexibility and performance is achieved with computer-interfaced pulsed operation of the detector and acquisition and processing of the resulting data. The photodetector of Fig. 9 (560 nm LED, HPG5566X) was used with the arrangement in Fig. 17. The interface board and associated components were located inside a 0.1 inch thick wall Al box to provide improved shielding. The information content of FIA or liquid chromatography systems are in a very low frequency domain, typically well below 1 Hz. The operation of the LED at a modest frequency (< 100 Hz) and the use of a low-pass filter as shown in Fig. 17 results in a system with significant immunity to high frequency noise (an appreciable amount can be contributed by video monitors in their usual location atop the CPU unit housing the interface board).

In operation, during the LED-off period (typ. 20–70 msec), after an initial brief wait period of 3 msec, the dark current levels from both the signal and reference photodetectors are alternatively and repeatedly sampled. At a sampling rate of 33 kHz, *ca.* 280 individual A/D conversions are made for reference and signal currents each within 20 msec, including the wait period. The reference and signal current values are then individually summed. The digital integration procedure thus results in a large and necessary increase in the effective resolution of the 12-bit interface board used (DAS-16G1, Metrabyte Corp., Taunton, MA). The average values of the reference and signal dark currents are then stored. The LED is then turned on (for a period of typically 20–70 msec) using the digital to analog output function of the interface board as a square wave generator. Generally the LED is driven at the maximum current at which it is rated for continuous duty (typically 50 mA). Again following a brief wait period (3 msec) for any ringing to subside (typically ≤ 1 msec), the signal and reference detector currents are alternately and repeatedly sampled. Software

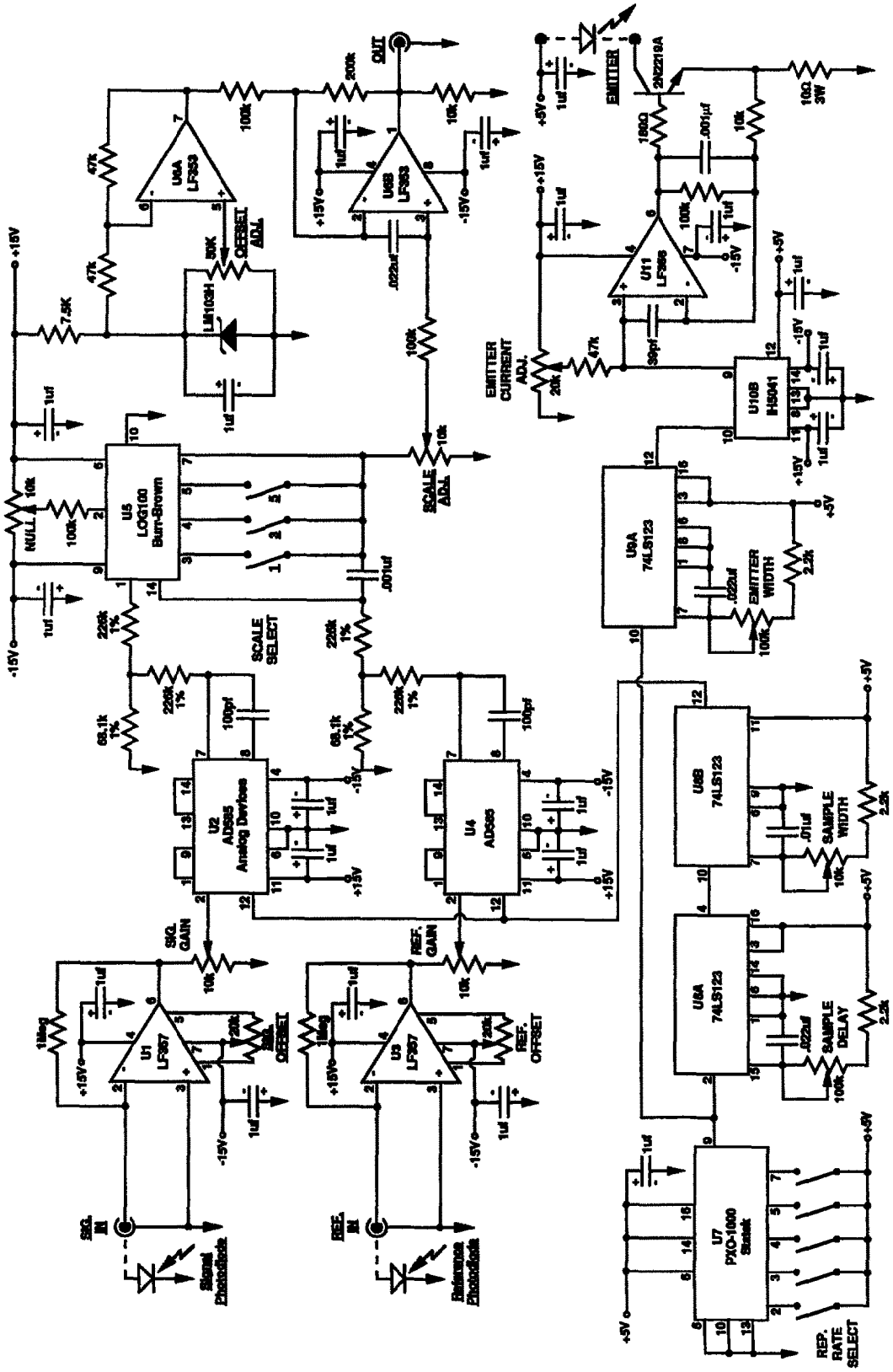

Fig. 15. Pulsed emitter photodetector schematic.

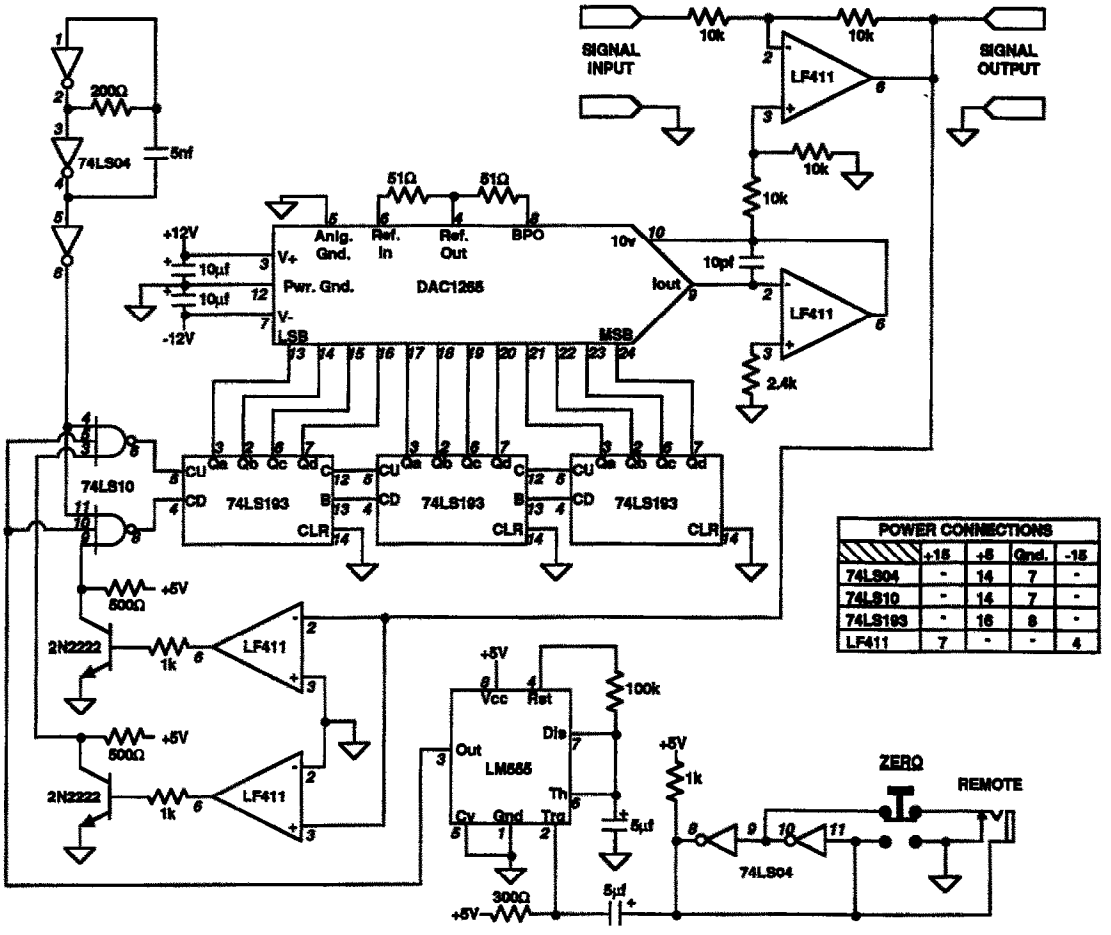

Fig. 16. Auto Zero Schematic.

(written in machine language) permit data acquisition rates up to 66.7 kHz on a 80386 processor based computer, close to the maximum sampling rate achievable by the A/D converter. The average dark current from the previous cycle is then subtracted from the corresponding average photocurrents from the LED-on period. The logarithm of the dark current corrected ratio value of the signal to the reference photodetector current is computed. The standard deviation (SD) of a number of such successive values (typically 30–50 are used) provides an index of the measurement stability (or precision). The peak to peak noise levels used in the rest of this paper are comparable to approximately twice this value. Figure 18 shows the improvement in measurement precision of measuring a blank solution (water) with increasing number of samples averaged (the effective integration period is indicated in the figure, a sampling rate of 22 kHz was used to generate these data). Little is gained beyond a sampling period of 500 msec but by this time the standard deviation of absorbance reaches $< 2 \times 10^{-6}$ absorbance; this is well beyond the performance capabilities of presently available commercial detectors. Note also that the slope of the best fit line in the log–log plot of Fig. 18 is -0.5, indicating correspondence to the theorem that the uncertainty of the measurement is reduced in direct proportion to the square root of the number of measurements, within the limits of the study. The measurement precision is also excellent with an absorbing solution in the cell, for 30 successive 66.7 msec measurements of a dye solution with a mean absorbance value of 0.430, the relative standard deviation was only 0.0026%. Note that the noise levels generated in FIA systems operated with peristaltic pumps are significantly greater than the intrinsic performance level of such a detector, the overall performance is limited by the flow/mixing noise in such systems.

Detector linearity was tested with a 605 nm LED and alkaline bromothymol blue as the test solution. Over a range of concentrations

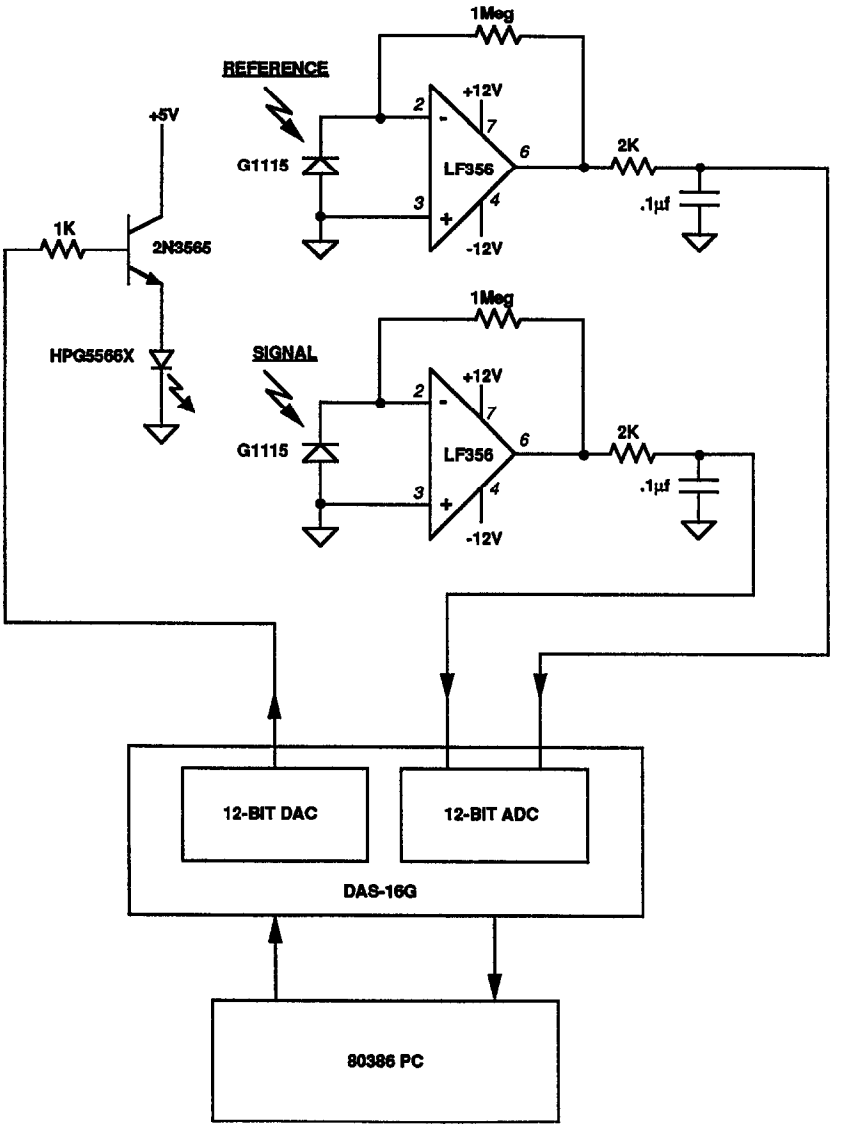

Fig. 17. Arrangement for computer interfaced pulsed detector.

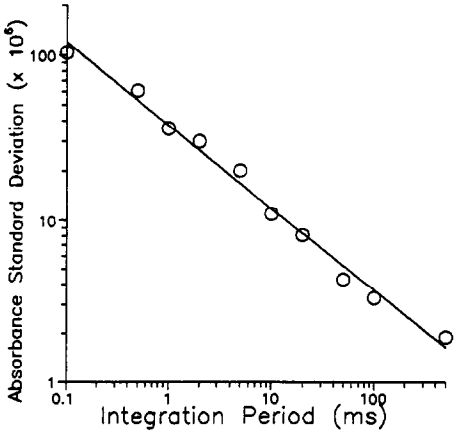

Fig. 18. Measurement precision as a function of the integration period for the computer-interfaced pulsed detector, sampling rate 22 kHz.

spanning two orders of magnitude, the absorbance–concentration relationship exhibited good linearity ($r^2 = 0.9997$, uncertainty of slope 0.78%).

CONCLUSIONS

LED-based optical detectors provide inexpensive high performance long life alternatives to continuum source detectors. For applications in which a reasonable match can be obtained between an LED wavelength and the analyte absorption, such detectors will generally outperform other available designs. If the chemical system can be so designed, a longer absorption wavelength is desirable because of the

availability of very high output sources. It is almost certain that the lower limit of the available LED wavelengths will continue to decrease for some time to come and thus broaden the scope of application of LED based optical detectors. Clearly, multiwavelength detectors containing a multiplicity of emitter LEDs can be made easily and may constitute a high light throughput alternative to continuum sources coupled to a diode array detector. Several sequentially turned on LEDs can be serially placed along a tube opposite correspondingly placed PDs, constituting a series of radial path detectors with unusual flexibility in making kinetic measurements. In essence, the low cost, small size and ease of fabrication of LED-based detectors hold unusual promise for those willing to experiment with them in unconventional ways.

Acknowledgement—This work spans several years of effort and has benefitted from the counsel of many people. In particular, we wish to acknowledge the help and interest of Steve Gluck, Dow Chemical Co.; Don Olson, Shell Development Co. and Doug Gjerde, Sarasep Inc.; Adrian Wade, University of British Columbia, is thanked for sharing his knowledge on the available literature on LED based detectors. This work was supported variously by grants from the Dow Chemical Co., Shell Development and by the Office of Basic Energy Sciences, U.S. Department of Energy through DE-FG05-84ER13281. However, this report has not been subject to review by any of the above agencies and no endorsement should be inferred.

REFERENCES

1. *Design Engineer's Data Book*, Industrial Devices Inc., Hackensack, NJ. 1989.
2. *Optical Semiconductors*, Mitsubishi Electric Corp., Torrance, CA. 1986.
3. J. Pawliszyn, *Rev. Sci. Instrum.*, 1987, **58**, 245.
4. H. Flaschka, C. McKeithan and R. M. Barnes, *Anal. Lett.*, 1973, **6**, 585.
5. T. Anfält, A. Granéli and M. Strandberg, *Anal. Chem.*, 1976, **48**, 357.
6. D. Betteridge, E. L. Dagless, B. Fields and N. F. Graves, *Analyst*, 1978, **103**, 897.
7. D. Betteridge, *Anal. Chem.*, 1978, **50**, 832A.
8. K. S. Johnson and R. L. Petty, *Limnol. Oceanogr.*, 1983, **28**, 1266.
9. K. S. Johnson, C. L. Beehler and C. M. Sakamoto-Arnold, *Anal. Chim. Acta*, 1986, **179**, 245.
10. M. Trozanowicz, W. Augustyniak and A. Hulanicki, *Mikrochim. Acta*, 1984, **II**, 17.
11. D. Betteridge, *Z. Anal. Chem.*, 1982, **312**, 441.
12. T. J. Sly, D. Betteridge, D. Wibberley and D. J. Porter, *J. Autom. Chem.*, 1982, **4**, 186.
13. D. Betteridge, W. C. Cheng, E. L. Dagless, P. David, T. B. Goad, D. R. Deans, D. A. Newton and T. B. Pierce, *Analyst*, 1983, **108**, 1.
14. G. J. Schmidt and R. P. W. Scott, *ibid.*, 1984, **109**, 997.
15. T. Imasaka, T. Kamikubo, Y. Kawabata and N. Ishibashi, *Anal. Chim. Acta*, 1983, **153**, 261.
16. P. J. Worsfold, J. R. Clinch and H. Casey, *ibid.*, 1987, **197**, 43.
17. J. R. Clinch, P. R. Worsfold and H. Casey, *ibid.*, 1987, **200**, 523.
18. J. R. Clinch, P. J. Worsfold and F. W. Sweeting, *ibid.*, 1988, **214**, 401.
19. H. Casey, R. T. Clarke, S. M. Smith, J. R. Clinch and P. J. Worsfold, *ibid.*, 1989, **227**, 329.
20. R. L. Benson, P. J. Worsfold and F. W. Sweeting, *ibid.*, 1990, **238**, 177.
21. M. Trojanowicz, P. J. Worsfold and J. R. Clinch, *Trends Anal. Chem.*, 1988, **7**, 301.
22. M. Trozanowicz and J. Szpunar-Lobinska, *Anal. Chim. Acta*, 1990, **230**, 125.
23. O. S. Wolfbeis, B. P. H. Schaffar and E. Kaschnitz, *Analyst*, 1986, **111**, 1331.
24. B. W. Smith, B. T. Jones and J. D. Winefordner, *Appl. Spectrosc.*, 1988, **42**, 1469.
25. J. A. Sweileh and P. K. Dasgupta, *Mikrochim. Acta*, 1986, **III**, 175.
26. J. A. Sweileh and P. K. Dasgupta, *Anal. Chim. Acta*, 1988, **214**, 107.
27. K. Petersen and P. K. Dasgupta, *Talanta*, 1989, **36**, 49.
28. K. Sonne and P. K. Dasgupta, *Anal. Chem.*, 1991, **63**, 427.
29. S. Dong and P. K. Dasgupta, *Talanta*, 1991, **38**, 133.
30. Z. Vecera and P. K. Dasgupta, *Anal. Chem.*, 1991, **63**, 2210.
31. B. G. Streetman, *Solid State Electronic Devices*, 3rd Ed., Prentice-Hall, Englewood Cliffs, New Jersey, 1991.
32. Y. Yamamoto (ed), *Coherence, Amplification and Quantum Effects in Semiconductor Lasers*, Wiley, New York, 1991.
33. H. Kressel and J. K. Butler, *Semiconductor Lasers and Heterojunction LEDs*, Academic Press, New York, 1977.
34. E. W. Williams and R. Hall, *Luminescence and the Light Emitting Diode*, Pergamon Press, 1978.
35. *Optoelectronics/Fiber Optics Applications Manual*, Hewlett Packard Co., Palo Alto, California, 1981.
36. H. Leidecker and C. Powers, *NASA Tech Briefs, 33–34*, 1991.
37. News release, Hewlett-Packard Co., *Photonics Spectra*, 1990, **24(11)**, 42.
38. K. Irgum, University of Umeå, Personal Communication, 1986.
39. News Release, 3M Co., *Photonics Spectra*, 1991, **25(10)**, 52.
40. N. Ishibashi and T. Imasaka, *Anal. Chem.*, 1990, **62**, 363A.
41. E. Unger and G. Patonay, *ibid.*, 1989, **61**, 1425.
42. J. Hicks and G. Patonay, *ibid.*, 1990, **62**, 1543.
43. P. Horowitz and W. Hill, *The Art of Electronics*, 2nd Ed., Cambridge University Press, Cambridge, Massachusetts, 1989.
44. *Linear IC Applications Handbook*, pp. 192–201. Burr-Brown Corp., Tempe, Arizona. 1988.
45. *Photodiodes*, Hamamatsu Corp., Bridgewater, New Jersey. 1991.
46. H. Poppe, *Anal. Chim. Acta*, 1980, **114**, 59.
47. *Idem, ibid.*, 1983, **145**, 17.
48. D. C. Stone and J. F. Tyson, *ibid.*, 1986, **179**, 427.
49. J. E. Stewart, *Appl. Optics*, 1981, **20**, 654.
50. *Idem, Proc. SPIE*, 1985, **492**, 529.

51. E. A. G. Zagatto, M. A. Z. Arruda, A. O. Jacintho and I. L. Matos, *Anal. Chim. Acta*, 1990, **234**, 153.
52. P. K. Dasgupta, J.-S. Rhee and E. L. Loree, *Spectroscopy*, 1987, **2(10)**, 39.
53. A. E. Bruno, E. Gassman, N. Pericles and K. Anton, *Anal. Chem.*, 1989, **61**, 876.
54. A. E. Bruno, R. Kuhn and H. M. Widmer, *Anal. Chim. Acta*, 1990, **234**, 259.
55. V. Kuban, P. K. Dasgupta and J. N. Marx, *Chem.*, 1992, 64, 36.
56. P. K. Dasgupta and K. Morris, *LC-GC Mag.*, 1992, 10, 149.

Talanta, Vol. 40, No. 1, pp. 75–80, 1993
Printed in Great Britain

0039-9140/93 $6.00 + 0.00
Pergamon Press Ltd

FLOW INJECTION DETERMINATION OF CHROMIUM(III) BY PYROGALLOL CHEMILUMINESCENCE

SHIGENORI NAKANO, MITSUNOBU FUKUDA and SHIZUKO KAGEYAMA
Chemical Institute, Faculty of Education, Tottori University, Koyama-cho, Tottori 680, Japan

HIDEYUKI ITABASHI and TAKUJI KAWASHIMA
Laboratory of Analytical Chemistry, Department of Chemistry, The University of Tsukuba, Ibaraki 305, Japan

(*Received* 26 *March* 1992. *Accepted* 4 *April* 1992)

Summary—A flow injection method is proposed for the determination of nanogram amounts of chromium(III) using a pyrogallol chemiluminescence system. It is based on its catalytic effect on the oxidation of pyrogallol with periodate at a neutral medium. The addition of 3-(*N*-morpholino)propanesulphonic acid to the reaction system increased the chemiluminescence signal for chromium(III). The present method allows the determination of 5–100 ng/ml of chromium(III). The relative standard deviation of 2.2% ($n = 10$) was obtained at 20 ng/ml of chromium(III) and the detection limit (signal-to-noise ratio = 2) was 1 ng/ml with the sampling frequency of 25/hr.

Kinetic methods of analysis using catalyzed reactions are powerful techniques for the determination of trace amounts of catalysts because they participate in the indicator reactions in a cyclic manner.[1,2] Further, the introduction of flow injection analysis makes kinetic–catalytic methods more attractive; the rapid and reproducible mixing of sample and reagents can be achieved.[3]

Some applications of chromium-catalyzed reactions including colour development and chemiluminescence (CL) for the determination of this element have been reported by several authors.[4–17] Table 1 shows the pertinent results of kinetic–catalytic methods for the determination of chromium at trace levels. Most of these methods required a separation step prior to analysis because co-existing ions interfered with the determination. The main problem in utilizing the catalyzed reactions for the assay of chromium lies in the selectivity.

The oxidation of pyrogallol (1,2,3-trioxybenzene) with molecular oxygen or hydrogen peroxide is accompanied by CL in aqueous alkali solutions;[18,19] the light emission was thought to be due to the excited singlet oxygen molecules. The reaction of pyrogallol with hydrogen peroxide has been applied to the assay of peroxidase activity[20,21] and cobalt(II).[22] Little attention have been paid to pyrogallol as a CL reagent and few papers have dealt with the CL oxidation of pyrogallol with other oxidants. The CL oxidation of gallic acid with hydrogen peroxide is thought to give similar results to the pyrogallol–hydrogen peroxide system and has been utilized for the determination of proteins,[23] formaldehyde,[19] silver(I) and cobalt(II).[24]

Recently, Evmiridis[25–27] has reported the CL flow injection determination of pyrogallol and periodate with a pyrogallol–periodate system. We found that chromium(III) enhanced the CL intensity resulting from the reaction of pyrogallol with periodate in a neutral pH region. Furthermore, the presence of 3-(*N*-morpholino)propanesulphonic acid (MOPS) in the reaction system markedly increased the CL signal for chromium(III). This paper describes the flow injection determination of nanogram levels of chromium(III) based on its catalytic effect on the CL oxidation of pyrogallol with periodiate in the presence of MOPS. As low as $10^{-8}M$ chromium(III) can be easily determined by measuring the intensity of the light produced. Total chromium can be determined by reducing chromium(VI) to chromium(III) with sulphite.

EXPERIMENTAL

Reagents

All chemicals used were of analytical-reagent grade and Millipore (Milli-Q) reagent grade demineralized water was used throughout.

Table 1. Kinetic-catalytic methods for the determination of chromium

Reaction system	Detection technique	Response	Detection limit, ng/ml	Additive	Ref.
o-Dianisidine/H_2O_2	Photometric	Cr(VI)	1.0	Ion exchange	4
		Cr(VI)	0.049	DMF*	5
I^-/BrO_3^-	Amperometric	Cr(VI)	5.0	Rotating Pt electrode	6
As(III)/IO_4^-	Photometric	Cr(III)	100		7
MBTH†/DMA‡/H_2O_2	Photometric	Cr(III)	0.4	EDTA	8
o-Tolidine/H_2O_3	Photometric	Cr(VI)	40	Ion exchange	9
Luminol/H_2O_2	CL	Cr(III)	0.025	EDTA	10
		Cr(III)	0.2	Br^-	11
		Cr(III)	0.1	IC§	12
		Cr(VI)‖	0.3	IC§	12
Lophine/H_2O_2	CL	Cr(VI)	0.3	Ion exchange	13
		Cr(VI)	20	Activated almina	14
Lucigenin/H_2O_2	CL	Cr(III)	5.0	CH_3OH	15
BSF#/H_2O_2	CL	Cr(III)	1.6	CH_3CN	16
FMN**/H_2O_2	CL	Cr(III) + Cr(VI)	2.6	TDBC††	17
Pyrogallol/IO_4^-	CL	Cr(III)	1.0	MOPS‡‡/EDTA	This work

*Dimethylformamide; †3-Methyl-2-benzothiazolinone hydrazone; ‡N,N-Dimethylaniline; §Ion chromatography; ‖Cr(VI) was reduced with sulphite; # Brilliant sulphoflavine; **Flavin mononucleotide; ††Tetradecyldimethylammonium chloride; ‡‡3-(N-Morpholino)propanesulphonic acid.

A chromium(VI) stock solution (1.00 mg/ml) was prepared by dissolving 1.414 g of potassium dichromate (primary standard, Wako Junyaku Co.) in 500 ml of water. A chromium(III) stock solution (0.50 mg/ml) in 0.1*M* hydrochloric acid was prepared by mixing the chromium(VI) stock solution, 6*M* hydrochloric acid and ethanol. The excess of ethanol was removed by boiling.

Pyrogallol from Kanto Kagaku was used without further purification. A pyrogallol stock solution (0.1*M*) was prepared by dissolving 1.26 g of the compound in $10^{-3}M$ hydrochloric acid, diluting to 100 ml with the same acid and filtering through a 0.45-μm Millipore filter. The stock solution was stable for at least a week if it was stored in a refrigerator. Generally, 250 ml of working solutions ($1.0 \times 10^{-4}M$) were prepared daily from the stock solution. A periodate solution ($6.0 \times 10^{-3}M$) was prepared by dissolving 0.690 g of potassium periodate (Nakarai Kagaku Co.) and diluting to 500 ml with water. A MOPS (Dojin Kagaku Co.) buffer solution ($8.0 \times 10^{-2}M$) involving ammonia (0.3*M*) and EDTA ($6.0 \times 10^{-3}M$) was also prepared; the pH of the solution was adjusted to about 7.0 with 3 and/or 0.1*M* hydrochloric acid when $1.0 \times 10^{-3}M$ hydrochloric acid was used as a carrier solution.

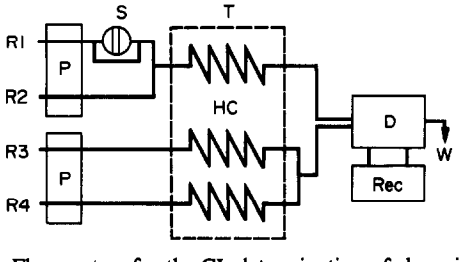

Fig. 1. Flow system for the CL determination of chromium(III). R1, HCl (1.0×10^{-3} or 0.1*M*); R2, MOPS ($8.0 \times 10^{-2}M$)/EDTA ($6.0 \times 10^{-3}M$)/NH_3 (0.3*M*); R3, pyrogallol ($1.0 \times 10^{-4}M$); R4, periodate ($6.0 \times 10^{-3}M$); P, micropump (0.7 ml/min); S, chromium(III) sample (321 μl); T, thermostated bath (30.0 ± 0.1°); HC, heating coil (1 m); D, CL detector; Rec, recorder; W, waste (pH 6.9).

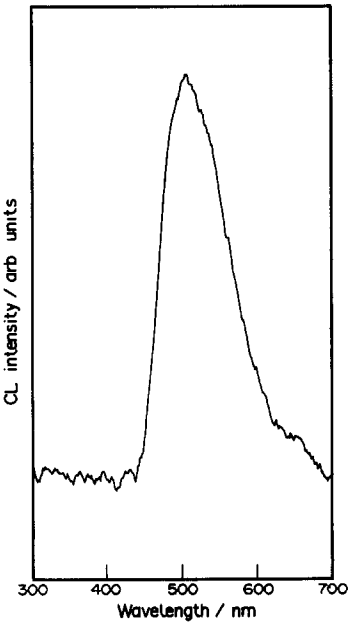

Fig. 2. CL spectrum of pyrogallol–periodate–chromium(III) system. Conditions: $C_{Cr(III)}$, 10 μg/ml; $C_{pyrogallol}$, $1.0 \times 10^{-3}M$; $C_{IO_4^-}$, $2.0 \times 10^{-2}M$; C_{MOPS}, $5.0 \times 10^{-2}M$; flow rate, 2.0 ml/min, pH 7.2, at room temperature. The chromium(III) solution was propelled from reservoir R1 and the spectrum was obtained by an integrating mode.

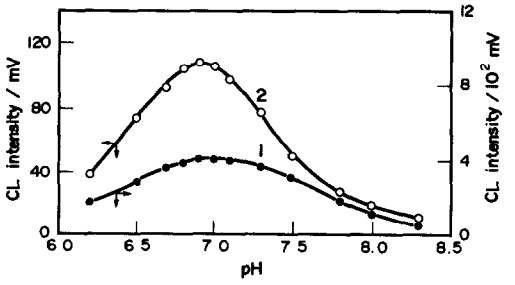

Fig. 3. Effect of pH on the CL intensity. 1, baseline; 2, 20 ng/ml chromium(III). Other conditions as in Fig. 1.

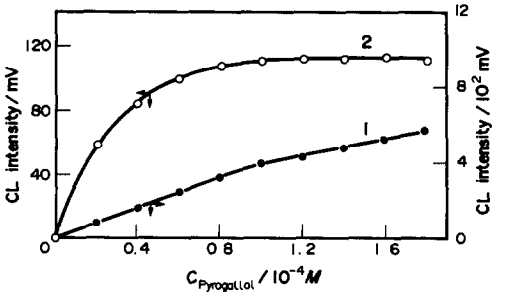

Fig. 5. Effect of pyrogallol concentration on the CL intensity. 1, baseline; 2, 20 ng/ml chromium(III). Other conditions as in Fig. 1.

Apparatus

The flow system is shown in Fig. 1. It consists of two double-plunger micropumps (Kurahashi Giken DLP-2000), a six-way injection valve (Sanuki Kogyo SVM-6M2) with variable sample volume, a circulating thermostated bath (Toyo LH-1000C), a CL detector (Soma Kogaku S-3400) equipped with a spiral type flow cell and a recorder (Rika Denki R-01). The flow cell was a 55-cm coil of Teflon tubing. All coils in the manifold are made from Teflon tubing (0.5 mm i.d.). Chemiluminescence spectra of the reaction system were obtained with a JASCO FP-777 spectrofluorometer installed with a Soma S-3400 CL flow cell over the wavelength range from 300 to 700 nm. A Toa Denpa Model HM-55 pH meter was also used.

Procedure

The carrier (R1, 1.0×10^{-3} or $0.1M$ hydrochloric acid), MOPS buffer (R2), pyrogallol (R3) and periodate (R4) solutions were propelled at a flow-rate of 0.7 ml/min. A 321-μl aliquot of sample solution was injected into the carrier stream, which was then mixed with the buffer solution. The mixed solution was sent to a heating coil (one metre) immersed in a water-bath at $30.0 \pm 0.1°$. Pyrogallol and periodate solutions heated at 30° were merged with the carrier stream in front of the flow cell. The emission light from the CL reaction was monitored with the detector without wavelength discrimination.

RESULTS AND DISCUSSION

Chemiluminescence spectra

The CL intensity from the reaction of pyrogallol with periodate was relatively weak compared with those produced by other CL reagents. Chromium(III) has a pronounced catalytic effect on this reaction at a neutral medium. Figure 2 shows the CL spectrum of the pyrogallol–periodate–chromium(III) system; an emission maximal peak exists at 507 nm. The rapid decrease in the CL emission light was observed; the CL emitting species with a high rate of formation had short lives.

Effect of reaction variables

The CL reaction of pyrogallol with periodate was studied as a fast assay method of chromium(III) with the flow injection technique. From the results of preliminary studies, the highly sensitive flow injection system shown in Fig. 1 was adopted and used in optimizing the variables such as flow-rate, the sampling loop,

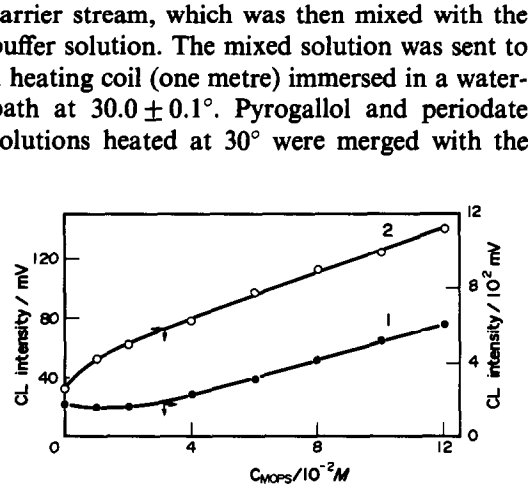

Fig. 4. Effect of MOPS concentration on the CL intensity. 1, baseline; 2, 20 ng/ml chromium(III). Other conditions as in Fig. 1.

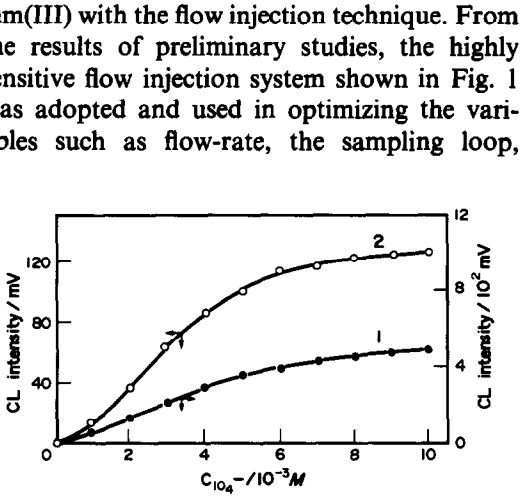

Fig. 6. Effect of periodate concentration on the CL intensity. 1, baseline; 2, ng/ml chromium(III). Other conditions as in Fig. 1.

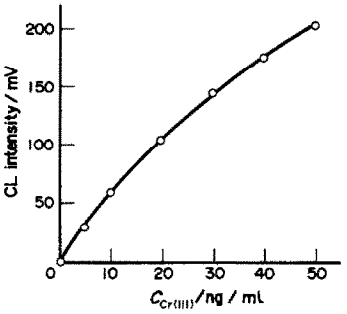

Fig. 7. Working curve for chromium(III). Other conditions as in Fig. 1.

Table 2. Determination of Cr(III) and Cr(VI) in the synthetic mixtures with and without sulphite

Taken, ng/ml		Cr(III) found* ng/ml	
Cr(III)	Cr(VI)	(I)†	(II)‡
0	30	0.0	30.1
5	25	5.6	29.8
10	20	10.8	30.0
15	15	15.2	30.2
20	10	20.2	30.4
25	5	25.4	30.0
30	0	30.0	30.1

*Average value ($n = 3$); †Without sulphite; ‡With sulphite ($1.0 \times 10^{-4}M$).

temperature and reagent concentrations that influenced the chromium(III)-enhanced and background CL intensity.

The effect of flow-rates of the carrier and reagent streams on the heights of peak and baseline was examined in the range 0.2–1.0 ml/min. With the increase in flow-rate up to 0.5 ml/min, the peak height increased; an almost constant peak remained at higher flow-rates. While the height of baseline was almost constant. A flow-rate of 0.7 ml/min was selected for the procedure.

The effect of the temperature on the CL intensity was studied by keeping the heating coils (1 m) at 20–50°. A constant and maximal peak height was obtained at 30–40°; the height of baseline increased with increasing temperature. A temperature of 30° was selected for further studies. Sample volumes varying from 110 to 460 μl of 20 ng/ml chromium(III) solution were injected into the system. The peak height increased with increasing injected sample volume up to 310 μl; at larger volumes it slightly increased. A 321-μl sample volume was adopted.

Preliminary experiments revealed that the catalytic effect of chromium(III) on the CL reaction was observed at a neutral medium and the optimum pH region was slightly shifted with the buffer agent used. For example, the maximal peak height was obtained at pH 7.3 and 7.7 in the presence of *N*,*N*-bis(2-hydroxyethyl)-2-aminoethanesulphonic acid (BES) and 2,4,6-trimethylpyridine (TMP), respectively. Thus, the effect of pH and buffer concentrations including imidazole, BES, MOPS, TMP, *N*-tris(hydroxylmethyl)methyl-2-aminoethanesulphonic acid (TES), *N*-2-hydroxyethylpiperazine-*N*′-2-ethanesulphonic acid (HEPES) and triethanolamine was examined by adding a constant concentration of ammonia and various amounts of hydrochloric acid. Of these, the maximal peak height was obtained in the presence of MOPS at pH 6.9 as shown in Fig. 3. The height of baseline was maximal at pH around 7. Figure 4 shows the effect of MOPS concentration on the heights of peak and baseline; they increased with increasing concentration of MOPS. This phenomenon cannot be explained at present and requires further investigation. On the other hand, the higher concentrations of the other buffers decreased the CL signal for chromium(III). From these results, the CL reaction was carried out at pH 6.9 in the presence of MOPS ($8.0 \times 10^{-2}M$). In order to optimize the concentration of ammonia, its initial concentration was varied in the range 0.01–0.8M, while keeping the concentrations of all other

Table 3. Maximum tolerance limits for diverse ions in the determination of 20 ng/ml chromium(III)

Tolerance limit, ng/ml	Ion added
10,000...	Al(III), As(V), Ba(II), Ca(II), Cd(II), Cu(II), Hg(II), Mg(II), Ni(II), Pb(II), Se(IV), Sr(II), V(IV), V(V), Zn(II), BO_3^{3-}, Br^-, ClO_4^-, CO_3^{2-}, F^-, NO_3^-, PO_4^{3-}, SO_4^{2-}, Citrate, Oxalate, Tartrate
1,000...	As(III), Te(IV), NO_2^-, I^-
100...	Ag(I), Ce(III), Ce(IV), Fe(II), Fe(III), Mn(II), Mo(VI), Ti(IV), Sn(II), W(VI)
50...	Bi(III), Sn(IV)
25...	Co(II)

ingredients constant. An ammonia concentration of 0.3M was chosen as optimal because it was maximal and a constant peak height was observed in the range 0.2–0.4M ammonia.

Figures 5 and 6 show the effect of the pyrogallol and periodate concentrations, respectively. The peak height was constant at pyrogallol concentrations above $0.8 \times 10^{-4}M$; the baseline height increased gradually. Thus, a $1.0 \times 10^{-4}M$ pyrogallol solution was used. As the heights of peak and baseline increased with increasing concentration of periodate, $6.0 \times 10^{-3}M$ periodate was selected taking account of the baseline stability.

Calibration graph

Calibration graphs were prepared by using the flow system shown in Fig. 1. The dynamic range for the chromium(III) determination was from 5 to 100 ng/ml at a sampling rate of 25/hr. Figure 7 shows a typical calibration graph for chromium(III) in the concentration range 5–50 ng/ml. Though the graphs were slightly curved, the reproducibility of the method was satisfactory; the relative standard deviations for 10 replicate determinations of 10, 20 and 50 ng/ml chromium(III) were 3.1, 2.2 and 1.9%, respectively. The detection limit (signal-to-noise ratio = 2) was 1 ng/ml.

Chromium(VI) at concentrations below 50 ng/ml was not detected by the present procedure. The method was tested for several synthetic mixtures of chromium(III) and chromium(VI) in the absence and presence of sulphite ($1.0 \times 10^{-4}M$) which hardly affected the chromium(III)-catalyzed reaction. The analytical results are given in Table 2. As can be seen, total chromium concentration can be determined by reducing chromium(VI) with sulphite; the chromium(VI) content is obtained by subtracting the chromium(III) content from total concentration of chromium.

Interferences

From preliminary experiments, some metal ions such as aluminum(III), iron(III) and zinc(II) at 100 ng/ml levels gave a negative error in the absence of a masking agent because of formation of their hydrolyzed species at the neutral medium; it was necessary to add a masking agent to the reaction system. It was expected that EDTA acted as an activator for chromium(III)[8] and could effectively suppress the interferences of diverse ions. Therefore, the effect of EDTA concentration on the chromium(III)-catalyzed reaction was examined over the range 0–$1.0 \times 10^{-2}M$. The peak height slightly increased with increasing concentration of EDTA up to $1.0 \times 10^{-3}M$; at higher concentrations, it was almost constant. Thus, a $6.0 \times 10^{-3}M$ EDTA solution was used.

The selectivity was tested by analyzing standard solutions containing 20 ng/ml chromium(III) and various amounts of diverse ions in the presence of EDTA. The tolerance limit was estimated with a 5% relative error. The results are summarized in Table 3. Most diverse ions did not interfere, at least at concentrations of 100 ng/ml. Negative interferences were observed from bismuth(III) and tin(IV) at concentrations higher than 100 ng/ml. But 50 ng/ml concentrations of these ions did not interfere. Cobalt(II) showed positive interference with a maximum tolerable concentration of 25 ng/ml because of its catalytic action on the CL reaction.

CONCLUSION

The proposed method, based on the catalysis of the CL oxidation of pyrogallol with peroxide in the presence of MOPS, provides a simple and sensitive approach for the determination of chromium(III) at nanogram levels. The dynamic range of the method is 5–100 ng/ml chromium(III) with the sampling frequency of 25/hr. The reproducibility of the method is satisfactory with the relative standard deviation of 2.2% ($n = 10$) at 20 ng/ml chromium(III) and the detection limit (signal-to-noise ratio = 2) is 1 ng/ml. The total chromium content can be determined by reducing Cr(VI) with sulphite.

REFERENCES

1. H. A. Mottola, *Kinetic Aspects of Analytical Chemistry*, Wiley, New York, 1988.
2. D. Perez-Bendito and M. Silva, *Kinetic Methods in Analytical Chemistry*, Horwood, Chichester, 1988.
3. J. Růžička and E. H. Hansen, *Flow Injection Analysis*, 2nd Ed., Wiley, New York, 1988.
4. B. M. Kneebone and H. Freiser, *Anal. Chem.*, 1975, **47**, 595.
5. I. F. Dolmanova, G. A. Zolotova, T. N. Shekhovtsova, V. D. Bubelo and N. A. Kurdyukova, *Zh. Anal. Khim.* 1978, **33**, 274.
6. C. M. Wolff and J. P. Schwing, *Bull. Soc. Chim. France*, 1976, 675.
7. D. P. Nikolelis and T. P. Hajiioannou, *Mikrochim. Acta*, 1978 **II**, 105.
8. S. Nakano, S. Hinokuma and T. Kawashima, *Chem. Lett*, 1983, 357.

9. F. Alba, J. M. Estela and V. Cerda, *Quim. Anal. (Barcelona)*, 1988, **7**, 219; *Chem. Abstr*, 1989, **111**, 108168k.
10. S. D. Hoyt and J. D. Ingle, Jr., *Anal. Chim. Acta*, 1976, **87**, 163.
11. C. A. Chang, H. H. Patterson, L. M. Mayer and D. E. Bause, *Anal. Chem.*, 1980, **52**, 1264.
12. T. Williams, P. Jones and L. Ebdon, *J. Chromatogr*, 1989, **482**, 361.
13. D. F. Marino and J. D. Ingle, Jr., *Anal. Chem.*, 1981, **53**, 294.
14. T. Kamidate, K. Yamaguchi, T. Segawa and H. Watanabe, *Anal. Sci.*, 1989, **5**, 429.
15. L. I. Dubovenko and A. M. Guta, *Izv. Vyssh. Uchebn. Zaved. Khim. Khim. Tekhnol.*, 1975, **18**, 1211; *Chem. Abstr.*, 1976, **84**, 38257m.
16. M. Yamada, A. Sudo and S. Suzuki, *Chem. Lett.*, 1985, 801.
17. H. Ohshima, M. Yamada and S. Suzuki, *Anal. Chim. Acta*, 1990, **232**, 385.
18. G. B. Meluzova and R. F. Vassil'ev, *Mol. Potochem.*, 1970, **2**, 251.
19. D. Slanwinska and J. Slawinski, *Anal. Chem.*, 1975, **47**, 2101.
20. R. Nilsson, *Acta Chem. Scand.*, 1964, **18**, 389.
21. G. Ahnström and R. Nilsson, *ibid.*, 1965, **19**, 313.
22. R. J. Miller and J. D. Ingle, Jr., *Talanta*, 1982, **29**, 303.
23. D. Balcerowicz, K. Balcerowicz, D. Slawinska and J. Slawinski, *Chem. Anal. (Warsaw)*, 1970, **15**, 479.
24. S. Stieg and T. A. Nieman, *Anal. Chem.*, 1980, **52**, 800.
25. N. P. Evmiridis, *Analyst*, 1987, **112**, 825.
26. *Idem, ibid.*, 1988, **113**, 1051.
27. *Idem, Talanta*, 1989, **36**, 357.

Talanta, Vol. 40, No. 1, pp. 81–87, 1993
Printed in Great Britain

0039-9140/93 $6.00 + 0.00
Pergamon Press Ltd

SEQUENTIAL INJECTION TECHNIQUE FOR AUTOMATION OF COMPLEX ANALYTICAL PROCEDURES: FLUOROMETRIC ASSAY OF FACTOR THIRTEEN

MIGUEL GUZMAN, CY POLLEMA, JAROMIR RŮŽIČKA and GARY D. CHRISTIAN
Department of Chemistry BG-10, University of Washington, Seattle, WA 98195, U.S.A.

(*Received* 11 *February* 1992. *Revised* 31 *March* 1992. *Accepted* 31 *March* 1992)

Summary—A non-segmented flow method is used to automate an analysis which involves five different reagents. The fluorometric assay for factor thirteen (FXIII) is performed by the sequential injection analysis (SIA) technique. Two reactions take place in a single line SIA system to produce the final fluorescing product. Because of its mechanical simplicity and versatility, the sequential injection (SI) technique is shown to be an attractive tool for automation of a complex analytical procedure. In addition to collecting quantitative and kinetic information, the SI system is illustratively used for optimization of the analysis and for obtaining validation information.

The sequential injection (SI) technique was developed to satisfy the demands for mechanically simple and robust, yet versatile, flow injection (FI) methodology.[1–4] The heart of a SI system is a selector valve which, in the simplest case, is used to connect a detector with the system and to introduce a wash solution, sample solution, and reagent(s) into a holding coil (Fig. 1). Sequential aspiration of solutions from specific ports of the selector valve leads to the formation of well-defined zones in the holding coil. Upon flow reversal, the entire contents of the holding coil are propelled towards a detector, and the zones penetrate each other due to combined axial and radial dispersion. The overlap of the reagent and sample zones triggers the formation of a reaction product. Propelling the product zone through an appropriate detector provides a signal similar to that obtained by conventional flow-injection analysis.[5]

The versatility of the SI manifold is a major advantage of the technique since each port of the selector valve allows a different operation to be performed. Although Fig. 1 illustrates a SI set-up for a simple one reagent analysis, the very same manifold (single pump, single valve) may be utilized for far more complex analytical procedures. This is achieved by assigning specific functions to free ports on a multiport valve and by designing an appropriate flow program. Thus, specific free ports are dedicated for introduction of different reagent solutions, while others allow introduction of a standard solution to the holding coil or connect a mixing chamber or a dilution coil to the SI system into which an aspirated sample may be introduced from the holding coil.[6] Computer control of the SI system is an essential prerequisite since an analytical procedure often requires a complex and highly reproducible flow pattern. Under the computer control, the flow rate and the direction of the flow can be varied at will and stopped flow often becomes an integral part of the analysis for monitoring slow reactions.

In contrast to conventional flow injection systems, the increasing complexity of the analysis will not sacrifice the mechanical simplicity of the SI manifold. In fact, most analyses performed in the SI mode can be applied to a single line, one pump, one valve configuration. Besides its versatility and mechanical simplicity, the SI technique offers additional advantages, namely the ability to change experimental parameters without physical restructuring of the manifold and the ability to control reaction time and the degree of zone dispersion.[2]

The significance of the two major disadvantages of the SI technique quoted in previous publications,[1–3] the lower sampling frequency and a requirement for a computer controlled system, will vary for different applications. For many applications, the positive aspects of the technique make, however, the SIA an attractive tool for development of automated analyses. To

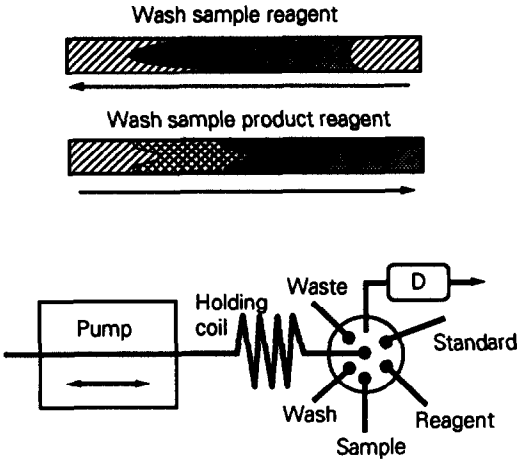

Fig. 1. Sequential injection analysis (SIA) system: zones are stacked sequentially in the holding coil. Substantial overlap of the zones occurs when the flow is reversed.

test this claim, SIA was used in this study for the development of an automated fluorometric assay of factor thirteen (FXIII), an analysis which involves a complex procedure and which, to date, has been performed exclusively in a manual model.

FXIII is an enzyme which plays an important role during the final stages of blood coagulation. A fluorometric assay[7] is used to determine its quality after it is produced by a fermentation process and after various stages of its purification. The fluorometric assay of FXIII is based on activation of the enzyme by thrombine followed by the active FXIII catalyzed condensation reaction between monodansyl cadaverine and *N,N*-dimethyl casein to form a fluorescing compound (Fig. 2). The amount of fluorescing product is directly related to the amount of the active FXIII formed during the activation period.

Two routinely performed assays include a single point measurement and a kinetic measurement of the FXIII activation.[7] In currently used methods, both measurements involve manual operations such as sample dilution, thermal equilibration of the reaction

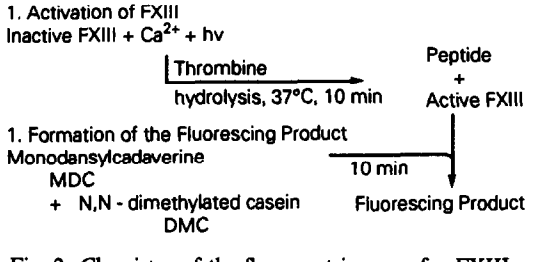

Fig. 2. Chemistry of the fluorometric assay for FXIII.

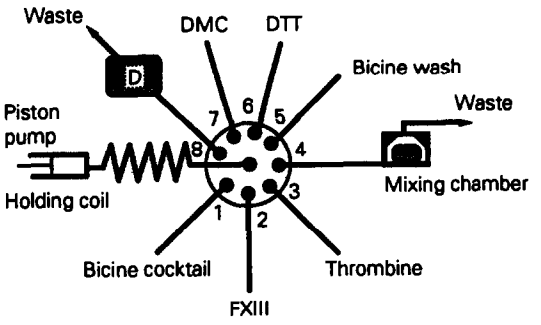

Fig. 3. System design for SIA of FXIII.

mixture, addition of reagents at specific times, monitoring of the reaction time and transportation of sample cuvets to the detection compartment. Each sample is run in duplicate to validate the results of the assay. The more concentrated samples require extensive dilution in order to bring the absorbance signal into the linear calibration range. As a result, some samples do not fall into the calibration range after the first dilution step and must be re-analysed.

Clearly, these manual operations and the inability to select the appropriate dilution factor for all samples on the first attempt make the analysis labor-intensive and time-consuming. This in turn prevents thorough investigation of the FXIII production. The automation of the assay by means of SI technology leads to significant improvement because the crucial operations are no longer performed manually, human bias is largely eliminated from the process, and the whole procedure is simpler.

The following studies describe the automation of the fluorometric assay by the SI technique. The experimental SI manifold and typical signal outputs resulting from the automated analysis of FXIII are shown and the ability of the SI system to provide a validation and diagnostic information is investigated.

EXPERIMENTAL

Chemicals

The concentration of standard FXIII solutions ranged from 0 to 50 μg/ml. The solutions employed included 0.05*M* bicine buffer at pH 10, 0.05*M* Tris buffer at pH 7.4, 0.4*M* calcium chloride in bicine buffer, 2% *N,N*-dimethyl casein (DMC), 100 NIHU/ml and 500 NIHU/ml thrombine, 0.2*M* dithriothreitol (DDT), and 4m*M* monodansyl cadaverine (MDC). In addition, a stock solution of bicine cocktail was prepared by mixing the bicine

buffer with MDC and calcium chloride in a 60:1:2.4 ratio.

Hardware

The SIA set-up consisted of an Alitea (S-2) piston pump (cam driven, sinusoidal flow) equipped with a 1-ml syringe, a Valco 8 port selector valve, an HP 1046A fluorescence spectrometer, an IBM personal computer, a water bath, a mixing chamber (0.75 ml internal volume), a stirring plate and PTFE (Teflon) tubing (0.5 mm internal diameter). Figure 3 shows the SI configuration. Ports 1 through 3 were used for introduction of bicine cocktail, FXIII, and thrombine solutions into the holding coil, respectively. Port 4 was connected to a mixing chamber by a 10-cm length of PTFE tubing of 0.5-mm internal diameter (20 μl volume). Ports 5 through 7 were used for injection of bicine wash, DTT (a component which quenches the FXIII activation), and DMC solutions into the holding coil, respectively. Port 8 was connected to the detector.

The pump, the valve and the detector were computer interfaced using a real time devices (RTD) board. A program written in Matlab software was used for controlling the pump and the valve, as well as for collecting, displaying and storing the signal output from the detector.

Procedure

The FXIII fluorescence assay requires injection of six different zones into the holding coil and then to the mixing chamber at specific stages of the analysis, using the SI configuration as depicted in Fig. 3. In the absence of a mixing chamber it would have been a difficult and impractical task to stack so many reaction zones in the holding coil and still ensure proper mixing with the sample. Obviously, a different approach is required. Connecting a mixing chamber to one of the ports is the most direct solution to the problem. The wash, sample and appropriate reagent solutions are sequentially aspirated in a specified order into the holding coil and then transferred into the mixing chamber at times selected suitable for the analysis. The contents of the mixing chamber are gently mixed, so that the reaction can take place. After the fluorescent product begins to form, a number of aliquots are withdrawn at selected times from the chamber and propelled through the detector thus providing both quantitative and kinetic information of the rate of fluorescing product formation, as well as allowing a wide dynamic range for analysis offered by measurements made at different reaction times of the fluorescing product formation.

The automated procedure consists of four stages: 1) sequential introduction of the bicine cocktail, FXIII sample and thrombine solutions into the mixing chamber which results in FXIII activation, 2) addition of DMC and DTT solutions into the mixing chamber which quenches FXIII activation and initiates formation of the fluorescing component, 3) a sampling cycle comprising aspiration of a sample aliquot from the mixing chamber and propelling the aliquot zone into the detector, and 4) washing out the system with bicine buffer. Although minor modifications accompanied the experimental procedure, this general outline was followed throughout the test period.

System preparation

First, all the solutions used in the assay were placed in a water bath and equilibrated to 37° and the syringe was filled with the wash solution. After 10 min, lines from ports 1, 2, 3, 5, 6 and 7 were filled with the appropriate solutions by selecting an appropriate port and aspirating 50 μl into the system for each solution. Since smaller volumes were required to fill the connecting lines, an excess of solutions was introduced into the holding coil. After all lines were filled, the excess solutions in the holding coil were propelled to waste. The mixing chamber and its connecting line remained empty at the beginning of each analysis. Next, the line connecting port 8 and the detector was flushed with bicine buffer and the spectrometer was set up for the measurement. The excitation wavelength was set to 350 nm and the emission wavelength was set to 500 nm. The lamp remained, however, off and was turned on only during the sampling stage to prevent excessive heating of the detector. A sinusoidal flow pattern provided an average flow rate of 21 μl/min over the working range of the pump and all volumes were approximated using this value.

Stage 1. Active FXIII was formed during the first stage of the analysis. After inputting two delay times (one for the hydrolysis activation of the FXIII and one for the development of the fluorescent product prior to the sampling stage cycle) and the number of sampling cycles into the computer, the analysis began by sequential aspiration of 210 μl of the bicine wash (port 5) and 210 μl of the bicine cocktail (port 1) into the holding coil. With flow reversal, 119 μl of the

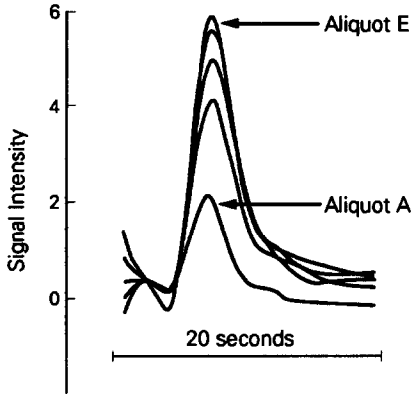

Fig. 4. Signals resulting from measurements of 50 μg/ml FXIII standard. Five aliquots were withdrawn from the mixing chamber in 67-sec sequences. Aliquot A provides the smallest signal because the fluorescence producing reaction time is shortest for this aliquot and the sample is, in addition, diluted by the dead volume of the line connecting the chamber and the valve.

holding coil content was expelled to the mixing chamber (port 4). The volumes are determined by the average flow rate and the time of aspiration. Bicine cocktail provided calcium ions used during the FXIII activation and MDC which was used later for the second reaction. Next, 42 μl of FXIII (port 2), and 10.5 μl of thrombine (port 3) were aspirated into the holding coil and 115 μl of the holding coil content was expelled to the chamber and mixed gently with the whole content. The hydrolysis of FXIII began and the length of the reaction was determined by delay time 1 which was selected prior the analysis.

Stage 2. At this stage the fluorescing product was formed in the mixing chamber. After the expiration of the delay time 1, 10.5 μl of DTT (port 6) and 42 μl of DMC (port 7) were sequentially aspirated into the holding coil and 115.5 μl of the holding coil content was injected into the mixing chamber and the valve was turned to port 8. At this stage, the mixing chamber was nearly filled to its capacity. The introduction of DTT quenched the activation process and the presence of DMC, MDT and active FXIII in the reaction mixture initiated the formation of the fluorescing product. The delay time 2 determined the time elapsed between introdution of DTT and DMC into the mixing chamber and first sample aliquot aspiration.

Stages 3 and 4. Following the delay time 2, the first sampling cycle was performed by sequential aspiration of 525 μl of the bicine wash (port 5) and a 63 μl aliquot from the mixing chamber (port 4) into the holding coil and expulsion of 588 μl of the holding coil content through the detector line (port 8) into waste. Signal collection was initiated at the time the liquid began to flow through the detector line. A signal in a form of a peak was obtained and the data were stored in the computer. The sampling cycle was then repeated with successive aspiration of equal aliquots from the mixing chamber, depending on the number of cycles selected prior to the analysis. Data for a total of three of five sample aliquots were collected and stored in presented experiments. Finally, all flow lines and the chamber were thoroughly flushed with the bicine wash and the system was prepared for injection of a new sample.

RESULTS AND DISCUSSION

Signal output profile

Figure 4 shows a typical signal output resulting from analysis of a 50-μg/ml FXIII standard sample. Five sampling cycles were selected for analysis of the sample, providing five peaks which, in Fig. 4, are shown overlapped to facilitate the graphical presentation. For each analysis, the first aliquot (aliquot A) provided the lowest peak and the last aliquot (aliquot E in this case) provided the highest peak, assuming the continuous formation of the fluorescing compound. Two features influence the changes in signal intensity: 1) for each consecutive aliquot the reaction time for formation of the fluorescent product increased by 67 sec, corresponding to a higher intensity signal and 2) aliquot A is diluted by the dead volume of the tube which connects the mixing chamber and the valve, which is reflected by proportionately lower signal for aliquot A. Using 150 sec for delay time 1, 194 sec for delay time 2 and five

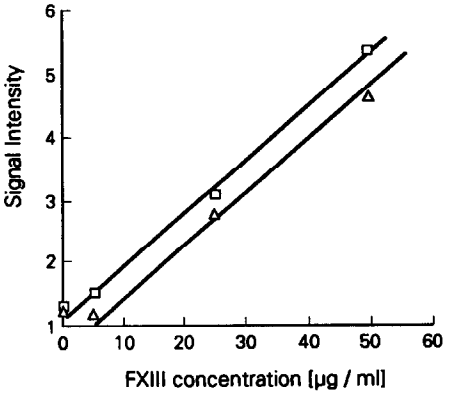

Fig. 5. Calibration curves constructed from measurement of four standards using two aliquots: △—aliquot B and □—aliquot C.

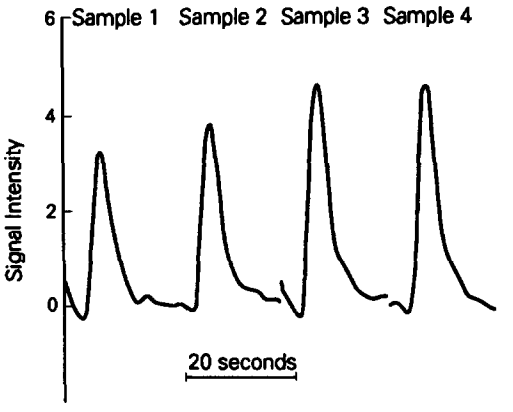

Fig. 6. The trend in the signal for aliquot C with successive doubling of the sample volume of a 50 μg/ml FXIII standard.

sampling cycles, the analysis of each sample took about 8 min.

Calibration curves

In the next experiment, four standards of FXIII in the concentration range from 0 to 50 μg/ml were measured in order to construct a calibration curve. Signal intensities of the peak heights resulting from monitoring aliquots B and C for each calibration sample are plotted against the concentration of the calibration samples (Fig. 5). A linear response was obtained with correlation coefficients of 0.98 and 0.99 for aliquots B and C, respectively. The importance of selecting the proper time for the measurement is illustrated by measuring the 5-μg/ml sample. For this sample, aliquot B does not provide a detectable signal but aliquot C, which was withdrawn 67 sec later, provides a readily detectable signal.

FXIII volume variation

The sample volume parameter was investigated. Only one stock solution, 50 μg/ml of FXIII, was used for generating data shown in Fig. 6. The concentration of inactive FXIII in the mixing chamber varied from sample to sample since the volume of FXIII sample was doubled for each consecutive injection of the analyte into the mixing chamber, starting with 21 μl and continuing with 42 μl, 84 μl and 168 μl while the total volume of reaction mixture in the mixing chamber was kept constant by decreasing the volume of bicine cocktail. The volumes of thrombine, DTT and DMC were kept constant throughout. Thus, the variables included concentration of FXIII, which was increasing, and concentrations of calcium ions and monodansyl cadaverin (MDC), which were decreasing. An increase of the signal can be observed for the first three samples, an expected trend since all the reagents are in excess and FXIII is the limiting reactant. The signal intensity is, however, increasing by only 15–20%, although the FXIII concentration was actually doubled. There are three primary reasons for this trend: 1) The blank (bicine buffer) provides a substantial background signal. The maximum signal intensities for the five aliquots of the blank are 0.68, 1.23, 1.35, 1.30 and 1.32 for corresponding sample aliquots A–E, respectively. 2) The decrease in MDC concentration affects the formation of the fluorescing compound. This is a known trend shown previously on manually performed assays, where measurements of the same FXIII sample using bicine cocktail solutions containing different MDC concentrations provided decreasing signal with decreasing MDC concentrations. 3) Similar experiments showed that decrease of calcium ion concentration also affects the kinetics of FXIII activation, but not as significantly as the MDC concentration if the molar concentration remains higher than the molar concentration of FXIII. The signal intensity for the fourth volume of analyte is actually slightly lower than for the previous volume, although the total FXIII concentration in the mixing chamber increased. Most likely, the MDC began to limit the reaction kinetics significantly.

Influence of delay times

The value of the delay time (1) selected for the SI procedure determines the success of the analysis. Too short a time results in too low a signal because the activation is not allowed to

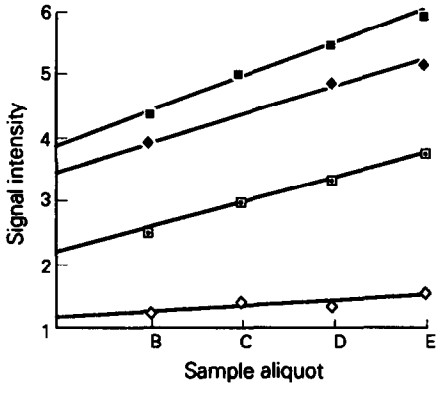

Fig. 7. Effect of variation in delay time (1): ◆—60 sec, blank, ⊡—60 sec, 50 μg/ml FXIII standard, ◆—300 sec, 50 μl/ml FXIII standard, and ■—450 sec, 50 μl/ml FXIII standard.

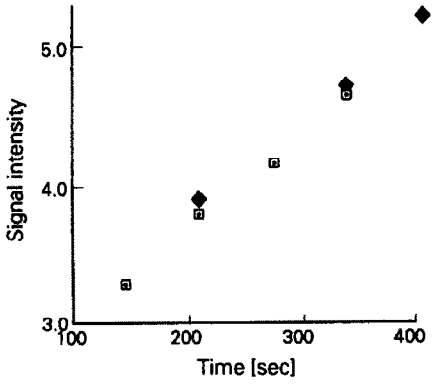

Fig. 8. Effect of variation in delay time (2): ⊡—60 sec, ◆—194 sec.

proceed to the desired degree, while too long a time will limit the sample throughput. Proper selection of the delay time (2) is easier since it determines the time for the aliquot sampling but does not influence the reaction process. In addition, the sampling occurs over a time period which is long enough for selection of an appropriate delay time (2) for all subsequent runs.

In one experiment, delay time (1) was varied from 60 to 450 sec while delay time (2) was kept at 194 sec for all samples. The results for aliquots B, C, D and E are presented in Fig. 7. For a given aliquot on the x-axis, the variation along the y-axis shows the effect of the increasing reaction time of protein activation. The lowest signal corresponds to the blank which was measured with delay time (1) set to 60 sec, while the other signals correspond to measurements of 50 μg/ml FXIII standard with varying delay (1) time. As important as an increase in absolute signal with increased delay time (1) is the relative signal intensity increase from aliquot to aliquot for each sample, because this parameter determines the sensitivity of the analysis. As Fig. 7 shows, the slope of the kinetic curve increases steadily over this time range, from a value of 0.38 for a 60-sec delay time to values of 0.45 and 0.52 for delay times of 300 and 450 sec, respectively. The delay time (1) was then set to 150 sec for subsequent experiments, a good compromise between the sensitivity factor and sampling frequency consideration.

The delay time (2) is less crucial since the second reaction is monitored over a certain time range and, therefore, the collected data provide more information about its kinetics. As a result, the appropriate sampling time can be easily selected. In one experiment, the same sample was injected twice, but with two different delay (2) times, 60 sec for the first injection and 194 sec for the second injection. Since all the other variables were kept constant and the first reaction was actually quenched by the addition of DTT solution, the signal intensity changes reflect the kinetics of the second reaction. In Fig. 8 the signal maximum for each aliquot from the two injections are plotted against the actual reaction time of the second reaction (time elapsed from the introduction of DMC and DTT into the chamber to the detection of an aliquot). As expected, the results suggest that the variation in delay time (2) has no effect on the activation process.

Temperature effect

Another important aspect of the assay is the temperature. In one experiment, all solutions were kept in the water bath at 37° for 9 hr. To investigate the effect of extended exposure to higher temperatures, the same sample was analyzed repeatedly during this period. The collected signals for a 50 μg/ml FXIII solution analyzed two hours apart provided comparable results and, therefore, indicated a reasonable stability of reagents and the sample over this time period. This was not the same, however, for extended periods. Figure 9 shows results for the sample containing 121 μg/ml FXIII which was analyzed at 1, 7, 8 and 9 hr after the reagents were immersed into the water bath. A definite steady decrease in the signal intensity is obvious. Thrombine, DMC and FXIII are likely to be most affected by the extended exposure to higher temperature. Thus, for process control applications it will be necessary to limit the time during which all the solutions are equilibrated. One possible solution is to thermostat the SI

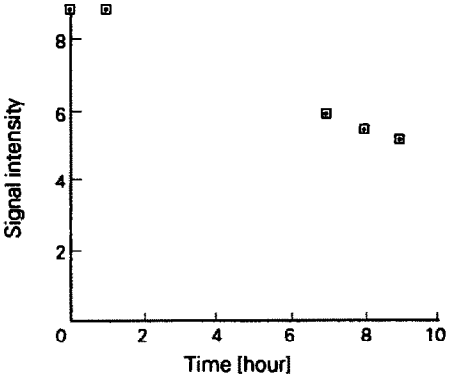

Fig. 9. Temperature effect on the analysis. Peak heights of aliquots E for a sample analyzed at 0, 1, 7, 8 and 9 hr after it was immersed together with all other solutions into a 37° water bath.

system and the bicine wash solution while the other solutions are kept at lower temperatures and perform thermal equilibration of them in the SI system. Considering small volumes of reagents and samples aspirated into the system and significant dilution in the bicine wash, it is likely that the resulting mixtures will require a short time for equilibration.

CONCLUSION

For the first time, a complex analytical assay was performed in the SIA mode. In the past, mentioned drawbacks of non-segmented flow systems often included the inability to perform an analysis involving a large number of reagents and extended reaction times. Furthermore, the mechanical complexity of the flow system was directly proportional to the increase in complexity of the analysis. Clearly, these objections are not valid for sequential injection methodology. In the presented example of FXIII assay, six different solution zones were introduced into the system at various times, two different reactions took place, appropriate dilutions were achieved and both quantitative and kinetic information was obtained. All this was performed with a single line, one pump, one valve system configuration.

When a SI method is being optimized, the parameters can be varied without physical restructuring of the system. The volumes of reagents and samples, the sequence of zones aspirated, the flow pattern and reaction times are varied interactively through the computer keyboard without a need to modify the system. Thus, once the SI system is properly assembled, an analyst can concentrate on the method development without involving hardware changes.

Collecting signal output for several sample aliquots from each sample provides both kinetic information (assuming the reaction takes place during the sampling period) and single point information (*i.e.*, the quantitative value for a particular reaction time). The concentration range of the analyte is extended since any of the aliquots can be used for calculating the quantitative values. Thus, for samples with high analyte concentration, an aliquot corresponding to shorter reaction time (aliquots A, B or C) can be used for quantitative prediction, while aliquots D and E are used for samples with very low analyte concentration. Of course, there is no objection to using all aliquots for the calculations if their signals fall within the calibration range.

As illustrated by the experiments, the SI system can be effectively used for method optimization, validation and diagnosis. Automation of an assay eliminates errors associated with manual manipulation, but one must exercise caution during the computer interfacing process to minimize other sources of errors. Precise timing and reproducibility of parameters such as flow rates, zone volumes and time delay will be crucial for successful analysis. For example, a sinusoidal flow piston pump (1) was used in these experiments to ensure pulse free flow and the flow was always stopped when the valve changed its position in order to avoid problems associated with back up pressure created if the flow continues during the valve rotation sequence. Clearly, for each hardware setup, it is important to identify the potential sources of errors and either eliminate or minimize them. Then the SI system can provide a powerful sample handling and sample pretreatment tool suitable for research, and clinical and process control applications.

Acknowledgments—The financial support for Miguel Guzman by Zymogenetics Inc. and Cy Pollema by National Institute of Health and technical assistance of John Fry are gratefully acknowledged.

REFERENCES

1. J. Růžička, G. D. Marshall and G. D. Christian, *Anal. Chem.*, 1990, **62**, 1861.
2. J. Růžička and T. Gubeli, *ibid.*, 1991, **63**, 1680.
3. T. Gubeli, G. D. Christian and J. Růžička, *ibid.*, 1991, **63**, 2405.
4. G. D. Christian, *J. Flow Inj. Anal.*, 1990, **7**, 86.
5. J. Růžička and E. H. Hansen, *Flow Injection Analysis*, 2nd Ed., Wiley, New York, 1988.
6. A. Baron, M. Guzman, J. Růžička and G. D. Christian, submitted for publication.
7. L. Lorand, O. M. Lockridge, L. K. Campbell, R. Myhrman and J. Bruner-Lorand, *Anal. Biochem.*, 1971, **44**, 221.

Talanta, Vol. 40, No. 1, pp. 89–93, 1993
Printed in Great Britain.

0039-9140/93 $6.00 + 0.00

FIA–FT–IR DETERMINATION OF IBUPROFEN IN PHARMACEUTICALS

SALVADOR GARRIGUES, MAXIMO GALLIGNANI and MIGUEL DE LA GUARDIA*
Department of Analytical Chemistry, University of València, 50 Dr Moliner St. 46100 Burjassot, València, Spain

(*Received* 25 *March* 1992. *Revised* 29 *April* 1992. *Accepted* 30 *April* 1992)

Summary—A method has been developed for the determination of Ibuprofen (2-[4-isobutylphenyl]-propionic acid) in pharmaceuticals by FT–IR, using the carbonyl band which this compound presents at 1710 cm^{-1} in carbon tetrachloride solutions. Samples are dissolved in carbon tetrachloride. In this solvent the excipients are not soluble and so the drug can be directly determined without any additional treatment. The use of a simple FIA manifold permits one to carry out this analysis with a low consumption of reagent and the FT–IR provides a continuous monitoring of the spectral base-line which permits an accurate determination of the maximum in the absorbance band. Also, the FIA system permits easy and fast sampling and cleaning of the measurement cell. The method has a dynamic range between 0.5 and 20 mg/ml with a sensitivity of 0.366 ± 0.004 au $\cdot$ $mg^{-1} \cdot ml \cdot mm^{-1}$ and a variation coefficient of 0.8% for 5 independent measurements of a real sample containing 200 mg of Ibuprofen per capsule. The developed procedure provides concentration values comparable with those found by UV spectrophotometry in the analysis of real samples but is free from matrix interferences.

Infrared spectrometry (IR) provides a useful way for the identification of drugs.[1–4] However, the traditional techniques employed to obtain the IR spectra, such as alkali halide disks, mulls and thin films, are not adequate for quantitative analysis, and because of this, ultraviolet spectrometry[5] is usually employed in the analysis of pharmaceuticals rather than IR.

The use of flow cells for handling appropriate solvents and with spacers opens the possibility of carrying out quantitative IR determinations of drugs in pharmaceuticals, especially for the development of automated procedures based on flow injection analysis (FIA).[6–9] There are few precedents in the use of FIA in infrared analysis[10–16] and until now only two papers have been applied to pharmaceutical analysis.[14,15]

Ibuprofen (2-[4-isobutylphenyl]-propionic acid) is a non-steroidal anti-inflammatory analgesic[1,2] commercialized under different propietary names, such as Amersol, Brufen, Ebufac, Fembil, Inabrin, Inflam, Librofem, Motrin, Nurofen, Poxofen, Proflex, Relcofen, Seclodin and Uniprofen. Ibuprofen is determined by chromatography,[17–22] spectrometry[2,23–25] and also titrimetric methods.[26] However, only one paper has been published concerning the determination of Ibuprofen by infrared spectrometry,[27] and this is a time consuming procedure.

In the present paper, a FIA-Fourier transform infrared procedure has been developed in order to determine Ibuprofen in capsules of ALTIOR™.

EXPERIMENTAL

Apparatus

A Perkin Elmer Fourier transform infrared spectrometer 1750 equipped with a temperature stabilized coated detector FR–DTGS was employed to carry out the absorbance measurements, with a resolution of 4 cm^{-1}.

The spectrometer is controlled by a 7700 data station and the absorbance continuously measured using a series of computer programs written in OBEY and BASIC, which permits us to obtain and store the FT–IR spectra as a function of time with a frequency of 17 sec, search the exact position of the absorbance maximum peak and correct the peak height absorbances from the base-line values, and record the FIA peaks. All these programs have been developed in our laboratory and can be supplied on request.

The scanning of a full interferogram is carried out in only two seconds and the software permits the storage on a micro floppy

*Author for correspondence.

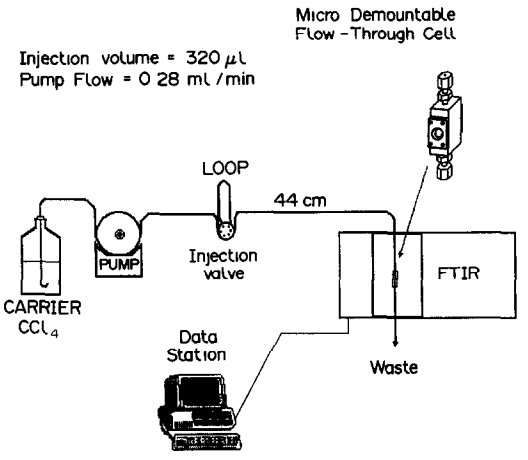

Fig. 1. Manifold.

disk in 15 sec. This process takes place during the FIA run and, after that, the corrected absorbance peak height values are established, the FIA recording obtained, and the calculations carried out.

The manifold employed (see Fig. 1) is a monochannel assembly with: a Gilson P-2 Minipulse peristaltic pump with solvent resistant Viton (Iso-versinic) 0.1 cm internal diameter pump tubes, a Rheodyne injection valve, type 50, with various fixed volume loops, PTFE connecting tubes with 0.8 mm internal diameter and a Spectra-Tech (Warrington, U.K.) microdemountable flow through cell.

Reagents

Ibuprofen (2-[4-isobutylphenyl]-propionic acid) standards were prepared from the crystalline compound (ESTEVE, Barcelona, Spain).

Analytical grade carbon tetrachloride (Panreac, Barcelona, Spain) was employed as carrier and also for the preparation of standards and samples.

IR spectroscopy grade potassium bromide (Merck, Darmstadt, Germany) was employed to obtain the FT–IR spectrum of Ibuprofen in pellet disks.

RESULTS AND DISCUSSION

FT–IR spectrum of Ibuprofen

The FT–IR spectrum of disks of Ibuprofen standards diluted in potassium bromide exhibits acid bands around 3000 cm^{-1} [see Fig. 2(A)], the transmittance band of the carbonyl group at 1710 cm^{-1}, and also the characteristic finger printing of the disubstituted aromatic hydrocarbons. Ibuprofen is very soluble in carbon tetrachloride and it has been confirmed that in the treatment of ALTIOR™ formulations with this solvent the drug is completely dissolved and the excipients remain undissolved. So, the transmittance IR spectra of standards and samples

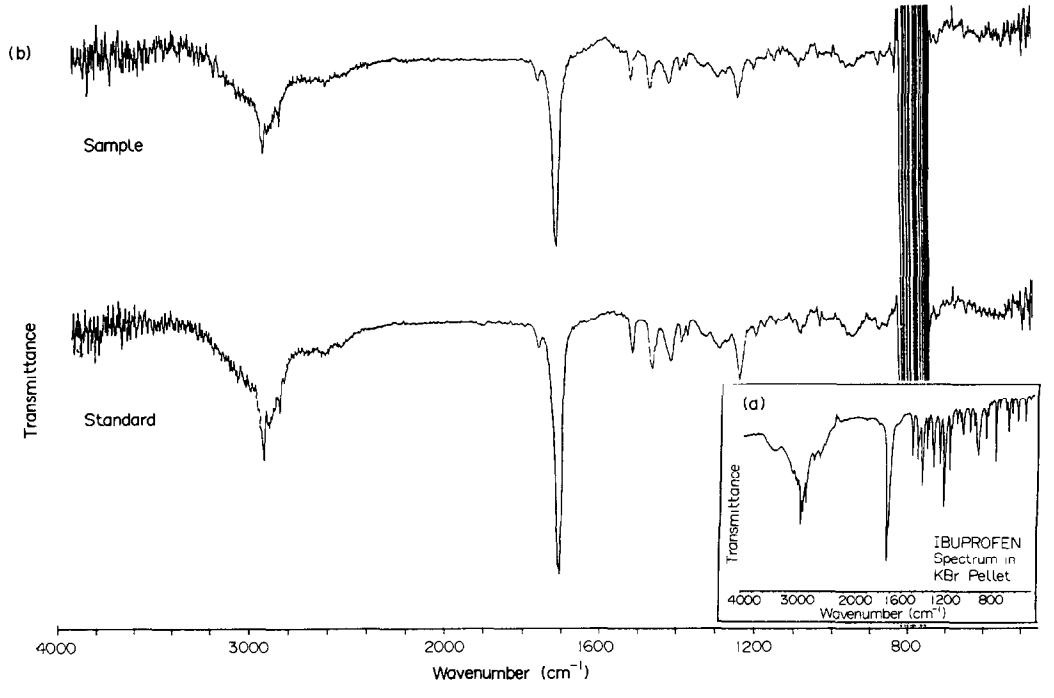

Fig. 2. FT–IR transmittance spectra of Ibuprofen in KBr disks (2A) and in CCl_4 solution (2B).

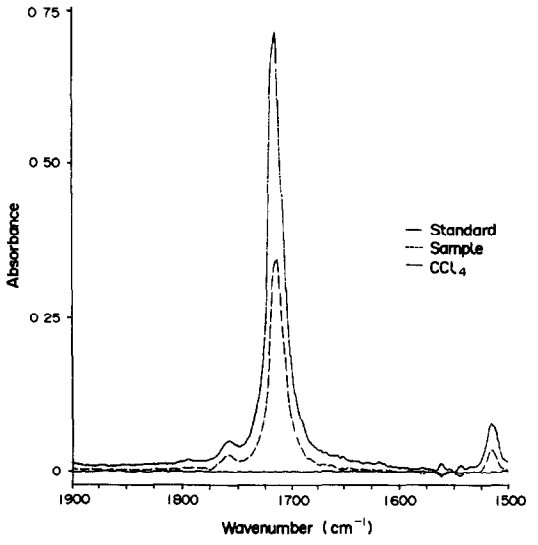

Fig. 3. FT–IR absorbance in the carbonyl region of blank solutions, sample and standard of Ibuprofen in CCl_4.

treated with carbon tetrachloride are identical and provide a way for the direct determination of Ibuprofen in pharmaceuticals [Fig. 2(B)].

In the present study the carbonyl band at 1710 cm^{-1} was selected for the quantitative determination of Ibuprofen because this band is very strong and appears in a transparent region of the CCl_4 (as can be seen in Fig. 3). The base-line of the absorbance spectrum was established between 1785 and 1650 cm^{-1}.

Effect of the FIA parameters on the absorbance of Ibuprofen

For a fixed concentration of 10 mg/ml Ibuprofen using a 0.1-mm cell (which provides a measurement volume of 1 μl) the effect of both the injection volume and the carrier flow were studied, in a univariate mode. Figure 4 indicates that an increase in the injected volume of sample provides an increase in the absorbance. However, this also increases the time required to carry out the analysis due to an increasing peak width. On the other hand (see Fig. 5), an increase in the carrier flow reduces drastically the absorbance readings and affects the precision of the measurements because, at the faster flow rates the sample does not remain in the cell at its maximum concentration for a long enough time to measure a full interferogram.

From these experiments a compromise value of 320 μl injection volume and 0.28 ml/min carrier flow were selected in order to obtain the highest sensitivity with good repeatability in the fastest experimental conditions.

Calibration of the system

Under the experimental conditions, previously selected, the absorbance of a series of 11 Ibuprofen standards dissolved in carbon tetrachloride was measured. A typical calibration equation of $A = -0.012 + 0.0358C$ (in mg/ml) was obtained with a regression coefficient R of 0.99959 [Fig. 6(B)].

Figure 6(A) shows the FIA recordings obtained by plotting the corrected absorbance peak height values found as a function of time, after the computer treatment of the monitored spectra.

Preparation of samples

As previously indicated, water soluble excipients are not solubilised in carbon tetrachloride and so Ibuprofen can be directly determined in pharmaceuticals, such as ALTIOR™, which does not contain other active ingredients. ALTIOR™ has a nominal content of 200 mg of

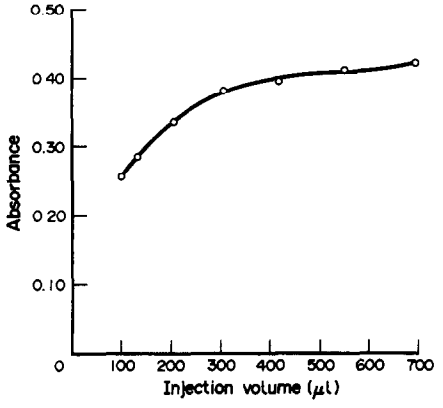

Fig. 4. Effect of the sample injection volume on the absorbance of Ibuprofen at 1710 cm^{-1}. Carrier flow: 0.28 ml/min.

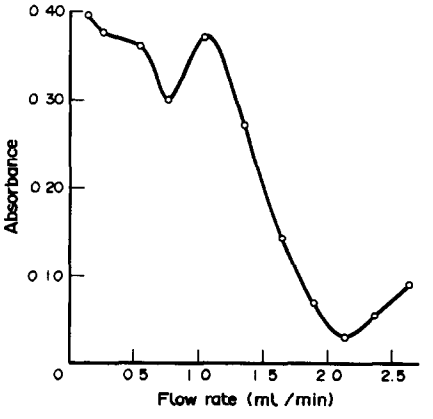

Fig. 5. Effect of the carrier flow on the absorbance of 320 μl of Ibuprofen. Concentration of Ibuprofen: 10 mg/ml.

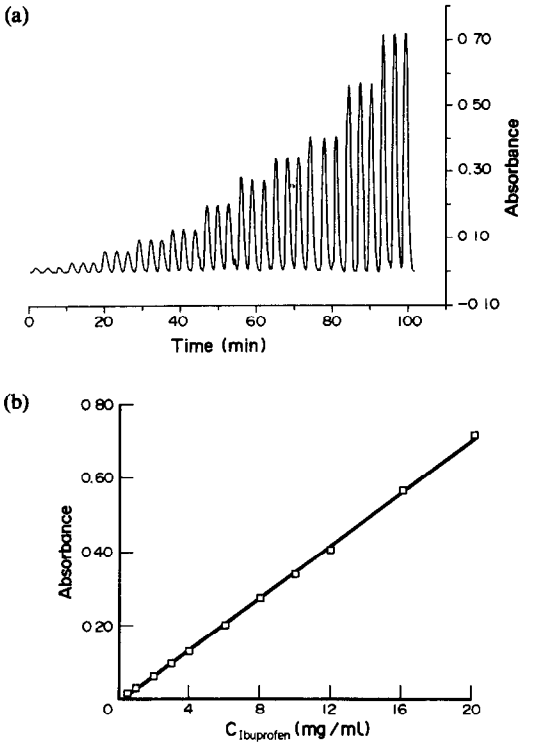

Fig. 6. FIA recording obtained from CCl_4 solutions of Ibuprofen (6A) for the FT–IR absorbance data of Ibuprofen solutions.

Ibuprofen per capsule and in order to obtain a good absorbance value, the following procedure is recommended.

Take five capsules of the pharmaceutical and grind to obtain a fine powder. Weigh accurately the amount of sample necessary to provide approximately 100 mg of Ibuprofen and extract with 10 ml of carbon tetrachloride. Filter to retain the excipient and inject 320 μl of the sample solution in the FIA manifold, using a carrier flow of 0.28 ml/min, and select the FT–IR spectrum between 1900 and 1500 cm^{-1}. Establish the spectral base-line from 1785 to 1650 cm^{-1} and record the absorbance, at the maximum of the carbonyl band, as a function of time. Interpolate the peak height of the FIA recording in the calibration graph, previously established from carbon tetrachloride solutions of pure Ibuprofen.

Analytical performance of the developed procedure

The sensitivity of the direct FIA–FT–IR analysis of Ibuprofen corresponds to a 0.366 ± 0.004 absorbance units $mg^{-1}.ml.mm^{-1}$ and this value could be increased using higher injection volumes or working in the stop flow mode. However these latter strategies diminish the sample frequency.

Using the recommended conditions, the limit of detection of the method (for a probability level of 95%) corresponds to a concentration of 0.08 mg/ml.

As compared with the method previously published for batch IR analysis of Ibuprofen in tablets,[27] the dynamic range obtained by us (from 0.5 to 20 mg/ml) is of the same order as that reported and the coefficients of variation, obtained for 5 independent measurements of a sample containing 10 mg of Ibuprofen per ml, is 0.8% in our case, five-fold lower than that reported by Husain *et al.*[27] The developed procedure could also be applied using a dispersive instrument working at a fixed wavenumber. However in this latter case the spectral base-line cannot be monitored and it produces a poorer linearity of the calibration lines and lower reproducibility.

The FIA–FT–IR method proposed has the inherent advantages of automated methods, such as speed, reproducibility and low consumption of reagents. Using the instrument described, it is possible to carry out 20 measurements per hour, which is a throughput 20-fold higher than that of the batch method of Husain *et al.*[27]

Compared with the UV reference method[2] the methodology developed provides matrix effect free measurements, because the excipient is not soluble in carbon tetrachloride and a higher dynamic range.

Analysis of real samples

Different lots of ALTIOR™ pharmaceutical, with a nominal content of 200 mg per capsule, have been analysed spectrophotometrically at 265 nm by a pharmaceutical laboratory and by the proposed FIA–FT–IR procedure. As can be seen in Table 1 results found are of the same order as those previously reported and compare well with the theoretical content.

The differences found with the UV analysis in terms of the t-test, could be due to the lack of information about the standard deviation of the spectrophotometric values, which avoids a more rigorous comparison. In this sense Table 1 shows that differences between values found by two different laboratories, using the same UV method, are higher than those between FT–IR and UV.

Table 1. Analysis of different lots of ALTIOR™ pharmaceutical

Sample	Ibuprofen found (mg/capsule)			
	FIA–FT–IR		UV Analysis	
	$\bar{X} \pm$ sec	t_{exp}	Lab 1 Reference	Lap 2
1	204 ± 3	1.10	207.3	196.2
2	209.0 ± 0.6	1.83	207.9	202.4
3	200.4 ± 1.5	0.47	201.1	213.6
4	206.7 ± 0.9	3.44	209.8	188.5
5	200.9 ± 0.7	9.57	194.2	204.1
6	201.0 ± 0.6	6.17	197.3	199.8
7	199.3 ± 0.9	4.89	203.7	215.7
8	202.8 ± 0.6	11.0	196.2	208.3
9	206.2 ± 0.3	15.33	201.6	190.8
10	195.6 ± 0.6	4.17	198.1	186.4

*Theoretical content: 200 mg per capsule.

t_{exp} values have been obtained from $(X - \bar{X})$/sec, X being the value obtained by the reference laboratory (Lab 1), $\bar{X}$ our average value for each sample and sec the standard deviation of three independent measurements. For a probability level of 0.95% and $n = 2$ and t_{theor} correspond to 4.303.

CONCLUSIONS

The FIA–FT–IR quantitative analysis of Ibuprofen in ALTIOR™ capsules can be carried out directly on carbon tetrachloride solutions of the pharmaceutical. In this solvent the excipient remains undissolved and so the only sample treatment is the dissolution of the drug and the filtration of the excipient. The injection of sample solutions in a carbon tetrachloride carrier stream provides very precise and accurate analysis of Ibuprofen with a good limit of detection and a sample throughput of 20/hr. The method requires low consumption of reagents and can be applied over a wide dynamic range. Results obtained in the analysis of real samples agree with those found by two independent laboratories using a UV reference method.

Acknowledgements—Salvador Garrigues acknowledges a grant from the Conselleria de Cultura Educació i Ciència de la Generalitat Valenciana, and Màximo Gallignani a grant from the Agencia Española de Cooperación Internacional, both for PhD studies. Authors acknowledge PENSA (Grupo ESTEVE, Barcelona, Spain) for the standards and samples supplied.

REFERENCES

1. *United States Pharmacopeia*, 22 revision, 1989 USP Convention Inc, Rockville, Md, U.S.A.
2. A. C. Moffat (ed.), *Clarke's Isolation and Identification of Drugs*, 2nd Ed, The Pharmaceutical Society of Great Britain, London, 1986.
3. M. J. de Faubert Maunder, *Practical Hints on Infrared Spectrometry with Particular Reference to Forensic Analysis*, Adam Hilger, London, 1971.
4. R. G. J. Miller and B. B. Stace, *Laboratory Methods in Infra-Red Spectrometry*, Heyden, Chichester, 1972.
5. S. Gorog, M. Renyei and B. Herenyi, *J. Pharm. Biomed. Anal.*, 1989, **7**, 1527.
6. J. Ruzicka and E. H. Hansen, *Flow Injection Analysis*, 2nd Ed., Wiley, New York, 1988.
7. M. Valcarcel and M. D. Luque de Castro, *Flow Injection Analysis. Principles and Applications*, Ellis Horwood, Chichester.
8. M. D. Luque de Castro and M. Valcarcel, *J. Pharm. Biomed. Anal.*, 1989, **7**, 1291.
9. J. C. Berridge, *ibid.*, 1989, **7**, 1313.
10. D. J. Curran and W. G. Collier, *Anal. Chim. Acta*, 1985, **177**, 259.
11. S. V. Olesick, S. B. French and M. Novotny, *Anal. Chem.*, 1986, **58**, 2256.
12. M. de la Guardia, S. Garrigues, M. Gallignani, J. L. Burguera and M. Burguera, *Anal. Chim. Acta*, 1992, **261**, 53.
13. M. Gallignani, S. Garrigues and M. de la Guardia, Communication Presented at XXVII CSI, B PO29, 1991, Bergen, Norway.
14. D. K. Morgan, N. D. Danielson and J. E. Katon, *Anal. Lett.*, 1988, **8**, 1979.
15. B. E. Miller, N. D. Danielson and J. E. Katon, *Appl. Spectrosc.*, 1988, **42**, 401.
16. M. Guzmán, J. Ruzicka, G. D. Christian and P. Shelley, *Vib. Spectrosc.*, 1991, **2**, 1.
17. B. M. Lampert and J. T. Stewart, *J. Cromatogr.*, 1990, **504**, 381.
18. S. Husain, A. S. R. K. Murty and R. Narasimha, *Indian Drugs*, 1989, **26**, 557.
19. J. H. Satterwhite and F. D. Boudinot, *J. Chromatogr. Biomed. Appl.*, 1989, **89**, 330.
20. G. Berner, R. Staab and H. M. Wagener, *J. Anal. Chem.*, 1990, **336**, 238.
21. P. J. Streete, *J. Chromatogr. Biomed. Appl.*, 1989, **87**, 179.
22. G. Geisslinger, K. Dietzel, D. Loew, D. Schuster, G. Rav, G. Lachmann and K. Brune, *J. Chromatogr. Biomed. Appl.*, 1989, **83**, 139.
23. C. S. P. Sastry, A. S. R. P. Tipirneni and M. V. Suryanarayana, *Analyst*, 1989, **26**, 704.
24. V. H. Bhalla, K. Krishnan, S. G. Deshpande and C. V. Shah, *Indian Drugs*, 1990, **27**, 580.
25. M. H. Abdel-Hay, M. A. Korany, M. M. Bedair and A. A. Gazy, *Anal. Lett.*, 1990, **23**, 281.
26. P. Parimoo, R. R. Sethuraman, A. Amalraj and N. Seshadari, *Indian Drugs*, 1989, **26**, 704.
27. S. Husain, A. S. R. K. Murty and A. R. Rao, *ibid.*, 1989, **26**, 185.

Talanta, Vol. 40, No. 1, pp. 95–99, 1993
Printed in Great Britain.

0039-9140/93 $6.00 + 0.00

POTENTIOMETRIC AND SPECTROPHOTOMETRIC DETERMINATION OF CALCIUM IN THE WET END OF PAPER MACHINES BY FLOW INJECTION ANALYSIS

JOHAN NYMAN and ARI IVASKA*
Laboratory of Analytical Chemistry, Åbo Akademi University SF-20500 Turku-Åbo, Finland

(*Received* 19 *February* 1992. *Revised* 18 *May* 1992. *Accepted* 18 *May* 1992)

Summary—A spectrophotometric and a potentiometric FIA method were used to determine calcium in samples of back water from paper mills. The spectrophotometric method used the complexation reaction between calcium and *o*-cresolphthalein complexon. Optimum pH for the method was calculated theoretically. An ion-selective calcium electrode based on neutral carrier was used in the potentiometric method. The spectrophotometric method had a linear range between 10 and 250 ppm calcium and the potentiometric method between 10 and 300 ppm. Samples were acidified to pH 4 either before or after filtration. Total calcium was determined by a d.c. plasma emission method. Significant amounts of calcium were found to be bound both to the solid matter and to soluble complexes in the samples. The spectrophotometric method gave higher values than the potentiometric method but both of them gave lower values than the d.c. plasma emission method. Calcium concentrations in the range 30–250 ppm were found in the samples.

Paper machine back water contains a wide variety of dissolved and colloidally dispersed detrimental inorganic and organic substances. The concentration of these substances, including calcium, is dependent on the degree to which the wet end of the paper machine is closed.[1,2] Fillers containing calcium, such as calcium carbonate are the main source of calcium in the circulating water in paper machines. Also reuse of discarded paper, containing gypsum ($CaSO_4$) as coater, from other stages in the manufacturing process and returned for reprocessing is a considerable source of calcium.[3]

Free ionized calcium can react in the back water with anions of fatty acids resulting in insoluble and sticky soaps. These soaps, forming pitch deposits, have negative effects on both the quality of the paper and running of the paper machine.[4] Due to these effects monitoring of calcium levels in the back water of paper machines has begun to gain interest in the paper industry. Calcium concentrations up to 300 ppm are usually of interest.

Various color forming reagents, *e.g.*, Eriochrome Black T,[5] chlorophosphonazo III,[6] calmagite[7] and *o*-cresolphthalein complexon (CPC),[8] have been used in the spectrophotometric determination of calcium by flow injection analysis (FIA). Among these, CPC is the most frequently used and will be studied in more detail in this work.

There are several ways of performing potentiometric calcium determination by the FIA technique. Calcium can be determined indirectly by using a copper wire electrode where the excess of EDTA in the carrier solution is measured.[9] Ion-selective electrodes (ISE), based on neutral carriers, *e.g.*, the ETH 1001 ionophore, are often based in direct determination of calcium in FIA.[10] Similar measurements have also been done with ISFETs.[11]

EXPERIMENTAL

Instrumentation

The central unit in the spectrophotometric and the potentiometric FIA system was a FIAstar® 5010 Analyser (TECATOR), featuring two 4-channel peristaltic pumps and injection valve. Appropriate reaction coil combinations were achieved with Chemifolds.

A FIAstar® 5023 Spectrophotometer (TECATOR), connected to the 5010 Analyser, was used in the spectrophotometric measurements. Absorbances were measured at 570 nm. A Schneider 386 PC was used to control the FIA system and to do data acquisition and evaluation.

*Author for correspondence.

Potentiometric determination of calcium by FIA was done with a small volume (20-μl), flow-through cell equipped with a Ca-selective electrode based on a neutral carrier. Potentials were measured against a flow-through Ag/AgCl reference electrode. Both electrodes were obtained from KONE Instruments, Finland. The 5010 Analyser was used as the pumping, injection and mixing unit. Data was gathered with a Perkin-Elmer strip chart recorder and the FIA system was operated manually.

Total calcium in samples was determined with dc-plasma emission spectroscopy (DCP). The instrument used was a SpectraSpan III B plasma emission spectrophotometer.

Chemicals

Calcium carbonate ($CaCO_3$) supra pure (Merck), $NaNO_3$ *p.a.* (Merck), NaOH *p.a.* (Merck), sulphuric acid *p.a.* (Merck), *o*-cresolphthalein complexon *p.a.* (Fluka), 2-amino-2-methylpropan-1-ol for synthesis (Merck), 8-hydroxyquinoline *p.a.* (Analar) and nitrilotriacetic acid (NTA) *p.a.* (Fluka) were used as received. Millipore water was used through the whole work.

Standards and samples

Standard solutions in the range 10–300 ppm Ca^{2+} were used and prepared by successive dilution of a 500 ppm Ca^{2+} stock solution prepared as described in the literature.[8] Slurries of back water from Finnish paper mills were used as samples. They were filtered through a paper filter prior to the analysis. Standards and samples were injected in triplicates.

RESULTS AND DISCUSSION

Spectrophotometric determination

Back water contains a large number of different inorganic compounds that may interfere in the spectrophotometric determination of calcium. Magnesium is the most severely interfering species due to its strong complexation with CPC:

$$\begin{aligned} Ca + L &\rightarrow CaL; \quad K_{CaL} = 10^{7.8} \\ Ca + CaL &\rightarrow Ca_2L; \quad K_{Ca_2L} = 10^{5.0} \end{aligned} \qquad (1)$$

$$\begin{aligned} Mg + L &\rightarrow MgL; \quad K_{MgL} = 10^{8.9} \\ Mg + MgL &\rightarrow Mg_2L; \quad K_{Mg_2L} = 10^{5.2} \end{aligned} \qquad (2)$$

where L represents CPC. Notations in this paper will follow the principles introduced by Ringbom.[12] Values of the stability constants are taken from Ref. 13, p. 340.

Interference of magnesium can be diminished by masking it with 8-hydroxyquinoline, 8-HQ:

$$Mg + X \rightarrow MgX; \quad K_{MgX} = 10^{4.7} \qquad (3)$$

where X stands for 8-HQ. The value of the stability constant, K_{MgX}, is taken from Ref. 13, p. 408. The masking reaction (3) can be considered by calculating the side reaction coefficient $\alpha_{Mg(X)}$:

$$\alpha_{Mg(X)} = 1 + [X'] \, K_{MgX}/\alpha_{X(H)} \qquad (4)$$

where [X'] stands for the total concentration of 8-HQ not bound to magnesium. In our application it is approximately $0.02M$. The protonation reaction of 8-HQ can be considered by introducing the side reaction coefficient $\alpha_{X(H)}$. Values for $\alpha_{X(H)}$ can be found in Ref. 13, p. 424. Concentrations of calcium and magnesium at the color transition point with CPC are denoted by $[Ca]_{trans}$ and $[Mg]_{trans}$ and their values can also be found in Ref. 13, pp. 426, 428. Effect of the masking reaction (3) on $[Mg]_{trans}$ can be calculated in the following way (Ref. 13, p. 233)

$$pMg'_{trans} = pMg_{trans} - \log \alpha_{Mg(X)} \qquad (5)$$

Values of pCa_{trans}, pMg_{trans}, $\log \alpha_{Mg(X)}$ and pMg'_{trans} between pH 9 and 11 are given in Table 1. Values of $\log \alpha_{Mg(X)}$ and pMg'_{trans} are calculated by using equations (4) and (5), respectively. The last row, ΔpM_{trans}, is the difference between pCa_{trans} and pMg'_{trans} and is a measure of the interference of magnesium on determination of calcium. The difference should be as large as possible in order to have minimum interference of magnesium. As can be seen in Table 1, pH 10–10.5 gives the maximum separation between the color transition points of the two metals. On the other hand the value of pCa_{trans} should be as large as possible in order to give a clear colour transition for calcium. Therefore, pH 10.5 is recommended. This is also the value used earlier by other workers[8] for

Table 1. Effect of pH and magnesium on the color transition point of the Ca–CPC complex. Magnesium is masked with $10^{-1.8}M$ 8-hydroxyquinoline

pH	9	10	10.5	11
pCa_{trans}	3.4	4.5	5.1	6.2
pMg_{trans}	3.6	4.7	5.7	7.3
$\log \alpha_{X(H)}$	1.0	0.3	0	0
$\log \alpha_{Mg(X)}$	2.0	2.7	3.0	3.0
pMg'_{trans}	1.6	2.0	2.7	4.3
ΔpM_{trans}	1.8	2.5	2.4	1.9

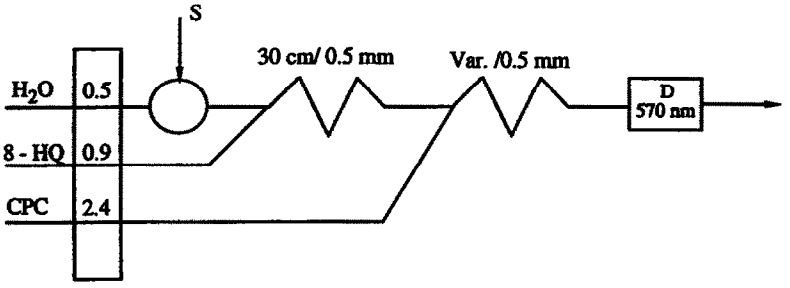

Fig. 1. The FIA manifold used in the spectrophotometric method with CPC. Flow rates are given in ml/min and the values for the coils are length/id.

the same determination. Their recommendation was obviously based on experimental results. The effect of soluble Ca-complexes, *e.g.*, sulphates, can be taken into consideration by introducing the side reaction coefficient log $\alpha_{Ca(SO_4)}$. This would slightly lower the pCa_{trans} values in Table 1, and give pCa'_{trans} when calculated according to equation (5). This effect, however, is only marginal at concentrations generally found in back waters and therefore is not considered here.

The FIA manifold used in the spectrophotometric determination is shown in Fig. 1 and is a modification of the one given in Ref. 8. Absorbance of the Ca–CPC complex was measured at 570 nm. Millipore water was used as the carrier solution. The masking solution for Mg^{2+} was 0.02*M* 8-hydroxyquinoline (8-HQ) buffered with 2-amino-2-methylpropan-1-ol to pH 10.5.

In order to find the optimum experimental parameters, the concentration of CPC was varied between 0.119 and 0.200m*M* while keeping the length of the second coil at 60 cm. When using a 0.119m*M* CPC solution, a linear calibration curve was found up to 100 ppm Ca^{2+}, whereafter the curve started to bend down. Concentrations of 0.15m*M* and higher gave a colour intensity which exceeded the working range of the spectrophotometer. By changing the length of the second coil to 30 cm and still keeping the reagent concentration of 0.15m*M* the dispersion was diminished to such a degree that the intensity of the color of the formed complex did not exceed the dynamic range of the spectrophotometer. When the reagent concentration was further increased to 0.20m*M* in this configuration the working range of the spectrophotometer was again exceeded. Based on these studies, a coil length of 30 cm and a CPC concentration of 0.15m*M* were used in this work. With these parameters the calibration curve was linear from 10 to 250 ppm Ca^{2+} ($r = 0.996$). The rsd was *ca.* 0.5% through the entire linear range.

Potentiometric determination by a calcium selective electrode

The manifold used in the potentiometric determination of calcium by FIA is shown in Fig. 2. A reagent stream of 0.28*M* $NaNO_3$ was used to give a constant ionic strength required for the potentiometric detection.

Interferences from the streaming potential were eliminated by grounding the inlet and outlet of the flow through electrode. The electrode showed linear response ($r = 0.997$) over the entire concentration range studied, 10–300 ppm Ca^{2+}. The slope of the line was 30 mV/pCa and the relative standard deviations were 0.6

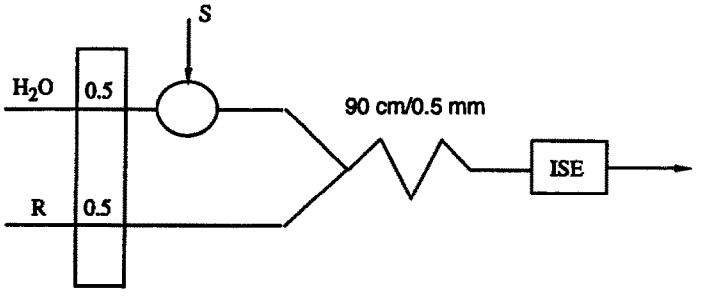

Fig. 2. The FIA manifold used in the potentiometric determination of calcium. Flow rates are given in ml/min and the values for the coils are length/id.

and 0.4% at the lower and the higher end of the curve, respectively.

Stability of the electrode response was tested by injecting 15 different back water samples in triplicate. During this process the slope of the calibration line decreased by 1 mV/pCa. This change in the slope was not irreversible and falls within variations of the slope when determined with standards on a daily basis.

Samples from paper mills

The spectrophotometric and the potentiometric methods were compared by determining calcium in two samples from paper mills. The results are given in Table 2. The spectrophotometric method had earlier been used in analysis of two samples from other mills. These results, #3 and #4, are also included in Table 2. All the samples were acidified to pH 4 by hydrochloric acid either (a) prior or (b) after filtering the solid matter. The purpose of acidification was to release the complex bound calcium. Acidification prior to filtering would release calcium bound both to solid matter and in soluble complexes. That procedure would therefore give the total calcium in the sample. Acidification after filtering effects only the soluble complexes. Calcium was also determined by a DCP method. Those results are included in Table 2 as well.

As can be seen in Table 2, higher calcium concentrations are found in the samples acidified prior to filtering indicating that significant amount of calcium is bound to the solid matter in the samples. The difference in the measuring principles of the DCP and ISE methods is that ISE gives the free, ionized amount of calcium, and DCP the total amount of calcium in the samples. The reason that higher calcium concentrations are found by the DCP method than by the ISE method, even after acidification of the samples, indicate that pH 4 is not acidic enough to break all calcium complexes in the samples, *e.g.*, sulfate complex or colloidal calcium oxalate. Due to the operating conditions of a paper machine pH values below 4 are not relevant in paper production and therefore were not used in this work.

Table 2. Calcium concentration in back water samples from paper mills determined by dc-plasma emission (DCP), potentiometric (ISE) and spectrophotometric methods. Samples were acidified to pH 4 with HCl (a) before and (b) after filtering

	Method					
	DCP		ISE		Spectroph.	
Sample no.	ppm	r.s.d., % $n = 3$	ppm	r.s.d., % $n = 3$	ppm	r.s.d., % $n = 3$
1(a)	102	1.2	69.1	0.2	77.5	0.6
2(a)	100	0.2	60.2	0.2	73.7	0.4
2(b)	65.5	1.5	30.2	0.3	43.5	0.1
3(a)					225	0.3
3(b)					170	0.3
4(a)					182	0.2
4(b)					78.2	0.4

Results in Table 2 show that the spectrophotometric method gives a higher calcium concentration than the ISE method. This discrepancy can be explained by considering how the principles of determination of these two methods differ. The ISE-method, as explained earlier, "senses" only the ionized calcium. The spectrophotometric method, however, uses a complexation reaction where calcium forms a stable complex with the reagent. Therefore calcium still bound to weaker complexes in the sample will be available to the spectrophotometric method.

CONCLUSIONS

With further development of the methods presented in this paper, *i.e.*, introducing a sampling and sample pretreatment system it would be possible to use the FIA methods in on-line applications for continuous analysis of back water. This would, in real time, give the concentrations of calcium in free form and also in weak, labile complexes to the process engineers running the paper machines and responsible of production and quality of the product.

As the results in this paper indicate, the ISE and the spectrophotometric methods give slightly different results due to the different principles of the two methods. By employing different sample pretreatment procedures in combination of different methods of determination it would also be possible to gain information of calcium speciation in the samples, if that is sought.

REFERENCES

1. W. J. Auhorn and J. Melzer, *TAPPI Papermakers Conference Proceedings*, Boston, April 9–11, 1979, 49.
2. W. J. Auhorn, *Wochenblatt für Papierfabrikation*, 1984, **2**, 37.
3. H. P. Hofmann, J. Weigl and A. von Raven, *ibid.*, 1990, **9**, 365.
4. L. H. Allen, *Tappi Journal*, pp. 61–64. January, 1988.
5. A. T. Haj-Hussein and G. D. Christian, *Microchemical Journal*, 1986, **34**, 67.

6. M. Zenki, K. Ohumo and K. Toei, *Z. Anal. Chem.*, 1990, **338**, 707.
7. N. Ishibashi and T. Imato, *ibid.*, 1986, **323**, 244.
8. E. H. Hansen, J. Růžička and A. K. Ghose, *Anal. Chim. Acta*, 1978, **100**, 151.
9. P. W. Alexander, M. Trojanowicz and P. R. Haddad, *Anal. Lett.*, 1984, **17**, 309.
10. H. Wada, T. Ozawa, G. Nakagawa, Y. Asano and S. Ito, *Anal. Chim. Acta*, 1988, **211**, 213.
11. A. U. Ramsing, J. Janata, J. Ruzicka and M. Levy, *ibid.*, 1980, **118**, 45.
12. A. Ringbom, *Complexation in Analytical Chemistry*, Wiley, New York, 1963.
13. E. Wänninen, Metallochromic Indicators, in Edmund Bishops (ed.), *Indicators*, Chap. 6B, pp. 340, 408, 424, 426, 428, 233. Pergamon Press, Oxford, 1972.

Talanta, Vol. 40, No. 1, pp. 101–106, 1993
Printed in Great Britain

0039-9140/93 $6.00 + 0.00
Pergamon Press Ltd

REVERSE FLOW INJECTION ANALYSIS OF COMPLEXING AGENTS AND ITS APPLICATION TO ESTIMATION OF COMPLEXING CAPACITY

NORIO TESHIMA, HIDEYUKI ITABASHI and TAKUJI KAWASHIMA*

Laboratory of Analytical Chemistry, Department of Chemistry, University of Tsukuba, Tsukuba 305, Japan

(*Received* 1 *May* 1992. *Accepted* 22 *May* 1992)

Summary—A redox reaction of copper(II) with iron(II) proceeds slowly in the presence of neocuproine, although the reaction would not take place in its absence. This reaction is accelerated by the presence of complexing agents such as EDTA, DTPA, CyDTA, EDTA-OH, NTA, citrate, pyrophosphate, producing a copper(I)-neocuproine complex ($\lambda_{max} = 454$ nm). A reverse flow injection analysis (r-FIA) method is presented for the determination of trace amounts of complexing agents by measuring the increase in absorbance at 454 nm. Complexing agents at the $10^{-6}M$ level can be determined at a rate of 120 samples/hr. By using this r-FIA system, a new procedure for the measurement of complexing capacity with metal ions such as Al(III), Cu(II), Zn(II), Cd(II) and Pb(II) has been developed. Complexing capacity for each metal ion can be measured at a rate of 120 samples/hr.

The effect of complexing agents such as aminopolycarboxylic acids and inorganic polyphosphates on environmental and biological cycles has been considered since these agents have been widely used in various industrial fields.[1] On the other hand, toxicity and bioavailability of trace metals in natural waters depend on the concentrations of various complexing agents because such metals form complexes with these complexing agents.[2–4] From this point of view, a concept of complexing capacity with metal ions was introduced for environmental assessment.[2,5] Several experimental procedures have been proposed for the measurement of complexing capacity of natural waters and have been reviewed by Florence[4] and Neubecker and Allen.[6] These methods can be classified into the following groups:[4,6] solubilization,[7] biological response,[2] ion-exchange,[8] voltammetric,[7,9] and ion selective electrode.[10,11] Recently, Akaiwa *et al.*[12] reported a method for the measurement of copper(II)-complexing capacity of natural waters by a back-extraction technique using bis(4,4,4-trifluoro-1-phenyl-1,3-butanedionato)copper(II). Taga *et al.*[13] also proposed a method for the complexing capacity of humic acids with copper by using a macroreticular weak-base anion exchanger, diethylaminoethyl Sephadex A-25 resin which can adsorb the metal-humic acids complex, but not the free metal ions. However, most of the methods are laborious and time consuming, and also no consistent relation can be found among the complexing capacity values obtained by these techniques.[7] Thus, reliable methods are still needed for measurements of complexing capacity in natural waters.

Recently, we showed that the redox reaction of copper(II) with iron(II) takes place in the presence of neocuproine.[14] In addition, this reaction was greatly accelerated by the presence of various complexing agents together with neocuproine, and a copper(I)–neocuproine complex ($\lambda_{max} = 454$ nm) was then produced. We have reported the flow injection analysis (FIA) of complexing agents such as EDTA, DTPA, CyDTA, EDTA–OH, NTA, citrate, pyrophosphate (diphosphate) by using this redox reaction.[15] The reverse flow injection analysis (r-FIA) method is known to be very valuable when a large volume of sample is available and reagent consumption should be minimized.[16] Thus, the present paper describes an indirect photometric determination of complexing agents by r-FIA based on the same reaction. By using this r-FIA system, a new procedure for the measurement of complexing capacity with metal ions such as Al(III),

*Author for correspondence.

Cu(II), Zn(II), Cd(II) and Pb(II) is also presented.

EXPERIMENTAL

Reagents

Stock solutions of iron(II) ($1.0 \times 10^{-2}M$), copper(II) ($1.0 \times 10^{-2}M$) and zinc(II) ($0.1M$) were the same as described previously.[14,15] An aluminum(III) solution ($0.1M$) was prepared by dissolving aluminum potassium sulfate dodecahydrate (potassium alum) in water. A cadmium(II) solution was prepared by diluting a stock standard solution for atomic absorption spectrophotometry with water. A lead(II) solution ($0.1M$) was prepared by dissolving lead(II) acetate trihydrate in water. Working solutions of metal ions were prepared by suitably diluting each stock solution with water and/or buffer solution. Neocuproine, ethylenediamine-*N,N,N',N'*-tetraacetic acid (EDTA), diethylenetriamine-*N,N,N',N'',N''*-pentaacetic acid (DTPA), *trans*-1,2-cyclohexanediamine-*N,N,N',N'*-tetraacetic acid (CyDTA), *N*-hydroxyethylethylenediamine-*N,N',N'*-triacetic acid (EDTA-OH), nitrilotriacetic acid (NTA), citrate and pyrophosphate solutions were the same as described previously.[14,15] Triphosphate solution ($0.1M$) was also prepared by dissolving an appropriate amount of sodium triphosphate in water.

All reagents used were of analytical reagent grade. Water used to prepare the solutions was purified by a Milli-Q water purification system (Millipore).

Apparatus

A schematic r-FIA diagram for the determination of complexing agents and of complexing capacity is shown in Fig. 1. Four double-plunger micro pumps (Sanuki Kogyo, DM2M-1026) and a six-way injection valve (Sanuki Kogyo, SVM-6M2) with a loop were used to assemble the system. The flow lines were made from Teflon tubing (0.5 mm i.d.). The absorbance change was monitored at 454 nm with a Soma Kogaku S-3250 spectrophotometer with a 10-mm micro flow cell (8 μl) and recorded on a Hitachi Model 056 recorder. A Corning Model 12 pH/mV meter was also used to monitor the pH of waste solution.

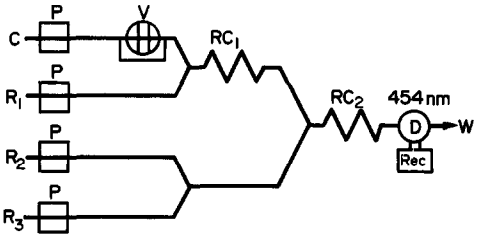

Fig. 1. Flow diagram of r-FIA for complexing agent and complexing capacity. Measurement of complexing agent; C, carrier solution ($0.05M$ acetate, pH 5.6); R_1, iron(II) ($1 \times 10^{-4}M$); R_2, R_3, sample solution (complexing agent); V, mixed solution of copper(II) ($1 \times 10^{-4}M$) and neocuproine ($5 \times 10^{-4}M$). Estimation of complexing capacity; C, carrier solution ($0.05M$ acetate, pH 5.6); R_1, sample solution (complexing agent); R_2, iron(II) ($1 \times 10^{-4}M$); R_3, mixed solution of copper(II) ($1 \times 10^{-4}M$) and neocuproine ($5 \times 10^{-4}M$); V, metal ion solution [Al(III), Cu(II), Zn(II), Cd(II) and Pb(II), $2 \times 10^{-5}M$]. The symbols P, RC, D, Rec and W are pump, reaction coil (0.5 mm i.d.), spectrophotometer (454 nm), recorder and waste, respectively.

Procedure for the measurement of complexing agent

In the flow system (Fig. 1), a buffer carrier solution (C), an iron(II) solution in reservoir R_1 and a complexing agent solution in reservoirs R_2 and R_3 were pumped at a flow rate of 2.3 ml/min. An aliquot (80 μl) of mixed solution of copper(II) and neocuproine was injected into the carrier stream. The reduction rate of copper(II) with iron(II) was accelerated by the presence of complexing agent and the copper(I)–neocuproine complex was produced in a reaction coil (0.7 m long) at room temperature. The absorbance of the complex produced was monitored continuously at 454 nm.

Procedure for the measurement of complexing capacity

In the flow system (Fig. 1), a buffer carrier solution (C), a complexing agent solution in reservoir R_1, an iron(II) solution in reservoir R_2 and a mixture of copper(II) and neocuproine in reservoir R_3 were pumped at a flow rate of 2.0 ml/min. An aliquot (200 μl) of metal ion such as Al(III), Cu(II), Zn(II), Cd(II) and Pb(II) was injected into the carrier stream. The metal ion reacts with the complexing agent to form a complex in a reaction coil RC_1 (0.5 m long): a decrease in absorbance at 454 nm was observed and monitored.

Table 1. Features of the calibration curves

Complexing agents	Intercept	Slope	Regression coefficient	r.s.d. (%) ($n = 10$)
EDTA	−0.0060	0.0052	0.999	1.2
NTA	−0.0011	0.0037	0.997	2.8
Citrate	−0.0003	0.0016	0.996	2.5
Pyrophosphate	−0.0041	0.0076	0.999	1.7

RESULTS AND DISCUSSION

Effect of reaction variables for the measurement of complexing agent

The optimum conditions for r-FIA were studied by propelling $1 \times 10^{-5}M$ EDTA solution in reservoirs R_2 and R_3. All measurements were carried out at room temperature.

The absorbance at 454 nm increased rapidly with increasing pH up to 5.1, and remained constant in the pH range 5.1–6.1. A pH value of 5.6 was used for the procedure.

The effect of iron(II) concentration was examined over the range 2×10^{-5}–$1 \times 10^{-3}M$. The absorbance increased with increasing concentration up to $7 \times 10^{-5}M$, and remained constant in the concentration range 7×10^{-5}–$1 \times 10^{-4}M$. At concentrations more than $1 \times 10^{-4}M$ the absorbance decreased gradually. A $1 \times 10^{-4}M$ iron(II) concentration was chosen for the procedure.

The effect of copper(II) concentration was examined over the range 2×10^{-5}–$7.5 \times 10^{-4}M$. The reproducibility of the flow signals became poorer at copper(II) concentrations more than $1 \times 10^{-4}M$, although maximum absorbance was obtained around $2 \times 10^{-4}M$. Hence, a $1 \times 10^{-4}M$ copper(II) concentration was chosen.

Maximum and constant absorbance was obtained over the concentration range 5×10^{-4}–$1 \times 10^{-3}M$ neocuproine. A $5 \times 10^{-4}M$ neocuproine concentration was selected.

The effect of reaction coil length was examined by varying coil length (RC_2, 0.1–5 m). The absorbance increased with increasing coil length and the absorbance showed maximum at 0.7 m, decreasing gradually beyond this length due to an increase in the degree of dispersion. A coil length of 0.7 m was used for the procedure.

Calibration graphs

The linear calibration graphs were obtained over the range 2×10^{-6}–$1 \times 10^{-5}M$ EDTA, NTA, citrate and pyrophosphate. The sampling rate of 120/hr is attained for the proposed method. The reproducibility of the method is satisfactory with low r.s.v. %. The features of the calibration graphs for each complexing agent are summarized in Table 1.

Interferences

The effect of foreign ions on the determination of $1 \times 10^{-5}M$ EDTA was studied. The tolerance limits for foreign ions are summarized in Table 2; a 5% error was considered to be tolerable. As can be seen from Table 2, Li(I), Na(I), K(I), Cl^-, NO_3^-, SO_4^{2-} and CH_3COO^- ($0.02M$), BO_3^{3-} ($0.01M$), CO_3^{2-} ($5 \times 10^{-3}M$), Mg(II) and Sr(II) ($2 \times 10^{-3}M$), Ca(II) and F^- ($1 \times 10^{-3}M$) showed no influence. However, Al(III), Co(II), Ni(II), Cu(II) and Zn(II) ($1 \times 10^{-5}M$) caused serious negative interferences because these ions reacted with EDTA to form stable complexes. Similar masking effects for these metal ions were also observed for DTPA, CyDTA, EDTA-OH and NTA.

Effect of reaction variables for the measurement of complexing capacity

In the flow system as shown in Fig. 1, a $1 \times 10^{-5}M$ EDTA and/or pyrophosphate solution was pumped as a model ligand and a

Table 2. Effect of foreign ions on the determination of $1 \times 10^{-5}M$ EDTA

Tolerance ratio [ion]/[EDTA]	Ion added
2000	Li(I), Na(I), K(I), Cl^-, NO_3^-, SO_4^{2-}, CH_3COO^-
1000	BO_3^{3-}
500	CO_3^{2-}
200	Mg(II), Sr(II)
100	Ca(II), F^-
<1	Al(III), V(IV,V), Mn(II), Fe(II), Co(II), Ni(II), Cu(II), Zn(II), Cd(II), Hg(II), Pb(II), Bi(III)

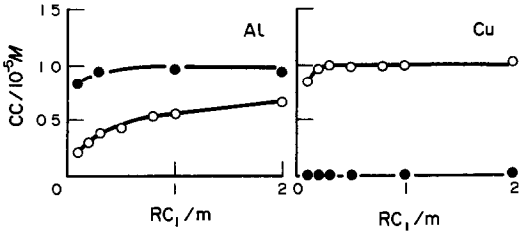

Fig. 2. Effect of reaction coil length (RC_1) for the measurement of complexing capacity. Complexing agents ($1 \times 10^{-5}M$): (○), EDTA; (●), pyrophosphate. Other conditions as in Fig. 1.

$2 \times 10^{-5}M$ metal ion concentration such as Al(III), Cu(II), Zn(II), Cd(II) and Pb(II) was injected into the carrier stream. The accelerating effect of complexing agents on the reduction of copper(II) with iron(II) is retarded by adding such metal ions. A decrease in absorbance at 454 nm corresponded to the concentration of each ligand in the presence of metal ion. By this phenomenon, a measurement of complexing capacity in natural water is also possible. The concentration of each model ligand solution was measured as a function of each metal ion such as Al(III), Cu(II), Zn(II), Cd(II) and Pb(II). Complexing capacities measured by using Al(III), Cu(II), Zn(II), Cd(II) and Pb(II) solutions are abbreviated as AlCC, CuCC, ZnCC, CdCC and PbCC. The concentrations of iron(II) ($1 \times 10^{-4}M$), copper(II) ($1 \times 10^{-4}M$), neocuproine ($5 \times 10^{-4}M$) and the reaction pH 5.6 were selected for the measurement of complexing capacity based on the above results. The reaction coil (RC_2) length of 0.7 m was also used.

The effect of reaction coil length of RC_1 was examined over the range 0.1–2 m (Fig. 2). Zn, Cd and Pb exhibited curves similar to those

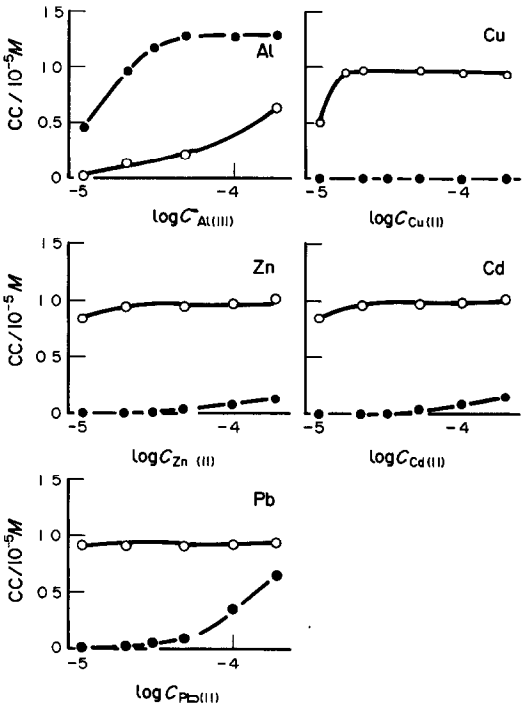

Fig. 3. Effect of metal ion concentration for the measurement of complexing capacity with each metal ion. Complexing agents ($1 \times 10^{-5}M$): (○), EDTA; (●), pyrophosphate. Other conditions as in Fig. 1.

for Cu. In the case of EDTA, maximum and constant values for CuCC, ZnCC, CdCC and PbCC were obtained at the reaction coil length greater than 0.3 m. The AlCC value increased gradually with increasing the reaction coil length and a lower CC value than the others was obtained. This is attributable to the fact that the rate of complex formation of Al(III) with EDTA is much slower than those of other metal ions.[17] In the case of pyrophosphate, the AlCC value increased with increasing reaction

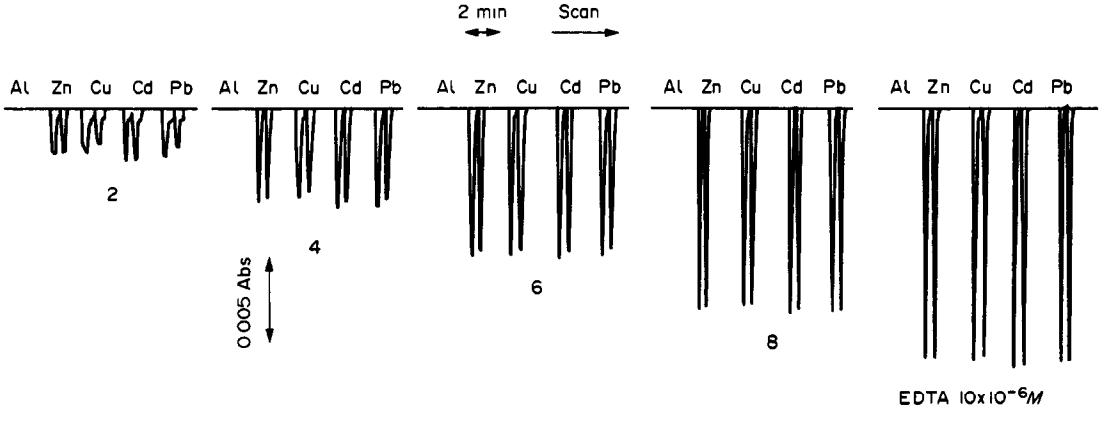

Fig. 4. Flow signals for complexing capacity with each metal ion at various concentrations of EDTA. Other conditions as in Fig. 1.

Table 3. Measurement of complexing capacity in river and lake waters

	Complexing capacity*/$10^{-7}M$				
	Extn method	Proposed method			
Sample	CuCC	AlCC	ZnCC	CdCC	PbCC
River water†					
A	3(<1)	5(<1)	5(1)	7(1)	4(1)
B	4(<1)	6(1)	4(1)	6(1)	4(2)
C	7(<1)	4(2)	3(1)	4(1)	2(1)
D	10(<1)	6(2)	5(2)	5(2)	8(3)
Lake water†					
A	3(<1)	4(<1)	3(1)	6(1)	1(<1)
B	4(<1)	4(<1)	4(1)	6(<1)	2(<1)
C	3(<1)	7(<1)	4(1)	5(1)	3(2)
D	3(<1)	5(1)	3(1)	4(1)	1(1)
E	3(<1)	5(2)	2(1)	4(1)	5(<1)

*Values determined in triplicate. ( ) = standard deviation.
†Collected at Tsukuba.

coil length. A maximum and constant AlCC value was obtained at a reaction coil length greater than 0.3 m, while CuCC, ZnCC, CdCC and PbCC values were very low.

The effect of metal ion concentration was examined at a constant concentration ($1 \times 10^{-5}M$) of EDTA and/or pyrophosphate. The results are shown in Fig. 3. In the case of EDTA, maximum and constant CuCC, ZnCC, CdCC and PbCC values were obtained at concentrations higher than $2 \times 10^{-5}M$. The AlCC value increased gradually with increasing concentration of aluminum(III) and the value was lower than those obtained for other metal ions. In the case of pyrophosphate, the maximum and constant AlCC value was obtained at greater than $5 \times 10^{-5}M$. The CuCC, ZnCC, CdCC and PbCC values were not obtainable over the range 1×10^{-5}–$3 \times 10^{-5}M$.

The effects of EDTA and pyrophosphate concentrations were examined by injecting $2 \times 10^{-5}M$ of each metal ion solution. The results for EDTA are shown in Fig. 4. The CuCC, ZnCC, CdCC and PbCC values were the same and the values increased linearly with increasing concentration of EDTA, while the AlCC value was not obtained. In the case of pyrophosphate, the AlCC value increased linearly with increasing concentration of pyrophosphate, while the CuCC, ZnCC, CdCC and PbCC values could not be obtained. Similar situations as for pyrophosphate were observed for triphosphate. From these results, a characterization of complexing agents in natural waters should be possible. Complexing capacity corresponding to the pyrophosphate type ligands would be obtained by injecting Al(III) solution. On the other hand, the CC value obtained by injecting other metal ions corresponds to the concentration of aminopolycarboxylic type ligands. Complexing capacities for each metal ion in natural waters at the 10^{-7}–$10^{-6}M$ level were determined at a rate of 120 times/hr by the proposed method.

Application to water samples

The applicability of the proposed method was evaluated by measuring complexing capacities of both river and lake waters. After the samples were filtrated with a 0.45-μm membrane filter, the measurement of complexing capacity was performed by the proposed method. The results, given in Table 3, are compared with those obtained by the extraction method.[12] Complexing capacities of the samples collected at the Tsukuba area were in the $10^{-7}M$ range. The values obtained by the proposed method were in the same order as those obtained by the extraction method. The ZnCC, CdCC and PbCC values should correlate with CuCC values obtained by the extraction method, corresponding to aminopolycarboxylic type ligands, while the AlCC values represent pyrophosphate type ligands. Although the proposed method was not evaluated in full detail, it can be seen from the results in Table 3 that it is useful for estimating two types of complexing capacity in natural waters.

REFERENCES

1. N. Yoza, T. Shuto, Y. Baba, A. Tanaka and S. Ohashi, *J. Chromatogr.*, 1984, **298**, 419.
2. E. W. Davey, M. J. Morgan and S. J. Erickson, *Limnol. Oceanogr.*, 1973, **18**, 993.
3. N. S. Fisher and D. Frood, *Mar. Biol.*, 1980, **59**, 85.
4. T. M. Florence, *Talanta*, 1982, **29**, 345.

5. M. S. Shuman and G. P. Woodward, *Anal. Chem.*, 1973, **45**, 2032.
6. T. A. Neubecker and H. E. Allen, *Water Res.*, 1983, **17**, 1.
7. P. G. C. Campbell, Marc Bisson, Robert Gagne and Andre Tessier, *Anal. Chem.*, 1977, **49**, 2358.
8. C. M. G. van den Berg and J. R. Kramer, *Anal. Chim. Acta*, 1979, **106**, 113.
9. K. W. Hanck and J. W. Dillard, *ibid.*, 1977, **89**, 329.
10. J. Buffle, France-Line Greter and W. Haerdi, *Anal. Chem.*, 1977, **49**, 216.
11. W. T. Bresnahan, C. L. Grant and J. H. Weber, *ibid.*, 1978, **50**, 1675.
12. H. Akaiwa, H. Kawamoto and H. Ogura, *Chem. Lett.*, **1986**, 605.
13. M. Taga, S. Tanaka and M. Fukushima, *Anal. Sci.*, 1989, **5**, 597.
14. H. Itabashi, K. Umetsu, K. Satoh and T. Kawashima, *ibid.*, 1990, **6**, 721.
15. H. Itabashi, K. Umetsu, N. Teshima, K. Satoh and T. Kawashima, *Anal. Chim. Acta*, 1992, **261**, 213.
16. K. S. Johnson and R. L. Petty, *Anal. Chem.*, 1982, **54**, 1185.
17. R. Pribil and V. Vesely, *Talanta*, 1962, **9**, 23.

Talanta, Vol. 40, No. 1, pp. 107–112, 1993
Printed in Great Britain

0039-9140/93 $6.00 + 0.00
Pergamon Press Ltd

DIRECT FIA–AS DETERMINATION OF POTASSIUM AND MAGNESIUM IN CEMENT SAMPLES BY USE OF THE SLURRIES APPROACH

R. MARTINEZ-AVILA, V. CARBONELL, A. SALVADOR and M. DE LA GUARDIA*

Department of Analytical Chemistry, University of Valencia, 50 Dr Moliner St., 46100 Burjassot, Valencia, Spain

(*Received* 25 *March* 1992. *Revised* 5 *June* 1992. *Accepted* 8 *June* 1992)

Summary—A direct procedure has been developed for the flame atomic determination of potassium and magnesium in cement samples. A 50-mg sample is dispersed in 25 ml of 0.13*M* nitric acid; 100 μl of this slurry is injected in a double channel FIA manifold simultaneously with 100 μl of a 10% (w/v) lanthanum solution. This procedure allows the rapid extraction of potassium and magnesium by leaching of the sample; nitric acid is not necessary if only potassium must be determined and the sample can be diluted with only distilled water. Aqueous standards are used. The manifold employed includes a well-stirred mixing chamber, which provides an adequate on-line dilution of the sample, in order to obtain emission or absorbance measurements in the dynamic range of the elements to be determined. The results obtained in the analysis of real samples agree with those found by flame atomic spectrometry after a previous alkaline fusion with lithium carbonate, and exhibit better precision. The limit of detection of the procedure is 0.007% for K_2O and 0.01% for MgO and the precision of the entire procedure corresponds to a relative standard deviation of 1%.

The analysis of cements by atomic spectrometry requires the dissolution of samples after a previous wet ashing or fusion procedure.[1,2] This is usually the most time consuming step and may introduce contamination or interelemental interferences, the latter caused by the total dissolution of all the sample components.

An alternative to the dissolution of solid samples for their analysis by atomic spectrometry is the direct introduction of slurries. Slurries are fine dispersions of powdered solids in water or other solvents. Previous work has shown that the use of slurries can be a convenient way to introduce solids into flames,[3–5] plasmas[6,7] and electrothermal atomization systems.[8–12]

The direct determination of mineral elements in slurries requires the use of solid particles of small diameter:[13] moreover, in some cases, problems related to inefficient volatilization of the elements from the solid phase may produce low results. In these cases, it is more suitable to treat the slurries in order to dissolve the elements to be determined. When the elements under study can be extracted from the suspended solid by a fast and easy way, direct analysis of the slurry by atomic spectrometry can be carried out without matrix separation.[14,15] So, losses or interelemental interferences can be avoided. The slurry sample introduction method has been applied to the determination of Na in standard reference cements using glycerol as a stabilizer for the dispersion and nitric acid as extractant agent.[16]

Recent studies in our laboratory have shown that slurries can be injected in flow systems and so Cu, Mn and Pb were determined in sewage sludge samples.[17]

In the present paper, the direct introduction of cement slurries has been carried out in a flow system for the determination of potassium and magnesium in real cement samples, with on-line dilution of the samples.

EXPERIMENTAL

Apparatus

A Perkin–Elmer 5000 atomic spectrophotometer equipped with a magnesium hollow-cathode lamp was used for absorbance measurements. Potassium was determined by flame emission spectrometry using a Varian SpectrAA-10 atomic absorption spectrophotometer. An air-acetylene flame was used in

*Author for correspondence.

both cases. All measurements were carried out without background correction.

A flow injection procedure was used to carry out the analysis, using the manifold indicated in Fig. 1. A Gilson P-2 Minipuls peristaltic pump with two 2.79 mm internal diameter polyvinylchloride tubes was employed to transport the aqueous carrier streams. Samples and lanthanum solutions were introduced using a double simultaneous injector constructed with two Rheodyne injection valves type 50 with fixed loops. A three way Y-shaped connector Omnifit, with an internal diameter of 0.8 mm, provides the merging point. A mixing chamber is connected after the merging point and before the nebulizer in order to obtain adequate dilutions of the samples. This chamber has a volume of 1 ml and the escape of any air bubbles can be assured by a slight dome in the upper part. A Teflon covered magnetic stirring bar assures an appropriate mixing in the dilution chamber. All the connecting tubes used were made of Teflon and with 0.8-mm internal diameter (Omnifit).

The dispersion coefficient provided by the manifold was 22. It was preferred to carry out the on-line dilutions of the samples than to use less sensitive instrumental conditions because FIA provides fast and reproducible dilutions and moreover, the analysis of real samples under conditions different than those providing the best sensitivity can be affected by matrix interferences.

Instrumental and flow injection parameters used in the analysis are given in Table 1.

Table 1. Instrumental and FIA parameters used in the determination of K and Mg in cement samples

Parameter	K	Mg
Wavelength/nm	766.5	285.2
Technique	FE	AA
Burner height*	0.5 cm	1.3 cm
Burner angle (°)	180	20
Qair/l/min	3.5	21
Qacetylene/l/min	1.5	1.3
Loop/μl	100	
Total flow rate/ml/min	8.4	
Mixing chamber volume/ml	1	

*The burner height being the distance below the focal point of the optical system.

FE: flame emission; AA: atomic absorption.

A Perkin–Elmer 5000 and a Varian SpectrAA-10 atomic spectrophometer were used for the measurement of absorbance of magnesium and emission of potassium respectively.

Reagents

A magnesium stock solution of 1000 ppm was prepared by dissolving 1 g of magnesium metal (Merk) in 50 ml of 5*M* hydrochloric acid and diluting to one litre with demineralized water.

Potassium stock solution of 1000 ppm was prepared from 1.9070 g of dry potassium chloride (Panreac) dissolved in one litre of demineralized water.

A 10% (w/v) lanthanum solution, prepared from lanthanum chloride ($LaCl_3 \cdot 7H_2O$) (Panreac), was used as a buffer solution to avoid anionic and ionization interferences.

Real cement samples were obtained from different Spanish and North African producers. Before the analysis, samples were ground in an agate ball mortar for half an hour in order to obtain a fine powder which was carefully homogenized.

All the reagents employed were analytical grade.

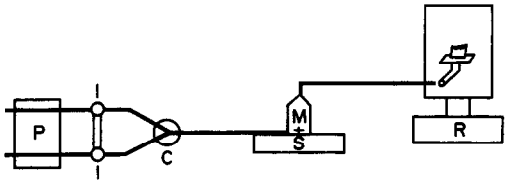

Fig. 1. FIA manifold employment in the analysis of potassium and magnesium in cement samples. P: peristaltic pump, I: injection valves, C: three-way connector, M: dilution chamber, S: magnetic stirrer and R: recorder.

Procedures

Recommended procedure

Preparation of slurries. The 50-mg sample was weighed into a standard flask and diluted up to 25 ml with 0.13*M* nitric acid. Homogenization of this dispersion can be achieved by introduction into an ultrasonic bath for 5 min. This procedure allows the rapid extraction of potassium and magnesium by leaching of the sample. If only potassium is to be determined, nitric acid is not necessary and distilled water is sufficient to extract it from the dispersed solids into the aqueous phase.

The size of 100% of the suspended particles determined by a laser diffraction system (Malvern Instruments, model 2600) was lower than 70 μm in all cases.

Flow injection analysis. Direct introduction of the dispersed sample is carried out without separation of the two phases, as follows:

One hundred microlitres of the slurry of the sample was injected in the double channel flow

injection system (Fig. 1) at the same time as one hundred microlitres of a 10% (w/v) lanthanum solution. Aqueous standards of K and Mg containing lanthanum and nitric acid were employed.

Reference method. Weigh 0.1 g of sample into a platinum crucible and add 1.5 g of lithium carbonate and 0.3 g of boric acid. Introduce the crucible into a muffle furnace, at 1100°; after 40 min, allow to cool to 700–800°. Transfer the molten contents of the crucible into a 250-ml porcelain evaporating basin. After cooling to room temperature, add 50 ml of hydrochloric acid (1 + 1 v/v) and stir until the solids are completely dissolved. Place the basin under an infrared lamp and evaporate to dryness at 130°. Add 5 ml of concentrated hydrochloric acid to re-suspend the silica and then dilute to 100 ml with hydrochloric acid (1 + 1 v/v). Filter using red-band (medium-textured) ashless Schuller filter-paper and dilute to 250 ml. Potassium and magnesium were determined by atomic spectrometric analysis of the filtered solution.

RESULTS AND DISCUSSION

Influence of the acidity of the medium

Preliminary experiments proved that atomic spectrometry determination of potassium in cement by direct injection of a discrete volume of a slurry containing 50 mg of sample dispersed in 25 ml of water in the FIA manifold provides results comparable to those found by analysis of samples using a previous alkaline fusion. However, the use of a 0.13*M* nitric acid medium for slurry preparation is necessary to obtain accurate results in the magnesium determinations as

Table 2. Effect of the concentration of nitric acid on the determination of Mg in cement samples

HNO_3 M	Sensitivity/au $mg^{-1}l$.	% MgO a	% MgO b
0	0.015	0.05 ± 0.01	0.03 ± 0.01
0.13	0.014	1.7 ± 0.1	1.67 ± 0.02
0.66	0.014	1.81 ± 0.03	1.73 ± 0.01
1.31	0.014	1.69 ± 0.03	1.73 ± 0.02
6.57	0.015	1.64 ± 0.05	1.68 ± 0.02
Real % MgO	1.72 ± 0.02%*		

Note: Percentage of MgO is expressed by the mean concentration of three analyses of each sample ± the standard deviation of the entire procedure.

a The appropriate volume of concentrated nitric acid was added directly to the solid sample and after that diluted with distilled water.

b Nitric acid was added in the concentration indicated.

*Data found after alkaline fusion.

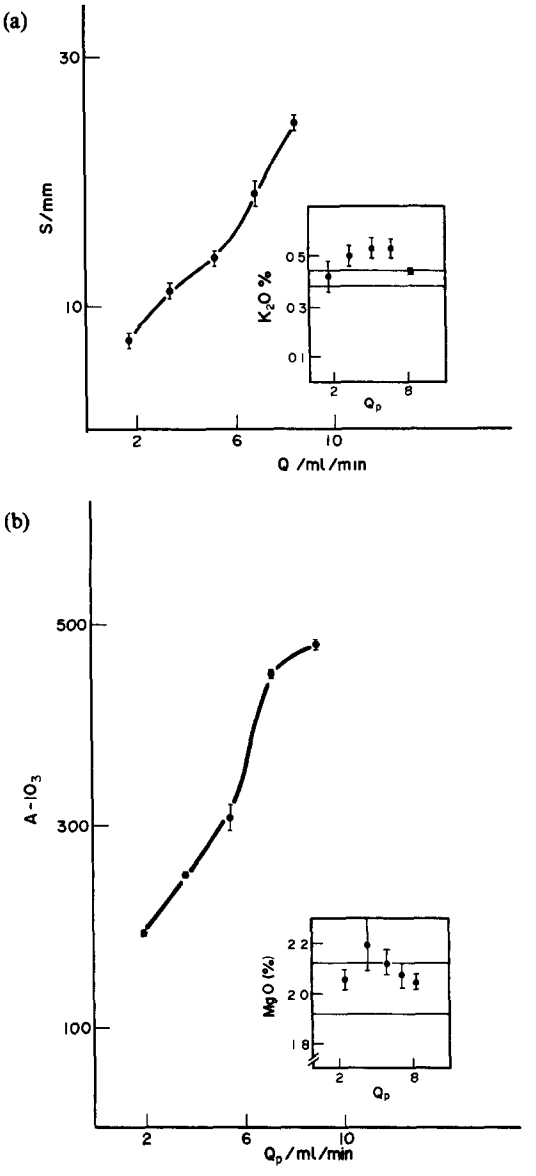

Fig. 2. Effect of the carrier flow on the sensitivity and accuracy of the determination of potassium (a) and magnesium (b) in cement. S: emission signal in mm; A: absorbance units. The horizontal lines in the insert correspond in both cases to the average value obtained for the analysis of these samples after an alkaline fusion ± the standard deviation.

can be seen in Table 2. The difference between the two analytes could be due to the high solubility in water of potassium salts that is sufficient to obtain complete extraction from the solid phase into the slurry, whereas an acid medium is required for the solubilization of magnesium. On the other hand, Table 2 shows that the analytical sensitivity for magnesium is not affected by the acid addition and that high concentrations of nitric acid are not required. The form of addition of nitric acid

(concentrated or diluted) is not important whereas the final concentration in the slurry is.

Effect of the FIA parameters

In order to study the influence of the FIA parameters on the analytical sensitivity and accuracy of the direct analysis of potassium and magnesium in cement, aqueous and acid slurries of 50 mg of a sample containing 0.4% (w/w) K_2O and 2.0% (w/w) MgO were prepared in a 25-ml volume. One hundred micolitres of slurry was injected in an aqueous carrier using different carrier flows, and the analytical measurements are shown in Fig. 2 (a and b).

The sensitivity of both determinations increases when the carrier flow rate increases. A carrier flow of 8.4 ml/min was selected for both cases because it provides an adequate sensitivity and also accurate values for both elements.

The inserts in Fig. 2 (a and b) represent the average values found for the direct analysis of the sample slurry at different values of the carrier flow. The average concentration values of samples, obtained after an alkaline

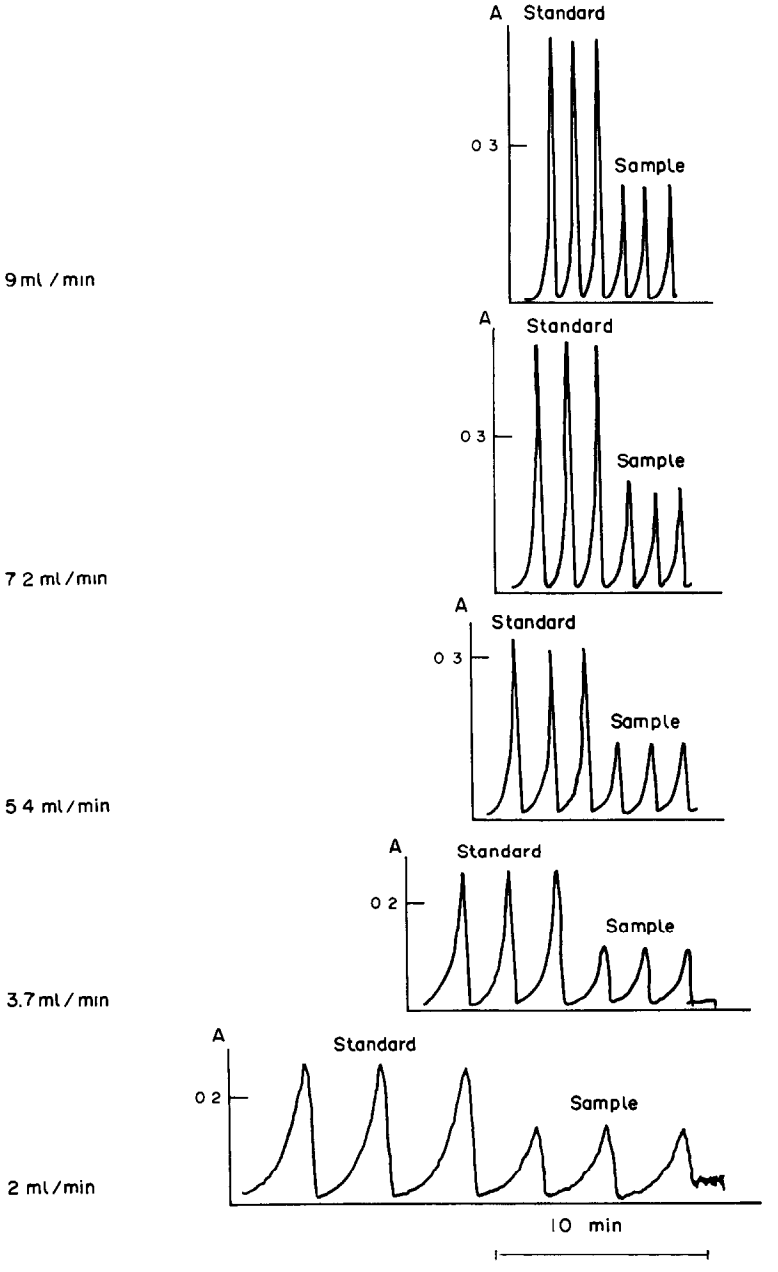

Fig. 3. FIA recording obtained for a standard of 10 μg/ml of magnesium and a sample containing 2.06% MgO as a function of the carrier flow.

fusion ± the standard deviation are represented by the horizontal lines. The comparison between these values provides an idea about the accuracy that could be obtained working at each carrier flow.

Flow injection recordings obtained from a magnesium standard of 10 μg/ml and a sample containing 2.06% MgO for different carrier flows, are shown in Fig. 3. The use

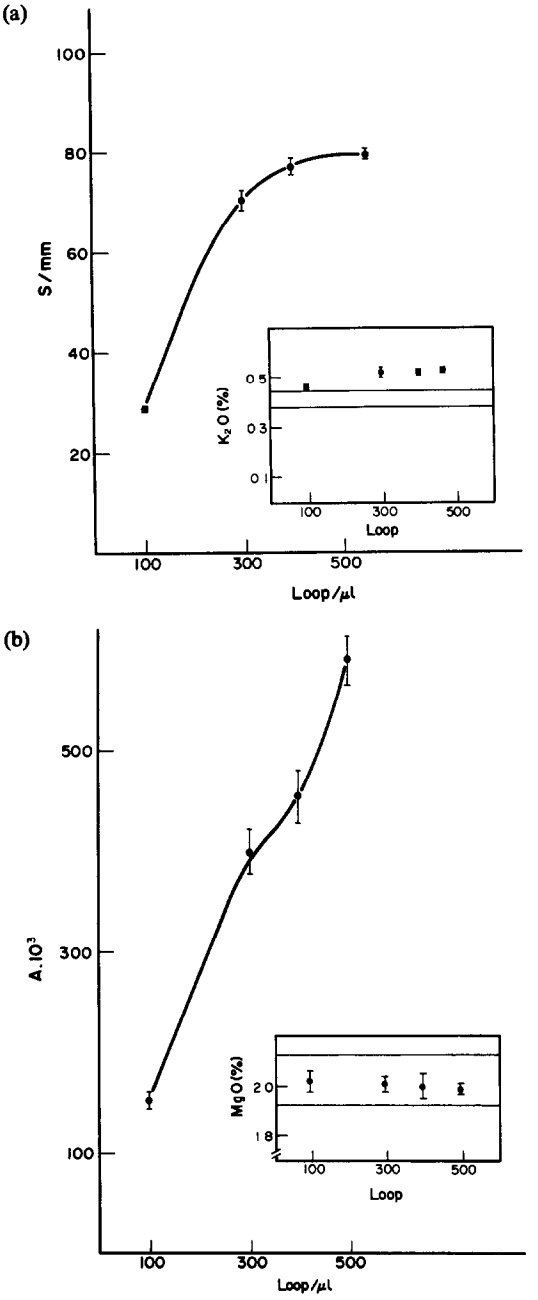

Fig. 4. Effect of the sample volume injected on the sensitivity and accuracy of the determination of potassium (a) and magnesium (b) in cement. S: emission signal in mm; A: absorbance units.

Table 3. Analysis of real cement samples

Sample	K_2O %		MgO %	
	Fusion	Slurry	Fusion	Slurry
1	0.82 ± 0.05	0.78 ± 0.01	1.41 ± 0.07	1.39 ± 0.03
2	0.40 ± 0.04	0.41 ± 0.01	1.7 ± 0.1	1.67 ± 0.07
3	0.80 ± 0.04	0.80 ± 0.01	—	—
4	0.54 ± 0.04	0.59 ± 0.01	2.0 ± 0.1	2.06 ± 0.05
5	—	—	1.7 ± 0.1	1.71 ± 0.02
6	0.19 ± 0.09	0.11 ± 0.01	1.0 ± 0.2	0.93 ± 0.03

Note: Percentage of K_2O and MgO are expressed by the mean concentration of three analysis of each sample ± the standard deviation of the entire procedure.

of high carrier flows provides a higher sensitivity and sample throughput with fast return to baseline. Samples may be injected at the rate of 48/hour compared with 10 samples/hour provided by dilution and continuous aspirations.

Figure 4 shows the effect of the sample volume injected on the sensitivity and accuracy of the determinations of potassium and magnesium. A 100-μl loop was selected (using the selected carrier flow rate) in order to obtain the best accuracy, although it provides a poorer sensitivity. The analytical sensitivity of the atomic spectrometric analysis of these elements is very high, and the content of K and Mg in cement samples is of the order of 0.5 to 1% (w/w). So, the use of low injection volume at high carrier flow rate provides a compromise between sensitivity and dynamic range of the potassium and magnesium determination with a high sample frequency.

Analysis of real samples

A series of real samples of cement were analysed by both the recommended and a reference method and Table 3 shows the results obtained for % K_2O and MgO. Results are comparable for both methods, as can be seen from the mean concentration data, taking into account the standard deviation values. The precision of the measurements by the proposed method is higher than the fusion procedure for both potassium and magnesium determinations; this could be due to the fact that the proposed method using slurries is direct, whereas the classical method requires several experimental operations.

Figure 5 shows a flow injection recording obtained from the injection of magnesium standards (from 4.8 to 30 μg/ml) and four acidified samples of cement. As can be seen, more than 48 injections can be carried out per hour.

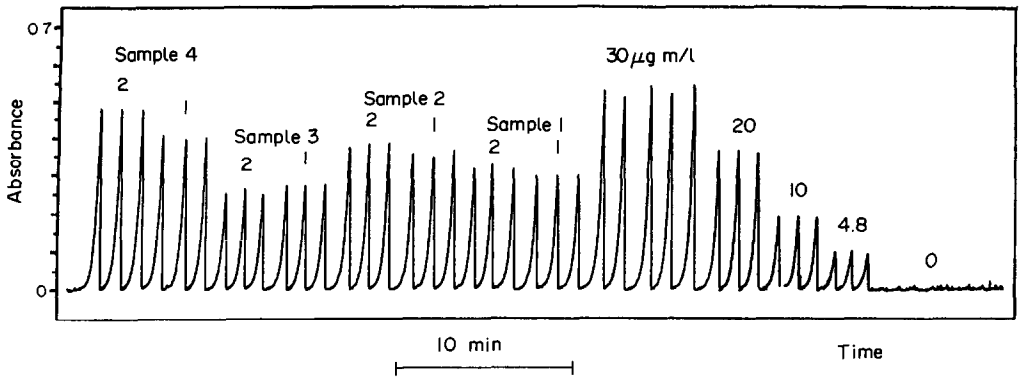

Fig. 5. FIA recording obtained for the injection of magnesium standards and acidified samples of cement.

Analytical performance of the developed procedure

Sensitivity is established from the slope of the calibration line. In the case of potassium, sensitivity has been determined for peak height values measured in cm, and is of the order of 0.20 $cm \cdot mg^{-1}$ l. The sensitivity for magnesium corresponds to 0.015 units of absorbance $\cdot mg^{-1}$ l. The regression coefficient of the calibration lines is 0.99995 for magnesium and 0.9994 for potassium, for a dynamic range up to 30 and 20 μg/ml respectively.

The limit of detection has been determined from ten measurements of the emission (potassium) or absorbance (magnesium) of a blank solution containing acid and lanthanum and it corresponds to the concentration of the element which provides an emission or absorbance value equal to twice the standard deviation of ten blank readings. A limit of detection of 0.15 mg/l. was obtained for potassium and 0.29 mg/l. for magnesium. These are concentrations of the elements in the slurry, corresponding to 0.007 K_2O and 0.01 MgO%, respectively, in the cement sample.

Precision has been derived from the relative standard deviation of ten analyses of a sample containing 0.54% of K_2O and 1.72% of MgO, respectively, and is of the order of 1% in both cases.

CONCLUSIONS

Using the recommended procedure, it is possible to take advantage of direct introduction of slurries in the flame flow injection analysis of solid samples, permitting an increase in the speed of the method, especially concerning the dilution of samples, and making possible the on-line addition of buffer solutions (as lanthanum) or other reagents, and decreasing the cost of the analysis.

REFERENCES

1. I. A. Voinovitch, *Analyse des sols roches et ciments. Méthodes choisies*, Masson Paris, 1988.
2. R. Bock, *A Handbook of Decomposition Methods in Analytical Chemistry*, Int. Textbook Comp., Glasgow, 1979.
3. J. Stupar and R. Aslec, *Analyst*, 1982, **107**, 144.
4. M. D. Wicman, R. Fjetkan and R. C. Fry, *Appl. Spectrosc.*, 1986, **40**, 233.
5. M. de la Guardia, A. Salvador, P. Bayarri and R. Farré, *Analyst*, 1986, **111**, 1375.
6. H. G. M. Parry and L. Ebdon, *Anal. Proc.*, 1988, **25**, 69.
7. M. E. Foulkes, L. Ebdon and S. Hill, *ibid.*, 1988, **25**, 69.
8. R. Karwowska and K. W. Jackson, *Spectrochim. Acta*, 1986, **41B**, 947.
9. L. Ebdon and A. Lechotycki, *Microchem. J.*, 1986, **34**, 340.
10. N. Carrion, Z. A. de Benzo, B. Moreno, A. Fernandez, E. J. Eljuri and D. J. Flores, *J. Anal. Atom. Spectrom.*, 1988, **3**, 479.
11. C. W. Fuller, R. C. Hutton and B. Preston, *Analyst*, 1981, **106**, 913.
12. M. L. Cervera, A. Navarro, R. Montoro, M. de la Guardia and A. Salvador, *J. Anal. Atom. Spectrom.*, 1991, **6**, 477.
13. J. B. Willis, *Anal. Chem.*, 1975, **47**, 1752.
14. A. Salvador, M. de la Guardia and A. Mauri, *At. Spectrosc.*, 1988, **9**, **6**, 195.
15. A. Morales, F. Pomares, M. de la Guardia and A. Salvador, *J. Anal. Atom. Spectrom.*, 1989, **4**, 329.
16. M. S. Epstein and T. A. Rush, *Applied Spectros.*, 1991, **45**, 1568.
17. R. Martinez-Avila, V. Carbonell, M. de la Guardia and A. Salvador, *J. Assoc. Off. Anal. Chem.*, 1990, **73**, 389.

Talanta, Vol. 40, No. 1, pp. 113–117, 1993
Printed in Great Britain

0039-9140/93 $5.00 + 0.00
Pergamon Press Ltd

DETERMINATION OF HYDROGEN PEROXIDE IN REACTOR MODERATOR SOLUTIONS BY FLOW INJECTION ANALYSIS

M. J. WHITAKER

Westinghouse Savannah River Company, Savannah River Site, Aiken, South Carolina 29808, U.S.A.

(*Received* 13 *January* 1992. *Revised* 2 *June* 1992. *Accepted* 4 *June* 1992)

Summary—A flow injection analysis (FIA) method for the determination of hydrogen peroxide in reactor moderator water has been developed and installed at the Savannah River Site (SRS) Water Quality Laboratory. The mode of detection is amperometric and the technique has an analytical range of 0.10–2.50 μg/ml with a sampling rate of 40 samples/hour. The calibration curve is linear with a correlation coefficient of 0.999 and the relative standard deviation is at the 0.50% level for both 0.10- and 2.50-μg/ml standards. When the FIA procedure is compared to the manual method previously used at the SRS Water Quality Laboratory for hydrogen peroxide analysis, it demonstrates a minimum twenty minute reduction in analysis time per sample and the total liquid waste generated per sample analyzed is reduced by 95%.

The moderator water used in the reactor at SRS is heavy water. For the reactor to function at an optimum, it is important that contaminants and radiolysis products be removed from the solution. Hydrogen peroxide is generated as an unwanted radiolysis product during normal reactor operations. Because of its corrosive nature it is imperative that the hydrogen peroxide be removed from the heavy water solution so that the delicate balance of this pristine system not be upset. Therefore, to ensure that the removal system is functioning properly, a variety of analyses are performed several times daily, of which, hydrogen peroxide is one.

This research project focused on the implementation of an automated analysis system for the determination of hydrogen peroxide in reactor moderator water. Flow injection analysis was selected as the technique of choice. Four major areas of development were investigated to improve the analysis of hydrogen peroxide over the existing methodology; (1) reduce the analysis time, (2) reduce the amount of radioactive waste, (3) reduce the analyst's length of contact and exposure time with the sample and, (4) develop a simple automated system and integrate it into the existing analyzer at the SRS Water Quality Laboratory.

The reduction in analysis time and total toxic liquid waste are extremely important issues in any analytical research or production laboratory. But, the importance of these particular issues takes on a much more significant role when the sample matrix is reactor moderator water and the sample is radioactive. For that reason, a great deal of effort was taken to reduce the analysis time and the amount of total radioactive liquid waste generated per sample analysis. The FIA method has reduced the analysis time per sample by a minimum of 20 min and the total radioactive sample waste by 95%. By accomplishing the first two objectives, 90% reduction of contact and exposure time of the analyst was also achieved.

To fulfill the final objective, the first step was to evaluate the various modes of detection that were available for hydrogen peroxide determination.[1–3] The criteria used in selecting a detector were that it must be simple and easy to operate, capable of measuring 0.10 μg/ml, small and compact, reliable, and reasonably priced. Reactor moderator water is extremely clean in terms of matrix interferences and hydrogen peroxide is the only electrochemically active species in the solution, thus it was determined that amperometric detection would be ideal for this particular application. The amperometric detector manufactured by Fiatron[4–6] for their modular FIA system was selected because it met all the criteria mentioned above.

The hydrogen peroxide procedure described in this paper is the second FIA method to be installed at the SRS Water Quality laboratory, the first of which was for the determination of

boron. To satisfy the objective of integrating the hydrogen peroxide system into the existing analyzer and to simplify the total system, the two FIA manifolds (boron and hydrogen peroxide) were integrated in such a way that switching from one method to the other would be a simple task and accomplished within a matter of a few minutes.

EXPERIMENTAL

Reagents and standards

All reagents and standards were of analytical-reagent grade quality and prepared in distilled, demineralized water from a Nanopure system (Barnstead/Thermolyne).

A 1% solution of sodium chloride in deionized water was used as the carrier and the electrolyte for the FI electrochemical (EC) detection system.

Stock and working standards were prepared from a 3% solution of hydrogen peroxide (Fisher Scientific CAS #7722-84-1) by adding the appropriate volume to each standard volumetric container and diluting to volume with demineralized water. Once stock standards were prepared, all solutions were refrigerated when not in use to reduce degradation. The working range of 0.10–2.50 μg/ml hydrogen peroxide were prepared daily to ensure accurate results.

Instrumentation

The flow injection analyzers used for this study were the Fiatron modular units. Each system includes a Fiatron SC-110 autosampler with a capacity of 120 samples, a FIA-Valve 2000 eight port sample injection valve equipped with a 58-μl sample loop, a FIA-Pump six channel peristaltic pump, and a master control module with a FIA-Zyme amperometric detection drawer. The FIA peaks were collected on a Cole-Parmer 100 millimeter strip chart recorder and a hard copy of the data results was printed on a Brother M-1109 dot matrix printer. A schematic diagram for the hydrogen peroxide FI manifold is shown in Fig. 1.

The master module unit of the Fiatron FI analyzer is the microprocessor controller where various timing parameters, sample and standard information, *etc.* are programmed and stored for each methodology. The unit is designed so it will accommodate several different detection techniques. Each technique is built into an individual detection drawer and only one detection device is functional at a time. The amperometric probe of the FIA–Zyme detector is a single constructed unit with a platinum working electrode and a silver/silver chloride reference electrode. It was determined when the probe was allowed to soak in 1% sodium chloride solution (carrier solution) overnight before use, it demonstrated better stability and reduced equilibration time at initial start-up.

This detection device is actually designed to analyze for various types of sugars. The sugar molecules react with a specific enzyme immobilized on the surface of a membrane to produce hydrogen peroxide as a reaction product, which is subsequently measured by the amperometric

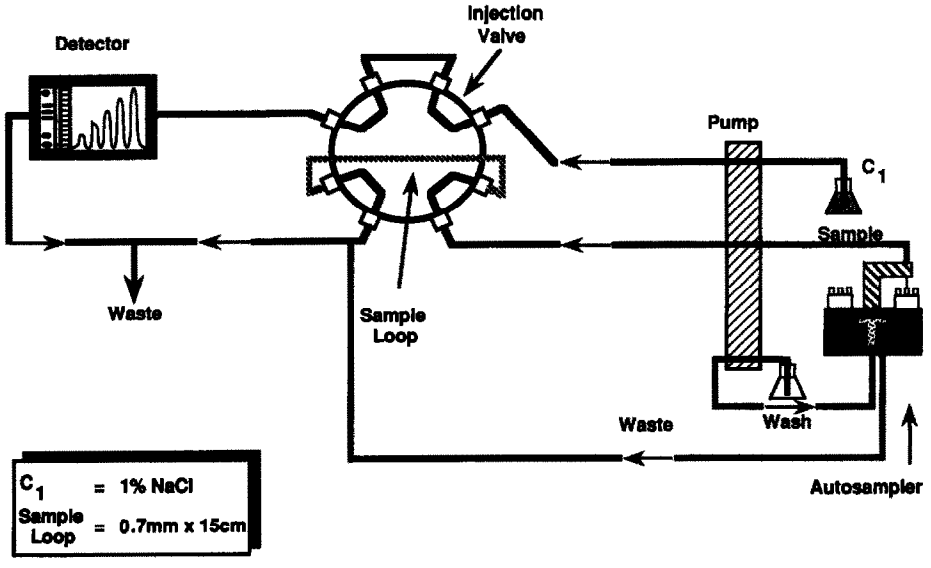

Fig. 1. Flow injection manifold for hydrogen peroxide.

Table 1. Experimental results of flow rate study using a 2.00-μg/ml hydrogen peroxide standard

Pump speed (%)	Flow rate (ml/min)	Analysis rate (min/sam)	Sample rate (sam/hr)	Response (Rel. Units)
14	0.70	3:36	17.00	109,000
18	0.90	3:05	19.00	107,700
22	1.10	2:30	24.00	100,900
24	1.20	2:15	27.00	96,400
26	1.30	1:59	30.00	95,200
28	1.40	1:51	32.00	85,700
30	1.50	1:44	35.00	85,000
32	1.60	1:40	36.00	82,200
34	1.70	1:35	38.00	81,200
36	1.80	1:30	40.00	78,600
38	1.90	1:21	44.00	75,500
40	2.00	1:16	47.00	73,600

probe. The potential of the probe is preset at the factory at 0.70 V. Hydrogen peroxide is a radiolysis by-product in reactor moderator water, therefore, it can be measured directly in the collected samples. Obviously, then, it was not necessary to utilize the immobilized enzyme membranes to generate hydrogen peroxide, so they were removed from the probe and only an o-ring remained to prevent leakage. Also, it was determined when using only a blank membrane (polycarbonate membrane without immobilized enzyme) sensitivity varied dramatically, probably due to variation in the thickness from one membrane to the next. Sensitivity and stability in the signal and the baseline improved considerably once the polycarbonate membrane material was removed.

RESULTS AND DISCUSSION

Flow rate study

A constant flow rate is a key parameter in the flow injection analysis technique and is determined by the size of the pump tubing used and the speed of the peristaltic pump. The pump tubing utilized for both the sample and carrier stream was Tygon tubing of 1.02 mm i.d., color coded as white/white.

The pump speed and size of pump tubing also affect the analysis rate, sample rate, and response factor of the sample or standard analyzed. Table 1 lists the data for a series of experiments in which the pump speed was increased from 14 to 40% of maximum velocity, giving the changes observed in flow rate, analysis rate, sample rate, and the response of a freshly prepared 2.00 μg/ml standard.

The flow rate ranged from 0.70 ml/min to 2.00 ml/min, with the corresponding responses ranging from 109,000 to 73,600 relative units. When the flow rate increases, the amperometric response decreases. A fixed sample loop of 0.7 mm × 15 cm dimensions was used to deliver a volume of 58 μl of standard into the FIA system for all flow rates studied in this series of experiments. The analysis time per sample includes loading of the sample loop, injection of sample, response, and return of signal to the baseline at a preset threshold, which decreases substantially with increased flow rate. The number of samples analyzed in one hour increases accordingly.

There are many reasons for automating sample analysis. One of the most obvious is reduction in man hours needed to accomplish the same job done manually. A much more important effect and impact when the samples are radioactive is reduction in exposure. To analyze one sample by the manual procedure at the SRS Water Quality Laboratory requires 20–30 min. Results of the time savings using the FIA method at different flow rates compared to an average 25 min for the manual method are illustrated in Fig. 2. The minimum time saved by the flow injection analysis technique at a flow rate of 0.70 ml/min is 21.40 min and the maximum time saved is 23.73 min when the flow rate is 2.00 ml/min. Of course, what is

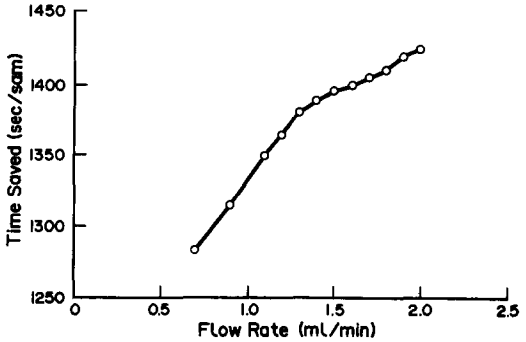

Fig. 2. Time savings per sample analyzed when using the FIA method at different flow rates, compared to an average 25 min analysis time for the manual method.

much more important here is that we have reduced the contact and exposure time of the analyst to the radioactive sample by more than 20 min, to 1–3 min per sample, a very significant improvement.

Sample volume study

The sample injection volume was varied by changing the length of the sample loops which were constructed from 1/16 inch Teflon tubing that had a 0.7 mm I.D., with the flow rate set at 1.80 ml/min. The results of analyzing various sample injection volumes of the upper limit standard of 2.50 μg/ml hydrogen peroxide are listed in Table 2. As expected, when the volume increases the response increases with each incremental enlargement in volume. It is important to realize that as the sample volume increases, so does the analysis rate (amount of time to analyze one sample), therefore a trade-off between sensitivity and analysis rate is created. The increased analysis rate is due to longer periods of time required to flush out the larger volumes of standard/sample introduced into the flow cell, plus the increase in response time with each volume enlargement. Because of the improved sensitivity achieved by removing the probe membrane, it was not necessary to use large volumes of standards/samples in this procedure. As a result, the 0.7 mm × 15 cm sample loop provided sufficient volume for analysis and was used for the remaining work.

pH Effects

The ideal operating pH range for reactor moderator water is 4.60–4.80. To determine the pH effects on the procedure described in this report a pH study was conducted. A 1.44 μg/ml hydrogen peroxide standard, prepared as described, has a measured pH of 4.45 and the carrier solution (1% sodium chloride) has a pH of 6.57. The pH of the 1.44 μg/ml standard was adjusted from 4.45 to 6.50 and analyzed after each adjustment to monitor the effects it might have on the FIA signal. The results of the pH experiments are listed in Table 3.

Table 2. Experimental results of sample volume study using a 2.50-μg/ml hydrogen peroxide standard

Sample loop (cm)	Sample volume (μl)	Response (Rel. Units)
15	58	201,000
20	77	213,400
25	96	261,600
30	115	286,200
35	135	312,900
40	154	347,600
45	173	406,500
50	192	418,900
55	212	432,300
60	231	452,400

Table 3. Experimental results of pH effects

pH	Response (Rel. Units)	Conc. (μg/ml)
4.45	202,900	1.44
5.00	204,300	1.45
5.90	206,500	1.46
6.50	209,800	1.48

It is noted that the difference in response from pH 4.45 to 6.50 is 6,900 relative units, in the order of 3%. It was therefore concluded, in the pH range studied, that pH has little effect on the amperometric detection of hydrogen peroxide when determined by this FIA methodology.

Calibration and reproducibility

The flow rate was set at 1.30 ml/min and the surface of the probe was freshly cleaned and prepared when calibration results were generated. The data are recorded in Table 4, demonstrating the linearity of the calibration curve which has a correlation coefficient of 0.999.

The precision of this procedure is excellent with relative standard deviations of 0.52% for 0.10 μg/ml and 0.34% for 2.50 μg/ml standards ($n = 5$).

Integration with the boron analyzer

A schematic diagram of the combined hydrogen peroxide and boron manifold is shown in Fig. 3. The combination manifold incorporates the two methods by adding four additional components to the hydrogen peroxide manifold to accommodate the boron method. These include a mixing coil, a 3-way valve to allow reagent to be added to the sample, a pump tube to deliver the reagent, and a colorometric detection drawer to replace the amperometric

Table 4. Calibration data with flow rate set at 1.30 ml/min

Conc. (μg/ml)	Response (Rel. Units)
0.10	19,200
0.25	40,450
0.50	72,600
1.00	138,900
1.50	212,400
2.00	271,100
2.50	325,100

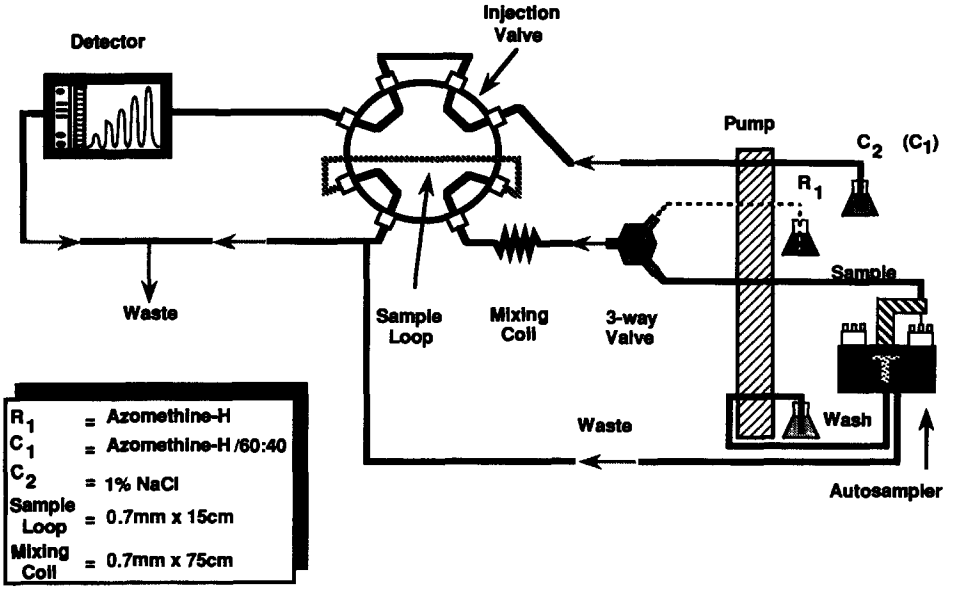

Fig. 3. Combined flow injection manifold for boron and hydrogen peroxide.

drawer. The illustration depicts the manifold as set for hydrogen peroxide analysis. This is indicated by the dashed line from R_1 to the 3-way valve, which represents there is no flow in the conduit, therefore no reagent is being delivered and the carrier solution is 1% NaCl (C_2). To change methods is a simple procedure, taking 2–3 min, requiring switching the detector drawers, adjusting the 3-way valve to the proper position, and using the appropriate carrier and reagent solutions.

CONCLUSION

The four major objectives established at the onset of this project were met and accomplished over and above expectations. Time required for analysis of an individual sample was reduced by 80%. The amount of liquid radioactive waste generated from the analysis of samples for hydrogen peroxide in reactor moderator water was reduced by 95%. The analyst's contact and exposure time with the radioactive samples was reduced by 90%. An automated system was developed, utilizing FIA technology, that was simplistic in design for ease of operation, and was integrated into the existing analyzer.

REFERENCES

1. L. Chen, M. S. Lin, M. Hara and G. A. Rechnitz, *Anal. Lett.*, 1991, **24**, 1.
2. Z. Genfa, P. K. Dasgupta, W. S. Edgemond, and J. N. Marx, *Anal. Chim. Acta*, 1991, **243**, 207.
3. P. A. Clapp and D. F. Evans, *ibid.*, 1991, **243**, 217.
4. *Flow Injection Analyzer Manual, Automated Sample Prep.*, Fiatron.
5. *Technical Application Notes, Peroxide (Active Oxygen) In Process Streams*, 1986.
6. J. C. Kutt and S. J. Vohra, *American Lab.*, December 1983.

Talanta, Vol. 40, No. 2, p. 119, 1993
Printed in Great Britain

0039-9140/93 $6.00 + 0.00
Pergamon Press Ltd

SPACE-AGE ANALYSIS: A GUIDE FOR AUTHORS AND REVIEWERS

The lead article in this issue by Professor R. A. Chalmers, retired Editor-in-Chief of *Talanta*, is taken from his invited lecture in the symposium on "The Status of Analytical Chemistry in the World" held at the 1992 Pittsburgh Conference. It reflects on his editorial experiences for over twenty years, and includes many words of wisdom that young and not so young researchers ought to take to heart. We, as his replacement editors—it takes two to do his job—asked him to publish it in *Talanta* because our readers should all benefit from and enjoy reading his comments. Our jobs as Editors-in-Chief and those of our referees would be made much easier if his guidelines for originality, usefulness and correctness were followed. Likewise, if referees would keep these guidelines in mind when evaluating manuscripts it would help assure the quality of publications we strive to maintain. Professor Chalmers addresses concerns about sources of error, use of statistics, basic chemical knowledge, and reference accuracy. We particularly direct readers to the section "Pluş a Change ...". All too few researchers fail to really justify why their work is important and ought to be published. It is easy to sweep dozens or hundreds of published methods under the rug with a broad claim that they are laborious, insensitive or non-selective, and then proceed to develop a presumably improved method where the real improvement is marginal or not made apparent. Often a work is presented with no attempt to even justify why it was done or what its advantages are, or only old or relatively inaccessible literature is cited.

We invite you to read Professor Chalmers' article. All should benefit from his words of wisdom.

Gary D. Christian
Elo H. Hansen

Talanta, Vol. 40, No. 2, pp. 121–126, 1993
Printed in Great Britain.

0039-9140/93 $6.00 + 0.00

SPACE-AGE ANALYSIS*

ROBERT A. CHALMERS
Department of Chemistry, University of Aberdeen, Old Aberdeen, Scotland

(*Received* 26 *June* 1992. *Accepted* 26 *June* 1992)

Summary—A survey is given of present-day analysis, from an editorial point of view, and suggests that though techniques have changed in order to meet the challenges of modern technological advances and materials, the fundamental character of analytical research and its publication has not.

The first task in any research project is to look at the history of the problem. If we do this in a survey of analytical chemistry as a whole, we find that in the past people sometimes knew what needed to be done, but did not have the equipment to do it, and sometimes had the equipment but did not see what to use it for. An example of the first is Faraday's testing of the pollution in the River Thames by dropping in pieces of white card and observing the depth at which they disappeared from view;[1] this was usually less than an inch, and the bottom of a card inserted vertically disappeared from sight before the top entered. The second is optoacoustics, examined by Alexander Graham Bell,[2] John Tyndall[3] and others, around 1880 (though Tyndall did indicate that the technique might be used for detecting methane in coalmines).

These two examples have one thing in common—technology—either as lack of it for use, or lack of technical problems to which to apply it. As the use of new materials and inventions increased, so did the problems and the technology and instrumentation needed to deal with them. Ideas that are often considered to be "modern" (which many regard as meaning post-World War II) appeared surprisingly early. An automatic carbon monoxide monitor had been reported by 1925,[4] and by 1928 no fewer than fourteen of them were in use for checking air quality in the Holland Tunnel in New York.[5] A quick look through the first twelve or so volumes of *Ind. Eng. Chem., Anal. Ed.* is very instructive and shows the shape of things to come. A thermal conductivity method for continuous recording of the carbon dioxide and oxygen levels in air was described in 1930,[6] for example, and so was an automatic photometric titrator.[7] A paper on what would now be called library searching or spectra matching appeared in 1938, with data for the X-ray diffraction patterns for 1000 substances.[8] A review by Ralph Müller in 1940 showed the very wide range of instrumentation even then available in the United States.[9]

THE INSTRUMENT REVOLUTION

It was evident that the main thrust in development of instrumentation arose in the USA, though there were notable contributions from Europe, such as polarography, which gave rise to an entire sub-discipline, electroanalytical chemistry, with its own specialist journals. All this is well described in the excellent A.C.S. publication "A History of Analytical Chemistry",[10] along with many other aspects of modern analytical chemistry. Some of these, such as Raman spectroscopy, were before their time and had to await the development of suitable instruments. FT–IR was another. Its principles were known to Michelson in 1891,[11] and he developed a mechanical harmonic analyser in 1898,[12] but the calculations were still extremely laborious, even with the aids developed later by Beevers and Lipson,[13] and the method really came into its own only with the arrival of the computer age, information theory and instrument science. An excellent account of this is given in a recent book.[14]

During the last two or three decades there has been an unprecedented display of ingenuity in devising instrumentation and computational

*This contribution is based on the opening lecture "Space-Age Analysis" in the Symposium on "The Status of Analytical Chemistry in the World" at the 1992 Pittsburg Conference, held in New Orleans, which in turn was partly based on earlier lectures.

methods for use in research and industrial analysis, catalysed by cross-fertilization of ideas between different disciplines. In particular, once a technique has been devised, a good deal of effort has gone into exploiting it to the full. Perhaps the prize examples are electrochemical stripping methods and flow-injection analysis, which are still being expanded in scope and versatility. These techniques also show well that the same idea may arise almost simultaneously in several different places.

As a result of the development of computers, microprocessors, robotics, chemometrics and so on, we now have the possibility of operating with very small quantities of material, with numerous data-points from a given experiment, and of exploring structure, structure–behaviour relationships, speciation, spatial distribution and so forth, to an extent never previously attainable.

"PLUS ÇA CHANGE ..."

All this is very exciting and full of promise, and it is all too easy to take the attitude "isn't science wonderful", without questioning its validity. As happens with almost all new techniques, however, we are carried along by the first flush of enthusiasm to believe that here at last we have the means to solve all problems, until further work begins to show up any shortcomings of the techniques and we find that the answers may be incomplete or even wrong.

If we survey the current literature, we quickly see that we have substantial dedicated groups of leading thinkers and innovators, working to extend the frontiers in their particular fields. Then we have a larger group of workers we might call "implementers", who apply these new techniques along with others to solving specific problems in industry or in research projects. Finally we have a possibly even larger group of those who, whether from choice or because of economic restrictions, continue to tread well-worn paths in analytical research, operating a kind of cottage industry to turn out methods that, though "new", are devoid of much originality and are hardly ever likely to be used. Take organic reagents for spectrophotometric determinations, for instance. Until about twenty years ago, research in this field involved finding fairly non-selective reagents and applying them to as much of the Periodic Table as possible, or finding reasonably selective (or even specific) reagents and then shunting various harmless substituents around the parent molecule to create "novel" reagents. The result was thousands of reagents, mainly for copper, cobalt, the palladium metals, iron and vanadium, that very seldom had any real advantages. The substituted hydroxamic acids developed as reagents for vanadium are a good example, and an entire book[15] has been devoted to reagents for copper. Then came the advent of micellar systems, so all these reagents were given a new lease of life as sources of "research" papers, and this was further extended by use of derivative spectrometry, solvent extraction and combinations of these and other ancillary techniques. Most of these authors were doubtless driven by the "publish or perish" syndrome, and perhaps did not realize that they could publish *and* perish.[16]

The resulting clutter in the literature could have been reduced if reviewers and editors had been far more critical in judging the value of such papers, as has been pointed out in various editorials.[17–19] After all, such reseach projects are quite suitable for *training* students in research methodology and to think analytically, but the results do not *have* to be published. Ph.D. examiners are usually asked whether the work *is* publishable, but not *where*, so may safely answer "yes". My plan for financing retirement would be to start a new journal called *Journal of Useless New Knowledge* (JUNK), with a page-charge and circulation only to authors (with one copy of the issue in which their paper appeared).

"A LITTLE LEARNING ..."

There is an unfortunate by-product of the computer/microprocessor age, however. Because the results are obtained automatically, the experimenter may come to believe they must automatically be correct, and take no thought about errors that may arise from the chemistry and methodology involved. Worse, the experimenter may run only a single experiment to obtain a large number of data points for interpretation, and forget that any mistake in setting up the experiment will invalidate the results.

The experimenter may be expected to be aware of the obvious sources of error, such as sample inhomogeneity, too small a sample, use of impure materials, failure to calibrate equipment or check commercial standards, non-linear instrumental response, noise, and so on, but

may well be unaware of some of the more subtle sources of error.

Adjustment of pH may seem a simple and trouble-free operation, but many factors can affect the relationship between the pH-meter reading and the effect of the hydrogen-ion concentration. As Kragten has pointed out,[20] if the adjustment is not done in the correct manner, and kinetically inert hydroxo-complexes are formed during it, the results obtained may not be as true as the operator thinks.

Some species used as buffering agents, or as auxiliary masking agents, may cause interference for totally unexpected reasons. Tartrate and citrate, for example, can form binuclear ligand-bridged kinetically inert complexes with two different metal ions, and if one of these is the ion of interest, it can be partially or even completely lost in the analysis.[21] If partial loss occurs, an analytical result will be obtained, but it will not be the correct one. On the other hand, as so often happens in analytical chemistry, what is a disadvantage in one situation can be turned into an advantage in another, and formation of such complexes can be used for masking purposes or even for determination of the bridging ligand. A further complication, however, is formation of mixed-ligand complexes of this type.[22] Another example is the effect of zirconium or hafnium on the hydrolysis of niobium and tantalum, where in certain pH-ranges the hydrolysis is inhibited by formation of soluble hydroxo-bridged polymeric mixed-metal species.[23]

Even established decomposition procedures may be suspect. It is well known that volatile compounds may be lost, or contamination occur, but there may be unsuspected problems. For example, prolonged heating of mixtures containing alkali-metal, aluminium, iron and sulphate ions can lead to insoluble jarosites—a fact well known to rock analysts, but probably not to analysts wet-ashing foodstuffs or other organic matter. Again, in many researches on determination of platinum metals, all the work is done with mixtures of solutions of pure salts in defined oxidation states, and no indication is given of how to get a real sample into solution with all the components in the desired oxidation states, and without formation of polymeric or kinetically inert species.

Interference tests are often too simplistic, being run with one species at a time, without regard to the compatibility of the oxidation states of different species, or the likelihood of appearance of these states. Interactive effects are hardly ever looked at, though they are known to occur in atomic-absorption spectrometry[24] and electrochemical stripping,[25] for example.

In equilibrium constant and speciation studies, some compounds used as background electrolytes may be significantly incompletely dissociated if used at too high a concentration, so ionic strength corrections may not be completely valid. Also, the anions of such electrolytes (notably nitrate) may form weak complexes with the metal ions of interest, and this can cause significant error if a high electrolyte concentration is used.[26]

A more subtle error may arise in computation of stability constants and speciation. The usual approach is to find the set of components which will give the lowest sum of the squares of the differences between the experimental and calculated data. Various combinations of components, with more added as the search progresses, are tested until the apparently best fit is obtained. Quite often a very similar fit is yielded by more than one set of components. It is then necessary to decide on chemical rather than statistical grounds which should be taken as "correct", and in such circumstances it would seem prudent to remember Occam's razor and employ it. Sometimes a major new species may be postulated on the basis of such calculations, but not independently verified or substantiated by repetition of the work or by other methods. It may, however, enter the literature compilations and be taken as gospel. Any subsequent work based on it will be in error if the species is in fact a bogus one. In this connection, utmost care in proof-reading papers on new species is of vital importance. In a recent case, the accidental omission of a subscript 2 from a chemical formula (one of eighteen listed in the source paper) led to a completely false set of results in a different work based on that erroneous formula.[27] The error was not easy to trace.

Editorial experience suggests that today's researchers may sometimes be unaware of the "hidden" sources of error such as those outlined above. This may be due to the fact that the increasing complexity of chemistry, together with the expectation that a chemist will be skilled in physics, statistics, computing science, electronics, economics, *etc.*, means that unless the student's course is lengthened, less will be taught about each topic. For graduate students this can be at least partly remedied by further instruction, but this is all too often restricted to

advanced material in the field of the research topic, and the student may remain only partly educated in other areas. This may seem a pessimistic outlook, but an editor sees not only the published papers, written by those whose work is scientifically sound, but also the papers which are rejected for some reason or other, and which raise such questions as "if this is how they do research, what do they teach their students?" Readers see only the papers that are accepted; reviewers will see some that are unacceptable, but only the editor will see the whole lot in both categories. Two examples of "question-raisers" may suffice as illustration. In one paper sodium was said to interfere when present at the 50-μg level, but in an application 1 ml of 1M sodium fluoride was added as a masking agent. In another it was stated that a chromium(VI) solution was used at pH 0–5.5, and that the chromium would be present in the tervalent state. This was supported by a reference to a well-known textbook, which actually said nothing of the sort—the passage referred to dealt with the equilibrium constants for the $Cr_2O_7^{2-}/HCrO_4^-/CrO_4^{2-}$ system. It is quite common to see references to use of buffers at pH-values where their capacity is practically zero, or of masking agents at pH-values where practically no free ligand would be present.

"STATISTICS MAY BE USED AS A DRUNK USES A LAMP-POST—MORE FOR SUPPORT THAN ENLIGHTENMENT"

Authors often quote more significant figures than can be justified by the experimentation or statistical needs, or produce a standard deviation on the basis of only two or three results. Sometimes the standard deviation is greater than the mean, but no comment is made on possible skewness of the distribution. Nowadays relative standard deviations of 2% are commonplace, and values of 10, 15 and even 20% seem acceptable to some authors, reviewers and editors. Papers on instrumental methods often compare the results with those of classical methods, usually claiming superiority. To anyone with long experience of the classical method used, such claims often seem untrue and to reflect only lack of classical experimental skill by the operator. Poor performers should practise and learn to do better! A typical case was a claim that a thermometric method (error $\pm$ 3%) was better than manual titration for iodometric determination of copper. Even a freshman can do better than that. An early robotics paper reported 0.6% relative standard deviation for titration of 1M hydrochloric acid.

Results are often compared by t and F tests and said to be equally as good, but it would sometimes be more correct to say "equally as bad". The precision of both the "new" and "standard method" results sometimes leaves much to be desired, and this can frequently be ascribed to the use of small samples and volumes, and an apparent lack of calibration of glassware.

Much is made of clinical tests as an aid to diagnosis of illness, but though these tests are undoubtedly useful when properly used, back-up by diagnostic skills is at least equally important, especially if the tests happen to have a high incidence of false positive or negative results. As some young physicians may never have seen clinical cases of certain illnesses and so be unable to recognize them, an inaccurate test result could have unfortunate consequences. This is perhaps even more the case with tests used in criminal investigation, where recent work on some old tests and development of new ones has shown that some prisoners have been convicted on the basis of highly questionable or at least equivocal evidence.

"ALTHOUGH THEY WROTE IT ALL BY ROTE, THEY DID NOT WRITE IT RIGHT ..."

The foregoing may be thought a rather jaundiced outlook, but editorial assessment of some 8000 papers has left the impression that a surprisingly large number of authors were apparently ignorant of some basic chemical facts or had not read the literature very carefully. It has also revealed that a great many authors fail to understand that language is a precise tool, and if misused can result in ambiguous or even erroneous information being conveyed. Some papers are so badly written that the reviewer is obliged to edit them before being able to assess them. Reading other journals in the course of checking manuscripts has shown that the standards of editing vary widely, and that some editors even manage to introduce errors themselves (to protect the guilty, no examples will be given). A frequent cause of annoyance in editing is error in references, and finding the correct version can take a great deal of time. Sometimes a reference may have nothing to do with the topic concerned (usually because the author has pulled out the wrong file card, or copied some-

one else's erroneous reference, having never tried to use it). In 23 manuscripts looked at early in 1991, there were 55 errors in authors' names, 3 in journal names, 2 in journal year, 5 in volume number, 3 in issue number (where this was necessary) and 5 in page number; 2 references were completely wrong and one was untraceable. There is no real excuse for such errors[28] (although even *Chemical Abstracts* can very occasionally be blamed). There are those who insist that editors do not need to check references and that the responsibility for correctness lies not just primarily, but absolutely, with the author. But how does the editor know references *are* correct, without checking them? It is, of course, always possible to blame the printer, but such errors can be corrected by means of a list of errata.

BACK TO THE FUTURE?

The thoughts above represent one person's view of the current scene in analytical chemistry. It would appear that the scene has changed only in range and technology since Lundell wrote his classic paper "The Chemical Analysis of Things as They Are" nearly sixty years ago,[29] but the chemistry sometimes seems only incidental in comparison with the instrumentation, and if the chemistry happens to be wrong ...

So what should we look for in the future? I would like to see an overhaul of teaching, with stronger emphasis on the chemical properties of elements and compounds, and preferably longer courses. Next I would like to see organization and co-ordination of research with a view to solving important and hitherto unresolved problems as a priority. This could not apply to all workers, of course, and I would like to see the cottage industry workers turning away from trivialities and achieving satisfaction by work such as obtaining more precise values for the equilibrium constants and other data that are basic to our understanding of chemistry and are needed for computerized speciation studies *etc.* Other useful pursuits for them might be in-depth studies of decomposition processes, explanation of anomalous results obtained in established methods, or critical comparison of alternative methods. Finally, a concerted effort by reviewers, publication committees and managing editors to raise the standard of published work by refusal to accept work that is fragmented, or offers no significant improvement over existing methods, or is based on inadequate experimentation. Aid with the last point might be achieved by publication of more guideline papers of the type pioneered by *Talanta* (Table 1). What is needed is better quality control.

Table 1. Research guideline papers

Topic	*Talanta* reference
Spectrophotometry	G. F. Kirkbright, 1966, **13**, 1
Gravimetry	L. Erdey, L. Pólos, R. A. Chalmers, 1970, **17**, 1134
Ion-selective electrodes	G. J. Moody, J. D. R. Thomas, 1972, **19**, 623
Titrimetry	A. Berka, J. Ševčík, R. A. Chalmers, 1972, **19**, 747
Kinetic methods	H. B. Mark, Jr, 1973, **20**, 705
Atomic-absorption spectrometry	J. Ramírez-Muñoz, 1973, **20**, 705
Stability constants	H. S. Rossotti, 1974, **21**, 809
Solvent extraction	Y. Marcus, 1976, **23**, 203
Polarography	L. Meites, B. H. Campbell, P. Zuman, 1977, **24**, 709
Ion-exchange (chromatography)	J. Inczédy, 1980, **27**, 143

What I *expect* to see is much the same scene as now, with a vanguard of innovators and explorers, and the main body of troops consolidating the ground won. There are still problems to be solved and advances to be made, however, and the programmes at meetings such as the Pittsburgh Conference always generate great hopes for the future.

REFERENCES

1. M. Faraday, *The Times (London)*, 5 July 1855.
2. A. G. Bell, *Phil. Mag.*, 1881, Ser. 5, **11**, 510.
3. J. Tyndall, *Proc. Roy. Soc.*, 1881, **31**, 307.
4. A. C. Fieldner, S. H. Katz and E. G. Meiter, *Eng. Rec.*, 1935, **95**, 423.
5. S. H. Katz and H. W. Frevert, *Ind. Eng. Chem.*, 1928, **20**, 564.
6. W. F. Hamilton, *Ind. Eng. Chem., Anal. Ed.*, 1930, **2**, 233.
7. H. M. Partridge, *ibid.*, 1930, **2**, 207.
8. J. D. Hanawalt, H. W. Rinn and L. K. Frevel, *ibid.*, 1938, **10**, 457.
9. R. H. Müller, *ibid.*, 1940, **12**, 571.
10. H. A. Laitinen and G. W. Ewing, *A History of Analytical Chemistry*, American Chemical Society, Washington D.C., 1977.
11. A. A. Michelson, *Phil. Mag.*, 1891, Ser. 5, **31**, 338; 1892, **34**, 280.
12. A. A. Michelson and S. W. Stratton, *ibid.*, 1898, Ser. 5, **45**, 85.
13. C. A. Beevers and H. Lipson, *ibid.*, 1934, Ser. 7, **17**, 855.

14. S. F. Johnston, *Fourier Transform Infrared*, Horwood, Chichester, 1991.
15. F. J. Welcher and E. Boschmann, *Organic Reagents for Copper*, Krieger, Huntington N.Y., 1979.
16. *Talanta*, 1984, **31**, No. 5, III.
17. *Ibid.*, 1979, **26**, No. 2, i.
18. A. J. Bard, *ChemTech*, 1986, **16**, 582.
19. C. A. Watson, *Analyst*, 1986, **111**, 1353.
20. J. Kragten, *Talanta*, 1977, **24**, 483.
21. C. G. Ramsay and B. Tamhina, *ibid.*, 1975, **22**, 437, and references therein.
22. D. A. Edwards, *Ph.D. Thesis*, University of Aberdeen, 1979.
23. E. Sørensen and A. B. Bjerre, *Talanta*, 1992, **39**, 529.
24. L. Pszonicki, A. Lechotycki and M. Krubiński, *ibid.*, 1988, **35**, 465.
25. P. Cofré and K. Brinck, *ibid.*, 1992, **39**, 127.
26. M. Štulíková, *ibid.*, 1991, **38**, 805.
27. B. W. Darvell and V. W.-H. Leung, *ibid.*, 1992, **39**, 1057.
28. *Ibid.*, 1981, **28**, No. 6, I.
29. G. E. F. Lundell, *Ind. Eng. Chem., Anal. Ed.*, 1933, **5**, 221.

Talanta, Vol. 40, No. 2, pp. 127–134, 1993
Printed in Great Britain.

0039-9140/93 $6.00 + 0.00

REVIEW

MICROBIAL CALORIMETRIC ANALYSIS (MCA) OF AQUEOUS ORGANIC COMPOUNDS

MARK L. FERREY and REX E. LOVRIEN
Biochemistry Department, University of Minnesota, 1479 Gortner Avenue, St Paul, MN 55108, U.S.A.

(*Received* 24 *February* 1992. *Accepted* 10 *June* 1992)

Summary—Adapted bacteria used in heat conduction calorimetry may be developed as 'analytical reagents' for compounds that can be metabolized by such bacteria. Adaption can be done by growing cells such as *E. coli* on the analyte of interest, for example a sugar. Samples to be analyzed are mixed with adapted cells which aerobically metabolize the sought-for analyte, producing heat. The method is called microbial calorimetric analysis, MCA. Average requirements are 2–200 nanomoles of analyte, "carbon", an excess of cells *ca.* 2–5 mg of cells, and 1–2 ml of air to maintain aerobicity. Heat production is usually completed in 300–600 sec at 25°. The combination of bacteria and heat conduction calorimetry is a sensor system having a sensitivity and selectivity dependent on bacterial adaption. The system is useful in analytical problems when analytes are in turbid suspension, are poor chromogens or not even prochromogenic. MCA takes advantage of the large aerobic heats usually generated by bacteria in active utilization of organic analytes. Typically from 20 to 70 kcal exothermic heat per mole of carbon atoms is generated, *e.g.*, (−)300 kcal/mole glucose. Heat conduction calorimeters, batch mixing instruments, measure 2–100 millicalorie heat with ±3% error in each run. Bacteria can be grown on many different kinds of compounds. Accordingly it is fairly easy to create diverse, specific 'analytical reagents' which function in MCA much as they function in their usual environment, in soils, *etc.* Intact, adapted bacteria have decided advantages over isolated enzymes as 'biosensors' for a number of practical reasons.

When bacterial cells are grown on carbon sources such as sugars or alcohols they adapt to metabolize the compounds on which they were grown. They become selective in their uptake of particular compounds, often quite narrowly selective. For example some bacteria metabolize ethanol but not methanol, yet others metabolize methanol but not ethanol.[1] Bacterial metabolism of organic carbon using oxygen, aerobic metabolism, tends to produce considerable heat. Bacterial aerobic metabolism of aqueous carbon commonly generates half or more of the heat generated by oxygen bomb calorimetric combustion of the dry compounds.[2] Such microbial metabolism (biological combustion) in a simple batch mixing calorimeter provides a means for analysis which is called microbial calorimetric analysis, MCA. Bacteria or yeast cells are the 'analytical reagents'. Dissolved oxygen is the main reactant in addition to the organic compounds in the aqueous sample. Figure 1 is an outline of the essentials of MCA.

Bacteria as reagents may seem odd as a basis for analysis. However bacterial cells together with heat conduction calorimetry have a few advantages that may be useful. For example MCA can accommodate turbid, even opaque samples such as a food slurry, not acceptable for direct spectrophotometric analysis. Bacteria can often continue to function under quite severe conditions that quickly denature isolated enzymes. This point is discussed more below.

Bacteria able to adapt and become selective are quite easily grown using the simplest equipment, shake-flasks. Several different kinds of bacteria effective in MCA may be stored in a frozen state to be used when wanted. Three of the most studied bacteria are *Pseudomonas*,[3] *Escherichia coli*[4] and *Salmonella*.[4] Hundreds of individual strains exist in each genus. Several Pseudomonads can metabolize and combust myriad carbon sources including petroleum and lignin fragment compounds. *E. coli* are enteric (intestinal) bacteria able to metabolize common sugars in foods and several fatty acid anions including acetate. It is not always necessary to use carefully identified bacteria as MCA reagents however. If one wants to analyze methanol in water a few milligrams of soil may be started with. The soil is added to a simple

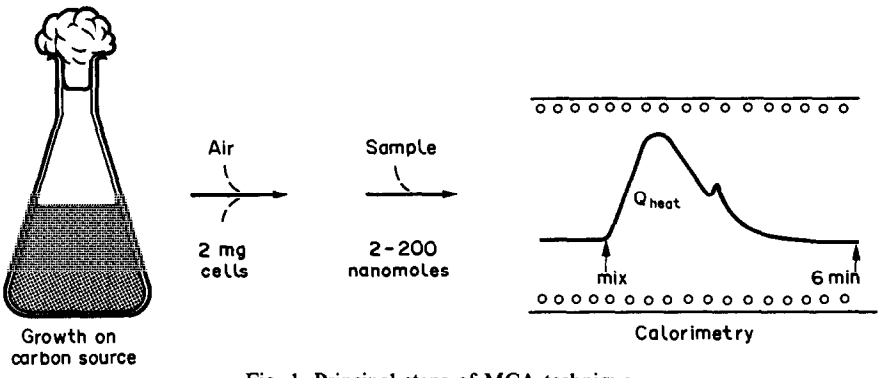

Fig. 1. Principal steps of MCA technique.

enrichment apparatus[5] through which air is bubbled. Small amounts of glucose are added to increase cell populations. Then glucose is withdrawn and methanol is added to *ca.* 0.2–0.6% methanol concentration. The surviving 'methylotrophs' although not identified, usually can combust a few dozen nanomoles of methanol, in 3–5 min. The resultant heats are proportional to the amount of methanol. Such an adaptive technique is not new; it is routine in several older analytical methods such as in measurement of biological oxygen demand, the B.O.D.[6] In order to take advantage of microbial biodegradative capacities, applying them to analysis, some points concerning bacteria may be reviewed.

Adapted bacteria develop quantities of enzymes, also porins and transport particles, to quickly absorb targeted compounds and metabolize them to get 'energy'. Adaption commonly raises concentrations of key enzymes 10X to 1000X[7] above concentrations seen under non-adapted conditions, 'constitutive enzymes'.[8] Bacterial adaption for MCA is simply use of processes occurring on a large scale in the environment and agriculture, biodegradation in soil, sewage, fermentation and silage making.

Of equal importance in MCA is the self-protection and self-maintenance which bacterial cells are able to do. Commonly it is suggested that biosensors can be devised using simply isolated enzymes in 'enzyme electrodes' to focus on reactions wanted to be transduced or biosensed such as an oxidation or a reduction. These biosensors frequently rely on an oxygen electrode for transduction to an electric signal.

Although such 'enzyme electrodes' are popular for research projects, they engender difficult practical problems. Many bacterial enzymes but especially those in redox (electron transfer) pathways are notably unstable when taken out of their protective cellular environment. Several prooxidative enzymes are destabilized on contacting dissolved oxygen.[9,10] These enzymes require intermediates, NADH, NADPH, *etc.* Therefore such biosensors have to be kept supplied with NADPH *etc.*, which may not be a trivial task. In contrast intact bacteria protect such enzymes, plus supply necessary flavin, NADPH intermediates. How bacteria do this, protect their enzymes, and also supply necessary intermediates, is not always well understood. *E. coli* bacteria for example, maintain about 2 m*M* reduced glutathione inside (intracellular GSH), to protect themselves against internal oxidative damage.[11] Many bacteria are endowed with rather remarkable survival capacities. But isolated or 'biosensor attached' enzymes usually are not so equipped.

When biosensors are constructed around oxygen electrodes the rough, fluctuating environments in real samples such as in fermenters knocks oxygen concentrations around so much that the baseline oxygen levels are hard to control. Oxygen electrodes can detect very small differences in oxygen concentrations, of the order of 5μM O_2/minute.[12] However in industrial environments the sensitivity of oxygen electrodes or enzyme-coupled oxygen electrodes are of little help when dissolved oxygen concentration fluctuations in baselines are larger than analyte concentrations. In contrast, MCA is 'carbon limited'. MCA is rather insensitive to oxygen concentration fluctuations so long as there is enough oxygen present to maintain aerobicity. Hence roughly fluctuating oxygen concentrations matter little, so long as there is enough to keep the system aerobic.

Bacterial response to 'carbon' is conventionally thought of as bacterial growth, which can be counted or otherwise measured. The MCA method is not based on cell growth, but avoids it. Not enough carbon as analyte is used to promote bacterial growth in the calorimeters. Bacterial doubling times—one

cycle of growth—usually require 20–60 min depending on the kind of cell and the temperature. Much more carbon has to be provided to obtain bacterial growth, than amounts of carbon needed to get an initial 'priming' pulse of heat in MCA's mode of operation, by a factor of about 10. When cells are adapted and in excess, their aerobic uptake and utilization of carbon is usually completed in a few minutes. No new cells are made nor wanted. The MCA method measures a burst of heat, proportional to the cells initial metabolism of the compound in question.

Summarizing so far, MCA or bacterial calorimetry uses *ca.* 0.5–1 ml of sample containing 10^{-6}–$10^{-4}M$ analyte. Measurement times after mixing cells and sample are 3–10 min. Oxygen concentrations usually need not be kept within narrow limits if there is enough oxygen available to keep the system aerobic through the analytical run. Namely 10–50% air saturation, equivalent to 10^{-3}–$10^{-4}M$ dissolved oxygen. Specificity is determined by the specificity with which cells can be adapted to absorb and metabolize the analyte. Microbial calorimetry takes advantage of microbial behaviour of a kind, that isolated enzymes coupled to sensors have considerable difficulty with. Namely enzyme protection, generation of needed intermediates, imperviousness to foreign compounds destructive to enzymes. Microbial calorimetry is quite like conventional wet chemistry analysis, in that the principal reagent or catalyst is discarded after each run. Bacteria in quantities needed for MCA are relatively inexpensive. About an hour's labour is sufficient to provide enough cells from sub-culture, for two to three days of use.

EXPERIMENTAL

Seebeck thermopile sensors and reaction vessels

The central parts for a batch mixing calorimeter are shown in Fig. 2. Thermoelectric devices which generate the Seebeck effect also exhibit the Peltier effect. Thermoelectrics used by us are sold primarily as Peltier pumps, *e.g.*, by the Melcor Company. They function with about 35% power efficiency, transducing heat to electric current and so are called Seebeck thermopiles when used in the Seebeck mode. Two Seebeck thermopiles are placed in good contact with the two faces of the mixing vessels and in contact with the aluminum metal heat sink as shown in Fig. 2. The heat sink which surrounds the assembly and contacts the outer faces of the

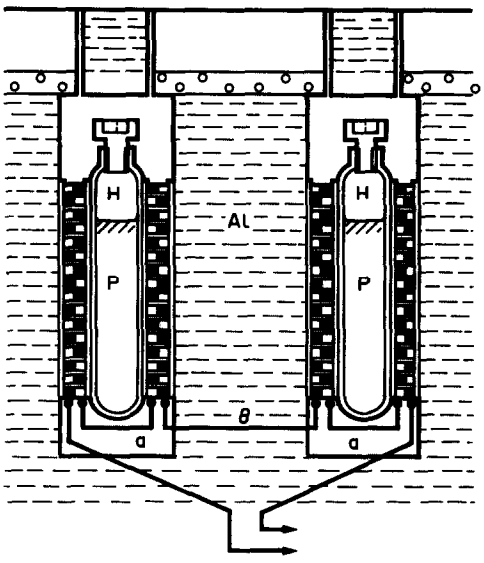

Fig. 2. Twin heat conduction batch mixing calorimeter using Seebeck thermoelectric sensors. Partition P divides the internal space in the lower part of both mixing vessels into two compartments, keeping reactants from mixing until the whole is inverted. Seebeck sensors are connected so a (=add) causes addition of voltages from the sensors within each pair. Connection o (=oppose) causes subtraction of the pairs of summed voltages from each other giving a net voltage (arrows) for transmittal to an external dc amplifier. Net voltage output is directly proportional to net power from the two vessels, reference and sample, with a figure of merit 7 μWatts net power (as heat) per μVolt net output signal. Al = aluminum heat sink, for promoting thermal equilibrium throughout before mixing and absorption of any heat from samples; H = headspace, air.

thermopiles weighs *ca.* 0.5 kg. Seebeck thermopiles are made mostly of metal, with thin ceramic face plates for electric insulation. Thus the path from the sample chamber is a good heat conduction path able to pass heat from the sample to the heat sink in a few seconds. About one third of such heat is transduced to electric power, a signal, by the Seebeck units. Thermopile resistances are *ca.* 1–2 ohms. Therefore signal source impedance is low, a distant advantage in low level dc amplification.

The mixing vessels are round in shape—short cylinders—about 35 mm in diameter and 4–6 mm thick, small versions of the 1927 design by Lipsett, Johnson and Maas.[13] A partition inside, about 20 mm long, keeps the reactants separated while the vessel is upright. Reactants (*e.g.*, microorganisms, and carbon analyte) are loaded in through a common port, using a syringe. After loading, each port is closed with a plastic screw. From 3 to 5 ml of air is left in the headspace of each mixing vessel. The system is left for 5–15 min to reach internal thermal equilibrium and disperse the thermal shock of

loading. Good thermal equilibrium—no heat being transmitted through any thermopile—appears as a flat baseline on the recorder or monitor. Net signal output is zero volts at that point. Then the assembly is inverted, mixing the reactants and also mixing in additional air from the headspaces.

The reference vessel is usually loaded with 2 ml of bacteria suspension on one side of the partition P indicated in Fig. 2, and 0.5–1 ml of solvent without carbon on the other side of the partition. The sample vessel is similarly loaded except the smaller aliquot contains the analyte, the compound or carbon source of interest. The method can thus be represented:

REFERENCE VESSEL	Microorganisms (2–5 mg, 2 ml) Excess cells	+	Buffer, no added carbon (1 ml)	Air ⇄ Mix	Heat of aerating bacteria, no added carbon	(1)
SAMPLE VESSEL	Microorganisms (2–5 mg, 2 ml) Excess cells	+	Buffer, include carbon, the analyte	Air ⇄ Mix	Heat of metabolism of carbon	(2)

The two Seebeck thermopiles belonging to the sample vessel are connected in series so their voltages add. Likewise, the two thermopiles interfacing the reference vessel are connected in series. However as Fig. 2 indicates, the common connection between the two pairs of thermopiles is chosen so these two sums oppose one another; subtract from each other. In effect the power from the reference is continuously subtracted from the sample's power, giving a net overall signal. The arrangement is similar to other 'differential' instruments such as spectrophotometers in which the signal from the reference subtracted from that of the principal sample. The net power, the difference signal between reactions (1) and (2) above is detected by the dc amplifier as a voltage. The amplifier is a 'single ended' amplifier that we construct, based on an Analogic Co. MP-221 chopper integrated circuit. It is fitted with gains from X100 to X3000 to cover various ranges of heat production. Amplifier outputs are displayed on a chart recorder or with a data logger-computer-monitor. The signal from the amplifier at any instant is proportional to net power from the sample and reference. Power is a rate of heat generation. Integrated over time, the area of the envelope under each curve (Fig. 3) is proportional to the overall heat of metabolic combustion of the analyte.

Seebeck calorimeters of this kind may be constructed with more than two mixing vessels, to make simultaneous measurements for two or more samples, referenced against a common control. Each mixing vessel requires its own pair of thermopiles and its own dc amplifier.

Precautions

The principal precaution in MCA, in solution–solution mixing calorimetry in general, pertains to H^+ transfer and H^+ titration heats. If solutions when first mixed have a pH mismatch, and considerable buffering capacity, hydrogen ions are shifted about. Considerable heat might be generated simply from mixing different buffers having different pHs. Most carboxylic and phosphate buffers have small ionization enthalpies, only one or two kcal/mole, or less. For example acetic acid ionization is (−)0.02 kcal/mole,[14] and $H_2PO_4^-$

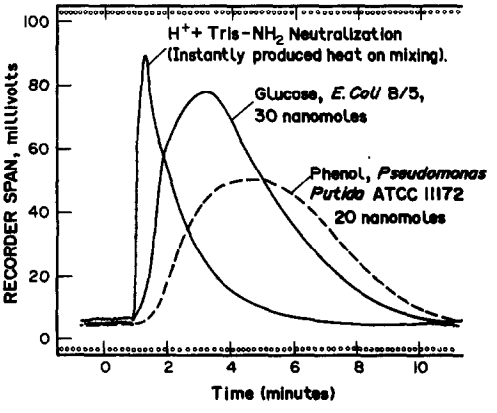

Fig. 3. Microbial calorimetry of metabolism by bacteria adapted to oxidize phenol, and glucose; calorimetric response to tris neutralization of H^+ in calibration of the instrument. The amplified voltages, the ordinate values are proportional to net power as heat generated by the sample at each instant. Integrated over time, the area under each envelope is proportional to the overall heat. Temperature = 25°, 1–2 ml reactant volumes.

ionization is (+)0.80 kcal/mole.[15] However amine buffers, tris, imidazole, and ammonium have large protonation and ionization enthalpies, from 5–15 kcal/mole magnitude. Elementary calculations based on volumes, buffer capacities, and ΔpH mismatches of from 0.2 to 2 pH units show that several dozen millicalories of heat can be generated from H^+ exchange. There are two means for dealing with this problem. (i) Use 0.15*M* sodium chloride or similar electrolyte as the solvent in which to suspend the bacteria after centrifuging them out of culture. The salt does not titrate so that if acids or H^+ sources are carried in by the sample upon mixing, they generate little if any neutralization heat. (ii) Heat generation of this kind is clearly seen because it is produced far more quickly (in a few seconds) than metabolism of any carbon compound. Figure 3 shows an example. H^+ titration heats can be subtracted out in effect, by deconvoluting them.

A second precaution pertains to sealing the reaction vessels. Port closers have to be gas tight. If they are not tight, water vapor may leak out. Water has a large, endothermic heat of vaporization, (+)540 cal/g H_2O. Even a few micrograms of water effusion causes severe drifting, and hence inability to reach a stable baseline. Heat conduction calorimeters respond to endothermic (cooling) heats with the same sensitivity as in exothermic heating, except with opposite signal polarity.

In some applications one may need to study anaerobic utilization of carbon *vs.* aerobic metabolism, particularly in fermentation analysis. Accordingly the vessels may be purged with nitrogen gas, so fairly rigorous anaerobicity can be maintained inside. Considerably less heat is usually produced in anaerobic utilization,[16] and more slowly than in aerobicity. Hence for MCA, aerobic conditions are used for three reasons: (i) convenience, only air is included, (ii) speed and (iii) sensitivity; heats of aerobic metabolism are large, often from 30–80 kcal/mole of carbon atom in various analytes studied so far.[17]

Dissolved oxygen for maintenance of aerobicity during MCA

Only limited amounts of analyte, *ca.* 2–200 nanomoles, are used in MCA. In case of glucose, probably nearly all bacteria for which careful measurements exist, produce close to (−)305 kcal/mole heat of glucose under MCA's conditions. That is, with an excess of cells and excess oxygen. About 15 millicalories of heat (exothermic) are expected from 50 nanomoles of glucose. Is there actually enough oxygen to maintain aerobicity?

If the sample and bacterial suspension were preequilibrated with air by simple exposure to air, usually they are 80–90% air saturated. Since air is 20% oxygen and its aqueous solubility is *ca.* 1.3×10^{-3} (25°), then 3 ml of solution has roughly 700–800 nanomoles of oxygen. Aerobic metabolism of hexoses usually requires *ca.* 3 moles O_2/mole hexose. Hence 150–200 nanomoles of O_2 are required for 50 nanomoles of a hexose such as glucose. Headspace oxygen is also available from the 3–4 ml of volume above the solutions in the mixing vessel. This provides several thousand additional nanomoles of O_2. Hence maintenance of aerobicity is ensured over nearly any reasonable range of carbon concentration, micromolar to submillimolar concentrations. As in more conventional analysis wherein reagents are kept in excess to drive consumption of the analyte, MCA likewise is suited to keep its two main reactants in excess; bacteria, and dissolved oxygen.

Rates of carbon utilization

Rates of carbon utilization and of heat production by bacteria are important because they govern the time needed for analysis. One might first expect that the many existing papers about carbon utilization should indicate the magnitudes of uptake rates in commonly studied cells such as *E. coli*, and thereby heat production rates. The two principal means for measuring carbon utilization rates have been developed over many years by observing microbial growth (the 'growth curve') and by oxygen uptake (Warburg manometry, later by the oxygen electrode). Several other means have been used; radioisotopes and trapping $^{14}CO_2$, and H^+ extrusion rates. The common ground under all these traditional means including heat production is metabolism. But large differences are seen in velocities so measured, from method to method when the same cells and carbon source are compared. Reasons for such differences cannot be reviewed here in detail, except for two points. (i) Microbial growth rates and their oxygen utilization rates depend on times necessary to entirely complete each microbial cell growth cycle for making new cells. Many bacteria have doubling times of 30–90 min even at optimum temperatures. (ii) In contrast,

velocities of *initial* carbon uptake and carbon metabolism by cells adapted to the targeted compound, are much larger than velocities or rates of growth. Priming metabolism heat generation mostly finishes in several seconds to a few minutes under conditions used for MCA. Namely, with excess cells, oxygen in excess, limited carbon.

Adapted bacteria take nutrient carbon compounds first into pathways variously called fueling reactions[18] and anaplerotic pathways. These are the Embden-Meyerhof-Parnas, the tricarboxylic acid, and the pentose phosphate cycles. It is in these early sectors of metabolism when carbon enters bacteria, that most of the heat and byproducts like CO_2 are produced. How exothermic they actually are depends on how well incoming compounds are fitted to the cell's pathways.[19] They make intermediates and cofactors, NADPH, carbon skeletons, several compounds necessary for the next tasks. Namely biosynthesis of cell material, provision of protecting compounds like GSH, etc. However this next tier of tasks is 10 to 100 times slower than priming metabolism, hardly exothermic, and not very heat productive. Priming metabolism heat production, being oxidative, is analogous to ordinary chemical reactions in one respect. Oxidative reactions in chemistry usually are much larger, roughly by a factor of 10, than heats of most other classes of reactions in water, molecular rearrangements, chelation, H^+ ionization, *etc.* Likewise, the kinds of aerobic metabolism and oxidation on which MCA hinges, are outstandingly exothermic. Commonly these metabolic molar heats are 50–70% as large as oxygen bomb combustion calorimetric heats taking compounds all the way to carbon dioxide and water. Thus heat production in the way MCA is carried out is generated with considerably larger magnitudes than those predicted by "indirect calorimetry" when it relies on cell growth, or on a mixture of cell growth and oxygen uptake.

A table of glucose uptake rates for aerobic *Escherichia coli* using data from our laboratory and a number of others was published in 1990.[20] Under MCA's conditions glucose is assimilated by *E. coli* at rates from about 2 to 20×10^{-19} mole glucose/bacterial cell/second. Using an average of 10×10^{-19} mole glucose/cell/second, 2 mg of cells (*ca.* 5×10^9 cells) might consume 20 nanomoles of glucose in about 5 sec. But this estimate is based on maintenance of the glucose concentration, whereas in fact it falls off rapidly under the normal conditions for using MCA; an excess of cells, carbon (glucose) is limited. Hence the rates seen after the initial burst of heat production fall off because the analyte depletes to concentrations below the K_m values for such cells which usually are approximately $0.1–1 \mu M$. Thus Fig. 3 represents average rate of heat production seen from many analytes, sugars, phenols, lower fatty acids and alcohols. In practice, when cells are adapted and in excess they usually oxidize limited amounts of carbon in 100–500 sec at 25°. All our work so far has been carried out at 25°, laboratory temperature. It is likely that 30–40° temperatures for assay would hasten microbial consumption of analytes, perhaps several fold. This aspect of MCA has not been investigated.

The figure of merit for Seebeck sensors of the kind we use (*e.g.*, Melcor C. P. 1.4-71-10 Peltier units) is close to a 7-μWatt power input/μVolt signal output. The sensor figure of merit enables estimation of the amplified signal one expects. For example, using 20 nanomoles of glucose, (−)300 kcal heat/mole, a 200-second combustion time to use all the sugar, an amplifier gain by a factor of 2000 and that there are 4.18 joules/calorie, an average amplified signal output of 36 mV is calculated.

RESULTS AND DISCUSSION

In order to compare microbial calorimetric analysis with a conventional analytic technique, Fig. 4 shows the behavior of phenol in MCA, and in Folin reagent spectrophotometry. *Pseudomonas putida* ATCC 11172 were adapted to

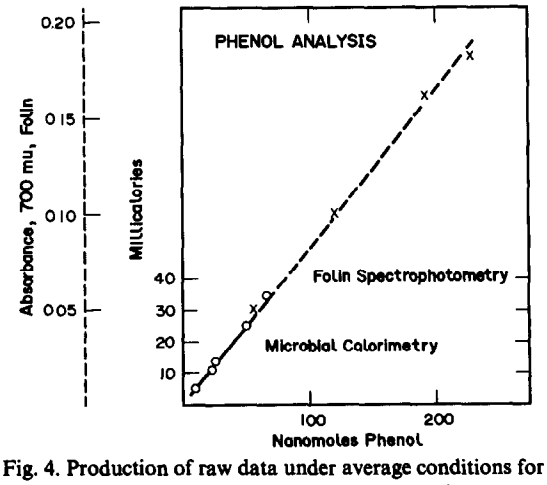

Fig. 4. Production of raw data under average conditions for the lower practical ranges for phenol analysis, in spectrophotometry (Folin–Ciocalteau reagent), and in microbial calorimetry using a bacteria adapted to phenol.

phenol by growing them on phenol, similar to growth on a series of lignin related fragments and cresols.[10] The vertical axes in Fig. 4 plot the minimal practical ranges of data production for both methods: zero–30 millicalories of heat in MCA, absorbance range 0.03–0.30 in spectrophotometric Folin analysis for a 1-cm pathlength and a 3-ml assay volume. Approximately 5–30 nanomoles of phenol suffices for MCA to span this heat production. A range of 30–100 nanomoles of phenol is required for such a spectrophotometric analysis. Thus in lower ranges of analytic capability for the two methods, MCA competes well with Folin spectrophotometry in the amount of phenol analyte required.

The slopes of such plots equal the parameters that characterize microbial calorimetry, and spectrophotometry. Namely the aerobic molar metabolic heat, $\Delta H_{a.m.} = (-)551 \pm 30$ kcal/mole, and the molar absorbance coefficient for Folin color, $\epsilon_{700} = 8460 M^{-1}cm^{-1}$ for phenol, respectively. Several cresol isomers and cogeners produce similar parameters in both methods, Folin spectrophotometry, and MCA technique using *P. putida*.[10]

Likewise several spectrophotometric analytic methods in which the analyte is a prochromogen, have value of $\epsilon_{\lambda max.} \sim 4000$ to $10{,}000 M^{-1}$ cm^{-1} when developed. Nelson–Somogyi analysis of reducing sugars[21] and ninhydrin analysis of amino acids are examples. Their four to seven carbon analytes give aerobic heat productions from a few hundred to several hundred kcal heat/mole of compound. Lower molecular weight analytes which are mostly not good prochromogens such as acetate, C_1–C_3 compounds like methanol, ethanol, glycerol, acetate, propanol yield from $(-)102$ to $(-)250$ kcal heat/mole in the MCA technique.[22] Therefore the relationship between conventional spectrophotometric analysis, where spectrophotometry can be used, and the MCA technique, illustrated in Fig 3, is expected to hold in many examples.

Microbial calorimetry is not expected to compete in sheer sensitivity with some modern techniques based on electrochemical detectors, or gas chromatography. However these techniques have requirements that make them labor intensive to use, despite the power of their instrumentation. For example it is possible to use gas chromatography of carbohydrates as a basis for analysis, but samples must be completely dry, derivatized, and extracted for G.C.'s purposes. A number of spectrophotometric and fluorimetric techniques are quite powerful in their way, but do not accept optically bad samples such as food or tissue slurries, very turbid solutions, nor analytes that are unreactive toward the reagent on which they rely to develop color. The MCA method is only of intermediate sensitivity. However MCA efficiently works with analytes in water that are poor chromogens or are not derivatizable to make color. Compounds that seriously interfere in other methods, foreign pigments and particles, are usually of little consequence in MCA, if a bacteria is available that can combust the sought-for analyte. If such a bacteria is not immediately at hand, usually one can be raised, adapted, by simply growing it on the sought for analyte. The MCA technique uses simple, inexpensive instrumentation. It allows the analyst to easily 'manufacture' as if it were, the necessary reagents by simply growing them via conventional microbiologic practice.

Acknowledgements—This work was supported by the Agricultural Experiment Station and by the Agricultural Utilization Research Institute of Minnesota.

REFERENCES

1. A. Balows and H. G. Truper in M. Dworkin, W. Harder and K. Heins-Sheifer (eds.) *The Prokaryotes*, 2nd Ed., Chap. 18, Vol. 1, Springer-Verlag, New York, 1991.
2. E. H. Battley, *Energetics of Microbial Growth*, Wiley, New York, 1987, 329.
3. R. Bayly, R. Jain, C. Poh and R. Skurray in S. Hagedown, R. Hanson and D. Kunz (eds.), *Microbial Metabolism and the Carbon Cycle*, Harwood, 1988, 359.
4. F. C., Neidhardt, in F. Neidhardt, J. Ingraham, B. Magasanik, K. Low and M. Schaechter (eds.), *Am. Soc. for Microbiol.*, pp. 3–6. Washington, D.C., 1987.
5. L. J. Andus, *Nature*, 1946, **158**, 149.
6. *Standard Methods for Examination of Water and Wastewater*, 16th Ed., *Am. Public Health Association*, p. 413. Washington, D.C. 1985.
7. G. Zubay, *Biochemistry*, Chap. 26. Addison-Wesley, Reading, Massachusetts, 1983.
8. D. V. Parke, *Enzyme Induction*, Chaps. 1–3. Plenum, New York, 1975.
9. J. L. Ingraham, O. Maaløe and F. C. Neidhardt, *Growth of the Bacterial Cell* pp. 132–148. Sinauer Assoc., Sunderland, Massachusetts, 1983.
10. R. Lovrien, M. Ferrey, T. Magnuson and R. Blanchette in N. G. Lewis and M. G. Paice (eds.), *Plant Cell Wall Polymers, Biogenesis and Biodegradation*, A.C.S. Symposium Series 399, pp. 544–558. Am. Chem. Soc. Publishers, Washington, D.C., 1989.
11. R. B. Roberts, D. B. Cowie, P. H. Abelson, E. T. Bolton, R. J. Britten, *Studies of Biosynthesis in* Escherichia coli. Carnegie Institution of Washington Pub. No. 607, pp. 318–405. Washington, D.C., 318–405, 1963.

12. H. N. Rasmussen, *Analyt. Biochem*, 1979, **95**, 416.
13. S. G. Lipsett, F. M. Johnson and O. Maas, *J. Am. chem. Soc.*, 1927, **49**, 925.
14. J. J. Christensen, R. M. Izatt and L. D. Hansen, *ibid.*, 1967, **89**, 213.
15. R. Alberty, *J. Biol. Chem.*, 169, **244**, 3292.
16. E. H. Battley, *Energetics of Microbial Growth*, p. 317. Wiley, New York, 1987.
17. R. Lovrien, G. Jorgenson, M. Ma and W. Sund, *Biotech, Bioeng.*, 1980, **22**, 1249.
18. J. Ingraham, O. Maaløe and F. C. Neidhardt, *Growth of the Bacterial Cell*, Sinauer Assoc. Sunderland, Massachusetts, pp. 134–170, 1983.
19. J. J. Anderson and S. Dagley, *J. Bacteriol*, 1980, **143**, 525.
20. I. Boe and R. Lovrien, *Biotech. Bioeng.*, 1990, **35**, 1.
21. R. E. Lovrien, K. K. Williams, M. L. Ferrey and D. A. Ammend, *App. Environ. Microbiol.* 1987, **53**, 2935.
22. R. E. Lovrien, M. L. Ferrey and I. N. Boe, *Thermochim. Acta*, 1990, **172**, 187.

Talanta, Vol. 40, No. 2, pp. 135–137, 1993
Printed in Great Britain.

0039-9140/93 $6.00 + 0.00

DETERMINATION OF VANADIUM: AN OPTIMIZATION OF THE GALLIC ACID PERSULPHATE METHOD

L. DARBHA and J. ARUNACHALAM
Analytical Chemistry Division, Bhabha Atomic Research Centre, Trombay, Bombay 400 085, India

(*Received* 16 *September* 1991. *Revised* 19 *March* 1992. *Accepted* 22 *March* 1992)

Summary—An optimization procedure for the gallic acid–persulphate method for the ultratrace determination of vanadium is reported. The optimization step has improved the sensitivity by a factor of three. The linearity range of the calibration graph is also extended.

The catalytic-photometric method involving the catalytic effect of vanadium (V) on the oxidation of gallic acid by ammonium persulphate reported by Fishman and Skougstad,[1] is accepted as a standard method for the determination of vanadium in water samples.[2] Qiang weiguo[3] had suggested some improvements in the analytical parameters to give better reproducibility. We report an optimization procedure which gives an improved sensitivity for the determination of vanadium.

Optimization of experimental parameters can be done by non-parametric as well as parametric methods. One of the popular non-parametric methods of optimizing experimental conditions is the simplex approach.[4] In the simplex method, a regular geometric figure known as simplex having n + 1 vertices is chosen, where n is the number of variables. The experiment is performed at the values of the parameters representing the vertices, and the process is continued until the desired optimum (maximum) is reached.

In the parametric approach, a set of experiments is carried out, usually based on factorial designs, to obtain an analytical expression (a function) relating the response with the experimental parameters. Among the parametric approaches, the Response Surface Method, coupled with the Method of Steepest Ascent, developed by Box,[5,6] is the most popular. In this method the response function is approximated, in a certain region of the factor space, by a polynomial, usually a second degree, in the form,

$$R = \beta_0 + \sum_{i=1}^{n} \beta_i X_i + \sum_{i,j=1}^{n} \beta_{ij} X_j X_j + \sum_{i=1}^{n} \beta_{ii} X_i^2 \quad (1)$$

where, R is the response, β are the coefficients and X are the experimental factors (variables).

The computation of the slope of the function reveals the variables that influence the response the greatest. At various new levels of this variable, the equation is solved for the others and the experiment is repeated at new values to locate the optimum in steps.

Assuming that the functional dependence of the response with the factors does not vary with the approach to the optimum, the coefficients of the parameters in the analytical function, obtained using the first set of experiments, can be examined to reveal the existence of a maximum or minimum. In such cases, it will be possible to obtain the values of the parameters that correspond to the maximum or minimum response.

In the present investigation a 3×3 (3^2) factorial design was used, with the concentrations of gallic acid and persulphate as the two variables, to obtain an analytical expression relating the concentration of the reactants to absorbance.

EXPERIMENTAL

Reagents and apparatus

All the reagents were prepared as suggested by Qiang weiguo.[3] Demineralized water was used in all the experimental steps. Gallic acid was recrystallized from hot water after the removal of any oxidized products by adding activated charcoal. A Hitachi 330 Model spectrophotometer was used for obtaining the absorbance. All the measurements were carried with 10-mm cells.

All the glassware used in the experiments was kept for a week in 10% nitric acid, and rinsed several times with demineralized water before use. Class A glassware was used throughout.

Procedure

3^2 Factorial design and optimization. The complete 2 variable at 3-level design used in the experiment is given in Table 1. The base level is denoted as 1 ml of 1% gallic acid and 1 ml of 5% persulphate. The upper and lower levels were obtained using a difference of ± 0.5 ml from the base level.

An aliquot of 20 ng of vanadium was pipetted into nine 10-ml standard flasks. Ammonium persulphate solution was pipetted into each of these bottles as given in the design. Required volumes of gallic acid solution were pipetted as given in Table 1, leaving an interval of 2 min between addition to each flask and the volumes were made up to the mark. Corresponding blanks were also run as per the design without the addition of vanadium. Maintaining a constant duration of one hour for the reaction to proceed at each level, the absorbances were measured for all the solutions. The increased absorbance due to the catalytic effect of vanadium for each experimental solution was obtained by subtracting the absorbance recorded for the corresponding blank. The values are given in Table 1.

RESULTS AND DISCUSSION

Optimal conditions

A second order polynomial function [equation (2)],

$$-0.008X^2 - 0.052Y^2 - 0.007XY + 0.076X + 0.134Y - 0.077 = 0 \quad (2)$$

(where X is the volume of 1% gallic acid and Y is the volume of 5% persulphate), was derived using the procedure (relative to the base point 1,1) discussed in Beveridge and Schechter,[4] relating the absorbance to the amounts of gallic acid and persulphate. The fitted response values are also given in Table 1 which show a very good agreement with the experimentally obtained responses.

Table 1. Factorial design used in the experiment

Exp. No.	Volume of 1% Gallic acid in ml	Volume of 5% persulphate in ml	Absorbance	
			Experiment	Fitted
1	1.0	1.0	0.066	0.067
2	1.5	1.5	0.090	0.088
3	1.5	0.5	0.068	0.069
4	0.5	1.5	0.039	0.039
5	0.5	0.5	0.010	0.012
6	1.0	1.5	0.060	0.066
7	1.0	0.5	0.043	0.042
8	1.5	1.0	0.087	0.092
9	0.5	1.0	0.038	0.038

Table 2. 2 × 2 Factorial design around the maximum

Exp. No.	Volume of 1% Gallic acid in ml	Volume of 5% persulphate in ml	Absorbance
1	3.7	0.5	0.058
2	3.7	1.5	0.074
3	4.7	0.5	0.068
4	4.7	1.5	0.057
5	4.2	1.0	0.106

The Lagrange's criteria for the existence of a maximum, minimum and a saddle point of the function are as follows.

$$\text{If} \quad D_1 > 0 \text{ and } D_2 > 0$$

a minimum exists, and,

$$\text{If} \quad D_1 < 0 \text{ and } D_2 > 0$$

a maximum exists, where,

$$D_1 = |\chi_{x1,x2}| \quad \text{and} \quad D_2 = \begin{vmatrix} \chi_{x1,x1}\chi_{x1,x2} \\ \chi_{x2,x1}\chi_{x2,x2} \end{vmatrix}$$

where χ is the partial derivative of the function with respect to variables X_1 and X_2. By applying these criteria, it is seen that a maximum exists for this function. This maximum was found algebraically, using the partial derivatives with respect to the two variables, and corresponds to 4.2 ml of 1% gallic acid and 1 ml of 5% persulphate.

Since the region of experimentation is far removed from the suggested maximum position, *i.e.*, 4.2 ml of (1%) gallic acid and 1 ml of (5%) persulphate, confirmatory experiments were carried out using 2 levels–2 factor experimental design using the same step size of 0.5 ml, around this optimum. The results are given in Table 2, confirming the suggested optium is the maximum.

Degree of enhancement

A set of experiments was performed with the suggested optimum quantities of gallic acid and persulphate with different amounts of vanadium. For comparison, the experiments were also performed with the quantities of the reagents suggested by Qiang weiguo,[2] for the same quantities of vanadium. The absorbances obtained in the two cases are given in Fig. 1. It is seen that the optimization has improved the sensitivity by a factor of 3. The response is also linear up to 70 ng of vanadium. Qiang wieguo[2] has indicated linearity only up to 35 ng of V (in

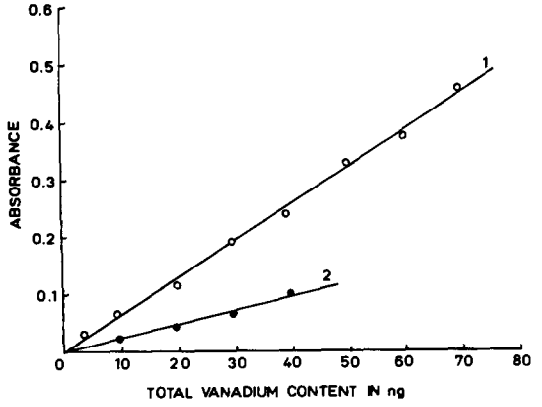

Fig. 1. Comparison of sensitivities of the present (optimized) method to the reported method. Curve 1. Absorbance obtained with the optimum values (4.2 ml of 1% gallic acid and 1 ml of 5% persulphate). Curve 2. Absorbance obtained with 1 ml of 1% gallic acid and 1 ml of 5% persulphate. Absorbances in both cases were measured with a 10-mm cell.

13 ml total solution) which might have been due to the use of 50-mm cells for the measurement of absorbance in his experiments.

The optimum volume of 4.2 ml of 1% gallic acid and 1 ml of 5% persulphate corresponds to equimolar concentrations of gallic acid and persulphate (0.022M for both gallic acid and ammonium persulphate, whereas the quantities of gallic acid suggested by other authors have been much lower (0.009M and 0.0045M in Ref. 1 and Ref. 2, respectively). Independent experiments carried out on different days showed that the absorbances are reproducible within $\pm 8\%$ at 2 ng/ml V.

REFERENCES

1. M. J. Fishman and M. W. Skougstad, *Anal. Chem.*, 1953, **25**, 604.
2. *Standard Method for the Examination of Water and Wastewater*, 16th Ed. (1985), American Public Health Association Procedure No: 327B.
3. Qiang weiguo, *Anal. Chem.*, 1983, **55**, 2043.
4. Gordon S. G. Beveridge and S. Schechter, *Optimization: Theory and Practice*, McGraw Hill, New York, 1970.
5. G. E. P. Box, *Biometrika*, 1964, **10**, 16.
6. O. L. Davies, *The Design and Analysis of Industrial Experiments*, 2nd Ed., Oliver and Boyd, London, 1960.

Talanta, Vol. 40, No. 2, pp. 139–142, 1993
Printed in Great Britain.

0039-9140/93 $6.00 + 0.00

OPTIMAL DESIGN OF DIFFUSIVE SAMPLERS

DWIGHT W. UNDERHILL
Department of Environmental Health Sciences, School of Public Health, University of South Carolina, Columbia, SC 29208, U.S.A.

(*Received* 16 *July* 1991. *Revised* 18 *May* 1992. *Accepted* 18 *May* 1992)

Summary—Some commercially available diffusive samplers use two layers of adsorbent placed in series. After sampling is completed, the time weighted average concentration of analyte is estimated from the weighted sum of the uptake of analyte on these two layers. It is known that such a division into layers can increase the permissible sampling time. Here the principles underlying this sampling procedure are analyzed through a fundamental application of the theory of diffusion. Using a trial and error procedure, the optimal division of adsorbent was calculated, and the increase in sampling time that such a division can give was confirmed theoretically. Also, should the uptake in the backup layer exceed a predetermined fraction of the total uptake, this will indicate misuse of the diffusive sampler.

Diffusive samplers are commonly used to determine the time weighted average concentrations of gases and vapors in both the workplace and the environment. Many such samplers contain two layers of adsorbent, and the concentration of analyte is determined from a weighted average of the uptakes on these two layers.[1-3] This paper develops a calculation for the optimal design of such diffusive samplers, and shows that an optimal use of the uptakes on these two layers can lead to a very significant increase in the useful sampling time for a diffusive sampler over what would be possible if only the total residue in the sampler were to be considered.

Mathematical analysis

Figure 1 gives a schematic diagram of the type of diffusive sampler considered here. In this sampler, the analyte diffuses into the sampler from the left, across the windscreen and air gap, to the adsorbent. The absorbent, which may be divided into two or more sections, serves as a sink for the analyte. The following are needed to describe the mass transfer in this diffusive sampler: 1) the sampler geometry, 2) the adsorption coefficient, 3) the diffusion coefficient of the analyte in air and in the sorbent, and 4) the ambient concentration of analyte as a function of time. These factors are accounted for in the following partial differential equations:
Transfer of analyte across the air gap:

$$\frac{1}{\alpha}\frac{\partial c}{\partial x_{(x=+0)}} = c_0 - c_{(x=-0)} \qquad (1)$$

Zero flux of analyte at the unexposed surface of adsorbate (an impervious backing)

$$\frac{\partial c}{\partial x_{(x=1)}} = 0 \qquad (2)$$

Diffusion within the adsorbent

$$\frac{\partial^2 c}{\partial x^2} = \alpha\frac{\partial c}{\partial \tau} \qquad (3)$$

where the above dimensionless factors are defined as follows:
Reduced Distance,

$$x = \frac{x}{W} \qquad (4)$$

Geometric Factor,:

$$\alpha = \frac{W}{\epsilon y L} \qquad (5)$$

Reduced Time, τ:

$$\tau = \frac{tD}{(1-\epsilon)LWK} \qquad (6)$$

Reduced Concentrations:

$$c = C/C_1 \qquad (7)$$

$$c_{(X=-0)} = C_{(x=-0)}/C_1 \qquad (8)$$

$$c_0 = C_0/C_1 \qquad (9)$$

The factors used in the above definitions are:

C = concentration of analyte in the interparticle void of sorbent pad, g/m^3
$C_{(X=-0)}$ = airborne concentration of analyte at the exposed surface of sorbent, g/m^3

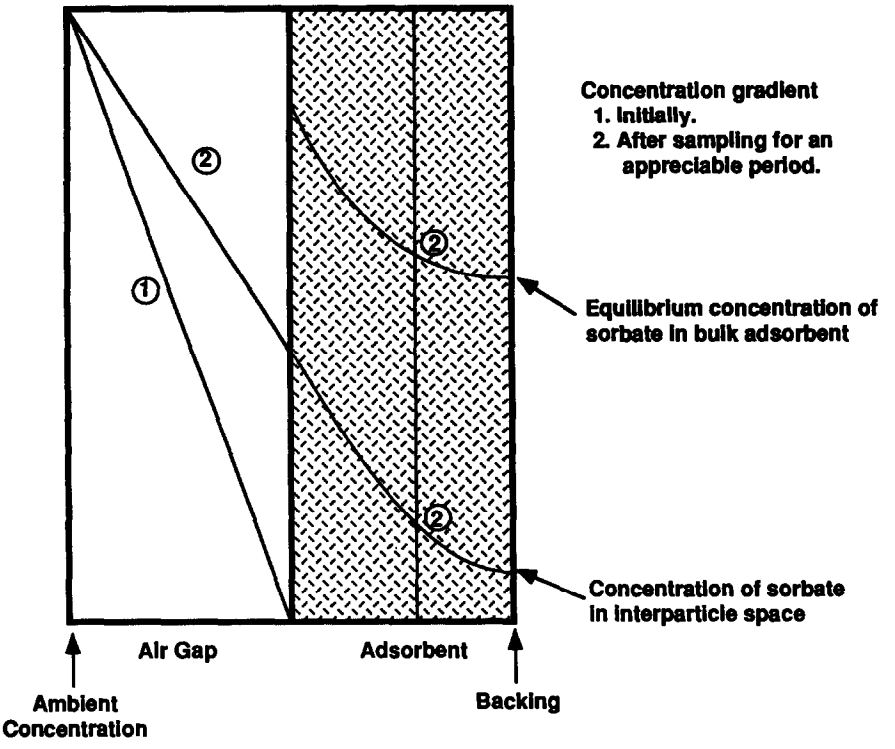

Fig. 1. Schematic diagram of a diffusive sampler.

C_0 = ambient concentration of analyte, g/m^3
C_1 = hypothetical unit concentration of analyte, 1 g/m^3
D = molecular diffusion coefficient for analyte in air, m^2/sec
K = partition coefficient for analyte-sorbent, defined as
$$= \frac{\text{(g analyte/m}^3\text{ compacted sorbent)}}{\text{(g analyte/m}^3\text{ ambient air)}}$$
L = width of air gap, m
t = sampling time, sec
W = thickness of the sorbent pad, m
X = distance into sorbent pad, m
y = tortuosity factor for interparticle diffusion, dimensionless
ϵ = fractional interparticle void volume, dimensionless

The reduced time is the actual sampling time divided by the time it would take the sampler to become saturated with analyte if exposed to a constant unit concentration of analyte (C_1), and the rate of uptake remained at the initial rate of input ($C_1 D/L$). The above equations can be solved to give analytical solutions that allow the relationship between exposure and uptake to be found in closed form.

The following two equations can be derived from Crank's[4] equation 4.50 by: 1) differentiation with respect to time to obtain the response from a pulse input; 2) integration with respect to bed depth to determine the amount of analyte in a layer of a given thickness. Because of the linearity of these equations, the order of these operations is immaterial. Then $m(\tau)$, the reduced uptake of analyte remaining in the sampler at a reduced time, τ, following a unit pulse input at $\tau = 0$, is

$$m(\tau) = \sum \frac{\alpha \exp(-\tau/\alpha)}{\vartheta_i^2(\vartheta_i^2 + \vartheta_i + \alpha)} \qquad (10)$$

The reduced uptake, $m_1(\tau)$, of the original analyte contained within the back-up section at a reduced time, τ, is:

$$m_2(\tau) = \sum \frac{\alpha \exp(-\tau/\alpha)\sin(\alpha x)}{\vartheta_i^2(\vartheta_i^2 + \vartheta_i + \alpha)\cos(\alpha)} \qquad (11)$$

where:

ϑ_i = the positive roots of $\vartheta_i \tan(\vartheta_i) = \alpha$

The reduced uptakes are defined as the actual uptake divided by the equilibrium uptake of analyte in the sampler exposed to a unit concentration of analyte (C_1). The quantity of analyte in the primary layer is the difference between the total residual uptake and the residue in the back-up layer.

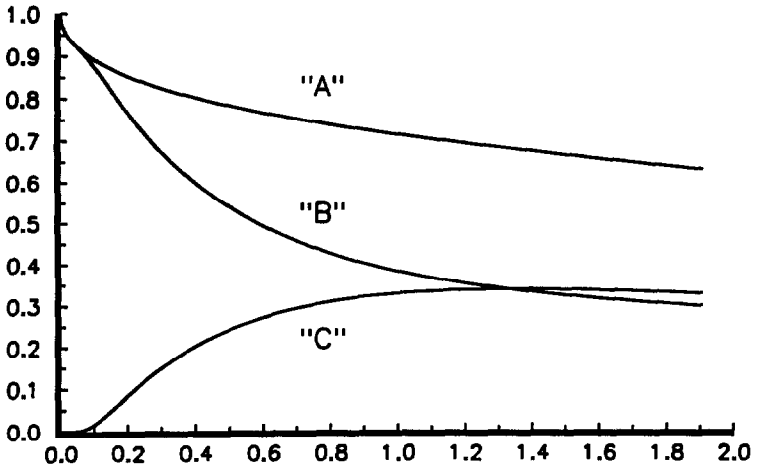

Fig. 2. Residue following a pulse input. A = Total residual analyte following a unit pulse input; B = Residue in primary layer; C = residue in secondary layer.

Also because of the linearity of the equations considered here, the solutions are additive. Thus equations (10) and (11) can be generalized to characterize the uptake from any possible exposure: any other input can be constructed as a series of pulses, so that the response to a pulse input can be generalized to include all other exposure scenarios.

RESULTS AND DISCUSSION

To demonstrate the applicability of this analysis to diffusive sampling, the residual analyte in a diffusive sampler was calculated assuming a geometric factor (α) of 0.7, a value that was chosen because it seems representative of commercially available diffusive samplers. In Fig. 2, lines "A", "B" and "C" show, respectively, the total amount of analyte, the analyte in the primary layer, and the analyte remaining in the back-up section of the sampler at a reduced time, τ, following a unit pulse input at a reduced time, $\tau = 0$. The treatment that follows, however, is independent of any particular value chosen for the geometric factor.

Here the "best" estimate of exposure is assumed to be the estimate that permits the sampler to sampler for the longest period of time within the error bounds cited for its accuracy. Figure 3 gives the results of using the residues shown in Fig. 2 to estimate within an absolute error of 5% the TWA exposure of the sampler. In this figure, the Y-axis gives the ratio of the estimated TWA to the true TWA. The X-axis gives (in units of the reduced time) the interval between the pulse input and time at which the

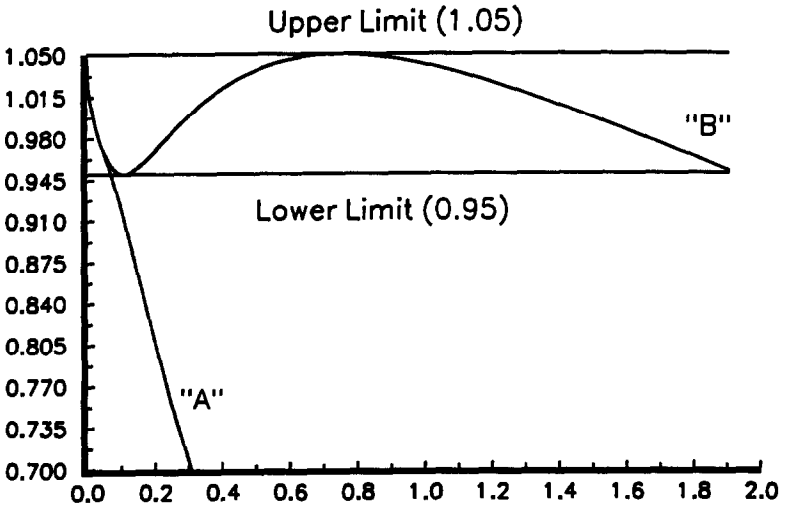

Fig. 3. Estimated uptake as a function of reduced time. A = calculated from total residue; B = calculated from the weighted sum of residues in the two layers of adsorbent.

residue in the sampler was determined. Line "A", which gives the "best" *i.e.*, longest satisfactory, estimate of the TWA exposure from the total residue in the sampler, is the total residue multiplied by a factor of 1.05. Thus a pulse input sampled just before the sampling period ended would be overestimated by 5%, and a pulse applied to a diffusive sampler given a unit pulse input at a reduced time of $\tau = 0.069$ before the sampling period ended, would be underestimated by a factor of 5%. Furthermore, any input sampled between these times would give an estimated TWA that lay between $\pm 5\%$ of the true TWA exposure of the diffusive sampler. Therefore for the criterion given above, the effective use time of the diffusive sampler, if only total uptake is considered, is for a reduced time of 0.069.

This effective use time can be extended considerably if adsorbent is divided into layers and a weighting factor applied to the uptake in each layer. In Fig. 3, line "B" shows the linear combination of primary and back-up layers giving the longest sampling time for which the estimated uptake remains within $\pm 5\%$ of the original input. The calculation giving the best division of the adsorbent bed into primary and back-up layers required sequential division of the adsorbent bed into hypothetical primary and back-up layers, and for each possible division, finding the maximum permissible sampling time. This process was continued until the optimal division and the weighting factors consistent with that division, were located. It was found for the sampler under consideration here (with a geometric factor of 0.7), that the longest sampling time consistent with a maximum absolute error of $\pm 5\%$, was obtained if the primary layer comprised 50.6 per cent of the total adsorbent, and further, if the residue on the primary layer was multiplied by a factor of 1.049 and added to the residue in the back-up layer multiplied by a weighting factor of 1.942. This gives a very significant extension of the permissible sampling time. The increase in the permissible sampling time, consistent with a maximum estimation error of $\pm 5\%$, is from a maximum value of the reduced time of $\tau = 0.069$ for the estimate from the total uptake, to a reduced time of $\tau = 1.91$, a factor of 28, for the estimate from the weighted sum of the uptakes on the primary and the backup layer.

These results are highly dependent on the value of the geometric factor, α. For example if the geometric factor has a value of 0.5 or less, then the adsorbent is so thin that equilibrium is rapidly established across the adsorbent as sampling progresses. With essentially the same concentration of analyte across the adsorbent, then very little is gained from dividing the adsorbent into primary and back-up layers and attempting to extract additional information from their linear combination. It was found that with a geometric factor of 0.2, the optimal division into primary and back-up layers was obtained if the primary layer contained 99.8% of the adsorbent. The increase in sampling time (still assuming a maximum absolute error of $\pm 5\%$) was only 19%.

Finally, the uptake on the back-up layer can serve as a warning of sampling error. After the sampling is concluded, there is an upper limit to the ratio of the residue in the back-up layer to the residue in the primary layer. For the first example considered here ($\alpha = 0.7$), if the ratio of the residue in the back-up layer exceeds 1.089 of the residue in the primary layer, this proves an error in either the design or the employment of the diffusive sampler.

CONCLUSION

A substantial increase in the effective use time of a diffusive sampler is possible through the selection of an appropriate sampler geometry, *i.e.*, the width of the air gap, the thickness of the adsorbent, and an optimal division of the adsorbent into primary and back-up layers. As shown here, the effect of these design parameters on the use time can be determined directly—and the use time of the sampler optimized—through equations derived from Fick's second law of diffusion.

REFERENCES

1. L. W. Anders, H. E. Mullens, and P. L. Sullivan, *Organic Vapor Monitor with Backup Section*; 3M Company Technical Paper R-3520TP, 1981.
2. *PRO-TECH Organic Vapor G-AA Air Monitoring Badge*; E. I. Du Pont de Nemours; Wilmington, DE, U.S.A., 1979.
3. *Vaporgard, Organic Vapor Dosimeter*; Mine Safety Appliances Co.; Pittsburgh, PA, U.S.A., 1985.
4. John Crank, *The Mathematics of Diffusion*, 2nd ed. Chap. 4, Clarendon Press: Oxford, U.K., 1975.

Talanta, Vol. 40, No. 2, pp. 143–146, 1993
Printed in Great Britain.

0039-9140/93 $6.00 + 0.00

ERROR BOUNDS IN DIFFUSIVE SAMPLING WITH REVERSIBLE ADSORPTION

DWIGHT W. UNDERHILL

Department of Environmental Health Sciences, School of Public Health, University of South Carolina, Columbia, SC 29208, U.S.A.

(*Received* 21 *November* 1991. *Revised* 20 *May* 1992. *Accepted* 20 *May* 1992)

Summary—Diffusive samplers are commonly used in the work place for compliance monitoring of gases and vapors. Because the workplace concentrations of analyte are not constant, the usual procedure of calibration of a diffusive monitor by exposure to a known constant concentration of analyte may lead to an unacceptable error. By considering the maximum possible error in the time weighted average (TWA) concentration, with no restrictions regarding the concentration as a function of time, a permissible sampling time is defined that is consistent with any possible concentration fluctuation.

Diffusive samplers are commonly used to determine the levels of toxic gases and vapors in the workplace. In the near future, most of what we think we know about worker exposure to noxious gases will probably be through the use of these devices. The National Institute of Occupational Safety and Health (NIOSH) is in the process of defining calibration procedures for diffusive samplers.[1] It is presumed that eventually the Occupational Safety and Health Administration (OSHA) will adopt these or similar procedures. It is important that the fundamental basis for the accuracy of diffusive sampling be established now so that future work with diffusive samplers will have an assured validity.

Many diffusive samplers currently used to monitor the time weighted average (TWA) exposure to gases and vapors in the work place have been calibrated using a constant concentration of contaminant.[2–4] Several theoretical analyses of the error in diffusive sampling also considered the uptake following exposure to a constant concentration of analyte.[5,6] Fluctuating concentrations of analyte have been considered in calculations of the effect of mass transport in the air gap in a diffusive sampler, but these analyses neglected the effect of a fluctuating concentration on the retention of analyte in the adsorbent, which is the area of primary concern in most diffusive samplers.[7,8]

Experience has shown that controlled constant exposures may reflect poorly the actual work place experience. In industry, there is the possibility of short duration, highly intense exposures that may occur, *inter alia*, during equipment failure. A calibration based on a constant exposure of contaminant may be significantly inaccurate when applied to the short duration, intense exposures that may occur anytime in a work shift.

This paper defines a procedure for determining the maximum effect of a fluctuating concentration of analyte on its measurement by a diffusive monitor. Using this procedure a "use time" for a diffusive sampler is defined such that the error in the TWA must be equal to or less than some predetermined value. The only general restriction on the calculations that follow is that the adsorption and diffusion coefficients are constant, thereby giving linear partial differential equations for mass transfer. This is not as severe a restriction as might first appear. Although at high concentrations, most adsorption isotherms are nonlinear, the adsorption of low airborne concentrations of many organic compounds, including chloroform, 1,1,1-trichloroethane, carbon tetrachloride, and benzene, on adsorbents such as Tenax can be described by linear adsorption isotherms. Under these conditions the adsorption is reversible, and, further, the mass transfer equations can be solved by standard methods.

Analytical solution to the transport equations

Figure 1 shows schematically the essential components of the diffusive sampler considered here. Ideally the rate of mass transport across

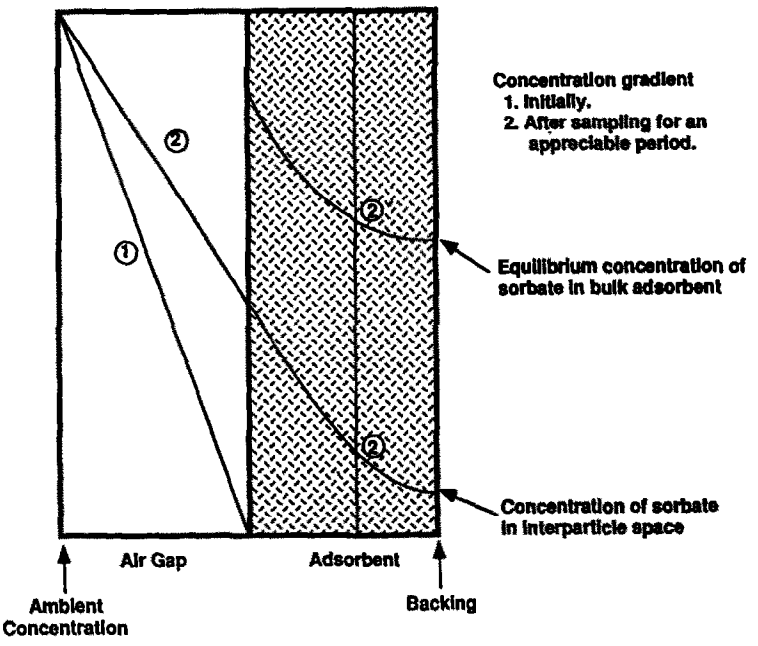

Fig. 1. Schematic diagram of a diffusive sampler. The analyte diffuses into the sampler from the left, across the windshield and the air gap, to the adsorbent. The adsorbent, which may be divided into two or more sections, serves as a sink for the analyte. The purpose of the windshield is to prevent any convective air currents from passing into the air gap and affecting the transport of analyte across the air gap.

the air gap is controlled by diffusion, and the overall uptake by the adsorbent is:

$$M = \frac{ADCt}{L} \tag{1}$$

where:

A = exposed surface of the diffusive sampler, cm^2
C = ambient concentration of analyte, g/cm^3
D = molecular diffusion coefficient for analyte in air, cm^2/sec
L = width of air gap between adsorbent bed and ambient atmosphere, cm
M = mass of samples analyte, g
t = sampling time, sec

Because physical adsorption is a reversible process, diffusive samplers that rely on physical adsorption are subject to loss of analyte by desorption and diffusion back to the atmosphere, and the overall uptake will be less than that given by equation (1).

The starting point for this analysis is to ask how long a diffusive sampler can remain open, adsorbing and desorbing analyte into the atmosphere until an unacceptable error occurs. This requires two steps, the first of which is to define what is meant by "an unacceptable error". The most common definition of exposure is the time weighted average exposure, defined as:

$$C_{twa} = \int_0^t C\,dt/t \tag{2}$$

where

C_{twa} = the time weighted average (TWA) ambient concentration of analyte, g/cm^3.

To show that this standard is met, a "successful" measurement must be within some predetermined value of the true TWA concentration.

Our objective is to determine the TWA within a predetermined error band for any fluctuating concentration of airborne analyte. Figure 2 shows the basic approach applied here. In this figure, the hypothetical concentration–time curve can be considered as a series of pulses, of equal duration but variable intensity. The residual analyte in the diffusion sampler can then be looked upon as the residue from each pulse. Because of the linearity of the diffusion equation, each pulse can be considered independently. The basic point is that as long as the error in estimating the magnitude of a pulse from its residue is within some predetermined value, then the TWA ambient

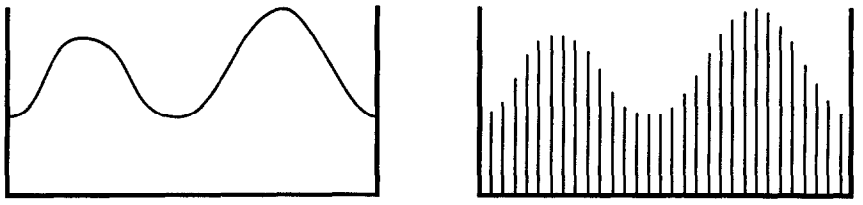

Fig. 2. Representation of a continuous input by a series of pulses. A = Continuous input; B = Pulse representation.

concentration of analyte can also be determined within this predetermined error.

The next step is to determine how long a diffusive sampler can be used to determine the TWA within a predetermined error band. The maximum high side error (overestimation) will occur for uptake at the end of the sampling period, and the maximum low side error (underestimation) will occur for the analyte sampled at the start of the sampling period. If the acceptable high side error in the estimate of the concentration is X%, and the corresponding acceptable low side error in the estimate in the concentration is Y%, then this standard can be met if the maximum percent loss of analyte during the sampling time is:

$$Z = 100\left\{1 - \frac{(100 - Y\%)}{(100 + X\%)}\right\} \tag{3}$$

To give specific examples, if it is desired to determine the TWA within an error band of ±5%, then sampling can continue until the residual analyte from a pulse is reduced by 9.53%, and for an error band of ±25%, the loss can be 40%.

Before determining the maximum time before an unacceptable loss of analyte by desorption can occur, it is necessary to estimate the rate at which the loss of analyte occurs. The required equations are well known, having been previously used to model surface diffusion from a sheet[9–11] before being applied to diffusive samplers.[4,5] Accordingly, the fraction of analyte remaining in the sampler following a pulse input is:

$$m(\tau) = \sum \frac{\alpha \exp(-\tau/\alpha)}{\vartheta_i^2(\vartheta_i^2 + \vartheta_i + \alpha)} \tag{4}$$

where:

ϑ_i = the positive roots of $\vartheta_i \tan(\vartheta_i) = \alpha$

and the two dimensionless parameters used in this calculation, α and τ, are defined as:

$$\alpha = \frac{W}{\epsilon\gamma L} \tag{5}$$

W = thickness of the sorbent bed, cm

γ = tortuosity factor for interparticle diffusion, dimensionless

ϵ = fractional interparticle void volume in the sorbent bed, dimensionless

$$\tau = \frac{tD}{(1-\epsilon)LWK} \tag{6}$$

K = equilibrium partition coefficient for analyte-sorbent, dimensionless, defined as

$$\frac{\text{(g analyte/m}^3\text{ compacted sorbent)}}{\text{(g analyte/m}^3\text{ ambient air)}}$$

Equations (3)–(6) permit the maximum use time, consistent with a predetermined error band, to be calculated. Figure 3 gives this same information graphically. There, the x-axis characterizes the geometry of the diffusive sampler (in terms of the geometric factor, α, and the y-axis gives the maximum sampling time, in terms of the reduced time, τ. Notice the very strong loss of sampling time as the error band is reduced from ±25 to ±5%, especially at high values of the geometric factor.

Application to laboratory validation of diffusive samplers

Laboratory validation of diffusive samplers, using the theory developed here, requires

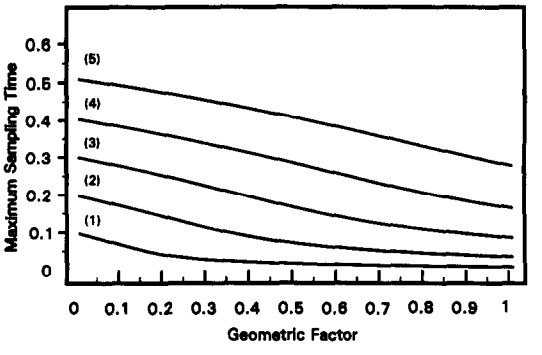

Fig. 3. Sampling time. Error bounds: (1) = ±5%; (2) = ±10%; (3) = ±15%; (4) = ±20%; (5) = ±25%.

measuring the retention of a pulse input by a diffusive sampler. One possible procedure is to expose a set of diffusive samplers to a high concentration of analyte for a short period of time, and then to analyze the retention in the samplers after various periods of time following this exposure. In a similar approach, the analyte lost from the sampler by desorption is collected and measured.[12] This latter procedure is better suited to determining small losses of analyte. In any case, the usual "validation" of diffusive samplers by exposure to a constant concentration of analyte does not seem appropriate if the criterion is that the estimated TWA be within a known error band following exposure to a variable concentration of analyte.

These results show what is ideally possible. Outside the laboratory, non-ideal effects from uneven packing, temperature fluctuations, co-adsorption of additional compounds (including water vapor), will reduce the performance calculated here. Because of the importance of diffusive sampling in monitoring worker exposures, it is important to determine how closely this idealized performance can be attained in the workplace.

REFERENCES

1. M. E. Cassinelli, R. D. Hull, J. V. Crable and A. W. Taess, *Protocol for the Evaluation of Passive Monitors*, in *Diffusive Sampling, An Alternative Approach to Workplace Air Monitoring*, A. Berlin, R. H. Brown, and K. J. Saunders (eds.), pp. 190–208. The Royal Society of Chemistry, Burlington House, London, England, 1987.
2. L. W. Anders, H. E. Mullens and P. L. Sullivan, *Organic Vapor Monitor with Backup Section*; 3M Company Technical Paper R-3520TP, 1981.
3. *PRO-TEK Organic Vapor G-AA Air Monitoring Badge*; E. I. Du Pont de Nemours, Wilmington, DE, U.S.A., 1979.
4. *Vaporgard, Organic Vapor Dosimeter*; Mine Safety Applicances Co.; Pittsburgh, PA, U.S.A., 1985.
5. R. W. Coutant, R. G. Lewis and J. Mulik, *Anal. Chem.*, 1985, **57**, 219.
6. D. W. Underhill, *ibid.*, 1989, **57**, 843.
7. F. Hearl and M. P. Manning, *Am. Ind. Hyg. Assoc. J.* 1980, **41**, 778.
8. D. W. Underhill, *Am. Ind. Hyg. Assoc. J.*, 1983, **44**, 237.
9. A. B. Newman, *Trans. Am. Inst Chem Engrs.*, 1931, **27**, 203.
10. H. S. Carslaw and J. C. Jaeger, *Conduction of Heat in Solids*, Clarendon Press, Oxford, 1959.
11. John Crank, *The Mathematics of Diffusion*, 2nd Ed., Chap. 4, Clarendon Press. Oxford, 1975.
12. G. Hourani and D. W. Underhill, in *Advances in Air Sampling*, Committee of the American Conference of Governmental Industrial Hygienists (eds.), Chap. 8, Lewis Publishers, Chelsea, MI, U.S.A., 1988.

Talanta, Vol. 40, No. 2, pp. 147–155, 1993
Printed in Great Britain.

0039-9140/93 $6.00 + 0.00

SUPERCRITICAL FLUID EXTRACTION OF 2,4-D FROM SOILS USING DERIVATIZATION AND IONIC MODIFIERS

ELIZABETH A. ROCHETTE and JAMES B. HARSH
Department of Crop and Soil Sciences, Washington State University, Pullman, Washington 99164-6420, U.S.A.

and

HERBERT H. HILL, JR
Department of Chemistry, Washington State University, Pullman, Washington 99164-4630, U.S.A.

(*Received* 2 *December* 1991. *Revised* 18 *May* 1992. *Accepted* 20 *May* 1992)

Summary—Supercritical fluid extraction (SFE) with CO_2, a clean and rapid alternative to conventional organic solvent extraction techniques, was investigated for the extraction of 2,4-D from soils using a variety of pre-extraction soil treatments to enhance extraction recoveries. Initial experiments with silylation, ion-pairing, methyl esterification, and ionic displacement are reported. Methyl esterification and ionic displacement during SFE proved to be the most promising approaches for quantitative extraction. Although the SFE procedures were not fully optimized, comparison between SFE and a standard Soxhlet extraction method demonstrated the potential for improving analytical measurement for highly polar pesticides in soil by modifying SFE–CO_2 extraction with derivatizing reagents and ionic solutions.

The herbicide 2,4-D (2,4-dichlorophenoxyacetic acid) is applied widely in the US and Canada, as well as in other countries, for the control of broadleaf weeds.[1–3] It is considered by the EPA to be a herbicide of heavy use which marginally leaches out of the root zone. It has been found in groundwater wells of at least two states in the US.[1]

Because of its polar nature, 2,4-D is difficult to extract from soils. One method used for the extraction of chlorinated hydrocarbons is Soxhlet extraction (EPA method 3540).[4] This method requires an 8–24-hr extraction with an acetone/hexane or methanol/toluene solution, followed by concentration in a Kuderna–Danish apparatus and a derivatization process before gas chromatographic analysis. This is a slow and organic solvent-consumptive method. An alternative method for chlorinated herbicides (EPA method 8150) involves acidifying the soil to pH 2 with HCl, shaking with acetone and then diethyl ether (each 3 times), placing the extract in a separating funnel, adding acidified sodium sulfate, readjusting the pH to 2, separating aqueous and organic layers, re-extracting the aqueous layer with diethyl ether, and evaporating the final extract in a Kuderna–Danish apparatus.[4] The final step, as in the Soxhlet method, is derivatization before gas chromatography.

A relatively new, solvent-efficient and rapid analytical extraction method is supercritical fluid extraction.[5] In this method, gases, such as CO_2 and N_2O, are heated and pressurized above their critical pressures and temperatures to produce supercritical extracting fluids. These fluids have densities intermediate to those of liquids and gases, with many solvating characteristics similar to liquids and diffusivities similar to gases.

To date, CO_2 is the supercritical extracting fluid of choice. It is non-toxic, relatively inexpensive and has conveniently low critical parameters. Unfortunately, while supercritical fluid CO_2 is a good solvent for nonpolar compounds,[5] it does not extract polar compounds well. Extraction recoveries of moderately polar pesticides such as diuron and linuron have been improved by modifying the CO_2 with a small amount of a polar additive such as methanol or ethanol.[6]

For highly polar compounds, modification of the extraction solvent with derivatizing reagents can be used to enhance extraction either by reaction with the solute or the matrix.[7] Hawthorne *et al.*, have investigated *in situ* chemical derivatization for the extraction of such polar analytes as fatty acids from whole cells, phenols from C_{18} sorbent disks, and 2,4-D from soils.[8] These promising results obtained

for the SFE extraction of 2,4-D from soil and sediment encourages further investigation. In this paper we report initial results on the development of sample derivatization and matrix modification methods for the SFE of 2,4-D from soil.

EXPERIMENTAL

Soil samples were spiked with 10 and 40 ppm of 2,4-D acid and extracted by SFE with CO_2 as the extracting fluid. Comparison of various sample treatments prior to extraction were made to determine relative extraction efficiencies of the various methods. These sample treatments included (1) silylation, (2) methyl esterification, (3) ion pairing and (4) ionic displacement. Finally, Soxhlet extraction was compared with SFE using an organic-rich soil containing 4.2% organic carbon.

Soils

One soil used for supercritical fluid extraction was from the 2C horizon of a Hoypus sandy loam collected in Island County, Washington. This soil had a pH of 6.6, electrolytic conductivity (EC) of 0.9 dS/m (saturation extract), and total organic carbon content of 0.3% as determined by wet combustion.[9]

The other soil was an organic-rich soil, the Ap horizon of the Coupeville soil also from Island County, Washington, which had a pH of 8.2, an EC of 0.05 dS/m, and an organic carbon content of 4.2% by weight.

All analyses were performed on air-dried soil.

Spiking procedure

Stocks of 2,4-D acid (purity 98.6%) and 2,4-D methyl ester (purity 97%) (Sigma Chemical Company, St Louis, Missouri) were prepared in acetone. Soils were spiked with 2,4-D acid in all cases, using acetone solutions of the herbicide and allowing the acetone to evaporate under an operating fume hood at laboratory conditions after application to the soil. Spike levels of 40 ppm 2,4-D on soil were achieved by applying 20 ml of a 5.6×10^{-2} g/l. solution of 2,4-D acid in acetone to 28 g of soil. The acetone-soil slurry was stirred and the acetone was allowed to evaporate. Spike levels of 10 ppm were achieved by applying 50 ml of a 1.2×10^{-2} g/l. solution of 2,4-D in acetone to 60 g of soil.

Supercritical fluid extractor

The supercritical fluid extractor is shown in Fig. 1. It was constructed by mounting 2 Valco HPLC/SFC valves (one 8-port and one 6-port) on a stainless steel block (17.5 cm × 7.5 cm ×

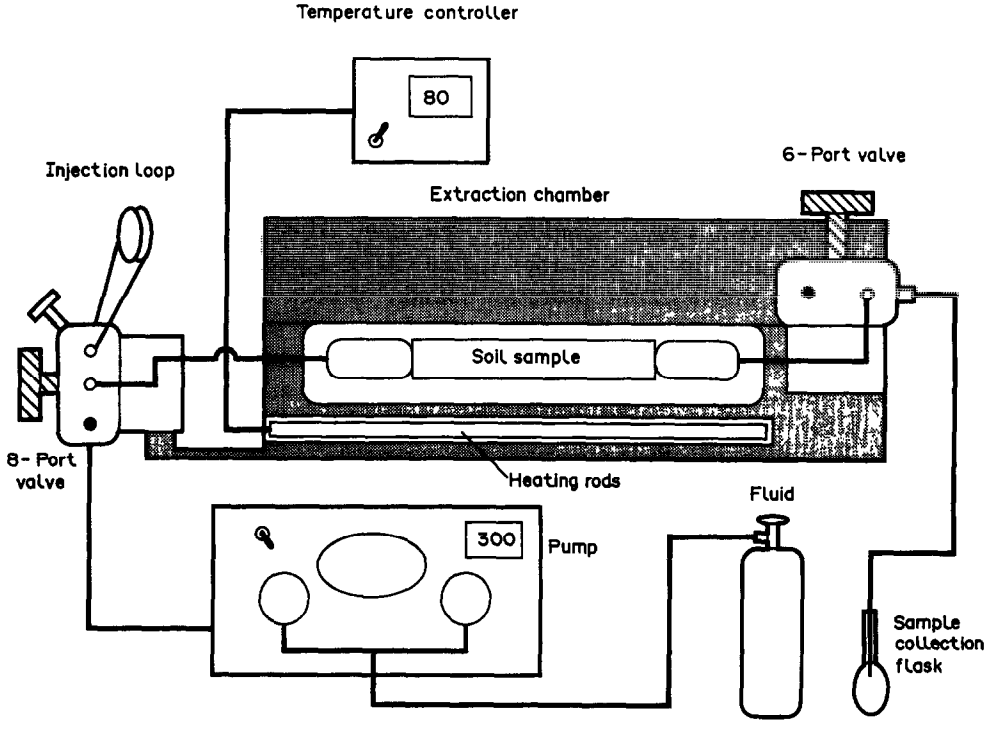

Fig. 1. Schematic of the supercritical fluid extractor.

2.5 cm). The stainless steel block, containing a trough (13.5 cm × 2.9 cm) to house the extraction cell, was heated with two 120 V Watlow heating rods (E4J30) controlled by an OMEGA CN 9000 temperature controller.

The 8-port valve was attached to an Altex Model 100A liquid chromatography pump, and precedes the extraction cell. The Altex pump could be set for specific pressures, though the pressure display showed some oscillation as the pistons alternated strokes. These pressure oscillations were typically from 5 atmospheres below the set pressure to 5 atmospheres above the set pressure. The flow rate of the pump was set at its maximum capability (9.99 ml/min). The 8-port valve was set up to allow injection of derivatizing reagents and solvents through an injection port and calibrated loop into the cell during extraction. The extractor was pressurized to roughly 85 atmospheres and heated to 80°. Injections of reagents were made with a glass syringe into the injection port of the 8-port valve while it was in the load position; the pressure was then raised to the desired level and the valve toggled to inject the solution. Meanwhile, the 6-port valve was in the closed position, stopping flow to the collection vessel.

Flow of CO_2 through a heated (80 to 90°) 60-μm fused-silica restrictor (roughly 0.5 m) was turned on or off with the 6-port valve. Static extractions (extractions in which the supercritical fluid is in contact with the matrix without fluid flow) were performed with the 6-port valve in a closed position. Dynamic extractions (extractions in which the supercritical fluid continuously flows through the matrix) were performed with the 6-port valve in an open position.

The extraction cell used was a Keystone Scientific 0.8-ml SFE cell made of stainless steel and sealed on each end with PEEK-rimmed, 2-μm stainless steel frits. PEEK unions were situated before and after the extraction cell to allow for easy removal and replacement of the extraction cell during sample loading and unloading. PEEK ferrules are replaceable and the wear problems of stainless steel are avoided.

For all methanol-based reagents added to the extractor, the SFE cell, 8-port valve, and tubing to the cell were rinsed with demineralized water and methanol as soon as possible after use; for the valve this involved making several injections of demineralized water followed by methanol. Hexane was used instead of methanol when Tri-Sil Concentrate was the additive. We believe that, with the possible exception of BF_3/methanol, this procedure has prevented degradation of the extractor.

Silylation

Silylations were performed using Tri-Sil Concentrate (Pierce, Rockford, IL, U.S.A.), which is a 2:1 mixture of hexamethyldisilazane (HMDS) and trimethylchlorosilane (TMCS). A volume of 200 μl was injected on to 1.2 g of soil, unless indicated otherwise. Samples treated with phosphate and hydrochloric acid, to be described, underwent SFE *in situ* silylation. Silylation extraction conditions were 380 atmospheres, 80°, in static mode for 15 min, followed by dynamic mode for 60 min at 340 atmospheres, unless stated otherwise. Extracts from silylation experiments were collected in 2 ml of hexane, and were injected directly into the GC after volume adjustments with hexane.

Extracts from extractions in which *in situ* silylation was not performed were derivatized in solution with 200 μl of Tri-Sil concentrate to 2 ml of solution, and a reaction time of at least 5 min at room temperature as recommended by the manufacturer. This procedure was followed for standards of 2,4-D acid to convert them to 2,4-D silyl esters.

Methyl esterification

Methyl esterification was performed using a BF_3 (14%)/methanol solution (Alltech Associates, Deerfield, IL, USA); this was used during extraction with SFE as well as for post-extraction derivatization as needed. Extraction conditions for methyl esterification were 300 atmospheres, 80°, for 10 min in the static mode, followed by dynamic extraction for 20 min at 300 atmospheres, 80°. Extracts were collected in 2 ml of methanol. Post-extraction treatment after *in situ* methyl esterification involved treatment of the extract with 1*M* aqueous sodium chloride solution and partitioning of the methyl ester into benzene before gas chromatographic analysis (1 extract:1 BF_3/methanol:1*M* sodium chloride:1 benzene, v:v:v:v). A standard, prepared from 2,4-D methyl ester powder, was dissolved in methanol and underwent the same treatment as the extract. The 2,4-D methyl ester powder was stored in a refrigerated (4°) desiccator; its low melting point (38°) precludes oven drying. Also, a standard prepared from 2,4-D acid powder was dissolved in methanol, underwent BF_3/methanol derivatization in solution for at least 5 min at roughly 60° in a sealed derivatization

vial, and then underwent the same treatment as the supercritical fluid extract (1 extract:1 BF_3/methanol:1*M* sodium chloride:1 benzene, v:v:v:v).

Ion pairing extraction

A 0.2*N* methanolic solution of m-trifluoromethylphenyl trimethylammonium hydroxide (TFTMFA) (Meth Prep 2, Alltech Associates, Deerfield, IL, USA) used for gas chromatographic on-column derivatization, was added during SFE. A volume of 300 μl of this solution was injected into the extraction cell and allowed to react with 1.1 g of soil under supercritical fluid conditions of 300 atmospheres, 80°, in static mode for 10 min, followed by dynamic mode for 20 min. The extracts were collected in 2 ml of methanol and were injected directly into the GC for analysis. Standards of 2,4-D methyl ester powder were prepared in methanol. Also, standards of 2,4-D acid powder were prepared in a 0.2*N* TFTMPA/methanol mixture (300 μl 0.2*N* TFTMPA to 2 ml of solution) and directly injected into the GC for analysis.

Methanol-modified extraction was identical to the TFTMPA extraction, except that 300 μl of methanol was injected onto the sample rather than TFTMPA. After the methanol-modified extraction, 300 μl of TFTMPA was added to the extract and the volume was adjusted to 2 ml.

Ionic displacement

Soil phosphate treatment involved addition of 0.2 ml of an aqueous solution of 1m*M* phosphate as phosphoric acid, adjusted to pH 4 with potassium hydroxide, to 1.2 g of soil. Addition of the phosphate solution was made to the soil in the SFE cell; the solution was allowed to evaporate for 7 hr under an operating fume hood, until the soil appeared dry by visual inspection. The coarse-grained nature of the soil allowed for relatively rapid drying. Extraction conditions were 380 atmospheres, 80°, 60 min in dynamic mode. The extract was treated in solution with Tri-Sil concentrate as was described in the silylation section. After 200 μl of Tri-Sil was added, the extraction conditions were 380 atmospheres, 80°, 15 min in static mode, followed by 45 min in dynamic mode at 340 atmospheres, 80°. Extracts were collected in 2 ml of hexane.

Soil hydrochloric acid treatment involved the addition of 0.2 ml of a 0.01*N* solution of hydrochloric acid in acetone to 1.2 g of soil to reduce the soil–acetone solution to a pH of roughly 2. The acetone was allowed to evaporate prior to silylation and extraction. Extraction conditions were 380 atmospheres, 80°, 15 min in static mode, followed by 40 min in dynamic mode, at 340 atmospheres, 80°. The hydrochloric acid-treated sample was treated *in situ* with 200 μl of Tri-Sil concentrate during extraction. The extract was collected in 2 ml of hexane, and injected directly into the GC for analysis after volume adjustments with hexane, as were extracts from silylation experiments.

Calcium chloride treatment involved adding $CaCl_2 \cdot 2H_2O$ dissolved in methanol (0.2*M*) to the extraction cell (300 μl to 1.1 g of soil) under supercritical fluid conditions. Extraction conditions were 300 atmospheres, 80°, 10 min in static mode, followed by 20 min in dynamic mode at 300 atmospheres, 80°. Extracts were collected in 2 ml of methanol. The extracts underwent BF_3/methanol derivatization in solution, and otherwise the same treatment (1*M* sodium chloride addition, partitioning into benzene) as that described for methyl esterification extracts. Likewise, the same 2,4-D methyl ester and 2,4-D acid standard preparation was performed as that of the methyl esterification experiment.

Some concern might be expressed regarding the use of chloride and its potentially corrosive effects on the high pressure stainless steel extractor and fittings. To date we have noticed no corrosive effects of methanolic calcium chloride treatment. The extractor, of course, was thoroughly cleaned after each use.

SFE collection efficiency

Lindane (γ-1,2,3,4,5,6 chlorocyclohexane) was used as a check on collection efficiency by placing 3 μl of a 1-ppm acetone solution onto the filter frit on the outlet end of the extraction cell, and allowing the acetone to evaporate before cell closure. Extraction conditions were 300 atmospheres, 80°, 10 min in static mode, followed by 20 min in dynamic mode under the same conditions. The lindane was collected in 2 ml of methanol. The recoveries obtained were 104, 94, 101 and 99% for four identical trials. Since lindane is more volatile (m.p. 112°) than 2,4-D (m.p. 138°), high collection efficiencies were assumed for 2,4-D.

Soxhlet extraction

Soxhlet extractions (EPA method 3540),[4] were performed using 6 g of soil placed in an acid-washed glass extraction thimble. The thimble was placed in the upper portion of an acid-

washed standard Soxhlet extractor with 300 ml of acetone/hexane (1:1) in the lower flask, heated in a heating mantle, and allowed to cycle for 24 hr. The extract was evaporated to 10 ml using an acid-washed 500-ml Kuderna–Danish apparatus and Snyder column, passed though 2 g of baked Na_2SO_4, which was further rinsed with 3 × 2-ml portions of acetone into the collection flask; the collected extract was quantitatively transferred using acetone to an acid-washed 40-ml Kuderna–Danish apparatus with a Snyder column, and further evaporated to a volume of approximately 0.5 ml. Soxhlet extracts, and standards of 2,4-D acid prepared in 0.5 ml of acetone/hexane (3:1) underwent BF_3/methanol derivatization (1 ml BF_3/methanol), 1*M* aqueous sodium chloride addition (1 ml), and partitioning into 5 ml of benzene. Standards of 2,4-D methyl ester were prepared in 0.5 ml of acetone/hexane (3:1), were mixed with 1 ml of methanol, 1 ml of 1*M* aqueous sodium chloride, and were partitioned into 5 ml of benzene.

This Soxhlet procedure gave recoveries of 98 and 96% of the 2,4-D acid added directly to the Soxhlet without a soil matrix.

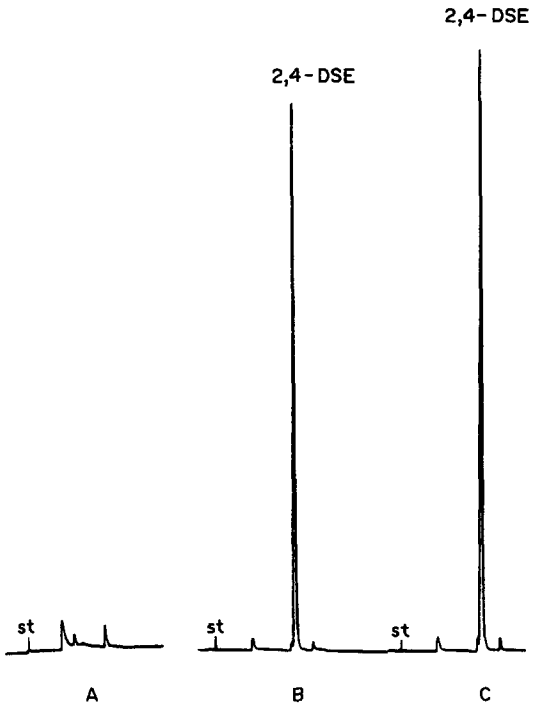

Fig. 2. Chromatograms of supercritical fluid extracts of 2,4-D silyl esters. A. SFE procedural blank prior to extraction B. B. Silylation in the SFE cell during extraction without soil present. C. Silylation under laboratory conditions using the same 2,4-D mass as B.

Chromatography

Analyses were performed with a Tracor gas chromatograph equipped with an 18-meter DB-5 capillary column, a split-mode injection system, and an electron capture detector (ECD). Analyses for silyl esters of 2,4-D were performed using a column temperature set at 190°, injector at 250°, column flow of 0.8 ml/min, and an ECD temperature set at 325°. For methyl esters of 2,4-D, the column temperature used was 180°, while all other conditions are the same as for silyl esters.

RESULTS AND DISCUSSION

Silyl esterification

Silylation of 2,4-D under supercritical fluid conditions was successful when a known amount of 2,4-D was placed in the cell in the absence of soil. Figure 2B shows a chromatogram of 2,4-D silylated under SFE conditions, and Fig. 2C shows a chromatogram of a standard of 2,4-D derivatized under laboratory conditions. This extraction without matrix recovered 91% of the 2,4-D as 2,4-D silyl ester.

When 1.2 g of 2,4-D-spiked soil (40 ppm) were placed in the extraction cell with no derivatizing reagent added, no 2,4-D was extracted using supercritical CO_2 (Fig. 3B). Addition of 200 μl of Tri-Sil Concentrate (which fills the soil pores with solution) recovered approximately 18% of the 2,4-D (Fig. 3C) from the spiked soil. Second and third subsequent additions of Tri-Sil concentrate recovered approximately 7 and 6%, respectively, of the original 2,4-D in the sample (Fig. 3D and 3E).

The average recovery for 6 independent extractions was 31% with a standard deviation of 9% (Table 1). For soils containing more moisture than the 0.4% of this sample, the use of silylating reagents is likely to be even more of a problem since water may interfere with silylation. Another disadvantage of making 2,4-D silyl esters is that these esters are not commercially available, making standard preparation a source of uncertainty in the results. However, 2,4-D methyl esters are commercially available and can be used to test recoveries from supercritical fluid extractions.

Methyl esterification

The methyl ester of 2,4-D was formed in the extraction cell using BF_3/methanol in soil spiked at the 10 ppm level. BF_3-catalyzed/methanol derivatization is commonly used for esterifying

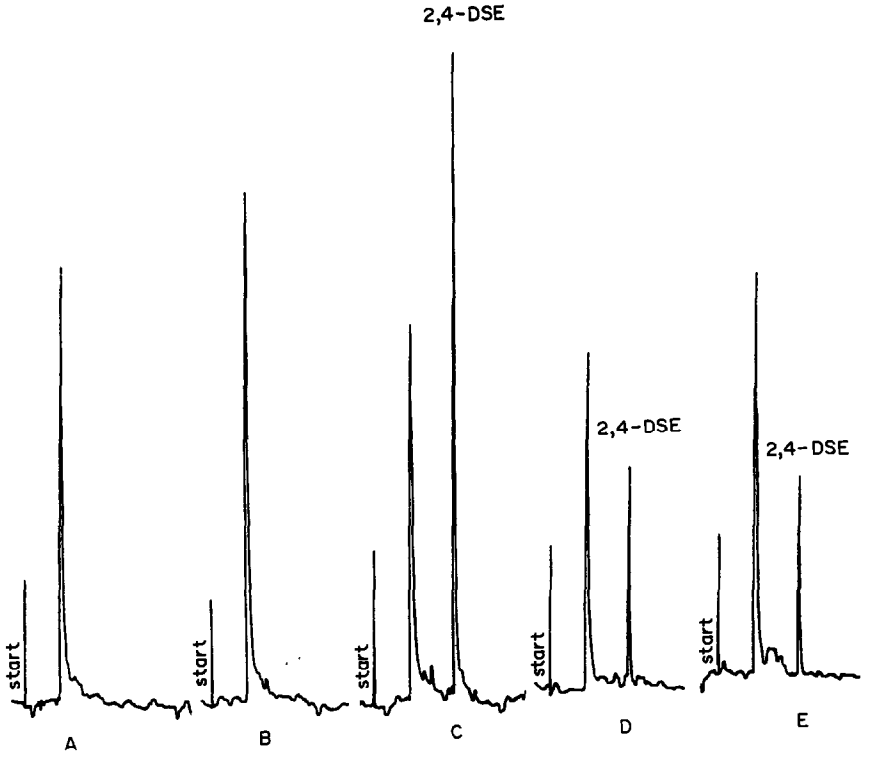

Fig. 3. Chromatograms of supercritical fluid extracts resulting from successive additions of Tri-Sil concentrate to 2,4-D-spiked soil in the extraction cell. A. Procedural blank prior to extraction B. B. Soil with no Tri-Sil added. C, D, E. First, second, and third increments (200 μl each) of Tri-Sil added to the soil, respectively.

2,4-D in solutions for gas chromatography,[11-16] and has been used by Hawthorne *et al.*, to recover 2,4-D from spiked and agricultural soil by supercritical fluid extraction.[8]

For solutions, BF_3/methanol is normally used at elevated temperatures (above the boiling point of methanol), and takes roughly 5 to 10 min. These conditions were met during SFE in the work of Hawthorne *et al.*,[8] and in ours; however, we found it necessary to destroy the BF_3 after extraction with an aqueous solution (such as 1*M* sodium chloride), and to partition the 2,4-D methyl ester into a non-polar solvent such as benzene for gas chromatography to prevent deterioration of the GC column. Initially when extracts and standards with BF_3/methanol were injected into our GC with a glass injector, 2,4-D methyl ester peaks were normal. However, use of the GC twenty-four hours later gave substantially broadened peaks. Peak widths at half maximum of 2,4-D methyl ester standards (not containing BF_3) were 2.3 times greater than before BF_3 injections. After the subsequent replacement of the glass injector and removal of roughly 0.3 m of the column, chromatographic efficiency was restored.

Another problem experienced with BF_3/methanol in the SFE was the development of holes at unions made of PEEK during the second extraction. This prevented multiple extractions and would make the routine use of BF_3 difficult and prompted us to abandon BF_3 as an *in situ* derivatizing reagent. During the first extraction, however, a recovery of 90% of the 2,4-D as its methyl ester was obtained (Table 1).

Table 1. SFE recoveries of 2,4-D from Hoypus sandy loam using various modifiers

CO_2 Modifier	No. trials	Recovery	Form of 2,4-D
No modifier added	5	0	Acid
Tri-Sil conc.	6	31 ± 9%	Silyl ester
0.2*M* $CaCl_2$/MeOH	2	86%, 87%	Acid
BF_3/MeOH	1	90%	Methyl ester
MeOH	2	6%, 6%	Acid
0.2*N* TFTMPA/MeOH	2	19%, 14%	Undetermined

Ion pairing

When an ion-pairing reagent, m-trifluoromethlphenyl trimethylammonium hydroxide (TFTMPA) was added to the soil sample during extraction, improved recoveries of 2,4-D were

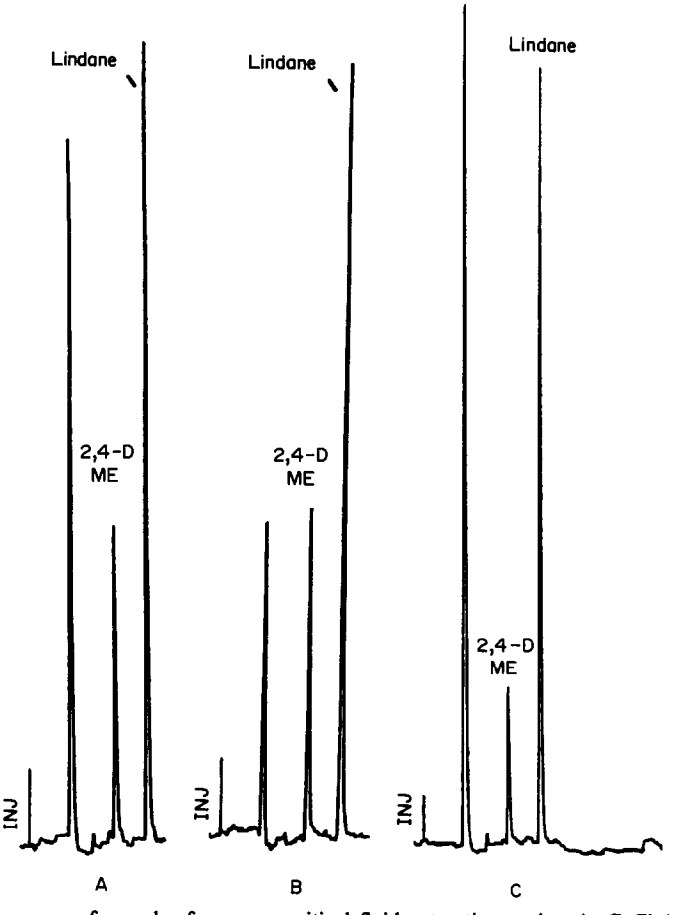

Fig. 4. Chromatograms of samples from supercritical fluid extractions using A. $CaCl_2$/methanol with post-extraction derivatization with BF_3/methanol, and B. BF_3/methanol derivatization during extraction (Hoypus zc). C. $CaCl_2$/methanol with post-extraction derivatization from the soil containing 4.2% organic carbon. Lindane was used as an internal standard.

obtained over those when the sample was extracted with methanol alone (Table 1). Apparently, TFTMPA extracts the 2,4-D acid by forming the trifluoromethylphenyl trimethylammonium salt, which dissolves into the supercritical fluid as an ion pair. Upon introduction into the hot gas chromatographic injector, the ion pair is thermally decomposed to form the methyl ester.[10,17] The use of TFTMPA or other quaternary ammonium additives provides an attractive alternative to BF_3/methanol treatment because the extracts require no post-extraction treatment. Unfortunately, the overall 2,4-D recoveries from SFE experiments in which TFTMPA was the additive were low compared to standards of 2,4-D methyl ester (14–19%).

Table 2. Comparison of standard Soxhlet extraction to $CaCl_2$-modified CO_2 SFE for the extraction of 2,4-D from organic-rich Coupeville Ap soil

Method	No. trials	Recovery	Form of 2,4-D
0.2*M* $CaCl_2$/MeOH on organic-rich soil	2	52%, 42%	Acid
Soxhlet on organic-rich soil	2	23%, 26%	Acid

Ionic displacement

In addition to ion pairing, TFTMPA may have been serving as an ion displacement reagent. Either the quaternary ammonium cation and/or its counterion may have displaced the acid or its conjugate base from active sites on the soil. To investigate this possibility in more detail, experiments with phosphate, hydrochloric acid and calcium chloride were made.

Because 2,4-D is a weak acid it may be dissociated and adsorbed by the soil as an anion. Thus, phosphate at a pH of 4 was chosen as an anion exchanging reagent. Under acidic conditions, phosphate is known to form inner-

sphere complexes with metal hydroxides by exchanging with anions in the soil to become irreversibly adsorbed.[18] The phosphate-treated soil was supercritically extracted with carbon dioxide. This extract was silylated after collection and analyzed for the 2,4-D silyl ester.

Unfortunately, the phosphate treatment produced an extraction of only about 19% of the adsorbed 2,4-D in the soil. However, remember that no 2,4-D can be extracted from this soil without some treatment, even though the acid form is soluble in supercritical carbon dioxide. After this extraction, 200 μl of the silylating reagent was added to the sample but only about 7% more of the original 2,4-D was recovered in this step for a total recovery of 26%. This was about the same as that observed for silylation alone. The addition of phosphate had little improvement on extraction efficiency from that of simple silylation.

The partial success of phosphate treatment indicated that perhaps some of the 2,4-D was adsorbed in the free acid form. Treatment with hydrochloric acid and silylation prior to extraction produced an enhanced recovery of 42%. We speculate that this was due to competitive displacement of hydrogen-bonded acid to hydroxy and/or anionic sites with protons to release the free acid which then formed the silyl ester.

Encouraged by these results, a strong cation displacing reagent, calcium chloride, was added to the soil during extraction. In this case the 2,4-D was extracted as the free acid and converted to the methyl ester for GC analysis after collection (Fig. 4). For two independent but identical experiments, extraction yields were 86 and 87%. Remember that when methanol without calcium chloride was used under the same conditions, only 6% yields of 2,4-D were obtained. The choice of calcium chloride was in part based on work by Cheng[19] in which a combination of methanol and calcium chloride was notably more efficient at extracting atrazine from soil than was methanol alone. This work was done using liquids only (not supercritical fluids).

Organic-rich soil

After these encouraging results, experiments with various soils were initiated. An example of these experiments is that of an organic-rich soil (4.2% organic carbon by weight). This soil was spiked with 2,4-D at the 10 ppm level. The results of duplicate experiments are shown in Table 1, including the results of comparative Soxhlet extractions. The recovery from this soil was 52 and 42% (Table 2). The Soxhlet extraction technique was notably less efficient, giving only 25 and 26% recovery of the 2,4-D. A lower Soxhlet recovery was also seen for the sandy soil, which gave a Soxhlet recovery of 47%.

Critique of methyl ester standard preparation

For experiments in which GC analyses involved methyl esters, the standard was prepared from 2,4-D methyl ester powder. For comparison, standards were also prepared from 2,4-D acid powder and then converted to the methyl ester as described in the experimental section. When 2,4-D acid standards derivatized with BF_3/methanol were used recoveries for the methanolic calcium chloride displacement experiment were 72 and 72%, rather than the 86 and 87% recoveries reported in Table 1 for the methyl ester powder standard. Similarly, the 2,4-D acid standard gave an 80% recovery compared to the 90% recovery determined with the methyl ester standard and reported in Table 1 for the BF_3/methanol modified extraction. The lower recoveries calculated using the 2,4-D acid standard relative to the 2,4-D methyl ester standard may have been due to partial hydrolysis of the methyl ester powder.

In contrast, recoveries determined using standards prepared from the methyl ester powder were substantially lower for the ion-pairing and methanol-modified experiments than those determined using standards prepared from the acid powder. For the methanol-modified experiment, SFE recoveries of 2,4-D determined with the 2,4-D acid standards were 11 and 15%, compared to the 6 and 6% reported in Table 1 based on the methyl ester standards. For the 0.2*N* TFTMPA-modified experiment, SFE recoveries determined with the 2,4-D acid standards were 69 and 71%, compared to the 19 and 14% reported in Table 1 based on the methyl ester standards. We attributed this to the low derivatization yield of 0.2*N* TFTMPA. Under the conditions used in this study, 0.2*N* TFTMPA converted only 24 to 33% of the 2,4-D acid standards in solution to the ester form. Thus, it is possible that the low extraction yields reported in Table 1 for the TFTMPA modifier may have been due to insufficient derivatization.

Hawthorne *et al.*, who obtained a recovery of 2,4-D >90% with TMPA (trimethylphenyl-

ammonium hydroxide), used a relatively high concentration of TMPA (about 20% in methanol) with a 15-min derivatization step and multiple extractions. Thus, with optimization of the esterification process in the GC, ion-pairing extraction followed by thermal decomposition esterification appears promising as an approach for the extraction and quantification of 2,4-D from soils.

CONCLUSIONS

This is the first report of the use of a salt solution to increase extraction efficiencies of polar compounds during SFE. The possibilities for salt-modified SFE look promising for the extraction of polar compounds. However, considerable optimization with respect to salt type, concentration and extraction time is needed before a final recommendation concerning this approach can be made.

Acknowledgements—The activities on which this report is based were financed in part by the Department of the Interior, U.S. Geological Survey, through the State of Washington Water Research Center. The contents of this publication do not necessarily reflect the views and policies of the Department of the Interior, nor does mention of trade names or commercial products constitute their endorsement by the United States Government. The SFE described was designed by R. Mark Worthington, who also contributed valuable technical advice for GC and SFE analyses. Several useful technical suggestions were provided by Michael Gallagher and Jeffrey Boyle. Editorial contributions were made by Andrew V. Ogram and Jeffrey L. Smith.

REFERENCES

1. J. A. Goodrich, B. W. Lykins and R. M. Clark, *J. Environ. Qual.*, 1991, **20**, 707.
2. A. E. Smith, *Weed Res.*, 1980, **20**, 355.
3. *Idem*, *ibid.*, 1978, **18**, 275.
4. U.S. EPA, *Test Methods for Evaluating Solid Wastes: SW-846*, Vol. I, U.S. Environmental Protection Agency, Office of Solid Waste and Emergency Response, Washington, D.C., 1986.
5. S. B. Hawthorne, *Anal. Chem.*, 1990, **62**, 633A.
6. M. E. P. McNally and J. R. Wheeler, *J. Chrom.*, 1988, **447**, 53.
7. J. W. Hills, H. H. Hill, Jr and T. Maeda, *Anal. Chem.*, 1991, **19**, 2152.
8. S. B. Hawthorne, D. J. Miller, D. E. Nivens and D. C. White, *ibid.*, 1992, **64**, 405.
9. D. W. Nelson and L. E. Sommers, *Indiana Acad. Sci. Proc.*, 1975, **84**, 456.
10. A. Darbre, In *Handbook of Derivatives for Chromatography*, K. Blau and G. S. King (eds.), Heyden and Sons, London, 1978.
11. J. Horner, S. S. Que Hee and R. G. Sutherland, *Anal. Chem.*, 1974, **46**, 110.
12. M. A. Baim and H. H. Hill, Jr., *J. Chrom.*, 1983, **270**, 631.
13. W. P. Cochrane, *J. Chrom. Sci.*, 1979, **17**, 124.
14. B. A. Olson, T. C. Sneath and N. C. Jain, *J. Agric. Food Chem.*, 1978, **26**, 640.
15. Y. Erner and C. W. Coggins, Jr., *J. Am. Soc. Hort. Sci.*, 1989, **114**, 846.
16. C. R. Sell and J. C. Maitlen, *J. Agric. Food Chem.*, 1983, **31**, 572.
17. D. K. McCreary, W. C. Kossa, S. Ramachandran and R. R. Kurtz, *J. Chrom. Sci.*, 1978, **8**, 329–331.
18. G. Sposito, *The Chemistry of Soils*, Oxford University Press, New York, 1989.
19. H. H. Cheng, *Intern. J. Environ. Anal. Chem.*, 1990, **39**, 165.

Talanta, Vol. 40, No. 2, pp. 157–165, 1993
Printed in Great Britain.

0039-9140/93 $6.00 + 0.00

ACID–BASE AND DISTRIBUTION EQUILIBRIA OF 5,7-DICHLORO-2-METHYL-8-HYDROXYQUINOLINE IN BRIJ-35 MICELLAR MEDIA SOLUTIONS

J. L. BELTRÁN,* R. CODONY, M. GRANADOS, A. IZQUIERDO and M. D. PRAT
Departament de Química Analítica, Universitat de Barcelona, Diagonal 647, 08028 Barcelona, Spain

(*Received* 2 *August* 1991. *Revised* 25 *May* 1992. *Accepted* 25 *May* 1992)

Summary—The acid–base equilibria of 5,7-dichloro-2-methyl-8-hydroxyquinoline (HQ) have been examined spectrophotometrically in aqueous micellar solution of the non-ionic surfactant Brij-35. The differences between apparent pK_a values at different surfactant concentrations can be quantitatively explained in terms of the extraction constants of the neutral species HQ and the ion-pair Na^+Q^-. Calculations have been performed by means of SPDIS program, developed in this work to handle multiwavelength spectrophotometric data in micellar systems.

Aqueous micellar media are widely used in different areas of analytical chemistry and several reviews concerning their analytical applications have been published.[1–4] One important property of micelles is their ability to solubilize a wide variety of compounds which are insoluble or slightly soluble in water. The incorporation of a solute into micellar systems can lead to important changes in its molecular properties. Surfactants usually affect spectral parameters: the intensity of the absorption bands can be increased and shifts in the absorption maxima of reagents and complexes are observed.[5,6] Moreover, the acid–base and complexation equilibria involved in these systems are also influenced by surfactants.[7,8]

Several theories have been proposed to account for the changes in spectral parameters and equilibria.[9–15] One of the most successful is the partition model,[12–15] in which it is assumed that micelles act as a separate phase uniformly distributed throughout the solution, and distribution of neutral species and ion associates between the aqueous phase and micelles can occur.

In this work the effect of the non-ionic surfactant polyoxyethylenlaurylether (Brij-35) on the apparent dissociation constants of 5,7-dichloro-2-methyl-8-hydroxyquinoline or chlorquinaldol (HQ) was studied by spectrophotometry. Interest in chlorquinaldol is related to its chelating ability towards metal ions and the enhancement of the fluorescence of some metal–chlorquinaldol complexes observed in non-ionic surfactant media.[16,17]

Although studies of equilibria in micellar media are usually carried out by means of uv–visible spectrophotometry,[5,8,18,19] to date no program has been able to calculate extraction and distribution constants from multiwavelength spectrophotometric data in these systems, where there is no physical separation between the two phases. Therefore, the constants were determined from data obtained at one wavelength and it was impossible to obtain the spectra of the species extracted into the micellar phase.

In order to improve the data treatment of this kind of system, the SPDIS program has been developed. It has been designed to handle spectrophotometric data taking into account the presence of distribution processes between aqueous and micellar phases.

By using SPDIS a quantitative assessment of the equilibria involved in the system studied has been obtained. The proposed model explains the differences observed between the apparent acid–base constants and the aqueous acid–base constants. Additionally, the effect of Brij-35 media on the fluorescence of chlorquinaldol has been studied and the variations in fluorescence intensity have been related with distribution equilibria between micellar and aqueous phases.

*Author for correspondence.

EXPERIMENTAL

Apparatus

The spectrophotometric measurements were carried out on a Beckman DU-7 instrument, using a 1.00-cm quartz cuvette. The spectrophotometer was connected to an IBM personal computer for data collection.

For fluorimetric measurements a Perkin Elmer LS-50 spectrofluorimeter, with a 1.00-cm quartz cuvette, was used.

The pH values were measured on a Radiometer PHM84 pH-meter, equipped with a Ross combined pH-electrode (Orion 81-02). The potentiometric system was calibrated prior to use with 4.008, 6.863 and 9.185 buffer solutions, prepared from Merck salts according to DIN 19266.

All spectrophotometric, fluorimetric and potentiometric measurements were made at $25.0 \pm 0.1°$.

Reagents

5,7-Dichloro-2-methyl-8-hydroxyquinoline (Supro, Troponwerke, Köln) was recrystallized twice from ethanol solution. Fresh $10^{-3}M$ solutions were prepared daily by dissolving the reagent in $0.02M$ hydrochloric acid. Brij-35 (Fluka) was used without further purification. All other chemicals were of analytical grade. Buffer solutions were prepared according to Perrin and Dempsey[20] from formic acid and sodium hydroxide, sodium dihydrogenphosphate and sodium hydroxide, and tris(hydroxymethyl)-aminomethane and hydrochloric acid. Ionic strength of the working solutions was kept constant at $0.1M$ by addition of sodium chloride.

Procedures

In order to determine the dissociation constants of chlorquinaldol, several series of solutions were prepared by adding hydrochloric solution of the reagent to 50-ml standard flasks, containing the buffer ($2 \times 10^{-3}M$), the ionic medium and the surfactant. Final concentration of chlorquinaldol was about $2 \times 10^{-5}M$. After thermic equilibration, spectra of the solutions were recorded, from 220 to 450 nm, at 5-nm increments, and finally the pH of the solutions was measured and converted into hydrogen ion concentration, according to the Davies equation.[20] (The activity coefficient calculated for the hydrogen ion was 0.771 at 25° and $0.1M$ ionic strength). Fluorimetric measurements were carried out at $\lambda_{ex} = 350$ nm and $\lambda_{em} = 530$ nm, using excitation and emission slit widths of 5 and 10 nm, respectively.

Data treatment

Dissociation constants. The dissociation constants of chlorquinaldol and the molar absorptivities of its pure species were determined using the program STAR.[21] This program was also used in the determination of "apparent" dissociation constants in micellar media, at different concentrations of surfactant. The apparent dissociation constants (K^*_{a1} and K^*_{a2}) are defined as:

$$K^*_{a1} = \frac{[HQ]^* \cdot [H^+]}{[H_2^+Q]^*} \quad K^*_{a2} = \frac{[Q^-]^* \cdot [H^+]}{[HQ]^*} \qquad (1)$$

where $[H_2Q^+]^*$, $[HQ]^*$ and $[Q^-]^*$ are the total concentration of the cationic, neutral and anionic species of chlorquinaldol, regardless of whether they are in the aqueous or micellar phase.

Taking into account that in micellar media the dissociation constants calculated by STAR are apparent, the molar absorptivities obtained with the program are also apparent. From the variation in the apparent dissociation constants and molar absorptivities, at different surfactant concentrations, the species that participate in distribution processes between the aqueous and micellar phases can be inferred.

Distribution equilibria. For the treatment of the extraction equilibria in micellar phases, the SPDIS program, based on the program STAR, was developed. As SPDIS is written in Turbo-PASCAL (5.0) for personal computers (IBM-PC/AT or compatible). The program was used for the determination of the extraction and distribution constants from absorbance data of micelle-containing solutions. The mathematical background is as follows: in a micellar medium, the volume of the micellar pseudophase (Vm) is given by:

$$Vm = (C_S - \text{cmc}) \cdot V \cdot V\phi \qquad (2)$$

where C_S is the total concentration of surfactant, cmc the critical micelle concentration (both in mole.l^{-1}), $V\phi$ the partial molar volume of micellar phase (l./mole), and V the total volume of the solution ($V = Vm + Vw$, Vw: volume of the aqueous phase). The ratio R, of the micellar volume to the total volume can be written as:

$$R = Vm/V = (C_S - \text{cmc}).V\phi \qquad (3)$$

The absorbance of a solution at a j determined wavelength (A_j) will be:

$$A_j = A_{j(w)} + A_{j(m)} \quad (4)$$

where $A_{j(w)}$ and $A_{j(m)}$ are the absorbances of the aqueous and micellar phases, respectively. Assuming a pathlength equal to 1.00 cm, these absorbances can be written as:

$$A_{j(w)} = \sum_{i=1}^{ni} C_{i(w)} \cdot \epsilon_{j,i(w)} \cdot Vw/V = \sum_{i=1}^{ni} C_{i(w)} \cdot \epsilon_{j,i(w)} \cdot (1 - R) \quad (5)$$

$$A_{j(m)} = \sum_{i=1}^{ni} C_{i(m)} \cdot \epsilon_{j,i(m)} \cdot Vm/V = \sum_{i=1}^{ni} C_{i(m)} \cdot \epsilon_{j,i(m)} \cdot R \quad (6)$$

where ni is the number of absorbing species, $C_{i(w)}$ and $C_{i(m)}$ are the concentrations of the i-species in aqueous and micellar phases, and $\epsilon_{j,i(w)}$ and $\epsilon_{j,i(m)}$ the molar absorptivities at the j-wavelength of the i-species in aqueous and micellar phases.

In this work, the values of R varied from 1.83×10^{-5} to 1.96×10^{-3}, thus the factor $(1 - R)$ in equation (5) can be assumed equal to unity ($V = Vw$).

If we consider that an extraction equilibrium takes place between aqueous and micellar phases we can write:

$$C_{i(m)} = K_{Di} \cdot C_{i(w)} \quad (7)$$

K_{Di} being the distribution constant of the i-species.

The program SPDIS was used for the determination of these distribution constants and the molar absorptivities of the species extracted in micellar phase, from absorbance data. For these calculations, previous knowledgement of the formation constants of the species in aqueous phase, and their molar absorptivities, are advisable.

The algorithms used for the refinement of equilibrium constants, and for the calculation of molar absorptivities, are the same as used in STAR. However, there is a minor change in the description of solution equilibria to take into account the extracted species. For each component of the solution (*e.g.*, the r-component), its total concentration (C_r), is equal to:

$$C_r = \sum_{i=1}^{ni} sc(i,r) \cdot C_{i(w)} \cdot \frac{Vw}{V} + \sum_{i=1}^{ni} sc(i,r) \cdot C_{i(m)} \cdot \frac{Vm}{V} \quad (8)$$

where $sc(i,r)$ is the stoichiometric coefficient of the r-component in the i-species.

Substituting the values $(Vw/V) = 1$ and $(Vm/V) = R$ the following equation is obtained:

$$C_r = \sum_{i=1}^{ni} sc(i,r) \cdot C_{i(w)} + \sum_{i=1}^{ni} sc(i,r) \cdot C_{i(m)} \cdot R \quad (9)$$

And, taking into account equation (7):

$$C_r = \sum_{i=1}^{ni} sc(i,r) \cdot C_{i(w)} + \sum_{i=1}^{ni} sc(i,r) \cdot C_{i(w)} \cdot K_{Di} \cdot R \quad (10)$$

On the other hand, the concentration of each species in aqueous phase is defined as:

$$C_{i(w)} = \beta_{i(w)} \cdot \prod_{k=1}^{nk} X_{k(w)}^{sc(i,k)} \quad (11)$$

Where nk is the number of components, $\beta_{i(w)}$ the formation constant of the i-species in aqueous solution, and $X_{k(w)}$ the free concentration of the k-component in aqueous phase. Rearranging equations (10) and (11) we obtain:

$$C_r = \sum_{i=1}^{ni} sc(i,r) \cdot \beta_{i(w)} \cdot \prod_{k=1}^{nk} X_{k(w)}^{sc(i,k)} + \sum_{i=1}^{ni} sc(i,r) \cdot \beta_{i(w)} \cdot K_{Di} \cdot R \cdot \prod_{k=1}^{nk} X_{k(w)}^{sc(i,k)} \quad (12)$$

In order to simplify computation, the second term on the right side of equation (12) can be treated as the definition of a system with $nk + 1$ components, where R is considered as the $nk + 1$ component, and $\beta_{i(w)} \cdot K_{Di}$ is the extraction constant of the extracted i-species. Therefore equation (12) can be written as:

$$C_r = \sum_{l=1}^{nl} sc(l,r) \cdot \beta_l \cdot \prod_{k=1}^{nk+1} X_k^{sc(l,k)} \quad (13)$$

where nl is the total number of species in aqueous phase and micellar phase.

The stoichiometric coefficient of R for the l-species, $sc(l, nk + 1)$, can only take two values: 0, for species present in the aqueous phase, and 1, for species present in micellar phase.

For any species the formation or extraction constant will be given by:

$$\beta_l = \beta_{l(w)} \cdot K_{Dl} \qquad \text{if } sc(l, nk+1) = 1$$

$$\beta_l = \beta_{l(w)} \qquad \text{if } sc(l, nk+1) = 0$$

The R value is used as a "free concentration", but it is calculated directly after equation (3). Furthermore, as the hydrogen ion concentration is known (as the pH of solution is measured), only $nk - 1$ mass balance equations have to be solved.

Once the mass balance equations have been solved, the program calculates the unknown molar absorptivities by multiple regression,[22] and the constants can be refined by the Gauss-Newton method.[23] As in STAR program, the minimized function is the sum of squared

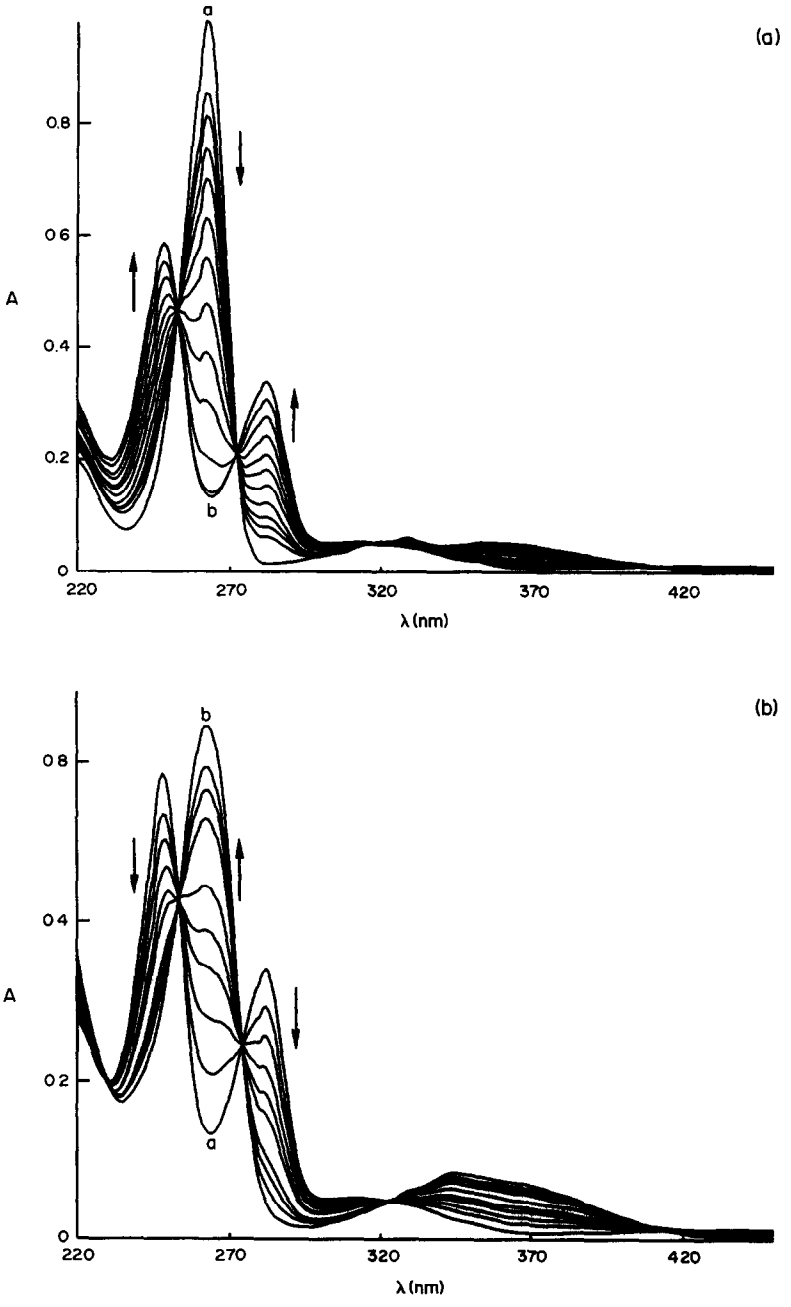

Fig. 1. Absorption spectra of chlorquinaldol (HQ) in aqueous solution as a function of pH. A: pH = 1.06 (a), 2.29, 2.95, 3.10, 3.24, 3.40, 3.54, 3.71, 3.90, 4.15, 4.54, 5.34 and 6.02 (b). B: pH = 6.02 (a), 7.24, 7.59, 7.85, 8.03, 8.21, 8.58, 8.81, 9.14 and 11.71 (b). $C_{HQ} = 1.98 \times 10^{-5} M$. Arrows indicate the spectral trends in changing the pH.

residuals of the absorbance of n solutions (a maximum of 200 in the SPDIS program) at nj wavelengths (up to 12).

RESULTS AND DISCUSSION

Dissociation constants in water

Chlorquinaldol shows two acid–base equilibria: the first is that of the heterocyclic nitrogen protonation, and the second corresponds to the dissociation of the hydroxyl group.

Chlorquinaldol absorption spectra in aqueous solution, in the absence of Brij-35, at several pH values are shown in Fig. 1. The protonated species exhibits an absorption maximum at 260 nm, the neutral species shows two absorption maxima, at 250 and 280 nm, and for the anionic form the absorption maximum is located at 265 nm. On the other hand all species shows broad bands at visible range, these bands being less sensitive than those in the UV range. The calculated pK_a constants are $pK_{a1} = 3.44 \pm 0.01$ and $pK_{a2} = 7.84 \pm 0.02$.

Apparent dissociation constants in the presence of Brij-35

In order to determine the influence of the non-ionic surfactant Brij-35, a series of experiments were run at different Brij-35 concentrations, above the cmc. The apparent pK_a values of the reagent for each Brij-35 concentration are given in Table 1. These results shows that as the surfactant concentration increases, from $1.1 \times 10^{-4} M$ to $1.9 \times 10^{-3} M$, the apparent pK_{a1} decreases from 3.34 to 2.37, whereas the pK_{a2} increases from 7.92 to 8.53.

The apparent spectra of the protonated form are independent of the surfactant concentration. Nevertheless, apparent spectra of the neutral form are strongly dependent on Brij-35 concentration. As its concentration increases, the intensity of absorption maximum at 280 nm decreases, and the intensity of the 250 nm maximum increases and shows a slight bathochromic shift. At high surfactant concentrations the apparent spectra of the neutral form show the same shape as those obtained when chlorquinaldol is dissolved in organic solvents like chloroform, benzene or isoamyl alcohol.[24] On the other hand, apparent spectra of the anionic species show a bathochromic shift of the maximum at 265 nm, and the band intensity slightly decreases as Brij-35 concentration increases. In Fig. 2 the apparent molar absorptivities, for each Brij-35 concentration, of the species HQ and Q^-, calculated by means of STAR program, are displayed.

Table 1. Apparent dissociation constants of chlorquinaldol in aqueous Brij-35 solutions

$C_{Brij\text{-}35}$ (M)	pK_{a1}*	pK_{a2}*	sigma
–	3.44 (0.01)	7.84 (0.02)	0.0055
1.07×10^{-4}	3.34 (0.02)	7.92 (0.03)	0.0065
1.53×10^{-4}	3.31 (0.02)	7.96 (0.02)	0.0044
1.92×10^{-4}	3.24 (0.02)	7.97 (0.03)	0.0071
3.21×10^{-4}	3.15 (0.02)	8.07 (0.02)	0.0052
6.50×10^{-4}	2.90 (0.02)	8.23 (0.02)	0.0049
1.07×10^{-3}	2.68 (0.02)	8.35 (0.02)	0.0053
1.91×10^{-3}	2.37 (0.02)	8.53 (0.02)	0.0051

*Values in ( ) are three times the estimated standard deviation of pK_a as given by the program.

Distribution equilibria in water-Brij-35 systems

According to the partition model, distribution of neutral species and ion associates between the aqueous solution and the micellar phase can take place. Since Brij-35 is a non-ionic surfactant, in this system ion-pairing can only occur between the charged species of the reagent, Q^- and H_2Q^+, and sodium and chloride ions, from the ionic medium. The effect of ions from buffers was neglected because their concentrations are much lower than those of the sodium chloride used to adjust the ionic strength.

Several equilibria models were checked with the SPDIS program. These models were chosen according to the variations observed in the spectral parameters and acid–base behaviour with the surfactant concentration. Thus, the variations observed in the apparent spectra of the neutral species, and in the apparent pK_a values (pK_{a1} decreases and pK_{a2} increases as Brij-35 concentration increases) suggest that HQ distributes between aqueous and micellar phases, as can be expected. On the other hand some variation in the apparent spectra of the anionic species was detected. In addition the extraction of ionic associates between the anionic form of oxine and derivatives and alkaline ions have been reported in several systems, including micellar solutions of non-ionic surfactants.[14,24] Finally, from the apparent spectra of cationic species obtained at different Brij-35 concentrations no inference can be made about the extraction into the micellar phase of an ion-pair of H_2Q^+. Nevertheless the extraction of this kind of ion-pair of oxine and derivatives into some organic solvents and micellar systems has been detected.[14,24]

In Table 2 the models assayed are listed. The models include, besides the dissociation

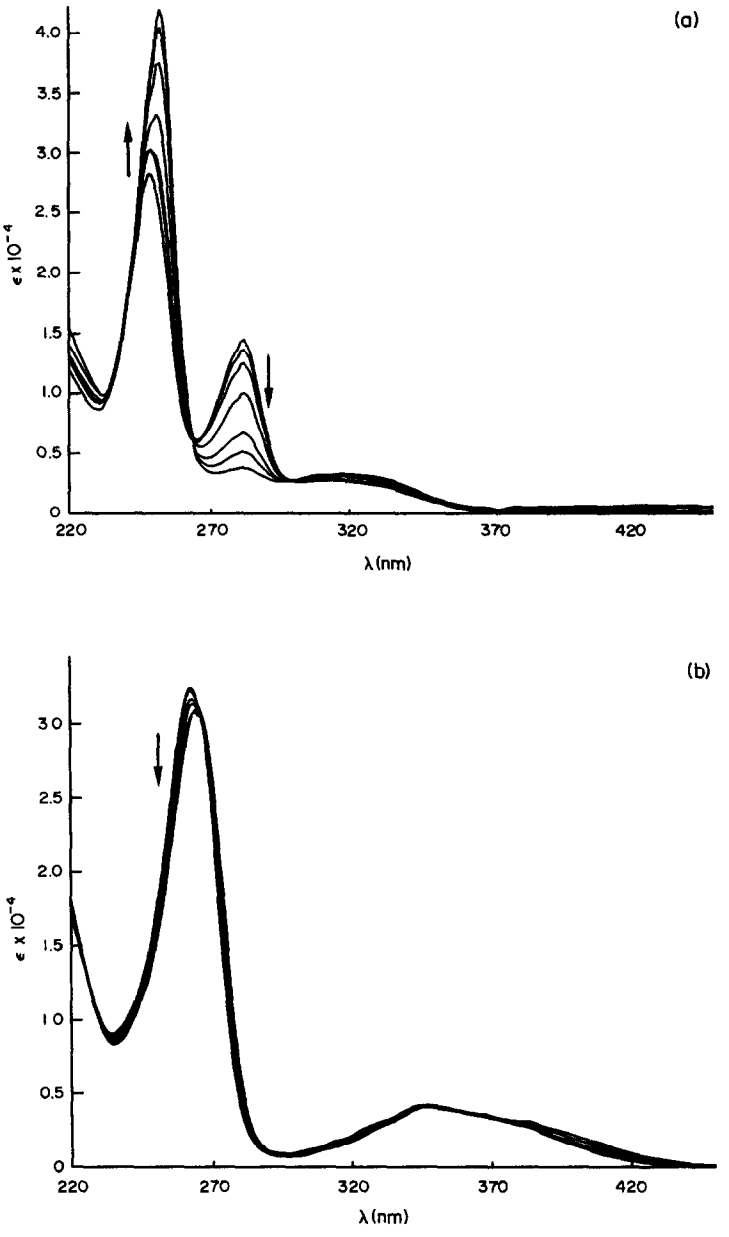

Fig. 2. Apparent molar absorptivities of the species HQ (a) and Q^- (b) as a function of $C_{Brij\text{-}35}$. Arrows indicate the spectrals trends in changing $C_{Brij\text{-}35}$ from 1.07×10^{-4} to $1.91 \times 10^{-3} M$.

Table 2. Model testing of chlorquinaldol distribution in aqueous Brij-35 solutions

Equilibria:

(A)	$H_2Q^+ \rightleftharpoons HQ + H^+$	K_{a1}
(B)	$HQ \rightleftharpoons H^+ + Q^-$	K_{a2}
(C)	$HQ \rightleftharpoons HQ_{(m)}$	K_D
(D)	$Na^+ + Q^- \rightleftharpoons Na^+.Q^-_{(m)}$	K_{E1}
(E)	$H_2Q^+ + Cl^- \rightleftharpoons H_2Q^+.Cl^-_{(m)}$	K_{E2}

Model	Equilibria considered	U	sigma D
1	A, B, C	0.461	0.0171
2	A, B, C, D	0.095	0.0078
3	A, B, C, D, E	0.085	0.0074

equilibria of the reagent in the aqueous phase, distribution equilibria of HQ, and of the ion associates $H_2Q^+.Cl^-$ and $Na^+.Q^-$. The fitting parameters obtained for each model are also given in Table 2. Calculations were carried out over 131 spectra, corresponding to Brij-35 concentrations between 1.53×10^{-4} and $1.91 \times 10^{-3} M$. Absorbance values were taken from 240 to 295 nm. This wavelength range includes the most characteristic bands of the different species. In the SPDIS data input surfactant partial molar volume and c.m.c. values are needed

Table 3. Survey of the equilibrium constants for the dissociation and extraction of chlorquinaldol in aqueous Brij-35 solutions

Equilibrium	Log K	Log D
$H_2Q^+ \rightleftharpoons HQ + H^+$	−3.44 (0.01)	
$HQ \rightleftharpoons H^+ + Q^-$	−7.84 (0.01)	
$HQ \rightleftharpoons HQ_{(m)}$	3.64 (0.01)	3.64
$Na^+ + Q^- \rightleftharpoons Na^+.Q^-_{(m)}$	3.77 (0.05)	2.77*

*$[Na^+] = 0.1M$.

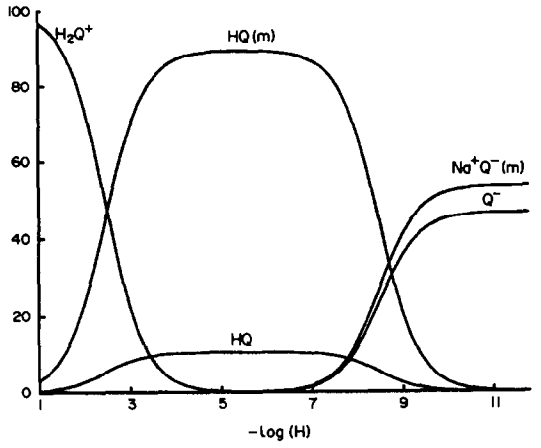

Fig. 3. Species distribution of chlorquinaldol ($2 \times 10^{-5}M$) as a function of pH, at $C_{Brij\text{-}35} = 1.9 \times 10^{-3}M$.

and they were taken as 1.070 l./mole[25] and $10^{-4}M$,[4,26] respectively.

If only distribution of the neutral species was considered (model 1) the standard deviation obtained was high (sigmaD = 0.0171) since large differences between experimental and calculated values were obtained, especially in the basic pH-range. When the extraction of the $Na^+.Q^-$ ion-pair was also taken into account (model 2) the fit with the experimental data was clearly improved (sigmaD = 0.0078). Finally model 3, which includes, besides the species of model 2, the extraction of $H_2Q^+.Cl^-$, was checked. Although a slight improvement of the fitting was obtained (sigmaD = 0.0074), the extraction constant of this ion-pair was ill-defined, and this species was found to be formed only to a maximum of 2%. Therefore the extraction of $H_2Q^+.Cl^-$ was not considered further and model 2 was adopted for this system. The calculated values of the constants and the distribution ratio D, defined as ratio of total concentration of chlorquinaldol in the micellar phase to that in aqueous phase, are given in Table 3. Figure 3 shows the species distribution as a function of pH, calculated from the obtained constants (by using a modified version of SOL1 program[27]), for a Brij-35 concentration equal to $1.91 \times 10^{-3}M$. Despite the high values obtained for the distribution ratios ($\log D$ = 3.65 and $\log D = 2.77$ for HQ and Q^-, respectively), the mass of chlorquinaldol in the micellar phase does not exceed 90% because of the low volume of the micellar phase, only 0.2% of the total volume.

The extraction of neutral and anionic species explains the observed differences in the spectra with increasing Brij-35 concentration. The calculated molar absorptivities of the species in micellar phases ($\lambda = 252$ nm; $\log \epsilon = 4.63$ for HQ and $\lambda = 263$ nm; $\log \epsilon = 4.50$ for Q^-) agree with those observed in organic solvents in which the extraction of the anionic species takes place, like isoamyl alcohol ($\lambda = 253$ nm; $\log \epsilon = 4.65$

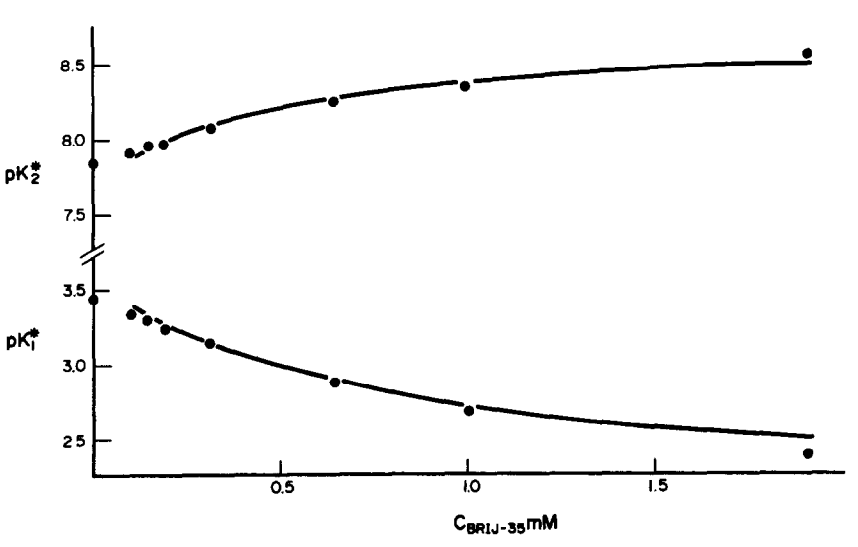

Fig. 4. Apparent dissociation constants as a function of $C_{Brij\text{-}35}$. (●): experimental values, (—): calculated curves using the constants given in Table 3.

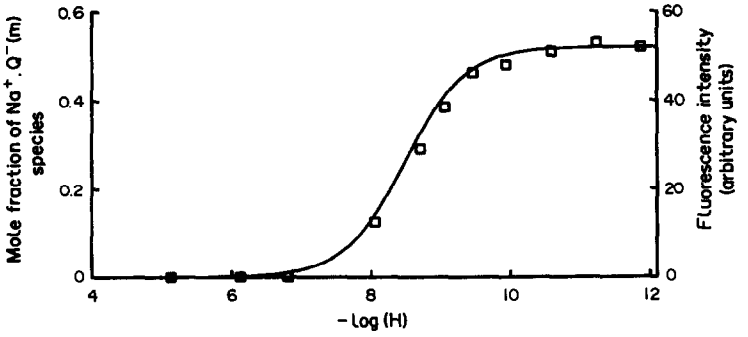

Fig. 5. Relative fluorescence intensities (□) of chlorquinaldol ($4 \times 10^{-5}M$) as a function of pH, at $C_{\text{Brij-35}} = 1.8 \times 10^{-3}M$. Solid line corresponds to molar fraction of $Na^+Q^-_{(m)}$.

for HQ and $\lambda = 260$ nm; $\log \epsilon = 4.51$ for Q^-). On the other hand, the fact that the ion-pair of the anionic form distributes between the two phases, but the cationic form does not, explains the finding that the shifting observed in pK_{a1} values is greater than that observed in pK_{a2} values.

From constant values given in Table 3, the apparent dissociation constants of the reagent, as a function of Brij-35 concentration, were determined. Theoretical and experimental apparent dissociation constant values are displayed together in Fig. 4. The good agreement between experimental and calculated "apparent" pK_a values shows that the proposed model provides a complete description of the effect of Brij-35 on the apparent dissociation constants of the reagent.

Fluorescence of chlorquinaldol in Brij-35 micellar solutions

It is well known that micellar media very often enhance fluorescence. This has been attributed to the solubilization of the fluorophore into the micelles. Preliminary experiments showed that chlorquinaldol does not fluoresce in aqueous solution in the whole pH range, but it does so when dissolved in basic aqueous micellar solutions of Brij-35 surfactant. In order to find a relationship between solubilization of chlorquinaldol into micelles and its fluorescence properties, the influence of pH and surfactant concentration on chlorquinaldol fluorescence was studied.

The pH dependence of the fluorescence intensity, at constant chlorquinaldol ($4 \times 10^{-5}M$) and Brij-35 ($1.8 \times 10^{-3}M$) concentrations is shown in Fig. 5. Points are the experimental relative fluorescence values whereas the solid line corresponds to mole fraction of $Na^+Q^-_{(m)}$ species in this micellar medium. This behaviour clearly indicates that the anionic form in the micellar phase is the only fluorescent species.

The influence of Brij-35 concentration (between 2×10^{-4} and $2 \times 10^{-3}M$) on fluorescence intensity was studied at constant pH (about 11) and chlorquinaldol concentration ($4 \times 10^{-5}M$). It was found that the relative fluorescence intensity is a linear function of the mole fraction of $Na^+Q^-_{(m)}(X_{NaQ})$.

The good correlation between observed fluorescence and calculated X_{NaQ} shows that solubilization of anionic form of chlorquinaldol into the micelles is a determining factor for fluorescence enhancement. Furthermore, the agreement between measured fluorescence intensity values and the proposed model for the equilibria of chlorquinaldol in Brij-35 micellar solutions confirms its validity.

Acknowledgement—The authors thank the CICYT (Project No. PB87-0059) for supporting this study.

REFERENCES

1. W. L. Hinze, in *Solution Chemistry of Surfactants*, W. L. Mittal (ed.), Vol. 1, p. 79. Plenum Press, New York, 1979.
2. E. Pellezeti and E. Pramauro, *Anal. Chim. Acta*, 1985, **169**, 1.
3. G. L. McIntire, *CRC Crit. Rev. Anal. Chem.*, 1990, **21**, 257.
4. L. J. Cline Love, J. G. Habarta and J. G. Dorsey, *Anal. Chem.*, 1984, **56**, 1133A.
5. J. Rosendorfova and L. Cermakova, *Talanta*, 1980, **27**, 705.
6. V. Kuban, I. Jancarova, J. Hedbavny and M. Vrchlabsky, *Collect. Czech. Chem. Commun.*, 1989, **54**, 70.
7. J. Jirasova, J. Bily and L. Cermakova, *ibid.*, 1990, **55**, 1491.
8. A. L. Underwood, *Anal. Chim. Acta*, 1982, **140**, 89.
9. G. S. Hartley and J. W. Roe, *Trans. Faraday Soc.*, 1940, **36**, 101.
10. P. Mukerjee and K. Banarjee, *J. Phys. Chem.*, 1964, **68**, 3567.

11. F. H. Quina and H. Chaimovich, *ibid.*, 1979, **83**, 1844.
12. L. S. Romsted, *ibid.*, 1985, **89**, 5107.
13. L. S. Romsted and D. Zanette, *ibid.*, 1988, **92**, 4690.
14. H. Hoshino, T. Saitoh, H. Taketomi, T. Yotsuyanaki, H. Watanabe and K. Tachikawa, *Anal. Chim. Acta*, 1983, **147**, 339.
15. S. Tagashira, *Anal. Chem.*, 1983, **55**, 1918.
16. R. Compañó, A. Grima, A. Izquierdo and M. D. Prat, *Anal. Chim. Acta*, 1989, **227**, 219.
17. R. Compañó, A. Izquierdo and M. D. Prat, *Quim. Anal.*, 1991, **10**, 27.
18. M. Macka and V. Kuban, *Collect. Czech. Chem. Commun.*, 1982, **47**, 2676.
19. J. Bily and L. Cermakova, *Anal. Lett.*, 1986, **19**, 747.
20. D. D. Perrin and B. Dempsey, *Buffers for pH and Metal Ion Control*, Chapman & Hall, London, 1974.
21. J. L. Beltran, R. Codony and M. D. Prat, submitted for publication.
22. P. C. Wang, *Numerical and Matrix Methods in Structural Mechanics*, John Wiley & Sons, New York, 1966.
23. E. Durand, *Solutions Numeriques des Equations Algébriques. Tome II: Systèmes de Plusieurs Equations*, Masson et Cie., Paris, 1972.
24. A. Izquierdo and R. Compaño, *Mikrochim. Acta*, 1983, **1**, 371.
25. M. Tanaka, S. Kaneshina and G. Sugihara, in *Solution Behaviour of Surfactants: Theoretical and Applied Aspects*, K. L. Mittal and E. J. Fendler (eds.), Vol. 1, p. 41, Plenum Press, New York, 1982.
26. M. G. Khaledi, *Trends Anal. Chem.*, 1988, **7**, 293.
27. A. Izquierdo and J. L. Beltrán, *J. of Chemometrics*, 1988, **3**, 209.

Talanta, Vol. 40, No. 2, pp. 167–172, 1993
Printed in Great Britain.

0039-9140/93 $6.00 + 0.00

CHEMILUMINESCENCE DURING THE OXIDATION OF ALCOHOLS BY PERMANGANATE: APPLICATION TO THE DETERMINATION OF ETHANOL IN GIN

S. I. MONTALVO* and J. D. INGLE, JR.†
Department of Chemistry, Oregon State University, Gilbert Hall 153, Corvallis, OR 97331-4003, U.S.A.

(*Received* 9 *April* 1992. *Revised* 26 *May* 1992. *Accepted* 26 *May* 1992)

Summary—Chemiluminescence is observed during the oxidation of ethanol with potassium permanganate under very acidic conditions. Factors affecting the chemiluminescence signal are discussed. Based on this chemiluminescence reaction, a method for the determination of alcohol in gin was developed. The method, which has a detection limit of 0.3% (v/v) and a relative standard deviation of about 1% at 40.0% (v/v), was used in the determination of ethanol in three different brands of gin with no sample preparation.

The oxidation of ethanol in acidic solutions by potassium permanganate is well known. This reaction is a two-electron process, which eventually gives acetic acid.[1] According to Banerji,[2] the permanganate-ethanol reaction stoichiometry is 4 to 5. With a large excess of the alcohol, the reaction kinetics are first order in permanganate and ethanol, and the rate of oxidation increases linearly with acid concentration.

Marino and Ingle[3] demonstrated that chemiluminescence (CL) is produced during the oxidation of humic material and polyphenols by permanganate ion in basic solutions. In our laboratory, it was discovered that oxidation of ethanol by permanganate ion produces weak CL and that the CL intensity is greater at very low pHs. Hence, the classic oxidation of simple aliphatic alcohols by acidic permanganate is a CL reaction.

Determination of ethanol (proof) in liquors is mandated by the Department of the Treasury (Bureau of Alcohols, Tobacco and Firearms).[4,5] The specified method, which is also recommended by the AOAC,[6] is based on hydrometer readings which are normalized to 60°F. Ethanol in other types of samples has been determined with many different methods including amperometry,[7] automated densitometry,[8] gas chromatography,[9,10] and titrimetry.[11]

This paper is concerned with using this new CL reaction for the determination of ethanol in gin. Spectral, optimization, and calibration data are discussed.

EXPERIMENTAL

Instrumentation

A discrete-sampling CL photometer described elsewhere[12,13] was used for all quantitative CL measurements. Briefly, it consists of a 1-cm pathlength spectrophotometer sample cell housed in an aluminum sample chamber. A brass temperature-controlled jacket around the same cell is connected to a thermostated water bath. The contents of the sample cell are mixed with a magnetic stirrer and a stirbar. The final reagent is delivered to the cell by means of an automatic pneumatically-activated syringe to initiate the reaction. A portion of the light emitted during the reaction is impingent on the photomultiplier tube (PMT). The resulting photoanodic current is converted to a voltage, electronically filtered, and displayed on a recorder.

Spectrophotometric data were obtained with a HP 8451A diode array spectrophotometer. Chemiluminescence spectra were acquired with a spectrometer based on an intensified diode array detector.[14]

Solution preparation

The water used for dilution of all aqueous solutions and rinsing was deionized water from a Millipore Milli-Q system connected to the house deionized water. All chemicals were

*Present address: Jefferson State Junior College, Brewton, AL 36426, U.S.A.
†Author for correspondence.

reagent grade. Potassium permanganate solutions (30m*M* and lower) were stored in black Teflon bottles in the dark. These bottles were washed and soaked with 1% (v/v) hydrochloric acid and then water to ensure the removal from the bottle walls of manganese dioxide formed during storage of previous permanganate solutions.

Measurement procedure

The general procedure followed for CL analysis involved the addition of 1.0 ml of sample, standard, or blank (water) and then 0.5 ml of acid to the sample cell with Eppendorf pipets. With the sample chamber lid closed and the PMT shutter open, 0.81 ml of the final CL reagent ($KMnO_4$) was injected into the sample cell using the pneumatic injector. CL peaks for the blank were negligible unless otherwise stated. Between runs the reaction cell was cleaned by adding 50% (v/v) hydrochloric acid, letting it stand for 2–3 min, and then rinsing ten times with water. Reaction mixtures and rinsing solutions were removed by vacuum aspiration.

All CL signals were reported as the maximum in the peak-shaped signal in Volts. Generally, the mean and the standard deviation of the CL signal from three or more repetitive runs are reported. The noise filter cut-off frequency was 0.5 or 1.0 Hz, and the cell temperature was controlled to 25°.

RESULTS AND DISCUSSION

Type of acid

The effect of the type of acid on the ethanol CL reaction was studied by using 0.5 ml of 50% (w/v) nitric, phosphoric, acetic, perchloric, or sulfuric acids or concentrated hydrochloric acid in the reaction mixture. Calibration curves over a concentration range of 1–50.0% (v/v) ethanol were obtained. No CL was observed with phosphoric or acetic acid. Apparently the pH of reaction mixture is too high with these acids for the reaction to proceed at a significant rate. The results for the other acids are summarized in Table 1. Hydrochloric acid provides the greatest signal and has the advantage of dissolving the MnO_2 formed during the reaction. However, the precision and linearity are poor. The detection limit with sulfuric acid is worse than that with some of the other acids. Also the reaction rate is slow and there is a potential explosion hazard of this acid when combined with potassium permanganate. The use of perchloric acid has two disadvantages, an imprecise blank signal and a potential explosion hazard when mixed with organic compounds. Nitric acid was finally chosen as the best acid because it yields a relatively high CL intensity, a relatively fast reaction rate, a reasonable detection limit, good precision, no blank signal, and a more linear response at lower ethanol concentrations.

Absorption and chemiluminescence spectra

A time sequence of the absorption spectra of a reaction mixture with ethanol in molar excess relative to permanganate revealed that in the visible wavelength range, MnO_4^- absorbs strongly from about 450 to 600 nm with a tail that extends to longer wavelengths and that most of the potassium permanganate is consumed in 30 sec. With Fe(II) added before injection of the oxidant, the CL signal is enhanced, and the absorbance due to MnO_4^- decreases much more rapidly than that without Fe(II) added due to the reduction of permanganate by this species.

To obtain a crude CL spectra, the CL signal was recorded with different cut-on filters between the reaction cell and the PMT in the CL photometer sample compartment. From the signal attenuations observed, it was esti-

Table 1. Effect of different mineral acids

Acid*	E_{CL},† V	RSD,† %	t_R,‡ min	DL,§ % (v/v)	Fit‖
HNO_3	0.13	0.8	1.3	1	2nd
HCl	0.32	28	2.5	1	2nd
$HClO_4$	0.21	2.8	0.9	1	2nd
H_2SO_4	0.033	0.9	4.4	3	No correlation

*All 50% (w/v) except conc. HCl; 10m*M* MnO_4^-.
†CL signal and RSD with 50% (w/v) ethanol.
‡Duration of CL (base width of CL peak).
§Approximate detection limit, smallest concentration tested that yielded a detectable peak.
‖The order of the polynomial yielding the best fit.

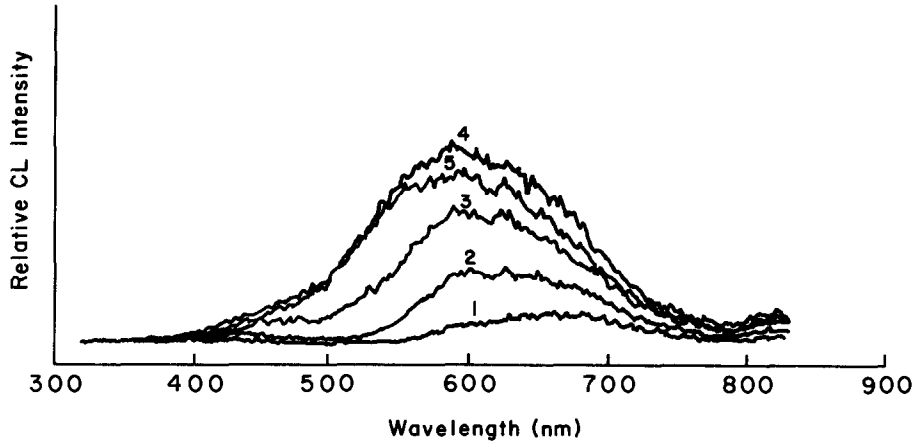

Fig. 1. Chemiluminescence spectra from the oxidation reaction of ethanol with $KMnO_4$. Spectra taken 1 sec apart with a 1-sec integration time and the numbers indicating the order. Reaction mixture: 2 ml of absolute ethanol, 0.5 ml of 95% (v/v) HNO_3, 0.81 ml of 10m*M* $KMnO_4$.

mated that the broad emission band begins at about 500 nm with an apparent maximum at about 660 nm.

For fast CL reactions, the intensified diode array provides a better means to obtain spectral information.[14,15] The successive CL spectra in Fig. 1 show that it takes about 4 sec for the reaction to reach its maximum intensity and the CL spectrum is quite broad. Note that the wavelength of maximum CL intensity (λ_m) shifts to shorter wavelengths as the reaction proceeds. After 1 sec, $\lambda_m \approx$ 650 nm, while $\lambda_m \approx 580$ nm after 4 sec. At 4 sec, the CL emission occurs over the 450–750 nm region. This apparent shift is attributed to the absorption of a fraction of the CL photons by permanganate whose absorption spectrum overlaps the CL spectrum. The strongest absorption occurs in the shorter wavelength region of the CL spectrum. As the reaction proceeds, the permanganate is consumed and the degree of absorption of CL photons of shorter wavelength decreases.

In the presence of Fe(II), the CL reaction proceeds about three times faster (*i.e.*, 1.5 sec to reach maximum intensity) as shown in Fig. 2. Note that λ_m is about 530 nm and emission occurs from about 380 to 800 nm. We postulate that this spectrum represents a truer picture of the CL spectrum. In this case, the Fe(II) reduces all the MnO_4^- almost immediately to lower Mn oxidation states [Mn(III) and Mn(IV)] which do not absorb the CL radiation as strongly but which we believe are responsible for oxidizing the ethanol.[16]

Optimization

In discussing the optimization of the $KMnO_4$ and HNO_3 concentrations, the stoichiometry and absorption of CL radiation by $KMnO_4$ should be kept in mind. If the oxidation proceeds to acetic acid it takes 0.8 moles of

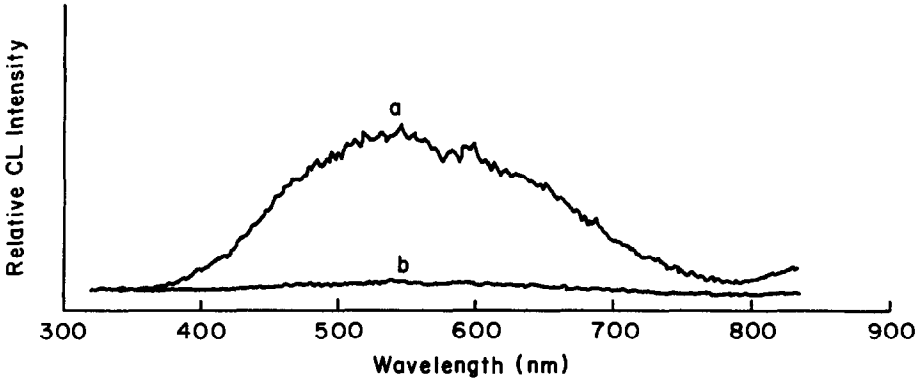

Fig. 2. Chemiluminescence spectra from the oxidation reaction of ethanol with $KMnO_4$ in the presence of Fe(II). Spectra taken 1.5 sec (a) and 3.5 sec (b) after injection. Reaction mixture: 1 ml of absolute ethanol, 1 ml of 0.1*M* Fe(II), 0.5 ml of 95% (v/v) HNO_3, 0.81 ml of 10m*M* $KMnO_4$.

permanganate to oxidize 1 mole of ethanol. If acetaldehyde is the oxidation product, 0.4 moles of permanganate is required to oxidize 1 mole of ethanol. The lowest concentration of ethanol used in the optimization studies was 1% (v/v) or 171m*M*. With 10m*M* permanganate, ethanol is in molar excess relative to permanganate in the reaction mixture by a factor of 21 or greater. Thus, it might be expected that the rate of oxidation and the CL signal would be proportional to the permanganate and ethanol concentrations. Because of the absorption of the CL photons by permanganate caused by the overlap between the CL spectrum and MnO_4^- absorption spectrum, it is also expected that attenuation effects will be more pronounced at higher permanganate concentrations.

The effect of nitric acid concentration on the CL signal for 12.5% (v/v) ethanol with different potassium permanganate concentrations is shown in Fig. 3. In all cases, the CL signal increases with higher acid concentrations. For a given nitric acid concentration, the CL signal increases as the potassium permanganate concentration increases from 1 to 10m*M*, but decreases when the oxidant concentration increases to 30m*M*. The potassium permanganate concentration yielding the highest CL signal depends upon the nitric acid concentration. Only for the case of a potassium permanganate concentration of 1.0m*M*, the dependence of the CL signal on the nitric acid concentration is approximately linear (pseudo-first order). However, at higher concentrations of potassium permanganate, a pronounced positive deviation is observed and is most obvious at 30m*M* potassium permanganate. The above behavior is attributed to the absorption of some of the CL radiation by unreacted potassium permanganate which is

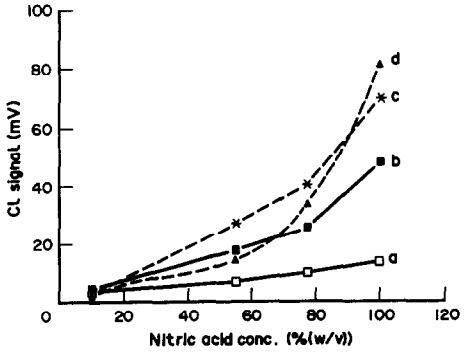

Fig. 3. Dependence of the CL signal on HNO_3 and $KMnO_4$ concentrations. $KMnO_4$ concentration: a, 1m*M*; b, 3.3m*M*; c, 10m*M*; d, 30m*M*; ethanol concentration, 12.5%.

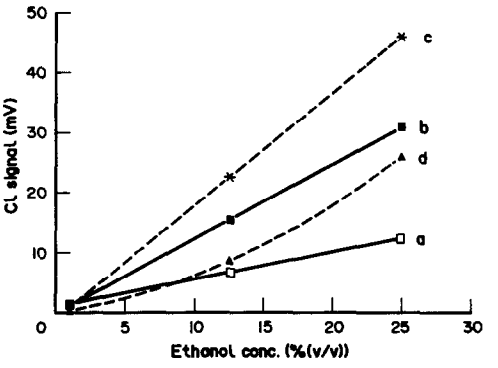

Fig. 4. Effect of $KMnO_4$ concentration on the shape of the calibration curve. a, 1m*M*; b, 3.3m*M*; c, 10m*M*; d, 30m*M*; HNO_3 concentration, 50% (v/v); ethanol concentration, 12.5%.

more significant at higher potassium permanganate concentrations and at lower nitric acid concentrations where the rate of consumption of potassium permanganate is slower. Note that the CL signal is largest with 30m*M* MnO_4^- only with 95% (w/v) nitric acid where the rate of reaction and the rate of disappearance of MnO_4^- is greatest.

Figure 4 shows calibration curves with different permanganate concentrations at a fixed nitric acid concentration of 50% (w/v). The slope of the calibration curve increases as the permanganate concentration increases from 1 to 10m*M*. However, the slope decreases when the permanganate concentration is further increased to 30m*M*. With 30m*M* MnO_4^-, nonlinearity is quite obvious and the calibration slope is less than that obtained with 3.3 or 10m*M* MnO_4^- due to greater absorption by the oxidant. At low ethanol concentrations, this attenuation effect is enhanced because the rate of disappearance of MnO_4^- is less. For example, for the lowest ethanol concentration tested [1% (v/v)], the CL signal with 10m*M* MnO_4^- is smaller than that observed with 1m*M* MnO_4^-. At higher ethanol concentrations, the opposite is true.

With 10m*M* potassium permanganate and 50% (w/v) nitric acid as a starting point, a three-dimensional simplex optimization was performed for a 1.0% (v/v) ethanol solution to find the nitric acid and potassium permanganate concentrations yielding the maximum CL signal. The optimum concentrations were found to be 10m*M* potassium permanganate and 95.0% (w/v) nitric acid. These conditions yielded a signal improvement of a factor of 12 relative to the starting vertex. The detection limit is 0.3%

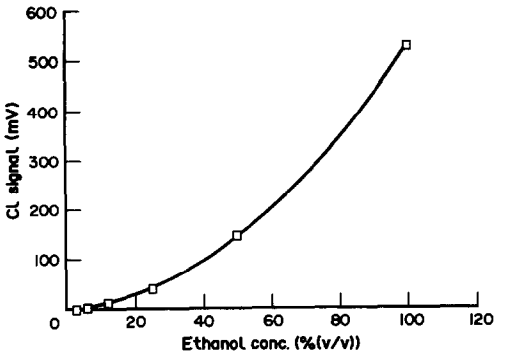

Fig. 5. Ethanol calibration curve with optimized reagent concentrations.

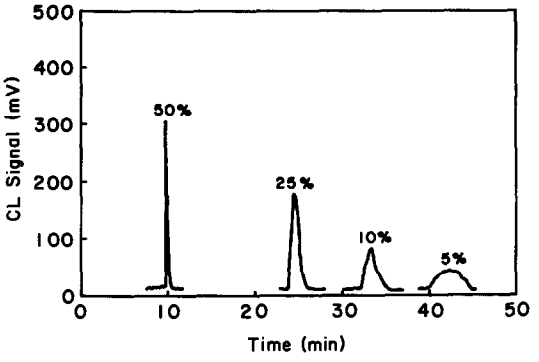

Fig. 6. Typical peak shapes. Numbers above the peaks indicate the %(v/v) ethanol.

(v/v) based on twice the standard deviation of the blank (dark) signal.

Calibration data

Figure 5 shows a typical ethanol calibration curve under the optimized conditions. Least squares fitting of the data with first, second, and third order polynomials revealed that the second order fit was the best (*i.e.*, minimum standard error). Over a small range of ethanol concentration (±5%), a linear fit may be used.

Figure 6 shows the typical peaks obtained from the ethanol CL reaction. At greater ethanol concentrations, the CL reaction is faster and the peak maximum is higher.

Ethanol determination in gin

Samples of three different brands of gin were analyzed without dilution. Standards with ethanol concentrations of 35.0, 40.0, 45.0, and 50.0% (v/v) were also run. The ethanol concentration in each sample was determined with a two-point calibration curve [two standards that bracketed the concentration in the sample and that differed by 5% (v/v) ethanol] and a three-point calibration curve over a range of 10% (v/v) ethanol. A linear fit was used in both cases.

The results are summarized in Table 2. The bracketing technique yielded excellent results as did the unweighted three-point calibration curve. The results with weighted calibration curves were more in error than the unweighted ones. The RSD in the CL signal for the standards and samples was about 1%.

The standard addition method was also attempted with dilution of the samples to work in the region where the calibration curve is more linear. The standard addition procedure is not recommended because it yielded poorer results because the calibration curve is not perfectly linear.

Wine and beer were briefly studied and their alcohol content determined. The alcohol concentrations found by CL were approximately two-fold that of the expected ones. Apparently other species in these samples were oxidized and contributed to the CL signal. Chemiluminescence is observed under similar conditions with polyphenols.[16]

It was also confirmed that the CL signal from 10% (v/v) ethanol was depressed by about a factor of 2 with 0.01% (w/v) glucose present. Apparently the permanganate concentration is

Table 2. Determination of ethanol in gin

Sample	Expected conc.; % (v/v)	Two-point calibration determined conc.,* % (v/v)	error, %	Three-point calibration determined conc.,† % (v/v)	error, %
Gordons	40.0	39.6 (1.3)	1.1	39.6	0.9
				39.6	1.0
Beefeater	47.0	47.1 (1.2)	0.2	47.0	<0.1
				47.5	1.0
Tanqueray	47.3	47.4 (0.8)	0.2	47.3	<0.1
				47.8	1.0

*RSD in parentheses based on RSD in sample signal.
†First value without weighting; second value with weighting.

reduced by reaction with the glucose and indicates that sugar would be a serious interferent for the determination of ethanol. The CL detection limit for glucose is about 0.5% (w/v) and the calibration curve is quite nonlinear.

CONCLUSIONS

The discovery of the chemiluminescence produced during the oxidation of ethanol by permanganate at low pH has lead to a new method to determine ethanol. This CL method is unique compared to most solution CL reactions in that the analyte is a necessary reagent for the CL reaction rather than an activator or acceptor that enhances the CL signal observed without the analyte. Although the CL reaction is class selective for hydroxide-containing compounds, it does not differentiate between many alcohols and phenols. Thus, it is best suited for samples in which the hydroxy-containing analyte is in sufficient excess with respect to other hydroxy-containing compounds or other species that react with permanganate. In this regard the CL determination of ethanol in gin proved to be a near ideal application of the technique. The accuracy was 1% or better with no sample preparation, even dilution, required. The method is rapid because the CL signal is obtained within 2 sec of adding the sample to the sample cell. The new CL reaction has the potential for use in determination of other alcohols or phenols. Some form of sample cleanup or prior oxidation of weaker reductants would be required in many cases. The CL reaction may also be suited for a post-column CL detection in HPLC.

Acknowledgements—We wish to thank M. Cecilia Yappert for obtaining the CL spectra. We also acknowledge the NSF (CHE-84-01784) for partial support of this research.

REFERENCES

1. J. W. Ladbury and C. F. Cullis, *Chem. Reviews*, 1959, **58**, 403.
2. J. Benerjee and K. Sengupta, *The Review of Physical Chemistry of Japan*, 1964, **34**(2), 81.
3. D. F. Marino and J. D. Ingle, Jr., *Anal. Chim. Acta*, 1981, **124**, 23.
4. U.S. Department of the Treasury, Bureau of Alcohol, Tobacco and Firearms, Title 27.
5. U.S. Dept. of the Treasury, Bureau of Alcohol, Tobacco, and Firearms, *Gauging Manual*, 1978.
6. S. Williams, ed., *Official Methods of Analysis of the Association of Official Analytical Chemists*, 14th Ed., Chapter 20, 1984.
7. E. L. Gulberg and G. D. Christian, *Anal. Chim. Acta*, 1981, **123**, 125.
8. R. G. Lidzey, B. M. Stockton and M. E. B. Brown, *J. Autom. Chem.*, 1981, **3**, 151.
9. Thomas P. J. Izod and J. A. Duisman, Union Carbide Corp., U.S. Patent 4,375,568,375,568, 1983; *Chem. Abstr.*, **98**, P160230j.
10. Su Tiansheng, *Fenxi Huaxue*, 1982, **10**, 240; *Chem. Abstr.*, **98**, 100507n.
11. V. L. Yarovenko, V. A. Yanson, T. P. Nikiforova, A. P. Rukhlyadeva and T. G. Filatova, *Fermentn. Spirt. Prom. St.*, 1983, **3**, 17; *Chem. Abstr.*, **98**, 214256k.
12. S. D. Hoyt and J. D. Ingle, Jr., *Anal. Chim. Acta*, 1976, **88**, 163.
13. L. A. Montano and J. D. Ingle, Jr., *Anal. Chem.*, 1979, **51**, 919.
14. M. C. Yappert and J. D. Ingle, Jr., *ibid.*, 1989, **61**, 593.
15. D. F. Marino and J. D. Ingle, Jr., *ibid.*, 1981, **53**, 455.
16. S. I. Montalvo, Ph.D. Thesis, Oregon State University, Corvallis, OR, U.S.A., 1986.

Talanta, Vol. 40, No. 2, pp. 173–177, 1993
Printed in Great Britain.

0039-9140/93 $6.00 + 0.00

SEPARATION OF THORIUM FROM LANTHANIDES BY SOLVENT EXTRACTION WITH IONIZABLE CROWN ETHERS

H. S. Du, D. J. Wood, Sadik Elshani and C. M. Wai*
Department of Chemistry, University of Idaho, Moscow, ID 83843, U.S.A.

(*Received* 28 *May* 1992. *Accepted* 30 *May* 1992)

Summary—Thorium and the lanthanides are extracted by α-(sym-dibenzo-16-crown-5-oxy)acetic acid and its analogues in different pH ranges. At pH 4.5, Th is quantitatively extracted by the crown ether carboxylic acids into chloroform whereas the extraction of the lanthanides is negligible. Separation of Th from the lanthanides can be achieved by solvent extraction under this condition. The extraction does not require specific counteranions and is reversible with respect to pH. Trace amounts of Th in water can be quantitatively recovered using this extraction system for neutron activation analysis. The nature of the extracted Th complex and the mechanism of extraction are discussed.

Thorium and the rare earth elements (REE) usually coexist naturally, *e.g.*, thorium is a common component of monazite and REE are generally present in thorite.[1] Separation of thorium from REE is therefore important for the analysis and production of these elements. Recent reports indicate that macrocyclic polyethers with a suitable cavity size and an attached ionizable functional group such as α-(sym-dibenzo-16-crown-5-oxy)acetic acid are selective for the extraction of trivalent lanthanide ions.[2] The extraction does not require specific counteranions and is reversible with respect to pH. In slightly acidic and neutral solutions, the extraction efficiencies of sym-dibenzo-16-crown-5-oxyacetic acid for the lanthanides are 2 to 3 orders of magnitude greater than the alkali metal and alkaline earth metal ions of similar size.[3] The crown ether carboxylic acid appears to behave like a bifunctional ligand which chelates with cations according to their size as well as their chemical nature. Chelation of ionizable crown ethers with thorium has not been reported in the literature. This paper compares the extraction behaviours of Th^{4+} and the two end members of the lanthanide series, La^{3+} and Lu^{3+}, with α-(sym-dibenzo-16-crown-5-oxy)acetic acid (**I**) and its phenyl substituted analogue α-(sym-dibenzo-16-crown-5-oxy)phenyl acetic acid (**II**) (Fig. 1). The nature of the extracted complexes and the conditions for the separation of Th from the lanthanide ions by solvent extraction with the crown ether carboxylic acids are discussed.

*Author for correspondence.

EXPERIMENTAL

α-(Sym-dibenzo-16-crown-5-oxy)acetic acid (**I**) was synthesized in our laboratory according to the procedure reported in the literature.[4,5] α-(Sym-dibenzo-16-crown-5-oxy)phenylacetic acid (**II**) was prepared from α-sym-hydroxydibenzo-16-crown-5 by reaction with α-bromophenylacetic acid in THF in the presence of sodium hydride as a base at room temperature for 24 hr. After that, water was added to destroy unconsumed sodium hydride and THF was evaporated in vacuo. The residue was dissolved in 100 ml of water and extracted with ether to remove unreacted crown alcohol. The water phase was acidified with 6*M* hydrochloric acid and extracted with methylene chloride. The methylene chloride phase was washed with water, dried with magnesium sulphate, and evaporated in vacuo to obtain the crown ether carboxylic acid (**II**). After recrystallization in ethylacetate-hexane, the final product is a white solid with a melting point range of 127–128.5°. Elemental analysis gave C, 67.46% and H, 5.67%, in good agreement with the calculated values for $C_{27}H_{28}O_8$ (C, 67.49%; H, 5.87%).

The nitrates of La^{3+} and Lu^{3+} were obtained from Alfa Chemical Company and that of Th^{4+} was from Mallinckrodt, Inc. All other chemicals used in the experiments were Baker Analyzed reagents. Demineralized water was prepared by

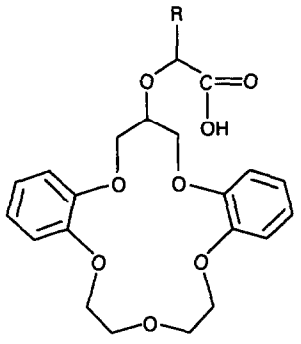

I. R=H α-(Sym-dibenzo-16-crown-5-oxy)acetic acid
II. R=C_6H_5 α-(Sym-dibenzo-16-crown-5-oxy)phenyl acetic acid

Fig. 1. Stuctures of the crown ether carboxylic acids: (I) α-(sym-dibenzo-16-crown-5-oxy)acetic acid and (II) α-(sym-dibenzo-16-crown-5-oxy)phenyl acetic acid.

passing distilled water through an ion exchange column (Barnsted Ultrapure Water Purification Cartridge) and a 0.2-μm filter assembly (Pall Corporation Utipor DFA).

Neutron activation analysis (NAA) was used to determine the concentrations of Th in the extraction experiments. Samples were generally irradiated for two hours in a TRIGA nuclear reactor with a steady flux of 6×10^{12} n/cm^2 sec. Neutron activation of ^{232}Th produces a short lived radioisotope ^{233}Th with a half life of 22.2 minutes. Its daughter product, ^{233}Pa ($t_{1/2} = 27$ days) further decays to ^{233}U with the emission of a 311 keV gamma which was used for quantitative determination of thorium. Radioisotope tracer techniques were used to measure the distribution of La^{3+} and Lu^{3+} in the extraction experiments. The nuclides ^{140}La ($t_{1/2} = 1.68$ days) and ^{177}Lu ($t_{1/2} = 6.74$ days) were produced by irradiation of La and Lu nitrates in the nuclear reactor. The 1596 keV gamma from ^{140}La and the 133 keV gamma from ^{177}Lu were used for quantitation. All samples were counted with a large volume ORTEC Ge(Li) detector with a resolution of 2.3 keV at 1332 keV gamma from ^{60}Co. The detector output was fed into an EG&G ORTEC ADCAM (Model 950A) multichannel analyzer and an IBM-XT computer was used for data processing. Details of the NAA procedures are given elsewhere.[6]

Extraction experiments usually involved 10 ml of a chloroform solution with a known concentration of the ligand and 10 ml of an aqueous solution containing the metal ions placed in a 30-ml Beckman polyvial with a fast-turn cap. The La and Lu solutions were spiked with the radioisotopes ^{140}La and ^{177}Lu, respectively. The mixture was shaken vigorously for 30 min with a wrist action mechanical shaker (Burrell model 75) at room temperature ($22 \pm 1°$). Dilute nitric acid and lithium hydroxide solutions were used for pH adjustment. The equilibrium pH of the aqueous phase was measured by an Orion model 701 pH meter with an Orion model 91-03 semimicro combination glass electrode. The distribution coefficients of La and Lu were determined by gamms counting 4-ml aliquots of the aqueous and organic phase which had been pipetted into 10-ml Beckmann polyvials. For NAA of Th in the aqueous phase, 1 ml of the aqueous solution was pipetted into a 2/5 dram polyethylene vial and heat sealed for neutron irradiation. A back-extraction procedure was used to remove Th from the organic phase into an acid solution prior to neutron activation. In this procedure, 4 ml of the organic phase was mixed with 4 ml of 1M nitric acid, and the mixture was shaken for 10 min to back-extract Th. Only 1 ml of the acid solution was placed in a 2/5 dram polyvial and heat sealed for neutron irradiation.

RESULTS AND DISCUSSION

The efficiency of extraction of Th^{4+}, La^{3+}, and Lu^{3+} from aqueous phase with α-(sym-dibenzo-16-crown-5-oxy)acetic acid in chloroform as a function of the equilibrium pH of the solution are given in Fig. 2(a). In these experiments, the concentration of the ionizable crown ether in the organic phase was fixed at $3 \times 10^{-3}M$, while that of Th^{4+} or trivalent lanthanide ions in the aqueous phase was $1 \times 10^{-4}M$. Sodium acetate at a concentration of $1 \times 10^{-3}M$ was used as a buffer in the aqueous solution. As shown in Fig. 2, the extraction of Th^{4+} occurs at a much lower pH than those of La^{3+} and Lu^{3+}. At pH < 2, Th^{4+} was not appreciably extracted, but the extraction efficiency increases rapidly at pH above 2. The extraction efficiency of Th^{4+} exceeds 95% at pH around 4 and is virtually quantitative at pH above 4.5. At pH above 7, however, the extraction efficiency for Th^{4+} tends to decrease. The extraction efficiencies of La^{3+} and Lu^{3+}, on the other hand, become appreciable at pH above 5 and reach a plateau around pH 6.5. The pH range for the extraction of trivalent lanthanide ions is shifted by approximately 3 pH units relative to that of Th^{4+}. This difference in pH constitutes a basis for their separation.

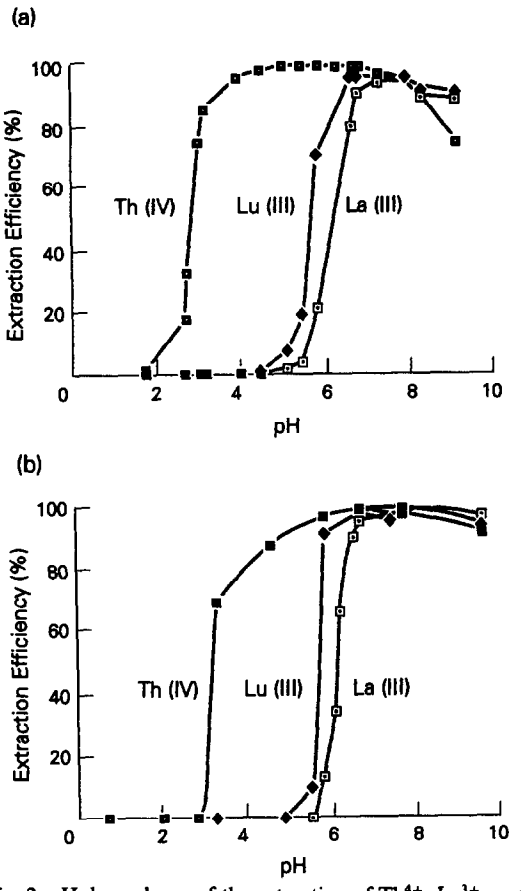

Fig. 2. pH dependence of the extraction of Th^{4+}, La^{3+}, and Lu^{3+} with (a) α-(sym-dibenzo-16-crown-5-oxy)acetic acid and (b) α-(sym-dibenzo-16-crown-5-oxy)phenyl acetic acid.

The cation to ligand ratio of the extracted species can be estimated from the variation of log *D vs.* log HL of the extraction experiments at a fixed pH, where *D* is the distribution coefficient and HL is the concentration of the ligand in the organic phase. Figure 3 shows the log *D vs.* log HL plots for Th^{4+} at pH 5 and for Lu^{3+} at pH 6.3. The slope for the Th^{4+} plot is 2.1 and that for the Lu^{3+} is 2.2, indicating that the ratio of cation to ligand of the extracted complexes is most likely 1:2 in both cases. Since the ligand carries one negative charge, the cationic species extracted into the organic phase must be doubly charged in order to satisfy the charge neutralization requirement. In the case of Th, it is known that hydrolysis of Th^{4+} occurs at pH around 3 leading to the formation of $Th(OH)^{3+}$ and $Th(OH)_2^{2+}$ species, with the latter being the major species in the pH range 3–5.[7] The extraction curve of Th corresponds to the pH range of the formation of $Th(OH)_2^{2+}$ species in the aqueous phase. The correlation suggests that the extracted form of Th is probably $Th(OH)_2L_2$. Hydrolysis of Lu^{3+} occurs at pH around 5–6 with the formation of $Lu(OH)^{2+}$ which also appears to be in the pH range for the extraction of Lu^{3+}. The extracted form of Lu is likely to be $Lu(OH)L_2$. The similarity in the extraction curves of Lu^{3+} and La^{3+} shown in Fig. 1 suggests that the trivalent lanthanide ions are probably all extracted by the ionizable crown ether via the same form.

The extraction curves for Th^{4+}, Lu^{3+} and La^{3+} with crown ether carboxylic acid (II) are given in Fig. 2(b). The results were obtained under experimental conditions similar to those described above for (I). Addition of phenyl group to the side arm of (I) changes the pK_a value and the solubility of the crown ether carboxylic acid in water. According to our measurements, the pK_a values for the crown ether carboxylic acids (I) and (II) are 4.7 and 5.2, respectively. Substitution of a phenyl group to acetic acid is known to lower the pK_a value from 4.77 to 4.31 because of the electron withdrawing of the phenyl group. The increase in

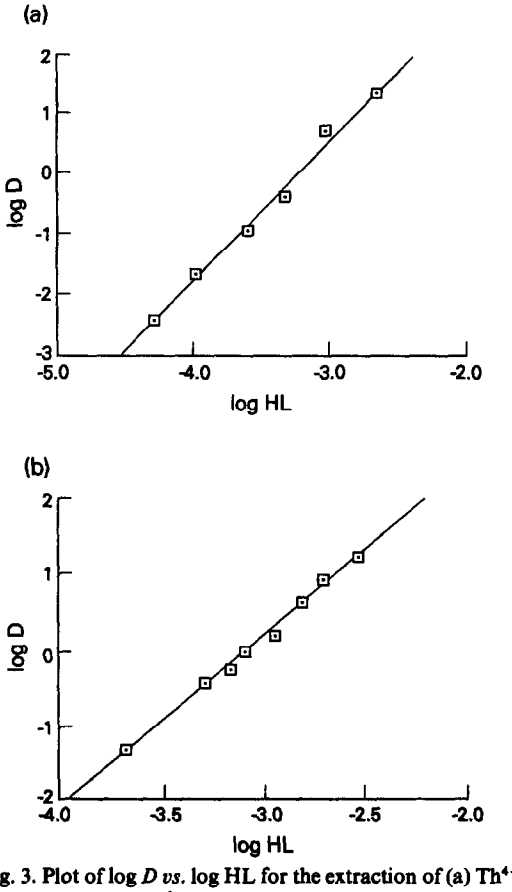

Fig. 3. Plot of log *D vs.* log HL for the extraction of (a) Th^{4+} (at pH 5) and (b) Lu^{3+} (at pH 6.3) with α-(sym-dibenzo-16-crown-5-oxy)acetic acid.

pK_a from (I) to (II) is opposite to the effect of α-substitution on the observed pK_a of acetic acid. It is possible that α-substitution in (II) tends to push the carboxylic acid group towards the cavity resulting in enhanced intramolecular hydrogen bonding with the cavity oxygen, thus increasing the strength of the O—H bond. This intramolecular hydrogen bonding must be stronger than the inductive effect of phenyl on the carboxylic acid. Substitution of phenyl in the side arm of (I) reduces the solubility of the macrocycle in water slightly. The solubility of (I) and (II) in distilled demineralized water at room temperature ($22 \pm 1°$) are $1.1 \times 10^{-4}M$ and $8.9 \times 10^{-5}M$, respectively, according to our experiments.

The extraction curve for Th^{4+} shifted slightly to higher pH from (I) to (II) and those for Lu^{3+} and La^{3+} showed little difference. At pH around 3–4 where Th^{4+} is extracted, the crown ether carboxylic acids should be present primarily in the organic phase. Thus, the extraction of Th^{4+} can be described by the following equation:

$$Th(OH)_2^{2+} + 2HL_{org} = Th(OH)_2L_2 + 2H^+ \quad (1)$$

The extraction constant (K_{ex}) according to equation (1) is given by

$$K_{ex} = [Th(OH)_2L_2]_{org}[H^+]^2/[Th(OH)_2^{2+}][HL]_{org}^2 \quad (2)$$

The concentration of $Th(OH)_2^{2+}$ is determined by the total Th species and the fraction of $Th(OH)_2^{2+}$ present in the aqueous phase. The fraction of $Th(OH)_2^{2+}$ can be calculated from the hydrolysis species of Th^{4+}, *i.e.*,

$$f = Th(OH)_2^{2+}/\Sigma Th(OH)_n^{(4-n)+} \quad (3)$$

with $n = 0$–4. In terms of stepwise hydrolysis constants (K_n) of Th^{4+}, f can also be expressed as

$$f = (K_1K_2/[H^+]^2)/(1 + K_1/[H^+] + K_1K_2/[H^+]^2 + \ldots) \quad (4)$$

The distribution coefficient D, which is the ratio of $[Th(OH)_2L_2]_{org}/\Sigma[Th(OH)_n^{(4-n)+}]_{aq}$, is related to pH and $[HL]_{org}$ by equation (5).

$$\log D = \log K + \log f - 2\log[H^+] + 2\log[HL]_{org} \quad (5)$$

According to equation (5), a plot of log D versus log $[HL]_{org}$ at a fixed pH should yield a straight line with a slope n which equals the ligand to Th ratio.

Both ionizable crown ethers (I) and (II) can be used for the separation of Th from the trivalent lanthanides. The difference in pH range for the extraction of Th and the lanthanides is slightly longer for (I). A suitable pH range for the separation of Th from the lanthanide ions using sym-dibenzo-16-crown-5-oxyacetic acid appears to be between 3–5 where Th is almost quantitatively extracted and the lanthanide ions are virtually not extractable. The best pH value for the separation is around 4.5 which can be easily controlled by means of an acetate buffer. To evaluate the separation efficiency under this condition, an experiment was performed with 50 ml of an aqueous solution at pH 4.5 containing $1 \times 10^{-4}M$ each of Th^{4+}, La^{3+} and Lu^{3+}. The aqueous solution was extracted with 20 ml of chloroform containing $3 \times 10^{-3}M$ α-(sym-dibenzo-16-crown-5-oxy)acetic acid in a separatory funnel. After phase separation, the organic phase was removed and washed with 10 ml of a pH 4.5 aqueous solution containing the acetate buffer. Both of the separated phases were analyzed for Th, Lu, and La by NAA. The purity of Th in the organic phase was found to be better than 99.9%. Only less than 0.1% of the lanthanides were found in the organic phase indicating essentially complete separation after one cycle of extraction. The Th extracted into the organic phase can be quantitatively stripped into a nitric acid solution, *e.g.*, 0.1–1M. For rapid back-extraction of Th from the organic phase for NAA, a 1M nitric acid solution was used.

The crown ether carboxylic acids can be used to preconcentrate trace amounts of Th from water for analytical purposes. To demonstrate this, between 100 and 400 μg of Th were spiked into 100-ml aliquots of a distilled water sample at pH 4.8. The solutions were extracted with 10 ml of chloroform containing $3 \times 10^{-3}M$ of α-(sym-dibenzo-16-crown-5-oxy)acetic acid. After shaking for 15 min, the organic phase was removed and washed. Thorium in the organic phase was back-extracted with 2 ml of a 1M nitric acid solution for NAA. The average recovery of Th was found to be $99.6 \pm 3.5\%$ based on the results of 5 samples. A preconcentration factor of 50 was obtained from this process. Higher preconcentration factors can be obtained by using a larger aqueous to organic phase ratio. Quantitative extraction of trace amounts of Th can be achieved if the aqueous to organic ratio does not exceed 20. The back-extraction step can provide further preconcentration. A total preconcentration factor of

4×10^2 can be easily achieved using the two-step extraction procedure.

This study demonstrates that crown ether carboxylic acids are capable of forming stable complexes with an actinide such as Th. The complexation depends on the oxidation state and hydrolysis species of the actinide present in the aqueous phase. The extraction efficiency thus is a strong function of pH which may be used as a basis for their separation. These types of ionizable crown ethers are potential selective chelating agents for solvent extraction separation of actinides and lanthanides.

Acknowledgements—This material is based upon work supported by the Idaho EPSCoR Program of the National Science Foundation under Grant No. RII-8902065.

REFERENCES

1. J. A. Katz, G. T. Seaborg and L. R. Lester, *The Chemistry of Actinide Elements*, 2nd Ed., Vol. 1, pp. 43–47. Chapman and Hall, N.Y., 1986.
2. J. Tang and C. M. Wai, *Anal. Chem.*, 1986, **58**, 3233.
3. C. M. Wai and H. S. Du, *ibid.*, 1990, **62**, 2412.
4. R. A. Bartsch, G. S. Heo, S. I. Kang, Y. Liu and J. Strzelbicki, *J. Org. Chem.*, 1985, **47**, 457.
5. J. Tang and C. M. Wai, *Talanta*, 1989, **36**, 1129.
6. W. M. Mok and C. M. Wai, *Anal. Chem.*, 1987, **59**, 233.
7. C. F. Baes and R. E. Mesmer, *The Hydrolysis of Cations*, Wiley, New York, 1976.

Talanta, Vol. 40, No. 2, pp. 179–183, 1993
Printed in Great Britain.

0039-9140/93 $6.00 + 0.00

SULPHATE ANALYSIS IN URANIUM LEACH IRON(III) CHLORIDE SOLUTIONS BY INDUCTIVELY COUPLED ARGON PLASMA SPECTROMETRY

I. NIRDOSH,* S. LAKHANI† and M. Z. MOHD YUNUS‡
Department of Chemical Engineering, Lakehead University, Thunder Bay, Ontario, Canada P7B 5E1

(*Received* 20 *January* 1992. *Revised* 2 *June* 1992. *Accepted* 3 *June* 1992)

Summary—Inductively coupled Argon Plasma Spectrometry is used for the indirect determination of sulphate in iron(III) chloride leach solution of Elliot Lake uranium ores via addition of a known amount of barium ions and analyzing for excess of barium. The ore contains ~7 wt% pyrite, FeS_2, as the major mineral which oxidizes to generate sulphate during leaching with Fe(III). The effects of pH, the concentrations of Fe(III) and chloride ions and for presence of ethanol in the test samples on the accuracy of analysis are studied. It is found that unlike the Rhodizonate method, removal of iron(III) from or addition of ethanol to the test sample prior to analysis are not required. Linear calibration curves are obtained.

For obtaining environmentally acceptable non-radiotoxic uranium mill tailings, aqueous solutions of iron(III) chloride acidified with the same concentration of hydrochloric acid have proved effective in the simultaneous leaching of radium-226 along with uranium from the ores.[1] These solutions contain nearly 5500 to 27,200 mg/l Fe(III) and 14,000 to 71,000 mg/l chloride. However, some ores contain high concentrations (~7 wt%) of sulphidic minerals, mostly pyrite, which are oxidized to sulphate by the Fe(III) present in the leach solution and concentration of sulphate in the solution gradually builds up upon repeated recycling of the solution for leaching of fresh ore.[1] This increase in the sulphate concentration causes the precipitation of radium sulphate or the coprecipitation of barium radium sulphate during leaching. The precipitate deposits on the finely divided solids whereby the mill tailings acquire low levels of radiotoxicity due to radium-226 and become environmentally hazardous, defeating the main purpose of leaching the ore with iron(III) chloride.

Nirdosh *et al.*[2] studied the removal of sulphate from iron(III) chloride leach solutions of Elliot Lake uranium ores using anion exchange. During this study sulphate was analyzed by the spectrophotometric method described by Vogel[3] wherein a known amount of barium is added to the test sample as aqueous barium chloride in quantities larger than that stoichiometrically needed for precipitating with sulphate. An ethanol matrix is maintained for the stability of the barium sulphate and sodium rhodizonate solution is added to give a coloured complex with the excess barium not precipitated with sulphate. The colour intensity is measured spectrophotometrically as 520 nm and the amount of the residual barium is determined from a calibration curve. The amount, and hence the concentration, of sulphate is then back calculated by difference. The calibration curve can also be plotted directly in terms of sulphate concentration.

Although straight forward, the method is tedious in that it requires complete removal of Fe(III) and other cations by ion-exchange prior to analysis in order to eliminate any possible interference by their coloured complexes such as the iron(III) rhodizonate.

Because this analytical method is primarily based on the quantitative measurement of barium ions in solution, it was thought worthwhile to explore if another simpler method of barium analysis by the Inductively Coupled Plasma Atomic Emission Spectrometry (ICP–AES) may be used without the need for the separation of interfering ions, such as Fe(III), from the test sample prior to analysis.

*Author for correspondence.
†Present Address: Environment Canada, 25 St Clair Avenue E., Toronto, Ontario, Canada M4T 1M2.
‡Present address: Petronas, Technical Services Department, PCSB, Petronas Office Complex, Kerteh 24300, Terengganu, Malaysia.

This paper presents investigations leading to a standardized analytical procedure for the quantitative determination of sulphate by ICP–AES in the presence of Fe(III) and chloride ions. The possible interference in analysis by only these ions was studied because of their usually high concentrations in the iron(III) chloride leach solutions of the Elliot Lake uranium ores, as noted above.

EXPERIMENTAL

A standard solution of barium containing 500 mg/l barium was prepared by dissolving barium chloride bihydrate in demineralized water. From this stock solution, samples were prepared containing varying amounts of barium by dilution with demineralized water. To some of these samples, a known (less than stoichiometric) quantity of ammonium sulphate was added to precipitate some barium as barium sulphate leaving a known residual barium concentration in solution. This was done to check if barium precipitated quantitatively. An Ashland unit model Jarrell Ash ICAP 9000 Inductively Coupled Argon plasma Spectrometer was used for analyzing barium in solution. The unit had an Argon purge of the optical path with other specifications as: forward power = 1000 watts; reflected power < 5 watts; plasma argon flow = 10 ml/min; auxiliary argon flow = 1.2 l/min; nebulizer argon flow = 0.6 l/min; sample uptake = 0.6 ml/min; and observation height = 15 mm above work coil. The analytical wavelength and detection limit for barium were respectively 493.41 nm and 10 μg/l (10 ppb). Calibration curves were prepared by plotting concentration of barium in the solution versus intensity ratio which is defined as the ratio of the intensity of light produced by the emission spectra to the instrument constant. The instrument constant is given by 1000/exposure time which is usually less than 10 sec. The effects of the addition of 95% ethanol, sample pH and the concentration of the Fe(III) or chloride ions in the sample were investigated by the methods outlined below. The concentration of Fe(III) and chloride were varied by adding iron(III) chloride hexahydrate or sodium chloride, respectively, to the standard barium solutions. All chemicals were Fisher Brand Analytical Reagent grade. The solid symbols in all the diagrams represent identical duplicate samples analyzed to check the reproducibility of results. Although many duplicate samples were prepared and analyzed, only a few have been added in the figures for the sake of clarity. In all the equations in the following sections the concentration of barium is expressed in the units of mg/l.

RESULTS AND DISCUSSION

The effect of ethanol addition

Varying amounts of the 500 mg/l barium standard solution in demineralized water were taken in 50 ml standard flasks so as to obtain barium concentrations between 0 to 100 mg/l in the final 50-ml solution. A 19-ml volume of 95% ethanol was added to each flask. This is the usual amount of ethanol added to samples for analysis via the rhodizonate method.[3] The volume was then made up to 50 ml with demineralized water. The flasks were repeatedly inverted to mix the contents and the samples were analyzed for barium.

The results are plotted in Fig. 1 and indicate a considerable scatter with no linear region in the calibration curve. During the course of analysis it was observed that ethanol caused a drift in the instrument which is considered to be due to the "memory effect", *i.e.*, the flame indicated the presence of ethanol (bright yellow flame) even up to 5 minutes after the sample had been analyzed. These results show that the presence of ethanol leads to interference and should be avoided.

The effect of pH

The suitability of the method was investigated at pH values 1 and 4. These pH values were selected because the iron(III) chloride leaching

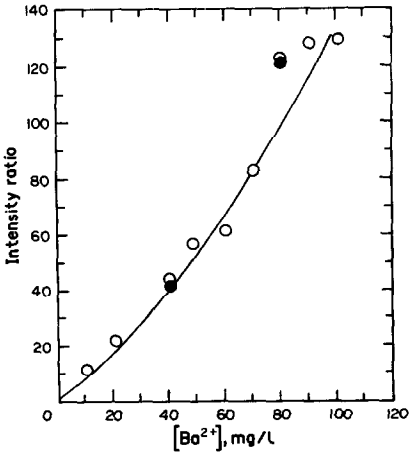

Fig. 1. Variation of intensity ratio with barium concentration in the presence of ethanol.

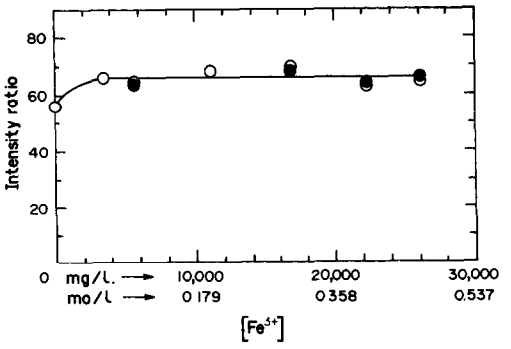

Fig. 2. Effect of Fe(III) concentration on the intensity ratio.

solutions of uranium ores are usually at pH $\leq$ 1 and the rhodizonate method of sulphate analysis works best at pH 4.[2] In each case, eleven test samples were prepared. Aliquots of the standard sulphate solution were taken in 50-ml standard flasks. Known excess amounts of the standard barium solution were then added to precipitate all the sulphate and leave free residual barium in solution. The volume was then made up with pH 1 or pH 4 solution of hydrochloric acid. The contents were thoroughly mixed by shaking the flasks. The precipitate was left to settle and then vacuum filtered using a Millipore unit with a 0.45-μm filter medium. The filtrate was then analyzed for barium. The results indicated that corresponding samples for both pH 1 and pH 4 gave intensity ratios of within $\pm$2–4 units of each other and, in the barium concentration range of 20–100 mg/l, the calibration curves could be described by the following linear equation:

$$\text{Intensity Ratio} = 4.51\ [Ba^{2+}]. \qquad (1)$$

This indicates that pH $\leq$ 4 has little effect on the analysis.

The effect of Fe(III)

Samples 5 ml of a 50 mg/l standard sulphate solution were taken in 50-ml flasks. Aliquots of 1*M* iron(III) chloride solution were added to give varying amounts of Fe(III) in the 50-ml solutions obtained. A 5-ml volume of the 500 mg/l barium standard solution was then added to each flask and the total volume was made up with demineralized water. The contents were mixed and the filtrates analyzed for barium. The results are plotted in Fig. 2. These results indicate that the intensity ratio is not significantly affected by the presence of Fe(III) in concentrations 3350–27,200 mg/l in the test samples.

Another set of calibration data were obtained by analyzing barium in two sets of standard samples. In one set, varying amounts of barium were used whereas in the second set, a fixed amount of 0.02*M* Fe(III) was added to the standard barium solutions of the same barium concentrations as in the first set. The results indicated that the intensity ratios for all the samples in both the sets were nearly the same and the calibration curves could be given by mutually superimposing linear lines given by the equation

$$\text{Intensity Ratio} = 1.08\ [Ba^{2+}]. \qquad (2)$$

These results confirm the findings obtained from Fig. 2 that between 3350–27,200 mg/l concentration range, the Fe(III) ions do not interfere with the analysis of barium.

The effect of chloride

The method was the same as described in Section 3.3 except that instead of the Fe(III) solution, varying amounts of a 3.9*M* standard sodium chloride solution were added to the flasks so as to give samples of chloride concentrations of 0 to 70,000 mg/l. The results are plotted in Fig. 3. A duplicate set of samples was prepared in an identical manner and barium was analyzed with the ICP–AES unit fitted with a high-solids' nebulizer instead of the usual cross-flow nebulizer. The results are included in Fig. 3 for comparison.

The results indicate that chloride ions showed a significant effect on the intensity ratio in the range of 0 to 20,000 mg/l for both types of nebulizers. The results with the cross-flow nebulizer indicate that the effect was more predominant up to a chloride concentration of 20,000

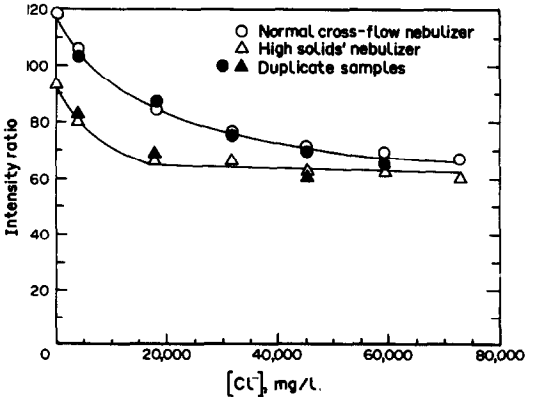

Fig. 3. Effect of chloride concentration on the intensity ratio.

Table 1. Comparison of $[SO_4^{2-}]_{analyzed}$ and the initially known $[SO_4^{2-}]_{known}$ values in demineralized water and aqueous solutions of 0.1M $FeCl_3$

$[SO_4^{2-}]_{known}$, mg/l	$[SO_4^{2-}]_{analyzed}$, mg/l		% Deviation	
	Demineralized water	$FeCl_3$ solution	Demineralized water	$FeCl_3$ solution
40	39	—	2.5	—
60	59	57	1.7	5.0
80	81	—	−1.3	—
100	100	104	0.0	−4.0
200	211	213	−5.5	−6.0
300	315	311	−5.0	−3.7
400	412	412	−3.0	−3.0
500	497	492	0.6	1.6

— = not done.

ml/l, after which there was a gradual tapering of the interference. However, with the high-solids' nebulizer, the interference was significantly reduced at chloride concentrations 20,000 mg/l, as is indicated by the lower curve in Fig. 3.

A separate set of calibration data were obtained with the cross-flow nebulizer by preparing samples that all had a chloride concentration of 30,000 mg/l. In this set of analyses, the instrument was flushed thoroughly after testing each sample. The results gave a linear calibration curve which could be described by the equation

$$\text{Intensity Ratio} = 1.31\ [Ba^{2+}]. \qquad (3)$$

These results indicate that high concentrations of chloride ions do not interfere with barium analysis provided a high-solids' nebulizer is used or with the cross-flow nebulizer, the instrument is flushed thoroughly after each test.

Sulphate analysis by the addition of barium ions

A 10-ml volume of a 1430 mg/l stock barium solution was taken in 100-ml standard flasks. To these, varying amounts of a 500 mg/l standard sulphate solution were added so as to obtain 40–500 mg/l sulphate. Two identical sets were prepared. The volumes were then made up with either demineralized water (first set) or a solution of 0.1*M* iron(III) chloride (second set). The barium sulphate was allowed to precipitate and the contents were filtered through a 0.45 μm filter medium. The filtrates were analyzed for barium by ICP–AES and barium concentrations were obtained from appropriate calibration curves. The concentration of sulphate was then calculated and the values, $[SO_4^{2-}]_{analyzed}$, are given in Table 1 along with the initial known sulphate concentrations, $[SO_4^{2-}]_{known}$, of the corresponding samples, and the percentage deviations.

These results indicate that (i) in general there is good agreement between the known and the calculated sulphate concentration values; and (ii) except for one sample containing 200 mg/l sulphate, the deviation is $\leq \pm 5\%$. Within the experimental errors, these deviations also indicate that barium sulphate precipitated quantitatively in the samples tested.

CONCLUSIONS

ICP–AES can be used for the quantitative determination of sulphate in iron(III) chloride leach solutions of uranium ores by precipitating the sulphate in the presence of known excess quantity of barium, analyzing for free barium and back calculating the sulphate concentration.

Interference by Fe(III) ions in concentrations of 3350–27,200 mg/l is insignificant and removal of Fe(III) from solution prior to analysis is not needed rendering the sample preparation much simpler than in the rhodizonate method.

Interference by chloride ions is insignificant at chloride concentrations 20,000 mg/l with a high-solids' nebulizer. When using a cross-flow nebulizer, flushing the instrument between each test is important to prevent interference by chloride.

Presence of ethanol in the test solution causes interference and should be avoided.

The reproducibility of results is within ± 2–4 intensity units and the accuracy is $\pm 5\%$.

The method can be used for aqueous solutions of pH < 4 and containing high concentrations of Fe(III) ($\approx$27,200 mg/l) and chloride ($\approx$71,000 mg/l) usually encountered in commercial oxidative iron(III) leach solutions of

ores with pyrite or other sulphides as significant gangue minerals.

Acknowledgements—Financial support from the Natural Sciences and Engineering Research Council of Canada and help in analyses by Mr A. Raitsakas of Lakehead University Instrument Laboratory are gratefully acknowledged.

REFERENCES

1. I. Nirdosh, M. H. I. Baird, S. V. Muthuswami and S. Banerjee, *Hydrometallurgy*, 1983, **10**, 265.
2. I. Nirdosh, A. Sirignano, C. R. Johnson and S. Lakhani, *Uranium*, **4**, 395.
3. A. I. Vogel, *A Text Book of Quantitative Inorganic Analysis*, 3rd Ed., p. 275. Longman and Green, London, 1961.

Talanta, Vol. 40, No. 2, pp. 185–193, 1993
Printed in Great Britain.

0039-9140/93 $6.00 + 0.00

DETERMINATION OF URINARY ARSENIC AND IMPACT OF DIETARY ARSENIC INTAKE

XIAO-CHUN LE, WILLIAM R. CULLEN* and KENNETH J. REIMER
Department of Chemistry, University of British Columbia, Vancouver, B.C., Canada, V6T 1Z1

(*Received* 7 *May* 1992. *Accepted* 2 *June* 1992)

Summary—An analytical method based on microwave decomposition and flow injection analysis (FIA) coupled to hydride generation atomic absorption spectrometry (HGAAS) is described. This is used to differentiate arsenite [As(III)], arsenate [As(V)], monomethylarsonic acid (MMA) and dimethylarsinic acid (DMA) from organoarsenic compounds usually present in seafood. Without microwave digestion, direct analysis of urine by HGAAS gives the total concentration of As(III), As(V), MMA and DMA because organoarsenic compounds such as arsenobetaine, usually found in most seafood, are not reducible upon treatment with borohydride and therefore cannot be determined by using the hydride generation technique. The microwave oven digestion procedure with potassium persulfate and sodium hydroxide as decomposition reagents completely decomposes all arsenicals to arsenate and this can be measured by HGAAS. Microwave decomposition parameters were studied to achieve efficient decomposition and quantitative recovery of arsenobetaine spiked into urine samples. The method is applied to the determination of urinary arsenic and is useful for the assessment of occupational exposure to arsenic without intereference from excess organoarsenicals due to the consumption of seafood. Analysis of urine samples collected from an individual who ingested some seafood revealed that organoarsenicals were rapidly excreted in urine. After the ingestion of a 500-g crab, a 10-fold increase of total urinary arsenic was observed, due to the excretion of organoarsenicals. The maximum arsenic concentration was found in the urine samples collected approximately between 4 to 17 hr after eating seafood. However, the ingestion of organoarsenic-containing seafoods such as crab, shrimp and salmon showed no effect on the urinary excretion of inorganic arsenic, MMA and DMA.

Arsenite [As(III)], arsenate [As(V)], monomethylarsonic acid (MMA), and dimethylarsinic acid (DMA) are widely present in the natural environment[1] and their relative toxicities are As(III) > As(V) > MMA > DMA.[2,3] Many organoarsenic compounds present in the biological system, however, are much less toxic. For example, arsenobetaine is found in many seafoods as the major arsenic compound and it is essentially non-toxic.[4,5] The ubiquitous presence of arsenic compounds in biological systems results in a need for methods that can accurately and easily assess their environmental impact.

A convenient approach to assess occupational exposure is through chemical analysis of urine because urine samples are readily obtained non-invasively. Such an analysis can provide important information about exposure to many chemical species and information about many of the body's metabolic functions. As early as 400 B.C., the Greek physician, Hippocrates, pointed out the importance of urine examinations in health and disease.[6–8] Diagnosing disease by visual examination of urine—referred to as uroscopy—was very popular among ancient medical practitioners. Although they lacked sophisticated equipment, they were able to obtain diagnostic information from such basic observations as color, volume, turbidity, viscosity, odor, and even sweetness. Interestingly, these same urine characteristics are still reported in today's clinical laboratories, although modern urinalysis includes not only the physical examination of urine, but also chemical analysis. In addition to routine chemical analysis, the determination of trace elements in urine has gained much attention[9–11] and has become a useful tool for health assessment.

Urinary excretion is the major pathway for the elimination of arsenic compounds from the body.[12–17] Therefore, urinary arsenic determination is important for assessing occupational exposure.[18–20] Excess exposure to arsenic can occur in occupations such as mining, smelting, glass making, and pesticide manufacture. In the work environment, the exposure to As(III) is mainly from As_2O_3 in non-ferrous smelters and in glass making. Exposure to arsenate arises

*Author for correspondence.

from its use in insecticides, cotton desiccants, and wood preservatives. Exposure to MMA and DMA is due to their use as selective herbicides. Rapid urine excretion of these arsenic compounds from humans,[13,14,17,20–22] monkeys,[15] dogs,[23] and hamsters[24] has been reported. The biotransformation of inorganic arsenic in the body, to DMA and MMA, has also been studied extensively.[13,21,24–29]

Unlike those from occupational exposure, dietary sources of arsenic, particularly from seafood, generally contain more complex organoarsenicals such as arsenobetaine, $(CH_3)_3As^+CH_2COO^-$. Arsenic ingested in this form is not metabolized and is excreted unchanged with a very short half-time.[5,12,16,17] Since arsenic compounds ingested from both occupational exposure and dietary sources contribute to the urinary arsenic excretion, the determination of total arsenic concentration in urine cannot be used to assess oocupational exposure to arsenic. In fact, it has been reported[18] that the total arsenic concentration in urine increased by a factor of 20–30 after ingestion of 100 g of shrimp. Because the two groups of arsenic species, from occupational exposure and from dietary intake of arsenic, are different, it should be possible to develop an appropriate analytical method to distinguish the contributions to urinary arsenic from these two sources. This was the objective of the present study.

In a previous publication,[30] we described a rapid method for arsenic determination based on the decomposition of organoarsenicals by potassium persulfate and sodium hydroxide with the aid of a microwave oven and subsequent determination by hydride generation atomic absorption spectrometry (HGAAS). The organoarsenicals were completely decomposed to arsenate. When the microwave oven was off, only As(III), As(V), MMA, and DMA were measured because organoarsenicals such as arsenobetaine are "hidden" and do not form hydrides upon treatment of borohydride under the commonly used analytical conditions. The difference between the two measurements with microwave power on or off accounts for the hidden organoarsenicals. This method is simple and rapid, with a sample throughput of approximately 100–120 analysis per hour and can be successfully applied to the decomposition of organoarsenicals in demineralized water and seawater. However, when arsenobetaine was spiked into a urine sample the recovery was approximately 40% due to incomplete decomposition. To solve this problem, we investigated simple approaches to achieve the complete decomposition of arsenic compounds in a complex matrix such as urine. Longer decomposition times and higher concentrations of decomposition reagents were found to be necessary. Therefore, a batch type digestion prior to the determination was developed to completely decompose the arsenic compounds in urine. Quantitative recoveries of organoarsenic and inorganic arsenic spiked into urine are achieved. The method developed here is successfully applied to the analysis of urinary arsenic. Urine samples from a research worker who ingested crab meat are analyzed and the excretion patterns of inorganic arsenic and organoarsenic compounds are compared.

EXPERIMENTAL

Instrumentation

A Varian Model AA-1275 atomic absorption spectrophotometer equipped with an air-acetylene flame atomizer, an open-ended T-shaped quartz tube (11.5 cm × 0.8 cm i.d.) mounted in the AA flame, a domestic microwave oven (Toshiba, Japan), and a lab-made new hydride generator as described previously[30] were used throughout this work. (Safety precaution: two holes drilled on one side of the microwave oven for sample inlet and outlet should be shielded with proper metal fittings to prevent any possible microwave leakage.) The experimental layout for flow injection analysis (FIA)/on-line microwave digestion coupled to HG AAS measurement is the same as discussed previously.[30] For most of the present work, however, a batch type microwave digestion was used, and the microwave oven was used off-line. Both the undigested and the digested samples were analyzed by using FIA/HGAAS.

Samples

Urine samples were collected from a 30-year old, healthy male working in an analytical chemistry research laboratory. Live crabs were purchased from a local fish market in Vancouver (Canada) and were steam cooked. After the cooked crab meat was eaten, urine samples were collected for the following 2–3 days. The samples were stored at 4° and were analyzed within 48 hr. No preservative was added.

Table 1. Experimental conditions for microwave digestion and hydride generation

	FIA/HGAAS Direct Analysis	Batch type microwave digestion FIA/HGAAS
Digestion	no	microwave digestion
Urine Samples	100 μl	40 ml
$K_2S_2O_8$	none	4.5 g
NaOH	none	2.7 g
Digestion time	none	5 × 3 min (for 6 samples)
HCl Conc.	0.70*M*	3.0*M*
HCl Flow Rate	3.4 ml/min	3.4 ml/min
$NaBH_4$ Conc.	0.65*M* in 0.1*M* NaOH	0.65*M* in 0.1*M* NaOH
$NaBH_4$ Flow Rate	3.4 ml/min	3.4 ml/min
Carrier Gas Flow	160 ml/min	160 ml/min
Cysteine	1.0%	none

Reagents

Standard solutions of As(III), As(V), MMA, DMA and arsenobetaine were prepared as described previously.[30] Sodium borohydride (Aldrich) solutions in 0.1*M* sodium hydroxide (BDH) were prepared fresh and filtered prior to use. Potassium persulfate (BDH) solutions in various concentrations of sodium hydroxide were prepared fresh daily for the FIA/microwave digestion/HGAAS determination. For the batch type microwave digestion, appropriate amounts of potassium persulfate and sodium hydroxide were directly added in their solid form into digestion vessels (Erlenmeyer flasks) containing sample solutions. Appropriate amounts of *L*-cysteine (Aldrich) were directly added and dissolved into the test solution when needed.

Procedures

FIA/HGAAS. A 100-μl sample was injected into a carrier stream (H_2O) by means of a Rheodyne six-port sample injection valve fitted with a 100-μl sample loop. The injected sample along with the carrier subsequently met with a continuously introduced hydrochloric acid stream and sodium borohydride stream. Upon mixing with sodium borohydride, hydride generation takes place and continues in the gas/liquid separator apparatus as discussed previously[30] in detail. Inside this apparatus, a continuous flow of carrier gas assists mixing and reaction and subsequently carries hydrides to the quartz tube mounted in the air-acetylene flame for the AA measurement. A peak signal was recorded by using an integrator (Hewlett–Packard 3390A) capable of both peak height and peak area measurements. It was found that the peak height measurement gave better reproducibility and lower standard deviation. Thus the peak height of the signal was measured for quantitation unless stated otherwise.

As(III), As(V), MMA, and DMA have been reported to have different sensitivities upon hydride generation;[31–33] and their maximum sensitivities appear at very different acid concentrations as reaction media. Although compromised acid conditions have often been used, considerable error was present particularly when one standard was used to represent the four species.[32,33] We have found that the use of cysteine in the reaction media shifts the optimum acid concentration to a much lower level;[34–36] and that under the same optimum acid concentration all the four arsenic species give the same maximum sensitivity.[37] Thus the determination error which otherwise arises from the use of compromised condition is eliminated. Upon optimization, 0.1 g of cysteine was added to every 10-ml of urine sample for the determination of As(III), As(V), MMA, and DMA in the urine. For the determination of total arsenic, the microwave decomposition was applied, and arsenic compounds were all converted to arsenate as confirmed previously[30] by using the molybdenum blue colorimetric method. Therefore there is no need to add cysteine in this case, and the optimum acid concentration for determining arsenate was chosen.

The experimental conditions are summarized in Table 1.

FIA/On-line microwave decomposition/HGAAS. A 100-μl sample was injected into the decomposition reagent stream containing potassium persulfate and sodium hydroxide. The stream carries the sample into a 3-m knotted Teflon coil (0.5 mm i.d.) located in the microwave oven which operates at full power (500 W). After microwave decomposition, the solution

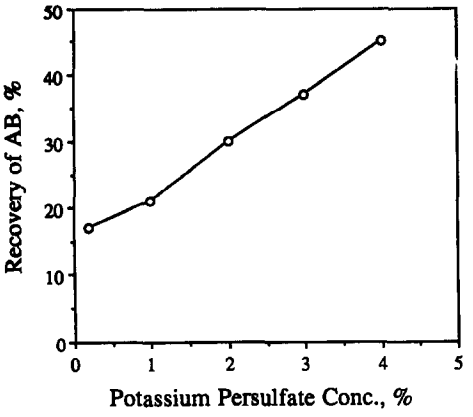

Fig. 1. Effect of $K_2S_2O_8$ concentration on recovery of arsenobetaine in urine by FIA/continuous microwave decomposition/HGAAS measurement.

flow mixes with the continuous acid and borohydride feeds. Hydride generation and gas/liquid separation take place and the evolved hydrides are introduced into the flame-heated quartz tube for AA measurement. The experimental conditions for this mode of operation are the same as described previously.[30]

Batch type microwave decomposition. A urine sample or standard solution (40 ml) and the appropriate amounts of potassium persulfate and sodium hydroxide (Table 1) were combined in a 125-ml Erlenmeyer flask. Six of such sample-containing flasks were placed in the microwave oven at one time. The microwave oven was then operated at full power for 3 min followed by a 2–3 min cooling period. This heating and cooling sequence was repeated for another four cycles. After the samples were cooled to room temperature, they were each diluted to 50 ml with demineralized water. The determination of arsenic was carried out by using FIA/HGAAS as described above. Note that excess potassium persulfate is used. This is not completely soluble in the urine sample prior to the digestion, however, the excess potassium persulfate decomposes in the presence of sodium hydroxide under microwave heating and there is no solid residue present after the decomposition is complete.

RESULTS AND DISCUSSION

By using the on-line microwave decomposition system described previously,[30] initial attempts to completely decompose organoarsenicals in a urine sample matrix were made by optimizing concentrations of the decomposition reagents, potassium persulfate and sodium hydroxide. Figures 1 and 2 show recoveries of spiked arsenobetaine (AB) into a urine sample, determined by HGAAS after on-line microwave decomposition using persulfate and sodium hydroxide of various concentrations. Recovery values were obtained by comparing signals from spiked AB with those of the same amount of an As(V) standard solution. As demonstrated in Fig. 1, increasing the concentration of potassium persulfate from 0.1 to 4% results in continuous improvement of recoveries with a maximum recovery of 45% when the potassium persulfate concentration is 4%. Further increase of persulfate concentration was not studied because of the limited solubility of potassium persulfate in water. Similarly, increasing the sodium hydroxide concentration from 0.1 to 2*M* also leads to higher recoveries in the determination of the spiked AB in the urine sample as shown in Fig. 2. Although recoveries are improved at these higher reagent concentrations, the desired quantitative recoveries are not achieved due to incomplete decomposition of AB. Therefore, in addition to higher concentrations of decomposition reagents, a longer decomposition time appears to be necessary in order to achieve complete decomposition of AB and thereby a quantitative recovery. Use of longer decomposition coils (5 m and 12 m as compared to 3 m used in the previous work) were studied in an attempt to achieve complete decomposition; and recoveries of spiked AB into urine were improved. However, with longer decomposition coils, a higher noise level and poorer signal stability were shown. To solve this problem, a batch mode

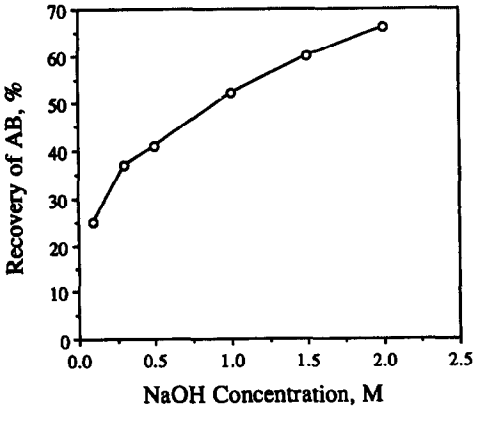

Fig. 2. Effect of NaOH concentration on recovery of arsenobetaine in urine by FIA/continuous microwave decomposition/HGAAS measurement.

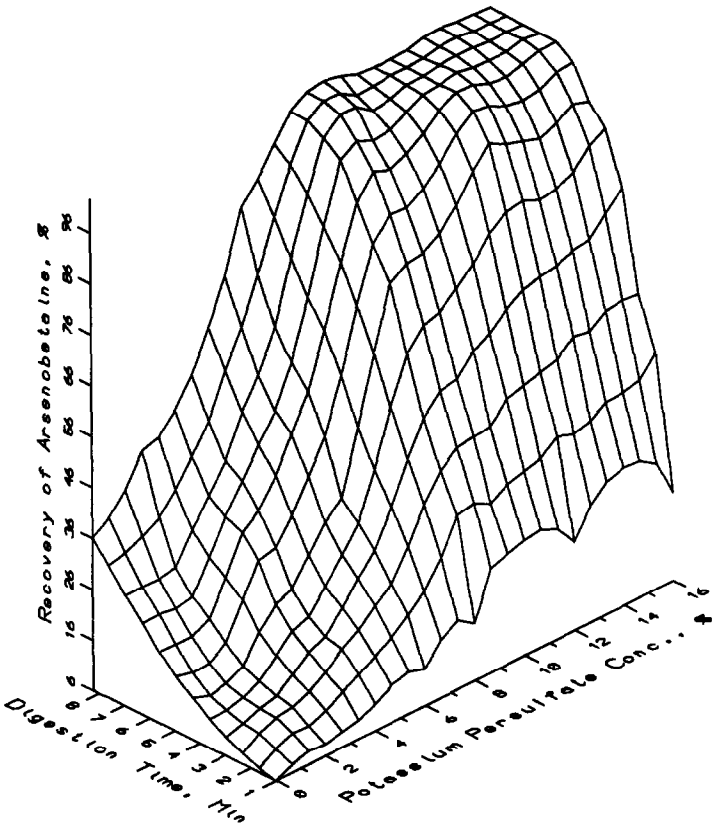

Fig. 3. Effect of microwave digestion time and $K_2S_2O_8$ concentration on recovery of arsenobetaine in urine by batch type microwave digestion and FIA/HGAAS determination.

microwave oven digestion followed by the determination by using FIA/HGAAS was chosen for the rest of this work.

Effect of decomposition time and concentrations of potassium persulfate and sodium hydroxide

Arsenobetaine (AB) is the major arsenic compound found in most seafood, it is excreted unchanged in urine after ingesting seafood, and it is one of the organoarsenic compounds that is most difficult to decompose to a form amenable to hydride generation. AB was chosen as a model compound in order to study the decomposition of organoarsenicals in urine. A measured amount of AB was spiked into a urine sample and the arsenic concentration was measured by using FIA/HGAAS after batch type microwave digestion in open vessels. Recovery was measured by comparing signals obtained from the spiked AB with those of the same amounts of an As(V) standard solution. For this optimization study, two samples at a time were placed in the microwave oven.

The effect of decomposition time and the amount of potassium persulfate on the recovery of AB spiked into a urine sample is shown in Fig. 3. By studying these two factors together, a possible dependence on each other would be revealed. In the present situation, increasing both the digestion time and the concentration of persulfate is beneficial to a quantitative recovery. As the decomposition time and the concentration of potassium persulfate increase, recoveries of AB approach unity. This is because a longer decomposition time and a higher concentration are useful for complete decomposition of AB in the urine sample. The decomposed arsenic product was confirmed to be arsenate,[30] an arsenic compound that readily forms arsine on treatment with borohydride. A contour diagram clearly showed that quantitative recoveries of AB are achieved when the amount of potassium persulfate added is in the range of 10–16 g per 100 ml of urine and the decomposition time is longer than 5 min.

The effect of the concentration of sodium hydroxide and the decomposition time was also studied by varying both of these factors, and the recovery results of AB are presented in Fig. 4. Similarly, recovery of spiked AB improves with

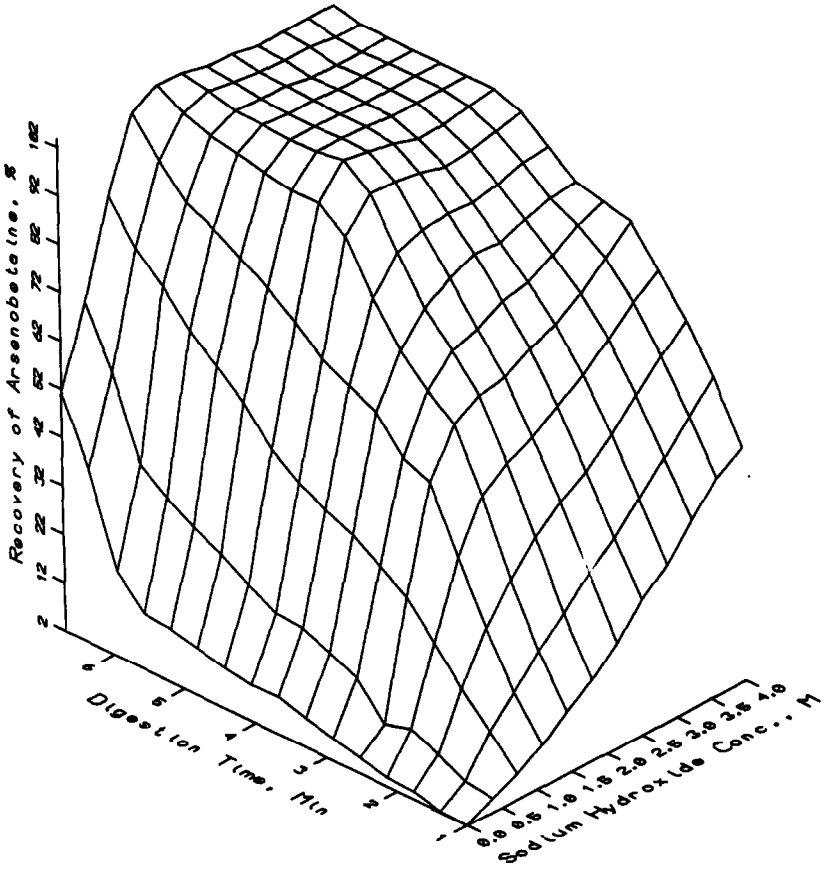

Fig. 4. Effect of microwave digestion time and NaOH cencentration on recovery of arsenobetaine in urine by batch type microwave digestion and FIA/HGAAS determination.

an increase of the sodium hydroxide concentration from 0.1 to 1.5*M* and the decomposition time from 0.5 to 4 min. Complete recovery is achieved with a sodium hydroxide concentration of above 1.5*M* and a microwave decomposition of longer than 4 min.

A six minute microwave decomposition time, 1.7*M* sodium hydroxide and 11% potassium persulfate were chosen as optimum for digesting two samples at one time to ensure complete decomposition and quantitative recoveries of organoarsenicals in urine samples. For a batch of 6 samples a total of 15 min proved to be sufficient and was adopted for further applications.

Calibration and standard addition

For comparison, both As(V) and AB were used as standards in obtaining calibration curves. As shown in Fig. 5, calibration curves obtained from As(V) and AB are superimposable, indicating that AB is completely decomposed to arsenate which forms arsine upon treatment with borohydride in the same way as does As(V). Therefore, either one of them can be used as standard for quantitative analysis. For convenience, As(V) was chosen.

To estimate any possible interference from the sample matrix, a standard addition study

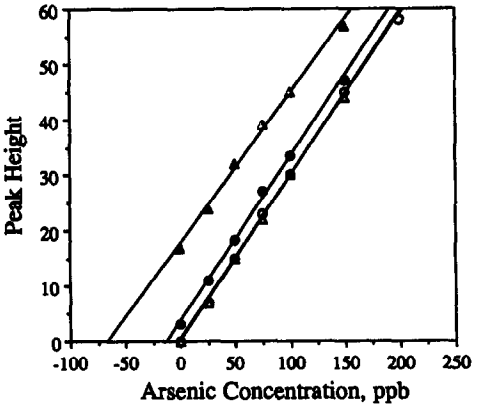

Fig. 5. Comparison of calibration curves of As(V) (○) and AB (△) and standard addition curves of As(V) (●) and AB (▲) spiked into a urine sample. For AB determination, both standards and spiked samples underwent microwave digestion; whereas no digestion was needed for As(V) determination.

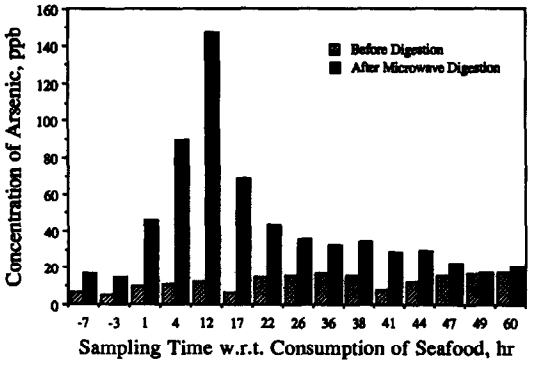

Fig. 6. Concentration of arsenic in urine samples collected from a person at various times with respect to his consumption of crab meat. (▨) sum of As(III), As(V), MMA and DMA, obtained directly by using FIA/HGAAS, without digestion of urine samples (■) total arsenic concentration obtained by using microwave digestion and FIA/HGAAS determination.

was conducted by separately spiking standard As(V) and AB of various concentrations into a urine sample. Samples spiked with As(V) were directly analyzed for arsenic by FIA/HGAAS, whereas the samples spiked with AB underwent microwave decomposition before being analyzed by the same FIA/HGAAS method. The two standard addition curves are also shown in Fig. 5 and they are essentially parallel to the calibration curves. These results demonstrate that there is no interference from the urine sample matrix in the determination of As(V) and AB. When As(III), MMA, DMA, and arsenocholine were spiked into the urine sample, quantitative recoveries were also obtained, indicating that there is no interference in the determination of these arsenic species in urine.

Analysis of a reference urine sample, UriChem (Urine Chemistry Control Level 1, Fisher Scientific), gives arsenic concentrations of 16.2 ± 1.0 ng/ml in the absence of microwave digestion and 26.4 ± 1.3 ng/ml after microwave digestion. No information on the arsenic species is available for comparison although the reference value for total arsenic concentration is 25 ± 19 ng/ml. Our results for total arsenic, 26.4 ± 1.3 ng/ml, is in good agreement with this value.

Standard deviation

Eleven aliquots (40 ml each) of a urine sample (collected approximately 5 hr after the ingestion of some crab meat) were analyzed for the sum of As(III), As(V), MMA, and DMA before microwave digestion and total arsenic concentration after microwave decomposition. Each decomposed sample was measured three times. The relative standard deviation (RSD) from the 11 replicate determinations of arsenic in the urine sample (mean arsenic concentration of 63.4 ng/ml) is 3.0% with peak height measurement and 4.9% with peak area measurement. The sum of As(III), As(V), MMA, and DMA measured before the microwave digestion of the same urine sample is 10.1 ng/ml.

Application

The method described above shows simplicity, accuracy, and is free from interference. Since the ingestion of seafood results in urinary excretion of increased levels of organoarsenic compounds, and the method developed is capable of differentiating these marine organoarsenicals from As(III), As(V), MMA and DMA, the method was used to analyze urine samples collected from a person before and after the consumption of some seafood.

Figure 6 shows the arsenic concentration in urine samples collected at various times encompassing the ingestion of crab meat from a 500-g steam cooked crab. The sum of As(III), As(V), MMA and DMA concentrations measured directly by FIA/HGAAS without digestion and the total arsenic concentration measured after microwave decomposition of the sample are compared. The difference corresponds to the organoarsenicals that normally do not form hydrides upon treatment with borohydride. As shown in Fig. 6, the ingestion of crab meat has very little effect on the concentration of As(III), As(V), MMA and DMA in urine. However, up to a 10-fold increase of total arsenic concentration is observed in urine samples collected after the ingestion of crab meat. This is expected as high concentrations of organoarsenicals such as arsenobetaine have been found in much seafood including crab,[16,25,38] and these organoarsenic compounds are eliminated by kidneys and excreted in urine. Obviously, measuring total urinary arsenic concentration is not acceptable for assessing occupational exposure when the subject has eaten seafood prior to the sampling. Roy[39] stated that the ingestion of seafood at 48–72 hours prior to the sampling would invalidate the use of urinary arsenic as a measure of occupational exposure if the dietary arsenic was not taken into account. In studies by Buchet *et al.*[21,22] the subjects were restricted from eating any seafood before their urine samples were collected. Foa *et al.*[18] and Chana and Smith[19] have further discussed the interference

from dietary arsenic on the biological monitoring of occupational exposure to arsenic. By using the analytical method developed here, however, we are able to differentiate the organoarsenicals due to dietary intake from As(III), As(V), MMA and DMA. Therefore, occupational exposure to inorganic arsenic can be easily assessed by measuring urinary arsenic concentration without interference from the consumption of seafood.

Figure 6 also shows that rapid urine excretion of these organoarsenicals occurs as early as one hour after eating seafood. The excretion of arsenic continues and maximum arsenic concentration appears between 4 and 17 hours after eating seafood. Reproducible excretion patterns were obtained from several replicate feeding experiments including the ingestion of some other seafood such as shrimp and salmon fish. Our results showing rapid urine excretion of organoarsenic compounds are in good agreement with Buchet *et al.*[25] who calculated that the half-time for urinary excretion following crab meat consumption was 18 hours. Freeman *et al.*[17] and Charbonneau *et al.*[15] have also reported that most of the arsenic ingested is excreted in the urine from both men[17] and monkeys[15] within two days of eating arsenic-containing fish. The urinary arsenic excretion pattern and the excretion rate vary with the different arsenic compounds ingested. While the excretion of organoarsenicals present in marine organisms is very fast as can be seen from this work and that of others,[15,17,40] the elimination of inorganic arsenic by the kidney is relatively slow. Buchet *et al.*[25] calculated a biological half-time of 30 hr for the urinary excretion of arsenic following a single ingestion of 3000 μg of arsenic as sodium arsenite. They also reported[21] that after the ingestion of 500 μg of arsenic in the form of arsenite, 45% of the dose was excreted within 4 days, of which 24% was as DMA, 10% as MMA and 11% as inorganic arsenic. Following ingestion of the same amounts of arsenic as MMA or DMA, however, approximately 75% of the dose was excreted in the urine within 4 days. Tam *et al.*[13] reported that in six human subjects who ingested 0.01 μg of arsenic as ^{74}As labelled arsenic acid, 38% of the dose was excreted in the urine within 48 hours and 58% within 5 days, of the latter excreted amount 30% was as DMA, 12% as MMA and 16% as inorganic arsenic. The difference in excretion rate between inorganic arsenic and seafood organoarsenic may be due to the fact that inorganic arsenic is metabolized by the human organism[13,21,25,26,28] whereas organoarsenic such as arsenobetaine is excreted unchanged in urine.[16]

It is also interesting to point out that a trace amount of organoarsenic is found in urine samples collected before the ingestion of seafood as shown in Fig. 6. In another set of experiments where urine samples were collected for 60 hr from the same person under a regular diet which did not include seafood, the arsenic concentration in every urine sample measured after the microwave digestion is higher than or at least equal to that obtained without the digestion. Therefore, this confirms the presence of organoarsenic compounds in the urine of people who do not regularly eat seafood. These results support the findings of Foa *et al.*[18] who reported that unknown organoarsenicals represented up to 70% of the total arsenic in urine samples of a reference population that does not have occupational exposure or does not ingest large amounts of seafood.

CONCLUSION

The present FIA/HGAAS method is rapid, sensitive and easy to use. In addition to the determination of As(III), As(V), MMA and DMA in urine samples described here, the method could be expanded to the analysis of other biological and environmental samples. The addition of cysteine into the sample enables As(III), As(V), MMA and DMA to give the same maximum sensitivity under the same condition. This eliminates the determination errors due to the choice of a compromised acid concentration for the four arsenic species; the optimum acid concentration for DMA is usually much lower than those for As(III), As(V) and MMA. The beneficial effect of cysteine is under further investigation.

Microwave oven decomposition is rapid and efficient. In the presence of potassium persulfate and sodium hydroxide, all arsenic species are converted to arsenate and therefore the total arsenic concentration is easily determined by using the hydride generation technique. The difference in arsenic concentrations obtained after the microwave decomposition and before the decomposition is a measure of the presence of complex organoarsenicals such as arsenobetaine.

Urinary arsenic due to occupational exposure usually consists of As(III), As(V), MMA and

DMA. Ingestion of seafood results in urinary excretion of organoarsenicals unchanged from their original forms present in the seafood. These two pools of arsenic compounds do not interchange. The present method is capable of differentiating these two pools of arsenic compounds and therefore can be used to distinguish the sources of urinary arsenic, occupational exposure or dietary intake.

Acknowledgements—This work is partly supported by the Natural Science and Engineering Research Council of Canada. The authors thank the Canada's Killam Trust and its Scholarship Committee for awarding a Killam Predoctoral Fellowship to X.C.L.

REFERENCES

1. W. R. Cullen and K. J. Reimer, *Chem. Rev.*, 1989, **89**, 713.
2. R. J. Lewis and R. L. Tatken, *Registry of Toxic Effects of Chemical Substances*, US Department of Health, Education and Welfare, Cincinnati, OH, U.S.A. 1978.
3. W. R. Penrose, *CRC Crit. Rev. Environ. Control*, 1974, **4**, 465.
4. T. R. Irvin and K. J. Irgolic, *Appl. Organomet. Chem.*, 1988, **2**, 509.
5. M. Vahter, E. Marafante and L. Dencker, *Sci. Total Environ.*, 1983, **30**, 197.
6. L. Gershenfeld, *Urine and Urinalysis*, 3rd Ed., pp. 17–24. Romanie Pierson Publishers, New York, 1948.
7. A. H. Free and H. M. Free, *Urinalysis in Clinical Laboratory Practice*, pp. 1–6. CRC Press, Ohio, 1975.
8. W. I. White, *Clin. Chem.*, 1991, **37**, 119.
9. K. S. Subramanian, *Prog. Analyt. Spectrosc.*, 1988, **11**, 511.
10. T. W. Clarkson, L. Friberg, G. F. Nordberg and P. R. Sager (eds.), *Biological Monitoring of Toxic Metals*, Plenum Press, New York, 1988.
11. S. Branch, H. M. Crews, D. J. Halls and A. Taylor, *J. Anal. At. Spectrom.*, 1991, **6**, 69R.
12. A. Chapman, *Analyst*, 1926, **51**, 548.
13. G. K. H. Tam, S. M. Charbonneau, F. Bryce, C. Pomroy and E. Sandi, *Toxicol. Appl. Pharmacol.*, 1979, **50**, 319.
14. C. Pomroy, S. M. Charbonneau, R. S. McCullough and G. K. H. Tam, *ibid.*, 1980, **53**, 550.
15. S. M. Charbonneau, K. Spencer, F. Bryce and E. Sandi, *Bull. Environ. Contam. Toxicol.*, 1978, **20**, 470.
16. E. A. Crecelius, *Environ. Health Perspect.*, 1977, **19**, 147.
17. H. C. Freeman, J. F. Uthe, R. B. Fleming, P. H. Odense, R. G. Ackman, G. Landry and C. Musial, *Bull. Environ. Contam. Toxicol.*, 1979, **22**, 224.
18. V. Foa, A. Colombi, M. Maroni, M. Buratti and G. Calzaferri, *Sci. Total Environ.*, 1984, **34**, 241.
19. B. S. Chana and N. J. Smith, *Anal. Chim. Acta*, 1987, **197**, 177.
20. J. P. Buchet and R. Lauwerys, in *Analytical Techniques for Heavy Metals in Biological Fluids*, S. Facchetti (ed.), pp. 75–90. Elsevier, Amsterdam, 1983.
21. J. P. Buchet, R. Lauwerys and H. Roels, *Int. Arch. Occup. Environ. Health*, 1981, **48**, 71.
22. J. P. Buchet, R. Lauwerys and H. Roels, *ibid.*, 1981, **48**, 111.
23. G. K. H. Tam, S. M. Charbonneau, G. Lacroix and F. Bryce, *Bull. Environ. Contam. Toxicol.*, 1979, **21**, 371.
24. H. Yamauchi and Y. Yamamura, *Toxicology*, 1985, **34**, 113.
25. J. P. Buchet, R. Lauwerys and H. Roels, *Int. Arch. Occup. Environ. Health*, 1980, **46**, 11.
26. T. H. Smith, E. A. Crecelius and J. C. Reading, *Environ. Health Perspect.*, 1977, **19**, 89.
27. M. Vahter and E. Marafante, *Chem. Biol. Interact.*, 1983, **47**, 29.
28. P. Mahieu, J. P. Buchet, H. Roels and R. Lauwerys, *Clin. Toxicol.*, 1981, **18**, 1067.
29. E. Marafante and M. Vahter, *Environ. Res.*, 1987, **42**, 72.
30. X.-C. Le, W. R. Cullen and K. J. Reimer, *Appl. Organomet. Chem.*, 1992, **6**, 161.
31. R. K. Anderson, M. Thompson and E. Culbard, *Analyst*, 1986, **111**, 1143.
32. T. A. Hinners, *ibid.*, 1980, **105**, 751.
33. M. H. Arbab-Zavar and A. G. Howard, *ibid.*, 1980, **105**, 744.
34. I. D. Brindle and X.-C. Le, *Anal. Chim. Acta*, 1990, **229**, 239.
35. I. D. Brindle, X.-C. Le and X.-F. Li, *J. Anal. At. Spectrom.*, 1989, **4**, 227.
36. X.-C. Le, W. R. Cullen, K. J. Reimer and I. D. Brindle, *Anal. Chim. Acta*, 1992, **258**, 307.
37. X.-C. Le, W. R. Cullen and K. J. Reimer, unpublished results.
38. K. A. Francesconi, P. Micks, R. A. Stockton and K. J. Irgolic, *Chemosphere*, 1985, **14**, 1443.
39. M. Roy, *Occup. Health Ontario*, 1983, 17.
40. G. K. H. Tam, S. M. Charbonneau, F. Bryce and E. Sandi, *Bull. Environ. Contam. Toxicol.*, 1982, **28**, 669.

Talanta, Vol. 40, No. 2, pp. 195–200, 1993
Printed in Great Britain.

0039-9140/93 $6.00 + 0.00

1-(2-PYRIDYLAZO)-2-NAPHTHOL (PAN) AS EXTRACTANT IN SOLID–LIQUID EXTRACTION OF SOME TRIVALENT RARE EARTH ELEMENTS*

JINZHANG GAO, GUANGLIN HU, JINWAN KANG and GUANGBI BAI
Institute of chemistry, Northwest Normal University, Lanzhou 730070, China

(*Received* 9 *April* 1992. *Accepted* 9 *June* 1992)

Summary—In the present paper, solid-liquid extraction behaviour of RE(III) (RE = La, Ce, Pr, Nd, Sm, Gd, Dy and Yb) by the use of 1-(2-pyridylazo)-2-naphthol (PAN, HL) as an extractant in paraffin (m.p. 48 ~ 50°) has been investigated at 80 ± 0.07°. The effect of equilibrium time, pH of aqueous phase, concentration of extractant in paraffin and solid diluent as well as buffer solution used on the extraction efficiency of RE(III) have been discussed. The extraction reacton is

$$RE^{3+} + 2HL_{(o)} + Cl^- \rightleftharpoons REL_2Cl_{(o)} + 2H^+$$

As a powerful chelant, 1–(2–pyridylazo)-2-naphthol (abbreviated as PAN or HL) can react with the majority of metal ions in the periodic table to form water-insoluble, coloured chelate complexes and has been applied widely to liquid–liquid extraction separation and extraction–photometric analysis in analytical chemistry.[1-3] Liquid–liquid extraction of RE(III) with PAN is reported in the literature.[4,5] Solid–liquid extraction by the use of molten paraffin as diluent has been paid close attention to because this method has some main merits such as no emulsification phenomenon and rapid phase separation and so on.[6,7] In this paper, a study on solid–liquid extraction behaviour of RE(III) (RE = La, Ce, Pr, Nd, Sm, Gd, Dy and Yb) with PAN in molten paraffin was described. The effect of equilibrium time, pH of aqueous phase and concentration of extractant in organic phase as well as solid solvent on the extraction efficiency of RE(III) has been observed.

EXPERIMENTAL

Reagents and apparatus

Preparation of 1-(2-pyridylazo)-2-naphthol (PAN) solution. A calculated amount of PAN (AR) was dissolved in pure acetone and stored in an amber bottle.

Paraffin with ceresin (PC, m.p. 48 ~ 50°) was purified according to the method in Ref. 8. Specific gravity is 0.772 g/ml at 80°.

Dibenyl (m.p. 68 ~ 70°) was of chemically pure grade without further purification.

Buffer solution (triethanolamine–hydrochloric acid) was used for pH adjustment. The ionic strength was maintained at 0.1 ± 0.01 with buffer.

Stock solutions of rare earth metals ($1.0 \times 10^{-2}M$) were prepared by dissolving calculated amounts of the pure oxide (99.99%) in an appropriate amount of $1M$ hydrochloric acid and diluting to the desired volume and then diluted to $1.0 \times 10^{-4}M$ when they were used.

All other chemicals used were of analytical grade.

All solid–liquid extraction experiments were carried out with the aid of the device below (see Fig. 1).

A Model DF-101B magnetic stirrer (Zhejiang, China), a super thermostat (Chongqing, China), model CS501, with an accuracy ± 0.07°, a model 721 spectrophotometer (Shanghai, China), a model U-3400 Hitachi spectrophotometer and a model PHS-10A digital acidity/ionometer (Xiaoshan, China) were also used.

Procedure

The solid–liquid extraction was carried out at 80 ± 0.07° as follows: an aliquot of the slightly acid solution containing definite amounts of

*Project supported by the National Natural Science Foundation of China.

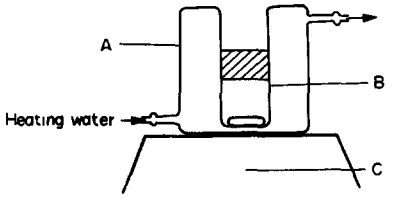

Fig. 1. Solid-liquid extraction device. A: water jacket; B: extraction vessel; C: magnetic stirrer.

rare earth ion was placed in the 30-ml extraction vessel and appropriate amount of PAN solution, buffer solution and solid solvent were added. The ionic strength of the aqueous phase was kept at 0.1 ± 0.01 and the phase ratio was 0.5 v/v. High temperature circulating water was then introduced into water jacket with a super thermostat. When the desired temperature was obtained, the magnetic stirrer was started. After 12 min, the stirring was stopped and the extraction vessel was allowed to cool to room temperature. Finally, the solidified solvent containing the complex extracted was separated.

The pH of the aqueous phase was measured on a pHS-10A digital acidity/ionometer. The amount of RE^{3+} contained in the aqueous phase was measured by Arsenzo III spectrophotometry. The amount of individual RE^{3+} in the organic phase was determined by means of the back-extraction method. Some preliminary results show that single back-extraction with 10 ml of 0.1*M* perchloric acid at 80° for 30 min can transfer completely the RE(III) to the aqueous phase.

RESULTS AND DISCUSSION

Determination of optimum conditions of solid–liquid extraction

Effect of pH. The effect of the pH of aqueous phase on the percentage extraction was examined in the pH range of 6.5 ~ 9.5 and the results are shown in Fig. 2. The extraction conditions were: PC as solid diluent; $(CH_2CH_2OH)_3N$–HCl as buffer; ionic strength 0.1 ± 0.01; extraction time 15 min; $C_{RE} = 2.0 \times 10^{-5}M$ and $C_{PAN(0)} = 2.5 \times 10^{-3}M$. Single solid–liquid extraction of La^{3+} and Ce^{3+} with PAN–PC performs quantitatively, and the pH ranges of quantitative extraction are 9.0 ~ 9.5 and 8.9 ~ 9.2 for La^{3+} and Ce^{3+}, respectively. When pH > 9.25, percentage extraction of Ce^{3+}, decreases rapidly. The percentage extraction of Pr^{3+}, Nd^{3+}, Sm^{3+}, Gd^{3+} and Yb^{3+} reaches the maximum at pH ~ 8.75, 8.20, 8.50, 7.90 and 7.70, respectively. When the pH of the aqueous phase in equilibrium is over the pH of maximum extraction, extraction efficiency of RE(III) (RE = Pr, Nd, Sm, Gd and Yb) decreases gradually. The percentage extraction of Dy^{3+} reaches the maximum at pH ~ 8.25 and decreases within the pH range 8.25 ~ 9.20 with pH increasing due to the hydrolysis of Dy^{3+} in the aqueous phase. When pH > 9.20 the amount of Dy^{3+} in the organic phase increases again due to part adsorption of water-insoluble, neutral

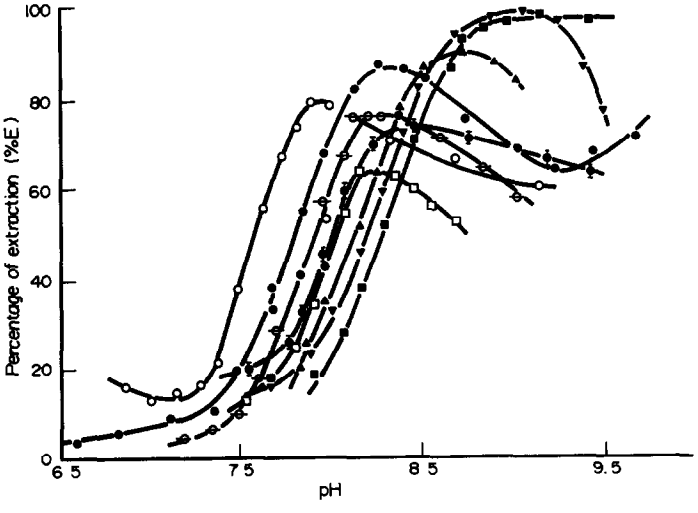

Fig. 2. Plots of %*E* vs pH of aqueous phase. PC as diluent, $(CH_2CH_2OH)_3N$–HCl as buffer, $C_{RE} = 2.0 \times 10^{-5}$ mol/l, $C_{PAN(0)} = 2.5 \times 10^{-3}$ mol/l. (■) La, (▼) Ce, (▲) Pr, (□) Nd, (♦) Sm, (⊖) Gd, (●) Dy, (○) Yb.

hydrolysate onto the surface of PC. The decrease in the percentage extraction when the pH of aqueous phase is over optimum pH is a direct consequence of hydrolysis and turbid phenomenon can be observed in the aqueous phase. Solubility products of $RE(OH)_3$ (RE = La, Ce, Pr, Nd, Sm, Gd, Dy and Yb) are 4.3×10^{-19}, 1.5×10^{-20}, 2.7×10^{-20}, 3.2×10^{-22}, 6.8×10^{-22}, 2.1×10^{-22}, 1.4×10^{-22} and 2.9×10^{-24}, respectively.[9–11] Thus at $C_{RE} = 2.0 \times 10^{-5} M$, precipitation of the hydroxides, without any complexing factors, should take place at pH ~ 9.40, 9.00, 8.40, 8.50, 8.34, 8.28 and 7.72, respectively. They are in essential agreement with the pH at which the percentage of the solid–liquid extraction of individual RE(III) with PAN–PC reaches the maximum, respectively.

Effect of stirring time. The effect of stirring time on the percentage extraction is shown in Fig. 3. In this series of experiments the pH of the aqueous phase was kept at 8.10 with $(CH_2CH_2OH)_3N$–HCl buffer solution and the solid–liquid extraction was carried out at $C_{Dy^{3+}} = 2.0 \times 10^{-5} M$ and $C_{PAN(0)} = 2.5 \times 10^{-3} M$. The equilibrium was established after 8 min. In the further tests 12 min was accepted as the equilibrium time for the extraction.

Effect of PAN concentration in PC. When the amount of $2.5 \times 10^{-3} M$ PAN–acetone solution was varied from 0.5 to 5.0 ml, at a constant pH of 8.20 and 3.86 g of PC (the volume of 3.86 g of PC is 5.00 ml at 80°), the percentage extraction increased, *i.e.*, the higher the initial amount of PAN, the higher the percentage extraction (Fig. 4). The initial concentration of PAN in PC was accepted as $2.5 \times 10^{-3} M$ in the further

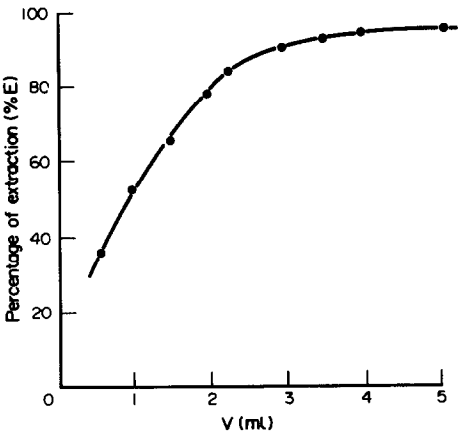

Fig. 4. Plot of the percentage of extraction (%E) vs amount of 2.5×10^{-3} PAN solution. PC as diluent, $(CH_2CH_2OH)_3N$–HCl as buffer, $C_{Pr^{3+}} = 2.0 \times 10^{-5}$ mol/l, pH = 8.20

experiments (except in the experiments discussed on the effect of $C_{PAN(o)}$ on the distribution ratio).

Effect of solid diluent. Paraffin with ceresin, naphthalene or diphenyl was used as solid diluent respectively and $(CH_2CH_2OH)_3N$–HCl buffer was used for the adjustment of the pH of aqueous phase. Figure 5 presents the relationships of the extraction percentage of Yb^{3+} in relation to the pH of the aqueous phase in the presence of different solid diluents. There is no emulsification phenomenon and phase separation is rapid when PC is used as diluent in solid–liquid extraction. Moreover, the extraction efficiency of Yb^{3+} with PAN–PC is higher than that in the presence of naphthalene or diphenyl due to the larger solubility of

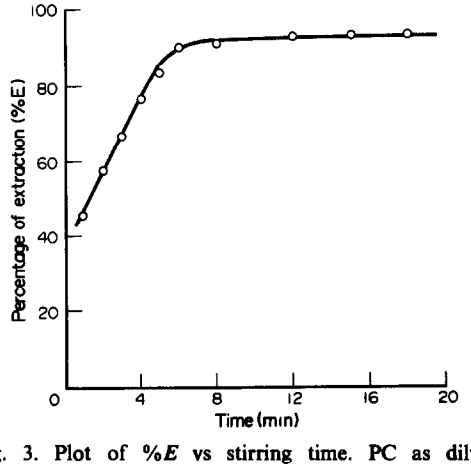

Fig. 3. Plot of %E vs stirring time. PC as diluent, $(CH_2CH_2OH)_3N$–HCl as buffer, pH = 8.10, $C_{Dy^{3+}} = 2.0 \times 10^{-5}$ mol/l, $C_{PAN(0)} = 2.5 \times 10^{-3}$ mol/l

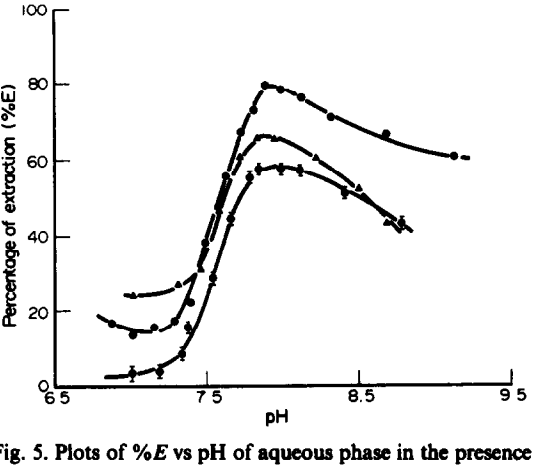

Fig. 5. Plots of %E vs pH of aqueous phase in the presence of different solid diluents. $(CH_2CH_2OH)_3N$–HCl as buffer, $C_{Yb^{3+}} = 2.0 \times 10^{-5}$ mol/l, $C_{PAN(0)} = 2.5 \times 10^{-3}$ mol/l. (●) Paraffin, (▲) diphenyl, (◆) naphthalene.

Yb^{3+}–PAN complex in molten PC. In the presence of naphthalene or diphenyl, solid–liquid extraction, however, has several drawbacks: naphthalene or diphenyl adheres to the extraction vessel after cooling and solidification and naphthalene solidified includes a part of aqueous phase. Hence, paraffin with ceresin was accepted as solid diluent in further experiments.

Effect of the used buffer. Finally, the effect of buffer solution on the percentage extraction of Dy^{3+} was investigated at PC as diluent, $C_{Dy^{3+}} = 2.0 \times 10^{-5} M$ and $C_{PAN(o)} = 2.5 \times 10^{-3} M$ for an extraction time of 12 min. Buffer solutions used for the adjustment of aqueous phase were NH_3–NH_4Cl, $(CH_2CH_2OH)_3N$–HCl and $(CH_2)_6N_4$–HCl, respectively. The results are shown in Fig. 6. The extraction efficiency was found to depend on the buffer that was employed in the following order: hexamethylenetetramine < triethanolamine < ammonia, this result is in agreement with liquid–liquid extraction.[12] The probable reason is that only smaller molecules can partake of coordination for steric hindrance of the big PAN anion. However, the rapid volatilization of ammonia under the experimental conditions decreases the buffer capacity of NH_3–NH_4Cl solution, thus causing difficulties in operation. Therefore, $(CH_2CH_2OH)_3N$–HCl buffer solution was accepted to adjust the pH of aqueous phase in our experiments. Furthermore, the use of $(CH_2CH_2OH)_3N$–HCl buffer solution can inhibit some ions such as Fe^{3+}, Al^{3+} and Mn^{2+} from extracting into organic phase because triethanolamine can form very stable water-soluble complexes with Fe^{3+}, Al^{3+} and Mn^{2+}.

Mechanism of solid–liquid extraction of RE(III) with PAN–PC

Determination of the composition of the extracted complex. Busev and Ivanov[13] had pointed out that, under various conditions of pH, ionic strength and concentration, PAN shows no intermolecular association. The concentration of RE(III) in the aqueous phase was always $2.0 \times 10^{-5} M$ in our experiments. Such concentrations of RE(III) in this phase can eliminate the possibility of polymerization of the RE(III)–PAN complex in the organic phase.[14] Hence, in RE^{3+} ($2.0 \times 10^{-5} M$/$CH_2CH_2OH)_3N$–HCl ($\mu = 0.1 \pm 0.01$)/PAN–PC system, the extraction process may be described by the following equation:

$$RE^{3+} + (x+y)HL_{(o)} + zCl^- \rightleftharpoons REL_x(HL)_y(Cl)_{z(o)} + xH^+ \quad (1)$$

where RE = La, Ce, Pr, Nd, Sm, Gd, Dy or Yb and (o) denotes organic phase.

The extraction constant (K_{ex}) is given by:

$$K_{ex} = [REL_x(HL)_y(Cl)_z]_o[H^+]^x / [RE^{3+}][HL]_o^{(x+y)}[Cl^-]^z \quad (2)$$

Based on the reported data,[15] the influence of ions and molecules present in the aqueous solution which can form non-extractable complexes with RE(III) can be neglected and thereby $[HL]_o$ is equal to the initial

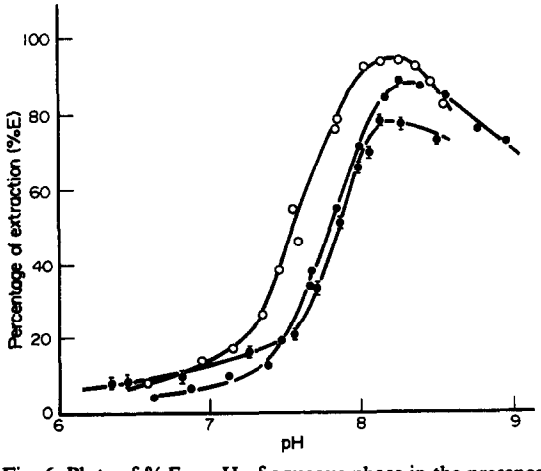

Fig. 6. Plots of %E vs pH of aqueous phase in the presence of different buffers. PC as diluent, $C_{Dy^{3+}} = 2.0 \times 10^{-5}$ mol/l, $C_{PAN(0)} = 2.5 \times 10^{-3}$ mol/l. (○) NH_3–NH_4Cl, (●) $(CH_2CH_2OH)_3N$–HCl, (◐) $(CH_2)_6N_4$–HCl.

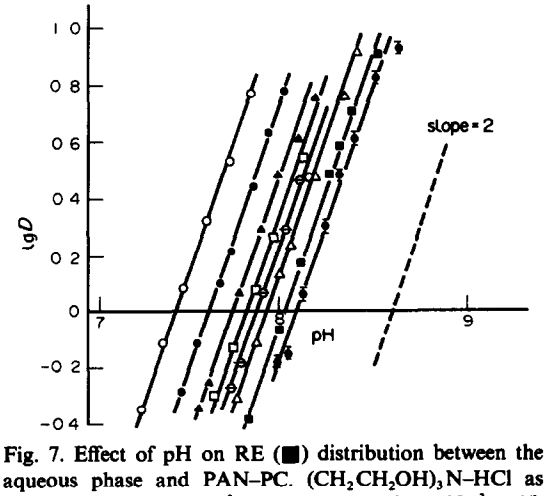

Fig. 7. Effect of pH on RE (■) distribution between the aqueous phase and PAN–PC. $(CH_2CH_2OH)_3N$–HCl as buffer, $C_{RE} = 2.0 \times 10^{-5}$ mol/l, $C_{PAN(0)} = 2.5 \times 10^{-3}$ mol/l. (◐) La, (■) Ce, (△) Pr, (⊖) Nd, (□) Sm, (▲) Gd, (●) Dy, (○) Yb.

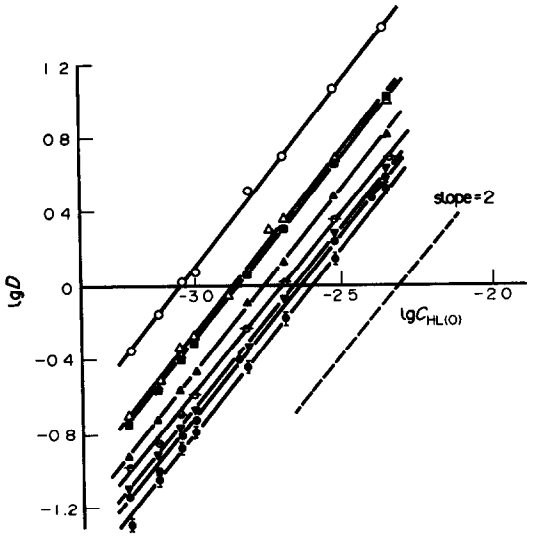

Fig. 8. Effect of the initial concentration of PAN on RE (■) distribution between the aqueous phase and PAN–PC. $(CH_2CH_2OH)_3N$–HCl as buffer; $C_{RE} = 2.0 \times 10^{-5}$ mol/l; La^{3+}: pH = 8.54; Ce^{3+}: pH = 8.30; Pr^{3+}: pH = 8.20; Nd^{3+}: pH = 8.05; Sm^{3+}: pH = 7.90; Gd^{3+}: pH = 7.86; Dy^{3+}: pH = 7.64; Yb^{3+}: pH = 7.50. (○) La, (△) Ce, (■) Pr, (▲) Nd, (▼) Sm, (⊖) Gd, (◐) Dy, (●) Yb.

concentration of PAN in the organic phase $C_{HL(o)}$. Equation (2) can be simplified:

$$K_{ex} = D\frac{[H^+]^x}{C_{HL(o)}^{(x+y)}[Cl^-]^z} \quad (3)$$

or

$$\log D = \log K_{ex} + x\text{pH} + (x+y)\log C_{HL(o)} + z\log[Cl^-] \quad (4)$$

where D denotes the distribution ratio of RE(III). From equation (4) the slope of a log D curve *vs.* pH at constant $C_{HL(o)}$ and $[Cl^-]$ gives the number of protons released on chelation, and the slope of log D *vs.* log $C_{HL(o)}$ at constant pH and $[Cl^-]$ gives the number of reagent molecules involved in the complex.

Figure 7 indicates the dependence of RE(III) extraction with PAN–PC on the pH of aqueous phase. The slope of log D *vs.* pH is approximately 2.0. This fact means that the distribution ratio of RE(III) is proportional to the minus second power of hydrogen ion concentration of the aqueous phase.

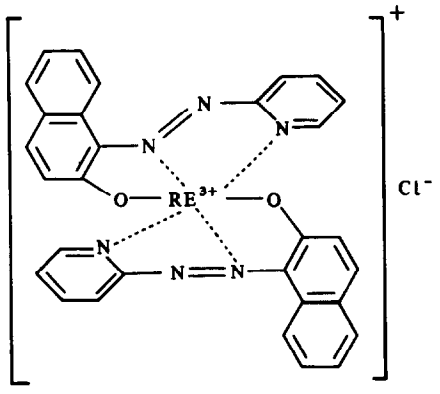

Scheme 1

Figure 8 shows the experimental results for extraction of RE(III) with various PAN concentrations in PC (from $6.0 \times 10^{-4}M$ to $8.0 \times 10^{-2}M$) at fixed pH values and $[Cl^-]$. log D *vs.* log $C_{HL(o)}$ give straight lines of slope 2.0. This indicates that two ligand molecules partake in the extraction process.

Within experimental error the results obtained suggest that 1:2 complexes of the rare earth metals with the reagent were formed. This is in accordance with the conclusion obtained in liquid–liquid extraction of RE(III) by Shibata.[4] Assume that only the neutral complexes can be extracted into PC since PC belongs to inert solvent and the affinity of PC is extreme small.[1] However, neutral complex $REL_2(OH)$ cannot be extracted into PC because of the hydrophilicity of $REL_2(OH)$ caused by a hydrogen bond between hydroxy in $REL_2(OH)$ and water molecule. Hence, the composition of the extracted species is proposed to be REL_2Cl. We believe that PAN is a tridentate ligand when PAN forms a complex with RE(III). The probable structure of the complex REL_2Cl is shown above.

The above results indicate that the mechanism of solid–liquid extraction reaction of RE(III) with PAN–PC may be expressed by the equation:

$$RE^{3+} + 2HL_{(o)} + Cl^- \rightleftharpoons REL_2Cl_{(o)} + 2H^+ \quad (5)$$

Table 1. Extraction parameters for the formation of REL_2Cl complexes (at $80 \pm 0.07°$, $\mu = 0.1 \pm 0.01$)

Parameter	Rare earth ions							
	La^{3+}	Ce^{3+}	Pr^{3+}	Nd^{3+}	Sm^{3+}	Gd^{3+}	Dy^{3+}	Yb^{3+}
log K_{ex}	−9.98	−9.85	−9.69	−9.58	−9.47	−9.32	−9.08	−8.72
$pH_{1/2}$ at $C_{PAN(o)} = 2.5 \times 10^{-3}M$	8.10	8.03	7.95	7.89	7.84	7.76	7.64	7.46

Calculation of the values of $pH_{1/2}$ and extraction constant (K_{ex}). Equation (4) can be simplified from equation (5):

$$\log D = \log K_{ex} + 2\text{pH} + 2\log C_{HL(o)} + \log[Cl^-] \quad (6)$$

$pH_{1/2}$ values are defined as the pH at which the distribution ratio (D) of the metal ion is equal to 1. Thus $pH_{1/2}$ is equal to the intercept of the abscissa axis of $\log D$ *vs.* pH (Fig. 6). With the aid of relation (6) the average $\log K_{ex}$ values were calculated by the least-squares method. The constants and $pH_{1/2}$ values at $C_{PAN(o)} = 2.5 \times 10^{-3} M$ are given in Table 1.

The comparison between solid–liquid extraction of RE(III) with PAN–PC and liquid–liquid extraction of RE(III) with PAN. The liquid–liquid extraction behaviour of RE(III) with PAN–CCl_4 or PAN–$CHCl_3$ has been reported in Ref. 5. The results show that under the same conditions and within the studied pH range, the RE(III) extraction efficiency decreases from the heavy RE to the light RE. Particular marked differences in the extraction efficiency of the light and the heavy RE occur when a solution of PAN in CCl_4 is applied to extraction. The light RE(La^{3+}, Ce^{3+} and Pr^{3+}) cannot be extracted into the organic phase, Nd^{3+}, Sm^{3+}, Gd^{3+} and Dy^{3+} can be partly extracted, while Yb(III) is extracted almost completely. PAN–CCl_4 can be used as the group reagent for the separation of RE(III) by the liquid–liquid extraction method. Regarding the RE(III) studied, a PAN solution in $CHCl_3$ is less efficient an extractant than a PAN solution in CCl_4. In the system of solid–liquid extraction, La^{3+} and Ce^{3+} can be extracted quantitatively at higher pH ranges because pH at the beginning of precipitation for La^{3+} and Ce^{3+} are more than those for the other RE(III). The solid–liquid extraction efficiency of RE(III) with PAN–PC is higher than that of liquid–liquid extraction with PAN–CCl_4 (except Yb^{3+}). Furthermore, extraction efficiency decreases slightly from the light RE to the heavy RE. The use of $(CH_2CH_2OH)_3N$–HCl buffer solution for pH adjustment can eliminate interference from Fe^{3+}, Al^{3+} or Mn^{2+}. Therefore, the solid–liquid extraction method with PAN–PC can be used for separation and purification of rare earth elements.

REFERENCES

1. J. Stary, *The Solvent Extraction of Metal Chelates*, Pergamon Press, Oxford, 1964.
2. R. G. Anderson and G. Nickless, *The Analyst*, 1967, **92**, 207.
3. Sunwei Zhang, Yongsheng Wu and Shaopu Liu, *Application of Organic Reagent in Analytical Chemistry*, Science Press, Beijing, 1981.
4. S. Shibata, *Anal. Chim. Acta.*, 1963, **28**, 388.
5. Natalia Pustelnik, Bozena Kuznik and Danuta M. Czakis-Sulikewska, *Acta Chim. Hung.*, 1985, **93**, 118.
6. Zulan Xu and Lixin Dai, *J. Anal. Chem.*, 1985, **13**, 784.
7. Li Cheng, Yunhui Yang, Mingrun Luo and Dingrong Zhang, *Chemical Reagent*, 1987, **9**, 265.
8. Guochang Zheng, *Microscopic Technique of Biology*, Education Press, 1978.
9. Y. Oka., *J. Chem. Soc. Japan*, 1938, **59**, 971.
10. T. Moeller and H. E. Kremers, *J. Phys. Chem.*, 1944, **48**, 395.
11. T. Moeller and N. J. Fogel, *J. Am. Chem. Soc.*, 1951, **73**, 4481.
12. K. L. Cheng, *Handbook for Organic Analysis*, Geology Press, Beijing, 1985, 55.
13. A. I. Busev and V. M. Ivanov, *Vest. Mosk. Gos. Univ., Ser. I*, 1964, **19**, 56.
14. L. I. Kononienko, R. A. Witkun and L. M. Burtnienko, *Chimija Procesow ekstrakcji, Izd. Nauka. Moskwa* (1972).
15. B. Kuznik, *J. Inorg. Nucl. Chem*, 1981, **43**, 3363.

Talanta, Vol. 40, No. 2, pp. 201–203, 1993
Printed in Great Britain.

0039-9140/93 $6.00 + 0.00

EXTRACTION SPECTROPHOTOMETRIC DETERMINATION OF MANEB WITH 1-(2′-PYRIDYLAZO)-2-NAPHTHOL (PAN)

A. L. J. Rao,* A. K. Malik and Jyoti Kapoor
Department of Chemistry, Punjabi University, Patiala-147002, India

(*Received* 21 *May* 1992. *Accepted* 9 *June* 1992)

Summary—A rapid, sensitive, simple and selective spectrophotometric method has been developed for the determination of micro-quantities of maneb (manganese ethylenebisdithiocarbamate) after extraction of the manganese–PAN complex in isobutyl methyl ketone (MIBK). The complex absorbs strongly at 550 nm. Beer's law is obeyed over the concentration range 0.37–3.75 μg/ml. The molar absorptivity was found to be 4.1×10^4 l.mole^{-1}.cm^{-1}. The developed method has been applied to the determination of maneb in commercial formulations, synthetic mixtures, grain and in the presence of various other dithiocarbamates.

Metallic salts of dithiocarbamic acid, such as nabam, ziram, zineb, ferbam and maneb are used as agricultural fungicides because of their low phytotoxicity and are applied in the rubber industry as vulcanization accelerators and antioxidants. Although several methods have been reported in the literature for estimating these fungicides, the method reported by Clarke[1] is of practical importance which is based on carbon disulphide evolution after decomposing these dithiocarbamates in acidic medium.[2–4] Hall has reported on a collaborative study of determination of maneb using modified versions of the methods of Clarke *et al.*[1] The results obtained from both the methods were inconsistent. Maneb was also determined by spectrophotometric methods,[5] a volumetric method with electrogenerated iodine[6] and by high performance liquid chromatography.[7] However all of the above mentioned methods are time consuming or have low sensitivity. This method is simple, sensitive and selective for the determination of maneb based on the extraction of the Mn–PAN complex into isobutyl methyl ketone. PAN has also been used to determine manganese in high purity Nb, Ta, Mo and W metals.[8]

EXPERIMENTAL

Equipment

An SP-20 Spectrophotometer for absorption measurement and a digital pH meter were used.

Reagents

Pure maneb was prepared by adding a solution of manganese(II) to a solution of disodium ethylenebisdithiocarbamate (Wilson Laboratories, Bombay). The precipitates so formed were filtered and dried over silica gel. The purity of maneb was checked by elemental analysis and by complexometric titration of manganese after decomposition using Thymolphthalexone as an indicator.[9] A 0.1-mg/ml solution of maneb was prepared in dimethyl sulphoxide (DMSO).

PAN solution, 0.1 mg/ml. PAN (LOBA) (10 mg) was dissolved in 100 ml of methanol.

Isobutyl methyl ketone. The purity of the isobutyl methyl ketone was checked spectrophotometrically before use.

Buffer solution. Boric acid and potassium chloride solutions (0.2*M*, 100 ml of each) were mixed, pH adjusted 9.2 with 0.2*M* sodium hydroxide and diluted to 500 ml.

Stock solutions. Stock solutions for interference studies were prepared by dissolving suitable salts in water. Synthetic samples were prepared by mixing suitable salts to give the required composition.

Procedure

To an aliquot containing 37.5 μg of maneb, 2 ml of boric acid buffer (pH 9.2) and 0.7 ml of PAN were added and the total volume was made up to 10 ml with doubly distilled water. The solution was allowed to stand for 2 min, then shaken exactly with 10 ml of isobutyl

*Author for correspondence.

methyl ketone. A second extract with another 10 ml of isobutyl methyl ketone gave negligible absorbance, so the absorbance of the first extract was measured at 550 nm against a reagent blank prepared under similar conditions.

RESULTS AND DISCUSSION

The absorption spectra of manganese–PAN complex in isobutyl methyl ketone were recorded against a reagent blank. The complex absorbs strongly at 550 nm whereas the reagent shows negligible absorbance. The absorbance of the complex was maximum when the pH of the aqueous phase was 8.0–11.0 and 0.7 ml of 0.01% PAN was used. The complex was extracted into isobutyl alcohol, chloroform, carbon tetrachloride, ethyl acetate, isobutyl methyl ketone, amyl alcohol and n-butyl acetate. Maximum absorbance was observed with isobutyl methyl ketone and hence this solvent was selected for the extraction of manganese–PAN complex. The absorbance of the complex remains practically constant for 24 hr.

The Job's method of continuous variation and mole-ratio methods indicated the formation of 1:2 (M:L) complex.

Analytical characteristics

Under the optimum conditions described above the calibration graph was linear over the concentration range 0.37–3.75 μg/ml of maneb at 550 nm. The molar absorptivity was found to be 4.1×10^4 $l \cdot mole^{-1} \cdot cm^{-1}$. Aliquots containing 37.5 μg of maneb gave a mean absorbance of 0.58 with a relative standard deviation of $\pm 0.3\%$.

Interferences

Sample solutions containing 37.5 μg of maneb, the interferences of various anions (as alkali-metal salts) and metal ions were studied after applying the general procedure. Of the anions examined, the amounts (mg) shown in parentheses are tolerable ($\pm 2\%$ error) for thiocyanate (4), orthophosphate (0.37), citrate (47), acetate (450), chloride (18), bromide (16), fluoride (120), sulphate (50), metabisulphite (5), but tartrate and EDTA interfered strongly. Of the metal ions examined Co(II) (0.03), Ni(II) (0.09), Bi (0.15), V(V) (0.2), Th(IV) (0.23), Mo(VI) (0.02) did not interfere. Cu(II), Pb(II), Hg(II), Zn(II) and Fe(II) interfered strongly but could be masked with 1.0 ml of 5% sodium fluoride solution.

Of the dithiocarbamates examined, nabam (sodium ethylenebisdithiocarbamate), dibam (sodium dimethyldithiocarbamate), vapam (sodium monomethyldithiocarbamate), sodium *N*-methylanilinecarbodithioate, *i.e.*, which do not contain any metal ion did not interfere in the determination of maneb. Ferbam, ziram and zineb could be masked with 1.0 ml of 5% sodium fluoride solution.

Simultaneous determination of ziram and maneb, or zineb and maneb

Ziram and maneb, zineb and maneb were taken in various proportions. Equal aliquots of the solution were analysed in the presence and absence of 1.0 ml of 5% sodium fluoride solution. The difference in the absorbance corresponded to the amount of zineb/ziram. The results are given in Table 1.

Applications

The proposed method is one of the most sensitive and selective methods for the determination of maneb and was applied to the determination of maneb in commercial formulations "Dithane M-45" (Indofil Chemicals) with pure samples taken as reference. Five dilutions of the stock solutions were prepared and in all cases the recoveries were between 72.5 and 72.9% by this method, where as the value reported was 73%.

Determination of maneb in grain

This procedure was applied for the determination of maneb in grain. A known amount of maneb was finely crushed with 20 g of grain and was shaken with 100 ml of acetonitrile for an hour. The mixture was filtered and residue was washed with three 10-ml portions of acetonitrile. The extract was evaporated at room temperature by a current of dry air. The residue was dissolved in dimethyl sulphoxide and the maneb content was analysed by general procedure. Untreated samples were taken as reference. The results are given in Table 2.

Table 1. Recovery of maneb from synthetic mixtures

Composition and percentage	Amount of Maneb (μg)		Recovery (%)
	Taken	Found	
Maneb:50	40.0	40.1	100.25
Ziram:50	45.0	44.9	99.7
	42.0	42.3	100.7
Maneb:50	30.0	30.2	100.6
Zineb:50	20.0	19.8	99.0
	35.0	35.0	100.0

Table 2. Recovery of maneb from grain

Amount of maneb added (μg)	Amount of maneb found (μg)	Recovery (%)
10	9.85	98.5
20	19.6	98.0
30	29.7	99.0
40	39.0	97.5
50	49.0	98.0

Comparison of sensitivity

The sensitivity of this method is better than that of the Lowen,[10] Cullen[11] and Chmiel[12] methods which are based on the determination of liberated CS_2. It is also more sensitive than the Rao *et al.*[13] method. According to the latter method a minimum of 2 μg/ml maneb could be determined but according to the present method a minimum of 0.37 μg/ml maneb could be determined. Moreover, this method is more selective since other pesticides like ziram, zineb, ferbam which usually interfere in other methods do not interfere in this method under the experimental conditions.

REFERENCES

1. D. G. Clarke, H. Baum, E. L. Stanley and W. E. Hester, *Anal. Chem.*, 1951, **23**, 1842.
2. R. Zaharadnik and P. Zuman, *Chem. Listy*, 1958, **52**, 231; *Coll. Czech. Chem. Comm.*, 1959, **24**, 11326.
3. J. Rosenthal, R. L. Carlsen and E. L. Stanley, *J. Assoc. Off. Agr. Chem.*, 1963, **36**, 1170.
4. W. K. Lowen, *ibid.*, 1953, **36**, 484.
5. S. Petrescu, *Rev. Chim. (Bucharest)*, 1966, **17**, 687.
6. D. Clyde, *J. Assoc. Off. Anal. Chem.*, 1983, **66**, 646.
7. K. H. Gustafsson and C. H. Fahlgren, *J. Agric. Food Chem.*, 1983, **31**, 461.
8. M. Elsie, P. Donaldson and W. R. Inman, *Talanta*, 1966, **13**, 489.
9. A. I. Vogel, *A Text Book of Quantitative Inorganic Analysis*, 3rd Ed., Longmans, London, 1969.
10. W. K. Lowen, *Anal. Chem.*, 1951, **23**, 1846.
11. T. E. Cullen, *ibid.*, 1964, **36**, 221.
12. Z. Chmiel, *Chem. Anal.*, 1979, **24**, 505.
13. A. L. J. Rao and N. Verma, *Rev. Roum. de Chimie*, 1990, **35**, 625.

Talanta, Vol. 40, No. 2, pp. 205–211, 1993
Printed in Great Britain

0039-9140/93 $6.00 + 0.00
Pergamon Press Ltd

DIRECT ZINC DETERMINATION IN COMMERCIAL SULPHURIC ACID BY DPASV. COMPARISON OF ROTATING DISC AND STATIONARY GRAPHITE ELECTRODES

IGNACY CUKROWSKI* and EWA CUKROWSKA
University of Transkei, Department of Chemistry, P/B X1, Umtata, Republic of Transkei, South Africa

(*Received* 11 *November* 1991. *Revised* 21 *April* 1992. *Accepted* 22 *April* 1992)

Summary—A striking gas technique employed made a direct Zn determination possible at extremely low pH in commercial acid solutions when a stationary impregnated graphite-based mercury film electrode was used. The original Zn(II) concentrations were determined quantitatively by differential pulse anodic stripping voltammetry on 0.5*M* and 1*M* sulphuric acid solutions by standard addition and were found to be $2 \times 10^{-8}M$ and $4.1 \times 10^{-8}M$, respectively. The influence of mercury ion concentration, pulse amplitude, potential step and pulse repetition time on analytical data was studied and optimized. A rotating disc graphite electrode was also used as a working electrode and was found unreliable for this purpose as hydrogen bubbles were not removed effectively and blocked the working electrode surface.

Stripping analysis, like many forms of ultratrace analytical techniques, is subject to interferences that affect accuracy and precision. The reliability and validity of the analytical data strongly depend on the degree to which contamination and/or loss of the analyte can be minimized. In this respect, the simplification of sample pretreatment steps and the restriction of their number is significant. It is desirable to operate at low pH as the rate of adsorption of metals onto the container and electrode surfaces is very pH-dependent, increasing considerably at high pH.[1] Robertson studied the adsorption of 11 elements in seawater onto various containers and indicated that optimum conditions for storing seawater were achieved by acidifying to pH 1.5 immediately after collection and storing in polyethylene containers.[2] Mart recommended deep-freeze (−20°) storage of the acidified sample to avoid leaching metals from the surface of a containter.[3] Scarponi *et al.* found,[4] investigating the contamination of seawater samples by cadmium, lead and copper during storage of samples, that conventional polyethylene containers can be used for long-term storage of samples at their natural pH (about 8) at 4°, but must be cleaned with acid for at least 1 week and conditioned with prefiltered seawater for at least 2 weeks. At the natural pH, samples were analyzed for labile heavy metals,[5] but the total concentration of metals was determined on rain and seawater samples acidified with concentrated hydrochloric acid to pH 1.5[5,6] or pH 2.[7] The increase in the peak currents observed upon acidification was explained as a result of the release of the metals from complexes[8] or labile complex formation that are "electrochemically available".[9] In addition, the presence of surfactants at low pH values did not affect peak current.[8]

It can be concluded from the above that for various environmental and industrial applications, the acidification of collected samples and direct determination was found to be the best procedure for minimizing contamination or loss of the trace metals. But in the case of the stripping Zn determination at solid electrodes the acidification results in a strong hydrogen evolution which can disable quantitative analysis. To overcome this problem, samples were buffered and Zn was measured at pH 5.8[10] or 4.6[11] while for most metals, seawater was acidified to pH 1.9.[10] DPASV at a GC rotating electrode was employed for Zn determination in Antarctic snow samples at pH 2.9 but further acidification resulted in steeper voltammetric baseline currents and loss of sensitivity for Zn.[12] SWV was found to be more sensitive in comparison with DPASV for Zn determination at SDME in strongly acidic media and for

*Author for correspondence.
New postal address: Univ. of the Witwatersrand, Dept of Chemistry, P.O. Wits 2050, Johannesburg, South Africa.

the determination of Zn lower than 10 μg/l. A 0.01*M* acid solution was recommended, but the highest SWV peak was obtained at pH 1.4.[13]

To acidify the real sample which is to be studied for zinc content one must know what the concentration of zinc is in a commercial acid. In our previous work we have presented the direct quantitative Zn determination at pH 2 by ASV at the epoxy-resin-impregnated graphite electrode (IGE).[14] In this paper, the extension to the DPASV technique with and without a background current correction is reported. The instrumental and analytical parameters were studied and optimized so that a direct Zn determination can be performed at pH ≅ 0, or even higher acid concentration (a calibration curve for Zn in 1*M* sulphuric acid is discussed) despite the solid and stationary electrode used. For comparison, some results of DPASV measurements at a rotating IGE will also be presented.

EXPERIMENTAL

Instrumentation and reagents

Analyses were done with a Polarecord E 506 in the differential mode with a polarography stand E 505 (both Metrohm). The voltammetric cell was a Metrohm universal measuring and titration vessel (6.1415.220) with a vessel lid (6.1414.010 – five electrode apertures). The working electrode (4 mm in diameter) was an epoxy-resin-impregnated graphite electrode for which production and preparation were described elsewhere.[15,16] From this electrode a tip was made which is of the exact shape and size required by Metrohm (6.1204) to fit a Metrohm E 628-50 rotating disc electrode (RDE) which was used in this paper as a RDE drive for a home made IGE disc. Once the working electrode was made no additional chemical, electrochemical or mechanical treatment was done during the whole study presented in this paper. The working electrode was used in two modes during the deposition step of a DPASV measurement: firstly, as a rotating disc (2100 rpm) and secondly, as a stationary one with the aid of the striking gas (SG) technique.[17] SG serves as the source of a metered stream of neutral gas which is used to deoxygenate the sample and stir the solution during the deposition stage. To achieve the latter an additional, two tubes holder was made and fixed in one of the vessel lid apertures. One tube was used to direct the metered gas stream towards the active surface area of the working electrode (the distance between a gas outlet and the electrode working surface was about 10 mm), and the second tube maintained an inert atmosphere over the solution being analyzed. A gas purge tube (Metrohm 6.1443.000) was used only when IGE worked in a rotating mode. Pure argon was used to deaerate and stir the solutions. All measurements were carried out in the three electrode system using a platinum wire counter electrode (Metrohm EA 285) and an Ag/AgCl saturated potassium chloride reference electrode (Metrohm EA 441/5) placed on the electrolyte vessel with a ceramic plug (Metrohm 6.1225.010). Solutions were prepared with analytical reagent grade chemicals and doubly distilled water. Standard solutions of sulphuric acid and metal ion concentrations were prepared by diluting stock solutions and were stored in polyethylene bottles rinsed with acid. Standard additions were made from fix Transferpettes and digital Transferpettors (Rudolf Brand GMBH, Germany). All experiments were done at room temperature 22 ± 2°.

Standard procedure

Except where specified, the experimental parameters and analytical procedure were as follows. A 50-ml volume of the solution to be studied was prepared directly in the voltammetric vessel by mixing appropriate volumes of doubly distilled water with the sulphuric acid, mercury nitrate and zinc nitrate solutions metered from 2.5*M*, $1 \times 10^{-2}M$ and $1 \times 10^{-4}M$ standard solutions, respectively. Samples were deaerated for 300 sec after which −1.4 V potential was applied to the IGE in the stirred solution for 180 sec. Then the potential was changed from −1.4 to 1.2 V and after 5 sec a rest period of 15 sec began during which sensitivity was adjusted from the pre-electrolysis position to a desired one. Scanning was from −1.2 to −0.85 V (E_{pulse} = 40 mV, E_{step} = 3 mV, pulse repetition time 0.4 sec) followed by stripping of any trace metal at 0.00 V for 30 sec in the stirred solution. Three consecutive curves were recorded in one sample and the last one was taken into consideration. The mercury film was removed by wiping the electrode gently with wet filter paper. Prior to the next measurement in a different sample the vessel and electrode system were rinsed with 0.1*M* sulphuric acid and water several times. If only the stirring solution mode was changed from RDE to SG only the mercury film was removed but the solution was unchanged in the vessel. A RDE rotation speed of 2100 rpm and

a gas outflow efficiency[17] of 2 l./min were the same for all experiments.

RESULTS AND DISCUSSION

Preliminary study

The primary aim at this stage was to find out whether any of the studied techniques, RDE and SG, are suitable for a direct Zn determination at extremely low pH using standard experimental parameters. A series of measurements was performed in which the concentration of Zn was kept constant, mainly $1 \times 10^{-7}M$, but mercury ion and sulphuric acid concentrations varied in the range of 5×10^{-7} to $5 \times 10^{-4}M$ and 0.005–2.5M, respectively. The results obtained are presented in Fig. 1 in the form of the bar graph and some selected voltammetric curves in Fig. 2. Despite the complexity of the system studied and the lack of obvious and clear (at the first view) relations presented in Fig. 1, some important conclusions and trends can be drawn up. It is seen that 2.5M sulphuric acid is not the one for the direct Zn determination for both techniques examined. On the other hand, the fact that with SG small peaks of zinc were recorded might suggest the possibility of quantitative analysis, but no attempt was made to do it. It is evident (see Fig. 2) that the Zn peaks recorded using SG are several times higher than those when the RDE mode was used. This fact can be explained by the IGE active electrode surface observations made during the deposition and rest stages. One may easily notice hydrogen bubbles which are not effectively removed during the electrode rotation. The amount of the gas increases with the acid concentration increase, the mercury ion concentration decrease and with a consecutive number of measurements of the same sample or for longer deposition times. Initially, many of these small bubbles are formed, but after several minutes they form a single big hydrogen bubble (rotating together with the electrode) which may cover the working surface of IGE even entirely. The fact of insufficient gas removal makes the RDE system uncertain and unreliable for quantitative analysis of Zn at very low pH. In the case of SG, the above described phenomenon does not take place. Only in 2.5M sulphuric acid during a rest stage, were small

Fig. 1. The influence of solution composition and solution stirring technique on zinc peak height. Blank bar—RDE; filled bar—SG. Zinc concentration: $1 \times 10^{-7}M$. Mercury concentrations: (a) $5 \times 10^{-4}M$; (b) $5 \times 10^{-5}M$; (c) $5 \times 10^{-6}M$; (d) $5 \times 10^{-7}M$. For standard procedure parameters see text. Question mark—no reproducible peak height (see text for full explanation).

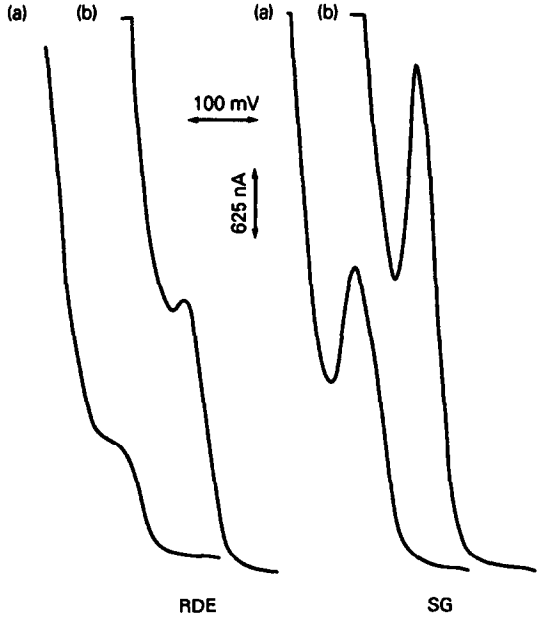

Fig. 2. DPASV peaks of zinc for selected measurements in 0.5M sulphuric acid. Zinc concentration: $1 \times 10^{-7}M$. Mercury concentrations: (a) $5 \times 10^{-5}M$; (b) $5 \times 10^{-4}M$. Standard parameters.

hydrogen bubbles observed. These were removed from the surface during the next deposition step. Even in $0.5M$ sulphuric acid and at the lowest mercury ion concentration studied no gas bubbles were observed during the rest step. For both stirring systems, the lower the pH, the lower the Zn peak height recorded for all mercury ion concentrations except $5 \times 10^{-4}M$, and the higher the mercury ion concentration the higher the Zn peak recorded for all sulphuric acid concentrations. In the solutions of $5 \times 10^{-4}M$ mercury ion and $5 \times 10^{-3}M$ acid, noise and the lack of reproducibility in peak height were observed when curves were recorded. The arrow and the question mark in Fig. 1 indicate a very low accuracy and uncertainty of the measurement performed in that solution, because the mercury nitrate partially played a role of a supporting electrolyte. Its concentration was only 10 times lower than that of the acid and any small vibration or shaking of solution caused the change of the current recorded from a diffusion to a diffusion-migration one. In addition, the superimposed hydrogen reduction and zinc oxidation currents made the system even more sensitive and unstable. The mercury ion concentration of $5 \times 10^{-4}M$ seems to be the best as not only the highest Zn peaks were recorded, but also the Zn peak in the $0.5M$ acid solution is higher than that in the $0.05M$ solution. This might suggest that the observed increase is caused by the Zn content present in the acid appearing as contamination. Furthermore, one may suppose that at such high mercury ion concentration levels, the amount of Hg(II) is a decisive factor when the sensitivity of a measurement is concerned. As a confirmation, the equal Zn peak heights, recorded by SG, in solutions of $5 \times 10^{-3}M$ sulphuric acid $+ 5 \times 10^{-5}M$ Hg^{2+} and $5 \times 10^{-2}M$ sulphuric acid $+ 5 \times 10^{-4}M$ Hg^{2+} may be used. This indicates that in both solutions the main source of Zn was the standard zinc solution added and not impurities in the sulphuric acid or the mercury nitrate standard solutions. For all other mercury concentrations studied, the pH of the solution (hence the acid concentration) limits the height of Zn peak—the lower pH, the lower peak recorded. It was also observed that Zn peaks recorded on acid solutions containing $5 \times 10^{-4}M$ Hg^{2+} are higher and narrower than those obtained at $5 \times 10^{-5}M$ Hg^{2+} or lower mercury ion concentration levels and at the same Zn and acid concentrations—compare two SG curve in Fig. 2.

Peak height assessment

An evaluation of voltammetric data when measurements of Zn content were performed at very low pH is not an easy task. The shape and size of the peak is strongly affected by a steep voltammetric baseline current from hydrogen evolution. In addition, the steepness of the baseline current depends on the acid and mercury ion concentrations, thickness of a mercury film as well as the sensitivity value pre-set before the curve is recorded, which very often must be changed when a standard addition technique is used. We found that at very low Zn(II) levels reliable results could be obtained only when the background current is recorded (without deposition step) just after each voltammetric measurement of Zn. A subtractive DPASV peak is not only much easier for interpretation but also higher, sometimes twice as high as that obtained using the tangent. The following demonstrates how substantial error can arise (the lower peak of metal, the more significant discrepancy) by tangent assessment of a DPASV peak height of zinc. Two experiments were performed on $0.5M$ sulphuric acid with $5 \times 10^{-5}M$ Hg^{2+} at the stationary IGE. The first one was the standard addition of zinc solution and the second one was the study of the height of zinc peak as a function of the deposition time, at $7 \times 10^{-7}M$ Zn^{2+} content. For both relationships straight lines were obtained but with negative values of y-axis interceptions. When corrected by taking the background current as baseline peak it results in curves that have positive y-axis intercepts, better correlation coefficients and larger gradients. For illustration purposes the interception, correlation coefficient and slope of calibration curves for tangent and background current correction were found to be -0.65; 0.975; 0.77 ± 0.06 and 0.10; 0.996; 0.89 ± 0.03, respectively. A tangent approximation of a hypothetical baseline is commonly used in a computerized equipment as it is an easy and quick way of peak height measurement.[13,18] One must realize that this method may often lead to large determination errors, which can be avoided by a subtractive method, or background current correction, or highly-developed mathematical analysis of the peak region.[19] In all further measurements backgrond current is taken into account for data evaluation.

Quantitative Zn determination

For zinc determination only the SG mode was used. The original Zn concentrations in $1M$

sulphuric acid solution with $5 \times 10^{-4}M$ Hg^{2+}, a deposition time of 10 min (sample A) and two $0.5M$ sulphuric acid solutions for 5-min deposition times and at different mercury concentration levels, mainly $5 \times 10^{-4}M$ (sample B) and $5 \times 10^{-5}M$ (sample C) were determined by the standard addition technique. In all cases, the relationships between the peak heights and the added Zn standards were linear but had different slopes. For samples A, B and C slopes were found to be 2.78, 4.48 and 3.81, respectively. The original concentrations of Zn in studied samples were in very good agreement; Zn contents in $1M$ and two $0.5M$ sulphuric acid solutions were found to be $4.1 \times 10^{-8}M$ and $2.0 \times 10^{-8}M$, respectively. The producer specification says that the maximum amount of Zn can be 5×10^{-5}% which corresponds to $3 \times 10^{-7}M$ Zn^{2+} in a $0.5M$ acid solution and is one order of magnitude more than the value found. One must notice the difference in the deposition times which were 5 and 10 min for the 0.5 and $1M$ acid solutions, respectively. From the analytical point of view, data obtained for both sulphuric acid solution concentrations, even when a 10-min deposition time had to be used in $1M$ acid to record peaks sufficiently high, well-shaped and suitable for quantitative determination of Zn, are regarded as fully satisfactory. This experiment also confirms that the higher the acid concentration, the lower the Zn peak recorded and the higher the mercury concentration, the higher the Zn peak recorded in the solution of the same pH, which results in a different slope of the calibration curve.

The effect of extremely low pH

The results of the preliminary study, especially the lack of a Zn peak in $2.5M$ sulphuric acid as well as a significant decrease in peak height in the $1M$ acid (sample A in quantitative Zn determination) suggested the need for a more detailed examination. A series of measurements was performed on one sample containing $2 \times 10^{-7}M$ Zn^{2+} and $1 \times 10^{-4}M$ Hg^{2+} with a stepwise standard sulphuric acid addition. After each acid addition the voltammetric curve was recorded and results obtained are presented in Fig. 3, where two curves are seen. The first one (lower curve) represents the real values of the peaks recorded and the second one (upper curve) was obtained when the dilution of Zn was taken into account. From this relation and the data presented in Fig. 1, where no decrease of Zn peak is observed in $0.5M$ acid solution with

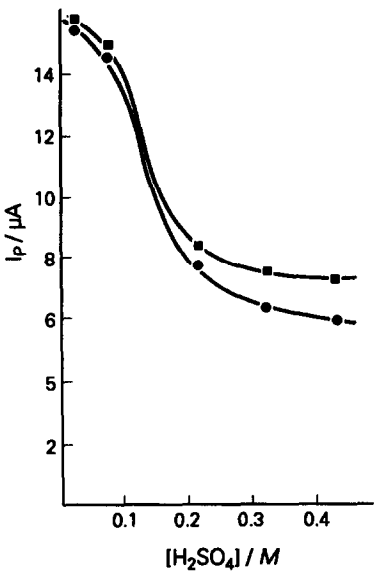

Fig. 3. The effect of acid concentration on zinc peak height. Mercury concentration: $1 \times 10^{-4}M$. Zinc concentration: $2 \times 10^{-7}M$. Standard instrumental parameters. (●) Zn peak recorded; (■) Zn peak recalculated (see text).

$5 \times 10^{-4}M$ Hg^{2+} addition it is clear, that there is no specific pH range at which the Zn peak height dramatically decreases. It depends not only on the acid to mercury ion concentration ratio but also on the working electrode or mode of solution stirring used and must be found experimentally for each system studied. For example, when the quantitative Zn determination

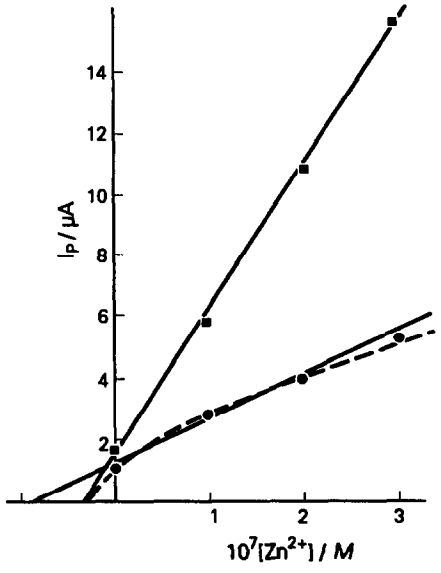

Fig. 4. Comparison of RDE (●) and SG (■) calibration curves for zinc, $0.5M$ sulphuric acid + $5 \times 10^{-4}M$ Hg^{2+}. Deposition time 5 min. Standard instrumental parameters. Dashed line = a real relationship for RDE (for explanation see text).

was performed using the RDE or SG modes in the same sample, two different relations were obtained even when the optimum composition of the solution for SG was chosen, mainly $5 \times 10^{-4}M$ Hg^{2+} in $0.5M$ acid (Fig. 4). One may see, that the original concentration of Zn in the acid solution estimated from RDE curve, presented as a solid line (●), is far too high—compare this result with those discussed in the previous section, *e.g.*, quantitative zinc determination. To explain this result, one must recall the hydrogen evolution phenomenon at RDE discussed earlier and under the circumstances the proper relationships for RDE is presented by a dashed line (●) in Fig. 4.

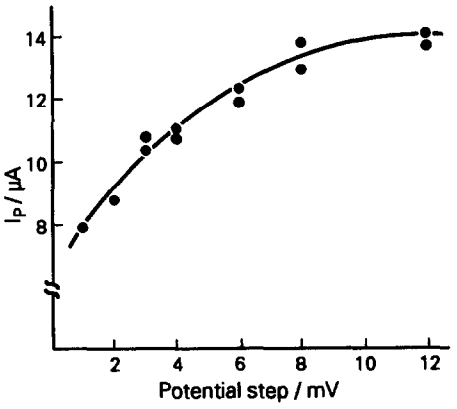

Fig. 6. The effect of potential step on Zn peak height. For details see Fig. 6.

The effect of instrumental parameters

The influence of the DPASV parameters on the analytical data was studied in $2.5 \times 10^{-2}M$ sulphuric acid (pH ≅ 1.6) containing $2 \times 10^{-4}M$ Hg^{2+}. It is not such a critical medium that pH must equal 0 but a very low pH is required and due to the striking gas technique employed we could record very well shaped Zn peaks. The estimated value of the Zn concentration in $2.5 \times 10^{-2}M$ sulphuric acid was found to be $1.07 \times 10^{-9}M$. This is in very good agreement with the results collected for 1 and $0.5M$ sulphuric acid but it was inconvenient, although possible, to study the effect of the instrumental parameters at such a low Zn level. By addition of $2 \times 10^{-7}M$ Zn^{2+} (about 200 times more than the original content) it was possible to obtain a high Zn peak (about 8 μA) at a deposition time of just 60 sec.

Under these conditions, *e.g.*, relatively low pH and relatively high mercury and zinc ions concentrations, one could expect a fairly stable and reliable performance of IGE in a SG mode, so all observed changes could be related to the instrumental parameter change. The influence of pulse amplitude, potential step and pulse repetition time on the peak height was studied. In each experiment, one parameter was varied while the others were kept constant. All measurements were performed in one sample solution. Prior to the series of measurements, a mercury film was plated in 180-sec steps followed by 60-sec steps (for total time of 16 min) to ensure that the electrode was reproducible. For all measurements, deposition potential, start potential and deposition time were −1.4 V, −1.2 V and 60 sec, respectively. The results are presented in Figs. 5–7. From data in Figs. 5 and 6 it is seen that the higher the scan rate the higher the peak recorded which is exactly opposite to the observation reported by Vos *et al.*[7] The pulse repetition time does not influence the peak height up to

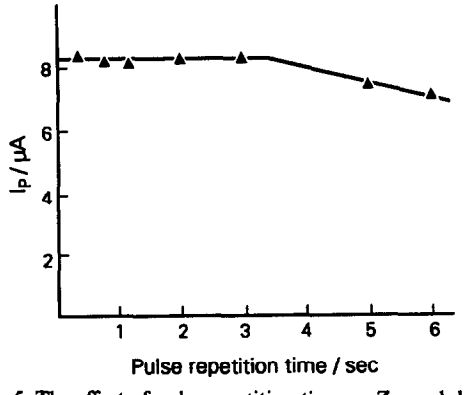

Fig. 5. The effect of pulse repetition time on Zn peak height in sulphuric acid solution. pH ≅ 1.6; mercury concentration $2 \times 10^{-4}M$; zinc concentration $2 \times 10^{-7}M$; deposition time 60 sec. For other instrumental parameters see text.

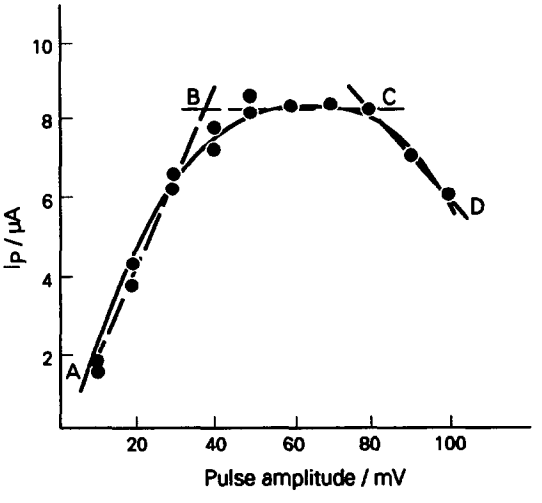

Fig. 7. The effect of pulse amplitude on Zn peak height. For details see Fig. 6.

3 sec. This is a very convenient relationship from the analytical point of view and allows the use of the shortest time available which makes the single measurement a relatively quick one. From the shape of the Zn peak recorded, when the influence of the potential step was studied and from the relation in Fig. 6, we recommend the use of 6 or 8 mV steps. This results in a 15- or 20-mV/sec scan rate at 0.4-sec repetition times. At these scan rate values the peak decreases only very slightly but its shape is much better than for 10 mV or higher steps because for a single Zn peak more points are recorded. In Fig. 7 three regions one may select and from them B–C one, *e.g.*, for pulse amplitude between 40 and 80 mV, which is the most suitable for use as the peak height does not depend on a pulse value and is the highest one. With the pulse amplitude increase, the DPASV zinc peak shifts towards more negative values, we recommend use of 50- or 60-mV pulse amplitudes (for 10 and 100 mV pulse amplitudes Zn peak potentials were -1050 and -1120 mV, respectively). The decrease of the Zn peak for higher pulse amplitude values (region C–D in Fig. 7) was also observed for a SWV zinc peak at SMDE, when the square wave amplitude was higher than 60 mV.[13]

During this study a significantly higher value of the gas outflow efficiency, 2 l./min, was used than that reported previously,[17] as it was necessary to remove effectively a huge amount of gas being evolved at the working surface of the IGE. Fortunately, even under these circumstances, *e.g.*, extremely low pH, very strong gas stream striking IGE and in addition at high mercury concentration (more than one order of magnitude higher than that used before[17]), hence for the thick mercury film formed, there was no single symptom observed which would indicate a destruction or failure of the working electrode and mercury film.

In conclusion, the method described provides a simple approach for direct determination of trace levels of zinc at extremely low pH in commercial acids used to acidify collected samples. Using optimized instrumental parameters, several hydrochloric and nitric acids solutions were analyzed for zinc at pH $\cong 0$ by standard addition. For all samples studied the Zn content was below the level specified by the producer. The detection limit of $1M$ acid solution and 10 min deposition time was estimated to be about $1 \times 10^{-9}M$. The results presented confirm that IGE combined with SG may be used successfully for this purpose and on the other hand, made it obvious that commercially available rotating disc electrodes are not suitable. Bearing in mind the results presented it is easy to explain why the loss of sensitivity for Zn at a pH lower than 2.9 was reported when GC as the working RDE was used (1500 rpm) at a $5 \times 10^{-5}M$ mercury ion concentration level.[12]

REFERENCES

1. R. Salim and B. Cooksey, *J. Electroanal. Chem.*, 1980, **106**, 251.
2. D. E. Robertson, *Anal. Chim. Acta*, 1968, **42**, 533.
3. L. Mart, *Talanta*, 1982, **29**, 1035.
4. G. Scarponi, G. Capodaglio, P. Cescon, B. Cosma and R. Frache, *Anal. Chim. Acta*, 1982, **135**, 263.
5. S. Daniele, M. A. Baldo, P. Ugo and G. A. Mazzocchin, *ibid.*, 1989, **219**, 19.
6. H. W. Nürnberg, *ibid.*, 1984, **164**, 1.
7. L. Vos, Z. Komy, G. Roggers, E. Roekens and R. Van Grieken, *ibid.*, 1986, **184**, 271.
8. P. Sagberg and W. Lund, *Talanta*, 1982, **29**, 457.
9. D. R. Turner and M. Whitfied, *J. Electroanal. Chem.*, 1979, **103**, 61.
10. T. M. Florence, *ibid.*, 1972, **35**, 237.
11. T. Rojahn, *Anal. Chim. Acta*, 1972, **62**, 438.
12. M. P. Landy, *ibid.*, 1980, **121**, 39.
13. P. Ostapczuk, P. Valenta and H. W. Nürnberg, *J. Electronal. Chem.*, 1986, **214**, 51.
14. E. Cukrowska and I. Cukrowski, *ibid.*, 1982, **131**, 341.
15. K. Sykut, I. Cukrowski and E. Cukrowska, *ibid.*, 1980, **115**, 137.
16. I. Cukrowski, Polish Patent No. 106555, 1980.
17. I. Cukrowski, E. Cukrowska and K. Sykut, *J. Electroanal.* 1981, **125**, 53.
18. Application Notes: P-2 and PLAT-9, EG&G Princeton Applied Research, USA.
19. Application Note Lab 2/88, vol. 17 and Metrohm's brochure "Measurement in Chemistry, 646 VA Processor", Metrohm, Switzerland.

Talanta, Vol. 40, No. 2, pp. 213–219, 1993
Printed in Great Britain.

0039-9140/93 $6.00 + 0.00

RAPID GAS ANALYSES FOR THE INVESTIGATION OF SPONTANEOUS COMBUSTION USING CAPILLARY GAS CHROMATOGRAPHY

W. J. HAVENGA
Research and Development, ISCOR Headquarters, P.O. Box 450, Pretoria 0001, South Africa

(*Received* 13 *April* 1992. *Revised* 10 *June* 1992. *Accepted* 10 *June* 1992)

Summary—A simple and fast but sensitive and precise gas chromatographic method is described for the quantitative determination of O_2, N_2, CO, CO_2, C1 and C2-hydrocarbons for coal research. Gas analyses are necessary to obtain parameters for modelling spontaneous combustion and to predict long term coal behaviour. The method is based on a single PLOT-type capillary column in a single channel gas chromatograph. Using a micro-volume TCD coupled in series with a FID detector containing a capillary methanizer it is possible to determine high and trace level gases simultaneously. Trace quantities of CO and CO_2 can be determined with a single analysis and the detection limits are improved significantly using the capillary methanizer. The detection limit of the described method is approximately ten parts per million CO_2 and one part per million CO. Using the same instrument configuration the O_2/N_2 ratios (major components), as parameter for coal reactivity, are also determined. The proposed approach is restricted to the determination of gases evolved during coal studies and the application to other gas mixtures is not considered.

Spontaneous combustion of coal is always undesirable as it can lead to atmospheric pollution and the loss of a valuable commodity or even life. The oxidation of coal (adsorption of oxygen) in which oxygen reacts with the coal to form what is termed an "oxycoal",[1] is the major source of heat in a heap. The oxycoal contains oxidation products such as carboxylic acids, humic acids, peroxides and hydroxides. These products decompose with time to release product gases such as CO and CO_2. Inherent CH_4 is released mainly due to desorption. These gases are released in relatively small concentrations compared to the total amount of oxygen adsorbed, and are expected to be present in trace levels at low temperatures.

The gas concentrations and temperatures in waste heaps is monitored to investigate the coal reactivity, toxic gas evolution and trace gas distribution in order to implement safety precautions and to make long term predictions. The release of CO is of particular importance as it is very toxic, has no smell and its emission from smouldering or burning heaps is a major hazard. Laboratory research programmes exploring the self-heating potential of coal[2] provide the latest information needed for the safe stockpiling, transportation and disposal of coal or waste material. A typical test is the determination of low temperature coal reactivity as well as the amounts of evolved gases. Typical gas concentrations, as found during laboratory experiments or in waste heaps, are indicated in Table 1.

The gases depicted in Table 1 are traditionally determined using two columns, namely a molecular sieve type packed column for O_2, N_2, CO and CH_4 and a Porapak Q for CO_2 and C2-C4 hydrocarbons. Mindrup[3] summarized most of the methods used for permanent gas and light hydrocarbon analyses. Single column applications, using temperature programming from sub-ambient temperatures[4] and dual column[5] or dual channel operation with column valving,[6–8] have been reported, but they are all complex or have long analysis times. All the above-mentioned techniques are based on thermal conductivity detection (TCD) for CO and CO_2 and therefore also lack the necessary sensitivity. Simplicity, efficiency, precision, sensitivity and ease of operation and ease of troubleshooting were considered important standards in developing an analytical technique for modelling of coal behaviour. Efficiency and resolution can be improved significantly using a capillary column.

The Carboplot 007 carbon molecular sieve type capillary column was employed in this investigation. Inorganic and light hydrocarbon gases can be separated and determined using this column and it was deemed possible to

Table 1. Typical expected gas concentrations

Component	Non-reactive waste heaps	Smouldering heaps	Laboratory low temperature experiments
CO	1–25 ppm	0.05–10%	100–5000 ppm
CO_2	0.05–1.5%	0.1–20%	0.05–2%
CH_4	<1	0.001–3%	10–5000 ppm
C_2H_4	<1	1–1000 ppm	<1
C_2H_6	<1	1 ppm–1%	<1

configure a system around a single column to suit the needs for coal research. This would eradicate the complications involved with dual column systems. A capillary methanizer, based on the principles described by Volman,[9] was used to improve the sensitivity for carbon monoxide and carbon dioxide. The efficiency, sensitivity and precision of this method, as well as its application to gas analysis in coal studies, was investigated.

EXPERIMENTAL

Instrument configuration

A Siemens Sichromat II gas chromatograph with a FID, a TCD with an internal cell volume of 20 μl and a gas sampling valve was used in this investigation. The TCD outlet was connected to the FID inlet using a 0.3-mm diameter fused silica capillary. The system was configured as illustrated in Fig. 1 and the FID capillary insert was packed with a cobalt catalyst as shown in Fig. 2. A CarboPLOT 007 capillary column (25 m × 0.53 mm), operated from ambient to 115°, and a helium carrier gas flow of 15 cm^3/min were employed.

A cobalt catalyst with a high surface area was prepared by soaking Chromosorb M (120 mesh) in a saturated cobalt nitrate solution. The excess liquid was removed by filtering under vacuum. The solid phase was dried overnight at 110° and then heated in air for 5 hours at 350° to obtain cobalt oxide with a high surface area. The catalyst was then packed into the quartz tube, as illustrated in Fig. 2, and installed in the FID of the gas chromatograph. The FID was heated overnight at 350° under a stream of helium gas to activate the catalyst.

Gas monitoring in experimental coal heaps

Gas samples are taken from heaps using gas sampling bulbs (250 cm^3), through probes installed at various points. The samples are introduced into the GC using the gas sampling valve with a fixed 0.25-cm^3 sample loop and analyzed for CO, CO_2, CH_4, C_2H_4 and C_2H_6.

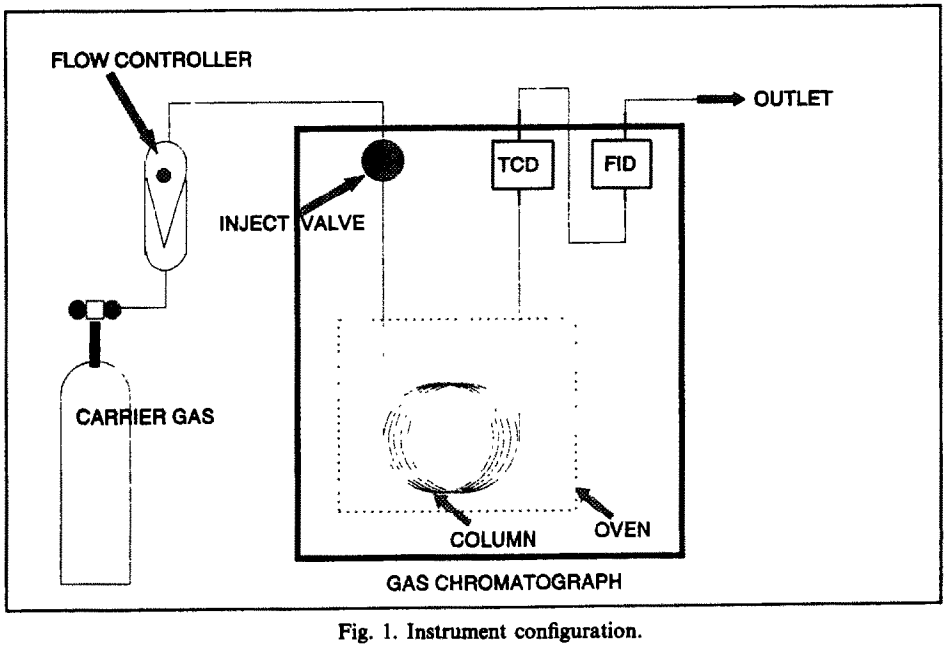

Fig. 1. Instrument configuration.

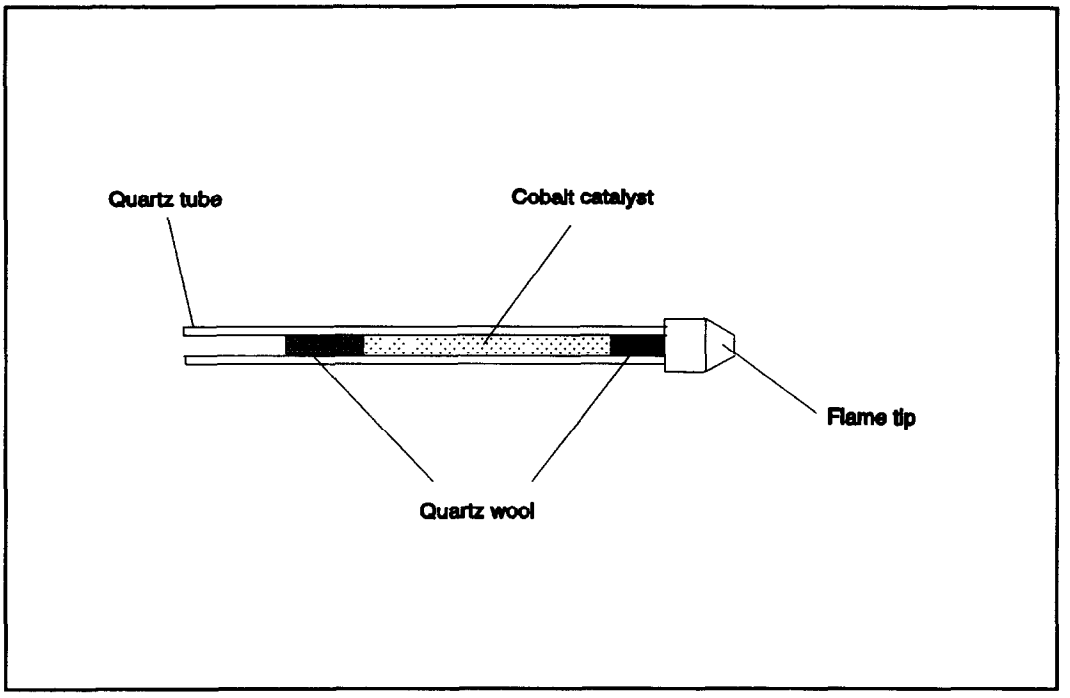

Fig. 2. Cross section of the glass insert in the FID.

The concentration of these gases may vary from trace levels to major components, depending on the temperature in the heap. The FID detector signal is used to quantify low concentration gases and the TCD detector signal for gas concentrations exceeding 1%. The results are expressed as parts per million or percent component present in a specific location in the heap.

Laboratory tests exploring the self heating potential of coal

Sample preparation. The air-dry samples were crushed to 25 mm, mixed, sieved and divided by means of a Jones-riffler to produce four kilogram samples of 1.0–6.3 mm coal particles. These samples were allowed to equilibrate with air at 35° in open trays for twenty four hours.

Apparatus. Reactivity determinations are based on the determination of the rate of oxygen adsorption. For this purpose high density PVC reaction vessels of *ca.* ten litre capacity are used. Each vessel is sealed by a polyurethane gasket located in a machined groove on the flange. The bolt-on lid contains a gas sampling port with a silicone rubber septum and an airtight stop-cock for pressure equalization. Experiments are carried out in a constant temperature room at $35 \pm 1°$ and *ca.* 30% relative humidity.

Method. The coal sample of known mass and density is placed in a reaction vessel of known volume, sealed, and placed in a rotator. The barometric pressure is recorded. Gas samples are removed at intervals through the septum and analyzed by the proposed gas chromatography method to determine the change of O_2/N_2 ratios with time and trace gas levels CO, CO_2 and CH_4 evolved. The test is continued until the O_2 level drops below 15%.

Calculation. The reaction constant of the material with oxygen is calculated from the change in gaseous oxygen content of the sealed container. The formula used is:

$$k = \frac{\ln \dfrac{O_{2i}}{O_{2f}}}{t} \qquad (1)$$

where O_{2i} and O_{2f} are respectively the initial and final O_2/N_2 mole ratio in the reaction vessel, t the time in days and k the rate constant of oxygen depletion (day^{-1}), assuming first order reaction. The reactivity of the material is expressed as normal cm^3 oxygen consumed per kilogram material per day. The formula used is:

$$\text{Reactivity} = k \cdot V_{O_{2i}} \qquad (2)$$

where $V_{O_{2i}}$ is the initial normal cm^3 volume of O_2 available per kilogram coal in the reaction vessel.

RESULTS AND DISCUSSION

System configuration

As indicated by Porter all the necessary conditions for conversion, except the catalyst, are present in the flame ionization detector. Complete conversion of CO and CO_2 to CH_4 is obtained at a FID operating temperature of 350°. Results obtained in this manner are found to be approximately 120 times more sensitive than those obtained employing a TCD. This methanizer configuration is only suitable for conversion of micro-quantities of gases and is therefore only applicable to capillary gas chromatography. The advantage of this method is improved efficiency when compared to traditional packed columns. Simultaneous determination of CO and CO_2 concentrations is also possible.

For simultaneous FID and TCD detection, the series coupling of the detectors was preferred above a parallel arrangement. The latter arrangement would reduce the already low flow rate through the TCD with a simultaneous decrease in resolution and sensitivity. It would also require the installation of a reliable outlet splitter with a very constant split ratio. In the case of the series arrangement it is necessary to use a micro volume TCD to eliminate the possibility of band broadening and resulting loss of resolution of the peaks detected with the FID.

The application of the method to the monitoring of gas concentrations in experimental coal heaps

Gas concentrations in coal waste heaps depend on factors such as the coal type, reactivity, age, moisture content (weather conditions), heap geometry and particle size. The concentration of these gases increase as a function of temperature. In burning heaps CO_2 concentration will typically increase to approximately

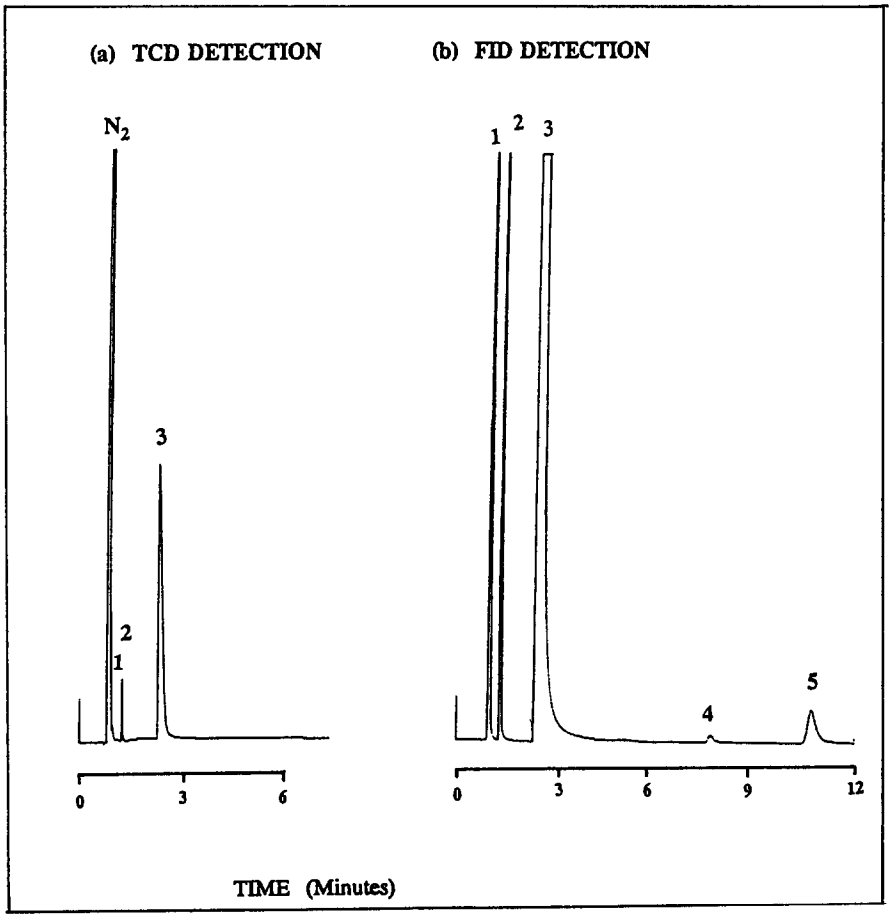

Fig. 3. Separation of gases from a smouldering heap. Column—Carboplot 007, 25 m × 0.53 mm; Oven temperature—90°; Carrier Gas—Helium, flow of 15 cm^3/min; Sample size—size 0.25 cm^3; Detection—TCD coupled in series with the FID, fitted with a capillary methanizer. 1 = 1.01% CO, 2 = 0.95% CH_4, 3 = 15.5% CO_2, 4 = 3.5 ppm C_2H_4, 5 = 43 ppm C_2H_6.

20 percent, methane to 2.5 percent and the C2-hydrocarbons to between 0.001 and 0.15 percent.

Using the Carboplot 007 column, base line separation of CO, CO_2 and CH_4 is achieved at an isothermal column temperature of 90° within an analysis time of 3 min. Ethylene and ethane can also be separated and detected using an extended analysis time of ten minutes, but these components are not normally present in samples and only occur in burning heaps or in high temperature experiments. A typical chromatogram of a sample collected from a waste heap at the Grootegeluk Coal Mine, is illustrated in Fig. 3.

As evident from Fig. 3(a) there is considerable interference (overlap) from the N_2 peak with the CO peak using TCD detection. This problem is solved when CO is converted to methane because the FID is insensitive to N_2 [Fig. 3(b)]. The relative signal intensity differences between Figs. 3(a) and (b) are also illustrated.

The application of the method to determine gas concentrations during controlled laboratory experiments

The low temperature adsorption of oxygen by coal is the main heat-generating step during the oxidation process of coal. The rate of oxygen adsorption, as a measure of coal reactivity, is determined by the gas chromatographic method and calculated according to equations (1) and (2). The reactivity is also used as a parameter for mathematical models used to predict the self-heating potential of coal. A reliable method for determining O_2/N_2 ratios during an experiment is therefore invaluable. For reliable reactivity calculations, the assumption of first order reaction must also be valid. Although a first order reaction is generally assumed for mathematical models of spontaneous combustion in coal stockpiles,[10,11] this is not necessarily the case. Stott[12] described the oxidation by a 0.5 power of the oxygen in the gas stream. Schmal[13] used an experimentally determined order of reaction (n) of 0.7 in the calculations with his moist coal model, and assumed $n = 1$ (as obtained from literature) for calculations with the dry coal model. The order of reaction was also investigated in our laboratory by plotting log O_{2f} versus time. The graphs were constructed from experimental data obtained for various coals and found to be linear. Under our experimental conditions we therefore accepted that chemisorption of oxygen by the coal particle surface proceeds according to a first-order reaction.

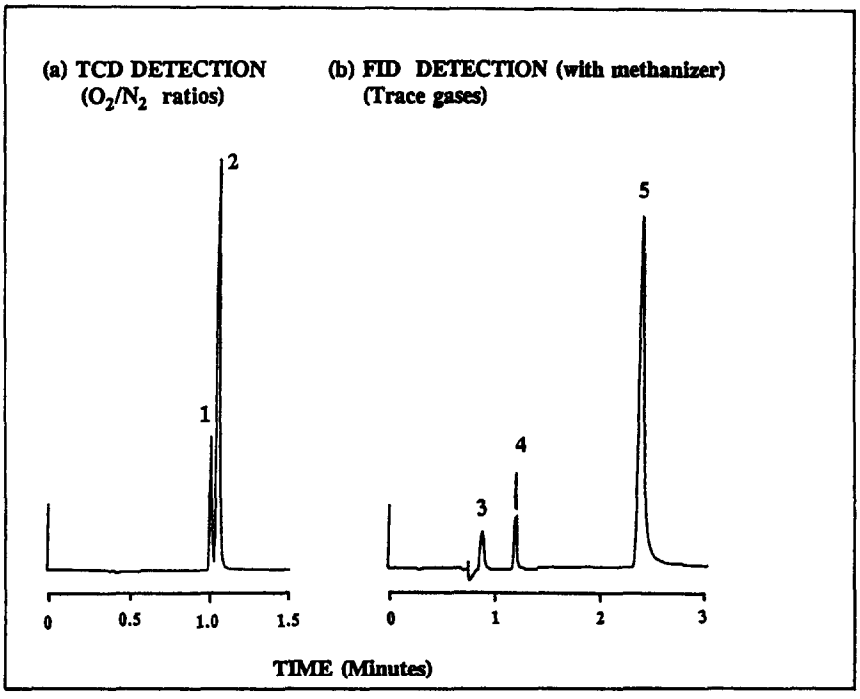

Fig. 4. Separation of gases during a controlled laboratory experiment. Column—Carboplot 007 column, 25 m × 0.53 mm; Carrier gas—helium with flow of 15 cm³/min; Sample size—(a) 10 μl, (b) 250 μl; Oven temp—(a) 30° (b) 90°; Coal sample—Obtained from the Syferfontein Coal Mine in the eastern Transvaal. 1 = 20.9% O_2, 2 = 79.0% N_2, 3 = 17 ppm CO, 4 = 27 ppm CH_4, 5 = 1448 ppm CO_2.

Table 2. Precision of reactivity and gas determinations during a typical laboratory experiment on a Syferfontein coal sample

	Average value X ($n = 11$)	Standard deviation	Coefficient of variation
O_2/N_2 ratios (O_{2i})	0.2562	—	—
O_2/N_2 ratios (O_{2f})*	0.2080	—	—
Reactivity	415 cm^3/kg/day	10.9	2.63
CO	17.8 ppm	0.44	2.49
CH_4	27.3 ppm	0.31	1.13
CO_2	1448 ppm	16	1.10

*Time elapsed = 0.177 days; $V_{O_{2i}} = 352.4$ cm^3.

Gas chromatographic results obtained on coal from the Syferfontein Mine in the eastern Transvaal, are illustrated in this paper. The $O_2:N_2$ ratios were determined using a Carboplot 007 column at ambient temperature and TCD detection. Almost baseline separation of O_2 and N_2 was achieved within an analysis time of under 1.5 minutes. A typical chromatogram is shown in Fig. 4(a).

Trace amounts of gases evolved during this experiment were also determined. A typical chromatogram of trace level gases is illustrated in Fig. 4(b). The final results of this experiment are given in Table 2.

Precision of the method

Data on precision studies was obtained by repeatedly analyzing the gases in the reaction vessel containing the Syferfontein coal (Table 2), as well as the gas sample collected from the Grootegeluk waste heap (Table 3).

As evident from Table 2, variation coefficients better than 2.5 percent were obtained in the case of the controlled laboratory experiment. As evident from the two sets of results obtained for the waste heap sample in Table 3, a considerable improvement is noticed in the case of FID detection. The CO peak could not be integrated on the TCD chromatogram due to overlap with the nitrogen peak. Furthermore the ethane and ethylene concentrations were too low for TCD detection. However, in the case of CO_2 present at a high concentration, the TCD results were found to be more precise. The lower value obtained on the FID could be due to the flattening out of the calibration curve at high gas levels. The combined results indicate that the precision is acceptable for the intended use of the method. Acceptable variation coefficients were obtained for all the trace gases, including the very low carbon monoxide concentration.

Linearity and detection limits

Multipoint calibration curves for each component were determined on the Carboplot 007 column using primary and secondary standards of different component concentrations. Relative response factors were calculated for each gas and were found to be linear over the concentration ranged indicated in Table 1. Other concentration ranges were not considered in this paper. The analytical working ranges for the FID and TCD, as well as the method detection limits (MDL) which can be expected for the trace gases, are indicated in Table 4.

The MDL is defined as the minimum concentration that could be measured with 99% confidence that the analyte concentration is greater than zero. The measurements were based on a maximum sample size of 250 μl that could be used to determine the trace gases with

Table 3. Precision of a gas determination on a reactive heap gas sample from Grootegeluk

	Results obtained on the FID			Results obtained on the TCD		
	Average concentration	Standard deviation	Coefficient of variation	Average concentration	Standard deviation	Coefficient of variation
CO	1.01%	0.003	0.31	p.o.	—	—
CO_2	15.5%	0.06	0.39	16.8%	0.05	0.30
CH_4	0.95%	0.003	0.28	0.94%	0.005	0.54
C_2H_4	3.5 ppm	0.83	23.7	n.d.	—	—
C_2H_6	43.5 ppm	0.79	1.82	n.d.	—	—

p.o.—Peak overlap, not integratable.
n.d.—Not detected.

Table 4. Suggested analytical working ranges for the TCD and FID

Component	Analytical working ranges	Type of detector	Method detection limits
O_2/N_2 ratios	0.1–0.26	TCD	—
CO	0–1%	FID (Methanized)	1 ppm
	1–10%	TCD	100 ppm
CH_4	0–1%	FID	1 ppm
	0.1–3%	TCD	100 ppm
CO_2	0–1%	FID (Methanized)	10 ppm
	1–20%	TCD	1000 ppm
C_2H_4	0–1%	FID	2.5 ppm
	0.1–3%	TCD	250 ppm
C_2H_6	0–1%	FID	2.5 ppm
	0.1–3%	TCD	250 ppm

this column, before observing the effects of overloading. Low enough detection limits were obtained with FID detection to allow reliable-results. Unacceptable detection limits were found on the TCD, thus illustrating the advantage of the FID and methanizer for reliable determination of evolved gases in coal research.

CONCLUSIONS

The Carboplot 007 capillary column used in the proposed configuration was found to exhibit superior performance compared to traditional methods. Separation and determination of O_2, N_2, CO, CO_2, CH_4, C_2H_4 and C_2H_6, as major or trace components, can be achieved with a single channel system built around a single column. Combining the efficiency and simplicity of the single capillary column with the detection capability of a capillary methanizer the following is achieved:

Separation of all the gases involved
Short analysis turnover time
Improved sensitivity for CO and CO_2
Wide linear working range of all the involved gases
Simplicity, ensuring ease of operation and ease of trouble shooting

The method can be applied to various investigations, covering a wide range of concentrations for the most important gases, by making inexpensive modifications. The method is particularly suitable for the monitoring of coal reactivity.

Acknowledgements—The authors wish to thank the management of Iscor for permission to publish this paper. Professor E. R. Rohwer is acknowledged for his expert advise during the project.

REFERENCES

1. D. Glasser and S. Bradshaw, *Report of the Dept of Chem Eng.*, Univ of Witwatersrand, 1989.
2. D. C. Farquharson, W. J. Havenga and A. L. M. Strauss, *Paper presented at the 6th National Meeting of SAChE*, Durban, August 1991.
3. R. Mindrup, *J. Chrom. Sci.*, 1978, **16**, 380.
4. P. Kusz, A. Andrysiak and J. Bobinski, *Chromatographia*, 1982, **15**, 297.
5. E. L. Obermiller and G. O. Charlier, *J. of Gas Chromatography*, 1968, **6**, 446.
6. L. E. Reed, *J. Chrom. Sci.*, 1987, **25**, 432.
7. J. L. Marchio, *ibid.*, 1971, **9**, 39.
8. A. Sood and R. B. Pannel, *ibid.*, 1982, **20**, 39.
9. K. Porter and D. H. Volman, *Anal. Chem.*, 1962, **34**, 748.
10. K. Brooks and D. Glasser, *Fuel*, 1986, **64**, 1035.
11. J. C. Edwards, *Report of the US BuMines*, 1990, **RI9296**, 8.
12. J. B. Stott, *Report of the US BuMines*, 1980, **OFR 113-81**, 59.
13. D. Schmal, J. H. Duyzer and J. W. van Heuven, *Fuel*, 1985, **64**, 963.

Talanta, Vol. 40, No. 2, pp. 221–224, 1993
Printed in Great Britain.

0039-9140/93 $6.00 + 0.00

DETERMINATION OF PLATINUM IN PLANTS BY EMISSION SPECTROMETRY AFTER PRECONCENTRATION ON MODIFIED SILICAGEL

VÍTĚZSLAV OTRUBA,* MARTA STRNADOVÁ and BLANKA SKALNÍKOVÁ
Department of Analytical Chemistry, Masaryk University, 611 37 Brno, Czech Republic

(*Received* 19 *February* 1992. *Revised* 10 *June* 1992. *Accepted* 10 *June* 1992)

Summary—Silicagel Separon SGX C18 (particle size 7 μm) was suitable for the preconcentration of 2–20 μg of Pt from 0.1*M* hydrochloric acid in the presence of cationic surfactants especially dimethyllaurylbenzylammonium bromide, with subsequent elution with 96% ethanol. The recovery was 86–110% for 2 μg of Pt. The sample matrix corresponding to 2.5 g of average plant ash does not interfere. The final emission spectrometry of platinum was carried out in 15 A dc-arc at Pt I 265.942 nm in the presence of Au as internal standard (Au I 267.595 nm). RSD was 6.3% in average.

The environmental platinum is often due to platinum dust coming from industrial and vehicles' catalyzers. Platinum contents of 37–680 μg Pt/kg were detected in roadside dust on dried plants.[1] Isolated samples of dried plants contained platinum levels of 100–830 μg/kg.[1] Among suitable methods for the determination of platinum the classical emission spectrometry,[2,3] the flame AAS,[4] ETA–AAS[4] or ICP–OES[5] were commonly used.[5] The absolute detection limits are reported to be usually 100 ng of Pt for the classical emission spectrometry[3] and the flame AAS,[4] 0.75 ng of Pt for ETA–AAS[4] or 30 ng of Pt for ICP–OES.[5] Thus, a preconcentration of platinum and its separation from the matrix is necessary when biologic samples are analysed.

Sufficiently low limits of detection can be achieved by using classical emission spectroscopy.

In this paper the simple preconcentration of platinum in the form of platinum(IV)–chlorocomplexes[7] with cationic surfactant on Separon SGX C18 column is used in combination with dc-arc-emission spectroscopy as detection. In this way the detection limit dropped to 10^{-7}% Pt for model samples.

EXPERIMENTAL

Instruments

Spectrograph PGS-2 of Carl Zeiss, Jena, supplied by two gratings, *i.e.*, with 651 lines/mm, blaze angle at 320 nm and reciprocal linear dispersion 0.737 nm/mm in the 1st order, or 1302 lines/mm, blaze angle 265 nm and reciprocate linear dispersion 0.184 nm/mm respectively if used in the 2nd order. A three-lens system with a 5-mm intermediate projection diaphragm was used, the entrance slit was 0.020 mm, the distance between carbon electrodes was 3 mm.

A UBI-1 generator of RFT supplying 15 A dc-arc was used. Carbon electrodes SU 326, SU 304 or SW 304 (carrier), SU 202 (counter electrode as cathode) and graphite powder SU 602 were used, all of Elektrokarbon Topolciany, CSFR.

Exposed photographic plates ORWO WU 2 and WU 3 (Germany) were evaluated on microphotometer MD-100, Zeiss with slit area 0.1 × 15 mm and under 20 times magnification using the P-transformation of characteristic curve and filters with 10% T(internal standard) or 100% T(platinum line).

AAS spectrometer Perkin–Elmer 306 with 10 cm burner, acetylene-air flames with flow rates 22.5 l./min for air and 1.4 l./min for acetylene. Hollow cathode lamp with Pt line 265.942 nm at 30 mA.

Membrane pump MP 2501 was from Laborinstruments Prague with stainless and teflon® fittings.

Chemicals

Standard solutions. Platinum solution (0.326 mg/ml) was prepared by dissolving the metal in *aqua regia* (1 + 9). $AuCl_3$ was prepared with 5.3 mg/ml Au in hydrochloric acid

*Author for correspondence.

(1 + 9). $ZrOCl_2$ was prepared in 1*M* hydrochloric acid with 3.0 mg/ml Zr and GeO_2 in water with 1.075 mg of Ge.

Brij 35 (Merck, Darmstadt). A 2.5% stock solution was used.

Butyltriphenylphosphonium bromide (BTPP). Recrystallized from ethanol.

Cetyltrimethylammonium bromide (CTMA) (Lachema Co., Brno).

Cetylpyridinium bromide (CPB) (Lachema, Brno).

Dimethyllaurylbenzylammonium bromide (Sterinol). 10% Aqueous solution (Galenius Co., Warsaw).

All other chemicals were of analytical grade quality. Matrix model solution: 2.6 g/l. Na (NaCl), 12.0 g/l. Ca ($CaCl_2$), 19.2 g/l. K (KCl), 3.6 g/l. Mg ($MgCl_2$), 1.0 g/l. Fe ($FeCl_3$) and 0.5 g/l. Al ($AlCl_3$) in 0.1*M* HCl. A 1-ml aliquot of such solutions corresponds to 0.1 g of average plant ash or 6.7 g of average plant material.[8]

Glass chromatographic columns 3 × 30 mm of Tessek Co., Prague filled with Separon SGX C18, particle size 7 μm.

RESULTS AND DISCUSSION

Determination of platinum with emission spectroscopy

For determination of platinum the line Pt I 265.942 nm and internal standards with Au I 267.595 nm, Ge I 265.1178 nm and Zr I 267.8636 nm were tested. Sodium carbonate was used as spectral buffer and Brij 35R as wetting agent.

Procedure for calibration. A 2-ml portion of 2.5% Brij 35R, 1 ml of 2.5% sodium carbonate and solutions containing 0–100 μg of Pt, 25μg of Au or 300 μg of Ge or 1000 μg of Zr were pipetted into 1 g of graphite powder in a Teflon® dish, the solution evaporated under an infra-red lamp, the residue thoroughly mixed and filled into carbon electrodes. Excited in 15 A dc-arc and exposed for 120 sec through the graduated gray filter onto plates WU 3 (grating 651 lines/mm) or WU 2 (grating 1302 lines/mm).

Sample procedure. Pipette 0.5 ml of 2.5% Brij 35R, solutions with 6.25 μg of Au, 75 μg of Ge or 250 μg of Zr, 0.25 ml of 2.5% sodium carbonate and a portion of the sample eluate in *aqua regia* into 0.25 g graphite powder in a Teflon® crucible and continue as above.

Best results were obtained when Au was used as internal standard. Using increased spectral resolution, one component of the structured background lies under the platinum line and interferes. Thus, in spite of steeper calibration plots for larger spectral resolution, the detection limit of 0.8 μg Pt/g graphite powder (0.1 μg of Pt in the electrode for determination) was identical in both cases and the grating with 651 lines/mm was observed as fully satisfactory. Some resulting data are collected in Table 1.

Preconcentration of platinum on dynamically modified Separon SGX C18

The column was initially washed with 30 ml of 70% ethanol and 100 ml of water and treated with 5 ml of aqueous solution of quarternary salt (0.33 ml/min) containing 1m*M* BTPP, 1m*M* CPB, 12.5m*M* CTMA or 2.7m*M* Sterinol. A 50-ml solution containing 20 μg of Pt in 0.1*M* hydrochloric acid and 1m*M* BTPP, 1m*M* CPB, 12.5m*M* CTMA or 2.7m*M* Sterinol passed through the column. The elution from the column followed with 70, 85 or 96% ethanol. The flow rate for the sorption and desorption

Table 1. Some parameters of the emission spectroscopy of platinum (Pt I 265.942 nm)

Internal standard	Reciprocal linear dispersion (nm/mm)	Slope of calibration plot*	Correlation† coefficient	RSD‡ %
Au I 267.595 nm	0.74	0.57	0.984	6.3
Ge I 265.118 nm	0.74	0.61	0.982	6.8
Zr I 267.863 nm	0.74	0.51	0.959	11.9
Au I 267.595 nm	0.18	0.89	0.989	7.8
Ge I 265.118 nm	0.18	0.95	0.981	8.1
Zr I 267.863 nm	0.18	0.83	0.975	9.8

*$P = f(\log c)$ in μg Pt/g graphite powder.

†Calibration plot between 2–100 μg Pt/g graphite powder.

‡Relative standard deviation for 30 μg Pt/g graphite powder and reciprocal linear dispersion 0.742 nm/mm or 10 μg Pt/g graphite powder and reciprocal linear dispersion 0.18 nm/mm.

Table 2. Effect of surfactants on the retention of platinum (20 μg) on Separon SGX C18 from 0.1*M* hydrochloric acid.

Surfactant	Surfactant concentration used, *m*M	Retained Pt (%)	Recovery (%)	Ethanol as eluent
BTPP	1	53	40	75%
CTAB	12.5	80	80–90	75, 85%
CPB	1	»95	86–100	85, 96%
Sterinol	2.7	»95	90–100	85, 96%

being limited by the available column pressure was 0.33 ml/min.

The behaviour of platinum on the sorbents was followed by AAS at Pt 265.942 nm in acetylene-air flames with flow rates 22.5 l./min for air and 1.4 l./min for acetylene respectively (Perkin-Elmer AAS, model 306). The determination limit was 3 μg Pt/ml.

In the presence of BTPP the sorption of platinum (20 μg of Pt) from 50 ml was poor and took place from 53% only and 40% of the total platinum amount was eluted with the first 5-ml fraction of 75% ethanol.

With CTMA the last three 10-ml fractions contained an average of 1.3 μg of Pt which is 6.5% of the total amount applied onto the column. The platinum elution resulted in the first two 5-ml fractions of 75% ethanol.

The sorbent was most effective in the presence of 1m*M* CPB or 2.7m*M* Sterinol and sorbed 20 μg of Pt from 50 ml of 0.1*M* hydrochloric acid quantitatively. Unfortunately 10–15 ml of 85 or 96% ethanol was necessary for the elution of platinum from the column covered by CPB, whereas in the presence of Sterinol the quantitative elution of Pt was already in the first ml of 96% ethanol and the recovery for 20 μg of Pt was 86–100%. Identical results were also obtained from 0.01*M* hydrochloric acid and 2.7m*M* Sterinol. Some results are given in Table 2.

Matrix effects were examined similarly but the solution with 20 μg of platinum in 0.1*M* hydrochloric acid and the quarternary salt in concentrations as above contained 5 or 25 ml of matrix model solution corresponding to 33.5 or 167.5 g of dry average plant material in the total volume of 50 ml. The eluate was evaporated with 0.25 g of powdered graphite. This represents approximately 10^{-7}% Pt in solution corresponding to 167.5 g of dry plant material, if the detection limit of 0.2 μg of Pt for 0.25 g of graphite is assumed.

From the 12.5m*M* CTMA solution with 5 ml of matrix model solution the recovery of platinum was 70–80% but 40% only in the presence of 25 ml of model matrix solution if eluted with 10 ml of 85% ethanol. Moreover the recovery of 2 μg of Pt in 50 ml was 20% only. For 1m*M* CPB and 20 μg of Pt in 50 ml the recoveries were 70–80% in the presence of 5 ml or 65% respectively in the presence of 25 ml of matrix model solution. The recovery of 2 μg of Pt was 50% only. A 10–15 ml amount of 85 or 96% ethanol was necessary for the elution of platinum from the column. Most suitable results were again observed with Sterinol (2.7m*M*). The recovery of even 2 μg of Pt in 50 ml was 100% in the presence of 25 ml of matrix model solution and the elution with 1 ml of 96% ethanol was satisfactory. Results are collected in Table 3.

Glycole–polymethacrylate gels such as Spheron DEAE 1000 (particle size 0.063–0.1 mm, Lachema INC, Brno) as anion exchanger showed no advantage against modified silicagel. Under similar conditions platinum was sorbed in more than 95% (flow rate 0.5 ml/min) from 0.1*M* hydrochloric acid but the recovery of platinum with 3 ml of 0.1*M* hydrochloric acid and 2*M* perchloric acid was 85% only.

The advantage of proposed method is in its high separation selectivity for platinum from accompanying main components of biological material. From the sample matrix, platinum(IV) chloro-complexes are retained only. The sorption of matrix macrocomponents such as aluminium or iron on Separon SGX C18 was

Table 3. Recoveries of minor platinum concentration from matrix model solution

Surfactant	Recovery		
	20 μg Pt for 5 ml*	2 μg Pt for 25 ml†	20 μg Pt for 25 ml†
CTAB	70–80%	20%	40%
CPB	70–80%	50%	65%
Sterinol	100%	100%	100%

*In the presence of 5 ml of matrix model solution (see the text).

†In the presence of 25 ml of matrix model solution.

not observed in contrast to anion exchanger Spheron DEAE 1000. The retention of platinum by Separon SGX C18 takes place from non-aggressive media of 0.1*M* hydrochloric acid and its elution with 85 or 96% ethanol respectively into small (1 ml) volumes of eluent is fast and quantitative. In this way the corrosion of stainless parts of membrane pumps is hindered which is not the case when using 2*M* perchloric acid as eluent from Spheron DEAE 1000.

Acknowledgement—Thanks are due to Professor L. Sommer for his deep interest and valuable comments.

REFERENCES

1. Platinum, Environmental Health Criteria 125, World Health Organization, Geneva, 1991.
2. S. I. Ginzburg, *Analytical Chemistry of Platinum Metal*, pp. 337, 338. Nauka, Moskva, 1972.
3. F. E. Beamisch, *The Analytical Chemistry of the Noble Metals*, pp. 487–500. Pergamon Press.
4. J. E. Cantle, *Atomic Absorption Spectrometry*, pp. 48, 366, 367. Amsterdam, 1982.
5. Anonym: ICP-Spectrometer Plasma II. Perkin Elmer Co., Norwalk 1990.
6. S. Kallmann, *Talanta*, 1987, **34**, 677.
7. F. Vlačil, I. Vinš, O. Malíček, *Collect. Czech. Chem. Commun.*, 1983, **48**, 2225.
8. N. G. Zirin, A. I. Obuchov, *Emission Spectroscopy of Soils, Plants and Other Biological Objects* pp. 184–185. Moscow University Publishing House, 1977.

Talanta, Vol. 40, No. 2, pp. 225–230, 1993
Printed in Great Britain.

0039-9140/93 $6.00 + 0.00

SIMULTANEOUS DETERMINATION OF WARFARIN AND BROMADIOLONE BY DERIVATIVE SYNCHRONOUS FLUORESCENCE SPECTROMETRY

S. PANADERO, A. GÓMEZ-HENS and D. PÉREZ-BENDITO

Department of Analytical Chemistry, Faculty of Sciences, University of Córdoba, E-14004 Córdoba, Spain

(*Received* 13 *April* 1992. *Revised* 12 *June* 1992. *Accepted* 12 *June* 1992)

Summary—By using second derivative synchronous fluorescence spectrometry the simple resolution of mixtures of the anticoagulant rodenticides warfarin and bromadiolone in the presence of β-cyclodextrin is accomplished, which causes a differential effect on the fluorescence intensity of these compounds. The determination method developed is simple, fast and inexpensive; in addition, measurements are performed in a single scan. Mixtures of warfarin and bromadiolone in ratios between 4:1 and 1:10 were satisfactorily resolved.

Warfarin[3-(3-oxo-1-phenylbutyl)-4-hydroxycoumarin] and bromadiolone{3-[3-(4-bromodiphenyl-4-yl)-3-hydroxy-1-phenylpropyl]-4-hydroxycoumarin} are two coumarin-based anticoagulants used as rodenticides. They impair blood coagulation, leading to hemorrhage as the ultimate cause of death. Warfarin is also extensively used as a clinically effective oral anticoagulant in man; on the other hand, bromadiolone has a much higher acute oral toxicity, so it is only used as a rodenticide. The interest on the determination of these compounds lies in the poisoning hazards for no-target animals owing to their toxicity to all mammals.

Because of their similar spectral features, the determination of these compounds in mixtures has so far been carried out by liquid chromatography[1–3] with fluorimetric detection. However, there are other approaches which allow the simple determination of compounds with overlapped spectra without prior separation. Synchronous spectrofluorimetry offers improved selectivity over conventional spectrofluorimetry thanks to the narrower spectral bandwidth, which in turn depends on the chosen $\Delta\lambda$ value (viz. the wavelength difference between emission and excitation monochromators). Also, derivative synthronous fluorescence spectrometry[4] has proved a highly useful analytical technique[5,6] for the direct resolution of mixtures of different compounds of clinical, biochemical and pharmaceutical interest.

Because the emission spectra of warfarin and bromadiolone are completely overlapped, direct use of derivative synchronous fluorescence spectrometry for their simultaneous determination is obviously precluded. We were thus to seek an alternative way of distinguishing the two compounds and found β-cyclodextrin to increase their fluorescence intensity to a different extent.

Cyclodextrins are reportedly interesting organized systems in terms of fluorescence and room-temperature phosphorescence of use for the determination of organic compounds.[7–10] Because of the internal cavity of these compounds, luminescent molecules can form stable inclusion complexes provided they fit in the cavities. The formation of these complexes is thus reliant on chemical and geometrical factors. The chief practical consequence of this association is that the luminescent molecules are isolated from the environment, so any quenching effects are avoided and their luminescence is enhanced. The inclusion complex of β-cyclodextrin with a coumarin (coumarin C540A) was previously studied[11] and β-cyclodextrin was used to improve the determination of warfarin by circular dichroism[12] and fluorimetry.[10] However, the differential effect of β-cyclodextrin on the fluorescent features of warfarin and bromadiolone is dealt with for the first time in this paper. The combination of this effect and derivative synchronous fluorescence spectrometry allowed the simple resolution of mixtures of these two compounds.

EXPERIMENTAL

Reagents

Stock warfarin and bromadiolone solutions (0.1 mg/ml) were prepared from warfarin (Aldrich) and bromadiolone (Chem. Ser.), respectively, in 0.1*N* sodium hydroxide, and stored at 0–4°. More dilute solutions of both were prepared daily by dilution with distilled water. A β-cyclodextrin solution, $10^{-2}M$, was prepared by dissolving β-cyclodextrin (Aldrich) in distilled water. A borate buffer of pH 9.5 was made from 0.1*M* boric acid and 0.4*M* sodium hydroxide. Reagent-grade chemicals and pure solvents were used throughout.

Apparatus

A Perkin–Elmer MPF-43A fluorescence spectrometer furnished with 1-cm quartz cells and a xenon source was used for fluorescence measurements. The cell compartment was thermostated by circulating water at 25° through it. A spectral band-pass of 8 nm was set for the excitation and emission monochromators. For synchronous fluorescence mesurements, both monochromators were interlocked and scanned simultaneously at 2 nm/sec. Derivative spectra were recorded by electronic differentiation of the signal from a Perkin–Elmer H 200-0507 derivative accessory. Of the six differential time constants available through the mode switch, position 6 was selected for all measurements. The spectrofluorimeter response (time constant) was set to 3 sec. A series of fluorescence polymer samples was used daily to adjust the spectrofluorimeter to compensate for changes in source intensity. A Perkin-Elmer LS-50 luminescence spectrometer controlled via a Hewlett-Packard Vectra computer, running the "Galactic" application program was used to obtain the contour plots.

Procedure

To a sample solution containing warfarin and bromadiolone in a final concentration range between 0.2 and 3.5 μg/ml of each were added 7 ml of $10^{-2}M$ β-cyclodextrin and 1 ml of 0.1*M* borate buffer (pH 9.5). The mixture was made up to 10 ml in a standard flask with distilled water. The second-derivative synchronous fluorescence spectrum was recorded by scanning both monochromators simultaneously while keeping an 85-nm constant difference between their wavelengths ($\Delta\lambda$). The excitation monochromator was scanned from 215 to 375 nm and the emission monochromator from 300 to 460 nm. The instrumental parameters were set as stated above. The second derivative peak-to-peak measurements[13] are given as the relative fluorescence intensity and expressed as ΔI. The derivative signal obtained at 348 nm (ΔI_1) was directly proportional to the bromadiolone concentration and the measurement obtained between 403 and 430 nm (ΔI_{2+3}) resulted from the contribution of both warfarin and bromadiolone. The difference between the total ΔI_{2+3} and ΔI_2, which can be ascribed to the bromadiolone concentration and was determined from a previously constructed calibration plot (ΔI_2 *vs.* bromadiolone concentration) is thus directly related to the warfarin concentration (ΔI_3).

RESULTS AND DISCUSSION

Optimization of variables

The emission spectra obtained in the absence of β-cyclodextrin are completely overlapped and have equal fluorescence intensity (Fig. 1). However, in the presence of β-cyclodextrin, the fluorescence of both compounds substantially enhanced and that of warfarin is higher than the fluorescence of bromadiolone. Both spectra remained stable for at least two hours, but they were also strongly overlapped, so that simultaneous determination of these compounds by conventional spectrofluorimetry was clearly

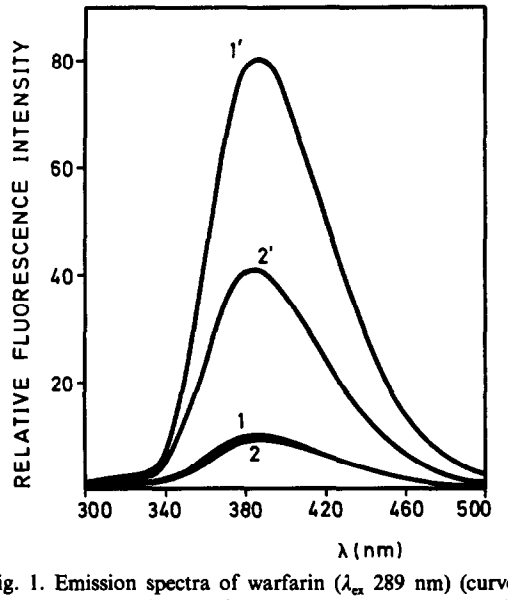

Fig. 1. Emission spectra of warfarin (λ_{ex} 289 nm) (curves 1,1') and bromadiolone (λ_{ex} 278 nm) (curves 2,2') in the absence (curves 1,2) and presence (curves 1,2') of β-cyclodextrin. [warfarin] = [bromadiolone] = 1 μg/ml.

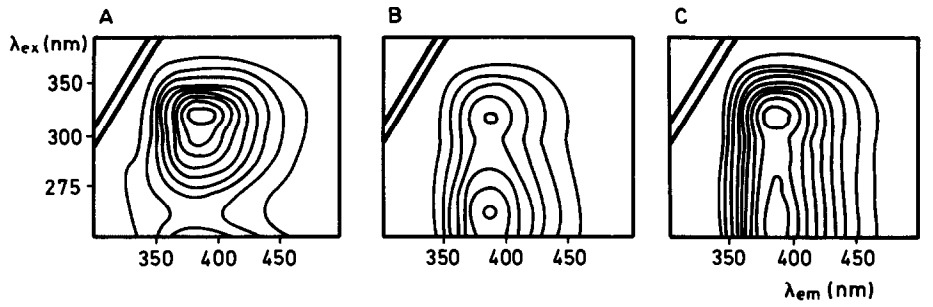

Fig. 2. Contour plots of warfarin (A), bromadiolone (B) and a mixture of both (C). Analyte concentrations as Fig. 1.

unfeasible and a different approach, such as synchronous spectrofluorimetry, was required for this purpose.

A simple way of determining the best $\Delta\lambda$ value for the resolution of a mixture by synchronous spectrofluorimetry involves obtaining the contour plots of the individual components and the mixture. These graphs allow one to choose the best synchronous trajectory to follow in order to avoid spectral overlap. Figure 2 shows these spectra for warfarin, bromadiolone and a mixture of both. As can be seen, warfarin yields a peak that overlaps with one of the two peaks of bromadiolone, so the resolution of this mixture by synchronous spectrofluorimetry is also unfeasible. This is quite apparent from Fig. 3, which shows the overlapped synchronous spectra obtained for the two compounds at $\Delta\lambda = 85$ nm, which according to the contour plots appears to be an appropriate path to use as it passes near the maxima of both compounds with no loss of sensitivity.

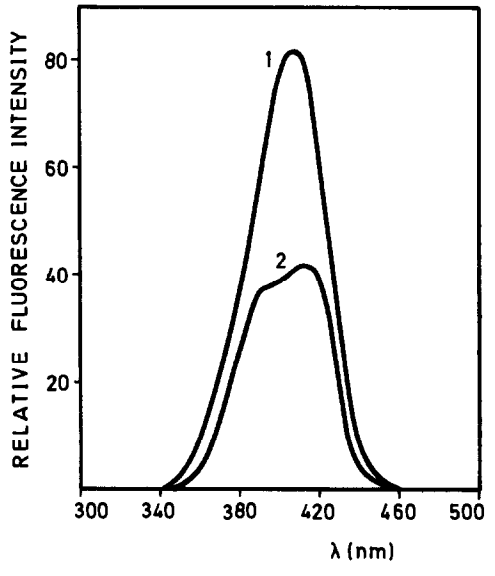

Fig. 3. Synchronous flourescence spectra of warfarin (curve 1) and bromadiolone (curve 2). $\Delta\lambda = 85$ nm. Analyte concentrations as Fig. 1.

In the event of strongly overlapped synchronous fluorescence spectra, as is the case with warfarin and bromadiolone, the technique calls for the additional resolution capability offered by derivative fluorescence spectrometry. Figure 4(A) shows the first-derivative synchronous fluorescence spectra obtained for warfarin, bromadiolone and a mixture of both. The signal obtained between the minimum at 390 nm and the maximum at 418 nm corresponds to the additive contribution of warfarin and bromadiolone, while the small shoulder at 356 nm is due to bromadiolone only. Although this approach could be used to resolve the mixture, the measurements at 356 nm might be inadequately precise. The second-derivative synchronous fluorescence spectra obtained for these compounds and a mixture of both [Fig. 4(B)] show that the bromadiolone concentration is correlated with the signal obtained at 348 nm (ΔI_1) and that the signal between the minimum at 403 nm and the maximum at 430 nm (peak-to-peak measurements) (ΔI_{2+3}) corresponds to the additive contribution of both compounds.

Because the signal-to-noise ratio (SNR) degrades as the derivative order is increased, we compared the SNR values obtained from the first- and second-derivative synchronous spectra. When electronic differentiation was used, the signal was derived with respect to time rather than the wavelength ($dI/d\lambda = dI/dt \times 1/c$, c being the wavelength scanning speed, which was kept constant during the scan), so all variables including the time factor markedly affected the SNR obtained. It was experimentally found that, in using electronic differentiation, the signal obtained from the second-derivative spectrum was higher than that from the first-derivative spectrum, the difference

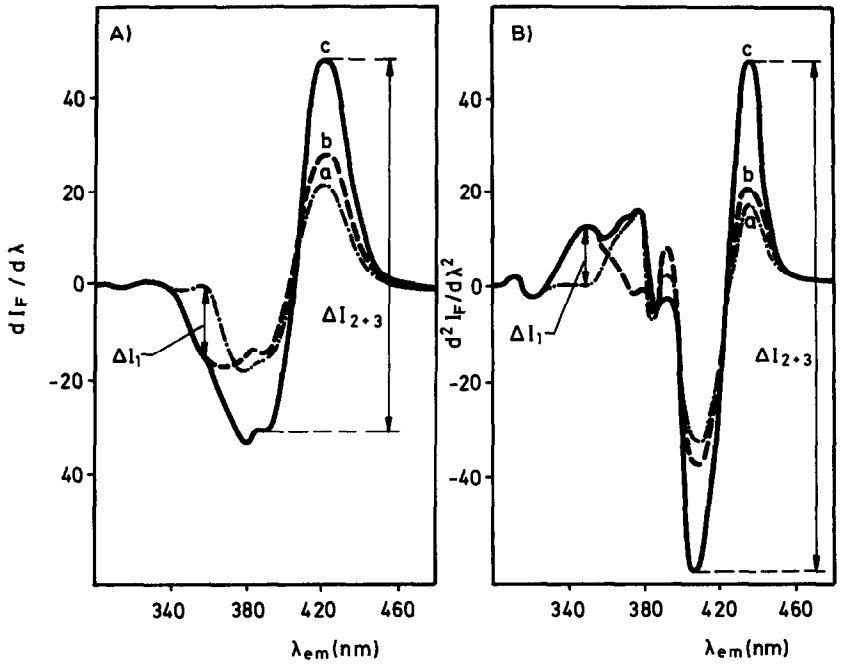

Fig. 4. First- (A) and second-derivative synchronous fluorescence spectra (B) of bromadiolone (curve a), warfarin (curve b) and a mixture of both (curve c). $\Delta\lambda$ = 85 nm. Wavelength scanning speed = 2 nm/sec. Analyte concentrations as Fig. 1.

increasing with increasing wavelength scanning speed.[14] At a scanning speed of 2 nm/sec noise increased from the first- to the second-derivative spectrum by about 30%, however, as the signal obtained from this spectrum was higher, the resulting SNR was only about 10% smaller. This led us to choose the second- instead of the first-derivative spectrum to resolve the warfarin–bromadiolone mixture, thus avoiding the potentially poor precision of the measurements made at 356 nm on the first-derivative spectrum.

Experimental variables were optimized according to the following criteria: 1) the fluorescent signal ΔI_1 should not depend on the warfarin concentration, 2) the fluorescence signal ΔI_{2+3} should be additive for the warfarin and bromadiolone concentrations, and 3) the fluorescence signal of each compound should be as tall as possible.

Instrumental variables ($\Delta\lambda$, wavelength scanning speed, differentiation constant, spectrofluorimeter time constant and slit widths) have a critical effect on the sensitivity and selectivity of the determination as they affect both the resolution and the signal because they modify the wavelength ranges and the number and relative intensity of the peaks making up the derivative synchronous fluorescence spectrum.

Figure 5 reflects the marked dependence of the second-derivative synchronous fluorescence spectra on the chosen $\Delta\lambda$ value. This variable affects the shape of these spectra, which show bathochromic shifts as $\Delta\lambda$ increases, and the ΔI value obtained. The resolution of the warfarin–bromadiolone mixture is only possible when $\Delta\lambda$ is in the range 80–90 nm, where ΔI_1 only depends on the bromadiolone concentration and ΔI_{2+3} is additive for the warfarin and bromadiolone concentrations. $\Delta\lambda$ value of 85 nm was thus chosen.

The shape of the derivative synchronous fluorescence spectra is also affected by the wavelength scanning rate, as it determines the dI/dt value obtained from the electronic differentiation accessory. This variable was studied in the range 0.5–8 nm/sec, and SNR was found to increase with increase in the scanning speed. However, it was impossible to use a high scanning speed because the signal ΔI_{2+3} was not additive for the warfarin and bromadiolone concentrations, so that a speed of 2 nm/sec was eventually chosen. The study of the effect of the differentiation constant showed that the optimization criteria were met at the minimum response speed (mode 6). The shape of the spectra did not change appreciably with the spectrofluorimeter time constant (0.3, 1.5 and 3.0 sec), but the spectra were cleaner when 3 sec

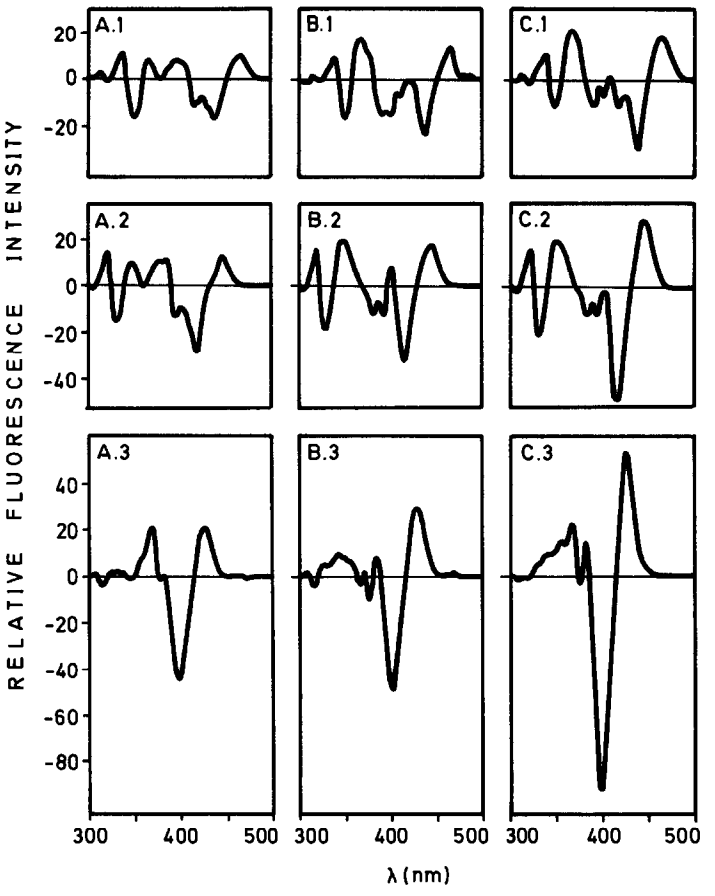

Fig. 5. Effect of $\Delta\lambda$ on the second-derivative synchronous fluorescence spectra of warfarin (A), bromadiolone (B) and a mixture of both (C). (1) 120 nm, (2) 100 nm, (3) 80 nm.

was used. From the different slit widths of the excitation and emission monochromators tested, a width of 8 nm for both monochromators was found to provide acceptable results.

The chemical and physico-chemical variables only affect the sensitivity of the method as they only alter the analytical signal (ΔI). The study of the effect of α- and β-cyclodextrin on the fluorescence of warfarin and bromadiolone showed this compound to raise the fluorescence of both compounds. On increasing the β-cyclodextrin concentration between 10^{-3} and $10^{-2}M$ the fluorescence intensity of both warfarin and bromadiolone increased; however, the effect was virtually negligible above a $8 \times 10^{-3}M$ concentration.

As shown elsewhere,[10] the fluorescence intensity of warfarin in the presence of β-cyclodextrin is constant over the pH range 6.8–11.0. We found the fluorescence intensity of bromadiolone in the presence of β-cyclodextrin to behave similarly towards pH, so we assayed two different buffers (boric acid–borate and ammonium–ammonia) and obtained the same fluorescence intensities. Also, the borate buffer concentrations assayed (5.0×10^{-3}–$2.5 \times 10^{-2}M$) were found to have no effect on this parameter. Decreasing the dielectric constant of the solutions by adding ethanol had no effect on the ΔI_{2+3} signal, but resulted in a loss of correlation between ΔI_1 and the bromadiolone concentration. The spectra were virtually independent of the temperature over the range 25–50°, so this was not a critical factor in choosing the best experimental conditions.

Features of the proposed methods

The main analytical features of the individual methods developed for warfarin and bromadiolone by using second-derivative synchronous fluorescence spectrometry are summarized in Table 1. The detection limits were calculated according to the IUPAC recommendation.[15] The detection limit for warfarin is similar to that achieved by conventional spectrofluorimetry.[9] This can be ascribed to the fact that even though the noise in the second-derivative synchronous spectrum is higher than that in the conventional

Table 1. Features of the individual determination of warfarin and bromadiolone

	Bromadiolone ΔI_1	Bromadiolone ΔI_{2+3}	Warfarin ΔI_{2+3}
Linear range ($\mu g/ml$)	0.5–6.0	0.2–3.5	0.2–3.5
Pearson correlation coefficient (r)	0.999	0.999	0.999
Detection limit	0.1	0.05	0.05
Precision*			
(1 μg/ml)	2.8	2.7	2.7
(3 μg/ml)	1.3	1.7	1.8

*% RSD ($P = 0.05$, $n = 11$).

spectrum, the signal obtained in the former by using electronic differentiation and the optimum instrumental variables is higher than that obtained in the conventional spectrum, so a small degradation of the SNR is the sole loss to be expected from using the second-derivative synchronous spectrum. The relative standard deviation obtained at two different concentrations (1 and 3 μg/ml) of both analytes was less than 3%. A brief study of the selectivity of these methods showed that other rodenticides such as dicoumarol and diphacinone are tolerated at the same concentration levels as warfarin and bromadiolone.

Simultaneous determination of warfarin and bromadiolone

Table 2 summarizes the results obtained in the resolution of synthetic mixtures of warfarin and bromadiolone by second-derivative synchronous fluorescence spectrometry. The determination was carried out in a single scan by using the calibration graphs obtained for each component. Mixtures of warfarin and bromadiolone in ratios between 4:1 and 1:10 were resolved.

Table 2. Determination of warfarin and bromadiolone in their mixtures

Warfarin/ bromadiolone ratio	Warfarin, $\mu g/ml$		Bromadiolone, $\mu g/ml$	
	Taken	Found*	Taken	Found*
4:1	0.80	0.76	0.20	0.18
2:1	2.00	1.90	1.00	1.04
2:1	1.00	0.95	0.50	0.50
1:1	1.00	0.96	1.00	1.05
1:2	0.25	0.25	0.50	0.48
1:2	0.50	0.54	1.00	1.00
1:2	1.00	0.94	2.00	1.95
1:3	1.00	1.04	3.00	2.88
1:4	0.50	0.48	2.00	2.00
1:8	0.50	0.50	1.60	1.64
1:10	0.20	0.21	2.00	2.00

*Average of three determinations.

The proposed method described could be applied to the analysis of animal tissues in cases of suspected poisoning. Liver is usually the most useful sample for diagnostic analysis; however, as it is a very complex matrix, previous extraction and clean-up processes would be required. Using liquid chromatography for the resolution of mixtures of coumarin anticoagulant rodenticides including warfarin and bromadiolone in animal tissues,[1-3] entails extraction into a chloroform–acetone mixture of ethanol and clear-up of the extracts by gel permeation chromatography or solid-phase extraction with silica columns. Similar separation procedures could be used before the derivative synchronous fluorimetric technique is applied for mixture resolution. The main advantages of the proposed method compared to chromatographic procedures, which call for dedicated and expensive instrumentation as well as, usually, elution gradient, are its great simplicity and low cost. All the synchronous technique requires is a simple switch for simultaneously scanning both monochromators, while the derivative technique can be implemented by incorporating a straightforward electronic accessory (electronic differentiation) or using computer software (numerical differentiation) to obtain derivative spectra.

Acknowledgements—CICyT is gratefully acknowledged for financial support.

REFERENCES

1. K. Hunter, *J. Chromatogr.*, 1983, **270**, 267.
2. K. Hunter, *ibid.*, 1983, **270**, 277.
3. W. Langseth and U. Nymoen, *J. Anal. Chem.*, 1991, **339**, 249.
4. P. John and I. Soutar, *Anal. Chem.*, 1976, **48**, 520.
5. S. Rubio, A. Gómez-Hens and M. Valcárcel, *Talanta*, 1986, **33**, 633.
6. P. Izquierdo, M. C. Gutiérrez, A. Gómez-Hens and D. Pérez-Bendito, *Anal. Lett.*, 1990, **23**, 487.
7. S. Scypinski and L. J. Cline Love, *Anal. Chem.*, 1984, **56**, 322.
8. A. M. Alak and T. Vo-Dinh, *ibid.*, 1988, **60**, 596.
9. O. Jules, S. Scypinski and L. J. Cline Love, *Anal. Chim. Acta*, 1985, **169**, 355.
10. J. C. Márquez, M. Hernández and F. García Sánchez, *Analyst*, 1990, **115**, 1003.
11. S. Scypinski and J. M. Drake, *J. Phys. Chem.*, 1985, **89**, 2432.
12. Y. Sato and Y. Suzuki, *Chem. Pharm. Bull.*, 1985, **33**, 4606.
13. T. C. O'Haver, *Clin. Chem.*, 1979, **25**, 1548.
14. C. Gutiérrez, S. Rubio, A. Gómez-Hens and M. Valcárcel, *Anal. Chem.*, 1987, **59**, 769.
15. G. L. Long and J. Winefordner, *ibid.*, 1983, **55**, 712A.

Talanta, Vol. 40, No. 2, pp. 231–235, 1993
Printed in Great Britain.

0039-9140/93 $6.00 + 0.00

SOLVENT EXTRACTION OF 8-QUINOLINOLATO–IRON(III) WITH THE AID OF VARIOUS PHENOLS AS HYDROGEN-BONDING DONORS

SHOICHI KATSUTA and NOBUO SUZUKI*
Department of Chemistry, Faculty of Science, Tohoku University, Sendai 980, Japan

(*Received* 26 *May* 1992. *Accepted* 16 *June* 1992)

Summary—Effect of various phenols (ArOH) on the solvent extraction of iron(III) with 8-quinolinol (HQ) has been investigated. Greatly enhanced extraction is found in the presence of ArOH, *e.g.*, the distribution ratio of iron(III) with HQ in carbon tetrachloride is increased 200,000-fold by 0.10*M* 3,5-dichlorophenol. From extraction equilibrium analysis, the enhanced extraction has been ascribed to the formation of association complexes of neutral iron(III) 8-quinolinolate (FeQ_3) with ArOH as $FeQ_3 \cdot n$ArOH (n = 1, 2, 3) in the organic phase, and the association constants ($\beta_{ass,n}$) have been determined. A linear relation is observed between logarithmic values of $\beta_{ass,n}$ and the acid-dissociation constant of ArOH. Existence of the hydrogen bond between FeQ_3 and ArOH is clearly shown by infrared spectroscopy.

While chelate extraction has been studied in depth, little attention has been paid to the role of hydrogen bond interaction between organic proton donors and metal chelates. The authors have recently discovered that halogenated phenols strongly interact with metal acetylacetonates through hydrogen bonding in organic solvents, and enhance the extraction of various metal ions with acetylacetone.[1–6] This novel enhancement effect of phenols as proton donors on the chelate extraction should be analytically important because it is expected to show quite different selectivity from the well-known synergistic enhancement effect of electron donors such as tributyl phosphate and trioctylphosphine oxide.[4–6] However, the effect of phenols has only been examined for the systems using acetylacetone and trifluoroacetylacetone[6] as chelating extractants. Further investigations concerning other chelating extractants are desired.

8-Quinolinol is one of the most familiar and widely used chelating extractants. In this paper, the effect of phenols on the extraction of iron(III) with 8-quinolinol is investigated. The extraction equilibria are analysed in detail, and the interaction between iron(III) 8-quinolinolate [tris(8-quinolinolato)iron(III)] and phenols is quantitatively evaluated. The existence of hydrogen bonding is examined by means of infrared (IR) spectroscopy.

*Author for correspondence.

EXPERIMENTAL

Reagents

The radioactive iron(III) solution labelled with ^{59}Fe was prepared as described previously.[4] 8-Quinolinol (Wako Pure Chemical) was recrystallized from ethanol and dried *in vacuo*. 3,5-Dichlorophenol (Wako Pure Chemical) was purified by vacuum sublimation at 35°. 4-Fluorophenol, 4-chlorophenol, 2,3-dichlorophenol, 2,6-dichlorophenol, 2,3-dimethylphenol, and 3,5-dimethylphenol (more than 97–99% purity, Aldrich or Tokyo Kasei) were used as obtained. Tris(8-quinolinolato)iron(III) was synthesied in the usual way, recrystallized from benzene–hexane and dried *in vacuo*, and its identity was established by elemental analysis. The organic solvents used were of spectroscopic grade. Water was doubly distilled. Other reagents used were of analytical grade.

Procedure

An aqueous solution of 1.0×10^{-6}–$1.0 \times 10^{-5}M$ radioactive iron(III) (5 ml) was placed in a 30-ml extraction vial together with an equal volume of an organic solution of $1.0 \times 10^{-2}M$ 8-quinolinol and $1.5 \times 10^{-4} - 2.0 \times 10^{-1}M$ phenol. The vial was mechanically shaken for 5–60 min at 330 strokes/min at 25°. After centrifugation, the equal-volume aliquots of both phases were pipetted out and their γ-activity was measured separately with an NaI(Tl) well-type scintillation counter. The distribution ratio

of iron(III) (D) was calculated as the radioactivity ratio. The pH of the aqueous phase was adjusted with 0.04–0.10M perchloric acid and measured with a glass electrode immediately after shaking. The ionic strength was maintained at 0.10 with perchloric acid and sodium perchlorate.

The distribution of 8-quinolinol, 4-fluorophenol and 4-chlorophenol between carbon tetrachloride and 0.10M sodium perchlorate was also investigated. The organic phase containing these compounds (1.0×10^{-4}–$8.3 \times 10^{-2}M$) was shaken with the aqueous phase for 15 min at 25°. The distribution ratio was determined by measuring the absorbance of the organic phase at 320 nm (8-quinolinol) or 289 nm (phenols) before and after shaking.

IR spectra of 0.10M 3,5-dichlorophenol and a mixture of 0.10M 3,5-dichlorophenol and 0.016M tris (8-quinolinolato)iron(III) in carbon tetrachloride were measured with Jasco IR-810 spectrophotometer using a cell with potassium bromide windows (layer thickness 0.1 mm) against air.

RESULTS AND DISCUSSION

The distribution ratio of iron(III) was independent of the shaking time (5–60 min) and the initial metal concentration (1.0×10^{-6}–$1.0 \times 10^{-5}M$). The recovery of radioactivity from the two phases was always confirmed to be quantitative.

In Fig. 1, the extraction of iron(III) with a mixture of 8-quinolinol (0.010M) and 3,5-dichlorophenol (0.050 or 0.10M) in carbon tetrachloride is shown as plots of log D *vs.* pH together with the extraction with 8-quinolinol alone. Greatly enhanced extraction is found in the presence of 3,5-dichlorophenol: in the whole pH region studied, the distribution ratio is increased 20,000- and 200,000-fold by 0.050 and 0.10M 3,5-dichlorophenol, respectively. This enhancement effect is much larger than that of the phenol on the extraction of iron(III) with acetylacetone previously reported.[4] The synergistic effect of the electron donor, tributyl phosphate (0.050M), was also examined on the extraction of iron(III) with 8-quinolinol, but no effect was observed.

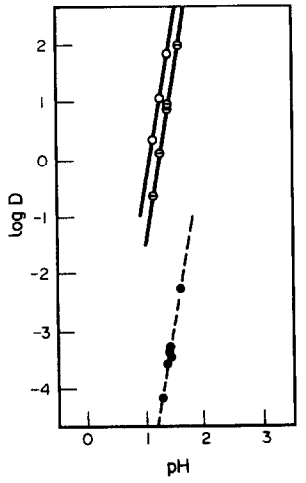

Fig. 1. Extraction of iron(III) with 8-quinolinol in carbon tetrachloride in the presence of 3,5-dichlorophenol. Initial phenol concentration in the organic phase (C_{ArOH}/M): (●) 0; (⊖) 0.050; (○) 0.10. Initial 8-quinolinol concentration in the organic phase (C_{HQ}/M): 0.010.

Table 1. Effect of various phenols (0.050M) on the extraction of iron(III) with 8-quinolinol (0.010M) in carbon tetrachloride at pH 1.40

Phenol	log D	log(D/D_0)*
4-Fluorophenol	−1.89	1.53
4-Chlorophenol	−0.72	2.70
2,3-Dichlorophenol	−2.06	1.36
2,6-Dichlorophenol	−2.86	0.56
3,5-Dichlorophenol	0.87	4.29
2,3-Dimethylphenol	−2.42	1.00
3,5-Dimethylphenol	−1.76	1.66

*D_0: Distribution ratio of iron(III) with 8-quinolinol alone; log $D_0 = -3.42$.

Table 1 shows the effect of various phenols (0.050M) on the extraction of iron(III) with 8-quinolinol (0.010M) in carbon tetrachloride at pH 1.40. All the phenols exert the enhancement effect, which increases in the following order: 2,6-dichlorophenol < 2,3-dimethylphenol < 2,3-dichlorophenol < 4-fluorophenol < 3,5-dimethylphenol < 4-chlorophenol < 3,5-dichlorophenol. The effect of 3,5-dichlorophenol is conspicuously large in the investigated phenols. The enhancement effect seems to be smaller when a chlorine atom or methyl group is present at the *ortho*-position of the phenol.

Table 2 shows the enhancement effect of 3,5-dichlorophenol (0.050M) on the extraction of iron(III) with 8-quinolinol (0.010M) in several organic solvents. The enhancement effect is remarkably influenced by the solvents and increases in the following order: chloroform < carbon tetrachloride < heptane. This solvent order is the same as that observed in the conventional synergistic extraction systems, *e.g.*, Zn(II)–thenoyltrifluoroacetone–tributyl phosphate system.[7,8] The solvent effect in the chelate extraction including the synergistic extraction has been throughly investigated.[7–11] It is striking that the inert solvents such as carbon

Table 2. Enhancement effect of 3,5-dichlorophenol (0.050*M*) on the extraction of iron(III) with 8-quinolinol (0.010*M*) in several organic solvents

Solvent	pH	log D_0^*	log D	log(D/D_0)
Chloroform	1.15	−2.05	−0.28	1.77
	1.25	−1.45	0.31	1.76
	1.40	−0.68	1.01	1.69
Carbon	1.14	†	−0.66	
tetrachloride	1.26	−4.2	0.08	4.3
	1.40	−3.42	0.87	4.29
	1.60	−2.28	1.99	4.27
Heptane	1.37	†	0.02	
	1.60	†	1.08	
	1.76	−4.2	1.58	5.8

*D_0: Distribution ratio of iron(III) with 8-quinolinol alone.
†The distribution ratio was too low to determine.

tetrachloride and heptane, which barely extract iron(III) with 8-quinolinol alone, can quantitatively extract iron(III) in the presence of 3,5-dichlorophenol.

Equilibrium analysis

Equilibrium analysis was carried out for the extraction of iron(III) with 8-quinolinol in carbon tetrachloride in the presence of 4-fluorophenol, 4-chlorophenol, and 3,5-dichlorophenol. The distribution ratio (D_0) of iron(III) with 8-quinolinol (HQ) alone can be expressed as

$$D_0 = \frac{\overline{[FeQ_3]}}{[Fe^{3+}] + \Sigma[FeQ_j^{(3-j)+}]} = \frac{K_{ex} P_{HQ}^3 [Q^-]^3}{K_{HQ}^3 (1 + \Sigma \beta_j [Q^-]^j)} \quad (1)$$

where the bar over the species denotes the organic phase, K_{ex} is the extraction constant defined as $[\overline{FeQ_3}][H^+]^3[Fe^{3+}]^{-1}[\overline{HQ}]^{-3}$, β_j is the overall stability constant of $FeQ_j^{(3-j)+}$ in the aqueous phase, and P_{HQ} and K_{HQ} are the partition coefficient and acid-dissociation constant of the neutral 8-quinolinol, respectively. In a region where the concentration of Q^- is low enough, the chelate species in the aqueous phase can be neglected, and equation (1) is then rewritten as

$$D_0 = \frac{\overline{[FeQ_3]}}{[Fe^{3+}]} = \frac{K_{ex} P_{HQ}^3 [Q^-]^3}{K_{HQ}^3}. \quad (2)$$

The equilibrium concentration of 8-quinolinolate anion Q^- in the aqueous phase is calculated from the following equation:

$$[Q^-] = \frac{C_{HQ} K_{HQ}}{[H^+](P_{HQ} + 1 + [H^+]/K_{H_2Q} + K_{HQ}/[H^+])}, \quad (3)$$

where C_{HQ} represents the initial concentration of 8-quinolinol, and K_{H_2Q} the acid-dissociation constant of the protonated 8-quinolinol H_2Q^+.

The P_{HQ}, K_{H_2Q} and K_{HQ} values were determined in the present study by investigating the distribution ratio of 8-quinolinol as a function of pH, *i.e.*, log $P_{HQ} = 2.02$, p$K_{H_2Q} = 5.03$, and p$K_{HQ} = 9.66$. These values are in good agreement with the literature values.[12,13]

In Fig. 2, a plot of log D_0 *vs.* log[Q^-] is shown. The plot gives a straight line with a slope of 3.0 as is expected from equation (2). The log K_{ex} value was determined to be 3.25 by a linear least-squares method, on the basis of equation (2).

In the presence of phenols (ArOH), if the association of tris(8-quinolinolato)iron(III) (FeQ_3) with ArOH in the organic phase is assumed, the distribution ratio (D) can be expressed as follows:

$$D = \frac{\overline{[FeQ_3]} + \Sigma\overline{[FeQ_3 \cdot n\mathrm{ArOH}]}}{[Fe^{3+}]} = \frac{K_{ex} P_{HQ}^3 [Q^-]^3}{K_{HQ}^3}(1 + \Sigma \beta_{ass,n} [\overline{\mathrm{ArOH}}]^n), \quad (4)$$

where $FeQ_3 \cdot n$ArOH denotes the association complex, and $\beta_{ass,n}$ the overall association constant in the organic phase defined as $[\overline{FeQ_3 \cdot n\mathrm{ArOH}}][\overline{FeQ_3}]^{-1}[\overline{\mathrm{ArOH}}]^{-n}$.

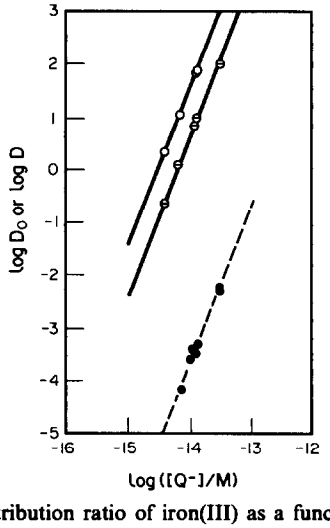

Fig. 2. Distribution ratio of iron(III) as a function of the equilibrium concentration of 8-quinolinolate anion in the aqueous phase. Organic solvent: carbon tetrachloride. C_{ArOH}/M: (●) 0; (⊖) 0.050; (○) 0.10. C_{HQ}/M: 0.010. pH: 1.1–1.6. The broken line indicates the calculated values from equation (2) and the solid lines from equation (4).

Figure 2 also shows plots of log D *vs.* log[Q^-] under the constant concentration of 3,5-dichlorophenol (0.050 and 0.10M). Each plot gives a straight line with a slope of 2.9, which is very close to the theoretical value 3 according to equation (4). This result indicates that the assumption leading to equation (4) is reasonable.

Dividing equation (4) by equation (2) gives

$$D/D_0 = 1 + \Sigma \beta_{ass,n}[\overline{ArOH}]^n. \quad (5)$$

Therefore, the enhancement of the extraction by phenols is quantitatively evaluated by the association constant. The association constants as well as the number of phenols in the association complexes can be obtained by analyzing the $\log(D/D_0)$ *vs.* $\log[\overline{ArOH}]$ plot according to equation (5).

The equilibrium concentration of phenols in the organic phase is calculated from the following equation:

$$[\overline{ArOH}] = \frac{C_{ArOH} P_{ArOH}}{P_{ArOH} + 1 + K_{ArOH}/[H^+]}, \quad (6)$$

where C_{ArOH}, P_{ArOH} and K_{ArOH} denote the initial concentration, partition coefficient and acid-dissociation constant of phenols, respectively. The P_{ArOH} values of 4-fluorophenol and 4-chlorophenol were determined in the present paper to be 0.555 ± 0.000 and 2.26 ± 0.06, respectively, given as the averages of data measured at 3 different phenol concentrations in the range 3.3×10^{-4}–$8.3 \times 10^{-2}M$; that of 3,5-dichlorophenol was previously determined[6] to be 11.6. The pK_{ArOH} values were reported to be 9.89 for 4-fluorophenol,[14] 9.37 for 4-chlorophenol, and 8.25 for 3,5-dichlorophenol.[15] The term $K_{ArOH}/[H^+]$ in equation (6) was practically negligible under the present pH conditions.

It should be pointed out that the equilibrium concentrations, [Q^-] and [$\overline{ArOH}$], can be affected if the mutual association between 8-quinolinol and phenols occurs. Previously, the association of acetylacetone with 3,5-dichlorophenol in the organic phase has been observed and quantitatively evaluated by the solvent extraction technique.[4,6] Therefore, the association of 8-quinolinol with the phenols was investigated in a similar manner, *i.e.*, by determining the distribution ratio of 8-quinolinol as a function of the phenol concentration in the organic phase. The distribution ratio of 8-quinolinol did not change in the presence of 4-fluorophenol and 4-chlorophenol, which indicates no association of 8-quinolinol with these phenols. On the other hand, 3,5-dichlorophenol somewhat enhanced the distribution ratio of 8-quinolinol, and the formation of 1 : 1 association complex of 8-quinolinol with 3,5-dichlorophenol in carbon tetrachloride was indicated. However, its association constant, determined to be 5.01, was relatively small. Consequently, the HQ-ArOH association could be neglected in the calculation of [Q^-] and [$\overline{ArOH}$] under the present pH conditions, 1.1–1.6, where most of 8-quinolinol exists in the aqueous phase as the protonated species.

In each phenol system, the D/D_0 was rapidly increased with an increase in [$\overline{ArOH}$]. The $\log(D/D_0)$ *vs.* $\log[\overline{ArOH}]$ plot for 3,5-dichlorophenol was an almost straight line with a slope of 3 in the higher concentration region of the phenol. In other phenol systems, although no such limiting slope could be observed, the slopes of the plots went up to higher than 2 at high concentrations of the phenols. These results indicate that the maximum number of phenol molecules able to associate with one molecule of tris(8-quinolinolato)iron(III) is 3, which is the same as that observed for the association of tris(acetylacetonato) complexes of scandium(III)[5] and iron(III)[4] with 3,5-dichlorophenol. The association constants were determined by a nonlinear least-squares method (SALS program, University of Tokyo) on the basis of equation (5), and are summarized in Table 3. Calculated D/D_0 values using these association constants were in good agreement with experimental values.

Very large association constants are obtained in the 3,5-dichlorophenol system. These values are larger than those of the association of tris(acetylacetonato)iron(III) with 3,5-

Table 3. Association constants of tris(8-quinolinolato)iron(III) with phenols in carbon tetrachloride at 25°

Phenol	$\log(\beta_{ass,1}/M^{-1})$	$\log(\beta_{ass,2}/M^{-2})$	$\log(\beta_{ass,3}/M^{-3})$
4-Fluorophenol	2.78	4.90	5.97
4-Chlorophenol	3.00	5.14	6.96
3,5-Dichlorophenol	3.55	6.00	8.32

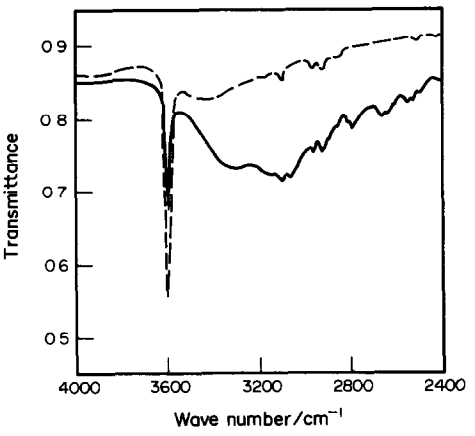

Fig. 3. IR absorption spectra in the O–H stretching vibration region of 0.10*M* 3,5-dichlorophenol (broken line) and a mixture of 0.10*M* 3,5-dichlorophenol and 0.016*M* tris(8-quinolinolato)iron(III) (solid line) in carbon tetrachloride.

dichlorophenol in carbon tetrachloride,[16] *i.e.*, $\log \beta_{ass,1} = 2.64$, $\log \beta_{ass,2} = 4.52$ and $\log \beta_{ass,3} = 5.73$.

The association constant is expected to correlate with the acid-dissociation constant of the phenols if the association is caused by hydrogen bonding of hydroxyl hydrogen of the phenols.[2,3] In a plot of the $\beta_{ass,n}$ ($n = 1$–3) values against the K_{ArOH} value of the phenols, either $\log \beta_{ass,n}$ value linearly increases with an increase in the $\log K_{ArOH}$ value as expected, which supports the existence of hydrogen bonding. Additionally, these linear relations will allow us to estimate the association constants of other various phenols from their K_{ArOH} values, except for *ortho*-substituted phenols. The *ortho*-substituted phenols should have the smaller association constants than expected from the linear plots because the substituents such as chlorine and methyl groups adjacent to the hydroxyl group may bring out the steric hindrance for the hydrogen bonding of the phenols to the chelate.[2,3]

More direct evidence for the hydrogen bonding can be obtained by IR spectroscopy. Figure 3 shows the IR absorption spectra in the O—H stretching vibration region of 3,5-dichlorophenol and a mixture of 3,5-dichlorophenol and tris(8-quinolinolato)iron (III) in carbon tetrachloride. By the addition of the chelate, the sharp band at 3600 cm^{-1} due to a free O—H of the phenol is reduced in intensity, and the broad band in the 3000–3500 cm^{-1} region due to a hydrogen-bonded O—H appears.[17] This is the first and definitive evidence for the hydrogen-bond acceptor ability of the 8-quinolinolato chelate. Since the only oxygen atom has a lone pair of electrons in the chelate, the hydroxyl hydrogen atom of the phenols probably interacts with the oxygen atom of the chelate. The maximum association number of the phenols, 3, is in agreement with the number of oxygen atoms in the chelate.

In conclusion, it was found that phenols form highly stable association complexes with iron(III) 8-quinolinolate through hydrogen bonding, and greatly enhance the extraction of iron(III) with 8-quinolinol. This study strongly suggests such the enhancement effect of phenols *via* chelate–phenol hydrogen bonding should be applicable to various chelate extraction systems.

REFERENCES

1. S. Katsuta, H. Imura and N. Suzuki, *Chem. Lett.*, 1991, 733.
2. H. Imura, S. Katsuta and N. Suzuki, *Polyhedron*, 1991, **10**, 1405.
3. S. Katsuta, H. Imura and N. Suzuki, *Bull. Chem. Soc. Jpn.*, 1991, **64**, 2470.
4. *Idem*, *J. Radioanal. Nucl. Chem.*, 1992, **157**, 255.
5. *Idem*, *Anal. Sci.*, 1991, **7**, 661.
6. S. Katsuta and N. Suzuki, *Talanta*, 1992, **39**, 849.
7. K. Akiba, N. Suzuki and T. Kanno, *Bull. Chem. Soc. Jpn.*, 1969, **42**, 2537.
8. S. Nakamura, H. Imura and N. Suzuki, *Inorg. Chim. Acta*, 1985, **109**, 157.
9. T. Omori, T. Wakahayashi, S. Oki and N. Suzuki, *J. Inorg. Nucl. Chem.*, 1964, **26**, 2265.
10. N. Suzuki and K. Akiba, *ibid.*, 1971, **33**, 1169.
11. N. Suzuki, J. Kodera and H. Imura, *Inorg. Chim. Acta*, 1987, **128**, 261.
12. J. Fresco and H. Freiser, *Anal. Chem.*, 1964, **36**, 631.
13. D. Dyrssen, *Svensk Kem. Tidskr.*, 1952, **64**, 213; *Chem. Abstr.*, 1952, **47**, 384h.
14. F. T. Crimmins, C. Dymek, M. Flood and W. F. O'Hala, *J. Phys. Chem.*, 1966, **70**, 931.
15. J. Drahonovsky and Z. Vacek, *Collect. Czech. Chem. Commun.*, 1971, **36**, 3431.
16. Unpublished data, determined by the method in Refs. 4–6.
17. E. F. H. Brittain, W. O. George and C. H. J. Wells, *Introduction to Molecular Spectroscopy Theory and Experiment*, p. 148. Academic Press, London, 1970.

Talanta, Vol. 40, No. 2, pp. 237–241, 1993
Printed in Great Britain.

0039-9140/93 $6.00 + 0.00

ION INTERACTION CHROMATOGRAPHY OF NITRILOTRIACETATOCOMPLEXES OF THE RARE EARTH ELEMENTS WITH POST-COLUMN REACTION DETECTION

ROKURO KURODA, TAKEHARU WADA, YOKO KOKUBO and KOICHI OGUMA
Laboratory for Analytical Chemistry, Faculty of Engineering, University of Chiba, Yayoi-cho, Chiba 263, Japan

(*Received* 17 *March* 1992. *Revised* 26 *June* 1992. *Accepted* 26 *June* 1992)

Summary—The chromatographic behaviour of nitrilotriacetatocomplexes of the rare earth elements (Sc, Y and lanthanides) on a reversed phase ODS column has been investigated in the presence of 1-octanesulphonate. There is a great difference in selectivity for the ODS among the rare earth nitrilotriacetatocomplexes. Concentration gradient elution with nitrilotriacetic acid (0.005–0.050*M*, pH 3.0) that contains 0.01*M* 1-octanesulphonate allows the rare earth elements to be separated from each other within 30 min at room temperature, except a Gd–Eu pair which is eluted together. Yttrium elutes at about 10 min between samarium and neodymium. Detection and quantitation of the rare earth elements can be achieved by post-column reaction with Chlorophosphonazo III in acid media at 700 nm.

Methods of separating the rare earth elements have been targets of investigation since their discovery. Increasing industrial utilization of the individual rare earth elements and their interest in geochemical roles have enhanced the development of methods for rapid, sensitive, selective determination of individual rare earth elements. Recent advances in the analytical methods for geological materials[1] and in analytical chromatography[2,3] have been reviewed. High performance liquid chromatography (HPLC) with polymer-based cation-exchange resins[4–9] and silica-based ion-exchangers[10–16] has been extensively used for the separation of individual rare earth elements with post-column reaction detectors. On account of the adjustable low ion-exchange capacity nature of ion-interaction chromatography (IIC) it gives more rapid, high resolution separation of the rare earths with gradient elution techniques.[17–25] α-Hydroxyisobutyric acid (HIBA) and lactic acid have been used most frequently as the complexing agent in the chromatographic modes above. One of the disadvantages of using HIBA or lactic acid is that the elution position of yttrium is very near to that of dysprosium or coincides with that of dysprosium.

Goetze and Bialkowski[26] separated the rare earth elements as anionic complexes with EDTA on a reversed phase C_{18} column with tetrahexylammonium chloride for the heavy rare earth group and tetrabutylammonium chloride for La, Nd, Pr and Sm. In this system independent runs are necessary for the heavy (Lu–Eu) and light (La–Sm) rare earth groups and Tb and Gd eluted together. Nitrilotriacetic acid has not been used as the complexing agent in conjunction with HPLC, although it received fairly wide acceptance as an eluting agent for rare earth separation.[27] However, its use was confined to production of large amounts of rare earth compounds.

In this work we report that on-column formation of nitrilotriacetatocomplexes of the rare earth elements in a reversed phase ODS column in the presence of 1-octanesulphonate will provide a high resolution chromatographic system for the separation of individual rare earth elements at room temperature.

EXPERIMENTAL

Apparatus

HPLC system consisted of a Hitachi L-6200 intelligent pump, a Rheodyne Model 7125 syringe loading valve with a 20-μl sample loop and a Hitachi L-4200 UV-VIS detector. Sample injection was made by a 10-μl microsyringe [MS-R25, Ito Co., Ltd., Shizuoka, Japan]. The detector output signal was fed into a Hitachi D-2500 Chromato-Integrator. For pumping the post-column reaction detection reagent,

Chlorophosphonazo III solution, a double plunger type of reciprocating pump [DMX-2300T, Sanuki Industry Co., Ltd., Tokyo] was used. The effluent and the post-column reagent were mixed via a low dead volume tee. The column was packed with ODS silica of 5-μm diameter (Hitachi ODS #3056, 150 × 4 mm i.d.) operated at 20°.

Reagents

All the chemicals used were of analytical reagent grade purity. Stock solutions of the rare earth elements were prepared from their oxides (99.9% purity, Wako Pure Chemical Industries Ltd., Osaka, Japan) to yield 0.1M metal solutions in 3M hydrochloric acid. These stock solutions were standardized by titration with EDTA–2Na using Xylenol Orange as a metal indicator. A mixed rare earth stock solution was 0.002M in each metal and 3M in hydrochloric acid. Sodium 1-octanesulphonate was obtained from Tokyo Kasei Kogyo Co., Ltd., Tokyo. Nitrilotriacetic acid (NTA, Dojindo Laboratories Co., Ltd., Kumamoto, purity >99%) was used for the preparation of eluent (0.005 to 0.05M). Chlorophosphonazo III [2,7-bis-(4-chloro-2-phosphonopheylazo)chromotropic acid, disodium salt] was used as post-column reaction detection reagent. A 0.0001M reagent solution in 0.05M hydrochloric acid was prepared and filtered through a 0.45-μm membrane filter before use.

Chromatographic separation and quantitation

Prior to the sample loading, the column was conditioned by passing 0.005M NTA–0.01M octanesulphonate solution (pH 3.0) for one hour. The mixed rare earths sample solution was prepared so that it contained 0.00005M of each rare earth and 0.01M octanesulphonate, the pH being adjusted to 3.0 with dilute ammonium hydroxide. A 10-μl volume of the prepared solution is loaded onto the column. A linear solvent program was run for the elution from 0.005–0.05M NTA(pH 3.0) usually over 25 min with the octanesulphonate concentration of 0.01M at a flow rate of 1 ml/min. A 0.0001M Chlorophosphonazo III–0.05M hydrochloric acid solution was delivered at a flow rate of 1 ml/min to join the effluent to achieve the post-column reaction detection at 700 nm. The calibration curves were constructed for each rare earth by plotting their concentrations against the peak area up to *ca.* 0.20, 0.23 and 0.26 mg/ml for La, Sm and Yb, respectively.

RESULTS AND DISCUSSION

In Fig. 1 the relationship between the retention time and NTA concentration is shown for La, Ce, Pr, Nd, Y, Dy, Lu and Sc, where 1-octanesulphonate and pH are kept constant at 0.01M and 3.0, respectively. As can be seen, the retention of the rare earth elements depends greatly on the NTA concentration and selectivity differences increase significantly with decreasing concentration of NTA. If concentration gradient elution is conducted, high resolution separation will be expected with low k' at higher NTA concentration, good separation factors (ratio of k' for two rare earth elements) and high plate number reflected by rapid mass transfer in IIC system. Hence, a linear NTA concentration gradient elution was attempted from 0.005 to 0.05M NTA with the gradient time of 15, 25 and 35 min. The chromatograms obtained for mixtures of La, Ce, Pr, Nd, Y, Sm, Eu, Gd, Tb, Dy, Ho, Er, Tm, Yb, Lu and Sc are illustrated in Fig. 2 for respective times. The Sc–NTA complex is not retained on the ODS coated with 1-octanesulphonate in this system, and exists as an anionic or neutral species, and its retention time coincides exactly with that of nitrate anion detected at the 301 nm characteristic

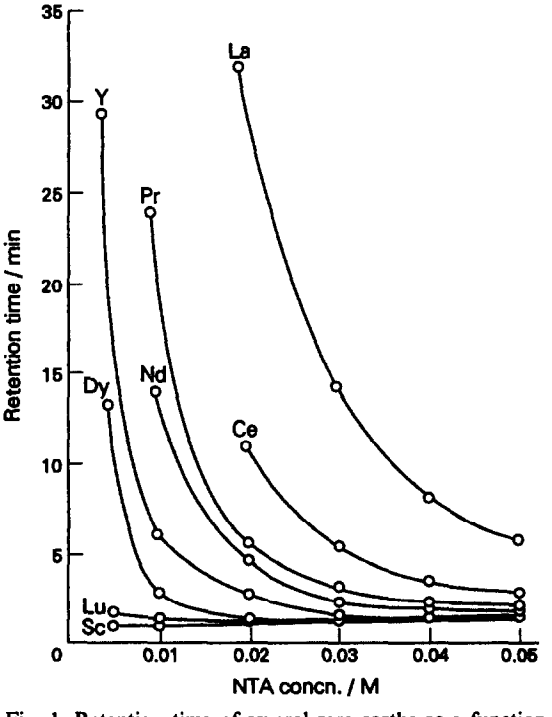

Fig. 1. Retention time of several rare earths as a function of NTA concentration (pH 3.0). Concentration of each rare earth: $5 \times 10^{-5}M$, 1-octanesulphonate concentration: 0.01M. Conducted at 20°.

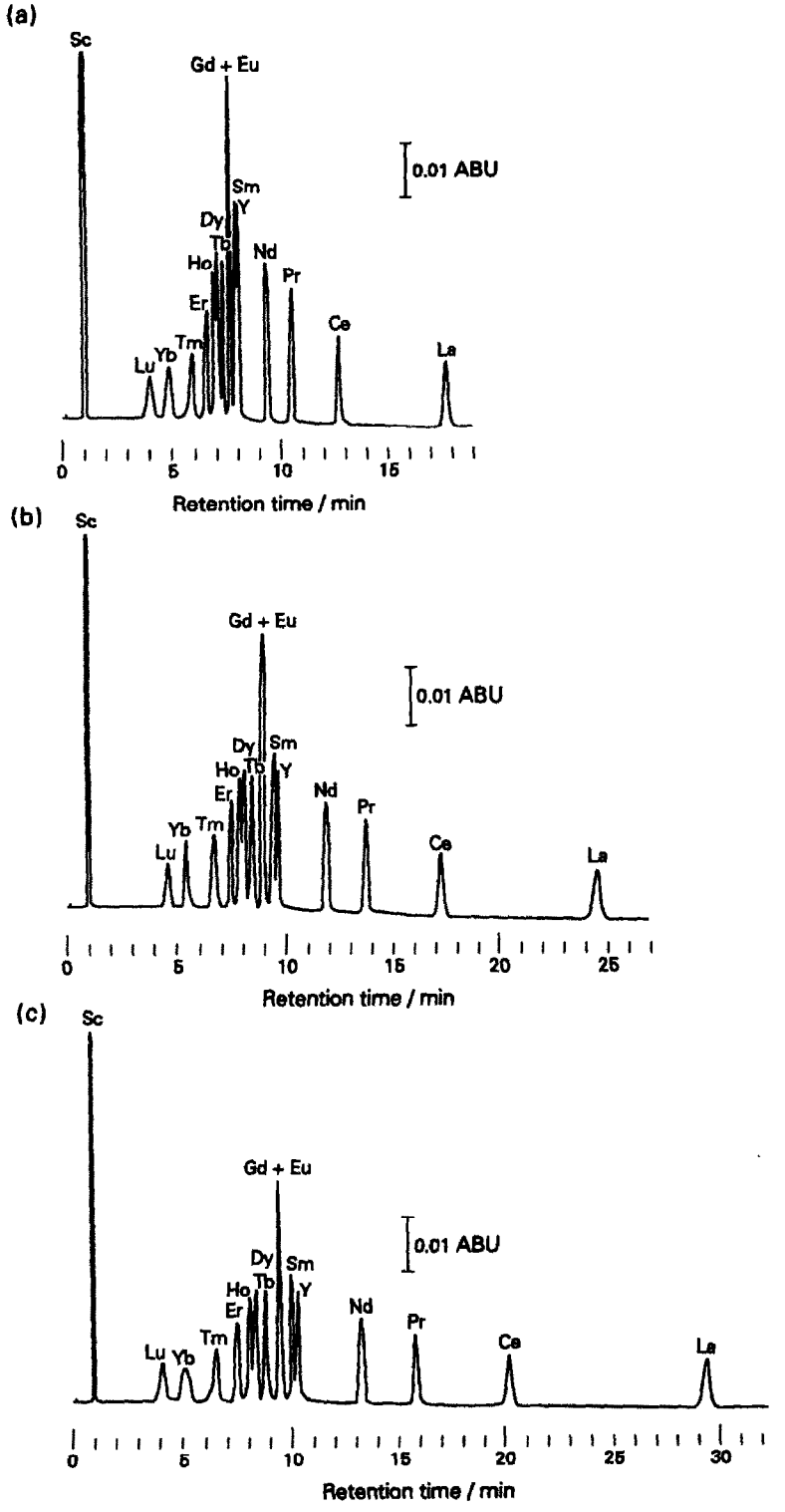

Fig. 2. Gradient elution runs. Concentration gradient elution run over 15, 25 and 35 min with 0.005–0.05*M* NTA (pH 3.0), 20°. Each rare earth concentration: $5 \times 10^{-5}M$. a: 15 min, b: 25 min, c: 35 min.

absorption band. With 25- and 35-min elution the adjacent rare earth elements can be resolved distinctly with the exception of the Eu–Gd pair. Y elutes between Sm and Nd, and this position is convenient for its detection and quantitation, because it usually behaves like heavy rare earth elements and often elutes together with Dy in most cation-exchange chromatography.

In this work 25-min elution was used for further study.

Since the hydrophobic ion, 1-octanesulphonate, interacts with the ODS, absorbs over its surface and controls the apparent ion-exchange capacity, its concentration in the mobile phase must affect the retention times of individual rare earth elements, *i.e.*, the speed of the chromatographic separations concerned. The effect of concentration of 1-octanesulphonate (0–0.03*M*) was thus examined on the retention time during the NTA gradient elution run, when the pH was kept at 3.0. The retention time increased rapidly with increasing concentration of 1-octanesulphonate, reaching a plateau at about 0.01*M* sulphonate for each rare earth. Its absence causes no retention of the rare earths on ODS. The concentration of 1-octanesulphonate exercises a great ion-exchange capacity function. Taking into consideration the selectivity differences, 0.01*M* concentration of 1-octanesulphonate was used.

The effect of pH of the eluent on retention was then tested. The retention times of some representative rare earth elements examined decreased with increasing pH values in the range 2.5–5.0. However, since lighter rare earth elements exhibit high retention times at pH 5 and selectivity differences are not profound as compared to those caused by NTA concentration changes, pH gradient elution would yield inferior results to concentration gradients both in terms of separation time and peak resolution, if it were tried. We used pH 3.0 as a safe value for use of ODS.

One of the factors which control the concentration of hydrophobic ion on the ODS surface is the presence of nonionic molecules such as methanol and acetonitrile in the mobile phase, which compete for the absorption sites on the ODS. The effect of methanol concentration on the retention time of NTA complexes was such that the retention of the complexes decreases with increasing methanol concentration. Methanol concentration gradient elution may be feasible, but increased viscosity of the methanolic mixed solvent media requires increasing the pressure applied to the chromatographic system. Therefore, only an aqueous eluent system was examined in the present study.

The present system provides an excellent medium particularly for the separation of adjacent La–Ce–Pr–Nd–Y–Sm–(Eu,Gd)–Tb–Dy–Ho–Er–Tm–Yb–Lu on a single run at room temperature; Eu–Gd pair is eluted together.

The mobile phase typically includes a complexing agent that can interfere with the post-column reaction detection of the rare earth elements. Commonly used colorimetric reagents for the rare earths are 4-(2-pyridylazo)-resorcinol, Xylenol Orange, Alizarin Red S, Arsenazo I and Arsenazo III,[2] but these reagents are not satisfactory to use in the presence of NTA, because of high stabilities of rare earth-NTA complexes with the conditions for their color development. Hence, Chlorophosphonazo III[28] was selected as the post-column reaction reagent, since it reacts with the rare earth elements in acid media. To avoid the reagent blank contributing to base line drift, detection was made at 700 nm where the detection sensitivity was somewhat lowered, but a stable constant base line level was guaranteed, as seen in Fig. 2.

The calibration curves were constructed for La, Sm and Tb by plotting the peak area against their concentration. The curves for La, Sm and Yb were linear up to 0.20, 0.23 and 0.26 mg/ml, respectively. Detection limits taken as corresponding to S/N ratio 3 are 77, 18 and 80 ng/ml, respectively, for La, Sm and Yb.

In the present IIC system the rare earth elements are introduced into the ODS column as simple ions, not the NTA complexes; the complexes are formed on the column from NTA in the eluent. If prepared complexes are loaded, peaks of early eluted heavy rare earths broaden, split (for Tb) and deteriorate the resolution, depending highly on the excess concentration of NTA. The system may provide an on-column derivatization ion-interaction chromatography for the rare earth elements.

REFERENCES

1. C. J. Kantipuly and A. D. Westland, *Talanta*, 1988, **35**, 1.
2. K. Robards, S. Clarke and E. Patsalides, *Analyst[London]*, 1988, **113**, 1757.
3. R. Kuroda, *Hyomen*, 1991, **29**, 240.
4. G. Zhao, S. Luo, S. Yao and S. Yu, *Bunseki Kagaku*, 1982, **31**, 63.
5. K. Yoshida and H. Haraguchi, *Anal. Chem.*, 1984, **56**, 2580.
6. M. Li, Y. Li and J. Feng, *J. Radioanal. Nucl. Chem.*, 1988, **123**, 613.
7. Y. Takata and G. Muto, *Bunseki Kagaku*, 1989, **38**, 293.
8. M. Vobecky, *J. Chromatogr.*, 1989, **478**, 446.
9. P. Dufek, M. Vobecky, J. Holik and J. Valášek, *ibid.*, 1988, **435**, 249.
10. S. Elchuk and R. M. Cassidy, *Anal. Chem.*, 1979, **51**, 1434.

11. J.-M. Hwang, J.-S. Shih, Y.-C. Yeh and S.-C. Wu, *Analyst[London]*, 1981, **106**, 869.
12. W.-N. Wang, Y.-J. Chen and M.-T. Wu, *ibid.*, 1984, **109**, 281.
13. A. Mazzucotelli, A. Dadone, R. Frache and F. Baffi, *J. Chromatogr.*, 1985, **349**, 137.
14. J. A. Tielrooy, J. C. Kraak, F. J. M. J. Maessen, *Anal. Chim. Acta*, 1985, **176**, 161.
15. J. A. Tielrooy, P. H. M. Vleeschhouwer, J. C. Kraak and F. J. M. J. Maessen, *Anal. Chim. Acta*, 1988, **207**, 149.
16. C. Tong, Z. Shan and P. Zhu, *Chromatographia*, 1989, **27**, 316.
17. C. H. Knight, R. M. Cassidy, B. M. Recoskie and L. M. Green, *Anal. Chem.*, 1984, **56**, 474.
18. R. M. Cassidy, S. Elchuk, N. L. Elliot, L. W. Green, C. H. Knight and R. M. Recoskie, *ibid.*, 1986, **58**, 1181.
19. D. J. Barkley, M. Blanchette, R. M. Cassidy and S. Elchuk, *ibid.*, 1986, **58**, 2222.
20. R. M. Cassidy, F. C. Miller, C. H. Knight, J. C. Roddick and R. W. Sullivan, *ibid.*, 1986, **58**, 1389.
21. R. M. Cassidy and C. Chauvel, *Chem. Geol.*, 1989, **74**, 189.
22. V. Kuban, L. Sommer and D. B. Gladilovich, *Zh. Anal. Chem.*, 1989, **335**, 588.
23. M. Adachi, K. Oguma and R. Kuroda, *Chromatographia*, 1990, **29**, 579.
24. R. Kuroda, M. Adachi, K. Oguma and Y. Sato, *ibid.*, 1990, **30**, 263.
25. R. Kuroda, T. Wada, G. Kishimoto and K. Oguma, *ibid.*, 1991, **32**, 65.
26. H.-J. Götze and D. Bialkowski, *Z. Anal. Chem.*, 1986, **323**, 350.
27. M. Marhol, *Ion Exchangers in Analytical Chemistry. Their Properties and Use in Inorganic Chemistry*, Elsevier, Amsterdam, Oxford, New York, 1982.
28. Z. Marczenko, *Separation and Spectrophotometric Determination of Elements*, p. 472. Ellis Horwood, Chichester, 1986.

Talanta, Vol. 40, No. 2, pp. 243–246, 1993
Printed in Great Britain.

0039-9140/93 $6.00 + 0.00

THE INVESTIGATION OF COMPLEX FORMATION EQUILIBRIA AT CONSTANT IONIC STRENGTH

G. ANDEREGG
Laboratorium für Anorganische Chemie, Eidgenössische Technische Hochschule, CH 8092 Zürich, Switzerland

(*Received* 17 *February* 1992. *Revised* 19 *June* 1992. *Accepted* 19 *June* 1992)

Summary—The inert salts used for the investigations of complex formation are briefly discussed in relation to the effects of their ions on the equilibria studied. In general, some association with the inert salt ions cannot be completely avoided. In case of very stable complexes measured at low ionic strength, their effects can be quantified even though they are not caused by the anion if NO_3^- or ClO_4^- are used. In the case of weak complexes, when ionic strengths $I \geq 1$ are used, the concentration of the complex of interest can be 1000 times lower than that of the associates of the same cation with the anion of the inert salt causing difficulties with the investigation of the latter systems. If the experimental results for K_1 of the alkaline-earth metal ions with fluoride in sodium perchlorate and sodium nitrate are correct, as their equilibrium constants have very similar values, it follows that the behavior of two anions is very similar. However, if NO_3^- associates with the above cations, as found, the same behavior is expected for ClO_4^-. A more accurate analysis can only be done if activity coefficients in these solutions are known.

The large volume of stability constant data of metal complexes ML_n in aqueous solution, expressed here for simplicity as K_n and β_n, reported in the last 40 years were obtained using a constant ionic medium in which an inert salt, *i.e.*, a supporting background electrolyte,[1] was introduced to adjust the ionic strength of the medium. This procedure was sometimes criticized because the components of the salt used (AX) are not inert but intervene in the investigated processes as reacting species. This was recently observed by Štulíková.[2] As the cation and the anion of the inert salt and the species studied M and L are charged species, electrostatic interactions with the ions of the inert salt with formation of associates are always possible, these can be either ion-pairs or complexes such as MX, AL and MLX. In a similar way the associate AX could be formed from the components of the inert salt especially at $I \geq 1$ as discussed, for sodium nitrate solutions. These interactions are particularly important in the investigation of weak complexes because the concentrations of the associates with the anion of the inert salt can be equal to or larger than those of the complexes investigated. The equilibrium constants obtained in the presence of an inert salt are concentration quotients as the corresponding activity coefficients are given the value one. With respect to the thermodynamic constants, the concentration quotients can also be considered as being thermodynamic, where the standard state is not pure water but the solution of the inert salt. The ionic strength I is calculated with the expression $I = 1/2\Sigma c_i z_i^2$, in which the sum is extended to all ions c_i present in solution, the concentration normally expressed in molarity (M) or molality (mol/Kg = m) and z_i is the electrical charge of the corresponding species. In the latter case this should be mentioned in order to avoid confusion (see Table 1). The most suitable salts for this purpose are those of univalent cations and anions since the above interactions are much weaker with respect to the case of ions of higher charge. Alkali metal cations and anions such as ClO_4^-, NO_3^-, ClO_3^-, *etc.* and the halide ions, whose conjugate acid should be strong, are used. If the hydrolysis of a metal ion is investigated, sodium perchlorate seems, for instance, to be the inert salt of first choice, because generally ClO_4^- is among the anions forming the weakest complexes. Nevertheless, the list of cations which interact with this anion is quite considerable. Thus, in the case of polyaminopolycarboxylates such as EDTA the above salt is not appropriate because of the formation of the sodium EDTA complex.[3] For this reason a potassium salt was used, but not the perchlorate because of its low solubility. Potassium chloride and nitrate were used and

Table 1. Log K_1 values for the equilibrium: $M^{2+} + F^- \rightleftharpoons MF^+$ at 25°, obtained with fluoride electrode measurements. The K_{18} values at I in molarity scale* are in dm³/mol or else in Kg/mol

Medium†	I [M $(NO_3)_2$]	Mg^{2+}	Ca^{2+}	Sr^{2+}	Ba^{2+}	Ref.
1*M* ($NaClO_4$)	0.09–0.3	1.318 (±0.020)	0.633 (±0.030)	0.146 (±0.035)	−0.222 (±0.230)	7
1*M* ($NaClO_4$)	0.03–0.15	1.380 (±0.019)	0.531 (±0.100)	0.114 (±0.050)	−0.155 (±0.155)	8
1 m ($NaNO_3$)	0.03–0.6	1.318 (±0.004)	0.568 (±0.011)	−0.027 (±0.025)	−0.377 (±0.050)	9
1 m ($NaNO_3$)	0.15–0.9	1.352 (±0.035)	0.682 (±0.023)	0.137 (±0.024)	−0.174 (±0.053)	10
1*M* (Na)NO_3	0.03–0.3	1.31 (±0.03)				11

*The conversion of log K_1 from the molarity to the molality scale[12] is done by substracting either 0.021 ($NaClO_4$) or 0.014 ($NaNO_3$) from each value in 1*M* medium and, for the opposite conversion, ($NaNO_3$) 0.020 is added to the data in molarity scale.

†Parentheses are used if the measurements are made at the given ionic strength reached by addition of the inert salt stated. The constant concentration of the substance or ion stated is given without parentheses.

the preference for the latter is due to its ability to form complexes which are weaker than those with Cl^-. The use of potassium chloride between 1940–1950 can be explained by the fact that its aqueous solution is normally present in the reference calomel (or AgCl) electrode. By using the same solution in the test cell it is possible to eliminate the diffusion potential, which is often the origin of erroneous potentiometric measurements. Perchlorate solutions during the measurements, in the presence of ligands such as 2,2′-bipyridyl, 1,10-phenanthroline or pyridine derivatives, cause the precipitation of insoluble (complex) salts. In the case of Pd(II) and the above ligands nitrate or chlorate were then preferred. The equilibria with Tl^{3+} had to be investigated potentiometrically in 1*M* perchloric acid and, in order to avoid the diffusion potential, a bridge with the same acid was prepared. A calomel reference electrode in 0.99*M* perchloric acid and 0.01*M* hydrochloric acid can be used.

In recent years inert salts containing organic cations with a very low tendency for complex formation were introduced: $N(CH_3)_4Cl$, $N(CH_3)_4NO_3$, $N(C_2H_5)_4ClO_4$, ..., but we have no corresponding substitutes for the anions. It is evident that the choice of a given salt is always the result of a compromise among several possibilities in relation to the system investigated. By using a given inert salt the equilibrium constants obtained refer to the standard state chosen and the species studied such as M, L, and ML_n can contain a variable number of medium components. Their relative concentrations are not affected by the equilibrium investigated and only their sum can be determined. For instance, the concentration of ML, obtained at a given I value attained with AX, is the sum of concentrations of all species

$$\sum_{i=0}\sum_{m=0}\sum_{n=0} [ML(H_2O)_iA_mX_n]$$

containing M and L in the ratio 1:1 and variable quantities of other components of the medium. Similar sums are valid for all complexes as well as for M and L. In order to obtain exact values for the equilibrium constants it is important that the concentrations of the species investigated are negligible with respect to those of the inert salt thus causing a minimal variation of the ionic strength I. This ensures that, when titrating the solution, the activity coefficients of the species studied remain practically constant. The value of the concentration quotient K_1 normally given in the literature corresponds to that obtained directly without corrections for the different species appearing in the three sums for ML, M and L. If K_1 has to be corrected for the presence of an A^+ complex, we have to obtain the corresponding constant in the same medium. The trivial case of different ML species with $n = m = 0$ in the above sum differing in the number of coordinated H_2O molecules and in the structure of ML in equilibrium is also possible and the concentrations of the ML species cannot be separately determined by potentiometric measurements.[4] In principle for a given ligand, for instance EDTA, we have the possible formation of species between A^+ and L^{4-}, HL^{3-}, *etc.* Among such species only those with the unprotonated ligand seem to be normally important as expected for electrostatic reasons because of its larger negative charge. Complex formation by a ligand is often accompanied by a pH decrease in the solution of the protonated ligand in the presence of a cation under study such as A^+. This is shown[3] by the decrease of the pK of HL^{3-} from 10.44 in 0.1 [$(CH_3)_4NCl$] to 10.24 in 0.1 (KNO_3), whereas the pK of H_2L^{2-} is the same in both media. While discussing this change, we have to realize that two different effects are operative and causing the variation of the pK of HL^{3-}: (a) change in the complexing cation of the inert salt

and (b) change in the activity coefficients of the ions and of water. If the I value is low, for instance 0.1, the ionic activity coefficients in the two salt solutions will have very similar values and the variation of the pK can be explained by the complex formation of A^+. In this way it is possible to estimate the value of K_1 for AL^{3-}. In the case of potassium as component of the inert salt, the constant K_1 for the EDTA complex on the basis of the above pK values is estimated[3] to be $10^{0.8} = 6.3$. This value can be used to estimate the reduction in the concentration of the unprotonated ligand $[L^{4-}]_0$ to $[L^{4-}]$ using a potassium salt as the inert salt: $[L^{4-}]_0 = [L^{4-}] + [KL^{3-}] = [L^{4-}](1 + 6.3[K^+]) = [L^{4-}]\Delta$. For instance inserting $[K^+] = 0.1$ one obtains: $[L^{4-}] = [L^{4-}]_0/(1 + 0.63) = [L^{4-}]_0/10^{0.21}$. This implies that the equilibrium constants corrected for potassium complex formation at $I = 0.1(KNO_3)$ are calculated multiplying their values by $\Delta = 1.63 = 10^{0.21}$ which takes into consideration the effective ligand concentration in the presence of the complexing metal ion of the inert salt. Clearly this estimate can be done more exactly if the constant in question has been evaluated more carefully. The effect of nitrate association in $0.1(KNO_3)$ for the EDTA complexes can be estimated using published data for their association with alkaline earth cations[5] and for the divalent first-row transition metal cations.[6] As the values of K_1 are close to 1, in view of the low nitrate concentration, one finds that the metal ion concentration should be divided by Δ values ranging from 1.07 ($=10^{0.03}$) to 1.146 ($=10^{0.06}$), *i.e.*, the corrected stability constant is to be multiplied by these values. Definitively one has an increase of the decimal logarithmic value of the stability constant K_{ML} from 0.03 to 0.06, an amount similar to the error of K_{ML}. Thus the association of nitrate in this case has no significant influence on the stability constants.

In the case of formation of alkaline-earth metal complexes with fluoride and chloride, investigated using sodium nitrate as inert salt, there can be no doubt that one can have a preference for a given medium but, as mentioned by Štulíková,[2] erroneous values for stability constants are obtained. An exact judgement of the situation is only possible if one knows the equilibrium constants for all species appearing in solutions of inert salts used and introduces them in equations like the sum given above, which allow one to quantify the interference of the different salt media. The results reported in references 7–11 at $I = 1$ for the fluorides are given in Table 1 and seem to be of the expected precision. One has two (or three) values available for log K_1 at $I = 1M$ ($NaClO_4$) or $1M$ ($NaNO_3$) medium as well as 1 m ($NaNO_3$) [$\cong 0.97M$ ($NaNO_3$)]. However, although these values are quite close it is not possible to find the same trend for each metal, which would be expected if NO_3^- forms more stable associates than ClO_4^-. It seems that the effects of side-reactions in the two media compensate one another and similar values of K_1 are obtained, although the activity coefficients in the two media are different. The large discrepancy of log K_1 of Mg^{2+} in $1M$ ($NaClO_4$) is commented on in the more recent reference 8 as "good agreement" Some doubts about the accuracy of the results of the first two references in sodium nitrate can be proposed because the concentrations of the reacting metal nitrates[9,10] are changed from values between 0.03 and 0.05 m to 0.2 and 0.3 m, respectively, by a corresponding decrease of the sodium nitrate concentration maintaining $I = 1$ m. The large changes in the concentration of the reacting metal nitrate, and consequently in the concentration of sodium nitrate, cannot ensure a constancy of the activity coefficients of the reacting species within the solutions used for the determination of the same constant K_1. A much lower medium change occurs using solutions with $I = 1M$ $(Na)NO_3$ in which, in accordance with this abbreviation, from 0.01 to $0.1M$ magnesium nitrate solutions sodium nitrate is added to reach $1M$ NO_3^- "maintaining the activity coefficients constant".[11] Among the values of Table 1 in sodium nitrate solutions the most accurate seems to be the last one for Mg^{2+} at $I = 1M$ $(Na)NO_3$ taking into consideration that in this case constant potential values with the fluoride electrode are obtained whereas at $I = 1$ m ($NaNO_3$) a potential drift is mentioned. This drift influences the values of the constants obtained. As Ba^{2+} forms fluoride complexes which are thirty times weaker than those of Mg^{2+}, in order to have the same concentration of BaF^+ as for MgF^+, one would need a $3M$ $Ba(NO_3)_2$ solution at the same free fluoride concentration Further, the above replacement of $NaNO_3$ with $M(NO_3)_2$ at $I = 1$ m ($NaNO_3$) occurs with decrease of the concentration of the nitrate ion from 1 in 1 m $NaNO_3$ to 0.7 in 0.3 m $M(NO_3)_2 + 0.1$ m $NaNO_3$. This could have some effects on the concentrations of the species in equilibrium if nitrate acts as ligand. On the

basis of recent investigations this seems to be the case, $M(NO_3)^+$ and $M(NO_3)_2$ have been detected in $NaClO_4$ solutions.[5] Also the sodium ion seems to associate with nitrate ($K_1 = 0.389$ dm^3/mol) and fluoride ($K_1 = 0.162$ dm^3/mol).[13,14] Considering these equilibria, it is possible to calculate: (a) the concentration of the reacting species M^{2+} and F^- after equilibration with NO_3^- and Na^+. In this calculation the formation of ternary or mixed complexes has not been considered because of the lack of reliable data. A correction factor Δ is then calculated for the published value for K_1; (b) the corrected ionic strength, after formation of the species $NaNO_3$, $M(NO_3)^+$ and $M(NO_3)_2$, NaF being negligible. These calculations have been done for Ba^{2+} because of the more effective nitrate association $\{K_1[M(NO_3)^+] = 1.45$ dm^3/mol; $\beta_2[M(NO_3)_2] = 0.93$ dm^6 mol$^{-2}\}$ in the presence of the lowest and largest quantities of $Ba(NO_3)_2$ in the measurements. The following results were obtained: (1) 0.05 m $Ba(NO_3)_2$: $[Na^+] = 0.66$ m, $[F^-] = 0.72 \times 10^{-3}$ m giving $\Delta = 10^{0.27}$, $[BaNO_3^+] \approx 0.02$ m and $I = 0.74$ m, (2) 0.3 m $Ba(NO_3)_2$: $[Na^+] = 0.086$ m, $[F^-] = 0.99 \times 10^{-3}$ m giving $\Delta = 10^{0.13}$, $[BaNO_3^+] \approx 0.1$ m and $I = 0.65$ m. The concentration of barium fluoride not exceeding 1×10^{-4} m, it seems evident that in these mixtures the side reactions are the more important. Of course the calculated concentrations are only estimates as they were obtained using the published values without correction for the different conditions, but they show that the investigation of weak association is very difficult and very often accompanied by large ionic strength changes as the inert salts form associates. The correction of K_1 is carried out multiplying the corresponding value of Table 1 by Δ. In general, it is expected that the actual value of K_1 is lower in presence of salts which associate with the components being investigated as long as the activity coefficients in the media are the same. In sodium nitrate one obtains K_1 values which are similar to those obtained in sodium perchlorate: it follows that in this latter medium an almost equally significant ClO_4^- association has to be considered. In conclusion, it is obvious that the investigation of weak complexes cannot be done in a reasonable way without taking into account the effects of the inert salt on the equilibria and on the ionic strength.

REFERENCES

1. F. J. C. Rossotti and H. Rossotti, *The Determination of Stability Constants*, McGraw-Hill Book Company, London, 1961.
2. M. Štulíková, *Talanta*, 1991, **38**, 805.
3. G. Anderegg, *Critical survey of Stability Constants of EDTA Complexes*, Pergamon Press, Oxford, 1977.
4. G. Anderegg and F. Wenk, *Helv. Chim. Acta*, 1971, **54**, 216.
5. V. A. Fedorov, A. M. Robov, I. I. Shmyd'ko, N. A. Vorontsova and V. E. Mironov, *Russ. J. Inorg. Chem.*, 1974, **19**, 950.
6. M. H. Hutchinson and W. C. E. Higginson, *J. Chem. Soc., Dalton Trans.*, 1973, 1347.
7. S. P. Tanner, J. B. Walker and G. R. Choppin, *J. Inorg. Nucl. Chem.* 1966, **30**, 2067.
8. A. M. Bond and G. Hefter, *J. Inorg. Nucl. Chim.*, 1971, **33**, 429.
9. Čadek, J. Veselý and Z. Šulček, *Collect. Czech. Chem. Commun.*, 1971, **36**, 3377. In Table 1 of this paper the K_1 values taken from literature are given in Kg/mol without the needed conversion from dm^3/mol data (Table 1)*.
10. V. Majer and K. Štulík, *Talanta*, 1982, **29**, 145. In this paper, as well as in the summary, the different tables and figures are given without mentioning the ionic medium used, *i.e.*, 1*M* ($NaNO_3$).
11. H. Gamsjäger, P. Schindler and B. Kleinert, *Chimia*, 1969, **23**, 229.
12. C. F. Baes Jr., R. F. Mesmer, *The Hydrolysis of Cations*, Wiley, New York, 1976.
13. R. A. Robinson, *J. Am. Chem. Soc.*, 1937, **59**, 84.
14. J. N. Butler and R. Huston, *Anal. Chem.*, 1970, **42**, 1308.

Talanta, Vol. 40, No. 2, pp. 247–254, 1993
Printed in Great Britain.

0039-9140/93 $6.00 + 0.00

DETERMINATION OF CHLORINATED HYDROCARBONS INTRODUCED INTO AIR/ACETYLENE FLAMES BY FOURIER TRANSFORM INFRARED EMISSION SPECTROSCOPY

ANTHONY R. KOEBELE and DAVID C. TILOTTA*

Department of Chemistry, The University of North Dakota, University Station, Box 7185, Grand Forks, ND 58202, U.S.A.

(*Received* 26 *March* 1992. *Revised* 23 *June* 1992. *Accepted* 23 *June* 1992)

Summary—A Fourier transform spectrometer is used to record the infrared emission from chlorinated hydrocarbons combusted in an air/acetylene flame. In this manner, the chlorinated hydrocarbons are determined by monitoring the infrared emission of hydrogen chloride at 2653 cm^{-1}. Discussion is presented of the air/acetylene flame background, and the potential spectral interference from the emission of deuterated species. Practical detection limits for chloroform, carbon tetrachloride and methylene chloride in acetone, methanol, and ethanol are solvent independent and are found to be 1.1, 0.80, and 1.0%, respectively. Calibration curves for these three analytes are linear from their detection limits to approximately 55% (v/v). In addition, evidence is presented that flame flicker-noise does not lead to a multiplex disadvantage when the Fourier transform instrument is used for data acquisition.

The acquisition of low-temperature infrared emission spectra from thermally excited materials is experimentally difficult due to low spectral emittance at low temperature. Because of this low emittance, Fourier transform spectrometers (FTSs) are generally used to increase the signal-to-noise ratios of the obtained spectra over conventional dispersive instruments. The throughput and multiplex advantages of the FTS allow a larger solid angle of collection and an increase in the detector irradiance, respectively, over dispersive instruments. Of course, these advantages are enjoyed in the infrared because it is assumed that detection noise, which is independent of the detector-irradiance, dominates over source (flicker) and photon noise.

In a recent paper, Tilotta *et al.* showed that a conventional FTS could be used to detect the infrared emission from the combustion products of organic molecules introduced into flames.[1] In their work, organic compounds were introduced into a hydrogen/air flame via a nebulizer for combustion and vibrational excitation. Since the hydrogen/air flame has been reported to have a temperature of 2380 K,[2] a commercially available FTS equipped with a room temperature tryglycine sulfate (TGS) detector proved to be satisfactory in recording the infrared emission from the flame. Cooled instrumentation, detectors, or special sample heat-transfer devices were not required.

Combustion flames, however, are atypical infrared sources and may be expected to have noise characteristics different from conventional infrared emission sources such as globars or Nernst glowers. It is well known from atomic spectroscopy, for example, that the spectral noise arising from combustion flames and nebulizers is multiplicative, *i.e.*, the noise is carried by the signal.[3] In terms of the application of Fourier transform spectrometry to atomic emission spectroscopy, there is evidence that flame-flicker noise effectively distributes itself across the transformed spectrum and leads to a multiplex disadvantage.[4,5] (It should be pointed out, however, that under some circumstances, an emission multiplex advantage can exist.[4,6])

To a large extent, organic compounds are detected indirectly in flames by the infrared emission from their combustion products. Of course for applications in chromatography or for screening methods for general non-metallic species, this operational principle is satisfactory. Previous studies of the analytical applications of infrared emission from combustion

*Author for correspondence.

flames have employed a miniature hydrogen/air capillary-head burner for combustion and vibrational excitation.[7-10] The hydrogen/air combustion flame was chosen in order to eliminate the spectral interference of CO_2 emission from hydrocarbon fuel gases. However for analysis by infrared emission from a combustion flame in which carbon or CO_2 is not the analyte, such as chlorine from a chlorinated hydrocarbon, a combustion mixture based upon a hydrocarbon fuel should be feasible.

The subject of this paper is the investigation of the application of Fourier transform spectrometry to the determination of chlorinated hydrocarbons by infrared emission from an air/acetylene flame. A commercially available Fourier transform spectrometer is optically coupled to a conventional atomic absorption laminar-flow slot-burner. Chlorinated hydrocarbons are introduced into the flame by a conventional concentric nebulizer and are monitored via their hydrogen chloride infrared emission signal. In addition, this paper investigates the Fellgett (multiplex) advantage when the infrared emissions of the flame are multiplexed by the Fourier transform instrument.

EXPERIMENTAL

Fourier transform spectrometer

All infrared emission measurements were conducted with a Nicolet Model 5-MX FTIR (Nicolet Instruments, Madison, WI., U.S.A.) The FTIR was modified for infrared emission spectroscopy by removing the conventional infrared source and installing a 4.3-cm diameter, f/1.5, aluminum concave reflecting mirror 13.0 cm from the original source location. Figure 1 shows the experimental design. Although the collection mirror was used off-axis, no significant aberrational defects were observed. The FTIR was operated at room temperature with its cover removed in order to admit the infrared emission from the flame into the optical path. In addition, the air circulation fan of the FTIR was disconnected so as not to cause flame turbulence.

A room temperature tryglycine sulfate (TGS) detector was used in the FTIR. All spectra, unless otherwise noted, are the result of 100 co-added scans and required a total scanning time of 3.75 min. Although this FTIR has a theoretically fixed resolution of 4 cm^{-1}, the experimentally observed resolution was approximately 6 cm^{-1}. A triangular

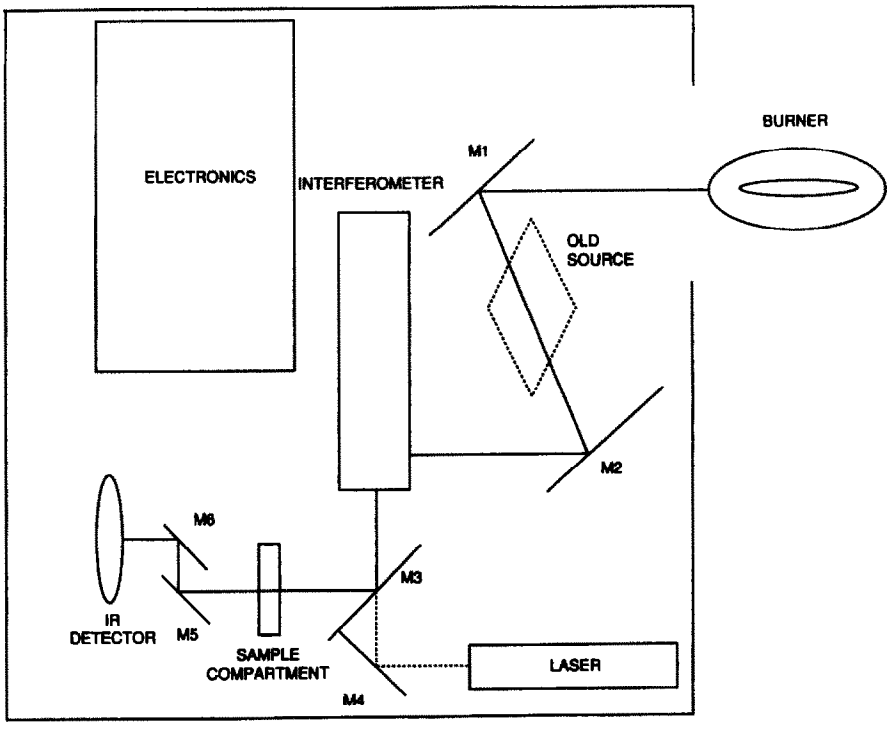

Fig. 1. Schematic diagram of instrumental set-up used to collect infrared emission from the air/acetylene flame. The old source was removed, and concave focusing mirror M1 was added to the optical bench in order to admit the infrared radiation into the interferometer. Mirrors M2, M3, M5 and M6 are concave mirrors and mirror M4 is planar. A 1-cm aperture was added to the sample compartment.

lar apodization function was employed and zero-filling was not utilized. All spectra were acquired with a 1-cm diameter aperture placed in the normal sample compartment. The spectra presented in this paper have not been corrected for the instrument response function.

Burner

A 10-cm long, laminar flow slot burner was obtained from a Perkin–Elmer model 403 atomic-absorption spectrometer (Perkin–Elmer Corporation, Norwalk, CT, U.S.A.) and positioned 30 cm from the FTIR collection mirror. Since the adjusting micrometers were retained, the slot burner could be precisely positioned along three axes. The infrared emissions were viewed over a 1.0-cm vertical section centered at a height of 4.0 cm above the slot-burner top.

The slot-burner utilized air and acetylene as its fuel and oxidant, respectively. Stoichiometric flame conditions were employed with an acetylene flow rate of 1000 ml/min. In order to increase flame stability, triple-stage regulation was utilized for both air and acetylene, and the acetylene tank was replaced when the pressure dropped to three-quarters its initial value. The aspirator uptake rate was 1.0 ml/min.

Reagents

All chemicals, with exception of acetone-d_6, were reagent grade (Fisher Scientific, Fairlawn, NJ, U.S.A.) and were used without further purification. The acetone-d_6 was 99.9% isotopically pure and was obtained from MSD Isotopes (Division of Merck-Frosst Canada Inc., Montreal, Canada). Calibration standards of chloroform were prepared to have concentrations of 5, 10, 20, 30, 50, 70 and 100 percent (v/v) by diluting the appropriate volume of chloroform with either ethanol, methanol, or acetone.

RESULTS AND DISCUSSION

Flame background

Figure 2 shows an infrared emission spectrum of the flame background in the region from 4200–400 cm^{-1}. As can be seen from Fig. 2, the major emission bands in the background spectrum are due to the asymmetric stretching vibration of CO_2 at 2261 cm^{-1} and the bending motion of CO_2 at 671 cm^{-1}. The infrared emission bands of water are significantly less intense than the CO_2 emission bands and occur in the 4075–3200 cm^{-1} and 2100–400 cm^{-1} spectral regions corresponding to stretching and bending motions, respectively. It should be noted, however, that this spectrum has not been corrected for the instrument response function and interspectral comparisons based on emission intensity are difficult. However from an experimental standpoint, the most intense emission band in any spectrum acquired from the air/acetylene flame is generally the asymmetric stretching vibration of CO_2 at 2261 cm^{-1}. During the course of these investigations, no other band was found with a greater intensity.

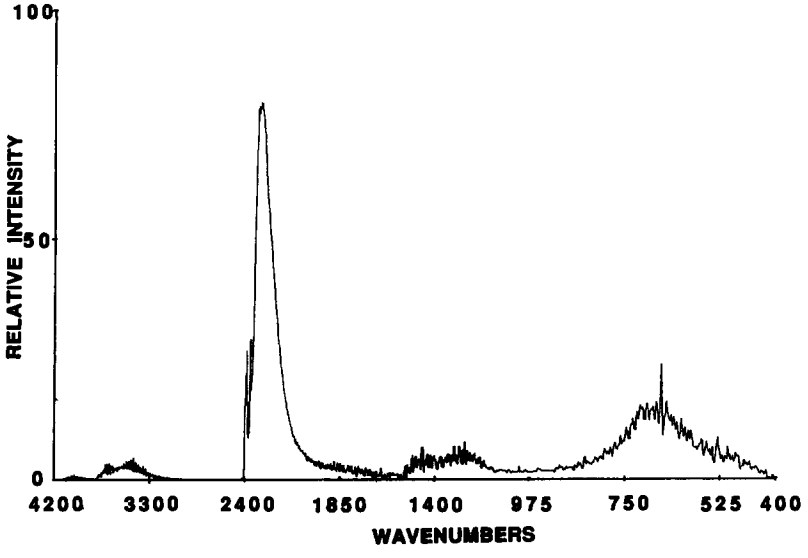

Fig. 2. Infrared emission spectrum of air/acetylene flame background.

It has been reported in the literature that the infrared absorption bands of CO_2 corresponding to the asymmetric stretching vibration and bending vibration occur at 2349 and 667 cm^{-1}, respectively.[11] In addition, a previous study on the infrared emission of CO_2 from a hydrogen/air flame reported the asymmetric stretching vibration to occur at 2262 cm^{-1}; the bending vibration was not observed.[1] The differences between the absorption and emission frequencies for the asymmetric stretching vibration of CO_2 have been accounted for by anharmonic distortion in the vibration, and absorption of the emitted radiation by atmospheric CO_2.[1,12] The presence of the bending vibration in the spectra from the air/acetylene flame (at 661 cm^{-1}) reflects the higher concentration of CO_2 over the hydrogen/air flame. The frequency shifts of the CO_2 bands in the air/acetylene flame (versus the hydrogen/air flame) may be due to a slight red shift because of anharmonicity in the bonds, and absorption of the radiation by atmospheric CO_2 (for the bending vibration at 667 cm^{-1}). However, exact conclusions are difficult to draw because of instrumental resolution considerations.

Flame and burner parameters

The air/acetylene burner may be oriented with its slot parallel to the optical axis or perpendicular to it. With the burner-slot oriented parallel to the optical axis, it may be anticipated that a larger signal would be observed because a larger number of emitting species would be in the optical path. In fact, with the slot burner oriented parallel to the optical axis, the emission intensities (measured by peak heights) were approximately 20% greater. This small improvement is expected because of the difficulty in collecting and imaging such a large amount of radiation from the source. No significant resolution loss due to off-axis radiation was observed.

The fuel/oxidant ratios are critical in flame infrared emission spectroscopy because the flame not only supplies vibrational energy but also thermally decomposes the organic analytes. Since a large number of analyses by flame infrared emission spectroscopy are based on the formation of an analyte derivatized for detection, the choice of flame conditions will depend on the emitting species. For example, the determination of Cl_2, Cl^-, or a chlorine-containing organic compound relies on the formation and emission of hydrogen chloride.[8] Thus, it is anticipated that fuel-rich flame conditions will promote the formation of hydrogen chloride.

It is well-known, however, that organic solvents introduced into air/acetylene flames may cause soot formation due to incomplete

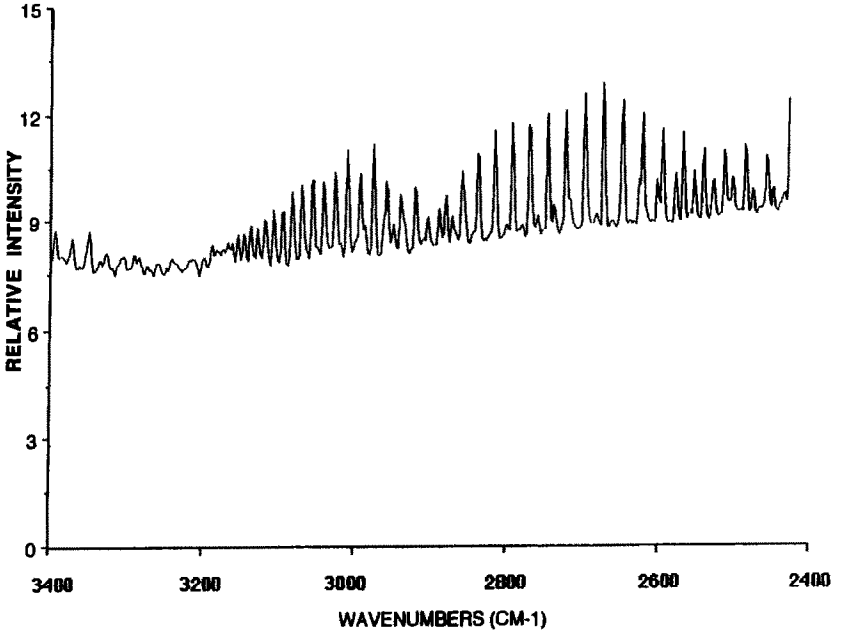

Fig. 3. Infrared emission spectrum of hydrogen chloride obtained when pure chloroform is aspirated into the air/acetylene flame. The baseline offset, to a relative value of 7.5, is due to blackbody radiation from soot particles in the flame.

combustion. In turn, the presence of soot particles in a flame may lead to blackbody radiation. Thus, a fuel-rich flame may interfere with calibration of the emission intensity because of the blackbody radiation from soot particles.

The effect of the fuel/oxidant ratio on the hydrogen chloride emission signal obtained from chloroform was studied by aspirating pure chloroform into the flame. Figure 3 shows the infrared emission spectrum from hydrogen chloride in the region 3600–2400 cm^{-1}. The baseline offset, at a relative value of about 7.5, is due to blackbody radiation from hot soot particles. The blackbody radiation does not affect the magnitude of the analytical calibration signal and can be removed by subtraction. However, it should be pointed out that the amount of blackbody radiation in each spectrum changes with respect to analyte/solvent composition, and it can affect the precision of the measurements because of associated noise.

The intensity of the hydrogen chloride emission line at 2653 cm^{-1} was observed as the air/acetylene ratio was varied. The intensity of this line was corrected for blackbody emission by subtracting the average background obtained from each side of the emission line (approximately ten wavenumbers from the 2653 cm^{-1} line). The most intense hydrogen chloride emission occurs at a fuel/oxidant ratio of 1:1.98 (acetylene:air) and reflects a fuel-rich flame, as expected. However, the adjustment of the air/acetylene ratio is not critical and the optimum ratio affords an hydrogen chloride emission intensity that is only 20% larger than at other ratios.

Noise studies

It is well known from statistical arguments that co-adding spectra leads to signal-to-noise ratio improvements dependent upon the square root of the number co-added, providing the noise is random. Conversely, deviation from this relationship is strong evidence of non-random noise properties. In order to establish the nature of the noise in the background emission bands of CO_2 and H_2O, a graph of the logarithm of the baseline noise (ordinate) versus the logarithm of the number of co-added scans (abscissa) was constructed for the case of 1, 10, 25, 81, and 100 co-added scans of the CO_2 emission band at 2261 cm^{-1}. If the noise is random, it can be shown that the slope of this graph should be equal to $-1/2$. Since, in fact, the slope of the experimentally determined graph was equal to -0.508 ($r = 0.99$), it can be inferred that the noise in the background emission band of CO_2 appears to be random over the range of instrumental parameters used in these experiments. Based on this result, it can be anticipated that the noise in all of the infrared emission bands from the flame is essentially random.

Since the flame utilizes acetylene as its fuel gas, the dominant emission bands in all spectra (even in the presence of analyte bands) are from CO_2 and H_2O. For example, when pure chloroform is aspirated into the flame, the intense emission line of hydrogen chloride at 2653 cm^{-1} is 1/20th the intensity of the CO_2 emission band at 2261 cm^{-1} (although the hydrogen chloride band is broader due to its rotational fine structure). From an experimental standpoint, the noise in the intense CO_2 emission bands significantly impairs the determination of carbon (as CO_2). However, the determination of chlorinated hydrocarbons may still be accomplished providing spectral interferences are negligible and the baseline noise in the spectral region of the analyte emission band is small. In Fourier transform spectrometry, however, the latter criterion may be influenced by the distribution noise of the multiplexing process. Since the air/acetylene flame background is spectrally rich (in fact, nearly continuous), noise localized around the bands and lines may effectively appear "white". Consequently, the noise in the background bands may influence the noise in the analyte bands.

In order to determine if the noise in the major emission bands distributes into the baseline, an experiment was conducted in which the amount of flame radiation reaching the detector was varied by the use of an aperture-stop placed immediately after the beamsplitter. The intensity of the background emission bands were monitored simultaneously with the magnitude of the baseline noise in a region considered to be free of spectral interferences. Since the baseline noise in that region should not directly arise from an infrared emission band, correlation of the signal-to-noise ratio (SNR) of the background emission bands with the optical throughput is strong evidence of detector noise-limited measurements.

The plot in Fig. 4 shows the relationship between the SNR of the CO_2 emission band and

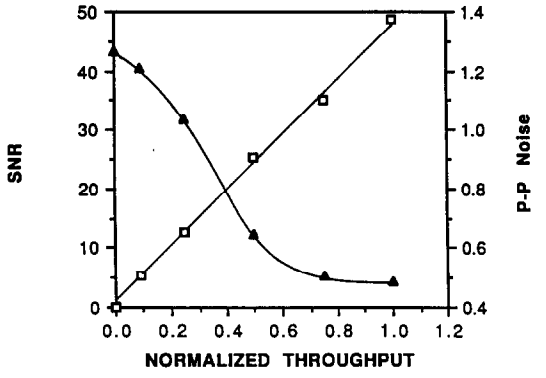

Fig. 4. Dependence of SNR of the CO_2 emission band (noise in the 4200–4300 cm^{-1} region) and peak-to-peak baseline noise on optical throughput. The line denoted by □ is the SNR of the CO_2 emission band and the line denoted by ▲ is the peak-to-peak baseline noise in the 4200–4300 cm^{-1} region. The optical throughput axis has been normalized, and best-fit lines have been drawn through the data points.

the optical throughput of the FT–IR spectrometer. For completeness, Fig. 4 also shows the absolute baseline noise (peak-to-peak) as a function of the optical throughput. The signal of the predominant background emission band at 2261 cm^{-1} was used as a measure of the intensities of all background emission bands, and the flame parameters were adjusted until this band had a relative standard deviation of 25% (constant for all measurements). The peak-to-peak noise in the region from 4300–4200 cm^{-1} was used because no discernible emission bands could be observed, even when 100 spectra were co-added. The SNR values in Fig. 4 are averages from ten single-scan spectra, and the optical throughput values were normalized to the largest value. It should be pointed out that the dynamic range of the CO_2 emission signals was limited by the maximum-attainable throughput of the infrared signal and the minimum detectable signal.

The plot of SNR versus throughput shown in Fig. 4 is quite linear ($r = 0.99$) and exhibits the kind of relationship between the SNR and throughput expected for the case of detector-noise limited measurements.[13] If substantial flicker noise were being distributed to the baseline, then an increase in the optical throughput would lead to virtually no change in the SNR, and, as a result, the slope of the line would decrease (ideally, to zero) at some point in this plot. Thus, it is believed that the dominant noise-source in this system is most likely the FT–IR spectrometer (TGS detector and/or electronics). Of course, other noise sources may also be present in this system and cannot be entirely ruled out. However, it is difficult to speculate on "other" noise sources because of the statistical uncertainty in the measurements. Nonetheless, Fig. 4 clearly shows that a true "multiplex disadvantage" is not present in this system using a TGS detector and $f/3$ collection optics.

Spectral observation windows and spectral interferences

As stated in a previous section, the air/acetylene flame has a number of emission bands due to excited CO_2 and H_2O. Furthermore, these bands are noisy to some degree because of flame turbulence. Thus, it is anticipated that some spectral regions of the air/acetylene flame will be more stable and noiseless than other spectral regions. Of course, those spectral "windows" with lower noise will yield superior detection limits over those windows with greater noise. Thus, an examination of the analytically useful wavelength regions in the air/acetylene flame is worthwhile.

As shown in Fig. 2, the flame background bands cover the entire mid-infrared region. However, clearly there exists certain wavelength regions in the background emission which are reasonably "clean" and can be used for analytical purposes. Based on the criterion of the absence of flame background emission bands, the useful infrared window in the air/acetylene flame occurs in the region of 3133–2400 cm^{-1}. Noise from either H_2O or CO_2 emission (produced by the flame) contributes to the wavelength regions outside of this window. In addition, absorption of radiation by atmospheric H_2O and CO_2 significantly reduce the intensity of emitting species in some regions. However based on experimentally determined results, analytical measurements can be acquired in the regions from 1700–1560 cm^{-1} and 1120–860 cm^{-1}. Of course, higher spectral resolution may be used to resolve the rotational fine structure.

The only species which has been found to give rise to infrared emission bands which overlaps those of the hydrogen chloride emission band are due to D_2O and HDO. As shown in Fig. 5, the infrared emission from D_2O and HDO (obtained by aspirating pure acetone-d_6 into the flame) is easily detected in the 3100–2420 cm^{-1} region. Because of the poor instrument resolution (6 cm^{-1}), assignment of the bands to either HDO or D_2O is

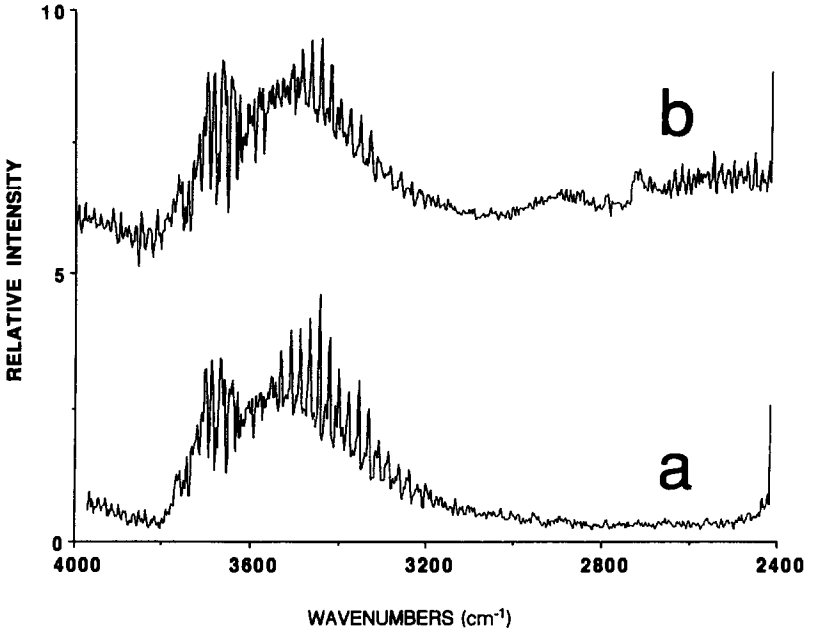

Fig. 5. Spectra showing location of D_2O and HDO infrared emission. Spectrum a is of the air/acetylene flame background and spectrum b is of the air/acetylene flame background when acetone-d_6 is aspirated into the flame (the emittance of spectrum b has been offset 5 arbitrary units). Infrared emission from D_2O and HDO is in the region of 3100–2420 cm^{-1}.

difficult. However, both molecular species are expected to exist at these flame temperatures because of hydrogen exchange.

As will be seen in the proceeding section, the hydrogen chloride infrared emission occurs in the 3100–2420 spectral region in the air/acetylene flame. Thus, the emission signals from D_2O and HDO potentially may spectrally interfere with the hydrogen chloride emission signal. Since elevated levels of deuterated species are generally not found with chlorinated species, this spectral interference should be minor. However, the interfering emission signal may be removed by subtraction as long as the noise in the signal does not significantly impair the precision of the measurement.

Matrix effects and calibration

Although it has been established that the intensity of an analytical emission band (*e.g.*, HCl, HF, CO_2, *etc.*) is directly proportional to analyte concentration, the use of infrared emission from flames as an analytical tool has been confined to detectors for gas chromatography and purge-and-trap analytical methods.[7–10] Since both these techniques isolate the analyte in an inert gas stream, the effect of different sample matrices on the analyte emission signal has not been studied. Figure 6 shows calibration curves for chloroform in ethanol, methanol, and acetone. The concentration axis has been expressed in terms of the percentage of solute in the total volume (percent v/v). Since a number of solvents were available, ethanol, methanol, and acetone were chosen as representative solvents.

The calibration curves of chloroform shown in Fig. 6 were background corrected for blackbody radiation (as described in a previous

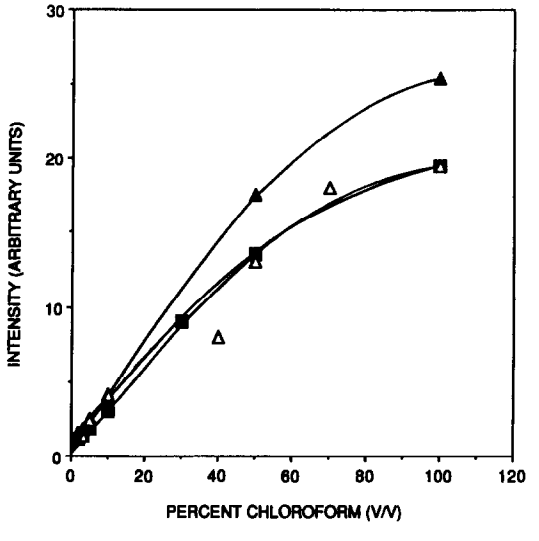

Fig. 6. Calibration curves of chloroform in acetone (△), methanol (▲), and ethanol (■).

section) and are linear from their detection limits to about 55%. Downward curvature at concentrations exceeding 55% is due to either self-reversal of the radiation by cooler hydrogen chloride molecules surrounding the flame, a loss of the hydrogen chloride emission signal from incomplete combustion from a lack of O_2, or a change in the flame conditions due to the introduction of large amounts of analyte. In addition, it is important to note that all curves have nearly the same slope at low concentrations. Thus for these three solvents, the signal from the chloroform (as hydrogen chloride) is approximately independent of solvent in dilute solutions. The detection limits of chloroform in all three solvents were statistically identical and were 1.10% (v/v). In addition, similar results were obtained for carbon tetrachloride and methylene chloride. The detection limits of CCl_4 and CH_2Cl_2 in these three solvents were 0.80 and 1.0%, respectively. Calibration curves for CCl_4 and CH_2Cl_2 were linear from their detection limits to 52% concentration and 60% concentration, respectively.

The detection limits of these chlorinated species in the air/acetylene flame are poor and are believed to be governed by the noise in the FT–IR spectrometer (most likely the TGS detector). A study of the SNR of the CO_2 emission band versus the optical throughput using the baseline noise in the 3000–2420 cm^{-1} region shows a dependence similar to that shown in Fig. 4. The poor detection limits may also be due to the noise present in the infrared emission band of water which slightly overlaps the emission of the HCl and the noise in the background blackbody emission. Further work is needed in order to gain a better understanding of the noise present in this system. Some improvements in the detection limits might be obtained by using a different burner or using a mercury cadmium telluride (MCT) detector. Of course, as shown above, spectral scans may be co-added to improve the detection limits. However, increasing the number of co-added scans increases the total scanning time.

CONCLUSIONS

It has been shown that a conventional Fourier transform infrared spectrometer coupled to an air/acetylene slot burner is suitable for determining chlorinated organic compounds in a variety of sample matrices. The organic compounds may be determined by the infrared emission from hydrogen chloride obtained upon combustion in the flame. The air/acetylene flame background, although spectrally rich, has several optical windows and does not interfere with the determination of the compounds. In addition, it has been shown that the Fourier transform instrument using a TGS detector does not lead to a multiplex disadvantage from flame flicker-noise. Although the detection limits for these chlorinated compounds are poor, it is believed that a better understanding of the noise aspects of this system could improve them.

REFERENCES

1. D. C. Tilotta, K. W. Busch and M. A. Busch, *Appl. Spectrosc.*, 1989, **43**, 704.
2. J. D. Ingle, Jr. and S. R. Crouch, *Spectrochemical Analysis*, p. 229. Prentice Hall, New Jersey, 1988.
3. J. D. Winefordner, R. Avni, T. L. Chester, J. J. Fitzgerald, L. P. Hart, D. J. Johnson and F. W. Plankey, *Spectrochim. Acta*, 1976, **31B**, 1.
4. G. Horlick, R. H. Hall and W. K. Yuen, in *Fourier Transform Infrared Spectroscopy* Vol. 3, pp. 37–81. Academic Press, New York, 1982.
5. E. Voigtman and J. D. Winefordner, *Appl. Spectrosc.*, 1987, **41**, 1182.
6. T. Hirschfeld, *ibid.*, 1976, **30**, 68.
7. S. W. Kubala, D. C. Tilotta, M. A. Busch and K. W. Busch *Anal. Chem.*, 1989, **61**, 1841.
8. *idim, ibid.*, 1989, **61**, 2785.
9. M. K. Hudson and K. W. Busch, *ibid.*, 1987, **59**, 2603.
10. S. Ravishankar, D. C. Tilotta, K. W. Busch and M. A. Busch, *Appl. Spectrosc.* 1990, **44**, 1247.
11. G. Herzberg, *Infrared and Raman Spectra of Polyatomic Molecules*, p. 274. Van Nostrand, New York, 1945.
12. E. K. Plyler, *J. Res. Nat. Bur. Stand.*, 1948, **40**, 113.
13. P. R. Griffiths and J. A. deHaseth, *Fourier Transform Infrared Spectrometry*, p. 253. Wiley, New York, 1986.

Talanta, Vol. 40, No. 2, pp. 255–260, 1993
Printed in Great Britain.

0039-9140/93 $6.00 + 0.00

SUPERSONIC JET SPECTROMETRY OF THERMALLY DECOMPOSED PRODUCTS FROM POLYSTYRENE AND POLYα-METHYLSTYRENE

TOTARO IMASAKA,* MASAMI HOZUMI and NOBUHIKO ISHIBASHI
Faculty of Engineering, Kyushu University Hakozaki, Fukuoka 812, Japan

(*Received* 14 *April* 1992. *Revised* 15 *June* 1992. *Accepted* 15 *June* 1992)

Summary—Polystyrene and polyα-methylstyrene are thermally decomposed, and the products are measured by fluorescence spectrometry and multiphoton ionization spectrometry. The monomers are found to be major products from both the polymers, but many other chemical species, including dimers and trimers, are also observed. The present instrument is applied to a mixture sample containing these two polymers, and the components included are selectively determined using this hyphenated technique.

Constituents of polymers are currently determined by mass spectrometry after pyrolysis of the sample using a heated insertion probe. Such an instrument is already commercially available and has been applied to many polymers, *e.g.*, polystyrene, polycarbonate, polyimide, *etc.*[1] More recently, a laser ablation technique has been used for vaporization of the sample,[2] which is especially useful for a polymer being easily carbonized at an elevated temperature. However, mass spectrometry has limited performance in differentiation of isomers, though some additional information is obtained from the mass fragment pattern, from the excess kinetic energy of ions, and from the daughter-ion mass spectrum obtained by mass spectrometry/mass spectrometry.

In order to overcome this problem, mass spectrometry is usually combined with a separation technique such as gas chromatography. However, standard chemicals are necessary for calibration of each column used. It is noted that each polymer has different characteristics, so that a few polymers are mixed to improve performance; *e.g.*, polyα-methylstyrene is added to polystyrene to improve the thermal properties of the polymer material. Thus a more selective analytical means is required, in order to clarify the constituents of the polymer.

Supersonic jet expansion cools a sample molecule and provides sharp spectral lines. Thus very high spectral selectivity is given by a combination with laser spectrometry.[3–6] This technique allows differentiation of even isomers and isotopes. However, only an analytical application has been reported so far for a polymer sample; polystyrene is measured by laser ablation/supersonic jet/fluorescence spectrometry.[7] In the laser ablation technique, two independent lasers are required, *i.e.*, ablation and excitation lasers, which makes the analytical system more complicated. Moreover, only fluorescence spectrometry has been applied, and therefore information available for assignment of the chemical species is quite limited.

In this study we describe supersonic jet spectrometry combined with fluorescence spectrometry and multiphoton ionization spectrometry. This hyphenated technique is applied to polystyrene, polyα-methylstyrene, and the mixture of these polymers.

EXPERIMENTAL

Apparatus

The supersonic jet spectrometer used in this study is reported in detail elsewhere, and is briefly described here.[8] The polymer sample was heated in a gas chromatograph chamber (Shimadzu, GC-8A). The thermally decomposed products were introduced into the vacuum system from a pulsed nozzle.[9] In the first chamber, the chemical species in a supersonic jet was excited by a dye laser (Quantel, YG581-C20, TDL-50, UVX-2). Fluorescence was measured by using a monochromator (Jasco, CT-25CP) equipped with a photomultiplier (Hamamatsu, R1477). A boxcar integrator (Stanford, SR-250) was used for measurement

*Author for correspondence.

of the signal. The second chamber is separated from the first chamber by a skimmer (Beam Dynamics, 1 mm i.d.). The chemical species in a molecular beam was multiphoton ionized by the same dye laser described above. The ion induced was extracted into the third chamber, *i.e.*, a time-of-flight tube, by a repulsive potential. The ion was detected by an assembly of three microchannel plates; this high-gain detector has a narrow pulse height distribution for a single ion and also removes an external amplifier. The transient signal, *i.e.*, the mass spectrum, was recorded by a waveform digitizer (Iwatsu, DM901). The signal was accumulated 1024 or 2048 times to improve the signal-to-noise ratio. A mass-selected multiphoton ionization spectrum was measured using the boxcar integrator by adjusting the delay time to monitor a specific ion.

Reagent

Styrene and polystyrene were obtained from Wako Pure Chemicals. Other chemicals such as α-methylstyrene and β-methylstyrene were supplied from Tokyo Kasei. Polyα-methylstyrene was purchased from Polyscience. Laser dyes were supplied from Lambda Physik and Exciton.

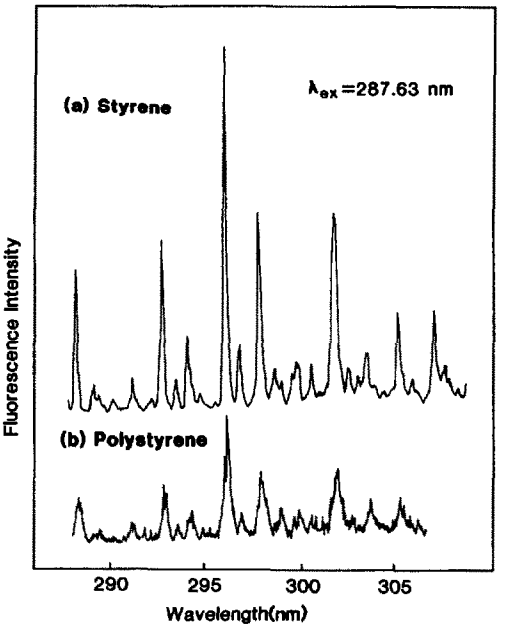

Fig. 2. Fluorescence spectrum for (a) styrene monomer (b) polystyrene; the exciting wavelength is indicated in the figure.

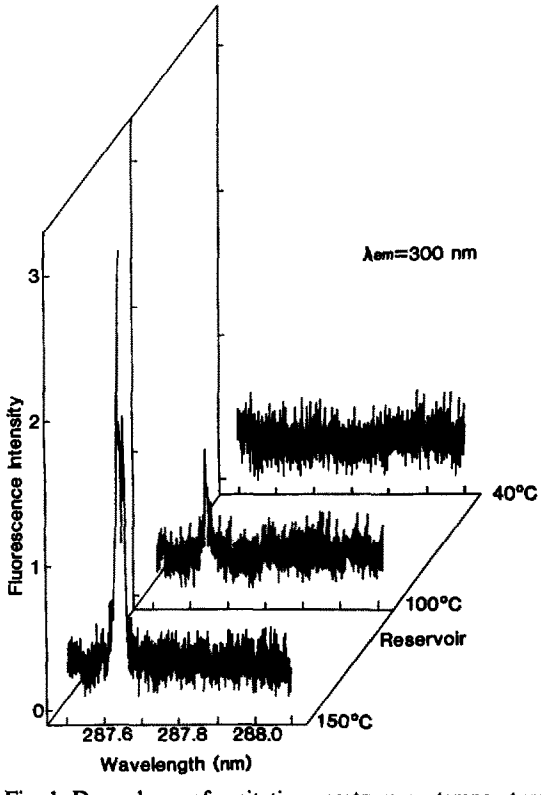

Fig. 1. Dependence of excitation spectrum on temperature for thermally decomposed products from polystyrene; the monitoring wavelength is indicated in the figure.

RESULTS AND DISCUSSION

Polystyrene

The excitation spectrum for thermally decomposed products from polystyrene were measured at various temperatures. The results are shown in Fig. 1. A sharp peak appears at 287.65 nm, which is readily assigned to the 0—0 transition of the styrene monomer from the database constructed by accumulating the data of 0—0 transition for many aromatic hydrocarbons.[10] It is noted that the signal is observed even below 100°. The ceiling temperature, at which the rate of thermal decomposition is equal to that of thermal polymerization, is 220° for polystyrene.[11] The lowest temperature at which the signal appears (100°) is much less than this ceiling temperature. Thus the styrene monomer observed might occur from the monomer included (or dissolved) in the polymer under reduced stagnation pressures (200 Torr). Presence of the styrene monomer in the thermally decomposed product is further confirmed by measuring the fluorescence spectrum, as shown in Fig. 2. The spectrum for polystyrene is identical to that for the styrene monomer. The signal intensity was rather small for a polymer sample, but it became almost identical to that for the

monomer at 350°. This is due to efficient generation of the monomer by thermal decomposition above the ceiling temperature.

Polyα-methylstyrene

The excitation spectrum for polyα-methylstyrene is shown in Fig. 3. The peak corresponding to the 0—0 transition is very weak and three characteristic progressions are observed in the spectrum, as reported.[12] These results are ascribed to the facts that there is a low-energy torsional motion of the methyl group, and that the configuration of the excited state is quite different from that of the ground state. The spectrum observed for the polymer is almost identical to that for the monomer. Thus a major component of the thermally decomposed product is a monomer of α-methylstyrene. The excitation spectrum recorded for β-methylstyrene in the similar spectral region is shown in Fig. 4. Since the band origin is located at longer wavelengths, many irregular peaks are observed in this spectral region, due to the transitions to high vibrational levels in the excited state. Thus the isomer is readily differentiated by the present instrument. The multiphoton ionization spectrum observed for polyα-methylstyrene is shown in Fig. 5, in which a parent ion is monitored. Spectral feature observed is almost

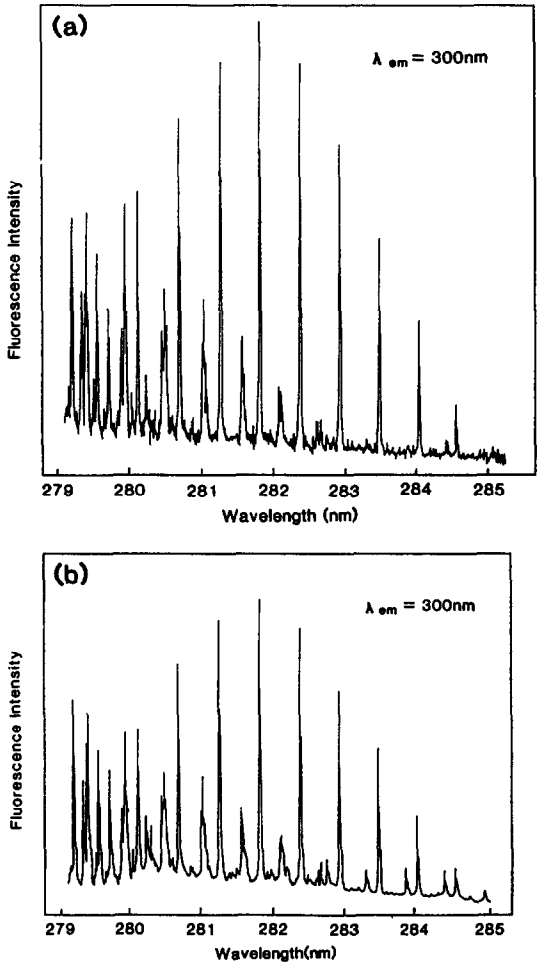

Fig. 3. Excitation spectrum for (a) polyα-methylstyrene (b) α-methylstyrene monomer; the monitoring wavelength is indicated in the figure.

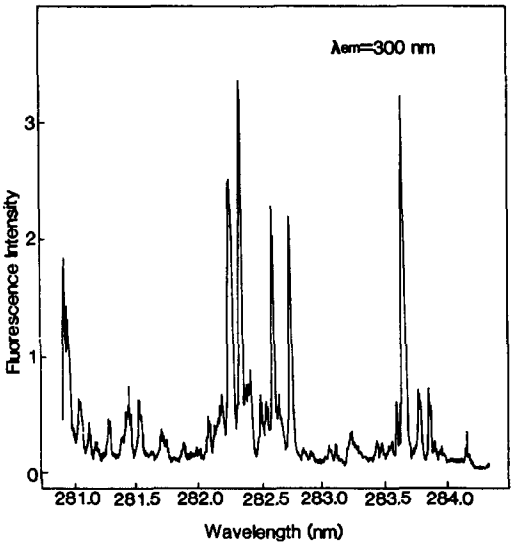

Fig. 4. Excitation spectrum for β-methylstyrene; the monitoring wavelength is indicated in the figure.

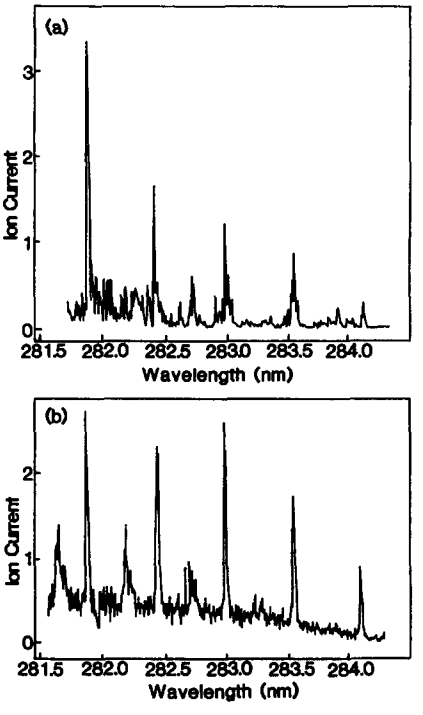

Fig. 5. Multiphoton ionization spectrum for (a) polyα-methylstyrene (b) α-methylstyrene monomer.

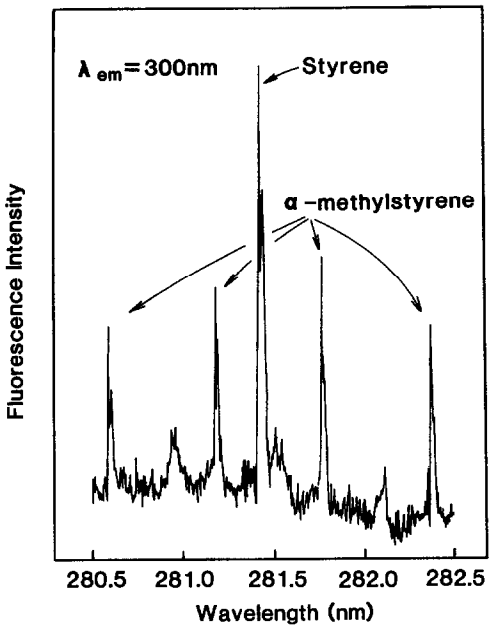

Fig. 6. Excitation spectrum for mixture sample containing polystyrene and polyα-methylstyrene.

identical to that observed in the spectrum for α-methylstyrene. Again, it indicates that α-methylstyrene occurs as a major product from polyα-methylstyrene. It is noted that the spectral shape is almost identical to that obtained in the excitation spectrum. This implies that the efficiency of multiphoton ionization is determined by the excitation step rather than the ionization step.

Mixture sample

In order to demonstrate the figure of merit of the present analytical instrument, a mixture sample containing polystyrene and polyα-methylstyrene was measured. The excitation spectrum obtained is shown in Fig. 6. Several peaks corresponding to the progressions for α-methylstyrene and a single peak corresponding to a transition to a high vibrational level for styrene are clearly observed. Thus the styrene and α-methylstyrene monomers are easily assigned. This assignment is further confirmed by measuring the multiphoton ionization spectrum by monitoring the parent ions at different delay times. As shown in Fig. 7, a sharp peak is observed at 281.55 nm when the ion is monitored between 10.2 ~ 10.6 μsec, corresponding to the parent ion of the styrene monomer (M.Wt. = 104). On the other hand several peaks (progression band) are observed, when the ion is monitored between 11.0 ~ 11.4 μsec, corresponding to the parent ion for the α-methylstyrene monomer (M.Wt. = 118). Thus each component is differentiated on the mass-selected multiphoton ionization spectrum. It is noted that a dip signal observed at 281.55 nm in Fig. 7(b) is attributed to a space charge effect (many styrene monomers are ionized and their charges scatter non-resonantly-ionized α-methylstyrene observed as a background signal) or to overloading the microchannel plate induced by a large number of styrene ions (a millisecond time interval is necessary to recover after the strong saturated signal). In order to avoid these effects, either the concentration of the styrene monomer or the laser power must be reduced. However, they decrease the signal intensity, and therefore the accumulation time should be increased to retain a sufficient signal-to-noise ratio.

A mass spectrum was measured by adjusting the laser wavelength to different values. The result is shown in Fig. 8. When the mixture sample is ionized at 282.04 nm under off-resonance conditions, many peaks appear in the spectrum. The largest peak, corresponding to M.Wt. = 104, is ascribed to the parent ion of the styrene monomer. However, many other peaks appear in the mass regions corresponding to dimers and trimers. When polystyrene is vaporized and ionized by a KrF laser (248 nm) and a ps-UV laser (290 nm),[13] an ArF laser (193 nm)

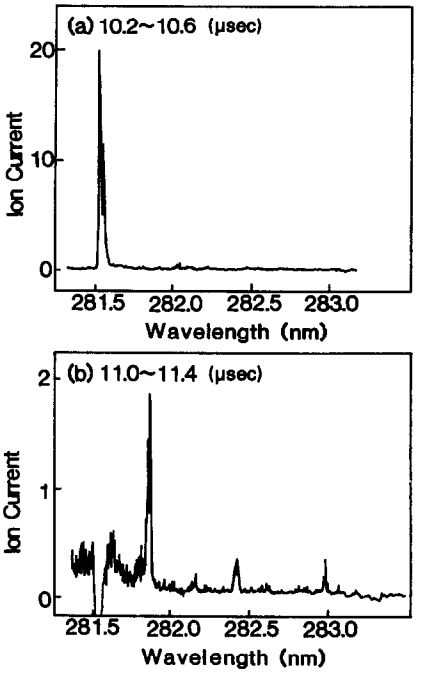

Fig. 7. Multiphoton ionization spectrum for mixture sample containing polystyrene and polyα-methylstyrene; the delay time specified in the figure is adjusted to monitor the parent ion of (a) styrene (b) α-methylstyrene.

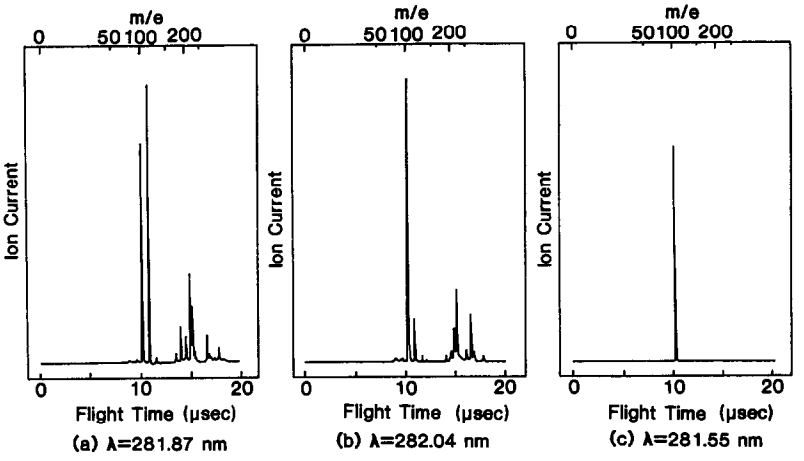

Fig. 8. Mass spectrum for mixture sample containing polystyrene and polyα-methylstyrene; the wavelength of the laser is indicated at the bottom of the figure; (a) on-resonance to α-methylstyrene (b) off-resonance (c) on-resonance to styrene; figure (c) is not presented to scale.

and a vacuum-UV laser (118 nm)[14] and Ar-ion sputtering and a vacuum-UV laser (118 nm),[15] a series of fragments, CnHx ($n = 4,6,\ldots,16$), is clearly observed. Thus thermal vaporization/supersonic jet/multiphoton ionization is more suitable for soft vaporization and ionization. When the mass spectrum is measured at 281.55 nm, which corresponds to the 0—0 transition for a styrene monomer, the peak at M.Wt. = 104 is strongly enhanced; almost a single peak is observed when this peak is presented not to scale out. Thus the strongest peak observed in Fig. 8(b) is confirmed to be due to a styrene monomer. When the laser wavelength is adjusted to 281.87 nm corresponding to one of the progression band for α-methylstyrene, the signal at M.Wt. = 118 becomes strongest among these signal peaks. This fact indicates that the peak at M.Wt. = 118 in Fig. 8(b) originates from a α-methylstyrene monomer. No other peak assignable to fragment species from polyα-methylstyrene is found in this spectrum. This is in contrast to the results obtained by a laser ablation/ionization technique (266 nm/248 nm, 266 nm/193 nm, 248 nm/266 nm); many fragment species are observed in these cases.[16] This result indicates soft vaporization/ionization in the present method, again.

CONCLUSION

As demonstrated in this study, supersonic jet spectrometry combined with a hyphenated spectrometric method is quite useful for determination of thermally decomposed products from polymers, especially for differentiation of the isomers. From the mass spectrum measured under non-resonant conditions, many candidates of the thermally decomposed products are proposed and can be ensured spectrometrically by measuring the mass-selected multi-photon ionization spectrum and excitation/fluorescence spectra. Unfortunately, many fragment species are remained unassigned in this study. In order to assign these chemical species, standard chemicals must be synthesized, since most of the candidates are not commercially available, now.

Acknowledgements—This research is supported by a Grant-in-Aid for Scientific Research from the Ministry of Education of Japan. The authors wish to thank Sanae Tagami and Masami Watanabe of Idemitsu Kosan Co. for gifts of the monomers and polymers used in this study.

REFERENCES

1. Application Data (C146-0064), *Thermal analysis/gas chromatograph-mass spectrometry*, Shimadzu, Kyoto, Japan.
2. R. Srinivasan and B. Braren, *Chem. Rev.*, 1989, **89**, 1303.
3. J. M. Hayes and G. J. Small, *Anal. Chem.*, 1983, **55**, 565A.
4. M. V. Johnston, *Trends Anal. Chem.*, 1984, **3**, 58.
5. D. M. Lubman, *Anal. Chem.*, 1987, **59**, 31A.
6. T. Imasaka and N. Ishibashi, *Prog. Quantum Electron.*, 1990, **14**, 131.
7. T. Imasaka, K. Tashiro and N. Ishibashi, *Anal. Chem.*, 1989, **61**, 1530.
8. C. H. Lin, M. Hozumi, T. Imasaka and N. Ishibashi, *The Analyst*, 1991, **116**, 1037.
9. T. Imasaka, T. Okamura and N. Ishibashi, *Anal. Chem.*, 1986, **58**, 2152.
10. N. Ishibashi and T. Imasaka, Report For Grant-in-Aid for Scientific Research from the Ministry of Education of Japan, Project No. 01470065.

11. L. A. Wall and J. H. Flynn, *Rubber Chem. Tech.*, 1962, **35**, 1194.
12. V. H. Grassian, E. R. Bernstein, H. V. Secor and J. I. Seeman, *J. Phys. Chem.*, 1990, **94**, 6691.
13. R. Larciprete and M. Stuke, *Appl. Phys. B*, 1987, **42**, 181.
14. D. Feldman, J. Kutzner, J. Laukemper, S. MacRobert and K. H. Welge, *ibid.*, 1987, **44**, 81.
15. J. B. Pallix, U. Schuhle, C. H. Becker and D. L. Huestis, *Anal. Chem.*, 1989, **61**, 805.
16. S. G. Hansen, *J. Appl. Phys.*, 1989, **66**, 1411.

Talanta, Vol. 40, No. 2, pp. 261–267, 1993
Printed in Great Britain.

0039-9140/93 $6.00 + 0.00

KINETIC SPECTROPHOTOMETRIC DETERMINATION OF Ga(III)–Al(III) MIXTURES BY STOPPED-FLOW INJECTION ANALYSIS USING PRINCIPAL COMPONENT REGRESSION

M. BLANCO,* J. COELLO, H. ITURRIAGA, S. MASPOCH, J. RIBA and E. ROVIRA

Departamento de Química, Unidad de Química Analítica, Universidad Autónoma de Barcelona, E-08193 Bellaterra, Barcelona, Spain

(*Received* 17 *February* 1992. *Revised* 22 *June* 1992. *Accepted* 29 *June* 1992)

Summary—A multivariate calibration method based on principal component regression analysis is applied to the resolution of mixtures by kinetic methodology. Gallium(III) and Al(III) were determined in mixtures on the basis of their different rate of reaction with 4-(2-pyridylazo)resorcinol in a slightly basic medium by using a stopped-flow injection procedure. Mixtures containing 1–5 mg/l. Ga(III) and 20–100 mg/l. Al(III) were successfully resolved with errors less than 10%.

Flow-injection analysis (FIA) is currently one of the most interesting analytical techniques on account of its potential for solving real problems in a variety of fields.[1,2] Even though all FIA methods are kinetic in nature, this adjective is only customarily employed in relation to those procedures relying on reaction rate measurements.[2] A host of kinetic methodologies are implemented by FIA. That of stopped flow is of special interest on account of its high potential.[3] However, such a potential has scarcely been exploited to date except for analytical determinations of a single analyte.

Mixtures of analytes have been resolved on the basis of their different rate of reaction by using the proportional-equation method[4] or, more recently, by least-squares fitting of kinetic curves[5] or by using the Kalman filter.[6] The inception of diode array spectrophotometers opened up new prospects in this context as they allow full UV–visible spectra to be recorded in a few-tenths of a second, an interval over which few kinetic reactions are bound to develop to a significant extent, so the net result is a simultaneous absorbance measurement at a number of different wavelengths. Rather than the typical (A_i, t_i) data pairs provided by conventional procedures, diode array spectrophotometers yield three-dimensional matrices of the form $(A_{j,w}, t_j, \lambda_w)$ and hence allow wealthier information to be obtained and complex mixtures unaffordable by conventional systems to be readily resolved.[7,8]

Every kinetic method entails a prior calibration. In the above-mentioned mixture resolution methods, such as calibration involves determining the reaction rate of each analyte in the mixture in order to subsequently determine its concentration in the mixture on the assumption that the experimental conditions are preserved, which may not hold inasmuch as the presence of a given analyte may influence the reaction rate of another and the analyte/reagent concentration ratio will not be the same for the analytes alone and in mixtures.

A general kinetic method for mixture resolution thus requires calibration to be carried out on mixtures concerned rather than the individual analytes. This type of calibration is frequently employed with time-independent chemical systems by using one of several procedures that are collectively known as "multivariate calibration procedures" (MCP).[9] Such procedures, however, have scarcely been used in connection with time-dependent reactions.[10]

In this work we used an MCP based on principal component regression (PCR) for the resolution of Ga(III)–Al(III) mixtures by complexation with 4-(2-pyridylazo)resorcinol in a basic medium.

*Author for correspondence.

THEORETICAL BACKGROUND

The absorbance of the product of a pseudo first-order reaction as a function of time is given by

$$A_{w,t} = a_w b C^0 (1 - e^{-kt}) + B_{w,C} \quad (1)$$

where a_w is the absorptivity coefficient at wavelength w, C^0 the initial concentration of the analyte, $B_{w,c}$ the absorbance when $t = 0$, (it includes the absorbance independent of the analytical reaction and the absorbance produced by the analytical reaction before the measurement starting point, consequently it depends both on the wavelength and on the analyte concentrations), b the lightpath and k the rate constant.

For a mixture of two analytes with additive absorbances in the absence of mutual interactions, equation (1) takes the form

$$A_{w,t} = a_{w,1} b C_1^0 (1 - e^{-k_1 t}) + a_{w,2} b C_2^0 (1 - e^{-k_2 t}) + B_{w,C} \quad (2)$$

which simplifies to

$$A_{w,t} = \sum_i K_{(i,w,t)} C_i^0 + B_{w,C} \quad (3)$$

Application of principal component regression (PCR) involves using principal component analysis (PCA) methodology[11] to draw analytically relevant information from the calibration data matrix obtained by recording the absorbance of m mixtures of known composition at n different wavelengths. For this purpose, the data matrix $\mathbf{A}(m,n)$ is broken down as follows:

$$\mathbf{A} = \mathbf{PT} + \mathbf{E} \quad (4)$$

where $\mathbf{P}(m,a)$ is the score matrix, $\mathbf{T}(a,n)$ the loading matrix, and $\mathbf{E}(m,n)$ the residual matrix, a being the number of principal components [$a \leq \min(m,n)$]. This procedure provides a calibration matrix, $\mathbf{B}$, by linear regression from the score matrix.

$$\mathbf{C} = \mathbf{PB} \quad (5)$$

$$\mathbf{B} = (\mathbf{P}^t\mathbf{P})^{-1}\mathbf{P}^t\mathbf{C} \quad (6)$$

The unknown mixture concerned is quantified by determining its scores, p_x, from its spectrum (a_x) and using the loading matrix obtained from the calibration samples. From the scores and matrix $\mathbf{B}$ the different mixture components are subsequently quantified by using the following equations:

$$a_x = p_x\mathbf{T} \quad (7)$$

$$a_x\mathbf{T}^t = p_x\mathbf{T}\mathbf{T}^t = p_x \quad (8)$$

$$C_x = p_x\mathbf{B} \quad (9)$$

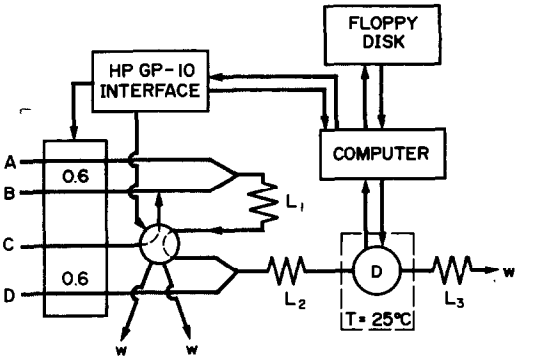

Fig. 1. Flow injection manifold. A: Borax buffer 0.1M, pH = 8.5. B: Bi-distilled water. C: unknown sample. E: PAR $10^{-3}M$. $V_t = 200$ μl; $L_1 = 2$ m, 0.5 mm i.d, $L_2 = 0.8$ m, 0.5 mm i.d, $L_3 = 2$ m, 0.3 mm i.d, D: spectrophotometric detector, W = waste.

EXPERIMENTAL

Reagents

Stock solutions of Ga(III) and Al(III) containing 1 g/l. of either in 1M hydrochloric acid were prepared from their nitrates (Merck *p.a.* grade chemicals) and standardized titrimetrically with EDTA[12].

A $10^{-3}M$ 4-(2-pyridylazo)resorcinol (PAR) solution was also prepared from its monohydrate monosodium salt (Merck, metallochromic indicator).

Finally, a 0.1M decahydrate disodium tetraborate buffer of pH 8.5 adjusted with nitric acid was made from Borax (Merck *p.a.* grade) and recrystallized twice in bi-distilled water.

Apparatus and manifold

The FIA manifold used (Fig. 1) consisted of a Gilson Minipuls 2 HP4 peristaltic pump; a Tecator V-200 variable-volume, two-channel injection valve; a quartz flow-cell of 18 μl inner volume and 10 mm lightpath that was thermostated at 25 ± 0.1°; and a Hewlett-Packard HP 8451A spectrophotometer. The peristaltic pump was connected to a relay and, together with the injection valve, was controlled via a GP-I0 interface connected to the switch of an HP 85 computer.

All tubes used and the injection loop were made of Teflon tubing of 0.5 mm bore.

Procedure

We recently developed a FIA-stopped flow system which allows samples to be injected and the flow to be halted by means of a commercially available Tecator V-200 injection valve.[13] Both the valve and the peristaltic pump were

Table 1. Composition (mg/l.) of the mixtures used for calibration and quantitation

Calibration samples							
	Mixture no.						
	1	2	3	4	5	6	7
[Ga]	2.47	0.00	1.48	2.47	3.45	3.94	4.93
[Al]	0.00	53.00	127.20	79.50	53.00	26.50	10.60
Quantitation samples							
	Mixture no.						
	8	9	10	11	12	13	14
[Ga]	0.99	1.23	1.48	1.97	2.96	4.44	4.44
[Al]	5.30	106.00	63.60	21.20	5.30	42.40	74.20

controlled by the computer of the spectrophotometer running a BASIC programme. On switching the valve, the metal solution was injected into the carrier which merged with the buffer and reagent stream solutions, and, once the plug had reached the detector cell, the flow was stopped and the spectra began to be recorded. Reference was recorded on the reagent stream solution, prior to the metal solution injection. In order to avoid wasting reagent, the peristaltic pump was also stopped.

The absorption spectra of the mixture were recorded over the wavelength range 490–540 nm at 2-sec intervals for 60 sec by using an integration time of 0.3 sec. Data were transferred to an IBM PC-XT computer via an HP/829339A RS232C interface for its mathematical treatment.

Fourteen solutions containing variable amounts of Ga(III) and Al(III) in the ranges 0–5 and 0–130 mg/l., respectively (Table 1), were injected in duplicate and the variation of the absorbance with time was monitored as described above. In order to simplify the calculations involved, the original data matrix was reduced to a representative portion, *viz.* that comprising the data corresponding to six wavelengths (500, 510, 518, 526, 532 and 540 nm) at five different times (6, 10, 14, 20 and 30 sec). The absorbances measured under these conditions were sorted as a function of time for each mixture and injection, and were processed by a principal component regression programme written by the authors that uses the NIPALS algorithm to break down the absorbance matrix.[14]

The values obtained for the five mixtures and the two solutions or pure metal ion were used to construct the calibration matrix, whereas those yielded by the other seven mixtures were employed for validation. Both calibration and validation were done by using the recordings obtained for the two injections.

RESULTS AND DISCUSSION

The kinetics of formation of the Ga(III)–PAR complex in an acid medium is well known.[15] However, the proposed mechanism does not hold for a basic medium owing to the presence of hydroxo complexes, which occur as the major species above pH 3.[16] In earlier work we derived the rate equation for this reaction in a slightly basic medium:[17]

$$v = k[\mathrm{Ga}]\,[\mathrm{H}^+]^{\frac{1}{2}}[\mathrm{PAR}] \qquad (10)$$

At pH 8.5 (Borax buffer) and a PAR concentration of $10^{-3}M$, the reaction can be assumed

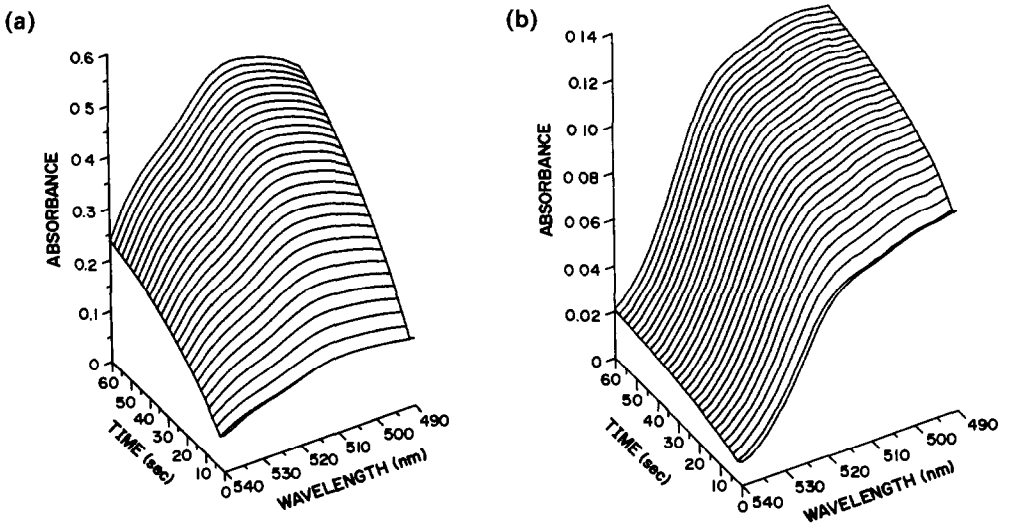

Fig. 2. (a) Kinetic curves of Ga-PAR complex obtained over the wavelength range 490-540 nm. (b) Kinetic curves of Al-PAR complex obtained over the same range.

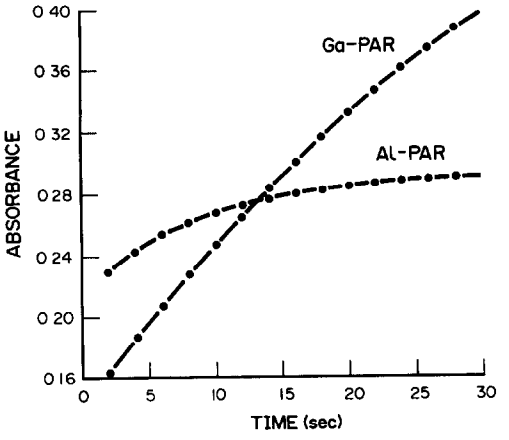

Fig. 3. Kinetic curves. Ga-PAR: 2.5 mg/l, Al-PAR: 100 mg/l. Dashed line: theoretical curve calculated using equation 1.

to be of pseudo first-order in the metal concentration, $v = k_{Ga}[Ga]$, so the corresponding rate constant is $k_{Ga} = (2.45 \pm 0.08) \times 10^{-2}$ sec^{-1}.

Under these conditions, the formation of the Al(III)–PAR complex is also of pseudo first-order in the metal concentration, and the rate constant is $k_{Al} = (9 \pm 1) \times 10^{-2}$ sec^{-1}, as determined by using the programme STATGRAPHICS 5.0 to fit the curves of seven solutions over the Al(III) concentration range 10.6–127.2 mg/l.

Figure 2 shows the variation with time and the wavelength of the absorbance of solutions containing 2.5 mg/l. Ga and 100 mg/l. Al. The corresponding kinetic curves obtained at 510 nm are shown in Fig. 3. The line is the theoretical curve corresponding to the model defined by equation (1) as fitted by STATGRAPHICS. As

Table 2. Variation of the residual variance with the number of principal components (a)

Components	1	2	3	4	5	6	7
$V_y(\cdot 10^4)$	7500	89	105	10	137	68	73

can be seen, the fit is quite good for both ions and thus indicative of pseudo first-order kinetics for the concentration of the two metal ions.

A plot of all the data recorded at the five times used in the calculations for pure solutions of Ga and Al is shown in Fig. 4., The wavelengths chosen for the quantitation of the mixtures are marked with an arrow. It must be remarked the cyclic structure of the data corresponding to the different times.

Determination of the number of principal components

Correct estimation of the number of principal components is crucial to the application of a PCR procedure. In this work we selected the number of factors by means of the cross-validation method.[18] For each factor, the total residual variance of the concentrations predicted by the model, (V_y), was calculated

$$V_{y_{\text{Total}}} = \frac{1}{NM} \sum_{i=1}^{M} \sum_{j=1}^{N} (\hat{C}_{(i,j)} - C_{(i,j)})^2 \qquad (11)$$

where N and M are, respectively, the number of analytes and samples used in the calibration set; $C_{(i,j)}$ denotes the experimental concentration of the analyte i in the sample j, and $\hat{C}_{(i,j)}$ refers to the calculated value. The variation of the residual variance with the number of PC is

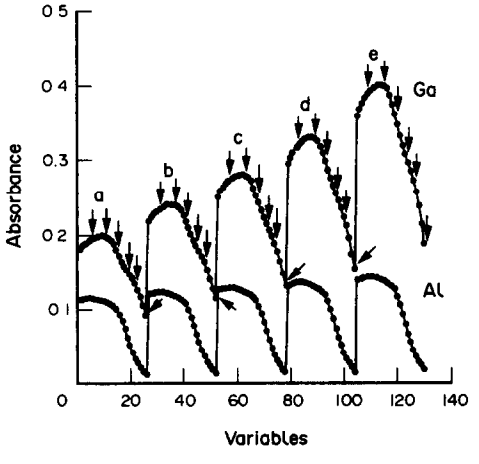

Fig. 4. Plot of measured data for Ga and Al solutions at 5 times (a: 6, b: 10, c: 14, d: 20 and e: 30 s) in the wavelength range 490–540 nm. The wavelengths chosen for the quantitation of the mixtures are marked with an arrow.

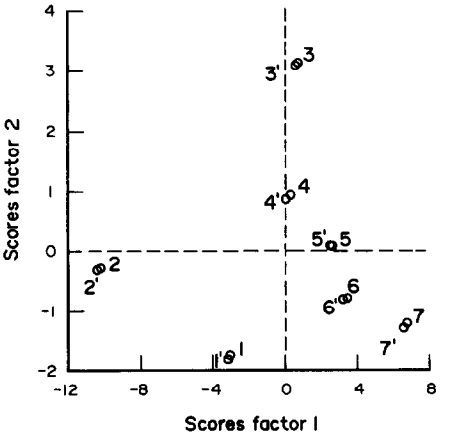

Fig. 5. PCR score plot, showing the position of the 7 calibration mixtures, two replicates of each one, on the first two factors, PC1 *vs.* PC2.

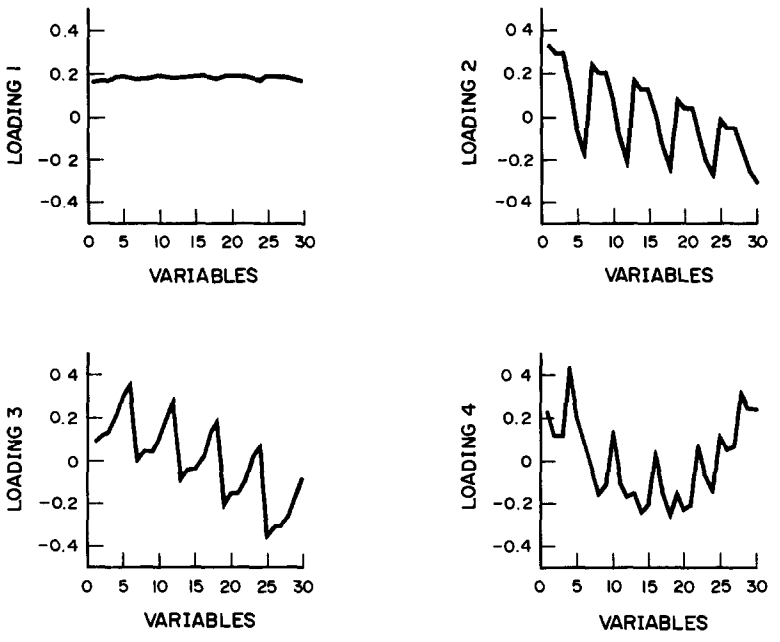

Fig. 6. Loading spectrum for factors PC1, PC2, PC3 and PC4.

shown in Table 2. It is observed that the minimum was found when four components were considered, increasing the value when more factors were used in the model.

Figure 5 shows the scores plot of the second PC versus the first PC; by comparison with data in Table 1, it is observed that PC1 scores increase with the concentration of Ga, whereas those of PC2 do it with the concentration of Al. The particular structure of the data in the calibration matrix, an ordered set of 6 measurements at each one of the 5 different times chosen, is reflected in the plot of the loadings of the four PC used to build the model, as is shown in Fig. 6. PC3 is associated to this cyclic structure, and the plot of the loading values of the 30 variables used for PC3 versus those of PC2 and PC1, Fig. 7, follows the same pattern as the original data. The relationship between PC4 and the data structure is more complex. Along the time, the absorbance recorded for a sample increases depending not only on the initial concentration of both metals but on the different values of the kinetic constants and the absorption coefficients of Ga–PAR and Al–PAR complexes as well. Figure 8 shows the loading values for PC4 at different wavelength versus each one of the 5 times selected and comparing with Fig. 3, it is seen that the minimum appears when the absorbance of Ga–PAR and Al–PAR are similar.

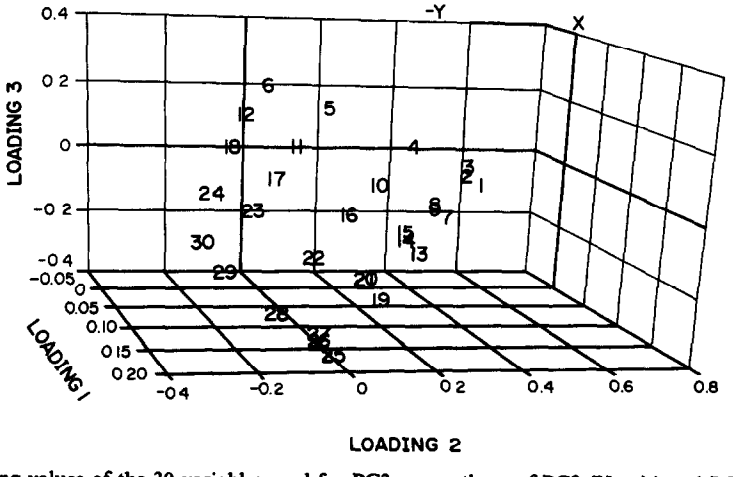

Fig. 7. Loading values of the 30 variables used for PC3 versus those of PC2 (Y axis) and PC1 (X axis).

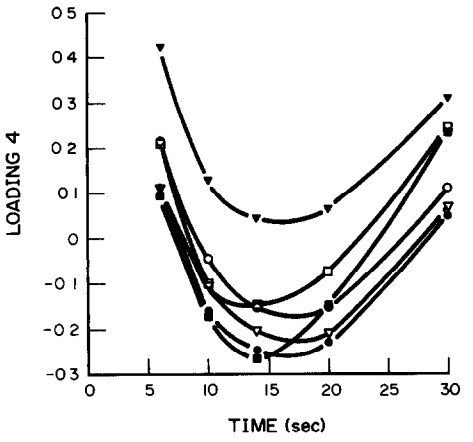

Fig. 8. Loading values for PC4 at different wavelengths (500 (●), 510 (○), 518 (▽), 526 (▼), 532 (□), 540 (■) nm) versus each one of the 5 times selected.

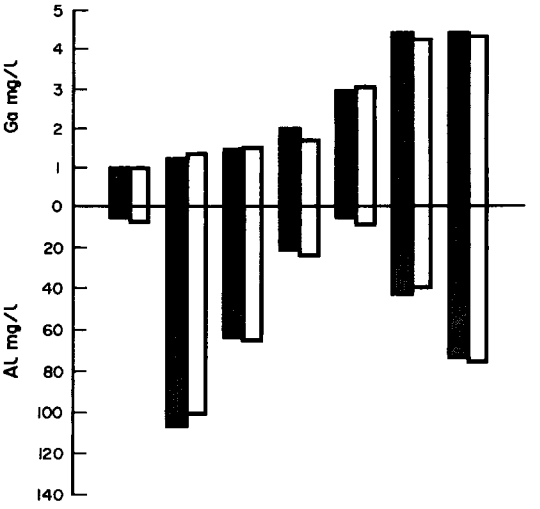

Fig. 9. Mixtures resolution. ■ Added, □ found.

Quantitation of the samples

Once the calibration model was established, analysis of the sample set was performed. The average values obtained are shown and compared with the added metal concentrations, Fig. 9. As can be seen, the mixtures were accurately resolved, with errors smaller than 10% in every case except for Al at concentrations below 20 mg/l., which can be attributed to the low sensitivity of its reaction with PAR under our experimental conditions.

The reproducibility of the proposed method, expressed as the mean relative standard deviation (MRSD), was estimated from the differences between the calculated values for two injections of each mixture according to the following equation,[19]

$$\%\text{MRSD} = 100 \times \frac{1}{\bar{C}}\left[\frac{\sum_{i}^{Z}\sum_{j}^{N}(C_{(i,j)1} - C_{(i,j)2})^2}{2Z}\right]^{\frac{1}{2}} \quad (12)$$

where N and Z are, respectively, the number of analytes and samples used in the validation set; $C_{(i,j)n}$ denotes the calculated concentration of the analyte i in the sample j and the determination n and $\bar{C}$ the mean concentration.

The MSRD was found to be 0.8% for Ga and 1.6% for Al.

We should emphasize that this procedure allows the highly accurate and precise simultaneous determination of GA–Al mixtures in which the latter metal is in a large excess (100:1) over the former.

The literature includes a few methods for the kinetic spectrophotometric resolution of Ga–In mixtures,[20,21] but none for Ga–Al mixtures, the resolution of which has so far been addressed by using spectrofluorimetric methods,[22–24] which obviously afford lower detection limits, but are applicable over narrower Ga/Al concentration ratio ranges (1:10).

In conclusion, multivariate calibration opens up new prospects for the resolution of mixtures on the basis of time-dependent chemical reactions. The procedures involved can be readily implemented in stopped-flow injection manifolds, which further increase the analytical potential of this technique.

Acknowledgements—The authors are grateful to the DGICyT for financial support granted for the realization of this work as part of Project PB87-0761.

REFERENCES

1. J. Ruzicka and E. H. Hansen, *Flow Injection Analysis*, Wiley, New York, 1981.
2. M. Valcárcel and M. D. Luque de Castro, *Flow-Injection Analysis. Principles and Applications*, Ellis Horwood, Chichester, 1987.
3. J. Ruzicka and E. H. Hansen, *Anal. Chim. Acta*, 1980, **114**, 19.
4. H. B. Mark Jr. and G. A. Rechnitz, *Kinetics in Analytical Chemistry*, Interscience, New York, 1968.
5. B. G. Willis, W. H. Woodruff, J. R. Frysinger, D. W. Margerum and H. L. Pardue, *Anal. Chem.*, 1970, **42**, 1350.
6. P. D. Wentzell, M. I. Kazayannis and S. R. Crouch, *Anal. Chim. Acta*, 1989, **224**, 263.
7. G. M. Ridderand and B. W. Margerum, *Anal. Chem.*, 1977, **49**, 2099.
8. M. C. Gutiérrez, A. Gómez-Hens and D. Pérez-Bendito, *Anal. Chim. Acta*, 1989, **225**, 115.
9. K. R. Beebe and B. R. Kowalski, *Anal. Chem.*, 1987, **59**, 1007A.

10. M. Otto, *Analyst*, 1990, **115**, 685.
11. J. Edward Jackson, *A User's Guide to Principle Components*, Wiley, New York, 1991.
12. G. Charlot, *Chimie Analytique Quantitative II. Méthodes Sélectionnées d'Analyse Chimique des Éléments*, Masson et Cie, Paris, 1974.
13. M. Blanco, J. Coello, H. Iturriaga, S. Maspoch and J. Riba, *J. Flow Inject. Anal.*, 1990, **7**, 3.
14. S. Wold, K. Esbensen and P. Geladi, *Chemometrics Intell. Lab. Syst.*, 1987, **2**, 37.
15. E. Mentasti, C. Baiocchi and L. J. Kirschembaum, *J. Chem. Soc., Dalton Trans.*, 1985, 2615.
16. C. F. Baes and R. E. Mesmer, *The Hydrolysis of Cations*, Wiley Interscience, New York, 1976.
17. M. Blanco, J. Coello, H. Iturriaga, S. Maspoch, J. Riba and E. Rovira, in the press.
18. S. Wold, *Technometrics*, 1978, **20**, 397.
19. G. E. P. Box, W. G. Hunter and J. S. Hunter, *Statistics for Experimenters*, Wiley, New York, 1978.
20. A. Marín, M. Silva and D. Pérez-Bendito, *Anal. Chim. Acta*, 1987, **197**, 77.
21. O. Abollino, E. Mentasti, C. Sarzanini and V. Porta, *Analyst*, 1991, **116**, 1167.
22. K. R. Vitense and L. B. MacGown, *ibid.*, 1987, **112**, 1273.
23. H. Heizo, M. Kiyotoshi and N. Yasaharu, *Anal. Chim. Acta*, 1978, **97**, 121.
24. J. M. Cano, A. García de Torres and M. E. Ureña, *Talanta*, 1990, **37**, 385.

Talanta, Vol. 40, No. 2, pp. 269–277, 1993
Printed in Great Britain.

0039-9140/93 $6.00 + 0.00

MULTIPARAMETRIC CURVE FITTING XIV*

MODUS OPERANDI OF THE LEAST-SQUARES ALGORITHM MINOPT

JIŘÍ MILITKÝ
Department of Textile Materials, Technical University, CS-461 17 Liberec, Czech Republic

MILAN MELOUN
Department of Analytical Chemistry, University of Chemical Technology, CS-532 10 Pardubice, Czech Republic

(*Received* 9 *December* 1991. *Revised* 29 *June* 1992. *Accepted* 29 *June* 1992)

Summary–Hybrid least-squares algorithm MINOPT for a nonlinear regression is introduced. MINOPT from CHEMSTAT package combines fast convergence of the Gauss–Newton method in a vicinity of minimum with good convergence of gradient methods for location far from a minimum. Quality of minimization and an accuracy of parameter estimates for six selected models are examined and compared with different derivative least-squares methods of five commercial regression packages.

In literature many regression algorithms and program packages for non-linear regression are described and classified.[1] According to their practical applicability in the chemical laboratory the program's modus operandi may be elucidated using a block structure classification:[2,3] regression program may be divided into functional blocks as INPUT, RESIDUAL SUM OF SQUARES, MINIMIZATION, STATISTICAL ANALYSIS, DATA SIMULATION, ADDITIONAL SUBROUTINES, *etc.* An amount of useful information achieved from program application, efficiency and reliability of results can be deduced from

(i) a numerical point-of-view which concerns ability to reach a minimum of the regression criterion (subroutines of a MINIMIZATION block);

(ii) a statistical point-of-view which concerns quality of statistical information (subroutines of STATISTICAL ANALYSIS block).

According to these two blocks the commonly used programs are not always reliable. Due to a great variability of regression models, regression criteria and data the effective algorithms enabling sufficiently fast convergence to a global extreme are not available. Some algorithms and programs often fail, *i.e.*, converge very slow or diverge.

In this paper we concentrate on procedures of derivative methods for the least-squares (LS) criterion which represents a very large group of methods today.[4] Some numerical aspects of the algorithm MINOPT are presented. Its numerical quality is examined and compared with other derivative methods on selected mathematical models usually found in problems of reaction kinetics and solution equilibria studies.

RESIDUAL SUM OF SQUARES BLOCK

In the classical setting the additive model of measurements is adopted

$$y_i = f(x_i; \beta) + \epsilon_i, \quad i = 1, \ldots, n \qquad (1)$$

In model (1) the y_i is the response (experimental quantity), x_i are non-stochastic explanatory variables (without detriment to generality, x is supposed to be scalar), $f(x_i, \beta)$ is a regression model containing the $(m \times 1)$ parameter vector β and ϵ_i is the so called (experimental) error.

The main task of regression is to find estimators, b, of an unknown parameter vector β. A process of parameter estimation is based on assumptions about errors ϵ: classical presumption requires the errors ϵ to be independent and identically distributed random variables having normal distribution $N(0, \sigma^2)$ with zero mean and constant variance σ^2. Based on these

*Part XIII, *Talanta*, 1988, **35**, 981.

assumptions the sufficient estimates $\hat{b} = \{b_1, \ldots, b_m\}$ can be obtained minimizing the least-squares criterion

$$U(\hat{b}) = \sum_{i=1}^{n} [y_i - f(x_i; \hat{b})]^2, \quad n \geqslant m \qquad (2)$$

MINIMIZATION BLOCK

For minimization of $U(\hat{b})$ criterion a lot of various derivative and non-derivative algorithms exist.[4-8] Derivative algorithms are useful for all model functions which are twice differentiable. In a sequel we concentrate on derivative methods and LS criterion only.

The main disadvantage of derivative methods is a local convergence which depends on a choice of an initial guess $\hat{b}^{(0)}$. All algorithms of this group are of iterative nature. In the i-th iteration a procedure starts from the estimates $\hat{b}^{(i)}$ to which a suitable increment vector $d^{(i)}$ is added:

$$\hat{b}^{(i+1)} = \hat{b}^{(i)} + d^{(i)} \qquad (3)$$

The vector $d^{(i)}$ is considered acceptable if

$$U(\hat{b}^{(i)} + d^{(i)}) \leqslant U(\hat{b}^{(i)}) \qquad (4)$$

Here, the increment vector can be expressed by relation

$$d^{(i)} = \alpha_i V \qquad (4a)$$

where V is directional vector and α is scalar. Some algorithms admit equality or even a small increase of $U(\hat{b}^{(i+1)})$ against $U(\hat{b}^{(i)})$. Procedure of a search of minimum $U(\hat{b})$ consists of the following four steps:

1. *Determination of initial guess of parameters* $\hat{b}^{(0)}$

This step is decisive for many algorithms for successful minimization. From a good initial guess $\hat{b}^{(0)}$ the simple algorithms usually converge. For a very poor initial guess a minimum cannot be found by any methods of this group.

2. *Determination of direction vector* V

Derivative of a LS criterion function $U(\hat{b})$ in a point $(\hat{b} + \alpha V)$ according a scalar α has form

$$\frac{\delta U(\beta)}{\delta \alpha} = \left[\frac{\delta U(\beta)}{\delta \beta}\right]^T \frac{\delta \beta}{\delta \alpha} \qquad (5)$$

For $\alpha \to 0$ we get from equation (5) so called directional derivative

$$S_D = \left.\frac{\delta U(\beta)}{\delta \alpha}\right|_{\alpha \to 0} = g^T V \qquad (6)$$

where g is the gradient vector of $U(\hat{b})$ whose elements g_j are equal to $\delta U(\hat{b})/\delta b_j$. The steepest decrease of a criterion function is in the direction $-g$. The condition of acceptability of the directional vector V requests that the directional derivative is not positive. Any direction for which an inequality $g^T V > 0$ holds is therefore inconvenient. Moreover, if the directional vector V is acceptable the positive regular definite matrix $\mathbf{R}$ exists so that

$$V = -\mathbf{R}g \qquad (7)$$

The directional derivative S_D is then equal to

$$S_D = -g^T \mathbf{R} g \qquad (8)$$

For a positive definite matrix $\mathbf{R}$ their quadrative forms are always positive so that S_D in equation (8) is negative.

3. *Calculation of minimization step* αV

For calculation of the minimization step (also called the optimal increment or the correction vector) $d = \alpha V$ in direction V the approximation of $U(\hat{b})$ by the Taylor series up to a quadratic term can be used. It leads to form

$$U(\hat{b} + \alpha V) \approx U(\hat{b}) + \alpha g^T V + \frac{\alpha^2}{2} V^T \mathbf{H} V \qquad (9)$$

where $\mathbf{H}$ is symmetric Hessian (matrix) having as elements the second derivatives of $U(\hat{b})$. Equation (9) assumes α to be approximately quadratic so that the optimal value of α may be estimated by putting the first derivative $U(\hat{b} + \alpha V)$ according to α to zero. Solving this equation will give

$$\alpha^* = -\frac{\delta U(\hat{b})}{\delta \alpha} \Big/ \frac{\delta^2 U(\hat{b})}{\delta \alpha^2} = -g^T V [V^T \mathbf{H} V]^{-1} \qquad (10)$$

and after substitution from equation (8) we obtain the so called Raleigh coefficient

$$\alpha^* = g^T \mathbf{R} g [g^T \mathbf{R}^T \mathbf{H} \mathbf{R} g]^{-1} \qquad (11)$$

The suitability of Raleigh coefficient α^* is restricted for a region in which the approximation (9) can be used.

For LS criterion $U(\hat{b})$ the gradient g can be expressed in the form

$$g = 2\mathbf{J}^T \hat{e} \qquad (12)$$

and the Hessian $\mathbf{H}$ in the form

$$\mathbf{H} = 2[\mathbf{J}^T \mathbf{J} - \mathbf{W}^T \hat{e}] = 2[\mathbf{J}^T \mathbf{J} - \mathbf{B}] \qquad (13)$$

Here $\hat{e}$ is the residual vector having components

$$\hat{e}_i = y_i - f(x_i; \hat{b}) \qquad (14)$$

$\mathbf{J}$ is the Jacobian (matrix) of dimension $(n \times m)$ with elements

$$J_{ij} = \frac{\delta f(x_i, \hat{b})}{\delta b_k}, \quad j = 1, \ldots, n; \quad k = 1, \ldots, m \quad (15)$$

and $\mathbf{W}$ is a three-dimensional array of dimension $(n \times m \times m)$ which is composed from n layers where the ith one is formed by the matrix $\mathbf{W}_i$ having elements

$$W_{i(j,k)} = \frac{\delta^2 f(x_i, \hat{b})}{\delta b_j \, \delta b_k} \quad (16)$$

4. *Termination of iteration process*

The natural criterion of an optimal estimate $\hat{b}$ is a zero value of the gradient g. Many methods of a minimum search terminate the iterative process when the norm of gradient

$$\| g \|^2 = \sum_{j=1}^{m} g_j^2 \quad (17)$$

is sufficiently small. It is possible to select a critical value of this norm, for example, equal to 10^{-4} *i.e.*, the limit under which the point $\hat{b}^{(i)}$ is considered as a local extreme. Often iterations terminate when too small changes of parameter estimates appear. None of these criteria enable a termination in a minimum. Minimization may terminate less heuristically. From the geometry of LS we get termination criterion as follows: the residual vector $\hat{e}$ is approximately perpendicular on columns of the matrix $\mathbf{J}$. This is equal to condition $\mathbf{J}^T\hat{e} = 0$. For cosines of angle α_j between the residual vector $\hat{e}$ and the j-th column J_j of a matrix $\mathbf{J}$ a simple relation is valid

$$\cos \alpha_j = \hat{e}^T J_j [J_j^T J_j \hat{e}^T \hat{e}]^{-1/2} \quad (18)$$

When a maximal value of $\cos \alpha_j$ is sufficiently small, *e.g.*, smaller than 10^{-9} it is supposed that a minimum $U(\hat{b})$ was reached. Some other termination criteria may be found in Ref. 7.

The following derivative algorithms seem to be dominant in nonlinear regression analysis today:

(a) Gauss–Newton methods;
(b) Marquardt methods;
(c) dog-leg method.

Gauss–Newton methods

For determination of a convenient directional vector V the quadratic approximation of a criterion function $U(\hat{b})$ may be used which also corresponds to equation (9) for $\alpha = 1$. From

$$\frac{\delta U(\hat{b} + V)}{\delta V_i} = 0 \quad (19)$$

the optimal direction vector $V_i = N_i$ in the form

$$N_i = -\mathbf{H}^{-1} g = (\mathbf{J}^T\mathbf{J} + \mathbf{B})^{-1} \mathbf{J}^T \hat{e} \quad (20)$$

is evaluated. Substituting into equation (11) we estimate that $\alpha^* = 1$. Therefore N_i is directly a minimization step d_i and the method is called the Newton–Raphson method. It is obvious that when the criterion $U(\hat{b})$ is a quadratic function (*i.e.*, an elliptic paraboloid) the minimum $\hat{b}$ will be reached in one step. For other forms of criterion function $U(\hat{b})$ and estimates $\hat{b}^{(0)}$ far from β, this method does not converge too fast. Moreover it requires knowledge of an array of second derivatives $\mathbf{W}_i$ for a determination of a matrix $\mathbf{B}$ in equation (13).

Neglecting matrix $\mathbf{B}$ is equivalent to a linearization of regression model and is theoretically acceptable for a case when a residual vector $\hat{e}$ is negligible. The corresponding directional vector L_i has the form

$$L_i = (\mathbf{J}^T\mathbf{J})^{-1} \mathbf{J}\hat{e} \quad (21)$$

and methods are called Gauss–Newton methods. They belong to the simple and the most frequently used procedures of nonlinear regression. When $\mathbf{H} \approx (\mathbf{J}^T\mathbf{J})$ is supplied into equation (11) it leads to $\alpha^* = 1$. From the practical point it is important that the Gauss–Newton method will work well, if some of the following conditions are fulfilled:

I. Residuals $\hat{e}_i = y_i - f(x_i, \hat{b})$ are small.

II. The model function $f(x, \beta)$ is nearly linear *i.e.*, the Hessian $\mathbf{H}$ has a small norm and its elements are nearly zero.

III. Residuals $\hat{e}_i$ have alternate signs so that $\mathbf{B}$ is approximately a zero matrix. It is valid in a vicinity of optimum $\hat{b}$.

Extending a region of convergence of this very simple method is possible to reach by different ways:

(a) The technique of an inversion of the matrix $\mathbf{J}^T\mathbf{J}$ and solution of a set of linear equations

$$(\mathbf{J}^T\mathbf{J})L = \mathbf{J}^T\hat{e} \quad (22)$$

(b) Improving a matrix $(\mathbf{J}^T\mathbf{J})$ in order to be close to Hessian $\mathbf{H}$.

(c) Choice of a suitable length of the step α.

Marquardt methods

The natural selection of a directional vector V_i is the direction of steepest descent $-g$. It corresponds to a matrix option $\mathbf{R} = \mathbf{E}$. For optimal coefficient α^* in this direction it is from equation (11) that

$$\alpha^* = g^T g [g^T \mathbf{H} g]^{-1} \approx g^T g [g^T (\mathbf{J}^T \mathbf{J})^{-1} g]^{-1} \quad (23)$$

The minimization step $d_i = -\alpha^* g$ corresponds to the gradient method.

The gradient methods converge often slowly in a vicinity of an optimum. On the other hand, in cases when $b^{(i)}$ is far from β it enables a direction leading to a minimum to be found. It is effective to use a combination of directions of the Newton method N_i or a direction of linearization L_i together with a direction $-g$ to a construction of the more robust procedures which are also called the hybrid procedures. Known representative is here the Marquardt method which calculates the directional vector $V_i(\lambda)$ by relation

$$V_i(\lambda) = (\mathbf{J}^T \mathbf{J} + \lambda \mathbf{D}_i^T \mathbf{D})^{-1} \mathbf{J}^T \hat{e} \quad (24)$$

where λ is the parameter and $\mathbf{D}_i$ is the diagonal matrix which eliminates an influence of various magnitudes of components of the matrix $\mathbf{J}$. Usually the diagonal elements D_{ii} are equal to diagonal elements of matrix $(\mathbf{J}^T \mathbf{J})$. Convenient selection of a parameter λ ensures:

(1) positive definiteness of a matrix $\mathbf{R} = (\mathbf{J}^T \mathbf{J} + \lambda \mathbf{D}^T \mathbf{D})$ which is necessary for its invertibility;

(2) a shortening step $V_i(\lambda)$ moving from a direction of linearization L_i;

(3) a possibility of a selection between a direction L_i and approximate direction $-g$. Step length in direction $-g$ is however equal to zero;

(4) a restriction of a magnitude of the incremental vector V_i to the certain "admissible" region in a vicinity of $b^{(i)}$.

The necessity of repeated matrix inversion for each λ is a disadvantage of this procedure which is rather time-consuming. Moreover a situation may happen that for large λ a magnitude V_i is too small. Therefore the maximal magnitude of λ is limited. Individual modifications of the Marquardt method differ especially in strategy of the adaptive setting of parameter λ.

Generally it is valid that methods of Marquardt type are for their robustness a standard part of library programs of most computer packages.

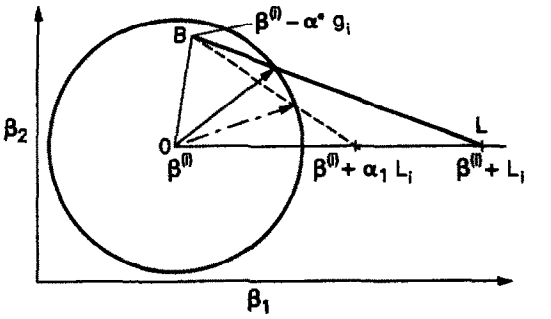

Fig. 1. Geometrical interpretation of dog-leg strategy. The circle shows admissible range of increments. Solid hypotenuse is $V(\mu)$ for $\alpha_1 = 1$ and dotted hypotenuse is $V(\mu)$ for $\alpha_1 = 1$.

Dog-leg methods

Among the main disadvantages of the Marquardt method are:

(a) a necessity of matrix inverse at change of parameter λ;

(b) a small length of vector $V(\lambda)$ for a large λ.

Both these disadvantages are removed in hybrid methods when the optimal directional vector $V(\mu)$ is the convex combination of vectors L and the vector $-\alpha^* g_i$. It holds that

$$V(\mu) = b^{(i)} + (1 - \mu) L_i \alpha_1 - \mu \alpha^* g_i \quad (25)$$

Here α^* is estimated from equation (23) and condition $0 \leqslant \mu \leqslant 1$ is valid. The function $V(\mu)$ for cases $\alpha_1 = 1$ and $\alpha_1 < 1$ on Fig. 1 hypotenuses of right angle triangles with dotted line for $\alpha_1 < 1$ and solid line for $\alpha_1 = 1$. Classical strategy of the Powell dog-leg method estimates an optimal vector $V_i(\mu)$ on the abscissa TB of a triangle defined by vertices $0 = b^{(i)}$; $T = b^{(i)} + L_i$; $B = b^{(i)} - \alpha^* g_i$ where α^* is defined by equation (23).

It is obvious that for $\mu = 0$ the vector $V(\mu)$ is identical with a linearization direction L_i and for $\mu = 1$ with a direction of negative gradient $-g$. The magnitude of a total increment in direction $-g$ correspond to the optimal value α^*.

Dennis and Mei[10] used the "shorter" vector $\alpha_1 L_i$ instead of a vector L_i. The parameter α_1 is determined that the increment in a linearization direction approximately corresponds to a Raleigh point, *cf.* Ref. 10.

$$\alpha_1 = 0.2 + 0.8 \, \|g_i\|^4 \times [g_i^T (\mathbf{J}^T \mathbf{J})^{-1} g_i g_i^T (\mathbf{J}^T \mathbf{J}) g_i]^{-1} \quad (26)$$

From Fig. 1 it is obvious that shortening $L_i \alpha_1$ leads to a directional vector $V_1^*(\mu)$ which is

closer to a linearization direction than the vector $V(\mu)$ calculated at option $\alpha_1 = 1$. MINOPT algorithm[11] uses $V_1^*(\mu)$ directional vector. For solution of matrix inverse problems a rational rank technique (*i.e.*, special pseudoinversion) is adopted. A special heuristic strategy for constraining a maximum step length based on quality of quadratic approximation of $U(\hat{b})$ is used here.

Other blocks as STATISTICAL ANALYSIS, GOODNESS-OF-FIT TEST, DATA SIMULATION, *etc.* will be described in the next contributions of this series.

Software

Program MINOPT from CHEMSTAT package carries out the numerical and statistical analysis of a non-linear regression model $f(x; \beta)$ with use of modified "double dog–leg" strategy. Input consists from the experimental data (x_i, y_i), $i = 1, \ldots, n$, and the initial guess of parameters estimates $\hat{b}^{(0)}$. The user supplies the regression model. All required derivatives are calculated numerically.

Program CHEMSTAT is available from authors on request.

RESULTS AND DISCUSSION

Comparison of some commercial packages for nonlinear regression

In a study of reaction kinetics and solution equilibria, the regression analysis of frequently used nonlinear models requires an estimation of unknown parameters of exponentials or parameter powers. To examine the reliability of MINOPT algorithm six testing problems have been chosen. Models I, II, and III are selected from literature. Models IV and VI are based on simulated data and Model V is based on experimental data. Testing models with their data and available initial guess of parameters are summarized below. To compare parameter estimates $\hat{b}$ and $U(\hat{b})$, no restart or repeated determination with new initial guess of parameters in divergence or failing were allowed. Commercial packages BMDP (*i.e.*, BMDP PC-90), SAS (*i.e.*, SAS version 6.03), SYSTAT (*i.e.*, SYSTAT version 5.01), SPSS (*i.e.*, SPSS PC+ version 3.1), ASYST (*i.e.*, ASYSTANT+ version 1.5), STATGR (*i.e.*, STATGRAPHICS version 5.0) and CHEMSTAT (*i.e.*, CHEMSTAT version 1.25) were used,[11,12] *cf.* Table 3.

Six tested models with data:

Model I. $y = \beta_1 + \beta_2 \exp(\beta_3 x)$

x	1	5	10	15	20	25	30	35	40	50
y	16.7	16.8	16.9	17.1	17.2	17.4	17.6	17.9	18.1	18.7

Model II. $y = \exp(\beta_1 x) + \exp(\beta_2 x)$

x	1	2	3	4	5	6	7	8	9	10
y	4	6	8	10	12	14	16	18	20	22

Model III. $y = \beta_1 \exp\left[\frac{\beta_2}{\beta_3 + x}\right]$

x	50	55	60	65	70	75	80	85
y	34780	28610	23650	19630	16370	13720	11540	9744

90	95	100	105	110	115	120	125
8261	7030	6005	5147	4427	3820	3307	2872

Model IV. $y = \beta_1 \exp(\beta_3 x) + \beta_2 \exp(\beta_4 x)$

x	7.448	7.448	7.969	8.176	9.284	9.439	7.552
y	57.544	53.546	19.498	16.444	4.305	3.006	45.290

7.877	8.552	9.314	7.607	7.847	8.176	8.523
27.952	11.803	4.764	51.286	31.623	21.777	13.996

8.903	9.314
7.727	4.999

Model V. $y = \beta_1 x^{\beta 3} + \beta_2 x^{\beta 4}$

x	12	13	14	15	16	17	18	19	20
y	7.31	7.55	7.80	8.05	8.31	8.57	8.84	9.12	9.40

21	22	23
9.69	9.99	10.30

Model VI. $y = \beta_1 [\exp(-\beta_2 x_1) + \exp(\beta_3 x_2)]$

x_1	0	0.6	0.6	1.4	2.6	3.2	0.8	1.6	2.6	4.0
x_2	0	0.4	1.0	1.4	1.4	1.6	2.0	2.2	2.2	2.2
y	40	10	5.0	2.5	2.5	2.0	1.0	0.7	0.8	0.7

1.2	2.0	4.6	3.2	1.6	4.2	4.2	3.2	2.8
2.6	2.6	2.8	3.0	3.2	3.4	3.4	3.8	4.2
0.4	0.4	0.3	0.22	0.22	0.1	0.05	0.07	0.03

4.2	5.4	5.6	3.2
4.2	4.4	4.8	5.0
0.03	0.03	0.02	0.01

Table 1. Initial guess of parameters estimated for six tested models

Model	$b_1^{(0)}$	$b_2^{(0)}$	$b_3^{(0)}$	$b_4^{(0)}$	$U(b^{(0)})$
I	1	1	1	—	$2 \cdot 10^{43}$
II	0.3	0.4	—	—	$4 \cdot 10^{3}$
III	0.02	4000	250	—	$1.7 \cdot 10^{9}$
IV	10^5	10^5	−1.679	−1.31	$1.12 \cdot 10^{4}$
V	100	0.1	2	10	$2.68 \cdot 10^{3}$
VI	12	1.0	25	—	226.9

Table 2. Best estimate of parameters of six various tested models

Model	b_1	b_2	b_3	b_4	$U(b)$
I	15.67	0.994	0.0222	—	$5.98 \cdot 10^{-3}$
II	0.2578	0.2578	—	—	124.34
III	0.005618	6180	345.2	—	87.9
IV	$8.315 \cdot 10^{7}$	$5.088 \cdot 10^{3}$	−1.95	−0.7786	134
V	3.802	$4.141 \cdot 10^{-3}$	0.223	2.061	$2.98 \cdot 10^{-5}$
VI	31.5	1.51	19.9	—	1.25

Table 3. Results of six analyzed models

Model I

Program	Method	Solution	Note	RSS
BMPD	3R-Gauss	False	Local minimum	3.68
	AR(DUD)	False	Local minimum	3.68
SAS	Gauss–Newton	False	Local minimum	1.903
	Marquardt	o.k.		5.987E-03
	Gradient	False	Local minimum	1.903
	DUD	False	Local minimum	2.036
SPSS	Marquardt	o.k.		5.986E-03
STATGR	Marquardt	Aborted	Overflow	4.011
ASYST	Gauss–Newton	False	Local minimum	67.76
	Var. metric	False	Divergence	
	Hybrid. method.	Aborted	System error	
SYSTAT	Var. metric	False	Local minimum	3.68
	Simplex	False	Local minimum	3.68
CHEMSTAT MINOPT		o.k.	28 iterations	5.986E-03

Model II

Program	Method	Solution	Note	RSS
BMDP	3R-Gauss	False	Local minimum	259.28
	AR(DUD)	False	Local minimum	1063.0
SAS	Gauss–Newton	False	Local minimum	3400
	Marquardt	o.k.	10 iterations	124.36
	Gradient	False	Very slow converg.	245.4
	DUD	DUD	Nearly o.k.	127.0
SPSS	Marquardt	o.k.		124.4
STATGR	Marquardt	o.k.	10 iterations	124.36
ASYST	Gauss–Newton	False	Program error	
	Var. metric	False	Program error	
	Hybrid. method	o.k.		124.36
SYSTAT	Var. metric	False	Local minimum	2000
	Simplex	o.k.	5 iterations	124.36
CHEMSTAT MINOPT		o.k.	10 iterations	124.36

continued

Table 3—*continued*

Model III

Program	Method	Solution	Note	RSS
BMDP	3R-Gauss	o.k.	11 iterations	87.95
	AR(DUD)	o.k.	160 iterations	87.95
SAS	Gauss–Newton	False	No convergence	1.6E + 09
	Marquardt	False	No convergence	6.9E + 06
	Gradient	False	No convergence	6.9E + 06
	DUD	o.k.	2.66 iterations	87.95
SPSS	Marquardt	o.k.		87.95
STATGR	Marquardt	False	Local minimum	9.0E + 04
ASYST	Gauss–Newton	False	No convergence	6.9E + 06
	Var. metric	False	Program error	
	Hybrid. method	False	Program error	
SYSTAT	Var. metric	False	Slow converg. err.	1.7E + 03
	Simplex	o.k.	160 iterations	87.95
CHEMSTAT MINOPT		o.k.	47 iterations	87.95

Model IV

Program	Method	Solution	Note	RSS
BMDP	3R-Gauss	False	No convergence	1.8E + 04
	AR(DUD)	False	Stack overflow	
SAS	Gauss–Newton	False	Local minimum	9.59
	Marquardt	False	No convergence	1.8E + 04
	Gradient	False	No convergence	1.3E + 04
	DUD	False	No convergence	1.8E + 04
SPSS	Marquardt	o.k.		3.18E − 04
STATGR	Marquardt	o.k.	28 iterations	3.179E − 04
ASYST	Gauss–Newton	False	No convergence	6.9E + 06
	Var. metric	False	Program error	
	Hybrid. method	False	Program error	
SYSTAT	Var. metric	o.k.	44 iterations	3.179E − 04
CHEMSTAT MINOPT		o.k.	37 iterations	3.179E − 04

Model V

Program	Method	Solution	Note	RSS
SPSS	Marquardt	False	Underflow error	
CHEMSTAT MINOPT		o.k.	47 iterations	128.98

Model VI

Program	Method	Solution	Note	RSS
SPSS	Marquardt	False	Very slow converg.	97.8
CHEMSTAT MINOPT		o.k.	51 iterations	2.98E − 05

Table 4. Performance index PI for tested packages

Package	PI[%] (tests 1–4)	PI[%] (tests 1–4)
BMDP	25	—
SAS	25	—
SYSTAT	37.5	—
STATGR	50	—
ASYST	8.3	—
SPSS	100	66.6
CHEMSTAT	100	100

Initial guess of parameters (Table 1), parameters estimates (Table 2) and results of convergence (Table 3) for six tested models are summarized. Detailed results may be found in the forthcoming[12] textbook or from the authors. For overall comparison of packages the Performance Index PI was computed

$$PI = \frac{100 * (\text{number of correct results})}{T * (\text{number of used methods in package})}$$

where T is the number of tests. From a numerical viewpoint the greater value of PI indicates the better package. Performance index PI for all tested packages are summarized in Table 4.

CONCLUSION

From this comparative study it can be deduced that the best results have been obtained using MINOPT procedure. Even this comparison may disappoint some users of standard statistical packages as it indicates that errors due to a false optimum, saddle points or a flat $U(b)$ function can often cause failure of the whole regression analysis.

REFERENCES

1. D. A. Ratkowsky, *Nonlinear Regression Modelling*, Marcel Dekker New York, 1983.
2. M. Meloun and M. Javůrek, *Talanta* 1985, **32**, 973.
3. M. Meloun, J. Havel and E. Högfeldt, *Computation of Solution Equilibria*, Ellis Horwood, Chichester, 1988.
4. P. E. Gill, W. Murray, M. M. Wright, *Practical Optimization*, Academic Press, London, 1981.
5. R. Schmidt, *Advances in Nonlinear Parameter Optimization*, Springer, Berlin, 1982.
6. A. R. Gallant, *Nonlinear Statistical Models*, Wiley, New York, 1987.
7. Y. Bard, *Nonlinear Parameter Estimation*, Academic Press, New York, 1974.
8. D. M. Bates and D. G. Watts, *J. Roy. Stat. Soc.* 1980, **B24**, 1.
9. J. E. Dennis and H. H. W. Mei, *J. Opt. Theor. Appl.*, 1979, **28**, 453.
11. J. Militký and J. Čáp, *Proc. Conf. CEF 87*, Taormina, Sicilia, May 1987.
12. M. Meloun, J. Militký and M. Forina, *Chemometrics in Instrumental Analysis*, Vol. 1, Solved Problems by IBM PC, Vol. 2. Interactive Model Building on IBM PC, Ellis Horwood, Chichester, 1992.

Talanta, Vol. 40, No. 2, pp. 279–285, 1993
Printed in Great Britain.

0039-9140/93 $6.00 + 0.00

MULTIPARAMETRIC CURVE FITTING XV

STATISTICAL ANALYSIS AND GOODNESS-OF-FIT TEST BY THE LEAST-SQUARES ALGORITHM MINOPT

JIŘÍ MILITKÝ
Department of Textile Materials, Technical University, CS-461 17 Liberec, Czech Republic

MILAN MELOUN
Department of Analytical Chemistry, University of Chemical Technology, CS-532 10 Pardubice, Czech Republic

(*Received* 9 *December* 1991. *Revised* 29 *June* 1992. *Accepted* 29 *June* 1992)

Summary—Estimation of nonlinear regression quality leads to examination of quality of parameter estimates, a degree of fit, a prediction ability of model proposed and quality of experimental data. Statistical analysis serves for computation of confidence intervals of parameters and confidence bands, the bias of parameters and bias of residuals. Goodness-of-fit test examines classical residuals using various diagnostics and identifies influential points. Mentioned topics of nonlinear model building and testing contained in MINOPT program from CHEMSTAT package are illustrated.

Practical applicability of regression algorithms and program packages for non-linear regression can be deduced from an ability to reach a minimum of a sum of squared residuals and from a quality and amount of statistical information. Structural classification of regression programs in blocks already introduced in ABLET programs of solution equilibria[1,2] and instrumental methods of analytical and physical chemistry concerns blocks INPUT, RESIDUAL SUM OF SQUARES, MINIMIZATION, STATISTICAL ANALYSIS, GOODNESS-OF-FIT TEST, DATA SIMULATION, *etc.* was also used here.

While a previous paper[3] of this series describes RESIDUAL SUM OF SQUARES and MINIMIZATION blocks, this paper brings a description of two other blocks of MINOPT structure, *i.e.*, STATISTICAL ANALYSIS and GOODNESS-OF-FIT TEST. Procedure of regression model testing[4] is illustrated.

THEORY

Statistical analysis block

Statistical analysis in nonlinear regression depends on an actual model used, measurement errors and a criterion function. Let us concentrate here on the method of maximum likelihood when the searched estimates $\hat{b}$ maximize the logarithm of the likelihood function $l(\beta) = \ln L(\beta)$. If for the additive model of measurement (*cf.* Ref. 3) the independent errors ϵ have the probability density function $p(\epsilon)$ then likelihood function $L(b)$ is defined as

$$L(b) = \prod_{i=1}^{n} p(y_i - f(x_i; b) \qquad (1)$$

In construction of confidence intervals of parameters β or in statistical hypotheses testing the linearization, Lagrange multipliers and likelihood ratio methods may be used.[5]

The least-squares (LS) method is the best case of an additive model of measurement and independent normally distributed measurement errors having constant variance. Gallant[5] shows that the least squares estimator $\hat{b}$ of true value of parameters β in the regression model has asymptotically m-dimensional normal distribution

$$\hat{b} \approx N[\beta, \sigma^2(\mathbf{J}^T\mathbf{J})^{-1}] \qquad (2)$$

Here σ^2 is error variance and $\mathbf{J}$ is the Jacobi matrix (definition, *cf.* ref. 3). The asymptotic normality of estimates $\hat{b}$ determined by the least-squares method does not require a normality of errors ϵ, Ref. 5.

For real experimental data the estimates $\hat{b}$ and other statistical characteristics are biased and therefore application of equation (2) is

limited. Statistical analysis of nonlinear regression models by the least-squares methods then depends on a magnitude of bias which describes a degree of nonlinearity of regression model.

Covariance matrix of parameter estimates. From equation (2) it follows that the asymptotic covariance matrix of estimate $\hat{b}$ is expressed by the relation

$$D(\hat{b}) = \sigma^2(\mathbf{J}^T\mathbf{J})^{-1} \tag{3}$$

where s^2 is estimator of σ^2. There exist many more accurate expressions,[6] but for practical calculations the asymptotic formula [equation (3)] is quite acceptable.

On the base of knowledge of a covariance matrix $D(\hat{b})$ either the variance of individual parameters $D(\hat{b}_j)$ or the correlation coefficients r_{ij} between estimates $\hat{b}_i$ and $\hat{b}_j$ may be estimated.

Bias of parameter estimates. The bias is given by

$$h = E(\hat{b} - \beta^*) \tag{4}$$

For the sake of simplicity we use an expression of parameter bias in the form[7]

$$h = (\mathbf{J}^T\mathbf{J})^{-1}\mathbf{J}^T d \tag{5}$$

where d is the $(n \times 1)$ vector with components

$$d_i = \frac{-\sigma^2 \operatorname{tr}[(\mathbf{J}^T\mathbf{J})^{-1}\mathbf{W}_i]}{2} \tag{6}$$

where tr[·] denotes a trace of matrix and $\mathbf{W}_i$ is the matrix of second derivatives of model function in the i-th point. The vector d is an expected value of difference between the linear and quadratic approximation of a model function.

Similarly the bias of residuals

$$\hat{e}_i = y_i - \mathrm{f}(x_i; \hat{b}) \tag{7}$$

can be defined. When $E(\epsilon) = 0$, the bias of residuals is equal to their mean value $E(\hat{e})$. The mean value of residuals vector

$$E = E(\hat{e}) \tag{8}$$

can be rewritten[7] as

$$E = (\mathbf{E} - \mathbf{P})\, d \tag{9}$$

where $\mathbf{P} = \mathbf{J}(\mathbf{J}^T\mathbf{J})^{-1}\mathbf{J}^T$ is the projection matrix and $\mathbf{E}$ is the unit matrix of order n.

For practical calculation the relative bias of parameter estimates is often used

$$h_{Rj} = \frac{h_j}{\hat{b}_j} 100 \quad [\%] \tag{10}$$

The bias of estimates is considered significant if $h_{Rj} > 1\%$ holds.[7] For such biased estimates the statistical analysis based on linearization of regression model cannot be correctly used.

For expressing the total bias of parameter estimates Box[8] proposed the scalar characteristic

$$\hat{M} = \frac{h^T(\mathbf{J}^T\mathbf{J})h}{m\hat{\sigma}^2} \tag{11}$$

The bias of parameters may be affected by a reparametrization.[9]

Interval estimates of parameters. Points estimates $\hat{b}$ of regression parameters β are, in the statistical view, worthless as they do not mention intervals in which a true value β may be expected. The estimates $\hat{b}$ are random quantities estimated on base of sample, $\{y_i, x_i\}$, $i = 1, \ldots, n$.

In nonlinear regression models for a construction of confidence regions and intervals a linearization is often used for which confidence regions are elliptic. However, a linearization is useful only in cases when a model is not strongly nonlinear and nonlinearity measures, for example, the parameter bias, are small. The more accurate confidence region calculated on the base of Lagrange multipliers or the likelihood ratio can also be constructed. They are generally non-elliptic and are not continuous.

For asymptotic normality of maximum likelihood estimates $\hat{b}$ it follows that the quadratic form

$$Q = (\beta - \hat{b})^T D(\hat{b})^{-1}(\beta - b) \tag{12}$$

has χ^2(m) distribution. The corresponding 100(1–α)% confidence region of parameters β forms a m-dimensional ellipsoid with boundaries expressed by

$$(\beta^* - \hat{b})^T D(\hat{b})^{-1}(\beta^* - \hat{b}) = \chi^2_{1-\alpha}(m) \tag{13}$$

where $\chi^2_{1-\alpha}(m)$ is the $100(1-\alpha)$%th quantile of $\chi^2(m)$ with m degrees of freedom. The center of this ellipsoid is in the point $\hat{b}$.

For the least-squares method the application of equation (13) leads to definition of confidence ellipsoid having the boundary

$$\Delta b^T(\mathbf{J}^T\mathbf{J})^{-1}\,\Delta b = m\hat{\sigma}^2 F_{1-\alpha}(m, n-m) \tag{14}$$

where $\Delta b = \beta - \hat{b}$ and $F_{1-\alpha}(m, n-m)$ is quantile of Fisher–Snedecor distribution.

When a bias of parameters h is calculated, instead of Δb the correction $\Delta b_0 = \hat{b} - h - \beta$ may be used.

For expressing a geometry of confidence ellipsoids the decomposition of the matrix $(\mathbf{J}^T\mathbf{J})^{-1}$ to eigenvalues L_i and eigenvectors Z_i may be introduced

$$(\mathbf{J}^T\mathbf{J})^{-1} = \mathbf{Z}\mathbf{L}\mathbf{Z}^T \tag{15}$$

where $\mathbf{Z}$ is a matrix containing eigenvectors in columns and diagonal matrix $\mathbf{L}$ contains eigenvalues $L_1 \geqslant L_2 \geqslant \cdots \geqslant L_m$ on a diagonal. Using this decomposition the new orthogonal set of coordinates $y = \mathbf{Z}\,\Delta b$ can be defined. This set has an important property that the axes of confidence ellipsoid are identical with the axes of the coordinate system. Introducing notation

$$p^2 = m\hat{\sigma}^2 F_{1-\alpha}(m, n-m) \tag{16}$$

the confidence ellipsoid can be expressed by simple formula

$$\sum_{i=1}^{m} \frac{Y_i^2}{L_i} = p^2 \tag{17}$$

The lengths of half-axes of the ellipsoid are equal to $p\sqrt{L_i}$. For a projection Δ_{jk} of the j-th half-axis into the axis of parameter β_k it holds that

$$\Delta_{jk} = p|Z_{kj}\sqrt{L_j}| \tag{18}$$

where Z_{kj} is the k-th elements of the vector Z_j which is the j-th column of matrix $\mathbf{Z}$.

When dimension of a parameter vector is $m > 2$, a partial confidence ellipsoid can be constructed.[5]

For building the confidence region the Lagrange multipliers or a likelihood ratio may also be used. For example, from properties of likelihood ratio the bound of $100(1-\alpha)\%$ confidence region can be defined by relation

$$2[\ln L(\hat{b}) - \ln L(\beta)] = \chi^2_{1-\alpha}(m) \tag{19}$$

For a least-squares criterion the relation (19) leads to the relation

$$U(\beta) - U(\hat{\beta}) = m\hat{\sigma}^2 F_{1-\alpha}(m, n-m) \tag{20}$$

The confidence region defined by this equation is not generally elliptical or continuous.

With the use of equation (13) the $100(1-\alpha)\%$th confidence interval of parameter β_j in the form

$$\hat{b}_j - \hat{\sigma}\sqrt{C_{jj}}\, t_{1-\alpha/2}(n-m) \leqslant \beta_j \leqslant \hat{b}_j + \hat{\sigma}\sqrt{C_{jj}}\, t_{1-\alpha/2}(n-m) \tag{21}$$

is direct analogy of confidence intervals of the parameters of linear models. An influence of other parameters is neglected. When all diagonal-off elements of the matrix $\mathbf{C} = (\mathbf{J}^T\mathbf{J})^{-1}$ are zero the relation (21) may be used. However, elements of the vector $\hat{b}$ are often mutually correlated so that intervals of equation (21) are under-estimated.

More suitable determination of the confidence interval of parameter β_k is based on the maximal length Δ_k of a projection Δ_{kj} into the parameter axis β_k. The confidence interval of a parameter β_k is then estimated by

$$\hat{b}_k - \Delta_k \leqslant \beta_k \leqslant \hat{b}_k + \Delta_k \tag{22}$$

Instead of projections it is simpler to search directly coordinates of extreme points on the confidence ellipsoid in directions of individual parameter axes.[2] The corresponding confidence interval of a parameter β_k is defined by inequality

$$\hat{b}_k - p\sqrt{C_{kk}} \leqslant \beta_k \leqslant \hat{b}_k + p\sqrt{C_{kk}} \tag{23}$$

holds. For $m = 1$ all confidence intervals[21-23] are identical. Increasing the number of regression parameters m the confidence intervals (22) and (23) are broader than those of (21). All confidence intervals are symmetrical. Using linearization the confidence intervals of prediction $f(x^*; \hat{b})$ and confidence bands can be simply derived.[4] The more accurate confidence bands may be constructed with the use of convenient reparametrization.[9]

Goodness-of-fit tests block

In many regression programs the statistical analysis of residuals represents the main diagnostic tool and a resolution criterion in a search of the "best" model when more than one are possible or proposed. The goodness-of-fit test (which is also called the fitness test) analyses the residual set and examines statistical characteristics.

To application of statistical analysis of classical residuals $\hat{e}$, it should be critically noted that the diagnostic use of classical residuals is not rigorous but of a rather approximate character. The classical residuals do not exhibit a zero mean, they are biased and they are a combination of errors ϵ. Moreover, they are dependent on true values of parameters β which are unknown.

Statistical analysis of classical residuals. Classical residuals are defined as the differences $\hat{e}$ between observation y_i and prediction $\hat{y}_i = f(x_i; \hat{b})$ by equation (7). Graphical and analytical examining residuals check the quality of a

nonlinear model.[4] The following plots are often used in nonlinear models examination:

(1) The overall diagram gives a first view of residuals. If the model is correct these residuals should resemble observations from a normal distribution with zero mean.

(2) Plot type I (also called the index plot) is a scatter plot of residuals $\hat{e}_i$ against an index i in the time order as occurred.

(3) Plot type II (also called the plot against an independent variable) is a scatter plot of residuals $\hat{e}_i$ against the independent variable x_j, $j = 1, \ldots, m$.

(4) Plot type III (also called the plot against a prediction) is a scatter plot of residuals against the prediction $\hat{y}_i$.

The following statistics are used in nonlinear models examination:

(1) The arithmetic mean of residuals known as the estimate of residuals bias, $E(\hat{e})$, should be equal to zero;

(2) The residual variance is calculated from the residual sum of squares

$$\hat{\sigma}^2 = U(\hat{b})/(n-m) \tag{24}$$

The square-root of a residual variance known as an estimate of the residual standard deviation, $s(\hat{e})$, should be of the same magnitude as the (instrumental) error $s_{\text{inst}}(y)$, of dependent variable (observation, measured quantity y), *i.e.*, $s(\hat{e}) \approx s_{\text{inst}}(y)$;

(3) The determination coefficient D^2 is computed from the relation

$$D^2 = 1 - \frac{U(\hat{b})}{\sum_{i=1}^{n} (y_i - \bar{y})^2} \tag{25}$$

where $\bar{y} = 1/n \, \Sigma_{i=1}^{n} y_i$ is the arithmetic mean of response variable. The determination coefficient is for linear models equal to the square of the multiple correlation coefficient. When the determination coefficient is multiplied by 100% we receive the regression rabat in percents, $100D^2$[%]. Determination coefficient D^2 is an increasing function of a number of parameters, therefore, it is not convenient to use as a resolution diagnostic for search of models of different numbers of parameters.

(4) To distinguish between various models proposed the Akaike information criterion AIC is more suitable to apply being defined by the relation

$$\text{AIC} = -\ln L(\hat{b}) + 2m \tag{26}$$

where $L(\hat{b})$ is the likelihood function. The "best" model is considered to be a model for which this criterion reaches a minimal value. Using the least-squares criterion the AIC may be expressed

$$\text{AIC} = n \ln\left[\frac{U(\hat{b})}{n}\right] + 2m \tag{27}$$

(5) The prediction ability of a model proposed may be examined by the mean quadratic error of prediction MEP being defined by the relation

$$\text{MEP} = \frac{1}{n} \sum_{i=1}^{n} (y_i - \text{f}(x_i; \hat{b}_{(i)})^2 \tag{28}$$

The symbol $\hat{b}_{(i)}$ denotes the estimator of parameter β computed without the point (x_i, y_i). Here instead of the parameter estimate $\hat{b}_{(i)}$, the one-step approximation $\hat{b}^1_{(i)}$ defined by following equation (29) may be used. Lower values of MEP criterion give better prediction ability of the model proposed.

Identification of influential points. Influential points can strongly affect some regression characteristics. The points affecting prediction $\hat{y}_i$, for example, may not be influential from the point of view of parameter variance. The degree of influence of individual points should be classified regarding which characteristics are affected.[4] While for linear models all the characteristics for identification of influential points are a function of residuals $\hat{e}$ and diagonal elements P_{ii} of the projection matrix $\mathbf{P} = \mathbf{X}(\mathbf{X}^T\mathbf{X})^{-1}\mathbf{X}^T$. For nonlinear regression models the parameter estimates and residuals cannot be expressed so simply as a linear combination of experimental data. When the Taylor type linearization of original nonlinear model is used, all methods of identification of influential points in linear models can be used here. Then in the nonlinear case the matrix $\mathbf{J}$ has the same role as $\mathbf{X}$ in the linear case. For a one-step approximation of the parameter estimate $\hat{b}_{(i)}$ computed without point (x_i, y_i) is valid

$$\hat{b}^1_{(i)} = \hat{b} - (\mathbf{J}^T\mathbf{J})^{-1} J_i \frac{\hat{e}_i}{1 - P_{ii}} \tag{29}$$

Here P_{ii} are elements of a projection matrix $\mathbf{P} = \mathbf{J}(\mathbf{J}^T\mathbf{J})^{-1}\mathbf{J}^T$. With use of equation (29) the variance estimate $\hat{s}^2_{(ii)}$ when leaving out the ith point is defined by

$$\hat{s}^2_{(i)} = \frac{U(\hat{b}) - \dfrac{\hat{e}_i^2}{1 - P_{ii}}}{n - m - 1} \tag{30}$$

Some characteristics of influential points based on linearization and used in program MINOPT are in Table 1. Interpretation of these characteristics may be found in Ref. 4.

To express an influence of individual points on parameter estimates the quadratic expansion of a regression model may be used, too.[10]

Nonlinear measure of an influence of the ith point on the parameter estimates is also represented by the likelihood distance

$$LD_i = 2[\ln L(\hat{b}) - \ln L(\hat{b})_{(i)})] \qquad (31)$$

In case of the least-squares the likelihood distance is expressed by

$$LD_i = n \ln\left[\frac{U(\hat{b}_{(i)})}{U(\hat{b})}\right] \qquad (32)$$

In both equations (31) and (32) the estimate $b_{(i)}$ is calculated by a nonlinear regression when the ith point is left out or the one-step approximation $\hat{b}^1_{(i)}$ of the parameter estimates is used. When inequality $LD_i > \chi^2_{1-\alpha}(2)$ holds, the ith point is strongly influential. The significance level α is usually chosen to be equal to 0.05.

Procedure of nonlinear model testing

A quality of nonlinear model proposed is examined using following criteria.

Quality of parameter estimates. Quality of parameter estimates $\hat{b}_j$ is considered according to their confidence intervals Δ_j, equation (18) and (21) and Δ_{Rj}, equations (22) and (23) or according to their standard deviations $s(\hat{b}_j)$, equation (3), the absolute bias h_j, equation (5) and the relative bias h_{Rj}, equation (10). Often an empirical rule of thumb is used: the parameter β_j is considered to be significant when its estimate $\hat{b}_j$ is greater than its 2 standard deviations, $2s(\hat{b}_j) < |\hat{b}_j|$. High values of parameter standard deviation $s(\hat{b}_j)$ is caused by termination of a minimization process before reaching minimum. Therefore, also inaccuracy of calculation of matrix **J** appears or a high nonlinearity of

Table 1. Three characteristics of influential points based on linearization. Critical level is the value of characteristic exceed this level, the corresponding point is denoted as highly outlying

Name	Form	Critical level
Cook distance D_i	$\frac{(\hat{b}-\hat{b}_i)^T \mathbf{J}^T \mathbf{J}(\hat{b}-\hat{b}_i)}{m\hat{\sigma}^2}$	1
DF_i	$\frac{(\hat{y}_i - \hat{y}_{(i)i})^2}{\hat{s}^2_{(i)} P_{ii}}$	$2\sqrt{m/n}$
Jackknife residual $\hat{e}_{Ji}$	$\frac{\hat{e}_i}{\hat{s}_{(i)}\sqrt{1-P_{ii}}}$	3

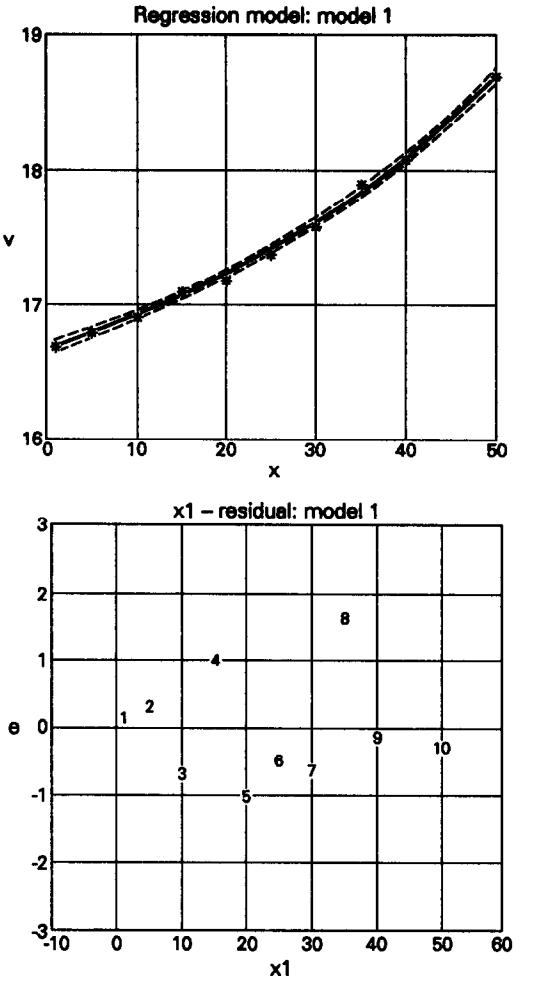

Fig. 1. Non-linear regression of data for Model I: (a) a curve-fitting, and (b) a scatter plot of type II of classical residuals.

regression model exists. The test of statistical significance of each parameter β_j, the null hypothesis $\beta_j = 0$ *vs.* the alternative one $\beta_j \neq 0$, is carried out.

Inter-dependence between parameters. Matrix of paired correlation coefficients of parameters, r_{ij}, expresses a measure of correlation or inter-dependence between two parameters β_i and β_j. If r_{ij} in absolute value is close to one, two parameters β_i and β_j are linearly dependent.

Quality of achieved model fitness. Agreement of proposed model with experimental data is examined by (i) the statistical analysis, and (ii) the goodness-of-fit test.

The statistical analysis of nonlinear regression contains following characteristics: the residual sum of squares $U(\hat{b})$, the regression rabat in percents 100 D^2[%], equation (25), the mean quadratic error of prediction MEP, equation (28), the Akaike information criterion AIC,

Table 2. Illustration of shortened output of MINOPT analysis of $\{x_i, y_i\}$ data for Model I

Quality of parameter estimates
Point and interval estimates of parameters

Parameter β_j	Point estimate $\hat{b}_j$	Standard deviation $s(\hat{b}_j)$	Absolute bias h_j	Relative bias $h_{R,j}$, [%]	Half-length of confidence interval Δj	$\Delta_{R,j}$
β_1	1.5673E + 01	1.7261E − 01	−0.0161	−0.1028	±0.6232	±0.6233
β_2	9.9925E − 01	1.5625E − 01	0.0160	1.5977	±0.5637	±0.5642
β_3	2.2222E − 02	2.1017E − 03	3.9E − 06	0.0176	±0.0075	±0.0076

Correlation (inter-dependence) between parameters
Matrix of paired correlation coefficient of parameters, r_{ij}

	β_1	β_2	β_3
β_1	1.0000E + 00	−9.9681E − 01	9.8629E − 01
β_2	−9.9681E − 01	1.0000E + 00	−9.9523E − 01
β_1	9.8629E − 01	−9.9523E − 01	1.0000E + 01

Quality of achieved curve-fitting
Statistical analysis and goodness-of-fit test of classical residuals

Independ. variable i	x	Response measured y	Prediction calculated $\hat{y}$	Standard deviation $s(\hat{y})$	Bias $h(\hat{y})$	Classical residual $\hat{e}$
1	1	1.6700E + 01	1.6695E + 01	1.9847E − 0	−1.2022E − 04	5.0684E − 03
2	5	1.6800E + 01	1.6790E + 01	1.5842E − 0	−1.7692E − 05	1.0093E − 02
3	10	1.6900E + 01	1.6921E + 01	1.2380E − 0	6.4131E − 05	−2.1134E − 02
4	15	1.7100E + 01	1.7068E + 01	1.1210E − 0	9.6718E − 05	3.2219E − 02
5	20	1.7200E + 01	1.7232E + 01	1.1897E − 0	8.5504E − 05	−3.1663E − 02
6	25	1.7400E + 01	1.7415E + 01	1.3105E − 0	4.0018E − 05	−1.4804E − 02
7	30	1.7600E + 01	1.7619E + 01	1.3837E − 0	−2.4973E − 05	−1.9465E − 02
8	35	1.7900E + 01	1.7848E + 01	1.3861E − 0	−8.8089E − 05	5.1821E − 02
9	40	1.8100E + 01	1.8104E + 01	1.4192E − 0	−1.1967E − 04	−3.7685E − 03
10	50	1.8700E + 01	1.8709E + 01	2.7266E − 0	8.4264E − 05	−8.5853E − 03

Statistical analysis

Residual sum of squares, $U(\hat{b})$:	5.9861E − 03
Regression rabat, $100D^2$, [%]:	9.9838E + 01
Akaike information criterion, AIC:	−6.4642E + 01
Estimate of standard deviation of prediction, $s(\hat{y}/x)$:	2.9243E − 02

Goodness-of-fit test

Estimate of residual variance, $s^2(\hat{e})$:	8.5516E − 04
Estimate of residual standard deviation, $s(\hat{e})$:	2.9243E − 02

Quality of experimental data
Indication of influential points (outliers and leverages):

Point i	Jackknife residual $\hat{e}_J$	Cook distance D	Diagonal elements H_{ii}	Normalized distance FDA	Likelihood distance LDA
1	7.0904E − 01	1.5852E − 02	4.6060E − 01	1.3469E − 03	8.8043E − 03
2	7.9083E − 01	2.3346E − 02	2.9349E − 01	5.8963E − 03	9.4152E − 03
3	−7.8569E − 01	4.6314E − 02	1.7922E − 01	2.0878E − 02	1.4915E − 02
4	1.1740E + 00	8.1704E − 02	1.4695E − 01	4.4161E − 02	4.7807E − 02
5	−9.9223E − 01	9.2870E − 02	1.6550E − 01	3.9056E − 02	4.2378E − 02
6	−6.3466E − 01	2.6862E − 02	2.0083E − 01	9.4246E − 03	9.4039E − 03
7	−7.5215E − 01	5.4890E − 02	2.2387E − 01	1.5231E − 02	1.1329E − 02
8	1.4315E + 00	3.9119E − 01	2.2466E − 01	2.6786E − 01	9.9158E − 01
9	−2.4752E − 01	2.2310E − 03	2.3554E − 01	7.5113E − 04	8.9988E − 03
10	−5.3222E − 01	1.4630E + 00	8.6934E − 01	4.1484E − 04	6.9048E − 03

Map of parameter sensitivity in model

Parameter j	Relative change $CjR(-5\%)$ [%]	Total sensitivity Cj	Relative change $CjR(+5\%)$ [%]
1	−1.1930E − 08	1.0000E + 00	2.8004E − 08
2	−7.0302E + 00	3.4946E + 00	7.6700E + 00
3	−1.7824E + 01	4.5182E + 03	2.1104E + 01

equations (26) and (27), the standard deviation of prediction $s(y/x)$, the total bias of parameter estimates M, equation (11), a graph of the confidence interval of prediction.

The goodness-of-fit contains: the table of the prediction calculated $\hat{y}$, the standard deviation of prediction $s(\hat{y})$, the residual bias $h(\hat{y})$, equation (9), and classical residuals $\hat{e}$, equation (7). Statistical characteristics describe classical residuals: the residual bias $E(\hat{e})$, equation (8), the norm of residual bias $\|E\|$, the mean of absolute residuals $E(|\hat{e}|)$, the mean of absolute values of relative residuals $100E(|\hat{e}_{rel}|)$ in percents, the estimate of residual variance $s^2(\hat{e})$, equation (24) and its square-root the residual standard deviation $s(\hat{e})$.

Prediction ability of model proposed. Prediction ability of model can be classified by the following procedure: data are divided on two groups, M_1 with indices $i = 1, \ldots, n/2$ and M_2 with indices $i = n/2 + 1, \ldots, n$. Denote estimates of parameters made from points of subgroup M_1 as $\hat{b}(M_1)$ and from subgroup M_2 as $\hat{b}(M_2)$. Prediction ability of the model is expressed by criterion

$$K = \frac{U(\hat{b})}{\sum_{i \in M_1} [y_i - f(x_i; b(M_2)]^2 + \sum_{i \in M_2} [y_i - f(x_i; b(M_1)]^2} \tag{33}$$

The prediction ability of the model is higher when the criterion K is close to one. The mean quadratic error of prediction MEP, equation (28), can also be calculated. The lower the value of MEP the better is the prediction ability of the proposed model.

Quality of experimental data. For examination of quality experimental data an identification of influential points by regression diagnostics is applied: the Jackknife residuals $\hat{e}_J$, the Cook distance D, the diagonal elements of projection (hat) matrix H_{ii}, the test criterion DSF, the normalized distance FDA, and the likelihood distance LD, equations (31) and (32).

Map of parameter sensitivity in model. The total sensitivity C_{Cj} for all parameters β_j and the relative changes caused by 5% change of parameters β_j are computed. Characteristics C_{Cj} and their interpretation are described in a forthcoming book.[4]

Graph of regression curve. A graph of regression curve fitted through given experimental points with the 95% confidence bands and two plots of classical residuals give a graphical overview of fitness achieved: the plot of type II and the plot of type III.

Physical meaning of parameter estimates. In proposed models some restrictions of physical meaning are given on parameter estimates. For example, concentrations or molar absorption coefficients are defined in a range of positive numbers only.

Software

Program MINOPT from CHEMSTAT package carries out the numerical and statistical analysis of a non-linear regression model $f(x; \beta)$ with use of modified "double dog–leg" strategy. This program contains all the above mentioned criteria of nonlinear model quality.

Program MINOPT is a part of CHEMSTAT package and is available from authors on request.

Illustrative examples

For illustration of MINOPT statistical characteristics the example of Model 1 from paper[3] was recomputed. Selected outputs are shown in Table 2.

CONCLUSION

Many problems in the chemical laboratory can be reduced to the problem of finding a correct mathematical model and its unknown parameters. It may be carried out by minimizing a difference between experimental and calculated data. The variety of regression diagnostics introduced here serves as an efficient tool in search of true model.

REFERENCES

1. M. Meloun and J. Čermák, *Talanta*, 1984, **11**, 947.
2. M. Meloun, J. Havel and E. Högfeldt, *Computation of Solution Equilibria*, Ellis Horwood, Chichester, 1988.
3. J. Militký and M. Meloun, *Talanta*, 1992, **39**,
4. M. Meloun, J. Militký and M. Forina, *Chemometrics for Analytical Chemistry*, Vol. 1: Interactive Data Analysis on IBM PC and Vol. 2: Interactive Model Building on IBM PC, Ellis Horwood, Chichester, 1992.
5. A. R. Gallant, *Nonlinear Statistical Models*, Wiley, New York, 1987.
6. J. R. Donaldson and R. B. Schnabel, *Technometrics*, 1987, **29**, 67.
7. R. D. Cook *et al.*, *Biometrika*, 1986, **73**, 615.
8. M. J. Box, *J. Roy. Stat. Soc.*, 1971, **B32**, 171.
9. G. P. Clarke, *J. Amer. Statist. Assoc.*, 1987, **82**, 221.
10. J. Militký, J. Čáp and K. Květon, *Proc. 2nd Int. Conference on Statistics*, Tampere, 1987.

Talanta, Vol. 40, No. 2, pp. 287–289, 1993
Printed in Great Britain.

0039-9140/93 $6.00 + 0.00

SHORT COMMUNICATION

DETERMINATION OF DIBENZO [*b*,*f*]-1,4-OXAZEPINE BY EXTRACTION SPECTROPHOTOMETRY

EMIL HALÁMEK, ZBYNĚK KOBLIHA and JAN SOUČEK
Department of Chemistry, Faculty of the Arms, Military University, 682 03 Vyškov, Czech Republic

(*Received* 29 *March* 1992. *Revised* 11 *June* 1992. *Accepted* 11 *June* 1992)

Summary—The spectrophotometric determination of the substance dibenzo [*b*,*f*]-1,4-oxazepine (CR) the form of an ionic associate with the anionactive dyes of the type of azo dyes, sulphonephthaleins and anthraquinones after extraction with chloroform was worked out. Conditional extraction constants K'_{ex} were calculated and equilibrium ratios D and extraction yields E of ionic associates were determined. On the basis of detection limit L_Q, the dyes Alizarine Black S (0.7 μg/ml) and Orange II (0.8 μg/ml) were recommended for extractive spectrophotometric determination of the substance CR.

INTRODUCTION

Dibenzo[*b*,*f*]-1,4-oxazepine (CR) represents a qualitatively higher degree in the development of substances with strongly irritating effects.[1,2]

The substance CR was identified by UV spectrophotometry,[3,4] NMR,[5] gas chromatography,[6] mass spectrometry,[7,8,10] HPLC[9] and—in the case of its metabolites—also by TLC. For the determination of CR, colorimetry and spectrophotometry[11] based on its diazotation splitting in an inorganic acid and organic solvent was used. On the same principle, a detector tube for the detection of CR in the air was designed.[12]

Dibenzo[*b*,*f*]-1,4-oxazepine is an organic heterocyclic base with a protonable nitrogen atom ($pK_H = 3.0$). So its cationic form can associate the anions of the dyes in acid solutions. Up to now, no attention has been given to this property of the substance CR.

The aim of this work is to investigate the formation of ionic associates of dibenzo[*b*,*f*]-1,4-oxazepine with some anionactive dyes[13–15] which may be extracted into chloroform and to elaborate a method of its determination by extraction spectrophotometry.

EXPERIMENTAL

Reagents and apparatus

Dibenzo[*b*,*f*]-1,4-oxazepine was synthesized in the army factory VOZ 072 at Zemianské Kostolany.[16] The azo dyes used [Calcon (C.I.15 705) (I), Eriochrome Black T (C.I. 14 645) (II) and Orange II (C.I. 15510) (III)], the sulphonephthaleins [Bromothymol Blue (IV) and Bromophenol Blue (V)] and a dye of the anthraquinone type [Alizarine Black S (C.I. 67 430) (VI)] were from Merck. The buffers (pH range 1.0–6.0, increments of 0.2 pH) were prepared according to the literature[17] and checked by means of an MV 870 pH-meter. (Präcitronic, Dresden). Chloroform was shaken three times with redistilled water and then distilled as an azeotropic mixture at 60°. The single-beam spectrophotometer Spekol 11 (Zeiss, Jena) was used for spectrophotometric measurements.

Procedures

The absorbance curves of the ionic associates obtained from measurements of the function $A = f(\lambda)$ were measured. A 1.8-ml portion of the pH 2.0 buffer, 0.2 ml of a methanolic solution of the dye ($c_L = 5mM$) and a methanolic solution of the substance CR ($c_{CR} = 5mM$: 100 μl for IV, V, 70 μl for VI, 50 μl for II, 30 μl for III and 20 μl for I) were pipetted into test tubes.

The extractions were performed by shaking the two phases (2 ml each) in glass test tubes at 20 ± 1° in the hand. The extraction time, which was 2 min, was chosen based on the study of the kinetic curves of extraction. The organic phase was measured spectrophotometrically against the blank.

Table 1. Parameters of the ionic associates of the substance CR with Calcon (I), Eriochrome Black T (II), Orange II (III), Bromothymol Blue (IV), Bromophenol Blue (V) and Alizarine Black S (VI)

Parameter*	Dye					
	I	II	III	IV	V	VI
λ_{max}, *nm*	531	513	480	410	413	500
pH_{opt}	2.0	1.2	1.2	1.5	1.0	†
c_L, m*M*	0.3	0.3	0.4	0.075	0.4	0.5
n_{CR}/nL	1	1	1	1	1	1
ϵ, $l \cdot mole^{-1} \cdot cm^{-1}$	6 600	4 100	18 100	9 600	4 400	26 700
ϵ', $l \cdot mole^{-1} \cdot cm^{-1}$	5 600	3 400	5 400	4 200	2 200	6 300
r	0.997	0.991	0.997	0.998	0.996	0.996
D	5.60	4.86	0.43	0.78	0.18	0.31
E, %	84.8	82.9	29.8	43.8	15.3	23.6
log K'_{ex}	6.09	5.98	4.19	4.28	3.73	3.91
L_D, μg/ml	0.6	0.9	0.6	1.2	1.1	0.4
L_Q, μg/ml	1.1	2.5	0.8	1.4	1.5	0.7

*λ_{max}—Absorption maximum of the ionic associate in chloroform, pH_{opt}—optimum pH for the extraction of the ionic associate into chloroform (†hydrochloric acid, $c_{HCl} = 0.8M$), c_L—optimum concentration of the dye in the aqueous phase, n_{CR}/n_L—mole ratio of the substance CR to the dye, corresponding to the composition of the ionic associate, ϵ—molar absorption coefficient under the conditions of quantitative extraction of the ionic associate, ϵ'—molar absorption coefficient of the ionic associate, r—correlation coefficient, D—distribution ratio, E—extraction yield, K'_{ex}—conditional extraction constant, L_D—detection limit, L_Q—limit of determination.[19]

The effect of the pH of the water phase was arranged similarly to the absorbance curves. The absorbance of the chloroform extracts of the ionic associates was measured for λ_{max} of each dye (see Table 1).

The composition of the ionic associates in the organic phase was determined by measurement of the dependence $A = f(x_L)$, where x_L is the molar ratio of the dye. Volumes ranging from 20 to 180 μl (in steps of 20 μl) of 5m*M* CR were pipetted and then completed to 200 μl with the 5m*M* solution of the dye; 2 ml of the buffer with pH_{opt} (see Table 1) were then added.

The optimum concentration of the dye in the water phase was determined from the dependence $A = f(c_L)$, $c_L = 0.5$ to 10.0m*M*. For the calculation of the molar coefficient ϵ, the dependence $A = f(c'_L)$ was determined. The amounts of 0.1–1 ml of the aqueous dye solution ($c_L = 50\mu M$) were pipetted into the test tubes, the volume was completed to 1 ml with pH_{opt} buffer and 1 ml of the solution of the substance CR ($c_{CR} = 5mM$) with pH_{opt} value was added. The calibration curves were determined by measurement of the dependence $A = f(c_{CR})$. The volumes of 1.8 ml of buffer solutions with pH_{opt} and 0.2 ml of methanolic dye solutions were pipetted into the test tubes. Then 10–100 μl of methanolic solution of the substance CR ($c_{CR} = 2.5mM$ for I, III, VI or 5m*M* for II, IV, V)—by steps of 10 μl—were added by means of the micropipette.

RESULTS AND DISCUSSION

The substance CR forms in the medium of a buffer with study dyes coloured ionic associate which may be extracted into chloroform. Their absorption curves are presented in Fig. 1.

The effect of the pH value of the aqueous solutions on the formation and the extraction of the substance CR is evident from Fig. 2. In dependence on the absorbance of the blank, the optimum pH values of the citrate buffers were

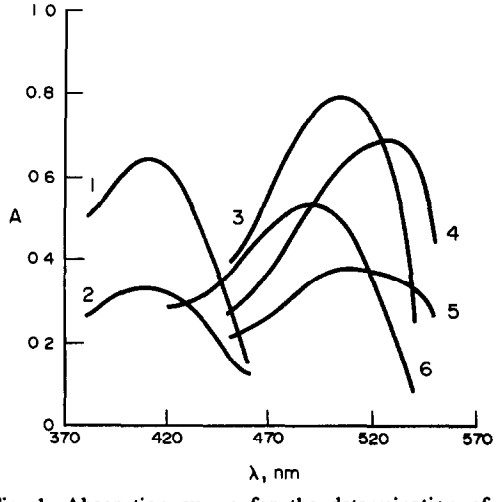

Fig. 1. Absorption curves for the determination of the substance CR with Bromophenol Blue (1) [$c_{CR} = 0.25mM$], Bromothymol Blue (2) [0.25m*M*], Alizarine Black S (3) [0.175m*M*], Calcon (4) [0.05m*M*], Eriochrome Black T (5) [0.125m*M*] and Orange II (6) [0.075m*M*]; $c_L = 0.5mM$, organic phase chloroform.

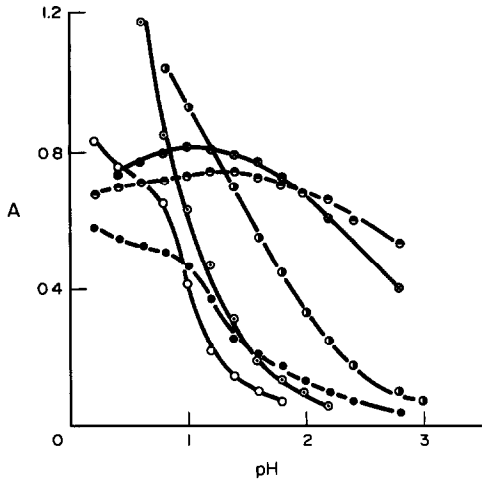

Fig. 2. Dependence of the absorbance of the ionic associate of the substance CR with Orange II (○) [$c_{CR} = 0.075 mM$, A_{480}], Bromothymol Blue (◓) [0.25mM, A_{410}], Alizarine Black S (●) [0.175mM, A_{500}], Eriochrome Black T (⊙) [0.125mM, A_{513}], Calcon (◑) [0.05mM, A_{531}] and Bromophenol Blue (⊗) [0.25mM, A_{413}], on the pH of the reaction medium; $c_L = 0.5 mM$.

determined for the dyes I–V, the optimum medium for VI was 0.8M hydrochloric acid (Table 1). It was found from the dependence of the absorbance variation on the molar ratio x_L of the dye that the substance CR forms ionic associates with all the other investigated dyes in the ratio 1:1.

The optimum concentration of the dye c_L in the reaction mixture is given in Table 1.

The ionic associates of the substance CR with the investigated dyes were extracted into chloroform in the surplus of the base. The molar absorption coefficients ϵ of the dyes (which may be considered constant at the maximum obtainable yield of the extraction) were determined by a simple linear regression. On the other hand, with a surplus of the dye a maximum yield of the extraction is not attained (in dependence on the conditions of the determination) in all cases. The resulting slope is not necessarily identical with the molar absorption coefficient ϵ. It could be considered as the conditional molar absorption coefficient and indicated as ϵ'.

The conditional extraction constants K'_{ex}, equilibrium ratios D and yields of the extraction were calculated according to Souček *et al.*[18]

In the investigated concentration range 25–250μM all measurements comply with the Lambert-Beer law. The extractive spectrophotometric method enables to determine 0.7 or 0.8 μg of substance CR in 1 ml of sample when using the dye III or VI.

REFERENCES

1. B. Ballantyne, D. Gall and D. C. Robson, *Med. Sci. Law*, 1976, **16**, 159.
2. V. N. Aleksandrov and V. I. Emelyanov, *Otravlyayushchie veshchestva*, p. 209. Voennoe izdatelstvo, Moscow 1990.
3. R. Higginbottom and H. Suschitzky, *J. Chem. Soc., II*, 1962, 2367.
4. B. Ballantyne, *Toxicology*, 1977, **8**, 347.
5. N. S. Narasimhan and P. S. Chandrachood, *Synthesis*, 1979, **8**, 589.
6. P. A. D'Agostini and L. R. Provost, *J. Chromatogr.*, 1982, 240, **243**.
7. D. N. Tripathi, R. C. Malhotra and A. Bratacharya, *ibid.*, 1984, **315**, 417.
8. E. R. J. Wils and A. G. Hulst, *ibid.*, 1985, **330**, 379.
9. C. D. Raghuveeran and R. C. Malhotra, *ibid.*, 1982, **240**, 243.
10. M. C. French, *Xenobiotica*, 1983, **13**, 345.
11. Pat. CSFR 2641, Military University, E. Halámek and V. Földeši, *The Analysis of Dibenzo[b,f]-1,4-oxazepine*, 1987.
12. Pat. CSFR 2702, Military University, E. Halámek and V. Földeši, *The detector Tube for the Detection of Dibenzo[b,f]-1,4-oxazepine in the air*, 1987.
13. Pat. CSFR 2731. Military University, E. Halámek, Z. Kobliha and J. Souček, *Extractive Spectrophotometric Determination of Dibenzo[b,f]-1,4-oxazepine by Anthraquinone Dyes*, 1988.
14. Pat. CSFR 2732, Military University, E. Halámek, Z. Kobliha and J. Souček, *Extractive Spectrophotometric Determination of Dibenzo[b,f]-1,4-oxazepine by Sulphonephtaleins*, 1988.
15. Pat. CSFR 2733, Military University, E. Halámek, Z. Kobliha and J. Souček, *Extractive Spectrophotometric Determination of Dibenzo[b,f]-1,4-oxazepine by Azo Dyes*, 1988.
16. Pat. CSFR 2677, Military University, V. Földeši, E. Halámek and J. Kubuš, *The Preparation of Dibenzo[b,f]-1,4-oxazepine*, 1987.
17. F. W. Küster and A. Thiel, *Chemical-Analytical Tables*, Academia, Prague 1988.
18. J. Souček, E. Halámek and R. Kysilka, *Collect. Czech. Chem. Commun.*, 1988, **53**, 1655.
19. K. Eckschlager, *Chem. Listy* 1989, **83**, 1009.

Talanta, Vol. 40, No. 2, pp. 291–298, 1993
Printed in Great Britain
Pergamon Press Ltd.

BOOK REVIEWS

Handbook of Inductively Coupled Plasma Mass Spectrometry: K. E. JARVIS, A. L. GRAY and R. S. HOUK, Blackie, Glasgow and London, and Chapman and Hall, New York, 1991. Pages xi + 380. £75.00.

It is a pleasant, if rare, experience to review a scientific text written by enthusiastic and knowledgeable authors who still manage to present an easy-to-read, informative and unbiased account of an analytical technique. Jarvis, Gray and Houk, assisted by inputs from I. Jarvis, J. W. McLaren and J. G. Williams, have managed to produce just such a book. A concise introductory chapter on the origins of ICP–MS sets the scene admirably, though it tends to assume a reasonable knowledge of various aspects of atomic spectrometry. This is followed by detailed and fully referenced chapters on instrumentation and on some of the options available to those ambitious enough to engage in development work. John Williams' chapter on sample introduction (other than by pneumatic nebulization) deserves wider readership than just those using ICP–MS, and includes a concise but useful summary of chromatography/plasma interfacing. The following chapter on interferences is up to date and commendably honest. Together with chapter 6 on calibration and data handling, and chapter 7 on sample preparation for ICP–MS, it provides excellent insight for existing or intending users. It is interesting to note that the authors have chosen to collect geological, environmental, nuclear, industrial and biological applications together in chapter 8, but dedicate a separate 22-page chapter to natural water analysis. This very fairly reflects the impact of ICP–MS in this field, where the full detection power, capacity for multi-element analysis and selectivity may be readily exploited. The final chapters are on solids analysis and isotope ratio determinations, the latter being especially valuable to anyone considering employing stable isotope tracer techniques. Some might think this is an expensive book, but if you buy an ICP–MS, this volume may prove to be the accessory providing best value for money. If you're still contemplating purchase, it may prove an even better investment!

M. S. CRESSER

Atomic Absorption Spectroscopy—Theory, Design and Applications: S. J. HASWELL (editor), Elsevier, Amsterdam, 1991. Pages: xx + 529. Dfl 345.00.

Volume 5 in the Analytical Spectroscopy Library (a series of books devoted to the application of spectroscopic techniques to chemical analysis) is a well-produced, comprehensive text which should become a standard handbook for practitioners in AAS. It is essentially a collection of 14 reviews preceded by 3 introductory chapters which deal with basic principles, instrumentation and practical techniques. The editor has not just compiled the reviews from the mainly UK and USA authors but has also written chapters 2 and 3. The close involvement of the editor has resulted in a text with only a minimum of repetition between contributors.

Areas of application covered are: waters, sewage and effluents (45 pages); marine analysis (33 pages); airborne particles (32 pages); food analysis (36 pages); ferrous metals (48 pages); non-ferrous metals (12 pages); geochemical (32 pages); petroleum (20 pages); glasses and ceramics (17 pages); clinical (flame techniques—21 pages, ETA—58 pages); forensic (24 pages); fine, industrial and other chemicals (52 pages) and polluted soils (12 pages).

All of the reviews contain numerous references (up to the year 1989) and a footnote appears on each odd-numbered page of the application chapters directing the reader to where the references are listed. I found this feature surprisingly useful. A subject index is included but it does not do justice to the comprehensive range of topics discusssd in the text, nor does it adequately refer the reader to all occurrences of a single topic. For example, ETA-AAS has advanced tremendously over the last decade and this text extols its virtues in almost every chapter but the index gives only 6 different page numbers for this topic. Another very minor gripe would be that the diagrams in chapter 1 are very small and Table 1 refers to mysterious λ-rays.

A common feature of the book is that it is full of practical details, some reviews such as that on elemental analysis of body fluids and tissues by ETA-AAS (Delves and Shuttler) are excellent, selective and critical. Others, e.g., on forensic science (Dale) and polluted soils (Cresser) are characterized by the ease at which the authors disseminate their extensive knowledge in the subject areas. The ubiquitous nature of samples and elements requiring analysis is shown in the chapter on food analysis (Rains) and extensive sample digestion methods for geochemical samples are given by Thompson and Banarjee. Indeed, there is something here to interest all those involved with AAS. It is a text to be highly recommended.

P. J. Cox

Glycerine—A Key Cosmetic Ingredient: E. JUNGERMANN and N. O. V. SONNTAG (editors), Dekker, New York, 1991. Pages xi + 460. $125.00 (U.S. and Canada), $143.75 (Elsewhere).

This book is the eleventh in Dekker's Cosmetic Science and Technology series and could well be sub-titled 'all you could possibly want to know about glycerine'! It presents a very comprehensive compilation of information about glycerine,

Talanta, Vol. 40, No. 2, pp. 291–298, 1993
Printed in Great Britain
Pergamon Press Ltd.

BOOK REVIEWS

Handbook of Inductively Coupled Plasma Mass Spectrometry: K. E. JARVIS, A. L. GRAY and R. S. HOUK, Blackie, Glasgow and London, and Chapman and Hall, New York, 1991. Pages xi + 380. £75.00.

It is a pleasant, if rare, experience to review a scientific text written by enthusiastic and knowledgeable authors who still manage to present an easy-to-read, informative and unbiased account of an analytical technique. Jarvis, Gray and Houk, assisted by inputs from I. Jarvis, J. W. McLaren and J. G. Williams, have managed to produce just such a book. A concise introductory chapter on the origins of ICP–MS sets the scene admirably, though it tends to assume a reasonable knowledge of various aspects of atomic spectrometry. This is followed by detailed and fully referenced chapters on instrumentation and on some of the options available to those ambitious enough to engage in development work. John Williams' chapter on sample introduction (other than by pneumatic nebulization) deserves wider readership than just those using ICP–MS, and includes a concise but useful summary of chromatography/plasma interfacing. The following chapter on interferences is up to date and commendably honest. Together with chapter 6 on calibration and data handling, and chapter 7 on sample preparation for ICP–MS, it provides excellent insight for existing or intending users. It is interesting to note that the authors have chosen to collect geological, environmental, nuclear, industrial and biological applications together in chapter 8, but dedicate a separate 22-page chapter to natural water analysis. This very fairly reflects the impact of ICP–MS in this field, where the full detection power, capacity for multi-element analysis and selectivity may be readily exploited. The final chapters are on solids analysis and isotope ratio determinations, the latter being especially valuable to anyone considering employing stable isotope tracer techniques. Some might think this is an expensive book, but if you buy an ICP–MS, this volume may prove to be the accessory providing best value for money. If you're still contemplating purchase, it may prove an even better investment!

M. S. CRESSER

Atomic Absorption Spectroscopy—Theory, Design and Applications: S. J. HASWELL (editor), Elsevier, Amsterdam, 1991. Pages: xx + 529. Dfl 345.00.

Volume 5 in the Analytical Spectroscopy Library (a series of books devoted to the application of spectroscopic techniques to chemical analysis) is a well-produced, comprehensive text which should become a standard handbook for practitioners in AAS. It is essentially a collection of 14 reviews preceded by 3 introductory chapters which deal with basic principles, instrumentation and practical techniques. The editor has not just compiled the reviews from the mainly UK and USA authors but has also written chapters 2 and 3. The close involvement of the editor has resulted in a text with only a minimum of repetition between contributors.

Areas of application covered are: waters, sewage and effluents (45 pages); marine analysis (33 pages); airborne particles (32 pages); food analysis (36 pages); ferrous metals (48 pages); non-ferrous metals (12 pages); geochemical (32 pages); petroleum (20 pages); glasses and ceramics (17 pages); clinical (flame techniques—21 pages, ETA—58 pages); forensic (24 pages); fine, industrial and other chemicals (52 pages) and polluted soils (12 pages).

All of the reviews contain numerous references (up to the year 1989) and a footnote appears on each odd-numbered page of the application chapters directing the reader to where the references are listed. I found this feature surprisingly useful. A subject index is included but it does not do justice to the comprehensive range of topics discusssd in the text, nor does it adequately refer the reader to all occurrences of a single topic. For example, ETA-AAS has advanced tremendously over the last decade and this text extols its virtues in almost every chapter but the index gives only 6 different page numbers for this topic. Another very minor gripe would be that the diagrams in chapter 1 are very small and Table 1 refers to mysterious λ-rays.

A common feature of the book is that it is full of practical details, some reviews such as that on elemental analysis of body fluids and tissues by ETA-AAS (Delves and Shuttler) are excellent, selective and critical. Others, e.g., on forensic science (Dale) and polluted soils (Cresser) are characterized by the ease at which the authors disseminate their extensive knowledge in the subject areas. The ubiquitous nature of samples and elements requiring analysis is shown in the chapter on food analysis (Rains) and extensive sample digestion methods for geochemical samples are given by Thompson and Banarjee. Indeed, there is something here to interest all those involved with AAS. It is a text to be highly recommended.

P. J. Cox

Glycerine—A Key Cosmetic Ingredient: E. JUNGERMANN and N. O. V. SONNTAG (editors), Dekker, New York, 1991. Pages xi + 460. $125.00 (U.S. and Canada), $143.75 (Elsewhere).

This book is the eleventh in Dekker's Cosmetic Science and Technology series and could well be sub-titled 'all you could possibly want to know about glycerine'! It presents a very comprehensive compilation of information about glycerine,

suitable substitutes and related materials. Such a broad spread is to be commended, but also has its drawbacks. One wonders, for example, if a cosmetic scientist requires 80 pages of detail on glycerine manufacture.

The book is well presented in 17 chapters written by a total of 13 authors. As may be expected with such a text, the style of writing varies and there are some minor overlaps of material.

After the introductory chapters, there are two chapters giving very detailed analysis of manufacturing methods and plants, especially in the USA. There follows chapters dealing with the chemical reactions of glycerine, its physicochemical properties, analysis and safety. Generally, these are comprehensive although it is surprising that no IR spectrum is included. Chapter 9 on economics may have sat more easily in the section on production. There follows 6 chapters dealing with aspects of the use and evaluation of glycerine in cosmetics. These are comprehensive, many taking the form of reviews of published work, although in chapter 13 the words 'speculate' and 'surmise' occur too frequently. The least successful chapter is the one dealing with monoglycerides where there are several mistakes, a tendency to repeat material and only 2 references post-1983. The book concludes with two chapters dealing with alternatives to glycerine and its non-cosmetic uses.

Throughout, the book is well referenced, enabling the interested reader to delve further into the subject. The editors have done a commendable job in producing such a text which will be a valuable resource for cosmetic, and other, scientists.

A. J. WINFIELD

Sampling: G. E. BAIULESCU, P. DUMITRESCU and P. GH. ZUGRAVESCU, Ellis Horwood, Chichester, 1991. Pages 184. £45.50.

Short, snappy titles may be eye-catching but they are not necessarily informative and can even be misleading. This is such a case. The authors state quite clearly that they consider the word sampling to apply to all the procedures prior to the measurement step, that is to include sample collection, handling, storage and preparation for analysis. That is acceptable, but the authors then all but ignore that very operation which most people would consider as "sampling"—the taking of a sample. This is admitted in a one paragraph appendix which gives a few references where readers will find relevant information.

Analysts seeking guidance on how to collect particular samples or even how to undertake the analysis will not find it in this book. Indeed it is neither practical nor a reference book but more of a philosophical discussion on the importance of correct sampling in the overall scheme of analysis. There are just five chapters with a few sub-divisions and as a consequence there are large blocks of unbroken text with few figures or tables. The philosophical approach means that there are no sub-divisions for types of analyis or instrumentation, or of an overall consideration of the requirements. Although one could not expect such a book to be comprehensive there are some surprising omissions. Spark source mass spectrometry appears in a list of eight techniques which the authors consider to be the only ones applicable to trace element analysis but there is no mention, here or elsewhere in the book, of other more modern techniques, for example ICP–mass spectrometry which is becoming widely used in multilement analysis. The tendency to simplicity can lead to misleading statements such as the "potted history of mass spectrometry" which appears in one sentence. There is no statistical treatment of the requirements for representative sampling.

In summary, this is a disappointing book. That is not to say it is not worth reading. It is written in a very easy style and would be a useful bed-time book for all analytical chemists because the authors hammer home the importance of sampling within the whole analytical scheme. There is a lot of background information, much of which will be in areas of study other than the reader's own. It will probably make the reader think about their own approach to carrying out analysis and it emphasises the importance of the role of the analyst. The authors repeatedly make the statement that "no analysis is better than the sample itself". If this comes across to the reader then the book is successful but the problem is that the process starts at the sample collection stage and if that is not done properly the rest is meaningless.

J. BACON

Techniques for Characterization of Electrodes and Electrochemical Processes: R. VARMA and J. R. SELMAN (editors), Wiley-Interscience, New York, 1991, Pages xii + 780. £89.70.

This volume collects together fifteen reviews, varying in size between 16 and 96 pages. The techniques covered are ellipsometry, photothermal deflection spectroscopy, surface x-ray absorption spectroscopy, surface enhanced Raman spectroscopy, neutron scattering, Mössbauer spectroscopy and laser interferometry as applied to electrode surfaces. Measurements *in situ* are stressed whenever possible. There are also two reviews on electrochemical impedance spectroscopy, two on modelling techniques, two general surveys (solid electrolytes and molten salts) and a short review on diffraction techniques for determining the structure of liquid electrolytes. To take the reader from fundamentals to applications in an average of some 50 pages is a tall order and I generally found it heavy going in style and content. I found myself wishing for a more elementary approach and an earlier appreciation of the relationship beween the electrochemical phenomena and the measured characteristic. Perhaps lack of space enforced a formal approach. As a whole, however, this volume has value as a substantial source-book for those interested in electrodes, but one would need more extensive texts before adopting these techniques. The electrochemistry is directed towards corrosion and electrode processes rather than analysis. Analytical interest, in a narrow sense, will thus tend to be in the applications of the techniques rather than the electrochemical results presented. The book will clearly have its uses in a large electrochemical research laboratory, but probably not in many analytical laboratories. I doubt if anybody who could use a library would think it *necessary* to have these reviews bound together.

D. MIDGLEY

suitable substitutes and related materials. Such a broad spread is to be commended, but also has its drawbacks. One wonders, for example, if a cosmetic scientist requires 80 pages of detail on glycerine manufacture.

The book is well presented in 17 chapters written by a total of 13 authors. As may be expected with such a text, the style of writing varies and there are some minor overlaps of material.

After the introductory chapters, there are two chapters giving very detailed analysis of manufacturing methods and plants, especially in the USA. There follows chapters dealing with the chemical reactions of glycerine, its physicochemical properties, analysis and safety. Generally, these are comprehensive although it is surprising that no IR spectrum is included. Chapter 9 on economics may have sat more easily in the section on production. There follows 6 chapters dealing with aspects of the use and evaluation of glycerine in cosmetics. These are comprehensive, many taking the form of reviews of published work, although in chapter 13 the words 'speculate' and 'surmise' occur too frequently. The least successful chapter is the one dealing with monoglycerides where there are several mistakes, a tendency to repeat material and only 2 references post-1983. The book concludes with two chapters dealing with alternatives to glycerine and its non-cosmetic uses.

Throughout, the book is well referenced, enabling the interested reader to delve further into the subject. The editors have done a commendable job in producing such a text which will be a valuable resource for cosmetic, and other, scientists.

A. J. WINFIELD

Sampling: G. E. BAIULESCU, P. DUMITRESCU and P. GH. ZUGRAVESCU, Ellis Horwood, Chichester, 1991. Pages 184. £45.50.

Short, snappy titles may be eye-catching but they are not necessarily informative and can even be misleading. This is such a case. The authors state quite clearly that they consider the word sampling to apply to all the procedures prior to the measurement step, that is to include sample collection, handling, storage and preparation for analysis. That is acceptable, but the authors then all but ignore that very operation which most people would consider as "sampling"—the taking of a sample. This is admitted in a one paragraph appendix which gives a few references where readers will find relevant information.

Analysts seeking guidance on how to collect particular samples or even how to undertake the analysis will not find it in this book. Indeed it is neither practical nor a reference book but more of a philosophical discussion on the importance of correct sampling in the overall scheme of analysis. There are just five chapters with a few sub-divisions and as a consequence there are large blocks of unbroken text with few figures or tables. The philosophical approach means that there are no sub-divisions for types of analyis or instrumentation, or of an overall consideration of the requirements. Although one could not expect such a book to be comprehensive there are some surprising omissions. Spark source mass spectrometry appears in a list of eight techniques which the authors consider to be the only ones applicable to trace element analysis but there is no mention, here or elsewhere in the book, of other more modern techniques, for example ICP–mass spectrometry which is becoming widely used in multilement analysis. The tendency to simplicity can lead to misleading statements such as the "potted history of mass spectrometry" which appears in one sentence. There is no statistical treatment of the requirements for representative sampling.

In summary, this is a disappointing book. That is not to say it is not worth reading. It is written in a very easy style and would be a useful bed-time book for all analytical chemists because the authors hammer home the importance of sampling within the whole analytical scheme. There is a lot of background information, much of which will be in areas of study other than the reader's own. It will probably make the reader think about their own approach to carrying out analysis and it emphasises the importance of the role of the analyst. The authors repeatedly make the statement that "no analysis is better than the sample itself". If this comes across to the reader then the book is successful but the problem is that the process starts at the sample collection stage and if that is not done properly the rest is meaningless.

J. BACON

Techniques for Characterization of Electrodes and Electrochemical Processes: R. VARMA and J. R. SELMAN (editors), Wiley-Interscience, New York, 1991, Pages xii + 780. £89.70.

This volume collects together fifteen reviews, varying in size between 16 and 96 pages. The techniques covered are ellipsometry, photothermal deflection spectroscopy, surface x-ray absorption spectroscopy, surface enhanced Raman spectroscopy, neutron scattering, Mössbauer spectroscopy and laser interferometry as applied to electrode surfaces. Measurements *in situ* are stressed whenever possible. There are also two reviews on electrochemical impedance spectroscopy, two on modelling techniques, two general surveys (solid electrolytes and molten salts) and a short review on diffraction techniques for determining the structure of liquid electrolytes. To take the reader from fundamentals to applications in an average of some 50 pages is a tall order and I generally found it heavy going in style and content. I found myself wishing for a more elementary approach and an earlier appreciation of the relationship beween the electrochemical phenomena and the measured characteristic. Perhaps lack of space enforced a formal approach. As a whole, however, this volume has value as a substantial source-book for those interested in electrodes, but one would need more extensive texts before adopting these techniques. The electrochemistry is directed towards corrosion and electrode processes rather than analysis. Analytical interest, in a narrow sense, will thus tend to be in the applications of the techniques rather than the electrochemical results presented. The book will clearly have its uses in a large electrochemical research laboratory, but probably not in many analytical laboratories. I doubt if anybody who could use a library would think it *necessary* to have these reviews bound together.

D. MIDGLEY

Liquid Chromatography Column Theory: R. P. W. SCOTT, Wiley, Chichester, 1992. Pages: xi + 279. £34.95.

Liquid Chromatographic Column Theory by R. P. W. Scott is a valuable addition to the Separation Science Series in that it deals at an essentially theoretical level with the quantitative relationships governing liquid chromatographic column performance. This is a welcome departure from many previous liquid chromatography texts which concentrate on particular applications of separations with no theoretical basis or even rationale for a given chromatographic analysis.

The main volume is free from typographical errors such as the incorrect spelling of theory in the Preface but the typeface used is not easy to read, particularly in terms of the interspersed algebra.

After an introductory chapter which briefly covers factors controlling retention, the physical nature of the column and nomenclature, subsequent chapters give complete coverage of the Plate and Rate Theories of chromatography together with extensions to these as proposed by several leading chromatographers. Chapters 3 and 10 are of particular interest in addressing the important variables of column dead volume and extra column band broadening.

The final four chapters deal with column design. Firstly, a general design protocol is suggested and this is followed by detailed consideration of the design requirements for packed columns, open tubular columns and columns for preparative liquid chromatography. In these chapters, previously derived relationships are applied to ascertain optimum column dimensions, stationary phase diameter and operating conditions. Listings of interactive BASIC computer programs are provided for the calculation of such optimised conditions for specified equipment.

This is not a book to be read but rather to be studied as required. It deals with the fundamental aspects of liquid chromatographic separations that many analysts, who rely heavily on this technique, largely ignore. It will be most useful to those working in analytical method development and may go some way to encouraging individual preparation of columns and to minimising acceptance of commercially offered components.

R. B. TAYLOR

Interfacial Phenomena in Biological Systems: M. BENDER, Dekker, New York, 1991. Pages xiv + 429. $135.00 (U.S. and Canada), $155.25 (Elsewhere).

This book covers some of the rather complicated interfacial aspects encountered in biological systems. The text is divided into five parts with further subdivision within each part. As the editor explains in the preface some physical and chemical principles are shared by more than one of these areas, and the arrangement of various chapters within the specific parts of the text is not always easy to follow.

The first part is titled "Biological surfaces" and includes chapters on the skin, the oral cavity, biomaterials, and plasma proteins. Each chapter reviews some of the current aspects of research within these areas and as throughout there are many useful and up-to-date references given at the end of each chapter to allow further reading and clarification of points where required.

The second part covers membranes, with the first two chapters on water stabilization and electromagnetic field influence being concise and easy to follow. The third chapter dealing with the "non-specific" adsorption of plasma proteins to erythrocytes is rather lengthy and may prove to be rather mathematical for most readers.

The two chapters in part three are covered under the heading "corpuscular" but they do appear to be rather isolated and could perhaps have been included in other parts of the text. Part four covers interactions, where the second chapter on supercomputer simulations again may be rather too specialized for most readers.

The final chapter on transport has two well written chapters, with the second in keeping with the title of the book covering many biological systems. The fact that proteins are covered extensively throughout the text emphasizes the important role they have in the structure of biological systems and also their involvement in transport and adhesion as well.

The text is rather specialized and as such will be of most benefit to researchers in the life sciences. It could also be useful for extended reading as part of certain undergraduate courses including medicine and dentistry. There is detailed coverage of the areas mentioned above but for those requiring even more information there are over 850 references, a large number being recent and published in the eighties.

K. I. CUMMING

Chemistry and Physics of Carbon: P. A. THROWER (editor), Dekker, New York, 1991. Pages xiii + 366. $165.00 (U.S. and Canada), $189.75 (Elsewhere).

Clearly, this well established series is set to "run" well into the future with the recent advances in Buckminster Fullerene and allied molecular carbon chemistry. The current volume 23 comprises four diverse topics in carbon science. This diversity may well appeal to carbon specialists, it will certainly not encourage those from outside this field to purchase this volume.

The first section addresses the characterization of structure and microstructure by magneto-resistance in various carbon materials including highly orientated graphites, cokes, carbon fibres and carbon/carbon composites. The second section reviews the electrochemical carbonization of fluoropolymers documenting chemical and electrochemical reduction of polytetrafluoroethane, and other fluoropolymers. The properties of the resulting electrochemical carbon, which is often electronically doped or contains electrolyte crystals, are discussed and its use in power sources and separation described. In the next section the methods of protection of carbon from oxidation at high temperatures are described. The limitations of the various coatings/incorporations are reported and the possibility of extending significant protection to temperatures above 1500° discussed. The final section addresses methods for assesssing the effectiveness for removing radioactive iodine from accidental nuclear emissions. In particular, the degradation in activity with weathering and/or ageing is considered.

Liquid Chromatography Column Theory: R. P. W. SCOTT, Wiley, Chichester, 1992. Pages: xi + 279. £34.95.

Liquid Chromatographic Column Theory by R. P. W. Scott is a valuable addition to the Separation Science Series in that it deals at an essentially theoretical level with the quantitative relationships governing liquid chromatographic column performance. This is a welcome departure from many previous liquid chromatography texts which concentrate on particular applications of separations with no theoretical basis or even rationale for a given chromatographic analysis.

The main volume is free from typographical errors such as the incorrect spelling of theory in the Preface but the typeface used is not easy to read, particularly in terms of the interspersed algebra.

After an introductory chapter which briefly covers factors controlling retention, the physical nature of the column and nomenclature, subsequent chapters give complete coverage of the Plate and Rate Theories of chromatography together with extensions to these as proposed by several leading chromatographers. Chapters 3 and 10 are of particular interest in addressing the important variables of column dead volume and extra column band broadening.

The final four chapters deal with column design. Firstly, a general design protocol is suggested and this is followed by detailed consideration of the design requirements for packed columns, open tubular columns and columns for preparative liquid chromatography. In these chapters, previously derived relationships are applied to ascertain optimum column dimensions, stationary phase diameter and operating conditions. Listings of interactive BASIC computer programs are provided for the calculation of such optimised conditions for specified equipment.

This is not a book to be read but rather to be studied as required. It deals with the fundamental aspects of liquid chromatographic separations that many analysts, who rely heavily on this technique, largely ignore. It will be most useful to those working in analytical method development and may go some way to encouraging individual preparation of columns and to minimising acceptance of commercially offered components.

R. B. TAYLOR

Interfacial Phenomena in Biological Systems: M. BENDER, Dekker, New York, 1991. Pages xiv + 429. $135.00 (U.S. and Canada), $155.25 (Elsewhere).

This book covers some of the rather complicated interfacial aspects encountered in biological systems. The text is divided into five parts with further subdivision within each part. As the editor explains in the preface some physical and chemical principles are shared by more than one of these areas, and the arrangement of various chapters within the specific parts of the text is not always easy to follow.

The first part is titled "Biological surfaces" and includes chapters on the skin, the oral cavity, biomaterials, and plasma proteins. Each chapter reviews some of the current aspects of research within these areas and as throughout there are many useful and up-to-date references given at the end of each chapter to allow further reading and clarification of points where required.

The second part covers membranes, with the first two chapters on water stabilization and electromagnetic field influence being concise and easy to follow. The third chapter dealing with the "non-specific" adsorption of plasma proteins to erythrocytes is rather lengthy and may prove to be rather mathematical for most readers.

The two chapters in part three are covered under the heading "corpuscular" but they do appear to be rather isolated and could perhaps have been included in other parts of the text. Part four covers interactions, where the second chapter on supercomputer simulations again may be rather too specialized for most readers.

The final chapter on transport has two well written chapters, with the second in keeping with the title of the book covering many biological systems. The fact that proteins are covered extensively throughout the text emphasizes the important role they have in the structure of biological systems and also their involvement in transport and adhesion as well.

The text is rather specialized and as such will be of most benefit to researchers in the life sciences. It could also be useful for extended reading as part of certain undergraduate courses including medicine and dentistry. There is detailed coverage of the areas mentioned above but for those requiring even more information there are over 850 references, a large number being recent and published in the eighties.

K. I. CUMMING

Chemistry and Physics of Carbon: P. A. THROWER (editor), Dekker, New York, 1991. Pages xiii + 366. $165.00 (U.S. and Canada), $189.75 (Elsewhere).

Clearly, this well established series is set to "run" well into the future with the recent advances in Buckminster Fullerene and allied molecular carbon chemistry. The current volume 23 comprises four diverse topics in carbon science. This diversity may well appeal to carbon specialists, it will certainly not encourage those from outside this field to purchase this volume.

The first section addresses the characterization of structure and microstructure by magneto-resistance in various carbon materials including highly orientated graphites, cokes, carbon fibres and carbon/carbon composites. The second section reviews the electrochemical carbonization of fluoropolymers documenting chemical and electrochemical reduction of polytetrafluoroethane, and other fluoropolymers. The properties of the resulting electrochemical carbon, which is often electronically doped or contains electrolyte crystals, are discussed and its use in power sources and separation described. In the next section the methods of protection of carbon from oxidation at high temperatures are described. The limitations of the various coatings/incorporations are reported and the possibility of extending significant protection to temperatures above 1500° discussed. The final section addresses methods for assesssing the effectiveness for removing radioactive iodine from accidental nuclear emissions. In particular, the degradation in activity with weathering and/or ageing is considered.

Overall, this volume contains a lot of useful information and is, generally, well presented. The sections on fluoropolymer reduction and oxidative protection contain a good deal of interesting science for the more general reader, whereas the other two sections are much more specialized.

J. T. S. IRVINE

Fourier Transform Raman Spectroscopy—Instrumentation and Chemical Applications: P. HENDRA, C. JONES and G. WARNES, Ellis Horwood, 1991. Pages 311. £53.00.

The yellow plastic duck on the cover is not merely to catch the eye. The illustration has been chosen for a very good reason—it sums up many of the advantages of FT Raman spectroscopy discussed in this book: for example, ease of sampling, and the ability to obtain spectra from coloured and fluorescent materials.

The contents fall into two distinct sections. The first third covers the background to vibrational spectroscopy, conventional laser Raman spectroscopy and the development of FT Raman instrumentation. The second two-thirds are used to discuss a large number of applications, stressing those areas where the FT method is superior to conventional laser Raman spectroscopy. Finally there is a fascinating appendix "the processing history of a spectrum—from ADC to VDU" which should be essential reading for anyone who uses FT IR spectroscopy seriously as well as users or potential users of FT Raman instrumentation.

The "applications" chapter covers a very wide range: organic chemistry (alkaloids, explosives, dyestuffs, pharmaceutical materials), polymers (including the duck!), biological samples (membranes, polypeptides, animal, wood and plant tissue), surfaces and catalysts, and inorganic compounds. The treatment, though didactic, is honest and the authors do not avoid the two negative aspects of the present FT Raman systems—sample heating leading to black-body emission and the difficulty of obtaining spectra from aqueous solutions. The chosen examples are well illustrated by spectra and I for one believe that the case is made for FT Raman as a routine analytical technique with wide applicability.

The introductory chapters are also excellent. "The vibration behaviour of molecules" is a good readable account (at senior undergraduate level) of IR and Raman spectroscopy while the chapter on conventional laser Raman spectroscopy contains very useful sections on such practical aspects of the technique as spectral bandwidth and signal-to-noise levels. The chapter on FT vibrational spectroscopy could be read with advantage by all students who use FT IR spectrometers.

I have only two complaints. The quality of the photographs is rather poor and some of them are unnecessary. The diagrams, on the other hand, are universally good—in many cases, however, they are over the page from the text. The publishers could well consider arranging the text so that diagrams and text could be read together without having to turn over the page.

In summary this is a very useful book, not only for those who are contemplating the purchase of an FT Raman instrument but for all users of vibrational spectroscopy. It should certainly be in all Chemistry Department libraries and many vibrational spectroscopists will want their own copy.

R. D. PEACOCK

Adenosine and Adenosine Receptors: M. WILLIAMS, Humana Press, Chichester, 1991. Pages xii + 512. £79.70.

This extremely competent volume edited by Michael Williams comprises five sections and thirteen chapters. The first section written by Michael Williams, himself, is a historical perspective starting with the paper by Drury and Szent-Gyorgyi published in *The Journal of Physiology* in 1929 first describing the physiological actions of adenosine compounds, continuing with the discovery of cyclic AMP in 1960's, nonadrenergic, noncholinergic transmission and ATP in the 1970's and further to the receptor classification of the 1980's. This is a short chapter but provides the reader with a simple introduction to the subject and to the more complicated information which follows in subsequent chapters. The second section is concerned with characterization of the receptor and its binding site. Michael Williams joins with Kenneth Jacobson in the first chapter in this section which is entitled "Radioligand Binding Assays for Adenosine Receptors". Following a brief description of the principles of radioligand binding, the chapter then becomes very technical. They catalogue the many agonist and antagonist radioligands which have been used and this is followed by a section on species differences, receptor autoradiography and the labeling of other adenosine recognition sites. I found this a difficult chapter to read, though the information is there for those who are interested. The second chapter in this section is by Bharat Trivedi, Alexander Bridges, and Robert Bruns and is entitled "Structure-Activity Relationships of Adenosine A_1 and A_2 Receptors". There is a short discussion on the two types of receptors and the chapter provides a copious list of adenosine analogues and their structure activity relationships.

Section three is called "Biochemical Mechanisms of Receptor Action" and contains four chapters. The first chapter in this section is by Dermot Cooper and Kevin Caldwell and is concerned with signal transduction mechanisms for adenosine. This is a long chapter of some thirty-seven pages covering a very large selection of topics. However, it is eminently readable and for this chapter alone, the whole volume is worth having. Thomas Dunwiddie writes a chapter on electrophysiological aspects of adenosine receptor function. The author points out that the physiological basis of responses to adenosine is much more complex than had first been suggested. He points out that there now seems to be several well established models in which adenosine can modulate ionic conductance, reduce calcium currents in some cells and activate potassium conductance in others. He states that at present there appear to be at least three or perhaps more receptors requiring to be postulated to account for the pharmacology observed in different systems. He then suggests how the answers to these questions can be provided. Adenosine release is discussed by Trevor Stone, Andrew Newby and Hilary Lloyd. The authors discuss the results of studies from various tissues in the body which have been shown to release adenosine and to differentiate between neuronal and non-neuronal release. This chapter also discusses the source of adenosine and the mechanisms thought to

Overall, this volume contains a lot of useful information and is, generally, well presented. The sections on fluoropolymer reduction and oxidative protection contain a good deal of interesting science for the more general reader, whereas the other two sections are much more specialized.

J. T. S. IRVINE

Fourier Transform Raman Spectroscopy—Instrumentation and Chemical Applications: P. HENDRA, C. JONES and G. WARNES, Ellis Horwood, 1991. Pages 311. £53.00.

The yellow plastic duck on the cover is not merely to catch the eye. The illustration has been chosen for a very good reason—it sums up many of the advantages of FT Raman spectroscopy discussed in this book: for example, ease of sampling, and the ability to obtain spectra from coloured and fluorescent materials.

The contents fall into two distinct sections. The first third covers the background to vibrational spectroscopy, conventional laser Raman spectroscopy and the development of FT Raman instrumentation. The second two-thirds are used to discuss a large number of applications, stressing those areas where the FT method is superior to conventional laser Raman spectroscopy. Finally there is a fascinating appendix "the processing history of a spectrum—from ADC to VDU" which should be essential reading for anyone who uses FT IR spectroscopy seriously as well as users or potential users of FT Raman instrumentation.

The "applications" chapter covers a very wide range: organic chemistry (alkaloids, explosives, dyestuffs, pharmaceutical materials), polymers (including the duck!), biological samples (membranes, polypeptides, animal, wood and plant tissue), surfaces and catalysts, and inorganic compounds. The treatment, though didactic, is honest and the authors do not avoid the two negative aspects of the present FT Raman systems—sample heating leading to black-body emission and the difficulty of obtaining spectra from aqueous solutions. The chosen examples are well illustrated by spectra and I for one believe that the case is made for FT Raman as a routine analytical technique with wide applicability.

The introductory chapters are also excellent. "The vibration behaviour of molecules" is a good readable account (at senior undergraduate level) of IR and Raman spectroscopy while the chapter on conventional laser Raman spectroscopy contains very useful sections on such practical aspects of the technique as spectral bandwidth and signal-to-noise levels. The chapter on FT vibrational spectroscopy could be read with advantage by all students who use FT IR spectrometers.

I have only two complaints. The quality of the photographs is rather poor and some of them are unnecessary. The diagrams, on the other hand, are universally good—in many cases, however, they are over the page from the text. The publishers could well consider arranging the text so that diagrams and text could be read together without having to turn over the page.

In summary this is a very useful book, not only for those who are contemplating the purchase of an FT Raman instrument but for all users of vibrational spectroscopy. It should certainly be in all Chemistry Department libraries and many vibrational spectroscopists will want their own copy.

R. D. PEACOCK

Adenosine and Adenosine Receptors: M. WILLIAMS, Humana Press, Chichester, 1991. Pages xii + 512. £79.70.

This extremely competent volume edited by Michael Williams comprises five sections and thirteen chapters. The first section written by Michael Williams, himself, is a historical perspective starting with the paper by Drury and Szent-Gyorgyi published in *The Journal of Physiology* in 1929 first describing the physiological actions of adenosine compounds, continuing with the discovery of cyclic AMP in 1960's, nonadrenergic, noncholinergic transmission and ATP in the 1970's and further to the receptor classification of the 1980's. This is a short chapter but provides the reader with a simple introduction to the subject and to the more complicated information which follows in subsequent chapters. The second section is concerned with characterization of the receptor and its binding site. Michael Williams joins with Kenneth Jacobson in the first chapter in this section which is entitled "Radioligand Binding Assays for Adenosine Receptors". Following a brief description of the principles of radioligand binding, the chapter then becomes very technical. They catalogue the many agonist and antagonist radioligands which have been used and this is followed by a section on species differences, receptor autoradiography and the labeling of other adenosine recognition sites. I found this a difficult chapter to read, though the information is there for those who are interested. The second chapter in this section is by Bharat Trivedi, Alexander Bridges, and Robert Bruns and is entitled "Structure-Activity Relationships of Adenosine A_1 and A_2 Receptors". There is a short discussion on the two types of receptors and the chapter provides a copious list of adenosine analogues and their structure activity relationships.

Section three is called "Biochemical Mechanisms of Receptor Action" and contains four chapters. The first chapter in this section is by Dermot Cooper and Kevin Caldwell and is concerned with signal transduction mechanisms for adenosine. This is a long chapter of some thirty-seven pages covering a very large selection of topics. However, it is eminently readable and for this chapter alone, the whole volume is worth having. Thomas Dunwiddie writes a chapter on electrophysiological aspects of adenosine receptor function. The author points out that the physiological basis of responses to adenosine is much more complex than had first been suggested. He points out that there now seems to be several well established models in which adenosine can modulate ionic conductance, reduce calcium currents in some cells and activate potassium conductance in others. He states that at present there appear to be at least three or perhaps more receptors requiring to be postulated to account for the pharmacology observed in different systems. He then suggests how the answers to these questions can be provided. Adenosine release is discussed by Trevor Stone, Andrew Newby and Hilary Lloyd. The authors discuss the results of studies from various tissues in the body which have been shown to release adenosine and to differentiate between neuronal and non-neuronal release. This chapter also discusses the source of adenosine and the mechanisms thought to

Overall, this volume contains a lot of useful information and is, generally, well presented. The sections on fluoropolymer reduction and oxidative protection contain a good deal of interesting science for the more general reader, whereas the other two sections are much more specialized.

J. T. S. IRVINE

Fourier Transform Raman Spectroscopy—Instrumentation and Chemical Applications: P. HENDRA, C. JONES and G. WARNES, Ellis Horwood, 1991. Pages 311. £53.00.

The yellow plastic duck on the cover is not merely to catch the eye. The illustration has been chosen for a very good reason—it sums up many of the advantages of FT Raman spectroscopy discussed in this book: for example, ease of sampling, and the ability to obtain spectra from coloured and fluorescent materials.

The contents fall into two distinct sections. The first third covers the background to vibrational spectroscopy, conventional laser Raman spectroscopy and the development of FT Raman instrumentation. The second two-thirds are used to discuss a large number of applications, stressing those areas where the FT method is superior to conventional laser Raman spectroscopy. Finally there is a fascinating appendix "the processing history of a spectrum—from ADC to VDU" which should be essential reading for anyone who uses FT IR spectroscopy seriously as well as users or potential users of FT Raman instrumentation.

The "applications" chapter covers a very wide range: organic chemistry (alkaloids, explosives, dyestuffs, pharmaceutical materials), polymers (including the duck!), biological samples (membranes, polypeptides, animal, wood and plant tissue), surfaces and catalysts, and inorganic compounds. The treatment, though didactic, is honest and the authors do not avoid the two negative aspects of the present FT Raman systems—sample heating leading to black-body emission and the difficulty of obtaining spectra from aqueous solutions. The chosen examples are well illustrated by spectra and I for one believe that the case is made for FT Raman as a routine analytical technique with wide applicability.

The introductory chapters are also excellent. "The vibration behaviour of molecules" is a good readable account (at senior undergraduate level) of IR and Raman spectroscopy while the chapter on conventional laser Raman spectroscopy contains very useful sections on such practical aspects of the technique as spectral bandwidth and signal-to-noise levels. The chapter on FT vibrational spectroscopy could be read with advantage by all students who use FT IR spectrometers.

I have only two complaints. The quality of the photographs is rather poor and some of them are unnecessary. The diagrams, on the other hand, are universally good—in many cases, however, they are over the page from the text. The publishers could well consider arranging the text so that diagrams and text could be read together without having to turn over the page.

In summary this is a very useful book, not only for those who are contemplating the purchase of an FT Raman instrument but for all users of vibrational spectroscopy. It should certainly be in all Chemistry Department libraries and many vibrational spectroscopists will want their own copy.

R. D. PEACOCK

Adenosine and Adenosine Receptors: M. WILLIAMS, Humana Press, Chichester, 1991. Pages xii + 512. £79.70.

This extremely competent volume edited by Michael Williams comprises five sections and thirteen chapters. The first section written by Michael Williams, himself, is a historical perspective starting with the paper by Drury and Szent-Gyorgyi published in *The Journal of Physiology* in 1929 first describing the physiological actions of adenosine compounds, continuing with the discovery of cyclic AMP in 1960's, nonadrenergic, noncholinergic transmission and ATP in the 1970's and further to the receptor classification of the 1980's. This is a short chapter but provides the reader with a simple introduction to the subject and to the more complicated information which follows in subsequent chapters. The second section is concerned with characterization of the receptor and its binding site. Michael Williams joins with Kenneth Jacobson in the first chapter in this section which is entitled "Radioligand Binding Assays for Adenosine Receptors". Following a brief description of the principles of radioligand binding, the chapter then becomes very technical. They catalogue the many agonist and antagonist radioligands which have been used and this is followed by a section on species differences, receptor autoradiography and the labeling of other adenosine recognition sites. I found this a difficult chapter to read, though the information is there for those who are interested. The second chapter in this section is by Bharat Trivedi, Alexander Bridges, and Robert Bruns and is entitled "Structure-Activity Relationships of Adenosine A_1 and A_2 Receptors". There is a short discussion on the two types of receptors and the chapter provides a copious list of adenosine analogues and their structure activity relationships.

Section three is called "Biochemical Mechanisms of Receptor Action" and contains four chapters. The first chapter in this section is by Dermot Cooper and Kevin Caldwell and is concerned with signal transduction mechanisms for adenosine. This is a long chapter of some thirty-seven pages covering a very large selection of topics. However, it is eminently readable and for this chapter alone, the whole volume is worth having. Thomas Dunwiddie writes a chapter on electrophysiological aspects of adenosine receptor function. The author points out that the physiological basis of responses to adenosine is much more complex than had first been suggested. He points out that there now seems to be several well established models in which adenosine can modulate ionic conductance, reduce calcium currents in some cells and activate potassium conductance in others. He states that at present there appear to be at least three or perhaps more receptors requiring to be postulated to account for the pharmacology observed in different systems. He then suggests how the answers to these questions can be provided. Adenosine release is discussed by Trevor Stone, Andrew Newby and Hilary Lloyd. The authors discuss the results of studies from various tissues in the body which have been shown to release adenosine and to differentiate between neuronal and non-neuronal release. This chapter also discusses the source of adenosine and the mechanisms thought to

be involved in its synthesis and release. Concluding this chapter, the authors state "the diverse aspects of adenosine's properties allow it to be viewed in many different ways and to be classified variously as hormone, neuromodulator, protective, or retaliatory metabolite. The overall concept must be that of an ubiquitous, arguably primitive molecule, importantly involved in homeostasis and the control of tissue function and integration". The last chapter in this section is by Jonathan Gieger and James Nagy, "Adenosine Deaminase and [^{3}H] Nitrobenzylthioinosine as Markers of Adenosine Metabolism and Transport in Central Purinergic Systems". This chapter is extremely long, comprising some sixty-four pages. This is a really comprehensive chapter dealing with such different things as sites and control of adenosin's actions in the central nervous system, metabolism of adenosines, its disposition within cells and cytotoxicity. The authors then deal with adenosine deaminase and suggest a possible role for this enzyme in the central nervous system and in the context of this enzyme, they also deal with its inhibition. This is followed with discussion on its cellular and ultrastructural localization and its species differences. The final part of the chapter is concerned with adenosine uptake and transport. Section Four is entitled "Physiological Functions of Adenosine Receptors" and concerns the effects of adenosine on the various systems of the body. This section is the heart of the volume and in a way it can be said that all the preceding sections have been leading up to this section.

Kevin Mullane and Michael Williams discuss the role of adenosine and cardiovascular function, both the direct effects on contractability and cardio arrhythmias and the indirect actions, such as inhibiting adrenergic responses and histamine H_2 mediated effects. The final section of this chapter deals with adenosine and pathophysiology of the cardiovascular system relating to hypertension and ischaemia. The chapter by Paul Churchill and Anil Bidani is concerned with adenosine and renal function and this chapter comprehensively deals with such topics as renal haemodynamics, with a discussion on the effects of adenosine on renal blood flow and glomerular filtration rate. Of particular interest are the sections on the interactions of adenosine with angiotensin II, and the prostaglandins and its involvement with renal secretion. The role of adenosine in respiratory physiology is in the chapter by Timothy Griffiths and Stephen Holgate and they detail the role of adenosine in the immune system with particular reference to the bronchial tree, the effects of adenosine on the central control of respiration, peripheral chemoreceptors and the pulmonary vascular responses. A very comprehensive chapter indeed. Michael Jarvis and Michael Williams have written the chapter on adenosine in central nervous system function. This is a chapter of over fifty pages long, is far ranging and very comprehensive. It covers too many topics to describe briefly here, however, it should be said that as with all the other chapters Michael Williams has had a hand in, this is an extremely lucid and well-written contribution.

In chapter twelve which is the only chapter in Section 5, Receptor Regulation, Bruce Cronstein and Rochelle Hirschhorn discuss adenosine and host defence. The chapter is primarily concerned with the adenosine receptors present in the immune system, and deals with these receptors on such cells as lymphocytes, monocytes and leucocytes and with the role of adenosine receptors in autoimmune disorders. In the final part of the chapter, the authors postulate that adenosine is a modulator on inflammation. The final section again consists of just one chapter, "Adenosine Receptors Future Vistas" is just three and a half pages of text and is another chapter written by Michael Williams. He points the finger forward to the possible development of adenosine and its derivatives in the clinic.

In summary, we have in this volume a very comprehensive coverage of the physiology, pharmacology, biochemistry and pathology of adenosine and its receptors. It is a book to delve into, not one to read all in one go. Some chapters are easy to read and are for a wide audience, others need a specialized background. The amount of information in this book is enormous and with a very comprehensive list of references at the end of each chapter. Anyone interested in the field has everything at their fingertips. Michael Williams must be congratulated for editing such a book. The effort which he must have put into this publication, particularly with his own several contributions, must have been considerable. A book for every University and Research Library and for the desk of those working with adenosine and adenosine receptors.

A. S. MILTON

Chemical Analysis in Complex Matrices: M. R. SMYTH, Ellis Horwood, Chichester, 1992. Pages 295. £50.00. ISBN 0-13-127671-9.

Many texts on chemical analysis minimize the importance of the analyte matrix and, as a result, overemphasize specialist determination techniques. In contrast, this book takes full account of the importance of the matrix in any analytical procedure. This is fully discussed in the initial short chapter describing general analytical strategy and the theme is carried through the subsequent chapters dealing with particular subject areas. These include bioanalysis of drugs, analysis in the brewing and adhesive industries and trace analysis of the atmosphere and of human and animal food.

It is a general rather than a specialist text on chemical analysis and as such it is a welcome addition to the chemical literature. This book may be read to obtain background information on the analytical requirements of various industries including the applications of bioanalysis and the source of atmospheric trace impurities. It also contains considerable analytical information appropriate to the specialist fields and industries included.

In some of the chapters very full accounts are given of the spectroscopic and chromatographic methods which are of general application and in others descriptions are given of more specialist techniques appropriate to the particular industry. While chromatography features strongly in many of the chapters there is no repetition throughout the book and each chapter provides complementary information on particular analytical problems.

The literary style of the book is uniform and clear and it is well produced. It provides a very readable source for a wide range of analytical information. It should be a very useful undergraduate text as well as one which could be profitably read by any analyst with a view to appreciating what is going on in adjacent fields of activity.

R. B. TAYLOR

be involved in its synthesis and release. Concluding this chapter, the authors state "the diverse aspects of adenosine's properties allow it to be viewed in many different ways and to be classified variously as hormone, neuromodulator, protective, or retaliatory metabolite. The overall concept must be that of an ubiquitous, arguably primitive molecule, importantly involved in homeostasis and the control of tissue function and integration". The last chapter in this section is by Jonathan Gieger and James Nagy, "Adenosine Deaminase and [^{3}H] Nitrobenzylthioinosine as Markers of Adenosine Metabolism and Transport in Central Purinergic Systems". This chapter is extremely long, comprising some sixty-four pages. This is a really comprehensive chapter dealing with such different things as sites and control of adenosin's actions in the central nervous system, metabolism of adenosines, its disposition within cells and cytotoxicity. The authors then deal with adenosine deaminase and suggest a possible role for this enzyme in the central nervous system and in the context of this enzyme, they also deal with its inhibition. This is followed with discussion on its cellular and ultrastructural localization and its species differences. The final part of the chapter is concerned with adenosine uptake and transport. Section Four is entitled "Physiological Functions of Adenosine Receptors" and concerns the effects of adenosine on the various systems of the body. This section is the heart of the volume and in a way it can be said that all the preceding sections have been leading up to this section.

Kevin Mullane and Michael Williams discuss the role of adenosine and cardiovascular function, both the direct effects on contractability and cardio arrhythmias and the indirect actions, such as inhibiting adrenergic responses and histamine H_2 mediated effects. The final section of this chapter deals with adenosine and pathophysiology of the cardiovascular system relating to hypertension and ischaemia. The chapter by Paul Churchill and Anil Bidani is concerned with adenosine and renal function and this chapter comprehensively deals with such topics as renal haemodynamics, with a discussion on the effects of adenosine on renal blood flow and glomerular filtration rate. Of particular interest are the sections on the interactions of adenosine with angiotensin II, and the prostaglandins and its involvement with renal secretion. The role of adenosine in respiratory physiology is in the chapter by Timothy Griffiths and Stephen Holgate and they detail the role of adenosine in the immune system with particular reference to the bronchial tree, the effects of adenosine on the central control of respiration, peripheral chemoreceptors and the pulmonary vascular responses. A very comprehensive chapter indeed. Michael Jarvis and Michael Williams have written the chapter on adenosine in central nervous system function. This is a chapter of over fifty pages long, is far ranging and very comprehensive. It covers too many topics to describe briefly here, however, it should be said that as with all the other chapters Michael Williams has had a hand in, this is an extremely lucid and well-written contribution.

In chapter twelve which is the only chapter in Section 5, Receptor Regulation, Bruce Cronstein and Rochelle Hirschhorn discuss adenosine and host defence. The chapter is primarily concerned with the adenosine receptors present in the immune system, and deals with these receptors on such cells as lymphocytes, monocytes and leucocytes and with the role of adenosine receptors in autoimmune disorders. In the final part of the chapter, the authors postulate that adenosine is a modulator on inflammation. The final section again consists of just one chapter, "Adenosine Receptors Future Vistas" is just three and a half pages of text and is another chapter written by Michael Williams. He points the finger forward to the possible development of adenosine and its derivatives in the clinic.

In summary, we have in this volume a very comprehensive coverage of the physiology, pharmacology, biochemistry and pathology of adenosine and its receptors. It is a book to delve into, not one to read all in one go. Some chapters are easy to read and are for a wide audience, others need a specialized background. The amount of information in this book is enormous and with a very comprehensive list of references at the end of each chapter. Anyone interested in the field has everything at their fingertips. Michael Williams must be congratulated for editing such a book. The effort which he must have put into this publication, particularly with his own several contributions, must have been considerable. A book for every University and Research Library and for the desk of those working with adenosine and adenosine receptors.

A. S. MILTON

Chemical Analysis in Complex Matrices: M. R. SMYTH, Ellis Horwood, Chichester, 1992. Pages 295. £50.00. ISBN 0-13-127671-9.

Many texts on chemical analysis minimize the importance of the analyte matrix and, as a result, overemphasize specialist determination techniques. In contrast, this book takes full account of the importance of the matrix in any analytical procedure. This is fully discussed in the initial short chapter describing general analytical strategy and the theme is carried through the subsequent chapters dealing with particular subject areas. These include bioanalysis of drugs, analysis in the brewing and adhesive industries and trace analysis of the atmosphere and of human and animal food.

It is a general rather than a specialist text on chemical analysis and as such it is a welcome addition to the chemical literature. This book may be read to obtain background information on the analytical requirements of various industries including the applications of bioanalysis and the source of atmospheric trace impurities. It also contains considerable analytical information appropriate to the specialist fields and industries included.

In some of the chapters very full accounts are given of the spectroscopic and chromatographic methods which are of general application and in others descriptions are given of more specialist techniques appropriate to the particular industry. While chromatography features strongly in many of the chapters there is no repetition throughout the book and each chapter provides complementary information on particular analytical problems.

The literary style of the book is uniform and clear and it is well produced. It provides a very readable source for a wide range of analytical information. It should be a very useful undergraduate text as well as one which could be profitably read by any analyst with a view to appreciating what is going on in adjacent fields of activity.

R. B. TAYLOR

The Periodic Table for Chromatographers: M. LEDERER, Wiley, Chichester, 1992. Pages v + 129. £60.00.

Although chromatography is often regarded as primarily a separation method for organic compounds, over the years it has played an important role in many inorganic separations. In this reference book Michael Lederer has brought together a collection of over 100 tables containing some 60,000 data values. These are usually presented in the format of the periodic table to illustrate the differences and similarities between the elements.

The values are principally drawn from previously published reports of extractions, ion-exchange separations, paper chromatography, electrophoresis and TLC, almost entirely from the 1960's and 1970's. There are sections on the distribution constants of the elements as undissociated molecules and as chelates with a range of reagents. The ion-exchange data are based on different resin columns and papers and eluent acids. The TLC values come from impregnated cellulose, silica and ion-exchanger phases and different liquid ion-exchange coatings. Finally there is one set of data from electrophoretic separations.

The author admits that the book is a result of a hobby of collecting chromatographic data. However, the problem with this book is that like many hobbies it represents material almost entirely for the specialist. The advent of ion chromatography, conductivity detection and specialised AED, ICP and AAS detection methods means that the separation of ions has advanced considerably over the last 10 years away from these traditional methods. Very few analysts would now contemplate separation of metal ions by TLC as a routine method and even less would think of paper chromatography. This book would therefore mainly appear to be valuable as a compilation of physical data of distribution and separation properties of the elements and their chelates and complexes. However, as the author notes in the Introduction, the values were collected under conditions that might be kinetically controlled rather than under equilibrium conditions.

R. M. SMITH

The Kirk-Othmer Encyclopedia of Chemical Technology: Volume 2, Fourth Edition. Alkanolamines to Antibiotics (Glycopeptides). J. I. KROSCHWITZ, M. HOWE-GRANT, L. C. HUMPHREYS and L. GRAY (editors), Wiley-Interscience, Chichester, 1992 Pages: xxviii + 1018. £135.00.

Inevitably, encyclopedias are referred to for specific items of interest rather than read from cover to cover. The easiest method of locating a desired topic in such a reference work is a simple search amongst items arranged in alphabetical order. Hence this volume, together with volume 1, covers topics beginning with the letter "A". Overall there are 27 volumes to be published, at the rate of one volume every 3 months, to extend coverage to the whole alphabet. A subscription price of 10% discount on individual volume list price is available. If information on a chemical substance is desired then here it is the most common correct name of the substance that is given (followed by its Chemical Abstracts Service Registry Number).

There are numerous topics in volume 2 involving contributions from several authors. Those topics covered at most length include aluminium and its alloys/compounds, amines, and various pharmaceutical agents such as analgesics, antiasthmatic agents and antibacterial agents. There are also extensive sections on amino acids and, ammonia and its compounds. Where appropriate methods of manufacture are covered and process diagrams are presented.

There is a small section on analytical methods which includes a survey followed by current trends and details of hyphenated instruments. This survey informs the reader of analytical techniques that are covered on other volumes of the encyclopedia (the names of the techniques appear in upper case to indicate a separate inclusion in the encyclopedia). The final section on antibiotics starts with a survey and then continues with various classes of antibiotics starting with aminoglycosides and continuing to the glycopeptides. The proposed volume 3 must, presumably, start with the lincomycin antibiotics.

I found browsing through this work and reading sections in depth to be both informative and enjoyable. These volumes will certainly enhance libraries in research, academic, industrial and other public institutions.

P. J. COX

Wilson & Wilson's Comprehensive Analytical Chemistry Vol. XXVII—Analytical Voltammetry: G. SVEHLA (editor), M. R. SMYTH and J. G. VOS (volume editors), Elsevier, Amsterdam, 1992. Pages xxv + 578. US$254.99. Dfl. 495.00. ISBN 0-444-88938.

This book is handsomely bound and properly printed, which is all too rare these days, and has contributions from 14 authors. A chapter by J. F. Cassidy on theory is well-judged for analytical users, with equations set at the right level for understanding without being too intimidating in number. The chapter on instrumentation is short (42 pp) and rather general, avoiding mention of any specific commercial instrumentation that an analyst might use. More space is devoted to modified electrodes than to computer software. I wonder if generalized circuit diagrams are really of any use to the average analyst and I also wish that suspended mercury reservoirs were seen as rarely in books as they are in the laboratory. There follows a chapter (37 pp, 241 references) devoted to "biological" molecules, *i.e.*, largely immunoassay, nucleic acids and proteins. Pharmacy (Bersier and Bersier) gets 184 pages of information on specfic molecules arranged by drug type: a very useful analytical compilation with 514 references. Environmental analysis is divided into inorganic (35 pp, 146 references) and organic and oganometallic (84 pp, 275 references). The former includes speciation, titration and stability constants; in fact there is rather little on direct analysis and that organized by neither sample type nor determinand. Two pages on metals in body fluids seem out of place here. The organics chapter covers air, water and (very briefly) soil analysis,

The Periodic Table for Chromatographers: M. LEDERER, Wiley, Chichester, 1992. Pages v + 129. £60.00.

Although chromatography is often regarded as primarily a separation method for organic compounds, over the years it has played an important role in many inorganic separations. In this reference book Michael Lederer has brought together a collection of over 100 tables containing some 60,000 data values. These are usually presented in the format of the periodic table to illustrate the differences and similarities between the elements.

The values are principally drawn from previously published reports of extractions, ion-exchange separations, paper chromatography, electrophoresis and TLC, almost entirely from the 1960's and 1970's. There are sections on the distribution constants of the elements as undissociated molecules and as chelates with a range of reagents. The ion-exchange data are based on different resin columns and papers and eluent acids. The TLC values come from impregnated cellulose, silica and ion-exchanger phases and different liquid ion-exchange coatings. Finally there is one set of data from electrophoretic separations.

The author admits that the book is a result of a hobby of collecting chromatographic data. However, the problem with this book is that like many hobbies it represents material almost entirely for the specialist. The advent of ion chromatography, conductivity detection and specialised AED, ICP and AAS detection methods means that the separation of ions has advanced considerably over the last 10 years away from these traditional methods. Very few analysts would now contemplate separation of metal ions by TLC as a routine method and even less would think of paper chromatography. This book would therefore mainly appear to be valuable as a compilation of physical data of distribution and separation properties of the elements and their chelates and complexes. However, as the author notes in the Introduction, the values were collected under conditions that might be kinetically controlled rather than under equilibrium conditions.

R. M. SMITH

The Kirk-Othmer Encyclopedia of Chemical Technology: Volume 2, Fourth Edition. Alkanolamines to Antibiotics (Glycopeptides). J. I. KROSCHWITZ, M. HOWE-GRANT, L. C. HUMPHREYS and L. GRAY (editors), Wiley-Interscience, Chichester, 1992 Pages: xxviii + 1018. £135.00.

Inevitably, encyclopedias are referred to for specific items of interest rather than read from cover to cover. The easiest method of locating a desired topic in such a reference work is a simple search amongst items arranged in alphabetical order. Hence this volume, together with volume 1, covers topics beginning with the letter "A". Overall there are 27 volumes to be published, at the rate of one volume every 3 months, to extend coverage to the whole alphabet. A subscription price of 10% discount on individual volume list price is available. If information on a chemical substance is desired then here it is the most common correct name of the substance that is given (followed by its Chemical Abstracts Service Registry Number).

There are numerous topics in volume 2 involving contributions from several authors. Those topics covered at most length include aluminium and its alloys/compounds, amines, and various pharmaceutical agents such as analgesics, antiasthmatic agents and antibacterial agents. There are also extensive sections on amino acids and, ammonia and its compounds. Where appropriate methods of manufacture are covered and process diagrams are presented.

There is a small section on analytical methods which includes a survey followed by current trends and details of hyphenated instruments. This survey informs the reader of analytical techniques that are covered on other volumes of the encyclopedia (the names of the techniques appear in upper case to indicate a separate inclusion in the encyclopedia). The final section on antibiotics starts with a survey and then continues with various classes of antibiotics starting with aminoglycosides and continuing to the glycopeptides. The proposed volume 3 must, presumably, start with the lincomycin antibiotics.

I found browsing through this work and reading sections in depth to be both informative and enjoyable. These volumes will certainly enhance libraries in research, academic, industrial and other public institutions.

P. J. COX

Wilson & Wilson's Comprehensive Analytical Chemistry Vol. XXVII—Analytical Voltammetry: G. SVEHLA (editor), M. R. SMYTH and J. G. VOS (volume editors), Elsevier, Amsterdam, 1992. Pages xxv + 578. US$254.99. Dfl. 495.00. ISBN 0-444-88938.

This book is handsomely bound and properly printed, which is all too rare these days, and has contributions from 14 authors. A chapter by J. F. Cassidy on theory is well-judged for analytical users, with equations set at the right level for understanding without being too intimidating in number. The chapter on instrumentation is short (42 pp) and rather general, avoiding mention of any specific commercial instrumentation that an analyst might use. More space is devoted to modified electrodes than to computer software. I wonder if generalized circuit diagrams are really of any use to the average analyst and I also wish that suspended mercury reservoirs were seen as rarely in books as they are in the laboratory. There follows a chapter (37 pp, 241 references) devoted to "biological" molecules, *i.e.*, largely immunoassay, nucleic acids and proteins. Pharmacy (Bersier and Bersier) gets 184 pages of information on specfic molecules arranged by drug type: a very useful analytical compilation with 514 references. Environmental analysis is divided into inorganic (35 pp, 146 references) and organic and oganometallic (84 pp, 275 references). The former includes speciation, titration and stability constants; in fact there is rather little on direct analysis and that organized by neither sample type nor determinand. Two pages on metals in body fluids seem out of place here. The organics chapter covers air, water and (very briefly) soil analysis,

mainly by literature reference. There is also a section on foodstuffs. Future developments are represented by a timely, but not immediately encouraging, review of modified electrodes by Forster and Vos (65 pp, 398 references) and a chapter on amperometric biosensors (40 pp, 207 references). References extend into 1988. The index is inadequate. This is undoubtedly a very useful volume for those concerned with organic analysis. Inorganic analysts will find it interesting, but not essential.

D. MIDGLEY

Trace Metal Analysis and Specification: I. S. KRULL (editor), Elsevier, Amsterdam, 1991. Pages: xvi + 302. Dfl. 240.00.

Although most analysts would first think of atomic-absorption spectroscopy or inductively-coupled plasma emission spectrometry when asked to analyse metal ions, these methods are non-species specific and only give total concentrations. However, in recent years there has been a greater realization of the importance of the form in which a metal is present in the sample. This has led to the rise of a range of coupled techniques in which a chromatographic separation, such as HPLC or GLC has been linked to an element specific detector and these form the backbone of this collection of reviews edited. Despite a larger number of research papers on this field little has been done previously to bring together inorganic chromatographic methods since Schwedt in 1981 and MacDonald in 1985.

The most important advances have been in the general application of plasma detectors, which have provided much greater sensitivity and specificity than ultraviolet spectroscopic detection. The book starts with a review of microwave induced plasma detection for GC by Uden with small sections on LC and SFC. Three chapters on environmental samples by Irgolic and interfacing by Heitkemper and Caruso and also by Houk and Jiang comprehensively cover coupled-LC and GC systems and although there is some overlap it is mainly in the samples being examined. Bilhorn, Pomery and Denton discuss the details of the instrumentation of plasma emission detectors and coupled direct current plasma instruments are described by Krull and Childress.

Alternative approaches are given in a review by Karcher and Krull on the use of complexation and derivatisation techniques and by Bond on electrochemical detection of metal ions. The more specific technique of ion chromatography is reviewed by Gjerde and Mehra.

Overall the book reflects the modern practice in metal ion analysis and emphasises the importance of coupling the more traditional spectroscopic and electrochemical methods with separation techniques. Each section includes numerous relevant examples of the applications of the techniques.

R. M. SMITH

Principles of Environmental Toxicology: S. F. ZAKRZEWSKI (editor), American Chemical Society, Washington, D.C., 1991. Pages xiii + 270. US$59.95 (Hardback) ISBN 0-8412-2125-1. US$ 44.95 (Softback). ISBN 0-8412-2170-7.

There is much more to this book than toxicology. Indeed, the amount of toxicology is disappointingly limited. The author starts by setting the scene in a chapter on world and environmental trends, and then looks at some basics of pharmacological concepts, metabolism of xenobiotics, factors that influence toxicity and chemical carcinogenesis and mutagenesis. As someone with little direct knowledge of toxicology I found these latter chapters quite interesting and useful, although without a background in biochemistry, some of the context is a little obscure. What disappointed me was that the book then went on to deal rather cursorily with air pollution, water and land pollution, pollution control, radioactive pollution, occupational toxicology and regulatory policies. As a specialist in some of these areas I found the treatment sadly limited. For example, the subjects of stratospheric ozone depletion and climate change are covered in a few pages each, without any real indication of toxicological consequences, be there any. The book, therefore, might more properly be called Principles of Environmental Pollution and Toxicology, being about 50% on each topic. The style is relatively light and easy to read and I can commend the book to the beginner in this field as providing a rather shallow but useful introduction to the subject. The book was derived from lectures given by the author and its primary use is likely to be as a teaching text. In this context, the shallowness of treatment of some areas will limit its value, and the discussion of regulatory policies purely in the context of United States law will severely limit the value of this chapter to those in other countries. In summary, a useful introductory level book, but do not be misled by the title.

R. M. HARRISON

Preparative and Process-Scale Liquid Chromatography: G. SUBRAMANIAN (editor), Ellis Horwood, 1991. Pages 286. £55.00.

If you take the papers presented at a short course on Preparative Chromatography and put them together do you get a book on Preparative Chromatography? All that you really obtain are the notes of speakers. As such, you have a very nice set of course notes, but not a book for others to read.

This book, Preparative and Process Scale Liquid Chromatography, is such a collection of course notes, and so, falls short of any target group of readers that would be interested in the subject, either as a novice, user or expert wanting to gain more knowledge of Preparative Liquid Chromatography.

Fourteen authors of different papers are gathered together. They cover a wide variety of subject matter from the design of preparative columns and preparative systems to the media used in the columns to the type of applications that are now being developed and run on preparative systems.

mainly by literature reference. There is also a section on foodstuffs. Future developments are represented by a timely, but not immediately encouraging, review of modified electrodes by Forster and Vos (65 pp, 398 references) and a chapter on amperometric biosensors (40 pp, 207 references). References extend into 1988. The index is inadequate. This is undoubtedly a very useful volume for those concerned with organic analysis. Inorganic analysts will find it interesting, but not essential.

D. MIDGLEY

Trace Metal Analysis and Specification: I. S. KRULL (editor), Elsevier, Amsterdam, 1991. Pages: xvi + 302. Dfl. 240.00.

Although most analysts would first think of atomic-absorption spectroscopy or inductively-coupled plasma emission spectrometry when asked to analyse metal ions, these methods are non-species specific and only give total concentrations. However, in recent years there has been a greater realization of the importance of the form in which a metal is present in the sample. This has led to the rise of a range of coupled techniques in which a chromatographic separation, such as HPLC or GLC has been linked to an element specific detector and these form the backbone of this collection of reviews edited. Despite a larger number of research papers on this field little has been done previously to bring together inorganic chromatographic methods since Schwedt in 1981 and MacDonald in 1985.

The most important advances have been in the general application of plasma detectors, which have provided much greater sensitivity and specificity than ultraviolet spectroscopic detection. The book starts with a review of microwave induced plasma detection for GC by Uden with small sections on LC and SFC. Three chapters on environmental samples by Irgolic and interfacing by Heitkemper and Caruso and also by Houk and Jiang comprehensively cover coupled-LC and GC systems and although there is some overlap it is mainly in the samples being examined. Bilhorn, Pomery and Denton discuss the details of the instrumentation of plasma emission detectors and coupled direct current plasma instruments are described by Krull and Childress.

Alternative approaches are given in a review by Karcher and Krull on the use of complexation and derivatisation techniques and by Bond on electrochemical detection of metal ions. The more specific technique of ion chromatography is reviewed by Gjerde and Mehra.

Overall the book reflects the modern practice in metal ion analysis and emphasises the importance of coupling the more traditional spectroscopic and electrochemical methods with separation techniques. Each section includes numerous relevant examples of the applications of the techniques.

R. M. SMITH

Principles of Environmental Toxicology: S. F. ZAKRZEWSKI (editor), American Chemical Society, Washington, D.C., 1991. Pages xiii + 270. US$59.95 (Hardback) ISBN 0-8412-2125-1. US$ 44.95 (Softback). ISBN 0-8412-2170-7.

There is much more to this book than toxicology. Indeed, the amount of toxicology is disappointingly limited. The author starts by setting the scene in a chapter on world and environmental trends, and then looks at some basics of pharmacological concepts, metabolism of xenobiotics, factors that influence toxicity and chemical carcinogenesis and mutagenesis. As someone with little direct knowledge of toxicology I found these latter chapters quite interesting and useful, although without a background in biochemistry, some of the context is a little obscure. What disappointed me was that the book then went on to deal rather cursorily with air pollution, water and land pollution, pollution control, radioactive pollution, occupational toxicology and regulatory policies. As a specialist in some of these areas I found the treatment sadly limited. For example, the subjects of stratospheric ozone depletion and climate change are covered in a few pages each, without any real indication of toxicological consequences, be there any. The book, therefore, might more properly be called Principles of Environmental Pollution and Toxicology, being about 50% on each topic. The style is relatively light and easy to read and I can commend the book to the beginner in this field as providing a rather shallow but useful introduction to the subject. The book was derived from lectures given by the author and its primary use is likely to be as a teaching text. In this context, the shallowness of treatment of some areas will limit its value, and the discussion of regulatory policies purely in the context of United States law will severely limit the value of this chapter to those in other countries. In summary, a useful introductory level book, but do not be misled by the title.

R. M. HARRISON

Preparative and Process-Scale Liquid Chromatography: G. SUBRAMANIAN (editor), Ellis Horwood, 1991. Pages 286. £55.00.

If you take the papers presented at a short course on Preparative Chromatography and put them together do you get a book on Preparative Chromatography? All that you really obtain are the notes of speakers. As such, you have a very nice set of course notes, but not a book for others to read.

This book, Preparative and Process Scale Liquid Chromatography, is such a collection of course notes, and so, falls short of any target group of readers that would be interested in the subject, either as a novice, user or expert wanting to gain more knowledge of Preparative Liquid Chromatography.

Fourteen authors of different papers are gathered together. They cover a wide variety of subject matter from the design of preparative columns and preparative systems to the media used in the columns to the type of applications that are now being developed and run on preparative systems.

mainly by literature reference. There is also a section on foodstuffs. Future developments are represented by a timely, but not immediately encouraging, review of modified electrodes by Forster and Vos (65 pp, 398 references) and a chapter on amperometric biosensors (40 pp, 207 references). References extend into 1988. The index is inadequate. This is undoubtedly a very useful volume for those concerned with organic analysis. Inorganic analysts will find it interesting, but not essential.

D. MIDGLEY

Trace Metal Analysis and Specification: I. S. KRULL (editor), Elsevier, Amsterdam, 1991. Pages: xvi + 302. Dfl. 240.00.

Although most analysts would first think of atomic-absorption spectroscopy or inductively-coupled plasma emission spectrometry when asked to analyse metal ions, these methods are non-species specific and only give total concentrations. However, in recent years there has been a greater realization of the importance of the form in which a metal is present in the sample. This has led to the rise of a range of coupled techniques in which a chromatographic separation, such as HPLC or GLC has been linked to an element specific detector and these form the backbone of this collection of reviews edited. Despite a larger number of research papers on this field little has been done previously to bring together inorganic chromatographic methods since Schwedt in 1981 and MacDonald in 1985.

The most important advances have been in the general application of plasma detectors, which have provided much greater sensitivity and specificity than ultraviolet spectroscopic detection. The book starts with a review of microwave induced plasma detection for GC by Uden with small sections on LC and SFC. Three chapters on environmental samples by Irgolic and interfacing by Heitkemper and Caruso and also by Houk and Jiang comprehensively cover coupled-LC and GC systems and although there is some overlap it is mainly in the samples being examined. Bilhorn, Pomery and Denton discuss the details of the instrumentation of plasma emission detectors and coupled direct current plasma instruments are described by Krull and Childress.

Alternative approaches are given in a review by Karcher and Krull on the use of complexation and derivatisation techniques and by Bond on electrochemical detection of metal ions. The more specific technique of ion chromatography is reviewed by Gjerde and Mehra.

Overall the book reflects the modern practice in metal ion analysis and emphasises the importance of coupling the more traditional spectroscopic and electrochemical methods with separation techniques. Each section includes numerous relevant examples of the applications of the techniques.

R. M. SMITH

Principles of Environmental Toxicology: S. F. ZAKRZEWSKI (editor), American Chemical Society, Washington, D.C., 1991. Pages xiii + 270. US$59.95 (Hardback) ISBN 0-8412-2125-1. US$ 44.95 (Softback). ISBN 0-8412-2170-7.

There is much more to this book than toxicology. Indeed, the amount of toxicology is disappointingly limited. The author starts by setting the scene in a chapter on world and environmental trends, and then looks at some basics of pharmacological concepts, metabolism of xenobiotics, factors that influence toxicity and chemical carcinogenesis and mutagenesis. As someone with little direct knowledge of toxicology I found these latter chapters quite interesting and useful, although without a background in biochemistry, some of the context is a little obscure. What disappointed me was that the book then went on to deal rather cursorily with air pollution, water and land pollution, pollution control, radioactive pollution, occupational toxicology and regulatory policies. As a specialist in some of these areas I found the treatment sadly limited. For example, the subjects of stratospheric ozone depletion and climate change are covered in a few pages each, without any real indication of toxicological consequences, be there any. The book, therefore, might more properly be called Principles of Environmental Pollution and Toxicology, being about 50% on each topic. The style is relatively light and easy to read and I can commend the book to the beginner in this field as providing a rather shallow but useful introduction to the subject. The book was derived from lectures given by the author and its primary use is likely to be as a teaching text. In this context, the shallowness of treatment of some areas will limit its value, and the discussion of regulatory policies purely in the context of United States law will severely limit the value of this chapter to those in other countries. In summary, a useful introductory level book, but do not be misled by the title.

R. M. HARRISON

Preparative and Process-Scale Liquid Chromatography: G. SUBRAMANIAN (editor), Ellis Horwood, 1991. Pages 286. £55.00.

If you take the papers presented at a short course on Preparative Chromatography and put them together do you get a book on Preparative Chromatography? All that you really obtain are the notes of speakers. As such, you have a very nice set of course notes, but not a book for others to read.

This book, Preparative and Process Scale Liquid Chromatography, is such a collection of course notes, and so, falls short of any target group of readers that would be interested in the subject, either as a novice, user or expert wanting to gain more knowledge of Preparative Liquid Chromatography.

Fourteen authors of different papers are gathered together. They cover a wide variety of subject matter from the design of preparative columns and preparative systems to the media used in the columns to the type of applications that are now being developed and run on preparative systems.

As such, there is a great deal of overlap from section to section. Sections written by manufacturers of equipment or packing materials are very biased to their equipment and materials. And in general, the data presented in these sections can be found in other journals, procedings of other conferences or even promotional material supplied by the manufacturers.

For me, the most interesting sections were those by industrial presenters who appear to be real users of preparative systems. Sections by Derek Hill, Kevin Connelly and Christopher Goward are well worth reading, as they give a real feel for Preparative Chromatography from real users of the systems, as opposed to people selling equipment or packing materials. In the sections from these presenters you can tell some of the major practical problems they have in Preparative Chromatography.

Overall, a nice set of course notes, but as a book it is lacking a target and so much material is repeated between different authors of different sections. It could also have done with another proof-read before being committed to print.

P. MYERS

Talanta, Vol. 40, No. 3, pp. 299–305, 1993
Printed in Great Britain.

0039-9140/93 $6.00 + 0.00

THE DETERMINATION OF ORGANOTIN COMPOUNDS IN EDIBLE OILS BY GAS CHROMATOGRAPHY-ATOMIC ABSORPTION SPECTROMETRY

D. S. FORSYTH, D. WEBER and K. DALGLISH

Food Research Division, Bureau of Chemical Safety, Food Directorate, Health Protection Branch, Health and Welfare Canada, Ottawa, Ontario, K1A 0L2, Canada

(*Received* 14 *May* 1992. *Revised* 4 *August* 1992. *Accepted* 4 *August* 1992)

Summary—An extraction method for butyl-, cyclohexyl-, octyl- and phenyltin compounds from edible oils was developed using 0.05% tropolone in 0.04*M* HCl/methanol. Cooling the methanol extracts in a dry ice/methanol bath removed approximately 64% of nonvolatile coextractives without affecting recoveries. Methyl derivatives formed by Grignard reaction were quantitated by gas chromatography-atomic absorption spectrometry. Edible oils sold in poly(vinyl chloride) containers had ng/g levels of dioctyl- and monooctyltin. GC–MS confirmed the presence of octyltin and did not detect any other organotin compounds in the extracts.

Organotin compounds are used in numerous applications including biocides, poly(vinyl chloride) (PVC) stabilizers and catalysts. Global consumption of PVC stabilizers accounted for 66–75% of all organotin production during the 1970s.[1] Currently, annual consumption is estimated to be 35×10^6 kg world wide.[2]

Dibutyltin is typically added as a heat stabilizer to rigid and semi-rigid PVC products used in industrial applications.

Dioctyltin compounds have low mammalian toxicity[3] and several are used by many countries as stabilizers in PVC drink containers and food packaging.[4] The monoalkyltin analogue is frequently blended with the dialkyltin to produce a synergistic effect in stabilizer performance.[4]

Recent analyses of Canadian wines for organotins[5,6] found butyltins in blended wine products containing imported wines which had been transported in containers constructed of butyltin-stabilized PVC. As edible oils are also shipped in these containers a survey was conducted to determine what alkytins were present in edible oils available to the consumer. Existing methods for determination of alkyltins in edible oil are primarily designed for migration studies using radiolabelled organotin stabilizers[7–9] of known composition or total tin determinations.[10,11] However, the methods found in the literature could not speciate unknown alkyltins in edible oils.

The purpose of this study was to develop a method capable of speciating a variety of alkyltins in edible oils using gas chromatography-atomic absorption spectrometry and to conduct a limited survey of edible oils available from retail outlets.

EXPERIMENTAL

Reagents and standards

Distilled-in-glass grade solvents (Caledon Laboratories Ltd., Georgetown, Ontario) and ACS reagent grade chemicals were used. The methylmagnesium chloride and tropolone were purchased from Aldrich Chemical Co., Inc. (Milwaukee, Wisconsin, U.S.A.). Dioctyltin dichloride (Oc_2SnCl_2) was obtained from MTM Research Chemicals (P.O. Box 1000, Windham, NH).

Dioctyldimethyltin was prepared from Oc_2SnCl_2 using the following procedure. Dioctyltin dichloride (10–20 mg) was weighed into a 10-ml screw cap centrifuge tube; tetrahydrofuran (1 ml) and 100-fold excess (molar basis) of methylmagnesium chloride were added under nitrogen. The reaction mixture was rotary tumbled at 25 rpm for 15 min and then cooled in ice. Hexane (3 ml) and prechilled 0.5*M* nitric acid were slowly added up to a 10-ml total sample volume. The aqueous layer was removed after tumbling (25 rpm, 2 min) and centrifugation (2000 rpm, 2 min). The organic layer was then tumbled (25 rpm, 2 min) once with approx. 8 ml of deionized (18 megohm/cm) water. The

pooled aqueous washings were extracted twice with 2-ml portions of hexane. The pooled organic extracts were then dried over anhydrous sodium sulphate. The dioctyldimethyltin was 97% pure (Sn basis). The source and purity of the other organotin standards have been described elsewhere.[5,12]

Instrumentation

Details of the gas chromatograph (GC)-atomic absorption spectrometer (AAS) system used in this study have been reported elsewhere.[13,14] GC operating conditions in the current study were as follows: glass column (1.8 m × 6 mm o.d., 2 mm i.d.), packed with 3% OV-7 on Chromosorb W, HP 100/120 mesh (Chromatographic Specialties Ltd., Brockville, Ont.); carrier gas, helium, 20 ml/min; transfer line, 0.8 m × 0.25 mm i.d. deactivated fused silica; transfer line temperature, 275°, column temperature program, 75° (0.5 min hold) to 130° (no hold) at 25°/min then to 155° (no hold) at 15°/min, then increased at 25°/min to 310° (5.0 min hold); injector temperature, 225°.

AAS operating conditions were: Hamamatsu Sn hollow cathode lamp (Hamamatsu Photonics K.K.); current, 15 mA; wavelength, 224.6 nm; bandpass, 0.5 nm; quartz T tube furnace temperature, 900°; furnace support gas flow rates, H_2 45 ml/min, air, 45 ml/min.

A Varian VISTA 6000 GC interfaced to a VG Analytical 7070EQ mass spectrometer with EBQQ configuration was used for GC-MS analysis. Using the conventional magnetic sector only, the system was operated in the electron impact mode (70 eV) at a mass resolution of 1000. GC operating conditions have been previously reported.[12] Selected ion monitoring was at m/z 205 and 207 for butyltrimethyltin ($BuMe_3Sn$), 225 and 227 for phenyltrimethyltin ($PhMe_3Sn$), 205 and 207 for dibutyldimethyltin (Bu_2Me_2Sn), 261 and 263 for octyltrimethyltin ($OcMe_3Sn$), 247 and 249 for tributylmethyltin (Bu_3MeSn), 231 and 233 for dicyclohexyldimethyltin (Cy_2Me_2Sn), 261 and 263 for dioctyldimethyltin (Oc_2Me_2Sn), 299 and 301 for tricyclohexylmethyltin (Cy_3MeSn), and 349 and 351 for triphenylmethyltin (Ph_3MeSn).

Analytical methods

Sample collection. A variety of edible oils were purchased from local supermarkets and stored at room temperature until analysis.

Extraction. Five grams of oil were weighed into a 50-ml centrifuge tube. Each sample was then tumbled for 20 min (65 rpm) with 10 ml of 0.05% tropolone in 0.04*M* hydrochloric acid/methanol. Following centrifugation (2000 rpm, 4 min), the sample was placed in a dry ice/methanol bath for 2 min and then briefly centrifuged (3000 rpm, 2 min). The methanol layer was collected with a Pasteur pipette. After the sample had warmed to room temperature, the extraction was repeated. The pooled extract was evaporated at 35° (Brinkmann RotoVapor-R, Brinkmann Instruments) to 1 ml over approx. 4 min. Chloroform (10 ml) was added and the volume reduced to 1 ml over 2–3 min. Hexane (15 ml) was then added and used to wash down the sides of the round bottom flask, and evaporated to 2 ml over approx. 3 min. Solvents were removed at these slow rates to prevent sample bumping and to ensure removal of the methanol, hydrochloric acid and chloroform during the transition to apolar solvent. The hexane was transferred to a 10-ml screw cap centrifuge tube with one 2-ml tetrahydrofuran rinse followed by two 2-ml rinses of hexane. The sample was placed in a water bath at 30° and the solvent volume reduced to 1 ml under a nitrogen stream. Pentane (5 ml) was then added and the sample evaporated to 1 ml.

Derivatization. Tetrahydrofuran (0.9 ml) and methylmagnesium chloride (0.7 ml) were added and the sample capped under nitrogen. After brief vortexing, the sample was rotary tumbled (10 min, 25 rpm). The sample was then cooled in ice and the volume adjusted to 10 ml with prechilled 0.5*M* nitric acid (added slowly initially). Isooctane (0.9 ml) was added, and the sample was tumbled (2 min, 25 rpm), and centrifuged briefly (up to 2500 rpm). The aqueous layer was removed and discarded and the acid wash repeated once. After discarding the aqueous layer, the organic volume was adjusted to 2.0 ml. Residual acid and water were removed by the addition of sodium bicarbonate and anhydrous sodium sulfate (approx. 300 mg each). The sample extract was then transferred to an autoinjector vial.

Analysis. Sample quantitation was by comparison to external standards using GC–AAS. A 10-μl sample volume was injected by autosampler. As a monooctyltin standard was unavailable, a Sn response factor determined from Bu_3MeSn standards was used to quantitate monooctyltin levels. Monooctyltin was identified in the samples by GC–MS. Reagent

blanks were run with each sample series. Method detection limits were 0.2 to 0.4 ng Sn/g (Table 1).

Recovery experiments. Samples of peanut or corn oil were spiked at 2 levels (3.2–5.6 or 16.2–28 ng/g) with $BuSnCl_3$, Bu_2SnBr_2, Bu_3SnBr, Oc_2SnCl_2, Cy_2SnBr_2, Cy_3SnBr and Ph_3SnCl. The percent recovery of each analyte was determined by dividing the mean peak area of the compound found in the spiked peanut or corn oil extracts by the mean peak area of the compound in blank peanut or corn oil extracts spiked just prior to derivatization.

Method development

Tropolone study. The effects of tropolone were evaluated by comparing recoveries from corn oil using (1) two 10-ml methanol extractions or (2) a methanol followed with 0.05% tropolone in methanol (10 ml each) extraction. No hydrochloric acid was added to these samples. Extraction conditions (minus methanol cooling with dry ice bath) were as given in the Extraction section. No chloroform was used during rotary evaporation. A 0.05% tropolone in hexane solution was used to rinse the round bottom flasks. Derivatization was as reported in the derivatization section except 18 megohm/cm water was used instead of the second 0.5*M* nitric acid wash and no sodium bicarbonate was added.

Hydrochloric acid addition. Spiked corn oil samples were extracted (minus methanol cooling step), and rotary evaporated as reported in the Extraction section. Derivatization was as reported in the tropolone study section. The hydrochloric acid content of the 0.05% tropolone/methanol solution was varied from 0 to 0.04*M*.

Sample cleanup. NaOH extraction. a) Nonvolatile Removal. Duplicate sample extracts from spiked peanut oil were taken to a constant volume under a nitrogen stream, desiccated under vacuum for 1 hr and then weighed. Hexane was added to obtain the original 2-ml volume and the sample extracted twice with 5 ml portions of 3% sodium hydroxide (tumbled 20 min, 65 rpm). After centrifugation, the aqueous layer was discarded. The hexane layer was dried over anhydrous sodium sulfate and transferred (with two 2-ml hexane washings) to a preweighed 125-ml round bottom flask, rotary evaporated, dessicated under vacuum and then weighed for comparison to the preextraction weight.

b) Chromatography. Two spiked 5-g peanut oil samples were extracted (minus methanol cooling) as reported in the extraction section. The samples were derivatized as described in the derivatization section with the following modifications. After removing the 0.5*M* nitric acid wash, the samples were extracted twice with 5-ml portions of 3% sodium hydroxide (tumbled 20 min, 65 rpm) followed by a 18 megohm/cm water wash (tumbling time 30 sec). The organic sample volume was adjusted to 2.0 ml, dried over anhydrous sodium sulfate and transferred to autoinjector vials to await analysis.

Dry ice-methanol cooling. Nonvolatile removal. Four 5-g samples of spiked peanut oil were extracted with 0.05% tropolone in 0.04*M* hydrochloric acid/methanol as described in the extraction section. Methanol extracts from two samples were cooled in dry ice/methanol. The pooled methanol extracts of

Table 1. Method detection limit (MDL)

Analyte	Mean $N_{p\text{-}p}$ (mV)*	N_{SD}(mV)†	Response factor‡	LOD§	MDL‖	
$BuMe_3Sn$	0.00854	0.00216	370.9	5.6	0.2 #	0.3**
Bu_2Me_2Sn	0.00850	0.00378	472.6	9.4	0.4	0.7
Bu_3MeSn	0.00935	0.00312	452.7	8.5	0.3	0.8
Cy_2Me_2Sn	0.00873	0.00314	388.8	7.1	0.3	0.7
Oc_2Me_2Sn	0.01069	0.00339	404.6	8.4	0.3	1.0
Cy_3MeSn	0.00912	0.00369	451.2	9.1	0.4	1.1
Ph_3MeSn	0.0090	0.00292	425.9	7.6	0.3	0.9

*Mean peak to peak baseline noise.
†Standard deviation of $N_{p\text{-}p}$.
‡Inverse of slope from linear regression (pg Sn/mV).
§Limit of dectection, (mean $N_{p\text{-}p} + 3N_{SD}$)*response factor (pg Sn).
‖Method detection limit, [((LOD inj./vol.)*extract vol.)/sample wgt.]*10^{-3}.
#as ng Sn/g.
**as ng $R_xSn^{(4-x)+}$/g, R = butyl, cyclohexyl or phenyl.

each sample were rotary evaporated, desiccated under vacuum and then weighed. The weights of the cooled sample extract residues were compared against those of the noncooled extracts.

RESULTS AND DISCUSSION

Extraction method

The method isolated the organotins with minimal coextractives without the expense and equipment requirements of gel permeation or other column chromatography. Recoveries of the organotins (excluding Cy_3SnBr results) from peanut and olive oil averaged 93 and 88% respectively (Table 2). The method also provided qualitative screening for tricyclohexyltin as recoveries were low but consistent (26–32%). Coextractives from the oil matrix did not affect derivatization yields.

The precision of the method, estimated from duplicate determinations of edible oil samples (Table 3), averaged 4.3% relative standard deviation (range 0.9–11.9%).

Initial work indicated the use of tropolone and hydrochloric acid were important factors affecting recovery efficiency. Tropolone (Fig. 1) improved the recoveries of monobutyltin and dicyclohexyltin from 36 to 96% and 29 to 46%

Table 2. Mean recoveries of organotins from oils

Analyte	Matrix	Spiking level (*ng/g*)	Mean* recovery (% ± SD)
$BuSnCl_3$	Peanut oil	22.5	97 ± 3
	Peanut oil	4.5	94 ± 5
	Olive oil	22.5	95 ± 2
	Olive oil	4.5	88 ± 4
Bu_2SnBr_2	Peanut oil	16.2	97 ± 2
	Peanut oil	3.2	98 ± 3
	Olive oil	16.2	97 ± 2
	Olive oil	3.2	85 ± 1
Bu_3SnBr	Peanut oil	28.0	91 ± 6
	Peanut oil	5.6	93 ± 3
	Olive oil	28.0	92 ± 2
	Olive oil	5.6	89 ± 3
Cy_2SnBr_2	Peanut oil	21.8	85 ± 3
	Peanut oil	4.4	88 ± 1
	Olive oil	21.8	88 ± 2
	Olive oil	4.4	74 ± 2
Oc_2SnCl_2	Peanut oil	22.8	91 ± 6
	Peanut oil	4.6	95 ± 1
	Olive oil	22.8	91 ± 2
	Olive oil	4.6	83 ± 3
Cy_3SnBr	Peanut oil	21.9	29 ± 3
	Peanut oil	4.4	32 ± 2
	Olive oil	21.9	32 ± 2
	Olive oil	4.4	26 ± 2
Ph_3SnCl	Peanut oil	25.4	93 ± 3
	Peanut oil	5.1	96 ± 2
	Olive oil	25.4	94 ± 2
	Olive oil	5.1	86 ± 4

*$N = 5$

Table 3. Alkyltin levels in edible oils

Oil type	Brand	Container material†	Analyte concentration (*ng/g*) $OcSn^{3+}$	Analyte concentration (*ng/g*) Oc_2Sn^{2+}
Sunflower	A	PVC	10.1‡ (10.0-10.2)	32.9‡ (32.5-33.2)
Sunflower	B	PVC	5.7‡ (5.5-5.8)	32.4‡ (31.9-32.9)
Peanut	A	glass	nd§	< 1.0
Peanut	C	PET	nd	< 1.0
Corn	C	PET	nd	< 1.0
Corn	D	PET	nd	< 1.0
Corn	D	PVC	26.9‡ (26.3-27.6)	118.4‡ (113.3-123.4)
Canola	C	PVC	6.1‡ (6.1-6.2)	30.8‡ (29.6-32.1)
Soya	E	PVC	nd	< 1.0
Soya	C	PVC	12.9‡ (12.4-13.5)	23.2‡ (21.3-25.2)
Sunflower	F	PVC	nd	< 1.0
Canola	G	PET	nd	< 1.0
Olive	C	glass	nd	< 1.0
Olive	H	glass	nd	< 1.0
Olive	I	PET	nd	< 1.0

*Uncorrected for recovery efficiencies.
†PVC- polyvinyl chloride; PET- polyethylene terephthalate.
§Not detected.
‡Average of duplicate determinations (range in brackets).

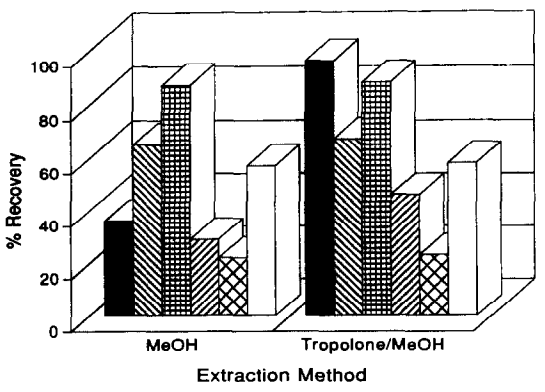

Fig. 1. The effect of tropolone on recovery of ■, monobutyltin; ▧, dibutyltin; ■, tributyltin; ▨, dicyclohexyltin; ⊠, tricyclohexyltin and □ triphenyltin.

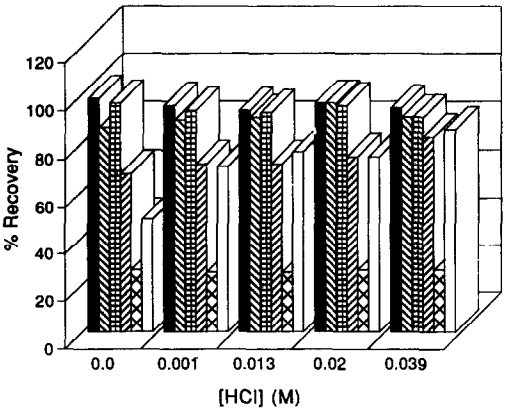

Fig. 2. The effect of HCl concentration on recovery of ■, monobutyltin; ▧, dibutyltin; ■, tributyltin; ▨, dicyclohexyltin; ⊠, tricyclohexyltin and □, triphenyltin.

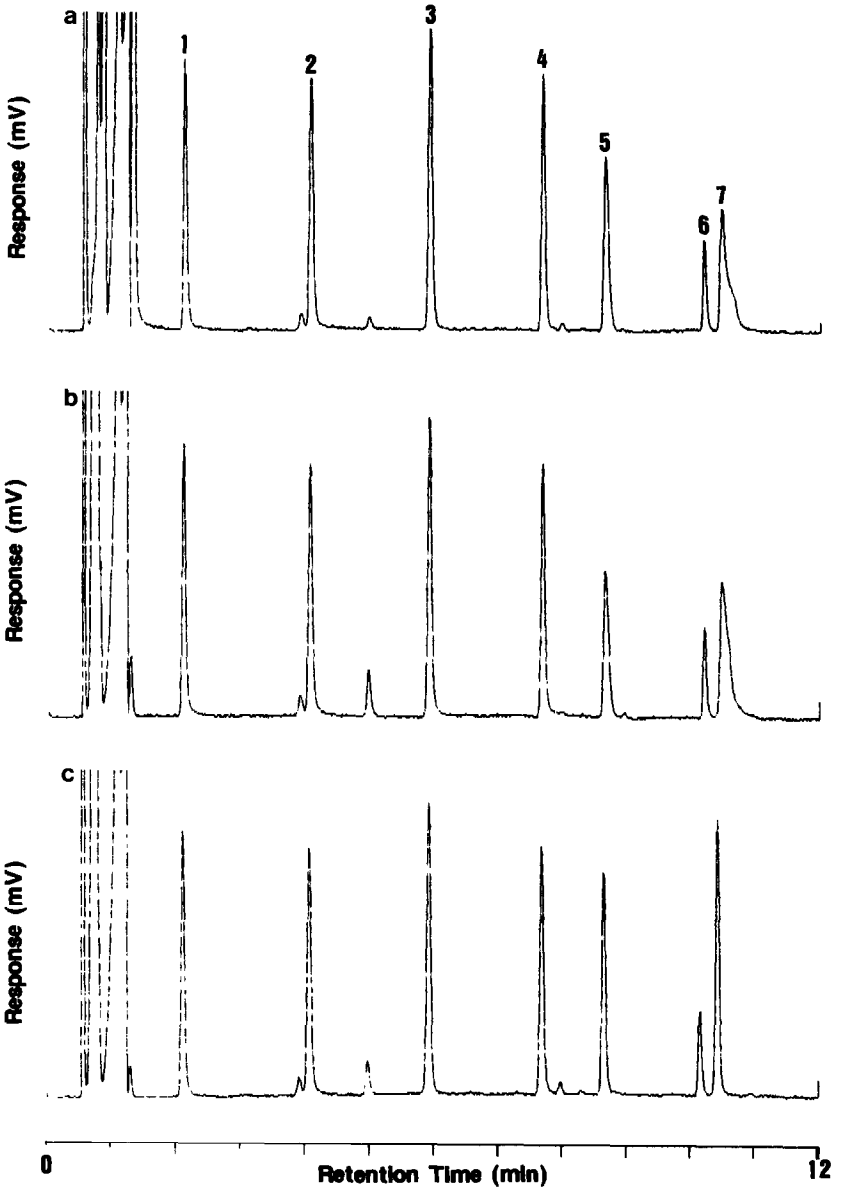

Fig. 3. GC-AAS chromatograms of oil samples containing (1) $BuMe_3Sn$; (2) Bu_2Me_2Sn; (3) Bu_3MeSn; (4) Cy_2Me_2Sn; (5) Oc_2Me_2Sn; (6) Cy_3MeSn; (7) Ph_3MeSn after (a) no sample cleanup (b) NaOH extraction and (c) MeOH extract cooling procedure.

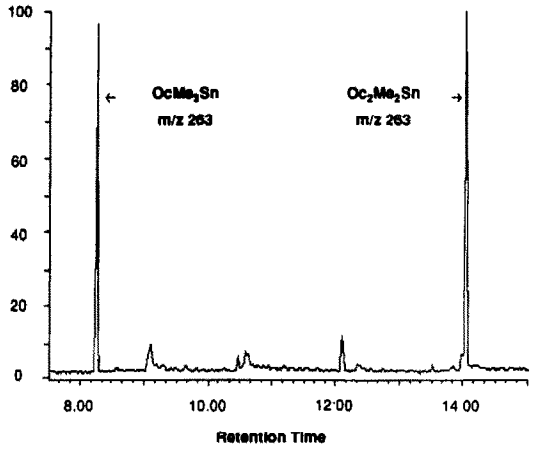

Fig. 4. GC-MS confirmation of sunflower oil containing monooctyltin (as $OcMe_3Sn$ (m/z 263 $[M\text{-}CH_3]^+$)), and dioctyltin (as Oc_2Me_2Sn (m/z 263 $[M\text{-}C_8H_{17}]^+$)).

respectively. The presence of hydrochloric acid (Fig. 2) increased recoveries of dicyclohexyltin and triphenyltin from 67 to 82% and from 48 to 85% respectively. Further improvements resulted from optimizing rotary evaporation and sample transfer steps in the procedure.

The derivatization method used previously[6] was modified by replacing 18 megohm/cm water with 0.5*M* nitric acid for the final sample wash to eliminate emulsion formation which occurred in some sample extracts.

Sample cleanup

GC column performance degraded rapidly during chromatography of initial (uncleaned) extracts, resulting in peak broadening of dioctyltin and tailing of triphenyltin [Fig. 3(a)]. The sodium hydroxide cleanup procedure, adapted from Martin-Landa *et al.*[15] removed only 1.2% of total nonvolatile coextractives and only slightly improved column performance [Fig. 3(b)]. However, cooling the methanol extract resulted in 63.6% reduction of nonvolatile coextractives present and improved the peak area/height ratio of both dioctyl- and triphenyltin [Fig. 3(c)]. Column performance could be easily maintained by silylation (using Silyl-8®) followed by a bake-out period (30 min) after every 20–30 injections with samples that had been prepared using the methanol extract cooling procedure.

Edible oil analyses

Monooctyl- and dioctyltin were found in 5 of the 15 oil samples with levels ranging from 5.7–26.9 ng/g and 23.2–118.4 ng/g respectively (Table 3). Canadian food regulations permit no more than 1 μg total octyltin/g.[16] No other alkyltins were found at levels exceeding the GC–AAS method detection limits.

GC–MS analysis of four oil samples confirmed the presence of monooctyltin [as $OcMe_3Sn$ (m/z 263 $[M\text{-}CH_3]^+$)], and dioctyltin [as Oc_2Me_2Sn (m/z 263 $[M\text{-}C_8H_{17}]^+$)] (Fig. 4). No other alkyltins were detected by GC–MS.

None of the oil samples purchased in glass or polyethylene terephthalate containers contained octyltins (Table 3). However, octyltins were present in most of the oils packaged in poly(vinyl chloride) containers (Table 3), indicating the octyltin source was probably the PVC container material. The absence of butyltins in the oil samples indicates that either the oil samples have not been in contact with PVC formulated with butyltin stabilizers or that the oils do not extract these organotin compounds from the PVC shipping containers efficiently.

CONCLUSIONS

Most of the tested organotins were quantitatively recovered from oil by extraction using 0.05% tropolone in 0.04*M* hydrochloric acid/methanol. Edible oil samples sold in PVC containers had monooctyl- and dioctyltin present. No other organotins were detected in the oil samples by GC–AAS or GC–MS.

REFERENCES

1. R. J. Maguire, *Water Poll. Res. J. Can.*, 1991, **26**, 243.
2. S. J. Blunden and C. J. Evans, *The Handbook of Environmental Chemistry*, Vol. 3, Part E, O. Huntzinger (ed.). pp. 1–44, 1991.
3. World Health Organization, *Tin and Organotin Compounds: A Preliminary Review*, Environmental Health Criteria 15, Geneva, Switzerland, pp. 109. 1980.
4. A. G. Davies and P. J. Smith, *Recent Advances in Organotin Chemistry, Advances in Inorganic Chemistry and Radiochemistry*, 1980, **23**, 1.
5. D. S. Forsyth, D. Weber and C. Cléroux, *Food Additives and Contaminants*, 1992, **9**, 161.
6. D. S. Forsyth, D. Weber and K. Dalglish, *J. Assoc. Off. Anal. Chem.*, 1992, **75**, 964.
7. A. D. Schwope, D. E. Till, D. J. Ehnthol, K. R. Sidman, R. H. Whelan and P. S. Schwartz, *Deutsche Lebensmittel-Rundschau*, 1986, **82**, 277.
8. H. Seidler, H. Woggon, M. Härtig and W.-J. Uhde, *Die Nahrung*, 1969, **13**, 257.

9. K. Figge, *Food and Cosmetics Toxicol.*, 1972. **10,** 815.
10. H. G. Carr, *Soc. of Plastic Eng.*, 1969, **25,** 72.
11. L. H. Adcock and W. G. Hope, *Analyst*, 1970, **95,** 868.
12. D. S. Forsyth and C. Cléroux, *Talanta*, 1991, **38,** 951.
13. D. S. Forsyth, *Total Environ.*, 1989, **89,** 299.
14. D. S. Forsyth and W. D. Marshall, *Anal. Chem.*, 1985, **57,** 1299.
15. I. Martin-Landa, F. Pablos and I. L. Marr, *Applied Organometallic Chem.*, 1991, **5,** 399.
16. Office Consolidation of the Food and Drugs Act and of the Food and Drug Regulations, B.23.003, Department of National Health and Welfare, Ottawa, Ontario.

Talanta, Vol. 40, No. 3, pp. 307–311, 1993
Printed in Great Britain.

0039-9140/93 $6.00 + 0.00

SEPARATION OF OXYANIONS OF PHOSPHORUS BY SINGLE COLUMN ION CHROMATOGRAPHY

DENISE HATTON and WILLIAM F. PICKERING
Chemistry Department, University of Newcastle, NSW 2308, Australia

(*Received* 4 *June* 1992. *Revised* 21 *July* 1992. *Accepted* 22 *July* 1992)

Summary—Separation of mixtures containing hypophosphite, phosphite, orthophosphate, chloride, nitrate and sulphate ions has been achieved using a Vydac 300 IC 405 column, refractive index detection and eluents which were 2m*M* in *p*-hydroxy benzoic acid or 4m*M* in *p*-amino benzoic acid (adjusted to pH 5.5). Calibration curves were linear over the concentration range 3 to 30 mg P/l.; and the precision (RSD for peak heights in mixtures) was $< \pm 10\%$. Using *p*-hydroxy benzoic acid, detection of eluted peaks by indirect UV absorption was equally satisfactory. In an initial survey, the elution behaviour of nine oxyanions of phosphorus (simple ions and condensed species) was examined, using eluents containing different organic carboxylic acids (six aliphatic and nine aromatic), present at levels of 1 to 5m*M*; with the pH adjusted to values between 3 and 8.6. No suitable conditions for separating mixtures containing condensed phosphates were identified.

A number of industrial processes produce wastes that contain mixtures of the oxyanions of phosphorus and many of the combinations have been analysed successfully using a dual column ion chromatograph and alkaline eluents, with detection of the eluted species being based (in most cases) on conductivity measurements. The mixtures of $H_2PO_2^-$, $H_2PO_3^-$ and $H_2PO_4^-$ found in plating baths have been analysed, for example, using eluents such as 3m*M* sodium carbonate (adjusted to pH 12 with sodium hydroxide[1] or a 3m*M* solution in sodium hydrogen carbonate; 2.4m*M* in sodium carbonate[2] (pH 10.3). To identify the different types of condensed phosphates found in foods elution with 80m*M* sodium hydroxide has been used.[3] Detection based on UV absorption by derivatives formed in post column reactions [*e.g.*, with Fe(III)] has been used in river water analysis (where the eluent was 1.5 to 8m*M* in sodium carbonate; 90m*M* in sodium hydroxide[4]) and in food analysis.[5]

Single column HPLC procedures have not become as well established. In this technique the eluents used are usually weak organic acid solutions and in these acidic conditions many phosphorus species, *e.g.*, hypophosphite, phosphite and orthophosphate, exist predominantly as monovalent ions. Separation of mixtures of these three oxyanions has been achieved using a Vydac 302 column, a conductivity detector and 20m*M* succinic acid (adjusted to pH 3) as the eluent;[6] and using a Hamilton PRP × 100 column, 4-amino-2 hydroxybenzoic acid (4m*M*, pH 5.5–6.5) as eluent and indirect ultraviolet absorption detection.[7] Mixtures of phosphoric, pyrophosphoric and tripolyphosphoric acids have been separated on a single column unit using an eluent composed of trimesic acid (pH 3.4) loaded with a chelating agent, *e.g.*, CyDTA.[8] For the determination of pyrophosphate and tripolyphosphate and detergent granules, an indirect UV detection method was found to be more sensitive than conductometric detection.[9]

Detection based on refractive index measurements appears to be an unexplored variant, hence in our single column ion chromatography study we elected to combine this detection system with separation on a short Vydac column. The eluents tested were a series of carboxylic acids which varied in structure, p*K*a, and pH (range 3–9).

EXPERIMENTAL

HPLC equipment

The unit used contained an ETP Kortech solvent pump (model K35M); a separating column (Vydac 300 IC 405); a sample loop (50 μl); a Refractive Index Detector (model ERC-7510); and a fast speed recorder (FSD 10 mV, operating at a paper speed of 1 cm/min). The eluent flow rate was adjusted to 1–2 ml/min. The room temperature was maintained at 22°.

For comparison studies using indirect UV absorbance detection, the column was connected into a Waters Associates Liquid Chromatograph fitted with a Lambda-Max Model 481 LC Spectro-photometer. The sample loop size in this unit was 10 μl.

Anion solutions

Stock solutions (1mM) of a series of phosphorus oxyanions [NaH_2PO_2; Na_2HPO_3; Na_2HPO_4; NaH_2PO_4; HPO_3; $(NaPO_3)_6$; $Na_5P_3O_{10}$; $Na_2H_2P_2O_7$; and $Na_4P_2O_7$] were prepared from A. R. grade chemicals dissolved in purified water obtained from a Millipore, Milli-Q reverse osmosis system.

Eluent solutions

The weak organic acid solutions listed below were pH adjusted before being filtered through a 0.45-μm membrane filter and degassed under vacuum. Each eluent was run at three pH values (3.5, 5.5 and 8.6), and where additional tests were warranted, solutions having intermediate pH values were prepared. The concentration of acid in the eluting solution was initially 1mM; but with some systems the levels were varied; and the additional concentrations (mM) tested are shown in brackets for (a) aliphatic carboxylic acids: acetic acid; succinic acid (0.5, 5, 20); adipic acid (5); maleic acid (5); fumaric acid (3); tartaric acid (2) and (b) aromatic carboxylic acids: benzoic acid (2); phenylacetic acid (5); *o*-hydroxy benzoic acid (5, 7.5, 10); *p*-hydroxy benzoic acid (2, 3, 4, 5); *p*-amino benzoic acid (2, 4); *o*-toluic acid (3); sulphosalicyclic acid (0.5, 4); phthalic acid (0.5, 2); and terephthalic acid (0.5).

RESULTS AND DISCUSSION

Eluent survey

The eluent strength of weak organic acid solutions tends to be a function of the molecular structure; the relative strength of the acid functional groups; and the system pH. Aliphatic acids have proved useful in some applications, but more widely used are aromatic mono- or di-carboxylic acids. The presence of substituent groups modifies the eluting power of these acids. For example, in a recent study[10] the effect of substituents on the separation of mixtures of monovalent (Cl^-, NO_2^-, Br^-, NO_3^-) and divalent (SO_4^{2-}, SeO_4^{2-}, $S_2O_3^{2-}$, $S_2O_6^{2-}$) inorganic ions was examined. For the pH range 5–7, it was found that the mobile phase eluent strength followed the order:

$$o\text{-sulfo} > o\text{-hydroxy} > p\text{-nitro} > p\text{-amino} > o\text{-amino} > m\text{-amino} = \text{benzoic acid.}$$

A change in pH can alter the affinity of the analyte species for the exchange sites on the column packing (by altering the degree of protonation) while simultaneously altering the level of displacing anion present in the eluent solution, hence in our investigation, we sought to utilise both effects by varying the pH of the acid eluent systems over a wide range (3–9).

Prediction of the effect of pH on elution patterns is difficult, due to the many competing equilibria involved, but many of the trends observed were as expected. For example, the elution times decreased on raising the system pH (or by increasing the eluent concentration) and when the level of displacing anions in the eluent became too high, the analyte species were swept through the column so rapidly that their detector signal became lost in the system peak observed on all chromatograms.

In the preliminary survey, the different oxyanions of P were introduced into the column as single component samples in order to confirm that the various species were being detected by the refractive index measurement unit. Systems or conditions worthy of more detailed study were then selected by comparing oxyanion elution times. A majority of the eluents tested proved to be unsuitable, due to P anions being eluted with the solvent front, or several oxyanions eluted at similar rates, or an analyte yielded multiple peaks. Only three of the organic acids (*para* substituted hydroxy- or amino benzoic acid; and *o*-phthalic acid) could be classified as potentially useful (*e.g.*, for separating mixtures containing $H_2PO_2^-$, $H_2PO_3^-$ and $H_2PO_4^-$) and these were then studied in more detail. Succinic acid was also subjected to further examination because it had been used successfully in an earlier study.[6] No suitable conditions for separating mixtures containing condensed phosphates were identified.

Separation of hypophosphite, phosphite and orthophosphate

Using p-amino benzoic acid or p-hydroxy benzoic acid. As shown on Fig. 1, separation of mixtures containing hypophosphite, phosphite, orthophosphate, chloride, nitrate and sulphate ions has been achieved using a Vydac 300 IC

405 column, refractive index detection and eluents which were 2m*M* in *p*-hydroxy benzoic acid or 4m*M* in *p*-amino benzoic acid (adjusted to pH 5.5). Using *p*-hydroxy benzoic acid, detection of eluted peaks by indirect UV absorption was equally satisfactory. Calibration curves (Fig. 2) were linear over the concentration range 3–30 mg P/l.; but the column was overloaded if mixtures contained more than 15 mg/l. of each component. Repeated analysis of this type of mixture was used to calculate the standard deviation of the various peak heights, and the precision was found to vary with the oxyanion involved. For example, the RSD values obtained using refractive index detection ranged from ±2% (hypophosphite) to ±10% (phosphite); with indirect UV detection (and *p*-hydroxy benzoic acid as eluent) the RSD values increased to < ±12%.

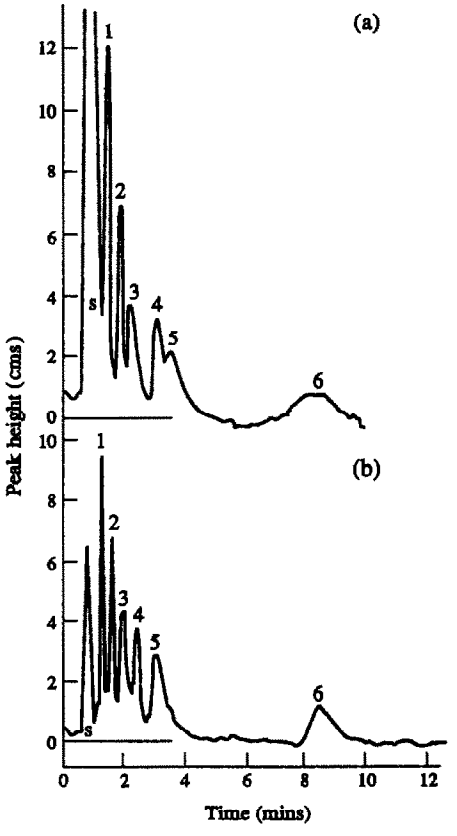

Fig. 1. Chromatograms showing the separation of mixtures containing 1. hypophosphite (250μ*M*); 2. chloride (125μ*M*); 3. orthophosphate (250μ*M*); 4. nitrate (125μ*M*); 5. phosphite (250μ*M*); and 6. sulfate (125μ*M*). s = system peak. Eluents used were (a). 4m*M* 4-amino benzoic acid (pH 5.5); (b). 2m*M* 4-hydroxy benzoic acid (pH 5.5). Flow rate 1.5 ml/min, Vydac 300 IC 405 column, column temperature 22°, refractive index detector. [With the instrument settings used, a peak height of 10 cms corresponds to 1×10^{-6} RI units].

The acid dissociation profiles of *p*-amino and *p*-hydroxy benzoic acid are somewhat similar (pK_a 4.6, 4.9), with both being weaker acids than the 4-amino-2-hydroxybenzoic acid (p*K*a 4.3) used by Mehra and Pelletier[7] for separating mixtures of a similar group of anions. The top phosphorus anion concentration studied by these investigators was 20 mg/l., and the precision achieved with this eluent (expressed as RSD values) was a little better than that achieved in our study.

Effective separation of phosphorous oxyanions by aromatic monocarboxylic acids appears to be influenced more by the type and position of substituents, than by the p*K*a value of the acid group. For example, benzoic acid has a p*K*a value similar to that of 4-amino-2-hydroxybenzoic acid but it did not selectively elute the various oxyanion species. Equally unsatisfactory as eluents were *o*-toluic acid, salicylic acid (p*K*a 3) and sulphosalicylic acid.

Using o-phthalic acid. Elution with *o*-phthalic acid has been reported[6] to yield poor separations of P oxyanions and most of the results obtained in our study were consistent with this opinion. For example, at pH 3.5 the P species signals tended to overlap and/or give dual peaks for a single species. At higher pH the $H_2PO_2^-$ ion travelled close to the solvent peak. It was found, however, that over a narrow pH range (5–5.5) there was separation of phosphite and orthophosphate ions, and with careful control of operating conditions (*e.g.*, 1m*M* eluent, being pumped through the column at 1.5 or 1.0 m/min) separation of the hypophosphite ion from the system peak was sometimes achieved, yielding a separation of the three anions. The sensitivity to operating parameters and overlap of the phosphorous peaks with chloride and nitrate ion signals led to curtailment of further studies on this eluent.

No suitable conditions for separating mixtures of P oxyanions were detected using the 1,4 isomer, terephthalic acid, as eluent.

Elution behaviour using aliphatic carboxylic acids

Succinic acid. Separation of $H_2PO_2^-$, $H_2PO_3^-$ and $H_2PO_4^-$ has been achieved[6] using 20m*M* succinic acid (adjusted to pH 3) as eluent, but small changes in pH were found to have a marked influence (*e.g.*, at pH 3.5 the three peaks totally overlapped). Since at pH 3, only about 8% of the diprotic acid would be ionized it was predicted that more dilute solutions (*e.g.*, 0.5, 1.0 or 2.0m*M*), adjusted to a slightly higher

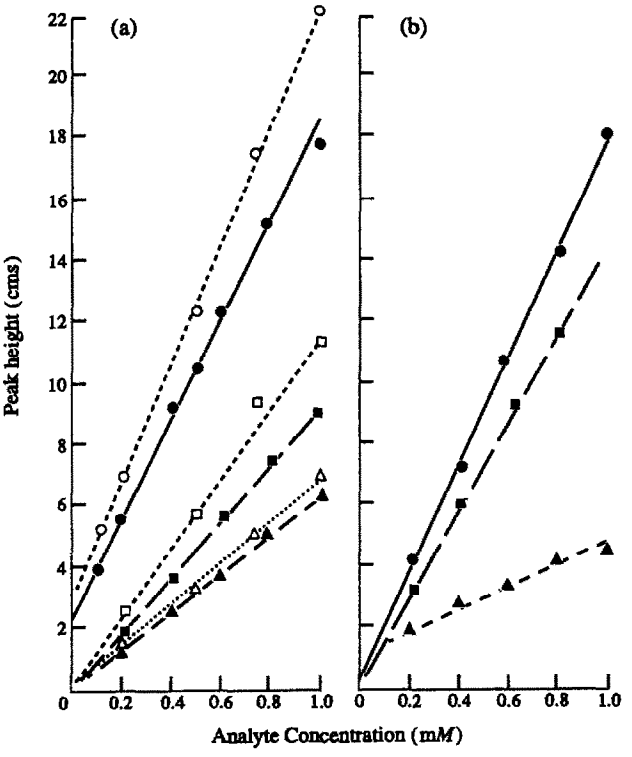

Fig. 2. Calibration curves for hypophosphite (●), orthophosphate (■) and phosphite (▲) ions; eluted at pH 5.5 from a Vydac column (300 IC 405) using an eluent flow rate of 2 ml/min. (a). Eluent, 4-hydroxy benzoic acid (2m*M*), refractive index detector; (indirect UV absorbance detection, dotted lines). (b). Eluent, 4-amino benzoic acid (4m*M*), refractive index detector. [With the instrument settings used, a peak height of 10 cm corresponds to 1×10^{-6} RI units or 2×10^{-3} absorbance units].

pH (*e.g.*, 3.5), could be equally effective. This proved to be a faulty premise, since in our study where we used these different conditions, the hypophosphite ion tended to come out with the solvent peak and the other oxyanions of phosphorus tested were rarely resolved.

Adipic, maleic, fumaric and tartaric acids. These four di-carboxylic acids showed no tendency to selectively elute the various phosphorous oxyanions, but the varied responses again showed the influence of molecular structure effects. For example, the dissociation constants for the two acid groups on adipic acid are reasonably similar to those of *o*-phthalic acid, but the absence of the aromatic ring resulted in greatly different elution behaviour. Tartaric acid has a species distribution pattern (as a function of pH) which is similar to fumaric acid, but these two acids yielded different (but equally unsatisfactory) elution patterns. Maleic acid and fumaric acid are the *cis* and *trans* isomers of the same basic molecule (HOOOC . CH = CH . COOH) but the p*K*a of the acid groups varies between the isomeric forms, and this was reflected in the eluting power.

Mono-carboxylic acid. The p*K*a value for acetic acid is similar to that of the two aromatic acids found to yield satisfactory separation of some P anions but the difference in size and chemical nature of the displacing ion led to completely different results. The introduction of a phenyl group into the base molecule altered elution behaviour, but did not facilitate separations.

Detection of oxyanions of phosphorus

In the survey of single analyte behaviour the refractive index detector yielded peaks for each of the anions tested, but those from condensed phosphates tended to be broad or distorted. The calibration graphs shown on Fig. 2 indicate the different responses observed for $H_2PO_2^{(-)}$, $H_2PO_3^{(-)}$ and $H_2PO_4^{(-)}$ ions and it can be seen that for these three oxyanions, the peak heights for 1m*M* (*i.e.*, 31 mg P/l.) solutions ranged from 0.5 to 2.0×10^{-6} RI units. Detector responses of similar magnitude were obtained using indirect UV detection (*cf.* Fig. 2). A similar type of calibration plot was obtained in an earlier study[7] which also used indirect UV absorbance as the detection mode, but where the eluent was

4-amino-2 hydroxy benzoic acid. As expected, peak width varied with the retention time, which in turn varied with system pH and nature of the eluent. There were occasions when an oxyanion of phosphorus yielded more than one peak, and no satisfactory explanation for this behaviour has been found.

General comments

Examination of the effect of pH on species distribution patterns for the various organic acids studied provided only limited guidance with respect to selecting operating conditions suitable for separating mixtures containing oxyanions of phosphorus. Despite the wide range of eluents tested and pH values used, this investigation did not find any system which effectively separated mixtures of condensed phosphate anions but it did discover two alternative reagent systems for separating hypophosphite, phosphite and orthophosphate mixtures. It also demonstrated that refractive index detection could be used in analyses of this type. The same detector mode proved useful in an earlier study of the separation of sulfite, sulfate and thiosulfate.[11]

Acknowledgements—This project was supported by funds made available by the Australian Research Committee, and the University of Newcastle Research Management Committee. This aid is gratefully acknowledged.

REFERENCES

1. Dionex, 1983. Application Note No. 49.
2. T. Tanaka, K. Hiiro, A. Kawahara and S. Wakido, *Bunseki Kagaku*, 1983, **32**, 771; *Chem. Abstr.*, 1984, **100**, 79028.
3. M. Chino and H. Sato, *Nipon Daigaku Nojuigakubu Gijutsu Kanku Hokoku*, 1990, **47**, 197; *Chem. Abstr.* 199ʊ, **113**, 150927.
4. P. Hoffman, I. Schmidtke and K. H. Lieser, *Z. Anal. Chem.*, 1989, **335**, 402.
5. A. M. Fitchett and A. Woodruff, *Liq. Chromatogr. HPLC Mag.*, 1983, **1**, 48; *Chem. Abstr.*, 1984, **100**, 131682.
6. D. S. Ryder, *J. Chromatogr.*, 1986, **354**, 438.
7. M. C. Mehra and C. Pelletier, *Chromatographia*, 1990, **30**, 337.
8. M. Nishimura, S. Imamuchi and A. Yamazaki, *Jpn. Kokai Tokkyo Koho*, 1990; *Chem. Abstr.*, 1990, **113**, 17212.
9. W. D. MacMillan, *HRC CC, J. High Resolut. Chromatogr. Commun.*, 1984, **7**, 102; *Chem. Abstr.*, 1984, **100**, 212093.
10. M. C. Mehra and C. Pelletier, *Anal. Sci.*, 1990, **6**, 431.
11. A. Beveridge, W. F. Pickering and J. Slavek, *Talanta*, 1988, **35**, 307.

Talanta, Vol. 40, No. 3, pp. 313–323, 1993
Printed in Great Britain.

0039-9140/93 $6.00 + 0.00

ELECTROCHEMICAL BEHAVIOR OF ZOPICLONE

J.-C. VIRÉ, H. ZHANG, G. QUARIN and G. J. PATRIARCHE
Free University of Brussels (ULB), Institute of Pharmacy, Campus Plaine, C-P. 205/6, Bd du Triomphe, B-1050 Brussels, Belgium

Z. SENTÜRK
University of Ankara, Faculty of Pharmacy, Department of Analytical Chemistry, 06100 Tandogan-Ankara, Turkey

G. D. CHRISTIAN
Department of Chemistry, BG-10, University of Washington, Seattle, WA 98195, U.S.A.

(*Received* 12 *June* 1992. *Revised* 15 *June* 1992. *Accepted* 16 *July* 1992)

Summary—The electrochemical properties of zopiclone, an anxiolytic and hypnotic drug, have been investigated by different techniques. The compound is reduced in two 2-electron steps in the pH range 0–12. The first step, which corresponds to the reduction of the pyrazine ring, is reversible in acidic and neutral solutions. Strong adsorption phenomena accompany the reduction process in acidic and neutral media. Zopiclone can be quantitatively measured over the entire pH range using DC polarography. However, the use of differential pulse and square-wave modes for quantitative measurements is more limited due to a slope modification in the current-concentration relationship. Adsorptive stripping voltammetry can be applied to the determination of low levels of the drug at pH 9, but only short deposition times may be used because large amounts of material accumulated under stirring conditions due to fast adsorption kinetics are rapidly released from the electrode surface. Detection limits are $1 \times 10^{-7} M$ and $2 \times 10^{-10} M$ for polarography and adsorptive stripping voltammetry, respectively. Only the first wave is of analytical interest for both techniques.

Zopiclone (4-methyl-1-piperazine carboxylic acid, 6-(5-chloro-2-pyridyl)-7-oxo-6,7-dihydro-5H-[3,4b]pyrrolo-5-pyrazinyl ester) is a new derivative of the cyclopyrrolone family. This compound has a chemical structure quite different from that of benzodiazepines but exhibits similar pharmacological effects, mainly anxiolytic and hypnotic properties,[1–3] which have often been compared with those of triazolam.[4–6] The piperazinyl carbamate moiety is important for the interaction of the drug at the receptor sites.[7]

A polarographic investigation of zopiclone has been carried out using direct current, differential pulse and square-wave techniques and cyclic and adsorptive stripping voltammetry. The electrochemical properties of the pyrazine ring, which is to be considered as a probable electroactive site of zopiclone, is well documented[8–14] but only the marked influence of small substituents has been investigated. The aim of this work is to determine the redox behavior of this more substituted pyrazine derivative in aqueous solutions and to compare the results with those presented in the literature.

From a pharmacological point of view, the knowledge of the electroanalytical properties of a drug is always of interest for further applications, in raw material or in biological fluids. The optimal conditions for its quantitative determination have also been developed. To our knowledge, only gas[15,16] and liquid[17] chromatographic techniques have been applied to the determination of zopiclone.

EXPERIMENTAL

Apparatus

DC polarographic analysis was performed using a PRG 34 Tacussel instrument equipped with a three electrode cell. The potentials are referred to the saturated calomel electrode (SCE), and unless otherwise stated, the following parameters were applied: drop time: 1.1 sec; scan rate: 5 mV/sec.

DP, SW and adsorptive stripping measurements were performed using a PAR 384B Polarographic analyzer equipped with an SMDE 303A stand and a Houston DMP 40 plotter, the following parameters being employed: DP

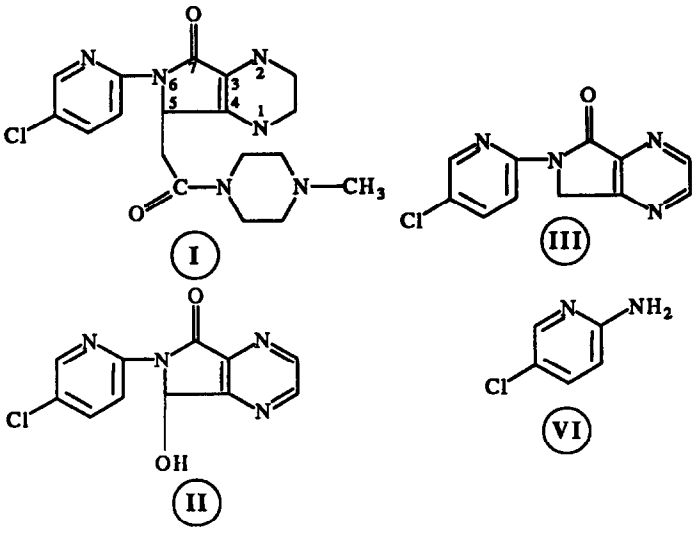

Fig. 1. Structures of Compounds Studied. I. Zopiclone (27.267 RP). II. 6-(5-Chloro-2-pyridyl)-5-hydroxy-7-oxo-6,7-dihydro-5H-[3,4b]pyrrolopyrazine (29.307 RP). III. 6-(5-Chloro-2-pyridyl)-7-oxo-6,7-dihydro-5H-[3,4b]pyrrolopyrazine (48.497 RP). IV. 2-Amino-5-chloropyridine (26.695 RP).

polarography: scan rate: 5 mV/sec, pulse height: 25 mV; SW voltammetry: pulse height 20 mV, frequency: 100 Hz, scan rate 200 mV/sec. Cyclic voltamperograms were recorded with a PAR 174A polarograph coupled with a PAR 175 programmer for scan rates up to 500 mV/sec and with a PAR 273 potentiostat monitored by an IBM XT computer for higher scan rates. These instruments were coupled with a PAR 303 and 303A stand, respectively. DP, SW and cyclic voltamperograms were plotted against a Ag/AgCl/saturated KCl reference electrode.

Reagents

Zopiclone and its precursors were graciously provided by Rhone-Poulenc, Brussels, Belgium. These compounds (Fig. 1) were used without further purification. A 0.1*M* Britton–Robinson buffer adjusted with sulfuric acid or sodium hydroxide was used, the absence of interaction between the investigated compound and each component of the buffer having been verified. A stock $2 \times 10^{-3}M$ solution, renewed daily, was prepared in 2-propanol. The working solutions were prepared by dilution of the stock solution and contained 10% 2-propanol.

RESULTS AND DISCUSSION

Influence of pH

Zopiclone was studied in the pH range 1–12. The drug is reduced at the dropping mercury electrode in two waves of about the same height (Fig. 2). Intensities of both waves decrease to about half of their initial values between pH 9.5 and 10.5 and recover their initial heights above pH 10.5. The first wave decreases slowly with a further increase in the pH. Between pH 9.5 and 10.5, three small additional waves appear before, between and after the main waves (Fig. 2).

First wave

The first wave corresponds to a two-electron transfer as indicated by controlled potential coulometry performed in both neutral and very alkaline solutions. Its half-wave potential is shifted towards more negative values with increasing pH up to pH 10, by 57 mV/pH unit (Fig. 3). A small break appears at this pH value and the slope becomes equal to 36 mV/pH unit at higher pH's.

Electrode mechanism. Logarithmic analysis of the wave in acidic medium exhibits two segments with slopes very close to 30 mV. This slope increases to 39 mV in neutral solution and 48 mV at pH 12.5, indicating that the process is reversible in acidic medium, becomes quasi-reversible at pH 7.0 and irreversible above pH 10. This behavior is confirmed by cyclic voltammetry (Fig. 4). In very acidic medium (1*M* perchloric acid), the well defined reduction peak gives rise to a re-oxidation peak but only at high scan rates, even when the scan is reversed after the first peak. The ratio i_{pa}/i_{pc} remains lower than unity, indicating an EC mechanism.

The linear increase of the reduction peak current with the square root of the scan rate and the independence of $i_p/v^{1/2}$ as a function of log

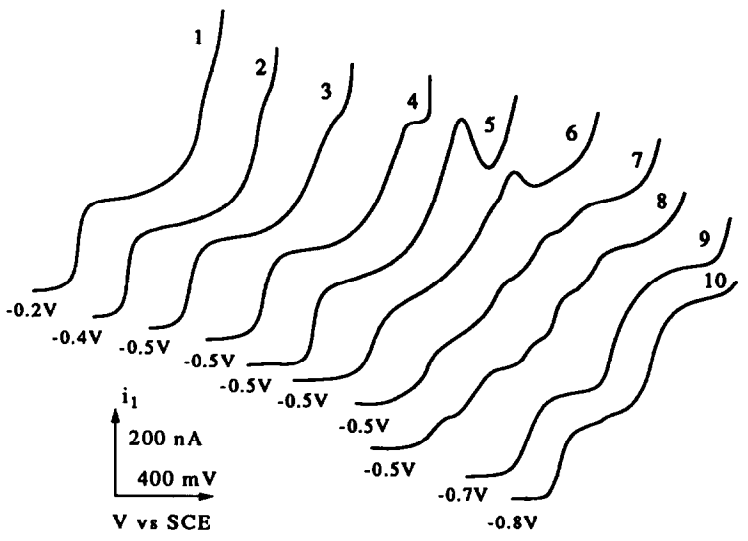

Fig. 2. DC Polarograms of $2 \times 10^{-4}M$ zopiclone in $0.1M$ Britton–Robinson buffer. pH = (1) 2.0; (2) 5.0; (3) 7.0; (4) 8.2; (5) 9.2; (6) 9.8; (7) 10.0; (8) 10.6; (9) 11.0; (10) $0.2M$ NaOH.

v shows the diffusion control of the process. However, adsorption appears at high scan rates (10 V/sec). Reversibility is confirmed by the independence of the peak potential against the scan rate.

Conducting similar experiments with solutions of increased pH shows that adsorption phenomena become more important and result from the adsorption of the reduced species. An adsorption peak precedes the reduction peak at pH 7 while the reoxidation peak becomes sharper [Fig. 4(B)]. The influence of adsorption can be minimized, but not eliminated, by addition of 40% ethanol to the solution [Fig. 4(C)]. The process remains reversible at pH 7 [Fig. 4(B),(C)] but the rate of the chemical reaction involved in the EC mechanism decreases with increasing pH and the i_{pa}/i_{pc} ratio is equal to unity at slow scan rates (< 50 mV/sec) and reaches 1.5 at higher scan rates (see below: second wave).

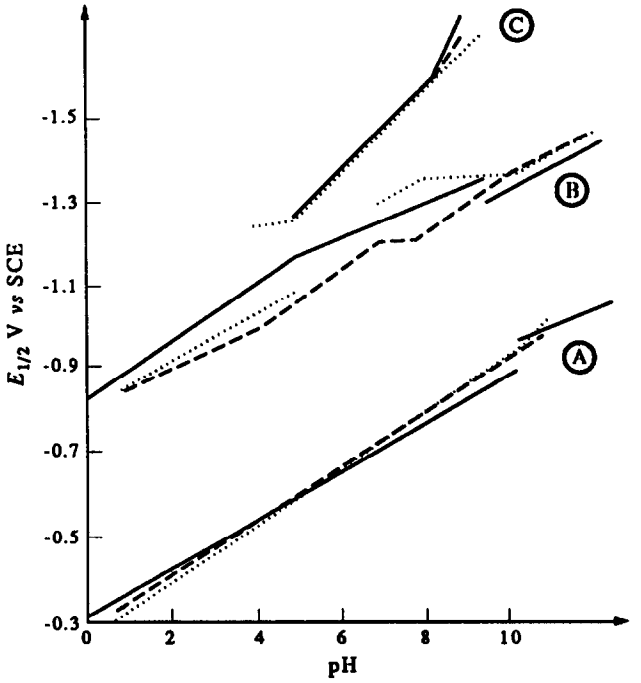

Fig. 3. Half-wave potentials as a function of pH. Zopiclone I, $2 \times 10^{-4}M$ —. Compound II, $2 \times 10^{-4}M$ · · ·. Compound III, $2 \times 10^{-4}M$ – – –. A: Wave 1; B: Wave 2; C: Wave 3.

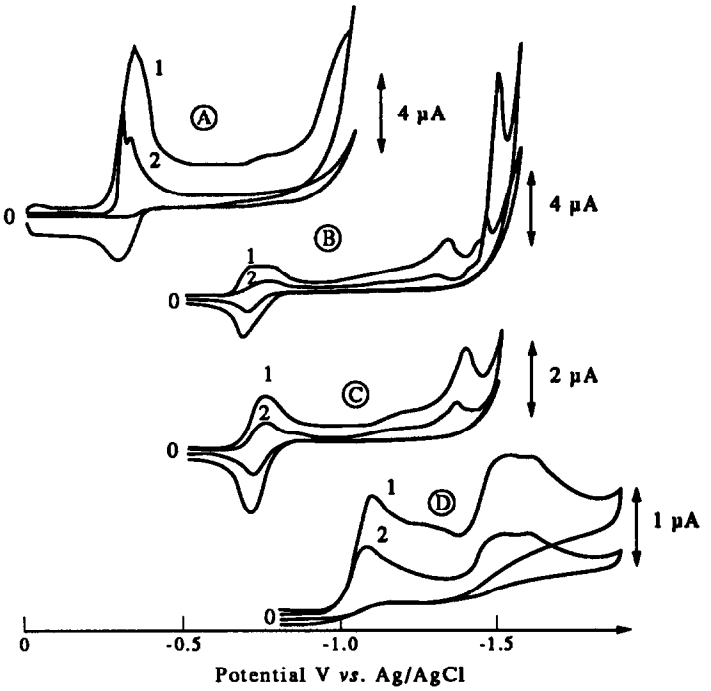

Fig. 4. Cyclic voltamperograms of $2 \times 10^{-4}M$ zopiclone. A: $1M$ $HClO_4$, (1) 500 mV/sec, (2) 100 mV/sec; B: pH 7, (1) 200 mV/sec, (2) 50 mV/sec; C: pH 7 and 40% ethanol, (1) 200 mV/sec, (2) 50 mV/sec; D: pH 12.5, (1) 200 mV/sec, (2) 50 mV/sec.

An inverse situation occurs at pH 12.5 [Fig. 4(D)]. The disappearance of the reoxidation peak and the negative shift of the reduction peak potential with increasing scan rate confirms the irreversibility established by the logarithmic analysis. The decrease of i_p *vs.* $v^{1/2}$ and of $i_p/v^{1/2}$ *vs.* log v with increasing scan rate shows a kinetic complication and the appearance of a CE mechanism. This corresponds to the reduction of the unprotonated form. Protonation takes place at the electrode surface before the electron transfer, as has been demonstrated elsewhere,[8,9] the pK value determination for zopiclone (pK = 10.25) being similar to those established by these authors for substituted pyrazines.

Reduction mechanism. The above described results indicate that the first wave can be attributed to the reduction of the pyrazine ring, giving rise to the corresponding 1,4-dihydropyrazine derivative, according to a reversible two-electron process.[10–13] It has been previously established that such a process is followed by a hydrolysis reaction of the formed 1,4-dihydropyrazine into an amino-aldehyde in acidic medium[13,14] which cannot be reoxidized [see disappearance of the reoxidation peak at slow scan rates, Fig. 4(A)]. By increasing the pH, the kinetics of the chemical reaction are decreased and reoxidation may occur, even at slow scan rates [$i_{pa}/i_{pc} = 1$, Fig. 4(B),(C)]. In alkaline solution, the process becomes irreversible due to a tautomerization reaction of the 1,4-dihydropyrazine into a less oxidizable 1,2- or 1,6-dihydropyrazine.[10,14]

Both the stability of the 1,4-dihydropyrazine and hence the reversibility of the process highly depend on the substituent on the pyrazine ring.[11,13] Electron-withdrawing substituents (pyrazinamide, pyrazine carboxylic acid) enhance the lifetime, while electron-releasing substituents (methylpyrazines) decrease this lifetime. Reversibility of this last group thus appears in a more restricted range of pH and/or scan rates.

In zopiclone, the pyrazine ring is substituted by a hydropyrrolone moiety which is itself substituted at the C5 and N6 atoms. Considering the extended reversibility of the reduction of zopiclone, as well as its reduction potential (intercept of the E–pH relationship at −0.300 V *vs.* SCE), which are similar to those of the unsubstituted pyrazine,[13] the behavior of zopiclone can be regarded as intermediate between pyrazinamide and methylpyrazine.[13] In fact, the hydropyrrolone substituent can be considered as an amido group on C3 and a methyl group on C4 of the pyrazine ring. This explains the stability and hence the wide pH range in which reversibility is observed for zopiclone.

It should be noted that substitution of the hydropyrrolone ring by the 4-methyl-1-piperazine carboxylate moiety does not modify the behavior of the first wave. This has been demonstrated by performing similar experiments on compounds II and III (E–pH relationships in Fig. 3). The main difference is in a more pronounced decrease of the first wave of compound II above pH 10.5 and its disappearance at pH 11.5.

Although most of the electrochemical characteristics of substituted pyrazines are encountered with zopiclone, two different behaviors are unusual. Pyrazine derivatives generally involve a protonation step before the $2e$–2H transfer occurs.[8-13] This appears in the E–pH relationship, the slope of which is about 90 mV/pH between pH 2 and 7. This preprotonation step does not occur or else it occurs in the bulk solution rather than at the electrode during reduction of zopiclone, since a slope of 57 mV/pH is observed between pH 0 and 10, indicating a classical $2e$–2H exchange. On the other hand, pyrazine compounds are often reduced in two one-electron steps in very acidic solutions, *i.e.*, the first wave splits into two separated one-electron waves.[10,12,13] This never occurs with zopiclone, even in 1M perchloric acid.

Second wave

Zopiclone exhibits a second wave over the entire pH range (Figs. 2 and 3). This ill-defined wave appears near the discharge of the supporting electrolyte. It becomes inhibited at pH 8 and exhibits a maximum between pH 8.5 and 10.0. Its intensity is somewhat higher than that of the first wave in acid and neutral medium and it decreases between pH 9.5 and 10.5, as does the first wave, and regains its initial value above pH 10.5. Its height remains constant when the pH is further increased. The half-wave potential of this wave is also shifted negatively with increasing pH [Fig. 3(B)] but the relationship exhibits two slopes, 67 and 41 mV/pH successively, with a break at pH 5. The potential becomes somewhat less negative above pH 10 (pK of the pyrazine ring) and then shifts by 52 mV/pH when pH is again increased.

Between pH 5 and 9 the second wave is immediately followed by a very steep third wave situated very closely to the supporting electrolyte discharge (not represented in Fig. 2). The height of this third wave is similar to that of the second wave and is constant between pH 5 and 8. It strongly decreases at pH 9 and disappears at pH 9.5. Its half-wave potential shifts negatively by 100 mV/pH with increasing pH [Fig. 3(C)]. In the presence of 40% ethanol, this third wave is completely removed and the second wave becomes better defined and of the same height as the first one.

Electrode mechanism. Logarithmic analysis of the second wave exhibits two slopes: 44 and 74 mV/log unit in acidic solutions and 50 and 68 mV/log unit in alkaline medium, demonstrating the irreversibility of the process at all pH values. Cyclic voltammetry confirms these results but brings some additional information. In acidic solutions, the second wave appears as a shoulder to the supporting electrolyte discharge current [Fig. 4(A)], but only at high scan rates (>0.5 V/sec in 1M perchloric acid, >0.2 V/sec at pH 3.25). No reoxidation peak can be seen before that of the first process. At pH 7, a flat peak corresponding to the second wave is followed by a sharp peak corresponding to the third wave [Fig. 4(B)]. This last peak disappears in the presence of 40% ethanol and the second wave becomes more defined and has the same intensity as the first one [Fig. 4(C)].

This means that the second process, developed in this last case with low interference from adsorption phenomena, also involves a two-electron transfer and that the higher intensity of the second wave as well as the presence of the third wave in the absence of ethanol result from adsorption phenomena. In fact, the third wave corresponds to the same process as the second one but from an adsorbed state. When the potential of the third wave is reached, the adsorbed molecules are desorbed and immediately reduced.

A study performed as a function of concentration shows that, if both the first and the second waves increase linearly with this parameter, the third wave appears only for relatively high concentrations. The lowest limit for which this third wave appears depends on the pH since adsorption increases with increased pH and the higher the pH, the lower will be the critical concentrations. Two peaks of similar height are recorded at pH 12.0 where adsorption problems are very low [Fig. 4(D)].

The negative shift of the peak potential with increasing scan rate confirms the irreversible character of the process. Analysis involving the peak current is not possible in acidic medium due to the disappearance of the peak at low scan rates. At pH 7, both the i_p *vs.* v and i_p/v *vs.* log v relationships show that strong adsorption

phenomena are involved but are lowered by ethanol additions. As with the first peak, the second peak exhibits a kinetic character at pH 12 due to a protonation reaction preceding the electron transfer.

Reduction mechanism. Very little information can be found about the second wave, whenever present, of pyrazine derivatives. Volke *et al.*[11] evoke a "probable" further reduction of the 1,4-dihydropyrazine ring leading to the tetrahydro derivative. Armand *et al.*,[14] working in alkaline medium, demonstrated that some 2,3-disubstituted pyrazines undergo a first reversible two-electron transfer giving rise to the 1,4-dihydro derivative, which is further irreversibly reduced to the 1,2,3,4-tetrahydro compound. Nevertheless, the phenomenon with zopiclone allows us to make some observations of the behavior of the second process, but the reduction site cannot be defined definitively.

The fact that the second peak only appears at high scan rates in acidic medium [Fig. 4(A)], meaning that time is too short to allow hydrolysis of the 1,4-dihydro derivative, shows that the second process is related to the pyrazine ring; a further reduction of 1,4-dihydropyrazine, or the reduction of another site (*i.e.*, the hydropyrrolone ring) is possible only when it is next to the intact 1,4-dihydropyrazine ring, but impossible when that ring has been hydrolyzed to the aminoaldehyde structure (in acid solution). A further reduction of the 1,4-dihydropyrazine is doubtful since such a process is irreversible and the reoxidation peak of the first process should be absent. This would mean that another site should be involved.

The structure of zopiclone allows consideration of only the cleavage of the hydropyrrolone ring. Such a reductive cleavage should occur between the C5 and N6 atoms, this bond having reduced stability in the hydro-pyrrolone ring, mainly when next to a rigid cycle (dihydropyrazine) instead of two separated groups (amino aldehyde). Such a behavior has been previously pointed out with piroxicam.[18,19] In such a case, the nature of the substituent at the C5 position should influence the reduction potential of the second wave.

In fact, the removal of the ester group (compound II) or its replacement by a hydroxy group (compound III) modifies the *E*-pH relationship [Fig. 3(B)]. Compound III remains more easily reduced than zopiclone up to pH 9.5, while compound II is reduced at less negative potentials in acidic solutions but at more negative values between pH 7 and 10.5. The wave disappears between pH 5 and 7, but the third wave remains. The third wave of the three compounds are superimposed [Fig. 3(C)], indicating that their reduction potentials are governed by the desorption process and that adsorption results from an identical part of the molecules, *i.e.*, the pyrrolopyrazine moiety.

The situation becomes more complex in alkaline medium where the second wave of each compound (I, II and III) appears at similar potentials and is shifted in the same manner with pH [Fig. 3(B)]. The first hypothesis which comes to mind is that zopiclone undergoes a hydrolysis of the ester function in alkaline solution, giving rise to compound III. This would mean that the hydroxy group has no more influence on the reduction potential between pH 10.5 and 12, in opposition to the marked influence exhibited between pH 7 and 10 [Fig. 3(B), compounds II and III]. While this hydrolysis of the ester function probably occurs, another chemical reaction would take place as indicated by the following experiments. Two samples of zopiclone were treated, respectively, with a pH 9 Britton–Robinson buffer and with 0.05*M* sodium hydroxide. Their dichloromethane extracts were submitted to thin layer chromatographic separation. Both samples show that zopiclone has completely disappeared. Neither compound II nor compound III can be detected, invalidating the above hypothesis, but aminochloropyridine (compound IV) has been formed. Chloropyridine is not detected.

A zopiclone solution treated with 0.05*M* sodium hydroxide has also been investigated polarographically as a function of pH. Two to four waves were recorded, depending on the pH, but they cannot be correlated to any wave of compounds I to III, of pyrazine carboxylic acid, nor those of pyrazinamide recorded under the same conditions. However, the first wave splits into two waves in very acidic solution and the reduction potential of this wave is shifted by 100 mV/pH up to pH 7, meaning that one or more simpler derivatives of pyrazine (*i.e.*, hydroxymethylpyrazine carboxylate) have been formed by a complex reaction involving the hydropyrrolone ring. In such a case, the second wave can no longer be attributed to the cleavage of this ring but to a further reduction of the dihydropyrazine resulting from the first electron transfer.[11,14] This would also explain the unusual positive shift in the potential of the second wave

Table 1. Characteristics of zopiclone calibration plots (Slopes in nA/$10^{-5}M$)

Medium	Technique	First Wave		Second Wave	
H_2SO_4, 0.1M	DC	1×10^{-6}–1×10^{-4}	$y = 49.1\,x + 1.3$ $r = 0.9997$, S.D. = 0.97%	Nonmeasurable	
	DP	1×10^{-6}–5×10^{-5}	$y = 16.5\,x - 0.9$ $r = 0.9991$, S.D. = 1.9%	Nonlinear	
		5×10^{-5}–2×10^{-4}	$y = 41.5\,x - 126$ $r = 0.9998$, S.D. = 1.5%		
	SW	1×10^{-6}–1×10^{-5}	$y = 199\,x - 8.5$ $r = 0.9954$, S.D. = 5.6%	Nonlinear	
		1×10^{-5}–2×10^{-4}	$y = 788\,x - 49$ $r = 0.9998$, S.D. = 0.90%		
pH 4.0	DC	1×10^{-6}–1×10^{-4}	$y = 44.5\,x + 3.5$ $r = 0.9997$, S.D. = 0.9%	Nonlinear	
	DP	1×10^{-6}–5×10^{-5}	$y = 13.9\,x - 0.66$ $r = 0.9989$, S.D. = 2.1%	1×10^{-6}–5×10^{-5}	$y = 15.5\,x + 3.6$ $r = 0.9993$, S.D. = 1.8%
		5×10^{-5}–2×10^{-4}	$y = 45.2\,x - 158$ $r = 0.9996$, S.D. = 1.9%		
	SW	1×10^{-6}–1×10^{-4}	Nonlinear	Nonlinear	
pH 8.0	DC	1×10^{-6}–1×10^{-4}	$y = 46.6\,x + 6.0$ $r = 0.9998$, S.D. = 0.78%	1×10^{-6}–1×10^{-5}	$y = 66.4\,x + 2.5$ $r = 0.9952$, S.D. = 5.7%
				1×10^{-5}–1×10^{-4}	$y = 50.7\,x + 22.7$ $r = 0.9996$, S.D. = 2.0%
	DP	1×10^{-6}–1×10^{-4}	Nonlinear	Nonlinear	
	SW	1×10^{-6}–1×10^{-5}	Nonlinear	Nonlinear	
pH 11.0	DC	1×10^{-6}–1×10^{-5}	$y = 61.6\,x + 14.2$ $r = 0.9979$, S.D. = 3.8%	1×10^{-6}–1×10^{-5}	$y = 70.9\,x + 15.5$ $r = 0.9983$, S.D. = 3.4%
		1×10^{-5}–1×10^{-4}	$y = 48.6\,x + 26.6$ $r = 0.9992$, S.D. = 2.8%	1×10^{-5}–1×10^{-4}	$y = 50.5\,x + 37.9$ $r = 0.9991$, S.D. = 3.1%
	DP	1×10^{-6}–1×10^{-5}	$y = 29.8\,x + 3.3$ $r = 0.9991$, S.D. = 2.5%	1×10^{-6}–1×10^{-5}	$y = 36.4\,x + 4.6$ $r = 0.9983$, S.D. = 3.4%
		1×10^{-5}–1×10^{-4}	$y = 20.7\,x + 10.3$ $r = 0.9965$, S.D. = 3.2%	1×10^{-5}–1×10^{-4}	$y = 24.6\,x + 11.8$ $r = 0.9987$, S.D. = 1.9%
	SW	1×10^{-6}–1×10^{-4}	$y = 98.7\,x + 27.5$ $r = 0.9991$, S.D. = 1.8%	1×10^{-6}–1×10^{-5}	$y = 274\,x + 41.2$ $r = 0.9517$, S.D. = 19%
				1×10^{-5}–1×10^{-4}	$y = 89.5\,x + 184$ $r = 9.9983$, S.D. = 3.4%

at pH 9.5 as the pH is increased when this chemical modification occurs [Fig. 3(B)].

Influence of concentration

The influence of zopiclone concentration on the polarographic response was investigated between $1 \times 10^{-6}M$ and $2 \times 10^{-4}M$. The drug can be determined quantitatively, but the results which are summarized in Table 1 depend highly on the pH and on the applied wave form. It can be deduced from Table 1 that DC polarography exhibits a better linearity for each investigated pH and over a wider concentration range, except at pH 11. DP and SW modes generally exhibit a slope modification in this relationship due to the adsorption phenomenon occurring with zopiclone. The higher concentrations offer higher slopes in acidic media, the opposite situation occurring at pH 11. The concentration at which this break in the slope appears depends on the applied wave form.

When it can be used, the SW mode provides a higher sensitivity. Except at pH 11, only the first wave is to be considered for analytical purposes, the second one giving rise in most cases to a non-linear increase of the current with increasing concentration. This is to be attributed to the strong adsorption of the compound produced in the first reduction step in acidic and neutral solutions.

Adsorptive stripping voltammetry

Adsorptive stripping measurements have been performed on the first reduction wave. Preliminary studies have demonstrated the usefulness of the square-wave mode which provides a hundred-fold enhancement in the response.

Influence of pH. An adsorptive study performed as a function of pH shows that the peak intensity remains very low below pH 6 and does not increase linearly with either the concentration or the deposition time. Above pH 6, a well defined peak is recorded, its intensity increasing regularly up to pH 9.5. It decreases abruptly above this value due to the degradation process which takes place. The degradation product of zopiclone is not accumulated in very alkaline medium. Since the solutions are stable enough at pH 9.0 (several hours) to perform adsorptive measurements, this pH value has been selected as providing the highest sensitivity. However, in order to verify that these results are not affected by the degradation process, the experiments on deposition and concentration were repeated at pH 7 where the compound is stable (see below).

Influence of the supporting electrolyte. The nature and the concentration of the supporting electrolyte may strongly influence the voltammetric response. Table 2 summarizes the peak potential and intensity and the half-peak width for seven buffered or unbuffered media. Compared with the values obtained with sodium sulfate or perchlorate from which low adsorption interference is expected, borate and acetate buffers partially inhibit the accumulation process while tris-HCl buffer enhances the peak height. The latter was selected for further investigations.

The highest sensitivity is provided by a $0.1M$ tris-HCl concentration. The peak height decreases below $0.05M$ and above $0.3M$. The same experiment repeated using a constant ionic strength demonstrates that the addition of as low as $1 \times 10^{-4}M$ tris-HCl in a $0.1M$ sodium sulfate solution enhances the peak current by a factor of two, the intensity becoming stable above $1 \times 10^{-3}M$. However, reproducibility is not as good as that observed with $0.1M$ tris-HCl alone.

This behavior may be attributed to a co-adsorption of the buffer molecules which increases the amount of accumulated zopiclone. At high tris-HCl concentrations (above $0.3M$), the adsorption of the buffer becomes competitive and inhibits accumulation of the drug.

Influence of the operating parameters. Maximum accumulation occurs between -0.4 and -0.6 V *vs.* Ag/AgCl for both pH 7 and 9 solutions. A deposition potential of -0.6 V has been selected for both pH values.

Unusual behavior has been observed from studying the influence of the deposition time (Fig. 5). At each investigated concentration, ranging from 1×10^{-9} to $1 \times 10^{-7}M$, at pH 9 a linear relationship exists between the peak current and the deposition time up to 30 sec only, the maximum response being obtained

Table 2. Adsorptive stripping voltammetry of $1 \times 10^{-7}M$ zopiclone. Influence of the nature of the supporting electrolyte ($0.1M$), pH = 7.0, $E_{acc} = -0.6$ V *vs.* Ag/AgCl, $t_{acc} = 30$ sec

	Acetate	Phosphate	Borate	Tris–HCl	$NaClO_4$	KCl	Na_2SO_4
E_p (V)	−0.854	−0.860	−0.790	−0.814	−0.924	−0.920	−0.926
i_p (nA)	601	1365	435	2872	1446	1179	1296
$\omega\frac{1}{2}$(mV)	55	54	90	50	75	88	85

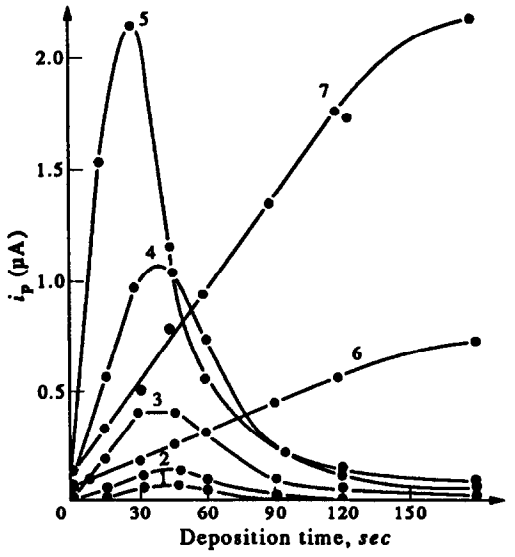

Fig. 5. Adsorptive stripping voltammetry of zopiclone. Peak current as a function of the deposition time. 0.1*M* tris-HCl buffer, $E_{acc} = -0.60$ V *vs.* Ag/AgCl, zopiclone concentration = (1) $1 \times 10^{-9}M$, (2) $3 \times 10^{-9}M$, (3) $1 \times 10^{-8}M$, (4) $3 \times 10^{-8}M$, (5) $1 \times 10^{-7}M$, (6) $3 \times 10^{-8}M$, (7) $1 \times 10^{-7}M$. 1–5: accumulation under stirring; 6, 7: accumulation without stirring.

between 30 and 45 sec. The current decreases rapidly above 45 sec to become negligible after 120 sec. A similar situation occurs at pH 7 using the same buffer; the maximum current is recorded between 30 and 45 sec and decreases after 45 sec as rapidly as observed at pH 9.

The fact that the current increases with the concentration but decreases with time indicates that the behavior is to be attributed to a release of the adsorbed material with time, not to a saturation of the electrode surface.

The same experiments repeated with a deposition step performed without stirring show that linearity is extended up to 120 sec (Fig. 5). With further accumulation time, the current levels off and does not decrease. This means that accumulation performed under stirring conditions gives rise to a metastable adsorbed layer, with a subsequent slow equilibrium provoking the release of a significant portion of the molecules instead of their rearrangement at the electrode surface to give a more stable adsorbed layer. The slower accumulation occurring in quiescent solution gives rise to a stable configuration of the adsorbed molecules. This behavior is observed at both pH 7 and 9.

The same experiment has been performed using three different supporting electrolytes: acetate buffer, sodium sulfate and sodium perchlorate. Again, the voltammetric response in stirred solution exhibits a maximum between 30 and 60 sec, depending on the nature of the supporting electrolyte, but lower currents are recorded (Table 2). This means that this unusual behavior must be attributed to zopiclone itself, not to a surface interaction of the tris-HCl buffer.

Effect of concentration. The above described behavior is also reflected in the plots of the peak current as a function of the concentration for different accumulation times. Tables 3 and 4 compare the characteristics of the calibration curves established at pH 7 and 9. It can be deduced that the neutral pH provides enhanced sensitivity (slope) but with lower precision. For each applied deposition time, a break appears in the linearity range with stirred solutions at $1 \times 10^{-9}M$ at pH 7 and at $1 \times 10^{-8}M$ at pH 9.

Table 3. Adsorptive stripping voltammetry of zopiclone. Calibration curves. 0.1*M* tris-HCl buffer, pH = 7.0, $E_{acc} = -0.6$ V *vs.* Ag/AgCl

t_{acc} (sec)	Linearity range (*M*)	Equation (slope in nA/$10^{-9}M$)	Correl. coeff.	s_b (%)
15	1×10^{-10}–1×10^{-9}	$y = 15.5x + 2.3$	0.998	3.5
	1×10^{-9}–1×10^{-7}	$y = 11.1x - 7.9$	0.999	1.2
30	1×10^{-10}–1×10^{-9}	$y = 25.8x + 1.1$	0.955	15.0
	1×10^{-9}–1×10^{-7}	$y = 15.2x - 12.9$	0.999	1.5
30*	1×10^{-9}–1×10^{-7}	$y = 5.5x + 5.5$	0.999	1.4
45	1×10^{-10}–1×10^{-9}	$y = 27.6x + 2.4$	0.945	17.3
	1×10^{-9}–1×10^{-7}	$y = 13.1x - 15.3$	0.999	1.3
60	1×10^{-10}–1×10^{-9}	$y = 26.7x - 0.8$	0.969	15.0
	1×10^{-9}–1×10^{-7}	$y = 8.1x - 8.8$	0.997	2.7
60*	1×10^{-9}–1×10^{-7}	$y = 7.7x + 8.3$	0.998	2.0
120	1×10^{-9}–1×10^{-8}	$y = 2.7x + 1.1$	0.999	2.4
	1×10^{-8}–1×10^{-7}	$y = 2.2x - 4.4$	0.997	4.1
120*	1×10^{-9}–1×10^{-7}	$y = 10.9x - 2.1$	0.100	0.7

*Accumulation performed without stirring.

Table 4. Adsorptive stripping voltammetry of zopiclone. Calibration curves. 0.1M tris-HCl buffer, pH = 9.0, $E_{acc} = -0.6$ V *vs.* Ag/AgCl

t_{acc} (sec)	Linearity range (M)	Equation (slope in nA/$10^{-9}M$)	Correl. coeff.	s_b (%)
15	1×10^{-9}–1×10^{-8}	$y = 13.6x + 0.2$	0.100	1.2
	1×10^{-8}–8×10^{-8}	$y = 18.0x + 4.2$	0.993	5.8
30	2×10^{-10}–1×10^{-8}	$y = 27.3x + 6.4$	0.999	1.4
	1×10^{-8}–8×10^{-8}	$y = 33.9x + 8.1$	0.998	2.8
30*	1×10^{-9}–1×10^{-8}	$y = 3.5x - 0.8$	0.998	2.8
	1×10^{-8}–8×10^{-8}	$y = 6.3x - 3.4$	0.996	5.4
45	4×10^{-10}–1×10^{-8}	$y = 29.6x + 0.1$	0.997	2.6
	1×10^{-8}–8×10^{-8}	$y = 35.0x + 9.8$	0.100	1.3
60	2×10^{-10}–1×10^{-8}	$y = 17.7x - 2.4$	0.999	1.4
	1×10^{-8}–8×10^{-8}	$y = 19.5x - 6.7$	0.100	0.4
60*	1×10^{-9}–1×10^{-8}	$y = 7.0x - 4.3$	0.999	2.5
	1×10^{-8}–8×10^{-8}	$y = 9.8x - 8.9$	0.999	1.6
120	1×10^{-9}–1×10^{-8}	$y = 3.6x - 0.8$	0.994	5.3
	1×10^{-8}–6×10^{-8}	$y = 3.2x + 1.7$	0.999	1.3
120*	1×10^{-9}–1×10^{-8}	$y = 17.4x - 8.4$	0.999	1.9
	1×10^{-8}–6×10^{-8}	$y = 19.1x - 17.3$	1.000	0.7

*Accumulation performed without stirring.

The slopes at the two pH values are similar before the break, but pH 9 provides a higher slope after the break, giving rise to a better sensitivity. This is attributed to a modification of the adsorption pathway which is strongly influenced by pH, as demonstrated above by polarography and cyclic voltammetry.

Despite the particular adsorptive behavior of zopiclone, the optimal analytical conditions can be summarized as follows: 0.1M tris-HCl buffer at pH 9 with an accumulation step of 30 sec performed at -0.6 V *vs.* Ag/AgCl under stirring conditions and a rest period of 5 sec. A 120-sec collection time without stirring provides a lower sensitivity but a higher precision. If it is required by the analysis conditions, a pH 7 tris-HCl buffer can be utilized with the same conditions but the lower limit is fixed at $1 \times 10^{-9}M$.

It is to be noted that the kinetics of the accumulation process are very fast at both pH values since very low concentrations (1 or $2 \times 10^{-10}M$) can be investigated using a short deposition time (30 sec). Most adsorptive procedures using similar convection conditions require longer times (120–300 sec) for measurements at these concentrations.[20–22] This fast kinetic behavior could be used to advantage to perform adsorptive voltammetric detection in flow injection analysis, as well as for the analysis of complex media (biological or environmental) in which an interfering compound is more slowly adsorbed.

Acknowledgements—The authors are indebted to Rhone-Poulenc Company (Brussels, Belgium) who generously provided zopiclone and its derivatives. H. Zhang was supported financially during this work by a Solvay S.A. (Belgium) grant to the Free University of Brussels. Thanks are also expressed to the "Fonds National de la Recherche Scientifique" (FNRS Belgium) for help to one of us (G. J. P.) and to the SPPS (Belgium Politic Research, ARC), Contract no. 86/91-89.

REFERENCES

1. A. Agnoli, V. Manna and N. Martucci, *Intern. J. Clin. Pharmacol. Res.*, 1989, **9**, 277.
2. B. Musch and F. Maillard, *Intern. Clin. Psychopharmacol.*, 1990, **5**, 147.
3. F. Kelly, J. O'Grady and Y. Champey, *Lancet*, 1990, **335**, 1033.
4. G. Hayoun and C. Bagot, *Curr. Therap. Res.—Clin. and Experim.*, 1989, **46**, 1236.
5. R. Aantaa, M. Salonen and T. Nyrke, *Eur. J. Clin. Pharmacol.*, 1990, **38**, 47.
6. R. Fontaine, P. Beaudry, P. Lemorvan, L. Beauclair and G. Chouinard, *Intern. Clin. Psychopharmacol*, 1990, **5**, 173.
7. M. Largeron, M. B. Fleury, *J. Pharm. Sci.*, 1989, **78**, 627.
8. J. A. Squella, L. J. Nunez-Vergara, M. Dominguez, T. Pineda and M. Blazquez, *Gazz. Chim. Ital.*, 1991, **121**, 117.
9. L. J. Nunez-Vergara, J. A. Squella, M. Dominguez and M. Blazquez, *J. Electroanal. Chem.*, 1988, **243**, 133.
10. H. Lund and M. M. Baizer, *Organic Electrochemistry*, 3rd Ed., p. 732. Marcel Dekker, New York, 1991.
11. J. Volke, D. Dumanovic and V. Volkova, *Coll. Czech. Chem. Commun*, 1965, **30**, 246.
12. L. N. Klatt and R. L. Rousseff, *J. Am. Chem. Soc*, 1972, **94**, 7295.
13. J. Swartz and F. C. Anson, *J. Electroanal. Chem.*, 1980, **114**, 117.
14. J. Armand, K. Chekir and J. Pinson, *Can. J. Chem.*, 1974, **52**, 3971.
15. S. Kennel, P. Kintz, A. Tracqui, P. Mangin, A. A. Lugnier and A. J. Chaumont, *J. Chromatogr.-Biomed. Appl.*, 1990, **527**, 169.
16. D. Debruyne, J. Lacotte, B. H. Deligny and M. Moulin, *J. Pharm. Sci.*, 1991, **80**, 71.

17. C. Fernandez, B. Baune, F. Gimenez, A. Thuilliez and R. Farinotti, *J. Chromatogr.-Biomed. Appl.*, 1991, **572**, 195.
18. J-M. Kauffmann, J-C. Viré, M. Gelbcke and G. J. Patriarche, *Anal. Lett.*, 1984, **17**, 2319.
19. J-C. Viré, J-M. Kauffmann, J. Braun and G. J. Patriarche, *Analusis*, 1985, **13**, 134.
20. J. Wang, *Stripping Analysis, Principles, Instrumentation and Applications*. VCH Publishers, Deerfield Beach, Florida, 1985.
21. R. Kalvoda and M. Kopanica, *Pure Appl. Chem.*, 1989, **61**, 98.
22. J-C. Viré, J-M. Kauffmann and G. J. Patriarche, *J. Pharm. Biomed. Anal.*, 1989, **7**, 1323.

Talanta, Vol. 40, No. 3, pp. 325–331, 1993
Printed in Great Britain.

0039-9140/93 $6.00 + 0.00

ADSORPTIVE STRIPPING BEHAVIOUR OF MITOXANTRONE ON CARBON PASTE ELECTRODES

JUAN CARLOS CORTINA VILLAR, AGUSTÍN COSTA GARCÍA and PAULINO TUÑÓN BLANCO*
Department of Physical and Analytical Chemistry, University of Oviedo, 33006 Oviedo, Principality of Asturias, Spain

(*Received* 5 *December* 1991. *Revised* 19 *June* 1992. *Accepted* 13 *July* 1992)

Summary—The electrooxidation of mitoxantrone (MXT) on carbon paste electrodes was studied using voltammetric techniques in adsorption conditions. The analyte was accumulated at the working electrode (a carbon paste electrode) under precisely controlled mass-transport conditions and stripped electrochemically in the same solution. An electrode pretreatment is proposed which shows good reproducibility of the analytical signal (0.81%). The stripping step was studied with alternating current voltammetry providing a linear response in the concentration range 5×10^{-11} to $7 \times 10^{-10} M$ in aqueous samples. Finally, a method using the medium exchange and AC phase-selective adsorptive stripping voltammetry technique was proposed for MXT analysis in urine samples.

Mitoxantrone [Fig. 1, 1,4-dihydroxy-5,8-bis (2-(2-hydroxyethl) amino]ethyl amino) 9,10-anthracenedione dihydrochloride] belongs to a new structural class of antineoplastic agents, the anthracenediones. A large series of analogues have been synthesized with structural features predicted to favour intercalation with DNA. After initial studies, MXT was selected for clinical trials on the basis of its potency and excellent antitumour activity in mice.[1–4]

Due to the continued use of MXT in clinical trials several analytical methods have been developed for its determination. The main emphasis has been on chromatographic[5–15] and immunoassay methods[16,17] of analysis. However, some fundamental electrochemical studies dealing with the polarographic behaviour of MXT in the presence of cuprous and cupric salts have been carried out, and a probable explanation of its antitumour activity was put forward.[18] Both electron spin resonance spectroscopy and electrochemical studies have been applied to obtain a better understanding of the metabolism of MXT.[19]

The use of carbon paste electrodes for electroanalysis has gained popularity. One of the primary reasons for this is their applicability to anodic oxidations and the lower charge current involved. Such electrodes thus permit important analytical applications which are not available to the HMDE. On the other hand, the effective utility of solid electrodes is generally hampered by a gradual fouling of the electrode surface. Such loss of electrode activity is usually attributed to the adsorption of reaction products, the analyte itself, or a large variety of electroinactive organic surfactants. A slow decrease in peak current or in extreme cases complete inhibition of the electron transfer may be observed. In these cases the method cannot be used for analysis. To overcome these negative effects, the electrode surface can be treated before the measurement step to obtain a reproducible surface and therefore a reproducible peak current similar to that obtained by the HMDE.[20–24]

In this paper, the electroactivity of MXT on carbon paste electrodes (CPE) was studied using adsorptive stripping voltammetry (ADSV). As far as we know this is the first fundamental work in which the adsorptive stripping signal at a carbon paste electrode is recorded using the alternating current technique. In previous works, other authors[25–28] have reported the differential pulse adsorptive stripping voltammetry of some selected molecules but a poor reproducibility between each measurement and

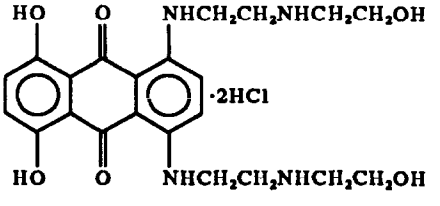

Fig. 1. Mitoxantrone structure.

*Author for correspondence.

higher detection limits were found (above $1 \times 10^{-9} M$).

As is well known, the advantage of ADSV on CPE's is that this technique is readily coupled with the "medium exchange" procedure as the accumulated species are rarely air sensitive. Using this procedure, after accumulation the working electrode can be easily transferred into a blank solution of appropriate composition, where the stripping step is carried out and the voltamperogram is recorded without interference from other non-accumulated electroactive species present in the original sample. Therefore, accumulation and stripping steps may take place under the optimum conditions for each process.[29,30] In this study the above procedure was applied to the analysis of MXT in urine samples to avoid interferences from uric acid. The results obtained showed that the proposed method constituted a valid alternative to others previously reported allowing meaningful physiological concentrations of MXT to be analysed.

This work provided the basis for an FIA method applied to the determination of MXT in urine.[31] The full automatized procedure included a voltammetric detector using AC voltammetry after adsorption of the analyte on CPE and proves to be a fast, reproducible and selective method of analysis.

EXPERIMENTAL

Apparatus

The experiments were carried out in an all-glass cell designed for a three electrode potentiostatic circuit. Linear sweep voltammetry (LSV) and cyclic voltammetry (CV) experiments were performed using a Metrohm E-611 potentiostat coupled to a Metrohm E-612 scanner. Voltamperograms were recorded on a Graphtec WX-4421 X-Y recorder. Alternating current voltammetry (AC) stripping measurements were made using a Metrohm Polarecord E-506. A carbon paste electrode was used as working electrode. The three-electrode cell design was completed with a calomel reference electrode and a platinum wire as the auxiliary electrode. A magnetic stirrer (Agimatic Selecta) and a stirring bar (1 cm long, 2 mm thick) provided the convective transport during the preconcentration step.

Reagents and procedure

MXT was kindly supplied by Lederle Laboratories Division. It is a hygroscopic dark solid normally supplied as a sterile aqueous solution containing mitoxantrone free base, with sodium chloride, sodium acetate and acetic acid as inactive ingredients. The product does not contain anti-bacterial preservatives. Solutions of MXT were prepared daily by dilution of an ampoule in demineralized water. The samples were stored in the dark at room temperature to avoid photochemical decomposition. As MXT reacts with phosphate and borate ions, several buffers (pH 3–11) composed of acetic acid/acetate, bicarbonate/carbonate were used. Alternatively perchloric acid and sodium hydroxide solutions were used when necessary. Carbon paste electrodes (geometric area 12.5 mm^2) which consisted of a teflon tube with an inner core containing a contact with a twist action, were prepared by mixing 1.8 ml of paraffin oil (Uvasol, Merck) with 5 g of spectroscopic grade graphite powder (Ultracarbon, Dicoex, Bilbao, Spain). The carbon paste was packed into the well of the working electrode to a depth of 1 mm and the surface was polished on a white paper sheet placed over a flat glass stand. All solutions were prepared using water purified by distillation and then passed through an ion exchanger. All chemical reagents employed were of analytical grade. Urine samples consisted of aliquots of pooled urine (from at least 15 healthy individuals) to which increasing amounts of MXT were added to give the desired concentrations.

Cyclic voltamperograms were recorded from $1 \times 10^{-6} M$ solutions of MXT in the pH range 0–14 using a preconcentration step of 30 sec and stirring in open circuit conditions. A fresh carbon paste surface was used for each experiment.

The preconcentration step was carried out as follows: 20 ml of buffer solution containing the desired amount of MXT and stirred at 1000 rpm until the solution was homogenous. The working electrode was then immersed into the cell and a preconcentration time in open circuit conditions was implemented. A quiescent period of 10 sec was then allowed before commencing the potential scan (the last 5 sec under electrolysis at the starting potential). Stripping voltammetric experiments in the AC mode were carried out using a fixed frequency of 75 Hz and a scan rate of 10 mV/sec, while in CV it was 100 mV/sec.

RESULTS AND DISCUSSION

Cyclic voltammetry experiments

Cyclic voltamperograms were recorded in the pH range 0–14 using the conditions outlined

above. A typical voltamperogram obtained in 0.1M perchloric acid is shown in Fig. 2, where two anodic peaks can be observed. When the cyclic scan is reversed before the second anodic peak potential is reached one can see a reduction peak corresponding to a reversible process.

The oxidation peak potentials shift to more negative values as the pH increases, following the equations:

1st process:

$$Ep/V = -5.87 \times 10^{-2}\ pH + 0.80;\ r = 0.9991$$
$$(pH = 1\text{–}14)\ (n = 13)$$

2nd process:

$$Ep/V = -6.30 \times 10^{-2}\ pH + 1.023;\ r = 0.9983$$
$$(pH = 1\text{–}13)\ (n = 12)$$

The slope was seen to be similar for both processes (Fig. 3). The first process increases at a rate of 58 mV per unit of pH, in close agreement with a reversible reaction involving two protons and two electrons.

The effect of the electrolyte support on the peak intensity was studied in order to find out the best analytical characteristics. The oxidation peak intensity shows two maximum values: in acid pH an absolute maximum and around pH 7 a relative maximum for both processes. At very alkaline pHs MXT undergoes a decomposition and all processes disappear, at pH 14 in 5 min. The relative signal improvement in acid pH was better than at other pHs (after 30 sec of preconcentration), an enhancement factor of 9.4 was obtained. Also, the difference between anodic and cathodic peak potentials is smaller

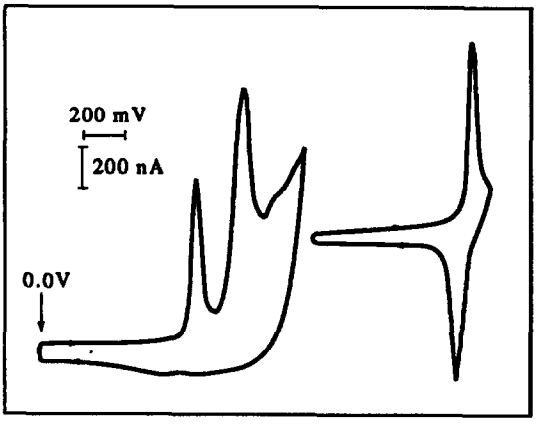

Fig. 2. Cyclic voltamperograms of $1 \times 10^{-6}M$ MXT in 0.1M perchloric acid.

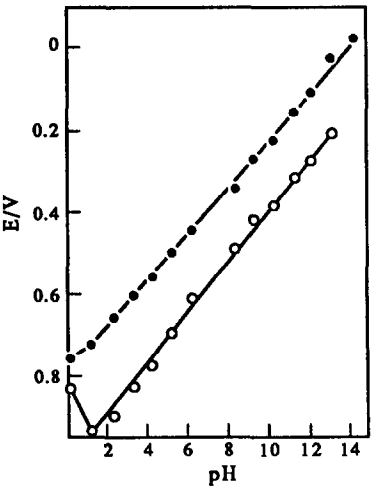

Fig. 3. Effect of pH on peak potential of the first (●) and the second(○) anodic process for a $1 \times 10^{-6}M$ MXT concentration. Scan rate 100 mV/sec.

than in other pHs (55 mV). Therefore, for all subsequent experiments 0.1M perchloric acid was chosen, as at this pH the intensity and morphology of both peaks were at an optimum.

There was no great effect on peak intensity if the preconcentration step was carried out in closed circuit conditions for a wide range of potentials assayed between −0.3 and +0.5 V.

The peak intensity of the first anodic peak increases linearly with the scan rate potential between 10 and 60 mV/sec following the equation:

$$I/\mu A = 0.012v/mV.sec^{-1} + 0.175;$$
$$r = 0.992\ (n = 5)$$

Due to the short range of scan rates where the linear dependence is found, no definitive conclusion about the effective control processes by adsorption can be made. Since from an analytical point of view it is necessary to prove that the molecule is effectively adsorbed on the electrode, the following medium exchange experiments were carried out. The CPE was immersed in a $4.5 \times 10^{-7}M$ solution of MXT for 30 sec while stirring in an open circuit. Then, the electrode was carefully cleaned and transferred to another cell containing only the background electrolyte. A cyclic voltamperogram recorded in the positive direction showed the same anodic processes as those observed when the analyte was in the cell, indicating that the drug had been adsorbed and transported to the new cell on the CPE.

When the analyte preconcentration step was carried out at a more positive potential than

that of the first oxidation peak, the subsequent scan in the negative direction in the blank cell produced a reduction peak which resembled that which had been obtained originally. From this it can be concluded that the product of the oxidation process is insoluble and that it is also adsorbed and transported on the electrode surface. Finally, a third experiment consisted of carrying out the preconcentration step in an open circuit and scanning in the negative direction. The observed reduction peak is similar, once more, to the one obtained in the presence of the analyte, but in this case the intensity of the peak was higher than in the last experiment, showing that the first product of electrooxidation is more soluble than MXT.

Electrode mechanism

In the pH ranges studied, the voltamperograms recorded show two anodic processes, the first almost reversible ($E_{pa} - E_{pc} = 55$ mV in 0.1M pechloric acid) when the scan was reversed before the second anodic process. So, one can expect that the two -OH groups are oxidized to produce the quinone which is in agreement with the 2 H^+ and 2 e^- transferred as shown by the cyclic voltammetric study and the consulted bibliography.[32,33] At higher potentials the amino aromatic groups are probably oxidized irreversibly.[34-36] Other reactions which break the molecule may occur on the electrode surface resulting in a loss of the reduction peak on the reverse scan. In order to confirm the electrode mechanism proposed, some experiments were carried out with N-methylaniline and 5,8-dihydroxy-1,4-naphtoquinone. Figure 4 shows three voltamperograms recorded using different solutions containing $6.3 \times 10^{-7}M$ MXT, $1.10^{-5}M$ N-methylaniline and $1 \times 10^{-6}M$ 5,8-dihydroxy-1,4-naphtoquinone prepared in 0.1M perchloric acid. In the case of 5,8-dihydroxyde-1,4-naphtoquinone a preconcentration step of 60 sec was carried out before starting the potential scan, since that a weak adsorption was observed previously in the study. N-methylaniline doesn't show affinity for the electrode surface.

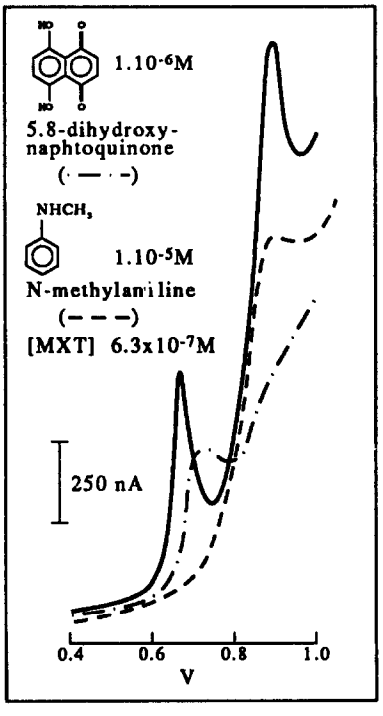

Fig. 4. Voltamperograms of $6.3 \times 10^{-7}M$ MXT, $1 \times 10^{-5}M$ N-methylaniline and $1 \times 10^{-6}M$ 5,8-dihydroxy-1,4-naphtoquinone solutions in 0.1M perchloric acid. Scan rate 100 mV/sec.

Electrode pretreatment

As previously mentioned, activation of carbon paste electrodes is an essential and fundamental part in any CPE study for analytical purposes. In our case, the analyte itself shows a strong adsorption on the electrode which is similar in both open or closed circuit conditions. Consequently, it has been shown that an *in situ* pretreatment in the presence of MXT was difficult. To clean or activate the electrode surface the following procedure was used: after each measurement the CPE was taken and immersed in another cell containing 0.1M perchloric acid. It was held for 30 sec with stirring at -1.5 V. Afterwards the CPE was dried carefully and was ready for the next measurement.

Operating in this way provided excellent reproducibility of voltammetric data and a relative standard deviation of 0.81% ($n = 10$) was obtained for the voltammetric signal. The following experiments were carried out using this activation step before each measurement.

Adsorptive stripping behaviour

In general, increasing amounts of MXT adsorbed on CPE raise the peak current. For the first process, a plot of peak current *vs.* preconcentration time for several concentrations in the range from 5×10^{-9} to $1 \times 10^{-7}M$, scanning with LSV is shown in Fig. 5. It can be seen that for short preconcentration times the peak intensity grows linearly with preconcentration time and the slopes of the linear portions are proportional to the assayed concentrations. For longer accumulation times, peak current stabil-

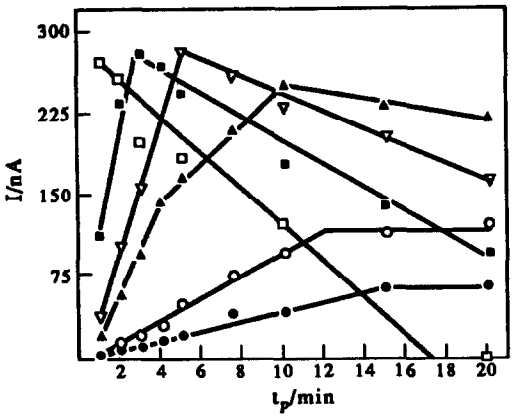

Fig. 5. Effect of preconcentration time upon weak intensity of the first anodic process for different MXT concentrations. (●) 5×10^{-9}, (○) 1×10^{-8}, (▲) 1.5×10^{-8}, (▽) 2.5×10^{-8}, (□) 5×10^{-8} and (□) $1 \times 10^{-7}M$.

ization was observed in all cases and for higher concentrations this decrease was directly proportional to the preconcentration time. This behaviour at low concentrations and low preconcentration time might be explained in terms of a linearized Langmuir isotherm. In fact it can be assumed in these conditions that the electrode surface is homogenous and no interactions between the adsorbed MXT occur. However at high solution activities, a saturation coverage of the electrode by adsorbate (*e.g.*, to form a monolayer) can occur. The decreasing peak intensity can be assumed as being due to the formation of a non-conducting layer of the analyte adsorbed on the electrode surface.

As for the first process, Fig. 6 shows a plot of current intensity *vs.* the product of accumulation time by MXT concentration. From this plot an increasing linear dependence between both parameters is found if the product assumes values less than 1×10^{-7} mol. l^{-1}. min showing that a wide range of concentrations and accumulation times could be used for analytical purposes. Therefore, for the first process a reasonable preconcentration time of 4 min meant that a large linear calibration range with fairly good sensitivity could be obtained.

Stripping with alternating current voltammetry

The first MXT anodic process is almost reversible and is of greater analytical interest. Therefore, the next experiment attempted was the stripping step on the CPE surface with alternating current voltammetry. Exploratory experiments were carried out to optimize the main parameter that controls alternating current voltammetry, that is the effect of the AC superimposed voltage. This was evaluated for a $2.5 \times 10^{-8}M$ MXT solution using a preconcentration time of 30 sec while stirring the solution in an open circuit. The same activation step was used as in the LSV technique. The results showed a linear dependence on the peak current in the range 5–20 mV following the equation:

$$I/\mu A = 0.035\ \triangle E/mV + 0.15;$$

$$r = 0.9980\ (n = 4)$$

At higher amplitude values the peak current remained constant. We also observed that the half-peak width was 55 mV for an amplitude of 20 and 45 mV for an amplitude of 10 mV, so the selectivity losses were small at an amplitude of 20 mV.

Calibration plots

The preconcentration of the drug by adsorption onto the CPE for 1 and 4 mins, in an open circuit under stirring conditions, produced calibration graphs that followed the equations:

1 min: I/nA

$$= 2.28 \times 10^{11}\ [MXT] - 255.0\ (n = 6)$$

$$r = 0.9990\ (1 \times 10^{-9}\text{–}1.5 \times 10^{-8}M)$$

Detection limit $1 \times 10^{-9}M$

4 min: I/nA

$$= 3.74 \times 10^{11}\ [MXT] + 50.4\ (n = 5)$$

$$r = 0.9990$$

1st linear range $(5 \times 10^{-11}\text{–}7 \times 10^{-10}M)$

Detection limit $5 \times 10^{-11}M$

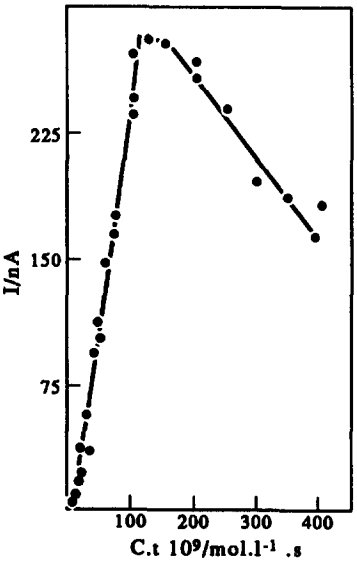

Fig. 6. Peak current *vs.* the product of accumulation time by MXT concentration.

I/nA

$= 7.29 \times 10^{10}$ [MXT] + 262.3 ($n = 4$)

$r = 0.9980$

2nd linear range (7×10^{-10}–$2 \times 10^{-9} M$

Analytical interference

In stripping voltammetry the preconcentration of MXT by adsorption can be hampered by the presence of other surfactants competing for the adsorption sites on the electrode. The influence of four different surfactants was studied using a preconcentration time of 60 sec at 1000 rpm, open circuit conditions and a MXT concentration of $1 \times 10^{-8} M$ (4.4 ppb). The stripping step was carried out with LSV. All of the surfactants suppressed the stripping signal of the drug. The anionic surfactant sodium lauryl sulphate (SLS) caused a greater decrease in the peak than a cationic surfactant such as cetyltrimethylammonium chloride (CTAC). A 29-ppm solution of SLS decreased the MXT peak current by 82% while 32 ppm of CTAC only decreased it by 62%. On the other hand, Triton X-100 (non-ionic nature) showed a strong effect, so 25 ppm caused a peak decrease of 80%. Gelatin was chosen as a model of the surfactants that may occur in biological media since it consists of a mixture of soluble proteins. 25 ppm of gelatin produced a 10% peak decrease and a 1000-fold excess (50 ppm), it being necessary to reduce the stripping peak by 36%. This could be due to the large molar mass of gelatin leading to a lower diffusion rate from the MXT solution to the electrode surface.

The effect of the molecules which interfere in biological fluids, might be reduced by adequate dilution of the sample providing samples in which the concentration of MXT is within the linear range of the method, whereas the concentration of interferents are below the threshold of interference.

Determination of MXT in urine samples

After optimization of the MXT adsorption and stripping steps, the method was applied to the determination of MXT in urine samples. The first experiment was carried out with blank urine sample, 100 μl of urine without any kind of pre-treatment was added to 20 ml of $0.1 M$ perchloric acid and then scanned anodically. The voltamperogram showed an anodic peak at the same potential as that of MXT and this was shown to be due to uric acid. The process was diffusion controlled and it was possible to avoid this interference by doing a "medium exchange" experiment, *i.e.*, the adsorption step and the stripping step were carried out in different solutions, the latter being done in $0.1 M$ perchloric acid without the drug. Following this procedure the interference caused by uric acid was removed. (Fig. 7). In five consecutive determinations of urine samples to which an MXT concentration of $5 \times 10^{-7} M$ had been added a mean concentration of $5.01 \times 10^{-7} M$ was obtained with a standard deviation of 1.51%. This was achieved by injecting 20 μl of the sample into the cell and by using a standard addition method. The estimated detection limit for a ratio s/n = 3 in urine samples following this procedure was $5 \times 10^{-8} M$.

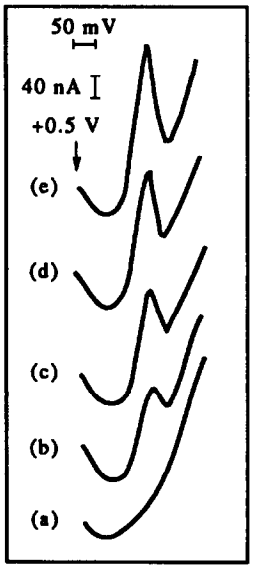

Fig. 7. Determination of MXT in urine samples. (a) Blank. (b) Addition of 20 μl of urine sample with MXT previously added. (c, d, e) Successive additions of 10 μl of $5 \times 10^{-7} M$ MXT standard.

Acknowledgements—The authors thank DGICYT (Spain) for economic support (Project No. PB 87/1041).

REFERENCES

1. K. C. Murdock, R. G. Child, P. F. Fabio, R. B. Angier, R. E. Wallace, F. E. Durr and R. V. Citarella, *J. Med. Chem.*, 1979, **22**, 1024.
2. I. E. Smith, *Cancer Treat Rev.*, 1983, **10**, 103.
3. R. Zee-Cheng and C. C. Cheng, *J. Med. Chem.*, 1978, **21**, 291.
4. R. E. Wallace, K. C. Murdock, R. B. Angier and F. E. Durr, *Cancer Res.*, 1979, **39**, 1570.
5. I. Peng, D. Ormberg, D. S. Alberts and T. P. Davis, *J. Chrom. Biomed. Appl.*, 1982, **22**, 235.

6. R. Hulhoven and J. P. Desager, *J. High Resol. Chrom. Commun.*, 1983, **6**, 512.
7. S. T. Houtpt and R. P. Baldwin, *Anal. Lett.*, 1983, **16**, 1343.
8. G. Ehninger, B. Proksch and E. Schiller, *J. Chrom. Biomed Appl.*, 1985, **43**, 119.
9. K. E. Choi, J. A. Sinkule, D. S. Han, S. C. McGrath, Daly and S. A. Larson, *ibid.*, 1987, **64**, 81.
10. B. Payet, P. Arnoux, J. Catalin and J. P. Cano, *ibid.*, 1988, **86**, 337.
11. S. J. P. Van Belle, T. J. Schoemaker, S. L. Verwey, A. C. A. Paalman and J. G. McVie, *J. Chrom. Biomed. Analysis*, 1985, **38**, 73.
12. M. J. Czejka, *Labor-Med.*, 1988. **11**, 8.
13. P. Chang, K. C. Chem and M. L. King, *Chem. Abs.*, 1990, **113**, 103518.
14. C. Wu. P. Guo and H. Song, *Huaxi Yike Daxue Suebao*, 1990, **21**, 39.
15. A. El-Yazigi and A. Yusuf, *J. Pharm. Biomed. Appl.*, 1989, **7**, 877.
16. G. Nicolau, V. Szucs-Myers, W. McWilliams, J. Morrison and A. Lanzilloti, *Invest. New Drugs*, 1985, **3**, 56.
17. S. V.Flavell and D. J. Flavell, *J. Immunol. Methods*, 1988, **115**, 179.
18. F. Baykut, R. Apak and E. Tutem, *Chim. Acta Turc.*, 1987, **15**, 169.
19. B. Nguyen and P. L. Gutierrez, *Chem. Biol. Interact.*, 1990, **74**, 139.
20. J. R. Barreira, A. Costa and P. Tuñón, *Electrochim. Acta.*, 1989, **34**, 957.
21. J. R. Barreira, A. Costa, A. J. Miranda and P. Tuñón, *Electroanalysis*, 1989, **1**, 529.
22. J. R. Barreira, A. Costa and P. Tuñón, *Analyst*, 1989, **114**, 939.
23. J. R. Barreira, V. Cabal, A. Costa and P. Tuñón, *ibid.*, 1990, **115**, 209.
24. M. T. Fernández, J. R. Barreira, A. Costa and P., Tuñón, *Electroanalysis*, 1991, **3**, 409.
25. E. N. Chaney Jr. and R. P. Baldwin, *Anal. Chem.*, 1982, **54**, 2556.
26. H. Y. Chaeng, L. Falat and R. L. Li, *ibid.*, 1982, **54**, 1384.
27. J. P. Hart and S. A. Wring, *Analyst*, 1989, **114**, 933.
28. N. E. Zoulis, D. P. Nikolelis and C. E. Efstathiou, *ibid.*, 1990, **115**, 291.
29. J. Wang, *Stripping Analysis*, p. 61. VCH, Deerfield Beach, Florida, U.S.A. 1985.
30. J. Wang and B. A. Freiha, *Anal. Chim. Acta*, 1988, **204**, 201.
31. J. C. Cortina, A. Costa and P. Tuñón, *ibid.*, 1992, **256**, 231.
32. E. Laviron, *J. Electroanal. Chem.*, 1984, **164**, 213.
33. *Idem, ibid.*, 1983, **146**, 15.
34. R. E. Parker and R. N. Adams, *Anal. Chem.*, 1956, **28**, 828.
35. L. H. Piete, P. Ludwig and R. N. Adams, *ibid.*, 1962, **34**, 916.
36. P. J. Elving and A. F. Krivis, *ibid.*, 1958, **30**, 1645.

Talanta, Vol. 40, No. 3, pp. 333–339, 1993
Printed in Great Britain.

0039-9140/93 $6.00 + 0.00

ADSORPTIVE STRIPPING VOLTAMMETRIC BEHAVIOUR OF MITOXANTRONE ON MERCURY ELECTRODES

JUAN CARLOS CORTINA VILLAR, AGUSTÍN COSTA GARCÍA and PAULINO TUÑÓN BLANCO*
Department of Physical and Analytical Chemistry, University of Oviedo, 33006 Oviedo, Principality of Asturias, Spain

(*Received* 5 *December* 1991. *Revised* 19 *June* 1992. *Accepted* 13 *July* 1992)

Summary—The electrochemical behaviour of mitoxantrone (MXT), an important antineoplastic agent, has been studied at mercury electrodes. The nature of the process taking place at the hanging mercury drop electrode (HMDE) was clarified. The electrochemical behaviour observed was in close agreement with theoretical predictions for an adsorbed molecule which is reversibly reduced. Both the molecule and its reduced product appeared to be adsorbed at the surface of the electrode. Adsorptive stripping voltammetry has been proven to be advantageous over any other assay technique, allowing 5×10^{-11} *M* MXT to be detected. The interference arising from surfactants competing for the adsorption sites at the electrode have been studied and the possibility of MXT determination in dilute urine samples has been shown. Some interesting data, such as the MXT adsorbing surface area and the kinetic constant of the associated coupled chemistry reaction were also determined.

Mitoxantrone, 1,4-dihidroxy-5,8-bis({2-[(2-hidroxyethyl)amino]ethyl} amino)-9,10-anthracenedione (Fig. 1) is a substituted anthraquinone with strong DNA binding properties similar to the anthracycline antibiotics.[1] The drug has shown activity *in vitro* and *in vivo* against solid tumours and leukaemia.[2–4]

As far as we know the elemental electrochemical study of MXT at mercury electrodes reported in previous work does not exist.[5] Since the MXT structure has important electroactive functional groups, we have previously reported its oxidation behaviour at the carbon paste electrode[5] and this work is devoted mainly to its reduction behaviour using mercury electrodes. The effect of some parameters such as accumulation time, potential, ionic strength, *etc.*, on the MXT adsorption process was evaluated. The influence of different models of scanning potential were also studied, which included linear sweep voltammetry (LSV), alternating current voltammetry (ACV) and square wave voltammetry (SWV). The AC mode applied to the stripping of the MXT adsorbed gave the most sensitive analytical response, and the preconcentration of the drug in open circuit allowed extended linear calibration plots to be drawn. Finally, two electroanalytical methods applied to the analysis of MXT in ampoules or urine samples have been proposed. In the case of urine samples, a reliable clean up sample procedure is necessary to avoid the interference arising from naturally occurring substances in urine.

EXPERIMENTAL

Apparatus

Linear sweep and cyclic voltammetric experiments were carried out using a Metrohm E-611 potentiostat coupled to a Metrohm E-612 scanner. Voltamperograms were recorded on a graphtech WX-4421 X-Y recorder. Alternating current stripping measurements were made using a Metrohm Polarecord E-506. The square wave voltammetric measurements were obtained using an Inelesca PDC 1212 potentiostat coupled to an Inelesca GOT 1018 scanner assisted by a computer model Acer 500+. As working electrodes for the stripping experiments, a Metrohm EA-410 hanging mercury drop electrode

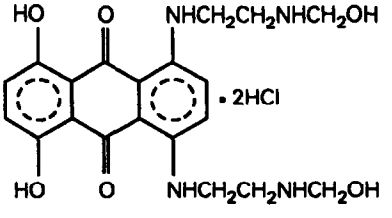

Fig. 1. Mitoxantrone structure.

*Author for correspondence.

(HMDE) and a Metrohm 663 static mercury drop electrode (SMDE) were used as indicated below. Unless otherwise stated, drop areas of 2.20 and 0.57 mm^2 were used with the HMDE and SMDE respectively. The three-electrode cell design was completed with a calomel saturated reference electrode and a platinum wire auxiliary electrode.

Reagents and procedure

The MXT in solid form (84% pure) as well as ampoule form was a generous gift from Lederle Division Laboratories, Cyanamid Iberica, and used as supplied. MXT is a hygroscopic dark blue solid supplied for clinical purposes as a sterile, aqueous solution containing mitoxantrone hydrochloride equivalent to 2 mg/ml ($4.5 \times 10^{-3} M$) mitoxantrone free base, with sodium chloride, sodium acetate and acetic acid as inactive ingredients. Stock solutions ($4.5 \times 10^{-3} M$) were prepared by dissolving the necessary amount of the solid product in water, and were kept at room temperature in the dark to avoid its crystallization and photochemical decomposition.

Several buffers composed of acetic acid, phosphoric acid and sodium hydroxide solutions were used. Also perchloric acid and sodium hydroxide solutions were used when necessary (pH below 3 and above 11). Buffers containing borate ions were excluded because they react chemically with the reduction product of MXT in such a way that the formation of the reversible pair is not allowed.

All reagents were of analytical-reagent grade and demineralized water was obtained by passing distilled water through an ion exchanger.

The background electrolyte (20 ml) was added to the cell and the dissolved oxygen was removed by passing oxygen free argon for 15 min. The stirring applied during the preconcentration step was the maximum allowed which did not produce oscillations of the HMDE or 3000 rpm in the case of the SMDE. A quiescent period of 10 sec was allowed before commencing the potential scan (the last 5 sec under electrolysis at the starting potential when the preconcentration step was done in the open circuit). Stripping voltammetric experiments in the AC mode were carried out using a fixed frequency of 75 Hz, a phase angle $\phi = 0°$ and a scan rate of 10 mV/sec.

The urine samples examined consisted of mixtures of human urine from healthy individuals. Samples consisted of aliquots of 10 ml of pooled urine to which appropriate amounts of MXT were added on order to achieve the desired final concentration.

Sample purification was accomplished by liquid–solid extraction according to the following procedure: 5 ml of urine with the desired amount of MXT previously added was passed through a reversed phase disposable C18 cartridge (Sep-Pak, Waters) previously activated by washing with pure methanol (10 ml) and water (20 ml). The effuent was disposed of, the cartridge washed with 20 ml of water containing 10% methanol, and the retained materials were eluted with 5 ml of acetonitrile:0.1M sodium hydroxide (50%).

RESULTS AND DISCUSSION

Cyclic voltammetry and nature of the electrode process

Cyclic voltamperograms were recorded from a $1 \times 10^{-7} M$ solution in the pH range 0–14. A typical voltamperogram obtained in 0.1M perchloric acid is shown in Fig. 2, where two cathodic peaks were observed; the first one, which is more useful from an analytical point of view, is found to be reversible over all pH ranges studied, when the cyclic scan is reversed before the second cathodic peak potential.

The reduction peak potential shifts to more negative values as the pH increases with different slopes and following the equations:

1st linear range:

$$Ep/V = -0.3 - 0.0844 \times \text{pH} \quad (n = 4)$$

$$\text{pH} = 0 - 3 \qquad r = 0.999$$

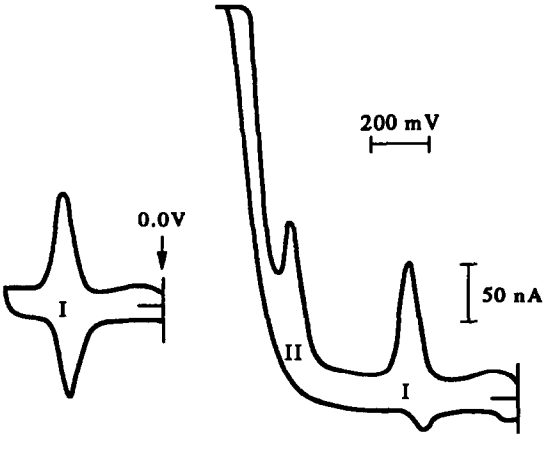

Fig. 2. Cyclic voltamperogram of $1 \times 10^{-7} M$ MXT solution in 0.1M perchloric acid.

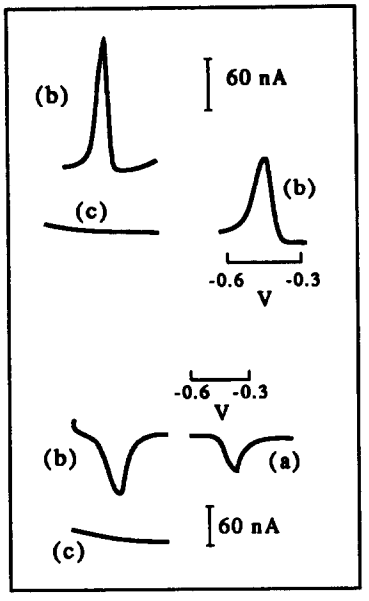

Fig. 3. Medium exchange experiments with a solution $5 \times 10^{-7}M$ of MXT in $0.1M$ perchloric acid. Voltamperograms before (a) and after (b) medium exchange. (c) Voltamperograms recorded in the new medium with a fress mercury drop.

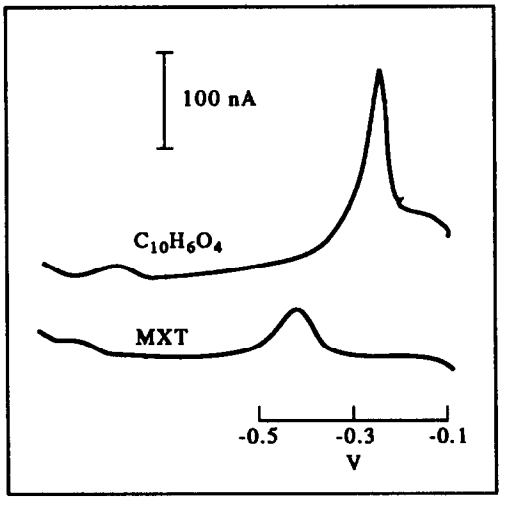

Fig. 4. Voltamperograms of $1 \times 10^{-4}M$ 5,8-dihydroxyde 1,4-naphtoquinone and $5 \times 10^{-7}M$ MXT solutions in $0.1M$ perchloric acid. Scan rate 100 mV/sec.

2nd linear range:

$$Ep/V = -0.4 - 0.048 \times \text{pH} \quad (n = 8)$$

$$\text{pH} = 3 - 12 \quad r = 0.997$$

3rd linear range:

$$Ep/V = -0.985 \quad (n = 3)$$

$$\text{pH} = 12 - 14 \quad r = 0.999$$

It can be seen that the slopes rate between the second and the first linear range is 1.75 (almost 2) indicating that in the first linear range two protons are implicated whereas in the second linear range only one proton is implicated. Similar behaviour was observed for the second process although a displacement of the potential of about 0.4 V is shown.

No strong influence of the pH on the current intensity of the first peak was found for a pH range from 0 to 6. In general, at higher pHs the peak current decreases slightly, and for this reason $0.1M$ perchloric acid was chosen for subsequent experiments.

Although the shape of the cyclic voltamperograms (CV) allows the prediction of an adsorption control of the electrode process, the effective adsorption of both MXT and its product of the electrode reaction on the HMDE was proven by carrying out two different medium exchange experiments. These were to keep the HMDE in contact with a solution $5 \times 10^{-7}M$ in MXT for 30 sec under stirring conditions and in an open circuit. Then, the medium exchange procedure was similar to that followed in previous work[5] and the CV which was started in the positive direction was recorded. The same experiment was carried out after preconcentration at a potential which was more negative than the first cathodic peak. The CV recorded after medium exchange in both cases showed identical peaks to those obtained in the MXT solutions under the same experimental conditions (Fig. 3), indicating that not only MXT but also its reduction product are adsorbed and placed on the electrode surface.

According to the experimental evidence described above, a linear dependence of the peak intensity upon the scan rate was found in the range 10–100 mV/sec and follows the equation:

$$I/\mu\text{A} = 0.53 \times v/\text{mV} \cdot \text{sec}^{-1} + 3.5 \quad (n = 10)$$

$$r = 0.998$$

$$[MXT] = 5 \times 10^{-7}M \quad \text{(SMDE)}$$

On the other hand, when the cyclic scan is reversed before the second cathodic peak potential, it was found that the cathodic peak intensity (I_{pc}): anodic peak intensity (I_{pa}) ratio decreases exponentially with the scan rate. A plot of I_{pa}/I_{pc} *vs.* the time transcurred between both electrochemical processes shows a linear dependence that follows the equation:

$$I_{pa}/I_{pc} = -1.61 \times 10^{-2} t/\text{s} + 0.9977 \quad (n = 8)$$

$$r = 0.997$$

So supposing a first order kinetic for the chemical reaction the corresponding kinetic equation is:

$$v = 0.0161 \times [\text{MXT}]$$

in $0.1M$ perchloric acid as background electrolyte.

Electrode mechanism

As reported previously, MXT shows two cathodic processes in the pH range studied. The first of these is reversible and at acid pHs corresponds to a transference of $2H^+$ and $2e^-$. The electrochemical reaction was attributed to the anthraquinone groups which are reduced to the dihydroxianthraquinone.[6-8] A ECE mechanism was found, *i.e.*, the product of the first cathodic process undergoes a chemical reaction whose products are then reduced in the second cathodic process. Other reactions which break the molecule may occur on the electrode surface resulting in a loss of the oxidation peak in the reverse scan.

In order to prove the main reduction peak of the MXT is due to the anthraquinone groups, the molecule 5,8-dihydroxyde-1,4-napthoquinone containing similar quinonic groups has also been studied. Figure 4 shows the voltamperogram of a $1 \times 10^{-4}M$ solution of 5,8-dihydroxyde-1,4-naphthoquinone prepared in $0.1M$ perchloric acid. In fact, the electrochemical process is similar but the displacement of the peak potential to less negative values occurs. This difference can be accounted for by having in mind that this molecule possesses one less aromatic ring. This results in a poorer adsorption and accordingly a higher energetic level that leads to an easier electrochemical reduction; and on the other hand, a concentration two orders of magnitude higher is necessary to obtain a similar peak intensity that comes to emphasize the better adsorption preconcentration of MXT.

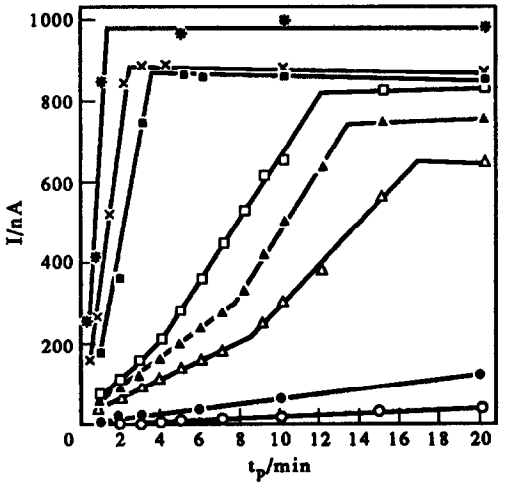

Fig. 5. Effect of preconcentration time upon first cathodic peak intensity for different MXT concentrations. (○) 1×10^{-8}, (●) $2{,}5 \times 10^{-8}$, (△) 5×10^{-8}, (▲) 7.5×10^{-8} (□) 1×10^{-7}, (■) $1{,}5 \times 10^{-7}$, (⊙) 2.5×10^{-7} y (⊖) $5 \times 10^{-7}M$.

Parameters affecting the adsorptive stripping signal

The peak current intensity of the first process is unaffected by changes in the concentration potential (range from -0.3 to $+0.2$ V) or by carrying out the preconcentration step in open circuit. So, the following experiments were carried out using a preconcentration step in an open circuit.

No significant influence on the stripping current was observed when the ionic strength of the background electrolyte was studied in the range 0.1–$0.5M$.

Accumulation curves

As is well known, the mass transport from the bulk of the solution to the electrode surface controls the overall rate of adsorption. When the mass transport is made convectively, *i.e.*, by stirring the solution, the rotation speed affects the magnitude of the stripping peak current. This effect was demonstrated for a $5 \times 10^{-7}M$ MXT solution by varying the rotation speed in the range 90–900 rpm and using a preconcentration time of 60 sec. The stripping current shows a linear dependence on the rotation speed (w) according to the equation:

$$I/\text{nA} = 4.2 \times 10^{-2} \times w/\text{rpm} + 61.24 \quad (n = 6)$$

$$r = 0.996$$

A plot of the peak current *vs.* the preconcentration time for eight different MXT concentrations, in which the preconcentration step was carried out in the open circuit under constant stirring conditions, is shown in Fig. 5. As expected, the peak intensity grows in direct proportion to increasing preconcentration time. At a certain peak current (about 200 nA), the cathodic stripping peak shifts a few millivolts to more negative potentials and becomes sharper. This sharper peak grows linearly with the preconcentration time, as shown in Fig. 6. The appearance of this phenomenon can be explained by Laviron in terms of interactions among the adsorbed molecules,[9] and has been described in other work also.[10]

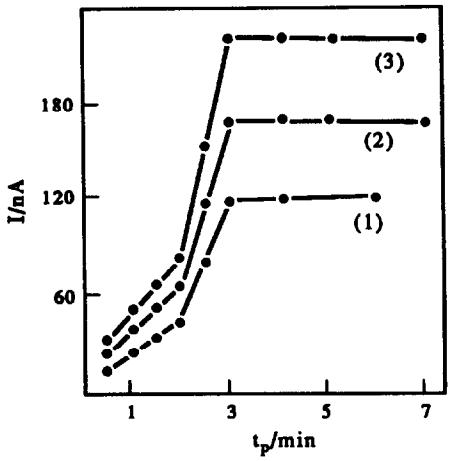

Fig. 6. Effect of preconcentration time upon peak intensity using three different electrode areas. (1) 0.29 mm², (2) 0.44 mm² and (3) 0.57 mm²

At longer preconcentration times, peak current stabilization was observed and we can assume that the electrode surface is saturated by the molecule adsorbed. So this stabilization was achieved at shorter preconcentration times for higher MXT concentrations.

The area of an adsorbed MXT molecule was calculated using a series of preconcentration experiments. These consist of studying the preconcentration time effect for three different drop sizes of the electrode (0.29, 0.44 and 0.57 mm²) and for a $5 \times 10^{-7}M$ MXT concentration. The results showed that for a preconcentration time of 180 sec a monolayer of adsorbed MXT was obtained (Fig. 6). Using Faraday's Law three values for the MXT adsorbed area were calculated (1.53, 1.66 and 1.51 nm²). The mean value was 1.57 nm² with a standard deviation of 5.2%, that is in agreement with others obtained for similar molecules using this method and reported in the literature[10] (folic acid 1.66 nm², blue methylene 1.28 nm²).

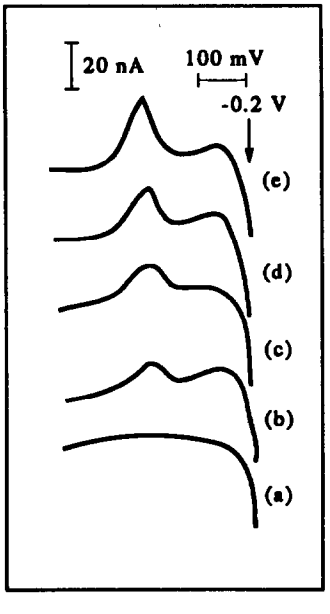

Fig. 7. Determination of MXT in urine samples. (a) Blank, (b) Addition of 1 ml of the organic extract, (c, d, e) Successive additions of 10 μl of $1 \times 10^{-5}M$ MXT standard.

Influence of other surface active compounds

The influence of some surfactants of different nature on the preconcentration-stripping process of MXT was studied in order to determine the optimum experimental conditions for carrying out adsorptive stripping measurements in the presence of a large excess of surface active compounds. A preconcentration time of 60 sec and a MXT concentration of $1 \times 10^{-7}M$ (44.4 ppb) were used in all experiments.

Competition for the adsorption sites of the electrode surface between MXT and gelatin (a known mixture of soluble proteins itself) is solved in favour of MXT; thus, the stripping response obtained in a 1000-fold excess of gelatin is 68% of its original value. The effect of an anionic surfactant, sodium laurylsulphate (SLS), and a cationic surfactant, cetyltrimethylammonium chloride (CTAC), was also studied. CTAC caused greater decreases in the peak than SLS, thus, a 2.6 ppm solution of CTAC or SLS decreased the MXT peak current to 84 and 70% of its original peak value, respectively. The cationic surfactant at bigger concentrations form a white precipitate and current peak increases. Finally, the effect of a non-ionic surfactant such as Triton X-100 was examined. A large excess of Triton X-100 (36 ppm) caused a peak increase of 32% of its original value. At the same time, a change in the peak width was observed. This sharper peak increases in direct proportion with the MXT concentration.

In conclusion, preconcentration in the presence of a large excess or surface active compounds has proved feasible, and well-defined relationships exist between the transferred charge, the preconcentration time and the analyte concentration in the background electrolyte.

Stripping of the MXT adsorbed with different voltammetric techniques

In order to ascertain the most sensitive adsorptive stripping response, several potential scan modes were assayed. Initial experiments were carried out with linear sweep voltammetry (LSV) when the analyte is preconcentrated for

one or five min at a HMDE in open circuit under a stirring rate of 1000 rpm. The intensity follows the equations:

$$I/\text{nA} = 5.94 \times 10^8\ [\text{MXT}] - 0.520\ (n = 8)$$
$$r = 0.9992$$
$$t_p = 1\ \text{min}\quad (5 \times 10^{-9}\text{–}3.5 \times 10^{-7} M)$$

$$I/\text{nA} = 2.76 \times 10^9\ [\text{MXT}] + 0.433\ (n = 4)$$
$$r = 0.9995$$
$$t_p = 5\ \text{min}\quad (1 \times 10^{-9}\text{–}1 \times 10^{-8} M)$$

The accuracy of this technique expressed in terms of the relative standard deviation is 0.53% at a concentration of $1 \times 10^{-7} M$ and using a preconcentration time of 1 min.

Stripping with square wave voltammetry (SWV)

SWV for analytical purposes was applied in the determination of other quinones at low levels by adsorptive stripping voltammetry.[11] Irreversible systems are in general, less attractive than reversible ones for the application of SWV, because of diminished sensitivity and resolution.[12] Therefore, it is possible to obtain good results with the first process of MXT.

The purpose of the first series of experiments was to optimize the parameters of the waveform, such as square-wave amplitude (Esw), potential step (Es) and frequency (f) for a MXT concentration of $1 \times 10^{-8} M$ and using 1 min as preconcentration time. Data obtained for different potential step, while maintaining other parameters of the waveform constant (Esw = 25 mV, f = 150 Hz), showed that for a value of 5 mV the peak intensity was the highest and that between 5 and 25 mV the intensity decreases and peak width increases. Then, voltamperograms for MXT were generated at seven different square-wave frequencies. A plot of peak current *vs.* frequency gave a maximum of between 150 and 165 Hz. At smaller and higher values the current peak quickly decreases. Finally, the effect of the square-wave amplitude upon peak current was shown to have a maximum of 25 mV.

These optimum values of Es and Esw are in close agreement with a reversible $2e^-$, $2\,H^+$ reduction to produce the corresponding hydroquinone.

Using these last optimized parameters and a preconcentration time of 60 sec, a calibration plot was carried out, providing a linear response between 1×10^{-9} and $1 \times 10^{-8} M$ that follows the equation:

$$I/\mu\text{A} = 9.01 \times 10^7\ [\text{MXT}] + 0.187\quad (n = 5)$$
$$r = 0.9996$$

The estimated detection limit ($s/n = 3$) was $3.2 \times 10^{-9} M$

Stripping with alternating current voltammetry (AC)

As is well known, the enhancement of sensitivity when the voltamperogram is recorded with AC mode has been theoretically predicted by Laviron for reversible redox couples with the reactant and product strongly adsorbed under Langmuir isotherm conditions.[13] Therefore, AC voltammetry was applied to the MXT stripping.

The peak current of the AC voltamperograms recorded from $5 \times 10^{-8} M$ MXT solutions, was found to be closely proportional to the superimposed voltage amplitude, ΔE, and no stabilization was observed, as expressed by the following equations:

1st linear range:

$$I/\text{nA} = 12.7 \times \Delta E/\text{mV} + 2.9\quad (n = 5)$$
$$r = 0.9997\quad (1 - 7.5\ \text{mV})$$

2nd linear range:

$$I/\text{nA} = 7.1 \times \Delta E/\text{mV} + 44.8\quad (n = 9)$$
$$r = 0.9990\quad (7.5 - 27.5\ \text{mV})$$

Finally, the effect of MXT concentration upon the peak current was studied using a superimposed voltage amplitude of 25 mV. The conditions and equations can be seen below:

$$I/\text{nA} = 5.6 \times 10^{10}\ [\text{MXT}]\text{–}39.7\quad r = 0.9999$$
$$t_p = 1\ \text{min}\quad (1 \times 10^{-9}\text{–}7.1 \times 10^{-9} M)$$
$$\text{L.D. } 1.5 \times 10^{-9} M$$

$$I/\text{nA} = 1.1 \times 10^{11}\ [\text{MXT}] + 3.5\quad r = 0.9995$$
$$t_p = 5\ \text{min}\quad (5 \times 10^{-11} - 2 \times 10^{-9} M)$$
$$\text{L.D. } 6.3 \times 10^{-11} M$$

Analytical applications

The first of these was the MXT determination in ampoules. A standard addition method using a stock solution $6.3 \times 10^{-3} M$ MXT was used. No preconcentration step was carried out. In these conditions, a linear calibration was done between 7.87×10^{-7} and $7.87 \times 10^{-6} M$, in which

the intensity *vs.* MXT concentration follows the equation:

$$I/\text{nA} = 5.9 \times 10^6\ [\text{MXT}] + 0.2 \quad (n = 7)$$

$$r = 0.9997$$

So, an adequate ampoule dilution was needed (5 μl in 20 ml 0.1M perchloric acid) for to work in the above linear range.

In five consecutive determinations, a mean concentration value of $5.04 \times 10^{-3}M$ was obtained, with a standard deviation of 1.37%.

The MXT determination in urine samples was carried out following the previously mentioned clean-up procedure and 1 ml of the organic extract was injected in 20 ml of 0.1M perchloric acid. A standard addition method was used and the voltapermograms recorded are found in Fig. 7. The recovery of the method was established by processing five urine samples to which MXT had been added and established at $94 \pm 12\%$.

Acknowledgement—The authors thank DGICYT (Spain) for economic aid (Project No. PB 87/1041).

REFERENCES

1. K. C. Murdock, R. G. Child, P. F. Fabio, R. B. Angier, R. E. Wallace, F. E. Durr and R. V. Citarella, *J. Med. Chem.*, 1979, **22**, 1024.
2. I. E. Smith, *Cancer Treat., Rev.*, 1983, **10**, 103.
3. R. Zee-Cheng and C. C. Cheng, *J. Med. Chem.*, 1978, **21**, 291
4. R. E. Wallace, K. C. Murdock, R. B. Angier and F. E. Durr, *Cancer Res.*, 1979, **39**, 1570.
5. J. C. Cortina, A. Costa García and P. Tuñón Blanco, *Talanta*, 1993, **40**, 325.
6. J. P. Hart, in *Electrochemistry Sensors and Analysis*, M. R. Smith and J. G. Vos (eds), *p.* 355. Elsevier, Amsterdam, 1986.
7. J. C. Vire and G. J. Patriarche, *Analysis*, 1978, **6**, 395.
8. G. J. Patriarche and J. C. Vire, in *Electroanalysis in Hygiene, Environmental, Clinical and Pharmaceutical Chemistry*, W. F. Smith (ed.), p. 209. Elsevier, Amsterdam, 1980.
9. E. Laviron, *J. Electroanal. Chem.*, 1975, **63**, 245.
10. J. M. Fernández, A. Costa, A. J. Miranda and P. Tuñón, *ibid.*, 1987, **255**, 241.
11. J. C. Vire, V. Lopez, G. J. Patriarche and G. D. Christian, *Anal. Lett.*, 1988, **21**, 2217.
12. E. J. Zachowski, M. Wojciechowski and J. Osteryoung, *Anal. Chim. Acta*, 1986, **183**, 47.
13. E. Laviron, *J. Electroanal Chem.*, 1979, **97**, 135.

Talanta, Vol. 40, No. 3, pp. 341–345, 1993
Printed in Great Britain.

0039-9140/93 $6.00 + 0.00

SANDWICH-TYPE FLOW-THROUGH FIBER-OPTIC CELLS FOR OPTICAL ABSORBANCE MEASUREMENTS

PURNENDU K. DASGUPTA,* HARVEY S. BELLAMY and HANGHUI LIU
Department of Chemistry and Biochemistry, Texas Tech University, Lubbock, TX 79409-1061, U.S.A.

(*Received* 10 *July* 1992. *Accepted* 10 *July* 1992)

Summary—The sandwich cell described by Pavon *et al.*[1] and a similar sandwich cell, except with angled (45°, confocal) single strand optical fibers and a conventional Z-type cell of 6-mm path length have been studied with respect to their performance for absorbance detection. Both sandwich cells show less susceptibility by one order of magnitude to artifact absorbance signals from RI changes than the Z-cell. The light throughput in the sandwich cells increase by an order of magnitude when an inert metallized reflector is used and this improves S/N. The overall light throughput is substantially greater for the angled entrance single strand fiber optic cell rather than the cell with the bifurcated fiber optic. Attainable limits of detection with these cells appear to be related to the pathlength for the cell dimensions studied.

Pavon *et al.*[1] have recently described in this journal a universal sandwich membrane flow-through cell which can be used for spectrophotometric or chemiluminescence measurements. For absorption measurements, light conducted by one leg of a bifurcated fiber optic cable is brought into the cell through the common leg, passes through the test solution, is reflected by a Teflon^R plate and is carried out back to a detector through the other leg of the fiber optic [Fig. 1(a)]. In some applications, the Teflon plate may be replaced by a porous hydrophobic membrane that can be part of a gas diffusion or phase separation device integral to a flow injection analyzer.

The authors rightly point out that the great virtue of this cell is its simplicity. This results in turn in robustness, and ease of construction, cleaning and repair. They have also indicated its relative freedom from bubble entrapment problems. The emphasis was placed on the versatility of the design in manifold applications rather than what performance limits can be expected. From a practical viewpoint of flow-through optical detection (whether for liquid chromatography or for flow injection analysis), the majority of applications involve straightforward optical absorbance measurement without gas diffusion or phase separation. We believe that the cell design described by Pavon *et al.*[1] is an important advance. Therefore we believe further that it is important to determine the performance limits of such a cell optimized for absorbance measurements and compare the same to the performance of flow-through cells of more conventional design and dimensions. It is of considerable interest, for example, to determine if the short path length of the cell results in a proportionate decrease in the attainable limit of detection (LOD, in terms of concentration), and the quantitative degree to which artifact signals from changes in refractive index may be reduced in this cell.

The purpose of the present note is to address these issues.

EXPERIMENTAL

The universal sandwich cell of Pavon *et al.*[1] was obtained in its commercial version from Alitea U.S.A. (Medina, WA, U.S.A.). This cell was used with a bifurcated fiber optic (common leg bundle diameter 1.6 mm, individual leg bundle diameter 1.1 mm; Dolan-Jenner Industries, Woburn, MA, U.S.A.). Reflective Mylar film (175 μm thick, Marlin P. Jones and Associates, Lake Park, FL, U.S.A.) and transparent Kel-F film (175 μm thick, American Durafilm Co., Natick, MA, U.S.A.) were obtained as indicated. Metallic aluminum was deposited on one side of the Kel-F film by vacuum deposition to form a highly reflective flexible mirror with an inert surface.

A variation of the Alitea sandwich cell was constructed by replacing the original cell front block FB (Fig. 1) with a different block in which

*Author for correspondence.

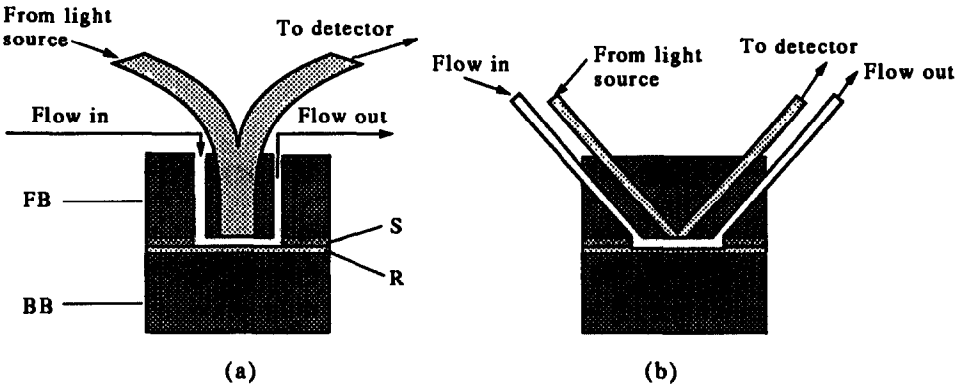

Fig. 1. Reflective sandwich cells: (a) Perpendicular light entrance cell with bifurcated fiber optic, (b) Angled light entrance cell with single strand fiber optic. FB: Front block, S: Spacer, R: Metallized reflector, BB: Bottom block.

two 1.0-mm holes were drilled at oppositely inclined angles [see Fig. 1(b)] to accommodate 1.0-mm diameter ESKA polymeric single strand optical fibers (Edmund Scientific, Barrington, NJ, U.S.A.) that were polished at the termini and ended flush at the interior surface of FB. The fibers were held in place by epoxy adhesive and jacketed outside with black heat-shrink poly(vinylchloride) tubing. The spacing between the fibers was such that they were confocal at the reflector surface. Experiments with both the original and the modified Alitea cell were conducted with the mylar/Kel-F reflector in place of the Teflon^R reflector supplied with the cell, except as mentioned. A third cell, used for comparison, utilized the common Z-geometry with illuminated dimensions of 6 mm × 1.0 mm ϕ. The cell was constructed of opaque poly(ether ether ketone) polymer with optically flat glass windows and also utilized fiber optic to transmit light back and forth from the cell. This latter cell has been described in more detail elsewhere.[2]

The same electronic and optical arrangement was used to test all three cells (Fig. 2). Except as stated, the light source was a 605-nm high brightness light emitting diode (LED, Stanley HAA5566X, AC Interface, Los Angeles, CA) driven by a 40-mA constant current source. The LED was referenced on the backplane by a photodiode R (S2007, Electronic Goldmine, Phoenix, AZ, U.S.A.) and the reflected/transmitted light was detected by photodiode D, identical to R. Both photodiodes were mounted on a circuit board containing a log ratio amplifier integrated circuit chip (LOG100JP, Burr-Brown, Tucson, AZ, U.S.A.). The optical fibers were directly coupled to the photodiodes. The optoelectronic assembly was enclosed in a metallic, essentially light tight enclosure. The cell and electronics were then further put in a 0.25″ thick-walled brass box to minimize external electromagnetic noise. Power ($\pm$12 V) was supplied by a wall-mounted supply and the amplifier was operated with a fixed gain of 5 V/absorbance unit.

The test arrangement consisted of a pneumatically pressurized reservoir pumping a carrier liquid at 1.1 ml/min through a loop injector (loop volume *ca.* 110 μl), a conduit (0.75 × 750 mm) and the detector. Experiments with bromothymol blue (BTB) were conducted by injecting various concentrations of the alkaline test solute (0.12–100 μg/ml) into an alkaline carrier. Refractive index effects were studied by injecting 50% (v/v) aqueous ethanol into a water carrier.

RESULTS AND DISCUSSION

Increasing light throughput

Replacing the white Teflon^R backplate with a metallized reflector increases light throughput by a factor of 8–10 as evidenced from the detector photocurrent. This results in improved signal/noise, particularly when the incident light intensity is low. For example, for a blue LED emitting at 470 nm the light output is very low and the system noise level was observed to be inversely related to the detector photocurrent. For direct photometric measurements where a membrane is not required, we therefore recommend the use of a metallized reflector. A Kel-F film (transparent down to *ca.* 210 nm) is to be preferred if aggressive reagents/solvents are to be used. Indeed, further use of such a film as the entrance window to the cell (placed between FB and S, Fig. 1, with appropriately

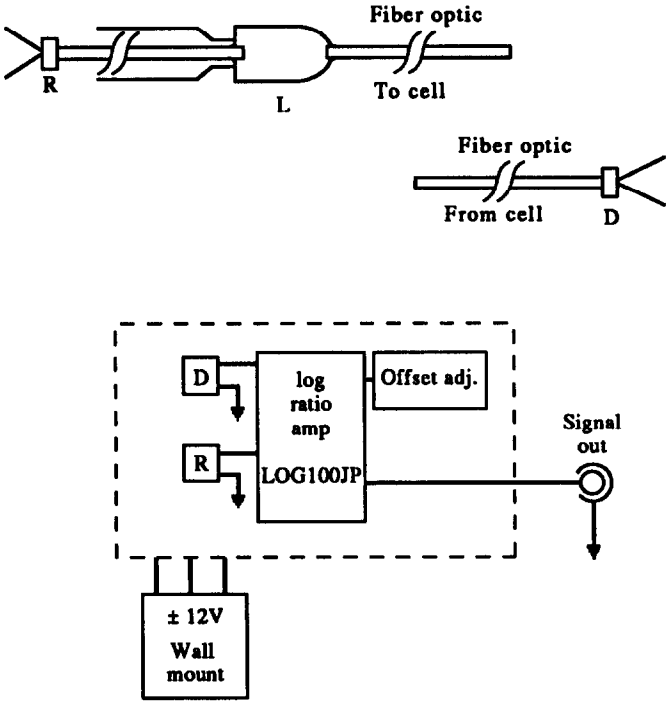

Fig. 2. Optoelectronic test arrangement. L: Light emitting diode; R, D: Reference and Signal Photodiodes.

placed holes punched in the flow path) can serve to prevent direct contact of the fiber optic to the test solutions.

Path length and detection limits

With a 1/32 in. (0.75 mm) spacer, the effective path length of the cell in Fig. 1(a) was 1.5 mm. The computed or nominal path lengths of all three cells studied are listed in Table 1 along with the observed performance parameters. The linear slopes for calibration with BTB correspond reasonably well with the anticipated path lengths, as may be expected. The slightly lower value of linear r^2 for the conventional geometry cell probably results from the higher absolute absorbance values measured by this cell and the lack of perfect correspondence between the relatively broadband emission of the LED and absorption by BTB. The absolute noise levels appear to be related to the overall light throughput for each cell rather than to the path length. In this respect, the angled entrance cell with the single strand fiber optics appears to do a much better job than the bifurcated fiber bundle. With water flowing through each cell, detector diode photocurrents were 45 nA and 360 nA for cells 1(a) and 1(b), respectively. Overall the angled cell thus results in a somewhat better LOD. The longer pathlength of the conventional cell allows it an LOD even lower. The absolute noise levels of the Z-cell and the angled entrance sandwich cell are the same, thus the detection limit is inversely related to the path length. However, quite respectable LODs are obtained by either sandwich cell.

The illuminated volume of the Z-cell is 4.7 μl. In the sandwich cells, the distance to the reflector is small, comparable to or less than the aperture of the light entrance/exit. Thus, if we presently ignore the lateral diffusion of light, the illuminated volumes are 1.5 and 1.3 μl for the straight and angled light entrance sandwich cells, respectively. Doubtless, the actual illuminated volume will be somewhat larger, but this is still very respectable.

Both sandwich cells were found to be immune to bubble entrapment problems.

Refractive index effects

When the injected fluid element has a different refractive index (RI) from that of the carrier stream, virtually all flow-through cells used for optical absorbance measurements produce an artifact signal not related to true absorption. Betteridge *et al.*[3] were the first to clearly illustrate that this occurs because the moving bolus of a fluid element of different RI forms a dynamically changing lens that affects the light transmitted through the illuminated volume. The degree to which a cell is susceptible to

Table 1. Performance comparison of cell designs

	Sandwich cell, perpendicular light entrance/exit	Sandwich cell, angled light entrance/exit	Z-geometry conventional cell
Nominal or calculated pathlength mm	1.5	2.1	6.0
Sensitivity to alkaline BTB (mAU/ppm)*	4.3	6.2	17.0
Linear r^2 to injected BTB over 2 orders of magnitude	1.0000	0.9999	0.9997
Absolute noise level (μAU, $\pm$SD†)	46.3 ± 4.6	35.5 ± 5.3	35.5 ± 2.7
Computed detection limit for BTB, ppb	32.0	17.0	6.3
Refractive Index Artifact Signal (mAU)‡	9.5	14.0	176

*Absorbance units per ppm bromothymol blue injected into FIA system.
†Pulseless, pressurized flow of water.
‡50% ethanol injected into water carrier in a FIA system, amplitude of signal from positive to negative excursion.

producing such artifact RI signals is dependent on the cell geometry—a large value for the ratio of the physical path length to the bore (called the aspect ratio) results in an increase in RI sensitivity. By imaging the source on the exit window with focusing optics and using tapered cell construction (light exit diameter < entrance diameter) it is possible to greatly reduce RI sensitivity,[4] albeit it cannot be eliminated altogether. It is also possible to correct for the artifact RI signal by using a second wavelength as a reference.[5] Nevertheless, it would be desirable to reduce the intrinsic sensitivity of a cell to RI changes in the first place. Consideration of the principles laid out by Betteridge *et al.*[3] clearly indicate that as long as the aspect ratio is not overly large (causing light loss to the cell wall), if the incident light goes not just through a single lens element but also through a second lens element oppositely placed, the RI effect can be largely cancelled. In previously unpublished work, we have observed that RI artifacts are indeed greatly reduced in a T-type cell geometry where the source and detector optical fibers are placed in the opposing arms of a tee. In this arrangement, the fluid enters through the short arms of the tee and flows at equal rates around and past the opposing fibers. Opposing lenses are thus created in the illuminated volume by a transient element of a different RI. The reflective sandwich cell of Pavon *et al.*[1] does this in a far simpler and elegant fashion, passing the light through the same optical element in two directions. The great reduction in RI sensitivity compared to a conventional cell is illustrated in Fig. 3. Note that dispersion is very limited in these experiments and the effects are larger than what would be observed in a typical analytical system where the injected plug will undergo greater dispersion in the carrier. While the RI artifact signals appear complex, they are nevertheless highly reproducible. Because alcohol has a refractive index closer to glass (or acrylate fiber) than does water and the overall dispersion in the system is low, the dominant feature is a negative absorbance signal because the presence of alcohol results in less reflection loss at the fluid–fiber or fluid/window interface.

The response of the angled light entrance sandwich cell is particularly complicated apparently because the injected bolus sequentially affects the probe volume of each of the fibers. However, the overall amplitude of the response is essentially the same as that of the original sandwich cell when the greater path length of the angled entrance cell is taken into account.

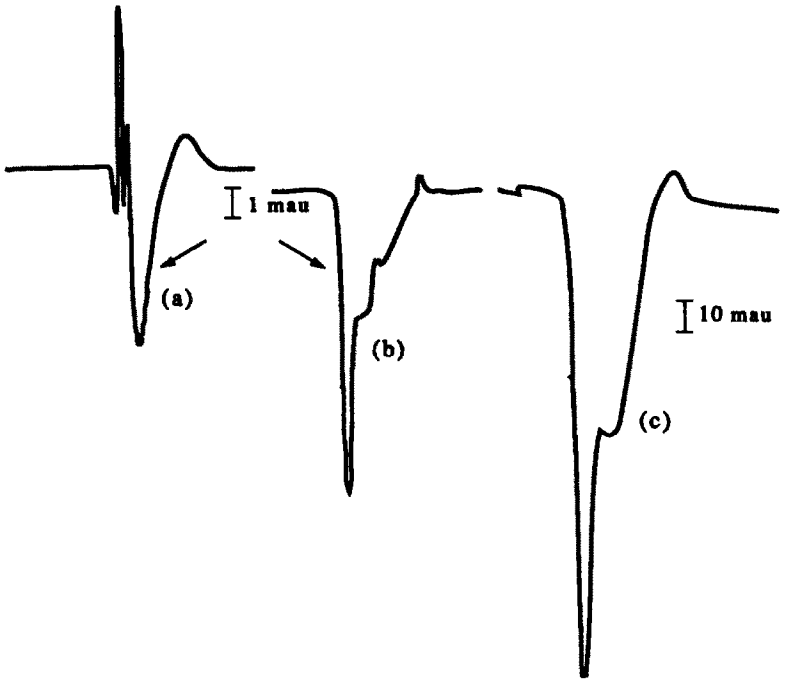

Fig. 3. Artifact absorbance signal arising from the injection of 50% ethanol into a water carrier. (a) Angled light entrance sandwich cell, (b) perpendicular light entrance sandwich cell, (c) Z-configuration cell. Note the order of magnitude different scale in (c).

CONCLUSIONS

In summary, the cell described by Pavon *et al.*[1] combined with a metallized reflective element provides attractive performance in terms of absolute concentration sensitivity, susceptibility to bubble entrapment and RI artifacts and ease of construction and cleaning. In its conceptually simplest embodiment, a thin-walled transparent conduit of glass or silica can be provided with in/out connecting tubes and an opaque enclosure, metallized on one exterior half with a bifurcated fiber optic probe from the other half. If measuring the exact dispersion patterns of a bolus without imposing the influence of the cell itself is important, such a design is expected to produce minimum changes in the flow pattern. The original sandwich design is more robust, however, and may be modified to have flow entrance/exits through the sides of the spacer S to achieve a no-disruption flow geometry. As to the single strand fiber optic pair angle light entrance/exit configuration, it is not a new concept.[6,7] Construction is somewhat more involved than the perpendicular geometry sandwich cell but otherwise it may be more attractive where source light levels are low or in uv applications where single strand 1-mm core silica fibers not only directly provide an inert window but are substantially less expensive than the corresponding bifurcated fiber optic bundles.

Acknowledgement—We thank Alitea U.S.A. for the gift of the sandwich cell. This work was supported by the Office of Basic Energy Sciences, U.S. Department of Energy through DE-FG05-84ER13281. However, this manuscript has not been subject to review by the DOE and no endorsement should be inferred.

REFERENCES

1. J. L. P. Pavon, E. R. Gonzalo, G. D. Christian and J. Ruzicka, *Anal. Chem.*, 1992, **64**, 923.
2. P. K. Dasgupta, H. S. Bellamy, H. Liu, J. L. Lopez, E. L. Loree, K. Morris, K. Petersen and K. A. Mir, *Talanta*, in the press.
3. D. Betteridge, E. L. Dagless, B. Fields and N. F. Graves, *Analyst*, 1978, **103**, 897.
4. J. E. Stewart, *Appl. Optics*, 1981, **20**, 654.
5. E. A. G. Zagatto, M. A. Z. Arruda, A. O. Jacintho and I. L. Mattos, *Anal. Chim. Acta*, 1990, **234**, 153.
6. J. Ružička and E. H. Hansen, *ibid.*, 1985, **173**, 3.
7. M. T. Jeppesen and E. H. Hansen, *ibid.*, 1988, **214**, 147.

Talanta, Vol. 40, No. 3, pp. 347–350, 1993
Printed in Great Britain.

0039-9140/93 $6.00 + 0.00

APPLICATION OF STANDARDLESS ANALYSIS IN GRAPHITE FURNACE ATOMIC ABSORPTION SPECTROMETRY: DETERMINATION OF CHROMIUM

YANSHENG ZHENG* and XINGGUANG SU
Department of Chemistry, Jilin University, Changchun 130023, P.R. China

(*Received* 15 *May* 1992. *Revised* 9 *July* 1992. *Accepted* 10 *July* 1992)

Summary—Influences of atomization temperatures on the characteristic mass and the atomic absorption coefficient of chromium were studied. The experimental results show that the values of characteristic mass have appeared to be stable to better than 10% when the analyte is atomized in the range of 2500–2800°. The standardless analysis was applied to the determination of chromium in standard sediment and geochemical reference samples and satisfactory results were obtained.

The idea of standardless or absolute analysis[1–4] has attracted attention of spectroscopic workers ever since Walsh's first paper on atomic absorption spectroscopy.[5] There are now several approaches that have been proposed for providing graphite furnace conditions approximate to those that are theoretically required for absolute analysis. Typically, these devices have been called "constant temperature furnaces", a name that seems to have been proposed by Woodriff.[6] However, the Woodriff furnace was very difficult to use for real analysis. At present, in discussions of the development of graphite furnace atomic absorption spectrometry (GFAAS), it is worth while to speak of the method which is known as the stabilized temperature platform furnace.[7] With this system, it has been demonstrated that it is possible to control the experimental conditions so tightly that a unique and constant calibration curve can be assumed as valid. However, any change of sample composition and the formation of stable molecules can be a source of larger errors for application of standardless analysis. Therefore, it is an important condition that a matrix modifier should be used to eliminate interferences for application of standardless analysis in real samples.

In atomic absorption spectrometry, the transient atomic absorption signal of a spectral line is the result of the time-dependent density distribution of the analyte atoms in the analysis volume. The equation which has been derived for GFAAS[1,2] is

$$A(t) = \frac{0.432\sqrt{4\pi \ln 2}e^2 g_i}{m_e c^2 Z(T)\Delta\nu_D s} \times \exp(-E_i/kT)\gamma'\delta f H(a,\omega)\, N(t) \quad (1)$$

Here m_e and e are the mass and the charge of the electron, c is the velocity of light in vacuum, f is the oscillator strength, g_i and E_i are the statistical weight and the energy of the lower level for the analytical line, γ' is a coefficient accounting for hyperfine splitting in the analytical line and the Doppler line width in the light source, δ is a correction factor for adjacent lines in the light source spectrum, $Z(T)$ is the partition function at temperature $T(K)$, k is the Boltzmann constant, $H(a,\omega)$ is the Voigt integral for the point of the absorption line centour distant from the line centre by $\omega = 0.72a$ (here a is the damping constant of the Voigt profile), s is the cross section of the tube, $N(t)$ is the total number of free analyte atoms in the analysis volume at time t.

The atoms need not be distributed homogeneously over the tube length, but they must maintain a homogeneous distribution in the plane perpendicular to the light beam, because otherwise the $A(t)$ measured will not be linearly related to $N(t)$.[8,9] The constant

$$K = \frac{0.432\sqrt{4\pi \ln 2}e^2 g_i \exp(-E_i/kT)\gamma'\delta f H(a,\omega)}{m_e c^2 Z(T)\,\Delta\nu_D} \quad (2)$$

will be called the atomic absorption coefficient.

*Author for correspondence.

In graphite furnace atomic absorption spectrometry, the sensitivity is usually expressed as the characteristic mass (m_0), *i.e.*, the mass of analyte in picogram corresponding to a peak area of 0.0044 $A \cdot s$. As long as the removal of free analyte atoms from the furnace is a first order process, we get for the peak area absorbance (A_i):

$$A_i = KN_0\tau_R/s \quad (3)$$

here N_0 is the total number of analyte atoms deposited in the furnace and τ_R is the average residence time of atoms in the optical path.

We recall that

$$N_0 = m \cdot N_A/M_a \quad (4)$$

Here m is the analyte mass, N_A is the Avogadro number, M_a is the molar mass of the analyte.

Substituting equation (4) into equation (3), we come to

$$A_i = KN_A\tau_R m/sM_a \quad (5)$$

For an absolute analysis, the constant K in equation (2) should be obtained from universal constants. However, it is possible to obtain τ_R experimentally if the process of atom generation is fast in comparison with the removal process.[8,10,11] Therefore, for all practical purposes it is more convenient to measure K in equation (5) from a known quantity of analyte, as is done for the measurement of the molar absorptivity in UV–Vis molecular spectroscopy. The characteristic mass (m_0) was calculated from the mean peak area from the following equation:

$$m_0 = (0.0044/A_i)m \quad (6)$$

Here m is the mass of analyte in picograms for the particular element. It can be seen from equation (5) that the relation between K and m_0 can be expressed as

$$K = 2.30 \times 10^{-14}M_a r^2/m_0\tau_R \quad (7)$$

Here r is the tube radius. If we assume that the temperature in the furnace is constant and that the removal proceeds exclusively via diffusion through the graphite tube ends, the residence time can be expressed as:

$$\tau_R = l^2/8D \quad (8)$$

Here l is the tube length and D is the diffusion coefficient.

Substituting equation (8) into equation (7), we come to

$$K = 1.84 \times 10^{-13}M_a Dr^2/m_0 l^2 \quad (9)$$

In this paper, the influences of atomization temperatures on the characteristic mass and the atomic absorption coefficient of Cr were studied. The method of standardless analysis was applied to the determination of chromium in standard sediment and geochemical reference samples; satisfactory results were obtained.

EXPERIMENTAL

Apparatus

A Hitachi 180–50 atomic absorption spectrometer with a GA-3 graphite furnace was used. Pyrolytically coated graphite tubes (made in China) and solid pyrolytic L'vov platforms and pyrolytic V-shaped boats[12] (made in our laboratory). The size of the graphite tubes used in our experiments is $r = 2.35$ mm and $l = 30$ mm. The slit width was 1.3 nm. A Cr hollow cathode lamp (made in China) was used as a light source and operated at 10 mA. A deuterium arc background system was used throughout. N_2 was used as the purge gas, due to its lower cost than Ar at a flow rate of 150 ml/min and the purge gas was stopped during the atomization step. The 357.9 nm line of Cr was employed for all measurements. The absorption signals were recorded with an XWT-164 (made in China) strip chart recorder. Sample solution was injected into graphite tube with a 20 ml Eppendorf micropipette. The temperature of the furnace was corrected using a MT-2 optical pyrometer (made in China). The graphite furnace operating parameters were as follows: dry 80–120°, 30 sec; ashing 800°, 30 sec; atomization 2700°, 7 sec; cleaning 2800°, 3 sec.

Reagents

Chromium stock solution (1 mg/ml) was prepared by dissolving a suitable amount of $K_2Cr_2O_7$ (analytical reagent grade) in quartz sub-boiling distilled water. The working standards were prepared by appropriate dilution with water prepared in a sub-boiling still.

A 5%(w/v) solution of the ammonium salt of EDTA was prepared by dissolving 5.00 g of EDTA (analytical reagent grade) in sub-boiling distilled water and adding 15 ml of 25% aqua ammonia (analytical reagent grade) and then diluting to 100 ml with water.

Procedure

Standard sediment and geochemical reference samples (made in China) were used in this study. Transfer a weighted amount of the sample into

Table 1. The experimental values of m_0 and K for Cr at various atomization temperatures

Temp. (°C)	m_0 (pg)			$10^{14} \times K$ (cm^2)		
	Wall	Platform	V-shaped boat	Wall	Platform	V-shaped boat
2200	4.9	5.9	5.0	1.82	1.07	1.40
2300	4.3	5.0	3.4	2.23	1.36	2.26
2400	3.5	3.9	2.7	2.87	1.81	2.99
2500	3.4	3.0	2.6	3.22	2.46	3.25
2600	3.2	2.9	2.5	3.55	2.76	3.65
2700	2.9	2.7	2.4	4.26	3.19	3.90
2800	2.9	2.9	2.3	4.47	4.10	4.19

a polyfluorotetraethylene crucible usually 0.1–0.2 g, carefully add 5 ml and 3 ml of concentrated nitric and perchloric acids, respectively. Heat on a sand bath until near dryness, again add 3 ml of perchloric acid, 5 ml of hydrofluoric acid and 0.5 ml of sulphuric acid and continuously heat to dryness. The residue dissolves in sub-boiling distilled water. Add 0.5 ml of 5% (w/v) ammonium salt of EDTA as a matrix modifier and make the final volume to 25 ml for the determination of chromium by GFAAS.

RESULTS AND DISCUSSION

Influences of atomization temperature on m_0 *and* K

There are parameters influencing the stability of standardless analysis by graphite furnace atomic absorption spectrometry in which the temperature of the atomization step is a main factor.[13] Frech and Baxter[14] have studied the temperature dependence of atomization efficiencies of some elements in the graphite furnace. They pointed out that the atomization efficiency for most elements reaches a plateau, often in the higher temperatures region. We observed the influences of atomization temperatures on the experimental values of m_0 and K when the sample was evaporated from the wall, using the platform and the V-shaped boat techniques. The results are listed in Table 1.

As shown in Table 1, the influences of atomization temperatures on the experimental values of m_0 and K showed basically the same tendency when the samples were evaporated in three different ways. The value of m_0 decreased with an increase in the atomization temperature, and then reached a stable value after 2500°. The stability of m_0 values obtained by vaporizing of the three different ways appeared to be better than 10% in the range of 2500–2800°. However, the m_0 values are the smallest in the V-shaped boat furnace and the m_0 values in the platform furnace are less than that for the wall of the furnace at temperatures higher than 2600°. On the other hand, the value of K increases with increasing atomization temperature in the range of 2200–2800°.

Standardless analysis of Cr

It can be seen from Table 1 that the values of m_0 for Cr appeared to be stable to better than 10% when the analyte was atomized in the range of 2500–2800°. Therefore, we investigated the determination of Cr without standards. The determination of Cr in the standard sediment and geochemical reference samples by the three

Table 2. Standardless determination of Cr in samples

Sample*	Calculating method of m_0		Calculating method of K		Calibration curve method		Expected value
	Content,† μg/g	RSD, %	Content,† μg/g	RSD, %	Content,† μg/g	RSD, %	μg/g
GSS-4	368.4	1.2	358.7	5.7	358.4	3.3	370
GSR-3	135.0	3.1	131.0	3.7	131.0	5.0	134
GSD-2	12.2	1.8	12.1	1.9	12.1	2.2	12.2
GSD-8	7.5	4.4	7.4	1.5	7.4	2.7	7.6

m_0 was 2.9 pg/0.0044 A.s K was 4.26×10^{-14} cm^2.

*GSS-4 and GSR-3 are Geochemical reference samples (China). GSD-2 and GSD-8 are drainage sediment samples (China).

†Values are the mean of five measurements.

methods with 2%(v/v) ammonium salt of EDTA as matrix modifier was carried out. The analytical results are listed in Table 2. They indicate that standardless analysis applied to determination of Cr in practical samples provides satisfactory results. But it must be emphasized that a frequent check of characteristic mass will be a key link which assures accurate analytical results and that use of a matrix modifier to eliminate the interferences will be a necessary condition for application of standardless analyses in a practical sample.

REFERENCES

1. B. V. L'vov, *Spectrochim. Acta*, 1990, **45B**, 633.
2. B. V. L'vov, V. G. Nikolaev, E. A. Norman, L. K. Polzik and M. Mojica, *ibid.*, 1986, **41B**, 1043.
3. B. V. L'vov, *ibid.*, 1978, **33B**, 153.
4. C. S. Rann, *ibid.*, 1968, **23B**, 827.
5. A. Walsh, *ibid.*, 1955, **7**, 108.
6. R. Woodriff, *Appl. Spectrosc.*, 1974, **28**, 413.
7. W. Slavin, *Graphite Furnace AAS. A Source Book*. Perkin–Elmer Corp., Norwalk, 2nd Ed., 1991.
8. W. M. G. T. van den Broek and L. de Galan, *Anal. Chem.*, 1977, **49**, 2176.
9. S. L. Paveri-Fontana, G. Tessari and G. Torsi, *ibid.*, 1974, **46**, 1032.
10. Y. S. Zheng, R. Woodriff and J. A. Nichols, *ibid.*, 1984, **56**, 1388.
11. Y. S. Zheng and Y. S. Liu, *Fenxi Huaxue* 1987, **15**, 162.
12. Y. S. Zheng and F. Zhu, *Jilin Daxue Ziran Kexue*, 1987, **1**, 103.
13. W. Slavin and G. R. Carnrick, *Spectrochim. Acta*, 1984, **39B**, 271.
14. W. Frech and D. C. Baxter, *ibid.*, 1990, **45B**, 867.

Talanta, Vol. 40, No. 3, pp. 351–354, 1993
Printed in Great Britain.

0039-9140/93 $6.00 + 0.00

ADSORPTIVE STRIPPING MEASUREMENTS OF TRACE ALUMINUM IN THE PRESENCE OF CUPFERRON

JOSEPH WANG,* JIANMIN LU and ROSSI SETIADJI
Department of Chemistry, New Mexico State University, Las Cruces, NM 88003, U.S.A.

(*Received* 30 *June* 1992. *Revised* 8 *July* 1992. *Accepted* 8 *July* 1992)

Summary—The adsorptive collection of the aluminum complex with cupferron is exploited for developing a highly sensitive stripping procedure for trace aluminum. Optimal experimental conditions include the use of $2 \times 10^{-4}M$ cupferron in PIPES buffer (pH 7.0), an accumulation potential of -0.40 V and a linear potential scan. With controlled accumulation for 2 min, a detection limit near 30 ng/l. aluminum is obtained. The relative standard deviation (at 5 μg/l.) is 2.9%. Possible interferences are evaluated. The analytical performance compares favourably with that of early adsorptive stripping schemes for aluminum.

Because of the environmental and biological significance of aluminum, a highly sensitive method is required for its reliable measurement. The extremely negative reduction potential of aluminum makes its direct voltammetric quantitation difficult. Indirect polarographic schemes, based on the distinct reduction wave of aluminum, in the presence of di-o-hydroxyazo dyes, have thus been developed (1–3). It is possible to couple this redox behavior with the spontaneous interfacial accumulation of the aluminum/azo-dye complex for developing a highly sensitive adsorptive stripping procedure.[4] A drawback of this procedure is the slow chelate formation that requires a 10-min heating period at 90°. The need to heat the sample (after the ligand addition) has been obviated through the use of another reagent, 1,2-dihydroxyanthraquinone-3-sulphonic acid (DASA).[5] The resulting adsorptive stripping voltammetric procedure permits quantitation down to the nanomolar level, but suffers from interferences due to coexisting zinc and antimony ions.

The present paper describes a highly sensitive adsorptive stripping procedure for determining aluminum by adsorption accumulation and reduction of its complex with cupferron. The cupferron-based procedure compares favourably—in terms of sensitivity, selectivity and simplicity—with earlier adsorptive stripping schemes for aluminum. The utility of cupferron for adsorptive stripping measurements of other trace metals have been reported recently.[6,7]

*Author for correspondence.

EXPERIMENTAL

Apparatus and reagents

The equipment used to obtain the voltamperograms (a PAR 264A analyzer with a PAR 303 static mercury drop electrode) has been described in detail elsewhere.[4,6] A medium-sized hanging mercury drop electrode (HMDE) with a 0.016-cm^2 surface area was employed.

All solutions were prepared with doubly distilled water. A 1000-ppm stock aluminum solution (atomic absorption standard, Aldrich) was diluted as required. Stock solutions (0.1M) of cupferron (Aldrich) were prepared weekly and were stored at 4°. A $1 \times 10^{-3}M$ PIPES buffer (pH 7.0) served as supporting electrolyte.

Procedure

Voltammetric stripping experiments were performed in the following matter. The blank solution (10 ml) was pipetted into the cell and purged with nitrogen for 8 min. The preconcentration potential (usually -0.40 V) was applied to a fresh mercury drop while the solution was stirred. Following the accumulation period, the stirring was stopped and after 15 sec the voltamperogram was recorded by applying a linear scan (at 100 mV/sec) in the negative direction; the scan was terminated at -1.55 V.

RESULTS AND DISCUSSION

Response characteristics

Figure 1 shows cyclic voltamperograms for 10 μg/l. (ppb) aluminum, in a medium containing

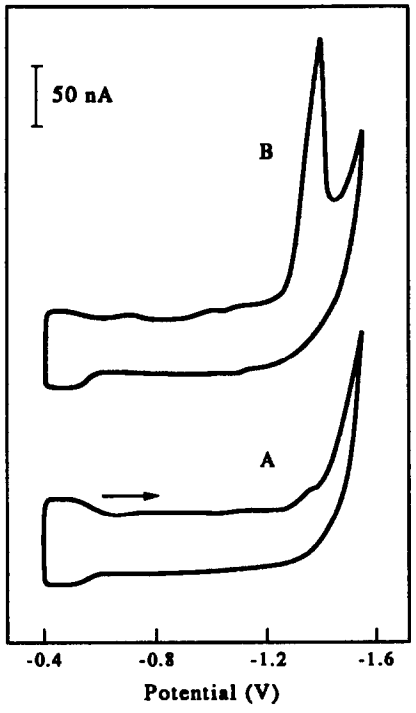

Fig. 1. Cyclic voltamperograms for 10 μg/l. aluminum after O (A) and 90 (B) sec stirring at -0.40 V. Scan rate, 100 mV/sec; solution, $1 \times 10^{-3}M$ PIPES buffer (pH 7.0), containing $2 \times 10^{-4}M$ cupferron.

$2 \times 10^{-4}M$ cupferron and $1 \times 10^{-3}M$ PIPES buffer (pH 7.0). In the absence of prior accumulation, only a small peak from the reduction of the aluminum/cupferron complex is observed at -1.39 V (A). When the experiment is repeated with a 90-sec stirring period (-0.40 V), a significantly (40-fold) larger cathodic peak is observed, indicating an interfacial accumulation of the complex (B). No peaks are observed upon scanning in the positive direction. The cathodic peak (following the stirring period) increased linearly with the potential scan rate (not shown), as expected for the surface-bound species. The peak also decreased rapidly upon repetitive scans, indicating rapid desorption of the complex from the surface. The fact that a well-defined cyclic voltammetric response is observed for μg/l. concentrations indicates the remarkable sensitivity associated with the interfacial accumulation process.

The spontaneous accumulation of the aluminum–cupferron complex can be exploited for effective preconcentration prior to the voltammetric scan. Figure 2 displays voltamperograms for 5.0 μg/l. aluminum after different preconcentration periods (0–60 sec, a–e). While quantitation is not possible without accumulation (a), well-defined peaks are observed after preconcentration. The peak increases rapidly with increasing preconcentration time, indicating (again) an enhancement of the complex concentration on the mercury surface. Also shown in Fig. 2 is the resulting peak-current *vs.* preconcentration time plot for 2.5 (A) and 5.0 (B) μg/l. aluminum. The rapid increase of the current observed at short preconcentration times, is followed by a levelling-off for longer periods. Such profiles reflect the kinetics of the adsorption process.

Various experimental variables affecting the adsorptive stripping response were evaluated and optimized. Figure 3(A) shows the dependence of the aluminum/cupferron peak on the ligand concentration. The peak height increases linearly with the cupferron concentration up to $2 \times 10^{-4}M$, after which it starts to level off. The dependence of the peak height on the accumulation potential is shown in Fig. 3(B). Such behaviour is attributed not only to the complex stoichiometry, but also to competition of the free ligand for adsorption sites. Larger peaks were obtained over the range from -0.40 to -0.50 V, *i.e.*, around the potential of zero charge; the peak decreased rapidly at lower and higher potentials. Other optimal conditions

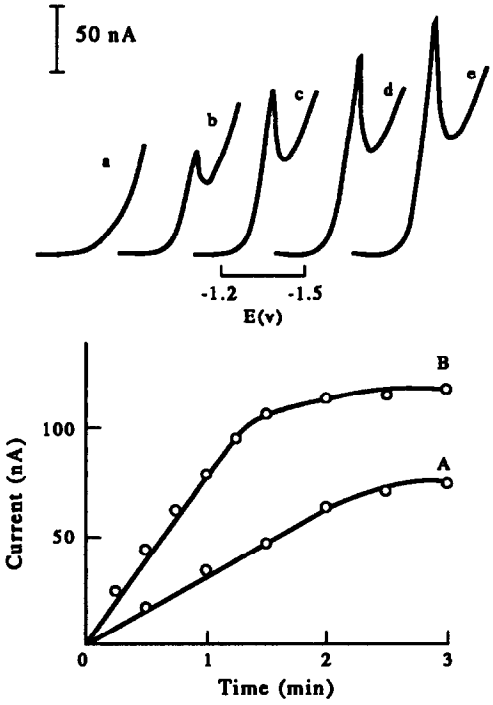

Fig. 2. Stripping voltamperograms for 5.0 μg/l. aluminum after preconcentration for 0 (a), 15 (b), 30 (c), 45 (d), and 60 (e) sec (at -0.40 V with 400 rpm stirring). Also shown are the resulting current *vs.* time plots for 2.5 (A) and 5.0 (B) μg/l. aluminum. Other conditions, as in Fig. 1.

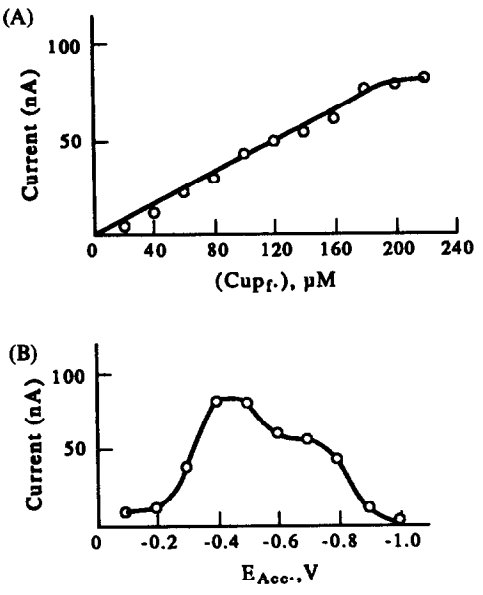

Fig. 3. Effect of cupferron concentration (A) and accumulation potential (B) on the response to 5.0 μg/l. aluminum. One-min accumulation. Accumulation potential (A), −0.50 V. Other conditions, as in Fig. 1.

include the use of pH 7.0 and of the linear potential scan mode (at 100 mV/sec).

Analytical performance

Figure 4 shows voltamperograms obtained after increasing the aluminum concentration in 2 μg/l. steps [(a)–(e)]. Well-defined peaks, proportional to the metal concentration, are observed using a 60-sec preconcentration period. Also shown are the resulting calibration plots following 30 (A) and 60 (B) sec of preconcentration. Both plots are highly linear over the entire range examined (slopes, 8.4 and 14.6 nA · l. · μg^{-1}, respectively; correlation coefficients, 0.998). A detection limit of 0.03 μg/l. ($1.1 \times 10^{-9} M$) was estimated from the signal-to-noise characteristics of the response for 0.25 μg/l. aluminum solution (120-sec accumulation). Such a detection limit is lower than that of the azo-dye based stripping procedure[4] and is similar to that of the DASA-stripping scheme.[5] Non-electrochemical methods for aluminum, such as inductively coupled plasma[8] and liquid chromatography[9] are characterised by significantly higher detection limits (of 0.3 and 0.2 μg/l. respectively). The adsorptive accumulation of the aluminum/cupferron complex results in reproducible stripping peak currents. For 22 successive measurements of 5 μg/l. aluminum, the mean peak current was 75.3 nA, with a range of 72.0–78.9 nA and a relative standard deviation of 2.9% [conditions, as in Fig. 2(e)].

The following metal ions (25 μg/l.) were tested and found not to affect the 5 μg/l. aluminum peak: Cu(II), Pb(II), Zn(II), Cd(II), Ni(II), Co(II), Sb(III), Fe(III), Bi(III), Tl(I), Mo(VI), Se(IV), Ga(III), In(III), Pd(II), Zr(IV), Te(VI), Ge(IV), W(VI), Ru(III), and Rh(III). Several of these ions [Cu(II), Pb(II), Cd(II), In(II), Ni(II) and Zn(II)] yielded cathodic peaks at lower potentials that did not affect the response of interest. Indeed, it was possible to simultaneously quantitate aluminum with 4 or 5 of these metals. In contrast, interfering overlapping signals were observed in the presence of U(VI), Cr(VI), and Ti(VI). An appropriate masking or separation step would be required in the presence of elevated levels of these ions. Hence, the cupferron-based procedure offers new selectivity dimensions compared to early adsorptive stripping schemes, that suffer from interferences due to Cu(II), and Fe(III)[4] or Zn(II) and Sb(III).[5] As noted above, these ions do not affect the aluminum/cupferron response.

In conclusion, the method described provides a highly sensitive approach to the determination of aluminum. Such use of cupferron offers an

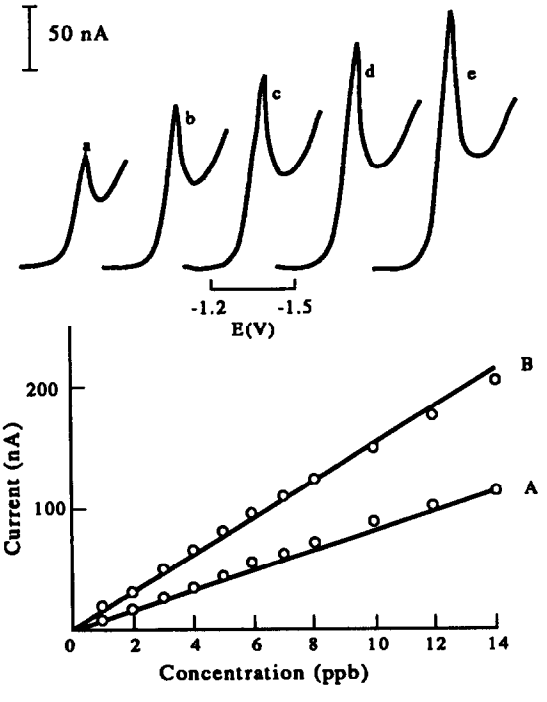

Fig. 4. Stripping voltamperograms for solutions of increasing aluminum concentrations: 2 (a), 4 (b), 6 (c), 8 (d), and 10 (e) μg/l. One-min accumulation at −0.40 V. Other conditions, as in Fig. 1. Also shown are the resulting calibration plots following 30 (A) and 60 (B) sec. accumulation.

alternative adsorptive stripping scheme, which compares favourably with the use of other ligands for the same task. The method successfully addresses the growing needs for measuring trace aluminum in environmental and clinical matrices. Such applications will require a prior removal/destruction of the organic matter. Speciation and on-line monitoring schemes based on this adsorptive stripping procedure are anticipated.

Acknowledgements—This work was supported by grants from Lawrence Livermore NL (Subcontract B160617) and Sandia NL (contract DE-AC04-76DP00789). R.S. acknowledges a fellowship from the National Atomic Energy Agency of Indonesia.

REFERENCES

1. H. Willard and J. Dean, *Anal Chem.*, 1950, **22**, 1264.
2. B. Cooney and J. Saylor., *Anal. Chim. Acta*, 1959, **21**, 276.
3. R. Romero, J. Tahan and A. Moronta, *ibid.*, 1992, **357**, 147.
4. J. Wang, P. A. M. Farias and J. Mohmoud, *ibid.*, 1985, **172**, 57.
5. C. M. G. van den Berg, K. Murphy and J. Riley, *ibid.*, 1986, **188**, 177.
6. J. Wang and R. Setiadji, *ibid.*, 1992, **264**, 205.
7. K. Jiao, W. Jin and H. Metzner, *ibid.*, 1992, **260**, 35.
8. Y. Mauras and P. Allain, *Anal. Chem.* 1985, **57**, 1706.
9. E. Kaneko, H. Hoshino, T. Yotsuyanagi, N. Gunji, M. Sato, T. Kikuta and M. Yuasa, *ibid.*, 1991, **63**, 2219.

Talanta, Vol. 40, No. 3, pp. 355–361, 1993
Printed in Great Britain.

0039-9140/93 $6.00 + 0.00

APPLICATION OF NONPARAMETRIC STATISTICS TO THE ESTIMATION OF THE ACCURACY OF MONTE CARLO CONFIDENCE INTERVALS IN REGRESSION ANALYSIS

JOSEPH S. ALPER* and ROBERT I. GELB
Department of Chemistry, University of Massachusetts–Boston, Boston, Massachusetts 02125, U.S.A.

(*Received* 16 *June* 1992. *Accepted* 6 *July* 1992)

Summary—Confidence intervals and their uncertainties for nonlinear regression parameters are obtained using nonparametric statistical methods. The confidence intervals are calculated by means of a Monte Carlo procedure. Their uncertainties depend on the confidence level desired and on the number of Monte Carlo simulations of the data set. They are obtained by calculating the uncertainties in the boundaries of the confidence intervals using a generalization of the nonparametric method used to calculate confidence intervals for medians. The method described here provides reliable confidence intervals at relatively low computational expense. It seems especially suited to the statistical analysis of nonlinear regression problems that are difficult to deal with using conventional methods.

Nonlinear regression analysis of experimental data[1–4] has become a standard procedure in chemistry. This analysis determines the values of the adjustable parameters in a set of model equations (nonlinear in the parameters) that result in the best fit of the model to the experimental data. In addition to the values of the parameters, it is important to obtain estimates of the uncertainty in each parameter value. For the general nonlinear problem, if the experiment were repeated many times, the distribution characterizing the set of values of any one of the parameters will not be normal as it would be in a linear problem. Consequently, traditional parametric estimates of the uncertainties, which rely on the assumption that the parameter values are normally distributed, may not be correct and can lead to significant errors. The appropriate measure of the uncertainty is a confidence interval at some chosen probability level.

In a recent paper, we described a simple nonparametric method for estimating confidence intervals for the values of parameters obtained from nonlinear regression analyses.[5] This method is based on Monte Carlo sampling[6,7] of the universe of possible data sets consistent with the one actually obtained from the experiment. Confidence intervals derived using this procedure are free from assumptions about the distributions of the calculated parameters and about covariances between them. It is the purpose of this paper to determine the number of Monte Carlo sampling points required to achieve any predetermined level of accuracy of the confidence intervals.

EXPERIMENTAL

Determination of confidence intervals

Our procedure for determining confidence intervals for parameters is straightforward. First, the set of experimental data together with estimates of their uncertainties is analyzed using a nonlinear regression algorithm. The algorithm provides optimized values of the adjustable parameters and the value of χ^2, the goodness-of-fit statistic. Assuming that the estimates of the uncertainties in the experimental data are correct, if the model serves as a correct description of the phenomena, then the value of χ^2 will be approximately equal to the number of degrees of freedom. The number of degrees of freedom is equal to the number of data points minus the number of adjustable parameters.

Second, the experimental data set is repeatedly and randomly manipulated to provide N simulated experimental data sets, where N is some suitably chosen number. In earlier work, we employed a Monte Carlo technique to generate these simulated data sets.[5,8] This technique is based on the assumption that the error in each

*Author for correspondence.

experimental datum is derived from some known probability distribution. A random number chosen from this distribution is added to the measured datum resulting in a new datum. A new data set is generated by repeating this process for each datum in the original data set.

The nonlinear regression algorithm is then applied to each of the simulated experimental data sets providing a new set of parameters for each data set. The N values of each parameter are characterized by a distribution which is an approximation to the distribution of the universe of values of that parameter. A confidence interval for each parameter can be obtained directly from the calculated set of values for that parameter by numerically ordering the set of values and then choosing an appropriate percentile to determine the boundary values of the confidence interval. For example, the boundary values at the 5th and 95th percentile levels of the values of an optimized parameter constitute a 90% confidence interval for that parameter.

The percentile method is a direct implementation of the definition of the confidence interval. Using the example given in the previous paragraph, if the experiment were repeated many times, in 90% of the experiments the value of the parameter determined by the nonlinear regression would be expected to lie in the 90% confidence interval bounded by the 5th and 95th percentiles. There are other procedures for generating a confidence interval from the distribution of a parameter, but the simplicity of the percentile method makes it, in our opinion, the method of choice.

Because the set of calculated values for a parameter represents only a finite and possibly non-representative sample of the universe of parameter values, the estimate of the confidence limits from that set of values is subject to error. The overall accuracy of confidence intervals obtained from the procedure outlined above depends on two factors: (1) the accuracy of the calculated parameter distribution obtained from the Monte Carlo simulations and (2) the accuracy of the determination of the location of the percentile levels.

The first factor derives from the inherent limitations in the Monte Carlo simulation. Even if an infinite number of simulations were performed, the calculated distributions might not be equivalent to the true distribution because of the experimental errors in the original data set. We will return to this point below.

We are primarily concerned in this paper with answering the question implicit in the statement of the second factor: assuming that the procedure for generating parameter distributions is correct, how many values, N, of a calculated parameter resulting from N simulations of the original data set are required to provide accurate percentile levels and thus, accurate confidence intervals?

In order to answer this question, we first note that percentiles are so-called "order statistics"; they involve only numbers of points (in this case, the set of calculated values of a parameter) rather than the actual values of these points. Simple nonparametric methods can be used to determine confidence intervals for these statistics.[9] In order to avoid confusion in the following discussion, we will refer to confidence intervals for the percentiles as "ranges". That is, the confidence interval for a given percentile level (which itself is the boundary of a confidence interval) will be called the range of the percentile.

Ranges for order statistics

The order statistics relevant to the study of the uncertainty in confidence intervals are the median and a generalization of the median. In the following discussion of these order statistics, we will assume that a set of values for each of the parameters has been obtained by some random manipulation of the experimental data.

The median. There is a straightforward procedure for determining the range (confidence interval) about the simplest of the order statistics, the median. Consider a set of N data points X_i, $i = 1, N$, randomly chosen from a large population with some unknown distribution. Let the median of the large population be M while that of the N member sample be X_m. The probability that exactly k of the N data points lie at or below the unknown population median is given by the binomial distribution:

$$P(N,k) = \binom{N}{k}\left(\frac{1}{2}\right)^N \tag{1}$$

We can calculate a symmetric range $[X_q, X_{N-q+1}]$ of level $1-\beta$ for the sample median by calculating the cumulative probability that at least q and no more than $N-q$ points lie below the true median. The interval is constructed so that $1-\beta$ is the probability that the population median M lies within the interval.

We thus chose q to be the largest integer such that

$$\sum_{k=q}^{N-q} P(N,k) \geqslant 1-\beta \qquad (2)$$

This interval is symmetric about the sample median X_m because the binomial distribution is symmetric if the probability of each elementary event is 0.5.

This procedure can be illustrated by means of a simple example. We consider a set of $N = 50$ points arranged in ascending numerical order and arbitrarily chose $1-\beta = 0.683$, the value equal to the one-sigma confidence level for a normally distributed variable. Using equation (1) we find:

$$P(50,25) = 0.1123$$
$$P(50,26) = P(50,24) = 0.1080$$
$$P(50,27) = P(50,23) = 0.0960$$
$$P(50,28) = P(50,22) = 0.0788$$
$$P(50,29) = P(50,21) = 0.0598$$

We interpret $P(50,k)$ to be the probability that the population median M lies in the closed interval $[X_k, X_{k+1}]$. This represents a conservative interpretation of the probability measure. The maximum value of q statisfying equation (2) is found to be 21. For this value of q the sum of the probabilities is 0.7975. This sum is the probability that M lies between the 21st and the 30th entries in the list of data points arranged in ascending order.

The interval $[X_{21}, X_{30}]$ constitutes the conservative 0.683 range for the population median. We note that this result is independent of the nature of the distribution of the population from which the sample is chosen and is also independent of the actual values of the members of the population. We now generalize this analysis and apply it to the percentile method for estimating confidence intervals.

The generalized median. The median divides the population so that 50% of the points lie at or below it. We define a generalization median, which we call the p-median, $0 < p < 1$, to be the point X_p such that a fraction p of the points lie below it. The probability that exactly k of a sample of N data points will lie at or below the p-median is given by

$$P(N,k,p) = \binom{N}{k} p^k (1-p)^{N-k} \qquad (3)$$

The binomial distribution is not symmetric about its maximum value if $p \neq 0.5$. Therefore, two integers q and r, $q < r$, are needed to define a confidence interval about a p-median. These integers were chosen so that they define an interval of minimum length (compared with intervals defined by any other pair of integers) while satisfying

$$\sum_{k=q}^{r-1} P(N,k,p) \geqslant 1-\beta \qquad (4)$$

We continue to interpret $P(N,k,p)$ in a conservative manner; the probability refers to the closed interval between the k^{th} and $k+1^{\text{st}}$ points. Consequently, the range for the p-median is given by the asymmetric interval $[X_q, X_r]$ about X_p.

We show in the next section that the p-median is ideally suited for determining the appropriate value of N, the number of values of each parameter needed to achieve some desired degree of accuracy.

Application of the p*-median to confidence intervals*

Suppose that a set of N values of each of the adjustable parameters is determined by the Monte Carlo simulation or some other method. The p- and $(1-p)$-medians of the numerically ordered set of values of each parameter define the $1-2p$ confidence interval for that parameter. For example, the $p = 0.05$ and $p = 0.95$ medians define the 90% confidence interval. For the case of N data points, the position of the upper median is $u = [N(1-p)]$, where $[r]$ denotes the integer part of r. In order that the confidence interval be symmetric with respect to the highest and lowest data point, we set the lower median X_1 at position $N-u+1$.

We now consider the uncertainty in the location of the upper and lower p-medians X_u and X_1. After choosing some arbitrary confidence level $1-\beta$ we calculate the range about X_u using the method described in the previous section. It is important to note that the position of the boundaries of this interval is independent of the actual values of the parameters and their distributions and so can be calculated once and for all. Ranges about the upper and lower p-medians are related by mirror reflection symmetry. If the upper median lies at position u and the confidence interval around it is $X_q \leqslant X_u \leqslant X_r$, then the corresponding range about the lower p-median is $X_{N-r+1} \leqslant X_{N-u+1} \leqslant X_{N-q+1}$. Representative ranges about p-medians for various values of p and N with $1-\beta = 0.683$ are given in Table 1.

Table 1. Positions of the upper p-medians and their 68.3% confidence intervals

Number of Monte Carlo simulations	Confidence levels for the parameters a_j		
	68.3% $p = 0.842$*	80% $p = 0.90$	90% $p = 0.95$
50	[40, 43, 46]†	[43, 45, 48]	[47, 48, 50]
100	[81, 85, 89]	[88, 90, 94]	[93, 95, 98]
200	[164, 169, 175]	[176, 180, 185]	[187, 190, 194]
300	[247, 253, 260]	[265, 270, 276]	[282, 285, 290]
400	[331, 338, 346]	[355, 360, 367]	[376, 380, 385]

*The $p = 0.842$ median is located at the upper bound of the 68.3% confidence interval for a parameter a_j.

†[40,43,46] means that the $p = 0.842$ median is found at position 43 and that the boundaries of the 68.3% confidence interval for this median are found at positions 40 and 46.

The (1–2p) confidence interval for a regression parameter a_j is given by $[X_l, X_u]$ since it is bounded by the lower and upper p-medians. The uncertainty in this confidence interval can be expressed in terms of the ranges in the positions of X_l and in X_u. Consider, as an example, the 90% confidence interval for a_j calculated using $N = 200$ Monte Carlo simulations. This interval is defined by the 0.05- and 0.95-medians and so is bounded by the 11th and 190th positions in the ordered list of the 200 values of a_j. At a confidence level of $1 - \beta = 68.3\%$ for the uncertainty in the position of each p-median, we see from Table 1 that the 0.95-median is uncertain by $-3, +4$ positions, while the 0.05-median is uncertain by $-4, +3$ positions.

These uncertainties mean that the lower p-median could lie as high as position 14 and as low as 7, while the upper p-median could lie as high as position 194 and as low as 187. Using positions 7 and 194 as the boundaries of a confidence interval implies a confidence level of 94% since 12 values have been struck from each end of the list of 200 values. Similarly, the interval bounded by positions 14 and 187 imply a confidence level of 87%.

We have thus found that the confidence interval $[X_{11}, X_{190}]$ corresponds to a confidence level of 90 $+4, -3$%. To the degree of accuracy required for our analysis of uncertainties, we can approximate the asymmetric uncertainty estimate by the symmetric uncertainty, $90 \pm 3.5\%$. This symmetrization will be applied to all the uncertainties calculated in this work.

We now determine the confidence level of this uncertainty of $\pm 3.5\%$. This confidence level depends only on the confidence level of the uncertainties in the p-medians which we have arbitrarily set at $1 - \beta = 68.3\%$. The probability that either p-median will lie outside its range is β. Since the positions of the 2 p-medians are independent, the probability that both will lie outside their respective ranges is β^2. As explained in the preceding paragraphs, the uncertainty in the 90% confidence interval for a_j was determined by considering the case where both p-medians lie outside the interval defined by positions 11 and 190 and the case where both lie inside. Assuming sufficient symmetry in the binomial distribution, the probability of the occurrence of either of these two cases is approximately $\beta^2/2 = 0.050$, which corresponds to a 95% confidence level.

We conclude that if $N = 200$ Monte Carlo simulations are performed, we can be 95% confident that the confidence level for the 90% interval $[X_{11}, X_{190}]$ is $90 \pm 3.5\%$. We emphasize again that this 95% confidence level depends only on the 68.3% uncertainty in the p-medians. It does not depend on the number of simulations nor on the confidence level or interval for a_j.

The results of this analysis for different values of N is given in Table 2. For each value of N, we show the 68.3, 80, and 90% confidence intervals for a_j as defined by the upper and lower p-medians and the uncertainties in each of these confidence levels.

Suppose we wish to calculate the confidence interval at the nominal level of 80% for the parameter a_j but would be satisfied knowing that the confidence level actually lies in the

Table 2. Boundaries of confidence intervals (as defined by the upper and lower p-medians) and the uncertainties (at the 95% level) in the confidence levels of these intervals

Number of Monte Carlo simulations	Confidence levels		
	68.3%	80%	90%
50	[8, 43]*	[6, 45]	[3, 48]
	±12%†	±10%	±6%
100	[16, 85]	[11, 90]	[6, 95]
	±8%	±6%	±5%
200	[32, 169]	[21, 180]	[11, 190]
	±5.5%	±4.5%	±3.5%
300	[48, 253]	[31, 270]	[16, 285]
	±4.3%	±3.7%	±2.7%
400	[63, 338]	[41, 360]	[21, 380]
	±3.8%	±3.0%	±2.3%

*[8, 43] means that the 68.3% confidence interval for any one of the adjustable parameters a_j is bounded by the 8th and 43rd values of that parameter.

†±12% is the uncertainty (at the 95% confidence level) in the 68.3% confidence interval, *i.e.*, the interval [8, 43] represents a confidence level of 68.3 ± 12%.

somewhat wider range 74–86%. Table 2 shows that if $N = 100$, there is a 6% uncertainty in the 80% confidence level. Thus, 100 values of each parameter are sufficient, and the nominal 80% bounds will appear at the 11th and 90th entries of the list of the 100 values of a_j.

There appears to be little practical difference between a nominal 80% confidence level and the range 74–86% obtained using 100 Monte Carlo simulations. Consequently, we conclude that 100 simulations are adequate for an estimation of 80% confidence intervals. Similarly, if the difference between a 68.3% confidence level and the range 60–76% is regarded as unimportant, then 100 simulations are adequate to accurately describe this confidence level. However, for the nominal 90% confidence level, 100 simulations yields a range of 85–95%. This represents a range in the odds from approximately 6:1 to 20:1. This range does seem to represent a significant difference and indicates that a larger number of simulations, say 200, is appropriate. As explained above, for $N = 200$, the nominal 90% level represents the range $90 \pm 3.5\%$ which appears adequately precise for most applications.

These results can be interpreted from a different point of view. Instead of focussing on the uncertainty in the confidence level, we can use the uncertainty in the position of the boundaries of the p-medians to determine the uncertainty in the confidence interval about the parameter. Using the same example, ($N = 200$, 90% confidence interval), we assume that the confidence level of 90% is correct but that there is uncertainty in the interval. This uncertainty can be calculated from the values of the parameters found at 4 positions higher and 3 positions lower from each of the boundaries of the original confidence interval. In constrasting the two points of view, we note that only the first, which analyzes the uncertainty in the confidence level, is independent of the statistical fluctuations involved in using the Monte Carlo for estimating the parameter distributions.

A specific chemical example illustrating the determination of the accuracy of a confidence interval for a parameter may clarify this discussion. We show that for this example, the procedure described above produces, for each regression parameter, a set of values that accurately reproduces the actual distribution of that parameter. Moreover, the procedure provides accurate percentile levels (boundaries of the confidence intervals).

A simulated differential kinetic analysis

A simulated mixture of substances X and Y is analyzed for both components by a differential kinetic method involving the measurement of absorbance versus time. The mixture is treated with a color developing reagent which reacts with the analytes at different rates. We will assume that the rates of product formation are first- or pseudo-first-order in both X and Y and that the products of the reactions involving X and Y are the only light absorbing species in the mixture. The time dependence of the absorbance is given by

$$A(t) = X(1 - e^{-at}) + Y(1 - e^{-bt}), \qquad (5)$$

where $A(t)$ is the absorbance at time t; X and Y are constants proportional to the concentrations of the analytes X and Y, and a and b are the first- or pseudo-first-order rate constants for the reaction of X and Y, respectively, with the color developer. Once values of X and Y are determined, the corresponding concentrations can be obtained from Beer's Law and the appropriate extinction coefficients.

We note that equation (5) is identical in form to one describing a controlled potential chronocoulometric determination of two electroactive species which are reduced or oxidized at different rates. Thus, the quantity of electricity $Q(t)$ passed at time t during the bulk electrolysis of a mixture of substances X and Y under conditions of constant stirring is given by

$$Q(t) = Q_X(1 - e^{-at}) + Q_Y(1 - e^{-bt}) \qquad (6)$$

where Q_X and Q_Y are the quantities of electricity required for complete oxidation or reduction of X and Y and a and b are the corresponding mass-transfer coefficients for these species, which are taken as constants.

An exact data set of $A(t)$ *vs.* t was constructed using 11 values of t: 0.0, 2.0, 4.0, . . . , 20.0. The values of the four parameters were chosen to be $X = 0.50$, $Y = 0.70$, $a = 0.05$, and $b = 0.20$. We simulated an experimental data set by adding to each exact value of $A(t)$ (which varied from 0.0 to approximately 0.9) a normally distributed random error with a mean of 0 and a standard deviation of 0.005.

The simulated experimental data set was analyzed using the Levenberg-Marquardt nonlinear regression technique as implemented by Press *et al.*[4] to obtain the values of the four parameters X, Y, a, and b that best fit the simulated experimental data set. We found $X = 0.518$,

$Y = 0.689$, $a = 0.0493$ and $b = 0.207$. The goodness-of-fit statistic, χ^2, was found to be 7.28, which is approximately equal to 7, the number of degrees of freedom in the regression analysis. Standard error estimates for each of the parameters are obtained from the diagonal elements of the covariance matrix. These error estimates, which we will refer to as parametric estimates, had values of 0.12, 0.50, 0.11 and 0.07 for X, Y, a and b, respectively.

Unfortunately, error estimates of regression parameters obtained from the covariance matrix are unreliable if the model equation is nonlinear in the parameters.[4,5] Examination of equation (5) reveals such a nonlinearity. In order to obtain accurate confidence intervals for the calculated parameters we employ a Monte Carlo simulation method.

In implementing this method, each value of $A(t)$ in the simulated experimental data set is scattered by adding a random normally distributed error with mean 0 and a standard deviation of 0.005. The resulting Monte Carlo data set is analyzed using the nonlinear regression algorithm and a new set of parameters is obtained. This procedure is repeated a total of N times. A confidence interval for each parameter is then derived from the N values of that parameter.[5]

As discussed above, our goal in this work is to determine the number N of Monte Carlo simulations required in order to obtain some predetermined degree of accuracy in the calculated confidence intervals. We examined the 68.3 and 90% confidence intervals for the differential kinetic example using three different values of N (50, 100 and 200). In order to evaluate the reproducibility of our results, we repeated each set of calculations six times. Finally, we made an additional calculation with $N = 4000$. We assume that the confidence interval obtained from this calculation is an accurate approximation of the "true" confidence interval that would be obtained in the limit as N goes to infinity.

The numerical results are summarized in Table 3. An entry in the first row of numbers listed below the value of N is the mean of the 6 Monte Carlo confidence interval half-widths for the specified parameter. The entry below this one is the standard deviation of the 6 values, and the corresponding entry in the third row is the maximum deviation from the mean. Thus, this entry indicates a typical worst value obtained for a confidence interval for a given value of N. For example, the mean of the 6 Monte Carlo 68.3% confidence half-intervals for parameter X calculated using $N = 50$ was 0.037. The standard deviation was 0.006 and the 6 half-interval values fell within the range 0.030 to 0.044.

Table 3. Confidence half-intervals and their uncertainties as a function of the number of Monte Carlo simulations for the differential kinetic analysis example*

68.3% confidence half-interval			
X	Y	a	b
	$N = 50$		
0.037	0.016	0.0030	0.0060
0.006	0.004	0.0005	0.0008
0.007	0.005	0.0008	0.0011
	$N = 100$		
0.036	0.016	0.0029	0.0053
0.005	0.005	0.0003	0.0008
0.006	0.006	0.0005	0.0010
	$N = 200$		
0.034	0.013	0.0028	0.0053
0.004	0.003	0.0004	0.0009
0.007	0.004	0.0005	0.0010
	$N = 4000$		
0.0333	0.0126	0.0029	0.0051
90% confidence half-interval			
X	Y	a	b
	$N = 50$		
0.062	0.050	0.0067	0.0124
0.009	0.009	0.0016	0.0023
0.012	0.012	0.0024	0.0040
	$N = 100$		
0.063	0.041	0.0053	0.0112
0.007	0.008	0.0005	0.0013
0.009	0.010	0.0012	0.0023
	$N = 200$		
0.060	0.040	0.0055	0.0108
0.006	0.007	0.0007	0.0012
0.008	0.010	0.0012	0.0030
	$N = 4000$		
0.0617	0.0401	0.0058	0.0115

*For each value of N, each number in the first row is the mean value of the confidence interval half-widths obtained from 6 independent Monte Carlo simulations. The corresponding number in the second row is the standard deviation. The number in the third row is the maximum deviation from the mean value.

RESULTS AND DISCUSSION

The Monte Carlo confidence intervals differ significantly from the parametric estimates, sometimes by a factor of ten or more. For example, the $N = 4000$ Monte Carlo 68.3% interval for parameter Y is 0.0126 which is to be compared with the parametric standard error estimate of 0.50. This discrepancy indicates that this example is one of the typical cases in which parametric estimates of the uncertainties in non-linear regression parameters are in error.

The results of Table 3 indicate that there is little value in extending the Monte Carlo

method beyond $N = 200$. Focussing on the 90% confidence interval for parameter X ($X = 0.52$ from the regression analysis), we find a mean half-width of 0.060 with a standard deviation of 0.006 and a range of values of 0.052 to 0.068. Suppose that the $N = 200$ calculation had been performed only once and that the extreme value of 0.052 had been obtained for the confidence interval half-width. Then, the value of parameter X would be 0.52 ± 0.05 with 90% confidence. There seems to be little or no practical difference between this value and the value of 0.52 ± 0.06 which was obtained using 4000 Monte Carlo simulations.

In order words, the standard deviations of the confidence intervals for $N = 100$ and $N = 200$ are generally only 10–20% of the half-widths of the interval values. The single exception is the $N = 100$ value for parameter Y, where the standard deviation is about 30% of the interval value. For $N = 200$ all of the half-interval standard deviations are less than 25% of the interval values and the extreme values are within 30% of the $N = 4000$ intervals.

As discussed above, the accuracy of a confidence interval can be directly estimated from the ordered set of values of the parameters. We consider the 90% interval for X and examine its values at the 14^{th} and 187^{th} positions and at the 7^{th} and 194^{th} positions. These values lead to minimum and maximum confidence interval half-widths of 0.055 and 0.066, respectively. The "exact" value of 0.617 falls within this range. The corresponding extreme and "exact" intervals for Y are 0.032, 0.050, and 0.0401. These results, together with numerous other similar comparisons, serve to confirm our estimate that the extreme values contain the exact result with about 95% probability.

This example thus illustrates our contention, based on the analysis of generalized p-medians given above, that even if only 100 or 200 simulations are employed, the Monte Carlo 68.3% and 90% confidence intervals provide accurate and practical estimates of the "true" confidence intervals. The relatively minor errors of 10–20% in the Monte Carlo confidence intervals seem especially insignificant in the view of the fact that the parametric estimates of confidence intervals for nonlinear regression parameters can be in error by an order of magnitude or more.

REFERENCES

1. G. A. F. Seber and C. J. Wild, *Nonlinear Regression*, Wiley, New York, 1989.
2. D. M. Bates and D. G. Watts, *Nonlinear Regression Analysis and its Applications*, Wiley, New York, 1988.
3. A. Gifi, *Nonlinear Multivariate Analysis*, Wiley, New York, 1990.
4. W. H. Press, B. P. Flannery, S. A. Teukolsky and W. T. Vetterling, *Numerical Recipes: The Art of Scientific Computing*; Cambridge University Press, Cambridge, 1986.
5. J. S. Alper and R. I. Gelb, *J. Phys. Chem*, 1990, **94**, 4747.
6. M. H. Kalos and P. A. Whitlock, *Monte Carlo Methods Volume I: Basics*, Wiley Interscience, New York, 1986.
7. M. P. Allen and D. J. Tildesley, *Computer Simulation of Liquids*, Oxford University Press, Oxford, 1987.
8. J. S. Alper and R. I. Gelb, *J. Phys. Chem*, 1991, **95**, 104.
9. M. H. Hansen, W. N. Hurwitz and W. G. Madow, *Sample Survey Methods and Theory, Volumes I and II*, Wiley, New York, 1953.

Talanta, Vol. 40, No. 3, pp. 363–379, 1993
Printed in Great Britain.

0039-9140/93 $6.00 + 0.00

STRUCTURAL CHARACTERIZATION OF POLY(*N*-ALKYL-4-VINYLPYRIDINIUM) TRIFLATES USING PYROLYSIS/TANDEM MASS SPECTROMETRY

TAPAN K. MAJUMDAR, ASOKA RANASINGHE, LING LU and R. GRAHAM COOKS*
Department of Chemistry, Purdue University, West Lafayette, IN 47906, U.S.A.

WILMER K. FIFE and MARTEL ZELDIN
Department of Chemistry, Purdue University, Indianapolis, IN 46205, U.S.A.

(*Received* 13 *May* 1992. *Revised* 2 *July* 1992. *Accepted* 2 *July* 1992)

Summary—Desorption chemical ionization (DCI) and desorption electron ionization (DEI) of homo- and co-polymers of *N*-alkyl-4-vinylpyridinium triflates having ethyl, n-hexyl and n-dodecyl groups as *N*-alkyl substituents, produce mass spectra that display oligomeric ions. These positively charged ions are singly-charged and result from cleavage of the polymer into neutral oligomers and the loss of a single triflate anion per oligomer. Analogous negatively charged ions, in which each neutral oligomer carries an extra triflate anion, are observed in the desorption chemical ionization mass spectra. Each oligomer within the available mass range is represented in the mass spectra. The formation of cluster ions in which a single, multiply-charged cation is associated with a number of singly-charged anions, as observed for these ammonium polysalts, is unusual. Five major and three minor series of positively charged ions are observed in DCI and DEI methods of ionization. Ions in the different series correspond either to cleavage at different bonds between the constituent monomers or to hydrogen transfer in different directions. Unique and structurally diagnostic fragmentation processes are observed in tandem mass spectrometry (MS/MS) experiments performed using collision activated dissociation of mass-selected oligomeric ions.

Although well-established methods exist for molecular weight determination of polymers,[1,2] there is a need for improved analytical methods for structural characterization. It would also be useful if, unlike the case for existing methods,[1,2] pure samples were not needed for such analyses. Mass spectrometry has increasingly been used for direct analysis of polymers,[3–11] including biopolymers, where tandem mass spectrometry[12,13] can provide structural information on compounds present in mixtures.[14,15] The recent increased use of mass spectrometry in polymer characterization followed the introduction of the desorption ionization[16] and, more recently, spray ionization, techniques.[17] Recent applications of tandem mass spectrometry in polymer chemistry include characterization and monomer sequence distribution of polyalkylisocyanates,[18] the determination of polymer additives,[19] analysis of chemical structures of ions generated from low molecular weight polyglycols,[20] and sequence analysis of polyamides,[21,22] and polyesters.[23] Some of these studies[21–23] utilize chemical degradation to produce suitably sized oligomers while in others,[18] thermolysis accompanies ionization. The work of Bennighoven, Hercules and their collaborators[4] stands out as accessing high molecular weight organic polymers. Fragmentation can be limited and in some cases[4,8] true molecular weight distributions are obtained. The advantages of pyrolysis tandem mass spectrometry include simplicity, speed and sample economy. The limitations of most pyrolysis/MS experiments are the complexity of the mass spectra and the inability to access higher oligomeric ions. However, rapid heating techniques such as desorption chemical ionization (DCI) are known to yield higher mass molecular ions without causing much fragmentation.[24] Therefore the combination of DCI and MS/MS might provide an excellent means of characterization of polymers. Recent successes[18] achieved in characterizing alkylisocyanates by a combination of pyrolysis tandem mass spectrometry and DCI encourage further application of this method to other types of copolymers.

*Author for correspondence.

Poly(*N*-alkyl-4-vinylpyridinium) salts have both hydrophilic and hydrophobic units in their structure and are useful as polyelectrolytes,[25-28] surfactants,[25-27] and artificial enzymes.[28-32] These polymers can be produced, either by direct heating of the monomers, or by an inverse-micro-emulsion process that consists of overnight heating at 45–55° of an emulsion containing a mixture of the monomers, a reaction initiator, and organic and aqueous solvents.[33,34] Despite their potential for various applications, very little is known about the structural characteristics of these polymers. Studies on polyvinylpyridines,[35] monomeric *N*-alkylpyridinium,[36-38] and related organic salts[39-42] using desorption ionization have been reported but there appear to have been no previous structural investigations on the polysalts by mass spectrometry.

The objectives of this study are (i) to develop mass spectrometric methods to ionize poly(*N*-alkyl-4-vinylpyridinium) salts, (ii) to acquire structural information and (iii) to investigate the gas-phase ion chemistry of the pyrolysis products formed from these polymers.

EXPERIMENTAL

Experiments were performed using a Finnigan TSQ 700 mass spectrometer. The samples were dissolved in either methanol or methylene chloride. A drop of sample solution was placed on the loop of rhenium wire which comprises the filament of the desorption probe and dried before introduction into the ion source. The amount of sample on the probe tip was approximately 0.5 μg. Samples were pyrolyzed by heating the probe from 30 to 500° at a rate of 10/sec. At this heating rate, desorption of the sample starts when the temperature of the filament is approximately 200° and continues until the temperature is 500°. The scan speed of the quadrupole is typically 1000 amu/sec. This allows the data system to average 3–5 scans covering a range of 1000 amu. The signal-to-noise ratio can be improved by narrowing the mass range and keeping the scan speed constant. Temperatures of the ion source and the manifold were 150 and 70° respectively. The electron energy was 20 eV during desorption electron impact (DEI), which was performed without reagent gas being present, and 150 eV during desorption chemical ionization (DCI). The emission current of the source filament was 0.2 mA. Isobutane was used as the reagent gas for chemical ionization at a source pressure of 0.5 torr. MS/MS product spectra were obtained by mass selecting a specific ion, using the first quadrupole, Q1, accelerating these ions to a nominal 10 eV in Q2 where collision-activated dissociation (CAD) was performed under multiple collision conditions with argon (2.0×10^{-3} torr) as the collision gas, and finally by performing mass analysis of the resulting fragments using the third quadrupole, Q3. MS/MS parent spectra were obtained similarly, except that Q1 was scanned instead of Q3 which was set to pass a selected fragment ion. An ion derived from the isobutane reagent gas, instead of the sample beam, was used to estimate attenuation because the sample ion beam is stable only for a short period (typically 2–3 sec) due to the rapid desorption. The reagent ion beam (m/z 57) was attenuated to 25% after introducing argon (2×10^{-3} torr) into the collison cell.

Homo and copolymers of *N*-alkyl-4-vinylpyridinium trifluoromethanesulphonates (triflates) containing ethyl, n-hexyl and n-dodecyl groups as the *N*-alkyl chains were examined in this study. Polymer-I, polymer-II and polymer-III are the homopolymers of *N*-ethyl-4-vinylpyridinium triflate, *N*-hexyl-4-vinylpyridinium triflate and *N*-dodecyl-4-vinylpyridinium triflate, respectively. The co-polymer, Polymer-IV was prepared using *N*-ethyl-4-vinylpyridinium triflate (0.83 mole) and *N*-hexyl-4-vinylpyridinium triflate (0.17 mole) monomers, polymer-V was prepared using *N*-ethyl-4-vinylpyridinium triflate (0.80 mole) and *N*-dodecyl-4-vinylpyridinium triflate (0.20 mole) monomers, by the microemulsion method.[33,34] The polymers were synthesized according to procedures described in refs 32, 33, 43, 44 and 45.

RESULTS AND DISCUSSION

Both 20-eV desorption electron ionization (DEI)* and isobutane desorption chemical ionization (DCI) mass spectra of the polymers show monomeric and oligomeric positively-charged ions formed by polymer cleavage and loss of a single triflate anion. Formation of intact cations (C^+) from pyridinium salts

*For brevity, many of the mass spectra are not shown. Interested individuals may request copies of those spectra from the authors.

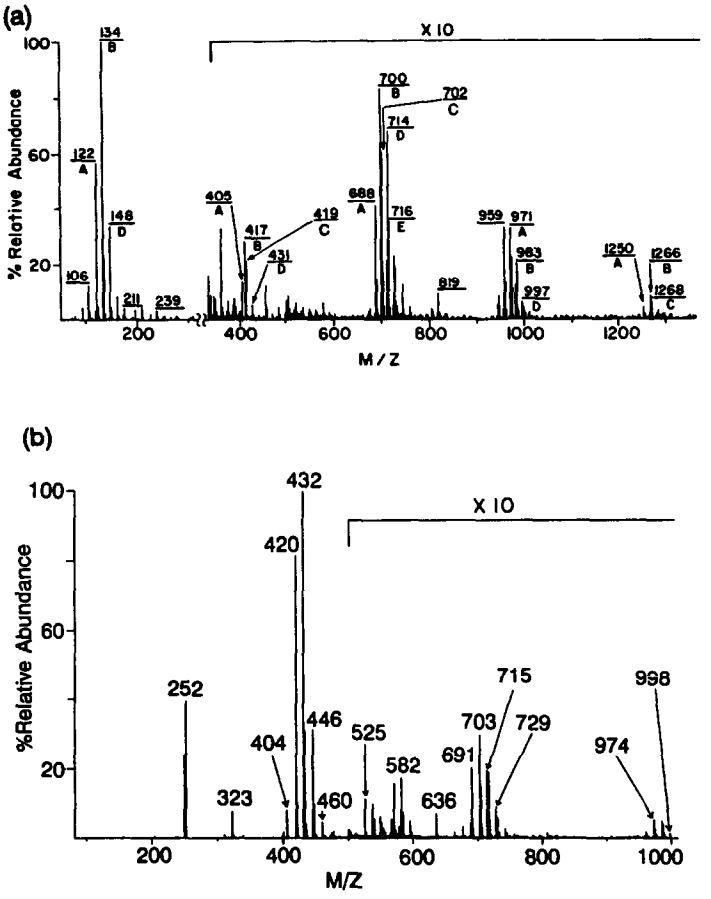

Fig. 1. Mass spectra of polymer-I obtained by (a) positive DCI and (b) negative DCI.

has been reported earlier[41] by both EI and ion bombardment. Thermal desorption of quaternary ammonium and phosphonium salts is well known.[46] The gas-phase ions observed from the present polymers are unique in that they are polycationic species. They include a polycation of n charges associated with $(n-1)$ triflate counter ions. As noted above, positive ion formation from poly(*N*-alkyl-4-vinylpyridinium)triflates occurs by the loss of only one triflate group from the pyrolyzed oligomer fragment. The corresponding negatively-charged ions are also observed and are polysalts with one additional triflate group. Multiply-charged ions formed by the loss or gain of more than one triflate anion are not observed in any of the experiments discussed here.

Typical positive and negative ion mass spectra obtained by DCI of polymer-I [poly(*N*-ethyl-4-vinylpyridinium triflate)] are shown in Fig. 1. The ions are observed as groups of oligomers; for example, the ions m/z 134, 417, 700, 983, and 1266, seen in Fig. 1(a) represent the series $n = 0$, 1, 2, 3, and 4 in the oligomer structure shown in Scheme 1(a). Other peaks are due to homologs and saturated forms of these ions, and they too occur as groups of oligomers as discussed below. Similarly, the negative ions m/z 432, 715, and 998 in Fig. 1(b) may be obtained by substituting $n = 1$, 2, and 3 in the structure shown in Scheme 1(b). Although, these characteristic series of ions may result from several processes, they can be explained by the simplified equations and structures displayed in Scheme 1. The same types of ions are formed by positive ion DCI and DEI except that the series extend to higher mass in the DCI experiments. Formation of higher mass ions during DCI compared to DEI may be due to several reasons, including collisional relaxation of the thermally excited ions in the high pressure CI source.

Since isobutane DCI provides access to higher oligomers, it was chosen for structural investigations discussed in the following sections. Positive ions were chosen over negative ions since they contain smaller contributions due to the triflate counter ion at a given mass.

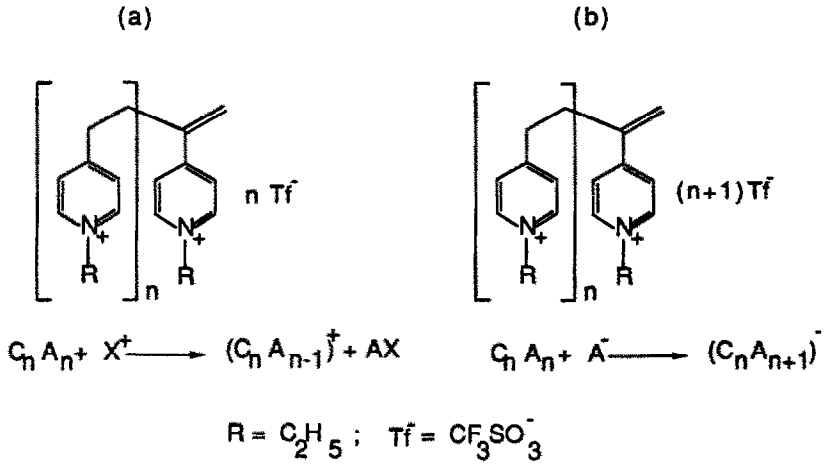

Scheme 1. Structures of poly(*N*-alkyl-4-vinylpyridinium) triflates and the general mechanism of formation of ions under DCI conditions; (a) formation of positive ions (b) formation of negative ions.

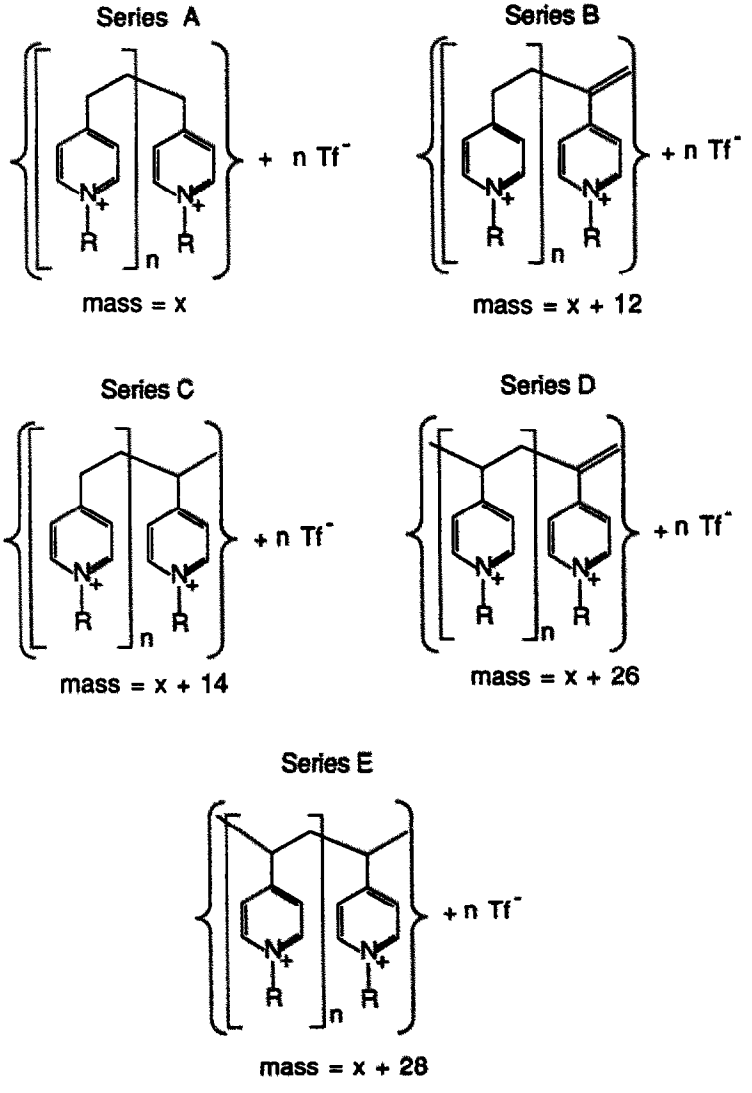

Scheme 2. Major series of positive ions observed under DCI conditions.

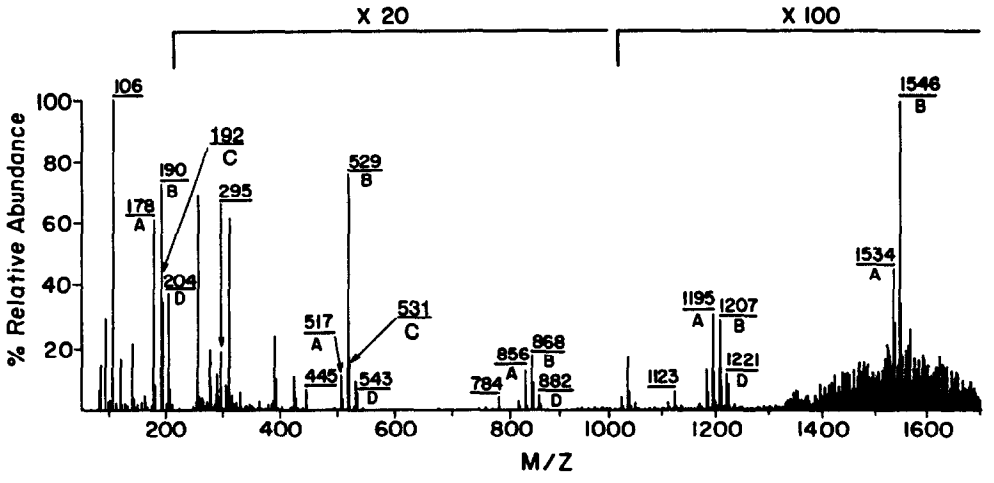

Fig. 2. DCI positive ion mass spectrum of polymer-II.

Five different series of monomer and oligomer ions, as well as their fragments, are observed in the DCI mass spectra and their structures and mass differences are summarized in Scheme 2. Successive members in each series are found to differ from each other by a fixed mass corresponding to the monomer unit, *N*-alkyl-4-vinylpyridinium triflate. In particular cases, structural assignments were confirmed by MS/MS parent and product spectra. The following discussion is subdivided according to the types of ions observed.

Series A ions

Figures 2 and 3 are the DCI mass spectra of polymer-II and polymer-V, respectively. Ions with m/z 178, 517, 856, 1195 and 1534 in the mass spectrum of polymer-II [poly(*N*-hexyl-4-vinylpyridinium triflate; Fig. 2] belong to series A. Structures for these ions may be obtained by substituting $n = 0$, 1, 2, 3, and 4 in the general structure for series A ions in Scheme 2. The MS/MS product spectrum of ion m/z 1195 (Table 1) shows that this ion fragments to produce series A ions of m/z 856, 517, 178 and series B ions of m/z 868, 529, and 190, respectively. Based on this information, fragmentation pathways for series A ions are shown in Scheme 3, using ion m/z 1195 as an example. The MS/MS parent spectrum of m/z 178 [Fig. 4(a)] confirms its origin from series A ions (m/z 517, 856, and 1195), as well as from series C ions (m/z 531 and 870) and another series of ions (m/z 505, 844, 1183).

One fragment ion seen in Scheme 3, m/z 106, is present in the DCI mass spectra of all the polymers and in the MS/MS product spectra of

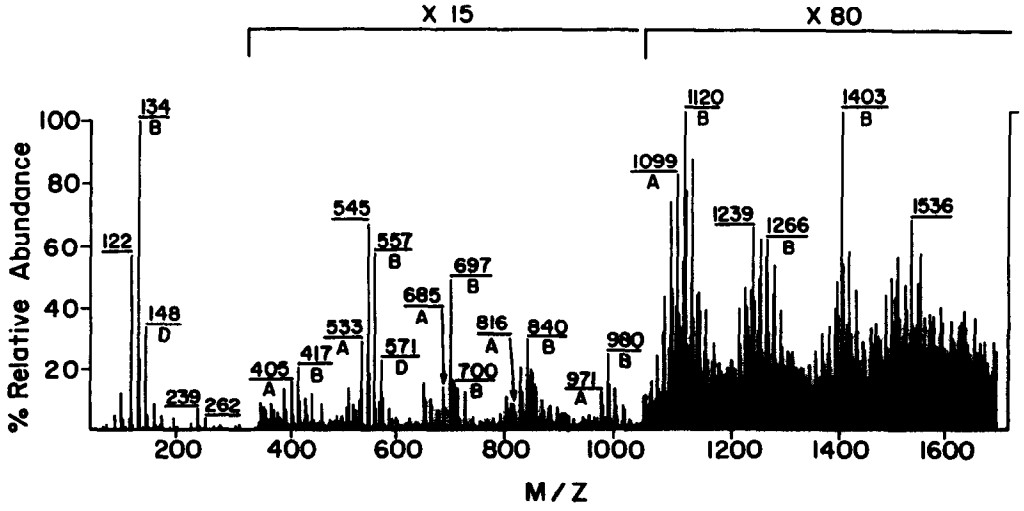

Fig. 3. DCI positive ion mass spectrum of polymer-V.

Table 1. MS/MS product spectra of selected ions

Polymer	Selected ion (m/z)	Product ions m/z (%RA)*
Poly(*N*-hexyl-4-vinyl pyridinium)triflate	1195 (A)	106 (5), 178 (15), 190 (53), 517 (95), 529 (100), 856 (16), 868 (13)
	1207 (B)	106 (6), 190 (45), 529 (100), 868 (30)
	1209 (C)	106 (12), 178 (5), 190 (64), 192 (7), 204 (15), 517 (21), 529 (100), 531 (10), 543 (16), 856 (4), 868 (10), 870 (37), 882 (5)
	1221 (D)	106 (12), 120 (3), 190 (37), 204 (12), 529 (82), 531 (3), 543 (100), 868 (11), 882 (40)
	884 (E)	106 (5), 178 (6), 190 (81), 192 (10), 204 (57), 206 (10), 529 (49), 531 (81), 543 (89), 545 (100)
Copolymer having *N*-ethyl and *N*-hexyl groups	1083 (A)	106 (14), 122 (4), 134 (21), 178 (7), 190 (66), 405 (36), 417 (27), 461 (84), 473 (100), 517 (33), 529 (44), 744 (13), 756 (16), 800 (34), 812 (25)
	1095 (B)	106 (10), 122 (4), 134 (17), 190 (24), 417 (26), 473 (100), 487 (3), 529 (25), 545 (3), 756 (6), 812 (7)
	1041 (C)	106 (16), 120 (6), 122 (11), 134 (41), 136 (8), 148 (16), 178 (6), 190 (38), 192 (4), 204 (14), 405 (31), 417 (63), 419 (52), 431 (46), 461 (48), 473 (100), 475 (67), 487 (73), 702 (14), 714 (6), 744 (10), 756 (19), 758 (50), 770 (31)
	1053 (D)	106 (16), 134 (37), 136 (8), 148 (11), 190 (38), 204 (21), 338 (14), 417 (77), 419 (18), 431 (82), 473 (98), 487 (100), 714 (28), 756 (19), 770 (93)
	1111 (E)	106 (26), 122 (18), 134 (30), 136 (23), 148 (14), 178 (15), 190 (40), 204 (23), 309 (15), 417 (13), 419 (12), 431 (18), 473 (32), 475 (44), 487 (24), 489 (30), 501 (38), 758 (16), 772 (18), 800 (11), 814 (12), 826 (12), 828 (13), 840 (25), 961 (10)
Copolymer having *N*-ethyl and *N*-dodecyl groups	1099 (A)	106 (14), 134 (23), 262 (57), 274 (20), 288 (29), 391 (20), 405 (51), 417 (23), 533 (31), 546 (20), 557 (54), 559 (40), 662 (26), 676 (31), 688 (31), 700 (29), 802 (29), 816 (69), 828 (100), 949 (43)
	1123 (B)	106 (37), 120 (11), 134 (33), 148 (12), 162 (12), 212 (11), 262 (24), 274 (56), 288 (24), 323 (12), 338 (13), 417 (24), 459 (18), 557 (19), 636 (55), 700 (100), 714 (33), 840 (25)
	1125 (C)	106 (84), 120 (70), 134 (95), 148 (50), 262 (55), 274 (98), 288 (60), 405 (44), 417 (52), 419 (70), 431 (75), 545 (65), 557 (88), 559 (93), 571 (51), 700 (85), 842 (77), 854 (100), 975 (64)
	994 (D)	106 (10), 134 (9), 148 (15), 274 (85), 288 (70), 507 (18), 557 (30), 571 (60), 697 (60), 711 (100), 723 (12), 844 (20)
	1139 (E)	134 (38), 136 (28), 148 (28), 262 (28), 274 (60), 276 (25), 288 (53), 302 (33), 405 (50), 417 (35), 431 (45), 433 (63), 445 (30), 545 (38), 559 (90), 571 (98), 573 (70), 714 (75), 716 (30), 728 (70), 842 (88), 854 (70), 856 (100), 868 (73), 989 (25)

*Ion abundances are normalized to the most abundant fragment ion in the MS/MS spectrum and are not corrected for isotopic contributions. The standard deviation of the relative ion abundances is 12%.

all five series of ions. It is proposed that this ion is formed by alkene elimination from the *N*-alkyl group of the monomer of Series B (m/z 190 in Scheme 3) as shown opposite.

Turning from polymer-II, we discuss first the other homopolymers and then the copolymers. This discussion continues to focus on A series ions. Series A ions in the DCI mass spectrum of polymer-I [Fig. 1(a)] occur at m/z 122, 405, 688, 971 and 1254, respectively. There appear to be two isomeric ions at m/z 122 and their probable structures and fragmentation pathways, as revealed by MS/MS experiments, are shown in Scheme 4. The product spectrum of ions m/z 122, generated from polymer-I, included m/z 79 (35%), 94 (100%) and 106 (20%) which indicate that these ions are mostly composed of the protonated *N*-ethyl-4-methylpyridine structure, shown in Scheme 4(a). The isomeric ion, protonated 4-isopropylpyridine, m/z 122 shown in

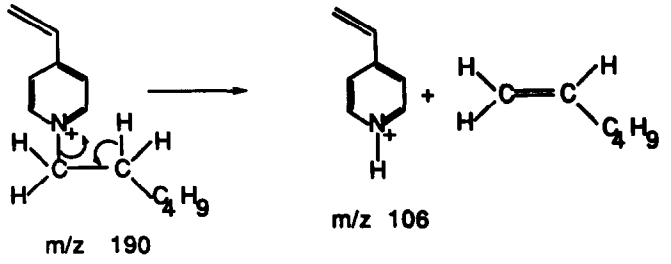

Scheme 4(b), appears to be formed in the DCI mass spectra of the polymers that do not contain the *N*-ethyl group. In these cases the product spectrum of this ion displays the fragments *m/z* 79 (100%), 94 (5%) and 106 (65%), which is consistent with its proposed structure. Note that the formation of the fragment ion, *m/z* 94, is much more favorable

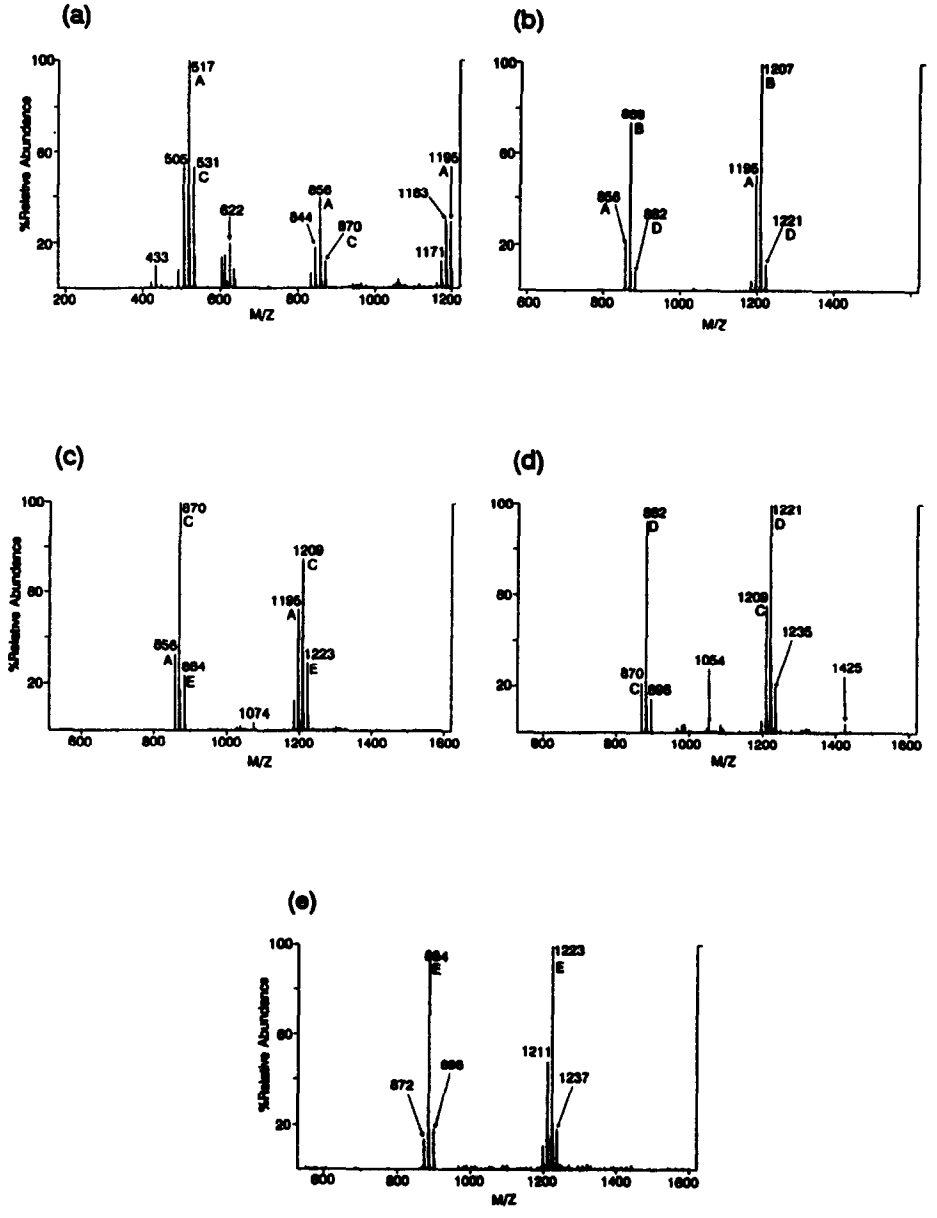

Fig. 4. MS/MS positive ion parent spectra of (a) series A ion *m/z* 178, (b) series B ion *m/z* 529, (c) series C ion *m/z* 531, (d) series D ion *m/z* 543 and (e) series E ion *m/z* 545 from polymer-II.

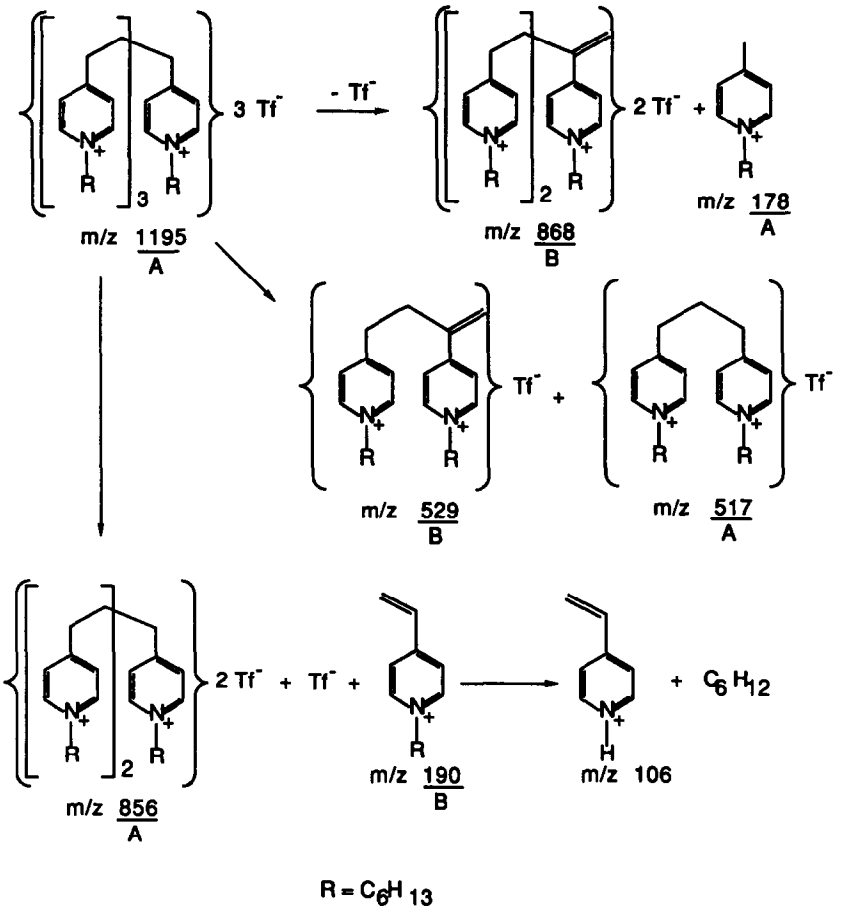

Scheme 3. Proposed fragmentation pathways for Series A ion, *m/z* 1195, determined by MS/MS scans under CAD conditions.

from protonated *N*-ethyl-4-methylpyridine [Scheme 4(a)] than from protonated 4-isopropylpyridine [Scheme 4(b)]. On the other hand, the formation of the fragment ions, *m/z* 106 and 79 is favored from protonated 4-isopropylpyridine [Scheme 4(b)], as indicated by the ion abundances in the product MS/MS spectra. The DCI mass spectrum of polymer-III [poly(*N*-dodecyl-4-vinylpyridinium triflate); not shown here] displays the series A ions *m/z* 262, 685 and 1108 corresponding to $n = 0$, 1 and 2, respectively, in the general formula for series A (Scheme 2).

The copolymers examined by DCI showed ions corresponding to both homo- and hetero-oligomers. For example, Polymer-IV displays the series A ions *m/z* 122, 178, 405, 461, 517, 688, 744, 800, 971, 1027, 1083, 1254 and 1310, respectively, in its DCI mass spectrum (not shown). Ions *m/z* 122, 405, 688, 971 and 1254 are the monomer and homo-oligomers having the *N*-ethyl-4-vinylpyridinium group, *i.e.*, they are the same ions as discussed above in connection with polymer-I, while ions *m/z* 178 and 517 are the monomer and homo-dimer containing the *N*-hexyl-4-vinylpyridinium group. The remaining ions are the hetero-oligomer ions *m/z* 461 (dimer), *m/z* 744 (trimer having two *N*-ethyl and one *N*-hexyl groups), *m/z* 800 (trimer having one *N*-ethyl and two *N*-hexyl groups), *m/z* 1027 (tetramer having three *N*-ethyl and one *N*-hexyl groups), *m/z* 1083 (tetramer having one *N*-ethyl and three *N*-hexyl groups) and *m/z* 1310 (pentamer having four *N*-ethyl and one *N*-hexyl groups), respectively.

Structural compositions of these ions are supported by the MS/MS experiments summarized in Table 1. For example, fragmentation of the ion *m/z* 1083 (Table 1) clearly shows that it consists of two *N*-ethyl and two *N*-hexyl groups. It produces the series A ions *m/z* 800, 744, 517, 461, 405, 178 and 128 having the compositions described earlier. It also produces series B ions at *m/z* 812, 756, 529, 473, 417, 190 and 134. The presence of all these ions in the MS/MS product spectrum of *m/z* 1083 (Table 1) supports the proposed structure for this ion and

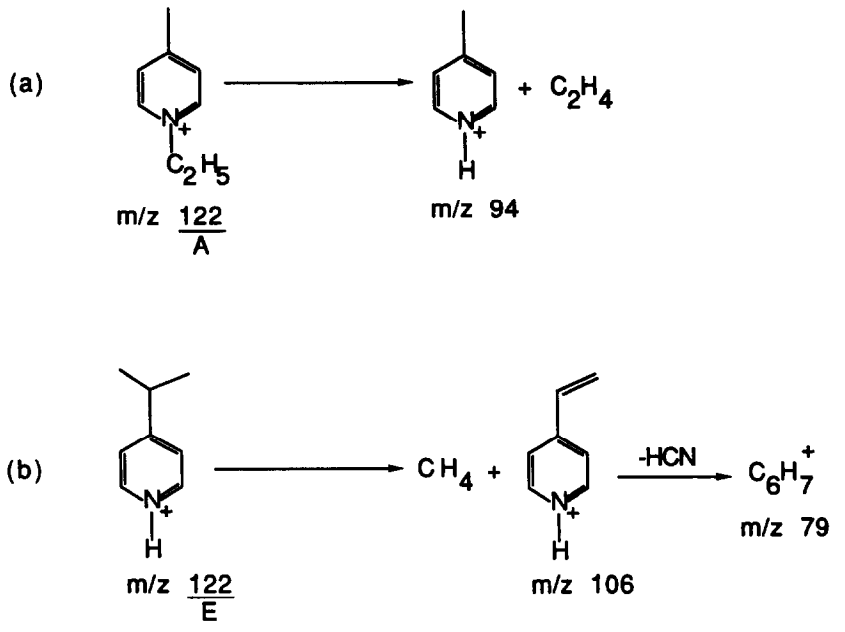

Scheme 4. Proposed structures of the two isomeric ions of *m/z* 122 and their fragmentation pathways, as suggested by MS/MS product scans.

is consistent with the general fragmentation pathways discussed earlier. The MS/MS parent spectrum of the hetero-dimer ion *m/z* 461 shows series A ions *m/z* 744, 800, 1027 and 1083; series C ions *m/z* 758, 1041 and 1097; and ions of the series *m/z* 732, 788, 1015 and 1071 as its precursors. This behavior is analogous to that of the A series N-hexyl ion, *m/z* 178, discussed above.

The DCI mass spectrum of polymer-V (Fig. 3) displays the series A ions *m/z* 122, 262, 405, 533, 685, 688, 816, 971, 1099 and 1239, respectively. The ions at *m/z* 122, 405, 688 and 971 are the homo-oligomers containing *N*-ethyl-4-vinylpyridinium groups, and their structures and compositions have already been discussed. Analogous ions, containing the *N*-dodecyl-4-vinylpyridinium group, appear at *m/z* 262 and 685. The hetero-oligomer ions are *m/z* 533 (dimer), 816 (trimer having two *N*-ethyl and one *N*-dodecyl groups), 1099 (tetramer having three *N*-ethyl and one *N*-dodecyl groups) and 1239 (tetramer having two *N*-ethyl and two *N*-dodecyl groups), respectively. Oligomers having the *N*-dodecyl group display more fragment ions compared to other oligomers due to the multiplicity of C—C linkages in the *N*-dodecyl substituent. The MS/MS product spectrum of the hetero-oligomer ion *m/z* 1099 (Table 1) shows the expected ions of series A and series B.

The mixed dimer ion *m/z* 533 shows series A ions *m/z* 816, 956, 1099 and 1239; series C ions *m/z* 830, 982, 1113, 1265; and the series B ions *m/z* 804, 944, 1087 and 1227 as its precursors in MS/MS parent spectrum (Fig. 5).

Series B ions

Ions of this series are the most abundant in the DCI mass spectra of all the poly(*N*-alkyl-4-vinylpyridinium triflates. These ions have a double bond whose position is not known definitively, but for convenience, it is shown in the original terminal position (Scheme 2) and a probable mechanism of formation, a 1,4 hydride shift followed by a 1,2 shift, is shown below:

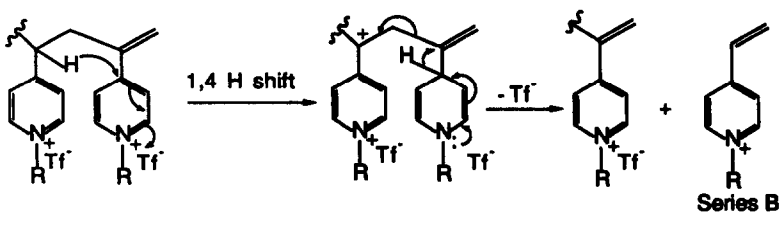

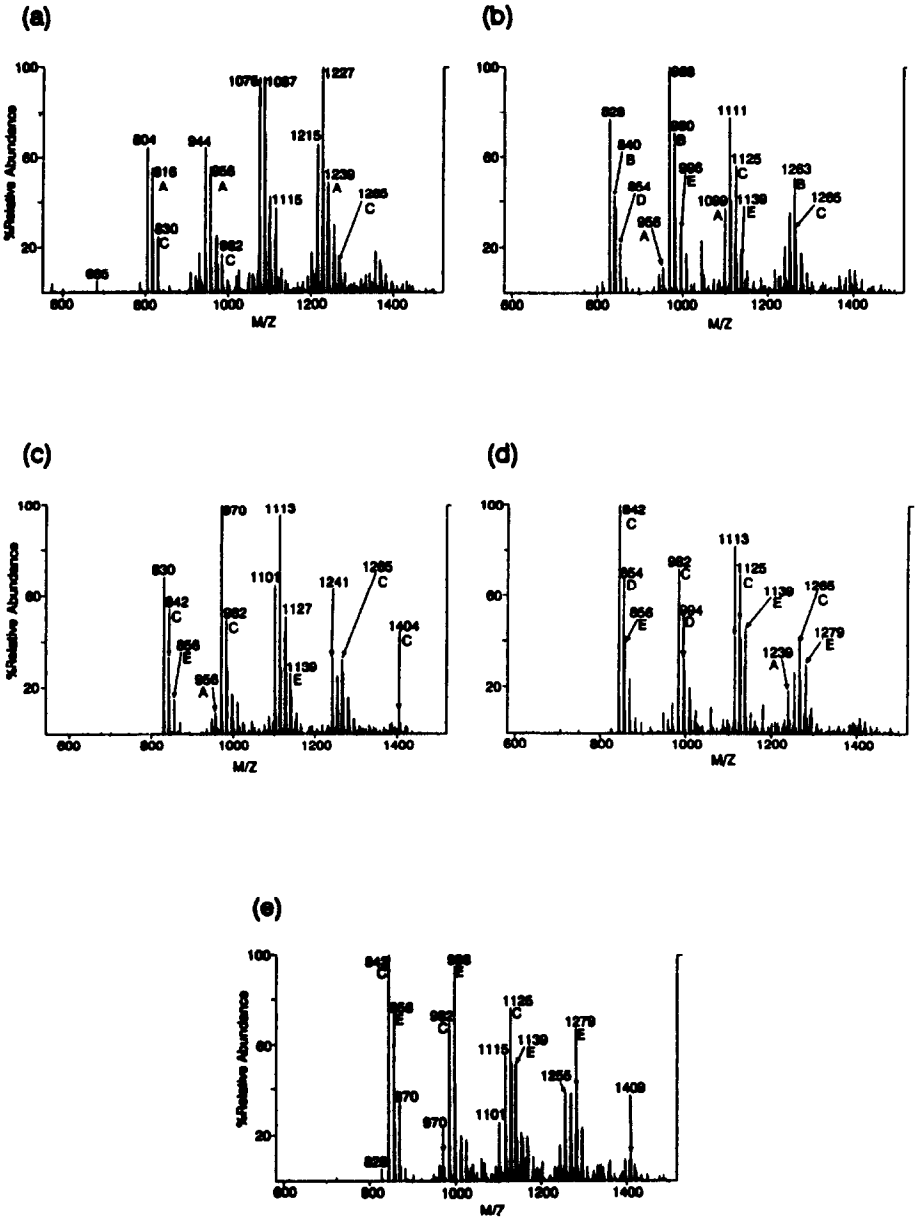

Fig. 5. MS/MS positive ion parent spectra of (a) series A ion m/z 533, (b) series B ion m/z 557, (c) series C ion m/z 559, (d) series D ion m/z 571 and (e) series E ion m/z 573 from polymer-V.

Each ion of this series has a mass 12 daltons higher than the corresponding ion of series A and the lowest member of the series is the monomeric *N*-alkyl-4-vinylpyridinium cation. The DCI mass spectrum of polymer-II (Fig. 2) shows series B ions m/z 190, 529, 868, 1207 and 1546 corresponding to the mono-, di-, tri-, tetra- and pentamer, respectively. Fragmentation pathways of series B ions are the simplest among the five series observed in the DCI mass spectra of the polymers because the series B ions generate mostly lower mass ions belonging to the same series. This is illustrated by the typical fragmentation pathway shown in Scheme 5. The ion m/z 1207 is chosen for this example and data from its MS/MS product spectrum are collected in Table 1. This ion fragments to produce ion m/z 106, the 4-vinylpyridinium cation and other series B ions m/z 190, 529 and 868, respectively. MS/MS parent spectra of series B ions show higher mass ions of series B as the major precursors in combination with ions from all other series. For example, the MS/MS parent spectrum of ion m/z 529, [Fig. 4(b)], shows series A ions at m/z 856 (23%) and 1195 (50%); series B ions at m/z 868 (74%) and 1207 (100%);

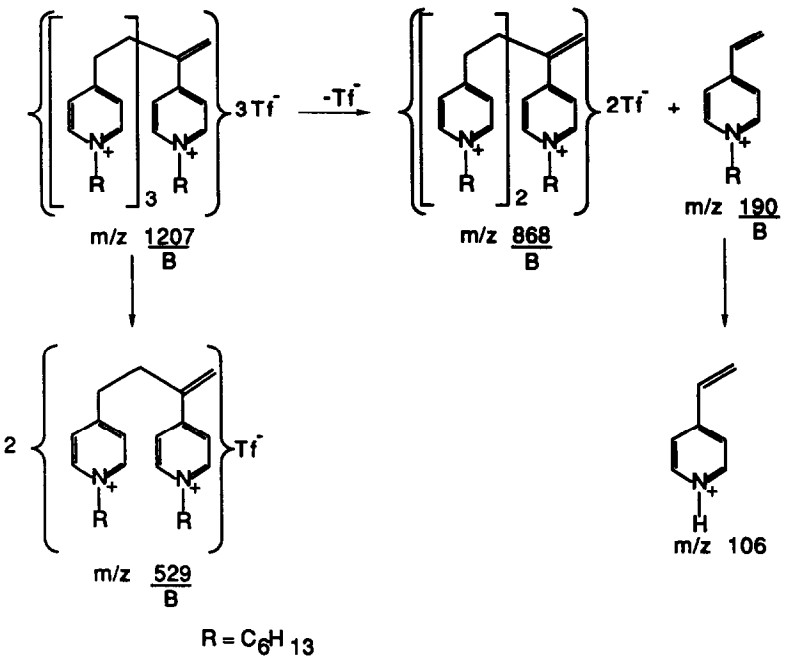

Scheme 5. Proposed fragmentation pathways for Series B ion, *m/z* 1207, determined by MS/MS scans under CAD conditions.

a series C ion at *m/z* 1209 (22%); series D ions at *m/z* 882 (10%) and 1221 (15%); and a series E ion *m/z* 1223 (5%) as its precursors. The ease of formation of series B ions from both saturated and unsaturated polymer chains as suggested below explains their high relative abundances in the DCI mass spectra of the polymers.

The DCI mass spectra of polymers I, III, IV and V show similar ions of B-series to those discussed for polymer II. MS/MS experiments showed many fragment ions in the case of *N*-dodecyl containing oligomers generated from polymer-V because of the ease of dissociation of the complex *N*-dodecyl group, as mentioned above. These fragment ions were again diagnostic of the structural compositions of the oligomers. For example, the MS/MS product spectrum of the ion *m/z* 1123 (Table 1) displays a series A ion at *m/z* 262; series B ions at *m/z* 134 (*N*-ethyl-4-vinylpyridinium monomer, *m/z* 274 (*N*-dodecyl-4-vinylpyridinium monomer), *m/z* 417 (dimer having *N*-ethyl groups); *m/z* 557 (hetero-dimer), *m/z* 700 (trimer having *N*-ethyl groups), *m/z* 840 (trimer consist of two *N*-ethyl and one *N*-dodecyl groups); series D ions at *m/z* 148, 288 and 714, respectively. It is evident from the product spectrum that three *N*-ethyl groups and one *N*-dodecyl group comprise the hetero-tetramer ion, *m/z* 1123. MS/MS parent spectrum of the hetero-dimer ion *m/z* 557 [Fig. 5(b)] shows the series A ions *m/z* 1099 and 1239; series B ions *m/z* 840, 980, 1123, 1263; series C ions 842, 982, 1125 and 1265; series D ions *m/z* 854 and 994; and series E ions *m/z* 996 and 1139, respectively.

Series C ions

This series is the saturated form (with respect to the main carbon chain) of series B and therefore the mass of each member of this series is 2 daltons higher than the corresponding ion of series B. Ions of series C in the DCI mass spectrum of polymer-II (homopolymer of *N*-hexyl-4-vinylpyridinium triflate; Fig. 2) include the monomer (*m/z* 192) through the pentamer (*m/z* 1548) corresponding to $n = 0$, 1, 2, 3 and 4 in the general structure shown in Scheme 2. Collision activated dissociation of these ions yields a rich spectrum with fragment ions belonging to series A, B, C, and D respectively. For example, the MS/MS product spectrum of *m/z* 1209 (Table 1) shows series A ions at *m/z* 178, 517, 856; series B ions at *m/z* 190, 527, 868; series C ions 192, 531, 870; and series D ions *m/z* 204, 543, and 882. The structures of the series A and B ions have already been discussed and the presence of these ions helps to confirm the structure of the C series tetramer, *m/z* 1209. Routes of fragmentation of this ion, *m/z* 1209, are shown in Scheme 6 and are typical of the series C ions.

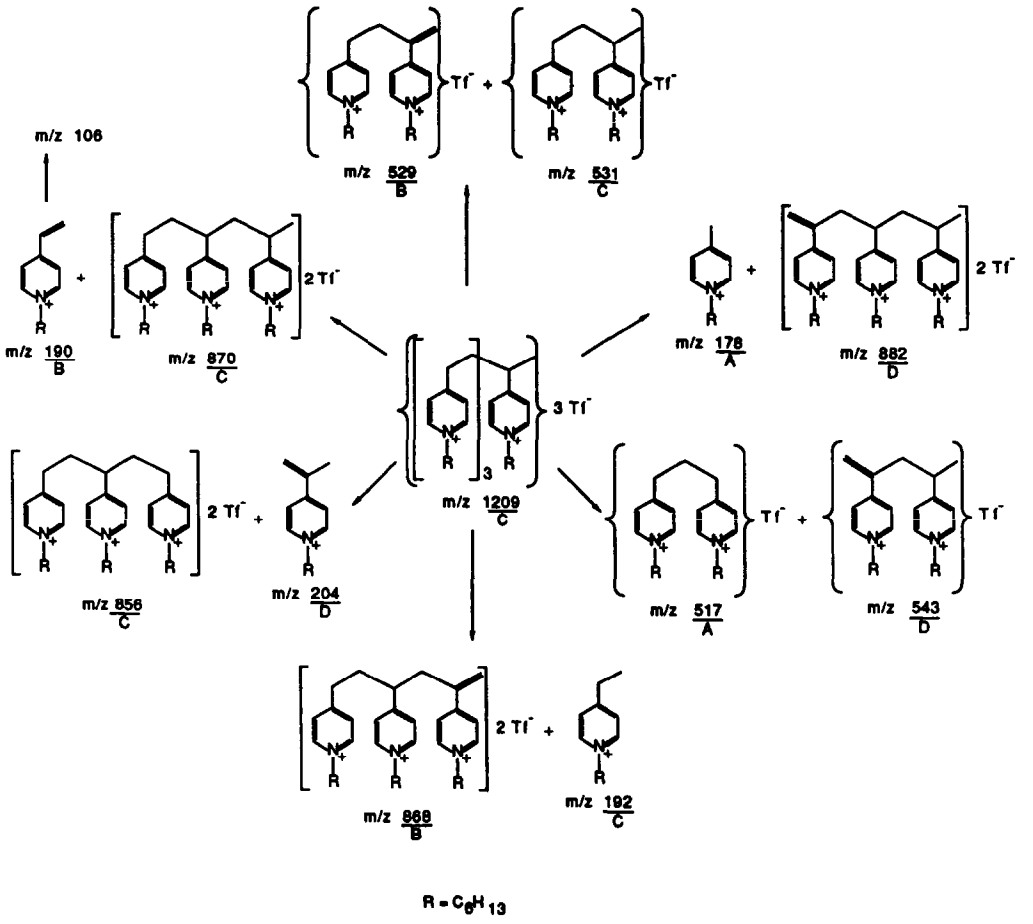

Scheme 6. Proposed fragmentation pathways for Series C ion, *m/z* 1209, determined by MS/MS scans under CAD conditions.

The MS/MS parent spectrum of the dimer ion *m/z* 531 [Fig. 4(c)] shows series A ions at *m/z* 856, 1195; series C ions at *m/z* 870, 1209; and series E ions at *m/z* 884 and 1223, respectively. The parent spectrum clearly proves that series C ions are only formed from series having saturated main chains. Major precursors of *m/z* 531 are the higher mass ions of series C. Polymers I, III, IV, and V show similar behavior with respect to series-C ions in their DCI mass spectra. Ions of series C in the DCI mass spectrum of polymer-V (Fig. 3) are the monomer and homo-oligomers *m/z* 136, 419, 702 and 985 containing *N*-ethyl-4-vinylpyridinium group; ions *m/z* 276, 699 and 1122 containing *N*-dodecyl-4-vinylpyridinium group; and the mixed-oligomer ions *m/z* 559 (mixed-dimer), *m/z* 842 (trimer composed of two *N*-ethyl and one *N*-dodecyl groups), *m/z* 982 (trimer having one *N*-ethyl and two *N*-dodecyl groups), *m/z* 1125 (tetramer comprised of three *N*-ethyl and one *N*-dodecyl groups), *m/z* 1265 (tetramer having two *N*-ethyl and two *N*-dodecyl groups) and *m/z* 1405 (tetramer comprised of one *N*-ethyl and three *N*-dodecyl groups). The MS/MS product spectrum of ion *m/z* 1125 (Table 1) is consistent with the proposed structure of the ion. The MS/MS parent spectrum of the co-dimer *m/z* 559 [Fig. 5(c)] displays high mass ions of series A, C and E as its precursors.

Series D ions

Ions of series D, like their homolog, series B, have a double bond in the main carbon chain. The probable location for the double bond is the terminal vinyl group in the main chain. The formation of these ions may involve a 1,2 hydride shift followed by 1,3 hydride shift as shown in the following tentative scheme, but this remains to be established.

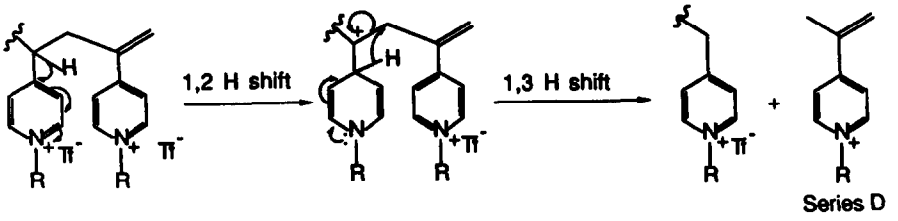

Ions with *m/z* 204, 543, 882 and 1221 corresponding to mono-, di-, tri- and tetramer in the DCI mass spectra of polymer-II (homopolymer having N-hexyl group; Fig. 2) belong to series D. Typical MS/MS fragmentation pathways for this series are shown in Scheme 7 using the tetramer, *m/z* 1221, as an example (Table 1). Ions *m/z* 120 and 106 in the MS/MS product spectrum of *m/z* 1221 are formed by loss of hexene from the *N*-alkyl group of ions *m/z* 204 and 190 as shown in Scheme 7. The ion at *m/z* 543 can be formed by two different channels (Scheme 7) during collision activated dissociation of *m/z* 1221, which helps explain why *m/z* 543 is the most abundant ion in the MS/MS product spectrum. Scheme 7 also shows formation of series B ions at *m/z* 190, 529, 868; a series C ion at *m/z* 531, and series D ions at *m/z* 204, 543, and 882. The MS/MS parent spectrum of the D ion *m/z* 543 [Fig. 4(d)] shows higher members of series D ions viz. *m/z* 882 (80%) and 1221 (100%) as its major precursors along with ion *m/z* 870 (20%) of series C and *m/z* 884 (18%) and *m/z* 1223 (36%) of series E, respectively.

The DCI mass spectrum of polymer-V (Fig. 3) shows series D ions *m/z* 148 (monomer having *N*-ethyl group), *m/z* 288 (monomer having *N*-dodecyl group), *m/z* 431 (dimer having *N*-ethyl group), *m/z* 571 (mixed-dimer), *m/z* 711 (dimer having dodecyl groups), *m/z* 714 (trimer having *N*-ethyl groups), *m/z* 994 (mixed trimer having one *N*-ethyl and two *N*-dodecyl groups), *m/z* 997 (tetramer composed of *N*-ethyl groups) and *m/z* 1134 (trimer composed of *N*-dodecyl groups) respectively. The presence of the ions at *m/z* 711 and *m/z* 571 in the product spectrum of ion *m/z* 994 (Table 1) confirms that the latter is

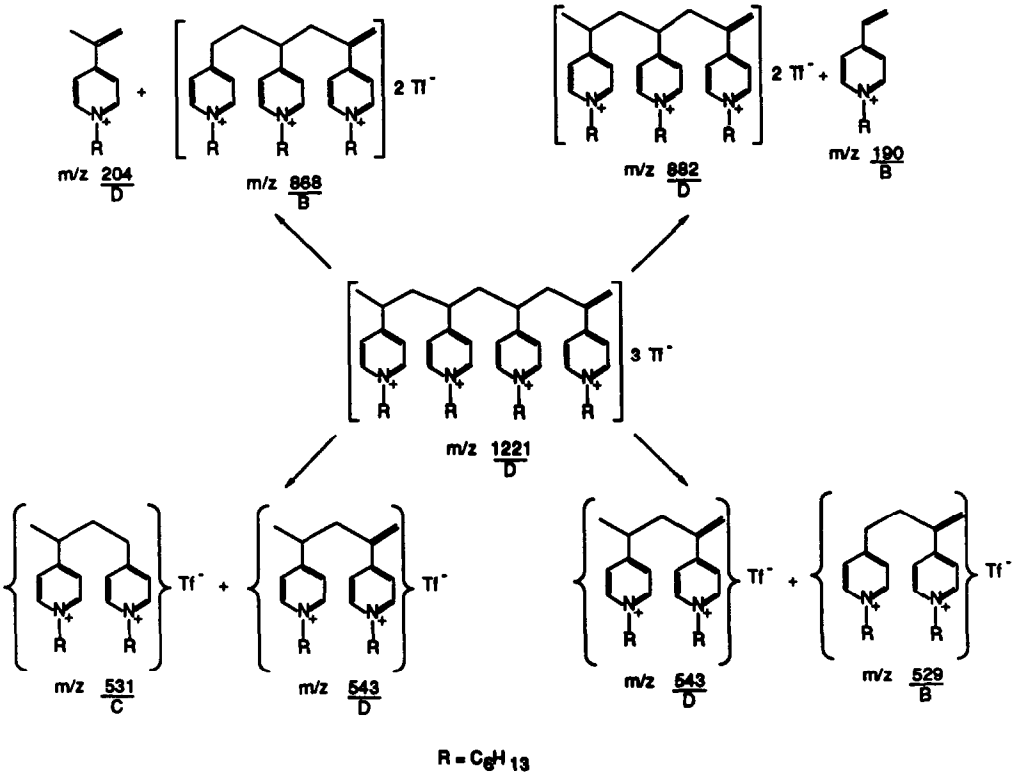

Scheme 7. Proposed fragmentation pathways for Series D ion, *m/z* 1221, determined by MS/MS scans under CAD conditions.

composed of a trimer having one *N*-ethyl and two *N*-dodecyl groups. The MS/MS parent spectrum of the mixed-dimer, *m/z* 571 [Fig. 5(d)] shows high mass ions of all five series as its precursors.

Series E ions

These ions are the saturated forms of the ions of series D. The DCI mass spectrum of polymer-II (homopolymer composed of *N*-hexyl groups; Fig. 2) displays series E ions *m/z* 206, 545, 884 and 1223 the structures of which can be obtained by substituting $n = 0$, 1, 2 and 3 in the general structure of series E ions (Scheme 2). Typical MS/MS fragmentation pathways for this series are shown in Scheme 8 using data taken from the MS/MS product spectrum (Table 1) of the trimer ion *m/z* 884. Ions of all five series are present in the MS/MS spectrum. The parent spectrum of *m/z* 545 [Fig. 4(e)] shows series C ions at *m/z* 870, 1209 and series E ions at *m/z* 884 and 1223 as its precursors. The homopolymers having *N*-ethyl group and *N*-dodecyl group show analogous behavior.

The DCI mass spectrum of polymer-V shows series E ions at *m/z* 150 (monomer having *N*-ethyl group), *m/z* 433 (dimer having *N*-ethyl group), *m/z* 573 (mixed-dimer), *m/z* 713 (dimer having *N*-dodecyl groups), *m/z* 856 (mixed-trimer composed of one *N*-dodecyl and two *N*-ethyl groups), *m/z* 996 (mixed-trimer having one *N*-ethyl and two *N*-dodecyl groups), *m/z* 999 (tetramer composed of *N*-ethyl group), *m/z* 1139 (mixed-tetramer composed of one *N*-dodecyl and three *N*-ethyl groups) and *m/z* 1282 (pentamer composed of *N*-ethyl group), respectively. Collision activated dissociation of *m/z* 1139 (Table 1) produces fragment ions *m/z* 716 (trimer composed of *N*-ethyl groups) and *m/z* 573 (mixed-dimer) among other ions, proving evidence for the structural composition of *m/z* 1139 as a tetramer having three *N*-ethyl and one *N*-dodecyl groups. The MS/MS parent spectrum of the mixed-dimer ion *m/z* 573 [Fig. 5(e)] displays mostly high-mass ions of series C and E respectively.

Other processes

The DCI mass spectra of the polymers display other ions besides those belonging to the five series discussed so far. Most of these ions are the result of simple fragmentation of the series ions. One such fragment ion series has as its lowest member the 4-vinylpyridinium ion, *m/z* 106,

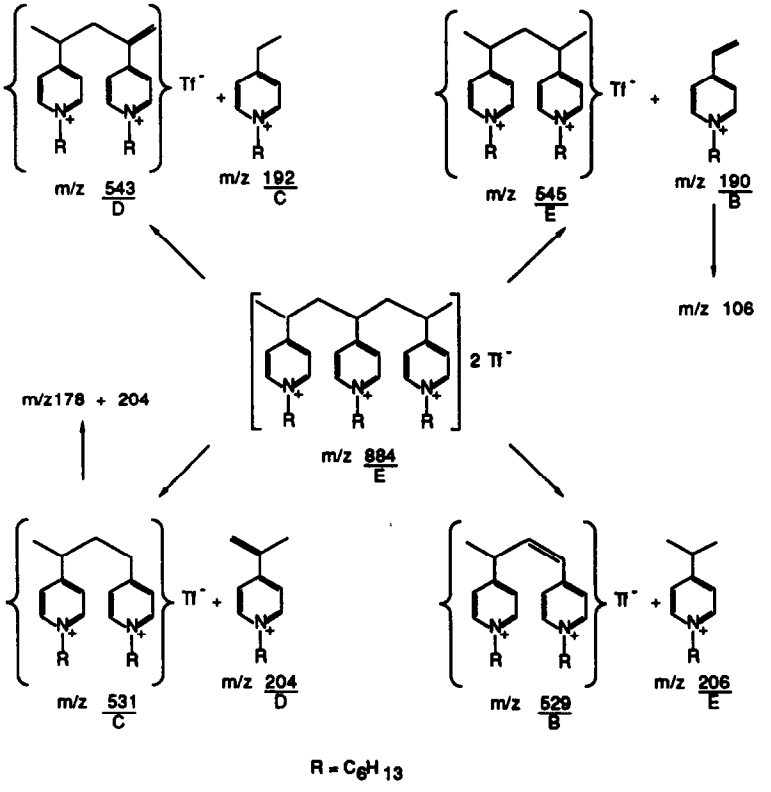

Scheme 8. Proposed fragmentation pathways for Series E ion, *m/z* 884, determined by MS/MS scans under CAD conditions.

shown in Scheme 5. These ions are formed by alkene loss from the *N*-alkyl group according to the mechanism shown in the discussion of series A ions. A similar mechanism has been proposed by Katritzky *et al.* for fragmentation of *N*-alkylpyridinium ions.[36-38] Higher members of this series are present in the DCI mass spectrum of polymer-II (homopolymer composed of *N*-hexyl groups; Fig. 2) and are due to loss of C_6H_{12} *m/z* 445 (series B dimer-C_6H_{12}), *m/z* 784 (series B trimer-C_6H_{12}) and *m/z* 1123 (series B tetramer-C_6H_{12}), respectively.

Another series of low abundance ions in the DCI mass spectra of the polymers are formed by the loss of both a triflate anion and the *N*-alkyl substituent as a carbocation, as shown in the following reaction. These ions have neutral 4-vinylpyridine groups in their structures.

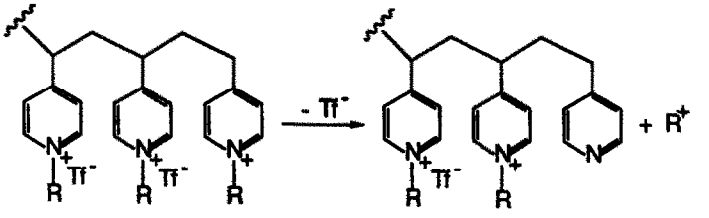

Formation of neutral pyridine and the corresponding carbocation during gas-phase fragmentation of *N*-alkylpyridinium ions has been reported in the literature.[36-38] Ions belonging to this series in the mass spectrum of polymer-I [Fig. 1(a)] are *m/z* 211 (4-vinylpyridinium ion + 4-vinylpyridine), *m/z* 239 (*N*-ethyl-4-vinylpyridinium ion + 4-vinylpyridine), and *m/z* 819 (series D trimer + 4-vinylpyridine). Ions, *m/z* 295 (*N*-hexyl-4-vinylpyridinium ion + 4-vinylpyridine) and *m/z* 634 (series B dimer ion + 4-vinylpyridine), in the mass spectrum of polymer-II (Fig. 2) also belong to this series. The presence of both the ion *m/z* 379 (*N*-dodecyl-4-vinylpyridinium ion + 4-vinylpyridine) and the carbocation *m/z* 169 ($C_{12}H_{25}^+$) in the DCI mass spectrum of polymer-III supports the mechanism proposed in the above reaction. Another minor series of ions having doubly unsaturated main chains corresponds to the unsaturated form of D ions and is also present in the DCI mass spectra of the polymers. These doubly unsaturated ions are clearly displayed at *m/z* 712 in the DCI mass spectrum of polymer-I (Fig. 1(a)), at *m/z* 709 in the DCI mass spectrum of polymer-III and *m/z* 569 in the DCI mass spectrum of polymer-V (Fig. 3). A general structure of these ions is suggested in the following reaction.

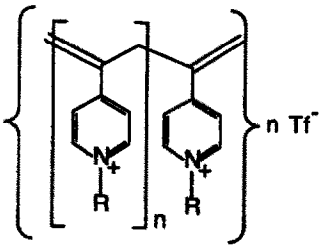

Ions two mass units different from the main series ions are apparent in the DCI mass spectra of the polymers. For example, the DCI mass spectrum of polymer I shows the ions at *m/z* 712 and *m/z* 981 which are two mass units below the main series ions, D and E, respectively. These types of ions might be formed by processes involving skeletal fragmentation with hydrogen transfer. These ions contribute isotope to the main series ions.

CONCLUSIONS

The capabilities of DCI mass spectrometry in producing characteristic oligomeric ions and of DCI MS/MS in characterizing the structures of these ions has been demonstrated. The ion chemistry described here should find application in methods for structural characterization of vinylpyridinium polymers. All five series of positive ions observed in the DCI pyrolysis/mass spectra of these polymers are stable species that yield structural information on their constituent monomers by CAD. Series A ions have a saturated main chain and yield mostly low mass ions of series A and series B on gas-phase fragmentation by CAD. The most abundant species in the DCI mass spectra of the polymers, ions of series B, have double bonds along their main chain and are produced as products of CAD of all five

series of ions. They themselves undergo simple fragmentation during CAD, principally forming lower mass ions of series B. Ions of series C are the saturated form of the corresponding ions of series B and form ions of series A, B, C, and D upon collision activated dissociation. These ions show ions of the saturated species, *viz.* series A, C and E, as precursors in their MS/MS parent spectra. Ions of series D and E are the homologs of series B and C ions respectively. DCI mass spectra of the poly(*N*-alkyl-4-vinyl-pyridinium) triflates also show other series of ions that are formed by simple fragmentation at the *N*-alkyl groups. One such series is formed by alkene loss from the *N*-alkyl group of the ions of the major series and another fragment series is found to be generated by loss of the *N*-alkyl group as carbonium ions, leaving a neutral pyridine-substituted oligomer. Another low intensity doubly unsaturated series of ions, corresponding to the unsaturated form of the D ions is also observed in the DCI mass spectra of the polymers.

Acknowledgements—The assistance of Prema Ranganathan, Yue Xin and Ying Hu in the synthesis of polymeric materials is acknowledged. This work was supported by the National Science Foundation (CHE 87 21768) and by the Office of Naval Research.

REFERENCES

1. D. C. Craver and T. Provder (eds.), *Polymer Characterization*; Advances in Chemistry, Symp. Series 227, *Am. Chem. Soc.*, Washington, D.C., 1990.
2. H. R. Allcock and F. W. Lampe, *Contemporary Polymer Chemistry*; Prentice Hall, New Jersey, 1990, 2nd Ed., pp. 335–497.
3. H.-R. Schulten and R. P. Lattimer, *Mass Spectrom. Rev.*, 1984, **3**, 231.
4. I. V. Bletsos, D. M. Hercules, V. D. Leyen, B. Hagenhoff, E. Niehuis and A. Benninghoven, *Anal. Chem.*, 1991, **63**, 1953.
5. G. Montaudo, E. Scamporrino and D. Vitalini, *Macromolecules*, 1989, **122**, 623.
6. B. Durairaj, A. W. Dimock, E. T. Samulski and M. T. Shaw, *J. Polym. Sci., Part A: Polymer Chemistry*, 1989, **27**, 3211.
7. H. Feld, A. Leute, R. Zurmühlen and A. Benninghoven, *Anal. Chem.*, 1991, **63**, 903.
8. L. M. Nuwaysir, C. L. Wilkins and W. J. Simonsick, Jr., *J. Am. Soc. Mass Spectrom.*, 1990, **1**, 66.
9. J. A. Moore, in *The Analytical Chemistry of Silicones*, A. L. Smith (ed.), Chapt. 13, pp. 421. Wiley, 1991.
10. J. T. Brenna and W. R. Creasy, *Applied Spec.*, 1991, **45**, 80.
11. R. B. Cody, A. Bjarnason and D. A. Weil, in *Lasers and Mass Spectrometry*, D. Lubman (ed.), Chap. 14, Oxford University Press, New York, 1990.
12. K. L. Busch and R. G. Cooks, in *Tandem Mass Spectrometry*, F. W. McIafferty (ed.), Chap. 2, Wiley, New York, 1983.
13. K. L. Busch, G. L. Glish and S. A. McLuckey, *Mass Spectrometry/Mass Spectrometry: Techniques and Applications of Tandem Mass Spectrometry*, VCH, New York, 1988.
14. H. R. Morris, A. Dell, M. Panico, J. Thomasoates, M. Rogers, R. McDowel and A. Chatterjee, in *Mass Spectrometry of Biological Materials*, Practical Spectroscopy Series, Vol. 8, p. 137. C. N. McEwen and B. S. Larsen (eds.), Marcel Dekker Inc., New York, 1990.
15. D. L. Lippstreu-Fisher and M. L. Gross, *Anal. Chem.*, 1985, **57**, 1174.
16. S. J. Pachuta and R. G. Cooks, *Chem. Rev.*, 1987, **87**, 647.
17. J. B. Fenn, M. Mann, C. K. Meng and C. M. Whitehouse, *Mass Spectrom. Rev.*, 1990, **9**, 37.
18. T. K. Majumdar, M. N. Eberlin, R. G. Cooks, M. M. Green, B. Muñoz and M. P. Reidy. *J. Am. Soc. Mass Spectrom.*, 1991, **2**, 130.
19. J. M. Richards, W. H. McClennen and H. L. C. Meuzelaar, *J. Appl. Polym. Sci.*, 1990, **40**, 1.
20. R. P. Lattimer, H. Münster and H. Budzikiewicz, *Int. J. Mass Spectrom. Ion Processes*, 1989, **90**, 119.
21. G. Montaudo, E. Scamporrino and D. Vitalini, *Macromolecules*, 1989, **22**, 623.
22. G. Montaudo, E. Scamporrino, G. Puglisi and D. Vitalini, *J. Polym. Sci. Polym. Chem. Ed.*, 1987, **25**, 475.
23. G. Montaudo, E. Scamporrino and D. Vitalini, *Macromolecules*, 1989, **22**, 627.
24. A. Guarini, G. Guglielmetti, N. Andriollo and M. Vincenti, *Anal. Chem.*, 1992, **64**, 204.
25. F. M. Menger, *Topics in Current Chemistry*, Vol. 136, Springer-Verlag, Berlin, 1986.
26. J. H. Fendler, *Surfactants in Solution* K. L. Mittal and B. Lindman (eds.), Vol. 3, pp. 1947–1989. Plenum Press, New York, 1982.
27. J. H. Fendler, *Membrane Mimetic Chemistry*, pp. 209–223. Wiley, New York, 1982.
28. U. P. Strauss and B. L. Williams, *J. Phys. Chem.*, 1961, **65**, 1390.
29. S. Shinkai, M. Hirakawa, M. Shimomura and T. Kunitake, *J. Org. Chem.*, 1981, **46**, 868.
30. T. Kunitake and S. Shinkai, *Adv. Phys. Org. Chem.*, 1980, **17**, 435.
31. T. Rodulfo, J. A. Hamilton and E. H. Cordes, *J. Org. Chem.*, 1974, **39**, 2281.
32. T. Okubo and N. Ise, *J. Am. Chem. Soc.*, 1973, **95**, 2293.
33. S. E. Friberg, G. Rong, C. C. Yang and Y. Yang, in *Polymer Association Structures: Microemulsions and Liquid Crystals*, A. Megda and E. Nokaly (eds.), Chap. 3, pp. 35. Am. Chem. Soc. Symp. Series 384, Washington, D.C., 1989.
34. F. Candau, in *Polymer Association Structures: Microemulsions and Liquid Crystals*, A. Megda and E. Nokaly (eds.), Chap. 4, pp. 47. Am. Chem. Soc. Symp. Series 384, Washington, D.C., 1989.
35. R. A. Fletcher and A. J. Fatiadi, *J. Trace Microprobe Tech.*, 1986, **4**, 215.
36. C. H. Watson, G. Baykut, Z. Mowafy, A. R. Katritzky and J. R. Eyler, *Anal. Instrum.*, 1988, **17**, 155.
37. A. R. Katritzky, C. H. Watson, Z. D. Szafran and J. R. Eyler, *J. Am. Chem. Soc.*, 1990, **112**, 2471.
38. *Idem, ibid.*, 1990, **112**, 2479.
39. R. Stoll and F. W. Röllgen, *Org. Mass Spectrom.*, 1979, **14**, 642.

40. A. Vincze, K. L. Busch and R. G. Cooks, *Anal. Chim. Acta*, 1982, **136**, 143.
41. K. L. Busch, B.-H. Hsu, K. V. Wood, R. G. Cooks, C. G. Schwarz and A. R. Katritzky, *J. Org. Chem.*, 1984, **49**, 764.
42. J.-C. Tabet and R. Cotter, *J. Anal. Chem.*, 1984, **56**, 1662.
43. W. K. Fife, P. Ranganathan and M. Zeldin, *J. Org. Chem.*, 1990, **55**, 5610.
44. P. Ranganathan, W. K. Fife and M. Zeldin, *J. Polym. Sci.: Part A: Polym. Chem.*, 1990, **28**, 2711.
45. Y. Xin, Thesis, Purdue University at Indianapolis, 1991.
46. R. Stoll and F. W. Röllgen, *J. Chem. Soc. Chem. Commun.*, 1980, 789.

Talanta, Vol. 40, No. 3, pp. 381–384, 1993
Printed in Great Britain.

0039-9140/93 $6.00 + 0.00

APPLICATION OF ION-EXCHANGE-RESIN PHASE SPECTROPHOTOMETRY TO FLOW INJECTION ANALYSIS SYSTEM—I. DETERMINATION OF TRACE ZINC IN HAIR OF CHILDREN

REN-MIN LIU, DAO-JIE LIU and AI-LING SUN
Department of Chemistry, Liaocheng Teachers College, Liaocheng, Shandong, P. R. China.

(*Received* 7 *January* 1992. *Revised* 2 *July* 1992. *Accepted* 2 *July* 1992)

Summary—A novel flow injection analysis system with ion-exchange-resin phase spectrophotometric detection is described in this paper. Zincon was presorbed on the ion-exchange resin. The resin was then added to a flow-through cell. When samples pass through the resin, the zincon presorbed on the resin reacts with zinc(II) to form the zincon–zinc(II) complex, which has an absorption maximum at 620 nm in solution, but at 650 nm in the resin phase. The measurements were made at 650 nm. High sensitivity and precision can be obtained by the proposed method. When 4.0 ml of sample solution was used, the sensitivity obtained was more than 10 times higher than that of the corresponding solution method. The proposed method has been successfully applied to the determination of zinc in the hair of children.

Ion-exchange resin phase spectrophotometry is based on the direct measurement of the degree of light absorption by an ion-exchange resin phase that has sorped a sample component. It combines the steps of preconcentration, separation and determination and provides a sensitivity several hundred times greater than that obtained with solution phase spectrophotometry. By direct application of the method, trace elements in water samples can be determined without additional preconcentration. Analytical methods for up to 20 elements have been developed and were summarized in a review.[1–9] Recently, ion-exchanger phase spectrophotometry has been applied to flow analysis.[10–12] This provides a novel means for studying ion-exchanger phase spectrophotometry.

In the present work, ion-exchange resin phase spectrophotometry was applied to a flow injection analysis (FIA) system. The purpose of this study was to apply chelating agent-loaded resin phase spectrophotometry to an FIA system. Zincon was presorbed on the ion-exchange resin. This formed the chelating agent-loaded resin. The resin was then added into a flow-through cell (Fig. 3). When samples pass through the resin beads, the immobilized zincon reacts with zinc(II) to form the zincon-Zn(II) complex, which has an absorption maximum at 650 nm in the resin phase. The proposed method has been applied to the direct determination of zinc in the hair of children.

EXPERIMENTAL

Reagents

Stock zinc solution, 1000 μg/ml.

pH Buffer solution. A 31-g weight of boric acid, 37 g of potassium chloride and 10 g of thiourea were dissolved in 800 ml of water and the pH was adjusted to about 9.0 with 20% sodium hydroxide, and the solution was diluted to 1000 ml.

Eluent solution. Hydrochloric acid (0.20*M*)

Zincon solution, 0.02%. A 0.020-g weight of zincon was dissolved in a 2 ml of 1*M* sodium hydroxide and the solution was diluted to 100 ml.

Ion-exchange resin. 201 × 4(100 ~ 160 mesh) anion-exchange resin in the chloride form (NanKai University) was used. It was conditioned, air-dried at 40° and stored in polyethylene containers.

All chemicals used were of analytical grade and were prepared with demineralized water.

Apparatus

The FIA system is shown in Fig. 1. The peristaltic pump was supplied by the Jiangsu Electroanalytical Instrument Plant. A six-way rotary valve with two PTFE tube loops was used for sample and eluent injection. The connection of the valve is shown in Fig. 2. Sample and eluent solutions were injected into the carrier solution alternately by an asynchronous injection technique. A 721

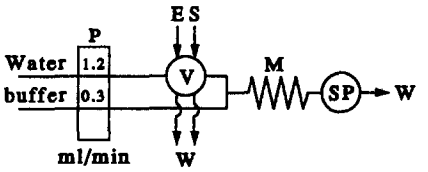

Fig. 1. Schematic diagram of the FIA system. P, peristaltic pump; V, six-way injection valve with two loops (one is 4.0 ml for sample injection the other is 1.0 ml for eluent injection); S, sample; E, eluent; M, mixing coil (100 cm, i.d. 1.0 mm); SP, spectrophotometer; W, waste.

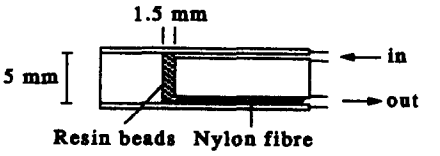

Fig. 3. Schematic diagram of the resin-filled flow-through cell.

spectrophotometer (The Third Analytical Instrument Plant of Shanghai) connected to a XWT-S platform recorder (The Third Automatic Instrument Plant of Shanghai) was used as the detector with a flow-through cell (Fig. 3). the cell had a black side, a 5 mm path and a diameter of 1.5 mm. In order to retain the resin in the cell, the cell was blocked with nylon fibre.

Procedures

Preparation of chelating resin loaded with zincon. One gramme of the anion-exchange resin was stirred with 20 ml of the zincon solution for 30 min and then the resin was collected. The amount of the zincon taken up was determined by measurement of the absorbance at 470 nm. About 7 μmoles of zincon was loaded on 1 g of the resin. The capacity for chelating metal is about 7 μmol/g resin. The chelating resin loaded with zincon has high stability. No zincon can be released even in 1.0*M* sodium chloride and 0.1*M* hydrochloric acid.

Determination. The FIA system is connected with PTFE tubing (1.0 mm i.d.) according to the arrangement shown in Fig. 1 and Fig. 2. Inject the sample solution (4.0 ml) into the carrier (water) solution flowing at 1.2 ml/min and merging with the buffer solution flowing at 0.3 ml/min. Allow the sample slug to pass through the flow-through cell, in which the colour-forming reaction takes place. Read the absorbance in the flow-cell at 650 nm. Inject the eluent solution into the carrier solution when the absorbance steady state has been recorded. When the recorder comes back to its baseline the next sample is then injected and determined as before.

Prepare a series of standard solutions of Zn(II). Inject these solutions into the carrier solution, as for sample solutions, before and after the sample runs.

Use the peak height (maximum absorbance) as a measure of absorbance throughout for the samples and calibrations runs.

RESULTS AND DISCUSSION

Zincon is a sensitive reagent for zinc. It reacts with zinc(II) to form a blue colour complex in the pH range 8.5–9.5. The complex decomposes immediately when the pH of the solution is below 6. As a result, a buffer solution of borate with a pH of 9.0 was employed for complex formation and a 0.20*M* hydrochloric acid solution was employed for the desorption of the zinc from the resin.

Effect of flow-rate

Figure 4 shows the influence of flow-rate (carrier solution and buffer solution together,

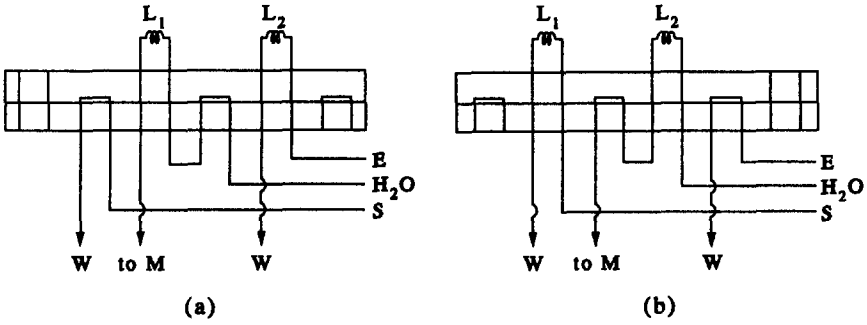

Fig. 2. Schematic diagram of the connection of the valve. (a), Sample injection position; (b), eluent injection position; E, eluent; S, sample; L1, loop for sample; L2, loop for eluent; M, to mixing coil; W, waste.

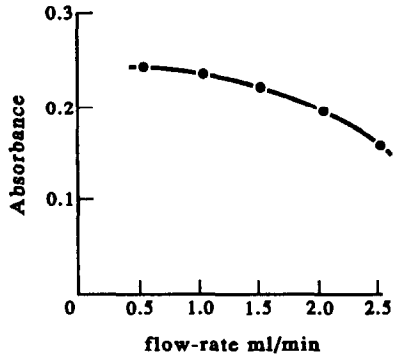

Fig. 4. Effect of flow-rate on sensitivity. Sample volume, 4.0 ml.

the ratio of them is 4:1) on the measurement of a 100 μg/l. Zn(II) solution. It can be seen that a change in the flow-rate from 0.5–2.5 ml/min decreased the sensitivity by 32%. However there was a linear relationship between the measured absorbance and the Zn(II) concentration determined at a constant flow-rate. Measurements at flow-rate lower than 0.6 ml/min took longer than 10 min. In all subsequent experiments, the total flow-rate was maintained at 1.5 ml/min.

Effect of sample volume

The increase of the sample volume resulted in a proportional increase of absorbance. Much higher sensitivity can be obtained by employing a larger volume of sample solution. But more time would be required for each determination. So the selection of sample volume should reflect a consideration of sensitivity and analysis speed.

Calibration and sensitivity

According to the proposed procedure, the calibration graph was established with standard solution of Zn(II) (Fig. 5). The calibration curve is reasonably linear in the concentration range

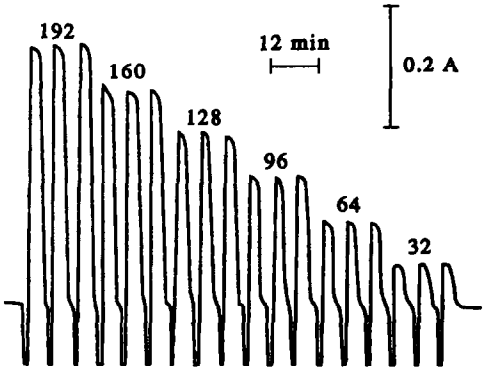

Fig. 5. Recorder signals for standard solution of Zn. Values above the peaks are concentrations of Zn in μg/l.

of 16–360 μg/l. The sensitivity of the proposed method has been compared with that of a conventional FIA method (Table 1). The sensitivity is more than 10 times higher than that of corresponding solution method for a 4.0 ml sample injection.

Precision and detection limit

Precision was measured with a sample solution of 32 μg/l. and 80 μg/l. in Zn(II), respectively. For 10 determinations, the relative standard deviations obtained were 1.4 and 1.1%, respectively. The detection limit, defined as the concentration that produces an absorbance equal to twice the magnitude of the fluctuation in the background was as low as 4.2 μg/l.

Effect of foreign ions

The following ions interfere in the determination of zinc when present in a molar ratio to zinc of 1:1 or more: aluminium, iron(III), chromium(III), cobalt(II), nickel(II), manganese(II), lead(II), molybdenum(VI), cadmium(II), mercury(II) and bismuth(III). These elements in hair samples were also determined by us. The maximum value of these elements in hair are as follows (ppm): aluminum (42.8), iron (37.6), chromium (0.19), cobalt (0.07), nickel (0.42), manganese (1.46), lead (9.72), molybdenum (0.31) and cadmium (0.21). They are not high enough to interfere in the determination of zinc in hair samples. Copper(II) interferes seriously. It can be masked by the addition of thiourea in the buffer solution.

Determination of zinc in hair of children

Hair is an excretive organ of the human body. The content of micro-elements in hair can reflect the cumulative status of micro-elements in the human body.[13] Zinc is an essential micro-element. So the determination of zinc in hair of children is of great interest in the evaluation of nutrient status. The present method has been applied to the determination of zinc in the hair of children. Hair was washed with acetone and

Table 1. Comparison of the sensitivity of FIA ion-exchange resin phase absorptiometry with that of FIA solution phase absorptiometry (metal concentration giving a final absorbance of 0.50)

FIA ion-exchange resin phase absorptiometry	308 μg/l. sample volume 2.0 ml 186 μg/l. sample volume 4.0 ml
FIA solution phase absorptiometry	1940 μg/l. sample volume 200 ul

Table 2. Determination of zinc in hair of children ($X \pm SD$, $\mu g/g$)

Age	Boys Number	Boys Data obtained	Girls Number	Girls Data obtained
1	62	81.8 ± 31.6	68	80.4 ± 31.3
		(79.6 ± 30.4)*		(78.7 ± 31.6)
2	71	81.2 ± 28.3	60	83.8 ± 25.9
		(81.7 ± 27.2)		(84.7 ± 25.1)
3	66	88.3 ± 34.5	76	90.7 ± 36.6
		(89.8 ± 32.9)		(90.2 ± 37.7)
4	68	93.9 ± 33.4	68	97.5 ± 29.8
		(92.0 ± 35.5)		(98.8 ± 27.4)
5	74	116.1 ± 37.6	64	108.2 ± 34.0
		(113.3 ± 40.1)		(105.6 ± 37.1)

*The values in the parenthesis were obtained by AAS method

de-ionized water to remove surface contamination and dry-ashed in a muffle furnace at 450°, and the residue was dissolved in nitric acid. The pH of the solution was adjusted to about 9.0 and diluted to 50 ml with demineralized water. The solution was then analysed by the proposed method and an AAS method. The results are listed in Table 2. Table 2 showed that the results of this method are in accordance with those of the AAS method.

REFERENCES

1. K. Yoshimura, H. Waki and S. Ohashi, *Talanta*, 1976, **23**, 449.
2. K. Yoshimura, Y. Toshimitsu and S. Ohashi, *ibid.*, 1980, **27**, 693.
3. K. Yoshimura, H. Waki and S. Ohashi, *ibid.*, 1978, **25**, 579.
4. Y. Toshimitsu, K. Yoshimura and S. Ohashi, *ibid.*, 1979, **26**, 273.
5. K. Yoshimura, S. Nigo and T. Tarutanl, *Talanta*, 1982, **29**, 173.
6. H. Wahi and J. Korkisch, *ibid.*, 1983, **30**, 95.
7. Ge Wueng-Xeng and Meng Li, *Anal. Chem. (China)*, 1978, **8**, 349.
8. Li Shi-Yu and Gao Wei-Ping, *Talanta*, 1984, **31**, 844.
9. K. Yoshimura and H. Waki, *ibid.*, 1985, **32**, 345.
10. K. Yoshimura, *Anal. Chem.*, 1987, **59**, 2922.
11. *idem.*, *Bunseki Kagaku*, 1987, **36**, 656.
12. *idem.*, *Analyst*, 1988, **113**, 471.
13. D. C. Hildrbrand, *et al.*, *Clin. Chem.*, 1974, **20**, 148.

Talanta, Vol. 40, No. 3, pp. 385–390, 1993
Printed in Great Britain.

0039-9140/93 $6.00 + 0.00

SPECTROPHOTOMETRIC DETERMINATION OF GADOLINIUM(III) WITH 2-(5-BROMO-2-PYRIDYLAZO)-5-DIETHYLAMINOPHENOL (5-Br-PADAP)

L. D. MARTINEZ, E. PERINO, E. J. MARCHEVSKY and R. A. OLSINA

Department of Analytical Chemistry, Faculty of Chemistry, Biochemistry and Pharmacy, National University of San Luis, P.O. Box 375, 5700-San Luis, Argentina

(*Received* 14 *November* 1991. *Revised* 2 *July* 1992. *Accepted* 2 *July* 1992)

Summary—Reaction between gadolinium(III) and 2-(5-bromo-2-pyridylazo)-5-diethylaminophenol (5-Br-PADAP) was studied for delineating optimal conditions for complexation. This reagent can be used for the spectrophotometric determination of Gd(III) in concentrations ranging from 0.04 to 1.2 ppm ($a = 1.76(\pm 0.03) \times 10^5$ (l.$^{-1}$ mole^{-1} . cm). The reaction takes place at a pH between 9.2 and 11.6. In the presence of Triton X-100 this complex is soluble in water. In order to overcome difficulties caused by the presence of other lanthanides, an ion exchange chromatographic technique was used.

For several years, the use of micellar media of ternary metal–chromophore–surfactant systems has been a common practice in the spectrophotometric determination of metal ions, with a view to enhancing sensitivity and/or selectivity.[1–3] The solubilizing power of micellar systems has allowed investigators to speed up and simplify many common analytical procedures when the chromophore or chelate formed is insoluble or only slightly soluble in water, thus avoiding costly and tedious extractions and allowing determination in a homogeneous medium.[4]

The growing importance of the rare-earths elements (REE) in advanced engineering and high-technology ceramics and in special glasses has made it necessary to develop simple and reliable analytical methods for determining traces of these elements.

The analytical application of 2-[(5-bromo-2-(pyridylazo)]-5-diethylaminophenol (5-Br-PADAP) (RH) compounds has been extensively studied. However since the metal chelates obtained are insoluble in water, the methods require aqueous alcohol media or extraction into non-polar solvents.

At present, 5-Br-PADAP can be used in the spectrophotometric determination of many rare earths,[5–9] but it has not been employed for the determination of Gd(III). In this paper, we describe the use of 5-Br-PADAP for the spectrophotometric determination of Gd(III).

The proposed method using the reagent 5-Br-PADAP produces an absorptivity of 1.76×10^5 l. mole^{-1} . cm^{-1} and it is the most sensitive, comparing it with other methods such as arsenazo[6,10] ($a = 5 \times 10^4$ l. mole$^{-1} \cdot$ cm^{-1}) and PAN[11] ($a = 7 \times 10^4$ l. mole$^{-1} \cdot$ cm^{-1}). This circumstance is important for the determination of trace elements in geological samples to solve petrogenesis problems. Selectivity is low, as happens with every chromogenic reagent for REE; a previous separation is unavoidable in any spectrophotometric method. Nevertheless these methods are frequently used for REE determination because of their simplicity, expeditiousness and low cost.

EXPERIMENTAL

Reagents

Standard solutions of Gd(III) were prepared by dissolution of suitable amounts of the oxide (99.99% pure, Aldrich) in small volumes of concentrated hydrochloric acid, followed by dilution with distilled water. Standardization was achieved as described in the literature.[12]

5-Br-PADAP standard solution. The reagent was purified by recrystallization twice from ethanol–water. A solution of the purified reagent ($2 \times 10^{-3} M$) was prepared by dissolution in ethanol. Lower concentrations were prepared by serial dilution.

Octylphenol poly(ethyleneglycol) ether (Triton X-100 Merck) solution. A 5% (v/v) surfactant solution in redistilled water was prepared.

Buffer solution. Ammonium nitrate–ammonia solutions were used for the pH adjustment.

Cation exchange resin. Dowex 50W-X4 (200–400 mesh) was used. All other reagents used were of analytical grade.

Apparatus

A Variant spectrophotometer (model 634-UV–Vis) with 10-mm optical path glass cells was used for the absorptiometric measurements. The pH values were measured with an Orion 701-A pH meter equipped with a glass combination electrode.

The apparatus used for the separation through ionic exchange is that described by Wolfsberg *et al.*[13]

Procedure

An aliquot of the standard metal solution was placed in a 50-ml standard flask. Next, 2.5 ml of an ethanolic solution of 5-Br-PADAP ($2.5 \times 10^{-3}M$), 5.0 ml of buffer solution (pH = 9.8) and 5 ml of surfactant solution (5% v/v) were added. The mixture was then made up to volume with distilled water and mixed well by shaking vigorously. The color intensity was determined against a blank as the reference solution at 580 nm.

The proposed method was applied to Gd(III) determination in standard samples of known composition rocks. The procedure developed was the following:

Take the sample (0.1–0.2 g) in a 50-ml platinum dish and heat gently to drive off moisture. Treat with 7 ml of hydrofluoric acid and 10 ml of nitric acid, cover and digest on the steam-bath. Add more hydrofluoric acid, if necessary, to complete the decomposition. The fluorides of rare earths and calcium are completely precipitated. Allow the precipitate to settle, filter it off on a Whatman No. 40 filter paper and wash with hot water. Transfer the precipitate to the original platinum dish and decompose the paper with nitric acid (steam-bath). Evaporate to dryness, add 5 ml of nitric acid and evaporate to a moist residue. After cooling, dissolve the residue in dilute nitric acid.

Then, continue with the procedures described by Stary[14] and Wolfsberg *et al.*[13] That is, solvent extraction was performed to remove the metals listed in Table 3, followed by ion exchange to separate gadolinium from the rare earths. The sample pH was adjusted to 3 prior to placing on the column. The fraction obtained was collected in the period between 6 and 7.5 hr. A hydrochloric acid–nitric acid solution was added and evaporated to dryness. The treatment was repeated with 5 ml of solution. Then, the residue was taken up with dilute hydrochloric acid solution. The operative conditions were adjusted and the spectrophotometric determination was carried out.

RESULTS AND DISCUSSION

An attempt has been reported to use the reagent 5-Br-PADAP in the determination of REE without finding a proper solution to the inconvenience due to hydrolytic decomposition of the complex. In our work, the coloured complexes were easily obtained by adding a few drops of an ethanolic solution of 5-Br-PADAP to an aqueous solution of metal ion. Different solvents were tried so as to select the best one with respect to its solubilization ability. An increase in the percent organic solvent always produced a loss of sensitivity. It was therefore necessary to introduce a surfactant into the reaction medium in order to solve the solubility difficulties while maintaining sensitivity.

The surfactant, Triton X-100, proved to be most suitable for our system, in a proportion of 0.5% (v/v). Figure 1 shows the influence of the surfactant percentage upon the absorbance of the Gd(III)–5-Br-PADAP complex.

The full purple color of the Gd(III)–5-Br-PADAP complex develops in a few minutes at

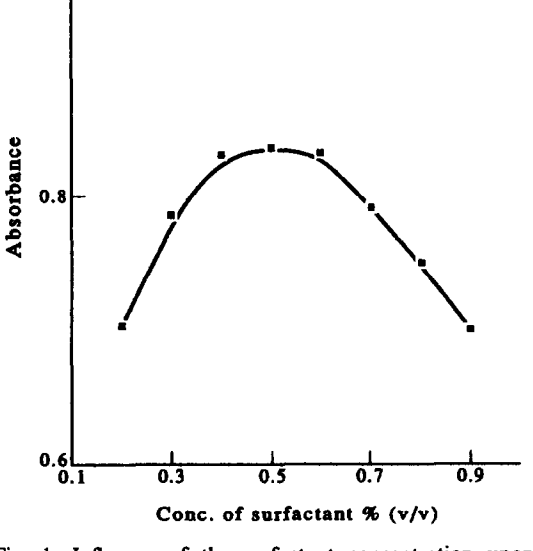

Fig. 1. Influence of the surfactant concentration upon absorbance of metal complex. $C_{Gd(III)} = 4.73 \times 10^{-6}M$, $C_{RH} = 9.5 \times 10^{-5}M$, pH = 9.8; Ethanol–water 5% (v/v); $\lambda = 580$ nm.

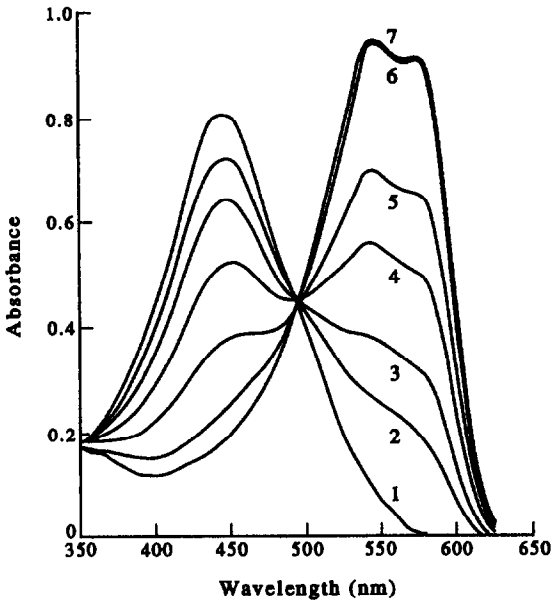

Fig. 2. Absorption spectra of Gd(III)–5-Br-PADAP in 5% (v/v) ethanol–water and 0.5% (v/v) Triton X-100 at various pH values. $C_{Gd(III)} = 1.85 \times 10^{-4}M$; $C_{RH} = 1.85 \times 10^{-5}M$; pH: 1 = 5.0; 2 = 7.6; 3 = 8.2; 4 = 8.8; 5 = 9.2; 6 = 9.6; 7 = 9.8–11.2.

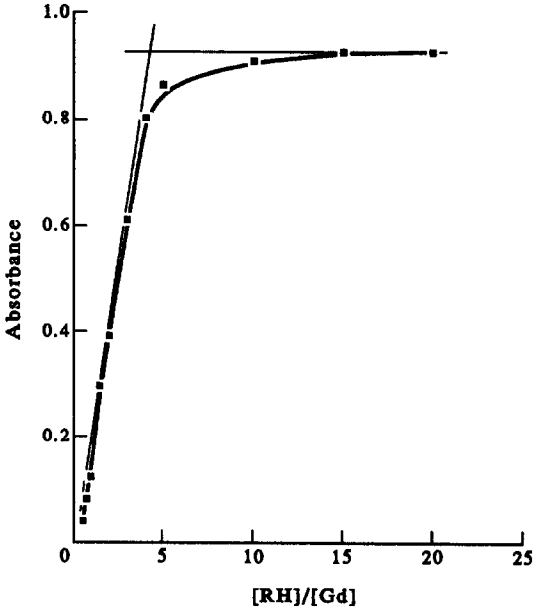

Fig. 4. Dependence of absorbance upon reagent to metal ratio. $C_{Gd(III)} = 5.2 \times 10^{-6}M$; pH = 9.8; λ = 580 nm; $\mu = 0.1$ ($NaClO_4$); Ethanol–water 5% (v/v); 0.5% (v/v) surfactant solution.

room temperature and its absorbance remains constant for up to 72 hr.

Figure 2 shows the absorption spectra of a mixture of reagent, Triton X-100 and Gd(III) at various pH values.

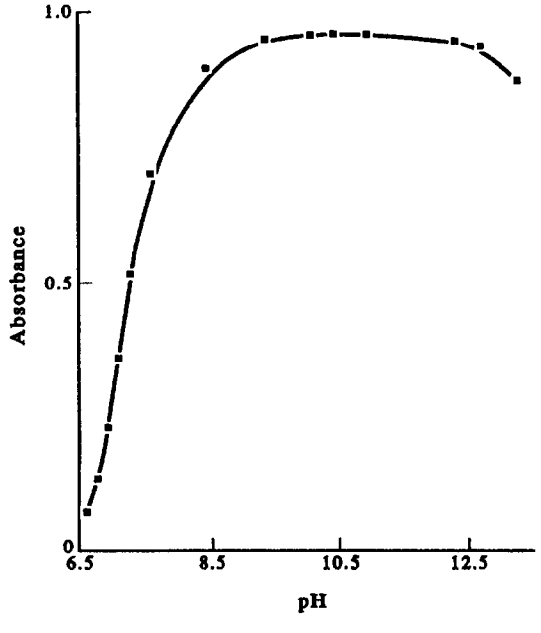

Fig. 3. Influence of the pH upon absorbance of metal complex $C_{Gd(III)} = 5.3 \times 10^{-6}M$; $C_{RH} = 1.1 \times 10^{-5}M$; Ethanol–water 5% (v/v); 0.5% (v/v) surfactant solution; $\mu = 0.1$ ($NaClO_4$).

Our experiments enabled us to determine the optimal pH range for complex formation. The results are shown in Fig. 3.

Reagent concentration and calibration curve

The reagent concentration appropriate for the quantitative work was evaluated by plotting the saturation curve (Fig. 4) at pH 9.8. The Gd(III) concentration was kept constant while the 5-Br-PADAP was changed between 7×10^{-6} and $5.6 \times 10^{-4}M$ with Triton X-100 and ethanol concentrations kept constant at 0.5 and 5.0%, respectively. The absorbance was read at λ_{max} 580 nm.

For a 1:10 Gd(III)–5-Br-PADAP molar ratio, the complete development of the complex is achieved and remains unaltered for proportions up to 1:50. The absorbance at pH 9.8 and ionic strength of $0.10M$, as well as the absorption spectrum, did not change over a 3-day period.

The stoichiometry of the complex was studied at pH 9.8. The method of continuous variations (Job) was used and as can be seen from Fig. 5, the ratio of Gd(III): reagent was 1:4. The mole ratio and slope ratio methods also confirmed this stoichiometric ratio.

Beer's law of the Gd(III)–5-Br-PADAP-Triton X-100 complex was linear in the Gd(III) concentration range of 0.04–1.2 mg/l.

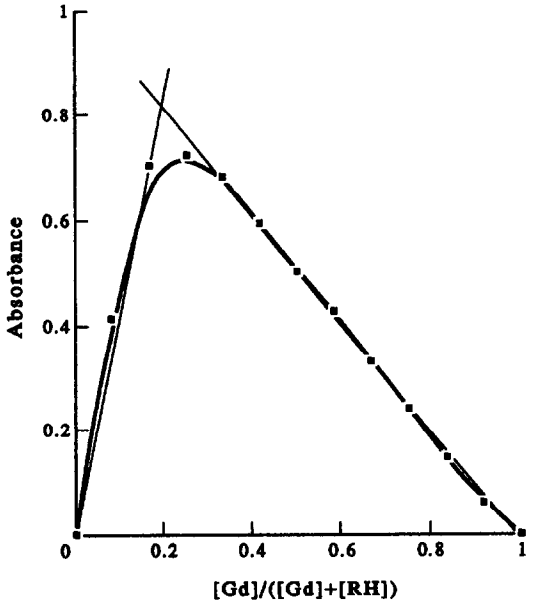

Fig. 5. Continuous variation plots. $C_{Gd(III)} = C_{RH}$; pH = 9.8; Ethanol–water 5% (v/v); 0.5% (v/v) surfactant solution.

Table 2. Tolerances for some common anions. Ethanol–water 5% (v/v); 0.5% surfactant solution

Ion	ION/Gd(III) Tolerated molar-ratio	ION/Gd(III) Tolerated mass-ratio	Error rel %
Bromide	1,000	610	−0.3
Chloride	10,000	2,270	−0.2
Carbonate	1,000	300	−0.5
Nitrate	10,000	3,970	0
Tetraborate	10,000	9,930	0
Sulfate	1,000	615	0
Iodide	1,000	813	−0.9
Phosphate	interf.	interf.	
Tartrate	1,000	1,327	−0.6
EDTA	interf.	interf.	
CDTA	interf.	interf.	
Oxalate	1,000	563	−1.9
Ascorbic acid	1,000	1,122	−1.8
Fluoride	500	61	−1.9
Nitrite	1,000	25	−1.7
Citrate	50	87	−1.8
Acetate	10,000	3,758	−0.3
Perchlorate	10,000	6,337	−0

Table 1 summarizes the optimal experimental conditions for the quantitative evaluation of Gd(III) ion with the reagent 5-Br-PADAP in the presence of the surfactant, Triton X-100.

Effects of concomitant ions

Under the optimum experimental conditions, the influences of some anions, cations and a number of complexing species that could be applied as selective masking agents were examined.

The influences were studied individually. The potential interferent and gadolinium(III) were put in pH 9.6 buffer solutions of ammonium nitrate–ammonia. The gadolinium(III) concentration was kept fixed while that of the possible interferent was increased until the magnitude of error was *ca.* ±2%, arbitrarily established as the maximum acceptable. Table 2 shows the admissible proportions of several anions and masking agents. EDTA, CTDA and phosphate interfere in a molar ratio lower than 1:1 with respect to gadolinium(III).

Under the conditions required to form the gadolinium(III)–5-Br-PADAP complex, Mn(II), Zn(II), Cd(II), Cu(II), Ni(II), Bi(III), Fe(III), Pb(II), Sb(III) and the elements belonging to the group of rare earths not only consume reagents, thus making the gadolinium(III) complexation incomplete or even null, but they spectrally disturb the spectrometric determination to a large extent. In order to increase tolerances up to values compatible with the composition of some concrete samples, several masking agents—cyanide, diethanolamine, ascorbic acid, tartaric acid, triethanolamine, were tried in their maximum admissible concentration. Results obtained for any of the above

Table 1. Experimental conditions for determination of gadolinium(III) with 5-Br-PADAP Definitions:[15] S = estimated standard deviation for $n = 6$, α = corresponds 95% confidence, CL = confidence limit

pH range	9.6–11.2
Buffer solution	Ammonium nitrate–ammonia, pH 9.8
Surfactant solution	Triton X-100, 0.5% (v/v)
Organic solvent	Ethanol, 5% (v/v)
Maximum of reagent absorption	445 nm
Maximum of complex absorption	580 nm
Bathochromic shift	135 nm
Fulfillment of Beer's law	0.044–1.25 mg/l.
Molar absorptivity	$1.76(\pm 0.03) \times 10^5$ l. mole$^{-1} \cdot$ cm^{-1} ($S = 2.150$; $\alpha = 0.05$) CL = $(1.733–1.786) \times 10^5$ l. mole$^{-1} \cdot$ cm^{-1}
Sandell's sensitivity	8.93×10^{-4} μg/cm^2
Stability of complex	3 days

Table 3. Tolerances for some common cations

Ion	ION/Gd(III) tolerated molar ratio	ION/Gd(III) tolerated mass ratio	Error rel %
Ca(II)	5,000	1,262	+1.7
K(I)	10,000	2,500	0
Ru(III)	50	32	+1.9
Rh(III)	50	33	+1.7
W(VI)	100	118	+0.9
Sr(II)	2,000	1,120	0
Mn(II)*	50	18	+1.2
Cr(III)	50	17	+1.2
Zn(II)*	100	42	+1.8
Cd(II)*	95	20	+1.6
Cu(II)*	100	41	+1.2
Ni(II)*	100	37	+2.1
Hg(II)*	100	128	+1.8
Li(I)	5,000	222	0
Bi(III)*	100	133	+1.9
Fe(III)*	100	36	+1.9
Pb(II)*	100	132	+2.1
Pd(II)*	100	68	+0.9
Mg(II)	1,000	158	0
Sb(III)*	100	78	+2.0
Al(III)	1,000	179	+0.7
Si(IV)	500	90	−1.8
Be(II)	300	17	+1.8
Te(IV)	100	82	+0.9
Zr(IV)	100	59	+1.7
Ba(II)	1,000	880	0
Re(V)	100	119	+0.9
Au(III)	1,000	1,262	0
As(III)	30	15	+1.7
Ce(III)†	30	27	+0.6
La(III)†	30	27	+0.4
Er(III)†	20	21	+0.1
Yb(III)†	20	22	+0.4
Sm(III)†	20	19	+0.3
Pr(III)†	20	19	+0.8
Eu(III)†	20	21	+0.2
Nd(III)†	20	18	+0.1
Y(III)†	30	17	+0.7
Dy(III)†	20	22	+0.4

*Two successive extractions ($Vo = Vw$), in aqueous phase of pH 5.5 with diethyldithiocarbamate 0.4M in carbon tetrachloride.

†Ion exchange chromatography—α-hydroxyisobutyric acid adjusted to different pH values was used as an eluent.

mentioned cations showed no significant modifications. Therefore we tested other separation techniques suitable for this case. Liquid–liquid extraction by means of diethyldithiocarbamate dissolved in carbon tetrachloride was chosen to separate interfering cations. The procedure employed was the one suggested by Stary,[14] using pH 5.5. Following extraction, the pH was readjusted to 9.6 and the spectrophotometric method followed. The admissible tolerances thus obtained are shown in Table 3. Most of the rare earth elements react with 5-Br-PADAP, resulting (with this method) in serious interference with the determination of Gd(III). Thus, a separation step must be conducted prior to the spectrophotometric determination of Gd using this method. In order to apply the method developed for the determination of Gd(III) to a mixture of rare earths, ion exchange chromatography was used to separate the constituents. The technique proposed by Wolfsberg[13] to separate a mixture of Eu, Sm, Nd, Ce, La and Gd was considered to be convenient. Synthetic samples of the mentioned ions of different composition were subjected to the separation using a 0.8 × 60 cm column of cation exchange resin and a flow rate of 9 ml/hr. In the initial step, 0.5 molar hydroxyisobutyrate adjusted to the desired pH values (3.4–4.2) by the addition of concentrated NH_4OH was used as an eluent. A value of 3.4 was selected as the initial pH of the eluent because at this pH an adequate separation of 10 mg of Y, 0.5 mg of Gd, and 10 mg of each other ion was achieved in less than 30 hr. Gadolinium is eluted between 6.5 and 7.5 hr after the start of column operation.

The elution of the three different ions was checked by X-ray fluorescence, using a preconcentration technique. The fraction containing Gd(III) was preconcentrated and then taken to a final volume of 50 ml. The spectrophotometric determination was carried out on an aliquot of this fraction with the reagent 5-Br-PADAP using the above-mentioned method. The results were highly satisfactory, obtaining in all cases an error less than 2%, as can be seen in Table 4.

Finally, the results of the method applied to Gd(III) determination in standard samples of known composition rocks are shown in Table 5.

Table 4. Determination of gadolinium(III) in mixtures of rare earths ($n = 6$)

Sample	Composition, % (w/w)	Gd(III) found %	Error rel %
Y	20	$\bar{x} = 1.01$	
La	29	$S = 1.07 \times 10^{-2}$	
Sm	20	CL = (1.00–1.03)	1
Ce	30	$\alpha = 0.05$	
Gd	1		
Y	30	$\bar{x} = 5.03$	
Sm	30	$S = 1.16 \times 10^{-2}$	
Nd	20	CL = (5.01–5.04)	0.6
La	15	$\alpha = 0.05$	
Gd	5		
Y	3	$\bar{x} = 4.96$	
Sm	30	$S = 1.03 \times 10^{-2}$	
Ce	30	CL = (4.95–4.97)	0.8
La	30	$\alpha = 0.05$	
Eu	2		
Gd	5		
Y	33.33	$\bar{x} = 33.29$	
Nd	33.33	$S = 1.41 \times 10^{-2}$	
Gd	33.33	CL = (33.28–33.31)	0.1
		$\alpha = 0.05$	

Table 5. Concentrations (μg/g) of Gd(III) in USGS reference materials

Sample USGS	Content Gd(III)	Gd(III) found	Error rel %
AGV-1	5.5	$\bar{x} = 5.6$ $S = 1.12 \times 10^{-2}$ CL = (5.45–5.56) $\alpha = 0.05$	1.8
G-2	5.0	$\bar{x} = 5.2$ $S = 1.01 \times 10^{-2}$ CL = (5.1–5.3) $\alpha = 0.05$	4.0
GSP-1	15.0	$\bar{x} = 15.3$ $S = 2.9 \times 10^{-2}$ CL = (15.1–15.4) $\alpha = 0.05$	2.0

CONCLUSIONS

The analytical applications of the reagent are an original contribution for gadolinium(III) spectrometric determination. Complexation is accompanied by a strong bathochromic effect, about 135 nm, providing a clear contrast between the colors of the free reagent and the one belonging to the gadolinium(III) complex.

The results obtained for a variety of geological reference materials demonstrate that the procedure allows precise and accurate analysis of geological samples for their REE and Y content. The total salt concentration is reduced and potentially interfering elements are eliminated.

The main advantage of the method proposed is the high sensitivity and the low cost of the equipment required.

REFERENCES

1. B. K. Chernova, *J. Anal. Chem. USSR*, 1977, **32**, 1171.
2. W. L. Hinze, I. L. Mittal (ed), *Solution Chemistry of Surfactants*, Vol. 1, p. 79, Plenum Press, New York, 1979.
3. E. Pelizzetti and E. Pramaruro, *Anal. Chim. Acta*, 1985, **169**, 1.
4. H. Watanabe, I. L. Mittal and E. J. Fendler (eds.), *Solution Behaviour of Surfactants. Theoretical and Applied Aspects*, Vol. II, Part VII, p. 1305. Plenum Press, New York, 1982.
5. X. Wang, *Chem. Abstr.*, 1984, **100**, 95652.
6. D. B. Gladilovich, V. Kuban and L. Sommer, *Talanta*, 1988, **35**, 259.
7. Abu Zuhri, Z. Ali and Salimradi, *Microchem J.*, 1984, **29**, 126.
8. Lin Chang Shan, Chang Hanchang and Zhao Guiwen, *Chem. Abstr.*, 1984, **100**, 114110.
9. D. B. Gladilovich, K. Vlastimil and H. Josef, *Chem. Abstr.*, 1988, **109**, 117078.
10. S. Savin, *Talanta*, 1961, **8**, 673.
11. S. Shibata, *Anal. Chim. Acta*, 1963, **28**, 388.
12. K. Marczenko, *Spectrophotometric Determination of Elements*, p. 441. Wiley, New York, 1976.
13. K. Wolfsberg, *Analytical Chemistry*, 1962, **34**, 518.
14. J. Stary, *The Solvent Extraction of Metal Chelates*, p. 157, Pergamon Press, New York, 1964.
15. A. L. Wilson, *Talanta*, 1970, **17**, 31.

Talanta, Vol. 40, No. 3, pp. 391–398, 1993
Printed in Great Britain.

0039-9140/93 $6.00 + 0.00

RAPID AUTOMATED DETERMINATION OF CONSTANTS OF SOLUBILITY PRODUCT AND CRITICAL MICELLE CONCENTRATIONS BY THE FLOW-RATE GRADIENT TECHNIQUE

JULIANA MARCOS, ANGEL RÍOS and MIGUEL VALCÁRCEL
Department of Analytical Chemistry, University of Córdoba, E-14004 Córdoba, Spain

(*Received* 30 *December* 1991. *Revised* 2 *July* 1992. *Accepted* 2 *July* 1992)

Summary—Several straightforward, rapid and automated methods for the determination of the constant of solubility product of various inorganic salts and hydroxides and the critical micelle concentrations of both anionic and cationic surfactants are reported. The underlying methodology relies on the establishment of flow-rate gradients in completely continuous flow systems including a conductometric or potentiometric detector. The results obtained are quite consistent with those reported in the chemical literature.

Unsegmented flow systems have proved to be powerful tools for automating some steps of the analytical process. A host of applications have been developed on the basis of this methodology, as shown in pertinent monographs.[1–3] Such applications usually involve constant experimental conditions where flow rate is one of the major variables. However, in some of the approaches reported in the last few years, manipulation of hydrodynamic conditions in unsegmented flow systems plays a crucial role in developing new automated determinations.[4] Thus, variable flow-rate methodologies allow the automated determination of acidity constants,[5] complex stoichiometries,[6] and the implementation of titrimetric procedures,[7,8] among others.

In variable flow-rate methodologies, the flow-rate is changed throughout the measurement step according to a linear or non-linear mathematical function, the first derivative of which defines the flow-rate gradient (Q) in each case. Linear flow rate–time functions provide constant flow gradients, while non-linear flow rate-time functions give rise to variable flow gradients. Every flow-rate gradient can be used to create a corresponding concentration gradient profile along the flow system. This is very important in as much as it allows one to automatically and gradually change the concentration of one of the analytes with time. Many chemical and physico-chemical properties are dependent on this variable, so one immediate application of this methodology is in the determination of certain parameters or in studying some properties.

In this work we used flow-rate gradients to determine constants of solubility product (K_{sp}) and critical micelle concentrations (cmc) by using a simple manifold in a rapid, automated fashion and monitoring conductivity or pH changes. Both parameters are related to the critical concentration of one reactant, above which dramatic changes in the properties of the system concerned occur (formation of a solid phase, constants of solubility product, or micelles, cmc).

EXPERIMENTAL

Reagents

Aqueous solutions of the following compounds were used at different concentrations and pH values.

Inorganic salts. Zinc(II) nitrate (Riedel), tin(II) chloride (Merck), nickel(II) nitrate (Merck), aluminium(III) nitrate (Riedel), potassium nitrate (Merck), disodium tartrate (Merck), cobalt(II) nitrate (Merck), copper(II) nitrate (Merck), sodium oxalate (Merck), calcium chloride (Merck), potassium iodate (Fluka), lead(II) nitrate (Riedel), and sodium fluoride (Riedel) were used.

Surfactants. A 0.10M sodium dodecyl sulphate solution (Aldrich), 0.010M sodium

Table 1. Constants of solubility product obtained by using the automated flow method with direct introduction of insoluble compound into the system

Compound	n(moles)*	Literature $pK_{sp}^{\dagger}$	pK_{sp} found	r.s.d.(%)
$CaSO_4$	6×10^{-3}	4.6	4.4	1.0
KH-Tartrate	10^{-2}	3.5	3.5	1.3
CoC_2O_4	1.6×10^{-3}	5.4	5.6	0.5
CuC_2O_4	2×10^{-4}	7.5	7.6	0.5
$Ca(IO_3)_2$	5×10^{-3}	6.2	6.4	0.6
PbF_2	6×10^{-3}	7.4	6.4	0.9

*Quantity of moles added to 100 ml of distilled water to prepare the suspension.
†From reference (9) (at 25°).

hexadecyl sulphate (Aldrich), 0.010*M* cetylpyridinium chloride (Serva), 0.010*M* cetyltrimethyl ammonium bromide (Serva), 0.4*M* dodecyltrimethyl ammonium bromide (Aldrich) and 0.010*M* sodium dioctyl sulphosuccinate (Aldrich) were prepared.

Preparation of the suspensions of the insoluble compounds. The insoluble compounds were previously precipitated in a flask, filtered and washed until no conductometric signal was obtained from the last water volumes used to wash the precipitate. Water was used as solvent to prepare those suspensions, taking a certain number of moles of each insoluble compound (see Table 1) for 100 ml of water.

Apparatus

A Gilson Minipuls-3 peristaltic pump controlled by a Commodore 64 microcomputer through a laboratory-made interface was used to set flow-rate gradients.[6] A Gilson Minipuls-2 peristaltic pump was used to provide a constant flow-rate. A YSI conductometer (model 3S) and a FIAtron 721 FIA cell equipped with a glass-calomel microelectrode and connected to a Radiometer pHM 62 pH-meter and a Radiometer REC 80 recorder were used as detectors. The potentiometric detection requires a calibration procedure. This was done by passing through the system standard buffers at pH 4.00 and 7.00. A Tecator TM II chemifold was also employed.

Manifold

The configuration used is depicted in Fig. 1. The two streams used are merged at point C. The programmable pump (PP) is controlled by the microcomputer and the flow rate of solution A is changed linearly with time. The conventional pump (CP) is operated at constant flow-rate. As a result, a flow gradient is created that gives rise to a concentration gradient arising from the different composition of solutions A and B.

The methodology used in this work is based on a completely continuous flow system in which the result of the concentration gradient established along reactor coil R (70 cm length and 0.5 mm i.d.) is continuously monitored with a conductometer or a glass-calomel microelectrode for pH measurements. The signal was automatically recorded on an x-t recorder at an appropriate chart speed to obtain graphically and accurately the parameter determined in each case.

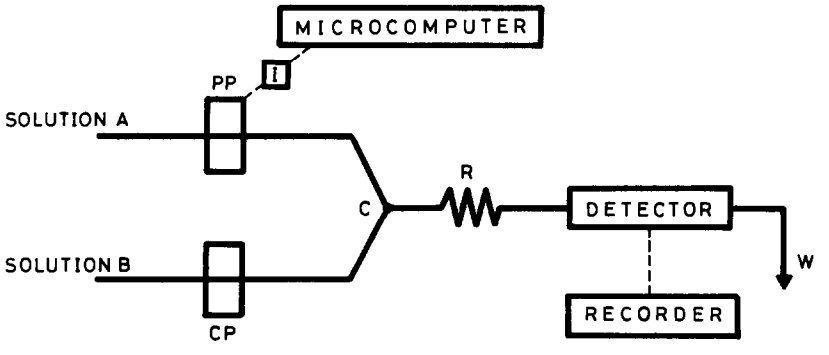

Fig. 1. Manifold used for solubility and critical micelle concentration determinations. [PP = programmable pump; CP = conventional pump; R = reactor coil (length = 70 cm; inner diameter = 0.5 mm); C = merging point; I = electronic interface].

The experiments were carried out at room temperature (18–25°) due to the difficulties to thermostatize all the system.

RESULTS AND DISCUSSION

The manifold in Fig. 1 was used to determine constants of solubility product and critical micelle concentrations, which are dealt with below in separate sections.

Determination of constants of solubility product

Constants of solubility product were determined by direct introduction of the insoluble compound into the system and by *in situ* formation of the compound in the manifold.

Direct introduction of the insoluble compound. A suspension of each insoluble compound studied was used as solution A in Fig. 1. The suspension was prepared as Experimental section reports and was continuously stirred to get the homogeneous suspension that was introduced into the system. The amounts were chosen in order to provide recordings where two zones (before and after K_{sp} value) were clearly shown, but different amounts, in the same range, can be used. The suspensions of those compounds were propelled by means of the programmable pump. To avoid the risk of blocking up the connections and the tubes of the flow manifold a flow-meter was placed at the end of the flow system for the continuous monitoring of the flow-rate. Solution B in Fig. 1 was distilled water in this case. As pump A was operated to obtain a linear positive flow-rate gradient, the insoluble compound concerned was partially dissolved after the mixing point, so the measured conductivity increased as a result of the gradual increase in the amount of insoluble compound dissolved in the system. Thus, as shown in Fig. 2, a linear conductivity-time relationship was obtained up to a point where the slope of the plot started to change. A constant conductivity would be expected after this point as a consequence of the constant dissolved ion concentration in the system when the constant of solubility product is reached. However, the small increase in conductivity in this region can be due to the intrinsic conductivity of the insoluble compound. The time at which the slope changes is denoted by t_p, and represents the situation in which the liquid phase from point C (Fig. 1) is saturated with ions from the precipitate. Therefore, this situation defines the solubility product (K_{sp}) and can be used to calculate it.

The hydrodynamic conditions in this system are determined by the flow-rate of solution A (q_A) which is changed according to the equation $q_A = Qt$ (Q is the flow gradient and t the time), whereas solution B is circulated at constant flow-rate (q_B). It should be noted that this

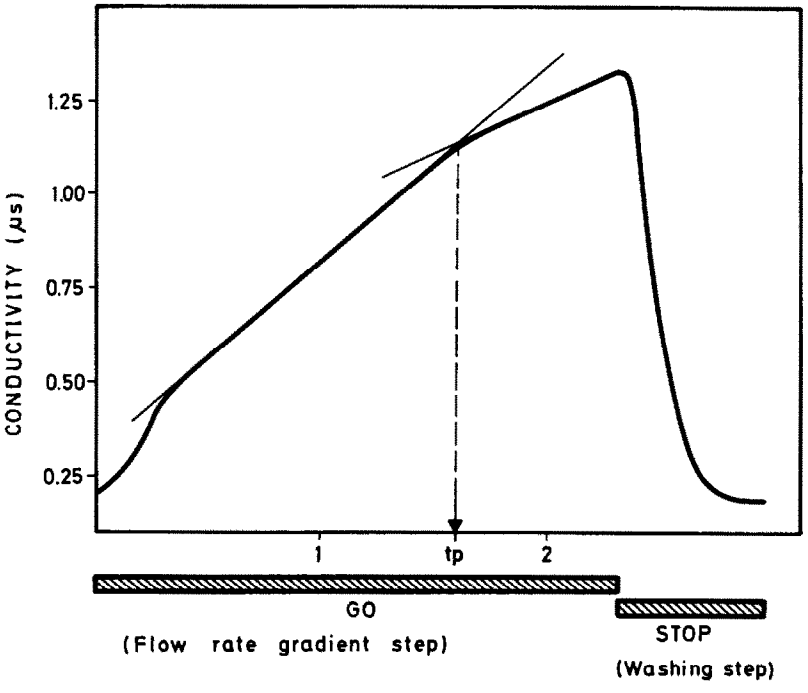

Fig. 2. Recording obtained for CoC_2O_4 by using a suspension of this compound as a solution A (Fig. 1).

methodology involves two different processes, namely: interaction between ions to form the precipitate and dilution through increase in the total flow-rate (q_T) throughout the experiment:

$$q_T = q_B + q_A = q_B + Qt \quad (1)$$

Therefore, the dilution factor (f) of the system will be:

$$f_A = q_A/(q_A + q_B) = Qt/(Qt + q_B) \quad (2)$$

If the maximum flow-rate of solution A[$(q_A)_{max}$] is of similar order than that of solution B, then a linear zone will be obtained only at the initial time period, when $q_A \ll q_B$:

$$f_A \approx q_A/q_B = Qt/q_B \quad (3)$$

However, this factor tends to 1 at great values of time, when q_A is much higher than q_B.

Figure 3 shows the variation of dilution factor with time under two different situations. In all cases the B stream flowed at constant flow-rate (1.5 ml/min); however, the flow-rate for the A stream was changed in the range $0 < q_A < 4.0$ (curve A) or $0 < q_A < 0.6$ (curve B). In practice, the latter conditions (*i.e.*, a linear change in Fig. 3) were required to prevent the dilution process from masking the conductometric signal yielded by the precipitation process. Thus, under this latter condition:

$$f_A = q_A/(q_A + q_B) \approx q_A/q_B = Qt/q_B = (Q/q_B)t \quad (4)$$

Therefore, for a salt of the general type N_mM_n whose solubility is characterized by:

$$K_{sp} = [N]^m[M]^n$$

the concentration of each ion at the time t_p is given by:

$$[\text{ion}] = xC_sq_A/(q_A + q_B) = xC_sQt_p/(Qt_p + q_B) \quad (5)$$

where x is the number of ions resulting from the dissolution of one molecule of salt ($x = m$ for N, and $x = n$ for M), and C_s is the "concentration" of the suspension introduced as solution A. Thus, provided the stoichiometry of the insoluble compound is known, K_{sp} can be calculated from the experimental data. This methodology allows the determination of constants of solubility product greater than 10^{-8}. Lower K_{sp} caused the level of dissolved ions to be too low to be clearly distinguished from the blank. Some of the K_{sp} values thus obtained are listed together with their literature counterparts in Table 1. According to the experimental procedure used the ionic strength within the flow system was very low in all cases, and it can be assumed to be close to zero in order to compare the experimental results with those reported in the literature. The precision of the method as r.s.d. was about $\pm 2\%$ ($n = 11$; $P = 0.05$) referred to pK_{sp}.

In situ *formation of the insoluble compound.* Most hydroxides are special insoluble compounds insofar as they can be generated by changing the pH within a flow system. Various

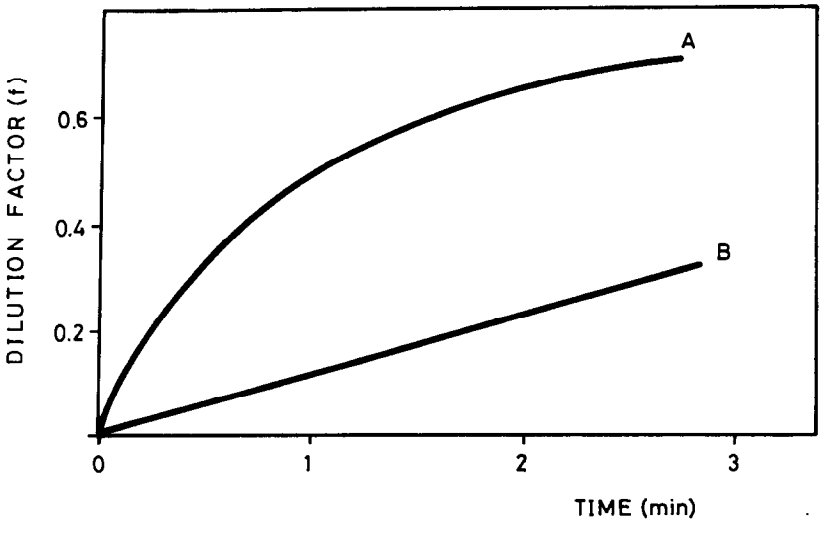

Fig. 3. Variation of the dilution factor (f) in the system as a function of the flow gradient used. Curve A: Q = 1.49 ml/min^2 (q_A changes from 0 to 4.0 ml/min). Curve B: Q = 0.22 ml/min^2 (q_A changes from 0 to 0.6 ml/min). q_B = 1.5 ml/min in all cases.

insoluble hydroxides were studied by using the manifold depicted in Fig. 1 and creating a pH gradient in the flow system. Thus, solution B contained one metal ion (0.010M) in acidic medium (HCl), while solution A was sodium hydroxide at different concentrations in each case (see Table 2). Those concentrations allowed the K_{sp} value to be reached during the experiment. The formation of soluble complexes [like $Al(OH)_4^-$] did not occur because the pH reached in the flow system was not high enough. Precipitates were formed under a pH gradient at a characteristic time dependent on the intrinsic solubility. The process was monitored conductometrically and yielded a recording such as that shown in Fig. 4 (curve A). The conductivity decreased dramatically through disappearance of H^+ ions (highly conductive) by neutralization with OH^- ions (part 1 in curve a). When the product of the ion concentrations equalled K_{sp}, the precipitate started to be formed and the conductivity decreased slowly (part 2 in the curve). Finally, once all the metal had precipitated, OH^- ions were in excess, so the conductivity started to increase (part 3 in the curve). The recordings obtained were quite different from those resulting from replacement of the dissolved metal ion with an acid solution at the same pH (curve B in Fig. 4), which in fact represents an acid–base conductometric titration.

As those precipitation reactions correspond to fast reactions, no kinetic effects were detected. Therefore, the same K_{sp} values were obtained by using different flow gradients. The parameter t_p was changed when the Q value was modified, keeping the constants of the solubility product the same by applying the equations described below.

The process can be better studied by using a conductometric and a potentiometric (pH) detector arranged in series, in order to obtain both conductometric and potentiometric information, as is shown in Fig. 5, where curves A′ and B′ were obtained in the presence of metal ion [0.010M solution of Zn(II) in HCl], whereas curves A and B were recorded in its absence. On comparing curves A and B, and A′ and B′, it is clear that t_p is the time at which the precipitation process starts, so it can be used to calculate the constant of the solubility product:

$$q_T = q_{OH} + q_H = Qt + q_H \qquad (6)$$

where q_{OH} and q_H are the flow-rates of solutions A and B, respectively. At $t = t_p$, $q_{OH} = Qt_p$ and, provided this flow-rate is known, the pH at this time can be readily calculated from the conductivity-time recording.

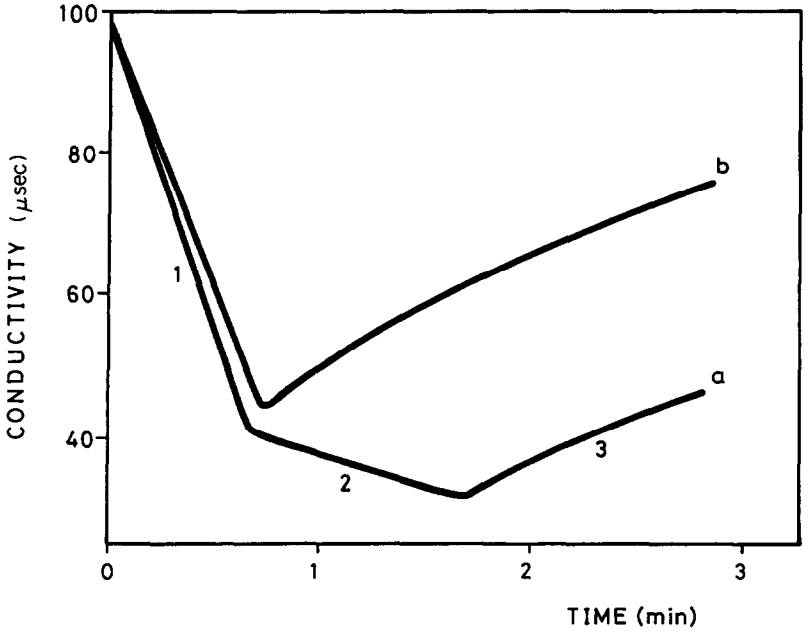

Fig. 4. Conductivity-time recordings obtained by using 0.0246M sodium hydroxide as solution A (Fig. 1), and $10^{-2}M$ $Zn(NO_3)_2$ in $6.3 \times 10^{-3}M$ HCl as solution B (curve a), or in $6.3 \times 10^{-3}M$ HCl alone as solution B (curve b).

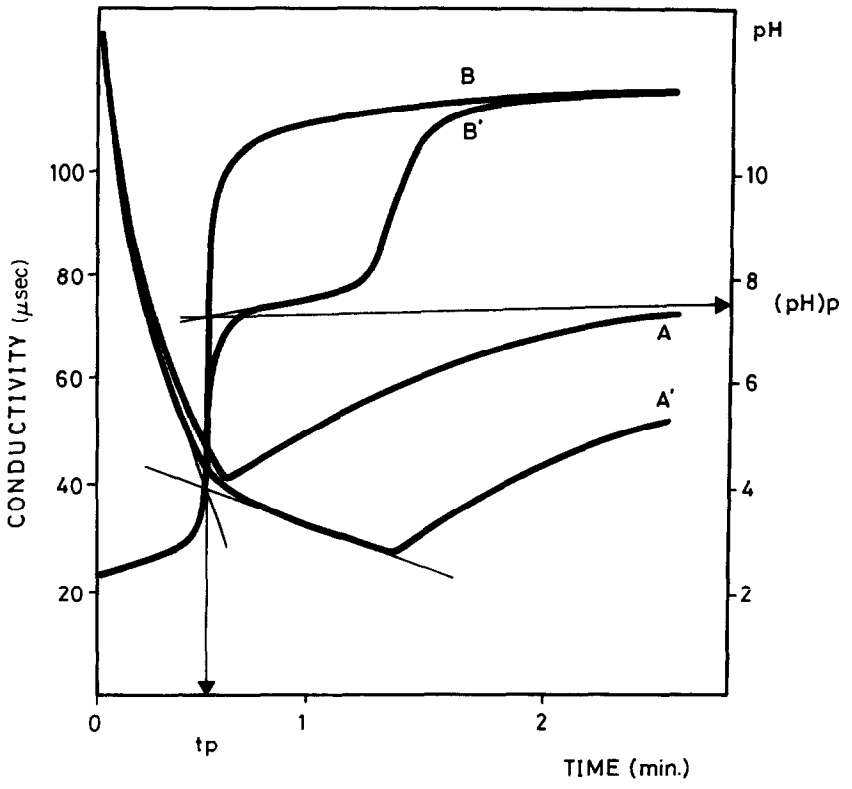

Fig. 5. Conductivity-time (curves A) and pH-time (curves B) recordings obtained for a $10^{-2}M$ $Zn(NO_3)_2 + 6.3\ 10^{-3}M$ hydrochloric acid mixture as solution B (curves A′ and B′), and for a $6.3\ 10^{-3}M$ HCl solution as solution B [curves A and B, which correspond to the experiment performed in the absence of Zn(II)]. $7.58 \times 10^{-3}M$ NaOH was used as solution A in all cases (see Fig. 1).

The concentrations of H^+ and OH^- at the mixing point are:

$$[H^+]_p = [H^+]_0 q_H/(Qt_p + q_H) \quad (7)$$

$$[OH^-]_p = [OH^-]_0 Qt_p/(Qt_p + q_H) \quad (8)$$

If $[H^+]_p \leqslant [OH^-]_p$ the concentration of OH^- after the confluence point is determined as:

$$[OH^-]_{tp} = [OH^-]_p - [H^+]_p \quad (9)$$

If $[OH^-]_p \leqslant [H^+]_p$ the concentration of H^+ after the mixing point is calculated as:

$$[H^+]_{tp} = [H^+]_p - [OH^-]_p \quad (10)$$

then, the OH^- concentration could be determined through:

$$[OH^-]_{tp} = 10^{-14}/[H^+]_{tp} \quad (11)$$

The metal ion concentration at t_p can be calculated from the equation:

$$[M]_{tp} = [M]_0 q_H/(Qt_p + q_H) \quad (12)$$

where $[M]_0$ is the metal ion concentration in solution B. So, the constant of solubility product will be given by:

$$K_{sp} = [M][OH^-]^m = [M]_{tp}[OH^-]^m_{tp}$$

where m is the stoichiometry of the hydroxide.

The use of potentiometric measurements has some advantages over conductometric ones in this case. Thus:

t_p is better defined in the graphs under all conditions.

The pH (concentration of the precipitating reagent) can be obtained directly from the graphs depending on the t_p value. Therefore, no algebraic calculation is required.

Table 2 summarizes the results obtained for three different insoluble hydroxides by using this methodology and two pH gradients along the flow system. The ionic strength was between 0.01 and 0.03 in all cases. As can be seen, the constants are quite consistent with those reported in the literature[9] (ionic strength, $I = 0$), from which the conditional constants were calculated taking into account the ionic strength.

Table 2. Constants of solubility product obtained by the automatic flow method with *in situ* formation of the insoluble compounds

			Constants of solubility product (pk_{sp})			
	Experimental conditions			Literature values		r.s.d. (%)
Compound	Solution A	Solution B*	Experimental values	$I = 0$	$I = 0.015$	Experimental values
$Ni(OH)_2$	pH = 8.60	pH = 5.20	15.5	15.8	15.4	1.0
	pH = 11.54	pH = 2.83	15.0			1.8
$Zn(OH)_2$	pH = 8.60	pH = 5.20	15.1	14.8	14.5	4.5
	pH = 11.64	pH = 3.03	15.6			2.0
$Al(OH)_3$	pH = 11.50	pH = 2.18	33.5	33.5	32.6†	0.2
	pH = 11.80	pH = 2.20	32.2			0.4

*The concentration of all metal ions was 0.01*M* in all cases.
†For $I = 0.03$

Determination of critical micelle concentrations

The critical micelle concentration (cmc) is a major physicochemical parameter of surfactant compounds which, like constants of solubility product, represents a point or range of concentrations beyond which dramatic changes in the properties of the compound solution occur. Surfactant micelles are of great chemical and biochemical interest in connection with catalysis of chemical reactions,[10] room-temperature phosphorimetry experiments on liquid samples,[11] studies on their similarities with membranes on globular proteins,[12] and solvents used in liquid chromatography.[13] All these uses required the cmc of the surfactant concerned to be known. It should also be noted that this characteristic parameter changes with the experimental conditions, so the literature values only apply under specified conditions and are thus only guidances.

Traditionally the cmc is determined by measuring some physical property related to the micelle formation (*e.g.*, surface tension, osmotic pressure, refractive index, conductivity[14]). Some cmc determinations are also based on the flow injection analysis with a dilution chamber.[15,16] The continuous flow system depicted in Fig. 1 allows the automated determination of the cmc of ionic surfactants in a straightforward manner. Solution A contains the surfactant at a high concentration (much higher than the cmc), while solution B is distilled water (*i.e.*, the situation is similar to that of the determination of constants of solubility product by introducing an insoluble compound into the flow system). A linear dilution factor is also used in this case. Therefore, a non-linear conductivity-time

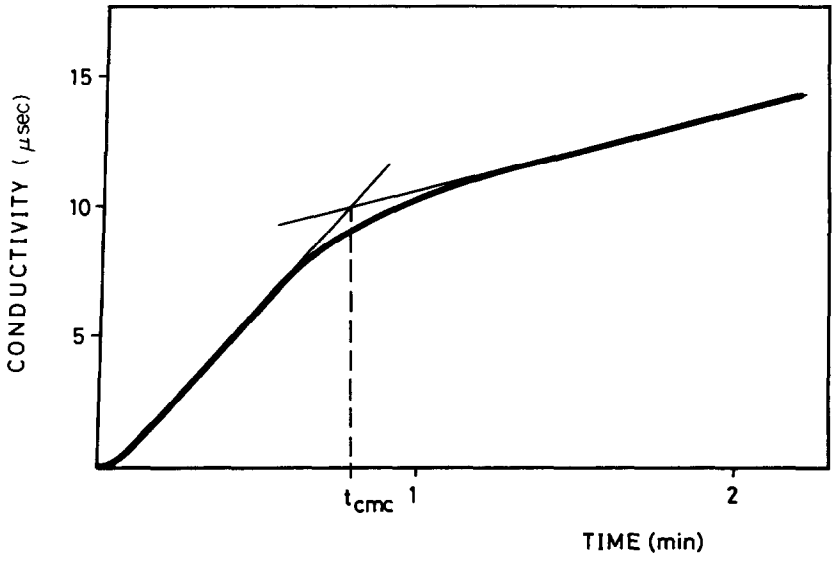

Fig. 6. Conductivity-time recording obtained for sodium dodecylsulphate by using a 0.1*M* solution of this compound as solution A.

Table 3. Critical micelle concentration obtained by using the automatic flow method and the batch procedure

Surfactant	Solution A concentration	cmc Found (m) Flow system	Batch procedure	Literature cmc (M)	r.s.d. (%)
Sodium dodecyl sulphate	0.10	8.4×10^{-3}	7.6×10^{-3}	8.2×10^{-3}	2.8
Sodium dioctyl sulphosuccinate	0.01	3.6×10^{-4}	—	6.8×10^{-4}	4.1
Sodium hexadecyl sulphate	0.01	9.2×10^{-4}	4.7×10^{-4}	7.0×10^{-4}	2.8
Cetylpyridinium chloride	0.01	9.1×10^{-4}	1.0×10^{-4}	9.0×10^{-4}	3.2
Cetyltrimethylammonium bromide	0.01	9.4×10^{-4}	8.6×10^{-4}	9.2×10^{-4}	1.7
Dodecyl trimethylammonium bromide	0.40	1.8×10^{-2}	1.3×10^{-2}	1.6×10^{-2}	5.0

response will be indicative of the occurrence of a process other than dilution, *viz.* micelle formation. Figure 6 shows a typical recording where the two zones of predominance of non-associated molecules surfactants and micelles can be clearly seen. The cmc is related to the time at which the two straight lines intercept (t_{cmc}). The flow-rates are:

$$q_A = Qt_{cmc} \quad \text{and} \quad q_B = \text{constant}$$

so

$$\text{cmc} = [\text{surfactant}]_0 q_A/(q_A + q_B)$$
$$= [\text{surfactant}]_0 Qt_{cmc}/(Qt_{cmc} + q_B)$$

where $[\text{surfactant}]_0$ is the concentration of surfactant in solution A.

The cmc values of various surfactants were determined in this manner and the results obtained are listed in Table 3 compared with those obtained by the batch procedure and those reported in the literature.[14] Under the experimental procedure the ionic strength had a negligible effect due to the low values for this variable. The precision of the automated flow gradient method was ± 2 and $\pm 3\%$ as r.s.d. ($n = 11$, $P = 0.05$).

CONCLUSIONS

As shown in this work, flow gradients in a continuous flow system can be used for the simple, rapid automated determination of physico-chemical parameters. This allows some classical batch determinations to be automated to obtain similar results. This strategy exploits the analytical potential of variable flow-rates in unsegmented flow systems compared to the conventional methods where the flow-rate is kept constant, and expands the possibilities of flow methodologies. The new applications are unaffordable by methods using constant flow-rates. The proposed methodology can also be used to study other properties of chemical systems dependent on the concentration of one of the reactants, as well as perform studies in solvents other than water, taking care of using tubes made out of solvent-compatible materials.

Acknowledgements—The CICyT is acknowledged for financial support (Grant No. PB90/0925). J. Marcos is also grateful to the Basque Government for financial support received through a personal fellowship.

REFERENCES

1. J. Ruzicka and E. H. Hansen, *Flow Injection Analysis*, 2nd Ed., Wiley, New York, 1988.
2. M. Valcárcel and M. D. Luque de Castro. *Flow Injection Analysis. Principles and Applications.*, Ellis Horwood. Chichester, 1987.
3. M. Valcárcel and M. D. Luque de Castro. *Non-Cromatographic Continuous Separation Techniques*, Royal Society of Chemistry. Cambridge, 1991.
4. A. Ríos and M. Valcárcel, *Talanta*, 1991 **38**, 1359.
5. J. Marcos, A. Ríos and M. Valcárcel, *Anal. Chem.*, 1990, **62**, 2237.
6. M. Agudo, J. Marcos, A. Ríos and M. Valcárcel, *Anal. Chim. Acta*, 1990, **239**, 211.
7. J. Marcos, A. Ríos and M. Valcárel, *ibid.*, 1992, **261**, 489.
8. *Idem, ibid.*, 1992, **261**, 495.
9. *Handbook of Chemistry and Physics*, 57 Ed., CRC Press, Cleveland, 1977.
10. M. L. Lunar, S. Rubio and D. Perez-Bendito, *Anal. Chim. Acta*, 1990, **237**, 207.
11. L. J. Cline-Love, M. Skrilec and J. G. Habarta, *Anal. Chem.*, 1980, **52**, 754.
12. R. B. Gennis and A. Jonas, *A. Ann. Rev. Biophys. Bioeng.*, 1977, **6**, 195.
13. M. G. Khaledi, J. K. Strasters, A. H. Rodgers and E. D. Breyer, *Anal. Chem.*, 1990, **62**, 130.
14. M. J. Rosen, *Surfactant and Interfacial Phenomena*. Wiley. New York, 1988.
15. S. H. Brooks, A. Berthod, B. A. Kirsch and J. G. Dorsey, *Anal. Chim. Acta*, 1988, **209**, 111.
16. A. Berthod, S. H. Brooks and J. G. Dorsey, *J. Colloid Interface Sci.*, 1988, **122**, 514.

Talanta, Vol. 40, No. 3, pp. 399–403, 1993
Printed in Great Britain.

0039-9140/93 $6.00 + 0.00

VOLTAMMETRIC AND AMPEROMETRIC DETERMINATION OF ASCORBIC ACID AT A CHEMICALLY MODIFIED CARBON FIBRE MICROELECTRODE

ZHIQIANG GAO* and ARI IVASKA†
Laboratory of Analytical Chemistry, Åbo Akademi University, SF-20500 Turku-Åbo, Finland

TAOXING ZHA, GUANGQING WANG,‡ PEIBIAO LI and ZAOFAN ZHAO
Department of Chemistry, Wuhan University, Wuhan 430072, P.R. of China

(*Received* 15 *May* 1992. *Revised* 30 *June* 1992. *Accepted* 30 *June* 1992)

Summary—A carbon fibre microelectrode was modified by electrodeposition of a thin copper-heptacyanonitrosylferrate (CuHNF) film on its surface. The film showed the ability to catalyse electrochemical oxidation of ascorbic acid. The catalytic reaction was limited either by diffusion, or by the electrochemical reaction of the catalyst. A linear, cyclic voltammetric response for ascorbic acid was obtained between 5.0×10^{-5} and $6.0 \times 10^{-3}M$. By amperometric measurements the linear range could be extended to 8.0×10^{-6}–$2.0 \times 10^{-3}M$. The modified electrode showed good stability and reproducibility.

There has been a lot of interest in developing different kind of biosensors over the recent years.[1–3] Electrochemical biosensors have a number of advantages in detection of biological substances, such as: simple and inexpensive instrumentation, simple sample treatment and fast response time. Electrochemical biosensors are suitable for both *in vivo* and *in vitro* applications, such as transducers in molecular recognition in biological systems.[4–6] Many attempts have been focused on miniaturization of biosensors, which is an important step in development of compact, high performance automatic analytical systems and sensing devices for artificial organs, especially *in vivo* applications. This trend is due to the attractive features these sensors possess. Firstly, the small electrode size and therefore low background current facilitate *in vivo* electrochemical detections,[7] and even detections in single cells.[8] Secondly, due to the small area of the electrode only very low currents will be measured (as low as 10^{-17}A), and therefore the electrodes can be used in high resistive solvents where electrodes of conventional size would encounter high uncompensated *iR* drops.[9] Low currents also allow the electrodes to be used in ultrafast cyclic voltammetry to study fast electrode processes.[10–13] A good number of papers have been published discussing the use of chemically modified microelectrodes as biosensors. Since the pioneering work of Adams the field of *in vivo* electrochemistry has been subject to considerable development.[14] A lot of efforts have been devoted improving the selectivity of neurotransmitter measurements.[15–19] These include the use of electrochemical pretreated, Nafion coated carbon fibre modified electrodes,[15–17] stearic acid modified microelectrodes,[18] or use of a poly(ester-sulphonic acid) coating to exclude anionic interferences from the electrode surface.[19] Hurrel and Abruña[20] employed polymer modified microelectrodes for amperometric determination of calcium. They reported submicromolar sensitivity for their electrodes and a dynamic range that extends over three orders of magnitude. The selectivity, especially toward magnesium was fairly good. Wrighton and co-workers developed a variety of sensors based on chemically modified microelectrode arrays sensitive to pH,[21] hydrogen and oxygen[22] as well as to other chemical species.[23,24] Kuwana *et al.* designed a microcarbon array enzyme glucose electrode that relied on the catalytic

*On leave from Henan University, Kaifeng 475001, P.R. of China.
†To whom correspondence should be addressed.
‡Present address: Department of Chemistry, Yan'an University, Yan'an Shanxi, P.R. of China.

monitoring of unconsumed oxygen.[25] Dong *et al.* have studied reduction of ascorbic acid with a Prussian Blue modified platinum microdisk electrode.[26]

We have recently reported how the overpotential of reduction and oxidation of hydrogen peroxide at glassy carbon electrode can be reduced by modifying the electrode surface with copper-heptacyanonitrosylferrate, CuHNF.[27] In this work we present the results obtained on electrocatalytic oxidation of ascorbic acid at a carbon fibre microelectrode modified by electrodeposition of a thin film of CuHNF.

EXPERIMENTAL

Chemicals

All chemicals used were of certified analytical grade and used without further purification. The solutions were prepared from double distilled water. Ascorbic acid solution was stored under nitrogen in a refrigerator. Potassium heptacyanonitrosylferrite solution was prepared daily.

Electrode and apparatus

Electrochemical experiments were performed with a low current–low noise potentiostat (Shanming Electronic Factory, Fujian, P.R. of China) equipped with a Type 3086 X-Y recorder (Yokogawa Hokushin Electric, Tokyo, Japan). A three-electrode system consisting of a chemically modified carbon fibre microelectrode (CMCFME), a platinum wire auxiliary electrode and a saturated calomel reference electrode (SCE) were used in all electrochemical measurements. All potentials given in this paper are measured *vs* the SCE. High purity nitrogen was used to remove oxygen from the solutions. Glass sealed carbon fibre microelectrodes were prepared according to the procedure described by Wightman and Vipf.[28] The fibre end is flush with the glass surface, making it easy to polish. Carbon fibres were obtained both from Union Carbide Co (New York) and Amoco Performance Products, Inc. (Greenville, SC).

Modification procedure

Before modification of the surface, the carbon fibre electrodes were polished first with fine polishing paper and then with 0.3- and 0.05-μm alumina. The electrodes were then cleaned in an ultrasonic bath with water and acetone for 10 min. The CuHNF film was then deposited on the surface of the electrodes by scanning them from 0.5 to -0.4 V in an oxygen free $4 \times 10^{-3}M$ $CuSO_4$–1.0M KCl solution with a scan rate of 20 mV/sec and then keeping the potential at -0.4 V for 30 sec. The electrodes were then removed from the solution, rinsed with water thoroughly and transferred into a $5 \times 10^{-3}M$ $K_2(Fe(CN)_5NO)$ solution where they were potential cycled for 10 min in the range of -0.4–0.5 V with a scan rate of 20 mV/sec. After rinsing thoroughly with water, the electrodes were ready for experiments.

RESULTS AND DISCUSSION

Evaluation of the quality of the electrode preparation

In order to obtain highly reproducible results, it is essential, after the electrode preparation, to evaluate the electrochemical behaviour of the electrode as well as its effective radius. Oxidation of hexacyanoferrate(II) at the electrodes in a 1M potassium chloride solution was selected as the evaluation reaction because the diffusion coefficient of this system is known.[29] Figure 1 illustrates a number of cyclic voltamperograms of glass sealed carbon fibre microelectrodes. At low scan rates the voltamperograms have sigmoidal shape due to the steady-state diffusion to the electrode surface and because a significant fraction of the current passes at the edges of the electrode.[28] Equation (1) describes the current under mass transfer limited, steady-state conditions at a microdisk electrode:[28]

$$i = 4nFDrC \qquad (1)$$

where n is the number of electrons transfered, F is the Faraday constant, D is the diffusion

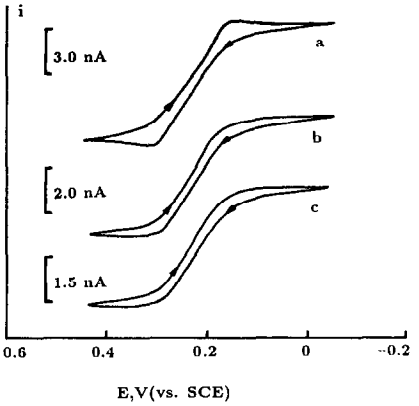

Fig. 1. Cyclic voltamperograms with 50 mV/sec scan rate of 1.0mM $K_3FeCN)_6$ in 1.0M KCl at carbon fibre microelectrodes of different radius: (a) 30, (b) 20 and 15 μm.

coefficient, r is the radius of the electrode and C is the bulk concentration of the depolarizer. Knowing the values of D, C, F, n and measuring the current, the effective radius of the electrode can be determined. In our studies we found the radius to be in good agreement with the values given by the carbon fibre manufacturers.

To study the effect of deposition time of copper at −0.4 V on the behaviour of the modified electrode the following experiment was conducted. After the linear scan from 0.5 to −0.4 V in a 4mM solution of copper sulphate the electrode was held for different lengths of time at −0.4 V before proceeding with the modification procedure as described in the Experimental section. The results of this study are shown in Fig. 2. As can be seen, 30 sec is enough to produce a film with reversible cyclic voltammeric behaviour. When longer deposition times or higher Cu(II) concentrations were used, the stability of the film as well as the amount of modifier on the electrode surface were decreased. With increased deposition time, the cyclic voltammetric response of the film became more sluggish. When a newly formed CMCFMF electrode was cycled in 1.0M potassium chloride, pronounced tailing at the negative end of the voltamperogram was observed. With increasing number of scans the tailing of the i-E curve disappeared gradually. This behaviour of the film may be due to migration of free Cu^{2+} from the lattice of the film to the solution. Due to the larger radius of Cu^{2+}, 3.25 Å, it is more difficult for these ions to be transported through the film than the smaller potassium ions with the radius of 1.25 Å.[30] After several cycles, all the interspatial Cu^{2+} is replaced by potassium ions and a typical steady-state i-E curve is obtained

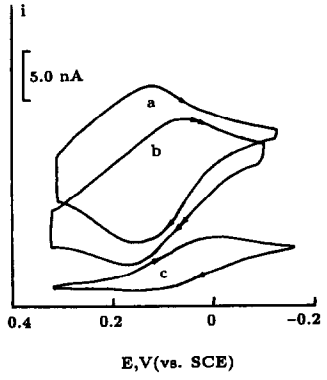

Fig. 2. Cyclic voltamperograms with 50 mV/sec scan rate of the CMCFME ($r = 25$ μm) under different deposition time in 4mM $CuSO_4$–1.0M KCl solution: (a) 30 sec, (b) 60 sec and (c) 240 sec.

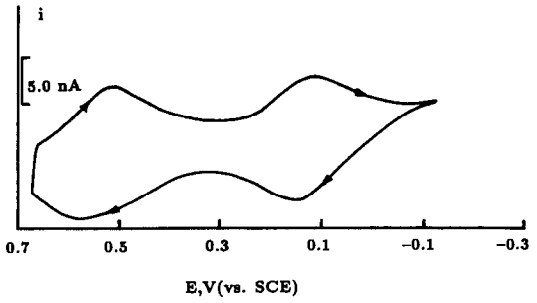

Fig. 3. Cyclic voltamperogram with 50 mV/sec scan rate of CMCFME ($r = 20$ μm) in 1.0M KCl solution.

as shown in Fig. 3. It can be seen that there are two couples of redox peaks in the potential range studied, one at 0.14 V and the other one at 0.59 V. Mössbauer spectra indicated that the redox couples at 0.14 V and 0.59 V are Cu(I)/Cu(II) and Fe(II)/Fe(III), respectively.[31]

It was interesting to notice that when the potential was scanned in the range of −0.5 V to 0.9 V the peak current of the redox couple at 0.14 V decreased markedly and disappeared after a dozen scans. But the peak current of the redox couple at 0.59 V remained unchanged.[27] The reason for this change is not clear yet. It might be that a new structure in the Cu(II)–Fe(III)$(CN)_5NO$ compound is formed and Cu(II) is not capable of undergoing redox reactions any more. As long as the potential, however, was kept less positive than 0.5 V the CMCFME did exhibit stable cathodic and anodic waves at 0.14 V. As will be discussed below, only the redox couple at 0.14 V has the catalytic effect on the oxidation of ascorbic acid. The catalytic ability of the film can be maintained as far as potentials less than 0.5 V are used.

The peak currents of our electrodes at 0.14 V were found to be proportional to the potential scan rate indicating that the modified microelectrode behaves exactly as could be expected of a reversible, surface immobilized redox couple.[32] The cyclic voltamperogram at a CMCFME with radius smaller than 5 μm, however, differed from that of an electrode with larger radius. The peak shaped voltamperogram disappeared and instead, a sigmoidal shaped voltamperogram was observed. In this case, however, it was very difficult to obtain a good CuHNF film on the electrode surface as well.

The electrode behaviour was not found to depend on pH within the range 2–8 in pure electrolyte solutions as long as the solution contained excess of potassium or sodium ions.

Although the shape of the wave at 0.14 V was slightly affected by the pH, the peak potentials were almost the same in pH 2 to 8. Beyond this pH range the CMCFME was unstable and the modified film was rapidly destroyed, especially in strong alkaline media.

Stability of the CMCFME upon scanning was tested in potassium or sodium containing solutions in the pH range 2–8, by performing 100 cyclic voltammetric scans with a scan rate of 50 mV/sec, in the range of −0.5 to 0.5 V. No significant changes either in cathodic or anodic current (<5%) could be observed. The electrode was found to possess additionally good mechanical stability when the solution was stirred with a magnetic stirbar.

Electrocatalysis of ascorbic acid at the CMCFME

The catalytic function of CMCFME upon oxidation of ascorbic acid is shown in Fig. 4. The cyclic voltamperogram obtained in 1*M* potassium chloride, curve (a), is changed in the presence of 0.6m*M* ascorbic acid, curve (b). When the oxidation of ascorbic acid is studied at a naked carbon fibre microelectrode a broad wave, however, is observed, indicating an irreversible electron transfer process.[26] In addition, the electrode reaction of ascorbic acid at a naked carbon fibre microelectrode depends on the electrode pretreatment as well.[33] The peak potential of ascorbic acid oxidation at the CMCFME is also about 200–300 mV less positive

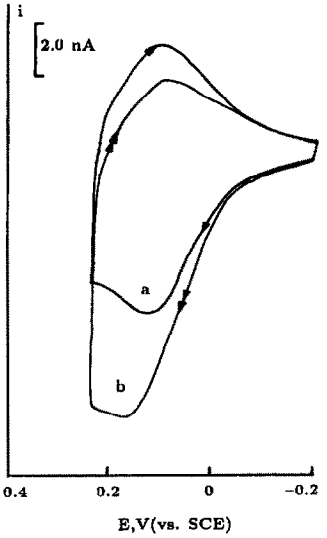

Fig. 4. Cyclic voltamperograms, 50 mV/sec scan rate, of a CMCFME ($r = 20$ μm) in (a) 1.0*M* KCl solution and (b) 0.6m*M* ascorbic acid + 1.0*M* KCl.

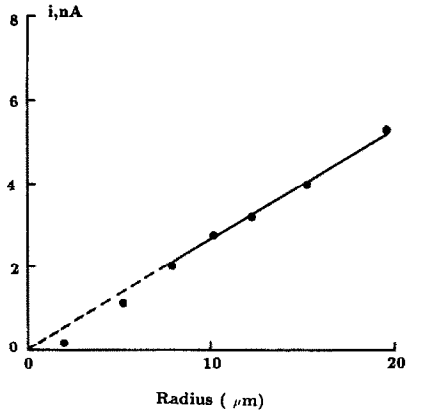

Fig. 5. Cyclic voltammetric peak current of ascorbic acid as function of the radius of the CMCFME in 1.0m*M* ascorbic acid and 1.0*M* KCl. The scan rate used was 10 mV/sec.

than that at the naked carbon fibre microelectrode. The catalytic activity of the redox couple at 0.14 V obviously mediates in the oxidation of ascorbic acid and reduces the high overpotential otherwise observed at solid electrodes. The peak potential of oxidation is not found to be affected by the ascorbic acid concentration.

At low potential scan rates, $v < 10$ mV/sec, the voltamperogram of ascorbic acid oxidation reached the steady state at the CMCFME. With increasing potential scan rate, however, a peak shape voltamperogram appeared indicating that only quasi steady state was reached. By using small radius microelectrodes ($r < 5$ μm) a steady state could be reached even at high potential scan rates. It was interesting to note that the limiting current of ascorbic acid oxidation at the CMCFME (5 μm) was lower than that at a naked carbon fibre microelectrode. This indicates that the overall reaction rate of the system is mainly controlled by the catalytic reaction, not by diffusion of ascorbic acid to the electrode. A similar result was obtained by Dong *et al.* in their studies on PB modified electrodes.[26,34] If oxidation of ascorbic acid at CMCFME is controlled solely by diffusion, the relationship between limiting current of ascorbic acid oxidation and the radius of modified microelectrode would follow equation (1), *i.e.*, the plot of the limiting current *i vs.* the radius *r* is a straight line. Figure 5 shows the plot of the limiting current of ascorbic acid oxidation as a function of the radius of the CMCFME. As can be seen the plot is no longer linear with electrodes with very small radii. This indicates that the overall process of ascorbic acid oxidation changes from diffusion controlled to

catalytic reaction controlled process with decreasing radius of the microelectrode. The same tendency was also observed when the concentration of ascorbic acid is increased but keeping the electrode radius constant.

For quantitative determination of ascorbic acid, a CMCFME with a relative large radius ($r = 20\ \mu m$) was used. Due to the mass transfer limited current of ascorbic acid oxidation at this electrode, a linear calibration curve could be expected. A linear, cyclic voltammetric response was obtained at a scan rate of 50 mV/sec with the ascorbic acid concentration from 5×10^{-5} to $6 \times 10^{-3} M$. A linear least square fit yielded the slope of 6.3 nA/mM with a correlation coefficient of 0.997. The relative standard deviations ($n = 10$) were 3.1 and 6.7% at the high end and at the low end of the calibration plot, respectively.

Amperometric determination of ascorbic acid at CMCFME

Quantitative determination of ascorbic acid was also done amperometrically in a stirred solution. Potential of the electrode was kept at 0.2 V corresponding to the beginning of the limiting current of ascorbic acid oxidation. The amperometric response was measured when a series of successive standard additions of ascorbic acid was made to the solution. Linear response was found in the concentration range 8×10^{-6}–$2 \times 10^{-3} M$. The slope of the calibration graph was 6.55 nA/mM and the correlation coefficient 0.998. The relative standard deviations ($n = 10$) were 2.3 and 5.1% at the high end and at the low end of the calibration plot, respectively.

CONCLUSIONS

Oxidation of ascorbic acid on naked carbon electrodes requires a high overpotential. Normally oxidation takes place in the range 0.4–0.5 V. This results in high background currents and interferences from other substances that are oxidized in this or lower potential range.[5] The CMCFME allows electrochemical detection of ascorbic acid at significantly lower potentials and therefore improves the selectivity of the determination as well as the sensitivity due to the higher signal-to-noise ratio. Amperometric determination of ascorbic acid at CMCFME certainly will find useful applications with biosensors.

REFERENCES

1. R. K. Kobos, *Trends in Anal. Chem.*, 1987, **6**, 6.
2. P. W. Carr and L. D. Bowers, *Immobilized Enzymes in Analytical and Clinical Chemistry*, Wiley, New York, 1980.
3. P. G. W. Brown, *Trends in Biotechnol.*, 1985, **3**, 200.
4. K. Morita and Y. Shimizu, *Anal. Chem.*, 1989, **61**, 159.
5. J. E. Frew and H. A. O. Hill, *ibid.*, 1987, **59**, 933A.
6. Y. Ikariyama, S. Yemauchi, T. Yukiashi and M. Ushioda, *J. Electroanal. Chem.*, 1988, **251**, 267.
7. R. M. Wightman, L. J. May and A. C. Michael, *Anal. Chem.*, 1988, **60**, 769A.
8. R. A. Wallingford and A. G. Ewing, *ibid.*, 1988, **60**, 1972.
9. R. M. Wightman, *ibid.*, 1981, **53**, 1125A.
10. K. B. Oldham, C. G. Zoski, A. M. Bond and D. A. Sweigart, *J. Electroanal. Chem.*, 1988, **248**, 467.
11. C. P. Andrieux, D. Garreau, P. Hapiot and J. M. Saveant, *ibid.*, 1988, **248**, 447.
12. J. O. Howell and R. M. Wightman, *J. Phys. Chem.*, 1984, **88**, 3915.
13. S. Pons and M. Fleischmann, *Anal. Chem.*, 1987, **59**, 1391A.
14. P. T. Kissinger, J. B. Hart and R. N. Adams, *Brain Res.*, 1973, **55**, 209.
15. M. P. Brazell, R. J. Kasser, K. J. Renner, J. Feng, B. Moghaddam and R. N. Adams, *J. Neurosci. Meth.*, 1987, **22**, 167.
16. G. A. Gerhardt, A. F. Oke, G. Nagy, B. Moghaddam and R. N. Adams, *Brain Res.*, 1984, **290**, 390.
17. P. Hulthe, B. Hulthe, K. Johannessen and J. Engel, *Anal. Chim. Acta.*, 1987, **198**, 197.
18. P. A. Broderick, *Brain Rev.*, 1989, **495**, 115.
19. J. Wang and M. S. Lin, *Electroanalysis*, 1990, **2**, 253.
20. H. C. Hurrel and H. D. Abruña, *Anal. Chem.*, 1988, **60**, 254.
21. M. J. Natan, T. E. Mallouk and M. S. Wrighton, *J. Phys. Chem.*, 1987, **91**, 648.
22. J. W. Thackeray and M. S. Wrighton, *J. Phys. Chem.*, 1986, **90**, 6074.
23. J. W. Thackeray, H. S. White and M. S. Wrighton, *ibid.*, 1985, **89**, 5133.
24. D. Belanger and M. S. Wrighton, *Anal. Chem.*, 1987, **59**, 1426.
25. S. Dong and T. Kuwana, *Electroanalysis*, 1991, **3**, 485.
26. S. Dong and G. Che, *J. Electroanal. Chem.*, 1991, **315**, 191.
27. Z. Gao, A. Ivaska, P. Li, K. Lui and J. Yang, *Anal. Chim. Acta*, 1992, **259**, 211.
28. R. M. Wightman and D. O. Wipf, in A. J. Bard (ed.), *Electroanalytical Chemistry*, Vol. **15**, Marcel Dekker, New York, 1989, p. 268.
29. K. Aoki and J. Osteryoung, *J. Electroanal. Chem.*, 1981, **125**, 315.
30. L. Meters, *Handbook of Analytical Chemistry*, McGraw-Hill Book Company, New York, 1963.
31. Z. Gao, PhD Dissertation, 1990, Wuhan University, Wuhan, China.
32. A. J. Bard and L. R. Faulkner, *Electrochemical Methods*, Wiley, New York, 1980.
33. F. G. Gonon, C. M. Fombariet, M. J. Buda and J. F. Pujol, *Anal. Chem.*, 1981, **53**, 1386.
34. F. Li and S. Dong, *Electrochim. Acta*, 1987, **32**, 1511.

Talanta, Vol. 40, No. 3, pp. 405–407, 1993
Printed in Great Britain.

0039-9140/93 $6.00 + 0.00

FLOW-INJECTION DETERMINATION OF 9,10-PHENANTHRENEQUINONE WITH CATALYTIC PHOTOMETRIC DETECTION

NOBUTOSHI KIBA, HIROSHI SUZUKI, EIICHI GOTO and MOTOHISA FURUSAWA
Department of Applied Chemistry and Biotechnology, Faculty of Engineering, Yamanashi University, Kofu 400, Japan

(*Received* 22 *April* 1992. *Accepted* 30 *June* 1992)

Summary—A catalytic photometric method with a flow-injection system is described for the determination of 9,10-phenanthrenequinone. It is based on the catalytic effect of 9,10-phenanthrenequinone on the redox reaction of 1,2-dinitrobenzene with formaldehyde under alkaline conditions. 9,10-Phenanthrenequinone at the 5.0×10^{-8}–$5.0 \times 10^{-6}M$ level can be determined at a rate of 20 samples/hr. The detection limit is 1.0×10^{-8} M (40 pg in a 10-μl injection).

9,10-Phenanthrenequinone (PQ) has been shown to possess photosensitivity and is used as a photoreceptor and photoinitiator in photoresistors.[1,2] The PQ content in photopolymers influences the sensitivity and stability of the resistors. PQ has been determined spectrophotometrically[3,4] and fluorimetrically,[5] but the methods were unsuitable for the rapid analysis of a large number of samples. PQ catalyses the reduction of 1,2-dinitrobenzene to nitrophenyl hydroxylamine dianion (λ_{max}: 560 nm) in the presence of formaldehyde. The reaction was used for the spot-test of PQ down to 2 ng.[6,7] The catalytic reaction was applied to the determination of catecholamines in alkaline dimethyl sulphoxide as solvent.[8]

Kinetic methods based on catalytic reactions are useful in trace analysis because of the sensitivity and selectivity. Though many batch techniques for kinetic catalytic analysis have been used, care must be exercised to control the reaction time. In a flow-injection system, the reaction time can easily be controlled by varying a flow-rate and length of reaction coil.[9]

In this paper, a flow-injection photometric method for the determination of PQ based on the catalytic effect on the reduction of 1,2-dinitrobenzene with formaldehyde is reported. The conditions for the catalytic reaction were studied in order to adapt it to a flow-injection system. This method was applied to the determination of PQ in photopolymer.

EXPERIMENTAL

Reagents

1,2-Dinitrobenzene (DNB) and 30% formaldehyde (FA), which were obtained from Nacalai Tesque (Kyoto, Japan), were used as received. Dimethyl sulphoxide (DMSO), which was from Wako Chemicals (Tokyo, Japan), was purified by a refrigeration method.[10] All other chemicals were of analytical-reagent grade.

Apparatus and procedure

A schematic diagram of the flow-system is shown in Fig. 1. A sodium hydroxide solution (3M) and reagent solution which consisted of 3mM DNB and 3M FA in DMSO were pumped by a reciprocating pump of the double plunger type (Kyowa Seimitsu, KHU-W-52)

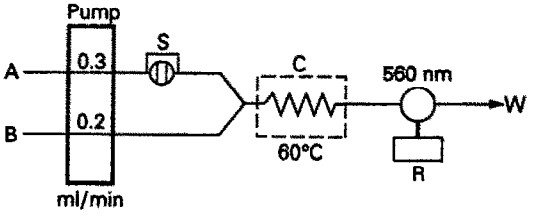

Fig. 1. Schematic diagram of the flow-injection system for the determination of 9,10-phenanthrenequinone. A: reagent solution (3mM 1,2-dinitrobenzene and 3M formaldehyde in DMSO), B: 3M NaOH, S: sample injector with 10-μl loop, C: reaction coil (10 m × 0.5 mm i.d.) kept at 60°, D: spectrophotometer, R: data processor, W: waste.

at a total flow-rate of 0.5 ml/min. Samples were introduced with an injection valve (Sanuki, SV1-SU7) with a 10-μl loop. The reaction coil (10 m × 0.5 mm) was kept at 60° in a water-bath. The absorbance at 560 nm was monitored with a spectrophotometer (Jasco, Uvidec-100-VI), the output being fed to a data processor (System Instrument, Chromatocorder II). The flow channel was assembled from 0.5-mm bore Teflon tubing and stainless steel connectors.

RESULTS AND DISCUSSION

Optimization

The effect of temperature on the reaction was examined over the range 50–70°. As shown in Fig. 2, the response was essentially constant from 60–65°. The decrease in response at higher temperature may be attributed to the thermal lability of the product.

The effect of sodium hydroxide concentration in the reaction coil was examined in the concentration range 0.4–1.2 *M*. The response increased exponentially according to the second power of the concentration (Fig. 3). Above the concentration of 1.3*M*, base line stability was poor because sodium hydroxide is slightly soluble in aqueous DMSO solution.

The response was dependent on the composition of aqueous DMSO solution. The total flow-rate was kept constant at 0.5 ml/min and the ratio of flow-rates for the sodium hydroxide solution and the reagent solution which contained 75% DMSO was changed from 0.5:4.5 to 4.5:0.5. The response increased gradually with increasing content of DMSO in the reaction medium. At higher flow-rates of the reagent solution, the base line was unstable because of incomplete mixing and poor sodium hydroxide solubility. A flow-rate of 0.2 ml/min for the sodium hydroxide solution and a flow-rate of 0.3 ml/min for the reagent solution were selected, as a compromise between sensitivity and base line stability.

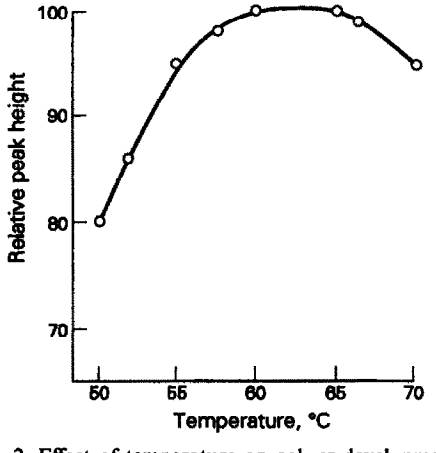

Fig. 2. Effect of temperature on colour development.

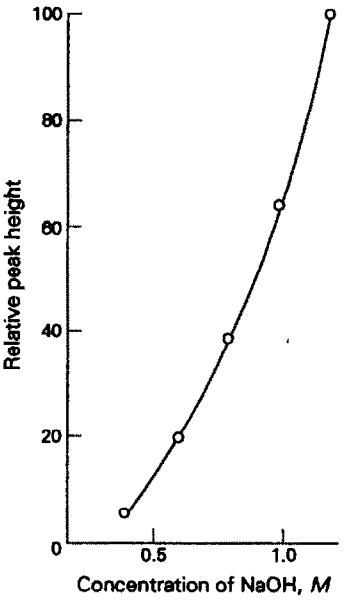

Fig. 3. Effect of NaOH concentration on colour development.

Since the catalytic reaction proceeds with the elapse of time, the peak height depends on the flow-rate and reaction coil length. The lower flow-rates gave higher peaks but the baseline reversion times were increased. A total flow-rate of 0.5 ml/min was selected, taking account of the sensitivity and the rate of sampling. Under the conditions the rate of sampling was 20/hr.

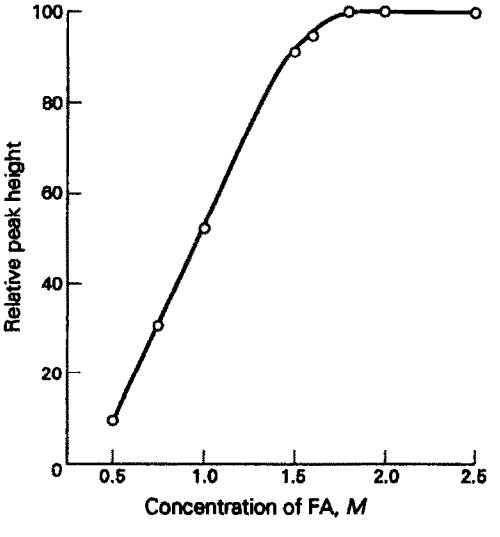

Fig. 4. Effect of concentration of formaldehyde on colour development

Table 1. Interference of various quinones on the determination of 5.0×10^{-7} *M* PQ

Quinones	Concentration ($\times 10^{-7}M$)	Error (%)	Response RSD (%)
1,2-Benzanthraquinone	50	0.0	1.0
Anthraquinone	50	0.0	0.91
1,2-Naphthoquinone	50	2.5	1.3
1,4-Naphthoquinone	50	15.6	1.9
	20	5.3	1.4
2-Methyl-1,4-naphthoquinone	50	5.3	1.5
	20	2.2	1.3
2,3-dichloro-1,4-naphthoquinone	50	3.8	1.4
	20	1.3	1.2

Table 2. Results for PQ in photosensitive resin

Content* %	Peak height† Absorbance	Found %
0.50	0.704 (1.1)	0.51
1.0	0.843 (0.88)	1.00
2.0	0.981 (0.98)	2.01
3.0	1.06 (0.97)	3.00
4.0	1.12 (1.2)	3.99
5.0	1.16 (1.4)	4.98

*Obtained from the data presented by manufacturers.

†All values are means ($n = 9$) with relative standard deviation (%) in parentheses.

The effect of FA concentration on the response is shown in Fig. 4. The response increased as the concentration increased and above the concentration of 1.8 *M* it was constant.

The reaction was found to be independent of the DNB concentration between 1.5–3.0m*M*.

Interference

The selectivity of the reaction was examined by studying the effect that $1.0 \times 10^{-6}M$ concentration of various quinones had on the determination of $5.0 \times 10^{-7}M$ PQ. The results, summarized in Table 1, show that the method provides good precision with relative standard deviation values of less than 2.0% in the absorbance measurements (7 replicates).

Calibration graph

The calibration graph was obtained from different concentrations of PQ under the same conditions as shown in Fig. 1. The graph was linear over the range 5.0×10^{-8}–$5.0 \times 10^{-6}M$. The linear regression equation was $y = 0.460x + 3.751$ with a correlation coefficient of 0.992 ($n = 21$), where y and x are absorbance and log[PQ concentration (M)], respectively.

Application

Table 2 shows the results for the determination of PQ in photosensitive resin prior to photoirradiation, which was coated in a 60-μm thick layer on circuit boards. The resin contains dimethylaminoethyl methacrylate–methyl methacrylate copolymer (56.0–60.5 wt%), pentaerythritol triacrylate (27%), tetraethylene glycol diacrylate (10%), tribromoethylphenyl sulphone (2%) and PQ (5.0–0.5%). The resin (0.1 mg) which was scraped from the boards was dissolved in 10.0 ml of DMSO. The solution (10 μl) was injected into the system.

It is concluded that the flow-injection system with catalytic reaction is useful for the sensitive, rapid and reliable measurement of PQ. The proposed method could easily be used for the determination of PQ in the photopolymer.

REFERENCES

1. K. Masaoka, Y. Minami and H. Kakumaru, *Jpn. Kokai Tokkyo Koho JP 01*, 1989, **177**, 535.
2. A. Moromoto, *Jpn. Kokai Tokkyo Koho JP 63*, 1988, **246**, 749.
3. E. Sawiki and W. Elbert, *Anal. Chim. Acta*, 1960, **22**, 448.
4. I. A. Aolotarevskaya and A. I. Kamneva, *Zh. Anal. Khim.*, 1972, **27**, 1227.
5. M. Tachibana, M. Hayakawa and M. Furusawa, *Bull. Chem. Soc. Jpn.*, 1982, **55**, 3520.
6. F. Feigl and C. C. Neto, *Anal. Chem.*, 1956, **28**, 397.
7. F. Feigl and V. Anger, *Spot Test in Organic Analysis*, 6th Ed., p. 330. Elsevier, Amsterdam, 1972.
8. N. Kiba, T. Mizuno and M. Furusawa, *J. Chromatogr.*, 1955, **329**, 147.
9. T. Yamane and N. Kiba, *Bunseki*, 1990, 357.
10. M. Tachibana and M. Furusawa, *Bull. Chem. Soc. Jpn.*, 1988, **61**, 2353.

Talanta, Vol. 40, No. 3, pp. 409–413, 1993
Printed in Great Britain.

0039-9140/93 $6.00 + 0.00

ATOMIC ABSORPTION DETERMINATION OF TRACES OF CADMIUM IN URINE AFTER ELECTRODEPOSITION ONTO A TUNGSTEN WIRE

GUIEN ZHANG, JINGHUA LI, DEXUE FU, DAQING HAO and PINGPING XIANG
Dept. of Chem., Henan Normal University, Xin Xiang, Henan, 453002, P.R. China

(*Received* 22 *April* 1992. *Revised* 30 *June* 1992. *Accepted* 30 *June* 1992)

Summary—A three-coil tungsten wire is used as electrode for the preconcentration of cadmium, which is then placed in a graphite tube for atomization and atomic absorption measurement. The heating parameters of the graphite furnace are optimized using the Modified and Weighted Centroid Simplex Method (MWCS), and computer program for automatic calculation. Sulphuric acid is selected as the supporting electrolyte for electrodeposition. The linear range of the calibration graph is 0.00–0.55 ng/ml. The detection limit is 0.01 ng/ml. For 0.1 ng/ml cadmium the coefficient of variation is 3.35% for ten parallel determinations. No interference occurs in the presence of more than 20 coexisting ions. Traces of cadmium in urine of normal people and in river water and the recoveries for cadmium are determined. The results are satisfactory.

There have been numerous reports on the determination of traces of metal ions using preconcentration by electrodeposition together with the graphite furnace atomic absorption method[1–9]. Earlier, researchers tried to increase the sensitivity by deposition on a metal wire followed by atomization in a fire, but that method is only equal in sensitivity for the level of solution sampling in a graphite tube. Czobik[16] placed the cathode with deposited metal directly into a graphite tube and successfully determined Cd of sea water and blood serum. Yet, because the tungsten wire length was limited, the effective area was small and the sensitivity was low. In this paper we present a new approach. Atomic absorption determination is performed using an electrode of tungsten wire with 3 coiled turnings matched with the graphite tube diameter with increased effective area and sensitivity.

The modified and weighted centroid simplex method

MWCS is used to optimize the conditions for the determination, performed automatically using a program on a PB-700 computer. Traces of cadmium in urine of normal people and river water have been determined.

EXPERIMENTAL

Instruments and reagents

The following materials were used: a Dao Jin AA-670 atomic absorption spectrometer, pyrolitically coated graphite tubes (Dao Jin catalog 200–54525-045), a HDV-7 Transistor potentiostat.

Cadmium standard solution, 1 mg/ml. Weigh 0.2282 g of specpure reagent 3 $CdSO_4 \cdot 8H_2O$, dissolve in 0.1*M* sulphuric acid and dilute to 100 ml with 0.1*M* sulphuric acid.

Electrodeposition equipment and procedure

The electrode is made of tungsten wire which is 0.3 mm in diameter and wound to 3 turnings. Before using it, burn the graphite furnace twice till its surface turns shiny. Its absorbance is then zero.

An HDV-7 potentiostat is used as the power source, the three-winding tungsten wire is the cathode, a platinum electrode is the anode, a saturated calomel electrode is the reference electrode, and saturated potassium chloride solution is contained in the reference cell. A potassium chloride salt-bridge connects the electrolysis and reference cell.

Add 20.0 ml of sample solution containing 0.1*M* sulphuric acid to the electrolysis cell, insert the electrodes and then stir the solution. The controlled cathode potential is −1.0 V (*VS.*SCE) and the preconcentration time is 2 min. Remove the electrode without interrupting the power. Use filter paper to carefully remove the electrolyte from the tungsten wire and then place it in the graphite tube in such a way that the light is parallel to the surface of the

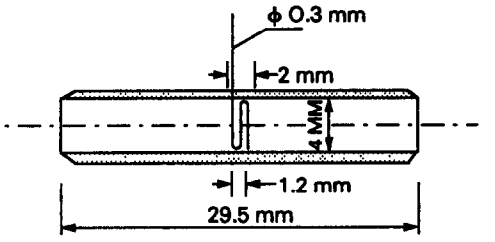

Fig. 1. Tungsten wire shape and match of wire and graphite tube.

three-winding tungsten wire, i.e. passes through the centre of the coil.

Initiate the heating cycle of the graphite furnace, and record the absorbance.

Conditions for atomic absorption measurement

Wave length: 228.8 nm, slit width: 0.3 nm, hollow cathode lamp electric current: 6 mA, argon flow: 1.5 l./min.

The heating program of the graphite furnace was as follows:

dry: 100°, 20 sec; ashing (ramp): 250°, 10 sec; atomization (stair): 1500°, 3 sec; cleaning: 2000°, 2 sec.

RESULT AND DISCUSSION

Study of the shape of the tungsten wire and match of the wire and the graphite tube

Tungsten wire can withstand high temperatures, is chemically stable and can form various shapes. Therefore, tungsten wire is used as the material for the cathode. In order to increase the sensitivity of the analysis and to enlarge the surface area for electrolysis, 3 windings wire are used. The coil is smaller than the diameter of the sampling hole of the graphite tube and its diameter is smaller than the inner diameter of the graphite tube, i.e., 4 mm high long and 1.2 mm wide (Fig. 1). This matches the graphite tube well (Fig. 1). In the graphite tube the surface with three wound wires is placed parallel to the light beam. The blank absorbance of this electrode is nearly zero. The experimental results show that this procedure has high sensitivity and good

Table 1. Effect on Absorbance from numbers of turnings of Tungsten wire (0.3 mm diameter wire)

Number of turnings	1	2	3
Absorbance	0.087	0.130	0.169
	0.088	0.131	0.168
	0.084	0.130	0.171
	0.085	0.129	0.172

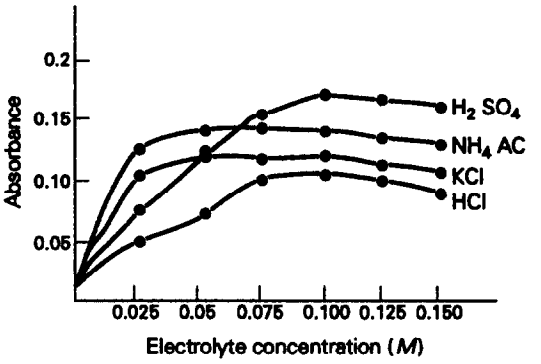

Fig. 2. Effect of different base electrolytes.

reproducibility for the determination of Cd. Table 1 lists the absorbance of Cd after its deposition onto W-wire with different numbers of turnings.

Selection of conditions for electrodeposition[10-15]

In order to optimize the electrodeposition of Cd, the following parameters were investigated.

Supporting electrolyte. Experiments were carried out with four electrolytes: H_2SO_4, HCl, HNO_3 and NH_4AC. The experiments show that at low concentration, absorbance increases with increasing electrolyte concentration, but the absorbance decreases when the concentration has reached a certain value. Interference from nitric acid is serious. In 0.1*M* sulphuric acid, the absorbance is largest and stable, as shown in Fig. 2. So 0.1*M* sulphuric acid is selected as the base electrolyte.

Cathode potential. The influence of the cathode potential between −0.4 and −1.4 V is shown in Fig. 3. For further investigations, the electrodeposition was carried out at −1.0 V.

Effect from electrodeposition time. The yield of the deposition depends strongly on electrolysis time. The absorbance increased from 0.05 at 0.5 min to 0.7 at 3.5 min, with a slight curvature dependence. In order to keep the analysis time

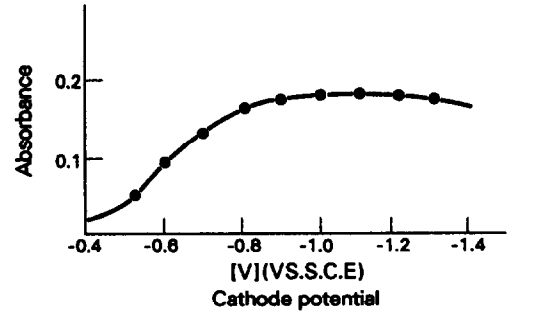

Fig. 3. Effect of cathode potential.

Table 2. Upper and lower limits of the factor studies

Factor	Ashing temp.	Ashing time	Atomization temp.	Atomization time
Upper limit	500°	15 sec	2000°	5 sec
Lower limit	100°	5 sec	1000°	1 sec

Table 3. The pushing process of MWCS

Point no	Point name	Vertex of forming the simplex	Ashing temp. (°C)	Ashing time (sec)	Atomiz. temp. (°C)	Atomiz. time (sec)	Absorbance (A)
1	Vertex		310	11	1620	3	0.426
2	Vertex		190	11	1620	3	0.392
3	Vertex		250	9	1620	3	0.465
4	Vertex		250	10	1500	3	0.480
5	Vertex	1,2,3,4,5	250	10	1380	2	0.385
6	Reflection		250	10	1758	4	0.420
7	Vertex	1,2,3,4,7	250	10	1486	3	0.475
8	Reflection		331	9	1464	3	0.380
9	Vertex	1,3,4,7,9	231	10	1575	3	0.480
10	Reflection		179	9	1462	3	0.340
11	Vertex	3,4,7,9,11	274	10	1576	3	0.460
	Best range		231–274	9–10	1486–1620	3	0.480
	Best point		250	10	1500	3	

short, a period of 2 min was chosen when the absorbance was 0.4 for the above Cd solution.

Effect of tungsten wire diameter. When tungsten wires of different diameters are examined, the absorbance increases linearly with increasing diameter, increasing from 0.025 at 0.2 mm to 0.33 at 0.6 mm. A wire with 0.3 mm diameter was used in further studies.

Effect of stirrer speed. In order to increase the mass transfer rate and decrease the concentration polarization, stirring is needed during the electrodeposition. After the speed reaches a certain value, the absorbance changes little. So 200 rpm is selected as the speed for stirring.

Selection of atomic absorption conditions

After investigating the effects on absorbance, 6 mA was chosen as the lamp electric current, 0.3 nm for the slit and 1.5 l./min for the argon flux.

Optimization of the condition of the graphite furnace

In order to optimize the measurement parameters for ETAAS, the MWCS technique was applied, using a PB-700 computer and a self-designed program. The parameter ranges and optimum values are shown in Tables 2–4.

Calibration curve

The calibration curve is linear up to 0.6 ng/ml Cd. The equation of the linear regression is $y = 1.647x - 0.0157$; the correlation coefficient is $r = 0.9998$. For 0.1 ng/ml Cd, the standard deviation is 3.35% ($n = 10$). The detection limit is 0.01 ng/ml.

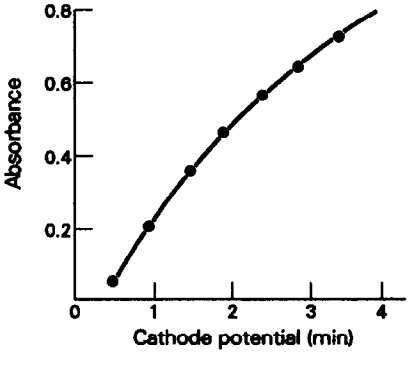

Fig. 4. Effect of electrodeposition time.

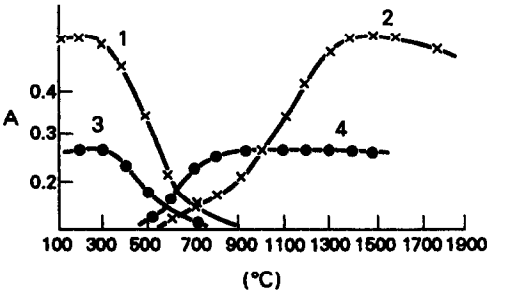

Fig. 5. Ashing and atomization curves for two methods. (1), (2): Ashing–atomization curves for solution deposited in the graphite tube. (3), (4): Ashing–atomization curves for electrodeposition–atomic absorption with a graphite furnace.

Table 4. Optimal analytical conditions

Lamp Current	Slit	Argon flux	Cathode potential	Base electrolyte	Electrodeposition time		Stirring speed
6 mA	0.3 nm	1.5 l./min	−1.0 V	0.1*M* H_2SO_4	2 min		200 rpm
drying temp.	drying time	ashing temp.	ashing time	atomization temp.	atomization time	cleaning temp.	cleaning time
100°	20 sec	250°	10 sec	1500°	3 sec	2000°	3 sec

Effect of coexisting ions

Experiments have been carried out with more than 20 coexisting ions. For errors smaller than 5%, the permitted amount of each coexisting ion is shown in Table 5.

Sample analysis

Determination of cadmium in urine of normal people. It is important to determine the cadmium content of urine of normal people in environmental sanitation monitoring. But it cannot be determined directly by ordinary graphite furnace AAS, due to the low concentration of cadmium. After decomposition of urine, Cd can be separated using electrodeposition and determined with ETAAS as described above.

Place 20 ml of urine in a beaker. Digest with one of two methods. Procedure 1: add 4 ml of concentrated perchloric acid and 4 ml of concentrated nitric acid to the sample. Procedure 2: add 10 ml of concentrated nitric acid to the sample. Each digestion requires two such additions of acid and heating. Heat it on an electric-heating plate and digest until white crystals appear and the excess of nitric acid is removed. Remove from the plate and cool. Dissolve and dilute the residue to 100 ml with 0.1*M* sulphuric acid. Take 20-ml portions for the electrodeposition of Cd. Recovery was determined by the standard addition method. The results are listed in Table 6.

Determination of the free cadmium in river water. The cadmium content of the canal of Xinxiang city was determined. Take 50 ml of water, add 5 ml of 1*M* sulphuric acid, to bring the concentration of sulphuric acid to 0.1*M*. Mix well and store overnight. Filter with quantitative filter paper. Take 2-ml filtered portions of liquid in five 100-ml standard flasks, add 0.00, 1.00, 2.00, 3.00, 4.00 ml of standard solution containing 10 ng/ml cadmium. Bring the volume up to 100 ml with 0.1*M* sulphuric acid and determine the Cd concentration by taking 20 ml of each bottle. The results are shown in Table 7.

Table 5. Effect from coexisting ions (Cd: 0.2 ng/ml, 20 ml)

Coexisting ions	Added as	Concentration of coexisting ion (μg/ml)	Ratio	Relative error (%)
Ni^{2+}	$NiSO_4$	15	7.5×10^4	−5.0
Th^{4+}	$ThO_2 + HCl$	15	7.5×10^4	1.0
Mn^{2+}	$MnSO_4$	15	7.5×10^4	−6.5
Cr^{3+}	$Cr_2(SO_4)_3$	15	7.5×10^4	−3.5
Cu^{2+}	$CuSO_4$	100	5×10^5	1.0
Sb^{IV}	$K(SbO)C_4H_4O_6 \cdot 1/2H_2O$	0.5	2.5×10^3	1.0
In^{3+}	$In + HCl$	10	5×10^4	−5.5
Ag^{1+}	$AgNO_3$	250	1.25×10^6	3.5
Zn^{2+}	$AnSO_4$	250	1.25×10^6	−3.5
Pb^{2+}	$Pb(NO_3)_2$	5.44	2.72×10^4	−5.0
Fe^{2+}	$FeSO_4(NH_4)_2SO_4 \cdot 7H_2O$	5	2.5×10^4	1.0
AS^{III}	AsO_3^{3-}	0.25	1.25×10^3	−5.0
Co^{2+}	$CoSO_4 \cdot H_2O$	50	2.5×10^5	−5.0
Bi^{3+}	$Bi + HNO_3$	15	7.5×10^4	1.0
Mg^{2+}	$MgCl_2$	25	1.25×10^5	−1.5
K^+	KCl	0.025*M*		−1.5
Na^+	Na_2SO_4	0.016*M*		0.0
NH_4^+	NH_4AC	0.05*M*		−4.0
NO_3^+		0.0005*M*		−5.0
Cl^-		0.025M		−2.5
Ac^-	NH_4AC	0.05*M*		−3.5
HPO_4^{2-}	$(NH_4)_2HPO_4$	0.016*M*		1.0
Hg^{2+}	$Hg(NO_3)_2$	1.5	7.5×10^4	4.0

Table 6. Result of Cd determination in the urine of normal people, and the recovery factor

Sample*	Determined value on urine sample (*ng/ml*)	Cd added (*ng/ml*)	Cd found (*ng/ml*)	Recovery (%)
1	0.135	0.200	0.326	95.4
2	0.137	0.200	0.328	95.6
3	0.120	0.200	0.313	96.4
4	0.128	0.200	0.320	95.9
5	0.096	0.070	0.164	97.8
6	0.096	0.160	0.252	97.6
7	0.096	0.200	0.294	98.9

*1 and 2 are $HClO_4 + HNO_3$ digests, 3–7 are HNO_3 digests.

Table 7. Results determined of Cd in water and the recovery factor

Sample	Value determined in water sample (*ng/ml*)	Cd added (*ng/ml*)	Cd found (*ng/ml*)	Recovery (%)
1	0.102	0.100	0.201	99.8
2	0.102	0.200	0.304	102
3	0.102	0.300	0.405	101
4	0.102	0.400	0.502	100

Atomization mechanism

Figure 5 compares the ashing and atomization curves for the normal solution ETAAS method (curves 1 and 2) with those using the electrodeposition method (curves 3 and 4). Ashing curve (3) has the largest absorbance at 100–300° and changes little in this range. This matches the melting point of Cd (320.9°). When the ashing temperature is above 300°, Cd begins melting, its volatization increases, and nearly all the atoms are lost at 800°; this matches the boiling point of Cd (765°).

Curve (4) in Fig. 5 is the atomization curve for electrodeposition–atomic absorption. Atomization starts at 400°. The absorbance increases with the temperature in the range 400–900°. In this range, partial atomization transforms to full atomization.

Note that ashing temperature effects are similar for both methods but atomization efficiency reaches a maximum at lower temperatures than with the solution deposited in the graphite tube.

REFERENCES

1. W. Lund and B. V. Larsen, *Anal. Chim. Acta*, 74 **70** 299.
2. M. P. Newtow and D. G. Davis, *Anal. Chem.*, 1975 **47** 2003.
3. Y. Hoshino, *Tokyo Inst. Technol.*, 1980 **5** 199.
4. X. Boxing, X. T. Ming, S. M. Neng and F. Y. Ahi, Talanta, 1985 **32** 1016.
5. Qing-ping Su, *Trace Analysis*, 1985 **3, 4** 82.
6. W. Lund and B. V. Larsen, *Anal. Chim. Acta*, 1976 **81** 319.
7. *Idem, ibid*, 1974 **72** 57.
8. W. Lund, Y. Thomassen and P. Doyle, *ibid.*, 1977 **93** 53.
9. E. W. Wolff, M. P. Landy and D. A. Peel, *Anal. Chem.*, 1981 **53** 1566.
10. A. Ciszewski, J. R. Fish, T. Malinski and R. E. Sioda, *ibid.*, 1989 **61** 856.
11. H. Marshall and J. A. Page, *Spectrochim. Acta*, 33B, **1978** 795.
12. R. E. Sioda and T. Z. Fahidy, *Anal. Chem.*, 1990 **62** 550.
13. J. C. Vidal, F. Monreal and J. R. Castillo, *Analyst* 1990 **115** 539.
14. M. Veber, S. Gomiscek and V. Stresko, *Anal. Chim Acta*, 1987 **193** 157.
15. J. Shiowatana and J. P. Matousek, *Talanta*, 1991 **38** 375.
16. E. J. Czobik and J. P. Matousek, *Spectrochimica Acta*, **35B**, 741.

Talanta, Vol. 40, No. 3, pp. 415–423, 1993
Printed in Great Britain.

0039-9140/93 $6.00 + 0.00

SIMULTANEOUS DETERMINATION OF BERYLLIUM AND ALUMINIUM IN MIXTURES USING DERIVATIVE SPECTROPHOTOMETRY

NARINDER KUMAR AGNIHOTRI, HAR BHAJAN SINGH,* RATTAN LAL SHARMA and VINAY KUMAR SINGH

Department of Chemistry, University of Delhi, Delhi 110007, India

(*Received* 16 *April* 1992. *Accepted* 25 *June* 1992)

Summary—The spectrophotometric determination of beryllium and aluminium with 5,8-dihydroxy-1,4-naphthoquinone in the presence of a non-ionic surfactant is reported. Absorption maxima, molar absorptivity and Sandell's Sensitivity of 1:2 (M:L) beryllium and aluminium complexes are, 585 nm and 598 nm, 1.63×10^4 l. mole^{-1}. cm^{-1} and 2.04×10^4 l. mole^{-1}. cm^{-1}, and 0.55 ng/cm^2 and 1.32 ng/cm^2 respectively. Beer's law is obeyed between $7.20–3.96 \times 10^2$ ng/ml beryllium and $1.08 \times 10^1–1.08 \times 10^3$ ng/ml aluminium. A method for simultaneous determination of beryllium and aluminium in their mixture using derivative spectra is described. The range $3.6 \times 10^1–3.6 \times 10^2$ ng/ml beryllium could be determined in the presence of $1.08 \times 10^2–1.08 \times 10^3$ ng/ml aluminium, and vice versa.

Toxicity of beryllium and aluminium as well as the need for sensitive and selective methods for determining these elements are well documented.[1] Several sensitive reagents exist for spectrophotometric determination of beryllium (Beryllon II, III, and IV, Quinalizarin, Erichrome Cyanine R) and aluminium (Chrome Azurol S, Erichrome Cyanine R, Pyrocatechol Violet, Aluminon). These reagents become selective in the presence of a suitable masking agent.[2] Acetyl acetone and 8-hydroxyquinone are the sensitive and selective reagents recommended and practised for extractive spectrophotometric determination of beryllium and aluminium respectively.[3]

Impact of micellar system[4–6] on the photometric parameters, and utility of derivatization[7–8] of normal absorption spectra on the selectivity and sensitivity of the spectrophotometric methods are well established. Simultaneous photometric determination of beryllium and aluminium is hampered due to spectral overlap of their complexes. In such cases spectrometry coupled with derivative techniques is useful in analysis of such mixtures.[9–11]

We now report a rapid, sensitive and inexpensive spectrophotometric determination of micro amounts of beryllium and aluminium using 5,8-dihydroxy-1,4-naphthoquinone (DHNQ), a bidentate ligand capable of forming polychelate(s),[12–14] as a chromogenic reagent, and Triton X-100, a non-ionic surfactant, to generate the requisite micellar medium. Simultaneous determination of beryllium and aluminium, without any pre-separation or masking, has also been carried out using derivative spectra.

*Author for correspondence.

EXPERIMENTAL

Instruments

Absorption measurements were made on a Shimadzu UV-260 recording spectrophotometer using 10-mm fused silica cells and a 1-nm band width taking water as reference. First and second order derivative spectra were recorded with $\Delta\lambda = 2$ and 4 nm respectively. The pH of solutions were measured on an EC digital pH-meter (Model pH 5662) fitted with a combined glass electrode.

Chemicals

All chemicals used were of analytical grade purity. Dilute solution of sulphuric acid and sodium hydroxide were used for pH adjustment. Stock solutions (0.01M) of Be(II) and Al(III) were prepared in decimolar sulphuric acid using $BeSO_4 . 4H_2O$ and $KAL(SO_4)_2 . 12H_2O$ respectively. As DHNQ is sparingly soluble in water, an appropriate amount (7.61 mg) was first dissolved in the minimum amount of 0.2*M* sodium hydroxide with stirring at 40°, which was followed by addition of 4.0 g of Triton

X-100 and acidification. The solution was diluted to 100 ml with water.

Procedure

To study the effect of varying H^+ concentration on the absorbance of each system, two sets of solutions in the pH range 2.0–11.5 were prepared. One of these contained $2 \times 10^{-4}M$ DHNQ, 2% w/v Triton X-100 and $0.01M$ ammonium acetate, while the other, in addition, contained $2 \times 10^{-5}M$ of the metal ion [Be(II) or Al(III)] as well.

The effect of varying surfactant concentration on the absorbance of the complex was studied by increasing the amount of Triton X-100 in a series of solutions, $2 \times 10^{-4}M$ in DHNQ, $2 \times 10^{-5}M$ in metal ion solution and $0.01M$ in ammonium acetate at the pH of maximum complex formation.

Beer's law was studied by adding increasing amounts of the metal ion to a $2 \times 10^{-4}M$ solution in DHNQ, 2% w/v in Triton X-100 and $0.01M$ in ammonium acetate, keeping the ratio $L:M \geqslant 10$.

Simultaneous determination of Be and Al

Concentrations of beryllium and aluminium ions were determined from first/second derivative spectra by measuring derivative amplitudes at isodifferential points and comparing the values with a calibration graph. The calibration graph for beryllium was prepared by measuring amplitudes of the first/second derivative spectra at isodifferential point of aluminium, and vice versa for aluminium.

RESULTS AND DISCUSSION

Absorption spectra and its dependence on pH

DHNQ exhibits maximum absorption at 490 nm which shows a bathochromic shift to 610 nm with pH on account of increasing dissociation of the phenolic groups. Formation of Be(II)–DHNQ–Triton X-100 and Al(III)–DHNQ–Triton X-100 complexes was studied in the pH range 2.0–11.5. The complex formation starts at 5.0 and 5.5 in the case of beryllium and aluminium respectively and increases up to pH 6.5 and 6.6 as evidenced by increase in absorbance. This remains constant from pH 6.5 to 7.4 and 6.6 to 7.6 in the respective cases and further increase in pH, results in decrease of absorbance in both cases. Beryllium and aluminium complexes show absorption maximum at 585 nm and 598 nm respecitvely at pH of maximum complexation. Subsequent studies have been carried out at these λ_{max} wavelengths and pH values (6.8 and 6.9 respectively).

Effect of surfactant

The surfactants investigated include cetyltrimethylammoniumbromide (CTMB), *N*-cetylpyridiniumchloride (CPC), sodiumlaurylsulphate (SLS), and triton X-100. As absorbance of the complex in each case was lesser in the presence of an ionic surfactant than in non-ionic surfactant, either due to increased deprotonation of the ligand or inhibition of complex formation, Triton X-100, a non-ionic surfactant was selected for micelle formation. Concentrations up to 2% (w/v) of surfactant is found to increase the extinction of the complex which decreases with a further increase in the case of both the metal ions. A 2% w/v concentration of Triton X-100 was, therefore, maintained in subsequent studies.

Reversibility of the complexation reaction

Complexation of Be(II) and Al(III) with DHNQ in the presence of Triton X-100 is reversible between pH 6.8 to 11.5, and 6.9 to 11.5 respectively. The colour of the ligand and that of complexes are stable up to twenty four and eight hours respectively at room temperature (20–25°).

Effect of reagent concentration

Absorbance spectra of solutions containing increasing amounts (4×10^{-6}–$2.8 \times 10^{-4}M$) of reagent and fixed amount of the metal ion showed an increase in absorbance at absorption maxima, 585 nm and 598 nm respectively for Be(II) and Al(III) complexes. Since the ligand also absorbs at λ_{max} of the complexes. The corrected absorbance at λ_{max} of each complex was plotted against molar ratio (L:M) of the reagent. The slope of the plot remains constant between 5:1 to 20:1 (L:M) in the case of the beryllium complex and 10:1 to 45:1 (L:M) in the case of the aluminium complex. The reagent concentration in subsequent studies has, accordingly, been kept within the above mentioned limits, wherever possible.

Number of chromogenic species and their composition

A computer program[15] based on matrix rank determination of an absorbance matrix has been used to determine the number of chromogenic

species present in solution. The rank is determined by triangularizing the matrix, based on the method of gaussian elimination and comparison of the diagonal elements with error matrix. Though on this basis three absorbing species (H_2L, HL^-, L^{2-}), are inferred to be present in the ligand solution in the pH range 2.0 to 11.5, existence of only the first two species are of significance up to 8.0 (pH of concern for the present investigation); error matrix $\geqslant 0.0026$. Three absorbing species are shown to be present in the solution of Be(II)/Al(III) complexes for error matrix $\geqslant 0.0030$.

Stoichiometry of the complexes were determined using the method of continuous variations. Plot of absorbance at λ_{max} of the complexes versus mole fractions of the metal ion shows a maximum at 0.33, suggesting the formation of a 1:2 (M:L) complex in each case. The complexes are, therefore, represented as $Be(HL)_2$ and $[Al(HL)_2]^+$, where H_2L represents the molecular form of DHNQ.

Effect of metal ion concentration

Absorbance of solutions having excess of ligand increased linearly with increase in metal (Be(II)/Al(III)) ion concentration [Fig. 1(a) and 2(a)]. Linear regression of absorbance on concentration gave equations with positive intercepts due to absorption by the ligand at λ_{max} of the complexes. The observed absorbance values have, therefore, been corrected in two ways giving corrected absorbances A_I and A_{II} as expressed in equations (1) and (2). These corrected absorbance values show improvement in linear fit (Table 1) which is evident from the regression coefficients.

$$A_I = (A)_{max(C)} - [(A)_{max(C)}/(A)_{max(L)}]_{L.BLK} \times (A)_{max(L)} \quad (1)$$

$$A_{II} = (A)_{max(C)} - [(A)_{max(C)}/V_L]_{L.BLK} \times (V_L - R \times V_M) \quad (2)$$

where $[(A)_{max(C)}/(A)_{max(L)}]_{L.BLK}$ is the ratio of absorbances of the ligand blank solution at λ_{max} of the complex and that of the ligand, V_L and V_M are volumes of equimolar solutions of ligand and metal ion respectively, and R is stoichiometry of the complex.

First and second derivative spectra of the above-mentioned solutions are shown in Figs. 1(b) and (c), and 2(b) and (c). The first derivative spectrum of beryllium shows a peak at 585 nm [Fig. 1(b)] and that of aluminium shows crossover point at 598 nm [Fig. 2(b)] corresponding to λ_{max} of the respective complexes. Heights of the peaks (PH) and depth of the troughs (TD) were measured from the base line of the ligand and plotted against the metal ion concentration. Relationship between PHs or TDs and increasing metal ion concentration at different wavelengths in each case show a good linear fit (Table 1) which is useful in determining these metal ions in solution. Be(II)–DHNQ–Triton X-100 and Al(III)–DHNQ–Triton and X-100 systems obey Beer's law from 7.20–72 ng/ml, 36–396 ng/ml and 10.8–108 ng/ml and 108–1.08 $\times 10^3$ ng/ml beryllium and aluminium ions respectively.

Table 1. Relationship between concentration of Be(II)/Al(III) ion (ng/ml) and absorbance or PH/TD

Be–DHNQ–Triton X-100 Straight line equation	*Al–DHNQ–Triton X-100* Straight line equation
Normal mode	
Absorption at 585 nm	Absorption at 598 nm
$[A] = 1.380 \times 10^{-3}C + 2.423 \times 10^{-1}$ (0.9941)	$[A] = 5.232 \times 10^{-4}C + 2.197 \times 10^{-1}$ (0.9983)
$[A_I] = 1.453 \times 10^{-3}C - 5.412 \times 10^{-3}$ (0.9944)	$[A_I] = 5.493 \times 10^{-4}C - 2.167 \times 10^{-3}$ (0.9984)
$[A_{II}] = 1.653 \times 10^{-3}C - 3.293 \times 10^{-3}$ (0.9958)	$[A_{II}] = 6.058 \times 10^{-4}C - 3.534 \times 10^{-3}$ (0.9988)
First Derivative mode	
$[TD]_{602\ nm} = 2.715 \times 10^{-1}C + 7.729$ (0.9835)*	$[TD]_{608\ nm} = 9.616 \times 10^{-2}C + 0.879$ (0.9925)*
$[TD]_{533\ nm} = 1.919 \times 10^{-1}C + 3.945$ (0.9908)*	$[TD]_{530\ nm} = 3.998 \times 10^{-2}C + 1.951$ (0.9885)
$[PH]_{585\ nm} = 1.914 \times 10^{-1}C - 3.519$ (0.9979)*	$[PH]_{592\ nm} = 3.831 \times 10^{-2}C - 2.029$ (0.9942)*
$[PH]_{538\ nm} = 1.698 \times 10^{-1}C - 1.675$ (0.9983)	$[PH]_{543\ nm} = 3.464 \times 10^{-2}C - 1.835$ (0.9975)
Second Derivative mode	
$[TD]_{592\ nm} = 2.268 \times 10^{-1}C - 4.102$ (0.9979)*	$[TD]_{601\ nm} = 8.805 \times 10^{-2}C + 2.469$ (0.9902)*
$[TD]_{545\ nm} = 1.372 \times 10^{-1}C + 1.577$ (0.9894)	$[PH]_{617\ nm} = 4.984 \times 10^{-2}C - 1.426$ (0.9934)*
$[PH]_{611\ nm} = 7.589 \times 10^{-2}C + 2.465$ (0.9776)	
$[PH]_{564\ nm} = 1.399 \times 10^{-1}C + 2.537$ (0.9928)*	

*Recommended for determination, A_I/A_{II} = Corrected absorbance, PH = Peak height, TD = Trough depth, C = Concentration of Be(II)/Al(III).

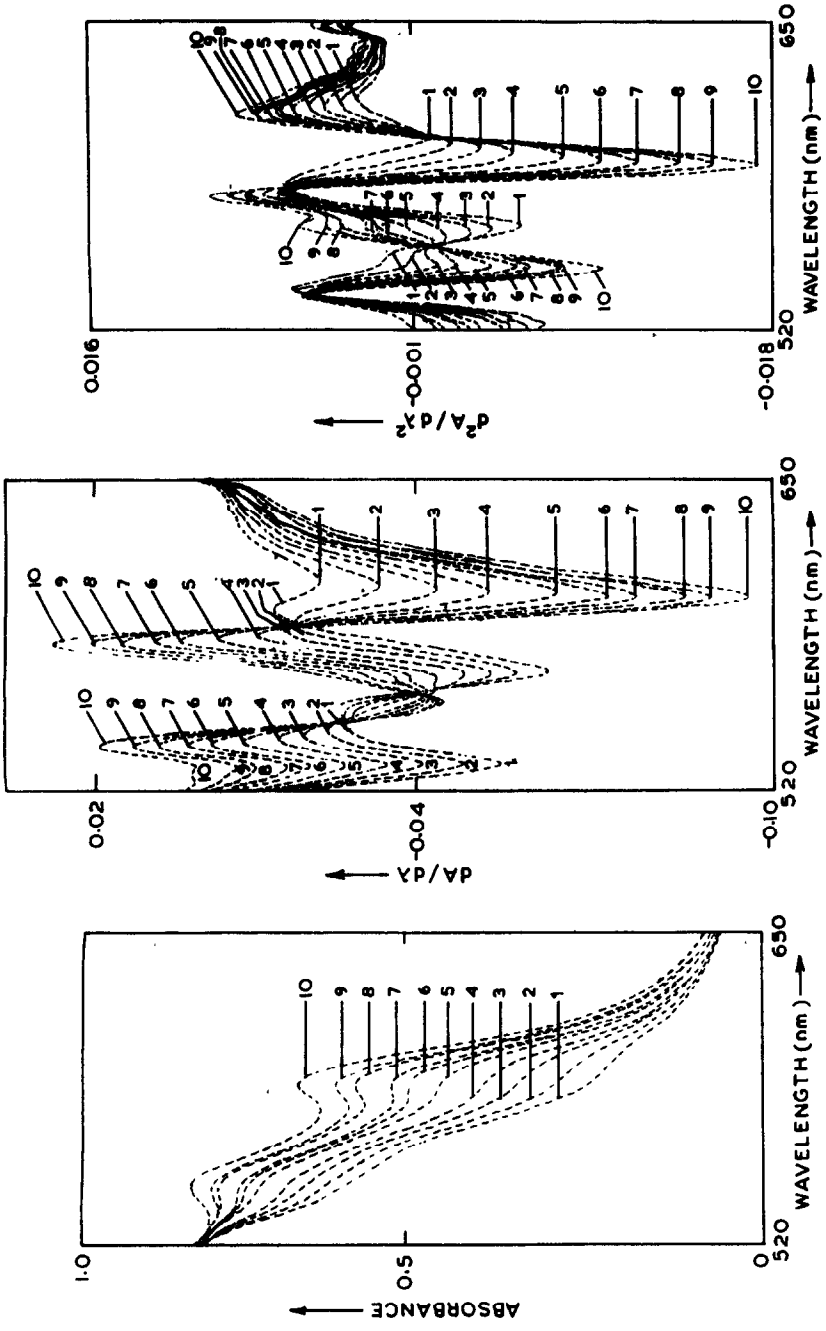

Fig. 1. Spectra of Be(II)–DHNQ–Triton X-100 system containing increasing amount (from 3.60×10^{1}–3.96×10^{2} ng/ml) of Be(II) (No. 2 to 10); No. 1 contains 2×10^{-4} *M* DHNQ (a) Normal, (b) First order and (c) second order derivative spectra.

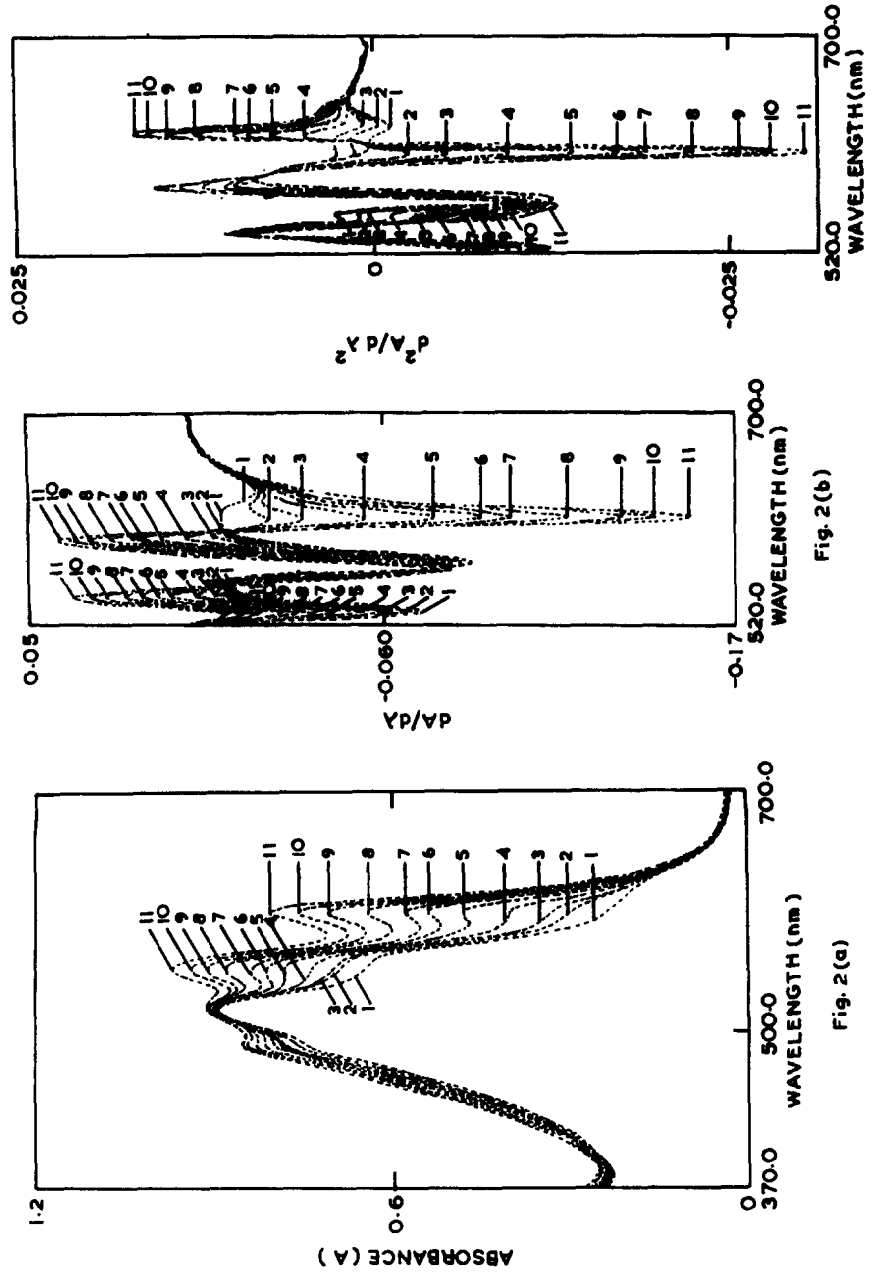

Fig. 2. Spectra of Al(III)–DHNQ–Triton X-100 system containing increasing amount (from 1.08×10^2–1.08×10^3 ng/ml) of Al(III) (No. 2 to 11); No. 1 contains 2×10^{-4} *M* DHNQ, (a) Normal, (b) First order and (c) second order derivative spectra.

Molar absorption coefficient (ϵ), specific absorptivity (a) and Sandell's sensitivity (S) of the complexes under optimal experimental conditions are found to be 1.63×10^4 l. mole^{-1}. cm^{-1} and 2.04×10^4 l. mole^{-1}. cm^{-1}, 1.81 ml g^{-1}cm^{-1} and 0.76 ml g^{-1}cm^{-1}, and 0.55 ng/cm^2 and 1.32 ng/cm^2 respectively. The IUPAC detection limits ($K = 3$)[16] are 0.5 ng/ml for beryllium and 1.0 ng/ml for aluminium.

Conditional stability constant

Conditional stability constants[17,18] of beryllium and aluminium complexes have been determined by taking the following equilibria

$$Be^{2+} + 2H_2L \rightleftharpoons [Be(HL)_2] + 2H^+$$

$$Al^{3+} + 2H_2L \rightleftharpoons [Al(HL)_2]^+ + 2H^+$$

The value of the conditional stability constant (k') for beryllium and aluminium complexes has been found to be 1.58×10^5 l. mole^{-1} and 2.69×10^5 l. mole^{-1} respectively; concentrations have been used instead of activity as the solutions are dilute and a non-ionic surfactant has been used.

Effect of diverse ions

Effect of the presence of diverse ions in the determination of Be(II) and Al(III) using DHNQ was studied under optimum conditions. The analytical results for a series of determinations are given in Table 2. When a precipitate appeared, it was removed by centrifugation before measuring the absorbance of the supernatant liquid. Absorbance measurement in the first and second derivative modes proved useful in overcoming interferences in a number of cases where masking agents like EDTA, tartrate, citrate, oxalate, F^- could not help. For example, very close absorption profiles due to Ce, Th, Au, Al, As, Cr, Fe, Ni and UO_2, and Th, Ce, Au, Cr, Fe, Ga, In, Be, Co, Ni, Sn and UO_2 in case of beryllium and aluminium complexes get resolved from those of the analytes [Be(II)/Al(III)] in higher order derivative modes enabling their determination in presence of such ions.

Simultaneous determination of Be and Al in mixtures

Since absorption spectra of beryllium and aluminium complexes overlap, their photometric determination in mixtures is difficult. Appropriate parameters were selected to record the first and second derivative spectra and determine the positions of isodifferential points.

Table 2. Tolerance limits* for diverse ions in the determination of (a) 1.80×10^2 ng/ml Be(II), (b) 5.40×10^2 ng/ml Al(III)

Diverse ion	*Ratio* ([Diverse ion]:[*M*]) (a)	(b)	Diverse ion	*Ratio* ([Diverse ion]:[*M*]) (a)	(b)
Cations					
Mo(VI)	50	100 (−)	Fe(III)	0.1 (−)	0.1 (−)
W(VI)	90	200 (−)	Au(III)	01 (−)	0.6
UO_2(II)	01	0.1	Ca(II)	200	70
Ce(IV)	0.3 (−)	0.8	Mg(II)	15	05
VO(II)	15	03	Sn(II)	06 (−)	02 (−)
Th(IV)	02 (−)	01	Pb(II)	50 (−)	04
Zr(IV)	100 (−)	150 (−)	Mn(II)	20 (−)	03
B(III)	60	50	Co(II)	50	0.8
Al(III)/Be(II)	0.1	0.03	Ni(II)	03	0.5
Ga(III)	02	0.5	Cu(II)	02 (−)	02
In(III)	40	01 (−)	Zn(II)	20 (−)	10
Tl(III)	90 (−)	08	Cd(II)	100	40
As(III)	04 (−)	02 (−)	Hg(II)	90	30
Bi(III)	10	20 (−)	Li(I)	05	01
Cr(III)	01 (−)	0.1 (−)	Ag(I)	02	150
Anions					
F^-	05	02 (−)	Tartrate	500	25
Cl^-	500	400	Citrate	03	01 (−)
Br^-	400	300	Oxalate	40 (−)	15 (−)
I^-	700	250	EDTA	02	0.8
SCN^-	25 (−)	15	Phosphate	40	06
Ascorbate	90 (−)	30 (−)	Borate	70	20

* ≤ 2.0% Deviation.
(−) Negative deviation.
_ Precipitation at higher concentration.

Be(II) and Al(III) complexes have one isodifferential point in each of the two derivative modes, *viz.*, B′, B″ and A′, A″ which are at 589.5 nm, 601.5 nm, and 597.5 nm, 608.5 nm respectively [Fig. 3(a) and (b)]. The isodifferential points at 601.5 nm, (B″) and 608.5 nm, (A″), are potentially useful for the determination of aluminium and beryllium respectively. Calibration graphs were then made by measuring the distances of the absorption profiles of one metal at the isodifferential point of the other. Figure 3(a) and (b) show the first and second order derivative spectrum of the two series of 24 solutions containing increasing amount of beryllium and aluminium ions. Linear plots are obtained for 3.60×10^{1}–3.60×10^{2} ng/ml beryllium and 1.08×10^{2}–1.08×10^{3} ng/ml aluminium [equations (3) and (4)].

$$D = 1.309 \times 10^{-1}\,[\mathrm{Al}] - 8.936 \quad (r = 0.9989) \text{ at B}'' \quad (3)$$

$$D = 1.005 \times 10^{-1}\,[\mathrm{Be}] + 1.524 \quad (r = 0.9919) \text{ at A}'' \quad (4)$$

Presence of beryllium in a solution of aluminium and that of aluminium in a solution of beryllium, changes the amplitude $d^2A/d\lambda^2$ in second derivative spectra respectively at A″ and B″, the isodifferential points of aluminium and beryllium complex [Figs. 4(a) and (b)]. Concentration of beryllium and aluminium ions is then read from the calibration curve. The results of simultaneous determination of beryllium and aluminium ions are given in Table 3. The mixture containing 3.60×10^{1}–3.60×10^{2} ng/ml beryllium and 1.08×10^{2}–1.08×10^{3} ng/ml aluminium can be analysed with a relative error of $<2.80\%$.

Procedure is developed for determination in aqueous phase of beryllium and aluminium when present either alone or in mixture. Simplicity, sensitivity, large range of linearity besides accuracy and precision are the main advantages of the developed methods.

Acknowledgements—The authors are thankful to U.G.C. for financial assistance to N.K.A. during this work.

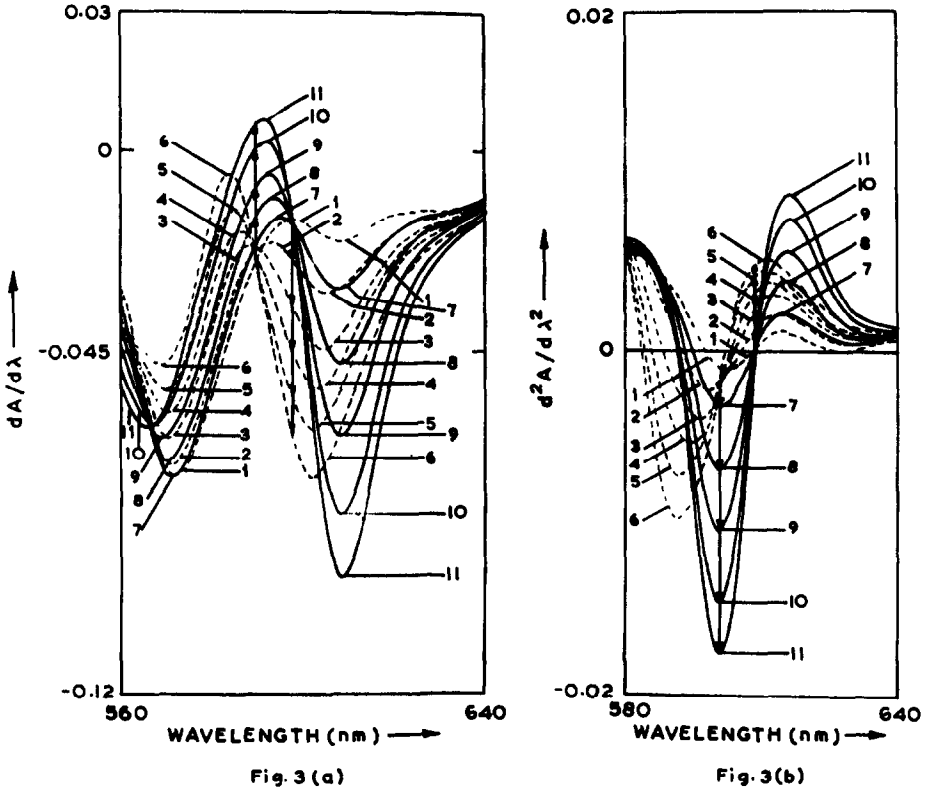

Fig. 3. Derivative spectra of two sets of solutions one containing increasing amounts (from 3.60×10^{1}–1.80×10^{2} ng/ml) of Be(II) (No. 2 to 6) and the other contain (1.08×10^{2}–5.40×10^{2} ng/ml) Al(III) (No. 7 to 11), and both having $2 \times 10^{-4}M$ DHNQ (No. 1), in Triton X-100; (a) First order and (b) second order derivative spectra.

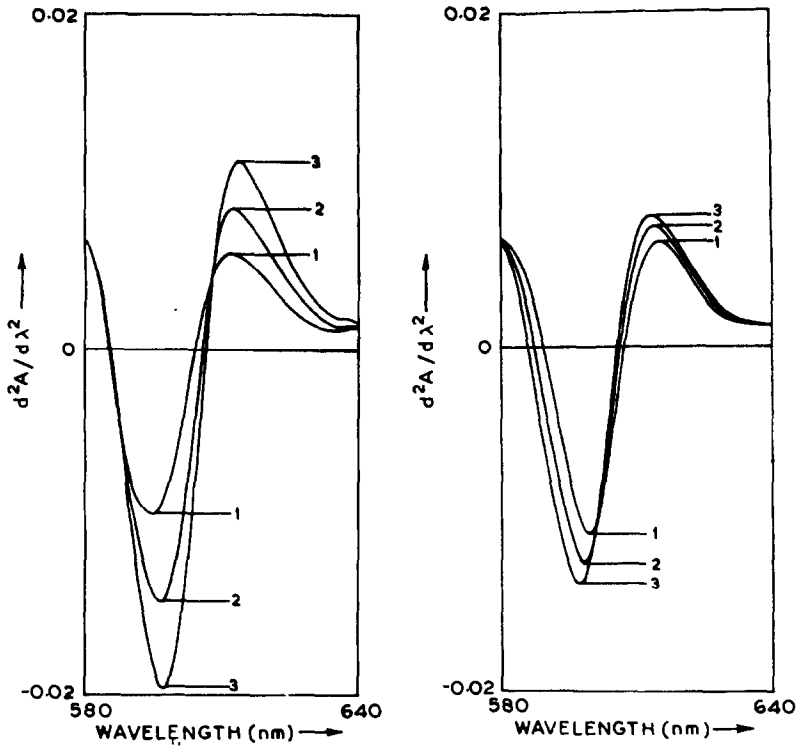

Fig. 4(a) Fig. 4(b)

Fig. 4. Second order derivative spectra of DHNQ complexes of Be(II) and Al(III) in Triton X-100; (a) Be(II) 144.0 ng/ml and 108.0 (1), 324.0 (2) and 540.0 (3) ng/ml Al (III); (b) Al(III) 324.0 ng/ml and 36.0 (1), 72.0 (2) and 108.0 (3) ng/ml Be(II).

Table 3. Quantitative determination of beryllium (3.60×10^1–3.60×10^2 ng ml^{-1}) and aluminium (1.08×10^2–1.08×10^3 ng/ml) in the mixtures

S. No.	Amount taken (*ng/ml*) Be(II)	Al(III)	Amount found (*ng/ml*) Be(II)	Al(III)	Relative error, % Be(II)	Al(III)
1.	036.0	108.0	036.5	106.6	1.39	−1.29
2.	036.0	324.0	035.6	323.4	−1.11	0.18
3.	036.0	540.0	035.0	551.0	−2.78	2.04
4.	108.0	216.0	107.6	217.1	−0.37	0.51
5.	144.0	432.0	144.8	431.2	0.55	−0.18
6.	180.0	648.0	181.2	649.2	0.67	0.18
7.	180.0	432.0	180.4	433.6	0.22	0.37
8.	288.0	648.0	287.7	648.6	−0.10	0.09
9.	288.0	864.0	288.6	866.3	0.21	0.27
10.	360.0	648.0	360.6	646.6	0.17	−0.22
11.	360.0	864.0	361.6	858.1	0.44	−0.68
12.	360.0	1080.0	351.0	1093.4	−2.50	1.24

REFERENCES

1. E. Berman, *Toxic Metals and Their Analysis*, Heyden, London, 1980.
2. Z. Marczenko, *Spectrophotometric Determination of Elements*, Ellis Horwood, Chichester, 1976.
3. E. B. Sandell and H. Onishi, *Photometric Determination of Traces of Metals*, Vol. 3, Part I, Wiley, New York, 1978.
4. L. J. C. Love, J. G. Habarta and J. G. Dorsey, *Anal. Chem.*, 1984, **56**, 1133A.
5. E. Pelizzetti and E. Pramauro, *Anal. Chim. Acta.*, 1985, **169**, 1.
6. E. Pramauro and E. Pelizzetti, *Trends in Anal. Chem.*, 1988, **7**, 260.
7. S. Shibata, M. Furukawa and K. Goto, *Anal. Chim. Acta*, 1973, **65**, 49.
8. V. A. Perfil'ev, V. T. Mishchenko and N. S. Poluéktov, *Zh. Anal. Khim.*, 1985, **40**, 1349.
9. B. Morelli, *Analyst*, 1983, **108**, 870.
10. S. Kus and Z. Marczenko, *ibid.*, 1987, **112**, 1503.
11. F. G. Sanchez, M. H. Lopez and J. C. M. Gomez, *Talanta*, 1987, **34**, 639.
12. R. S. Bottei and P. L. Gerace, *J. Inorg. Nucl. Chem.*, 1961, *23*, 245.

13. H. D. Coble and H. F. Holtzclaw, Jr., *ibid.*, 1974, **36**, 1049.
14. C. G. Pierpont, L. C. Francesconi and D. N. Hendrickson, *Inorg. Chem.*, 1978, **17**, 3470.
15. R. M. Wallace and S. M. Katz, *J. Phys. Chem.*, 1964, **68**, 3890.
16. IUPAC, Nomenclature, Symbols, Units and Their Usage in Spectrochemical Analysis, Pure Appl. Chem., 1976, **45**, 105.
17. A. Ringbom, *J. Chem. Educ.*, 1958, **35**, 282.
18. L. G. Sillen and A. E. Martell, *Stability Constants of Metal Ion Complexes*, Vol. 1, Vol. 2, Chemical Society London, 1964, 1971.

Talanta, Vol. 40, No. 3, pp. 425–430, 1993
Printed in Great Britain.

0039-9140/93 $6.00 + 0.00

BIOLUMINESCENT FLOW SENSOR FOR *L*-PHENYLALANINE DETERMINATION IN SERUM

S. GIROTTI,* E. FERRI, S. GHINI and R. BUDINI
Institute of Chemical Sciences, University of Bologna, via S. Donato, 15-40127 Bologna, Italy

GIACOMO CARREA and ROBERTO BOVARA
Institute of Hormone Chemistry, CNR, Via M. Bianco, 9-20131 Milano, Italy

SANDRO PIAZZI and ROBERTO MERIGHI
St. Orsola Hospital, Via Massarenti, 9-40127 Bologna, Italy

ALDO RODA
Department of Pharmaceutical Sciences, Via Belmeloro, 6–40126 Bologna, Italy

(*Received* 14 *May* 1992. *Revised* 24 *June* 1992. *Accepted* 15 *July* 1992)

Summary—A highly sensitive and rapid bioluminescent flow sensor was developed for the determination of the content of *L*-phenylalanine (Phe) in serum by monitoring the reduced form of nicotinamide adenine dinucleotide (NADH), produced by immobilized phenylalanine dehydrogenase (PheDH), with bacterial bioluminescent enzymes immobilized on a separate nylon coil. The L-PheDHs extracted from *Bacillus badius*, *Bacillus sphaericus* and *Rhodococcus sp. M*4 were investigated and the performances of the three immobilized L-PheDH's were analysed. The *B. badius* reactor was found to give higher transformation rate and better sensitivity; the response was linear from 1 to 100μM at 25°, with a detection limit of 10 pmoles (0.5μM). The intra- and inter-assay coefficients of variation were less than 5% and recoveries ranged from 90 to 101%. The results agreed well with those obtained with a chromatographic method for the Phe determination in serum and with the normal reference values.

L-Phenylalanine (*L*-Phe), an essential amino acid for mammals, is of great interest in many fields, occurring naturally in blood, saliva, urine, milk and other body fluids.[1,2] Aberrations of *L*-Phe metabolism lead it to accumulate in the blood of hyperphenylalaninemic patients.[1–4] Therefore, a simple, rapid and sensitive method for the determination of *L*-Phe in very small samples is essential for screening of neonatal diagnosis[3] and dietary management of hyperphenylalaninemic patients[4] and, to this end, a variety of methods have been designed. Among the chromatographic ones, there are high performance liquid (HPLC), ion-exchange with postcolumn derivatization with ninhydrin,[5,6] narrow-bore reversed-phase with precolumn derivatization with *o*-phthalaldehyde (absorbance) or 9-fluorenylmethyl chloroformate (fluorescence),[7] reversed-phase without derivatization,[8] reversed or normal-phase with *p*-nitrobenzoyl and 3,5-dinitrobenzoyl derivatization,[9] and chiral thin-layer chromatography.[10] The chromatographic methods are reliable, but require expensive instrumentation or result in high cost per analysis. Also spectrophotometric methods can be used with second derivative to enhance specificity.[11] However, the most specific methods make use of enzymes such as Phe hydroxylase,[1] *L*-Phe oxidase,[12] amino acid oxidase[13] and *L*-phenylalanine dehydrogenase.[14–19]

Recently several *L*-phenylalanine dehydrogenases were detected and isolated from several microorganisms such as *Bacillus badius*, *Bacillus sphaericus*, *Nocardia*, *Termoactinomyces intermedius* and *Rhodococcus sp. M4*[14–19] and this allowed us to develop several enzymatic assays.[18–20]

Bioluminescent flow sensors have been developed previously for several analytes and enzymes,[21] including lactate dehydrogenase (LDH)[22] and, more recently, *L*-lactate and *D*-lactate present in biological fluids.[23,24] When

*Author for correspondence.

an immobilized enzyme is used in a continuous-flow system, manual handling is minimized and the reproducibility is enhanced, making the analytical system[25] simple and cheap.

In this work, the assay of *L*-Phe was based on bioluminescent monitoring of the reduced form of nicotinamide adenine dinucleotide (NADH), produced by *L*-PheDH immobilised into a nylon coil that preceded the bioluminescent detection coil [see equations (1), (2) and (3)].

$$L\text{-Phenylalanine} + NAD^+ + H_2O \xrightleftharpoons{L\text{-PheDH}} L\text{-Phenylpyruvate} + NADH + H^+ + NH_4^+ \quad (1)$$

$$NADH + FMN + H^+ \xrightleftharpoons{NADH\ oxred} NAD^+ + FMNH_2 \quad (2)$$

$$FMNH_2 + RCHO + O_2 \xrightleftharpoons{luciferase} FMN + H_2O + RCOOH + LIGHT \quad (3)$$

EXPERIMENTAL

Reagents

Luciferase from *Photobacterium fischeri* (EC 1.14.14.3; 15 mU/mg protein), NAD(P)H:FMN oxidoreductase from *Photobacterium fischeri* (EC 1.6.8.1; 100 U/mg protein), NAD^+ (lithium salt), FMN were purchased from Boehringer (Mannheim). n-Decanal and Dithiothreitol (DTT) were obtained from Sigma (St. Luis, MO). *L*-Phenylalanine dehydrogenase from *Bacillus badius* (E.C. 1.4.1.; 34 U/mg protein/3.5 U/mg lyophilized) and *Bacillus sphaericus* (E.C. 1.4.1.; 35 U/mg protein/7.3 U/mg lyophilized) were a gift from Central Glass Co. (Tokyo, Japan), whereas PheDH from *Rhodococcus sp.* M4 (E.C. 1.4.1.; 90 U/mg protein) was from Calbiochem (San Diego, CA). Nylon-6 tubes, 1 mm i.d., were obtained from Portex Ltd (Hythe, U.K.). All other reagents and compounds were analytical-reagent grade.

Preparation of solutions

The working bioluminescent solution was 0.1μM potassium phosphate buffer (pH 6.75), containing 10μM FMN, 27μM decanal and 0.5mM DTT. The solution was prepared 20–30 min before analysis. Decanal was previously dissolved in propanol-2-ol (0.05%, v/v) and was stable for at least 6 weeks at 4°. The working bioluminescent solution showed no detectable degradation after 8–10 hr in the dark at room temperature. Because NAD^+ is unstable in alkaline media, 1mM NAD^+ had to be reconstituted daily with water.

Immobilization of enzymes on nylon

The dehydrogenases (2 mg/ml of phosphate buffer) and bioluminescent enzymes were immobilized on nylon coils that had been activated with triethyloxonium tetrafluoroborate, 1,6-diaminohexane and glutaraldehyde as described previously.[20–23] After removal of the enzyme solutions, the tubes were washed thoroughly with potassium phosphate buffer and stored in 0.1M potassium phosphate buffer (pH 7.0), with 1% m/v bovine serum albumin (BSA), 1mM DTT and 0.02% (w/v) sodium azide, −20° for long-term storage and at 4° for short-term storage.

The activity and the protein content of free and immobilized enzymes were measured as described previously.[20–23] The stability of the immobilized enzymes was determined by measuring the residual activity of PheDH after intermittent use of the coils (analysis at room temperature and storage at 4°) over a period of 4 months.

Apparatus

The manifold developed for bioluminescent continuous-flow determination of *L*-phenylalanine is shown in Fig. 1 and it is similar to those described previously.[21–24]

Chromatographic assay

Analysis of free amino acids in serum was made according to classical Moore's method[5,6]

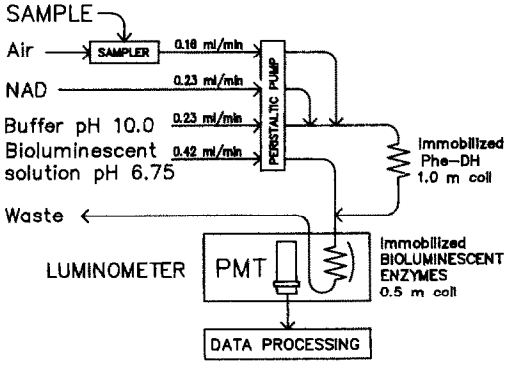

Fig. 1. Manifold for bioluminescent continuous-flow assay of *L*-pheynlalanine.

Table 1. Michaelis constants of free and immobilized enzymes, obtained from Lineweaver-Burke plot

Enzyme	Substrate or coenzyme	K_m of free enzyme, mM	K_m of immob. enzyme, mM
NAD(P)H:FMN	FMN	0.042 ± 0.005*	0.039 ± 0.004
oxidoreductase	NAD	0.41 ± 0.06	0.37 ± 0.05
PheDH from	Phe	0.085 ± 0.007	0.093 ± 0.008
B. badius	NAD	0.14 ± 0.04	0.18 ± 0.03
PheDH from	Phe	0.24 ± 0.05	0.29 ± 0.04
B. sphaericus	NAD	0.15 ± 0.02	0.20 ± 0.03
PheDH from	Phe	0.22 ± 0.06	0.28 ± 0.05
Rodococcus sp. M4	NAD	0.12 ± 0.03	0.16 ± 0.02

*Standard deviation.

using a 3A30 automatic analyzer equipped with a 3AR/1C/6/10-Li 12 cm ion exchange column (Carlo Erba Instruments, Milano).

Sample treatment

Blood collected from veins without stasis and strictly avoiding haemolysis or standard control sera were used. When the bioluminescent flow sensor was used the serum samples were diluted 1 + 9 to 1 + 49 without deproteinization with the 0.02M pyrophosphate buffer (pH 10.0) used to supply external dehydrogenase reactor. The phenylalanine content was evaluated comparing the samples with graphs obtained by pooled sera treated as above. Three different pooled sera at three Phe levels (42, 136 and 916nM, respectively) were used to determine Phe with respect to the reference interval (0–69nM) and pathological values (>69nM). The standards were stable for 6 days if stored at +4°, and for at least 4 months at −20°.

For the chromatographic method the serum was deproteinized with sulphosalicyclic acid (30/40 mg per ml serum), centrifuged at 3500 rpm for 15 min, stored at −20° and analysed within 6–7 days.

Comparison for phenylalanine content was also made with the spectrophotometric determination,[14] using 0.1M glycine buffer, pH 10.4

RESULTS AND DISCUSSION

Enzyme immobilization

Under the described conditions of coupling 60–70% of added PheDHs (considering both activity and protein content) was bound to the matrix in all the three cases. Apparent Michaelis constant (K_m) values of the immobilized enzyme for substrates and coenzymes were not markedly different from those of the free enzymes (Table 1), and activity recovery (5% for *Bacillus badius* and 4% for *Bacillus sphaericus* and *Rhodococcus sp. M4*) was in agreement with previously published data on nylon-immobilized enzymes.[21–25] Immobilized PheDHs maintained *ca.* 50% of their original activity after 60–90 days of intermittent use. This was to be expected owing to the stability of the covalent bond between the enzyme and the matrix and also to the intrinsic stability of the enzymes.

For short-term storage, the reactors were filled with storage buffer and kept at 4°; for long-term storage they were kept at −20°; in this case they retained the original activity almost completely even after 18 months. Repetitive freeze-thaw cycles, however, should be avoided.

Optimization of experimental conditions

The conditions for maximum light emission for the three PheDHs were selected after preliminary testing including reagent concentration, flow rate, pH and composition of the buffer solutions, and reaction temperature. This also made it possible to optimize precision and peak separation, as reported previously for other analytes.[21–24]

The pH and ionic strength of solutions are important parameters in the continuous-flow system. Experiments were made to establish the optimum pH (about pH = 10.5 for oxidative deamination in batch analysis[15–19]) for the determination of phenylalanine in several buffers (tris[hydroxymethyl]-aminomethane (Tris), *N*-[tris(hydroxy-methyl)-methyl]glycine (Tricine), glycylglycine, pyrophosphate). The influence of coenzyme concentrations was also studied.

The highest activity of immobilized PheDHs was obtained at pH 10 as shown in (Fig. 2) for *Bacillus badius* and *Bacillus sphaericus* in 0.02M pyrophosphate buffer. The nature of the buffer significantly influenced the reactor response with the best results obtained in pyrophosphate buffer (Fig. 3). PheDH from *Bacillus badius*

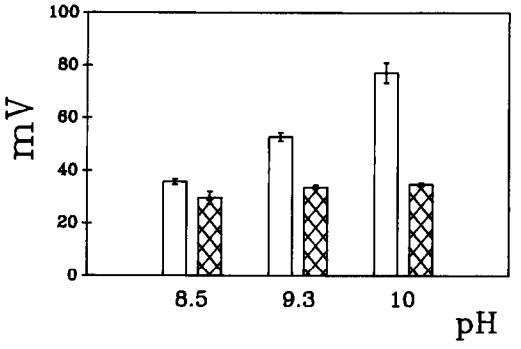

Fig. 2. Effect of pH (0.02*M* pyrophosphate buffer) on the light emission for phenylalanine dehydrogenases from *Bacillus badius* (white) and *Bacillus sphaericus* (hatched), at 1m*M* Phe level.

gave a higher light emission than that of *Bacillus sphaericus* and *Rhodococcus sp. M*4. Therefore pyrophosphate was the buffer of choice and the PheDH from *B. badius* was normally used especially when low Phe concentrations have to be determined.

The pH of the luminescent buffer solution was kept at 6.5 (0.1*M*); the optimum pH for the bacterial luciferase, *ca.* pH 7.0, was achieved on mixing it with the alkaline buffer solution for the Phe determination (pH 10, 0.02*M*).

There was an increase of PheDH activity by increasing the coenzyme concentration in the range of 0.5–10m*M*. However 1m*M* NAD^+ was routinely used in order to reduce cost and because the assay sensitivity was satisfactory also at this concentration.

The transformation yield of the PheDH coil was determined at 1m*M* of Phe and compared with the light emitted from an equal concentration of NADH in different buffers. NADH

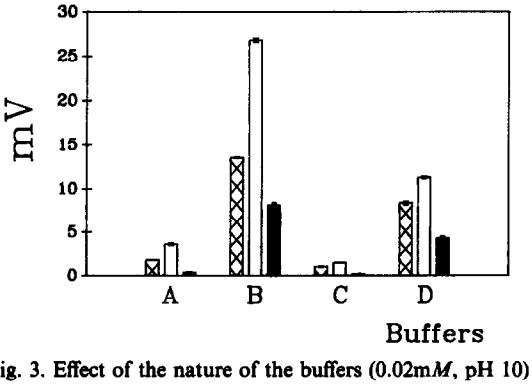

Fig. 3. Effect of the nature of the buffers (0.02m*M*, pH 10) on the light emission for phenylalanine dehydrogenases from *Bacillus sphaericus* (hatched), *Bacillus badius* (white) and *Rhodococcus sp. M*4 (black), at 0.1m*M* Phe level. buffers: A: Tris; B: Pyrophosphate; C: glycilglycine; D: Tricine.

was analysed with the same manifold and in the same conditions as phenylalanine and the transformation yield was taken as the ratio between the response (mV) obtained for Phe and that obtained for NADH. The yields were not very high (maximum 10%) owing to non-equilibrium conditions of analysis and to an unfavourable equilibrium constant.

Determination of L-*phenylalanine*

Using the PheDH reactor, the detection limit of the assay (3σ) was 0.5μM for an injected sample volume of 20 μl. The response, for freshly prepared phenylalanine standard solutions, obtained by the measurement of peak height, was linear between 1 and 100μM; $y = 1.01 \pm 0.02$ mV $(M)^{-1} + 9.09 \pm 0.15$ mV; correlation coefficient $(r) = 0.995$, number of analysis $(n) = 8$; probability (P) < 0.001. The non-zero y intercept for the calibration curve was caused by the background of nylon coil, *i.e.*, light emission when only the working bioluminescent solution flows into the nylon coil.

The relative standard deviation (R.S.D) of the method in the analytical range of Phe was below 5%. The recoveries were between 90 and 101% when phylalanine standards (1–50μM) were added to serum samples of known phenylalanine concentration (916μM) diluted 1 + 19 with pyrophosphate buffer.

The specificity of *Bacillus badius* PheDH coil for a variety of substrates (tested at two different concentrations) is shown in Table 2. Although it was reported that PheDH can catalyze the oxidative deamination of a number of amino acids such as methionine (8% relative activity to *L*-phenylalanine), *L*-tyrosine (9%), *L*-norleucine (19%), *etc.*[19,16] at 10m*M* level, we found no or low activity with the above-mentioned amino acids and also with others (Table 2). Only DL-thienylalanine, normally not present in the serum, gave a high response (33–49%). This suggests that the enzyme recognizes the back of the skeleton of the two molecules, which is similar in two cases.

Serum

L-Phe is generally very stable and freezing-thawing does not change Phe concentration in serum;[1] and it is also possible to analyse Phe without pre-treatment or deproteinization with sulphosalicyclic acid. It should be noted that the use of sulphosalicylic acid would inhibit reactor response and need buffers at high ionic strength to keep the optimal pHs.

Table 2. Specificity for *L*-Phenylalanine reaction catalysed by *L*-PheLDH

ACID	Concentration, *m*M	Light, *mV*	Substance (mV)/Phe (mV), %
L-Phenylalanine	1	22,1	
L-Phenylalanine	0,1	7,1	
DL-Phenylglycine	1	—*	—
DL-Phenylglycine	0,1	—	—
DL-Thienylalanine	1	7,3	33
DL-Thienylalanine	0,1	3,5	49
Glycil-*L*-phenylalaline	1	0.04	0.2
Glycil-*L*-phenylalaline	0,1	0.01	0.1
D-Tyrosine	1	—	—
D-Tyrosine	0,1	—	—
L-Tyrosine	1	—	—
L-Tyrosine	0,1	—	—
DL-Tryptophan	1	—	—
DL-Tryptophan	0,1	—	—
L-Arginine	1	—	—
L-Arginine	0,1	—	—
L-Valine	1	0,3	1.4
L-Valine	0,1	—	—
L-Methionine	1—	—	—
L-Methionine	0,1	—	—
L-Histidine	1	0,1	0.5
L-Histidine	0,1	—	—
L-Alanine	1	—	—
L-Alanine	0,1	—	—
L-Aspartic acid	1	—	—
L-Aspartic acid	0,1	—	—
L-Glutamic acid	1	—	—
L-Glutamic acid	0,1	—	—
L-Leucine	1	—	—
L-Leucine	0,1	—	—
L-norleucine	1	—	—
L-norleucine	0,1	—	—
4-Hydrophenyl-pyruvic	1	—	—
4-Hydropheynl-pyruvic	0,1	—	—
Phenylpyruvic acid	1	0.33	1.5
Phenylpyruvic acid	0,1	0.1	1.4
Indole-3-pyruvic acid	1	0.1	0.1
Indole-3-pyruvic acid	0,1	—	—
Imidazolepyruvic acid	1	—	—
Imidazolepyruvic acid	0,1	—	—
α-Ketoisocaproic acid	1	—	—
α-Ketoisocaproic acid	0,1	—	—

* No signal detected

With samples diluted 1 + 1 − 1 + 4 with pyrophosphate buffer a slight inhibition of the luminescent enzymes was observed and the calculated *L*-Phe concentrations are quite different. At higher dilutions (1 + 9 − 1 + 99) little or no interference was found for sera, while *L*-Phe diluted in acid showed a greater inhibition.

Constant addition of 50μM *L*-phenylalanine to different serum diluted from 1 + 19 to 1 + 199 gave a good recovery (87–104%) both with addition after dilution, and addition before dilution. Variable additions of *L*-Phe (10–500μM) to serum constantly diluted to 1 + 19 or to buffer alone gave the same good correlation.

The results of within-day and between-day reproducibility studies with the two sera (normal and pathological) gave R.S.D. values of $< 5\%$. These satisfactory results are also due to the use of an automatic diluter—injector in the treatment and preparation of the sample.

The content of *L*-phenylalanine was assayed with the ion-exchange chromatographic method performed automatically with deproteination and compared with the continuous-flow system. The results obtained with the bioluminescent method agreed well with those from the reference method giving, for normal and pathological *L*-phenylalanine concentrations, the correlation equation: $y = 0.90 \pm 0.02 \times + 0.23 \pm 0.08$; $r = 0.947$, $n = 59$; $P < 0.001$, for the chromatographic (x) *vs.* the bioluminescent (y) method (Fig. 4). Moreover we used the Wilcoxon Test for coupled, not parametric data

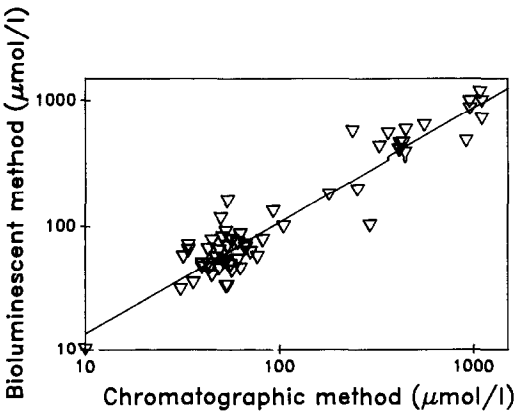

Fig. 4. Comparison between determination of *L*-phenylalanine using bioluminescent flow sensor (y) and chromatographic method (x). Reference range: 0–69μM Phe.

which shows ($P = 0.19$) that the results obtained from the two methods were not statistically different.

CONCLUSIONS

The lifetime and operational stability of immobilized enzymes were satisfactory. The residual activity of the whole enzymic system after 2 months of use and analysis of more than 40 samples per day was *ca.* 50% of the original. The lifetime of the proposed sensor, defined as the time during which accurate results can be obtained within the full calibration range, was about 4 months.

The direct use of serum, without extraction with chaotropic agents such as perchloric, metaphosphoric or sulphosalicylic acid, allows exclusion of the pre-instrumental work-up (only dilution has been made).

Recently Wendel *et al.*[20] have developed a batch method for the control of phenylketonuric patients using PheDH from *Rhodococcus sp. M4*, with a good sensitivity. However the method requires an extraction step from serum with perchloric acid and incubation at 21° for 15 min, which made the procedure more complex and time consuming than that of the luminescent one. The flow sensor makes it possible to reduce the analysis time (1–2 min) in comparison to chromatographic analysis (20–30 min).

The present data agreed well with those reported by other workers[15–19] and the automation of the whole system should allow the use of the bioluminescent flow sensor for the continuous monitoring of *L*-Phe in blood and in foodstuffs. For instance the direct determination of *L*-Phe in paper disc (sent by mail) with blood from newborn for neonatal screening of hyperphenylalaninaemia, or dietary management of phenylketuronic patients should be possible, as well as the quality control of aspartase of which *L*-Phe is a hydrolysis product.

Acknowledgements—This work was supported by grants from MURST (Ministero della Università e della Ricerca Scientifica e Tecnologica) and CNR (Consiglio Nazionale delle Ricerche, Comitato Nazionale Biotecnologie e Biologia Molecolare (Grant n. 90.01349.CT14)). Dr. Y. Hibino and Central Glass Co. Ltd are gratefully acknowledged for the gift of PheDH.

REFERENCES

1. R. Shen and C. W. Abell, in H. U. Bergmeyer, *Method of Enzymatic Analysis*, Vol. VIII, p. 405. Verlag Chemie, Weinheim, 1985.
2. C. R. Scriver and L. E. Rosemberg, *Amino Acids Metabolism and its Disorders*, Vol. 10, *Major Problems in Clinical Pediatrics*, p. 290. W. B. Saunders & Co., London, 1973.
3. A. Ponzone, O. Guardamagna, S. Ferraris, S. Biasetti, G. Bracco and A. Niederwieser, *Eur. J. Ped.*, 1987, **146**, 93.
4. P. L. Chang, S. Lewis, J. Heathcote and D. T. Whelan, *J. Int. Feder. Clin. Chem.*, 1991 **3**, 58.
5. S. Moore, D. H. Spackman and W. H. Stein, *Anal. Chem.*, 1958, **30**, 1185.
6. C. R. Scriver, S. Mackenzie, C. L. Clow and E. Devin, *Lancet*, 1971, **i**, 310.
7. H. Godel, P. Seitz and M. Verhoef, *LC-GC Intl.*, 1992, **5**, 44.
8. N. D. Atherton, *Clin. Chem.*, 1989, **35**, 975.
9. A. J. Bourque and I. S. Krull, *J. Chromatogr.*, 1991, **537**, 123.
10. G. Toth, M. Lebl and V. J. Hruby, *ibid.*, 1990, **504**, 450.
11. Y. Nozaky, *Arch. Biochem. Biophys.*, 1990, **277**, 324.
12. H. Koyama, *Clin. Chim. Acta*, 1984, **136**, 131.
13. T. Yao and T. Wasa, *Anal. Chim. Acta*, 1988, **209**, 259.
14. W. Hummel, N. Weiss and M.-R. Kula, *Arch. Microbiol.*, 1984, **137**, 47.
15. Y. Asano, K. Endo, A. Nakazawa, Y. Hibino, N. Okazaki, M. Ohmori, N. Nuamo and K. Kondo, *Agric. Biol. Chem.*, 1987, **51**, 2621.
16. L. de Boer, M. van Rijssel, G. J. Euverink and L. Dijkhuizen, *Arch. Microbiol.*, 1989, **153**, 12.
17. N. Okazaki, Y. Hibino, Y. Asano, M. Ohmori, N. Numao and K. Kondo, *Gene*, 1988, **63**, 337.
18. T. Ohshima, H. Sugimoto and K. Soda, *Anal. Letters*, 1988, **21**, 2205.
19. Y. Asano, A. Nakazawa, K. Endo, Y. Hibino, M. Ohmori, N. Numao and K. Kondo, *Eur. J. Biochem.*, 1987, **168**, 153.
20. W. Wendel, W. Koppelkamm and W. Hummel, *Clin. Chim. Acta*, 1991, **201**, 95.
21. A. Roda, S. Girotti, S. Ghini and G. Carrea, *J. Biolumin. Chemilumin.*, 1989, **4**, 423.
22. S. Girotti, C. Bassoli, M. L. Cascione, S. Ghini, G. Carrea, R. Bovara, A. Roda, R. Motta and R. Petilino, *ibid.*, 1989, **3**, 41.
23. S. Girotti, B. Grigolo, E. Ferri, S. Ghini, G. Carrea, R. Bovara, A. Roda, R. Motta and R. Petilino, *Analyst*, 1990, **115**, 889.
24. S. Girotti, S. Ghini, G. Carrea, R. Bovara, A. Roda and R. Budini, *Anal. Chim. Acta*, 1991 **255**, 259.,
25. P. V. Sundaram, *Methods Enzymol.*, 1988, **137**, 288.

Talanta, Vol. 40, No. 3, pp. 431–444, 1993
Printed in Great Britain.

0039-9140/93 $6.00 + 0.00

INVESTIGATION OF RELATIVE HUMIDITY EFFECTS ON THE RESPONSE BEHAVIOR OF A pH INDICATOR-BASED OWG VAPOR SENSOR

DANIEL CALLAHAN and DAVID S. BALLANTINE, JR.*
Chemistry Department, Northern Illinois University, DeKalb, IL 60115, U.S.A.

(*Received* 21 *April* 1992. *Revised* 21 *May* 1992. *Accepted* 15 *July* 1992)

Summary—The response of a pH indicator-based optical waveguide sensor was characterized with respect to the effects of relative humidity (RH) on the magnitude of the sensor response, and on the rate of response to both hydrochloric acid and ammonia/ammonium hydroxide vapors. Water vapor constitutes both a chemical and a systematic (optical) interference for the OWG sensor response to hydrochloric acid. Swelling of the polymer films upon exposure to water vapor results in a decrease in the loss of light at the polymer/air interface, resulting in an increase in the sensor signal. In addition, high RH conditions decrease the bromothymol blue indicator response to hydrochloric acid vapor. In contrast, the bromothymol blue indicator response to ammonia increases as the RH increases. High RH levels also increases the rate of diffusion (transport) of hydrochloric acid into (and out of) Nafion films, but does not affect the diffusion rate for poly(vinyl alcohol) polymer films. The RH does not appear to have any significant effect on the rate of transport of ammonia in any of the polymer films studied.

Due to the advantages of microsensor technologies (low cost, rapid and sensitive detection, and portability), there is increasing interest in the development of these devices for a variety of chemical sensing applications. In order to optimize a sensor for detection of a given analyte (or class of analytes) a thorough characterization of the sensor response behavior is required. Such characterization includes evaluation of the coating/reagent materials and their effects on the sensor performance, as well as the sensor response to potential interferences.

A multiple internal reflection optical waveguide (MIR-OWG) sensor for the detection of acidic and alkalescent vapors was recently reported.[1] This sensor employed a pH indicator (bromothymol blue) suspended in an ionic polymer, Nafion. During the initial evaluation of this sensor a dramatic interference from water vapor was noted. In order to eliminate or correct for this interference, the nature of the interference with respect to the response mechanism must be determined. The work reported herein is intended to address this problem. Specifically, the effects of water vapor on the rate and magnitude of sensor response were investigated. The implications of the results reported herein are discussed with respect to the design and construction of similar OWG sensors.

*Author for correspondence.

EXPERIMENTAL

Materials

The two indicators studied during this work were thymol blue and bromothymol blue. Both are sulfonic acid-type pH indicators, with structures and effective transition ranges in aqueous solution included in Fig. 1. Thymol blue was obtained from Aldrich, and bromothymol blue was obtained from Fisher Scientific. Both materials were of >95% purity and were used as received. These materials were dissolved in methanol to obtain solutions that were approximately 2 mg (indicator)/ml (solution).

Poly(vinyl alcohol) samples were selected to represent a broad range of molecular weight ranges as well as varying degrees of hydrolysis as indicated in Table 1. Nafion was obtained as a 5% solution from Solution Technologies, Mendenhall, U.S.A.; all other polymers were obtained from Aldrich and were used as received. Solutions were prepared by dissolving the polymers (or in the case of Nafion, by dilution) in methanol/water solution to obtain final polymer concentrations of 2 mg/ml.

Solutions for coating the OWGs were prepared by mixing equal volumes of the selected

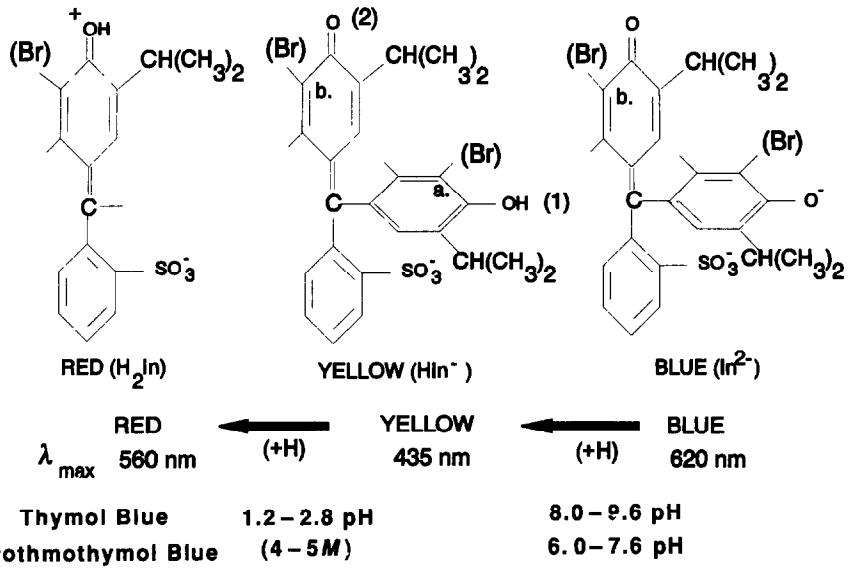

Fig. 1. Representation of the three forms of the pH indicators, thymol blue and bromothymol blue; (a) and (b) indicate sites of the bromines for the BT indicator.

polymer and indicator solutions to obtain final concentrations of 1 mg/ml in each component. These solutions were cast onto either quartz slides, for single-pass spectroscopic measurements, or onto cylindrical quartz capillary tubes for the MIR spectroscopy measurements as described below. The quartz capillaries (100 mm × 0.87 mm o.d.; wall thickness 0.065 mm) were obtained from ChemGlass, Inc. (New Jersey).

Procedures

In the previous study sensor response measurements were performed using the LED-OWG electronics module described previously.[1] Additional measurements during this work were performed using the Minichrom Monochromator system (Optometrics Corp., Ayer MA), equipped with a tungsten lamp source and a photo-multiplier (PMT) detector. Two experimental set-ups were used during these studies and are illustrated in Figs. 2 and 3. Figure 2 represents the single-pass system. The indicator/polymer film was cast onto a thin quartz slide which was, in turn, placed in a flow cell inside the spectrophotometer as indicated. Because light only passes through the sample film once before reaching the PMT detector, the sensitivity of this configuration is limited. Figure 3 represents the MIR-OWG set-up. Light is introduced to one end of the waveguide via optical fibers which are connected to the exit port of the monochromator. Light propagates along the waveguide via internal reflection and exits the opposite end of the waveguide, where it is transmitted to the PMT via a second set of optical fiber couplers. The light may be reflected at more than one interface, as indicated in the inset in Fig. 3. If the refractive index of the polymer is less than that of the waveguide substrate then reflection can occur at the substrate/film interface if the incident angle, θ, is greater than the critical angle, θ_c, determined from Snell's Law. If the refractive index of the polymer is greater than that of the substrate then light is transmitted through the substrate/polymer interface, where it may either be reflected at the film/air interface or lost via transmission through the interface.

Table 1. Polymeric materials

Polymer	PolymerID	MW Range	% Hydrolysis
poly(vinyl alcohol)	PVA-H	105,000–110,000	100%
	PVA-M	31,000– 50,000	98%
	PVA-L1	13,000– 23,000	89%
	PVA-L2	9,000– 10,000	80%
poly(vinyl acetate)	PVAc	High Mol Wt.	0%
Nafion	NAF	—	—

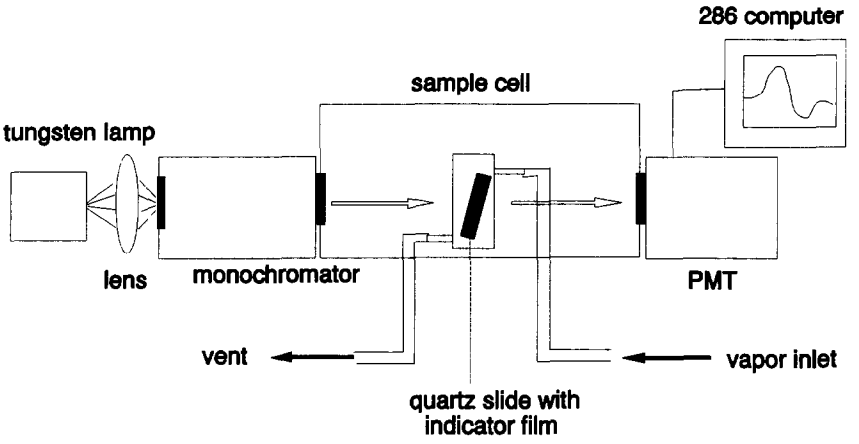

Fig. 2. Instrumental setup used to collect single-pass spectral data for the indicator/polymer films using the Minichrom system.

The Minichrom system was interfaced to a Hyundai 286 personal computer via an RS-232 port. The system is fully programmable and can obtain absorbance spectra in the visible region (300–750 nm), or to monitor PMT voltage at a given wavelength as a function of time. Voltage data from PMT and from the LED-OWG module were collected by computer via an IBM data acquisition and control adapter (DACA) card.

Hydrochloric acid and ammonia vapors were generated by bubbling dry $N_2(g)$ through an aqueous solution of hydrochloric acid or ammonium hydroxide. The vapor output from the bubbler could be sent directly to the quartz slide or the MIR-OWG sample cells illustrated in Figs. 2 and 3, or could be mixed with diluting air/vapor from a VG-400 Vapor Generator System (Microsensor Systems, Inc., Bowling Green KY) before being directed to the sample cells.

RESULTS AND DISCUSSION

Indicator/PVA films were cast onto quartz slides, and spectra were obtained using the

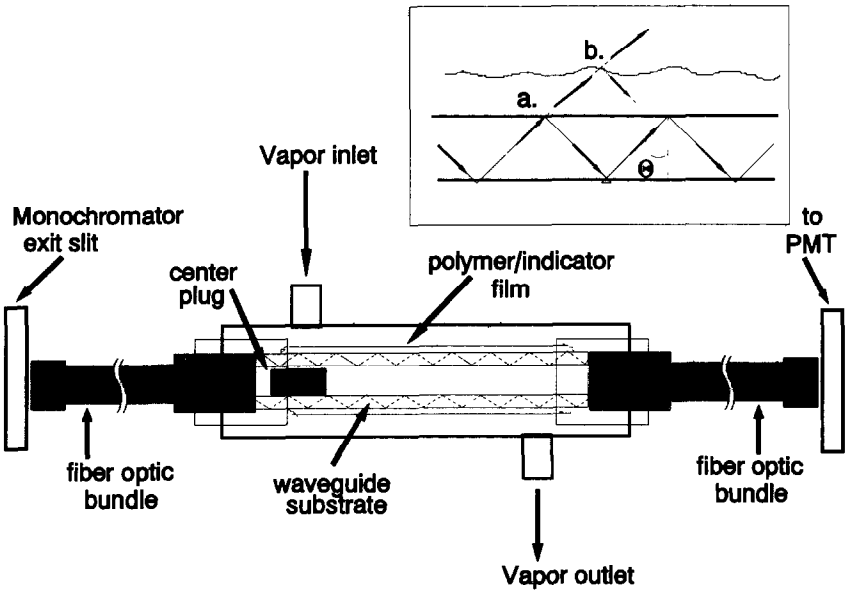

Fig. 3. Fiber optic coupler adaptation used to collect MIR-OWG data using the Minichrom system. The insert illustrates reflection(s) and losses at a) the substrate/film interface and b) the film/air interface.

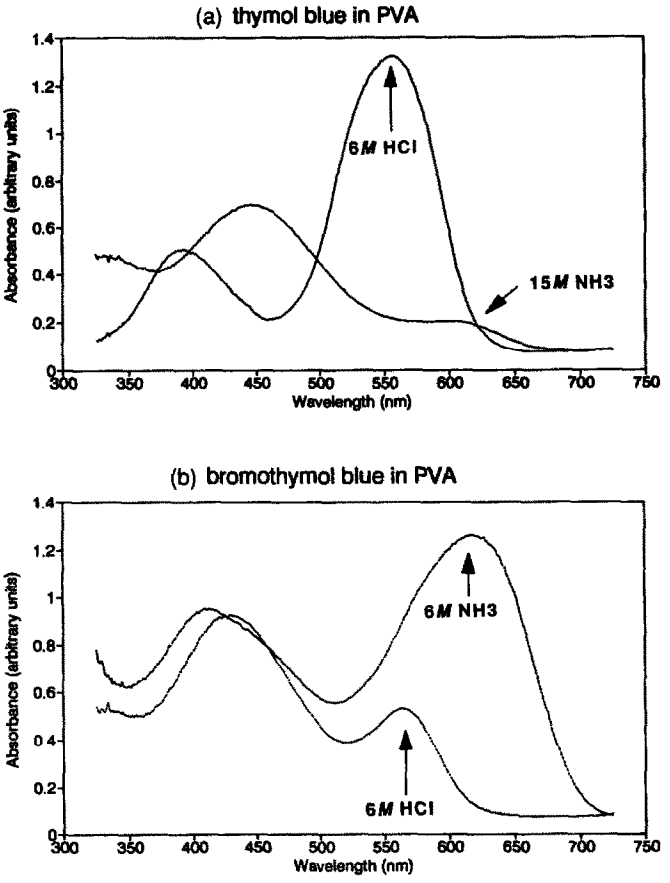

Fig. 4. Single-pass spectra for a) a TB/PVA film (solid lines) and b) BT/PVA film (dashed lines) upon exposure to HCl and NH_3 vapors, as indicated in figure.

single-pass optical configuration in Fig. 2. Typical absorbance spectra for the TB/PVA and BT/PVA films are presented in Fig. 4(a) and (b). Separate spectra were obtained for each film exposed to hydrochloric acid and ammonia vapors from solutions of various concentrations, as indicated in the Figure captions. Note that both indicators exhibit three characteristic forms (H_2In, HIn^-, and In^{2-}), with the predominant form being dependent on the acidity or basicity of the film. Spectral studies for the indicators in Nafion films yielded similar results.

The initial color of the indicator films varied depending on the indicator and the polymer matrix. The bromothymol blue (BT) indicator suspended in PVA polymer exhibited an initial yellow color, typical of the HIn^- form of the indicator. Thymol blue (TB)/PVA films were initially red in color, indicative of the H_2In form; exposure to NH_3 vapors converted the TB to the HIn^- (yellow) form which persisted for long periods of time after removal of the NH_3 vapor. The TB/NAF film also dried in the red form. Exposure to NH_3 vapors could shift the equilibrium temporarily to the HIn^- form, but the indicator reverts to the H_2In (red) form upon removal of NH_3 vapors. This is likely due to the acidic nature of the sulfonic acid groups in the Nafion polymer. The Nafion solution was treated with sodium hydroxide to convert the sulfonic acid sites to the sodium salt before preparation of some NAF/indicator films. In these Na-salt Nafion films, the HIn^- form of the TB indicator was more stable. The TB could then be converted to the H_2In form upon exposure to HCl vapors. In general, the TB indicator films exhibited irreversible response to the HCl vapors; the red color indicative of the H_2In form persisted long after removal of the HCl vapor. It was possible, however, to regenerate the HIn^- (yellow) form of the TB in the Na-salt Nafion film by exposure to NH_3 vapor. The BT/NAF films also dried in the red (H_2In) form, but could be readily converted to the yellow (HIn^-) form by exposure to NH_3, or prolonged exposure to water vapor. Once converted to the HIn^- form, the BT films

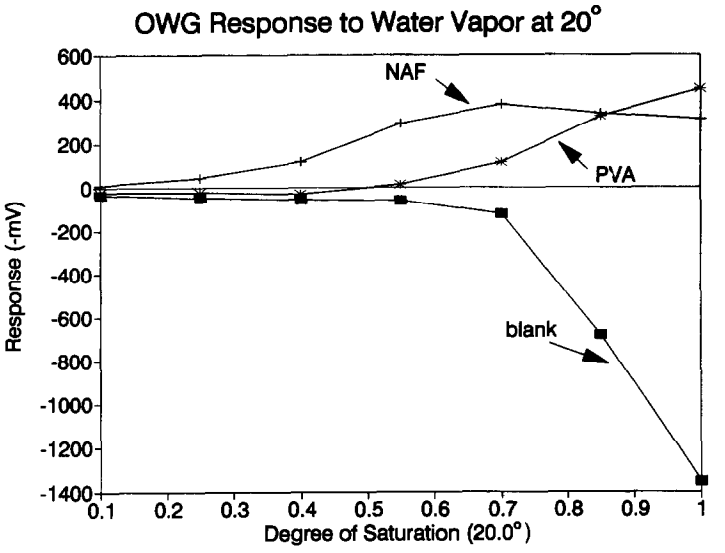

Fig. 5. LED-OWG Response to water vapor at 20° *vs.* % saturation (P/P°) for a blank waveguide and waveguides coated with Nafion and PVA films.

exhibit spontaneously reversible response to both hydrochloric acid and ammonia vapors.

As indicated in the spectra in Fig. 4, the TB films exhibited minimal spectral response to ammonia, but sensitive response to hydrochloric acid vapors. The BT films, on the other hand, exhibited very sensitive response to ammonia and lesser sensitivity to hydrochloric acid vapors. These differences are readily explained by the differences in structure (see Fig. 1) and are consistent with the relative pH transition ranges observed for these indicators in aqueous solution. The spectral behavior of the indicators seemed to be independent of the molecular weight or the % hydrolysis of the PVA polymers. While there was some variation in the intensity of the absorbance peaks, the position of indicator equilibrium (determined as the ratio of the H_2In and HIn^- peaks) seemed fairly consistent in all the PVA and PVAc polymers.

Water vapor effects

The presence of water vapor affects the sensor response in a variety of ways. The observed effects can be generally classified as systematic (optical), chemical, or kinetic effects, as discussed below.

Systematic response effects. In our initial report dealing with an LED-OWG acid vapor sensor it was noted that exposure of the sensor to nearly saturated water vapor resulted in a significant increase in transmittance (*i.e.*, photodetector voltage). Previous experimental results indicated that this effect was due to the water vapor/polymer interactions, and was not due to any change in the absorbance spectra of the indicator.[1] Since this increase in signal is in the opposite direction than the acid–indicator response this effect constituted a systematic interference. We initially proposed a differential approach (dual wavelength or dual sensor) to compensate.[1] As part of the current work this phenomenon was investigated further to determine the source of the effect and to identify other possible means to either compensate for or eliminate the interference.

Typical response data for uncoated (blank) and polymer-coated waveguides exposed to water vapor (using the LED-OWG sensor configuration from Ref. [1]) are summarized in Fig. 5. The data as presented represent the change (increase or decrease) in the photodetector signal upon exposure of the waveguide to water vapor. For the uncoated waveguide the detector signal decreases, whereas for the polymer-coated waveguides the signal increases.

Table 2. Refractive indices for experimental materials

Material	Refractive index (at 589 nm)*
Poly(vinyl alcohol)	1.49–1.53
	1.50
Nafion	—
Borsilicate glass	1.52
Quartz (fused)	1.46
air (@20°)	1.00
water (@20°)	1.33

The refractive index range in the table is from Ref. 2; the value of 1.50 is the value given by Aldrich for the high MW PVA polymer used for the majority of the reported studies. All other values were obtained from Ref. 4. A refractive index for Nafion was unavailable.

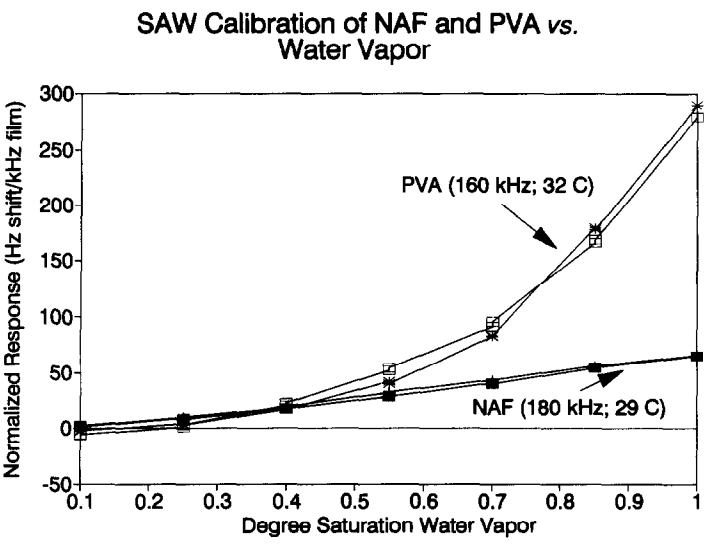

Fig. 6. Normalized response of polymer-coated 158 MHz SAW devices to water vapor between 10 and 100% saturated.

These data can be explained in part by referring to Snell's Law and the refractive indices for the waveguide sensor materials in Table 2. Using the refractive index values (n_i) for the glass capillary and air we obtain a critical angle of 41°. Light having an incident angle *less* than the critical angle will be transmitted through the glass/air interface and lost, whereas light having an incident angle *greater than* this value will be reflected at the interface and will propagate through the waveguide to the detector. The introduction of water vapor will change the effective n_i value of air at the interface; for adsorbed or condensed water vapor, having an n_i value of 1.33, we obtain a critical angle of 61°. This increase in the critical angle translates into a decrease in the cone of acceptance, which would readily account for the observed decrease in the detector signal for the bare waveguide exposed to water vapor.

The polymer-coated LED-OWG response is not as easily explained. For all practical purposes, the refractive indices of the substrate materials and the PVA are close enough in value that nearly all light will be transmitted through the substrate/polymer interface, except for incident angles approaching the grazing angle (90°). A glass capillary coated with PVA, for example, has a critical angle of 80.7°. For such cases the polymer/air interface becomes the reflecting interface. Because the polymer film surface is most likely not as smooth as the glass surface, greater scattering and transmission losses would be expected at this interface. An increase in detector signal upon exposure to water can only result from a reduction in the amount of light lost at this interface. A number of possibilities exist to explain the observed behavior. First, swelling of the polymer results in both a thicker film and, possibly, a smoother film surface. A smoother surface would decrease the amount of scattering and transmission losses. A thicker film would decrease the total number of reflections and thereby decrease the number of opportunities for loss of light at this interface.

In order to quantify the amount of water absorbed into the polymer, surface acoustic wave (SAW) studies were performed. SAW devices were coated with polymer films, and the frequency of the devices were observed while the coated devices were exposed to varying concentrations of water vapor. Results of these studies are presented graphically in Fig. 6. The sensor responses (frequency shift in Hz) are plotted *vs.* the vapor pressure of water (fraction of saturation, P/P°). Note that the sensor responses (frequency shift) have been normalized *vs.* the amount of polymer coating, reported in kHz of frequency shift. Thus the values plotted in the figure represent a *relative* increase in mass; the actual % increase in mass would be equal to the relative increase divided by a factor of 1000. If we assume that the entire SAW response is due to added mass of water vapor, then the polymer swelling can be estimated as follows. Treating the adsorbed vapor as a condensed liquid, the increase in volume can be approximated as the volume of an equivalent amount of this vapor in its liquid form, *i.e.*, from the reciprocal of the liquid density, ρ_L. The %

Table 3. Polymer swelling estimated from SAW sorption data

Water vapor (Rel. sat.)	Poly(vinyl alcohol) (160 kHz film)		Nafion (180 kHz film)	
	Norm. response (*Hz/kHz*)	Estimated % Swelling*	Norm. response (*Hz/kHz*)	Estimated % Swelling
0.10	—	—	2.1	0.21 (0.05)
0.25	2.78	0.28 (0.07)	9.3	0.93 (0.23)
0.40	19.0	1.9 (0.5)	18.2	1.8 (0.45)
0.55	46.9	4.7 (1.2)	30.3	3.0 (0.75)
0.70	87.9	8.8 (2.2)	41.8	4.2 (1.1)
0.85	173	17.4 (4.4)	55.4	5.6 (1.4)
1.00	284	28.5 (7.1)	65.3	6.6 (1.7)

*Figures in parenthesis are corrected for estimated SAW response due to elastic effects.

swelling is then calculated as the product of the % mass increase and $1/\rho_L$. Estimated percent swelling for various water vapor saturation levels are given in Table 3. Swelling for Nafion films is relatively small, with a maximum at saturation of only 6.6%. This is a reasonable estimate when compared to swelling estimates of 13% for Nafion membrane samples in aqueous solution.[5] For PVA the estimated swelling appears to be more significant, approaching 29% when exposed to saturated water vapor.

These estimates should be considered as upper limits only. According to SAW theory, changes in the mass or in the elastic modulus of the coating will produce a shift in the resonant frequency of the device. The increase in mass due to the sorption of water vapor into the polymer film will produce a corresponding decrease in the SAW frequency. If the sorption of water vapor causes swelling of the polymer, with an accompanying decrease in the elastic modulus, then there will be an additional decrease in the SAW frequency. A recent report concluded that the contribution of swelling effects to the observed SAW frequency shift may exceed the mass loading effect by a factor of 4–6.[6] If we take into consideration the contribution of swelling effects the frequency shift due to mass loading is smaller than the total observed frequency shift by a factor of 4 or more, and the actual swelling for PVA is on the order of 7%. These more conservative estimates of swelling are given in parenthesis in Table 3.

Using the swelling data from Table 3, we can estimate the refractive index for the swollen polymer film by considering the volume percents of the polymer and water in the swollen film, such that

$$n_{\text{swelled}} = \left(\frac{V_{\text{PVA}}}{V_{\text{total}}}\right) \cdot n_{\text{PVA}} + \left(\frac{V_{\text{water}}}{V_{\text{total}}}\right) \cdot n_{\text{water}} \quad (1)$$

As noted above, the critical angle for a PVA-coated glass capillary (calculated from Snell's Law) is 80.7°. For a PVA film swelled by 29% a refractive index of 1.44 is calculated using equation 1, with a corresponding decrease in the critical angle to 71°. For the more conservative swelling estimate of 7%, the refractive index and corresponding critical angle are 1.49 and 78.6°, respectively. This reduction in the critical angle implies that more light would be reflected at the substrate/polymer interface, which translates into an increase in the detector signal consistent with the observed OWG responses. This change in the critical angle is rather small, $\approx 2°$–$10°$ for PVA and significantly less for the NAF. Any increases in light due to this phenomenon will likely be too small to account for the large observed increases in detector signal. Therefore, it is proposed that the observed signal increases are predominantly the result of decreases in scattering and transmission losses at the film/air interface due to swelling, as discussed above, with only minor increases due to changes in refractive index.

Since this effect is most likely the result of a decrease in losses at the polymer/air interface, this potential systematic interference may be minimized or avoided by controlling the reflecting interface. The above experiments were repeated using the MIR-OWG configuration of Fig. 3. The fiber-optic couplers introduce light to the waveguide at angles much closer to the grazing angle compared to the LED; using this configuration there is a greater chance for reflection at the substrate/polymer interface. As seen in Fig. 7, the increase in signal of the MIR-OWG upon exposure to water vapor is much smaller, in the order of 10–20 mV. This small increase is consistent with what would be expected due to refractive index changes as a result of swelling, as discussed above.

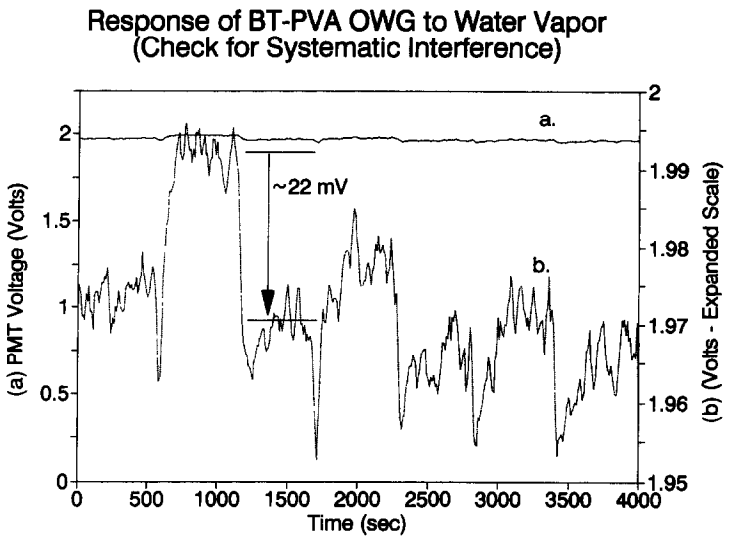

Fig. 7. Response of polymer-coated MIR-OWG sensor to water vapor, illustrating decreased response to water vapor compared to LED-OWG.

Selection of substrate and polymer materials, based on refractive indexes, and the introduction of light into the waveguide can thus be controlled so that the majority of light propagates by reflection at the substrate/polymer interface. Such an OWG sensor will still respond to changes in the absorbance properties of the reagent film via the evanescent wave, but changes in signal due to losses at the film/air interface will be avoided or minimized.

Kinetic effects. In our initial investigation it was reported that the addition of water vapor to the sensor increased the rate of recovery (return to baseline) for a BT-NAF OWG sensor exposed to hydrochloric acid vapor. In order to investigate the effect of water vapor on sensor response time the indicator/polymer films were exposed to hydrochloric acid and ammonia vapors mixed with diluting air from the VG-400 containing varying amounts of water vapor.

Figure 8 summarizes the results for a TB-NAF (base-treated) film exposed to hydrochloric acid vapor from a 0.33*M* hydrochloric acid solution maintained at room temperature (23°). This vapor produced from this solution has an estimated hydrochloric acid concentration of 20 ppb (see calculations and discussion in Ref. 1). The flow rate from the bubbler was approximately 100 ml/min. The bubbler output was mixed with diluting air streams from

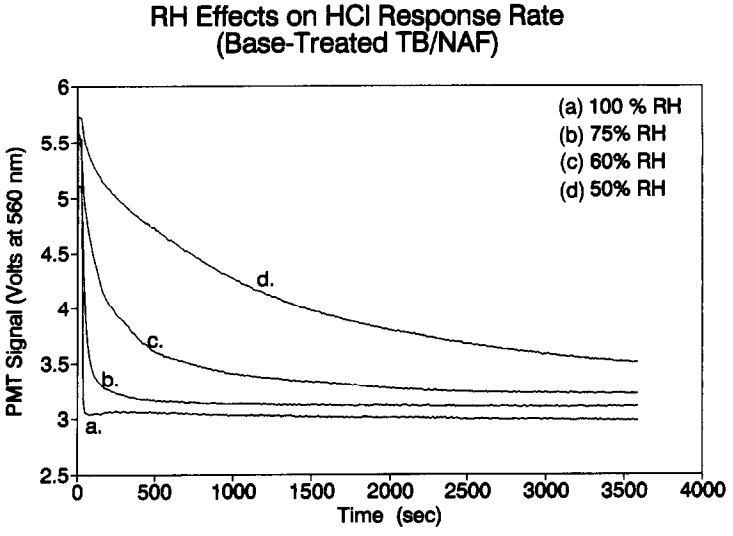

Fig. 8. Rate of response of a TB-NAF (base-treated) film to HCl vapor as a function of RH using the single-pass configuration. PMT signal at 560 nm was monitored during acid vapor exposure.

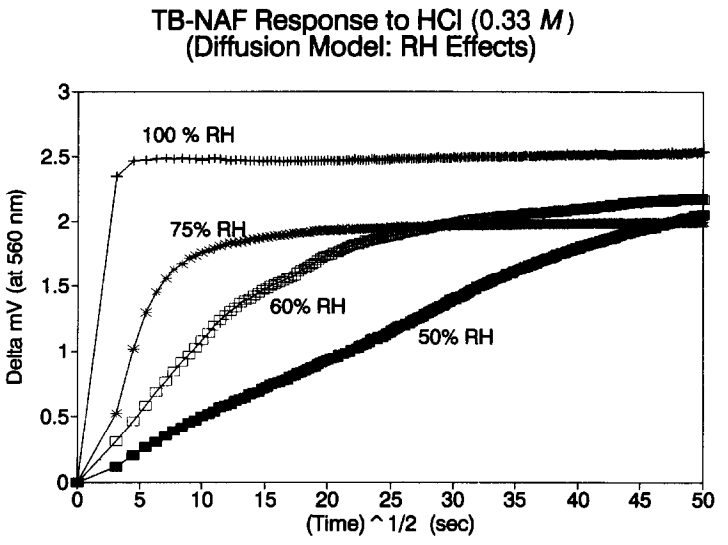

Fig. 9. Data from Figure 8 plotted *vs.* $\sqrt{t}$, indicating the diffusion limited response of the indicator film.

the VG-400 (100 ml/min) that were 100, 50, 20 and 0% saturated in water vapor. Assuming that the bubbler output was saturated with water vapor, then the relative humidity (RH or % saturation) of the resulting streams was 100, 75, 60 and 50% RH, respectively, and the concentration of hydrochloric acid vapor was 10 ppb. These vapor streams were introduced to a TB-NAF film on a quartz slide and signal intensity at 560 nm (in volts) was monitored as a function of time using the single pass configuration in Fig. 2. The results clearly indicate the increase in response rate with increased RH.

If we assume that the indicator response is fast compared to the rate of diffusion then we can characterize the response of the sensor by way of a diffusion model. For a film of uniform thickness the concentration of analyte at some depth in the film as a function of time, $C(x,t)$, can be described using the one-dimensional Fick's Law,

$$\frac{\delta^2 C}{\delta t} = D \frac{\delta C}{\delta x^2} \tag{2}$$

where D is the diffusion coefficient. Assuming that the film response is directly proportional to the vapor absorbed into the film, and that the rate of the indicator reaction is fast compared to the rate of diffusion, then the incremental response (ΔmV) is proportional to $\sqrt{t}$ until the concentration of solution in the film reaches

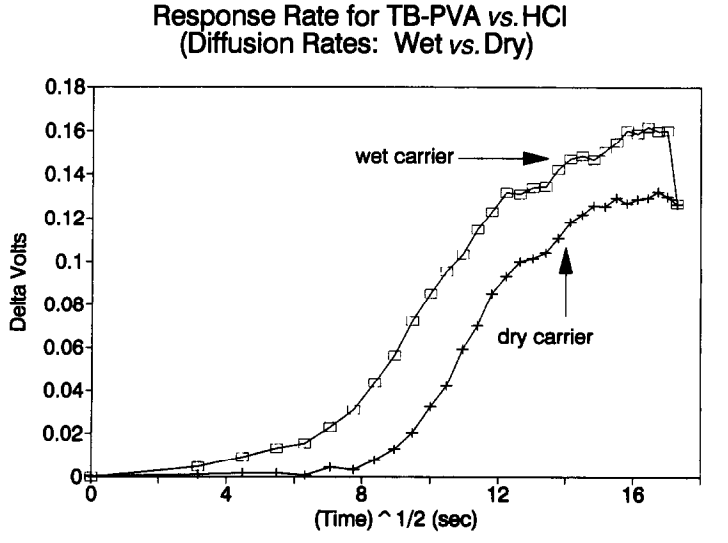

Fig. 10. Response for MIR-OWG TB-PVA film plotted *vs.* $\sqrt{t}$, indicating that rate of response of the PVA films to HCl vapor are not dependent on RH.

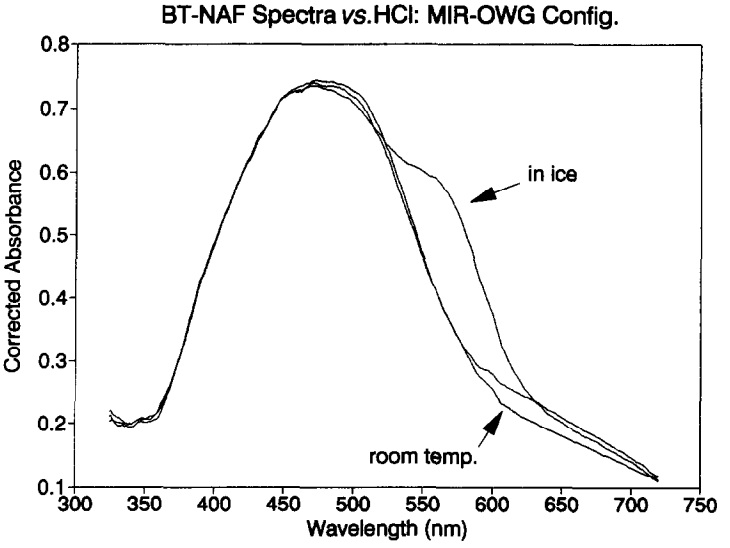

Fig. 11. Spectra for BT/NAF film exposed to water vapor, and HCl vapor from 0.165 M HCl bubbler solution at 0° and 23° as indicated. Spectra were collected using the MIR-OWG configuration from Fig. 3.

approximately 60% of the equilibrium film concentration.[7] Plotting the response data in Fig. 8 as ΔmV *vs.* $\sqrt{t}$ produces the data presented in Fig. 9. The linear initial slopes for the plots in Fig. 9 indicate that the diffusion model fits the observed responses, and that the rate of diffusion of hydrochloric acid into the Nafion film is humidity-dependent. Previous work has demonstrated that gas diffusivity in Nafion polymer films increases as the degree of film hydration increases,[8] which supports the observations reported above.

Similar experiments for hydrochloric acid *vs.* PVA films indicate that the diffusion of hydrochloric acid into these films is not sensitive to humidity. This unique behavior observed for the HCl/NAF system may be explained by the cation-exchange properties of Nafion. When these response studies were performed using the fiber-optic configuration of Fig. 3 the results represented in Fig. 10, plotted as ΔmV *vs.* $\sqrt{t}$, were obtained. The response profiles for the 50 and 100% RH conditions are similar in appearance (although slightly offset in time) indicating that the diffusion of hydrochloric acid into the PVA film is not sensitive to RH. It is worth noting that, unlike the data in Fig. 8, the initial slopes of the ΔmV *vs.* $\sqrt{t}$ plots in Fig. 10 are not linear. This is due to differences in the optical configurations used to collect these data. The data in Fig. 9 were obtained using the single pass configuration, whereas the data in Fig. 10 were obtained using the MIR-OWG configuration. For the single-pass configuration the observed signal is an integrated response through the entire film. As soon as hydrochloric acid diffuses into the film there is a net decrease in the detector signal; as the concentration of hydrochloric acid in the film increases the signal at 560 nm decreases proportionately. In contrast, for the MIR-OWG configuration most of the light is reflected at the substrate/polymer interface, as discussed previously, and probes the film via the evanescent wave. The sensor response arises from interactions of the evanescent wave with the indicator in the film. The effective probing depth of the evanescent wave is generally small compared to the average thickness of the film, so that there is no indicator response until the hydrochloric acid diffuses far enough into the film to be sensed at the substrate/polymer interface.

For the BT-polymer sensors, the rate of response to ammonia vapor was observed to be independent of RH for both the NAF and the PVA films. The magnitude of response, however, was significantly affected by RH for both ammonia and hydrochloric acid. These observations are discussed in the next section.

Chemical (interference/synergistic) response effects. A series of experiments was performed to investigate the effect of water vapor on the indicator response of the OWG sensor. To differentiate between the systematic effects of water discussed previously, complete absorbance spectra were obtained for polymer/indicator films on a quartz capillary tube using

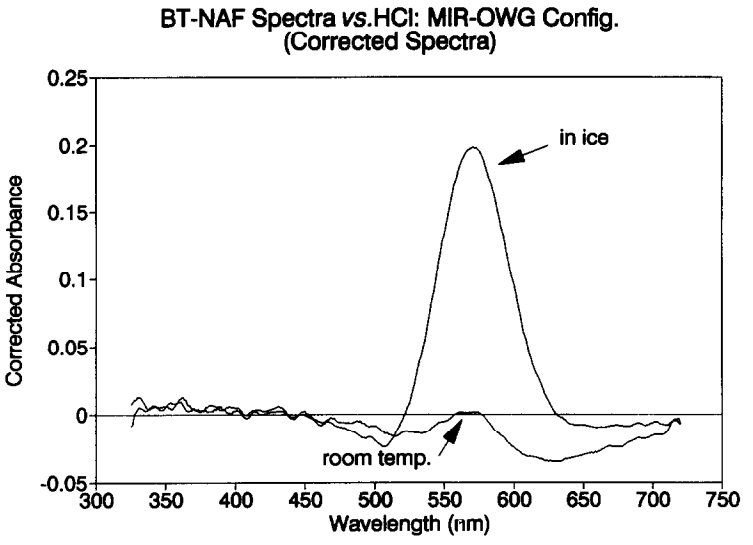

Fig. 12. Corrected spectra for a BT-NAF OWG sensor exposed to HCl vapor as indicated. Spectra were obtained by subtracting the baseline spectra (water vapor) from the HCl vapor spectra in Fig. 11.

the fiber-optic configuration in Fig. 3. Systematic effects will increase the sensor signal at all wavelengths, whereas changes in the indicator response (chemical interferences) will only be observed at the λ_{max} in the absorbance spectra for the relevant indicator form(s).

Complete spectra were collected for a BT/NAF coated waveguide using the MIR-OWG configuration. Spectra were collected for the waveguide exposed to water vapor (no acid), to vapors from 0.165*M* hydrochloric acid solution at room temperature (23°), and to vapors from the same hydrochloric acid solution maintained in an ice bath (0°). These spectra are given in Fig. 11. It should be noted that the optical bandpass using the fiber optic couplers is much larger than the bandpass using the single-pass configuration (exit slit width = 300 μm), which results in a broadening (and shifting) of the spectral features (*i.e.*, absorbance bands). As seen in Fig. 11, the majority of the BT indicator is in the HIn^- (yellow) form, indicated by the broad peak at $\approx$450 nm. Exposure to the relatively small hydrochloric acid vapor concentration (in ice) produces a slight shoulder at 560 nm, but this shift toward the red H_2In form is too small to see a sizable decrease in the 450 peak. At higher hydrochloric concentrations, the decrease in the HIn^- form is readily observed as the response at 560 increases.

To make it easier to identify changes in the absorbance spectra in Fig. 11, corrected spectra were obtained by subtracting the baseline spectra (water vapor) from spectra obtained upon exposure to hydrochloric acid vapors. The corrected spectra for the BT/NAF OWG exposed to hydrochloric acid vapor are given in Fig. 12. It should be noted that, since the large peak due to the yellow form has been subtracted, small increases or decreases in the red (H_2In) form are readily seen in the corrected spectra. Increasing the temperature of the hydrochloric acid bubbler solution should increase the concentration of both hydrochloric acid and water vapor sent to the OWG sensor. Although there is an *increase* in hydrochloric acid vapor, there is a marked *decrease* in the sensor absorbance at 560 nm. As the concentration of water in the polymer increases there will be a slight decrease in the concentration of indicator due to swelling of the polymer, but this factor is too small ($\approx$7%) to account for the factor of 2 observed decrease in absorbance. Similar behavior was observed for BT/PVA response to hydrochloric acid.

The vapor pressures of water at 0° and 23° are 4.6 torr and 21.1 torr, respectively, so that the increase in the bubbler solution temperature represents an increase in water vapor concentration by a factor of 5. The increase in water sorbed into the polymer films can be estimated from the SAW data discussed previously. At an average SAW sensor temperature of 30° the vapor pressure of water is 31.8 torr; vapor pressures of 4.6 torr and 17.5 torr represent saturation levels of 14.5 and 66%, respectively. According to the SAW responses represented in Fig. 6, this 5-fold increase in water vapor concentration translate into a 6–8 fold increase in

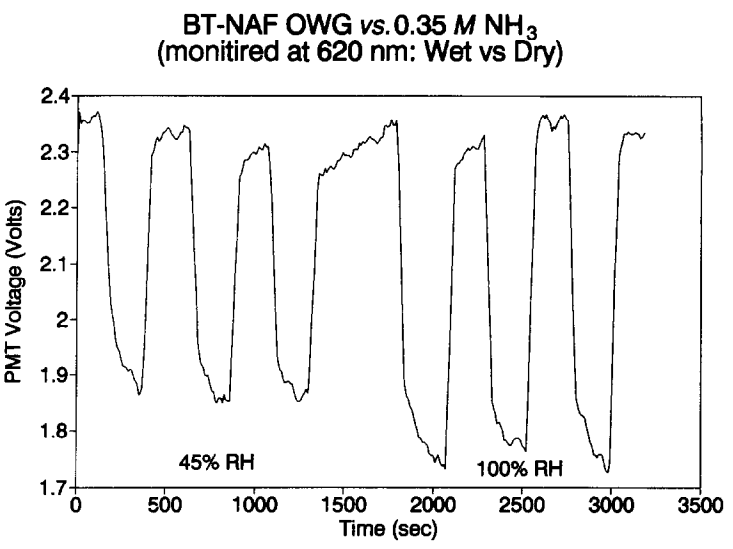

Fig. 13. Response of BT-NAF OWG to vapor from 0.35*M* NH_3 solution mixed with a) dry carrier gas, and b) carrier gas saturated with water vapor.

water in the Nafion film, and a nearly 50-fold increase for PVA. It is suggested that the presence of water in the polymer film acts as a chemical interference by affecting the equilibrium between the hydrochloric acid(g) and the BT indicator. No comparable chemical interference was observed for the TB-polymer films studied.

This behavior can be explained by making reference to the levelling effect of water. Briefly, levelling refers to the fact that strong acids in aqueous solvent will donate protons to water, *e.g.*,

$$HCl + H_2O \longleftrightarrow H_3O^+ + Cl^- \quad (3)$$

so that hydronium (H_3O^+) becomes the strongest acid in the system. This levelling effect is quite apparent for the BT indicator in aqueous solution, where very acidic conditions (4–5*M*) are necessary to protonate the indicator. In the dry polymer films, however, very small concentrations of hydrochloric acid are sufficient to produce the H_2In form. As the concentration of water increases, however, H_3O^+ becomes the predominant species; since H_3O^+ is a weaker acid than the hydrochloric acid, a greater concentration of acid is required to shift the indicator to the H_2In form.

The acid response of the TB *vs.* the BT indicator can be explained by considering the relative ability of the two indicators to act as a base (proton acceptor). Using the p*K* values for the indicator transitions in Fig. 1, then K_a and K_b values for the HIn^- form of the indicators can be calculated for these equilibria in aqueous solution. The ability of TB to act as a base (proton acceptor), is nearly 4 orders of magnitude larger than for BT. This may explain the irreversible formation of the H_2In form under mildly acidic conditions for TB, and the reversible behavior for the BT indicator under similar conditions in the polymer films.

To evaluate the effect of water vapor on the response to NH_3 vapors, various solutions of NH_3 were placed in the bubbler (at room temperature) with a bubbler flow rate of 90 ml/min. The vapor output from the ammonia bubbler was mixed with diluting air from the VG-400 at 100 ml/min. The diluting air was alternated between dry air and saturated water vapor. Again assuming that the output from the bubbler was nearly saturated in water vapor, then the RH of the vapor streams to the sensor were 40% RH (when diluting air was dry air) and 100% RH (when diluting air was saturated water vapor). Typical responses for a BT-NAF film using the MIR-OWG configuration are given in Fig. 13. The responses represent changes in PMT signal at 620 nm while the sensor is exposed to vapor from a bubbler solution of 0.35*M* ammonium hydroxide. The first three responses are in dry diluting air (45% RH), and the second three responses are in saturated water vapor (100% RH). Similar exposures were performed using 0.05, 0.10 and 0.35*M* ammonium hydrochloride solutions, and results for 100% RH and 45% RH conditions are plotted in Fig. 14. Responses to ammonia in 100% RH are generally 15–20% greater than

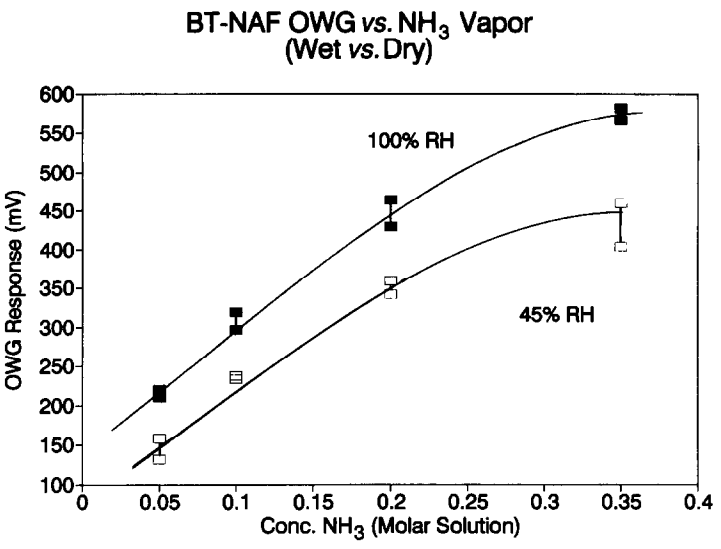

Fig. 14. Calibration curves for BT-NAF OWG response to NH_3 at 45% RH and 100% RH.

responses in 45% RH. Similar ammonia response behavior was observed for BT/PVA films.

This increased ammonia response in the presence of water vapor is interpreted as a chemical effect rather than an optical effect for several reasons. First, optical (systematic) effects would be evident as an *increase* in photodetector signal; this would translate into an increase in the baseline of the sensor when the RH was increased to 100%, whereas the baseline remains fairly constant for the data collected in Fig. 13. Second, there is a net *decrease* in signal when ammonia is introduced, indicating an increase in absorbance at 620 nm, consistent with a chemical effect. Third, the data were collected using the MIR-OWG configuration; as noted earlier, systematic effects are minimized using this configuration.

There are several possible explanations for the observed chemical effect of water on ammonia response behavior. First, water in the polymer film increases the K_a of the indicators, *i.e.*, solvation of the indicators increases their ability to donate protons to the base (ammonia). As the activity of water in the hydrated film increases, the In^{2-} species become more stable than in a dry (non-polar) film and the indicator equilibrium shifts in favor of the blue form. Alternatively, the presence of water increases the solubility of ammonia in the film, increasing the indicator response as a direct consequence.

CONCLUSIONS

The results of the above study have significant ramifications with regard to the design of indicator-based OWG sensors. These considerations are listed below:

1. In the LED-OWG, light is primarily reflected at the film/air interface, whereas for the MIR-OWG light is reflected at the substrate/film interface. The systematic interference from water vapor may be avoided by constructing the OWG sensor to utilize evanescent wave interactions as the predominant response mechanism. In this way losses at the film/air interface are minimized.

2. PVA films would be preferable to the Nafion films to avoid kinetic effects since the response times, *i.e.*, diffusion rates, in PVA are independent of relative humidity.

3. The OWG sensitivity to acidic and/or basic vapors is determined largely by the choice of indicator. For acid vapor sensing, TB-PVA films provide better sensitivity at the expense of reversibility. BT-polymer films provide both sensitive and reversible response to both hydrochloric acid and ammonia vapors. Because humidity tends to decrease the response of the BT-polymer films to hydrochloric acid (at low hydrochloric acid vapor levels), some means of humidity control would be required for reliable trace detection.

Acknowledgements—The authors wish to thank Mr. Charles Caldwell of the NIU Chemistry Electronics shop, Mr. Ed Hyland and Mr. Dan Edwards of the NIU Chemistry Glass

shop, and Mr. Larry Gregerson of the NIU Chemistry Machine shop for their assistance in the construction of various components for the experimental apparatus used in this study. This work was supported in part by a Grant-in-Aid from the Society of Analytical Chemists of Pittsburgh. Portions of this work were presented at the FACSS Meeting in Anaheim, CA, October 1991.

REFERENCES

1. D. S. Ballantine, Jr., D. Callahan, G. J. Maclay and J. R. Stetter, *Talanta*, in the press.
2. J. Brandup and E. H. Immergut, (eds.), *Polymer Handbook*, 3rd Ed., Wiley, New York, p. VI–461 (1989).
3. Aldrich Chemical Company, 1990–91 catalog.
4. R. C. Weast, *CRC Handbook of Chemistry and Phvsics*, 55th Ed., CRC Press, Cleveland, pp. E-222—E-223 (1974).
5. G. Gebel, P. Aldebert and M. Pineri, *Macromol*, 1987, **20**, 1425.
6. J. W. Grate, M. Klusty, R. A. McGill, M. H. Abraham, G. Whiting and J. Andonian-Haftvan, *Anal. Chem*, 1992 **64**, 610.
7. J. Crank, *The Mathematics of Diffusion*, Clarendon Press, Oxford, Chap. 4, 1975.
8. T. Sakai, H. Takenaka and E. Torikai, *J. Electrochem. Soc.*, 1986, **133**, 88.

Talanta, Vol. 40, No. 3, pp. 445–451, 1993
Printed in Great Britain.

0039-9140/93 $6.00 + 0.00

ELECTROPOLYMERISED *o*-PHENYLENEDIAMINE FILM AS MEANS OF IMMOBILISING LACTATE OXIDASE FOR A *L*-LACTATE BIOSENSOR

EITHNE DEMPSEY* and JOSEPH WANG†
Department of Chemistry, New Mexico State University, Las Cruces, NM 88003, U.S.A.

MALCOLM R. SMYTH
School of Chemical Sciences, Dublin City University, Dublin 9, Ireland

(*Received* 5 *May* 1992. *Revised* 10 *June* 1992. *Accepted* 14 *July* 1992)

Summary—The immobilisation of *L*-lactate oxidase at a platinum electrode was achieved by entrapping the enzyme within an *o*-phenylenediamine film at 0.65 V (*vs.* Ag/AgCl). Anodic detection of the product of the enzymatic reaction, i.e., hydrogen peroxide, at 0.75 V (*vs.* Ag/AgCl) was employed for the quantification of *L*-lactate using amperometric batch and flow injection methods. This technique allows the enzyme to be entrapped in a strongly adherent thin membrane. The sensor exhibits a very fast response time, an active enzyme loading of 5 mU/cm^2 electrode surface, and high sensitivity with a detection limit of $2.46 \times 10^{-7}M$. A sample throughput of 180/hr, precision of 3.53% for 25 injections and linearity up to 1.5m*M* were obtained in flow injection analysis studies. The one-step procedure for sensor preparation requires 20 min, and the discriminative properties of the polymer film show great promise as a means of excluding interfering compounds commonly found in serum.

Polymeric coatings have recently become of increasing interest in the modification of electrode surfaces.[1] By appropriate choice of monomer and experimental conditions for film preparation, polymer films with particular desired properties may be achieved. Heineman *et al.*[2] have reported that *o*-phenylenediamine forms polymeric films upon electrochemical oxidation in solutions of neutral/slightly acidic pH, and that the electrode exhibits a nearly Nernstian response with changes in pH.[3,4] The selective permeability can be varied with the nature of the ions dissolved in solution.[5]

Polymer coated electrodes have several attractive features, such as being a convenient means of immobilising an electrocatalyst near the electrode surface in high concentration,[6,7] while preventing interferences and electrode fouling.[8] The electrochemical method of immobilisation permits a controlled method of localisation of biologically active molecules at electrode surfaces. Therefore by this approach the spatial distribution of the enzyme may be readily controlled and thickness of the enzyme film easily varied. The usefulness of sensors based on immobilised enzymes depends on several factors such as the immobilisation method, thickness and stability of the entrapped enzyme, the response time and storage conditions required.

Despite uncertainties as to the mechanism of entrapment, electrochemical deposition offers advantages over the more traditional methods of enzyme immobilisation, particularly in the simplicity and reproducibility of the one-step construction process. Conventional enzyme electrodes employing discrete macroscopic membranes (to overcome problems associated with interferences and electrode fouling) suffer in lack of reproducibility and response times.[9,10]

It has recently been demonstrated that immobilisation of glucose oxidase with an electrochemically generated *o*-phenylenediamine film can be used for the amperometric detection of glucose.[11] A fast and permselective response was thus reported. The objective of the present work was to explore the *o*-phenylenediamine electropolymerisation scheme for effective immobilisation of lactate oxidase.

The determination of *L*-lactate is important in the diagnosis of respiratory insufficiencies, heart disease[12,13] and also in sport medicine. The

*Permanent address: Dublin City University, Glasnevin, Dublin 9, Ireland.
†Author for correspondence.

relevant lactic acid concentration in blood occurs in the range 0.3–1.5m*M*.[14] Determination of *L*-lactate also plays an important role in the food industry, *e.g.*, wines and dairy products.[15]

Previous methods for determination of *L*-lactate have involved enzyme reactors,[16] co-immobilisation of lactate oxidase and lactate dehydrogenase in enzymatic amplification schemes,[10] entrapment of the enzyme behind a semi-permeable membrane.[9]

The immobilisation of *L*-lactate oxidase in poly(vinyl alcohol) has also been reported[17] following gamma-irradiation. These methods result however in slower response time, interference problems and prove to be more complicated than the method described here. This paper describes a simple and easily controlled enzyme immobilisation procedure that has application in the development of sensors for this biologically important compound.

EXPERIMENTAL

Apparatus

Amperometric measurements and electropolymerisation of *o*-phenylenediamine were carried out in a 3-electrode cell (Model VC-2, BAS), containing 10 ml of 0.05*M* phosphate buffer as supporting electrolyte. Reference and counter electrodes were Ag/AgCl (Model RE-1, BAS) and platinum wire, respectively. A platinum disk electrode served as the working electrode and all three joined the cell through holes in its Teflon cover. The three-electrode system was then connected to an EG&G PAR Model 264A polarographic Analyser, the output of which was displayed on a strip chart recorder (Model 4500 Microscribe, The Recorder Co.). A magnetic stirrer and bar provided the convective transport. The flow injection system used was equipped with a carrier reservoir, a platinum thin-layer detector (Model TL-10A, BAS) a Rainin Model 5041 sample injection valve (20 μl loop) and interconnecting tubing. A flow rate of 2.0 ml/min was employed throughout.

Reagents

All experiments were conducted at room temperature in 0.05*M* phosphate buffer pH 7.4, and all solutions were prepared with doubly-distilled water. Lactate oxidase (activity 38 Units/mg), *L*-lactate, glucose, nicotinamide adenine dinucleotide (reduced form), uric acid and acetaminophen were obtained from Sigma Chemical Co., St. Louis, MO. The ascorbic acid was obtained from J. T. Baker Inc., Phillipsburg, NY and the *o*-phenylenediamine dihydrochloride from Aldrich, Milwaukee, WI. The cellulose dialysis membrane (MW cutoff 12–14 k) was purchased from Spectrum Medical Industries, Los Angeles, CA. Stock solutions of glucose were allowed to mutarotate at room temperature for 24 hr before use. The nitrogen used to obtain a controlled atmosphere in the electrochemical cell was of high purity grade.

Electrode preparation

Prior to electropolymerisation the platinum disk working electrode was polished firstly with 3 μm of alumina followed by 0.05 μm, after which it was sonicated in distilled water for 5 min to remove any residual alumina. Lactate oxidase/*o*-phenylenediamine films were electrochemically grown on platinum electrodes from a fresh solution of 1m*M* *o*-phenylenediamine and 3.42 units of enzyme in 0.05*M* phosphate buffer, (pH 7.4). Electropolymerisation was initiated by applying a constant potential of 0.65 V (*vs.* Ag/AgCl) in deaerated unstirred solutions for 20 min. The enzyme electrode was thoroughly rinsed with doubly-distilled water after preparation and stored in phosphate buffer pH 7.4 at 4° when not in use.

Procedure

Amperometric responses of the lactate oxidase/*o*-phenylenediamine (LOX/o-PD) electrode to *L*-lactate were measured in batch and flow experiments by application of a fixed potential of 0.75 V to the enzyme electrodes. The background current was allowed to decay before aliquots of the stock *L*-lactate solution were added and the oxidation current due to hydrogen peroxide measured.

An estimation of the activity of enzyme entrapped in the polymer film was carried out amperometrically. A clean polished platinum electrode was held at 0.75 V (*vs.* Ag/AgCl) in stirred solution containing 1.0m*M* *L*-lactate in phosphate buffer, pH 7.4. When a steady state current was achieved, a known activity of lactate oxidase was injected and the current response noted for the production of hydrogen peroxide. A calibration curve was constructed and the activity of each LOX/o-PD electrode expressed as equivalent activity in solution. Enzyme stability within the film was ascertained by measuring the current response over a 20 day period. While not in use, the electrode was stored in phosphate buffer pH 7.4.

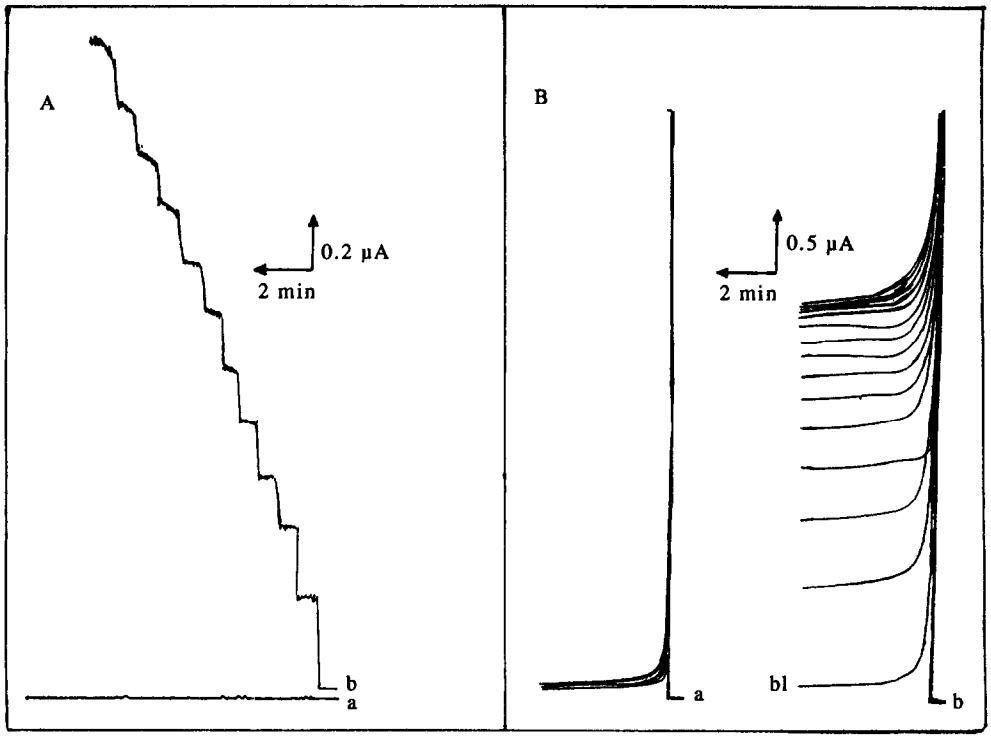

Fig. 1. (A) Current–time response for successive $5 \times 10^{-5}M$ injections of *L*-lactate obtained at (a) unmodified and (b) modified enzyme surfaces in batch. Operating potential 0.75 V with 400 rpm stirring rate and electropolymerisation solution containing 1m*M* *o*-phenylenediamine and 3.42 Units enzyme (5 mU/cm^2 electrode) for 20 mins at 0.65 V. Electrolyte, 0.05*M* phosphate buffer pH 7.5 (B) Chronoamperometric response to 1.25×10^{-4} *L*-lactate increments again at (a) unmodified and (b) modified surfaces. Other conditions as (A).

RESULTS AND DISCUSSION

Lactate oxidase catalyses the reaction shown below and electrochemical biosensing is based on the amperometric monitoring of the hydrogen peroxide produced.

$$\text{LOX(FAD)} + L\text{-LACTATE} + O_2$$

$$\Leftrightarrow \text{LOX(FADH}_2\text{)} + \text{PYRUVATE} + H_2O_2$$

The response of the LOX/*o*PD electrode to successive additions of *L*-lactate at the bare and modified surfaces, using both amperometric and chronoamperometric measurements, is shown in Fig. 1. Steady state currents were achieved within 15 sec and 2 mins respectively, with high sensitivity for μM concentrations of substrate and a detection limit of $2.46 \times 10^{-7}M$ for both techniques.

The effects of many experimental variables were investigated in order to optimise analytical performance. Optimisation of enzyme loading in the polymer film is shown in Fig. 2. Linearity and response increased with increasing biocatalytic activity in the film, the optimum activity being achieved with 3.42 Units in solution (1.6 mU/electrode). The response to 50μM additions of *L*-lactate resulted in a slope of 4.5 nA/μM and a correlation coefficient of 0.99975 when the electropolymerisation solution contained 1m*M* *o*-phenylenediamine and 3.42 units lactate oxidase.

The effect of operational potential (A) and pH (B) for amperometric experiments is shown in Fig. 3. An increase in oxidation current for hydrogen peroxide, resulting from 0.25m*M* injections of *L*-lactate occurred as the applied potential increased from 0.2 to 0.8 V with a decrease at higher potentials. An optimum current response to 0.5m*M* injections of *L*-lactate was achieved at pH 7.4 and therefore this pH was taken as that providing maximum activity for the operation of this enzyme electrode.

Figure 4(A) shows the effect on anodic response with increasing concentration of *o*-phenylenediamine in the electropolymerisation solution, keeping both enzyme activity and time

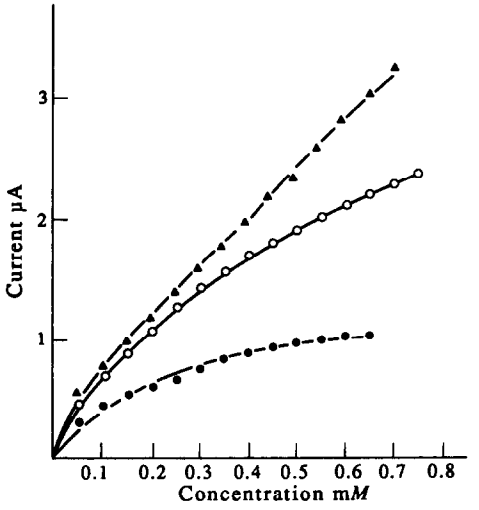

Fig. 2. Current dependance on *L*-lactate oxidase loading in the electropolymerised film upon injection of $5 \times 10^{-5}M$ *L*-lactate. Polymerisation carried out in 1m*M* *o*-phenylenediamine and (▲) 3.42 Units, (○) 2.28 Units and (●) 1.14 Units enzyme activity. Other conditions as in Fig.1(A).

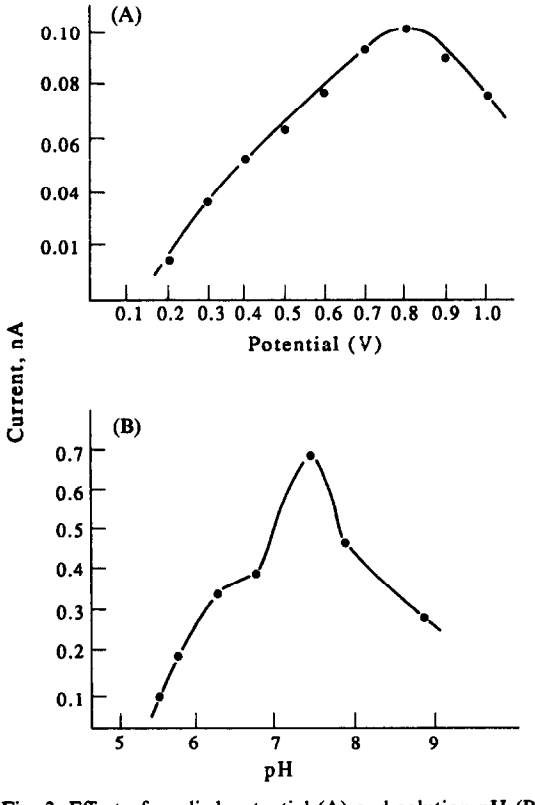

Fig. 3. Effect of applied potential (A) and solution pH (B) on response to $2.5 \times 10^{-4}M$ and $5 \times 10^{-4}M$ injections of *L*-lactate respectively. Electropolymerisation solution containing 10m*M* (A) and 5m*M* (B) *o*-phenylenediamine with 3.04 Units enzyme activity. Enzyme loading-5 mUnits/cm^2. Other conditions as in Fig. 1(A).

constant. The greatest current was observed for the film prepared with 1m*M* monomer solution. A subsequent decrease in response was observed up to 5m*M*, followed by an increase once more up to 10m*M*. A thicker film implies a slower response time and a lowering of sensitivity but results in a wider linear range. A thinner film appears to incorporate more enzyme resulting in a greater response. The diffusion of the product hydrogen peroxide through the film may be the limiting factor as the thickness is increased, the enzymatic reaction occurs more readily in the outer portions of the polymer layer near the solution side than in the interior of the film.

The effect of the electropolymerisation potential on current response is shown in Fig. 4(B). An optimum value was found to be 0.65 V, but

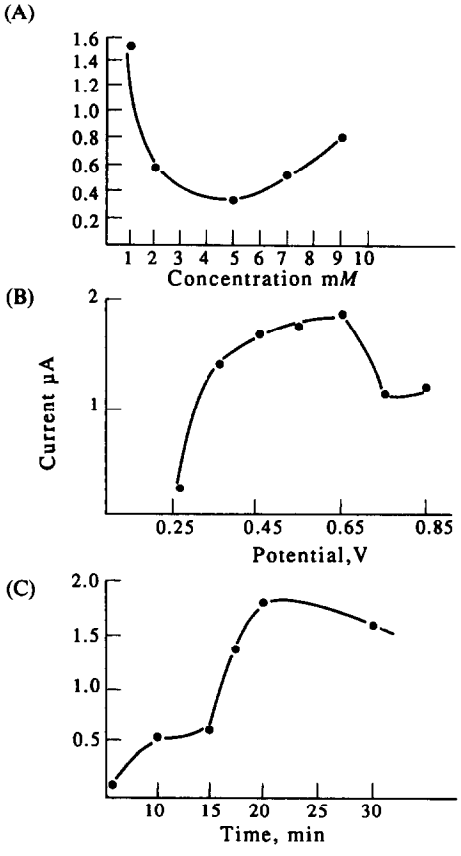

Fig. 4. (A) Effects of *o*-phenylenediamine concentration on response to $5 \times 10^{-4}M$ injections of *L*-lactate. Enzyme activity constant at 5 mU/cm^2 electrode. (B) Dependance of current on electropolymerisation potential in 1m*M* *o*-phenylenediamine and 3 Units enzyme for 20 min. Injection of $5 \times 10^{-4}M$ *L*-lactate. (C) Current-electropolymerisation time response to $5 \times 10^{-4}M$ *L*-lactate. Electropolymerisation solution as in (B) and amperometric detection at 0.75 V.

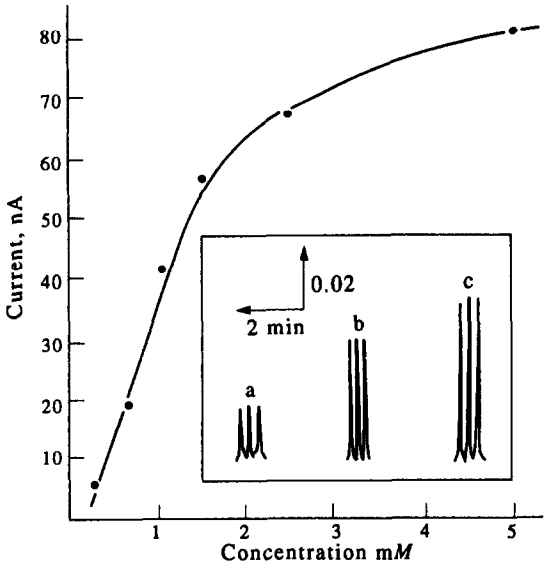

Fig. 5. Flow injection detection of *L*-lactate. Calibration plot over the 2.5×10^{-4}–$5 \times 10^{-3}M$ range with typical peaks for (a) 0.5m*M* (b) 1.0m*M* (c) 1.5m*M* *L*-lactate. Flow rate 2 ml/min. Sample and carrier—phosphate buffer pH 7.5. Other conditions as in Fig. 1(A).

as the anodic potential was increased above this value, the amperometric response decreased. A decrease in conductivity in the film and a loss of activity occurs at high potentials. Destruction of the polymer may be attributed to irreversible deterioration of the film by formation of electroinactive polymer films on the surface. Figure 4(C) shows the effect of polymerisation time on performance of the sensor. The form of the current *vs.* time curve implicates a nucleation and phase growth process in the mechanism of deposition of *o*-phenylenediamine, similar to that of the growth of *m*-toluidine on gold.[18] The monomer appears to oxidise more readily on the poly(*o*-phenylenediamine) film than on the platinum itself. Initial growth requires 5–10 min followed by a rapid increase in current with increasing thickness of polymer film. Saturation of enzymatic activities above 20 min may result in the conformational arrangements of the enzyme within the film. Due to release of protons in the course of polymerisation, the acidic environment produced may lead to denaturation of lactate oxidase at longer electropolymerisation times.

The fast response and stability of the LOX/o-PD electrode makes it an attractive choice in dynamic flow systems. Figure 5 illustrates flow injection peaks for 20-μl samples of increasing *L*-lactate concentration. The peak width of 6 sec allows a sample throughput of 180 samples/hour, with linearity observed up to 1.5m*M* and a limit of detection of $1 \times 10^{-4}M$. Twenty five successive injections of a 5m*M* *L*-lactate solution showed a precision of 3.54%. Under optimum conditions, a precision study employing 10 consecutive separate batch additions of 50μM *L*-lactate resulted in a RSD of 3.23% (not shown).

The potential required to oxidise hydrogen peroxide is sufficiently anodic that several other interfering compounds may contribute to the signal. However, the electropolymerised *o*-PD film appears to be very effective in preventing interferences while allowing hydrogen peroxide to pass through the film. Due to its permselectivity the access of substances such as ascorbate to the electrode surface is blocked. Similar improvements were reported for analogous sensing of glucose.[11]

The selectivity of the LOx/*o*-PD electrode was studied by monitoring the response to 0.5m*M* *L*-lactate alone and in the presence of relevant compounds at the 1.0m*M* level which may interfere by direct electrode oxidation (Table 1). In the case of polypyrrole films[19] anionic species showed enhanced electrochemistry due to the electrostatic interaction with the polymer matrix which contained cationic fixed sites. The relatively high response to uric acid in the case of the *o*-PD polymer was further decreased by an additional cellulose membrane (12–14 k MW cutoff) over the electrode. The polymer film proved effective in further reducing the current signal due to uric acid, ascorbic acid, NADH, and glucose (all at the 1.0m*M* level) while retaining 90 and 64.3% of the *L*-lactate response (0.5m*M*), with and without cellulose membrane respectively.

The oxidation of *o*-phenylenediamine in phosphate buffer shows a completely irreversible oxidation peak at 0.35 V using cyclic

Table 1. Percentage interference response compared to that of analyte (A) without membrane and (B) with cellulose membrane. All interferences at the 1.0m*M* level in presence of 0.5m*M* *L*-lactate. Electropolymerisation solution containing 4.54 Units and 10m*M* *o*-phenylenediamine. All other conditions as in Fig. 1(A)

Interference	(A)%	(B)%
Glucose	0	0
NADH	5.5	4.1
Ascorbate	19.0	11.0
Uric Acid	94.0	50.0

voltammetry, which with continuous scanning between 0.2 and 0.7 V resulted in a decrease in peak current until eventually no current flowed. This behavior is indicative of a non-conductive polymeric film coating the electrode until eventually access of the monomer to the surface is blocked resulting in the formation of a very compact and insulating layer.[20]

The mechanism by which the enzyme is entrapped is uncertain; however adsorption of the lactate oxidase at the platinum surface prior to electropolymerisation could play an important part. Initial film formation is that of a conducting organic film and subsequent formation of a non-conducting film then occurs. *o*-Phenylenediamine forms polymeric films during oxidation at almost all pH values. Most organic electrochemical oxidations of this type form a monocation as the initial electrolysis product, which is involved in the follow-up chemical reaction. The insulating film could then possibly be formed by the polymerisation of the dication formed upon disproportionation. Poly(*o*-phenylenediamine) contains phenazine rings as electroactive sites. The ladder polymer is partially ring opened and involves moieties of the oxidised forms of the quinone-imine type.[21] Under optimum conditions, 5 mUnits/cm^2 electrode surface equivalent to 1.52 Units/ml in the electropolymerisation solution may be incorporated into the film. The estimation of enzyme activity on the surface was carried out by comparison to the rate of hydrogen peroxide production when the enzyme was in solution in the presence of excess substrate. This assumed that the solution kinetics are equivalent to those when the enzyme is in the immobilised form, which is not true due to mass transfer limitations resulting from immobilisation. The activity within the film may be estimated however from the plot of current *vs.* activity in solution.

The upper limit of the electrode response may be improved by placement of a cellulose membrane onto the LOX/*o*-PD film. This restricts the diffusion of *L*-lactate to the underlying enzyme layer and as a result extends linearity. The improvement in linear response was accompanied by a significant decrease in the noise level for injections of μM quantities of substrate. In the presence of cellulose membrane the response has mass transfer as opposed to kinetic limitations, the latter resulting in a levelling off at lower substrate concentrations. This restricts the diffusion of *L*-lactate to the underlying enzyme layer and as a result extends linearity. A LOX/*o*-PD polymer electrode prepared from 1.14 Units enzyme activity and 1m*M* *o*-phenylenediamine solution resulted in an i_{max} (the maximum current, obtained from the intercept of the Lineweaver-Burk plot of 1/current *i* *vs.* 1/[Substrate]) of 1.236 μA and apparent Michaelis-Menten constant (K_m app, calculated from the slope of the graph) of 117.3μM. The same electrode covered with cellulose membrane showed an i_{max} of 1.3528 μA and K_m app of 342.2μM. The additional diffusional restrictions imposed as a result of the membrane causes alteration of basic catalytic properties and results in a shift in the apparent K_m app. The increase in K_m app in the case of the membrane indicates that the immobilisation process generates a loss of affinity to the substrate due to the additional environmental constraints placed on the enzyme.[22] However, this method is useful from the analytical point of view due to extension of the upper limit.

An improvement in linearity was also observed using 10m*M* monomer in the electropolymerisation solution and after film formation, polymerisation once more in the same solution. Linearity in this case was extended up to 1.5m*M* again at the expense of lower sensitivity and slower response time.

The stability of the LOX/*o*-PD electrode with storage at 4° in phosphate buffer (pH 7.5) was investigated. Responses were measured as the oxidation of resultant hydrogen peroxide caused by the addition of 0.5m*M* *L*-lactate at 24-hourly intervals. A 50 and 93% decrease in response was observed after 5 and 20 days respectively.

CONCLUSION

Electrochemically initiated polymerisation has recently received great attention in the modification of electrode surfaces. Polymer film electrodes offer higher inherent chemical and physical stability, higher surface activity and a very sensitive electrochemical response. The electropolymerisation of *o*-phenylenediamine provides simultaneous immobilisation of lactate oxidase and offers the advantage of producing a very thin and self insulating film that can be coated on any conducting surface. The sensor is found to reject physiologically important compounds, *e.g.*, ascorbic acid while incorporating a significant amount of lactate oxidase. The very fast response time, together with the high sensitivity and high sample throughput, are further distinctive features of the described sensor.

The stability and dynamic bahavior of the film allows for application in flowing streams.

REFERENCES

1. J. Wang, *Electroanalysis*, 1991, **3**, 255.
2. W. R. Heineman, H. J. Wieck and A. M. Yacynych, *Anal. Chem.*, 1980, **52**, 345.
3. A. Make and D. H. Geske, *J. Chem. Phys.*, 1960, **33**, 825.
4. H. B. Mark and F. C. Anson, *Anal Chem.*, 1963, **35**, 722.
5. Y. Ohnuki, H. Matsuda, T. Ohsaka and N. Oyama, *J. Electroanal. Chem.*, 1983, **158**, 55.
6. S. V. Sasso, R. J. Pierce, R. Walla and A. M. Yacynych, *Anal. Chem.*, 1990, **62**, 1111.
7. A. L. Nguyen, J. H. T. Luong and A. M. Yacynych, *Biotech. Bioeng.*, 1991, **37**, 729.
8. R. J. Geise, J. M. Adams, N. J. Barone and A. M. Yacynych, *Biosensors and Bioelect.*, 1991, **6**, 151.
9. W. J. Blaedel and R. A. Jenkins, *Anal. Chem.*, 1976, **48**, 1241.
10. F. Schubert, J. Lutter and F. Scheller, *Anal. Chim. Acta*, 1991, **243**, 17.
11. C. Malisesta, F. Palmisano, L. Torsi and P. G. Zambonini, *Anal. Chem.*, 1990, **62**, 640.
12. M. Mascini, D. Moscone and G. Palleschi, *Anal. Chim. Acta*, 1984, **157**, 45.
13. J. B. Toffaletti, *Clin. Chem. News*, 1989, **9**, 14.
14. J. Wandrup, K. Tvede, J. Grinsted and H. Jordening, *Clin. Chem.*, 1989, **35/8**, 1740.
15. G. H. Aschor and J. Weily, *J. Chromatogr.*, 1984, **287**, 452.
16. E. H Hanson, A. Arndal and L. Norgaard, *Anal. Letts.*, 1990, **23**, 22.
17. K. Hajizadeh, H. B. Halsali and W. R. Heineman, *Anal Chim. Acta*, 1991, **243**, 23.
18. P. Herrasti and P. J. Ocon, *Appl. Electrochem.*, 1990, **20**, 640.
19. M. Freund, L. Bodalbhai and A. Brajter-Toth, *Talanta*, 1991, **38**, 95.
20. A. M. Yacynych and H. B. Mark, *Electrochem. Soc.*, 1976, **123**, 1346.
21. K. Chiba, T. Ohnaki, Y. Ohnuki and N. Oyama, *J. Electroanal. Chem.*, 1987, **219**, 117.
22. E. Gonzalez, F. Pariente, E. Lorenzo and L. Hernandoz, *Anal. Chim. Acta*, 1991, **242**, 267.

Talanta, Vol. 40, No. 3, pp. 453–457, 1993
Printed in Great Britain.

0039-9140/93 $6.00 + 0.00

NON-ENZYMATIC OPTICAL SENSOR FOR PENICILLINS

HUARUI HE,* HONG LI, GEORG URAY and OTTO S. WOLFBEIS†
Institute of Organic Chemistry, Karl-Franzens University, Heinrich St. 28, A-8010 Graz, Austria

(*Received* 31 *March* 1992. *Accepted* 12 *June* 1992)

Summary—We report on the first penicillin-sensitive fluorosensor not based on the use of an enzyme. Rather, the recognition process relies on the use of an anion carrier (which carries the penicillin anion from the aqueous sample into the membrane), a proton receptor (lipophilic nile blue which accepts the proton, thereby undergoing a change in fluorescence intensity), and a new lipophilic hydroxylic plasticizer material (which facilitates ion transport). All materials are contained in a dyed poly(vinyl chloride) membrane whose fluorescence is monitored. The optical sensor fully reversibly responds to penicillin V over the 0.01–10m*M* concentration range, and to penicillin G from 0.03 to 10m*M*. Potential interferences by about 20 other anions have been investigated. Nitrate, salicylate, and ascorbate were found to interfere significantly. These species are, however, usually not present in penicillin bioreactors or drug formulations where penicillin sensing is most important. The sensor does not respond to penicillins containing an aliphatic amino group (such as amoxicillin). The method has been applied for determination of penicillin G in pharmaceutical formulations.

In view of the large scale production of penicillins there is a considerable interest in continuous sensing of penicillin both during biotechnological production and in quality control. Another attractive application is on-line monitoring of penicillins *in vivo* during therapy and pharmacokinetic studies. Methods for determination of penicillin include flow injection analysis,[1,2] HPLC,[3,4] potentiometry,[5] and spectrophotometry.[6,7] An optical sensor for penicillin and its analogs has been reported by two groups.[8,9] In these, the enzyme penicillinase rather unspecifically hydrolyzes all kinds of penicillins to give penicillic acids. The corresponding decrease in pH is monitored using an optical fiber pH sensor. While this is a promising approach for on-line sensing and has all the advantages of fiber optic biosensors,[10] it suffers from two limitations: the observed pH change also strongly depends on the buffer capacity (which in biological samples can vary to a considerable extent), and the enzyme loses activity with time and at low pH. An alternative and more reliable method was therefore sought.

In a search for non-enzymatic alternatives for optically sensing penicillins, we have found a method which exploits the phenomenon of co-extraction[11] of both an ion and its counter-ion into a PVC membrane. The extraction of organic cations has been described several times in the past two years, but there is only a limited number of reports on the extraction of organic anions into lipid phases.[5,12,13] We report here that penicillin anions can be extracted as well, provided suitable receptor/carriers and plasticizers are incorporated into the membrane.

EXPERIMENTAL

Apparatus

Measurements were performed using an Aminco SPF 500 spectrofluorometer equipped with a tungsten halogen lamp as a light source. Data were transferred onto a HP 9825A desk calculator and plotted. All fluorescence spectra are uncorrected. Sample solutions were pumped through a 100-μl flow-through cell containing the sensing membrane at a rate of 1.5 ml/min, using a Ventilomat autosampler (Fa. Ziegler, Graz, Austria). pH measurements were performed with a Metrohm pH meter (Metrohm, Buchs, Switzerland) calibrated with Aldrich pH standards of pH 4.00 and 7.00.

The flow injection equipment comprises autosampler (Besta, Heidelberg, Germany), pump (Gilson, France), fiber optic photometer (Oriel 3090, Chelsea Instruments, London, UK), data

*On leave of absence from Department of Chemistry, Nankai University, CN-300071 Tianjin, P.R. China.
†Author for correspondence.

acquisition unit (Keithley 575, Taunton, USA), and personal computer. Sample solutions were pumped through the flow-through cell containing the sensing membrane using the autosampler. Fluorescence intensity was measured with the photometer and data were transferred to an acquisition unit controlled by the PC.

Reagents

Penicillin G potassium salt was obtained from Fluka AG (Buchs, Switzerland), while penicillin V and amoxicillin (Fig. 1) were purchased from a pharmacy. For the membrane preparation, poly(vinyl chloride) (high molecular grade) (PVC) bis(2-ethylhexyl) phthalate (DOP), bis(2-ethylhexyl) sebacate (DOS), 2-nitrophenyl octyl ether (NPOE), tri(2-ethylhexyl) phosphate (TOP), tridodecylmethylammonium chloride (TDMAC) and tetrahydrofurane (THF) were obtained from Fluka AG. The new plasticizer (WM3, Fig. 1) was synthesized by Dr. Kriessmann (Fa. VIANOVA, Graz) and was found to be of sufficient purity. The lipophilic N-octadecanoyl nile blue (ODNB) was prepared according to the published procedure.[14] The samples, Penicillin G-Natrium, Antipen, and Retarpen (all from Biochemie GmbH, Vienna, Austria) were purchased from a drug store.

Membrane preparation

The membranes were prepared from a batch of 2.4 mg of PVC, 0.2 mg of TDMAC, 0.6 mg of ODNB and 6.0 mg of WM3. The mixture was dissolved in 1.5 ml of freshly distilled tetrahydrofurane. 0.1 ml of this solution was pipetted onto a 12 × 50-mm dust-free glass plate (Menzel-Gläser, Germany) which was located in THF-saturated atmosphere in a desiccator. After about 5 hr the glass plate with the sensing membrane on it was removed and placed in ambient air for 15 min to dry completely. From the amount of materials used we estimate the membrane to have a thickness of around 1.0–1.5 μm. Before measurements, the sensor membrane was placed, for 10 min, in a freshly prepared 0.1M solution of penicillin G in pH 6.00 buffer (50mM sodium citrate and 50mM sodium tartrate), and another 10 min in plain buffer of pH 6.00 for activation.

Experimental procedure

The glass plate with the PVC membrane of about 1-μm thickness was mounted in a flow-through cell. The measuring system was arranged according to Ref. 15. Standard solutions, freshly prepared from distilled water, were pumped over the sensing membranes, and fluorescence intensity was continuously recorded at excitation/emission wavelengths set to 520/670 nm, respectively.

Optical selectivity coefficients were determined by using a method similar to the separate-solution method (SSM) frequently applied in ion-selective electrodes.[14,16] Solutions of potentially interfering compounds were prepared in proper concentrations (C_I^{n-}), and the fluorescence of the sensing membranes was

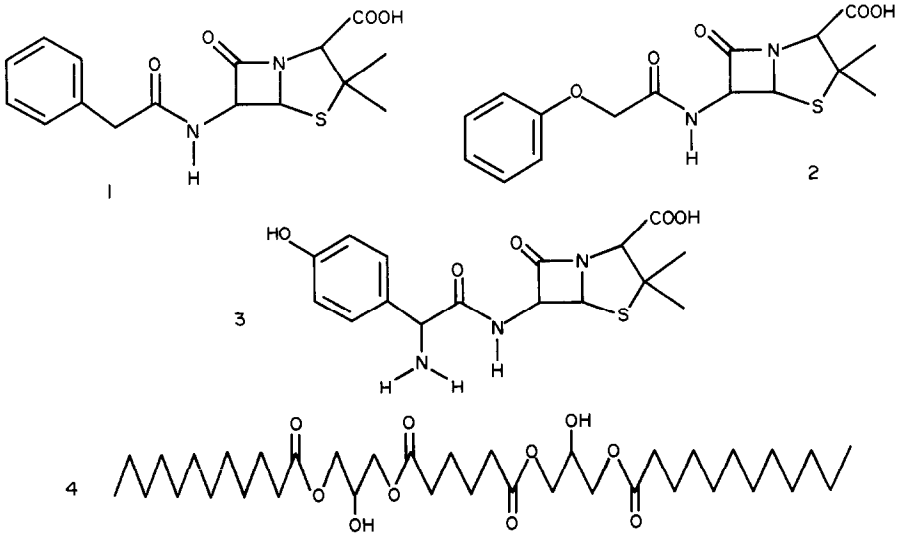

Fig. 1. Chemical structures of the penicillins studied in this work, and of plasticizer WM3. 1: penicillin G, 2: penicillin V, 3: amoxicillin, 4: WM3.

measured under experimental conditions identical to those when establishing the calibration curve. The fluorescence intensities thus obtained were related to the concentration of penicillinate anion ($C_{pncl.}^-$).

The drug samples—three kinds of dry (powdered) penicillin contained in an ampoule—were pretreated according to the following procedure: 40 mg of Penicillin G-Natrium or 80 mg of Retarpen (containing benzathine-penicillin G and polypyrrolidon K 17) or 17 mg of Antipen (containing clemizole-penicillin G and sodium penicillin G) were suspended in 70 ml of a pH 5.50 buffer solution composed of 50m*M* sodium citrate and 50m*M* sodium tartrate. The solution was stirred at room temperature until clear. It was then diluted to 100 ml with the same buffer solution. This solution was used directly for the measurements.

RESULTS AND DISCUSSION

Selection of the plasticizer

In order to function properly, PVC-based membranes for use in either electrochemical and optical sensing require the addition of a plasticizer. It is well known that the type of plasticizer has a dramatic effect on the response behavior of such "liquid membranes". Five plasticizers (DOS, DOP, TOP, NPOE, WM3) with different polarities have been investigated in an initial study.[17] The results showed that tri-dodecyl-methylammonium chloride (TDMAC) along with the plasticizer WM3, whose chemical structure is shown in Fig. 1, is a viable carrier/plasticizer combination for sensing penicillin. Optical transduction is achieved via the PVC-soluble *N*-octadecanoyl nile blue (ODNB). Hence, the membrane whose fluorescence responds to penicillin consists of PVC, TDMAC, ODNB, and WM3 only.

Fluorescence spectra of lipophilized nile blue in plasticized PVC

Figure 2 shows the uncorrected excitation and emission spectra of lipophilized nile blue in a WM3-plasticized PVC membrane as it is used in practice. The emission maximum of the base form is at 670 nm. The maxima are similar to those given in the literature, differences probably arising from the fact that spectral maxima strongly depend on the nature of the additives contained in the membrane material. The red base form of nile blue has a much larger Stokes' shift than the blue (acid) form so that interferences by straylight can be kept to a minimum. Given the longwave absorption and emission of the dye used, the sensor obviously is fully compatible with solid-state opto-electronic components such as LEDs.

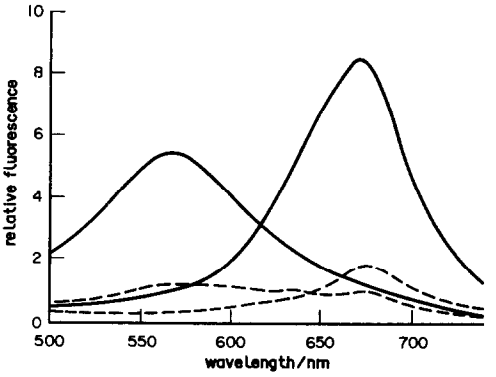

Fig. 2. Uncorrected excitation and emission spectra of lipophilized nile blue in a WM3-plasticized PVC membrane. Fluorescence intensity is given in arbitrary units.

The response of the optrode membrane

The sensing membrane contains an anion exchanger (TDMAC) and a chromo-ionophore (ODNB). When, at any pH between 5.3 and 6.0, the penicillin carboxylate anion is transported into the PVC membrane by the anion carrier, a proton will be co-extracted (rather than a chloride released). The conjugate base form of nile blue contained in the membrane acts as a chromogenic proton carrier. On protonation, it undergoes a significant change in fluorescence intensity. Hence, it also acts as the optical transducer. The response function can be related to the product of the activities of two ions.[11,18] The signal depends only on the activity of the analytes if the pH value of the sample

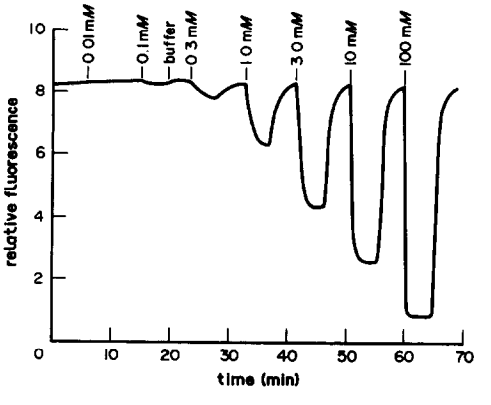

Fig. 3. Response time, relative signal change, and reversibility of the penicillin-sensitive sensor membrane at pH 5.50, with excitation/emission wavelengths set to 520/650 nm.

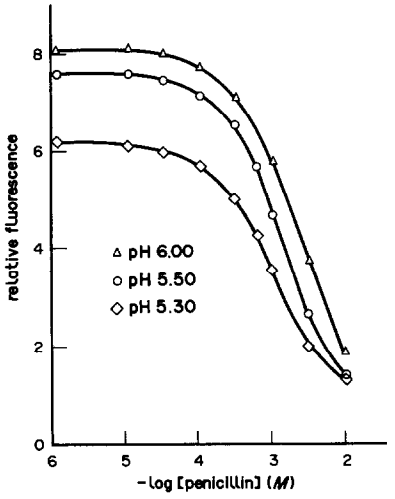

Fig. 4. Calibration curves for the penicillin-sensitive membrane at pH's of 6.00, 5.50 and 5.30 and excitation/emission wavelengths set to 520/650 nm.

solution is kept constant. When exposed to increasing levels of penicillin G, the sensor membrane undergoes a fully reversible colour change from red to blue. Figure 3 shows the response curve of the penicillin G sensor. Response times are about 3 min in the forward direction, but 5 min for the reverse response. The rather sluggish response is due to slow mass transfer in the membrane rather than to the dead volumes of flow-through cell and tubings, respectively.

The fluorescence intensity is a specific function of the analyte (penicillin G) only if the pH value of the sample solution is kept constant. Figure 4 shows the calibration curves of the sensor at different pH values. Clearly, the response is highly pH dependent since the recognition process is coupled to a proton transport mechanism. The dynamic range is shifted to a lower concentration range at lower pH, while the total signal change becomes smaller. The dynamic range is from 30μM to about 10mM, with a detection limit of about 10μM.

Figure 5 shows the response and calibration curves of the penicillin-sensitive membrane plasticized by WM3 and tested with a flow injection analyzer.[19] The linear range is 1–60mM concentration. A comparison with the results of the measurement using the flow-through cell of the fluorometer (see Fig. 4) shows the dynamic range to be shifted to a higher concentration range. This can be attributed to the dilution effect of the flow injection analysis.

The possible response mechanism

The mechanism of the interaction between penicillin, TDMA, and WM3 probably involves (a) formation of hydrogen bonds between the amido groups of penicillin and the hydroxy groups of the plasticizer, and (b) electrostatic attraction between the ammonium ion (TDMAC) and the penicillinate anion. We find only membranes plasticized by some kind of hydroxylated plasticizers (with a ratio of hydroxy groups to carbon atoms in the chain being around 10) to respond to penicillins. Similar effects were found in case of fluorescence-based optical sensors for alkali ions[20] and in other sensors based on the use of synthetic carriers.[17]

Selectivity tests

Interferences by 18 compounds have been investigated using the established method.[12] Optical selectivity coefficients (K^{opt}), defined as the logarithm of the concentration of an interfering species that gives the same response, are summarized in Table 1. They show salicylate,

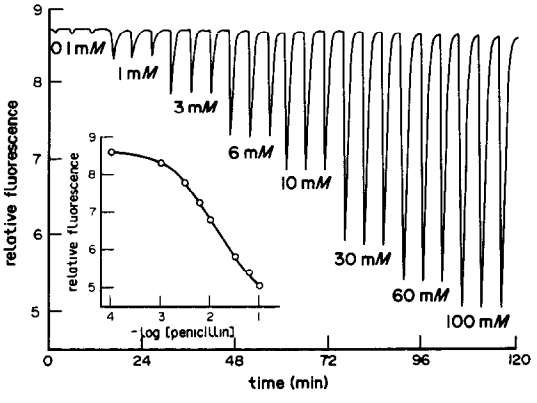

Fig. 5. Response curve of the penicillin-sensitive membrane plasticized by WM3, tested with the flow injection analyzer, and resulting calibration plot (insert).

Table 1. Optical selectivity coefficients (K^{opt}) of the penicillin-selective optical sensor for potentially interfering ions at pH 5.50

Interferent	log K^{opt}
Salicylate	0.30
Nitrite	0.20
Ascorbate	0.15
Benzoate	−0.45
Nitrate	−0.74
Iodide	−1.08
Chloride	−1.83
Acetate	−2.53
Oxalate, phenylalanate	−2.70
Glycinate	−2.80
Glutamate, amoxicillin	< −3
Lactose, glucose	< −3
Sulphate, phosphate, carbonate	< −3

Table 2. Results of 5 replicate determinations of penicillin in 3 kinds of penicillin formulations. SC, specified concentration (in m*M*); AV, average measured value (in m*M*); SD, standard deviation; RSD (%), relative standard deviation; RE (%), relative error

Sample	SC	AV	SD	RSD(%)	RE(%)
Penicillin G-Natrium	1.14	1.17	0.02	1.58	2.93
Retarpen	0.87	0.82	0.02	−2.34	−6.13
Antipen	0.31	0.29	0.01	2.42	−4.68

ascorbate and nitrite to strongly interfere, while nitrate, iodide and chloride have moderate effects. Interestingly, penicillins containing a basic amino group (such as amoxicillin, see Fig. 1) display no response. This high selectivity may be exploited for distinguishing aminopenicillins from other penicillins.

Determination of penicillin G in injection ampoules

Retarpen and Antipen contain benzathine–penicillin and clemizol–penicillin, respectively. Benzathine and clemizol are relative lipophilic organic ammonium ions and capable of forming strong ion-pairs with penicillinate anion. As a result, they are hardly soluble in water. Furthermore, dissolved benzathine and clemizol were expected to interfere due to their much higher lipophilicity than the proton. In order to avoid any errors caused by the co-extraction of benzathine or clemizol with penicillinate anion, they must be masked prior to assay. In earlier work[21] it has been shown that tartrate can form a complex with organic ammonium, and this can be exploited for masking the lipophilic organic ammonium and to keep it in the water phase. Consequently, all measurements were performed in a 50m*M* tartrate medium. The results are summarized in Table 2.

The experimental data are slightly lower than the specified concentrations for Retarpen and Antipen. We think that this is due to the interference of residual benzathine and clemizol cation, both of which may not completely be masked by the tartrate anion in the buffer solution. For Penicillin G-Natrium, the data are slightly higher. The highest relative error observed is −6.1%. If dealing with samples which do not significantly vary from batch to batch (such as in pharmaceutical quality control), this may be corrected for by a correction factor).

Acknowledgement—This work was financially supported by the Austrian Science Foundation within project S5701-PHY which is gratefully acknowledged.

REFERENCES

1. T. D. Yerian, G. D. Christian and J. Ruzicka, *Anal. Chem.*, 1988, **60**, 1250.
2. B. Olsson, *Anal. Chem. Acta*, 1988, **209**, 123.
3. J. Haginaka and J. Wakai, *Anal. Biochem.*, 1988, **168**, 132.
4. P. D. Rice, Y. Y. Shao and D. R. Bobbitt, *Talanta.*, 1989, **36**, 985.
5. S. J. Yao, J. Shiao and L. H. Nie, *ibid.*, 198, **36**, 1249.
6. B. Morelli, *Annal. Chem. Acta*, 1988, **209**, 175.
7. H. F. Askal, G. A. Saleh and N. M. Omar, *Analyst*, 1991, **116**, 387.
8. T. J. Kulp, I. Camins, S. M. Angel, C. Munkholm and D. R. Walt, *Anal. Chem.*, 1987, **59**, 2849.
9. M. R. S. Fuh, L. W. Burgess and G. D. Christian, *ibid.*, 1988, **60**, 433.
10. O. S. Wolfbeis (ed.), *Fiber Optic Chemical Sensors and Biosensors.*, CRC Press, Boca Raton, Florida, 1991, vols. 1 and 2.
11. W. E. Morf, K. Seiler, B. Lehrmann, Ch. Behringer, K. Hartmann and W. Simon, *Pure & Appl. Chem.*, 1989, **61**, 1613.
12. V. V. Cosofret and R. P. Buck. *Pharmaceutical Applications of Membrane Sensors*, CRC Press, Boca Raton, Florida, 1992. pp. 22–30.
13. R. L. Solsky, *Anal. Chem.*, 1990, **62**, 21R.
14. W. E. Morf, K. Seiler, B. Rusterholz and W. Simon, *ibid.*, 1990, **62**, 738.
15. O. S. Wolfbeis and B. P. H. Schaffar, *Anal. Chim. Acta*, 1987, **198**, 1.
16. G. J. Moody and J. D. R. Thomas, *Selective Ion Sensitive Electrodes*, p. 12. Merrow, Hertfordshire, England, 1971.
17. H. He, G. Uray and O. S. Wolfbeis, *Fresenius J. Anal. Chem.*, 1992, **343**, 313–318.
18. W. E. Morf, K. Seiler, P. R. Sörensen and W. Simon, *Ion Selective Electrodes*, 1989, **5**, 141.
19. B. Weigl, in Chemical, Biochemical, and Environmental Fiber Sensors III, R. A. Lieberman (ed.), *Proc. SPIE*, 1991, **1587**, 288–295.
20. H. He and O. S. Wolfbeis, *ibid.*, 1990, **1368**, 165.
21. H. He, G. Uray and O. S. Wolfbeis, *Anal. Chim. Acta*, 1991, **246**, 251.

Talanta, Vol. 40, No. 3, pp. 459–460, 1993
Printed in Great Britain

0039-9140/93 $6.00 + 0.00
Pergamon Press Ltd

BOOK REVIEWS

Advances in Coal Spectroscopy: H. L. C. MEUZELAAR (editor), Plenum, New York, 1992. Pages xx + 416. US $85.00. ISBN 0-306-43796-1.

This publication, the latest in the Modern Analytical Chemistry series, is based on the keynote lectures given at a Utah symposium on coal spectroscopy in June, 1989. The literature of the last 3 years, therefore, is not covered except in a few isolated instances.

The publication has the usual characteristics of symposium proceedings, being disparate and somewhat unfocussed, but providing the reader with accounts of the application of a series of analytical techniques to structural investigations of coals and coal-derived products. In 15 chapters somewhat more recent work in well-established techniques such as proton and ^{13}C NMR, mass spectrometry and gas chromatography are presented along with accounts of work using more specialized techniques such as SEM, XAFS, and laser spark emission spectroscopy. Maceral analysis by fluorescence microspectrophotometry forms the subject of one chapter, while another gives an interesting account of the use of computer-enhanced mass spectrometry in the investigation of coal structure. While the overall emphasis in the book is on the organic structure of coal, ash analysis and combustion behaviour also receive some attention.

The standard of presentation in "Advances in Coal Spectroscopy" is generally good, but the literature surveys are by no means exhaustive, and the work is essentially a series of individual snap-shots of the topics covered. Its readership, therefore, is likely to be drawn from those who are already active in or on the edge of coal chemistry research. At the price set it is also likely to be a library purchase. It can be recommended as a moderately useful institutional acquisition.

W. STEEDMAN

Electroorganic Synthesis—Festschrift for Manuel M. Baizer: R. D. LITTLE and N. L. WEINBERG (editors), Dekker, New York, 1992. Pages xxxiii + 434. $150.00 (US and Canada), $172.50 (elsewhere). ISBN 0-8247-8584-3.

Manuel M. Baizer (1914–1988) was recognised as the foremost international authority on organic electrosynthesis, and this book is a tribute to his memory. The contents comprise the published proceedings of the Manuel M. Baizer Memorial Symposium, held as part of the 177th meeting of the Electrochemical Society in Montreal, May 1990.

However, unlike many conference proceedings in which individual contributions do not always mesh together to give a coherent treatise on a particular subject, this book can be viewed as an excellent review of developments across the range of organic electrosynthesis. This reflects not only Baizer's all-encompassing interest in the subject but also the standing of the contributors, who represent a world-wide theatre.

The book is packed with detail, and after a suitable introduction to Baizer's career and publications enlivened with personal anecdotes there are 48 papers grouped into sections. These papers cover an expansive range of topics including direct electroreductions and electrooxidations, indirect and mediated systems, modified electrodes, alternative electrode materials, biochemical, biomass and natural product systems, mechanistic studies, electrogenerated bases; conducting polymers and electrochemical ion-exchange. The editors are to be congratulated on the tight, condensed style of the papers, which are well referenced; and many are almost mini-reviews of their topics. This book therefore represents a résumé of the current state-of-the-art and as such is invaluable to anyone wishing to assess the present situation.

Baizer's best-known contribution to the subject was his pioneering work at Monsanto on the commercialisation of the electrohydrodimerisation of acrylonitrile to adiponitrile. Since then it is arguable that industrial exploitation of electroorganic processes has failed to attain hoped-for levels, reflecting the particular difficulty in this discipline of scaling up systems that appear promising in the laboratory. Baizer showed that perspicacity and perseverance could overcome these developmental problems and it is to be hoped that the contents of this book will attract others to consider this technology.

This packed little book is not cheap, and it may be that a more lasting monument to Baizer for the general chemist and for newcomers to the field of electrochemistry will be his seminal textbook, edited with Henning Lund: 'Organic Electrochemistry' (Dekker) now in the 3rd edition. However, this Festschrift volume is not only a fitting tribute to a fine scientist, but is also a valuable review in its own right.

D. J. WALTON

Data Fitting in the Chemical Sciences: P. GANS, Wiley, Chichester, 1992. Pages xii + 258. £29.95. ISBN 0-471-93412-7.

The full title of this book is *Data Fitting in the Chemical Sciences by the Method of Least Squares* and this conveys a much clearer picture of its contents than the shorter title which appears on the front cover. The earlier chapters contain a discussion of the application of the method of least squares to both linear and non-linear problems. I was impressed by the wide range of different least squares techniques described and with the thoroughness of their presentation. Model selection and testing are then considered. The later chapters illustrate the application of these ideas in fitting polynomials,

Talanta, Vol. 40, No. 3, pp. 459–460, 1993
Printed in Great Britain

0039-9140/93 $6.00 + 0.00
Pergamon Press Ltd

BOOK REVIEWS

Advances in Coal Spectroscopy: H. L. C. MEUZELAAR (editor), Plenum, New York, 1992. Pages xx + 416. US $85.00. ISBN 0-306-43796-1.

This publication, the latest in the Modern Analytical Chemistry series, is based on the keynote lectures given at a Utah symposium on coal spectroscopy in June, 1989. The literature of the last 3 years, therefore, is not covered except in a few isolated instances.

The publication has the usual characteristics of symposium proceedings, being disparate and somewhat unfocussed, but providing the reader with accounts of the application of a series of analytical techniques to structural investigations of coals and coal-derived products. In 15 chapters somewhat more recent work in well-established techniques such as proton and ^{13}C NMR, mass spectrometry and gas chromatography are presented along with accounts of work using more specialized techniques such as SEM, XAFS, and laser spark emission spectroscopy. Maceral analysis by fluorescence microspectrophotometry forms the subject of one chapter, while another gives an interesting account of the use of computer-enhanced mass spectrometry in the investigation of coal structure. While the overall emphasis in the book is on the organic structure of coal, ash analysis and combustion behaviour also receive some attention.

The standard of presentation in "Advances in Coal Spectroscopy" is generally good, but the literature surveys are by no means exhaustive, and the work is essentially a series of individual snap-shots of the topics covered. Its readership, therefore, is likely to be drawn from those who are already active in or on the edge of coal chemistry research. At the price set it is also likely to be a library purchase. It can be recommended as a moderately useful institutional acquisition.

W. STEEDMAN

Electroorganic Synthesis—Festschrift for Manuel M. Baizer: R. D. LITTLE and N. L. WEINBERG (editors), Dekker, New York, 1992. Pages xxxiii + 434. $150.00 (US and Canada), $172.50 (elsewhere). ISBN 0-8247-8584-3.

Manuel M. Baizer (1914–1988) was recognised as the foremost international authority on organic electrosynthesis, and this book is a tribute to his memory. The contents comprise the published proceedings of the Manuel M. Baizer Memorial Symposium, held as part of the 177th meeting of the Electrochemical Society in Montreal, May 1990.

However, unlike many conference proceedings in which individual contributions do not always mesh together to give a coherent treatise on a particular subject, this book can be viewed as an excellent review of developments across the range of organic electrosynthesis. This reflects not only Baizer's all-encompassing interest in the subject but also the standing of the contributors, who represent a world-wide theatre.

The book is packed with detail, and after a suitable introduction to Baizer's career and publications enlivened with personal anecdotes there are 48 papers grouped into sections. These papers cover an expansive range of topics including direct electroreductions and electrooxidations, indirect and mediated systems, modified electrodes, alternative electrode materials, biochemical, biomass and natural product systems, mechanistic studies, electrogenerated bases; conducting polymers and electrochemical ion-exchange. The editors are to be congratulated on the tight, condensed style of the papers, which are well referenced; and many are almost mini-reviews of their topics. This book therefore represents a résumé of the current state-of-the-art and as such is invaluable to anyone wishing to assess the present situation.

Baizer's best-known contribution to the subject was his pioneering work at Monsanto on the commercialisation of the electrohydrodimerisation of acrylonitrile to adiponitrile. Since then it is arguable that industrial exploitation of electroorganic processes has failed to attain hoped-for levels, reflecting the particular difficulty in this discipline of scaling up systems that appear promising in the laboratory. Baizer showed that perspicacity and perseverance could overcome these developmental problems and it is to be hoped that the contents of this book will attract others to consider this technology.

This packed little book is not cheap, and it may be that a more lasting monument to Baizer for the general chemist and for newcomers to the field of electrochemistry will be his seminal textbook, edited with Henning Lund: 'Organic Electrochemistry' (Dekker) now in the 3rd edition. However, this Festschrift volume is not only a fitting tribute to a fine scientist, but is also a valuable review in its own right.

D. J. WALTON

Data Fitting in the Chemical Sciences: P. GANS, Wiley, Chichester, 1992. Pages xii + 258. £29.95. ISBN 0-471-93412-7.

The full title of this book is *Data Fitting in the Chemical Sciences by the Method of Least Squares* and this conveys a much clearer picture of its contents than the shorter title which appears on the front cover. The earlier chapters contain a discussion of the application of the method of least squares to both linear and non-linear problems. I was impressed by the wide range of different least squares techniques described and with the thoroughness of their presentation. Model selection and testing are then considered. The later chapters illustrate the application of these ideas in fitting polynomials,

exponentials and various other functions to experimental data. A chapter on Fourier transform techniques is included and a rather specialised chapter on least squares interpretation of potentiometric titrations, a topic clearly dear to the author's heart, provides a conclusion.

The statistical theories which underpin the techniques discussed are presented, but in a rather unsystematic way: propagation of error formulas are given in Chapter 2 but the reader is referred to an Appendix for a derivation and the Central Limit Theorem makes only a fleeting appearance on page 107. Most readers are likely to apply the methods discussed by acquiring a computer program rather than by writing one but there is no guide to selection of suitable routines from the large number of program packages now commercially available. Crystallography, something of an adventure playground for the least squares specialist, gets only a passing mention.

I strongly recommend this book to research workers who already have some experience of least squares methods, possibly through use of an applications package, and who want a more detailed and wider understanding of what these methods can deliver. The complete novice and anyone with a dislike for matrix algebra should look elsewhere.

K. W. MUIR

High Performance Liquid Chromatography: Second Edition. S. LINDSAY, Wiley, Chichester, 1992. Pages xxii + 337. Softback £17.50, ISBN 0-471-93115-2. Hardback £39.93, ISBN 0-471-93180-2.

The appearance of the second edition of Sandie Lindsay's text is both timely and appropriate. As part of the Thames Polytechnic Analytical Chemistry by Open Learning (ACOL) series, this highly revised edition will be welcomed by students and practitioners of High Performance Liquid Chromatography. One particularly annoying fault in the first edition—and indeed in a number of first edition texts in the ACOL series—the lack of an index, has been rectified.

For those unfamiliar with the ACOL philosophy, it is "... a convenient and flexible way of studying for people who, for a variety of reasons, cannot use conventional education courses." At various stages in the text the reader is asked to answer questions, draw graphs or perform calculations. Self assessment questions (SAQs) are also included to enable the reader to establish whether or not he or she has understood what has been studied. The author's response to each SAQ is provided at the end of each chapter. Summaries, and lists of objectives respectively keep the reader abreast of important points covered, and of goals to be achieved.

The number of pages has been increased by almost one hundred over the first edition, and the number of chapters has doubled from five to ten. More important of course, is the new arrangement and content of these chapters. For example, "Columns" and "Detectors" now appear, rightly so, as independent chapter headings. Other new chapter headings are "Retention and peak dispersion", "Solvent delivery and sample injection", "The mobile phase", and "Method development". The tenth chapter is a short one on additional topics such as small bore columns, enantiomer separation, flash chromatography, preparative HPLC, SFC, and LC–MS.

Chapter 6 on "The mobile phase" is particularly useful in that it describes methods (sequential, predictive, iterative) of mobile phase optimization in ternary and quaternary systems. This is undoubtedly one aspect of HPLC which has progressed considerably since the first edition of this book was published, thanks to advances in computing, and its inclusion is not only valuable but essential. Indeed, the important contribution of microcomputers to HPLC is rather underplayed, here and in other sections of the book, for example when discussing photodiode array detectors. This, however, is a minor criticism.

The book is well written, is pitched at the correct level for its intended readership, is certainly good value for money, and can be thoroughly recommended.

D. F. RENDLE

exponentials and various other functions to experimental data. A chapter on Fourier transform techniques is included and a rather specialised chapter on least squares interpretation of potentiometric titrations, a topic clearly dear to the author's heart, provides a conclusion.

The statistical theories which underpin the techniques discussed are presented, but in a rather unsystematic way: propagation of error formulas are given in Chapter 2 but the reader is referred to an Appendix for a derivation and the Central Limit Theorem makes only a fleeting appearance on page 107. Most readers are likely to apply the methods discussed by acquiring a computer program rather than by writing one but there is no guide to selection of suitable routines from the large number of program packages now commercially available. Crystallography, something of an adventure playground for the least squares specialist, gets only a passing mention.

I strongly recommend this book to research workers who already have some experience of least squares methods, possibly through use of an applications package, and who want a more detailed and wider understanding of what these methods can deliver. The complete novice and anyone with a dislike for matrix algebra should look elsewhere.

K. W. MUIR

High Performance Liquid Chromatography: Second Edition. S. LINDSAY, Wiley, Chichester, 1992. Pages xxii + 337. Softback £17.50, ISBN 0-471-93115-2. Hardback £39.93, ISBN 0-471-93180-2.

The appearance of the second edition of Sandie Lindsay's text is both timely and appropriate. As part of the Thames Polytechnic Analytical Chemistry by Open Learning (ACOL) series, this highly revised edition will be welcomed by students and practitioners of High Performance Liquid Chromatography. One particularly annoying fault in the first edition—and indeed in a number of first edition texts in the ACOL series—the lack of an index, has been rectified.

For those unfamiliar with the ACOL philosophy, it is "... a convenient and flexible way of studying for people who, for a variety of reasons, cannot use conventional education courses." At various stages in the text the reader is asked to answer questions, draw graphs or perform calculations. Self assessment questions (SAQs) are also included to enable the reader to establish whether or not he or she has understood what has been studied. The author's response to each SAQ is provided at the end of each chapter. Summaries, and lists of objectives respectively keep the reader abreast of important points covered, and of goals to be achieved.

The number of pages has been increased by almost one hundred over the first edition, and the number of chapters has doubled from five to ten. More important of course, is the new arrangement and content of these chapters. For example, "Columns" and "Detectors" now appear, rightly so, as independent chapter headings. Other new chapter headings are "Retention and peak dispersion", "Solvent delivery and sample injection", "The mobile phase", and "Method development". The tenth chapter is a short one on additional topics such as small bore columns, enantiomer separation, flash chromatography, preparative HPLC, SFC, and LC–MS.

Chapter 6 on "The mobile phase" is particularly useful in that it describes methods (sequential, predictive, iterative) of mobile phase optimization in ternary and quaternary systems. This is undoubtedly one aspect of HPLC which has progressed considerably since the first edition of this book was published, thanks to advances in computing, and its inclusion is not only valuable but essential. Indeed, the important contribution of microcomputers to HPLC is rather underplayed, here and in other sections of the book, for example when discussing photodiode array detectors. This, however, is a minor criticism.

The book is well written, is pitched at the correct level for its intended readership, is certainly good value for money, and can be thoroughly recommended.

D. F. RENDLE

Talanta, Vol. 40, No. 4, pp. 461–477, 1993
Printed in Great Britain.

0039-9140/93 $6.00 + 0.00

REVIEW

AMPEROMETRIC GAS SENSORS

S. C. CHANG,*
Department of Chemistry, IIT, Chicago, IL 60616, U.S.A.

J. R. STETTER
Transducer Research, Inc. 1228 Olympus Dr. Naperville, IL 60540, and Department of Chemistry, IIT, Chicago, IL 60616, U.S.A.

C. S. CHA
Deptartment of Chemistry, Wuhan University, Wuhan, 430072 People's Republic of China.

(*Received* 1 *December* 1991. *Accepted* 25 *July* 1992)

The earliest successful amperometric gas sensor of modern design was the Clark electrode used for oxygen determination.[1,2] A detailed description of various types of Clark electrodes and their applications can also be found elsewhere.[3,4] While the analytical reactions for many toxic gases like SO_2, Cl_2, Br_2, NO_2 and HCN at solid electrodes has been known,[5] practical gas sensors were not constructed because there was no convenient way to package the electrodes and electrolytes for field or laboratory use.

A breakthrough came in the late 60s as the result of the development of fuel cell technology. The use of Teflon-bonded noble metal catalyzed gas-diffusing electrodes to constrain the aqueous electrolytes made modern amperometric gas sensors possible for a wide range of toxic gases. In addition, the use of a Pt/air reference electrode by Oswin in 1969[6] significantly simplified sensor design and led to practical field gas sensors for alcohol,[7] CO,[8–10] nitrogen oxides,[10,12] H_2S,[11] and SO_2[13] that were introduced in the 70s. A variety of two- and three-electrode amperometric gas sensors were introduced during the same period. For example, SO_2,[14] H_2CO,[15] ozone,[16] cyanide,[17,18] ammonia[19] and hydrazine[20–22] sensors have been addressed, as well as variations on these sensors.

A combination of the Teflon-bonded gas-diffusion electrode and a solid polymer electrolyte (SPE) membrane (*e.g.*, Nafion) was used to provide an alternative design for the amperometric gas sensor. Sensors for H_2,[23] CO[23–25] and nitrogen oxides[24,25] were introduced and, later, a sensor for O_2.[26] Recent studies of the electrochemistry of the SPE system indicate that CO_2[27] and alcohol[28] sensors are possible.

Amperometric gas sensors with non-aqueous electrolytes have been reported for Cl_2,[29] CH_4[30,31] and CO_2.[32,33] Commercial non-aqueous sensors have been available since the mid 70s. The amperometric gas sensor has seen widespread use in industrial hygiene and safety,[34] environmental and medical applications, and, recently, indoor air pollution studies.[35]

The amperometric gas sensor is often described in the literature using terms such as polarographic, electrolytic, voltammetric, amperometric, or micro-fuel cell. This use of diverse and sometimes inappropriate nomenclature confuses the method of sensor operation, the description of the sensor design, and the application. Most amperometric gas sensors are not polarographic because they do not contain a mercury electrode. Many are not electrolytic but rather are galvanic cells and none generate sufficient power to be called a fuel cell. The method most frequently employed in these gas sensors is "constant potential amperometry". Therefore, the term "amperometric gas sensor" is preferred and it can be modified by an appropriate adjective to yield a precise description of the method of operation of the electrochemical sensor. The name "amperometric gas sensor" will also distinguish the "current"

*Present address: Dow Chemical Company, Midland, MI 48640, U.S.A.

measurement from the "potential" measurement in potentiometric systems and "amperometric gas sensor" will be used throughout this discussion.

AMPEROMETRIC GAS SENSOR

An amperometric gas sensor is a device designed to measure the concentration of gaseous compounds. The gas sensor is an electrochemical cell and the detection of gases and vapors is performed either by electro-oxidation or electro-reduction of the compound at an electrode surface that is in contact with a liquid, solid polymer, or gel electrolyte. Typically, the sensing electrode is a noble metal catalyzed gas-diffusing electrode which is capable of keeping the electrolyte in the cell and yet is porous enough to allow the gas phase to diffuse to the electrode/electrolyte interface.

By choice of a suitable geometry for gas exposure and electrolyte confinement, materials for membranes, electrolytes, electrocatalysts, and useful operating conditions (*e.g.*, electrode potentials and sample flow rates), the sensor can be made quite sensitive for a particular gas component and quite insensitive to others.

A potentiostat is usually applied to provide a fixed or controlled potential for the sensing or working electrode relative to a reference electrode which is placed in the same electrolyte. In a three-electrode system the potentiostat is employed to energize and control the electrochemical cell as well as amplify the sensor's signal. The three-electrode configuration allows for precise operation even with microelectrodes. The reference electrode is used to maintain the sensing electrode at a known electrochemical potential and must be stable in the electrolyte of the sensor. The sensor is designed such that the magnitude of the current generated by the electrochemical reaction of the analyte is directly proportional to the analyte concentration in the gas stream being sampled. Some work has been performed using the cyclic voltammetric technique for gas detection, but the success of this approach for gas sensors is not well documented.[22]

In amperometric gas sensors, a sampling system, usually a pump or diffusion tube, is used to transport the reactive gas to the sensing electrode. A major problem often exists in obtaining a representative aliquot of the sampled environment so that the observed sensor current has analytical significance. It is not critical that efficient sampling take place; however, repeatable sampling is required to make the sensor signal a meaningful representation of the concentration.

A membrane is often employed to cover and protect the sensing (working) electrode. The membrane can also slow the diffusion of unwanted gases to the sensing electrode and decrease the flow rate dependence of signal magnitude. In a number of cases, the rate of mass transfer through the membrane is the main factor controlling the limiting current output of amperometric gas sensors.

The counter electrode completes the electrochemical cell by performing the half cell reaction, the nature of which is preferably in opposition to the sensing electrode reaction in order to minimize net chemical changes in sensors. Two electrode systems for O_2 and CO are common and in these sensors the counter (or auxiliary) electrode serves as both counter and reference electrode.

The electrolyte should be chosen carefully. It must carry the ionic current efficiently, solubilize the analyte effectively, support both counter and sensing electrode reactions, form a stable reference potential with the reference electrode, and be compatible with the materials of construction. Sensor signals are often observed to decay as electrolytes evaporate. Such instabilities often can be controlled by a judicious choice of the electrolyte and the operating conditions of the system.

SENSOR STRUCTURE

Figure 1 is a schematic diagram of an amperometric gas sensor system. The sensor may consist of six major parts (see Fig. 1); filter, membrane (or capillary), working or sensing electrode, electrolyte, counter electrode, and reference electrode. Each part of the sensor influences the overall performance and analytical characteristics of the sensor. Choosing appropriate materials for sensor construction and selecting an efficient sensor geometry is critical to sensor operation. The "minor" details of sensor design can have a profound influence on the accuracy, precision, response time, sensitivity, background current, noise, stability, lifetime and selectivity of the resulting sensor. Often the choice of optimum sensor materials and geometry for a given application are not obvious.

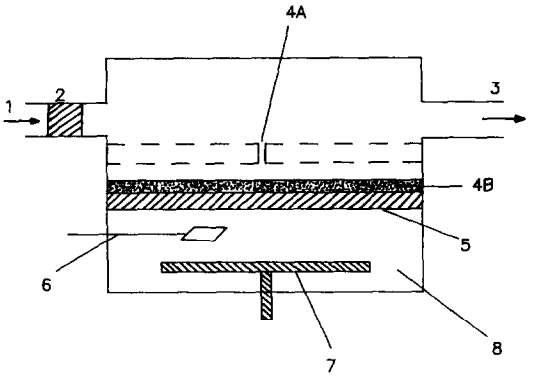

Fig. 1. Schematic diagram of the amperometric gas sensor system.

Definite relationships must exist among materials of construction, sensor geometry, specific electroanalytical method employed, and the performance characteristics of gas/vapor sensors. However, such relationships are still poorly defined. An adequate general model of the amperometric gas sensor does not exist and guidance in the design and application of these sensors is still very much an art.[36] Insight into the mechanism of the amperometric gas sensor, however, can be obtained by examining the reactivity of specific sensor systems.

Various types of amperometric sensor structures can be classified in different ways. The simplest way would be to classify them as two-electrode or three-electrode systems. However, such classification gives no insight into the nature of the sensing electrode and the main process controlling the magnitude of the sensor signal. In the following sections, sensor structures are classified according to the type of sensing electrode employed and the geometry of the gas-permeation path and the ion-conducting phase (electrolyte).

Membrane-covered planar electrode system (Clark sensor)

The Clark sensor is the most published and widely used membrane-covered planar electrode amperometric gas sensor. It usually works as a two-electrode system, although three-electrode configurations of the same sensor are also feasible.

The Clark sensor was first introduced to measure oxygen fugacity in medical applications. A schematic diagram of the Clark cell[1,2] is illustrated in Fig. 2. The container houses the electrolyte, the cathode, and anode. The external electrical circuit consists of a variable voltage source and a current meter to measure any current flowing between the two electrodes. A gas permeable membrane separates the electrolyte from the oxygen sample. When the cathode is made negative enough with respect to the anode (by adjusting the circuit), dissolved oxygen molecules at the cathode are electrochemically reduced and a current flows in the external circuit. The magnitude of this current is a measure of the concentration of oxygen in the sampled gas.

A practical illustration of a typical Clark sensor[37] is given in Fig. 3. The membrane fits closely over the end of the electrode, leaving a thin layer of electrolyte (typically 5 μm–15 μm thick) between the cathode surface and the membrane. Suitable membrane materials are polypropylene, polyethylene, Teflon, or Mylar. In general, polypropylene or polyethylene are the materials of choice, and the membrane thickness is typically 20–25 μm. Both plastic membrane materials are good electrical insulators and their permeability to oxygen is practically unchanged in the presence of water vapor.[38] This makes them ideal in medical applications where relative humidities may vary substantially from sample to sample.

The reference/counter electrode in the Clark sensor is most frequently a silver–silver chloride electrode and the electrolyte is typically a buffer solution with the addition of some sodium

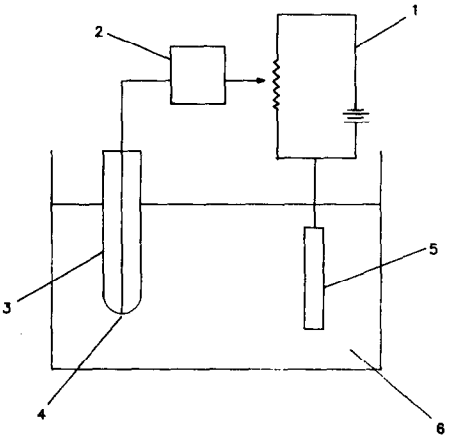

Fig. 2. The basic outline of an amperometric oxygen cell.

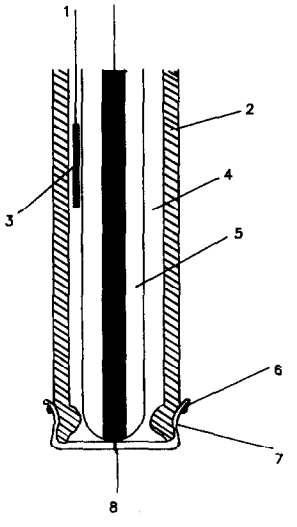

1. To current measuring circuit
2. Insulating container
3. Ag/AgCl reference electrode
4. Electrolyte
5. Glass insulating rod
6. O-ring
7. Plastic membrane
8. Pt wire cathode

Fig. 3. Schematic outline of a practical Clark amperometric oxygen cell.

chloride to stabilize the potential of the reference/counter electrode. The electrolyte can be a potassium chloride solution and, in industrial applications, glycol can be added to reduce the possibility of electrolyte freezing. Gelling agents (*e.g.*, methacrylate) can be added to enable convenient handling of the electrolytes. In medical applications, an electrolyte of pH = 7 is generally chosen[39] and the complete system is thermostated at 37° so that the blood–gas pO_2 measurements are made at normal body temperature.[40]

Gas-diffusion electrode gas sensor system

Gas-diffusing electrodes used in amperometric gas sensor systems are usually[7] of the semi-hydrophobic type. These electrodes are prepared by mixing Teflon emulsion with high surface area noble metal catalyst powder, and then depositing the slurry on a metal wire screen or on the surface of a totally hydrophobic porous Teflon film or a hydrophillic SPE membrane. The resulting gas-diffusing electrode consists of highly interlocked matrices of gas pores, electrolyte channels, electronically conducting paths and electrocatalytic surfaces. It is porous enough to effect efficient gas permeation, has sufficient metal catalyst to be a good electronic conductor, and is hydrophilic enough to make intimate contact with the electrolyte for ionic conduction and electrochemical reactions involving gases. Gas-diffusing electrodes are especially valuable in those cases when the kinetics of electrochemical reaction are very slow, such as the oxidation of hydrocarbons.

Free electrolyte sensor. Figure 4 illustrates the structure of a gas sensor that uses a Teflon-bonded gas-diffusion electrode.[31] The gas chamber that exposes the working electrode to the analyte stream allows easy pnuematic connections for the sample. For convenience, the working and counter/reference electrode are often positioned vertically and located at opposite ends of the electrolyte chamber. The vented gas exposure chamber for the counter and reference electrode insures a nearly constant reference potential, since the counter and reference electrode reactions may also involve the reaction or production of a gas, such as the evolution or reduction of oxygen. In other cases, metal/metal oxide (such as Pb/PbO) or metal/metal halide (such as Ag/AgCl) electrodes are used as counter and reference electrodes, and a gas-diffusing electrode is employed only as the sensing electrode. The primary reasons that the Pt/Air reference electrode is used in most industrial sensors are that: (1) it is a convenient size, (2) can be made rugged (no glass), and (3) its reference potential (about 1.0 V *vs.* NHE), even though not reversible, is stable (constant) enough to be used as a reference electrochemical voltage for the three-electrode sensor! The fully enclosed Pb/PbO_2 electrode may come close to these features but is consumed during operation and therefore, not catalytic.

One of the principal benefits of the free electrolyte sensor is the high buffering capacity of the electrolyte, which helps to keep the composition and pH value of the electrolyte

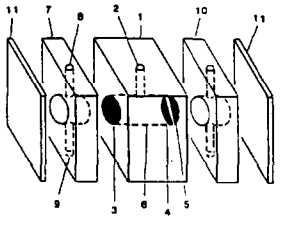

1. Main compartment
2. Solution inlet
3. Working electrode
4. Reference electrode
5. Counter electrode
6. Solution reservoir
7. Gas chamber for working electrode
8. Gas inlet
9. Gas outlet
10. Gas chamber for counter–reference electrodes
11. Cover

Fig. 4. Basic sensor design.

nearly constant over a long period of continuous operation. In addition, the position of the "three-phase boundaries" within the gas-diffusing electrode are more stable when the latter is in contact with the free electrolyte. However, localized changes at the sensing electrode (dehumidification, carbonization, pH change, *etc.*) may still occur in pores adjacent to the gas chamber. Carbonization of alkaline electrolyte is especially harmful since precipitation of crystallites of carbonates not only weaken the hydrophobic character of the electrode, but also form crystals that pierce it. Therefore, the long-term performance of sensors employing gas-diffusion electrodes is usually better when an acidic or neutral salt electrolyte is used.

Solid polymer electrolyte (SPE) sensors. A problem of the free electrolyte sensor is possible electrolyte leaks. Attempts to by-pass this situation include stabilization of the electrolyte in various porous matrices or gels. By far the most successful attempt seems to be the use of a solid polymer electrolyte (SPE) membrane for the electrolyte and the Nafion membrane is commonly employed for this purpose.[24,25,41]

Nafion is a copolymer of polytetrafluoroethylene (PTFE) and polysulfonylfluoride vinyl ether containing sulfonic acid groups. The sulfonic acid groups are chemically bound to the perfluorocarbon backbone as illustrated in Fig. 5(a).

The equivalent weight (EW) of an ion-exchange resin is defined as the weight of resin which neutralizes one equivalent of base. Ion exchangers are also characterized by their ion exchange capacity (IEC) and the IEC is given by the milli-equivalents (meq) of sulfonic acid/dry weight of membrane. The relationship between IEC and EW can be expressed as:

$$\text{IEC} = 1000/\text{EW}$$

Generally, IEC is determined by titration of the resin with base and measurement of the gravimetric weight. Upon exposure to water, the sulfuric acid groups are solvated, the mobility of proton is enhanced, and the Nafion becomes a good proton conductor, *i.e.*, an acidic electrolyte.

In the Nafion electrolyte sensor design, a thin Nafion solid polymer film is used both as the electrolyte and as a support for the electrode structure. The electrodes can consist of high surface area metal powder together with

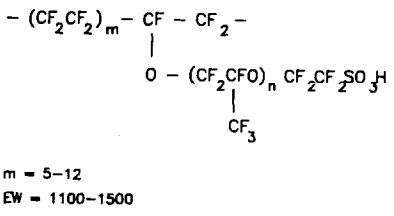

Fig. 5(a). Structural formula of Nafion (1000 series).

some form of current collector attached to the Nafion substrate using heat or chemical bonding techniques. The specific design [see Fig. 5(b)], construction, and performance of the Nafion system have been described in the literature.[24,25,41]

Apparently, a good contact between catalyst particles and the "solid" polymer membrane is vital to the performance of the electrode. The contact area could be improved either by impregnation of the catalyst layer with a Nafion solution,[42,43] or by *in-situ* formation of crystallites of a noble metal catalyst within the surface layer of the membrane.[44–46] The noble metal catalyst/Nafion membrane interface is chemically very stable, which seems to be the main reason for the long-term stability of some sensor designs employing a Nafion membrane. However, the water content of the membrane must be carefully controlled in order to avoid drowning or drying-out of the electrode-membrane assembly. Under- or over-humidification will not only influence the ionic conductivity of the SPE membrane, but also affect the coverage and thickness of liquid film on the surface of the catalyst, resulting in deterioration of the

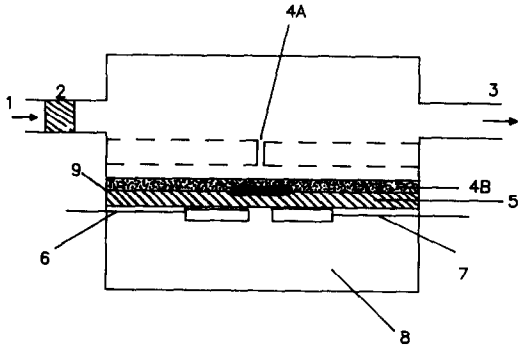

Fig. 5(b). Schematic diagram of sensor using a thin sheet of Nafion as the electrolyte.

analytical characteristics of the sensing electrode. Usually, a water reservoir, as shown in Fig. 5(b), can insure a constant humidification of the system.

BASIC OPERATING MECHANISM OF THE AMPEROMETRIC GAS SENSOR

General mechanism of electrochemical gas reactions

The response of an amperometric gas sensor can be described by the following eight steps in light of the Fig. 1 schematic:

1. Introduction of the gas or vapor phase compound to the sensor through the filter. [The filter can act to enhance the selectivity of the sensor system by removing unwanted electroactive contaminants and protect the sensing electrode from particulate contamination.]
2. Transfer of the reactant from the gas chamber to the back of the sensing electrode and diffusion to the gas/electrolyte interface. [Laminar flow characteristics dominate in gas chambers of typical geometries. There may be a membrane or capillary somewhere between the gas chamber and the electrode, and transfer across the membrane or capillary is usually characterized as a diffusion process.]
3. Dissolution of the electroactive species in the electrolyte. [Rate of mass transfer across the gas/liquid boundary and solubility of the gas in the electrolyte can affect sensor sensitivity and response time.]
4. Diffusion of the analyte to the electrode/electrolyte interface (in the liquid phase).
5. Adsorption onto the electrode surface.
6. Electrochemical reaction.
7. Desorption of the products
8. Diffusion of the products away from the reaction zone to the bulk of electrolyte or gas phase.

Any of these steps can be rate limiting, thus determining the ultimate response characteristics of the amperometric sensor. The parameters that most frequently influence the observed analytical characteristics of a sensor include: sample flow rate, working electrode composition, type and amount of electrolyte, membrane porosity and permeability, and the electrochemical potential of the sensing electrode. By controlling these parameters, the sensor engineer can often achieve the desired and/or optimum sensor response characteristics for a particular compound in a given situation.

Steps 5, 6 and 7 in the proposed mechanism are especially important since they involve the electrocatalytic phenomena. It is often appropriate to consider steps 5, 6 and 7 as a single but rather complex electrocatalytic event. The precise mechanism of the electrochemical process can be worked out by careful analysis of the transient and steady-state current response and the build-up of intermediate and final reaction products. The response of an electrode may also be complicated by electrode poisoning processes and/or auto-catalytic reactions (observed as a change of steady-state signal response time and magnitude).

In addition, the electrochemical reaction mechanism may change with sensor operating conditions. For example, at low analyte sampling rates, the sensor may electro-oxidize all of the available analyte and act as a coulometric device being limited by the supply of analyte. Conversely, at high analyte flows, diffusion through the electrolyte may limit response; and at low electrocatalytic activity, the rate of reaction at the electrode surface may limit the observed current (*i.e.*, signal). Before an appropriate model can be developed for the sensor, the nature of the rate-limiting step must be determined.

Theory of the limiting current: steady-state sensor response

It is usually preferable that a sensor works in the "limiting current region" in which the magnitude of the sensor signal is practically independent of the electrode potential. In theory, the limiting current region can be achieved in any case when the rate-limiting step is a step prior to electron transfer. In sensor design, diffusion-limited current operation is by far the most commonly employed for analytical applications in the field.

There are several possibilities for realization of diffusion limited current. First, the rate of electrode reaction may be limited by the rate of diffusion through a membrane or a capillary which is placed somewhere between the gas stream containing the analyte and the catalyst layer of the electrode. The limiting current, i_{lim}, (not current density), according to equation (1), can be written as

$$i_{lim} = \frac{nFD_s AC_s^0}{\delta} \tag{1}$$

where n is the number of electrons involved in the electrochemical reaction per molecule of the

diffusing species, F is the value of the Faraday, A is the effective area of the membrane or the cross section of the capillary, and δ is the thickness of the membrane or the length of the capillary. The diffusion constant also represents the gaseous diffusion constant for s in the medium of the membrane or capillary.

Second, the current can be limited by the rate of diffusion across the diffusion layer in solution. An expression similar to equation (1) can be used to calculate the current. However, in this case A in equation (1) is the effective surface area of the electrode, D_s is for diffusion of s in solution, and δ is the thickness of the diffusion layer in solution at the electrode surface (this is the typical interpretation of Fick's equation in polarography).

There are other ways to realize a potential independent limiting current which is not governed by the diffusion process. The current may be limited by transport to the sensor from the outside world. In this case, 100% of the electroactive species that enters the gas sensor reacts and the limiting current is related to the sample in a "coulometric" way. This method of sensor operation has been used successfully to determine the electrochemical characteristics for several gas sensor reactions.[9,47,48]

If the rates of diffusion processes are much faster than the rate of reaction at the electrode surface, then the current is controlled by the rate of the electrode kinetics. In this case an expression for the current will take the form

$$i = nFKA[P]^n[Q]^m \exp(\alpha nF/RT\eta) \qquad (2)$$

where K represents the standard rate constant, n and m represent the order of the reaction for concentration of reactants P and Q respectively, α and η are the transfer coefficient and overvoltage of the electrode reaction. This behavior has been observed for an NO_2 gas sensor with a very low surface area electrode[49] in acid electrolyte.

Theoretically, the above model has several interesting consequences. If the kinetics of transport of reactant to the electrode surface (up to step 5) are significantly slower than all other steps, the limiting current should be potential independent. Conversely, a strong potential dependence should be observed for sensors wherein the electrocatalytic reaction limits the observed current and this "electrode-reaction" limited sensor should produce limiting currents that are independent of external events such as analyte flow rate. These predictions have been recently confirmed for the electrochemical reaction on NO_2 at a gold electrode in acid electrolyte.[41]

To appreciate the differences in the limiting current mechanisms, it is useful to discuss specific sensors and several are presented in the following sections.

The Clark cell (oxygen sensor)

The Clark oxygen gas sensor is probably the most widely used, most thoroughly studied, and best characterized of the amperometric gas sensors. Figure 6 represents the one-dimensional model, showing the transport of oxygen from the sample (concentration C_s) to the cathode surface of a Clark sensor. Assuming an even distribution of current density at the electrode surface, it is easy to prove that the steady-state limiting diffusion current density at the cathode of the Clark sensor can be expressed as

$$I_{lim} = (1/I_{lim(m)} + 1/I_{lim(l)})^{-1} \qquad (3)$$

where $I_{lim(m)}$ and $I_{lim(l)}$ represent the limiting diffusion current densities across the membrane (m) and thin electrolyte film (l) respectively:

$$I_{lim(m)} = \frac{nFD_m C_m}{\delta_m} \qquad (4)$$

$$I_{lim(m)} = \frac{nFD_l C_l}{\delta_l} \qquad (5)$$

where δ_m and δ_l represent the thicknesses of membrane and electrolyte layer respectively, and subscripts "m" and "l" are used to denote parameters D and C in different layers.

I_{lim} in equation (3) may be predominantly determined by either $I_{lim(m)}$ or $I_{lim(l)}$ if one of them is significantly smaller than the other. In most sensor designs found in industrial applications,

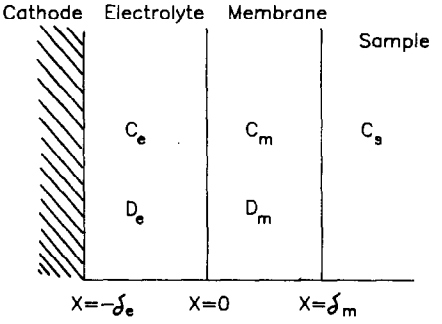

Fig. 6. The one-dimensional diffusion model, showing the transport of oxygen from the sample (concentration C_s) to the cathode surface, where it is electrochemically reduced.

the rate of mass transport across the membrane is the limiting factor, and $I_{lim(l)} > I_{lim(m)}$.

Mancy *et al.*[50] have provided a comprehensive solution for the E *vs.* t behavior of this sensor by solving the transient form of Fick's law of diffusion for the system shown in Fig. 6. The main conclusions of their work can be summarized as follows.

Within a very short time interval after the start of polarization, diffusion in the electrolyte layer alone is rate limiting and the current density at the cathode is given as:

$$I = nF\frac{K_b}{K_o}C_s\left(\frac{D_e}{\pi t}\right)^{1/2} \times\left[1+2\sum_{n=1}^{\infty}\exp\left(\frac{-n^2\delta_l^2}{D_e t}\right)\right] \quad (6)$$

where K_o is the distribution coefficient for the electrolyte-membrane interface, and K_b is the distribution coefficient for the sample-membrane interface.

Since typically δ_l is about 10 μm and D_e is 0.1 m^2/sec, equation (6) will only hold for $t < 0.1$ sec, since the diffusion layer must be confined to the electrolyte film. In this short initial time interval ($t < 0.1$ sec) the exponential terms in equation (6) can be neglected, so we have

$$I \cong nF\left(\frac{K_b}{K_o}\right)C_s\left(\frac{D_e}{\pi t}\right)^{1/2} \quad (7)$$

After that short initial time interval, the diffusion layer enters the membrane and, if we assume $\delta_m/\sqrt{D_m} \gg \delta_e/\sqrt{D_e}$, the rate of mass transfer within the membrane will soon turn out to be the predominant rate limiting step and the current density equation becomes

$$I = nFK_bC_s\left(\frac{D_m}{\pi T}\right)^{1/2} \times\left[1+2\sum_{n=1}^{\infty}\exp\left(\frac{-N^2\delta_m^2}{D_e t}\right)\right]^{1/2} \quad (8)$$

This equation can be reduced to a simpler form by noting that typical values for δ_m and D_m are <20 μm and 10^{-3} m^2/sec, respectively. Thus, for $t < 10$ sec,

$$I = nFK_bC_s\left(\frac{D_m}{\pi t}\right)^{1/2} \quad (9)$$

Because, in both cases, it is diffusion transport alone which controls the magnitude of the observed current density, equations (9) and (7) are similar.

At longer time intervals, the diffusion layer will spread into the membrane layer, approaching the outer face of the membrane. Under these conditions, the current density is given by

$$I = nFK_bC_s\frac{D_m}{\delta_m} \times\left[1+2\sum_{n=1}^{\infty}\exp\left(-\frac{n^2\pi^2D_m t}{\delta_m 2}\right)\right] \quad (10)$$

After 20 or 30 sec, the exponential term becomes negligible and equation (10) reduces to steady-state current density:

$$I = \frac{nFK_bC_sD_m}{\delta_m} \quad (11)$$

which is the same ($c_m = K_bC_s$) as equation (4) since only transport in the membrane is of importance.

Other investigators have developed models to explain the precise shape of the i *vs.* E behavior of the Clark oxygen gas sensor. Mochizuki[51] developed a much simplified one-dimensional model which included a reaction rate term to describe the destruction of oxygen at the cathode surface. Hahn[52] further developed this model to include not only one-dimensional but spherical and cylindrical coordinate steady-state geometries. Using this approach, Hahn was able to produce oxygen concentration profiles in the electrolyte and membrane layers as well as at the cathode surface at various polarizing voltages. A complete representation of the theroetical i *vs.* E behavior was obtained in this manner and compared well with experimental observations.

However, the basic assumption of the one-dimensional model, *i.e.*, uniform distribution of current density at the surface of the sensing electrode, could hardly be totally realized at Clark electrodes of practical size. If the diameter of the electrode exceeds 1–2 mm, lateral ionic conduction through the thin electrolyte film and removal of reaction products from the central part of the electrode would be difficult, so the current density near the center of the electrode could be lower. On the other hand, for very small electrodes, the "edge effect" can enhance the rate of mass transfer at the periphery of the electrode. Limiting current density at an electrode with a radius smaller than 100 μm can be significantly higher than that predicted by the one-dimensional model.[53–55]

Sensors using gas-diffusion electrodes

Analysis of the polarization behavior of gas-diffusion electrodes has been performed.[56,57] When a diffusion barrier (membrane or capil-

lary) is placed somewhere between the gas stream and the catalytic layer of the gas-diffusion electrode, potential independent limiting current may appear if the kinetics of the electrochemical reaction are much faster than the rate of mass-transfer through the diffusion barrier. Such a diffusion barrier can make amperometric sensors more stable. If the reaction is fast over a range of potentials, no potential control is required in the gas sensor. A simple two-electrode system provides adequate analytical performance because, even though the thermodynamic potential can drift during sensing, no change in the analytical signal (the steady-state current) is observed. When the electrode reaction is slow, the potential of the sensing electrode must be precisely controlled (as in the three-electrode system) to avoid drift in the sensor current.

The gas-diffusion electrode can be an efficient electrochemical device and, often consumes a significant portion of the gaseous reactant by Faradaic reaction. When this condition exists, the magnitude of the sensor's signal will vary with the flow-rate (or input) of the gas stream. Sedlak and Blurton[9] studied the limiting current in a three-electrode amperometric gas sensor by measuring the flow rate dependence of the sensor signal for carbon monoxide at various concentrations. They reported an empirical analysis of these data that included consideration of both the mass transfer and electrochemical processes occurring in the gas sensor. The overall mass transfer equation for the electrochemical reaction in the sensor was given as:

$$\frac{dc}{dt} = -V\left(\frac{dc}{dx}\right) - k\int\frac{\delta c}{\delta t}\,dt \qquad (12)$$

where c denotes the concentration of reactant, V represents the linear velocity of the gas stream, and k is the overall rate constant for transfer of reactant to the catalytic electrode. The first term on the right hand side of equation (12) refers to the convectional transport of the gaseous analyte and the second term refers to ("unsteady-state") mass transfer of gaseous reactant through the electrode and membrane structure. The solution to this differential equation for a gas path geometry as defined in Fig. 7 is given

$$c(x,t) = c^{\circ}[1-\exp(-\lambda t)] \times \exp[(\lambda - k)whx/G] \qquad (13)$$

where c° denotes the initial concentration of the reactant, λ is a time constant arising from

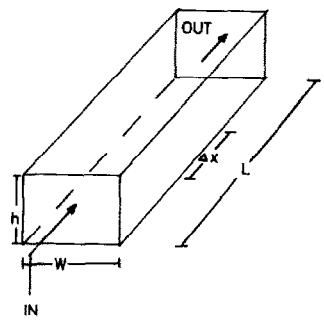

Fig. 7. Schematic of gas pathway in sensor. The gas-diffusion electrode is placed at downside of the box.

solution of the continuity equation, and G is the volumetric gas flow-rate ($G = whV$).

Faraday's law must apply to the sensor current (if no gas losses or side reactions are assumed to occur in the sensor and the effect of build-up of concentration in the gas chamber can be ignored), then the observed current, i, is

$$i(t) = -(nFG/V)[C(L,t) - C(0,t)]$$

and

$$i(t) = (nFC^{\circ}F/V)[1-\exp(\lambda - t) \times (1-\exp[(\lambda - k)whL/G])] \qquad (14)$$

The steady state value of i is attained at sufficiently large values of $\lambda\, t$:

$$i = (nFC^{\circ}G/V) \times (1-\exp[(\lambda - k)whL/G]) \qquad (15)$$

Equations (14) and (15) were sufficient to describe the experimental data that they reported but the physical significance of the constants is not entirely clear. This approach does not offer a plausible mechanism of response. Critical examination of these data can be revealing.

Figure 8 (curve a) shows a response time curve for 48 ppm CO using a flow rate of 700 cm^3/min. As predicted by equation (15), the sensor signal increases with time to a steady-state value at large values of t. Figure 8 (curve b) shows the current decay with time after the CO analyte flow through the sensor had ceased. The rapid return of the current to zero supports the assumption used in the derivation of equation (16) that all the CO migrating through the porous electrode is electro-oxidized. Curve (c) illustrates the data for a curve plotted in the form $-\log(1 - i/i_{lim})$ *vs.* t. The slope of this plot equals λ. The values calculated from these data gave $\lambda = 0.18 \pm 0.02$ sec^{-1} for $300 < G < 1500$ cm^3/min. Similar semi-logarithmic plots were obtained with the current decay results and they

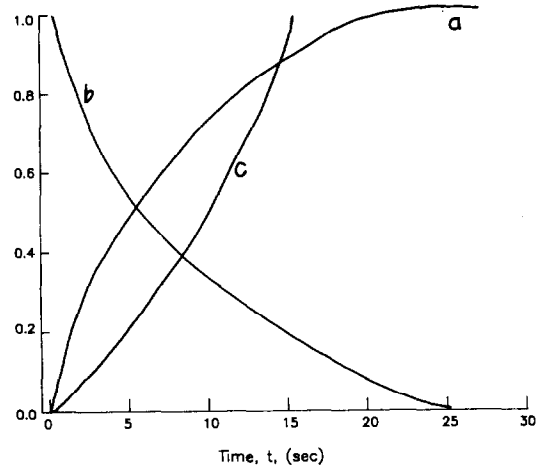

Fig. 8. Sensor response characteristics: (a) I/Ilim vs t(sec) for signal rise; (b) I/Ilim vs t (sec) for signal decay; (c) $-\log(1 - I/Ilim)$ vs t (sec) for signal rise. Ilim: limiting current.

gave a value of $\lambda = 0.16 \pm 0.02\ \text{sec}^{-1}$ in the same flow-rate range. Thus, the time constants for rise and decay of the sensor signal are essentially equal and are independent of flow rate supporting the first order response model for the transient current.

Sedlak and Blurton[10] also measured current *vs.* flow rate behavior for 39 ppm NO and compared the current to the theoretically predicted values (if 100% oxidation of analyte in the electrode is assumed for all flow rates). It follows from equation (15) that, as $G \to 0$,

$$\lim(i/G) = nFC^{\circ}/V \qquad (16)$$

Thus, as the flow rate is decreased, a point is reached at which all of the NO entering the sensor reacts. Therefore, current measurements at very low flow rates permit calculation (or estimation) of C° at known n or n at known C° (concentration). Notice that equation (16) describes the analyzer current only when oxidation or reduction of the sample gas is obtained with "perfect" Faradaic efficiency. This method has been used to determine "n" for several gaseous reactions[10,21] using an amperometric gas sensor.

At the typical flow rates used in the amperometric gas sensor, coulometric reaction efficiency is rarely achieved and sometimes as little as 2% of the gas is reacted during its passage through the gas sensor. However, the fraction of analyte reacted in the sensor is always constant as long as conditions (*e.g.*, flowrate, geometry, potential, *etc.*) are held constant. One need not achieve quantitative reaction to use the sensor as a quantitative analytical tool. However, suitable calibration of the steady-state current must be performed regularly, since the performance of the gas-diffusion electrode can change gradually with time. These changes may be due to losses in electrocatalyst activity, electrolyte concentration changes or contamination, or even clogging of the pores of the gas porous diffusion membrane.

For many gas sensor designs, it is reasonable to assume that all of the analyte entering the electrolyte is consumed with Faradaic efficiency and the current is limited by mass transport of gas across the membrane separating the gas sample chamber and the electrode/electrolyte interface. This was confirmed by several studies of CO, NO_2, and hydrazine reactions and the "coulometric" characteristics of the "steady-state" current was observed during sensor operation.[21,47,48]

Equation (16) can also be used to describe the mass transport limited response of the solid polymer electrolyte sensor. However, if the surface reaction of analyte is slow or the effective surface area of the electrode is small, then the response of the electrochemical sensor will be limited by the rate of the electrocatalytic (electrode) reaction and the observed limiting current will be proportional to the surface area of the electrode. In this case, equation (16) will be inadequate to describe the flowrate *vs.* i and i *vs.* concentration behavior of the sensor.

Low surface area Au electrodes have been examined for an NO_2 reduction reaction.[49] The limiting currents were compared to a high surface area Au electrode. The i *vs.* E behavior was different for these two different surface area sensing electrodes. The results illustrated that the observed current is limited by diffusion to the high surface area electrode. At the low surface area electrode, the observed current is dependent upon the rate of the electrochemical reaction at the electrocatalyst surface, and in this case:

$$i_{\text{lim}} = K[NO_2][O_2][A] \qquad (17)$$

where A is the surface area of the catalyst. Equation (17) is a typical expression of the kinetics of a chemical reaction and K is the Arrhenius constant and contains the temperature dependence of the reaction.

Concluding remarks on limiting currents and sensor models

An accurate model of sensor response should include the ability to describe all of the obser-

vations in all regions of sensor performance. Such a model does not yet exist. However, it is clear that the signal (time dependent and steady-state parts) of any gas sensor is limited by either Fickian diffusion, membrane mass transport (permeation and/or diffusion), or the kinetics of the electrocatalytic process. Each of these can be viewed as a "resistance" to current passage that must be overcome to generate the observed sensor signal. The controlling resistance for the system can then be expressed as follows:

$$1/R(\mathrm{s}) = 1/R(\mathrm{d}) + 1/R(\mathrm{m}) + 1/R(\mathrm{k}) \quad (18)$$

where $R(\mathrm{s})$ represents the system resistance, $R(\mathrm{d})$ is diffusion resistance, $R(\mathrm{m})$ is membrane (electrolyte solubility and mass-transport) resistance, and $R(\mathrm{k})$ is the resistance of the electrocatalytic reaction.

Equation (18) allows for any of the processes to be dominant and ultimately control the rate of the reaction in the sensor. Each of these terms may be expressed in terms of the parameters previously described for the sensor current.

Usually, all the $R(\mathrm{d})$, $R(\mathrm{m})$ and $R(\mathrm{k})$ terms are inversely proportional to the concentration of reactant C°, so the reciprocal of the resultant resistance $R(\mathrm{s})^{-1}$ is directly proportional to C°. Therefore, linear response to the concentration of reactant could be realized regardless of whether the kinetics of the electrode process is controlled by a single step or controlled simultaneously by several steps. However, it would be much easier to design and predict the sensor response under various circumstances if the kinetics of the sensing electrode is governed by a single step, wherein the rate of that step is independent of the electrode potential.

APPLICATIONS AND EXAMPLES OF AMPEROMETRIC GAS SENSORS

Amperometric gas sensors have been used to design instruments for chemical detection, and a wide variety of both portable and fixed-site toxic gas monitors are now commercially available. These instruments have found applications in monitoring industrial atmospheres, medical gases, compressed air lines, process streams, and pipe line gas. Gas chromatographic instrumentation, ventilation controllers, energy management systems, environmental pollutant control equipment, chemical research instrumentation, and analytical laboratory gas analyzers also utilize amperometric gas sensors. The sensors are found everywhere from space shuttles to the rim of volcanoes.

The practical capabilities of some present day industrial electrochemical gas sensors are summarized in Table 1. The first sensors were developed for the more common atmospheric pollutants namely CO, NO, NO_2, H_2S and SO_2. Sensors have also been developed for some special cases such as the hydrazines,[20,21] Cl_2,[29] CH_4,[30] O_3[16] and alcohol,[7] and, of course, the medical application for the detection and measurement of N_2O,[33,58,59] O_2, CO_2[32] and $CHClBrCF_3$.[33] Table 2 lists several classes of compounds which have been analyzed in real-time using commercially available electrochemical sensors and associated instrumentation.

Commercial instrumentation with ppm-level sensitivity has already been developed for the detection and measurement of CO, NO, H_2S, SO_2, O_2, N_2H_4, $(CH_3)N_2H_2$ and $(CH_3)2N_2H_2$. Other candidates for analysis by amperometric gas sensors (many of which have been performed) include all electrochemically active compounds like acetylene, alcohols, aldehydes (acetone), phosphine, arsine and phosgene. These compounds are often encountered as interferences on present day commercial instruments.

The application of amperometric sensors has been extended to compounds (like benzene, methane, pyridine, and trichloroethylene) electrochemically inactive at the potentials traditionally used in gas sensors.[50] Thus, the ultimate applications are only limited by the imagination of the analyst. However, the analytical characteristics of each individual sensor will determine the ultimate success of the specific application. Analysis for selected compounds has been extended into the ppb range.[10,11,29,35,41,49,60]

Examples of the electrochemical reactions that are used as the basis for analyzing gases in amperometric sensors are given in Table 3. Reactions for NO_2, N_2O, CO_2 and O_2 analyses

Table 1. Exemplary capabilities of electrochemical detectors

Detection principle	Gas/vapor measured	Approximate detection level (ppm)	Ref.
Constant potential Amperometry	CO	1–3000	8
	NO	1–100	61
	NO_2	1–500	60
	H_2S	1–5000	14
	SO_2	1–100	15
	Cl_2	0.1–50	29
	MMH	0.1–500	20, 21

Table 2. Classes of gaseous compounds analyzed amperometrically

1	Hydrocarbons and carbon/oxygen compounds	CO, CO_2, C_2H_4, C_2H_5OH, EtO
2	Oxides of nitrogen	NO, NO_2, N_2O
3	Sulfur compounds	H_2S, CH_3SH, C_2H_5SH, SO_2
4	Reduced nitrogen	NH_3, N_2H_4, $(CH_3)N_2H_3$, $(CH_3)_2N_2H_2$
5	Other	O_2, H_2, Cl_2, O_3, PH_3, As_3, HCN, $CHClBrCF_3$

are electrochemical reductions while the other examples utilize electro-oxidation to produce the analytical signal. The complementary reaction at the counter electrode with oxidation at the working electrode is typically oxygen reduction:

$$O_2 + 4H^+ 4e^- = 2H_2O$$

while the reverse reaction may occur at the counter electrode during reduction reactions of analyte at the sensing electrode. The cell reactions and specific mechanism are not well defined for all sensor systems and this is an area that requires study in the future.

ANALYTICAL CHARACTERISTICS OF SPECIFIC SENSOR SYSTEMS

The amperometric sensor requires only small amounts of power and is relatively small. This makes it ideal for portable and fixed-site analyzer applications. The four characteristics that limit the successful application of the amperometric gas sensor technology are: (1) stability of the electrochemical system with time and with environmental fluctuations, (2) the response time, (3) the specificity or selectivity (*i.e.*, degree to which one reaction occurs relative to the others which occur in the same sensor), and (4) the lower detection limit [*i.e.*, signal to noise (S/N) and/or signal to background (S/BKG) ratio]. The following discussion addresses the relationship between the desired analytical characteristics and sensor design as well as suggesting ways that have been used to overcome sensor limitations. The response time of the sensor has been discussed in previous sections.

Lower detection limit

The lower detectable limit for a particular gaseous compound is related to several factors including mass transport of the compound within the detection system, electrocatalytic activity (the catalyst material, form, and potential of operation), Faradaic equivalents per mole transferred during reaction, analyte solubility and mobility in the electrolyte, the physical geometry of the sensor, and the "method" of operation (including semipermeable membranes or filters). It is the optimization of these parameters which leads to the maximum S/N for a given analytical system.

Sensitivity is typically not limited by the Faradaic or electrocatalytic signal. For example, using Faraday's law [equation (16)], the current achieved (*i.e.*, sensitivity) by reacting a one ppm CO/air mixture at 1% efficiency in a

Table 3. Examples of amperometric gas sensor reactions

Gas analyzed	Electrochemical reaction proposed	Electrocatalyst	Ref.
NO_2	$NO_2 + 2H^+ + 2e = NO + H_2O$	Au	60
CO	$CO + H_2O = CO_2 + 2H^+ + 2e$	Pt	8
H_2	$8\ H_2 + 4H_2O = 8\ O_4^{2-} + 10H^+ + 8e$	Au	14
MMH	$(CH_3)N_2H_3 + 4OH^- = CH_3OH + N_2 + 3H_2O + 4e$	Au	21
NO	$NO + 2H_2O = NO_3^{2-} + 4H^+ + 3e$	Au	61
O_2	$1/2\ O_2 + 2H^+ + 2e = H_2O$	Au, Ag, Pt	62, 63
CO_2	$CO_2 + H_2O + 2e = HCOO^- + O - H^-$	Ag	32, 33
N_2O	$N_2O + H_2O + 2e = N_2 + 2OH^-$	Ag,Pt	33, 59

gas stream of 600 cm^3/sec would be *ca* 1 μA. Clearly, a current of 1 μA can be easily measured with existing electronic capabilities. However, the background current and fluctuations thereof cause most sensors to have a detection limit in the low ppm range. Thus, the practical lower detection limit for most sensors is the relatively large magnitude of the background and noise current and not the size of the signal.

The possible causes of background current in amperometric gas sensors can include:

1. impurities in the electrolyte such as traces of dissolved oxygen, and/or slow oxidation or reduction of solvent at the sensing electrode, such as the slow evolution of hydrogen or oxygen from an aqueous solution,
2. corrosion of the electrode, such as the slow growth of the oxide layer on the surface of a noble or passivated metal electrode catalyst in the anodic potential range, and
3. diffusion of the reactant or reaction products from the counter electrode, such as the diffusion of dissolved peroxide toward the sensing electrode from an oxygen-reducing counter electrode.

Lower detection limits for current amperometric gas sensors has been extended to ppb levels for certain analytes like NO_2,[10,35,41,49,60] Cl_2,[29] and H_2S.[11]

Selectivity

Typically, ppm levels are easily analyzed by an amperometric gas sensor. Interferences can be generally kept to an acceptable level either by selecting the proper electrocatalytic conditions or by using a selective adsorbent in the instrument inlet to remove undesirable electrochemically active contamination. The selectivity of amperometric gas sensors can be improved by careful manipulation of thermodynamic and/or kinetic reaction parameters. Examples have been discussed[8,11] and a brief example is offered here. Carbon monoxide oxidation occurs on a platinum electrocatalyst at 0.9–1.5 volts *vs.* NHE. However, the CO reaction proceeds 100 to 1000 times slower on a gold electrocatalyst. On the contrary, H_2S reactivity is high for both Au and Pt electrocatalysts. Thus, H_2S can be monitored even in the presence of CO by using a gold electrocatalyst. This is an example of kinetic selectivity. The NO oxidation reaction on gold does not occur at potentials below about 1.0 volt *vs.* NHE, but NO_2 can be reduced at potentials about 0.8 volts *vs.* NHE. Thus, NO_2 can be detected even in the presence of NO using a gold electrocatalyst operated at 0.8 volts *vs.* NHE. This is an example of thermodynamic selectivity with the constant potential amperometric gas sensor. Favorable kinetics or thermodynamics are the only two sources of inherent sensor selectivity. All methods of achieving selectivity can be put into these categories except those involving external devices (*e.g.*, pre-filtration or pre-treatment of the gaseous analyte prior to sensor entry).

Precision and accuracy

The accuracy of amperometric gas sensors is typically limited by the preparation of standards while the precision is a function of the operating conditions, the concentration of analyte, and the care taken by the operator.

In field monitoring situations there is often no opportunity for repeat readings and, indeed, the sensor must often operate unattended gathering data over a long period of time. Instrument precision must be known in order to quantify the analyte and assess the reliability of each independent measurement. The precision of amperometric gas sensors for a variety of gases has been evaluated and for signals that are 10–100 times larger than the background current, precision is typically within 1% of the signal.[7,11,20]

The accuracy of an individual datum point is often limited by the ability to calibrate the instrument. Calibration is achieved when an unambiguous relationship between the instrument signal and the actual gas concentration is established. For an electrochemical sensor system we may assume that the response *vs.* concentration function is linear (if the sensor materials and geometry are properly chosen) over about two orders of magnitude. Typical least squares representations of signal *vs.* concentration data produce nearly ideal slopes and intercepts with correlation coefficients of near unity.[55,64]

The range of linear response of the sensor varies with the particular gas or vapor being monitored. In most cases linear response is observed in the low ppm range and may extend to as high as 5000 and 10,000 ppm. For example, the linear response of a hydrogen sulfide sensor was evaluated[11] in the concentration range 0–0.277 ppm and 0–153 ppm and the signal is directly proportional to the H_2S concentration.

Often determinations of linearity are limited by the ability to synthesize an accurate calibration for gas mixtures. For highly reactive gas mixtures such as hydrazine, it is difficult to prepare an accurate gas mixture even under ideal laboratory conditions. NBS gas standards are available with an accuracy certified as $\pm 2\%$ for certain mixtures such as CO/air.

In conclusion, the accuracy, precision, and typical linear response of the amperometric gas sensor system is very important because it makes the following possible:

1. reliable and accurate instrument calibration with only a single datum point, *i.e.*, only one standard gas sample is necessary making field use simple,
2. simplified electronic design to measure, amplify, record, manipulate, and report (display) the output signal, and
3. simple additivity of responses when used in a sensor array where one records responses to various compounds and simple mixtures of compounds.

Stability

The stability of an amperometric gas sensor relates to its ability to retain its original response characteristics over long time intervals and under changing environmental conditions. Stability is generally divided into short-term fluctuations and long-term fluctuations. The stability for certain sensors has been reported.[10,11,20,21]

The causes of zero drift (*i.e.*, drift in background current) and span drift (*i.e.*, fluctuations in signal magnitude or changes in the steady-state current) are not well characterized. It is known that drift can be caused by temperature fluctuations, sensor operation at extreme relative humidities over long time periods (under or over-humidification of the membrane or the gas-diffusion electrode), catalyst degeneration or fouling, and electrolyte contamination. Besides, if the counter electrode reaction consumes an electroactive substance of limited supply (such as the metal/metal oxide electrode), the lifetime of the sensor will be limited and extreme drift can be observed near the end of the sensor life. Even the input current of an operational amplifier can exhaust the capacity of a small size reference electrode after long term continuous operation.[65] In spite of such problems, amperometric sensors may last many years in demanding industrial environments and retain good analytical performance.

RECENT ADVANCES AND FUTURE POSSIBILITIES

It is inevitable that advanced amperometric gas sensors will be designed which provide improvements in practical detection limits, stability, and selectivity as well as in the total number of compounds which can be measured.[62] The improvements will be a result of an extension of our knowledge about these sensors as well as improvements in the materials, geometries, and electroanalytical methods that become known and used.

Electrochemical sensor arrays

Amperometric gas sensors respond to a limited number of compounds and each one responds with its own characteristic selectivity. One way to overcome these limitations and improve the sensor's versatility and selectivity is to construct sensor arrays made from sensors with the most orthogonal response possible.[66,67]

Information is created in a sensor by its reaction to a chemical stimulus. This reaction of the sensor to the type of chemical and its concentration creates an analytical signal that is transduced into an electronic signal by the sensor. More specifically, if chemicals are to be identified on the basis of their relative electrochemical reactivities, then the sensor array must be designed so that the information necessary to accomplish this task is generated. It must contain sensors that record a different electrochemical response for each chemical species. Thus, to achieve the most effective array for a given problem, the sensor array and the analytical problem must be considered together.

A sensor array consisting of four electrochemical sensors and two hot wire filaments has been evaluated.[68–70] The array was constructed to both identify and quantify a toxic chemical vapor in a few minutes using a portable, battery-operated, lightweight instrument. The electrochemical sensors are combined with a heterogeneous catalyst (which transforms non-electroactive compounds into electroactive fragments) that allows the electrochemical sensors to respond to a very broad range of chemicals. The four electrochemical sensors were chosen to have two working electrodes of Au and two of Pt. One Au and one Pt electrode are operated at anodic potentials to facilitate oxidations and one of each catalyst are operated at cathodic potentials to facilitate reductions. By comparing the signals from the sensors in the array, one can tell whether the sample contains electro-

oxidizable or electro-reducible constituents. The size of the signal is related to the analytes electrokinetic processes, pyrolysis kinetics in the filament reactor, and the analyte concentration. Thus, the signals from these sensors provide a set of chemical parameters related to the vapor's catalytic and electrocatalytic properties. Hence, the term "chemical parameter spectrometry" or CPS was chosen to describe this technique. The term "pyrolysis amperometry" has also been used[71] in connection with the detection of gases and vapors by this technique, however, "catalytic oxidation" followed by amperometric detection of the products is actually occurring.

It is possible to "tune" the array for sensitivity to specific reagents by choosing appropriate sensors and useful operating conditions. The technique of utilizing sensor arrays is effective when coupled with computer data acquisition and algorithms for data analysis[72] (*e.g.*, pattern recognition methods). Multivariate statistical methods can be used to evaluate how well the array can identify compounds and suggest improved approaches as well as be an operational tool for field instrumentation. Recent sensor arrays have been combined with neural networks to simulate an artificial nose.[73]

Coulometry

Amperometric gas sensors produce data that can be interpreted coulometrically. The theory and method of a "dynamic" coulometric technique using amperometric gas sensors has been discussed.[47,48] It can take several forms, but usually uses two amperometric gas sensors (a and b) with sample chambers connected in series with a means for reversing the direction of gas flow through the sensors. By measuring the steady-state (currents) signals from both sensor electrodes with the gas flow first in a forward and then in a reverse direction, the absolute concentration of the reactant species can be calculated by using the following equation:

$$X_{af} = CI_{af}I_{br}(I_{af} + I_{bf})/(I_{af}I_{br} - I_{ar}I_{bf}) \quad (19)$$

where $C = RT/nFPV$ and the subscripts f and r refer to the forward and reverse flow directions, I is the measured current, P is the sample pressure, V is the volumetric flowrate, and X_{af} is the concentration of species X entering sensor "a" in the forward direction, and so forth.

The technique assumes 100% Faradaic efficiency for all analyte arriving at the sensing electrode and proportionality of the current signals to the reactant concentration for both sensors, *i.e.*, linear sensor response *vs.* concentration. This method is a fast and simple way to use the gas sensor to determine the concentration in an unknown sample gas. Since the concentration is determined from a coulometric calculation, it eliminates the need for a reference gas standard and can serve as a primary method of measurement of concentration for unknown gas samples. The method can be applied in modified form to the analysis of various electrochemically active species in electrolyte solutions.

Future possibilities

The continuing publications concerning chemical sensors and in particular, amperometric sensors[74–76] underscore the continuing importance of this electroanalytical approach in the fabrication of practical gas sensors. Advanced amperometric gas and vapor monitors will be designed which incorporate improvements in present practical detection limits as well as in the total number of compounds which can be measured.[62] The field of sensors is interdisciplinary and future advances are likely to occur by combinations of advanced technologies in other fields with the known useful electrochemistries.

Microelectronics has produced a variety of physical and chemical sensors but only very few can be considered amperometric and these structures usually do not contain the electrolyte. Most microsensors are potentiometric and the more common amperometric gas sensors (*e.g.*, CO, H_2S, NO, NO_2, *etc.*) have not yet been microfabricated. It is believed that microelectronic fabrication techniques are well suited for the production of amperometric gas sensors. The need for a geometrically well-defined sensing electrode surface area is well-recognized. Photolithographic reduction and other mask making techniques can be used to produce identical, highly uniform and well-defined electrode structures. Thin and thick film metallization as well as sputtering techniques can be applied to produce the metallic electrode elements. Chemical and plasma etching techniques can be used to delineate geometrically well-defined electrode surfaces. These microelectronic fabrication techniques provide a fruitful way to prepare sensors with specific geometries. These techniques have only begun to be explored at this time.[54]

Sensor arrays are not well developed but hold promise to vastly improve sensor selectivity especially when combined with advanced computational techniques like neural networks. New electrolyte materials must be found so that integrated sensor structures can be built. This is an exciting time for sensor research and, in the near future, amperometric sensors will be more sensitive, more selective, smaller, and less expensive.

REFERENCES

1. L. C. Clark, R. Wolf, D. Granger and Z. Taylar, *J. Appl. Physiol.*, 1953, **6**, 189.
2. L. C. Clark, *Trans. Am. Soc. Art. Int. Org.*, 1956, **2**, 41. US Patent No. 2,913,386, 1959.
3. I. Fatt, *The Polarographic Oxygen Sensor*, CRC Press, 1974.
4. Y. H. Lee and G. T. Tsao, *Adv. Biochem. Engineering*, 1979, **13**, 35.
5. D. T. Sawyer, R. S. George and R. C. Rhodes, *Anal. Chem.*, 1959, **31**, 2.
6. H. G. Oswin and K. F. Blurton, US Patent No. 3,776,832, *Electrochemical Detection Cell*, Dec. 4, 1973.
7. H. W. Bay, K. F. Blurton, H. C. Lieb and H. G. Oswin, *Nature*, 1972, **240**, 52.
8. K. F. Blurton and J. M. Sedlak, *J. Electrochem. Soc.*, 1974, **121**, 1315.
9. H. W. Bay, K. F. Blurton, J. M. Sedlak and A. M. Valentine, *Anal. Chem.*, 1974, **46**, 1837.
10. J. M. Sedlak and K. F. Blurton, *J. Electrochem. Soc.*, 1976, **123**, 1476.
11. *Idem*, *Talanta*, 1976, **23**, 445.
12. J. M. Sedlak and K. F. Blurton, *ibid.*, 1976, **23**, 811.
13. K. F. Blurton and J. R. Stetter, *J. Chromatogr.*, 1978, **155**, 35.
14. Dynasciences Corp., US Patent No. 3,622,488, Nov. 23, 1971.
15. R. V. Marcote, R. Chand and T. H. Johnston, *Proc. ISA Analys. Instr. Symp. Instrument Soc. of America*, p. 31. Pittsburgh, 1973.
16. C. Fabian, *Electrochim. Acta*, 1985, **20**, 863.
17. B. Premysl and S. Bruckenstein, *Anal. Chem.*, 1980, **52**, 1183.
18. *Idem*, *ibid.*, 1989, **52**, 2207.
19. D.-M. Pfenning, J. Deprez and D. Kitzelmann, *Ber. Bunsen. Phys. Chem.*, 1990, **94**, 988.
20. J. R. Stetter, K. A. Tellefsen, R. A. Saunders and J. J. DeCorpo, *Talanta*, 1979, **26**, 799.
21. J. R. Stetter, K. F. Blurton, A. M. Valentine and K. A. Tellefsen, *J. Electrochem. Soc.*, 1978, **125**, 1804.
22. J. C. Schmidt, C. S. Sands and D. N. Campbell, US Patent No. 4,500,391, Feb. 19, 1985.s
23. A. B. LaConti and H. J. R. Maget, *J. Electrochem. Soc.*, 1971, **118**, 506.
24. A. B. LaConti, M. E. Nolan, J. A. Kosek and J. M. Sedlak, ACS Symposium Series No. 149, *Chemical Hazards in the Workplace* (ed.), by Chondhary G., p. 551 (1981).
25. A. B. LaConti, R. M. Dempsey and M. E. Nolan, US Patent No. 4,171,253, Oct. 16, 1979, *Chem. Abstr.*, **90**, 60474a; A. B. LaConti, US Patent No. 4,025,412, May 24, 1977, *Chem. Abstr.*, **87**, 87843h.
26. H. Yen and J. Lu, *Sensors and Actuators*, 1989, 19.
27. R. L. Cook, R. C. MacDuff and A. F. Sammells, *J. Electrochem. Soc.: Electrochemical Science and Technology*, 1988, **135**, 1470.
28. O. J. Enea, *Electrochem. Soc.: Accelerated Brief Comm.*, p. 1601, June 1988.
29. M. L. Langhorst, *Am. Ind. Hyg. Assoc. J.* 1982, 43.
30. T. Otagawa, S. Zaromb and J. R. Stetter, *Sensors and Actuators*, 1985, **8**, 65.
31. *Idem*, *J. Electrochem. Soc.*, 1985, **132**, 2951.
32. W. J. Albery and P. Baron, *J. Electroanal. Chem.*, 1982, **138**, 87.
33. W. J. Albery and G. D. Haggett, *Electrochem. Detectors*, T. H. Ryan (ed.), p. 1. Plenum Press, 1984.
34. J. R. Stetter, *Instrumentation to Monitor Chemical Exposure in the Synfuel Industry*, Annals American Conf. of Governmental and Industrial Hygienists 11, 225–269, 1984.
35. W. R. Penrose *et al.*, Proc. EPA/AWMA Symposium on Total Exposure Assessment Methodology, Tropicana Hotel, Las Vegas, NV, Nov. 27.30 (1989).
36. Z. Cao, W. J. Buttner and J. R. Stetter, *Electroanalysis*, 1992, **4**, 253.
37. C. E. W. Hahn, *J. Phys. E.: Sci. Instrum*, 1980, **13**, 470.
38. A. W. Myers, J. A. Mayer, C. E. Rogers, V. Stannetl and M. Szware, Tappi. Monograph Series, Vol. 23, 1962.
39. H. Heitmann, R. G. Buckles and M. B. Laver, *Respir. Physiol.*, 1967, **3**, 380.
40. M. B. Laver and A. Seifen, *Anesthiol.*, 1963, **26**, 73.
41. S. C. Chang and J. R. Stetter, *Electroanalysis*, 1990, **2**, 359.
42. E. A. Ticianelli, C. R. Derouin, A. Redondo and S. Srinivasan, *J. Electrochem. Soc.*, 1988, **135**, 2209.
43. W. Poir, T. E. Springer and S. Srinivasan, *ibid.*, 1989, **136**, 644.
44. A. Katayama-Aramata, H. Nakajima, K. Fujikawa and H. Kita, *Electrochim. Acta*, 1983, **28**, 777.
45. H. Kita, K. Fujikawa and H. Nakajima, *Electrochim. Acta*, 1984, **29**, 1721.
46. H. Nakajima, Y. Takakuwa, H. Kikuchi, K. Fujikawa and H. Kita, *ibid.*, 1987, **32**, 791.
47. J. R. Stetter and S. Zaromb, *J. Electroanal. Chem.*, 1983, **148**, 271.
48. J. R. Stetter, S. Zaromb and D. O'Gorman, *J. Electroanal. Chem.*, 1983, **148**, 279.
49. J. R. Stetter and S. C. Chang, *Portable Monitor for the Measurement of Indoor NO_2 Concentrations*, Proc. Indoor Air '87, Berlin, West Germany, August, 1987.
50. K. H. Mancy, D. K. Okon and C. N. Reilley, *ibid.*, 1965, **4**, 65.
51. M. Mochizuki, *Monograph Series Res. Inst. Appl. Electron* 1951, **2**, 39.
52. C. E. W. Hahn, PhD Thesis, University of Oxford, 1974.
53. O. J. Jensen, T. Jacobsen and K. Thomson, *J. Electroanal. Chem.*, 1978, **87**, 203.
54. J. R. Stetter, G. J. Maclay and W. J. Buttner, *Microfabricated Amperometric Gas Sensor*, IEEE Trans. on Electron Devices 35(6), 793 (1988).
55. P. H. Rieger, *Electrochemistry*, Prentice Hall, Englewood Cliffs, N.T., 1987.
56. C. Berger, *Handbook of Fuel Cell Technology*, Prentice-Hall, 1968.

57. J. O. M. Bockris and S. Srinivasan, *Fuel Cells: Their Electrochemistry*, McGraw-Hill, 1969.
58. W. N. Brooks, S. P. Gibson and C. E. W. Hahn, *J. Appl. Physiol.*, 1978, **45**, 637.
59. C. S. Cha, P. F. Liu, Z. B. Chou, Z. G. Wu and W. Y. Lu, *J. Electroanal. Chem.*, 1988, **248**, 69.
60. Dynasciences Corp., US Patent No. 3,622,487, Nov. 23, 1971.
61. D. Dutta and D. Lundolt, *J. Electrochem. Soc.*, 1972, **119**, 1320.
62. J. R. Stetter, ACS Symposium Series No. 309, p. 299. 1986.
63. W. J. Baker, J. F. Combs, T. L. Zinn, A. W. Woting and R. F. Wall, *Ind. Eng. Chem.*, 1959, **51**, 727.
64. D. A. Skoog, D. M. West and F. J. Holler, *Fundamentals of Analytical Chemistry*, pp. 1–47. Saunders, Philadelphia, U.S.A., 1988.
65. J. Y. Lucisano, J. C. Armour and D. A. Gough, *Anal. Chem.*, 1987, **59**, 736.
66. J. R. Stetter, S. Zaromb and M. W. Findlay, Jr., *Sensors and Actuators*, 1984, **6**, 269.
67. J. R. Stetter and S. Zaromb, *Sensors and Actuators*, 1984, **6**, 225.
68. J. R. Stetter, S. Zaromb, W. R. Penrose, M. W. Findlay, T. Otagawa and A. J. Sincali, *Proc. Hazardous Materials Spills Conf.*, J. Ludwigson (ed.), 1984.
69. J. R. Stetter, W. R. Penrose, S. Zaromb and J. O. Stull, *Anal. Instrum.*, 1985, **21**, 163 (1985).
70. J. R. Stetter, W. R. Penrose, S. Zaromb, D. Christian and T. Otagawa, *Proc. 2nd Annual Tech. Seminar on Chem. Spills*, 1985.
71. J. Unwin and P. T. Walsh, *Sensor and Actuators*, 1989, **17**, pp. 575–581.
72. J. R. Stetter, P. C. Jurs and S. L. Rose, *Anal. Chem.*, 1986, **58**, 860.
73. J. R. Stetter, in *Sensors and Sensory Systems for an Electronic Nose*, J. W. Gardner and P. N. Bartlett (eds.), Kluwer Academic Pubs., Dordrecht, The Netherlands, pp. 273–301. 1992 [ISBN 0-7923-1693-2].
74. T. T. Moriizumi, I. Takatsu and K. Ono, *Proc. of the 2nd Int. Meeting on Chemical Sensors*, 1986, p. 647.
75. *Chemical Sensors*, T. E. Edmonds (ed.), Chapman and Hall, N.Y., 1988.
76. *Biosensors Fundamentals and Applications* by A. R. F. Turner, I. Karado and S. Wilson, Oxford University Press, Oxford, England, 1987.

Talanta, Vol. 40, No. 4, pp. 479–484, 1993
Printed in Great Britain.

0039-9140/93 $6.00 + 0.00

ESTIMATION OF pH AND AUTOPROTOLYSIS CONSTANTS IN MIXTURES OF ALIPHATIC AMIDES WITH WATER: MEDIUM EFFECT ON THE 4-AMINOAZOBENZENE SYSTEM

AGUSTIN G. ASUERO,* MARIA A. HERRADOR and A. GUSTAVO GONZALEZ
Department of Analytical Chemistry, Faculty of Pharmacy, The University of Seville, 41012-Seville, Spain

(*Received* 24 *March* 1992. *Revised* 14 *August* 1992. *Accepted* 26 *August* 1992)

Summary—Correction factors to the glass electrode and autoprotolysis constants of mixtures of aliphatic amides with water: *N,N*-dimethylformamide (DMF), *N,N*-dimethylacetamide (DMA), *N*-methylformamide (NMF), *N*-methylacetamide (NMA), formamide (F) and acetamide (A), have been determined. The acidity constants of 4-aminoazobenzene referred to the standard state of the mixtures of these aliphatic amides with water as well as the medium effect on the 4-aminoazobenzene system have been evaluated from spectrophotometric measurements.

Amide–water mixtures are useful polar reaction media and solvents for a variety of purposes. In spite of this, there is relatively little data[1–4] available on the analytical use of mixtures of aliphatic amides with water. Correction factor to be made to the glass electrode, autoprotolysis constants and acidity constants of 4-aminoazobenzene (HB) in mixtures of aliphatic amides with water: *N,N*-dimethylformamide (DMF), *N,N*-dimethyl-acetamide (DMA), *N*-methylformamide (NMF), *N*-methylacetamide (NMA), formamide (F) and acetamide (A), have been evaluated in this paper. An attempt has been made to interpret the medium effects on the basis of hydrophobic interactions.

EXPERIMENTAL

Apparatus

All titrations were made with a Crison digilab 517 pH-meter and an Ingold electrode (order No. 0402311) assembly (glass–AgCl/Ag) (CH-8902 Urdorf/Switzerland). In order to avoid the glass membrane dehydration, the electrode was soaked in water when not in use. Prior to the measurement of pH, the electrode was soaked in a solution of the desired solvent composition. Titration vessels used consisted of tall beakers sealed into a water jacket through which water circulated from a Techne C-100 water bath. Temperature was controlled at $25 \pm 0.1°$ by means of a Selecta 320-R water bath. Titrations were carried out by using 2.0-ml micro burette with magnetic stirring. In the determination of densities, a Paar DMA 60 densimeter fitted with a Paar DT 100-20 densitothermometer, a Tecam 1000 heat interchanger and a Techne C-400 circulator were employed.

A Spectronic 2000 Bausch & Lomb spectrophotometer equipped with silica cells of 1-cm path length was used for the absorbance measurements. 4-Aminoazobenzene was synthesized according to the method indicated by Vogel.[5] The crude product was recrystallized from methanol and its melting point was 127° (reported value 128°). The purity of the dye was checked by thin layer chromatography as described by Vytras *et al.*[6] Solutions of 4-aminoazobenzene at 0.1% v/v in the various pure liquid amides were prepared. In the case of acetamide, a solution containing 50 mg of 4-aminoazobenzene in 50 ml of 10*M* acetamide in water was employed.

Reagents

N,N-Dimethylformamide, *N,N*-dimethylacetamide, *N*-methylformamide and *N*-methylacetamide (E. Merck Darmstadt), acetamide (Merck Schuchardt) and formamide (Normasolv, Ferosa, Barcelona) were stored in 4 Å molecular sieves for at least one week. Analytical reagent potassium monohydrogenphthalate (Riedel–Häen) was used in the

*Author for correspondence.

Table 1. Relative permittivities[8] of different water–aliphatic amide mixtures at 25°

%, v/v	DMF	NMF	F	DMA	NMA	%, mol.	A
10	77.32	80.73	82.82	76.62	79.27	4.96	81.67
20	74.86	83.62	87.43	74.62	79.96	9.83	84.49
30	72.40	87.11	93.20	72.30	81.36	14.60	86.79
40	69.52	91.47	97.23	69.47	83.42	19.30	88.33
50	65.95	96.93	101.79	66.39	86.18	23.90	88.49
60	61.74	103.89	105.12	62.70	89.92	28.45	90.25
70	56.73	113.04	110.00	57.99	95.93	32.90	90.64
80	51.04	126.77	111.28	52.46	105.88		

standardization of alkaline solutions. Potassium chloride (Merck, Darmstadt) was used for the adjustment of ionic strength.

Procedures

Correction factors. In 50-ml standard flasks prepare three solutions containing a suitable volume (or weight in the case of acetamide) of amide, 1, 2.5 and 5 ml of a 0.01064*M* solution of hydrochloric acid, respectively, and distilled water to the mark. Measure the pH at $25 \pm 0.1°$.

Autoprotolysis constants. In a 100-ml standard flask add a suitable volume (or weight in the case of acetamide) of amide, 10 ml of 1*M* potassium chloride, 1.3 ml of 1*M* hydrochloric acid and distilled water to the mark, at $25 \pm 0.1°$. Transfer 75 ml of this solution to the titration vessel and titrate with 1*M* potassium hydroxide. Measure the pH at $25 \pm 0.1°$.

Procedure for the evaluation of acidity constants. Solutions for absorbance and pH measurements were prepared in 25-ml standard flasks by mixing 1 ml of $7.61 \times 10^{-4}M$ stock solution of 4-aminoazobenzene in the appropriate amide, 2.5 ml of 1*M* potassium chloride, the necessary volume of pure amide to give the required solvent composition in the final mixture, a few drops of hydrochloric acid or sodium hydroxide at different concentrations and distilled water to the mark. Absorbance was measured at 489, 496 and 505 nm, against a solvent blank and the pH checked after the absorbance measurements. The temperature was kept at $25 \pm 0.1°$.

RESULTS AND DISCUSSION

Reversibility of electrode assembly

Plots of potential cell against pH-meter reading (in mV) for each solvent mixture at the various acid concentrations and ionic strength tested give straight lines whose slope values (from 60.15 to 58.32) are very close to the theoretical nernstian slope (k) value of 59.16. By using the t-test[7] on the slopes one may assume that the behavior of the electrode is reversible.

Correction factors

The relative permittivity of the mixtures of amides with water have been previously reported[8] (Table 1). The amide molar fraction X_{AM} was determined from

$$X_{AM} = \frac{1}{1 + \left(\frac{100 d_m}{V_{AM} d_{AM}} - 1\right)\frac{MW}{18}} \qquad (1)$$

where d_{AM} and d_m are the densities of the pure amide[9] and the mixture containing V_{AM} percentage v/v of amide, respectively, and MW is the amide relative molar mass. The d_{AM} values obtained for the different mixtures studied are compiled in Table 2.

The correction factors to the glass electrode, δ, for transforming the pH-meter readout, R, (when the calibration is done with aqueous buffers) in the logarithm of the proton activity in the studied medium, pH*, $\delta = R - pH^*$, obtained for the different

Table 2. Density of different water–aliphatic amide mixtures at 25° (d_4^{25})

%, v	DMF†	NMF	F	DMA	NMA	%, mol.	A
10	0.9964	0.9984	1.0128	0.9951	0.9957	4.96	1.0032
20	0.9961	0.9998	1.0282	0.9956	0.9967	9.83	1.0096
30	0.9959	1.0012	1.0427	0.9963	0.9984	14.60	1.0155
40	0.9956	1.0026	1.0561	0.9972	0.9999	19.30	1.0215
50	0.9950	1.0040	1.0693	0.9968	1.0002	23.90	1.0273
60	0.9928	1.0054	1.0823	0.9953	0.9980	28.45	1.0329
70	0.9878	1.0068	1.0950	0.9886	0.9931	32.90	1.0384
80	0.9789	1.0082	1.1060	0.9790	0.9849		

†Taken from Ref. 2.

Table 3. Correction factors to the glass electrode for several water–aliphatic amide mixtures at 25°

%, v/v	DMF*	NMF	F	DMA	NMA	%, mol.	A
10	0.088 ± 0.099	0.820 ± 0.025	1.815 ± 0.580	0.030 ± 0.004	0.021 ± 0.010	4.96	0.178 ± 0.011
20	0.093 ± 0.006	1.169 ± 0.040	2.656 ± 0.618	0.150 ± 0.014	0.176 ± 0.040	9.83	0.299 ± 0.029
30	0.182 ± 0.018	1.513 ± 0.070	3.244 ± 0.522	0.342 ± 0.007	0.358 ± 0.004	14.60	0.603 ± 0.061
40	0.309 ± 0.005	1.803 ± 0.099	3.645 ± 0.437	0.509 ± 0.008	0.525 ± 0.003	19.30	0.813 ± 0.035
50	0.386 ± 0.010	2.167 ± 0.134	4.063 ± 0.333	0.683 ± 0.005	0.735 ± 0.010	23.90	1.091 ± 0.147
60	0.476 ± 0.011	2.539 ± 0.156	6.504 ± 0.144	0.854 ± 0.010	0.958 ± 0.010	28.45	1.062 ± 0.114
70	0.536 ± 0.007	2.978 ± 0.155	4.766 ± 0.111	1.019 ± 0.008	1.182 ± 0.030	32.90	1.152 ± 0.103
80	0.491 ± 0.009	3.460 ± 0.175	4.917 ± 0.223	1.098 ± 0.012	1.425 ± 0.040		

*Taken from Ref. 2.

solvent mixtures assayed are compiled in Table 3. The relatively small standard deviation observed in most cases indicates that the liquid junction potential is practically constant[10] for each solvent composition tested. However, the reproducibility of measurements in formamide–water mixtures is somewhat poor, and measurements in water–NMF and water–A at high v/v amide to water ratio (or w/v in the case of A) also suffer some dispersion.

This behavior may be qualitatively explained because all mixtures studied are more basic than pure water; the hydrogen ion is expected to be more stabilized in these media, owing to specific interactions between the hydrogen ions and the basic amides. The free standard energy of transfer from water to the mixed solvent, $\Delta G_t^0(H^+)$, will be negative and hence, the medium effect, $\log f_H$, also $[\Delta G_t^0(i) = 2.303\ RT \log f(i)]$.

The presence of alkyl substituents on a nitrogen atom enhances its basicity. Therefore, the theoretical order of basicity of amides studied—which is based in the facility to donate the electron pair of the nitrogen atom—should be

$$\text{DMF} > \text{NMF} > \text{F} \quad \text{DMA} > \text{NMA} > \text{A}.$$

However, an opposite arrangement is found, surprisingly, if we take into account "the virtual basicity" indicated by the values of δ

$$\text{DMF} < \text{NMF} < \text{F} \quad \text{DMA} \simeq \text{NMA} < \text{A}.$$

This fact may be attributed to some other interactions that take place between the hydrogen ions and the various solvent species such as ion–multipole interactions, structural effects or other solvatation effects. Nevertheless, a positive value of δ does not necessarily imply a negative medium effect on the hydrogen ions since the liquid junction potentials are unknown.

Autoprotolysis constants

The pK_s values obtained for the different amide–water mixtures are compiled in Table 4. In the case of water–F mixtures, the cologarithm of the autoprotolysis constant passes through a minimum as the percentage of liquid amide in the mixed solvent increases, unlike the behaviour shown by the other water–amide mixed-solvent mixtures.

The standard deviations of the pK_s values were smaller than 0.04. It can be shown (as expected) that a minimum in the pK_s value is found between pure water and 10% v/v of amide composition (0.0–4.96% molar in the case of acetamide) with the exception of the water–F system. The influence of the relative permittivity of the medium on the autoionization of mixed aliphatic solvents has been envisaged. Several different types of correlation[11,12] between the autoprotolysis constants and acidity constants of weak acids, respectively, and solvent composition have been suggested. The Born equation[13] predicts a

Table 4. Cologarithm of the autoprotolysis constants of water–aliphatic amide solvents

%, v/v	DMF	NMF	F	DMA	NMA	%, mol.	A
10	13.77	13.98	13.50	13.60	13.75	4.96	13.72
20	13.90	14.25	13.27	13.65	13.94	9.83	13.80
30	14.13	14.32	11.68	13.91	14.07	14.60	13.92
40	14.45	14.46	11.72	14.09	14.19	19.30	14.02
50	14.85	14.79	12.04	14.42	14.45	23.90	14.17
60	15.35	15.15	12.20	14.82	14.77	28.40	14.32
70	16.14	15.68	12.42	15.50	15.22	32.90	14.44
80	17.28	15.92	12.71	16.36	15.72		

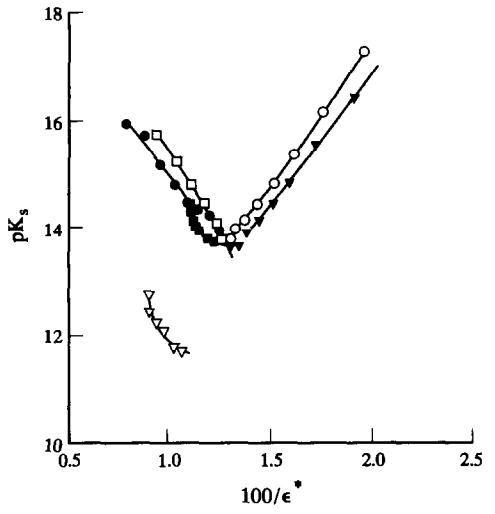

Fig. 1. Dependence of pK_s with the reciprocal value of the permittivity for several water–formamide derivative mixtures: (○) water–DMF mixtures, (●) water–NMF mixtures, (▽) water–F mixtures, (▼) water–DMA mixtures, (□) water–NMA mixtures and (▼) water–A mixtures.

linear relationship when the pK_s is plotted against the reciprocal of the permittivity. Plots of this kind are depicted in Fig. 1, showing a linear behavior with the exception of the A and F–water mixtures. Thus, in a first approach this fact may suggest a predominance of electrostatic effects on the ionization of aqueous mixtures of DMF, NMF, DMA and NMA.

Evaluation of acidity constants

4-Aminoazobenzene may undergo a prototropic tautomeric solvent dependent azonium-ammonium[14] equilibria

$$\underset{\mathbf{I}}{H_3N^+ - C_6H_5 - N = N - C_6H_5} \rightleftarrows \underset{\mathbf{II}}{H_2N - C_6H_5 - N = N^+H - C_6H_5}.$$

The S-shaped form of the absorbance versus pH* graphs obtained in all cases suggests a single ionization process. According to the basic properties of the mixed solvents studied and the greater facility of protonation of the amine–nitrogen with respect to the azonitrogen form I seems to be stabilized. Previous UV–visible and H^1 NMR spectra[15] of 4-aminoazobenzene and similar azodyes in polar solvents such as water–amide mixtures also indicates the potentially tautometric dye exists as true aminoazo species.

4-Aminoazobenzene in its ionization is quite strong and it is not entirely cationic even at pH 1. The pK_a^* (K_a^* being the acidity constant at the standard state of the mixed solvent) values in the media studied are collected in Table 5 and were spectrophotometrically evaluated[1] taking into account that the limiting absorbance of HB^+ is unavailable. The standard deviations were smaller than 0.06 except for the case of acetamide– and formamide–water mixtures whose values were somewhat superior.

Estimation of the medium effect

The solvent effect in the dissociation process of HB^+ can be expressed as follows[16]

$$\Delta G_t\,|HB^+/B|_{sys} = \Delta G_t^0(H^+) + \Delta G_t^0(B) - \Delta G_t^0(HB^+) = 2.303RT \log f\,|HB^+/B|_{sys}. \quad (2)$$

If we assume that the electrostatic effects may be estimated by using the Born model,[17] we have

$$\log f\,|HB^+/B|_{sys} = \log f_{non}\,|HB^+/B|_{sys} + \frac{Ne^2}{2}\left(\frac{1}{r_{H^+}} - \frac{1}{r_{HB^+}}\right) \times \left(\frac{1}{\epsilon^*} - \frac{1}{\epsilon}\right) = pK_a^* - pK_a \quad (3)$$

where $\log f_{non}\,|HB^+/B|_{sys}$ is the non electrostatic contribution to the medium effect.

Table 5. Acidity constants (pK_a^*) of the 4-aminoazobenzene system in water–aliphatic amide mixtures

%, v/v	F	NMF	DMF†	NMA	DMA	%, mol	A
10	1.02	1.83	—	2.65	2.61	2.90	2.64
20	0.19	1.47	2.45	2.46	2.30	5.80	2.50
30	−0.34	1.40	2.21	2.18	1.95	8.70	2.45
40	−0.87	0.81	1.99	2.01	1.65	11.60	2.31
50	−1.11	0.31	1.79	1.86	1.33	14.50	2.14
60	−1.62	0.00	1.56	1.37	0.98	17.40	2.10
70	−1.97	−0.50	1.20	1.21	0.53	20.30	1.92
80	−2.15	−1.14	1.07	0.95	0.14–0.05	23.20	1.73

†Taken from Ref. 1.

Table 6. Medium effects ($-\Delta pK_a$) on the AAB system† in the water-aliphatic amide mixtures studied

%, v/v	F	NMF	DMF§	NMA	DMA	%, mol.	A
10	1.93	1.12	—	0.30	0.34	2.90	0.31
20	2.76	1.48	0.50	0.49	0.65	5.80	0.45
30	3.29	1.55	0.74	0.77	1.00	8.70	0.50
40	3.82	2.14	0.96	0.94	1.30	11.60	0.64
50	4.06	2.64	1.16	1.09	1.62	14.50	0.81
60	4.57	2.95	1.39	1.52	1.96	17.40	0.85
70	4.92	3.45	1.75	1.74	2.42	20.30	1.03
80	5.10	4.09	1.88	2.00	2.81–2.90	23.20	1.22

†The pK_a value of aminoazobenzene in water was found to be 2.95.
§Taken from Ref. 1.

The medium effects in the various mixtures studied are reported in Table 6. The permittivity contribution depends on the difference in the ion sizes of H^+ and HB^+ ions. That the permittivity plays such a minor role in the dissociation process is confirmed by plotting ΔpK_a against the difference of reciprocal permittivity values $(1/\epsilon^* - 1/\epsilon)$ (Fig. 2). In the case of acetamide derivatives and DMF, non linear graphs are obtained. Nevertheless, though in the case of F and NMF solutions a linear plot is observed, the estimation of r_{HB}^+ (given that $r_H^+ = 1.7$ Å) yields meaningless results. This behaviour indicates that the non-electrostatic interactions will play a primary role. Since all ΔpK_a values in the different media are negative ($pK_a^* < pK_a$), taking into account the predominance of the non electrostatic terms, we may assume that

$$\log f_{non}\,|HB^+/B|_{sys} < 0 \qquad (4)$$

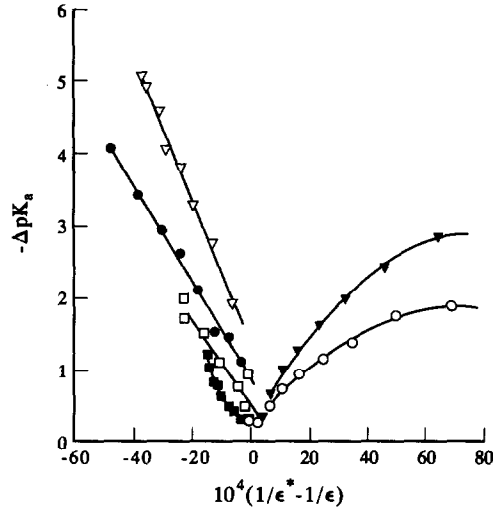

Fig. 2. Dependence of $-\Delta pK_a$ (medium effect) against 10^4 $(1/\epsilon^* - 1/\epsilon)$ for several water–formamide derivative mixtures: (○) water–DMF mixtures, (●) water–NMF mixtures, (▽) water–F mixtures, (▼) water–DMA mixtures, (□) water–NMA mixtures and (■) water–A mixtures.

and then

$$\Delta G_t^0(H^+) + \Delta G_t^0(B) - \Delta G_t^0(HB^+) < 0. \qquad (5)$$

The $\Delta G_t^0(H^+)$ values are negative because of the major basicity of partially aqueous mixtures with respect to pure water. Assuming[17] that the liquid junction potential is $\ll \delta$ we may calculate the $\Delta G_t^0(B) - \Delta G_t^0(HB^+)$ values. In all cases $\Delta G_t^0(B) < \Delta G_t^0(HB^+)$. Thus, the neutral species B is more stable than the charged one HB^+ in the solvent mixtures studied.

The 4-aminoazobenzene is sparingly soluble in water, but soluble in the water–aliphatic amide mixtures studied. Though a theoretical discussion concerning the specific solvation by part of the mixed solvents exceeds the frame of this paper, a brief discussion on the basis of the basic nature of cosolvent and hydrophobic interactions would explain the results obtained in a qualitative way.

According to the virtual basicity of cosolvents indicated above, and considering that this feature plays a capital role in the solvation process, the more basic the solvent mixture the more the 4-aminoazobenzene would display its acidic features (less pK_a value). Thus, at a first insight the acidity of 4-aminoazobenzene is expected to be in the same arrangement as the virtual basicity of cosolvents. This is found for the formamide family

$$F > NMF > DMF.$$

However, in the case of acetamide derivatives the sequence is

$$DMA > NMA > A.$$

In consequence, some other effects in addition to solvent basicity seem to play an important role in this context. The virtual basicity of the formamide family is hierarchically greater than that of the acetamide one. Accordingly so, the basicity may be considered as the most

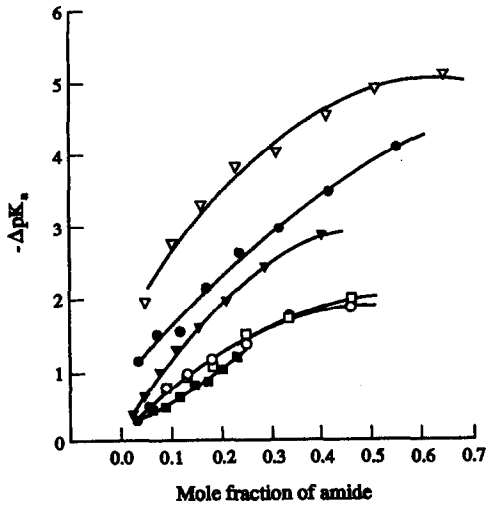

Fig. 3. Dependence of $-\Delta pK_a$ (medium effect) with the mole fraction of amide for several water–formamide derivative mixtures: (○) water–DMF mixtures, (●) water–NMF mixtures, (▽) water–F mixtures, (▼) water–DMA mixtures, (□) water–DMA mixtures and (■) water–A mixtures.

important factor for explaining the acidity of 4-aminoazobenzene in mixtures of F, NMF and DMF with water. Conversely, in the acetamide family, hydrophobic interactions would be competitive against basicity and the outcome agrees with the experimental arrangement.

Hydrophobic interactions contribute to a more negative value of medium effects.[1] These hydrophobic interactions occur between the "aniline moiety" of the uncharged 4-aminoazobenzene (B) and the methyl groups of the acetamide derivative (hydrophobic interactions cancel with the left hand ring in HB^+ and B species). Accordingly, the acidity of 4-aminoazobenzene will increase as the number of methyl groups in the amide molecule increases and therefore agrees well with the experimental sequence. Consequently, by hook or by crook the presence of aliphatic amides as cosolvents enhances the acidity of the 4-aminoazobenzene system. The plots of pK_a^* versus mole fraction of amide were non linear in all instances as shown in Fig. 3.

Acknowledgements—The financial assistance of the "Dirección General de Investigación Científica y Técnica de España" through Project PB-89-0630 is gratefully acknowledged.

REFERENCES

1. A. G. González, M. A. Herrador and A. G. Asuero, *Anal. Chim. Acta*, 1991, **246**, 429.
2. A. G. González, D. Rosales, J. L. Gómez-Ariza and A. G. Pérez, *Talanta*, 1986, **33**, 105.
3. A. G. González, D. Rosales, J. L. Gómez-Ariza and J. Fernandez Sanz, *Anal. Chim. Acta*, 1990, **228**, 301.
4. A. G. González., M. C. Mochón, J. L. Gómez-Ariza and A. G. Pérez, *ibid.*, 1991, **224**, 109.
5. A. I. Vogel, *A Textbook of Practical Organic Chemistry*, 4th Ed., p. 720. Longman, 1978.
6. K. Vytras, J. Kalous and J. Cerna-Frybortova, *Talanta*, 1990, **37**, 1025.
7. J. B. Kennedy and A. M. Neville, *Basic Statistics Methods for Engineers and Scientists*, 2nd Ed., Harper & Row, New York, 1976.
8. P. Rohdewald and M. Möldner, *J. Phys. Chem.*, 1973, **77**, 373.
9. The Merck Index, 8th Ed., Merck and Co., Rahway, New Jersey 1968.
10. K. Das, A. K. Das and K. K. Kundu, *Electrochim. Acta*, 1981, **22**, 54.
11. L. Sůcha and St. Kotrlý, *Solution Equilibria in Analytical Chemistry*, Van Nostrand Reinhold, London, 1972.
12. E. J. King, *Acid-Base Equilibria, The International Encyclopedia of Physical Chemistry and Chemical Physics*, p. 250. Pergamon Press, New York, 1965.
13. J. O'M Bockris and A. K. N. Reddy, *Modern Electrochemistry*, Vol. 1, Plenum Press, New York, 1973.
14. R. L. Reeves, *J. Am. Chem. Soc.*, 1966, **88**, 2240.
15. L. Skulski, W. Waclawek and A. Szurowska, *Bull. Acad. Pol. Sci., Ser. Sci. Chim.*, 1972, **20**, 463.
16. K. P. Ang, *J. Sol. chem.*, 1975, **4**, 949.
17. A. L. De, *Electrochim. Acta*, 1984, **29**, 471.

Talanta, Vol. 40, No. 4, pp. 485–490, 1993
Printed in Great Britain.

0039-9140/93 $6.00 + 0.00

MIXED HYDROXIDE COMPLEX FORMATION AND SOLUBILITY OF BISMUTH IN NITRATE AND PERCHLORATE MEDIUM

J. KRAGTEN and L. G. DECNOP-WEEVER
Laboratorium voor Analytische Chemie, Universiteit van Amsterdam, Amsterdam, The Netherlands

P. GRÜNDLER
Labor für Analytische Chemie, Universität von Rostock, Germany

(*Received* 16 *March* 1992. *Revised* 3 *August* 1992. *Accepted* 26 *August* 1992)

Summary—From the precipitation borderlines in the pBi′–pH diagram, determined experimentally under CO_2-free conditions, the stability constants of bismuth hydroxide, bismuthoxynitrate and bismuthoxyperchlorate have been established. The following values have been found

Nitrate-medium:	Perchlorate-medium:
$\log {}^*K_{s0}(OH) = 5.2$	$\log {}^*K_{s0}(OH) = 5.2$
$\log {}^*K_{s0}(NO_3) = -1.2$	$\log {}^*K_{s0}(ClO_4) = -0.9$
$\log {}^*\beta_2 = -4.0$	$\log {}^*\beta_2 = -4.1$
$\log {}^*\beta_3 = -10.0$	$\log {}^*\beta_3 = -9.9$
$\log {}^*\beta_4 = -21.5$	$\log {}^*\beta_4 = -21.5$
$\log {}^*\beta_{1,0,1} = 1.2$	$\log {}^*\beta_{1,0,1} = 3.5$

The constants refer to precipitates equilibrated for 30 min, prepared at room temperature ($23 \pm 0.5°$) in sodium perchlorate or sodium nitrate medium with an ionic strength of 1.00 ± 0.01. Concerning error propagation it is stated that pBi′ values calculated with these constants will have a standard deviation of about 0.1 log unit.

The hydrolysis of bismuth (III) has been studied by many authors.[1–8] The hydroxide-complex formation constants were estimated from the difference between the amount of hydroxide added and the hydroxide found (pH) after equilibrating. A disadvantage of such a procedure is that the measurements are performed in small limited pBi′–pH regions. Formation constants of hydroxide complexes present only outside such a region cannot be determined. Complexes formed at low concentration inside such a pBi′–pH region easily escape observation because of the limited accuracy inherent to the procedure in which pH-measurements have to be converted into H_3O^+ concentrations. Usually a restricted number of hydrolysis constants is found in this way.

A better procedure appeared to be the determination of the precipitation area in the pBi′–pH diagram. The theory has been described in previous publications,[4,9] but is extended in this paper for the more complex case in which two precipitates may be formed. The simple procedure has been applied successfully to the determination of the complete set of the hydrolysis constants of seven tervalent lanthanides Ce(III), Sm(III), Gd(III), Yb(III), Er(III), Nd(III) and La(III), of which constants were unknown hitherto.[9–16]

Faced with erroneous results in the determination of Bi(III) in 1*M* nitrate medium we supposed that the hydrolysis constants of Bi(III) and especially the solubility product of Bi-oxynitrate found in the literature[17] were disputable.

Recalculation of the solubility product of $BiONO_3$ from the original publication of Swinehart and Garrett[17] showed that they made a mistake with the introduction of the ion-activity coefficients and moreover they did not consider the possible formation of $BiNO_3^{2+}$ ions in solution. $\text{Log } {}^*K_{s0} = 0.25$ was found (instead of -2.55). Swinehart and Garrett[17] did not perform their experiments at constant ionic strength and constant nitrate concentration, but this fact cannot explain the large discrepancy in the log values above.

We decided to determine the formation constants of the bismuth-oxy-compounds with

nitrate, perchlorate and chloride (and to check the constants of bismuth hydroxide if possible) applying our precipitation technique that was so successful for the lanthanides.

In the following it will be shown that there is no reason to doubt the solubility product of $Bi(OH)_3$ and the formation constants of the complexes $Bi(OH)_3$ and $Bi(OH)_4^-$.

The formation constants of BiOCl could not be determined as the rather strong formation of Bi-chloride in solution interfered in the photometric complex formation titration of Bi.

THEORY

The reactions for hydroxide formation can be written as follows:

$$\begin{array}{ccccccc} & & BiOA_{solid} & & & & \\ & & \downarrow\uparrow & & & & \\ BiA^{2+} & \rightleftharpoons & BiOA & & & & \\ \downarrow\uparrow & & \downarrow\uparrow & & & & \\ Bi^{3+} & \rightleftharpoons & BiOH^{2+} & \rightleftharpoons & Bi(OH)_2^+ & \rightleftharpoons & Bi(OH)_3 \rightleftharpoons \cdots \\ & & \downarrow\uparrow & & & & \downarrow\uparrow \\ & & Bi_6(OH)_{12}^{6+} & & & & Bi(OH)_{3\ solid} \end{array}$$

In this reaction scheme A stands for the anions nitrate, perchlorate and chloride. First we will only consider the side reactions with hydroxide. The side reactions with the anion A will be considered later in this paper.

The above system has two independent variables. The concentrations of the various species depend on the total concentration of Bi and the pH. If an additional constraint is set, only one degree of freedom remains which implies that a relationship exists now between metal ion concentration and pH. A curve reflecting the particular constraint can be drawn in the pBi′–pH plot. Areas with predominating species so arise in the pBi′–pH diagram: by setting $[Bi(OH)_i] = [Bi(OH)_{i+1}]$ for different values of i, we get the borderlines of the regions of predominance of the various $Bi(OH)_i$ species; by setting $p.[Bi_p(OH)_q] = [Bi(OH)_i]$ for different values of i, p and q, the borderline for polynuclear complex formation is obtained; and by restricting $Bi(OH)_3$ to a maximum value assuming that excess of $Bi(OH)_3$ precipitates and that the remaining $Bi(OH)_3$ is in equilibrium with the precipitate, we get the precipitation line as function of the pH.

According to Ringbom[18] a system of coexisting equilibria can be described with one main reaction and competitive side-reactions, covering all other reactions. The parameter [Bi′] the total concentration of Bi in solution, is much more useful than the concentration $[Bi^{3+}]$ of the free metal ion, to which it is related by Ringbom's side-reaction coefficient

$$\alpha_{Bi} = [Bi']/[Bi^{3+}]. \quad (1)$$

By substituting in equation (1) the relevant equilibria equations in the so-called H-form (defined in accordance with the IUPAC notation):

$$^*\beta_i = [Bi(OH)_i][H]^i/[Bi^{3+}] \quad (2)$$

this leads to the general equation for only OH side reactions:

$$\alpha_{M(OH)} = 1 + 10^{(pH + \log {}^*\beta_1)} + 10^{(2pH + \log {}^*\beta_2)} + \cdots + 10^{(mpH + \log {}^*\beta_m)} \quad (3)$$

The pH-range can be divided into distinct regions with one of the hydroxide complexes predominating in each region. In each particular region the corresponding term in equation (3) will be the largest. For this particular area in the pBi′–pH plot the side reaction coefficient can be approximated by

$$\log \alpha_{Bi} = i\,.\,pH + \log {}^*\beta_i \quad (4)$$

In the case when a polynuclear complex like $Bi_6(OH)_{12}$ [which can be written in the general form $Bi_p(OH)_q$] predominates the equation can be written as[4]

$$\log \alpha_{Bi} = [q\,.\,pH + \log({}^*\beta_{qp}) + \log(p) - (p-1)\,.\,pBi']/p \quad (5)$$

This principle can be extended if other species—*e.g.*, $Bi(NO_3)_j$—are formed in solution. This component may be considered as a special case ($p = 1, q = 0$) of the more general form: $Bi_p(OH)_qA_j$.

If its formation constant is defined as $^*\beta_{jqp}$ analogously to equation (2) the equation will be:

$$\log \alpha_{Bi} = [q\,.\,pH + \log({}^*\beta_{jqp}) + \log(p) - (p-1)\,.\,pBi' - j\,.\,pA]/p \quad (6)$$

In practice we deal with a mixture of species with the general formula $Bi_p(OH)_qA_j$.

For every species defined by (p, q, j) equation (6) can be written down. The value of $\log \alpha_{Bi}$ is in good approximation equal to the largest value of all possible combinations of p, q and j. Its exact value is found by taking the logarithm of the sum of powers of 10 with the rightside of equation (6) as the exponent [see also equations (15) and (16)].

The precipitation of $Bi(OH)_3$

The uncharged species $Bi(OH)_3$ has a limited solubility. If a precipitate is present in solution under equilibrium conditions, a maximum is set to the concentration of $Bi(OH)_3$ in solution, hence to $[Bi^{3+}]$ and consequently to the overall concentration [Bi']. Using $^*\beta_3$ and maximizing $Bi(OH)_3$ we find: $pBi^{3+} = -\log(^*K_{so}) + 3pH$ from which follows together with equation (1):

$$pBi'_{max} = -\log(^*K_{so}) + 3pH - \log \alpha_{Bi} \quad (7)$$

Substitution of equation (6) in (7) gives

$$pBi'_{max} = (3p - q) \cdot pH - p \cdot \log(^*K_{so}) - \log(^*\beta_{qpj}) - \log(p) + j \cdot pA \quad (8)$$

Equation (8) gives rise to a set of straight lines in the pBi'–pH diagram. Each line represents an equilibrium between the $Bi(OH)_3$ precipitate and the species $Bi_p(OH)_qA_j$ in solution.

From equation (7) and the fact that we have to take the maximum value of $\log \alpha_{Bi}$ it follows that the real value of pBi'_{max} is the minimum value given by the set of straight lines (8). The lines enclose the precipitation region of $Bi(OH)_3$ in the pBi'-pH plot. A line only contributes as borderline if the species predominates in solution; not all lines are involved. If $Bi_p(OH)_qA_j$ predominates in solution in that particular pH region, line (8) will be the borderline in that pH region (Figs. 1 and 2).

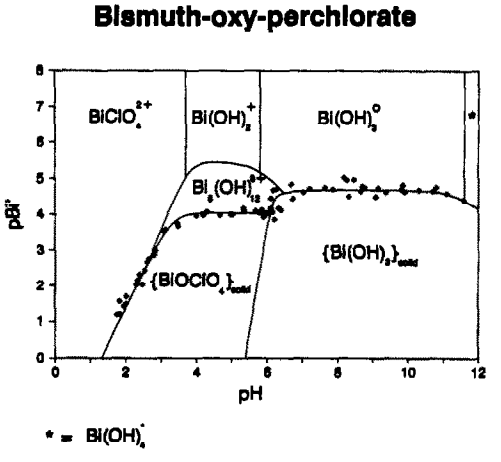

Fig. 1. The pBi'–pH diagram for bismuth in the presence of 1*M* perchlorate. The dots denote the experimental results. The envelope curves of the precipitation regions of $Bi(OH)_3$ and $BiOClO_4$ are found by adapting the curves to the experimental points. From the resulting equilibrium constants follows the position of the regions of predominance above the precipitation regions. The regions are indicated with the respective predominating ions.

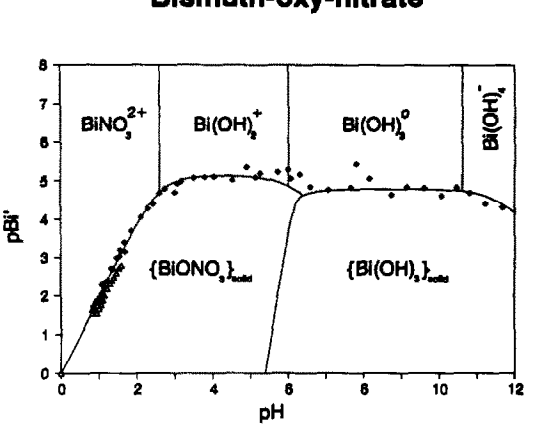

Fig. 2. The pBi'–pH diagram for bismuth in the presence of 1*M* nitrate. The dots denote the experimental results: ◆: own results, △: results of Swinehart and Garrett.[17] The envelope curves of the precipitation regions of $Bi(OH)_3$ and $BiONO_3$ are found by adapting the curves to the experimental points. From the resulting equilibrium constants follows the position of the regions of predominance above the precipitation regions. The regions are indicated with the respective predominating ions.

The precipitation of the mixed hydroxide $Bi(OH)_2A$

It is known that Bi(III) forms precipitates of the composition BiOA in which A stands for nitrate, perchlorate or chloride. For the equilibrium considerations it is not a restriction to write $Bi(OH)_2A$ instead of BiOA. The uncharged species $Bi(OH)_2A$ has a limited solubility. If a precipitate is present in solution under equilibrium conditions, a maximum is set to the concentration of $Bi(OH)_2A$, hence to $[Bi^{3+}]$ and consequently to the overall concentration [Bi']. Using $^*\beta_{121}$ for the formation constant of $Bi(OH)_2A$ and maximizing its concentration we find:

$$pBi^{3+} = -\log(^*K_{so}) + 2pH - p[A] \quad (9)$$

from which follows together with equation (1):

$$pBi'_{max} = -\log(^*K_{so}) + 2pH - p[A] - \log \alpha_{Bi} \quad (10)$$

Substitution of equation (6) into (10) gives

$$pBi'_{max} = (2p - q) \cdot pH - p \cdot \log(*K_{so}) - \log *\beta_{qpj} - \log p + (j - p) \cdot pA \quad (11)$$

Equation (11) gives rise to a set of straight lines in the pBi′–pH diagram. Each line that participates in shaping the precipitation region, represents an equilibrium between the precipitate $Bi(OH)_2A$ and the species $Bi_p(OH)_qA_j$ predominantly present in solution. Again not all lines may be involved [similar to the previous case for $Bi(OH)_3$].

EXPERIMENTAL

At low and moderate concentrations of nitrate and perchlorate Bi(III) does not form complexes with these ions. Under these conditions the regions of predominance in solution are restricted to the species Bi^{3+}, $Bi(OH)^{2+}$, $Bi(OH)_2^+$, $Bi(OH)_3$, $Bi(OH)_4^-$ and $Bi_6(OH)_{12}^{6+}$ and only one precipitate $Bi(OH)_3$ is formed.

At higher concentration (1*M* nitrate or 1*M* perchlorate) a second precipitate is formed of which the precipitation region lies on the acid side of the other precipitation region. The precipitate has a different appearance with a fine crystalline structure. For perchlorate and nitrate the ratio bismuth:oxygen:anion is 1:1:1. If this precipitate was filtered off and then brought into a basic solution, a slow recrystallization into $Bi(OH)_3$ was observed.

Depending on the experimental conditions only one of the two possible precipitates will be in equilibrium with the solution.

The formation of the precipitate was equal to the procedure as described for gadolinium.[11] In a glove box under nitrogen a CO_2-free sodium hydroxide solution is added slowly and carefully to the acid solution of bismuth. The experimental conditions are 1*M* NO_3^- or 1*M* ClO_4^-. The ionic strengths are kept at 1.00 ± 0.01. The temperature was kept constant at $23.0 \pm 0.5°$. The time left to the system to reach equilibrium was kept at 30 min, after which the precipitate was removed by centrifugation. Preliminary experiments revealed that after 30 min changes of both pH and pBi′ in one batch were negligible compared to the reproducibility of the precipitate formation.

The pH-meter was calibrated in concentration units.[9,11,14] Hence if pH is written, actually $-\log[H^+]$ is meant and not the activity of H^+. It implies that the determined formation constants are full concentration products. The Bi concentration has been determined in the supernatant centrifuged solution by complex formation titration with EDTA as the titrant with photometric endpoint detection using Semi-Xylenol Orange as the indicator.[19,20]

RESULTS

For both $BiONO_3$ and $BiOClO_4$ the precipitation regions have been determined. The experimental results are presented as points in Figs. 1 and 2. The precipitation region of the $Bi(OH)_3$ species is enclosed by the following three straight lines in the pBi′–pH plot:[4]

$$pBi'_{max} = 4.75 \quad (12)$$

$$pBi'_{max} = -pH + 16.30 \quad (13)$$

$$pBi'_{max} = 6pH - 32.33 \quad (14)$$

The other lines from the set as described by equation (8) do not contribute; they lie at least 1 log unit higher in the diagram. The lines (12)–(14) hold for both 1*M* nitrate and 1*M* perchlorate solutions. It implies that the hydroxide formation constants are the same in both experiments.

Initially we assume that the value for $Bi_6(OH)_{12}^{6+}$ ($\log *\beta_{6,12} = 0.33$) is correct ($I = 0.1$ and 3).[5–8] Introducing this value in equation (8) and setting $j = 0$ we conclude with equation (14) for $\log *K_{so} = 5.20$. From this and the equations (12) and (13) follows: $\log *\beta_3 = -9.95$ and $\log *\beta_4 = -21.50$. These data are not very dependent on errors in $\log *\beta_{6,12}$ [a change of 0.3 has a negligible influence (0.05) on the other data]. The data found for $*K_{so}$, $*\beta_3$ and $*\beta_4$ are in agreement with the literature data ($I = 0.1$).[5–8] Because of this confirmation we adopt the literature values of $\log *\beta_1 (-1.4)$ and $\log *\beta_2 (\approx -4)$ as holding for both matrices. (The value of $\log *\beta_1$ could not be confirmed from our experimental data; $\log *\beta_2$ has later been selected as 4.0 and 4.1 for better fits to the data for nitrate and perchlorate media respectively.)

The precipitation region of the $BiOClO_4$ precipitate is enclosed by the lines:

$$pBi'_{max} = 4.09 \quad [\text{in equilibrium with } Bi_6(OH)_{12}^{6+}] \quad (15)$$

$$pBi'_{max} = 2pH - 2.63 \quad (\text{in equilibrium with } BiClO_4^{2+}) \quad (16)$$

The precipitation region of the $BiONO_3$ precipitate is enclosed by the lines:

$$pBi'_{max} = 4.9 \quad \text{[in equilibrium with } Bi(OH)_2^+\text{]} \quad (17)$$

$$pBi'_{max} = 2pH \quad \text{(in equilibrium with } BiNO_3^{2+}\text{)} \quad (18)$$

The set of constants presented in Table 1 turned out to be the only set with which it is possible to get a fit to the experimental data for both the nitrate experiments and for the perchlorate experiments with nearly the same set of constants for hydroxide formation.

Deducing these constants from all lines which can be drawn in the pBi'–pH plot is like solving a puzzle. The lines which arise after substitution of the constants in equation (8) and (11) should either be borderlines of the precipitation region or lie at least one log unit higher.

In Table 2 a survey is given of all possible lines which originate from equation (8) and (11) for the perchlorate system in which we deal with two possible precipitates $Bi(OH)_3$ and $BiOClO_4$.

The real curves in Figs. 1 and 2 for the precipitates regions have been found with the mathematically correct equations:

$$pBi'_{max} = -\log[10^{-3pH+5.2} + 10^{-2pH+3.8} + 10^{-pH+1.1} + 10^{-4.7} + 10^{pH-16.3} + 10^{-6pH+32.33} + 10^{-3pH+8.70}]. \quad (19)$$

$$pBi'_{max} = -\log[10^{-2pH-0.87} + 10^{-pH-2.27} + 10^{-4.97} + 10^{pH-10.77} + 10^{2pH-22.37} + 10^{-4.09} + 10^{-2pH+2.63}] \quad (20)$$

In Table 2 asterisks (*) indicate which predominating ion is in equilibrium with the specific precipitate. The equations (*) in the right column of Table 2 are equivalent to equations (15) and (16). The corresponding terms in equation (20) predominate and determine the shape of the precipitation region. The same holds for the equations in the left column, which lead to dominating terms in equation (19). It should be noted that all equations are mutually dependent on each other as all constants appear in all equations. It is surprising that the system actually has only one satisfactory set of constants.

An analogous set of equations hold for the nitrate system.

Table 1.

Nitrate-medium	Perchlorate-medium
$\log {}^*K_{so}(OH) = 5.2$	$\log {}^*K_{so}(OH) = 5.2$
$\log {}^*K_{so}(NO_3) = -1.2$	$\log {}^*K_{so}(ClO_4) = -0.9$
$\log {}^*\beta_1 = -1.4$	$\log {}^*\beta_1 = -1.4$
$\log {}^*\beta_2 = -4.0$	$\log {}^*\beta_2 = -4.1$
$\log {}^*\beta_3 = -10.0$	$\log {}^*\beta_3 = -9.9$
$\log {}^*\beta_4 = -21.5$	$\log {}^*\beta_4 = -21.5$
$\log {}^*\beta_{6,12} = 0.3$	$\log {}^*\beta_{6,12} = 0.3$
$\log {}^*\beta_{1,0,1} = 1.2$	$\log {}^*\beta_{1,0,1} = 3.5$
Ionic strength = 1.00 ± 0.01	Temperature = $23 \pm 0.5°$

DISCUSSION

In Fig. 2 the jump in experimental points near pH 6 indicates that before that pH value the $BiOClO_4$ precipitate is present and while above pH 6 the Bi $(OH)_3$ precipitate occurs.

Both precipitates are formed by neutralizing the acidic bismuth solutions with hydroxide. This implies that the $BiOClO_4$ precipitate is formed first in the experiments. The precipitate converts into the $Bi(OH)_3$ precipitate after reaching higher pH values. The reaction proceeds slowly because of its heterogeneous character. Near pH 6 it takes hours to reach equilibrium in an acceptable way and in that region the position of the experimental points will be less precise compared to the experimental points related to lower and higher pH.

This consideration holds also for the nitrate system although it is less obvious from Fig. 2 as the horizontal parts of both precipitation lines lie approximately at the same level (≈ 5); there is no jump detectable in the experimental points.

Table 2.

$Bi(OH)_3$-precpt		$BiOClO_4$-precpt	
$pBi'_{max} = 3.pH - 5.20$:	Bi^{3+}	$pBi'_{max} = 2.pH + 0.87$:	Bi^{3+}
$= 2.pH - 3.80$:	$Bi(OH)^{2+}$	$= pH + 2.27$:	$Bi(OH)^{2+}$
$= pH - 1.10$:	$Bi(OH)_2^+$	$= +4.97$:	$Bi(OH)_2^+$
$= +4.70$:	$^*Bi(OH)_3$	$= -pH + 10.77$:	$Bi(OH)_3$
$= -pH + 16.30$:	$^*Bi(OH)_4^-$	$= -2.pH + 22.37$:	$Bi(OH)_4^-$
$= 6.pH - 32.33$:	$^*Bi_6(OH)_{12}^{6+}$	$= +4.09$:	$^*Bi_6(OH)_{12}^{6+}$
$pBi'_{max} = 3.pH - 8.70$:	$Bi(ClO_4)^{2+}$	$pBi'_{max} = 2.pH - 2.63$:	$^*Bi(ClO_4)^{2+}$

In principle the horizontal parts of BiOA precipitation lines can also be explained by assuming that $Bi(OH)_2A$ is the predominating species in solution. However, this is unlikely as then $Bi_6(OH)_{12}^{6+}$ should not be present and this complex is essential for explaining the jump in the precipitation lines near pH 6 in Fig. 1.

The experimental points found by Swinehart and Garrett[17] are also drawn in Fig. 2. Obviously these points do not deviate much from our measurements. This is remarkable as they did not work at constant ionic strength; their experiments were performed at a different temperature and 2–3 weeks were used to let the system reach chemical equilibrium.

Concerning the accuracy, the position of the individual experimental points has a precision of ± 0.5 log units in the pBi′ (vertical) direction if the borderline is (nearly) horizontal. The points have a precision of ± 0.5 log units in the pH direction if the borderline is (nearly) vertical. The borderlines themselves are close to the mean position of the points and hence are defined more precisely. The standard deviation of the line position may be estimated by 0.1 log unit. The sets of constants in Table 1 are deduced from the position of these lines, but as many constants work together in defining one line, the constants are not mutually independent in a statistical sense. Actually a covariance matrix should be given, but this is difficult to estimate from the calculation procedure and makes no sense. More relevant is to conclude that for a given pH value a pBi′ value calculated using the set of constants will have a standard deviation of about 0.1 log unit.

Attempts to determine a similar way the constants of the Bi–Cl system were finally given up. The solubility of BiOCl is very low while at the same time soluble strong BiCl complexes interfere in the titrimetric determination of Bi. Determinations are only possible at chloride levels below $0.07M$. Perhaps the determination of Bi in the presence of Cl will succeed with atomic spectroscopic techniques like ICP–AES or AAS, but no attempts have been made.

For direct application in an analysis procedure the precipitates $BiONO_3$ and $BiOClO_4$ are not of interest. Knowledge about precipitate formation however is of indirect value in analytical chemistry. Colloidal formed BiOA reacts rather slowly and even behaves rather inert when it sticks to the vessel wall. It explains why in some related cases bismuth escapes from being analysed. It also explains why bismuth and its alloys sometimes dissolve very slowly in strong acid. It is then passified by a layer of BiOA on its surface.

Acknowledgements—We are indebted to Annelies de Wit, Pauline Lobé and Renata Tel for their meticulous contribution to the time-consuming determination of the experimental points in the diagrams.

REFERENCES

1. Ju. Ju. Luré, *Spravočnik po analitičeskoj*, chimii, Moskow, 1979.
2. I. Muylder and M. Pourbaix, Proc. 9th Meeting Intern. Comm. Electrochem. Thermod. Kinet., Paris, 1957.
3. T. F. Bidleman, *Anal. Chim. Acta*, 1971, **56**, 221.
4. J. Kragten, *Atlas of Metal-Ligand Equilibria in Aqueous Solution*, Ellis Horwood, Chichester, 1978.
5. *Stability Constants of Metal-Ion Complexes*, Part A, IUPAC Chem. Data Series No 21, Oxford, 1982.
6. L. G. Sillén and A. E. Martell, *Stability Constants of Metal-Ion Complexes*, Special Publication No. 17, The Chemical Society, London, 1964.
7. *Idem, ibid.*, Special Publication No. 25, The Chemical Society, London, 1971.
8. C. F. Baes, Jr. and R. E. Mesmer, *The Hydrolysis of Cations*, Wiley, New York, 1976.
9. J. Kragten and L. G. Decnop-Weever, *Talanta*, 1978, **25**, 147.
10. *Idem, ibid.*, 1979, **26**, 1105.
11. *Idem, ibid.*, 1980, **27**, 1047.
12. *Idem, ibid.*, 1982, **29**, 219.
13. *Idem, ibid.*, 1983, **30**, 131.
14. *Idem, ibid.*, 1983, **30**, 134.
15. *Idem, ibid.*, 1984, **31**, 731.
16. *Idem, ibid.*, 1987, **34**, 861.
17. D. F. Swinehart and A. B. Garrett, *J. Am. Chem. Soc.*, 1951, **73**, 507.
18. A. Ringbom, *Complexation in Analytical Chemistry*, Interscience, New York, 1963.
19. J. Kragten, *Z. für Anal. Chemie*, 1973, **264**, 356.
20. *Idem, Mikrochimica Acta, 1971*, 821.

Talanta, Vol. 40, No. 4, pp. 491–494, 1993
Printed in Great Britain

0039-9140/93 $6.00 + 0.00
Pergamon Press Ltd

LIQUID CHROMATOGRAPHIC DETERMINATION OF THE KNOWN LOW LEVEL IMPURITIES IN LOVASTATIN BULK DRUG: AN APPLICATION OF HIGH–LOW CHROMATOGRAPHY

ANTHONY HOUCK, SCOTT THOMAS and DEAN K. ELLISON
Merck Sharp & Dohme Research Laboratories, P.O. Box 2000, Rahway, NJ 07065, U.S.A.

(*Received* 11 *February* 1992. *Revised* 20 *August* 1992. *Accepted* 20 *August* 1992)

Summary—High–low chromatography in combination with gradient elution and multiple wavelength detection is a rapid and sensitive technique that can be used to assay low level impurities in lovastatin. The method is reproducible and can be applied to samples containing as little as 0.1% of any known impurity.

Monitoring low levels of impurities in pure bulk drugs is a critical but often difficult task.[1] Lovastatin, an effective cholesterol reducing agent,[2] is an example of a highly purified drug which contains a number of known low level impurities (see Fig. 1). The production of pure lovastatin involves isolation and purification from a complex fermentation broth.[3] Impurities which are shown in Fig. 1 are either carried over from the fermentation process or produced during the isolation procedure. As a result, these impurities must be routinely monitored throughout the production process. Assaying each impurity individually against reference standards would take a significant amount of time and also require a large supply of analytical standard for each impurity. Rather than optimize analytical methodology for the assay of each individual impurity, we have applied a novel combination of high–low chromatography, gradient elution and multiple wavelength detection to monitor these impurities.[4] To our knowledge, this is the first time this combination of chromatographic techniques has been reported. We demonstrate here that we can obtain reproducible and quantitative results in a short period of time for monitoring known low level impurities in the drug lovastatin.

EXPERIMENTAL

General

HPLC-grade acetonitrile and reagent grade phosphoric acid were purchased from Fisher Scientific and J.T. Baker Chemical Company, respectively. The standards L-154,803, L-154,819, L-637,312, L-642,257, L-154,883, L-665,624, were obtained from the Merck Sample Collection located in Rahway, N.J. Asterric acid was kindly provided by Dr Tom Verhoeven, Merck and Co.

Chromatographic instrumentation

The HPLC system for the high–low impurity assay consisted of a Spectra Physics Model 8700 pump, a Spectra Physics Model SP8500 dynamic mixer, a Spectra Physics Model 8710 autosampler fitted with a 10 microliter injection loop, and two Kratos Model 757 variable wavelength detectors connected in series. A Hatachi column heater, Model 655A-52, was used to maintain the column temperature at 30°.

Lovastatin chromatographic procedure

Reversed-phase separation of impurities in lovastatin was accomplished using a 25.0-cm × 4.6-mm i.d. column packed with C-8 chemically bonded silica (5 micron) Partisil (Whatman) Column. The following gradient system was used: 40:60 water (0.1% v/v H_3PO_4, pH = 2.2):acetonitrile to 20:80 in four minutes, then 10:90 in three minutes and hold for five minutes. The flow was 1.5 ml/min with dual wavelength detection at 200 and 238 nm. All samples were diluted in acetonitrile at a concentration of 2.0 mg/ml.

Quantitation

Two injections of lovastatin standard (0.3 mg/ml) were followed by two injections of

sample (2 mg/ml). Impurities in the sample are identified by retention times and the area counts for each impurity are averaged. The impurity percentages in the sample are then calculated as follows:

$$\text{Wt\% impurity} = \frac{\text{RFS} \times 100}{\text{RFST} \times \text{RRF}}$$

Where: RFS, the response factor of a given impurity in the sample, is calculated by dividing the average area count of impurity in the sample by the concentration of the sample (typically 2.0 mg/ml); REST, the response factor of the lovastatin standard, is calculated by dividing the average area count of the lovastatin standard by its concentration (typically 0.3 mg/ml). This response factor was checked approximately every 10 injections; and RRF, the relative response factor, is a correction factor which accounts for a difference in response (both a function of retention time and UV characteristics of a given impurity) between a given impurity and the lovastatin standard. The RRF is calculated by dividing the response factor of a given impurity by the response factor of standard. This factor must be determined experimentally using authentic samples of impurities. We typically check the RRF daily using a

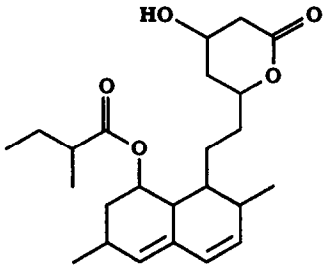

I
Lovastatin
(L-154, 803)

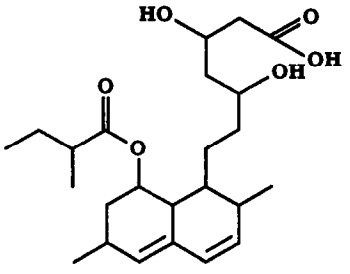

II
Hydroxy Acid Lovastatin
(L-154, 819)

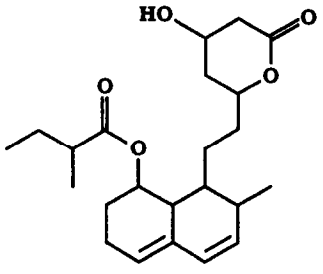

III
Compactin
(L-637, 312)

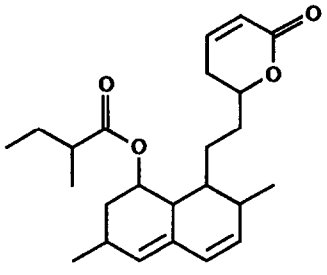

IV
Dehydrolovastatin
(L-642, 257)

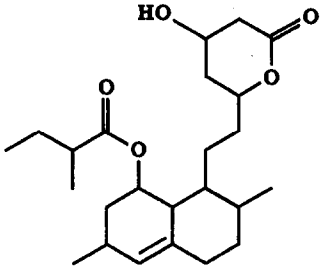

V
Dihydrolovastatin
(L-154, 883)

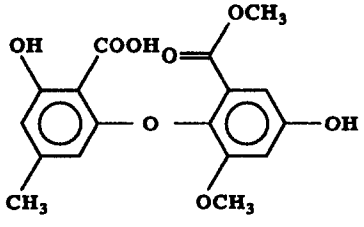

VII
Asterric Acid

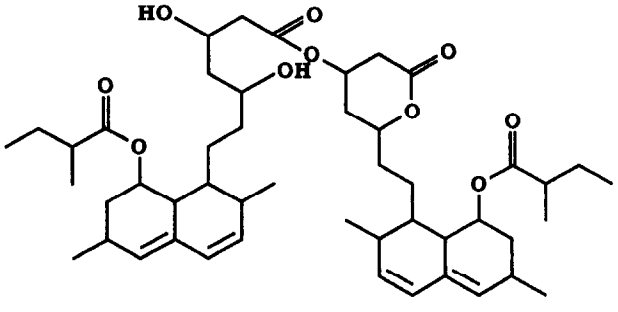

VI
Lovastatin Dimer
(L-665, 624)

Fig. 1. Structure and nomenclature of lovastatin and known impurities in lovastatin.

Table 1. Average area response for lovastatin impurities shown in Fig. 1. Each individual impurity was injected at the 0.02-μg level five consecutive times and the average value and %RSD for the five injections presented. Impurities V and VII were monitored at 200 nm while all other impurities were monitored at 238 nm

Compound	Area counts	%RSD
V	3528	1.3
VI	13075	1.1
II	14299	1.5
III	16474	1.1
IV	19952	1.0
VII	39599	0.5

lovastatin sample which contains a known amount of each impurity.

RESULTS AND DISCUSSION

To routinely monitor low level impurities in lovastatin, it was important to develop a rapid and sensitive analytical method for detecting low level impurities (see Fig. 1). The assay would be useful for release testing of the pure bulk drug and monitoring impurity levels throughout the lovastatin production process.

Wavelength selection

Lovastatin has a strong absorption band in the UV range with an A 1% 1 cm of 634 at its wavelength of maximum absorbance, 238 nm. This absorption is attributed to the diene conjugation (Fig. 1). All of the impurities, with the exception of asterric acid and dihydrolovastatin, contain the same diene functional group and also have a maximum absorbance at 238 nm. As a result, UV detection at this wavelength should provide adequate sensitivity for the impurities with the diene system. The dihydro and asterric acid have very little absorbance at 238 nm, but each does absorb significantly at 200 nm (see response in Table 1). Consequently, we chose to monitor 200 nm also, in order to detect these two impurities with improved sensitivity.

Separation

Our initial reverse phase separations indicated that each impurity could not be base line resolved from each other in a reasonable amount of time using isocratic conditions. This is consistent with the wide range of polarities which exist among the various impurities (see Fig. 1). Gradient chromatography, however, allowed us to base line resolve each impurity within a short chromatographic run-time (see Fig. 2). There are unknown impurities which appear on the chromatogram between known impurities I and III and between known impurities VII and II. These impurities are occasionally detected in some samples, however, because the levels are much less than 0.05%, these impurities have not been identified.

Detection limit

We needed a limit of quantitation (LOQ) of less than 0.1% for each impurity.[5] Our approach was to determine the LOQ for each impurity and then use that value to determine

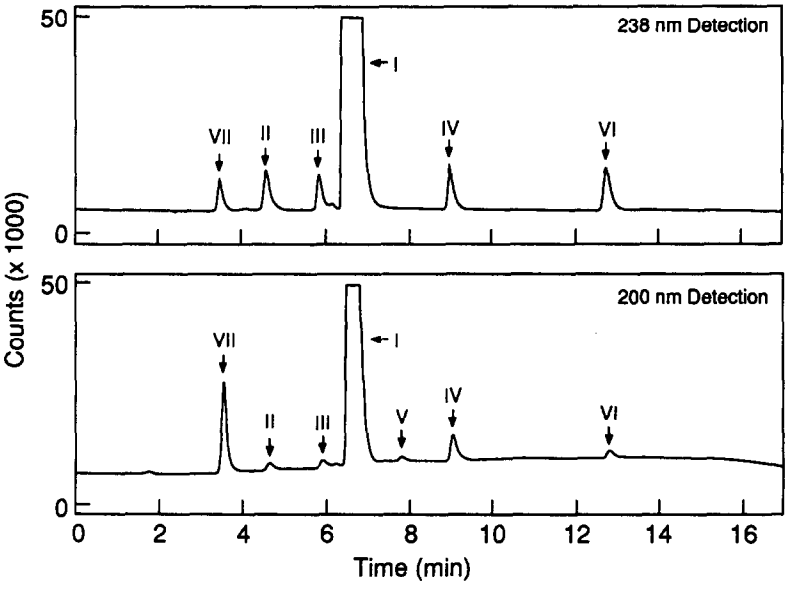

Fig. 2. Chromatographic separation of known impurities spiked at the 0.5% level in a 2-mg/ml lovastatin sample. Conditions are as described in the experimental section.

the amount of sample which would be needed to be injected onto the column. For example, we determined our LOQ to be $\geqslant 3000$ area counts. The average area count responses for each impurity are shown in Table 1. The dihydrolovastatin gives the least sensitive response, 3528 area counts for a 0.02-μg on-column injection because it has low UV absorption even at 200-nm detection (no diene chromaphore). This 0.02-μg level of dihydrolovastatin corresponds to a 20-μg level on column injection of sample in order to get 0.1% quantitation limit. All other impurities are well above the 3000 area count criteria at the 0.02-μg injection level.

Linearity

The area count response of the dihydrolovastatin impurity as a function of concentration is linear across the concentration range of 0.002–0.2 mg/ml (correlation coefficient greater than 0.9999). This concentration range of 0.002–0.2 mg/ml corresponds to a weight percent ([weight of impurity/weight of sample] $\times$ 100%) of 0.1–10% for a 2-mg/ml sample concentration. We selected this concentration range because our experience with lovastatin has suggested that no impurity will be above the 10% range. We performed an identical linearity test with the other impurities shown in Fig. 1 and in each case the correlation coefficient was better than 0.9999.

Reproducibility

The percent relative standard deviation as a function of impurity is also shown in Table 1. The standard deviation was calculated using five successive injections of each solution. In all cases the % RSD was below the 3% level. We consider percent relative standard deviations of less than 20% acceptable for assaying low level impurities in bulk drugs.

Advantages

We have noted three significant advantages of using this method of analysis as compared to methods which routinely employ reference standards for assaying each known impurity; 1) high sensitivity, 2) shorter analysis time, and 3) less frequent use of impurity standards. Because we are able to load more sample on to the column without worrying about going above the linear range of the main component, lovastatin, our sensitivity towards low level impurities in lovastatin is increased by more than five times. A significant amount of time is saved by quantitating each impurity relative to a lovastatin standard, as opposed to assaying each impurity individually. This feature also avoids the excessive use of standards which are often available in limited quantity.

REFERENCES

1. R. K. Gilpin and L. A. Pachla, *Anal. Chem.*, 1989, **61**, 191R.
2. J. A. Tobert, R. V. Zupkis and T. M. Gutwein, *J. Am. Med. A.*, 1988, **260**, 359.
3. A. W. Alberts, J. Chen, G. Duron, V. Hunt, J. Huff, C. Hoffman, J. Rothrock, M. Lopez, J. Joshua, E. Harris, A. Harris, A. Patchett, R. Monaghan, S. Currie, E. Stapley, G. Albers-Schonberg, O. Hensens, J. Hirhfield, K. Hoogsteen, J. Liesch and J. Springer, *Proc. Natl. Acad. Sci.*, 1980, **77**, 3957.
4. E. L. Inman and H. J. Tenbarge, *J. Chromatogr. Sci.*, 1988, **26**, 89.
5. Subcommittee report on Environmental Analytical Chemistry, *Anal. Chem.*, 1980, **52**, 2242.

Talanta, Vol. 40, No. 4, pp. 495–501, 1993
Printed in Great Britain.

0039-9140/93 $6.00 + 0.00

CHROMATOGRAPHIC DETERMINATION OF COPPER SPECIATION IN JET FUEL

DANIEL B. TAYLOR and ROBERT E. SYNOVEC*
Department of Chemistry, BG-10, University of Washington, Seattle, Washington 98195, U.S.A.

(*Received* 22 *July* 1992. *Revised* 19 *August* 1992. *Accepted* 19 *August* 1992)

Summary—A method is described that allows one to distinguish and quantitate two different classes of copper compounds in the same hydrocarbon sample. This will enable the study of the effects of different copper compounds on the performance and stability of petroleum samples. Copper *N,N'*-disalicylidene-1,2-propylenediamine (CuDMD) and several copper carboxylates were preconcentrated from a hydrocarbon matrix using a column packed with polyvinylpyrrolidone, $(C_6H_9NO)_x$, a novel polymeric stationary phase. The copper complexes were then sequentially eluted using a step gradient program beginning with hexane/isopropyl alcohol as the eluent and ending with an acetic acid/isopropyl alcohol eluent. The copper complexes were detected by serial UV absorbance and flame atomic absorbance (FAA) detection. With on-column preconcentration and FAA detection, the limits of detection were 7 and 40 ppb copper for CuDMD and the copper carboxylates respectively. With this method, it was possible to distinguish between the two different classes of copper compounds in the same hydrocarbon sample, which will help to provide an understanding of the catalytic activity of different copper compounds, leading to a better understanding of the factors causing fuel instability. The method promises to be a valuable tool in the analysis and characterization of copper compounds in petroleum samples.

INTRODUCTION

Recently there have been several articles about the speciation of metals in aqueous samples.[1–4] For the purpose of this report, speciation will be defined as the distribution of a metal among different ligands to form complexes. The speciation of a metal is defined by the ligands attached to the metal, therefore, if two metal atoms have different ligands attached, the metals have different speciation. Metal speciation is also important for petroleum systems like jet fuel but the methods used to determine the speciation of metals in aqueous samples cannot be used for petroleum samples. Metal complexes in hydrocarbon matrixes are not retained, relative to the major constituent of the fuel, by the reversed-phase columns typically used to determine the speciation of metals in aqueous samples, but are eluted by the non-polar components in the fuel. Thus, reversed-phase chromatography cannot be used to preconcentrate and separate the copper compounds in petroleum samples. In this manuscript we describe a normal-phase chromatographic method for the determination of copper speciation in jet fuel.

The presence of copper in jet fuel, even at concentrations as low as 40 ppb, can have a detrimental effect on fuel stability.[5,6] It is believed that the copper dissolved in jet fuel degrades the stability of the fuel by acting as a catalyst for the free radical oxidation of the fuel, which leads to the formation of varnishes, gums and sediments.[7,8] This is especially noticeable when the fuel is in contact with hot surfaces, such as heat exchangers. The gums and sediments can cause many problems when they form within an engine. They can clog fuel filters, reduce the efficiency of heat exchangers causing engines to overheat or thermal break down of cooling oil, and clog nozzles in the combustion chambers of engines and change the fuel spray pattern.[7,8] The adverse effect of copper on fuel stability can be reduced by adding DuPont Metal Deactivator (DMD) to the fuel.[6,7] The active ingredient in DMD is *N,N'*-disalicylidene-1,2-propylenediamine which chelates all of the copper in the fuel, and thus, reduces its catalytic activity. The chemical structure of DMD and the CuDMD complex are shown in Fig. 1.

In order to determine whether the copper present in a jet fuel sample will degrade the stability of the fuel, one needs to be able to differentiate between CuDMD and the other forms of copper which will catalyze fuel oxidation. An analytical technique that can

*Author for correspondence.

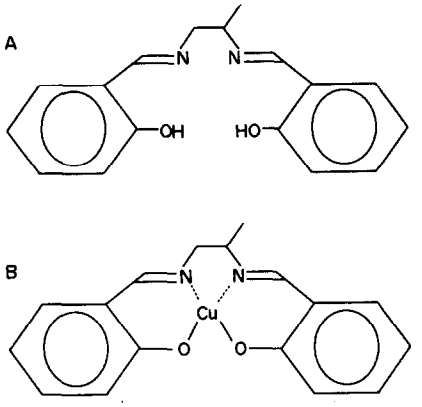

Fig. 1. Chemical structures of (A) the active ingredient in DuPont Metal Deactivator (DMD) and (B) the copper DMD complex.

accomplish this differentiation is needed. A technique that can determine both the speciation and concentration of copper at low parts per billion (ppb) concentrations is needed, because both copper concentration and speciation determine how the dissolved copper will affect fuel stability.

We have developed a method capable of distinguishing between CuDMD and the catalytically active copper carboxylates. The method has enabled us to separate the copper complexes into two classes: strongly bound copper of the CuDMD complex, and the weakly bound copper of the copper carboxylates. This method is significant, because it makes it possible to distinguish between the copper that will have a detrimental effect on fuel stability and cause the fuel to degrade, and the copper which has been "passivated" by DMD and will not affect fuel stability. The technique we have developed for determining the speciation of copper involves preconcentrating and separating the different classes of copper compounds using normal-phase chromatography. The copper compounds are detected by serial ultra-violet absorbance and flame atomic absorption (FAA) detectors. It is important that the speciation is not disturbed during the preconcentration or separation of the two classes of copper compounds, because if the speciation of the copper is changed the information about the catalytic activity of the copper in the jet fuel is lost.

Initially the suitability of the traditional stationary phase alumina for the normal-phase preconcentration and separation of the copper compounds in jet fuel was investigated. The copper in hexane solutions was retained by the alumina, but could not be eluted unless strong acid was added to the eluent. The acidic eluent eluted all of the copper species at the same time. The eluted copper, regardless of its original speciation, had the same response factor for the UV absorbance detection at 300 nm. We interpreted this to mean that alumina acts as an ion-exchanger that displaces the native ligands when the copper adsorbs on the stationary phase. All of the copper was being eluted as the same compound, which is why the response factor was the same for every copper compound. We had developed a method capable of preconcentrating copper from jet fuel with a limit of detection of 0.07 ppb, but all information about copper speciation was lost. So, the method would not be useful in determining the effect of copper speciation on fuel stability.

Alumina could not be used as a stationary phase for the determination of the speciation of copper in jet fuel, because alumina was too polar, and acidic eluents converted it into an ion-exchange phase. We were also concerned about silica based packing materials because of their similarity to alumina. Even the derivatized packing materials have residual silanol groups that could retain the copper. A stationary phase polar enough to allow preconcentration and elution of the copper complexes in the jet fuel, but not polar enough to act as an ion-exchanger and displace the native ligands, was needed. One such stationary phase is polyvinylpyrrolidone[9] (PVP), $(C_6H_9NO)_x$. The chemical structure of the PVP polymer is shown in Fig. 2. A column was packed in house with commercially available packing material with a nominal diameter of 50 μm, because traditional HPLC columns packed with PVP are not commercially available. The column was used to evaluate the feasibility of using PVP as a stationary phase in the normal-phase chromatographic separation of copper complexes in jet fuel. On-column preconcentration of copper complexes and maintenance of their speciation was studied with the PVP stationary phase. Future work should employ smaller diameter PVP particles, to minimize peak broadening.

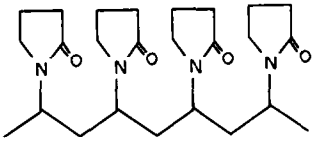

Fig. 2. Chemical structure of the stationary phase material polyvinylpyrrolidone (PVP).

Table 1. Flame atomic absorbance spectrophotometer operating conditions

Lamp current:	25 mA
Slit:	1 mm, 0.7 nm
Wavelength:	326.4 nm
Flame:	Air–acetylene
Gas flow rates:	46–30
Nebulizer type:	Spoiler
Burner type:	10.5 cm, 3-slot

EXPERIMENTAL

Reagents

N,N'-disalicycline-1,2-propylenediamine, active ingredient in DMD, was purchased from Pfaltz & Bauer, Inc. Technical grade copper naphthenate was purchased from Chem Service. The copper cyclohexanebutyrate was purchased from Pfaltz & Bauer. Reagent grade copper acetate was purchased from Aldrich. Copper powder was purchased from J. T. Baker. Because the copper naphthenate and cyclohexanebutyrate were of unknown purity, solutions of all three carboxylates were made and the copper content was determined by FAA. The isopropyl alcohol, and hexane were Baker Analyzed HPLC Reagent grade solvents (J. T. Baker). The water was purified in house using a Milli-Q Reagent Waters System (Millipore Corporation, Bedford, MA, U.S.A.). The jet fuels analyzed in this study were provided by the Fuels Research Branch at Wright-Patterson Air Force Base (Dayton, OH, U.S.A.).

Column

The column was a 5 cm × 4.3 mm PEEK column with ultra-high molecular weight polyethylene frits (Upchurch Scientific Inc. Oak Harbor WA, U.S.A.). The PVP stationary phase came from Dionex Onguard-P solid phase extraction cartridges (Dionex Corp. Sunnyvale, CA, U.S.A., p/n 039597). The average nominal diameter of the PVP was reported to be 50 μm. The column was packed by slurrying the PVP with isopropyl alcohol, and transferring the slurry into the column with an eyedropper. The excess isopropyl alcohol was removed by a small pump (Fluid Metering Inc. Oyster Bay, NY).

Apparatus

The HPLC system was a Dionex BioLC system with a variable wavelength absorbance detector. The system provides a metal-free eluent flow path which has ensured no sample contamination by the chromatographic system and a low baseline. The HPLC was coupled to the FAA spectrophotometer by connecting the variable wavelength absorbance detector outlet tubing to the FAA nebulizer with an 18 gauge blunt tip needle and 20 gauge Teflon tubing.

A Perkin–Elmer 403 flame atomic absorbance spectrophotometer (Norwalk, CT, U.S.A.) with manual controller, a spoiler nebulizer and 10.5 cm 3-slot burner was used as an element specific detector. The operating conditions for the FAA are listed in Table 1.

The final solvent program was: 0–3 min, 30% hexane, 70% isopropyl alcohol, with a 1.25-ml sample injection at 0.5 min. The eluent from 3 min to the end of run was 5% acetic acid and 0.5% water in isopropyl alcohol.

Data acquisition and control

The data acquisition and system control were done using an IBM AT computer with an IBM DACA board (Boca Raton, FL, U.S.A.). The data acquisition and system control software was written in-house using Microsoft Quick Basic. (Microsoft Corp., Bellevue, WA, U.S.A.).

RESULTS AND DISCUSSION

The PVP stationary phase was evaluated by injecting hexane solutions of the copper complexes listed in Table 2 onto the PVP column.

Table 2. Capacity factor (k') *vs.* percent acetic acid, by volume, on a PVP stationary phase

Species	LOG stability constant[11]	Percent acetic acid in eluent by volume 0	1	2	3	5
Copper acetate	3.63	*	3.0	2.5	2.1	2.4
Copper cyclohexanebutyrate	2.98	*	3.1	2.7	2.4	2.3
Copper naphthenate	†	*	3.2	2.4	2.2	2.4
CuDMD	20.5	0.8	0.6	0.5	0.4	0.5

*The copper carboxylates had a capacity factor greater than 40 for eluents without any acetic acid.

†The stability constant of copper naphthenate is unknown but should be in the same range as the copper acetate and copper cyclohexanebutyrate.

We needed to determine whether the copper compounds would be retained by PVP. If they were retained, we then needed to determine how strongly they were retained and under what conditions they were eluted. It was also important to determine whether the copper speciation was preserved or whether the ligands were displaced from the copper during retention and elution, specifically, if the same copper compound injected was eluted, or if ligand loss or exchange had occurred during retention and separation. This can be substantiated by comparing the ratio of UV and FAA responses for different compounds.

The CuDMD complex was used as a test compound, because it is the dominant copper compound present in fuels containing copper that have been treated with DMD. Figure 3 shows the capacity factor, k', of the CuDMD complex on PVP for different combinations of isopropyl alcohol and hexane. From Fig. 3 we can see that the retention time of the CuDMD complex increases as the hexane concentration increases and the mobile phase becomes less polar. This means the CuDMD complex will be strongly retained by the PVP as long as the mobile phase is non-polar. Since jet fuel is nearly as non-polar as hexane, the capacity factor of CuDMD can be estimated from Fig. 3 to be near 100 when jet fuel flows through the PVP column, which means on-column preconcentration will be feasible.[10]

The other copper compounds investigated in this study were copper carboxylates. Copper carboxylates are copper compounds which might be present in jet fuel that would degrade fuel stability. The copper carboxylates tested had a capacity factor greater than 40 on PVP for all the combinations of hexane and isopropyl alcohol. The copper carboxylates were effectively eluted by a mixture of acetic acid, water and isopropyl alcohol. The water appeared to be necessary for UV detection of the copper carboxylates, which undergo an absorbance shift when hydrated, but changes in the concentration of water in the eluent did not affect the capacity factors of the copper compounds. When the concentration of water in the eluent was greater than 3%, the column back pressure became excessive. The pressure increase is thought to be due to water induced swelling of the PVP.

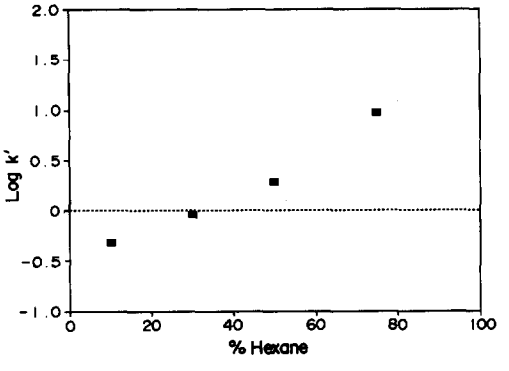

Fig. 3. Log k' of CuDMD complex as a function of percent hexane (by volume) in isopropyl alcohol, where k' is the capacity factor.

The capacity factors of the copper compounds for different combinations of acetic acid and isopropyl alcohol are listed in Table 2. None of the copper carboxylates eluted unless the eluent contained acetic acid. The data in Table 2 indicates all of the copper carboxylates have similar capacity factors for each acetic acid concentration. We believe this is because all the copper carboxylates were eluting as the same species: copper acetate. It seems the copper complexes were intact when they adsorbed on the PVP, but the copper carboxylates underwent ligand exchange during elution. Changing the concentration of acetic acid in the eluent did not significantly change the capacity factors of the copper carboxylates. The peaks just got wider as the acetic acid concentration decreased. This result is thought to be due to the kinetics of the ion exchange process.

The first column in Table 2 lists the logarithms of the stability constants in water,[11] of the copper compounds studied in this investigation. Stability constants, K_s, or formation constants, K_f, describe the strength of a metal ligand complex. The smaller the stability constant of a metal complex, the more likely the complex is to dissociate into metal and ligand ions. This information is significant, because it provides an indication of the likelihood the copper will dissociate while it is being separated. The logarithms of the stability constants listed are for metal complexes in water. The copper complexes should be less prone to dissociate in the solvent systems used in the separation, because they do not support ions as well as water. The CuDMD complex is several orders of magnitude more stable than the copper carboxylates. The copper carboxylates all have similar stability constants, because all the ligands are bound to the copper ion by the same functional group. This is significant, because the stability constant of a copper complex may be related to its

catalytic activity in jet fuel.[5-8] The stability constant of a copper complex may be inversely correlated with the catalytic activity of the copper in jet fuel, because the copper of the more labile species is more available to interact with the components in the fuel, is not as stabilized in one oxidation state, and can act as a catalyst.

Once we had demonstrated that the copper compounds were adequately retained by the PVP to effect a separation, while the majority of the non-polar constituents of jet fuel passed through essentially unretained, we developed a separation of the two classes of copper compounds using the information in Table 2 and Fig. 3. The separation enabled us to distinguish between the copper that would adversely affect fuel stability and the copper that would not. The separation uses a mixture of hexane and isopropyl alcohol to carry the sample to the column and elute the CuDMD. Then a step gradient to a 3% acetic acid in isopropyl alcohol is used to elute the other copper compounds in the sample. Figure 4 is the absorbance chromatogram at 280 nm of a 1.25-ml hexane injection that illustrates the solvent program used to separate the copper compounds. The disturbance between 1 and 3 min is the injection disturbance and the refractive index effects due to the hexane passing through the system. Since acetic acid absorbs weakly at 280 nm, the increase in absorbance between seven and eight minutes is proportional to the acetic acid concentration. This solvent program enabled us to separate the copper complexes into two classes:

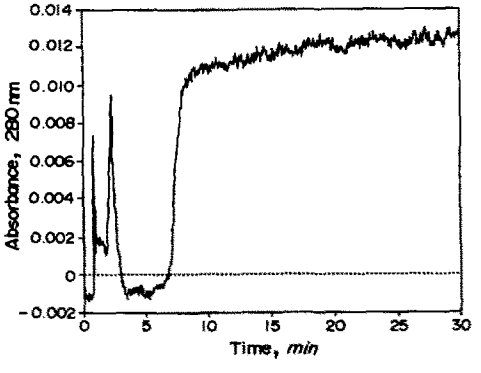

Fig. 4. Solvent program used in normal-phase separation of copper complexes in jet fuel. Absorbance of mobile phase at 280 nm is proportional to the concentration of acetic acid present. The program was 70% isopropyl alcohol/30% hexane from 0–3 min, with sample injection at 0.5 min, 3-end of run was 5% acetic acid and 0.5% water in isopropyl alcohol. The disturbance between 2–3 min is explained in the text.

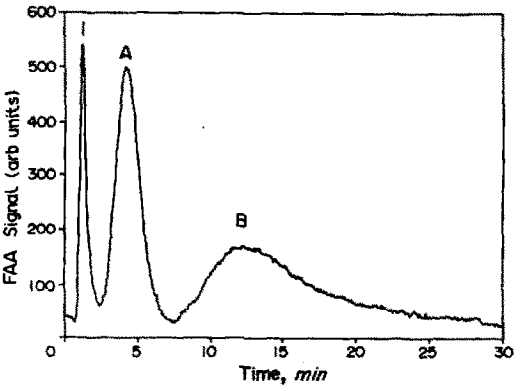

Fig. 5. Normal-phase separation of on-column preconcentrated copper complexes in hexane followed by FAA detection of the Cu signal: (A) CuDMD and (B) Copper carboxylate with (I) injection disturbance explained in text.

CuDMD and the copper carboxylates. This is significant because it enabled us to distinguish, for the first time, the weakly bound copper complexes that would have a detrimental effect on fuel stability from the strongly bound copper complex (CuDMD) that does not affect fuel stability.

Figure 5 shows the separation of two copper compounds in a hexane solution with copper-specific FAA detection. The peak at 4 minutes is CuDMD, the peak at 12.5 min is a copper carboxylate, and the spike at one minute is due to the combustion of the hexane plug, which makes the flame richer; the soot particles of the hexane flame scatter the light.

Having established that the test copper complexes can be separated with a PVP stationary phase, we needed to lower the limit of detection (LOD) to the point where we could detect copper at an adequate level to detect copper concentrations that would cause stability problems. We considered on-column preconcentration,[10] since the copper complexes are readily preconcentrated at high k' while the non-polar constituents of the fuel pass through at low k'. On-column preconcentration was accomplished by injecting a larger volume of jet fuel. Table 3 shows the detected volume of the copper peaks for two different injection volumes. Injecting a

Table 3. On-column preconcentration study: effect of injected volume on eluted peak volume at the base

Volume Injected	25.0 μl	1.25 ml
Peak width, CuDMD	1.61 ml	3.0 ml
Peak width, copper acetate	6.20 ml	13 ml

Table 4. Limit of detection (LOD) for copper carboxylates and copper DMD

Copper complex	Conc. LOD, *ppb*	Mass LOD, *ng*	Relative response factor*	Peak width, *min*
CuDMD	7	9	1.00	3
$Cu(OAc)_2$†	40	50	0.14	13

*This ratio indicates the relative response of the flame AA detector to a copper solution after separation.[12]
†$Cu(OAc)_2$ is copper acetate

sample volume fifty times greater only increased the peak width by a factor of two. This loss of column efficiency is acceptable for the method, because more than adequate chromatographic resolution is achieved with the solvent program to distinguish between the different classes of copper compounds. Thus, the limit of detection (LOD) was substantially improved by on-column preconcentration of a large sample volume.

The injected concentration and mass LODs for the different copper complexes are listed in Table 4. The LODs were the concentrations of copper required to give a signal three times the standard deviation of the baseline noise. The LODs for the different copper species were influenced by the width of the peak and the solvent used for elution.[12-14]

Once we had demonstrated the method could separate and detect the two classes of copper complexes at sufficiently low concentrations to be useful in the evaluation of the stability of fuels, the method was used to analyze several jet fuel samples in order to demonstrate its ability to identify and quantitate strongly and weakly bound copper complexes in real samples. The chromatograms of the jet fuel samples are shown in Fig. 6. Figure 6(A) shows the FAA signal for a fuel sample that has been double clay treated (DCT), a process which removes all the metals from the fuel. This is consistent with the chromatogram that does not indicate the presence of copper. This sample was taken as the baseline, and subtracted from the subsequent fuel samples. Figure 6(B) shows the

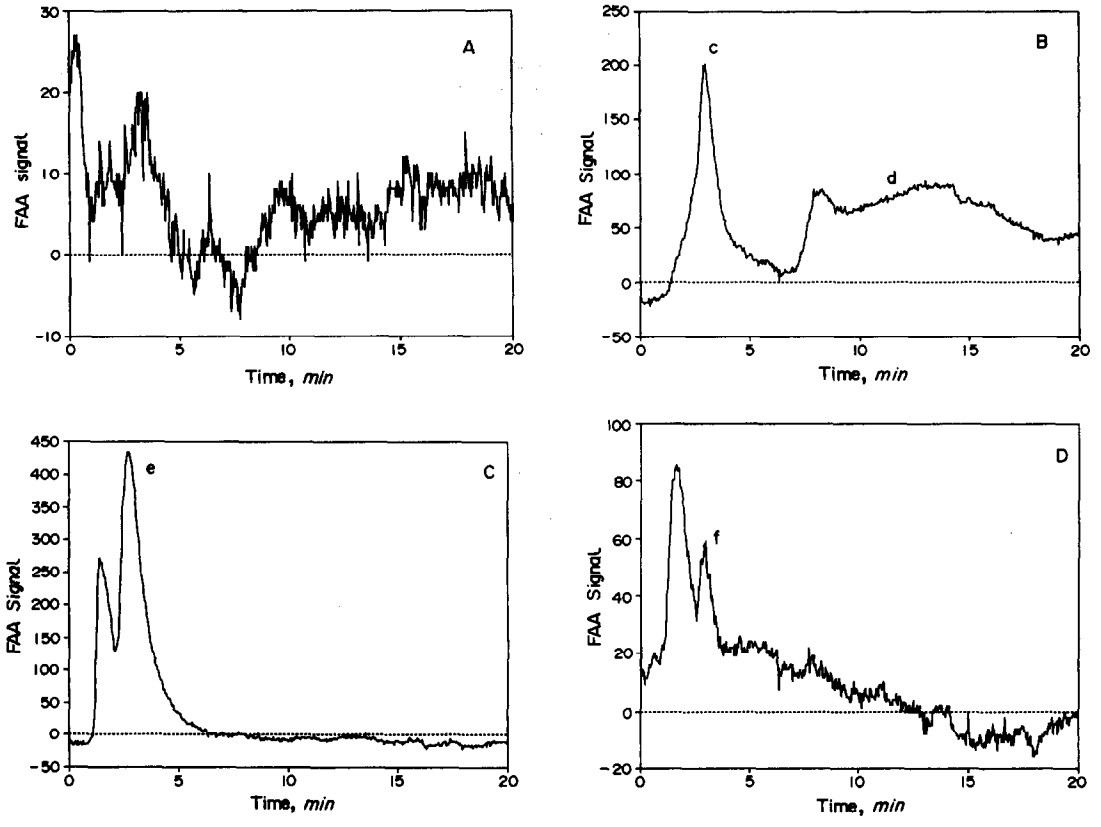

Fig. 6. FAA detection of the normal-phase separation of on-column preconcentrated jet fuel samples run as in Fig. 5, with quantitative results summarized in Table 5 for the labeled features: (A) chromatogram of double clay treated JP-8 with all metals removed, (B) chromatogram of JP-8 that had been standing over copper for 18 hours, (C) chromatogram of Mobil Oil Co. jet fuel, (D) chromatogram of POSF-2691, JP-4.

Table 5. Concentration of copper complexes in jet fuel

	Strongly bound copper*	Weakly bound copper†
Retention time range (*min*):	2–7	7–20
Concentration	ppb	ppb
Double clay Treated JP-8	0	0
JP-8 over Cu Powder	95‡	300‡
Mobil Oil Co., Tarrance, CO	200§	0
POSF-2691, JP-4	14‖	0

*Strongly bound copper elutes between 2–7 min, as defined in Fig. 5.

†Weakly bound copper elutes between 7–20 min, as defined in Fig. 5.

‡Quantitation features shown in Fig. 6(B).

§Quantitation for peak shown in Fig. 6(C), with injection disturbance preceding it.

‖Quantitation for peak shown in Fig. 6(D), with injection disturbance preceding it.

chromatogram of a JP-8 sample that had been standing over copper powder for 18 hours. The chromatogram shows almost 400 ppb of copper was solvated by the fuel, with 95 ppb Cu solvated into a strongly bound form similar to CuDMD and 300 ppb as weakly bound copper. This shows the propensity of jet fuel to solvate any copper with which it is in contact. Figure 6(C) shows the chromatogram of a Mobil Oil Company JP-5 sample from Tarrance Co. The chromatogram shows that the fuel contains 200 ppb of tightly bound copper, probably CuDMD. Figure 6(D) shows the chromatogram of the JP-4 sample POSF-2691, which contains 14 ppb copper in a form similar to CuDMD. Table 5 is a summary of the information about the copper complexes found in the fuel samples.

CONCLUSIONS

We have developed a method capable of differentiating between the copper species that will cause fuel instability and the copper that has been passivated by DMD, with LODs of 40 and 7 ppb respectively. This is the first reported analytical method capable of determining copper near the level where it can cause stability problems while differentiating between the copper that will cause stability problems and the copper that is no longer catalytically active.

Acknowledgements—The authors would like to acknowledge the U.S. Air Force Fuels Research Branch at Wright-Patterson AFB for supporting this research, especially Steve Anderson and Ron Butler.

REFERENCES

1. D. J. Mackey, *J. Chromatogr.*, 1988, **436**, 243.
2. *Idem, ibid.*, 1982, **242**, 275.
3. A. Mazzucotelli, R. Frache, A. Viarengo, C. Martino, *Talanta*, 1988, **35**, 693.
4. B. P. Karcher and I. S. Krull, *J. Chromatogr. Libr.*, Vol. 47, p. 123. Amsterdam, The Netherlands, 1991.
5. C. J. Pederson, *Oil Soluble Complexing Agents as Metal Deactivators*, Dupont Product Literature, 1955.
6. *DMD and DMD-2 Petroleum Additives*, Dupont Product Literature, 1987.
7. R. H. Clarke, *3rd International Conference on Stability and Handling of Liquid Fuels*, p. 283. 1988.
8. Coordinating Research Council, *Literature Survey on the Thermal Oxidation Stability of Jet Fuel*, April 1979, CRC Report No. 509, 1, 53.
9. E. V. Hort, *Encyclopedia of Chemical Technology*, 1978, **23**, 967.
10. B. F. Johnson, J. Bramlage and J. G. Dorsey, *Anal. Chim. Acta*, 1991, **255**, 127.
11. A. E. Martell and R. M. Smith, *Critical Stability Constants*, Vol. 3, Plenum Press, New York, 1977.
12. A. S. Attiyat, *Microchem. J.*, 1987, **36**, 228.
13. I. Kojima and C. Iida, *J. Anal. At. Spectrosc.*, 1987, **2**, 463.
14. A. S. Attiyat, *Can. J. Spectrosc.*, 1987, **32**, 118.

Talanta, Vol. 40, No. 4, pp. 503–506, 1993
Printed in Great Britain.

0039-9140/93 $6.00 + 0.00

SPECTROPHOTOMETRIC STUDY OF Co(II), Ni(II), Cu(II), Zn(II), Cd(II) AND Pb(II) COMPLEXES WITH SOME CROWN ETHERS IN DIMETHYLSULPHOXIDE SOLUTION USING MUREXIDE AS A METALLOCHROMIC INDICATOR

NAADER ALIZADEH
Department of Chemistry, Tarbiat Modarres University, Tehran, Iran

MOJTABA SHAMSIPUR*
Department of Chemistry, Shiraz University, Shiraz, Iran

(*Received* 1 *June* 1992. *Revised* 19 *August* 1992. *Accepted* 19 *August* 1992)

Summary—The complexation reactions between Co(II), Ni(II), Cu(II), Zn(II), Cd(II) and Pb(II) ions and benzo-15-crown-5, dicyclohexyl-18-crown-6, dibenzo-18-crown-6 and 1,10-diaza-18-crown-6 have been studied in dimethylsulphoxide solution at 25° by means of a competitive spectrophotometric method using murexide as a metallochromic indicator. With the exception of Pb(II)(benzo-15-croqn-5)$_2$ the stoichiometry of the resulting complexes was found to be 1:1. The formation constants of the complexes were determined, and found to follow the Irving–Williams rule for the cations of the first transition series. It was found that the metal ion-18-crown interactions are strongly dependent on the nature of the substituents on the ring.

Since Pedersen's discovery of macrocyclic polyethers (crowns) capable of forming stable and selective complexes with the alkali and alkaline earth cations,[1] the studies of these ligands and their complexes become an import field of research. During the past two decades, intensive efforts have been undertaken to understand the factors which control the thermodynamic and kinetic stability and selectivity of the resulting complexes in solution.[2–6] However, most of the investigators have concentrated their efforts on the study of alkali and alkaline earth-crown ether complexes, and the corresponding macrocyclic complexes with transition and heavy metal ions, especially in non-aqueous solutions, have received much less attention.[6]

Because of the low stabilities of most crown ether complexes with the cations of the first transition series,[4,6] as well as the serious interference by hydrolysis of these cations in aqueous crown and cryptand solutions,[7] we chose to study the corresponding complexation reactions in dimethylsulphoxide (DMSO) solution. Using DMSO as a dipolar aprotic solvent removes difficulties associated with transition metal ion hydrolysis.[8] Moreover, in this solvent, the different transition metal salts and crown ethers used are readily soluble and, more importantly, the resulting murexide solutions in DMSO are quite stable (in contrast to the corresponding aqueous solutions).

We have recently reported a spectrophotometric method for the study of the murexide complexes with Co(II), Ni(II), Cu(II), Zn(II), Cd(II) and Pb(II) ions in dimethylsulphoxide solution.[9] In this paper, we employed murexide as a metallochromic indicator to study the resulting complexes between these cations and benzo-15-crown-5 (B15C5), dicyclohexyl-18-crown-6 (DC18C6), dibenzo-18-crown-6 (DB18C6) and 1,10-diaza-18-crown-6 (DA18C6) in dimethylsulphoxide solution by means of a competitive spectrophotometric method.

EXPERIMENTAL

Reagent grade cobalt chloride, nickel chloride, copper chloride, zinc chloride, cadmium nitrate and lead nitrate (all from Merck) were dehydrated and dried as described elsewhere.[9] Reagent grade tetraethylammonium perchlorate (TEAP, Fluka) and murexide (Mu, Merck) were of the highest purity available and were used without further purification except for vacuum

*Author for correspondence.

drying over P_2O_5 for 72 h. Crown ethers B15C5, DC18C6, DB18C6 and DA18C6 (all from Merck) were purified and dried by the previously described methods.[10,11] Spectroscopic grade dimethylsulphoxide (DMSO, Merck) was used as received. All spectra were obtained with a Model 2100 Shimadzu UV-Vis spectrophotometer at $25 \pm 1°$.

The formation constants of the resulting complexes between the crown ethers and metal ions used were determined by the absorbance measurements, at λ_{max} of each murexide–metal ion complex,[7] of solutions in which varying concentration of metal ions (2.0×10^{-4}–$1.0 \times 10^{-3} M$) were added to a fixed concentration of murexide ($2.0 \times 10^{-5} M$) and crown ethers (0.005–$0.03 M$) in DMSO. The ionic strength of all solutions was kept constant at $0.1 M$ using TEAP. All solutions were neutral and, hence, the ligand existed in its monovalent form throughout.[9,12] Attainment of equilibrium was checked by the observation of no further change in the spectra after several hours. It should be mentioned that none of the transition metal complexes with crown ethers used show any absorption band in the visible region in the concentration ranges studied.

As it was pointed out before,[9] in the case of 1:1 complex formation between murexide and a metal ion, M, the following linear relation exists between $(A/A_0 - 1)/C_M$ and A/A_0

$$(A/A_0 - 1)/C_M = \epsilon_{Mu}/\epsilon_{MMu} K'_{MMu} - K'_{MMu} A/A_0 \quad (1)$$

where $A_0 = \epsilon_{Mu} C_{Mu}$ and A, ϵ_{Mu}, ϵ_{MMu}, C_{Mu}, C_M and K'_{MMu} are the absorbance at λ_{max} of complex, molar absorptivity of murexide, molar absorptivity of complex, total concentration of murexide, total concentration of metal ion and apparent formation constant of MMu, respectively. It should be noted that under the neutral conditions used, murexide exists only in its monovalent form[12] and can only form 1:1 complexes with metal ions;[9,13,14] thus, when no other complexing agent is present, K'_{MMu} would be actually equal to the absolute formation constant K_{MMu}. According to equation (1), the value of K'_{MMu} could be obtained from the intercept of the linear plot of $(A_0/A - 1)/C_M$ *vs.* A_0/A.

However, in the presence of a crown ether, as a buffer ligand, the metal ion can also form 1:1 and 2:1 (ligand to metal) crown ether complexes with respective stepwise formation constants

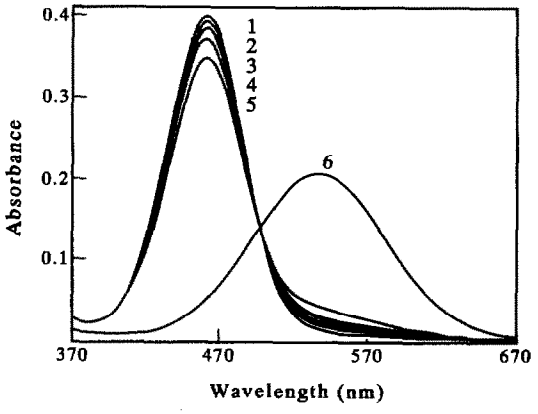

Fig. 1. Plots of $(K_{MMu}/K'_{MMu} - 1)/C_{B15C5}$ *vs.* C_{B15C5}. MMu: 1, Pb–murexide: 2, Zn–murexide.

K_{MC} and K_{MC_2}. In this case, the murexide–metal ion apparent formation constant, K'_{MMu}, can be related to its absolute formation constant, K_{MMu}, by

$$K'_{MMu} = K_{MMu}/\alpha_M \quad (2)$$

Under the experimental conditions $C_C \gg C_M \gg C_{Mu}$, that is the fraction of free metal α_M is given by

$$\alpha_M = 1 + K_{MC} C_C + K_{MC_2} C_2^2 \quad (3)$$

where C_C is the total concentration of crown ether.

Combination of equations (2) and (3) results in

$$\frac{1}{K'_{MMu}} = \frac{1}{K_{MMu}} + \frac{1}{K_{MMu}} (K_{MC} C_C + K_{MC_2} C_C^2) \quad (4)$$

Rearrangement of equation (4) then gives

$$(K_{MMu}/K'_{MMu} - 1)/C_C = K_{MC} + K_{MC_2} C_C \quad (5)$$

According to equation (5), a plot of $(K_{MMu}/K'_{MMu} - 1)/C_C$ *vs.* C_C provides information about the stoichiometry and stability of the metal ion–crown ether complexes. The existence of a linear relation between $(K_{MMu}/K'_{MMu} - 1)$ and C_C reveals the formation of both 1:1 and 2:1 complexes in solution, from the intercept and slope of which K_{MC} and K_{MC_2} could be obtained, respectively. While in the cases where only a 1:1 complex is formed, the (K_{MMu}/K'^{-1}_{MMu}) *vs.* C_C plots give horizontal lines, the intercept of which is equal to K_{MC} (Fig. 1).

RESULTS AND DISCUSSION

The spectra of murexide and its complexes with Co(II), Ni(II), Cu(II), Zn(II), Cd(II) and

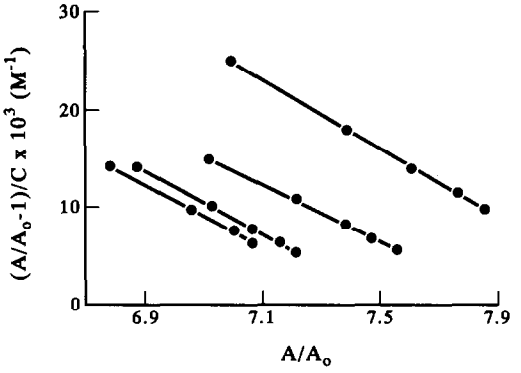

Fig. 2. Visible region spectra for titration of $2.0 \times 10^{-5}M$ murexide with Zn(II) in the presence of $0.01M$ B15C5 and ionic strength of $0.1M$ in DMSO. [Zn(II)]: 1, $4.0 \times 10^{-4}M$; 2, $5.9 \times 10^{-4}M$; 3, $7.9 \times 10^{-4}M$; 4, $9.9 \times 10^{-4}M$; 5, $1.2 \times 10^{-3}M$; 6, murexide alone.

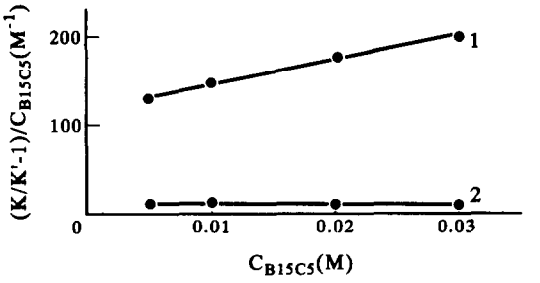

Fig. 3. Plots of $(A/A_0 - 1)/C_M$ *vs.* A/A_0 for Zn(II)–murexide at different concentrations of B15C5 in DMSO. C_{B15C5}: 1, $0.005M$; 2, $0.01M$; 3, $0.02M$; 4, $0.03M$.

Pb(II) ions in DMSO solution are reported elsewhere.[9] All of the resulting complexes are distinguished by a strong spectral shift of about 18–73 nm toward shorter wavelengths, in comparison to the free murexide. In order to determine the stoichiometry and stability of metal ion complexes with B15C5, DC18C6, DB18C6 and DA18C6, the spectra of a series of solutions of fixed murexide and crown ether concentrations and varying amounts of the metal ions were recorded. All spectra presented satisfactory isobestic points. The deviations of spectra from isobestic points were at the most $\pm 5\%$. The spectra of mixtures of murexide and zinc ion in the presence of B15C5 in DMSO solution are shown in Fig. 2 and the corresponding $(A/A_0 - 1)/C_M$ *vs.* A/A_0 plots are given in Fig. 3. The apparent formation constants of metal–murexide complexes were obtained from the slopes of such linear plots. The stoichiometry and stability of different metal–crown ether complexes were determined using the corresponding plots of $(K_{MMu}/K'_{MMu} - 1)$ against C_C. Two samples of the resulting plots are shown in Fig. 1.

With the exception of Pb(II)–B15C5 system, all metal ion–crown ether complexes examined showed a 1:1 stoichiometry. However, in the case of Pb(II) ion, evidences for the formation of both 1:1 and 2:1 (ligand to metal) complexes in DMSO solution was observed. B15C5 has a cavity size (1.7–2.2 Å)[15] that is too small for Pb(II) ion (2.38 Å).[16] Therefore, the cation can only partially penetrate inside the cavity of the ligand and, consequently, a second ligand can approach the cation from the other side to form a 2:1 sandwich complex.[17] In all other cases studied, the size of the cations used (Table 1) are smaller than the cavity size of the three 18-crowns tried (2.6–3.2 Å)[15] and, therefore, the formation of 1:1 complexes is not unexpected.

All calculated formation constants of the resulting complexes between the cations and crown ethers used in DMSO solution are summarized in Table 1. The previously reported stability constants for Cu(II) and Pb(II) complexes with DA18C6 in DMSO are also included for comparison.[18] It should be noted that the Ni(II)–DA18C6 and Zn(II) DA18C6 systems in DMSO showed an unexpected spectrophotometric behaviour (probably due to the

Table 1. Log K_f of different metal ion–crown ether complexes in DMSO

	Log K_f					
Ligand	Co(II)(0.75)*	Ni(II)(0.69)*	Cu(II)(0.77)*	Zn(II)(0.74)*	Cd(II)(0.95)*	Pb(II)(1.19)*
Murexide†	4.56 ± 0.03	5.45 ± 0.05	5.65 ± 0.03	4.27 ± 0.04	4.63 ± 0.03	4.52 ± 0.03
DA18C6	1.82 ± 0.04	—	3.02 ± 0.03	—	2.61 ± 0.03	3.43 ± 0.04
			3.00 ± 0.10‡			4.22 ± 0.02‡
DC18C6	1.48 ± 0.03	2.19 ± 0.04	2.71 ± 0.03	1.70 ± 0.03	1.82 ± 0.03	2.23 ± 0.04
CB18C6	0.80 ± 0.05	1.29 ± 0.03	2.24 ± 0.03	1.46 ± 0.03	0.36 ± 0.05	1.35 ± 0.03
B15C5	0.92 ± 0.05	2.04 ± 0.05	2.78 ± 0.04	0.96 ± 0.05	1.35 ± 0.03	2.07 ± 0.04(1:1)
						1.38 ± 0.05(2:1)

*Ionic radius in angstroms.[14]
†Data from reference 7.
‡Data from reference 18.

existence of a third equilibrium in solution) and, therefore, the corresponding formation constants cannot be determined by the proposed method. As it is seen, the sequence of stability of the first transition series with all crown ethers tried (*i.e.*, Co(II) < Ni(II) < Cu(II) > Zn(II)) follows the Irving–Williams order,[19] which generally holds for the equilibrium constants of transition metals. On the other hand, Pb^{2+} ion forms more stable complexes[5] than Cd(II) ion with 18-crowns used, mainly because of the better fitting condition of this cation inside the macrocyclic ligands' cavity.

Comparison of the data given in Table 1 shows that among 18-crowns used, where the ring frame remains the same, metal ion–crown ether interaction is strongly a function of the nature of substituents on the ring which control both the electron-pair donicity and the flexibility of the ligand molecules. It is seen that DA18C6 forms the most stable complexes and DB18C6 the least stable ones in the series. The two nitrogen atoms of DA18C6 ring, as soft bases, would interact more strongly with the transition metal ions as soft or intermediate acids[20] than oxygen atoms, as hard bases. It should be noticed that DA18C6 has also the most flexible structure among the 18-crowns used, so that the macrocyclic molecule can easily wrap itself around the cations, inducing more stability to the resulting complexes.

Table 1 shows that, substitution of two benzo groups on the 18C6 ring lowers the stability of the resulting complexes in comparison to DC18C6. This behaviour may be attributed to some combination of the electron-withdrawing property of benzo groups which weakens the electron-donor ability of the oxygen atoms of the ring, and reduced flexibility of the ligand which prevents the macrocyclic molecule wrapping itself around the cation.[10,11]

REFERENCES

1. C. J. Pedersen, *J. Am. Chem. Soc.*, 1967, **89**, 7017.
2. I. M. Kolthoff, *Anal. Chem.*, 1979, **51**, 1R.
3. J. D. Lamb, R. M. Izatt, J. J. Christensen and D. J. Eatough, in G. A. Melson(Ed.), *Coordination Chemistry of Macrocyclic Compounds*, Chap. 1, Plenum, New York, 1979.
4. R. M. Izatt, S. J. Bradshaw, S. A. Nielsen, J. D. Lamb, J. J. Christensen and D. Sen, *Chem. Rev.*, 1985, **85**, 271.
5. M. Shamsipur, *Iranian J. Chem. Eng.*, 1988, 59.
6. R. M. Izatt, K. Pawlak, J. S. Bradshaw and R. L. Bruening, *Chem. Rev.*, 1991, **91**, 1721.
7. B. G. Cox, P. Firman and H. Schneider, *Inorg. Chem.*, 1982, **21**, 2320.
8. R. Pizer and R. Selzer, *Inorg. Chem.*, 1983, **22**, 1359.
9. M. Shamsipur and N. Alizadeh, *Talanta*, in the press.
10. S. Kashanian and M. Shamsipur, *Inorg. Chim. Acta*, 1989, **155**, 203.
11. A. Semnani and M. Shamsipur, *J. Electroanal. Chem.*, 1991, **315**, 95.
12. K. L. Cheng, K. Ueno and T. Imamura, *CRC Handbook of Organic Analytical Reagents*, p. 291, CRC Press, Boca Raton, Florida, 1982.
13. S. Kashanian, M. B. Gholivand, S. Madaeni, A. Nikrahi and M. Shamsipur, *Polyhedron*, 1988, **7**, 1227.
14. M. Shamsipur, S. Madaeni and S. Kashanian, *Talanta*, 1989, **36**, 773.
15. C. J. Pedersen, *J. Am. Chem. Soc.*, 1970, **92**, 386.
16. R. D. Shannon, *Acta Crystallogr. Sect. A.*, 1976, **32**, 751.
17. J. Massaux, G. Roland and F. Desreux, *Inorg. Chim. Acta*, 1982, **60**, 129.
18. F. Arnaud-Neu, B. Spiess and M. J. Schwing-Weill, *J. Am. Chem. Soc.*, 1982, **104**, 5641.
19. H. Irving and R. J. P. Williams, *J. Chem. Soc.*, 1953, 3192.
20. R. G. Pearson, *J. Am. Chem. Soc.*, 1963, **84**, 3533.

Talanta, Vol. 40, No. 4, pp. 507–510, 1993
Printed in Great Britain.

0039-9140/93 $6.00 + 0.00

SPECTROPHOTOMETRIC DETERMINATION OF URANIUM USING ASCORBIC ACID AS A CHROMOGENIC REAGENT

K. K. GUPTA, P. G. KULKARNI, GEORGE THOMAS, N. VARADARAJAN, R. K. SINGH* and M. K. T. NAIR

Fuel Reprocessing & Nuclear Waste Management Group, PREFRE Plant, B.A.R.C., Tarapur, India

(*Received* 9 *April* 1992. *Revised* 19 *August* 1992. *Accepted* 19 *August* 1992)

Summary—A spectrophotometric method has been developed for the determination of uranium(VI) using ascorbic acid. Uranium in the hexavalent state forms a reddish-brown coloured complex with ascorbic acid. The colour intensity of the complex is maximum at pH 4.2–4.5 and is stable for 24 hr. The absorbances of uranium(VI)–ascorbic acid complex at 360 and 450 nm are used for its quantification. Uranium in the range 8–200 μg/ml has been determined with good precision. The method allows the determination of uranium in the presence of many metal ions present as impurities. The described method is simple, accurate and applicable to uranium concentration relevant to the PUREX process and thus can be used for analytical control purposes.

The PUREX process is employed commercially to recover uranium and plutonium by reprocessing spent nuclear fuels. The uranium concentration is determined in various streams for process control in plant operations. Spectrophotometric methods are the most commonly and widely used analytical techniques for uranium determination. In general, these methods are based on the colour reaction of U(VI) with two types of chromogenic reagents. These are intensely coloured organic reagents forming chelate types of complexes and inorganic reagents containing oxygen and sulphur donors, forming simple coordination complexes with U(VI). Methods based on the former type of reagents like dibenzyolmethane (DBM), 1-(2-pyridylazo)-2-napthol (PAN), 5-dimethylamino-2-(2-thiazolyazo) (TAM), arsenazo(III) and 8-hydroxyquinoline are highly sensitive but less specific and therefore have poor tolerance for trace level impurities present in the sample.[1–5] In the application of such methods the prior chemical separation of U(VI) is, therefore, mandatory. The chemical separation steps are often time consuming and tedious in nature, making such methods unsuitable for process control analysis purposes.[6] On the other hand methods based on the latter type of chromagenic reagents are relatively simple and rapid. Two such methods currently in use are based on the colour reactions of uranyl ion with hydrogen peroxide and alcoholic ammonium thiocyanate.[7,8] The peroxide method finds limited application owing to its poor sensitivity and selectivity. The alcoholic ammonium thiocyanate method has relatively good sensitivity and selectivity. However, the waste generated in this procedure causes serious concern. The corrosive nature and relatively high concentration of thiocyanate pose typical waste management problems. The alcohol fraction of the waste constitutes a fire hazard and necessitates additional precautions, while storing or disposing. To circumvent these problems, a new spectrophotometric method has been developed for the estimation of uranyl ion in aqueous as well as organic streams of the PUREX process. The method involves the use of ascorbic acid as a chromogenic reagent for uranyl ion in aqueous media. The results of analysis of some synthetic samples and actual PUREX process samples are reported here.

EXPERIMENTAL

Apparatus

Absorbance measurements were made with a Shimadzu UV–Vis-160 double beam microcomputer-controlled recording spectrophotometer with 1 cm path glass cells. A glass electrode pH meter was used for pH measurements.

*Author for correspondence.

Reagents

Standard uranium solution. A uranium(VI) stock solution (5 mg/ml) was prepared by dissolving nuclear pure grade U_3O_8 powder (obtained from Uranium Metal Plant, B.A.R.C.) in 1:1 nitric acid and standardized by a modified Davis & Gray method using potentiometric end point detection.[9]

Ascorbic acid solution. *L*-Ascorbic acid, $C_6H_8O_8$ (Polypharm, Bombay), was dissolved in distilled water to make a 1*M* solution and filtered through Whatman 41 paper.

Sodium carbonate solution. Sodium carbonate, Na_2CO_3 (Qualigens fine Chemicals, Bombay), was dissolved in distilled water to make a 0.5*M* solution.

Chromogenic reagent. Chromogenic reagent was prepared as and when needed by mixing 1*M* ascorbic acid solution, 0.5*M* sodium carbonate solution and distilled water in the proportion 7:4:9 to the required total volume.

All chemicals used were of analytical reagent grade.

Preparation of synthetic acidic uranium sample. Fixed aliquots of U(VI) standard solution were evaporated to dryness in different vials. The residue of each of these vials was dissolved in nitric acid of varying strength keeping the volume constant.

Procedure and calibration

A weighed or volumetric aliquot of the sample solution up to 0.5 ml in volume and containing not more than one milli equivalent of nitric acid was transferred quantitatively into a 25 ml capacity standard flask. The solution was made up to the mark with freshly prepared chromogenic reagent. The content of the flask was mixed well by shaking and the absorbance of the resultant solution was measured at 360 nm (0.2–1.0 mg U) or 450 nm (1–5 mg U) against a reagent blank. The amount of uranium present in an aliquot can be computed with the following equations:

$$U = 1.4887\ A_1 + 0.0098 \text{ (360 nm)}$$

or

$$U = 4.2696\ A_2 + 0.0001 \text{ (450 nm)}.$$

Here U is the uranium amount (mg) present in the sample aliquot and A_1 and A_2 are the measured absorbances at 360 nm and 450 nm, respectively.

Ten weighed aliquots of the standard uranium solution covering the range from 0.2–5 mg were evaporated to dryness into separate beakers and the content of each beaker was

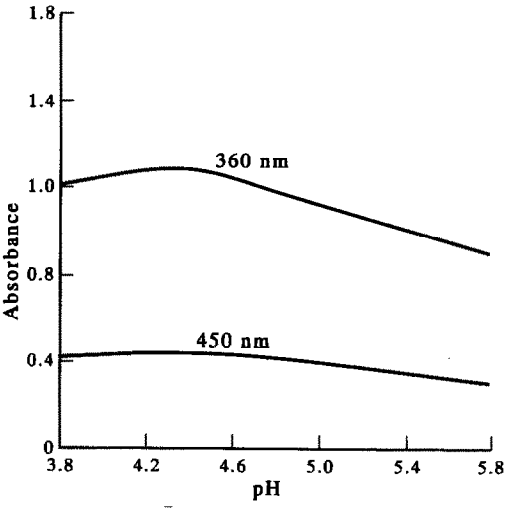

Fig. 2. Effect of pH.

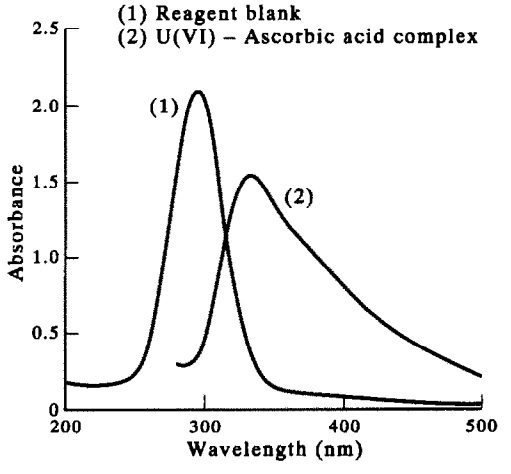

Fig. 1. Absorbance spectra.

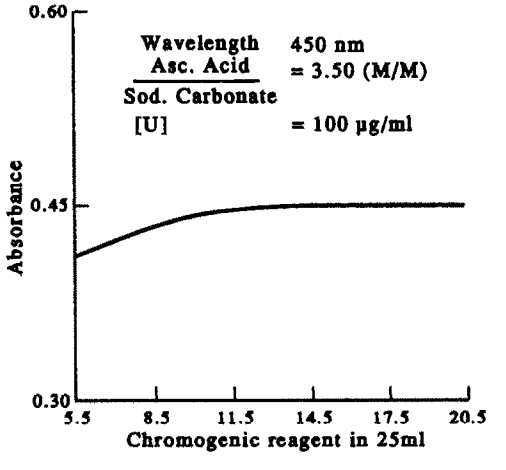

Fig. 3. Optimization of amount of chromogenic reagent.

Table 1. Uranium determination by ascorbic acid (synthetic samples)

	360 nm			450 nm		
	Uranium (*mg*)			Uranium (*mg*)		
	Taken	Found	Relative error (%)	Taken	Found	Relative error (%)
1.	0.173	0.168	−2.9	1.048	1.038	−1.0
2.	0.467	0.479	+2.5	2.167	2.173	+0.3
3.	0.621	0.610	−1.8	3.170	3.189	+0.6
4.	0.836	0.842	+0.7	4.276	4.261	−0.4
5.	1.079	1.088	+0.8	4.982	5.011	+0.6

transferred quantitatively into separate 25 ml standard flasks using chromogenic reagent. The absorbance of the developed colour was measured according to the procedure described earlier. The calibration equations were obtained by regression analysis.[10]

RESULTS AND DISCUSSION

Absorption spectra

Uranium forms a 1:1 complex with ascorbic acid. The instability constant of the complex $[UO_2HA]^+$ at 20° is 3.3×10^{-3} as reported.[11] The complex has the maximum absorption at 335 nm (Fig. 1). At this wavelength the chromogenic reagent itself has significant absorption and hence absorbance measurements are made at 360 and 450 nm which obey Beer's law. The complex has a molar extinction coefficient of about 4000 at 360 nm and 1400 at 450 nm. The complex is stable for 24 hours.

Effect of pH

The complex formation and its absorbance is influenced by the pH of the medium (Fig. 2). At the pH range 4.2–4.5 the absorbance is constant. There is no need for preneutralization of acidic samples since the chromogenic reagent itself acts as a buffer possessing sufficient buffer capacity, hence the system needs no external buffer for pH control.

Amount of chromogenic reagent

At the fixed ratio of ascorbic acid to sodium carbonate, the optimum amount of the chromogenic reagent necessary for the quantitative complexation of uranium is evaluated (Fig. 3).

Analysis of the synthetic samples

Analysis results of synthetic samples are reported in Table 1.

Interferences

Iron, zirconium and plutonium are the potential interferents expected in the uranium determination in PUREX process stream samples. The effects of these metal ions has been studied and the results are listed in Table 2. It can be seen from the data that Zr and Fe do not interfere up to a 1:1 ratio (w/w). The method is also free from Pu interference up to a 1:2 ratio (w/w). Nitric acid influence on uranium estimation has been studied and the results are summarized in Table 3. No significant interference is observed up to 1 meq. nitric acid in the sample aliquot. Interference caused by some anions like sulphate, phospate and fluoride has been reported.[10] These ions are rarely encountered in significant amount in PUREX process streams and hence were not tested in this work.

Table 2. Determination of uranium in the presence of foreign metals

Uranium taken (*mg*)	Element present (*mg*)	Uranium found (*mg*)	Relative error (%)
2.092	Zr	2.062	−1.43
2.023	0.214	2.012	−0.54
2.133	0.535	2.166	+1.54
2.026	1.070	2.019	−0.34
2.000	2.140	1.989	−0.55
2.131	Fe	2.161	+1.40
2.161	0.210	2.196	+1.62
2.092	0.416	2.010	−3.92
2.131	0.521	2.112	−0.89
2.016	1.021	1.998	−0.89
2.109	2.021	2.186	+3.65
1.842	Pu	1.821	−1.14
1.804	0.100	1.820	+0.89
1.926	0.200	1.954	+1.45
2.142	0.250	2.124	−0.84
2.153	0.500	2.211	+2.69
1.986	1.000	1.996	+0.50

Analysis of actual PUREX process samples

The method was tested with some process samples preanalysed by isotopic dilution mass spectrometry (IDMS)[12] and potentiometry[9], after suitable dilution. The comparative results are given in Table 4 and are in good agreement.

Table 3. Influence of nitric acid on uranium estimation, Uranium standard conc. = 83.399 mg/g

Nitric acid added (*meq.*)	Uranium found (*mg/g*)	Relative error (%)
—	83.987	+0.7
0.25	84.431	+1.2
0.50	83.401	+0.0
0.75	82.827	−0.7
1.00	82.043	−1.6

Table 4. Analysis of actual PUREX process samples

Sample	Uranium analysis by method (*g/l*) A	B	Relative error (%)
Feed 1	213.59*	216.89*	+1.5
Feed 2	94.32*	93.17*	−1.2
O.S. 1	89.40	90.72	+1.5
O.S. 2	85.33	84.61	−0.8
O.S. 3	80.21	81.03	+1.0
O.S. 4	78.53	79.19	+0.8
U.P. 1	85.62	84.56	−1.2
U.P. 2	81.74	82.59	+1.0
U.P. 3	243.95	241.63	−1.0
U.P. 4	205.65	204.08	−0.8
U.P. 5	315.35	317.90	+0.8
U.P. 6	404.60	408.34	+0.9

A—IDMS/Potentiometry Method
B—Present Method
O.S.—Organic Stream
U.P.—Uranium Product
*Value in mg/g.

Reliability

Aged ascorbic acid solution introduces a bias in the method. To avoid this, ascorbic acid solution should be prepared daily.

The precision of the method (RSD, 11 determinations) is found to be ±2% and ±1% at 0.5 and 5 mg levels respectively.

Acknowledgements—The authors express their sincere thanks to Shri A. N. Prasad, Director, F.R. and N.W.M. Group for his keen interest and encouragement given during the work. The authors are also thankful to the members of the mass spectrometry group and Shri Pintu Sen for their help and cooperation provided at various stages of the work.

REFERENCES

1. Yoe J. H. *et al. Anal. Chem.* 1953, **25**, 1200.
2. K. L. Cheng *et al. Ibid.*, 1953, **27**, 782.
3. E. Sorensen, *Acta Chem. Scand.*, 1960, **14**, 965.
4. V. I. Kuznetsov, *Radiokhim*, 1960, **2**, 689, *Anal. Abstr.*, 1961, 4613.
5. K. Motozima *et al. Anal. Chem.*, 1961, **32**, 1083.
6. F. Baumgartner *et al. Journal of Radioanalytical Chemistry*, 1980, Vol. 58.
7. I. M. Kolthoff *et al.* (ed.): *Treatise on analytical chemistry*, Part II, p. 100. Interscience 1962.
8. Carl E. Crouthamel *et al. Anal. Chem.*, 1952, **24**, 1780.
9. F. P. Roberts *et al.* (ed.), NUREG/CR-3584, Method 3.0, 1984.
10. Edward L. Bauer, *A Statistical Manual for Chemists*, Academic Press, 1971.
11. P. N. Palei, (ed.) *Analytical Chemistry of Uranium*, Israel Program for Scientific Translations, Jerusalem, 1963.
12. A. D. Moorthy *et al. B-8, Third National Symposium on Mass Spectrometry*, Hyderabad, 1985.

Talanta, Vol. 40, No. 4, pp. 511–514, 1993
Printed in Great Britain.

0039-9140/93 $6.00 + 0.00

SIMULTANEOUS DETERMINATION OF MULTICOMPONENTS BY FLOW INJECTION ANALYSIS

DETERMINATION OF COPPER AND ZINC IN SERUM BY USING ZINCON AS COLOURING REAGENT

REN-MIN LIU, DAO-JIE LIU and AI-LING SUN

Department of Chemistry, Liaocheng Teachers College, Liaocheng, Shandong, People's Republic of China

(*Received* 5 *March* 1992. *Revised* 19 *August* 1992. *Accepted* 19 *August* 1992)

Summary—A flow injection system is described for the simultaneous determination of copper and zinc with a single detector. Two sample plugs are injected into the same carrier stream sequentially. One is for zinc determination and the other is for the sum of copper and zinc. For zinc determination, copper masking reagent is simultaneously injected into a parallel carrier stream and merged with the sample plug by using the merging zone technique. Zincon is used as the colour reagent for the spectrophotometric determination of copper and zinc. The results for the analysis of serum by the proposed method correspond well with those obtained by an AAS method. The rate of analysis is about 45 samples/hr.

Flow injection analysis (FIA) has increasingly been used in various fields, owing to its high sample throughput, cost effective performance and versatility. Whereas in the initial development of FIA, methods were focussed on finding selective methods of detection, a recent trend has been the design and optimization of measuring systems for the simultaneous determination of two or more components, *e.g.*, multicomponent determination.[1–5]

Copper and zinc are essential micro-elements in the human body. The determination of copper and zinc, especially their ratio, in serum is of great interest in clinical chemistry.[9] Several FIA atomic spectroscopy methods have been reported for the simultaneous determination of copper and zinc in serum,[6–8] whereas few methods have been based on spectrometric detection.

Zincon is a sensitive reagent for copper and zinc. In the present work, zincon is used as the reagent for the determination of copper and zinc by using a flow injection analysis system. A three-loop system is used to sequentially inject two samples, one of which is merged with a copper masking solution. In this manner, two FIA peaks are sequentially recorded, one the sum of copper and zinc, the other zinc only.

EXPERIMENTAL

Reagents

Standard stock solution of copper. 1.0 mg/ml.

Standard stock solution of zinc. 1.0 mg/ml.

Copper masking reagent. A 5% (m/V) solution of thiourea.

Buffer solution (carrier). A 12.4-g weight of boric acid, 13 g of potassium chloride, 3.1 g of sodium citrate, 1.5 g of sodium triphosphate and 0.13 g of 1,10-phenanthroline were dissolved in 800 ml of water and the pH was adjusted to 9.0. The solution was then diluted to 1000 ml.

Zincon solution. 0.05% aqueous solution.

Apparatus

The flow injection manifold used is shown in Fig. 1. A Hitachi 220A spectrophotometer equipped with a flow cell was used as the detector. A dual six-way rotary valve (provided by Yellow Sea Fisheries Research Institute, Chinese Academy of Fisheries Sciences) with three loops was used for sample and copper masking reagent injection. The connection of the valve was shown in Fig. 2.

Procedure

The FIA system is connected up with PTFE tubing (1.0 mm i.d.) according to the arrange-

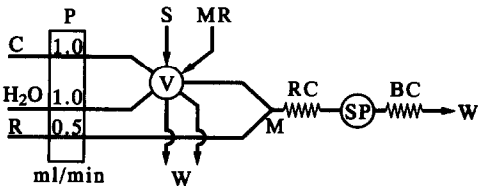

Fig. 1. Schematic diagram of FIA system. C, carrier (buffer solution); R, zincon solution; P, peristaltic pump; S, sample; MR, copper masking reagent; V, injection valve (PTFE); M, confuence point; RC, reaction coil (1.0 mm i.d., 120 cm long); BC, back-pressure coil (0.5 mm i.d., 2.0 m long); SP, spectrophotometer; W, waste.

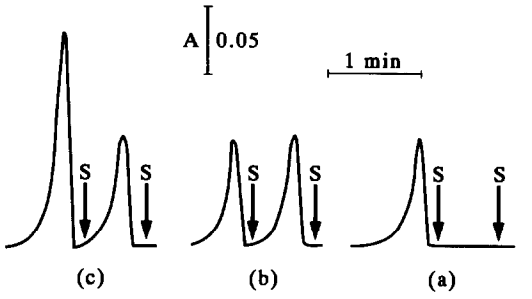

Fig. 3. Typical recordings for copper and zinc, (a) 1.0 μg/ml copper alone; (b) 1.0 μg/ml zinc alone; (c) 1.0 μg/ml copper and 1.0 μg/ml zinc in a mixture. The first (right) peak is for the sample in loop 2 and the second is for the sample in loop 3. S marks the time of injection for each sample plug.

ment shown in Fig. 1. The connection and operation of the injection valve is shown in Fig. 2. Three loops are mounted on the injection valve. Two are for samples and one is for the copper masking reagent. The sample plugs are injected into the carrier solution sequentially for separate spectrophotometric measurements. One is for zinc determination and the other is for the sum of copper and zinc. For zinc determination, the copper masking reagent is simultaneously injected into another carrier (water) and merges with the sample plug by the merging zones technique. The absorbance is red in the flow-cell at 606 nm. Two peaks are observed for the two separate injections, shown in Fig. 3(b). The first peak corresponds to zinc and the second to the sum of copper and zinc. Using the peak height as a measure of absorbance, copper absorbance can be calculated by the difference between the two peaks.

Prepare a series of mixed standard solutions of Cu(II) and Zn(II). Inject these solutions into the carrier solution as described for sample solutions, before and after the sample runs.

RESULTS AND DISCUSSION

FIA manifold for simultaneous determination

In the present approach, two sample plugs were injected into the same carrier solution sequentially. The second is injected after the signal for the first is recorded. One is for zinc determination and the other for the sum of copper and zinc. For the determination of the sum of copper and zinc, only the sample plug was injected into the carrier, and for the determination of zinc, the copper masking reagent was merged with the sample. A 120-cm reaction coil for colour-reaction was found to be suitable both for the determination of zinc and the sum of copper and zinc. The peak separation of the two sample plugs can be controlled by adjusting the interval of the injections. Good separation of the two peaks as shown in Fig. 3 can be obtained when the injection interval is 30–40 sec.

Determination of zinc and copper with zincon.

Zincon reacts with zinc and copper to form blue complexes. The absorption spectra of these

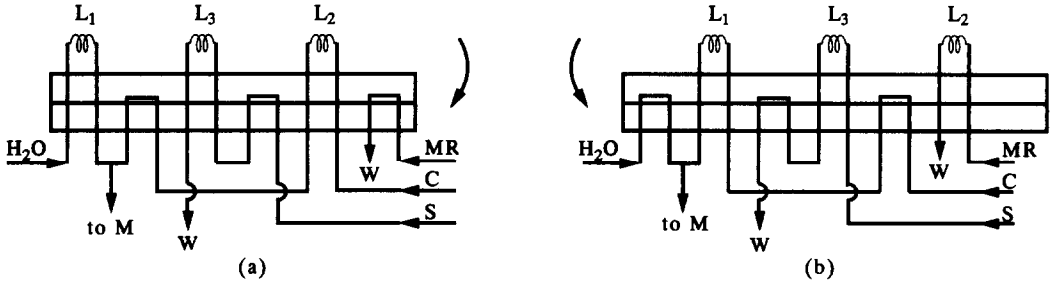

Fig. 2. Injection valve and loop configurations, (a) state of determination of zinc; (b) state of determination of the sum of copper and zinc; L1, loop for copper masking reagent injection (120 μl); L2, loop for sample injection in determination of zinc (80 μl); L3, loop for sample injection in determination of the sum of copper and zinc (80 μl). Other symbols are as for Fig. 1.

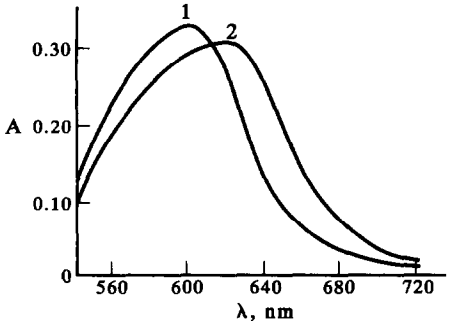

Fig. 4. Absorption spectra of Cu(II)–zincon and Zn(II)–zincon complexes, (1) 0.8 μg/ml of copper; (2) 0.8 μg/ml of zinc.

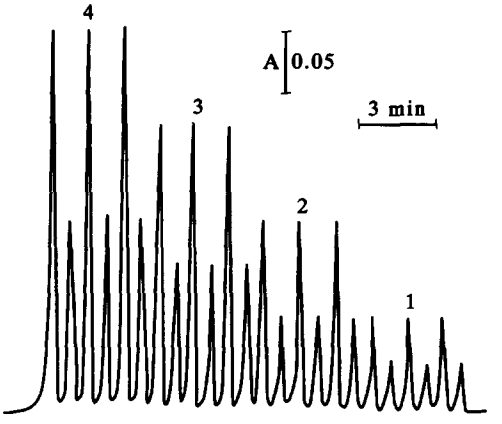

Fig. 5. Recorded signals of mixed standard solutions of copper and zinc. The first (right) peak corresponds to zinc and the second to the sum of copper and zinc. 1, 0.5 μg/ml copper and 0.5 μg/ml zinc; 2, 1.0 μg/ml copper and 1.0 μg/ml zinc; 3, 1.5 μg/ml copper and 1.5 μg/ml zinc; 4, 2.0 μg/ml copper and 2.0 μg/ml zinc.

complexes, as shown in Fig. 4, intersect at 606 nm, at which their absorption coefficients are equivalent ($a_{Cu} = a_{Zn} = a$). The absorbance at this point in the zinc determination in the FIA system can be described as:

$$A = a_{Zn} \cdot b \cdot C_{Zn} = a \cdot b \cdot C_{Zn}$$

The absorbance in the determination of the sum of copper and zinc can be described as:

$$A = a_{Zn} \cdot b \cdot C_{Zn} + a_{Cu} \cdot b \cdot C_{Cu}$$
$$= a \cdot b(C_{Zn} + C_{Cu})$$

A wavelength of 606 nm was chosen both for measurement of zinc and the sum of copper and zinc.

For this simultaneous determination, it was desirable for the zinc signal to be obtained separately in addition to the signal of the sum of copper and zinc. It was decided to mask copper with thiourea. Experiments at pH 9.0 with borate solution indicated that copper could be masked by thiourea since only one peak was obtained when the solution containing only copper was injected [Fig. 3(a)].

Zincon reacts with copper at pH 5–9.5 and zinc at 8–9.5.[10] The effect of the concentration of buffer solution was also studied. Maximum peak heights can be obtained when 0.20*M* borate solution was used. As a result, a pH of 9.0 for complex formation and a buffer solution of 0.20*M* borate were employed.

The effect of the concentration of zincon on the peak height was studied by injecting a mixed solution of 2 μg/ml zinc and 2 μg/ml copper. The peak height was found to be almost independent of the concentration of zincon in the range 0.025–0.075%. A 0.05% solution of zincon was chosen for this study.

Calibration

Under the conditions described, mixed standard solutions of zinc and copper (mass ratio 1:1) were measured (shown in Fig. 5). The calibration graph was linear in the range 0–5 μg/ml for the sum of copper and zinc. The linear ranges of the individual elements are also 0–5 μg ml.

Mixed standard solutions of different ratios of copper and zinc between 0/50 and 50/0 were also measured. The slopes of the calibration curves for copper and zinc were in good agreement with those of the corresponding calibration graphs for the individual elements. Recoveries of copper and zinc in synthetic mixtures were determined (Table 1). Table 1 indicates good recoveries of zinc and copper in synthetic mixtures can be obtained, even at

Table 1. Recovery of copper and zinc in synthetic mixtures

Cu added (μg/ml)	Zn added (μg/ml)	Cu found (μg/ml)	Zn found (μg/ml)	Recovery(%) Cu	Zn
0	2.00	0	2.02		101
0.40	1.60	0.41	1.58	103	98.8
0.80	1.20	0.78	1.19	97.5	99.2
1.20	0.80	1.22	0.80	102	100
1.60	0.40	1.57	0.41	98.1	103
2.00	0	1.97	0	98.5	

Table 2. Determination of copper and zinc in serum of healthy people and leukosis patients (μg/ml)

Sample	Number	Age	Cu	Zn	Cu/Zn
Healthy	18	35–42	0.98 ± 0.06	1.07 ± 0.08	0.92 ± 0.05
Leukosis	18	35–42	1.07 ± 0.21	0.82 ± 0.16	1.30 ± 0.28

Table 3. Results for four samples analysed by the proposed method and an AAS method

	Metal ion found (μg/ml)			
	Proposed method		AAS method	
Sample no.	Cu	Zn	Cu	Zn
1	0.98 (0.67)*	1.12 (0.56)	0.96	1.09
2	0.95 (0.62)	1.07 (0.52)	0.97	1.03
3	1.21 (0.81)	0.84 (0.58)	1.15	0.87
4	1.16 (0.77)	0.87 (0.64)	1.16	0.89

*Values in the parentheses are the relative standard deviations in percent of six determinations.

differing ratios. The relative standard deviations for 0.5 μg/ml copper and zinc in a synthetic mixture were 0.9 and 0.7%, respectively.

Interference

Iron(III), manganese(II), nickel(II), cobalt (II), aluminum(III) and cadmium(II) interfere in the determination.[11] The interference of these elements at levels present in serum can be masked by the addition of sodium citrate, sodium triphosphate and 1,10-phenanthroline in the carrier solution.[11] Iron(III), aluminum(III), manganese(II), and cadmium(II) can be masked by citrate and triphosphate. Cobalt(II), nickel(II) and cadmium(II) can be masked by 1,10-phenanthroline.

Application

The proposed FIA method was applied to the determination of zinc and copper in serum samples of healthy people and leukosis patients. Mix 1.0 ml of serum and 1.0 ml of 2.0*M* hydrochloric acid. Shake and allow to stand for 10 min. Then add 0.5 ml of 20% trichloroacetic acid and heat for 10 min in a 90–95° water-bath with continued stirring. Cool with water and centrifuge at 3000 rpm. Adjust the pH of the supernatant liquid to about 7.0 and analyse by the proposed method. The results are listed in Table 2.

Table 2 shows that the ratio of Cu/Zn of healthy people and leukosis patient had a significant difference.

The samples listed in Table 2 were also determined by an AAS method. The results of the proposed method were in good agreement with those of the AAS method. The results of four samples are listed in Table 3.

REFERENCES

1. K. Oguma and R. Kuroda, *J. Flow Inject. Anal.*, 1985, **2**, 98.
2. S. Motomizu and M. Onoda, *Anal. Chim. Acta*, 1988, **214**, 298.
3. K. Cammann, *Z. Anal. Chem.*, 1988, **329**, 691.
4. S. Kozuka, K. Saito, K. Oguma and R. Kuroda, *Analyst*, 1990, **115**, 431.
5. T. Yamane and E. Goto, *Talanta*, 1991, **39**, 139.
6. B. F. Rocks, R. A. Sherwood, L. M. Bayford and C. Riley, *Ann. Clin. Biochem.*, 1982, **19**, 338.
7. C. W. McLeod, P. J. Worsfold and A. G. Cox, *Analyst*, 1984, **109**, 327.
8. A. N. Araujo and J. L. F. C. Lima, *J. Trace Elem. Electrolytes Health Dis.*, 1989, **3(2)**, 97.
9. X. Kong, *The Nutritional, Physicological and Clinical Significance of Essential Micro-elements*, pp. 177 and 234. Anhui Scientific and Technical Press, Hefei, 1983.
10. Y. Zeng, H. Zhang and Z. Cheng, *Handbook of Modern Chemical Reagents*, Fourth Section, *Color Reagents of Inorganic Ions*, p. 639. Chemical Industry Press, Beijing, 1989.
11. Y. Pan and J. Wang, *Physical Testing and Chemical Analysis*, 1991, **27**, 235.

Talanta, Vol. 40, No. 4, pp. 515–520, 1993
Printed in Great Britain.

0039-9140/93 $6.00 + 0.00

EQUILIBRIA AND SPECTROELECTROCHEMICAL STUDIES ON THE FORMATION OF MULTIBRIDGED TRIS(BIPYRAZINE) RUTHENIUM(II) COMPLEXES WITH RUTHENIUM–EDTA GROUPS

HENRIQUE E. TOMA* and ROSANA L. SERNAGLIA
Instituto de Química, Universidade de São Paulo, Caixa Postal 20780, CEP 01498, São Paulo, SP, Brazil

(*Received* 30 *June* 1992. *Revised* 18 *August* 1992. *Accepted* 18 *August* 1992)

Summary—The tris(bipyrazine) ruthenium(II) complex forms a series of complexes containing $[Ru^{II/III}EDTA]^{2-/-}$ groups coordinated to the peripheral nitrogen atoms of the bipyrazine bridging ligand. These groups exhibit similar redox potentials ($E^0 = 0.38$ V *vs.* SHE) and a very weak electronic coupling through the central complex. When the peripheral Ru(III) groups are reduced to the Ru(II) state, strong charge-transfer bands appear at 490 and 670 nm and the stability constants increase by 7 orders of magnitude due to d_π–p_π^* back-bonding interactions involving the peripheral ions and the bipyrazine ligand.

Binding of ruthenium–EDTA and related complexes to a central bridging unity such as the meso-tetrapyridylporphyrin, TPyP,[1–4] has provided a useful approach for the design of multibridged systems displaying unusual chemical and electrocatalytical properties. Another interesting system is the multibridged complex $[Ru(bpz)_3\{Fe(CN)_5\}_n]^{2-3n}$ (bpz = bipyrazine), which exhibits photoinduced multinuclear charge-transfer reactivity[5] when confined in modified nickel-electrodes. In this work we report the analytical characterization and determination of the equilibrium constants of a new series of multibridged species (Fig. 1) obtained from the reaction of $[Ru(bpz)_3]^{2+}$ with $[(EDTA)Ru(III)/(II)]^{-/2-}$ complexes.

EXPERIMENTAL

The complexes $[Ru(bpz)_3]Cl_2$ and $[Ru(HEDTA)(H_2O)]$ were prepared by literature methods.[6–8] The $[Ru(bpz)_3(RuEDTA)_n]^{2-n}$ complexes were generated in aqueous solution, under an argon atmosphere, by the reaction of $[Ru(bpz)_3]Cl_2$ and $[Ru(HEDTA)(H_2O)]$, using appropriate amounts of each species. The pH of the solutions was kept at 4.7 using acetate buffer. Sodium trifluoroacetate (NaTFA) was used as supporting electrolyte, and to keep the ionic strength around 0.25*M*.

The electronic spectra were recorded on a Hewlett-Packard 8452A diode-array spectrophotometer. Cyclic voltammetry was carried out with a Princeton Applied Research Corp. (PARC) instrumentation, consisting of a model 173/179 potentiostat and a model 175 universal programmer. A glassy carbon working electrode was employed for the measurements, with use of a Luggin capillary arrangement with a Ag/AgCl (1M KCl) reference electrode. The measured potentials were converted to the SHE scale by adding 0.222 V. For the spectroelectrochemical measurements, the PARC potentiostat was used in parallel with the HP 8452A spectrophotometer. A three electrode system was designed for a rectangular quartz cell of 0.025 cm optical path length. A gold minigrid was used as transparent working electrode, in the presence of

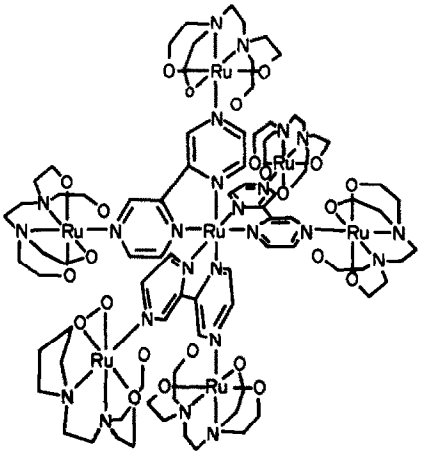

Fig. 1. The $[Ru(bpz)_3(RuEDTA)_6]^{4-}$ complex.

*Author for correspondence.

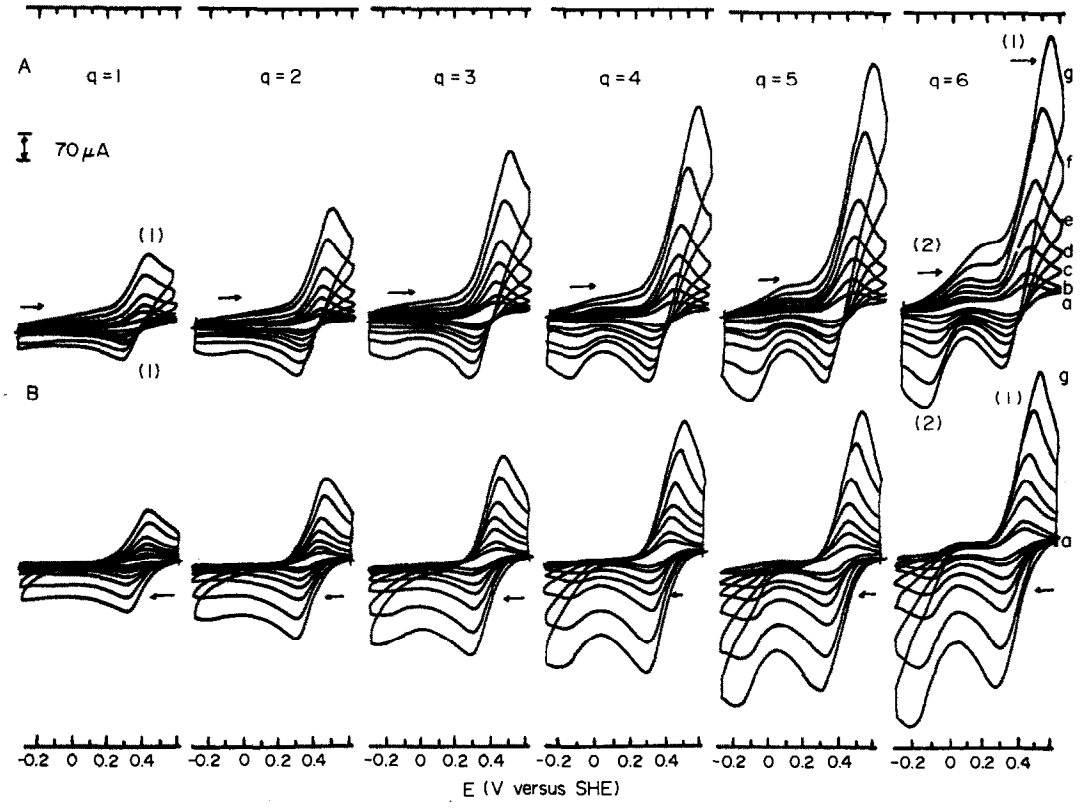

Fig. 2. Cyclic voltamperograms of the $[Ru(bpz)_3(RuEDTA)_n]^{2-n}$ complexes (2mM) in aqueous solution, for several values of $q = [RuEDTA^-]/[Ru(bpz)_3^{2+}]$; (A) starting from cathodic potentials; (B) starting from anodic potentials. Scan rates = (a) 10, (b) 20, (c) 50, (d) 100, (e) 200, (f) 500 and (g) 1000 mV/sec, [NaTFA] = 0.25M, pH 4.5 (acetate buffer), 25°.

a small Ag/AgCl reference electrode and a platinum auxiliary electrode.

RESULTS AND DISCUSSION

The $[Ru(bpz)_3]^{2+}$ (Ru_c) and $[RuEDTA]^-$ (P^-) complexes react yielding a series of multibridged $[Ru^{II}(bpz)_3(Ru^{III}EDTA)_n]^{2-n}$ species, here denoted $[Ru_cP_n]^{2-n}$, containing $[Ru^{III}EDTA]^-$ groups attached to the peripheral nitrogen atoms of bipyrazine. The reaction leads to an enhancement of the absorption band at 298 nm ascribed to internal $\pi \rightarrow \pi^*$ transitions in the bpz ligand, and of the absorption bands at 412 and 442 nm ascribed to Ru_c(II)-to-bpz, $d_\pi \rightarrow p_\pi^*$ charge-transfer transitions.[6] These bands are shifted to 436 and 474 nm in the presence of excess of $[RuEDTA]^-$ ions.

Spectrophotometric titration exhibited no evidence of saturation in the absorbance versus concentration plots, even in the presence of a fifteen times excess of $[RuEDTA]^-$ (around 15mM) over $[Ru(bpz)_3]^{2+}$.

Electrochemical behavior of the reduced species

The cyclic voltamperograms of the polymetallated complexes are shown in Fig. 2. The characteristic wave with $E_{1/2} = 0.38$ V *vs.* SHE was ascribed to the $[Ru(bpz)_3(Ru^{III/II}EDTA)_n]$ redox couples. The redox potential of the $[Ru(bpz)_3]^{2+/3+}$ center is higher than 2.0 V and the corresponding redox waves can not be observed in aqueous solution.[6] A broad, irreversible wave was observed around −0.9 V, involving the reduction of the bipyrazine ligands.

Starting from the reduced complexes at −0.3 V, the anodic peak currents $i_a(1)$ corresponding to the peripheral $[RuEDTA]^{2-}$ groups in the polimetallated species increased almost linearly with the ratio $q = [Ru^{III}EDTA^-]/[Ru(bpz)_3^{2+}]$, as shown in Fig. 3(A). Some dissociation of the polymetallated complexes can be detected above $q = 4$ from the rise of the small anodic wave (2) at 0 V, corresponding to the free $[Ru^{II}EDTA]^{2-}$ species as well as from the deviations of linearity in Fig. 3(a). On the other hand, saturation is observed slightly above $q = 6$, indicating that

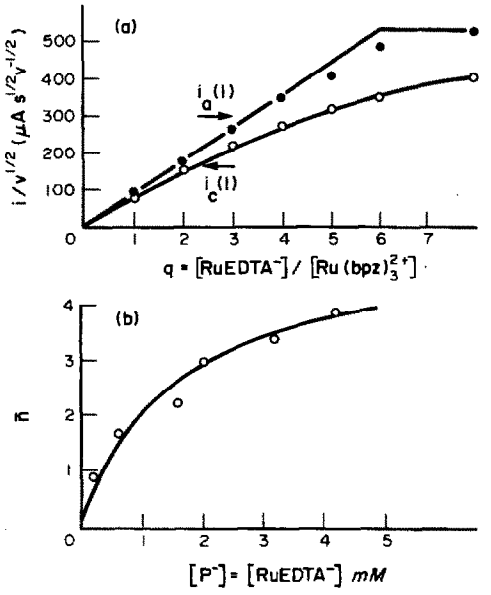

Fig. 3. (a) Plots of the anodic and cathodic peak currents from Fig. 2(A) and 2(B), *vs.* the molar ratio q, including additional points above $q = 6$; (b) plot of $\bar{n}$ versus [RuEDTA$^-$], employed for the evaluation of the equilibrium constants.

the formation of the reduced species is almost quantitative.

The increase of $i_a(1)$ with the number of coordinated [Ru^{III}EDTA$^-$] ions is consistent with the general behavior observed for polynuclear and polymeric systems[9] containing identical, non-interacting redox groups. In this case, it has been shown that the current–potential responses exhibit the same shape as that obtained with the corresponding molecule containing a single center, but the magnitude of the current is enhanced by the presence of additional electroactive centers.

Electrochemical behavior of the oxidized species

In the reverse scan, as shown in Fig. 2(B), the cathodic peak (1) was followed by a second peak around −0.1 V, corresponding to the reduction of [Ru^{III}(EDTA)(H$_2$O)]$^-$ species generated from the dissociation of the oxidized polymetallated complexes.

The voltamperograms of the oxidized complexes involve a series of equilibrium reactions, expressed by equation (1),

$$[Ru(bpz)_3]^{2+} + n[Ru^{III}EDTA]^- \overset{\beta_n}{\rightleftharpoons} [Ru(bpz)_3(Ru^{III}EDTA)_n]^{2-n} \quad (1)$$

In order to evaluate the equilibrium constants β_n, we started at 0.6 V, as shown in Fig. 2(B), with the polynuclear complexes in equilibrium condition. In contrast to the case of the reduced complexes, the plot of the cathodic peak currents, $i_c(1)$ *vs.* q (Fig. 3) exhibited no evidence of saturation, indicating that the oxidized complexes are rather weak.

The use of the relative intensities of the successive waves, $i_c(1)$ and $i_c(2)$, in Figure 2(B) for calculation of β_n is rather complicated, requiring a careful deconvolution of the voltamperograms. For this reason, we preferred to calculate the equilibrium constants based on the difference of $i_a(1)$ in Fig. 2(A), for the [Ru^{II}(bpz)$_3$(Ru^{II}EDTA)$_n$]$^{2-2n}$ species, and the corresponding cathodic peak currents, $i_c(1)$ shown in Fig. 2(B). In both cases the starting solutions are in equilibrium condition and in the absence of dissociation, these two currents would be equivalent, because of the expected similarity between the diffusion coefficients of the oxidized and reduced complexes. It should be noted that kinetic effects become important at low scan rates, *e.g.*, < 100 mV/sec, due to the lability of the [Ru^{III}EDTA] species.[10] However, at scan rates above 500 mV/sec, the ratios of the cathodic peak currents $i_c(1)$ and $i_c(2)$ become constant within 5%. Therefore, the kinetic effects can be neglected at high scan rates. For this reason, a scan rate of 1000 mV/sec, was employed in the equilibrium calculations.

The peak currents are proportional to the number of peripheral groups. In Fig. 2(A), $i_a(1)$ should correspond to the total amount of [RuEDTA]$^-$, since the dissociation of the reduced complexes is negligible, at least when $q < 5$. As q approaches 6, this is only approximate, and extrapolated currents, $i'_a(1)$, from the linear plot in Fig. 3(a), would be better employed in the calculations, in order to correct for the dissociation process. In this way, the concentration of free [Ru^{III}EDTA$^-$] ions, or [P$^-$], can be evaluated from the difference of the extrapolated currents, $i'_a(1)$, and $i_c(1)$ in Fig. 3(a).

The successive equilibria (1) can be analysed based on the Bjerrum[11] function $\bar{n}$,

$$\bar{n} = \frac{[P^-_{total}] - [P^-_{free}]}{[Ru_c]} \quad (2)$$

which is given by

$$\bar{n} = \frac{\beta_1[P^-] + 2\beta_2[P^-]^2 + 3\beta_3[P^-]^3 + \cdots}{1 + \beta_1[P^-] + \beta_2[P^-]^2 + \beta_3[P^-]^3 + \cdots} \quad (3)$$

The plot of $\bar{n}$ against [P$^-$] is shown in Fig. 3(b), indicating that when $q = 6$, the

average number of attached $[Ru^{III}EDTA]^-$ groups is smaller than 4.

Equation (3) can be rearranged in the following way:

$$\frac{\bar{n}}{(1-\bar{n})[P^-]} = \beta_1 + \beta_2\frac{(2-\bar{n})}{(1-\bar{n})}[P^-] + \beta_3\frac{(3-\bar{n})}{(1-\bar{n})}[P^-]^2 + \cdots \quad (4)$$

From the linear plot of $\bar{n}/(1-\bar{n})[P^-]$ against $(2-\bar{n})[P^-]/(1-\bar{n})$ shown in Fig. 4(a), β_1^{III} was estimated as $4 \times 10^3/M^{-1}$ (intercept) and $\beta_2^{III} = 8 \times 10^6 M^{-2}$ (slope).

A second rearrangement of equation (3) leads to

$$\frac{\bar{n}-(1-\bar{n})\beta_1[P^-]}{(2-\bar{n})[P^-]^2} = \beta_2 + \beta_3\frac{(3-\bar{n})}{(2-\bar{n})}[P^-] + \cdots \quad (5)$$

The plot of equation (4) shown in Fig. (4b) is practically linear. From this plot, β_2^{III} and β_3^{III} were estimated as $8.0 \times 10^6 M^{-2}$, and $8 \times 10^9 M^{-3}$ respectively. Based on the linear trend observed for β_1^{III}, β_2^{III} and β_3^{III}, the extrapolated values for β_4^{III}, β_5^{III} and β_6^{III} were $4 \times 10^{12} M^{-4}$, $1.0 \times 10^{15} M^{-5}$ and $1.3 \times 10^{17} M^{-6}$ respectively.

In the case of the reduced complexes, the equilibrium constant β_1^{II} can be calculated from the thermodynamic cycle:

$$\begin{array}{ccc} [Ru^{II}EDTA]^{2-} + [Ru(bpz)_3]^{2+} & \overset{\beta_1^{III}}{\rightleftharpoons} & [Ru^{II}EDTARu(bpz)_3] \\ \Big\downarrow E^0[Ru^{III}EDTA]^- & & \Big\downarrow E^0[Ru^{III}EDTARu(bpz)_3]^+ \\ [Ru^{III}EDTA]^- + [Ru(bpz)]_3^{2+} & \overset{\beta_1^{III}}{\rightleftharpoons} & [Ru^{III}EDTARu(bpz)_3]^+ \end{array}$$

where

$$E^0[Ru^{III}EDTARu(bpz)_3]^+ = E^0[Ru^{III}EDTA]^- + 0.0591 \log \frac{\beta_1^{II}}{\beta_1^{III}}$$

The calculated β_1^{III} is comparable to that report by Matsubara and Creutz[10] for the related pyrazine complex, *e.g.*, $1.0 \times 10^4 M^{-1}$.

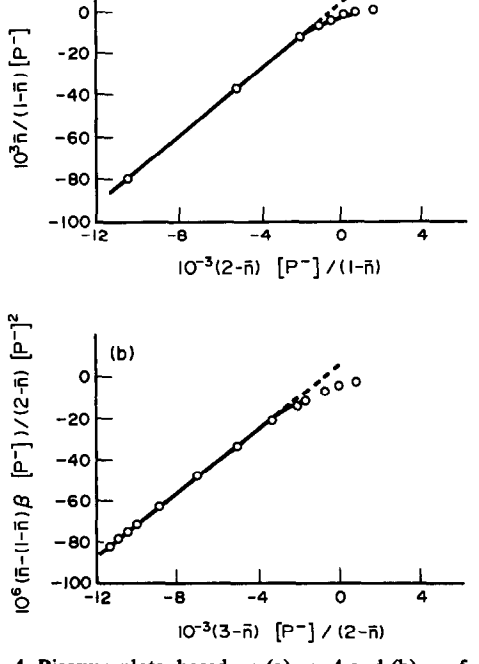

Fig. 4. Bjerrum plots, based on (a) eq. 4 and (b) eq. 5, for the evaluation of β_1, β_2 and β_3.

Since $E^0[Ru^{III}EDTARu(bpz)_3]^- = 0.38$ V, $E^0[Ru^{III}EDTA]^- = 0.04$ V, and $\beta_1^{III} = 4 \times 10^3 M^{-1}$, one can calculate $\beta_1^{II} = 5 \times 10^{10} M^{-1}$. This result is slightly higher than that reported in the literature[10] for the $[Ru^{II}EDTA(pyrazine)]^{2-}$ complex, *e.g.*, $1.7 \times 10^8 M^{-1}$. The difference of 7 orders of magnitude in the stability constants of the Ru^{III} and Ru^{II} species, reflects the importance of π-backbonding interactions in the [Ru^{II}EDTA–bipyrazine] moiety. A similar behavior is expected for the successive β_n^{II} constants, with respect to β_n^{III}.

Spectroelectrochemical behavior

The polynuclear complexes exhibit reversible spectroelectrochemical behavior in aqueous solution, a shown in Fig. 5. The reduction of the $[Ru^{II}(bpz)_3(Ru^{III}EDTA)_n]^{2-n}$ complexes around 0.38 V, is responsible for the rise of two strong absorption bands at 490 and 670 nm. These bands were ascribed to charge transfer transitions from the peripheral $Ru^{II}EDTA^{2-}$ groups to the π_1^* and π_2^* levels of the bridging bipyrazine ligand, by analogy to the systems previously reported in the literature.[12] The plots of absorbance against $q = [RuEDTA^-]/[Ru(bpz)_3^{2+}]$ were typically linear, exhibiting a

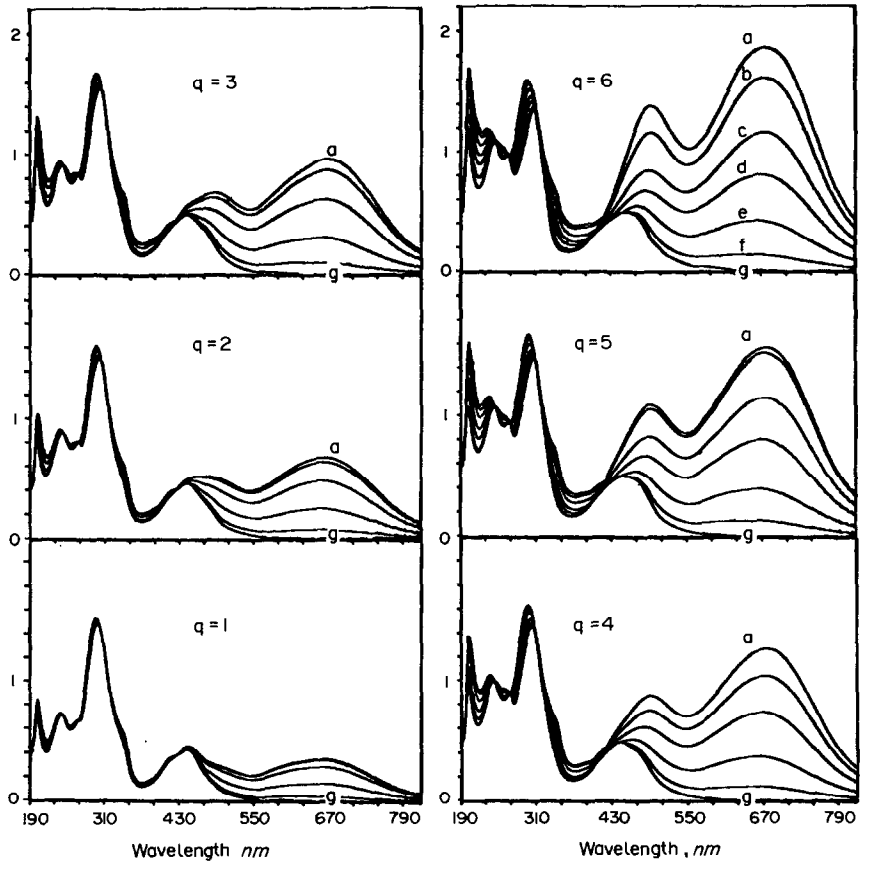

Fig. 5. Spectroelectrochemical behavior of the $[Ru(bpz)_3(RuEDTA)_n]^{2-n}$ complexes (1m*M*) in aqueous solution, for several values of $q = [RuEDTA^-]/[Ru(bpz)_3^{2+}]$. Applied potentials: (a) −578, (b) 172, (c) 272, (d) 322, (e) 372, (f) 422 and (g) 622 mV; [NaTFA] = 0.25*M*, pH 4.5, 25°.

saturation point when this ratio is 6, corresponding to the hexametallated species. The titration plot confirms that the reduced species $[Ru^{II}(bpz)_3(Ru^{II}EDTA)_n]^{2-2n}$ are quite stable, and that metallation reaction is nearly quantitatively under the conditions of this work, in agreement with the electrochemical results.

The Nernst plots, (*E vs.* log [ox]/[red]), for the several values of q employed in the experiments were linear. When $q = 1$, the Nernst slope coincided with the theoretical value of 0.059 V/decade, for a monoelectronic redox equilibrium, with $E^0 = 0.36$ V, in agreement with the cyclic voltamperograms. However, for $q = 2$, 3, 4, 5 and 6, the Nernst slopes were 0.071, 0.077, 0.088, 0.104 and 0.132 V/decade, and the corresponding E^0 were 0.35, 0.34, 0.33, 0.32 and 0.30 V, respectively.

The trends observed in the E^0 values are consistent with the statistical considerations for equivalent multisite redox processes reported in the literature.[9] The increase of the Nernst slope as a function of q cannot be explained in terms of the number of electrons involved, since the cyclic voltamperograms were consistent with $n = 1$. This type of behavior is determined by the dissociation equilibrium involving the oxidized polymetallated complexes. As a matter of fact, by using a fifteen times excess of $[Ru^{III}(EDTA)(H_2O)]^-$ over $[Ru^{II}(bpz)_3]^{2+}$ in order to repress the dissociation of the $[Ru^{II}(bpz)_3(Ru^{III}EDTA)_n]^{2-n}$ species, the Nernst slope decreased from 0.132 ($q = 6$) to 0.100 ($q = 15$) V/decade.

CONCLUSION

The chemistry of the $[Ru^{II}(bpz)_3(RuEDTA)_n]^{2-n}$ complexes is characterized by a complex dynamic equilibrium in solution, and by a very weak interaction between the peripheral [RuEDTA] groups. The stability of the polynuclear complexes is strongly enhanced in the reduced state, as a consequence of the d_π–p_π^* backbonding interactions involving the

peripheral ruthenium(II) groups and the bipyrazine bridging ligand.

Acknowledgements—The support from FAPESP and PADCT is gratefully acknowledged.

REFERENCES

1. H. E. Toma and K. Araki, *J. Chem. Res.*, 1990, 82.
2. K. Araki and H. E. Toma, *J. Electroanal. Chem.*, 1991, **297**, 301.
3. *Idem*, *Inorg. Chim. Acta*, 1991, **179**, 293.
4. C. Shi and F. C. Anson, *J. Am. Chem. Soc.*, 1991, **113**, 9564.
5. C. Hidalgo-Luangdilok and A. B. Bocarsly, *Inorg. Chem.*, 1990, **29**, 2894.
6. R. J. Crutchley and A. B. P. Lever, *J. Am. Chem. Soc.*, 1980, **102**, 7218.
7. Y. Yoshino, T. Uehiro and M. Saito, *Bull. Chem. Soc. Jpn.*, 1979, **52**, 160.
8. M. Mukaida, H. Okuno and T. Ishimori, *Nippon Kagaku Sasshi*, 1965, **86**, 589.
9. J. B. Flanagan, S. Margel, A. J. Bard and F. C. Anson, *J. Am. Chem. Soc.*, 1978, **100**, 4248.
10. T. Matsubara and C. Creutz, *Inorg. Chem.*, 1979, **18**, 1956.
11. F. J. C. Rossotti and H. Rossotti, *The Determination of Stability Constants*, McGraw-Hill, New York, 1961.
12. H. E. Toma, P. S. Santos and A. B. P. Lever, *Inorg. Chem.*, 1988, **27**, 3850.

Talanta, Vol. 40, No. 4, pp. 521–526, 1993
Printed in Great Britain.

0039-9140/93 $6.00 + 0.00

CALCIUM BINDING BY FULVIC ACIDS STUDIED BY AN ION SELECTIVE ELECTRODE AND AN ULTRAFILTRATION METHOD

ANDREW S. MATHUTHU
Department of Chemistry, University of Zimbabwe, P.O. Box MP 167, Mount Pleasant, Harare, Zimbabwe

JAMES H. EPHRAIM
Department of Water and Environmental Studies, Linköping University, S-581 83 Linköping, Sweden

(*Received* 21 *February* 1992. *Revised* 18 *August* 1992. *Accepted* 18 *August* 1992)

Summary—The interaction between Ca^{2+} and two well-characterized fulvic acids (Armadale and Laurentide FA) has been studied at 0.100 and 0.010*M* sodium nitrate using a fixed concentration of fulvic acid (100 ppm) and varying amounts of calcium (0.005–0.020 mmoles). Free calcium concentration was determined by *in situ* measurements employing a calcium electrode. For Armadale FA, free calcium was additionally determined via an ultrafiltration technique followed by atomic absorption measurements. For both fulvic acids, Ca^{2+} binding was observed to be decreased by an increase in the ionic strength of the system. At the lower ionic strength, the tendency for binding is dependent on the fulvic acid-to-metal ratio while at the higher ionic strength, the binding is insensitive to changes in the fulvic acid-to-metal ratio (an observation corroborating the contention that calcium binding to humic substances is primarily electrostatic). Comparison of the computed overall complex formation functions shows that values obtained from the ultrafiltration method were higher than those obtained using the calcium electrode. The binding of calcium was similar for the two fulvic acids.

The interaction between Ca^{2+} ions and humic substances has normally been considered in the light of the influence of Ca^{2+} on the binding of other heavy metal ions (e.g., Pb^{2+}, Cu^{2+}, Cd^{2+} and Zn^{2+}) by humic substances.[1,2] To predict the competitive role of Ca^{2+} ions in the binding of other heavy metal ions by humic substances, one has to understand how Ca^{2+} itself is sequestered by these organic acids. A number of earlier researchers have sought to achieve this objective,[3–5] but even though it has been postulated that Ca^{2+} binding by humic substances is primarily electrostatic, their studies have predominantly been performed at only a single ionic strength (0.100*M*). In this paper, the binding of Ca^{2+} by humic substances has been studied as a function of metal-to-fulvic acid ratio, pH and ionic strength for two well characterized fulvic acids using a calcium electrode. For one of the fulvic acids, an additional method involving the separation of the free metal from the complex was employed. The results have been analysed both as the fraction of metal bound and the overall complex formation function varying pH, ionic strength and metal-to-fulvic acid ratio.

EXPERIMENTAL

Materials and instrumentation

Two well characterised fulvic acids, Armadale Horizons Bh fulvic acid, AFA and Laurentide fulvic acid, LFA, isolated from peat, were obtained from Concordia University, Canada.[6–8] Results of the titratable acidic moieties (the active sites involved in metal interactions) are presented in Table 1. A further discussion of these results has been reported by Ephraim *et al.*[7] Standard sodium hydroxide was prepared from analytical concentrates obtainable from J. T. Baker Chemicals and standardized using potassium hydrogen phthalate. Analytical grade NaCl, $NaNO_3$ and $Ca(NO_3)_2$ were supplied by J. T. Baker Chemicals. An Amicon Model 8050 ultrafiltration cell (cell capacity = 50 ml; hold-up volume 0.5 ml) using an Amicon Diaflo membrane YM2 (diameter 43 mm) was used to

Table 1. Comparison of acidic capacities of Armadale Bh Horizons fulvic acid and Laurentide fulvic acid

FA Sample	Titratable acid, meq/g FA			
	Aqueous	Non-aqueous		
		−COOH	−OH	Total
Armadale FA	5.60 ± 0.15	4.15 ± 0.05	1.84 ± 0.06	5.99 ± 0.03
Laurentide FA	7.72 ± 0.05	5.60 ± 0.01	2.13 ± 0.01	7.73 ± 0.01

separate free Ca^{2+} from FA bound calcium and free FA. A Perkin-Elmer Model 503 Atomic Absorption spectrophotometer was used to determine free Ca^{2+} after ultrafiltration. An Orion ionanalyzer, Model 901, was used for pH and pCa measurements employing, respectively, a glass combination pH electrode and a model F2112 Ca, calcium-ion selective electrode from Radiometer A/S.

Procedure

The binding of Ca^{2+} to Armadale and Laurentide FAs was studied at 0.010 and 0.10*M* sodium nitrate using a calcium ion-selective electrode and an ultrafiltration technique.[9] In the ion selective electrode technique (ISE), two approaches were used. In the first approach, the removal of Ca^{2+} in solution was measured during neutralization of FA with base starting with a fixed initial ratio of FA to Ca^{2+}. In the second approach, the initial degree of dissociation of the FA was fixed by adding an appropriate amount of base and the ratio of FA to Ca^{2+} was changed stepwise by titration with calcium. A calibration curve was prepared (at the desired bulk electrolyte concentration) just before and immediately after each experiment.

A complete description of the ultrafiltration method and its adaptation to metal–humate binding studies is given elsewhere.[9] In a typical ultrafiltration experiment, a batch approach was employed where a number of solutions (volume = 50 ml) each containing known concentrations of FA and Ca^{2+} at a defined ionic strength (0.010 and 0.10*M* sodium nitrate) were adjusted to desired pH values with standard base and allowed to equilibrate by placing them at ambient temperature in a dessicator for about 24 hr. The solutions were allowed to equilibrate in a dessicator containing ascarite to ensure a CO_2-free atmosphere. After equilibration, the pH of each solution was determined and 10% of the solution was removed by ultrafiltration under pressure of 3.5 bars. The first 5% of the filtrate was discarded and the next 5% collected for Ca^{2+} ion concentration determination using the Atomic Absorption Spectrophotometer. Total filtrate was limited to 10% of the solution to minimize disturbance of the system. To obtain reliable results, both the calcium electrode and the ultrafiltration membrane were specially handled.

Special handling of the calcium electrode

At pHs between 5 and 8.5 the response of the calcium electrode was independent of pH and followed the Nernstian relationship, but below pH 5, the mV reading decreased progressively as the pH was lowered. To obtain meaningful results at PHs below 5, it was necessary to prepare special calibration curves. A family of calibration curves was prepared by following the response of the electrode at a fixed calcium concentration as a function of pH in the pH range 3–8.5. A typical set of these curves is shown in Fig. 1(a) and (b). Plots of potential *vs.* pCa indicate that the electrode response was Nernstian even at pH 4.0. By using these continuous calibration curves it was possible to extend the study pH range to as low as 4.0 with reproducible results. The calibration curves were obtained at the desired ionic strengths (0.10 and 0.010*M* sodium nitrate) and no significant effect of Na^+ ions on the electrode readings was observed.

Conditioning of the ultrafiltration membrane

An unconditioned YM2 membrane, molecular weight cut-off of 1000 Daltons, selectively retained Ca^{2+} while allowing easy passage of water. A bigger pore-size membrane, YM5 with a molecular weight cut off of 5000 Daltons was permeable to FA molecules as well. Proper conditioning of the YM2 membrane was attained for use in the experiment by filtering $Ca(NO_3)_2$ through it until its retention coefficient for Ca^{2+} was zero [Fig 2(a) and (b)] while that for FA was determined to be unity via the use of an UV–Vis spectrophotometric method.[9]

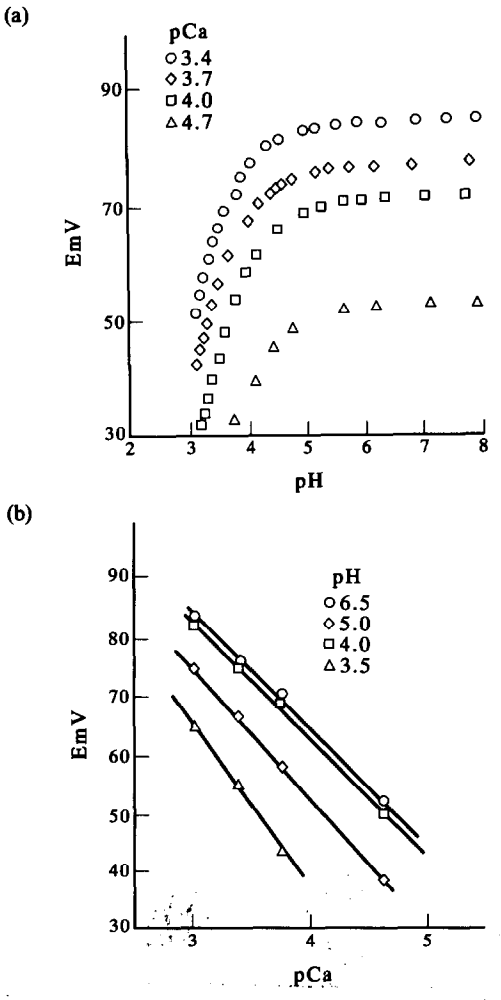

Fig. 1. (a) The response of the calcium electrode as a function of pH for different concentrations of Ca(II). (b) The Nernstian response of the calcium electrode at different pHs, points picked from Fig. 1(a). (Temperature = 23°; ionic strength = 0.10M $NaNO_3$.)

RESULTS AND DISCUSSION

Results of calcium binding to AFA and LFA expressed as fraction of calcium bound, Ca_b/Ca_t, where Ca_b is calcium bound and Ca_t is total calcium, as a function of pH are shown in Figs 3–5. Table 2 gives a detailed relationship between the logarithm of the complex formation function (log β_{ov}) and pH, where β_{ov} has been defined as follows:

$$\beta_{ov} = \{(\Sigma M_b)\gamma_{Mb}\}/\{(M_f\gamma_{Mf})(\Sigma A^- \gamma_{A-})\} \quad (1)$$

In the above equation, ΣM_b and M_f are the total metal bound and free metal respectively, γ_{Mb} is the activity coefficient of the metal-fulvate complex, γ_{Mf} is the single ion activity coefficient of the free metal ion obtained from Kielland,[10] ΣA^- is the total ionized free form of the fulvic acid at the given pH and γ_{A-} is the activity coefficient of the fulvate ion. To facilitate the resolution of the above expression [equation (1)], it is assumed that the activity coefficients of the metal–fulvate complex, γ_{Mb}, and the fulvate ion γ_{A-} are equal thus allowing their cancellation to yield the following:

$$\beta_{ov} = \{(\Sigma M_b)\}/\{(M_f\gamma_{Mf})(\Sigma A^-)\} \quad (2)$$

In Table 2, column 1 describes the composition of the solution studied and the method used, column 2 indicates the pH range studied, column 3 gives the complex formation function arrived at by linear regression analysis, column

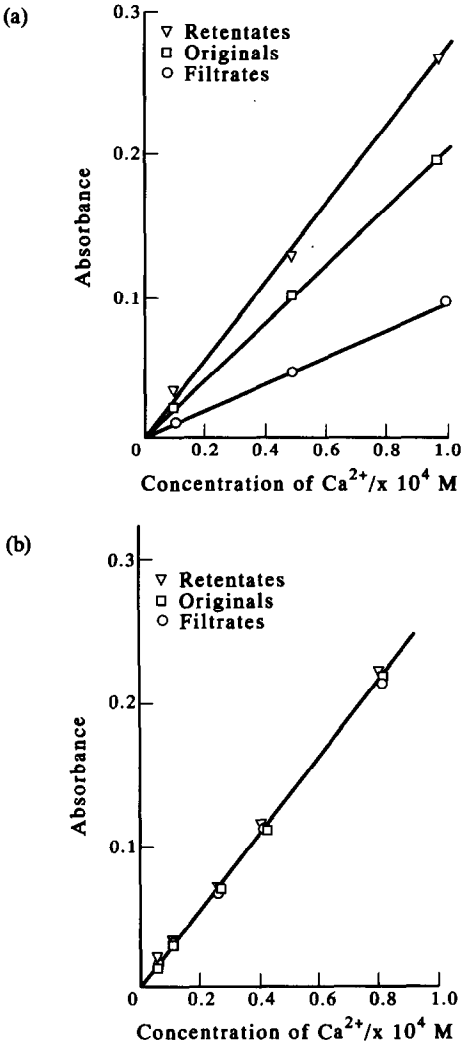

Fig. 2. (a) The effect of ultrafiltration on the concentrations of free Ca^{2+} in the filtrates and retentates. (b) A comparison of the concentrations of free Ca^{2+} in the filtrates, retentates and the original standard solutions after membrane conditioning. (Ultrafiltration cell = Amicon Model 8050; Membrane = YM2; ionic strength = 0.10M $NaNO_3$; temperature = 23°; pressure = 3.5 bars.)

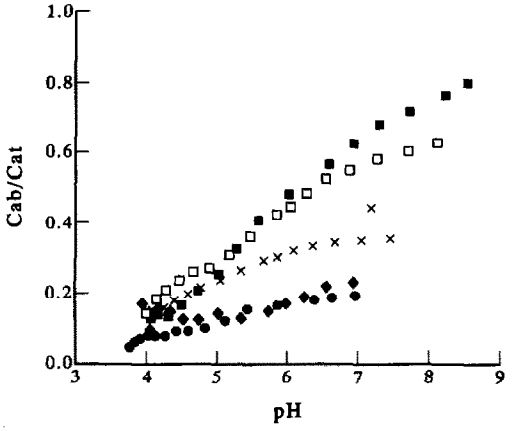

Fig. 3. Fraction of Ca bound as a function of pH, FA-to-metal ratio and ionic strength for Armadale Horizon Bh fulvic acid; method = ISE: Cab = calcium bound = $Ca_{total} - Ca_{free}$; Cat = total calcium. ■ $FA/Ca^{2+} = 6/1$; $I = 0.010$, □ $FA/Ca^{2+} = 3/1$; $I = 0.010$, × $FA/Ca^{2+} = 1.5/1$; $I = 0.010$, ◆ $FA/Ca^{2+} = 3/1$; $I = 0.10$, ● $FA/Ca^{2+} = 1.5/1$; $I = 0.10$.

4 gives the correlation coefficient and the last column gives the number of points used in the analysis. Generally, the complex formation function was found to be dependent on pH and ionic strength of the medium and the values agreed appreciably well with other reports.[5] There was a similar positive dependence on pH for both the ISE and ultrafiltration methods even though the ultrafiltration method gave slightly higher values. The log β_{ov} values which averaged from 2.8 to 3.1 in the pH range 4 to 8 are comparably lower than the log β_{ov} for a strongly complexing cation like Cu^{2+} to FA which is about 8 at pH 5.[11,12]

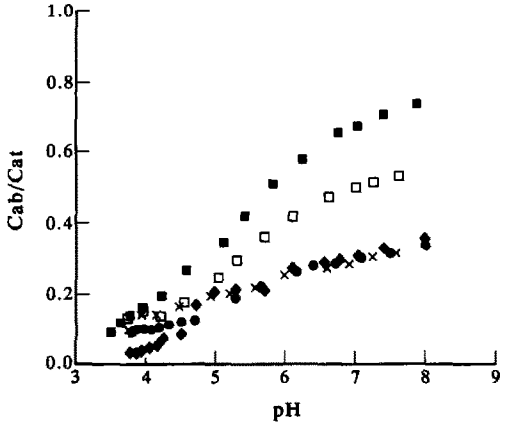

Fig. 4. Fraction of Ca bound as a function of pH, FA-to-metal ratio and ionic strength for Laurentide fulvic acid; method = ISE: ■ $FA/Ca^{2+} = 7.7/1$; $I = 0.010$, □ $FA/Ca^{2+} = 3.8/1$; $I = 0.010$, × $FA/Ca^{2+} = 1.9/1$; $I = 0.010$, ◆ $FA/Ca^{2+} = 7.7/1$; $I = 0.10$, ● $FA/Ca^{2+} = 3.8/1$; $I = 0.10$.

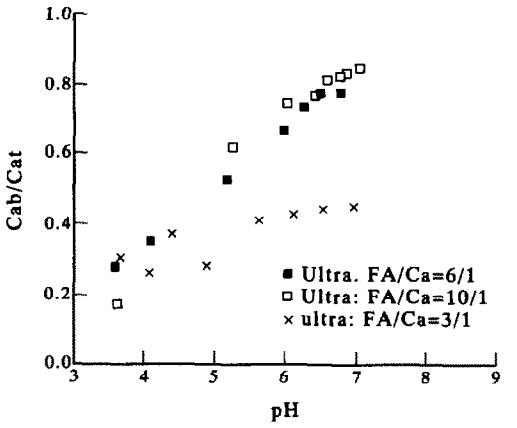

Fig. 5. Fraction of Ca bound as a function of pH, FA-to-metal ratio and ionic strength for Armadale Horizon Bh fulvic acid; method = ultrafiltration: ■ $FA/Ca^{2+} = 6/1$; $I = 0.010$, □ $FA/Ca^{2+} = 10/1$; $I = 0.010$, × $FA/Ca^{2+} = 3/1$; $I = 0.010$.

Effect of FA to Ca^{2+} ratio

For both FAs, the fraction of calcium bound, Ca_b/Ca_t, increased significantly with increase in the ratio of FA to calcium in 0.010*M* sodium nitrate solutions especially at pH values greater than 5 for low FA/Ca ratio and greater than 6 for high FA/Ca ratio (Figs 3 and 4). This could be attributed to an increase in the binding sites relative to Ca^{2+} concentration. At the higher ionic strength, 0.10*M* sodium nitrate, the fraction bound seemed to have no dependence on the ratio of Fa to Ca^{2+} because even though there is an increase in binding sites with an increase in the FA/Ca^{2+} ratio, the Ca^{2+} ions are not effectively bound because of screening by the Na^+ ions.

Effect of ionic strength

The fraction of calcium bound was distinctly higher in 0.010*M* sodium nitrate than in 0.10*M* solutions. A high concentration of Na^+ ions seemed to reduce the accessibility of the binding sites on the FA to Ca^{2+} and hence the observed reduction in the fraction bound. This would suggest that Ca^{2+} binding to FA is mainly in the form of weak electrostatic associations comparable to Na^+–FA associations. This conclusion is further supported by the apparent insensitivity of the fraction of Ca^{2+} bound at high bulk electrolyte concentrations (0.10*M* sodium nitrate) with increasing ratios of Ca^{2+} to fulvic acid. This behavior mimics an ion exchange mechanism where Ca^{2+} ions exchange with Na^+ ions already on the polymer surface. The counterion concentrating properties of the fulvic acid molecule are not considered in this paper.

Table 2. Complex formation functions for Ca^{2+} binding to Armadale (AFA) and Laurentide (LFA) fulvic acids. $\beta_{ov} = \Sigma M_b/\{M_f \gamma \Sigma A^-\}$ (Eq^{-1})

System	pH range	Log β_{ov}-pH relationship	r	n
AFA; Ultra; $Ca^{2+} = 1.0 \times 10^{-4} M$; $I = 0.010 M$ $NaNO_3$.	3.6–6.8	$\log \beta_{ov} = 2.70 + 0.20$ pH	0.990	7
AFA; Ultra; $Ca^{2+} = 6.0 \times 10^{-5} M$; $I = 0.010 M$ $NaNO_3$.	5.0–7.1	$\log \beta_{ov} = 2.89 + 0.18$ pH	0.990	8
AFA; Ultra; $Ca^{2+} = 2.0 \times 10^{-4} M$ $I = 0.010 M$ $NaNO_3$.	3.7–6.7	$\log \beta_{ov} = 3.49 \pm 0.14$	—	8
AFA; ISE; $Ca^{2+} = 1.0 \times 10^{-4} M$; $I = 0.010 M$ $NaNO_3$.	4.0–8.5	$\log \beta_{ov} = 1.78 + 0.28$ pH	0.993	15
AFA; ISE; $Ca^{2+} = 2.0 \times 10^{-4} M$ $I = 0.010 M$ $NaNO_3$.	4.0–8.1	$\log \beta_{ov} = 2.38 + 0.18$ pH	0.978	16
AFA; ISE; $Ca^{2+} = 4.0 \times 10^{-4} M$; $I = 0.010 M$ $NaNO_3$.	4.0–7.4	$\log \beta_{ov} = 2.69 + 0.11$ pH	0.979	15
AFA; ISE; $Ca^{2+} = 2.0 \times 10^{-4} M$; $I = 0.100 M$ $NaNO_3$.	3.9–6.9	$\log \beta_{ov} = 3.07 \pm 0.11$	—	13
AFA; ISE; $Ca^{2+} = 4.0 \times 10^{-4} M$; $I = 0.100 M$ $NaNO_3$.	3.7–7.0	$\log \beta_{ov} = 2.83 \pm 0.15$	—	15
AFA; ISE; $Ca^{2+} = 7.9 \times 10^{-4}$–$7.9 \times 10^{-4} M$; $I = 0.010 M$ $NaNO_3$.	6.2–6.7	$\log \beta_{ov} = 3.35 \pm 0.18$	—	19
LFA; ISE; $Ca^{2+} = 1.0 \times 10^{-4} M$; $I = 0.010 M$ $NaNO_3$.	3.5–7.8	$\log \beta_{ov} = 1.81 + 0.28$ pH	0.988	14
LFA; ISE; $Ca^{2+} = 2.0 \times 10^{-4} M$; $I = 0.010 M$ $NaNO_3$.	3.7–7.6	$\log \beta_{ov} = 2.08 + 0.20$ pH	0.981	12
LFA; ISE; $Ca^{2+} = 4.0 \times 10^{-4} M$; $I = 0.010 M$ $NaNO_3$.	3.7–7.5	$\log \beta_{ov} = 2.62 + 0.08$ pH	0.991	11
LFA; ISE; $Ca^{2+} = 1.0 \times 10^{-4} M$; $I = 0.100 M$ $NaNO_3$.	3.8–8.0	$\log \beta_{ov} = 1.28 + 0.31$ pH	0.915	17
LFA; ISE; $Ca^{2+} = 2.0 \times 10^{-4} M$; $I = 0.100 M$ $NaNO_3$.	3.8–8.0	$\log \beta_{ov} = 2.31 + 0.14$ pH	0.975	16
LFA; ISE; $Ca^{2+} = 4 \times 10^{-5}$–$7.5 \times 10^{-4} M$; $I = 0.010 M$ $NaNO_3$.	6.2–6.6	$\log \beta_{ov} = 3.52 \pm 0.08$	—	19
LFA; ISE; $Ca^{2+} = 1.6 \times 10^{-4}$–$5.9 \times 10^{-4} M$; $I = 0.100 M$ $NaNO_3$.	6.9–7.0	$\log \beta_{ov} = 3.03 \pm 0.44$	—	12

Note: Ultra. = ultrafiltration; ISE = ion selective electrode; AFA = Armadale FA; LFA = Laurentide FA; r = correlation coefficient; n = number of points; 100 ppm of FA was used for all trials.

Comparison of Armadale FA and Laurentide FA

There was no significant difference in the binding of calcium to the two fulvic acids as long as the ratio of FA to calcium was high but as the proportion of calcium increased the fraction bound to AFA tended to be higher than the fraction bound to LFA (Figs 3 and 4). The apparent extra binding affinity of calcium to AFA might be attributable to the extra acidity that was observed in the non-aqueous titrations of AFA.[7] This extra acidity was not observed in LFA (Table 1). It is, therefore, being postulated that the enhanced binding in AFA could be due to this extra acidity. The log β_{ov} values were, however, identical within the limits of experimental error. This is despite the fact that the acid–base capacities of the two fulvic acids are significantly different (LFA = 7.7 and AFA = 5.6 meq/g). A careful comparison of Figs 3 and 4 shows that the effect of ionic strength on the fraction of calcium bound was more pronounced in AFA than in LFA.

Comparison of the ultrafiltration and the ISE methods

The ultrafiltration method indicated slightly higher binding as compared to the ISE method, *i.e.*, the log β_{ov} obtained by ultrafiltration were greater than those obtained by the ion selective electrode by 0.5 log units in the pH range of 4–5. This difference, $[\log \beta_{ov,(ultra)} - \log \beta_{ov,(ise)})]$, reduces to ~0.25 around pH 7 (Fig. 6). The fraction of Ca^{2+} bound, (Ca_b/Ca_t), obtained by both methods showed a similar dependence on pH and the ratio of FA/Ca^{2+}. The discrepancy between binding constants obtained from the two methods (Fig. 6) which was similarly observed in Cd^{2+}/FA binding studies has been attributed to the intrinsic problems of determining free metal ion concentration associated with each method.[13–15] The ion selective electrode technique determines free metal ion concentration *in situ* while in the ultrafiltration, free metal is separated from the complex before its analysis. The narrow detection limit of the ion

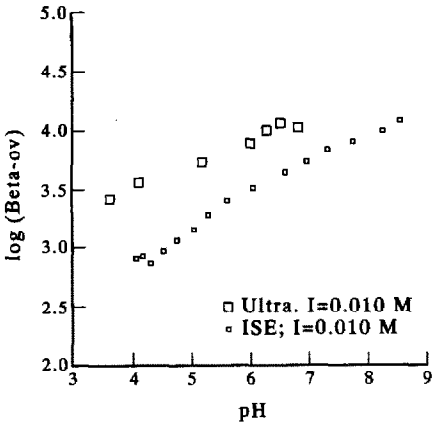

Fig. 6. Comparison of overall complex formation function obtained from ultrafiltration and ion selective electrode methods

specific electrode (not lower than $1.0 \times 10^{-6}M$) and the fact that the method is limited only to ions for which an ion selectrode is available, offer a limited application of the method to metal–humate systems that are close to environmental conditions. On the other hand, the ability to study metal–humate interactions with low concentrations of both fulvic acid and metal ions coupled with the fact that it can be used in studies involving most metal ions for which no easy *in situ* analyses of the free metal ion are available make the ultrafiltration technique a promising technique to complement studies of metal–humate interactions.

CONCLUSION

The log β_{ov} values which are presented in Table 1 are in good agreement with earlier published results.[3,4,5,16,17] The exact magnitude of the values obtained can be affected by the method employed, *e.g.*, with the ultrafiltration method the log β_{ov} values on the average ranged from 3.6 to 4.1 as compared to 2.8 to 3.5 for the ISE method. The low log β_{ov} values suggest that Ca^{2+} will have minimal interference in the interactions of strongly complexing heavy metals like Cu^{2+} with FA, but could reduce the binding of weak complexing metals like Cd^{2+} and Zn^{2+}.

Artefacts in metal–humate binding studies may be identified, reduced or eliminated by employing different methods for the study of the same metal–humate system. Under ideal conditions, different methods used in studies of the same metal–humate system must yield similar results if the methods are measuring the same kind of reaction. Discrepancies in results of well-adapted methods to metal–humate interactions might lead to insight into the existence of different "windows" of the reaction sequence. In this respect, it is suggested that the ion selective electrode and the ultrafiltration techniques may be used as complementary methods rather than as mutually exclusive methods.

Acknowledgements—Financial support from the National Science Foundation, USA, the Swedish Natural Science Council, NFR and the Swedish Institute (for ASM during visit to Sweden) are gratefully acknowledged.

REFERENCES

1. A. Wolf, K. Bunzl, F. Dietl and W. F. Schmidt, *Chemosphere*, 1977, **6**, 207.
2. J. G. Hering and F. M. M. Morel, *Environ. Sci. Technol.*, 1988, **22**, 1234.
3. G. R. Choppin and P. M. Shanbhag, *J. Inorg. Nucl. Chem.*, 1981, **43**, 921.
4. M. Schnitzer and E. H. Hansen, *Soil Sci.*, 1970, **109**, 333.
5. N. Paxeus and M. Wedborg in B. Allard, H. Boren and A. Grimvall (eds.), *Lecture Notes in Earth Sciences*, 33, **287**, 1991.
6. D. S. Gamble, *Can. J. Chem.*, 1970, **48**, 2662.
7. J. Ephraim, S. Alegret, A. Mathuthu, M. Bicking, R. L. Malcolm and J. A. Marinsky, *Environ. Sci. Technol.*, 1986, **20**, 354.
8. Z. D. Wang, B. C. Pant and C. H. Langford, *Anal. Chim. Acta*, 1990, **232**, 43.
9. J. H. Ephraim and J. A. Marinsky, *ibid.*, 1990, **232**, 171.
10. J. Kielland, *J. Am. Chem. Soc.*, 1937, **59**, 1675.
11. M. Schnitzer and S. I. M. Skinner, *Soil Sci.*, 1966, **102**, 361.
12. *Idem, ibid.*, 1967, **103**, 247.
13. J. H. Ephraim and H. Xu, *Sci. Total Environ.*, 1989, **81/82**, 625.
14. J. Buffle, P. Deladoey, F. Greter and W. Haerdi, *Anal. Chim. Acta*, 1980, **116**, 255.
15. J. Buffle and C. Staub, *Anal. Chem.*, 1984, **56**, 2837.
16. B. A. Dempsey and C. R. O'Melia. In R. F. Christman and E. T. Gjessing (eds.), *Aquatic and Terrestrial Humic Materials*, p. 239. Ann Arbor, Ann Arbor Science, 1983.
17. R. F. C. Mantoura, A. Dickson and J. P. Riley, *Estuar. Coast. Mar. Sci.*, 1978, **6**, 387.

Talanta, Vol. 40, No. 4, pp. 533–540, 1993
Printed in Great Britain.

0039-9140/93 $6.00 + 0.00

A NEW METHOD FOR THE EVALUATION OF THE OXIDIZING EQUIVALENT OF MANGANESE IN SURFACE FRESHWATERS

DAVID JOHNSON and BARRY CHISWELL
Department of Chemistry, University of Queensland, Qld 4072, Australia

(*Received* 19 *February* 1992. *Revised* 30 *July* 1992. *Accepted* 30 *July* 1992)

Summary—The suitability of application of a number of previously used methods for the evaluation of the oxidizing equivalent (OE) of manganese in natural waters is compared with a new method, which depends upon colour development of the dye *N,N'*-diethyl-*p*-phenylenediamine (DPD) upon oxidation by oxidized forms of manganese. The effect of introducing a commonly used metabolic poison, azide, into the most reliable of these determinations of OE has also been assessed.

It is found that, although the methods described by other workers involving redox titrations (*viz.* oxalic acid and iodometric) gave good results when undertaken upon a synthetically prepared (concentrated) manganese (IV) oxide colloid, all such methods involving colour development by oxidation of dyes gave poor results. On the other hand, the new DPD colorimetric method gave results comparable with the titration methods, but was found to be much more sensitive and faster than either titration technique.

All of the methods, apart from the new DPD method, give poor results upon manganese samples in tests undertaken on naturally occurring waters with high OE values.

The importance of microorganisms in mediating change in the oxidation state of manganese in natural waters has been a topic of wide discussion for some years. In work undertaken in our laboratories to assess the relative importance of microbiological and chemical oxidation/reduction of manganese in dam waters, out of necessity, we have developed methods of calculating the oxidation state of manganese in natural waters. In this work we have assessed the methods previously used to arrive at a statement of the oxidation speciation of the manganese and developed a new method of determining the manganese oxidizing equivalents (O.E.).

In natural waters, manganese exists in the oxidation states, II, III and IV. As the oxidation states III and IV cannot be distinguished by redox or colorimetric methods, they are usually expressed together as the sum total oxidising equivalents, which themselves are measured by redox titration or colour forming ability with a colorimetric reagent. A measure of the ratio O/Mn can be obtained as a value x by using equation (1). The total manganese

$$x = 1 + \frac{\frac{1}{2}[\text{O.E.}]}{[\text{MnOx}_{\text{tot}}]} \qquad (1)$$

where $[\text{OE}] = 2[\text{Mn(IV)}] + [\text{Mn(III)}]$ and $[\text{MnOx}_{\text{tot}}] = [\text{Mn}_{\text{tot}}] - [\text{Mn(II)}]$; concentration ($\text{Mn}_{\text{tot}}$) can be obtained by atomic absorption spectroscopic measurements of acidified solutions of the sample, while the manganese(II) concentration can be found by analysis of the dissolved manganese in the sample by use of the colorimetric reagent $\alpha,\beta,\delta,\gamma$-tetrakis(4-carboxyphenyl)porphine [T(4-CP)P].[1]

Equation (1) can only provide the average oxidation state of the manganese present in the sample and there are no commonly accepted methods of determining the individual manganese(IV) and manganese(III) concentrations. The O/Mn ratio has the values 1.0, 1.5 and 2.0 for pure samples of manganese(II), (III) and (IV), respectively.

Since techniques such as atomic absorption spectrometry, voltammetry and neutron activation analysis, traditionally used for elemental analysis of naturally occurring waters, are incapable of distinguishing between the reduced manganese(II) species on one hand and mixed higher oxidation state manganese species on the other hand, the most suitable techniques for such a problem are necessarily redox or colorimetric, the latter using redox dyes.

Table 1. Common redox methods

Redox method	References
Ferrous iron	2–4
Iodate	4, 5–7
Oxalate	4, 8–11

Table 1 lists the most commonly used redox methods for the determination of the oxidation state of manganese oxides, while Table 2 lists common colorimetric reagents used by researchers for the determination of manganese oxidation state. Many such colorimetric reagents, although accurate in laboratory situations, suffer severe interference when used in the analysis of natural waters.

Various colorimetric dyes react stoichiometrically with oxidized manganese, and in such reactions the triphenylmethane dyes such as leuco Berbelin Blue (LBB) and leuco Crystal Violet (LCV) undergo two electron oxidations to form the dyes Berbelin Blue and Crystal Violet. The *p*-aminobiphenyl dyes *o*-tolidine and benzidine also undergo instantaneous two electron oxidations to their coloured forms.[28]

It is the purpose of this paper to evaluate redox and colorimetric methods currently available for manganese oxidation state determination and to compare them with a new colorimetric method using *N,N* diethyl-*o*-phenylenediamine (DPD), a dye not previously used for the determination of the oxidation state of manganese.

EXPERIMENTAL

Reagents

1M *Potassium fluoride.* A 5.81-g weight of potassium fluoride was dissolved in 100 ml of Milli-Q water.

1M *Manganese(II) sulphate.* A 84.51-g weight of manganous sulphate monohydrate was dissolved in 500 ml of water.

2.5×10^{-2}M *Potassium permanganate.* A 0.3951-g weight of potassium permanganate was dissolved in 100.0 ml of Milli-Q water.

2.75×10^{-1}M *Sodium thiosulphate.* A 6.82-g weight of sodium thiosulphate was dissolved in one litre of Milli-Q water.

5×10^{-3}M *Sodium thiosulphate.* A 1.24-g weight of sodium thiosulphate (Aldrich) was dissolved in one litre of Milli-Q water.

3.341×10^{-4}M *Potassium iodate.* A 7.14976-g amount of potassium iodate (Aldrich), previously dried in an oven at 120°, was dissolved in one litre of Milli-Q water to give the stock solution. A 10.0-ml portion of this solution was then further diluted to one litre.

7.5×10^{-4}M *Oxalic acid.* A 1.35054-g weight of oxalic acid (Aldrich) was dissolved in 100.0 ml of Milli-Q water. This solution was then diluted by 1 in 200 to provide the final concentration, approximately $7.5 \times 10^{-4}M$.

DPD Reagent. A 0.10-g weight of *N,N*-diethyl-*p*-phenylenediamine (Aldrich) was dissolved in 30 ml of Milli-Q water and 0.8 ml concentrated perchloric acid and then diluted to 100.0 ml. The solution was stable in light for at least two weeks.

Acetate buffer. A 250-ml amount of glacial acetic acid (AnalaR, Ajax Chemical) was diluted to one litre and titrated to pH 4.0 with 5*M* sodium hydroxide.

1×10^{-3}M *Sodium bicarbonate.* A 0.084-g sodium bicarbonate was dissolved in 50 ml of Milli-Q water and diluted to one litre.

LCV Reagent. A 0.10-g amount leuco Crystal Violet (Aldrich) was dissolved in 30 ml of Milli-Q water and 0.80 ml of concentrated perchloric acid and then diluted to 100.0 ml. The solution was stable in light for up to one month.

o-*tolidine reagent.* A 0.20-g amount of *o*-tolidine (Aldrich) was dissolved in 200.0 ml of Milli-Q water.

T-(4-CP)P reagent[1]. This was prepared directly by refluxing a propionic acid solution, 0.24*M* in both 4-carboxybenzaldehyde and pyrrole, for two hours. Upon cooling, purple crystals of T(4-CP)P separated out and were recrystallized from a methanol/chloroform mixture.

2×10^{-4}M *T-(4-CP)P solution.* A 79.1-mg weight of reagent was dissolved in 5 ml of 0.1*M* sodium hydroxide and diluted to 500 ml with Milli-Q water. The solution is stable for up to six months if stored in a darkened container.

6×10^{-4}M *Cadmium(II) solution.* A 0.0505-g weight of cadmium(II) chloride was dissolved in 500 ml of water.

Table 2. Common colorimetric reagents for OE determination

Colorimetric dye	References
o-tolidine	4, 12–15
Leuco Crystal Violet	4, 14, 16, 17
Leuco Berbelin Blue	18–22
Benzidine	21, 23–26
Leuco Malachite Green	13, 27

Borate buffer (pH 8.0/0.15M *in imidazole).* A 50-ml portion of $2.5 \times 10^{-2}M$ (9.525 g/l)-sodium tetraborate was added to 20 ml of $0.1M$ hydrochloric acid in a 150-ml beaker. A 1.0212 g weight of imidazole in 25 ml of water was added and the pH adjusted to 8.0 using $0.1M$ hydrochloric acid. The solution was transferred to a 100.0-ml standard flask and made up to the mark.

Preparations

Manganese(III) fluoride.[29] The $1M$ potassium fluoride and manganous sulphate solutions were mixed with 250 ml of $4M$ sulphuric acid and 50 ml water, and $2.5 \times 10^{-2}M$ potassium permanganate solution was added slowly with constant stirring. This yielded a solution containing approximately $0.01M$ manganese(III) fluoride as determined by iodometric titration using $0.275M$ sodium thiosulphate. Appropriate dilution of the solution was made prior to use. It should be noted that this solution contains an excess of Mn(II).

Colloidal manganese(IV) oxide. A stock manganese(IV) oxide suspension was prepared by the method of Murray *et al.*[4] The total concentration of manganese in the colloidal solution prepared was found to be 2.01 mg/l. by atomic absorption analysis of acidified aliquots; the colloid was shown to have an oxidizing equivalent of 4.01 as determined by iodometric titration using $5 \times 10^{-1}M$ sodium thiosulphate. Analysis for the presence of Mn(II) in solution using the colorimetric reagent $\alpha,\beta,\gamma,\delta$-tetrakis(4-carboxyphenyl)porphine gave a zero result, and the colloidal solution was calculated by equation (1) to have a value of $x = 1.99$.[11] At this concentration and pH, the suspension was stable for more than two years with no evidence of flocculation, as confirmed by periodic standardization. Standardization using $7.5 \times 10^{-4}M$ oxalic acid was also undertaken; this method gave a value of x for the MnO_x colloid of 2.

Murray *et al.*[4] have characterised this MnO_x product by X-ray photoelectron spectroscopy and have shown it to have values of x between 1.90 and 1.98.

Instrumentation

UV–Vis spectrophotometer. Optical densities of LCV, DPD and *o*-tolidine solutions were measured on a Hewlett-Packard HP845OA, UV–Vis spectrophotometer using 1-cm quartz cuvettes.

Calibration of the HP-845OA was undertaken using colloidal manganese dioxide oxidized DPD, LCV, or *o*-tolidine standards prepared by appropriate dilutions of a 2 mg/l. stock manganese(IV) oxide suspension. Concentrations were determined by colorimetry, by comparison against the calibration curve prepared from these standards.

Atomic absorption spectrometer. Atomic absorption spectroscopy determinations of manganese were made using a Varian AA 875 spectrometer or a Varian SpectrAA 300 spectrometer. An oxidizing air-acetylene flame was used and the wavelength was selected according to concentration. For manganese in the range 10–2000 μg/l., 279.5 nm was used, and for concentrations in the range 2–10 mg/l., 403.2 nm was used.

Calibration standards were prepared by appropriate dilutions from commercial, 1000 mg/l., AAS standard (BDH) supplied in $1M$ nitric acid.

Determination of total manganese concentrations ($[Mn_{tot}]$)

These values were determined for the standard colloidal manganese(IV) oxide and dam water samples by the use of AAS, following acidification of the sample to pH 1.0 using concentrated hydrochloric acid.

Determination of manganese(II) concentrations [Mn(II)]

These were found for the standard colloidal manganese(IV) oxide colloid (effectively a blank) and dam water samples by the following method: 5.00 ml of sample solution was placed into 25-ml standard flasks which had been painted black except for 0.5 cm either side of the volume mark. A 1.0-ml aliquot of $2 \times 10^{-4}M$ T-(4-CP)P solution and 1.0 ml of borate buffer were then added followed by 3.0-ml of $6 \times 10^{-4}M$ cadmium(II) solution. The absorbance at 468 nm was measured between 5 and 20 min after mixing.[30]

Determination of oxidising equivalents of colloidal manganese(IV) oxide, manganese(III) fluoride and of dam water samples

Oxalic acid method. In each determination the value of OE is the mole value of either the titrant used, or the dye consumed in the reaction. As noted above, this method was used to standardize the colloidal MnO_2. The method

was also applied to 100-ml aliquots of dam water samples.

Iodometric method. A 100-ml volume of the colloidal manganese(IV) oxide, Mn(III) fluoride, or the dam water sample were used. An excess of potassium iodide (Ajax) was added to this aliquot followed by 5 ml of 0.1*M* sulphuric acid. The liberated iodine was determined by titration against $5 \times 10^{-3}M$ thiosulphate previously standardized against $3.341 \times 10^{-4}M$ potassium iodate. The end-point determination was aided by the addition of starch solution late in the titration.

Leuco Crystal Violet (LCV) method. Suitable aliquots of the stock manganese(IV) oxide colloid, or dam water samples were added to approximately 12.5 ml of sodium bicarbonate solution in 25-ml standard flasks. To each sample, 0.50 ml of LCV reagent was added followed by 1.0 ml of buffer solution. The solution was mixed and stood for 5 min before making up to the mark with reagent water. The 1 cm absorbance was determined at 590 nm against a reagent blank.

o-*Tolidine method.* Measured volumes of manganese(IV) oxide colloid were added to 100-ml standard flasks. A 25-ml volume of 3*M* perchloric acid and 10 ml of *o*-tolidine solution were added and solutions made up to the mark after mixing. The 1-cm absorbance of the yellow solution was measured at 440 nm.

N,N-*Diethyl*-p-*phenylenediamine (DPD) method.* Suitable aliquots of stock manganese(IV) oxide colloidal suspension or 5.00 ml of unknown samples were added to approximately 12.5-ml aliquots of the sodium bicarbonate in 25-ml standard flasks. To each sample, 0.50 ml of DPD reagent was then added followed by 1.0 ml of buffer solution. The solution was then mixed and left to stand for at least five minutes. The resulting pink coloured solutions were made up to the mark with reagent water and the 1-cm absorbance was determined at 552 nm against a reagent blank.

RESULTS AND DISCUSSION

Determination of OE

Oxalic acid method. The oxalate method involves the addition of a known amount of excess oxalic acid to the sample, with subsequent back titration of the non-oxidized oxalate with permanganate at 60°. Murray *et al.*[4] found that this method gave results for samples of his synthetic MnO_x of $x = 1.99 \pm 0.02$. Results from this study for the analysis of the colloidal manganese (IV) oxide agreed well, with $x = 1.98 \pm 0.01$.

This method was tested, on a series of natural water samples. On all occasions samples consumed more permanganate than did the oxalate standard alone, giving titration results up to 117% of the oxalate standard value.

Because of its interaction with many components present in natural waters, other than manganese, permanganate has to be considered as being too powerful as an oxidizing agent to determine the oxidizing equivalents in such cases; for this reason the oxalate method was not investigated further.

Iodometric method. The iodometric method had similar success to the oxalate method for Murray *et al.*,[4] yielding typical values of x of 1.98 ± 0.05. Although this technique uses the much weaker reducing agent, iodide ion, when the same series of dam samples that were used in the oxalic acid method were measured by iodometric titration using 100-ml volumes, problems were encountered in determination of the end-point. The samples were yellow/brown in colour because of the presence of colloidal organic material and MnO_x, which lead to total inability to detect any end-point.

Leuco Crystal Violet (LCV) method. The method of Kessick and Morgan[12] was used in this investigation.

Figure 1 shows the results of a kinetics experiment measuring the stability of the colour of crystal violet when reacted with standard MnO_2 and manganese(III) fluoride. Thermodynamics predict that both manganese(IV) and (III) will

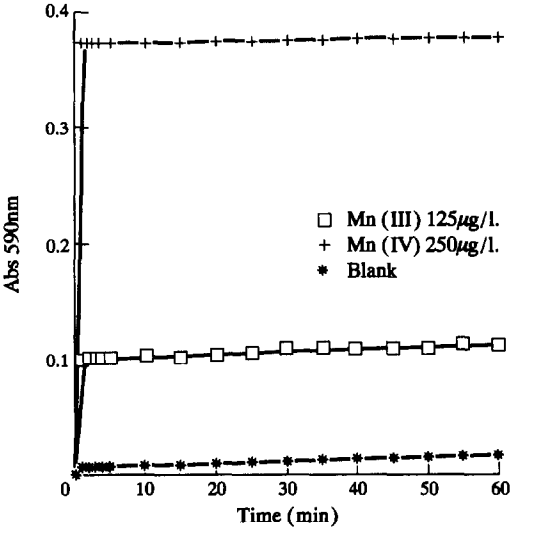

Fig. 1. Reaction of LCV with Mn(III) fluoride and Mn(IV) oxide.

oxidize LCV, however some evidence exists that the kinetics of such reactions may differ. Morgan and Stumm[13] have stated that manganese(III) reacts somewhat more slowly with *o*-tolidine than does manganese(IV).

From Fig. 1 it can be seen that both Mn(III) and Mn(IV) immediately oxidize LCV to a maximum absorbance. The absorbance values remained relatively constant over the period of 1 hour with no real increase observed, indicating that the dye does not react slowly with synthetic MnO_2 or manganese(III) compounds, nor does atmospheric oxidation play any significant role. No difference in stability of colour is observed between the reactions of manganese(III) and (IV).

De Vitre *et al.*[31] have used the method of Kessick *et al.*[12] and compared it with two other methods for the determination of MnO_x concentrations in lake samples; they found it to have three major drawbacks:

(i) the measured absorbance is a function of the kinetics of the reduction of MnO_x by LCV (from Murray's[4] data),
(ii) analysis of turbid samples required scattering corrections of up to 80% of the measured value, and,
(iii) when sulfide concentrations are significant, the LCV forms polymeric solutions resulting in the formation of a cloudy suspension.

In the study undertaken in work reported in this paper, point (i) was found to be insignificant if measurements were taken in under one hour. Point (ii) was found only to be a problem when sediment samples or samples very close to the sediment were taken; scattering caused by analysis of water column samples was measured and found to be negligible; measurement of OE in sediments was not undertaken. Point (iii) was found to be the major problem and was particularly prevalent during periods of stratification. This phenomenon also occurred frequently in samples from other levels of the dam. LCV could therefore not be used at all to measure OE in hypolimnetic samples.

A further problem associated with the use of LCV to determine OE was encountered when azide was used in our experiments to poison and thus prevent microbiological oxidation. Azide is often used as a poison in such work where one wishes to distinguish microbial from chemical reactions; its operation appears to be as a relatively non-specific block on the operation of terminal oxidases within cytochrome chains.[32]

Azide interference was found to be high when measuring the concentration of MnO_x by the LCV method. Two solutions containing the same concentration of colloidal MnO_x standard, one of which contained 15 m*M* NaN_3 and one without the poison, were measured and compared by the LCV method. Figure 2(A) presents the typical visible spectrum of the leuco Crystal Violet dye, oxidized by MnO_2. In the presence of 15 m*M* azide, (Fig. 2(B)) the spectrum is very clearly altered, and marked interference, and complete disappearance of the 591 nm peak, is observed. Such background interference appears to be due to the formation in the LCV

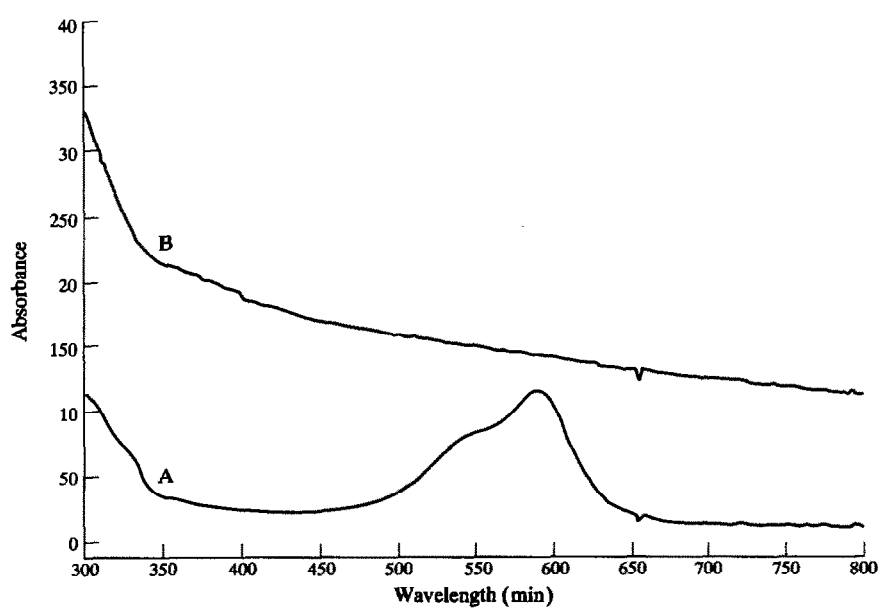

Fig. 2. Absorption spectrum of LCV (A) without azide, and (B) with azide.

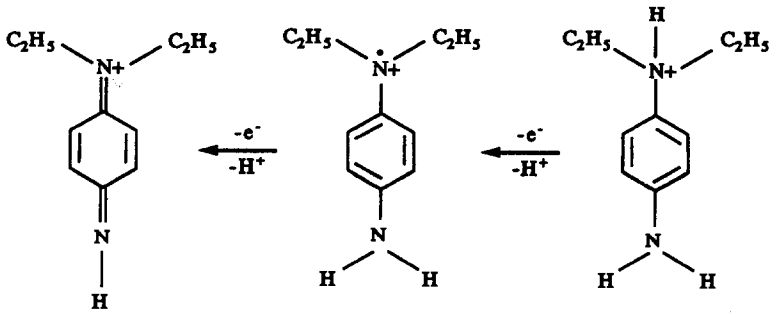

Fig. 3.

solution of a cloudy suspension in the presence of azide.

A number of papers describe the use of the dyes leuco Berbelin Blue (LBB) and LCV to measure OE in the presence of the metabolic inhibitor, azide. In such cases, failure to observe an absorbance peak at 591 nm for LCV and similar peak LBB, has been interpreted in terms of the poison inhibiting microbial oxidation and consequent non-production of oxidized manganese to oxidize the dye and produce the absorbance. Thus, in a study into the oxidation of manganese by cells of *Leptothrix Discophora* SS1, Boogerd and De Vrind[20] measured MnO_2 concentration colorimetrically using LBB, showed that azide inhibited the influence of this strain on the oxidation process. As LBB is of similar structure to LCV, it is clearly likely that azide reacted similarly with LBB, to give a suspension which led to light scattering and no observable absorbance peak.

De Vrind *et al.*[22] in an investigation into manganese oxidation by spore coats of a marine *Bacillus* species, found that the spores oxidized manganese to MnO_2, as measured by LBB. When NaN_3 was present no oxidation could be measured. Again, if the reaction of azide with LBB is similar to that with LCV, one would expect that no absorption peak would be obtained.

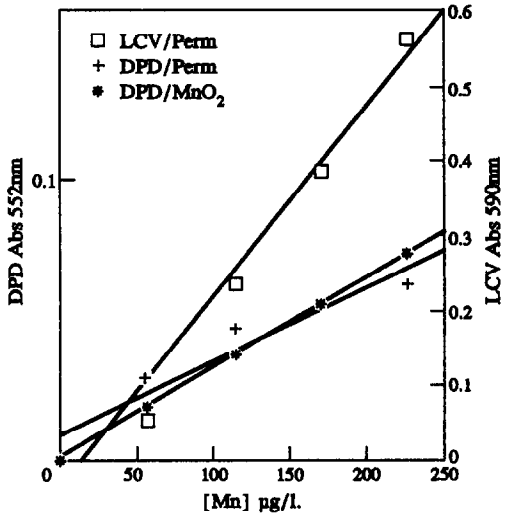

Fig. 4. Standardization of DPD and LCV. LCV/Perm., $r = 0.9898$; DPD/Perm., $r = 0.9582$; DPD/MnO_2, $r = 0.0008$.

o-*Tolidine method.* The method of Morgan and Stumm[13] using *o*-tolidine to determine manganese OE in a colloidal manganese(IV) oxide suspension was attempted in this work on several occasions, but the reagent appeared to react non-quantitatively with standard MnO_2 suspension, providing calibration coefficients of no better than 0.97. Although the purity of the reagent used may be responsible for the deviation from linearity, no attempt was made to purify the reagent as previous experience has shown this to be very time consuming, with very limited improvements.[33] Furthermore, being a *p*-aminophenyl molecule, as is LCV, NaN_3 may also interfere in similar experiments. For these reasons no further work was attempted using *o*-tolidine to determine OE.

N,N-*diethyl*-p-*phenylenediamine, (DPD) method.* DPD is most often currently used for the determination of chlorine residuals in treated water.[34] Figure 3 illustrates the sequential oxidation reactions that DPD undergoes at pH 4.0.

In contrast to LCV, LBB and *o*-tolidine, DPD initially undergoes a one electron oxidation. The semiquinoid intermediate product is a cationic radical, and it is this species, known as Wurster's dye,[35] that provides the pink colour when oxidation of DPD occurs.

DPD provided much improved stoichiometrical results upon colloidal manganese(IV) oxide suspensions compared with those obtained using *o*-tolidine; commonly, correlation coefficients of 0.9999 were achieved. Being only a one electron oxidation, one mole of MnO_2 is able to provide two moles of the cationic radical; this somewhat offsets the lower molar absorptivity.

Table 3. Comparison of Redox and Colorimetric Methods for the Determination of MnO_x

Method	"x" value
LCV	1.65 ± 0.06
o-tolidine	2.36 ± 0.06
LBB	2.13 ± 0.08
Oxalate	1.99 ± 0.05
Iodine	1.98 ± 0.05
DPD	1.98 ± 0.03
Iodine	1.98 ± 0.04

Comparison of the DPD, LCV and iodometric methods

In a comparison of the DPD and LCV methods it was first concluded that permanganate is unsuitable for use as a standard for both reagents. Figure 4 shows that Beer's law plots, using permanganate to standardize both dyes, are far from linear. Significant deviation from linearity occurs indicating that MnO_4^- is being consumed by impurities present in the dyes. It is also possible that the high oxidation state of manganese in MnO_4^- provides problems when used as a redox/colorimetric standard. The reduction of MnO_4^- occurs stepwise, through to the stable IV oxidation state. Full reduction to the Mn(II) state occasionally may not occur rapidly on the timescale required for measurements to be made.

The deviation from linearity is not observed when colloidal MnO_2 is used as the standard in corresponding concentrations.

DPD shows vast superiority in reproducibility over *o*–tolidine and LCV, when used to measure MnO_2 concentration, the standard deviation for measurement of 100 μg/l. MnO_2 being only 5 μg/l.

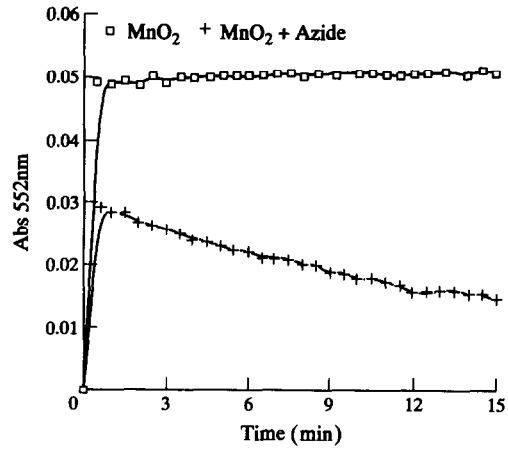

Fig. 5. Stability of DPD absorbance in the presence of azide.

One mole of permanganate should be capable of oxidizing five moles of DPD and thus should give absorbances $\frac{5}{2}$ those of the corresponding MnO_2 concentrations. However, this was not observed. The extinction coefficient of the permanganate line, 1.49×10^4 $l \cdot mole^{-1}$ cm^{-1}, is only $\frac{3}{4}$ that for the MnO_2 line, 1.97×10^4 $l \cdot mole^{-1} \cdot cm^{-1}$. It is worth noting in this context that Tipping *et al.*[35] found that permanganate gave an extinction coefficient of only 2.5×10^4 $l \cdot mole^{-1} \cdot cm^{-1}$ with *o*-tolidine, compared to 3.3×10^4 $l \cdot mole^{-1} \cdot cm^{-1}$ when a synthetic manganese(IV) oxide was used. This discrepancy, according to Tipping, almost exactly accounted for the high oxidizing equivalents obtained by Murray *et al.*[4]

Since permanganate cannot be used as a colorimetric standard it is necessary to use MnO_2 standards for the DPD method. To compare the iodine and DPD methods it was

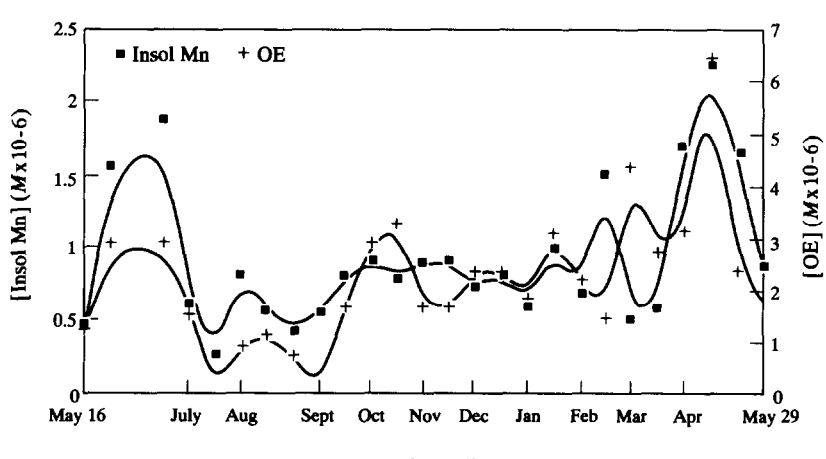

Fig. 6. OE values by DPD method and insoluble manganese concentrations for freshwater dam samples over one year.

therefore necessary to standardize the stock MnO_2 colloidal suspension using the oxalate method. The iodine and DPD methods could then be compared by analysis of a second synthetic MnO_2 colloidal suspension.

Results showed great consistency. The second colloidal suspension was found to be 2020 ± 15 μg/l. using the iodine method and 2010 ± 20 μg/l. using the DPD method.

Table 3 lists the results of Murray *et al.*[4] for the determination of the x value of a synthetic MnO_x suspension and compares them to the results for DPD obtained in this work.

It is clear that DPD is an excellent dye for use in these circumstances. Results compare extremely favourably with the redox titration methods and with other colorimetric methods. It has advantages over the redox methods in sensitivity, time required for each determination, ease of performance and only small sample volumes are required.

To investigate the effect of the poison NaN_3 on the DPD determination of OE, an experiment was run that involved the measurement of a known amount of MnO_2 in the presence of azide by comparison of the absorbance value at 552 nm against a series of standards. The absorbance values used were taken less than 30 sec after DPD had been added to the samples. The final value obtained of 295 μg/l., an average of five individual readings, was within 1.7% of the desired value, 300 μg/l. Figure 5 illustrates the effect of leaving the DPD to react for 15 min with 15 mM NaN_3. It is seen that the DPD colour is again very stable for at least this time period in the absence of azide, but when azide is added the colour is rapidly removed. However, if a measurement is taken within one minute, a value within 1% can be obtained in the presence of azide.

The method was used to find the OE of freshwater dam samples, collected from a depth of three metres, over the year May 1990–May 1991. Figure 6 shows the results obtained and offers a comparison between OE and concentration of insoluble manganese (defined as being retained by a 0.05-μm filter membrane) in the water sample. At this water depth, the majority of the oxidized manganese will be associated with the insoluble fraction of the metal, however it is not necessarily the case that a high OE and a large concentration of insoluble manganese should occur together. Further analysis of this relationship will be taken up in continuing studies.

REFERENCES

1. B. Chiswell and K. R. O'Halloran, *Talanta*, 1991, **38**, 641; B. Lowe, Honours Thesis, University of Queensland, 1990.
2. E. Tipping, D. W. Thompson and J. H. Davison, *Chem. Geol.*, 1984, **44**, 359.
3. E. V. Grill, *Geochim. Cosmochim. Acta*, 1982, **46**, 2435.
4. J. W. Murray, L. S. Balistrieri and B. Paul, *ibid.*, 1984, **48**, 1237.
5. D. Hastings and S. Emerson, *ibid.*, 1986, **50**, 1819.
6. S. Kalhorn and S. Emerson, *ibid.*, 1984, **48**, 897.
7. L. F. Adams and W. C. Ghiorse, *ibid.*, 1988, **52**, 2073.
8. S. M. Bromfield, *Plant and Soil*, 1958, **9**, 325.
9. J. D. Hem and C. J. Lind, *Geochim. Cosmochim. Acta*, 1983, **47**, 2037.
10. J. D. Hem, *ibid.*, 1981, **45**, 1369.
11. D. Z. Piper, J. R. Basler and J. L. Bischoff, *ibid.*, 1984, **48**, 2347.
12. M. A. Kessick and J. J. Morgan, *Environ. Sci. Tech.*, 1975, **9**, 157.
13. J. J. Morgan and W. Stumm, *J. Am. Wat. Works Assocn.*, 1965, **57**, 107.
14. J. J. Delfino and G. F. Lee, *Environ. Sci. Tech.*, 1968, **2**, 1094.
15. E. Tipping, *Geochim. Cosmochim. Acta*, 1984, **48**, 1353.
16. S. Emerson, S. Kalhorn, L. Jacobs, B. M. Tebo, K. H. Nealson and R. A. Rosson, *ibid.*, 1982, **46**, 1073.
17. W. C. Ghiorse, *Bacterial Transformations of Manganese in Wetland Environments*, in: *Current Perspectives in Microbial Ecology* (eds.), C. A. Reddy, M. J. King, *Am. Soc. Microbiol.*, Washington D.C., 1984.
18. W. E. Krumbein and H. J. Altmann, *Helgolander wiss. Meersunters.*, 1973, **25**, 347.
19. W. C. Ghiorse and P. Hirsch, *Iron and Manganese Deposition by Budding Bacteria*, in: *Environmental Biogeochemistry and Geomicrobiology*, Vol 3, W. E. Krumbein (ed.), p. 897. 1978.
20. F. C. Boogerd and J. P. M. De Vrind, *J. Bacteriol.*, 1987, **169**, 489.
21. K. H. Nealson and J. Ford, *Geomicrobiol. Jl*, 1980, **2**, 21.
22. J. P. M. De Vrind, E. W. De Vrind-De Jong, J. W. H. De Voogt, P. Westbroek, F. C. Boogerd and R. A. Rosson, *Appl. Environ. Micro.*, 1986, **52**, 1096.
23. S. D. Chapnick, W. S. Moore and K. H. Nealson, *Limnol. Oceanog.*, 1982, **27**, 1004.
24. F. Fiegl, *Spot Tests in Inorganic Analyses*, Elsevier, 1958.
25. K. H. Nealson, The Isolation and Characterisation of Marine Bacteria which Catalyse Manganese Oxidation, in: *Environmental Biogeochemistry and Geomicrobiology*, Vol 3, Ed. W. E. Krumbein, Ann Arbour Science, 1978, p. 847.
26. A. C. Greene and J. C. Madgwick, *Geomicrobiol. Jl*, 1988, **6**, 119.
27. J. G. Ormerod, *Limnol. Oceanog.*, 1966, **11**, 635.
28. A. Berka, M. Korinkova and J. Barek, *Microchem. Jl*, 1976, **21**, 38.
29. J. Barek, A. Berka and H. Skokankova, *Microchem. Jl*, 1982, **27**, 393.
30. K. R. O'Halloran, Honours Thesis, University of Queensland, 1987.
31. R. R. De Vitre, J. Buffle, D. Perret and R. Baudat, *Geochim. Cosmochim. Acta*, 1988, **52**, 1601.
32. R. C. Aller and P. D. Rude, *ibid.*, 1988, **52**, 751.
33. G. Rauchle, M.Sc. Thesis, University of Queensland.
34. L. J. Michaelis, *J. Am. Chem. Soc.*, 1931, **53**, 2953.
35. E. Tipping, J. G. Jones and C. Woof, *Arch. Hydrobiol.*, 1985, **105(2)**, 161.

Talanta, Vol. 40, No. 4, pp. 541–544, 1993
Printed in Great Britain.

0039-9140/93 $6.00 + 0.00

SPECTROPHOTOMETRIC METHOD FOR THE DETERMINATION OF VANADIUM IN URANIUM RICH HYDROGEOCHEMICAL SAMPLES USING PYRIDYL AZO RESORCINOL (PAR)

G. CHAKRAPANI,* D. S. R. MURTY, B. K. BALAJI and R. RANGASWAMY
Chemical Laboratory, Atomic Minerals Division, Department of Atomic Energy, Nagarbhavi, Bangalore 560072, India

(*Received* 1 *June* 1992. *Revised* 23 *July* 1992. *Accepted* 23 *July* 1992)

Summary—A simple and precise method has been developed for the determination of traces of vanadium(V), using 4-(2 pyridyl azo) resorcinol, in natural water samples, containing very high concentrations of uranium. CDTA–pyrophosphate buffer has been used for masking interferants, including uranium which otherwise interferes above 125 ppb. The reaction of vanadium with PAR in the presence of buffer requires a waiting period of 45 min. The Sandell sensitivity of the method is 0.003 μg/ml, at 545 nm at an optimum pH of 6.5 ± 0.2. The precision of the method is ±15% at the 100 ppb level of vanadium(V). The method has been successfully applied to a number of natural water samples during hydrogeochemical exploration.

The determination of vanadium in hydrogeochemical samples assumes significance, as it is a path finder[1] element for identifying uranium deposits. The presence of vanadium in potable water, in trace quantities has been found to have beneficial effects on the health of individuals.[2] In general, the vanadium in natural water samples varies up to a maximum of 1400 ppb.[3] Various methods that have been reported[4–7] for the determination of vanadium in traces, mostly involving preconcentration, are either cumbersome or the tolerance limits for various ions are poor or their determination levels high. In the method reported for vanadium(V) using PAR and CDTA,[8,9] uranium interferes seriously. Amongst others, uranium(VI) also forms a complex with PAR,[9,10] under identical conditions and thus acts as a major interferant in the determination of traces of vanadium in water samples containing high uranium. During the course of hydrogeochemical surveys in the Cuddapah basin, Andhra Pradesh, India, natural water samples showed anomalous uranium values varying up to a maximum of 5550 ppb.[11] Therefore, a simple and precise analytical procedure for the estimation of vanadium in the presence of high uranium, in hydrogeochemical samples has been developed and the results are presented in this paper.

*Author for correspondence.

EXPERIMENTAL

Instrumentation

A Shimadzu UV-240 graphicord double beam spectrophotometer with 10-mm path length quartz cells and an Orion analyser model 407 A pH meter were used.

Reagents

Vanadium solution. (1 ml = 100 μg of V). Dissolve 0.2309 g of ammonium metavanadate A.R (Renna, Budapest, Hungary) in water, add 15 ml of 1:1 nitric acid and dilute to 1000 ml. From this, prepare a fresh vanadium standard solution of 1 ml = 1 μg of V.

CDTA (0.014M)–pyrophosphate (0.4M) (buffer). Dissolve 1.25 g of 1,2 amino cyclohexane *NNNN*-tetra acetic acid, CDTA (Pro analysis, Merck) in a minimum amount of dilute sodium hydroxide and adjust to pH 6.5 (solution 1). Dissolve 44.69 g of tetra sodium pyrophosphate (Analar, BDH) in a minimum amount of dilute nitric acid and adjust to pH 6.5 (solution 2). Mix solutions 1 and 2 and make up to 250 ml.

PAR solution (0.004M). Prepare 0.1% 4-(2 pyridylazo) resorcinol by dissolving 0.1 g of the sodium salt of PAR (Loba Chemie GR) in distilled water and adjust the pH between 6.5 and 7.0. All the other reagents used are of Analar grade.

Table 1. Tolerance limits in μg for various ions in the determination of 3 μg of vanadium in the presence of CDTA pyrophosphate

Interferant	μg/Aliquot*
K^+	48,000
Na^+	40,000
Ca^{+2}	10,000
Mg^{+2}	10,000
Mo^{+6}	5,000
Zn^{+2}	300
UO_2^{+2}	300†
Cu^{+2}	100
Fe^{+3}	20†
Mn^{+2}	500
As^{+3}	10
Ni^{+2}	100
Pb^{+2}	1,000
SeO_4^{-2}	3
Cl^-	80,000
SO_4^{-2}	40,000
HCO_3^-	25,000
F^-	50

*The interference effect beyond the concentration given was not studied.

†Fe^{+3} and UO_2^{++} interfere beyond the concentration given. Aliquot, maximum 10 ml; Buffer, 10 ml of 0.4*M*; PAR 2 ml of 0.1%; total volume of 25 ml.

Procedure

To an aliquot of a natural water sample (maximum 10 ml) containing 1–10 μg of vanadium(V), add 10 ml of CDTA–pyrophosphate buffer, adjust to pH 6.5 ± 0.2 if necessary, and add 2 ml of PAR at the end. Dilute to 25 ml and after 45 min measure the optical density of the solution at 545 nm. Draw a calibration graph by treating 1, 2, 3 and 5-μg vanadium standards in a similar way. Beer's law is obeyed in the range of 40–400 ppb of vanadium.

RESULTS AND DISCUSSION

The sequence of addition of reagents, should be the addition of CDTA pyrophosphate buffer, followed by pH adjustment, where necessary, and addition of PAR at the end. Any precipitate formed after the addition of buffer dissolves while adjusting to pH 6.5 ± 0.2. However, in a situation where the precipitate does not dissolve, if Ca is present in >1000 ppm, smaller aliquots are to be taken.

The CDTA reagent is a well known complexing agent.[12] The presence of CDTA prevents the reaction of many metal ions like Ca, Mg, Al, Mn, Mo, Co, Cr, Cu, Zn, Pb, Ni, *etc.*[8,13] with PAR, making the method one of the most selective for the determination of vanadium. The selective masking reaction of CDTA was attributed to its thermodynamic effect.[14] CDTA has a special action towards the vanadyl ion, in that it does not form a stable complex, in contrast to other metal ions.[15,16] The reaction of vanadium with PAR in the presence of buffer is not instantaneous and requires a waiting period of 45 min. Probably the lower stability constant[14] of the VO_2–CDTA complex ($K = 10^{16.59}$) eventually paves the way for the formation of the more stable VO_2-PAR complex ($K = 10^{18.81}$), thus requiring a waiting period of about 45 min.

$$VO_2 - CDTA + PAR \leftrightharpoons VO_2 - PAR + CDTA^{14}$$

The stability of the VO_2–buffer–PAR complex alone and in the presence of various cations and anions was studied from 45 min to 4 hr. During the period of study the complex was found to be stable. Thus, various metal ions and other anions as indicated in Table 1 do not interfere, during this period.

The tetra sodium pyrophosphate is a well known complexing agent and has been used in the determination of uranium in water samples, using laser induced fluorimetry.[17]

The complexing/buffering property of pyrophosphate for uranium has been made use of as

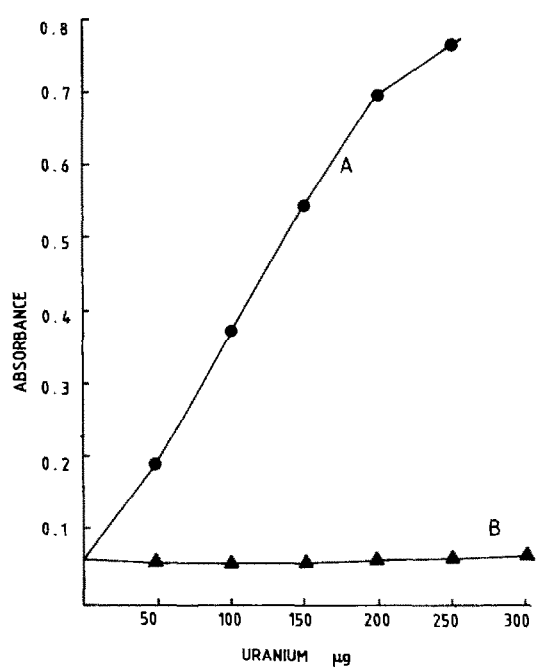

Fig. 1. Effect of uranium on vanadium determination; 3 μg of vanadium with varying concentration of uranium in a total volume of 25 ml. A, in the presence of 10 ml of 0.014*M* CDTA only. B, in the presence of 10 ml of 0.014*M* CDTA–0.4*M* pyrophosphate buffer.

Table 2. Recovery studies for vanadium on synthetic water samples

Synthetic water samples	Composition in 25-ml volume	Vanadium added (in 25 ml)	Vanadium found (in 25 ml)
SYWS-1	Ca and Mg (10 mg each) Cl, SO_4, Na and K (40 mg each)	3 μg	2.85 μg
SYWS-2	SYWS-1 + HCO_3 (25 mg) added at pH 6.5	3 μg	2.90 μg
SYWS-3	SYWS-1 + F (50 μg)	3 μg	3.25 μg
SYWS-4	SYWS-3 + Zn (300 μg) Cu (100 μg) Fe (20 μg) Mn (500 μg) As (10 μg) Ni (100 μg) Pb (1000 μg) Se (3μg)	3 μg	3.30 μg

a masking effect in the proposed spectrophotometric determination of vanadium in the presence of high concentrations of uranium. Thus, the shortcoming of the V–PAR method[8] in which uranium interferes even in the presence of CDTA has been overcome by using pyrophosphate buffer. While determining vanadium in the presence of uranium using PAR, the reaction due to U-PAR is completely suppressed by pyrophosphate, and not by CDTA (Fig. 1). Because of the excellent buffering capacity of pyrophosphate, there is no need to adjust the pH of natural water samples, whose pH will generally be around 6.5–8.5.

The concentrations of various cations and anions, as given in Table 1, were fixed, for interference studies, keeping in view the anomalous values for cations and anions that are likely to be present in anomalous natural water samples. The interference effects of these ions beyond the concentrations given in Table 1, were not studied, except in the case of Fe(III) and U(VI); studies indicate that if Fe(III) is present in more than 20-μg amounts in 10 ml of water sample, it interferes seriously. U(VI) also interferes, if present in more than 300 μg/10 ml. The tolerance limits were fixed as being able to accommodate 5% change in the standard value. As Pb is a general co-existent of uranium, it is probable that Pb will often occur with uranium and hence its interference effect has been studied up to 1000 μg/10 ml. Lead does not interfere even at this high concentration. Fe, U, Pb and other cations and anions are not likely to exist in natural waters above the levels indicated in Table 1.

The optimum concentration of CDTA (0.014*M*) and pyrophosphate (0.4*M*) has been fixed, keeping in mind the natural water samples containing anomalous concentrations of cations and anions as given in Table 1. Uranium present in water samples above 125 ppb interferes in the determination of vanadium, if not masked. Uranium at 100 ppb gives a value equivalent to 15 ppb vanadium.

In Fig. 1, the interference effect of uranium (from 50 μg to 300 μg) on the determination of vanadium (3 μg) is shown in the presence of 0.014*M* CDTA alone and in the presence of both 0.014*M* CDTA and 0.4*M* pyrophosphate buffer mixture. It is very clear from the graph that in the absence of pyrophosphate buffer and in the presence of CDTA alone, uranium interferes seriously [see rising line (A)] *i.e.*, increasing absorbance values for the same concentration of vanadium (3 μg) with an increase in uranium concentration. On the contrary, the interference effect of uranium is not seen in the presence of CDTA–pyrophosphate buffer, as shown by the flattened line (B). Thus, the studies indicate that 10 ml of 0.4*M* pyrophosphate buffer can completely mask uranium (either as UO_2^{2+}, U^{4+} or both) up to 300 μg and CDTA plays no role in complexing uranium. Hence, vanadium can be determined in water samples containing anomalous concentrations of uranium even in the order of 10,000 ppb and greater without interference from it.

In the absence of the naturally available water samples, having anomalous concentrations of various ions as given in Table 1, synthetic water samples were prepared in order to study the recoveries by the present method. Good recoveries of vanadium have been obtained (>90%) on synthetic water samples, SYWS-1, SYWS-2, SYWS-3, and SYWS-4, as given in Table 2.

Natural water samples (Bore well waters), having a very high concentration of uranium (approx. from 1000 to 5000 ppb) have been selected for the determination of vanadium, so as to indicate the extent of uranium interference on vanadium, in the presence of only CDTA and in the absence of pyrophosphate buffer. The vanadium values in these samples,

Table 3. Analytical data of vanadium and uranium in geochemical exploration water samples

Sample No.	By ICP–AES[18] (V in ppb)	By present† method (V in ppb)	% RSD	With only CDTA–PAR (V in ppb)	Uranium[17] in ppb
AMD-1	87	80*	20	424	2280
AMD-2	112	95*	15	265	1136
AMD-3	108	120	11	528	2725
AMD-4	102	108	15	940	5550
AMD-5	96	89*	18	330	1620
AMD-6	146	134	11	589	3086
AMD-7	110	114	12	319	1438
AMD-8	94	99*	15	637	3539

*Vanadium determined after preconcentration by evaporation.
†Vanadium values given are the average of six determinations.

determined by the present method and by ICP–AES,[18] are tabulated in Table 3 for comparison. The values given in ppb are the average of six determinations. In the same samples, vanadium values, determined by using only CDTA, are very high due to interference from uranium. This explains clearly the role of the buffer. The uranium values in the above samples were determined by laser induced fluorimetry.[17] The relative standard deviation of the method at 100 ppb vanadium is within ±15%.

Two separate aliquots of natural water samples were taken and one portion of it was analysed after treating with an oxidizing agent, keeping both V and U in +5 and +6 states respectively. Another portion of it was analysed directly without adding any oxidizing agent. The vanadium values obtained in both cases were found to be the same and hence the addition of an oxidizing agent is not essential. It is also reported that vanadium[19,20] and uranium[21] mostly exist in +5 and +6 states respectively.

CONCLUSIONS

The present method is simple and precise, involving only the addition of CDTA-pyrophosphate buffer and PAR to natural water samples. Vanadium down to 100 ppb can be determined in the presence of high concentrations of uranium and dissolved solids, without preconcentration and/or isolation from interferants.

Acknowledgements—The authors are highly thankful to Dr R. K. Malhotra, for suggesting the problem and for his valuable guidance throughout this work. The authors are also thankful to the late Shri. B. N. Tikoo, Shir. K. P. Cheria and Shri. S. G. Vasudeva for the encouragement and to Dr S. Viswanathan, Director, Atomic Minerals Division for permission to publish this paper.

REFERENCES

1. R. W. Boyle, *Geochemical Prospecting for Thorium and Uranium Deposits* p. 498. Elsevier Publishing Co., Amsterdam, 1982.
2. L. S. Clesceri, A. E. Greenberg and R. R. Trussel, *Standards Method for Examination of Water and Waste Water*, 17th Ed., pp. 3–151. APHA Publication, 1989.
3. K. H. Wadepohl, *Handbook of Geochemistry;* Vol. 11–2, 1970, New York, 23–1.
4. S. C. Shone, *Anal. Chem.*, 1951, **23**, 1186.
5. K. Naito and Sugawara, *Bull. Chem. Soc. Japan*, 1952, **30**, 799.
6. P. E. Rayem, *Analyst*, 1960, **85**, 569.
7. M. J. Fishmen and M. W. Skougstad, *Anal. Chem*, 1964, **36**, 1643.
8. O. Budevsky and L. Johnova, *Talanta*, 1965, **12**, 291.
9. Hiroshi Onishi, *Photometric Determination of Traces of Metals*,, Vol. 3, Part 11B, 4th Ed., p. 625. Wiley-Interscience, 1989.
10. I. Broic, E. Polla and M. Rodosemic, *Microchim, Acta*, 1985, **11**, 187.
11. Atomic Minerals Division, DAE, India, Achievements for Field Season, p. 54. 1989–90.
12. F. D. Snell, *Photometric and Fluorimetric Methods of Analysis Metals*, Part 2, pp. 1226, 1227. Wiley Interscience, 1978.
13. T. Yotsuyanagi, J. Itoh and K. Aomura, *Talanta*, 1969; **16**, 1611.
14. J. Itoh, T. Yotsuyanagi and K. Aomura, *Anal. Chim. Acta*, 1975, **77**, 229.
15. D. Budevsky and R. Pribil, *Talanta*, 1964, **11**, 1313.
16. W. J. Geary and C. N. Larsson, *SA.C Conference*, Heffer, Cambridge, 1965.
17. R. K. Malhotra and B. N. Tikoo, *Proceedings of the Fifth National Symposium Held at Hyderabad (India)*, Indian Society of Analytical Scientists, 1988.
18. M. Thompson and J. N. Walsh, *A Handbook of Inductively Coupled Plasma Spectrometry*, p. 201. Blackie, 1983.
19. *Surficial Uranium Deposits, International Atomic Energy Agency*, Vienna, IAEA-TECDOC-322, 146, 1984.
20. V. M. Goldsmith, *Geochemistry*, Alex Muir (ed.), p. 491. Oxford 1954.
21. Geochemical Exploration for Uranium, International Atomic Energy Agency, Technical Reports Series No. 284, p. 16. Vienna, 1988.

Talanta, Vol. 40, No. 4, pp. 545–549, 1993
Printed in Great Britain.

0039-9140/93 $6.00 + 0.00

DETERMINATION OF ABSOLUTE CONFIGURATIONS FROM VIBRATIONAL RAMAN OPTICAL ACTIVITY: *TRANS*-2,3-DIMETHYLTHIIRANE

PRASAD L. POLAVARAPU,* SIMEON T. PICKARD, HOWARD E. SMITH* and THOMAS M. BLACK
Department of Chemistry, Vanderbilt University, Nashville, TN 37235, U.S.A.

LAURENCE D. BARRON* and LUTZ HECHT
Chemistry Department, The University, Glasgow G12 8QQ, U.K.

(*Received* 17 *June* 1992. *Accepted* 22 *July* 1992)

Summary—Experimental and theoretical vibrational Raman optical activity (VROA) spectra of (2*R*,3*R*)-2,3-dimethylthiirane in the 200–1500 cm^{-1} region are presented. The level of agreement obtained for the observed and predicted VROA signs suggests that the absolute configurations of chiral molecules can be determined confidently using VROA.

Raman optical activity in vibrational transitions, known as vibrational Raman optical activity (VROA), was theoretically formulated[1,2] and experimentally observed[3] in the early 1970's. However, as the effect is very small (usually a few parts in 10^4 units of ordinary Raman cross sections, which themselves are weak) and the phenomenon is one of higher order perturbations, the experimental measurements remained difficult and theoretical predictions appeared hopeless. Two recent developments[4–11] have changed this gloomy situation and the course of VROA spectroscopy. It was recognized that VROA can be predicted[4–10] from first principles using *ab initio* quantum theoretical methods and at about the same time the VROA instrumentation in Glasgow has been improved dramatically so that VROA spectra can be obtained routinely with excellent signal-to-noise ratios.[11] As a result, important chemical problems are beginning to be addressed now using VROA spectroscopy. One of these is the determination of absolute configurations of chiral molecules. Since optical activity is being probed in the vibrational transitions and since each vibrational transition of a chiral molecule in principle can exhibit VROA, the informational content in a VROA spectrum contains the complete stereochemistry of a molecule in the solution phase. Extraction of this information from a given experimental spectrum is not quite straightforward and in this context the reliability of the theoretical models employed plays a key role. In order to be able to use VROA spectroscopy as a practical tool for stereochemical studies, VROA research at this time is directed towards establishing this reliability. As part of this development we investigated the experimental and theoretical VROA of enantioenriched *trans*-2,3-dimethylthiirane. These results are presented and critically analysed in this paper.

*Authors for correspondence.

THEORY AND EXPERIMENTAL

The enantioenriched *trans*-2,3-dimethylthiirane used in the present study was characterized earlier[12] and had $[\alpha]^{23-25}D + 105°$ (neat). Thus, based on the highest rotatory power reported for either enantiomer, this sample of thiirane had an enantiomer excess of 81%. The VROA spectra were obtained on a second new Raman spectrometer developed at Glasgow which will be described in detail elsewhere (this is a 90°-scattering version, for small organic molecules, of the backscattering VROA instrument for biological samples described in Ref. 11).[13] A brief description is as follows. The incident laser beam from an Ar^+ laser, at 488 nm with ~750 mW power at the sample, is modulated between right and left circular polarizations using a KD*P electro-optic modulator at ~1 Hz. The depolarized light scattered in the 90° direction with polarization in the

scattering plane was collected and dispersed on to a CCD detector by a 0.25-meter spectrograph (JY HR250S). A holographic notch filter (Kaiser Optical Systems) enabled the spectra to be measured down to ~ 100 cm^{-1}. The detector is a Peltier-cooled back thinned CCD camera (Wright Instruments Ltd. Model AT1) with an exceptional quantum efficiency ($\sim 80\%$). The light scattered during the left circular polarization excitation was subtracted from that during the right circular polarization excitation and this difference spectrum represents the depolarized VROA, $I_z^R - I_z^L$. For comparison of magnitudes with the theoretical predictions this difference is normalised with the corresponding sum, $I_z^R + I_z^L$, and the normalized circular intensity difference is denoted Δ_z. Typical exposure time was 0.8 sec with total data acquisition time of one hour. The experimental difference and sum spectra are displayed in Fig. 1.

The *ab initio* quantum theoretical predictions of Δ_z were obtained from the expression[1,14]

$$\Delta_z = \frac{I_z^R - I_z^L}{I_z^R + I_z^L} = \frac{24(\gamma^2 - \delta^2/3)}{12\ \beta^2} \qquad (1)$$

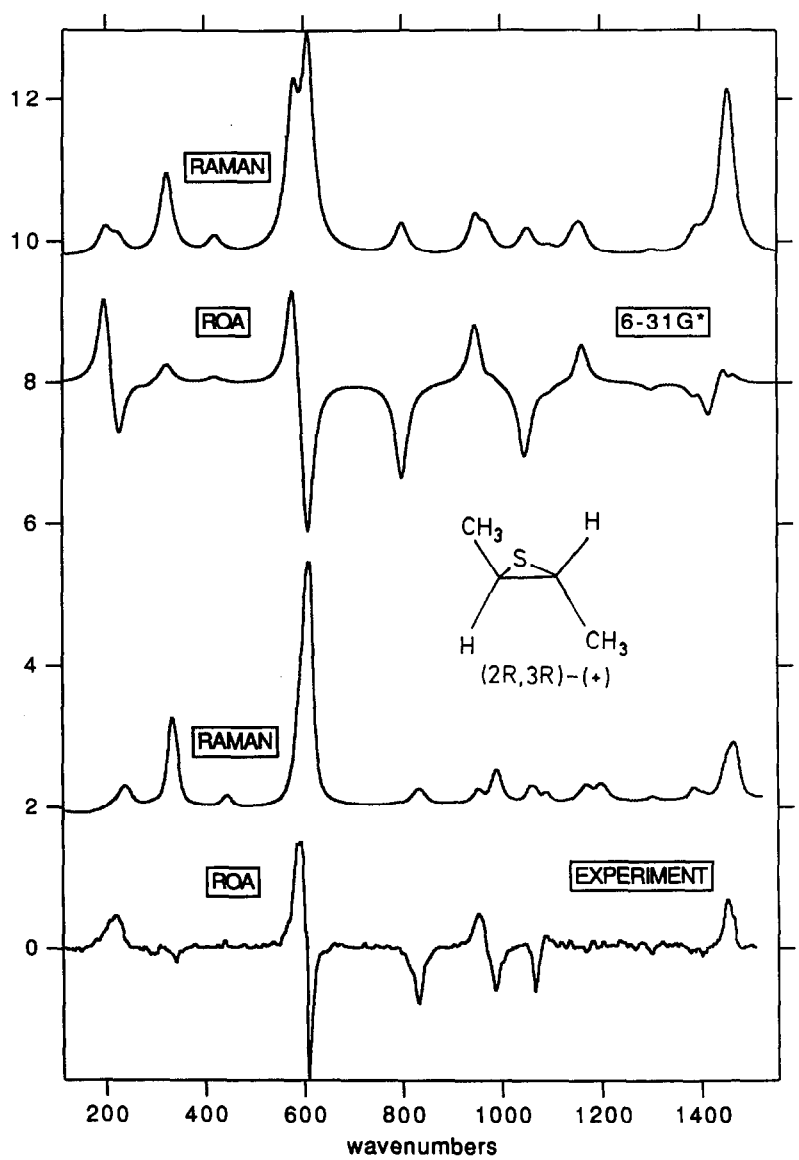

Fig. 1. Experimental (bottom two traces) and *ab initio* theoretical (top two traces) Raman and VROA spectra for (+)-*trans*-2,3-dimethylthiirane and (2*R*,3*R*)-2,3-dimethylthiirane, respectively. The theoretical spectra were obtained with the 6-31G* basis set and the calculated frequencies were multiplied by 0.89 to bring them closer to the experimental frequencies. All spectra are presented on arbitrary intensity scales.

where

$$\gamma^2 = \frac{1}{2}\left[3\frac{\partial\alpha_{\alpha\beta}\partial G'_{\alpha\beta}}{\partial Q\ \partial Q} - \frac{\partial\alpha_{\alpha\alpha}\partial G'_{\beta\beta}}{\partial Q\ \partial Q}\right] \quad (2)$$

$$\delta^2 = \frac{\omega}{2}\frac{\partial\alpha_{\alpha\beta}\partial A_{\gamma\delta\beta}}{\partial Q\ \partial Q}\epsilon_{\alpha\gamma\delta} \quad (3)$$

$$\beta^2 = \frac{1}{2}\left[3\frac{\partial\alpha_{\alpha\beta}\partial\alpha_{\alpha\beta}}{\partial Q\ \partial Q} - \frac{\partial\alpha_{\alpha\alpha}\partial\alpha_{\beta\beta}}{\partial Q\ \partial Q}\right] \quad (4)$$

by evaluating the polarizability derivatives $\partial\alpha_{\alpha\beta}/\partial Q$, $\omega^{-1}\ \partial G'_{\alpha\beta/\partial 2}$, $\partial A_{\alpha\beta\gamma}/\partial Q$ numerically. Here Q is the vibrational normal coordinate; $\alpha_{\alpha\beta}$ is the electric dipole electric dipole polarizability, $G'_{\alpha\beta}$ is the electric dipole magnetic dipole polarizability and $A_{\alpha\beta\gamma}$ is the electric dipole electric quadrupole polarizability. These tensor derivatives were obtained in the static limit by evaluating the tensors at the equilibrium geometry and at the geometries displaced by 0.005 Å along each cartesian coordinate. The procedure for obtaining the $\omega^{-1}\ G'_{\alpha\beta}$ tensor in the static limit is due to Amos[15] as implemented in the CADPAC program[16] which simultaneously evaluates the $\alpha_{\alpha\beta}$ and $A_{\alpha\beta\gamma}$ tensors. The above mentioned tensor derivatives were obtained with the 6-31G* basis set[17] at the fully optimized geometry. Vibrational frequencies and normal mode descriptions were also obtained[12] with the same basis set. The predicted spectra were simulated with Lorentzian band shapes using 12 cm^{-1} half-width at half-height. The resulting theoretical spectra are compared to the corresponding experimental spectra in Fig. 1 where the theoretical frequencies are multiplied by 0.89 to bring them closer to the experimental frequencies. The experimental Δ_z values corrected to 100% enantiomeric excess are given in Table 1.

RESULTS AND DISCUSSION

The experimental data for the (+)-*trans*-2,3-dimethylthiirane and the theoretical data for the enantiomer with the 2*R*,3*R* configuration are used in the following discussion. Also the theoretical frequencies cited in the discussion are those scaled down by 0.89.

The two resolved experimental Raman bands at 1458 and 1446 cm^{-1} are composed of four

Table 1. Vibrational raman optical activity in (2*R*,3*R*)-2,3-dimethylthiirane

	6-31G*					Experiment¶		
Sym	Freq (cm^{-1})	Scaled‡	$45\alpha^2 + 7\beta^2$	dep. ratio	$\Delta_z \times 10^4$	Freq (cm^{-1})	$\Delta_z \times 10^4$	Assignment†
A	1641	1460	15.5	0.72	13.6	1458	2.6	CH_3 def
B	1640	1460	20.5	0.75	−10.7	1458		CH_3 def
A	1633	1453	7.1	0.74	−0.8	1446	4.0	CH_3 def
B	1629	1450	19.3	0.75	2.2	1446		CH_3 def
A	1592	1417	4.2	0.48	−12.4	1398	−5.2	—C*—H bend + CH_3 def
B	1566	1394	3.7	0.75	3.7	1380	−1.3	CH_3 Umb
A	1559	1388	2.6	0.70	−7.5	1380		CH_3 Umb
B	1462	1301	1.1	0.75	−5.7	1297	−5.3	—C*—H bend
A	1307	1163	13.6	0.25	5.6	1198	0.4	C*—C* str + —C*—H bend
A	1290	1148	3.8	0.75	−1.6	1170	−1.7	—C*—H bend + CH_3 rock
B	1233	1097	1.4	0.75	−3.2	1089	4.9	—C*—H bend + CH_3 rock
A	1189	1058	3.8	0.74	−1.3	1052	1.8	—C*—H bend + CH_3 rock
B	1179	1049	2.4	0.75	−21.6	1068	−13.0	C*—C str + CH_3 rock
A	1102	981	1.9	0.05	30.8	991	−6.4	—C*—H bend + CH_3 rock
B	1092	972	4.3	0.75	−1.8	991		C*—C str + CH_3 rock
B	1066	949	6.9	0.75	5.9	953	10.0	—C*—H bend + CH_3 rock
A	900	801	14.3	0.17	−10.2	837	−14.3	C*—C* str + C*—CH_3 str
B	685	610	22.7	0.75	−2.8	611	−2.2	C*—S str
A	651	579	23.8	0.36	3.0	593	3.3	C*—S str
A	473	421	3.9	0.14	1.1	450	+1.8	C*—C*—C bend
B	365	325	3.9	0.75	0.7	342	−0.7	S—C*—C bend
B	320	285	0.0	0.75	§	309	−6.3	C*—C*—C bend
A	254	226	0.5	0.60	−16.1	246		S—C*—C bend
B	239	213	0.1	0.75	−21.0	246	2.2	CH_3 torsion
A	224	199	0.6	0.73	14.3	224	14.3	CH_3 torsion

†From Ref. 12.

§Very small Raman intensity.

‡Scaling factor is 0.89.

¶The experimental Δ_z values are the averages of two measurements and are corrected to 100% enantiomeric excess and thus the listed values are for the pure enantiomer.

normal modes arising from the bending motions of the methyl groups. A single positive VROA envelope is observed for these two bands but if the bands could be resolved better, the predictions indicate a positive-negative-negative-positive substructure in this region. Although the order of the predicted modes here cannot be verified from the available experimental data, the predictions indicate net positive VROA in agreement with the experimental observation. The experimental band at 1398 cm^{-1}, associated with a methyl bending motion coupled to CH_3 bending, has weak negative VROA. This is also the sign predicted for this mode. The predicted VROA intensities differ somewhat from the observed values for the bands discussed above. The two umbrella type bending modes of the CH_3 groups are associated with the unresolved experimental band at 1380 cm^{-1}. These two modes are predicted to have opposite VROA signs cancelling each other due to their overlap and giving a net negative VROA. This is also the sign seen in the experimental spectrum for the 1380 cm^{-1} band. The 1297 cm^{-1} band in the experimental spectrum has weak negative VROA which is supported by the theoretical predictions for the corresponding theoretical mode at 1301 cm^{-1} associated with a —C*—H bending motion.

The C*—C* stretching motion is associated with the experimental band at 1198 cm^{-1}. The VROA associated with this band is weak and positive. Although the same sign is predicted for the corresponding theoretical mode at 1163 cm^{-1}, the predicted intensity is somewhat higher. The neighboring experimental Raman band at 1170 cm^{-1} has weak negative VROA which again is in agreement with the theoretical predictions for the corresponding mode at 1148 cm^{-1}. The predicted and observed VROA signs do not agree for the two experimental bands at 1089 and 1052 cm^{-1} which are associated with —C*—H bending motions. However, since the intensities associated with these two bands are small the predictions can probably be improved here if higher levels of theory are utilized. The experimental Raman band at 1068 cm^{-1} is associated with the C*—C stretch coupled to CH_3 rocking motion and is seen to have significant VROA. This observation is faithfully reproduced in the predicted spectrum where the corresponding theoretical mode is situated at 1049 cm^{-1}. The C*—C stretching coupled to CH_3 rocking motion mode and a —C*—H bending mode are predicted to be responsible for the 991 cm^{-1} experimental Raman band. While this experimental Raman band has negative VROA of substantial intensity, correspondingly large negative VROA is not found for the theoretical modes. Out of the two theoretical modes associated with the 991 cm^{-1} experimental Raman band, the one at 981 cm^{-1} is strongly polarized and has very weak Raman intensity while the other at 972 cm^{-1} is depolarized and has somewhat higher Raman intensity. Therefore the observed VROA at 991 cm^{-1} is most likely due to the calculated mode at 972 cm^{-1} which has negative but weak VROA. Therefore the predicted and observed VROA signs also match here but the intensities differ substantially. The positive VROA at 953 cm^{-1} and the negative VROA at 837 cm^{-1} in the experimental spectrum match very nicely with those of the corresponding theoretical modes at 949 and 801 cm^{-1}, respectively, in both signs and intensities.

The unresolved Raman band at 600 cm^{-1} is associated with the symmetric and antisymmetric C*—S stretching modes. The VROA spectrum however clearly shows bisignate bands here indicating the importance of VROA spectroscopy in yielding additional information. The antisymmetric stretch is associated with the negative part and the symmetric stretch is associated with the positive part of this bisignate couplet. The negative band is slightly more intense than the positive and both are much stronger than any other band in the 200–1500 cm^{-1} region of the VROA spectrum. The theoretical predictions here match with the experimental observations quite satisfactorily, and this agreement is by far the most reliable test for verifying the theoretical model employed.

In the region below 500 cm^{-1}, the experimental spectrum has six Raman bands, but only the band assigned to the symmetric methyl torsion mode has significant VROA. The sign and magnitude for this VROA band are seen to match with those in the predicted spectrum. As discussed elsewhere,[18] methyl torsion VROA is particularly useful for stereochemical deductions. The predicted VROA spectrum also shows strong negative VROA for the two modes at 213 and 226 cm^{-1}, but the experimental spectrum does not have the corresponding feature. This appears to be the only strong disagreement between the predictions and experimental observations.

CONCLUSIONS

The experimental VROA spectrum for (+)-*trans*-2,3-dimethylthiirane is seen to compare remarkably well with that predicted for 2*R*,3*R* configuration, but some differences between the observed and predicted intensities are noticed. As in our earlier studies of alanine[8,9] and tartaric acid,[10] the best agreement between calculations and experiment is found in skeletal vibrations in the range ~ 500–$1000\ cm^{-1}$ which are dominated by stretch coordinates and which reflect the stereochemistry most directly. For the purpose of predicting the absolute configurations, however, it is essential that the signs for corresponding experimental and calculated VROA bands be the same, but differences in relative intensities for corresponding bands are less important. Since observed VROA signs indeed match with the predicted ones for a majority of the bands, this agreement then establishes the reliability for utilizing VROA as a valuable new technique for stereochemical studies.

Acknowledgements—Grants from the National Institutes of Health (GM29375), the National Science Foundation (CHE 8808018), the Science and Engineering Research Council, the Wolfson Foundation and the Deutsche Forschungsgemeinschaft (Habilitandenstipendium II C1-He 1588/3-1) supported this work.

REFERENCES

1. L. D. Barron and A. D. Buckingham, *Mol Phys.*, 1971, **10**, 1111.
2. *Idem*, *ibid.*, *Ann. Rev. Phys. Chem.*, 1975, **26**, 381.
3. L. D. Barron, M. P. Bogaard and A. D. Buckingham, *J. Am. Chem. Soc.* 1973, **95**, 603.
4. P. K. Bose, L. D. Barron and P. L. Polavarapu, *Chem. Phys. Lett.*, 1989, **155**, 423.
5. P. K. Bose, P. L. Polavarapu, L. D. Barron and L. Hecht, *J. Phys. Chem.*, 1990, **94**, 1734.
6. T. M. Black, P. K. Bose, P. L. Polavarapu, L. D. Barron and L. Hecht, *J. Am. Chem. Soc.* 1990, **112**, 1479.
7. P. L. Polavarapu, *J. Phys. Chem.*, 1990, **94**, 8106.
7. P. L. Polavarapu, *Chem. Phys. Lett.*, 1990, **174**, 511.
8. L. D. Barron, A. R. Gargaro, L. Hecht and P. L. Polavarapu, *Spectrochim. Acta* 1991, **47A**, 1001.
9. L. D. Barron, A. R. Gargaro, L. Hecht and P. L. Polavarapu, *ibid.* 1992, **48A**, 261.
10. L. D. Barron, A. R. Gargaro, L. Hecht, P. L. Polavarapu and H. Sugeta, *Spectrochim. Acta A*, 1992, **48A**, 1051.
11. L. Hecht, L. D. Barron, A. R. Gargaro, Z. Q. Wen and W. Hug, *J. Raman Spectrosc.*, 1992, **23**, 401.
12. P. L. Polavaraup, S. T. Pickard, H. E. Smith, T. M. Black, A. Rauk and D. Yang, *J. Am. Chem. Soc.*, 1991, **113**, 9747.
13. L. Hecht and L. D. Barron, unpublished work.
14. L. D. Barron, *Molecular Light Scattering and Optical Activity*, *Cambridge University Press*, 1982.
15. R. D. Amos, *Chem. Phys. Lett.* 1982, **87**, 23.
16. R. D. Amos and J. E. Rice, *CADPAC: Cambridge Analytic Derivative Package*, Cambridge, 1987.
17. P. C. Hariharan and J. A. Pople, *Theor. Chim. Acta* 1973, **28**, 213.
18. L. D. Barron, L. Hecht and P. L. Polavarapu, *Spectrochim. Acta A*, 1992, **48A**, 1193.

Talanta, Vol. 40, No. 4, pp. 557–563, 1993
Printed in Great Britain.

0039-9140/93 $6.00 + 0.00

SPECTROSCOPIC ANALYSIS AND DRUG-BINDING STUDIES OF THE CNBr FRAGMENTS OF HUMAN SERUM ALBUMIN

JIAN WANG, THILIVHALI T. NDOU* and ISIAH M. WARNER†
Department of Chemistry, Emory University, Atlanta, Georgia 30322, U.S.A.

CHOU-PONG PAU
Division of HIV/AIDS, National Center for Infectious Diseases, Centers for Disease Control, Atlanta, Georgia 30333, U.S.A.

(*Received* 18 *May* 1992. *Revised* 21 *July* 1992. *Accepted* 21 *July* 1992)

Summary—Three large fragments (A, B and C) of human serum albumin (HSA) were produced by cyanogen bromide digestion of HSA in order to investigate the specific binding sites. The fragments were isolated by use of gel filtration, followed by high performance ion exchange chromatography. The isolated fragments were examined by use of UV/Vis, steady-state fluorescence, and circular dichroism spectroscopy. The study was extended to examine the interactions of bilirubin and two anionic drugs, warfarin and naproxen, with HSA and the three fragments. The primary bilirubin binding site on HSA molecule appeared to be located between fragment A and fragment C. The results also suggest the binding sites of the two anionic drugs to most likely be located in fragment C of HSA molecule.

Human serum albumin (HSA) is the most abundant plasma protein in the body. A large number of low molecular weight compounds, including several drugs, bind reversibly to HSA, which functions as the major transport protein in the body. In certain instances, the albumin binding of a drug is a significant factor for the pharmacokinetics, and the displacement of one drug by another from the albumin binding sites can contribute to the phenomenon of synergistic drug interaction. Knowledge of the HSA binding sites is important for rational understanding of albumin binding and for any approach to systematize such interactions. Furthermore, detailed knowledge about the specific location of the ligand-binding sites of HSA will improve the understanding of general mechanisms of ligand-protein interactions since the number of binding sites of the HSA molecule is rather small. For example, HSA is the dominant transport protein for acidic drugs, and it is believed that there are two main binding sites for acidic drugs.[1,2] It is well established that aromatic-acidic drugs that bind to site I are mostly bulky heterocyclic molecules with a negative charge at the center of a large nonpolar molecule. In contrast, drugs that bind to site II have an extended configuration, and the negative charge is located at one end of the molecule, away from the nonpolar region. One possible approach to locate binding sites on HSA is to cleave the HSA into several fragments and study the ligand binding to various fragments of HSA. Thus, the necessary information about the microenvironment of the binding sites on HSA may be obtained. There are two main protein fragmentation methods: (1) enzymic cleavage and (2) chemical cleavage. One of the most widely used methods is chemical cleavage, which cleaves proteins at the methionine residues using cyanogen bromide. In this method, relatively large fragments, high selectivity, and high cleavage yield are obtained.[3] Several studies of protein structure and drug-binding sites have been performed by use of this fragmentation method.[4–9] Sjöholm and Liungstedt[8] used the low ultraviolet region of circular dichroism spectral data of HSA CNBr fragments to calculate the quantitative contribution of the α helical and β structure in the fragments. They found that large parts of the ordered structures in HSA are preserved in the fragments. Thus this cleavage method should be a meaningful tool for studying the protein conformation and ligand binding sites.

*Present address: Gillette Research Institute, Gaithersburg, MD 20879, U.S.A.
†Author for correspondence.

Bilirubin is one of the most important compounds in the human body that binds to HSA. A high concentration of free bilirubin normally causes jaundice for newborn babies, and this risk decreases when the molecule is bound to HSA. Several studies investigating the binding properties of bilirubin with HSA[10-16] have been reported. The binding site is reported to be specific, and there is some evidence about the location of the bilirubin binding site on the HSA molecule. However, there is no conclusive information in this regard.[16]

Although its amino acid sequence has already been elucidated, and the crystallographic data[17,18] revealing some information about the three dimensional structure of HSA, the binding mode of HSA to certain therapeutic drugs is still not well-understood. Numerous experimental approaches have so far been unable to fully clarify the detailed tertiary structure of HSA and its influence on the binding properties of HSA. Although the detailed high resolution three dimensional structure of HSA is still not available, the crystallographic studies have provided us with more evidence of the physical properties of HSA.[17,18] However, if the detailed structure of certain crystalline forms of HSA is revealed, the real tertiary structure of HSA in solution may not be the same as observed in crystalline form. Therefore, without the exact knowledge of the tertiary structure of HSA both in crystalline form and in solution, the ligand-HSA binding modes can be explained in various ways. Many ligand-HSA binding models are based on the three-domain model proposed by Brown,[19] which has been recently confirmed by Carter.[17] Using crystallographic methods Carter[17] has demonstrated the binding of HSA to small molecules to be within the subdomains IA and IIA. However, this model does not provide sufficient evidence for the binding properties of bulkier ligands such as bilirubin.[20]

In this paper, we report the use of cyanogen bromide to cleave human serum albumin into three main fragments. These fragments were isolated by use of size exclusion and ion exchange chromatography. The three fragments were then examined using UV/Vis, fluorescence, and circular dichroism spectroscopic methods. Furthermore, bilirubin and two acidic drugs, warfarin and naproxen, were used as probe molecules to investigate the complexing ability of the isolated fragments. In particular, warfarin and naproxen were chosen because of their reported preference to bind specifically at site I and site II of HSA, respectively.[1,2] The ligand–protein interactions were monitored by use of fluorescence and circular dichroism spectroscopic techniques. The binding characteristics were compared with those of the intact albumin molecule with the aim of specifying the location of the various binding sites.

EXPERIMENTAL

Materials

Human serum albumin (crystallized and lyophilized), cyanogen bromide, formic acid (99%), propionic acid (99%), bilirubin, warfarin, and naproxen were all purchased from Sigma Chemical Co. (St Louis, MO). Sephadex G-25, G-100 media and mono S HR5/5, mono Q HR5/5 and Fast Flow Sephorose Q XK16/20 ion exchange columns, and a Gel Filtration LMW calibration kit were purchased from Pharmacia LKB Biotechnology Inc., (Piscataway, NJ).

Apparatus

The analytical scale ion-exchange separations were conducted on a high performance ion-exchange chromatography (HPIC) system. This system contains a Bio-Rad model 700 gradient module and workstation equipped with a 2-ml injection loop and a model 1706 UV/Vis detector. The preparative ion-exchange separations were performed on a chromatographic system containing two Beckman 114 pumps, a Beckman 141 gradient controller, a Dionex UVM fixed wavelength UV/Vis detector and an HP 7450 integrator. The absorbance measurements were obtained using a Shimadzu UV/Vis scanning spectrophotometer. Fluorescence studies were performed by use of a Spex model F2T21I spectrofluorometer equipped with a thermostated cell housing and a cooled photomultiplier tube. The circular dichroism (CD) spectra were obtained on a Jasco J-600 spectropolarimeter. All measurements were conducted at $20 \pm 0.1°$.

Methods

Cleavage reaction. The CNBr cleavage reaction was performed following the procedure reported by McMenamy *et al.*[5] Briefly, HSA was dissolved in 80% formic acid and reacted with an equivalent weight of CNBr in the dark at 0–4° for 24 hr. Fragments consisted of residues 298-584, 1-123 and 124-297 of the primary structure of HSA and were labelled as A, B and C, respectively.[5]

Isolation of the fragments. The digested solution was passed through a G-25 column (2 × 8 cm) in 1% propionic acid to remove the salts, and 50 mg (2 ml) of the protein was fractionated on a Sephadex G-100 column. Three fractions (I, II, and III) were collected [Fig. 1(a)] The molecular weight calibration was conducted by use of a gel filtration LMW calibration kit, which covered the molecular weight range of 13,700–67,000. The elution fraction I collected from G-100 column contained the aggregate and monomer of HSA. The elution fraction II containing fragment A was dialyzed against Tris-HCl buffer (20m*M*, pH = 7.5). Fragment A was further purified by using an anion exchange Mono Q column [Fig. 1(b)], and then the fragment was scaled up to preparative quantity by using the Fast flow Sephorose Q column. The elution fraction III was dialyzed against citric acid buffer (20m*M*, pH = 5.0), and fragments B and C were separated by injecting fraction III onto a mono S HR5/5 cation exchange column [Fig. 1(c)].

Characterization and ligand-binding of the fragments. All of the isolated fragments were dialyzed against phosphate buffer (20m*M*, pH = 7.5). As a comparative study, the ligands and the fragments were mixed on a 1:1 ratio by volume at pH 7.5. In addition, the original HSA ($1.54 \times 10^{-5}M$) was used in the complexing studies with the ligands. All ligand-fragment mixture solutions were buffered at pH 7.5 using the phosphate buffer. The concentrations of the ligands were 3.8×10^{-5}, 5.0×10^{-5}, and $2.7 \times 10^{-6}M$ for bilirubin, warfarin, and naproxen, respectively. The UV, circular dichroism, and fluorescence spectroscopic measurements were used to determine the

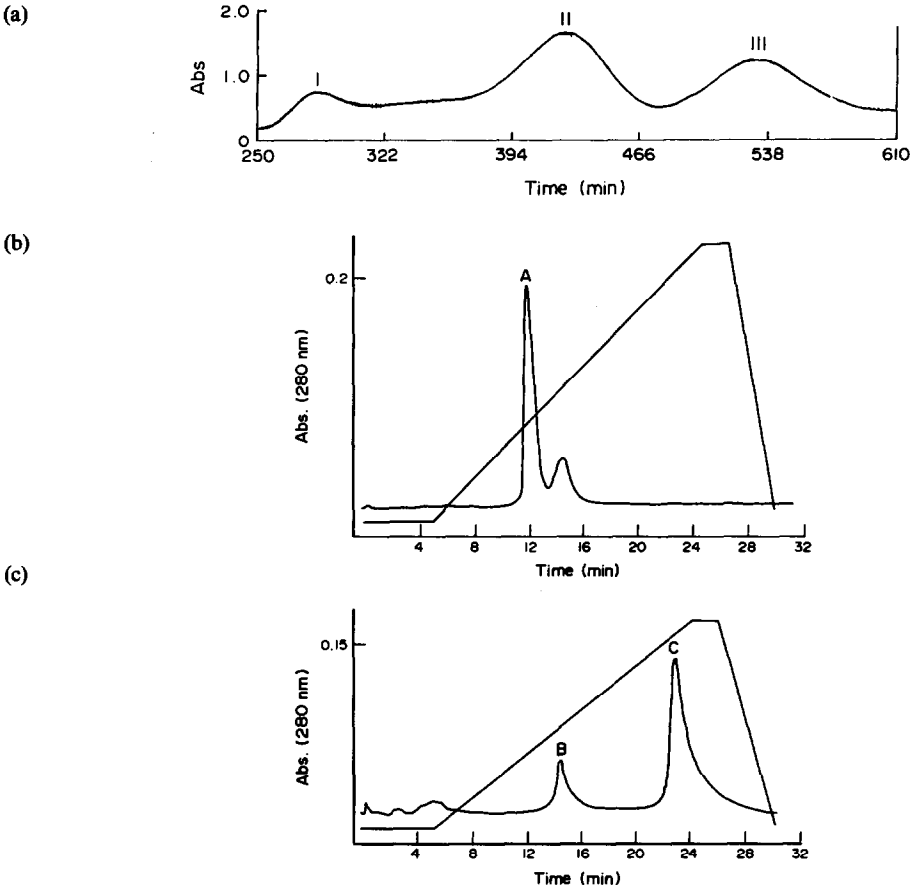

Fig. 1. (a) Elution of CNBr fragments of HSA (50 mg of HSA digest) from a Sephadex G-100 column (2.5 × 50 cm) with 5% propionic acid, 0.1*M* NaCl, flow rate 15 ml per hour. The components in the II and III fractions were further isolated by high performance ion chromatography (HPLC) [See Fig. 1.(b) and 1.(c)]. (b) Isolation of fraction II [from Fig. 1.(a)] on a Mono Q column (0.5 × 5 cm), 0–1.0*M* NaCl gradient in 20m*M* Tris-HCl, pH 7.5, flow rate 1.0 ml/min. (c). Isolation of fraction III (from Fig. 1.(a)) on a Mono S column (0.5 × 5 cm), 0–1.0*M* NaCl gradient in 20m*M* citric Acid, pH 5.0, flow rate 1.0 ml/min.

characteristics and ligands binding of the fragments. In fluorescence measurements, the emission spectra of the fragments are subtracted.

RESULTS AND DISCUSSIONS

Isolation of the fragments

Figure 1(a) shows the chromatogram of the fragments obtained from the size exclusion chromatography column (Sephadex G-100). The molecular weight calibration study suggests that the molecular weight of fragment A is approximately 37,000 and those of fragments B and C are approximately 18,000. McMenamy *et al.*[5] have reported observing the presence of impurities from the commercial HSA used in their study. In this study, the chromatogram of the commercial HSA does not show the presence of impurities compared with that obtained using fresh HSA. Hence, results in this study were conducted using HSA from Sigma. HPLC was used for further isolation of the fragments from the gel filtration column, in order to improve the resolution of the fragments and separation time. A better resolution and a shorter separation time was achieved when using HPLC, compared with a separation using a soft gel ion exchange column[5] [Fig. 1(a) and (b)]. As the separation time decreased, the fragments were concentrated after elution from the HPLC columns. For example, after injecting 8 ml of the fraction III sample on mono S column, the elution volume of fragments B and C were about 1 and 2 ml, respectively.

Spectroscopic properties of the fragments

The concentrations of the fragments were estimated from UV spectral data, and the values were 3.2×10^{-5}, 5.0×10^{-5}, and $3.6 \times 10^{-5} M$ for fragments A, B and C, respectively, using molar absorptivities reported by Gamblir and McMenamy.[7] As we expected, fluorescence is well suited for distinguishing these fragments. According to the amino acid sequence of HSA, fragment C contained the only tryptophan amino acid residue in HSA. Thus, the fluorescence spectrum showed predominately the spectrum of tryptophan. Fragment A contained some tyrosine amino acid residues, and thus, had a predominate tyrosine fluorescence spectrum. Fragment B contained fewer aromatic amino acid residues, and had almost no fluorescence. Circular dichroism (CD) studies were conducted to better understand the conformation of the fragments, especially, the secondary structure. Knowledge of the conformation of the fragments is important for predicting and better understanding the interactions between HSA and the fragments with the drugs in solution. The CD spectra of the fragments were similar in all respect to that of pure HSA molecule, regardless of the concentrations. This in turn suggests that the fragments still retained some secondary structure of the native HSA molecule.

Ligand-fragment binding study

Bilirubin-fragment interaction. Neither pure bilirubin nor HSA solution show a CD signal between 350–550 nm region. However, when HSA is added to a bilirubin solution, the HSA-bilirubin complex has a negative and a positive band at 410 and 460 nm, respectively. This suggests a strong HSA-bilirubin interaction giving rise to induced CD signals. To ascertain whether the specific binding center was limited to any of the CNBr fragments, the CD spectra of bilirubin-fragment complexes were measured in the same region as that of the bilirubin-HSA complex (Fig. 2). The interaction of the fragments with bilirubin seemed to be significantly different from that of the bilirubin–HSA complex. Upon addition of fragment A to bilirubin, a small positive band and a large negative band at 460 and 495 nm were observed, respectively. In contrast, fragment C induced a positive band and a broad negative band at 415 and 460 nm, respectively. The interaction of bilirubin and fragment B induced only a very weak CD signal. These marked differences between the CD spectra of HSA and bilirubin and that of the fragments with bilirubin suggest that the integrity of the original binding site of HSA is not contained in any of the individual CNBr fragments.

The above data suggest that the interaction mechanism in the native HSA molecule, which is probably responsible for the spatial configuration of the binding sites, is lost in bilirubin-fragment interactions. In addition, the induced CD signal of bilirubin with the fragments indicates that the fragments are still active in the binding of bilirubin. The weak intensity of the induced CD signals suggests that the interaction of fragment B probably does not correspond to the high affinity binding site of HSA. This interaction may represent the secondary site of the HSA molecule, which binds bilirubin after saturation at the main binding site. This also suggests that the binding site of bilirubin involves a region of the tertiary structure on the

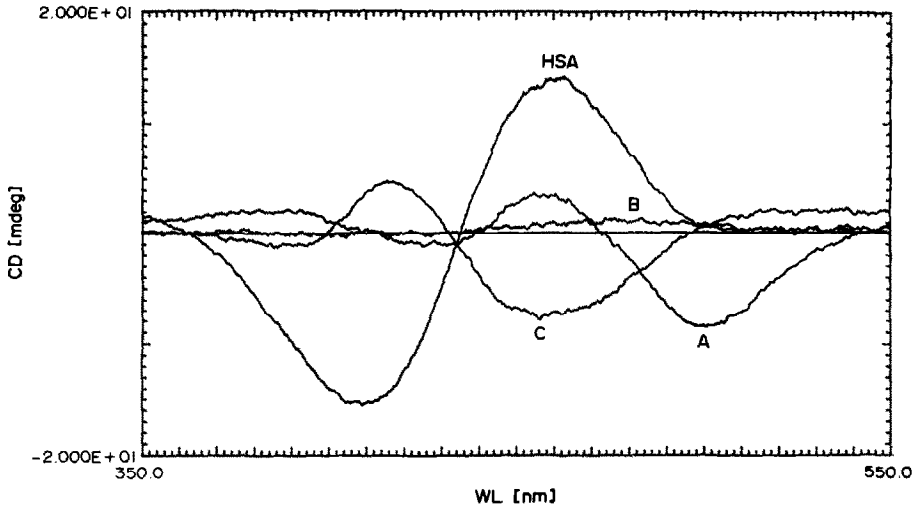

Fig. 2. Circular dichroism spectra of bilirubin with HSA and HSA fragments, respectively, in 20m*M* sodium phosphate, pH 7.5.

HSA molecule which is most likely located between the regions of fragments A and C. In contrast, the results reported by several other studies[12,13,15,16] concluded that bilirubin is most likely bound to the region of residues 180–250. This region is located only in fragment C of the CNBr digestion.

Fluorescence measurements were conducted in an attempt to obtain more evidence of the location of the binding site of bilirubin on HSA. Bilirubin is a weak fluorophore and upon addition of HSA, the fluorescence intensity increases dramatically. Figure 3 clearly shows the influence of fragments A and C on the fluorescence emission of bilirubin. Upon addition of fragment A or C to a solution containing bilirubin, the fluorescence emission of bilirubin is enhanced. Gitzelmann-Cumarasamy *et al.*[10] reported the presence of two HSA peptides labelled with a reactive bilirubin analogue (residues 124–297 and residues 446–547) located in fragments C and A, respectively. Geisow and Beaven[13] concluded that the labelling region of residues 446–547 by bilirubin could represent one of the weaker binding sites in the HSA molecule. In contrast, the results obtained in this study support the assumption that the high affinity binding site of bilirubin on HSA is located between fragments A and C. In summary, both the CD and fluorescence data suggest a strong association between bilirubin and HSA molecule. However, according to Brown's model,[19,20] the bulky bilirubin molecule cannot completely penetrate into the cavity of the helix cylinder of HSA. Therefore, our results could be explained in terms of partial insertion of the bilirubin molecule inside the cavity of HSA helix cylinder. In addition, because of the homologous structure of the domains II and III,[18] and the folding of protein in solution, it is most likely for bilirubin to interact with both domains II and III. This in turn will result in the

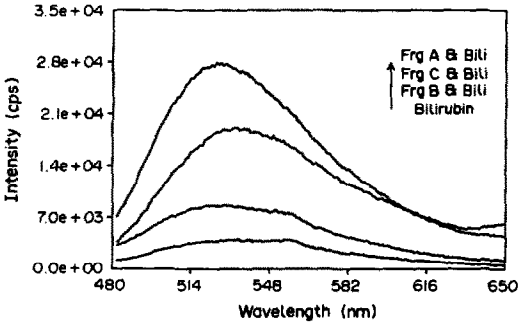

Fig. 3. Fluorescence spectra of bilirubin with HSA and HSA fragments, respectively, in 20m*M* sodium phosphate, pH 7.5, $\lambda_{ex} = 450$ nm.

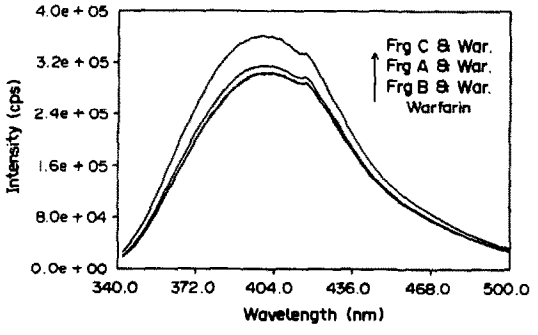

Fig. 4. Fluorescence spectra of warfarin with HSA fragments, respectively, in 20m*M* sodium phosphate, pH 7.5, $\lambda_{ex} = 320$ nm.

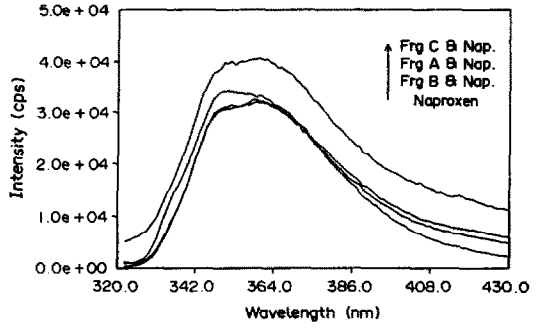

Fig. 5. Fluorescence spectra of naproxen with HSA fragments, respectively, in 20m*M* sodium phosphate, pH 7.5, $\lambda_{ex} = 310$ nm.

formation of an integral binding center, which changes its symmetry and flexibility, giving rise to a CD signal and enhanced fluorescence emission. In contrast, after fragmentation, domain II and III are separated into two different fragments, C and A, which binds bilirubin differently with the intact HSA molecule.

Anionic drug-fragment interaction

The HSA molecule has at least two different anionic binding sites.[1,2] For site I, warfarin is a typical binding drug. Chignell[21] has observed an increase in the fluorescence quantum yield of warfarin upon binding to HSA molecule. When we added fragment C to solutions containing warfarin, the intensity of the fluorescence emission spectrum of warfarin was enhanced (Fig. 4). In contrast, upon addition of fragment A or B in solutions containing warfarin, no significant changes of its fluorescence emission was observed. This also suggests that binding site I is located in fragment C of HSA.

Naproxen is reported to bind favorably to site II of the HSA molecule.[1] The addition of fragment C to a solution containing naproxen showed an increase in the fluorescence intensity of naproxen (Fig. 5); no significant change in the narpoxen spectrum was observed upon addition of either fragment A or B. This suggests that binding site II is also located in fragment C of HSA. The fluorescence signals of the fragments are weaker compared to that of the native HSA molecule.

CONCLUSION

There are several different binding sites on HSA for different types of drugs. To specify more closely the sites, we used the CNBr cleavage method to cleave HSA into three main fragments: A, B, and C. These fragments were isolated employing size exclusion and ion exchange chromatography and then examined by use of UV, fluorescence, and circular dichroism. The fragments were easily distinguished by using fluorescence measurements. Our CD data showed the fragments still retained some secondary structure of HSA. Finally, we investigated the interaction of bilirubin and two anionic drugs (warfarin and naproxen) with the fragments. The bilirubin data suggest that the binding site of bilirubin might be formed by a cooperative effect between the A and C fragments. The anionic-drugs suggest that both binding site I and II on HSA could be in the same fragment, *i.e.*, fragment C. The weaker interaction observed from our fragment-drug data also shows a drawback for using the fragment-drug interaction to locate binding sites in complex protein. From this study and others,[8,12,13] it could be inferred that the drug-binding mechanism in the native HSA molecule is probably a result of a combination of several types of forces, such as electrostatic, hydrogen bonding, and hydrophobic interactions. Most likely, the combination of these forces is destroyed during fragmentation; hence, only a weak fluorescence signal is observed for the fragments. Alternatively, the binding center is totally destroyed during the fragmentation process, and the fragments probably rearrange to form a new binding site that does not exist in the native HSA molecule. However, this binding site has a lower affinity than the native HSA, and hence, weaker interaction for the drugs is observed.

Acknowledgement—The authors acknowledge the support of an NIH grant (Grant No. GM 39844).

REFERENCES

1. G. Sudlow, D. J. Birkett and D. N. Wade, *Molec. Pharmac.*, **11**, 824.
2. *Idem. ibid.*, *1976*, **12**, 1052.
3. A. Fontana and E. Gross, *Practical Protein Chemistry*, A. Darbre Ed., pp. 84–88. Wiley, New York, 1986.
4. E. Gross and B. Witkop, *J. Am. Chem. Soc.*, 1961, **83**, 1510.
5. R. H. McMenamy, H. M. Dintzis and F. Watson, *J. Biol. Chem*, 1971, **246**, 4744.
6. B. Meloun, M. A. Saber and J. Kusnir, *Biochim. Biophys. Acta*, 1975, **393**, 505.
7. K. K. Gamblir and R. H. McMenamy, *J. Biol. Chem.*, 1973, **248**, 1956.
8. Ingvar Sjöholm and Ingrid Ljungstedt, *ibid.*, 1973, **248**, 8434.
9. J. R. Morrison, N. H. Fidge and B. Grego, *Anal. Biochem.*, 1990, **186**, 145.

10. N. Gitzelmann-Cumarasamy, C. C. Kuenzle, and K. J. Wilson, *Experientia*, 1976, **32**, 768.
11. C. C. Kuenzle, N. Gitzelmann-Cumarasamy and K. J. Wilson, *J. Biol. Chem.*, 1976, **251**, 801.
12. T. Sjödin, R. Hansson and I. Sjöholm, *Biochim. Biophys. Acta*, 1977, **494**, 61.
13. M. J. Geisow and G. H. Beaven, *Biochem. J.*, 1977, **163**, 477.
14. A. A. Lamola and J. Flores, *J. Am. Chem. Soc.*, 1982, **104**, 2530.
15. T. Peters, Jr. *Adv. Protein Chem.*, 1985, **37**, 161.
16. U. Kragh-Hansen, *Dan. Med. Bull.*, 1990, **37**, 57.
17. D. C. Cater, X-M. He, S. H. Munson, P. D. Twigg, K. M. Gernert, M. B. Broom and T. Y. Miller, *Science*, 1989, **244**, 1195.
18. D. C. Cater, X-M. He, *Science*, 1990, **249**, 302.
19. J. R. Brown, *Albumin: Structure, Biosynthesis, Function*, T. Peters, Jr. and I. Sjöholm (eds.), pp. 1–10. Pergamon Press, Oxford, 1977.
20. J. R. Brown and P. Shockley, *Lipid-Protein Interaction*, P. C. Jost and O. H. Griffith (eds.), pp. 25–28. Wiley, Vol. 1, 1982.
21. C. F. Chignell, *Molec Pharmac.*, 1970, **6**, 1.

Talanta, Vol. 40, No. 4, pp. 565–569, 1993
Printed in Great Britain.

0039-9140/93 $6.00 + 0.00

DYNAMIC COATING ION-INTERACTION CHROMATOGRAPHIC SEPARATION OF SOME TRACE IMPURITIES IN OXYGEN-FREE ELECTRONIC COPPER (OFEC) BY PRE-COLUMN CHELATION WITH 4-(2-THIAZOLYLAZO)RESORCINOL

RAJANANDA SARASWATI and T. H. RAO

Instrumental Analysis Division, Defence Metallurgical Research Laboratory, Kanchanbagh P.O., Hyderabad, 500 258, India

(*Received* 23 *March* 1992. *Revised* 16 *June* 1992. *Accepted* 16 *June* 1992)

Summary—Deleterious trace impurities like Mn, Fe, Co, Ni, Zn, Bi and Pb in oxygen-free electronic copper (OFEC) were separated and determined by dynamic coating ion-interaction chromatography (IIC) with spectrophotometric detection using pre-column reaction methods. 4-(2-Thiazolylazo)resorcinol (TAR) was used as pre-column chelating agent. The requirements for sample preparation and the conditions for pre-column chelation reaction are discussed. The optimum conditions for the sensitive detection of these trace metal ions after ion-chromatographic separation are set. The pH of the chelating medium and the eluent, the concentration of TAR and the composition of the eluent were investigated. The detection limits achieved were 2.0, 2.8, 0.6, 0.8, 1.2, 2.6 and 3.0 ng for Mn, Fe, Co, Ni, Zn, Bi and Pb, respectively. The results obtained by IIC methods compare well with those of graphite furnace atomic-absorption spectrometry and the certified values of Mur Bundy Hamil (MBH Analytical Ltd, U.K.).

Studies on the influence of various impurities on the annealability and electrical conductivity of oxygen-free electronic copper have shown that the higher the impurities the higher will be the softening temperature and the lower will be the electrical conductivity.[1–5] For example, the presence of every 5 ppm of lead content in 0–25 ppm range reduces the electrical conductivity of copper by about 0.1% in the international annealed copper society standard (IACA). Similarly, every increment of 5 ppm antimony content in the 0–25 ppm range lowers the conductivity by 0.15% IACS. The presence of Fe in the order of 0.001% (at Cu purity 99.999%) will result in intergranular fracture due to microcracks and micropores and results in embrittlement of Cu at even low stress levels. Therefore, the accurate determination of trace impurities in Cu has become increasingly important. Several schemes for the systematic analysis have been described in the literature.[6] None of the schemes includes the determination of all trace impurities in a single sample, although several independent procedures have been proposed. With the advent of atomic-absorption spectrometry, many procedures for the determination of trace impurities in copper have appeared. However, the detection limits of AAS procedures are severely restricted by matrix effects. In this context, the ion-interaction chromatography (IIC) separation and detection technique seems to be one of the promising tools.

In recent years, this technique has become an attractive method for trace metal determinations.[7–10] The advances that have taken place in column and detection techniques[11–15] have explained the capability of IIC to characterize a wider range of anions and cations. Since individual metals and metal compounds form distinct ions with differing retention times, it is possible to analyze several of them in a single run. The separation and simultaneous determination of metal ions as their chelates with organic reagents by IIC has received much attention. A wide variety of organic reagents have been used to complex metal ions prior to separation.[10,16,17] 4-(2-Thiazolylazo)resorcinol (TAR) is one such reagent which has been used extensively for the spectrophotometric determination of numerous ions. TAR and its chelates with metal ions are insoluble in water. However, they are readily soluble in some solvents that are miscible with water and they can be extracted into solvents that are immiscible with water. Therefore, most metal chelates with TAR can be separated by IIC and can be detected spectrophotometrically.

Though several ion chromatographic methods are available for the separation of transition metals, no reports on the separation and detection of trace impurities in oxygen-free electronic copper as chelates with TAR using IIC have been reported.

In previous communications,[18–20] the separation of transition and rare earth metals present in low-alloy and stainless steel samples using PAR and Arsenazo-III as post-column chelating agents are discussed. Our current research efforts, as described here, are focused on the separation and determination of trace impurities in OFE copper (MBH CRM 17867B, 17868B, 17869B and 17870B) in a single sample by dynamic coating ion-interaction chromatography using TAR as a pre-column chelating agent.

EXPERIMENTAL

Apparatus

The Waters Ion Chromatography system consists of Model 501 pumps with a Waters U6K injector. A Spherisorb S-5 ODS I separation column was employed. A Waters 486 tunable absorbance UV-Vis spectrometric detector with a 12-μl flow cell was used to monitor the effluent from the column. A Waters maxima 820 chromatography workstation along with a printer was employed.

The labware was used after conditioning in an ultrasonic cleaner and equilibrating in reagent grade water (18 Ω resistance) from a Millipore Milli Q water system, having total metallic impurities less than 1 ppb.

Reagents and solutions

High-purity 'Suprapure' grade chemicals from Merck were used. Solvents were further purified using isothermal sub-boiling distillation in a laminar flow fume hood having class 100 condition with a total lab facility maintained at class 10,000 level to overcome dust and particulate contamination. Pure metals from Johnson Matthey (JMC) and Certified Reference Materials from Mur Bundy Hamil (MBH) were used for the preparation of standard solutions and eluents.

Standard solutions of ions were prepared by dissolving known amounts of pure metals and diluting to the required levels. Elution was performed with $1 \times 10^{-3}M$ sodium octane-1-sulphonate (54 mg in 250 ml)–$0.023M$ tartaric acid solution at a flow rate of 1 ml/min. Calibration graphs were obtained with the chosen parameters with injecting standards separately and in mixtures and recording the peak heights for the respective ions.

Sample preparation and matrix separation

A 10-g sample (which was previously washed with methanol and dried with an IR lamp) was dissolved in a requisite amount ($\sim$40 ml) of nitric acid (1 + 1), covering the beaker and heating below the boiling point. After the sample was dissolved, the solution was boiled to get rid of nitrogen oxides. The solution was cooled and then diluted to approximately 100 ml. The sample solution obtained contains a high concentration of copper matrix. This may have a detrimental effect on the chromatographic column and the separation of impurities. Therefore, separation of the copper matrix is a prerequisite for achieving reliable trace element determinations when IC procedures are used. This matrix separation was achieved by subjecting the sample solution to electrolysis at 0.6A using platinum gauze electrodes and a magnetic stirrer. The solution was covered and heated on an electrothermal plate to concentrate it by evaporation, and then the solution was made up to the mark of a 25-ml standard flask and diluted further if required. A 20-μl portion of the solution was used for injection after filtering this solution through a 0.45-μm filter.

Preparation of metal chelates

A 10.0-ml portion of $1.0M$ tartrate buffer (pH 6.0), 4.0 ml of TAR ($5 \times 10^{-3}M$) solution and 4.0 ml of methanol were mixed with a known volume of the above sample solution. The mixture was diluted up to 25.00 ml with water. In order to accelerate the colour development of the chelates such as Fe–TAR and Bi–TAR the solution had to be heated in a boiling water bath. A time study at different temperatures with a mixture of the metals show that 20–25 min at 60–75° is required for the colour development of all the chelates. Then the solution was cooled to room temperature before injection.

Separation of the chelates and reagent

The ODS column was equilibrated with sodium octanesulphonate ($1 \times 10^{-3}M$)–water (50:50 v/v containing $0.023M$ tartrate buffer, pH 6.0). A 20-μl aliquot of the prepared test solution was injected into the ODS column and the complexes were eluted at a flow rate of 1.0 ml/min. The detection wavelength was set at 580 nm.

Table 1. Comparison of results (wt%) [mean ± r.s.d (%) $n = 5$] obtained by IIC, GFAAS and the certified values of MBH*

	17867B	17868B	17869B	17870B
Mn	0.008 ± 2.1	0.0215 ± 2.6	0.0286 ± 2.0	0.040 ± 3.8
	[0.008 ± 4.2]	[0.0215 ± 6.2]	[0.0288 ± 4.9]	[0.040 ± 7.8]
	(0.009)	(0.0216)	(0.030)	(0.0405)
Fe	0.0120 ± 4.2	0.028 ± 0.8	0.037 ± 1.9	0.053 ± 2.5
	[0.0125 ± 6.1]	[0.026 ± 1.2]	[0.037 ± 7.2]	[0.055 ± 6.8]
	(0.0125)	(0.029)	(0.038)	(0.055)
Co	0.035 ± 4.5	0.030 ± 1.2	0.016 ± 1.8	0.001 ± 2.5
	[0.032 ± 3.8]	[0.030 ± 5.2]	[0.018 ± 7.6]	[0.001 ± 6.6]
	(0.037)	(0.030)	(0.016)	(0.001)
Ni	0.039 ± 6.1	0.0336 ± 2.9	0.020 ± 1.3	0.0048 ± 2.1
	[0.035 ± 9.8]	[0.0333 ± 8.6]	[0.021 ± 3.2]	[0.005 ± 6.1]
	(0.040)	(0.0340)	(0.020)	(0.005)
Zn	0.030 ± 5.2	0.0241 ± 5.7	0.0130 ± 5.0	0.0020 ± 1.6
	[0.035 ± 9.2]	[0.0245 ± 10.6]	[0.0130 ± 5.5]	[0.002 ± 12.8]
	(0.030)	(0.0245)	(0.0135)	(0.0022)
Bi	0.011 ± 1.1	0.0290 ± 1.8	0.035 ± 5.0	0.054 ± 3.6
	[0.011 ± 9.6]	[0.0290 ± 4.4]	[0.038 ± 5.3]	[0.055 ± 4.5]
	(0.011)	(0.0295)	(0.0385)	(0.055)
Pb	0.012 ± 4.2	0.024 ± 4.0	0.0380 ± 6.9	0.046 ± 7.2
	[0.015 ± 8.1]	[0.025 ± 7.6]	[0.0389 ± 5.8]	[0.049 ± 4.1]
	(0.013)	(0.025)	(0.0385)	(0.048)

*Values in [ ] are obtained by GFAAS; and values in ( ) are the MBH certified values.

Instrumental methods

A GBC Model 902 atomic absorption spectrophotometer was used, equipped with a GBC Model GF 2000 graphite furnace. A deuterium lamp was used for background correction. Visimax II hollow cathode lamps were used as light sources. Solutions were injected by a GBC PAL-2000 auto-sampling system. All absorbances were measured as peak heights and were recorded with an Epson Lx-800 printer. The system was operated by a Philips Model P-3105 data station connected on line.

A 1-g amount of sample was dissolved in 5 ml of dilute nitric acid (1 + 1), and the solution was made up to 100 ml with water, and further diluted as required, for atomic-absorption spectrometry.

RESULTS AND DISCUSSION

The results for four sample materials are presented in Table 1. For comparison, the values (wt%) obtained by graphite furnace atomic-absorption spectrometry (GFAAS), and the certified values from MBH are also given. The agreement between the results is excellent as are the relative standard deviations.

Several organic solvents, such as methanol, ethanol, acetonitrile, tetrahydrofuran, isopropyl-alcohol and sodium ocatanesulphonate combined with water, were investigated as binary and ternary mobile phases. A simple methanol–water, ethanol–water or acetonitrile–water binary system mobile phase gave tailing peaks and low sensitivities, and the unreacted reagent appeared as two peaks which overlap with the peaks of Ni^-, Cu^- and Fe–TAR chelates. However, the sodium octanesulphonate–tartaric acid system gave excellent peak shapes and high sensitivities for the separation of Mn, Fe, Co, Ni, Cu, Zn, Bi and Pb metal chelates with TAR which was found to be a good colour forming pre-column reagent. The effect of the concentration of sodium octanesulphonate in the mobile phase on the retention of the chelates is shown in Fig. 1. The chromatograms were recorded at 580 nm as all chelates showed significant adsorption at this wavelength. However, below this wavelength there was an indication of overlap of the peaks of the unreacted reagent and the Ni–TAR chelate peak.

As the pH of the mobile phase shows, the absorption spectra were recorded under mild acidic conditions and it was observed that the absorption of these metal–TAR red chelates was influenced by the hydrogen ion concentration. The absorption of these chelates was found to be maximum around pH 6.0. Below this pH there is marked decrease in the absorption which may be due to protonation equilibria as found in the case of the Cr–PAR chelates.[21]

Various buffers like tartrate, oxalate, citrate, KH_2PO_4–Na_2HPO_4, and Tris-(hydroxymethyl)-aminomethane (Tris) were used to determine

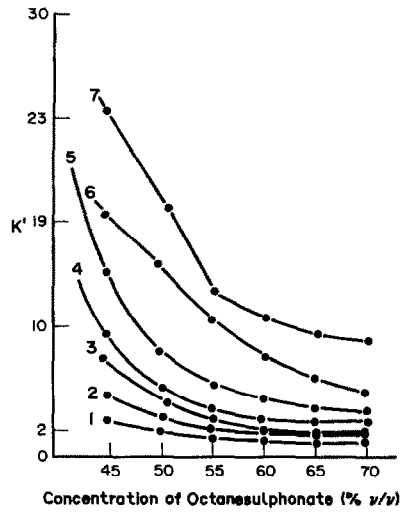

Fig. 1. Effect of sodium octane-1-sulphonate concentration on the retention times of the TAR chelates; buffer, tartrate ($2.308 \times 10^{-2}M$); pH 6.0; flow rate 1 ml/min; TAR ($2.5 \times 10^{-4}M$); column length, 300 × 3.9 mm ID (Spherisorb S-5 ODS-I); detection wavelength, 580 nm.

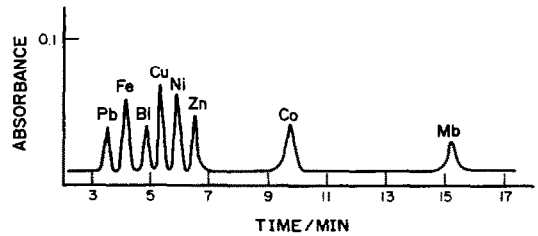

Fig. 2. Separation of some trace elements in OFE copper sample (CRM 17867B) by IC using TAR as pre-column chelating reagent. Octanesulphonate ($10^{-3}M$) with tartrate buffer ($2.308 \times 10^{-2}M$) mobile phase; pH 6.0; flow rate, 1 ml/min; TAR ($2.5 \times 10^{-4}M$); column length, 300 × 3.9 mm ID (Spherisorb S-5 ODS-I); detection wavelength, 580 nm.

the optimum pH range of the mobile phase. Tartrate was found to improve the peak shapes and produce higher peak heights for the TAR chelates of Fe, Co, Ni, Mn and Cu. Tris and KH_2PO_4–Na_2HPO_4 had no beneficial effect on the separation, and the retention of these metal–TAR chelates changed very little, but that of Fe^{-} and Co–TAR chelates increased markedly in the pH range 6.0–7.0. The effect of buffers like tartrate, oxalate, and citrate on the absorbance of these chelates is given in Table 2. As can be seen, the maximum absorption was obtained in the tartrate buffer. It was also found that the absorption of the metal–TAR chelates was influenced by the concentration of tartrate added. With the increase in tartrate concentration, the absorption increases progressively and then decreases. A possible explanation is, in a weakly acidic medium, the concentration of hydroxy groups would be low; hence the hydroxy groups coordinated to metal ions could be replaced by tartrate. As a result, coloured ternary (M–tartrate–TAR) complexes would be formed. Therefore, the absorbance increases as the tartrate concentration increases. However, at high concentrations of tartrate, the coordinated TAR would be replaced by tartrate which would lead to a decrease in the absorbance. The optimum concentration for the maximum absorption of M–TAR chelates was obtained when the concentration of tartrate was about $2.3 \times 10^{-2}M$ and the concentration of TAR was kept at $2.5 \times 10^{-4}M$.

Table 2. Absorption characteristics of the metal–TAR chelates in various buffers

Chelate	Tartrate	Oxalate	Acetate
	(molar absorptivity/10^4 l^3 mol^{-1}. cm^{-1})		
Pb–TAR	3.2	2.1	2.5
Fe–TAR	4.3	2.6	1.9
Bi–TAR	3.5	2.4	2.3
Cu–TAR	4.6	3.0	2.8
Ni–TAR	4.4	2.1	1.8
Zn–TAR	4.5	2.2	2.4
Mn–TAR	4.0	2.1	1.5
Co–TAR	4.2	2.9	2.0

Buffer concentration, $2.3 \times 10^{-2}M$; pH 6.0; flow rate 1 ml/min; TAR ($2.5 \times 10^{-4}M$); column length, 300 × 3.9 mm ID (Spherisorb S-5 ODS-I); detection wavelength, 580 nm.

The chromatograms obtained for some of the trace impurities are illustrated in Fig. 2. Based on the spectrophotometric studies described above, the complete separation of these elements requires about 15 min. Pb was separated at about 3 min 30 sec, followed by Fe (4 min 10 sec), Bi (4 min 50 sec), Cu (5 min 25 sec), Ni (5 min 50 sec), Zn (6 min 30 sec), Co (9 min 30 sec) and Mn (15 min 15 sec).

As the optimum performance of silica based bonded columns occurs in the pH range 3.5–7.0, the effect of variation of the pH of the eluent was carefully studied within this range. It was observed that the retention time increases with a decrease in pH. This may be because increased acidity decreases the ionization of tartrate, which in turn decreases the degree of metal complexation, thereby increasing retention times.[22] It was found that a pH of 6.0 gave the best separation and detection.

The peaks that appearing in the chromatograms were identified by spiking with authentic (*i.e.*, known) metal ion solutions. Quantitative measurements were done by plotting calibration

graphs for individual elements, taking peak heights at different concentrations and comparing with the result for samples. The absolute detection limits, calculated as the amount of injected metal ion that gave a signal that was three times the background noise (*i.e.*, signal-to-noise ratio of 3:1) were 2.0, 2.8, 0.6, 0.8, 1.2, 2.6 and 3.0 ng for Mn, Fe, Co, Ni, Zn, Bi and Pb, respectively.

The other trace elements that are normally present in OFE copper are Se, Te, Mg, Sb, As and Sn and are not detectable using TAR.

No significant change in peak width was observed during the separation of ions using the same sample solution volumes, indicating excellent column performance throughout the analysis.

CONCLUSION

By using TAR as a pre-column chelating agent, some of the trace impurities in OFE copper can be successfully separated and determined by ion-interaction chromatography. This method is fairly selective and sensitive and can be applied to other metallurgical samples for trace analysis at sub-ppm levels.

Acknowledgements—The authors are grateful to Professor Dr P. Rama Rao and Shri S. L. N. Acharyulu for providing facilities and permission to publish this work.

REFERENCES

1. Y. T. Hsu and B. O. Reilly, *J. Metals*, 1977, **12**, 21.
2. S. Nakahara and Y. Okinaka, *Scripta Metal.*, 1985, **19(4)**, 517.
3. L. K. Bigelow, *Metal Trans.*, 1976, **7 B(4)**, 661.
4. W. P. Riley and H. V. Maker, *Conserv. Recycling*, 1986, **4**, 315.
5. D. C. Abbas, *Diss. Abstr. Int.*, 1978, **38(10)**, 121.
6. I. M. Kolthoff and P. J. Elving, *Treatise on Analytical Chemistry*, Part 2, Vol. 3. InterScience, New York, 1981.
7. B. R. Willford and H. Veening, *J. Chromatogr.*, 1982, **251**, 61.
8. G. Nickless, *ibid.*, 1985, **313**, 129.
9. B. Steinbrech, *ibid.*, 1987, **10**, 1.
10. K. Robards, P. Starr and E. Patsalides, *Analyst*, 1991, **116**, 1247.
11. F. Vlacil, L. Vins and J. Coupek, *J. Chromatogr.*, 1987, **391**, 119 and 113.
12. J. S. Fritz, D. J. Gjerde and R. M. Becker, *Anal. Chem.*, 1980, **52**, 1519.
13. J. S. Fritz and G. J. Sevenich, *ibid.*, 1983, **55**, 12.
14. J. F. Jen, K. E. Daugherty and J. G. Tarter, *J. Chromatogr.*, 1988, **436**, 86.
15. Z. Hu and Y. Tans, *Analyst*, 1988, **113**, 179.
16. Chang-shan Lin, Ziao-song Zhang and Zue-zhu Liu, *ibid.*, 1991, **116**, 277.
17. Liu Qiping, Zhang Huashan and Cheng Jieke, *Talanta*, 1991, **38(6)**, 669.
18. R. Saraswati, N. R. Desikan, S. V. Athavale and T. H. Rao, *Anal. Chim. Acta.*, 1990, **237**, 325.
19. R. Saraswati and T. H. Rao, *Analyst*, 1992, **117**, 735.
20. R. Saraswati, N. R. Desikan and T. H. Rao, *Mikrochim. Acta*, 1992, **109**.
21. R. G. Anderson and G. Nickless, *Analyst*, 1967, **92**, 207.
22. P. R. Haddad and P. E. Jackson, *Ion Chromatography: Principles and Application*, pp. 103 and 186. Elsevier, Amsterdam, 1990.

Talanta, Vol. 40, No. 4, pp. 571–576, 1993
Printed in Great Britain.

0039-9140/93 $6.00 + 0.00

SPECTROPHOTOMETRIC METHODS FOR THE DETERMINATION OF TOLNAFTATE

C. S. P. SASTRY,[1]* B. S. SASTRY,[2] J. VENKATESWARA RAO[2] and R. RAMA KRISHNA[3]

[1]Foods, Drugs and Water Laboratories, School of Chemistry, Andhra University, Visakhapatnam 530 003, India
[2]Dept. of Pharmaceutical Sciences, Andhra University, Andhra, India
[3]Asst. Drug Controller, Air Cargo Complex, Sahar, Bombay, India

(*Received* 28 *October* 1991. *Revised* 12 *February* 1992. *Accepted* 22 *February* 1992)

Summary—Two simple and sensitive visible spectrophotometric methods (methods A and B) for the determination of tolnaftate in bulk samples and formulations are described. Method A (λ_{max} 490 nm) involves the reaction of tolnaftate with 2,6-dichloroquinone-4-chlorimide (DCQC: Gibb's reagent), while method B (λ_{max} 530 nm) is based on a similar reaction of the drug with *p*-*N*,*N*-dimethylphenylene diamine in the presence of chloramine-T. Both these methods are applicable to pure samples as well as formulations of the drug.

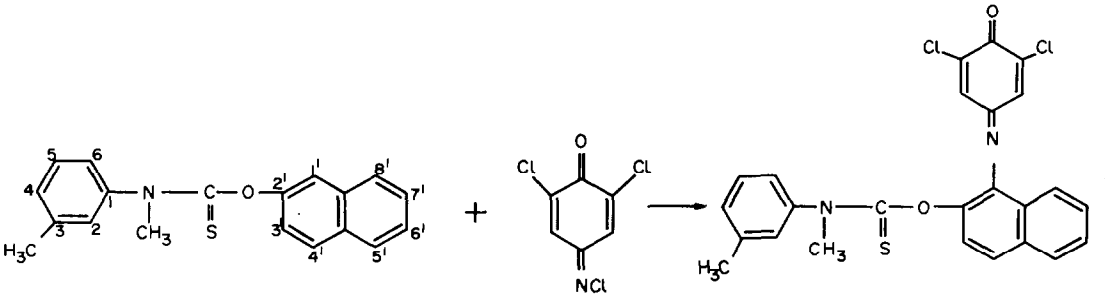

Scheme 1

Tolnaftate (TNF), (*o*-2-naphthyl *N*-methyl-*m*-tolyl thiocarbamate, Scheme 1) finds wide use in the form of topical solutions and creams in the treatment of cutaneous mycoses caused by a number of organisms belonging to the genera trichophyton, epidermophyton, microsporum and malassezia. It is ineffective against candida. The drug is less effective in the presence of hyperkeratotic leisons. It is often formulated in combination with other antibacterial and antifungal agents such as gentamycin and iodochlorohydroxyquinoline and steroid drugs such as betamethasone.

Tolnaftate is officially listed in B.P.[1] and U.S.P.[2] UV spectrophotometric determination at 258 nm is the basis of both the official methods. A survey of literature revealed that no visible spectrophotometric methods are reported so far for the estimation of tolnaftate. Two such methods (methods A and B) now developed are described in this paper. Method A utilises the oxidative coupling reaction of tolnaftate with 2,6-dichloroquinone-4-chlorimide (DCQC), the well known Gibb's reagent,[3] to produce a chromophore with λ_{max} at 490 nm. In method B, tolnaftate undergoes a similar coupling reaction with the *N*-chloroquinone diimine (NCQDI) [produced *in situ* by the action of chloramine-T (CAT) on *p*-*N*,*N*-dimethylphenylene diamine (DMPD)] to give a coloured product with λ_{max} at 530 nm. The two methods now proposed are applicable to bulk samples as well as formulations of TNF.

EXPERIMENTAL

Apparatus

A Systronics model 106 digital visible spectrophotometer with 1-cm matched glass cells was used for absorbance measurements in the visible region. A Milton Roy spectronic 1201 UV–Vis spectrophotometer was used for absorbance measurements in the UV region. An Elico model LI-120 digital pH meter was used for pH measurements.

*Author for correspondence.

Reagents

All aqueous solutions were prepared with doubly distilled water. All the chemicals and solvents used were of Analytical Reagent Grade.

Aqueous solutions of DMPD dihydrochloride (0.1% w/v) and CAT (0.1% w/v) and isopropanolic solution of DCQC (0.1% w/v) were prepared. They can be used for one week when stored at 5°. Buffer (pH 7.0) was prepared by mixing 612 ml of 0.067*M* disodium hydrogen phosphate solution with 388 ml of 0.067*M* potassium dihydrogen phosphate solution and adjusting the pH to 7.0.

Standard drug solutions. A stock solution of tolnaftate (500 μg/ml) was prepared in methanol. Working standard solutions (40 μg/ml for method A and 100 μg/ml for method B) were prepared by appropriate dilution of the stock solution with methanol.

Procedure for bulk samples. Method A. Aliquots of standard drug solution ranging from 0.5–4.0 ml (representing 20–160 μg of the drug) were pipetted out into a series of 10-ml standard tubes. The volume in each tube was adjusted to 4.0 ml by the addition of the appropriate amount of methanol to each tube. A 1-ml portion of DCQC reagent was added to each tube and the tubes were heated in a water bath at 80° until complete evaporation of the solvent in all the tubes (approximately 20 min). The tubes were then taken out, cooled and the residue in each tube was dissolved in isopropanol and the volume adjusted to the mark with the same solvent. The absorbances of the red coloured solutions were measured against a reagent blank after 5 min and before 50 min. The amount of the drug was calculated from its calibration graph.

Method B. Aliquots of standard tolnaftate solution ranging from 0.5–4.0 ml (representing 50–400 μg of the drug) were pipetted out into a series of 20-ml standard flasks. The volume in each flask was adjusted to 4.0 ml by the addition of an appropriate amount of methanol to each flask. A 9-ml portion of pH 7.0 buffer was added to each flask followed by 0.5 ml of DMPD solution and 1 ml of CAT solution. The volume was made up to the mark with distilled water. The contents of each flask were well mixed. The stoppered flasks were stored for one hour to allow full colour development. The absorbances were measured within the next 60 min at 530 nm against a reagent blank prepared simultaneously by omitting the drug solution. The amount of drug was calculated from the calibration graph.

Procedure for formulations. A quantity of cream or a volume of solution meant for topical use, equivalent to about 20 mg of TNF, was dissolved in about 50 ml of chloroform and transferred to a separating funnel. The chloroform solution was washed successively with 0.1*N* sodium hydroxide (2 × 25 ml), 0.1*N* hydrochloric acid (2 × 25 ml) and distilled water (1 × 25 ml). The chloroform solution in the separating funnel was then filtered into a 250-ml beaker through a chloroform washed cotton plug. The aqueous layer was extracted with chloroform (2 × 25 ml) and each chloroform extract was filtered into the same 250-ml beaker. The solvent in the beaker was evaporated and the residue dissolved in 40 ml of methanol and carefully transferred into a 100-ml standard flask. The beaker was washed with methanol (3 × 10 ml) and the washings were added to the standard flask. The volume in the flask was made up to 100 ml to obtain a solution of about 200 μg/ml of TNF. This stock sample solution was diluted stepwise with methanol to provide working sample solutions containing about 100 μg/ml (method B) and 40 μg/ml (method A) of TNF.

The sample solutions were then analysed by the procedures of the methods A and B.

RESULTS AND DISCUSSION

The absorption spectra of the reaction products in methods A and B show characteristic λ_{max} values (Figs 1 and 2). The reaction conditions were established by varying one parameter at a time and observing its effect on the absorbance of the coloured species.

In method A, addition of 1 ml of DCQC reagent and a heating time of 15–20 min at 80° was found to give maximum colour intensity. The suitability of organic solvent medium for colour development using methanol, acetone, isopropanol or dioxane as solvent was studied, as aqueous medium did not give a clear solution. A stable colour with maximum intensity was attained only with isopropanol and so it is preferred. The coloured species was found to be stable up to 45 min. In method B, constant absorbance values were noticed when the volume of DMPD solution added ranged from 0.25–0.75 ml and the volume of CAT solution from 0.5–1.5 ml. Volumes of 0.5 ml of DMPD

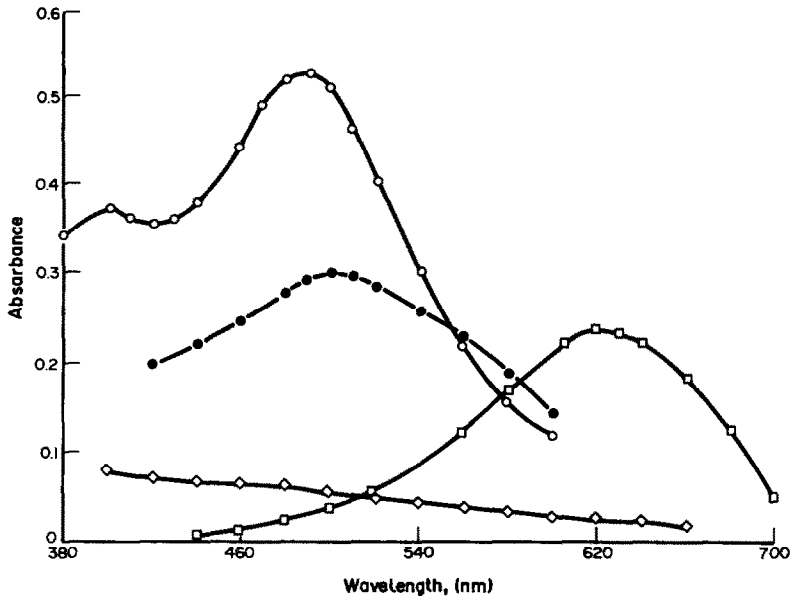

Fig. 1. Absorption Spectra of TNF (○——○); reagent blank *vs.* distilled water (◇——◇), β-naphthol (●——●) and *N*-methylaniline (□——□) with DCQC systems (concentrations of TNF $4.553 \times 10^{-5}M$; β-naphthol $3.468 \times 10^{-5}M$; *N*-methylaniline $4.665 \times 10^{-5}M$; DCQC $4.760 \times 10^{-4}M$).

and 1 ml of CAT were fixed as the optimum amounts to be added. Addition of 9 ml of buffer solution was found to be necessary to maintain the pH at 7.0 for maximum colour development. The colour intensity was found to increase up to one hour and then remained stable for a period of one hour.

The optical characteristics such as Beer's law limits (subject to an absorbance of at least 0.04 and a deviation of 2% from the linear portion in a plot of absorbance *vs.* concentration, μg/ml) molar absorptivity, Sandell's sensitivity (number of μg converted to the coloured product, which in a column

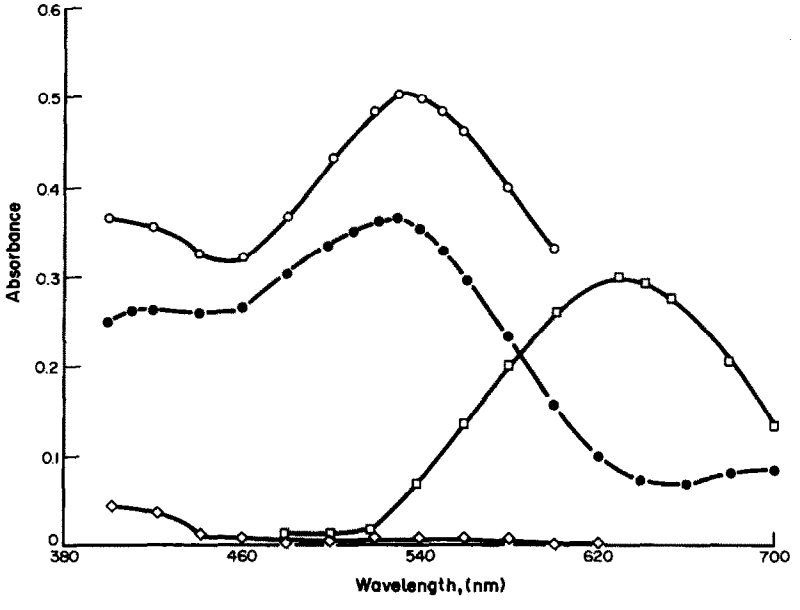

Fig. 2. Absorption spectra of TNF (●——●); reagent blank *vs.* distilled water (◇——◇), β-naphthol (○——○) and *N*-methylaniline (□——□) with DMPD–CAT systems (concentrations of TNF $6.505 \times 10^{-5}M$; β-naphthol $6.936 \times 10^{-5}M$; CAT $2.195 \times 10^{-4}M$; pH 7.0; *N*-methylaniline $6.997 \times 10^{-5}M$; DMPD $1.170 \times 10^{-4}M$).

Table 1. Optical characteristics, precision and accuracy of the proposed methods for tolnaftate

Data	DCQC A	DMPD–CAT B
λ_{max} (*nm*)	490	530
Beer's law limits ($\mu g/ml$, x)	2.0–14.0	2.5–20.0
Molar absorptivity (l.mole^{-1}.cm^{-1})	1.155×10^4	5.72×10^3
Sandell's sensitivity ($\mu g/cm^2$/0.001 adsorbance unit)	0.026	0.053
Optimum photometric range (μg/ml)	3.0–7.0	8.0–20.0
Regression equation ($mx + b$)		
Slope (m)	3.75×10^{-2}	1.86×10^{-2}
Intercept (b)	-1.73×10^{-3}	-1.19×10^{-3}
Correlation coefficient (r)	0.9999	0.9999
% RSD*	0.74	0.62
% Range of error (confidence limits)		
0.05 level	0.78	0.65
0.01 level	1.23	1.02
% Error in bulk samples† (tolnaftate without additives usually present in formulations)	+0.51	−0.42

*Calculated from six determinations.

†Average of three determinations considered. Taken 1 mg each time and diluted suitably.

solution of cross section 1 cm^2 shows an absorbance of 0.001) and optimum photometric range (calculated as μg/ml from linear portion in a plot of percent transmission *vs.* logarithm of the concentration) are given in Table 1. The regression equation and the correlation coefficient obtained by linear least squares treatment of the results in each case are also recorded in Table 1. The precision of the two methods was tested by estimating six replicates of the drug within Beer's law limits (100 μg/10 ml for method A and 400 μg/20 ml for method B). The percent relative standard deviation and the percent range of error at 95% confidence level are given in Table 1.

Commercially available formulations (creams and topical solutions) of TNF were successfully analysed by the proposed methods. The values obtained by the proposed and reference methods are given in Table 2. Application of t- and F-tests to the results obtained by the proposed and reference methods revealed no significant differences between the calculated and theoretical values (95% confidence limit) thus establishing their close similarity in precision and accuracy. The results of the recovery experiments by the proposed methods are also listed in Table 2.

The following additives generally used in the formulations of creams and solutions were found not to interfere in the colour development of methods A and B when added in excess fold (compared to the drug) as mentioned in parentheses; stearic acid (70), cetyl alcohol

Table 2. Assay of tolnaftate in pharmaceutical formulations

Formulations	Labelled amount, *mg/g*	Found by proposed methods, %* A	Found by proposed methods, %* B	Found by reference method, %*	Recovery of the proposed method,† %* A	Recovery of the proposed method,† %* B
CREAM TNF–10 mg/g	10	99.0 ± 0.63 t = 0.81 F = 1.3	98.9 ± 0.77 t = 1.24 F = 2.01	99.3 ± 0.55	98.7 ± 0.42	98.3 ± 0.54
CREAM TNF–10 mg/g	10	98.6 ± 0.63 t = 1.53 F = 1.05	100.4 ± 0.92 t = 0.58 F = 1.28	99.0 ± 0.65	98.5 ± 0.74	101.0 ± 0.64
SOLUTION TNF–10 mg/g	10	97.8 ± 0.69 t = 1.3 F = 1.2	100.0 ± 0.73 t = 0.69 F = 1.41	98.2 ± 0.75	97.9 ± 0.69	98.5 ± 0.56

*Average ± standard deviation of six determinations; the t- and F-values refer to comparison of the proposed methods with the reference method. Theoretical values at 95% confidence limit, $t = 2.57$, $F = 5.05$.

†After adding 10 mg to each pharmaceutical formulation, each value is an average of three determinations.

(10), glyceryl monostearate (50), sodium lauryl sulphate (10), propyl paraben (5) and glycerin (25). Betamethasone valerate, gentamycin and iodochlorohydroxyquinoline often included in some of the commercial formulations of TNF were found not to interfere in the two proposed methods.

Thus the proposed procedures constitute at the first reported visible spectrophotometric methods for the determination of TNF in pure samples and formulations. Among the two proposed methods, method A is more sensitive than method B, while the λ_{max} is found to be higher for method B. The stability period of the coloured species was also found to be greater in method A.

Chemistry of the coloured species

The reactions of amines and phenols with *N*-halosubstituted quinoneimines to yield coloured coupling products are well known.[4,5] Since TNF possesses both substituted toluidine and substituted naphthol moieties, it can be expected to undergo similar coupling reactions to give the coloured coupling products as follows.

Method A. In tolnaftate there are two possible sites for the coupling reaction to take place, namely position 4 of the *N*-methyl-*m*-toluidine moiety (which is para to the substituted amino grouping) and position 1′ of the naphthyl moiety (which is ortho to the substituted hydroxyl grouping). It is rather difficult to predict which of the two possible products is being formed under the experimental conditions. It is, however, reasonable to assume that only one of the two possible products is being formed during the course of the reaction since the coloured species exhibits only one well defined maximum at 490 nm. In order to settle the point of attachment during coupling, Gibb's reagent was treated with β-naphthol and *N*-methyl aniline separately under the experimental conditions of the reaction. The product in the former case exhibited a λ_{max} at 500 nm (which is very close to the 490 nm shown by the TNF: Gibb's reagent product) while the latter had λ_{max} only at 620 nm. This strongly suggests the involvement of naphthyl moiety (through position 1′) of TNF in the formation of the coloured coupling product as shown in Scheme 1.

Method B. The reaction of TNF with DMPD requires the presence of an oxidant. Among the various oxidants (IO_4^-, $S_2O_8^-$, CAT, $Cr_2O_7^{-2}$) tried in conjunction with DMPD, only CAT is able to generate the coloured species. It is therefore reasonable to assume the initial *in situ* formation of *N*-chloroquinone diimine (NCQDI) by the reaction of DMPD with CAT (as already reported in the case of *p*-aminophenol and sodium hypochlorite in the estimation of dulcin[4]) and the subsequent coupling of NCQDI with TNF. The point of coupling of TNF and NCQDI was settled as in the case of method A by examining the reaction products of β-naphthol and *N*-methyl aniline with DMPD–CAT reagent. As in the case of method A, the spectral characteristics of the reaction product of β-naphthol are very similar to those of the coloured species of method B (530 nm), while *N*-methylaniline reaction product had a λ_{max} only at 630 nm. Thus the generation of the coloured species in method B may be depicted as shown in Scheme 2.

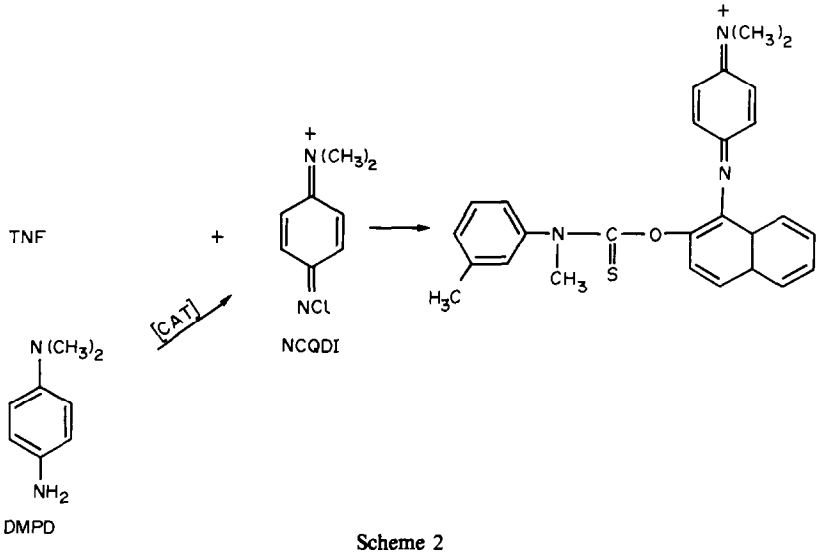

Scheme 2

The proposed methods are found to be simple, selective (when compared to the reported UV method) and sensitive and can be used for routine determination of tolnaftate in pure samples and formulations. The greater sensitivity and the stability observed in method A may be attributed to the presence of the electron withdrawing halogen atoms in the Gibb's reagent which enhance its oxidative coupling tendency. The procedure of method A is simpler in that it requires no oxidizing agent whereas the reaction mixture of method B contains NCQDI, unreacted DMPD and excess oxidant besides the other drug and non drug components of the formulation. None of the additives existing in solution (in methods A and B) and cream (in method A) formulations of tolnaftate interfere, even when the sample solution was prepared as under the bulk sample. However, some of the additives existing in creams separate out in method B (being aqueous medium) and so cause interference. It can be avoided by removal of such interfering components. The recommended procedure for formulations was designed keeping this in view. None of the components in the blank of cream (*i.e.*, without tolnaftate) produced colours with the proposed reagents.

Acknowledgements—The authors are grateful to BPL Pharmaceuticals Pvt. Ltd, Bombay for generously providing gift samples of tolnaftate and also to the University Grants Commission for JRF to one of us (J. V. Rao).

REFERENCES

1. *British Pharmacopoeia*, Vol. II, p. 578. Her Majesty's Stationery Office, London, 1988.
2. *United States Pharmacopeia*, XX, p. 806. The United States Pharmacopoeial Convention, New York, 1980.
3. H. D. Gibbs, *J. Biol. Chem.*, 1927, **71**, 445.
4. M. V. Rao, O. P. Kapur and C. S. P. Sastry, *Food Chemistry*, 1983, **12**, 109.
5. D. Svobodova, P. Krenek, M. Fraenkl and J. Gasparic, *Mikrochim. Acta*, 1977, **1**, 251.

Talanta, Vol. 40, No. 4, pp. 577–583, 1993
Printed in Great Britain

0039-9140/93 $6.00 + 0.00
Pergamon Press Ltd

BROMOMETRIC DETERMINATION OF CARBIMAZOLE

M. G. EL-BARDICY, Y. S. EL-SAHARTY and M. S. TAWAKKOL
Department of Analytical Chemistry, Faculty of Pharmacy, Cairo University, Kasr-El-Aini, 11562, Egypt (A.R.E.)

(*Received* 8 *August* 1991. *Revised* 29 *November* 1991. *Accepted* 20 *February* 1992)

Summary—Direct bromometric titration of carbimazole using *N*-bromosuccinimide (NBS) in the presence of methyl red as indicator and three indirect titrations using NBS, potassium bromate and dibromohydantoin (DBH) are developed. The direct procedure can be adopted for quantities of carbimazole ranging from 2–12 mg with mean accuracies of 100.2 ± 0.5. The indirect procedures can be used for quantities of the drug ranging from 1–6 mg using NBS and DBH and 2–16 mg using potassium bromate with mean accuracies of 100.11 ± 0.3, 100.49 ± 0.31 and 100.26 ± 0.51 respectively. The proposed procedures have been successfully applied for the analysis of the drug in tablet form and their validity has been checked using the standard addition technique. The reaction products were separated by TLC methods and their structure was elucidated using IR and NMR spectroscopy. The stoichiometry and the possible pathways of the reaction were postulated and presented.

Carbimazole, ethyl-3-methyl-2-thioxo-4-imidazoline-1-carboxate, Neo thyrostate, is an antithyroid drug used in the treatment of thyrotoxicosis or Graves' disease.[1] It produces its effect by blocking the biosynthesis of thyroxines T_3, T_4.[2]

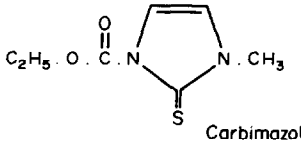

Carbimazole

Several spectrophotometric methods were applied to the determination of the drug in pure and tablet forms.[3–5] A direct titrimetric method, using ceric sulphate as titrant and 5,7 diiodo-8-quinolinol as indicator was reported.[6] Various chromatographic procedures were used for the detection and determination of carbimazole and its metabolite.[7–9]

The present work describes simple, rapid, inexpensive and accurate procedures for the determination of carbimazole and its tablet form, moreover excipients and additives do not interfere. The method is based on the reaction of the drug with various brominating reagents using direct or indirect titrations. The indirect procedures depend on the addition of a known excess of the brominating reagent to the drug and determining the excess reagent iodometrically.

EXPERIMENTAL

Samples

Authentic sample of carbimazole, BP batch No. 97609, was kindly supplied by Nicholas Laboratories Ltd, London. It was dried and its purity was proved to be 100.7% according to BP 1988[3] (Table 1).

The pharmaceutical formulation "Neo-mercazole" consists of tablets; each tablet is claimed to contain 5 mg of carbimazole, batch No. 1089114, 389110 and 389111 manufactured by CID Co., Cairo, A.R.E.

Stock solutions of carbimazole are prepared to contain 0.2 mg/ml and 0.4 mg/ml of carbimazole in water.

Apparatus

^{1}H NMR spectra were recorded on EM-390 90 MHz varian NMR spectrometer.

Infra-red spectra were made on Pye-unicam IR sp 1100 spectrophotometer.

A 5-ml semimicroburette accurate to 0.02 ml was used.

Materials and reagents

Standard potassium bromate; 0.1N.

Standard NBS, 0.01M, standardized against 0.01N sodium thiosulphate.

Potassium iodide solution, 10% w/v.

Table 1. Determination of carbimazole in pure form and in pharmaceutical preparation by both proposed and official BP (1988) methods

Samples*	NBS titration		Bromate–bromide titration	DBH titration	Official method BP (1988)
	Direct	Indirect			
Authentic	100.2 ± 0.5	100.1 ± 0.0	100.3 ± 0.5	100.5 ± 0.3	100.7 ± 0.1
Carbimazole tablets batch No. (1089114)	99.8 ± 0.8	99.5 ± 0.7	100.1 ± 0.4	99.9 ± 0.3	99.5 ± 0.3
Carbimazole tablets batch No. (389110)	99.3 ± 0.3	99.1 ± 0.9	100.5 ± 0.9	99.8 ± 0.0	99.6 ± 0.4
Carbimazole tablets batch No. (389111)	100.2 ± 0.4	100.0 ± 0.3	100.9 ± 0.3	100.7 ± 0.1	100.3 ± 0.4

*Average of five different experiments.

Sodium thiosulphate solutions, 0.01N and 0.05N. Standardized against 0.01*N* and 0.05*N* potassium dichromate.

Starch solution. Prepared freshly.

Methyl red indicator. According to BP 1988.[3]

Potassium iodobismuthate. Dilute solution, according to BP 1988.[3]

Silica gel G; PLC plates (20 × 20 cm, 2 mm thickness).

Procedures

Bromometric determination of carbimazole using N-*bromosuccinimide.* Direct procedure. Measure accurately an aliquot of the stock solution (0.4 mg/ml) equivalent to 2–12 mg of carbimazole into a 500-ml conical flask, complete to 30 ml with distilled water, add 20 ml of hydrochloric acid, 10 drops of methyl red indicator and mix well. Titrate with continuous stirring using 0.01*M* NBS solution till the red colour of the indicator disappears.

Calculate the amount of carbimazole from the equivalent factor each one millilitre of 0.01*M* NBS = 0.6207 mg of carbimazole. The results obtained are presented in Table 2.

Indirect procedure. Measure accurately an aliquot of the stock solution (0.2 mg/ml) equivalent to 1–6 mg of carbimazole into a 500-ml glass stoppered conical flask, complete to 30 ml with distilled water, then add 20 ml of hydrochloric acid and 25 ml of 0.01*M* NBS. Moisten the stopper with potassium iodide and allow to stand at room temperature for 1–5 min, then add 10 ml of 10% potassium iodide; and wash the stopper with 20 ml of water. Titrate with 0.01*N* sodium thiosulphate using starch as indicator. Simultaneously, carry out a blank experiment.

Calculate the concentration of carbimazole from the equivalent factor, one millilitre of 0.01*M* NBS = 0.6207 mg of carbimazole. The results are illustrated in Table 2.

Bromometric determination of carbimazole using bromate–bromide. Measure accurately an aliquot of the stock solution (0.4 mg/ml) equivalent to 2–16 mg of carbimazole into a 500-ml glass stoppered conical flask, complete to 40 ml with distilled water, add 10 ml of 0.1*N* potassium bromate, 5 ml of 10% potassium bromide and 20 ml of hydrochloric acid. Moisten the stopper with potassium iodide and allow to stand at room temperature for about 15–20 min. Add 20 ml of 10% potassium iodide, wash the stopper with 20 ml of water and titrate with 0.05*N* sodium thiosulphate using starch as indicator. Simultaneously, carry out a blank experiment.

Calculate the concentration of carbimazole from the equivalent factor, each one millilitre of 0.1*N* potassium bromate = 3.1033 mg of carbimazole. The results obtained are shown in Table 2.

Bromometric determination of carbimazole using dibromohydantoin. Measure accurately an aliquot of the stock solution (0.2 mg/ml) equivalent to 1–6 mg of carbimazole into a 500-ml glass stoppered conical flask, complete to 30 ml with distilled water. Add 20 ml of hydrochloric acid and 50 ml of DBH reagent. Moisten the stopper with potassium iodide and allow to stand at room temperature for 1–5 min. Add 10 ml of 10% potassium iodide and wash the stopper with 20 ml of water. Titrate with 0.01*N* sodium thiosulphate using starch as indicator. Simultaneously, carry out a blank experiment.

Each one millilitre of $2.5 \times 10^{-3}M$ DBH equivalent to 0.3103 mg of carbimazole. The results obtained are shown in Table 2.

Determination of carbimazole in tablet form. Weigh 20 tablets and calculate the average weight of a tablet. Take the calculated needed weight of the powdered tablets to prepare stock solutions containing 0.2 mg/ml of carbimazole.

Apply the prementioned procedures as given before.

The results obtained are shown in Table 1.

Table 2. Determination of authentic samples of carbimazole using NBS, bromate–bromide and DBH

NBS procedures						Bromate–bromide procedure			DBH procedure		
Direct titration			Indirect titration								
Taken, mg	Found,* mg	Recovery, %	Taken, mg	Found,* mg	Recovery, %	Taken, mg	Found,* mg	Recovery, %	Taken, mg	Found,* mg	Recovery, %
2	1.99	99.50	1	1.00	100.00	2	2.00	100.00	1	1.005	100.50
4	4.00	100.00	2	2.00	100.00	4	4.03	100.75	2	2.000	100.00
6	6.05	100.83	3	3.02	100.67	6	6.05	100.83	3	3.010	100.33
8	8.04	100.50	4	4.00	100.00	8	8.04	100.50	4	4.020	100.50
10	10.02	100.20	5	4.99	99.80	10	9.98	99.80	5	6.050	100.80
12	12.00	100.00	6	6.01	100.17	12	12.02	100.17	6	6.050	100.83
						14	14.09	100.64			
						16	15.90	99.38			
Mean ± S.D.	100.2 ± 0.5			100.1 ± 0.3			100.3 ± 0.5			100.5 ± 0.3	

*Average of five different experiments.

RESULTS AND DISCUSSION

The direct titration of carbimazole with NBS was successful in hydrochloric acid medium using methyl red as indicator, in addition the indirect titration was suitable for any of the previously mentioned brominating reagents.

The different factors affecting the indirect titration of carbimazole, such as acidity of the medium and the duration of the reaction were studied.

It was found that 20 ml of 20% (v/v) hydrochloric acid in a total volume of about 55 ml in the bromate–bromide procedure, while 20 ml of 20% (v/v) hydrochloric acid in a total volume of about 55–80 ml in the NBS or DBH procedure were optimal. A big change in the concentration of the acid will lead to irreproducible results.

The reaction time between carbimazole and the reagents is critical. It was found that 15–20 min in contact with bromate–bromide mixture and 1–5 min in contact with NBS or DBH were optimal. Lower or higher results are obtained if the reaction proceeds for less or more than the specified period.

Adequate results were obtained with all procedures by allowing the reaction to proceed at room temperature; higher temperature would lead to lower results.

The volume of excess reagent to be added in the bromate–bromide and DBH procedures should be at least double that consumed in the reaction; low results would otherwise be obtained.

Under the experimental conditions used, the molar ratios relating carbimazole to bromate, NBS and DBH were found to be 1:1, 1:3 and 2:3 respectively. It was of interest to note that NBS reacts with carbimazole either indirectly or directly by the same ratio.

When the proposed methods were applied to the determination of authentic carbimazole, the results demonstrate good precision as shown from Table 2 where the average recoveries were 100.3 ± 0.5 for carbimazole adopting the bromate–bromide titration, 100.3 ± 0.5 and 100.1 ± 0.3 applying the direct and indirect titrations with NBS respectively and 100.5 ± 0.3 using DBH titration.

Table 3. Determination of carbimazole in "Neo-mecazole" tablets by applying the standard addition technique to the proposed titrimitric procedures

Preparation	Direct NBS titration: Labelled carbimazole, *mg*	Authentic added, *mg*	Recovery of added, %	Indirect NBS titration: Labelled carbimazole, *mg*	Authentic added, *mg*	Recovery of added, %
Carbimazole	5.0	—	—	2.00	—	
tablets	5.0	2.00	100.50	2.00	2.00	101.00
batch No.	5.0	4.00	100.25	2.00	3.00	99.67
(1089114)	5.0	6.00	100.00	2.00	4.00	100.75
	5.0	8.00	100.00	2.00	5.00	100.60
Mean ± S.D.		100.2 ± 0.2			100.5 ± 0.6	
	Bromate–bromide tritration			DBH titration		
Carbimazole	6.0	—	—	2.00	—	
tablets	6.0	2.00	100.00	2.00	2.00	100.00
batch No.	6.0	4.00	99.00	2.00	3.00	100.67
(1089114)	6.0	6.00	100.67	2.00	4.00	100.50
	6.0	8.00	99.38	2.00	5.00	100.40
Mean ± S.D.		99.8 ± 0.7			100.4 ± 0.3	

*Average of five different determinations.

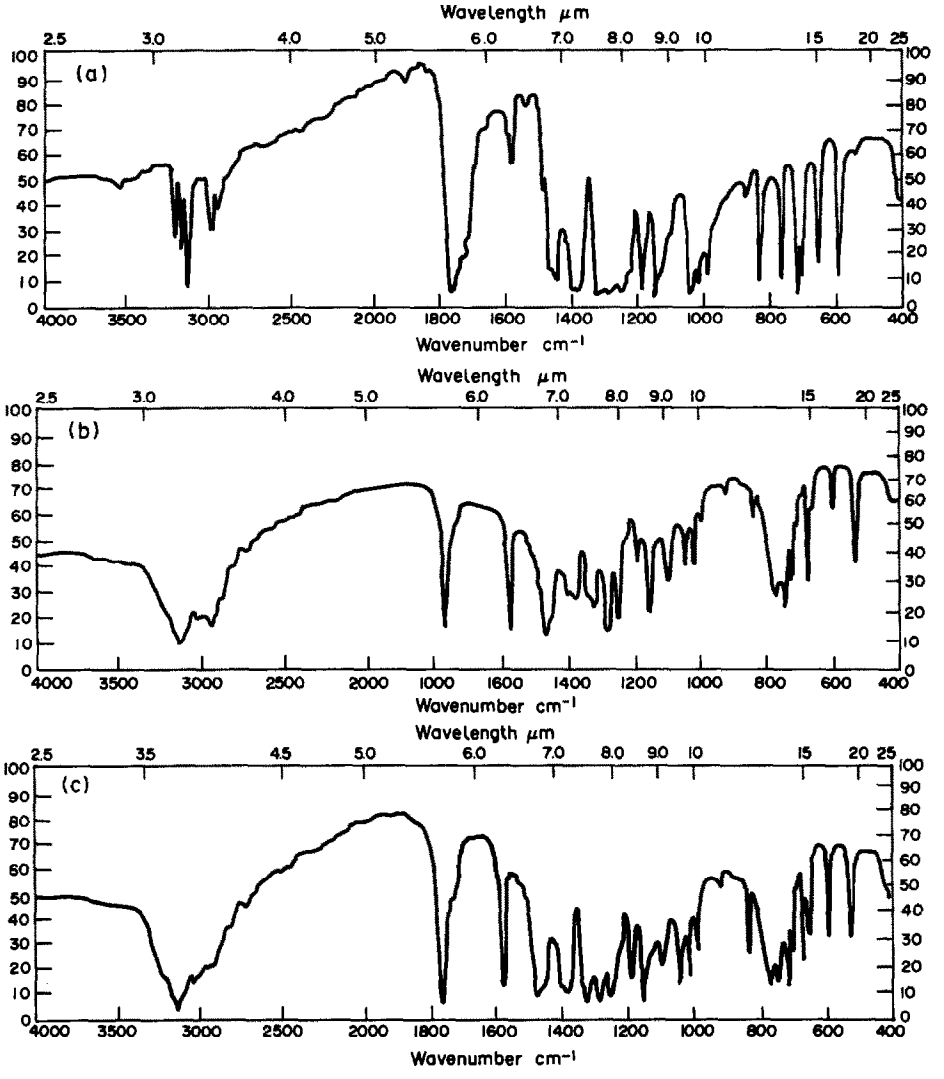

Fig. 1. IR spectra of (a) carbimazole, (b) major product and (c) minor product in KBr.

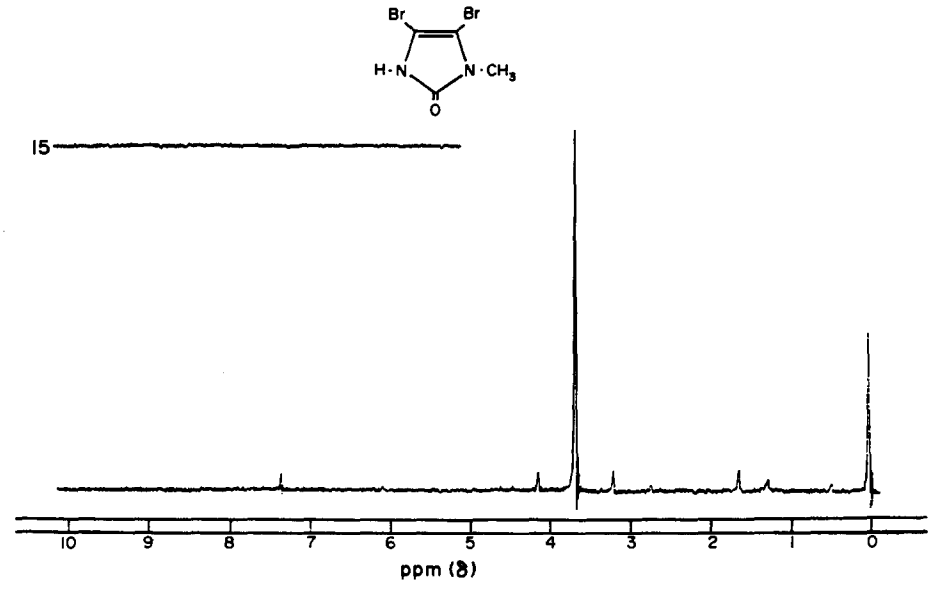

Fig. 2. ^{1}H-NMR of the major product, in $CDCl_3$.

Carbimazole (Neo-mercazole) tablets were analysed for carbimazole content by the proposed titrimetric procedures, before and after filtration from insoluble excipients and additives. It was found that the determination of a suspension of carbimazole powdered tablets gave more or less similar results to that obtained using filtered extracts of tablets. This means that excipients and additives used for their manufacture do not interfere with the proposed procedures. Nevertheless, filtration was preferred for all determination to ensure complete extraction and accuracy of the final volume, providing more clear detection of the end point, and this was adopted in Table 1.

The validity of the proposed procedures was assessed by applying the standard addition technique. The results obtained are presented in Table 3. Further comparative determination of carbimazole in its tablet form by the proposed titrimetric methods and the official BP 1988

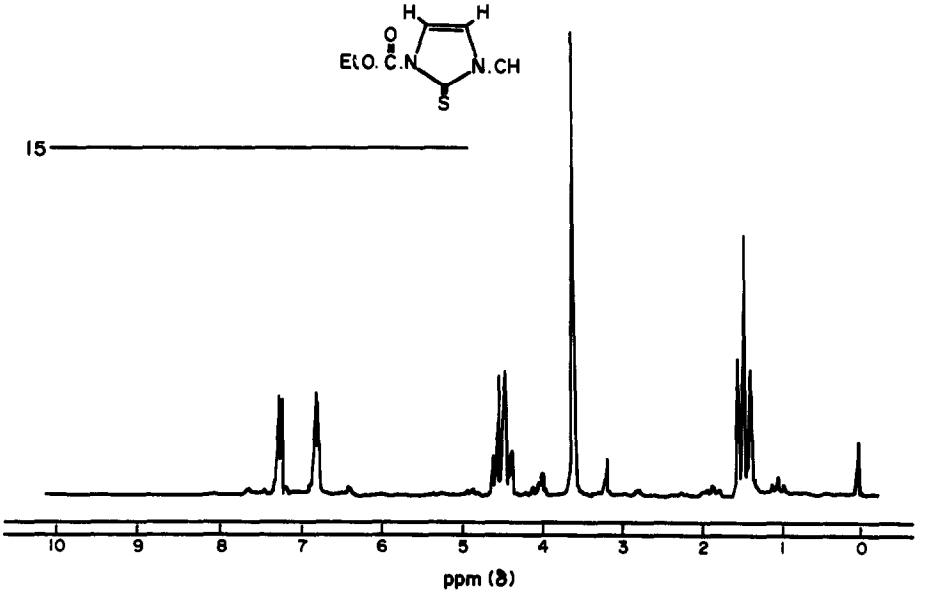

Fig. 3. Effect of reagent concentration.

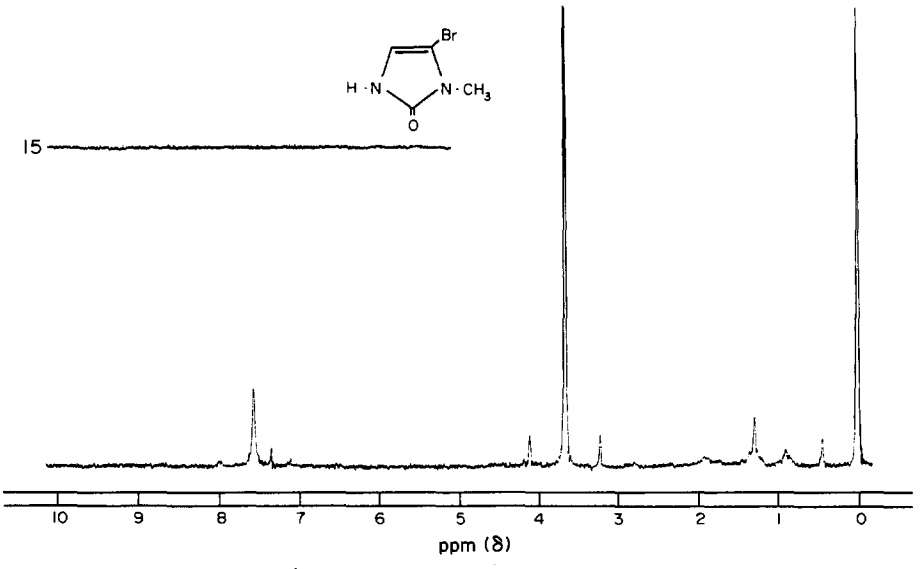

Fig. 4. ^{1}H-NMR of the minor product, in $CDCl_3$.

method has been done. The results obtained were illustrated in Table 2.

The studies of the reaction products, after applying the different bromometric procedures were carried out. The reaction products obtained from each bromometric procedure were compared on TLC plates with a spot of the authentic material. Different developing

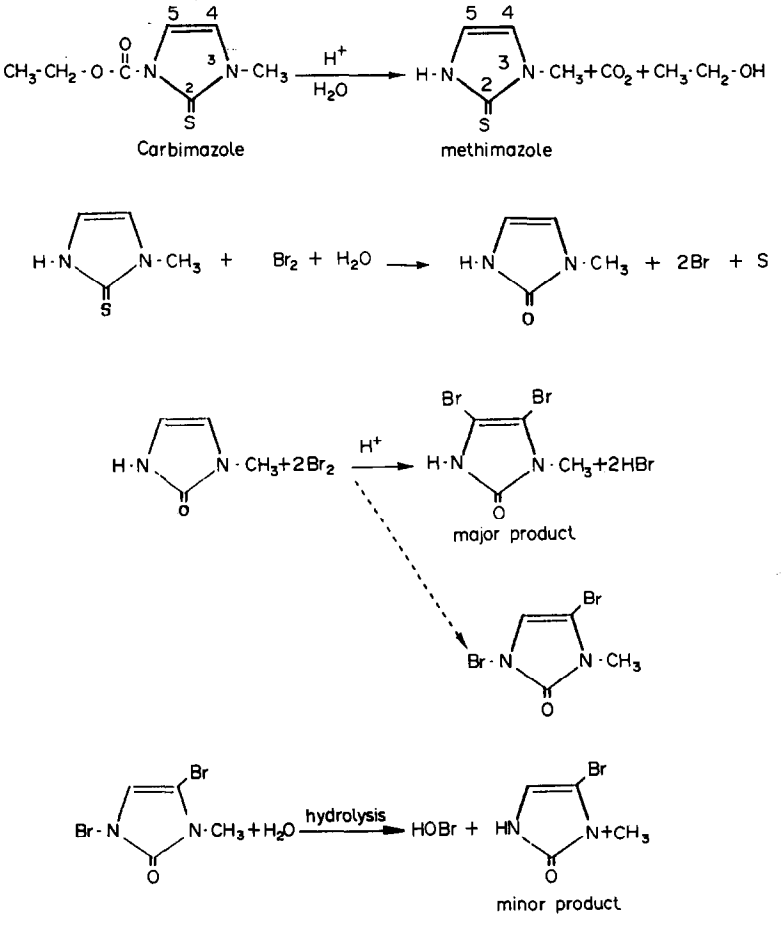

systems were tried[7] and chloroform–acetone (4:1) was found to be the most suitable one. Various methods for visualization were studied[10,11] and the most suitable one being dilute solution of potassium iodobismuthate. It was found that all the procedures gave the same products.

Isolation of the reaction products

The bromate–bromide procedure was carried out as before using 80 mg of carbimazole and suitable needed amounts of the other reagents. The reaction between carbimazole and bromine was then stopped after 15 min using concentrated ammonia solution. The products were extracted with chloroform, evaporated, then separated on PLC plates using chloroform–acetone (4:1) as solvent system. The spots were visualized using dilute potassium iodobismuthate solution. The bands corresponding to the products were scratched and then extracted with chloroform. The products obtained after evaporation of the chloroformic extract were identified by IR, Fig. 1, and NMR, Figs 2–4.

Mechanism of the reaction

According to the molar ratios of the reaction and from IR and NMR data it may be suggested that the reaction proceeds (on p. 582).

^{1}H-NMR Fig. 2 of the major product in comparison with that of the parent compound, Fig. 3 showed no ethyl function and no aromatic protons, a fact which suggests that the starting material was subjected to hydrolysis followed by decarboxylation and bromination at positions 4 and 5 to give 4,5 dibromo-3-methyl-2-oxo-4-imidazoline.

^{1}H-NMR of the minor product (4-bromo-3-methyl-2-oxo-4-imidazoline), Fig. 4 showed a singlet at 7.6 p.p.m. corresponding to (^{1}H, 5-H).

Considering the absence of ethyl function from ^{1}H-NMR and the presence of a carbonyl absorption band in IR at 1760 cm^{-1}, Fig. 1, we might suggest that desulpherization of the starting compound occurs during the course of the reaction. In addition, IR spectrum showed an absorption band at 3120 cm^{-1} which could be an —NH or —OH. Furthermore, detection of sulphur in the products by Lasaigne sodium test,[12] proved to be absent.

REFERENCES

1. A. G. Gilman, L. S. Goodman and F. Murad (eds.), *The Pharmacological Basis of Therapeutics*, 7th Ed., Macmillan Publ. Co., New York, 1985, 1389.
2. A. Burger, *Burger's Medicinal Chemistry*, 3rd Ed., p. 852. Part II, Wiley, New York, 1970.
3. British Pharmacopoeia, Her Majesty's Stationary Office, London, 1988.
4. A. E. Szabe, G. Stajer and E. Vinkler, *Pharmazie*, 1974, **29**, 615.
5. C. E. Searle, *J. Appl. Chem.*, 1955, **5**, 313.
6. K. Sriramam, N. R. Sastry, B. V. S. Sastry and G. N. L. Prasuna, *Indian Drugs*, 1984, **21**, 520.
7. P. Owen, A. Pendleburg and A. C. Moffat, *J. Chromatogr.*, 1978, **161**, 187.
8. G. G. Skellern, B. I. Knight, L. C. K. Low, W. D. Alexander, D. G. McLarty and W. J. Kalk, *Br. J. Clin. Pharmacol.*, 1980, 137.
9. G. G. Skellern, *Analyst*, 1981, **106**, 1071.
10. E. Stahl, in *Thin Layer Chromatography*, Springer Verlag, New York, 1969.
11. H. Weichsel, *Mikrochim. Acta.*, 1965, **325**.
12. F. G. Mann and B. C. Saunders, *Practical Organic Chemistry*, 4th Ed., p. 325. Longman Inc., New York, 1960.

Talanta, Vol. 40, No. 4, pp. 585–588, 1993
Printed in Great Britain

0039-9140/93 $6.00 + 0.00
Pergamon Press Ltd

SPECTROPHOTOMETRIC DETERMINATION OF KETOPROFEN IN PHARMACEUTICAL PREPARATIONS BY MEANS OF CHARGE TRANSFER COMPLEX FORMATION

M. EL-SADEK, S. EL-ADL, M. ABOU-KULL and S. M. SAKR
Pharmaceutical Chemistry Department, Faculty of Pharmacy, Zagazig University, Zagazig-Egypt

(*Received* 27 *May* 1991. *Revised* 27 *September* 1991. *Accepted* 30 *September* 1991)

Summary—A spectrophotometric determination of ketoprofen based upon oxime formation followed by charge transfer complexation with *o*-chloranil has been developed. Different variables affecting the complexation process have been studied. Beer's law is obeyed in the concentration range 10–80 μg/ml. The method has been successfully applied to the determination of ketoprofen in pure form and in pharmaceutical dosage forms in the presence of its impurities.

Ketoprofen is an anti-inflammatory anti-rheumatic agent widely used in pharmaceutical practice. Many methods were reported for its determination including titrimetry,[1] spectrophotometry,[2,3] polarography[4] and chromatography.[5–7] Most of the aforementioned methods are not sufficiently selective for the determination of ketoprofen in pharmaceutical preparations in the presence of its degradation products and impurities during the manufacturing process. In order to obtain the necessary sensitivity and selectivity, the proposed method is developed based on the reaction of hydroxylamine with the ketonic group of ketoprofen to form ketoprofen oxime. Upon reaction with *o*-chloranil, a charge transfer complex is formed. Although the proposed method is more complicated than the existing procedures, it distinguishes itself by the required characters and therefore, promises to be a valuable achievement in practical application.

EXPERIMENTAL

Apparatus

A Schimadzu UV–Vis self-recording spectrophotometer with 1-cm quartz cuvettes was used.

Materials and reagents

Ketoprofen; profenid capsules: labelled to contain 50 mg of ketoprofen per capsule; profenid vials: labelled to contain 100 mg of ketoprofen per vial (Rhone Poulenc, France); *o*-chloranil; hydroxylamine hydrochloride; sodium acetate; chloroform; pure ketoprofen oxime solution (100 mg g/50 ml in chloroform) and *o*-chloranil solution ($10^{-4}M$ in chloroform).

Procedures

Oximation procedure. To a 50-mg ketoprofen sample, 10 ml of hydroxylamine hydrochloride and 25 mg of sodium acetate was added and the mixture was dissolved in 30 ml of methanol (75%). The mixture was refluxed for 30 min, cooled and extracted with three successive 10-ml portions of chloroform; the chloroformic extract was collected in a 50-ml standard flask and diluted to volume.

Complexation with o-*chloranil.* A suitable aliquot of ketoprofen oxime equivalent to 0.1–0.8 mg was transfered into a 10-ml standard flask, 5 ml of *o*-chloranil was added and the mixture was allowed to stand for 5 min and then diluted to volume with chloroform. The absorbance was measured at 530 nm against a blank prepared in the same way but in the absence of ketoprofen.

Pharmaceutical dosage forms. The contents of 20 capsules or 6 vials were throughly mixed and a quantity equivalent to 50 mg of ketoprofen was added. The procedure was completed as mentioned for the above procedures.

RESULTS AND DISCUSSION

Due to the presence of the ketonic functional group in ketoprofen, it interacts with hydroxylamine hydrochloride to form ketoprofen oxime.

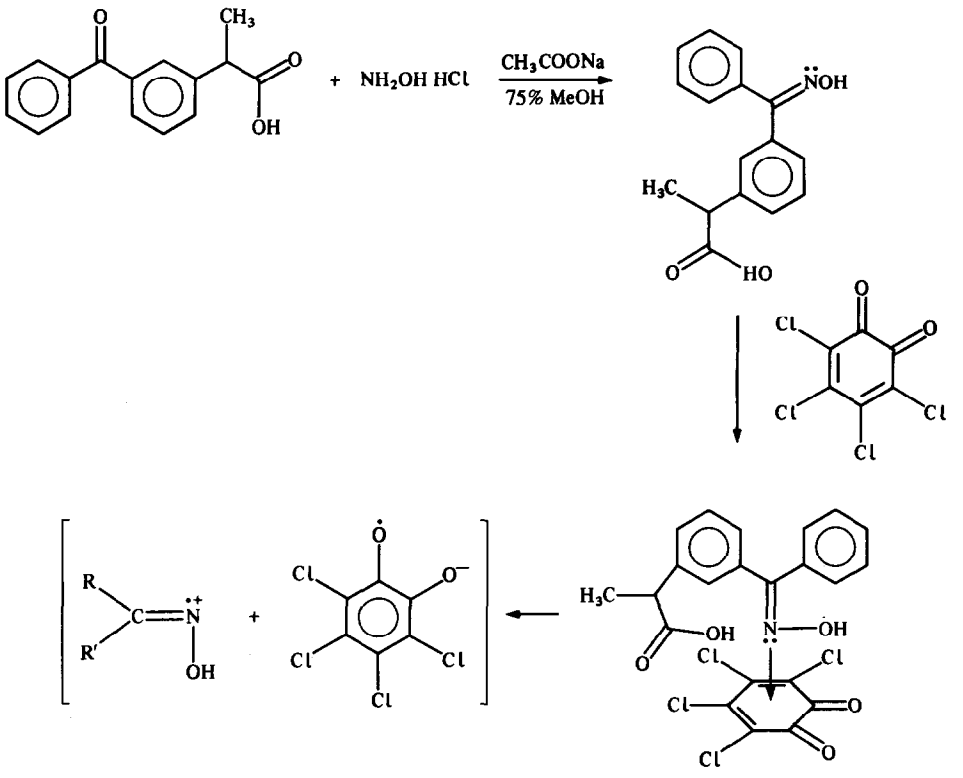

Scheme 1

The formed ketoprofen oxime has an iminic group with a lone pair of electrons on the nitrogen atom, thus it acts as an electron donor (n-donor). On the other hand, *o*-chloranil (3,4,5,6-tetrachloro-*o*-benzoquinone) is highly reactive as an electron acceptor (π acceptor), so it forms an n-π charge transfer complex with ketoprofen. The outer intermediate complex is formed immediately within 60 sec after mixing donor and acceptor. This intermediate is stable in the dark under a nitrogen atmosphere and in a non-polar solvent. It changes to the inner complex in light and in the presence of a relatively polar solvent (chloroform). From elemental and spectroscopic analyses the pathway is proposed in Scheme 1.

Upon studying the absorption curves for ketoprofen, ketoprofen oxime, *o*-chloranil and the ketoprofen oxime–*o*-chloranil complex, different maxima were exhibited at 260, 325, 240 and 530 nm in chloroform respectively; another indication of charge transfer complex formation.

Variable parameters affecting the complexation process were studied. The effect of reflux

Table 1. Determination of ketoprofen powder by the proposed method compared with the official B.P. 1982

	Proposed method		Official method		
Taken, *mg*	Found, *mg*	Recovery,* %	Taken, *mg*	Found, *mg*	Recovery,* %
0.200	0.196	98.00	200.00	208.00	104.00
0.300	0.302	100.66	300.00	306.00	102.00
0.400	0.399	99.75	400.00	406.00	101.50
0.500	0.504	100.80	500.00	503.00	100.60
0.600	0.601	100.16	600.00	595.00	99.16
Mean ± S.D.		99.87 ± 1.12			101.45 ± 1.78
N		5			5
V		1.271			3.193
S.E.		0.504			0.799
t					1.672 (2.31)
F					2.512 (6.39)

*Average of 3 experiments.

Table 2. Determination of ketoprofen in profenid capsules by the proposed method compared with the official B.P. 1988 method

	Proposed method		Official method		
Taken, *mg*	Found, *mg*	Recovery,* %	Taken, *mg*	Found, *mg*	Recovery,* %
0.200	0.204	102.00	0.200	0.201	100.50
0.300	0.294	98.00	0.300	0.293	97.66
0.400	0.405	101.25	0.400	0.395	98.75
0.500	0.508	101.60	0.500	0.499	99.80
0.600	0.593	98.83	0.600	0.595	99.16
Mean ± S.D.		100.33 ± 1.79			99.17 ± 1.07
N		5			5
V		3.231			1.155
S.E.		0.803			0.480

*Average of 3 experiments.

Table 3. Determination of ketoprofen in profenid vials by the proposed method compared with the official B.P. 1988 method

	Proposed method		Official method		
Taken, *mg*	Found, *mg*	Recovery,* %	Taken, *mg*	Found, *mg*	Recovery,* %
0.400	0.393	98.25	0.400	0.393	100.50
0.500	0.489	97.80	0.500	0.502	100.40
0.600	0.607	101.17	0.600	0.585	97.50
0.700	0.689	98.43	0.700	0.692	98.85
0.800	0.810	101.25	0.800	0.793	99.75
Mean ± S.D.		99.38 ± 1.68			99.40 ± 1.24
N		5			5
V		2.844			1.561
S.E.		0.754			0.558

*Average of 3 experiments.

time on the oximation processs was examined and it was found that reflux for 30 min afforded complete oximation when using the TLC technique. Also, 5 ml of $10^{-4}M$ *o*-chloranil achieves maximum colour intensity which is stable for up to 40 min. The molar ratio of ketoprofen oxime and *o*-chloranil by the continuous variation method[8] was found to be 1:1.

Beer's law is obeyed in the range 10–80 μg/ml, with the least square method. The absorption graphs were described by the following regression equation:

$$A_{530nm} = 0.002 + 1.233X$$

where X is the concentration in μg/ml in the final solution.

The proposed method was successfully applied to the determination of pure ketoprofen, the results obtained were compared with the official titrimetric method[1] (Table 1). Statistical analysis of the results revealed that there is no significant difference between them.

The effect of degradation products and impurities which may be present: 2-(4-aminophenyl)propionic acid, 2-(4-mercaptophenyl)-propionic acid, 2-iodobenzoic acid and 2-(3-carboxyphenyl)propionitril was experimentally studied and results obtained showed no interference, indicating selectivity of the method.

Pharmaceutical preparations containing ketoprofen were analysed by the proposed method and the results were compared with UV spectrophotometric method[9] (Tables 2 and 3). Statistical analysis of the results showed both methods are equally precise and accurate.

The above study shows that the proposed method is more sensitive than the official B.P. 1980 method. It is sensitive down to 10 μg/ml compared with 200 μg/ml for the official method. Also, the proposed method is a selective one depending upon the presence of an intact molecule and not the hydrolytic products, so it can be used as a stability-indicating assay for ketoprofen in the presence of its impurities for different pharmaceutical dosage forms.

REFERENCES

1. *British Pharmacopoeia, H.M.S.O.* p. 69. London, Addendum 1982.
2. B. Unterhalt, *Pharm. Ztg.*, 1978, **123**, 1801.
3. B. Lotti, *Boll. Chim. Farm.*, 1975, **114**, 351.

4. P. Populaire, B. Terlain, S. Pascal, B. Decouvelaire, G. Leberton, A. Renard and J. P. Thomas, *Ann. Pharm. Fr.*, 1973, **31**, 679.
5. R. Ballerini, A. Cambi, P. Del Soldato, F. Melani and A. Meli, *J. Pharm. Sci.*, 1979, **68**, 366.
6. P. Stenberg, T. E. Joensson, B. Nilssen and F. Wollheim, *J. Chromatogr.*, 1979, **177**, 145.
7. R. Farinotti and G. Mahuzier, *J. Pharm. Sci.*, 1979, **68**, 484.
8. J. Rose, *Advanced Physicochemical Experiments*, p. 54. Pitman, London, 1964.
9. *British Pharmacopoeia*, *H.M.S.O.*, p. 639. London, 1988.

Talanta, Vol. 40, No. 4, pp. 589–590, 1993
Printed in Great Britain

0039-9140/93 $6.00 + 0.00
Pergamon Press Ltd

BOOK REVIEWS

Element Specific Chromatographic Detection by Atomic Emission Spectroscopy: P. C. UDEN (editor), American Chemical Society, Washington, D.C., 1992. Pages x + 350. U.S. $74.95. ISBN 0-8412-2174-X.

Increasing demand on trace analysis of complicated samples have fuelled the developments of 'hyphenated' systems. One basic requirement of a 'hyphenated' system is the successful interfacing of component techniques within the system. The same applies to 'chromatograph–atomic emission spectroscopy' systems in which the most common problems lie in ensuring the efficient transfer of the separated analyte to the AES detector and in maintaining a good detector response in a chromatographic environment (e.g., with respect to mobile phase and eluted forms of the analyte).

This book is developed from the 1990 ACS symposium at Boston. It consists of 19 chapters covering mainly gas chromatography–atomic emission spectroscopy (11 chapters), high performance liquid chromatography–atomic emission spectroscopy (3 chapters), supercritical fluid chromatography–atomic emission spectroscopy (2 chapters) and gas chromatography/high performance ligand chromatography–mass spectrometry (3 chapters). Some are review chapters but most chapters are specific discussions of particular aspects, illustrated with studies from the authors' own laboratories. These include discussions on the modes of excitation (mainly on microwave-induced plasma but a few on inductively-coupled plasma and one chapter each on direct current plasma and alternative current plasma) and on detector optics (including a chapter on photo-diode array detection and another on fibre-optic sensor specific to chlorine).

The book is a timely publication of the state-of-the-art of element-specific detection for chromatographic systems. The book is contributed to by researchers, many of whom are experts in the field of chromatographic science, from a variety of backgrounds (academic, industrial and instrument manufacturers) and countries (*e.g.*, US, Germany, Japan). Although some subject areas (*e.g.*, microwave-induced plasma excitation) are common, the emphasis in the papers is sufficiently varied to make the book a comprehensive account of diversed aspects (*e.g.*, technical, fundamental and applied) of a 'hyphenated' technique. Examples are chapter 6 which is more technical on solving optic problems, chapter 9 (technical) on the instrumentation of capacitively coupled plasma, chapter 2 (fundamental) on the development of LC/SFC–AES for non-metals and chapter 15 (applied) on analysis of Se in food and water sample. The diversity is enhanced by the inclusion of discussions on less commonly used techniques such as chapter 8 on a 'doubly-hyphenated' system (GC–AES–MS), chapter 11 on surface-wave plasma and chapter 12 on He discharge detector.

The scientific quality of the chapters is generally high although the first two-thirds of the book appears to be better than the rest. The papers were submitted camera-ready but generally the typeface and chapter formats are quite consistent throughout and quite good too, except for a few chapters which used crowded pitch and single line spacing, making reading rather difficult. The text in the chapters are usually adequately illustrated, well referenced and current. The tables, diagrams and figures are generally clear and well presented.

Overall, this book is informative, up-to-date, well presented and reasonably priced. It should be useful to all those who work with chromatography-element specific detection systems.

S. C. TAM

Precision and Resolution in Spectroscopic Model Fitting: J. H. SWARTE, Delft University Press, Delft, The Netherlands, 1992. Pages xiii + 198. ISBN 90-6275-756-6 (Softback).

The Dutch PhD thesis is a model most countries would do well to follow: the final product is a compact paperback book with all the obvious advantages. Some theses are subsequently distributed as books, and this volume is one of them. It is concerned with the problem of obtaining accurate peak positions, and resolving peak overlaps in any one dimensional spectroscopic problem.

It begins with a survey of traditional methods of obtaining peak parameters, and is suitably provocative particularly concerning Fourier transform and second-order derivative techniques. This section is followed by a short chapter on the use of model fitting to obtain peak parameters. There are then two chapters concerning precision and resolution in spectroscopy; the first of these is qualitative, the next a more mathematical approach exclusively concerned with non-linear least squares. The final theory section deals with the incorporation of measurement errors into non-linear least squares model fitting, and chapter 6 applies this theory to a series of 22 spectroscopic problems. Finally there are two short chapters containing discussion and conclusions.

The whole work is quite clear, the English is competent, but I am very surprised that maximum entropy methods received no mention anywhere. There are good theoretical reasons for preferring them to non-linear least squares, and they should at least appear in discussions in a publication of this sort. This aside, the book will provide interesting, specialist reading for spectroscopists concerned with quantitative analysis.

C. J. GILMORE

Contemporary Electroanalytical Chemistry: A. IVASKA, A. LEWENSTAM and R. SARA (editors), Plenum, New York, 1990. Pages x + 458. US$120.00. ISBN 0-306-43818-6.

This book contains 53 papers presented by 106 authors at the ElectroFinnAnalysis Conference at Turku-Åbo, Finland, in June 1988. The papers have been grouped into seven sections, though the allocation in some cases has been made quite arbitrarily.

The first section, headed 'Electrochemical Instrumentation and Methods', contains eight papers, half of which deal with 'fast' techniques, i.e., fast electrochemistry, FT-faradaic admittance, fast potentiostats, and FFT-filtering, whilst the other four papers deal with photoelectroanalytical chemistry, reverse pulse voltammetry, multiple sensor arrays, and simultaneous ESR-electroanalytical investigations. Regardless of one's particular interest, most electrochemists will find this section of interest for the papers highlight the advances being made in several techniques. The second section deals with 'Industrial Applications' of electroanalytical techniques to process and product control, and environmental monitoring; products cited include sodium hydroxide, explosives, and those from fermentation and plating processes.

Although most of the papers in this book deal with sensors in one form or another, the ten papers in the section 'Electrochemical Sensors' deal with the structures and responses of solid-state devices, such as ISFETs, SFETs, MOSFETs, and chemically-modified electrodes and ion-selective membrane electrodes. The papers in the fourth section, 'Electrochemical Flow Analysis', concentrate mainly on flow injection analysis, and the modification of electrode systems for use in flow analysis.

Most of the papers in the sections 'Clinical Applications' and 'Pharmaceutical Applications' deal with the use of ion-selective electrodes and adsorptive stripping voltammetry. In the final 'General' section, there are more papers dealing with the use of adsorptive stripping voltammetry, and some with differential pulse polarography.

With the large number of papers, it is inevitable that the quality of the publications varies, but, on the whole, the quality is reasonably good. All of the papers are clearly written, informative, and up-to-date at the time of the conference: there are a number of mis-spellings but these do not diminish the overall quality of the book. This book can be recommended to those who wish to be aware of the progress made in the many related fields of electroanalytical chemistry.

J. B. CRAIG

The Kirk-Othmer Encyclopedia of Chemical Technology: Volume 3, Fourth Edition. Antibiotics (β-Lactams) to Batteries. J. I. KROSCHWITZ and M. HOWE-GRANT (editors), Wiley-Interscience, Chichester, 1992. Pages xxviii + 1121. £135.00. ISBN 0-471-52671-1 (v. 3).

A review of the first volume of the fourth edition of this encyclopedia appeared in *Talanta*, 39, 1063. The current volume completes an extensive section on antibiotics (continued from volume 2) and the contents then proceed alphabetically to a 158-page dissertation on batteries. As with the two previous volumes numerous authors from industry and academia have contributed to this tome.

Elements and compounds of antimony, arsenic and barium are covered in a concise manner with details of production and economics. Much general chemistry associated with these elements is also included. The importance of pharmaceutical compounds is very much in evidence for as well as the section on antibiotics there are details of antiobesity drugs, antiparasitic agents and antiviral agents. Indeed, almost half of this volume is concerned with pharmaceutical agents.

There is a small section on automated instrumentation which is devoted to descriptions of analysers used in clinical chemistry and hematology. Analysis is also mentioned in the section concerning asbestos. An attempt to locate atomic-absorption spectroscopy in the encyclopedia results in a referral to the section on spectroscopy in a future volume. Some of the other topics in volume 3 include antifreezes, antioxidants, atmospheric modelling, azo dyes, bakery processes and barrier polymers.

Overall the volume maintains the high standard of previous volumes with many up-to-date references, competent and easy-to-understand descriptions of technological processes and much interesting chemistry.

P. J. Cox

Talanta, Vol. 40, No. 4, p. 591, 1993
Pergamon Press Ltd. Printed in Great Britain

CORRIGENDUM

Wu Lixin and He Huannan, Determination of absorption efficiencies of carbon dioxide absorbents by gas chromatography. *Talanta*, **39**, 1081–1087, 1992.

Thomas Scientific would like to point out that Ascarite II® is a trademark registered in the United States Patent and Trademark Office, Reg. No. 1,134,932 and also a trademark registered in The Trade Marks Registry, Patent Office of Great Britain and Northern Ireland, Reg. No. 1,106,141; both in the name of Arthur H. Thomas Co. Furthermore, the production of Ascarite II® is under the sole jurisdiction of the Arthur H. Thomas Co., doing business as Thomas Scientific.

Talanta, Vol. 40, No. 5, pp. 707–711, 1993
Printed in Great Britain.

0039-9140/93 $6.00 + 0.00

SPECTROPHOTOMETRIC DETERMINATION OF CHROMIUM WITH IODONITROTETRAZOLIUM CHLORIDE AND TETRAZOLIUM VIOLET

M. KAMBUROVA
Department of Chemistry, Higher Institute of Agriculture, 4000 Plovdiv, Bulgaria

(*Received* 5 *December* 1991. *Revised* 9 *March* 1992. *Accepted* 21 *April* 1992)

Summary—The interaction of Iodonitrotetrazolium chloride and Tetrazolium Violet with chromium(VI) has been studied and the formation of ion-associates with a 1:1 composition in hydrochloric acid medium established. Extraction photometric methods for determination of chromium in steels and soils have been developed.

A characteristic feature of chromium as a transition element is its ability to form a great number of complex compounds of different structure and chromium oxidation state.[1–4] Various reagents have been suggested for photometric determination of chromium, and solvent extraction of ion-pairs of Cr(VI) anions with organic cations has been described by several authors.[5–14] Several of the organic reagents for spectrophotometric determination of chromium were mentioned in an earlier paper on determination of chromium(VI) by extraction with Methylene Blue;[15] others that have been proposed include sodium 2′-bromo-4′,5′-dihydroxyazobenzene-4-sulphonate,[16] fluphenazine hydrochloride,[17] 4-(2′-thiazolylazo)resorcinol,[18] 4-(2-pyridylazo)resorcinol,[19] *o*-hydroxyquinolphthalein,[20] *o*-nitrophenylfluorone[21] and gallacetophenone.[22] Diphenylcarbazide is considered to be one of the most sensitive spectrophotometric reagents for chromium,[23] but suffers from various interferences.

Tetrazolium salts have been used to provide cations for the formation of ion-associates of various anions in the determination of a number of metals, including Co, Zn, Au, Sb, Nb, Mo, W, Re, Tl and Ga,[24–34] but only triphenyltetrazolium chloride has so far been used as a reagent for determination of chromium.[13,35,36] Here we report on the use of Iodonitrotetrazolium chloride (INT) and Tetrazolium Violet (TV) as counter-ions for formation of ion-association complexes with the chlorochromate anion (CrO_3Cl^-) and determination of chromium(VI).

EXPERIMENTAL

Apparatus

A Zeiss VSU 2-P spectrophotometer and a Specord UV-VIS spectrophotometer were used with 1-cm light-path cuvettes.

Reagents

Iodonitrotetrazolium chloride (INT), $1 \times 10^{-4}M$; Tetrazolium Violet (TV), 1×10^{-5} and $1 \times 10^{-4}M$; potassium chromate, 1×10^{-4} and $1 \times 10^{-5}M$; sulphuric acid, 18 and $0.18M$; hydrochloric acid, 12 and $1.2M$; nitric acid, 17 and $1.55M$; perchloric acid, $9M$; hydrofluoric acid, concentrated; 1.2-dichlorethane.

Procedure

In a 100-ml separatory funnel, $1.2M$ hydrochloric acid (1.2 ml for INT or 0.9 ml for TV), 2 ml of $1 \times 10^{-4}M$ INT or 1 ml of $1 \times 10^{-4}M$ TV and a known amount of chromium(VI) were mixed and the solution was diluted to 10 ml with distilled water and then shaken with 3 ml of dichlorethane for 1 min. The organic layer was transferred through a dry filter paper into a 1-cm cuvette and its absorbance measured at 250 nm for INT or 230 nm for TV. Corresponding blanks containing the same solutions but no chromium were prepared.

RESULTS AND DISCUSSION

Optimization of conditions

With chromium(VI), in hydrochloric acid medium, Iodonitrotetrazolium chloride and

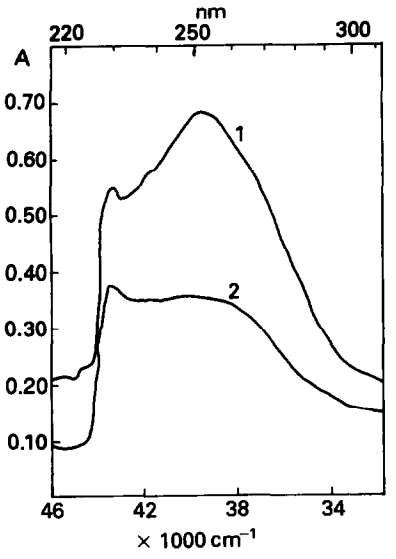

Fig. 1. Absorption spectra (in dichlorethane) of ion-association complex of Cr(VI) with INT (1) and of INT (2); $C_{Cr(VI)} = 1 \times 10^{-5}M$, $C_{INT} = 1 \times 10^{-5}M$, $C_{HCl} = 0.14M$.

Tetrazolium Violet form ion-associates with compositions $INT^+ \cdot CrO_3Cl^-$ and $TV^+ \cdot CrO_3Cl^-$ respectively. This composition is in agreement in earlier reports on the nature of chromium(VI) complexes in hydrochloric acid media.[37-41].

Our studies show that the ion-associate of Cr(VI) with INT or TV is quantitatively extracted into dichlorethane. With other solvents, such as chloroform, benzene, nitrobenzene, ether, the compound is not extractable.

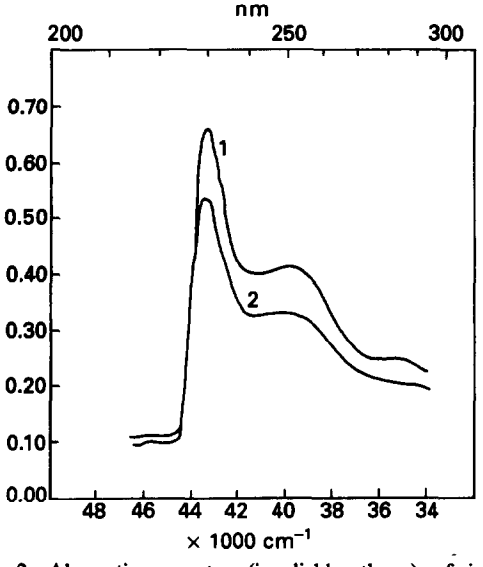

Fig. 2. Absorption spectra (in dichlorethane) of ion-association complex of Cr(VI) with TV (1), and of TV (2); $C_{Cr(VI)} = 7 \times 10^{-6}M$, $C_{TV} = 7 \times 10^{-6}M$, $C_{HCl} = 0.01M$.

The INT ion-associate has absorption maxima at 230 and 250 nm (Fig. 1). The intensity of the second maximum is considerably the higher so 250 nm is used as the working wavelength. The TV ion-associate has an absorption maximum at 230 nm (Fig. 2).

Maximum extraction of the chromium ion-associates is reached with a shaking time of 30 sec, and the ion-associates are stable for five days.

The composition of the ion-association complexes was determined by the Asmus, molar ratio and equilibrium shift methods,[42] and found to be 1:1. Under the optimal conditions the molar absorptivities, determined by the Komar method[42] were $\epsilon_{250} = (8.8 \pm 0.05) \times 10^4$ $1.mole^{-1}.cm^{-1}$ (for INT) and $\epsilon_{230} = (1.22 \pm 0.03) \times 10^5$ $1.mole^{-1}.cm^{-1}$ (for TV). Beer's law is obeyed over the chromium concentration 0.02–0.3 μg/ml. From these data it is seen that the reaction of chromium with INT and TV is highly sensitive.

To establish the optimal conditions for extraction and complexation we studied the relationship between light-absorption and the concentration of the tetrazolium salts INT and TV (Fig. 3). The optimal concentration of tetrazolium salt for formation and extraction of the associate was found to be $[INT] \geq 2 \times 10^{-5}M$, and $[TV] \geq 1 \times 10^{-5}M$, for 3 μg of chromium.

The acidity of the aqueous phase and the nature of the acid are also important conditions in extraction of these two ion-association complexes, especially the nature of the acid. The influence of hydrochloric, sulphuric, nitric and perchloric acids on the extraction process was studied (Fig. 4). The light-absorption was

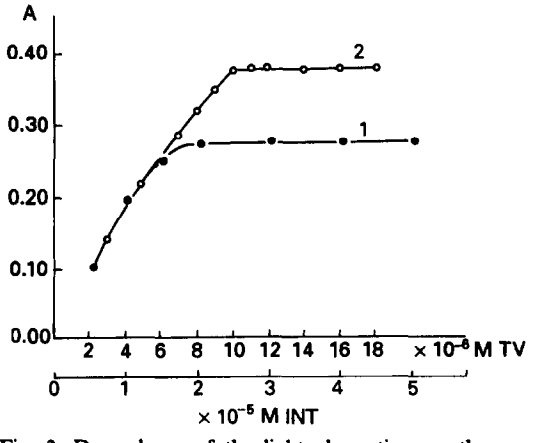

Fig. 3. Dependence of the light absorption on the concentration of (1) INT and (2) TV; (1) $C_{Cr(VI)} = 0.3$ μg/ml, $C_{HCl} = 0.14M$; (2) $C_{Cr(VI)} = 0.3$ μg/ml, $C_{HCl} = 0.11M$.

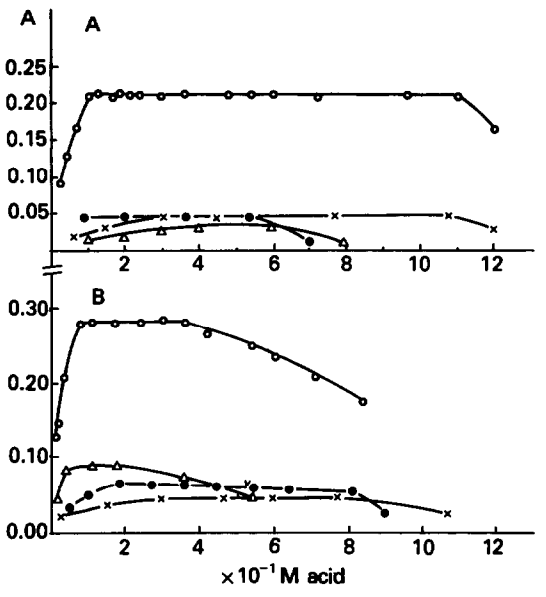

Fig. 4. Investigation of the influence of acidity and acid type on the extraction of Cr(VI) with (A) INT, $C_{INT} = 1 \times 10^{-5}M$, $C_{Cr(VI)} = 7 \times 10^{-6}M$ and (B) TV, C_{TV} lw = $7 \times 10^{-6}M$, $C_{Cr(VI)} = 7 \times 10^{-6}M$. ○—HCl, ●—$HClO_4$, ×—$HNO_3$, △—$H_2SO4$.

greatest when hydrochloric acid was used. CrO_3Cl^- is quantitatively formed in the solution,[37-40,43-45] and the best results were obtained with 0.07–0.36M hydrochloric acid for TV and 0.1–1.1M hydrochloric acid for INT. Use of too high an acidity leads to a decrease of the light absorption because of some reduction of Cr(VI) to Cr(III).

Interferences

Table 1 lists the effects of certain elements and complexing agents on the determination of 2 μg of Cr(VI). Most of the ions studied did not interfere, but Hg(II), Al(III), Ca(II), Na(I) and Br^- interfered in the determination of chromium(VI) with INT, and Hg(II) interfered in the determination of chromium(VI) with TV. As masking reagents, ammonium fluoride, tartaric acid and ascorbic acid were used. The method for determination of chromium with INT was found to be selective in the presence of W(VI) and Mo(VI). The method with TV was found to be selective in the presence of Fe(III) and V(V). We should point out that in the determination of chromium with diphenylcarbazide[23] (the most sensitive and selective method), these four ions interfere.

Table 1. Effect of foreign ions on determination of 2 μg of chromium

Ion	Limiting amount, *mg*		Ion	Limiting amount, *mg*	
	INT	TV		INT	TV
K(I)	8.0	3.0	Na(I)	0.100	0.120
Cd(II)	8.0	10.0	Ca(II)	0.080	0.090
W(VI)	7.0*	0.066	Ag(I)	0.050	0.090
Mo(VI)	3.0*	1.20*	Al(III)	0.005	0.100
Fe(III)	3.0*	40.0*	Hg(II)	0.002	0.002
Cu(II)	1.00	0.80	CO_3^{2-}	1.00	7.0
Mg(II)	1.00	1.20	Cl^-	0.70	5.0
V(V)	1.00*	7.1*	SO_4^{2-}	0.20	3.0
Ni(II)	1.00	0.50	$C_2O_4^{2-}$	0.100	0.50
Co(II)	0.60	0.050	PO_4^{3-}	0.080	0.80
Zn(II)	0.50	5.0	NO_3^-	0.040	0.070
Mn(II)	0.100	7.0	Br^-	0.010	0.90

*In the presence of masking reagents (ascorbic acid and ammonium fluoride).

On the basis of the data obtained we have developed two methods for determination of chromium, and applied them to steels and some selected soils. The comparatively low tolerance ratios for sodium and calcium restrict the soil analysis application to soils of podzolic type.

Analysis of soils

The methods were applied for the determination of chromium in five soil samples: lessive cinnamonic, pseudopodzolic, gray forest, brown, and black.

Sample preparation. Weigh 4 g of the soil into a platinum crucible, then heat it for 3 hr in a muffle furnace at 550°. After cooling, transfer the sample into a platinum basin, add 2 ml of doubly distilled water, 1 ml of concentrated sulphuric acid and 10 ml of concentrated hydrofluoric acid, and heat on a sand-bath until vapours of SO_3 appear. Dissolve the residue in 5 ml of doubly distilled water acidified with hydrochloric acid to pH 3.[46] Raise the pH of the solution to ~10 by addition of concentrated ammonia solution to precipitate the iron and aluminium. Filter off the precipitate with a suitable filter paper and wash it with three 3-ml portions of doubly distilled water. Evaporate the filtrate to ~20 ml, cool, acidify the solution to pH 3 with hydrochloric acid, transfer it into a 25-ml standard flask and dilute to the mark with water. Take a 2.5-ml or other suitable aliquot of this solution and oxidize the chromium(III) to chromium(VI)[23] by adding 5 ml of 1M sulphuric acid and 1.5 ml of 1-mg/ml potassium permanganate solution and boiling for 3 min. Cool, then add 0.1 ml of saturated thiourea solution and 0.5 ml of 100-mg/ml potassium nitrite solution, and dilute to volume in a 25-ml standard flask. Take an aliquot of this solution for analysis. Run a reagent blank.

Table 2. Determination of chromium in soils and steels

Soil*	Cr, 10^{-4} %			RSD† %	
	INT	TV	Atomic absorption	INT	TV
Black	9.35	9.33	9.37	0.5	0.7
Pseudopodzolic	5.82	5.80	5.80	0.5	0.5
Lessive cinnamonic	4.15	4.18	4.17	0.7	0.5
Gray forest	3.72	3.69	3.70	0.7	0.6
Brown	3.51	3.54	3.53	0.7	0.5

Steel	Certified chromium content, %	Chromiun found, %		RSD† %	
		INT	TV	INT	TV
38 × 2CO in 14a	1.84	1.83	1.83	0.5	0.4
CO-C 37	17.6	17.6	17.6	0.6	0.7

*The soils contained 0.018–0.049% sodium and 0.015–0.041% calcium.
†Relative Standard Deviation.

Determination of chromium. Add to the aliquot sample solution 1.2 ml of 1.2*M* hydrochloric acid and 2 ml of $1 \times 10^{-4}M$ INT (or 0.9 ml of 1.2*M* hydrochloric acid and 1 ml of $1 \times 10^{-4}M$ TV) and 2 ml each of saturated solutions of ascorbic acid and ammonium fluoride, and dilute to 10 ml with water. Shake the solution for 1 min with 3 ml of dichlorethane. Filter the extract through a dry filter paper and measure the absorbance at 250 nm (for INT) or 230 nm (for TV). Correct for the absorbance of the blank.

The concentration of Cr(VI) is determined from a calibration graph.

Analysis of steels

Two standard samples were studied: 38 × 2 CO-C 14a contains (%) C 0.364, Si 0.50, Mn 0.305, Cr 1.84, Ni 0.162, W 0.292, V 0.208, Cu 0.128, Al 0.56, S 0.0058, P 0.0074, and CO-C 37 contains (%) C 0.05, Si 0.5, Mn 1.35, Cr 17.6, Ni 12, Cu 0.2, Nb 1.2.

Dissolve a 0.1-g sample in 30 ml of a 1:3 v/v mixture of 1:1 v/v nitric acid and 1:1 v/v hydrochloric acid; add 10 ml of concentrated sulphuric acid and evaporate the solution until vapours of SO_3 appear. Transfer the solution into a 100-ml standard flask and dilute to the mark with distilled water. Take a suitable aliquot and oxidize the Cr(III) to Cr(VI) as described for soil samples. Complete the analysis as described for soils.

Results

The results of the soil and steel analyses are given in Table 2 and the accuracy of the methods was checked by atomic-absorption spectrometry. There was good agreement between the results obtained by the three methods.

REFERENCES

1. M. Udy, in *Chromium*, Vol. 1, p. 113. Reinhold, New York, 1956.
2. F. A. Cotton and G. Wilkinson, *Inorganic Chemistry*, 2nd Ed., Interscience, New York, 1966.
3. D. D. Perrin, *Organic and Analytical Reagents*, Mir, Moscow, 1967.
4. V. M. Rao and M. N. Sastri, *Talanta*, 1980, **27**, 771.
5. G. H. Morrison and H. Freiser, *Anal. Chem.*, 1964, **36**, 93R.
6. R. Bock and C. Hummel, *Z. Anal. Chem.*, 1963, **198**, 176.
7. R. Bock and J. Jainz, *ibid.*, 1963, **198**, 315.
8. M. Ziegler and K.-D. Pohl, *ibid.*, 1964, **204**, 413.
9. E. I. Savichev, E. I. Iskhakova and L. F. Flyazhnikova, *Zavodsk. Lab.* 1962, **28**, 412.
10. V. P. Zhivopistsev, A. A. Minin, L. L. Milyutina, E. A. Selezneva and V. Kh. Aitova, *Tr. Komis. po Analit. Khim.*, 1963, **14**, 133.
11. W. J. Maeck, M. E. Kussy and J. E. Rein, *Anal. Chem.*, 1962, **34**, 1602.
12. G. Winkhaus and H. Uhrig, *Z. Anal. Chem.*, 1964, **200**, 14.
13. J. Hála, O. Navrátil and V. Nechuta, *J. Inorg. Nucl. Chem.*, 1966, **28**, 553.
14. G. K. Schweizer and S. W. McCarty, *ibid.*, 1965, **27**, 191.
15. M. Kamburova, *Talanta*, 1992, **39**, MS EH91164 (in the press).
16. Y. Wakamatsu, *Bunseki Kagaku*, 1983, **32**, E143.
17. H. S. Gowda and J. B. Raj, *J. Indian Chem. Soc.*, 1982, **59**, 1398.
18. B. Subrahmanyam and M. C. Eshwar, *Mikrochim. Acta*, 1976, **II**, 579.
19. W. B. Ferng and G. A. Parker, *Z. Anal. Chem.*, 1980, **304**, 382.
20. I. Mori, Y. Fujita and T. Enoki, *Bunseki Kagaku*, 1979, **28**, 707.
21. W.-B. Qi and L.-Z. Zhu, *Talanta*, 1986, **33**, 694.
22. P. N. Rao and K. A. Reddy, *J. Indian Chem. Soc.*, 1980, **57**, 402.
23. E. B. Sandell, *Colorimetric Determination of Traces of Metals*, 3rd Ed., Interscience, New York, 1959.
24. A. Aleksandrov and M. Kamburova, *Mikrochim. Acta*, 1976, **II**, 357.
25. *Idem*, *ibid.*, 1976, **II**, 61.

26. A. Dimitrova, A. Aleksandrov and A. Dimitrov, *Natura (Plovdiv)*, 1972, **5**, No. 1, 57.
27. A. Aleksandrov and S. Kostova, *Z. Anal. Chem.*, 1981, **306**, 125.
28. *Idem.*, 1984, **83**, 247.
29. A. Aleksandrov and M. Hagieva, *Nauch, Tr. Khim., Plovdiv Univ.*, 1979, **17**, 11.
30. A. Aleksandrov and A. Dimitrov, *Mikrochim. Acta*, 1972, 680.
31. T. Pukas, *Chem. Anal. (Warsaw)*, 1960, **5**, 513.
32. A. Dimitrov, A. Aleksandrov, A. Hrdlicka and M. Vrchlabský, *Scripta Fac. Sci. Nat. Univ. Purk. Brun.*, 1983, **13**, Nos 3–4, 117.
33. A. Aleksandrov and B. Milusheva, *Natura (Plovdiv)*, 1974, **7**, No. 1, 69.
34. A. Aleksandrov and G. Simeonova, *Nauchn. Tr. Plovdiv. Univ.*, 1978, **16**, No. 3, 39.
35. M. Kamburova, unpublished work.
36. *Idem, Zh. Analit. Khim.*, 1990, **45**, 678.
37. A. K. Lavrukhina and L. V. Yukina, *Analytical Chemistry of Chromium*, Izd. Nauka, Moscow, 1970.
38. D. G. Tuck and R. M. Walters, *J. Chem. Soc.*, 1963, IIII.
39. V. M. Rao and M. N. Sastri, *Talanta*, 1980, **27**, 771.
40. C. Deptuła, *Rocz. Chem.*, 1968, **42**, 725.
41. A. A. Minin and L. L. Khlyupina, *Uch. Zap. Perm. un-ta*, 1974, No. 324, 194.
42. M. I. Bulatov and I. P. Kalinkin, *A Practical Manual of Photocolorimetric and Spectrophotometric Methods of Analysis*, 3rd Ed., Khimiya, Leningrad, 1972.
43. H. Specker, *Z. Anal. Chem.*, 1963, **197**, 109.
44. L. S. Khintibidze and G. D. Supatashvili, *Izv. Akad. Nauk Gruz. SSR, Ser. Khim.*, 1982, **8**, 96.
45. R. Shanker and K. S. Venkateswarlu, *J. Inorg. Nucl. Chem.*, 1970, **32**, 2369.
46. I. G. Vazhenin, *Methods for Determination of Trace Elements in Soils, Plants and Waters*, Kolos, Moscow, 1974.

Talanta, Vol. 40, No. 5, pp. 713–717, 1993
Printed in Great Britain.

0039-9140/93 $6.00 + 0.00

SPECTROPHOTOMETRIC DETERMINATION OF CHROMIUM (VI) WITH METHYLENE BLUE

M. KAMBUROVA

Department of Chemistry, Higher Institute of Agriculture, 4000 Plovdiv, Bulgaria

(*Received* 24 *October* 1991. *Revised* 9 *March* 1992. *Accepted* 17 *April* 1992)

Summary—The interaction of Cr(VI) and the thiazine dye Methylene Blue has been examined. The ion-associate formed is extractable into 1,2-dichlorethane. The optimum conditions have been established, and values obtained for the conditional extraction constant K'_{ex}, distribution constant K'_D and association constant β'. A sensitive and selective method for determination of microquantities of Cr(VI) in soils and alloys is suggested.

The determination of microquantities of chromium in soils and other naturally occurring materials is of particular importance in connection with the growing interest in environmental problems. It is known that an increase in the content of this element in soils makes them infertile, and that the toxic effect depends, to some extent, on the chromium oxidation state.[1] On the other hand, it has also been established that the introduction of chromium salts into soils has some positive effects, such as an increase in sugar content and yields, favourable changes in chemical composition, and activation of some biochemical processes.[2–5] Obviously, the concentration and oxidation state of chromium, like those of other microelements, are of great significance for its physiological action.

The reagents suggested for determination of chromium include: diantipyrylmethane,[6] diphenylcarbazide,[7] diantipyrylstyrylmethane,[8] Chromethylpyrazole and Chrompyrazole I,[9] triphenyltetrazolium chloride,[10] *N*-*m*-tolyl-*p*-methoxybenzohydroxamic acid,[11] antipyrine basic dyes,[12] Chrome Azurol S,[13,14] α-methyl-2,4-dihydroxybenzylidene-2-aminoaniline,[15] bis-(2,4-diaminophenyl)phosphonate,[16] (1-naphthylmethyl)triphenylphosphonium,[17] 2, 2′-bipyridyl[18] and 3-hydroxyflavone.[19] The most sensitive and selective of these is diphenylcarbazide, but V(V), Mo(VI), Fe(III) and Hg(II) interfere with the Cr(VI) determination.

The goal of the present work was to use the thiazine dyestuff Methylene Blue (MB) for determination of microquantities of chromium by an extraction photometric method.

EXPERIMENTAL

Reagents

Methylene Blue (MB), 1×10^{-4} and $1 \times 10^{-5}M$ solutions; potassium chromate, 1×10^{-4} and $1 \times 10^{-5}M$ solutions; hydrochloric acid, $1{,}2M$; perchloric acid, $9M$; 1,2-dichlorethane. Analytical-reagent grade or equivalent chemicals were used.

Apparatus

Zeiss VSU 2-P and Specord UV-VIS spectrophotometers were used, with 1-cm path-length cuvettes.

Procedures

Calibration. In a 100-ml separatory funnel place 1.5 ml of $1.2M$ hydrochloric acid, 1 ml of $1 \times 10^{-4}M$ Methylene Blue, and a known volume of chromium(VI) solution containing up to ~5 μg of chromium. Dilute to 10 ml with distilled water and shake with 3 ml of dichlorethane for 1 min. Transfer the organic layer through a dry filter paper into a 1-cm cuvette and measure the absorbance at 295 nm against a reagent blank similarly prepared.

Determination of chromium in soils. Weigh a 4-g sample into a platinum crucible and heat it at 500–550° for 3 hr. Cool the crucible, add 2 ml of doubly distilled water, 1 ml of concentrated sulphuric acid and 10 ml of concentrated hydrofluoric acid, and evaporate until fuming has ceased. Cool, and dissolve the residue in 5 ml of doubly distilled water acidified to pH 3 with hydrochloric acid.[20] Add concentrated ammonia solution to precipitate iron and aluminium at

pH 10, filter off the precipitate, and wash it with three 3-ml portions of doubly distilled water, then evaporate the filtrate and washings to about 20 ml. Cool the solution, acidify it to about pH 3 with hydrochloric acid, and make up to the mark in a 25-ml standard flask. Take a 2.5-ml or other suitable aliquot of this solution and oxidize the chromium(III) to chromium(VI)[21] by adding 5 ml of 1*M* sulphuric acid and 1.5 ml of 1-mg/ml potassium permanganate solution and boiling the mixture for 3 min. Cool, then add 0.1 ml of saturated thiourea solution and 0.5 ml of 100 mg/ml potassium nitrite solution, and dilute to volume in a 25-ml standard flask. To a suitable aliquot of this solution add 1.5 ml of 1.2*M* hydrochloric acid, 1 ml of $1 \times 10^{-4}M$ Methylene Blue and 2 ml each of saturated solutions of ascorbic acid, tartaric acid and ammonium fluoride (to mask any interfering ions). Dilute to 10–12 ml with water and shake for 1 min with 3 ml of 1,2-dichlorethane. Filter the organic phase through a dry paper into a 1-cm cuvette and measure the absorbance at 295 nm against a reagent blank run by the same procedure. Prepare a calibration graph with chromium(VI) standards similarly treated.

Determination of chromium in steels. Dissolve a 0.1-g sample of the steel in 30 ml of a 1:3 v/v mixture of 1:1 v/v nitric acid and 1:1 v/v hydrochloric acid. Cool, add 10 ml of concentrated sulphuric acid and evaporate until SO_3 fumes appear. Cool, take up the salts in water, and dilute to volume in a 100-ml standard flask. Oxidize a suitable aliquot as described above for soil samples. To a suitable aliquot of the resultant solution add 1.5 ml of 1.2*M* hydrochloric acid, 2 ml of $1 \times 10^{-4}M$ Methylene Blue and dilute to ~10 ml with saturated ammonium fluoride solution (to mask any interfering ions). Extract the ion-associate and complete the determination as for soil analysis.

RESULTS AND DISCUSSION

The solubility of the ion-associate in various organic solvents was investigated. The most effective for extraction of the compound was found to be 1,2-dichlorethane. The absorption spectra of the ion-associate and the dye in 1,2-dichlorethane and chloroform are given in Fig. 1. The absorption spectrum of the associate in dichlorethane has maxima at 230 and 295 nm. At 230 nm the dye also absorbs strongly, so 295 nm was selected as the working wavelength. The absorption spectrum of the associate in chloroform has only one maximum, at 245 nm.

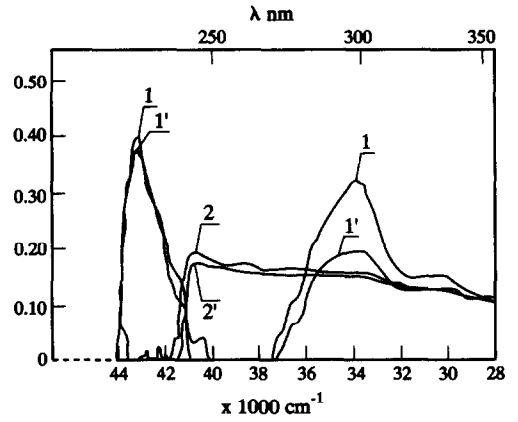

Fig. 1. Absorption spectra of $MB^+ \cdot CrO_3Cl^-$ in (1) $C_2H_4Cl_2$ and (2) $CHCl_3$, and of MB in (1′) $C_2H_4Cl_2$ and (2′) $CHCl_3$; $C_{Cr(VI)} = 4 \times 10^{-6}M$, $C_{HCl} = 0.18M$, $C_{MB} = 4 \times 10^{-6}M$.

The ion-associate formed from the cation of the dye (MB^+) and Cr(VI) in hydrochloric acid medium may be ascribed the formula $MB^+ \cdot CrO_3Cl^-$, in agreement with earlier reports.[22–25]

The Job,[26] Bent and French,[27] and Asmus[28] methods all showed that the extracted species was a 1:1 ion-associate of the dye cation and the chlorochromate anion. Equilibrium between the two phases, aqueous and organic, was reached in 30 sec. The ion-associate is stable for over 36 hr. Its molar absorptivity was determined by the method of Komar[29] and Klotz and Ming[30] and found to be $(8.33 \pm 0.04) \times 10^4$ l · mole^{-1} · cm^{-1} at 295 nm.

To find the optimum conditions for extraction of the ion-associate, the influence of pH and the concentrations of Methylene Blue and chromium(VI) was studied.

The acidity of the aqueous phase is a major factor in the determination. The influence of hydrochloric, sulphuric, nitric and perchloric acids on the extraction equilibrium was investigated. Only in the presence of hydrochloric or perchloric acid was the ion-associate extracted. Figure 2 indicates that not only the concentration but also the nature of the acid has an effect on the extraction equilibrium. Maximum absorbance is achieved in hydrochloric acid medium, in the acid range 0.18–0.6*M*. A higher concentration of the acid causes some reduction of Cr(VI) to Cr(III) and a decrease in light-absorption by the organic phase.

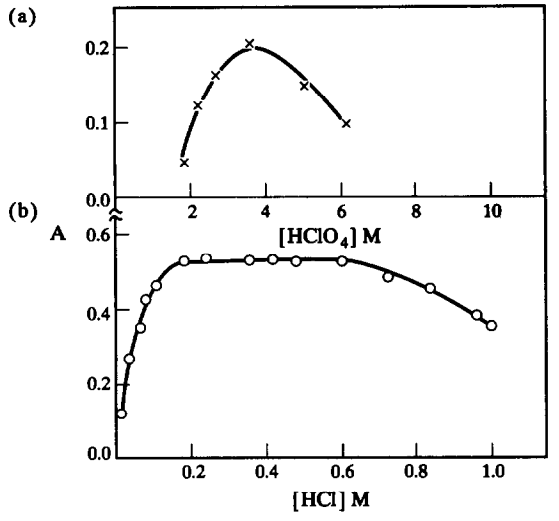

Fig. 2. Investigation of the influence of acidity on the extraction of Cr(VI) with Methylene Blue: $C_{Cr(VI)} = 5 \times 10^{-6}M$, $C_{MB} = 1 \times 10^{-5}M$; (A) $HClO_4$, (B) HCl.

Table 1. Effect of diverse ions on determination of 2 μg of chromium

Foreign ion	Limiting amount, *mg*
Ni(II)	55
K(I)	40
V(V)	32.5*
Sr(II)	30
W(VI)	30*
Fe(III)	3.5*
Mo(VI)	3*
Cu(II)	2
Cd(II)	1
Mn(II)	1
Zn(II)	1
Al(III)	1*
Pb(II)	0.5
Co(II)	0.2
Na(I)	0.2
Ca(II)	0.08
Hg(II)	interferes at any level

*In the presence of ascorbic acid, ammonium fluoride and tartaric acid as masking agents.

Optimization of the concentration of Methylene Blue is essential in the determination of chromium; for 0.2 μg/ml Cr(VI) the absorbance of the extract is maximum with MB concentration $\geq 1 \times 10^{-5}M$ and for 0.5 μg/ml Cr(VI),[MB] $\geq 2.5 \times 10^{-5}M$ is necessary (Fig. 3).

Beer's law is obeyed over the Cr(VI) concentration range from 0.01 to 0.54 μg/ml in the 10 ml of aqueous phase.

Interferences

The data in Table 1 show that mercury(II) must be absent from the test solution, and that calcium and sodium must be present in only small amounts, which places a restriction on the types of sample that may be analysed for chromium by the proposed method. Several potentially interfering ions can easily be masked with suitable reagents. The method offers better selectivity than the diphenylcarbazide method with respect to vanadium(V), molybdenum(VI) and iron(III).

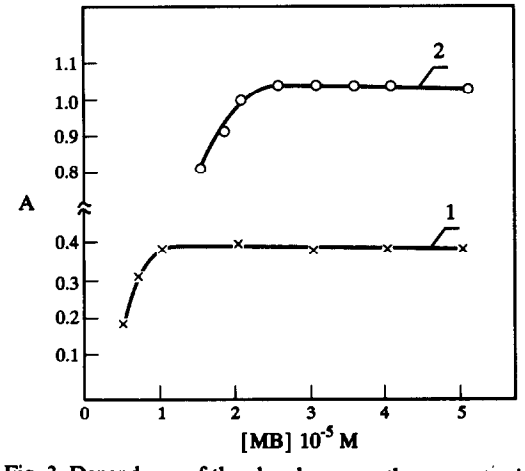

Fig. 3. Dependence of the absorbance on the concentration of Methylene Blue: (1) $C_{Cr(VI)} = 0.2$ μg/ml; (2) $C_{Cr(VI)} = 0.5$ μg/ml; $C_{HCl} = 0.18M$.

Extraction equilibria

The following equilibria should be taken into account for the system of chromium(VI), Methylene Blue, hydrochloric acid, water and 1,2-dichlorethane.

1. Formation of the ion-association complex in the aqueous phase, and the corresponding equilibrium constant:

$$\beta = \frac{[MB^+ \cdot CrO_3Cl^-]}{[MB^+][CrO_3Cl^-]}. \qquad (1)$$

2. Distribution of the complex between the aqueous and organic phases, and the corresponding distribution constant:

$$K_D = \frac{[MB^+ \cdot CrO_3Cl^-]_{org}}{[MB^+ \cdot CrO_3Cl^-]}. \qquad (2)$$

3. The entire extraction process and the corresponding extraction constant:

$$K_{ex} = \frac{[MB^+ \cdot CrO_3Cl^-]_{org}}{[MB^+][CrO_3Cl^-]} = K_D\beta. \qquad (3)$$

The system is much more complicated than this, however, since the formation constant for

CrO_3Cl^- and the distribution constant for $MB^+ \cdot Cl^-$ between the organic and aqueous phases also need to be taken into account, and in consequence the constants listed above are apparent (or conditional) constants.

A conditional constant was obtained for the distribution coefficient of the ion-associate by taking 5 ml of $1 \times 10^{-4}M$ Methylene Blue, 1.5 ml of $1.2M$ hydrochloric acid and various amounts of chromium(VI), diluting to 15 ml with water and shaking the mixture for 1 min with 3 ml of 1,2-dichlorethane in a separatory funnel, then diluting the extract to volume in a 25-ml standard flask with 1,2-dichlorethane. The absorbance (A) was measured, against a reagent blank prepared in the same way (without chromium present), in 1-cm cuvettes at 295 nm. For each solution containing chromium an exact duplicate was prepared, and this was extracted with three 3-ml portions of dichlorethane, the extracts being combined and diluted to volume in a 25-ml standard flask; the absorbance (A_{max}) was then measured against the reagent blank already prepared. As a constant amount of Methylene Blue is used, the change in absorbance is due to the ion-associate. The value of the conditional distribution coefficient $D'_{MB/Cr}$ is then given by

$$D'_{MB/Cr} = A/(A_{max} - A).$$

The results were evaluated by plotting log $D'_{MB/Cr}$ against log $C_{Cr(VI)}$ (Fig. 4). According to the model used by Aleksandrov *et al.*,[31] the intercept of the horizontal part of the curve on the ordinate gives log K'_D and the intercept of the extrapolated slope of the curve gives log K'_{ex}

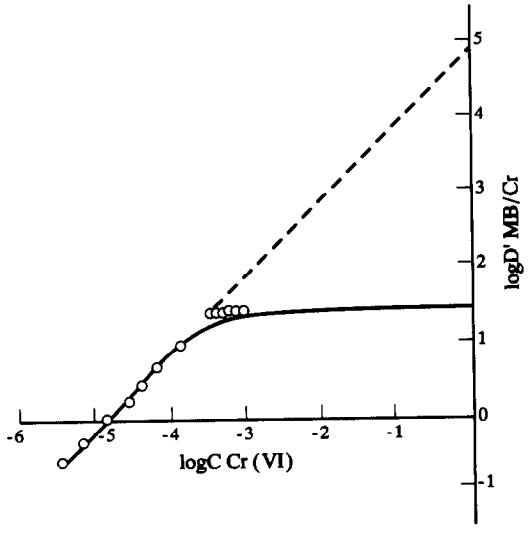

Fig. 4. Determination of $D'_{MB/Cr}$, K'_D and K'_{ex}.

Table 2. Determination of chromium in selected soils and steels

Soil*	Cr, 10^{-4}% Methylene Blue method	Atomic absorption	RSD*, %
Leached chernozem	2.40	2.38	0.6
Podzolized black	2.50	2.54	0.5
Brown	3.53	3.54	0.5
Gray forest	3.70	3.67	0.6

Steel	Certified chromium present, %	Chromium found, %	RSD, %
38 × 2 CO-C 14a	1.84	1.85	0.4
CO-C 37	17.6	17.6	0.5

*The soils contained 0.024–0.036% sodium and 0.019–0.030% calcium.
†Relative Standard deviation (based on 3 determinations).

(where primes indicate conditional constants). From equation (3) the value of β' can then be obtained. The theoretical curve can be calculated[31] from

$$D'_{MB/Cr} = K'_D\beta'[Cr]/(1 + \beta'[Cr]) \quad (4)$$

and is also shown in Fig. 4. The slope of 45° confirms that a 1:1 ion-associate is formed. The conditional constants obtained were

$$K'_{ex} = (7.94 \pm 0.22) \times 10^4;$$

$$K'_D = 26.99 \pm 0.08;$$

$$\beta' = (2.94 \pm 0.09) \times 10^3.$$

Applications

Soil analysis. As is evident from Table 1, the method is applicable only to soils with sufficiently low calcium and sodium contents, *e.g.* soils of bodzol type. As a test of its validity the method was applied to some selected soils, and the chromium was also determined by atomic-absorption spectrometry. The results are shown in Table 2.

Steel analysis. An advantage of the method for steel analysis is that it is applicable to steels containing large amounts of vanadium or molybdenum relative to chromium, in contrast to the diphenylcarbazide method, where these elements interfere. Typical results are given in Table 2.

REFERENCES

1. *Nouveau traité de chimie minérale*, Vol. XIV, 1959.
2. H. Bukreeva, *Nauch. Tr. Sverdl. Gos. Ped. In-ta*, 1972, **31**, 161.
3. O. K. Dobrolyubskii and G. M. Viktorova, *Agrokhimiya*, 1974, No. 10, 135.

4. M. Andrzejewski, *Rocz. Nauk. Roln., Ser. A*, 1971, **97**, No.2, 75.
5. D. Bertrand and A. de Wolf, *C. R. Acad. Sci. Paris*, 1965, **261**, 5616.
6. A. A. Minin and L. L. Khlyupina, *Uch. Zap. Permsk. Univ.*, 1974, No. 324, 194.
7. P. G. Jeffery, *Chemical Methods of Rock Analysis*, 1st Ed., Pergamon Press, Oxford, 1970.
8. A. N. Tananaeva and V. N. Podchainova, *Primen. Org. Reagentov. Anal. Khim.*, 1974, 43; *Chem. Abstr.*, 1977, **86**, 830984.
9. L. S. Khintibidze and G. D. Supatashvili, *Izv. Akad. Nauk. Gruz. SSR. Ser. Khim.*, 1982, **8**, 96.
10. M. Kamburova, *Zh. Analit. Khim.*, 1990, **45**, 678.
11. S. B. Gholse, B. K. Deshmukh and P. J. Anokar, *J. Indian Chem. Soc.*, 1984, **61**, 465.
12. L. S. Khintibidze, G. D. Supatashvili and M. E. Mdinaradze, *Reagenty v Analit. Khimii, Perm*, 1983, No.5, 123.
13. H. Nishida and T. Nishida, *Bunseki Kagaku*, 1984, **33**, 333.
14. G. Fang and J. Luo, *Fenxi Huaxue*, 1985, **13**, 769.
15. S. Srinivasan and V. Seshagiri, *J. Indian Inst. Sci.*, 1981, **63**, 153.
16. H. Mori, Y. Fujimura and Y. Takegami, *Bunseki Kagaku*, 1981, **30**, 652.
17. D. T. Burns and S. Kheawpintong, *Anal. Chim. Acta*, 1985, **177**, 253.
18. P. Uma, P. K. Rao and M. N. Sastri, *Indian J. Chem.*, 1985, **24A**, 539.
19. A. Cabrera Martin and S. Rubio Barroso, *Quim. Anal. (Barcelona)*, 1986, **5**, 443.
20. I. G. Vazhenin, *Methods for Determination of Microelements in Soils, Plants and Waters*, Kolos, Moscow, 1974.
21. E. B. Sandell, *Colorimetric Methods for Determination of Traces of Metals*, 3rd Ed., Interscience, New York, 1959.
22. A. K. Lavrukhina and L. V. Yukina, *Analytical Chemistry of Chromium*, Izd. Nauka, Moscow, 1970.
23. D. G. Tuck and R. M. Walters, *J. Chem. Soc.*, 1963, 1111.
24. C. Deptula, *Rocz. Chem.*, 1968, **42**, 725.
25. V. M. Rao and M. N. Sastri, *Talanta*, 1980, **27**, 771.
26. P. Job, *Ann. Chim. Phys. (Paris)*, 1928, **9**, 113.
27. H. E. Bent and C. L. French, *J. Am. Chem. Soc.*, 1941, **63**, 1568.
28. E. Asmus, *Z Anal. Chem.*, 1960, **178**, 104.
29. N. P. Komar, *Dokl. Akad. Nauk SSSR*, 1950, **72**, 535.
30. I. M. Klotz and W. C. L. Ming, *J. Am. Chem. Soc.*, 1953, **75**, 4159.
31. A. Aleksandrov, O. Budevski and A. Dimitrov, *J. Radioanal. Chem.*, 1976, **29**, 243.

Talanta, Vol. 40, No. 5, pp. 719–723, 1993
Printed in Great Britain.

0039-9140/93 $6.00 + 0.00

SPECTROPHOTOMETRIC DETERMINATION OF MERCURY IN SOILS WITH TRIPHENYLTETRAZOLIUM CHLORIDE

M. KAMBUROVA
Department of Chemistry, Higher Institute of Agriculture, 4000 Plovdiv, Bulgaria

(*Received* 18 *June* 1991. *Revised* 19 *September* 1991. *Accepted* 7 *October* 1991)

Summary—The formation of the acidocomplex of mercury(II) with triphenyl-tetrazolium chloride is studied spectrophotometrically in water–organic media. The composition of the complex is established as TTC:Hg:I = 1:1:1. The molar absorptivity $\epsilon_{255} = (6.45 \pm 0.12) \times 10^4$ l mole$^{-1} \cdot$ cm^{-1} is determined. The selectivity of the reaction is studied and the method for determination of mercury(II) 0.1–0.8 μg/ml is shown. Extraction investigations of the system discussed were carried out. The characteristic values for the extraction equilibrium and the equilibrium in the aqueous phase was determined: extraction constant $K_{ex} = 3.16 \times 10^4$, distribution constant $K_D = 20.67$, and association constant = 1.53×10^3. A rapid and sensitive extractive–photometric method for determination of mercury(II) in soil was developed. The determination was carried out without preliminary elimination of mercury.

Getting into soil, mercury has a negative effect upon the development of crop plants. This necessitates some more detailed studies of this chemical element in soils. Various methods for determination of mercury have been published.[1] They require expensive equipment and highly qualified analysts.[2,3] Atomic absorption spectrophotometry[4–11] and analyses with some other reagents are used.[12–29]

No data about determination of mercury with tetrazolium salts can be found in the literature. The tetrazolium salt (triphenyltetrazolium chloride) we suggest is a new reagent for determination of microquantities of mercury(II). It is known that mercury has an extremely high affinity towards iodide ion. Hg(II) forms stable acidocomplexes with I^-. This can be used in developing an extraction–photometric method for determination of mercury. The nature of the interaction between the acidocomplex of Hg(II) with the cation of the tetrazolium salt should be studied. The present paper represents the conditions needed for determination of mercury with triphenyltetrazolium chloride (TTC). This is an extremely simple and direct extraction for determination of microquantities of mercury.

The goal is to develop an extraction–photometric method using TTC for determination of mercury, superior, in some respects, to the existing methods. For example, no preliminary isolation or concentration of mercury is required as in some of the other methods.[19,20,29] To be superior in sensitivity to methods reported in the literature[16,17,24,27,28] the organic extract needs to be stable for a long time, and not only for a few hours as it is in the method of Mudakavi and Ramaswamy.[25]

EXPERIMENTAL

Apparatus

Spectrophotometer VSU 2-P, Carl Zeiss Jena, DDR, $\lambda = 255$ nm, 1 cm light path cuvette; Specord UV–VIS, DDR.

Reagents

2,3,5-Triphenyltetrazolium chloride (TTC) ($5 \times 10^{-4}M$, Merck), mercury acetate, p.a.—2 μg/ml Hg(II), $1 \times 10^{-5}M$ Hg(II); Sulphuric acid, p.a.—$2M$; Potassium iodide, p.a.—$1 \times 10^{-3}M$, Chloroform, merk.

Procedure

Sulphuric acid 1 ml $2M$, KI 1 ml $1 \times 10^{-3}M$ and TTC 0.5 ml $5 \times 10^{-4}M$ are added to an aliquot of the sample solution containing 1–8 μg of mercury in a separating funnel. It is diluted to aqueous phase volume of 10 ml with distilled water and extracted with 3 ml of chloroform for 30 sec. The organic layer is then transferred through filter paper into a 1-cm cuvette and recorded on a photometer VSU 2-P spectrophotometer at 255 nm. A blank, containing the same solutions without mercury, is prepared.

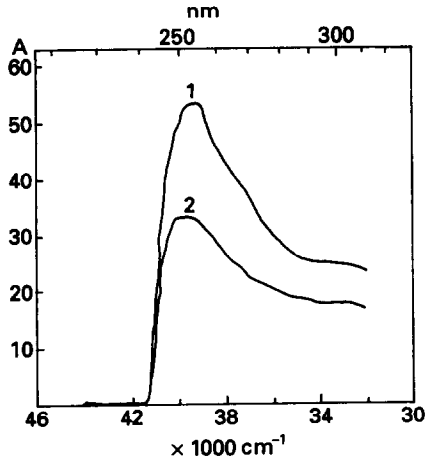

Fig. 1. Absorption spectra in chloroform of ion-association complex (1) and triphenyltetrazolium chloride (2); $C_{Hg(II)} = 0.2$ μg/ml, $C_{H_2SO_4} = 0.2M$, $C_{KI} = 5 \times 10^{-5}M$, $C_{TTC} = 5 \times 10^{-5}M$.

RESULTS AND DISCUSSION

The light absorption of the solutions of mercury acidocomplexes with TTC reaches its maximum immediately after mixing and does not change for 2 days. To clear out the possibility of extracting the ion associate a number of different types of solvents were tested: hydrocarbons (benzene and toluol), ketones, ethers, alcohols, chloroform, dichlorethane and tetrachlorethane. The studies showed that the associate is best dissolved in chloroform. The absorption spectra of equimolar solutions of tetrazolium salt and ion-association complex in sulphuric acid show that the absorption maxima are around 255 nm (Fig. 1). The absorption additivity, without a significant shift in the absorption maximum, is an indication of a formation of an ion-association complex.

The stoichiometric coefficients of the associate formation were established by various methods.[30] The ratio $Hg:I^-$ in the complex was established by the isomolar series and molar ratio methods. The ratio $TTC:[HgI_3]^-$ was proved by the methods of Bent–French, molar ratios, isomolar series and the method of Assmuss. The pH remained constant and optimal ($0.2M$ sulphuric acid) in all the assays. The results for the light absorption of the extracts at 255 nm showed that the associate was formed at a ratio $TTC:Hg:I = 1:1:3$.

The ion-associate of Hg(II) was completely extracted in a single extraction of only 5 sec. The molar absorptivity of the associate, calculated by the method of Komar–Tolmatchov,[30] was $\epsilon_{255} = (6.45 \pm 0.12) \cdot 10^4$ l mole^{-1} · cm^{-1}. This indicates the high sensitivity of the given reaction. The detection limit is 0.1 μg/ml Hg(II). Under optimum reaction conditions ($C_{TTC} = 2.5 \cdot 10^{-5}M$, $C_{H_2SO_4} = 0.2M$), the Beer's law was obeyed in the concentration range of 0.1–0.8 μg/ml Hg(II).

The effect of the acidity of the solution on the extraction of the ion associate of mercury is given in Fig. 2. The optimum acidity of the extraction was over a rather wide range: pH 1–9 and 0.1–4.5M H_2SO_4. At pH > 9, a hydrolysis occurs and the light absorption of the ion associate decreases. The effect of various acids (H_2SO_4, HCl and HNO_3) on the extraction equilibrium was studied. The light absorption of the extracts showed constant and maximum values when using H_2SO_4 (0.1–4.5M) or HCl (0.1×10^{-1}–$3.8 \times 10^{-1}M$).

A large excess of potassium iodide is needed for formation and extraction of the mercury complex with I^-. The chloroform extracts

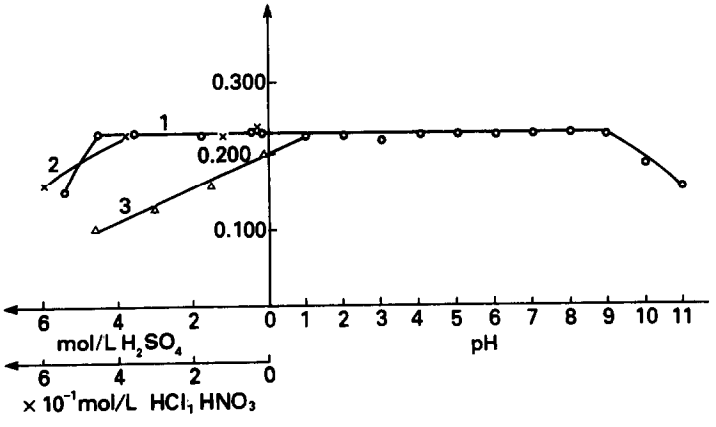

Fig. 2. The influence of acidity on the extraction of Hg(II) using TTC: 1—H_2SO_4, 2—HCl, 3—HNO_3; $C_{Hg(II)} = 2 \times 10^{-6}M$, $C_{TTC} = 2.5 \times 10^{-5}M$, $C_{KI} = 5 \times 10^{-5}M$.

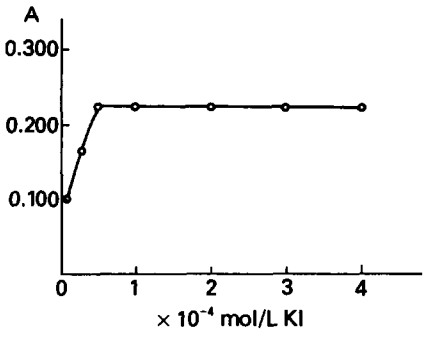

Fig. 3. Dependence of the absorbance change on the concentration of KI; $C_{Hg(II)} = 2 \times 10^{-6}M$, $C_{H_2SO_4} = 0.2M$, $C_{TTC} = 2.5 \times 10^{-5}M$.

have maximum value at a concentration of KI $> 0.5 \times 10^{-4}M$ (Fig. 3).

The extraction also depends strongly on the reagent TTC. A complete extraction of mercury(II) was achieved at a 10-fold excess of TTC (Fig. 4).

The effect of some ions upon the extraction–photometric determination of mercury(II) under optimum conditions was studied. The ratios of the accompanying ions at which the deviations in the results reached $S_r = 0.02$ ($n = 3$) are given in Table 1. The results obtained show the possibility of extractive–photometric determination of Hg(II) in the presence of numerous ions without separating Hg(II) from the accompanying ions. When an extraction with chloroform is used, Hg(II) could be determined in the presence of various amounts of the ions mentioned because the complexes they form cannot be extracted in chloroform. Ascorbic acid and NaF were used to eliminate the interference of Fe(III), Mo(VI) and W(VI). The determination is only interfered with by S_2O_3.

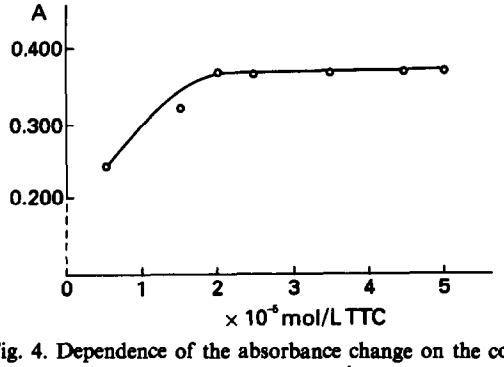

Fig. 4. Dependence of the absorbance change on the concentration of TTC; $C_{Hg(II)} = 4 \times 10^{-6}M$, $C_{H_2SO_4} = 0.2M$, $C_{KI} = 1 \times 10^{-4}M$.

A study of the extraction equilibrium

The values characterizing the extraction equilibrium K_{ex}, K_D, β were determined by a chemical model.[31]

We consider the equilibrium in the extraction system of triphenyltetrazolium chloride–mercury iodide–chloroform.

1. The formation of the ion associate in aqueous phase is characterized by the corresponding equilibrium constant

$$\beta = \frac{TTC[HgI_3]}{[TTC^+] \cdot [HgI_3^-]}. \quad (1)$$

2. Distribution of the ion associate between the aqueous and the organic phases and the corresponding distribution constant

$$K_D = \frac{\{TTC[HgI_3]\}_0}{TTC[HgI_3]}. \quad (2)$$

3. The entire process of the extraction in the system considered is described by the corresponding equilibrium constant which is regarded as the extraction constant

$$K_{ex} = \frac{\{TTC[HgI_3]\}_0}{[TTC^+] \cdot [HgI_3^-]} = K_D \cdot \beta. \quad (3)$$

Table 1. Effect of foreign ions $C_{Hg(II)} = 0.33$ μg/ml, $C_{KI} = 8.33 \times 10^{-5}M$, $C_{H_2SO_4} = 0.16M$, $C_{TTC} = 4.10 \times 10^{-6}M$

N	Foreign ion	*Limiting ratio* C_X/C_{Hg}, *mg*	*Limiting conc. of* foreign ion, *mg*
1	Ni(II)	50000:1	200
2	K(I)	50000:1	200
3	Ca(II)	20000:1	80
4	Fe(III)	17500:1	70*
5	Na(I)	12500:1	50
6	Cd(II)	7500:1	30
7	Pb(II)	5000:1	20
8	Mg(II)	5000:1	20
9	Sr(II)	5000:1	20
10	Zn(II)	3750:1	15
11	Co(II)	2500:1	10
12	Cu(II)	2500:1	10
13	Mn(II)	2500:1	10
14	Al(III)	1500:1	6
15	Mo(VI)	60:1	0.24*
16	Bi(II)	25:1	0.1
17	W(VI)	25:1	0.1*
18	Ag(I)	2.5:1	0.01
19	Cr(VI)	2.5:1	0.01
20	BO_2^-	18750:1	75
21	SO_4^{2-}	18750:1	75
22	PO_4^{3-}	18750:1	75
23	EDTA	5000:1	20
24	Br^-	2500:1	10
25	$C_2O_4^{2-}$	2500:1	10
26	Cl^-	2500:1	10
27	NO_3^-	500:1	2
28	CO_3^{2-}	500:1	2
29	SCN^-	125:1	0.5
30	$S_2O_3^{2-}$	interfere	

*In the presence of maskings reagents.

The distribution coefficient determined at a constant concentration of TTC and variable concentration of Hg(II) in the system studied gives the form:

$$D_{TTC} = \frac{\Sigma(TTC)_0}{\Sigma(TTC)} = \frac{\{TTC[HgI_3]\}_0}{[TTC^+] + TTC[HgI_3]}. \quad (4)$$

The following solutions are introduced into 100-ml separating funnels: 1 ml of $5 \times 10^{-4}M$ TTC, 1 ml of $2M$ H_2SO_4, 5 ml of $1 \times 10^{-3}M$ KI and the corresponding amounts of Hg(II). The volume of the aqueous phase is brought to 10 ml with distilled water. It is extracted with 3 ml of $CHCl_3$ for 30 sec. After the stratification of the two phases the organic phase is transferred through filter paper into a standard flask of 25 ml and is diluted up to the mark with chloroform. The light absorption of the organic phase is measured at $\lambda = 255$ nm with a 1-cm light path cuvette.

To determine the distribution coefficient of tetrazolium salts TTC, the absorptions obtained are compared to the one obtained after three times the extraction of the aqueous layer:

$$D_{TTC} = A/(A_{max} - A)$$

A—light absorption for a single time extraction
A_{max}—light absorption for three times extraction.

The experimental data are represented graphically by log D_{TTC}/log $C_{Hg(II)}$ (Fig. 5). The distribution constant is determined graphically by extrapolation of the straight line parallel to the x-axis up to the point of intersection with the y-axis. Using this graphical dependence we can also determine the extraction constant K_{ex} and the association constant β. They are determined by the slope of the figure up to the point of its intersection with the ordinate axis. The slope of the straight line (Fig. 5) is 45°. It means that the molar ratio of the reacting ions TTC^+ and $[HgI_3]^-$ is 1:1.

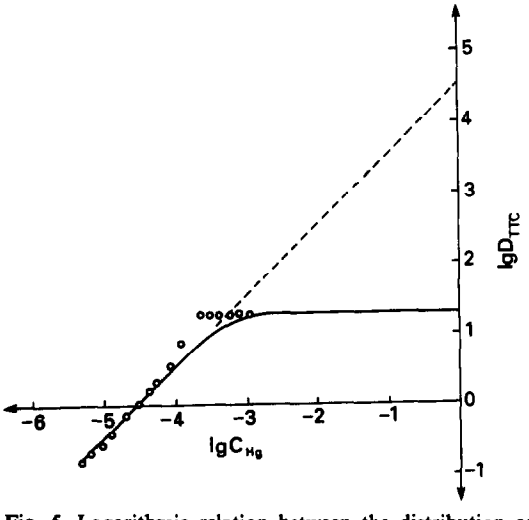

Fig. 5. Logarithmic relation between the distribution coefficient of TTC and the concentration of Hg(II).

The check-up for the fidelity of the experimental data has been performed according to the following formula:

$$D_{TTC} = \frac{K_D \cdot \beta \cdot [Hg]}{1 + \beta[Hg]}. \quad (5)$$

A curve is built, by the values calculated for D_{TTC}, where $C_{Hg(II)}$ is arbitrary changed and β and K_D are found experimentally. The curve obtained in this way is shown in Fig. 5. A good agreement is seen between the experimental data and the theoretical curve.

The ion associate $TTC[HgI_3]$ is characterized by the following equilibrium constants determined graphically:

$$K_D = 20.67 \pm 0.10$$

$$K_{ex} = 3.16 \times 10^4 \pm 0.08 \times 10^4$$

$$\beta = 1.53 \times 10^3 \pm 0.21 \times 10^3.$$

Determination of mercury in soils

The method was applied to determination of microquantities of mercury in various types of soils. The samples were collected from a depth of 0–20 cm.

Dissolving the sample. A 2-g weight of soil, 5–7 ml of conc. H_2SO_4 and an excess of $KMnO_4$ are placed into a flask equipped with a reflux condenser. The crystals of $KMnO_4$ are added slowly in small portions, while stirring. It is heated until vapours of SO_3 are evolved. After cooling down, 10 ml of distilled water are added. The excess of $KMnO_4$ and manganese oxides are eliminated by adding H_2O_2. Iron is isolated by precipitation as hydroxide. After filtration the solution is transferred into a standard flask of 25 ml and the volume is brought to the mark with distilled water. Aliquots of this solution are taken for analysis.

Extraction and determination of mercury. The following solutions were transferred into separating funnels: 12 ml of the corresponding type of soil solution and 1 ml of $2M$ H_2SO_4, 1 ml of $1 \times 10^{-3}M$ KI, 0.5 ml of $5 \times 10^{-4}M$ TTC and 5 ml of a saturated solution of NaF (to mask the interfering ions). Extracted with 3 ml of $CHCl_3$ for 30 sec. Then the organic phase was recorded

Table 2. Content of mercury in soil samples

N	Soil samples	Mercury, %		Accuracy (E_r%)*	Precision (RSD %)†
		Triphenyltetrazolium chloride	Dithizone		
1	Black	2.4×10^{-5}	2.6×10^{-5}	+0.9	0.5
2	Podzolized black	13.1×10^{-5}	13.0×10^{-5}	−0.8	0.3
3	Gray forest	5.0×10^{-5}	5.2×10^{-5}	+1.1	0.9

*Relative error.
†Relative Standard Deviation.

at $\lambda = 255$ nm. A blank, containing the same solutions without the corresponding type of soil, is prepared. The concentration of mercury was determined by a standard curve.

The results for mercury(II), obtained using triphenyltetrazolium chloride, were compared to those obtained by the dithizone method (Table 2). The results of both methods show a good agreement. The method with TTC we developed, is sensitive, selective and rapid. Moreover, the reagent used in this method does not suffer the lack of stability which is the case for the dithizone extraction of mercury.

REFERENCES

1. V. Gladichev, S. Levischka and L. Filipova, *Analitical Chemistry of Mercury, publ. "Science"*, 1974.
2. K. Samsahl, *Anal. Chem.*, 1967, **39**, 1480.
3. S. Tong, W. Gutenman and D. Lisk, *ibid.*, 1969, **41**, 1872.
4. W. Hatch and W. Ott, *ibid.*, 1968, **40**, 2085.
5. N. Sevova, S. Alexandrov and S. Sevov, *God. Sofiisk. univ. Him. fac.*, 1984, **78**, 203.
6. K. Robinson, *Int. J. Environ. Anal. Chem.*, 1989, **36**, 111.
7. J. Sneddon, *Spectrosc. Lett.*, 1987, **20**, 527.
8. G. Doshi and S. Joshi, *Indian J. Technol.*, 1987, **25**, 371.
9. V. Krishnasamy and K. Ayyadurai, *J. Indian Inst. Sci.*, 1988, **68**, 207.
10. V. Toshio, A. Masaru and M. Soichiro, *Bunseki kagaku, Bunseki Kagaku*, 1981, **30**, 740.
11. Ö. Einarsson, G. Lindstedt and T. Bergström, *J. Autom. Chem.*, 1984, **6**, 74.
12. E. Sandell, *Colorimetric Determination of Traces of Metals*, Interscience, New York, 1959.
13. E. Hakkila and G. Waterbury, *Anal. Chem.*, 1960, **32**, 1340.
14. C. Merrit, H. Hershenson and L. Rogers, *ibid.*, 1953, **25**, 572.
15. I. Kressin and J. Coleman, 22nd Annual Southwest Regional Meeting, ACS, 1967.
16. S. Lebedeva and E. Ovsepan, *Himiya i him. tehnol. Erevan*, 1989, **N5**, 145.
17. B. Raman and V. Shinde, *Analyst*, 1990, **115**, 93.
18. J. Shufu and J. Niangin, *Phys. Test. Chem., Anal. B.*, 1989, **25**, 279.
19. Z. Marczenko and R. Lobinski, *Chem. Anal.*, 1989, **34**, 87.
20. Y. Agrawal and G. Mehd, *J. Inst. Chem. (India)*, 1989, **61**, 139.
21. S. Maspoch and M. Blanco, *Quim. Anal.*, 1987, **6**, 68.
22. F. Capitan, P. Espinosa, M. Bosque-Sendra and M. Francisca, *Ann. Chim.*, 1987, **77**, 945.
23. G. Bing and Z. Zhuang, *Acta sci., natur. univ. Jilinensis*, 1987, **N3**, 91.
24. S. Savvin and N. Roeva, *Determination Components in Natural Waters, M.*, 1987, 42.
25. J. Mudakavi and Y. Ramaswamy, *J. Indian Inst. Sci.*, 1986, **66**, 155.
26. R. Sharma and H. Singh, *Talanta*, 1989, **36**, 457.
27. M. Popescu, *Rev. Chim.*, 1989, **40**, 147.
28. N. Maslei and L. Oxitisch, Uzgorod. University Uzgorod. 1988, Dep. v Ukr. NIINTI, N 2344.
29. G. Zhang and L. Bin, *Anal. Chem.*, 1987, **15**, 912.
30. M. Bulatov and I. Kalinkin, *Practical Manual of Photocolorimetric and Spektrophotometric Methods Analysis, L., Chemistry* 1972.
31. A. Alexandrov, O. Budevski and A. Dimitrov, *Radioanal. Chem.*, 1976, **29**, 243.

Talanta, Vol. 40, No. 5, pp. 725–728, 1993
Printed in Great Britain.

0039-9140/93 $6.00 + 0.00

IODNITROTETRAZOLIUM CHLORIDE—A NEW ANALYTICAL REAGENT FOR DETERMINATION OF CHROMIUM

M. KAMBUROVA
Department of Chemistry, Higher Institute of Agriculture, 4000 Plovdiv, Bulgaria

(*Received* 25 *April* 1991. *Revised* 25 *July* 1991. *Accepted* 2 *August* 1991)

Summary—The extraction of chromium (VI) with iodnitrotetrazolium chloride (INT) was studied spectrophotometrically. The basic spectrophotometric characteristics of the ion associated formed were determined. Using different methods it was found that the ratio between chromium and INT was 1:1. The molar absorptivity of the associate is $\epsilon_{250} = (3.70 \pm 0.08) \times 10^4$ l · mole^{-1} · cm^{-1}. Performing the reaction in acid medium (0.1–1.1*M* hydrochloric acid) allowed the determination of chromium in the presence of large amounts of W(VI), Mo(VI), Fe(III) and V(V). Hence INT is suggested as a sensitive and selective reagent for extractive–spectrophotometric determination of microquantities of chromium(VI).

Tetrazolium salts appear as highly sensitive reagents for extractive–spectrophotometric determination of a number of elements, *viz.* Co(II), Zn(II), Au(I), Sb(V), Nb(V), Mo(VI), W(VI), Re(VII), Tl(III), Ga(III).[1–11] The methods for determination of chromium with tetrazolium salts are particularly interesting. In earlier studies we have established that under certain conditions triphenyltetrazolium chloride[12] and tetrazolium violet[13] form ion-association complexes with chromium, which are extractable in organic solvents.

The known methods of determination of chromium are of low sensitivity.[23,24] The most sensitive and selective is the method with diphenylcarbazide.[21] It is the best reagent for determination of small amounts of chromium. A disadvantage of this method appears to be the labour-consumption of the preparatory works. Another disadvantage is the instability of the aqueous solution of diphenylcarbazide and its preparation in acidified acetone.

In the present work we show the possibility of using iodnitrotetrazolium chloride (INT) for determination of chromium to demonstrate that in the determination of microquantities of chromium, the tetrazolium salt is superior to diphenylcarbazide in some respects. The reagent we used is available and has good chemical–analytical parameters. The complexation and extraction of chromium(VI) with this tetrazolium salt was studied as well as the effect of various factors upon the extraction of the ion associate of chromium. Its basic chemical–analytical characteristics were determined. The possibility of using INT as a reagent for spectrophotometric determination of microquantities of chromium(VI) is demonstrated in assays of this species in steel and soil samples.

EXPERIMENTAL

Reagents

Iodnitrotetrazolium chloride (INT), Fluka, $1 \times 10^{-4}M$; potassium chromate, *p.a.* $1 \times 10^{-4}M$ Cr(VI); hydrochloric acid, *p.a.* 1.2*M*; 1.2 dichlorethane, *p.a.*

Apparatus

A Carl Zeiss VSU 2-P spectrophotometer (Jena, DDR) was used with 1-cm light path quartz cells with measurement at 250-nm. A Specord UV–VIS (DDR) was also used.

Procedure

Corresponding amounts of the solution containing chromium, 1.2 ml of 1.2*M* hydrochloric acid and 2 ml of $1 \times 10^{-4}M$ INT are introduced into separating funnels. The mixture is diluted with distilled water to an aqueous phase volume of 10 ml and extracted with 3 ml of dichlorethane for one minute. The organic layer is then transferred through filter paper into a 1-cm cell and measured at $\lambda = 250$ nm. A blank is prepared in a similar manner, without the presence of chromium.

RESULTS AND DISCUSSION

With chromium, in hydrochloric acid medium, Iodnitrotetrazolium chloride forms an ion associate with chromium in hydrochloric acid medium of composition INT $H[CrO_3Cl]$. This composition has been confirmed in earlier reports.[14-18]

Our studies showed that the ion associate of Cr(VI) with INT was quantitatively extracted into dichlorethane. In other solvents, such as chloroform, benzene, nitrobenzene and ether, the compound is not extractable.

The analysis of the absorption spectra of the ion associate obtained from the interaction of Cr(VI) and INT showed that the compound had maximum light absorption at $\lambda = 230$ nm and $\lambda = 250$ nm (Fig. 1). The intensity of the second maximum was considerably higher. We therefore chose 250 nm as a working wavelength.

The maximum extraction of chromium as an ion associate in the organic phase was reached after extraction for 30 sec. The ion associate is stable for five days.

The molar ratios of the constituents in the associate were established by the method of equilibrium shift.[19] The tangent of the slope angle was 1, *e.g.*, the ratio INT:Cr = 1:1. This ratio was confirmed with the method of Asmuss.[20] Under optimal conditions the molar absorptivity had the value of $\epsilon_{250} = (3.70 \pm 0.08) \times 10^4\ l \cdot mole^{-1} \cdot cm^{-1}$.[20] The light absorption of the associate depended linearly on the concentration of chromium in the range 0.02–0.3 μg/ml. From these data it is seen that the reaction of chromium with INT is highly sensitive.

The basic parameters studied which characterize the qualities of INT as a reagent are concentration parameters.

To establish the optimal conditions for extraction and complexation we studied the relationship between light absorption and the concentration of the tetrazolium salt (Fig. 2). The optimal concentration of INT for formation and extraction of the associate was found to be [INT] $\geqslant 2 \times 10^{-5} M$.

The stability and character of the compound formed depend considerably on the acidity of the aqueous phase. The effect of the acids upon the extraction of the ion associate of chromium is given in Fig. 3 where it can be seen that the nature of the acids studied (HCl, H_2SO_4, HNO_3 and $HClO_4$) contributes substantially to the maximum extraction of chromium as an ion associate. The best results were obtained in hydrochloric acid medium in the range 0.1–1.1M hydrochloric acid.

When the acidity of the aqueous phase is high, the extraction of the ion associate decreases because of the reduction of Cr(VI) to Cr(III).

The effect of foreign elements and complexing substances was studied during the determination of 2 μg of Cr(VI). It was found that most of the studied ions did not interfere with the determination of chromium as an ion associate. The experimental data are given in Table 1. Hg(II), Al(III), Ca(II), Na(I) and Br^- all interfered in the determination. Sodium fluoride, tartaric acid and ascorbic acid were used as

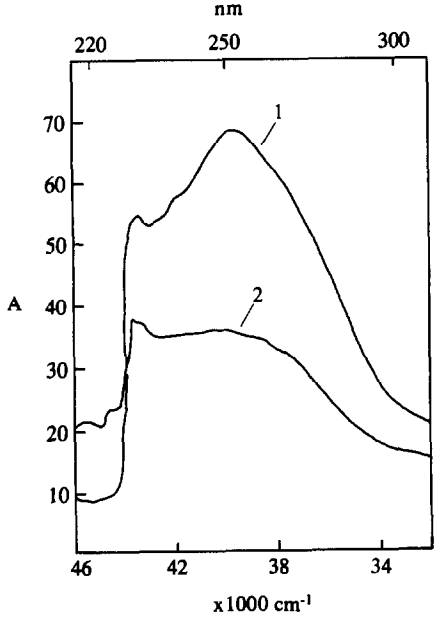

Fig. 1. Absorption spectra in dichlorethane of the ion-association complex of Cr(VI) with INT(1) and INT(2).

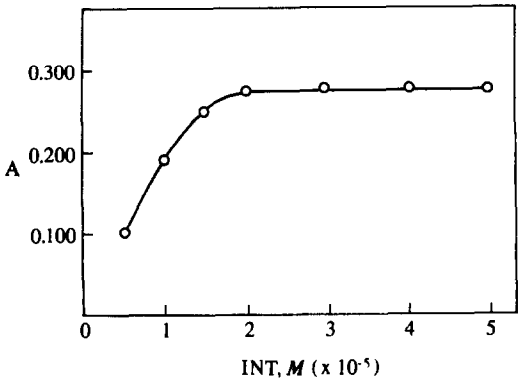

Fig. 2. Dependence between light absorption and the concentration of INT; $C_{Cr(VI)} = 0.3$ μg/ml, $C_{HCl} = 0.14M$.

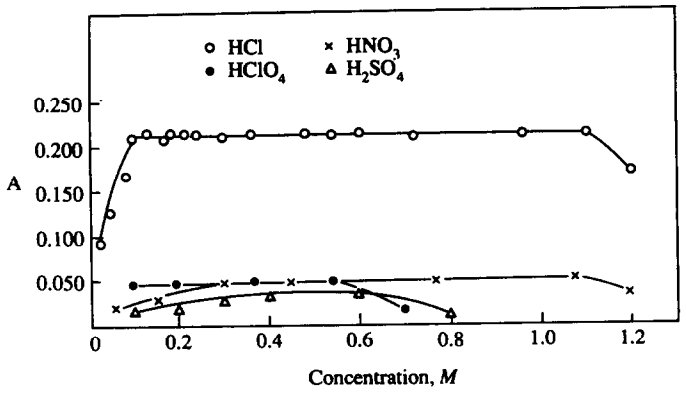

Fig. 3. Dependence between light absorption and pH of the solution; $C_{INT} = 1 \times 10^{-5} M$, $C_{Cr(VI)} = 7 \times 10^{-6} M$.

masking reactions. The method with INT for determination of chromium was found to be selective in the presence of W(VI), Mo(VI) and Fe(III).

On the basis of the data obtained we developed a method for determination of chromium. The sensitivity of the method according to Sandell[21] is $W_S = 0.0014$ $\mu g/cm^2$. Its practical applicability was demonstrated by application to analysis of steels and soils containing chromium.

Application to determination of chromium in steels

Sample dissolution. Steel (0.1 g) is weighed and dissolved in a 30-ml mixture (1:3) of HNO_3(1:1) and HCl(1:1). Concentrated sulphuric acid (10 ml) is added and the mixture is evaporated until SO_3 vapour is noticed. The solution is transferred into a 100-ml standard flask and is diluted to the mark with distilled water.

Table 1. Effect of foreign ions

N	Foreign ion,	μg	Chromium(VI) Taken, μg	Found, μg	$C_M/C_{Cr(VI)}$
1	K(I)	8000	2	1.98	4000
2	Cd(II)	8000	2	1.99	4000
3	W(VI)	7000	2	1.97	3500*
4	Mo(VI)	3000	2	1.99	1500*
5	Sr(II)	3000	2	1.99	1500
6	Fe(III)	3000	2	2.02	1500*
7	Cu(II)	1000	2	2.00	500
8	Mg(II)	1000	2	2.00	500
9	V(V)	1000	2	2.02	500*
10	Ni(II)	1000	2	2.00	500
11	Co(II)	600	2	2.01	300
12	Zn(II)	500	2	1.99	250
13	Mn(II)	100	2	2.01	50
14	Ag(I)	50	2	2.00	25
15	Na(I)	10	2	2.00	5
16	Ca(II)	8	2	2.01	4
17	Al(III)	5	2	1.99	2.5
18	Hg(II)	2	2	interference	
19	CO_3^{2-}	1000	2	2.01	500
20	Cl^-	700	2	1.99	350
21	SO_4^{2-}	200	2	1.98	100
22	NO_3^-	40	2	2.01	20
23	Br^-	10	2	2.01	5

*In the presence of maskings reagents.

The oxidation of Cr(III) to Cr(VI) is performed with potassium permanganate in a sulphuric acid medium.[21]

Determination of chromium. Aliquots of the prepared solution of alloyed steel, 1.2 ml of 1.2*M* hydrochloric acid, 2 ml of $1 \times 10^{-4} M$ INT are introduced into separating funnels. Saturated solutions of 2 ml of sodium fluoride and 2 ml of ascorbic acid are introduced (to mask the interfering ions). The solutions are extracted with 3 ml of dichlorethane for 1 min. The organic layer is then transferred through filter paper into 1-cm cell and measured at $\lambda = 250$ nm.

The quantity of chromium in the aliquot is determined by a standard curve. The results of the chromium determination in steels are given in Table 2.

Application to analysis of soils

The method was applied to the determination of chromium in five soil samples: lessive cinnamonic, pseudopodzolic, gray forest, brown and black soil.

Sample dissolution. A 4-g soil sample is weighed and introduced into a platinum crucible, heated for 3 hr in a muffle furnace at 550°. After cooling, the sample is transferred into a platinum bowl and 2 ml of bidistilled water, 1 ml of concentrated sulphuric acid and 10 ml of hydrofluoric acid are added. It is evaporated on a sand bath until SO_3 vapour is evolved. The dry residue is dissolved in bidistilled water acidified with hydrochloric acid.[22]

Table 2. Determination of chromium in steels

N	Steel	Content of chromium by certification list, %	Chromium found, % (*n*)
1	38 × 2I–O CO–C 14a	1.84	1.83 ± 0.02 (5)
2	CO–C 37	17.6	17.58 ± 0.01 (5)

38 × 2I–O CO–C 14a (%): C—0.364; Si—0.50; Mn—0.350; Ni—0.162; Cr—1.84; W—0.293; V—0.208; Cu—0.128; Al—0.56; S—0.0058; P—0.0074; CO–C 37 (%): C—0.05; Si—0.5; Mn—1.35; Cr—17.6; Ni—12; Cu—0.2; Nb—1.2.

Table 3. Determination of chromium in soils

N	Soil	$Cr \times 10^{-4}$ %		Relative error, %
		Iodnitrotetrazolium chloride	Atomic absorption	
1	Lessive cinnamonic	4.35	4.37	0.45
2	Pseudopodzolic	5.62	5.62	0.00
3	Gray forest	3.10	3.12	0.64
4	Brown	3.11	3.12	0.32
5	Black	9.35	9.37	0.21

After the precipitation of iron and aluminium the solution was transferred into a 25-ml standard flask and diluted up to the mark with bidistilled water. Aliquots from this solution were taken for analysis.

Determination of chromium. Hydrochloric acid (1.2-ml, 1.2*M*), 2 ml of $1 \times 10^{-4}M$ INT and equal volumes of saturated solutions of ascorbic acid and ammonium fluoride are added to the sample solution. A 10-ml portion of the aqueous phase is extracted for 1 min with 3 ml of dichlorethane. A blank is run in parallel in the absence of soil sample.

The concentration of Cr(VI) is determined with a standard curve. The accuracy of the method was checked with an atomic absorption method. The experimental data (Table 3) show good agreement between the results obtained by the two methods.

The method with iodnitrotetrazolium chloride can be successfully applied to the determination of chromium in various objects. Its features are high accuracy, selectivity and sensitivity.

REFERENCES

1. A. Alexandrov and M. Kamburova, *Mikrochim. Acta*, 1976, 357.
2. *Idem, ibid*, 1976, 61.
3. A. Dimitrova, A. Alexandrov and A. Dimitrov, *Natura, Universite de Plovdiv*, Bulgarie, 1972, **5**, 57.
4. A. Alexandrov and S. Kostova, *Z. Anal. Chem.*, 1981, **306**, 125.
5. *Idem, J. Radioanal. Chem.*, 1984, **83**, 247.
6. A. Alexandrov and M. Hagieva, *Nauch. Tr. PU"P. Hilendarski"*, Plovdiv, 1979, **17**, 11.
7. A. Alexandrov and A. Dimitrov, *Mikrochim. Acta*, 1972, 680.
8. T. Pukas, *Chemia Analityczna*, 1960, **5**, 513.
9. A. Dimitrov, A. Alexandrov, D. Dimova and M. Vrchlabsky, *Scripta Fac. Sci. Nat. Univ. Purk. Brun.*, 1983, **13**, 117.
10. A. Alexandrov and B. Milusheva, *Natura, Universite de Plovdiv*, Bulgarie, 1974, **7**, 69.
11. A. Alexandrov and G. Simeonova, *Nauch. Tr. PU"P. Hilendarski"*, Plovdiv, 1978, **16**, 39.
12. M. Kamburova, *Mikrochim. Acta*, in the press.
13. M. Kamburova, A. Alexandrov and T. Popov, *ibid.*, in the press.
14. L. Hintibidze, G. Supatashvilly and M. Mdinaradze, *Organicheskie reagentov v analyt. chimii, Perm*, 1983, 123.
15. C. Deptula, *Rocz. Chem.*, 1968, **42**, 725.
16. *Idem, Chem. Anal. (Warsaw)*, 1968, **13**, 211.
17. *Idem, J. Inorg. Nucl. Chem.*, 1968, **30**, 1309.
18. A. Minin and L. Hlupina, *Uchen. zap. Permsk. in-ta*, 1974, **324**, 194.
19. A. Babko, *Fiziko-himicheskii analiz kompleksnih soedinenii v rastvorah*, Kiev, Izd. AN USSR, 1955.
20. M. Bulatov and I. Kalinkin, *Prakticheskoe rukovodstvo po photokolorimetricheskim i spektrophotometricheskim metodom analiza, L.*, Himiya, 1972.
21. E. Sendel, *Kolorimetricheskie metodi opredelenya sledov metalov, M.*, Mir, 1964.
22. I. Vagenin, *Metodi opredelenya mikroelementov v pochvah, rastenyah i vodah*, Moskva, 1974.
23. A. Lavruhina and L. Ukina, *Analytisheskaya himiya chroma, M.*, Nauka, 1970.
24. M. Tataev and L. Anisimova, *Sb: Ispolzovanie organiscsheskih reagentov v analytisheskoi himii, M.*, 1978.

Talanta, Vol. 40, No. 5, pp. 729–735, 1993
Printed in Great Britain.

0039-9140/93 $6.00 + 0.00

ANNOTATION PAPER

INTERFERENCE BY VOLATILE NITROGEN OXIDES IN THE DETERMINATION OF MERCURY BY FLOW INJECTION COLD VAPOR ATOMIC ABSORPTION SPECTROMETRY

INGE ROKKJÆR, BOY HOYER* and NINA JENSEN
Department of Chemistry, Aarhus University, Langelandsgade 140, 8000 Aarhus C, Denmark

(*Received* 11 *May* 1992. *Revised* 7 *July* 1992. *Accepted* 3 *August* 1992)

Summary—The determination of mercury by the title method with sodium tetrahydroborate as reducing agent can be interfered with by volatile nitrogen oxides which inhibit the reduction of mercury by scavenging the reducing agent. The nitrogen oxides are formed as reduction products of nitric acid during sample decomposition. The interference effect was encountered in the determination of mercury in sewage sludge digests, and the main symptom was poor reproducibility of the shape of the mercury peak. The area of the mercury peak is more resistant to the interference than the peak height. The nitrogen oxide interference did not cause any systematic error in the mercury determination when calibration was done by standard addition. The interference can be easily remedied by purging the sample with argon.

The coupling of flow injection (FI) with cold vapor atomic absorption spectrometry (CVAAS) for the determination of mercury has many significant advantages in comparison with the conventional batch CVAAS technique. These advantages include[1] lower sample and reagent consumption, higher sample throughput, ease of automation and superior resistance to metals which cause solution-phase interferences (*e.g.* Ni, Cu and Ag). When sodium tetrahydroborate is employed as reducing agent in FI–CVAAS it is generally used in lower concentration than in batch CVAAS,[1,2] and the determination of mercury by the latter technique is therefore more susceptible to interferences from sample constituents which scavenge the reducing agent. The present paper describes an interference of this type which was encountered in the determination of mercury by FI–CVAAS in digests of sewage sludge. The interference effect could be attributed to volatile nitrogen oxides which were formed during the decomposition of the sample.

To the authors' knowledge, the interference from nitrogen oxides in the determination of mercury by batch CVAAS has only been described in one paper,[3] and the interference therefore appears to be rare in this technique. Stuart[4] and Wigfield *et al.*[5] have previously shown that the peak area is generally less susceptible to matrix effects and interferents than the peak height in the determination of mercury by batch CVAAS.

*Author for correspondence.

EXPERIMENTAL

Apparatus

All atomic absorption measurements were made with a Perkin–Elmer ZL 4100 spectrometer equipped with a 16.6-cm quartz flow-through cell heated to 200°. Operating conditions were as follows: wavelength, 253.7 nm; monochromator wavelength interval, 0.7 nm; mercury hollow cathode lamp current, 6 mA. Sample introduction was performed by a Perkin–Elmer FIAS 200 flow injection system, of which a schematic diagram is shown in Fig. 1. The gas–liquid separator was a vertical tube with the sample inlet placed above the waste outlet and the gas outlet in the top.[6] The internal volume of the gas–liquid separator was 4.1 ml, and it was filled with spherical glass beads with a diameter of 3 mm. The 1-mm i.d. tube connecting the gas–liquid separator and the quartz cell was one metre long. The carrier was a 10% (v/v) hydrochloric acid

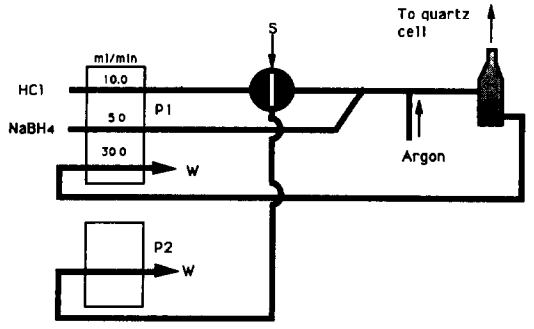

Fig. 1. Schematic diagram of flow injection system for mercury determination. P1, P2: peristaltic pumps; S: sample inlet; W: waste.

solution, while the reductant, unless stated otherwise, contained 0.2% (v/w) sodium tetrahydroborate stabilized with 0.04% (v/w) sodium hydroxide. The flow rates were as follows: carrier, 10 ml/min; reductant, 5 ml/min; waste, 30 ml/min; argon, 75 ml/min. The amalgamation accessory was a Perkin–Elmer system in which the gas from the gas–liquid separator passes through a wash bottle and a magnesium perchlorate drying filter prior to collection of mercury on a platinum-gold gauze. Mercury is subsequently liberated by rapid heating of the gauze to 600°. In the experiments with the amalgamation technique, the argon flow through the gas–liquid separator was 300 ml/min, while the collector was purged with a 75 ml/min argon stream during heating. The volume of the sample loop was respectively 500 μl in the direct flow injection measurements and 200 μl in the measurements with the amalgamation technique. The pressure digestion bomb (Berghof model DAB III) was made of stainless steel with a 250-ml Teflon insert.

Reagents and samples

Solutions were prepared from triply distilled water and Merck Suprapur chemicals except for sodium tetrahydroborate and potassium dichromate which were of Merck analytical grade with low mercury content. The anti-foaming agent was Merck no. 7743 silicone oil. Mercury standards were prepared in a stabilizing medium containing 5% (v/v) nitric acid and 0.05% (w/v) potassium dichromate. Sludge samples were supplied from a local sewage treatment plant. The type I sludge was sampled from the aerobic stage of the treatment while the type II sludge originated from an anaerobic digester. The total solid content of sludge I and II was respectively 2.8 and 4.0%.

Procedure

Sludge samples were decomposed by mixing 20 ml of concentrated nitric acid and approximately 20 g wet sludge in the pressure digestion bomb and heating it to 140° for 4 hr. After cooling, the digest was transferred to a standard flask and the volume made up to 100 ml with water. The nitric acid concentration of this solution determined by acid–base titration was $2.9 \pm 0.1M$ for both sludge types. Before mercury determination, the type II sludge digest was further diluted tenfold with water. Volatile nitrogen oxides were removed from the digests by purging with an argon stream (75 ml/min) in a sample tube (15 mm i.d.).

Quantitation of mercury was done by standard addition. It has been shown that precision is improved by use of a single, large addition with the number of measurements equally distributed between sample and spiked sample.[7] This approach was adopted in the present study, and the mercury concentration was approximately tripled by the addition. In separate experiments it was verified that the linear part of the instrument response function was not exceeded by the addition. Four replicate measurements were performed on the unspiked as well as the spiked sample. A blank signal measured in $0.1M$ nitric acid was subtracted from all absorption curves. Signals were smoothed with a 5-point Savitsky-Golay algorithm prior to peak height evaluation. The peak integration time was 20 sec unless stated otherwise. Signals were evaluated by peak height in the amalgamation technique.

RESULTS AND DISCUSSION

In Fig. 2, a series of absorption curves obtained by repetitive mercury measurements on the type I digest is shown. The technique employed is FI–CVAAS without amalgamation. Obviously, the peak shape can vary considerably between individual replicates. Although a gradual decrease of peak height is seen in Fig. 2, it was generally observed that the variations in peak shape were random. The relative standard deviation of the peak height and peak area were respectively 11.5 and 2.4% for the signals in Fig. 2 which are typical values for repetitive measurements on the type I digest. Thus, precision is substantially improved by using the peak area instead of the peak height as the analytical signal.

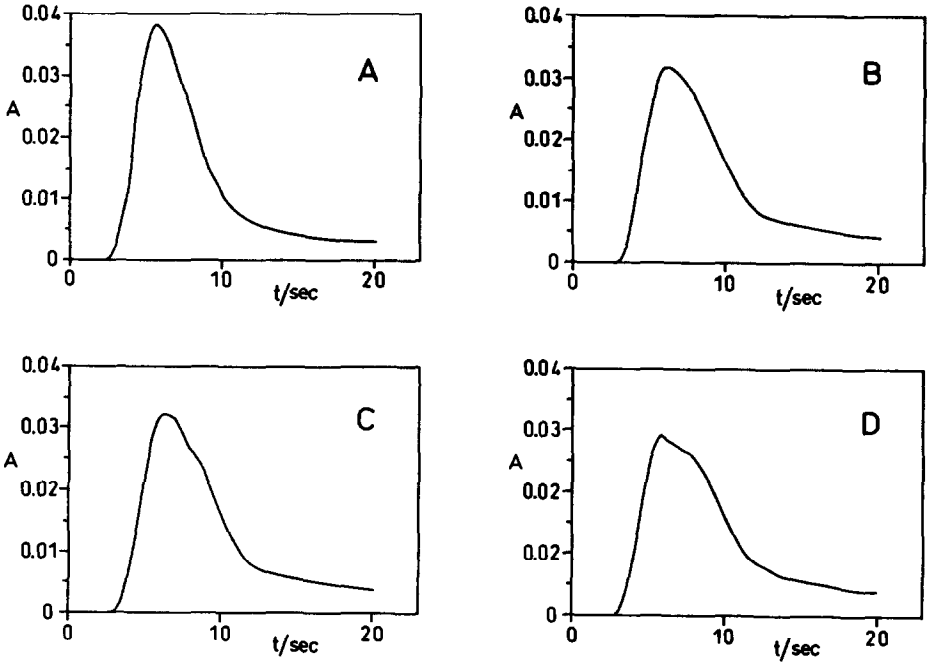

Fig. 2. Absorption peaks for mercury obtained by repetitive measurements on the type I sludge. The peak heights (absorbance) and areas (absorbance·s) are respectively: (A) 0.038, 0.203; (B) 0.032, 0.214; (C) 0.032, 0.204; (D) 0.029, 0.207.

Initially it was believed that the poor reproducibility of the absorption peak of mercury was due to segmentation of the sample stream by the formation of hydrogen gas which takes place at the confluence point of the sample and the reductant stream. From this hypothesis it follows that the shape and the reproducibility of the mercury peak should be improved by decreasing the concentration of sodium tetrahydroborate. However, as shown in Fig. 3 the

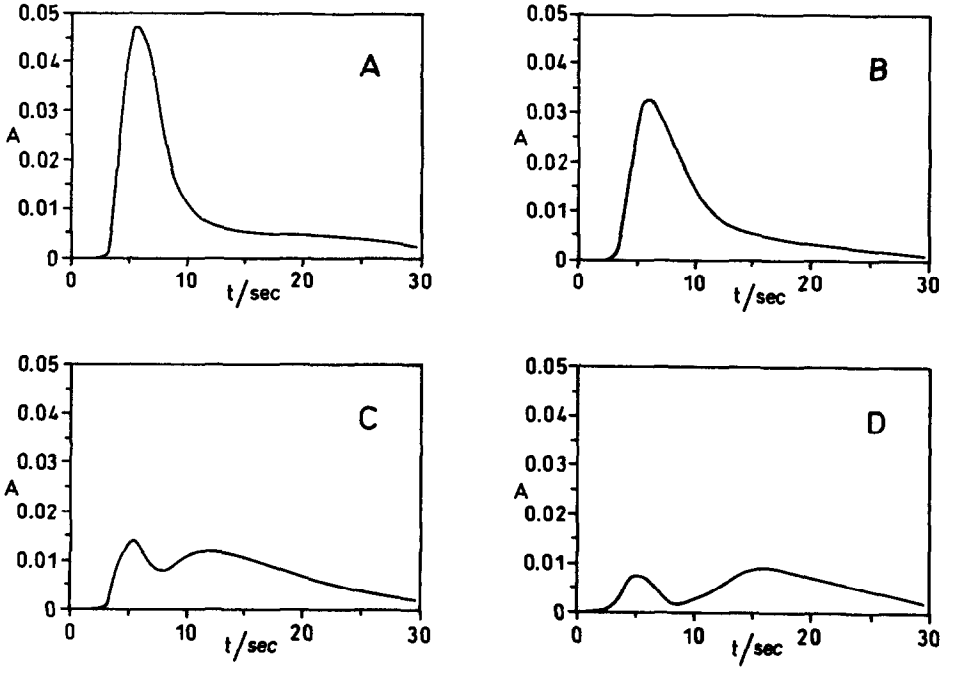

Fig. 3. Influence of the reductant concentration on the mercury signal measured in a type I digest by FI–CVAAS without amalgamation. Sodium tetrahydroborate concentration [% (v/w)]: (A) 0.2; (B) 0.15; (C) 0.1; (D) 0.05.

mercury peak was suppressed, broadened and even split when the strength of the reducing solution was decreased. In a similar experiment, a mercury standard prepared in a nitric acid medium of equal strength as the type I digest was used as sample. In this case, it was found that the concentration of sodium tetrahydroborate could be reduced from 0.2% (v/w) to at least 0.012% (v/w) without any significant change of the mercury signal. Therefore, a constituent of the type I sample matrix interferes with the reduction of mercury or the separation of the elemental mercury into the gas phase. In Fig. 4 it is shown that purging of the type I digest with argon greatly improves the shape of the mercury absorption peak, and the interferent must therefore be volatile. This is in agreement with previous work[8] which showed that nitrogen oxides generated by reduction of nitric acid during sample decomposition can inhibit the formation of the hydrides of arsenic and selenium in the hydride generation atomic absorption technique. Signal suppression by nitrogen oxides has also been reported in the determination of mercury by batch CVAAS in samples which were decomposed by a mixture of nitric, sulphuric and hydrochloric acid.[3] The decomposition was done in an open flask heated by a boiling water bath, and it would be expected that the volatile nitrogen oxides escaped under such conditions. However, concentrated sulphuric acid reacts with nitrogen oxides, *e.g.*,[9]

$$N_2O_4 + 3H_2SO_4 \leftrightarrow NO^+ + NO_2^+ + 3HSO_4^- + H_3O^+$$

and their solubility is therefore increased. This is in agreement with the fact that no interference from nitrogen oxides was observed when nitric acid was used on its own for decomposition.[3]

The extent of the interference from nitrogen oxides in the type I digest was related to the age of the digest. In one digest, which had been kept for four months in a half full bottle, no interference was observed at all, and a reduction of the concentration of sodium borohydride from 0.2% (v/w) to 0.003% (v/w) only caused a slight broadening of the mercury peak, while the integrated absorbance was unaffected. Usually, 2 or 3 days passed between sample decomposition and the FI–CVAAS measurement. In this case the degree of interference was typically as shown in Fig. 1. The mercury signal was strongly suppressed and resembled Fig. 2C when the measurement was performed immediately after the sample was transferred from the pressure bomb. These observations can all be attributed to the volatility of the interferent. In all cases, it was found that 10 min of argon

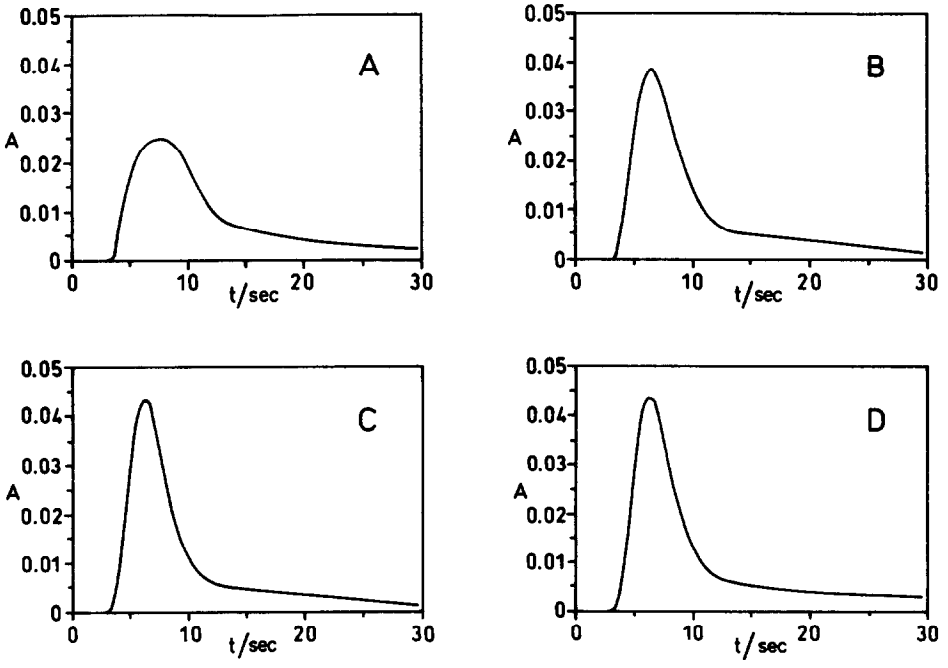

Fig. 4. Influence of the argon purging time on the mercury signal measured in a type I digest by FI–CVAAS without amalgamation. Sodium tetrahydroborate concentration: 0.2% (v/w). Purging time (min): (A) 0; (B) 2; (C) 4; (D) 6.

purging was sufficient for complete elimination of the interference. No further change of the mercury signal occurred when the purging time was increased to 60 min, and the amount of mercury lost by the purging is therefore insignificant.

The most plausible explanation[3] of the interference effect appears to be that the reduction of nitric acid during sample decomposition yields a volatile product (the interferent) which is further reduced by sodium tetrahydroborate. The rate of the latter reaction must be so fast that tetrahydroborate is consumed before the reduction of mercury is complete. Naturally, the suppression of the mercury evolution can only be complete when the interferent is in stoichiometric excess of tetrahydroborate. The scavenging of the reductant and the concomitant inhibition of mercury evolution will be most pronounced in the central part of the sample zone where the concentration of the interferent is highest. This effect explains the splitting of the mercury peak at low reductant concentrations which is seen in Fig. 3.

The main products of the reduction of nitric acid when used as oxidant in high concentration are[9] NO, NO_2, N_2O_4 and NO_2^-. On the basis of the present work it is not possible to determine which species is the actual interferent. Argon purging will also remove nitrite from the sample according to the reaction[9]

$$3HNO_2 \leftrightarrow HNO_3 + H_2O + 2NO\uparrow.$$

An attempt was made to eliminate the interference from nitrogen oxides by increasing the strength of the reductant solution, which normally contained 0.2% (v/w) sodium tetrahydroborate. However, this was not possible in practice with the digests of the type I sludge because the formation of aerosol in the gas–liquid separator became excessive, and the moisture carried into the quartz cell condensed on the end windows. Moderate foaming occurred in the gas–liquid separator when mercury was determined in the type I digest. Addition of anti-foaming agent to the carrier solution did not reduce the foaming significantly, whereas some suppression of the foaming was obtained by adding anti-foaming agent to each sample. However, this measure did not improve the reproducibility of the mercury signal, and further use of the anti-foaming agent was given up.

The data given in Fig. 2 and Fig. 5 indicate that the area of the mercury peak is less susceptible to the interference from nitrogen oxides than the peak height. In order to investigate this matter further, the results obtained by the direct FI method and the amalgamation method were compared. In the latter, the collection of mercury prior to the measurement step yields a signal which corresponds to the total quantity of mercury evolved during the reduction step, and this signal is not sensitive to variations in the shape of the mercury concentration transient emerging from the gas–liquid separator. The amalgamation method will also be affected by interference from nitrogen oxides if the evolution of mercury is inhibited to such an extent that a significant amount of unreacted, ionic mercury is pumped to waste from the gas–liquid separator. However, the measurements reported in the following were performed on digests which were at least 2 days old (see above), and purging of the digest with argon did not affect the mercury signal obtained with the amalgamation method. This result implies that the interference from nitrogen oxides is not so severe that it reduces the efficiency of the transfer of mercury from the sample to the collector. Mercury was determined in twelve separate digests of the type I sludge by the direct FI as well as the amalgamation method, and the concentration (as determined by the latter method) ranged from 4.6 μg/l. to 6.3 μg/l. When the FI signals were evaluated by peak height, the ratio $R = [Hg]_{TOT(FI)}/[Hg]_{TOT(AMALGAM)}$ ranged from 82 to 105%, with mean and standard deviation of respectively 96 and 6%. For the peak area evaluation of the FI signals, the corresponding values for R were: range, 95–105%; mean, 99%; standard deviation, 3%. Again, precision is improved by use of peak integration. A t-test showed that the mean value of R obtained by either form of signal

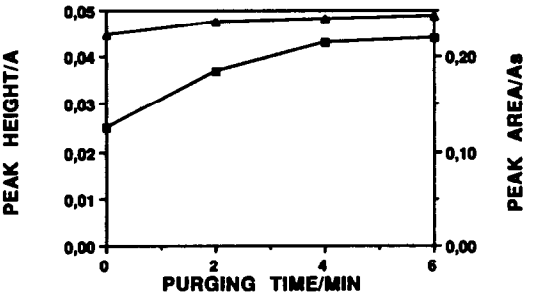

Fig. 5. Influence of the argon purging time on the peak height (■) and the peak area (▲) of the mercury signal measured in a type I digest by FI–CVAAS. Experiment conditions as in Fig. 4. Each point is the average of 3 replicates.

evaluation did not differ from 100% at a 95% confidence level. Therefore, it cannot be concluded from the data that the interference from nitrogen oxides causes systematic errors in the direct FI mercury determination. However, it must be emphasized that quantitation of mercury was carried out in a manner that yields a high precision (see above). If fewer replicates and a smaller standard addition is used, as would be expected in a routine application, the variations in peak shape can cause serious scatter of the results in the direct FI method when signal evaluation is based on peak height.

The high mercury content of the type II sludge digest necessitated a further tenfold dilution prior to measurement. In this matrix, no signal distortion was observed, and the relative standard deviation of the peak height as well as the peak area was typically 2%. For this sludge type the accuracy of the direct FI method was also verified by comparison with the amalgamation technique. Eleven digests were analysed, and the mercury content in the diluted digests ranged from 4.3 to 7.1 μg/l. The values for R (defined above) were: (a) peak height evaluation of FI signals: mean, 100%; standard deviation, 3%; (b) peak area evaluation: mean, 99%; standard deviation, 3%. In this case, there is little to choose from the two ways of quantifying the signal in agreement with the reproducible FI peak shapes.

As discussed above, the precision of the determination of mercury by FI-CVAAS without amalgamation in the type I digest was improved by evaluating the signal by peak area instead of peak height. However, it is possible that signal evaluation by peak area results in a poorer detection limit as the best signal-to-noise ratio (S/N) is found at the peak maximum. On the other hand, the noise is averaged by signal integration, and it is not possible to determine *a priori* whether it is peak height or peak area that yields the best detection limit. This matter was not investigated experimentally, but an estimate can be given as follows. If the noise level N is assumed to be independent of absorbance at low absorbance levels, one obtains:

$$(\mathrm{S/N})_{\text{peak h}} = \frac{A_{\text{peak}}}{\mathrm{N}}.$$

In practice, the peak area is evaluated by numerical integration of I absorbance readings taken with constant time interval Δt, and S/N for the peak area is approximately

$$(\mathrm{S/N})_{\text{peak a}} = \frac{\Delta t \sum_{i=1}^{I} A_i}{\Delta t \cdot \mathrm{N}\sqrt{I}}$$

if the noise is "white". Thus,

$$\frac{(\mathrm{S/N})_{\text{peak h}}}{(\mathrm{S/N})_{\text{peak a}}} = \frac{\sqrt{I} \cdot A_{\text{peak}}}{\sum_{i=1}^{I} A_i}.$$

Moreover,

$$I = \frac{\text{integration time}}{\Delta t} = \frac{20\ \text{sec}}{18\ \text{msec}} = 1110.$$

It is reasonable to assume that the shape of the signal is independent of concentration at low signal levels, or, in other words, that the ratio between peak height and peak area is constant. In a typical signal (*cf.* Fig. 2), the values for the peak height and the peak area were respectively 0.038 A and 0.20 $A \cdot s$, and

$$\frac{A_{\text{peak}}}{\sum_{i=1}^{I} A_i} = \frac{\text{peak h}}{(\text{peak area})/\Delta t} = 0.0034.$$

Therefore,

$$\frac{(\mathrm{S/N})_{\text{peak h}}}{(\mathrm{S/N})_{\text{peak a}}} = 0.11$$

which indicates that the best detection limit with the given experimental conditions is obtained by evaluating the signal by peak area. However, it must also be taken into account that $(\mathrm{S/N})_{\text{peak h}}$ is improved by the Savitsky–Golay smoothing.

In conclusion, there is a risk of interference from volatile nitrogen oxides when mercury is determined by FI–CVAAS in digests of samples which have been decomposed by nitric acid. This acid is prescribed for sample decomposition in, *e.g.*, the Danish[10] and Swedish[11] standard methods for mercury determination in waters, sludges and sediments. The interference effect is easily eliminated by purging the sample with argon. Alternatively, the nitrogen oxides can be reduced by sulphamic acid.[8] The interference is more likely to occur in FI–CVAAS than in batch CVAAS as the concentration of sodium tetrahydroborate used in the latter method is higher. For example, the concentration of sodium

tetrahydroborate in the present study was approximately 0.07% (v/w) after the merging point of the sample and reductant streams. In batch CVAAS, the concentration of sodium tetrahydroborate in the reaction vessel is typically[1,2] 0.6% (v/w) assuming complete mixing of the reductant and the sample. Both estimates disregard acidic hydrolysis of tetrahydroborate. It is also likely that the risk of interference from nitrogen oxides on the mercury determination can be decreased by use of tin(II)chloride as reductant instead of sodium tetrahydroborate. Typically, a 10% (v/w) tin(II)chloride solution is used as reductant[12] in FI–CVAAS which has a much higher stoichiometric reduction capacity than the corresponding 0.2% (v/w) sodium tetrahydroborate reductant. Consequently, it is less likely that the tin(II)chloride reductant is consumed by nitrogen oxides.

In the present work, the continuous variation of the mixture ratio between the interferent and the reductant created by the dispersion of the sample zone proved useful in the elucidation of the interference mechanism. Therefore, this article also exemplifies the diagnostic power of flow injection analysis.

Acknowledgements—The authors thank B. T. Jensen and K. Zambach for inspiring discussions.

REFERENCES

1. B. Welz and M. Schubert-Jacobs, in *Colloquium Atomspekrometrometrische Spurenanalytik*, B. Welz (ed.), Vol. 5, p. 327. Perkin Elmer, Überlingen, 1989.
2. B. Welz and M. Schubert-Jacobs, *Fresenius Z. Anal. Chem.*, 1988, **331**, 324.
3. S. B. Adeloju and T. F. Mann, *Anal. Lett.*, 1987, **20**, 985.
4. D. C. Stuart, *Anal. Chim. Acta*, 1979, **106**, 411.
5. D. C. Wigfield, S. M. Croteau and S. L. Perrins, *J. Anal. Toxicol.*, 1981, **5**, 52.
6. B. Welz and M. Schubert-Jacobs, *Atom. Spectrosc.*, 1991, **12**, 91.
7. J. P. Franke, R. A. de Zeeuw and R. Hakkert, *Anal. Chem.*, 1978, **50**, 1374.
8. R. M. Brown, R. C. Fry, J. L. Moyers, S. J. Northway, M. B Denton and G. S. Wilson, *ibid.*, 1981, **53**, 1560.
9. F. A. Cotton and G. Wilkinson, *Advanced Inorganic Chemistry*, 4th Ed., pp. 422–432. John Wiley, New York, 1980.
10. Danish Standard, *Determination of metals in water, sludge and sediment*. General guidelines for determination by atomic absorption spectrophotometry in flame, DS 259, Dansk Standard, Copenhagen 1982.
11. Swedish Standard, *Metal content of water, sludge and sediment by flameless atomic absorption spectrometry—Special guidlines for mercury*. SS 02 81 75, Standardiseringskommisionen i Sverige, Stockholm, 1989.
12. Technical Summary. Perkin–Elmer FIAS-200 Flow Injection System for Atomic Spectroscopy. *Recommended Analytical Conditions and General Information for Mercury/Hydride Analyses*. TSAA-10, Perkin–Elmer, Überlingen, 1990.

Talanta, Vol. 40, No. 5, pp. 737–740, 1993
Printed in Great Britain.

0039-9140/93 $6.00 + 0.00

POTENTIOMETRIC DETERMINATION OF SACCHARIN IN DIETARY PRODUCTS USING MERCUROUS NITRATE AS TITRANT

ORLANDO FATIBELLO FO* and ANTONIO JOSÉ MORAES GUARITÁ DOS SANTOS

Departamento de Quimica, Universidade Federal de São Carlos, C.P. 676, CEP 13565-905, São Carlos, S.P., Brazil

Instituto de Fisica e Quimica de São Carlos, Universidade de São Paulo, C. P. 369, CEP 13560-970, São Carlos, S.P., Brazil

(*Received* 20 *August* 1992. *Revised* 6 *November* 1992. *Accepted* 8 *November* 1992)

Summary—A rapid, precise and low cost method for saccharin determination in dietary products is proposed. Saccharin in several samples is potentiometrically titrated with mercurous nitrate solution using a silver wire coated with a metallic mercury film as the working electrode, and the end point was found using a Gran's plot. The detection limit of sodium saccharin was 0.5 mg/ml and the best pH range was from 2.0 to 3.5. Sucrose, glucose, aspartame, sodium cyclamate, sorbitol, fructose, benzoic acid, salicylic acid and lactose do not interfere even in significant amounts. The interference due to the presence of chloride and/or phosphate ions can be eliminated by previous solvent extraction of this sweetener. Recovery of saccharin from various dietary products gave from 95.2 to 103.2% of the label claim.

Saccharin (o-benzoic sulfimide, $C_6H_4COSO_2NH$) and its salts are white crystalline powders, odorless and in diluted solution are about 400–500 times[1] sweeter than sucrose. Due to their characteristics, they are widely used in medicine and several dietary products. There are several analytical procedures cited in the literature for determining saccharin such as gravimetry,[2,3] polarography,[4,5] fluorimetry,[6] ultraviolet spectrophotometry,[7,8] infrared spectrophotometry,[9] thin-layer chromatography,[10] gas–liquid chromatography,[11–13] high-performance liquid chromatography,[14,15] visible spectrophotometry using tris-(1,10-phenanthroline)-iron(II) chelate,[16] methylene blue,[17] phenothiazine,[18] phenosulphonaphthalein,[19] chlorophenothiazine,[20] azure B[21] and azure C[22] and potentiometry by using a liquid membrane electrode based on the formation of ion association between this sweetener with iron(II)-bathophenanthroline chelate.[23] Nevertheless most of these methods are time-consuming and laborious.[2–5,10,16–22] while others either need costly equipment[4–6,11–15] or have limitations in selectivity and/or sensitivity.[2,3,6–10,16–23]

In this paper, a new potentiometric method for saccharin determination in dietary products is proposed, based on the low solubility of mercurous saccharinate. Saccharin was potentiometrically titrated with $Hg_2(NO_3)_2$ solution and the remaining Hg_2^{2+} was monitored by a silver electrode coated with a metallic mercury film. After the equivalence point, a small excess of the titrant causes a potentiometric jump that was treated by a Gran's plot to give a precise and accurate end point determination. The proposed method is rapid, precise, accurate, inexpensive and does not need previous preparation to remove interferring substances. Only samples containing chloride and/or phosphate ions need be extracted with ethyl acetate in order to quantitate saccharin.

EXPERIMENTAL

Apparatus

Potentiometric measurements were carried out using a Micronal potentiometer, model B374 with 1 mV precision. The indicator electrode used was a silver wire (Aldrich, 99.9%) of 1 mm diameter and 15 mm length coated with a metallic mercury film and the reference electrode was a silver–silver chloride electrode in a 0.1*M* KCl solution with a 3.0*M* $NaNO_3$ bridge.

All potentiometric measurements were made in a 25 ml glass vessel and the temperature was kept at 25 ± 1°C by circulation of water from a

*Author for correspondence.

Veb ML W Prufgerate-Werb Medingem/Sitz Freital thermostatic bath, model U2C.

Reagents

All reagents used were of analytical grade. Saccharin stock solution was prepared by dissolving 4.580 g of saccharin (Aldrich, 99%) in 25–30 ml 0.1*M* NaOH solution and diluted to 250 ml. The reference solutions were prepared from the stock solution. The ionic strength and pH of these solutions were adjusted to 0.2*M* with sodium nitrate and to pH 3 with nitric acid.

The mercurous nitrate solution was prepared by dissolving 2.6260 g of $Hg_2(NO_3)_2$ (Aldrich, 99%) in $10^{-3}M$ HNO_3. The ionic strength of this solution was adjusted to 0.2*M* with $NaNO_3$ and the volume was made up to 1000 ml with water. This 0.005*M* solution was then standardized with 0.01*M* potassium chloride solution by potentiometric titration. A silver wire coated with mercury was used as an indicator electrode.

Sample preparation

Doce Menor powder and Assugrin liquid sweetener (Vepê Indústria Alimenticia Ltda., São Bernardo do Campo, S. P., Brazil), Sucaryl liquid sweetener (Abbott Laboratórios do Brasil Ltda., São Paulo, S. P., Brazil), Dietil liquid sweetener (Nutricia S. A., Rio de Janeiro, R. J., Brazil), and Diet Coke (Refrescos Ipiranga Ltda., Ribeirão Preto, S. P., Brazil) were purchased from a local food store.

(a) Liquid sweeteners

A volume of 1.0 ml of each liquid sweetener sample was diluted to 25.0 ml in a volumetric flask with 0.2*M* $NaNO_3$ made to pH 3 with nitric acid. Then. 5.0 ml of this solution was directly titrated with $5.4 \times 10^{-3}M$ $Hg_2(NO_3)_2$ solution.

(b) Powder sweeteners

An accurately weighed amount of 1.0–1.6 g of the solid sweetener was transferred to a 20.0 ml volumetric flask and the sample was dissolved and diluted to volume with 0.2*M* $NaNO_3$, pH 3 solution. An aliquot containing 10–80 mg of saccharin was transferred to the glass vessel and titrated as described with liquid sweeteners.

(c) Low calorie soft drinks

An aliquot of 250 ml of low calorie soft drink was transferred into a 500 ml separator funnel. An aliquot of 2 ml of concentrated HNO_3 was added and the saccharin content was extracted three times with 50, 30 and 10 ml of ethyl acetate, respectively. The layers were allowed to equilibrate for at least 3 min after each extraction. The organic phases were transferred to a 150 ml beaker and ethyl acetate was evaporated in a current of hot air. To the residue was added sufficient 0.1*M* NaOH solution to dissolve it, the pH adjusted to 3, and the solution was transferred to a 20 ml volumetric flask. The solution was made up to volume with 0.2*M* $NaNO_3$ solution and an aliquot of 5.0 ml was taken for titration as previously described.

RESULTS AND DISCUSSIONS

Life-time of the electrode

After about 10 titrations it is necessary to wash the electrode with distilled water to remove the precipitate. The mercury film must be renewed daily.

Effect of pH

The effect of the pH on the determination of $9.52 \times 10^{-3}M$ saccharin by $5.40 \times 10^{-3}M$ mercurous nitrate was studied. The optimum pH values for the titration of this sweetener was found to be from 2.0 to 3.5. There is a decrease of the potentiometric jump at a pH of less than 2.0 due either to the partial decomposition of saccharin to ammonium o-sulfobenzoic acid by acid hydrolisis[1] and/or protonation of the saccharinate anion (pKa = 1.6).[24] The decrease also occurs at a pH of above 3.5 due to the hydrolysis of mercurous cation to Hg_2O. A 0.2*M* $NaNO_3$ solution at pH 3 was then chosen for further work.

Potentiometric titration

Figure 1(a) shows a typical titration curve of 5 ml of $9.52 \times 10^{-2}M$ saccharin with $5.4 \times 10^{-3}M$ mercurous nitrate at 0.2*M* ionic strength and pH 3.0. Figure 1(b) shows the Gran's Method[25,26] applied to determine the equivalence point of this titration, using the equations for precipitation titrations in which the electrode responded to the titrant (Hg_2^{2+}). For this kind of reaction, Gran's Function, F_2, is equal to $(V_o + V) \times 10^{-mE/nK}$ before the equivalence point, and equal to $(V_o + V) \times 10^{E/K}$ after the equivalence point, where V_o is the initial volume of saccharin solution, V is the added volume of mercurous nitrate solution, E the observed EMF, K the calibration slope of the indicator electrode, and m and n are equal to 1 and 2, respectively. The precision was estimated

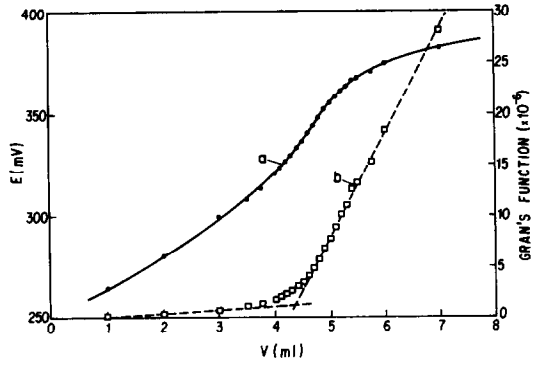

Fig. 1. (a) Typical titration curve of saccharin with mercurous nitrate at ionic strength 0.2*M*, pH 3 and 25°C. (b) Gran's method applied to determine the equivalence point of this titration.

from six titrations for 5 ml aliquots of $9.52 \times 10^{-3}M$ saccharin with mercurous nitrate. The standard deviation of the added volume of $Hg_2(NO_3)_2$ at the equivalence point and the relative standard deviation were 0.025 ml and 1.21%, respectively. The detection limit of the method performed by addition of saccharin in sugar containing soft drink (Coke) was $8 \times 10^{-4}M$.

Analytical curve

The analytical curve obtained [$V_e = 0.0285 + 0.4649m_{sac}$(mg)] from five different titrations of saccharin with $5.40 \times 10^{-3}M$ of mercurous nitrate and the good linearity ($r = 0.9993$) between the equivalence volume (V_e) and the amount of titrated saccharin (mg), demonstrated the usefulness of the proposed method.

Effect of foreign substances

Several potential organic and inorganic interferents which would be expected to exist in dietary products such as sucrose, fructose, glucose, aspartame, sodium cyclamate, sorbitol, benzoic acid, salicylic acid, lactose, citric acid, sodium chloride and sodium phosphate were investigated in a concentration range of at least 50 times higher than that of saccharin. Of those substances, only sodium chloride and sodium phosphate have strong interference, while sodium cyclamate has little interference, except at high concentrations. However, the interference due to chloride and/or phosphate ions can be eliminated with previous solvent extraction of the sweetener from aqueous medium with ethyl acetate. Figure 2 shows the effect of cyclamate concentration (0.10; 0.20 and 0.50*M*) on the titration of 1.0 ml of $9.52 \times 10^{-3}M$ of saccharin with $5.40 \times 10^{-3}M$ of mercurous nitrate. It can be seen from the curves that this method can be successfully applied to the determination of saccharin, even in the presence of cyclamate in a concentration range of 20 times that of saccharin. Nevertheless, 0.50*M* cyclamate solution (50 times) has a strong effect.

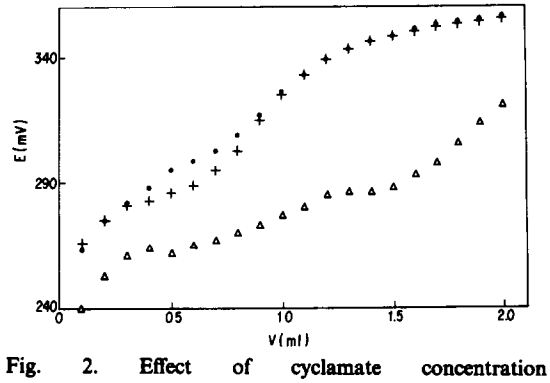

Fig. 2. Effect of cyclamate concentration (...:0.10; +++:0.20 and △△△:0.50*M*) on the determination of $9.52 \times 10^{-3}M$ saccharin with $5.40 \times 10^{-3}M$ of mercurous nitrate solution.

Determination of saccharin in dietary products

The results presented in Table 1 show a recovery of 95.2–103.2% of saccharin from three dietary products. In this study 1.89; 3.89; 5.78 and 7.74 mg/ml of saccharin were added to several diet products.

Table 2 presents a comparison between a UV spectrophotometric method, reported as one of the most used methods for saccharin determination,[7] and that proposed in this paper. Sucaryl was also analysed by the standard addition method and the result obtained is very similar to that obtained by Gran's method. The results are in close agreement with those reported and within an acceptable range of error. The adaptation of this method in flow injection analysis is underway.

Table 1. Recovery of saccharin from various dietary products

Sample	Saccharin (*mg/ml*) Added	Found	Recovery (%)
Assugrin	1.89	1.80	95.2
	3.89	3.99	102.6
	5.78	5.92	103.1
	7.74	7.62	98.5
Sucaryl	1.89	1.95	103.2
	3.89	3.78	97.2
	5.78	5.55	96.0
	7.74	7.53	97.3
Doce Menor	3.89	3.91	100.5
	5.78	5.75	99.5
	7.74	7.81	100.9

Table 2. Potentiometric determination of saccharin in dietary products using Gran's method

Sample	Saccharin content (*mg/ml*), (*mg/gl*)* or (*mg/290 ml*)†		Rel. error %	Coefficient of variation
	Spectrophotometric	Potentiometric‡		
Assugrin	57.2	55.8 ± 3.0	−2.4	5.4
Dietil	50.1	48.0 ± 1.0	−4.2	2.1
Sucaryl	58.7	61.2 ± 3.0	+4.3	4.9
Sucaryl§	58.7	59.5 ± 0.5	+1.4	1.0
Doce Menor*	24.8	26.2 ± 0.5	+5.6	1.9
Diet Coke†	15.2	15.7 ± 0.7	+3.3	4.5

‡Assay values represent the average of six ($n = 6$) determinations per sample with a confidence level of 95%.

§Determined by standard addition method.

CONCLUSIONS

The potentiometric method for determination of saccharin reported in this paper is rapid, precise and of low cost. It is suitable for routine analysis of this sweetener in various dietary products.

Acknowledgements—The financial support of CNPq (Conselho Nacional de Desenvolvimento Cientifico e Technológico, Process 50.1638/91.1), FAPESP (Fundação de Amparo à Pesquisa do Estado de São Paulo, Process 91/2637-5) and also the scholarship furnished by CNPq to A.J.M.G.S. are gratefully acknowledged.

REFERENCES

1. *THE MERCK INDEX—An Encyclopedia of Chemicals and Drugs*, 8th ed., pp. 927–928, Merck & Co., INC, New Jersey, 1968.
2. M. S. Oakley, *J. Assoc. Off. Agric. Chem.*, 1947, **30**(3), 492.
3. AOAC Official Methods of Analysis, 1984, Method 20202, 405.
4. A. M. Lasheen, *Proc. Am. Soc. Hort. Sci.*, 1961, **77**, 135.
5. G. Sontag and K. Kral, *Frezenius Z. Anal. Chem.*, 1979, **294**(4), 278.
6. Y. Nakamura, *J. Fdhyg. Soc. Jpn*, 1975, **16**(6), 368; *Anal. Abstr.* 1977, **32**, 2F10.
7. M. M. Hussein, H. Jacin and F. B. Rodriguez, *J. Agric. Food Chem.*, 1976 **24**(1), 36.
8. P. P. Losada, J. S. Lozano and J. S. Gandara, *Anal. Bromatol.*, 1989, **XLI-1**, 177.
9. D. Coppini and A. Albasini, *Mitt. Geb. Lebensmitteluntersters Hyg.*, 1968, **59**(3), 239; *Chem. Abstr.*, 1969, **70**, 76503g.
10. T. Korbelak, *J. Assoc. Off. Anal. Chem.*, 1969, **52**, 487.
11. H. Koenig, *Fresenius' Z. Anal. Chem.*, 1971, **225**, 123.
12. J. Robert, *J. Assoc. Off. Anal. Chem.* 1971, **54**, 1140.
13. E. M. Ratchik and V. Viswanathen, *J. Pharm. Sci.*, 1975, **64**(1), 133.
14. C. J. Argoudelis, *J. Chromatogr.*, 1984, **303**(1), 256.
15. J. T. Hann and I. S. Gilkison, *J. Chromatogr.*, 1987, **395**, 317.
16. Y. Yamamoto, T. Kumamaru, Y. Hayashi, M. Yamate, T. Kobayashi and R. Tanaka, *J. Pharm. Soc. Jpn.*, 1968, **88**, 28.
17. Y. A. Beltagy, S. M. Rida and A. Issa, *Pharmazie*, 1974, **29**, 64.
18. A. Tanaka, N. Nose, T. Suzuki, S. Kobayashi and A. Watanabe, *Analyst*, 1977, **102**, 367.
19. E. Fernandez-Flores, A. A. Johnson, B. Leber, D. Larry and S. Lerner, *J. Assoc. Off. Anal. Chem.*, 1973 **56**(6), 1411.
20. P. G. Ramappa and H. Sanke Gowda, *Fresenius Z. Anal. Chem.*, 1978, **292**, 413.
21. P. G. Ramappa and A. N. Nayak, *Analyst*, 1983, **108**, 966.
22. A. Thimme Gowda, N. M. Made Gowda and K. S. Rangappa, *Anal. Lett.*, 1984, **17**(B18), 2129.
23. N. Hazemoto, N. Kamo and Y. Kobatake, *J. Assoc. Off. Anal. Chem.*, 1974, **57**(5), 1205.
24. A. Albert and E. P. Serjeant, *The Determination of Ionization Constants: A Laboratory Manual*, 3rd ed., p. 173, Chapman and Hall, New York, 1984.
25. M. Mascini, *Ion-Selective Electrode*, 1980, **2**, 17.
26. D. Midgley and K. Torrance, *Potentiometric Water Analysis*, pp. 86–97, John Wiley, New York, 1978.

Talanta, Vol. 40, No. 5, pp. 741–747, 1993
Printed in Great Britain.

0039-9140/93 $6.00 + 0.00

PRECONCENTRATION AND CATALYSIS IN REDUCTION OF ALIPHATIC ORGANOHALIDES USING SURFACTANT-COATED ELECTRODES*

HEPING ZHANG and JAMES F. RUSLING†
Department of Chemistry, Box U-60, University of Connecticut, Storrs, CT 06269-3060, U.S.A.

(*Received* 10 *August* 1992. *Revised* 16 *September* 1992. Accepted 21 *September* 1992)

Summary—Voltammetric reductions of several organohalide pollutants in films of didodecyldimethylammonium bromide (DDAB) and clay-DDAB cast onto pyrolytic graphite electrodes were examined. Direct reduction data show that the amount of accumulation in these liquid crystal films was larger for relatively nonpolar analytes such as trans-1,2-dibromocyclohexane than for chlorinated acids. The vicinal dibromides are probably taken up by hydrophobic regions of the films. Chlorinated acids were accumulated and reduced in DDAB films, but their direct reduction was partly blocked by the clay-DDAB films. Catalytic reductions using films containing metal phthalocyanines had good efficiencies for all substrates studied and shifted reduction potentials positive by 200–550 mV.

Solutions of dispersions of water-insoluble surfactants can be cast onto solid supports to make ordered films.[1–21] Results of X-ray diffraction, electron microscopy, and gel-to-liquid crystal transition temperatures close to those of bilayer vesicle suspensions of the same surfactants have been used to propose stacked, wavy multiple bilayer structures for these films.[1–15,19,20] A partially disordered structure of adjacent bilayer domains has been deduced on the basis of phase transition and electron microscopy studies of dialkyldimethylammonium films,[20] and a similar structure was proposed for phospholipid films based on electrochemistry of incorporated amphiphilic probes.[20] Surfactant films with multiple bilayer structures can also be prepared as intercalates between clay[8,17,20] or linear ionic polymer layers.[9–14]

Insoluble surfactants used for cast films typically have two or three hydrocarbon chains of 12 or more carbons. Permeability of these surfactant films is controlled by their phase. Neutral, water soluble solutes pass through films that are in the liquid crystal state, but permeability is poor in the solid-like gel phase.[8–13]

Ordered surfactant films have many potential uses in analytical chemistry.[15,16–20] They show permselectivity. Films of didodecyldimethylammonium bromide (DDAB) are impermeable to multiply charged hydrophilic cations in aqueous solution,[16] and DDAB-clay films are relatively impermeable to multiply charged anions and cations in solution.[18] Anionic redox catalysts in aqueous solutions can be introduced by ion exchange into liquid crystalline films of DDAB from aqueous solutions. Films incorporating anionic metal macrocyclic tetrasulfonates on electrodes[17] and clay-surfactant composite films containing neutral metal phthalocyanines have been used to catalyze reductions of trichloracetic acid.[18] Charge transport rates were much better for both types of films in liquid crystal phases than in solid-like gel states. Surfactant films loaded with metal phthalocyanine tetrasulfonates[19] or intercalated with clay colloids[18] gave stable signals for several weeks or more in aqueous electrolyte solutions. DDAB films without such stabilizing anions were usable for about a week.[16]

Since liquid crystal films of cationic surfactant are permeable to neutral or anionic organics, there are two components to electrochemical catalysis using them. The first is the usual electrochemical catalytic cycle. Represented in its simplest form:

$$P + e = Q \quad E^{\circ\prime}_{P/Q} \text{ (at electrode)} \qquad (1)$$

$$2\,Q + RX \rightarrow 2\,P + \text{Products (in film, rds)} \qquad (2)$$

in which the reduced form of the catalyst Q formed at the electrode reduces organohalide substrate RX at potential $E^{\circ\prime}_{P/Q}$, which is typically significantly positive of the potential of

*Part 12 of the series: Electrocatalysis in Organized Media.
†Author for correspondence.

direct, irreversible reduction of substrate RX. The current at $E^{\circ\prime}_{P/Q}$ is increased by the catalytic cycle in rough proportion to the square of the rate of the bimolecular rate-determining step (rds), equation (2). The film may also preconcentrate substrate RX. Enhanced RX concentration in the films would produce larger currents in the direct reduction than at bare electrodes, and perhaps increase rates of catalytic reductions via enhancement of the rate of the bimolecular rds.[22]

In this paper, we compare direct and catalytic reductions of several small, aliphatic organohalide molecules in DDAB and clay-DDAB films, with the aim of surveying possible voltammetric applications. DDAB was chosen because its films are liquid crystalline at ambient temperature,[8,16] and should be permeable to and perhaps preconcentrate the organohalides. In contrast, films of longer chain alkylammonium surfactants, such as dioctadecyldimethylammonium bromide, are in the solid-like gel state below 44–50°C, and show poor permeability and charge transport at ambient temperature.

Aliphatic organohalide molecules that are completely dehalogenated by reduced metal phthalocyanine catalysts were chosen. These compounds are "activated" by having a $-$COOH or another carbon-halogen group adjacent to a carbon-halogen bond attacked in the reaction.[23,24] The specific compounds studied were trichloroacetic acid, formed in water chlorination,[25] 3-chloroacrylic acid, a hydrolysis product of the soil fumigant Vorlex (1,3-dichloropropylene),[26] and two vicinal dihalides that serve as models for many aliphatic fumigants and pesticides.

EXPERIMENTAL

Chemicals

Didodecyldimethylammonium bromide (DDAB, 99+%) and cobalt phthalocyanine (CoPc) were from Eastman Kodak and used as received. Nickel phthalocyanine tetrasulfonic acid tetrasodium salt (NiPcTS), *trans*-3-chloroacrylic acid (CAA), 1,2-dibromobutane (DBB) and *trans*-1,2-dibromocyclohexane (DBCH) were from Aldrich. Trichloroacetic acid was from Janssen Chimica. Butanol was from Burdick & Jackson. Bentonite clay (Bentolite H) was from Southern Clay Products, cation-exchange capacity 80 mequiv/100 g. Other chemicals were analytical reagent grade.

Apparatus

Cyclic and square-wave voltammetry were done in three-electrode cells using a basal plane pyrolytic graphite (HPG-99, Union Carbide) cylinder as a working electrode, a platinum-wire as a counter electrode, and a saturated calomel electrode (SCE) as reference. The potentiostat was a BAS-100 electrochemical analyzer. Cells were thermostated at 25°C. PG cylinders ($A = 0.20$ cm^2) were sealed into heat shrinkable teflon tubes, as described previously.[17,19] Pyrolytic graphite (PG) electrodes were abraded to a rough finish with 400-grit SiC paper before coating.

Preparation of films

DDAB films were prepared by pipetting 10 μl of 0.1 *M* DDAB/chloroform onto a freshly abraded PG electrode, as described previously.[16] Chloroform was evaporated overnight in air. DDAB electrodes loaded with nickel phthalocyanine tetrasulfonate were prepared by soaking DDAB-PG electrodes in 1 m*M* NiPcTS solution overnight, then washing with distilled water. Clay-DDAB films and CoPc-Clay-DDAB films were cast from chloroform suspensions as described previously.[18]

Voltammetry

Procedures included compensation of the cell's ohmic drop and were described previously.[16–18]

RESULTS

Direct reductions

Scans by cyclic voltammetry after coated electrodes were equilibrated in solution for 10 min or more showed larger peak currents on DDAB coated electrodes than on bare PG [Fig. 1 (a)], as illustrated for 1,2-dibromobutane (DBB). Repetitive cyclic scans of the same equilibrated electrode gave much diminished peak currents [Fig. 1 (b)] on second and subsequent scans, consistent with the chemically irreversible reduction of DBB in the film. DBB is converted to olefin[27] which cannot be oxidized on the reverse scan to regenerate DBB. Thus, the film is depleted of DBB during the scan and an additional equilibration period is required to reload the film with analyte and regenerate the signal.

In general, the largest current enhancements were obtained with DDAB-PG electrodes and

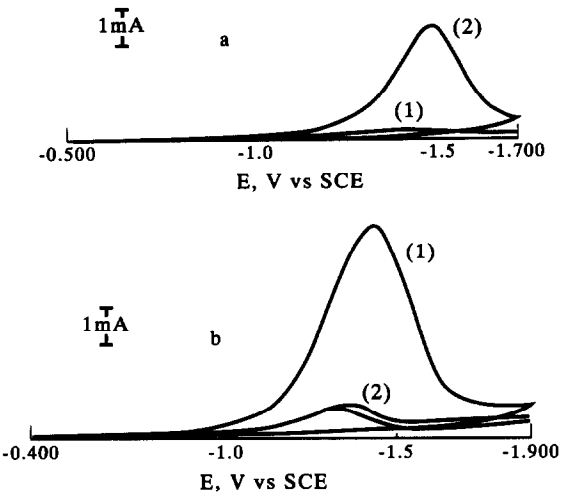

Fig. 1. Cyclic voltamperograms at 0.10 V/sec in 0.1*M* KBr solution containing 0.2 *M* 1-butanol and saturated with DBB (*ca.* 2.5 m*M*): (a) (1) bare PG electrode; (2) DDAB–PG electrode after equilibration; (b) Multiple scans on a different DDAB–PG electrode: (1) first scan; (2) scans 2–5.

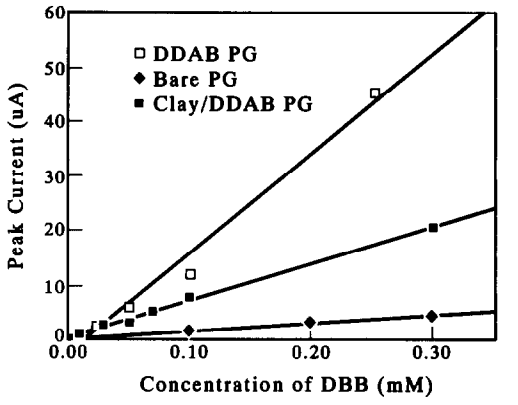

Fig. 2. Influence of concentration of DBB on peak current at 0.10 V/sec in 0.1 *M* KBr/0.2 *M* 1-butanol on bare PG, clay–DDAB–PG, and DDAB–PG electrodes.

the neutral DBB and *trans*-1,2-dibromocyclohexane (DBCH) analytes. DBCH gave the largest enhancement in peak currents compared to bare electrodes (Table 1), consistent with having the largest oil/water partition coefficient of the two dibromides.[28] Peak currents on clay–DDAB electrodes for DBCH and DBB were intermediate between those on DDAB–PG and bare electrodes.

Less dramatic current increases were found for trichloroacetic acid (TCA) and chloroacrylic acid (CAA) on DDAB electrodes (Table 1). The clay–DDAB electrodes gave smaller peak currents for these acids than bare electrodes.

Good linearity was found in plots of peak current *vs.* concentration in the 5 μM–1 m*M* range. This is illustrated for DBB in the lower concentration range (Fig. 2). Sensitivities were best for the neutral vicinal dihalides, with typical correlation coefficients of 0.994–0.998 for both types of coated electrodes.

Catalytic reductions

These reactions were done with NiPcTS–DDAB and CoPc–clay–DDAB electrodes, which had been used to catalyze reduction of trichloroacetic acid in earlier work.[17,18] All of the substrates were catalytically reduced by both electrodes.

Cyclic voltammetry of a NiPcTS–DDAB electrode clearly shows a nearly reversible, one-electron reduction peak[19] centered around −0.7 V (Fig. 3, top). The direct, irreversible reduction peak of TCA on a non-catalytic DDAB electrode can be seen at about −1.4 V (Fig. 3, middle). The use of a NiPcTS–DDAB electrode in a solution containing TCA gave a broad peak (Fig. 3, bottom) about 400 mV positive of the direct reduction. This new "catalytic" peak is larger than the peak for the NiPcTS–DDAB electrode in solutions without TCA, and has no anodic complement. This is because the reduced form of NiPcTS has reacted with TCA to regenerate NiPcTS in the film (cf. Scheme I) in a catalytic cycle. Similar results were obtained with CAA (Fig. 4), and catalytic and direct reduction peaks are of about equal heights. Catalysis shifts the peaks to more positive potentials.

Table 1. Voltammetric characteristics of direct reductions of organohalides*

Compound (Conc., m*M*)	DDAB–PG $-E_p$ (*V vs.* SCE)	DDAB–PG i_p (*mA*)	Clay–DDAB–PG $-E_p$ (*Vvs.*SCE)	Clay–DDAB–PG i_p (*mA*)	Bare PG $-E_p$ (*Vvs.*SCE)	Bare PG i_p (*mA*)
DBCH (< 1)†	1.48	0.25	1.30	0.18	1.42	0.007
DBB (2.5)†	1.60	0.29	1.30	0.07	1.43	0.03
TCA (5)	1.45	1.0	1.30	0.14	1.40	0.25
CAA (5)	1.50	0.29	1.65	0.08	1.40	0.20

*Scan rate 0.10 V/sec, 0.1 *M* KBr in water; DBCH and DBB solutions were 0.2*M* in butanol.
†Estimated concentrations for saturated solutions.

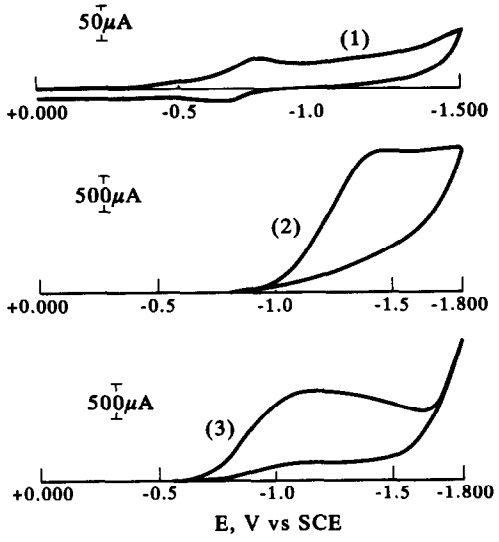

Fig. 3. Cyclic voltamperograms at 0.10 V/sec in 0.1 *M* NaCl solution: (1) NiPcTS–DDAB electrode after loading in 1 m*M* NiPcTS; (2) DDAB–PG electrode with 10 m*M* TCA in solution; (3) NiPcTS–DDAB electrode with 10 m*M* TCA in solution.

As observed previously, currents for CoPc in CoPc–clay–DDAB films are quite small.[18,20] The Co(II)/Co(I) reduction can be observed by square wave voltammetry at about −0.45 V, with a second wave due to ligand reduction at about −1.2 V [Fig. 5 (a)]. Large catalytic waves were found when these electrodes were used in solutions of any of the analytes [Fig. 5 (b)].

Electrochemical catalytic reactions can be characterized by their catalytic efficiencies, *i.e.*, the ratio of catalytic peak or plateau current (i_{cat}), to the peak current of the catalyst (i_d) in the absence of a reducible substrate. This quantity is roughly proportional to the square of the rate constant of the reaction of reduced catalyst with substrate.[22] Voltammetry with the two types of coated catalytic electrodes gave good efficiencies for all the organohalides studied (Table 2). The catalytic reductions were at potentials about 200–550 mV more positive than direct reductions of the substrates on the same electrodes (Table 2). For the vicinal dibromides,

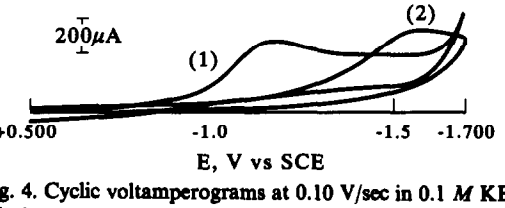

Fig. 4. Cyclic voltamperograms at 0.10 V/sec in 0.1 *M* KBr solution containing 5 m*M* 3-chloroacrylic acid: (1) NiPcTS–DDAB electrode; (2) DDAB–PG electrode.

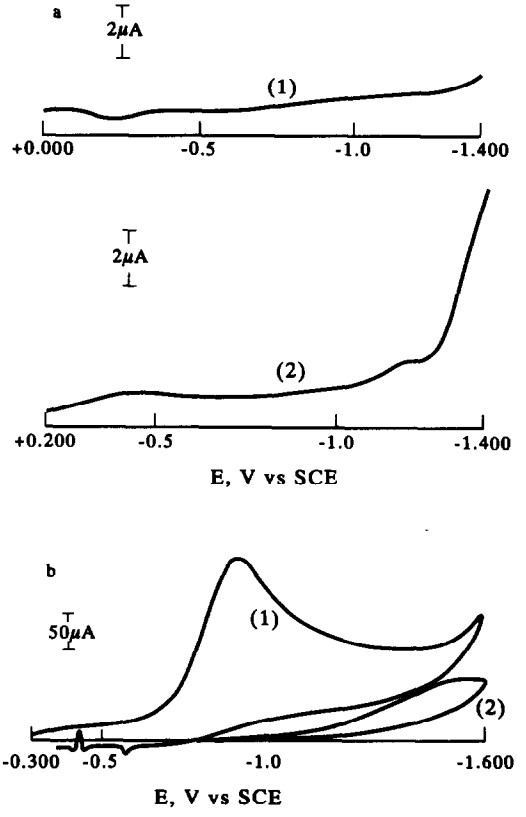

Fig. 5. Voltamperograms in 0.1 *M* KBr/0.2 *M* butanol solutions: (a) square wave voltamperograms at 15 Hz, 25 mV pulse amplitude, 4 mV step: (1) PG electrode; (2) CoPc–clay–DDAB electrode. (b) cyclic voltamperograms at 0.10 V/sec in solutions saturated in DBB: (1) CoPc–clay–DDAB electrode; (2) clay–DDAB electrode.

catalytic reductions on the CoPc–clay–DDAB electrodes were about 250 mV positive of those on NiPcTS–DDAB electrodes. Catalytic efficiencies on the two types of electrodes are not directly comparable because the peak current of the CoPc–clay–DDAB electrode is so small in the absence of a reducible substrate. Catalytic currents on the NiPcTS–DDAB electrodes were larger than on the CoPc composite electrodes.

A peak for catalytic reduction of TCA at CoPc–clay–DDAB electrodes was also found at about −0.6 V, as reported previously.[18] It is likely that this reaction, as well as those of the vicinal dibromides, involves the Co(II)/Co(I) redox couple of Co(II)Pc. Catalytic reductions at −1.1 V in these films may involve addition of two electrons to the catalyst. Reductions catalyzed by NiPcTS–DDAB films probably involve addition of electrons to the ligand of the catalyst, as found for similar reactions in microemulsions.[29]

Coated electrodes were used for several days with no gross loss in performance. However,

Table 2. Potentials and efficiencies for catalytic reductions of organohalides*

Compound (m*M*)	NiPcTS–DDAB $-E_p$ (*V vs.* SCE)	NiPcTS–DDAB i_{cat} (*mA*)	NiPcTS–DDAB i_{cat}/i_d	CoPc–Clay–DDAB–PG $-E_p$ (*V vs.* SCE)	CoPc–Clay–DDAB–PG i_{cat} (*mA*)	CoPc–Clay–DDAB–PG i_{cat}/i_d
DBCH (< 1)†	1.15	0.51	4	0.90	0.17	177
DBB (2.5)†	1.20	0.76	7	0.95	0.21	218
TCA (5)	1.10	0.58	7	(0.6)‡,1.1	0.12	125
CAA (5)	1.15	0.33	4	1.1	0.13	135

*Scan rate 0.10 V/sec, 0.1 *M* KBr in water; DBCH and DBB solutions were 0.2 *M* in butanol.
†Estimated concentrations for saturated solutions. ‡Catalytic peak at −0.6 V reported previously, see Ref. 17.

day to day reproducibility was not satisfactory, and such electrodes would need daily calibration in real analytical situations.

Influence of alcohol

Butanol was used in DBB and DBCH solutions to improve solubilities. Coated electrodes in solutions containing butanol may deteriorate a bit faster, but the effect was not dramatically noticeable. Also, alcohol was previously shown to increase the fluidity of surfactant films, giving larger currents for ferrocyanide incorporated into DDAB films.[16] This was also observed in the present work (Fig. 6), as illustrated for DBB. Linear increases in peak current with butanol concentration were found.

DISCUSSION

Direct reductions

Aliphatic vicinal dihalides undergo two-electron reductions at cathodes to yield olefins.[27] Halogenated carboxylic acid derivatives are reductively dehalogenated, with hydrogen replacing halogen.[30] Both are two-electron irreversible reductions. The organohalide analytes need to enter the films before being reduced. After reductions at relatively low scan rates, the films appear to be depleted of the analyte, and further equilibration is needed to restore the signal.

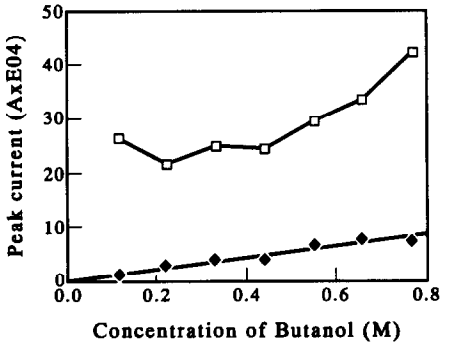

Fig. 6. Influence of butanol on peak current in 0.1 *M* KBr/0.2 *M* butanol solutions saturated in DBB (□) cyclic voltammetry at 0.10 V/sec at DDAB–PG electrodes; (◆) square wave voltammetry at NiPcTS–DDAB electrodes, 15 Hz, 25 mV pulse amplitude, 4 mV step.

Peak currents for direct reductions in the films compared to those on bare electrodes can be taken as a measure of the relative amount of organohalide accumulated during equilibration. For DDAB films, the amount of accumulation of analytes followed the order DBCH > DBB > TCA > CAA. Results for the vicinal dibromides are in line with oil/water partition coefficients, which for DBCH is an order of magnitude larger than for DBB.[28] This suggests that the vicinal dibromides reside at relatively hydrophobic sites in the DDAB films, probably in the vicinity of the hydrocarbon tails of the surfactant bilayers. Chlorinated acids could enter the films either in the anion or acid forms. Since the neutral acid forms are still quite polar, their hydrophobic interactions with the hydrocarbon tails of the surfactant are expected to be weak. The anions, on the other hand, need to compete with Br^- ions to enter the films by ion exchange.

The order of accumulation of analytes was the same for the clay–DDAB and DDAB films. Currents for TCA and CAA were smaller on clay–DDAB electrodes than on bare electrodes, indicating that access to the electrode is partly blocked by the composite film. Clay–DDAB films do not act as ion exchangers. Therefore, this blocking effect is consistent with TCA and CAA having entered the DDAB films, which *are* anion exchangers,[16] mainly by an ion exchange process.

In a practical sense, the best enhancement in sensitivity was found for the neutral DBCH and DBB, although a four-fold increase in current compared to bare electrodes was also found for TCA with DDAB electrodes. Good linearity of voltammetric peak current was found in the micromolar concentration range. Thus, these films show promise for the determination of relatively hydrophobic electroactive species in

water. Addition of butanol to the solution can be used to enhance sensitivity, although perhaps at some expense to long term stability. However, the film casting procedure is so simple that coated electrodes can be made readily by the user on demand.

Catalytic reductions

The main advantage to catalytic reductions in the films are shifts to less reducing (*i.e.*, more positive) potentials. Peak currents in the catalytic reductions were comparable to those in direct reductions, so that sensitivities would not be much better than for direct reductions. However, the positive potential shift from the catalysis might remove the peak from interfering peaks that might occur at the more reducing potential of the direct reduction of the analyte.

The low current for the CoPc–clay–DDAB electrodes in the absence of reducible substrate has been traced to crystallization of CoPc within the composite film matrix.[20] Thus, all of the catalyst in the film may not be available for reaction. On the other hand, concentrations of up to 0.3 *M* NiPcTS can be achieved in DDAB films, leading to the higher observed catalytic currents. From a practical point of view, catalytic clay-composite films may be more suitable in some situations. Even though the catalytic currents are somewhat smaller, they are measured against the background of the very low current of the composite films.

A better surfactant coated electrode for activated organohalides might be prepared with a catalyst with a much lower reduction potential. This should further decrease the possibility of encountering reducible interferences in real samples. This type of electrode, probably with a much thinner catalytic film, might also be useful on a larger scale for treatment of contaminated water. Work along these lines is currently underway in our laboratories.

CONCLUSIONS

This work shows that neutral alkyl vicinal dihalides can be preconcentrated in easily prepared liquid crystal films of insoluble surfactants and clay-surfactant composites on electrodes, giving larger voltammetric sensitivities. Trichloroacetic acid can be preconcentrated in surfactant films, but not in the composites. In practice, such electrodes would probably require daily calibration. In principle, preconcentration of neutral organohalides could also be done with appropriate polymeric coatings.[31] Similarly, phospholipid films on electrodes[32–35] should have preconcentration properties in their liquid crystal states. However, to our knowledge, preconcentration of organohalides has not been studied for polymer or phospholipid-coated electrodes.

Analytes gave signals at significantly less negative potentials by using surfactant films with incorporated catalysts, which may be useful in avoiding easily reducible interferences. DDAB films are impermeable to multiply charged anions,[16] while composite films reject multiply charged ions of both signs.[18] Thus, film permeabilities combined with catalysis may provide desirable selectivity in some analytical applications.

Acknowledgements—This work was supported by U.S. PHS grant No. ES03154 awarded by the National Institute of Environmental Health Sciences.

REFERENCES

1. N. Nakashima, R. Ando and T. Kunitake, *Chem. Lett.*, 1983, 1577–1580.
2. T. Kunitake, M. Shimomura, T. Kajiyama, A. Harada, K. Okuyama and M. Takayanagi, *Thin Solid Films*, 1984, **121**, L89–91.
3. Y. Ishikawa and T. Kunitake, *J. Am. Chem. Soc.*, 1986, **108**, 8300–8302.
4. I. Hamachi, S. Noda and T. Kunitake, *ibid.*, 1990, **112**, 6744.
5. I. Hamachi, T. Honda, S. Noda and T. Kunitake, *Chem. Lett.*, 1991, 1121.
6. I. Hamachi, S. Noda and T. Kunitake, *J. Am. Chem. Soc.*, 1991, **113**, 9625.
7. Y. Ishikawa and T. Kunitake, *ibid.*, 1991, **113**, 621.
8. Y. Okahata and A. Shimizu, *Langmuir*, 1989, **5**, 954.
9. M. Shimomura and T. Kunitake, *Polymer J.* 1984, **16**, 187.
10. T. Kunitake, A. Tsuge and N. Nakashima, *Chem. Lett.*, 1984, 1783.
11. N. Nakashima, M. Kunitake, T. Kunitake, S. Tone and T. Kajiyama, *Macromolecules*, 1985, **18**, 1515.
12. Y. Okahata, G. Enna, K. Taguchi and T. Seki, *J. Amer. Chem. Soc.*, 1985, **107**, 5300.
13. Y. Okahata and G. Enna, *J. Phys. Chem.*, 1988, **92**, 4546.
14. Y. Okahata, G. Enna and K. Takenouchi, *J. Chem. Soc. Perkin II*, 1989, 835.
15. Y. Okahata and H. Ebato, *Anal. Chem.*, 1991, **63**, 203.
16. J. F. Rusling and H. Zhang, *Langmuir*, 1991, **7**, 1791.
17. J. F. Rusling, N. Hu, H. Zhang, D. Howe, C.-L. Miaw and E. Couture, in *Electrochemistry in Microheterogeneous Fluids*, R. A. Mackay, and J. Texter, (eds.), VCH Publishers, New York, 1992, pp. 303–318.
18. N. Hu and J. F. Rusling, *Anal. Chem.*, 1991, **63**, 2163.
19. N. Hu, D. J. Howe, M. F. Ahmadi and J. F. Rusling, *ibid.*, 1992, **64**, 3186.
20. J. F. Rusling, N. Hu and M. F. Ahmadi, *Langmuir*, 1992, **8**, 2455.

21. M. T. Rojas, M. Han and A. E. Kaifer, *ibid.*, 1992, **8**, 1627.
22. J. F. Rusling, *Accts Chem. Res.*, 1991, **24**, 75.
23. T. F. Connors, J. V. Arena and J. F. Rusling, *J. Phys. Chem.*, 1988, **92**, 2810.
24. J. F. Rusling, C. L. Miaw and E. C. Couture, *Inorg. Chem.*, 1990, **29**, 2025.
25. E. Pelizzetti, C. Minero and V. Maurino, *Adv. Coll. Interface Sci.*, 1990, **32**, 271.
26. T. F. Connors, J. D. Stuart and J. B. Cope, *Bull. Environ. Contam. Toxicol.*, 1990, **44**, 288.
27. J. Casanova and H. R. Rogers, *J. Org. Chem.*, 1974, **39**, 2408.
28. A. Owlia, Z. Wang and J. F. Rusling, *J. Am. Chem. Soc.*, 1989, **111**, 5091.
29. G. N. Kamau, N. Hu and J. F. Rusling, *Langmuir*, 1992, **8**, 1042.
30. P. J. Elving and C.-S. Tang, *J. Am. Chem. Soc.*, 1950, **72**, 3244.
31. J. Wang, in *Electroanalytical Chemistry*; Vol. 16, pp. 1–88. A. J. Bard, (ed.), Marcel Dekker; New York, 1989.
32. O. Chastel, J.-M. Kauffmann, G. J. Patriarche and G. D. Christian, *Anal. Chem.*, 1989, **61**, 170.
33. O. J. Garcia, P. A. Quintela and A. E. Kaifer, *ibid.*, 1989, **61**, 979.
34. J.-M. Kauffmann, O. Chastel, G. Quarin, G. J. Patriarche and M. Khodari, *Bioelectrochem. Bioenergetics*, 1990, **23**, 167.
35. J. Wang and M. Ozsoz, *Analyst*, 1990, **115**, 831.

Talanta, Vol. 40, No. 5, pp. 749–756, 1993
Printed in Great Britain.

0039-9140/93 $6.00 + 0.00

ORGANICALLY-DOPED SOL–GEL BASED TUBE DETECTORS: DETERMINATION OF IRON(II) IN AQUEOUS SOLUTIONS

I. KUSELMAN* and O. LEV

Division of Environmental Sciences, School of Applied Science and Technology, The Hebrew University of Jerusalem, Jerusalem 91904, Israel

(*Received* 14 *July* 1992. *Revised* 18 *September* 1992. *Accepted* 18 *September* 1992)

Summary—A novel type of disposable sensor for the determination of iron(II) in aqueous solution is described. The iron sensor serves to exemplify a new class of disposable field tests for field analysis of water pollutants. The sensors are comprised of capillary glass tubes filled with porous sol–gel silica powder doped with *o*-phenanthroline. When a sample solution is passed through a tube detector the iron ions are complexed by the immobilized *o*-phenanthroline and a stained section of the capillary develops. Metrological characteristics of these detectors including precision and accuracy and chemical interferences by heavy metals and humic acids are discussed.

Length of stain sensors are frequently used by occupational health and indoor air practitioners for the detection of air borne pollutants.[1,2] The tube detectors are comprised of glass tubes, filled with silica powder impregnated with specific photometric reagents. Leaching of the impregnated reagents hinders their application for water diagnosis. In principle, direct chemical derivatization of silica glass by photometric reagents may be used to circumvent this obstacle and improve the stability and shelf life of these detectors. Indeed, synthesis of porous glass derivatized with several colorimetric reagents has been reported.[3–6] However, complexation capacity of such glasses is relatively low and the ability to form multiple ligand complexes with metal ions is hindered by the tight bonding of the reagents to the glass. For example, iron(II) forms—almost exclusively—a triple ligand complex with *o*-phenanthroline, while Zaytsev and Trophymchuk[6] report a two ligand complex of *o*-phenanthroline derivatized silica with divalent iron. Alterations in coordination stoichiometry affect the complexation capacity and specificity of such potential detectors. Recently, the sol–gel doping procedure has evolved as an efficient method to encapsulate organic compounds in silica glass.[7,8] The method is based on the introduction of the organic dopants with the reaction precursors during the hydrolysis/polycondensation of alkoxisilanes to form silica glass.[9] Application of this method for the preparation of colorimetric[10,11] and fluorometric sensors[12,13] and prototypes of on-line fibre optic sensors have been reported.[14,15] In a recent paper[16] we demonstrated that sol–gel technology can be used to mold organically doped silica powder for length of stain detectors suitable for water analysis. In this paper a systematic study of a representative type of water detector is undertaken, in order to evaluate potential utilization in water analysis.

Iron is a widespread pollutant, with a special relevance to the water industry because it frequently serves as a flocculation agent. Recommended[17] procedures for its aqueous determination include atomic absorption spectroscopy, inductively coupled plasma and polarographic techniques. These techniques are very sensitive but require complex analytical instruments and therefore are less suitable for field analysis. Future field instruments may rely on the evolution of electrochemical methods using modified electrodes, which promise high sensitivity and simple instrumentation.[18–20] Currently, however, most rapid field tests rely on the colorimetric determination of the orange–red chelate of divalent iron with *o*-phenanthroline under reducing conditions. This is a reliable and pH insensitive technique, which is approved by the Standard Methods.[17] However, even this technique requires a comparator and a certain level of wet chemistry. Another relevant

*Current address: National Physical Laboratory, Jerusalem 91904, Israel.

procedure for determiantion of iron(III) in aqueous solution is based on complexation of iron with soluble *o*-phenanthroline and subsequent filtration of the complex through a fixed bed of silica gel grains.[21] This technique comes a step closer to length of stain detectors but does not eliminate the need for "wet chemistry" and therefore is less amenable for field testing. In this paper we evaluate the characteristics of iron sol–gel tube detectors, that will serve to model this new class of field tests.

EXPERIMENTAL

Reagents

Analytical grade reagents and triply distilled water were used unless stated otherwise. Tetramethoxysilane was purchased from ABCR. Iron(II) stock solution (10m*M*) was prepared by dissolving the required amount of $FeSO_4 \cdot 7H_2O$ in distilled water. Hydroxylamine hydrochloride (1.3m*M*) was used to prevent oxidation of divalent iron. Sample solutions were buffered to pH = 4 by 0.1m*M* acetate buffer. Interference studies were conducted using $NiSO_4 \cdot 6H_2O$, $Zn(CH_3COO)_2 \cdot 2H_2O$, $Cr(NO_3)_3 \cdot 9H_2O$, $Hg(CH_3COO)_2$, $CdCl_2 \cdot H_2O$, $AgNO_3$, $(NH_4)_6Mo_7O_{24} \cdot 6H_2O$, $Bi(NO_3)_3 \cdot 5H_2O$ and humic acid sodium salts (Aldrich).

Glass preparation

The experiments were carried out using doped sol–gel glasses prepared according to standard sol–gel procedures:[9,22] *e.g.*, 2.5 ml of tetramethoxysilane, 3.0 ml of 0.1% *o*-phenanthroline in methanol and 2.9 ml of 0.5m*M* sodium hydroxide were mixed, allowed to gel for approximately three days and dried to constant weight (*ca.* 2.0 g) at 41° for approximately two weeks. The final concentration of *o*-phenanthroline in the dry glass is *ca.* 0.15%. After drying, the glasses were crushed in a porcelain cup, sieved by a sieve shaker and selected fractions were collected for further experiments.

Preparation of tube detectors

Glass capillaries (0.7-mm inside diameter and 10-cm length) were filled to *ca.* 75% of their length with sol–gel grains and stoppered at both ends by 3-mm filter paper to hold the glass bed in place. In some experiments plastic tubes (2-mm inside diameter and 20-cm length) were connected to the downstream side of the glass capillaries in order to hold the excess volume of solution that passed through the sensor (Fig. 1). Plastic tubes permit accurate determination of the sampled volume by a simple length measurement with no need for analytical scale and with minimal evaporation loss.

Measurement procedure

In the simplest measurement procedure one end of the tube detector is immersed *ca.* 2-mm deep in a sample solution and capillary forces drive the solution upward through the tube detectors. As the colorless front of the sampled solution advances upwards, a second red front marking the upper end of the stained portion of the sol–gel doped glass ascends (Fig. 1). The length of the stained portion of the sol–gel glass can be measured after an adequate amount of solution has passed through the sensor. Hydrostatic pressure or external pumping were applied in order to sample larger volumes through the sensor. To achieve this, the tube detectors (the capillaries connected with the plastic tubes) were dipped into vertical tubes filled with the sample solutions [Fig. 1(b)]. In some experiments a home made pumping device comprising a plastic syringe connected to a simple piston mechanism was used in order to inject the sample slowly through the detecting capillary [Fig. 1(c)]. The measuring procedure currently takes 15 min or more, depending on the sampled volume and grain size.

Interference evaluation

Evaluation of chemical interferences was conducted by repeating iron analysis in the presence of each of the interfering species mentioned in the Standard Methods[17] and comparing the results with a measurement of a blank solution containing iron with no interfering substance. All the solutions were prepared according to the reagent preparation procedures above.

RESULTS AND DISCUSSION

Calibration

A calibration curve for determination of iron can describe the length of stain formed after either constant sampling time or constant sampled volume. In practice, constant volume calibration curves are more accurate since they eliminate flow rate drifts. On the other hand, constant volume techniques require careful monitoring (or manual attendance) of the volume in order to terminate the analysis before an excess volume is sampled. A third, intermediate

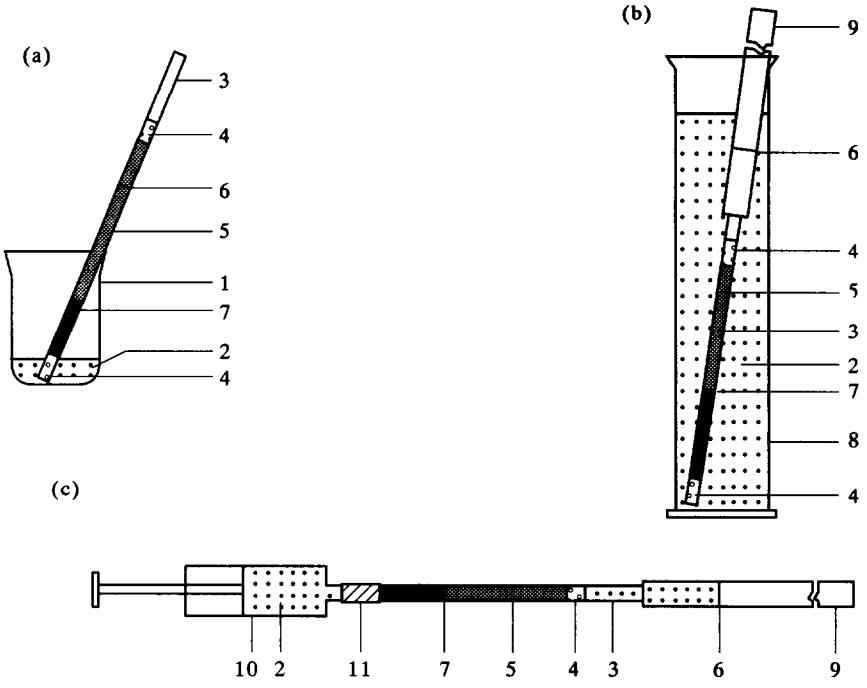

Fig. 1. Schemes of tube detectors using alternative sampling modes: a. capillary force; b. hydrostatic pressure; c. external pumping. 1. beaker, 2. sample solution, 3. capillary tube, 4. paper plug, 5. sol–gel glass powder, 6. solution front, 7. color front, 8. cylinder, 9. auxiliary (plastic) tube, 10. syringe, 11. rapid connector, 12. positioning mechanism.

procedure can be employed when the evolution of the length of stain is proportional to the sampled volume, *i.e.*, measure the length of stain after constant sampling time and correct the result for differences in the sampled volumes. The auxiliary plastic tubes (Fig. 1) are convenient tools that accumulate and measure the sampled volume. When an auxiliary tube with radius r_a filled to a level l_a, is connected to a capillary of length l_c and radius r_c, the sampled volume can be expressed as

$$V = 3.14(l_c\, r_2^c\, v_f + l_a\, r_a^2) \qquad (1)$$

where v_f represents the void fraction (dimensionless) of the packed capillaries. Now, taking $v_f = 1$, V can be approximated by:

$$V = 3.14\ (l_c\, r_c^2 + l_a\, r_a^2) \qquad (2)$$

Figure 2 depicts a typical dependence of the length of stain S (mm) propagation on the sampled volume. These experiments were conducted using capillary suction of 3.0mM divalent iron solution through a detector filled with 0.1–0.2 mm glass grains doped with 1.7% *o*-phenanthroline (sampling duration = 15 min). After an initial evolution time the front stablizes and propagation velocity becomes proportional to the sampled volume, indicating equilibrium control. Therefore, it is convenient to express the calibration curves as a relative length of stain R_l versus the concentration of the analyte: R_l is defined as the ratio (in percent) between the volume of the coloured bed and the sampled volume:

$$R_l = 100\ S\ r_c^2/(l_c\, r_c^2 + l_a\, r_a^2) \qquad (3)$$

When capillary suction is the only driving force, the sample fills only the volume of the packed bed, auxiliary tubes are not needed and equation (4) can be used directly:

$$R_l = 100\ S/l_c \qquad (4)$$

l_c now stands for the length of the packed bed section. Thus, calibration curves depicting S *vs.* C at constant l_c can be used.

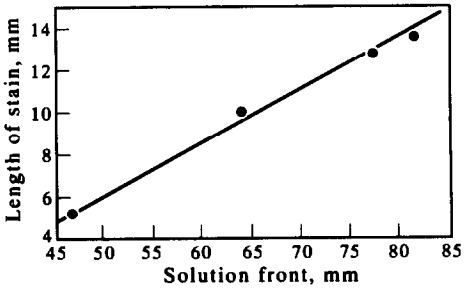

Fig. 2. Evolution of the length of stain. The sampled volume is expressed in units of length of wetted section.

Analysis of calibration data

Figure 3 (after data reproduced from[16]) depicts two calibration curves describing the relative length of stain as a function of iron concentration in two working ranges: Fig. 3(a) depicts a calibration curve of a sensor operated under capillary forces at relatively high concentrations (0.5–10.0mM) the sensor comprises glass grains (smaller than 0.1 mm) doped with 1.7% o-phenanthroline. Approximately 0.02 ml of solution were sufficient to produce such a response. Curve B depicts sensor response in the low concentration range (0.01–0.1mM). Larger samples (*ca.* 0.5 ml) were required to produce significant coloured sections and therefore hydrostatic driving force (0.05 atm) was applied. Glass powder (0.1–0.2 mm) doped with 1.0% o-phenanthroline was used. The concentration of o-phenanthroline in the glass was set as a compromise between considerations regarding the length of the coloured section (favoured by lower o-phenanthroline concentrations) and colour contrast, which becomes more intense, when higher concentrations of ligand are used. Leaching of the reagent becomes significant at exceedingly high concentrations of o-pehnanthroline and then a pretreament to wash the easily leachable molecules of dopant may be required prior to packing of the capillaries. At the level of o-phenanthroline, used in this experiment, the colour fronts were sharp, could be clearly distinguished within $+/-0.1$ cm and leaching pretreatment was not required. The size of the glass grains was determined as a compromise between resolution (favouring smaller grains) and analysis time (favouring larger grains). When large particles and a short analysis period are used intraparticle diffusion becomes significant and affects the selection of the optimal particle dimensions.

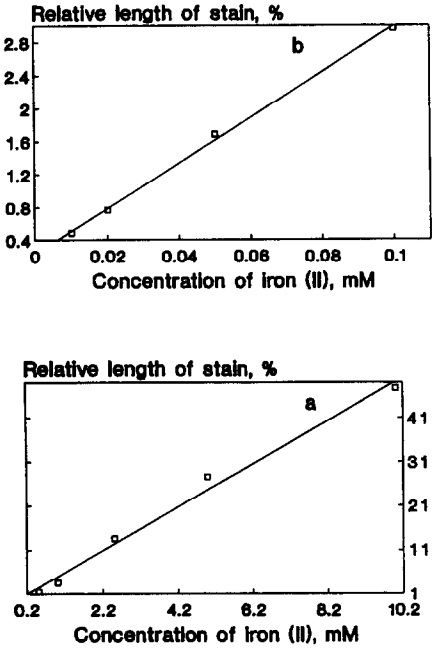

Fig. 3. Calibration curves of iron tube detectors: a. 0.5–10mM; b. 0.01–0.1mM.

The values of R_l in the high iron concentration range [Fig. 3(a)] are best fitted by

$$R_l = 0.07 + 4.91C \quad (5)$$

with standard deviation $S_{ad} = 2.2\%$ and correlation coefficient $R = 0.989$, where C represents iron concentration in mg/l. The values of R_l in the low iron concentration range [Fig. 3(b)] are best fitted by

$$R_l = 0.23 + 27.6C \quad (6)$$

with $S_{ad} = 0.06\%$ and $R = 0.998$.

Precision

Repeatability evaluation[23] in the two working ranges was based on 24 identical measurements at $C = 10$mM and 25 repeated measurements at $C = 0.1$mM. The tube detectors were prepared using the same procedure used for the preparation of the calibration curves in Fig. 3. Frequency histograms depicting the percent of measurements falling in the corresponding R_l ranges are presented in Fig. 4(a) and (b). For $C = 10$mM [Fig. 4(b)] the mean relative stain length, $R_{l,av} = 50.04\%$. The relative standard deviation of the measurements is $S_r = 1.35\%$. The histogram in Fig. 4(b) summarizes the measurements conducted at 0.1mM. Here, $R_{l,av} = 3.03\%$ and $S_r = 2.65\%$. By comparison, the reliability of visual determination using nessler tubes is approximately 5–10% and for photometric determination (using a pectrophotometer) it is approximately 3%.[17]

The histograms of Fig. 4 deviate from normal distribution and are skewed towards high R_l values. This phenomenon although barely noticeable in the high concentration range [Fig. 4(b)] is indeed significant at $C = 0.1$mM. This asymmetry can be attributed to a mechanism shift from equilibrium domination to one influenced by intraparticle diffusion. Therefore, the deviation from the normal distribution is more significant when larger grains and external driving force are used.

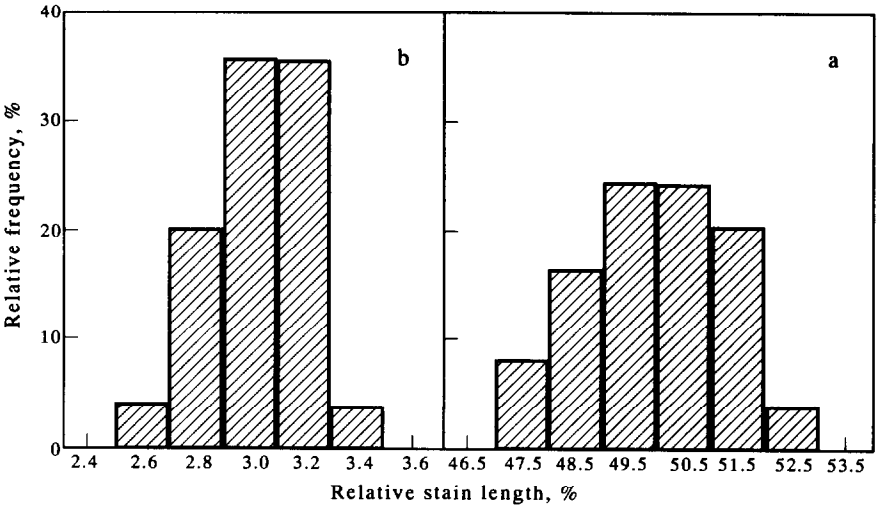

Fig. 4. Frequency histograms for iron determination by tube detectors: a. 10mM; b. 0.1mM.

Bias and accuracy

The frequency histograms of Fig. 4 can be used to estimate the bias[23] of the technique. Since the "true" concentrations of iron(II) are known ($C_t = 0.1$mM or 10mM) the sample bias (B) can be calculated by $B = C_{av} - C_t$ where C_{av} = average concentration. From Fig. 4(a) and equation (5), $C_{av} = 10.18$mM and the standard deviation of the determined concentration $S_c = 0.27$mM. By analogy $C_{av} = 0.101$mM and $S_c = 0.006$mM for Fig. 4(b) and equation (6). The relative error in the preparation of the standard solution is approximately 2%, since hydrated iron salts were used for the stock solutions (*i.e.*, the standard deviation of C_t is $S_{st} = 0.2$mM at $C = 10$mM and $S_{st} = 0.002$mM at $C = 0.10$mM). Analytical techniques are considered to be sufficiently accurate when the difference between the systematic error of analysis and the random error in the preparation of the standard solutions are insignificant relative to the random error of the analysis.[24] It has recently been demonstrated[25] that this condition is guaranteed, at 95% confidence level, for normalized standard deviation $S_{st}/S_c = 0.8$ when $B/S_c < 0.7$ and for $S_{st}/S_c = 0.4$ when $B/S_c < 0.3$. The results of Fig. 4(a) indicate that $S_{st}/S_c = (0.2/0.27) = 0.8$ (approximated to a larger value) and $B/S_c = 0.18/0.27 = 0.67$. Likewise, Fig. 4(b) indicates that $S_{st}/S_c = 0.4$ and $B/S_c = 0.17$. Therefore, in both cases the accuracy demands are easily met.

The metrological characteristics of this method are particularly encouraging since the repeated experiments (for construction of Fig. 4) were independent of the calibration experiments. These experiments were conducted using different batches of doped sol–gel glasses, prepared by two different experimenters, and in fact more than 6 months elapsed between the construction of the calibration curves and the metrological studies.

Interferences

Interferences to the colorimetric determination of iron by phenanthroline chelate are well studied,[26,27] thermodynamic chelation data are available[28,29] and detailed procedures to mask some of the interferences have been devised.[17] Tube detectors and liquid photometry employ the same chelates but since the underlying mechanism of tube detectors is more complex, different effects of interfering species are to be expected. The study included the species mentioned in Standard Methods.[17] Each interference analysis was repeated at three interference levels: identical to the molar concentration of ferrous ions; five times this concentration; and 10 or 25 times (molar ratio) larger. The results of the interference studies are described in Table 1 along with the relevant thermodynamic complexation values. In some cases (*e.g.*, copper and nickel) the tube detectors exhibit better characteristics than liquid analysis and in others (*e.g.*, chromium and zinc) the effect of interfering species is more significant than the corresponding liquid analysis.

Classification of modes of interference may help gain a better insight into the reason for the different role of competing chemical specieson tube detection and conventional liquid colorimetry (or photometry). Five different

Table 1. Interferences and stability constants of metals and humic acids

Interfering compound	Relative interference						Stability constants				Recommended interference threshold[18]
	Fe [M]	%i	[M]	%i	[M]	%i	$^{-}pK_1$	$^{-}pK_2$	$^{-}pK_3$	$^{-}p\beta_3$	
Fe(II) ~								5.8		21.5	
Ni(II) ~ 5 m*M*	5.ppm	NS	25.ppm	NS	250ppm	11%	8.7	8.2	7.8	24.7	2.ppm
Co(II) ~ 5 m*M*	5.ppm	NS	25.ppm	11%	250ppm	22%	7.2	6.7	6.0	19.9	5.ppm
CU(II) ~ 5 m*M*	5.ppm	NS	25.ppm	NS	250ppm	11%	9.1	6.8	5.0	20.9	5.ppm
ZN(II) ~ 1 m*M*	1 m*M*	NS	5 m*M*	250%	10 m*M*	316%	6.5	5.6	5.0	17.1	> 10 × [Fe]
Cr(III) ~ 1 m*M*	1 m*M*	180%	5 m*M*	220%	10 m*M*	240%					> 10 × [Fe]
Bi(II)*1 m*M*	1 m*M*	NS	5 m*M*	NS	10 m*M*	NS					precipitate
Cd(II)*1 m*M*	1 m*M*	NS	5 m*M*	NS	10 m*M*	NS	5.8	4.8	4.2	14.8	"
Hg(II)*1 m*M*	1 m*M*	NS	5 m*M*	NS	10 m*M*	NS		19.6	3.7	23.3	"
Mo(II)*1 m*M*	1 m*M*	NS	5 m*M*	NS	10 m*M*	−50%					"
Ag(I)*1 m*M*	1 m*M*	NS	5 m*M*	NS	10 m*M*	−15%	5.0	7.0		"	
Humic acids ~ 1 m*M*	56ppm	NS	280ppm	NS	560ppm	NS					

~ glasses doped by 1% *o*-phenanthroline; *glasses doped by 0.15% *o*-phenanthroline, %i = .
NS = not significant.
ppm = mg/L.
$K_1 = ([M^{2+}]\,[L])/[ML^{2+}]$
$K_2 = ([ML^{2+}]\,[L])/[ML_2^{2+}]$
$K_3 = ([ML_2^{2+}]\,[L])/[ML_3^{2+}]$
$\beta_3 = K_1\,K_2\,K_3$
stability constants after.[28,29]

classes of interferences may be distinguished: interferences due to complexes of iron with other ions, such as pyrosulphate and cyanide; coloured background of the solution, *e.g.*, high concentrations of humic acids; consumption of *o*-phenanthroline by other cations to form uncoloured chelates, *e.g.*, nickel and cadmium; coloured chelate formation with cations such as Cu(II) and Cu(I); precipitation of phenanthroline—mixed metal chelates forming a milky, opaque solution, *e.g.*, silver and molybdenum. In the following section, the significance of each mode of interference is discussed and exemplified by the data of Table 1.

Iron chelate with other chemical species. A pretreatment is recommended in order to release the iron ions from the competing chelate prior to the colorimetric determination. This mode of inteference affects tube detection and photometric methods in the same manner and therefore is not exemplified here.

Coloured solution. Filtration is usually recommended in order to eliminate suspended solids and colloid interferences. In the presence of dissolved coloured substances, comparative colorimetry is not recommended and instrumental analyses, using a suitable reference, may partially overcome this mode of interference. Tube detectors are less sensitive to effects of suspended interferences since interfering particles are filtered out by the glass bed. Tube detectors are also less sensitive to dissolved colours because the location of the front, and not colour intensity is measured. The low interference of humic acids (Table 1) even when their concentration is ten times larger than iron exemplifies this characteristic.

Formation of an uncoloured chelate. Addition of excess phenanthroline is sufficient to eliminate such interferences and since phenanthroline does not absorb visible light, excess phenanthroline has no effect on the background colour of the solution. Tube detectors are particularly sensitive to this mode of interference, because downstream to the colour front virtually all the phenanthroline is consumed. Competition of other metals for the same ligand may cause misleading, large colour stains. Fortunately, the tube detectors operate in a displacement chromatography mode, and therefore the competition between the cations is significant only when iron and the interfering caton have similar affinity to the ligand. When the chelate of the interfering metal (*e.g.*, nickel) with phenanthroline is more stable than ferroine it displaces the red stain to a higher position without affecting its length. When the competing ligand has a much lower affinity to phenanthroline its own band will be displaced upstream with no significant interference. This is the reason why the stable nickel–phenanthroline and the less stable cadmium–phenanthroline have relatively little effect on iron determination with tube detectors, while copper and cobalt (which have intermediate stability constants) give misleading high readings.

Formation of coloured chelates. Metals that form phenanthroline chelates that absorb light in the visual range affect the selectivity of colorimetric determination, particularly when their molar absorptivity (e) is large. For example, copper(I) with is formed during the reduction of iron(III) with hydroxylamine yields an intense red chelate with *o*-phenanthroline. Tube detectors are affected by such interferences only when the stability constants of such chelates are similar to that of ferroine. Otherwise, a displacement mechanism will separate the two colour bands.

Precipitation of mixed complexes. Bismuth, cadmium, mercury, molybdate and silver form stable metal–ligand salts with common anions such as chloride and nitrate. The resulting solution is often milky, turbid and interferes with photometric or colorimetric determination of iron. A filtration step is often necessary prior to the photometric measurement. Table 1 reveals that these interferences are often less significant for iron determination by tube detectors. The formation of a solid precipitate is hindered by the competition of the labile and stable iron chelate. However, in some cases (*e.g.*, molybdate and silver) a mixed precipitate of interfering metal/iron salts appears and diminishes the size of the coloured ferroine section (here, of course, the immobilized phenanthroline does not take part in the reaction).

The analyses and classification presented here are sufficient to explain tube detector interferences which operate under pseudo equilibrium conditions. When high flow rates and large particle sizes are used the selectivity of the tube detectors will be influenced also by intraparticle diffusion and the relative lability of the competing chelates.

CONCLUSIONS

The iron length of stain detector demonstrates the advantages and current shortcomings of tube detectors based on doped sol–gel silica sensors for water analysis. Operator convenience, easy implementation and good precision and accuracy are significant advantages, particularly for a technology in its current initial stage of development. However, techniques to mask interferences and to further reduce measurement time should be developed. Currently the disposable tube detectors still do not eliminate wet chemistry since buffering (with acetate buffer) and reduction of iron(III) to iron(II) are still required prior to the final quantitation by the tube detectors. However, these pretreatments may be performed by inserting additional precolumns comprised of modular disposable segments, before the length of stain detector. Such precolumns, may be designed to perform specific pretreatments such as iron reduction, buffering or absorption of specific interfering substances, in a similar way to flow injection analysis. Work, in these directions is currently underway.

Acknowledgements—The research is supported by the Ministry of Science and Technology, Israel and the Forschungszentrum fuer Umwelt and Gesundheit (GSF) GmbH Neuherberg and the Szold Foundation of the P.E.F. Israel Endowment Funds Inc. We are grateful for the collaboration of Professors D. Avnir and M. Ottolenghi.

REFERENCES

1. NIOSH, *Manual of Analytical Methods*, 3rd Ed., NIOSH, Washington, DC, 1984.
2. P Roper, *Am. Ind. Hyg. Assoc. J.* 1971, **32**, 405.
3. J. O. W. Norris, *Analyst*, 1989, **114**, 1359.
4. G. Gubitz, P. Van Zoonen, C. Gooijer, N. H. Velthorst and R. W. Frei, *Anal. Chem.*, 1985, **57**, 2071.
5. W. R. Seitz, *CRC Crit. Rev. Anal. Chem.*, 1988, **19**, 135.
6. V. N. Zaytsev and A. K. Trophymchuk, *Ukrainian Chem. J.*, 1984, **50**, 1126.
7. D. Avnir, S. Braun and M. Ottolenghi, in *Superamolecular Architecture in Two and Three Dimensions*, T. Bein (Ed.), ACS Symp. Series, No. 499, Chap. 27, 1991.
8. D. Avnir, D. Levy and R. Reisfeld, *J. Chem., Phys.*, 1984, **88**, 5956.
9. C. J. Brinker and G. W. Scherer, *Sol Gel Science*, Academic Press, New York, 1990.
10. R. Zusman, C. Rottman, M. Ottolenghi and D. Avnir, *J. Non-Cryst. Solids*, 1990, **122**, 107.
11. O. Lev, B. Iosefzon-Kuyavskaya, I. Gigozin, M. Ottolenghi and D. Avnir, *Fresenius Z. Anal. Chem.*, 1992, **343**, 370.
12. B. Isoefzon-Kuyavskaya, I. Gigozin, M. Ottolenghi, D. Avnir and O. Lev, *J. Non-Cryst. Solids*, 1992, **147**, 808.
13. M. Eyal, R. Gvishi and R. Reisfeld, *Journal De Physique*, 1987, **48**, C7–471.
14. E. T. Knobbe, B. Dunn and M. Gold, SPIE vol 906, *Optical Fibers in Medicine III*, 1988.
15. K. T. V. Grattan, G. E. Badini, A. W. Palmer and A. C. C. Tseung, *Sensors and Actuators A*, 1991, **25–27**, 483.
16. C. Rottman, M. Ottolenghi, R. Zusman, O. Lev, M. Smith, G. Gong, M. L. Kagan and D. Avnir, *Mat. Lett.*, 1992, **13**, 293.
17. I. Kuselman, B. Iosefzon-Kuyavskaya and O. Lev, *Anal. Chim. Acta*, 1992, **256**, 65.
18. APHA, WPCF, AWWA, *Standard Methods For The Examination Of Water and Wastewater*, 17 Ed., APHA, New York, NY, APHA, 1989.
19. Z. Gao, P. Li and Z. Zhao, *Talanta*, 1991, **38**, 1177.
20. A. R. Guadalupe and H. D. Abruna, *Anal Chem.*, 1985, **57**, 142.
21. A. P. Doherrty, R. J. Forster, M. R. Smyth and J. G. Vos, *ibid.*, 1992, **64**, 572.

22. F. Vydra and V. Markova, *Talanta*, 1962, **9**, 449.
23. R. A. Nadkarni, *Anal. Chem.*, 1991, **63**, 675A.
24. National system of assurance of uniformity of measurements. Confidence and Requirements for verification of measuring instrument, Procedural Rules MI 187–86, MI 188–86, Moscow, Izd, Standartov, 1987.
25. I. Kuselman, *Talanta*, 1993, **40**, 1.
26. J. O. Hibbits, W. F. Davis and M. R. Menke, *ibid.*, 1961, **8**, 163.
27. W. B. Fortune and G. E. Mellon, *Ind. Eng. Chem., Anal. Ed.*, 1938, **10**, 60.
28. W. A. E. McBryde, A critical Review of Equilibrium Data for Proton- and Metal Complexes of 1,10-Phenanthroline, 2,2′-Bipyridil and Related Compounds, IUPAC, Chemical data series, No. 17, Pergamon Press, Oxford, 1975.
29. A. A. Schilt, *Analytical Applications of 1,10-Phenanthroline and Related Compounds*, Pergamon Press, Oxford, 1969.

Talanta, Vol. 40, No. 5, pp. 757–760, 1993
Printed in Great Britain.

0039-9140/93 $6.00 + 0.00

AIR-GAP FIBER-OPTIC AMMONIA GAS SENSOR

SATYAJIT KAR and MARK A. ARNOLD*
Department of Chemistry, University of Iowa, Iowa City, IA 52242, U.S.A.

(*Received* 1 *August* 1992. *Revised* 14 *August* 1992. *Accepted* 11 *September* 1992)

Summary—A novel fiber-optic gas sensing arrangement based on an air-gap design is evaluated. In this arrangement, a small gap of air separates the internal solution from the sample. In addition, a second air-gap separates the internal solution from a fiber-optic probe which measures the fluorescence of the internal solution. A series of gas sensors for ammonia is used to investigate several critical design parameters. The length of the air-gap between the internal solution and the fiber-optic probe affects the magnitude of response. The length of the air-gap separating the internal and sample solutions has minimal effect on either magnitude or rate of response. As with membrane-type gas sensors, thickness of the internal solution and concentration of the indicator dye are the most important sensor parameters to consider when designing a fiber-optic gas sensor.

Fiber-optic ammonia sensors capable of nanomolar detection have been developed and the use of these devices to investigate neurochemical events has been proposed.[1] The utility of such a device for biomedical research depends to some extent on the dimensions of the sensing tip. Smaller sensing tips will permit greater spatial resolution, thereby enhancing the information content of the measurement.

Ammonia gas sensing electrodes based on potentiometric pH detection have been miniaturized with tip sizes as small as 10 microns.[2,3] An air-gap design was used to fabricate these sensors. The air-gap is constructed by silanizing a short region inside a drawn out glass capillary. Sensor construction is completed by placing a small volume of internal solution above this hydrophobic region and then positioning a small pH/reference electrode pair in the internal solution. Additionally, the corresponding micro-biosensors have been demonstrated by covalently attaching urease to the outer surface at the tip of the glass capillary.[4]

We have characterized a series of miniature fiber-optic ammonia sensors based on this same air-gap design. Instead of using a pH electrode to measure the pH of the internal solution, a set of optical fibers is used in combination with a fluorescent pH indicator dye. Our intention has been to identify sensor parameters that most strongly influence the analytical characteristics of air-gap fiber-optic gas sensors. Sensors with tip sizes from 0.2 to 0.5 mm have been constructed. The sensor design parameters considered in this investigation include the positioning of the internal solution relative to both the optical fibers and the sample solution, volume and length of the internal solution, and concentration of the indicator dye.

*Author for correspondence.

EXPERIMENTAL

Sensor fabrication

Sensor bodies were constructed from glass capillary tubes (Kimble Products, Skokie, II) in the following manner. First, the closed end of the tube was removed and then the tube was cleaned by placing it into boiling water for approximately 30 min followed by a thorough rinsing with water. Cleaned capillaries were dried in a 115° oven. Sensing tips were formed by drawing out the capillary when the glass became red-hot under a normal gas flame. In this way, two sensor bodies were produced from each capillary with tip sizes ranging from 0.2 to 0.5 mm. Tips were silanized individually by dipping each into a 4% solution of dichlorodimethyl silane in carbon tetrachloride. The solution that occupied the tip was allowed to evaporate in air. Each tip was dipped between 6 and 10 times and the treated tips were placed in an 80° oven for 1 hr. Silanized tips were stored under nitrogen.

Sensors were constructed by placing a small volume of the internal solution inside a sensor

body between the silanized region and a fiber-optic probe. Figure 1 shows the sensor tip schematically. The fiber-optic probe was constructed by packing four plastic optical fibers (Super Eska type EK-10 fibers from Mitsubishi Rayon America, New York, NY) into a narrow bore glass capillary. This capillary fit snugly in the sensor body by matching the outer diameter of the capillary with the inner diameter of the untreated end of the sensor body. The optical fibers were held in the inner capillary with an adhesive sealant. A needle was used to place a small volume of the internal solution in position. The fiber-optic probe was then placed in the sensor body until its tip butted against the tapered portion at the drawn tip. A low temperature dental wax (Sybron-Kerr, Romulus, MI) was used to seal the top of the sensor and to hold the fiber-optic probe in place. As illustrated in Fig. 1, there was a short gap between the internal solution and the tip of the fiber-optic probe. As specified below, several internal solution compositions were used throughout this investigation. Internal solution volumes were calculated from differential weights obtained by weighing the sensor body before and after placement of the internal solution.

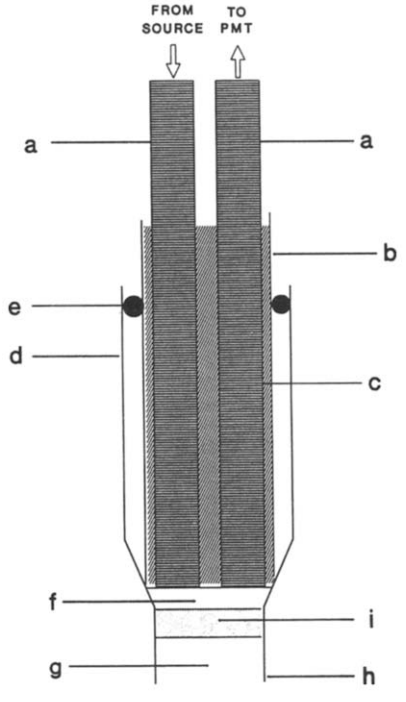

Fig. 1. Schematic representation of the air-gap fiber-optic ammonia sensor showing a, optical fibers; b, fiber-optic probe body; c, epoxy; d, gas sensor body; e, wax seal; f, air-gap; g, air-gap; h, sensor tip; i, internal solution.

Fluorescence measurements

Fluorescence from the internal solution was measured through the fiber-optic probe by using an instrumental arrangement similar to that reported previously.[1] Basically, the incident radiation was selected from a 100 watt tungsten halogen lamp by a 490 nm narrow band pass filter and then launched into two of the four plastic fibers of the fiber-optic probe. Emission was collected by the remaining fibers and directed toward the detection optics which consisted of a 540 nm interference filter and a photomultiplier tube (PMT).

Sensor calibrations

Sensors were calibrated by immersing the sensor tip in a 10.0-ml aliquot of a 0.01*M* sodium hydroxide solution that contained 0.105*M* sodium chloride. The required levels of ammonia were obtained by adding a series of microliter additions of an ammonium chloride standard solution. The steady-state sensor response was recorded after each change in the ammonia concentration. Response times were measured as the time required to achieve 95% of the final steady-state response.

Reagents

Both 5(and 6)-carboxyfluorescein (CF) and 5(and 6)-carboxy-4′,5′-dimethylfluorescein (CDMF) were used as received from Molecular Probes, Inc., Eugene, OR. All other reagents were analytical grade quality and were purchased from common suppliers. Freshly distilled-deionized water from a Milli-Q three house purification unit was used for all solutions.

RESULTS AND DISCUSSION

The position of the internal solution is a critical parameter in terms of both the magnitude and rate of sensor response. A small air gap between the fiber-optic probe and internal solution was found to be necessary to prevent the internal solution from climbing between the outer wall of the fiber-optic probe and the inner wall of the sensor body (see Fig. 1).

The size of gap between the fiber-optic probe and internal solution has important optical consequences in terms of both the intensity of the incident radiation hitting the internal solution and the efficiency of the fibers to collect the emitted radiation. Both parameters are

adversely affected by increasing this distance. As a result, a larger gap lowers the sensitivity of the measurement. For example, the effect of increasing the gap distance from 0.6 to 3.2 mm was measured for a sensor with an internal solution composed of 0.112M ammonium chloride and 1.0μM CF. In this experiment, the sensor response was measured for a zero to 10μM concentration step and the volume of the internal solution was 0.5 μl throughout. The magnitude of response decreased approximately 4-fold when the gap distance was increased, yet there was no significant difference in sensor response times.

The position of the internal solution was unstable when the chamber holding this solution was not sealed (see Fig. 1). Slight changes in ambient atmospheric pressure caused movement in the internal solution, thereby altering the sensor response. Another problem encountered with unsealed sensors was evaporation of the internal solution. Evaporation affected the sensor response in two ways. First, a decrease in the volume of the internal solution resulted in an increase in the distance between the fiber-optic probe and the internal solution which altered the fluorescence measurement. Second, evaporation altered the sensor response by concentrating the components in the internal solution. The small volumes of internal solution resulted in rather dramatic evaporation effects which demanded sealing the chamber before reproducible responses could be obtained.

The length of the air-gap region at the sensor tip was less critical than the length of the internal solution. The length of the internal solution affects both the magnitude and rate of response. These effects are illustrated by the data plotted in Fig. 2 which presents both the magnitude and rate of response measured for an ammonia concentration step from zero to 10μM. The internal solution used in this experiment was composed of 0.02M ammonium chloride and 10μM CF and the air-gap at the sensor tip was 3 mm. Increases in the length correspond to increases in the optical path length which provides higher sensitivity and larger responses. As the length approaches 2.5 mm, the response becomes insensitive to solution length, thereby defining the maximum optical path length in terms of the fluorescence measurement. Unfortunately, response times also increase as a function of solution length. Response times increased by a factor of 4.5 as the length was varied from 0.8 to 2.5 mm. Extrapolation to zero length gives the minimum response time based on the other parameters of the sensor design, most notably the length of the air-gap region. The effect of air-gap length was minimal when internal solution lengths ranged from 1 to 5 mm. Under these conditions, the rate of diffusion through the internal solution is rate limiting and controls the sensor response time. Similar results have been obtained for fiber-optic ammonia gas sensors with microporous Teflon membranes as the gas-permeable barrier.[1,5]

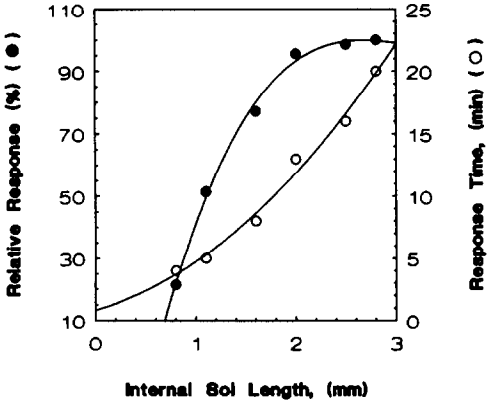

Fig. 2. Effect of internal solution length on the magnitude of response (right axis) and response time (left axis).

Both the magnitude and rate of response are also strongly influenced by the concentration of the indicator dye. These effects were examined by recording responses for a zero to 10μM concentration step as a function of the concentration of CF. Besides the indicator, the internal solution contained 0.1M ammonium chloride. As has been observed for sensors with Teflon membranes,[1,5] both the magnitude of response and response times increase as the dye concentration increases. By increasing the dye concentration from 2 to 10μM, the magnitude of the response increased by a factor of 2.5 and the response time increased from 4 to 11 min. Both effects are caused by a need for more ammonia to enter the internal solution to achieve equilibrium at higher dye concentrations.

Response curves for miniature air-gap fiber-optic ammonia sensors have the same nonlinear shape as the larger, membrane-type sensors. Figure 3 provides a sample response curve for a sensor with approximately 0.3μl of an internal solution composed of 2.0mM ammonium chloride and 0.1mM CDMF. The curve shape matches that predicted by the response function which has been derived for fiber-optic ammonia sensors.[5,6] Relative

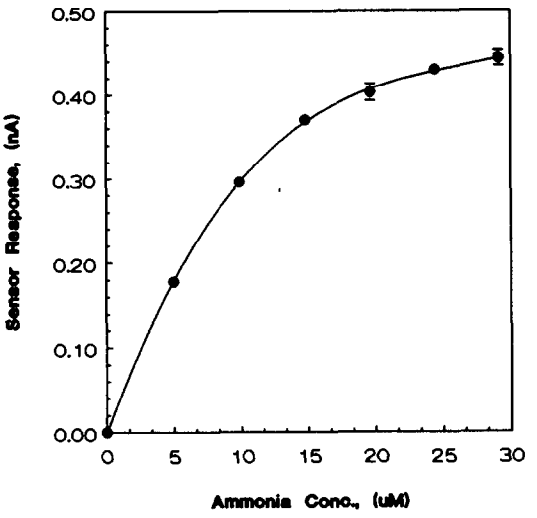

Fig. 3. Sample calibration curve for an air-gap fiber-optic ammonia sensor.

standard deviations for this sensor range were from 1 to 4% over the 5 to 30μM concentration range. Response times varied from 3 to 10 min over this same concentration range with longer response times recorded at lower ammonia concentrations. The limit of detection was calculated to be 0.5μM (S/N = 3) which is similar to that obtained for a membrane-based sensor with the same internal solution.

CONCLUSION

The response properties of fiber-optic ammonia sensors based on an air-gap design are similar to those for the larger, membrane-based sensors. The results of this investigation indicate that miniaturization is possible without adversely affecting the sensitivity, limit of detection or response time of the fiber-optic ammonia sensor. Overall, the thickness of the internal solution and the concentration of the indicator dye are the critical parameters that determine analytical performance.

Acknowledgements—This work was supported by grants from the National Science Foundation (BNS-8716769) and the National Institutes of Health (GM-35487).

REFERENCES

1. S. Kar and M. A. Arnold, *Anal. Chem.*, 1992, **64**, 2438.
2. C. P. Pui, R. F. Miller and G. A. Rechnitz, *ibid.*, 1978, **50**, 330.
3. J. P. Joseph, *Mikrochim. Acta*, 1984, **2**, 473.
4. J. P. Joseph, *Anal. Chim. Acta*, 1985, **169**, 249.
5. T. D. Rhines and M. A. Arnold, *Anal. Chem.*, 1988, **60**, 76.
6. M. A. Arnold and T. J. Ostler, *ibid.*, 1986, **58**, 1137.

Talanta, Vol. 40, No. 5, pp. 761–764, 1993
Printed in Great Britain.

0039-9140/93 $6.00 + 0.00
Pergamon Press Ltd

VOLTAMMETRIC DETERMINATION OF INDIUM IN ALUMINA SUPPORTED CATALYSTS

P. V. C. RAO and V. J. KOSHY
Research Centre, Indian Petrochemicals Corporation Ltd, Baroda-391346, India

(*Received* 2 *June* 1992. *Revised* 14 *July* 1992. *Accepted* 2 *September* 1992)

Summary—A sensitive and rapid method for the estimation of trace levels of indium in alumina supported catalysts using square wave voltammetry (SWV) is discussed. The SWV method for indium in the alumina matrix is standardized using synthetic samples and good recoveries were obtained. Calibration graphs are linear in the range 1–5 μg/ml and the detection limit is 3.57×10^{-8} g/ml. In order to determine the accuracy of the proposed method, the results obtained have been compared with those given by atomic absorption spectrophotometry (AAS). Statistical analysis shows no significant bias between the two methods. This technique is found suitable for the estimation of indium in the range 0.1–1.0% (w/w) in the catalyst samples with an RSD < 1.5%.

Alumina supported noble metal catalysts have the ability to rearrange and transform the molecular structure of hydrocarbons: hence they have become very important in the petrochemical industry.[1] It is well known that various promoter elements are added to the alumina support in order to improve the activity and selectivity of the catalyst.[2] Indium is used as such and decreases the number of electron acceptor centres characterizing Lewis acidity of alumina by the neighbouring centre effect.[3] It is therefore important to monitor the level of indium in the catalysts during the preparation as well as usage in commercial plants.

In our laboratory, X-ray fluorescence,[4] electrothermal atomic absorption spectrometry,[5] electron probe micro analysis[6] and spectrophotometry[7] are the techniques reported for the estimation of minor constituents in catalysts. In the present study, the possibility of using square wave voltammetry for the determination of indium in alumina supported catalysts is investigated. This technique has been widely used for the estimation of indium in other matrices[8–10] but is rarely used for quantification of catalysts. In such investigations, the sensitivity and selectivity is much affected by the composition of the matrix. In the presence of large amounts of alumina, techniques based on atomic spectrometry suffer from atomization interferences.[11] The proposed voltammetric method is free from such problems and offers good sensitivity for the determination of trace levels of indium in the alumina supported catalysts.

EXPERIMENTAL

Apparatus

A Princeton Applied Research (PAR) Model 384B polarographic analyser system together with PAR 303A static mercury drop electrode were used for all square wave voltammetric measurements and the voltamperograms were recorded on a Houston DMP-40 digital plotter. Potentiostatic control of the electrode potential was established by means of a three electrode system consisting of a static mercury drop working electrode, a platinum wire counter electrode and an Ag–AgCl–KCl (satd) reference electrode. The SWVs are recorded at 10^5NA whereas the CVs are recorded at 10^3NA current settings.

A GBC model 902 atomic absorption spectrophotometer, equipped with deuterium arc background corrector, a 10 cm laminar flow air–acetylene burner, indium hollow cathode lamp and Epson LX-800 printer were used for all AAS measurements. An IBM PS/2 computer system with Lotus 1-2-3 was used for all plots and computations.

Reagents

All reagents used were of analytical grade and water purified by means of a Milli-Q system was used for preparing all the solutions. Standard

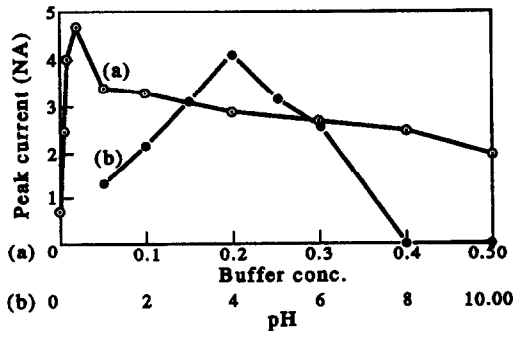

Fig. 1. Plot of buffer concentration (a) + pH (b) *vs.* peak current of indium(III) system.

In(III) solution has been prepared by dissolving 1.000 g of indium metal (99.99%) in 30 ml (2:1) hydrochloric acid by refluxing in a round-bottomed flask. After complete dissolution, the contents are cooled and transferred to a 100-ml standard flask and made up to volume with double distilled water. This solution is standardized with respect to indium AAS standard (1000 μg/ml) from Aldrich. Acetate buffer (1*M*) was prepared by mixing appropriate amounts of sodium acetate and acetic acid.

Procedure

Synthetic solutions are made by accurately weighing 1.000-g portions of finely ground powdered and dried (<200 mesh, 200° for 2 hr) γ-alumina was then taken in six separate 100-ml round bottom flasks. To each of them, the stock solution was added to achieve final concentrations of indium in the range of 0.1–1.0% (w/w). Subsequently the other concomitant solutions have been added in the following range (μg/ml): copper (10–100), zinc (10–100), Re (10–100), Sn (20–120), Li (40–120), Na (10–40), Ni (10–100) and Pd (10–100). Later, 30 ml of 2:1 hydrochloric acid was added and digested under reflux for 2 hr. After complete dissolution, the contents are quantitatively transferred to a 50-ml standard flask and the volume brought up to the mark with deionised water.

In the case of laboratory prepared catalysts also, 1.000-g portions are digested with 30 ml of 2:1 hydrochloric acid and diluted to 50 ml, as mentioned above.

Preparation of samples

To the standard or sample solution of 0.2 ml, add 1.0 ml of 1*M* acetate buffer and dilute the solution to 10 ml with water. After 4 min of deaeration, the square wave voltamperograms were recorded from −0.50 to −0.80 V (*vs.* Ag/AgCl) and the height of the peak is measured at −0.64 V. The blank substraction mode in the 384B was applied for all the samples. Each sample was then determined for indium by the standard addition method.

For atomic absorption spectrophotometric (AAS) analysis of indium, calibration solutions were prepared from their AAS standard solutions in the range 10–50 (μg/ml) using the following parameters: lamp current, 5 mA; flame, air–acetylene; wavelength, 325.6 nm; distance of the burner below optical axis, 6 mm. Matrix matching was carried out using reagent blank depending upon the sample dilution.

RESULTS AND DISCUSSION

Selection of experimental conditions

The experimental conditions have been optimized using 8 μg/ml of indium(III) in the synthetic solutions. The effects of pH and buffer concentration on the peak height are shown in Fig. 1. The optimum pH is about 4.0 and the buffer concentration of 0.1*M* was fixed for all further investigations.

Calibration

In order to ascertain the accuracy of the methods developed, synthetic solutions (S-1–S-5) of known compositions were prepared and used for voltammetric studies. A typical square wave voltamperogram of a laboratory prepared sample before and after the indium spike is shown in Fig. 2. The analysis has been carried out by the standard additions method. The regressed plots of successively spiked solutions shows good linearity as seen in Fig. 3. The

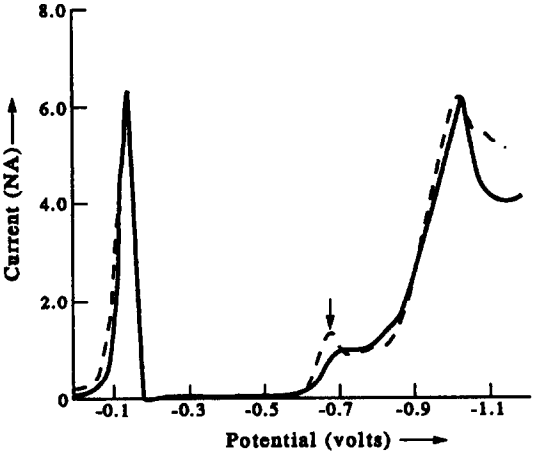

Fig. 2. Square wave voltamperogram of indium in alumina digest (—) and with an indium spike (– – –).

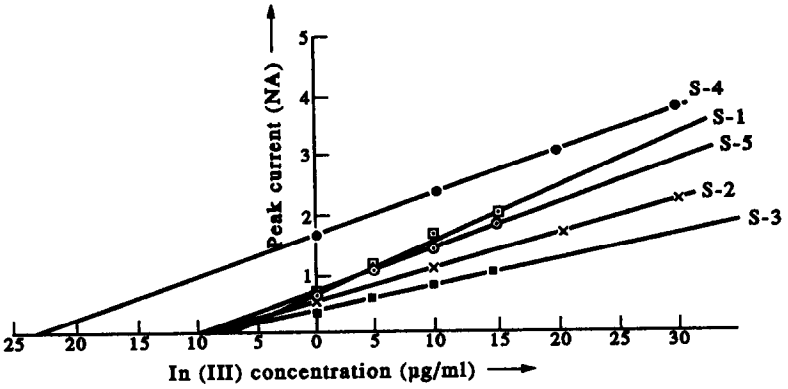

Fig. 3. Typical graphs obtained using standard addition method.

calibration characteristics of indium in synthetic solutions are given in Table 1. The percentage recovery for indium tested for different samples lies between 99 and 101%. Under the optimum conditions, the detection limit[12] of indium in the alumina matrix was found to be 3.57×10^{-8} g/ml.

Interference study

The possible interference of other concomitant elements, present as active element, promoter element or impurity, carried forward during the sample digestion processes were studied by adding increasing amounts of interferent to a fixed concentration of indium(III) solution (8 μg/ml) and measuring the peak currents under optimal conditions after each addition. The results are summarized in Table 2. It can be observed that the increase in the metal to concomitant ratio (>1:10) causes considerable interference (Pt and Sn) in the analysis of indium, but in the present study most of the catalyst compositions fall within these limits. The main interference is due to Fe(III).

Cyclic voltammetry

The cyclic voltammetry of the system was investigated wtih model 384B polarographic analyser with a static mercury drop electrode. The cyclic voltamperograms have been recorded at a scan rate of 50 mV/sec in acetate buffer: indium standard solution (a), synthetic sample (b) and catalyst digest (c) are shown in Fig. 4. Reversible peaks were obtained for indium in acetate buffer, whereas the peaks were not discernible in the case of catalyst digest, indicating the irreversible nature of indium reduction in the presence of other catalyst elements.

Sample analysis

The acquisition of data for the laboratory prepared samples was carried out by following the same procedure as that used for synthetic solutions. Recovery assays of indium in the digests of laboratory prepared samples (S-6–S-11) were carried out separately by SWV and AAS methods and the results are given in Table 3. The relative standard deviation of the order of 1.5% in indium content shows good reproducibility of the method. The results obtained by SWV and AAS were subjected to an *F*-test, and at the 95% confidence level the calculated

Table 1. Concentrations and statistical data for indium

	S-1	S-2	S-3	S-4	S-5
Concentration, Mean (μg/ml)	8.089	6.127	3.945	2.068	9.925
Standard deviation	0.148	0.042	0.092	0.065	0.106
Coefficient of variation	1.83	0.68	2.33	3.14	1.07
Recovery,					
Added (μg/ml)	4.00	4.00	4.00	4.00	4.00
Found (μg/ml)	4.01	4.07	4.01	3.97	4.07
% Recovery	100.25	101.75	100.25	99.25	101.75
Correlation coefficient	0.999	0.998	1.000	0.999	0.999

Table 2. Determination of 8 μg/ml of indium in the presence of foreign ions

Ion added	Amount (μg/ml)	Error (%)	Interference
Al^{3+}	2000	0.52	+
Cu^{2+}	100	1.20	+
Fe^{3+}	10	2.55	–
Li^{+}	100	0.15	+
Ni^{2+}	80	1.20	+
Pb^{2+}	1000	1.80	–
Pd^{2+}	100	0.36	–
Pt^{4+}	80	2.20	+
Re^{7+}	100	0.63	–
Sn^{2+}	80	5.20	+
Zn^{2+}	100	1.90	+
Cl^{-}	1000	2.60	+
NO_3^{-}	1000	1.05	–
SO_4^{2-}	1000	1.88	–

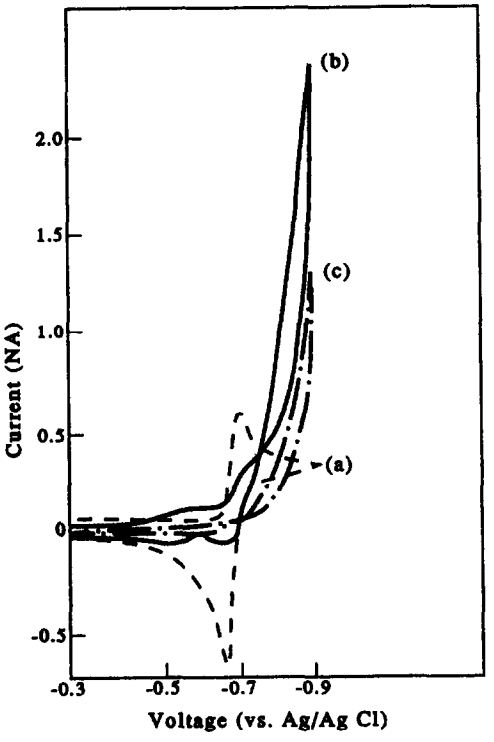

Fig. 4. Cyclic voltamperogram of indium(III) in (a) 0.1*M* acetate buffer, (b) in synthetic solution, (c) in the catalyst digest.

F-value did not exceed the tabulated value, indicating the absence of any significant error. The same method was extended to the analysis of real catalyst samples (CAT1–CAT5) and the results obtained by SWV compare well with AAS results (Table 4).

CONCLUSIONS

The results obtained indicate that the SWV method has proved its usefulness for the determination of indium in the presence of other active elements. SWV serves as an alternative for AAS method and its reliability is shown by the recovery studies performed and by the satisfactory determination in the laboratory prepared samples. The proposed method gives good sensitivity and lower detection limits compared to AAS. In addition to Fe, concomitants like Pt and Sn can cause interference at higher concentrations. In conclusion, the procedure is rapid and simple for the determination of indium in the alumina supported catalysts.

Table 3. Results of recovery assays of indium in the laboratory prepared samples by SWV and AAS methods

Sample	Metal added (μg/ml)	Total metal found (μg/ml) SWV*	AAS	% Recovery SWV	AAS
S-6	20.00	20.55	20.28	100.25	101.40
S-7	40.00	39.45	41.00	98.63	102.50
S-8	60.00	61.20	60.90	102.11	101.50
S-9	80.00	80.89	80.54	101.11	100.68
S-10	81.00	81.60	81.15	100.74	100.20
S-11	100.00	101.72	101.90	101.72	101.90
			MEAN:	100.76	101.36

*RSD ≤ 1.5%.

Table 4. Indium content of catalysts determined by SWV and AAS methods

Sample	Indium found, % (w/w) SWV	AAS
CAT-1	0.103	0.101
CAT-2	0.197	0.205
CAT-3	0.306	0.304
CAT-4	0.404	0.402
CAT-5	0.408	0.405

Acknowledgements—The authors wish to thank Dr. I. S. Bhardwaj, Director (R&D), IPCL for granting permission to publish this work. The technical assistance of Mr N. R. Shah is gratefully acknowledged.

REFERENCES

1. M. Sittig, *Handbook of Catalyst Manufacture*, Noyes Data Corporation, New Jersey, 1978.
2. M. N. Edgar, in *Applied Industrial Catalysts*, B. E. Leach (ed.), Vol. 1, p. 137. Academic Press, New York, 1983.
3. S. B. Kogan, A. M. Morz, O. M. Oranskaya, I. V. Semenskaya, I. V. Gordetskaya and N. R. Bursian, *Zhur. Prik. Khimi*, 1983, **56**, 1975; *Chem. Abstr.*, **99**, 182186q.
4. P. V. C. Rao, G. Kalpana, V. J. Koshy, N. V. R. Apparao, M. C. Jain and R. V. Patel, *Analyst*, 1991, **116**, 847.
5. G. Kalpana and V. J. Koshy, *Indian J. Chem.*, 1992, **31A**, 39.
6. V. J. Koshy, K. V. Rao, G. Kalpana and V. N. Garg, *Talanta*, 1992, **39**, 17.
7. V. J. Koshy and V. N. Garg, *Talanta*, 1987, **34**, 905.
8. W. Gruner and M. Radtke, *Z. Anal. Chem.*, 1986, **325**, 611.
9. T. Kurotu, *Anal. Chim. Acta*, 1991, **233**, 325.
10. L. Sin-ru and F. Q. Sheng, *Analyst*, 1984, **109**, 97.
11. E. M. Donaldson, CANMET Report No. 83-4E, 1983.
12. Analytical Methods Committee, *Analyst*, 1987, **112**, 199.

Talanta, Vol. 40, No. 5, pp. 765–768, 1993
Printed in Great Britain.

0039-9140/93 $6.00 + 0.00
Pergamon Press Ltd

A FAST RESPONSE MEMBRANE-BASED pH INDICATOR OPTODE

TERENCE J. CARDWELL, ROBERT W. CATTRALL, LESLIE W. DEADY,* MARIA DORKOS and GREGORY R. O'CONNELL

Centre for Scientific Instrumentation, La Trobe University, Bundoora, Victoria 3083, Australia

(*Received* 15 *June* 1992. *Revised* 11 *August* 1992. *Accepted* 12 *August* 1992)

Summary—A cellulose acetate based optode membrane containing 4-dimethylamino-4′-octylazobenzene as an acid–base indicator is described. Other essential components of the membrane for a fast-responding and durable sensor are diethyl phthalate, triethyleneglycol and potassium tetrakis(4-chlorophenyl)borate. Factors affecting the sensor behaviour are discussed and an application in a flow-cell is demonstrated.

There is much current interest in the development of optical sensors (optodes) for a variety of analytical purposes. For example, a number of indicators have been immobilized in polymer films and used as pH sensors.[1] A considerable amount of work has dealt with poly(vinyl chloride) based membranes and Morf and coworkers have described the mechanisms which lead to successful optical sensors.[2] However, PVC based membranes tend to suffer from a slow response time, in the order of seconds to minutes, which is not too different from their potentiometric counterparts. A rapid colour change is essential if a film is to be used in an acid/base titration and, for repeated use, the indicator must not leach out of the membrane. Among the most successful attempts at achieving a fast response for optode membranes has been the incorporation of an unmodified "direct dye" such as Congo Red into a modified cellulose acetate film.[3]

Our work in this field is related in that cellulose acetate was found to be the best polymer from which to construct a water-permeable membrane, but we have modified a standard indicator to make it more polymer-compatible and less prone to leaching in aqueous solutions. We have also developed a simple formulation for a membrane sensor which has a fast response to pH change and which does not require an ultra-thin film. This paper reports studies on factors critical to the response time and the use of the optode in a flow system.

*Author for correspondence.

EXPERIMENTAL

4-Dimethylamino-4′-octylazobenzene

A solution of sodium nitrite (0.12 g) in water (1 ml) was added, dropwise with stirring, to a solution of 4-octylaniline (0.25 g) in water (3 ml) and concentrated hydrochloric acid (1.2 ml) at $<5°$. After 15 min at 5°, this was added, slowly with stirring, to a solution containing an excess of *N*,*N*-dimethylaniline and sodium acetate in aqueous ethanol. The yellow solid which separated was filtered, washed with water, and recrystallized from acetonitrile to give orange-yellow flakes, m.p. 80–81° (found: C, 78.6; H, 9.4; N, 12.7. $C_{22}H_{31}N_3$ requires C, 78.3; H, 9.2; N, 12.5%).

Construction of membrane

A typical composition was (weight %): cellulose acetate (Aldrich-acetate content 39.8%), 50; diethyl phthalate, 10; triethylene glycol, 34.7; dye, 0.3; sodium tetraphenylborate, 5. This mixture (100 mg) was dissolved in *ca.* 2 ml of tetrahydrofuran (which was purified by passage through a short alumina column), a coating applied to the appropriate surface and the solvent allowed to completely evaporate. In some circumstances, the membrane was heated briefly to improve the transparency. Coated in this way were a glass microscope slide and plastic coated stirrer bar (for qualitative testing), the inside of a normal 1-cm quartz cuvette (for visible spectroscopy), and the walls of a 14-mm × 2.3-mm diameter tunnel (roughened with a diamond drill to improve adhesion of the plastic) in a 7.5-mm diameter glass cylinder (for use in the flow-cell). The membrane when separated from

a glass surface was quite robust. The thickness of the membrane in both the glass cylinder and on a flat glass surface was typically *ca.* 50 μm, measured by micrometer, which is considerably thicker than the fast response examples of Porter.[3]

Spectroscopy

The membrane coated cuvette was used and gave λ_{max} values of 420 nm (free base) and 545 nm (conjugate acid). A standard spectroscopic technique[4] was applied to determine the pK of the dye in this membrane. In spite of a non-uniform coating, the membrane gave useable values within $\pm$ 1 pH unit of the pK, determined as 3.8. This compares with the value of 2.96 reported by Yeh and Jaffé,[5] obtained in 25% ethanol–sulphuric acid for the parent dimethylaminoazobenzene. The values reported by Yeh and Jaffé are not true pK_a values, since tautomeric forms are possible for the protonated species.

Flow-cell measurements

The Discontinuous Flow Analyser used has been described previously.[6] In this work, the indicator application was demonstrated by the titration of 0.1M sodium hydroxide or potassium hydroxide with 0.1M hydrochloric acid, the membrane coated glass cylinder (i.d., 2.3 mm) providing the flow channel and the optical window for a yellow LED (emission λ_{max} = 580 nm).

RESULTS AND DISCUSSION

Composition of the sensor

There are five necessary components of the successful sensor:

1. Cellulose acetate was the polymer support of choice for making a water-permeable membrane. Cellulose triacetate, polyvinyl acetate, polyvinyl pyrrolidone, and polyvinyl chloride were much less satisfactory. A noteworthy feature was that the optode worked with much thicker membranes than are normally specified for sensors, so that casting the membrane required no special technique.

2. Diethyl phthalate (5–20%) was included as plasticizer and this improved the transparency of the membrane. Slow drying, as from inside a cuvette, gave a more transparent membrane; one cast on a glass slide was opaque initially but gentle heat for a short time gave a clear membrane.

3. During early fabrication attempts it was noted that, if the membrane retained any of the water miscible tetrahydrofuran used to initially dissolve the components, the response time was much reduced. This essential feature has been incorporated in the final formulation by including the non-volatile triethylene glycol as "wetting-agent". About 10% by weight seemed to be necessary and up to 50% was used.

4. This first study has only considered a single indicator (I) which is a simple azo-dye to which is attached the long-chain octyl group. This was prepared by standard chemistry and the compound at 0.3% was miscible with the polymer and did not leach from the membrane on repeated use.

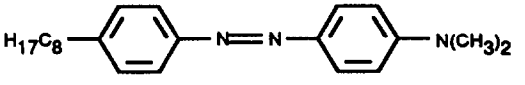

(I)

5. For this dye, which goes from a yellow neutral form in base to a red cationic form in acid, it was essential to have an ion-balance reagent (IBR) present and sodium tetraphenylborate (NaTPB) and potassium tetrakis(4-chlorophenyl)borate (KTKB) were each used. Without the IBR, no reaction occurred in aqueous hydrochloric acid. To maintain ionic balance in these conditions, it is necessary for an anion to be taken into the membrane with the proton and it was evident that the hydrophilic chloride anion would not transport along with the proton into this membrane. The IBR provided mobile metal cations in the membrane to exchange with the incoming protons to overcome this problem. A molar excess (with respect to the dye) was necessary for rapid response. However, too much gave an opaque/crystalline membrane, and 5% by weight (*ca.* 10-fold molar excess) was a good working amount. It emerged that the response time was affected by the nature of the IBR reagent, as described below.

The membranes with NaTPB as the IBR, though thicker than those reported previously,[3] were characterized by a rapid response to pH change in either direction. For a coated slide immersed in the appropriate solution, the colour change to red was "instant" and to yellow, marginally slower, but too fast to measure quantitatively in a batch type experiment. A more quantitative answer is available

from flow-cell experiments (below). The colour change could be quantitatively related to pH by visible spectroscopy only over *ca.* a 2-unit range about the pK value of 3.8. Thus, this dye is more appropriate for an indicator of pH change rather than for a measure of pH value.

Flow-cell application

The application of this pH-optode to use in a discontinuous flow analysis system[6] was demonstrated. The optode membrane (*ca.* 50 μm thick) was incorporated into the flow-cell of the instrument as described in the experimental section. Figure 1(a) shows a typical DFA acid–base titration curve for a membrane with NaTPB as the IBR. At A, the liquid in the flow-cell is 0.1M hydrochloric acid. At B, the titration cycle of the instrument provides a rapid flush of 0.1M sodium hydroxide and the indicator immediately turns yellow. The actual titration begins at C as acid is added and the observable colour change back to red commences at about D. The end-point E is indicated by the rapid change in the detector signal and is defined in the DFA instrumental method by taking the first derivative. The times for the colour changes can be estimated from the time-bar in the figure, which refers to the speed of rotation of the instrument cam. These times are virtually identical to the case where a water-soluble indicator is introduced separately into the flowing stream.[6]

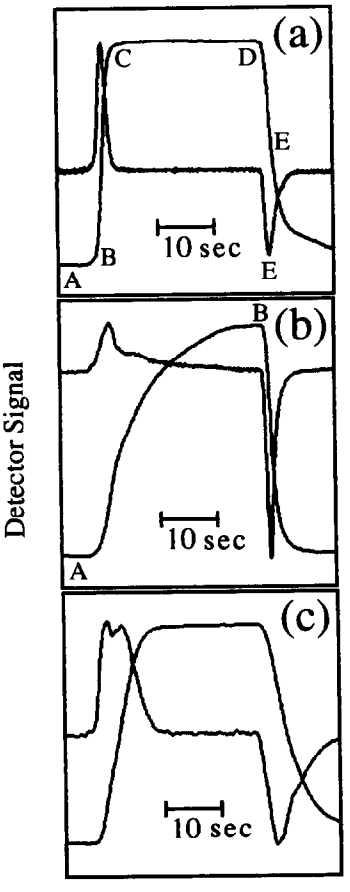

Fig. 1. DFA titration of 0.1M HCl with base. (a) Base, 0.1M NaOH; IBR, NaTPB. (b) Base, 0.1M NaOH; IBR, KTKB. (c) Base, 0.1M KOH; IBR, KTKB. The time-bars relate to the instrument cam speed.

The behaviour is ideal for the DFA application, which requires a rapid colour change at the end-point. Unfortunately, NaTPB as IBR slowly leached from the membrane and the optode ceased to function after about ten titration cycles (though the coated glass slide lasted many more batch changes of acid and base, probably because there is much less agitation of the membrane surface than in the DFA cell). This problem was overcome by the use of the less hydrophilic KTKB as IBR and there was no perceptible deterioration in the membrane performance after more than forty cycles. However, with sodium hydroxide as the base, there was now an unacceptably slow response for the acid to base change (but no effect on the reverse). This is seen in Fig. 1(b) as a very slow rise, A, in the detector signal to the maximum, B, which is reached just before the change back to the acid form.

Clearly, the movement of the various ions involved in the indicator colour change, across the membrane/solution interface, is a complex process. The tetrakis(4-chlorophenyl)borate anion apparently has a lower affinity for a sodium ion in the membrane than does the unsubstituted tetraphenylborate anion and the replacement of a proton by a sodium ion is slower. The situation, however, is also cation dependent and, when potassium hydroxide was used as the base, the response times in both directions were quite acceptable. The membrane was stable indefinitely and Figure 1(c) shows the titration sequence in these conditions after seventy cycles.

This DFA application represents an advance on the previous example using photometric end-point detection, where an indicator had to be added in reasonably high concentrations to the flow system.[6] Compound I, while being a quite satisfactory indicator for a strong acid–strong base titration, has limited potential because of its low pK_a value. We are currently investigating compounds applicable to other pH

regions and which will be compatible with the polymer system.

Acknowledgements—We thank the Australian Research Council for financial support.

REFERENCES

1. S. M. Stole, T. P. Jones, L.-K. Chau and M. D. Porter, in *Chemical Sensors and Microinstrumentation*, R. W. Murray, R. E. Dessy, W. R. Heineman, J. Janata, W. R. Seitz (eds), Chap. 19, ACS, Washington DC, 1989.
2. W. E. Morf, K. Seiler, B. Lehmann, Ch. Behringer, S. Tan, K. Hartman, P. R. Sørensen and W. Simon, in *Ion-selective Electrodes, 5*, E. Pungor (ed.), p. 115. Pergamon Press, Oxford, 1989.
3. T. P. Jones and M. D. Porter, *Anal. Chem.*, 1988, **60**, 404.
4. A. Albert and E. P. Serjeant, *Ionization Constants of Acids and Bases*, Methuen, London, 1962.
5. S. J. Yeh and H. H. Jaffé, *J. Am. Chem. Soc.*, 1959, **81**, 3283.
6. T. J. Cardwell, R. W. Cattrall, G. J. Cross, G. R. O'Connell, J. D. Petty and G. R. Scollary, *Analyst*, 1991, **116**, 1051.

Talanta, Vol. 40, No. 5, pp. 769–770, 1993
Printed in Great Britain.

0039-9140/93 $6.00 + 0.00
Pergamon Press Ltd

BOOK REVIEWS

The Kirk–Othmer Encyclopedia of Chemical Technology: Volume 4, Fourth Edition. Bearing Materials to Carbon. J. I. KROSCHWITZ and M. HOWE-GRANT (editors), Wiley–Interscience, Chichester, 1992. Pages: xxx + 1117. £150.00. ISBN 0-471-52672-X (v. 4).

The first three volumes of this encyclopedia have recently been reviewed in *Talanta* and the current volume continues to report on a variety of chemical topics. The chemical elements covered together with associated compounds are beryllium, bismuth, boron, bromine, cadmium and calcium. Technological aspects of the different solid state forms of carbon are mentioned at the end of the volume and carbides are dealt with in a separate section.

Several other diverse topics, as well as the expected elements and compounds, are included. Some of these are beer, benzene, biosensors, bleaching agents, butadiene, butylenes, caprolactam and carbohydrates. The standard of the previous volumes is maintained and the topics are dealt with at a level which is informative, interesting, and easy to understand. My own favourite gems in this volume include (1) the different ways of sawing logs of trees into slabs, (2) a definition of Scotch whisky, (3) the use of biopolymers in chiral chromatography, and (4) problems associated with developing artificial blood.

Other short sections cover biphenyl and terphenyls, brake linings and clutch facings, butyl alcohols and carbamic acid. The topic of biotechnology is stated to be dispersed throughout various articles but a concise overview is included in this volume. Extensive and up-to-date bibliographies are given after each article and the whole work is extremely well edited. This is an encyclopedia which every good science library should obtain.

P. J. Cox

The Elements: Second Edition, J. EMSLEY, Oxford University Press, Oxford, 1991. Pages: vii + 251. £11.95 (softback). ISBN 0-19-855568-7.

This is a marvellous book of data about all the elements up to atomic number 104. The first edition was published in 1989 and proved extremely popular. The main additions in the second edition are sections on what the author calls Environmental Properties.

The first nine pages explain the type of data provided and the sources of information. Thereafter, the data are arranged per element in alphabetical order, with two pages devoted to each element. The preliminary information given includes the atomic number, relative atomic mass, the derivation of the name and the date and place of discovery. This is followed by a section on Chemical Properties such as reactivity towards air, water, acids and alkalis, values of the atomic and ionic radii, the electronegativity and effective nuclear charge. The standard reduction potentials and oxidation states are also listed. The next section concerns Physical Properties such as the melting and boiling points, thermodynamic properties, density, thermal conductivity, electrical resistance, mass magnetic susceptibility, molar volume, crystal structure and X-ray diffraction mass absorption coefficients.

The section on Nuclear Properties contains the thermal neutron capture cross-section, the number of isotopes and isotope mass range and details about the key isotopes. Details relevant to NMR spectroscopy are also given including relative sensitivity, receptivity, magnetogyric ratio, quadrupole moments and frequency in MHz. The Electron Shell Properties listed are the ground state electron configuration, the term symbol and the electron affinity in kJ mol^{-1}. The main lines in the atomic spectrum are given along with ionisation energies for sequential loss of up to 10 electrons.

The new sections on Environmental Properties will be of interest to geologists and those involved in the life sciences. The abundance of the element in the sun, the earth's crust and the oceans are listed along with geological data concerning the principal ores, world production of the element or its minerals and an indication of the estimated reserves available. Data in the subsection on the biological role of the element includes typical levels found in human muscle, bone and blood. Normal daily dietary intake is given along with comments on the toxicity of the element and whether or not it is essential to healthy human existence.

There are 20 supplementary tables of properties of the elements in order of the element and in ranking order of property. For example, there is a table on the dates of discovery of the elements in chronological order. Other tables give the melting and boiling points of the elements in order of temperature.

The cost of the paperback version is extremely reasonable and I consider this book to be excellent value for money. Anyone who is interested in elemental properties should have a copy of this book on their library shelves. This must be one of the most concise yet comprehensive collections of data about the elements. I do not know how I managed to survive without it!

D. LITTLEJOHN

Solution Mining—Leaching and Fluid Recovery of Materials: R. W. BARTLETT, Gordon & Breach Science Publishers, Philadelphia, 1992. Pages: xxxii + 276. $29.00 £16.00. ISBN 2-88124-546-3.

Anyone who has been shown around a cyanide treatment plant for extracting gold from mining wastes by aerial oxidation assisted by complexation of the gold cannot fail to have been impressed by the simplicity and the cheapness of the process. Similarly, the recycling of leachates from old mining residue tips to extract workable levels of copper and other metals obviously makes not only economic but also environmental sense. But that the value of materials extraction by solution mining exceeded two billion dollars in the US alone in 1990, accounting for between 20% (for boron) through 35% (for gold), 75% (for uranium) to 85% (for magnesium) of that country's total production came as a big surprise to me. The author of this book has been responsible for a number of large development programmes, for recovery of copper, gold and precious metals, and boron. Based on this experience he has introduced an advanced level course on the topic for which this is the textbook.

Both surface mining, of old mining residues, and deep mining, of new deposits following initial mechanical removal of 15–25% of the ore body, are discussed. The need for the introduction of some rather formidable mathematical equations becomes clear when the last chapter, computer simulation of solution mining operations, is reached. Optimisation of a commercial process depends on a sound knowledge of the permeability of the rock, the lump sizes, the dimensions of the ore heap, the flow of the eluting acid, and the kinetics of the process.

Environmental aspects of solution mining are also discussed. Handling large amounts of cyanide solution presents obvious hazards, while slightly less obvious is the possible percolation of acid leachates into ground water. Dust and noise from mechanical mining are probably more serious threats to the environment.

This is an interesting book, though written for a rather specialised market. It is readable, well illustrated, (with both photographs and line drawings) and contains useful bibliographies at the end of each chapter. It is certainly good value for money.

I. MARR

Capillary Electrophoresis—principles, practice and applications: S. F. Y. LI, Elsevier, Amsterdam, 1992. Pages: xxvi + 582. Dfl 395.00. ISBN 0-444-89433-0.

This is a very comprehensive text which deals in detail with the several modes of capillary electrophoresis.

Chapter one is a readable introduction to the range of individual techniques associated with CE. It will be particularly useful in acquiring a basic knowledge of the different modes of use. Chapters two and three deal with injection and detection techniques in considerable detail. Both are very comprehensive and provide a wealth of information on lesser known methods as well as those more generally appreciated.

A very complete overview of column technology is given in Chapter four dealing in particular with methods of capillary coating and attributes of gel-filled capillaries. Chapter five gives an exhaustive coverage of electrolyte systems used including the functions of simple buffer systems and organic modifiers. The effects and uses of more complex additives are also well covered in particular the use of surfactants in MEKC. Chapter six is a collection of diverse methods and techniques associated with CE ranging from fraction collection through isoelectric focusing and isotachophoresis and concluding with a review of combination methods.

Chapter seven lists a multitude of CE applications. Amino-acid and biopolymer separations are comprehensively covered and the utilisation of CE in various diverse areas is reviewed. At the end of this chapter there is a very useful summary of separation conditions for different analytes in various matrices which will provide useful starting points for new applications. The review of commercial equipment which is also included in this chapter will prove invaluable for first time users of the technique. The last chapter attempts to cover recent advances and to indicate possible future developments.

This volume is a very useful addition to the literature of separation science encompassing, as it does, all aspects of this rapidly emerging family of methods. It is almost encyclopaedic in its coverage and all chapters are extremely well referenced. This will facilitate any search for original information on any aspect of CE.

R. B. TAYLOR

Talanta, Vol 40, No 6, pp 771–774, 1993
Printed in Great Britain

0039-9140/93 $6 00 + 0 00

SPECTROPHOTOMETRIC DETERMINATION OF TRACE AMOUNTS OF CADMIUM IN HIGH PURITY ZINC MATERIALS WITH IODIDE AND RHODAMINE 6G

S KARTIKEYAN, T PRASADA RAO*, C S P IYER and A. D DAMODARAN
Regional Research Laboratory (CSIR), Trivandrum 695 019, India

(*Received* 13 *August* 1992 *Revised* 18 *November* 1992 *Accepted* 21 *November* 1992)

Summary—A highly selective and sensitive spectrophotometric procedure for the determination of cadmium is developed This is based on the interaction of rhodamine 6G with tetraiodocadmate (II) anion to form a pink product which absorbs maximally at 575 nm that is stable for 24 hr when stabilized with gelatin Cadmium concentrations as low as 0 01 ppm can be readily determined The method is precise and has been applied to synthetic sea water samples and high purity zinc materials

Cadmium is one of the priority pollutants and is usually associated with zinc materials. Various methods have been described for the last one decade for trace determination of cadmium. These procedures are applicable to the determination of cadmium in river water,[1] natural water[2–5] and waste water.[6–8] Since, zinc has a relatively low tendency to form complexes with iodide ($pK_4 = -2\,3$) compared to cadmium ($pK_4 = 6.1$), this has been utilized with advantage to devise methods for cadmium after reaction with rhodamine B[6] ($\varepsilon l = 4.2 \times 10^4$ l.mole^{-1}.cm^{-1}) and pyronine G[10,11] ($\varepsilon l = 9.0 \times 10^4$ l.mole^{-1}.cm^{-1}). However, the former method is less sensitive and the latter has a drawback in the sense that pyronine G is an impure commercial dye consisting of ~80% rhodamine S and ~20% of pure pyronine[12] (where rhodamine S is the main reacting molecule). Hence, it is essential to devise a procedure to determine traces of cadmium in high purity zinc materials with a reagent of definite composition. This paper describes the studies on the interaction of anionic iodo complex of cadmium with rhodamine 6G that provides a basis for a highly selective spectrophotometric method for the determination of cadmium. This method finds application in the determination of cadmium at levels down to 1 μg/g of high purity zinc materials.

*Author for correspondence

EXPERIMENTAL

Reagents

All reagents used were of analytical reagent grade unless otherwise stated. All solutions were prepared with double distilled water.

Standard cadmium solution, 500 ppm: Dissolve 0.2854 g of cadmium sulphate (3 $CdSO_4$.8 H_2O) in 250 ml of water and standardize titrimetrically using EDTA. Prepare working standards (5 ppm) by suitable dilution.

Citrate buffer solution, 0.8*M*, pH 3.5: Prepare the citrate buffer (0.8*M*) by dissolving 21.04 g of citric acid monohydrate and 29.41 g of trisodium citrate in water and adjust the pH to 3.5 using either HCl or NaOH and diluting to 250 ml.

Rhodamine 6G (BDH, Poole, U.K.) solution, 0.01%: Dissolve 0.025 g of rhodamine 6G in 250 ml of water.

Potassium iodide solution, 10%: Dissolve 10 g of potassium iodide in 100 ml of water.

Gelatin solution, 1%: Dissolve 1 g of gelatin in 100 ml of water.

Apparatus

A microcomputer based Hitachi Model 220 double beam spectrophotometer with extended program was used. An ELICO LI-120 digital pH meter was used for pH adjustment.

Procedure

Mix 2.5 ml of citrate buffer in an aliquot of sample solution containing not more than

0.6 ppm of cadmium in a 25-ml volumetric flask, mix and adjust the pH to 3.5 using HCl or NaOH under a pH meter. Mix 2 ml of potassium iodide and 5 ml of rhodamine 6G followed by 1 ml gelatin and dilute to the mark with distilled water using 10-mm quartz cells Measure the absorbance at 575 nm against a reagent blank and establish the concentration by reference to a calibration graph prepared for 0–0.6 ppm of cadmium using standard cadmium solutions, by following the above procedure

Analysis of high purity zinc materials

Dissolve 5 g of high purity zinc materials in 10 ml of 1·1 HCl and dilute to 100 ml with water. Add 2 ml of 20% solution of sodium citrate to a 10-ml aliquot and adjust the pH to 3.5, as described above. Transfer the solution to a 25-ml volumetric flask and establish the concentration of cadmium as described above.

RESULTS AND DISCUSSION

The pink ternary complex that resulted, on the addition of rhodamine 6G to the aqueous solution of cadmium containing iodide, was unstable and gradually precipitated on standing. This ternary complex (Cd–I⁻–rhodamine 6G) was found to be stable for 24 hr on the addition of gelatin.

Absorption spectra and spectral characteristics

Figure 1 shows the absorption spectra of 4 ml of $10^{-4}M$ rhodamine 6G (curve A) with 1 and

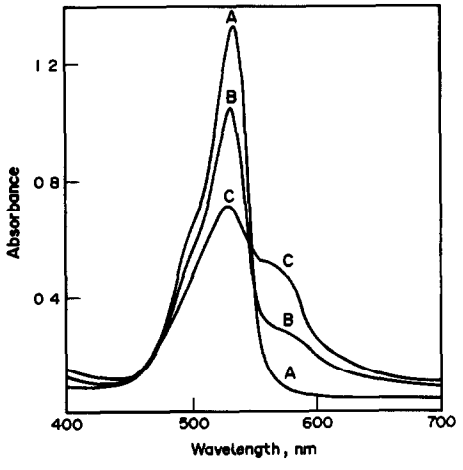

Fig 1. Absorption spectra of the cadmium–iodide-rhodamine 6G complex, width of cells, 10 mm, reference, water, pH 3 5 Curve A 4 ml of $1 \times 10^{-4}M$ rhodamine 6G + buffer and 2 ml of 10% KI solution + 1 ml of 1% gelatin in 25 ml of final solution Curves B & C as in A but with the addition of 1 and 4 ml of $1 \times 10^{-4}M$ cadmium solution

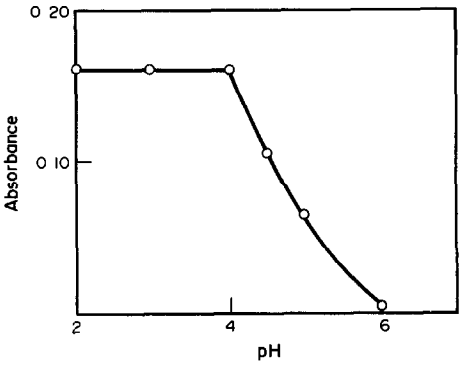

Fig 2 Effect of pH on the absorbance at 575 nm (0 2 ppm of cadmium, 2 ml of 10% KI, 5 ml of 0 01% rhodamine 6G, total volume = 25 ml, 10 mm quartz cells)

4 ml of $1 \times 10^{-4}M$ (curves B and C, respectively) amounts of cadmium in the presence of potassium iodide and gelatin. It is evident from Fig. 1 that the interaction of the iodo complex of cadmium with rhodamine 6G proceeds with a considerable bathochromic shift. the ternary complex has a maximum absorption at 575 nm compared with that of the dye at 530 nm.

Optimization of experimental conditions

It was found that the ternary complex was fully formed in the pH range 2–4 (Fig. 2) Studies at higher acidities were not considered because liberation of I_2 increases the blank value. Citrate buffer (pH 3.5) was preferred to phthalate or acetate buffer as its presence removes the interference of 200-fold amounts of Pb^{2+}, Cu^{2+}, WO_4^{2-}, Sn^{2+} and Sb^{3+}. The results of the investigation on the effect of iodide and rhodamine 6G showed that, for constant and maximum absorbance, the solution should contain at least 3 ml of 5% potassium iodide

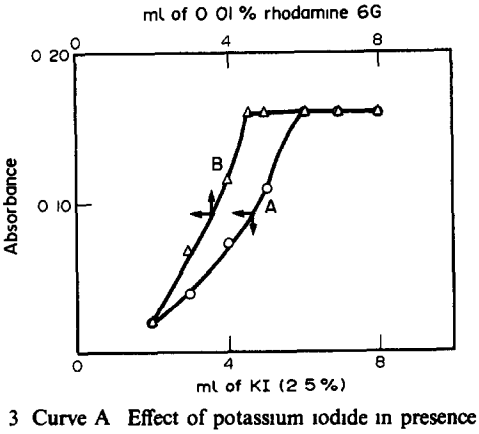

Fig 3 Curve A Effect of potassium iodide in presence of 5 ml of 0 01% rhodamine 6G Curve B Effect of rhodamine 6G in presence of 2 ml of 10% KI (0 2 ppm of cadmium, pH 3 5, total volume = 25 ml, 575 nm, 10 mm quartz cells)

Table 1 Results of interference studies

Interference	Remarks
Li^+, Na^+, K^+, Ca^{2+}, Sr^{2+}, Ba^{2+}, Pb^{2+}, Sn^{2+}, Cu^{2+}, Zn^{2+}, Fe^{2+}, Co^{2+}, Be^{2+}, Ni^{2+}, Mn^{2+}, UO_2^{2+}, Cr^{3+}, Fe^{3+}, Al^{3+}, Sb^{3+}, Tl^{3+}, La^{3+}, Ce^{4+}, Zr^{4+}, Th^{4+}, Se^{4+}, Sb^{5+}, AsO_4^{3-}, AsO_3^{3-}, VO_4^{3-}, MoO_4^{2-}, WO_4^{2-}, SO_3^{2-}, $S_2O_3^{2-}$, $B_4O_7^{2-}$, F^-, SCN^-, oxalate and tartrate	No interference
Hg^{2+}, Pd^{2+}, Bi^{3+} and Pt^{4+}	Interfere by enhancing the absorbance
NO_2^-	Interferes by oxidizing rhodamine 6G

(*cf.* curve A, Fig. 3) and 4.5 ml of 0.01% rhodamine 6G (*cf.* curve B, Fig. 3). Under these optimal conditions, the colour development was instantaneous and remains stable for 24 hr. The order of addition of reagent solutions was found not to be critical provided that the gelatin solution was added after the addition of other reagent solutions.

Calibration graph and precision

The colour system obeys Beer's law in the range 0–0.6 ppm of cadmium in a final volume of 25 ml. The molar absorptivity (*el*) at 575 nm was calculated to be 8.9×10^4 $l.mole^{-1}.cm^{-1}$. Ten replicate determinations on standard solutions that contained 5 μg of cadmium showed a mean recovery of 98.6% with a coefficient of variation of 1.39%.

Nature of the complex

The combining ratio of cadmium to rhodamine 6G was established to be 1:2 from mole ratio and continuous variation methods. These methods were unsuccessful when applied to the determination of the combining ratio of cadmium to iodide as no colour development took place when they were present in molar proportions. However, the equilibrium shift method indicates a ratio of 1:4 for cadmium to iodide. Hence, the ternary complex has the empirical composition $(Cd\ I_4)^{2-}R_2^+$ where R^+ represents the rhodamine 6G cation.

Interference studies

The interfering effects of various ions at 40 ppm level on the determination of 0.2 ppm of cadmium by the proposed method are summarized in Table 1.

The addition of 2 ml of 5% thiourea overcame the interference due to Pd^{2+} and Pt^{4+} and addition of 2 ml 5% oxalic acid eliminated the interference due to Bi^{3+}. The interference of mercury(II) was eliminated by reduction with 2.5 ml of 2% $SnCl_2$ and centrifuging of the turbid solution prior to the addition of reagent solutions. The addition of 2 ml 5% urea overcame the interference due to nitrite.

Analysis of synthetic samples

The results in Table 2 show that the presence of similar or even larger concentrations of metal ions either alone or in combination, had no effect. The method can therefore be used for the determination of cadmium in real samples such as steel and high purity zinc materials.

Table 3 presents the results of the analyses of synthetic sample solutions of various forms of sea water after overcoming the interferents as described above. The results clearly show that the method can find use in trace determination of cadmium in polluted sea water samples.

Analysis of high purity zinc materials

Table 3 shows the results of the determination of cadmium in zinc sulphate and zinc oxide samples by the proposed method. The results were compared with those obtained by atomic absorption spectroscopy. The data obtained on samples spiked with known amounts of cadmium are presented. The results show good agreement between the two methods.

Table 2. Analysis of synthetic samples (cadmium concentration = 0 1 ppm in a final volume of 25 ml)

Composition of solution	Absorbance
NaCl (2 g)	0 080
Fe (200 ppm) + Cu (80 ppm) + Cr (40 ppm)	0.078
Fe (200 ppm) + Cr (120 ppm) + Ni (80 ppm)	0 080
Fe (200 ppm) + Mn (40 ppm)	0 080
Fe (200 ppm) + Mo (40 ppm) + W (40 ppm)	0 078
Zn (200 ppm) + Pb (200 ppb) + Cu (80 ppm)	0 082

Table 3 Analysis of sea water samples

S No	Composition of the sample	Aliquot taken (*ml*)	Cadmium added (*μg* in 25 *ml* of final solution)	Absorbance
1	None	—	1 0	0 032
		—	2 5	0 080
2	NaCl (20%)	10	—	0 000
		10	1 0	0.033
		10	2 5	0 080
3	Sea water			
	Na (1 05%), K (0 04%),	10	—	0 001
	Mg (0 13%), Ca (0 04%),	5	2 5	0 078
	Cl (1 89%)	10	1 0	0 032
4	Deep sea water*			
	Na (3 2%), K (0.64%), Mg (3.67%), Ca (1 3%),	10	—	0 000
	Cl (17%)	10	1 0	0 034
		10	2 5	0 085

Table 4 Analysis of high purity zinc materials

Sample solution	Amount of Cd added (*μg/g*)	Aliquot taken (*ml*)	Cadmium found (*μg/g*) Proposed method	AAS
(A) Zinc sulphate*	—	10 0	1 60	1.60
(5 g/100 ml)	1 0	10 0	2 58	2 60
	2 0	5 0	3 65	3 60
(B) Zinc oxide†	—	10 0	5 70	5.70
(5 g/100 ml)	2 5	10 0	8 20	8 25
	5 0	5 0	10 60	10 65

*AnalaR BDH Chemicals Ltd, India
†S D Fine Chemicals Ltd, India

CONCLUSION

The method described provides a simple and reliable means of determining trace amounts of cadmium by spectrophotometry. Though it is of similar sensitivity as that of pyronine G procedure,[10] it is superior to other methods in terms of selectivity and is readily applicable to the analysis of high purity zinc materials. The method also has the advantage of virtual freedom from 200-fold amounts of various extraneous ions and can therefore serve as an alternative to atomic absorption spectrophotometry for rapid and precise determination of cadmium in steel, in polluted sea water, waste water and high purity zinc materials.

Acknowledgement—The authors wishes to thank the Department of Ocean Development, New Delhi, for providing funds in carrying out this work

REFERENCES

1 K Kanamura and S Igarashi, *Anal Sci*, 1988, **4**, 175
2 S. Wang, C Xu and H Lu, *Fenxi Shiyanshi*, 1988, **7**, 13
3 X. Liu, *Fenxi Shiyanshi*, 1986, **5**, 41
4. Z. Huang, S He and J Lu, *Fenxi Huaxue*, 1986, **14**, 454
5 S Li and Y Xie, *Fenxi Huaxue*, 1986, **14**, 938
6 C Hsu, W Wang, L Yang, J Pan and Y Wang, *Micro-chim Acta*, 1989, **5–6**, 313
7 X. Liu, Z Kou and T Chen, *Lihua Jianya Huasche Fence*, 1989, **25**, 149
8 N Shen, F Wei and Q Qi, *Anal Lett*, 1981, **14**, 1565.
9 S. Liu, Y Liu and Z Liu, *Mikrochim Acta*, 1983, **II**, 35
10 T Prasada Rao and T V Ramakrishna, *The Analyst*, 1982, **107**, 704
11 W He, *Lihua Jianya Huasche Fence*, 1987, **23**, 220
12. C A Watson, *The Analyst*, 1970, **95**, 131

Talanta, Vol 40, No 6, pp 775–780, 1993
Printed in Great Britain

0039-9140/93 $6 00 + 0 00

HIGH-SPEED CHROMATOGRAPHIC ANALYSIS OF HIGH-FRUCTOSE CORN SYRUP FOR PROCESS MONITORING

DARREN R DUNPHY and ROBERT E SYNOVEC
Department of Chemistry, BG-10, University of Washington, Seattle, WA 98195, U S A

(*Received* 23 *September* 1992 *Revised* 20 *November* 1992 *Accepted* 20 *November* 1992)

Summary—High-speed chromatography is coupled with numerical methods for analyzing unresolved chromatograms and applied to a process analysis of high-fructose corn syrup A column selection process is demonstrated where a minimum amount of resolution is sacrificed in order to decrease analysis time from over 5 min to 25 sec. Two data analysis methods, linear least squares regression and the sequential chromatogram ratio technique coupled with sequential suppression, are compared for their ability to quantitate the poorly resolved chromatograms Both methods fit pure component analyte chromatograms, collected on a computer, to a sample chromatogram with unknown concentrations of each analyte For a high-fructose corn syrup sample with a nominal fructose concentration of 55%, linear least squares analysis gave a fructose concentration percentage of $57\,2 \pm 0\,9\%$ The sequential chromatogram ratio algorithm gave a fructose concentration percentage of $57\,9 \pm 0\,7\%$

Liquid chromatography involves a balance between analysis time, separation ability, and complexity of instrumentation.[1] In many applications, analysis time becomes critical. High-speed chromatography[2] (where the eluent dead-time is around 10 sec) and super-speed chromatography (where eluent dead-time is less than a second) sacrifice either resolution or instrumental simplicity. Traditional attitudes toward high-speed chromatography favor the loss of the latter over the former.[3] However, in certain applications, such as process analysis and control, it is desirable to keep instrumentation as simple as possible.[4] In such cases it is advantageous to sacrifice resolution for analysis time. Davis and Giddings have shown that as the number of components in a chromatogram increase, the probability of interference between an analyte and an unknown also increases.[5,6] This situation is essentially the same as when one sacrifices resolution while reducing analysis time. For process chromatography, however, this is less a problem, as most of the components are generally known, and chromatograms, sequential in time, are fairly constant while the process is under control. Yet, any data analysis algorithm must first support accurate qualitative analysis prior to, or in conjunction with, quantitative analysis. Quantitation remains a problem, as traditional data analysis techniques such as integration or peak height do not work well with unresolved or poorly resolved chromatograms.

Two methods that are useful for the quantitation of poorly resolved chromatograms are linear least squares regression,[7,8] and the sequential chromatogram ratio (SCR) technique.[9–11] Both are computer-based methods that fit analyte standard peaks to the chromatogram to be analyzed. Linear least squares regression, the better known of the two, is limited to cases where all components of a region of interest in a chromatogram are known. The SCR technique does not have this limitation, however, and can also be used to provide qualitative information on analyte purity and identity using a statistical value obtained from a pure analyte standard.[10] The SCR technique is not able to quantify totally unresolved analytes unless coupled with sequential suppression,[11] in which the signal contribution of an interfering component is mathematically removed.

The following paper will demonstrate the application of high-speed chromatography to an analysis important to process monitoring, where resolution is forsaken in order to decrease analysis time. For this particular application it is advantageous to go from a 5 min chromatogram to less than 30 sec. The particular analysis examined will be that of high-fructose corn syrup. Special attention will be given to the choice of an appropriate column, as the packing

material used for the separation is sensitive to high pressure The high-fructose corn syrup separation is accomplished at approximately 80°C, thus special attention to efficiently heating the high-speed column is necessary to avoid radial thermal gradients that lead to severe peak broadening.[12] The adverse effects of a radial thermal gradient in the high-speed regime is avoided by using a column with a bore that is significantly more narrow than conventional column widths.[13,14] Both linear least squares regression and the SCR technique, coupled with suppression, will be applied to analyze the poorly resolved high-speed chromatogram, obtained in less than 30 sec. Results from the analysis will show that both methods give similar results in terms of quantitative precision and accuracy.

THEORY

Given a certain resolution, R_S, the minimum analysis time required, t_R, is

$$t_R = 16R_S^2\left(\frac{\alpha}{\alpha-1}\right)^2\frac{(k'_B+1)^3}{(k'_B)^2}\frac{H}{u}, \qquad (1)$$

where k'_B is the capacity factor for the latest eluting analyte, α is the selectivity factor of the two analytes, H is the plate height, and u the linear mobile phase velocity.[2] A comparison of the resolution change between two columns, labeled with subscripts 1 and 2, differing only in analysis time but not in thermodynamics, may be made using equation (1)

$$R_{S,1} = R_{S,2}\left(\frac{t_{R,1}(H/u)_2}{t_{R,2}(H/u)_1}\right)^{1/2}, \qquad (2)$$

where column 1 may correspond to a high-speed column, and column 2 to a normal-speed column. The minimum analysis time is also equal to

$$t_R = \frac{L}{u}(1+k'), \qquad (3)$$

where L is the column length and k' is the capacity factor of the last analyte.[3] For high-speed chromatography,

$$H \approx Cu \propto \frac{d_p^2 u}{D_m}, \qquad (4)$$

where d_p is the packing material diameter, and D_m is the analyte diffusion coefficient.[2] Substituting equations (3) and (4) into equation (2) leads to the relationship between resolution, column length, mobile phase velocity and particle diameter

$$R_{S,1} = R_{S,2}\left(\frac{L_1 u_2 d_{p,2}^2}{L_2 u_1 d_{p,1}^2}\right)^{1/2}. \qquad (5)$$

For chromatography using soft packing materials such as a polymer gel, pressure becomes an important limitation. The pressure drop ΔP across a packed column is given by

$$\Delta P = \frac{\phi\eta u L}{d_p^2}, \qquad (6)$$

where u is the mobile phase velocity, ϕ is a structural parameter dependent on packing material geometry, and η the viscosity of the mobile phase.[2] For the sake of discussion, one can set the constraint that the pressure drop must be kept constant for both separations

$$1 = \frac{u_1 L_1}{u_2 L_2}\left(\frac{d_{p,2}}{d_{p,1}}\right)^2. \qquad (7)$$

This constraint keeps the instrumental performance requirements constant in terms of pump reliability. If one of the parameters is adjusted, then at least one other parameter must be changed to maintain the identity of equation (7). Thus, equation (5) must be worked within the context of equations (3) and (7), and in terms of analysis time, equation (5) becomes

$$\frac{R_{S,1}}{R_{S,2}} = \left(\frac{t_{R,1}d_{p,2}^2}{t_{R,2}d_{p,1}^2}\right)^{1/2}. \qquad (8)$$

Under the constraint of equation (7), speeding up an analysis by changing particle size is not the best method. If one increases particle size, then either the column length must be lengthened (which actually increases analysis time), or the mobile phase linear velocity must be increased. However, the velocity would have to be changed by a factor equal to the square of the particle size change, leading to an undue loss of resolution. By decreasing particle size, either the column length would have to be shortened, or the mobile phase velocity decreased, which again would increase analysis time. Although decreasing column length by an amount necessary to preserve the identity of equation (7) decreases the analysis time by a factor equal to the square of the particle size change (equation 8), resolution is not sacrificed (equation 5). Moreover, extremely short columns have limited commercial availability.

Decreasing column length and speeding up the mobile phase linear velocity is the most acceptable method of decreasing analysis time

while sacrificing a minimum of the resolution and keeping pressure drop constant. By decreasing column length by a factor of M, the mobile phase linear velocity may be increased M times (equation 7). This leads to a decrease in resolution equal to a factor of M (equation 5) and a decrease in analysis time equal to a factor of M^2 (equation 8).

The above discussion assumes that an unresolved chromatogram can be quantified. Two computer analysis methods that can be used to analyze unresolved chromatograms are linear least squares regression,[7,8] and the sequential chromatogram ratio technique.[9-11] Both methods determine the best fit of a calibration standard to an analysis. For least squares analysis of N analytes, analyte concentrations are given as a $1 \times N$ row vector $\mathbf{x}$, computed as follows

$$\mathbf{x} = \mathbf{y}\beta^T(\beta\beta^T)^{-1}, \tag{9}$$

where $\mathbf{y}$ is the response vector (expressed as a row) and β is a calibration matrix predicted by

$$\beta = X^{-1}Y, \tag{10}$$

where Y is the calibration set containing N rows for N pure component standards, and X is an $N \times N$ diagonal matrix containing the concentrations of the pure component standards.

Linear least squares regression works well when all the components of a chromatogram are known. However, if a component in a chromatogram is an unknown, or a standard for that component is not available, then this method is not usable. A technique that can analyze unresolved chromatograms even when unknowns are present is the sequential chromatogram ratio (SCR) technique. The SCR technique involves the point-by-point ratio of two chromatograms differing only in the relative concentrations of one or more analytes.[9] For a linear detector, the sequential ratio of analyte j is computed by

$$R(t) = \frac{U(t)}{S(t)} = \frac{C_{j,U}}{C_{j,S}}, \tag{11}$$

where $U(t)$ and $S(t)$ are two sequential chromatograms expressed as data vectors, recorded under the same conditions, and $C_{j,U}$ and $C_{j,S}$ are the injected concentrations of analyte j for each respective chromatogram. A plot of the sequential ratiogram will be flat where there exists a pure elution region for analyte j. If the injected concentration of analyte j is known for either $U(t)$ or $S(t)$, the concentration of j in the other chromatogram may be determined from the flat ratiogram. The sequential chromatogram ratio may also be used to provide qualitative information on peak purity, or for analyte identification. The ratio of the chromatogram with a pure component standard chromatogram of the analyte (or suspected analyte) in question is examined. The presence of a flat ratiogram, whose boundaries are determined by comparison of a flatness statistic S_w, obtained from the ratiogram in question, to S_w obtained from replicate standard runs, indicates a pure elution region of an analyte common to both the chromatogram and the standard.[10] The sequential chromatogram ratio may be used to determine concentration changes in chromatograms with resolution as small as 0.1.[9] To quantitate totally unresolved analytes, or to improve the quantification of poorly resolved analytes, it is possible to algebraically remove an interfering component using sequential suppression.[11] Sequential suppression, like the SCR technique, uses two sequential chromatograms, each containing the component to be suppressed. All that needs to be known is the concentration change of that analyte between the two chromatograms. Sequential suppression creates a third chromatogram, $S_{supp}(t)$, lacking the signal contribution of the suppressed component

$$S_{supp}(t) = S(t) - kU(t). \tag{12}$$

The suppression constant k is the ratio of concentrations of the component to be suppressed, obtained from equation (11). If $U(t)$ is a pure component standard, then the signal contributions of all other analytes are unaffected.

EXPERIMENTAL

The mobile phase pump consisted of an ISCO LC-2600 syringe pump (ISCO, Inc., Lincoln, Nebraska) with a volumetric flow rate of 0.75 ml/min for the high-speed analysis, and 0.66 ml/min for the normal-speed analysis. Note that it is not the volumetric flowrate, specifically, that defines the analysis time regime, but rather the linear flow velocity and column dead time.[2] The detector was a Bio-Rad refractive index monitor (Bio-Rad Laboratories, Richmond, CA) with a 10 μl flow cell. Sample injection was accomplished with a Rheodyne 9125 manual injection valve (Rheodyne Inc., Cotati, CA) with a 5 μl sample loop. For the normal-speed analysis, a 100×7.8 mm, 9 μm particle diameter polystyrene-divinyl benzene sulfonated ion

exclusion column in the Pb^{2+} form (Bio-Rad Laboratories, Richmond, CA) was used. The high-speed column was a 35 x 3.2 mm, 10 μm particle diameter polystyrene–divinyl benzene sulfonated ion exclusion column in the Ca^{2+} form (Alltech Associates, Inc., Deerfield, IL). Both columns were heated to 78°C in a hot water bath.

The mobile phase was 100% HPLC-grade water (J.T. Baker Inc., Phillipsburg, NJ). The fructose (Alfa Products, Danvers, MA), dextrose (J.T. Baker, Phillipsburg, NJ), and maltose (Aldritch Co., Inc., Milwaukee, WI) standards were at concentrations of 0.01, 0.0083 and 0.005 g/ml, respectively. Two high-fructose corn syrup samples, one at 55% nominal fructose concentration, and the other at 42% nominal fructose concentration, were diluted 500 times in water.

Data collection was accomplished through the use of an IBM XT personal computer (Boca Raton, FL), equipped with a DASH-16 data acquisition board (Metrobyte Corp., Taunton, MA). Data collection was performed at the rate of 250 points per sec which were box-car averaged down to 50 points per sec. The data were processed using Matlab (The Mathworks, Inc., South Natick, MA). A variance-weighted ratio algorithm was used to calculate all ratios.[9]

Each corn syrup sample was run five times All analyte standards were run four times, twice before the corn syrup samples, and twice after

RESULTS AND DISCUSSION

Before choosing a column for high-speed chromatography it is necessary to examine a conventional analysis, and compare it to the goals of the high-speed separation. Figure 1 is of a chromatogram of high-fructose corn syrup, with a total analysis time of 5.5 min. A reasonable goal is to speed up the analysis to under 30 sec, a 12-fold decrease in analysis time. Although pressure drop across the column was an important consideration, the constraint of equation (7) was not entirely necessary, but should be kept in mind, as the pressure drop of the slow separation (600 psi) was well below the recommended maximum of 1500 psi. Assuming constant volumetric flowrate, the mobile phase linear velocity was increased by a factor of 5.9 by going to a 3.2 mm i.d. column, instead of the 7.8 mm i.d. column used for the slow separation. Column diameter was decreased in this manner in order to lessen the effects of any radial thermal gradients in the heated column at the higher linear flow velocity, and thus maintain the separation efficiency.[12] Microbore columns (1 mm i.d.) easily eliminate any radial thermal gradient,[13,14] but any column with less than 3.2 mm i.d. would have lead to significant extra-column band broadening from the detector available for analyte peaks less than 10 times the detector flow cell volume. The separation efficiency achieved with the high-speed (3.2 mm i.d.) column indicated that radial thermal gradients were not significant with this column at 78°C and a linear flow velocity of 3 mm/sec. To decrease analysis time further, the column length was decreased from 10 to 3.5 cm. Thus, the column dead time was about 11 sec, which was in the high-speed regime.[2] Theoretically, at constant volumetric flowrate, all the changes in column diameter and length result in the analysis time decreasing by a factor of 17.0 (equation 3), with an increase in pressure by 2.1 times (equation 6). Also, the resolution should be $\sqrt{17.0}$ times worse, or a factor of 4.1.

Figure 2 shows two chromatograms of high-fructose corn syrup using the high-speed column, nominally at 42% fructose (HF-42)

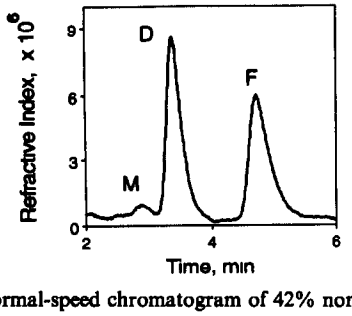

Fig. 1 Normal-speed chromatogram of 42% nominal fructose concentration high-fructose corn syrup M—maltose, D—dextrose, F—fructose. For chromatographic conditions, see text.

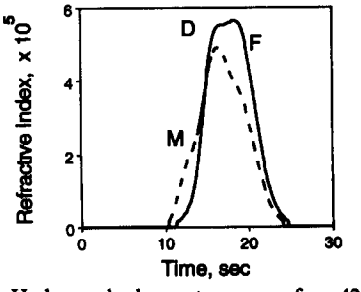

Fig. 2. High-speed chromatograms of a 42% nominal fructose concentration high-fructose corn syrup (dashed line) labeled HF-42 in Table 1 and text, and a 55% nominal fructose high-fructose corn syrup (solid line) labeled HF-55 in Table 1 and text: M—maltose, D—dextrose, F—fructose. For chromatographic conditions, see text.

and 55% fructose (HF-55). The experimental parameters, such as pressure and analysis time, are within acceptable bounds of the values predicted in the above discussion of going from a normal-speed separation to a high-speed separation. Actual agreement was not expected, as the above discussion, using equations (3), (5), (6) and (8), assume that the thermodynamics between the separations remains constant. This was not precisely the case, as the fast column packing material differs slightly in particle diameter and counterion (as reported in the experimental section). Also, by using a smaller diameter column, the thermal gradients present in the heated column were minimized. Total analysis time has been decreased by a factor of over 13, relative to Fig. 1, to under 25 sec. Resolution of the three sugars in the high-speed chromatograms was determined from injections of individual standards, shown in Fig. 3. Resolution between the fructose and the dextrose has decreased from 2.2 in the normal-speed chromatogram to 0.8 in the high-speed chromatogram; resolution between dextrose and maltose has decreased from 1.0 to 0.3. Finally, the pressure drop across the column has been increased to 1100 psi in the high-speed runs, from 600 psi in the normal speed run.

As all components of the sample mixture were known, it was possible to apply least squares regression (equations 9 and 10) to quantitate the poorly resolved chromatograms, using the analyte standards in Fig. 3. The results, shown in Table 1, agree well the nominal percentages of each sugar one might expect in a corn syrup sample, especially the fructose percentage. Precision was also good, with the standard deviation being better than 2% on average for fructose, the primary analyte of interest. By using an automated injection system, precision could be further improved to below 1%.

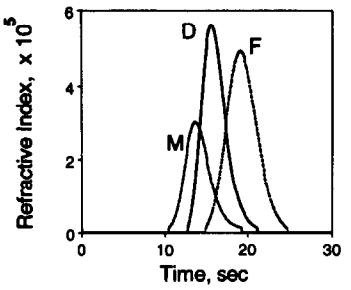

Fig 3 High-speed pure-component chromatograms for the major components of high-fructose corn syrup· M—maltose, D—dextrose, F—fructose For chromatographic conditions, see text

The SCR technique works in a similar fashion to linear least squares regression, but has the added advantage that not all of the components in a chromatogram need be known (high-fructose corn syrup can be expected to contain up to 1.5% unknown higher saccharides).[9-11] Figure 4 is a ratiogram between the HF-55 corn syrup sample and a pure fructose standard (Fig. 3), obtained from applying equation (11). The ratiogram is flat from 20 to 23 sec, indicating a pure elution region for fructose. This constitutes the qualitative analysis of fructose, and can be substantiated by applying a flatness statistic comparison of apparent pure elution regions between replicate standards and the data in Fig. 4.[10] From this flat region the ratio of concentrations between the two chromatograms may be calculated. Below 20 sec, the ratiogram rapidly increases due to a mixed elution region of fructose and dextrose. This mixed elution region in no way interferes with the analysis of fructose. Even if an unknown component co-eluted with the dextrose or maltose, it would still be possible to calculate the concentration of fructose, as a flat ratiogram would still exist. Maltose may also be analyzed by repeating the above procedure, using a pure maltose standard of known concentration.

Table 1 Quantitative comparison of the determination of the primary components in high-fructose corn syrup by linear least squares regression and the SCR technique coupled with suppression

Sample label	Nominal fructose (%)	Method of analysis*	Maltose (%)	Dextrose (%)	Fructose (%)
HF-42	42	LLSR	18.5 ± 0.2	43.4 ± 0.5	38.1 ± 0.5
		SCR	18.1 ± 0.4	42.8 ± 1.2	39.0 ± 1.2
HF-55	55	LLSR	1.9 ± 0.5	40.7 ± 0.7	57.2 ± 0.9
		SCR	1.4 ± 0.6	40.3 ± 0.4	57.9 ± 0.7

All values are the average of five runs, and are listed ±1 S.D.

*LLSR—Linear least squares regression. SCR—Sequential chromatogram ratio technique coupled with sequential suppression

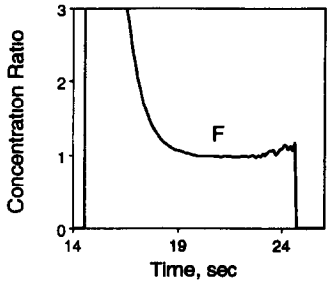

Fig. 4 Ratio of injected concentrations, obtained from applying equation (11) to the chromatograms of the 55% nominal concentration high-fructose corn syrup (Fig. 2) and the pure fructose standard chromatogram (Fig 3) The flat concentration ratio for fructose, F, is used for positive identification and quantification

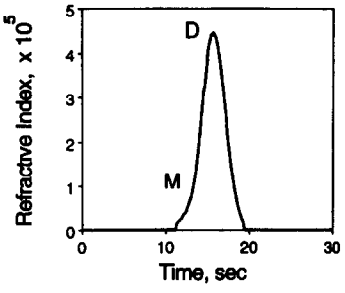

Fig 5 High-speed chromatogram of 55% nominal concentration high-fructose corn syrup after fructose has been mathematically suppressed using equation (12) and the pure component fructose chromatogram (Fig 3)

However, it is not possible to quantitate dextrose without suppression of maltose or fructose, as no pure elution region exists for this sugar as is clear from Fig. 3. One must first mathematically remove the signal contribution of either maltose or fructose, using sequential suppression. Figure 5 is the same chromatogram of the above high-fructose corn syrup (HF-55), only with the signal contribution of fructose removed, using equation (12). The suppression constant, k, was calculated from the ratiogram in Fig. 4. There now exists a pure elution region for dextrose, with which the SCR technique was applied. The results of the analysis using the SCR technique may be compared with the results of the analysis using least squares in Table 1. Again, precision could be improved with the use of an automated injection system to better than 1%. The results of the two methods are comparable with each other.

By using an appropriate data analysis method, it is possible to sacrifice resolution in order to speed up an analysis, and not give up significant accuracy or precision of the results. Linear least squares analysis is a simple algorithm which requires that all components of a chromatogram be known. The sequential chromatogram ratio technique does not have this limitation, and provides results comparable with classical least squares.

Acknowledgement—The authors would like to thank Michael J Blackburn and Cargill, Inc for providing a refractive index detector, the normal-speed column, and the high-fructose corn syrup samples

REFERENCES

1 R P W Scott, in *Gas Chromatography*, A Goldup (ed), p 125 Institute of Petroleum, London, 1965
2 C N Renn and R E Synovec, *Anal Chem*, 1988, **60**, 200
3 P Kucera and N. Licago, in *HPLC in the Pharmaceutical Industry*, G W Fong and S K Lam (eds), p. 3 Marcel Dekker, Inc , New York, 1991
4 J B Callis, D L Illman and B R Kowalski, *Anal Chem*, 1987, **59**, 624A
5 J. M Davis and J C Giddings, *Anal Chem*, 1983, **55**, 418
6 J M. Davis and J C Giddings, *Anal Chem*, 1985, **57**, 2178
7 M M. Sharaf, D L Illman and B R Kowalski, *Chemometrics*, p 48, Wiley-Interscience, New York, 1986
8 K. R. Beebe and B R Kowalski, *Anal. Chem.*, 1987, **59**, 1007A
9 R E Synovec, E L Johnson, T J Bahowick and A W Sulya, *Anal Chem*, 1990, **62**, 1597
10 T. J Bahowick and R E Synovec, *Anal Chem*, **64**, 1992, 489
11 D R Dunphy, T J Bahowick and R E Synovec, *J. Chrom*, submitted for publication, 1993
12 H Poppe, J C. Kraak, J F K Huber and J H M van den Berg, *Chromatographia* **14**, 1981, 515
13 C N Renn and R E Synovec, *Anal Chem*, 1991, **63**, 598
14 C N Renn and R E Synovec, *Anal Chem*, 1992, **64**, 479

Talanta, Vol 40, No 6, pp 781–784, 1993
Printed in Great Britain

0039-9140/93 $6 00 + 0 00

SPECTROPHOTOMETRIC DETERMINATION OF SELENIUM WITH 6-AMINO-1-NAPHTHOL-3-SULPHONIC ACID (J-ACID) AND ITS APPLICATION IN TRACE ANALYSIS

K N RAMACHANDRAN, R. KAVEESHWAR and V. K. GUPTA*
School of Studies in Chemistry, Pt Ravishankar Shukla University, Raipur, M P, 492 010, India

(*Received* 9 *September* 1992 *Revised* 18 *November* 1992 *Accepted* 18 *November* 1992)

Summary—A selective procedure for spectrophotometric determination of selenium with 6-amino-1-naphthol-3-sulphonic acid (J-acid) is described In acidic conditions selenium forms a yellow complex with J-acid which has an absorption maximum at 392 nm The molar absorptivity is $1\,48 \times 10^4$ 1 $mol^{-1}cm^{-1}$ Beer's law is obeyed for selenium in the range of 0 08–0 8 mg/l The method has been applied to the determination of trace amounts of selenium in water, polluted water, plant material and steel plant dust The proposed method is sensitive, rapid, simple and accurate

Selenium is one of the widely distributed non-metallic elements with considerable significance.[1,2] The maximum tolerance limit for human beings is 0.1 mg/m^3 in air and 4 mg/l for water.[2] Several methods based on different techniques have been reported for the determination of selenium.[3–7] Of the numerous methods reported for spectrophotometric determination of selenium, only a few of them have sensitivity, selectivity and simplicity. The most popular reagents reported include 3,3′-diaminobenzidine,[8] dithiozone,[9] o-phenylenediamine,[10] and chromotropic acid.[11] Methods using o-diamines require long reaction times, acidity maintenance, *etc.* while most of the other reported reagents are non-selective. Here, 6-amino-1-naphthol-3-sulphonic acid (J-acid) is proposed as a new reagent for photometric determination of selenium(IV). The sensitivity for the determination of selenium (IV) is superior to that of other reported reagents. The conditions of the formation of the Se (IV)–J-acid complex were studied in detail. In the pH range of 1–2.5, J-acid reacts instantaneously with Se (IV) to form a yellow 2.1 complex.

The Se–J-acid complex exhibits maximum absorption at 392 nm with a molar absorptivity of $1\,48\ (\pm 0.01) \times 10^4$ 1 $mol^{-1}cm^{-1}$. Beer's law is valid over the concentration range of 0.08–0.8 mg/l of Se (IV). The colour reaction is free from interference from more than 25 ions investigated. The proposed method has been applied to the spectrophotometric determination of trace amounts of Se (IV) in environmental samples and offers advantages of simplicity, sensitivity, rapidity and stability of the coloured solution without heating.

EXPERIMENTAL

Apparatus

Absorption spectra and the absorbance were recorded using a Varian DMS 100 S UV–visible spectrophotometer, with matched silica cells. A Systronics pH meter model No. 331 was used to measure the pH. Standard glassware was used for volumetric measurements.

Reagents

All chemicals used were of analytical reagent grade unless otherwise stated. Deionized double distilled water was used.

Standard selenium solution (100 mg/l): dissolve 100 mg of elemental selenium in 5 ml concentrated nitric acid by gently heating and evaporate to dryness and dilute with distilled water to 100 ml. Dilute further to obtain a 1 mg/l working standard solution.

J-acid (Wilson): dissolve 500 mg of 6-amino-1-naphthol-3-sulphonic acid (J-acid) in 100 ml of concentrated sulphuric acid, and store in an amber coloured bottle.

Sulphuric acid: 18M.

*Author for correspondence

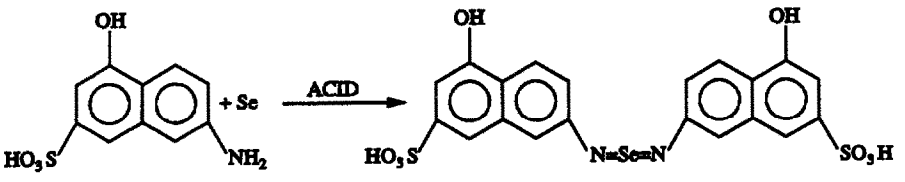

J-ACID J-ACID-Se-COMPLEX (λmax, 392 nm)

Scheme 1

Acid mixture: mix 80 ml of concentrated nitric acid with 20 ml of 60% perchloric acid.

EDTA: 0.05M.

3,3′-Diaminobenzidine hydrochloride: dissolve 500 mg of the reagent in 100 ml water.

Hydroxylammonium chloride solution: dissolve 2.5 g of the reagent in 100 ml of water.

Sodium hydroxide: dissolve 10 g of the reagent in 100 ml of water.

Potassium bromide, bromine water, saturated solution of bromine in distilled water.

Recommended procedures

Procedure for the study of the colour reaction of selenium. Take a test solution containing not more than 20 μg of selenium in a 25 ml calibrated flask, add 2 ml of J-acid, mix well and successively dilute to the mark with sulphuric acid. Measure the absorbance at 392 nm against a reagent blank.

Procedure for the determination of selenium in water and polluted river water. Take an aliquot of test solution in a distillation flask, add 5 ml sodium hydroxide solution and distill the mixture under vacuum to concentrate the selenium content. Discard the distillate and then add 0.7 g potassium bromide and 10 ml sulphuric acid treated with 8–10 drops of saturated bromine water to the concentrate. Connect the condenser of the distillation flask to a receiver flask containing 10 ml of 2.5% hydroxylammonium chloride solution to collect the distillate containing $SeBr_4$. Now distil the sample under vacuum until white copious fumes of SO_3 vapours are evolved. Make the distillate to a fixed volume (25 ml). Take 10 ml of it and then follow the recommended procedure described above for determination of selenium.

Procedure for the determination of selenium in plant materials. Take 5 g of plant material in a 100 ml Kjeldahl flask, add 10 ml nitric acid and heat for 20 min. Then add 0.5 ml perchloric acid and heat for another 10 min or until the evolution of ample fumes of perchloric acid, whichever is earlier. Add 10 ml water to the cooled residue and heat for 10 min. Add 5 ml of HCl and heat for 10 min. Then dilute the contents to 50 ml after adding 10 ml EDTA solution and then follow the above recommended procedure for determination of selenium.

Procedure for determination of selenium in steel plant dust. Place the filters containing dust from the steel plant in 100 ml beaker, add 10 ml acid mixture for digestion and evaporate to 2 ml. Cool the contents and boil with 10 ml HCl for 10 min. Again cool the contents and dilute to 25 ml with water. Analyse 5 ml of the solution for selenium as recommended above.

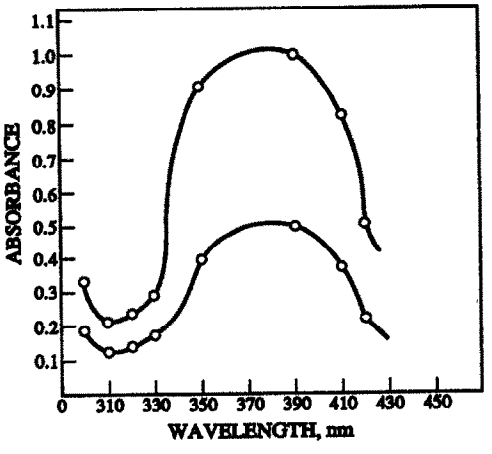

Fig 1 Absorption spectra of dye A Concentration of selenium = 5 μg/25 ml B Concentration of selenium = 10 μg/25 ml

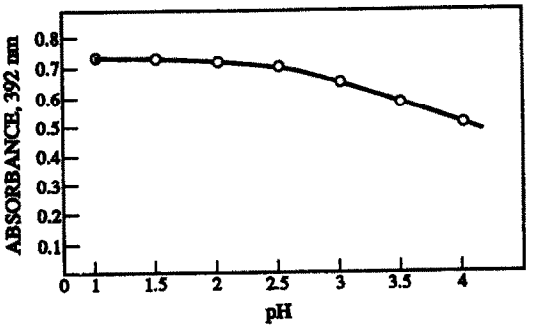

Fig. 2 Effect of pH on colour development concentration of selenium = 10 μg/25 ml.

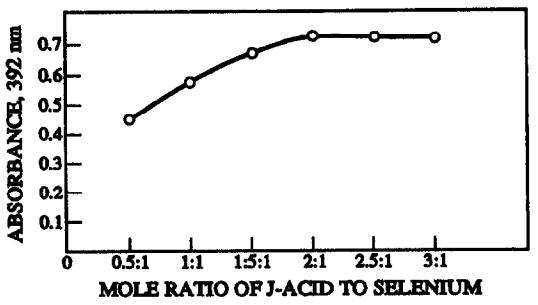

Fig 3 Effect of J-acid on colour reaction concentration of selenium = 10 μg/25 ml.

Table 1. Effect of diverse ions concentration of Se(IV)—0 4 mg/l

Diverse ions	Tolerance limit* mg/l
Fe^{2+}, Fe^{3+}, V^{5+}	10,000
Ca^{2+}, Ba^{2+}, Be^{2+}, Cl^-, Br^-, SO_3^{2-}	5000
Mg^{2+}, CN^-, SO_4^{2-}, NH_4^+, CO_3^{2-}, Zn^{2+}	2500
Al^{3+}, Zr^{4+}, Cr^{3+}	6000
Sn^{2+}, Te^{4+}	1000
Cu^{2+}, Ni^{2+}	500
NO_3^-, NO_2^-	50

*Tolerance limit may vary the results by $\pm$2%

RESULTS AND DISCUSSION

Absorption spectra

The absorption spectra of the Se (IV) J–acid complex is shown in Fig. 1. The absorption maximum of the complex is at 392 nm.

Adherence to Beer's law and sensitivity

The absorbance is a linear function of selenium concentration in the range of 0.08–0.8 mg/l of solution. The apparent molar absorptivity is 1.48×10^4 l $mol^{-1}cm^{-1}$. The Sandell sensitivity is 0.005 $\mu g/cm^2$

Reproducibility

The relative standard deviation of the sample containing 0.4 mg/l of selenium for seven replicate analyses is $\pm$ 2.26%. The percentage recovery of spiked samples is 96–98%.

Conditions for the colour development

The absorbance of the complex depends on the pH of solution as shown in Fig. 2. The maximum and constant absorbance was attained in the pH range 1–2.5.

Under the conditions employed the volumes of 0.5% J-acid required to obtain constant absorbance for 0.8 mg/l selenium was 2 ml. Hence 2 ml of J-acid solution was introduced.

The colour reaction was instantaneous and requires no heating. In the solution of pH 1–2 5 the absorbance reached its maximum immediately and remained stable for at least 24 h Normal variations in temperature have no effect on the complex.

Composition of the complex

The composition of the complex was determined by the continuous variation method and mole ratio method. The ratio of Se–J-acid was 1:2 in the complex by both methods (Fig. 3).

Effect of foreign ions

The effect of various ions on the determination of selenium was studied and their tolerance limits are shown in Table 1 It was found

Table 2. Application of the method

Samples	Natural water[a] ($\mu g/ml$)	Polluted river[b] water ($\mu g/ml$)	Steel plant[c] dust ($\mu g/g$)	Plant materials[d] ($\mu g/g$)
Se(IV) added	0 100	—	0 200	—
	0 150	—	0 500	—
	0 200	—	1 000	—
Se(IV) found*				
(a) Present method	0 098	0.380	0 198	0 324
	0 145	0.460	0 491	0 450
	0 195	0 520	0 950	0 478
(b) Reported method	0 097	0 360	0 193	0 322
	0.147	0.420	0 489	0.450
	0 192	0 530	0 958	0 480
Recovery %				
(a) Present method	98.0	—	99.0	—
	96 6	—	98 1	—
	97 5	—	95 0	—
(b) Reported method	97 0	—	96 5	—
	98.0	—	97.8	—
	96 0	—	96.0	—

*Mean of three replicate determinations

a—Amount of sample taken, 5 ml; b—amount of sample taken, 5 ml; c—amount of sample taken, 27 3 mg, d—amount of sample taken, 5 mg

Table 3 Comparison with other spectrophotometric methods

Reagents	Medium/pH	λ_{max} (*nm*)	Beer's law range (*μg/ml*)	Remarks
3,3′-Diaminobenzidine[8]	Aqueous pH 2–3	420	0 1–10 0	Coloured salts, oxidants, Bi^{3+}, Te^{4+}, Cr^{3+}, Mo^{4+}, V^{5+}, etc interfere
4,5-Diamino-6-thiopyridine[12]	Aqueous pH 1 5–2 5	380	0 1–2 5	Fe^{3+}, Fe^{2+}, Cu^{2+}, $S_2O_3^{2-}$, SO_3^{2-}, ClO_3^-, *etc* interfere
1-Phenylthiosemicarbazide[13]	Butanol + $CHCl_3$ 0 05–2*M* HCl	380–400	1 0–2 0	Cu^{2+}, V^{5+}, Fe^{3+}, Bi^{2+}, Te^{4+}, Mn^{2+} interfere
2,3-Diaminonaphthalene[14]	Aqueous 1 5–2 5	380	1 0–12 0	Fe^{2+}, Fe^{3+}, Mn^{2+}, V^{5+} and other oxidants as well as reductants interfere
Dithio-oxamide[15]	Aqueous 3–4*M* HCl	410–415	0 2–2	Cr^{3+}, As^{5+}, Cu^{2+}, Fe^{3+}, Te^{4+} interfere
o-Phenylenediamine[10]	Toluene 1 5–2 5	335	Up to 4	1–3 hr for reactions, Fe^{3+}, Bi^{2+}, Mn^{2+} interfere
4-Nitrophenyl hydrazine + 8 quinolinol[16]	Aqueous 9–11	550	0 28-1 8	Fe^{3+}, Cu^{2+}, V^{5+}, Mn^{2+}, interfere
6-Amino-1-naphthol-3-sulphonic acid (J-acid) (Present method)	Aqueous 1–2 5	392	0.08–0 8	Te^{4+}, V^{5+}, Fe^{3+}, Cu^{2+}, do not interfere

that tellurium^{4+}, manganese^{2+}, vanadium^{5+}, iron^{2+}, iron^{3+} and copper^{2+}, which interfere strongly with most of the other reported methods did not interfere. Thus, the selectivity and sensitivity of the method is appreciable and can be applied to the determination of trace amounts of selenium.

APPLICATION

The method has been applied for the determination of selenium in several samples of water, polluted river water, plant materials and steel plant dust. The results obtained are present in Table 2 and are in agreement with those obtained by the 3,3′-diaminobenzidine method.

Comparison with other reagents

J-acid is proposed as one of the most sensitive reagents available for the spectrophotometric determination of selenium. The proposed method is simple, rapid and accurate as compared to other published methods. The sensitivities of various reagents are listed in Table 3 for comparison.

Acknowledgements—The authors are grateful to the Head of the School of Studies in Chemistry, Pt Ravishankar Shukla University, Raipur for providing laboratory facilities. One of the authors, K N R, is thankful to Ravishankar University, Raipur for providing a fellowship and the other, R K, is thankful to the C S I R, New Delhi for providing a fellowship

REFERENCES

1 J R Shapira, in D L Klayman and W H Gunther (eds), *Organic Selenium Compounds, Their Chemistry, and Biology*, p 701, Wiley Interscience, New York, 1971
2 F A Patty, *Industrial Hygiene and Toxicology*, Vol 2, p 886, Wiley Interscience, New York, 1962
3 J Tan and Y Huang, *J Water, Air Soil Poll*, 191, **57–58**,59
4 H Robberecht and R V Grieken, *Talanta*, 1982, **29**, 824
5 L Danhong and Z Yongxi, *Chem Abstr*, 1992, **116** (4), 33,492d
6 Qi Wenbin and X Xiaomei, *Chem Abstr*, 1991, **115** (15), 154,262s
7 D Karel, K Jana and P Ladislave, *Chem Abstr*, 1991, **115** (17), 178867u
8. B G Russel, *Talanta*, 1967, **14**, 957
9 A D Campbell and A H Yshaya, *Anal Chim Acta*, 1980, **119**, 171
10 J Hon, S Cheng and B Soo, *Anal Abstr*, 1987, **59**, 10B78
11 S C Lavale and M Dave, *J Ind Chem Soc*, 1989, **66**, 974
12 L Frank-Chan, *Talanta*, 1964, **11**, 1019
13 A I Busev, *ibid*, 485
14 M J Rankin, *Environ Sci Technol*, 1973, **7**, 823
15 N B Lebed and R P Pantaler, *Zh Anal Khim*, 1986, **41** (12), 2224
16 A Bhat and V K Gupta, *J Ind Chem Soc*, 1982, **59**, 888

Talanta, Vol 40, No 6, pp 785–790, 1993
Printed in Great Britain

0039-9140/93 $6 00 + 0 00

CONVECTIVE TRANSPORT IN DIFFUSIVE SAMPLERS

DWIGHT W. UNDERHILL
School of Public Health, University of South Carolina, Columbia, SC 29208, U S A

(*Received* 16 *June* 1992 *Revised* 18 *November* 1992 *Accepted* 18 *November* 1992)

Summary—Convective transport in diffusive samplers was determined by the loss of a dilute dye solution from these samplers while held in a water bath The water flow in the bath was adjusted to give the same Reynolds number had the diffusive sampler been exposed to an airborne analyte at a predetermined flow velocity By numerical analysis, estimates were made of the degree of interference of convection on sampler performance. The results indicate an enormous difference between commercial diffusive samplers with respect to the effect of convection on the transport of analyte into the sampler

Many diffusive samplers are seriously affected by ambient air currents, and experiments in which the uptake of analyte is determined at different air flow velocities are an important part of a proposed procedure to "validate" the performance of diffusive samplers.[1–5] However, because diffusive effects predominate in these samplers, determining the added effect of convection has a high experimental error. This difficulty in seeing the convective transport against a much larger background of diffusive transport could be resolved if the effect of diffusion could be reduced to where the major mode of mass transfer is convection.

By holding these samplers in a water bath, the diffusion coefficient for the analyte (in this study a dilute solution of methylene blue, a dye) is reduced to a negligible level, and the mass transport by convection can be determined independently of molecular diffusive effects. The suppression of molecular diffusion by this procedure is quite effective because the rate of diffusion of dyes in water is about 1000 times lower than that of organic analytes in air

Water bath models have been used before in studies of the airborne mass transfer of contaminants, for example to simulate the performance of an impinger, to model the transport by thermal currents of toxic matter during a fire, or to define operational parameters for local ventilation systems to exhaust ethylene oxide.[6–8] In these prior examples the major component of mass transport is convection, so that the use of a water bath model for this study, where the major component of mass transfer is diffusion, may appear novel.

THEORY

The water flow was adjusted to give the same Reynolds number had the diffusive sampler been exposed to air at a predetermined velocity. This maintains the same flow patterns around and *through* the diffusive sampler that would be observed in an atmospheric environment at the same Reynolds number. The Reynolds number (Re) is defined as:

$$Re = dV/v \tag{1}$$

where:

d = characteristic linear dimension of the flow channel in centimeters,
V = fluid velocity in centimeters per second,
v = kinematic viscosity of the flowing fluid.

Listed below are the necessary steps in applying data from a water bath experiment to the diffusive sampling of airborne contaminants.

Step 1: determining the appropriate scaling factors

At 25°C, the kinematic viscosities of air and water, v_a and v_w, are 0.155 and 0.0084 cm^2/sec, respectively. To maintain the same Reynolds number in water as in air (and hence the same flow patterns), the ratio of the flow of water to the flow of air should be the ratio of these kinematic viscosities, which is a factor of 0.0542.

Because the actual diffusive samplers, and not models, are used in these experiments, there is no need to provide scaling factors for any dimensional changes.

Step 2: determining the "exposure time"

In order to obtain the same flow of water as of air, the sampler must be in the water bath longer than in a corresponding air chamber. The ratio of the two exposure times for an equivalent amount of flow is the ratio of the kinematic viscosities, v_a/v_w, which is approximately a factor of 18. Thus to estimate the effect of convection on the sampling of an analyte from air at the same Reynolds number and for the same total flow, the time durations for the measurements in the water bath should be divided by a factor of 18.

For these results to be valid, the duration of the water bath test should be either until nearly all the dye is lost from the sampler, or for a time period significantly longer than $(v_a/v_w)L^2/D_m$, where L is the width of the air gap, and D_m is the diffusion coefficient of the analyte in air. The significance of the grouping, L^2/D_m, is that it describes the mean time required for an analyte to pass across the air gap.

Step 3: determining the eddy diffusion

After the rate of loss of an aqueous solution of methylene blue by convection from the sampler was measured, these results were used to quantify the eddy diffusion inside the diffusive sampler. To do this, the diffusive sampler was treated as consisting of a series of strips, with the mass transfer across each strip calculated using the Crank–Nicolson finite difference equation:[9]

$$\frac{C_{i,j+1}-C_{i,j}}{\delta T}=\frac{D_e}{2\delta X^2}\left\{\frac{C_{i+1,j}-2C_{i,j}+C_{i-1,j}+C_{i+1,j}}{\delta X^2}+C_{i+1,j+1}\frac{-2C_{i,j+1}+C_{i-1,j+1}}{\delta X^2}\right\} \quad (2)$$

where:

$C_{(i,j)}$ = concentration in the ith strip at the jth time in grams per cubic centimeter,
δT = time increment in seconds,
δX = width of strip in centimeters,
D_e = eddy diffusion coefficient in square centimeters per second.

It is assumed that the concentrations at the jth time are known, and the unknowns are the concentrations at the next time row, $j+1$. If this model assumes n strips, then there are n equations with $n+2$ unknowns, which can be reduced to n unknowns once the boundary conditions are defined. The two boundary equations appropriate for this model are:

$$C_{i=1}=0 \text{ (negligible dye concentration at opening)} \quad (3)$$

and

$$C_{i=n-1}=C_{i=n} \text{ (no diffusion out of back of sampler).} \quad (4)$$

Further, it is assumed that the sampler is initially evenly filled with dye, so that at time $t=0$ (*i.e.* $j=0$) the initial concentration of dye is:

$$C_{j=0}=K. \quad (5)$$

Combining equations (2)–(5) leads to a series of equations that comprise a tridiagonal matrix. A well-known numerical method leads to the solution of such matrices in a number of arithmetic operations proportional to "n".[10]

The eddy diffusion will be strongest at the exposed surface and drop off rapidly in intensity with respect to the depth in the sampler. Here it was assumed that the eddy diffusion obeyed a power function of the form,

$$D_e=aX^b \quad (6)$$

where:

X = distance from the back of the diffusive sampler

allowing us to find by trial and error the coefficients "a" and "b" for the eddy diffusion coefficient, D_e, that best give the measured outflow of dye as a function of time.

Step 4: calculating the effect of eddy diffusion on uptake

Next, the mass transport of airborne analytes by the combined effects of convection and molecular diffusion can be determined by adding the molecular diffusion coefficient to the eddy diffusion coefficient, *i.e.*

$$D=D_m+D_e \quad (7)$$

where:

D = combined diffusion coefficient,
D_m = molecular diffusion coefficient and
D_e = eddy diffusion coefficient, all in square centimeters per second

This is the same procedure used in the van Deemter equation for mass transport in a gas chromatography column.[11]

Assuming that the eddy diffusion coefficient is not constant across the sampler, then the mean diffusion coefficient across the air gap, if calculated using equation (9.15) of Crank, will be.[9]

$$D_{ave} = L\left(\int_0^L \frac{dX}{D}\right)^{-1}. \quad (8)$$

If the average diffusion coefficient, D_{ave}, differs appreciably from the molecular diffusion coefficient, D_m, then the sampling rate has been affected by the eddy diffusion, and the percent increase in the sampling rate brought about by eddy diffusion is given by the factor, $100(D_{ave}/D_m - 1)$.

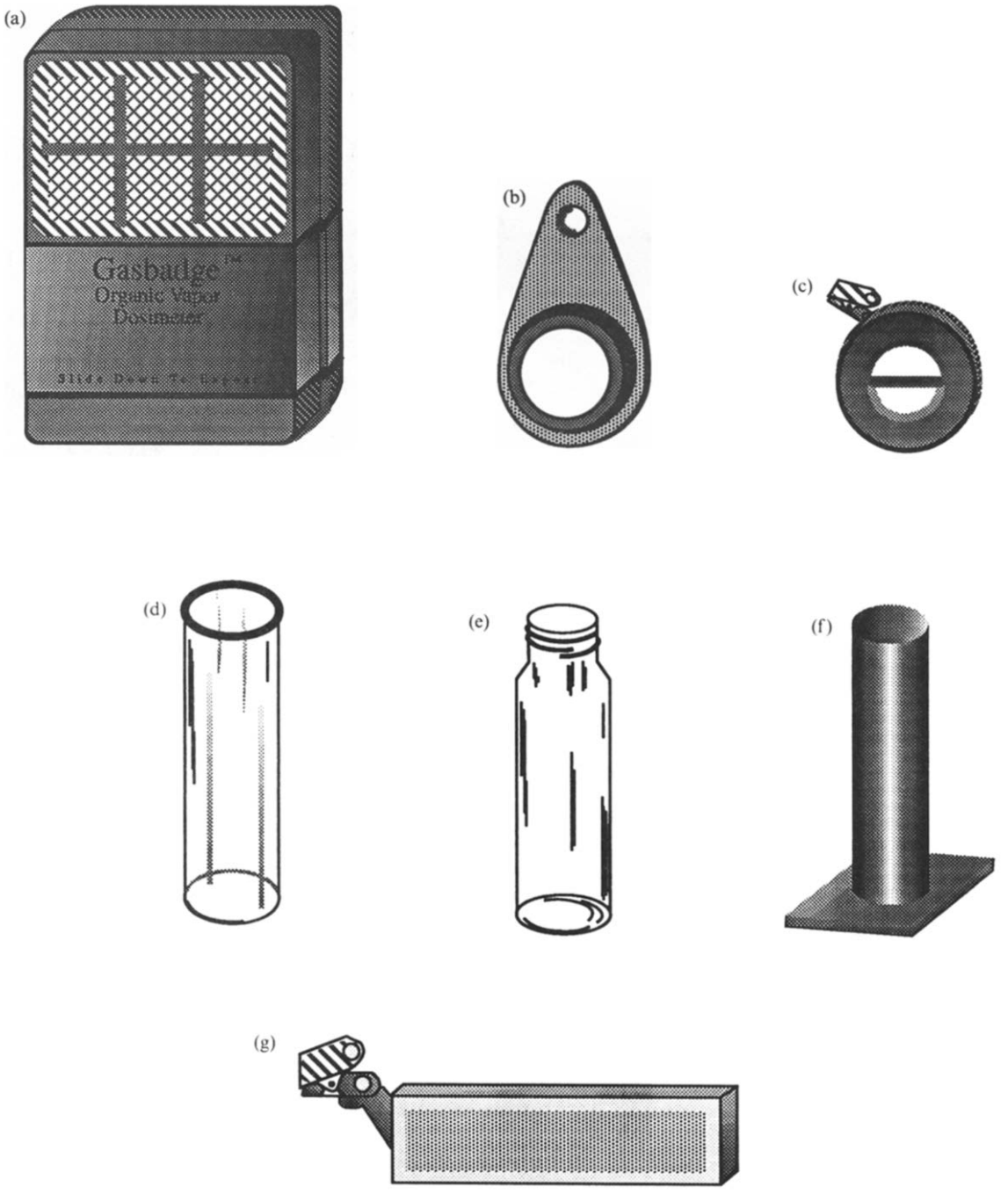

Fig 1 The diffusive samplers (a) The *Gasbadge Organic Vapor Dosimeter*; (b) The 3*M Brand Air Sampling Monitor*, (c) Advanced Chemical Sensors Co. *Formaldehyde Monitor*; (d) the *PF-1 Formaldehyde Monitor*, (e) the *HOMEcheck Mobile Home Odor (Formaldehyde) Test Kit*, (f) The *Palmes' Tube*, (g) the *Pro-Tek Air Monitoring Badge*

Table 1 Physical dimensions of examined diffusive samplers

1	The *3M Brand Air Sampling Monitor*, #3550 is a badge type sampler in which the diffusion barrier is 3 *cm* in diameter, and 0 9 *cm* deep A thin continuous membrane is placed at the end of the diffusion barrier to reduce the effect of external convection currents.[16]
2	The *Formaldehyde Monitor*, Advanced Chemical Sensors Co is also a badge type sampler The diffusion barrier is 2 4 *cm* in diameter, and 0 5 *cm* deep As with the 3M diffusive sampler, a thin continuous membrane is placed at the end of the diffusion barrier to reduce the effects of external convection currents [15]
3	The *Gasbadge Organic Vapor Dosimeter* is a badge type sampler, having a diffusion passage 4 8 *cm* wide, 3 7 *cm* high, and 1 3 *cm* deep The convection barrier is a course ($\approx$25 openings per cm^2) light plastic screen [14]
4	The *HOMEcheck Mobile Home Odor (Formaldehyde) Test Kit* is a glass cylinder 7 *cm* high At its base the outside diameter is 2 *cm* and the inside diameter is 1 8 *cm* In use, solution is to be placed in it Its fill line is 2 *cm* over the base It has a screw top $\approx$0 5 *cm* in height The inside diameter at the screw top is 1 5 *cm* [20]
5	The *Palmes' Tube* used in these experiments was fashioned from an aluminum cylinder 7 *cm* high, closed at one end, and having an outside diameter of 1 4 *cm* and an inside diameter of 0 9 *cm* [19]
6	The *PF-1 Formaldehyde Monitor*, distributed by Air Quality Research, Inc , Berkeley, CA, is a glass cylinder 9 3 *cm* deep (measured internally), having an outside diameter of 2 5 *cm*, an internal diameter of 2 3 *cm*, and is closed at one end [21]
7	The *Pro-Tek Air Monitoring Badge* [12] is a badge-shaped diffusive sampler that is unusual in that both sides of the sampler, after the covers have been removed, can participate in the sampling process The diffusion space on either side is 0 8 *cm* wide, 6 5 *cm* in length, and 0.3 *cm* deep The actual diffusion takes place through a set of small holes ($\approx$15 cm^{-2}) placed in the plastic cover

EXPERIMENTAL RESULTS

Samplers having a high degree of flow induced convection

Many commercial diffusive samplers are shaped like film badges and are conveniently used to assess worker exposure by being attached to the worker's collar during his or her workday. Because in such samplers, the wide, thin region across which mass transport takes place is very vulnerable to the sampling rate being altered by convection, these diffusive samplers must be furnished with some means to reduce convection. The first two samplers tested, the Pro-Tek Air Monitoring Badge and the Gasbadge Organic Vapor Dosimeter, have a solid surface permeated with small holes, and a porous plastic screen, respectively, placed at the exterior of the sampler to reduce convective flow.[12-14] Figure 1 gives drawings of representative diffusive samplers. Additional details of the diffusive samplers used in these tests are given in Table 1 In our tests these diffusive samplers were filled with a dilute solution of methylene blue and placed in a water bath, 11.5 cm wide, 13 cm high, and 30 cm long (see Fig. 2). At a flow rate of 0 11 cm/sec, the loss of methylene blue was so rapid that its loss could not be quantified Even stopping the water flow, placing the closed sampler into the water bath, carefully opening the sampler and restarting the water flow, gave irreproducible results In the few seconds required to establish an even water flow in the recirculating water bath, much of the dye was lost from the samplers

Our inability, even with care, to place these diffusive samplers into a water bath and starting the flow of water without their losing a sizable fraction of the methylene blue dye contained within, indicates (even though no numerical

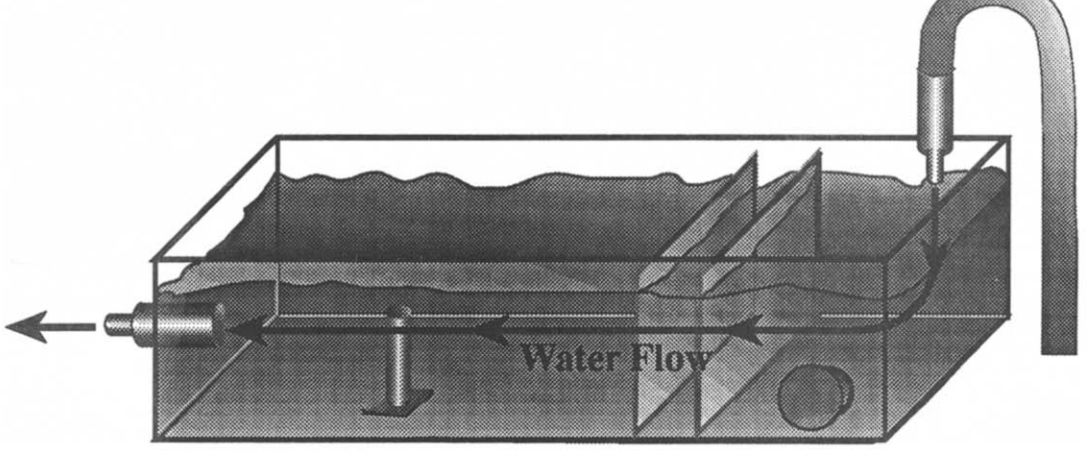

Fig 2 The test system

values could be obtained) a strong effect of convection on their performance.

In the absence of numerical data, the numerical analysis developed above could not be applied to these samplers.

Samplers having a low degree of flow induced convection

The other two "film badge" type of diffusive samplers, the Formaldehyde Monitor, Advanced Chemical Sensors Co., and the 3M Brand Air Sampling Monitor, #3550, both contain a thin plastic membrane across the exterior of the diffusive sampler.[15,16] For both samplers, under the same conditions as described above, less than 1% of the methylene blue was lost from the sampler over a 24 hr test period. In these diffusive samplers, the convective flow from the sampler was reduced by such an extent that it could not be conveniently measured. In these latter two samplers, any measurable convective effects should only be in the external air film that is found across any impervious surface placed in an air stream.

Again, no numerical values are presented for this case, but this time because the mass transfer of the dye (and presumably all convective effects as well) was blocked by a continuous membrane placed between the air gap and the ambient environment. Nevertheless this is useful knowledge, for if the external film does control any flow induced effects, then the analysis of flow effects on mass transfer is reduced to calculations involving the Schmidt and Reynolds numbers that are familiar to chemical engineers and that have already been applied successfully to the effect of the air film on the performance of diffusive samplers.[17,18]

Samplers having a moderate degree of flow induced convection

A large family of diffusive samplers are patterned after the Palmes' tube, and geometrically are essentially long tubes with an adsorbent or reactive material placed at the closed end of the tube.[19] Very often there is no wind shield placed over the open end of the sampler, for the very length of the tube is thought to provide sufficient protection against an unacceptable amount of convection.

In the tests that are described next, three of these samplers, *i.e.* a HOMEcheck Mobile Home Odor (Formaldehyde) Test Kit, PF-1 Formaldehyde Monitor, and a Palmes' tube were filled with a dilute solution of methylene blue and placed in the water bath.[20] Table 2 gives the fraction of a dilute solution of methylene blue remaining in the samplers after they were opened in the water bath, at various times and water flow velocities.

In carrying through these tests it is essential that the solution inside the sampler be at the same temperature as the water in the water bath, or else flotation effects confound the convection effects. For if the solution in the samplers were only a few degrees centrigrade warmer than the water in the bath, then a chimney effect resulted in rapid loss of solution and the subsequent results were irreproducible. To eliminate thermal effects, these tube-shaped samplers were allowed to thermally equilibrate in the bath for an hour with rubber stoppers placed over their openings, before the stoppers were lifted away and the test begun.

Note from Table 2 that the higher the flow velocity, the more rapid the loss of dye solution by convection. Note also that the wider the diameter of the sampler, the more rapid the loss. One characteristic of the Palmes' tube was a very rapid loss of a small fraction ($\approx$20%) of the dye, followed by a period of comparatively small loss.

As described earlier, these data can be analysed to give estimates of the effect of eddy

Table 2 Fraction of dye retained in diffusive samplers after being opened in water bath

Mean water velocity	Elution time, (*hr*)	Palmes' tube sampler	HOME check sampler	PF-1 Formaldehyde Monitor
Slow	1	0 699	0 890	0 858
flow·	3	0 676	0 717	0 720
0 070 *cm/sec*	10	0 633	0 692	0 670
	24	0 607	0.633	0 530
Medium	1	0 713	0 824	0 700
flow	3	0 697	0 723	0 514
0 23 *cm/sec*	10	0 681	0 497	0 133
	24	0 554	0 280	0 033
Fast	0 25	0 773	0 811	0 353
flow	1	0 753	0 747	0 273
0 70 *cm/sec*	3	0.607	0 649	0 047
	10	0 503	0 090	0 007
	24	0 444	0 005	0.000

These water flow velocities of 0 07, 0.23, and 0 7 *cm/sec* match the Reynolds number of air flow velocities of 1 26, 4 14, and 12 6 *cm/sec*, respectively As Cassinelli *et al* suggest "validating" diffusive samplers at air flow velocities of 10 and 150 *cm/sec*, these samplers were tested at the low range of possible air flow velocities in the work environment [5] However, it should be noted that both the HOMEcheck Mobile Home Odor (Formaldehyde) Test Kit and the PF-1 Formaldehyde Monitor are intended for home use in the absence of strong air currents

Table 3 Calculated percent increase in sampling rate due to added effect of eddy diffusion

Flow velocity	Palmes' tube sampler	HOME-check sampler	PF-1 Formaldehyde Monitor
Fast	15	27	121
Medium	11	17	40
Slow	11	9	14

diffusion on the sampling rate of representative analytes. It was found by trial and error that the observed loss of dye by convection from the Palmes' tube, at the lowest flow velocity, could be matched very closely ($\pm 1.2\%$) by assuming coefficients of 0.0305 cm^2/sec and 18.86 for the coefficients "a" and "b" in equation (6). The corresponding coefficients for loss assuming the same Reynolds number in air are 0.549 cm^2/sec and 18.86 (the coefficient "b" remains unchanged). Further, if it is assumed that the analyte being sampled has a molecular diffusion coefficient of 0.1 cm^2/sec in air, then from equations (7) and (8) the percent increase in the sampling rate brought about by the added presence of eddy diffusion is 11%.

Table 3 shows the results of applying this algorithm to the data in Table 2. Note that the diffusive sampler having the widest diameter would be expected to be affected the most by convection. At the highest flow velocity examined (0.7 cm/sec), the sampling rate would be expected to be affected the most by convection. At the highest flow velocity examined (0.7 cm/sec), the sampling rate would be expected to be increased by 121%, indicating that at this velocity the rate of uptake was controlled by eddy diffusion, rather than by molecular diffusion, thus invalidating the basic assumption assumed in the use of this type of sampler. This limits the use of this sampler to quiescent areas where air flow velocities are very low.

CONCLUSIONS

This work shows an enormous difference between commercial diffusive samplers with regard to convection affecting the transport of analyte. Most importantly, placing a plastic membrane impervious to flow across the face of the diffusive sampler, as was done in two of these samplers, can attenuate this effect to a very low level. Given the uncertainties caused by convection, it certainly seems appropriate that this preventative step be taken. However, should the diffusive sampler have no protective membrane, then in the design and testing of such diffusive samplers, a simple aqueous dye experiment can be used to determine the degree to which convection is likely to confound their calibration.

REFERENCES

1 L Pozzoli and D Cottica, in A Berlin *et al* (ed), *Diffusive Sampling, An Alternative Approach to Workplace Air Monitoring*, pp 119–130, R. H Brown and K J Saunders The Royal Society of Chemistry, Burlington House, London, 1987
2 K -H. Pannwitz, *ibid*, pp. 157–162
3 B -O Hallberg, *ibid*, pp 149–151
4 B Sammi, *ibid*, pp. 166–169.
5 M E Cassinelli, R D Hull, J V Crable and A W Taess, *ibid*, pp 190–208
6 V A Marple, *A Fundamental Study of Inertial Impactors*, Ph D. Dissertation, University of Minnesota, Particle Technology Laboratory Pub No 144, 1970
7 E Epstein, *J Heat Transfer*, 1988, **110**, 885
8 P Roy, *Use of a Water Tank Model for Demonstration of Ventilation Controls for Hospital Ethylene Oxide Sterilization Operations*, a paper presented at the American Industrial Hygiene Conference, Boston, MA, 3 June 1992
9 J. Crank, *The Mathematics of Diffusion*, 2nd Ed, Oxford University Press, London, 1975
10 J Westlake, *A Handbook of Numerical Matrix Inversion and Solution of Linear Equations*, Wiley, New York, 1968
11 J. J van Deemter, F J Zuiderweg and A Klinkenberg, *Chem Engng Sci*, 1956, **5**, 271
12 Pro-Tek, Inc, 95 Brownstone Ave, Portland, CT 06480
13 R H Brown and M L Woebkenberg, in S. V Herring (ed.), *Air Sampling Instruments* 7th Ed, American Conference of Governmental Industrial Hygienists, Cincinnati, OH, 1989
14 Abcor GasBadge Organic Vapor Dosimeter, National Mine Service Co., West Oakdale, PA 15071
15 Advanced Chemical Sensors Co, Pompano Beach, FL
16 3M Organic Vapor Monitor #3500—Instructions for Use Occupational Health and Safety Products Division/3M, P O Box 33125, St Paul, MN 55133
17 W M Edwards, in R H Perry and D W Green (eds), *Perry's Chemical Engineers' Handbook*, 6th Ed, McGraw-Hill, New York, 1984
18 D W Underhill and C E Feigley, *Anal Chem*, 1991, **63**, 1011
19 E D. Palmes and G D Gunnison, *Am Ind Hyg Assn J.*, 1973, **32**, 78
20 Instructions for Using your HOMEcheck Mobile Home Odor (Formaldehyde Test Kit), Air Technology Labs, Inc, 815 Harbour Way South, Richmond, CA 94804
21 Air Quality Research, Inc, Berkeley, CA

Talanta, Vol 40, No 6, pp 791–797, 1993
Printed in Great Britain

0039-9140/93 $6 00 + 0 00
Pergamon Press Ltd

DETERMINATION OF NOBLE METALS IN SILICATE ROCKS, ORES AND METALLURGICAL SAMPLES BY SIMULTANEOUS MULTI-ELEMENT GRAPHITE FURNACE ATOMIC ABSORPTION SPECTROMETRY WITH ZEEMAN BACKGROUND CORRECTION*

J G. SEN GUPTA
Geological Survey of Canada, Ottawa, Ontario, Canada K1A OE8

(*Received* 27 *July* 1992 *Revised* 13 *November* 1992 *Accepted* 15 *November* 1992)

Summary—A new method has been developed for rapid determination of μg/g and ng/g amounts of noble metals in silicate rocks, ores and metallurgical samples by attacking with hydrofluoric acid and aqua regia, preconcentration by ion-exchange chromatography and measuring in a simultaneous multi-element graphite furnace atomic absorption spectrometer equipped with a polarized Zeeman background correction device which eliminated interferences from any incompletely separated common elements The method was tested for Ru, Rh, Pt, Ir, Pd, Ag and Au with three Canadian certified reference materials, and then applied to the determination of ng/g amounts of these elements in four new Canadian candidate reference materials

The quantitation of trace and ultra-trace amounts of noble metals in geological and metallurgical samples is fraught with the difficulty of not only selection of a suitable method for decomposition and preconcentration but also application of a sufficiently rapid and sensitive method for accurate determination.

Although fire assay preconcentration of noble metals involving collection in lead, tin or nickel sulphide button has found useful application in some Government and large commercial laboratories,[1] wet-chemical decomposition and preconcentration by solvent extraction or ion-exchange separation procedure is still the preferred choice of small geochemical laboratories where space limitation and high cost of fire assay equipment inhibit application of the former.

In the past, for graphite furnace atomic absorption spectroscopic (GFAAS) determination of precious metals in geological, metallurgical and meteoritic materials decomposition of samples by heating with HF–aqua only were used by several workers.[2–7] Except for the works of Kritsotakis and Tobschall[3] and Branch and Hutchison,[4] who used ion-exchange separations, preconcentration of precious metals were effected by tellurium co-precipitation.[2,6,7] Thus, Sighinolfi *et al.*[2] observed aqua regia solubilization of precious metals except platinum which was completely attacked by HF–aqua regia, their results for precious metals in HF–aqua regia digest of SARM-7 were reasonably good compared to the certified values. Kritsotakis and Tobschall[3] also obtained good results for Au, Pt, Pd, Rh and Ir in SARM-7, and, excepting Pt and Rh values which were somewhat low, their results for Au, Pd and Ir in PTM-1 and PTC-1 were comparable with the certified values.

Using sodium peroxide fusion method, Branch and Hutchison[4] noted losses of only 1% Pt and 2% Pd in the residue of a sample of PTO-1 (ultrabasic rock) after HF–aqua regia digestion. Because of these insignificant losses, these workers omitted determination of Pt and Pd in the residues after HF–aqua regia digestion of PTA-1, PTC-1 and PTM-1.[4] For vegetation samples, use of an ashing temperature of 900°C prior to treatment with HF–aqua regia improved GFAAS results for Au, Pt and Pd, which compared favorably with those of nickel sulphide fire assay/neutron activation.[7]

In the present work, a new method has been developed for determination of the noble metals which involves decomposition of samples by attack with HF–aqua regia followed by ion-exchange preconcentration and simultaneous measurement of four elements using a multi-element graphite furnace atomic absorption spectrometer equipped with Zeeman background

*Paper presented at *37th Canadian Spectroscopy Conference*, Ottawa, Ontario, 12–14 August 1991 Geological Survey of Canada Contribution NO 22992

correction device. The method was found satisfactory for determination of Ru, Rh, Pt, Ir, Pd, Ag and Au in three certified reference materials of Canadian Certified Reference Materials Project (CCRMP). Application was then made to the determination of these elements in four new candidate reference materials (two rocks, one mineralized rock and one sulphide mineral) of CCRMP.

EXPERIMENTAL

Instruments and reagents

Hitachi Model Z-9000 simultaneous multi-element atomic absorption spectrometer, fitted with a pyrolytically-coated tube (Part No. 190–6003), argon gas (UHP, 99 999%, exit pressure regulated to 44 psi and predried by passing through a Matheson Gas Purifier Model 6406) and cooling water, was used in this work. The cooling water was supplied by a Neslab Cooflow Model CFT-33 Refrigerated Recirculator and the temperature was maintained at 17°C In addition to the built-in plotter of the Hitachi Z-9000 instrument, an IBM compatible PC computer was used for data recording and storage. A Radiometer pH meter was used for all pH measurements.

Standard solutions of ruthenium, rhodium, palladium, iridium, platinum and gold (100 ng/ml each) were prepared by diluting 1000 μg/ml of the Plasma-Chem ICP standard solutions of these elements (Delta Scientific Ltd, Mississauga, Ontario Supplier) with 1*M* hydrochloric acid. A standard solution of silver was prepared by dissolving a weighed amount of silver grain (Johnson Matthey "Specpure") in hot dilute nitric acid, cooling and diluting to a definite volume. An aliquot was diluted with 1*M* nitric acid to obtain a concentration of 100 ng/ml. All silver standard solutions were stored in dark bottles inside a cupboard to prevent decomposition by light. Mixtures of calibration standards containing 10–100 ng/ml of noble metals were prepared by mixing appropriate aliquots of these stock standard solutions and diluting to definite volumes with 1*M* hydrochloric acid, and stored in nalgene bottles fitted with screw-caps.

Ultrapure water, prepared by reverse osmosis with a Millipore apparatus, and Seastar ultrapure acids were used throughout this work.

Ion-exchange columns

A series of 12 ion-exchange resin columns,[8] each 30 cm long and 1.8 cm I.D., were prepared and packed with Dowex 50W-X8 cation exchange resin (50–100 mesh). The columns were washed with 3*M* hydrochloric acid until the effluents were free from Fe^{+3} (tested with drops of 1% ammonium thiocyanate solution on a spot plate), and then with deionized water until the washings were neutral to blue litmus paper

Procedure

To a 100-ml Teflon beaker, previously cleaned by heating with HF–aqua regia, 5 g of finely powdered (−200 mesh) and homogenized sample was transferred. The sample was moistened with water and carefully treated with a total of 25 ml of hydrofluric acid (48–51%), adding a small quantity at a time and stirring with a Teflon rod and immediately covering with a Teflon cover until the vigorous reaction subsided. The bottom side of the cover and the upper inner wall of the beaker were washed with small quantity of a jet of water to dislodge adhering solid particles of the sample, using a policeman if necessary After adding 25 ml of a freshly prepared aqua regia solution and mixing, the beaker was covered and heated overnight on a steam-bath. The following morning, the cover was removed and the beaker was heated on the groove of a medium-hot iron plate until the solution was evaporated to dryness. After cooling, 25 ml of concentrated nitric acid was added, the lumps were broken with the Teflon rod and the solution was evaporated to dryness again To the residue, brought to room temperature, 1 ml of 20% (w/v) sodium chloride (Note 1) solution and 25 ml of freshly prepared aqua regia were added, the beaker was covered and heated with frequent stirring and dislodging the solid until the solution became clear The cover was removed and the solution was evaporated to incipient dryness. The residue was treated with 10 ml of concentrated hydrochloric acid, and after stirring with the rod to a syrupy liquid the solution was evaporated to dryness on the steam-bath (Note 2). The evaporation process was repeated once more with an additional 10 ml of concentrated hydrochloric acid (steam-bath).

To the residue 10 ml of concentrated hydrochloric acid was added, and after stirring with the rod the beaker was covered and heated briefly on the groove of the hot plate to dislodge the solid from the bottom. After adding 60–70 ml of water, the beaker was heated on the hot plate with frequent stirring until a clear or near clear solution was obtained (Note 3). When the solution was clear, the beaker was cooled to room

temperature and the solution was transferred to a 100-ml standard flask. The beaker was rinsed with 2% hydrochloric acid and the volume was made up to the mark with the same acid. When any undissolved material was noticed, the solution was allowed to stand several hours to settle the solid particles and then filtered through a 11-cm Whatman No. 40 filter paper. The residue and the filter paper were washed thoroughly with a hot solution of 2% hydrochloric acid until the paper was free from any stain of iron, nickel or copper. The solution was transferred to a 100-ml standard flask, the beaker was rinsed with 2% hydrochloric acid and the volume was made up the mark with the same acid. The solution was stored in a nalgene bottle fitted with a screw-cap (solution A). Any insoluble residue was separately treated by the procedure described under Results and Discussion.

Ion-exchange separation

A 40-ml aliquot of the above stock solution A was transferred to a 600-ml borosilicate beaker and diluted to ~350 ml with deionized water to attain pH 1 5 ± 0.3 (tested with a pH meter). The solution was passed through the ion-exchange column at a rate of 2 ml/min, and the effluent was collected in a 800-ml borosilicate beaker. The beaker and the column were washed with a total of 350 ml of water acidulated to pH 1.5 with hydrochloric acid, and the washings were collected in the same beaker containing the effluent. After adding 1 ml of 2% (w/v) sodium chloride solution (Note 1) to the effluent, the beaker was placed on a hot plate and the solution was evaporated to ~5 ml. The solution was transferred to a 20-ml borosilicate beaker by rinsing with hot 3*M* hydrochloric acid and evaporated first on a hot plate to ~0 5 ml, then on a steam bath to a moist residue. The salts were dissolved in hot 3*M* hydrochloric acid, the solution was transferred to a 10-ml borosilicate beaker and evaporated to near dryness (steam bath). In the case of a syrupy residue, which indicated the presence of sulphuric acid formed by oxidation of sulphides during decomposition of the sample with nitric acid, it was evaporated further to dryness on a hot plate until no more white fumes appeared. The inside of the beaker was rinsed with water and the solution was evaporated again. The residue was treated with 4 ml of aqua regia, the beaker was covered with a watch glass and heated to dissolve the salts. When the reaction subsided, the cover was removed and its bottom was rinsed with water into the beaker, and the solution was evaporated to a moist residue on the steam-bath. The salts were dissolved in 0.5 ml of 1*M* hydrochloric acid by warming briefly on the steam-bath and, depending on the concentration of the noble metals expected, the solution was transferred to a suitable standard flask (1–5 ml) and the volume was made up with the same acid. In case a white residue (hydrated TiO_2) separated out from some silicate rock samples, it was filtered out through a 4-cm glass fiber filter paper, the beaker and the paper were rinsed with small quantity of 1*M* hydrochloric acid and the filtrate was made up to a definite volume

Table 1 Instrumental parameters

Element	Wavelength (nm)	Varian hollow-cathode lamp current (mA)
Ru	349 9	8
Rh	343 5	5
Pd	244 8	5
Ag	328 1	3
Ir	208 9	10
Pt	266 0	10
Au	242 8	4

Spectral bandwidth fixed at 0 8 nm in the Hitachi Z-9000 instrument

Instrumental determination

Using the instrument operating parameters of Tables 1 and 2 and standard solutions (40 μl of each) containing the analytes in concentrations from 0 to 100 ng/ml, calibration curves were prepared for Ru, Rh, Pt and Ir (Fig. 1). Employing the instrument parameters of Tables 1 and 3 and five standard solutions (10 μl of each) of similar concentrations (except silver concentrations which ranged only from 0 to 75 ng/ml because of its much higher sensitivity than other elements), calibration curves for Ag, Au and Pd were prepared (Fig. 2).

Table 2 Temperature programme for simultaneous determination of Ru, Rh, Pt and Ir

No	Stage	Temperature (°C) Start	End	Time (sec)
1	Dry	75	75	10
2	Dry	90	90	60
3	Dry	120	130	20
4	Ash	850	850	20
5	Ash	1400	1400	10
6	Atom	3000	3000	10
7	Clean	3000	3000	5

Monitoring stage 1–7
Check stage 1–7
Carrier gas 200 ml/min
Interrupted gas 0 ml/min

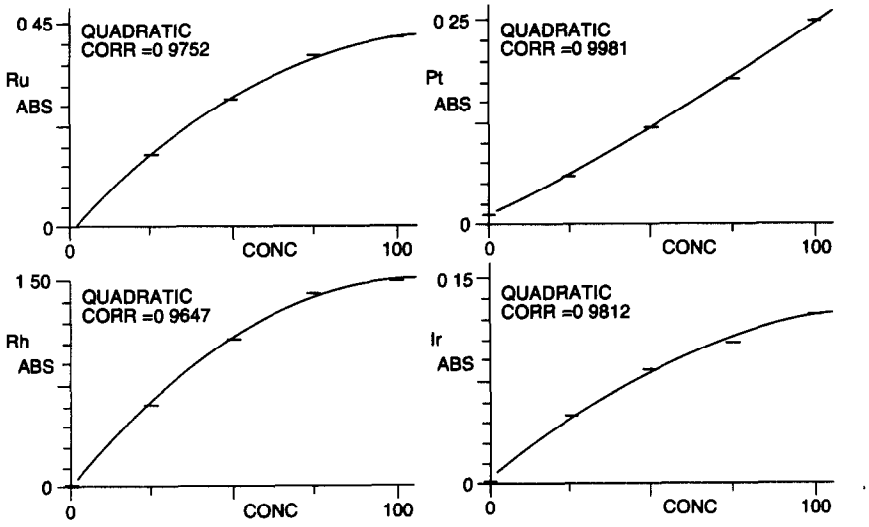

Fig 1 Calibration curves for ruthenium, rhodium, platinum and iridium at atomization temperature of 3000°C (concentration in ng/ml)

For silicate rocks and minerals, Ru, Rh, Pt and Ir were determined from 20–40 μl of a solution containing 0.5–2 g sample/ml, and Ag, Au, and Pd from 10–20 μl of a solution containing 0.2–1 g sample/ml or after suitable dilution with 1*M* hydrochloric acid, as necessary.

Table 3 Temperature programme for simultaneous determination of Ag, Au and Pd

No	Stage	Temperature (°C) Start	End	Time (sec)
1	Dry	75	75	10
2	Dry	90	90	60
3	Dry	120	130	10
4	Ash	800	800	20
5	Atom	2700	2700	10
6	Clean	2800	2800	5

Monitoring stage 1–6
Check stage 1–6
Carrier gas 200 ml/min
Interrupted gas 0 ml/min

For sulphide ores or metallurgical samples, Ru, Rh, Pt and Ir were determined from 10–40 μl of a solution containing 0.1–0.2 g sample/ml, and Ag, Au and Pd from 10–20 μl of a solution containing 0 1–0.2 g sample/ml or after suitable dilution with 1*M* hydrochloric acid, as required.

Notes

1. Sodium chloride was added to form chlorocomplexes of the noble metals to prevent their decomposition to free metals and losses to the walls of the beaker during evaporation steps.

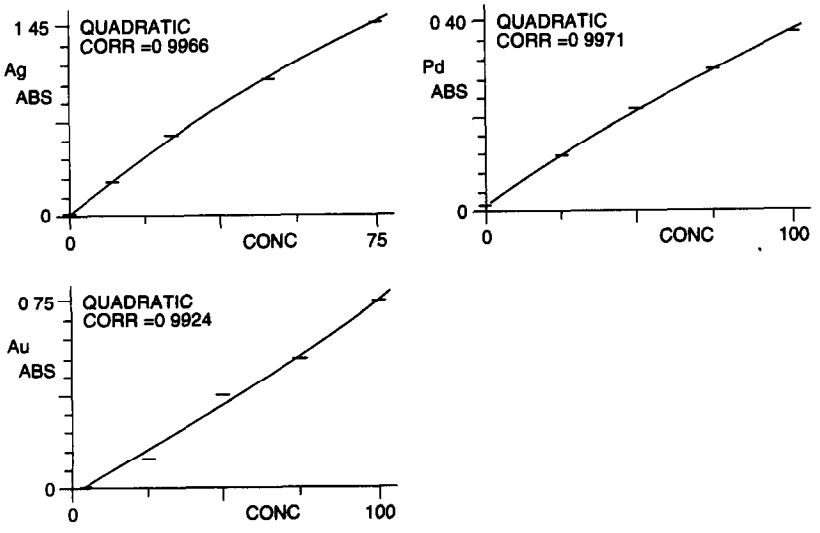

Fig 2 Calibration curves for silver, gold and palladium at atomization temperature of 2700°C (concentration in ng/ml)

2. Heating on the steam-bath instead of a hot plate prevented decomposition of the noble metal salts to free metals, particularly gold and platinum.

3. Sulphide minerals gave clear solutions at this stage.

RESULTS AND DISCUSSION

Sensitivity

The sensitivities of the noble metals on pyrolytically-coated graphite furnace in the Hitachi Z-9000 multi-element atomic absorption spectrometer are given in Table 4 and compared with those obtained previously[9] by using a Varian single-element graphite tube atomizer (Model GTA-95) in combination with a Varian AA-475 spectrometer. Compared to the Varian AA-475 coupled with GTA-95, higher temperatures are found necessary for the noble metals with the Z-9000 instrument to obtain sufficiently high sensitivities for useful analytical applications. This is probably due to the fact that Hitachi Z-9000 spectrometer has a restricted spectral bandwidth of 0.8 nm for all elements, whereas spectral bandwidth of <0.8 can be used with Varian AA-475.

For ruthenium, rhodium, platinum and iridium an atomization temperature of 3000°C, and for silver, gold and palladium an atomization temperature of 2700°C were found satisfactory in the Hitachi Z-9000 instrument.

With the Hitachi Z-9000 instrument four elements could be determined simultaneously in one firing and the instrument could be programmed for determination of up to eight elements automatically in two firings. However, in this work, based on the sensitivities and atomization temperatures, the noble metals were divided into two groups containing four elements in Group 1 and three elements in Group 2 for simultaneous determinations as follows:

Group 1—Ru, Rh, Pt and Ir.

Group 2—Ag, Au and Pd.

Table 4 Sensitivities of noble metals on pyrolytically-coated graphite-furnace in Hitachi Z-9000 simultaneous multi-element atomic absorption spectrometer

Element	Atomization temperature (°C)	Sensitivity* (pg)	
		This work†	Previous value with Varian GTA-95‡
Ru	3000	26	30 at 2700°C
Rh	3000	7	10 at 2600°C
Pd	2700	11	7 at 2600°C
Ag	2700	2	1 at 2000°C
Ir	3000	92	40 at 2700°C
Pt	3000	74	80 at 2700°C
Au	2700	6	3.7 at 2400°C

*Defined as the weight of the element in picogram (pg) which produces a change, compared with a pure solvent or blank, of 0 0044 absorbance unit

†Average of several determinations using different concentrations of the element

‡Sen Gupta [9]

Analyses of reference materials for noble metals

The results for noble metals as obtained in this work for three CCRMP reference materials SU-1a (Ni–Cu–Co ore), PTM-1 (noble metals bearing Ni–Cu matte) and UMT-1 (ultramafic ore tailings) are given in Table 5 and compared with the certified or other values.[9,10] For UMT-1 "recommended" values for some noble metals are now available in the "Certificate of Analysis" sheet. These and other "provisional" or "information" values for this sample are compared with the results of this work in Table 5. Good agreement is found in most cases indicating completeness of recovery.

Silver was not determined in PTM-1 because a previous work[9] showed that most of the high silver from this sample was lost by precipitation as silver chloride during sample decomposition steps.

For four other reference materials (diabase rock, gabbro rock, mineralized gabbro and massive sulphide mineral), the results of this work are compared in Table 5 with those obtained by independent method(s) and/or supplied by the Coordinator of CCRMP. Reasonably good agreement is found between the results of this work with other values, where available.

In order to test any loss of precious metals in the residues after HF–aqua regia dissolution of the samples of Table 5, the filter paper containing the residue was transferred to a porcelain crucible and after charring the paper at 450°C the residue was ignited to oxides at 800°C. After cooling, the oxides were finely ground by the tip of an agate pestle and then transferred to a zirconium crucible and intimately mixed with 5 g Na_2O_2. The crucible was covered by a zirconium lid and placed on a claypipe triangle enclosed by a chimney which was supported by a tripod stand, and the mixture was fused over a Méker burner for 2–3 min with occasional swirling. The melt was cooled to room temperature, small quantities of concentrated hydrochloric acid were gradually added and the dissolved mass was quickly transferred to a 100-ml borosilicate beaker with a jet of water. More concentrated

Table 5 Multi-element GFAAS determination of noble metals in CCRMP reference materials after dissolution by HF + aqua regia digestion and preconcentration by ion-exchange chromatography (unit of results specified under sample)

Sample	Ru		Rh		Pd		Ag		Ir		Pt		Au	
	This work	Other values	This work	Other values	This work	Other values	This work	Other values	This work	Other values	This work	Other values	This work	Other values
Ni–Cu–Co ore, SU-1a (μg/g)	0.1	(0 1, 0 2)* 0 1†	0 08	0 1* 0 08‡	0 36	(0 4, 0.34)* (0 37 ± 0 03)‡ 0 35†	4 4	(4 3 ± 0 3)‡	0 03	0 03* 0 02†	0 45	(0 41 ± 0 06)‡	0 16	(0 2, 0 17)* 0 15‡
Ni–Cu-matte, PTM-1 (μg/g)	0 7	(0 63–0 7)*	0 7	(0 9 ± 0 2)‡	7 8	(8 1 ± 0 7)‡ 7 6†	—		0 1	0 2*	5 6	(5 8 ± 0 4)‡ 5 6*	1 8	(1 8 ± 0 2)‡ 1 8*
Ultramafic ore tailings, UMT-1 (ng/g)	6	7§‖, 9¶	10	(9 8 ± 2 9)**	93	(104 2 ± 5 9)**	470	490††	<25	5§‖ (8 73 ± 0 35)¶	120	(128 3 ± 9 8)**	52	(48 2 ± 4 4)**
Diabase rock (ng/g)	5	—	2	2§	25	30§, 17‖, 22‡‡	74	—	<25	<5§, 0 7‖	38	—	14	—
Gabbro rock (ng/g)	<5	<5§, 0 2‖	0 7	0 7§, <1‖	21	22§, 20‡‡	56	—	<25	<5§, 0 7‖	42	60§‖	20	—
Mineralized gabbro (μg/g)	0 10	—	0 05	—	0 34	—	0 31	—	0 13	—	0 72	—	0 10	—
Massive sulphide mineral (μg/g)	0 1	—	0 2	—	1 1	1 0‡‡	0 7	—	0 2	—	2 0	2 0‡‡	0 2	0 2‡‡

*Sen Gupta [9]

†Sen Gupta and Grégoire [11]

‡Steger[10] (recommended value)

§Determined by single element GFAAS from the concentrate obtained by tellurium co-precipitation of noble metals from HF + aqua regia digest combined with Na_2O_2 fusion of the residue (Analyst Sen Gupta)

‖Determined by ICP-MS from the concentrate obtained by tellurium co-precipitation of noble metals from HF + aqua regia digest combined with Na_2O_2 fusion of the residue (Analysts Sen Gupta & Grégoire)

¶"Provisional value" in the certificate of analysis sheet for UMT-1

**"Recommended value" in the certificate of analysis sheet for UMT-1

††"Information value" in the certificate of analysis sheet for UMT-1

‡‡Initial approximate value supplied by the Co-ordinator of CCRMP with samples

hydrochloric acid was added and the beaker was heated on a hot plate until the solution became clear or near clear and no more evolution of gas bubbles occurred. A very small amount of gritty matter was filtered off through a glass fiber filter paper and washed with 1*M* hydrochloric acid. The solution was diluted to 60 ml with water, 5 ml of 1 mg Te/ml solution was added and a freshly prepared stannous chloride solution was added in excess to coprecipitate any precious metals with the added tellurium. After boiling, the coagulated precipitate was filtered off through a Millipore Type HA 0.45 μm filter disk and washed with 1*M* hydrochloric acid. The disk was placed in the original beaker and decomposed by concentrated nitric acid and aqua regia as described in an earlier paper.[9] The final solution was evaporated on the steam-bath in a 10-ml beaker in the presence of 1 mg sodium chloride. The salts were dissolved in 0.5 ml of 1*M* hydrochloric acid by warming the beaker on the steam-bath, the solution was transferred quantitatively to a 1-ml standard flask and the volume made up to the mark with the same acid. A reagent blank was taken throughout the whole procedure. An aliquot of 40 μl of this solution was transferred to a new graphite tube in the Hitachi Z-9000 spectrometer and after drying and ashing as usual (*cf.* Table 2) the sample was atomized at 3000°C for determining Ru, Rh, Pt and Ir. From another aliquot of 40 μl the sample was dried, ashed and atomized at 2700°C (*cf.* Table 3) for determining Ag, Au and Pd. The amounts, if any, of these elements were quantified from calibration curves. The precious metals were found to be either nil or negligibly small in these solutions.

Acknowledgements—The author is indebted to the Coordinator of CCRMP for supplying the reference materials used in this work, and to D C Grégoire for providing ICP-MS data on some samples reported in this work

REFERENCES

1 J G. Sen Gupta, *Prog Analyt Spectrosc*, 1989, **12**, 403
2. G P Sighinolfi, C. Gorgoni and A. H Mohamed, *Geostand. Newsletter*, 1984, **8**, 25
3 K Kritsotakis and H J Tobschall, *Fresenius Z Anal Chem.*, 1985, **320**, 15
4 C H Branch and D Hutchison, *J Anal At Spectrom*, 1986, **1**, 433
5 G E. M Hall and G F Bonham-Carter, *J Geochem Expl*, 1988, **30**, 255
6 C E. Dunn, G E M Hall and E Hoffman, *ibid*, 1989, **32**, 211
7 G E M. Hall, J.-C Pelchat and C E Dunn, *ibid*, 1990, **37**, 1
8. J G Sen Gupta, *Talanta*, 1984, **31**, 1045
9. *idem*, *ibid*, 1989, **36**, 651.
10 H F. Steger, CANMET Report **80-6E**, 1980
11 J G Sen Gupta and D C Grégoire, *Geostand Newsletter*, 1989, **13**, 197

Talanta, Vol 40, No 6, pp 799–803, 1993
Printed in Great Britain

0039-9140/93 $6 00 + 0 00

DETERMINATION OF MANGANESE, IRON AND COPPER IN SODIUM BY CHEMICAL MODIFICATION/GRAPHITE FURNACE ATOMIC ABSORPTION SPECTROMETRY

YUKIHIRO KOSHINO and AKIR NARUKAWA

Materials Analysis Laboratory, Corporate Research and Development Group, NGK Insulators, Ltd, 2-56 Suda-cho, Mizuho-ku, Nagoya-shi, Aichi 467, Japan

(*Received* 1 *September* 1992 *Revised* 13 *November* 1992 *Accepted* 15 *November* 1992)

Summary—Trace Mn, Fe and Cu in sodium were determined by chemical modification/graphite furnace atomic absorption spectrometry The sodium sample was changed into NaOH in a desiccator by room temperature water vapor generated under reduced pressure, then the NaOH was dissolved in water and HNO_3 was added to give a clear solution. The solution was analysed by chemical modification/graphite furnace atomic absorption spectrometry A nickel nitrate modifier was effective in improving integrated absorbance signals and the reproducibility of measurement Analytical results for Mn, Fe and Cu were 170, 970 and 210 ng/g and relative standard deviations ($n = 5$) were 3 5, 5 8 and 6 7%, respectively These results agreed with the values obtained from a chelating resin preconcentration/ICP-AES method

When sodium is used as a coolant for fast reactor systems, analysis of impurities in it is very important. Metal impurities in sodium are analysed by flame atomic absorption spectrometry or ICP–AES after decomposing by water vapor or alcohol and treating with HCl, but detection limits with these methods are at the microgram per gram level because a great quantity of NaCl matrix is present.

On the other hand, graphite furnace atomic absorption spectrometry (GFAAS) is a highly sensitive technique. Since it is easily influenced by the matrix, the interferences are removed by various methods, *e.g.* solvent extraction,[1,2] or ion-exchange.[3–5] However, these methods require complicated procedures. In recent years, elimination of matrix interference has been investigated using chemical modifiers. Chemical modification methods have the advantage that no complicated procedures are required and there is no concern of contamination from vessels used for separation or preconcentration of analyte elements. Chloride matrix interference is eliminated by addition of HNO_3 or NH_4NO_3 because the generated nitride can be decomposed at about 400°C before the ash step.[6,7] Mg $(NO_3)_2$ and Ni $(NO_3)_2$ are used as modifiers for the determination of Mn and Al.[8,9]

This paper describes the determination of Mn, Fe and Cu in sodium by chemical modification/GFAAS. Mg $(NO_3)_2$ and Ni $(NO_3)_2$ were investigated as chemical modifiers in accordance with previous reports.[8–11] Sodium was changed into NaOH in a desiccator by room temperature water vapor generated under reduced pressure, then treated with HNO_3. The resulting solution was analysed by GFAAS using Ni $(NO_3)_2$ modifier. Nanogram per gram levels of Mn, Fe and Cu in sodium were determined accurately.

EXPERIMENTAL

Apparatus

A Perkin-Elmer Model Z5100 atomic absorption spectrophotometer equipped with a Zeeman background corrector, an AS-60 autosampler and a ZHGA-600 atomizer were used. A Perkin-Elmer model 7700 computer was used to control furnace conditions and the amount of solution injected. Hollow-cathode lamps of Mn, Fe and Cu were used as the radiation sources. A pyrolytic graphite coated graphite tube and pyrolytic graphite L'vov platform were used throughout. A Nippon Jarrell Ash, ICAP 575-II inductively coupled plasma atomic emission spectrometer (ICP-AES) was used in the chelating resin preconcentration experiment to check the accuracy of the established method. A Miwa Seisakusho, argon atmospheric glove box capable of maintaining the concentration of both moisture and oxygen below 1 μl/l was used to treat sodium samples. A METTLER AE-163 balance was used.

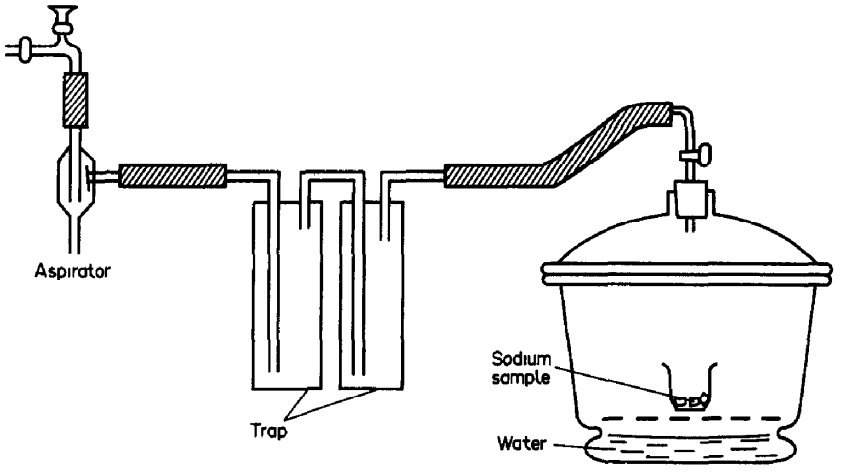

Fig. 1 Decomposition system for sodium

Reagents

Metal stock standard solutions (1000 mg/l) were prepared by dissolving 0.2500 g of high purity metals (Mn;99.99%, Cu; 99.99%, Katayama Chemical Industries Co. Ltd., Japan, Fe; 99.99%, Wako Pure Chemical Industries Co. Ltd., Japan) in 5 ml of HNO_3 and diluting to 250 ml with water. These resulting solutions were stored in polyethylene bottles. Metal–$NaNO_3$ solutions (20 ng/ml Mn, Fe and Cu, $1^m/_v$% Na) were prepared by dissolving 3.70 g of $NaNO_3$ (Merck Suprapur) in $0.2^m/_v$% HNO_3 and adding 2000 ng of Mn, Fe and Cu, then diluting to 100 ml with $0.2^m/_v$% HNO_3. These solutions contain 1.0 g of sodium in 100 ml. Calibration standards were prepared in the same manner using metal–$NaNO_3$ solutions containing 0–2000 ng of analyte elements. Mg modifier solution was prepared by dissolving 1.000 g of Mg $(NO_3)_2$ $6H_2O$ (Merck Suprapur) in water and diluting to 100 ml. Ni modifier solution was prepared by dissolving 1.000 g of Ni $(NO_3)_2$ $6H_2O$ (Kojundo Kagaku Kenkyuujo, Japan, 99.9%) in water and diluting to 100 ml. A Cica-Merck Ultra Pure HNO_3 was used. A Bio-Rad Laboratory Chelex-100 chelating resin (200–400 mesh) was used to concentrate and separate analyte metals. Distilled water was purified with Milli-Q purification system.

Table 1 Optimum operating conditions for graphite furnace AAS

Parameter	Element		
	Mn	Fe	Cu
Wavelength (nm)	279 5	248 3	324 8
Slit width (nm)	0.2	0.2	0.7
Lamp current (mA)	20	30	15
Drying (°C)	120	120	120
[Ramp(s)–Hold(s)]	(1–60)	(1–60)	(1–60)
Ash (°C)	1100	1300	1100
[Ramp(s)–Hold(s)]	(10–30)	(10–30)	(10–30)
Atomization (°C)*	2100	2400	2400
[Ramp(s)–Hold(s)]	(0–8)	(0–5)	(0–5)
Clean up (°C)	2800	2800	2800
[Ramp(s)–Hold(s)]	(1–3)	(1–3)	(1–3)

Ar flow rate 300 cm^3/min.
*Ar flow was stopped in this step

Analytical procedure

After removing oxidized surfaces of sodium samples using a ceramic knife and polytetrafluoroethylene (PTFE) coated tweezers in the glove box. 1 g of sample was weighed into a PTFE evaporating dish. The dish was taken out from the glove box, and placed into a desiccator containing water at the bottom. The sodium sample was changed into NaOH by water vapor generated under reduced pressure for 5 hr using an aspirator. A schematic drawing of sodium decomposition system is shown in Fig. 1. The resulting NaOH was dissolved in 20 ml of water and 3 ml of HNO_3 added, followed by dilution to 100 ml with water. Twenty microlitres of the solution and 20 μl of Ni modifier solution were injected into the furnace and the integrated absorbance signal was measured with the conditions given in Table 1. Calibration graphs are constructed by a series of calibration standards.

RESULTS AND DISCUSSION

Investigation of ash and atomization temperatures without modifier

The effect of ash and atomization temperatures on the signals for Mn, Fe and Cu were investigated without modifier. The signals

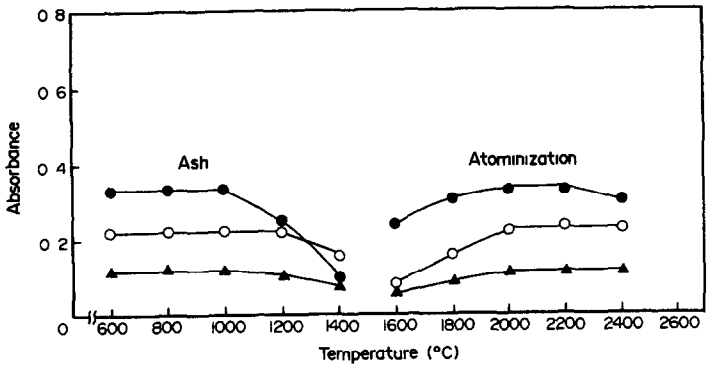

Fig. 2 Effects of ash temperature (atomization at 2000°C for Mn, 2400°C for Fe and Cu) and atomization temperature (ash at 1000°C) on the absorption signal for Mn, Fe and Cu in metal–$NaNO_3$ solution
● Mn 400 pg, ○ Fe 400 pg, ▲ Cu 400 pg

obtained are shown in Fig. 2 as a function of ash and atomization temperatures. First, ash temperature was studied. Twenty microlitres of metal–$NaNO_3$ solution was injected into the furnace, followed by application of an ash temperature of 600–1400°C, and an atomization temperature of 2000°C for Mn, 2400°C for Fe and Cu. Other conditions were according to Table 1. Signals were maximum and constant at an ash temperature of 600–1000°C for Mn and Cu, 600–1200°C for Fe. From these results, an ash temperature of 1000°C was selected for the atomization study. Second, atomization temperature was examined at 1600–2400°C. Since maximum signal was obtained an atomization temperature of 2000–2200°C for Mn (0.327), and above 2000°C for Fe (0.225) and Cu (0.114), respectively, 2100°C for Mn and 2400°C for Fe and Cu were selected as atomization temperatures.

Investigation of ash and atomization temperatures with Ni modifier

Ash and atomization temperatures using Ni modifier were investigated by injecting 20 μl of Ni modifier solution and 20 μl of metal–$NaNO_3$ solution into the furnace. Signals obtained are shown in Fig. 3. The signal for Mn was maximum and constant at an ash temperature of 600–1200°C, and an atomization temperature of 1900–2200°C. For Fe and Cu, maximum and constant signals were obtained at ash temperatures of 1200–1400°C and 600–1200°C, respectively, and an atomization temperature of 2200–2600°C for both. From these results, Ni modifier gave a higher ash temperature than only the metal–$NaNo_3$ solutions examined. The maximum absorbance for Mn, Fe and Cu was 0.630, 0.248 and 0.140, respectively. These maximum values were 1.9 times for Mn, 1.1 times for Fe and Cu in comparison to values found without Ni modifier. Mean integrated absorbances and relative standard deviations of five repeated runs on metal–$NaNO_3$ solutions in the case of with and without Ni modifier are shown in Table 2. Since the relative standard deviations for Mn, Fe and Cu using Ni modifier were within 2%, this was effective in improving the reproducibility.

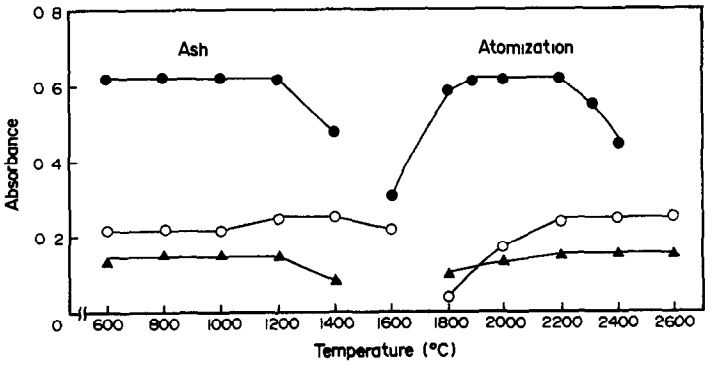

Fig 3 Effects of ash temperature (atomization at 2000°C for Mn, 2400°C for Fe and Cu) and atomization temperature (ash at 1000°C for Mn and Cu, 1300°C for Fe) on the absorption signal for Mn, Fe and Cu in metal–$NaNO_3$ solution in addition of Ni modifier ●: Mn 400 pg, ○ Fe 400 pg, ▲ Cu 400 pg.

Table 2 Effect of Ni modifier on reproducibility

NI modifier	Absorbance Mn	Fe	Cu
With*	0 655 (0 7)	0.250 (0 9)	0 135 (1 3)
Without	0 331 (3 7)	0 229 (2 2)	0 119 (4 9)

*1 m/v% $Ni(NO_3)_3$ $6H_2O$ 20 m μl was added
The amount of Mn, Fe and Cu tested was 400 pg, respectively The percentage relative standard deviation ($n = 5$) is given in parentheses

Effect of concentration of nitric acid

The effect of the concentration of nitric acid on the integrated absorbance signal was examined. Twenty microlitres of 0–3M HNO_3 metal–$NaNO_3$ solution was injected into the furnace and treated following the conditions given in Table 1. The signals were constant at a range of 0–3M HNO_3, and hence HNO_3 did not have an affect on absorption signals.

Investigation of modifiers

Some modifiers were examined for eliminating the $NaNO_3$ interference. The concentration of HNO_3 in the test solution was fixed 0.2 m/v%, because 0–3M HNO_3 did not have an affect on the signals. Twenty microlitres of modifier solution and 20 μl of metal–$NaNO_3$ solution were sucked into the autosampler, then injected into the furnace and treated following the conditions given in Table 1. Although Mg $(NO_3)_2$, Ni $(NO_3)_2$, Pd $(NO_3)_2$, NH_4NO_3, $(NH_4)_2HPO_4$ and $NH_4H_2PO_4$ were examined as modifiers, only Mg $(NO_3)_2$ and Ni $(NO_3)_2$ gave good peak profiles. Accordingly, these two modifiers were tested in detail. Peak profiles for Mn are shown in Fig. 4. Integrated absorbance signals for Mn obtained with metal–$NaNO_3$ solutions, and with added Mg modifier solution and Ni modifier solution were 0.330, 0.638 and 0.655, respectively. With Mg and Ni modifiers the Mn signal increased about 1.9 times. Since Mn forms an alloy with Mg and Ni having higher melting points in this order than Mn only, the atomization time was delayed in the order of Mg and Ni. Therefore, Mg and Ni modifiers were effective in preventing vaporization of Mn in the ash step. Mg modifier caused peak split. The reason ascribed was the disagreement of valence of Mn. The result of the same examination for Fe is shown in Fig. 5. The signals obtained with metal–$NaNO_3$ solutions, and with Mg modifier solution and Ni modifier solution were 0.224, 0.248 and 0.249, respectively. Though the increase in the signal was about 10% when Mg and Ni modifiers were used, peak split was not observed. Copper showed the same behavior as Fe. The results of these examinations show that the Ni modifier gave the largest absorption signals and good peak profiles for Mn, Fe and Cu. Further, the optimum amount of Ni modifier solution is in the range of 5–50 μl, with the largest signal found for 20 μl. From these results, ash and atomization temperatures were investigated with the optimum amount, *i.e.* 20 μl, of Ni modifier. The results are shown in Fig. 3.

Lower detection limit

The lower detection limits were 30, 50 and 50 ng/g for Mn, Fe and Cu, respectively, equal to 0.010, 0.006 and 0.004 the absorbance signal,

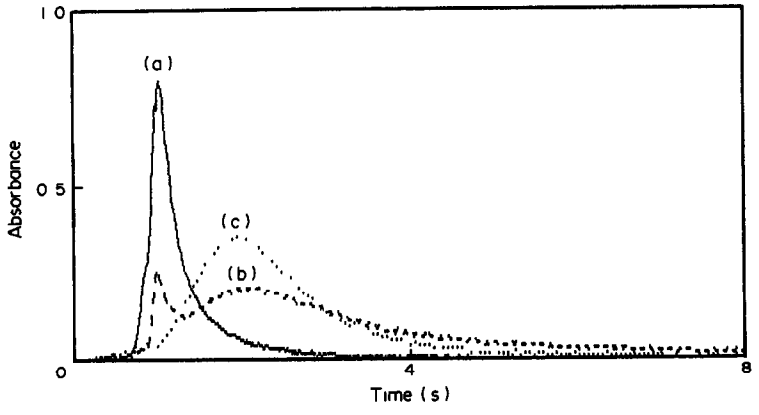

Fig. 4. Investigation of chemical modifier for Mn The amount of Mn tested was 400 pg (a) Metal–$NaNO_3$ solution 20 μl. (b) Metal–$NaNO_3$ solution 20 μl and Mg modifier 20 μl. (c) Metal–$NaNO_3$ solution 20 μl and Ni modifier 20 μl

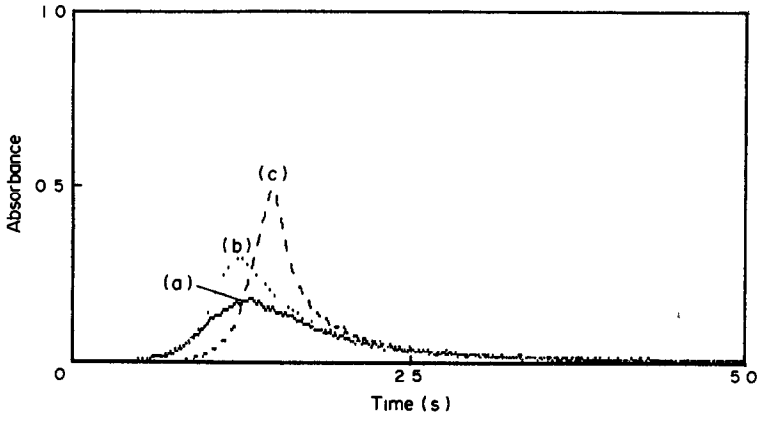

Fig 5 Investigation of chemical modifier for Fe. The amount of Fe tested was 400 pg. (a) Metal–$NaNO_3$ solution 20 μl. (b) Metal–$NaNO_3$ solution 20 μl and Mg modifier 20 μl (c) Metal–$NaNO_3$ solution 20 μl and Ni modifier 20 μl.

defined as three times the standard deviation of procedural blanks ($n = 3$).

Results of the analysis

The analytical results for Mn, Fe and Cu in a sodium sample using the proposed method and a preconcentration/ICP-AES method are summarized in Table 3. The procedure of preconcentration/ICP-AES was as follows; the NaOH generated by decomposing sodium was dissolved in 50 ml of water, and the pH was adjusted to 8.0 by adding dropwise HCl (1 + 100). The solution was passed through a column loaded in the H form Chelex-100 resin at a flow rate of 1 ml/min, then the adsorbed Mn, Fe and Cu were eluted with 20 ml of 2M HNO_3, and determined by ICP-AES. The results agreed with the values obtained from preconcentration/ICP-AES, and percentage relative standard deviations ($n = 5$) were within 10%. The time required for the determination of Mn, Fe and Cu was about 8 hr, including 5 hr sample decomposition time.

Table 3. Determination of Mn, Fe and Cu in sodium metal

Method	Found (ng/g) Mn	Fe	Cu
Proposed	170 (3.5)	970 (5.8)	210 (6.7)
Preconcentration/ ICP-AES	160	1010	200

The percentage relative standard deviation ($n = 5$) is given in parentheses.

REFERENCES

1 Y. Shinjo, T Shimizu and T Tsunoda, *Anal Sci*, 1989, **5**, 69
2 K. Ueda, S. Kitahara, K Kubo and Y Yamamoto, *Bunseki Kagaku*, 1987, **36**, 728
3 R Kobayashi and K Imaizumi, *Anal Sci*, 1989, **5**, 61.
4 T. Shimizu, K Ichikawa and M Shijo, *Bunseki Kagaku*, 1988, **37**, 164
5. Y. Shijo, T Shimizu and Tsunoda T, *Anal Sci*, 1989, **5**, 65
6 B Welz, G. Schelmmer and J R Mudakavi, *Anal Chem*, 1988, **60**, 2567
7 M Taga, O. Sakurada and H. Takahashi, *Bunseki Kagaku*, 1988. **37**, 164
8 W. Salvin, G R Carnick and D. C Manning, *Anal Chem*, 1982, **54**, 621.
9 T Nakamura, R Sasagawa and J Sato, *Bunseki Kagaku*, 1992, **41**, 89
10 B. Welz, G Schlemmer and J R Mudakavi, *J Anal. At. Spectrom*, 1988, **3**, 93.
11. K. K. Roe and P N Froelich., *Anal Chem*, 1984, **56**, 2724.

Talanta, Vol 40, No 6, pp 805–809, 1993
Printed in Great Britain

0039-9140/93 $6 00 + 0 00
Pergamon Press Ltd

SYNERGISTIC EXTRACTION OF COBALT(II) FROM CESIUM CONTAINING AQUEOUS SOLUTIONS WITH MIXTURES OF 4-ACYL-PYRAZOL-5-OLS AND CROWN ETHERS

B RUSDIARSO, A. MESSAOUDI and J P BRUNETTE*

Laboratoire de Chimie Minerale et Analytique, E H I C S, C N R S URA 405, 1, Rue Blaise Pascal, 67008 Strasbourg Cedex, France

(*Received* 3 *August* 1992 *Revised* 5 *October* 1992 *Accepted* 10 *November* 1992)

Summary—The synergistic extraction of cobalt(II) from aqueous solutions loaded with cesium chloride or nitrate, with mixtures of 1-phenyl-3-methyl-4-acyl-pyrazol-5-ols (HL) [acyl = benzoyl (HPMBP), para-*tert* -butyl-benzoyl (HPMB'P), stearoyl (HPMSP)] and crown ethers E = B15C5, 18C6, DC18C6, DB18C6 and DB24C8 (DC = dicyclohexano, B = benzo, DB = dibenzo), in $CHCl_3$, CH_2Cl_2 and $ClCH_2CH_2Cl$, has been studied The experimental data agree with the extracted species E_2CsCoL_3 (E = B15C5), $ECsCoL_3$ (E = DB18C6) and CoL_2E (E = DB24C8) The extraction yields follow the orders 18C6 ≥ DC18C6 > DB18C6 > B15C5 > DB24C8, HPMBP > HPMB'P > HPMSP, and $ClCH_2CH_2Cl > CH_2Cl_2 > CHCl_3$ In spite of the better complexation of potassium than cesium with "18C6" type crown ethers, the extraction of ECsCo $(PMBP)_3$ is generally higher than the EKCo$(PMBP)_3$ one Except in the case of DB24C8, loading the aqueous phase with Cs^+, K^+, Sr^{2+} or Ba^{2+} improves the synergistic extraction of cobalt

Added to acidic chelating extractants (HL) crown ethers (E) can act as neutral oxo-donor synergistic agents in the extraction of numerous metal cations (M^{m+}), *e.g.*, trivalent actinides and rare earths generally extracted with HL = HTTA (thenoyltrifluoroacetone),[1–3] HPMBP (1-phenyl-3-methyl-4-benzoylpyrazol-5-ol),[4,5] HPMTFP (1-phenyl-3-methyl-4-trifluoroacetyl-pyrazol-5-ol)[5,6] as ML_3E or ML_3E_2 species, technetium as TcO (OH).TTA.E[7] and cobalt as Co $(TTA)_2E$.[8] Likewise, in previous papers,[9,10] it has been shown that cobalt, nickel, cadmium and zinc are extracted from sodium or lithium aqueous solutions with HPMBP and crown ethers as $M(PMBP)_2E$ species, but E_eK^+,M $(PMBP)_3^-$ ion pairs were extracted from potassium solutions. The present paper deals with the synergistic extraction of cobalt(II) from cesium solutions, with mixtures of 4-acyl-pyrazol-5-ols and crown ethers. The role of cesium in the synergistic effect is compared to the role of potassium and other similar cations.

EXPERIMENTAL

Chemicals

4-Acyl-pyrazol-5-ols were prepared following Jensen's procedure.[11] Crown ethers, Aldrich chemicals of analytical grade, were used without further purification: dicyclohexano-18-crown-6 was a mixture of the *syn-cis* and *anti-cis* isomers.

Metal extraction and analytical procedure

The experimental data obtained were of type $\log D_{Co}$ *vs.* pH ($D_{Co} = [Co]_{org}/[Co]_{aq}$) at various constant extractant concentrations. The organic phases were prepared by dissolving weighted amounts of acyl-pyrazolol and crown ether in the solvent freshly washed with distilled water (extractant concentrations from 0 to 0.06*M*). Initial cobalt concentration in the aqueous phase, before contact with the organic phase, was $10^{-3}M$, and the ionic strength was fixed at 1*M* (generally $[CsNO_3] = 1M$ or $[CsCl] = 1M$, and, in particular experiments, $[CsCl] + [LiCl] = 1M$). The distribution measurements were performed in a thermostated vessel (25.0 ± 0.2°C) using a batch technique· two volumes (40 ml) of aqueous phase and one volume (20 ml) of organic phase were shaken. For each experimental point, the pH (measured with a digital pH meter and combination glass-reference electrode) was adjusted to a given value (between 3 and 5) by adding small volumes of acidic or basic solutions of suitable composition to keep constant ionic strength and cesium concentration of the aqueous phase.

*Author for correspondence

After at least 15 min shaking, time enough to reach equilibrium, the phases were separated by gravity, and equal aliquots of both phases (0.5 to 1 ml) were withdrawn and centrifuged. Cobalt concentrations were determined, after suitable dilution ($\frac{1}{10}$ or $\frac{1}{5}$), by atomic absorption measurements with a Perkin Elmer 2380 spectrophotometer (The organic aliquot was contacted with 10 or 5 ml of 0.1*M* HNO_3 to strip and dilute cobalt before determination.) Before shaking phases for a new experimental point, at another pH, the aqueous and organic phase volumes were completed up to 40 and 20 ml.

RESULTS AND DISCUSSION

Cobalt extraction from 1M CsCl (or $CsNO_3$) aqueous solutions with HPMBP and crown ethers (E) in chloroform

In the presence of dibenzo-24-crown-8 (DB24C8), a weak synergistic effect occurs, and the extraction curve (Fig. 1) is a straight line of slope 2 as in the extraction performed with HPMBP alone [extraction of Co $(PMBP)_2$ with $\log K_{2,0} = -6.88$]. The synergistic effect is more and more improved with benzo-15-crown-5 (B15C5), dibenzo-18-crown-6 (DB18C6), dicyclohexano-18-crown-6 (DC18C6, commercial mixture) and 18-crown-6 (18C6) crown ethers, and the slope 3 of the curves indicates a significant change in the extraction process. Varying $[HPMBP]_{org}$ at constant pH and $[E]_{org}$, leads to $\log D_{Co}$ *vs.* $\log[HPMBP]_{org}$ curves which are also straight lines of slope 2 (E = DB24C8) or 3 (E = "18C6" type crown ethers or B15C5) (Fig. 2). These results indicate the extraction of $Co(PMBP)_2$ moieties with DB24C8 and Co $(PMBP)_3^-$ moieties with other crown ethers. The slopes of the curves $\log D_{Co}$ *vs.* $\log[E]_{org}$ at constant pH and $[HPMBP]_{org}$ are 1, 2 and 1 for E = DB24C8, B15C5 and "18C6" crown ethers, respectively (Fig. 3). Thus, the experimental data are in agreement with the extraction of $Co(PMBP)_2DB24C8(B15C5)_2Cs^+$, $Co(PMBP)_3^-$, and ("18C6") Cs^+, Co $(PMBP)_3^-$ species. Attempts to measure the cesium concentrations in organic phases did not lead to accurate conclusions owing to its high concentration in the aqueous phase and to its possible extraction, independently of the cobalt one. Nevertheless, analogous species [Co $(PMBP)_2DB24C8$, $(B15C5)_2K^+$, $Co(PMBP)_3^-$ and ("18C6") K^+, $Co(PMBP)_3^-$] were previously extracted from 1*M* KCl aqueous medium.[9,10] Moreover, the extraction of CoL_3^- anions in B^+, CoL_3^- ion pairs with B^+ = high molecular weight ammoniums and HL = 4-acyl-pyrazol-5-ols, is rather common.[12]

Table 1 Cobalt extraction from 1M CsCl medium with 4-acylpyrazol-5-ols and crown ethers in $CHCl_3$ at 25°C

HL	E	Extracted species	$\log K^*_{i,j}$
HPMSP	B15C5	E_2CsCoL_3	−7.15
HPMB'P	B15C5	E_2CsCoL_3	−5.77
HPMBP	B15C5	E_2CsCoL_3	−5 38
HPMSP	DB18C6	$ECsCoL_3$	−8 49
HPMB'P	DB18C6	$ECsCoL_3$	−6 93
HPMBP	DB18C6	$ECsCoL_3$	−6.57
HPMBP	DC18C6	$ECsCoL_3$	−5.90
HPMBP	18C6	$ECsCoL_3$	−5 80
HPMSP	DB24C8	CoL_2E	−5.69
HPMB'P	DB24C8	CoL_2E	−4.75
HPMBP	DB24C8	CoL_2E	−4.53

$^*\log K_{i,j} = \log D_{Co} - i\log[HL]_{org} - j\log[E]_{org} - i\text{pH}$
$\Delta\log K_{i,j} \pm 0\,05\text{–}0\,10$

Taking arbitrarily $\log[Cs^+] = 0$, conditional extraction equilibrium constants have been determined. They are summarized in Table 1. No noticeable effect was observed by replacing CsCl by $CsNO_3$.

Comparison of cobalt extraction from 1M CsCl medium with those performed from other similar media (KCl, NaCl, LiCl, $SrCl_2$, $BaCl_2$)

The extraction of $Co(PMBP)_2DB24C8$ does not depend on the aqueous medium (CbCl,

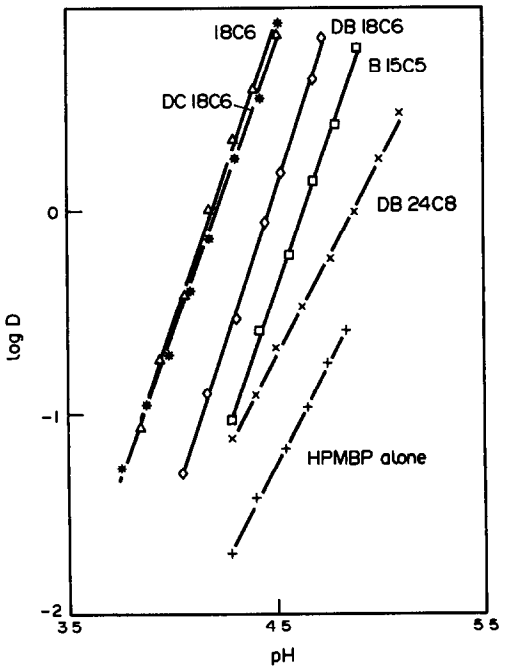

Fig 1. Distribution curves of cobalt from 1*M* CsCl aqueous medium with HPMBP (0.02*M*) and crown ethers (0.02*M*) in chloroform. pH effect

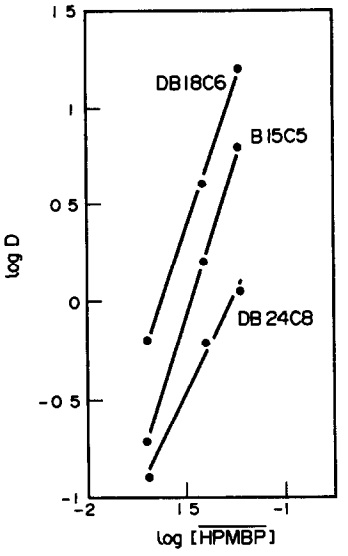

Fig 2. Distribution curves of cobalt from 1*M* CsCl aqueous medium at pH 4 4 with HPMBP and crown ethers (0 02*M*) in chloroform. [HPMBP] effect

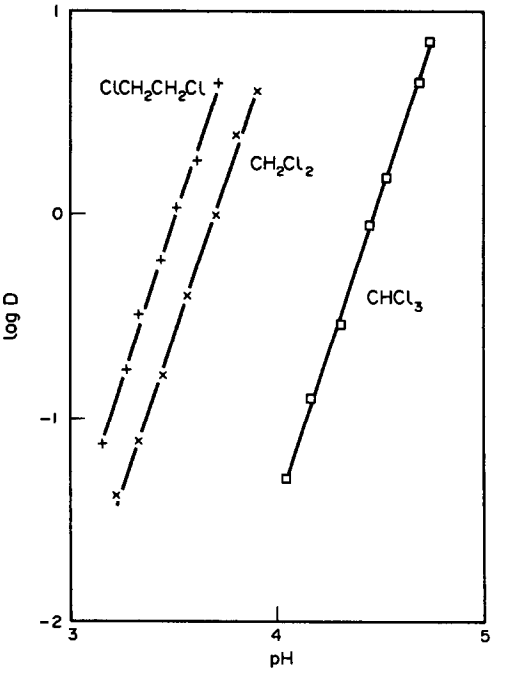

Fig 4 Distribution curves of cobalt from 1*M* CsCl aqueous medium with HPMBP (0.02*M*) and crown ethers (0 02*M*) in chloroform, dichloromethane and 1,2-dichloroethane pH effect

KCl, NaCl or LiCl): $\log K_{2,1}$ (−4.53) lies between values determined with linear polyethers, *e.g.* −4.17 with Triton X-100 and −4.82 with Butex,[13] which shows that there is no obvious cavity effect.

Like K^+[10] (ionic diameter 2.66 Å), Cs^+ (ionic diameter 3.34 Å) likely forms $(B15C5)_2Cs^+$ "sandwich" cationic complexes with B15C5 (cavity diameter 1.7–2.2 Å), which are co-extracted as ion pairs with Co $(PMBP)_3^-$ anions: the extractions performed from CsCl and KCl media ($\log K_{3,2} = -5.38$ and −5.40, respectively) are quite similar, which can be related with the close complex formation constants of Cs^+ and K^+ with "15C5" type crown ethers.[14] The extraction is higher than that performed from LiCl medium [extraction of Co $(PMBP)_2B15C5$ with $\log K_{2,1} = -4.8$].[10]

The cavity size of "18C6" type crown ethers (diameter 2.6–3.2 Å) allows the formation of

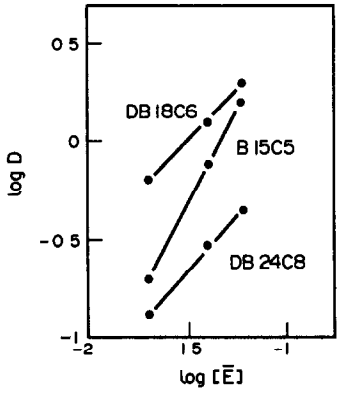

Fig 3. Distribution curves of cobalt from 1*M* CsCl aqueous medium at pH 4.4 with HPMBP (0.02*M*) and crown ethers in chloroform: [crown ether] effect.

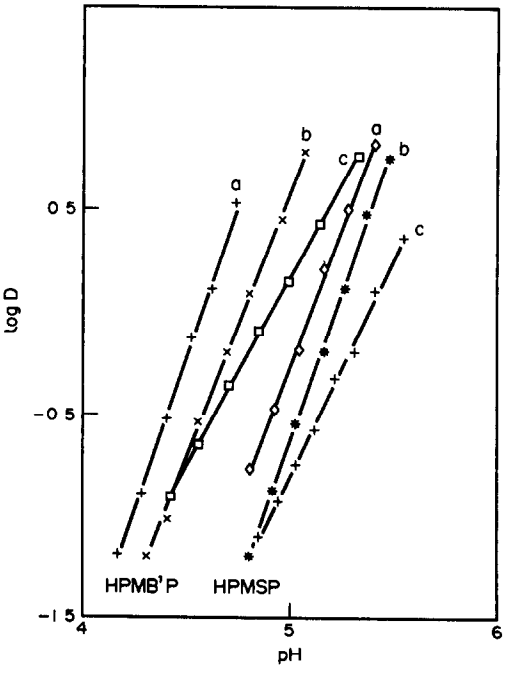

Fig. 5 Distribution curves of cobalt from 1*M* CsCl aqueous medium with HPMB'P or HPMSP (0 02*M*) and crown ethers (0.02*M*) in chloroform· pH effect (a = DB18C6, b = B15C5, c = DB24C8).

stable inclusion complexes with K^+ whereas Cs^+ is slightly too large to enter into the cavity, which leads to lower complex formation constants K_f: for example, in water, $\log K_f$ (18C6, K^+) = 2.03 whereas $\log K_f$ (18C6,Cs^+) = 0.99.[15] Thus, a better extraction of ("18C6")K^+, $Co(PMBP)_3^-$ than ("18C6")Cs^+,$Co(PMBP)_3^-$ could be expected. In fact, the opposite is observed emphasizing the better extractability (lipophilicity + ion pair stability) of the cesium containing ion pairs. The cobalt extraction from CsCl aqueous medium with HPMBP and "18C6" crown ethers is minimum with DB18C6, that is the weakest complexing agent towards Cs^+ [$\log K_f$ (DB18C6,Cs^+) = 0.83],[15] but also the least flexible ligand From LiCl and NaCl media, only Co $(PMBP)_2$DB18C8 species are extracted (40% of extracted cobalt at pH = 5, with $[DB18C6]_{org} = [HPMBP]_{org} = 0.02M$). It results in a lower cobalt extraction than those performed from 1*M* CsCl and KCl media (95 and 91%, respectively). Loading aqueous phases with Sr^{2+} or Ba^{2+} also improves cobalt extraction (80 and 65% from 0.33*M* $SrCl_2$ and $BaCl_2$ media, respectively.

Influence of cesium concentration on cobalt extraction

In order to estimate the influence which the variation of cesium concentration exercises on cobalt extraction with mixtures of HPMBP and DB18C6, extraction experiments have been performed from ([CsCl] + [LiCl] = 1*M*) aqueous solutions with increasing [CsCl] from 0 to 1*M*, the cobalt extraction is progressively improved, and the DB18C6Cs^+,$Co(PMBP)_3^-$ extraction is characterized by an increase of $\log D_{Co}$ *vs.* pH curve slope from 2 [extraction of Co $(PMBP)_2$ DB18C8 alone] to 3. At pH = 5, with $[HPMBP]_{org} = [DB18C6]_{org} = 0.02M$, the extracted cobalt ratios are 40, 48, 58, 72 and 95% at [CsCl] = 0, 0.01, 0.05, 0 1 and 1*M*, respectively.

Diluent effect (*Fig.* 4)

Replacing chloroform by 1,2-dichloroethane and dichloromethane, leads to better synergistic extractions of cobalt from 1*M* CsCl solutions. Stoichiometries of extracted species remain unchanged, *i.e.* $Co(PMBP)_2$DB24C8 ($\log K_{2,1} = -3.07, -3.33$, respectively), DB18C6, Cs^+,$Co(PMBP)_3^-$ ($\log K_{3,1} = -3.77, -4.30$, respectively), and $(B15C5)_2Cs^+$,$Co(PMBP)_3^-$ ($\log K_{3,2} = -2.55, -3.15$ respectively). The extraction order, $ClCH_2CH_2Cl > CH_2Cl_2 > CHCl_3$, is that of diluent dielectric constants.

Effect of the acyl group of 4-acyl-pyrazol-5-ols on the extraction

Among 4-acyl-pyrazol-5-ols, HPMBP is certainly the most studied as a metal extractant. Nevertheless, its unsufficient lipophilicity limits its applications Thus, it was interesting to substitute its acyl = benzoyl group with more lipophilic para-*tert.*-butylbenzoyl and stearoyl groups, which leads to the more lipophilic, but less acidic HPMB'P and HPMSP chelating acidic extractants. Slope analysis of cobalt distribution curves (Fig 5) performed with mixtures of HPMB'P or HPMSP and B15C5, DB18C6 or DB24C8 crown ethers in chloroform has shown that the extracted species have the same composition as those extracted with HPMBP The extraction constants are given in Table 1. For each crown ether, they follow the order HPMBP > HPMB'P > HPMSP which is the decreasing order of the acidic character of the compounds, that means that the lack of acidity of HPMB'P and HPMSP is not counterbalanced by an increase of lipophilicity. The variations of $\log K_{3,1}$ (extraction of DB18C6, Cs^+,CoL_3^-) and those of $\log K_{3,2}$ [extraction of $(B15C5)_2Cs^+$,CoL_3^-] between HPMBP, HPMB'P and HPMSP, are close to those observed previously in the extraction of B^+, CoL_3^- where B^+ = methyl-tri-*n*-octylammonium,[12] which can be explained mainly by the CoL_3^- complex formation: indeed, these variations are weaker (by $\frac{2}{3}$) in the extraction of CoL_2DB24C8 species that involve only two L^- per cobalt.

CONCLUSIONS

The presence of cesium in aqueous phases can strongly enhance the extraction of cobalt (II) with mixtures of 4-acyl-pyrazol-5-ols (HL) and crown ethers (E): it is the case when sufficiently stable complexes are formed between Cs^+ and crown ethers, *e.g.* 18C6,Cs^+, DC18C6,Cs^+, DB18C6,Cs^+, and $(B15C5)_2Cs^+$, which are coextracted with CoL_3^- as ion pairs In spite of the better complexation of K^+ than Cs^+ with "18C6" type crown ethers, a greater synergistic effect is achieved in extractions from cesium containing solutions. When the crown ether cavity is too large in comparison with the Cs^+ size (DB24C8), only a weak synergistic effect is observed, due to extraction of CoL_2E complexes. In all cases, extractions are higher in diluents of high dielectric constant, and with HPMBP, more acidic but less lipophilic than

HPMB'P or HPMSP. Results herein emphasize how important the aqueous phase composition is, in extraction systems involving mixtures of acidic chelating extractants and crown ethers.

Acknowledgements—The author B Rusdiarso is indebted to the Indonesian Government for financial support during his stay in Strasbourg

REFERENCES

1 H F Aly, S M Khalifa, J D Navratil and M T Saba, *Solvent Extr Ion Exch*, 1985, **3**, 623
2 G M Nair and D R Prabhu, *J Radioanal Nucl Chem*, 1988, **121**, 83
3 Y Meguro, H Muto and Z Yoshida, *Anal Sci*, 1991, **7**, 39
4 C Yonezawa and G R Choppin, *J Radioanal Nucl Chem*, 1989, **134**, 233
5 J N Mathur, *Solvent Extr Ion Exch*, 1990, **8**, 629
6 J N Mathur and P K Khopkar, *Solvent Extr Ion Exch*, 1988, **6**, 111
7 M Le Tuong and T Lengyel, *J Radioanal Nucl. Chem*, 1989, **136**, 225
8 H F Aly, M M El Dessouky, S M Khalifa, J D Navratil and F A Shehata, *Solvent Extr Ion Exch*, 1985, **3**, 867
9 M Lakkis, J P Brunette, M J F Leroy and J Alstad, *Solvent Extr Ion Exch*, 1986, **4**, 287
10 A M Sastre, A Sahmoune, J P Brunette and M J F Leroy, *Solvent Extr Ion Exch*, 1989, **7**, 395
11 B S Jensen, *Acta Chem Scand*, 1959, **13**, 1668
12 M Lakkis, Z Lakkis, G J Goetz-Grandmont and J P Brunette, *Monatsh Chem*, 1991, **122**, 9
13 N E Kroutchinina, A Sahmoune, J P Brunette and M J F Leroy, *Solvent Extr Ion Exch*, 1987, **5**, 73
14 Y Takeda, *Top Curr Chem*, 1984, **121**, 1
15 R M Izatt, J S Bradshaw, S A Nielsen, J D Lamb and J J Christensen, *Chem Rev*, 1985, **85**, 271

Talanta, Vol 40, No 6, pp 811–817, 1993
Printed in Great Britain

0039-9140/93 $6 00 + 0 00

SIMULTANEOUS DETERMINATION OF AMOXYCILLIN AND DICLOXACILLIN IN CAPSULES BY POTENTIOMETRIC TITRIMETRY AND HIGH-PERFORMANCE LIQUID CHROMATOGRAPHY

EZZAT M ABDEL-MOETY,* MOHAMMAD A. ABOUNASSIF, EL-RASHEED A GAD-KARIEM and NASHAAT A. KHATTAB

Pharmaceutical Chemistry Department, College of Pharmacy, King Saud University, P O Box 2457, Riyadh-11451, Saudi Arabia

(*Received* 24 *October* 1991 *Revised* 10 *November* 1992 *Accepted* 10 *November* 1992)

Summary—Direct potentiometric titration and two HPLC conditions for the simultaneous determination of amoxycillin and dicloxacillin in their capsules have been developed One-run titration utilizing 0 05*M* acet. $HClO_4$ enables the quantification of both antibiotics The HPLC-separation could be undertaken on reversed phase, LiChrosorb RP-18 (10 μm), and LiChrospher 100 RP-18 (5 μm), columns by using mobile phases containing acetonitrile + 1% aq, acetic acid, in proportions of 47·53 or 39 61 (v/v), respectively, at a flow rate of 1 5 ml/min with UV-detection at 240 nm Recoveries of the individual drugs by the application of each described method were found to be fairly satisfactory

INTRODUCTION

Synergistic activity of some penicillin combinations was reported for gram-negative bacteria.[1-4] Combined penicillins provide a broader spectrum of antibacterial activity and may be advantageously prescribed in cases of β-lactamase-producing strains. Synergy between amoxycillin (I) and dicloxacillin (II) has been demonstrated against clinical isolates of some β-lactamase-producing and non-producing strains.[5,6] Pharmaceutical preparations containing both the mentioned β-lactam antibiotics are now normally found in the market.

There have been some different procedures of analysis proposed for the determination of amoxycillin, including spectrophotometric measurement of the copper chelate[7] or the penicillenic acid formed by reaction with H^+/Cu^{2+},[8] spectrofluorometry (Ex: 366 nm and EM: 430 nm) after reaction with formaldehyde, in addition to high-performance liquid chromatography (HPLC),[9] which is also the method of choice for dicloxacillin.[10] The British Pharmacopoeia 1988[11] recommends a titrimetric method for the determination of amoxycillin in bulk form using standard mercuric nitrate with potentiometric detection of the equivalent complex,

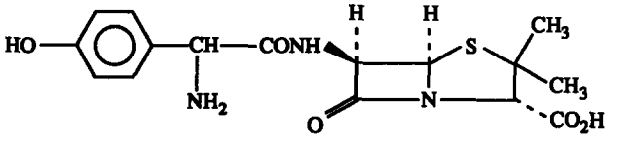

I Amoxycillin

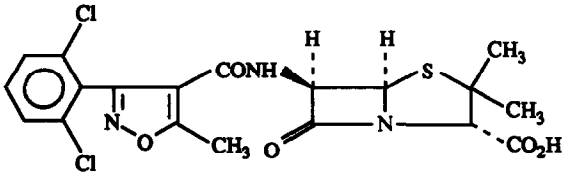

II Dicloxacillin

*Author for correspondence.

and a colorimetric one using imidazole mercury reagent at 325 nm in the case of capsules containing the drug. No official procedure has yet been approved for dicloxacillin, although the method described for amoxycillin seems to be applicable Quantification of the individual penicillins in their binary combinations cannot be achieved by adopting the BP 1988 procedure. The applicability of the derivative spectrophotometry for simultaneous determination of amoxycillin and dicloxacillin in their mixtures and in capsules has been recently investigated.[12] Preliminary separation of amoxycillin from dicloxacillin, by dissolving in 0.1 mole/l hydrochloric acid, where only amoxycillin goes into solution leaving dicloxacillin, followed by adopting the ferric hydroxamate method[13] is recommended by one of the manufacturers for the determination of each separated penicillin [14]

The present work describes a potentiometric titrimetry and two HPLC procedures for simultaneous determination of amoxycillin and dicloxacillin in pharmaceutical formulations. The stability-indicating characteristics, *i.e* determination of the intact drug substance in the presence of its degradation product(s), and statistical evaluation of the results have been discussed.

EXPERIMENTAL

Apparatus

Potentiograph model E576, equipped with Dosimat E575 and magnetic stirrer E649 (Metrohm, Herisau, Switzerland), and combined glass–calomel electrodes were used for recording potentiometric titration curves

Varian model 5000 Liquid Chromatograph equipped with a variable Varian UV-50 detector set at 240 nm, a Rheodyne model 7125 injector with a 20 μl sample loop, and a Varian model 9176 strip recorder (chart speed 0.5 cm/min), were used. The chromatographic parameters were controlled by a Varian Data System model CDS 111L. Two different columns, namely a Hibar prepacked LiChrosorb RP-18 (10 μm), 25 cm × 4 mm ø, and a Hibar prepacked LiChrospher 100 RP-18 (5 μm), 12.5 cm × 4 mm ø (E. Merck, Darmstadt, Germany), were utilized. Eluting solvent mixtures containing CH_3CN + 1% aq CH_3COOH, 47·53 (v/v), in case of LiChrosorb, and 39.61 (v/v), in case of LiChrospher, were kept isocratic at a rate of 1.5 ml/min.

Materials

Amoxycillin trihydrate. The drug was used as supplied (Gist-Brocades, Amsterdam, The Netherlands). Purity was assessed by the BP 1988 method[11] and found to be 99.1% (the water of crystallization content 12.6%).

Dicloxacillin monohydrate. The drug was utilized without further treatment, the claimed purity was 99.6% (the water of crystallization content 3.9%) (Gruppo Lepetit, S.p.A., Milan, Italy). The reference substances and dosage formulations containing them were stored in a dry cool place in tightly closed and moisture-proof containers.

Pharmaceutical preparations

Amoclox capsules are products of Memphis Chem Co., El-Zeitoun, Cairo, Egypt, BN490013; each capsule contains 250 mg amoxycillin (as trihydrate) and 250 mg dicloxacillin (as sodium monohydrate) and Miclox 250 capsules, produced by Misr Co. Pharm. Ind., S.S.A., El-Mataria, Cairo, Egypt, BN R127; each capsule contains 125 mg amoxycillin (as trihydrate) and 125 mg dicloxacillin (as sodium monohydrate)

HiPer Solv acetonitrile for HPLC (BDH-Chemicals, Poole, U.K.), and all-glass distilled water were used for preparing the mobile phase. All other chemicals were of analytical grade

Standard solutions

Acetic acid, 0.05*M* $HClO_4$ was prepared by adding 4.2 ml $HClO_4$ (72%, w/w) to about 900 ml glacial acetic acid, followed by 32 ml acetic anhydride and then cooling to room temperature (~22°C) before completing the volume to 1l with glacial acetic acid. The moisture content was checked by the micromethod of Karl–Fischer, and was adjusted to 0.01–0.2% by adding either acetic anhydride or water. Standardization of the freshly prepared solution was carried out against 0 5 g KH phthalate to get the correction factor (f).

Analytical procedures. Potentiometric titrimetry

Authentic amoxycillin or dicloxacillin. An aliquot of the drug (50–75 mg) was weighed and dissolved in 25 ml glacial acetic acid. The titration curve was recorded using standard 0.05*M* acetic $HClO_4$. The amount C (mg) of penicillin was computed from the expressions:

$$C \text{ (mg) amoxycillin (anhydrous)} = V \times f \times 18.270 \quad (1)$$

where V is the volume of titrant (protonation of the amino group) and f is the correction factor. The equivalent factor (F) 18.270 is the amount (milligrammes) of anhydrous amoxycillin equivalent to each millilitre of the titrant. The F-value for the trihydrated base is 20.970.

$$C \text{ (mg) dicloxacillin (anhydrous)} = V \times f \times 23.516 \quad (2)$$

where, V is V_1 or V_2 which are the volumes at EP_1 (protonation of the carboxylate group) and EP_2 (protonation of the basic nitrogen in the isoxazole at the 2-position), respectively. For pure dicloxacillin, the millilitres of V_1 equals exactly that of V_2. The equivalence value 23.516 is milligrammes of dicloxacillin equivalent to each millilitre of the titrant.

Authentic binary mixtures. A mixture containing equialiquots (50 mg each) of amoxycillin and dicloxacillin sodium was dissolved in 25 ml glacial acetic acid and the titration was completed with 0.05M acetic $HClO_4$. The V_1 [end point equivalent to the sum of the amino group (amoxycillin) and the carboxylate group (dicloxacillin)] and V_2 [end point corresponding to the basic centre in the isoxazole ring at position-2 (dicloxacillin alone)] were located. The content of amoxycillin and dicloxacillin can be calculated as follows:

$$C \text{ (mg) amoxycillin (anhydrous)} = (V_1 - V_2) \times f \times 18.270 \quad (3)$$

$$C \text{ (mg) dicloxacillin (anhydrous)} = V_2 \times f \times 23.516. \quad (4)$$

Sample determination. The content of at least 10 capsules was weighed and thoroughly mixed. From the powder, aliquot portions containing about 50–75 mg of each drug were taken and dissolved in 25 ml glacial acetic acid. Recording the titration curves was undertaken by using 0.05M acetic $HClO_4$ and applying equations (3) and (4) for computing the amounts of both penicillins

Recovery experiments. To one of two equal amounts of the capsule content, an accurately weighed aliquot of the drug to be evaluated was added and mixed. Each powder, with or without addition, was dissolved separately in 25 ml glacial acetic acid. The procedure described for sample determination was followed for getting the quantities of the component drugs. The volume increases of the titrant due to the added drug could be used for determination of the recovered amount in relation to the known added amount.

HPLC methods

Standard mixtures and series. For each drug substance, 25 mg was dissolved in the mobile phase up to 100 ml to get the stock solutions, *i.e.* 250 μg/ml. Mixtures containing both drugs were prepared by mixing equal amounts of the stock solution followed by proper dilution to obtain the required concentrations. From the stock solutions, different working solutions (25–125 μg/ml) were prepared by diluting aliquots with the mobile phase. Standard plots of each antibiotic were made by injecting replicates

Sample preparation and determination The content of at least 20 capsules was weighed and the average content weight of a capsule was computed. Aliquots containing 25 mg of each drug were transferred into 100 ml volumetric flasks, and about 80 ml of the mobile phase added followed by mechanical shaking for 10 min before completing to volume with mobile phase. From each well-mixed solution, 3 ml portions were diluted with mobile phase into 10 ml. Triplicate injections of each sample were done alternatively with similar standard working solution in order to enable reliable sample-standard comparisons. Calculation of drug contents was undertaken either by matching the standard curves and/or adopting the following formula:

$$C \text{ (mg capsule)} = \frac{A_1 \times D \times C\% \times W_1}{A_2 \times W_2}$$

where A_1 and A_2 are the areas for amoxycillin or dicloxacillin in sample and standard, respectively, D is the dilution factor, W_1 and W_2 are the average weight (milligrammes) per capsule and the taken weight (milligrammes), respectively, and $C\%$ is the concentration (percent) of standard solution in the final dilution.

Recovery and reproductivity. Different ratios of standard to sample, namely 1:2, 2:3, 3·2 and 2:1, were prepared by diluting aliquots of the stock solutions with mobile phase. Triplicate injections of each solution mixture were done to ensure the degree of recovery of the added amounts of each drug. The reproducibility was tested by 12 consecutive injections of a standard solution equivalent to full amounts of each component based on the theoretical quantities

Chromatographic conditions. Two different HPLC-conditions, LiChrosorb RP-18 (10 μm) and LiChrosphere RP-18 (5 μm) columns

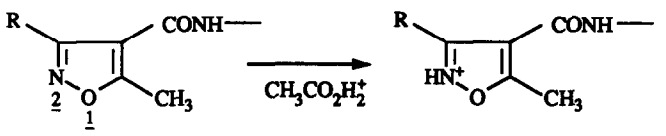

Scheme 1

utilizing different proportions of CH_3CN and 1% aq. CH_3COOH as the mobile phases, have been investigated and evaluated for their stability-indicating characteristics. The flow rate was 1.5 ml/min, the UV-detection was fixed at 240 nm, and the CDS-attenuation was 16 (5 mV/Fs) at 0.5 cm/min chart speed, in the two conditions.

RESULTS AND DISCUSSION

The application of the BP-1988[11] procedure, described for the determination of amoxycillin capsules, has been tried on specimen capsules containing amoxycillin and dicloxacillin combinations. The reaction products of the imidazole-mercury reagent with dicloxacillin exhibit overlapping maxima at the wavelength specified for amoxycillin. Even the binary mixtures containing both studied penicillin exhibit considerable UV-band overlap. At the practically justified λ_{max} for amoxycillin (227 and 274 nm), dicloxacillin exhibits considerable effective UV absorbance at about 275–280 nm, which makes the direct UV spectrophotometric determination of one penicillin in the presence of the other quite impracticable.

The potentiometric titrimetry described here depends on the fact that the amino groups of amoxycillin and the carboxylate groups of dicloxacillin are readily protonated together differentially from the dicloxacillin isoxazole basic ring, when treated with acetic perchloric acid. The direct linking of the heteroatoms N and O in the isoxazole ring of dicloxacillin has a base-weakening effect (pka 2.03), which is about 3 pka units weaker than oxazole. The lone pair of electrons on the nitrogen of 1,2-azole is not part of the aromatic sextet and is therefore available for salt formation without disruption of the aromaticity. Scheme 1 demonstrates the protonation pattern of the substituted isoxazole; The HPLC separation of the two component penicillins has been tried on the basis of finding out not only an accurate quantitative method but also one with good stability-indicating characteristics. Two different reverse-phase (RP) columns, namely LiChrosorb and LiChrospher, have revealed validity. Table 1 gives the LC parameters of the HPLC methods. Figures 1 and 2 illustrate the HPLC resolution of both penicillins and their degradation products, on the LiChrosorb and the LiChrospher columns, respectively. It is clear that the intact drug substances were resolved quite away from both of the solvent peaks and those of the degradation products. The selected chromatographic conditions seemed to be the best for indicating the drug stabilities. Table 2 collects and matches the obtained results of assay, recovery and reproducibility testing of the proposed three methods. Variations in results between the two different techniques, namely potentiometric protonation and liquid chromatography, are only in the drug assay of capsules. No clear explanation can be suggested, but it may be due to the variability of the capsules matrices or the poor stability-indicating characteristics of the potentiometric method. The high-performance liquid chromatography has achieved a pronounced advantage over some other techniques in being the most stability-indicating. Both the described HPLC methods have proved their advantage in the capability of finding the accurate contents of each

Table 1 HPLC parameters for resolved amoxycillin and dicloxacillin

	HPLC method			
Column	(LiChrosorb)		(LiChrospher)	
Drug	Amoxycillin	Dicloxacillin	Amoxycillin	Dicloxacillin
Capacity factor (k')	3 16	2 2	1 75	6 46
Resolution (R)	3 34		11 93	
Tailing factor (peak asymmetry factor)	1 70	1 70	1 63	1 33
SDrel(replicates)*	⩽2 0%		⩽2 0%	
Stability indication	valid		valid	

*Relative standard deviation

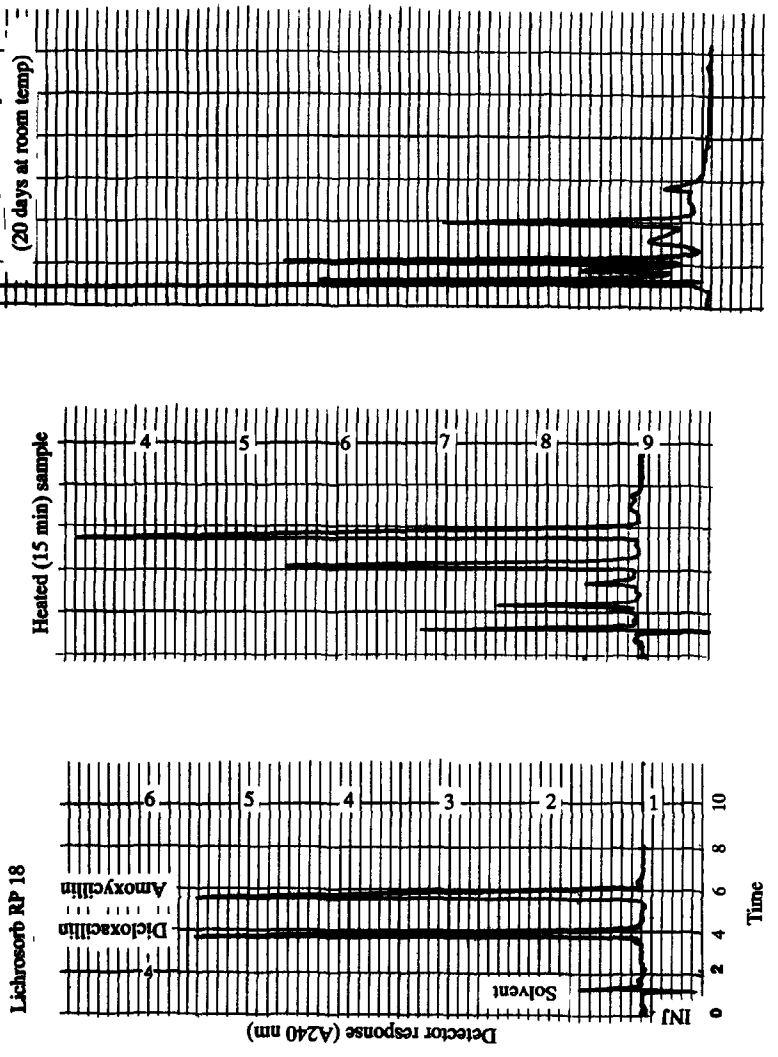

Fig. 1 HPLC chromatographic separation on LiChrosorb RP18 column of fresh, heated [at 80°C (15 min)] and normally degraded (20 days at ~22°C) samples of amoxycillin and dicloxacillin.

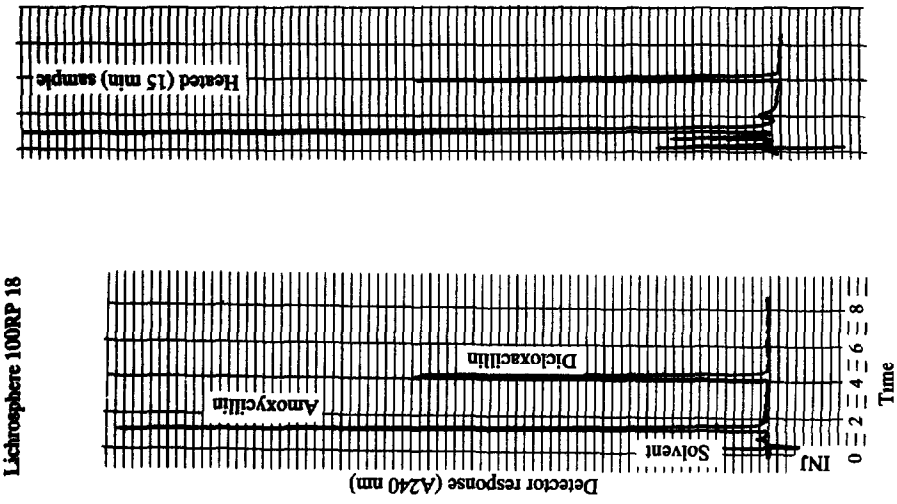

Fig. 2. HPLC chromatographic elution on LiChrospher 100RP18 column of fresh and heated [at 80°C (15 min)] samples of amoxycillin and dicloxacillin.

Table 2 The assay, recovery and reproducibility on the application of the proposed potentiometric titrimetry and HPLC methods

	Potentiometric titrimetry ($HClO_4$-titration)		HPLC methods (LiChrosorb)		(LiChrospher)	
	Amoxycillin	Dicloxacillin	Amoxycillin	Dicloxacillin	Amoxycillin	Dicloxacillin
1. *Assay*						
Amoclox capsules						
$X^* \pm SD$	80 6 ± 2 6	110.0 ± 2 5	83 9 ± 2 3	93 7 ± 1 6	84 3 ± 1 4	93 5 ± 1 2
$CV(n)^+$	1 9 (5)	1 4 (5)	1 6 (6)	1 7 (6)	1 7 (6)	1 2 (6)
Miclox capsules						
$X \pm SD$	105 6 ± 1 4	88 5 ± 1 7	101 4 ± 1 7	83 0 ± 1 6	100 5 ± 1 3	81 9 ± 1 3
$CV(n)$	1 4 (4)	2.0 (4)	1 7 (6)	1.9 (6)	1 3 (6)	1 6 (6)
2 *Recovery*						
Amoclox capsules						
$X \pm SD$	100.8 ± 0 9	100.2 ± 0 7	100.1 ± 0 5	99 7 ± 1.0	100 1 ± 0 5	100 0 ± 1 0
$CV(n)$	0.9 (9)	0.7 (7)	0 5 (4)	1 0 (4)	0.5 (4)	1.0 (4)
	Student's T (tab. T-value)		1 91 (2 20)	0 83 (2 26)	1.91 (2 20)	0 25 (2 26)
Miclox capsules						
$X \pm SD$	—	—	100 1 ± 0.7	100 3 ± 0 8	100.1 ± 0 7	100 0 ± 1 1
$CV(n)$	—	—	0 7 (4)	0 8 (4)	0 7 (4)	1 1 (4)
3 Reproducibility						
$X \pm CV(n)$	100.9 ± 1 0 (4)	100.1 ± 0.6 (6)	100.0 ± 0 8 (12)	100 0 ± 0.7 (12)	100 0 ± 1.0 (12)	100 0 ± 0.8 (12)

*Arithmetic mean

^+n = the average mean of at least two determinations of each encountered experiment

drug substance in the presence of its degradation products, although no justification of the decay products have been done in this study. Moreover, the quantification of both intact penicillins can be carried out simultaneously without possible interferences from the presence of the degradation fragments of both drug substances. The recovery testing of all the proposed methods indicates the good accuracy and precision. The statistical evaluations of the obtained recoveries demonstrate that there are no significant differences between the potentiometric method and each of the liquid chromatographic methods proposed in the present communication. Good reproducibilities of all the investigated methods have been observed for different replicates, as reflected in the relative low coefficient of variations.

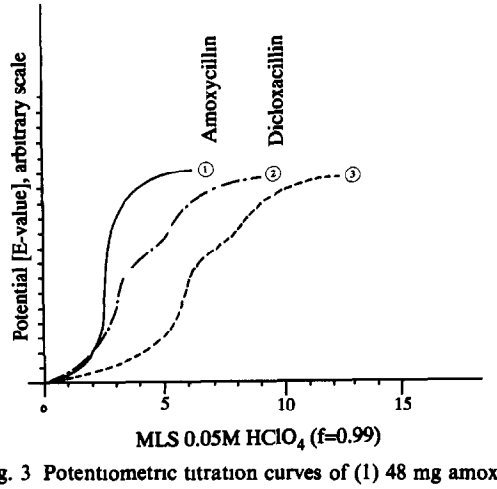

Fig. 3 Potentiometric titration curves of (1) 48 mg amoxycillin, (2) 54 mg dicloxacillin, and (3) a mixture of (1) and (2) against standard 0.05M (f = 0 99) acetic $HClO_4$.

It can be concluded that the demonstrated methods for the simultaneous quantification of amoxycillin and dicloxacillin in their mixtures and/or dosage formulations are simple, rapid and accurate. The relative cheapness of the apparatus beside the simplicity of the procedure of the non-aqueous potentiometry demonstrate its advantageous characteristics. The liquid chromatographic techniques described in the present work have the clear advantage of indicating the drug stability in addition to their high accuracy and confidence.

Acknowledgements—The authors would like to thank Dr S A Ismaiel, Research Directorate, Misr Co for Pharm Ind S A A, El-Matania, Cairo-ET, for providing reference amoxycillin trihydrate and dicloxacillin monohydrate

REFERENCES

1. R. Sutherland and F R. Batchelor, *Nature*, 1964, **201**, 868
2. L D Sabath, C E. McCall, N. H Steighbigel and M Finland, *Antimicrob. Agents Chemotherapy*, 1967, **149**
3 C H. O'Callaghan, P. W Muggleton, S M Kirby and D M. Ryan, *Antimicrob Agents Chemotherapy*, 1967, **337**
4. L. D. Sabath, M. Jago and E P Abraham, *Biochem J*, 1965, **96**, 739

5. R. T. Yousef, G. Tawil and H. Abou-Shleib, *Pharmazi*, 1985, **40**, 650
6. J E. F. Renold (eds), *Martindale The Extra Pharmacopoeia*, 29th Ed., pp 112 and 215, The Pharmaceutical Press, London, 1989
7. J D Doadrio and A Doadrio, *An R Acad Farm.*, 1983, **49**, 69, through *Anal Abstr*, 1984, **46-9E20**, 869
8 D. Marini, *Rass Chim*, 1976, **28**, 35, through *Chem Abstr*, 1976, **85**, 83296
9 P K Bhattacharyya and W M Cort, in K Florey (ed), *Analytical Profiles of Drug Substances*, Vol 7, p 37 Academic Press, FL, 1978
10. G. Laurault, D. V. C Awang and D Kindack, *J Chromatogr*, 1984, **283**, 449
11. *The British Pharmacopoeia* 1988, pp 37 and 625, HMSO, London, 1988
12. E. M Abdel-Moety, *J Pharm Biomed Anal*, 1991, **9**, 1987
13 *The British Pharmaceutical Codex* 1973, p 737, The Pharmaceutical Press, London, 1973
14 S A Ismaiel, *Misr Co for Pharm Ind*, *S A A* personal communication
15 D A Doule and G F Smith (eds), *Heterocyclic Chemistry*, p 321, Van Nostrand Reinhold Co, London, 1976

Talanta, Vol 40, No 6, pp 819–825, 1993
Printed in Great Britain

0039-9140/93 $6 00 + 0 00

JESS, A JOINT EXPERT SPECIATION SYSTEM—III*. SURROGATE FUNCTIONS

PETER M. MAY
School of Mathematical and Physical Sciences, Murdoch University, Murdoch, Western Australia 6150, Australia

KEVIN MURRAY
Division of Water Technology, CSIR, Pretoria, South Africa 0001

(*Received* 25 *November* 1991 *Revised* 2 *November* 1992 *Accepted* 3 *November* 1992)

Summary—A new, general method of coupling calculations of equilibria with those of other chemical effects and processes is described The method, based on the use of simple empirical functions, is demonstrated by applying it to changes of ionic strength and temperature in speciation modelling

One of the most persistent criticisms of speciation models is that they are too simplistic: many systems, especially physiological or environmental systems,[1] it is said, are chemically much more complicated than we can, at present, properly simulate. Leaving aside the lack of understanding of scientific modelling often reflected by this kind of criticism, it is undeniable that equilibrium calculations are currently somewhat limited.[2] As outlined in Part I of this series,[3] they suffer from inadequacies in several thermodynamic respects, including how best to deal with changing conditions of temperature and ionic strength. Moreover, profound difficulties can arise when applications involve relationships between chemical species other than equilibrium interactions.[4,5] Kinetically-controlled systems fall into this category, as do biological or industrial processes regulated by feedback mechanisms.

The reason why speciation calculations are presently so limited is simple. Programs cannot be expanded indefinitely to cope with extra complexity. This is even though the various processes may be well understood and can be satisfactorily described in mathematical terms. The problem is to solve simultaneously multiple systems of equations that are inherently diverse, and sometimes very large. Not only is it theoretically difficult to amalgamate such different types of calculation but efforts to do so in a general way tend to overwhelm whatever computational capacity is available.

Accordingly, progress in coupling equilibrium with other calculations has been slow, despite the fact that this has been the focus of much research.[6] Resorting to brute force seems unlikely to yield, at least in the foreseeable future, the comprehensive modelling capabilities which motivated our development of JESS.[3]

This paper describes a general method for speciation calculations of complicated chemical systems which require extension beyond just solving conventional mass balance equations. As a specific case, it outlines how we have applied this method to overcome the difficulties which have hitherto restricted calculations of changing temperature and ionic strength. It should be noted that details of the algorithm used below are of secondary importance and are likely to be improved in future. Subsequent papers will detail the method's application to metal ion binding by macromolecules and to other complicated effects.

GENERAL METHOD

Partitioning the numerical computation of the solution of a heterogeneous set of non-linear equations implies an iterative approach in which successive, improving approximations are substituted into each of the equation subsets in turn. Such calculations yield a simultaneous, overall solution by convergence, *i.e.*, changes in the tentative solution produced by a full iterative cycle become negligible, as defined by some pre-determined tolerances. Whatever methods are used to improve the tentative solution from initial estimates to final values, the calculation

*Part II is *Talanta*, 1991, **38**, 1419[8]

performed in respect of each part of the iterative process should not counteract the progress made elsewhere. Otherwise, convergence becomes slow or, in the extreme, the iteration diverges

In essence, coupling calculations of equilibria with those of other chemical effects and processes can be simplified if the different types of equation can be partitioned, and evaluated separately, without compromising the chances, or the rate, of achieving convergence. This is not straightforward: attempts to evaluate equation subsets in isolation fail to converge except in special cases where the propagation of errors in any tentative solution is controlled. These well-behaved cases are, in general, difficult to derive rigorously, particularly if this must be done *a priori* Consequently, attempts to tackle complicated calculations by partitioning the system's equations are frequently unsuccessful.

A general method which helps to overcome this problem of partitioning is now being implemented in our JESS package for speciation calculations.[3] This is based on empirical expressions that we call "surrogate functions". These surrogate functions have four main characteristics:

(i) they are simple in form;
(ii) they are constructed to represent the main effects of selected subsets of equations,
(iii) their parameters are determined empirically, sometimes by optimization of data obtained from the behaviour of the subset of equations scanned over a range of conditions;
(iv) they are easily incorporated into the solution of the equations in the equilibrium calculations.

By substituting surrogate functions into other parts of a complicated calculation, the effects of their respective subset of equations can be emulated. In this way, error propagation in that stage of the iterative cycle can be substantially reduced and the likelihood of convergence failure through the partitioning of the calculation suppressed.

In addition to the simplification of calculations achieved by partitioning, there are other advantages to using surrogate functions. The most important of these is that the equation solving code can be generalized. This is because the simple form of the surrogate function can, over a suitably narrow range, stand in place of equations of considerably greater intricacy. The benefit of avoiding a tailor-made code is not only that standard, well-tried equation-solving methods can be applied but also that any subsequent alterations are much easier to implement because the highly specific segments of the program are well isolated. Another advantage of surrogate functions is that they can be applied directly to experimental data, even when the functional behaviour of the data has not been satisfactorily characterized

Much work has been done in the past on response surface analysis and experimental design.[7] There are some parallels between these approaches and surrogate functions in that both involve empirical data fitting, reduction in the number of empirical parameters and similar methods of choosing suitable functions. However, the key difference proposed here is in the use of the surrogate function to incorporate complicated effects into the solution of another, application-specific, set of equations (in this case for equilibrium modelling).

So far, we have experienced surprisingly few difficulties in implementing surrogate functions in JESS. Of course, the best way to formulate the empirical functions must be worked out in each particular case. It is necessary to decide on the variables to use, the number and the make-up of the terms to include and the number of degrees of freedom to permit. The initial range over which the surrogate function is to interpolate must be decided. Often this must be done arbitrarily in the first instance, but then information for making better choices tends to become available naturally after the first iterative cycle is complete. Significantly, the range may be narrowed as convergence approaches.

A SPECIFIC IMPLEMENTATION

The practical problems of modelling equilibria which must take account of changes in ionic strength (I) and temperature (T) were discussed in detail in Part I of this series [3] These stem mainly from the large number of correction methods available, especially for changes in ionic strength. This diversity makes it highly unsatisfactory to perform such corrections by interspersing conventional formulae within the body of the equilibrium calculations. To do so would introduce serious inflexibilities through lack of modularity in programming. It would also generate very bulky and cumbersome code. Moreover, the simulation procedure would

sometimes become prohibitively time-consuming: certain models involve many thousands of equilibrium constants and, to investigate the influence of ionic strength and temperature, would require all of them to be repeatedly recalculated.

For these reasons, JESS applies the user's choice of correction methods in a separate stage prior to the equilibrium calculations themselves. This isolates and minimizes the impact of what is necessarily a tedious step in the modelling procedure. It also permits JESS to offer a wide selection of approaches to ionic strength correction. Any desired combination of methods is possible because each reaction can be treated individually beforehand. The fact that particular methods of correction do not need to be "hardwired" into the speciation program code is therefore a tremendous advantage.

A set of computer programs has been developed to take data from any standard JESS Thermodynamic (JTH) database.[8] The information concerning how each equilibrium constant changes with respect to I and T is evaluated and expressed as a surrogate function. The surrogate functions employ a set of nine empirical parameters we call the "Constant Correction Coefficients" or CCCs. These are then passed on, via intermediate databases, to the equilibrium calculations. Thus, equilibrium constants (as $\log K$) can be obtained *at any required* I *and* T (within user-specified ranges) in an extremely efficient and flexible way during subsequent stages of the modelling procedure.

The major practical limitation of this approach is that users must nominate, at an early stage, the ranges of I and T over which they will later wish to perform their equilibrium calculations. The accuracy of the corrections is lessened if ranges are given which are either wider or narrower than those actually explored later on. However, the likely ranges of I and T are usually set by the overall context of the modelling and are mostly evident to users from the outset.

The surrogate functions for equilibrium constant correction

From the ranges of I and T specified by the user, JESS creates a two-dimensional grid of 3×3 points. A grid of nine points was considered to be adequate from two points of view. First, real changes of $\log K$ as a function of I and T are sufficiently smooth over fairly wide ranges. Secondly, in practice there will seldom exist sufficient primary data to justify a denser grid. JESS then applies the correction methods specified by the user to determine values of the equilibrium constants at each of the corresponding nine pairs of I and T values, as described below. The position of the midpoints is based on the available data and the ranges required and need not necessarily be in the middle of the ranges. A two-dimensional empirical function is then fitted exactly to the surface created by these nine points. This function can be described as follows.

At constant T, the function is

$$\log K = P_1 + \frac{P_2 I^{\frac{1}{2}}}{1 + I^{\frac{1}{2}}} + P_3 I$$

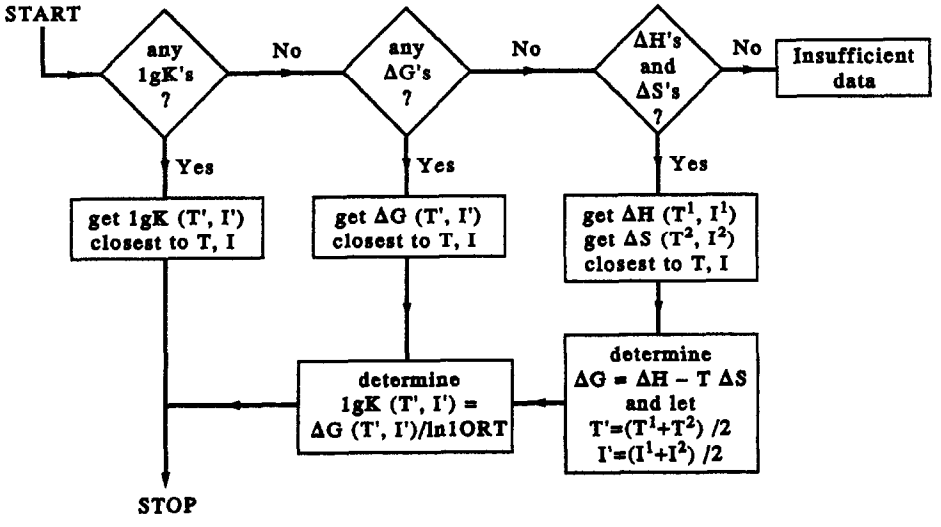

Fig. 1

This functional form was chosen to reflect an underlying theoretical model (of a Debye–Hückel type). Although it may not be accurate over large ranges it is almost certainly preferable to a simpler quadratic or cubic function.

The assumption is then made that, at constant I, each coefficient, P, is a quadratic function in T. This form was chosen because it is well known that a linear model is often adequate for modelling the change of $\log K$ with T and that by simply including a quadratic term its flexibility would be greatly enhanced. In this respect, it is relevant to note that "thermodynamics does not define [a] quantitative relationship between K and T"[9] and that a very wide variety of functional forms have been applied in the literature,[9] with little to favour any one in particular. Thus, we put

$$P_j = C_{1j}T^2 + C_{2j}T + C_{3j}.$$

Substituting the nine pairs of I and T values and their corresponding $\log K$s into these equations results in a system of linear equations which is solved to give the nine coefficients C_{ij}.

Algorithms for obtaining constants under given conditions

Although, for any given reaction, data can be stored in the thermodynamic database at many different Is and Ts, the data available are unlikely to fall precisely on the nine points required for the CCC grid. To obtain the $\log K$ for a particular grid point, the present algorithm simply selects the constant nearest to the I and T of the grid point and corrects it. The details are given in the following sections.

- Selecting the $\log K$ closest to a specified I and T
  If no $\log K$ values are found explicitly in the database, an attempt is made to determine an approximation from other thermodynamic parameters (free energy, enthalpy and entropy changes). The algorithm currently in use is shown in Fig. 1.

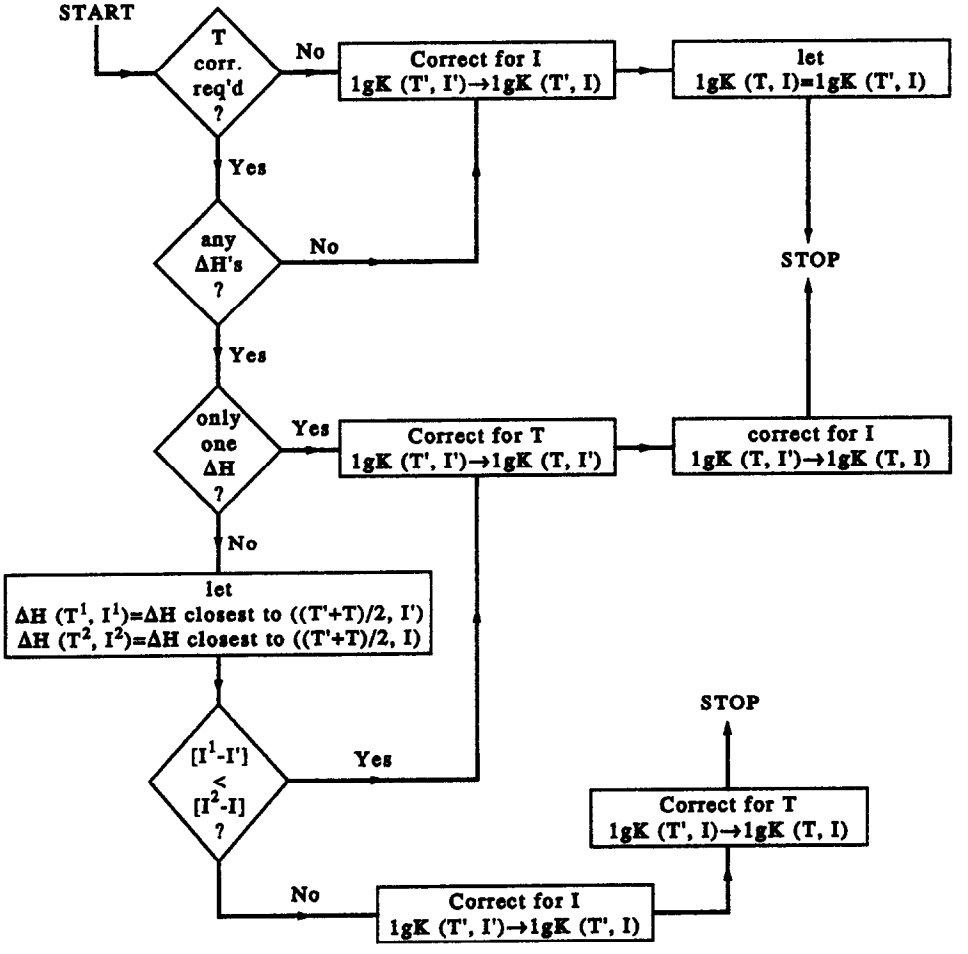

Fig. 2

If a series of constants (of any particular type) are found, the following objective function is evaluated to decide which value should be used.

$$U = |T - T'|/60 + |I - I'|$$

where I and T refer to the required conditions and I' and T' refer to the conditions under which the constant in the database applies. If the constant in the database refers to a range of conditions, I' and T' assume the upper or lower limit, whichever is closest to I and T. The constant with the lowest value of U is taken.

- Correcting a log K for I and T

Once the value of the equilibrium constant closest to the required conditions has been obtained, it is corrected using the methods selected for this purpose by the user. The user can specify activity coefficient calculation methods for individual species in the Thermodynamic database. It is possible either to invoke these or to override them with a global method. Figure 2 shows the current algorithm for correcting from (I', T') to (I, T).

RESULTS

To investigate the accuracy of interpolations using the above Constant Correction surrogate function, data for the following five reactions were examined.

$$H^+ + OH^- = H_2O \quad (1)$$

$$H^+ + F^- = HF \quad (2)$$

$$Zn^{2+} + F^- = ZnF^+ \quad (3)$$

$$H^+ + Phthalate^{2-} = HPhthalate^- \quad (4)$$

$$H^+ + Acetate^- = HAcetate \quad (5)$$

Tables 1–5 summarise the results obtained. When constants were corrected for ionic strength, the Davies equation was used to calculate the activity coefficient for all charged species:

$$-\log \gamma = \frac{Az^2\sqrt{I}}{1+\sqrt{I}} + 0.3Az^2$$

where A was calculated as in Ref. 10.

The following formula was used for uncharged species:

$$-\log \gamma = -0.1I$$

Table 1 Interpolation results for reaction (1) T range 10–50°; I range. 0–3, Medium NaCl

log K = 1 7500E-4T**2 − 0 042000T + 14.943
+[9 4574E-4T**2 − 0 058268T
−0 30502]*[sqrt(I)/(1 + sqrt(I))]
+[−2 2273E-4T**2 + 0.013438T + 0 046917]*I

T	I	ΔH	log K (obs)	log K (calc)	Difference
10	0 0		14 54*[a]	14 54	0 00
20	0 0		14 17[a]	14.17	0 00
25	0.0	−13 3*[d]			
30	0.0		13 84*[a]	13 84	0 00
40	0 0		13 55[a]	13 55	0 00
50	0.0		13 28*[a]	13 28	0 00
25	0.1		13.71[b]	13 75	0.04
25	0.5		13 67*[b]	13.64	−0.03
25	1 0		13.71[b]	13 66	−0.05
25	3.0		13.99*[b]	13 99	0.00
35	1.0	−13 5*[c]			

*Used in determination of CCC function

[a]A. Albert and E. P. Serjeant, *The Determination of Ionization Constants*, Chapman & Hall, London, 1984

[b]P Verhoeven, G. T. Hefter and P M May, *Min & Metall Process.*, 1990, 173

[c]V P. Vasilev and L D. Shekhanova, *Zh Neorg. Khim*, 1974, 19, 2969 (E· 1623).

[d]R. M. Smith and A E Martell, *Critical Stability Constants*, Vol 4, Plenum, N Y , 1976.

Table 2. Interpolation results for reaction (2) T range 10–50°; I range. 0 5–4; Medium· $NaClO_4$. All data from A M Bond and G. T Hefter, *IUPAC Chem. Data Ser.*, 27, Pergamon, Oxford, 1980

log K = −2 7874E-5T**2 + 8 3207E-3T + 2.7222
+[9 1211E-6T**2 + 1 4524E-3T
−0 25761]*[sqrt(I)/(1 + sqrt(I))]
+[−6.5785E-7T**2 − 1 0477E-4T + 0.19573]*I

T	I	ΔH	log K (obs)	log K (calc)	Difference
25	0 5		2 92*	2 92	0 00
25	1.0	3 1*	2 97	3 00	0 03
25	2.0		3 13*	3 17	0 04
25	3 0		3 31	3 35	0.04
25	4 0		3 54*	3 54	0.00

*Used in determination of CCC function

Table 3. Interpolation results for reaction 3 T range 25°; I range. 0–1, Medium· $NaClO_4$ All data from G T Hefter, N H. Tioh and C B Chan, *Polyhedron*, 1990, 9, 901

log K = 0.0T**2 + 0 0T + 1.2000
+[0 0T**2 + 0.0T − 1.8266]*[sqrt(I)/(1 + sqrt(I))]
+[0 0T**2 + 0.0T + 0.25328]*I

T	I	log K (obs)	log K (calc)	Difference
25	0.0	1.20*	1 20	0 00
25	0.01	1 1	1.04	−0.06
25	0 02	0 98	0 98	0 00
25	0.05	0 83	0 88	0.05
25	0.1	0 72	0.79	0.07
25	0 2	0.66*	0 69	0.03
25	0 5	0.56	0 57	0 01
25	1.0	0 54*	0.54	0 00

*Used in determination of CCC function.

Table 4 Interpolation results for reaction (4) T range 15–55°, I range 0–1, Medium $(C_2H_5)_4NI$ A. De Robertis, C De Stefano, C Rigano and S Sammartano, *J Soln Chem*, 1990, 19, 569

log K = 5.7506E-5T**2 − 1 7755E-3T + 5 4197
+[− 1 2649E-5T**2 + 8 6239E-4T
− 1 4037]*[sqrt(I)/(1 + sqrt(I))]
+[2 5733E − 6T**2 + 3.8064E-3T + 0 66715]*I

T	I	log K (obs)	log K (calc)	Difference
15	0 0	5.406*	5 406	0 000
15	0 36	5 124*	5 144	0 020
15	1 0	5 434*	5 434	0 000
25	0 0	5 410	5 411	0 001
25	0 04	5 144	5 210	0 066
25	0 16	5 079	5 136	0 057
25	0 36	5 141	5 165	0 024
25	0 64	5 285	5 282	−0 003
25	1 0	5 479	5 480	0 001
35	0 0	5 428*	5 428	0 000
35	0 36	5 171*	5 196	0 025
35	1 0	5 537*	5 537	0 000
45	0 0	5 457	5 456	−0 001
45	0 04	5 193	5 258	0 065
45	0 16	5 134	5 194	0 060
45	0 36	5 211	5 239	0 028
45	0 64	5 379	5 378	−0 001
45	1 0	5 605	5 604	−0 001
55	0.0	5.496*	5 496	0 000
55	0 36	5 261*	5 291	0 030
55	1 0	5 683*	5 683	0 000

*Used in determination of CCC function

Table 5 Interpolation results for reaction (5) T range 15–55°, I range 0–1, Medium $(C_2H_5)_4$ NI A De Robertis, C De Stefano, C Rigano and S Sammartano, *J Soln Chem*, 1990, 19, 569

log K = 5 3750E-5T**2 − 2 4875E-3T + 4 7792
+[− 1 7227E-6T**2 − 1 5450E-4T
−0.73973]*[sqrt(I)/(1 + sqrt(I))]
+[2 1165E-6T**2 + 1 3645E-3T + 0 30527]*I

T	I	log K (obs)	log K (calc)	Difference
15	0 0	4 754*	4 754	0 000
15	0 36	4 592*	4 593	0 001
15	1 0	4 709*	4 709	0 000
25	0 0	4 750	4 751	0 001
25	0.04	4.614	4 640	0 026
25	0 16	4 573	4 592	0 019
25	0 36	4 591	4 594	0.003
25	0 64	4 645	4 638	−0 007
25	1 0	4.718	4 719	0 001
35	0 0	4 758*	4 758	0 000
35	0 36	4 603*	4 606	0 003
35	1 0	4 740*	4.740	0 000
45	0 0	4 777	4 776	−0 001
45	0 04	4 642	4 666	0 024
45	0 16	4 602	4 621	0 019
45	0 36	4 626	4 628	0 002
45	0 64	4 688	4 680	−0 008
45	1 0	4 773	4 772	−0 001
55	0 0	4 805*	4 805	0 000
55	0.36	4 657*	4 662	0 005
55	1 0	4 815*	4 815	0 000

*Used in determination of CCC function

Temperature corrections were made with the following formula.

$$\ln K_2 = \ln K_1 + \frac{\Delta H}{R}\left(\frac{1}{T_1} - \frac{1}{T_2}\right)$$

where R = gas constant.

Since the purpose of this exercise was to investigate how well CCC functions fit observed data (not how well constants can be corrected), the T and I ranges were chosen such that inaccuracies due to correction of constants (for T and I) were minimized. Accordingly, the following two conditions were satisfied wherever possible. First, the limits were set at points for which measured data were available. Secondly, reactions were selected such that there were sufficient intermediate points against which the interpolated constants could be directly compared These points were necessarily other than those whose data were used in the determination of the CCC function. The CCC functions, determined for each reaction (with T in °C), are given in Tables 1–5 in the Fortran format displayed by JESS.

CONCLUSION

The increasing use of chemical simulation for such purposes as optimizing industrial process streams, understanding molecular mechanisms of biochemistry and making decisions for environmental regulation must inevitably create demand for ever more sophisticated modelling capabilities. The method described in this paper based on surrogate functions is intended to facilitate such developments. How successful it will be in general is still unclear, although preliminary investigations of several possibilities appear promising.

It would seem that the surrogate function approach is particularly well-suited to correction of constants for I and T. This is probably because, on the whole, the change in a constant over quite significant (and useful) ranges can be adequately described by quite simple functions. Indeed, this provides one criterion by which to judge the suitability of any other potential application to the surrogate function method. Another is that the surrogate function should be easily incorporated into, and mathematically compatible with the solution of, the equations in the main application

The results presented here demonstrate that satisfactory interpolated values can be obtained from the proposed Constant Correction surrogate function. This is despite the fact that

particularly wide ranges of conditions were chosen. In real applications these ranges would usually be considerably smaller and thus the interpolations would probably be even more precise (assuming that satisfactory corrections for T and I were possible).

As might be expected, the deviations are greatest for interpolations at low ionic strengths when I ranges from zero to a high value ($1M$ and above). Here again, such extreme ranges would not normally be necessary in practice. One would generally know the approximate ionic strength of the system under investigation. Then, for example, one could choose ranges which were confined to one side or the other of the Debye–Hückel minimum (say between 0.0–0.3M and 0.3–3.0M for low and high ionic strength solutions, respectively). In such cases one might reasonably anticipate very satisfactory interpolations.

Finally, it is important to record that the particular methods of selecting constants described above are likely to change in the near future. For instance this will occur when, as foreshadowed,[3] we implement the JESS programs that modify observed and estimated thermodynamic values to achieve intermediate databases with better internal consistency However, we see no reason why these changes would negate the conclusions about surrogate functions that are drawn in this paper.

REFERENCES

1 M M Jones, A D Weaver and M A Basinger, *J Inorg Nucl Chem*, 1981, **43**, 2175
2 T J Wolery, K J Jackson, W L Bourcier, C J Bruton, B E Viani, K G Knauss and J M Delany, in *Am Chem Soc Symp Ser 416*, D C Melchior and R L Bassett (eds), pp 104–116 *Am Chem Soc*, Washington DC, 1990
3 Part I P M May and K Murray, *Talanta*, 1991, **38**, 1409
4 I Bodek, W J Lyman, W F Reehl and D H Rosenblatt, *Environmental Inorganic Chemistry, Properties, Processes, and Estimation Methods*, Pergamon Press, New York, 1988
5 C W Miller, in *Mat Res Soc Symp Proc*, Vol 15, pp 481–488 1983
6 R L Bassett and D C Melchior, in *Am Chem Soc Symp Ser 416*, D C Melchior and R L Bassett (eds), pp 1–14 Am Chem Soc, Washington DC, 1990
7 J W Frazer, L P Rigdon, H R Brand, C L Pomernacki and T A Brubaker, *Anal Chem*, 1979, **51**, 1747
8 Part II P M May and K Murray, *Talanta*, 1991, **38**, 1419
9 M J Blandamer, J Burgess, R E Robertson and J W Scott, *Chem Rev*, 1982, **82**, 259
10 P M May and K Murray, *Talanta*, 1985, **32**, 483

Talanta, Vol 40, No 6, pp 827–830, 1993
Printed in Great Britain

0039-9140/93 $6 00 + 0 00

ION-PAIR CHROMATOGRAPHIC DETERMINATION OF CHROMIUM(VI)

A. V. PADARAUSKAS* and L G KAZLAUSKIENE
Department of Analytical Chemistry, University of Vilnius, 2734 Vilnius, Lithuania

(*Received* 18 *June* 1992. *Revised* 13 *October* 1992 *Accepted* 27 *October* 1992)

Summary—Ion-pair chromatography (IPC) with conductometric detection was investigated as a precise and selective analytical method for the determination of chromium in electro-plating solutions and waste waters. Chromatographic parameters were optimized for separation of Cr(VI) and SO_4^{2-} The analytical column (100 × 6 mm) was packed with 10 μm silasorb C_{18} (Czechoslovakia) Tetrabutylammonium butyrate (TBAB), at pH 7 0 in acetonitrile–water (18·82 v/v) mixture, was used as the eluent. Two samples of solution are taken for the analysis In the first of them the amount of Cr(VI) is determined, in the second one Cr(III) is oxidized to Cr(VI) with H_2O_2 in alkaline medium and the total amount of Cr is determined From the difference of the two obtained results the concentration of Cr(III) is calculated The detection limit of Cr(VI) is 0.1 μg/ml and the relative standard deviation (at the 1 0 μg/ml) is 4 0%. The IPC results for chromium agreed closely with these obtained by spectrophotometry

At present chromium is widely used in industry. Electroplating solutions containing Cr(III) salts, chromates or bichromates are suitable for chrome-plating and for etching and passivation of metallic details. Further, Cr(III) is less toxic than Cr(VI). Thus, when electroplating solutions and waste waters are controlled it is important to determine the concentration of both forms of chromium.

Precipitation[1,2] and titrimetric[3] analysis are used for determination of chromium in electroplating solutions most of all. However, the precipitation methods is time consuming and non-selective. Further, chemical methods of analysis are not sensitive enough for analysis of waste waters. Thus more sensitive spectrophotometry[4,5] or atomic-absorption spectrometry[6] (AAS) are used to determine chromium in waste waters. Fe(III), Cu(II), Hg(II), Mo(VI) and V(VI) interfere in the spectrophotometry determination of chromium with diphenylcarbazide. Iron can be masked with EDTA and vanadium, copper and molybdenum can be extracted into chloroform as oxine complexes, while mercury can be masked with chloride.[7,8] The additional operations prolong the analysis. AAS is non-selective for chromium forms.

Recently, ion-chromatography (IC)[9] has been very popular for anion determination in aqueous solution. Suppressed[10] and single column[11,12] IC have been used for the detection of Cr(VI), but these ions are very strongly retained in anion-exchange columns and so the chromatographic peaks obtained were very broad, which made accurate quantification difficult.

As an alternative to IC methods, is ion-pair chromatography (IPC).[13] It is more efficient and selective than IC and so is applicable to separate and determine inorganic, as well as organic and complex, ions.[14] With the help of IPC, in most cases chromium is determined as a chelate with 4-(2-pyridylazo)resorcinol using a spectrophotometric detector.[15,16] This technique is very sensitive and is used for the analysis of natural waters. However, this method is insufficiently selective because of the capability of a great number of metals to form analogous chelates.

In industrial waters it is more convenient to determine chromium in the form of CrO_4^{2-} when many of the other metals are in the form of cations and do not interfere in chromium determination. Furthermore, a conductometric detector can be used.

The objective of this study was to develop a IPC method for the determination of chromium in electroplating solutions and waste waters.

EXPERIMENTAL

Instrumentation

The work was done with an HPLC chromatograph manufactured in Russia (Tsvet 3006) and

*Author for correspondence.

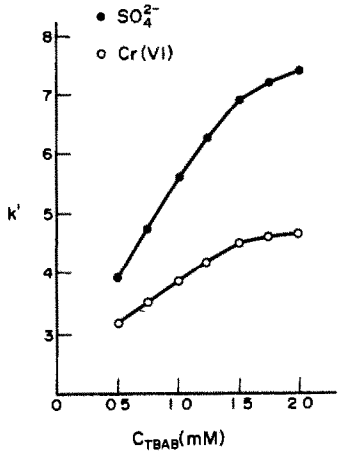

Fig 1 Effect of TBAB concentration on the capacity factor (k') Eluent conditions TBAB, 80% H_2O, 20% CH_3CN, pH 7 0

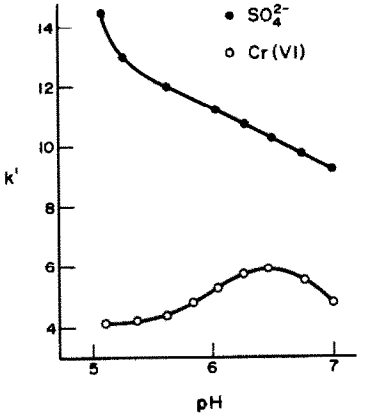

Fig 3 Effect of eluent pH on the capacity factor (k') Eluent conditions 1mM TBAB, 1mM butyric acid, 82% H_2O, 18% CH_3CN

equipped with a conductometric detector. The analytical column (100 × 6 mm) was packed with 10-μm silasorb C_{18} (Czechoslovakia)

The absorbances of standard and sample solutions were measured at 540 nm with KFK-2 photometer. The diphenylcarbazide method[5] was used.

Reagents and solutions

All chemicals were of analytical-reagent grade. The mobile phase was prepared by dissolving tetrabutylammonium hydroxide and butyric acid (TBAB) in mixtures of specified volumes of "pure for chromatography" grade acetonitrile and demineralized water. The eluent was filtered with a 0.22-μm membrane GS filter before use. Proper pH of the eluent was obtained with sodium hydroxide solution. The flow-rate was 2 ml/min

Analyte solutions were prepared by dissolving potassium chromate, chromium sulphate and potassium sulphate in demineralized water. The Cr(VI) and SO_4^{2-} standards were prepared daily from a standard stock solution. All analytes were determined on an elemental basis.

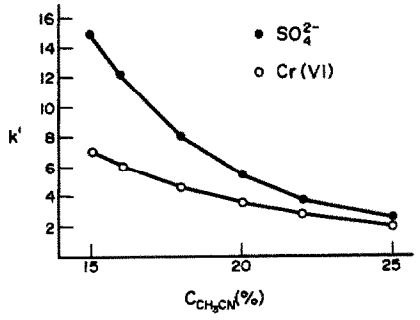

Fig. 2. Effect of CH_3CN concentration on the capacity factor (k') Eluent conditions 1mM TBAB, pH 7 0

RESULTS AND DISCUSSION

Influence of TBAB and acetonitrile concentration on Cr(VI) and SO_4^{2-} resolution

The influence of some inorganic anions which are generally present in water samples on Cr(VI) determination has been estimated first of all. According to our investigation single-charge anions F^-, Cl^-, NO_2^-, NO_3^-, $H_2PO_4^-$ at given conditions (mobile phase—1mM TBAB,75% H_2O, 25% CH_3CN, pH 7.0) are slightly retained and do not effect the determination of Cr(VI). Anions of W(VI) and Mo(VI) also do not interfere. But the selectivity of separation of SO_4^{2-} and Cr(VI) is bad, hence an optimization of the resolution of the anions has been made.

Figure 1 illustrates the effect of ion-pair reagent concentration in the mobile phase on the

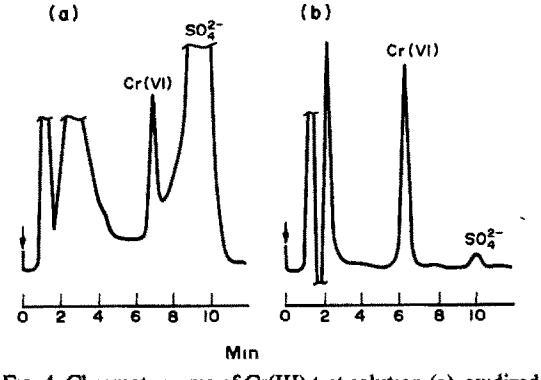

Fig 4 Chromatograms of Cr(III) test solution (a) oxidized with ammonium persulphate, (b) oxidized with hydrogen peroxide Eluent conditions 1mM TBAB, 82% H_2O, 18% CH_3CN, pH 7 0

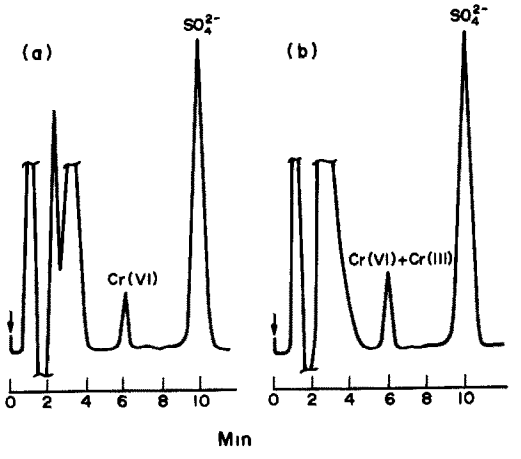

Fig 5 Chromatograms of waste water Eluent conditions as in Fig 4

retention of Cr(VI) and SO_4^{2-}. According to the results the retention and the selectivity of resolution increases with increasing TBAB concentration. The optima ion-pair reagent concentration in the mobile phase is 1.0–1.5 m*M*.

In Fig. 2 the dependence of retention of Cr(VI) and SO_4^{2-} upon CH_3CN concentration in the mobile phase is shown. The selectivity of resolution of anions tested increases with decreasing CH_3CN concentration and is optimal in the acetonitrile concentration range 15–20%.

Influence of eluent pH

Figure 3 illustrates the effect of mobile phase pH on the retention of anions tested. Retention of SO_4^{2-} ions increases with decreasing mobile phase pH. The explanation of the fact can be the decrease of mobile phase elution strength because of the protonation of the ion-pair reagent anion (butyrate) with increasing acidity (butyric acid's pK = 4.8).

There are two species of Cr(VI) in neutral medium—CrO_4^{2-} and $HCrO_4^-$ (chromic acid pK = 6.5). With increasing mobile phase acidity the equilibrium $CrO_4^{2-} + H^+ \leftrightarrows HCrO_4^-$ moves to the right, *i.e.*, the quantity of $HCrO_4^-$ ions increases. Competition of two contrary processes takes place in the system. Protonation of butyrate ions increases the retention of Cr(VI) ions. On the other hand protonation of Cr(VI) ions goes on too, therefore their charge and retention at the same time decreases. Besides that at pH < 6.5 the signal of Cr(VI) ions begins to decrease. That indicates dimerization of $HCrO_4^-$ ions with forming bichromate. Hence the dependence of Cr(VI) retention on mobile phase pH is determined by three factors: (1) protonation of butyrate ions; (2) protonation of chromate ions; (3) dimerisation of protonated chromate ions.

The optimal eluent for Cr(VI) determination is 1m*M* TBAB, 82% H_2O, 18% CH_3CN and pH 7.0.

Characteristics of Cr(VI) determination

The limit of detection of Cr(VI) was calculated as the concentration equivalent to three times the baseline noise (S/N = 3, sample injection volume of 100 μl) and is 0 1 μg/ml. The sensitivity of detection can be increased by increasing the sample loop size. The calibration plot for Cr(VI) peak area against concentration is linear in the range 0 15–20 μg/ml. Ten standard solutions containing 1.0 μg/ml Cr(VI) were analysed by the proposed method. The results had a relative standard deviation of 4.0%.

Oxidation of Cr(III) to Cr(VI)

In most cases the oxidation of Cr(III) to Cr(VI) is carried out by treating chromium with ammonium persulphate in acidic medium or with hydrogen peroxide in alkaline medium. Chromatograms of Cr(III) test solutions oxidized with ammonium persulphate (a) and with hydrogen peroxide (b) are shown in Fig. 4. If the oxidation with persulphate is carried out, a big quantity of SO_4^{2-} ions forms and the chromatographic column is overloaded. On the other hand hydrogen peroxide and it's reduction products do not interfere with the Cr(VI) determination.

Determination of Cr(III) and Cr(VI) in chromium electroplating solutions and waste waters

Two samples of solution were taken for the analysis. The first one was adjusted to pH 7–8 (if required), filtered and the amount of Cr(VI) was determined. The second one was adjusted to pH 9–10, and 0.1–0.5 ml of 30% H_2O_2 were added, the solution was boiled for 1–2 min, diluted, filtered, and the total amount of Cr(III) and Cr(VI) was determined. From the difference between the two results obtained the concentration of Cr(III) in the tested solution was calculated. Electroplating solutions were diluted 50–1000 times, and waste waters 2–5 times, or not at all. In Fig. 5 chromatograms of waste water from a television set plant are shown. Table 1 shows results of Cr(III) and Cr(VI) determination in chromium

Table 1 Cr(III) and Cr(VI) content in electroplating solutions and waste waters determined by IPC and spectrophotometric analysis

Sample	Element	Number	IPC	Spectrophotometry
Chromium electroplating solutions, *g/l*	Cr(VI)	1	12.7	12 9
		2	16.4	16 0
		3	10 5	10 2
		4	5.4	5.4
	Cr(III)	1	5 4	5 3
		2	3 9	4 1
		3	6 1	6 3
		4	1 6	1 7
Waste waters, *mg/l*	Cr(VI)	1′	6.5	6 6
		2′	4 3	4 3
		3′	2 8	3.0
		4′	4.6	4 4
	Cr(III)	1′	0 84	0.80
		2′	1 26	1 33
		3′	0 60	0 53
		4′	0 94	0 96

The chromatography time was 20 min The results obtained in this study show that the proposed IPC method can be used to determine Cr(III) and Cr(VI) in electroplating solutions and waste waters

electroplating solutions and waste waters by IPC and spectrophotometry.

REFERENCES

1. J R Rao and M S Sastri, *Z Anal Chem*, 1972, **259**, 286.
2. K. Varughese and V G Vaidya, *Anal Chim. Acta*, 1970, **50**, 176
3. N. S Frumina, E G Tregub and L. N Charlamova, *Zavodsk. Lab.*, 1969, **35**, 1297
4. T. Yamamoto, S Kadowaki and J H Carpenter, *Geochem J.*, 1974, **8**, 123.
5. Yu Lurje, *Analiticzeskaya Khimiya Promishlennych stocznych vod*, Khimiya, Moscow, 1984
6. G. G Welcher and O H Kriege, *Atom Absorpt. Newsletter*, 1969, **8**, 97
7. Z. Marczenko, *Spectrophotometric Determination of Elements*, Ellis Horwood, Chichester, 1976
8. B Salzman, *Anal Chem*, 1952, **24**, 1016.
9. H Small, T S Stevens and W S Bauman, *ibid.*, 1975, **47**, 1801.
10. Yu A. Zolotov, O A Shpigun and L A Bubchikova, *Z Anal Chem* 1983, **316**, 8
11. F. J Saleh, J H Huang and R V Lewis, *J Chromatogr Sci*, 1989, **27**, 480
12. A R Timerbaev, *Zavodsk Lab*, 1990, **56**, 19
13. R Modin and G. Schill, *Talanta*, 1975, **22**, 1017
14. A V. Padarauskas, I K Stulgene, R M Kazlauskas and O M. Petrukhin, *Zh Analit Khim*, 1991, **46**, 1169.
15. H. Hoshino and T Yotsuyanagi, *Anal Chem*, 1985, **57**, 625
16. S X. Zhang, P X Zha and S C Lin, *Talanta*, 1986, **33**, 838

Talanta, Vol 40, No 6, pp 831–840, 1993
Printed in Great Britain

0039-9140/93 $6.00 + 0.00

COMPARISON OF PHOTOMETRY AND CONDUCTOMETRY FOR THE DETERMINATION OF TOTAL CARBONATE BY GAS PERMEATION FLOW INJECTION ANALYSIS

VLASTIMIL KUBÁŇ* and PURNENDU K. DASGUPTA†
Department of Chemistry and Biochemistry, Texas Tech University, Lubbock, TX 79409-1061, U.S.A.

(*Received* 27 *October* 1992 *Accepted* 27 *October* 1992)

Summary—The experimental system involves the permeative preconcentration of CO_2 from an acidified sample through a tubular silicone rubber membrane into a suitable receptor. Procedures for measuring the CO_2 collected in the receptor by the absorbance change of an acid–base indicator incorporated in the receptor or by the conductance change of the receptor are compared. Previous theoretical considerations of the photometric system are augmented for numerical modeling and the theoretical behavior of the conductometric system is considered in detail. Experimental data generally conform to theoretical expectations. Based on either reproducibility or sensitivity, the conductometric measurement method using a solution of 1–10m*M* tris(hydroxymethylamino)methane as receptor is recommended. The interference from sulfite or sulfide can be eliminated by adding acidic permanganate to the sample, considerably more involved arrangements are necessary to eliminate interferences from cyanide.

The determination of total carbonate carbon is a crucially important measurement in a diverse variety of samples ranging from natural waters to beverages to physiological fluids. (For many real samples, total carbonate carbon is essentially the same as dissolved CO_2.) Unfortunately, specific chemistry to determine carbonate does not really exist. One reported procedure[1] utilizes the catalysis of the reaction between Cr(III) and edta by carbonate; however, even the catalyzed reaction is quite slow. This restricts the lower determination limit to $\sim 10\mu M$ and there may be interferences from chelating agents present in natural waters. Virtually all other existing procedures rely on adjustment of the sample pH to convert total carbonate to the free acid form, transport of a reproducible fraction of the CO_2 to a suitable receptor across an appropriate membrane and measurement of the transferred CO_2 via potentiometry[2], spectrophotometry[3–7] or conductometry.[8,9] Indeed, for the determination of CO_2 in biological fluids, this membrane-differentiated procedure has been in vogue since such a method was introduced for segmented flow analyzers. In many samples, most notably physiological fluids, carbonate species represent by far the dominant anions derived from a volatile weak acid and although the measurement itself is nonselective, no significant interferences are encountered. In potentiometric measurements, the transferred CO_2 changes the pH of the receptor and this pH change is directly sensed. Altogether, this measurement strategy is essentially the same as that of a potentiometric gas sensing electrode. It is obvious that the desired analytical performance parameters such as sensitivity and linear response range are dependent on the choice of the receptor. Compromises in one or the other parameter may be necessary in making such a choice, Van der Linden[10] has outlined the theoretical considerations. Photometric measurements of the pH change are less direct and further require the consideration of the choice of a suitable indicator, both in terms of its pK_a and spectral properties, as well as its concentration. These considerations have been outlined as well[10] and Cresol Red (CR) is the most commonly used indicator for this purpose. A fiber optic based fluorescence sensor using a receptor buffer and hydroxypyrene trisulfonate as the acid–base indicator has also been described.[11]

The conductometric measurement strategy is only indirectly related to a change in pH of the

*Permanent address: Department of Analytical Chemistry, Masaryk University, Kotlarska 2, CS-61137 Brno, Czechoslovakia.
†Author for correspondence

receptor. Considerations relating to the choice of a suitable buffer for conductometric sensing have never been outlined and will be considered in the next section.

Further alternatives to the above approaches are limited in scope. Precipitation as $CaCO_3$ and subsequent determination of the calcium by atomic absorption spectroscopy[12] has obvious sensitivity limitations. A polypyrrole electrode responds to carbonate[13] but it is neither completely selective nor stable in an aerobic environment.

Interferences may not be a problem in some sample types in the membrane differentiated approach, but in some others they are. Among the more common anions that can be potentially present in real samples, sulfite, sulfide and cyanide are the principal species derived from parent acids that are sufficiently volatile to be transferred across the membrane. Especially, the concurrent presence of sulfite and carbonate is common in many beverages. Linares *et al*[2] chose, for example, to determine the sum of carbonate and sulfite by potentiometry after membrane differentiated gas transfer, sulfite by an independent specific colorimetric procedure and carbonate by the difference of the two above results. Even in the absence of a specific colorimetric reaction for sulfite, it should be reasonably simple to differentiate this analyte from carbonate because SO_2 is a much stronger acid than CO_2 and by choosing a donor pH appropriately intermediate between the respective pK_a values, SO_2 transport can be vastly reduced. Differentiating CO_2 from H_2S or HCN, gases of comparable or weaker acid strength, is considerably more difficult. Adjustment of acceptor pH to limit ionization and thus discriminate against a weaker acid is of little value for gases like HCN which have a high intrinsic solubility in the unionized form.[14] To what extent it is possible to remove or minimize these interferences based on the different redox or complexing properties of these ions relative to carbonate, has not been reported.

The purpose of the present paper is to (a) delineate the theoretical considerations on the membrane-differentiated conductometric measurement technique as to the choice of a receptor, (b) compare the optimized conductometric technique with an optimized colorimetric technique and make recommendations as to the preferred procedure based on the observed results, and (c) explore the possibilities of minimizing the effects of the potential interferents.

PRINCIPLE OF THE CONDUCTOMETRIC METHOD

For simplicity, we shall consider a stationary receptor into which the CO_2 is transferred. Let us assume that the amount of the CO_2 absorbed and the receptor volume is such that there is a net increase of C_TM in total carbonate carbon in the receptor. We further assume that during the measurement cycle, the receptor solution is propelled to the detector and the peak signal is measured essentially without dispersion. There are two possible extreme compositions of the receptor: (a) water[8,9] and (b) a strong alkali such as NaOH. In the first case, the blank is negligible and the net signal may be given by:

$$S_{H_2O,net} = 1000([H^+]\lambda_{H^+} + [HCO_3^-]\lambda_{HCO_3^-} + 2[CO_3^{2-}]\lambda_{CO_3^{2-}} \quad (1)$$

where λ_i is the equivalent conductance of species i, concentrations are expressed in molar units and S is in units of μS/cm and

$$[HCO_3^-] = [H^+]K_1C_T/Q \quad (2)$$

$$[CO_3^{2-}] = K_1K_2C_T/Q \quad (3)$$

$$Q = [H^+]^2 + K_1[H^+] + K_1K_2 \quad (4)$$

K_1 and K_2 being the first and second dissociation constants of H_2CO_3. $[H^+]$ may be computed from an equation derived from the requirements of charge and mass balance:[15]

$$[H^+]^4 + K_1[H^+]^3 + (K_1K_2 - C_TK_1 - K_W)[H^+]^2 - K_1(2C_TK_2 + K_W)[H^+] - K_1K_2K_W = 0 \quad (5)$$

Figure 1(a) shows the expected signal as a function of C_T. Use of water as absorber results in high initial sensitivity and a negligible background conductance but very pronounced nonlinear response behavior. A nonlinear response behavior may be undesirable but by itself it is not the sole determinant of the utility of a method in an era where the exact response behavior can be easily stored in a computer's memory. The real problem is that the accuracy of the estimation depends acutely on the initial CO_2 content of the receptor because of the steep initial portion of the response. This initial content cannot be assumed simply from the background conductance of the receptor because in many real situations, CO_2 may not be the only adventitious impurity in the receptor water. Moreover, Fig. 1(a) assumes the efficiency of transport is independent of C_T. Because of poor ionization of CO_2 in pure water, in most real situations transmembrane transfer efficiency will decrease with increasing C_T and the overall

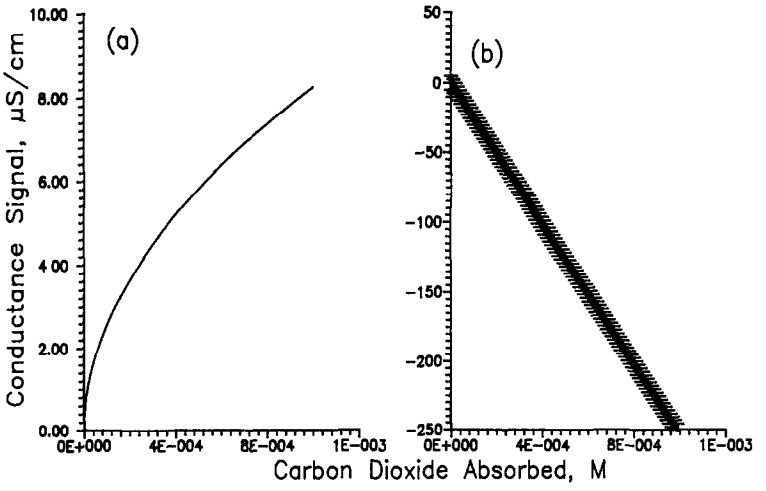

Fig 1 (a) Expected conductance signal with pure water as absorber, (b) expected conductance signal with pure NaOH as absorber

nonlinearity in response behavior would be much larger.

In contrast, the use of an absorber like NaOH results in conversion of the absorbed C_T into carbonate. If the original concentration of NaOH in the receptor is $C_{NaOH}M$, the background conductance $S_{Blank,NaOH}$ is given by

$$S_{Blank,NaOH} = 1000(\lambda_{Na^+} + \lambda_{OH^-})C_{NaOH} \quad (6)$$

When C_TM CO_2 is absorbed and $2C_TM$ NaOH is converted to Na_2CO_3 (obligatorily, $C_{NaOH} > 2C_T$), the sample conductance is:

$$S_{sample,NaOH} = 1000(\lambda_{Na^+}C_{NaOH} + \lambda_{OH^-}(C_{NaOH} - 2C_T) + 2\lambda_{CO_3^{2-}}C_T) \quad (7)$$

The net signal is therefore

$$S_{net,NaOH} = 2000(\lambda_{CO_3^{2-}} - \lambda_{OH^-})C_T \quad (8)$$

Note that not only is the net signal strictly linear with C_T, but the presence of adventitious impurities like NaCl or Na_2CO_3 in the receptor NaOH would make no difference in equation (8). It should also be noted that $\lambda_{OH^-} > \lambda_{CO_3^{2-}}$ *i.e.* S_{net} is negative. The necessity to cover some minimum range of C_T requires that some minimum concentration of NaOH be used as absorber. NaOH is highly conductive and results in a high background conductance. Consequently, although the sensitivity (slope of the calibration plot) given by equation (8) is high, the noise is also high and limits of detection are not necessarily improved. If we assume a noise equivalent of 1% of the background conductance, the situation is depicted in Fig. 1(b) for a 2mM NaOH absorber and the expected noise is shown as an error bar.

It is now obvious that a desirable absorber should have a low initial background conductance, good sensitivity and preferably linear response behavior. Can this be achieved with an appropriate buffer or weak base solution? Let us consider the solution of a weak base B with a dissociation constant K_a for its conjugate acid. The background conductance of such a receptor is shown in Fig. 2 as a function of pK_a and concentration. For clarity, the results are shown both in linear and logarithmic scales. It is obvious that too large a background conductance is detrimental in terms of achieving a good S/N. Therefore we consider next the effect of absorption of CO_2 by an absorber B with the pK_a of BH^+ being $\leqslant 9$. The conductance of the absorber solution after absorption of C_TM CO_2 is given by

$$S_{sample,B} = 1000(\lambda_{BH^+}[BH^+] + \lambda_{OH^-}[OH^-] + \lambda_{H^+}[H^+] + \lambda_{HCO_3^-}[HCO_3^-] + 2\lambda_{CO_3^{2-}}[CO_3^{2-}]) \quad (9)$$

The individual species concentrations are given by the standard acid–base equilibrium expressions:

$$[BH^+] = C_B[H^+]/(K_a + [H^+]). \quad (10)$$

where C_B is the total concentration of B and K_a is the dissociation constant of BH^+, and $[HCO_3^-]$ and $[CO_3^{2-}]$ have been given by equations (2) and (3). The relevant polynomial in $[H^+]$ can be solved by numerical iteration from the charge balance equation

$$[H^+] + [BH^+] - [OH^-] - [HCO_3^-] - 2[CO_3^{2-}] = 0 \quad (11)$$

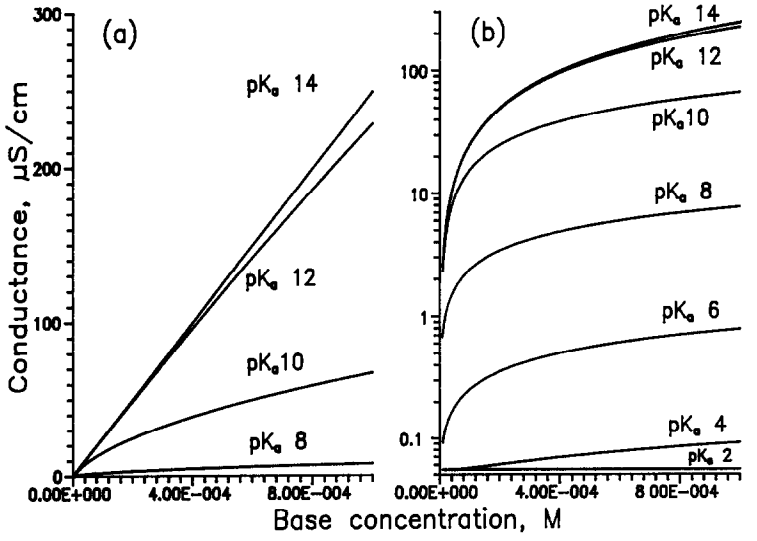

Fig. 2. Background conductance values of different base solutions as receptor as a function of pK$_a$ of the conjugate acid BH$^+$ and concentration The equivalent conductance of BH$^+$ is assumed to be 50 (a) Linear ordinate, (b) logarithmic ordinate

and the value of equation (9) can thus be computed. The net signal can be computed to be

$$S_{\text{net,B}} = S_{\text{sample,B}} - S_{\text{Blank,B}}. \qquad (12)$$

where $S_{\text{Blank,B}}$ is the value of equation (9) at $C_T = 0$. $S_{\text{sample,B}}$ is shown plotted in Fig. 3 for different pK$_a$ values, C_B was assumed to be $0.005M$ and λ_{BH^+} was assumed to be 50. The results indicate that in terms of linearity of response and background conductance, experimentation with bases with the pK$_a$ value of BH$^+$ being in the range of 6–8 may be recommended. However, it is actually inappropriate to assume that the blank receptor solution contains no absorbed CO_2. In a real situation, it is more practical to assume that the original receptor contains some initial dissolved CO_2, to the extent of $C_{T,i}$ molar To this, the sample adds additional CO_2 to the extent of C_T molar. Thus in computing $S_{\text{sample,B}}$ and $S_{\text{Blank,B}}$, respectively,

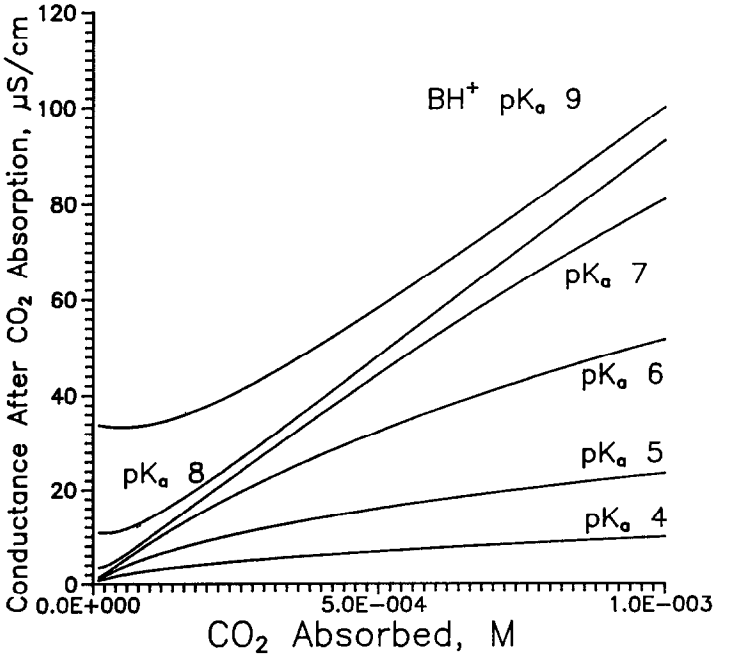

Fig. 3. Conductance of base receptor solutions upon CO_2 absorption The base concentration is assumed to be 5mM, λ_{BH^+} is assumed to be 50 and the pK$_a$ of BH$^+$ is indicated

$C_{T,i} + C_T$ and $C_{T,i}$ need to be substituted for C_T in equations (9)–(12). Consideration of Fig. 3 will indicate that the presence of some initial dissolved CO_2, up to the extent of *ca.* $2 \times 10^{-4}M$, will actually improve the linearity of response to further additions of CO_2 for receptors with conjugate acid pK_a values of $\geqslant 7$. It should also be noted that in Fig. 3 absorption efficiency has not been considered as a function of receptor pK_a. The pH of a 1mM solution of a weak base receptor varies from 8.5 to 9.5 as the pK_a varies from 6 to 8. At the low end of this pH scale, efficient absorption of CO_2 may not occur due to saturation of the solution at the membrane–receptor interface.

EXPERIMENTAL

Chemicals

Neutral Red (NR) and CR, were obtained from Aldrich Chemical and used without further purification. Buffer substances included 4-methylpyridine (4-Picoline, pK_a 6.1), bis-(2-hydroxymethyl)-imino-tris(hydroxymethyl)-methane (Bis–Tris, pK_a 6.5), 1,3-bis[tris(hydroxymethyl)methylamino]propane (BTP, pK_{a1} 6.8, pK_{a2} 9.0), morpholinopropanesulfonic acid (MOPS, pK_a 7.2), Tris(hydroxymethyl)-aminomethane (Tris, pK_a 8.1), and sodium carbonate/bicarbonate (all from Sigma/Aldrich Chemical). For unbuffered receptor solutions, carbonate free NaOH was added to 20–50μM indicator solutions to attain the desired pH or to water until the desired background conductivity was reached. For the donor stream, phthalate (0.05M, pH 4) and acetate (0.1M, pH 4.9) and 0.5M H_3PO_4 were tested.

Equipment

The manifold for the flow injection determination is shown in Fig. 4. All systems used the membrane permeation-preconcentration mode. In the colorimetric detection scheme, the sample and the modifier/conditioning reagent (0.5M H_3PO_4) are pumped together (model XV peristaltic pump, Alitea U.S.A., Medina, WA), mixed in a mixing coil MC and proceed through the jacket of a silicone membrane permeation device PU to waste. The active element of PU is a silicone membrane tube 120 mm long, 0.4 mm in i.d. and 0.6 mm in o.d.[16] PU constitutes the loop of the injection valve V and when it is switched to the inject position, the contents of PU are flushed by the receptor/indicator solution to the optical detector (Kratos Model 757). The amount of sample injected is dependent on the length of time the valve is in the load mode; except as indicated, load periods of 1 and 5 min were, respectively used to obtain the data reported here for the conductometric and photometric procedures. All conduit tubing were 0.7 mm in i.d.

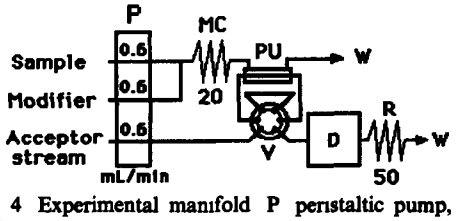

Fig. 4 Experimental manifold P peristaltic pump, MC: mixing coil, PU: silicone membrane permeation unit, V: six-port rotary valve, D: detector, R: restriction tubing, W: waste. Tubing length in cm is indicated (0.7 mm i.d.)

The conductometric detection manifold is identical, except that the membrane length was 18 cm unless otherwise noted and a model CDM-I conductivity detector (Dionex Corp.) was used. In experiments pertaining to the elimination of potential interferences, a solution of 100 mg/l $KMnO_4$ in 0.1M H_2SO_4 was used as the conditioning reagent. Depending on the quality of the H_2SO_4 used, it may be necessary to boil this solution to remove volatile acid gases before the addition of $KMnO_4$.

Software

MINSQ (Micromath Scientific Software, Salt Lake City, UT), a nonlinear least squares fitting routine that utilizes the Marquardt–Levenberg algorithm, was used for model fitting. The results were exported to GRAPHER (Golden Software, Golden, CO) for graphical presentation.

RESULTS AND DISCUSSION

Photometric determination

Based on considerations previously outlined,[6,14] the receptor pH should be minimally 2 pK_a units above that of the (first) dissociation constant of the permeant acid gas of interest. The pK_1 of H_2CO_3 being 6.3, a carbonate–bicarbonate buffer with a pH of *ca.* $\geqslant 8.3$ is therefore commonly used as receptor. Sensitivity considerations dictate that pK_{In} should not be drastically different from the receptor pH. Indeed, CR, the most common indicator used for the determination of CO_2, has a pK_{In} of 8.3. The base form of CR ($\lambda_{max} = 572$ nm)

absorbs more strongly than the acid form ($\lambda_{max} = 434$ nm). Monitoring a decrease in absorbance due to CO_2 transfer by following the absorption at 572 nm is more sensitive than monitoring an increase in absorbance at 434 nm. However, the background absorbance and baseline noise is also higher. In principle, NR has more desirable spectral characteristics for this application because the acid form ($\lambda_{max} = 530$ nm) absorbs more strongly than the base form ($\lambda_{max} = 450$ nm) and the increase in absorption due to CO_2 absorption can therefore be more sensitively monitored by measuring the acid form. However, NR has a pK_{In} of ~7, lower than that optimally desired. It has been previously reported[17] that the pK_{In} of NR is increased in the presence of anionic surfactants—the effective pK_{In} is 7.30, 7.82, 8.03 and 8.25, respectively in the presence of 1, 3, 5 and 10m*M* sodium dodecylsulfate (SDS) in a medium containing 10% ethanol. We experimented therefore with a receptor solution containing NR and 1m*M* SDS. Although the sensitivity did increase relative to a receptor without SDS, the extent was marginal (*ca.* 10%) and additional problems appeared because of vastly enhanced tendencies of bubble formation within the conduits or the permeation device. This in turn increased baseline noise and deteriorated reproducibility. It is interesting to note that the lack of a greater increase in sensitivity could be traced back to slower kinetics of the overall indicator reaction in the micellar medium. This avenue of investigation was therefore abandoned and further experiments continued with receptor buffers containing CR without any surfactant.

The high permeability of silicone membranes to carbon dioxide and oxygen is well known. When dimethylsilicone membranes were first introduced by General Electric Co., a particularly well publicized experiment showed the prolonged survival of rodents put in cages completely covered with silicone membrane, even when the latter were put under water.[18] A high permeability of the membrane to the analyte gas results in membrane limited transport only at high donor flow rates. Indeed, this is experimentally observed. As Fig. 5(a) indicates, the system does not become membrane transport limited until the donor flow is well in excess of 0.5 ml/min.

The membrane permeation system shows relatively rapid response, as indicated in Fig. 5(b). When the sample is changed from a blank to standard or vice-versa, full plateau response is attained by the second injection. The short term reproducibility of repeat injections of the same sample is excellent (rsd = 0.2%, $n = 15$). These characteristics are independent of the (colorimetric or conductometric) detection mode used.

The response of the buffer/indicator reaction system was studied at 50μ*M* indicator concentration at a constant total buffer concentration of 1m*M* (sodium carbonate + bicarbonate) with varying pH and also at a constant buffer pH of 9.0 with varying buffer concentration of

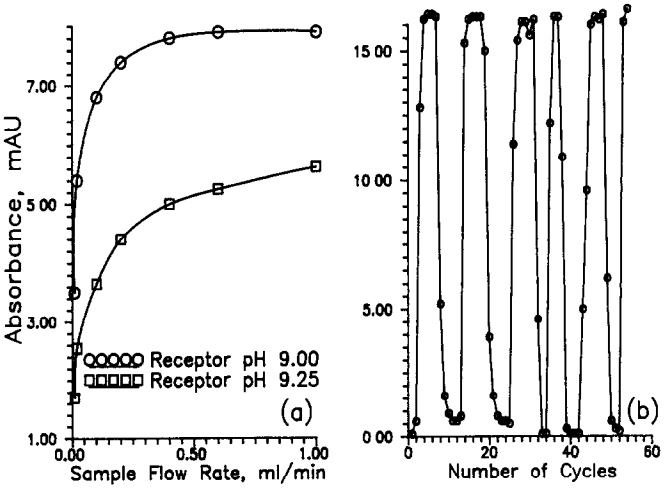

Fig. 5. Colorimetric determination system (a) Response as a function of donor flow rate, 1m*M* carbonate buffer of indicated pH, 50μ*M* CR, 3 min preconcentration of sample containing 1m*M* C_T, detection at 434 nm (b) Temporal response pattern for repeated analysis and alternation between a sample (0.25m*M* in C_T) and a blank Successive points plotted are 3 min apart Other conditions same as above

0–5mM. The results are shown in Fig. 6. The system can also be modeled numerically:

$$[Na^+] = C_{T,in}(K_1[H^+]_{in} + K_1K_2)/([H^+]_{in}^2 + K_1[H^+]_{in} + K_1K_2) + K_w/[H^+]_{in} + [In^-]_{in} - [H^+]_{in} \quad (13)$$

Where the subscript in denotes initial conditions, $C_{T,in}$ being the initial buffer concentration. The total indicator concentration C_{In} is distributed as

$$[In^-] = C_{In}K_{In}/([H^+] + K_{In}) \quad (14)$$

$$[HIn] = C_{In}[H^+]/([H^+] + K_{In}) \quad (15)$$

After the absorption of CO_2, the final concentration of total carbonate is

$$C_{T,fin} = C_{T,in} + [C_{T,analyte}]f \quad (16)$$

where a fraction f of the analyte C_T is transferred to the receptor. This fraction f can also be presumed to include the effects of dispersion in the flow injection system. $[H^+]_{fin}$ is then computed from

$$[H^+]_{fin} = C_{T,fin}(K_1[H^+]_{fin} + 2K_1K_2)/([H^+]_{fin}^2 + K_1[H^+]_{fin} + K_1K_2) + K_w/[H^+]_{fin} + C_{In}K_{In}/([H^+]_{fin} + K_{In}) - [Na^+] \quad (17)$$

and thence the absorbance signal can be computed:

$$Abs = C_{In}([H^+]_{fin}/(K_{In} + [H^+]_{fin}) - [H^+]_{in}/(K_{In} + [H^+]_{in}))\Delta\epsilon \quad (18)$$

where $\Delta\epsilon$ is the difference in molar absorptivities of the indicator in the acid and base forms, respectively at the wavelength of interest. Two of the data sets in each of Fig 6(a) and (b) were subjected to nonlinear least squares fitting with f and $\Delta\epsilon$ being adjustable parameters. Note that in each case, the two experimental data sets were treated collectively as one and the results shown are from a single fit. These results illustrate the general agreement of experimental results with theoretical expectations and also point out the problems inherent in photometric measurement of this type: nonlinear response and an acute dependence of the response on buffer concentration and its initial pH. In our experience, it is very difficult to reproduce the response behavior on a day-to-day basis, because of unavoidable CO_2 absorption by the receptor buffer. Accordingly, it is also difficult to quantitatively reproduce the results as new receptor solutions are made.

Conductometric determination

Figure 7(a) shows the results of experiments with the receptor being pure water and NaOH solutions of two different concentrations. The predicted linear response behavior was observed for the higher concentration NaOH absorber (the approximate concentration of the NaOH receptor in millimolar can be obtained by dividing the cited background conductance by 250; however, since some CO_2 contamination is unavoidable, it is more convenient to cite it in

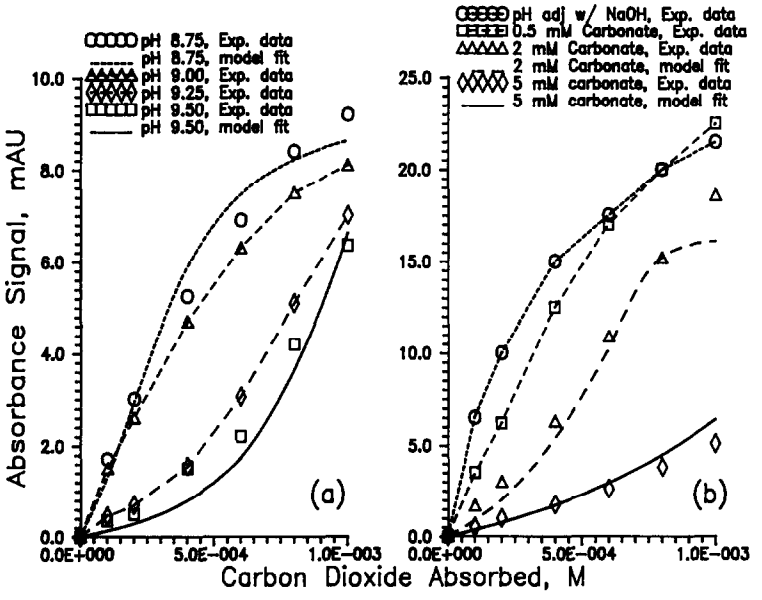

Fig. 6. Colorimetric system, conditions as in Fig 5 except 5 min preconcentration time (a) 1mM carbonate buffer, pH as indicated; (b) pH 9.0 carbonate buffer, concentration as indicated.

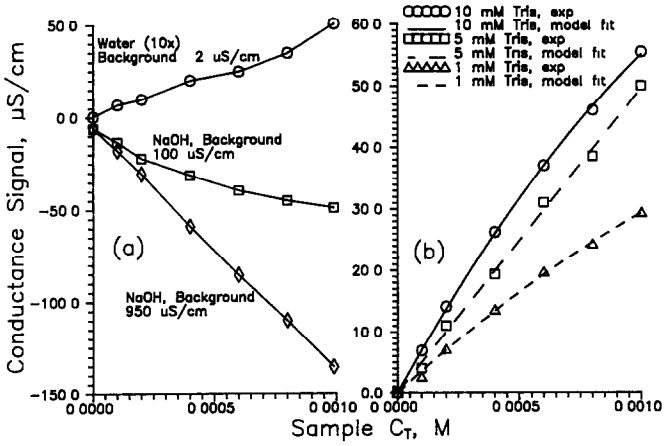

Fig 7 Conductometric system (a) Response using pure water and NaOH solutions as absorber (12 cm membrane) Note that the response is magnified by 10 for the water absorber (b) Response using different concentrations of Tris as absorber The lines shown are the best model fits to the experimental data shown as the points

terms of background conductance), over the C_T range studied but the absolute noise level was also high, as expected. With the lower concentration NaOH absorber, the response is linear only at low concentrations of C_T and even then the CO_2 already present in the absorber leads to a lower calibration slope than for the higher concentration absorber. At higher C_T values, C_T exceeds the absorber concentration and response nonlinearity becomes very pronounced. Day-to-day reproducibility of the signal with a low concentration absorber is also poor. The same problems relating to reproducibility and linearity of response also plagues the use of pure water as absorber. However, in this case even though the absolute sensitivity at higher C_T levels is quite low (note that the response is plotted with tenfold magnification), the background conductance is so low that background noise is very small; if the limit of detection was the only criterion, pure water should be the absorber of choice

Figure 7(b) shows the experimental results at three different concentrations of Tris as absorber, the most useful of the weak base absorbers studied, as detailed below. The points plotted are the experimental observations and the lines drawn represent best fit of the data to the model represented by equations (9)–(12) and (16) as modified by the allowance of a finite initial concentration of CO_2 already present in the absorber ($C_{T,i}$, *vide supra*). The CO_2 transfer efficiency through the membrane, [f, see equation (16)] and $C_{T,i}$ are the adjustable parameters the best fit values of which are obtained by the fitting procedure. It would appear that a satisfactory agreement exists between the model expectations and the observed results (λ_{BH^+} was assumed to be 40). However, the best fit values for f also consistently increase with increasing absorber concentration (that concomitantly results in higher initial absorber pH); this is not part of the model assumptions. The reason for this behavior is considered below along with the results observed for other absorbers. Meanwhile, although the absolute value of the response with a Tris absorber is substantially smaller than with NaOH, baseline noise is so much improved that relative reproducibility in the determination range tested is significantly better (rsd 0.5–1% for Tris *vs.* $\geqslant$2% for the higher concentration NaOH absorber). Comparable reproducibilities are also observed with other weak base absorbers. The response with the Tris absorbers are also very close to linear. We made no special efforts to determine limits of detection because the preconcentration protocol used in the present system can easily be extended to greater sampling periods for improving detection limits. It should be noted, however, that because of surface stagnation (*vide infra*), the relationship between the preconcentration period and the observed signal is not linear.

Figure 8(a) shows the experimental results obtained with several different receptors of different pK_a, all at a concentration of 1m*M*. Note that all the absorbers other than MOPS are of the free base type, thus the conductance is relatively low when the free base is put in solution (BTP is a diprotic base with a pK_2 of 9, the background conductance in this case is

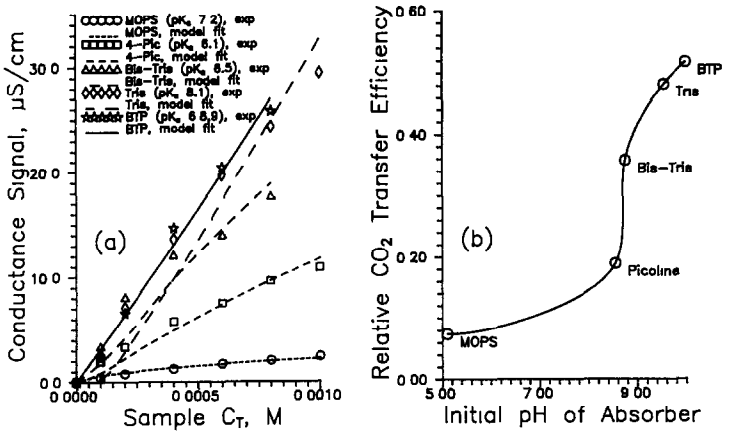

Fig 8 Conductometric system (a) Response using 1mM solutions of different weak bases (MOPS is used in zwitterionic form) as absorber (b) The best model fit values of the CO_2 transfer efficiency [f, equation (16)] as a function of the initial absorber pH

not negligible; the model equations were also modified for BTP to take into account its diprotic nature). MOPs, on the other hand, is a zwitterionic substance. The base form (*e.g.* the alkali metal salt) has a high background conductance and is not attractive. Experiments were therefore conducted with the zwitterionic form itself, even though it was recognized that this would result in a slightly acid absorber pH. Again, in most cases the experimental data (shown as the points) were reasonably fitted by the model (λ_{BH+} was assumed to be 40, 40, 35 and 30 for 4-picoline, Tris, Bis–Tris; λ_{BH+} was assumed to be 60 for BTP and the mobility of either the cationic or anionic form of MOPS was assumed to be 30). The best fit values of f are shown in Fig. 8(b) as a function of the initial absorber pH. The sigmoid dependence of the transfer efficiency on this parameter is clear. This suggests strongly that boundary layer stagnation can occur at the membrane–receptor interface. Such a dependence of f on the initial absorber pH would not have been observed if liquid phase diffusion within the receptor was sufficiently fast relative to the membrane-permeated flux of CO_2 for homogeneous equilibrium to exist in the receptor phase.

Interferences

If no measures are taken, sulfite, sulfide and cyanide all interfere in either the colorimetric or the conductometric procedure. However, the extent of response is not equal on an equimolar basis because of differences in the pK_a of the different acids as well as their different permeabilities through silicone rubber. For example, in the colorimetric procedure using 0.5M H_3PO_4 as the modifier, 1mM $NaHCO_3$ produces a signal of 15.7 mAU (3 min preconcentration, 2mM $NaHCO_3$ receptor) while the same signal is elicited by 0.68mM Na_2S. For KCN, 3.8mM produces a signal of 26 mAU and 0.75mM $NaHSO_3$ produces a much smaller signal of 2.15 mAU Similarly in the conductometric procedure using 1 mS/cm NaOH as absorber and 0.5M H_3PO_4 modifier, $NaHCO_3$, Na_2S, KCN and $NaHSO_3$ (all at 1mM concentration) respectively elicited signals of 149, 103, 17.1 and 17 μS/cm.

The use of a higher pH modifier, *e.g.* a 0.05M pH 4 potassium acid phthalate buffer, did not perceptibly reduce the signal from an $NaHCO_3$ sample. However, it was effective in reducing the interference from $NaHSO_3$ (by 75%, as measured by the colorimetric method), signals from cyanide or sulfide were predictably undiminished. It is noteworthy that the background signal was perceptibly affected when an acetate buffer (0.1mM, pH 4.9) was used as the modifier, presumably due to the permeation of volatile acetic acid. Further experiments to reduce the influence of interferents were limited to the conductometric procedure using 10mM Tris as the receptor. The interference from both sulfide and sulfite was completely eliminated using H_2SO_4–$KMnO_4$ as the modifier. However, the interference from cyanide continued unabated. Using a modifier of H_2O_2 (1 g/l) was found to be equally ineffective for cyanide. By adding an additional pumping channel to pump a metal salt [1mM $NiSO_4$ or $Fe_2(SO_4)_3$] at the same rate as the sample (0.6 ml/min) and merging this with the sample, followed by an 0.7 × 500 mm mixing coil prior to the existing

manifold shown in Fig. 4 (which then adds H_3PO_4 and so on), a study was carried out to see if the cyanide could be effectively removed by chelation. The reaction with Fe(III) was too slow to be of much utility; however, the use of Ni(II) eliminated >90% of the initial signal. Unfortunately, if sulfide is present, NiS is precipitated in the manifold, leading to complications. We find that cyanide can be effectively removed by oxidation only under alkaline conditions. To adopt this successfully in the present case, a relatively complex manifold is required. Alkaline permanganate prepared *in situ* in the manifold (the reagent is unstable; alkaline ferricyanide is ineffective and alkaline hypochlorite itself leads to volatile acid gases upon subsequent acidification), is added to the sample and this mixture is acidified before preconcentration. Details of this approach will be described in a subsequent publication addressing the measurement of CO_2 in process gases in the presence of SO_2, H_2S and HCN. It may also be noted that based on the differences between the pK of HCN and pK_1 of H_2CO_3, a two stage pH-based discrimination[14] between carbonate and cyanide is also possible. However, the required arrangement is not simple, either.

CONCLUSIONS

Measurement of total dissolved CO_2 in aqueous samples can be accomplished by a procedure involving acidification of the sample, permeation of the CO_2 through a silicone rubber membrane, and collection in a suitable receptor. Relative to the use of a photometric method utilizing an indicator solution in a carbonate–bicarbonate buffer, a conductometric procedure with a weak base receptor solution provides better day-to-day reproducibility, sensitivity and detection limits. A number of different weak bases may be useful for the purpose; based on our experience and its inexpensive availability in a pure form, Tris solutions (1–10m*M*) are recommended. The interference from sulfide and sulfite can be eliminated by using H_2SO_4–$KMnO_4$ as the sample acidifying/oxidizing agent. Significantly more elaborate efforts are required to eliminate the interference from cyanide

Acknowledgements—This work was supported by an unrestricted grant from Shell Development, Houston, TX. We appreciate the inputs of Randy Shearer and Don Olson of Shell Development. We also gratefully acknowledge the help of Charles J. Patton, U.S. Geological Survey, Arvada, CO for help in locating the literature on early continuous flow procedures for the measurement of dissolved CO_2. Research on the use of membranes for the analysis of ionic/ionizable substances is also partially supported by the office of Basic Energy Sciences, U.S. Department of Energy (USDOE) through DE-FG05-84ER13281. However, this manuscript has not been subject to review by the USDOE and no endorsements should be inferred.

REFERENCES

1 V. I. Shlyamin, O. N. Obrezkov, O. A. Shpigun and Yu. A. Zolotov, *Zh. Anal. Khim.*, 1991, **46**, 76
2 P. Linares, M. D. Luque de Castro and M. Valcárcel, *Anal. Chim. Acta*, 1989, *225*, 443
3 W. J. Seifert, E. Seifter, D. Kamboses and A. Chenas, *Advances in Automated Analysis*, Technicon International Congress, 1970, p. 509, Thurman Associates, Miami, FL, 1971
4 M. A. Kenny and M. H. Cheng, *Clin. Chem.*, 1972, **18**, 352.
5 H. Baadenhuijsen and H. E. H. Seuren-Jacobs, *Clin. Chem.*, 1979, **25**, 443
6 W. E. van der Linden, *Anal. Chim. Acta*, 1983, **151**, 359
7 S. Motomizu, K. Toei, T. Kuwaki and M. Oshima, *Anal. Chem.*, 1987, **59**, 2930
8 R. M. Carlson, *Anal. Chem.*, 1978, **50**, 1528
9 J. J. R. Rohwedder and C. Pasquini, *Analyst*, 1991, **116**, 841
10 W. E. van der Linden, *Anal. Chim. Acta*, 1983, **155**, 273
11 O. S. Wolfbeis, L. J. Weis, M. J. P. Leiner and W. E. Ziegler, *Anal. Chem.*, 1988, **60**, 2028
12 F. T. Esmadi, M. A. Kharoaf and A. S. Attiyat, *Talanta*, 1990, **12**, 1123.
13 Y. Ikariyama and W. R. Heineman, *Anal. Chem.*, 1986, **58**, 1803
14 V. Kubáň and P. K. Dasgupta, *Anal. Chem.*, 1992, **64**, 1106
15 W. Stumm and J. J. Morgan, *Aquatic Chemistry*, 2nd Ed., p. 138, Wiley, New York, 1981
16 V. Kubáň, P. K. Dasgupta and J. N. Marx, *Anal. Chem.*, 1992, **64**, 36
17 J. Jurasová and V. Kubáň, *Coll. Czech. Chem. Commun.*, 1987, **52**, 2401
18 *General Electric Permselective Membranes*, Bulletin GEA-8685A, General Electric Co., Schenectady, NY, 1970

Talanta, Vol 40, No 6, pp 841–844, 1993
Printed in Great Britain

0039-9140/93 $6 00 + 0 00

IODOMETRIC MICROGRAM DETERMINATION OF CHROMIUM(III) AND (VI) BY USE OF CHEMICAL AMPLIFICATION REACTIONS

A M EL-WAKIL, A B FARAG and M. S EL-NAHAS
Department of Chemistry, Faculty of Science, Mansoura University, Mansoura, Egypt

(*Received* 27 *April* 1992 *Revised* 6 *October* 1992 *Accepted* 23 *October* 1992)

Summary—A simple, rapid and sensitive method is described for the iodometric determination of microgram amounts of chromium(III), based on the oxidation of chromium(III) with periodate at pH 3 2, removal of the unreacted periodate by masking with molybdate and subsequent iodometric determination of the liberated iodate Chromium(VI) can be determined by this method after prior reduction to chromium(III) with sodium sulphite The method can also be used for the analysis of organochromium compounds

The determination of chromium(III) and (VI) in environmental and biological systems is of considerable interest.[1–3] Chromium(VI) may enter the drinking water distribution system from the corrosion inhibitors used in water pipes.[3] Chromium(III) and (VI) may also exist in very low concentrations in natural waters.[4]

Although some instrumental methods have been described [2–4] for the estimation of trace concentrations of chromium, iodometric amplification procedures, with their simplicity and sensitivity, [5–11] are still of special attraction and Besada[12] has described such a method for the determination of chromium(III).

The aim of the present study was to develop a rapid and accurate iodometric method for the determination of microgram amounts of chromium(III) and (VI) in aqueous solution and to explore the critical role of pH in the reactions used.

EXPERIMENTAL

Reagents

Unless otherwise specified, all reagents were of analytical reagent grade.

Ammonium molybdate solution. A 100-mg/ml aqueous solution of $(NH_4)_6Mo_7O_{24}.4H_2O$.

Potassium periodate solution. Prepared by dissolving 1.75 g of the recrystallized reagent in 500 ml of distilled water containing 3 ml of saturated borax solution.

*Sodium thiosulphate solution, 0.005*M. Standardized against potassium iodate solution.

Sodium sulphite solution. A saturated aqueous solution of the anhydrous salt.

Buffer solution, pH 3.2. Prepared by mixing 150 ml of glacial acetic acid with ~100 ml of water, then adjusting the pH with concentrated sodium acetate solution and diluting with water to 500 ml.

Chromium(VI) stock solution. Prepared by dissolving 0.2450 g of potassium dichromate in water acidified with two drops of concentrated sulphuric acid and diluting to volume in a 500-ml standard flask. Test solutions were prepared by further dilution.

Chromium(III) stock solution. Prepared by adding 0.5–1 ml of saturated sodium sulphite solution to a standard solution of chromium(VI), acidifying with 1 ml of 5*M* sulphuric acid, then removing the excess of sulphurous acid by boiling for 1–2 min. The pH was adjusted to around 3 with dilute sodium hydroxide solution.

Procedures

Determination of chromium(III). Transfer a known volume of chromium(III) solution (0.5–5 ml, containing 20–310 μg of Cr) to a 100-ml conical flask. Add 5 ml of potassium periodate solution, immediately adjust the pH to 3.0–3.2 by adding the buffer solution directly, and keep the solution for 0.5 hr at room temperature (20–27°). This method is easier and faster, but suffers from slightly higher blank values than those obtained by the alternative method, which is a little time-consuming, of

Table 1 Determination of various amounts of Cr(III) in aqueous media

Cr taken, μg	Cr* found, μg	Note
20 8	21 1 ± 0.8	Determination of Cr(III) after reduction of
41 6	41 0 ± 0 8	of Cr(VI) with sulphite
104 0	104 3 ± 0 7	
208 0	208.3 ± 0 9	
312 0	311 7 ± 0 7	
25 0	25 1 ± 0 8	Determination of Cr(III) in presence of Cr(VI)
50 0	50 3 ± 0 7	Cr(III) = 25–300 μg
100 0	100 2 ± 0 8	Cr(VI) = 100 μg
200.0	199.6 ± 0 7	
300 0	300 1 ± 0 6	
25 0	24 9 ± 0 6	Cr(III) = 25 μg, Cr(VI) = 25–300 μg
100 0	100 0 ± 0 6	Cr(III) = 100 μg; Cr(VI) = 25–300 μg
300 0	300 1 ± 0 6	Cr(III) = 300 μg, Cr(VI) = 25–300 μg

*Average ± standard deviation (5 determinations)

adjustment to pH 3.0–3.2 with dilute sulphuric acid and/or sodium hydroxide solution and then leaving the reaction mixture for 0.5 hr at room temperature. At the end of this interval, in either case add 2 ml of the acetate buffer before adding 2 ml of the ammonium molybdate solution to mask the unreacted periodate. It should be remembered that heating increase the rate of oxidation of chromium(III) to chromium(VI) but also causes a concomitant increase in the blank values. Add a few crystals (20–40 mg) of solid potassium iodide and after a few minutes titrate the liberated iodine with sodium thiosulphate solution. Run a blank under the same conditions and apply any correction necessary.

Determination of chromium(VI). To a known volume of chromium(VI) solution (1–10 ml) containing up to 310 μg of chromium, in a 100-ml conical flask, add 0.5–1 ml of saturated sodium sulphite solution followed by 1 ml of 5*M* sulphuric acid. After about 1 min, boil the solution for 1 min to remove the excess of sulphurous acid. Adjust the pH to ~3 with dilute sodium hydroxide solution and determine the chromium(III) as above.

Analysis of chromium(III) and (VI) mixtures. Analyse an aliquot of the mixture according to the chromium(III) procedure; the volume of standard sodium thiosulphate solution required (*A* ml) is equivalent to the chromium(III). Treat another aliquot as for determination of chromium(VI), to obtain the sum of Cr(III) + Cr(VI) from the volume of standard sodium thiosulphate required (*B* ml). The volume of thiosulphate equivalent to the chromium(VI) present in the original mixture will be *B*–*A* ml.

Determination of chromium in organic compounds. Weigh accurately about 2 mg of sample, and digest it with 5 ml of saturated potassium chlorate solution and 5 ml of concentrated nitric acid, then evaporate the solution to dryness. Take up the salts in 5 ml of distilled water and follow the procedure for determination of chromium(VI).

RESULTS AND DISCUSSION

Besada[12] has published a method for iodometric determination of chromium(III), based on oxidation of Cr(III) to Cr(VI) with potassium periodate, masking the unreacted periodate with molybdate and subsequent iodometric determination of the chromium(VI) and iodate.

The oxidation of chromium(III) with periodate proceeds according to

$$2Cr^{3+} + 3IO_4^- + 4H_2O = Cr_2O_7^{2-} + 3IO_3^- + 8H^+ \quad (1)$$

which indicates that the reaction will be promoted by the use of low acidity. The iodate and

Table 2 Determination of sum of Cr(III) and Cr(VI) in aqueous media

Cr(III) + Cr(VI) taken, μg	Cr* found, μg
25 + 100	125 1 ± 0 8
50 + 100	150 5 ± 0 7
100 + 100	199.9 ± 0 8
200 + 100	299 9 ± 0 8

*Average ± standard deviation (5 determinations)

chromium(VI) liberated can oxidize iodide according to

$$IO_3^- + 5I^- + 6H^+ = 3I_2 + 3H_2O \quad (2)$$

$$Cr_2O_7^{2-} + 6I^- + 14H^+ = 2Cr^{3+} + 3I_2 + 7H_2O. \quad (3)$$

If both reactions (2) and (3) can occur, each initial chromium(III) ion leads to the liberation of 12 atoms of iodine. It has been found that reaction (1) is complete at room temperature within 0.5 hr in the pH range 3.1–5.5, but the rate of oxidation is lower at pH 2.9 and markedly decreased at pH 2.2. In addition, in reaction (2) the release of iodine for subsequent determination is remarkably slow at pH $\geq$ 4 but quantitative at pH $\sim$ 3. A comprehensive study on the critical role of pH in reaction (3) revealed some facts which are worth mentioning and should be considered in any similar investigations. Reaction (3) is strongly pH-dependent, as can be predicted from the standard redox potentials concerned, and is very slow at pH $\geq$ 2. It is quantitative and instantaneous at pH $\leq$ 1, but under these conditions the molybdate–periodate complex is at least partially decomposed,[13] and erroneously high results are obtained because of reaction of the liberated periodate with iodide. Aerial oxidation of iodide can also occur under these conditions. The blanks will be high and variable. However, reaction (3) (in acetate media) proceeds slowly at pH 2.2, taking a relatively long time for completion ($\sim$2.5 hr) and being accompanied by increased blank values, and proceeds extremely slowly at pH $\geq$ 3.1. It is interesting that in acidic media free from acetate ion and with pH adjusted with sulphuric acid, reaction (3) is even slower at pH 2.2. than the same reaction at pH 2.2. in the presence of acetate buffer. A pH around 3.2 is the best choice, giving a reasonable rate for reaction (1), meeting the recommendations of Burnel for the masking reaction[13] and allowing completion of the determination at a pH at which reaction (3) is not operative. There will then be only 9 atoms of iodine released per Cr(III) ion, but the method can be employed for the determination of chromium(III) in the presence of chromium(VI), or for the sum of the two after reduction of the chromium(VI) to the tervalent state.

Alternatively, the chromium(VI) could be directly determined iodometrically at pH $\sim$ 1 on the basis of equation (3). In the method based on reoxidation to chromium(VI), sodium sulphite was found to be the most suitable reducing agent for use in the prior reduction method, as its excess can be easily eliminated by boiling the solution. The procedures finally developed have been used for the determination of various microgram amounts of chromium(III) and/or chromium(VI), with the results shown in Tables 1 and 2.

Moreover, the proposed method has been successfully employed for the determination of chromium in organochromium compounds after their decomposition by acid digestion (or oxygen-flask combustion).[14] Representative results are given in Table 3.

The clear advantages of the proposed method are that it is not only applicable for the determination of chromium(III) in the presence of chromium(VI), but can also be used for the determination of both oxidation states in a mixture.

Table 3 Determination of chromium ion in organic compounds

Compound	Sample weight, *mg*	Theoretical Cr content, %	Cr found, %	Decomposition method
Sodium bis(1-cysteinato)	1 972	14.89	14 9	Oxygen-flask
chromate(III) dihydrate,[15]	2 072		14 9	Oxygen-flask
$C_6H_{14}CrN_2NaO_6S_2$	2 097		14 9	Wet digestion
	2.037		14.9	Wet digestion
Chromium oxinate,	2.152	10 74	10 7	Oxygen-flask
$Cr(C_9H_6ON)_3$	1 921		10.8	Oxygen-flask
	1 940		10.7	Wet digestion
	2 284		10 8	Wet digestion
Chromium acetylacetonate,[16]	1.980	14 89	14 9	Oxygen-flask
$Cr(C_5H_7O_2)_3$	1.746		15 0	Oxygen-flask
	2 067		15 0	Wet digestion
	1 438		14.9	Wet digestion

REFERENCES

1 K G Stollenwerk and D B Grove, *J Environ Qual*, 1985, **14**, 396
2. K S Subramanian, *Anal Chem*, 1988, **60**, 11
3. E Orvini, T Zerlia, M Gallorini and M Spezial, *Radioanal Lett*, 1980, **43**, 173
4. S Osaki, T Osaki and Y Takashima, *Talanta*, 1983, **30**, 683
5 R. Belcher, *ibid*, 1968, **15**, 357
6. S K Tobia, Y A Gawargious and M F El-Shahat, *Z Anal Chem*, 1973, **265**, 23
7 Y A Gawargious, L S Boulos and A Besada, *Analyst*, 1976, **101**, 458
8 A Besada, Y A Gawargious and S Y Kareem, *Talanta*, 1976, **23**, 392
9 A. B Farag, A M El-Wakil, H. N A. Hassan and A F. Abdel-Aziz, *Indian J Chem*, 1985, **24A**, 896.
10 A B Farag, H N. Hassan, A M. Khalil and A. F Abdel-Aziz, *Analyst*, 1985 **110**, 1265
11. A M El-Wakil, A B Farag and M S. El-Shahawi, *Talanta*, 1989, **36**, 783.
12 A Besada, *Z Anal Chem*, 1974, **271**, 368
13 D Burnel, *C R Acad Sci, Paris*, 1965, **261**, 1982
14 E A Kalinovskaya and L S Sil'vestrova, *Zavodsk Lab*, 1968, **34**, 30
15 P. de Meester, D J Hodgson, H C Freeman and C J Moore, *Inorg Chem*, 1977, **16**, 1494
16 R P Sharma and K K Bhasin, *Polyhedron*, 1986, **5**, 667

Talanta, Vol 40, No 6, pp 845–849, 1993
Printed in Great Britain

0039-9140/93 $6 00 + 0 00

DETERMINATION OF TRACE THORIUM USING CATALYTIC–ADSORPTIVE STRIPPING VOLTAMMETRY OF THE THORIUM–CUPFERRON COMPLEX

ROSSI SETIADJI, JOSEPH WANG* and GILBERTO SANTANA-RIOS
Department of Chemistry and Biochemistry, New Mexico State University, Las Cruces, NM 88003, U S A

(*Received* 8 *September* 1992 *Accepted* 22 *October* 1992)

Summary—A sensitive stripping voltammetric procedure for trace measurement of thorium, based on the catalytic-adsorptive peak of the thorium–cupferron complex, is reported Optimal experimental conditions include the use of 1m*M* BES buffer solution (pH 5 5), containing 20μM cupferron, an accumulation potential of −0 80 V (*vs* Ag/AgCl), and a differential pulse potential scan The resulting stripping procedure offers improved sensitivity over a previous stripping scheme for thorium The limit of detection after 5 min preconcentration is 50 ng/l ($2 \times 10^{-10} M$), the response is linear up to $8 \times 10^{-8} M$, and the relative standard deviation at the $2\ 1 \times 10^{-8} M$ level is 4 4% Possible interferences are evaluated

Because of the importance of thorium in the nuclear industry, a sensitive and yet simple method for its determination is required. Spectrophotometric or neutron activation measurements of trace levels of thorium usually require lengthy procedures as well as expensive instrumentations.[1,2] Because of the extremely negative reduction potential of thorium, it cannot be determined by direct polarographic analysis.[3] However, indirect polarographic procedures based on complexation[4] or displacement[5] reactions have been reported. Lower detection limits can be achieved by adsorptive stripping voltammetry, based on coupling the complexation of thorium with Mordant Blue 9, with an adsorptive accumulation of the complex.[6]

The present paper describes an extremely sensitive stripping voltammetric procedure for trace measurements of thorium, based on the coupling of adsorptive accumulation and catalytic effects. This procedure relies on the role of cupferron as both a chelating agent and an oxidizing agent for thorium. A similar role of cupferron has been exploited recently for analogous measurements of trace molybdenum[7] and chromium.[8] The dual (adsorptive/catalytic) amplification effects result in improved sensitivity over a previous adsorptive stripping procedure for thorium. These improvements, as well as detailed optimization and characterization, are reported below.

*Author for correspondence.

EXPERIMENTAL

Apparatus and reagents

An EG&G PAR 264A voltammetric analyzer, a PAR 303A static mercury drop electrode and a PAR 0073 X-Y recorder were used to obtain the voltamperograms. All solutions were prepared from double-distilled water. Chemicals used were of analytical grade. The thorium and other metal atomic standard solutions (1000 mg/l.) were purchased from Aldrich. A 0.01*M* stock solution of cupferron (Aldrich) was prepared daily. An aqueous pH buffer stock solution containing 0.5*M* BES [*N*,*N*-bis(2-hydroxyethyl)-2-amino ethanesulfonic acid] (Aldrich) and 0.4*M* sodium hydroxide was prepared.

Procedure

A 10-ml volume of doubly distilled water was pipetted into the voltammetric cell. Next, 20 μl of the BES pH buffer (final concentration 1.0m*M*) and 20 μl of 0.01*M* cupferron stock solution (final concentration 20μM) were added. The pH of the solution was then adjusted to 5.50. After deaeration of the solution (by purging with nitrogen) for 8 min, an accumulation potential of −0.80 V (*vs.* Ag/AgCl) was applied to a fresh mercury drop, while the solution was stirred, for a predetermined period of time. Following the accumulation step, the stirring was stopped and after 15 sec, the background voltamperogram was obtained by ap-

plying differential pulse negative-going scan terminating at -1.40 V. A scan rate of 10 mV/sec and pulse amplitude of 50 mV were used. A known volume of thorium standard was then added and the accumulation-stripping cycle was repeated with a new mercury drop.

RESULTS AND DISCUSSION

Cyclic voltammetry

Figure 1 illustrates typical cyclic voltamperograms for 10 μg/l. ($4.3 \times 10^{-8} M$) thorium, in the presence of $2 \times 10^{-5} M$ cupferron recorded following 0 (a) and 60 (b) sec stirring at -0.80 V (*vs.* Ag/AgCl) in a medium containing 1.0mM BES buffer solution (pH 5.5). In the absence of prior accumulation, a small cathodic peak, associated with the reduction of the thorium-cupferron complex, is observed at -1.27 V. The reduction peak, observed also in the anodic branch (at a similar potential), is indicative of a catalytic process. No reductive response was observed for the free ligand under these conditions. A substantial increase of the cathodic peak is observed after the stirring period, indicating a significant accumulation onto the surface. Subsequent scans exhibit a substantial diminution of the complex cathodic peak (not shown), indicating rapid desorption of the complex from the surface. The fact that a well-defined cyclic voltammetric response is observed for μg/l. concentrations illustrates the remarkable sensitivity associated with the coupling of adsorptive accumulation and catalytic processes. Such processes can be summarized as follows.

$$[\text{Th(IV)-cupferron}]_{sol} \rightarrow [\text{Th(IV)-cupferron}]_{ads} \quad (1)$$

$$[\text{Th(IV)-cupferron}]_{ads} + e^- \rightarrow [\text{Th(III)-cupferron}]_{ads} \quad (2)$$

$$\text{cupferron}_{(red)} \qquad \text{cupferron}_{(ox)}$$

Reaction 2 corresponds to an EC mechanism which results in the catalytic-adsorptive wave. Hence, cupferron acts as both the complexing agent and the oxidizing agent, in a manner similar to that reported for analogous measurements of molybdenum[7] and chromium.[8] Such self-catalytic behavior eliminates the need for adding another oxidizing agent for performing the catalytic regeneration.

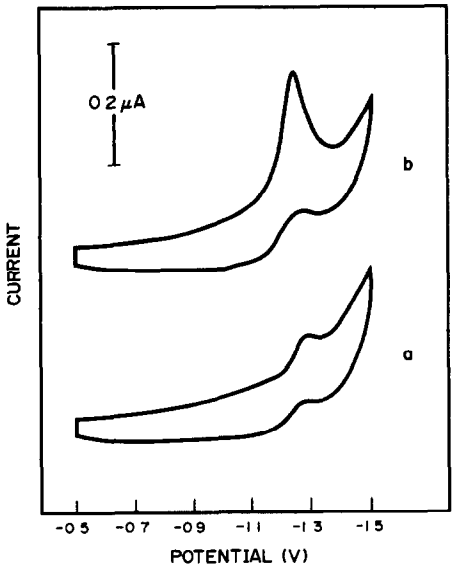

Fig 1 Cyclic voltamperograms for 10 μg/l. thorium in the presence of 20μM cupferron following 0 (a) and 60 (b) sec accumulation at -0.50 V (*vs.* Ag/AgCl) with 300 rpm stirring Scan rate, 50 mV/sec Electrolyte, 1mM BES (pH 5.5)

Optimized experimental conditions

The effective accumulation of the thorium–cupferron complex prior to the voltammetric scan can be exploited for a highly sensitive determination of thorium. Figure 2 displays stripping voltamperograms for 2.5 μg/l. of thorium following different preconcentration periods [0–120 sec, (*a*)–(*e*)]. The peak increases rapidly with increasing accumulation time, indicating an enrichment of surface concentration of the complex. The inherent sensitivity of the cupferron based procedure is indicated also from the well-defined response observed without accumulation (*a*). Figure 2 inset exhibits the resulting peak current *vs.* accumulation time plot for 2.5 (A) and 5.0 (B) μg/l. thorium. The peak current increases rapidly and linearly with the time at first and starts to level off at longer periods.

Other experimental variables affecting the adsorptive stripping response were studied and optimized. The dependence of the complex peak current on the ligand concentration is shown in

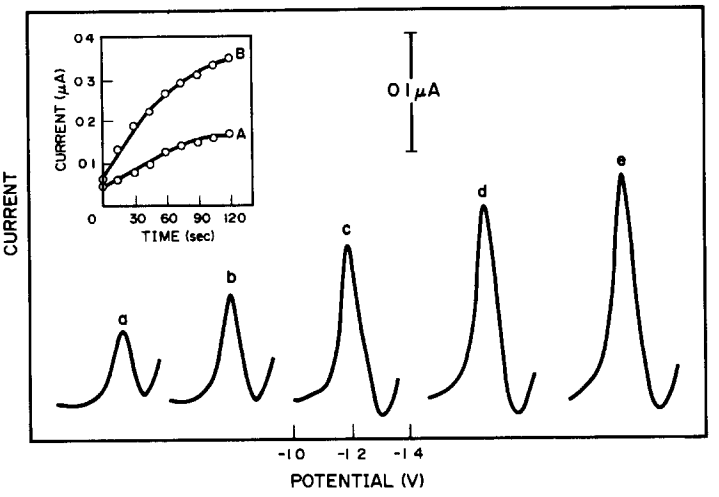

Fig 2 Voltamperograms for 2 5 μg/l thorium following 0 (a), 30 (b), 60 (c), 90 (d) and 120 (e) sec accumulation at −0 80 V Inset are the resulting current–accumulation time plots for 2 5 (A) and 5 0 (B) μg/l thorium Differential pulse waveform with 50 mV amplitude and 10 mV/sec scan rate Other conditions as in Fig 1

Fig. 3(A). The current increases linearly with the cupferron concentration up to 16μM and then it starts to level off. A concentration of 20μM cupferron was chosen for subsequent experiments. At higher cupferron concentration, high background current is observed owing to the fact that cupferron is electroactive and exhibits a well-defined peak at −1.24 V. The pH of the solution has a significant effect on the response of both cupferron and its thorium complex. Figure 3(B) illustrates the effect of pH on the stripping current. At pHs lower than 5.0, a large and stable cupferron reduction peak, which interferes with the complex quantitation, is observed. Such a peak is expected based on the known electroactivity of cupferron in acidic media.[9] Furthermore, the complex formation is slower at a more acidic solution. At pHs higher than 6.0, the response of the complex is smaller and rather unstable due to competitive hydroxide formation. All subsequent work used a 1mM BES pH buffer solution (pH 5.5). Other solutions tested, including an acetate buffer (0.25M, pH 5.5), 0.01M NH_4Cl, 0.01M PIPES, and 0.01M HEPES (all at pH 6.0), yielded inferior responses.

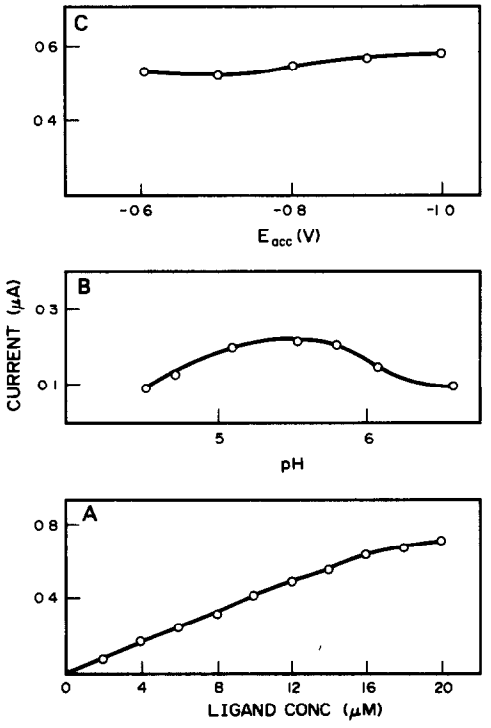

Fig. 3 Effect of cupferron concentration (A), solution pH (B), and accumulation potential on the response of 20 (A,C) and 10 (B) μg/l thorium. Accumulation time, 60 (A,C) and 30 (B) sec at −0 80 V (A,B). Other conditions as in Fig 2

The dependence of the complex peak current on the accumulation potential is shown in Fig. 3(C). The peak current increases slowly over the accumulation potential range from −0.60 to −1.00 V (*vs.* Ag/AgCl). The peak decreases rapidly at accumulation potentials higher than −1.10 V (not shown) which approach the reduction potential of the complex. Other optimal conditions include the use of differential pulse waveform with a 50 mV pulse height, 0.2 sec drop time, and a scan rate of 10 mV/sec.

Analytical performance

The analytical utility of the adsorptive stripping procedures depends on achieving a wide

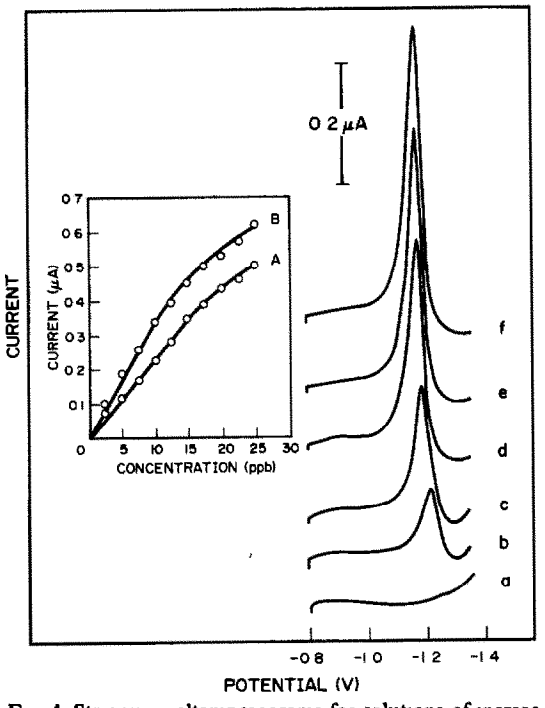

Fig 4 Stripping voltamperograms for solutions of increasing thorium concentration over the range 0–25 μg/l (a)–(f) Accumulation for 15 sec Inset are current–concentrations plots for 15 (A) and 45 (B) sec preconcentration Other conditions are as in Fig. 2

linear dynamic range, high sensitivity, good selectivity and high accuracy and precision. Figure 4 shows the voltammetric stripping response for solutions of increasing thorium concentration in 5 μg/l. steps (a)–(f). Well defined stripping peaks, which are proportional to thorium concentration, are observed following a short (15 sec) accumulation period. The resulting calibration plots, obtained with accumulation period of 15 (A) and 45 (B) sec, are also shown in Fig. 4 (inset). While the response recorded after 15 sec accumulation is linear over the range from 0 to 20 μg/l. thorium, the 45 sec data exhibit linearity only up to 15 μg/l. Both plots indicate curvature at higher thorium concentrations. The sensitivity of the procedure over the linear portion of the current–concentration plots is 21.4 and 28.7 nA l. μg^{-1} for 15 and 45 sec, respectively (correlation coefficients, 0.998). A detection limit of 0.05 μg/l. ($2.0 \times 10^{-10} M$) was estimated based on the signal-to-noise characteristics ($S/N = 3$) of the response to 0.5 μg/l. thorium following 5 min accumulation. This detection limit is lower than that of the Mordant Blue 9 stripping procedure.[6] Figure 5 compares adsorptive stripping voltamperograms for 0.5 (a) and 5.0 (b) μg/l. thorium, using cupferron (A) and Mordant Blue 9 (B) as the complexing agent. The inherent sensitivity of the cupferron-based procedure is apparent from a comparison with the azo dye based one. Notice, in particular, that the use of Mordant Blue 9 does not permit quantitation of 0.5 μg/l., while cupferron offers a well-defined response at this level.

The adsorptive accumulation of the thorium–cupferron complex results in reproducible stripping currents. The precision was estimated from 20 successive measurements of 5.0 μg/l. thorium following a 60-sec accumulation step. The mean peak current was 270.7 nA, with the range from 252.5 to 287.5 nA, and a relative standard deviation of 4.4%. Recovery experiments using river water spiked with known concentration of thorium yielded 96.4% accuracy.

No interference was observed upon adding 50 μg/l. of the following metals ions to a 5 μg/l. thorium solution: Bi(III), Cd(II), Cu(II), Fe(III), Hf(IV), Hg(II), La(III), Mn(II), Pb(II), Sb(V), and Sn(IV). Although additions of 25 μg/l. Nb(V), Te(IV), and Zn(II) resulted in the

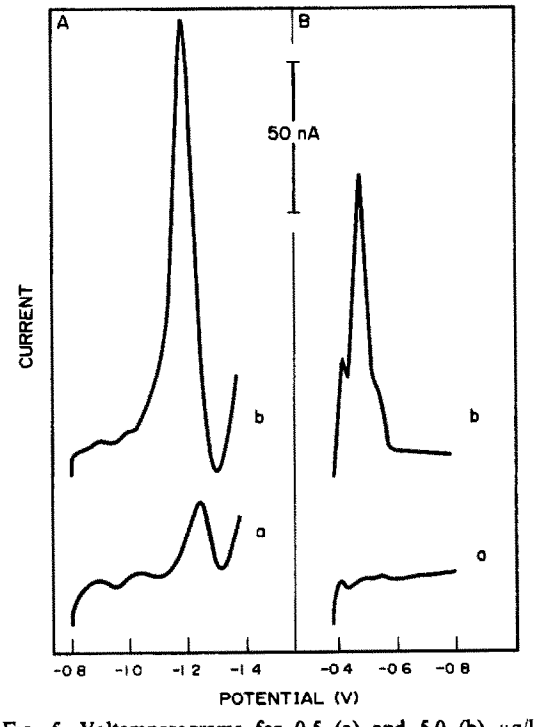

Fig. 5 Voltamperograms for 0 5 (a) and 5 0 (b) μg/l thorium, with cupferron (A) and Mordant Blue 9 (B), obtained following 5 (a) and 1 (b) min accumulation Solutions (A), 1m*M* BES pH 5 5 and 20μ*M* cupferron, and (B) 0.05*M* acetate buffer pH 6.5 and 2μ*M* Mordant Blue 9 Other conditions, (A) as in Fig. 2, (B) linear scan with 50 mV/sec, accumulation potential −0 38 V

appearance of new peaks (at −0.87, −0.97, and −0.98 V, respectively), only zinc and niobium cause *ca.* 50% diminution of the 5 μg/l. thorium peak. Al(III), Sc(III), and U(VI) resulted in overlapping peaks with thorium. Addition of 25 μg/l. Cr(VI), Ni(II), Ti(IV), V(V), W(V) and Zr(IV) caused the disappearance of the 5 μg/l. thorium peak. As a consequence, thorium should be isolated from these interfering elements prior to its determination. Severe interference from relevant ions such as Al(III), U(VI) or Ti(IV) characterize also the quantitation of thorium in the presence of Mordant Blue 9.[6]

In conclusion, under the optimum conditions, trace levels of thorium can be determined rapidly with a simple approach using the catalytic–adsorptive stripping peak of the thorium–cupferron complex. Such coupling of interfacial and catalytic processes offers higher sensitivity and a lower detection limit over a previously reported procedure. The attractive performance characteristics of the cupferron-based procedure, along with its instrumentation portability and low cost operation, should find wide applicability for measuring trace thorium in environmental and nuclear matrices. Such applications may require a prior removal of interfering elements.

Acknowledgements—This work was supported by the Battelle Pacific Northwest Laboratory (subcontract No 095985-A-P1) and Lawrence Livermore National Laboratory (subcontract B160617) R S acknowledges a fellowship from the National Atomic Energy Agency of Indonesia.

REFERENCES

1 A Ramesh, J Khrisnamacharyulu, L K Ravindranath and S B Rao, *Analyst*, 1992, **117**, 1037
2 C A Huh and M P Bacon, *Anal Chem*, 1985, **57**, 2138
3 I M Kolthoff and J J Lingane, *Polarography*, Vol. II, p 446 Interscience, New York, 1952
4 Z Zao, X Cai, P Li and H Yang, *Talanta*, 1986, **33**, 623
5 G A Mazzocchin and S Daniele, *ibid*, 1990, **37**, 317
6 J. Wang and J M Zadeii, *Anal Chim Acta*, 1986, **188**, 187
7 K Jiao, W Jin and H Metzner, *ibid.*, 1992, **260**, 35.
8 J Wang, J Lu and K Olsen, *Analyst*, 1992, **117**, 1913
9 I M Kolthoff and A Liberti, *J Am Chem Soc*, 1948, **70**, 311

Talanta, Vol 40, No 6, pp 851–853, 1993
Printed in Great Britain

0039-9140/93 $6 00 + 0 00

USE OF *P*-DIMETHYLAMINOBENZALHYDE AS A COLOURED REAGENT FOR DETERMINATION OF GENTAMYCIN

HUAIYOU WANG,* JIANCHENG REN and YICI ZHANG†
Analysis and Test Centre, Shandong Teachers' University, Jinan 250014, People's Republic of China

(*Received* 2 *September* 1992 *Accepted* 22 *October* 1992)

Summary—Spectrophotometric determination of gentamycin is described. Gentamycin reacts with *p*-dimethylaminobenzalhyde in acetic acid/acetate buffer solution to form a Schiff base, a yellow complex, and its maximum absorption wavelength is 405 nm Effects of pH, kanamycin, streptomycin, beneylpenicillin, lincomycin and foreign ions on the determination of gentamycin have been examined. The absorbance for gentamycin from 0 to 74 40 μg/ml obeys Beer's law The linear regression equation of the calibration graph is $C = 103A - 0\,264$, with a linear regression correlation coefficient of 0.9997, and recovery from 97 to 101% The results obtained by this method agreed with those of the microbiological method This method is rapid and simple, and can be used for the determination of gentamycin in injection solutions of gentamycin sulphate

Gentamycin is a broad spectrum aligosaccharide antibiotic produced by *Micromonospora purpurea*. The present USP,[1] UP[2] and CP[3] requirements for this antibiotic estimate the total potency by a microbiological method. Wilson *et al.*[4] published a chemical method for quantitating the total potency of gentamycin after separation of impurities by TLC. However, the procedure is inconvenient. The determination of gentamycin by a colorimetric method based on gentamycin reaction with Cu^{2+} in basic medium to form an orange complex has been reported,[5,6] but the sensitivity is too low in these methods. Although the official microbiological assay estimates total potency, many foreign ions and biologically active impurities in drugs may interfere.[7]

This paper reports a rapid spectrophotometric method for estimating the total potency of gentamycin, which is based on a Schiff reaction,[8] *i.e.*, *p*-dimethylaminobenzalhyde reacts with amino of gentamycin molecule to form a Schiff base, a yellow complex. The principal advantage of this method is high sensitivity, which is two orders higher than that of the previous colorimetric method.[6]

EXPERIMENTAL

Apparatus

All the spectrophotometric measurements were made with a SHIMADZU UV-265 UV-vis recording spectrophotometer with matched 1-cm quartz cells. In order to compare all spectrophotometric measurements and ensure reproducible experimental conditions, the UV-265 spectrophotometer was checked daily. An acidimeter (Model pHS-3C, Shanghai Leici instruments factory, China) was used for pH adjustments.

Reagents

Gentamycin sulphate (624 μg/mg), kanamycin sulphate (784 μg/mg), streptomycin sulphate (741 μg/mg), beneylpenicillin (1607 μg/mg), lincomycin hydrochloride (838 μg/mg) were used as standards. (*Drugs and Biological Products Examination Bureau of China*). All reagents were of analytical-reagent grade, unless stated otherwise. Double-distilled water was used in all experiments.

Gentamycin sulphate standard solution. 1560 μg/ml. An accurately weighed 0.1250-g standard sample of gentamycin sulphate was dissolved in water, transferred into a 50-ml standard flask and diluted to the mark with water. It is stable for 5 days at 5°.

p-*Dimethylaminobenzalhyde solution*, 1% (v/w). *(Chemical Reagent Factory of Shanghai, China).* Accurately weighed 0.5000 g of *p*-dimethylaminobenzalhyde was dissolved in 25 ml of glacial acetic acid and diluted to the mark in a 50-ml standard flask with pH 4.1 acetic acid/acetate buffer solution. The solution was prepared fresh daily.

*Author for correspondence.
†Present address Department of Physics, Shandong Teachers' University, Jinan, People's Republic of China.

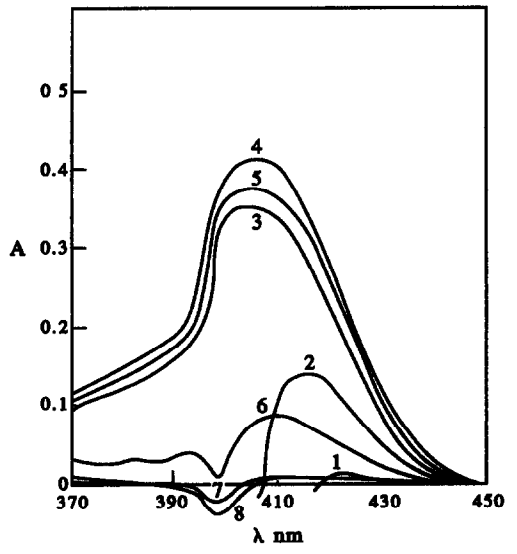

Fig 1 Effect of pH on the absorption spectrum of gentamycin complex

1 pH = 1 00	5 pH = 5 01
2 pH = 2 01	6 pH = 8 29
3 pH = 3 04	7 pH = 9 91
4 pH = 4 01	8 pH = 12 00

Procedure

A 0.50-ml portion of standard gentamycin sulphate solution was transferred into a 25-ml standard flask, and 2.0 ml of 1% *p*-dimethylaminobenzalhyde solution and 5 ml of pH 4.1 acetic acid/acetate buffer solution were added. The mixture was shaken and heated for 2 min in a boiling water bath, and then cooled to room temperature at once, diluted to the mark with water and mixed well. The absorbance of the gentamycin complex was measured at 405 nm against a reagent blank prepared with the same reagent concentration, but no gentamycin sulphate.

Absorption spectrum of gentamycin complex

A gentamycin complex solution prepared according to the procedure was scanned with the spectrophotometer and the absorption spectrum was recorded. The maximum absorption wavelength is 405 nm.

RESULTS AND DISCUSSION

Effect of pH

Comparative tests at various pH values show that the maximum absorption wavelength of the gentamycin complex changes with pH (Fig. 1). Variation of the pH from 1 to 12 was investigated. λ_{max} of the gentamycin complex is 405 nm in the range of pH 3 ~ 12, but the absorbance is different under the different pH conditions. The λ_{max} is 423 nm and 426 nm at pH 1 and 2, respectively. In addition, the absorbance spectrum was measured in the range of pH 3.7 ~ 4.5 at intervals of 0.2 pH using *p*-dimethylaminobenzalhyde prepared with glacial acetic acid. It was found that the maximum absorption wavelength is also 405 nm in the range of pH 3.7 ~ 4 5. Therefore, a pH 4.1 acetic acid/acetate buffer system was employed. The reasons for the negative absorbances at pH 9.9 and 12 are possibly due to refractive index effects or a pH-dependence of a blank constituent

Stability of gentamycin complex

According to the procedure, the gentamycin complex solution was heated for different times in a boiling water bath and the absorbance measured. The results are shown in Table 1. The colour formation of the gentamycin complex is slow at room temperature, but when heated for 2 min in a boiling water bath the absorbance reached its maximum. Heating for 2 min was selected as optimum. The absorbance of the complex remained stable for at least 8 hr at room temperature.

Effect of foreign ions

A systematic study was made of the effect of the ions commonly found, on the determination of 32.1 μg/ml gentamycin sulphate. A 500-mg/l. level of each potentially interfering ion was tested first. If interference occurred, the ratio was reduced progressively until interference ceased. The tolerance level was defined as an error not exceeding ±5% in the determination of the analyte. The results are summarized in Table 2.It is emphasized that under the selected conditions, kanamycin reacts with *p*-dimethylaminobenzalhyde to form a complex. The absorption spectra of the kanamycin and gentamycin complexes strongly overlap (Fig. 2).

Effect of amount of p-*dimethylaminobenzalhyde*

It was found that addition of 2.0 ml of 1% *p*-dimethylaminobenzalhyde was sufficient for

Table 1. Effect of heating time on formation of gentamycin complex

Heating time (*min*)	2	4	6	8	10	15	20
Absorbance	0 343	0.342	0 336	0.352	0.302	0 294	0 290

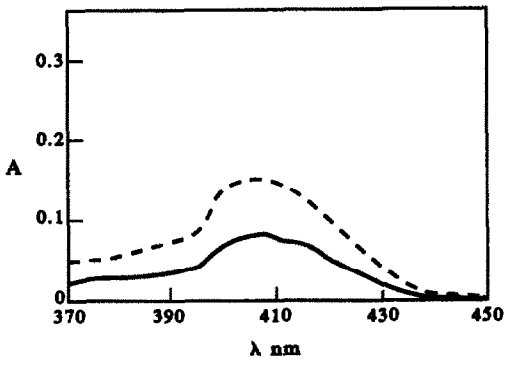

Fig 2 Comparison of gentamycin and kanamycin spectra Dashed line = absorption spectrum of gentamycin complex (14 3 μg/ml) Solid line = absorption spectrum of kanamycin complex (27 4 μg/ml)

Table 2 Effect of foreign ions on the determination of 32 1 μg/ml gentamycin

Foreign ions or species	Tolerance level, μg/ml
Benzylpenicillin, streptomycin, lincomycin, K^+, Na^+,	500
Zn^{2+},Cu^{2+}, Mg^{2+},Mn^{2+}, Ni^{2+}	300
Al^{3+},Cr^{3+},Pb^{2+},Co^{2+}	200
Fe^{3+},Fe^{2+},Hg^{2+}	100
Ca^{2+}	50
NH_4^+	20
Cl^-,Ac^-,SO_4^{2-}, NO_3^-,CO_3^{2-},BO_3^{3-}	500
Br^-,I^-	40
Kanamycin	5

determining gentamycin up to 74.4 μg/ml (upper limit of linear range). Therefore, 2.0 ml of 1% *p*-dimethylaminobenzaldhyde solution is recommended.

Relationship between concentration of gentamycin and absorbance

Under the selected conditions, a linear relation was obtained between absorbance and concentration of gentamycin in the range of 0 ~ 74.40 μg/ml. The linear regression equation of the calibration graph is $C = 103A - 0.264$, with a correlation coefficient of linear regression of 0.9997.

Recovery of gentamycin

The recovery of gentamycin added to three different injection gentamycin sulphate solutions is shown in Table 3. The recovery is from 97.4 to 101%.

Table 3 Results for the recovery of gentamycin from injection of gentamycin sulphate

Sample No	Sample content, μg/ml	Gentamycin added, μg/ml	Gentamycin found, μg/ml	Recovery, %
1	29 1	12 5	41 3	97 6
2	25 6	37 4	63 0	100 0
3	25 2	25 0	50 5	101 2

Table 4 Results of determination by spectrophotometric and microbiological method

Sample No	Spectrophotometric methods mg/ml	Microbiological method,* mg/ml
1	40 8	40 7
2	40 2	40 5
3	40 0	39 8
4	39 9	40 3
5	40 1	40 0

*Results obtained by Shandong Drugs Examination Bureau, China

Analysis of sample

A 1.0-ml portion of injection solution of gentamycin sulphate was transferred into a 50-ml standard flask, diluted to mark with water and mixed well. According to the procedure, 1.0 ml of this solution was transferred into a 25-ml standard flask, reacted and measured. The results are shown in Table 4.

Reproducibility

The same batch number of gentamycin sulphate injection solutions was measured 10 times, under the previously selected conditions. The mean value was 40 7 mg/ml with a standard deviation of 0.54 and relative standard deviation of 1.3%.

REFERENCES

1 *The United States Pharmacopoeia*, 22nd Revision, p 603, 1990
2 *The British Pharmacopoeia*, Vol II, pp 266, 267, 1988
3 *The Chinese Pharmacopoeia*, 5th Ed, Vol II, pp 696–698, 1990
4 William J Wilson *et al*, *J Pharm Sci*, 1973, **62**, 282
5 Pete Tarbotton, *Am J Pharm*, 1987, **44**, 115
6 Jiang Kaiyu *et al*, *Chin J Pharm Anal*, 1989, **9**, 368
7 Guo Du *et al*, *Chin J Pharm*, 1989, **24**, 312
8 M M *Chine Rev*, 1940, **26**, 297

Talanta, Vol 40, No 6, pp 855–861, 1993
Printed in Great Britain

0039-9140/93 $6 00 + 0 00

KINETIC ENZYMATIC DETERMINATION OF ETHANOL/METHANOL MIXTURES BY THE STOPPED-FLOW TECHNIQUE

EVA FÓRSTER,* MANUEL SILVA, MATHIAS OTTO* and DOLORES PÉREZ-BENDITO
Department of Analytical Chemistry, Faculty of Sciences, University of Córdoba, 14004 Córdoba, Spain

(*Received* 26 *June* 1992 *Revised* 20 *October* 1992 *Accepted* 20 *October* 1992)

Summary—The analytical use of the enzymatic oxidation of alcohols by alcohol oxidase was assessed applying the stopped-flow technique for mixing sample and reagents, and the DTNB (5,5′-dithiobis-(2-nitrobenzoic acid))/*L*-cysteine system as a new chromogenic reagent The oxidation reaction was monitored by measuring the rate of absorbance decrease at 412 nm, the wavelength of maximum absorption of the reduced form of DTNB The calibration graphs for the individual determination of the alcohols were linear over the range 1.0×10^{-6}–$1\ 0 \times 10^{-5}M$, and the precision ranged between 2.1 and 4 8% A differential rate principle was applied to the determination of ethanol/methanol mixtures involving mutual kinetic effects which allowed mixtures in molar ratios between 25 1 0 and 1 0 1 0 to be accurately resolved with good precision (r s d less than 9 and 5%, respectively) Compared to the flow-injection analysis method, the proposed approach offers higher sensitivity and sample throughput, as well as the wider concentration ratio range for mixture resolution

Ethanol is a major compound in chemistry and biochemistry and a very important ingredient of various groceries and beverages as well as cosmetics, medicines, cleaning fluids, *etc.* Ethanol is commonly associated to methanol, which introduces some hazards owing to the toxic effects of the latter, so the determination of both alcohols in mixtures is of great interest. In recent years, several methods for the resolution of this mixture at very different concentration levels have been reported. Of these, gas chromatographic methods are quite commonplace, and headspace gas analysis[1,2] is particularly useful for these determinations. In general, analyses can be performed in a few minutes over wide dynamic ranges,[1,3,4] even though the sensitivity achieved is not correspondingly high (in any case lowest concentration determined from the calibration graphs was *ca.* $10^{-4}M$). These chromatographic methods have been used for the determination of methanol and ethanol in foods[5,6] and plasma.[4] Spectrophotometric methods have also been used for this purpose. Thus, methanol and ethanol reduce cerium(IV) in a $HClO_4$ medium, forming complexes at different reaction rates that can be determined spectrophotometrically.[7] Mixtures of these alcohols in ratios from 3:7 to 7:3 can thus be resolved. Also, a flow-injection system with a column of immobilized alcohol oxidase was used for the simultaneous determination of these alcohols using the *p*-rosaniline/Na_2SO_3 system as chromogenic reagent for the aldehydes formed in the enzymatic reaction.[8] The method allows the resolution of ethanol/methanol mixtures at the microgram per millilitre level in the ratio range 3.3:1.0 to 1.0:1.3.

In this work we used the above-mentioned enzymatic reaction for the determination of lower straight-chain alcohols such as methanol, ethanol, propanol and butanol, as well as for the resolution of methanol/ethanol mixtures based on the stopped-flow technique, which allows the photometric monitoring of the fast reaction between the hydrogen peroxide released in the enzymatic reaction and the DTNB (5,5′-dithiobis(2-nitrobenzoic acid))/*L*-cysteine system used as chromogenic reagent. The use of the stopped-flow technique and the DTNB/*L*-cysteine system (employed here for the first time as a developer system for this enzymatic reaction) allows for a faster determination of these alcohols at the nanogram per millilitre level. The method is also suitable for the accurate resolution of binary mixtures of methanol and ethanol subject to mutual kinetic effects and compares favourably with its flow-injection

*Present address. Bergakademie Freiberg, Department of Chemistry, 9200 Freiberg, Germany

counterpart in terms of sensitivity, alcohol concentration ratios that can be assayed and sample throughput.

EXPERIMENTAL

Reagents

All reagents used were of analytical grade Alcohol solutions (methanol, ethanol, propanol and butanol) were prepared from standards of absolute grade (Merck) by appropriate dilution with bidistilled water. A 1.6 mg/ml alcohol oxidase (AO, candida boidinii, Sigma) solution was prepared by dissolving 16 mg of the lyophilized powdered enzyme (which features a protein activity of 4–10 units/mg) in 10 ml of 0.1*M* tris(hydroxymethyl)aminoethane (Tris) buffer of pH 8.55 A stock solution of 5,5′-dithiobis(2-nitrobenzoic) acid (DTNB) ($1.0 \times 10^{-3}M$) was prepared by dissolving 40 mg of chemical (Merck) in 100 ml of 0.1% sodium citrate. A stock L-cysteine solution ($1.24 \times 10^{-2}M$) was prepared by dissolving 37.5 mg of reagent (Merck) in 25 ml of bi-distilled water. The 0.1*M* Tris buffer (pH 8.55) was prepared by dissolving 13.28 g of sodium chloride and 12.1 g of Tris in about 850 ml of bidistilled water, the pH then being adjusted to 8.55 with 1*M* hydrochloric acid and the mixture diluted to one litre with further bidistilled water. All solutions were stored in a refrigerator in order to minimize degradation.

Apparatus

Absorbance measurements were made on a Philips PU 8625 UV–visible spectrophotometer fitted with a device for stopped-flow measurements[9] and a Netset PC-AT 16-Mhz compatible computer equipped with a PC-Multilab PCL-812PG 12-bit analog-to-digital converter for acquisition and treatment of kinetic data. The software required for application of the initial reaction-rate method was written by the authors themselves. A Hanna HI 8418 pH-meter was also used.

Procedures

Individual kinetic determinations of the alcohols. Two solutions were mixed in the stopped-flow cell by simultaneous injection from two drive syringes, one of which was filled with a solution prepared by mixing 2.0 ml of sample containing between 1.0×10^{-6}–$1.0 \times 10^{-5}M$ alcohol in the final volume, 3.0 ml of $1.0 \times 10^{-3}M$ DTNB, 2.0 ml of $1.24 \times 10^{-2}M$ *L*-cysteine and 3.0 ml of 0.1*M* Tris buffer (pH 8.55) in a 10-ml standard flask, and the other with a solution made by diluting 2.0 ml of 1.6 mg/ml alcohol oxidase with 8.0 ml of 0.1*M* Tris buffer (pH 8.55). The reaction was monitored at 412 nm and the temperature was kept constant at $25 \pm 0.1°$. The computer system recorded the full signal *vs.* time curve at a data acquisition rate of 100 msec per point and calculated the initial rate (over a period of *ca.* 2 sec) and the concentrations of the alcohols from the corresponding calibration graph.

Resolution of methanol/ethanol mixtures. Synthetic samples containing micromolar concentrations of methanol and ethanol were analysed in two kinetic runs. A volume of 1.0 ml of $2.5 \times 10^{-3}M$ ethanol was added to 1.0 ml of sample containing 2.0–$6.0 \times 10^{-6}M$ methanol and 5.0×10^{-6}–$5.0 \times 10^{-5}M$ ethanol in a final volume of 10 ml and the above-described procedure was followed for the determination of ethanol in the mixture based on initial rate measurements because methanol was not affected under these conditions. In the second experiment, two calibration graphs were constructed for methanol (initial rate and final absorbance *vs.* methanol concentration) in the range 8.0×10^{-7}–$4.0 \times 10^{-6}M$ in the presence of the ethanol concentration found in the previous experiment. Then, an aliquot of the mixture was reacted under the same conditions as for the individual kinetic determinations of the alcohols the concentration of methanol in the sample was determined from the measured initial rate or final absorbance.

RESULTS AND DISCUSSION

The enzymatic oxidation of lower straight-chain alcohols with alcohol oxidase is widely used; the reaction is generally monitored via a coupled reaction in which the aldehyde formed in the enzymatic reaction is reacted with an appropriate reagent in order to obtain a chromogenic product.[10] The proposed method for the determination of these alcohols relies on the above-mentioned enzymatic reaction and the DTNB/*L*-cysteine system as chromogenic reagent for the hydrogen peroxide released in the enzymatic oxidation of the alcohols. This chromogenic reaction was used for the first time in this work as coupled to the enzymatic determination of these alcohols, for which the following reaction scheme is suggested. In a first step,

hydrogen peroxide is formed by enzymatic oxidation of the alcohols:

$$\text{R-OH} + \text{Alcohol oxidase} \rightarrow \text{R-CHO} + H_2O_2$$

and the chromogenic reagent is formed by reaction between DTNB and *L*-cysteine according to

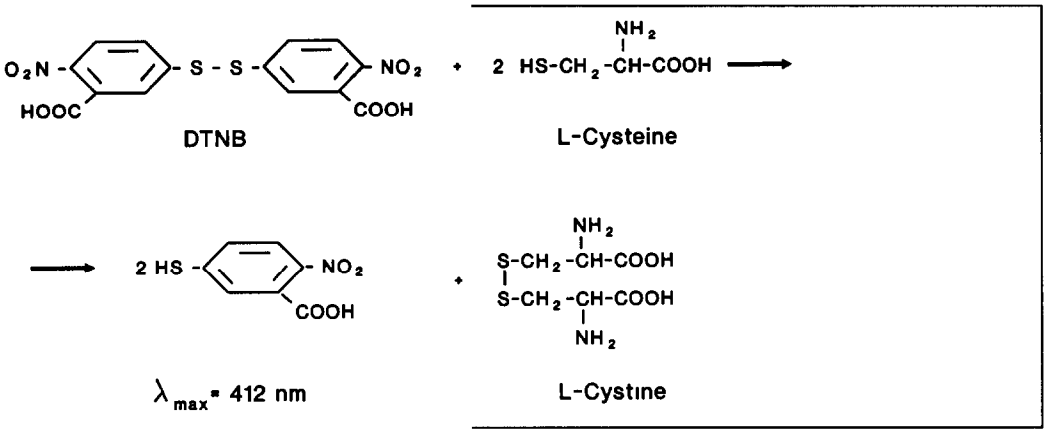

The sulphur derivative of 2-nitrobenzoic acid (a sulphide or mercaptan) is responsible for the colour, which shows maximum absorption at 412 nm. In the final step, this compound reacts with hydrogen peroxide to yield DTNB (colourless) again.

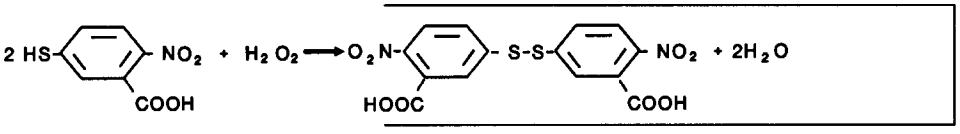

This reaction scheme is consistent with literature data on the reversible oxidation of mercaptans.[11] In fact, these compounds can be oxidized to sulphoxides and even to sulphones by using concentrated hydrogen peroxide, whereas dilute solutions of this oxidant readily oxidize mercaptans to disulphides. On the other hand, disulphides can be reduced to mercaptans by mild reducing agents such as *L*-cysteine, so interconversion between *L*-cysteine and *L*-cystine using this sulphide/disulphide system is very important in biochemistry.

These reactions develop to completion in a few seconds, which calls for the use of the stopped-flow technique for making kinetic measurements. Figure 1 shows the stopped-flow kinetic curve (absorbance at 412 nm *vs.* time) provided by the spectrophotometer and processed by the data acquisition system which is the basis for development of the proposed kinetic method for the determination of lower straight-chain alcohols. Even though the proposed method is based on signal decrease *vs.* time measurements, reaction rates are usually positive, so all graphs and calculations in this work are conformant to this criterion.

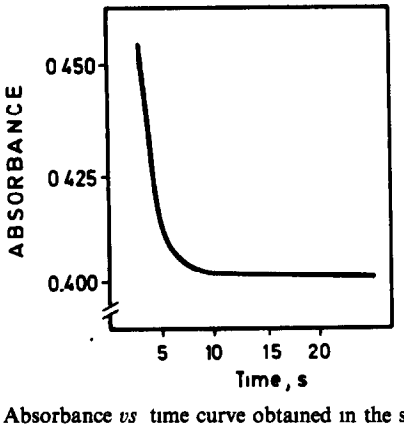

Fig 1 Absorbance *vs* time curve obtained in the stopped-flow determination of $5.0 \times 10^{-6} M$ ethanol Experimental conditions as described under Procedure

Influence of variables

The working conditions for application of the proposed method were selected by using ethanol only to examine the influence of variables on both the enzymatic and the chromogenic reaction. The conditions arrived at for ethanol were then applied to the other alcohols. In this study, all concentrations stated are initial concentrations in the syringes (twice the actual concentrations in the reaction mixture at time zero after mixing) and kinetic data (averages of three measurements) were obtained from the initial rate/concentration plots.

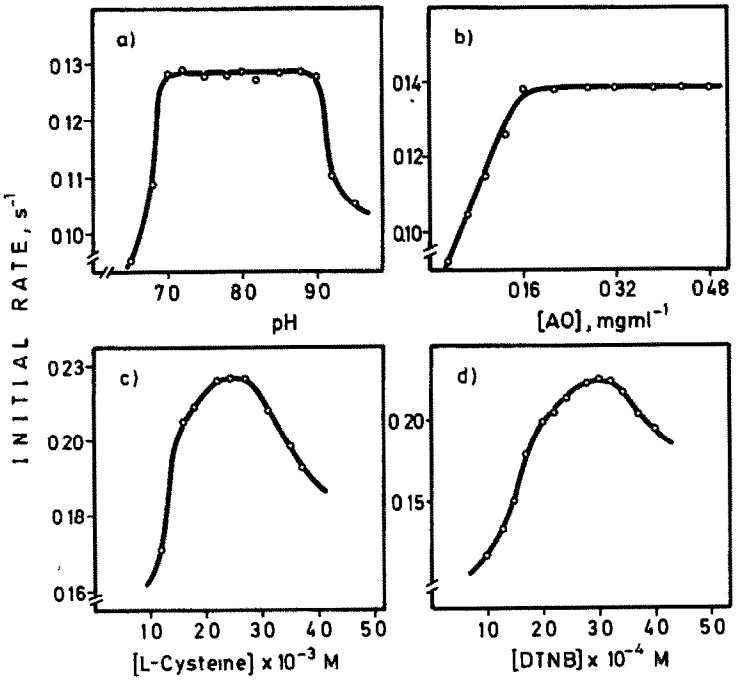

Fig 2 Effect of (a) pH, and (b) the alcohol oxidase, (c) *L*-cysteine and (d) DTNB concentrations on the kinetic determination of $1.0 \times 10^{-6}M$, (a) and (b), and $5.0 \times 10^{-6}M$, (c) and (d), ethanol (conditions described under Experimental)

The effect of the temperature on the reaction rate was examined between 15 and 45°. The absorbance *vs.* time curves show an increase in reaction rate with increase in temperature up to 20°, above which the initial rate remained constant up to 40°. At higher temperatures, the reaction rate decreased owing to the enzyme denaturation. A temperature of 25° was selected.

The influence of the pH was studied over the range 6.5–9.5. As can be seen from Fig. 2(a), a pseudo zero-order region occurred between pH 7.0 and 9.0, above which the reaction rate decreased, probably owing to the enzyme denaturation. A pH of 8.55 was chosen for further experiments, which was adjusted and kept constant by using a $0.1M$ Tris buffer. The influence of the alcohol oxidase concentration on the reaction rate was studied over the range 0.032–0.48 mg/ml [Fig. 2(b)], its dependence being of zero-order at concentrations above 0.16 mg/ml; therefore, 0.32 mg/ml alcohol oxidase was selected for further experiments in order to ensure the presence of an excess and avoid unnecessary consumption of the enzyme.

The effect of the *L*-cysteine concentration on the reaction rate at an ethanol concentration of $5 \times 10^{-6}M$ is illustrated in Fig. 2(c). As can be seen, a $2.48 \times 10^{-3}M$ *L*-cysteine solution (2.0 ml of $1.24 \times 10^{-2}M$ solution in 10 ml) yielded the maximum initial-reaction rate, so it was chosen for implementation of the proposed procedure. The influence of the DTNB concentration on the analytical signal is shown in Fig. 2(d). The initial rate increased with increasing DTNB concentration up to $2.8 \times 10^{-4}M$ and the reaction became nearly zero-order with respect to DTNB over a narrow range, $2.8–3.2 \times 10^{-4}M$, above which it started to decrease. A DTNB concentration of $3.0 \times 10^{-4}M$ was selected.

Kinetic enzymatic determination of alcohols

The initial rates derived from the absorbance *vs.* time curves for solutions containing different concentrations of the alcohols under the selected conditions, were linearly related to the alcohol concentration. The analytical features of the proposed stopped-flow methods are summarized in Table 1. As can be seen, the alcohols can be determined at the nanogram per millilitre level with good precision (between 2.1 and 4.8% as RSD). We should note the relatively large values of the intercepts in the linear regression equations. In fact, lower alcohol concentrations resulted in decreased initial rates, however, the net absorbance changes in the kinetic curves were very small, so the analytical results were quite irreproducible. The dynamic linear ranges

Table 1 Analytical figures of merit of the determination of alcohols by the stopped-flow technique

Alcohol	Dynamic linear range M	Dynamic linear range ng/ml	Linear regression equation*	Correlation coefficient ($n = 10$)	Precision† (RSD), %
Methanol	1.0×10^{-6}–1.0×10^{-5}	32–320	$IR = 5.61 \times 10^{-2} + 3.37 \times 10^{3}\ C$	0.9994	4.49
Ethanol	1.0×10^{-6}–1.0×10^{-5}	46–460	$IR = 1.34 \times 10^{-1} + 1.50 \times 10^{4}\ C$	0.9995	2.71
Propanol	1.0×10^{-6}–1.0×10^{-5}	60–600	$IR = 1.35 \times 10^{-1} + 1.62 \times 10^{4}\ C$	0.9998	2.13
Butanol	1.0×10^{-6}–1.0×10^{-5}	74–740	$IR = 2.81 \times 10^{-2} + 3.52 \times 10^{3}\ C$	0.9995	4.83

*IR = initial rate (absorbance/sec), C = molar concentration.
†Obtained from 11 samples containing $5 \times 10^{-6} M$ of the alcohol

obtained in this work allow the kinetic determination of these alcohols with a higher reliability. The analytical sensitivity to the alcohols varied from compound to compound in the following sequence:

propanol ≅ ethanol > butanol ≅ methanol.

We thus selected the ethanol/methanol couple in order to test the performance of the proposed kinetic enzymatic method in the resolution of mixtures of the alcohols.

At this point it is worth comparing the performance of the proposed kinetic enzymatic method for the determination of alcohols with others reported in the literature also based on the use of alcohol oxidase. Two recently reported methods were selected for this purpose: one in which alcohol oxidase is immobilized in a gelatin matrix and the electrode formed from the membrane is used in a continuous-flow system,[12] and the other based on a flow-injection system including a column of immobilized alcohol oxidase and using the *p*-rosaniline/Na_2SO_3 system as a coupled reaction for spectrophotometric detection.[8] Table 2 shows the performance of the methods as applied to the determination of ethanol and methanol only, compared to the proposed stopped-flow method, which offers higher sensitivity, inasmuch as it allows the determination of these alcohols at lower concentrations by at least two orders of magnitude, and lower analysis time (it was considered to be the time elapsed between insertion of the sample into the system and the end of data processing for delivery of the analytical signal). Even though the use of immobilized enzyme obviously reduces analytical cost, the low enzyme concentrations used in this procedure partly avoids the need to work in homogeneous medium (the estimated cost per analysis was $10 per 100 triplicate determinations. On the other hand, alcohol oxidase solutions prepared as described above are stable for at least 4 hr (the longest time assessed).

Resolution of methanol/ethanol synthetic mixtures

The first step in the resolution of mixtures of species involves checking whether the reaction rates of the species concerned are independent of one another or, in other words, if the presence of one component has no effect on the kinetic behaviour of the others. We thus constructed several calibration plots of initial rate *vs.* methanol concentration in the present of different fixed concentrations of ethanol. The results obtained are shown in Fig. 3. As can be seen, the initial rate decreased with an increase in the methanol concentration owing to the presence of ethanol. In summary, the occurrence of strong negative mutual kinetic effects was detected in the resolution of methanol/ethanol mixtures, consistent with previous reports.[8]

The occurrence of this mutual kinetic effect precluded use of classical differential reaction-rate methods for resolution of these mixtures, so a new methodology must be developed in order

Table 2 Comparison of the figures of merit of the proposed stopped-flow method for the determination of alcohols with those of other recently reported methods using alcohol oxidase

Method	Methanol Dynamic range, M	Methanol Precision, %	Ethanol Dynamic range, M	Ethanol Precision, %	Time for analysis, sec
Stopped-flow	1.0×10^{-6}–1.0×10^{-5}	4.49	1.0×10^{-6}–1.0×10^{-5}	2.71	10
Continuous-flow*	5.0×10^{-4}–1.5×10^{-2}		1.0×10^{-2}–3.0×10^{-1}		<120
Flow-injection†	3.1×10^{-4}–1.9×10^{-3}	2.29	2.2×10^{-4}–6.5×10^{-3}	3.46	30–180

*Ref 12
†Ref 8

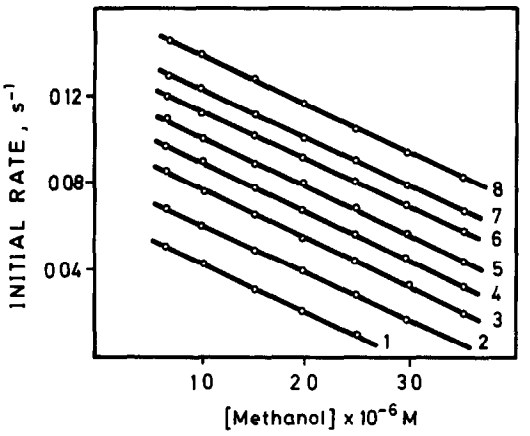

Fig 3 Calibration plots of initial rate *vs* methanol concentration obtained in the presence of the following amounts of ethanol curves (1)–(8) 1·0–8·0 × $10^{-6}M$ ethanol Reaction conditions as described under Procedure

to take account of this effect as in previously reported cases.[13–15] Even though the intercepts of the curves shown in Fig. 3 depend on the concentration of ethanol, their relationship cannot be used to assess the mutual kinetic effect because, if an unknown mixture is added with increasing amounts of methanol, a linear dependence is indeed found, yet the intercept of the straight line depends on the concentration of both ethanol and methanol in the mixture. It is therefore indispensable to establish a set of experimental conditions under which the mutual kinetic effect does not occur in order to be able to determine one of the mixture components. For this purpose, we prepared various samples of methanol containing increasing concentrations of ethanol and found that, at ethanol concentrations above 2·0 × $10^{-4}M$, methanol concentrations of the order of $10^{-6}M$ had no effect on the measured initial rate of ethanol. Under these conditions, ethanol could be determined in the presence of methanol. Thus, at a fixed ethanol concentration of 2.5 × $10^{-4}M$, the above-mentioned linear dependence held over the range 5.0 × 10^{-6}–5.0 × $10^{-5}M$ for ethanol and the straight line obtained conformed to the following regression equation

$$IR = 0.464 + 2.60 \times 10^{3}[\text{ethanol}] (r = 0.992). \quad (1)$$

Under these conditions, the resolution of methanol/ethanol mixtures can be accomplished by using the following procedure· the amount of ethanol required to obtain a concentration of 2.5 × $10^{-4}M$ in this alcohol was added to an aliquot of the unknown sample and the mixture is reacted as described for the individual determination of the alcohols. Substitution of the measured initial rate into equation (1) yields the concentration of ethanol in the unknown sample. Once such a concentration is known, a calibration graph for methanol is constructed in the presence of the determined ethanol concentration (Fig. 3). Then, a new aliquot of the unknown mixture is reacted and the measured initial rate allows the methanol contents in the sample to be determined from the previously run calibration graph. Obviously, this procedure only permits the resolution of methanol/ethanol mixtures with ethanol contents not lower than those of methanol, which is the normal situation in real samples. On the other hand, applying the proposed method to these samples would call for further investigations as

Table 3 Analysis of synthetic mixtures of methanol and ethanol by the stopped-flow technique

Taken, $10^{-6}M$		Ethanol, $10^{-6}M$		Methanol, $10^{-6}M$			
				Initial rate		Final absorbance	
Ethanol	Methanol	Found	Error, %	Found	Error, %	Found	Error, %
50.0	2·00	49·4	−1·2	2·09	4·5	1·92	−4·0
40·0	2·00	41·0	2·5	2·10	5·0	2·08	4·0
30·0	2·00	29·4	−2·0	2·13	6·5	2.11	5·5
20·0	2·00	20·6	3·0	1.87	−6·5	1.88	−6·0
15·0	2·00	15·7	4·7	1·84	−8·0	1·87	−6·5
6·00	1·00	6·16	2·7	1·14	14·0	0·92	−8·0
5·00	1·00	4·80	−4·0	1·15	15·0	1·06	6·0
6·00	2·00	6·33	5·5	2·21	10·5	1.85	−7·5
5·00	2·00	5·20	4·0	2·20	10·0	1·87	−6·5
6·00	3·00	6·20	3·3	3·29	9·7	2·76	−8·0
5·00	3·00	4·81	−3·8	3·25	8·3	3·26	8·7
5·00	3·80	4·80	−4·0	4·02	5·8	3.92	3·1
5·00	5·00	5·10	2·0	5·30	6·0	4·70	−6·0

regards sample pretreatment in order to avoid potential interferences.

The results obtained for several synthetic mixtures of methanol and ethanol are summarized in Table 3. As can be seen in the table, methanol was determined from two calibration curves: initial rate and net absorbance change *vs.* methanol concentration. Equilibrium measurements resulted in smaller errors in the determination of this alcohol, so they were chosen to analyse for it in this type of sample. Thus, the determination of ethanol/methanol mixtures was feasible over the concentration ratio range 25·1–1:1. When the recommended procedure was applied to a series of 11 samples containing (a) $5.0 \times 10^{-6}M$ ethanol and $3.0 \times 10^{-6}M$ methanol; (b) $2.0 \times 10^{-5}M$ ethanol and $2.0 \times 10^{-6}M$ methanol, and (c) $5.0 \times 10^{-5}M$ ethanol and $2\,0 \times 10^{-6}M$ methanol, the average relative standard deviations (for both species) were 3.86, 5.05 and 4.61%, respectively.

Compared with other methods for the resolution of ethanol/methanol mixtures based on the same enzymatic reaction [*e.g.*, the simultaneous determination of these alcohols by flow-injection analysis[8]] the proposed stopped-flow method can be applied to higher ethanol/methanol ratios and is more precise: the flow-injection method allows the resolution of ethanol/methanol mixtures in the weight ratio range of only 3.3:1.0–1.0:1.3, with a precision (RSD) between 6.0 and 7.1%.

Acknowledgements—The authors gratefully acknowledge financial support from the DIGICyT (Spain) (Project No PB91–0840), as well as from the Deutscher Akademischer Austauschdienst in Bonn and the Institut für Analytische Chemie of the Mining Academie Freiberg (Germany)

REFERENCES

1 R M Anthony, C A Suitheimer and I Sunshine, *J Anal Toxicol*, 1980, **4**, 43
2 J P Camelbeeck, D M Comberbach, J Goossens and P Roelants, *Biotechnol Tech*, 1988, **2**, 183
3 D Ge, J Wang, J Guo and B He, *Sepu*, 1989, **7**, 384
4 S T Cheung and W N Lin, *J Chromatogr Biomed Appl*, 1987, **58**, 248
5 H Tanner and H Limacher, *Fleuss Obst*, 1984, **35**, 182
6 K Isshiki, *Shokuhin-Eiseigaku-Zasshi*, 1985, **26**, 39
7 M Ignaczak and J Dziegiec, *Chem Anal (Warsaw)*, 1982, **27**, 505
8 A Maqueira, M D Luque de Castro and M Valcárcel, *Michrochem J*, 1987, **36**, 309
9 A Loriguilo, M Silva and D Pérez-Bendito, *Anal Chim Acta*, 1987, **199**, 29
10 H A Mottola, *Kinetic Aspects of Analytical Chemistry*, Wiley, New York,1988
11 J. March, *Advanced Organic Chemistry Reactions, Mechanisms, and Structure*, 3rd Ed, pp 1089, 1092 and 1110 Wiley, New York, 1985
12 H Belghith, J L Romette and D Thomas, *Biotechnol Bioeng*, 1987, **30**, 1001
13 A Ríos, M Silva and M Valcárcel, *Z Anal Chem*, 1985, **320**, 762
14 A Marín, M Silva and D Pérez-Bendito, *Anal Chim Acta*, 1987, **197**, 77
15 A Loriguillo, M Silva and D Pérez-Bendito, *ibid*, 1988, **212**, 233

Talanta, Vol 40, No 6, pp 863–866, 1993
Printed in Great Britain

0039-9140/93 $6 00 + 0 00

ASSIGNMENT OF STANDARD pH VALUES [pH*(s)] TO BUFFERS IN 50 MASS % METHANOL + WATER FROM 288.15 TO 308.15 K

H. A. AZAB

Chemistry Department, Faculty of Science, Assiut University, Assiut, Egypt

(*Received* 26 *June* 1992 *Revised* 20 *October* 1992 *Accepted* 20 *October* 1992)

Summary—The secondary dissociation constants of *o*-phthalic and phosphoric acids have been determined in methanol + water (50 mass %) from reversible e m f measurements of the cell of the type Pt, H_2(1 atm)|M_2A(m), MHA(m), MCl|AgCl, Ag at different temperatures (288 15–308 15 K) and at different ionic strengths To minimize the unsteadiness in potential measurements palladium coated platinum electrodes have been used The large set of such e m f values has been analyzed in terms of a multi-linear regression method recommended in recent IUPAC documents The thermodynamic values $\Delta G°$, $\Delta H°$ and $\Delta S°$, for the respective equilibria, were estimated Standard pH values [pH*(s)] have been assigned to buffers in methanol + water (50 mass %) at temperatures between 288 15 and 308 15 K

The study of the dissociation equilibria of phosphoric and *o*-phthalic acids in water[1–5] has permitted the combination of a series of standard aqueous buffer solutions. The standardization of pH* measurements in mixed solvents, needs similar studies regarding the dissociation equilibria of certain adequate electrolytes in these solvents.[6,7] In the present work the second-stage dissociation constant of phosphoric and *o*-phthalic acid in methanol + water (50 mass %) have been determined as part of a program to develop standard buffer solutions.[5,8]

EXPERIMENTAL

All reagents used were of AnalaR (BDH) grade. All stock solutions were prepared in doubly-distilled air free conductivity water. Methanol + water (50 mass %) was prepared by mixing appropriate amounts of analytical grade methanol, fractionally distilled before use, with conductivity water. Owing to the low solubility of dipotassium phosphate in the given solvent, disodium phosphate was used. *o*-Phthalic acid, potassium chloride and certified ULTREX Baker potassium hydrogen phthalate were dried at 383.15 K before use. The potentiometric measurements, the preparation and standardization of the silver–silver chloride electrode were carried out as described earlier.[8] The values of the standard potential of the Ag/AgCl electrode ${}_sE°_{AgCl}$, in methanol + water H_2O (50 mass %) from 288.15 to 308.15 K have been determined and are given in Table 1. Each measured e.m.f. value was corrected to 1 atm (101,325 Pa) pressure of hydrogen from the barometric pressure and the vapor pressure of the solution, the latter being taken as the same as the vapor pressure of the solvent.[9–11] An average of about four independent cells were measured at each electrolyte molality and at each temperature The large set of such e.m.f. values has been analyzed in terms of a multi-linear regression method recommended in recent IUPAC documents.[12]

RESULTS AND DISCUSSION

Electrochemical cells without liquid junction potentials of the type:

$$\text{Pt}|H_2(1\text{ atm})|M_2A(m),\ \text{MHA(m)},\ \text{MCl(m)}|\text{AgCl}|\text{Ag} \quad (1)$$

were used to determine pK_{a_2} values of *o*-phthalic and phosphoric acid in methanol + water (50 mass %) from 288.15 to 308.15 K.

A represents the $C_6H_4(COO)_2^{2-}$ and HPO_4^{2-} anions and M^+ the Na^+ or K^+ cations.

For the equilibrium

$$HA^- \rightleftharpoons A^{2-} + H^+$$

$$K_2 = \frac{a_H^+ \cdot m_A^{2-} \cdot \nu_A^{2-}}{m_{HA^-} \cdot \nu_{HA^-}} \quad (2)$$

Table 1 Standard potential ($E°$) of the Ag/AgCl electrode in methanol + water (50 mass %) at different temperatures (288 15–308 15 K)

T, K	$E°$, V
288 15	0 1975
293 15	0 1935
298 15	0 1893
303.15	0 1850
308 15	0 1802

when the concentrations are such that $m_{Cl^-} = m_{HA^-} = m_A^{2-}$ relationship (3) can be derived[8]

$$pKa_2 + \beta I = \left(\frac{(E - E°)F}{2.303\ RT}\right) + \log m + \frac{2AI^{1/2}}{1 + Ba°I^{1/2}} \quad (3)$$

where A and B are the constants of the Debye–Hückel equation for the respective solvent which were derived for methanol + water (50 mass %) from the expressions given by Robinson and Stokes:[13]

β is the salting-out parameter and $a°$ is an "ion-size" parameter which has been assigned the widely used value of 4.4 Å. Electric permittivities (ϵ), for the solvents containing methanol were not available in the literature for temperatures other than 298.15 K.[14] However, it was observed from the data of Akerlof[15] that the relationship between the log of the electric permittivity and temperature is linear and that the gradients of the lines for various organic solvents and their aqueous mixtures are essentially parallel. This provided an acceptable method for extrapolating the measured electric permittivities for methanol + water (50 mass %). An equation for the least-squares regression line for the relationship between $\log \epsilon_{H_2O}$ and temperatures was derived from the data given by Hamer[16]

$$\log \epsilon = 0.00197\ t + 1.9431 \quad (4)$$

where t is expressed in °C.

The Debye–Hückel constants for methanol + H_2O (50 mass %) at temperatures other than 298.15 K were calculated using electric permittivities estimated from the known difference between ϵ_{H_2O} and the electric permittivity for the mixed solvent at 298.15 K by extrapolating the difference to different temperatures.

By representing the right hand side of equation (3) vs. concentration (m) graphically, a straight line intersecting the ordinates at pKa_2 is obtained.

Table 2 Experimental data obtained by electrochemical cell (1) for $KH_2PO_4(m) + Na_2HPO_4(m) + NaCl(m)$ in methanol + water (50 mass %)

T, K	m	I	E, V	$P_s(a_H\ \nu_{Cl^-})$	$-\log \nu_{Cl^-}$	pH*(s)
	0.001	0 005	0 845	8.324	0 0534	8 271 ± 0.001
	0 002	0 010	0 825	8 275	0 0723	8 203 ± 0 002
288 15	0 003	0 015	0 812	8 224	0 0857	8 138 ± 0 001
	0 004	0 020	0 803	8 192	0 0964	8 096 ± 0 001
	0 005	0 025	0 796	8 166	0 1054	8.061 ± 0 002
	0.001	0 005	0 851	8 303	0.0535	8 249 ± 0.002
	0 002	0 010	0 830	8.243	0.0726	8.170 ± 0.001
293 15	0 003	0 015	0 818	8 212	0 0860	8 126 ± 0 002
	0.004	0 020	0 808	8 165	0 0967	8 068 ± 0 001
	0 005	0 025	0.801	8.142	0.1057	8.036 ± 0.002
	0 001	0 005	0 857	8.287	0 0541	8 233 ± 0 001
	0 002	0 010	0 836	8 233	0 0733	8 160 ± 0 002
298.15	0 003	0 015	0 823	8 189	0 0869	8 102 ± 0 001
	0 004	0 020	0.813	8 145	0 0977	8 047 ± 0 002
	0.005	0 025	0 806	8 124	0.1067	8.017 ± 0.002
	0 001	0 005	0 862	8 255	0 0545	8 200 ± 0 001
	0 002	0 010	0 842	8 223	0 0738	8 149 ± 0.001
303.15	0.003	0 015	0 829	8 183	0 0875	8.095 ± 0.002
	0 004	0.020	0.819	8.142	0 0984	8 044 ± 0.002
	0.005	0 025	0 811	8 106	0.1075	7 998 ± 0 001
	0 001	0 005	0 868	8 248	0 0549	8 193 ± 0 001
	0 002	0 010	0 848	8 222	0 0743	8 148 ± 0 002
308.15	0 003	0 015	0 834	8 169	0 0880	8.081 ± 0.002
	0 004	0 020	0.824	8.131	0 0990	8 032 ± 0.001
	0 005	0 025	0 816	8.097	0 1081	7 989 ± 0 002

Table 3 Experimental data obtained by electrochemical cell (1) for $C_6H_4(COOK)_2(m) + HKC_6H_4(COO)_2(m) + KCl(m)$ in methanol + water (50 mass %)

T, K	m	I	E, V	$P_s(a_H \nu_{Cl^-})$	$-\log \nu_{Cl^-}$	pH*(s)
	0.002	0 01	0 783	7 541	0 0723	7 469 ± 0 001
	0.004	0 02	0 761	7 457	0 0964	7 361 ± 0 002
288.15	0 006	0 03	0 746	7 371	0 1131	7 258 ± 0 001
	0 008	0 04	0 736	7 321	0 1262	7 195 ± 0 002
	0.010	0 05	0 727	7 202	0 1369	7 065 ± 0 001
	0 002	0 01	0 789	7 538	0.0726	7 465 ± 0.002
	0.004	0.02	0 766	7.443	0 0967	7 346 ± 0 001
293 15	0 006	0 03	0 752	7.379	0 1135	7 266 ± 0 002
	0 008	0 04	0 741	7.315	0 1266	7 188 ± 0 001
	0 010	0.05	0 731	7 239	0 1374	7 102 ± 0 001
	0 002	0 01	0 794	7 523	0 0733	7 450 ± 0 001
	0 004	0 02	0 771	7 435	0 0977	7 337 ± 0 002
298 15	0.006	0 03	0 756	7.358	0 1146	7 243 ± 0 002
	0 008	0 04	0.745	7 296	0.1278	7 168 ± 0 001
	0 010	0 05	0 736	7 241	0 1387	7 102 ± 0 001
	0 002	0 01	0 799	7 508	0 0738	7 434 ± 0 002
	0 004	0.02	0 777	7.444	0 0984	7 346 ± 0 002
303 15	0 006	0 03	0.762	7 370	0.1154	7 255 ± 0.001
	0 008	0.04	0 751	7 312	0 1287	7 183 ± 0 001
	0.010	0 05	0.741	7 243	0 1387	7 103 ± 0 001
	0 002	0 01	0.804	7 502	0.0742	7 428 ± 0.002
	0 004	0 02	0 780	7 411	0 0990	7 312 ± 0 002
308 15	0.006	0 03	0 765	7 342	0 1161	7 226 ± 0 002
	0 008	0 04	0 753	7 271	0 1294	7 142 ± 0.001
	0.010	0.05	0.744	7 220	0 1405	7 079 ± 0 001

Seven cell solutions containing hydrochloric acid at molalities ranging from 0.05 to 0.005 *m* were used to determine the standard potential of the silver–silver chloride electrode. The standard potential, on the molality scale was obtained by extrapolation of

$$E^\circ = E + 2k \log m - \frac{2k A m^{1/2}}{1 + B a^\circ m^{1/2}} \quad (5)$$

to $m = 0$.

This function is derived from the Nernst equation, where a Debye–Hückel expression has been included to approximate the mean activity coefficient of HCl. The term k is written for RT ln $10/F$ and the Debye–Hückel constant A and B were calculated as mentioned above.

The acidity function $P_s(a_H \cdot \nu_{Cl})$ has been obtained from the e.m.f. of the hydrogen–silver chloride cell (1) containing the standard solutions (with added chloride) in methanol + water medium.[17]

$$P_s(a_H \cdot \nu_{Cl}) = \frac{(E - E^\circ)F}{2.303RT} + \log m_{Cl} \quad (6)$$

and then pa_{H^*} by the non-thermodynamic step

$$pa_{H^*} = P_s(a_H \cdot \nu_{Cl}) + \log {}_s\nu_{Cl} \quad (7)$$

Data for the experimental measurements of e.m.f. of cell (1) at different temperatures (288.15–308.15 K) and different ionic strengths are given in Tables 2 and 3 for both *o*-phthalic and phosphoric acid in methanol + water (50 mass %). As the concentration of the supporting electrolyte increased, a salting out effect is observed. This is because the activity coefficient of the uncharged particles present in solution is changed on increasing the concentration of the dissolved salt.

Table 4 pKa_2 values of *o*-phthalic acid in methanol + H_2O (50 mass %) at different temperatures and ionic strengths

288.15 K		293 15 K		298 15 K		303 15 K		308 15 K	
I	pKa_2	I	pKa_2	I	pKa_2	I	pKa_2	I	pKa_2
0	7 735 ± 0.002	0	7 723 ± 0.002	0	7 710 ± 0 004	0	7 690 ± 0.003	0	7.684 ± 0.004
0.002	7 671 ± 0.003	0.002	7 659 ± 0 003	0.002	7.646 ± 0 003	0 002	7.626 ± 0.004	0 002	7.620 ± 0.003
0.004	7.646 ± 0.004	0.004	7.634 ± 0 004	0.004	7.621 ± 0.002	0 004	7 601 ± 0.004	0.004	7 595 ± 0.002
0.006	7 628 ± 0.003	0.006	7 616 ± 0 003	0.006	7.603 ± 0 004	0 006	7 583 ± 0.003	0 006	7 577 ± 0.003
0.008	7.612 ± 0.002	0.008	7.600 ± 0 004	0.008	7.587 ± 0.003	0 008	7 567 ± 0.002	0.008	7 561 ± 0.002
0.010	7.599 ± 0.003	0.010	7.587 ± 0.002	0 010	7 574 ± 0 002	0.010	7 554 ± 0.004	0.010	7 548 ± 0.003

Table 5 pKa_2 values of phosphoric acid in methanol + H_2O (50 mass %) at different temperatures and ionic strengths

288 15 K		293 15 K		298 15 K		303 15 K		308 15 K	
I	pKa_2	I	pKa_2	I	pKa_2	I	pKa_2	I	pKa_2
0	8 430 ± 0 002	0	8 418 ± 0 003	0	8 410 ± 0 003	0	8 397 ± 0 003	0	8 389 ± 0 003
0.001	8.384 ± 0 003	0.001	8 372 ± 0 004	0 001	8 364 ± 0 004	0 001	8 351 ± 0 004	0 001	8 343 ± 0 002
0.002	8 366 ± 0.003	0.002	8 354 ± 0 004	0 002	8.346 ± 0 004	0 002	8 333 ± 0 004	0 002	8 325 ± 0 003
0.003	8 352 ± 0.004	0 003	8 340 ± 0 002	0 003	8 332 ± 0 004	0 003	8 319 ± 0 004	0 003	8 311 ± 0 004
0.004	8.341 ± 0 004	0 004	8 329 ± 0 003	0 004	8 321 ± 0 002	0 004	8 308 ± 0 002	0 004	8 300 ± 0 002
0 005	8 331 ± 0 004	0 005	8 319 ± 0 004	0 005	8.311 ± 0 003	0 005	8 298 ± 0 003	0 005	8 290 ± 0 002

Table 6 Thermodynamic parameters for the secondary dissociation of *o*-phthalic and phosphoric acid in methanol + H_2O (50 mass %)

Acid	T, K	ΔG° (kJ/mole)	ΔH° (kJ/mole)	$-\Delta S^\circ$ (Jk^{-1} mole^{-1})
	288 15	42.65 ± 0 002	2 38 ± 0 02	139 73 ± 0 05
	293 15	43 32 ± 0 002	2 46 ± 0 01	139 38 ± 0 04
o-Phthalic	298 15	43 99 ± 0 004	2 55 ± 0 01	138 99 ± 0 06
	303 15	44 61 ± 0 003	2 64 ± 0 02	138 44 ± 0 04
	308 15	45 31 ± 0 003	2 72 ± 0 02	138 21 ± 0 03
	288 15	46 48 ± 0 002	3 81 ± 0 01	148 08 ± 0 04
	293 15	47 22 ± 0 003	3 94 ± 0 02	147 63 ± 0 05
Phosphoric	298 15	47 98 ± 0 003	4 07 ± 0 01	147 27 ± 0 04
	303.15	48 71 ± 0 003	4 21 ± 0 02	146 79 ± 0 05
	308 15	49 47 ± 0 003	4 35 ± 0 01	146 42 ± 0 04

The secondary dissociation constants of *o*-phthalic and phosphoric acids in methanol + water (50 mass %) at different temperatures (288.15–308.15 K) and at different ionic strengths are given in Tables 4 and 5. Values of pKa_2 at different ionic strengths have been calculated using a convenient form of the Debye–Hückel equation, such as that due to Davies.[18] Values of the thermodynamic parameters ΔG°, ΔH° and ΔS° for the second dissociation stage of *o*-phthalic and phosphoric acid have been calculated and are given in Table 6.

The need for reliable pH measurements at different temperatures in mixed solvents such as methanol and water has become increasingly apparent in different biological studies. The data obtained in the present report can be used for preparing standard buffer solution for pH*(s) measurements in methanol + water (50 mass %) at different temperatures (288.15–308.15 K) as shown in Tables 2 and 3.

REFERENCES

1 W J Hamer and S F Acree, *J Res Nat Bur Stand*, 1944, **32**, 215
2 *Idem*, *ibid*, 1945, **35**, 381
3 G G Manov, N J Delollis, P W Lindwal and S F Acree, *ibid*, 1946, **36**, 543
4 R G Bates, V E Bower, R G Miller and E R Smith, *ibid*, 1951, **47**, 433
5 H. A Azab, *Bull Soc Chim France*, 1987, **2**, 265
6 M Paabo, R A Robinson and R G Bates, *J Am Chem Soc*, 1965, **87**, 415
7 R N Roy, J J Gibbons, B Kennan and F Steven, *J Chem Soc*, *Faraday Trans*, 1984, 80, 3167
8 H A Azab, *Talanta*, 1992, **39**, 913
9 R G Bates, *Determination of pH*, p 282 Wiley, New York, 1973
10 M Sankar, J B Macaskill and R G Bates, *J Soln Chem*, 1979, **8**, 887
11 A Patterson and W A Felsing, *J Am Chem Soc*, 1942, **64**, 1478
12 S Rondinini, P R Mussini and T Mussini, *Pure Appl Chem*, 1987, **59**, 1549
13 R A Robinson and R H Stokes, *Electrolyte Solutions*, 2nd Ed, Butterworths, London, 1968
14 D Dobos, *Electrochemical Data*, p 140 Akademiai Kiado, Budapest, 1975
15 G Akerlof, *J Am Chem Soc*, 1932, **54**, 4125
16 W J Hamer, *Handbook of Chemistry and Physics*, R S Weast (ed), 52nd Ed, Chemical Rubber Co, Cleveland, Ohio, 1971
17 R G Bates, *Determination of pH Theory and Practice*, p 225 Wiley, New York, 1964
18 C W Davies, *J Chem Soc*, 1938, 2093

Talanta, Vol 40, No 6, pp 867–878, 1993
Printed in Great Britain

0039-9140/93 $6.00 + 0.00

DESIGN AND PERFORMANCE OF A NEW CONTINUOUS-FLOW SAMPLE-INTRODUCTION SYSTEM FOR FLAME INFRARED-EMISSION SPECTROMETRY: APPLICATIONS IN PROCESS ANALYSIS, FLOW INJECTION ANALYSIS, AND ION-EXCHANGE HIGH-PERFORMANCE LIQUID CHROMATOGRAPHY

CHRISTOPHER K. Y. LAM, YUNKE ZHANG, MARIANNA A. BUSCH and KENNETH W BUSCH*
The Department of Chemistry, P.O Box 97348, Baylor University, Waco, TX 76798–7348, U S A

(*Received* 31 *July* 1992. *Revised* 15 *October* 1992. *Accepted* 15 *October* 1992)

Summary—A new sample introduction system for the analysis of continuously flowing liquid streams by flame infrared-emission (FIRE) spectrometry has been developed. The system uses a specially designed purge cell to strip dissolved CO_2 from solution into a hydrogen gas stream that serves as the fuel for a hydrogen/air flame. Vibrationally excited CO_2 molecules present in the flame are monitored with a simple infrared filter (4.4 μm) photometer The new system can be used to introduce analytes as a continuous liquid stream (process analysis mode) or on a discrete basis by sample injection (flow injection analysis mode). The key to the success of the method is the new purge-cell design The small internal volume of the cell minimizes problems associated with purge-cell clean-out and produces sharp, reproducible signals Spent analytical solution is continuously drained from the cell, making cell disconnection and cleaning between samples unnecessary. Under the conditions employed in this study, samples could be analyzed at a maximum rate of approximately 60/h. The new sample introduction system was successfully tested in both a process analysis- and a flow injection analysis mode for the determination of total inorganic carbon in Waco tap water. For the first time, flame infrared-emission spectrometry was successfully extended to non-volatile organic compounds by using chemical pretreatment with peroxydisulfate in the presence of silver ion to convert the analytes into dissolved carbon dioxide, prior to purging and detection by the FIRE radiometer. A test of the peroxydisulfate/Ag^+ reaction using six organic acids and five sugars indicated that all 11 compounds were oxidized to nearly the same extent. Finally, the new sample introduction system was used in conjunction with a simple filter FIRE radiometer as a detection system in ion-exchange high-performance liquid chromatography. Ion-exchange chromatograms are shown for two aqueous mixtures, one containing six organic acids and the second containing six mono-, di-, and trisaccharides

Although the analytical application of gas-phase infrared emission is well documented for the case of remote sensing of pollutants in smokestack plumes[1–5] and gases in jet engine exhaust,[6] its use as a means of routine quantitative analysis in the laboratory is relatively new.[7–9] When flame/furnace infrared-emission (FIRE) spectrometry is employed in the laboratory, samples are introduced into a heated environment (such as a small flame[10] or electrically heated furnace[11,12]) where they are typically converted into small, thermally-stable, vibrationally-excited molecules.[13,14] The characteristic infrared bands emitted by these molecules are generally well resolved and can be detected with a simple infrared filter photometer.[7]

Because FIRE spectrometry is a relatively new analytical technique, much of the previous work has concentrated on improving instrumental performance.[10,11,15–19] Although it is clear from previous studies that gas-phase infrared emission from selective radiators could be useful analytically in a number of significant areas,[7] the key to the analytical success of the technique depends on the availability of a reliable means of sample introduction.[20–23] In particular, the ability to determine analytes present in continuously flowing liquid streams would be useful for applications involving process analysis,[24] flow injection analysis (FIA),[25] and high-performance liquid chromatography (HPLC).[26]

One way to introduce a liquid sample into a flame or furnace on a continuous basis is in the form of a fine spray. Although both thermospray and pneumatic nebulization show

*Author for correspondence.

some promise as means of analyzing liquid streams on a continuous basis, the sensitivity achieved by spraying aqueous samples directly into a small flame or furnace has been relatively disappointing to date.[27,28] Poor sensitivity can be attributed to cooling of the excitation source by liquid evaporation. (Evaporation of as little as 1 ml/min of an aqueous stream by a microflame or low thermal-mass furnace of the type used in FIRE spectrometry will produce a measurable depression in the excitation temperature of the source [27]) When the power to the thermospray nebulizer was increased to completely vaporize the liquid stream prior to introduction into the source, the relatively large amount of water vapor diluted the analyte and significantly increased the magnitude of the water background emission in the FIRE spectrum.[27] Regardless of the type of nebulizer used, small fluctuations in nebulizer efficiency gave rise to increased background noise resulting from changes in excitation temperature, source background, or a combination of both.[28]

Compared with FIRE-HPLC applications involving direct introduction of liquid into the source,[28] FIRE-GC applications involving direct introduction of gas-phase samples into the source have produced improved detection limits which are typically in the low ng/sec range.[10] Improved detection limits for liquid samples have been obtained in some FIRE applications[21-23] through the use of purge tubes, which permit the sparging of volatile analytes out of the liquid and into the flame. The major disadvantages with previous sparging approaches[21-23] have been, (1) the large internal volume introduced by the purge tube, (2) the relatively long time period between samples (about 3–6 min) due to disconnection of the sample purge tube for cleaning and refilling, (3) the additional purge tube and valving system required to maintain gas flow and stabilize the flame during cleaning of the sample cell, and (4) the limitation of the technique to relatively volatile, dissolved analytes.

In spite of the disadvantages associated with the earlier use of purge tubes, the improved detection limits obtained by sparging discrete samples from liquids[21-23] (compared to direct introduction of liquid into the source[27,28]), suggested that a sparging approach might be useful in improving the sensitivity of FIRE spectrometry for liquid samples. This paper reports a new sample introduction sample for FIRE spectrometry that is highly versatile and can be used to analyze liquid streams on a continuous basis. The key to this system is a specially designed purge tube which introduces less than 2 ml of internal volume and does not require disconnection between samples.

To demonstrate the potential of the new sample introduction system, the specially designed purge tube was used for the determination of total inorganic carbon (TIC) by FIRE spectrometry in both a process analysis and a flow injection analysis mode. Finally, an improved FIRE-HPLC detector, which uses the new purge tube, is described. This detector, which, in principle, should be universal for all oxidizable organic compounds, was used to monitor organic acids and sugars which had been separated by ion-exchange HPLC.

EXPERIMENTAL

FIRE radiometer

A standard, single-channel, filter FIRE radiometer of the type described previously[7] was used for these studies. The radiometer consisted of a flame excitation source, a chopper, calcium fluoride collection optics, a bandpass filter, a lead selenide detector, and a preamplifier. Signal from the preamplifier was fed to a lock-in amplifier (Model #HP3962, Ithaco, Inc., Ithaca, NY) whose output was monitored with a recorder/integrator (Model #3396A, Hewlett-Packard Corp., North Hollywood, CA). A bandpass filter with a transmission band at 4.4 μm (Part #58300, Oriel Corp., Stratford, CT) was used to select the antisymmetric stretching vibration of CO_2 from the other infrared radiation emitted by the flame.[22]

An improved two-tube burner, described previously,[10] was used as the excitation source. In this study, the inner stainless steel capillary was replaced with a nickel capillary [Part #31313, Alltech Associates, Inc., Deerfield, IL; i.d. 0.51 mm (0.020 in.); o.d., 1.59 mm (1/16 in.)] because of its superior resistance to attack by hydrochloric acid. The inner nickel capillary was centered and positioned so that its tip was 1 mm above the outer stainless steel tube (Part #2-0384, Supelco, Inc., Bellefonte, PA) using a glass wool plug. A diffusion flame was maintained on the burner by flowing hydrogen gas up the central nickel capillary and air up

the outer stainless steel tube. The flow rate of H_2 was maintained with a flow controller (Part #8148, Alltech Associates, Inc.), and air flow was controlled with a rotameter (Part #03216–18, Cole Palmer, Chicago, IL).

Purge cell

Figure 1 shows a schematic diagram of the purge cell used in this study. The lumen of the cell had an inside diameter of 10 mm, a length of 30 mm, and a total volume of 2.4 cm^3. The top portion of the cell was sealed with a Teflon® [poly(tetrafluoroethylene)] stopper, TC [Fig. 1(A)], which was fitted with an O-ring [O, Fig. 1(A)]. A length of Teflon® tubing [Part #123814, Spectrum Scientific, Los Angeles, CA; o.d., 3 17 mm (1/8 in.); i d., 0.79 mm (1/32 in)] served as the sample conduit and was passed into the cell through a hole drilled in the center of the Teflon® stopper. The bottom end of the purge cell was connected to the purge gas supply through a gas dispersion tube, G (Part #9435-09, Ace Glass, Vineland, NJ; o.d., 5 mm). The gas dispersion tube was held in place by two Nylon nuts, N (Part #NY-402-1, Swagelok Co., Solon, OH) that compressed O-rings against the dispersion tube when tightened to the two ends of a Nylon union, U (Part #NY-400-1-4, Swagelok Co.). The side arm of the purge cell (o.d., 6.35 mm; i d , 3.96 mm) was located just below the bottom of the Teflon® stopper [Fig. 1(B)]. The porous end of the gas dispersion tube, F, and the end of the Teflon® tube that served as the sample conduit were adjusted so that they were separated by about 1 mm, and the vertical distance from the top of

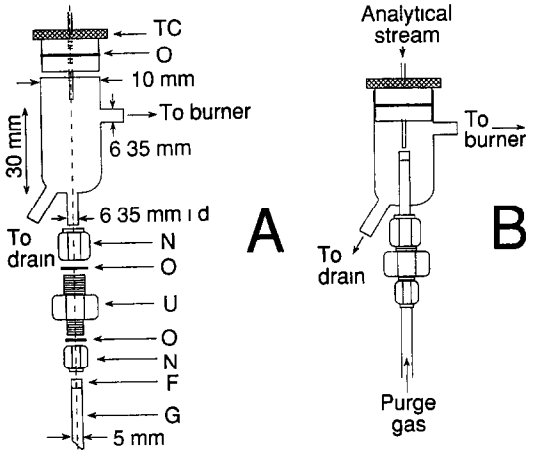

Fig 1 Schematic diagram and dimensions for the continuous-flow purge cell (A) Exploded view (B) Assembled TC, Teflon® cap, O, O-ring, N, nylon nut, U, nylon union, F, porous glass frit, G, gas dispersion tube

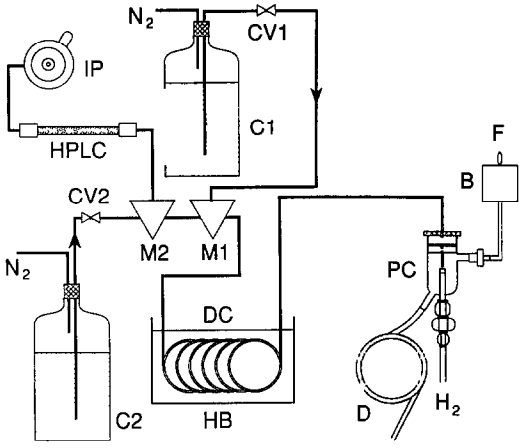

Fig 2 Schematic diagram of the continuous-flow sample delivery system configured for high-performance liquid chromatography IP, injection port of the liquid chromatograph, HPLC, chromatographic column, M1, M2, multiport valves, C1, C2, glass carboys, CV1, CV2, check valves, DC, delay coil, HB, hot bath, PC, continuous-flow purge cell, D, drain, B, two-tube burner, F, hydrogen/air flame, N_2, nitrogen gas inlet, H_2, hydrogen gas inlet Air supply for the hydrogen/air flame not shown

the gas dispersion tube to the center axis of the side arm of the purge cell was approximately 5–6 mm.

The purge cell was connected to the two-tube burner (Fig 2) by mean of Teflon® tubing [o.d., 3.17 mm (1/8 in.), i.d., 1.59 mm (1/16 in.)]. This tubing was connected to the side arm of the purge cell by means of a 1/4–1/8 in. reducing union (Part #B-400-6-2, Swagelok Co.) and to the central capillary of the burner by means of a 1/8–1/16 in reducing union (Part #B-200-6-1, Swagelok Co.).

A length of Tygon® tubing (Part #6409-18, Norton Co, Worcester, MA; o.d., 11 mm; i.d., 8 mm) was connected to a tube at the bottom of the purge cell by means of a hose clamp and allowed the spent liquid in the purge cell to drain into a waste container. The diameter of this tubing was selected so as to introduce the smallest possible volume while still allowing the liquid to drain freely A loop, formed in the Tygon® tubing and filled with solution (Fig. 2), prevented the escape of gas through the drain.

Hydrogen gas was used to purge the analytical stream. A cylinder of hydrogen gas was connected to the gas dispersion tube with Tygon® tubing (Part #6409-25, Norton Co., o.d., 8 mm; i d., 4.8 mm) which was held in place with a hose clamp.

Purge cell performance was evaluated as a function of several design parameters and operating conditions. These included the effect of

reagent- and purge-gas flow rates, reagent concentrations and three different frit porosities in the gas dispersion tube.

Sample introduction

Liquid streams were introduced into the purge cell through a length of Teflon® tubing. One end of this tubing passed through the Teflon® stopper of the purge cell, as described previously, and the other end was connected to the sample delivery system. Three sample delivery systems were studied.

HPLC mode. Figure 2 shows a diagram of the delivery system used for HPLC applications. Two separate nitrogen gas cylinders were used to pressurize two heavy-walled glass carboys (2-l. capacity, catalog #45-3203, Rainin Instrument, Woburn, MA, 5-l. capacity, catalog #45-3205, Rainin Instrument), equipped with special caps to which tubing could be connected. The pressure, which was controlled by standard, two-stage regulators, was typically maintained at 7–14 kPa above atmospheric (1–2 psig), but in no case exceeded the rating of the glass carboys (10 psig). Each outlet from the two carboys was connected to its own check valve (Part #J-6468-80, Cole Palmer) and then to its own three-way connector (Part #OM-1003, Chrom Tech Inc., Apple Valley, MN) which served as a mixer. One three-way connector (M2, Fig. 2) mixed the effluent from the chromatograph (Varian 5000 Liquid Chromatograph, Varian, Sunnyvale, CA) with the contents of carboy C2. The other connector (M1, Fig. 2) permitted addition of reagent from carboy C1 to the liquid stream. A delay coil, which could be maintained at a fixed, constant temperature by means of a hot bath, could be inserted after the two mixers. Teflon® tubing [catalog #6468-08, Cole Palmer; i.d., 0.79 mm (1/32 in.)] was used for all connections.

A sample injection loop of 20 μl (Model #00-997182-04, Varian) or 50 μl (Model #00-997182-05, Varian) volume was employed. All samples were injected onto the HPLC column manually using a 100-μl syringe (Model #00-997074-04, Varian).

Ion-exchange HPLC of a mixture of organic acids (butyric, formic, fumaric, oxalic, propionic, and tartaric) dissolved in deionized water (Continental Water System Co., Austin, TX) was performed using an ORH-801 column (Interaction Chemicals, Mt. View, CA) packed with cation-exchange polymer in the hydrogen form. The 30-cm long by 6.5-mm diameter column was maintained at 37° by means of a water jacket (Model #9502, Alltech Associates) connected to a circulating water bath (Model Type MS, Lauda, Westbury, NY). A GC-801 IonGuard® guard column (Interaction Chemicals) was connected between the injector and the analytical column. Separation was performed using 0.01*N* nitric acid (ACS reagent grade, Fisher Scientific, Pittsburgh, PA) in HPLC-grade water (Fisher Scientific) as the mobile phase at a flow rate of 0.8 ml/min.

Ion-exchange HPLC of a mixture of sugars (fructose, galactose, glucose, mannitol, raffinose, and sucrose) dissolved in deionized water was performed using a CHO-620 carbohydrate column (Interaction Chemicals) packed with a cation-exchange polymer in the Ca^{2+} form. The 30-cm long by 6 5-mm diameter column was maintained at 90° by means of the same water jacket and recirculating water bath employed in the separation of organic acids. A precolumn filter (Model #A-318, Upchurch Scientific, Oak Harbor, WA) and GC-620 IonGuard® guard column (Interaction Chemicals) were placed between the injector and the analytical column. Separation was performed using HPLC-grade water as the mobile phase at a flow rate of 0.5 ml/min.

FIA mode. In this arrangement, the separation channel, consisting of the injection port, HPLC column, and the mixer, M2, was removed, and a septum injector (Part #OM-3301, Chrom Tech Inc.) for sample introduction was interposed between the check valve, CV2, and the remaining three-way connector, M1. Samples were injected manually using either a 25- or 250-μl syringe (catalog #725SNR and #702SN, Hamilton Co., Reno, NV). Both carboys were pressurized as described previously, with flow for the carrier provided by pressurization of carboy C2.

Process analysis mode. This arrangement was similar to the FIA mode, but the septum injector was not used, and the sample was introduced continuously from a carboy Carboy C1 in Fig. 2 was replaced by three, 2-litre carboys connected in parallel, which were used for the introduction of blank, sample, and analytical standard, as desired. The three carboys connected in parallel were pressurized from a single nitrogen gas supply, and a four-way valve (Part #45-1118, Rainin Instrument), which was located ahead of the check valve, CV1, was used to select the desired solution.

Sample pretreatment

Determination of total inorganic carbon (TIC) required addition of hydrochloric acid (Fisher Scientific) to the sample stream prior to purging, while organic acids and sugars required addition of sodium peroxydisulfate ($Na_2S_2O_8$, Sigma, St Louis, MO) and a catalyst. Silver nitrate ($AgNO_3$, Thorn Smith Laboratories, Beulah, MI), cupric sulfate ($CuSO_4$, Mallinckrodt, Inc., St Louis, MO), and ferric chloride ($FeCl_3$, EM Science, Gibbstown, NJ) were each evaluated as a catalyst in the peroxydisulfate method. The effect of three different temperatures on the peroxydisulfate reaction was examined by adjusting the temperature of the hot bath (Fig. 2) to 21, 59, and 89°. Four different lengths and inside diameters of the delay coil were evaluated: 3.05 m (10 ft.) × 0.79 mm (1/32 in.), internal volume of 1.5 ml; 2.13 m (7 ft.) × 0.79 mm (1/32 in.), internal volume of 1.0 ml; 2.13 m (7 ft.) × 1.6 mm (1/16 in), internal volume of 4.3 ml; and 4 27 m (14 ft.) × 1.6 mm (1/16 in.), internal volume of 8.6 ml A delay coil was not employed for TIC determinations.

Reagents

Stock solutions of K_2CO_3 (Analytical Grade, J. T. Baker, Phillipsburg, NJ) were prepared by drying primary standard K_2CO_3 at 110° for 24 hr prior to dissolution in distilled, deionized water. A 0.25*M* solution of hydrochloric acid was prepared by dilution of the concentrated reagent using deionized water. Solutions of sodium peroxydisulfate were prepared by dissolving the solid reagent in deionized water. Solutions containing mixtures of organic acids and sugars were prepared by weighing and dilution with deionized water. Organic acids, sugars, and all reagents not already specified were obtained from typical commercial sources and used without additional purification.

RESULTS AND DISCUSSION

Purge-cell performance

The purge cell is the most critical component of the sample introduction system, and the design shown in Fig. 1 represents the best of several tested. The performance of this purge cell was evaluated using the FIA mode of sample delivery. In this procedure, carboy C1 was filled with a dilute solution of hydrochloric acid, and carboy C2 was filled with deionized water. An aliquot of standardized carbonate (K_2CO_3) solution was injected into the flowing aqueous stream using a 250-μl syringe and converted to CO_2 on mixing with the flowing hydrochloric acid stream. Dissolved CO_2 was liberated from solution at the gas dispersion tube and swept into the hydrogen/air flame by the purge gas (H_2), where it was vibrationally excited and detected by the FIRE radiometer configured in the carbon mode (4.4 μm filter)

In these studies, location of the gas dispersion tube with respect to the side arm of the cell [Fig. 1(B)] did not prove to be critical For convenience, the tube was positioned adjacent to the cell side arm, with the end of the Teflon® sample delivery tube close to, but not touching the tip of the porous frit.

Cell performance was found to vary with frit porosity in the gas dispersion tube. Figure 3(A) shows signals obtained by making replicate 250-μl injections of 12.5m*M* K_2CO_3 solution and acidifying with 0.25*M* hydrochloric acid. These results show that of the three frits tested, the 10–20 μm frit gave the best performance in terms of peak height and average RSD (4–8 μm frit: 35 mm ± 3.3%, 10–20 μm frit: 43 mm ± 3.3%; 25–50 μm frit. 30 mm ± 4.0%). As a result, a frit porosity of 10–20 μm was employed in all further studies.

The effect of hydrochloric acid concentration was also studied. According to the pK_1 and pK_2

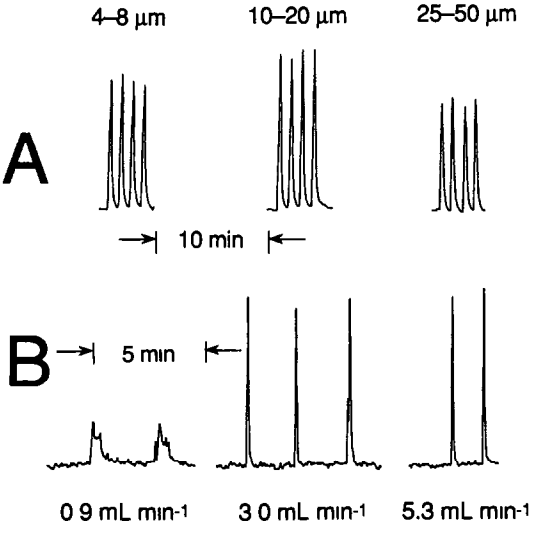

Fig 3. Peak profiles obtained with the sample delivery system configured for flow injection analysis (A) Influence of frit porosity in the gas dispersion tube Injections of 250 μl of 12.5m*M* K_2CO_3 solution mixed with 0 25*M* HCl (acid flow rate, 3.15 ml/min) (B) Influence of HCl flow rate for 10–20 μm frit porosity Injections of 25 μl of 0 241*M* K_2CO_3 solution Deionized water flow rate for (A) and (B), 5 30 ml/min

of carbonic acid (6 37 and 10.25, respectively) a final pH of less than 3.9 should be sufficient to convert all carbonate and bicarbonate in the sample into dissolved carbon dioxide. For samples with a relatively low acid-neutralizing capacity, 0.25*M* hydrochloric acid was used. For samples with a higher acid-neutralizing capacity, the concentration of hydrochloric acid was adjusted accordingly.

The influence of acid flow rate on purging efficiency was also studied. Different flow rates of hydrochloric acid were obtained by using Teflon® delivery tubes with different inside diameters and by adjusting the valve in the carboy cap. Figure 3(B) shows the injection profiles obtained from replicate 25-μl injections of 0.241*M* potassium carbonate solution followed by acidification with 0.25*M* hydrochloric acid. As can be seen from Fig. 3(B), if the flow rate of the hydrochloric acid stream was too slow, purging efficiency was poor, and serious peak broadening and distortion were evident. In general, narrow, symmetric peaks were obtained as long as the hydrochloric acid flow rate exceeded 3 ml/min

Because the purge gas (H_2) also provided fuel for the hydrogen/air flame, selection of the purge gas flow rate was an important factor affecting flame stability, as well as purging efficiency For optimal system performance, a hydrogen flow rate of about 50–70 ml/min was found to be satisfactory While higher flow rates produced stronger signals (as expected for a mass-flow rate detector), baseline fluctuations also increased Ultimately, the maximum hydrogen flow rate that could be used was limited by the internal pressure produced within the purge cell. If the flow rate produced an internal pressure much above one atmosphere, the spent liquid in the 8-mm Tygon® drain loop was expelled, allowing the purge gases to escape.

Because of the nature of the burner used, air flow rates were not particularly critical. As found in previous studies,[10] air flow rates between 100–200 ml/min produced satisfactory results. In general, both the hydrogen and air flow rates were adjusted to obtain optimal burner and purge-cell performance for each analytical application

Compared with the purge cell used in previous studies,[21–23] the new cell design (Fig. 1) offers several advantages. Since the internal free volume of the cell (internal cavity volume minus the volume of the gas dispersion tube) was less than 2 ml, flushing of the purged analyte into the flame was quite rapid, purge-cell clean-out problems were virtually eliminated, and peaks were sharp with minimal tailing [Fig. 3(A)] Since the new cell design continuously drained the spent analytical solution, cell disconnection and cleaning between samples were unnecessary. Therefore, the extra valves and reference purge cell required in the previous purge system[21–23] could be eliminated, and the total analysis time for a large number of samples was considerably shortened. Figure 3(A) shows that samples could be reproducibly injected at a rate of approximately 60/hr, compared with 10–20 samples/hr using the old purge system.[21–23]

Total inorganic carbon

Total inorganic carbon (TIC) in water is defined as the sum of all dissolved carbonates, bicarbonates and carbon dioxide present in the sample.[29] Because the level of TIC affects the pH and mineral content of the water, the measurement of TIC is important in many environmental and industrial areas including oceanography,[30] water resource management,[31] and water/wastewater treatment.[32]

Total inorganic carbon in water is typically determined indirectly from alkalinity titrations and a knowledge of the initial pH of the sample.[29] This indirect procedure depends on two measurements and can produce errors when the sample contains significant, but unsuspected levels of noncarbonate bases that increase the acid-neutralizing capacity of the water sample In contrast to alkalinity measurements, FIRE spectrometry has been shown to offer a sensitive, reproducible, accurate, and direct means of determining TIC, with few interferences.[22] In this earlier FIRE method, demountable purge tubes, requiring disconnection and cleaning between samples, were employed To demonstrate the versatility of the new sample introduction system, TIC in samples of Waco tap water was determined by FIRE spectrometry using both the process analysis and FIA modes of continuous sample delivery

FIA mode. In the FIA application, carboy C2 (Fig. 2) contained deionized water, and carboy C1 contained 0.25*M* hydrochloric acid Using this experimental configuration, a series of five replicate, 250 μl-injections of each of five standard potassium carbonate solutions was made, and the results are shown in Fig. 4(A). As can be seen from these recorder tracings, baseline stability was quite good, and replicate injections could be made with high precision (2.4%

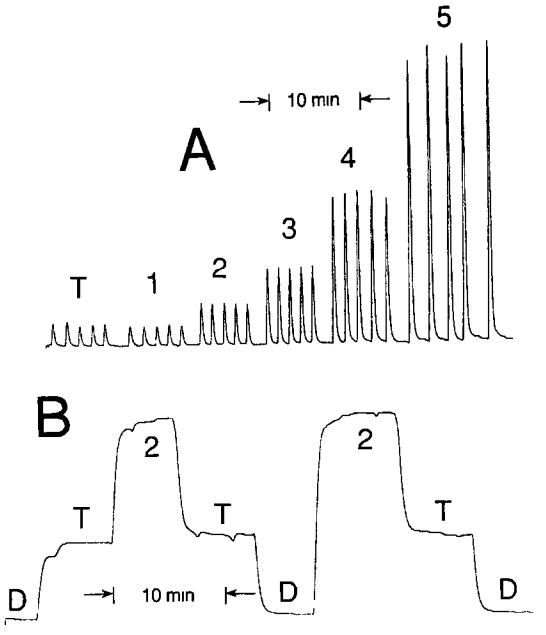

Fig 4 Peak profiles obtained with the sample delivery system configured for (A) flow injection analysis and (B) process analysis (A) Injections of 250 μl of (1) 3 12mM, (2) 6 25mM, (3) 12 5mM, (4) 25 0mM, and (5) 50mM K_2CO_3 solution, and (T) Waco tap water, each mixed with 0 25M HCl Flow rates deionized water, 5 34 ml/min, HCl, 3 59 ml/min (B) Signal obtained for continuous delivery of (D) deionized water, (T) Waco tap water, and (2) 6 25mM K_2CO_3 solution, each mixed with 0 25M HCl Flow rates deionized water plus HCl, 8.42 ml/min, Waco tap water plus HCl, 7 38 ml/min, K_2CO_3 solution plus HCl, 7 94 ml/min

average RSD for a single measurement) over the time period required for the analysis. Using this same data, a plot of average peak height vs. potassium carbonate concentration gave a highly linear calibration curve with a correlation coefficient of 0.99990. From this calibration curve, the TIC of a sample of Waco tap water was estimated from the five replicate injections, T, shown in Fig. 4(A) as equivalent to 3.1 ± 0.3mM potassium carbonate, a value which compares well with the TIC levels (2–4mM potassium carbonate) typical of the natural waters making up the municipal water supply.[22]

Process analysis mode. In this application, carboy C1 (Fig. 2) was replaced with three carboys, connected in parallel, which contained either deionized water [the blank, D in Fig. 4(B)], Waco municipal water [the sample, T in Fig. 4(B)], or a 6.25mM solution of potassium carbonate [the standard, 2 in Fig. 4(B)]. Carboy C2 (Fig. 2) contained 0.25M hydrochloric acid. Figure 4(B) shows the excellent reproducibility of the signal obtained using the FIRE radiometer when the four-way valve was repeatedly switched between blank, sample and standard.

On the basis of a single-standard calibration curve, constructed from the results shown in Fig. 4(B), the TIC of a sample of domestic water (taken on a different day) was estimated as equivalent to 2.4 ± 0.1mM potassium carbonate. The difference between the TIC values obtained from Fig. 4(A) and Fig. 4(B) undoubtedly reflects a number of factors including the natural variation in water quality and the difference between a single- and multi-point calibration procedure It should also be noted that in the process analysis mode, small differences in solution flow rate from the three carboys (blank, sample, and standard) were sometimes observed, even though the carboys were all pressurized from the same nitrogen cylinder. Since the rate of solution flow into the purge cell determines the magnitude of the signal, solution flow rate from these three carboys must be controlled as precisely as possible for good quantitative work

Nonvolatile organics

The measurement of TIC by FIRE spectrometry is made possible by the acidification step that converts non-volatile carbonates and bicarbonates to dissolved carbon dioxide, which can be readily purged from solution and excited in the FIRE source.[22] Nonvolatile organics in aqueous solution can, in principle, also be converted to carbon dioxide by chemical reaction prior to the purge step, if a suitable oxidizing agent can be found Sodium peroxydisulfate, one of the strongest chemical oxidizing agents known [$E°_{red}(S_2O_8^{2-}/SO_4^{2-}) = +2.010$ V; $E°_{red}(S_2O_8^{2-}/HSO_4^{-}) = +2.123$ V][33] was selected for this initial study, despite the fact that reactions involving this species are typically slow at room temperature and generally require a catalyst [34] Silver(I) and copper(II) are among the catalysts that have been investigated most extensively,[34] although peroxydisulfate reactions employing iron(III) chloride have also been reported.[35] In the silver catalyzed reaction, peroxydisulfate is thought to react with Ag^+ to form a higher valent silver species (Ag^{2+}, or possibly even Ag^{3+}), which subsequently oxidizes the substrate.[34] In the copper catalyzed reaction, the active oxidizing species is believed to be copper(III).[34]

The FIA mode of sample delivery was used to determine the best concentrations of sodium peroxydisulfate (carboy C2, Fig. 2) and catalyst (carboy C1) for the FIRE procedure. Of the

three metal salts investigated, silver nitrate was found to be the best catalyst for this application. In neutral media, cupric sulphate was an effective alternative to silver nitrate, especially under conditions in which silver formed an insoluble precipitate. In acid media (0.01*N* sulphuric acid), however, cupric sulphate appeared to lose much of its catalytic activity and was ineffective in promoting the oxidation of acetic, propionic, or butyric acids under the conditions employed in this study. Iron(III) chloride did not appear to exhibit any catalytic activity under the reaction conditions tested.

The effectiveness of sodium peroxydisulfate over a concentration range of 0.5–5% was also investigated. Peroxydisulfate concentrations greater than 2% caused the reaction to become so vigorous that considerable foaming of the liquid in the purge cell was produced. If the reaction occurred too rapidly, solution was forced out of the purge cell and into the Teflon® tube leading to the burner. This produced an unstable baseline and, in some cases, the flame was completely extinguished. At lower peroxydisulfate concentrations, the reaction proceeded more slowly, but a stable baseline could be obtained. A 1% sodium peroxydisulfate concentration was found to produce a reasonably rapid reaction, without excessive foaming, and represented a good compromise.

Concentrations of silver nitrate catalyst in the range from 0.1–10% were also examined. At high silver concentrations, excessive foaming in the purge cell was observed. A 0.25% silver nitrate solution was found to produce a reasonably rapid reaction rate, as well as a stable baseline, and was used for most peroxydisulfate reactions.

The peroxydisulfate reaction could also be accelerated by heating, and three different delay coil temperatures (Fig. 2) were investigated (21, 59 and 89°). At a bath temperature of 89°, the formation of bubbles could be observed in the delay coil as a result of substrate oxidation. Below 89°, no visible evidence of oxidation was observed.

Aqueous solutions of non-volatile organic acids, and mono- and disaccharides were used to test the peroxydisulfate pretreatment procedure The FIA mode of sample delivery was employed with carboy C1 containing a 0.25% silver nitrate solution, carboy C2 containing a 1% sodium peroxydisulfate solution, the hot bath maintained at 89°, and a total liquid flow rate of 10 ml/min. Samples containing individual compounds were injected sequentially into the flowing reagent stream using a 25-μl syringe. Figures 5(A) and (B) show the results obtained for the organic acids and the mono- and disaccharides, respectively. In both recordings, excellent baseline stability and peak shape are evident.

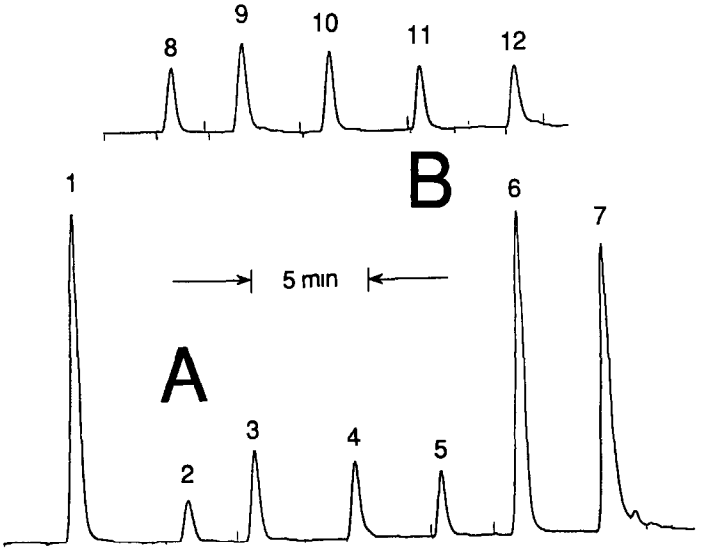

Fig 5. Peak profiles obtained for aqueous solutions of (A) carboxylic acids and (B) sugars, with the sample delivery system configured for flow injection analysis Interface conditions 1% sodium peroxydisulfate solution, 0 25% $AgNO_3$ solution; total liquid flow rate, 10 ml/min; delay coil, 3 05 m × 0 79 mm, water bath, 89°. Quantities injected. (1) 1 μl, 100% formic acid, (2) 5 μl, 2 0% malic acid, (3) 10 μl, 2 0% malic acid; (4) 10 μl, 1 8% citric acid (5) 5 μl, 0.34*M* acetic acid; (6) 1 μl, 100% propionic acid, (7) 1μl, 100% butyric acid, (8) 10 μl, 2 0% glucose; (9) 10 μl, 1 8% galactose, (10) 10 μl, 1 5% maltose, (11) 10 μl, 1 0% sucrose, (12) 10 μl, 1 5% fructose.

Table 1 gives the FIRE signal (peak height) obtained per mole of carbon injected into the sample delivery system. For the 11 compounds studied in this experiment, these values are fairly similar and range from a low of 1.8×10^6 mm/mole C for butyric acid to a high of 5.0×10^6 mm/mole C for acetic acid. An analysis of the numbers in Table 1 suggests that the extent of peroxydisulfate oxidation of the four aliphatic acids is a function of the chain length of the acid, with the two-carbon chain (acetic acid) giving the best results. Malic acid (a four-carbon, dicarboxylic acid) and citric acid (a six-carbon, tricarboxylic acid) may give a better response than butyric acid because the extra functional groups already make these molecules more highly oxidized

Table 1 suggests that the variation in signal per mole of carbon reflects differences in the kinetics of the oxidation process rather than thermodynamic factors, with conversion of analyte to carbon dioxide probably limited by the relatively short reaction time employed in the experiment. In this application, a 3.05 m (10 ft.) x 0.79 mm (1/32 in.) delay coil, having an internal volume of 1 5 ml, was selected to avoid excessive peak broadening. For a total reagent flow rate of about 10 ml/min and a heating coil volume of about 1.5 ml, the sample remains in the heating coil for only about 9 sec before entering the purge cell. If the extent of oxidation is governed by kinetics, the heating coil should be made as long as possible to ensure complete oxidation of the organic analyte. For process stream applications where the concentration of organic analyte may not vary dramatically with time and mixing of adjacent solution volumes is not a problem, very long coil lengths or stop flow techniques could be used to extend the reaction time of the sample.

HPLC mode

The generation of purgeable carbon dioxide by the oxidation of organic acids and sugars in a flowing liquid stream (Table 1) suggested that peroxydisulfate/Ag^+ pretreatment might be useful in the development of an improved FIRE detector for HPLC. Such a detector would be especially useful in applications involving the separation of nonvolatile organic compounds that do not have a conveniently accessible UV chromophore and are present at concentrations where changes in refractive index are small. Ion-exchange HPLC with an aqueous mobile phase was selected to avoid the large background associated with the oxidation of an organic mobile phase.

Figure 6(A) shows the chromatogram obtained for a 50-μl injection of an aqueous mixture of six sugars, separated on an ion-exchange column in the Ca^{2+} form. In this application, a 1% solution of peroxydisulfate was pumped from carboy C2 (Fig. 2) at a flow rate of 4.5 ml/min, and a 0.25% solution of silver nitrate catalyst was pumped from carboy Cl at 3.4 ml/min. The flow rate of the mobile phase (HPLC-grade water) through the ion exchange column was maintained at 0.5 ml/min. A 2 13 m (7 ft.) x 1.6 mm (1/16 in.) delay coil, having an internal volume of 4.3 ml, was immersed in a water bath at a temperature of 89°.

Figure 6(B) show the chromatogram obtained for a 50-μl injection of an aqueous mixture of six organic acids, separated on a column packed with cation-exchange polymer in the hydrogen form. In this application, a 1% solution of

Table 1 FIRE response (4.4 μm filter) using peroxydisulfate/Ag^+ pretreatment

Compound	Formula weight,* g/mole	C injected, mole x 10^6	peak height, mm	Signal/mole, C, mm/mole C x 10^{-6}
Formic acid	46.0	26 0	88 5	3 3
Acetic acid	60 0	3 4	17 0	5 0
Propionic acid	74 1	40.0	87 0	2 2
Butyric acid	88 1	44 0	77 0	1 8
Malic acid	134 1	3 0	11 0	3 7
Citric acid	192.1	5 6	20 5	3 6
Fructose	180 2	5 0	16 5	3 3
Glucose†	198.2	6.1	17 0	2 8
Galactose†	198 2	5 5	23 0	4 2
Sucrose	342 3	3 5	17 0	4 8
Maltose†	360 3	5.0	21 0	4 2

*Ref 36
†Monohydrate

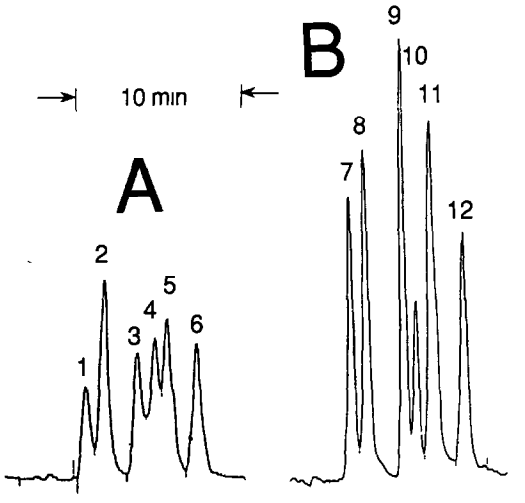

Fig 6 Peak profiles obtained for an aqueous mixture of (A) sugars and (B) carboxylic acids with the sample delivery system configured for ion-exchange high-performance liquid chromatography Sugars separated on a CHO-620 Carbohydrate column, mobile phase, HPLC-grade water, flow rate, 0 5 ml/min through the column, column temperature, 90°, 50-μl injection Interface conditions 1% sodium peroxydisulfate solution, 4 5 ml/min, 0 25% $AgNO_3$ solution, 3 4 ml/min, delay coil, 2 13 m × 1 6 mm, water bath, 89° Carboxylic acids separated on an ORH-801 Organic Acid column, mobile phase, 0 01N HNO_3, flow rate, 0 8 ml/min through the column, column temperature, 35°, 50-μl injection Interface conditions 1% sodium peroxydisulfate solution, 4 5 ml/min, 0 25% $AgNO_3$ solution, 5 7 ml/min, delay coil, 3 05 m × 0 79 mm, water bath, 89° Quantities injected (1)(96 μg raffinose, (2) 137 μg sucrose, (3) 122 μg glucose, (4) 117 μg galactose, (5) 120 μg fructose, (6) 122 μg mannitol, (7) 273 μg oxalic acid, (8) 290 μg tartaric acid, (9) 180 μg formic acid, (10) 185 μg fumaric acid, (11) 165 μg propionic acid, (12) 79 μg butyric acid

sodium peroxydisulfate was pumped from carboy C2 at 4.5 ml/min, and a 0.25% silver nitrate solution was pumped from carboy C1 at 5.7 ml/min. The flow rate of the mobile phase (0.01N nitric acid) through the ion exchange column was maintained at 0.8 ml/min. A 3.05 m (10 ft.) × 0.79 mm (1/32 in.) delay coil, having an internal volume of 1.5 ml, was immersed in a water bath at a temperature of 89°.

Figure 6 demonstrates that the FIRE-HPLC detector has good baseline stability and responds rapidly enough to follow the analytes as they elute from the column At the solution flow rates used, the carboxylic acids remained in the heated delay coil for only about 8 sec and the sugars for only about 30 sec. In the case of the sugars, a smaller diameter (1/32 in) delay coil resulted in such a short residence time in the heating bath that the signals decreased significantly The dependence of signal on residence time in the bath suggests that the extent of the reaction is controlled by the kinetics of the peroxydisulfate oxidation. A more detailed study of the parameters affecting the peroxydisulfate oxidation of organic analytes with the new purge system is currently underway in this laboratory.

While the HPLC column represents the major source of chromatographic band broadening when a UV- or RI detector is employed,[37] band broadening in the FIRE-HPLC chromatogram can also be caused by mixing with the peroxydisulfate and silver nitrate solutions, as well as by flow of the chromatographic effluent through the delay coil and other components which make up the FIRE-HPLC interface. In order to estimate the relative importance of these additional sources of band broadening, the band variances, σ^2, resulting from different components in the HPLC–FIRE interface were estimated (Table 2) from the baseline widths, W, of

Table 2 Approximate contributions of FIRE-HPLC components to band broadening

FIRE-HPLC components	Measured baseline band width, W, sec	Standard deviation, σ, sec	Band variance, σ^2, sec^2
(1) Flow, two mixings*	41*	10†	100
(2) Flow, two mixings, delay coil‡	55‡	14†	190
(3) Delay coil§	—	9 5	90§
(4) Flow, two mixings, delay coil, HPLC column, connecting tubing‖	67‖	17†	290
(5) HPLC column, connecting tubing#	—	10	100#
(6) HPLC column, RI detector**	30**	7 5†	56

*From peaks numbered 5, Fig 4A
†Calculated from $\sigma = W/4$, assuming Gaussian profile Ref 37
‡From peak 6, Fig 5A 3 05 m × 0 79 mm delay coil
§Calculated from $\sigma_2^2 = \sigma_3^2 + \sigma_1^2$, where subscripts refer to row numbers
‖From peak 11, Fig. 6B 3 05 m × 0 79 mm delay coil
#This data Calculated from $\sigma_4^2 = \sigma_5^2 + \sigma_2^2$, where subscripts refer to row numbers
**Manufacturer's data RI detector Ref 38

several FIRE peaks assuming a Gaussian band shape.[37]

The band variance resulting from mixing with two reagents and flow through the HPLC–FIRE interface in the absence of both the delay coil and HPLC column (Table 2, row 1) was estimated from the FIRE response for injections of 50m*M* potassium carbonate solution [peaks 5, Fig. 4(A)]. In this experiment, the HPLC column and its connecting tubing had been removed, and injections were made manually through a septum located at M2 in Fig. 2. No delay coil was employed, but mixing occurred with the carrier (distilled water) from carboy C2 and with 0.25*M* hydrochloric acid introduced from carboy C1.

Peak 6 in Fig. 5 was used to estimate the band variance resulting from mixing with two reagents and flow through the HPLC–FIRE interface with the delay coil in place (Table 2, row 2). In this experiment, a 1-μl injection of 100% propionic acid was made manually through the septum injector. Mixing occurred with peroxydisulfate solution from carboy C2 and silver nitrate solution from carboy C1. A 3.05 m × 0.79 mm delay coil was used to promote the formation of carbon dioxide. Once this variance had been determined, band broadening due to the delay coil alone (Table 2, row 3) could be estimated by subtracting the band variance in row 1 from that in row 2.

Peak 11 in Fig. 6(B) (propionic acid) was used to estimate the total band variance for the complete HPLC–FIRE detector (Table 2, row 4). In this experiment, a mixture containing several organic acids was chromatographed on an ORH-801 Organic Acid column under conditions essentially identical to those recommended by the manufacturer.[38] Mixing occurred with peroxydisulfate solution from carboy C2 and silver nitrate solution from carboy C1 A 3.05 m × 0.79 mm delay coil was used to promote the formation of CO_2. Once the total variance had been determined, band broadening due to the HPLC column and the tubing which connected it to the multi-port valve M2, could be estimated (Table 2, row 5) by subtracting the variance in row 2 from that in row 4.

A comparison of the results in Table 2 indicates that band broadening in the complete FIRE-HPLC detector [including the column and delay coil (290 sec^2, row 4)], is nearly three times that resulting from the HPLC column and its connecting tubing alone (100 sec^2, row 5). Approximately half of the additional broadening results from the delay coil (90 sec^2, row 3) and approximately half from reagent mixing and flow through the remainder of the interface (100 sec^2, row 1). The band variance calculated indirectly for the HPLC column (our data, 100 sec^2, row 5) is reasonable when compared to the band variance estimated from the manufacturer's literature[38] for propionic acid under nearly the same chromatographic conditions (56 sec^2, row 6). [Some of the difference between these two values undoubtedly reflects the additional tubing required to connect the HPLC column to valve M2 (Fig. 2), as well as errors in estimating the variance in row 5 due to small differences in liquid flow rate for rows 1, 2 and 4.] The approximate agreement between the variances in rows 5 and 6 provides some verifications of the calculational procedure. These calculations have also suggested several design modifications for the FIRE-HPLC interface, which are currently being implemented in this laboratory.

CONCLUSIONS

A new liquid sampling system which employs a specially designed purge cell is described for use in continuous-flow FIRE spectrometry. The new analytical system represents a major improvement over the discrete-sampling purge system used in previous studies.[21–23] The small internal volume of the new cell promotes rapid flushing of the purge analyte into the flame, thereby minimizing problems associated with purge cell clean-out and resulting in sharp, reproducible signals. Spent analytical solution is continuously drained from the cell. Since cell disconnection and cleaning between samples is no longer necessary, total analysis time for a large number of similar samples is considerably reduced.

The new purge cell is highly versatile and was successfully tested in both a process analysis- and a flow injection analysis mode for the determination of TIC in Waco tap water. Other samples which have proven amenable to FIRE spectrometry using the new purge cell include carbonated beverages, bleaches, and volatile organic compounds (VOCs).[20] Some of these applications[20] employed a simple, single-channel FIRE photometer configured in the chlorine mode[7] (3.8-μm bandpass filter).

In this study, flame infrared-emission spectrometry was successfully extended to non-

volatile organic compounds, using chemical pretreatment with peroxydisulfate in the presence of silver ion to convert the analyte to carbon dioxide, prior to purging and detection by the FIRE radiometer. Pretreatment of six organic acids and five sugars with peroxydisulfate and silver ion at 89° for approximately 9 sec gave results which indicated that all 11 compounds were oxidized to nearly the same extent.

Chemical pretreatment avoids the introduction of large amounts of unwanted sample matrix into the flame, thereby minimizing dilution of analyte in the excitation source and reducing flame background noise. When pretreatment with peroxydisulfate and silver ion was applied to aqueous solutions of organic acids and sugars eluting from a liquid chromatograph, the FIRE radiometer could be used as a convenient detection system for ion-exchange HPLC.

Acknowledgements—This work was supported by Baylor University Research Grant 0100-032-1510 Infrared-Emission Research. The authors express their appreciation to Mr Jeff Riemenschneider and Mr Larry G White of the Texas State Technical College in Waco for help in fabricating the glass purge cell Portions of this paper were presented at Pittcon'92, March 1992, New Orleans, LA, Paper No 275, and were taken from the Ph D. dissertation of Christopher K. Y Lam

REFERENCES

1 S. H Chan, C C Lin and M J D Low, *Environ Sci Tech.*, 1973, **7**, 424.
2 P. R Griffiths, *Amer Lab*, 1975, **7**, 37
3 W F. Herget and J D Brasher, *Appl Opt*, 1979, **18**, 3404
4. *Idem*, *Opt. Eng.*, 1980, **19**, 508
5 W F Herget, *Appl Opt*, 1982, **21**, 635
6 R D. Hudson, Jr, *Infrared System Engineering*, Wiley, New York, 1969
7 M A Busch and K. W Busch, *Spectrochim Acta Rev*, 1991, **14**, 303
8 *Idem*, *Amer Lab.*, 1991, **23**, 18
9 K. W Busch, M A Busch, D C Tilotta, S W Kubala, C K Y Lam and R. Srinivasan, *Spectroscopy*, 1989, **4**, 22
10 Y. Zhang, K W Busch and M A Busch, *Appl Spectrosc*, 1992, **46**, 930
11. *Idem*, *ibid.*, 1992, **46**, 631.
12. D C Tilotta, M. A Busch and K W.Busch, *ibid.*, 1991, **45**, 178
13 *Idem*, *ibid*, 1989, **43**, 704
14. Y Zhang, M A Busch and K W Busch, *ibid.*, 1992, **46**, 1673
15 S Ravishanker, D C Tilotta, K W Busch and M A Busch, *ibid*, 1990, **44**, 1247
16 S Ravishankar, D C Tilotta, S W. Kubala, M A Busch and K W Busch, *Anal Chem*, 1990, **62**, 1604.
17 K W Busch, M A Busch, D C Tilotta, S W Kubala and S Ravishankar, *Appl Spectrosc*, 1991, **45**, 964
18 S Ravishankar, D C Tilotta, K W Busch and M A Busch, *ibid*, 1991, **45**, 1684
19 M A. Busch and K W Busch, *ibid*, 1991, **45**, 546
20 C K Y Lam, Ph D Dissertation, Baylor University, Waco, TX, 1992
21 S W Kubala, D C Tilotta, M A Busch and K W Busch, *Talanta*, 1991, **38**, 589
22 *Idem*, *Anal Chem.*, 1989, **61**, 1841
23 S W Kubala, D C Tilotta, M A Busch and K W Busch, *ibid*, 1989, **61**, 2785
24 H H Willard, L. L Merritt, Jr, J A Dean and F A Settle, Jr, *Instrumental Methods of Analysis*, 6th Ed, Chap 31, Van Nostrand, New York, 1981
25 J. Růžička and E H Hansen, *Flow Injection Analysis*, 2nd Ed, Wiley, New York, 1988
26 L R Snyder and J J Kirkland, *Introduction to Modern Liquid Chromatography*, 2nd Ed, Wiley, New York, 1979
27 D C Tilotta, K W Busch, M A Busch and S Ravishankar, *15th Annual Meeting of the Federation of Analytical Chemistry and Spectroscopy Societies*, Oct 1988, Boston, MA, Paper No D74
28 M A Busch, C K Y Lam, D C Tilotta and K W Busch, *41st Pittsburgh Conference on Analytical Chemistry and Applied Spectroscopy*, March 1990, New York, NY, paper No 483
29 W Stumm and J J Morgan, *Aquatic Chemistry*, Wiley, New York, 1981
30 T Almgren, D Dyrssen and S Fonselius, *Methods of Seawater Analysis*, 2nd Ed, K Grasshoff, M Ehrhardt and K Kremling (eds), Chap 8 Verlag Chemie, Weinheim, Germany, 1983
31 A E Greenberg, J J Connors and D Jenkins, *Standard Methods for the Examination of Water and Wastewater*, 15th Ed., American Public Health Association, Washington, DC, 1981
32. *Introduction to Water Treatment Principles and Practices of Water Supply Operations*, American Water Works Association, Denver, CO, Vol 2, 1984, Vol 4, 1982
33 N N Greenwood and A Earnshaw, *Chemistry of the Elements*, p 846. Pergamon, Oxford, 1984
34 D. A House, *Chem Rev*, 1962, **62**, 185
35 S. P Srivastava and S Ghosh, *Z Physik Chem*, 1956, **205**, 332
36. *The Merck Index*, 11th Ed, Merck & Co, Rahway, NJ, 1989
37 B. L. Karger, L R Snyder and C Horvath, *An Introduction to Separation Science*, pp 135–146 Wiley, New York, NY, 1973
38 *ORH-801 Organic Acids Column, Instruction Manual*, p 10 Interaction Chemicals Inc, 1615 Plymouth Street, Mountain View, CA 94043, 1989

Talanta, Vol 40, No 6, pp 879–882, 1993
Printed in Great Britain

0039-9140/93 $6 00 + 0 00

OPTIMIZATION OF A SIMULTANEOUS MULTI-ELEMENT ATOMIC ABSORPTION SPECTROMETER*

KIMBERLY S FARAH
Department of Chemistry, University of Massachusetts Lowell, Lowell, MA 01854, U S A

JOSEPH SNEDDON†
Department of Chemistry, McNeese State University, Lake Charles, LA 70609, U S A

(*Received* 7 *July* 1992 *Revised* 9 *October* 1992 *Accepted* 13 *October* 1992)

Summary—A variable-size simplex procedure was used to optimize the overall response of a simultaneous multi-element flame atomic absorption spectrometer Seven factors (air to fuel ratio, slit width, height above the burner head, and four hollow cathode lamp currents) were optimized for copper, iron, manganese, and zinc atomic absorption A univariate search procedure was used to determine the effect of individual factors on response The results of the optimization showed that a comprise set of operating conditions must be used when performing multi-element determinations The atomic absorption sensitivity of the multi-element determination as compared to single-element determination was reduced by a factor of no more than two

Convention flame or furnace atomic absorption spectrometry (AAS) has generally been considered to be a single-element technique. In the last decade, multi-element systems using sequential or simultaneous techniques,[1,2] including continuum sources[3] and lasers,[4] have been developed. Simultaneous multi-element AAS studies require that a single set of operating conditions, such as flame type, hollow cathode lamp current, and slit width be used for analysis. For optimum performance, a compromise in operating conditions between those of a single-element determination to a multi-element determination must be employed.

Univariate searches, which vary one factor at a time while holding other factors constant, have been used to optimize operating conditions. A drawback to this approach is that it does not take into account interactions between the factors being varied, and requires many experiments to optimize conditions. Another technique employed for system optimization is the "simplex" method A simplex is a geometric figure that has a number of vertexes equal to one more than the number of dimensions in the factor space: for example, a three-dimensional simplex is a tetrahedron.[5] Each variable being studied in the optimization process will add one dimension to the simplex. The simplex rapidly attains an experimental optimum guided by calculations and decisions that are rigidly specified.[6] The sequential simplex method as introduced by Spendley *et al.*,[7] uses a multi-factor, empirical strategy for optimizing experimental conditions.

Optimization of experimental factors in atomic absorption spectrometry was studied by Parker *et al.*,[8] and also by Borszeki *et al.*[9] They showed that by changing experimental factors, such as fuel and oxidant flow rates and burner height, the overall system response could be improved for a single element. Michel *et al.*,[10] and Sneddon[11] performed simplex optimization of experimental factors for microwave electrodeless discharge lamps. Johnson *et al.*,[12] used a simplex in the computer controlled study of pulsed hollow cathode lamps.

In this paper, a sequential simplex has been used to optimize the operating conditions for a multi-element measurement of copper, zinc, manganese, and iron using flame atomic absorption spectrometry. The factors that were varied include the slit width, hollow cathode lamp currents of each element, air to fuel ratio, and height above the burner head.

*Presented, in part, at FACSS XIX Philadelphia, PA, U S A, 20–25 September 1992
†Author for correspondence

EXPERIMENTAL

Instrumentation

A Smith-Hieftje 8000 atomic absorption spectrometer (Thermo Jarrell Ash, Franklin, MA, U.S.A.) was used with an air/acetylene flame. The instrument was operated in the simultaneous mode which allows for analysis of up to four elements at a time. The system uses a galvanometer driven grating in its monochromator A galvanometer driven mirror is used to select lamps. This mechanism allows the instrument to scan the full spectrum (190–800 nm) in 20 milliseconds. Visimax II hollow cathode lamps were used. Measurements were performed with no background correction. Wavelengths for the four elements used were· 279.5 nm (manganese), 248.3 nm (iron), 324.7 nm (copper) and 213.9 nm (zinc).

Preparation of the standard

A standard solution containing 0.5 μg/ml zinc, 3.0 μg/ml copper, 4 0 μg/ml iron, and 2.5 μg/ml manganese was prepared from 1000 μg/ml certified atomic absorption solutions of zinc, copper, iron and manganese (Fisher Scientific Co, New Jersey). Concentrations were chosen by preliminary experimentation so that the signal generated was between 0.2 and 0.3 absorbance units and were based on previously established calibration curves which showed the approximate linear working range for each of the individual elements. Distilled/deionized water was used for making dilutions.

Procedure for the simplex

The simplex rules used in this study are based on the modified simplex introduced by Nelder and Mead.[13] These rules allow the simplex to expand in regions of favorable response and contract in regions of unfavorable response. An IBM^{tm}-compatible 286 computer was used for all calculations. A program was incorporated into Quattro Pro 3.0 Borland to calculate the reflection, expansion, and contraction points. Boundary conditions for the simplex were based on the operating limits of the instrument (*e.g.*, height above the burner head could not be below zero). If a new vertex contained an instrumental parameter which was beyond the boundary limits, or if the absorbance for any individual element was less than 0.1 absorbance units, a response of -1 was assigned.

The experimental factors include the air to fuel ratio, the height above the burner head, the slit width, and the hollow cathode lamp currents for each of the four elements (Mn, Cu, Zn and Fe). The system was auto-zeroed prior to each analysis. Four repeats were performed for each set of instrumental factors. The response at each vertex was taken to be the sum of the absorbance readings for each of the four elements. The best, next-to-worst and worst responses were ranked for each simplex move. The worst response was discarded in the next simplex move while a new calculated vertex was added (either a reflection, expansion or contraction) This procedure was continued until the overall response of the vertices varied by less than the experimental deviation.

Univariate experiment

Once the region of optimum response was found, a univariate search was conducted over a wide range of values for each instrumental factor. All factors were held constant at their simplex optimum value except for the factor of interest. Four repeats of each standard were conducted at the factor of interest. A sample uptake rate was maintained at 3 ml/min throughout the experiment.

RESULTS AND DISCUSSION

Simplex optimization

The simplex experiment was used to achieve the maximum overall absorbance for a simultaneous determination of the four elements listed above. The factors chosen each affect the overall absorbance of the system. The simplex was halted after 22 vertexes. Figure 1 shows improvement in overall response as the simplex increased. The coordinates for the final accepted

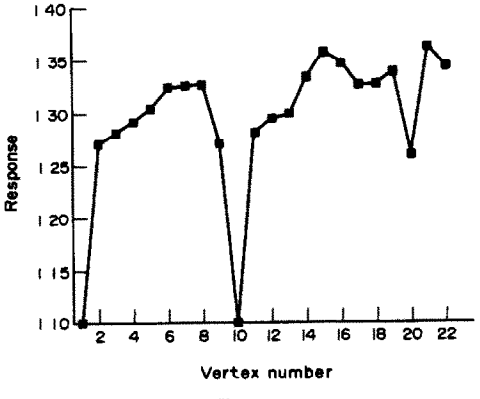

Fig 1

Table 1. Optimum operating conditions for multi-element flame AAS measurement of Cu, Fe, Mn and Zn obtained by simplex and univariate experiments

Operating parameters	Simplex optimum	Univariate optimum
Air/Fuel ratio (SCFH)	2 53—3 1	1.9–2.11 2 92–3 45
Slit width (nm)	0 4	0 4
Burner height (mm)	8.9–9 4	8 0–13 4
Copper lamp (mA)	2 0–3 0	2 0–5 5
Iron lamp (mA)	5.0–5 5	5 5–9 0
Manganese lamp (mA)	4 8–5.2	3 9–6 0
Zinc lamp (mA)	2 0–3 1	1.5–3.4

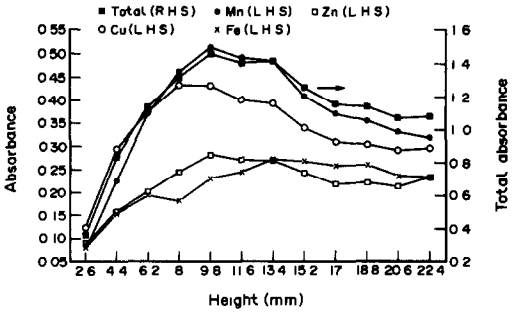

Fig 3

vertex (number 21), which produced the highest overall response, were taken as the optimum instrumental operating conditions. The eight initial vertices were based on the acceptable operating conditions for single element analysis. As such, the optimum response was achieved relatively quickly. Table 1 lists the results of optimum values which the simplex and univariate experiments obtained for each of the seven factors studied. Univariate experiments for each factor, in the region of the optimum, assisted in verifying that the optimum lay near the simplex value.

Air to fuel ratio optimization

The optimum values for the air to fuel ratio are listed in Table 1. Figure 2 illustrates the results of the univariate search for optimum air to fuel ratio. A univariate search was conducted to find the region of highest overall absorbance and the region for the maximum absorbance of the individual elements. There are two regions of optimum absorbance, the first at 3.16:1 and the second at 2:1. The two different regions of optimum occur due to the variation in absorbances for the individual elements. Copper, zinc and manganese have higher absorbances when the flame is fuel rich (lower air to fuel ratio). Iron, however, has a higher absorbance when the flame is fuel lean.

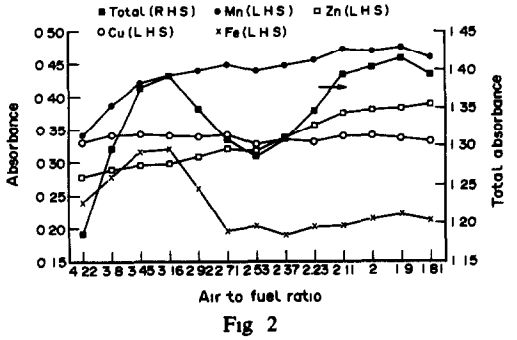

Fig 2

Height above the burner head optimization

Figure 3 shows the results of the univariate search for absorbance vs. height above the burner head. The height, given in mm, is the height from the tip of the burner head to the center of the hollow cathode lamp light. A maximum total absorbance was found at a height of 9.8 mm. Maximum absorbances for the individual elements occurred at slightly different heights above the burner head. No attempt was made to investigate potential interferences between elements which may have resulted as the height above the burner head was changed.

Slit-width and hollow cathode lamp current optimization

Five possible values of the slit width were available for the optimization: 0.08 nm, 0.15 nm, 0.4 nm, 1.0 nm and 2.0 nm. The simplex converged rapidly to the 0.4-nm slit width. At a slit width of 0.08 nm, insufficient light from the hollow cathode lamp reached the detector. While at the larger slit widths of 1 nm and 2 nm, the photomultiplier tube (PMT) used for iron became saturated with light. For the optimization of copper in a single element determination, a slit width of 1 nm is preferred. In the multi-element situation, however, this was not possible due to saturation of the PMT. These results again show that a compromise in operating conditions is required for multi-element determinations.

The range of optimum hollow cathode lamp currents is given in Table 1. Absorbances over the range of each of the lamp currents varied by less than 15%. Preferred lamp currents for individual element determinations did not vary from those of the multi-element determinations. The results for the single element determination are in agreement with those of Parker *et al.*,[8] who demonstrated that changing the lamp

Table 2. Comparison of atomic absorption sensitivity for single element determination *vs* multi-element flame AAS determination

Element	Sensitivity for single element μg/ml	Sensitivity for multielement μg/ml
Copper	0 065	0 085
Iron	0 08	0 167
Manganese	0 04	0 055
Zinc	0 015	0 016

current for calcium did not cause a statistically significant difference upon response.

Atomic absorption sensitivity

The atomic absorption sensitivity, defined as the concentration or mass which yields 1% absorption of $A = 0.0044$[14] was determined for each element individually and for the multi-element solution. Operating factors for the individual elements were determined from simplex optimization and univariate searches. For the multi-element standard, the instrumental parameters attained from the best response in the final simplex worksheet were used. Table 2 lists the atomic absorption sensitivities for the individual elements as compared to the multi-element case. In each case, the multi-element determination showed reduced sensitivity. Sensitivity was not decreased by more than a factor of two for any of the elements. The reduced sensitivity for iron in the multi-element analysis was caused by the use of an air to fuel ratio which was optimum for the other elements but which was not the optimum ratio for iron.

CONCLUSION

Multi-element atomic absorption requires a compromise in operating conditions from those of a single element determination. The modified simplex algorithm allows for rapid optimization of multi-element atomic absorption spectrometry. Once the optimum region has been attained, univariate searches can be used to verify that the simplex values are in the region of true optimum. Univariate searches can also provide some information about the effect of different operating conditions on single elements being analysed in a multi-element analysis. Using simplex optimized operating conditions, it can be seen that sensitivity is only slightly less for multi-element determinations for the elements used in this study

Acknowledgements—The authors gratefully acknowledge the generous support of Thermo Jarrell Ash Corporation, in particular, Gerald R Dulude and John J Sotera

REFERENCES

1 M Retzik and D Bass, *Am Lab*, 1988, **20**, 70
2 G R Dulude, *Can Chem News*, 1991, **43**, 31
3 J M Harnly, T C O'Haver, B Golden and W R Wolf, *Anal Chem* 1979, **12**, 2007
4 K C Ng, H A Abdalla, T E Barber and J D Winefordner, *Appl Spectrosc*, 1990, **44**, 849
5 J Sneddon, *Spectroscopy*, 1990, **5**, 33
6 F H Walter, L R Parker, S L Morgan and S N Deming, *Sequential Simplex Optimization*, CRC Press, Florida, 1991
7 W Spendly, G Hext and F Himsworth, *Technometrics*, 1962, **4**, 441
8 L R Parker, S L Morgan and S N Deming, *Appl Spectrosc*, 1975, **29**, 429
9 J Borszeki, K Doerffel and E Gegus, *Magy Kem Foly*, 1980, **86**, 207
10 R G Michel, J Coleman and J D Winefordner, *Spectrochim Acta*, Part B, 1978, **33B**, 195
11 J Sneddon, *Developments in the Application of Atomic Fluorescence Spectrometry to Clinical Analysis*, Ph D Thesis, University of Strathclyde, 1980
12 E R Johnson, C K Mann, and T J Vickers, *Appl Spectrosc*, 1976, **30**, 415
13 A Nelder and R Mead, *Computer J*, 1965, **7**, 308
14 J D Ingle and S R Crouch, *Spectrochemical Analysis*, p 299 Prentice Hall, New Jersey, 1988

Talanta, Vol 40, No 6, pp 883–889, 1993
Printed in Great Britain

0039-9140/93 $6 00 + 0 00

RESIN PHASE SPECTROPHOTOMETRY OF BERYLLIUM BY AN OPTICAL FIBER AND BERYLLON II

XU YANJUN, CHEN XINGGUO and HU ZHIDE*
Department of Chemistry, Lanzhou University, Lanzhou, 730000, People's Republic of China

(*Received* 3 *June* 1991 *Revised* 20 *June* 1991 *Accepted* 10 *October* 1992)

Summary—We have developed a resin phase spectrophotometric method to determine the amount of beryllium by detecting a change in absorbance of the resin phase 8-Hydroxynaphthalene-3,6-disulphonic acid–(1-azo-2′)-1′,8′-dihydroxynaphthalene-3′,6′-disulphonic acid tetrasodium salt (beryllon II) immobilized by a strong base anion-exchange resin on the end of a bifurcated optical fiber bundle was chosen as a material sensitive to beryllium Experiments were made using a home-made optical fiber spectrophotometer The properties of the resin phase proved to be good for continual use of 350 times during a month The reaction order between immobilized beryllon II and beryllium in solution was determined by kinetic theory and experiments This method was also used to determine the amount of beryllium in beryllium–copper alloy, the response was linear from 0.43 to 2 60 μg/ml at pH 12 5 and 676 nm. The effect of interfering ions on the determination of beryllium was studied at the same time

Many reagents have been proposed for the spectrophotometric determination of beryllium.[1] The two most important reagents for routine spectrophotometric determination of beryllium are chrome azurol S and beryllon II.[2–8] We immobilized the two colour reagents on a strong base anion-exchange resin and found that chrome azurol S and beryllon II immobilized on the resin formed colour complexes with beryllium in solution under proper conditions. The resin with beryllon II was attached to the common end of a bifurcated optical fiber bundle. We carefully studied the interaction between beryllium in solution and beryllon II in a resin phase and established a new analytical method by detecting a change of resin phase absorbance.

Our interest is in the development of new resin phase spectrophotometric methods which have a greater precision than conventional methods for the measurements of elements. In this paper we report our preliminary studies using an optical fiber spectrophotometer to assist the development of a new resin phase spectrophotometric method.

In comparison with conventional liquid phase spectrophotometry, a very small amount of colour reagent is consumed in measurements. In addition, the selectivity and sensitivity of this method is enhanced because of the separation and enrichment function of the resin.[11] In our experiments, because the resin phase with beryllon II interacts with dissolved beryllium for only a short time, there is no remarkable effect on enrichment.

Our method was based on detecting a change of absorbance in the resin phase; beryllon II was chosen as a material sensitive to beryllium. The absorbance of the Be-immobilized beryllon II complex was proportional to the beryllium concentration in solution. The method was also used to determine the amount of beryllium in beryllium–copper alloy Good results were obtained.

In general, it is convenient to establish such a method by using proper colour reagents and an optical fiber spectrophotometer.

EXPERIMENTAL

Apparatus

The optical fiber spectrophotometer is composed of a bifurcated optical fiber bundle and an ordinary spectrophotometer, Model 721, manufactured by the Shanghai No.3 Analytical Instruments Factory, China. Two arms of a bifurcated optical fiber bundle were fixed between the monochromator and the detector of the spectrophotometer.

A bifurcated optical fiber bundle is composed of many single strands of optical fiber. The effective sectional area of the bundle is 0.3 × 0.3 cm^2

*Author for correspondence

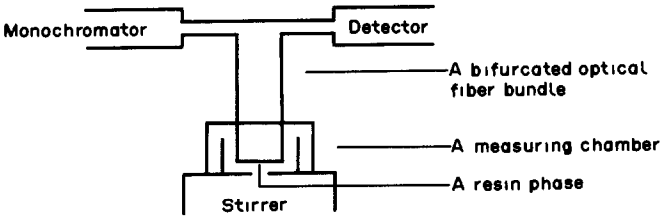

Fig 1 Measuring device

with two arms and a common end. Probe radiation is transported through one arm of the bifurcated bundle. Detected radiation is then transported through the other arm to a detector.[12] The measuring device is shown in Fig. 1.

The light source is a 10 V, 75 W tungsten lamp. The power supply voltage must be stabilized by a voltage-regulating transformer.

A pH meter, Model PHS-2, manufactured by the Shanghai No.2 Analytical Instruments Factory, China, was used to measure pH with a saturated calomel electrode (Type 232) and a glass electrode (Type 231) manufactured by the Shanghai Dian Guang Device Works, China. The solutions of various pH values were made by adding various volumes of sodium hydroxide solution to analytical solutions.

Absorbance was measured with a UV-240 spectrophotometer manufactured by Shimadzu Corporation, Japan.

Reagents

A beryllium stock solution was prepared by dissolving 0.2710 g of 99.99% pure beryllium metal in a minimum amount of concentrated hydrochloric acid and by diluting the solution to 250 ml with water. Less concentrated standard solutions were prepared by dilution from the stock solution. The 99.99% pure beryllium metal was provided by Professor Wang Huaigong of the Department of Chemistry, Lanzhou University.

Other reagents used were 5.0% EDTA solution, 10.0% sodium hydroxide solution, 10.0% ascorbic acid solution and 0.10% beryllon II solution. EDTA, sodium hydroxide, ascorbic acid and beryllon II were manufactured by the Peking Chemical Works, China.

Strong base anion-exchange resin (717) [R-N$(CH_3)_3$Cl] was manufactured by the Shanghai Resin Works, China. Its exchange capacity is 3.0 mmol/g. It possesses 7% cross-linking, the cross-linking agent being divinylbenzene (DVB). A general equivalent of 717 resin is Dowex I made in the U.S.A.

Polystyrene (average molecular weight about 10^5) was manufactured by Lanzhou Chemical Industry Company.

All reagents were analytical grade.

Procedures

Immobilization procedure. After 717 resin was ground in a grinder to 180 mesh size, the beryllon II was immobilized by soaking 1.0 g of 717 resin in a 10.0 ml, $1.8 \times 10^{-3}M$ beryllon II solution for half an hour and stirring. The resin with immobilized beryllon II was filtered through a funnel with filter paper, washed with water and dried by heating. Draw a certain amount of filtered, undiluted solution to determine the concentration of beryllon II in the filtered solution by spectrophotometry at 546 nm. The amount of beryllon II bound to the resin phase can be calculated through the change of beryllon II concentration in solution before and after adding the resin to the beryllon II solution. The amount of beryllon II bound to the resin was 1.4×10^{-5} mole/g.

A 6-ml toluene solution of polystyrene was mixed with 1.0 g of resin with immobilized beryllon II. The concentration of polystyrene in the toluene solution was 1.0 g of polystyrene in 50 ml of toluene. The 0.1 ml toluene solution

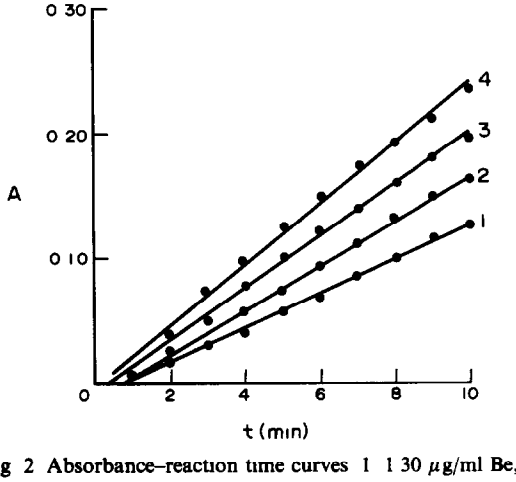

Fig 2 Absorbance–reaction time curves 1 1 30 μg/ml Be, 2 1 73 μg/ml Be, 3 2 17 μg/ml Be, 4 2 60 μg/ml Be

of polystyrene without resin phase was dropped to the common end of a bifurcated optical fiber bundle. After the toluene evaporated, the 0.1 ml toluene solution of polystyrene with resin phase was dropped to the common end of a bifurcated bundle. The resin phase could be used for measurement after toluene was evaporated completely About 16 mg of resin with beryllon II was attached to the common end of the bifurcated optical fiber bundle

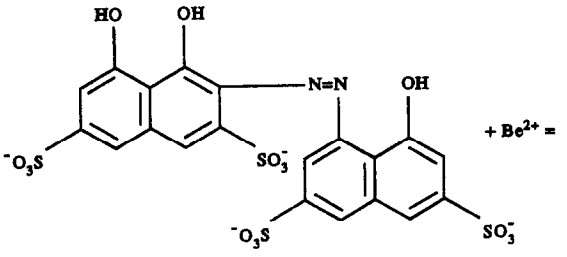

Beryllon II was immobilized in a resin phase by combining RSO_3^- groups of beryllon II with $R\text{-}N(CH_3)_3^+$ groups of resin by electrovalent bonds.

Measurement of absorbance–time curves. Absorbance–time curves shown in Fig. 2 were measured using a home-made optical fiber spectrophotometer and beryllon II resin on the common end of the optical fiber bundle. A stirrer was used during the measurements.

Spectrum measurements. The absorption spectra of blank resin and resin–beryllon II without beryllium shown in Fig. 3(a) were obtained with a UV-240 spectrophotometer. During measurements, the blank resin and resin–beryllon II were suspended in pure glycerol.

The absorption spectrum in Fig. 3(b) were obtained with a home-made optical fiber spectrophotometer according to the analytical procedure.

Analytical procedure A 2.0-ml volume of 10.0% ascorbic acid, 5.0 ml of 5.0% EDTA, 2.0 ml of 10.0% sodium hydroxide and a certain amount of beryllium were added to a 50-ml standard flask and diluted to the mark. The resin phase was immersed in the solution, and the absorbance was measured at 676 nm.

After detection, the resin phase was soaked in 3.0*M* hydrochloric acid for 3 min to remove beryllium in the resin phase. Because the colours of beryllon II vary with acidities in solution, the resin phase soaked in a 3.0*M* hydrochloric acid must be immersed in a reagent reference solution for 5–10 min to make beryllon II develop the color at the measuring pH value. By so doing, the zero point of a spectrophotometer can be regulated accurately before each measurement.

RESULTS AND DISCUSSION

Reaction order between beryllium in solution and beryllon II in the resin phase

By the reaction

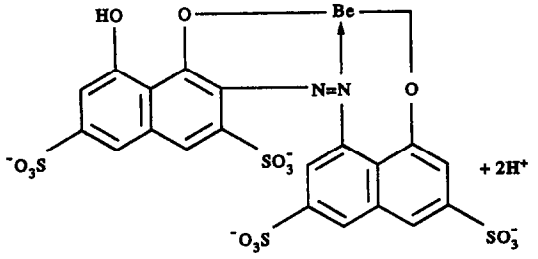

we can obtain the reaction rate equation

$$dC/dt = K_1 C_L C_{Be} \quad (1)$$

where C is the concentration of the Be–beryllon II complex in the resin phase; t is time. C_L is the concentration of beryllon II in the resin phase; C_{Be} is the beryllium concentration in solution and K_1 is a constant. Because the concentration of the Be–beryllon II complex in the resin phase is proportional to the complex absorbance in the resin phase, we substitute the complex absorbance for the complex concentration in equation (1) and obtain equation (2)

$$dA/dt = K_2 C_L C_{Be} \quad (2)$$

where A is the complex absorbance in the resin phase. Because beryllon II is a solid, within a certain reaction time only beryllon II on the resin phase surface reacts with beryllium in solution; therefore, C_L can be considered constant during the reaction process. For the above reason, we can obtain equation (3)

$$dA/dt = K_3 C_{Be} \quad (3)$$

where $K_3 = K_2 C_L$.

In experiments, the beryllium amount in solution was considerable, up to 65–130 μg/50 ml. The amount of beryllium reacting with beryllon II in the resin phase accounts for a very small part of the total amount of beryllium in solution. So C_{Be} can also be considered constant during the reaction process. For the above reason, we can obtain equation (4)

$$dA/dt = K_4 \quad (4)$$

where $K_4 = K_3 C_{Be} = K_2 C_L C_{Be}$.

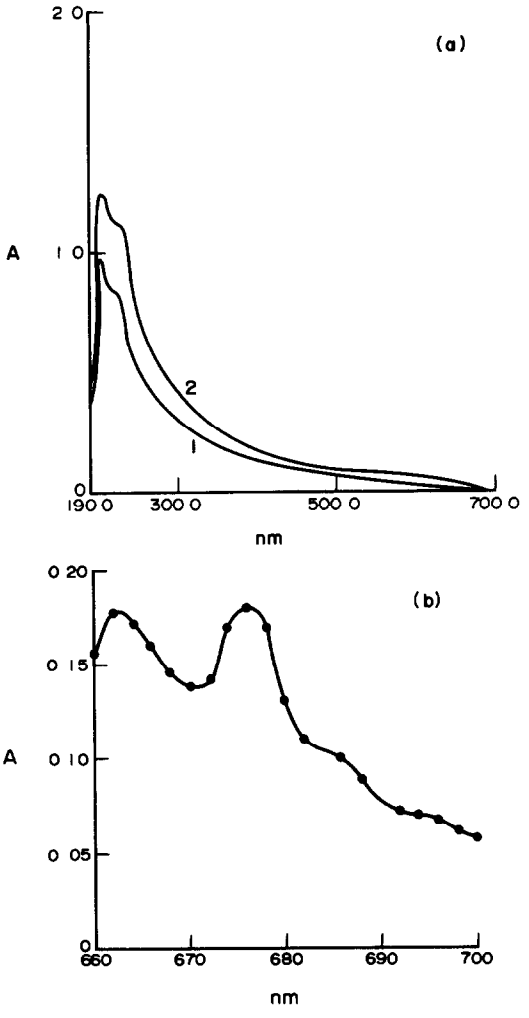

Fig 3 (a) Absorbance–wavelength curves 1 Blank resin, 2 resin–beryllon II (b) Absorbance–wavelength curve Reaction time = 5 min Be concentration = 2 17 μg/ml

Equation (4) is a rate equation of a pseudo-zero-order reaction. We integrate equation (4) to obtain equation (5)

$$A = K_4 t + B \qquad (5)$$

where B is a constant. Equation (5) is a kinetic equation of a pseudo-zero-order reaction. It shows that the Be–beryllon II complex absorbance in a resin phase is proportional to the reaction time between beryllium in solution and beryllon II in a resin phase only if the total amount of beryllium in solution is much greater than the total amount of beryllon II in the resin phase and only beryllon II on the surface of the resin phase reacts with beryllium in solution.

We conducted a series of experiments and found that the relation between the complex absorbance and the reaction time is linear, shown in Fig. 2. The change in absorbance with time was not influenced by the rate of stirring. By kinetic theory and experiments, we come to the conclusion that the reaction between beryllium in solution and beryllon II in a resin phase is a pseudo-zero-order reaction under our experimental conditions.

Because K_4 is equal to $K_3 C_{Be}$ and K_4 stands for the slopes of every curve in Fig. 2, K_4 increases with C_{Be} and can be determined by the slopes of every curve in Fig. 2. When the concentrations of beryllium in solution are 1 30, 1.73, 2.17 and 2.60 μg/ml, K_4 values in equation (5) are 0.014, 0.018, 0.021 and 0.025, respectively. In Fig 2, the Y-intercepts of curves 1, 2, 3 and 4 are 0.011, −0.015, −0.0081 and −0.0051

Figure 2 indicates that the A–t curves cannot pass through the origin because a certain time is needed for a change in beryllium concentration. Before beryllium in solution forms a complex with beryllon II in the resin phase, it must pass through the interface between the resin phase and solution. This mass transfer process takes some time. As the beryllium concentration in solution increases, the time decreases. When beryllium concentration is 1.30, 1 73, 2.17 and 2.60 μg/ml and absorbance values reach 0.1 unit, the time is 8.1, 6.5, 5 2 and 4.3 min, respectively.

Spectra

Figure 3(a) shows the absorption spectra of the blank resin and resin–beryllon II without beryllium.

Curve 1 has two absorption maxima at 204.8 and 222.3 nm. They are the E1 and E2 absorption bands of benzene rings in the resin Curve 2 also has two absorption maxima at 208.3 and 233.5 nm and we believe they are also E1 and E2 absorption bands of benzene rings in the resin. Because beryllon II was combined with resin, a red shift in absorption maxima was produced. It is reported that the absorption maxima of beryllon II in aqueous solution is 546 nm at pH 6–7.[7] After beryllon II was combined with resin, the absorption maxima at 546 nm disappears. We cannot yet explain the phenomenon.

It is reported in by Lukin and Zavarickhina[7] that the maximum absorption wavelength of the Be–beryllon II complex in aqueous solutions if 600 nm,[7] but Fig 3(b) shows that the maximum absorption wavelength of Be–immobilized beryllon II complex is 676 nm under our experimental conditions. Immobilization leads

to a maximum absorption wavelength shift from 600 to 676 nm. This red shift of the complex in the resin phase is attributed to a higher ligand concentration in the resin phase than one in the solution of a conventional wet method.[9-11] So, the Be–beryllon II complex has a higher coordination number in the resin phase.[9,11] However, no experimental evidence was provided to prove this point.

Effect of pH

Figure 4 shows the effect of pH on the absorbance of the Be-immobilized beryllon II complex. From pH 12.4 to 12.6, the absorbance of the complex is constant. At pH values higher than 12.6 and lower than 12.4, absorbance decreases rapidly. Absorbance is sensitive to a pH change. We chose pH 12.5 as a measuring pH value to obtain a higher absorbance. We cannot explain why the useful pH range is so narrow; perhaps at pH values more than 12.6, the dissolved beryllium forms a $Be(OH)_2$ precipitate while at pH values lower than 12.4, the Be-immobilized beryllon II complex on the resin phase may dissociate. In our study, no experiments were made on this aspect.

Acidity to remove beryllium from resin phase

We removed beryllium from resin phase using $1M$, $2M$, $3M$ and $6M$ hydrochloric acid. In order to ensure the removal of beryllium from the resin phase, we used $3M$ hydrochloric acid during our experiments.

Effect of ionic strength on absorbance

The effect of variation of ionic strength on the absorbance of the Be-resin–beryllon II complex was investigated adding a certain amount of sodium chloride to vary the ionic strength; it was observed that the absorbance of the Be-resin–beryllon II complex was independent of variation in ionic strength in the range 0–0.01M sodium chloride.

Calibration

Figure 2 shows that the slope of the absorbance–time curve is proportional to Be concentration in solution which means that the Be concentration can be related on the absorbance at a fixed time after the reagents are mixed. In our paper, reaction time was fixed to 5 min in sample analysis.

Since the method is used in the rate mode determining the reaction time is very important. If the reaction time is too long the resin phase

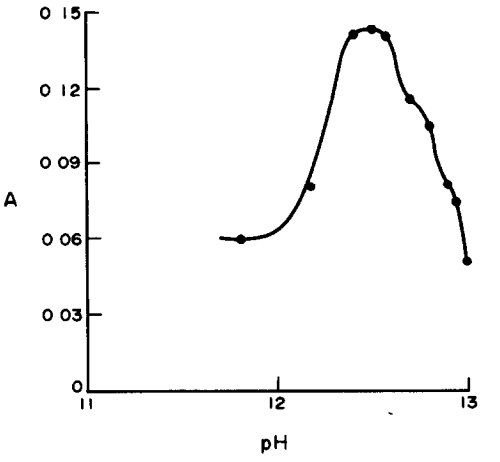

Fig 4. Absorbance–pH curve Reaction time = 5 min Be concentration = 2 17 μg/ml

is easily saturated and the linear range becomes narrow; at the same time, the analysis rate decreases. If the reaction time, is too short absorbance readings are too low and greater measuring errors occur.

In order to have a wider measuring linear range and shorter measuring time, we chose curve 2 (Fig. 5) as a calibration curve in sample analysis. Its slope is 0.0514, Y-intercept −0.0121 and correlation coefficient 0.9970. The linear range of curve 2 is 0.43–2.60 μg/ml. The reaction time of curve 2 is 5 min.

Experiments showed that response was linear from 0.43 to 2.60 μg/ml at pH 12.5. At this pH, the maximum absorption wavelength of the Be–beryllon II complex was 676 nm. By kinetic theory and experiments, we found that the reaction between beryllium in solution and beryllon II in the resin phase was a pseudo-zero-order reaction under our experimental

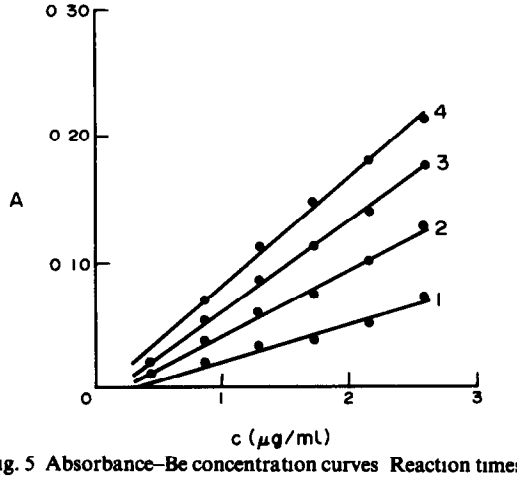

Fig. 5 Absorbance–Be concentration curves Reaction times of curves 1–4 are 3, 5, 7 and 9 min, respectively

Table 1 Effect of interfering ions on the determination of Be

Interfering ions	Concentration of interfering ions, μg/ml	Concentration of beryllium, μg/ml	Recovery rate of beryllium, %
F^-	240	2.17	104
Cl^-	400	2.17	100
NO_3^-	80	2.17	100
SO_4^{2-}	1920	2.17	93
PO_4^{3-}	760	2.17	93
Fe(III)	40	2.17	100
Co(II)	400	2.17	96
Ni(II)	800	2.17	100
Cu(II)	60	2.17	100
Mg(II)	60	2.17	103
Ca(II)	40	2.17	104

conditions. The stability of the resin phase was satisfactory for a continual use of 350 times during a month.

Effect of interfering ions

Table 1 shows the effect of interfering ions on the determination of beryllium.

Solutions of cation and anion for the interfering studies were made from the sulphates of copper(II), nickel(II), iron(III), the chlorides of cobalt(II), calcium(II) magnesium(II), sodium salts of fluoride, chloride, sulphate, phosphate and potassium salt of nitrate.

Many elements form coloured beryllon II complexes (*e.g.*, Fe^{3+}, Cu^{2+}, Mg^{2+}, Ca^{2+}, *etc.*) but in the presence of EDTA their interference is considerably masked.

Ascorbic acid was used to reduce iron(III) to iron(II) because, when a 10.0% sodium hydroxide was added, colloidal iron(III) hydroxide was formed which affected absorbance readings. Ascorbic acid can be omitted if iron is absent.

The relation between recovery rate of Be and Be concentration was not studied in our paper. Generally speaking, in a certain range of Be concentration, the recovery rate of Be does not vary with Be concentration.

Sample analysis

A beryllium–copper alloy sample solution was prepared by dissolving a 0.2518 g sample in 8 ml of 1:1 hydrochloric acid and by dropping 30% H_2O_2 as the solution was being heated. Surplus H_2O_2 was removed by heating. The sample solution was then transferred into a 100-ml standard flak and diluted to the mark.

Results of sample analysis are shown in Table 2.

Table 2 shows that the method is suitable for determining the amount of beryllium in beryllium–copper alloy and obtaining good results.

Precision was evaluated by measuring the absorbance at 676 nm four times for a sample. The Be concentration in the sample solution was determined from the second calibration curve of Fig. 5. Be content in sample and standard deviation were 2.02% and 0.03%.

This method is different from conventional resin phase spectrophotometry.[9-10] The resin phase with beryllon II need not be replaced for a long time. After beryllon II in a resin phase reacts with beryllium in solution, the resin phase is soaked in a 3.0*M* hydrochloric acid and the Be–beryllon II complex in the resin phase dissociates. Only beryllium in the resin phase comes off and beryllon II is still kept in the resin phase. In other words, after every measurement, the function of the resin phase can be entirely restored by soaking in hydrochloric acid. Because the resin phase has been attached to the common end of a bifurcated optical fiber bundle and need not be replaced, every measurement is made in the same resin phase; therefore, there

Table 2 Results of sample analysis

Be content in sample, %	Determined Be content, %	Standard deviation, % ($n = 4$)	Added Be amount, μg	Recovery rate of beryllium, % ($n = 4$)
2.12	2.02	0.03	21.68	104

is greater precision in this method than in a conventional resin phase spectrophotometric method.

REFERENCES

1 L E Smythe and R N Whittem, *Analyst*, 1961, **86**, 83
2 P Pakalns, *Anal Chim Acta*, 1964, **31**, 576
3 L Sommer and V Kuban, *ibid*, 1969, **44**, 333
4. J H Callahan and K D Cook, *Anal Chem*, 1982, **54**, 59
5 G Kwapulinska and F Buhl, *Mikrochim Acta*, 1984, **1(5–6)**, 333
6 Shi Huiming and Li Jinhe, *Huaxue Shiji (China)*, 1983, **5(2)**, 65
7 A M Lukin and G B Zavarikhina, *Zh Analit Khim*, 1956, **11**, 393
8 G G Karanovich, *ibid*, 1956, **11**, 400
9 Wang Rui, *Fenxi Shiyanshi (China)*, 1982, **1**, 64
10 K Yoshimura and H Waki, *Talanta*, 1976, **23**, 449.
11 Yang Quansheng, *Physical Testing and Chemical Analysis (Chemical Analysis) (China)*, 1988, **1**, 55
12 W R Seitz, *Anal Chem*, 1984, **56**, 16A

Talanta, Vol 40, No 6, pp 891–895 1993
Printed in Great Britain

0039-9140/93 $6 00 + 0 00

POTENTIOMETRIC DETERMINATION OF IRON USING A FLUORIDE ION-SELECTIVE ELECTRODE—THE APPLICATION OF THE APPLE II-ISE INTELLIGENT ION ANALYZER

BINGYAO SUN,* YINGZHI YE, HONGWU HUANG and YAN BAI†
Department of Chemistry, Zhengzhou University, Zhengzhou, Henan, 450052, People's Republic of China

(*Received* 16 *July* 1992 *Revised* 24 *August* 1992 *Accepted* 10 *October* 1992)

Summary—A new method for determining iron is based on both nonlinear regression calibration plots and parabolic interpolation using a fluoride ion-selective electrode (ISE) and the Apple II-ISE intelligent ion Analyzer developed by ourselves The experimental conditions for determining iron are discussed The appropriate acidity of the experimental solution is pH 3, controlled by total ionic strength adjustment buffer (TISAB) that is composed of glycine (aminoacetic acid), nitric acid and sodium nitrate The suitable total concentration of fluoride is equal to the highest concentration of iron in the standard series Because the mathematical model of the method coincides with the experimental data the Apple II-ISE intelligent ion Analyzer can perform data acquisition and data processing, and the performance of fluoride electrode is excellent, the new method for determination of iron is fast and accurate This method has been used successfully in the determination of iron in mineral samples

Methods for determining iron include spectrophotometry,[1,2] titrimetry including redox titration[3] and complexometric titration,[4,5] photometric complexometric titration,[6,7] atomic absorption spectrometry (AAS),[8,9] polarized Zeeman AAS,[10] precolumn chelation liquid chromatography,[11] flow injection analysis,[12] oscillopotentiometric titration,[13] *etc.* In addition, there have only been a few reports on potentiometric methods[14,15] and kinetic potentiometric methods.[16,17] But there haven't been any reports on determining iron with a fluoride-ISE. Because several complexes can be formed from iron(III) and fluoride, the difficulty lies in establishing the stoichiometric ratio between fluoride and iron in their complexes during the analytical experiment. The stepwise stability constants are not markedly different in order of magnitude, so potential breaks at the equivalence point are not evident in potentiometric titration with fluoride as the titrant and fluoride-ISE as the indicator electrode. However it was found here that there is a smooth relationship between the potential of the fluoride-ISE and the amount of iron(III) in a standard series containing a constant quantity of fluoride. Furthermore, it was shown that the mathematical model, $y = ax^2 + bx + c$, coincides with the experimental data by the quadratic regression. Thus, both the quadratic regression calibration plot and the parabolic interpolation are satisfactory for the determination of iron.

*Author for correspondence
†Present address Department of Traditional Chinese Medicine, Henan College of Traditional Chinese Medicine, Zhengzhou, Henan, 450003, People's Republic of China

EXPERIMENTAL

Reagents

Standard solution of iron(III) [$C(Fe^{3+}) = 0.1000M$] was prepared by dissolving reduced iron powder, that had been dried for two hours at 393 K and weighed accurately after cooling, in an appropriate amount of nitric acid. After the iron powder reacted completely it was necessary to remove the nitrogen dioxide from the solution by evaporation Then the solution was transferred to a volumetric flask, diluted to the mark with water and mixed. Dilute standard solutions of iron were prepared from the stock solution as above by diluting with water as necessary.

Total ionic strength adjustment buffer (TISAB) [$C(NaNO_3 + NH_2CH_2COOH + 0.18\ HNO_3) = 0.50M$] pH 3, was prepared by dissolving 37.5 g of glycine and 42.5 g of sodium nitrate in appropriate amounts of water, adding 6.2 ml of nitric acid during agitation, (calculated

on the basis of. $NH_3^+CH_2COOH$; $pK_{a1} = 2.35$[3], HNO_3: 66%, $\rho = 1.40$ g/cm^3), then the solution was diluted with water to 1000 ml. Other TISAB, pH 2 and pH 4, *etc.*, were prepared by altering the added amount of nitric acid.

Sodium fluoride solution [C(NaF) = 1.0M] was stored in a polyvinyl chloride (PVC) flask. Dilute sodium fluoride solutions were obtained by dilution.

All reagents used were of analytical grade and doubly distilled water was used throughout.

Apparatus

The fluoride-ISE was a Model 201 electrode (made in Jiangsu Electroanalyzer Factory), with $10^{-3}M$ sodium fluoride saturated by silver chloride as the interal solution. The reference electrode was a Model 217 double-junction saturated calomel electrode (made by Shanghai Electrophotodetector Factory) with a 1M sodium nitrate as the bridging solution. The test solution was in the PVC plastics beaker and stirred with a PVC-coated magnetic bar during the experiment. Both the stirring speed and electrode distance were kept constant throughout all measurements. The cell potentials were measured with the Apple II-ISE intelligent ion Analyzer (0.1 mV resolution), which has nine functions as follows:[18] (1) method of calibration plot; (2) single standard addition method; (3) double standard addition method; (4) Gran's method; (5) sample addition method; (6) comparison method and determination of pH; (7) determination of selectivity; (8) potentiometric titration; (9) digital potentiometer, and cannot only discriminate and acquire the equilibrium potential of electrode automatically, but also process data quickly. There are linear and quadratic regression and parabola interpolations in the method of the calibration plot. The principles of quadratic regression and parabola interpolation are explained in the following two sections.

Quadratic regression. Suppose the quadratic equation is

$$y = ax^2 + bx + c \tag{1}$$

If n pairs ($n \geqslant 3$) of data are acquired from experiments: x_i, $y_i (i = 1, 2, \ldots, n)$, then n simultaneous linear equations in three unknowns are obtained:

$$\begin{cases} ax_1^2 + bx_1 + c = y_1 \\ ax_2^2 + bx_2 + c = y_2 \\ \cdots \\ ax_n^2 + bx_n + c = y_n \end{cases} \tag{2}$$

Solving the simultaneous linear equations, we can find a, b, c and the quadratic equation by substituting a, b, c into equation (1). For the determination of iron with the fluoride-ISE, y is the potential of fluoride-ISE, x is the concentration of iron: $C(Fe^{3+})$, or its logarithm: $\log C(Fe^{3+})$.

Parabolic interpolation. Given n experimental points. x_i, $y_i (i = 1, 2, \ldots, n)$, and in order of: $y_i < y_{i+1}$, take three near-points to the point interpolated and calculate according to the formula as follows, that is, three-node Lagrange's interpolation formula:

$$\begin{aligned} x = {} & \frac{(y - y_i)(y - y_{i+1})}{(y_{i-1} - y_i)(y_{i-1} - y_{i+1})} x_{i-1} \\ & + \frac{(y - y_{i-1})(y - y_{i+1})}{(y_i - y_{i-1})(y_i - y_{i+1})} x_i \\ & + \frac{(y - y_{i-1})(y - y_i)}{(y_{i+1} - y_{i-1})(y_{i+1} - y_i)} x_{i+1} \end{aligned} \tag{3}$$

then, we can obtain x from y

For a given y, the three near-points can be selected in the following way.

$$i = \begin{cases} 2 & \text{at } y \leqslant y_2 \\ k-1 & \text{at } y_{i-1} < y \leqslant y_k \\ & \quad \text{and } |y - y_{k-1}| \leqslant |y - y_k| \\ k & \text{at } y_{k-1} < y < y_k \\ & \quad \text{and } |y - y_{k-1}| > |y - y_k| \\ n-1 & \text{at } y \geqslant y_{n-1} \end{cases} \tag{4}$$

The block diagram of the computer program for this calculation was referred to the previous work of authors.[19]

Procedure

Pipette 1.0, 2.0, ..., n ml of standard solution of iron into a series of 50-ml volumetric flasks successively, add equal volumes of sodium fluoride solution and 5 ml of TISAB solution, dilute to the mark with water and mix Transfer them in the proper order into a series of 100-ml dried plastics beakers, measure the cell potentials with Apple II-ISE Analyzer in order of decreasing iron concentration *i.e.*, increasing fluoride concentration. At the same time, enter the concentrations of iron corresponding to the various solutions. If the quadratic regression calibration plot was adopted, as soon as data acquisition was complete, the calibration plot would be displayed on the screen and printed out simultaneously on the floppy disk to use for

determining the sample. If the parabola interpolation was adopted, then the interpolation table would be arranged and written on the floppy disk.

Determination of iron in iron ore sample. The solution of mineral sample was prepared in a similar way as the standard solution of iron. Pipette an appropriate amount of sample solution into a 100-ml volumetric flask, add TISAB and an equal amount of sodium fluoride solution to the standard series and the sample. After measuring the potential, the result was displayed and printed out immediately.

RESULTS AND DISCUSSION

Effect of pH

Acidity influences both the potential response of fluoride-ISE and the complexation of iron (III) with fluoride.

Generally speaking, we should use the fluoride-ISE in the intermediate pH range 4–8.[20] If the pH is less than 4, the protonation results in the formation of hydrogen fluoride, to which the electrode is insensitive. However, it was shown that the electrode still retains good linear response of potential and the same experimental slope, $-59.3\ \text{mV} \cdot \text{pF}^{-1}$, in acidic solution by our experiments. This result is in agreement with Radic and Bralic.[21] In terms of theory, if we define C as the total concentration of fluoride and hydrogen fluoride δ_F as the fraction of concentration of fluoride, or distribution coefficient of fluoride, then:

$$[F^-] = \delta_F C = \frac{K_a}{[H^+] + K_a} C \tag{5}$$

$$a = \gamma_F [F^-] = \frac{\gamma_F K_a}{[H^+] + K_a} C \tag{6}$$

where, K_a is the dissociation-constant of hydrogen fluoride, a and γ_F are the activity of fluoride and its activity coefficient, respectively. After substituting formula (6) into the following equation:

$$E = E^0 + S \log a \tag{7}$$

we can obtain the potential of the fluoride electrode expressed in terms of γ_F, K_a, $[H^+]$ and C as follows:

$$E = E^0 + S \log \frac{\gamma_F K_a}{[H^+] + K_a} + S \log C \tag{8}$$

If the solution is sufficiently buffered, the ionic strength and pH are fixed. This can readily be realized by adding TISAB. Then, in equation (8), the second term,

$$S \log \frac{\gamma_F K_a}{[H^+] + K_a}$$

is constant. Consequently, the sum of the standard electrode potential E^0 and the second term is also constant. We can define the sum as the conditional potential and express it as $E^{0'}$, that is.

$$E^{0'} = E^0 + S \log \frac{\gamma_F K_a}{[H^+] + K_a} \tag{9}$$

substituting formula (9) into (8), a similar equation to (7) can be obtained:

$$E = E^{0'} + S \log C \tag{10}$$

Here, the linear relationship between E and $\log C$ is shown clearly. Because the conditional potential $E^{0'}$ is not a fixed constant but depends on the experimental conditions, the calibration plot will be shifted parallel when altering the experimental conditions. From the above discussion, we concluded that if necessary the fluoride-ISE can be used in acidic solution, but the experimental conditions, such as acidity, ionic strength, *etc.*, must be strictly controlled.

For the determination of iron, the acidity had to be controlled. We had prepared several standard series that contained the same total fluoride concentration, $2.0 \times 10^{-3} M$, and the same iron concentration range, $2.0 \times 10^{-4} \sim 1.0 \times 10^{-3} M$, only at different pH values. The experimental results are shown in Table 1.

The results illustrate that at pH 2 and 4 the variations of potential are less than pH 3. At pH 4 the hydrolysis and the formation of polyhydroxy complexes of iron(III) influence the complexation reactions of iron(III) with fluoride. At pH 2, the protonation of fluoride as a

Table 1. Effect of pH on potentials

$C(Fe^{3+})/M$	1.0×10^{-3}	8.0×10^{-4}	6.0×10^{-4}	4.0×10^{-4}	2.0×10^{-4}	R/mV
pH 2	103.7	94.8	86.4	78.7	71.2	32.5
3	84.7	72.3	60.7	50.2	40.7	44.0
4	53.8	49.9	44.6	37.5	28.5	25.3

*The numerical values in the table are potentials.

Table 2. The coefficients of the acid effect at different pH values (HF. $K_a = 6.8 \times 10)^4$

pH	$\alpha_{F(H)}$	$\log \alpha_{F(H)}$	$6 \log \alpha_{F(H)}$
2	15 71	1.196	7 176
3	2 47	0 393	2 358
4	1.15	0 061	0 366

side reaction is not neglected. If we introduce the coefficient for the acid $\alpha_{F(H)}$, as a coefficient for the side reaction:[22]

$$\alpha_{F(H)} = \frac{[F^{-\prime}]}{[F^-]} \tag{11}$$

$$\alpha_{F(H)} = 1 + \frac{[H^+]}{K_a} \tag{12}$$

and consider the effect of pH on the overall formation constant β_6 ignoring the other side reactions, then, from

$$\beta_6 = \frac{[FeF_6^{3-}]}{[Fe^{3+}][F^-]^6} \tag{13}$$

we can obtain:

$$\beta_6' = \frac{\beta_6}{\alpha_{F(H)}^6} \tag{14}$$

where β_6' is the conditional formation constant, the logarithmic form as follows:

$$\log \beta_6' = \log \beta_6 - 6 \log \alpha_{F(H)} \tag{15}$$

Some results calculated are arranged in Table 2. It is clear that at pH 2 the conditional formation constant β_6' is decreased by seven orders of magnitude compared to the overall formation constant β_6. But, at pH 3 the effect of acid is not serious, or can be neglected.

In summary, the optimum acidity for determining iron is pH 3.

Effect of fluoride concentration

Figure 1 shows the variation of potential when the standard series contains the same iron concentration range, $2.0 \times 10^{-4} \sim 1.0 \times 10^{-3} M$, but different total fluoride concentration, all at pH 3. The figure shows that the less the amount of fluoride the greater the variation of potential when the amount of fluoride is larger than one-fold amount. If the amount of fluoride is too much, such as seven-fold amount, the curve becomes gentle, that is, the variation of potential is not obvious. Therefore, to employ less fluoride is advantageous for increasing the sensitivity and accuracy of the determination of iron. But if the amount of fluoride is too little, less than one-fold amount, on the contrary, the variation of the potential begins to decrease and the potential response of the fluoride electrode becomes unsteady with poor reproducibility. A suitable amount of fluoride is just one-fold.

TISAB

Several buffer systems were used in the experiments. The system composed of glycine, nitric acid and sodium nitrate is better than others. Nitric acid and nitrate are better than hydrochloric acid and chloride, because chloride can complex with iron, and so influences the determination. A suitable concentration of TISAB is $0.05M$, but the effect of TISAB concentration is not as important as acidity and the fluoride concentration.

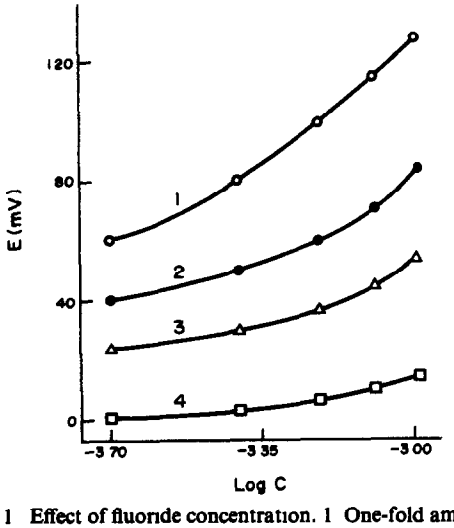

Fig. 1 Effect of fluoride concentration. 1 One-fold amount fluoride; 2. twice ~, 3. three-fold ~, 4. seven-fold ~

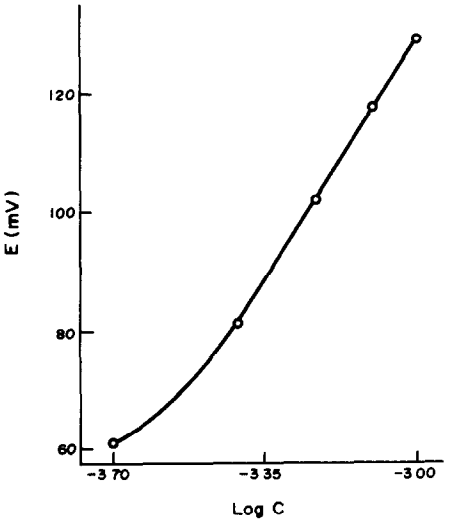

Fig 2 A quadratic regression calibration plot

Table 3 Several standard series

$C(Fe^{3+})/M$	1.0×10^{-2}	8.0×10^{-3}	6.0×10^{-3}	4.0×10^{-3}	2.0×10^{-3}	R/mV
E/mV	130.9	118.0	98.0	69.4	39.7	91.2
$C(Fe^{3+})/M$	1.0×10^{-3}	8.0×10^{-4}	6.0×10^{-4}	4.0×10^{-4}	2.0×10^{-4}	
E/mV	128.4	117.6	101.9	81.4	60.9	67.5
	128.9	117.3	101.0	80.2	58.5	70.1
	127.0	115.6	100.5	78.8	58.2*	68.8
	127.3	115.7	100.6	78.8	58.3*	69.0
$C(Fe^{3+})/M$	1.0×10^{-4}	8.0×10^{-5}	6.0×10^{-5}	4.0×10^{-5}	2.0×10^{-5}	
E/mV	128.9	123.4	119.5	114.9	110.0	18.9

*Obtained by measuring the same standard series twice at interval of 10 hours after preparation

Range of determination

Table 3 lists the measured results of several standard series prepared in suitable experimental conditions at pH 3, with a one-fold amount of fluoride and 0.05M TISAB. The results show that the range for determining iron is $2.0 \times 10^{-5} \sim 1.0 \times 10^{-2}M$ and the optimum range is $2.0 \times 10^{-4} \sim 1.0 \times 10^{-2}M$. The measurement of potential showed that the solution can be steady for a long time after preparation.

Interferences

Every substance that can complex with fluoride will be possible interferences of the method, such as aluminium, silicon and zirconium. On the other hand, all substances being able to complex with iron except fluoride also influence the determination of iron, such as thiocyanate, oxalate and tartrate, Strictly speaking, during the determination the interferences should not be present, but it was shown in the experiments that if the interference concentrations are far less than iron, the method is not influenced.

A quadratic regression calibration plot is shown in Fig. 2. It is obvious that the mathematical quadratic regression calibration plot and parabola interpolation method have high accuracy and precision.

REFERENCES

1 L L Stookey, *Anal Chem*, 1970, **42,** 779
2 H Hoshino and T Yotsuyanagi, *Talanta*, 1984, **31,** 525
3 D C Harris, *Quantitative Chemical Analysis*, W H Freeman and Company, 1982, 383, 666
4 M Fujimoto, I Shirotoni and Y Nakatsukasa, *Mikrochim Acta*, 1971, **1,** 121
5 H Yamada, T Maeda and I Kojima, *Anal Chim Acta*, 1974, **72,** 426
6 D Nonova and N Lihareva, *Talanta*, 1976, **23,** 439
7 Y Chen and H Chen, *Chem J Chin Univ*, 1982, **3,** 319
8 M T Glenn and J Savory, *Anal Chem*, 1973, **45,** 203
9 A Li, W Ren and Y Liao, *ibid*, 1984, **12,** 286
10 J He and Y Tang, *Chem J Chin Univ*, 1985, **6,** 689
11 D A Roston, *Anal Chem*, 1984, **56,** 241
12 H Cui and Z Fang, *ibid*, 1984, **12,** 759
13 Y Chen, J Weng, W Xu and H Gao, *ibid*, 1987, **15,** 820 (in Chinese)
14 R W Cattrall and Pui Chin-poh, *ibid*, 1975, **47,** 93
15 Y Zhu, S Huang and S Liu, *Chem Sensor*, 1989, **9,** 44
16 L A Lazarou and T P Hadjioannou, *Anal Chem.*, 1979, **51,** 790
17 Y Feng, Z Chen, S Zhou and R Yu, *ibid*, 1989, **17,** 1022
18 Y Ye, B Sun and F Wang, *Chem Researches*, 1991, **2,** 54
19 B Sun and Y Ye, *Bull Anal Test* 1990, **9,** 26.
20 H Freisor, *Ion-Selective Electrodes in Analytical Chemistry*, Vol 1, p 321 Plenum Press, New York and London, 1978
21 Njegomir Radic and Marija Bralic, *Analyst*, 1990, **115,** 737
22 I M Kolthoff and Philip J Elving (ed), *Treatise on Analytical Chemistry, Part 1, Theory and Practice*, Vol 2, 2nd Ed, p 462 Wiley, New York, 1979

Talanta, Vol 40, No 6, pp 897–899, 1993
Printed in Great Britain

0039-9140/93 $6 00 + 0 00

SIMULTANEOUS THIRD-DERIVATIVE SPECTROPHOTOMETRIC DETERMINATION OF COPPER AND NICKEL IN IRON ALLOYS AND ALUMINIUM ALLOY

WANG NAIXING and LIANG WEIAN
Department of Chemistry, Shandong University, Jinan, 250100, People's Republic of China

QI PING
Shandong Analysis and Test Center, Jinan, 250014, People's Republic of China

(*Received* 20 *July* 1992 *Revised* 7 *October* 1992 *Accepted* 8 *October* 1992)

Summary—A method is proposed for the simultaneous determination of copper and nickel by third-derivative spectrophotometry based on the absorption spectra of their complexes with cyanide ion in the ultraviolet range The method allows the determination of 0 55–5 8 μg/ml of copper and 0.55–6.8 μg/ml of nickel. The relative standard deviation for 11 determinations of 1 5 μl/ml of copper and nickel were 0.78 and 0.72%, respectively. The detection limits were 0.10 μg/ml for nickel and 0 13 μg/ml for copper The method has been applied to direct determination of copper and nickel in iron alloys and an aluminium alloy without any separation

Many methods have been reported for the spectrophotometric determination of nickel[1–5] and copper.[6–10] None of these is entirely specific for nickel and copper in the same sample.

The cyanide ion forms square tetracyanonickelate anion with nickel or copper in basic media. Buck *et al.*[11] demonstrated the potential application of ultraviolet spectroscopy for the measurement of nickel and copper.

In this paper the absorption spectra of nickel and copper complexes with cyanide ion are investigated using zero-order and derivative spectrophotometry. The suggested third-derivative spectrophotometry has been applied successfully to the analysis of copper and nickel in some iron alloys and an aluminium alloy without any separation.

EXPERIMENTAL

Apparatus

A Shimadzu UV-3000 double-beam spectrophotometer with 1.0 cm quartz cells was used.

Reagents

Stock solutions of copper and nickel, 5 mg/ml. Prepared from the sulphates. The exact concentrations were determined gravimetrically by ammonium thiocyanate and dimethylglyoxime method,[12] respectively, and further diluted as required.

Ammoniacal sodium cyanide solution containing 1.0 g of NaCN and 20 ml of concentrated ammonium hydroxide per 100 ml of solution is prepared.

All experiments were performed with analytical-reagent grade chemicals. Distilled water was used throughout.

Procedure

Transfer a known volume of sample solution containing 6.0–55 μg of copper and nickel into a 10 ml calibration flask. Add 0.15 ml of 1.0% NaCN solution, and dilute the mixture to the mark with distilled water. Record the third-derivative spectrum against a reagent blank. Determine the copper and nickel contents from the third-derivative spectrum by measuring the peak to valley signals at 242(+) nm - 234(−) nm for copper and at 271(+) nm - 283(−) nm for nickel, respectively, and comparing the value with an appropriate calibration graph.

Decomposition of sample

Dissolve 0.3 g of sample in 10 ml of hydrochloric acid (1 + 1) in a 50-ml beaker. Iron is oxidized by a few drops of concentrated nitric acid and the solution evaporated nearly to dryness. The residue is dissolved in 10 ml of

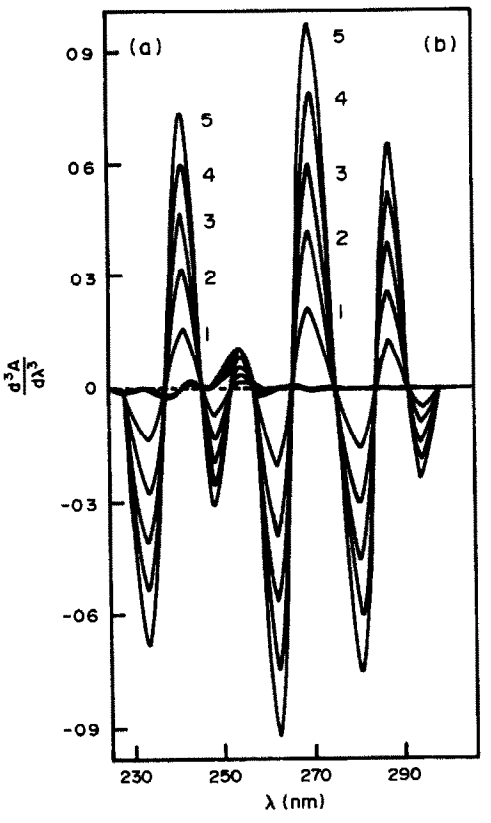

Fig 1 Calibration spectral curves $[CN^-] = 3.0 \times 10^{-3}M$, $\Delta\lambda = 6.3$ nm, scan rate = 50 nm/min, band pass = 1.0 nm, 1.0 cm cell (a) Cu, (b), Ni 1, 0.55, 2, 1.10, 3, 1.65, 4, 2.20, 5, 2.75 μg/ml

water. This solution with insoluble silicic acid is transferred to a 50-ml measuring flask. The iron (or aluminium) is precipitated by adding 25 ml of ammonium hydroxide (1 + 1) containing 5.0 g ammonium chloride and mixed thoroughly in the cold. The solution is diluted to the 50-ml mark with distilled water. Determine the copper and nickel concentrations in a suitable aliquot.

RESULTS AND DISCUSSION

Absorption spectra

The absorption spectrum of copper complex which has an absorption maximum at 238 nm; the absorption spectrum of the corresponding nickel complex has an absorption maximum at 268 nm; and both have sharp absorption patterns. However, they have slight interference on each other, when they are present in the same solution. To overcome this problem, derivative spectrophotometry can be used. The use of derivative spectra is not only simple and selective, but also improves the sensitivity.[13–15] Hence, their derivative spectras were investigated.

A study of the second-, third- and fourth-derivative spectra of the copper complex and nickel complex demonstrated that the third-derivative spectrum gave the lowest detection limits or highest sensitivity. The significant amplitudes are at 242(+) nm - 234(−) nm for copper and at 271(+) nm - 283(−) nm for nickel, respectively (Fig. 1).

Selection of optimum instrument conditions

The main instrumental parameters affecting the shape of the derivative spectra are the wavelength scan rate, the wavelength increment over which the derivative is obtained ($\Delta\lambda$) and the response time Therefore, various values of $\Delta\lambda$ were tested and 6.3 nm was selected, as the optimum, in order to give a satisfactory signal-to-noise ratio. The scan rate of the monochromator has no effect on the derivative signal obtained. Hence, a fast wavelength scan rate (*ca.* 50 nm/min) was selected The response time is automatically selected by the spectrophotometer in accordance with optical energy and the scan rate.

Optimization of reaction conditions

The effect of the cyanide ion concentration was studied. The experimental results found that the cyanide ion concentration ranges that gave the greatest derivative signals were 2.0×10^{-4}–$5.5 \times 10^{-3}M$ for copper and greater than $2.0 \times 10^{-4}M$ for nickel. So, $3.0 \times 10^{-3}M$ CN^- solution was selected.

The complexes formed quickly and the derivative absorption was stable for at least 6 h.

Calibration graphs,precision and detection limits

Using the optimum instrumental parameters and reaction conditions established above, linear calibration graphs were obtained by plotting the amplitudes measured for third-derivative spectra for copper and nickel in the concentration ranges 0.55–5.8 μg/ml and 0.55–6.8 μg/ml, respectively (in the final solution) The

Table 1 Effect of foreign ions on the simultaneous determination of copper and nickel Concentration [Ni] = [Cu] = 1.0 μg/ml

Ion	Ion/Ni or Cu, weight ratio
Mg^{2+}, Ca^{2+}, Ba^{2+}, Cl^-, SO_4^{2-}, NO_3^-, ClO_4^-	1000
Zn^{2+}, Al^{3+}, Cd^{2+}, Hg^{2+}	200
Fe^{3+}, Pb^{2+}	80
Mo^{6+}, Ti^{4+}, Cr^{3+}, Mn^{2+}, Sn^{4+}, V^{5+}	40
Co^{2+}, Cr^{6+}	15

Table 2 Simultaneous determination of copper and nickel in reference materials*

Sample No	Composition, % Certified value	Found†, % nickel	Found†, % copper	RSD,‡ % nickel	RSD,‡ % copper
Iron alloy-1	C 2.51, Cr 0 4, Si 2 62, Mo 0 68, P 0 193, S 0 046, Cu 0 68, Ni 0 24, V 0 032, Co 0 014, Sb 0 00043	0 244	0.671	0.86	0 70
Iron alloy-2	V 0.036, Co 0 014, Cu 0 123, Cr 1 10, Mo 0 002, Mn 1 07, Ti 0 094, Ni 0 027, Sb 0 00041	0 0276	0 128	0 96	0 90
Iron alloy-3	Co 0 237, Si 0 205, Mn 0 407, P 0 024, S 0 0315, Cr 0 24, Cu 0 38, Ni 0 207, Mo 0 315, Ti 0 113	0 211	0 386	1 0	0 80
Aluminium alloy	Si 747, Fe 0 39, Mg 0 305, Mn 0 16 Ni 0 064, Cu 5 74, Zn 0 66	0 067	5.84	0 92	0 51

*From Metallurgical Research Institute, Shandong, China
†Average of five determinations
‡Relative standard deviation ($n = 5$)

representative third-derivative spectral curves are shown in Fig. 1 The proposed procedure showed good precision, the relative standard deviation (RSD) for 11 determinations of 1.5 μg/ml of copper and nickel being 0.78 and 0.72%, respectively. The detection limits, corresponding to a signal-to-noise ratio (SNR) of 2, were found to be 0.13 μ/ml and 0.10 μg/ml for copper and nickel, respectively.

Interference studies

The effects of various cations and anions on the simultaneous determination of copper and nickel were investigated. The tolerance limit was taken as the amount that caused $\pm 5\%$ error. Cations were added as solutions of the their chlorides, nitrates or sulphates. Anions were added as solution of their sodium, potassium or ammonium salts. The results is given in Table 1.

Analytical application

The method can be applied to the determination of copper and nickel in iron and aluminium alloys. The results of analysis in comparison with certified values of several alloys are given in Table 2, indicating that the procedure provides accurate and precise results without the necessity of chemical separation.

REFERENCES

1 H Ishii, T. Odashima and T. Hashimoto, *Anal Sci*, 1987, **4**, 347
2 S L C Ferreira, *Talanta*, 1988, **6**, 485
3 F S Wei, P. H Qi, N K. Shen and F Yin, *ibid*, 1981, **3**, 189
4 K Kasiura and Z. Sytniewska, *Chem. Anal*, 1968, **13**, 177
5 Z Marczenko, *Spectrophotometric Determination of Elements*, pp 370–373 Horwood, Chichester, 1976.
6 K Hayashi, Y Sagashia and K Hirata, *Anal Chim. Acta*, 1987, **198**, 271.
7 T Fukasawa, S Kawakubo and L Tan *Analyst*, 1987, **112**, 1247
8 B Tamhina, *Mikrochim J*, 1980, **25**, 235
9 M. Roman, J J Berzas and A Espcyanate, *ibid*, 1983, **28**, 69
10. S. P Arya, J. L Malla and V. Slathia, *Talanta*, 1987, **2**, 293.
11 R. P Buck, Samang Singhadeja and L B Rogers, *Anal Chem*, 1954, **7**, 1240
12 A. I Vogel, *Quantitative Inorganic Analysis*, 3rd Ed, Longmans, London, 1961
13 N X Wang, W A Liang, S F Zhou and P Qu, *Anal Chim Acta*, 1992, **2**, 253
14 José A. Murillo, José M. Lemus, Arsenio Muñoz de lo Peña and Francisco Salinas, *Analyst*, 1988, **9**, 1439.
15 A L Jiménez, F Jiménez and J J Arias, *ibid.*, 1989, **1**, 93

Talanta, Vol 40, No 6, pp 901–907, 1993
Printed in Great Britain

0039-9140/93 $6 00 + 0 00

FLUORESCENCE PROPERTIES OF 1-NAPHTHOL, 2-NAPHTHOL AND 1,2,3,4-TETRAHYDRONAPHTHOL IN AQUEOUS ALCOHOL SOLVENTS WITH AND WITHOUT β-CYCLODEXTRIN

DAN WU* and ROBERT J. HURTUBISE
Department of Chemistry, University of Wyoming, Laramie, WY 82071, U S A

(*Received* 29 *July* 1992 *Revised* 6 *October* 1992 *Accepted* 6 *October* 1992)

Summary—The fluorescence properties of 1-naphthol, 2-naphthol and 1,2,3,4-tetrahydronaphthol were obtained in binary aqueous–alcohol solvents with and without β-cyclodextrin. The fluorescence of both the molecular and anionic forms of 1-naphthol and 2-naphthol were observed in the binary solvents without β-cyclodextrin Only the fluorescence of the molecular form of 2-naphthol appeared in the binary solvents with β-cyclodextrin present, and its fluorescence was quenched with increasing amounts of β-cyclodextrin However, the fluorescence intensity of the molecular form of 1-naphthol increased with an increasing amount of β-cyclodextrin in the binary solvents The fluorescence intensity of 1,2,3,4-tetrahydronaphthol decreased with an increase in the amount of β-cyclodextrin The fluorescence results were interpreted with the Stern-Volmer equation and a modified Stern-Volmer equation

INTRODUCTION

A considerable amount of work has been carried out in investigating the interactions of guest molecules with cyclodextrins with water as a solvent.[1,2] However, very little work has been performed with binary aqueous–organic solvents. Nakajima[3] studied the effects of ethanol on the inclusion complex formation of pyrene with β-cyclodextrin (β-CD). It was found that the intensity ratio of the third vibronic band to the first vibronic band of pyrene decreased with the addition of ethanol. This implied that pyrene experienced a less polar environment in the presence of ethanol. Warner and coworkers[4,5] further investigated this phenomenon. They found that in the presence of alcohols the fluorescence intensity of pyrene was enhanced compared to that with no alcohols present. They also found that the largest increase was achieved in aqueous solution with a small amount of *t*-butanol. The intensity peak ratio also showed that with the *t*-butanol present in solution, pyrene experienced a more hydrophobic environment than in other alcohol solutions. They proposed that the alcohol molecule was a third component which participated in the complex formation. In other work, the fluorescence lifetimes of pyrene were measured in a γ-CD solution in the presence of alcohols, and the pyrene complex had a longer lifetime than the free pyrene.[6,7] Upon addition of alcohol, the lifetime and the formation constant of pyrene–γ-CD complexes were increased with respect to that in aqueous solution. Patonay *et al.*[8] also studied the quenching of pyrene in γ-CD aqueous solution. A modified Stern-Volmer equation was derived and applied to their experimental data. Nelson and Warner[9] have also investigated the fluorescence quenching of naphthalene and pyrene cyclodextrin complexes with iodide in the presence of alcohols. De la Pena *et al.*[10] considered the influence of alcohol addition on the γ-CD:pyrene complex. Hamai[11] has reported on the inclusion complexes of γ-CD with coronene in aqueous methanol, and also on exciplex formation between perylene and *N,N*-dimethylaniline in a ternary inclusion compound with γ-CD in a water–ethanol mixture. Also, Hamai[12] investigated the complexes of γ-CD with coronene in aqueous methanol. Recently, Huang *et al.*[13] reported the effects of aliphatic alcohol cosolvents on the nature of the cyclodextrin inclusion complexes of 2-anilinonaphthalene-6-sulfonic acid using steady-state and time resolved fluorescence spectroscopy.

In this work, the fluorescence properties of 1-naphthol, 2-naphthol, and 1,2,3,4-tetrahydro-

*Present address Department of Chemistry, Purdue University, West Lafayette, IN 47907, U.S.A

1-naphthol were investigated in binary organic–aqueous solvents with and without β-CD. It was important to investigate the fluorescence properties of these compounds without β-CD to help distinguish the change in the fluorescence properties of the model compounds in the binary solvents with and without β-CD present. In addition, by investigating two hydroxyl aromatics that are structural isomers, and a hydroxyl aromatic in which the hydroxyl group was substituted on a hydroaromatic ring, important insights were gained about the interactions of these compounds in binary solvents with and without β-CD present.

EXPERIMENTAL

Reagents

Ethanol was purified by distillation. Water was HPLC grade and obtained from Burdick and Jackson Co. (Muskegon, MI, U.S.A.) and used as received. Methanol and isopropanol (HPLC Grade) were purchased from Baker Inc. (Phillipsburg, NJ, U.S.A.) and used without further purification.

1-Naphthol (99%), 2-naphthol (99%), 1,2,3,4-tetrahydro-1-naphthol (99%) and β-cyclodextrin hydrate (β-CD) were purchased from Aldrich Chemical Co. (Milwaukee, WI, U.S.A.) and used as received.

Instrumentation

Fluorescence spectra were recorded on a Perkin-Elmer LS-5 spectrofluorimeter (Norwalk, CT, U.S.A.) which had a xenon lamp pulsed at line frequency (50–60 Hz) and f/3 Monk-Gillieson type monochromators. A 1 × 1-cm quartz cell was used for handling the sample solutions. Slits were set at 5 nm for the excitation monochromator and 3 nm for the emission monochromator for all fluorescence spectra measurements. The spectrofluorimeter was interfaced with a Perkin-Elmer 3600 data station. The data collection and manipulation were achieved by using the Perkin-Elmer computer software (PECLS). A Perkin-Elmer model 660 thermal printer was used for plotting the spectra. An ultrasonic cleaner (Cole-Parmer, Chicago, IL, U.S.A.) was used to mix the solutions.

Procedures

The model compounds were dissolved in binary solvents with different percentages of organic solvents and in the absence of β-CD for the initial set of experiments. For the other major set of experiments, the model compounds were dissolved in the binary solvents with a fixed organic solvent to water volume ratio, but with various amounts of β-CD. Different amounts of β-CD were added to a series of 10-ml standard flasks, and then the contents of the standard flasks were sonicated to ensure that all the β-CD dissolved. For all the solvent systems investigated for fluorescence, aliquots from a stock solution of a given model compound were added to the standard flasks prior to diluting with the appropriate solvent to the final volume. The stock solutions were prepared by dissolving a weighed amount of model compound in a 1 1 organic:aqueous solvent with no β-CD present and then diluting to volume. The final concentration of the model compounds used in the experiments were 3 μg/ml for 2-naphthol, 1 μg/ml for 1-naphthol and 5 μg/ml for 1,2,3,4-tetrahydro-1-naphthol.

Solution fluorescence excitation and emission spectra of the model compounds in the binary solvents in the absence and presence of β-CD were obtained with the Perkin-Elmer LS-5 spectrofluorimeter. A scan rate of 240 nm/min and response factor of 2 were used to obtain the spectra. Since the excitation and emission maxima of the model compound shifted slightly with the volume ratio changes of the binary solvents, the excitation and emission monochromators were set at the wavelength corresponding to maximum fluorescence intensities.

In order to compensate for instrumental variation and obtain accurate intensity readings, the intergradation mode of the Perkin-Elmer LS-5 was used, and a *p*-terphenyl fluorescence standard bar was employed (Wilmad Glass Co., Buena, NJ, U.S.A.). The fluorescence standard bar was rectangular shaped and had *p*-terphenyl embedded in a polymethyl methacrylate (PMMA) matrix. The excitation and emission wavelengths used for *p*-terphenyl were 295 and 338 nm, respectively. Each time the standard bar was placed in the sample holder at the same position to ensure reproducible fluorescence signals. To obtain an intensity reading, the quartz cell containing the sample solution was placed in the sample holder, and the monochromators were set at the corresponding excitation and emission wavelengths. The signal was integrated for 4 sec and the intensity reading of the sample (I_{sample}) was displayed. Then, the fluorescence standard bar was switched into the excitation light path, and the excitation and emission

monochromators were set at 295 and 338 nm, respectively. By using the integration mode, the intensity reading of the standard bar (I_{std}) was obtained. The corrected intensity was calculated by using the following equation:

$$I_{corr} = (I_{sample}/I_{std})20$$

This equation shows that all the sample readings were arbitrarily corrected to the value which corresponded to an I_{std} of 20.

RESULTS AND DISCUSSION

Fluorescence properties of 2-naphthol, 1-naphthol, and 1,2,3,4-tetrahydro-1-naphthol in binary organic–aqueous solvents in the absence of β-cyclodextrin

The fluorescence properties of 2-naphthol in water have been extensively studied.[14–16] 2-Naphthol in the lowest excited singlet state is a stronger acid than in its ground state, and it undergoes excited state ionization in water. In this work, the emission spectra of 2-naphthol in water, 0.1*N* hydrochloric acid and 0.1*N* sodium hydroxide solution were obtained so that the fluorescence spectra of the anionic and molecular forms of 2-naphthol would be available. The emission spectra of 2-naphthol in 0.1*N* hydrochloric acid and 0.1*N* sodium hydroxide were due to the emission of molecular and anionic species of 2-naphthol, respectively. The emission spectrum of 2-naphthol in pure H_2O had two major bands which corresponded to molecular and anionic forms of 2-naphthol with the band for the anionic species appearing at longer wavelengths. Because very little work has been published on the influence of binary aqueous–organic solvents on the fluorescence of organic compounds, and in particular, for compounds with similar structures, the fluorescence properties of the three model compounds were obtained in several binary solvents. Three alcohol:H_2O binary solvent systems were studied over a wide range of compositions. The solvent systems were methanol (MeOH):H_2O, ethanol (EtOH):H_2O, and isopropyl alcohol (IPA):H_2O. The fluorescence results for 2-naphthol in MeOH:H_2O solvent will be discussed as a representative example. Figure 1 gives the emission spectra of 2-naphthol in H_2O, MeOH, and MeOH:H_2O solvents. It can be seen that the intensities of emission bands changed with addition of MeOH. The pronounced change in emission spectra was due to the anionic peak gradually decreasing with an increasing content

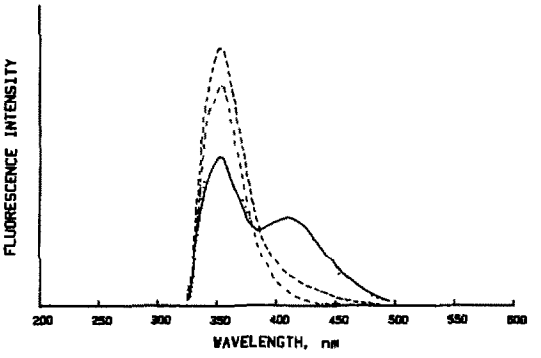

Fig 1 Representative fluorescence emission spectra of 2-naphthol in MEOH H_2O solvents in the absence of β-CD H_2O (——), MeOH H_2O (1 9) ( ), MeOH H_2O (1 1) (----), MeOH (- - -)

of MeOH. In pure MeOH, only the molecular form existed at 354 nm. Lee *et al.*[17] reported similar results for 2-naphthol in MeOH:H_2O. The excitation spectra showed red shifts of 0.5 nm and the emission spectra red shifts of 2.5 nm on changing from pure water to pure MeOH.

The relative fluorescence intensities of the molecular form of 2-naphthol and the anionic form of 2-naphthol *vs.* volume fraction of alcohol were compared, and the results for the molecular form are given in Fig. 2. The trends for intensity changes in the three alcohol:H_2O systems were similar to each other. As indicated in Fig. 2, the fluorescence intensities of the molecular form initially increased with addition of alcohols. At a IPA volume fraction of 0.5, a MeOH volume fraction of 0.7, and a EtOH volume fraction of 0.7, the intensities approximately reached maximum values, and then relative intensities decreased (Fig. 2) As more and more alcohol was added to the water, the fraction of the molecular form increased. Lee *et al.*[17] have shown that in greater than 50% methanol

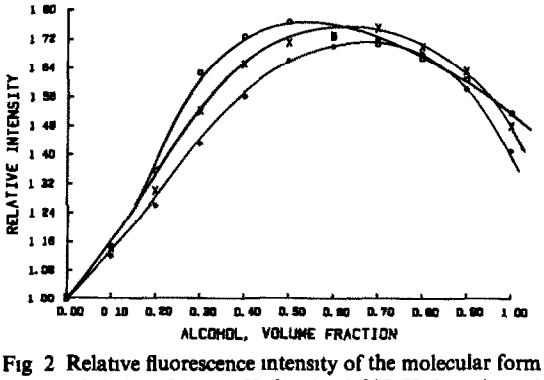

Fig 2 Relative fluorescence intensity of the molecular form of 2-naphthol in MeOH·H_2O (•), EtOH:H_2O (×), and IPA·H_2O (○) solvents *vs* volume fraction of alcohol to water

only emission from the molecular form of 2-naphthol was observed. In our work, fluorescence intensities of the anionic form in the different alcohol:water solvents decreased with addition of alcohols.

1-Naphthol undergoes excited state ionization in both neutral aqueous and acidic aqueous solutions. Excitation and emission spectra of 1-naphthol were obtained in H_2O, acidic and basic solutions. In the three types of solution, the emission band was the same and was due to the anionic form. In H_2O and acidic solution, the excitation bands corresponded to the ground state molecular form of 1-naphthol. In basic solution, the excitation peak originated from the ground state anionic form. Only in pure organic solvent could the fluorescence emission of only the molecular species be observed.

The fluorescence study of 1-naphthol was carried out in the same solvent systems as for 2-naphthol. Excitation and emission spectra of 1-naphthol in MeOH·H_2O solvents were obtained, and with increasing amounts of MeOH, the anion intensities, measured at 465 nm decreased, and intensities of molecular peaks at 328 nm increased In the solvents containing MeOH:H_2O, the emission spectra of both the molecular form and the anionic form were obtained. The excitation peak for 1-naphthol in MeOH was red-shifted by 4 nm relative to H_2O, and the emission band at 462 nm was blue-shifted by 3 nm relative to water. The spectra obtained in EtOH:H_2O and IPA:H_2O showed similar trends to that in MeOH.H_2O.

Plots of the relative fluorescence intensities of the molecular and anionic forms of 1-naphthol in the three alcohol·H_2O solvents *vs.* volume fraction of alcohol were acquired. The fluorescence intensities of the molecular form increased very slowly with larger amounts of alcohol, and then rapidly increased near a volume fraction of alcohol of 0.9. The maximum fluorescence intensity was reached in pure alcohol. The intensities from the anionic form had relatively constant values from pure H_2O to a volume fraction of alcohol of 0.3, then the intensities decreased with an increase in the amounts of the alcohol.

The fluorescence spectra of 1,2,3,4-tetrahydro-1-naphthol were obtained only in MeOH:H_2O and EtOH:H_2O binary solvents. As shown below, the structure of 1,2,3,4-tetrahydro-1-naphthol was different from 1-naphthol and 2-naphthol, in that, the hydroxyl group was bonded to an aliphatic ring. In addition, it does not undergo excited state ionization. The excitation and emission spectra of 1,2,3,4-tetrahydro-1-naphthol had one band each, and they appeared at 260 and 287 nm, respectively. The excitation bands red-shifted by 2 nm upon addition of MeOH, but the emission band did not shift. The fluorescence intensities increased with addition of alcohol. The maximum fluorescence values were obtained in a volume fraction of methanol of 0.6 MeOH:H_2O (6·4) and a volume fraction of ethanol of 0.5, and then the fluorescence intensities decreased beyond these volume fractions.

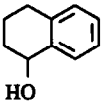

Fluorescence spectra of model compounds in organic–aqueous solvents with a fixed organic-aqueous composition in the presence of various amounts of β-cyclodextrin

The organic–aqueous solvent systems used in this part of the research were MeOH:H_2O (1:1), EtOH·H_2O (1:1) and IPA:H_2O (1·1) for 2-naphthol; MeOH.H_2O (1:9), EtOH·H_2O (1:9), and IPA.H_2O (1:9) for 1-naphthol; MeOH:H_2O (1:1) EtOH:H_2O (1:1) for tetrahydro-1-naphthol. The criteria used to select the solvents were a relatively high solubility of β-CD in the solvent and a relatively large change in the fluorescence intensity of the solute in the solvent in the presence of β-CD compared to the solute in the solvent without β-CD.

The emission spectra of 2-naphthol in EtOH:H_2O (1:1) were obtained with 0.00, 1.07, 4.54, 9 08 and 12 70 m*M* β-CD. The spectra showed only a molecular band at 355 nm, and the intensity of the 355 nm band decreased with the addition of β-CD. The emission spectra for 2-naphthol obtained in MeOH:H_2O (1·1) and IPA:H_2O (1:1) had similar spectral patterns as those obtained in EtOH:H_2O. A plot of fluorescence intensity of 2-naphthol in EtOH:H_2O *vs.* concentration of β-CD gave a straight line with a negative slope The same types of plots were also obtained with MeOH:H_2O and IPA:H_2O.

The emission spectra of 1-naphthol in EtOH:H_2O (1:9) are shown in Fig. 3. The emission spectra of 1-naphthol in all the binary solvents studied with β-CD gave molecular and anionic bands. The intensity of the molecular

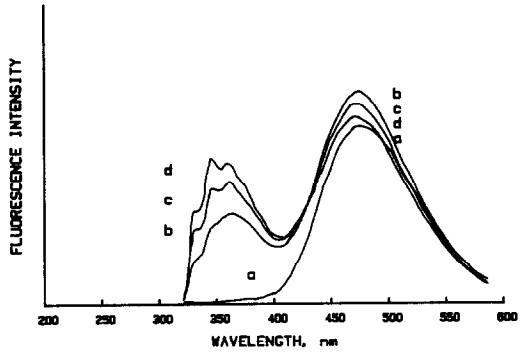

Fig 3 Fluorescence emission spectra of 1-naphthol in EtOH H_2O (1.9) with various amounts of β-CD (a) 0 00 mM, (b) 4 32 mM (c) 8 84 mM (d) 14 1 mM

form of 1-naphthol *vs.* concentration of β-CD is given in Fig. 4. As Fig. 4 shows, as the amount of β-CD increased, the fraction of the molecular form of 1-naphthol increased, and the intensity increased in a nonlinear fashion with the addition of β-CD. The intensity changes for 1-naphthol in MeOH:H_2O and IPA.H_2O were similar to that in EtOH:H_2O for the molecular species.

The fluorescence excitation and emission spectra of 1,2,3,4-tetrahydro-1-naphthol in binary solvents in the presence of various amounts of β-CD were relatively simple. There was only one emission peak, and the position of the spectra did not shift. The fluorescence intensity of this compound in EtOH:H_2O and MeOH:H_2O water decreased with the addition of β-CD, and linear relationships were obtained for fluorescence intensity *vs.* concentration of β-CD.

In summary, for 2-naphthol and 1,2,3,4-tetrahydro-1-naphthol in all the solvent systems studied, the intensities decreased with the addition of β-CD. In MeOH:H_2O, EtOH:H_2O, and IPA:H_2O the fluorescence intensity increased for the molecular form of 1-naphthol.

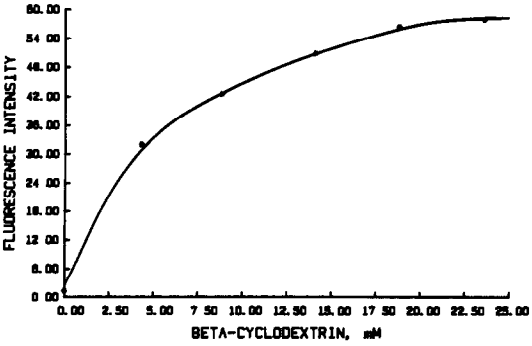

Fig 4 Fluorescence intensity of the molecular form of 1-naphthol in EtOH H_2O (1·9) *vs.* concentration of β-CD.

Fluorescence quenching of model compounds in binary solvents with various amounts of β-CD

The dynamic fluorescence quenching model is described by the Stern-Volmer equation:[18]

$$I_0/I = 1 + k_q\tau_0[Q] = 1 + K_{sv}[Q] \quad (1)$$

where I_0 and I are fluorescence intensities in the absence and presence of quencher, respectively, $[Q]$ is the concentration of the quencher, k_q is the bimolecular quenching constant, and τ_0 is the lifetime of the fluorophore in the absence of quencher. The Stern-Volmer constant is defined as K_{sv} and is equal to $k_q\tau_0$. Frequently, a plot of I_0/I *vs.* $[Q]$ gives a linear relationship, and the slope of the line is equal to the Stern-Volmer constant K_{sv}. As indicated in equation (1), if the lifetime of the fluorophor is known, the bimolecular quenching constant can be calculated.

If complex formation occurs with the ground state fluorophore and quenching results, the process is called static quenching. However, there are other mechanisms that can cause static quenching. An equation which has the same form as equation (1) is also used to describe the quenching mechanism [equation (2)].

$$I_0/I = 1 + K_s[Q] \quad (2)$$

where I_0, I, and $[Q]$ have the same meaning as in equation (1) In equation (2), K_s is the association constant of the complex in the ground state. According to this equation, a plot of I_0/I *vs.* $[Q]$ would also give a linear relationship. In this work, dynamic and static quenching could not be distinguished because lifetime measurements were not made.

As discussed earlier, the fluorescence signals of 2-naphthol and 1,2,3,4-tetrahydro-1-naphthol decreased with the addition of β-CD. Stern-Volmer plots of 2-naphthol in MeOH·H_2O, EtOH.H_2O and IPA:H_2O solvents were obtained, and all the curves gave linear relationships. The slopes of the curves were 16.4, 26.2, and 15.9 for MeOH:H_2O, EtOH:H_2O and IPA:H_2O, respectively. The linear relationships obtained for the curves indicated that either dynamic or static quenching processes were occurring. Based on the trends for the Stern-Volmer slopes, the fluorescence quenching of 2-naphthol by β-CD in the three alcohol:H_2O solvents was EtOH:H_2O > MeOH:H_2O > IPA:H_2O.

Stern-Volmer type plots of the molecular form of 1-naphthol data for water, MeOH:H_2O, and EtOH:H_2O did not represent quenching phenomena because the intensities of 1-naphthol in these solvents were enhanced. Thus, the normal Stern-Volmer plot could not be used to describe the data. However, a modified Stern-Volmer equation has been developed by Patonay *et al.*[4,8] that is useful in situations where the fluorescence signal is either enhanced or diminished. This equation was first used to explain the quenching of pyrene in β-CD solutions,[8] and it was assumed that the β-CD:pyrene complex might have a different quantum yield from the free molecular form. In their equation, Patonay and co-workers[4,8] defined the factors d and e as the quantum yield change of the cyclodextrin complex and the free molecule, respectively, and the ratio of fluorescence intensity could be expressed as:

$$(I_0-I)/I=[(1-e)+KC(1-d)]/(e+KCd) \quad (3)$$

where I_0 and I are fluorescence intensity of the compound in the absence and presence of quencher, or complexing agent, respectively. The term C is the concentration of the quencher, or complexing agent, and K is the equilibrium constant for the reaction of solute with cyclodextrin. If the quantum yield of the free molecular form does not change, which means e is equal to one, the equation (3) becomes:

$$(I_0-I)/I=[KC(1-d)]/(I+KCd) \quad (4)$$

Equation (4) can be rearranged to give.

$$I(I_0-I)=1/[K(1-d)C]=d/(1-d) \quad (5)$$

A plot of $I(I_0-I)$ *vs.* $1/C$ would give a linear relationship, and from the slope and intercept, the values of d and K can be obtained. As mentioned above this equation is not limited to describing quenching processes, but it can also be applied to cases where the fluorescence is enhanced.[4]

In this work, the fluorescence intensity of the molecular form of 1-naphthol increased in solutions with β-CD. It was assumed that the β-CD did not affect the fluorescence quantum yield of the molecular form of 1-naphthol, and thus equation (5) was valid. In addition, because only the fluorescence emission of the molecular form of 1-naphthol was measured, the fluorescence emission of the anionic form of 1-naphthol did not directly affect the fluorescence of the molecular form of 1-naphthol. The plots of $I(I_0-I)$ *vs.* $1/C$ of 1-naphthol for water, MeOH:H_2O, and EtOH:H_2O have good linear relationships with correlation coefficients of 0.995, 0.999, and 0.975, respectively. However, the same type of plot was also obtained for IPA:H_2O, and a linear relationship was not obtained. The equilibrium constants for the 1-naphthol:β-CD complex that were obtained from the plots were 1134, 859, and 171 for water, MeOH:H_2O and EtOH:H_2O, respectively. The d values were 34.3, 29.6 and 51.0 for water, MeOH:H_2O and EtOH:H_2O, respectively. The d values are rather large and indicate the substantial increase in the fluorescence intensity of the molecular form of 1-naphthol. This was due to the formation of a greater fraction of the molecular form of 1-naphthol as the amount of β-CD increased (Fig. 3). In MeOH:H_2O, the K value was larger than in EtOH:H_2O, which indicated in MeOH:H_2O more 1-naphthol reacted with β-CD than in EtOH:H_2O. This is reasonable because the association constant for EtOH with β-CD is 2.9 times as large as that in MeOH:H_2O.[19] Thus, 1-naphthol in EtOH:H_2O would not interact as readily with β-CD because EtOH would compete somewhat more effectively than MeOH for β-CD.

The Stern-Volmer plots of 1,2,3,4-tetrahydro-1-naphthol in MeOH:H_2O and EtOH:H_2O gave linear relationships, and the slopes of the plots with MeOH:H_2O and EtOH·H_2O were 47.1 and 54.5, respectively. The larger slope with EtOH:H_2O indicates more effective quenching in this solvent system and may be related to the fact that EtOH reacts more with β-CD than does MeOH.

Comparison of results

In water, the molecular and anionic forms of 2-naphthol were present. With the addition of alcohol, the extent of excited state ionization decreased, and only the molecular form emitted at relatively high concentrations of alcohol. For example, with ethanol, only the molecular form was present at 50% ethanol and greater. With 1-naphthol, only the anionic form emitted in water, and with the addition of alcohol both the molecular and anionic forms of 1-naphthol appeared, but the molecular form only started to appear in relatively large amounts of alcohol. This indicated that 1-naphthol had a greater tendency to undergo excited ionization than did 2-naphthol in alcohol water solvents. For 1,2,3,4-tetrahydro-1-naphthol it did not undergo excited state ionization, and its

fluorescence intensity reached maximum values in alcohol solvents that contained a sizeable amount of water.

Because of the very large range of solvents that could be used for the binary alcohol:water solvents, a wide range of binary solvents that contained β-CD were not investigated. Nevertheless, some very interesting results were obtained. Only the molecular form of 2-naphthol was present in the alcohol:water solvents containing β-CD, but the fluorescence intensity of 2-naphthol decreased in a linear fashion with the addition of β-CD. In contrast, the fluorescence intensity of the molecular form of 1-naphthol increased with the addition of β-CD while the fluorescence intensity of the anionic form of 1-naphthol decreased with increasing amounts of β-CD. The results obtained for the two hydroxyl aromatics indicated that they interacted differently with the alcohol:water β-CD systems. Because 2-naphthol did not show the anionic form, then it was possible that the hydroxyl group was inside the β-CD or protected from water, and thus did not undergo excited state ionization.[20,21] In the alcohol:water solvents with β-CD, 1-naphthol gave fluorescence emission from both the molecular form and the anionic forms. Thus, the hydroxyl group was not buried in the β-CD cavity and could undergo ionization with a sizeable amount of β-CD present Interestingly, 1,2,3,4-tetrahydro-1-naphthol is structurally similar to 1-naphthol, but its fluorescence intensity decreased with the addition of β-CD.

The results of this work indicate that more detailed photophysical experiments are needed to elucidate the interactions of the three model compounds with β-CD in binary alcohol:water solvents. However, the results of this work form the basis for the development of analytical methodology for the determination of mixtures of 1- and 2-naphthol in alcohol:water solvents in the presence of β-CD. In addition, the results can be used in the fluorescence detection for the separation of the hydroxyl aromatics by high-performance liquid chromatography with alcohol based mobile phases that contain β-CD.

Acknowledgement—Financial support for this project was provided by the Department of Energy, Division of Basic Energy Sciences, Grant No DE-FG02-86ER13547

REFERENCES

1 J Szejtli, *Cyclodextrins and Their Inclusion Complexes*, Akademiai Kiade, Budapest, 1982
2 *Idem, Cyclodextrin Technology*, Kluwer Academic Publishers, Dordrecht, 1988
3 A Nakajima, *Bull Chem Soc Jpn*, 1984, **57**, 1143
4 G Patonay, K. Fowler, A Shapira, G Nelson and I M Warner, *J Incl Phenom*, 1987, **5**, 717
5 G Nelson, G Patonay and I M Warner, *ibid*, 1988, **6**, 277
6 *Idem, Anal Chem*, 1988, **60**, 274
7 *Idem, Talanta*, 1989, **36**, 199
8 G Patonay, A Shapira, P Diamond and I M Warner, *J Phys Chem*, 1986, **90**, 1963
9 G Nelson and I M Warner, *ibid*, 1990, **94**, 576
10 A M de la Pena, T T Ndou, J B Zung, K L Greene, D H Live and I M Warner, *J Am Chem Soc*, 1991, **113**, 1572
11 S Hamai, *Bull Chem Soc Jpn*, 1991, **64**, 431
12. *Idem, J Incl Phenom*, 1991, **11**, 55
13 J Huang, G C Catena and F V Bright, *Appl Spectrosc*, 1992, **64**, 606
14 E Djoufac-Woumfo, N Arnaud and J Georges, *Analyst*, 1988, **113**, 447
15 D M Hercules and L B Rogers, *Anal Chem*, 1958, **30**, 96
16. R Boyer, G Deckey, C Marzzacco, M Mulvaney, C Schwab and A Halpern, *J Chem Educ*, 1986, **63**, 181
17 J Lee, R D Griffin and G W Robinson, *J Chem Phys*, 1985, **82**, 4920
18 M R Eftink and C A Ghiron, *Anal Biochem* 1981, **114**, 199
19 K Kano, I Takenoshita and T Ogawa, *J Phys Chem*, 1982, **86**, 1833
20 T Yorozu, M Hoshino, M. Imamura and H Shizuka, *J Phys Chem*, 1982, **86**, 4422
21 D F Eaton, *Tetrahedron*, 1987, **43**, 1551

Talanta, Vol 40, No 6, pp 909–912, 1993
Printed in Great Britain

0039-9140/93 $6.00 + 0.00

GRAVIMETRIC DETERMINATION OF FREE CARBON AND SILICON CARBIDE IN SILICA FUME

S. DYE, D. PHILLIPS* and D. WOODFORD
School of Applied Chemistry, Curtin University, P.O. Box U1987, Perth, Western Australia 6001, Australia

I. BARROW
Chemistry Centre WA, 125 Hay Street, East Perth, Western Australia 6004, Australia

(*Received* 20 *July* 1992 *Revised* 5 *October* 1992 *Accepted* 5 *October* 1992)

Summary—Silica fume is formed as a by-product in the manufacture of silicon from quartzite. This paper describes an analytical method for the determination of free carbon and silicon carbide in silica fume. The silicon carbide was determined after removal of free carbon, amorphous silica, crystalline silica, graphite and silicon from the fume. The free carbon content was found to vary from 2 to 8% while the silicon carbide content ranged from 1 to 5%. X-ray diffraction, thermal analysis, scanning electron microscopy and Fourier Transform infrared spectroscopy were used to validate the steps used in the analytical procedure. The purpose of determining the free carbon and silicon carbide content of the fume is to help understand the efficiency of the reduction process and mechanism of the reaction.

Silica fume is formed as a by-product in the manufacture of silicon from quartzite by reduction with charcoal, coal or coke at temperatures of up to 1780° using graphite electrodes in an electric arc furnace. While there are a few less important reactions, the following represents the main reaction sequence.[1]

Molten quartz reacts with reductant:

$$SiO_2(l) + C(s) \xrightarrow{1780^\circ} SiO(g) + CO(g) \quad (1)$$

Gaseous SiO reacts with reductant:

$$SiO(g) + 2C(s) \xrightarrow{1570^\circ} SiC(s) + CO(g) \quad (2)$$

SiC reacts with molten quartz:

$$SiC(s) + SiO_2(l) \xrightarrow{1780^\circ} Si(s) + SiO(g) + CO(g) \quad (3)$$

The silica fume forms when SiO in the vapour phase reacts with oxygen:

$$2SiO(g) + O_2(g) \longrightarrow 2SiO_2(s)$$

Any unreacted carbon reductant and intermediate SiC will be carried through in the fume. Some fragments of the quartzite burden are also carried through with the fume, together with low levels (<1%) of graphite fragments from the electrodes. Low levels (<1%) of elemental silicon may also be detected in the fume. There have been no previous attempts to analyse SiC as a minor component in silica fume or other such matrices. Julietti[2,3] has developed procedures for the analysis of SiC in silicon carbide refractories.

A knowledge of the free carbon and SiC content of the fume is of important in assessing the efficiency of the reduction process and understanding the reaction mechanism.

EXPERIMENTAL

Samples

Approximately 150 g samples were taken at regular intervals from the fume discharge line to the baghouse over two periods. They were numbered 1–12 and 13–27 corresponding to the day, month and time of sampling. All samples were dried at 110° for 1 h prior to analysis. Samples of silicon and graphite electrodes were also taken for analysis.

Reagents

Hydrofluoric acid 70% Flukka Grade. Nitric acid 70%, AR Grade. Silicon carbide, LR Grade. Quartz, AR Grade.

Instruments

X-ray Diffraction measurements were made on a Philips PW 1820 diffractometer. DTA measurements were carried out on a Stanton

*Author to whom correspondence should be addressed.

Table 1 Dissolution characteristics of fume components

Acid	Quartz	SiC	Graphite	Silicon	Amorphous Silica
HF	CS	CI	CI	CI	CS
HNO_3	CI	CI	PS	CI	CI
HF/HNO_3	CS	CI	PS	CS	CS

CS = completely soluble, CI = completely insoluble, PS = partly soluble

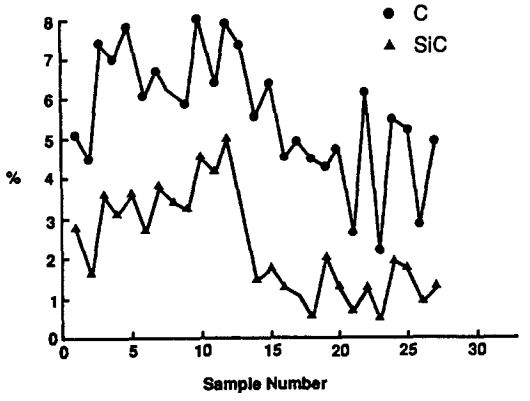

Fig 1 Free carbon and SiC content

Redcroft STA-780 in air at a heating rate of 20°/min. Fourier Transform Infra Red measurements were made on a BioRad FTS-40. Scanning Electron Microscopy measurements were made on gold coated samples using a Leica Cambridge Stereoscan 360.

Qualitative tests

Triplicate samples of SiC, graphite, quartz and silicon were treated with HF, HNO_3 and a HF/HNO_3 mixture to confirm the steps used in the analytical procedure. One-gram samples were dissolved in 50 ml of acid corresponding to the conditions to be used in the analytical procedure. The percentage weight losses were recorded for each test.

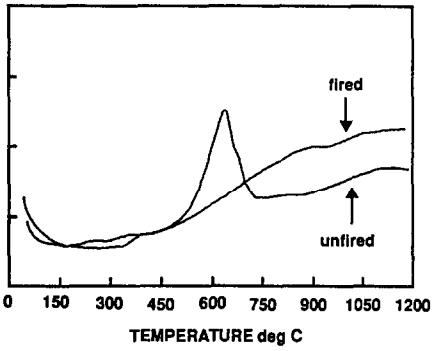

Fig 2. Differential thermograms of fired and unfired fume

Firing

One silica fume sample was heated at a series of temperatures for various periods of time to establish that there was no oxidation of SiC under such conditions. The relative intensities of the SiO_2 and SiC peaks were determined by X-ray diffraction.

Method for free carbon and SiC

A 10-g portion of silica fume sample was heated in a platinum crucible at 750° for 1 h The crucible was cooled and weighed. Two 5-g halves of sample, were treated separately with 50 ml of 1:1 HF in a Teflon beaker at 180° for 1 h and taken to dryness. A mixture of 10 ml of HNO_3 an 15 ml of HF was added and the sample again taken to dryness. A further 10 ml of HF was added to ensure the complete removal of silica. A 25 ml volume of HNO_3 was

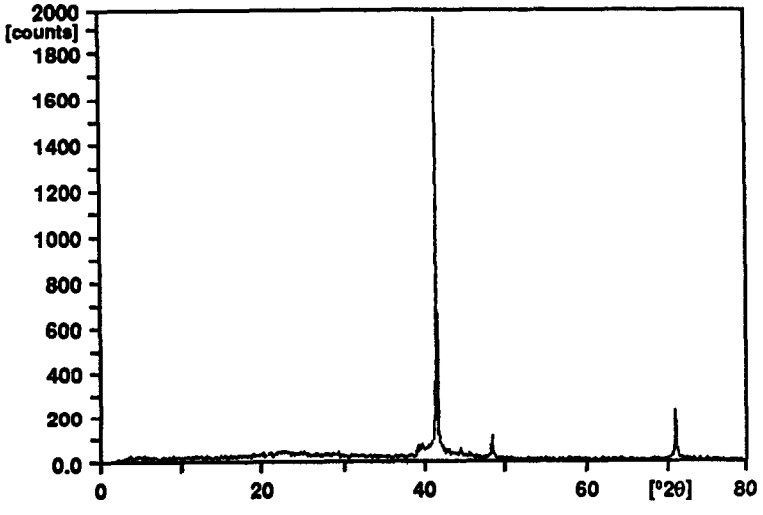

Fig 3. XRD trace of a SiC residue.

Table 2 X-ray diffraction of fired samples

Temperature (°C)	Time (min)	SiO_2 SiC Peak intensity
0	0	3 0
400	60	2 7
500	60	2 7
600	20	2 9
600	60	2 6
750	60	3 1

added, the beaker covered with a watchglass and the sample boiled for 4 h. The solution was diluted with 50 ml of deionized water and the grey residue filtered through a previously weighed 0.8 μm millipore filter paper. The paper and residue were dried at 110°, cooled and weighed as SiC. One SiC residue was sonicated for 30 min, treated with 5 ml of HNO_3 at 140° for 30 min and thermally analysed in air to check for complete removal of free carbon from the sample.

RESULTS AND DISCUSSION

Qualitative tests

The dissolution characteristics for the components of the fume are shown in Table 1.

Free carbon and silicon carbide content

The results for the free carbon and SiC content of the silica fume samples are shown in Fig. 1. The RSD for the free carbon determination was $\pm 1\%$ while that for the SiC determination was $\pm 3\%$.

The similar variation between the free carbon and SiC content is evidence for the proposed reaction mechanism. Some free carbon will be found in the fume due to incomplete reaction of the carbonaceous raw materials in equation (1). The diffusion of gaseous SiO through the highly porous carbon will result in both the complete conversion of carbon to SiC and the formation of some incompletely reacted SiC-coated carbon particles. The greater the number of these SiC-coated carbon particles, the higher will be the apparent free carbon content when the fume is fired at 750°. The results are thus evidence for equations (1) and (2) of the proposed reaction mechanism. Any carbon not oxidized at 750° will be removed during the concentrated nitric acid treatment in the analytical procedure.

Discussion of the analytical method

Differential thermograms of an unfired silica fume sample and one fired at 1000° for 1 h are shown in Fig. 2. The disappearance of the 600° exotherm indicates that all free carbon was removed by heating the sample at 750° for 1 h.

An X-ray diffractogram of a SiC residue is shown in Fig. 3. The only peaks found were those for SiC at 42°, 49° and 71° (2θ), respectively

X-ray diffraction data for the unfired and fired samples are shown in Table 2. The results

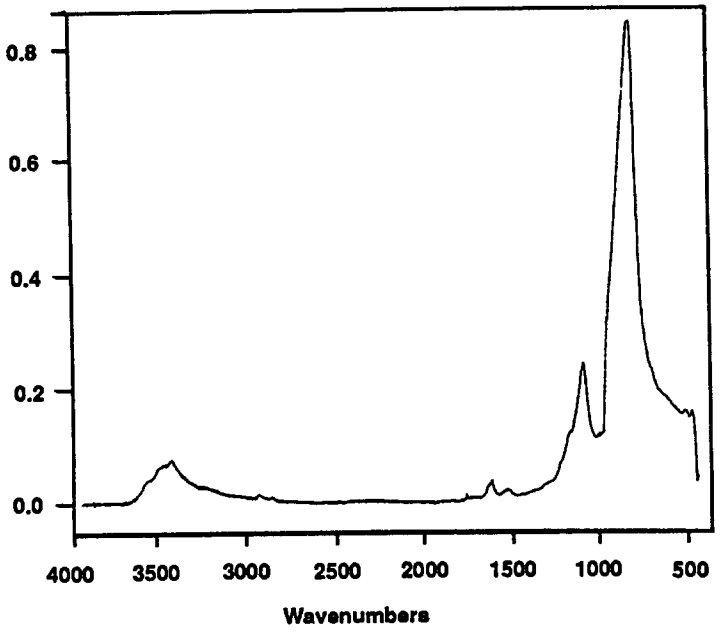

Fig 4 FTIR spectrum of a SiC residue

indicate that no significant oxidation of SiC occurred when the samples were fired at 750° for 1 h. This supports the findings of Julietti[2] and Ramanathan and Muraleedharan[4] where no significant oxidation of SiC was found below 800°.

Scanning electron microscopy studies on a typical final residue from the analytical method showed that SiC was the only phase present in the residue.

An FTIR spectrum of a SiC residue is shown in Fig. 4 where the typical antisymmetric SiC peak was revealed at 780 cm^{-1}. A small quartz peak occurred at 1080 cm^{-1} due to grinding the sample prior to analysis as reported by Falk and Karunanithy.[5]

Differential thermal analysis of a typical SiC residue in air showed no exotherm at 600° indicating that all carbon had been removed from the particles during the HNO_3 treatment.

CONCLUSION

A reliable method has been developed for the analysis of free carbon and SiC in silica fume. The free carbon and SiC content of the fume can be used as a measure of the efficiency of the furnace operation. At the time that these samples were taken, the furnace was operating much more efficiently and reproducibly during the second sampling period. The analytical results go part of the way to confirming the proposed reaction mechanism.

REFERENCES

1 D M Spratt, R. A Leupen and P A Bibby, *Conference of the Australasian Institute of Mining and Metallurgy*, Perth, 1988
2 R J. Julietti, *Trans J Brit Ceram Soc*, 1981, **80**, 175
3 R J Julietti and B. C E. Reeve, *ibid.*, 1991, **90**, 85.
4. S Ramanathan and R V Muraleedharan, *Interceram*, 1992, **41**, 79
5 M. Falk and S. Karunanithy, *Mat Sci Eng*, 1989, **114**, 209

Talanta, Vol 40, No 6, pp 913–917, 1993
Printed in Great Britain

0039-9140/93 $6 00 + 0 00

LIQUID–LIQUID EXTRACTION OF NIOBIUM(V) IN THE PRESENCE OF OTHER METALS WITH HIGH MOLECULAR MASS AMINES AND ASCORBIC ACID

MANJUSHA A KARVE and SHRIPAD M. KHOPKAR*
Department of Chemistry, Indian Institute of Technology, Bombay 400 076, India

(*Received* 16 *July* 1992 *Revised* 2 *October* 1992 *Accepted* 2 *October* 1992)

Summary—A novel method is proposed for the solvent extraction of niobium(V) A 0 1*M* solution of Aliquat 336S in xylene quantitatively extracts microgram quantities of niobium(V) from 0 01*M* ascorbic acid at pH 3.5–6 5 Niobium from the organic phase is stripped with 0 5*M* nitric acid and determined spectrophotometrically in the aqueous phase as its complex with TAR The method permits separation of niobium not only from tantalum(V) but also from vanadium(IV), titanium(IV), zirconium(IV), thorium(IV), chromium(III), molybdenum(VI), uranium(VI), iron(III), *etc* Niobium from stainless steel was determined with a precision of 0.42%

Solvent extraction separation of niobium with high molecular mass amines has been carried out from oxalic,[1–5] tartaric[6–8] and dicarboxylic acids.[9–11] Niobium was separated in oxalate media from tungsten, molybdenum, however titanium and zirconium showed strong interference. The separation from tartrate media needed specific diluents[7,8] such as chlorex when chloroform suppressed the extraction. Malonate media permitted group separation of niobium from tantalum while succinate[10] and glutarate[11] were not very effective. However, the systematic studies of extraction from ascorbate media are lacking. Therefore, such studies are reported in this paper. The proposed method facilitates the separation of niobium from titanium, zirconium, thorium, tantalum, chromium and molybdenum. The method was extended to the determination of niobium in stainless steel.

Apparatus and reagents

A digital pH meter with combined glass and calomel electrodes, Model GS866C spectrophotometer with matched 10-mm Corex glass cuvettes and a wrist-action flask-shaker were used.

The stock solution of niobium was prepared by fusing 0.1 g of niobium pentoxide with 5 g of potassium bisulphate in a platinum crucible. The cooled mass was extracted with 5 ml of 20% tartaric acid, and was made up to 100 ml with distilled water. The solution was standardized gravimetrically with *N*-benzoyl-*N*-phenyl hydroxyl amine.[12] It contained 1 mg/ml niobium. The diluted solution containing 30 μg/ml niobium was prepared by appropriate dilution.

Amberlite LA-1 (*N*-dodecyl (trialkylmethyl) amine), Amberlite LA-2 (*N*-lauryl (trialkylmethyl) amine), Primene JMT (a mixture of primary amines in the C_{18}–C_{22} range) (Rohm and Hass, Philadelphia, PA, U.S.A.), Aliquat 366S (tricaprylmethylammonium chloride) (General Mills Ltd., U.K.), Trioctylamine (Riedel de Haen, Hannover, Germany) were used without further purification. The exchangers were converted into the ascorbate form as per the procedure described earlier.[13]

A buffer solution of pH 5.4 was prepared by dissolving 80 g of ammonium acetate in 7 ml of glacial acetic acid and diluting to 1 l. with distilled water. TAR (4-(2-thiazolylazo) resorcinol) (Fluka AG, Buchs, Switzerland), 0.2% solution in methanol, was also used.

General procedure

To an aliquot of solution containing niobium(V), 1 ml of 0.01*M* ascorbic acid was added and its pH was adjusted to 4.5 by addition of dilute ammonium hydroxide or ascorbic acid. The resulting solution was made up to 10 ml with distilled water. The solution was transferred into a separating funnel and it was equilibrated with 10 ml of 0.1*M* Aliquat 336S in xylene. After allowing the phases to settle and

*Present address: Chemical Engineering Division, Department of Chemical Technology, University of Bombay Matunga, Bombay-400019 India

separate, niobium(V) was stripped from the organic phase with 0.5*M* nitric acid. Niobium in the aqueous phase was determined spectrophotometrically at 540 nm as its complex with 4-(2-thiazolylazo) resorcinol.[14]

RESULTS AND DISCUSSION

Extraction as a function of pH

The pH for the quantitative extraction of niobium(V) was ascertained by extracting it with 4% quantities of different liquid anion exchangers in xylene in the pH range of 1.0–8.0 (Fig. 1). The phase volume ratio was maintained at 1:1. The best pH ranges for the quantitative extraction were 3.5–6.5 (Aliquat 336S), 3.0–5.0 (Amberlite LA-1), and at 3.0 (Amberlite LA-2) and 6.0 (Primene JMT). The extraction was only 75.1% with trioctylamine. Aliquat 336S was preferred as the extractant as it permitted extraction over broader pH range.

Extraction as a function of Aliquat 336S concentration

With all other factors constant the extraction was carried out with different concentrations of Aliquat 336S (Table 1). The extraction was quantitative with 0.075–0.1*M* Aliquat 336S in xylene. Therefore 0.1*M* Aliquat 336S was used throughout the investigations.

Effect of varying ascorbic acid concentration

The best concentration of ascorbic acid for complete complexation of niobium(V) was ascertained by extracting niobium(V) with 0.001–0.05*M* ascorbic acid (Table 2). Thus 0.01*M* ascorbic acid was adequate for complete complexation of niobium(V).

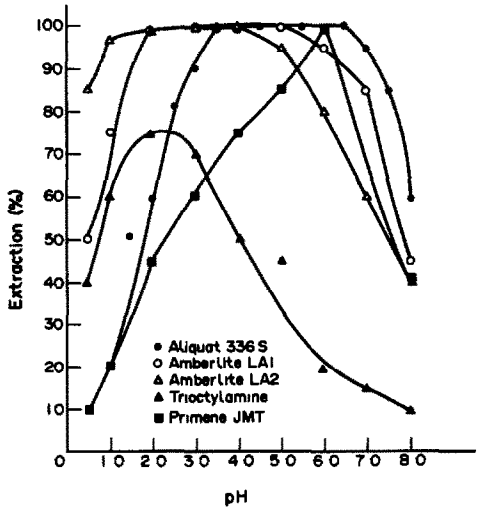

Fig. 1 Extraction of niobium(V) as a function of pH with various liquid anion exchangers

Table 1 Effect of Aliquat 336S concentration

Aliquat 336S concentration, *M*	Extraction, %	Distribution ratio, *D*
0 005	40 0	0 66
0 01	56 0	1 2
0 02	62 0	1 6
0.03	69 0	2 2
0 04	74 0	2 8
0 05	80 0	4 0
0 06	89 0	8 0
0.07	95 0	19 0
0 075–0 10	99 6	24 9

Effect of extracting solvent

Various nonpolar solvents like benzene, toluene, xylene, hexane, cyclohexane, chloroform and carbontetrachloride were tested as extractants (Table 3). The phase volume ratio was maintained at 1.1. The extraction was quantitative with toluene and xylene. Xylene alone was preferred as it was non-toxic in nature, offered clear phase separation and did not exhibit phenomenon of emulsification.

Period of equilibration

The extraction was carried out on a wrist-action flask-shaker for various periods of shaking of 1, 2, 4, 5, 7 and 10 min. The corresponding magnitude for the extraction in percentage was 40, 65, 80, 95, 99.6 and 99.6, respectively. Thus a 10-min period of equilibration was adequate.

Nature of extracted species

The probable composition of the extracted species was ascertained by plotting the graph of log *D vs.* log [Aliquat 336S] at a fixed ascorbic acid concentration and by plotting of log *D vs.*

Table 2 Effect of ascorbic acid concentration

Ascorbic acid concentration, $10^{-3}M$	Extraction, %	Distribution ratio, *D*
1 0	35.0	0 53
2 0	42 0	0 72
3 0	50 0	1 0
4 0	61 0	1 5
5 0	68 0	2 1
6 0	75 0	3 0
7.0	86 0	6 1
8.0	95.0	19 0
9 0	99 0	99 0
10 0–50 0	99 6	249

Table 3 Effect of various extracting solvents Aliquat 336S (0·1*M*) in suitable solvent

Solvent	Dielectric constant, *E*	Extraction, %	Distribution ratio, *D*
Benzene	2.28	95·6	21.7
Toluene	2·38	99·6	249.0
Xylene	2·30	99·6	249.0
Hexane	1.89	90.0	10·0
Cyclohexane	2.05	87·0	6·6
Chloroform	4·8	60·0	1.5
Carbontetrachloride	2·24	50.0	1.0

log [ascorbic acid] with a fixed Aliquat 336S concentration. The corresponding slopes were 2.9 and 3.1, respectively. Therefore, the probable species which was extracted was $[(R_4N)_3NbO(asc)_3]$. Similar inferences were noted in earlier work.[9]

Effect of stripping agents

After extraction of niobium(V), it was stripped with 10 ml of various mineral acids (Table 4). Sulphuric acid and hydrobromic acids were poor stripping agents while 0.5–7.0*M* nitric acid and 2.0–6.0*M* hydrochloric acid were satisfactory. Therefore, 0.5*M* nitric acid was used as the stripping agent.

Separation of niobium(V) from binary mixtures

Niobium(V) was extracted in the presence of various ions (Table 5). The tolerance limit was set as the amount of foreign ion required to cause ±2% suppression in the recovery of niobium(V). As the alkali, alkaline earths, aluminium(III), thallium(I, III), copper(II) and zinc(II) were not extracted they were tolerated in ratios exceeding 1:100. Gallium(III), indium(III) and molybdenum(VI) were coextracted, so niobium(V) was first stripped with 6*M* hydrochloric acid followed by stripping of these elements with 1*M* nitric acid. Titanium(IV), zirconium(IV) and hafnium(IV) were separated by stripping them first with 0.2*M* hydrochloric acid containing 0.6% hydrogen peroxide.[9] It should be noted that 0.2*M* hydrochloric acid is a poor stripping agent and in the presence of 0.6% hydrogen peroxide it quantitatively strips titanium, zirconium and hafnium but could not strip niobium. Similarly, scandium(III) and vanadium(IV) were separated by first stripping them with 0.01*M* oxalic acid–1*M* hydrochloric acid, followed by stripping of niobium with 0.5*M* nitric acid. Thorium(IV) and uranium(VI) were strongly complexed with ascorbic acid and hence could be stripped after niobium.

Table 4 Effect of stripping agents

Stripping agent, *M*	% of Stripping							
	0·5	1	2	3	4	5	6	7
HCl	80.0	85·0	99.6	99.6	99·6	99·6	99.6	80.0
HNO_3	99·9	99·6	99.6	99·6	99·6	99.6	99.6	99.6
H_2SO_4	10·0	20·0	25.0	30.0	25·0	21·0	20.0	20.0

Sequential separation of vanadium(IV), niobium(V) and tantalum(V)

The group separation of vanadium(IV), niobium(V) and tantalum(V) was possible in various ratios.

After extraction of the mixture, vanadium(IV) was stripped with 0.01*M* oxalic–1*M* hydrochloric acid followed by stripping of niobium(V) with 0.5*M* nitric acid. During such separation tantalum(V) was not extracted and remained behind in the aqueous phase. With various ratios of vanadium:niobium:tantalum,

Table 5 Separation of niobium from binary mixtures Nb(V) = 30 μg/10 ml = 0·032*M*, Nb(V) = 30 μg/10 ml = $32 \times 10^{-3}M$

Foreign ion	Added as	Tolerance limit $1 \times 10^{-3}M$
Li^+	LiCl	60
Na^+	NaCl	10
K^+	KCl	10
Ca^{2+}	$Ca(NO_3)_2$	12
Mg^{2+}	$MgSO_4\ 7H_2O$	16
Sr^{2+}	$Sr(NO_3)_2$	5
Ba^{2+}	$Ba(NO_3)_2\ 3H_2O$	32
Al^{3+}	$Al(NO_3)_3\ 9H_2O$	2
Ga^{3+}	$GaCl_3$	1
In^{3+}	$InCl_3$	4
Tl^+	$TlNO_3$	4
Tl^{3+}	$Tl_2(SO_4)_3$	2
Pb^{2+}	$Pb(NO_3)_2$	5
Sc^{3+}	$Sc(NO_3)_3$	0.8
Ti^{4+}	$Ti(SO_4)_2$	0.6
Zr^{4+}	$Zr(NO_3)_4$	0·5
Hf^{4+}	$Hf(NO_3)_4$	3
Ta^{5+}	Ta_2O_5	6
V^{4+}	$VOSO_4\ 5H_2O$	0·8
Th^{4+}	$Th(NO_3)_4$	1.7
Cr^{3+}	$Cr(NO_3)_3 \cdot 9H_2O$	1.5
$Mo_7O_{24}^{6-}$	$(NH_4)_6Mo_7O_{24}\ 12H_2O$	0·5
UO_2^{2+}	$UO_2(NO_3)_2\ 6H_2O$	1.8
Mn^{2+}	$MnSO_4$	1.7
Fe^{3+}	$FeCl_3$	1·1
Co^{2+}	$Co(NO_3)_2 \cdot 6H_2O$	1.6
Ni^{2+}	$Ni(NO_3)_2 \cdot 6H_2O$	1.1
Cu^{2+}	$CuSO_4 \cdot 5H_2O$	1·2
Zn^{2+}	$ZnSO_4\ 7H_2O$	1·2
Cl^-	HCl	1·1
NO_3^-	$NaNO_3$	1.7
SO_4^{2-}	Na_2SO_4	7
$C_2O_4^{2-}$	Oxalic acid	6
Mal^{2-}	Malonic acid	9
Cit^{3-}	Citric acid	4
$Tart^{3-}$	Tartaric acid	5

Table 6. Separation from multicomponent mixtures

No	Mixture	Taken, μg	Found, μg	Recovery, %	Stripping agent	Reagent	λ_{max}, nm
1.	Nb(V)	30	29.8	99.6	6*M* HCl	TAR	540
	Mo(VI)	100	99.6	99.6	1*M* HNO_3	Tiron	390
	Cr(III)	100	99.8	99.4	Unextracted	s-Diphenyl carbazide	570
2	Nb(V)	30	29.8	99 6	6*M* HNO_3	TAR	540
	Th	40	39 8	99 6	2*M* HCl	Arsenazeo III	650
	Fe(III)	100	99.4	99.4	Unextracted	1,10-phenanthroline	510
3	Nb(V)	30	29.8	99.6	6*M* HNO_3	TAR	540
	U(VI)	100	99.1	99.1	0.5*M* NaOH	Arsenazo III	665
	Ag	100	99.6	99.6	Unextracted	Dithiazone	460
4	Ti(IV)	100	99 6	99.6	0.1*M* HCl + 0.6% H_2O_2	Tiron	380
	Nb(V)	30	29.8	99.6	0 5*M* HNO_3	TAR	540
	Ni	100	99.6	99.6	Unextracted	PAR	510
5	Zr	40	39 8	99.5	0.1*M* HCl + 0.6% H_2O_2	Arsenazo III	650
	Nb(V)	30	29 8	99.6	0.5 HNO_3	TAR	540
	Mn	100	99.6	99.6	Unextracted	Formaldoxime	450
6	Nb(V)	30	29.8	99.6	6*M* HNO_3	TAR	540
	Th	50	49.7	99.5	6*M* HCl	Arsenazo III	650
	U(VI)	100	99.5	99.5	0.5*M* NaOH	Arsenazo III	665
	Fe(III)	100	99.6	99.6	Unextracted	1,10-phenanthroline	510

1:1:1 to 1:2:1 or 2:1:1, such separations were possible.

Separation of multicomponent mixtures

Niobium(V) was separated from several multicomponent mixtures (Table 6). Thus, it is interesting to note that 6*M* hydrochloric or nitric acid strips out niobium(V) but not molybdenum(VI), thorium(IV) or uranium(VI) as they form either anionic chloro or nitro complexes and get reextracted. Further metals like chromium(III), iron(III), silver(I), nickel(II) and manganese(II) are not extracted by Aliquat 336S under any conditions and can be thus separated while 0.1*M* hydrochloric acid in the presence of 0.6% hydrogen peroxide can easily strip out titanium(IV) or zirconium(IV) but not niobium(V). Therefore these differences were exploited to develop novel separations of niobium from multicomponent mixtures. Further these separations were confirmed from the knowledge of separation factors of various ions[15] (Table 7).

Table 7 Separation factor for various metal ions

Metal	Distribution ratio, *D*	Separation factor (α)
Nb	249	—
Ga	249	1 0
In	∞	—
Sc	332 3	0 74
Ti	249	1 0
Zr	110 1	2 2
Hf	124	2.0
V	165.6	1 5
Th	332.3	0.74
U	99	2.5
Mo	249	1.0

Most of the metals after stripping were determined spectrophotometrically with appropriate chromogenic ligand.

Determination of niobium in steel (BCS No. 261)

A 0.5-g sample was dissolved in a mixture of hydrochloric and hydrofluoric acids (2:1). The solution was evaporated almost to dryness, the residue was dissolved in 2 ml of concentrated hydrochloric acid containing 2 ml of 20%

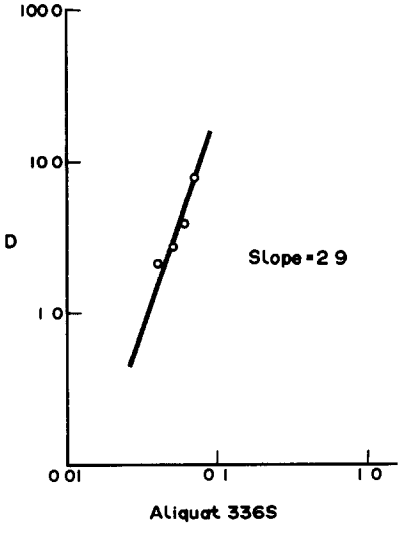

Fig 2 Distribution ratio *vs* Aliquat 336S concentration.

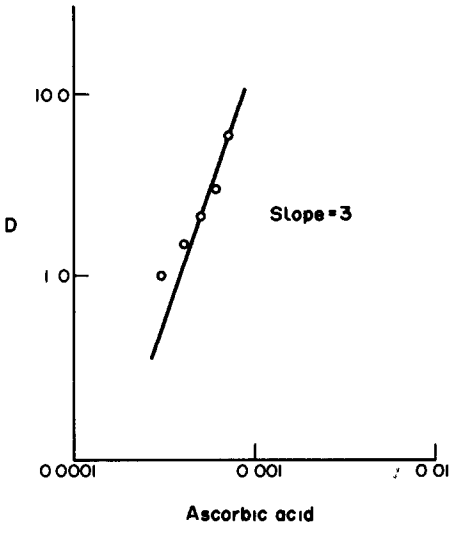

Fig. 3 Distribution ratio *vs* ascorbic acid concentration.

taric acid and the resulting solution was diluted to 50 ml with distilled water.

A known aliquot of solution was taken and was extracted as per the general procedure. Iron, chromium and molybdenum were co-extracted and were stripped with appropriate stripping agents as described earlier. The amount of niobium was found to be 0.900%, compared to the certified value of 0.920%. The precision of the determination was ±0.42% based on six determinations.

The significant feature of the proposed method is that it permits the separation of niobium from titanium(IV), vanadium(IV), tantalum(V), chromium(III), manganese(II), iron(III) and nickel(II) which are generally associated with it in steel. The method provides excellent sequential separation of vanadium(IV), niobium(V) and tantalum(V) in any ratio.

Acknowledgements—The author (MAK) is grateful to the Council of Scientific and Industrial Research, India for awarding her a Senior Research Fellowship

REFERENCES

1 L Rigali and P G Barbano, *Energia Nuclear*, 1967, **14**, 168
2. H. Green, *Metallurgia*, 1968, **407**, 143
3. V A Tayurskii, Z. N Shastina and V A. Pronin, *Z Anal Khim.*, 1978, **33**, 192
4. C. Djordjevic, H. Gorican and S. L Tan, *J Less Common Metals*, 1966, **11**, 342
5. A S Abdel-Gawad, A A Abdel-Rassoul, H B. Maghrawai and S A Sherif, *Ind. J Chem*, 1970, **8**, 293
6 A N Nevzorov and L A Bychkov, *Z Anal Khim.*, 1964, **19**, 1336.
7. V A Pronin, V A. Tayurskii, V A Khomutnikov and V O Dykhanskii, *Z Neorg Khim.*, 1976, **21**, 1288, *Chem Abstr*, 1985, **85**, 167,328
8 V A Pronin, V A Tayurskii and V O Tsykhanskii, *Z. Anal. Khim*, 1976, **31**, 58.
9 R R Rao and S M Khopkar, *Anal Lett*, 1984, **17**, 523
10 S D. Shete and V M Shinde, *Anal Chim Acta*, 1981, **125**, 165
11 G K Nurtseva and F. I Sobanov, *Z. Neorg Khim.*, 1986, **31**, 742; *Chem. Abstr.*, 1987, **104**, 156,722.
12 A K Majumdar and A. K Mukherjee, *Anal Chim Acta*, 1958, **19**, 23
13 M. A Karve and S. M. Khopkar, *Bull Chem. Soc Jpn*, 1991, **64**, 556
14. V Patrovsky, *Talanta*, 1956, **12**, 971.
15 M A Karve, Ph D Thesis entitled *Solvent Extraction Separation of Chemically Similar Elements with High Molecular Mass Amines from Ascorbate Solutions*, IIT, Bombay, August 1992

Talanta, Vol 40, No 6, pp 919–923, 1993
Printed in Great Britain

0039-9140/93 $6 00 + 0 00

DIFFERENCE SPECTROPHOTOMETRIC ASSAY OF BENZALDEHYDE IN BENZYL ALCOHOL

ISMAIL I. HEWALA

Department of Pharmaceutical Analytical Chemistry, Faculty of Pharmacy, University of Alexandria, Alexandria 21521, Egypt

(*Received* 1 *June* 1992 *Revised* 22 *September* 1992 *Accepted* 22 *September* 1992)

Summary—A simple and rapid procedure is described for the selective determination of benzaldehyde in benzyl alcohol intended for use in the manufacture of parenteral dosage form The assay is based upon the measurement of the difference absorbance between two equimolar solutions of benzaldehyde in buffer solution pH 5 75, one of which also contains sodium bisulphite The difference absorbance which has a maximum at 248 nm is due to the different spectral characteristics of benzaldehyde and its adduct form with sodium bisulphite is proportional to concentration of benzaldehyde. The accuracy, precision, sensitivity and specificity of the procedure are discussed Application of the assay is described for different batches of benzyl alcohol The results are compared with the official (BP) GLC method

The technique of difference spectrophotometry has proved to be useful for eliminating both non-specific matrix interference and specific interference from co-formulated drugs and decomposition products in a wide variety of formulations.[1] Procedures involving alteration of pH,[2] oxidation,[3] reduction,[4] competitive condensation[5] and ester formation[6] reactions have been successfully used in pharmaceutical analysis. The use of this technique for the detection of decomposition products has been described.[7]

Benzyl alcohol is commonly used in the manufacture of parenterals. Thus, the British Pharmacopoeia monograph for benzyl alcohol stated that benzyl alcohol intended for use in the manufacture of parenteral dosage form contains not more than 0.05% of benzaldehyde and described a GC method for the determination of the contents of benzaldehyde.[8] However, the limit test in the United States Pharmacopoeia monograph of benzyl alcohol for benzaldehyde, which involves the addition of hydroxylamine hydrochloride and titration with sodium hydroxide, is not specific for benzaldehyde and is designated as a test for aldehyde.[9]

In the present paper a new difference spectrophotometric procedure is described for the assay of benzaldehyde in benzyl alcohol. The method includes the measurement of the difference in absorbance between two equimolar solutions of benzaldehyde in buffer pH 5.75, one of which contains sodium bisulphite reagent. Sodium bisulphite forms an addition product with benzaldehyde and consequently destroys its strong UV absorption. The difference absorbance spectrum possesses the characteristic UV absorption band of benzaldehyde in the range 230–300 nm with a maximum at 248 nm and is free from interference due to benzyl alcohol.

EXPERIMENTAL

Reagents

Benzaldehyde (Sigma Chemical Co. U.K.), benzyl alcohol, sodium bisulphite (BDH, U.K.), dibutyl phthalate (Sigma Chemical Co., U.S.A.), were of analytical reagent quality.

Buffer solutions were prepared using substances of analytical reagent grade according to published formulae:[10] buffers pH 2 (potassium chloride and hydrochloric acid); pH 3, 4, 5, 6 and 7 (citric acid and disodium hydrogen phosphate); pH 8, 9 and 10 (potassium chloride, boric acid and sodium hydroxide).

Apparatus

Absorption and difference absorption spectra of solutions in 1-cm silica quartz cells were recorded using a Perkin-Elmer 550 S UV-visible spectrophotometer. The spectral band width was 2 nm, the scan rate 1 nm/sec and the response (time constant) one sec. The difference absorbance values of the standard, sample and blank solutions at 248 nm were read from the digital display under non-scanning conditions.

Gas chromatography was performed on a Pye-Unicam series 304 Gas chromatograph equipped with a flame-ionization detector. A 2-m length, 2-mm internal diameter glass column packed with 3% OV-17 (Phase separation Ltd) on Gas Chrom Q (80–100 mesh; Phase separation Ltd) was used. The temperature programming procedure described in the British Pharmacopoeia[8] under the monograph for benzyl alcohol was used for determination of benzaldehyde using dibutyl phthalate as an internal standard.

Procedures

Standard solutions. A standard solution of benzaldehyde was prepared by dissolving approximately 100 mg, accurately weighed, in 100 ml of ethanol (I). A 2-ml aliquot of solution I was transferred to a 50-ml standard flask and diluted to volume with ethanol (II) A 5-ml aliquot was transferred to two 50-ml standard flasks. The content of one flask was diluted to 50 ml with pH 5.75 buffer and the content of the second was diluted to 50 ml with 0.05% w/v sodium bisulphite solution prepared in pH 5.75 buffer. The difference absorption spectrum of the sodium bisulphite untreated solution in the sample cell was recorded relative to that of the solution treated with sodium bisulphite, in the reference cell.

Test solution. A sample solution of benzyl alcohol was prepared by dissolving approximately 100 mg, accurately weighed, in 25 ml of ethanol. A 3-ml aliquot was transferred to two 50-ml standard flasks and the procedure was continued as described above for standard solution from the words "The content of one flask was diluted . . . . . ." . The concentration of benzaldehyde in benzyl alcohol was calculated from the standard solution.

RESULTS AND DISCUSSION

Development of the method

Figure 1(A) shows the UV absorption spectra of benzaldehyde in the presence and absence of sodium bisulphite and their difference absorption spectrum. The bisulphite addition product of benzaldehyde eliminates the strong and weak UV absorption band of benzaldehyde around 248 and 280 nm, respectively. The difference absorption spectrum shows a λ_{max} at 248 nm and an isosbestic point (wavelength at zero ΔA because of the equal absorptivity of sodium

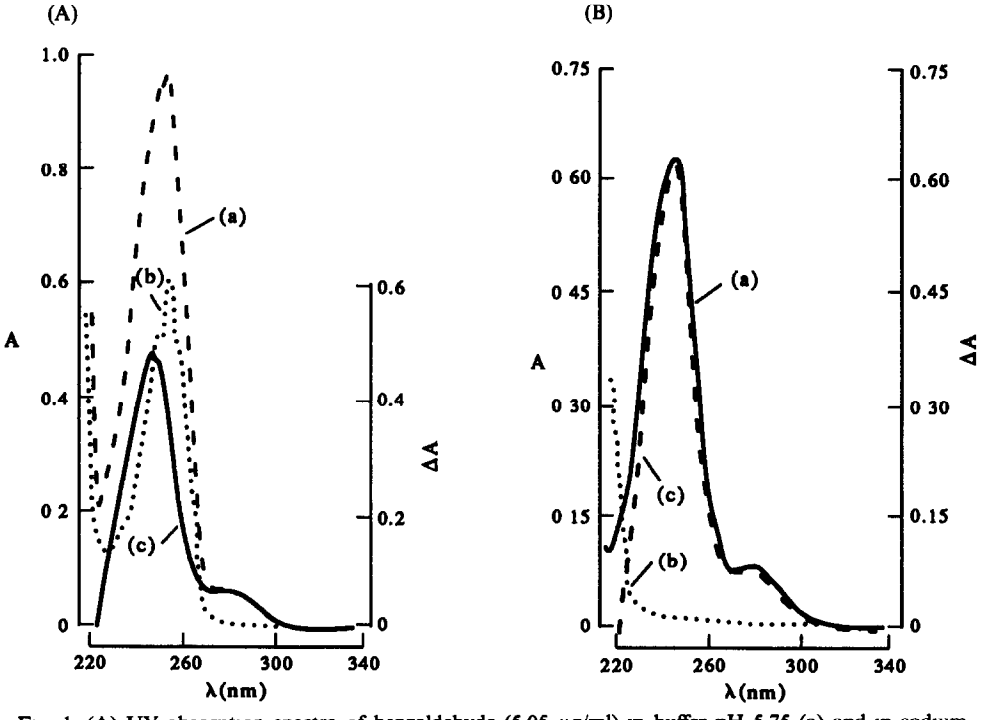

Fig 1 (A) UV absorption spectra of benzaldehyde (5.05 μg/ml) in buffer pH 5.75 (a) and in sodium bisulphite pH 5.75 solution (b) and the difference absorption spectrum (c) of solution (a) relative to solution (b) (B) UV absorption spectra of a sample of benzyl alcohol (0.353 mg/ml) in buffer pH 5 75 (a) and in sodium bisulphite pH 5 75 solution (b) and the difference absorption spectrum (c) of solution (a) relative to solution (b).

bisulphite non-treated and treated benzaldehyde) at 223 nm. The change in spectral properties of benzaldehyde by addition of sodium bisulphite is due to the destruction of dienone chromophore of benzaldehyde I to yield the diene chromophore II results from the classical addition of a nucleophile to the carbonyl system.[11]

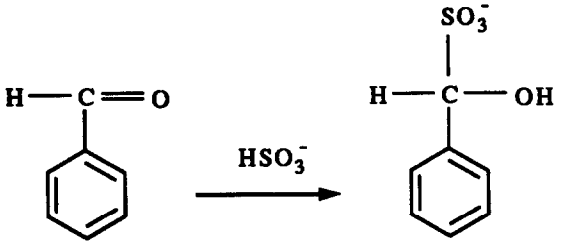

I II

The difference absorption spectrum closely resembles the UV-absorption spectrum of benzaldehyde between 340 and 230 nm (maximum at 248 nm).

The effect of pH was investigated by measuring the absorbance at 248 nm (A_{248}) of a solution of benzaldehyde that had been buffered to various pH values in the range 1–10 using buffer and sodium bisulphite treated benzaldehyde prepared in the same buffer. Figure 2 shows that the absorbance of benzaldehyde is not dependent on pH and that the reaction is pH dependent. The reaction is almost quantitative in solution adjusted to pH values between 5.5 and 6.0 as the A_{248} was maximum and the bisulphite treated solution has an absorption reading which is almost the same as the reagent, *i.e.*, has negligible absorption.

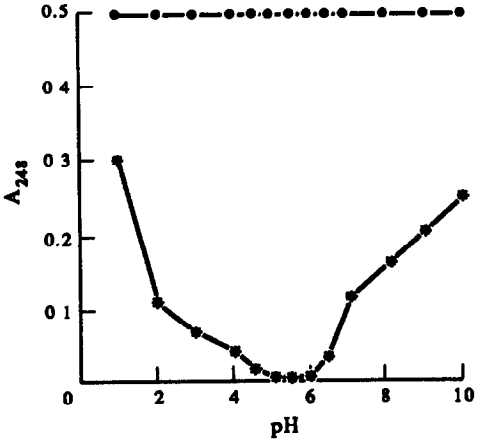

Fig. 2. The effect of pH on the absorbance of benzaldehyde (4 04 μg/ml) in the presence (—•—•—•) and absence (—·—·— — —) of sodium bisulphite

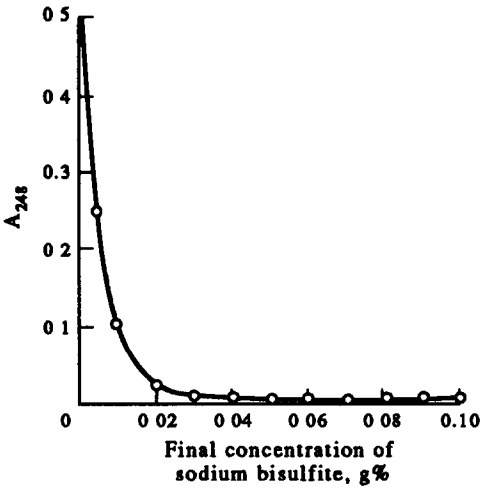

Fig. 3 The effect of concentration of sodium bisulphite on the absorbance of benzaldehyde (4 04 μg/ml) at pH 5 75

The effect of concentration of sodium bisulphite reagent was investigated and it was found that a concentration above 0.02% is enough for complete derivatization of benzaldehyde. A solution of 0.05% was chosen throughout the assay as sodium bisulphite has almost no absorption in the range up to 0.1% (0.004 absorbance units). It was found that increasing the concentration of sodium bisulphite (0.3–0.5% w/v) reduces the ΔA reading which could be due to the considerable absorption of bisulphite concentrated solution. Figure 3 shows the effect of bisulphite concentration on the absorbance of benzaldehyde at 248 nm.

Adherence to Beer's Law

Beer's law graphs for benzaldehyde showed that a rectilinear relationship exists between the measured ΔA_{248} and the concentration of benzaldehyde in the range 0–7 μg/ml. The regression equation was $Y = 0.12193\ X - 0.0012$ where Y is the ΔA_{248} in a 1-cm cell and X μg/ml is the concentration of benzaldehyde (correlation coefficient 0.9999 for $n = 6$). An almost identical line ($Y = 0.12188\ X - 0.0019$; correlation coefficient 0.9998 for $n = 6$) was obtained for a similar series of solutions of benzaldehyde containing benzyl alcohol (200 μg/ml).

Specificity, accuracy, precision and limit of detection

To assess further the specificity of the method, a series of solutions containing benzaldehyde at 10 μg/ml and increasing concentrations of benzyl alcohol (0–4 mg/ml), were assayed by the proposed procedure; the final

Table 1 Assay of benzaldehyde in standard mixtures of benzaldehyde and benzyl alcohol using the proposed method

Concentration of benzaldehyde in benzyl alcohol, added μg/g	20	50	100	200	400	500
Concentration of benzaldehyde in benzyl alcohol, found μg/g	19 70	49 40	99 90	200 10	399.80	500 20
Accuracy, %	98 50	98 80	99.90	100 05	99 95	100 04

concentration of benzaldehyde in each solution being 1 μg/ml. The ΔA of all solutions containing benzyl alcohol fell within 98.8–100.2% of that of the standard solution of benzaldehyde containing no benzyl alcohol. This confirms that the ΔA method is independent of the level of benzyl alcohol (Table 1).

The standard deviations of the difference absorbance given by a solution of benzyl alcohol (1 mg/ml) and benzaldehyde (1 μg/ml) (S_A) and a similar solution of benzyl alcohol without the addition of benzaldehyde (S_B), each assayed 10 times by the proposed procedure, were found to be 2.70×10^{-3} and 9.47×10^{-4}, respectively. The relative standard deviation, calculated from the corrected standard deviation,[12], was 0.57% and the limit of detection ($2S_B$) of benzaldehyde in benzyl alcohol corresponded to a concentration of 7.7×10^{-5}% m/m. These results show that the proposed method is accurate, precise and sensitive.

Analysis of commercial samples

In order to test the application of the method, the concentrations of benzaldehyde were measured in samples of benzyl alcohol intended for use in the manufacture of parenterals. Figure 1(B) shows the absorption spectrum of benzyl alcohol before and after treatment with sodium bisulphite and their difference absorption spectrum. The spectra illustrated that, whereas a direct measurement of A_{248} [Fig. 1(B), a)] of the solution is subject to interference from benzyl alcohol, the ΔA_{248} [Fig. 1(B), c] is selective for benzaldehyde. To prove further the absence of interference, the standard addition method was used to calculate the recovery of added benzaldehyde (2 μg/ml). The results (Table 2) show good recovery of the added benzaldehyde and consequently benzaldehyde is assayed without interference from any related substances[8] that may exist in commercial samples.

Table 2. Recovery of benzaldehyde added to diluted solutions of benzyl alcohol

	Concentration of benzaldehyde (μg/ml)		Recovery
Sample No	Without added benzaldehyde	With added (2μg/ml) benzaldehyde)	(As % of added benzaldehyde
Batch A	3 441	5 424	99 150
Batch B	5 621	7 625	100 200
Batch C	2 950	4.927	98 850
Batch D	4 632	6.626	99 700

Table 3 Concentration of benzaldehyde in commercial samples of benzyl alcohol

			Concentration of benzaldehyde μg/g		% m/m	
Sample	Approximate age (month)	Treatment	ΔA_{248}	GLC	ΔA_{248}	GLC
A	New	—	170	164	0 017	0 016
A	New	SF	168	165	0 017	0 017
A	New	SA	178	179	0.018	0.018
B	3	—	212	217	0 021	0 022
B	3	SF	212	218	0 021	0 022
B	3	SA	224	223	0 022	0 022
C	5	—	130	126	0.013	0.013
C	5	SF	133	136	0 013	0 014
C	5	SA	136	137	0 014	0 014
D	12	—	280	278	0 028	0 028
D	12	SF	278	271	0 028	0 027
D	12	SA	296	298	0 030	0 030

SF = Sterilization by filtration

SA = Sterilization by autoclaving at 121° for 15 min.

The proposed procedure was applied for the determination of four different batches of commercial benzyl alcohol described for use in manufacture of parenterals. For comparison, the concentrations of benzyl alcohol were also assayed by the GLC procedure described in the British Pharmacopoeia monograph for benzyl alcohol.[8] The results in Table 3 show good agreement between the two methods and confirm that the difference spectrophotometric procedure is both accurate and selective.

Parenteral dosage forms containing benzyl alcohol are sterilized either by filtration or autoclaving. The effect of such treatment on the concentration of benzaldehyde in benzyl alcohol was investigated. The results (Table 3) show that heat sterilization increases the concentration of benzaldehyde by approximately 5% of its original content. It is recommended that samples of benzyl alcohol (pharmaceutical grade) containing relatively high concentrations of benzaldehyde (stored samples) be sterilized by filtration.

REFERENCES

1 T. D Doyle and F R Fazzari, *J Pharm Sci*, 1974, **63**, 1921
2 A G Davidson and J B Stenlake, *Analyst*, 1974, **99**, 476
3 A G Davidson, *J Pharm. Pharmacol*, 1976, **28**, 795
4 *Idem, ibid*, 1978, **30**, 410.
5 *Idem, Analyst*, 1982, **107**, 422
6 *Idem, J Pharm Sci*, 1984, **73**, 1582
7 I I Hewala, Ph.D Thesis, 1989, University of Strathclyde, Glasgow, U K.
8 British Pharmacopoeia, Her Majesty's Stationery Office, London, 1988
9 United States Pharmacopoeia XXII, Mack Publishing Co, Easton, PA, 1990
10 H A. M. Mckenzie, *Data for Biochemical Research*, R M C Dawson, D C Elliot, W. H Elliot and K M Jones (eds), pp 475–504 Oxford University Press, U K 1968
11 T W G Solomons, *Organic Chemistry*, pp 681–735. John Wiley, New York, 1976
12 A L Wilson, *Analyst*, 1961, **86**, 72

Talanta, Vol 40, No 6, pp 925–929, 1993
Printed in Great Britain

0039-9140/93 $6 00 + 0 00

SPECTROPHOTOMETRIC DETERMINATION OF EQUILIBRIUM CONSTANTS OF TWO MUTUAL COMPETITIVE REACTIONS BY THE METHOD OF ISOSBESTIC POINTS

JIE ZHOU*, SHI-FU ZOU and WEI-AN LIANG†
Department of Chemistry, Shandong University, Jinan, Shandong, People's Republic of China

(*Received* 15 *July* 1992. *Accepted* 25 *August* 1992)

Summary—We have developed a method that makes use of dual isosbestic points in a dual ligand, single metal system that allows the determination of the equilibrium constants of complexes in which two ligands compete for the same metal ion, and one complex is colourless The competition of methyl thymol blue and citrate was used to test the model.

The method of corresponding solutions competition[1] can be used in the determination of equilibrium constants of two mutual competitive reactions and is useful in studying the chemical equilibria of complicated systems, such as speciation analyses.[2] However, the method is only applicable to the case in which two metal ions compete for the same ligand, whereas it is not suitable when two ligands compete for the same metal ion. New approaches are still required for the latter case. Based on the distribution of species in a competitive system, and making use of the characteristics of the isosbestic points found as system compositions vary, we have developed a method to determine the stability constants of complexes formed by two mutual competitive reactions. The method has been used in the system in which 3,3′-bis[*N*,*N*′-di(carboxymethyl)aminomethyl]-thymolsulphophthalein(methyl thymol blue) competes with 2-hydroxypropane-1,2,3-tricarboxylic acid (citric acid) for aluminium(III), and satisfactory results are obtained.

THEORY

Suppose that the reactions in which two ligands R and L compete for the same metal ion are as follows (the charges are omitted for simplicity)

$$M + R = MR, \quad \beta_1 = [MR]/[M][R] \qquad (1)$$

$$M + 2R = MR_2, \quad \beta_2 = [MR_2]/[M][R]^2 \qquad (2)$$

$$M + nL = ML_n, \quad \beta_L = [ML_n]/[M][L]^n \qquad (3)$$

Suppose the reaction (M + R) is a coloured reaction and the other reaction (M + L) is a colourless reaction in a competitive system. The absorption spectra of relevant species chosen in this study are shown in Fig. 1. The absorbance of the solution is expressed as

$$A = \epsilon_0[R] + \epsilon_1[MR] + \epsilon_2[MR_2] \qquad (4)$$

where ϵ_0, ϵ_1 and ϵ_2 are the molar absorptivities of R, MR and MR_2, respectively. Two isosbestic points exist in the spectra. According to earlier workers' discussion about the characteristics of isosbestic points,[3–5] we obtain $\epsilon_2 = 2\epsilon_1$ at the wavelength of the isosbestic point (λ_q). If λ_q is selected as the measurement wavelength, equation (4) becomes

$$\begin{aligned} A &= \epsilon_0[R] + \epsilon_1[MR] + 2\epsilon_1[MR_2] \\ &= \epsilon_1 C_0^R - (\epsilon_1 - \epsilon_0)[R] \\ &\quad + (C_0^R = [R] + [MR] + 2[MR_2]) \end{aligned} \qquad (5)$$

By rearrangement of equation (5), we obtain

$$\begin{aligned} [R] &= (\epsilon_1 C_0^R - A)C_0^R/(\epsilon_1 C_0^R - \epsilon_0 C_0^R) \\ &= (A_q - A)C_0^R/(A_q - A_0) \qquad [5(a)] \\ &\quad (A_q = \epsilon_1 C_0^R, A_0 = \epsilon_0 C_0^R) \end{aligned}$$

A_q is the absorbance of the isosbestic point q, A_0 is that of the reagent R at λ_q. They are constant and can be measured directly as C_0^R is fixed.

*Present address. Department of Basic Sciences, Shandong Agricultural University, Taian, Shandong, People's Republic of China
†Author for correspondence

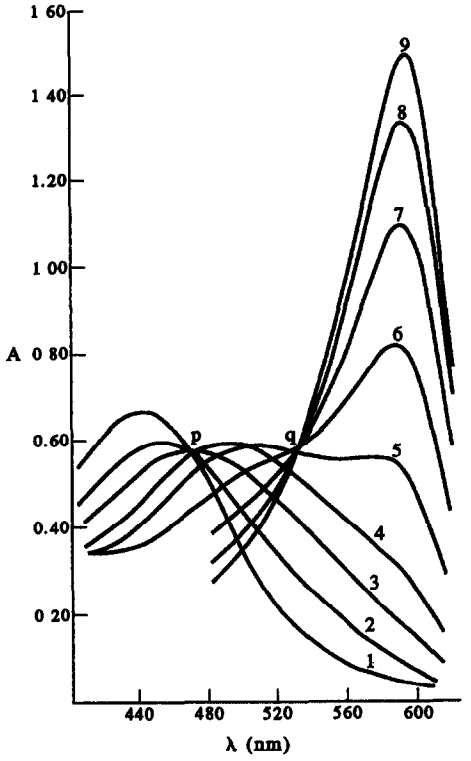

Fig 1 Absorption spectra for Al–MTB system at different C^{Al} $C_0^R = 1\ 70 \times 10^{-5}M$, pH = 4 95, 2-cm cells, with distilled water as the reference, C^{Al} ($\times 10^{-5}M$) curves 1—0 00, 2—0 40, 3—0 80, 4—1 20, 5—1 60, 6—2 00, 7—2 40, 8—2 80, 9—3 20

Therefore after the absorbance of each solution is measured, [R] is evaluated form equation [5(a)].

It should be noted, the values of [R] are almost close to zero for any of the curves across the point q, therefore, equations (5) and [5(a)] are useless under such circumstances.

After the values of [R] are obtained, from the definition of Bjerrum's function, we obtain

$$\bar{n} = (C_0^R - [R])/C^M \qquad (6)$$

$$\bar{n} = (\beta_1[R] + 2\beta_2[R]^2)/(1 + \beta_1[R] + \beta_2[R]^2) \qquad [6(a)]$$

$\bar{n}$ can be evaluated from equation (6). Substituting each pair of values ($\bar{n}$, [R]) of solutions into equation [6(a)], homologous linear equations are obtained. Two of the arbitrary equations compose simultaneous equations, and β_1 and β_2 can be evaluated.

Equation [6(a)] can be rewritten in the form

$$\frac{2-\bar{n}}{\bar{n}}[R]^2 = \frac{\bar{n}-1}{\bar{n}}[R]\frac{\beta_1}{\beta_2} + \frac{1}{\beta_2} \qquad [6(b)]$$

A linear plot of $(2-\bar{n})[R]^2/\bar{n}$ *vs.* $(\bar{n}-1)[R]/\bar{n}$ is obtained from equation [6(b)] (Fig. 2), the slope

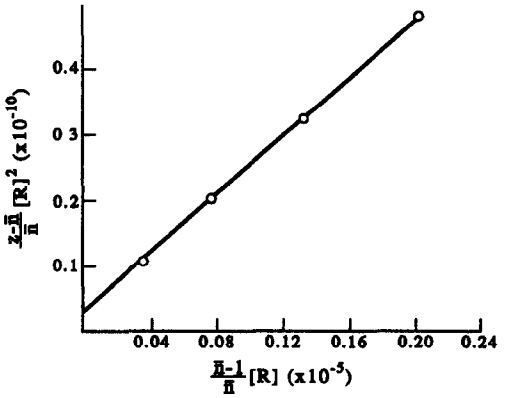

Fig 2 Graphs of $(2-\bar{n})[R]^2/\bar{n}$ *vs* $(\bar{n}-1)[R]/\bar{n}$

and the intercept of the line are β_1/β_2 and $1/\beta_2$, respectively. Thus β_1 and β_2 are evaluated.

When there is only the reaction (M + R) in a solution, equation (6) is used directly. If there is also the competitive reaction (M + L) simultaneously, equation (6) should be corrected. Because C^M is divided into two parts, ΔC^M is used in the reaction (M + L). So as to evaluate ΔC^M, we prepare two series of solutions. First, C_0^R is fixed and C^M is gradually increased, Secondly, $C_0^R + C_0^L$ is fixed and C^M is gradually increased. The absorbances of these solutions are measured as λ_q and [R] is evaluated from equation [5(a)]; the graphs of [R] *vs.* C^M are shown in Fig. 4.

In Fig. 4, a line parallel with the abscissa is drawn. It intersects with the curves *a* and *b* at a_1 and b_1. The solutions corresponding to the points a_1 and b_1 have the same [R]. From the material balance relation and the expression of equilibrium constants, we can derive that the solutions also have the same [M], [MR] and [MR_2], while C^M is different. The solutions include the following material balance equations

$$C_a^M = [M] + [MR] + [MR_2] \qquad (7)$$

$$C_b^M = [M] + [MR] + [MR_2] + [ML_n] \qquad (8)$$

$$C_a^R \text{ or } C_b^R = [R] + [MR] + 2[MR_2] \qquad (9)$$

$$C_b^L = [L] + n[ML_n] \qquad (10)$$

Subtracting equation (7) from equation (8), yields

$$C_b^M - C_a^M = \Delta C^M = [ML_n] \qquad (11)$$

Substituting equation (11) into (10), yields

$$[L] = C^L - n\,\Delta C^M \qquad (12)$$

According to the above discussion, β_1 and β_2 can be evaluated from equation [6(a)]. Whether there is the competitive reaction (M + L) or not, C_a^M has to be used in the calculation of β_1 and β_2. If the value of C_b^M at b_1 is used, ΔC^M consumed in the reaction (M + L) has to be deducted.

It is very convenient to evaluate the stability constant of ML_n by its distribution coefficient. We define

$$\delta_{ML_n} = [ML_n]/C_b^M = \Delta C^M/C_b^M \qquad (13)$$

δ_{ML_n} can be evaluated from equation (13). Substituting equations (1), (2), (3) and (8) into (13) yields

$$\delta_{ML_n} = \beta_1[L]^n/(1 + \beta_1[R] + \beta_2[R]^2 + \beta_L[L]^n \qquad [13(a)]$$

[R], β_1 and β_2 can be evaluated in advance. If n is known or evaluated by another method, substituting these known values into equation [13(a)] provides β_L.

EXPERIMENTAL

Apparatus

A Shimadzu UV-3000 double-beam spectrophotometer and a pHs-2 acidimeter were used.

Reagents

A $1.00 \times 10^{-3}M$ stock solution of aluminium-(III) was prepared by dissolving the calculated amounts of $KAl(SO_4)\cdot 12H_2L$(G.R.) in a solution of $1.0 \times 10^{-4}M$ hydrochloric acid. The working standard solutions were obtained by diluting the stock solution. A $1.213 \times 10^{-4}M$ solution of methyl thymol blue(MTB) was prepared from commercial MTB which was purified by DEAE-cellulose column chromatography,[7] and its accurate concentration was determined by a spectrophotometric method.[8] Citric acid solution (cit, $1.000 \times 10^{-3}M$), HOAc/NaOAc buffer solution (pH 5.0) and $1M$ potassium nitrate were prepared with analytical-reagent grade chemicals, respectively.

Procedure

To each of a series of 50-ml beakers, add 5 ml of buffer solution, 3.50 ml of MTB solution, 1.00 ml of cit solution, 2.5 ml of $1M$ potassium nitrate and a different volume of Al solution, respectively, dilute to 20 ml with distilled water, heat for five min in a boiling water-bath, and cool to room temperature. Transfer each of the solutions to a 25-ml standard flask, respectively, dilute to the mark with distilled water and mix, stand for 10 min and measure their absorption spectra or absorbances.

Selection of pH of solution

Based on the earlier studies, the range of pH selected was 4.5–5.0 for formation of the coloured complexes.

RESULTS AND DISUSSION

Determination of stability constants of the complexes for the Al–MTB system

When pH and C^{MTB} were fixed and C^{Al} was gradually increased, a series of solutions resulted with the absorption spectra shown in Fig. 1. Figure 1 shows Al can form two complexes with MTB. Their maximum absorption wavelengths are 492 and 585 nm, respectively. In addition, two isosbestic points exist in Fig. 1. According to the literature,[9] the compositions of the complexes with maxima at 492 nm and 585 nm are $Al(MTB)_2$ (1:2) and Al(MTB) (1:1), respectively. In the presence of a higher concentrations of Al(III), the formation of 1:1 complexes predominates, conversely, the formation of 1.2 complexes predominates. The first isosbestic point p is at 463 nm and the second isosbestic point q is at 532 nm at pH 4.95.

According to the above discussion, we measure A at 532 nm (λ_q) and evaluate [R] from equation [5(a)]. Substituting the values of [R] obtained into equation (6), we can evaluate $\bar{n}$. Then the values of $(2-\bar{n})[R]^2/\bar{n}$ and $(\bar{n}-1)[R]/\bar{n}$ are calculated, respectively. The values of relevant parameters obtained are shown in Table 1. A linear plot of $(2-\bar{n})[R]^2/\bar{n}$ *vs.* $(\bar{n}-1)[R]/\bar{n}$ is shown in Fig. 2. The values of β_1 and β_2 obtained from Fig. 2 are: $\beta_1 = 6.57 \times 10^6$ and $\beta_2 = 2.94 \times 10^{11}$, respectively.

Determination of stability constant of ML_n for Al–cit system

Similar to Fig. 1, the absorption spectra for Al–MTB–cit system at different C^{Al} are shown in Fig. 3. In Figs 3 and 1, C^{MTB} is the same. On

Table 1 Values of relevant parameters obtained for Al–MTB system at different C^{Al}($C_0^R = 1.70 \times 10^{-5}M$, $A_q = 0.600$, $A_0 = 0.175$)

$C^{Al}(\times 10^{-5}M)$	0 60	0.80	1.00	1.20
$[R](\times 10^{-5}M)$	0 932	0 720	0.528	0 360
$\bar{n}$	1 280	1.225	1.172	1 117
$(2-\bar{n})[R]^2/\bar{n}(\times 10^{-10})$	0.489	0 328	0 197	0 102
$(\bar{n}-1)[R]/\bar{n}(\times 10^{-5})$	0 204	0.132	0.077	0 038

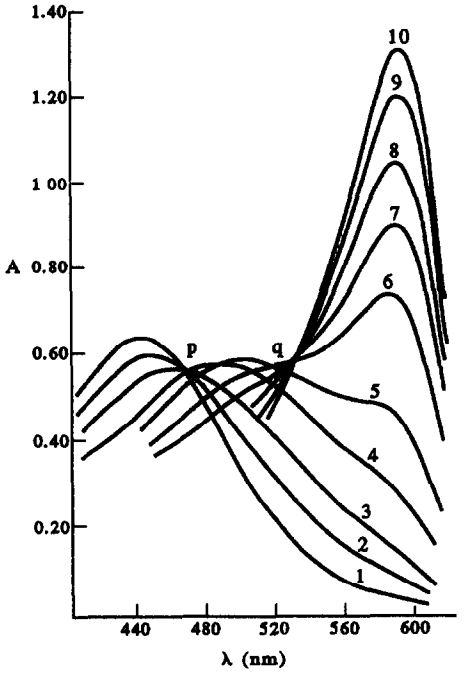

Fig. 3. Absorption spectra for Al–MTB–cit system at different C^{Al} $C^{L} = 4.00 \times 10^{-5}M$, C^{Al} ($\times 10^{-5}M$) Curves 1—0 00, 2—0.40, 3—0 80, 4—1.60, 5—3 20, 6—4 80, 7—5.60, 8—6.40, 9—7 20, 10—8.00; other conditions as for Fig 1

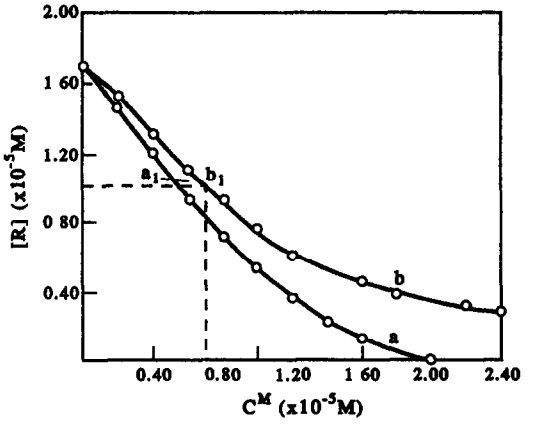

Fig 4 Graphs of [R] *vs* C^{Al} for two series of solutions corresponding to Fig 1(a) and Fig 3(b)

comparing the two figures, λ_{max} of the complexes formed between MTB and Al(III) is the same, as are λ_p, λ_q and A_q, A_p, respectively. But as C^{Al} is increased, the curves differ (the rate of change is diminished). Cit competes with MTB for Al(III) and a part of C^{Al} is consumed in the formation of the complexes Al(cit). It is preliminarily estimated that ternary complexes are not formed.

According to the report of the literature,[10] Al(III) can form 1:1 complexes (AlHL) with cit under acid conditions, so we consider n to be 1. Thus β_L can be evaluated. The absorbances of two series of solutions corresponding to Figs 1 and 3 are measured at λ_q, then [R] is evaluated from equation [5(a)] (Table 2). The graphs of [R] *vs.* C^{Al} are shown in Fig. 4. A line parallel with the abscissa is drawn at a fixed value of [R]. It intersects with the two curves at a_1 and b_1. [R] is the same at the two points a_1 and b_1, C^{Al} is evaluated from C_a^{Al} and C_b^{Al}, corresponding to a_1 and b_1. Then $[ML_n]$, [L] and δ_{ML_n} are evaluated from equations (11), (12) and (13), respectively. Thus β_L can be evaluated from equation [13(a)]. The values of relevant parameters and β_L are shown in Table 3. The average value of β_L obtained from Table 3 is 6.06×10^5 (log $\beta_L = 5.78$). Studies of the equilibrium relations for the Al–MTB system are limited. The only literature[9] we found reported log $\beta_1 = 3.88$, log $\beta_2 = 9.9$. Our results differ from them, because our experimental conditions are different from those of the literature.[9] For the Al–cit log system, after correcting our results by alpha coefficients (at pH 5, log $\alpha_{L(H)}$ and log $\alpha_{Al(OH)}$ are 1.2 and 0.4,[11] respectively), we calculated the

Table 2. Values of A for two series of solutions in the presence and in the absence of cit($A_q = 0.600$, $A_0 = 0\ 175$)*

C^{Al}($\times 10^{-5}M$)	0 00	0.20	0 40	0.60	0 80	1 00	1 20	1 40	1 60	1 80	2 00	2 20	2 40
A_a	0 175	0.238	0 300	0.367	0 420	0 468	0 510	0.545	0 570	—	0 600	—	—
$[R]_a$($\times 10^{-5}M$)	1 700	1.448	1 200	0.932	0 720	0.528	0 360	0.220	0 120	—	0 000	—	—
A_b	0 175	0 220	0 275	0.325	0 370	0.410	0 450	—	0 488	0 505	—	0.520	0 530
$[R]_b$($\times 10^{-5}M$)	1.700	1.520	1 300	1 100	0 920	0.760	0 600	—	0 448	0 380	—	0.320	0 280

*Subscripts a and b represent the presence and the absence of cit($C^{L} = 4\ 00 \times 10^{-5}M$), respectively

Table 3 Values of relevant parameters and β_L obtained from Fig. 4

[R]($\times 10^{-5}M$)	C_a^{Al}($\times 10^{-5}M$)	C_b^{Al}($\times 10^{-5}M$)	ΔC^{Al}($\times 10^{-5}M$)	[L]($\times 10^{-5}M$)	δ_{ML}	β_L($\times 10^5$)
1 000	0.550	0 700	0 150	3 850	0.214	6 80
0.920	0.610	0 800	0.190	3 810	0 238	7.07
0.830	0 690	0 900	0.210	3 790	0 233	6.07
0.760	0 760	1 000	0 240	3.760	0 240	5.70
0.680	0.850	1 100	0 250	3.750	0 227	4.64

stability constant to be $\log \beta_L = 7.38$. This is basically the same as the value of the literature ($\log \beta_L = 7.0$).[10] Because the latter calculation uses the former constants, it can be seen that the method developed in this paper is quite reliable.

REFERENCES

1 H Irving and D H Mellor, *J Chem Soc*, 1955, 3457
2 N C F Velloso, E A Neves and I G R Cutz, *Polyhedron*, 1985, **4**, 2043
3 S Kida, *Bull Chem Soc Japan.*, 1956, **29**, 805
4 S. F Zhou and W A Liang, *Talanta*, 1984, **31**, 837
5 S F Zhou and L J Dai, *Acta Chim. Sin*, 1980, **40**, 33.
6 J Bjerrum, *Metal Ammine Formation in Aqueous Solution*, Copenhagen, P Haase and Son, 1941.
7 H Sato, Y Yokoyama and K Momoki, *Anal Chim Acta*, 1977, **94**, 217
8 T Yoshino, H Imada and T Kuwano, *Talanta*, 1969, **16**, 151
9 N D Lukomskaya, T V Mal'koval and K. B Yatsimirskii, *J Inorg Chem* (*Russ*), 1967, **12**, 1299
10 C Bertin-Batsch, *Ann Chim* (*France*), 1952, **7**, 481
11 Z H Pong and X Y Zhang, *Principle of Complexometric Titrations*, p 117 Beijing University Press, Beijing, 1981

Talanta, Vol 40, No 6, pp 931–934, 1993
Printed in Great Britain

0039-9140/93 $6 00 + 0 00

PRECONCENTRATION AND DETERMINATION OF Ce, La AND Pr BY X-RAY FLUORESCENCE ANALYSIS, USING AMBERLITE XAD RESINS LOADED WITH 8-QUINOLINOL AND 2-(2-(5 CHLOROPYRIDYLAZO)-5-DIMETHYLAMINO)-PHENOL

A. N. MASI and R A OLSINA

Department of Analytical Chemistry "Dr. B. Marone", Faculty of Chemistry, Biochemistry and Pharmacy, National University of San Luis, San Luis, Argentina

(*Received* 9 *December* 1991 *Revised* 17 *April* 1992 *Accepted* 23 *August* 1992)

Summary—8-Quinolinol (oxine) and 2-(2-(5 chloropyridylazo)-5-dimethylamino)-phenol (5ClDMPAP) were immobilized on the non ionic sorbents Amberlite XAD-4 and XAD-7 These loaded resins were used for the preconcentration of Ce, La and Pr High preconcentration factors were obtained in each case After the retention of these rare earths, the resins were measured as thin films by x-ray fluorescence spectrometry Up to 50 ppm of REEs can be retained on these thin films

The analytical treatment of rare earth elements is not performed on the individual elements because they form a closely related group of elements.[1] It is usually necessary to preconcentrate and separate them from the matrix, especially for trace analysis. Chemists have proposed different procedures for preliminary enrichment and separation of trace REEs such as: coprecipitation,[2] ion exchange[3–5] and solvent extraction.[6]

The rare earths have been determined by many instrumental techniques, but are affected by spectral interferences. Thus, when they are determined by these techniques, separation and preconcentration steps are necessary. X-ray fluorescence analysis is a useful and versatile method for determination of rare earths[7–9] in a variety of materials. As with other instrumental methods, XRF is subject to spectral and other modes of interferences, which can be corrected.[10]

Absorption-enhancement effects are negligible in thin film type specimens because neither primary nor analyte line x-rays are significantly absorbed in the extremely thin layer.

We propose for the preconcentration and separation of Ce, La and Pr, the immobilization of two organic reagents on the adsorbent resins: 8-quinolinol (oxine) and 2-(2-(5 chloropyridylazo)-5-dimethylamino)-phenol (5ClDMPAP). With the proper conditions, the elements of interest can be retained on these. The resins which contain the retained ions are presented to the x-ray spectrometer as thin films. This technique has many advantages in the determination of the REEs.

EXPERIMENTAL

Reagents and apparatus

The Amberlite XAD-4 (Rohm & Haas) had a specific surface area of 750 m^2/g, pore diameter 50 Å and bead size 20–50 mesh; and XAD-7 had a specific surface area of 450 m^2/g, pore diameter 80 Å and bead size 20–50 mesh.

5ClDMPAP reagent was synthesized by the technique of Shibata and Furukawa.[11] This reagent is slightly soluble in water but easily soluble in ethanol.

Ce standard solution was prepared by dissolving $Ce(NO_3)_3$ in water. La standard solution was prepared with $La(NO_3)_3$ in 0.1*M* HCL. A Pr standard solution was prepared by dissolving Pr_4O_{11} in 0.1*M* HCl.

Membrane filter papers were Millipore of 0.47-μm pore size.

All other chemicals were analytical grade and doubly distilled water was used throughout.

A Philips PW1400 x-ray spectrometer was used for Ce, La and Pr Lα line measurement. The parameters were appropriately selected.

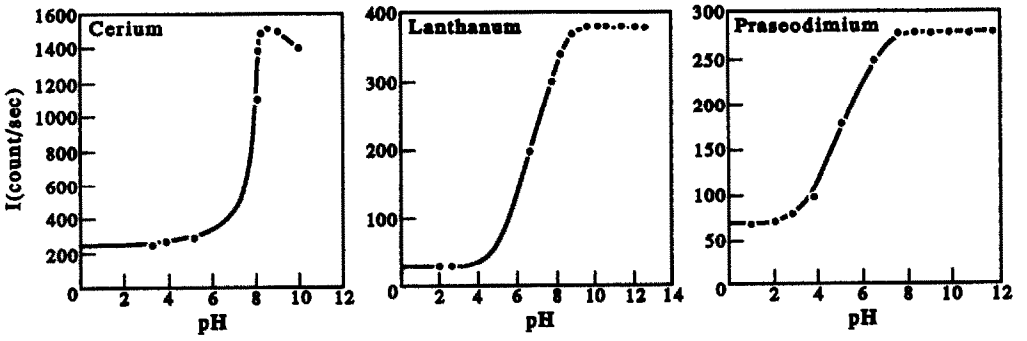

Fig 1 Retention of Ce, La and Pr on SCIDMPAP-XAD-4 as a function of pH

A Varian UV-Visible Spectrometer was used with 10-mm path length glass cells.

pH of solutions were measured in an Orion 701-A pH meter with a Ag–AgCl electrode.

The filtrations were performed in a special filtration apparatus with a vacuum pump.

Preparation of resins

The XAD resins were ground with an acetone–water mixture in a ceramic mortar and sieved with a mesh sifter to obtain 100–200 mesh grains. Then the resins were soaked with methanol–4*M* HCl (1:1) overnight and washed with water.[12]

Preparation of loaded resins

Using the optimum adsorption conditions,[13] the organic reagents were loaded on the ground resins (XAD-4 and XAD-7). One gram of each was shaken for 10 hr with solutions of 600 mg/l. 5ClDMPAP and 0.02*M* oxine both in 0.01*M* HCl.

Retention of Ce, La and Pr as a function of pH

Solutions containing 10 ppm Ce and 5% Triton were adjusted to the desired pH with sodium hydroxide or hydrochloric acid and shaken with 10-mg portions of each resin for 1 hr. Resins were filtered using a vacuum pump on Millipore paper. These papers were covered with Mylar and each analyte Lα line was recorded by an x-ray spectrometer. The same procedure was carried out with solutions of 10 ppm La and 10 ppm Pr. The graphs of retention as a function of pH are shown in Fig. 1.

Determination of critical thickness

Solutions containing 10 ppm Ce(III) were shaken with 10, 15, 20, 25, 30, 35 and 40-mg portions of loaded resins at the proper pH. Solutions were filtered on Millipore paper and then covered with Mylar. Ce lines were read with an x-ray spectrometer (Fig. 2).

Evaluation of the interelement effects in the thin film

Solutions containing a mixture of Ce and La in the ratio 1:6, 6:1 and Ce–Pr 1:6, 6:1 were prepared and Ce, La and Pr were determined by the same method.

Determination of total adsorption capacity

Each rare earth was retained at the proper pH on each loaded resin. With this purpose, 10 ml of REE solution between 0 and 80 ppm was shaken for 30 min with 10 mg of resin. Solutions were filtered on Millipore paper, covered with Mylar and REEs Lα lines were measured in an x-ray fluorescence spectrometer.

Preconcentration of Ce, La and Pr

Solutions containing 0–10 and 0–50 ppm Ce, La and Pr were shaken with 10 mg of each

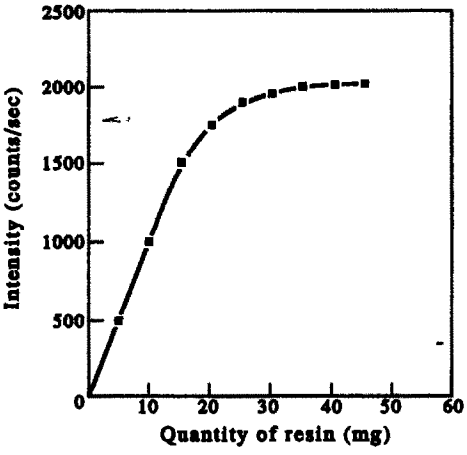

Fig. 2. Determination of critical thickness (critical quantity of resin in the film)

Table 1. Determination of Ce, La and Pr in different samples A and B are synthetic samples with the same composition as the standards of the NBS G2 and SDC-1, respectively Loaded resins 1 Oxine-XAD-4 2 Oxine-XAD-7 3 5ClDMPAP-XAD-4 4 5ClDMPAP-XAD-7

Contents in ppm			Loaded	Quantity found			Error %			Variation coeff		
Ce	La	Pr	Resin	Ce	La	Pr	Ce	La	Pr	Ce	La	Pr
10	10	10	4	9 91	9 80	9 86	0 85	2 00	1 20	1 50	1 47	2 37
10	10	10	1	9 62	10 40	9 79	3 67	4 00	2 10	2 30	1 23	2 34
10	5	25	4	10 20	4 79	25 30	2 00	4 20	1 20	3 26	2 98	1 05
10	5	25	1	9 96	5 08	24 80	0 40	1 60	1 40	1 47	2 51	1 38
10	25	5	4	10 10	24 83	4 82	1 00	0 68	3 60	1 28	1 11	3 68
10	25	5	1	9 71	25.22	4 80	2 90	0.88	4 00	1 45	0 956	5 26
25	10	5	4	25 11	9 88	5 16	0 48	1 20	3 20	0 51	2 93	6 12
25	10	5	1	24 50	10 17	5 04	2 00	1 70	0 80	0 56	1 10	5 38
5	10	25	3	5 05	10 17	24 88	1 00	1 70	0 48	2 42	1 76	0 84
5	10	25	2	5 01	10 22	24 50	0 20	2 20	2 00	3 61	2 10	1 28
5	25	10	3	5 20	24 70	9.88	4 00	1 20	1 20	2 93	0 52	2 35
5	25	10	2	4 86	25 10	9 80	2 80	0 40	2 00	3 46	0 93	2 66
5	30	—	1	5 00	29 78	—	0 00	0 73	—	5 32	0 36	—
5	—	30	1	4 82	—	29 80	3 60	—	1 20	2 70	—	0 83
30	5	—	4	29 98	4 84	—	0 06	3 20	—	0 51	3 26	—
30	—	5	4	30 50	—	4 91	1 60	—	1 70	0 41	—	5 18
15	9 6	1 9[A]	3	15 20	9 87	1 85	1 30	2 30	2 20	0 98	1 38	5 18
10 4	15	0 8[B]	2	10 60	15 30	0 85	2 00	2 00	5 10	1 23	1 11	26 30

loaded resin at maximum adsorption pH (7.5 in each case) for 30 min. Resins were filtered with a vacuum pump on Millipore paper. Thus, a thin film was obtained and covered with Mylar.

Calculation of enrichment coefficients

Ce, La and Pr solutions were agitated with loaded resins at maximum adsorption pH for 30 min. In filtered liquids the rare earth amounts were determined spectrometrically by the Arsenazo I[14] method (using triethanolamine buffer of pH 7.2) at 580 nm.

Determination of Ce, La and Pr by x-ray fluorescence spectrometry

Standards were measured in the x-ray fluorescence spectrometer. Measurement parameters were: 79.025° 2θ for Ce Lα, 82.930° 2θ for La Lα and 68.240° 2θ for Pr Lβ, Cr tube, 50 kV, 50 mA, LiF (200) crystal, 75–25 window width, counting time 100 sec, gas proportional-scintillation counter in tandem.

The reproducibility in the adsorption of Ce, La and Pr was assessed by repeating the same procedure, six times.

Analysis of samples

Samples containing Ce, La and Pr in different concentrations were prepared. Some were in the same proportions as the standard samples G2 and SDC-1 (USGS). A 10-ml portion of these samples was preconcentrated and determined by this method. Results are presented in Table 1.

RESULTS AND DISCUSSION

The adsorption behaviour of Ce, La and Pr as a function of pH was examined and results are presented in Fig. 1. As can be seen Ce and La adsorption begins in every case at pH 6 and is maximum at pH 8. For Pr the adsorption begins at pH 5, but the maximum retention is at pH 8. These REE cannot be separated by this method but they can be determined without interferences by preparing a thin film for measurement by x-ray fluorescence spectrometry.

In order to prepare the thin films with the loaded resins, the critical thickness was determined. Results showed that films prepared in this way allowed up to 20 mg of loaded resin (Fig 2).

The presentation of standards to an x-ray spectrometer as thin films permits determination free from interferences. Thus Ce, La and Pr together can be determined by this method, without modifying its line intensities. Under the experimental conditions the only interference detected was on measuring Pr Lα (75.42° 2θ). Because of the La Lβ_1 line (75.27 2θ), the resolution of the LiF 200 dispersing crystal did not allow a separation of these two lines. Therefore, Pr was determined by measuring its Lβ line (68.24° 2θ)

The rare earths not retained on the resins were spectrometrically determined by the Arsenazo I method. These experiments indicated that the adsorption is almost quantitative within 20 min of shaking. Consequently, all data were obtained after a shaking period

Table 2. Detection limits (in ppm) for the determination of Ce, La and Pr retained on each loaded resin

Resin	Ce	La	Pr
Oxine-XAD-4	0 36	0 42	0 71
Oxine-XAD-7	0 47	0 45	1 07
5ClDMPAP-XAD-4	0.47	0 53	0 94
5ClDMPAP-XAD-7	0 42	0 43	1 07

of 30 min to ensure complete equilibrium. Practically 100% retention of each element was obtained.

So, with these working conditions 10 mg of each resin adsorbs almost quantitatively up to 50 ppm of each element studied. Considering that 10 mg of loaded resin occupies 20 mm^3 and 10 ml of the REE solution were agitated with this quantity of resin, the enrichment factor is 500 in every case, which is highly satisfactory if the determination is made by x-ray fluorescence spectrometry.[15]

Synthetic calibration standards of individual rare earths were prepared over a concentration range between 0 and 80 ppm. The correlation found between measured intensity (corrected for background) and the concentration of an element was linear up to 50 ppm (maximum capacity of retention) in every case.

Synthetic samples with different concentrations of Ce, La and Pr were prepared due to the lack of suitable references samples with certified REE contents. In case of having these certified samples, they can be treated following Sen Gupta's procedure,[16] before performing the adsorption of the REEs on the loaded resins. The results for the determination of Ce, La and Pr in each of these samples are shown in Table 1.

The concentration at the detection limit is defined[10] as:

$$C_{DL} = (3/m)\ I_B^{1/2},$$

where:

m: is the slope of the calibration curve

I_B: is background intensity (counts/sec)

and was calculated for each case and presented in Table 2.

CONCLUSIONS

Amberlite XAD-4 and XAD-7 loaded with Oxine and 5ClDMPAP have proved to offer a simple preconcentration technique for determination of trace amounts of Ce, La and Pr by x-ray fluorescence analysis.

Acknowledgements—This work was supported by CONICET and the National University of San Luis

REFERENCES

1 D Ryachikov and V Ryabukhin, *Analytical Chemistry of Yttrium and the Lanthanide Elements*, Ann Arbor, 1970
2. I S Kalmykova and N Uklanova, *Z Anal Khimii*, 1980, **35**, 12, 2320.
3 A Hirose, K Kobori and D Ishii, *Anal Chim Acta*, 1978, **97**, 303
4 J Crock, F Lichte, Riddle G and C Beech, *Talanta*, 1986, **33**, 7, 601
5 I Roelandts, *Anal Chem*, 1981, **53**, 676
6 G Hubbard and T Green, *Anal Chem*, 1966, **38**, 428
7 G Hartmann, H Klenk, H Projahn and K Bächmann, *Z Anal Chem*, 1986, **325**, 105
8 L Chandola and P Khanna, *Mikrochim Acta*, 1985, **3**, 191
9 Z Gregorowicz, H Stec and J Ciba, *Z Anal Chem*, 1981, **307**, 412
10 E. Bertin, *Principles and Practice of X-Ray Spectrometric Analysis*, Plenum Press, New York, 1984
11 S Shibata and M Furukawa, *Bunseki Kagaku*, 1974, **23**, 1412
12 K Isshiki and E Nakayama, *Anal Chem*, 1987, **59**, 291
13 A Masi and R Olsina, in press
14 Z. Marczenko, *Spectrophotometric Determination of Elements*, Wiley, New York, 1976
15 A Mizuike, *Enrichment Techniques for Inorganic Trace Analysis*, Springer-Verlag, Berlin, 1983
16 J G Sen Gupta, *Talanta*, 1976, **23**, 343

Talanta, Vol 40, No 6, pp 935–942, 1993
Printed in Great Britain

0039-9140/93 $6 00 + 0 00

SPECTROSCOPIC STUDIES OF A NEAR-INFRARED ABSORBING pH SENSITIVE AMINODIENONE–CARBOCYANINE DYE SYSTEM

G PATONAY, G. A. CASAY, M. LIPOWSKA and L. STREKOWSKI
Department of Chemistry, Georgia State University, Atlanta, GA 30303, U S A

(*Received* 1 *September* 1992 *Revised* 13 *November* 1992 *Accepted* 15 *November* 1992)

Summary—Synthetic red and near-infrared absorbing dyes may be used as probe molecules in a large number of applications. Dyes exhibiting spectral changes with hydrogen ion concentration are useful as pH probes. Those dyes which have their absorption and fluorescence maxima in the long wavelength region of the visible spectral region are especially valuable because of decreased interference and semiconductor laser applications In this paper we have evaluated an aminodienone dye 1 which demonstrates pH dependent absorption and fluorescence spectra as well as solvent polarity dependence. In organic solvents the long wavelength absorption band of the dye is in the reduced interference region The absorption maximum is at 535 nm in neutral or alkaline solutions in methanol The absorption spectra undergo a strong bathochromic shift in the presence of acids (λ_{max} = 709 nm) with a concomitant change in the fluorescence spectra This pH sensitive dye was found to be especially useful for organic solvents The analytical utility of this and similar near-infrared absorbing dyes is discussed

The determination of hydrogen ion concentration (pH) is an important part of many analytical procedures. In previous years numerous dyes have been studied as to their potential for use as acid/base indicators. Sometimes only the color change is utilized, but more sophisticated methods use absorption or fluorescence spectroscopy. A large number of available weak organic acids and bases exhibit different absorption/fluorescence spectra or colors when in undissociated and ionic forms. The color changes or variations in absorption and fluorescence spectra are usually associated with the alteration in the degree of conjugation upon ionization of the functional groups present in the indicator molecule. The pH region of utility is usually determined by the pK_a of the indicator molecule.

Peterson was the first to report the use of an indicator that related the change in the absorption spectra to pH.[3] Seitz used a pH indicator based on changes in the fluorescence spectra of fluoresceinamine.[4] Fluorescence has become the preferred method because of its selectivity and sensitivity. Selectivity arises from the fact that not all chromophores that absorb will fluoresce, which is especially true in the NIR region where only a few classes of compound exhibit fluorescence. The use of fluorescent dyes as pH indicators, mostly azo or fluorescein derivatives, is well documented in the literature.[5–10] Applications include analysis of blood,[5] spinal cord tissue,[6] brain pH[7] and more.[8–10]

The utility of the indicator is often greatly enhanced if the pH change has a large effect on the fluorescence quantum yield of the indicator. Fluorescent indicators can be especially valuable in determining the pH of samples which have significant absorbance. In particular, the near-infrared spectral region of the electromagnetic spectrum has proven to be useful in the characterization of biological samples. The long wavelength red and short-wave near-infrared spectral region of 650–1000 nm exhibits minimal interference from biological matter. This attractive feature of the spectral region has intensified interest in development of new probe molecules. The analytical applications related to NIR absorbing chromophores have increased dramatically during the last few years. The use of semiconductor lasers as light sources further enhances the advantages of this spectral region.

The absorption and fluorescence properties of many pH sensitive indicators have been investigated in the past, including their use as fiber optic probes. Most of these dyes are weak acids or bases with ionizable functions such as carboxylic acid, phenol or amine. The appropriate pH indicator dye must have pH sensitive functional groups that reversibly change from the ionized to the non-ionized form with a

concomitant change in the degree of conjugation of the double bonds in the molecule as the hydrogen ion concentration changes. The use of pH indicators that are suitable for tissue and blood pH measurements in the physiological range has become of interest since their first application in the late 1970s.[1-4]

The chemistry of pH sensitive molecules has been of immense interest. One group of fluorescent dyes, however, that has not been fully investigated as pH indicators is the aminoenones.[11,12] Junek reported in 1973 the synthesis and properties of dialkyl aminomethylene substituted tetralones, indanediones and indanones.[11] In the following year he reported these dyes as a new group of pH indicators.[12] Nevertheless, few reports have addressed the use of aminoenone indicators that can be useful in the physiological range.[13,14]

We report here the spectral characteristics and the pH dependence of a new symmetrical aminodienone dye system **1** in methanol and in a series of organic solvents. The data presented reveal dramatic effects of protonation of the dye on its spectral characteristics. The dye is stable in alcohols under acidic and basic conditions and the dye spectra are dependent on the solution pH. Also, the dye exhibits high spectral sensitivity to the presence of protons in aprotic organic solvents.

EXPERIMENTAL

Reagent and chemicals

The chemical structure of the pH sensitive dye, 2,6-Bis[2′-(1″-ethyl-3″,3″-dimethylindolin-2″-ylidene)ethylidene]cyclohexanone (**1**, $C_{34}H_{40}ON_2$, MW = 492.68) used in this study, is shown in Fig. 1. We recently presented an efficient synthesis of **1** and its purification.[15] A sample of **1** used in this work was homogenous by TLC on silica gel with several mobile phases, gave good microanalytical results (C, H, N), and its 400 MHz proton NMR spectrum was fully consistent with the high purity of the dye.

For the experiments, spectrophotometric grade methanol was obtained from Baker Chemical Co. Isopropyl alcohol, dimethyl sulfoxide, dichloromethane, tetrahydrofuran, acetonitrile, hydrochloric acid, sodium hydroxide and buffer components were obtained from Fisher Scientific Co. The absorbance data were determined by using a disposable PS cuvette (Fisherbrand). The fluorescence intensity was determined in a quartz cuvette (Fisherbrand).

Method

Stock solutions of the dye (10^{-3} M) were prepared in spectrophotometric grade methanol, isopropanol and DMSO (Baker analyzed). For the pH studies, small amounts of stock solution were diluted to arrive at the desired concentrations for absorbance and fluorescence measurements. Since the dye is less soluble in water, the aqueous solutions were prepared by dissolving the dye in methanol and then diluting with water to obtain dye solutions in a methanol/water (1:9) mixture. No spectral differences were observed in the presence of up to 10% methanol.

Dye **1** is stable in methanol/water at room temperature for 24 hr. If kept in the dark at −20°C the dye solutions are stable for up to 20 days; however, they would turn orange if exposed to excessive sunlight. Dye **1** is stable in acetonitrile for 10 days, but undergoes slow

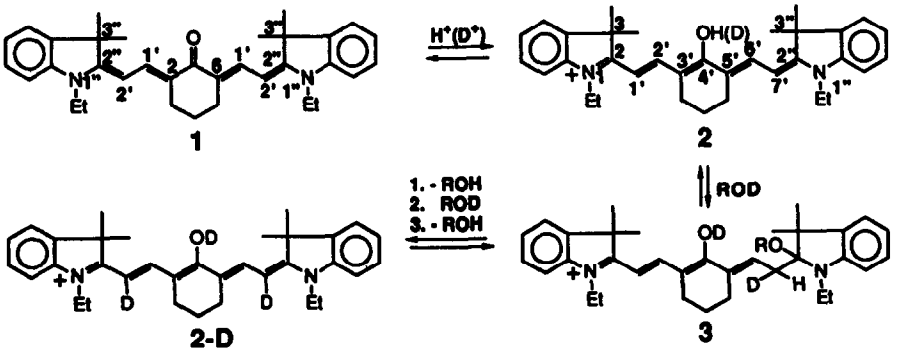

Fig. 1 Structures of a neutral form of the pH sensitive dye **1** and its protonated form **2**. A suggested mechanism for the selective hydrogen–deuterium exchange in positions 1′ and 7′ of the dye under acidic conditions is also shown. Note different numbering schemes for the disubstituted cyclohexanone derivative **1** and the cyanine dye **2**, as required by chemical names of these systems

decomposition in dimethyl sulfoxide, even in the dark. Accordingly, fresh working solutions were prepared for each experiment.

The solution pH was varied by slowly adding small amounts of hydrochloric acid or sodium hydroxide in a methanol–water mixture. The absorption spectra of the dye were taken before and after the pH measurements to examine the stability of the dye. The visual transition of color from basic (pink) to acid conditions (green) occurred at pH 3.0. Buffer solutions were used to calibrate the pH glass electrode (Fisher Scientific).

Instrumentation

Solution pH was determined by using an Orion Research Model 701A digital ionalyzer. A Perkin–Elmer Lambda 2 UV/Vis/near-IR spectrophotometer interfaced to a Zenith 286 PC was used to obtain absorption measurements. The PECSS program supplied with the instrument was used to analyze, store and retrieve data. An SLM 8000 spectrafluorometer interfaced to a PS/2 IBM PC was used for fluorescence measurements, and the fluorescence spectra were stored on floppy disks for later analysis. The pK_a values were determined using a Schott Geraete Model 250 autotitrator and model T90/10 autoburet interfaced to a PC.

RESULTS AND DISCUSSION

Absorbance

Representative absorption spectra of the pH sensitive dye **1** in methanol under acidic and basic conditions are shown in Fig. 2. Under basic conditions (dark pink solution), the dye is in a ketone form and shows a broad absorbance band with a maximum at 531 nm (Fig. 2B). The intensity of the 531 nm peak decreases with decreasing pH. At around pH 3 the dye solution turns a pale pink color. As the pH of the dye solution is decreased further, the color becomes pale green with the concomitant appearance of a narrow peak with a maximum absorbance at 709 nm (Fig. 2A). The intensity of the peak at 709 nm increases as the solution pH is lowered further while the color of the dye solution turns dark green. The change in the absorption spectra is attributed to the protonation of the oxygen atom to yield a cationic enol from **2** (Fig. 1). The formation of the enol function at the polymethine chain results in the development of a longer conjugated system. More specifically, the protonation results in the formation of a cationic cyanine dye systems **2**. This structural change is responsible for the observed, large bathochromic shift. It is known from the chemistry of the polymethine cyanine dyes that the two major determining factors in the absorption maximum wavelength are the extent of conjugation and presence of a quaternary nitrogen in the heterocyclic moiety. Those dyes that have no quaternary nitrogen, commonly referred to as dye bases, have much lower absorption wavelength maxima than a similar molecule with quaternary nitrogen in the heterocyclic terminus. The absorption of the cationic form **2** is typical for a heptamethine cyanine dye system.[16]

Two forms of the dye, thus, are an aminodienone **1** and a cationic heptamethine cyanine system **2**. The symmetrical cationic species **2** is the predominating form under acidic conditions. Dye **1** is more stable in acid conditions than in basic conditions, including light sensitivity. Under basic conditions the molecule undergoes deprotonation to form the neutral aminodienone **1**. The dye can be converted back and forth between the two forms simply by adjusting the solution pH, and these changes are fully reversible.

The dye is sparingly soluble in pure aqueous solutions; however, in the presence of a small amount of alcohol, the dye becomes soluble and it is stable in such a solvent system. The spectral behavior of the dye is markedly different in aqueous media. Under acidic conditions a broad absorbance peak with a maximum at 423 nm can be observed, while under basic conditions a very broad peak with a maximum absorbance of 484 nm is present. The molar absorptivity measured at pH 6 and pH 2, respectively, and other spectral properties of the dye are tabulated in Table 1. The different

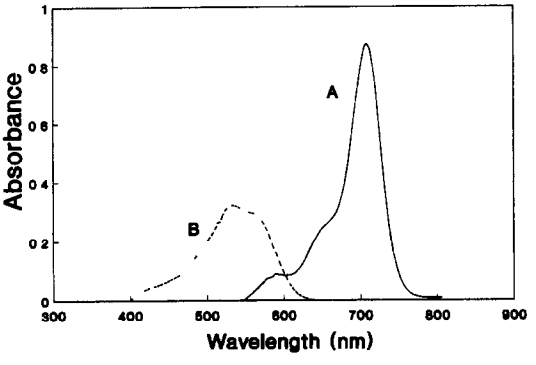

Fig 2 Absorbance spectra for the pH sensitive dye 1 in methanol under acidic (A), pH 2 (——) and basic (B), pH 6.5 (····) conditions

Table 1 Absorbance for 1

	Absorbance					
	Methanol		Water*		Isopropanol	
pH	λ (nm)	ϵ (l mol^{-1} cm^{-1})	λ (nm)	ϵ (l mol^{-1} cm^{-1})	λ (nm)	ϵ (l mol^{-1} cm^{-1})
Acidic	709	2 082E + 5	425	2.651E + 4	709	1 537E + 5
Basic	535	7 760E + 4	484	3 438E + 4	520	6 218E + 4

*10% Methanol/90% water

spectral behavior in aqueous systems might be attributed to two factors, namely, dimerization or higher order aggregation of the molecules in a less hydrophobic environment and covalent hydration of the dye system or dye aggregate under acidic conditions (Fig. 1). However, the absorbance spectra of dye **1** at concentrations $\leqslant 10^{-8}M$ showed no dimerization effect.

The hydration would result in shortening of the dye chromophore with a concomitant blue shift in the absorption spectra, as observed. This blue shift would be especially large for hydration of the cationic form **2**, due to a facile nucleophilic addition reaction with the polyunsaturated cationic chromophore.[15,16] The changes between the aqueous and organic solutions are fully reversible, however. After the aqueous solution of **1** was extracted with dichloromethane, the spectra of the organic extract taken under different pH conditions exhibited the same behavior as the spectra of a freshly prepared solution of **1** in dichloromethane. The same results were obtained with the extracts from alkaline and acidic solutions.

The addition reaction of water to position 2(2″) of the indoline of dye **2** to give an adduct **3** (R = H) can be suggested (Fig. 1). Absorption maximum around 400 nm was estimated[17,18] for **3**, which is in reasonable agreement with the experimental value of 423 nm. With methanol the equilibrium **2** + $CH_3OH \rightleftarrows$ **3** must favor the substrate **2** because the increased steric hindrance destabilizes the adduct **3** (R = Me) in comparison to its hydroxy analog (R = H). As a result, the absorption maximum of **2** in methanol is shifted to longer wavelengths relative to the absorption in aqueous media.

Strong experimental support for the suggested addition reactions was obtained from proton NMR studies. The spectrum of **1** taken in deuterochloroform exhibited a characteristic AB pattern for H1′ and H2′ at δ 5.46 and 8.17, respectively, with a coupling constant of 13.2 Hz.[15] Upon acidification of the 1 ml sample solution in the NMR tube with 2 equivalents of HCl in 0.05 ml of methanol, a similar absorption pattern was observed at δ 8.58 and 5.79, provided the spectrum was obtained immediately following acidification of the sample. The deshielding effect is attributed to the formation of cation **2**. With deuterium chloride instead of HCl a highly selective deuteration at positions 1′ and 7′ was observed to give **2-D** (note a different numbering scheme for this compound), as evidenced by the appearance of a singlet for H2′ (6′) at δ 8.58 and lack of absorption at δ 5.79. This fast deuteration was complete within 5 min, a minimum time period necessary for obtaining the NMR spectrum. No additional changes in integration of the spectral signals were observed after the sample had been allowed to stand at 23°C for 24 hr. The facility of this acid-catalyzed hydrogen–deuterium exchange was further stressed by the isolation of non-deuterated **1** after the sample of **2-D** had been treated with silica gel, a weak acid. These results are fully consistent with the proposed mechanism (Fig. 1) in which the adduct **3** is an intermediate product for **2-D.**

The NMR signals of the samples discussed above were gradually broadened with time, and no further broadening was observed after 1 hr after the addition of acid in methanol-d_4 to the solutions in deuteriochloroform. The period of time required to reach the final line shapes at 23°C decreased with increased amount of methanol-d_4 in the solution and was 15 min for pure methanol-d_4 in the presence of 2 equivalents of acid. Unfortunately the NMR spectra in aqueous acidic methanol-d_4 could not be obtained due to low solubility of the dye under these conditions. Interestingly, the neutral dye **1** gave sharp NMR signals regardless of the concentration, time, and solvent composition.

The NMR signal broadening is indicative of a relatively slow aggregation of the hydrophobic dye molecules in a hydrophilic environment, a typical property of most carbocyanine dyes.[19] It should be noted that in all cases dye **1** was isolated quantitatively from solutions used for NMR studies.[19]

In aqueous or methanol environment, under the influence of atmospheric oxygen, especially in the presence of intense sunlight, the dye decomposes and a color change can be observed with the absorption maximum changes from 535 nm (pink) in methanol (or 484 nm in aqueous solutions) to 445 nm (orange) in 25 min. The absorbance spectra of the dye in a 50% (v/v) methanol–water solution is shown in Fig. 3. This type of light sensitivity is typical for several members of the carbocyanine dye family and can be attributed to the reaction of the molecular oxygen with the conjugated system in the presence of short wavelength radiation. Accordingly, special care was taken not to expose our solutions to excessive sunlight during experiments.

In isopropanol the dye showed properties similar those in methanol. Under basic conditions the dye gave an absorbance peak at 520 nm which is only slightly lower than the absorbance shown in methanol. In acid conditions the dye showed an absorbance band at 709 nm. These results are in good agreement with the general observation about carbocyanine dyes that alcohols are usually good solvent systems for studying electronic spectroscopic properties of cyanine dyes and there is very little variation from alcohol to alcohol

The absorption properties of the dye were also examined in dichloromethane and tetrahydrofuran. When the solution was made acidic with the addition of acetic acid, a narrow peak with an absorption maximum at 709 nm was observed. This result is consistent with the formation of a cationic dye system **2**. The intensity of this absorption increased with increased acetic acid concentration in both solvents.

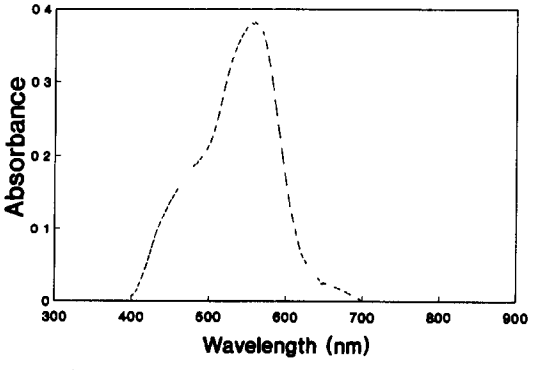

Fig. 3 Absorbance spectra for the pH sensitive dye **1** in a 50% methanol–water solution

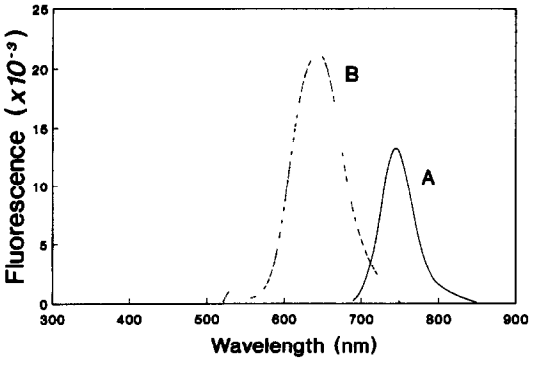

Fig 4 Fluorescence for the pH sensitive dye **1** in methanol under acidic (A), pH 2 (——) and basic (B), pH 6 5 ( ) conditions

Fluorescence

Changes in the fluorescence spectra of dye **1** in methanol were studied under acidic and basic conditions. The representative spectra under basic conditions, shown in Fig. 4(B), exhibited a broad peak with a maximum emission at 606 nm ($\lambda_{EX} = 534$ nm). The spectra under acidic conditions with an emission maxima at 743 nm, ($\lambda_{EX} = 709$ nm) is shown in Fig. 4(A). As can be seen, the emission spectra are determined by the solution pH. A plot of fluorescence intensity as a function of solution pH is shown in Fig. 5. The fluorescence emission was monitored at a constant wavelength of $\lambda_{EM} = 620$ nm ($\lambda_{EX} = 530$ nm) for the basic peak (Fig. 5B) and at $\lambda_{EM} = 740$ nm ($\lambda_{EX} = 709$ nm) for the acidic peak (Fig. 5A). The fluorescence emission intensity for dye **1** in the cationic enol form is not as intense as in the ketone form.

The fluorescence properties of the dye were found to be different in aqueous solutions compared to alcohols. Under basic conditions, the

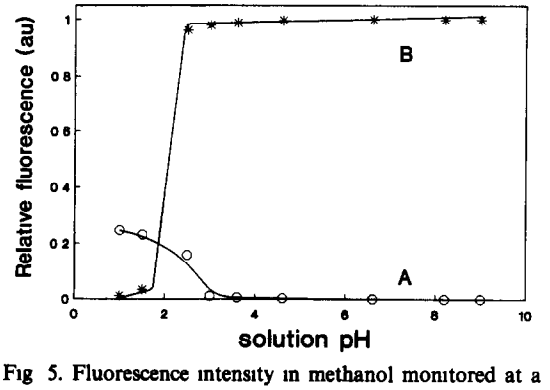

Fig 5. Fluorescence intensity in methanol monitored at a constant wavelength of $\lambda_{EM} = 620$ nm ($\lambda_{EX} = 530$ nm) for the basic peak (B) and at $\lambda_{EM} = 740$ nm ($\lambda_{EX} = 709$ nm) for the acidic peak (A)

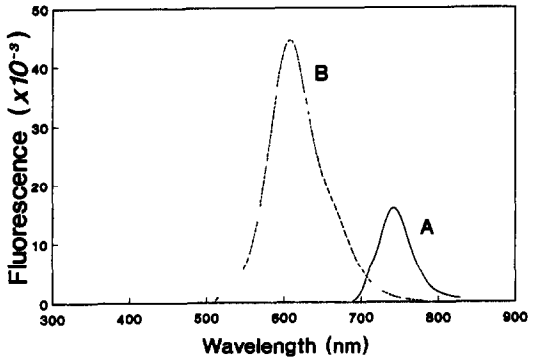

Fig. 6 Fluorescence for the pH sensitive dye 1 in isopropanol under acidic (A), pH 2 (——) and basic (B), pH 6 ( ) conditions

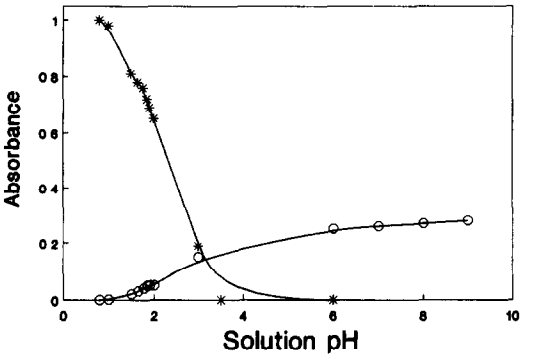

Fig 7 The pH dependence of the visible and NIR absorption peaks for dye 1 in methanol

dye showed a weak emission at $\lambda_{EX} = 495$ nm ($\lambda_{EX} = 425$ nm) while in the presence of acid a weak emission at $\lambda_{EM} = 660$ nm ($\lambda_{EM} = 545$ nm) could be observed. The solvent hydrophobicity dependence of fluorescence spectra was also studied using different methanol–water mixtures. The fluorescence intensity was the highest at high methanol concentrations indicating higher fluorescence quantum yield in alcohols (up to 100-fold). No significant change in the fluorescence intensity was observed up to 10% water concentration. The fluorescence intensity decreased at higher water concentrations; the fluorescence quantum yield was very low above water concentrations higher than 70% in methanol (v/v).

The fluorescence emission maximum of dye 1 in isopropanol was at 741 nm ($\lambda_{EX} = 709$ nm) under acidic conditions (Fig. 6A), while under basic conditions fluorescence maximum was at 606 nm (Fig. 6B). The dye fluorescence was also studied in dimethyl sulfoxide, acetonitrile and dichloromethane, and the results are shown in Table 2. These data indicate that the fluorescence spectra of this NIR dye are strongly dependent on the hydrophobicity of the solvent.

pK_a

The pK_a value for the dye was measured in 50%/50% water–methanol mixture with an automated titrator using NaOH dissolved in 50%/50% water–methanol mixture. The titration curves were analyzed with first and second order derivatives and only one pK_a was observed for the solution at 6.91. This value indicates that protonation is not the only factor that brings about changes in the absorption and fluorescence spectra of the dye with changing pH. When Figs 5 and 7 are compared to the pK_a value of the dye we can see that there is very little effect due to excited state deprotonation. Solvent effect may be the dominating factor as evidenced by spectral dependence on hydrophobicity. One possible explanation is the effect of pH on the dye aggregation.

Dye 1 as pH probe in organic solvents

The data presented here indicate that the dye is suitable as a pH probe in organic solvent medium. The advantages of this dye over other pH probes are a significant change in color and a relatively long absorption wavelength of the principal absorption band. Both the visible or the NIR bands can be used for determining the

Table 2. Fluorescence for 1

	Solution pH conditions					
	Acidic*			Pure solvent†		
	λ_{EX} (nm)	λ_{EM} (nm)	Int (E + 04)	λ_{EX} (nm)	λ_{EM} (nm)	Int (E + 04)
Methanol	709	744	1 28	520	606	4 54
Water	545	660	0 0353	425	495	0.0250
Isopropanol	709	742	1 7	520	606	4 5
Acetonitrile				505	571	1 1
Dichloromethane				469	544	0 0578
Dimethyl sulfoxide				515	574	2 6

*HCl

†λ_{EX} correspond to the absorbance maximum measured in the pure solvent

pH of the environment around the dye molecule. Figure 7 can be used as a calibration curve for determining pH using the NIR absorption peak. Figure 7 (circles) indicates that this peak is not present in the dye spectra in basic solutions. In basic solutions, however, the visible absorption appears and the intensity of the peak increases with increasing basicity of the solution and levels off at pH 6–7. The appearance of this shorter wavelength absorption peak corresponds to a decrease in the NIR absorption peak (Fig. 2A), clearly indicating the removal of the positive charge from the dye molecule. The dye base ketone which forms during this process has significantly lower absorption wavelength and blue shifted absorption maximum. The hypsochromic shift in absorption maximum is a result of two effects, less extensive conjugation and lack of positive charge in the chromophore. The combination of these two effects results in a significant spectral shift, which may be very advantageous when observing pH change. This large spectral shift and the pH range of spectral change indicate that additional processes have an influence on the dye spectral behavior. Further studies are under way to fully characterize this process.

Dye 1 as hydrophobicity probe

The NIR dye **1** also exhibits spectral changes as the hydrophobicity of the solvent is changed. The utility of this application was demonstrated for the determination of water content in alcohols. Most likely the observed change in the absorption spectra with changing water concentration is a result of dimer formation. The dimerization property of carbocyanine dyes has been documented in the literature.[19] As the water concentration increases, the carbocyanines tend to form dimers or higher aggregates because of the strong dispersion forces associated with the high polarizability of the polymethine chain. However, in most cases, the dimer or higher aggregate band is not too well resolved from the monomer band, hindering the application. The utility of our NIR dye as a hydrophobicity probe is illustrated in Fig. 8. It shows a typical calibration curve obtained using the NIR pH sensitive probe as a hydrophobicity probe using a methanol–water mixture as the model solvent. It is important to point out, however, that the researcher must make sure that the two effects, pH and hydrophobicity, do not interfere.

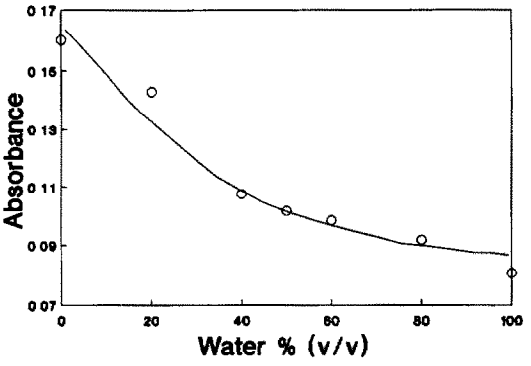

Fig 8 Typical calibration curve for determining water concentration in methanol by using dye **1** as a probe.

CONCLUSIONS

In summary, the NIR absorbing carbocyanine dye discussed in this paper can be valuable in determining analytical properties. The data presented illustrate the utility of this dye for determining pH and solvent hydrophobicity. The well separated absorption peaks of the protonated and non-protonated forms of the dye further enhance the analytical utility of this probe molecule. The dye is an especially useful probe organic solvents, e.g alcohols for the determination of pH. We are currently synthesizing and investigating similar NIR dyes for other probe and labeling applications. As a result of these studies the design of new, improved NIR absorbing probes may be available.

Acknowledgements—This work was supported in part by grants from the National Science Foundation (CHE-890456 and CHE-8409599) and the National Institutes of Health (AI-28903) Acknowledgement is also made to the donors of the Petroleum Research Fund, administered by the American Chemical Society, for partial support of this research

REFERENCES

1 L A Saari and W R. Seitz, *Anal Chem*, 1982, **54**, 823–824
2 J I Peterson and G G Vurek, *Science*, 1984, **224**, 123–128
3. J I Peterson, S R. Goldstein, R V Fitzgerald and D K Buckhold, *Anal. Chem.*, 1980, **52**, 864–868
4. W R. Seitz, *Anal Chem*, 1984, **56**, 16A
5 D. W. Luebbers and N Opitz, *Anal. Chem Symp Ser*, 1983, **17**, 609–619
6 S C Delheimer, R. E. Anderson and T M Sundt, *J Neurochem*, 1980, **31**, 1514–1519
7 T M Sundt, R E Anderson and R A Van Dyke, *J Neurochem.*, 1978, **31**, 627–635
8 R Pal, W. A. Petri, Y Barenholz and R R Wagner, *Biochim. Biophys. Acta.*, 1983, **729**, 185–192
9. L. Brown, P I. Halling, G A. Johnston and C. J. Suckling, *Tetrahedron Lett.*, 1990, **31**, 5799–5802
10. C G. Knight and A. Matthews, *Biochim Biophys Acta*, 1989, **985**, 75–80

11 H. Junek and W Remp, *Monatsh Chem*, 1973, **104**, 433–446
12. P Ollinger, W Remp and H Junek, *Monatsh Chem*, 1974, **105**, 346–353
13 A. E Boyer, M Lipowska, J -M Zen and G. Patonay, *Analyt Lett*, 1992, **25**, 415–428
14 S H. Makin, L I Boiko and O A Shavnygino, *Zh Org Khim*, 1977, **13**, 1189–1194
15 L Strekowski, M Lipowska and G. Patonay, *Synth Commun.*, 1992, **22**, 2593–2598
16 L Strekowski, M. Lipowska and G. Patonay, *J Org. Chem*, 1992, **57**, 4578–4580
17 A. G Cook, in *Enamines· Synthesis, Structure and Reactions* A G Cook (ed.), 2nd Ed, p 66 Marcel Dekker, New York, 1988.
18 P W. Hickmott, B. J Hopkins and C T Yoxall, *J Chem Soc (B)*, 1971, 205–211
19 G Patonay, M D Antoine, S. Devanathan and L. Strekowski, *Appl Spectrosc*, 1991, **45**, 457–461

Talanta, Vol 40, No 6, pp 943–948, 1993
Printed in Great Britain

0039-9140/93 $6 00 + 0 00

ELECTROCATALYSIS AND DETERMINATION OF HYDRAZINE COMPOUNDS IN LIQUID CHROMATOGRAPHY AT A MIXED-VALENT COBALT OXIDE/CYANOCOBALTATE FILM ELECTRODE

JIANXUN ZHOU and ERKANG WANG*

Laboratory of Electroanalytical Chemistry, Changchun Institute of Applied Chemistry, Chinese Academy of Sciences, Changchun, Jilin 130022, P R China

(*Received* 30 *July* 1992 *Revised* 5 *November* 1992 *Accepted* 8 *November* 1992)

Summary—A glassy carbon electrode coated with an electrodeposited film of mixed-valent cobalt oxide/cyanocobaltate (Co–O/CN–Co) enabled hydrazine compounds to be catalytically oxidized at the greatly reduced overpotential and in a wide operational pH range (pH 2.0–7 0) Electrocatalytic activity at the Co–O/CN–Co modified electrode was evaluated with respect to solution pH, film thickness, supporting electrolyte ions, potential scan rate, operating potential, concentration dependence and other variables The Co–O/CN–Co film electrode was completely compatible with a conventional reversed-phase liquid chromatographic (RP-LC) system. Practical RP-LC amperometric detection (RP-LCEC) of hydrazines was performed. A dynamic linear response range over three orders of magnitude and a detection limit at the pmol level were readily obtained The Co–O/CN–CO film electrode exhibited excellent electrocatalytic stability in the flowing streams

Liquid chromatography (LC) with amperometric and voltammetric detection (EC) represents a powerful tool for sensing and monitoring easily oxidizable species with high sensitivity and excellent selectivity. Unfortunately, hydrazine compounds which are of industrial and environmental significance exhibit such a large overpotential toward electrooxidation at ordinary carbon surfaces that they are not ideally suited for the quantitation with conventional LCEC approaches. Previous efforts toward enhancing the amperometric detection of hydrazines include the application of a preanodized glassy carbon electrode,[1] which enabled the hydrazines to be monitored at a modest positive potential (+0.50 V *vs.* Ag/AgCl). Chemically modified electrodes (CMEs) offer a promising approach for minimizing the overpotential effects, and various CMEs have been constructed and applied in LCEC of hydrazine sensing. These include cobalt phthalocyanine (CoPC) modified carbon paste electrodes,[2,3] a cobalt tetraphenylporphyrin modified electrode with heat treatment (HCME)[4] and an oxymanganese film modified electrode (MnCME).[5] In particular, intense research has been devoted recently to the preparation and characterization of mixed-valent inorganic catalytic centers,[6–20] of which the major advantages are the efficient electrocatalysis and inherent stability as needed for practical analysis; and various inorganic surface matrices based on mixed metal–hexacyano complexes, Prussian Blue (PB) and its analogues, have been successfully constructed and applied in electrocatalysis and determination of organic and inorganic species with LC amperometric detection. A Prussian Blue (PB) [iron (III) hexacyanoferrate (II)] film[6] and a mixed-valent ruthenium cyanide film[7] modified electrode have recently been prepared and used in flow injection amperometric detection of hydrazines. A PB filmed electrode has also recently been prepared and used in flow catalytically amperometric detection of sulfhydryl compounds (cysteine, *N*-acetylcysteine and glutathione),[8] upon which the catalytic reduction of dioxygen,[9] hydrogen peroxide,[9] CO,[10,11] hexacyanoferrate (III), iron (III) and $IrCl_6^{2-}$,[12] and the catalytic oxidation of ascorbic acid[13] have been previously reported. Nickel (II) hexacyanoferrate film modified electrodes have been devised and used in catalytic oxidation of reduced nicotinamide adenine dinucleotide (NADH) and the catalytic reduction of iron (III) in both batch and flow systems.[14–16]

*Author for correspondence.

Mixed-valent ruthenium cyanide film electrodes have been made and applied in the electrocatalysis and determination of As (III),[17] thiocyanate,[18] insulin,[19] cysteine and glutathione.[20]

In practical LCEC, the compatibility between the LC separation system and the EC detection unit is of great importance; and the media pH is the most crucial factor. Several of the above CMEs prepared, though successfully applied in flow-system detection of hydrazines, are limited to a relatively narrow operational pH range, or have not been broadly tested. Some of them[2,3,5] are limited to basic solution, and some others[4,6] to acidic media, making these CMEs of restricted use with conventional reversed-phase LC systems. The demonstration of a highly stable electrocatalytic surface with a broad operational pH range is therefore desirable for LCEC measurements of hydrazines.

The present work demonstrates that a glassy carbon electrode coated with an electrodeposited film of mixed-valent cobalt oxide/cyanocobaltate (Co–O/CN–Co), an analogue of Prussian Blue, enables the electrooxidation of hydrazines to proceed effectively at significantly low potential and in a wide pH range. The stable modified surface maintains long-term catalytic activity and is highly suitable for reversed-phase LCEC of the analytes. Features are characterized regarding several variables.

EXPERIMENTAL

Reagents and apparatus

Analytical reagent hydrazine sulfate (HZ) was from the Beijing Institute of Chemicals, and methylhydrazine (MHZ) and 1,2-dimethylhydrazine (DMHZ) were obtained from Merck. Stock solutions (0.1*M*) were prepared with doubly distilled water, and stored at 4°C in the dark. Standard working solutions in flow analysis were obtained by serial dilution of these stock solutions with the mobile phase used. $CoCl_2$ and $K_2Fe(CN)_6$ of analytical grade (Beijing Chem. Corp.), together with hydrazines, were used as received. All other reagents were of analytical grade; doubly distilled water was used for the preparation of all the solutions.

The chromatographic system consisted of a Model 510 pump, and a U6K injection valve. The analytical column was uBondapak C_{18} (5μm)250 × 4 mm i.d. (Waters Assoc., U.S.A.). The electrochemical detector was a BAS TL-5A thin-layer cell, with the potential monitored by a laboratory—made bipotentiostat.

Cyclic voltammetric experiments were performed with a laboratory-made potentiostat in a conventional three-electrode system cell, using a glassy carbon disk working electrode (with an area of 12 mm^2) in conjunction with a Ag/AgCl reference electrode and a platinum wire counter electrode.

Procedures

Prior to its modification, the glassy carbon (GC) electrode surface was polished with 0.05 μm α-alumina suspension, rinsed with water and ultrasonicated in an ethanol and a water bath, alternately, each for 2 min. The electrode was placed in a freshly prepared 2 m*M* $CoCl_2$/2 m*M* $K_3Fe(CN)_6$ solution in 0.5*M* KCl containing 10 m*M* HCl and subjected to potential sweep between −0.4 and 1.0 V at 50 mV/sec for 30 min (terminated at 0.0 V). The electrode was then removed from the solution and flushed with doubly distilled water; and a dark green film was clearly visible on the electrode surface. The modified electrode was scanned in 0.5*M* KCl (pH 4.0, adjusted with HCl) between −0.4 and 1.0 V at 50 mV/sec for several cycles until a steady-state current–voltage profile was observed.

RESULTS AND DISCUSSION

Electrocatalysis in a conventional cell

Figure 1A shows cyclic voltammograms of the Co–O/CN-Co film electrode in the solution of 0.5*M* KCl at pH 4.0. The Co–O/CN–Co film underwent a well-defined two-step oxidation at

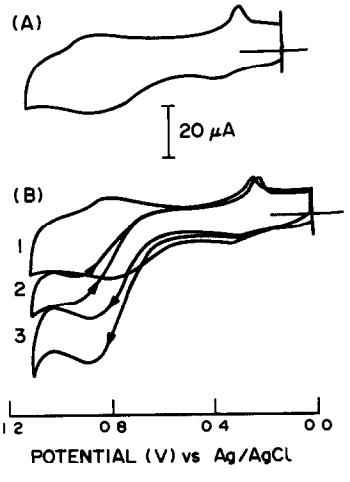

Fig 1 Cyclic voltammograms of Co–O/CN–Co film electrode in 0.5*M* KCl (pH 4 0) without [curve A and B(1)] and with the addition of 1 m*M* [curve B(2)] and 2 m*M* [curve V(3)] hydrazine Scan rate, 50 mV/sec

potentials of 0.34 and 0.85 V, respectively; and the oxidized film showed two-step reduction at potentials of 0.85 and 0.26 V.

So far, few studies have been reported concerning the formation of $Co^{2+}/Fe(CN)_6^{3-,4-}$ complexes, especially on a glassy carbon substrate which is commonly available in commercial electrochemical detectors. From previous literature,[21-25] there seems to be two possible mechanisms for the film formation of Co analogue to PB. Neff[21,22] and Itaya[23,24] suggested that PB and its analogues were formed mainly by the electrostatic interaction of the transition metal cations [Fe(II/III), Ru(III/IV), *etc.*] with the negatively charged $Fe(CN)_6^{3-,4-}$ to produce sparingly soluble mixed-valent metal deposits. Typical systems investigated include PB and Ruthenium Purple. Kulesza[25] has showed that a Ru analogue was converted to a mixed-valent Ru (III, IV) oxide crosslinked by cyanide during the modification procedure in 1:1(m*M*/m*M*) $RuCl_3$:$K_4Ru(CN)_6$, 0.5*M* KCl at pH 2. Surface measurements with X-ray photoelectron spectra (XPS) are helpful for the investigation of the mechanism concerning the film formation.

During the modification procedure, a gray–brown precipitate was readily formed in the $CoCl_2/K_3Fe(CN)_6$ mixture. A modified electrode was prepared, dispersed with the precipitate which had been treated with preliminary steps including filtering, rinsing with distilled water and air-drying, using the approach proposed by Dong and Kuwana[26] by rotating the GC surface under slight hand pressure over the slurry of the precipitate on a polishing paper. The voltammetric response of the resulting modified electrode was examined and was found to be virtually identical to that shown in Fig. 1A. It is plausible to hypothesize that Co analogue deposits formed on the electrode surface and in the solution are basically the same. Subsequently the solution-forming precipitate was applied to XPS measurements. XPS measurements were performed with a ESCALAB-MK II electron spectrometer (VG Scientific Limited, U.K.). A 20 mA at 14 KV $Al_{K\alpha}$ beam was used for excitation. XPS gave Co, O, C, N and K peaks, indicating that a CN group must be present in the coating. The absence of a Cl peak suggests that Cl^- did not play a significant role in the film formation, although it was present at a level of 0.5*M* in the solution for electrodeposition. Semi-quantitative analysis gave the approximate ratios of the atomic concentration: Co:O:CN as 1:7:10. These studies suggest that electrode coating was formed largely through the formation of mixed-valent Co oxo-bridges crosslinked by cyanide produced by the decomposition of $Fe(CN)_6^{3-}$, which is consolidated by the absence of an XPS Fe peak at Eb around 710–720 eV (not shown). The modified electrode surface can thus be best expressed as Co–O/CN–Co.

The anodic and cathodic peak currents increased linearly with potential scan rate up to 400 mV/sec, indicating essentially the surface behavior of the film electrode as in the case of PB and its analogues modified surfaces. The Co–O/CN–Co coating on the glassy carbon substrate was very stable in a wide pH range (2.0–7.0). For example, no obvious change was observed in the CVs at the modified electrode during at least a 1 hr period of continuous potential scanning between 0.0 and 1.0 V at 50 mV/sec in 0.5*M* KCl solution, corresponding to 90 cycles.

Figure 1B shows cyclic voltammograms of the Co–O/CN–Co film electrode in 0.5*M* KCl (pH 4.0) in the absence (curve 1) and in the presence of 1.0 m*M* (curve 2) and 2.0 m*M* (curve 3) hydrazine. Upon the addition of hydrazine, the anodic peak current of the second redox couple (at 0.85 V) increased, in proportion to the analyte concentration, and the corresponding cathodic wave disappeared. Such behavior is exactly what would be expected for an electrocatalytic CME oxidation.

The electrocatalytic capability of the Co–O/CN–Co film electrode toward MHZ and DMHZ was also determined and is shown in Fig. 2 (curves 2 and 3). An increased anodic and a decreased cathodic peak current were observed on CVs of the redox pair at 0.85 V with the addition of 2 m*M* MHZ (curve 2) and DMHZ (curve 3). The catalytic oxidation peak potential shifted negatively compared with that of the surface wave on the film electrode (from 0.85 to 0.80 and 0.65 for MHZ and DMHZ, respectively). The interaction of the analytes with the Co–O/CN–Co film may account for the peak potential variations. These analytes can not be effectively oxidized at the bare GC surface up to 1.2 V, as also illustrated in Fig 2 (dotted line).

Cyclic voltammetric experiments also provided other useful items of information preliminary to LCEC detection. First, there is no marked effect of media pH on either the peak potential (Fig. 3C, curve a) or the peak current (curve b) for catalytic oxidation of hydrazine at

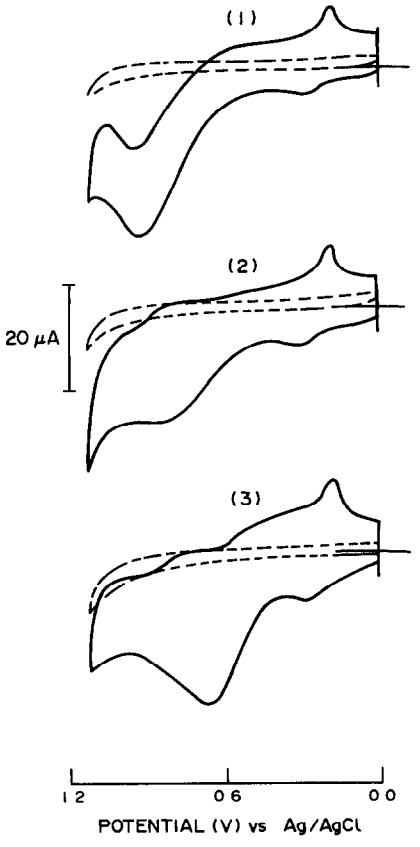

Fig 2 Cyclic voltammograms of 2 mM each of HZ (curve 1), MHZ (curve 2) and DMHZ (curve 3) at the Co–O/CN–Co film electrode (solid line) and the bare GC surface (dotted line) Scan rate, 50 mV/sec

the Co–O/CN–Co film electrode. This indicates that the electrocatalysis proceeds efficiently in a wider pH range (from acidic to neutral media) compared with previously reported catalytic surfaces,[2–7] and on the other hand, this pH effect can greatly favor the reproducibility of current measurements in LCEC detection, as the electrochemical detector is not sensitive to fluctuation of either the operating potential or the mobile phase pH during analysis. Second, the catalytic peak current as a function of the square root of the potential scan rate is linear over the range 5–360 mV/sec (Fig 3A), indicating a diffusion-controlled oxidation and a rapid reaction between the ferrocyanide species in the Co–O/CN–Co film and hydrazine.

Considering the fact that there exist channels in Prussian Blue and its analogues[14–25] favoring transport of K^+ during redox transitions, one could expect that K^+ concentration plays an important role in electrocatalysis of hydrazines at the Co–O/CN–Co film electrode. The cyclic voltammetric experimental results agree with this expectation. By the dilution of KCl electrolyte from 2.0 to 0.02M, the catalytic peak potential of 1 mM hydrazine at the Co–O/CN–Co film electrode surface shifted negatively (from 0.89 to 0.75 V); and then reduced sharply with lowering of the KCl concentration to less than 0.1M. Further, successive potential cycling produced deteriorated CV peaks at the Co–O/CN–Co film electrode in KCl electrolyte less than 0 1M (*eg.* 0.05M). These indicate that the long-term stability of the Co–O/CN–Co coating and efficient catalysis could only be practical when K^+ is present at a level higher than 0.1M in the supporting electrolyte and/or mobile phase.

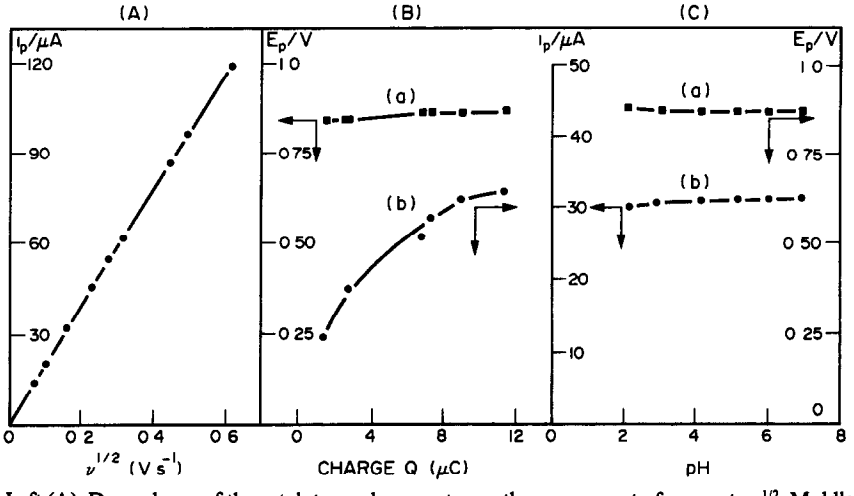

Fig 3 Left (A) Dependence of the catalytic peak current i_p on the square root of scan rate $v^{1/2}$ Middle (B) Film thickness effect on catalytic peak potential (curve a) and peak current (curve b) Right (C). The dependence of catalytic peak potential (curve a) and peak current (curve b) on pH from CVs of 1 mM hydrazine at the Co–O/CN–Co film electrode in 0 5M KCl, pH 4 0 (A and B) at scan rate of 50 mV/sec (B and C)

Cyclic voltammetric experiments also demonstrated that using either 0.5*M* KCl, 0.5*M* KH_2PO_4, 0.5*M* KNO_3, or 0.5*M* $KClO_4$ changed neither the peak potential (within 15 mV) nor the peak current (within 8%) for the catalytic oxidation of hydrazine by the Co–O/CN–Co film electrode. The effect of film thickness of the catalyst on the electrocatalytic response toward hydrazine was studied by cyclic voltammetry, with results as shown in Fig. 3B. The film thickness was estimated by charge consumed within the potential scan over the second anodic wave (at 0.85 V) (*ca.* 0.6–1.0 V) by calculating the peak area of the current–voltage profile at the Co–O/CN–Co film electrode in 0.5*M* KCl electrolyte. The catalytic peak potential (curve a) was virtually unchanged with film thickness, whereas the peak current (curve b) increased significantly with increased thickening of the film, the extent of which became less marked after 8.6 μC, that is 7.8×10^{-9} mol/cm^2; the corresponding time period required for film coating was *ca.* 25 min. Prolonging the modification time further contributed slightly to the electrocatalytic activity. Therefore, the modification time is selected as 30 min for the reproducible preparation of the Co–O/CN–Co film electrode. This is of analytical advantage in the reproducibility of both the current measurements and the electrode preparations. Five consecutive preparations beginning with bare glassy carbon substrate yielded charges of 8.3, 8.7, 8.5, 8.2 and 8.6 μC. The Co–O/CN–Co film was much thinner than the reported Prussian Blue deposits on glassy carbon. Since these inorganic film species have fairly high resistivities,[21] a modification procedure that produced a very thin film was important for applications to electrocatalysis and flow detection.

Chromatographic detection

The operating potential was optimized by hydrodynamic voltammograms (HDVs) of the analytes on the Co–O/CN–Co film electrode, as shown in Fig. 4A. Hydrazine and methylhydrazine (MHZ) exhibited peak-shaped HDVs at the modified surface, as seen for other electrocatalytic surfaces,[2-7] reaching their maximal levels at around 0.8 V. DMHZ, however, presented S-shaped HDV behavior up to 1.0 V. The sensitivity of current measurements follows the order HZ > MHZ > DMHZ. The amine groups might be responsible for these differences. No useful currents were obtained for the analytes on a bare GC surface up to 1.0 V under the same

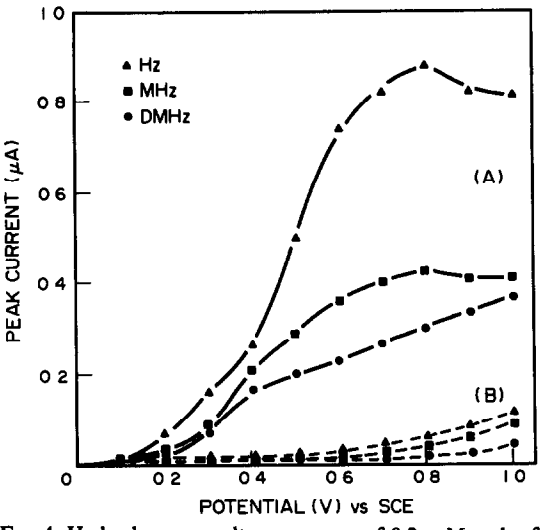

Fig. 4. Hydrodynamic voltammograms of 0.2 m*M* each of HZ, MHZ and DMHZ at the Co–O/CN–Co film electrode (curve A) and the bare GC surface (curve B) Column, μBondapak C_{18} (5 μm)250 × 4 mm i.d , mobile phase, pH 7.0, 0 1*M* KH_2PO_4 at flow rate of 1 0 ml min Injection volume, 10 μl

solution conditions (curve B). Based on the compromise among high sensitivity, selectivity and low background current, 0.80 V was selected for LC amperometric detection.

By virtue of the wide operational pH range available on the Co–O/CN–Co film electrode

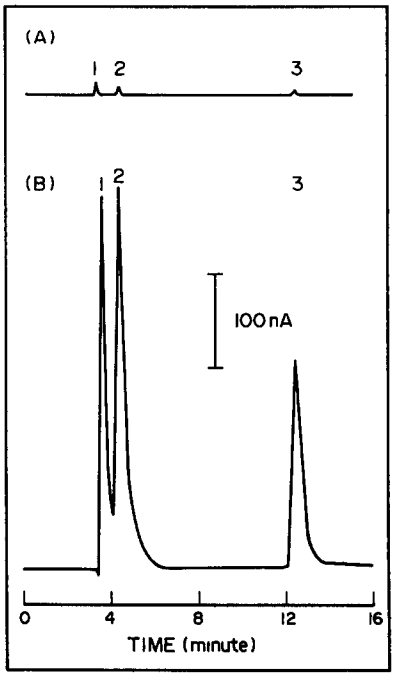

Fig. 5. Chromatograms of 0.2 m*M* HZ (1), 0 4 m*M* MHZ (2) and 0.26 m*M* DMHZ (3) at the Co–O/CN–Co film electrode (curve B) and the bare GC surface (curve A). Potential applied at 0 80 V *vs.* SCE Flow conditions as in Fig. 4

for electrocatalytic oxidation of hydrazines, practical RP-LCEC has been performed with a conventional ODS column, using pH 7.0, 0.1M KH_2PO_4 as mobile phase. Using higher concentration KH_2PO_4 was mobile phase is of a disadvantage for the maintenance of proper operating pressure and column efficiency, though contributing a little to the current response sensitivity. Well-defined and resolved chromatographic peaks were obtained as shown in Fig. 5, with the operating potential monitored at 0.80 V. Ten replicate injections of stock solutions containing 0.02 mM HZ, 0.04 mM MHZ and 0.026 mM DMHZ were carried out to determine the precision. The coefficient of variation of the peak heights was 1.7% for HZ, 2.5% for MHZ and 3.2% for DMHZ.

Under such conditions, LCEC of hydrazines at the Co–O/CN-Co film electrode gave dynamic linear response ranges of 3×10^{-7} to $7.5 \times 10^{-4}M$ for HZ, 6×10^{-7} to $9 \times 10^{-4}M$ for MHZ and 8×10^{-7} to $8 \times 10^{-4}M$ for DMHZ, with correlation coefficient greater than 0.99. The corresponding detection limit (based on three times the S/N ratio) was 1.5×10^{-4} mM, 3×10^{-4} mM and 5×10^{-4} mM for HZ, MHZ and DMHZ; that is 1.5, 3 and 5 pmol, respectively (10 μl loop).

The Co–O/CN–Co film coated electrode exhibited excellent stability for the continuous use in flowing streams. After 2 days service in the chromatographic system, during which working solutions containing 0.4 mM each of HZ, MHZ and DMHZ were injected at intervals, at least 80% of the initial current response level was obtained for hydrazines in LCEC with the Co–O/CN–Co film electrode; and the concentration dependence on the peak current was still linear up to two orders of magnitude. These features suggest that such a Co–O/CN–Co coating electrode is promising as an effective indicator for routine LCEC analysis of hydrazines.

CONCLUSIONS

A new inorganic catalytic electrode has been successfully constructed by electrodeposition on the glassy carbon surface of a Co–O/CN–Co film. The Co–O/CN–Co film electrode provides stable and efficient catalysis toward hydrazine compounds in a wide operational pH range, making it perfectly compatible with conventional reversed-phase liquid chromatographic systems. When used in LCEC, wide dynamic linear response range over three orders of magnitude and low detection limit at the pmol level are readily obtained. The Co–O/CN–Co coating shows acceptable long-term stability for continuous catalytic service in flow-through analytical systems. Moreover, the Co–O/CN–Co coated glassy carbon electrode offers the possibility of extending voltammetric techniques to hydrazine compounds otherwise poorly suited to electroanalysis at conventional carbon substrates.

Acknowledgements—The support of the National Natural Science Foundation of China and the Basic and High-Tech Research Division of the State Commission of Science and Technology is gratefully acknowledged

REFERENCES

1. K Ravichandran and R P Baldwin, *Anal Chem.*, 1983, **55**, 1782.
2. K. M Korfhage, K. Ravichandran and R P Baldwin, *Anal. Chem*, 1984, **56**, 1514
3. J. Wang, T Golden and R Li, *Anal Chem*, 1988, **60**, 1642
4. W Hou, J Hua and E. Wang, *Chin Sci Bull*, 1991, **36**, 785
5. Z. Taha and J Wang, *Electroanalysis*, 1991, **3**, 215
6. W Hou and E Wang, *Anal Chim. Acta*, 1992, **257**, 275
7. J Wang and Z. Lu, *Electroanalysis*, 1989, **1**, 517
8. W. Hou and E Wang, *J Electroanal Chem*, 1991, **316**, 155.
9. K Ogura, N. Shoji and I Uchida, *J Am Chem Soc*, 1984, **106**, 3423
10. K. Ogura and S Yamasaki, *J Chem Soc*, *Faraday Trans I*, 1985, **81**, 267
11. K Ogura and M Kaneko, *J Mol Catal*, 1985, **31**, 49
12. K. Itaya, I. Uchida and S Toshima, *J Phys Chem*, 1983, **87**, 105
13. F Li and S Dong, *Electrochim Acta*, 1987, **32**, 1511
14. A. B Bocarsly and S Sinha, *J Electroanal Chem*, 1982, **137**, 157
15. B. F Y. Y Hin and C R Lowe, *Anal Chem*, 1987, **59**, 2111
16. P J Kulesza, K Brajter and E Dabek-Zlotorzynska, *Anal. Chem.*, 1987, **59**, 2776
17. J. A. Cox and P. J. Kulesza, *Anal Chem.*, 1984, **56**, 1021
18. J A Cox, T J Gray and K R Kulkarni, *Anal Chem*, 1988, **60**, 1710
19. J A Cox and T J Gray, *Anal Chem*, 1989, **61**, 2462
20. J A. Cox and T J Gray, *Electroanalysis*, 1990, **2**, 107
21. D Ellis, M Eckhoff and V D Neff, *J Phys Chem*, 1981, **85**, 1225
22. K. P. Rajan and V. D Neff, *J. Phys Chem*, 1982, **86**, 4361
23. K Itaya, T. Ataka and S Toshima, *J Am Chem Soc*, 1982, **104**, 3751
24. K Itaya, T Ataka and S Toshima, *J Am Chem Soc*, 1982, **104**, 4767
25. P J. Kulesza, *J Electroanal Chem*, 1987, **220**, 295
26. S. Dong and T Kuwana, *J Electrochem Soc*, 1984, **131**, 813

Talanta, Vol 40, No 6, pp 949–955, 1993
Printed in Great Britain
Pergamon Press Ltd

BOOK REVIEWS

TrAC—Trends in Analytical Chemistry: Reference Edition, Volume 10, 1991. Elsevier, Amsterdam, 1992 Pages 372 Dfl. 545 00. ISBN 0-444-89503-5

This book is a compilation of the 10 issues of TrAC for the year 1991 and like all the 'Trends in' Reference Editions, is arranged in order of issue publication. Only the book reviews and news items are excluded The book finishes with a cumulative author and subject index for volumes 6–10

Each issue is divided into a number of subsections (meeting reports, monitor, computer corner, feature, observer, trends) that are not always distinguishable from one another. Attempts have not been made to divide articles up into general areas of analytical chemistry although one issue (Nov/Dec) is entirely devoted to environmental concerns

TrAC covers all areas of analytical chemistry and fills an important niche between specialized journals and text books The articles are intended for a wide readership and are accessible to the non-specialist whilst providing comprehensive references for those who need to look further TrAC is also a quick enjoyable way of keeping abreast with recent developments that are peripheral to your reading list or research interests

Elsevier have not wasted any time in publishing this reference edition. Coupled with a well balanced choice of articles from authors at the 'cutting edge' of their fields makes this a very useful update It is an invaluable source of teaching material and of new ideas for research

The price is apparently rather prohibitive, but hides the fact that for only a little more (Dfl 800 this year) your library can take all issues of TrAC and receive the reference edition when it is published. For the individual subscriber TrAC is very good value at Dfl 181 so there are few readers who would consider it necessary to purchase this reference edition

This book is available from the Amsterdam address or in the USA/Canada from Elsevier Science Publishing Company Inc , P.O Box 882, Madison Square Station, New York NY10159, U S A

B A McGaw

Fig. P, Version 6: BIOSOFT, Cambridge, 1991. £280, US$499

This scientific graphics software package for IBM PC/PS2 and compatibles is a major upgrade from the previous version, and is now a very powerful tool. Almost any type of graph that a scientist might want can be produced. The user has full control over the nature of the axes, the positioning of the tick marks, the choice and positioning of the labels, etc Graphs may be annotated with text, boxes, circles, ellipses and arrows as desired, and a suitable size and font can be chosen for each piece of text Multiple figures can be produced on the same page Figures can be produced in colour if desired Output drivers are included for many printers and HPGL plotters, including HP Paintjet and Laserjet III Curve-fitting and statistical tests are also included The output quality is extremely good, even with a nine-pin dot-matrix printer, but especially with a laser printer or a Matrix slide camera

The manual has 420 pages, of which 20 give a quick overview, 56 give tutorial instruction, 280 comprise sample figures with brief instructions for their production but no data, and 68 the reference section I found the tutorial less helpful than I had expected instead of detailed step-by-step instructions, it starts by giving a summary of the items to be entered, then goes off into explanations of all the possibilities, then returns to entry instructions Thus, a lot of reference information is presented in the tutorial section The reference section, too, did not have the usual format Indeed, it seemed to consist mainly of "tutorial" sections on the advanced topics not covered earlier in the manual As a result, the best way to learn to make full use of the program seems to be to work through the instructions for the sample figures However, this would have been easier if the data values for the samples had been included either in the handbook or on the disc

Fairly comprehensive instructions were given on screen, with context-sensitive help, and I actually found it easier to learn to use the program from this than from the manual

In conclusion, I believe this is an excellent package for computer-literate scientists who wish to produce their own diagrams in a form suitable for publication It is less well suited for use by students or technicians, who are likely to be baffled by its complexities

M. Masson

Patterson's German-English Dictionary for Chemists—4th Ed.: J C. Cox and G E Condoyannis (Eds.). Wiley, Chichester, 1992. Pages liii + 890 £52.00 ISBN 0-471-66991-1

There cannot be many of the present older generation of English-speaking chemists who have not at one time or another had recourse to *Patterson* in its 3rd edition dating from 1950 While the German chemists of the turn of the century indulged

Talanta, Vol 40, No 6, pp 949–955, 1993
Printed in Great Britain
Pergamon Press Ltd

BOOK REVIEWS

TrAC—Trends in Analytical Chemistry: Reference Edition, Volume 10, 1991. Elsevier, Amsterdam, 1992 Pages 372 Dfl. 545 00. ISBN 0-444-89503-5

This book is a compilation of the 10 issues of TrAC for the year 1991 and like all the 'Trends in' Reference Editions, is arranged in order of issue publication. Only the book reviews and news items are excluded The book finishes with a cumulative author and subject index for volumes 6–10

Each issue is divided into a number of subsections (meeting reports, monitor, computer corner, feature, observer, trends) that are not always distinguishable from one another. Attempts have not been made to divide articles up into general areas of analytical chemistry although one issue (Nov/Dec) is entirely devoted to environmental concerns

TrAC covers all areas of analytical chemistry and fills an important niche between specialized journals and text books The articles are intended for a wide readership and are accessible to the non-specialist whilst providing comprehensive references for those who need to look further TrAC is also a quick enjoyable way of keeping abreast with recent developments that are peripheral to your reading list or research interests

Elsevier have not wasted any time in publishing this reference edition. Coupled with a well balanced choice of articles from authors at the 'cutting edge' of their fields makes this a very useful update It is an invaluable source of teaching material and of new ideas for research

The price is apparently rather prohibitive, but hides the fact that for only a little more (Dfl 800 this year) your library can take all issues of TrAC and receive the reference edition when it is published. For the individual subscriber TrAC is very good value at Dfl 181 so there are few readers who would consider it necessary to purchase this reference edition

This book is available from the Amsterdam address or in the USA/Canada from Elsevier Science Publishing Company Inc , P.O Box 882, Madison Square Station, New York NY10159, U S A

B A McGaw

Fig. P, Version 6: BIOSOFT, Cambridge, 1991. £280, US$499

This scientific graphics software package for IBM PC/PS2 and compatibles is a major upgrade from the previous version, and is now a very powerful tool. Almost any type of graph that a scientist might want can be produced. The user has full control over the nature of the axes, the positioning of the tick marks, the choice and positioning of the labels, etc Graphs may be annotated with text, boxes, circles, ellipses and arrows as desired, and a suitable size and font can be chosen for each piece of text Multiple figures can be produced on the same page Figures can be produced in colour if desired Output drivers are included for many printers and HPGL plotters, including HP Paintjet and Laserjet III Curve-fitting and statistical tests are also included The output quality is extremely good, even with a nine-pin dot-matrix printer, but especially with a laser printer or a Matrix slide camera

The manual has 420 pages, of which 20 give a quick overview, 56 give tutorial instruction, 280 comprise sample figures with brief instructions for their production but no data, and 68 the reference section I found the tutorial less helpful than I had expected instead of detailed step-by-step instructions, it starts by giving a summary of the items to be entered, then goes off into explanations of all the possibilities, then returns to entry instructions Thus, a lot of reference information is presented in the tutorial section The reference section, too, did not have the usual format Indeed, it seemed to consist mainly of "tutorial" sections on the advanced topics not covered earlier in the manual As a result, the best way to learn to make full use of the program seems to be to work through the instructions for the sample figures However, this would have been easier if the data values for the samples had been included either in the handbook or on the disc

Fairly comprehensive instructions were given on screen, with context-sensitive help, and I actually found it easier to learn to use the program from this than from the manual

In conclusion, I believe this is an excellent package for computer-literate scientists who wish to produce their own diagrams in a form suitable for publication It is less well suited for use by students or technicians, who are likely to be baffled by its complexities

M. Masson

Patterson's German-English Dictionary for Chemists—4th Ed.: J C. Cox and G E Condoyannis (Eds.). Wiley, Chichester, 1992. Pages liii + 890 £52.00 ISBN 0-471-66991-1

There cannot be many of the present older generation of English-speaking chemists who have not at one time or another had recourse to *Patterson* in its 3rd edition dating from 1950 While the German chemists of the turn of the century indulged

in a heavy literary style to describe their achievements in science, those of our generation have turned to a simpler style to aid international understanding But their efforts have been thwarted by those of others intent on developing an endless stream of new words, not to be found in our old *Pattersons* As it happens, the difficulties of going *into* German are confounded by the number of technical words which are *not* translated from the English but are used as such

Having struggled through German stock inventories and been able to translate them only with the help of illustrated English catalogues, I am very appreciative of the approach of the present two editors of *Patterson*, who have, over the years, been compiling their own glossaries out of their own experience in technical translating. Technical dictionaries abound good ones are rare

So, how does the 4th edition of *Patterson* score? Very well indeed Many older trivial names are still included—Blausäure, Hirschhornsalz—along with culinary delights—Müsli, Steinpilz—older and newer spellings—Cadmium/Kadmium (but not Ton/Thon)—care with foreign names—Mékerbrenner—and so on. Then the eternal problem of the German compound words is dealt with extensively, verbs with many different prefixes, nouns with extensions—Mehrwegbehalter, Dauerbiegefestigkeit—idiomatic phrases—letzten Ende,—sei dem wie es sei—more difficult parts of verbs—ging(gehen)—and so on In short, this is an excellent revision which will give pleasure to the user because he will always find more than he seeks, not just a question answered but a lesson learned This new dictionary deserves a place, not merely on the bookshelf, but on the workdesk of every chemist who reads German scientific literature

I L MARR

Trace and Ultratrace Analysis by HPLC: S AHUJA, Wiley–Interscience, New York, 1992 Pages xi + 419 £59.00 ISBN 0-471-51419-5

The title suggests that this book attempts to focus on the utility of high-performance liquid chromatography (HPLC) for the analysis of small quantities of compounds. In reality, however, the author has done more than this in producing a comprehensive all-embracing text on HPLC, containing nine substantial well-referenced chapters

After having outlined the scope of the book in the first chapter, illustrated by selected examples demonstrating the applicability of the technique for the analysis of macro-molecules and small molecules, the following chapter describes the fundamental concepts of chromatography, relating them to instrument and column performance There follows two chapters devoted to instrumentation comprising solvent delivery systems, microcolumn HPLC and a full description of all the available detectors suitable for trace analysis Chapter 5 describes in detail the various possible approaches for sample preparation varying from solvent extraction to solid-phase extraction systems

Obviously the core of any analysis is the selection of the appropriate stationary and mobile phases These topics are comprehensively dealt with in chapters 6 and 7 which in parts are repetitive. There is a full description of reversed-phase systems including ion-pair chromatography This is followed by a chapter on optimization which brings together a lot of the topics dealt with earlier Throughout the book there are examples of applications to illustrate the chapter topics but there is also a concluding chapter dealing solely with applications from the areas of pharmaceuticals, food and the environment. Whilst the applications are cross-referenced in the index they are not always readily accessible

This book, which contains some factual and typographical errors, is not a beginners' text, assuming as it does in parts that the reader has a biological and chromatographic background. However, the author has included in appropriate chapters useful descriptions of some of the newer developments and understanding of analyte separation mechanisms The synoptic nature of the book tends to make it somewhat prosaic in parts

G G. SKELLERN

Gas–Liquid–Solid Chromatography: V G BEREZKIN, Dekker, New York, 1991 Pages viii + 231 $99 75 (U S and Canada), $114.50 (elsewhere) ISBN 0-8247-8425-1

The fundamental approach of this treatise is that separation in "gas–liquid" chromatography not only involves the two bulk phases, the gaseous mobile phase and the non-volatile liquid stationary phase, but is influenced by the interfaces between the gas and the liquid, and between the liquid and solid support Hence, the stationary phase is regarded as a binary system in gas–liquid–solid chromatography with gas–liquid chromatography an important, but limited case of gas–liquid–solid chromatography

Berezkin's book discusses up-to-date concepts in gas–liquid–solid chromatography. Theoretical principles, calculation procedures and experimental methods developed to estimate the effects of adsorption phenomena on retention are described in the nine chapters of the book

Chapter 1 outlines the evolution of gas–liquid–solid chromatography. In Chapters 2–4, factors effecting the retention of analysed compounds are considered including a discussion of the influence of adsorption on relative retention times and the effect of the solid support on the efficiency of separation. In Chapter 5, the effects of the stationary liquid phase to solid absorbant phase ratio on the characteristics of chromatographic resolution are considered for packed and capillary columns. Irreversible or quasi-irreversible absorption of solutes on the solid support is discussed in chapter 6, along with the effects of chemical transformation at the solid support surface The next two chapters consider the contributions that gas–liquid–solid chromatography has made to physicochemical measurements Chapter 7 considers equilibrium parameters of the absorption (partition) interaction between solutes and the liquid phase, whereas Chapter 8 is devoted to the

in a heavy literary style to describe their achievements in science, those of our generation have turned to a simpler style to aid international understanding But their efforts have been thwarted by those of others intent on developing an endless stream of new words, not to be found in our old *Pattersons* As it happens, the difficulties of going *into* German are confounded by the number of technical words which are *not* translated from the English but are used as such

Having struggled through German stock inventories and been able to translate them only with the help of illustrated English catalogues, I am very appreciative of the approach of the present two editors of *Patterson*, who have, over the years, been compiling their own glossaries out of their own experience in technical translating. Technical dictionaries abound good ones are rare

So, how does the 4th edition of *Patterson* score? Very well indeed Many older trivial names are still included—Blausäure, Hirschhornsalz—along with culinary delights—Müsli, Steinpilz—older and newer spellings—Cadmium/Kadmium (but not Ton/Thon)—care with foreign names—Mékerbrenner—and so on. Then the eternal problem of the German compound words is dealt with extensively, verbs with many different prefixes, nouns with extensions—Mehrwegbehalter, Dauerbiegefestigkeit—idiomatic phrases—letzten Ende,—sei dem wie es sei—more difficult parts of verbs—ging(gehen)—and so on In short, this is an excellent revision which will give pleasure to the user because he will always find more than he seeks, not just a question answered but a lesson learned This new dictionary deserves a place, not merely on the bookshelf, but on the workdesk of every chemist who reads German scientific literature

I L MARR

Trace and Ultratrace Analysis by HPLC: S AHUJA, Wiley–Interscience, New York, 1992 Pages xi + 419 £59.00 ISBN 0-471-51419-5

The title suggests that this book attempts to focus on the utility of high-performance liquid chromatography (HPLC) for the analysis of small quantities of compounds. In reality, however, the author has done more than this in producing a comprehensive all-embracing text on HPLC, containing nine substantial well-referenced chapters

After having outlined the scope of the book in the first chapter, illustrated by selected examples demonstrating the applicability of the technique for the analysis of macro-molecules and small molecules, the following chapter describes the fundamental concepts of chromatography, relating them to instrument and column performance There follows two chapters devoted to instrumentation comprising solvent delivery systems, microcolumn HPLC and a full description of all the available detectors suitable for trace analysis Chapter 5 describes in detail the various possible approaches for sample preparation varying from solvent extraction to solid-phase extraction systems

Obviously the core of any analysis is the selection of the appropriate stationary and mobile phases These topics are comprehensively dealt with in chapters 6 and 7 which in parts are repetitive. There is a full description of reversed-phase systems including ion-pair chromatography This is followed by a chapter on optimization which brings together a lot of the topics dealt with earlier Throughout the book there are examples of applications to illustrate the chapter topics but there is also a concluding chapter dealing solely with applications from the areas of pharmaceuticals, food and the environment. Whilst the applications are cross-referenced in the index they are not always readily accessible

This book, which contains some factual and typographical errors, is not a beginners' text, assuming as it does in parts that the reader has a biological and chromatographic background. However, the author has included in appropriate chapters useful descriptions of some of the newer developments and understanding of analyte separation mechanisms The synoptic nature of the book tends to make it somewhat prosaic in parts

G G. SKELLERN

Gas–Liquid–Solid Chromatography: V G BEREZKIN, Dekker, New York, 1991 Pages viii + 231 $99 75 (U S and Canada), $114.50 (elsewhere) ISBN 0-8247-8425-1

The fundamental approach of this treatise is that separation in "gas–liquid" chromatography not only involves the two bulk phases, the gaseous mobile phase and the non-volatile liquid stationary phase, but is influenced by the interfaces between the gas and the liquid, and between the liquid and solid support Hence, the stationary phase is regarded as a binary system in gas–liquid–solid chromatography with gas–liquid chromatography an important, but limited case of gas–liquid–solid chromatography

Berezkin's book discusses up-to-date concepts in gas–liquid–solid chromatography. Theoretical principles, calculation procedures and experimental methods developed to estimate the effects of adsorption phenomena on retention are described in the nine chapters of the book

Chapter 1 outlines the evolution of gas–liquid–solid chromatography. In Chapters 2–4, factors effecting the retention of analysed compounds are considered including a discussion of the influence of adsorption on relative retention times and the effect of the solid support on the efficiency of separation. In Chapter 5, the effects of the stationary liquid phase to solid absorbant phase ratio on the characteristics of chromatographic resolution are considered for packed and capillary columns. Irreversible or quasi-irreversible absorption of solutes on the solid support is discussed in chapter 6, along with the effects of chemical transformation at the solid support surface The next two chapters consider the contributions that gas–liquid–solid chromatography has made to physicochemical measurements Chapter 7 considers equilibrium parameters of the absorption (partition) interaction between solutes and the liquid phase, whereas Chapter 8 is devoted to the

in a heavy literary style to describe their achievements in science, those of our generation have turned to a simpler style to aid international understanding But their efforts have been thwarted by those of others intent on developing an endless stream of new words, not to be found in our old *Pattersons* As it happens, the difficulties of going *into* German are confounded by the number of technical words which are *not* translated from the English but are used as such

Having struggled through German stock inventories and been able to translate them only with the help of illustrated English catalogues, I am very appreciative of the approach of the present two editors of *Patterson*, who have, over the years, been compiling their own glossaries out of their own experience in technical translating. Technical dictionaries abound good ones are rare

So, how does the 4th edition of *Patterson* score? Very well indeed Many older trivial names are still included—Blausäure, Hirschhornsalz—along with culinary delights—Müsli, Steinpilz—older and newer spellings—Cadmium/Kadmium (but not Ton/Thon)—care with foreign names—Mékerbrenner—and so on. Then the eternal problem of the German compound words is dealt with extensively, verbs with many different prefixes, nouns with extensions—Mehrwegbehalter, Dauerbiegefestigkeit—idiomatic phrases—letzten Ende,—sei dem wie es sei—more difficult parts of verbs—ging(gehen)—and so on In short, this is an excellent revision which will give pleasure to the user because he will always find more than he seeks, not just a question answered but a lesson learned This new dictionary deserves a place, not merely on the bookshelf, but on the workdesk of every chemist who reads German scientific literature

I L MARR

Trace and Ultratrace Analysis by HPLC: S AHUJA, Wiley–Interscience, New York, 1992 Pages xi + 419 £59.00 ISBN 0-471-51419-5

The title suggests that this book attempts to focus on the utility of high-performance liquid chromatography (HPLC) for the analysis of small quantities of compounds. In reality, however, the author has done more than this in producing a comprehensive all-embracing text on HPLC, containing nine substantial well-referenced chapters

After having outlined the scope of the book in the first chapter, illustrated by selected examples demonstrating the applicability of the technique for the analysis of macro-molecules and small molecules, the following chapter describes the fundamental concepts of chromatography, relating them to instrument and column performance There follows two chapters devoted to instrumentation comprising solvent delivery systems, microcolumn HPLC and a full description of all the available detectors suitable for trace analysis Chapter 5 describes in detail the various possible approaches for sample preparation varying from solvent extraction to solid-phase extraction systems

Obviously the core of any analysis is the selection of the appropriate stationary and mobile phases These topics are comprehensively dealt with in chapters 6 and 7 which in parts are repetitive. There is a full description of reversed-phase systems including ion-pair chromatography This is followed by a chapter on optimization which brings together a lot of the topics dealt with earlier Throughout the book there are examples of applications to illustrate the chapter topics but there is also a concluding chapter dealing solely with applications from the areas of pharmaceuticals, food and the environment. Whilst the applications are cross-referenced in the index they are not always readily accessible

This book, which contains some factual and typographical errors, is not a beginners' text, assuming as it does in parts that the reader has a biological and chromatographic background. However, the author has included in appropriate chapters useful descriptions of some of the newer developments and understanding of analyte separation mechanisms The synoptic nature of the book tends to make it somewhat prosaic in parts

G G. SKELLERN

Gas–Liquid–Solid Chromatography: V G BEREZKIN, Dekker, New York, 1991 Pages viii + 231 $99 75 (U S and Canada), $114.50 (elsewhere) ISBN 0-8247-8425-1

The fundamental approach of this treatise is that separation in "gas–liquid" chromatography not only involves the two bulk phases, the gaseous mobile phase and the non-volatile liquid stationary phase, but is influenced by the interfaces between the gas and the liquid, and between the liquid and solid support Hence, the stationary phase is regarded as a binary system in gas–liquid–solid chromatography with gas–liquid chromatography an important, but limited case of gas–liquid–solid chromatography

Berezkin's book discusses up-to-date concepts in gas–liquid–solid chromatography. Theoretical principles, calculation procedures and experimental methods developed to estimate the effects of adsorption phenomena on retention are described in the nine chapters of the book

Chapter 1 outlines the evolution of gas–liquid–solid chromatography. In Chapters 2–4, factors effecting the retention of analysed compounds are considered including a discussion of the influence of adsorption on relative retention times and the effect of the solid support on the efficiency of separation. In Chapter 5, the effects of the stationary liquid phase to solid absorbant phase ratio on the characteristics of chromatographic resolution are considered for packed and capillary columns. Irreversible or quasi-irreversible absorption of solutes on the solid support is discussed in chapter 6, along with the effects of chemical transformation at the solid support surface The next two chapters consider the contributions that gas–liquid–solid chromatography has made to physicochemical measurements Chapter 7 considers equilibrium parameters of the absorption (partition) interaction between solutes and the liquid phase, whereas Chapter 8 is devoted to the

determination of physicochemical parameters for adsorption of solutes at the interfaces between the gas and liquid stationary phase and between the liquid phase and the solid support. the final chapter considers practical aspects of the effect of the solid support on the conditioning and ageing of columns.

Throughout the book, theoretical models and practical experiments are used in equal measure to guide the reader through a fairly detailed consideration of adsorption phenomena Emphasis is placed on understanding the basis of the technique rather than on specific applications in particular areas of analysis Numerous equations are presented, but often the reader has to look back several pages to be reminded of the definition of symbols A comprehensive table of definitions would have been a helpful addition to the text. All the chapters contain useful illustrations and tables of relevant data. Some of the figures have been reproduced directly from initial publications and are not of a high quality One would have thought that it would have been possible to redraw some of the graphs without too much difficulty. Each chapter has its own list of references, covering the literature up to the mid 1980s, although some of the papers in east European journals may not be easily accessible

The importance of adsorption phenomena in gas–liquid chromatography has been recognised for many years, so the topics considered in this book are not entirely new The author claims that this is the first time that an attempt has been made to consider consistently gas–liquid chromatography and gas–liquid–solid chromatography Whether or not this is true does not really matter The main point is that a text has been produced which considers, in some detail, theoretical and practical aspects of gas–liquid–solid chromatography and so it should be helpful to scientists interested in the fundamental basis of chromatographic separations

D LITTLEJOHN

Potentiometric Water Analysis, Second Edition: D MIDGLEY and K. TORRANCE, Wiley, Chichester, 1991 Pages xiv + 586 £65.00. ISBN 0-471-92983-2

This is a welcome revision of Midgley and Torrance's authoritative text first published in 1978 The format of the first edition has been maintained, but the content has been updated to include recent developments in electrode technology and potentiometric methods of importance in water analysis This is very much a practical textbook where the authors have tried to provide enough information to enable the analyst to use commercially available ion-selective electrodes without having to undertake extensive method development

Part I provides a theoretical and practical background to potentiometry and Part II contains almost 400 pages of analytical methods for water analysis Separate chapters in Part I cover electrochemical principles, potentiometric instrumentation and methodology The theory of electrochemistry is covered in sufficient detail to allow the analyst to understand the practical importance of the principles and relationships which affect activity, electrode potentials, liquid junction potentials, etc The fundamental basis of different types of ion-selective electrodes (ISE) are described, but without a detailed explanation of the mechanisms of electrode response Similarly, the chapter concerned with instrumentation describes what can be achieved with modern potentiometric equipment without labouring the technicalities In contrast, the authors have taken the trouble to point out the importance of establishing the analytical viability of a method and many readers will find the chapter on the statistical evaluation of data extremely helpful Many papers published on potentiometric analysis fail to give details of accuracy and precision and omit a discussion of errors The authors have tried to compensate for those deficiencies by providing a realistic indication of the performance of various types of electrodes when applied in water analysis

The value of the book to many readers will be the extensive notes on over 35 separate ISE applications given in Part II Not only are the apparatus, reagents and procedures described in adequate detail, but sources of error and electrode performance are discussed, comments on the lifetime of electrodes, typical response times and comparisons with other methods, where appropriate.

The ability of potentiometry to provide low-cost measurements in field and laboratory applications, as well as in on-line monitoring, has made the technique very important in water analysis Midgley and Torrance have provided an up-to-date review of methods and procedures which is clearly written and easy to read Each chapter is accompanied by a list of references covering developments up to 1990

Although the text does not contain all that many figures, it has numerous tables of useful information on electrochemical data, electrode comparisons and analytical methods. There is also a list of manufacturers of potentiometric equipment Anyone interested in potentiometry or water analysis should obtain a copy of this book

D LITTLEJOHN

Spectrochemical Analysis by Atomic Absorption and Emission: L. LAJUNEN Royal Society of Chemistry, Cambridge 1992 £18.50 (softback) Pages xii + 242 ISBN 0-851-86873-8

This book is very timely, coming on the market, as it does, when the modern analytical atomic spectroscopies such as ICP–MS are becoming firmly established necessitating their inclusion with more than a passing reference in our training courses Substantial chapters deal with Theory of atomic spectroscopy, Atomic absorption, Plasma atomic emission, ICP–MS, Atomic fluorescence, Sample preparation, while some smaller chapters cover the Histological background and Comparisons Flame emission is dismissed in two sides, so the book cannot be described as long-winded!

The author's practical experience comes over on many occasions through his comments on the practical consequences and the relevance of this or that aspect of theory and so on The author has included numerous diagrams, some his own,

determination of physicochemical parameters for adsorption of solutes at the interfaces between the gas and liquid stationary phase and between the liquid phase and the solid support. the final chapter considers practical aspects of the effect of the solid support on the conditioning and ageing of columns.

Throughout the book, theoretical models and practical experiments are used in equal measure to guide the reader through a fairly detailed consideration of adsorption phenomena Emphasis is placed on understanding the basis of the technique rather than on specific applications in particular areas of analysis Numerous equations are presented, but often the reader has to look back several pages to be reminded of the definition of symbols A comprehensive table of definitions would have been a helpful addition to the text. All the chapters contain useful illustrations and tables of relevant data. Some of the figures have been reproduced directly from initial publications and are not of a high quality One would have thought that it would have been possible to redraw some of the graphs without too much difficulty. Each chapter has its own list of references, covering the literature up to the mid 1980s, although some of the papers in east European journals may not be easily accessible

The importance of adsorption phenomena in gas–liquid chromatography has been recognised for many years, so the topics considered in this book are not entirely new The author claims that this is the first time that an attempt has been made to consider consistently gas–liquid chromatography and gas–liquid–solid chromatography Whether or not this is true does not really matter The main point is that a text has been produced which considers, in some detail, theoretical and practical aspects of gas–liquid–solid chromatography and so it should be helpful to scientists interested in the fundamental basis of chromatographic separations

D LITTLEJOHN

Potentiometric Water Analysis, Second Edition: D MIDGLEY and K. TORRANCE, Wiley, Chichester, 1991 Pages xiv + 586 £65.00. ISBN 0-471-92983-2

This is a welcome revision of Midgley and Torrance's authoritative text first published in 1978 The format of the first edition has been maintained, but the content has been updated to include recent developments in electrode technology and potentiometric methods of importance in water analysis This is very much a practical textbook where the authors have tried to provide enough information to enable the analyst to use commercially available ion-selective electrodes without having to undertake extensive method development

Part I provides a theoretical and practical background to potentiometry and Part II contains almost 400 pages of analytical methods for water analysis Separate chapters in Part I cover electrochemical principles, potentiometric instrumentation and methodology The theory of electrochemistry is covered in sufficient detail to allow the analyst to understand the practical importance of the principles and relationships which affect activity, electrode potentials, liquid junction potentials, etc The fundamental basis of different types of ion-selective electrodes (ISE) are described, but without a detailed explanation of the mechanisms of electrode response Similarly, the chapter concerned with instrumentation describes what can be achieved with modern potentiometric equipment without labouring the technicalities In contrast, the authors have taken the trouble to point out the importance of establishing the analytical viability of a method and many readers will find the chapter on the statistical evaluation of data extremely helpful Many papers published on potentiometric analysis fail to give details of accuracy and precision and omit a discussion of errors The authors have tried to compensate for those deficiencies by providing a realistic indication of the performance of various types of electrodes when applied in water analysis

The value of the book to many readers will be the extensive notes on over 35 separate ISE applications given in Part II Not only are the apparatus, reagents and procedures described in adequate detail, but sources of error and electrode performance are discussed, comments on the lifetime of electrodes, typical response times and comparisons with other methods, where appropriate.

The ability of potentiometry to provide low-cost measurements in field and laboratory applications, as well as in on-line monitoring, has made the technique very important in water analysis Midgley and Torrance have provided an up-to-date review of methods and procedures which is clearly written and easy to read Each chapter is accompanied by a list of references covering developments up to 1990

Although the text does not contain all that many figures, it has numerous tables of useful information on electrochemical data, electrode comparisons and analytical methods. There is also a list of manufacturers of potentiometric equipment Anyone interested in potentiometry or water analysis should obtain a copy of this book

D LITTLEJOHN

Spectrochemical Analysis by Atomic Absorption and Emission: L. LAJUNEN Royal Society of Chemistry, Cambridge 1992 £18.50 (softback) Pages xii + 242 ISBN 0-851-86873-8

This book is very timely, coming on the market, as it does, when the modern analytical atomic spectroscopies such as ICP–MS are becoming firmly established necessitating their inclusion with more than a passing reference in our training courses Substantial chapters deal with Theory of atomic spectroscopy, Atomic absorption, Plasma atomic emission, ICP–MS, Atomic fluorescence, Sample preparation, while some smaller chapters cover the Histological background and Comparisons Flame emission is dismissed in two sides, so the book cannot be described as long-winded!

The author's practical experience comes over on many occasions through his comments on the practical consequences and the relevance of this or that aspect of theory and so on The author has included numerous diagrams, some his own,

determination of physicochemical parameters for adsorption of solutes at the interfaces between the gas and liquid stationary phase and between the liquid phase and the solid support. the final chapter considers practical aspects of the effect of the solid support on the conditioning and ageing of columns.

Throughout the book, theoretical models and practical experiments are used in equal measure to guide the reader through a fairly detailed consideration of adsorption phenomena Emphasis is placed on understanding the basis of the technique rather than on specific applications in particular areas of analysis Numerous equations are presented, but often the reader has to look back several pages to be reminded of the definition of symbols A comprehensive table of definitions would have been a helpful addition to the text. All the chapters contain useful illustrations and tables of relevant data. Some of the figures have been reproduced directly from initial publications and are not of a high quality One would have thought that it would have been possible to redraw some of the graphs without too much difficulty. Each chapter has its own list of references, covering the literature up to the mid 1980s, although some of the papers in east European journals may not be easily accessible

The importance of adsorption phenomena in gas–liquid chromatography has been recognised for many years, so the topics considered in this book are not entirely new The author claims that this is the first time that an attempt has been made to consider consistently gas–liquid chromatography and gas–liquid–solid chromatography Whether or not this is true does not really matter The main point is that a text has been produced which considers, in some detail, theoretical and practical aspects of gas–liquid–solid chromatography and so it should be helpful to scientists interested in the fundamental basis of chromatographic separations

D LITTLEJOHN

Potentiometric Water Analysis, Second Edition: D MIDGLEY and K. TORRANCE, Wiley, Chichester, 1991 Pages xiv + 586 £65.00. ISBN 0-471-92983-2

This is a welcome revision of Midgley and Torrance's authoritative text first published in 1978 The format of the first edition has been maintained, but the content has been updated to include recent developments in electrode technology and potentiometric methods of importance in water analysis This is very much a practical textbook where the authors have tried to provide enough information to enable the analyst to use commercially available ion-selective electrodes without having to undertake extensive method development

Part I provides a theoretical and practical background to potentiometry and Part II contains almost 400 pages of analytical methods for water analysis Separate chapters in Part I cover electrochemical principles, potentiometric instrumentation and methodology The theory of electrochemistry is covered in sufficient detail to allow the analyst to understand the practical importance of the principles and relationships which affect activity, electrode potentials, liquid junction potentials, etc The fundamental basis of different types of ion-selective electrodes (ISE) are described, but without a detailed explanation of the mechanisms of electrode response Similarly, the chapter concerned with instrumentation describes what can be achieved with modern potentiometric equipment without labouring the technicalities In contrast, the authors have taken the trouble to point out the importance of establishing the analytical viability of a method and many readers will find the chapter on the statistical evaluation of data extremely helpful Many papers published on potentiometric analysis fail to give details of accuracy and precision and omit a discussion of errors The authors have tried to compensate for those deficiencies by providing a realistic indication of the performance of various types of electrodes when applied in water analysis

The value of the book to many readers will be the extensive notes on over 35 separate ISE applications given in Part II Not only are the apparatus, reagents and procedures described in adequate detail, but sources of error and electrode performance are discussed, comments on the lifetime of electrodes, typical response times and comparisons with other methods, where appropriate.

The ability of potentiometry to provide low-cost measurements in field and laboratory applications, as well as in on-line monitoring, has made the technique very important in water analysis Midgley and Torrance have provided an up-to-date review of methods and procedures which is clearly written and easy to read Each chapter is accompanied by a list of references covering developments up to 1990

Although the text does not contain all that many figures, it has numerous tables of useful information on electrochemical data, electrode comparisons and analytical methods. There is also a list of manufacturers of potentiometric equipment Anyone interested in potentiometry or water analysis should obtain a copy of this book

D LITTLEJOHN

Spectrochemical Analysis by Atomic Absorption and Emission: L. LAJUNEN Royal Society of Chemistry, Cambridge 1992 £18.50 (softback) Pages xii + 242 ISBN 0-851-86873-8

This book is very timely, coming on the market, as it does, when the modern analytical atomic spectroscopies such as ICP–MS are becoming firmly established necessitating their inclusion with more than a passing reference in our training courses Substantial chapters deal with Theory of atomic spectroscopy, Atomic absorption, Plasma atomic emission, ICP–MS, Atomic fluorescence, Sample preparation, while some smaller chapters cover the Histological background and Comparisons Flame emission is dismissed in two sides, so the book cannot be described as long-winded!

The author's practical experience comes over on many occasions through his comments on the practical consequences and the relevance of this or that aspect of theory and so on The author has included numerous diagrams, some his own,

many taken from the publications of the major manufacturers Comparisons of performance and statements on interferences and other problems are illustrated by tables or figures, well referenced Nebulisers and sample introduction, Electrothermal atomization, Background correction, Hydride generation, Cold-vapour technique, Optics of spectrometers, all receive thorough treatment in this book.

It is suggested that this book is for undergraduates and lecturers would that we have sufficient time in undergraduate courses to deal so thoroughly with this topic and others in analytical chemistry. However, for advanced Diploma and Masters courses this could become a welcome course text, at a size and price appropriate to the market There are a few minor errors in text and in figures—even in fact, as when the temperature of the nitrous oxide flame is said to be only a little *lower* than that of the air–acetylene flame—but these do not detract from the considerable value of this book. The balance of the discussion is good, the illustrative detail is good, and the presentation is clear

I L. MARR

Biosensor Principles and Applications: L J BLUM and P R COULET (Eds), Dekker, New York, 1991 Pages x + 357 £125.00 (US and Canada), $143 75 (elsewhere) ISBN 0-8247-8546-0

This is the 15th volume in the series on Bioprocess Technology by W. C McGregor

For those who are already involved in the multi-disciplined biosensor field or about to embark into this field this book will serve as a comprehensive, up-to-date, reference source.

Every major type of biosensor is included The main emphasis is on the enzyme based types and fiberoptic biosensors But many others such as immunosensors, microbial biosensors, *in vivo* biosensors are all given separate chapters The presentation and language used to explain how a particular biosensor works is not too technical yet is sufficient to enable the reader to understand how it works, the characteristics of its performance and its limitations Considering the large number of contributors involved from different countries, a high standard of presentation is maintained throughout the 14 chapters As expected there are one or two isolated instances of variation, e g., Fig 3 on p 73 and the equation on p 250 are difficult to read—possibly because of size reduction problems

All authors uniformly make the reader aware that despite the advances in biosensor technology over the last 20 years, this field of endeavour is still in its infancy and has yet unfulfilled potential Those wishing to obtain a foretaste of achievable future developments in industrial, environmental and health monitoring need go no further than to read the final chapter In so doing there is no doubt that the rest of the text will be read and the book recognised as a valuable general reference source for biosensors

R R MOODY

Standardization Within Analytical Chemistry: P KIVALO, Akadémiai Kiadó, Budapest, 1989 Pages 155 + appendices US $36

As a scientific discipline, analytical chemistry is a branch of metrology As Lord Kelvin pointed out, " when you can measure what you are speaking about and express it in numbers, you know something about it " The expression of analytical information in numbers unfortunately cannot always be referred uniquely to the basic physical constants For this reason it is often necessary to specify in detail how the measurement is to be performed Uniform procedures are essential if the highest reliability and repeatability are to be attained The requisite definitions, procedures, and calculations are collectively embodied in the standardization for each particular measurement

This book discusses in detail the several aspects of standardization and the steps in their development Standard methods or techniques are based on sound scientific principles Nevertheless, standardized or test methods for specific purposes or commercial products must often take into account the individual characteristics of the material to be analysed in order to ensure quality control and fitness for the intended purpose. In these instances, "pure" analytical chemistry becomes "applied" analytical chemistry in the development of protocols and certified reference materials. This process, the domain of numerous national and international standardizing bodies, is traced with logic and clarity in the seven chapters of the book.

Following an introduction, the history of analytical chemistry and the development of metrology are reviewed briefly In Chapters 3 and 4, the reader is introduced to early international standardization efforts, especially through ISO and IEC (of which Lord Kelvin was the first president), and the International Union of Pure and Applied Chemistry (IUPAC) Chapter 5 contains 53 pages and is the longest in the book, it is devoted to such matters as terminology, sampling and quality assurance, collaborative studies, and standard reference materials The latter subject may merit more attention than it receives in the few pages allotted to it. Reference standards are currently available in a variety of forms, and they may be certified for composition or for many different properties critical to special analytical problems The short final chapters discuss legal aspects and future trends in standardization

Especially commendable is the inclusion, among the appendices, of the 49-page ISO Guide 2—1986, "General terms and their definitions concerning standardization and related activities". Terms relating to all aspects of standardization are defined in English, French, and Russian, while the equivalent terms in German, Spanish, Italian, Dutch and Swedish are listed

This book is recommended to all who are concerned with the development, nature, and application of analytical standards.

R G BATES

many taken from the publications of the major manufacturers Comparisons of performance and statements on interferences and other problems are illustrated by tables or figures, well referenced Nebulisers and sample introduction, Electrothermal atomization, Background correction, Hydride generation, Cold-vapour technique, Optics of spectrometers, all receive thorough treatment in this book.

It is suggested that this book is for undergraduates and lecturers would that we have sufficient time in undergraduate courses to deal so thoroughly with this topic and others in analytical chemistry. However, for advanced Diploma and Masters courses this could become a welcome course text, at a size and price appropriate to the market There are a few minor errors in text and in figures—even in fact, as when the temperature of the nitrous oxide flame is said to be only a little *lower* than that of the air–acetylene flame—but these do not detract from the considerable value of this book. The balance of the discussion is good, the illustrative detail is good, and the presentation is clear

I L. MARR

Biosensor Principles and Applications: L J BLUM and P R COULET (Eds), Dekker, New York, 1991 Pages x + 357 £125.00 (US and Canada), $143 75 (elsewhere) ISBN 0-8247-8546-0

This is the 15th volume in the series on Bioprocess Technology by W. C McGregor

For those who are already involved in the multi-disciplined biosensor field or about to embark into this field this book will serve as a comprehensive, up-to-date, reference source.

Every major type of biosensor is included The main emphasis is on the enzyme based types and fiberoptic biosensors But many others such as immunosensors, microbial biosensors, *in vivo* biosensors are all given separate chapters The presentation and language used to explain how a particular biosensor works is not too technical yet is sufficient to enable the reader to understand how it works, the characteristics of its performance and its limitations Considering the large number of contributors involved from different countries, a high standard of presentation is maintained throughout the 14 chapters As expected there are one or two isolated instances of variation, e g., Fig 3 on p 73 and the equation on p 250 are difficult to read—possibly because of size reduction problems

All authors uniformly make the reader aware that despite the advances in biosensor technology over the last 20 years, this field of endeavour is still in its infancy and has yet unfulfilled potential Those wishing to obtain a foretaste of achievable future developments in industrial, environmental and health monitoring need go no further than to read the final chapter In so doing there is no doubt that the rest of the text will be read and the book recognised as a valuable general reference source for biosensors

R R MOODY

Standardization Within Analytical Chemistry: P KIVALO, Akadémiai Kiadó, Budapest, 1989 Pages 155 + appendices US $36

As a scientific discipline, analytical chemistry is a branch of metrology As Lord Kelvin pointed out, " when you can measure what you are speaking about and express it in numbers, you know something about it " The expression of analytical information in numbers unfortunately cannot always be referred uniquely to the basic physical constants For this reason it is often necessary to specify in detail how the measurement is to be performed Uniform procedures are essential if the highest reliability and repeatability are to be attained The requisite definitions, procedures, and calculations are collectively embodied in the standardization for each particular measurement

This book discusses in detail the several aspects of standardization and the steps in their development Standard methods or techniques are based on sound scientific principles Nevertheless, standardized or test methods for specific purposes or commercial products must often take into account the individual characteristics of the material to be analysed in order to ensure quality control and fitness for the intended purpose. In these instances, "pure" analytical chemistry becomes "applied" analytical chemistry in the development of protocols and certified reference materials. This process, the domain of numerous national and international standardizing bodies, is traced with logic and clarity in the seven chapters of the book.

Following an introduction, the history of analytical chemistry and the development of metrology are reviewed briefly In Chapters 3 and 4, the reader is introduced to early international standardization efforts, especially through ISO and IEC (of which Lord Kelvin was the first president), and the International Union of Pure and Applied Chemistry (IUPAC) Chapter 5 contains 53 pages and is the longest in the book, it is devoted to such matters as terminology, sampling and quality assurance, collaborative studies, and standard reference materials The latter subject may merit more attention than it receives in the few pages allotted to it. Reference standards are currently available in a variety of forms, and they may be certified for composition or for many different properties critical to special analytical problems The short final chapters discuss legal aspects and future trends in standardization

Especially commendable is the inclusion, among the appendices, of the 49-page ISO Guide 2—1986, "General terms and their definitions concerning standardization and related activities". Terms relating to all aspects of standardization are defined in English, French, and Russian, while the equivalent terms in German, Spanish, Italian, Dutch and Swedish are listed

This book is recommended to all who are concerned with the development, nature, and application of analytical standards.

R G BATES

Chromatography, 5th Edition—fundamentals and applications of chromatography and related differential migration methods: E HEFTMANN (editor), Elsevier, Amsterdam, 1992 Part A· fundamentals and techniques. Pages xxxvi + 552 Dfl 350 00 Part B· applications. Pages xxxii + 630. Dfl 370 00 Parts A and B set price Dfl 650.00

The fifth edition comprising Part A, on fundamentals and techniques, and Part B, on applications, is a completely revised edition of an important text on chromatography with contributions from 38 authors. Chapters on countercurrent chromatography, supercritical fluid chromatography, affinity chromatography and field flow fractionation have been added to Part A In Part B, chapters on proteins on peptides, nucleic acids and their constituents and pharmaceuticals have been strengthened

Chapter 1 is an excellent introduction, providing an overview of the theory of chromatography with emphasis on a simplified treatment of the more practical chromatographic concepts The theory of chromatography has evolved to such an extent that no single volume, let alone a single chapter, could address this topic satisfactorily but to compensate for this fact, a number of valuable general references are listed amongst the 142 references for this chapter

Chapter 2 deals with countercurrent chromatography (CCC) The principles of the two basic systems of CCC, *i e* , the hydrostatic and hydrodynamic systems, are described together with the design and capability of 10 selected CCC instruments and a table of recent applications

Planar chromatography (PC) is the subject of the next chapter in which there are sections on classification of techniques, principal factors affecting separations, instrumentation, preparative PC and special PC techniques such as TLC/FID, a technique of growing importance in which separations take place on rods of adsorbent which, after development, are passed at constant speed through a flame ionization detector

Chapter 4, a very practical one on column liquid chromatography (CLC), is concerned mainly with the most widely used type of CLC—namely HPLC There are sections on solvent delivery systems, sample handling, columns and connectors, detectors, *etc.*, and a section on some new forms of liquid chromatography.

A comprehensive chapter on ion-exchange chromatography covers the synthesis and properties of ion-exchange resins, ion chromatography and variations of the ion-exchange technique such as ion-exclusion, ion-pair and ligand-exchange chromatography

Size exclusion chromatography (also variously known in the earlier literature as gel filtration, gel permeation chromatography, *etc.*) is dealt with in Chapter 6 in which there is a good balance of theoretical and practical aspects The next chapter on affinity chromatography is, not surprisingly, almost exclusively concerned with biospecific iterations and there is only a mention of the expansion of the method to include other types of interaction ,

Supercritical fluid chromatography (SFC), the subject of Chapter 8, was first applied in 1963 but, due to the rapid development of the instrumentally less challenging technique of HPLC, SFC has not progressed at the pace one might have expected However, many of the early problems associated with instrumentation and columns have been overcome and so the popularity of SFC is growing and it appears to have a bright future Since operating temperatures are typically much lower in SFC than in GC, it is suitable for thermolabile solutes such as explosives and for samples that are not sufficiently volatile for GC Furthermore, because on decompression, supercritical fluids turn into gases, typical GC detectors such as the FID may be used This is a very useful chapter which covers principles, columns, instrumentation and detectors

Gas chromatography, undoubtedly the principal method of analysis of volatile, thermally stable organic compounds present in mixtures, is the subject of the next chapter in which all the important aspects, from column type, carrier gas selection, instrumentation, detectors *etc* , are covered, although the chapter concentrates mainly on recent developments and trends There is a nice section on stationary phase selection including a consideration of chiral stationary phases and liquid crystal stationary phases

The penultimate chapter of Part A concerns field flow fractionation (FFF). The classification and treatment of the various techniques is well done but with a multitude of terms such as flow FFF (FFFF) and sedimentation/floatation focusing FFF (SFFFFF!) one is thankful for the comprehensive list of abbreviations provided at the beginning of the volume

The treatment of electrophoresis including immunoelectrophoresis, which forms the final chapter of Part A, is comprehensive, although in view of the growing importance of capillary zone electrophoresis, perhaps a little more space could have been devoted to that particular technique

In Part B there are chapters on the applications of the various techniques dealt with in Part A, to the separation and analysis of an assortment of compounds including inorganic species, amino acids and peptides, proteins, lipids, carbohydrates, nucleic acids, porphyrins, phenolic compounds, drugs, fossil fuels, synthetic polymers, pesticides and environmentally important samples

A useful feature of the work is a list of names and addresses of manufacturers and suppliers of chromatography and electrophoresis materials and equipment There are approximately 200 clear, good quality figures and 100 tables throughout this volume All chapters are well referenced—for example, three chapters have chosen 500 and 600 references and only two chapters have less than 100—the average being about 250.

Taken together, Parts A and B provide an incomparable source of reference for any worker engaged in the use of chromatographic methods

A K DAVIES

Emulsion Polymer Technology: R. D. ATHEY, Dekker, New York, 1991 Pages viii + 304. $110 00 (US and Canada), $126 50 (elsewhere).

The flavour of this book is accurately indicated in the first line of the preface where the author states that "there is a real need for a book on emulsion polymers that speaks directly to the users The need is not so much for erudition, but

Chromatography, 5th Edition—fundamentals and applications of chromatography and related differential migration methods: E HEFTMANN (editor), Elsevier, Amsterdam, 1992 Part A· fundamentals and techniques. Pages xxxvi + 552 Dfl 350 00 Part B· applications. Pages xxxii + 630. Dfl 370 00 Parts A and B set price Dfl 650.00

The fifth edition comprising Part A, on fundamentals and techniques, and Part B, on applications, is a completely revised edition of an important text on chromatography with contributions from 38 authors. Chapters on countercurrent chromatography, supercritical fluid chromatography, affinity chromatography and field flow fractionation have been added to Part A In Part B, chapters on proteins on peptides, nucleic acids and their constituents and pharmaceuticals have been strengthened

Chapter 1 is an excellent introduction, providing an overview of the theory of chromatography with emphasis on a simplified treatment of the more practical chromatographic concepts The theory of chromatography has evolved to such an extent that no single volume, let alone a single chapter, could address this topic satisfactorily but to compensate for this fact, a number of valuable general references are listed amongst the 142 references for this chapter

Chapter 2 deals with countercurrent chromatography (CCC) The principles of the two basic systems of CCC, *i e* , the hydrostatic and hydrodynamic systems, are described together with the design and capability of 10 selected CCC instruments and a table of recent applications

Planar chromatography (PC) is the subject of the next chapter in which there are sections on classification of techniques, principal factors affecting separations, instrumentation, preparative PC and special PC techniques such as TLC/FID, a technique of growing importance in which separations take place on rods of adsorbent which, after development, are passed at constant speed through a flame ionization detector

Chapter 4, a very practical one on column liquid chromatography (CLC), is concerned mainly with the most widely used type of CLC—namely HPLC There are sections on solvent delivery systems, sample handling, columns and connectors, detectors, *etc.*, and a section on some new forms of liquid chromatography.

A comprehensive chapter on ion-exchange chromatography covers the synthesis and properties of ion-exchange resins, ion chromatography and variations of the ion-exchange technique such as ion-exclusion, ion-pair and ligand-exchange chromatography

Size exclusion chromatography (also variously known in the earlier literature as gel filtration, gel permeation chromatography, *etc.*) is dealt with in Chapter 6 in which there is a good balance of theoretical and practical aspects The next chapter on affinity chromatography is, not surprisingly, almost exclusively concerned with biospecific iterations and there is only a mention of the expansion of the method to include other types of interaction ,

Supercritical fluid chromatography (SFC), the subject of Chapter 8, was first applied in 1963 but, due to the rapid development of the instrumentally less challenging technique of HPLC, SFC has not progressed at the pace one might have expected However, many of the early problems associated with instrumentation and columns have been overcome and so the popularity of SFC is growing and it appears to have a bright future Since operating temperatures are typically much lower in SFC than in GC, it is suitable for thermolabile solutes such as explosives and for samples that are not sufficiently volatile for GC Furthermore, because on decompression, supercritical fluids turn into gases, typical GC detectors such as the FID may be used This is a very useful chapter which covers principles, columns, instrumentation and detectors

Gas chromatography, undoubtedly the principal method of analysis of volatile, thermally stable organic compounds present in mixtures, is the subject of the next chapter in which all the important aspects, from column type, carrier gas selection, instrumentation, detectors *etc* , are covered, although the chapter concentrates mainly on recent developments and trends There is a nice section on stationary phase selection including a consideration of chiral stationary phases and liquid crystal stationary phases

The penultimate chapter of Part A concerns field flow fractionation (FFF). The classification and treatment of the various techniques is well done but with a multitude of terms such as flow FFF (FFFF) and sedimentation/floatation focusing FFF (SFFFFF!) one is thankful for the comprehensive list of abbreviations provided at the beginning of the volume

The treatment of electrophoresis including immunoelectrophoresis, which forms the final chapter of Part A, is comprehensive, although in view of the growing importance of capillary zone electrophoresis, perhaps a little more space could have been devoted to that particular technique

In Part B there are chapters on the applications of the various techniques dealt with in Part A, to the separation and analysis of an assortment of compounds including inorganic species, amino acids and peptides, proteins, lipids, carbohydrates, nucleic acids, porphyrins, phenolic compounds, drugs, fossil fuels, synthetic polymers, pesticides and environmentally important samples

A useful feature of the work is a list of names and addresses of manufacturers and suppliers of chromatography and electrophoresis materials and equipment There are approximately 200 clear, good quality figures and 100 tables throughout this volume All chapters are well referenced—for example, three chapters have chosen 500 and 600 references and only two chapters have less than 100—the average being about 250.

Taken together, Parts A and B provide an incomparable source of reference for any worker engaged in the use of chromatographic methods

A K DAVIES

Emulsion Polymer Technology: R. D. ATHEY, Dekker, New York, 1991 Pages viii + 304. $110 00 (US and Canada), $126 50 (elsewhere).

The flavour of this book is accurately indicated in the first line of the preface where the author states that "there is a real need for a book on emulsion polymers that speaks directly to the users The need is not so much for erudition, but

for simple explanation of operating mechanisms involved in the physics and chemistry of polymers and colloids as they apply to emulsion polymer manufacture and use".

There are four sections in this book which are sub-divided into essentially stand-alone chapters The first section contains a discussion of formulation for various industries, a very basic introduction to colloid science, an even more basic introduction to polymer chemistry and concludes with a useful discussion of emulsion polymerization procedures on the laboratory and pilot-plant scales. The second section is titled "The Monomers" It is sub-divided into the vinyl monomers, styrenes, acrylates and methacrylates, diene monomers, waterborne condensation polymers and by-products in the latex Each section is well referenced from both the patent and the scientific literatures The next section deals with analysis and testing which includes discussions of viscometry, surface tension measurements, particle size analysis, mechanical stability, electrophoretic mobility, residual monomer measurement and molecular weight determination. The final section contains a discussion of colloidal stabilizers, rheology modifiers, curatives, heat and UV stabilizers, biocides and of fillers, pigments and reinforcing agents

The book, which is well indexed, will be primarily of use to those readers who work in industry Although it is not aimed at the academic researcher, some parts would serve as useful introductions to specific topics such as particle size analysis Given its rather high price, it is likely to find itself predominantly on library shelves

D J HOURSTON

HyperChem—Release 2 for Windows: 1992: AUTODESK Ltd , Cross Lanes, Guildford, Surrey, U K £500 00 (Educational users), £2000 00 (Other users)

HyperChem is a suite of programs for the generation and examination of molecular images on a personal computer It consists of two discs, three manuals and a hardware lock (dongle) which are all delivered in a large box If you lose the dongle the whole package must be purchased again so take great care that it stays firmly attached to the back of the computer. A free demonstration disc is also available The basic PC requirements are 4MB of memory, a 386 (or 486) with a maths co-processor, 20MB of hard disc space and preferably a colour monitor (VGA) HyperChem operates under Microsoft's Windows (version 3, at least) so a mouse is also required.

The manuals are, on the whole, very extensive and very helpful and the program suite loads easily into the PC On starting Windows a HyperChem icon consisting of a green liquid in a beaker appears, double clicking on this icon starts the show I tried HyperChem with a Cyrix 486 processor (an Intel chip is the standard processor) and Windows version 3 1—no problems were encountered

The "Getting Started" manual contains several tutorials for new users of the system and I was able to follow all of these with ease Details on how to drive HyperChem from Excel and Visual Basic are also given The "Computational Chemistry" manual is a good basic introduction to both molecular mechanics and quantum mechanics Compared to some other molecular graphic systems, I found it very easy to create images of molecules on the screen and one of my research students was manipulating 3D images within minutes of using the program suite Molecules are first drawn in 2D and then by a mere click of the mouse—hey presto—a 3D structure appears with hydrogens added automatically This is very impressive but care should be taken to realize that molecules will have been given standard geometrical values and, *e g* , staggered hydrogen arrangements if appropriate. Chirality also needs to be checked HyperChem then allows more realistic geometries to be generated by energy minimization. Measuring features of the molecular images was very simple—bond lengths, non-bonded distances, valency and torsion angles were all included in the available options.

HyperChem is especially helpful for those wishing to examine proteins and amino-acids as a library of such fragments is included Brookhaven protein database files can also be used and some of these files are included in the package

I was particularly interested in the molecular mechanics capabilities of HyperChem and the MM+, AMBER, BIO+ and OPLSA force fields are provided. Semi-empirical methods (Extended Huckel, CNDO, INDO, MINDO/3, MNDO and AM1) are also available I was pleased to see that the user may change or add parameters to the MM+ (based on Allinger's MM2) force field The appropriate files are available as text files and can hence be edited All atom types are available in MM+ and up-to-date references of parameters are given in the manuals and the programs When the potential energy of a molecular representation is minimized it must be remembered that we are dealing with just a sophisticated model of the system (generated by mathematical manipulations not actual experimental data) and that some "molecules" will be more accurately modelled than others When accurate structures of small molecules are already known from X-ray crystallographic studies the user should be able to import these (*e g.*, from the CSSR database) into HyperChem. In this respect the manuals do not explain how to use atom coordinates based on fractions of unit cell edges, but, as Brookhaven file can be read, this should presumably be a possibility. The user should also be warned that molecular mechanics studies involving, for example, heavy atom molecules are less accurate than those involving hydrocarbons as the latter are associated with better characterized parameters

The graphics are impressive and a student is in danger of believing that reality is being displayed but molecular chemistry in 3D is not the only way to view the subject

Molecular mechanics normally gives an insight into molecular conformations in a hypothetical isolated state at absolute zero However, with HyperChem molecular dynamics simulations can be performed in the presence of a box of water molecules

Investigations involving electrons requires the use of the semi-empirical options and plots of electron density and molecular orbitals can be obtained All of the semi-empirical calculations are best performed on small molecular systems as the computer time required can run into hours In this respect a powerful PC is recommended as such calculations are normally performed on more powerful machines—such as Cray supercomputers!

for simple explanation of operating mechanisms involved in the physics and chemistry of polymers and colloids as they apply to emulsion polymer manufacture and use".

There are four sections in this book which are sub-divided into essentially stand-alone chapters The first section contains a discussion of formulation for various industries, a very basic introduction to colloid science, an even more basic introduction to polymer chemistry and concludes with a useful discussion of emulsion polymerization procedures on the laboratory and pilot-plant scales. The second section is titled "The Monomers" It is sub-divided into the vinyl monomers, styrenes, acrylates and methacrylates, diene monomers, waterborne condensation polymers and by-products in the latex Each section is well referenced from both the patent and the scientific literatures The next section deals with analysis and testing which includes discussions of viscometry, surface tension measurements, particle size analysis, mechanical stability, electrophoretic mobility, residual monomer measurement and molecular weight determination. The final section contains a discussion of colloidal stabilizers, rheology modifiers, curatives, heat and UV stabilizers, biocides and of fillers, pigments and reinforcing agents

The book, which is well indexed, will be primarily of use to those readers who work in industry Although it is not aimed at the academic researcher, some parts would serve as useful introductions to specific topics such as particle size analysis Given its rather high price, it is likely to find itself predominantly on library shelves

D J HOURSTON

HyperChem—Release 2 for Windows: 1992: AUTODESK Ltd , Cross Lanes, Guildford, Surrey, U K £500 00 (Educational users), £2000 00 (Other users)

HyperChem is a suite of programs for the generation and examination of molecular images on a personal computer It consists of two discs, three manuals and a hardware lock (dongle) which are all delivered in a large box If you lose the dongle the whole package must be purchased again so take great care that it stays firmly attached to the back of the computer. A free demonstration disc is also available The basic PC requirements are 4MB of memory, a 386 (or 486) with a maths co-processor, 20MB of hard disc space and preferably a colour monitor (VGA) HyperChem operates under Microsoft's Windows (version 3, at least) so a mouse is also required.

The manuals are, on the whole, very extensive and very helpful and the program suite loads easily into the PC On starting Windows a HyperChem icon consisting of a green liquid in a beaker appears, double clicking on this icon starts the show I tried HyperChem with a Cyrix 486 processor (an Intel chip is the standard processor) and Windows version 3 1—no problems were encountered

The "Getting Started" manual contains several tutorials for new users of the system and I was able to follow all of these with ease Details on how to drive HyperChem from Excel and Visual Basic are also given The "Computational Chemistry" manual is a good basic introduction to both molecular mechanics and quantum mechanics Compared to some other molecular graphic systems, I found it very easy to create images of molecules on the screen and one of my research students was manipulating 3D images within minutes of using the program suite Molecules are first drawn in 2D and then by a mere click of the mouse—hey presto—a 3D structure appears with hydrogens added automatically This is very impressive but care should be taken to realize that molecules will have been given standard geometrical values and, *e g* , staggered hydrogen arrangements if appropriate. Chirality also needs to be checked HyperChem then allows more realistic geometries to be generated by energy minimization. Measuring features of the molecular images was very simple—bond lengths, non-bonded distances, valency and torsion angles were all included in the available options.

HyperChem is especially helpful for those wishing to examine proteins and amino-acids as a library of such fragments is included Brookhaven protein database files can also be used and some of these files are included in the package

I was particularly interested in the molecular mechanics capabilities of HyperChem and the MM+, AMBER, BIO+ and OPLSA force fields are provided. Semi-empirical methods (Extended Huckel, CNDO, INDO, MINDO/3, MNDO and AM1) are also available I was pleased to see that the user may change or add parameters to the MM+ (based on Allinger's MM2) force field The appropriate files are available as text files and can hence be edited All atom types are available in MM+ and up-to-date references of parameters are given in the manuals and the programs When the potential energy of a molecular representation is minimized it must be remembered that we are dealing with just a sophisticated model of the system (generated by mathematical manipulations not actual experimental data) and that some "molecules" will be more accurately modelled than others When accurate structures of small molecules are already known from X-ray crystallographic studies the user should be able to import these (*e g.*, from the CSSR database) into HyperChem. In this respect the manuals do not explain how to use atom coordinates based on fractions of unit cell edges, but, as Brookhaven file can be read, this should presumably be a possibility. The user should also be warned that molecular mechanics studies involving, for example, heavy atom molecules are less accurate than those involving hydrocarbons as the latter are associated with better characterized parameters

The graphics are impressive and a student is in danger of believing that reality is being displayed but molecular chemistry in 3D is not the only way to view the subject

Molecular mechanics normally gives an insight into molecular conformations in a hypothetical isolated state at absolute zero However, with HyperChem molecular dynamics simulations can be performed in the presence of a box of water molecules

Investigations involving electrons requires the use of the semi-empirical options and plots of electron density and molecular orbitals can be obtained All of the semi-empirical calculations are best performed on small molecular systems as the computer time required can run into hours In this respect a powerful PC is recommended as such calculations are normally performed on more powerful machines—such as Cray supercomputers!

Overall a very impressive package which will become more important as the power of PCs improves I recommend it to all who are interested in molecular chemistry Those academics with access to enterprise funds should include this package in their software requests.

P J Cox

Talanta, Vol. 40, No. 7, pp. 957–967, 1993
Printed in Great Britain.

0039-9140/93 $6.00 + 0.00

RESPONSES OF H^+ SELECTIVE SOLVENT POLYMERIC MEMBRANE ELECTRODES FABRICATED FROM MODIFIED PVC MEMBRANES

ERNÖ LINDNER, VASILE V. COSOFRET, ROBERT P. KUSY and RICHARD P. BUCK
Department of Chemistry, The University of North Carolina at Chapel Hill, Chapel Hill, NC 27599-3290, U.S.A.

THOMAS ROSATZIN, ULRICH SCHALLER and WILHELM SIMON†
Department of Organic Chemistry, Swiss Federal Institute of Technology (ETH), Universitätstraße 16, CH-8092 Zürich, Switzerland

JUDIT JENEY, KLÁRA TÓTH and ERNÖ PUNGOR
Department of General and Analytical Chemistry, Technical University of Budapest, 1111 Budapest, Szent Gellért tér 4, Hungary

(*Received* 14 *December* 1992. *Accepted* 28 *January* 1993)

Summary—Potentiometric responses of a novel class of pH sensitive ionophores, namely several phenoxazine derivatives, were tested in different modified PVC matrices. The ionophores were compounded into liquid membranes as usual or were covalently coupled to the polymeric matrix. The general analytical performance of the membranes and other membrane characteristics (*i.e.*, resistance and response time, as measures of membrane decomposition or structural changes) were followed in time. The transient responses of membranes with mobile ionophores in high molecular weight (HMW) and carboxylated PVC (PVC–COOH) were compared to those with immobilized ionophores. The response time of membranes with immobilized ionophores was found to be between those with mobile ionophores in HMW (fast response) and PVC–COOH (sluggish response). Accordingly, the rate of response was correlated primarily to the –COOH content of the membranes.

To utilize the advantages of the existing semiconductor and microelectronics technologies and their potential for development of ion-selective microelectrode arrays for biological applications, attempts have been made to apply chemically sensitive membranes directly on to the surface of microelectronic devices.[1–4] Unfortunately, reducing the size of the sensor and changing the classical membrane electrode construction (internal reference electrode/internal filling solution/ion-selective membrane) to a planar sensor arrangement without a large liquid internal contact, brought several problems to light concerning the potential stability, reproducibility, response time and life time of these sensors, due to the stringent requirements in this field. Besides these, factors such as membrane biocompatibility and low membrane resistance became decisive in membrane optimization.

To reach the goal of microelectronically fabricated electrodes we were guided by existing information. Potentiometric sensors are useful when rapid direct signal transformation is needed, as in continuous monitoring and flow-through analysis.[5,6] The precision, reliability, short and long term stability, as well as the short response time of membrane-based sensors, make them attractive for biological applications.[6–13] Ionophore-based alkaline and alkaline earth ion-selective PVC membranes already proved their outstanding properties in different fields of potentiometric analysis.[10–17] Thus, we focus on two topics achieving (I) long sensor life time and (II) rapid response times.

(I) The sensor life time of planar microelectrodes is determined primarily by the dissolution of the membrane ingredients into the sample solution and by the adhesion of the membrane to the wafer (problems of encapsulation). In the recent past, ion-selective ionophore loaded PVC membranes have been extensively used for preparation of ion and molecule selective optical sensors.[18–23] Loss of membrane con-

stituents in these "bulk optodes" is even more important to be avoided, since, in contrast to the potentiometric sensors, the optical signal is directly dependent on the concentration of the components in the membrane.

Possibilities for elimination, or the slowing down of the process of leaching of membrane ingredients are: (1) use of ionophore and/or plasticizer free membranes;[24-30] (2) attachment of the ionophores to the matrix by covalent coupling;[31,32] (3) increasing the distribution coefficient of the components by introducing adequate structural elements (*e.g.*, large alkyl chains) or selecting membrane matrices of more advantageous partition properties;[33,34] (4) replacement of the low molecular weight mobile ionic additives (such as sodium tetraphenyl borate) with more lipophilic derivatives {*e.g.*, potassium tetrakis *p*-chlorophenyl borate or-sodium tetrakis[3,5-bis(trifluoromethyl)phenyl]-borate};[35,36] and (5) use of PVC compatible polymers as fixed site additives[37-39] instead of the lipophilic salts.[31]

(II) Recently, PVC membrane based calcium selective bulk optodes with immobilized phenoxazine derivatives as chromoionophores were described.[31] An important enhancement in sensor life time could be achieved by immobilizing the chromoionophore. However, the response time of these bulk optical sensors with immobilized ionophores was increased as well. Since phenoxazine derivatives have proven to be excellent ionophores in potentiometric pH sensors[40] it was of interest to study the effect of ionophore immobilization on the response of potentiometric electrodes, known as surface sensors. PVC matrix pH sensors with extended life time may be serious competitors to pH sensitive glass electrodes in some special fields of applications[24-26,40-44] such as cardiology.

This paper describes the responses of large numbers of H^+ selective electrodes tested as possible candidates to prepare planar ion-selective microelectrodes for cardiovascular applications. The membranes were fabricated from different modified and compounded PVC membranes since our aim was to select an optimal membrane composition for acute and chronic applications in cardiology. Accordingly, we compared the responses of the different matrices, studied changes of the membrane properties during a long period of time, and noted alterations of the dynamic responses as a function of membrane matrix modifications. Aminated and carboxylated PVC (PVC–NH_2 and PVC–COOH, respectively) were selected for these studies primarily as a consequence of their excellent adhesion properties[45-47] (crucial in the preparation of planar electrodes) while hydroxylated PVC (PVC–OH) seemed to be attractive since it has been reported as having no interference from serum proteins.[48]

Theoretical and experimental evidence for membrane component loss, solvent uptake and response time degradation

The conclusions from extensive theory and experiments[49-55] on bathed ion exchange membranes include the following.

(1) Interfacial potential differences (pds) depend thermodynamically on external bathing ion activity when the ion is previously incorporated in the membrane at constant activity. For example, aminated PVCs containing added TPB^- at exactly the same concentration as amine sites, should provide an ideal system: $RNH_3^+TPB^-$ (and ion pairs in equilibrium) that should maintain constant proton activity in the membrane.
(2) Any extraneous processes including (a) exchange of TPB^- for any other bathing solution anions; (b) water uptake to dilute the interior proton activity; (c) loss of plasticizer to concentrate the site density and thereby change the proton activity, will perturb the interfacial pds.
(3) Factors in (2) shift each interfacial pd, and if the system does not respond exactly "symmetrically", there will be a shift in the asymmetry potential, *e.g.*, a shift in E°.
(4) Uptake of water or loss of plasticizer causes formation of surface layers of different composition compared with the bulk composition. The interfacial pds are then complicated by diffusion pds between the outer membrane surface and the interface between the perturbed layer and the original, homogeneous bulk. Thus, time dependent responses to activity steps in solution are predicted. As surface layers become thicker, time responses are longer.

These conclusions follow from studies of response mechanisms of ion-selective electrodes using different transient techniques.[27,56-59] The results for several ion-selective electrodes demonstrated high resistance surface film formation[27,56,58] from plasticizers and impurities in plasticizers and/or membrane matrix materials

such as PVC. In the case of glass electrodes, high resistance surface layers are formed by hydrolysis of the glass to form silica gel, and, if dried, partly silica layers.[60] Morf has shown that when the surface region has a different selectivity coefficient for each species, compared with the membrane bulk, there is a voltage off-set.[61] On the basis of his model, long term changes of electrode response to primary ion activity steps and interfering cation activity changes could be explained.

In polymers with positively or negatively charged groups,[45,46] uptake of water is expected by unbalance of osmotic pressure. This uptake may be accompanied by the formation of hydrophilic (colloidal) water droplets,[62–64] by membrane hydrolysis or by the formation of ion–dipole clusters.[65,66] The probability of formation of such "inhomogenities" (hydrophilic or hydrophobic domains) is considerably larger in modified PVC matrices with high concentrations of sites compared to high molecular weight PVCs of low ion exchange capacity. The process may start at the membrane surface as a consequence of aqueous solution contact, and is thought to be prolonged in time as water penetrates into the bulk of the membrane. Along with these structural changes, alterations of the selectivity coefficients and increases in the total membrane resistance and in the response time are expected.[26]

For the quantitative evaluation of the potential–time transients, the following two equations were used:[59,67]

$$E(t) = E_2 + S \log\left(1 - \left(1 - \frac{a_{i,1}}{a_{i,2}}\right) e^{-t/\tau_1}\right) \quad (1)$$

and

$$E(t) = E_2 + S \log\left(1 - \left(1 - \frac{a_{i,1}}{a_{i,2}}\right) \frac{1}{\sqrt{t/\tau_2 + 1}}\right), \quad (2)$$

where $E(t)$ is a time dependent potential at time t following a sudden change of the sample solution activity; E_2 is the final steady-state potential; $a_{i,1}$ and $a_{i,2}$ are the solution activities before and after the activity change in the sample, respectively; τ_1 and τ_2 are time constants and S is the experimentally determined slope of the EMF–log a_i calibration curve.

Equation (1) was suggested as an approximate description of the potential–time transients when diffusion/equilibration processes within the aqueous boundary layer are assumed to be rate determining. Equation (2) applies when transport processes within the membrane are thought to be decisive in determining the rate of response.[59,67] The time constant of equation (2) depends on the diffusion coefficients in the membrane and in the aqueous boundary layer, on the thickness of the boundary layer and on the partition parameter K. The partition parameter K was found to depend on the equilibrium constant (K_{ex}) of the dominant extraction reaction [equation (3)] and on the concentration of free ligand within the membrane.[67]

$$M^{z+}(aq) + zX^-(aq) + kR^-(m) + rL(m) \leftrightarrows ML_l^{z+}(m) + kR^-(m) + zX^-(aq) + (r - l)L(m). \quad (3)$$

Accordingly, the polarity of a membrane has a direct influence on τ_2.[67] Higher polarity (PVC membranes containing –COOH, –OH, $-NH_2$ or $-SO_3H$ functional groups) result in slower responses.[58,68] Furthermore, the formation of surface layers with different properties from the bulk (hydrophilic or hydrophobic regimes) as a consequence of aqueous solution contact, is more likely in high site density modified PVCs compared to more conventional HMW PVCs. The increase in response time values for modified PVC as a function of solution contact (hydration) is consistent with the expectations.[9]

EXPERIMENTAL

Chemicals

For all experiments, deionized water doubly distilled in Pyrex glass and chemicals of puriss or pa grade were used.

Buffer solutions

For the determination of the pH sensitivity and potentiometric selectivites of the electrodes, the following buffer solutions were used:[40] (I) citrate–borate buffer with 60mM Li^+ ion background; (II) a TRIS buffer with 140.0mM Na^+ ion background; (III) a TRIS buffer with 200.0mM K^+ ion background, (IV) a Britton–Robinson buffer with or without 140mM NaCl (see Table 10.47 in Ref. 69). The pH of the solutions was adjusted by means of a hydrogen ion-selective glass electrode (Orion model 91–57) by the addition of hydrochloric acid or sodium hydroxide to the stock buffer solutions.

Membranes

The solvent polymeric membranes were prepared according to Ref. 70. Their most common

Table 1. Characterization of ETH 3531 and ETH 3534 by gel permeation chromatography. The relative amount of each component was calculated from the respective peak area (SD; $n = 3$)

Form of Nile Blue	ETH 3531	ETH 3534
Immobilized	95.3 ± 1.0%	86.6 ± 1.2%
Mobile	4.0 ± 1.0%	12.9 ± 1.3%
Other derivatives	0.7 ± 0.2%	0.5 ± 0.2%

composition was 1 wt % ionophore, 64–66 wt % plasticizer and 33 wt % PVC and 70 mole % (compared to the ionophore) potassium tetrakis (*p*-chlorophenyl) borate (KT*p*ClPB) as lipophilic salt additive. However, in some cases membranes without ionophore (mainly aminated PVC membranes) were also cast.

All ionophores and plasticizers were products of Fluka AG (Buchs, Switzerland) or synthesized in our laboratories: tridodecylamine (TDDA) (Fluka 95292); ETH5294 (Fluka 27086); ETH 2439 (Fluka 27087); 2-nitrophenyl octylether (o-NPOE) (Fluka 73741); Bis(2-ethylhexyl) sebacate (DOS) (Fluka 84818); ETH 5350 was synthesized as described in Ref. 31. As polymeric membrane materials, several commercially available products were tested: poly(vinyl chloride) (PVC, high molecular weight, HMW), Fluka 81392, carboxylated PVC (PVC–COOH, with 1.8% COOH groups), Aldrich, 18955 and hydroxylated PVC (PVC–OH), a copolymer of 91% vinyl chloride, 3% vinyl acetate and 6% vinyl alcohol, Fluka 27827. The latter could not be used alone for membrane casting (as a consequence of the bad mechanical properties of the membrane), but only as a 1:1 mixture with HMW. The 1,4-diamino butane and piperazine modified PVC samples were prepared in our laboratories with the reaction scheme suggested by Ma and Meyerhoff.[25] The H^+ sensitive ETH 3531 and ETH 3534 membrane matrices were synthesized as described in Ref. 31.

Synthesis and analysis of ETH 3531 and ETH 3534

The synthesis of Nile Blue directly bound to carboxylated PVC (ETH 3534) and to carboxylated PVC through a spacer (ETH 3531) is described in detail by Rosatzin *et al.*[31] The efficiencies of the conversions were followed by elemental analysis and absorption measurements[31] and the products were characterized by gel permeation chromatography (Table 1). The equipment used for gel permeation chromatography was a LiChroGraph® HPLC System (Merck, Darmstadt, Germany) including a gradient pump L-6200 and a D-6000 HPLC Manager Chromatography Data Station Software. A Kontron Uvikon LCD 725 (Kontron, Zürich, Switzerland) served as a detector. The column (600 × 7.5 mm I.D.) was a PLgel 5μ 100Å (Polymer Laboratories Ltd, Shropshire, U.K.) and THF with 1% (v/v) 0.02*M* $NaOCH_3$ in methanol was used as solvent at a flow rate of 2.0 ml/min.

EMF measurements

Cell voltages were measured at room temperature with an Orion Expandable Ion Analyzer (Model EA 920). As a reference electrode an Orion model 90-02 Ag/AgCl double junction reference electrode was used throughout. The readings were made when the potential changes were less than 0.2 mV/min.

Determination of the internal resistance of the cells

The internal resistances of the cells were determined by the voltage divider method using known shunts.[71,72] The potential drop at $t = 0$ (ΔE_Ω) was used to evaluate the ohmic resistance (R_Ω).

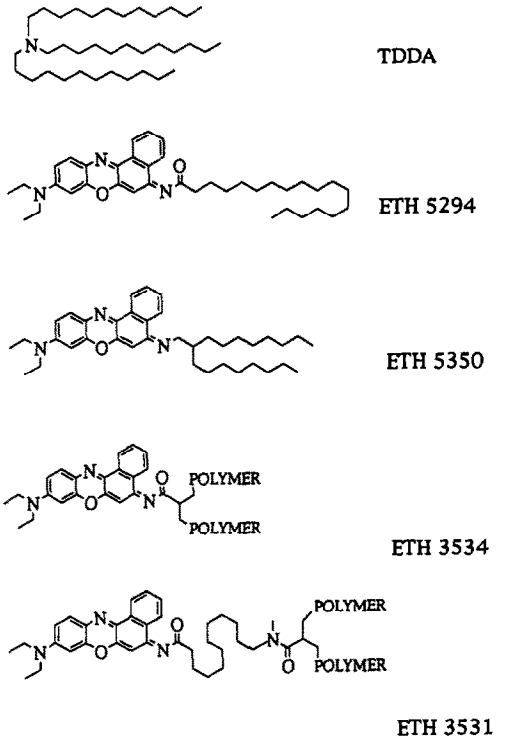

Fig. 1. The chemical structure of hydrogen sensitive ionophores discussed.

Table 2. Membrane compositions, response ranges, slopes*

Electrode No.	Matrix	H^+ ionophore	Plasticizer	Linear pH range	Slope (*mV/decade*)
1a	HMW†	ETH 5294	o-NPOE	(2.5)‡ 4.0–12	(58.9)‡ 59.3
b	HMW†	ETH 5350	o-NPOE	(2.5)‡ 4.5–12	(57.6)‡ 57.5
c	HMW†	TDDA	o-NPOE	4.0–12	59.7
2a	HMW†	ETH 5294	DOS	(2.5)‡ 4.0–11	(56.4)‡ 57.4
b	HMW†	ETH 5350	DOS	(2.0)‡ 3.5–12	(57.7)‡ 58.3
3a	PVC–COOH§	ETH 5294	o-NPOE	4.0–12	58.5
b	PVC–COOH§	ETH 5350	o-NPOE	(2.5)‡–12	57.6
4a	PVC–COOH§	ETH 5294	DOS	(2.5)‡–8.0	54.1
b	PVC–COOH§	ETH 5350	DOS	3.5–10	54.5
5	HMW + PVC–OH‖	ETH 5294	o-NPOE	4.0–12	58.5
6	PVC–NH_2(1,4-DAB)**	no ionophore	o-NPOE	4.0–10	54.9
7	PVC–NH_2(1,4-DAB)**	no ionophore	DOS	(2.5)‡–5	44.5
8	PVC–NH_2(1,4-DAB)**	ETH 5350	DOS	3.0–12	58.2
9	PVC–NH_2(PIP)††	no ionophore	o-NPOE	4.0–11	58.0
10	PVC–NH_2(PIP)††	no ionophore	DOS	4.0–10	53.3
11a	PVC–NH_2(PIP)††	ETH 5294	o-NPOE	(2.5)‡ 4.0–12	(57.5)‡ 59.1
b	PVC–NH_2(PIP)††	TDDA	o-NPOE	4.0–12	58.8
12	PVC–NH_2(PIP)††	ETH 5294	DOS	4.0–11	53.9
13	PVC–CO-Nile Blue‡‡	ETH 3534‡‡	DOS	5.5–10	54.3
14	PVC–CO-R-Nile Blue§§	ETH 3531§§	DOS	6.5–10	53.6

*The data were determined after a short period of conditioning time, generally after 1–3 days. All the membranes were fabricated with additional KTpClPB (10–70 mole % with respect to the ionophores or active sites).
†Membranes were prepared from Aldrich or Fluka HMW PVC but no difference was found.
‡The data in parentheses were determined in the Britton–Robinson buffer.
§Aldrich carboxylated PVC (PVC–COOH) with 1.8% COOH content.
‖1:1 mixture of Aldrich Very High Molecular Weight PVC and Fluka PVC–OH.
**1,4-diamino butane modified PVC, synthesized at the TU Budapest according to Ref. 25.
††Piperazine based aminated PVC, synthesized at the Medical School of the UNC Ref. 26.
‡‡Nile blue modified PVC–COOH synthesized at the ETH Zürich[31] see Fig. 3.
§§Nile blue modified PVC–COOH with "spacer" synthesized at the ETH Zürich[31]; see Fig. 1.

Response time measurements

To determine the dynamic response of different electrodes a switched wall jet arrangement was used.[59,73] The standard deviation of $t_{90\%}$ data as well as the rise times of the measuring electronics are given elsewhere.[58] All response time measurements were carried out in the presence of a background electrolyte of constant ionic strength in order to minimize the effect of streaming and diffusion potentials in the streaming sample solution.

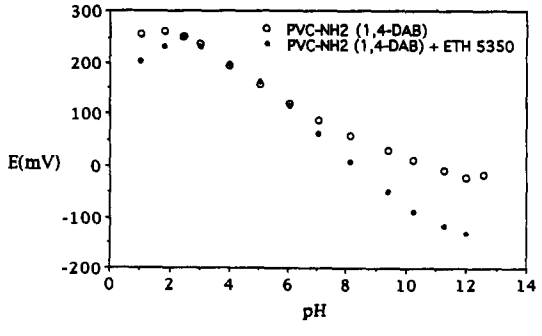

Fig. 2. pH response of a 1,4-diamino-butane based PVC–NH_2 electrode (7 and 8 in Table 2) after 1 month continuous contact with aqueous solution. ○ Ionophore free membrane; ● ETH 5350 compounded membrane.

RESULTS AND DISCUSSIONS

Response ranges and slopes

In the course of this work a large number of modified PVCs were compared on the basis of their potentiometric behavior. The chemical constitutions of the ionophores used in this work are summarized in Fig. 1 while the membrane compositions and some of the relevant parameters of the H^+ sensitive membrane electrodes are given in Table 2. Comparing the analytical parameters (selectivity coefficients, stability and reproducibility) of mobile ionophores (ETH 5294, ETH 5350) loaded into membranes cast from different PVCs (HMW, PVC–COOH, PVC–NH_2, PVC–OH), no significant differences were found, and the data were the same as published earlier for HMW membranes.[40] The linear response range can be extended to lower pH values using PVC–COOH as the matrix and DOS as the plasticizer. The properties of ionophore free H^+ selective

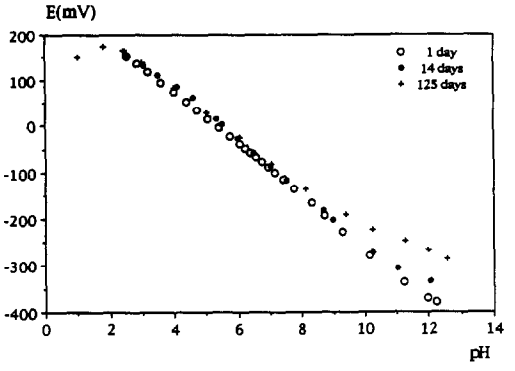

Fig. 3. EMF response of the ETH 5294 ionophore based pH electrode (3a) in the PVC–COOH matrix.

membranes (PVC–NH_2) are dependent on the chemical structure of the amine (basicity) as well as on several parameters related to the synthesis (*e.g.* N content and glass transition temperature of the aminated product *etc.*).[26] The analytical performance of the ionophore free membranes could be improved by the addition of mobile ionophore (Fig. 2). This improvement becomes more visible with elapsed time. The parameters of ETH 5350 compounded PVC–NH_2 membranes remain approximately constant, in contrast to the ionophore-free membranes where a slight decrease of the slope and a shift in detection limit to lower pH values were observed.[26] Similar loss of sensitivity was experienced with ETH 5294 compounded PVC–COOH electrodes in alkaline solutions after about 2 weeks (Fig. 3).

Time dependent membrane resistances

Information on the structural changes of the different membrane matrices as a function of aqueous solution contact is crucial in design of sensors for chronic applications. Accordingly, parallel to the analytical tests, membrane resistances were followed as a function of time by the voltage divider method (Table 3).[71,72] The electrodes were kept in a pH = 7.00 Tris buffer solution between the tests. The resistances of ETH 5294 based membranes increased significantly with time except with PVC–OH as the matrix. The largest increase in the bulk membrane resistance (R_Ω) was observed with PVC–NH_2 thereafter with PVC–COOH, HMW and PVC–OH membranes. These data correlate nicely with preliminary dissolution data carried out on modified PVC membranes containing the basic form of Nile Blue A as the ionophore. The amount of ionophore dissolved from different PVC membranes was the smallest for PVC–OH and the largest when PVC–NH_2 and PVC–COOH were used as matrices.[74]

The changes of membrane resistances with time (Table 3) substantially correspond with alterations of other membrane parameters as well. These changes are manifest in: (1) a shift of the lower limit of detection to higher hydrogen ion activities (Fig. 3); (2) changes of selectivity coefficients to larger values; (3) shift of the offset voltage of the cell ($E°$);[47] (4) slower time responses to step activity changes.[9,26]

No resistance increase was observed with TDDA compounded membranes during a 2 month period of time. In agreement with this result, the basic analytical parameters of these membranes were found to be constant.[47] Accordingly, we assume that the long term deterioration of ETH 5294 based sensor responses is mainly due to the loss of ionophore following its decomposition within the membrane. Naturally, the rate of decomposition is heavily influenced by several parameters like: (i) the pH of the sample solution, (ii) the energy and intensity of

Table 3. Membrane resistances (R_Ω) ($M\Omega$) as a function of contact time with the sample solution

Time (*Days*)	(1a)* HMW ETH-5294	(1c)* HMW TDDA	(3a)* PVC–COOH ETH-5294	PVC–COOH TDDA†	(7)* PVC–OH ETH-5294	(9)* PVC–NH_2 (PIP)	(11a)* PVC–NH_2 (PIP) ETH-5294	(11b)* PVC–NH_2 (PIP) TDDA
1	0.15	0.1	0.2			0.1	0.1	0.1
2				0.08	0.2			
12			0.9			1.0	1.2	0.4
15	0.85	0.3						
23					0.2			
30	3.6	0.6	7.3			6.9		
35							9.4	1.2
40	3.9	0.7						
50					0.2			
60			21.3	0.1	0.3	13	21.5	1.1

*Numbers in the first row correspond with the membrane numbers in Table 1.
†Membrane was fabricated with o-NPOE as plasticizer and 70 mole % KTpClPB.

Table 4. Compositions, slopes and $t_{90\%}$ response time data of pH sensitive membranes with mobile and immobilized H^+-ionophores. All membranes contained 1 wt% ionophore (or equivalent amounts immobilized), 66 wt% DOS, 33 wt% polymer and 10 mol % KTpClPB (in respect to the amount of ionophore)

Electrode No./ ionophore	Matrix (wt%) HMW PVC	Matrix (wt%) PVC–COOH	Response time, $t_{90\%}$ (ms) pH range 8.4→7.4	Response time, $t_{90\%}$ (ms) pH range 7.4→8.4	Slope (mV/pH) Solution I* pH range 8.4→7.4	Slope (mV/pH) Solution I* pH range 6.0→5.0	Slope (mV/pH) Solution II† pH range 6.0→5.0
Glass					58.0	58.0	56.0
2a/ETH 5294	33.5		36	31	58.4	56.8	53.7
4a/ETH 5294		33.5	510	335	49.0	57.9	52.8
13/ETH 3531	12.1	22.5	280	275	53.1	32.0	47.9
14/ETH 3534	22.0	12.6	105	105	58.4	36.4	39.9

*Solution I: 0.13*M* NaCl in 0.01*M* Tris/0.01*M* NaOH with pH 8.4 or pH 7.4.
†Solution II: 0.12*M* NaCl in 0.01*M* malonic acid/0.02*M* NaOH with pH 6.0 or pH 5.0.

illumination of the membrane, (iii) the pH of the matrix, *etc.* The pH of the matrix is quite acidic in the case of PVC–COOH or basic in PVC–NH_2. In addition to this the partition coefficient of the ionophore between the aqueous solution and PVC membrane may be different for the different modified PVCs.

Dynamic responses

Upon selecting ETH 5294 as a proton carrier for thin layer optical membranes[18] or planar micro pH electrode construction[47] the loss of membrane components from certain matrices seemed to be decisive in determining the corresponding sensor properties. To avoid problems connected with gradual changes in the membrane matrix composition, Nile Blue (the active ingredient) was bound directly or through a spacer to the carboxylated PVC matrix (Fig. 1; ETH 3531 and ETH 3534).[31] The efficiency of the conversion related to the available carboxyl groups was about 21% (ETH 3531) or 23% (ETH 3534) calculated from the elemental analysis.[31] The result of the gel permeation chromatography analysis showed that only a minor amount of the original ionophore (Nile Blue) was not covalently immobilized to the polymer (Table 1). All other reaction products of Nile Blue-like lipophylized derivatives were found to exist in concentrations smaller than 1%. The steady state and dynamic properties of membranes containing mobile ETH 5294 in HMW and PVC–COOH were then compared to the relevant characteristics of ETH 3531 and ETH 3534-based membranes. In this part of the work DOS was used as plasticizer. As a consequence, a considerable interference was experienced at relatively high pH values (Table 4).

The response times of membrane system 2a and 2b (mobile ETH 5294 or ETH 5350 in HMW (Table 2)) were found to be short and practically independent of the concentration of the sample solution. The same ionophores in carboxylated PVC (membranes 4a and 4b)

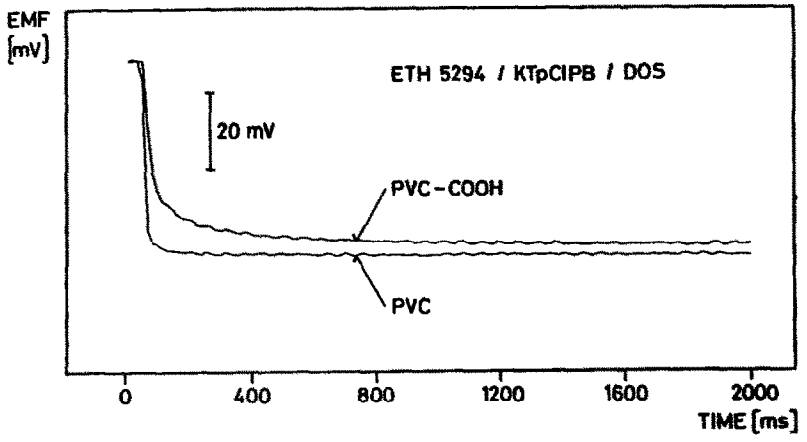

Fig. 4. The effect of the membrane matrix on the dynamic response curves of ETH 5294 ionophore based pH sensor fabricated from high molecular weight (2a) and carboxylated PVC (4a) as matrix (see Tables 2 and 4).

Table 5. $t_{90\%}$ values and time constants τ_1 and τ_2 of HMW and PVC–COOH membranes with the H^+-selective ionophore ETH 5294

Electrode No./ matrix	$t_{90\%}$ (*ms*) pH change Sol. I 7.4→8.4†	Sol. II 5.0→6.0†	Fitting parameters Eq. (1)* τ_1 (*ms*)	RMSD (*mV*)	Fitting parameters Eq. (2)* τ_2 (*ms*)	RMSD (*mV*)	$t_{90\%}$ (*ms*) pH change Sol. I 8.4→7.4†	Sol. II 6.0→5.0†
2a/HMW	31		3.70	0.48	0.01	0.26	36	
		58	5.50	1.24	0.10	0.39		91
4a/PVC–COOH	335		23.90	1.29	3.94	0.15	510	
		175	14.90	2.31	1.10	0.63		270

*During the measuring time of 1 sec, 1650 values were recorded and each 20th value (78 data points) was used for curve fitting.

†The numbers represent the negative logarithm of the activities of the solutions, $a_{i,1}$ and $a_{i,2}$ [Eqs (1) and (2)]. The arrows indicate the direction of the activity step.

showed a considerably slower response (Fig. 4 and Tables 4 and 5). Some increase in response time was expected on the basis of earlier literature findings.[9,58,68] However, in the activity range of pH = 8.4→7.4 the rate of response was 10–15 times slower for PVC–COOH membranes compared to HMW membranes. In the high pH ranges the effect of cation interference may make an important contribution to the rate of response (see the decreased slope values in the case of PVC–COOH membranes), but PVC–COOH based membranes had about a 3 times slower response in the pH range pH = 6.0→5.0 as well, where no interference is expected. In addition to this, equation (2) gave a much better fit (smaller RMSD data) to the transients recorded with PVC–COOH based membranes compared to equation (1) (Table 5) suggesting diffusional phenomena in the membrane phase.

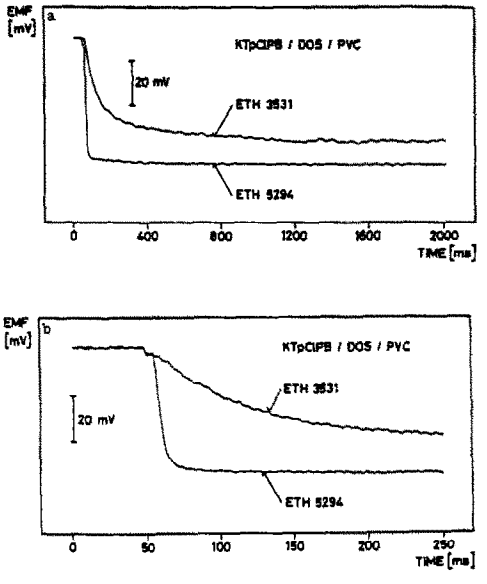

Fig. 5. Effect of ionophore immobilization on the dynamic response curves of pH sensitive liquid membranes in two different time domains (5a: 0–2000 ms; 5b: 0–250 ms). The membranes used for the response time studies contained the same amount of ionophore (mobile or immobilized) and the same PVC/plasticizer ratio.

The $t_{90\%}$ data (and in general the dynamic behavior) of membranes with covalently coupled active sites (ETH 3531 and ETH 3534) were found to be larger than those evaluated with mobile ETH 5294 in HMW (Figs 5a and b) but smaller compared to values determined with ETH 5294 in PVC–COOH. A comparison of the response time data summarized in Table 4 (for an activity step, pH = 8.4→7.4) suggests that the increase of response time is in close correlation with the free –COOH concentration of the membranes. The PVC–COOH concentration of membrane 4 (Table 2) is 33.5 wt % (the –COOH concentration ~134m*M*) while of membranes 13 and 14 (Table 2) 22.5 wt % (~95m*M*) or 12.6 wt % (~31m*M*), respectively. It is remarkable that the selectivity coefficients also vary in parallel with the –COOH content of the membranes (see the slopes in Table 4 in the range of pH = 7.4 and 8.4). The membrane with the highest –COOH content shows the most serious cation interference and so on. It is known that the rate of response of ion-selective electrodes becomes slower in the presence of considerable interference.[75] In addition the character of the response time curves proved to be more exponential with decreasing –COOH content [better fit to equation (1)—smaller RMSD values—compared to equation (2); see Table 6]. The increasing exponential character suggests that surface processes become more dominant with decreasing –COOH content. Consequently, the most dominant influence on the rate of response of H^+ selective membranes with covalently coupled ionophores cannot be attributed to the chemical structure or constitution of the ionophore–matrix coupling,

Table 6. Characteristic data of the response time curves ($t_{90\%}$ values) as well as of fitted theoretical equations (time constants τ_1, τ_2 and RMSDs), of membranes with mobile- and immobilized H^+-ionophores

	Matrix (wt%)		pH change 8.4→7.4*				
				Fitting parameters Eq. (1)†		Fitting parameters Eq. (2)†	
Electrode No./ ionophore	HMW PVC	PCV–COOH	$t_{90\%}$ (ms)	τ (ms)	RMSD (mV)	τ (ms)	RMSD (mV)
2a/ETH 5294	33.5		36	11.2	0.34	1.06	0.46
4a/ETH 5294		33.5	510	128	1.07	500	0.28
13/ETH 3531	12.1	22.5	280	145	0.65	684	1.54
14/ETH 3534	22.0	12.6	105	68.2	0.59	102	1.60

*The numbers represent the negative logarithm of the activities of the solutions, $a_{i,1}$ and $a_{i,2}$ [Eqs (1) and (2)]. The arrows indicate the direction of the activity step.

†During the measuring time of 1 sec, 1650 values were recorded and each 20th value (78 data points) was used for curve fitting.

but to the –COOH content of the membranes. It is primarily interesting in comparison to the transient response of bulk optodes with the same immobilized ionophores where the increased response times were attributed to changes in the membrane bulk transport properties.[31]

CONCLUSIONS

H^+-selective PVC membranes, fabricated from various modified PVCs, exhibit different short (response time) and long time (life time) behavior. The long time behavior of membranes with mobile ionophores is determined by the leaching out of membrane ingredients and is reflected in changes of the analytical performances (slopes and selectivities), electrical properties (bulk resistance and polarization) and dynamic response ($t_{90\%}$ response and response function) of the electrodes. These changes are related to the properties of the membrane matrix which is determined by the chemical character and the concentration of the various functional groups (–OH, –COOH, $-NH_2$) in modified PVCs. The immobilization of the ionophore extends the sensor life time. However, the concentration of the remaining functional groups (–COOH groups not converted in the immobilization reaction) proved to be decisive in the dynamic response behavior of membranes with covalently attached ionophores. The response times of membranes with immobilized ionophores decrease with decreasing –COOH content and approach the response time of membranes with mobile ionophores. By decreasing the –COOH content of the membranes to a minimal amount it should be possible to construct a pH sensitive microelectrode with an immobilized ionophore, having fast response and extended life time.

Acknowledgement—This work is partly supported by the North Carolina Biotechnology Center in support of the Duke–North Carolina Center for Emerging Cardiovascular Technologies.

REFERENCES

1. J. Janata and R. J. Huber, *Ion-sel. Electrode Rev.*, 1979, **1**, 31.
2. J. Janata and R. J. Huber, in H. Freiser (ed.), *Ion-selective Electrodes in Analytical Chemistry*, Vol. 2, Chapter 3. Plenum Press, New York, 1978.
3. P. Bergveld and A. Sibbald, "Analytical and biomedical applications of ion-sensitive field effect transistors" in G. Svehla (ed.), *Wilson and Wilson's Comprehensive Analytical Chemistry*, Vol. XXIII. Elsevier, Amsterdam, 1988.
4. J. Janata, *Principles of Chemical Sensors*. Plenum Press, New York, 1989.
5. E. Pungor, K. Tóth and A. Hrabéczy-Páll, *Trends Anal. Chem.*, 1984, **3**, 28.
6. K. Tóth, J. Fucskó, E. Lindner, Zs. Fehér and E. Pungor, *Anal. Chim. Acta*, 1986, **179**, 359.
7. P. C. Meier, D. Ammann, W. E. Morf and W. Simon, in J. Koryta (ed.) *Medical and Biological Applications of Electrochemical Devices*. John Wiley, Chichester, 1980.
8. U. Oesch, P. Anker, D. Ammann and W. Simon, in E. Pungor (ed.) *Ion-selective Electrodes*, 4. Akadémiai Kiadó, Budapest, 1985.
9. D. M. Band and T. Treasure, in A. K. Covington (ed.) *Ion-selective Electrode Methodology*. CRC Press, Boca Raton, FL, 1979.
10. U. Oesch, D. Ammann and W. Simon, *Clin. Chem.*, 1986, **32**, 1448.
11. M. E. Meyerhoff, *Clin. Chem.*, 1990, **36**, 1567.
12. W. Simon and U. E. Spichiger, *Internat. Lab.*, 1991, **21**, 35.
13. J. Jeney, K. Tóth, E. Lindner and E. Pungor, *Microchem. J.*, 1992, **45**, 232.
14. T. P. Byrne, *Selective Electrode Rev.*, 1988, **10**, 107.
15. B. M. Buckley and L. J. Russell, *Ann. Clin. Biochem.*, 1988, **25**, 447.

16. V. V. Cosofret and R. P. Buck, *Pharmaceutical Applications of Membrane Sensors*. CRC Press, Boca Raton, FL, 1992.
17. Z. R. Zhang and V. V. Cosofret, *Selective Electrode Rev.*, 1990, **12**, 35–135.
18. K. Seiler, *Ionenselektive Optodenmembranen*. Fluka AG, Buchs, Switzerland, 1991.
19. K. Seiler, K. Wang, E. Bakker, W. E. Morf, B. Rusterholtz, U. E. Spichiger and W. E. Simon, *Clin. Chem.*, 1991, **36**, 1350.
20. K. Seiler, W. E. Morf, B. Rusterholtz and W. Simon, *Anal. Sci.*, 1989, **5**, 557.
21. K. Wang, K. Seiler, W. E. Morf, U. E. Spichiger, W. Simon, E. Lindner and E. Pungor, *Anal. Sci.*, 1990, **6**, 715.
22. W. E. Morf, K. Seiler, B. Rusterholtz and W. Simon, *Anal. Chem.*, 1990, **62**, 738.
23. S. J. West, S. Ozawa, K. Seiler, S. S. S. Tan and W. Simon, *Anal. Chem.*, 1992, **64**, 533.
24. S. C. Ma, N. A. Chaniotakis and M. E. Meyerhoff, *Anal. Chem.*, 1988, **60**, 2293.
25. S. C. Ma and M. E. Meyerhoff, *Mikrochim. Acta I*, 1990, 197.
26. V. V. Cosofret, E. Lindner, R. P. Buck, R. P. Kusy and J. Q. Whitley, *J. Electroanal. Chem.*, 1993, **45**, 169.
27. E. Lindner, Zs. Niegreisz, K. Tóth, E. Pungor, T. R. Berube and R. P. Buck. *J. Electroanal. Chem.*, 1989, **259**, 67.
28. J. Pick, K. Tóth, E. Pungor, M. Vasak and W. Simon, *Anal. Chim. Acta*, 1973, **64**, 477.
29. I. A. Mostert, P. Anker, H.-B. Jenny, U. Oesch, W. E. Morf, D. Ammann and W. Simon, *Microchim. Acta, I*, 1985, 33.
30. H.-B. Jenny, C. Reiss, D. Ammann, B. Magyar, R. Asper and W. Simon, *Microchim. Acta, II*, 1980, 309.
31. Th. Rosatzin, P. Holy, K. Seiler, B. Rusterholtz and W. Simon, *Anal. Chem.*, 1992, **64**, 2029.
32. S. Daunert and L. G. Bachas, *Anal. Chem.*, 1990, **62**, 1428.
33. P. M. Gehrig, B. Rusterholtz and W. Simon, *Chimia*, 1989, **43**, 377.
34. P. M. Gehrig, B. Rusterholtz and W. Simon, *Anal. Chim. Acta*, 1990, **233**, 295.
35. H. Kobayashi, T. Sonoda, A. Sonoda and K. Fujiki, *J. Fluorine Chem.*, 1991, **54**, 61.
36. H. Nishida, N. Takada, M. Yoshimura, T. Sonoda and H. Kobayashi, *Bull. Chem. Soc. Jpn*, 1984, **57**, 2600.
37. O. Kedem, M. Perry and R. Bloch, *IUPAC International Symposium on Selective Ion Sensitive Electrodes*, paper 44, Cardiff, 1973.
38. E. Lindner, E. Gráf, Zs. Niegreisz, K. Tóth, E. Pungor and R. P. Buck, *Anal. Chem.*, 1986, **60**, 295.
39. Th. Rosatzin, E. Bakker, K. Suzuki and W. Simon, in preparation.
40. V. V. Cosofret, T. M. Nahir, E. Lindner and R. P. Buck, *J. Electroanal. Chem.*, 1992, **327**, 137.
41. P. Anker, D. Ammann and W. Simon, *Microchim. Acta, I*, 1988, 237.
42. D. Erne, D. Ammann and W. Simon, *Chimia*, 1979, **33**, 88.
43. D. Ammann, F. Lanter, R. A. Steiner, P. Schulthess, Y. Shijo and W. Simon, *Anal. Chem.*, 1981, **53**, 2267.
44. U. Oesch, Z. Brzozka, A. Xu, B. Rusterholtz, G. Suter, H. V. Pham, D. H. Welti, D. Ammann, E. Pretsch and W. Simon, *Anal. Chem.*, 1986, **58**, 2285.
45. T. Stachwill and D. J. Harrison, *J. Electroanal. Chem.*, 1986, **202**, 75.
46. D. J. Harrison, L. L. Cunningham, X. Li, A. Teclemariam and D. Perman, *J. Electrochem. Soc.*, 1988, **135**, 2473.
47. E. Lindner, V. V. Cosofret, S. Ufer, R. P. Buck, R. P. Kusy, R. B., Ash and H. T. Nagle, *J. Chem. Soc. Faraday Trans.*, 1993, **89**, 361.
48. L. F. Dürselen, D. Wegmann, K. May, U. Oesch and W. Simon, *Anal. Chem.*, 1988, **60**, 1455.
49. R. P. Buck, "Chemical sensor mechanisms—a progress report", in E. Pungor (ed.) *Ion-selective Electrodes*, 4, pp. 3–31. Adadémiai Kiadó, Budapest, 1985.
50. R. P. Buck, "Electrochemistry of ion-selective electrodes", in R. E. White, J. Bockris, B. Convay and E. Yeager (eds) *Comprehensive Treatise of Electrochemistry*, Vol. 8, Chapter 3, pp. 137–248. Plenum Pub., New York, 1984.
51. R. P. Buck and P. Vanysek, *J. Electroanal. Chem.*, 1991, **297**, 19.
52. M. L. Iglehart and R. P. Buck, *Talanta*, 1989, **36**, 89–98.
53. R. G. Bates, *Determination of pH Theory and Practice*, pp. 289–314. John Wiley, New York, 1964.
54. W. E. Morf, *The Principles of Ion-selective Electrodes and of Membrane Transport*. Elsevier, Amsterdam, 1981.
55. F. Helfferich, *Ion Exchange*, Chapter 7, pp. 323–336. McGraw-Hill, New York, 1962.
56. J. R. Sandifer and R. P. Buck, *J. Electroanal. Chem.*, 1974, **56**, 385.
57. K. Tóth, E. Gráf, G. Horvai, E. Pungor and R. P. Buck, *Anal. Chem.*, 1986, **58**, 2741.
58. M. Huser, P. M. Gehrig, W. E. Morf, E. Lindner, J. Jeney, K. Tóth and E. Pungor, *Anal. Chem.*, 1991, **63**, 1380.
59. E. Lindner, K. Tóth and E. Pungor, *Dynamic Characteristics of Ion-selective Electrodes*. CRC Press, Boca Raton, FL, 1988.
60. B. Karlberg, *J. Electroanal. Chem.*, 1973, **42**, 115.
61. W. E. Morf, *Anal. Lett.*, 1977, **10**, 87.
62. G. Horvai, V. Horváth, A. Farkas and E. Pungor, in E. Pungor (ed.), *Ion-selective Electrodes*, 5, p. 397. Akadémiai Kiadó, Budapest, 1989.
63. G. Horvai, E. Gráf, K. Tóth, E. Pungor and R. P. Buck, *Anal. Chem.*, 1986, **58**, 2735.
64. X. Li, S. Petrovich and D. J. Harrison, *Sensors Actuators*, 1990, **B1**, 275.
65. S. G. Cutler, *Polym. Preps., Am. Chem. Soc., Div. Polym. Chem.*, 1978, **19**, 330.
66. R. D. Lundberg, H. S. Makowski and L. Westerman, *Polym. Preps., Am. Chem. Soc., Div. Polym. Chem.*, 1978, **19**, 310.
67. W. E. Morf, E. Lindner and W. Simon, *Anal. Chem.*, 1975, **47**, 1596.
68. K. Tóth, E. Lindner, J. Jeney, E. Gráf, M. Horváth, E. Pungor, I. Bitter, T. Meisel, B. Ágai, L. Töke, R. P. Buck and R. Kellner, in E. Pungor (ed.), *Ion-selective Electrodes*, 5, p. 18. Akadémiai Kiadó, Budapest, 1989.
69. D. D. Perrin and B. Dempsey, *Buffers for pH and Metal Ion Control*. Chapman and Hall, London, 1974.
70. G. J. Moody, R. B. Oke and J. D. R. Thomas, *Analyst*, 1970, **95**, 910.
71. D. Ammann, E. Pretsch, W. Simon, E. Lindner, A. Bezegh and E. Pungor, *Anal. Chim. Acta*, 1985, **171**, 119.

72. D. Ammann, *Ion-selective Microelectrodes; Principles, Design and Application*, Chapter 18. Springer, Berlin, 1986.
73. E. Lindner, K. Tóth, E. Pungor, T. R. Berube and R. P. Buck, *Anal. Chem.*, 1987, **59**, 2213.
74. E. Lindner, V. V. Cosofret, T. M. Nahir and R. P. Buck, Characterisation of stability of modified PVC membranes for microfabricated ion-selective electrode arrays in biomedical applications, in A. M. Usmani (ed.) *Polymeric Materials in Biosensors and Diagnostics*, *Amer. Chem. Soc.*, Washington DC, 1993, in press.
75. B. Fleet, T. H. Ryan and M. J. D. Brand, *Anal. Chem.*, 1974, **46**, 12.

Talanta, Vol. 40, No. 7, pp. 969–974, 1993
Printed in Great Britain.

0039-9140/93 $6.00 + 0.00

INVESTIGATION OF THE COMPOSITION OF COMPLEXES AND THE STOICHIOMETRY OF NON-COMPLEX REACTIONS BY FLOW INJECTION METHOD

JINGFU LIU and HUICHANG MA*
Research Center for Eco-Environmental Sciences, Academia Sinica, P.O. Box 2871, Beijing 100085, China

(*Received* 2 *December* 1992. *Revised* 7 *November* 1992. *Accepted* 8 *December* 1992)

Summary—Combining the Asmus straight-line method with the flow injection (FI) technique, a new FI–straight-line method is established to investigate the formulas of the blue, the purple and the red complexes formed by iron(III) and Tiron in different pH solutions. Using the proposed FI–straight-line method, the stoichiometries of cyanide and barbituric acid for producing the intermediate and the final product of the chromogenic reaction of cyanide with pyridine–barbituric acid reagent are also studied.

Various spectrophotometric methods have been established to investigate the empirical formulas of colored complexes in solution. Among them the Asmus straight-line[1] method has the advantages of being more suitable for determining the composition of weak complexes and applicable for complex systems where ligands are not pure and precise ligand concentration is not known.

The straight-line method is conventionally performed by a manual procedure which does not allow investigation of the composition of unstable products of intermediate of some complicated reactions. It has been adapted to a flow technique by Martinez *et al.*[2] The method is based on the merging of two solutions (metal and reagent), keeping the flow rate of one of them constant and increasing the other stepwise.

The flow injection (FI) technique has many advantages. One of them is that it allows fast reactions to be investigated. In the present study, the straight-line method was combined with the flow injection technique to measure complex formulas, determine the stoichiometry of non-complex reactions and to investigate the mechanism of complicated reactions.

PRINCIPLE

The straight-line method was initially established by Asmus to determine the composition of mononuclear complexes. Later, it was expanded to measure the composition of polynuclear complexes by Klausen *et al.*[3] The principle of the method can be expressed as follows.

For the reaction of the form

$$m\mathrm{M} + n\mathrm{L} = \mathrm{M}m\mathrm{L}n (m, n \geqslant 1). \quad (1)$$

Constant volume of a standard solution of M (concentration C_{M}^0) and varying volumes (V_{L}) of a standard solution of L (concentration C_{L}^0) are added into a series of volumetric flasks of volume V, the pH is adjusted and an inert salt solution is added. Then the mixtures are diluted to volume and the absorbance (A) is measured at a suitable wavelength. Assuming

$$[\mathrm{M}m\mathrm{L}n] \ll C_{\mathrm{L}} \quad (2)$$

$$\epsilon_{\mathrm{M}} = \epsilon_{\mathrm{L}} = 0 \quad (3)$$

where the brackets refer to the equilibrium concentration. C to the analytical or total concentration and ϵ to molar absorptivity. Expressing $1/(C_{\mathrm{L}})^n$ graphically as a function of $1/A$ for different sets of n, a straight line will be expected for the correct value of n. Similarly, if a constant concentration of L and different amounts of M are applied, a straight line would be obtained for the correct value of m by plotting $1/(C_{\mathrm{M}})^m$ against $1/A$ for different sets of m. If the complex formed during the determination of n is the same as that formed during the determination of m, the complex can be represented by $\mathrm{M}m\mathrm{L}n$.

When the straight-line method was adapted for a flow injection system, the flow system can be designed as following: A carrier stream composed of a buffer and an unreacting electrolyte is propelled to the system to control the pH and the ionic strength of the system. Component M

*To whom correspondence should be addressed.

is introduced into the system at a constant concentration. A series of L are injected into the system as samples. The sample zone merges with reagent M to form the colour species and the peak absorbance (A), corresponding to C_L^{max} (the analytical concentration of L at peak maximum), is detected.

In FIA, a chemical reaction is usually non-equilibrated. Namely,

$$C_{MmLn}^{max} \leqslant [MmLn]^{max} \quad (4)$$

in which C_{MmLn}^{max} represents the peak maximum concentration of the produced $MmLn$ when the peak absorbance (A) is detected. $[MmLn]^{max}$ is the equilibrium concentration of $MmLn$ at the peak maximum.

When

$$[MmLn]^{max} \ll C_L^{max}. \quad (5)$$

From equations (4) and (5), we have

$$C_{MmLn}^{max} \ll C_L^{max}. \quad (6)$$

Assuming

$$\epsilon_M = \epsilon_L = 0$$

a straight line will be obtained for the correct value of n if $1/(C_L^{max})^n$ is graphically expressed as a function of $1/A$ for different sets of n.

If the volume and the concentration of the injected L are S_v and C_L^0, respectively, then according to FIA theory,[4]

$$C_L^{max} = C_L^0/D_L^m = C_L^0/(2\pi^{3/2}R^2D_f^{1/2}T^{1/2}/S_v), \quad (7)$$

where D_L^{max} is the dispersion coefficient of L at peak maximum, D_f is the axial dispersion coefficient, R is the tube radius and T is the residence time. They are all constants for a certain manifold. Therefore,

$$C_L^{max} = KC_L^0Sv \quad (8)$$

in which K is a constant. If Sv is kept constant, then

$$C_L^{max} = K_1C_L^0 \quad (9)$$

$$1/(C_L^{max})^n = K_1'/(C_L^0)^n, \quad (10)$$

where K_1 and K_1' are constants.

It is well known that C_L^{max} will, for $D_L^{max} \geqslant 2$, increase linearly with increase of Sv. If C_L^0 remains unchanged and D_L^{max} is controlled in the region of $D_L^{max} \geqslant 2$, then from equation (8) we have

$$C_L^{max} = K_2Sv \quad (11)$$

$$1(C_L^{max})^n = K_2'/(Sv)^n. \quad (12)$$

According to equations (10) and (12), it is seen that a straight line will be obtained at the correct set of n by plotting $1/(C_M^0)^n$ against $1/A$ or by plotting $1/(Sv)^n$ against $1/A$. Similarly, if various concentrations or volumes of M are injected and a constant concentration of L is pumped into the flow system, the value of m can be obtained by plotting $1/(C_L^0)^m$ against $1/A$ or by plotting $1/(Sv)^m$ against $1/A$.

If $\epsilon_M \neq \epsilon_L \neq 0$, the absorbance of the excess ligand should be corrected. This can be done easily by the stopped-flow FIA technique if the reaction rate is not very fast. Unfortunately, the reaction of iron(III) and Tiron is too fast to use the stopped-flow FIA method. In the present study, absorbance was corrected simply by adjusting the baseline to $A = 0$.

EXPERIMENTAL

Reagents

Unless otherwise stated, analytical reagents from Beijing Chemical Factory were used throughout.

Iron(III) solution: A 0.1000M iron(III) stock solution was prepared by dissolving 0.5590 g of iron powder in 15 ml of 6M HCl, adding 3 g of $KClO_3$, and diluting to 100 ml with water. Working solutions were made by diluting this stock solution with 0.1M hydrochloric acid.

1,2-Dihydroxybenzen-3,5-disulfonate (trade name Tiron, chemical pure, Shanghai Chemical Reagent Factory) solution: A $5.0000 \times 10^{-2}M$ Tiron stock solution was prepared by dissolving 1.661 g of Tiron in 100 ml of water. Working solutions were made by diluting this stock solution with water.

Pyridine solution: Add 12 ml of concentrated hydrochloric acid in 60 ml of pyridine, dilute to 250 ml with water.

Pyridine–barbituric acid reagent: Place 8.205 g of barbituric acid in a 250 ml standard flask and add just enough water to wash the flask wall and wet the barbituric acid. Add 60 ml of pyridine and mix. Then 12 ml of concentrated hydrochloric acid is added and mixed. Dilute to volume with water and mix when the mixture has cooled to room temperature. This stock contains 0.20M barbituric acid. Working solutions were prepared by diluting this stock with the above prepared pyridine solution.

Chloramine-T solution: Dissolve 0.5 g of chloramine-T in 100 ml of water.

Standard cyanide solution: Standard cyanide solutions were prepared from a stock solution of potassium cyanide (1000 μg CN^-/ml, pH 11) with 1 g/l sodium hydroxide solution.

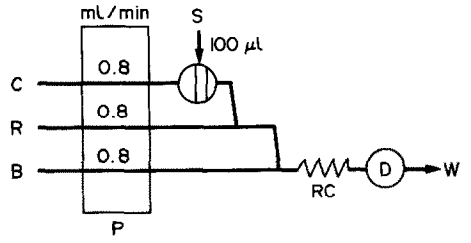

Fig. 1. Manifold used for determining formulas of complexes formed by iron(III) and Tiron in different pH solutions. C, water carrier; S, samples of Tiron or iron(III); R, iron(III) or Tiron solution; B, buffer solutions of pH 4.0, 5.9 or 9.0; RC, reaction coil (120 cm long, 0.7 mm i.d.); D, spectrophotometer, wavelength set at 620 nm, 560 nm or 480 nm; P, peristaltic pump; W, waste.

Buffer solution of pH 4.0: Dissolve 7.94 g of anhydrous sodium acetate in 100 ml of water, add 47 ml of acetic acid and dilute to 500 ml with water.

Buffer solution of pH 5.9: Dissolve 78 g of sodium dihydrogen phosphate in 1000 ml of water, and adjust to pH 5.9 with concentrated sodium hydroxide solution.

Buffer solution of pH 9.0: Dissolve 35 g of ammonium chloride in 100 ml of water, add 24 ml of ammonia solution (contains about 28% (w/v) ammonia, and dilute to 500 ml with water.

A FIA-91 flow injection analyzer (Shanghai No. 3 Analytical Instrument Factory) was used. This is an integrated instrument which consists of two 4-channel peristaltic pumps, a 16-port value, a grating spectrophotometric detector, a Laser PP40 4 color X–Y printer plotter and a microcomputer system. Program control and data processing are conducted automatically by the microcomputer system.

RESULTS AND DISCUSSION

Determination of composition of Fe(III)–Tiron complex

Ferric ions produce three different colored complexes with Tiron, depending on the pH of the solution. According to Harrey *et al.*,[5] the colors of the three complexes are blue (pH < 5.6), purple (pH 5.7–6.9) and red (pH > 7.0), and their metal–ligand molar ratios are 1:1, 1:2 and 1:3, respectively. The present study is to investigate the composition of the three complexes by the proposed FI–straight-line method.

The manifold depicted in Fig. 1 was designed to measure the formulas, represented by $Fe_m(Tir)_n$, of the three complexes. In the first series of experiments, the blue complex formed at pH 4.0 was investigated. To determine the value of n, a series of different concentrations of Tiron ($C^0_{Tir} = 0.8–2.0 \times 10^{-3} M$) were injected into water carrier, while a constant concentration of iron(III) ion ($C^0_{Fe} = 1 \times 10^{-3} M$) and a buffer of pH 4.0 were propelled into the flow system. Absorbance was detected at 620 nm, the peak absorbance wavelength of the blue complex, and the results are shown in Fig. 2(A), which was obtained by plotting $1/(C^0_{Tir})^n$ against $1/A$ for different sets of n. The value of m was determined similarly, the only difference being that the Tiron solution is introduced at a constant concentration ($C^0_{Tir} = 6 \times 10^{-3} M$) and various concentrations of ferric ion ($C^0_{Fe} = 0.6–1.8 \times 10^{-3} M$) were injected into the system. The curves obtained for the determination of m are shown in Fig. 2(B). Figure 2 indicates that a straight line occurs for $n = 1$ or $m = 1$. As

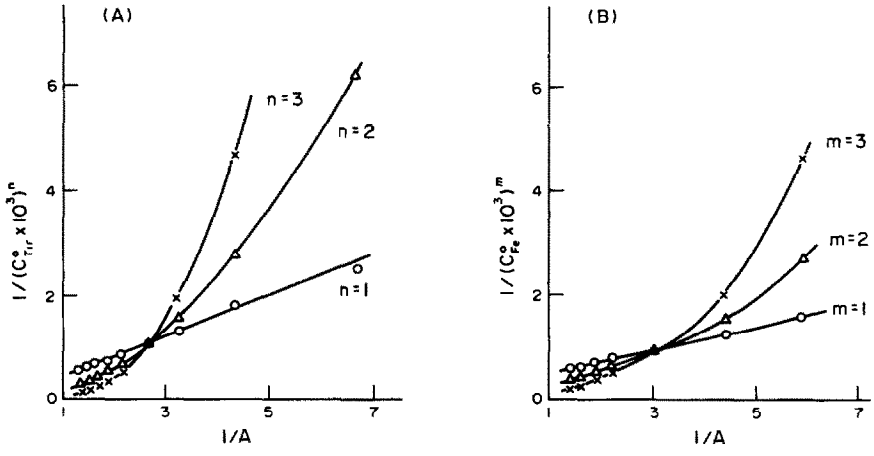

Fig. 2. The use of the FI–straight-line method for determining the formula of the blue complex formed by iron(III) and Tiron in a buffer solution of pH 4.0: (A) determination of n, $C^0_{Tir} = 0.8–2.0 \times 10^{-3} M$, $C^0_{Fe} = 1.0 \times 10^{-3} M$; (B) determination of m, $C^0_{Tir} = 6.0 \times 10^{-3} M$, $C^0_{Fe} = 0.6–1.8 \times 10^{-3} M$.

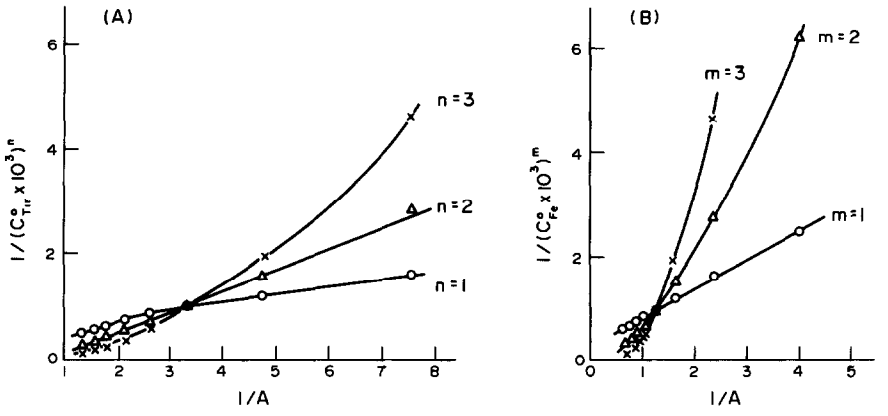

Fig. 3. The use of the FI–straight-line method for determining the formula of the purple complex formed by iron(III) and Tiron in a buffer solution of pH 5.9: (A) determination of n, $C^0_{Tir} = 0.6$–$2.0 \times 10^{-3}M$, $C^0_{Fe} = 1.0 \times 10^{-3}M$; (B) determination of m, $C^0_{Tir} = 6.0 \times 10^{-3}M$, $C^0_{Fe} = 0.4$–$1.8 \times 10^{-3}M$.

only one kind of complex is produced by iron(III) and Tiron in a buffer solution of pH 4.0,[5] the formula of the blue complex is Fe(Tir).

The compositions of the purple and the red complexes are measured similarly. For investigating the purple complex, a buffer of pH 5.9 was adopted and the absorbance was detected at 560 nm. Results are shown in Fig. 3. For producing the red complex, a buffer of pH 9.0 was adopted. Absorbance was detected at 480 nm and the resulting curves are shown in Fig. 4. From Figs 3 and 4 it is seen that the compositions of the purple and the red complexes are $Fe(Tir)_2$ and $Fe(Tir)_3$, respectively.

The formulas of the blue, the purple and the red complex obtained above agree well with the metal–ligand molar ratios obtained by Harrey *et al.*[5] This fact indicates that the FI–straight-line method is suitable for determining the composition of complex.

Reaction mechanism of cyanide with pyridine–barbituric acid

Cyanide is usually determined by the pyridine–barbituric acid method based on the Koning synthesis. Determination is conventionally conducted by detecting the final product of the reaction at 580 nm. In our previous study,[8] an intermediate of the reaction with a peak absorbance at 494 nm was found and was applied to determine cyanide successfully by FIA. In the present study, we measured the molar ratios of cyanide to barbituric acid for producing the intermediate and the final product, in order to propose a more detailed mechanism of the reaction.

This above-mentioned reaction is a complicated reaction, in which cyanide first reacts with chloramine-T or bromine water to produce cyanogen chloride or bromide. The produced cyanogen chloride or bromide quantitatively oxidizes pyridine to glutaconicaldehyde which condenses with barbituric acid to form a colored polymethine dye. The overall stoichiometry of cyanide and barbituric acid is 1:2.[7] Unfortunately, the stoichiometry of cyanide and barbituric acid for producing the intermediate is not clear. Obviously, a more detailed reaction

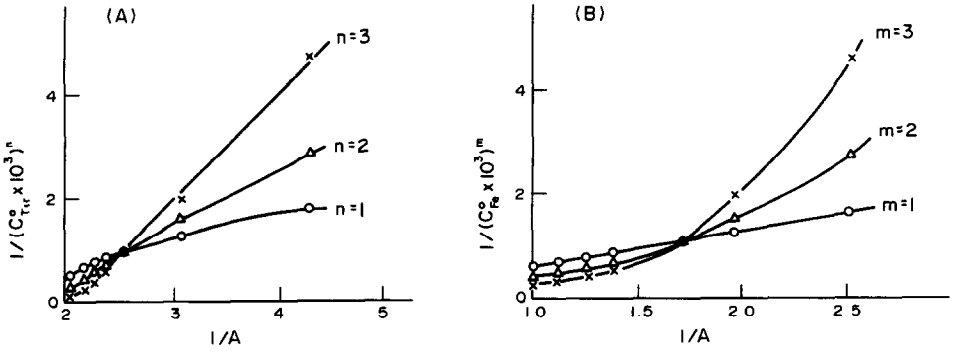

Fig. 4. The use of the FI–straight-line method for determining the formula of the red complex formed by iron(III) and Tiron in a buffer solution of pH 9.0: (A) determination of n, $C^0_{Tir} = 0.6$–$1.8 \times 10^{-3}M$, $C^0_{Fe} = 1.0 \times 10^{-3}M$; (B) determination of m, $C^0_{Tir} = 6.0 \times 10^{-3}M$, $C^0_{Fe} = 0.6$–$1.8 \times 10^{-3}M$.

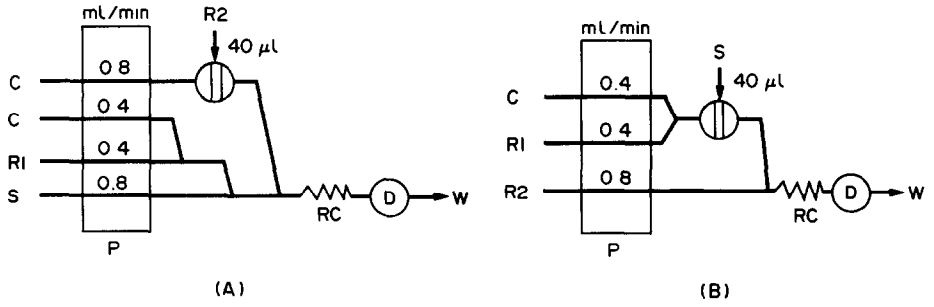

Fig. 5. Manifold used for investigating the stoichiometry of cyanide and barbituric acid during the formation of the intermediate and the final product: (A) determination of n; (B) determination of m; C, sodium dihydrogen phosphate buffer solution (pH 5.9): R1, chloramine-T solution; R2, pyridine–barbituric acid reagent; S, cyanide; RC, reaction coil (30 cm long, 0.7 mm i.d. or 270 cm long, 0.7 mm i.d.); D, spectrophotometer, wavelength set at 494 nm or 580 nm; P, peristaltic pump, W, waste.

mechanism could be acquired if the stoichiometry is determined. The stoichiometry of cyanide and barbituric acid could be measured by the FI–straight-line method if the concentration of chloramine-T and pyridine were constant and in sufficient excess. Assuming that cyanide and barbituric acid have a stoichiometry of $m:n$, then the value of m and n can be determined respectively by the proposed FI–straight-line method.

The manifolds shown in Fig. 5 were adopted. When the intermediate was investigated, the reaction coil was 30 cm long and absorbance was detected at 494 nm. However, the coil length and the detected wavelength were changed to 270 cm and 580 nm, respectively, when the final product was investigated. Figure 5(A) shows the manifold employed to determine the value of n for producing the intermediate and the final product, in which various concentrations of pyridine–barbituric acid reagent (C^0_{Barb} = 0.08–0.2M) were injected into the system while cyanide was propelled into the system at a constant concentration ($C^0_{CN^-} = 7.6 \times 10^{-5}M$). Results are shown in Fig. 6, which indicates that the values of n were 1 and 2, respectively, for producing the intermediate and the final product.

From Fig. 6(B) it can be concluded that the reaction molar ratio of cyanide to barbituric acid for producing the final product is 1:2, which agrees with results reported in literature.[5] This fact demonstrates that the FI–straight-line method can be applied to determine the stoichiometry of non-complex reactions.

Although the stoichiometries of cyanide and barbituric acid for producing the intermediate and the final product have been obtained, the reaction mechanism is not clear because the molecular number of cyanide for forming one molecule of the intermediate or the final product is still uncertain. A manifold shown in Fig. 5B was designed to determine the consumed molecular number of cyanide the value of m. In this manifold cyanide was injected at various concentrations ($C^0_{CN^-} = 0.2$–$1.4 \times 10^{-4}M$) while

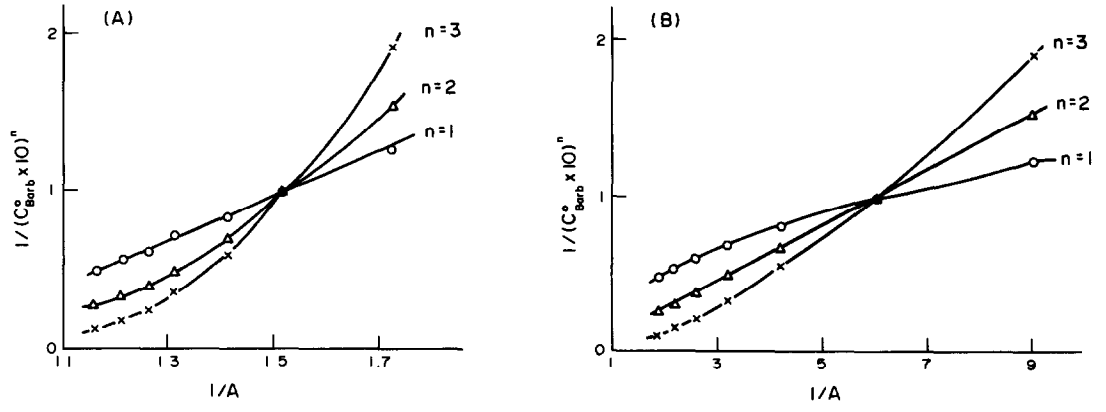

Fig. 6. Determination of the reaction molar ratios of cyanide to barbituric acid for producing the intermediate and the final product by the FI–straight-line method: (A) for investigation of the intermediate; (B) for investigation of the final product. $C^0_{Barb} = 0.08$–$0.2M$; $C^0_{CN^-} = 7.6 \times 10^{-5}M$.

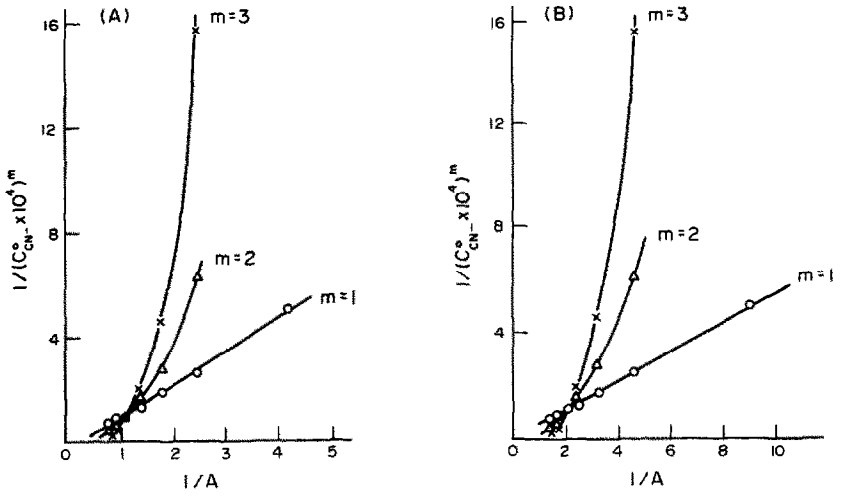

Fig. 7. Determination of the consumed molecular number of cyanide for producing one molecule of the intermediate and the final product by the FI–straight-line method: (A) for investigation of the intermediate; (B) for investigation of the final product. $C^0_{Barb} = 0.1M$; $C^0_{CN^-} = 0.2$–$1.4 \times 10^{-4}M$.

barbituric acid was introduced at a constant concentration ($C^0_{Barb} = 0.1M$). The results are shown in Fig. 7 which indicates that for both the intermediate and the final product a straight line was obtained by setting $m = 1$, *i.e.* only one molecule of cyanide was consumed for producing one molecule of the intermediate or the final product. As barbituric acid was always in large excess during the measurement of n and m, the intermediate and the final product formed during the determination of n must be the same as that formed during the determination of m. Therefore, we conclude that for producing one molecule of the intermediate and the final product, the consumed cyanide is one molecule while the consumed barbituric acid is one and two molecules respectively.

CONCLUSIONS

A new FI–straight-line method was established by combining the Asmus straight-line method with the flow injection technique. The proposed method is suitable for investigating compositions of stable and unstable complexes, especially unstable complexes which cannot be investigated by conventional methods. The method can also be applied to determine stoichiometries of some non-complexing reactions. Since it can be used to measure stoichiometry of reactants when an unstable intermediate is formed, the proposed method has great significance in investigating mechanisms of some complicated reactions.

REFERENCES

1. E. Asmus, *Z. Anal. Chem.*, 1960, **178**, 104.
2. J. Martinez Calatayud, P. Campins Falco and M. C. Pascual Marti, *Analyst*, 1986, **111**, 1317.
3. K. S. Klausen and F. J. Langmyhr, *Anal. Chim. Acta*, 1963, **28**, 501.
4. J. Ruzicka and E. H. Hansen, *Flow Injection Analysis*, 2nd Edn., p. 29. Wiley, New York, 1988.
5. A. E. Harrey, Jr and D. L. Manning, *J. Am. Chem. Soc.*, 1950, **72**, 4488.
6. H. Ma and J. Liu, *Anal. Chim. Acta*, 1992, **261**, 247.
7. W. J. Williams, *Handbook of Anion Determination*. Butterworths, London, 1979.

Talanta, Vol. 40, No. 7, pp. 975–979, 1993
Printed in Great Britain.

0039-9140/93 $6.00 + 0.00

THE DETERMINATION OF MOLYBDENUM IN A SEA WATER CANDIDATE REFERENCE MATERIAL BY INDUCTIVELY COUPLED PLASMA-MASS SPECTROMETRY

F. VANHAECKE,[1] J. GOOSSENS,[1] R. DAMS[1] and C. VANDECASTEELE[2]

[1]Laboratory of Analytical Chemistry, Ghent University, Institute for Nuclear Sciences, Proeftuinstraat 86, B-9000 Ghent, Belgium, [2]Department of Chemical Engineering, Katholieke Universiteit Leuven, de Croylaan 46, B-3001 Heverlee, Belgium

(*Received* 26 *November* 1992. *Revised* 12 *January* 1993. *Accepted* 12 *January* 1993)

Summary—In the framework of a certification campaign organized by BCR (Bureau Communautaire de Référence, Commission of the European Communities, Brussels) molybdenum was determined in a sea water candidate reference material (BCR CRM 403) using inductively coupled plasma-mass spectrometry. The determination was hampered by both non-spectral (signal suppression) and spectral interferences. Ten-fold dilution of the sea water and the use of a carefully selected internal standard allowed accurate correction for the signal suppression. Spectral interferences on Mo nuclides could mainly be attributed to BrO^+ and $BrOH^+$ ions. At the level of spectral overlap encountered, these interferences could be corrected for with sufficient accuracy by matrix matching of the blank for Br or by application of a mathematical correction method involving resolvation of a pair of simultaneous equations. Results obtained after application of anion exchange to separate Br from Mo confirmed the results obtained using the correction methods, proving the validity of the latter. A good agreement is established by comparison of the ICP-MS result with those obtained by other techniques in other laboratories.

Inductively coupled plasma-mass spectrometry (ICP-MS) is a powerful and versatile technique that has proven its utility in the analysis of water samples of different origin.[1–23] Due to its complex matrix and high salt content (salinity: *ca.* 35 g/kg), the accurate determination of (ultra-)trace elements in sea water is a difficult and challenging task for the analyst. High levels of dissolved solids not only cause orifice clogging of, and solid deposition on, the sampling cone,[24] but are also on the origin of severe matrix effects. In addition, the complexity of the sea water matrix leads to many spectral interferences.

For interference-free elements present at relatively high concentrations, dilution of the sea water can be sufficient to allow accurate determination.[18] In most cases however, the literature reports on the necessity of a separation (and preconcentration) step prior to ICP-MS analysis. This separation/preconcentration step can, *e.g.*, involve solvent extraction,[19] electrodeposition,[12] cation exchange[1,5,7,14] and anion exchange.[13] These procedures are often time-consuming and are not without risk for Mo due to the complex chemistry of this element.[5,25] In the present paper it is shown that ten-fold dilution and careful application of correction methods for both spectral and non-spectral interferences were sufficient to allow accurate determination of Mo in the sea water candidate reference material (BCR CRM 403).

EXPERIMENTAL

Instrumentation

The instrument used is a VG PlasmaQuad ICP-mass spectrometer (VG Elemental, Winsford, UK) equipped with a Fassel torch, a Gilson Minipuls-2 peristaltic pump, a Meinhard type Tr-30-A3 concentric glass nebuliser and a double pass Scott-type spray chamber with surrounding liquid jacket, the temperature of which is controlled with a recirculating refrigeration–heating system. Sampling cones (1.0 mm orifice) and skimmer cones (0.75 mm orifice) are made of nickel. Operation conditions are summarized in Table 1. The settings of the electrostatic lenses were optimized in order to obtain maximum signal intensity for $^{115}In^+$.

Reagents and solutions

For the quantitation of Mo in the sea water CRM, the sample pretreatment was limited to a

Table 1. PlasmaQuad operation conditions

Plasma RF power:	Forward:	1350 *W*
	Reflected:	<5 *W*
Gas flow rates:	Plasma:	13.5 *l/min*
	Auxiliary:	0.5–1 *l/min*
	Nebuliser:	0.725–0.750 *l/min*
Sample uptake rate:		0.9 *ml/min*
Spray chamber temperature:		10°*C*
Ion sampling depth:		10 *mm* (from load coil)
Vacuum:	Expansion stage:	2.4 *hPa* (*mbar*)
	Intermediate stage:	10^{-4} *hPa* (*mbar*)
	Analyser stage:	4.8×10^{-6} *hPa* (*mbar*)

ten-fold dilution using 0.14*M* HNO_3 and the addition of an appropriate internal standard (10 μg/l In in blank, sample and standard solutions); 0.14*M* HNO_3 solutions (with 10 μg/l In as an internal standard) were used as blanks for the standard solutions in all cases and for the sample solutions when using the mathematical correction method. For correction for the spectral interferences by matrix matching of the blank, simulated blank solutions for the sample were prepared by adding an equal amount of Br ($NaBrO_3$, analytical reagent grade, UCB) as determined in the ten-fold diluted CRM (*ca.* 6.75 mg/l) to the original blanks. As the ICP-MS response is known to be linear over a very wide range, standard solutions of only one concentration level, prepared at least in triplicate, were used for calibration. Since it is our experience that Mo causes severe memory effects,[26] the concentration of the standard solutions was kept limited to *ca.* 10 μg/l. These standard solutions were obtained by successive dilution of 1 g/l solutions prepared from Mo foil (Goodfellow Metals, 99.9% purity) or MoO_3 (UCB, 99% purity). In order to improve the stability, stock solutions (10 mg/l), from which standard solutions were prepared, contained 1% HF. By comparing results for "fresh" and "old" standard solutions, 10 μg/l Mo solutions were proven to be stable for over one month.

Anion exchange for the removal of Cl- and S-containing anions is described in detail in a previous publication.[27] In order to separate Br from Mo, this procedure was slightly modified with respect to the eluent concentration and elution rate. Fifteen millilitres of the sea water was mixed with 100 μl 0.2*M* $SnCl_2$ (analytical reagent grade, RPL) solution and 1.5 ml 1.4*M* HNO_3. After 1 min stirring the solution was brought on top of the anion exchange resin column (Dowex-1, converted to nitrate form). $SnCl_2$ is used as a reductant in order to convert possible present Mo(VI), retained as $Mo_xO_y^{z-}$ on the anion exchanger,[25] to lower oxidation states in order to ensure complete elution[27,28] and to reduce possibly present BrO_3^- to Br^-, which is likely to be retained more strongly by the resin.[29] After this pretreatment, Br^- is retained on the column (>99.5%), whereas Mo is eluted at 3 ml/min with 100 ml of 0.07*M* HNO_3 and collected in the effluent. Finally, Rh was added as an internal standard and the effluent was diluted to volume (150 ml) using 0.14*M* HNO_3.

Measurements

Measurements were done using the mass scanning mode of data acquisition (mass range: 90–120 u, number of channels: 512 or 1024, dwell time per channel: 320 μs, number of sweeps: 400). The total measuring time depended on the number of channels and was *ca.* 1 or 2 min. Every blank, sample or standard solution was measured three times. Solutions were measured in a sequence that avoided memory effects as much as possible. Where necessary, the sample introduction system was rinsed for 2 min with 0.14*M* HNO_3.

RESULTS AND DISCUSSION

Correction for non-spectral and spectral interferences

As a result of the high level of dissolved solids (salinity *ca.* 35 g/kg) it is necessary to dilute the sea water matrix in order to avoid orifice or nebuliser clogging and matrix effects too severe to allow accurate determination. A ten-fold dilution brought the signal suppression to acceptable levels, whereas the concentration of Mo in the diluted samples was still high enough (*ca.* 1 μg/l) to allow quantitation.

An earlier study of matrix effects in ICP-MS[30] showed that, in all cases studied, the magnitude of the signal suppression or enhancement depends in a regular way on the mass number. Hence, accurate correction for non-spectral interferences is only possible using an internal standard with mass number close to that of the

analyte element(s). This study also pointed out that the use of an internal standard with mass number closely matching that of the analyte also improves the precision. For both accuracy and precision, the ionization potential of the internal standard was established not to be of major importance. Hence, In was chosen as the internal standard for this determination. Only for the quantitation of Mo in sample solutions obtained after anion exchange, Rh was used instead of In as the internal standard due to the presence of Sn (isobaric overlap with $^{115}In^+$).

The quantitation of Mo in the sea water CRM was not only hampered by non-spectral, but also by spectral interferences. Mo has 7 isotopes: ^{92}Mo (14.8%), ^{94}Mo (9.1%), ^{95}Mo (15.9%), ^{96}Mo (16.7%), ^{97}Mo (9.5%), ^{98}Mo (24.4%) and ^{100}Mo (9.6%). The nuclides ^{92}Mo, ^{94}Mo and ^{96}Mo can suffer from an isobaric interference arising from the corresponding Zr nuclides, while an isobaric interference on ^{96}Mo, ^{98}Mo and ^{100}Mo from the corresponding Ru nuclides is also possible. Spectral interferences from BrO^+ and $BrOH^+$ ions were experimentally observed. Since Br has two isotopes, ^{79}Br (50.7%) and ^{81}Br (49.3%), the signals of ^{95}Mo, ^{96}Mo, ^{97}Mo and ^{98}Mo are affected to the largest extent. Polyatomic ions, such as *e.g.* $ArKO^+$ and KKO^+ (mainly affecting the signal of $^{95}Mo^+$ and $^{94}Mo^+$, respectively), were also observed[31] and finally $^{100}Mo^+$ is coincident with $^{84}SrO^+$. Careful study of the relevant part of the mass spectrum for the diluted sea water indicated that an additional interference at (m/q) = 97 was present. As a result, the latter nuclide was not used for quantitation. Comparison of the spectrum with and without the use of anion exchange prior to the measurement pointed out that the polyatomic ion on the origin of this interference contains an element present in anionic form in the sea water. Therefore it is strongly suspected that the interference on $^{97}Mo^+$ is due to $NaKCl^+$.

For the first correction method it was assumed that ^{98}Mo, the most abundant Mo nuclide only suffers from a spectral interference from $^{81}Br^{16}OH^+$ and $^{81}Br^{17}O^+$. The Br concentration of the diluted sea water was determined experimentally to be *ca.* 6.75 mg/l. Simulated blank solutions with an equal Br concentration were used for correction. Although the authors were aware of the possible influence of the matrix on the level of MO^+ an MOH^+ formation,[32] a systematic study of the influence of the sea water matrix on the levels of BrO^+ and $BrOH^+$ species was not carried out due to the relatively low level of spectral overlap (*ca.* 5%), while the results obtained were also checked by comparison with those obtained using the mathematical correction method.

For the mathematical correction method, it was assumed that the interferences on the signals of $^{95}Mo^+$ and $^{98}Mo^+$ were mainly to be attributed to $^{79}Br^{16}O^+$ and $^{81}Br^{16}OH^+$, respectively. Indeed, measurements of Br standard solutions showed that the signals at (m/q) = 96 and 98 necessarily have to be mainly attributed to $^{79}Br^{16}OH^+$ and $^{81}Br^{16}OH^+$, respectively, since the signal intensities observed were substantially higher than expected on the basis of the signal intensities for the corresponding $Br^{16}O^+$ ions and the relative abundances of ^{16}O and ^{17}O. The ratio ($^{81}BrOH^+/^{79}BrO^+$) was expected to be sufficiently constant and was determined experimentally by measuring Br standard solutions of various concentrations. Hence, the following pair of simultaneous equations could be resolved:

$$\begin{cases} {}^{95}S_{samp}(\text{total}) = {}^{95}S_{samp}(Mo^+) + {}^{95}S_{samp}(BrO^+) \\ {}^{98}S_{samp}(\text{total}) = {}^{98}S_{samp}(Mo^+) + {}^{98}S_{samp}(BrOH^+), \end{cases}$$

where S_{samp} is the net signal at the (m/q) value and of the origin specified, normalized to the signal of the internal standard ($^{115}In^+$). In a first approximation, the contribution of $^{81}BrOH^+$ to the total signal at (m/q) = 98 was neglected, allowing to predict the value for $^{95}S_{samp}(Mo^+)$ on the basis of $^{98}S_{samp}$(total) and the abundances of both Mo isotopes involved. Hence, the contribution of $^{79}BrO^+$ to the total signal at (m/q) = 95 could be estimated:

$$\begin{aligned} {}^{95}S_{samp}(BrO^+) &= {}^{95}S_{samp}(\text{total}) - {}^{95}S_{samp}(Mo^+) \\ &= {}^{95}S_{samp}(\text{total}) - \left[{}^{98}S_{samp}(\text{total}) \times \frac{\Theta^{95}Mo}{\Theta^{98}Mo} \right], \end{aligned}$$

where Θ is the isotopic abundance of the nuclide specified.

The ratio [$^{81}BrOH^+/^{79}BrO^+$] was determined experimentally to be *ca.* 0.025. The relatively limited importance of $BrOH^+$ justifies the approximation used. Application of this ratio allowed an estimation of the contribution of $^{81}BrOH^+$ to the total signal at (m/q) = 98:

$$\begin{aligned} {}^{98}S_{samp}(BrOH^+) = {}^{95}S_{samp}(BrO^+) \\ \times [{}^{81}BrOH^+/{}^{79}BrO^+]_{stand}, \end{aligned}$$

Table 2. ICP-MS results obtained after subtraction of a simulated blank solution, mathematical correction and anion exchange prior to the analysis

Applied method	Mean result (S.D.) (*nmole/kg*)
Subtraction of simulated blank	104.2 (4.3)
Mathematical correction	112.1 (5.3)
Anion exchange	110.5 (5.3)

so that this interference could be corrected for. Although this correction method offers the possibility for iteration, no attempt was made to improve the accuracy of the correction in this way, due to the relatively limited importance of the spectral interference. Finally, the possible presence of Ru was checked, since this would lead to an additional (isobaric) interference on $^{98}Mo^+$. Careful survey of the spectrum, taking into account the contribution of $NaKCl^+$ and SrO^+ signals, did not reveal any significant level of Ru. Of course, for routine determinations, this correction method can easily be automated by computer programming.

Quantitation

The quantitation of Mo in the sea water CRM was carried out during a certification campaign. Two bottles of the CRM were supplied by BCR. Analyses were carried out on 10 samples on different days. For each individual determination one of the two correction methods cited was used. Both methods lead to comparable corrections (*ca.* 5%). Results obtained after the use of anion exchange prior to the analysis confirmed the results obtained using the correction methods, proving the validity of the latter. Results are presented in Table 2. No significant difference (t-test, 95% confidence level) between the results obtained using the different methods could be established. Also the precision was seen to be comparable (F-test, 95% confidence level) for each of the methods applied.

As a mean result a Mo concentration of 109.4 nmole/kg with a standard deviation of 5.7 nmole/kg was obtained. This result can be compared with those obtained by other techniques/laboratories taking part in the certification campaign (Table 3). Since only two other laboratories were able to give results, the possibilities for comparison are rather limited. However, since these results were obtained using independent and totally different techniques, 103 ± 20 nmole/kg was certified as Mo concentration in CRM 403.[33]

Table 3. Results obtained by various analytical techniques/laboratories for the determination of Mo in the sea water candidate reference material (BCR CRM 403)

Analytical technique	Mean result (S.D.) (*nmole/kg*)
ZETAAS	104.4 (7.3)
CSV	94 (11)
ICP-MS, this work	109.4 (5.7)

ZETAAS: Zeeman Electrothermal Atomic Absorption Spectrometry.
CSV: Cathodic Stripping Voltammetry.

CONCLUSION

In every case a trace or ultra-trace element has to be accurately determined in a complex, realistic sample using low resolution ICP-MS, the utmost attention must be paid to both matrix effects and possible spectral interferences. Ten-fold dilution of the sea water matrix and careful application of correction methods for both spectral and non-spectral interferences were shown sufficient to allow accurate determination of Mo in BCR CRM 403. In cases where the extent to which the Mo^+ signals are affected by BrO^+ and $BrOH^+$ is larger, the possibility for accurate quantitation is maintained by the use of an anion exchange resin column prior to the analysis. Mathematical correction on the other hand is less time consuming and reduces the possibility of sample contamination as a result of the limited amount of sample preparation and can hence be preferred at relatively low levels of spectral overlap or for routine analysis.

REFERENCES

1. J. W. McLaren, A. P. Mykytiuk, S. N. Willie and S. S. Berman, *Anal. Chem.*, 1985, **57**, 2907.
2. D. W. Boomer and M. J. Powell, *Can. J. Spectrosc.*, 1986, **31**, 104.
3. J. R. Garbarino and H. E. Taylor, *Anal. Chem.*, 1987, **59**, 1568.
4. D. Beauchemin, J. W. McLaren, A. P. Mykytiuk and S. S. Berman, *Anal. Chem.*, 1987, **59**, 778.
5. D. Beauchemin, J. W. McLaren, A. P. Mykytiuk and S. S. Berman, *J. Anal. At. Spectrom*, 1988, **3**, 305.
6. G. E. M. Hall, C. W. Jefferson and F. A. Michel, *J. Geochem. Explor.*, 1988, **30**, 63.
7. D. Beauchemin and S. S. Berman, *Anal. Chem.*, 1989, **61**, 1857.
8. J. R. Garbarino, H. E. Taylor and W. C. Batie, *Anal. Chem.*, 1989, **61**, 793.

9. C. Haraldsson, S. Westerlund and P. Öhman, *Anal. Chem.*, 1989, **221,** 77.
10. J. M. Henshaw, E. M. Heithmar and T. A. Hinners, *Anal. Chem.* 1989, **61,** 335.
11. D. W. Boomber, M. J. Powell and J. Hipfner, *Talanta*, 1990, **37,** 127.
12. N.-S. Chong, M. L. Norton and J. L. Anderson, *Anal. Chem.*, 1990, **62,** 1043.
13. K. K. Falkner and J. M. Edmond, *Anal. Chem.*, 1990, **62,** 1477.
14. D. C. Gregoire, *J. Anal. At. Spectrom.*, 1990, **5,** 623.
15. E. M. Heithmar, T. A. Hinners, J. T. Rowan and J. M. Riviello, *Anal. Chem.*, 1990, **62,** 857.
16. T. Kato, S. Nakamura and M. Morita, *Anal. Sci.*, 1990, **6,** 623.
17. M. E. Ketterer, *Anal. Chem.*, 1990, **62,** 2522.
18. G. P. Klinkhammer and L. H. Chan, *Anal. Chim. Acta*, 1990, **232,** 323.
19. M. B. Shabani, T. Akagi, H. Shimizu and A. Masuda, *Anal. Chem.*, 1990, **62,** 2709.
20. J. Toole, K. McKay and M. Baxter, *Anal. Chim. Acta*, 1991, **245,** 83.
21. E. Johansson and T. Liljefors, in *Applications of Plasma Source Mass Spectrometry*, G. Holland and A. N. Eaton (Eds), p. 34. The Royal Society of Chemistry, Cambridge, 1991.
22. E. Veldeman, L. Van't dack, R. Gijbels, M. Campbell, F. Vanhaecke, H. Vanhoe and C. Vandecasteele, in *Applications of Plasma Source Mass Spectrometry*, G. Holland and A. N. Eaton (Eds), p. 25. The Royal Society of Chemistry, Cambridge, 1991.
23. F. Vanhaecke, C. Vandecasteele and R. Dams, *Anal. Lett.*, 1992, **25,** 919.
24. D. J. Douglas and L. A. Kerr, *J. Anal. At. Spectrom.*, 1988, **3,** 749.
25. N. Stalica, in *Standard Potentials in Aqueous Solutions*, A. J. Bard, R. Parson and J. Jordan (Eds), p. 462. Marcel Dekker, New York, 1985.
26. H. Vanhoe, C. Vandecasteele, J. Versieck and R. Dams, *Anal. Chem.*, 1989, **61,** 1851.
27. J. Goossens and R. Dams, *J. Anal. At. Spectrom.*, 1992, **7,** 1167.
28. J. P. Faris and R. F. Buchanan, *Anal. Chem.*, 1964, **36,** 1157.
29. S. Peterson, *Ann. N.Y. Acad. Sci.*, 1954, **57,** 144.
30. F. Vanhaecke, H. Vanhoe, R. Dams and C. Vandecasteele, *Talanta*, 1992, **39,** 737.
31. H. Vanhoe, personal communication.
32. F. E. Lichte, A. L. Meier and J. G. Crock, *Anal. Chem.*, 1987, **59,** 1150.
33. Ph. Quevauviller, K. J. M. Kramer, K. Vercoutere and B. Griepink, *The Certification of the Contents of Cd, Cu, Pb, Mo, Ni and Zn in Sea Water (CRM 403)*, Commission of the European Communities, Community Bureau of Reference, EUR report 14601 EN, 1992.

Talanta, Vol. 40, No. 7, pp. 981–988, 1993
Printed in Great Britain.

0039-9140/93 $6.00 + 0.00

SPECTROPHOTOMETRIC DETERMINATION OF H_2O_2 WITH 1-ANILINONAPHTHALENE-8-SULFONIC ACID AND 4-AMINOANTIPYRINE WITH HEMATIN AS CATALYST

HYUNG-KEUN CHUNG, PURNENDU K. DASGUPTA* and JOHN N. MARX
Department of Chemistry, Texas Technical University, Lubbock, TX 79409-1061, U.S.A.

(*Received* 16 *November* 1992. *Received* 9 *December* 1992. *Accepted* 9 *December* 1992)

Summary—A spectrophotometric flow injection method for the determination of H_2O_2 in aqueous solution is presented. The technique is based on the oxidative condensation reaction between 1-anilinonaphthalene-8-sulfonic acid (ANSA) and 4-aminoantipyrine (AAP) in the presence of H_2O_2. Hematin is a good peroxidatic catalyst for this reaction; its effectiveness is significantly enhanced in an ammoniacal medium. If the yellow product formed in the alkaline medium is acidified, a blue chromophore (λ_{max} 592 nm) is formed; a surfactant is necessary to keep the blue compound in solution. Chemical and instrumental parameters for FIA were evaluated and optimized. A detection limit of 0.3μM was achieved with a linear dynamic range extending to 50μM. The typical relative standard deviation is 1.5% or better. The structure of the reaction product has been identified.

Many determination procedures for H_2O_2 are based on enzymatic reactions and colorimetry. In the presence of peroxidase, various organic species are oxidized by H_2O_2 to form colored products. Such reaction substrates include *o*-dianisidine,[1] *o*-tolidine,[2] 2,6-dichlorophenol,[3] *etc.* Although these methods are adequately sensitive, the absorption maxima of the reaction products occur at relatively low wavelengths (< 500 nm) where the potential for interference from indigenous species present in real samples is much higher.[4,5]

Methods based on the oxidation of 4-methoxy-1-naphthol[6] or oxidative coupling between phenol and *N,N*-dimethyl-*p*-phenylenediamine[7] result in products that absorb at longer wavelengths (620 and 650 nm, respectively). However, for both these methods, we have found that the rate of the blank reaction is relatively fast. These methods can be successfully used to assay the activity of a catalyst. For the analytical determination of H_2O_2, poor reproducibility and sensitivity result. Methods based on a two-component substrate, notably those involving the oxidative condensation reaction of a hydrogen donor with AAP, have been developed. These methods combine good selectivity and reproducibility. Usually a mixture of AAP and phenol[8] or phenolic derivatives[9] is oxidized by H_2O_2 in the presence of peroxidase to produce quinonoid dyes. These methods are otherwise attractive but the product absorption maxima range from 500 to 520 nm. If phenol is replaced in this reaction with aniline derivatives, the resulting products exhibit more intense absorption and absorption maxima at longer wavelengths. Tamaoku *et al.*[10] synthesized various water-soluble aniline derivatives such as *N*-ethyl-*N*-sulfopropylaniline, *N*-ethyl-*N*-sulfopropyl-*m*-toluidine, and *N*-ethyl-*N*-sulfopropyl-*m*-anisidine. These were recommended as good substitutes for phenolic derivatives. Relative sensitivities obtained with the above anilines were about 2–3 times greater than that with phenol and the absorption maxima ranged from 540 to 561 nm. Generally equilibrium-based procedures involving incubation at a certain temperature (e.g. 37°C) have been reported. The condensation reaction between AAP and *N*-ethyl-*N*-sulfopropylaniline in the presence of peroxidase has been adopted to develop a FIA method for the determination of H_2O_2 in rainwater with a limit of detection (LOD) of 0.14μM and a linear dynamic range up to 40μM.[11]

Saito *et al.*[12,13] suggested the use of manganese–tetrakis (sulphophenyl) porphine immobilized on anion exchange resins as a substitute for immobilized peroxidase. They applied this solid catalyst for the determination of H_2O_2 using the condensation reaction of AAP with phenol and of AAP with *N,N*-diethylaniline. Recently,

*To whom correspondence should be addressed.

hematin has been shown to be a stable, inexpensive and highly effective catalyst in ammoniacal media for the determination of H_2O_2. However, only fluorometric procedures have thus far been reported.[14] In the present work, various phenol and aniline derivatives that are oxidized by H_2O_2 in conjunction with AAP were investigated. The aim was to devise a reaction that results in products absorbing at wavelengths longer than 550 nm, to form the basis of an improved colorimetric FIA method. Further modification was considered by replacing horseradish peroxidase by hematin as catalyst. Among tested reagents, the hematin catalyzed reaction of 1-anilinonaphthalene-8-sulfonic acid (ANSA), AAP and H_2O_2 showed the most promising results. A colorimetric flow injection procedure based on this principle is described.

EXPERIMENTAL

Apparatus

A Hewlett–Packard 8451A diode array spectrophotometer was used for batch experiments. A block diagram of the FIA system used in most studies is shown in Fig. 1. The FIA manifold consists of a multichannel peristaltic pump, a sample injection valve, a first stage reaction coil and an acidification reaction coil, and an absorbance detector. The sample injection valve (six-port rotary valve, type 5020P, Rheodyne Inc.) was operated by a microprocessor controlled timer (DVSP-4, Valco, Houston, TX) and the sample loop (200 μl) was filled by aspiration. Except as specified, absorbance measurements were made with a Spectroflow 757 absorbance detector (Kratos/Schoeffel, Applied Biosystems, Ramsey, NJ). In some experiments, a home built flow-through absorbance detector (6 mm length, 11 ul volume, glass windows) was used. This detector consists of a high intensity 605 nm GaAs light emitting diode as a light source (Stanley HAA5566X, Component Technology Corp., Richardson, TX), a reference and a detector silicon photodiodes (type S2007, Electronic Goldmine, Phoenix, AZ) (see Fig. 9 in Dasgupta *et al.*[16]) and a log-ratio amplifier. Gas chromatography–mass spectrometry (GC–MS) of the hydrolytic decomposition product of the blue analytical product was conducted on a Hewlett–Packard 5988A instrument.

Reagents

All chemicals were reagent grade. Solutions of AAP (2m*M*), ANSA or other chromogenic reagents (15m*M*), and Hematin (100μ*M* in 0.1*M* NH_4OH) were prepared and stored at ~4°C when not in use. The reagent carrier stream was prepared by dilution of these stock solutions in 0.2*M* NH_3/NH_4Cl buffer solution. Stock solutions of 1*M* HCl and 20m*M* surfactant (lauryl sulfate (LS) or Triton X-100 (TX100)) were used to prepare more dilute working solutions. Hydrogen peroxide (3%, Mallinckrodt) stock solutions were standardized by titration with secondary standard $KMnO_4$ solution and lower concentrations of H_2O_2 were prepared by dilution of this stock solution immediately before measurement. All water used in the preparation of solutions and carrier streams was distilled and then deionized by a Nanopure system.

Procedure

In initial batch experiments, 2 ml of a reagent mixture (AAP and one of the chromogenic reagents shown in Table 1), 2 ml of hematin in NH_3/NH_4Cl buffer solution, and 2 ml of a H_2O_2 standard were transferred to a test tube. The formation of a colored reaction product and its apparent rate of formation were visually screened. Reactions that appeared promising

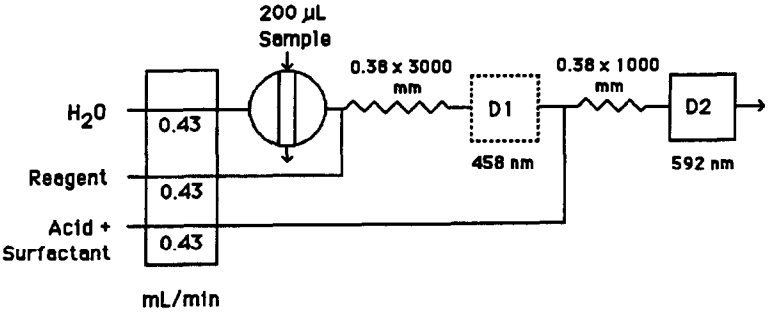

Fig. 1. Flow injection system schematic. Reagent: 10μ*M* hematin, 0.2m*M* AAP, 1.5m*M* ANSA and 2m*M* lauryl sulfate in 0.2*M* NH_3–NH_4Cl buffer. Acid/surfactant: 0.25*M* HCl, 5m*M* lauryl sulfate.

Table 1. Color produced by the reaction of H_2O_2, AAP and various chromogenic substrates*

Substrate tested	Color produced (absorption maximum, *nm*)
Phenol	red (505 *nm*)
4-Ethylphenol	red (490 *nm*)
4-Chlorophenol	red (510 *nm*)
Cresol	red (496 *nm*)
2-Naphthol	blue–purple (584 *nm*)
Chromotropic acid	purple–blue (560 *nm*)
6,7-Dihydroxynaphthalene-2-sulfonic acid	purple–blue (560 *nm*)
Aniline (HCl)	red–purple (550 *nm*)
N,N-diethyl-1,4-phenylenediamine	red (478 *nm*)
1-Anilinonaphthalene-8-sulfonic acid	yellow in basic (458 *nm*) blue–purple in acid (575 *nm*)

*Each test was performed in pH 10 ammoniacal buffer solution.

for flow injection adaptation were further studied by spectrometry. For the AAP–ANSA reaction system, the initial product in basic medium (stable at least for a day) was acidified by the addition of 2 ml of HCl to produce a blue product. Absorption spectra for the final product were taken immediately. In flow injection studies of the AAP–ANSA reaction system, two-step optimization procedures were employed. Preliminary experiments were performed in a basic media. A reagent solution, including hematin, was prepared in NH_3/NH_4Cl buffer solution. Standard solutions of H_2O_2 were injected in a water carrier to which the reagent was merged. The resulting reaction product was monitored at a wavelength of 458 nm. The latter optimization study included the acidification step in which an acid solution was introduced to react with the initial reaction product. The final product was monitored at 592 nm. Samples were injected minimally in triplicate and thus all reported data represent means from at least three runs.

RESULTS AND DISCUSSION

Initial studies

Oxidative condensation reactions between AAP and a number of potentially useful chromogenic reagents were examined. We deliberately limited this study to commercially available reagents. The reagent mixture, including hematin as a catalyst, was dissolved in a 0.1*M* NH_3/NH_4Cl (pH 10) buffer solution. To initiate the reaction, an aliquot of 1m*M* H_2O_2 was added. Many phenol and aniline derivatives undergo the desired hematin catalyzed oxidative coupling reaction with AAP in basic medium. In addition to the reagents shown in Table 1, mono and dinitrophenols were studied. They do not react. *N,N*-dialkylanilines ($R = CH_3$, C_2H_5) were also found to be inapplicable due to limited solubility. As may be expected, water soluble naphthalene derivatives with hydroxyl or amino groups acting as auxochromes result in products that exhibit absorption maxima at longer wavelengths and also display greater absorption intensity. In particular, 2-naphthol, chromotropic acid and 6,7-dihydroxynaphthalene-2-sulfonic acid react relatively fast, forming products with $\lambda_{max} > 560$ nm. However, alkaline solutions of phenolic reagents are particularly susceptible to alkaline degradation and the products also tend to be unstable.

When aniline derivatives are used with AAP, the resulting products display absorption maxima at longer wavelengths and absorb more intensely than phenolic derivatives. Most such compounds (e.g. *N,N*-dimethylaniline), however, are too poorly soluble in alkaline solutions. *N,N*-dialkyl-1,4-phenylendiamines ($R = CH_3$, C_2H_5) are sufficiently soluble and produce a relatively stable product. Nevertheless, the absorption maxima for these products are below 550 nm.

The AAP–ANSA reaction system

ANSA was chosen for study because of the functional groups and its stability in solution. Among all the tested reagents, ANSA was unusual in that the reaction product behaved as an acid–base indicator. The product initially formed in ammoniacal solution was yellow (λ_{max}, 458 nm). It readily forms an intense blue color in acidic medium (λ_{max}, 575 nm). Such a large bathochromic shift in absorption in a base to acid transition is relatively rare. Although the yellow product formed in basic solution was stable over at least day-long periods, the blue material displayed limited aqueous solubility

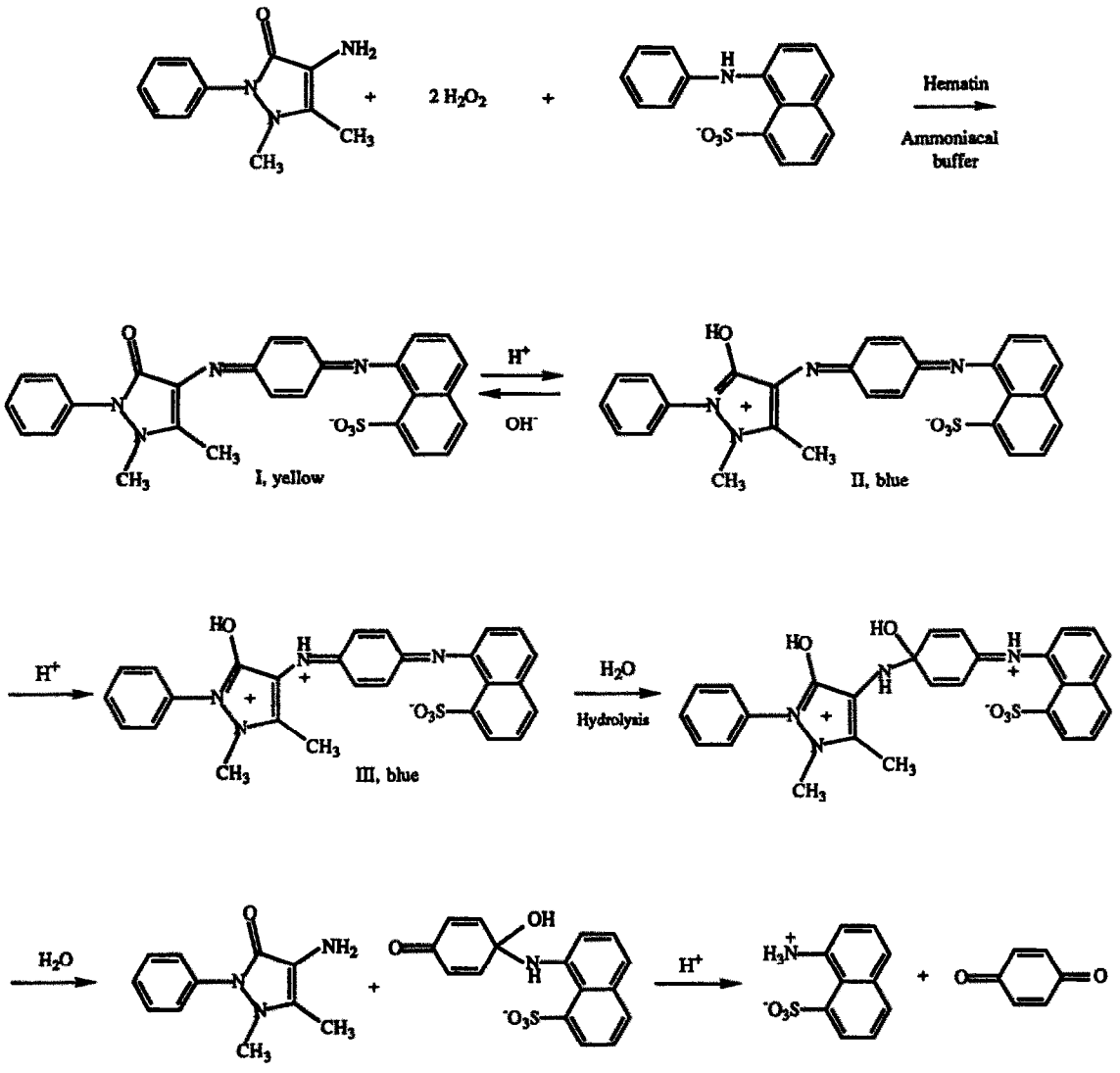

Fig. 2. The AAP–ANSA reaction scheme. The yellow product I initially formed is protonated to form the blue product II which undergoes acid hydrolysis as shown.

and was also hydrolyzed in an acid solution. The reaction itself did not proceed in acidic solutions. In analogy with previous studies involving AAP and chromogenic substrates,[12,13] we believe the structure of the yellow product to be I (Fig. 2) and that of the blue product to be II. Hydrolysis in acid medium of the blue product is believed to proceed according to the pathway shown in Fig. 2, resulting in 1-aminonaphthalene-8-sulfonic acid, benzoquinone and AAP. Benzoquinone was unambiguously identified in the acid hydrolyzate by GC–MS in comparison with an authentic sample (identical chromatographic retention time, parent mass and fragmentation pattern). The blue dye was synthesized in a milligram scale by scaling up the analytical procedure. The solid sample was acid hydrolyzed and the solution then made alkaline (pH 11). A chloroform extract of this sample was analyzed by GC–MS. AAP was unambiguously identified in this extract. 1-Aminonaphthalene-8-sulfonic acid cannot be analyzed by GC and such a procedure was not attempted. However, there remains little doubt that both the product structural identification and the hydrolytic pathways are as shown in Fig. 2.

The reaction itself does not proceed in acidic medium. Whereas the product formed in basic solution is soluble and stable, the protonated blue product has limited solubility probably because of its zwitterionic structure. Addition of surfactants increase solubility. In a medium containing micellar concentrations of LS, the

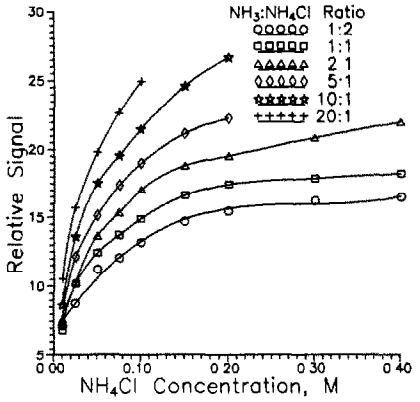

Fig. 3. Dependence of the peroxidatic activity of hematin on the buffer composition. Standard deviation of the results are less than the dimensions of the symbols plotted.

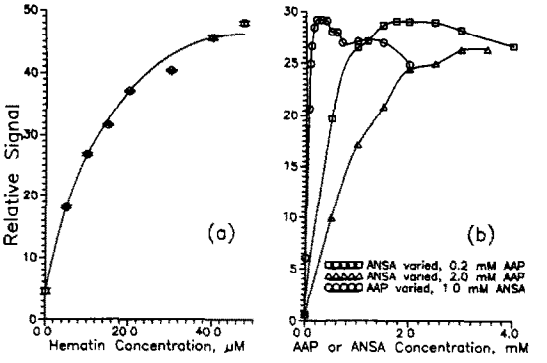

Fig. 4. Effect of reagent composition on system performance, 100μM H_2O_2 injected. (a) Variation of hematin concentration, 0.2mM AAP, 1.5mM ANSA, standard deviation of data are shown as error bars; (b) variation of AAP concentration, 1.0mM ANSA, 10μM hematin; variation of ANSA concentration, 10μM hematin, 0.2 and 2mM AAP; standard deviation of results are less than the dimensions of the points plotted.

absorption maximum of the blue product undergoes a bathochromic shift to 592 nm. Since the reagents show no appreciable absorption above 590 nm and the molar absorptivity in acidic surfactant containing solutions is more than four times that in basic solution, it was of interest to pursue the development of a new automated colorimetric method based on this principle.

Effect of NH_3/NH_4Cl buffer composition on hematin peroxidatic activity

Peroxidatic activity of horseradish peroxidase[17] or hematin[14] has been observed to be stimulated by NH_3, possibly due to the ligation of the nitrogen base to the metalloenzyme. The effect of NH_3 and NH_4Cl concentration on the peroxidatic activity of hematin was studied in the pH range of 8.5–10.5 with the flow injection system. Figure 3 shows that for a given pH (or ratio of NH_3 to NH_4Cl), the absorbance due to the product initially increases steeply as the buffer concentration increases and eventually becomes less dependent of the buffer concentration. At higher buffer concentrations ($<ca.$ 0.2M), it is clear that hematin peroxidatic activity depends mainly on NH_3 concentration. For further studies, a 0.2M NH_3/0.2M NH_4Cl buffer was chosen because buffering capacity is adequate at this composition, the dependence of the reaction rate on variation of the buffer components is minimal and relatively dilute acid can be used for later acidification.

Effect of hematin concentration

The effect of hematin concentration on product formation was studied with 100μM H_2O_2 as sample in the range of 0–45μM hematin. Figure 4(a) shows that the measured absorbance increases with increasing hematin concentration. However, the observed absorbance increases less than a factor of two as the hematin concentration is increased from 10 to 40μM while increased hematin concentrations were found to accelerate the decomposition of ANSA. A 10 μM hematin concentration was therefore used for further studies. With $<10\mu M$ hematin, the reagent mixture is stable for at least one day at room temperature (*ca.* 22°C). It should also be noted that hematin itself is colored and the baseline absorbance increases linearly with increasing hematin concentration.

Effect of substrate concentration

The effect of AAP concentration on product formation was studied with 100μM H_2O_2 in the range of 0–2 mM AAP. Figure 4(b) shows that the measured absorbance increases markedly up to an AAP concentration of about 0.15mM and then becomes relatively independent of the AAP concentration. Above 0.5mM AAP, the absorbance actually begins to decrease slightly.

The effect of ANSA concentration was studied in the range of 0–3.5mM with 0.2 and 2mM AAP (Fig. 4b). When AAP concentration is 0.2mM, the maximum absorbance was obtained at >1.5mM ANSA. With 2mM AAP, the maximum observed absorbance is ~20% less than that with 0.2mM AAP and is attained with >3mM ANSA. Hence 0.2mM AAP and 1.5mM ANSA were selected.

Acidification studies

If the effluent stream from the first stage is acidified without further measures, the blue product precipitates or is strongly adsorbed onto the flow injection system components including the optical window; this causes serious increase in baseline absorbance and noise levels. Addition of a surfactant into the acidifying carrier stream prevents such adsorption and has the additional benefit of shifting the absorption maximum to a longer wavelength with an attendant increase in molar absorptivity. To test the effect of pH on the formation of the final blue product, HCl or citric acid solutions in 10m*M* TX100 were used as the acidifying carrier stream. The absorbance at 592 nm as a function of pH is shown in Fig. 5. Maximum absorbance was attained at pH <3. A concentration of 0.25*M* HCl was chosen; at the flow rates used this was sufficient to attain a final pH of 2.5. In protonating the yellow product (I, Fig. 2), based on the basicity of the available sites, the carbonyl oxygen should be protonated first. The ring to which it is connected thence becomes a 6π-electron cationic system with considerable aromatic character. This results in a large bathochromic shift and enhanced absorptivity. With increasing acidity, one of the quinononoid *N* atoms will be protonated. This is expected to result in only a relatively minor increase in absorptivity over the monoprotonated form. Protonation here would also eventually result in hydrolytic cleavage of the bond, as indicated in Fig. 2. If the blue color is due solely to a monoprotonated form, the system may be modeled as:

$$\text{signal} = Q[\epsilon_{HA}[H^+]/(K_1 + [H^+]) + \epsilon_A K_1/(K_1 + [H^+])]. \quad (1)$$

Where Q is a proportionality constant, ϵ_{HA} and ϵ_A are the absorptivities of the protonated and non-protonated forms, respectively, at 592 nm and K_1 is the acid dissociation constant of the protonated form. If the blue color is due to both a mono- and a diprotonated form, the system may be modeled as:

$$\text{signal} = Q(\epsilon_{H2A}[H^+]^2 + \epsilon_{HA}[H^+]K_1 + \epsilon_A K_1 K_2/R \quad (2)$$

where

$$R = [H^+]^2 + K_1[H^+] + K_1K_2 \quad (3)$$

and ϵ_{H2A} is the absorptivity of the diprotonated form, K_1 and K_2 being the first and second acid dissociation constants of this form, respectively. Figure 5 shows the best fits of the experimental results to equations (1) and (2), respectively. It is clear that the diprotic acid model results in a much better fit. This model results in the best fit values of 3.6 and 5.5 for pK_1 and pK_2 a ratio of 1.53 for $\epsilon_{H2A}/\epsilon_{HA}$ and a negligible value for ϵ_A.

The effect of surfactants was studied with cetyltrimethylammonium chloride (CTAC), TX100 and LS solutions (cationic, non-ionic and anionic surfactant, respectively). The use of CTAC resulted in immediate precipitation of the blue product, probably due to ion pair formation with the sulfonate end of the molecule. The use of the other surfactants inhibited precipitation/wall adsorption. These effects take place only at surfactant concentrations sufficient to form micelles. Presumably the blue product partitions to the micelle. The significant increase of the molar absorptivity and the bathochromic shift indicates that the blue product either undergoes further aggregation within the micelle or participates in charge-transfer interactions with the surfactant molecules or both. As shown in Fig. 6, maximum absorbance is reached at >10m*M* TX100 and at >5m*M* LS. Since the use of LS gives about 20% higher signal than TX100 and prevents adsorption problems more effectively, the use of LS was adopted.

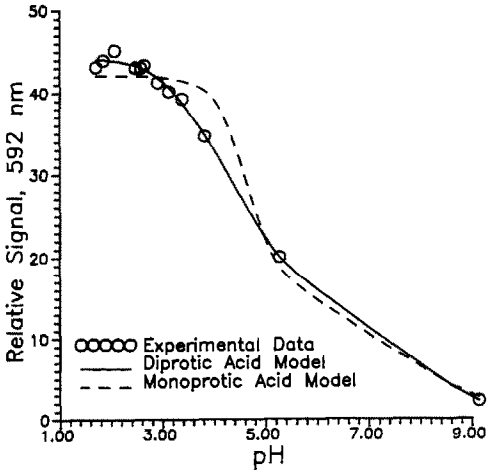

Fig. 5. The absorbance of the final blue product as a function of pH. The standard deviation of individual points is less than the dimension of the symbols plotted.

System performance

With experimental conditions optimized as described above, typical system output is shown in Fig. 7. The peak height response is linear in

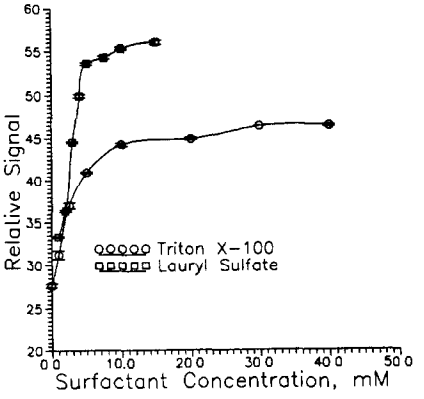

Fig. 6. Effect of surfactant concentration (added to 0.25*M* HCl solution), 10μM hematin, 0.2m*M* AAP, 1.5m*M* ANSA, 100μM H_2O_2.

the 1–50μM range; the best fit equation is given by:

$$\text{signal (AU)} = 6.1(\pm 0.061) \times 10^{-4}\ \text{C, } (\mu M) - 6.5(\pm 5.8) \times 10^{-6}. \quad (4)$$

Response becomes nonlinear at higher concentration, the signal for 100μM H_2O_2 is 13% below that predicted by the above equation. This is possibly due to saturation of the catalyst binding sites. Based on three times the noise level of the baseline divided by the calibration slope, the LOD is 0.30μM. The typical RSD for the entire 1–100μM range studied was $<1.5\%$.

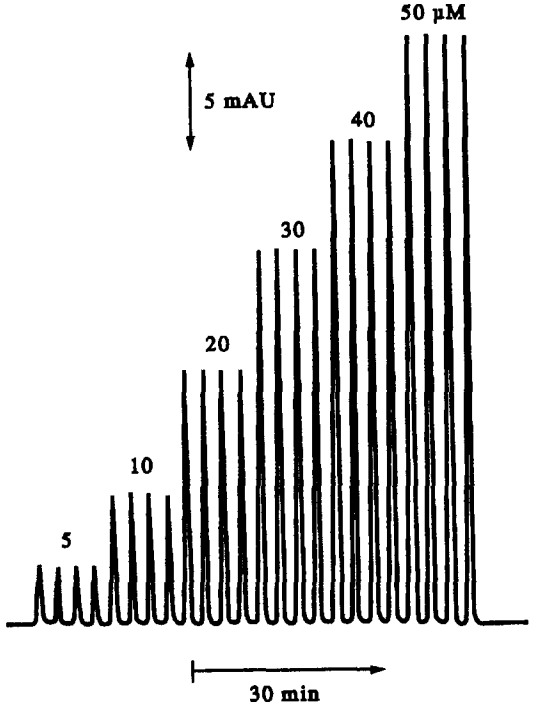

Fig. 7. Typical system output, conditions as in Fig. 1, 200 μl samples of 5–50μM H_2O_2.

Table 2. Effect of foreign species*

Substance	Added (μM)	Absorbance (mAU)	% Error
PO_4^{3-}	100	8.30	0
NO_2^-	10	17.7	110
HCO_3^-	100	8.28	0.24
HSO_3^-	100	8.34	0.48
Mn^{2+}	100	8.28	0.24
Ca^{2+}	100	8.08	2.65
Fe^{3+}	100	14.4	73.5
	50	11.1	33.3
OCl^-	100	8.22	0.96

*Total measured absorbance after addition of 10μM H_2O_2; in all cases, relative standard deviations were $\leq 0.8\%$.

When the LED-based detector was employed, the absorbance signal decreases by *ca.* 45% compared to the commercial detector (Spectroflow 757) because of the shorter pathlength of the LED-based detector cell. The RSD at 10μM H_2O_2 for this detector was 1.3%.

To test the effect of foreign species in the system, an excess amount (100μM in most cases) of such potential interferents were added to the H_2O_2 standard before determination by this procedure. The results presented in Table 2 show that only Fe^{3+} and especially NO_2^- seriously interfere with the determination. Both species react with ANSA itself to form blue products in acidic medium. However, no reaction due to NO_2^- ion occurs in basic medium. If acidification is omitted and the condensation product in basic medium is monitored at 458 nm, NO_2^- is no longer an interferent, at the expense of losing sensitivity. The use of sulfamic acid as masking agent for NO_2^- was tested. Addition of sulfamic acid into the reagent does not prevent blue color formation due to NO_2^-. However, addition of sulfamic acid to the sample prior to determination completely eliminates interference from NO_2^-. Except if ambient air samples containing HONO are scrubbed into an aqueous medium, H_2O_2 and NO_2^- are not expected to co-occur in the same sample. These measures are therefore not expected to be necessary for most real samples. Similarly, interference of Fe^{3+} may be prevented by addition of F^- but such measures are not expected to be necessary for real samples.

REFERENCES

1. G. I. Meerov, *Zh. Anal. Khim.*, 1966, **21**, 128.
2. R. Thompson, *Clin. Chim. Acta.*, 1966, **13**, 133.
3. L. A. Dobrick, *J. Biol. Chem.*, 1958, **231**, 4032.

4. B. H. Billing. *J. Clin. Pathol.*, 1955, **8**, 126.
5. G. W. Stevenson, S. L. Jacobs and R. J. Henry, *Clin. Chem.*, 1964, **10**, 95.
6. G. G. Guilbault and D. N. Kramer, *Anal. Chem.*, 1964, **36**, 2495.
7. D. N. Kramer and E. B. Hackley, *Anal. Lett.*, 1971, **4**, 223.
8. M. A. Pesce and S. H. Bodourian, *Clin. Chem.*, 1977, **23**, 757.
9. P. Fossati, L. Prencipe and G. Berti, *Clin. Chem.*, 1980, **26**, 227.
10. K. Tamaoku, Y. Murao, K. Akiura and Y. Ohkura, *Anal. Chim. Acta*, 1982, **136**, 121.
11. B. C. Madsen and M. S. Kromis, *Anal. Chem.*, 1984, **56**, 2849.
12. Y. Saito, M. Mifune, S. Nakashima, J. Odo, Y. Tanaka, M. Chikuma and H. Tanaka, *Anal. Sci.*, 1987, **3**, 171.
13. Y. Saito, M. Mifune, S. Nakashima, J. Odo, Y. Tanaka, M. Chikuma and H. Tanaka, *Talanta*, 1987, **34**, 667.
14. Z. Genfa and P. K. Dasgupta, *Anal. Chem.*, 1992, **64**, 517.
15. Z. Genfa and P. K. Dasgupta, *Anal. Chim. Acta*, 1992, **260**, 57.
16. P. K. Dasgupta, H. S. Bellamy, H. Liu, J. L. Lopez, E. L. Loree, K. Morris, K. Petersen and K. A. Mir, *Talanta*, in press.
17. I. Fridovich, *J. Biol. Chem.*, 1963, **238**, 3921.

Talanta, Vol. 40, No. 7, pp. 989–994, 1993
Printed in Great Britain.

0039-9140/93 $6.00 + 0.00
Pergamon Press Ltd

ISOLATION AND IDENTIFICATION OF IMPURITIES IN L-696,229 DRUG SUBSTANCE

S. V. PRABHU, J. M. BALLARD, R. A REAMER and D. K. ELLISON
Merck Research Laboratories, P.O. Box 2000, Rahway, NJ 07065–0900, U.S.A.

(*Received* 13 *November* 1992)

Summary—Two low level impurities in 3-[2-(2-benzoxazolyl)ethyl]-5-ethyl-6-methyl-2(1H)-pyridinone drug substance (L-696,229) have been isolated by a combination of preparative HPLC, solid-phase extraction and liquid–liquid extraction. They were identified as 3-[2-(2-benzoxazolyl)ethyl]-5-ethyl-6-(2-phenylethyl)-2(1H)-pyridinone (I) and 6,6′-(2-phenyl-1,3-propanediyl)bis[3-[2-(2-benzoxazolyl)ethyl]-5-ethyl-2(1H)-pyridinone] (II) by mass spectrometry and by their ^{13}C and ^{1}H-NMR spectra.

INTRODUCTION

3-[2-(2-Benzoxazolyl)ethyl]-5-ethyl-6-methyl-2(1H)-pyridinone (L-696,229) belongs to a class of compound which exhibits potent *in vitro* inhibition of human immunodeficiency virus type 1 reverse transcriptase.[1,2] L-696,229, which is presently undergoing safety and pharmacokinetic evaluation in humans,[2] contains an ethylene linkage between a benzoxazole group and a substituted pyridone (Fig. 1).

In the development of new drugs, one analytical challenge is to quickly develop rugged methods for quality evaluation. The determination of the purity of a drug candidate is important in order to establish the acceptability of batches for safety assessment and clinical trials. Ideally the total amount of impurity, as well as the quantity of each individual impurity, should be monitored in the bulk drug. A serious attempt should be made to identify each individual impurity present at 0.1% area (or greater) of the main peak in the LC/UV impurity profile.

Several different methods have been used for the HPLC analysis of L-696,229. A column-switching system, in which multiple HPLC columns are interconnected by a switching valve, has been used as an alternative to gradient elution to eliminate interferences from late-eluting species.[3] We have developed a simple, 0.1% aqueous phosphoric acid/acetonitrile gradient system to routinely monitor the purity and stability of L-696,229. Two late-eluting impurities were detected in some batches of L-696,229 using this method. Identification of both of these impurities was attempted because they exceeded the 0.1% level in some samples.

This paper describes the isolation and concentration of these impurities using sequential preparative HPLC, solid-phase extraction and liquid–liquid extraction. The identification of these impurities as 3-[2-(2-benzoxazolyl)ethyl]-5-ethyl-6-(2-phenylethyl)-2(1H)-pyridinone and 6,6′-(2-phenyl-1,3-propanediyl)bis[3-[2-(2-benzoxazolyl)ethyl]-5-ethyl-2(1H)-pyridinone] was achieved by mass spectrometry and by comparison of their NMR spectra to those of precursors.

EXPERIMENTAL

Apparatus

The preparative HPLC system consisted of a Rabbit™ solvent delivery system with a Dynamax-60A, C-8 column (250 × 21.4 mm; Rainin Instr., Woburn, MA), a Model 201 fraction collector (Gilson Medical Electronics, Middleton, WI), a Spectroflow Model 757 UV detector (Kratos Analytical, Ramsey, NJ) and a Model TYP7025 stripchart recorder (Linseis Inc., Princeton Junct., NJ). The analytical HPLC system consisted of a Model SP8700XR liquid chromatography pump with a built-in column heater (Spectra-Physics Analytical, Fremont, CA), a Model 759A UV detector (Applied Biosystems, Foster City, CA) and a Zorbax RX-C8 column (250 × 4.6 mm; Mac-Mod Analytical, Chadds Ford, PA). Data were collected with an Access* Chrom Vax-based chromatography data system (PE Nelson, Cupertino, CA). Solid-phase extractions were performed using Model SPE-21 vacuum manifolds (J. T. Baker Inc., Phillipsburg, NJ) with Bond Elut C-8

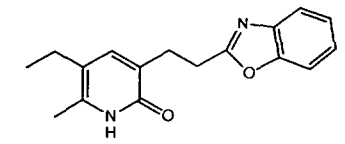

L-696,229

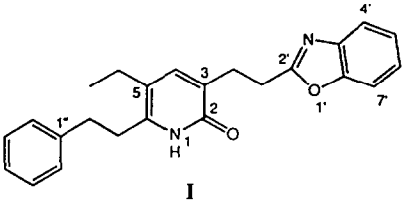

I

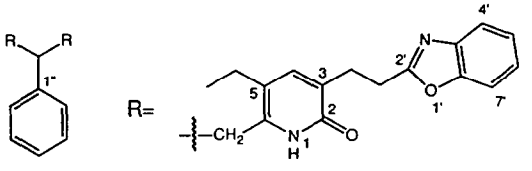

II

Fig. 1. Structure of L-696,229 and impurities I and II.

cartridges (6 ml) and adapters (Varian Sample Prepn. Prods., Harbor City, CA).

Chromatographic conditions

The mobile phase for preparative HPLC was acetonitrile/water (40:60 v/v) at a flow rate of 20 ml/min. The column was at ambient temperature and 5 ml injections were made; the UV detector was set at 234 nm. For analytical HPLC, 10 μl injections were made into the column held at 40°C and the mobile phase was acetonitrile/water (50:50 v/v) at a flow rate of 1.0 ml/min.

Isolation of impurities

Preparative HPLC. A sample of L-696,229 (2.2 g), enriched in impurities at the 1–2% level, was dissolved in 100 ml of acetonitrile/water (80:20 v/v). Aliquots (5 ml) of the solution were injected repetitively into the preparative HPLC system and appropriate fractions were combined to isolate each impurity. The final volume collected was approximately 600 ml for each impurity.

Solid-phase extraction. The acetonitrile/water ratio of the two cuts collected by preparative HPLC was adjusted to 20:80 v/v by the addition of water to give a final volume of about 1500 ml for each impurity. Three solid-phase extraction cartridges, connected in series using adapters, were conditioned with acetonitrile (15 ml) followed by water (15 ml) prior to use. Each impurity was concentrated separately on the cartridges by passing about 500 ml of the dilute impurity solution through the cartridges. Very little breakthrough of the impurity was detected when the eluate was monitored by analytical HPLC. The retained impurity was eluted with 10 ml of acetonitrile/water (95:5 v/v). This procedure was repeated with 2 × 500 ml portions of the dilute solutions and the combined washings totalled about 30 ml for each impurity.

Liquid–liquid extraction. The 30 ml solution of each impurity was concentrated to about 10 ml under nitrogen. Water (5 ml) and dichloromethane (15 ml) were added, the mixture was shaken for 2 min and then centrifuged for 2 min. The organic layer was removed and the extraction was repeated with a second 15 ml aliquot of dichloromethane. The combined organic layers were concentrated to dryness under a stream of nitrogen at room temperature to obtain impurity I (10 mg) and impurity II (14 mg).

Each impurity was analysed by thermospray ionization LC/MS and by electron ionization (EI) using a direct insertion probe. LC/MS was performed by injection of the sample into a Zorbax RX-C8 column (250 × 4.6 mm) with aqueous 0.1*M* ammonium acetate/acetonitrile (50:50 v/v) at a flow rate of 1.0 ml/min as the mobile phase. The LC column was coupled to a Finnigan MAT TSQ 70B mass spectrometer *via* a TSP2 thermospray interface held at 119°C; the ion source block was at 300°C. Positive ion mass spectra were acquired repetitively over the range 200–700 μ. Electron ionization (EI) mass spectra were recorded at 70 eV over the range 40–700 μ on a Finnigan 4500 mass spectrometer, using a fast-heating direct exposure probe, at a source temperature of 150°C.

NMR spectra were run in $CDCl_3$ on a Bruker AM-400 spectrometer. Proton spectra were observed at 400.13 MHz and were referenced to residual $CHCl_3$ at 7.27 ppm. Carbon-13 spectra (100.61 MHz) were referenced to $CDCl_3$ at 77.0 ppm. Impurity I: ^{1}H NMR ($CDCl_3$) δ 12.69 (br, H_1), 7.69 (m, $H_{4'}$), 7.45 (m, $H_{7'}$), 7.30 (overlapping m, $H_{5'}$, $H_{6'}$, $H_{2'',6''}$), 7.20 (m, $H_{3'',5''}$), 7.18 (s, H_4), 7.10 (m, $H_{4''}$), 3.33 (t, J = 7.6, 2′-CH_2), 3.16 (t, J = 7.6, 3-CH_2), 2.96 (m, 6-CH_2), 2.85 (m, 1″-CH_2), 2.30 (q, J = 7.5, CH_2CH_3), 1.00 (t, J = 7.5, CH_2CH_3).

^{13}C NMR ($CDCl_3$) δ 166.8 ($C_{2'}$), 164.2 (C_2), 150.8 ($C_{7'a}$), 142.5, 141.4, 140.8 ($C_{1''}$, C_6, $C_{3'a}$), 141.6 (C_4), 128.5, 128.4 ($C_{2'',6''}$, $C_{3'',5''}$), 127.7 (C_3), 126.2 ($C_{4''}$), 124.4, 124.0 ($C_{5'}$, $C_{6'}$), 119.5

($C_{4'}$), 118.7 (C_5), 110.3 ($C_{7'}$), 36.0, 32.7, 28.1, 27.5 ($4 \times CH_2$), 27.5 (CH_2CH_3), 15.4 (CH_2CH_3).

Impurity II: ^1H NMR ($CDCl_3$) δ 12.17 (br, H_1), 7.60 (m, $H_{4'}$), 7.35 (m, $H_{7'}$), 7.23 (m, $H_{5'}$, $H_{6'}$), 7.19 (m, $H_{2'',6''}$), 7.13 (t, J = 7.2, $H_{3'',5''}$), 7.07 (m, $H_{4''}$), 7.03 (s, H_4), 3.60 (m, 1''-CH), 3.26 (m, 2'-CH_2), 3.05 (overlapping m, 3-CH_2, 6-CH_2), 2.00 (m, CH_2CH_3), 0.67 (t, J = 7.5, CH_2 CH_3). ^{13}C NMR ($CDCl_3$)δ 166.7 ($C_{2'}$), 163.7 (C_2), 150.7 ($C_{7'a}$), 141.3 ($C_{3'a}$), 141.0 (C_4), 140.6 (br, C_6), 128.5, 127.7 ($C_{2'',6''}$, $C_{3'',5''}$), 128.1 (br, C_3), 127.0 ($C_{4''}$), 124.3, 123.9 ($C_{5'}$, $C_{6'}$), 119.4 ($C_{4'}$), 119.3 (br, C_5), 110.2 ($C_{7'}$), 46.3 (br, CH), 37.4 (br, CH_2), 27.9, 27.5 (CH_2CH_2), 22.6 (CH_2CH_3), 14.8 (CH_2CH_3). Several signals are broad (as noted) and $C_{1''}$ is not observed.

RESULTS AND DISCUSSION

Since related by-products due to the reaction between a benzyloxy precursor and benzaldehyde contamination of benzyl alcohol had been identified at an earlier stage of the synthesis,[4] a sample of L-696,229 enriched in the final product impurities at about 1–2% each was prepared to facilitate the isolation work. Although preparative HPLC is a well established technique for the isolation of pure compounds from mixtures, it suffers from the disadvantage that the desired compound is often obtained in a rather large volume of the mobile phase. Concentration of this solution, usually on a rotary evaporator, can be time-consuming and is potentially harmful to thermally labile materials. Solid-phase extraction cartridges provide a convenient, alternative method for stripping the solvents from the HPLC fractions;[5,6] the material retained on the cartridge may then be eluted with a minimum volume of a suitable mobile phase, with subsequent procedures (*e.g.*, concentration, chromatography, extraction) being easier to perform.

An isocratic reverse phase separation with acetonitrile/water (50:50 v/v) was found to be ideal for the resolution and stability of the two impurities [Fig. 2*A*] and a similar mobile phase (40:60 v/v) was used for the preparative LC work. Isolation of the two impurities from L-696,229 was achieved using a series of preparative HPLC injections and collection of appropriate fractions. The amounts of impurity I and II present in the starting material and in the individual pools throughout the isolation process were monitored by analytical reverse phase

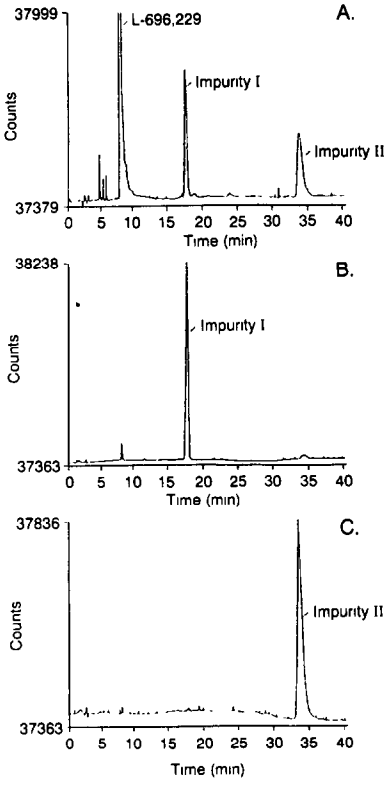

Fig. 2. Typical chromatograms of impurity-enriched sample and isolated impurities on analytical HPLC. *A*. Enriched L-696,229 sample. *B*. Chromatogram of isolated impurity I. *C*. Chromatogram of isolated impurity II. Chromatographic conditions: see Experimental.

HPLC. The initial preparative HPLC served as a rapid means of isolating the impurities from the bulk drug. Concentration of these impurities was then achieved by a combination of solid-phase extraction and liquid–liquid extraction. The isolated impurities I and II were better than 98% pure, as judged by HPLC area percentage and their retention times matched those of the low level impurities in typical batches of L-696,229 [see Figs 2*B* and 2*C*, respectively, for chromatograms].

Impurity I

The thermospray mass spectrum of impurity I contained the base peak at m/z 373 corresponding to $[M + H]^+$ of a compound with a molecular weight 90 u (C_7H_6) greater than L-696,229. A very low intensity peak at m/z 423 of unknown origin was also observed. The EI spectrum (Fig. 3) showed strong peaks at m/z 372 ($M^{+\cdot}$) and 91 ($C_7H_7^+$), the latter being characteristic of a benzyl group. The presence of a benzyl group was further indicated by the intense peak at m/z 281 $(M\text{-}C_7H_7)^+$ and the location of the benzyl group on the pyridone

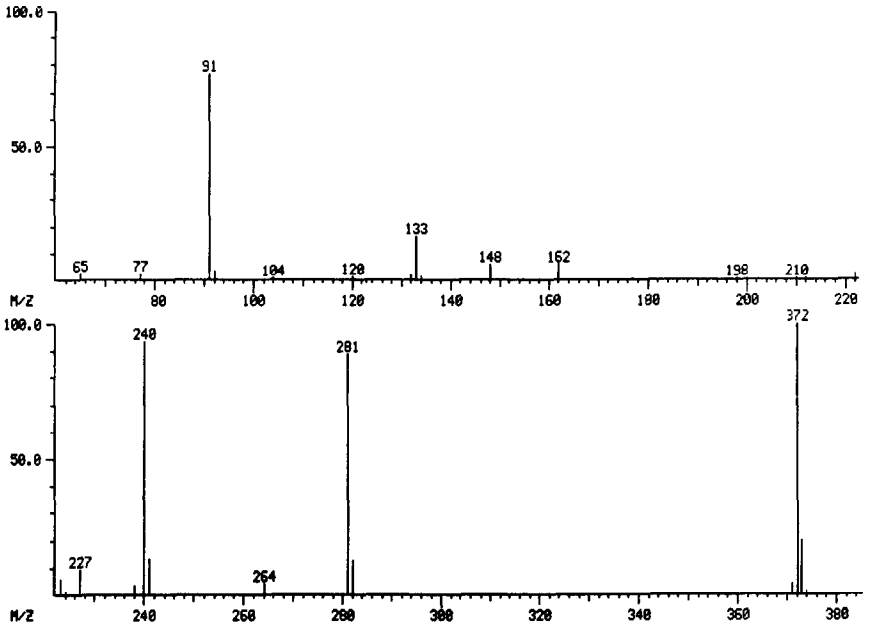

Fig. 3. EI mass spectrum of impurity I.

portion of the molecule was shown by the ion at m/z 240, which was 90 μ higher than the corresponding fragment ion (m/z 150; base peak) in the EI spectrum of L-696,229. The ions at m/z 240 and 133 can be ascribed to cleavage of the central CH_2-CH_2 bond between the benzoxazole and pyridone rings. The high field region of the proton NMR spectrum [see Fig. 4(*C*) and Experimental] of impurity I was similar to that of L-696,229 except for the absence of the 6-methyl group and the addition of a 1,2-substituted ethylene group. This was supported by the ^{13}C-NMR spectra [Figs 4(*A*,*B*); ^{1}H decoupled ^{13}C and APT[7] experiments] where five methylene groups and one methyl group were observed. The aromatic region of the ^{1}H and ^{13}C-NMR spectra supported the presence of an additional monosubstituted phenyl group. Taken together the data support the structure given in Fig. 1 for impurity I.

Impurity II

As an impurity I above, a methyl group is also missing from the proton NMR spectrum [see Fig. 5(*B*) and Experimental] of impurity II. Integrated intensities in the proton spectrum and ^{13}C-NMR experiments indicated the presence of an aliphatic methine. The aromatic region of the ^{13}C-NMR spectrum also showed a monosubstituted phenyl group. Unlike impurity I, the ratio of the monosubstituted phenyl to the pyridone/benzoxazole groups is 1:2. The ^{13}C-NMR spectrum of impurity II [see Fig. 5(*A*) and Experimental] has some unexplained broadening (not observed in the simpler analogue with a protected pyridone) but is consistent with the structure shown. Impurity II gave a thermospray mass spectrum which contained only the peak due to the $[M + H]^+$ ion at m/z 653. The molecular weight (652 μ) and the required even number of nitrogen atoms derived from the

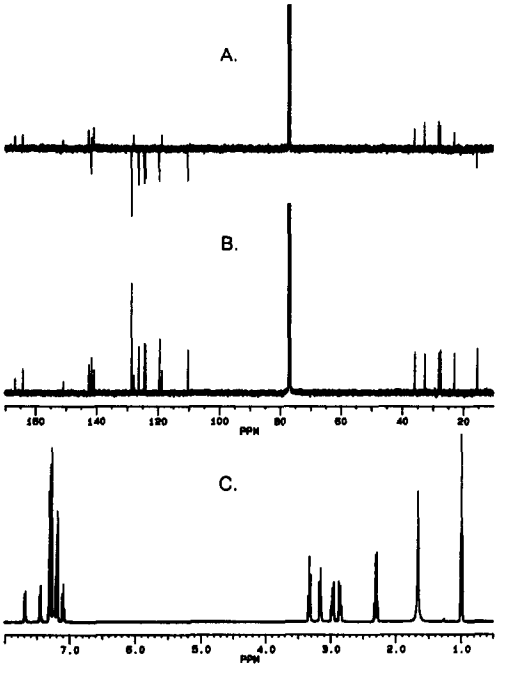

Fig. 4. *A*. ^{1}H decoupled ^{13}C, *B*. ^{13}C APT, and *C*. ^{1}H NMR spectra of impurity I.

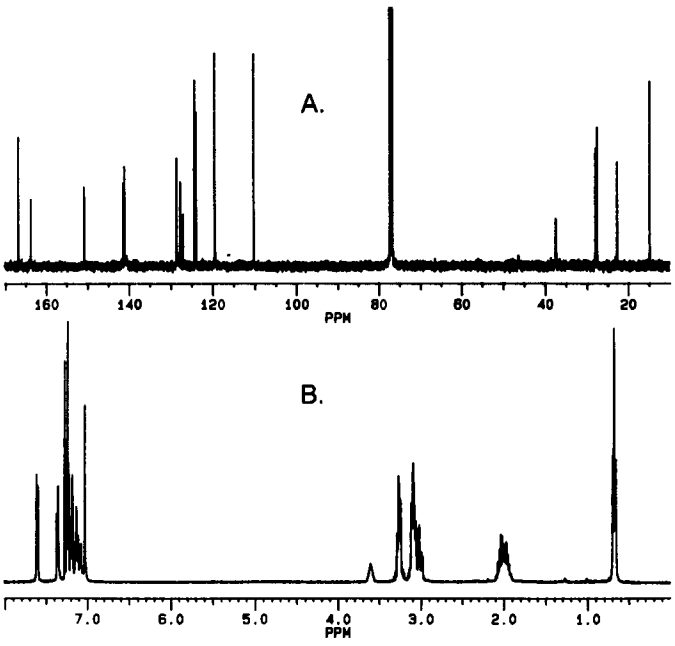

Fig. 5. *A*. ^{13}C,and *B*. ^{1}H NMR spectra of impurity II.

$[M + H]^+$ value are both consistent with the structure deduced from the NMR data. The EI spectrum (Fig. 6) showed a very weak molecular ion at m/z 652 together with peaks at m/z 371 and 282 due to cleavage of the bond between the benzylic carbon and the pyridone methylene group; as above, the ion at m/z 133 is ascribed to cleavage of the CH_2—CH_2 bond linking a benzoxazole group to the remainder of the molecule.

It should be noted that the structural characterization of related precursors[4] greatly

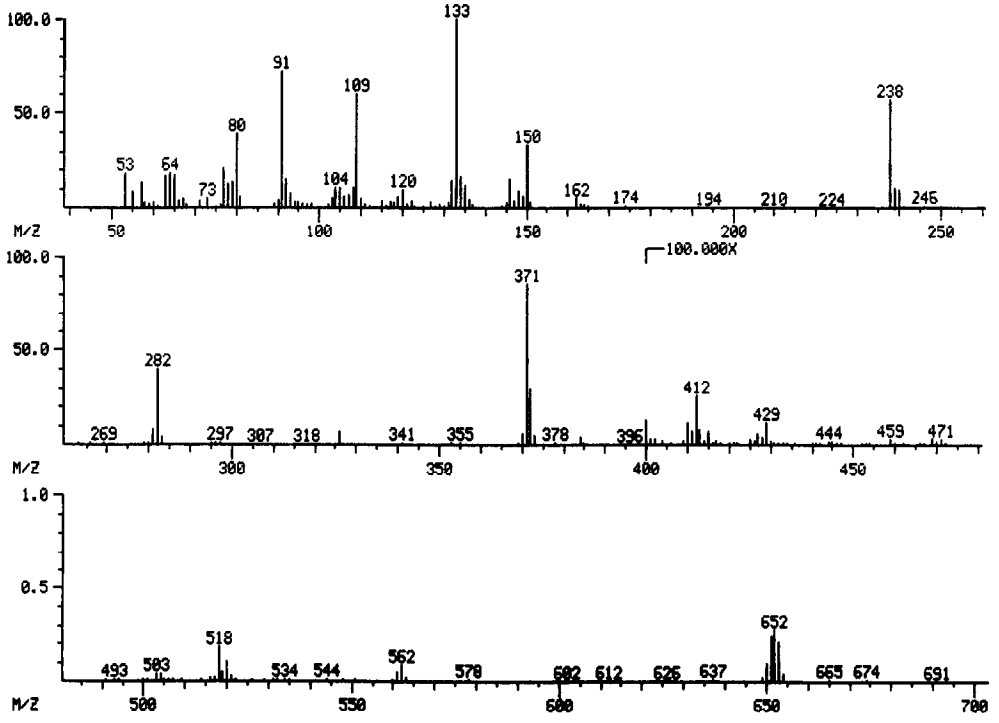

Fig. 6. EI mass spectrum of impurity II.

facilitated the identification of both of the isolated impurities.

CONCLUSION

The combination of sequential preparative HPLC, solid-phase extraction and liquid–liquid extraction has proved to be an effective and rapid strategy for the isolation of low level impurities from L-696,229 bulk drug substance. The isolated impurities were at least 98% pure. The structural characterization of these impurities was performed by NMR and MS.

Acknowledgements—Drs I. Houpis and J. Lynch are thanked for helpful discussions regarding the chemistry of formation of these impurities and for preparation of the impurity-enriched sample of L-696,229.

REFERENCES

1. W. S. Saari, J. M. Hoffman, J. S. Wai, T. E. Fisher, C. S. Rooney, A. M. Smith, C. M. Thomas, M. E. Goldman, J. A. O'Brien, J. H. Nunberg, J. C. Quintero, W. A. Schleif, E. A. Emini, A. M. Stern and P. S. Anderson, *J. Med. Chem.*, 1991, **34**, 2922.
2. M. E. Goldman, J. A. O'Brien, T. L. Ruffing, J. H. Nunberg, W. A. Schleif, J. C. Quintero, P. K. S. Siegl, J. M. Hoffman, A. M. Smith, and E. A. Emini, *Antimicrobial Agents and Chemotherapy*, 1992, **36**, 1019.
3. E. J. Woolf and B. K. Matuszewski, *Pharmaceutical Research*, 1993, **10**, 56.
4. I Houpis, T. M. H. Liu, J. Lynch and A. Molina, personal communication.
5. In *Handbook of Sorbent Extraction Technology*, K. C. VanHorne (ed.), p.110. Analytichem International, Harbor City, CA, 1985.
6. M. Zief and R. Kiser in *Solid Phase Extraction for Sample Preparation*. J. T. Baker Inc., Phillipsburg, NJ, 1990.
7. S. L. Patt and J. H. Schoolery, *J. Mag. Res.*, 1982, **46**, 535.

Talanta, Vol. 40, No. 7, pp. 995–998, 1993
Printed in Great Britain.

0039-9140/93 $6.00 + 0.00

FLOW-INJECTION DETERMINATION OF L-TYROSINE IN SERUM WITH IMMOBILIZED TYROSINASE

NOBUTOSHI KIBA, HIROSHI SUZUKI and MOTOHISA FURUSAWA

Department of Applied Chemistry and Biotechnology, Faculty of Engineering, Yamanashi University, Kofu 400, Japan

(*Received* 2 *November* 1992. *Revised* 21 *December* 1992. *Accepted* 22 *December* 1992)

Summary—A flow-injection method for the determination of the serum L-tyrosine is described. The method involves the conversion of tyrosine into dopaquinone by reaction of tyrosinase, followed by derivation of the dopaquinone with fluorogenic agent 1,2-diphenylethylenediamine. Serum was deproteinized with tungstic acid. Sample solution was injected into a reactor (50 × 4 mm i.d.) packed with glass beads on which tyrosinase was immobilized. The fluorescence was detected at 480 nm (excitation at 350 nm). The calibration graph was linear for 5×10^{-7}–2×10^{-4} *M* L-tyrosine; the detection limit was 2×10^{-7}*M*.

The concentration of tyrosine in serum is a useful indicator of disorders of metabolism (*e.g.*, phenylketonuria[1] and tyrosinosis[2]), and of disturbances in an organism (*e.g.*, hepatitis[3] and thyroid diseases[4]). The determination of tyrosine has been based on liquid chromatographic (LC) techniques.[5] However, the methods designed to quantify all serum amino acids are unnecessarily lengthy. A rapid and selective method is needed in order to provide the correct diagnosis.

Compounds with 1,2-dioxo moieties readily form fluorescent derivatives with 1,2-diaryle thylenediamines.[6] 1,2-Diphenylethylenediamine (DPE) has been used in a post-column reaction system in high performance liquid chromatography for the determination of catechol compounds,[7] in which a coulometric technique was used for the oxidation of the compounds to the corresponding *o*-quinones.

Tyrosinase (EC 1.14.18.1) catalyses the hydroxylation of L-tyrosine to L-dopa and the dehydrogenation of the L-dopa to L-dopaquinone[8] according to the reactions:

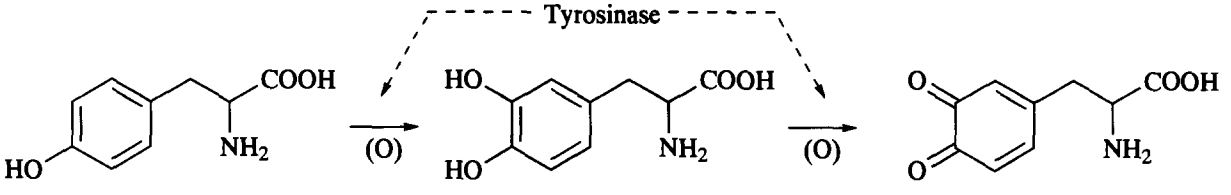

L-Tyrosine L-Dopa Dopaquinone

A highly fluorescent derivative was obtained by a condensation reaction to dopaquinone with DPE under mild conditions in a pre-column derivation procedure[9] according to the reaction[10]:

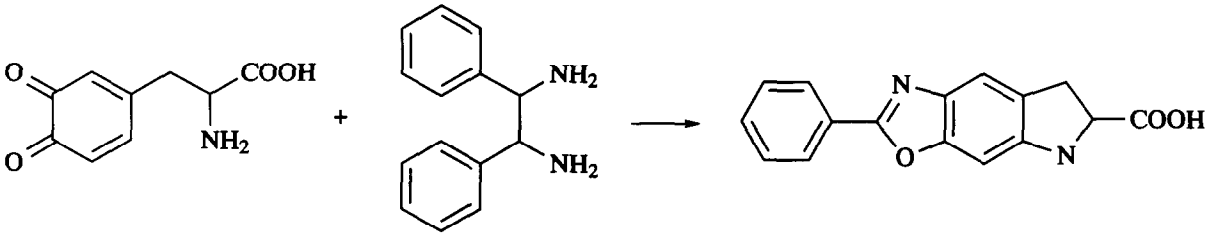

Dopaquinone DPE Ex = 350 nm
Em = 480 nm

This paper describes a flow-injection method for the determination of L-tyrosine with immobilized tyrosinase reactor followed by fluorescence detection after the addition of DPE. The method was used for the determination of L-tyrosine in serum.

EXPERIMENTAL

Materials and reagents

Tyrosinase (2400 U/mg, from mushroom) and L-tyrosine were purchased from Sigma Chemical (St Louis). Aminopropyl-CPG (pore size 59 nm, particle size 200–400 mesh) was from CPG Inc. (Fairfield). DPE was synthesized using the method of Irving and Parkins.[11] All other reagents used were of analytical-reagent grade. DPE solution was prepared by dissolving 0.32 g of DPE in 15 ml of 0.6*M* hydrochloric acid and diluting to 50 ml with ethanol. The preparation of the immobilized tryosinase reactor was described in detail in the previous paper.[12] The immobilized enzyme was packed into a stainless steel column (50 × 4 mm i.d.).

Apparatus and procedure

A flow diagram of the FIA system is shown in Fig. 1. A 0.2*M* phosphate buffer (pH 7.2) was pumped by a double plunger pump (Kyowa Seimitsu, KHU-W-52) at a flow rate of 0.4 ml/min. The DPE solution was pumped by a LC pump (Hitachi, L-6000) at a flow rate of 0.3 ml/min. The immobilized tyrosinase reactor, reaction coil (PTFE, 1000 × 0.5 mm i.d.) and cooling coil (stainless-steel, 100 × 0.5 mm i.d.) were thermostatted at 15, 105 and 15°C, respectively. Sample solution (30 μl) was injected into the carrier stream by a loop injector (Sanuki, SVI-5U7). The separation column (40 × 4 mm i.d.) was packed with Capcell 120 C_{18} (5 μm) (Shiseido, Tokyo). The fluorescence was measured at 480 nm (excitation 350 nm) with a spectrofluorimeter (Jasco, FP-200) connected to a chart recorder (TOA, FBR 251A).

Serum (10 μl) was deproteinized by adding 5% (w/v) sodium tungstate solution (10 μl) and 0.15*M* sulphuric acid (30 μl). The mixture was filtered through an Airpress-30 filter [a filter with an ultrafiltration membrane (nominal molecular weight cut-off 30,000)] (Tosoh, Tokyo) and a 30 μl of the filtrate was injected into the carrier stream.

RESULTS AND DISCUSSION

Reactor performance

The properties of immobilized tyrosinase were evaluated, with the dopaquinone produced in the reaction being monitored at 475 nm with a spectrophotometer (Jasco, Uvidec-100-VI). The influence of pH on the enzymatic reaction was studied over the pH range 6.0–8.0. A standard solution of L-tyrosine (0.5 m*M*) was injected into the carrier stream (water) and mixed with 0.2*M* phosphate buffer at various pH values prior to elution through the enzyme reactor. The total flow-rate through the enzyme reactor was 0.4 ml/min. Other conditions were identical to those shown in Fig. 1. The optimum pH for the enzymatic reaction was about 7.2. The reactor was placed in a water bath and the temperature was varied between 10 and 30°C. The reactor exhibited the highest activity at 15°C. The reactor was used by repeated injections of tyrosine solution (0.5 m*M*) at a sample speed of 15/h. The activity decreased gradually and remained at 80% of the initial value after 800 injections. The decrease in the activity of tyrosinase occurs during the course of reaction and is known as reaction inactivation.[13]

Condensation reaction

The reaction conditions were examined with respect to the temperature, the concentration of

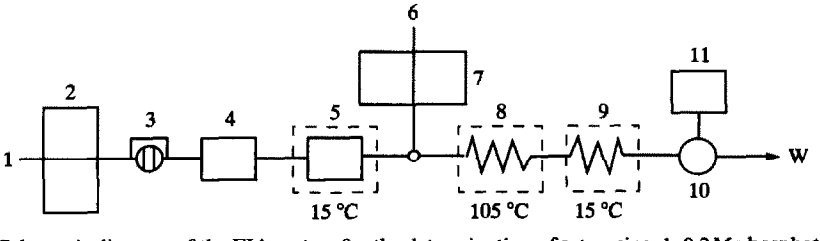

Fig. 1. Schematic diagram of the FIA system for the determination of L-tyrosine. 1: 0.2*M* phosphate buffer (pH 7.2); 2: pump (0.4 ml/min); 3: injector with 30 μl loop; 4: separation column (40 × 4 mm); 5: immobilized tyrosinase reactor (50 × 4 mm); 6: 30 m*M* DPE solution; 7: pump (0.3 ml/min); 8: reaction coil (1000 × 0.5 mm); 9: cooling coil (100 × 0.5 mm); 10: spectrofluorimeter (Ex = 350 nm, Em = 480 nm); 11: recorder, W: waste.

DPE, the kind of aqueous solvent systems, and the length of reaction coil. DPE solution was prepared by neutralizing with hydrochloric acid and diluting with organic solvent. Therefore, the reaction medium for the condensation reaction was adjusted to pH 7.2 by mixing the DPE solution with the carrier stream [0.2*M* phosphate buffer (pH 7.2)] which emerged from the reactor.

The effect of temperature on the reaction was examined over the range 80–110°C. The response increased linearly with an increase in temperature, but about 106°C bubbles generated in the reaction coil interfered with the measurement of the fluorophore. The effect of DPE concentration at a tyrosine concentration of 200 μM was examined from 10 to 50 m*M*. The response increased in the range 10–30 n*M* and became constant above 30 m*M*, where the DPE concentration in the reaction coil is about 13 m*M*. The response was dependent on the composition of the aqueous ethanol solution. The ethanol content in the DPE solution was changed from 40 to 90% (v/v) at a total flow rate of 0.7 ml/min. As shown Fig. 2, the maximum response was found at about 70% ethanol solution; at the maximum response, ethanol content in the reaction coil is about 30%. Various aqueous solvent systems were examined for their effect on the condensation reaction. The results are shown in Table 1. In ethanol, the response was higher than in other solvent systems. The changes in peak height as a function of the length of the reaction coil (0.5 mm i.d.) at a flow rate of 0.7 ml/min (0.4 ml/min carrier stream + 0.3 ml/min DPE solution) are shown in Fig. 3. The maximum response was obtained with a reaction coil of about 10 m. With increasing length of the reaction coil, the peak height decreased, but the peak area increased. The longer the reaction time, the nearer the conversion efficiency approaches 100%. The conversion efficiency was measured by using the fluorophore which was isolated by the method of Nohta *et al.*[10] Under the conditions shown in Fig. 1, the conversion efficiency of L-tyrosine (100 μM) to the fluorophore was 15%; in this case, it was assumed that L-tyrosine was converted to L-dopa in a 100% yeild. The sampling speed was 15/h.

Table 1. Effect of aqueous organic solvent on the condensation reaction

Solvent	Relative peak height
ethanol:water (7:3, V:V)	100
ethanol:DMSO:water (3.5:3.5:3)	66
ethanol:LDMF:water (3.5:3.5:3)	73
1,4-dioxane:water (7:3)	6
ethylene glycol:water (7:3)	3

DMSO:dimethyl sulfoxide.
DMF: *N*,*N*-dimethylformamide.

Specificity and interference

The responses to L-tyrosine and related compounds are shown in Table 2. This system exhibits low specificity for the compounds. As the concentrations of the compounds in serum are normally far lower than that of L-tyrosine, this system is not subject to interference from the compounds. Other L-amino acids normally found in proteins did not give any response.

In the presence of equimolar concentration of cysteine or ascorbic acid the peak height of tyrosine was depressed by about 50%. The interferences from the compounds (up to 1 m*M* each) were avoided by using on-line a separation column of ODS. Retention times of cysteine or ascorbate and tyrosine were 2.0 and 3.8 min, respectively.

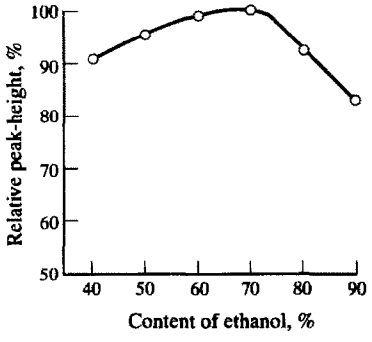

Fig. 2. Effect of ethanol content on the condensation reaction.

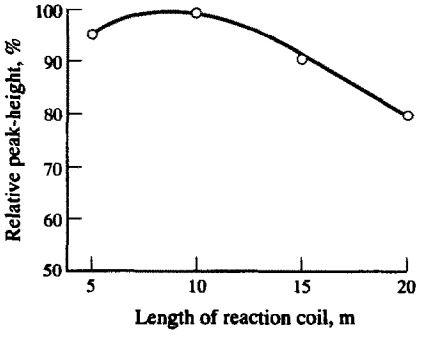

Fig. 3. Effect of length of reaction coil on the condensation reaction.

Table 2. Relative peak height for L-tyrosine and related compounds

Compound	Relative peak height
L-tyrosine	100
D-tyrosine	14
L-dopa	100
Dopamine	14
Epinephrine	13
norepinephrine	14
Tyr-Ala	45
Tyr-Glu	79
Tyr-Gly	36
Tyr-Leu	5
Tyr-Gly-Gly	79

Tyr-Ala: L-tyrosyl-L-alanine, Tyr-Glu: L-tyrosyl-L-glutamic acid, Tyr-Gly: L-tyrosylglycine, Tyr-Leu: L-tyrosyl-L-leucine, Tyr-Gly-Gly: L-tyrosylglycylglycine.

Calibration

Under the working conditions, the peak heights were plotted against the concentrations of L-tyrosine. A linear calibration graph was obtained for the range 1–200 μM. The least-square calibration equation was $y = 5.05x - 0.02$ with a linear correlation coefficient of $r = 0.997$ (9 data points), with the fluorescence intensity of 200 μM, tyrosine being taken as 1000 divisions, where y is peak height and x is tyrosine concentration. The detection limit (signal-to-noise ratio = 3) was 0.2 μM tyrosine (1 ng in a 30 μl injection).

Precision and reproducibility

Pooled human sera were repeatedly analysed during 10 days. The system was used for the analyses of 80 samples in a day and the immobilized tyrosinase reactor was stored in a refrigerator when not in use. In order to correct the variation of the conversion efficiency, standards were measured at 80-sample intervals. The immobilized tyrosinase reactor was renewed every 400 determinations. This system gave satisfactorily precise and reproducible results for serum containing 64 μM (11.60 mg/l) tyrosine, the within-day relative standard deviation (r.s.d.) was 0.97% and day-to-day r.s.d. was 1.8%.

Recovery

A sample of pooled human sera of known tyrosine concentration was supplemented with tyrosine to give final concentration of 70–985 μM. The recoveries were in the range 98–105%.

Comparison

Serum tyrosinase results ($n = 25$, range 61–210 μM) obtained using this system compared well with results obtained using amino acid analyser (Kyowa Seimitsu, K-201). The calculated linear regression and correlation coefficients were $y = 1.05x + 0.09$ and $r = 0.9798$, respectively.

CONCLUSION

An amino acid analyser for the determination of tyrosine is time-consuming. A flow-injection method, based on the fluorimetric detection of the dihydroxyindol produced in tyrosinase reaction, has been reported.[12] In the method, the use of a concentrated solution of potassium hydroxide (5M) caused poor reproducibility and poor dependability. The proposed method is three times more reproducible than the previous flow-injection method[12] and can easily be used for routine assay of tyrosine. The sensitivity and specificity of this method are sufficient to monitor concentrations of tyrosine in serum. The method has good recovery and within-run r.s.d. and between-run r.s.d.

REFERENCES

1. R. A. Roesel, P. R. Blankenship and F. A. Hommes, *Clin. Chim. Acta*, 1986, **156**, 91.
2. K. Sakai and T. Kitagawa, *Jikeikai Med.*, 1957, **4**, 1.
3. Y. Hijikata, Y. Shiozaki and Y. Sameshima, *J. Clin. Chem. Clin. Biochem.*, 1985, **23**, 259.
4. J. V. Hodge and J. A. Kilpatrick, *N. Z. Med. Jl*, 1968, **67**, 350.
5. F. Lottspeich and A. Henschen, in *High Performance Liquid Chromatography in Biochemistry*, A. Henschen, K.-P. Hupe, F. Lottspeich and W. Voelter (eds), pp. 141–164. VCH, Weinheim, 1985.
6. Y. Umegae, H. Nohta and Y. Ohkura, *Anal. Chim. Acta*, 1988, **208**, 59.
7. H. Nohta, E. Ymaguchi, Y. Ohkura and H. Watanabe, *J. Chromatogr.*, 1989, **467**, 237.
8. F. C. Brown and D. N. Ward, *J. Biol. Chem.*, 1958, **233**, 77.
9. M. Lee, H. Nohta, K. Ohtsubo, B. Yoo and Y. Ohkura, *Chem. Pharam. Bull.*, 1987, **35**, 235.
10. H. Nohta, T. Yukisawa and H. Ohkura, *Proceedings of the 40th Annual Conference of Japanese Society for Analytical Chemistry*, 1991, **400**.
11. M. N. H. Irving and R. M. Parkins, *J. Inorg. Nucl. Chem.*, 1965, **27**, 270.
12. N. Kiba, M. Ogi and M. Furusawa, *Anal. Chim. Acta*, 1989, **224**, 133.
13. Y. Tomita, A. Hariu, C. Mizuno and M. Seiji, *J. Invest. Dermatol.*, 1980, **75**, 379.

Talanta, Vol. 40, No. 7, pp. 999–1003, 1993
Printed in Great Britain.

0039-9140/93 $6.00 + 0.00

THERMODYNAMICS OF COMPLEXATION OF MAGNESIUM AND CALCIUM IONS WITH DICHLOROMETHYLENEDIPHOSPHONATE

L. KAILA, L. H. J. LAJUNEN, E. N. RIZKALLA* and J. ELORANTA
Department of Chemistry, University of Oulu, SF 90570, Oulu, Finland

(*Received* 29 *October* 1992. *Revised* 12 *January* 1993. *Accepted* 12 *January* 1993)

Summary—Thermodynamic parameters for the complexation of Ca^{2+} and Mg^{2+} ions by dichloromethylenediphosphonate (clodronate) ligand were obtained by potentiometric and calorimetric techniques. The measurements were conducted at an ionic strength of 0.10*M* [$(CH_3)_4NCl$]) and at 25°C. The potentiometric data were consistent with a model involving the presence of ML^{2-} MHL^- and M_2L species (L = tetranegative clodronate anion). The enthalpies of formation of the ML^{2-} and MHL^- complexes were obtained from calorimetric data. Attempts to determine the enthalpies of formation of the M_2L species were unsuccessful due to the limited solubilities of these species.

Organophosphonates are quite interesting both from fundamental and applied points of view.[1] Their role in water decalcification[2] and stabilization of peroxide solutions[3,4] has long been recognized. *In vitro* studies[5–8] indicated that *gem* diphosphonates have high biological activities particularly in inhibiting bone lysis and in the treatment of malignant hypercalcemia. The operative mechanism seems to involve calcium ion complexation by the ligand anion.

This paper summarizes the results obtained for the complexation of magnesium and calcium ions by the therapeutically active dichloromethylenediphosphonate (Cl_2MDP) anion. The investigation was conducted as a series of potentiometric and calorimetric titrations, and ^{31}P-NMR measurements in aqueous tetramethylammonium chloride media. Earlier measurements of the complexation of Li^+ Na^+ K^+, Rb^+ and Cs^+ by a homologous series of alkalidiene diphosphonates were interpreted as to reflect dominance of the electrostatic interactions to the bonding. This was apparent from the linear dependence of log β_{101} for the reaction;

$$M^+ + H_nL^{n-4} \Leftrightarrow MH_nL^{n-3};$$

$$\beta_{101} = [MH_nL]/[M][H_nL]$$

on the cation radius (r_M).[9,10] Moreover, plots of log β_{101} for the individual cations across the *gem* diphosphonate series against the polar substituent constant, σ^*[11] for the alkyl groups attached to the bridging methylene group were also linear. The slope of the latter correlations, ρ^* was found to decrease with increasing the cation radius. Since, ρ^* reflects the susceptibility of a given series of interactions to the degree of transmission of the inductive effects from the attached substituents, it was suggested[10] that such trend is associated with a drop in the strength of the metal–ligand interactions. By contrast, this rationale did not hold for the binding of calcium and magnesium ions by the same ligands.[12] The explanation offered was based on the short range repulsive forces predicted upon grouping the two phosphonate groups around the metal ion.

EXPERIMENTAL

Reagents and solutions

All reagents were of AR grade. Metal solutions were prepared from the corresponding chloride salts and the exact molarities were determined by complexometric titrations in the presence of the appropriate indicator.[13] Tetramethylammonium chloride was used as such without further purification. The disodium salt of dichloromethylenediphosphonate, $Na_2H_2Cl_2MDP \cdot 4H_2O$ was kindly donated by Leiras Ltd, Finland. The concentration of the stock ligand solutions were determined by pH titrations.

*Present address: Faculty of Science, Ain Shams University, Abbassia, Cairo, Egypt.

Measurements

The potentiometric titrations were carried out using a Radiometer PHM64 pH meter fitted with calomel and glass (Orion Research 91-01) electrodes. The glass electrode was calibrated by standard acid–base titration to read directly—log $[H^+]$ and to self correct for the liquid–junction potential at high acidity.[14] In each run, 30 ml aliquot of the metal–ligand mixture was titrated with standard $(CH_3)_4NOH$ (0.01*M*). All solutions were adjusted to 0.10*M* ionic strength by the addition of $(CH_3)_4NCl$ and maintained at 25°C with constant-temperature water circulated through a sealed jacketed cell. All measurements were obtained in a nitrogen atmosphere.

Calorimetric measurements were obtained using a semiadiabatic home-built Peltier-cooled titration calorimeter interfaced to a computer.[15] The calorimeter was calibrated electrically after four incremental additions and the change in temperature was sensed with a 20 KΩ thermistor. In a typical run, 50 ml of the ligand solution or the metal–ligand mixture, adjusted to the proper buffer region and an ionic strength of 0.10*M* $[(CH_3)_4NCl]$ and thermostatted to 25.0°C was titrated by a total of 4–5 aliquots of 0.10*M* HCl. The heats of dilution of the ligand and its metal complexes were determined in separate runs.

^{31}P-NMR spectra were obtained using a Jeol GX-400 FT NMR spectrometer. The shifts were recorded relative to an external standard of H_3PO_4.

RESULTS AND DISCUSSION

^{31}P-NMR spectrum of the clodronate anion displayed a simple doublet with a baricenter chemical shift depends not only on the medium pH but also on the total sodium content. Figure 1 shows a plot of the observed shift as a function of the amount of sodium ion in solution. In all measurements, the ionic strength of the medium was adjusted to 1.00*M* by adding the appropriate amount of $(CH_3)_4NCl$. The pH of the measured solutions was adjusted to *ca.* 14 where the ligand is fully deprotonated and slight perturbations of the medium pH would not reflect on the measured shift. As indicated in Fig. 1, increasing the amount of sodium caused a downfield shift which levelled off at approximately $[Na^+] = 1.0M$. The deshielding effect is attributed to sodium ion complexation by the ligand anion. Fonong *et al.*[16] reported

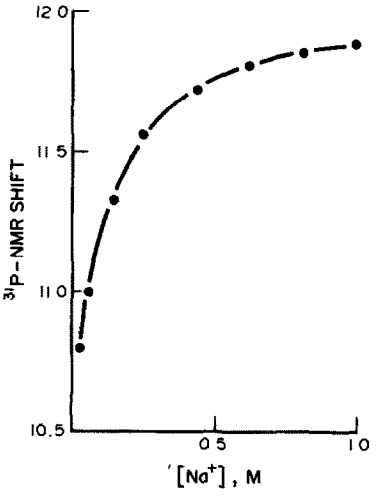

Fig. 1. Plot of the ^{31}P-NMR shift of the free Cl_2MDP^{4-} as a function of sodium ion concentration. $[Cl_2MDP^{4-}] = 24.2$ mM, pH ≃ 14.

a value of 1.28 for the formation of NaL^{3-} ($L = Cl_2MDP^{4-}$) in 0.10*M* NH_4Cl. Formation of $NaHL^{2-}$ species was also detected with other *gem* diphosphonate systems.[10,12] To avoid ambiguity, the present measurements were obtained in tetramethylammonium chloride.

The titration curve of the free ligand shows the presence of two distinct inflections corresponding to the liberation of two and three protons, respectively. Table 1 lists the p*K* values together with those obtained for other related ligands. The calculated constants are in excellent agreement with those reported in Refs 16 and 17 under similar experimental conditions. The entropies of protonation are larger than those reported for *gem*-dicarboxylates[18] presumably reflecting a larger degree of solvation of the free anion associated with the higher charge on these class of ligands.

The stability constants of the various metal complexes were refined by rigorous least squares using a modified version of the computer program SCOGS-2 written in this laboratory.[19,20] The program minimizes the sum of the square residuals between the observed and calculated hydrogen ion concentrations for a particular set of fitted stability constants. The program allows for the presence of different possible protonated and polynuclear species. In the present system, best fit was obtained when MHL and M_2L species were considered in addition to the normal ML complex.

The enthalpies of complexation were computed by fitting the observed heat changes, after correction for dilution effects, to the number of

Table 1. Thermodynamics of protonation of Cl_2MDP and other related ligands, $T = 298$ K; $I = 0.10M$ [$(CH_3)_4NCl$]

Reaction	log β	ΔH, kJ mole^{-1}	ΔS, J.K^{-1}.mole^{-1}
1. Cl_2MDP			
$H^+ + L^{4-} \Leftrightarrow HL^{3-}$	9.49 ± 0.01	-3.3 ± 0.3	170 ± 1
$H^+ + HL^{3-} \Leftrightarrow H_2L^{2-}$	5.96 ± 0.02	-2.2 ± 0.2	107 ± 1
$H^+ + H_2L^{2-} \Leftrightarrow H_3L^-$	2.18[16]		
$H^+ + H_3L^- \Leftrightarrow H_4L$	1.69[16]		
2. F_2MDP*			
$H^+ + L^{4-} \Leftrightarrow HL^{3-}$	8.16[16]		
$H^+ + HL^{3-} \Leftrightarrow H_2L^{2-}$	5.78[16]		
$H^+ + H_2L^{2-} \Leftrightarrow H_3L^-$	2.14[16]		
$H^+ + H_3L^- \Leftrightarrow H_4L$	1.46[16]		
3. EHDP*			
$H^+ + L^{4-} \Leftrightarrow HL^{3-}$	11.19[16]		
$H^+ + HL^{3-} \Leftrightarrow H_2L^{2-}$	7.03[16]		
$H^+ + H_2L^{2-} \Leftrightarrow H_3L^-$	2.78[16]		
$H^+ + H_3L^- \Leftrightarrow H_4L$	1.73[16]		
4. MDP*			
$H^+ + L^{4-} \Leftrightarrow HL^{3-}$	10.57[17]		
$H^+ + HL^{3-} \Leftrightarrow H_2L^{2-}$	7.00[17]		
$H^+ + H_2L^{2-} \Leftrightarrow H_3L^-$	2.78[17]		
$H^+ + H_3L^- \Leftrightarrow H_4L$	1.70[19]†		

*F_2MDP = difluoromethylenediphosphonic acid; EHDP = 1-hydroxyethane-1,1-diphosphonic acid; and MDP = methylenediphosphonic acid.

†In $(CH_3)_4NBr$.

moles of ML^{2-} and MHL^- complexes formed. The latter were calculated using the non-linear SIMPLEX program DELTA-H. In all cases, the concentration ranges were chosen as to minimize the formation of M_2L species. Attempts to determine the enthalpies of formation of these dinuclear species in separate runs were unsuccessful due to their limited solubilities. A sample set of the results obtained is shown in Table 2 and a summary of all the results is listed in Table 3. The errors given in Table 3 are based on the agreement between repetitive runs.

Table 2. Calorimetric data for the complexation of calcium ion by dichloromethylenediphosphonate, $T = 298$ K; $I = 0.10M$ [$(CH_3)_4NCl$]

Vol., ml	ΣQ_{cor}, mJ*	ΣQ_{calc}, mJ	[Ca^{2+}], 10^4M	[L^{4-}], 10^5M	[H^+], 10^8M
0.15	53.8	53.1	0.110	72.713	0.181
0.30	91.8	90.8	0.165	47.934	0.290
0.45	151.0	145.7	0.279	27.897	0.520
0.60	209.3	192.0	0.486	15.452	0.963
0.75	282.0	257.2	0.770	9.299	1.618
0.90	339.6	327.5	1.089	6.219	2.427
1.05	410.0	398.8	1.420	4.486	3.363
1.20	488.2	470.4	1.755	3.401	4.424
1.35	535.1	541.7	2.091	2.666	5.618
1.50	600.6	612.5	2.425	2.138	6.961
1.65	680.1	682.5	2.757	1.743	8.471
1.80	754.7	751.5	3.088	1.438	10.173
1.95	827.5	819.5	3.418	1.196	12.093
2.10	890.9	896.3	3.746	1.001	14.265
2.25	961.8	951.8	4.075	0.841	16.725
2.40	1025.3	1017.9	4.404	0.708	19.515
2.55	1086.1	1078.6	4.734	0.597	22.683

*Heat observed corrected for dilution effects.

Experimental conditions: Cup contents: [Ca^{2+}] = 4.8017 mM; [ligand] = 9.5694 mM; [H^+] = 3.8338 mM; volume = 52.25 ml; Titrant = 0.10M HCl.

Computed constants: $\Delta H_{101} = 5.1$ kJ mole^{-1} and $\Delta H_{111} = 2.0$ kJ mole^{-1}.

In Fig. 2, the values of log β_{101} of some calcium and magnesium diphosphonate complexes are plotted as a function of the total ligand basicity, Σ pK_a. The values for EDP (ethane-1,1-diphosphonate) and PDP (propane-2,2-diphosphonate) were reported at 0.5M [$(CH_3)_4NCl$] ionic strength[1] and have been normalized to the 0.10M ionic strength. The linearity observed in both cases emphasizes the dominance of ionic interactions in these systems. The value of Ca^{2+}–PDP complexation is greater than that predicted from the pK_a value. Replacement of the two protons in MDP by the bulky methyl groups in PDP is expected to strain the P–C–P angle and leads, probably to a stronger interaction with the metal ions. The same phenomenon has been observed with the carboxylate analogues.[18] No explanation is offered, however, for the destabilization below the "norm" in the case of Ca–F_2MDP and Ca–MP complexation (MP = methylphosphonic acid). The only difference is that, these measurements[16] were obtained in NH_4Cl rather than $(CH_3)_4NCl$ medium. Stability constants for the

Table 3. Thermodynamic parameters for the complexation of calcium and magnesium by dichloromethylenediphosphonate, $T = 298$ K; $I = 0.10M$ [$(CH_3)_4NCl$]

Reaction	$\log \beta$	$-\Delta G$, kJ mole^{-1}	ΔH, kJ mole^{-1}	ΔS, J.K.mole^{-1}
1. Cl_2MDP				
$Mg^{2+} + L^{4-} \Leftrightarrow MgL^{2-}$	6.20 ± 0.01	35.37 ± 0.06	12.8 ± 2.0	162 ± 7
$Mg^{2+} + HL^{3-} \Leftrightarrow MgHL^{-}$	3.15 ± 0.01	17.97 ± 0.06	9.1 ± 1.1	91 ± 4
$2Mg^{2+} + L^{4-} \Leftrightarrow Mg_2L$	(8.74)			
$Ca^{2+} + L^{4-} \Leftrightarrow CaL^{2-}$	5.77 ± 0.01	32.92 ± 0.06	5.1 ± 1.1	128 ± 4
$Ca^{2+} + HL^{3-} \Leftrightarrow CaHL^{-}$	3.09 ± 0.02	17.63 ± 0.11	5.3 ± 1.2	77 ± 4
$2Ca^{2+} + L^{4-} \Leftrightarrow Ca_2L$	(8.85)			
2. F_2MDP				
$Ca^{2+} + L^{4-} \Leftrightarrow CaL^{2-}$	4.36[16]			
$2Ca^{2+} + L^{4-} \Leftrightarrow Ca_2L$	5.92[16]			
3. HEDP				
$Mg^{2+} + L^{4-} \Leftrightarrow MgL^{2-}$	7.28[21]			
$Mg^{2+} + HL^{3-} \Leftrightarrow MgHL^{-}$	3.72[21]			
$2Mg^{2+} + L^{4-} \Leftrightarrow Mg_2L$	10.70[21]			
$Ca^{2+} + L^{4-} \Leftrightarrow CaL^{2-}$	6.62[21]			
$Ca^{2+} + HL^{3-} \Leftrightarrow CaHL^{-}$	3.54[21]			
$2Ca^{2+} + L^{4-} \Leftrightarrow Ca_2L$	12.20[21]			
4. MDP				
$Ca^{2+} + L^{4-} \Leftrightarrow CaL^{2-}$	6.02[22]	34.35	0.0[22]	92[22]

complexation by HCl_2MP^{3-} were found to fit these relationships, if the assumption is made that both phosphonate groups are bound to the metal ion and that the proton is bound to one of the remote free oxygens.

The entropy data can roughly be compared to those obtained for complexation by adenosine-5′-mono (AMP), di- (ADP) and triphosphate (ATP).[23] For both Mg^{2+} and Ca^{2+} ions, the ΔS value for MADP complexation was twice as much as that observed for MAMP complexation. This was taken as an evidence for the formation of a single M–O–P bond in the case of MAMP and two of such bonds in MADP. The average ΔS for the formation of an M–O–P bond was determined to be 60 and 51 J.K^{-1}.mole^{-1} for Mg^{2+} and Ca^{2+} ions, respectively. By analogy, the entropy changes for $MgCl_2MDP^{2-}$ and $CaCl_2MDP^{2-}$ supports chelation in both cases.

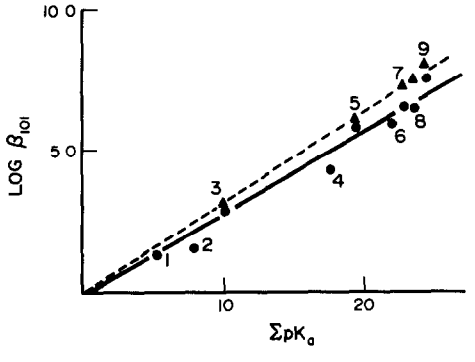

Fig. 2. Relationship between log β_{101} for the formation of some Ca^{2+} (solid line) and Mg^{2+} (dotted line) complexes with substituted methylenediphosphonates and the total acidity constant, ΣpK_a. (1) Cl_2MP; (2) MP; (3) HCl_2MDP; (4) F_2MDP; (5) Cl_2MDP; (6) MDP; (7) EHDP; (8) EDP; and (9) PDP.

REFERENCES

1. E. N. Rizkalla, *Rev. Inorg. Chem.*, 1983, **5**, 223.
2. G. H. Nancollas, *Adv. Colloid Inorg. Sci.*, 1979, **10**, 215.
3. S. Croft, B. C. Gilbert, J. R. Lindsay Smith, J. K. Stell and W. R. Sanderson, *J. Chem. Soc. Perkin Trans.*, 1992, **2**, 153.
4. E. N. Rizkalla, M. N. Ramsis, L. H. Khalil and S. S. Anis, *J. Coord. Chem.*, 1988, **17**, 359.
5. A. Jung, *Amer. J. Med.*, 1982, **72**, 221.
6. C. S. B. Galasko, A. N. Samuel, S. Ruston and E. Br. Lacey, *J. Surg.*, 1980, **67**, 493.
7. A. Jung, B. Mermillod, C. Barras, M. Baud and B. Courvoisier, *Cancer Res.*, 1981, **41**, 3238.
8. E. S. Siris, W. H.Sherman, D. C. Baquiran, J. P. Schlatterer, E. F. Osserman and R. E. Canfield, *New Engl. J. Med.*, 1980, **302**, 310.
9. R. R. Irani and K. Moedritzer, *J. Phys. Chem.*, 1962, **66**, 1349.
10. R. L. Caroll and R. R. Irani, *Inorg. Chem.*, 1967, **6**, 1994.
11. (a) R. W. Taft, Jr. *J. Amer. Chem. Soc.*, 1952, **74**, 3120; 1953, **75**, 4231; *J. Chem. Phys.*, 1957, **26**, 93; (b) M. S. Newman, *Steric Effects in Organic Chemistry*, Ch. XIII. Wiley, New York, 1956.
12. R. L. Caroll and R. R. Irani, *J. Inorg. Nucl. Chem.*, 1968, **30**, 2971.
13. T. S. West, *Complexometry with EDTA and Related Reagents*. Broglia Press, London, 1969.
14. L. H. J. Lajunen, E. Aitta and S. Parhi, *Talanta*, 1982, **28**, 277.
15. M. S. Caceci and G. R. Choppin, *Comput. Chem.*, 1982, **6**, 161.

16. T. Fonong, D. J. Burton and D. J. Pietrzyk, *Anal. Chem.*, 1983, **55**, 1089.
17. R. J. Grabenstetter, O. T. Quimby and T. J. Flautt, *J. Phys. Chem.*, 1967, **71**, 4194.
18. R. M. Smith and A. E. Martell. *Critical Stability Constants*, Vol. 3. Plenum Press, New York, 1977.
19. I. G. Sayce, *Talanta*, 1968, **15**, 1397.
20. K. Pieniniemi and L. H. J. Lajunen, to be published.
21. H. Wada and Q. Fernando, *Anal. Chem.*, 1972, **44**, 1640.
22. R. R. Irani and K. Moedritzer, *J. Phys. Chem.*, 1962, **66**, 1349.
23. S. M. Shanbhag and G. R. Choppin, *Inorg. Chim. Acta.*, 1987, **138**, 197.

Talanta, Vol. 40, No. 7, pp. 1005–1008, 1993
Printed in Great Britain.

0039-9140/93 $6.00 + 0.00

COMPLEXOMETRIC DETERMINATION OF MAGNESIUM OXIDE IN FLYASH BLENDED CEMENT

KA-KEUNG CHOI and SHIU-FAI LUK
Laboratory, China Cement Company, Tap Shek Kok, Tuen Mun, NT, Hong Kong

(*Received* 27 *October* 1992. *Revised* 11 *January* 1993. *Accepted* 12 *January* 1993)

Summary—A complexometric titration method is proposed to determine magnesium oxide in flyash blended cement. A 0.50 g of sample was heated with hydrochloric acid for 10 min. The solution was diluted to 500 ml, and 50 ml was pipetted and heated to boiling with 2.5 ml of 5% ammonium oxalate solution. The solution was then made alkaline by ammonium hydroxide. The suspension was cooled and filtered. The filtrate was titrated by standard 0.002*M* EDTA solution. The concentration of MgO in sample was calculated. The flyash content of the sample was determined by British Standard method and the recovery factor (f) was calculated by the equation of $f = 100/(99 - 0.315 \times \%FA)$. Concentration of MgO in sample was corrected by multiplying the recovery factor with concentration initially found by EDTA titration. The precision of the method is better with more time saving than the official methods.

Flyash blended cement is formed by grinding clinker with controlled proportions of flyash and gypsum. For simplicity it can be considered as made up of two components, namely, flyash (FA) and ordinary Portland cement (OPC). According to British Standard,[1] the magnesium oxide must not be greater than 4% because too much magnesium oxide may cause long-term expansion of concrete which may result in the cracking of a hardened concrete slab. There must be a method to determine the amount of magnesium oxide in a sample.

The BS method[1] requires hydrofluoric acid and perchloric acid to leach out the magnesium from the sample and uses atomic absorption spectrometry to determine its concentration. This method takes time to dissolve all the insoluble silica and requires special fume hoods for ventilation. The ASTM[2] method involves sodium carbonate fusion and is time consuming. Hence both official methods are not suitable for those laboratories that have many samples to be analysed.

Problems faced in the determination of magnesium oxide in blended cement include the quantitative extraction of magnesium and the interference from excessive amounts of calcium ions. Few methods[1,2] are reported to determine magnesium oxide in blended cement. Methods found to determine the magnesium in the presence of calcium include complexometric titration,[3–8] visible spectrophotometry,[9] polarography,[10,11] amperometric titration,[12] atomic absorption spectrophotometry,[1] X-ray fluorescence spectrometry[13,14] and inductively coupled plasma atomic emission spectrometry.[16] In cement or blended cement, the ratio of calcium oxide to magnesium oxide is usually more than 30:1. Complexometric titration is not possible to determine magnesium oxide directly without involving tedious sample preparation.[5] Yet it has been applied to cement where magnesium oxide was found by first determining the sum of CaO and MgO and then the CaO alone at higher pH. This approach is expected not to have satisfactory precision and accuracy because if 30 ml of titrant is for CaO alone, the amount for CaO and MgO is expected to be around 31 ml. Hence errors in these two separated titrations may cause MgO found to have a relative error greater than 10% which is outside of tolerance levels.

Instrumental methods have a greater tolerance to calcium concentration and they are more suitable to the analysis of blended cement because they are more time saving and have greater accuracy. Because of the expensive investment for such instrumentation, there is a need for a simple titration method to determine the magnesium oxide in blended cement. It is important especially to those cement plants in developing countries where there are difficulties in purchasing instruments, *e.g.* X-ray fluorescence spectrometer and atomic absorption spectrophotometer.

In this paper, a titration method is described with purification steps mentioned in ASTM[2] being simplified and the fusion procedure replaced by a leaching procedure with a recovery factor which depends on the percentage flyash in the sample. The method is simple, much quicker than both official methods, and has comparable accuracy.

EXPERIMENTAL

Analytical reagent grade chemicals and distilled water were used throughout the procedure.

Reagents

32% Hydrochloric acid
0.1% Methyl red indicator solution
12% Ammonium hydroxide solution, 1 vol. of distilled water mixed with 1 vol. of 25% ammonium hydroxide solution
5% Ammonium oxalate solution
50% Triethanolamine solution
1% Erichrome black T indicator solution, 0.2 g erichrome black T in 5 ml absolute ethanol and 15 ml of triethanolamine
0.002*M* Standard ethylenediamine tetraacetic acid solution
0.01*M* Standard ethylenediamine tetraacetic acid solution
Murexide indicator, 0.5 g murexide ground with 100 g sodium chloride.

Procedure

A 0.500 g of sample was accurately weighed into a 250-ml beaker and 50 ml of boiling distilled water was added. Then 10 ml of concentrated hydrochloric acid was added. The mixture was stirred by a glass rod and covered by a watch glass. The solution was kept boiling for 10 min to digest the sample. The solution was then diluted to 500 ml using a volumetric flask.

Fifty ml of sample was pipetted into a 250-ml beaker and 2.5 ml of 5% ammonium oxalate solution was pipetted into the beaker. Two drops of 0.1% methyl red indicator was added. The solution was heated to boiling. The solution was neutralized by 12% ammonium hydroxide and was made alkaline with 3–4 drops of ammonium hydroxide. The solution was boiled further for 10–15 sec.

The solution was cooled and filtered. The filtrate was collected and the residue was washed for several times with distilled water. To the filtrate, 10 ml of 50% triethanolamine and 20 ml of 12% ammonium hydroxide were added. The solution was then titrated by 0.002*M* standard EDTA solution using erichrome black T as indicator. The concentration of magnesium oxide was calculated as

$$\% \text{ MgO in sample} = f \times 40 \times 100 \times M \times V/(50 \times 2 \times m)$$

$$= f \times 40 \times M \times V/m$$

$$= f \times 80 \times M \times V \text{ for m} = 0.500 \text{ g}$$

m = sample mass
f = recovery factor
$= 100/(99 - (0.315 \times \%$ FA in sample))
M = molarity of standard EDTA solution
V = volume of titrant.

If the % FA is not known, to calculate the recovery factor, the % FA in sample was determined according to the BS method.[1] Twenty-five ml of the sample solution was pipetted out and filtered. The filtrate was collected. Ten ml of 50% triethanolamine solution was added and adjusted to a pH of 12. The CaO in sample was then titrated by 0.01*M* standard EDTA solution using murexide as indicator. The % FA was calculated by the following equation.

$$A \times \% \text{ FA} + B \times (100 - \% \text{ FA}) = \% \text{ CaO in sample}$$

A = % CaO in FA, can be taken as 2.0 if data not available[1]

B = % CaO in OPC, can be taken as 64.5 if data not available[1].

RESULTS AND DISCUSSION

In this method, the analyte is leached out by hydrochloric acid. The interferents which can complex with EDTA include iron, aluminium and calcium. The aluminium and iron are removed by adjusting the pH to around 10 and precipitating in the form of hydroxides. The main interferent, calcium, is removed by precipitation as calcium oxalate. As from Table 1, for 50 ml of sample solution, 2.0–4.0 ml of 5% oxalate solution gave a recovery of magnesium oxide from 103 to 92%. 2.5 ml of 5% oxalate solution was recommended to give recovery of magnesium oxide to be around 100%. Beyond 2.5 ml addition, the recovery decreases gradually which can be accounted as precipitation of magnesium as the oxalate. Any variation in the

Table 1. Effect of oxalate solution addition

Volume of 5% oxalate solution added (*ml*)	MgO found (%)	Recovery (%)
0.0	47.70	
1.0	22.27	2062.0
1.5	5.90	546.3
2.0	1.10	102.0
2.5	1.07	99.0
3.0	1.06	98.1
4.0	1.00	92.6
5.0	0.97	89.8
10.0	0.80	74.1

volume of oxalate added (*e.g.* 2.5 ± 0.5 ml) does not affect the recovery significantly.

Flyash blended cement is considered as composed of FA and OPC. The % MgO to be leached from FA and OPC by proposed method were studied. It was found that $99 \pm 2\%$ and $67.5 \pm 15.0\%$ of MgO could be extracted out from OPC and FA, respectively. A recovery factor is required to correct the incomplete extraction of magnesium oxide from the flyash component and this factor should be related to flyash content of sample. It is calculated as

$$f = \frac{100}{[\text{fractional recovery of OPC} \times (100 - \%\text{FA})] + [\text{fractional recovery of FA} \times \%\text{FA}]}$$
$$= 100/[99 - (0.315 \times \%\ \text{FA})].$$

Since the standard deviation in the % recovery of FA was great, its affect to accuracy may be significant. With theoretical approach, the recovery factor f for different recoveries from FA are calculated and are shown in Table 2. From British Standard,[1] the % FA in blended cement ranges from 15 to 35% and in Table 2, with the FA content at the upper limit, the relative error arised from the recovery of FA is about 6%. This is in the acceptable range and few cement samples have the FA content close to this value. Samples were prepared by using various standards of OPC and FA (from various regional sources). The known magnesium oxide concentrations were calculated based on the claimed values of standards. They were analysed by the proposed method. The results are listed in Table 3. The recoveries seem to be constantly low and it is attributed to low recovery of MgO from the flyash standards. The average recovery of MgO for FA as mentioned in preceding paragraph was the average of FA from different sources including USA, Australia, China and Indonesia. Most of flyash standards used in Table 3 were the standards from NIST and recoveries of these standards were at the lower side of the average. Hence the factor f was underestimated giving rise to negative deviation however, the errors observed were still within the tolerance level.

Table 2. Effect of variation in recovery factor at different recoveries from flyash

	15% FA		35% FA	
Recovery from FA* (%)	Calc. recovery factor	Relative error (%)	Calc. recovery factor	Relative error (%)
82.5	1.036	−2.4	1.073	−5.6
67.5	1.061	0.0	1.137	0.0
52.5	1.087	2.5	1.209	6.0

*% recovery from FA is calculated as $x \pm 6$ that is 67.5 ± 15.0.

Table 3. Accuracy analysis

Flyash content	MgO concentration (%) Known	Found	Relative error (%)
4.28	1.46	1.41	−3.4
5.46	3.77	3.52	−6.6
7.88	1.74	1.72	−1.1
9.65	2.22	2.13	−4.1
10.25	1.26	1.20	−4.8
10.50	2.24	2.15	−4.0
11.00	1.09	1.03	−5.5
13.10	0.68	0.69	1.5
13.18	1.06	1.06	0.0
13.38	3.55	3.41	−3.9
14.24	2.78	2.78	0.0
14.46	1.25	1.15	−8.0
15.76	1.21	1.15	−4.9
17.40	1.48	1.51	2.0
17.80	1.59	1.49	−6.2
18.81	1.19	1.19	0.0
19.23	2.04	1.90	−6.9
22.87	1.70	1.73	1.8
23.74	2.32	2.14	−7.7
28.78	3.59	3.46	−3.6
32.40	1.10	1.03	−6.4
35.64	2.92	2.88	−1.4
36.30	2.70	2.66	−1.5

In real sample analysis, the results were checked by either X-ray fluorescence spectrometry or BS method.[1] With the match pair technique, the calculated t-values are less than the theoretical values. It can be concluded that there is little difference between the proposed method with either the XRF or BS method. In the precision analysis, with triplicate determinations, the standard deviation of the method is less than the BS method.

Table 4. Sample analysis

Flyash content (%)		MgO concentration (%) Proposed	XRF	BS[1]
0		1.04		1.02
		1.19		1.13
6		1.33	1.34	1.42
12		1.48	1.54	
		1.57 ± 0.02	1.58	1.52
		2.60 ± 0.02	2.58 ± 0.13	2.67 ± 0.31
		1.09	1.10	1.11
		1.34	1.29	1.27
		1.20		1.16
		1.29		1.33
22		1.83	1.76	
		1.82	1.74	1.79
		1.24	1.22	1.24 ± 0.01
		1.34	1.33	1.32
		2.59 ± 0.02	2.59 ± 0.19	2.49 ± 0.05
		0.73		0.68
		0.72		0.80
30		1.34		1.38
t value	Calculated		1.576	0.451
	Theoretical		2.228	2.131

The method has several advantages over the BS method. It can be completed within an hour while the BS method usually takes more than 2 hr to complete the digestion. Second, it does not involve the use of hydrofluoric acid, perchloric acid, platinum crucibles or the expensive instrumentation. Therefore this method is suitable to be carried out by less experienced technicians. According to ASTM,[15] the difference between the extreme values in three results should be less than 0.15 and in the present work, the maximum difference is about 0.03. This satisfies the ASTM requirement and shows that this method has good reproducibility.

CONCLUSION

A simple and rapid method has been developed to determine the magnesium oxide in flyash blended cement. As compared with the official methods, it does not require tedious sample preparation procedures, hazardous chemicals, or sophisticated instrumentation, *e.g.* atomic absorption spectrophotometer is needed. The reagents used are common and inexpensive. Although this method sometimes requires an additional titration to find out the % flyash content, it does not increase the work load of the technician, because in usual practice, the determination of % FA in the sample must be included in routine blended cement analysis. This method is suitable for those laboratories with a lot of routine samples to be analysed.

REFERENCES

1. *British Standard*, British Standard Institution, BS 6588, 1985.
2. *Annual Book of ASTM Standards*, American Society for Testing and Materials, 1980, Part 13, C595-79.
3. M. do Rosario Tavares Cravo, *Tecnica Lisb.*, 1964, **38**, 121; *Anal. Abstr.*, 1966, **13**, 1296.
4. B. C. Sinha and S. Dasgupta, *Talanta*, 1978 **25**, 693.
5. B. C. Sinha and S. K. Roy, *Analyst*, 1982, **107**, 965.
6. J. Stabryn, *Zh. Analit. Khim.*, 1976, **31**, 2263; *Anal. Abstr.*, 1977, **32**, 5B50.
7. P. Stiglitz and J. Cornet, *Rev. Matér. Constr.*, 1963, 271; *Anal. Abstr.*, 1965, **12**, 138.
8. M. D. Alvarez Jiménez, J. A. Pérez-Bustamante and F. Burriel Martí, *Anal. Chem.*, 1975, **47**, 512.
9. G. Banerjee, S. K. Kanji and S. Mandal, *Z. Anal. Chem.*, 1976, **282**, 47.
10. J. An, J. Zhou and X. Wen, *Talanta*, 1985, **32**, 479.
11. X. Wang, S. Lui and Y. He, *Fenxi Huaxue*, 1985, **13**, 853.
12. A. Roueche and D. Monnier, *Anal. Chim. Acta*, 1964, **31**, 426.
13. R. F. Gebhardt (Ed.), *Rapid Methods for Chemical Analysis of Hydraulic Cement*, pp. 31–54. American Society for Testing and Materials, 1988.
14. P. M. Van Dyck, Szabina B. Torok and R. E. Van Grieken, *Anal. Chem.*, 1986, **58**, 1761.
15. *Annual Book of ASTM Standards*, American Society for Testing and Materials, 1980, Part 13, C114–80.
16. M. L. Fernández Sánchez, J. Palacio Suarez E. Fernández Molina and A. Sanz Medel, *J. Anal. At. Spectrom.*, 1987, **2**, 491.

Talanta, Vol. 40, No. 7, pp. 1009–1011, 1993
Printed in Great Britain.

0039-9140/93 $6.00 + 0.00

FLUORIMETRIC DETERMINATION OF NITRITE

NIANQIN JIE, JINGHE YANG and FANQIN MENG
Department of Chemistry, Shandong University, Jinan, People's Republic of China

(*Received* 19 *October* 1992. *Revised* 11 *January* 1993. *Accepted* 13 *January* 1993)

Summary—A sensitive and rapid fluorimetric method for the determination of nitrite is described. The method is based on the reaction of nitrite with tryptophan to form a highly fluorescent compound in alkaline medium. The method has been applied in the determination of nitrite in water and food samples.

Determination of trace amounts of nitrite is of importance, particularly in the fields of environmental and food chemistry. Many spectrophotometric methods for the determination of nitrite have been reported.[1–5] Electrometric methods are also available,[6–7] as well as HPLC of the free ion.[8–9] However, some of these methods require close control of conditions, and some, which are too complex and time-consuming, are unsuitable for routine application.

Fluorimetric methods have also been reported for the determination of nitrite.[10–14] This paper describes a fluorimetric procedure, based on the reaction between nitrite and tryptophan. This method is very simple, rapid and suitable for the determination of nitrite in water and food samples.

EXPERIMENTAL

Apparatus and reagents

An RF-540 spectrofluorometer (Shimadzu, Kyoto, Japan) was used.

All reagents used were of analytical grade and all water used was demineralized and doubly distilled.

L-Tryptophan stock solution: 0.2 mg/ml.

Standard solution of sodium nitrite. A 100 μg/ml nitrite stock solution was made by dissolving 0.150 g of sodium nitrite, previously dried for 2 h at 100°C, in distilled water, and diluting accurately to 1000 ml. Diluted solution should be prepared fresh daily.

Hydrochloric acid: 0.24*M*. Sodium hydroxide solution: 0.75*M*.

Procedure

A 0.8 ml of *L*-tryptophan solution (0.2 μg/ml), 0.8 ml of hydrochloric acid solution (0.24*M*) and 1 ml of working nitrite solution (0.16 μg/ml) were added sequentially to a 25-ml volumetric flask. The contents of the flask were mixed, then the flask was placed in a boiling-water bath for 15 min. Add 2.5 ml of sodium hydroxide solution (0.75*M*) into the reaction mixture. Dilute to mark with water and measure the fluorescence intensity at an excitation wavelength of 320 nm and an emission wavelength of 385 nm.

RESULTS AND DISCUSSION

Fluorescence spectra

The excitation and emission spectra of the system investigated is shown in Fig. 1. The fluorescent species has excitation and emission maxima at 320 and 380 nm, respectively.

Effect of L-*tryptophan concentration*

The effect of *L*-tryptophan concentration on the fluorescence intensity of the system was studied. When the concentration of *L*-tryptophan was between 5.6 and 8.0 μg/ml, the fluorescence intensity reached a maximum and remained constant. An *L*-tryptophan concentration of 6.4 μg/ml was selected. Effect of hydrochloric acid concentration in the reaction.

Experiments indicated that the maximum and constant intensity was obtained for HCl concentration in the range 0.005–0.010*M*. The fluorescence intensity decreased for values outside this range. An HCl concentration of 0.008*M* was chosen.

Effect of sodium hydroxide solution in the final system

The optimum sodium hydroxide solution concentration is 0.075*M*. The tolerance range is 0.06–0.09*M*. In addition, it was shown that the

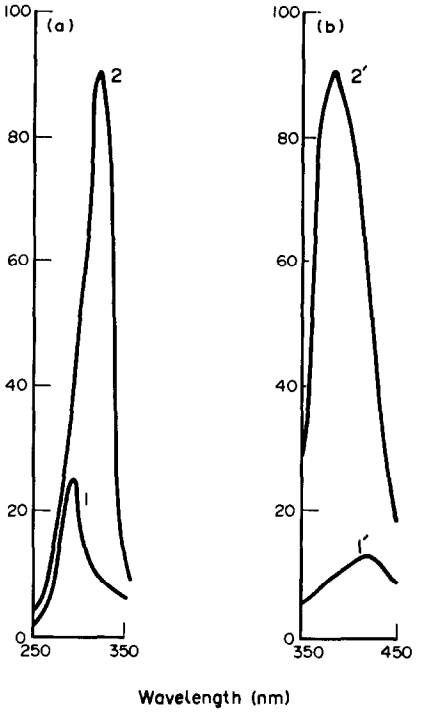

Fig. 1. Fluorescence spectra: (a) excitation, 320 nm; (b) emission, 385 nm. 1 and 1', tryptophan–NaOH system (reagent blank); 2 and 2', tryptophan–NO_2^--NaOH system; conditions: (tryptophan) = 6.4 μg/ml; (NO_2^-) = 0.16 μg/ml. There is tryptophan in the reagent blank. The tryptophan is a fluorescing substance, therefore in the absence of nitrite (reagent blank) an appreciable fluorescence signal was observed.

fluorescence intensity of the system reached a maximum after heating at 100°C for 15 min, and remained stable for 80 min.

Calibration graph

The calibration graph for the determination of nitrite was constructed under the optimum conditions. Good linearity obtained over the range 0.01–0.20 μg/ml. The detection limit is 0.001 μg/ml with the signal to noise ratio (S/N) value of 3.

Table 1. Tolerance of the method towards interference ions (amount of nitrite taken, 2 μg)

Ion	Ratio of ion to NO_2^- (μg/μg)		Ion	Ratio of ion to NO_2^- (μg/μg)
Al(III), Zn(II)	750		Fe(III)	1 15*
Ni(II)	500		NO_3^-	400
Mg(II)	400		PO_4^-	300
NH_4^+	200		F^-	200
Ba(II)	40		I^-	10
Ca(II)	30	60*	BrO_3^-	2
Cu(II)	2	10*		

*In the presence of 0.3 mg EDTA.

Table 2. Results for the determination of nitrite in water

Sample	NO_2^- found (μg)	NO_2^- added (μg)	Recovery (%)	Content (μg/ml)
Tap water	0.50	0		
(1 ml)	0.50	0		0.020
	1.50	1.0	100	
	1.50	1.0	100	
Water of a	1.55	0		0.062
lake (1 ml)	1.57	0		0.063
	2.55	1.0	100	
	2.62	1.0	105	

Interference of other ions

The interference of various cations and anions normally found in association with nitrite was studied. The amount of the diverse ion which brings about 5% variation in fluorescence was taken as its tolerance limit. Table 1 shows that only Fe(III), Cu(II) and BrO_3^- caused a severe interference, but Fe(III) and Cu(II) can be masked by adding EDTA. The presence of Fe(III) and BrO_3^- increased the fluorescence intensity owing to their oxidizing nature. Because Cu(II) exhibits a complexing ability, Cu(II) and tryptophan probably form a compound which is of stronger fluorescence. Hence in the presence of Cu(II), the fluorescence intensity of the system is increased.

Determination of nitrite in water and food samples

Transfer 1.0 ml of tap water into a 25-ml volumetric flask, then add 0.3 mg EDTA. Complete the determination by the procedure described above. The results obtained are given in Table 2.

The proposed method was also used to determine nitrite in sausage and milk samples. A 10-ml portion of spiked milk or 2.5 g sausage sample was placed into 200-ml standard flask and freed from proteins and fat according to a standard method,[15] then 1 ml of filtrate obtained was used for the fluorimetric determination of nitrite. The results are summarized in Table 3. The recoveries of nitrite were found to be 95.0–100%.

Table 3. Determination of nitrite in food samples

Sample	Found (μg/g)*	Standard deviation (μg/g)	Reference value†
Sausage 1	42.7	0.42	41.9
Sausage 2	33.5	0.23	33.4
Whole milk	15.9	0.30	15.6

*National Standard of China for nitrite in food sample: ≤0.03 g/kg.

†Obtained by the method reported by Shoji Motomizo *et al.*[10]

Mechanism of the reaction

The possible reaction between *L*-tryptophan and nitrite is:[16]

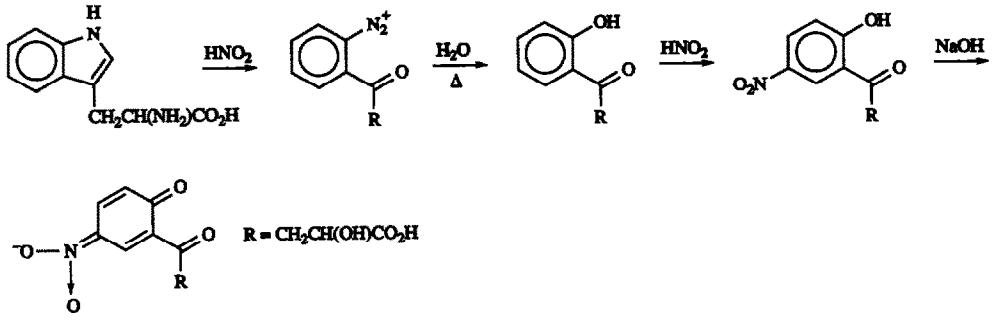

Based on the reaction, the conjugative effect in the reaction product is stronger than that in tryptophan, therefore the reaction product is of greater fluorescence intensity than tryptophan.

Acknowledgement—This work was supported by the National Science Foundation of Shandong, China.

REFERENCES

1. M. Okad, H. Mjyata and K. Toei, *Analyst*, 1978, **103**, 1195.
2. M. F. Gine, H. Bergamin F., E. A. G. Zagatto and B. F. Reis, *Anal. Chim. Acta.*, 1980, **114**, 191.
3. R. A. Nicholas and J. B. Fox, *J. Assoc. Off. Anal. Chem.*, 1973, **56**, 992.
4. V. Raman and M. S. Dabbas, *Microchem. J.*, 1989, **40**, 242.
5. A. Aamer and Al-hatim, *Int. J. Environ. Anal. Chem.*, 1990, **38**, 617.
6. L. Ganghan and Y. Shenglai, *Anal. Lett.*, 1989, **22**, 1743.
7. Z. Gao and Z. Zhao, *Anal. Chim. Acta*, 1990, **241**, 161.
8. R. G. Gerrise, *J. Chromatogr.*, 1979, **171**, 527.
9. H. J. Cortes, *ibid.*, 1982, **234**, 517.
10. S. Motomizo, H. Mikasa and K. Toei, *Talanta*, 1986, **33**, 729.
11. H. D. Axelrod and N. A. Engel, *Anal. Chem.*, 1975, **47**, 922.
12. J. H. Wiersma, *Anal. Lett.*, 1970, **3**, 123.
13. Nakamura M., *Anal. Lett.*, 1980, **13**, 771.
14. Y. Mukai *et al.*, *Bunseki Kagaku*, 1991, **40**, 105.
15. International Dairy Federation, FIL-IDF 50 A, 1980.
16. K. K. Verma, A. Jain and J. Gasparic, *Talanta*, 1986, **35**, 35.

Talanta, Vol. 40, No. 7, pp. 1013–1017, 1993
Printed in Great Britain.

0039-9140/93 $6.00 + 0.00

SIMPLIFIED DATA PROCESSING FOR THE SIMULTANEOUS DETERMINATION OF CATALYSTS BY CATALYTIC KINETICS

ZHONG-LIANG ZHU, ZHI-CHENG GU* and XIAN-DE WANG
Department of Chemistry, Tongji University, Shanghai, 200092, People's Republic of China

(*Received* 16 *October* 1992)

Summary—An approximate equation for data processing is proposed for the simultaneous determination of catalysts by catalytic kinetics. On applying the equation to the reaction between two reactants catalyzed by two catalysts, the calculation is simplified to that of only one reactant, simplifying the experiment and data processing. The equation was used to treat the simultaneous determination of ruthenium and osmium with Ce(IV)–As(III) as the indicator reaction, with the results in good agreement with those using the exact equation.

Because of their interference with each other, it is usually difficult to catalytically determine trace elements simultaneously when they catalyze a common indicator reaction. For example, while I^-, Ru and Os can be determined by their catalytic effect on the reaction between Ce(IV) and As(III) as the indicator reaction,[1,2,7] a prior separation is necessary if the others coexist when one is to be determined. Rodriguez described a method for the determination of Os and I^-, using Ag^+ or Hg(II) to mask the iodide.[3] Pardue proposed a method to determine Ru and Os based on their differences in their kinetic behaviour on the same indicator reaction.[4] It is necessary to carry out two kinetic runs to determine two elements in Rodriguez and Pardue's work. Gu has demonstrated the possibility for the simultaneous determination of catalysts with a single kinetic run, based on kinetic differences of catalysts on the indicator reaction.[5] As the kinetic behavior of the reactions between Ce(IV) and As(III) catalyzed by Ru and Os are quite different,[4,6] it is possible to determine the two elements simultaneously through a single kinetic run. In this paper Ru and Os are determined satisfactorily and an approximate equation is given, in which the experiment and the data processing for the reaction between two reactants catalyzed by two elements can be simplified as those for one reactant.

*To whom correspondence should be addressed.

THEORY

In general, an indicator reaction between A and B in the determination of several catalysts $C_1, C_2, \ldots, C_n$ by catalytic kinetics may be written stoichiometrically as:

$$aA + bB \xrightarrow{C_1, C_2, \ldots, C_n} xX + yY$$

and the reaction rate equation for the ith catalyst is:

$$v_i = -\mathrm{d}[A]/\mathrm{d}t = (-a/b)\,\mathrm{d}[B]/\mathrm{d}t = k_i[A]^{p_i}[B]^{q_i}[C_i] (i = 1, 2, \ldots, n), \quad (1)$$

where p_i and q_i are the reaction orders of A and B, respectively. According to the stoichiometric relationships, the concentration of B can be expressed as

$$[B] = [B]_0 - (b/a)([A]_0 - [A]), \quad (2)$$

where $[A]_0$ and $[B]_0$ are the initial concentrations of A and B. Substituting equation (2) into equation (1), we have:

$$v_i = k_i[C_i][A]^{p_i}\{[B]_0 - (b/a)([A]_0 - [A])\}^{q_i}. \quad (3)$$

In a system with n catalysts which catalyze a common indicator reaction, when the behaviors of the catalysts are independent, the reaction rate may be written as follows,

$$v' = v'_0 + \Sigma k_i[A]^{p_i}[B]^{q_i}[C_i] = v'_0 + \Sigma k_i[A]^{p_i}\{[B]_0 - (b/a)([A]_0 - [A])\}^{q_i}[C_i]. \quad (4)$$

If $[A]_0$, $[B]_0$, p_i and q_i are known and p_i and q_i are different, $[C_i]$ can be calculated by multiple linear regression of v_i on $[A]^{p_i}[B]^{q_i}$. In the following, only two catalysts are considered, i.e. $n = 2$. Equation (4) may be simplified as:

$$v = v' - v'_0 = k_1[A]^{p_1}[B]^{q_1}[C_1] + k_2[A]^{p_2}[B]^{q_2}[C_2], \quad (4')$$

where p_1, p_2, q_1 and q_2 and the initial concentration of each reactant must be available. This would require a great number of experiments. For the sake of simplification, an approximate equation is proposed:

$$[B]^{q_i} = \{[B]_0 - (b/a)([A]_0 - [A])\}^{q_i} = T[A]^{p''_i}, \quad (5)$$

where T is a constant, called the model conversion coefficient. And equation (1) becomes:

$$v_i = k'_i[A]^{p'_i}[C_i] \quad (i = 1, 2), \quad (6)$$

where $k'_i = k_iT$, $p'_i = p_i + p''_i$ and p''_i is called "the reduced fractional reaction order". Taking the logarithm, equation (6) becomes:

$$\ln v_i = p'_i \ln[A] + \ln k'_i[C_i], \quad (7)$$

p'_i and k'_i can be obtained from the plot of the $\ln v_i$ *vs.* $\ln[A]$ by calibration with standard solutions of C_i. For a two-component mixture

$$v = \Sigma k'_i[A]^{p'_i}[C_i] = \Sigma f_i[A]^{p'_i} \quad (8)$$

f_1 and f_2 can be obtained by two linear regressions of v *vs.* $[A]^{p'_1}$ and $[A]^{p'_2}$ and $[C_i]$ can be solved from f_i and k'_i.

Unlike equation (4), when equation (8) is used, only two kinetic runs are needed to obtain p'_1 and p'_2. Furthermore, the exact initial concentrations of reactants need not necessarily be known, provided the amounts of them added in each experiment remain constant. In practice, Ru and Os are determined as the catalysts to the reaction between Ce(IV) and As(II).

EXPERIMENTAL

Apparatus

F7230 spectrophotometer equipped with a thermostat; IBM microcomputer.

Reagent

As(III) *solution.* Prepare a 0.20*M* As(III)–2*M* H_2SO_4 solution by dissolving 4.95 g As_2O_3 in 20 ml 1*M* NaOH and adding 2*M* H_2SO_4 to 250 ml. The solution was diluted to $1.8 \times 10^{-3}M$ with 2*M* H_2SO_4 (solution B).

Ce(IV) *solution.* Prepare a 0.039*M* Ce(IV)–2*M* H_2SO_4 solution by dissolving $(NH_4)_4Ce(SO_4)_4 \cdot 2H_2O$ in 2*M* H_2SO_4.

Stock standard Ru *solution.* Prepare a $5.00 \times 10^{-4}M$ solution by dissolving $RuO_2 \cdot H_2O$ in H_2SO_4. Dilute this stock solution as required before use.

Stock standard Os *solution.* Prepare a $5.00 \times 10^{-4}M$ solution by dissolving OsO_4 in water. Dilute this stock solution as required before use.

All the chemicals used were of analytical reagent grade. Redistilled water was used.

Procedures

A 5.0 ml portion of Ce(IV) solution was mixed with sample solution containing Ru and Os and diluted to 25 ml with water (solution A). Both solutions A and B were mixed with a proportion of 1:2 in a cell as quickly as possible. The absorbance change with time was measured at 418 nm against water. The absorbance at intervals of 10 sec was recorded automatically.

Data processing

The reaction rate v was calculated by the Savitzky–Golay method[8] from the A *vs.* t plot. Based on Beer's law, the absorbance A was used in equation (6) instead of [Ce(IV)]. Similar to the Savitzky–Golay convolution, the following equation was used.

$$v_j = -dA/dt = -\left(\sum_{i=-m}^{m} q_iA_{i+j}\right) \Big/ (\Delta t.N),$$

where Δt is the interval of sampling time, N is the normalization factor, q_i is the convolution coefficient and $2m + 1$ is points used for smoothing. When the reaction rate was obtained from square polynomials of first order,

$$N = 2\sum_{i=1}^{m} i^2$$

and

$$q_i = i \quad (i = -m, -m+1, \ldots, 0, 1, \ldots, m).$$

Experimentally, a smooth plot of v *vs.* t could be obtained by $m \geqslant 5$, and $m = 5$ was specified.

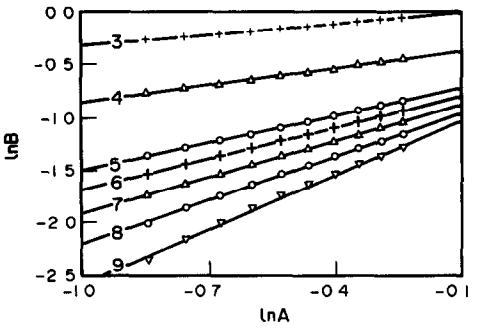

Fig. 1. The ln A–ln B relations. Simulated curves for different values of B_0 as given in Table 1.

RESULTS AND DISCUSSION

Confirmation of the approximate equation

From the logarithm of equation (5):

$$\ln[B] = p_i'' \ln[A]/q_i + \ln T/q_i.$$

Equation (5) can be tested when the ln[B] *vs.* ln[A] plot is linear. As an example, in the reaction between Ce(IV) and As(III) catalyzed by Ru and Os, $a = 2$, $b = 1$, and letting $q_i = 1$, equation (2) can be written as:

$$[B] = [B]_0 - 1/2([A]_0 - [A]).$$

The ln[B] *vs.* ln[A] plot computed by simulation is shown in Fig. 1. It is linear over a wide range of concentration; the values of p_i'' and T were obtained from the slope and the intercept. The data, as well as the correlation coefficients, are listed in Table 1. The correlation coefficients approach 1 in quite a wide range of reactant ratios. It means that equation (5) can be used extensively. Two special cases should be noted.

(a) When $[A]_0$ and $[B]_0$ are in stoichiometric ratio, equation (5) becomes exact. Hence $p_i'' = q_i$, $T = (b/a)^{q_i}$.

(b) When $[B]_0 \gg [A]_0$, while p_i'' approaches 0 and T approaches $[B]_0^{q_i}$ the reaction becomes a "pseudo p_i-order reaction".

Table 1. The result of linear regression of ln A *vs.* ln B

No.	A_0	B_0	p_i''	T	r
1	0.900	50.000	0.01	50.00	0.9966
2	0.900	5.000	0.06	5.01	0.9969
3	0.900	1.000	0.35	1.02	0.9985
4	0.900	0.700	0.54	0.73	0.9992
5	0.900	0.490	0.88	0.53	0.9999
6	0.900	0.450	1.00	0.50	1.0000
7	0.900	0.410	1.16	0.47	0.9999
8	0.900	0.370	1.39	0.44	0.9994
9	0.900	0.330	1.74	0.43	0.9979

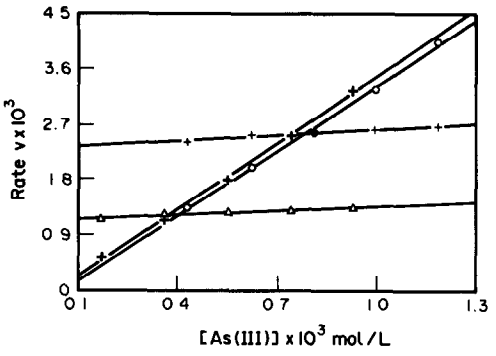

Fig. 2. Effect of [As(III)] on reaction rate. + [Ru] = 8.0×10^{-8}, [Ce(IV)] = $1.8 \times 10^{-3}M$; △ [Ru] = 8.0×10^{-8}, [Ce(IV)] = $1.3 \times 10^{-3}M$; ○ [Os] = 6.7×10^{-8}, [Ce(IV)] = $1.8 \times 10^{-3}M$; + [Os] = 6.7×10^{-8}, [Ce(IV)] = $1.3 \times 10^{-3}M$.

Reaction conditions

The reaction between Ce(IV) and As(III) catalyzed by Ru and Os did not change much in the range of 1.0–2.0M H_2SO_4. Hence 1.7M H_2SO_4 was specified in the procedure.

The effects of As(III) on the reaction rate is shown in Fig. 2 and the effect of Ce(IV) is shown in Fig. 3. In agreement with Refs 4 and 6, it was found that the osmium catalyzed reaction was dependent upon the As(III) concentration, but almost independent of the Ce(IV) concentration; on the other hand the ruthenium catalyzed reaction was dependent upon the [Ce(IV)] but almost independent of the [As(III)]. q_{Ru}, q_{Os}, p_{Ru} and p_{Os} were obtained by regressing ln v on ln[As(III)] and ln v on ln[Ce(IV)]; the values of which were 0.09, 1.08, 1.91 and −0.10, respectively. The great differences between both q_{Ru} and q_{Os} and p_{Ru} and p_{Os} made it possible to determine Ru and Os simultaneously. Reactants at $1.23 \times 10^{-3}M$

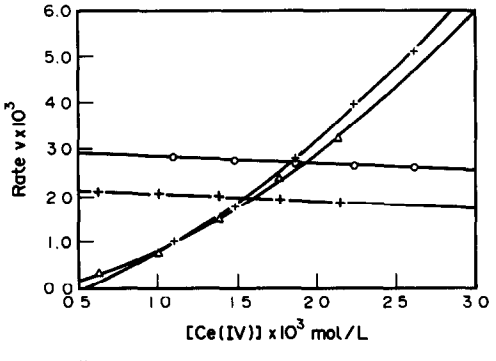

Fig. 3. Effect of [Ce(IV)] on reaction rate. + [Ru] = 8.0×10^{-8}, [As(III)] = $8.4 \times 10^{-4}M$; △ [Ru] = 8.0×10^{-8}, [As(III)] = $6.0 \times 10^{-4}M$; ○ [Os] = 6.7×10^{-8}, [As(III)] = $8.4 \times 10^{-4}M$; + [Os] = 6.7×10^{-8}, [As(III)] = $6.0 \times 10^{-4}M$.

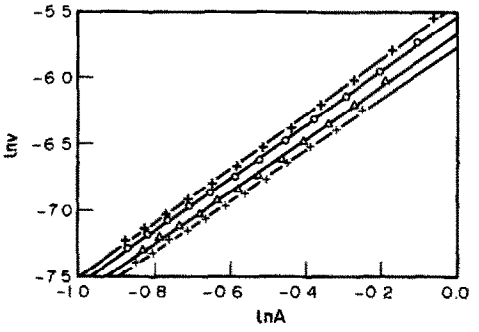

Fig. 4. p'_{Ru} dependence on initial concentration ratio of [Ce(IV)]/[As(III)] ([Ru] = $8.0 \times 10^{-8}M$).

p'_{Ru}	Initial ratio
+ 1.91	1.6:1
△ 1.98	1.9:1
○ 2.01	2.2:1
+ 2.06	2.5:1

As(III) and $2.59 \times 10^{-3}M$ Ce(IV) were specified in the procedure.

The plots of $\ln v$ *vs.* $\ln A$ of Ru and Os catalyzed reactions are shown in Fig. 4 and Fig. 5, respectively. The slopes of the plots refer to the apparent reaction order, i.e. p'_{Ru} and p'_{Os}. With an increase in the initial ratio of reactants, p'_{Ru} remained almost unchanged while p'_{Os} increased quite obviously.

The effect of temperature on reaction rate is shown in Fig. 6. The influence of temperature on the Ru catalyzed reaction was more serious than for the Os catalyzed one. A temperature of 28.0°C was specified in the procedure.

Reaction rate curves

The A *vs.* t plot and the v *vs.* t plot are shown in Figs 7 and 8, respectively. The patterns of the

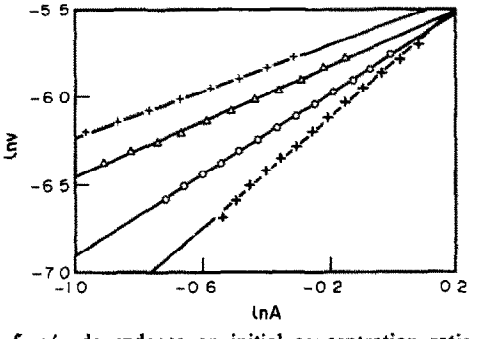

Fig. 5. p'_{Os} dependence on initial concentration ratio of [Ce(IV)]/[As(III)] ([Os] = $6.7 \times 10^{-8}M$).

p'_{Os}	Initial ratio
+ 0.66	1.6:1
△ 0.78	1.9:1
○ 1.14	2.2:1
+ 1.55	2.5:1

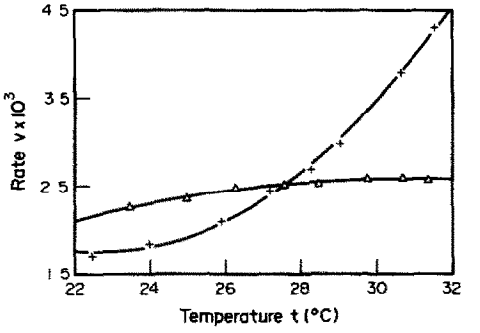

Fig. 6. Effect of temperature on reaction rate [Ce(IV)] = 1.8×10^{-3}, [As(III)] = $8.1 \times 10^{-4}M$. + [Ru] = $8.0 \times 10^{-8}M$; △ [Os] = $6.7 \times 10^{-8}M$.

curves for Ru and Os were different. This supports that the mechanism of the indicator reaction catalyzed by Ru and Os at the above conditions are different.

As shown in Fig. 9, linearity was observed in the experimental range for the reaction rate to be a function of the concentration of Ru and Os.

The reaction order p'_i *and rate constant* k'_i

The values of p'_i were obtained with Ru and Os, respectively, under the conditions mentioned above. The results are shown in Table 2.

In order to reduce the possibility of the interaction of Ru and Os, the reaction rate constants k'_i were determined with a mixture of Ru and Os with known concentrations. The results obtained are also listed in Table 2.

Determination of Ru *and* Os *mixtures*

A set of Ru(IV) and Os(VIII) mixtures were determined. The results calculated by

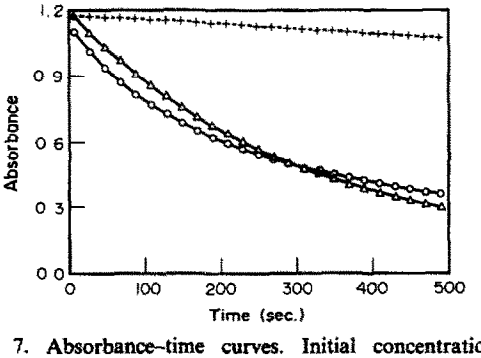

Fig. 7. Absorbance–time curves. Initial concentration of reactants: [Ce(IV)] = 2.59×10^{-3}, [As(III)] = $1.20 \times 10^{-3}M$; + blank; △ [Os] = $6.7 \times 10^{-8}M$; ○ [Ru] = $8.0 \times 10^{-8}M$.

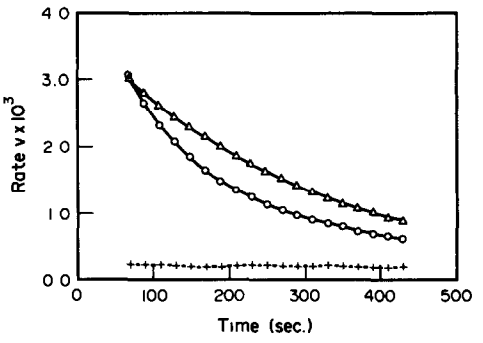

Fig. 8. Reaction rate–time curves. Initial concentration of reactants: [Ce(IV)] = 2.59×10^{-3}, [As(III)] = $1.20 \times 10^{-3}M$; + blank; △ [Os] = $6.7 \times 10^{-8}M$; ○ [Ru] = $8.0 \times 10^{-8}M$.

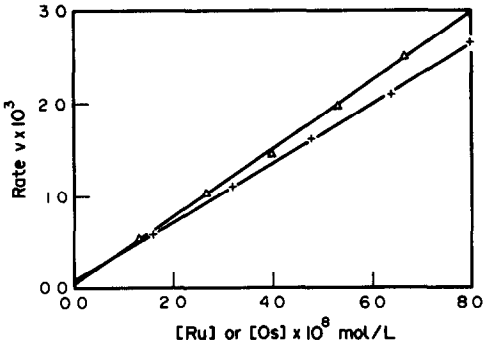

Fig. 9. Reaction rate dependence on Ru and Os [Ce(IV)] = 1.8×10^{-3}, [As(III)] = $8.1 \times 10^{-4}M$; + Ru; △ Os.

Table 2. Reaction order and rate constant

[Ru] × 10^8 (M)	p'_{Ru}	[Os] × 10^8 (M)	p'_{Os}	[Ru] × 10^8 (M)	[Os] × 10^8 (M)	$k'_{Ru} \times 10^5$	$k'_{Os} \times 10^5$
8.00	2.06	6.67	1.17	6.40	1.33	5.10	4.68
8.00	2.02	6.67	1.14	4.80	2.67	5.24	4.45
8.00	2.00	6.67	1.12	4.00	3.33	5.11	4.54
6.00	2.03	4.00	1.16	3.20	4.00	5.34	4.31
6.00	1.98	4.00	1.10	1.60	5.33	5.16	4.59
Mean	2.02		1.14			5.23	4.51

Table 3. Analysis of mixtures of Ru and Os

	[Ru] × 10^8M					[Os] × 10^8M			
Added	$Found_1$	$\%E_1$	$Found_2$	$\%E_2$	Added	$Found_1$	$\%E_1$	$Found_2$	$\%E_2$
0.00	0.21	—	−0.02	—	6.67	6.65	−0.3	6.75	1.2
1.20	1.27	6.0	1.29	7.4	5.67	5.67	0.1	5.67	0.1
1.60	1.75	9.2	1.75	9.4	5.33	5.27	−1.3	5.26	−1.3
2.40	2.33	−3.0	2.37	−1.1	4.67	5.09	9.1	5.11	9.5
3.20	3.21	0.4	3.27	2.1	4.00	3.84	−4.0	3.84	−4.0
4.00	3.84	−4.0	3.90	−2.4	3.33	3.35	0.4	3.34	0.2
4.80	4.73	−1.5	4.80	−0.1	2.67	2.72	2.0	2.71	1.5
5.60	5.44	−2.9	5.52	−1.5	2.00	2.01	0.4	1.99	−0.6
6.40	6.14	−4.1	6.22	−2.8	1.33	1.29	−3.4	1.26	−5.4
8.00	8.05	0.6	8.16	1.9	0.00	−0.26	—	−0.24	—

both equation (8) ($found_1$) and equation (4) ($found_2$) are listed in Table 3. The results calculated by approximate equation and the exact equation were coincident. This demonstrates that the approximate equation is accurate.

The method proposed in this paper has an advantage in that the result is independent of the initial time of reaction. Good results can be obtained, provided that A *vs.* t is recorded in the same range of reactant concentrations. In this paper the data of absorbance changing with time was recorded in the range of 0.70–0.40.

Acknowledgement—This work was supported in part by the National Science Foundation of P.R. China.

REFERENCES

1. R. D. Sauerbrumn and E. B. Sandell, *Mikrochim Acta*, 1953, **22**.
2. C. Surasiti and E. B. Sandell, *Anal. Chim. Acta*, 1960, **22**, 261.
3. P. A. Rodriguez and H. L. Pardue, *Anal. Chem.*, 1969, **41**, 1376.
4. J. B. Worthington and H. L. Pardue, *Anal. Chem.*, 1970, **42**, 1157.
5. Z. C. Gu and C. Xu, Selected Papers of 80th Anniversary of Tongji University, Vol. 3, p. 62. Tongji University Press, Shanghai, 1987.
6. R. L. Habig, H. L. Pardue and J. B. Worthington, *Anal. Chem.*, 1967, **39**, 600.
7. E. B. Sandell and I. M. Kolthoff, *J. Am. Chem. Soc.*, 1953, **56**, 1426.
8. A. Savitzky and M. J. E. Golay, *Anal. Chem.*, 1964, **36**, 1627.

Talanta, Vol. 40, No. 7, pp. 1019–1022, 1993
Printed in Great Britain.

0039-9140/93 $6.00 + 0.00

DETERMINATION OF ACTIVITY COEFFICIENTS OF TERMOLECULAR COMPLEX FORMATION

W. REGENSTEIN
Fachbereich Physik, Universität Potsdam, Am Neuen Palais 10, Potsdam D-O-1571, Germany

(*Received* 8 *October* 1992. *Revised* 7 *January* 1993. *Accepted* 12 *January* 1993)

Summary—The activity coefficients of CT-complexes exhibiting termolecular complex formation due to donor excess are determined. Since the solutions can be regarded as binary systems with respect to their activities the cases of non-volatile and volatile solutes in volatile solvents are considered here.

So far there is little information given in the literature[1–3] regarding the influence of the activity coefficients on termolecular complex formation of CT (Charge Transfer) complexes in case of high initial concentrations.

Whereas Childs *et al.*[2,4] combine spectroscopic with solubility measurements we apply spectroscopic and vapour pressure measurements to determining the equilibrium constants and activity coefficients, respectively.

DETERMINATION OF EQUILIBRIUM CONSTANTS

The formation of CT-complexes is controlled by the general scheme of reactions

$$qD + pA \overset{K}{\rightleftharpoons} D_qA_p. \tag{1}$$

Neglecting the activity coefficients and with the help of the law of mass action the equilibrium constant amounts to

$$K = c_i(c_D^q c_A^p)^{-1} \tag{2}$$

with c_i = complex concentration of stoichiometry q, p,
c_D, c_A = donor and acceptor concentration, respectively, at the state of equilibrium, and the initial concentrations

$$c_D^0 = c_D + qc_i \quad \text{and} \quad c_A^0 = c_A + pc_i.$$

In addition to 1:1-(termolecular) complexes there are also 2:1-complexes occurring under high donor concentrations. As Carter[5] has shown the coupled equilibriums now become

$$D + A \overset{K_1}{\rightleftharpoons} DA \tag{3}$$

and

$$D + DA \overset{K_2}{\rightleftharpoons} D_2A \tag{4}$$

with equilibrium constants

$$K_1 = c_1(c_D^0 - c_1 - 2c_2)^{-1}(c_A^0 - c_1 - c_2)^{-1}, \tag{5}$$

$$K_2 = c_2(c_D^0 - c_1 - 2c_2)^{-1}(c_1)^{-1}, \tag{6}$$

and the complex concentrations, respectively,

$$c_1 = R + (R^2 - 4K_1^2(c_A^0 c_D^0 - 2c_A^0 c_2 - c_D^0 c_2 + 2c_2^2))^{1/2}(2K_1)^{-1}, \tag{7}$$

where R is nondimensional,

$$c_2 = K_2(c_D^0 c_1 - c_1^2)(2K_2 c_1 + 1)^{-1} \tag{8}$$

$$R = K_1 c_A^0 + K_1 c_D^0 - 3K_1 c_2 + 1. \tag{9}$$

Provided the additivity of the extinctions E_i, and using the optical densities $E' = E/d$, where d denotes the layer thickness of the cuvette, the optical density is

$$E' = \epsilon_D c_D + \epsilon_A c_A + \epsilon_1 c_1 + \epsilon_2 c_2. \tag{10}$$

Application of data processing enables utilising complete information based on the total spectrum of specified points for computing the equilibrium constants. For that purpose Beer's law is written in matrix formulation

$$A = CE. \tag{11}$$

Let for instance the acceptor, the DA, and the D_2A complex be absorbing over the investigated spectral region, without loss of generality, and the spectra of m mixtures with l wave-

length are to be evaluated, then equation (12) is obtained

$$\begin{pmatrix} a_{11} & a_{12} & \cdots & a_{1l} \\ \cdot & \cdot & & \cdot \\ \cdot & \cdot & & \cdot \\ \cdot & \cdot & & \cdot \\ \cdot & \cdot & & \cdot \\ \cdot & \cdot & & \cdot \\ a_{m1} & a_{m2} & \cdots & a_{ml} \end{pmatrix} = \begin{pmatrix} c_{1A} & c_{11} & c_{12} \\ \cdot & \cdot & \cdot \\ \cdot & \cdot & \cdot \\ \cdot & \cdot & \cdot \\ \cdot & \cdot & \cdot \\ \cdot & \cdot & \cdot \\ c_{mA} & c_{m1} & c_{m2} \end{pmatrix} \begin{pmatrix} \epsilon_{A1} \cdots \epsilon_{Al} \\ \epsilon_{11} \cdots \epsilon_{1l} \\ \epsilon_{21} \cdots \epsilon_{2l} \end{pmatrix}. \quad (12)$$

The matrix of concentration includes the unknown equilibrium constants as non-linear parameters. There are several methods for the evaluation of the matrix equation given in literature.[6,7]

The equilbrium constants found with equation (12) are correct on the condition that the solutions are ideal. Yet, because of the acceptor's low solubility donor excess has frequently been applied. The relatively high donor concentrations do not permit looking upon the solutions as ideal any more. Instead of concentrations in equation (12) activities

$$a_i = \gamma_i c_i \quad (13)$$

have to be inserted. Then, and with low concentrations the activity coefficients tend to 1 whereas otherwise they may become greater or smaller than 1. Thus, for 1:1 and 1:2 complex formation the thermodynamical equilibrium constants arise as

$$K_1^{th} = c_1\gamma_1(c_D c_A \gamma_D \gamma_A)^{-1} = K_1\Gamma_1, \quad (14)$$

$$K_2^{th} = c_2\gamma_2(c_D c_1 \gamma_D \gamma_1)^{-1} = K_2\Gamma_2. \quad (15)$$

The Γ_i allow for the influence of the activity coefficients and permit a correction of the traditionally determined equilibrium constants. Besides, the activity coefficients can be derived through methods that are independent of the determination of equilibrium constants.

From the methods represented[8] vapour pressure decreasing proved appropriate for the investigations. The activity of the solvent can be found from the vapour pressure decrease according to Raoult's first law

$$a_s = p/p_{0s} \quad (16)$$

by vapour pressure measurements at different concentrations of the solvent. This method is bound to binary liquid solutions with no detectable vapour pressure developed by the solute, and provided that the magnitude of vapour pressure of the pure solvent at temperature is known. By means of the Gibbs–Duhem equation and the thus determined activity coefficients as well as taking into account the influence of the mol fractions of the solute x_i and the solvent x_s it is now possible to compute the activity coefficient of the solute by numerical integration of the equation

$$\lg a_i = -\int_{x_i'}^{x_i} x_s/x_i \, \mathrm{dlg}\, a_s + \lg a_i \quad (17)$$

through plotting x_s/x_i *vs.* $-\lg a_s$. The symbol a_i stands for the activity of the lowest measured mol fraction x_i. If the integral is referred to as A the equation turns by some transforming to

$$\lg(\gamma_i/\gamma_i') = A - \lg x_i + \lg x_i'. \quad (18)$$

Supposed that $\gamma_i = 1$ when $x_i' = 0$, the γ_i can be determined. For that purpose the quotient in equation (18) has to be plotted for a constant x_i and a variable x_i'. The quotient and hence the unknown activity coefficient[9] are found by extrapolation.

It seems to be more intricate to determine the activity coefficients γ_i of binary systems with two volatile components the vapour pressure of which is composed of the partial pressures of the components and the vapour phase being a non-ideal mixture. A detailed account of how to find the partial pressure by methods of non-statistical thermodynamics can be looked up in the monograph of Hildebrand and Scott.[10] Extensive data collections have been compiled and computed in Kraetsch's thesis.[11]

RESULTS

The measurements were carried out by using a vapour pressure osmometer of Knauer. The problem that emerges in evaluating CT-complexes consists in that there are not only two- but four- up to six-component-systems occurring depending on whether 2:1-complexes are formed and solvent mixtures are used. It could be shown, however, that the vapour pressure decreases of the solutions become negligibly small in case of the considered CT-complexes and within the frame of limited solubilities of the complex components. Merely the naphthalene–methylcyclohexane system makes an exception (see Table 1).

Table 1. Vapour pressures and activity coefficients of naphthalene in methylcyclohexane computed according to equations (16) and (18) at T = 298 K and $p_{0_2} = 6{,}27$ kPa

$x_1 = x_D$	c_D(M)	p(kPa)	γ_s	γ_D
0.006	0.05	6.248	1.00	2.15
0.013	0.1	6.228	1.00	3.24
0.026	0.2	6.186	1.01	4.61
0.039	0.3	6.142	1.02	5.37
0.052	0.4	6.091	1.02	6.0
0.065	0.5	6.043	1.03	6.66

The benzene–tetrachloromethane system clearly exemplifies that the slight differences in vapour pressures are not only caused by the limited solubility (see Table 2). Despite unlimited solubility the activity coefficients turn out to be approximately 1 over the total concentration range. Measurable differences in vapour pressure arise mainly from the donor. The influence of the other components (acceptor, complexes) remain negligible.

Thus the equlibrium constant of the 1 : 1-complex formation is obtained in accordance with Martire *et al.*[3] and Lane[2] by the activity coefficient of the donor

$$K_1^{th} = K_1/\gamma_D. \tag{19}$$

The measured vapour pressures of the benzene–TCNE (tetracyanoethylene) complex in tetrachloromethane and the activity coefficients computed from them were put together in Table 2.

Applying a regression program the vapour pressure of the binary benzene–tetrachloromethane system is described herein by the equation proposed in Barker's theory[12]

$$p \approx x_1 p_1^0 \exp\{(1-x_1)^2(A + Bx_1 + Cx_1^2)\} + (1-x_1)p_2^0 \exp\{x_1^2[(A - B/2) + (B - 2C/3)x_1 + Cx_1^2]\} \tag{20}$$

Table 2. Vapour pressures and activity coefficients of benzene in tetrachloromethane computed according to equations (21) and (22) at $T = 298$ K

$x_1 = x_D$	c_D(M)	p(kPa)	γ_2	$\gamma_1 = \gamma_D$
0.1	1.1	12.210	1.0	1.1
0.2	2.25	12.103	1.0	1.1
0.3	3.5	11.890	1.0	1.09
0.4	4.9	11.743	1.0	1.07
0.5	6.5	11.623	1.01	1.06
0.6	8.1	11.477	1.03	1.04
0.7	10.0	11.290	1.06	1.03
0.8	12.3	11.170	1.1	1.01
0.9	14.7	10.517	1.16	1.0

for known vapour pressures of the pure components p_1^0 and p_2^0 and with adaptation of the unknown coefficients A, B, C. From that the activity coefficients are found as

$$\ln \gamma_1 \approx (1 - x_1^2)(A + Bx_1 + Cx_1^2 + \cdots), \tag{21}$$

$$\ln \gamma_2 \approx x_1^2[(A - B/2) + (B - 2C/3)x_1 + (C - 3D/4)x_1^2 + \cdots]. \tag{22}$$

The vapour pressures of benzene $p_1^0 = 10.25$ kPa and tetrachloromethane $p_2^0 = 12{,}37$ kPa at $T = 298$ K for adaptation have been drawn from literature. The coefficients were calculated by non-linear compensation to $A = 0.213$, $B = -0.324$, $C = -0.049$ and $D = 0$. For calculation at least six datapoints are necessary. When the second number past point is not changing the computation was interrupted.

The vapour pressure measurements of the system naphthalene in methylcyclohexane with the non-volatile complex component compiled in Table 1 were determined by means of Raoult's law given in equation (16) and the Gibbs–Duhem equation (17).

CONCLUSIONS

The determination of activity coefficients of multiple-component systems such as, *e.g.* CT-complexes present today, is still a difficult and not yet satisfactorily solved problem. We could confirm by our system with aid of vapour pressure measurements, that the donor in access gets the most activity.

Using the benzene–TCNE in methylcyclohexane we could show that by unlimited solubility from donor-benzene the activity is not essential. The calculation of activity coefficients for the system with two volatile components was done by Barker's equation (20).

The experimental data show significant deviations from the UNIQUAC (Universal–Quasichemical),[13] UNIFAC (Universal group Activity Coefficients)[14] and NRTL (non random two-liquid)[15] equations which were derived on the basis of the grid model.

REFERENCES

1. G. Briegleb, *EDA-Komplexe*, Springer, Berlin, 1961.
2. E. H. Lane, S. D. Christian and J. D. Childs, *J. Amer. Chem. Soc.*, 1974, **96**, 38.
3. M. W. Hanna and D. G. Rose, *J. Amer. Chem. Soc.*, 1972, **94**, 2601.

4. J. D. Childs and S. D. Christian, *J. Amer. Chem. Soc.*, 1972, **94**, 5657.
5. S. Carter, *J. Chem. Soc. (A)*, 1968, 404.
6. P. J. Lingane and Z. Z. Hugus, Jr., *Inorg. Chem.*, 1970 **9**, 757.
7. H. Gampp, M. Meader, C. J. Meyer and A. D. Zuberbühler, *Talanta*, 1986, **33**, 943.
8. K. Schwabe, *Physikalische Chemie*, Akademie-Verlag, Berlin, 1986.
9. E. Kretschmer, *Physikalische Chemie—Grundkurs Chemie für Lehrer*, Vol. 6, pp. 2, berichtigte Ausgabe, VEB Dt. Verl. der Wissenschaften, Berlin, 1976.
10. J. H. Hildebrand and R. L. Scott, *Regular Solution*. Prentice-Hall, Englewood Cliffs, NJ, 1962.
11. H. Kraetsch, Numerische Untersuchungen über thermodynamische Zusatzfunktionen binärer Nichtelektrolytmischungen, Diss. (A), Martin-Luther-Universität, Halle/Wittenberg, 1967.
12. J. A. Barker, *Aust. J. Chem.*, 1953, **6**, 207.
13. D. S. Abrams and J. M. Prausnitz, *AIChE-J.*, 1975, **21**, 116.
14. A. Fredenslund, R. L. Jones and J. M. Prausnitz, *AIChE-J.*, 1975, **21**, 1086.
15. H. Renon and J. M. Prausnitz, *AIChE-J.*, 1968, **14**, 135.

Talanta, Vol. 40, No. 7, pp. 1023–1029, 1993
Printed in Great Britain.

0039-9140/93 $6.00 + 0.00

COLORIMETRIC DETERMINATION OF ISONIAZID AND ITS PHARMACEUTICAL FORMULATIONS

NADIA M. A. MAHFOUZ[1] and KAMLA M. EMARA[2]

[1]Department of Pharmaceutical Medicinal Chemistry, [2]Analytical Pharmaceutical Chemistry, Faculty of Pharmacy, University of Assiut, Assiut, Egypt

(*Received* 22 *September* 1992. *Revised* 30 *December* 1992. *Accepted* 12 *January* 1993)

Summary—Two colorimetric methods for the estimation of isoniazid are developed. The first method depends on coupling of isoniazid with diazotized 1-amino anthraquinone zinc chloride salt (fast red AL salt) to form a red colour (λ_{max} 510 nm). The second one is based on the formation of a green complex (λ_{max} 655 nm) between the acid hydrazide and 2,6-dimethoxy-1,4-benzoquinone (DMBQ). All measurements of the two procedures were carried out in the presence of sodium hydroxide at room temperature (20 ± 3°C). The two methods are applied for the determination of isoniazid in presence of congenial drugs, vitamins and additives normally encountered with it in pharmaceutical dosage forms. The reliability of these methods was established by parallel determination with the reported and official methods.

Isoniazid (INH), the antitubercular drug, has been determined by titrimetric[1–3] ultraviolet spectrophotometric,[4] Colorimetric,[5–8] fluorimetric,[9] polarographic,[10] paper or thin layer chromatographic,[11,12] and HPLC[13] methods. The compendial methods for the assay of isoniazid, in authentic and dosage forms, involve HPLC,[14] nitritimetric[14] and bromimetric titrations.[15]

In the present work, two spectrophotometric methods for the assay of isoniazid with fast red AL salt and DMBQ were described. The methods are sensitive, rapid and adopted for the assay of isoniazid in pure form and its pharmaceutical formulations.

EXPERIMENTAL

Apparatus

Uvidec-320 spectrophotometer (JASCO, Tokyo, Japan).

Infrared spectrophotometer (Perkin–Elmer 298) using potassium bromide disc.

^{1}H-NMR Spectra Varian EM 360A (60 MHz). The ^{1}H-NMR chemical shifts were measured against TMS = 0.0 ppm and compared with TMS = $CDCl_3$—7.289 ppm.

Melting points were determined on "Buchi-Gerat" in capillary tubes and were uncorrected.

Thin layer chromatography (TLC) was carried out using fluorescent silica get plates polygram -G UV_{254} (Macherey and Nagel, Duren). The spots were detected with UV at 254 nm.

Reagents and materials

Fast red AL salt solution, (Aldrich Chemical Co., Inc., USA). A 0.2% (w/v) aqueous solution was used, freshly prepared and protected from sunlight.

Sodium hydroxide, 0.4% (w/v) and 10% (w/v) aqueous solutions were used.

Isoniazid (Analar grade) (BDH, Poole, Dorset, UK).

2,6-Dimethoxy-1,4-benzoquinone reagent, A 0.1% w/v ethanolic solution was used. It was synthesized according to Hamblock[16] and Baker[17] procedures. Its purity and structure were confirmed by TLC ($CHCl_3$/MeOH 9:1), mp (254–255°C),[17] IR and ^{1}H-NMR spectra. IR (Fig. 1) revealed the presence of characteristic stretching bands, *viz.*, C—H (3070 and 2940/cm), C=O (1690 and 1640/cm), C=C conjugated (1590/cm), C—O—C (1260 and 1105/cm), in addition to one out of plane bending band at 880/cm corresponding to tetrasubstituted benzene. ^{1}H-NMR (Fig. 2) showed the presence of six protons at δ 3.86 ppm (singlet), corresponding to the methoxy functions and two aromatic protons at δ 5.85 ppm (singlet). The upfield shift of the latter protons was attributed to the shielding anisotropic effect of the ortho-carbonyl function.

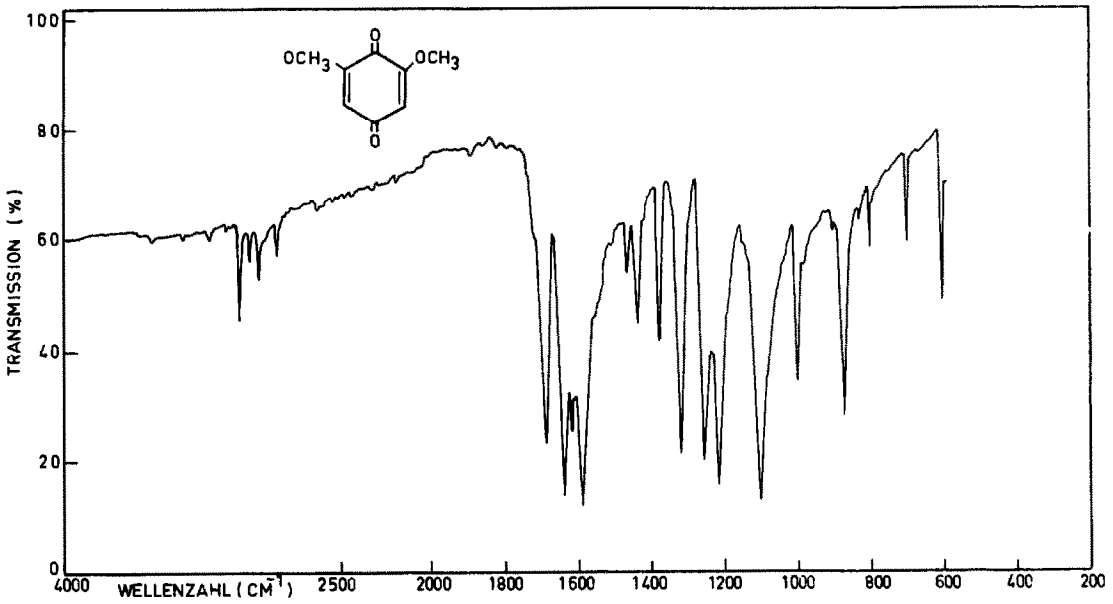

Fig. 1. IR spectrum of DMBQ (KBr disc).

All solvents and reagents were of analytical grade (Merck).

Pharmaceutical preparations

The following isoniazid commercial formulations were used:

(1)—Isocid tablets (CID, Egypt) contain 50 mg of isoniazid per tablet.

(2)—Isocid forte tablets (CID, Egypt) contain 200 mg of isoniazid per tablet.

(3)—Inhibex tablets (Misr, Egypt) contain 50 mg of isoniazid, 5 mg of nicotinamide and 5 mg of vitamin B_6 per tablet.

Method

Preparation of sample solutions. Isoniazid powder: Weigh 50 mg isoniazid and dissolve it in water and complete to 50 ml. Dilute this solution stepwise with water to obtain drug concentration 0.1 mg per ml. Use 1-ml aliquot of this solution for the procedure (fast red AL salt–isoniazid complex). For DMBQ–isoniazid

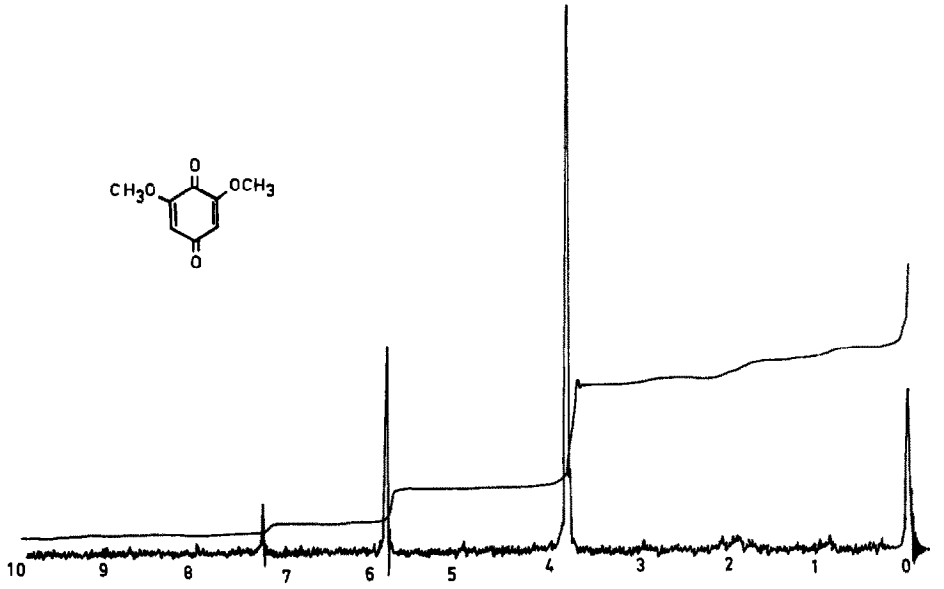

Fig. 2. ^{1}H-NMR spectrum of DMBQ.

complex; ethanolic solution of isoniazid was prepared similarly and diluted with the same solvent to obtain drug concentration 0.05 mg per ml. Use 1-ml aliquot of this solution for the procedure.

Tablets. Mix the contents of 20 tablets thoroughly. Weigh an amount equivalent to 50 mg of isoniazid into 50 ml calibrated flask, extract with 30 ml water (3 × 10 ml), filter and complete to 50 ml with water. Dilute this solution with water to contain 0.1 mg/ml of the drug. Use 1 ml of this solution for the procedure (for fast red AL salt–isoniazid complex). Similarly, for DMBQ–isoniazid complex, ethanolic solution of isoniazid tablets was diluted to obtain drug concentration 0.05 mg/ml and use 1 ml of this solution for the procedure.

Procedure

For fast red AL salt–isoniazid complex. To a 10 ml calibrated flask, add 1 ml of the sample solution, 2 ml of fast red AL salt solution, mix and stand for 10 min. Add 1.0 ml of sodium hydroxide solution (10% w/v). Make up to the mark with ethanol, mix and measure the absorbance at 510 nm against a reagent blank prepared similarly.

For DMBQ–isoniazid complex

Into 10 ml volumetric flask, transfer 1 ml of the sample solution, 1.5 ml of 2,6-dimethoxy-1,4-benzoquinone and 0.1 ml of sodium hydroxide solution (0.4% w/v). Mix the contents and leave for 10 min at room temperature (20 ± 3°C). Dilute the mixture to volume with ethanol and measure the absorbance at 655 nm against a reagent blank treated similarly.

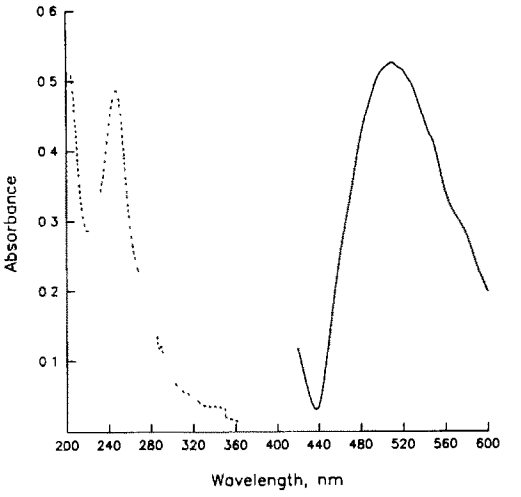

Fig. 3. Absorption spectra of fast red AL salt–isoniazid complex (——) and fast red AL salt (–·–·–), final drug concentration; 8.4 μg/ml.

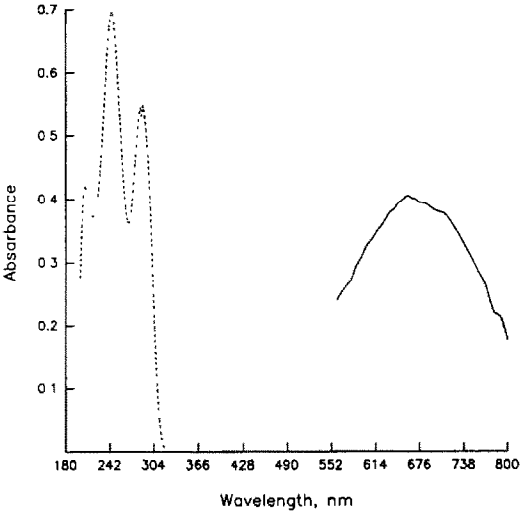

Fig. 4. Absorption spectra of DMBQ–isoniazid complex (——) and DMBQ (–·–·–), final drug concentration; 7 μg/ml.

RESULTS AND DISCUSSION

Absorption spectra

Isoniazid reacts with fast red AL salt in presence of sodium hydroxide in an aqueous ethanolic medium to form a red colour (λ_{max} 510 nm).

A green complex is formed when isoniazid is allowed to react with 2,6-dimethoxy-1,4-benzoquinone in presence of sodium hydroxide in an aqueous ethanolic solution. The absorption spectra of the two complexes are shown in Figs 3 and 4. Their spectral characteristics are summarized in Table 1.

Optimum conditions

To achieve maximum colour development, the reaction mixture of isoniazid and fast red AL salt must allowed to stand for 10 min before

Table 1. Spectral characteristics of the fast red AL salt–INH and DMBQ–INH complexes

Complex	λ_{max} (nm)	ϵ_{max} ($l \cdot mole^{-1} \cdot cm^{-1}$)	INH Linear range (μg/ml)	Quantitative parameters Intercept	Slope	Correlat. coeff.
Fast red Al salt–isoniazid	655	8.5×10^3	2–15	0.0126	0.0589	0.9993
DMBQ–isoniazid	655	1.6×10^4	1–10	0.0105	0.0584	0.9988

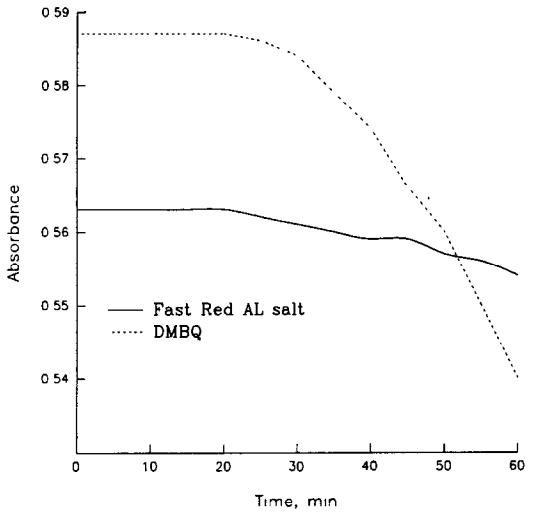

Fig. 5. Stability time of fast red AL salt–isoniazid and DMBQ–isoniazid complexes final drug concentrations 9.0 and 5.0 μ/ml, respectively.

Table 2. Effect of the amount of the reagents on the coloured complexes

Volume of reagent (*ml*)	Fast red AL salt–INH complex* A_{510}	DMBQ–INH complex† A_{655}
0.5	0.179	0.268
1.0	0.354	0.473
1.5	0.512	0.585
2.0	0.626	0.576
2.5	0.616	0.535
3.0	0.600	0.515

*Final drug concentration, 10 μg/ml.
†Final drug concentration, 5 μg/ml.

addition of sodium hydroxide solution. The formed red colour was stable for 20 min at room temperature (20 ± 3°C) (Fig. 5). For complete formation of DMBQ–isoniazid complex, it is necessary to stand for 10 min, in presence of sodium hydroxide, before dilution. The maximum absorbance readings remain constant for ~20 min (Fig. 5).

Table 3. Effect of sodium hydroxide concentration on colour intensity

Fast red AL salt–INH complex*		DMBQ–INH complex†	
10% sodium hydroxide (*ml*)	A_{510}	0.4% sodium hydroxide (*ml*)	A_{655}
0.5	0.508	0.025	0.501
1.0	0.616	0.050	0.534
1.5	0.600	0.100	0.585
2.0	0.580	0.150	0.568
2.5	0.550	0.200	0.530
3.0	0.520	0.300	0.477

*Final isoniazid concentration, 10 μg/ml.
†Final isoniazid concentration, 5 μg/ml.

Table 4. Effect of diluting solvent on the coloured products

Solvent	Fast red AL salt–INH complex* λ_{max}	A	DMBQ–INH complex† λ_{max}	A
Methanol	510	0.378	655	0.435
Ethanol	510	0.616	655	0.589
Acetone	505	0.198	660	0.230
Dimethyl formamide	505	0.510	665	0.354
Isopropanol	510	0.417	660	0.451
Dioxane	495	0.365	650	0.073

*Final isoniazid concentration, 10 μg/ml.
†Final isoniazid concentration, 5 μg/ml.

It is clear from the data reported in Table 2 that isoniazid needs 2 ml of 0.2% fast red AL salt or 1.5 ml of 0.1% 2,6-dimethoxy-1,4-benzoquinone for the reactions to complete.

Different alkalies were tested for both methods, sodium hydroxide is the best one and 1 ml of 10% sodium hydroxide and 0.1 ml of 0.4% sodium hydroxide are recommended for the formation of fast red AL salt—isoniazid and DMBQ–isoniazid complexes, respectively (Table 3).

Methanol, ethanol, isopropanol, acetone, dimethyl formamide and dioxane were tested as diluting solvents in the two methods. The results revealed that ethanol was the best solvent (Table 4).

Interference

No interference was observed from the presence of other drugs, vitamins, commonly encountered excipients and additives when isoniazid was determined by the two methods (Table 5).

Quantification

Beer's law holds good over the ranges 2–15 and 1–10 μg/ml by fast red AL salt–INH and

Table 5. Determination of isoniazid in the presence of other drugs, vitamins and excipients

Substance	Amount (*mg*)	Recovery (% ± SD)† Fast red AL salt–INH complex	DMBQ–INH complex
Pyridoxine	5	99.9 ± 1.04	100.7 ± 0.95
Nicotinamide	50	99.7 ± 1.29	99.9 ± 0.85
Glucose	10	100.3 ± 1.11	99.6 ± 1.12
Lactose	10	99.3 ± 0.96	99.8 ± 0.91
Gum acacia	10	99.4 ± 0.86	100.4 ± 0.92
Magnesium stearate	20	99.9 ± 0.55	99.1 ± 0.89
Microcrystalline cellulose	20	100.0 ± 0.78	100.4 ± 0.78
Starch	20	98.8 ± 1.03	99.4 ± 0.93

*Added per 10 mg isoniazid.
†Average of five determinations.

Table 6. Assay of isoniazid powder by the suggested and reported colorimetric methods

Isoniazid, mg†	Fast red AL salt–INH complex	DMBQ–INH complex	Reported method*
10	100.7	98.8	100.9
20	98.9	99.6	98.6
30	99.3	101.8	98.5
40	100.2	99.9	101.1
50	99.8	100.1	99.9
60	101.4	100.5	98.7
Mean ± SD	100.1 ± 0.84	100.1 ± 0.92	99.6 ± 1.08

*Ref. 6.
†Average of three experiments.

DMBQ–INH complexes, respectively. Correlation coefficient, intercepts and slopes for the calibration data of isoniazid by the two suggested methods are given in Table 1.

To examine the precision of both procedures, eight replicate analyses were performed on the same solution containing 10 and 5 μg per ml of the drug, and relative standard deviations of 1.43% and 1.55% were obtained by fast red AL salt–INH and DMBQ–INH complexes, respectively.

Table 7. Determination of isoniazid and its pharmaceutical preparations

Sample	Recovery (% ± SD)* Fast red AL salt–isoniazid complex	DMBQ–isoniazid complex	Official method†
Isoniazid powder	99.8 ± 0.88 F‡ = 1.12 t§ = 0.26	100.1 ± 1.26 F‡ = 2.31 t§ = 0.69	99.7 ± 0.83
Isocid tablets‖	100.8 ± 1.137 F‡ = 1.07 t§ = 0.19	101.0 ± 1.18 F‡ = 1.00 t§ = 0.07	100.9 ± 1.18
Isocid forte tablets‖	100.8 ± 1.21 F‡ = 1.26 t§ = 0.15	100.9 ± 1.29 F‡ = 1.11 t§ = 0.02	100.9 ± 1.36
Inhibex tablets‖	99.2 ± 1.29 F‡ = 1.05 t§ = 0.22	99.2 ± 1.31 F‡ = 2.02 t§ = 0.29	99.0 ± 1.31

*Averge of five determinations.
†Ref. 15.
‡Tabulated F for (4,4) degrees of freedom at $P = 0.05$ is 6.39.
§Tabulated t for 4 degrees of freedom at $P = 0.05$ is 2.776.
‖Details in Experimental section.

Applications

The proposed procedures were used to determine isoniazid in authentic and pharmaceutical

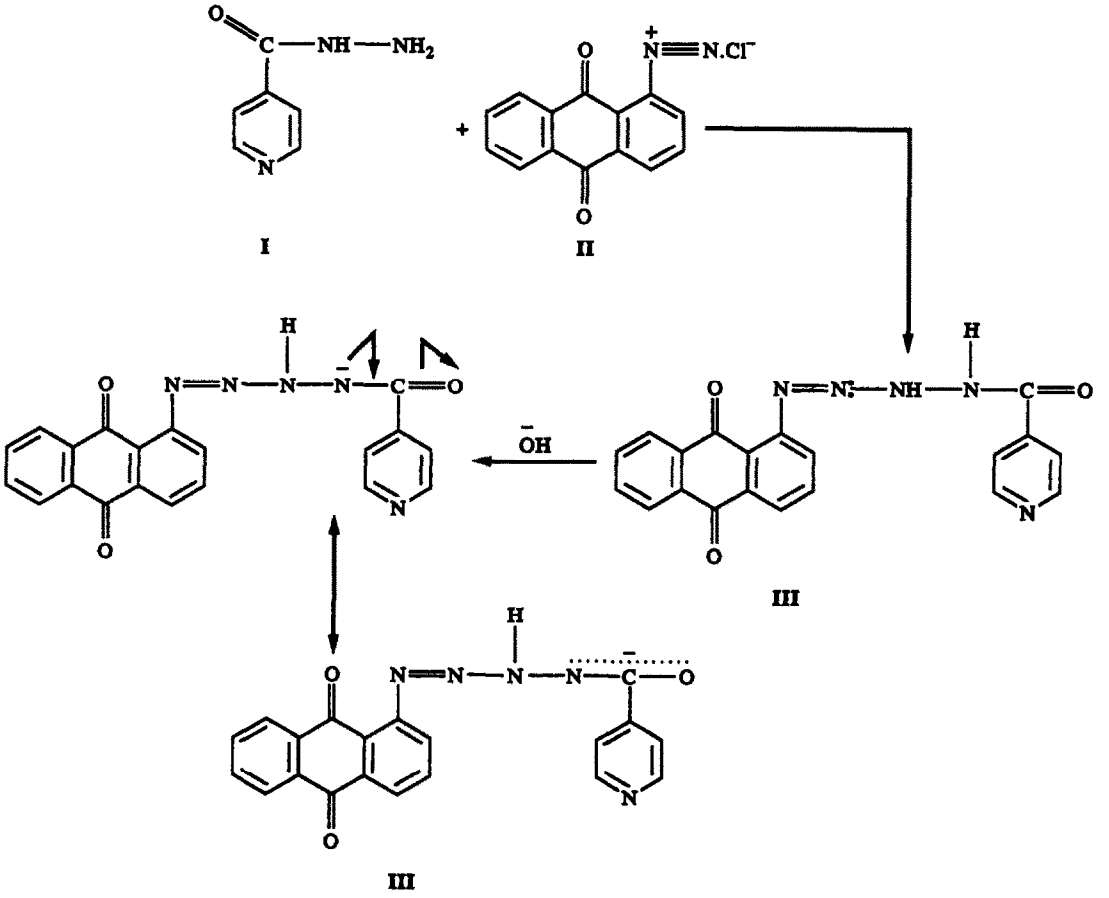

Scheme 1.

preparations. The results obtained are comparable to those given by the reported and official methods, Tables 6 and 7. Student *t*- and *F*-test show no significant differences between the proposed, and official methods. In addition, the suggested methods have the advantages of rapidity and simplicity.

Reaction involved

Fast red AL salt (I), in presence of sodium hydroxide, reacts with isoniazid (II) (molar ratio 1:1) to form a red colour with maximum absorption at 510 nm in aqueous ethanolic medium. The mechanism of the reaction may be interpreted as shown in Scheme 1.

A characteristic green coloured product (λ_{max} = 655 nm) is formed when isoniazid is allowed to react with DMBQ in presence of sodium hydroxide in aqueous medium. Under the experimental conditions, the suggestion that acid hydrazides form hydrazones with the carbonyl function of the reagent is excluded due to the failure of some aromatic amines, *e.g.* *p*-aminophenol, sulfonamide, dapsone, hydroxylamine and semicarbazide to give green colour with DMBQ. This negative response reveals that under a mild reaction condition no azomethine derivatives are formed.

However, quinones are easily reduced to hydroquinone derivatives by different reducing agents, *e.g.* hydrazine.[18,19] It was reported[18] that reduction of *p*-benzoquinone in alkaline medium give a deep green compound which formed from equimolar amount of *p*-benzoquinone and hydroquinone (charge-transfer or donor–acceptor complex).[18] In addition, it was reported[19] that aryl hydrazines are easily oxidized by benzoquinone (Q) to give aryldiimide and hydroquinone (QH_2)[19]

$$Ph\text{-}NHNH_2 + Q \rightarrow Ph\text{-}N = NH + QH_2$$

Moreover, isoniazid as hydrazine derivative can be attacked by oxidizing agents especially in presence of alkali solution.[18] Consequently the mechanism of formation of the green coloured product when isoniazid I reacts with DMBQ II may proceed through reduction of II into hydroquinone derivative III and formation of quinone: hydroquinone charge transfer or donor–acceptor complex IV (Scheme 2).

A preliminary chemical test to confirm the formation of hydroquinone derivative as a by-product was carried out by addition of few drops of ferric chloride T.S., disappearance of the green colour took place. This indicates the decomposition of the complex with oxidation of the hydroquinone derivative into 2,6-dimethoxy-1,4-benzoquinone with formation of a yellow colour.

In addition, the continuous molar variation for the reaction between isoniazid and DMBQ reveals that the interaction between these two compounds occurs at a ratio of 1:2. This provides further evidence for the suggested mechanism shown in Scheme 2. All attempts to separate the green coloured product IV failed.

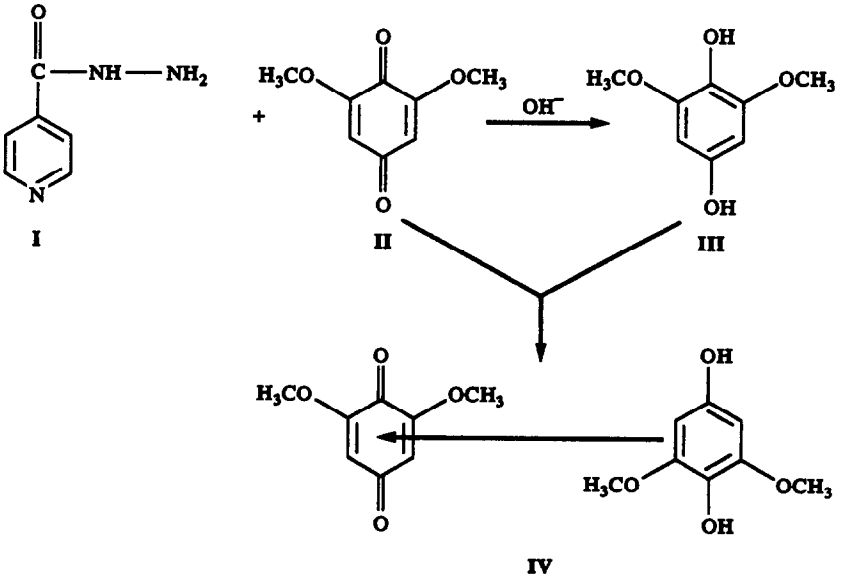

Scheme 2.

REFERENCES

1. U. Muralikrishna and K. Subrahmanyam, *Indian Drugs*, 1984, **21**, 356.
2. B. B. Karamkar, *J. Inst. Chem. (India)*, 1983, **55**, 153.
3. M. Sarwar, A. Malik and U. A. Khan, *Anal. Lett.*, 1989, **22**, 853.
4. B. N. Sarkar, *Indian J. Pharm.*, 1972, **24**, 58.
5. Z. H. Mohamed, L. El-Sayed and A. M. Wahbi, *Egypt. J. Pharm. Sci.*, 1989, **30**, 43.
6. M. E. El-Kommos and A. S. Yanni, *Analyst(London)*, 1988, **113**, 1091.
7. A. Abou-Ouf, A. Taha, and M. Saidham, *J. Pharm. Sci.*, 1973, **62**, 1700.
8. L. P. Pavlyuchenkova and M. A. Veksler, *Formatsiga (Mosco)*, 1974, **23**, 29 through Ref. 17.
9. P. C. Ioannou, *Talanta*, 1987, **34**, 857.
10. J. J. Vallon, A. Badinand and C. Bichon, *Anal. Chim. Acta*, 1975, **78**, 93.
11. L. Reio, *J. Chromatogr.*, 1970, **47**, 60.
12. R. M. De Sagher, A. P. De Leenheer and A. E. Claeys, *J. Chromatogr.*, 1975, **106**, 357.
13. J. T. Stewart, I. L. Honigberg, J. P. Brant, W. A. Murray, J. L. Webb and J. B. Smith, *J. Pharm. Sci.*, 1976, **65**, 1536.
14. *United States Pharmacopeia XXII, National Formulary XXI*, pp. 728, 729. US Pharmacopeial Convention, Rockville, MD, 1990.
15. *British Pharmacopoeia* 1988, pp. 317, 812 and 957. HMSO, London, 1988.
16. H. Hamblock, Ph. D. Thesis Bonn 1982.
17. W. Baker, *J. Chem. Soc.*, 1941, 662.
18. H. J. Roth, K. Eger and R. Torschütz, *Arzneistoff analyse. Readtivitat-Stubilitat-Analytik.*, p. 79. George Thieme Verlag, Stuttgart, 1981.
19. Hans-Dieter Becker, in *The Chemistry of Quinonoid Compound*, S. Patai (ed.) Part 1, p. 403. John Wiley, London, 1974.

Talanta, Vol. 40, No. 7, pp. 1031–1039, 1993
Printed in Great Britain.

0039-9140/93 $6.00 + 0.00

PERFORMANCE OF AN ION TRAP MASS SPECTROMETER MODIFIED TO ACCEPT A DIRECT INSERTION MEMBRANE PROBE IN ANALYSIS OF LOW LEVEL POLLUTANTS IN WATER

SCOTT J. BAUER and R. GRAHAM COOKS
Department of Chemistry, Purdue University, West Lafayette, IN 47907, U.S.A.

(*Received* 17 *September* 1992. *Revised* 20 *November* 1992. *Accepted* 20 *November* 1992)

Summary—Modifications to a Finnigan ITS40 ion trap mass spectrometer are described which allow its use with a direct insertion probe. Details are given of the fabrication of a membrane probe for such an instrument. The membrane probe, which includes facilities for heating the fluid, employs a tubular membrane which is located just outside the electrode structure of the ion trap. Direct analysis of organic compounds in aqueous solution is demonstrated using a silicone membrane, with compounds such as benzene, chlorobenzene and dichloroethene being studied below the 1 ppb level. The effects of operating parameters including probe temperature, ion trap temperature, solution flow rate, mass spectrometer scan speed, and instrument tune procedures are explored in detail. Optimum performance characteristics are identified and trace level detection of eight organic compounds in the parts per trillion range is demonstrated. In seven of the eight cases studied, detection limits are below the EPA practical limit of quantitation levels. It is shown that the most sensitive mode of operation is when steady state passage of the analyte across the membrane is achieved, however, the time required for this is long in the case of some samples, and a dynamic flow injection analysis procedure is then favored. Use of the modified inlet system for solid sample introduction via a standard solids probe is also demonstrated.

The objective of this work was to develop an inexpensive mass spectrometer for use in screening organic compounds of environmental interest in drinking or ground water by membrane introduction mass spectrometry (MIMS).[1] It is well known that over 95% of the water samples that are tested in a typical environmental laboratory contain no detectable organic contaminants of environmental interest. However, verification of this requires the long and costly process of extracting 1–2 l. of water three times with either methylene chloride or diethyl ether, dehydration of the extract over sodium sulfate, evaporation of the extract in a Kuderna Danish apparatus down to 1 ml, solvent exchange to an appropriate GC medium such as hexane, and injection of the sample into a gas chromatograph for a 20–60 min temperature programmed run, depending on the analytes of interest.[2] The many steps involved in this process are costly in both material and manpower and are themselves potentially damaging to the environment through the loss and disposal of organic solvents. Clearly, a system that could effectively screen water samples for the presence of organic compounds by MIMS would be valuable since it would require that the traditional analysis be conducted only on the small fraction of the samples that were found to contain compounds of interest during the screening.

The direct analysis of organic pollutants in water by MIMS has been the subject of intense activity. Westover and co-workers detected and quantified organic analytes directly from aqueous solution using a silicone membrane probe coupled to their mass spectrometer in 1974.[3] Since then, many variations of the membrane inlet system have been applied to the task of analyzing a broad range of aqueous organic analytes at low detection limits.[4–10] Among the more successful methods, is the flow-through method in which a capillary or other membrane is placed within or in close proximity to the ion source of the mass spectrometer, and the aqueous solution is passed across this membrane.[9] In this type of procedure, transportation of the solution is conveniently done using a peristaltic pump and flow injection methods of sample handling extend to quantitation using external standard solutions.[9] In earlier experiments in this laboratory, a simple flow-though MIMS system was used with an ion trap and it gave encouraging results, even though the analyte was not heated and the probe was located some distance from

the ion trap electrodes.[8] In this as in most other MIMS work, silicone polymers were used since they allow passage of a large number of relatively non-polar organics into the spectrometer while excluding all but a trace of the water. The limitations of the silicone polymers to hydrophobic compounds of low molecular weight have led to the recent development of new MIMS techniques that allow the analysis of some polar organic compounds using microporous membranes.[11]

A Finnigan ITS40 ion trap GC/MS was chosen for this work because of its wide use, light weight, rugged construction and low cost. The ITS40 was modified to allow sample introduction via a standard 1/2 in. diameter direct insertion probe. A tubular membrane probe was constructed to allow organic analytes to be examined directly from aqueous solution. The inlet system was constructed in such a way that the gas chromatographic capability of the instrument was not compromised. Early experiments had demonstrated the need to place the membrane as close to the spectrometer source as possible, in order to minimize analyte loss through condensation or dilution in transfer lines, and to minimize memory effects and instability caused by contamination in the transfer lines.[12] When the probe is installed in the new inlet system, the membrane is positioned 1/2 in. from the ion trap providing greatly improved performance over earlier designs.

These modifications to the ITS40 allow it to be used in a number of applications that were previously the domain of much more expensive dedicated mass spectrometers. Such uses include analysis of industrial process and waste streams though flow injection analysis,[13] on-line monitoring of chemical reactions,[14,15] analysis of water samples for environmentally significant contaminants[8,16] and solid sample introduction by a direct insertion solids probe. The multiple capabilities of the modified instrument, coupled with its light weight and compact size, may also make it a viable choice for on-site environmental or industrial analysis.

EXPERIMENTAL

Ion trap modification

The ion trap was removed from the Finnigan ITS40 GC/MS and a 3/4 in. hole was bored through the instrument outer case. A KF-16 quick flange nipple was welded in place in the 3/4 in. hole. Viewed from the top of the instrument, the flange was located 72.8° counter clockwise from the GC inlet and located in such a way that the center was aligned vertically (along the z-axis) with the GC inlet line. This alignment was critical as the new entrance into the trap was designed to match the manufacturer's GC entry vertical dimensions and the rotation was necessary to avoid interference from the ion trap tie bolts. A flat stainless steel disk was welded into the end of the quick flange and a 5/32 in. hole drilled in it to accept and align a Teflon transfer line. A 5/32 in. hole was then drilled into the ion trap to provide an entrance for the Teflon transfer line between the ring electrode and the bottom endcap electrode. This hole was drilled in two parts to match the factory GC inlet location and required that 2/3 of the hold diameter be drilled through the stainless steel exit end cap and 1/3 of the hole diameter be located in the lower Teflon spacer ring. A Teflon transfer line was then fabricated to provide a direct analyte passage into the internal volume of the ion trap. The inner bore of the transfer line was threaded to facilitate its insertion and removal during maintenance. The existing manifold heating unit was also modified to accommodate the new inlet port. A 1 in. wide slot was cut into the bottom of the manifold that would allow the heating unit to be installed in its normal position with the new inlet in place. A Norcal bellows valve was installed with a 3/4 in. quick flange on one end and a 1/2 in. Cajon fitting on the other. This mated to the KF-16 flange on the ion trap manifold and also sealed the probe when inserted in the mass spectrometer. A 1/4 in. stainless steel line was welded in place just behind the Cajon fitting for inlet rough pumping controlled through a Nupro level valve. This completed the modification of the ion trap. The design is relatively simple but requires accurate machining to accomplish proper alignment of all the parts when assembled. Helium buffer gas is introduced into the trap through the GC transfer line and there is no need to disconnect the GC capillary when operating in the membrane introduction mode. This makes changing from GC operation to direct insertion probe operation a simple matter of inserting or removing the probe. Detailed blueprints and a description of the modifications are available.[17]

Membrane probe

The membrane probe was constructed according to the plan in Fig. 1. It is designed exclusively for capillary membranes but it accommodates a variety of lengths as might be dictated by future

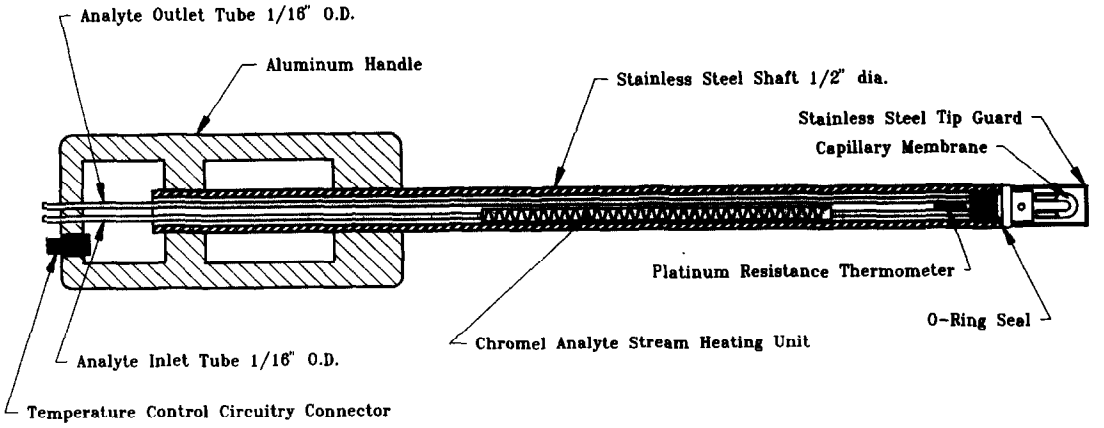

Fig. 1. Design of the tubular membrane probe.

experiments. The probe was constructed from an old Finnigan TSQ ion volume insertion tool. The inner parts were removed from the insertion tool and the end cut off. A probe tip was manufactured according to the plan in Fig. 1. The outer diameter of the probe tip matches the diameter of the probe tube to ease insertion through the inlet system Cajon fitting. Fluid transfer to the membrane is through two stainless steel 1/16 in. tubes welded into the back of the probe tip. Two 18 gauge needles were then welded into the end of the probe tip to accept the membrane tubing. A removable stainless steel guard was constructed to protect the membrane from damage when the probe is inserted into the instrument. A nichrome heating element and a platinum temperature sensor were installed on the inlet feed line to control the temperature of the inlet analyte stream. Electrical insulation between the heating element and the stainless steel inlet line was accomplished with Teflon shrink wrap applied to the tube surface. Heat insulation between the heating element and the internal wiring consisted of a layer of ceramic tape applied over the heating element which was covered in turn by a ceramic tube. All the internal wiring was routed to the probe handle end cap into a quick disconnect plug that matches the standard Finnigan solids probe heating controller. This control system was found to give fast heating and to result in stable temperatures over long periods of time. Passage of ana lyte through the membrane is strongly temperature dependent and small temperature fluctuations can cause baseline oscillations that may be unacceptable when doing trace analysis work.

Note that the design of the probe is such that it can be used in the modified ITS40 or also in any other spectrometer that will accept a 1/2 in. diameter probe. The probe length and electrical connections were also designed to provide maximum interchangeability.

With the probe installed in the ion trap as in Fig. 2, water is pumped through the probe by a

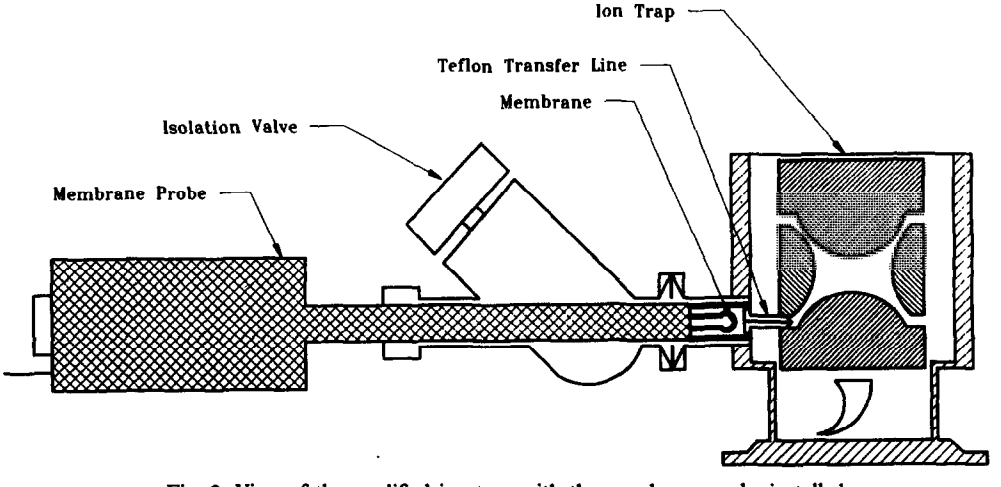

Fig. 2. View of the modified ion trap with the membrane probe installed.

peristaltic pump. Analyte solutions are injected into the mass spectrometer by simply switching the inlet line to the analyte solution. Note that the pump is located on the downstream side of the membrane probe and pulls water through the probe rather than pumping it through on the feed side. This was done as it was found that some compounds are adsorbed from solution by the tubing of the peristaltic pump itself. It was noted early in our experiments that more consistent results were obtained if the analyte stream did not pass through the pump on its way to the probe.[18]

Methods

Preliminary studies with the new membrane probe interface used a Dow Corning (Midland, MI) Medical Grade Silastic tubular membrane of 0.025 in. ID × 0.047 in. OD. The membrane was installed on the probe with approximately 1/2 in. exposed length. Instrument performance checks were made with aqueous solutions of three different organic compounds with different physical properties in order to assure that any results obtained were not compound specific. The analytes selected were benzene (860 pptr), THF (516 ppb), and *trans*-dichloroethene (8.8 ppb). Instrument parameters were varied to identify the optimum operating conditions, that is those where sensitivity was maximized and noise was minimized. The main factors explored systematically were:

1. Probe temperature.
2. Ion trap temperature.
3. Flow rate.
4. Scan rate.
5. Instrument tune parameters.

Trace analysis of several compounds was at- tempted using the optimized parameters identified in the performance studies. For the trace analysis work the following conditions were used: probe temperature 30°C, trap temperature 50°C, and solution flow rate 2 ml/min. The mass spectrometer was operated so as to scan a single diagnostic ion at 1 sec/scan, and helium buffer gas was introduced into the ion trap at a rate optimized during the tuning procedure. Most experiments were conducted by recording 600 scans, where the baseline was first recorded for 150 scans, the analyte solution was then injected for 250 scans to obtain a stable maximum signal, and the system was allowed to return to baseline conditions over the next 200 scans. We used single ion scans only to conserve disk space due to the large number of scans recorded per experiment. The large number of scans were required to cover the time period necessary for the analyte to reach its equilibrium flow rate through the membrane where the maximum response is obtained. Full spectra were obtained in later experiments to compare instrument performance. All analyte solutions were made up using reagent grade chemicals. Solutions were prepared in de-ionized water by weight and diluted to part per billion or part per trillion levels by serial dilutions. Duplicate tests were performed on separate days using freshly prepared solutions to verify the results. Tests of the probe interface were also done using a Finnigan solids probe operated at room temperature. Solid samples of acridine, phenanthridine, and 7,8-benzoquinoline were examined.

RESULTS AND DISCUSSION

Membrane probe performance

Initial tests were performed to identify optimum operating conditions for the analysis of aqueous solutions of organic analytes using the membrane probe. It was found that several operating parameters for the ion trap were quite different from those appropriate for membrane introduction into quadrupole instruments.[9] The main factors that affected performance in the analysis of aqueous organic analytes at low levels using the ITS40 are outlined below.

Probe temperature. The signal-to-noise ratio was found to be strongly dependent on the temperature of the analyte stream passing through the membrane probe. Temperature effects had been demonstrated previously on a triple quadrupole mass spectrometer,[5,8,18] where it was found that the analyte signal is enhanced at higher temperatures. Bier *et al.* demonstrated that as the temperature of the probe was raised more analyte passed through the membrane and signal was enhanced right up to a temperature of 100°C.[19] Surprisingly, in the case of the ion trap mass spectrometer, the temperature dependence is inverted. As the temperature was raised the signal-to-noise ratio decreased. Figure 3 shows how the signal-to-noise ratio depends on probe temperature over the range from 30 to 70°C. The experiment was done by monitoring the molecular ions of benzene, tetrahydrofuran (THF), and *trans*-dichloroethene (DCE) near the detection limits. All three compounds displayed substantial gains in S/N ratio at lower temperatures. As an illustration of the

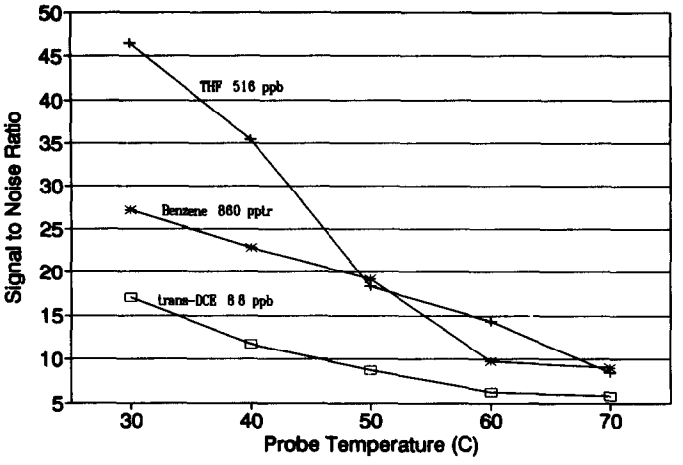

Fig. 3. Graph showing the signal-to-noise (S/N) for low level aqueous solutions as a function of probe temperature.

the raw data, Fig. 4 shows the ion current profiles recorded when monitoring m/z 78 from benzene at five temperatures. The inverse temperature dependence found for the ion trap spectrometer is due to the way the spectrometer handles ions compared to the quadrupole spectrometers. In the case of the quadrupole spectrometer, the ions pass immediately through the spectrometer and are pumped away as they are formed. A higher probe temperature increases the flow of analyte across the membrane and signal is enhanced. The increased flow of water that accompanies the analyte across the membrane is pumped away and does not interfere with the detection process. In the ion trap however, the ions are trapped as they are formed and a significant amount of the water that passes through the membrane with the analyte is also ionized and trapped. In this case the excess water at higher temperatures significantly interferes with detection of analyte ions as the instrument automatic gain control function decreases the ionization time to maintain a constant ion population. The high water ion concentration would otherwise result in space charging conditions with loss in sensitivity and resolution. Not only the rate of water passage but the rate of analyte diffusion through the membrane depends strongly on the probe temperature. Figure 5 displays this effect by plotting the time required to achieve maximum signal *vs.* probe temperature. Benzene and *trans*-dichloro- ethene diffusion rates are affected minimally as the time to maximum signal only differs by approximately 100 seconds between 30 and 70°C. THF on the other hand is affected dramatically. The time to reach maximum signal for THF at 30°C was 625 sec compared to 165 sec at 70°C. The result of this was the need for an extraordinarily long analysis time for the THF solution at 30°C, the temperature one would prefer to use in order to minimize contributions from water. Figure 6 shows the ion current profile for the response of the molecular ion of THF at temperatures between 30 and 70°C. All the ion current profiles in Fig. 6 are on the same time scale and the analysis of THF at 30°C requires nearly 30 min compared to less than 10 min at 70°C. Analysis-can be done by establishing a stable baseline, injecting the analyte until the maximum signal

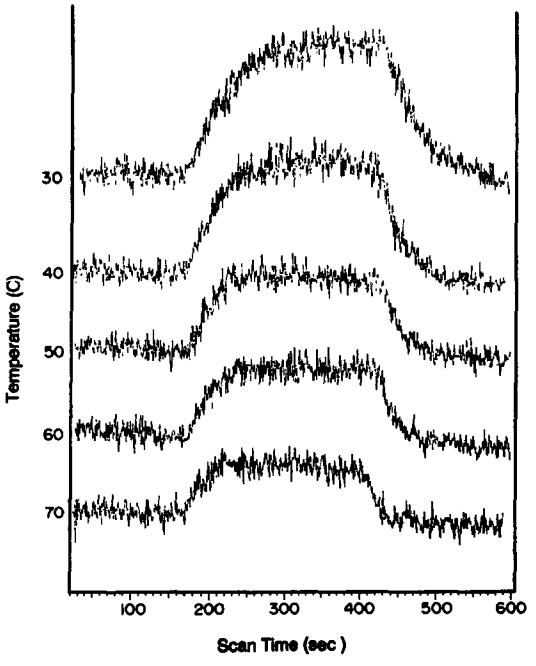

Fig. 4. Ion current profiles for m/z 78 for a 860 ppt benzene solution at probe temperatures of 30–70°C.

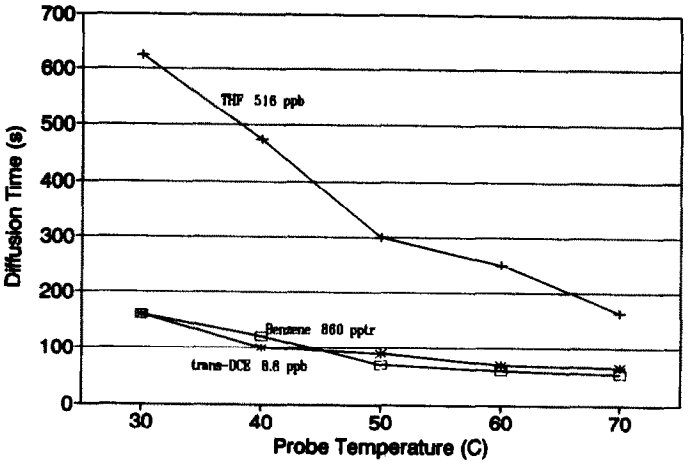

Fig. 5. Dependence of the analyte diffusion rate through the membrane on the probe temperature.

is reached and then examining the return to baseline conditions after the analyte solution is replaced by water. The minimum detection limits are estalished in this way. Using flow injection, analytes can also be quantitated without reaching the maximum response but concentrations must then be higher to obtain a measurable baseline deflection that can be compared to a standard. Clearly the type of compound analyzed must be considered when selecting the probe temperature and a balance must be struck between the desire to reach the lowest detection limits and the need for rapid quantitative analysis.

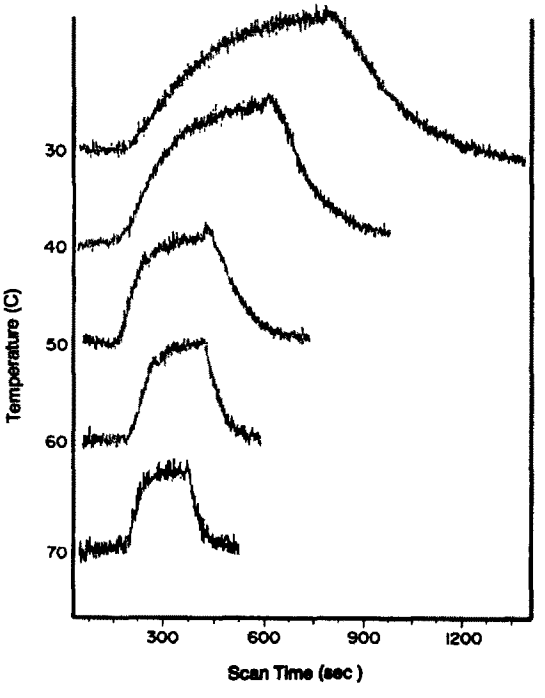

Fig. 6. Ion current profiles for m/z 82 for 516 ppb THF solution showing the time required to reach maximum signal at temperatures ranging from 30 to 70°C.

Ion trap temperature. In addition to the effects of probe temperature, the signal-to-noise depends on the ion trap temperature. Again the best signal-to-noise ratio was obtained at lower temperatures. Figure 7 plots the measured signal to noise ratios *vs.* ion trap temperature for the three test solutions 516 ppb THF, 860 pptr benzene, and 8.8 ppb *trans*-dichloroethene. All three compounds showed an increase in signal-to-noise ratio at lower temperatures. The S/N gains associated with changes in the temperature of the ion trap are not as dramatic as those associated with probe temperature but are significant and probably arise from the same cause. For the trace analysis studies reported in this paper, we chose a trap temperature of 50°C. This seemed to be a good low temperature where we could take advantage of the S/N enhancement without totally sacrificing the advantage of higher temperatures in desorbing contaminants that collect on the inner surfaces during routing use.

Analyte flow rate. The flow rate of the analyte solution through the membrane probe has an impact on the ability to detect analytes at very low concentrations. High flow rates deliver a higher number of analyte molecules to the inner surface of the membrane per unit time and signal is enhanced. Figure 8 shows how the S/N ratio changes with flow rate for a 500 pptr solution of chlorobenzene. The ratio is maximized at 3 ml/min. The flow rate enhancement undoubtedly depends on the nature of the analyte molecule and therefore will differ somewhat for different classes of molecules. We chose a standard flow rate of 2 ml/min for the trace analysis work as

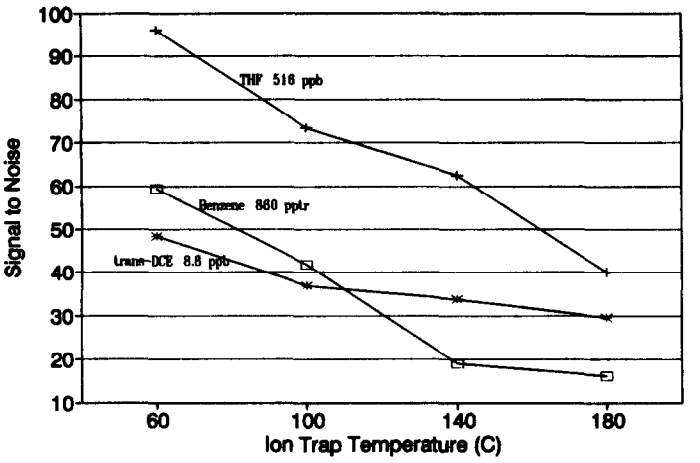

Fig. 7. The effect of ion trap temperature on the S/N ratio for the molecular ions of benzene, dichloroethene (DCE), and tetrahydrofuran (THF) at low levels in water.

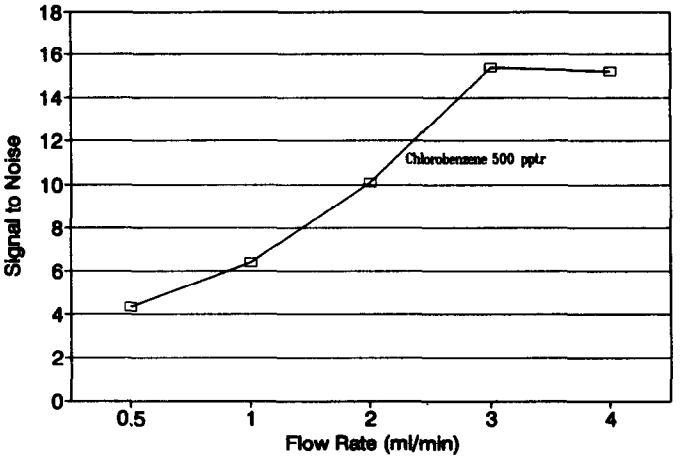

Fig. 8. The effect of analyte flow rate on S/N ratio for chlorobenzene (500 pptr in water).

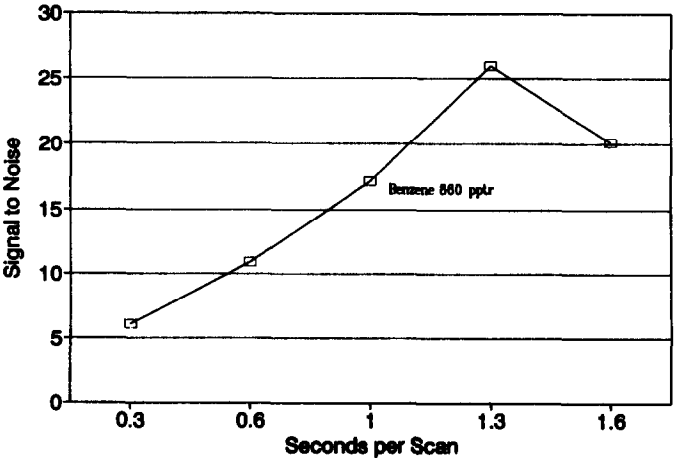

Fig. 9. The effect of scan speed on the S/N ratio for the molecular ion of benzene (860 pptr in water).

this seemed to provide good results for a wide range of organic analytes.

Scan speed. It was found that a mass spectrum scan rate such that a single ion scan at a rate of 1.3 sec per scan produced the most stable baseline. Figure 9 displays the effects of scan speed *vs.* signal-to-noise ratio for single ion monitoring of m/z 78 from a 860 pptr aqueous benzene sample.

Instrument tune factors. It was found that the instrument auto-tune set up conditions were not suitable for MIMS work and manual tuning had to be performed to optimize the results. Some of the manual tune factors changed slightly from day to day as would be expected under normal running conditions to achieve suitable peak shapes and mass assignments, but others were constant from day to day. Among these were segment RF settings which had to be set to 250 for all four segments with automatic gain control (AGC) in operation so that masses below 40 amu were continually swept from the trap. This eliminated much but not all of the very large ion load imposed on the trap by the presence of water which passes through the membrane continually. Other tune criteria, such as AGC prescan factors, AGC target values, and multiplier voltage, were set daily according to the needs of the experiment being run. These factors were optimized to provide maximum signal strength without inducing space charge effects in the trap. It was found that the best conditions were obtained in the shortest period of time if the instrument was tuned to FC-43 with the helium buffer gas on and the probe inserted in the instrument with deionized water running through it at the desired temperature.

Trace analysis of organic compounds in aqueous solution

Using the optimum conditions identified in the performance studies, we analyzed five organic analytes in aqueous solution in the parts per trillion range. Table 1 lists the analytes and their associated detection limits. The detection limits are based on a signal-to-noise ratio of three at maximum signal for the ion current obtained for the diagnostic ion of the analyte. The table also shows the practical quantitation limits (PQL) according to the EPA ground water monitoring list.[20] PQLs are the lowest concentrations of analytes in ground waters that can be reliably determined within specified limits of precision and accuracy by standard methods under routine laboratory operating conditions. Using these values as a guide, seven of the eight compounds tested were detected below the PQL. While the PQL provides a low limit goal that one may

Table 1. Detection limits for aqueous solutions obtained using the modified ITS40 MIMS system

Analyte	Detection limit (ppb)	EPA PQL (ppb)
Benzene	0.21	2
Trichlorofluoromethane	0.60	10
Chlorobenzene	0.16	2
trans-Dichloroetheane	0.81	1
Chloroform	0.58	0.5
cis-1,3-Dichloropropene	0.60	20
Hexachloroethane	0.28	0.5
Carbon tetrachloride	0.60	1

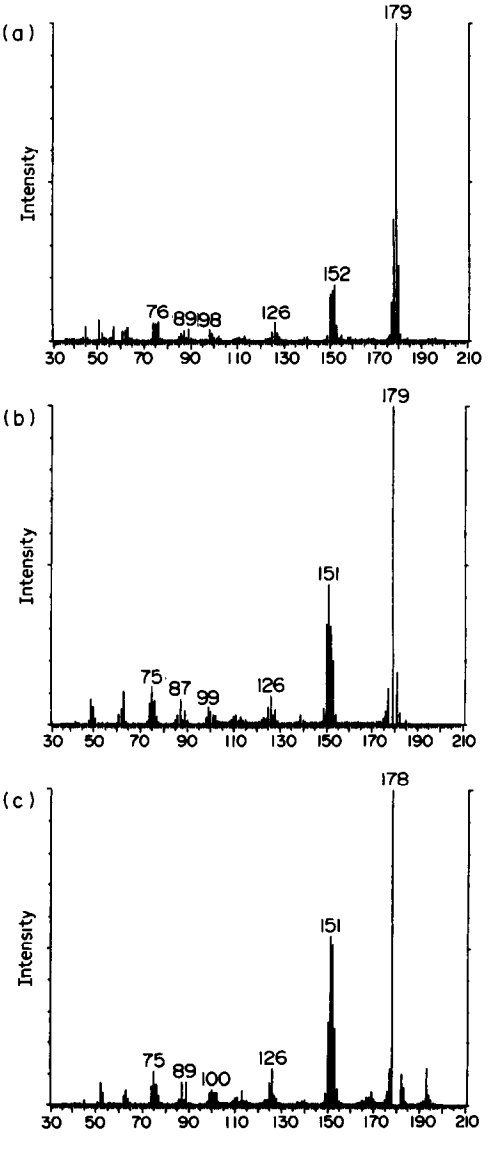

Fig. 10. Mass spectra obtained in the solids probe experiments using (a) phenanthridine, (b) 7,8-benzoquinoline and (c) acridine.

want to equal or exceed in experimental studies with new analytical methods, a more realistic question is whether or not a new method is applicable to routine daily analysis. The focus of routine work in a water quality laboratory is in assurance that the water sample being tested is free of contaminants above the maximum contamination level (MCL). The MCL in many cases is a regulatory limit that is often orders of magnitude greater than the PQL. Clearly this MIMS instrument has the ability to act as a very effective screening system for environmental or industrial applications.

Solids probe experiments

The modified inlet system was tested for its applicability to the analysis of solid samples using a standard solids probe. The experiment examined the fragmentation pathways of three isomeric compounds phenanthridine, acridine, and 7,8-benzoquinoline. The probe was operated at room temperature which provided a rate of sample vaporization which was large enough to necessitate lowering of the AGC target value to 1000 in order to avoid resolution losses due to trap overload. The system was therefore surprisingly sensitive in solid sample analysis. Figure 10 displays the mass spectra for the three compounds. The results of this experiment indicate that this inlet system may be used very effectively as a solid sample analysis system. The solids probe could be heated if necessary using the same temperature control system we use for the membrane probe as the heating and control circuits in the membrane probe were designed to match those of the standard Finnigan solids probe.

CONCLUSION

The experiments done here indicate that a simple quadrupole ion trap, after a few relatively simple modifications, can be used very effectively as a membrane introduction mass spectrometer. The instrument is also useful for analysis of solid samples and the modifications do not affect the original utility as a gas chromatograph/mass spectrometer. Remarkably good performance, including detection limits below 1 ppb, is achieved in the analysis of trace organic pollutants in water. The performance tests indicate that the operating conditions must be selected carefully to optimize analysis time and detection limits according to the type of compounds tested.

An instrument such as this could be used for rapid low-level screening of water samples by membrane introduction mass spectrometry. The size and weight of the instrument make *in situ* analysis a distinct possibility. One limitation in the dissemination of techniques based on MIMS is the need for new EPA standard methods which use this technology. The advent of new membrane materials that are more selective toward specific classes of compounds should improve performance further. Tests are underway in this laboratory to identify other useful membrane materials and to expand the list of compounds that can be analyzed at detection limits comparable with those achieved by existing purge and trap and other EPA methods.

Acknowledgements—This work was supported by the US Environmental Protection Agency (EPA CR815747) and by BP America through the Chemistry Department's Industrial Associates Program. Weldon Vaughan is thanked for skilful technical assistance.

REFERENCES

1. T. Kotiaho, F. R. Lauritsen, T. K. Choudhury, R. G. Cooks and G. G. Tsao, *Anal. Chem.*, 1991, **63**, 875A.
2. *Guidelines Establishing Test Procedures for the Analysis of Polutants*, CFR 40, Part 136, Appendix A, 1991, p. 312.
3. L. B. Westover, J. C., Tou and J. H. Mark, *Anal. Chem.*, 1974, **46**, 568.
4. D. Wenhu, C. Kuangnan, L. Jianli and D. Zhenying, *Mass Spectrosc. (Tokyo)*, 1987 **35**, 122.
5. B. J. Hartland, P. J. D. Nicholson and E. Gillings, *Wat. Res.*, 1987, **21**, 107.
6. M. LaPack, J. C. Tou and C. Enke, *Anal. Chem.*, 1990 **62**, 1265.
7. J. S. Brodbelt and R. G. Cooks, *Anal Chem.*, 1985, **57**, 1153.
8. A. K. Lister, K. V. Wood, K. Noon and R. G. Cooks, *Biomed. Environ. Mass Spectom.*, 1989, **18**, 1063.
9. M. E. Bier, T. Kotiaho and R. G. Cooks, *Anal. Chim. Acta*, 1990, **231**, 175.
10. L. E. Slivon, M. R. Bauer, J. S. Ho and W. L. Budde, *Anal. Chem.*, 1991, **63**, 1335.
11. F. R. Lauritsen, T. K. Choudhury, L. E. Dejarme and R. G. Cooks, *Anal. Chim. Acta*, in press.
12. W. J. Schmidt, H.-D. Meyer, K. Schugerl, W. Khulman and K.-H. Belgardt, *Anal. Chim. Acta*, 1984, **163**, 101.
13. M. J. Hayward, T. Kotiaho, A. K. Lister, R. G. Cooks, G. D. Austin, R. Narayan and G. T. Tsao, *Anal. Chem.*, 1990 **62**, 1798.
14. T. Kotiaho, M. J. Hayward and R. G. Cooks, *Anal. Chem.*, 1991, **63**, 1974.
15. D. Favretto, P. Traldi, C. A. Benassi and A. Bettero, *Biol. Mass Spectrom.*, 1991, **20**, 669.
16. A. Sturaro, L. Doretti, G. Parvoli, F. Lecchinato, G. Frison and P. Traldi, *Biomed. Environ. Mass Spectrom.*, 1989, **18**, 707.
17. S. J. Bauer, Masters Thesis, Aug. 1992, Purdue Univ.
18. S. J. Bauer, M. J. Hayward, D. E. Riederer, T. Kotiaho, R. G. Cooks and G. D. Austin, Unpublished results.
19. M. E. Bier and R. G. Cooks, *Anal. Chem.*, 1987, **59**, 597.
20. *Standards for Owners and Operators of Waste Treatment, Storage and Disposal Facilities*, CFR 40, Part 264, Appendix IX, 1991, p. 149.

Talanta, Vol. 40, No. 7, pp. 1041–1047, 1993
Printed in Great Britain.

0039-9140/93 $6.00 + 0.00

STUDY ON CATALYTIC FLUORIMETRIC DETERMINATION OF TRACE MANGANESE

GUIEN ZHANG, DING XI CHENG and SULING FENG
Department of Chemistry, Henan Normal University, Henan XiXiang 453002, People's Republic of China

(*Received* 14 *September* 1992. *Accepted* 14 *November* 1992)

Summary—A new kinetic fluorimetric method has been proposed for the determination of trace manganese. The method is based on the catalytic oxidation of rhodamine 6G with potassium periodate in the presence of nitrilo triacetic acid as activator, in near neutral media. The detection limit for manganese is 0.018 ng/ml. The linear range of the determination is 0.04–1.00 ng/ml. The proposed method suffers from few interferences in the presence of more than 30 foreign ions. The method has been used to determine trace manganese in hair, urine, fish and water samples. The results are satisfactory.

INTRODUCTION

There have been reports on the determination of manganese by catalytic fluorimetric photometry [1–7], mainly based on the catalytic fluorimetric reaction with alkaline, hydrogen peroxide or dissolved oxygen as oxidants, but the sensitivity has been unsatisfactory. Some reports on catalytic fluorimetry with potassium periodate as oxidizing agent in acid medium, list higher sensitivity, but interference is more serious. So far there has been no report on the determination of manganese by catalytic fluorometry using rhodamine 6G in a neutral medium.

In our experiments, we use nitrilo triacetic acid as activator in near neutral medium, and manganese catalyzes potassium periodate oxidation of rhodamine 6G to produce fluorescence. On the basis of this, a detailed study of appropriate conditions for the indicated reaction was conducted, and the best reagent doses were determined according to the controlled and weighed centroile simplex method. We measured fluorescence at a fixed time and found a new way to determine manganese content with high sensitivity and high selectivity, the detection limit being 1.8×10^{-2} ng/ml and the linear range 0.04–1.00 ng/ml. Generally, common ions did not interfere with the determination. Satisfactory results have been achieved in the determination of the manganese content in biological specimens, human hair and urine, fish and water samples.

EXPERIMENTAL

Reagents and instruments

Standard manganese solution: dissolve 0.3904 g manganese sulfate monohydrate in water and dilute to 100 ml. The solution contains 1.006 mg/ml manganese and should be properly diluted as required before use.

Potassium dihydrogen phosphate-sodium hydroxide buffer solution, pH 6.8. Dissolve 1.36 g potassium dihydrogen-phosphate in 150 ml water, then use 0.2*M* sodium hydroxide solution to adjust the pH to 6.8 and dilute with water to 200 ml.

Nitrilo triacetic acid (NTA) solution: $5.0 \times 10^{-3}M$;
Rhodamine 6G solution: $1.0 \times 10^{-4}M$;
Potassium periodate solution: $5.0 \times 10^{-4}M$;
Mixed solution of three acids: (HNO_3:H_2SO_4:$HClO_4$ = 10:1:4);
RF-540 fluorophotometer;
Model 930 fluorophotometer;
Model 501 super constant temperature meter;
PH S-2 acidimeter.

All the reagents for the experiment were analytical reagent grade or guaranteed, and redistilled water was used to prepare solutions.

Procedure

Add 2.70 ml of pH 6.8 buffer solution, 2.35 ml of $5.0 \times 10^{-3}M$ nitrilo triacetic acid and

0.32 ml of $1.0 \times 10^{-4}M$ rhodamine 6G to a 25 ml measuring flask, add water up to 20 ml, and shake well. Then add 2.85 ml of $5.0 \times 10^{-4}M$ potassium periodate and the proper amount of standard manganese solution into the flask, dilute up to the mark before shaking, and heat in a thermostatted water bath (70 ± 0.2°C) for 10 min. Then cool the solution to room temperature with flowing water for 3 min, and determine its fluorescence value F with a fluorimeter, with an excitation wavelength of 348.4 nm and an emission wavelength of 548.3 nm.

RESULTS AND DISCUSSION

Rhodamine 6G is a triphenylmenthane dye and emits very strong yellow–green fluorescent light. When oxidized by such strong oxidizers as potassium periodate, its molecular structure is destroyed and the fluorescence disappears, but the reaction is very slow due to the difficulty of direct electron acceptance and the effect of steric hindrance. When trace manganese exists in the system, the reaction speeds up, illustrating that manganese catalyzes the reaction of potassium periodate with Rhodamine 6G. When activator nitrilo triacetic acid exists, the reaction accelerates very quickly, as shown in Fig. 1. On the basis of this, we have further studied the experimental conditions for the determination of trace manganese.

[Mn(II)] = 10.06 ng/ml
1–1′: Rh 6G aqueous solution;
2–2′: KH_2PO_4–NaOH, Rh 6G;
3–3′: KH_2PO_4–NaOH, NTA, Rh 6G;
4–4′: KH_2PO_4–NaOH, NTA, KIO_4, Mn(II);
5–5′: KH_2PO_4–NaOH, Rh 6G, KIO_4;
6–6′: KH_2PO_4–NaOH, Rh 6G, KIO_4, MN(II);
7–7′: KH_2PO_4–NaOH, NTA, Rh 6G, KIO_4;
8–8′: KH_2PO_4–NaOH, NTA, Rh 6G, KIO_4 Mn(II).

Choice of the best experimental conditions (with manganese concentration being 0.40 ng/ml under all conditions)

Influence of the property and acidity of the buffer solution. Having compared the five buffer solutions of tartaric acid–sodium tartrate, acetic acid–sodium acetate, potassium hydrogen phthalate–hydrochloric acid, potassium hydrogen phthalate–sodium hydroxide, potassium dihydrogen phosphate–sodium hydroxide, we have found that among the buffer medium of tartaric acid–sodium tartrate, manganese can hardly catalyze the reaction of potassium periodate oxidization of rhodamine 6G, probably because the complexation of tartrate with manganese makes manganese lose its catalytic activity. Among the buffer medium of acetic acid–sodium acetate, the reagent blank fades quickly, *i.e.*, the background value of the uncatalyzed reaction is very high, which makes it hard to accurately determined the result of the experiment and is not fit for practical analysis. Potassium hydrogen phthalate–hydrochloric acid, potassium hydrogen phthalate–sodium hydroxide and potassium dihydrogen phosphate–sodium hydroxide have about the same property. The background values of their uncatalyzed reactions are very low and the

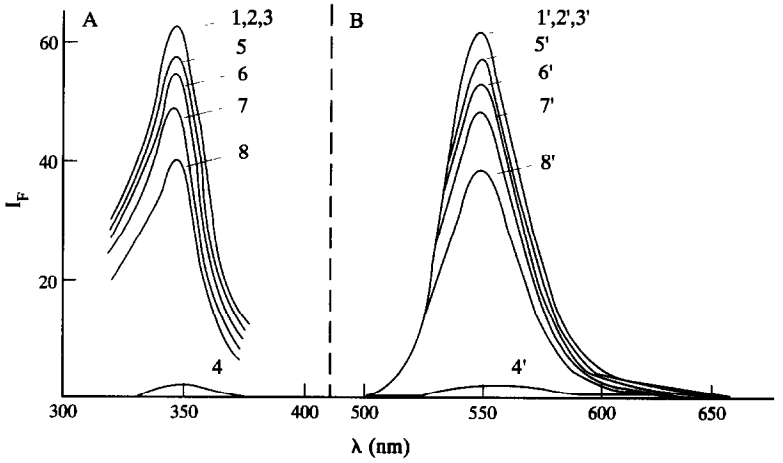

Fig. 1. Excitation and emission spectra of Rhodamine 6G in the presence of different reagents. Measurements made following heating for 10 min and cooling for 3 min.

Table 1. Simplex shifting process

Point number	Retention point	Simplex shifting mode	Simplex number	KH_2PO_4–NaHO *ml*	NTA *ml*	Rh6G *ml*	KIO_4 *ml*	ΔIF
1				3.10	3.10	0.38	3.10	15
2				1.90	3.10	0.38	3.10	11
3				2.50	1.90	0.38	3.10	16
4				2.50	2.50	0.22	3.10	15
5			1	2.50	2.50	0.30	1.90	17
6	5, 3, 4, 1, 2	reflection	2	3.35	1.90	0.26	2.60	12
6′	5, 3, 4, 1, 2	contraction	2′	3.00	2.20	0.29	2.72	17
7	5, 6′, 4, 3, 1	reflection	3	2.10	1.40	0.22	2.55	14
7′	5, 6′, 3, 4, 1	contraction	3′	2.84	2.68	0.34	2.96	16
8	5, 6′, 3, 7′, 4	reflection	4	2.94	2.16	0.42	4.0	12
8′	5, 6′, 3, 7′, 4	reflection	4′	2.61	2.42	0.27	2.42	18
9	8′, 5, 6′, 3, 7′		5	2.69	2.34	0.32	2.86	20

measurement sensitivity is high. With these solutions, a series of buffer solutions of different acidity with pH = 2.0–8.0, respectively, were prepared, and with their reagent blanks as references, experimental responses at different pH values were measured, and the results are shown in Fig. 2. From Fig. 2 it can be seen that when the heating time is fixed at 10 min, there are three plateaus appearing with increasing pH value on the ΔIF acidity curve, and the third plateau has the highest test sensitivity, with the relative pH value being 6.6–7.0 in the potassium dihydrogen phosphate–sodium hydroxide system. So potassium dihydrogen phosphate–sodium hydroxide buffer solution with pH = 6.8 is the best choice.

Choice of activator. The study of the influence of the 8 complexing agents—nitrilo triacetic acid, triethylenetetramine, triethanolamine, tetraethylenepentamine, EDTA, 8-hydroxyquiroline, thiourea, and phenanthroline upon the catalytic system shows that only nitrilo triacetic acid and phenanthroline can serve as activators and nitrilo triacetic acid does better and brings about better results. It is our best choice for activating agent.

Choice of the best dose of different reagents by controlled and weighted centroid simplex method. On the basis of conditional experiment 1 and 2, we experimented with the proper dose of buffer solutions, nitrilo triacetic acid, rhodamine 6G and potassium periodate, and determined the scope of their dose before choosing the best dose by controlled and weighted centroid simplex method. Simplex shifting was conducted 12 times, as shown in Table 1.

When simplex shifting reached 8′, it would meet the expected requirement, the relative deviation of the experiment response value of the five retention points was $R = 4.6\% < 5\%$, and the process stopped, with 9 being centroid of the five retention points.

Influence of reaction temperature. The system is very sensitive to the temperature change. Low temperature results in very slow catalyzed and uncatalyzed reactions. With the temperature increasing, the catalyzed reaction speeds up and ΔIF value increases with the rise of temperature from 45°C to 70°C. When the temperature is higher than 70°C, the uncatalyzed reaction speeds up as well, and is even faster than catalyzed reaction. ΔIF value drops more than at 70°C and analytical sensitivity decreases. For the results see Fig. 3. So the reaction temperature was fixed at 70°C and a model 501 super constant temperature meter was used to control temperature.

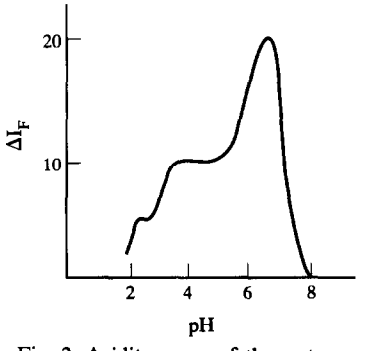

Fig. 2. Acidity curve of the system.

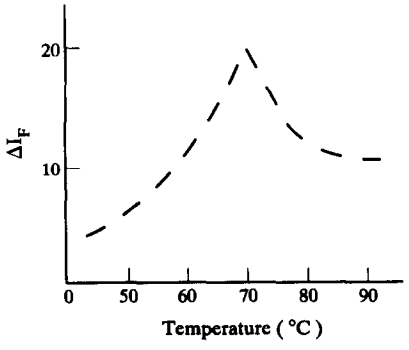

Fig. 3. Influence of temperature upon fluorescence intensity.

Influence of reaction time. After the study of influence of reaction time upon fluorescence intensity (with relevant reagent blank as reference), as shown in Fig. 4, it can be seen that between 2 and 12 min ΔIF–t is of linear relation and 10 min is taken as the reaction time.

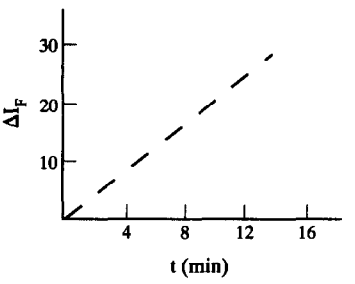

Fig. 4. ΔIF-Reaction time curve of the system.

Relation between manganese and IF

According to the described experiment method, we determined the value of fluorescence intensity IF (with manganese concentration being 0.04–1.20 ng/ml) and found the calibration graph, as shown in Fig. 5. It can be seen that within the scope of 0.04–1.0 ng/ml, IF value and manganese concentration suggest a linear relation, with the linear regression equation being $IF = 100.03 - 49.07x$ and correlation coefficient $r = 0.9999$.

Coexistence ions' interference

Under the chosen experiment condition, an interference experiment was conducted on more than 30 common ions. When the permitted relative deviation from the IF value is $\pm 5\%$, the interference is as listed in Table 2.

Sensitivity and accuracy of the method

Eleven parallel experiments were made on the following test solutions. The results are as follows:

IF value of reagent blank test: 99.6, 99.3, 100.0, 99.3, 100.4, 99.8, 100.3, 100.5, 100.0, 100.4, 99.7, standard deviation SD = 0.29, detection limit: 0.018 ng/ml.

Measured IF value of 0.40 ng/ml manganese: 80.6, 80.3, 80.2, 79.5, 80.6, 80.5, 81.0, 80.2, 80.8, 80.1, 79.9, standard deviation: 0.43, of coefficient of variation 2.2%.

Measured IF value of 0.80 ng/ml manganese: 62.3, 60.9, 61.0, 60.6, 61.2, 60.8, 60.0, 60.3, 60.1, 60.2, 61.4, standard deviation: 0.67, coefficient of variation: 1.7%.

Sample analysis

Determination of trace manganese in human hair. Get some hair cut from hind-brain scalp, have it soaked in 3% "White Cat" Brand detergent for 30 minutes, well stirred, washed clean in deionized water, baked dry under infrared lamp, and cut it into 0.5–1 cm segments with stainless steel blade. Take 0.3 g of this sample, put it into a 50 ml dry beaker before adding 5.0 ml mixed acid (HNO_3:$HClO_4$ = 3:5), cover it with a surface dish, put the beaker in a vent cabinet and keep it there overnight, then have it resolved for 40 minutes at a low temperature the next day. Remove the surface dish and heat it until almost dry at a low temperature (to get rid of the excess mixed acid), shift it into a 50 ml measuring flask, have it water-diluted to the mark (at this time the solution becomes transparent). At the same time a blank test is conducted. Take 0.50–1.00 ml aliquots of this sample solution into a 25 ml measuring flask and have the solution adjusted into neutral solution with 0.02M sodium hydroxide solution, determine the IF value using the experiment method. Ascertain the Mn(II) content from the calibration graph accordingly. After subtracting the reagent blank, convert it into manganese content in the sample and do recovery test for the results (see Tables 3 and 4).

Determination of trace manganese in human urine. Get 25.00 ml morning urine, have it digested, shifted into a 25 ml measuring flask, and water-diluted to the mark. Then get 2.5 ml and put it into another 25 ml measuring flask, have it adjusted to the neutral with 0.2M sodium hydroxide solution, determine the fluorescence intensity IF value using the experiment method, at the same time conduct a blank test, deduct the blank value, work out manganese content in the urine sample and do addition recovery test. The result is shown in Tables 5 and 6.

Determination of manganese content in skinned fish. Get 50 g skinned fish baked for

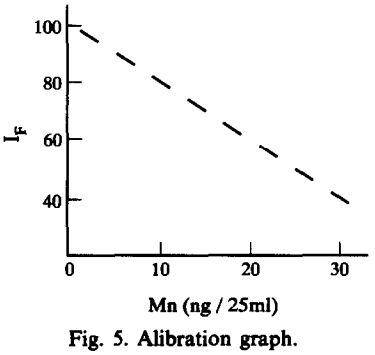

Fig. 5. Alibration graph.

Table 2. The influence of coexistence ions. $[Mn^{2+}] = 10.06$ ng/25 ml (0.4 ng/ml)

Coexistence ions	Addition form	Concentration of coexistence ions	Ratio [ion]/[Mn^{2+}]	IF value change, %
K^+	KCl	1.68 *mg/ml*	4.2×10^6	6.0
Cl^-	KCl	1.52 *mg/ml*	3.8×10^6	6.0
Na^+	NaF	0.88 *mg/ml*	2.2×10^6	4.2
F^-	NaF	0.72 *mg/ml*	1.8×10^6	4.2
Ni^{2+}	$NiSO_4$	4.32 *μg/ml*	1.08×10^4	−4.8
W(VI)	Na_2WO_4	10.24 *μg/ml*	2.56×10^4	−6.0
Mo(VI)	$(NH_4)_2MoO_4$	0.48 *μg/ml*	1.2×10^3	−5.4
Co^{2+}	$Co(NO_3)_2$	20.6 *ng/ml*	51.5	−3.6
Cu^{2+}	$CuSO_4$	0.48 *μg/ml*	1.2×10^3	−4.5
BrO_3^-	$NaBrO_3$	1.28 *mg/ml*	3.2×10^6	6.6
ClO_3^-	$KClO_3$	27.28 *μg/μl*	6.82×10^4	4.6
NO_3^-	KNO_3	6.14 *mg/ml*	1.54×10^7	−6.0
SO_4^{2-}	K_2SO_4	1.10 *mg/ml*	2.75×10^6	6.6
Br^-	KBr	13.45 *μg/ml*	3.36×10^4	−5.1
NO_2^-	$NaNO_2$	4.32 *ng/ml*	10.8	−4.2
Se	metal Se (HNO_3 dissolution)	40.4 *ng/ml*	1.01×10^2	4.8
Cr^{3+}	$Cr_2(SO_4)_3$	2.24 *ng/ml*	5.6	6.0
Cr(VI)	K_2CrO_4	8.24 *ng/ml*	20.6	3.0
Ag^+	$AgNO_3$	4.2 *ng/ml*	10.5	−4.8
Bi^{3+}	metal Bi (HNO_3 dissolution)	3.66 *ng/ml*	9.2	−6.0
Zr(IV)	Acylzirconium chloride	0.33 *μg/ml*	8.3×10^2	−5.4
Fe^{3+}	$NH_4Fe(SO_4)_2$	64 *ng/ml*	1.6×10^2	5.4
Zn^{2+}	metal Zn (HCl dissolution)	0.90 *μg/ml*	2.2×10^{-3}	−6.0
Cd^{2+}	metal Cd (HCl dissolution)	7.22 *μg/ml*	1.8×10^4	5.4
Pb^{2+}	$Pb(NO_3)_2$	0.84 *μg/ml*	2.1×10^3	−4.8
Sb(III)	metal Sb (H_2SO_4 dissolution)	15.7 *ng/ml*	39	−6.0
As(III)	As_2O_3 (10% NaOH dissolution)	5.46 *μg/ml*	1.4×10^4	−4.8
Ge^{4+}	metal Ge (H_2O_2 dissolution)	8.00 *ng/ml*	20	4.2
Si^{+4}	SiO_2 (unhydrated sodium carbonate high temperature dissolution)	0.38 *μg/ml*	9.5×10^2	−5.0
I^-	KI	1.53 *μg/ml*	3.8×10^3	−4.6
Hg^{2+}	$Hg(NO_3)_2$	0.8 *μg/ml*	2.0×10^3	4.8
$C_2O_4^{2-}$	$Na_2C_2O_4$	0.33 *mg/ml*	8.2×10^5	4.5
Mg^{2+}	$MgSO_4$	3.2 *μg/ml*	8.0×10^3	5.1
ClO_4^-	$KClO_4$	29 *μg/ml*	7.2×10^4	−4.8
Ca^{2+}	$CaCO_3$ (HCl dissolution)	1.00 *μg/ml*	2.5×10^3	−6.6
Sn^{+4}	metal Sn (HCl dissolution)	0.11 *μg/ml*	2.8×10^2	−4.8
V(v)	NH_4VO_3	3.4 *μg/ml*	8.5×10^3	−6.0

24 hours at 105°C, then ground into powder. Get 2.00 g and put it into a 250 ml Erlenmeyer flask, add 20 ml concentrated HNO_3 and 3–4 glass beads, cover the flask with a short neck funnel. When the digestion reaction slows, put the Erlenmeyer flask into the vent cabinet and

Table 3. Measured results of trace manganese content in human hair

Hair sample	Sample weight	Sample amount *ml*	Manganese content worked out with regression equation *ng/25 ml*			Measured value of manganese content (*μg/g*)			Average value	RSD %
I	0.3006	1.00	18.88	17.85	18.35	3.14	2.97	3.05	2.97	4.0
	0.2989	1.00	17.32	17.60	16.80	2.90	2.94	2.81		
II	0.2268	1.00	7.65	7.40	8.18	1.69	1.63	1.80	1.78	5.8
	0.2468	1.00	9.18	8.68	9.45	1.86	1.76	1.91		
III	0.2944	0.50	12.75	12.25	13.25	4.33	4.16	4.50	4.32	3.9
	0.2484	0.50	10.72	11.22	10.20	4.32	4.52	4.11		

Table 4. Recovery test on human hair sample

Hair sample	Sample weight g	Sample amount ml	Manganese content in the sample ng/25 ml	Added manganese amount ng/25 ml	Measured content ng/25 ml	Recovery %
I	0.3006	0.30	5.35	5.03	10.02	96.4
	0.2989	0.30	5.32	5.03	10.10	95.0
II	0.2268	0.50	4.02	5.03	9.18	102.6
	0.2468	0.50	4.40	5.03	9.70	105.4
III	0.2944	0.30	7.62	5.03	12.50	97.0
	0.2484	0.30	6.45	5.03	11.23	95.0

Table 5. Measured results of trace manganese content in human urine

Urine sample	Sample amount ml	Manganese content worked out with regression equation ng/25 ml			Measured value of manganese content μg/l			Average value	RSD %
I	2.50	6.22	5.98	5.98	2.49	2.39	2.39	2.42	3.4
	2.50	6.22	6.22	5.72	2.49	2.49	2.29		
II	2.50	5.25	5.48	5.25	2.10	2.19	2.10	2.13	4.6
	2.50	5.25	5.00	5.72	2.10	2.00	2.29		
III	2.50	3.72	4.00	3.48	1.49	1.60	1.39	1.49	6.3
	2.50	4.00	3.72	3.48	1.60	1.49	1.39		

let it stay overnight—for cold nitrification, then raise the temperature for high temperature nitrification. When solid granules are digested, take the flask out for cooling, then add 10 ml triple acid mixed nitrified solution for 2 hours at a low temperature digestion until a lot of white smog appears. This is followed by high temperature heating until digested liquid becomes colorless, transparent wet-salted state. After that, get it cooled, dissolved with hot distilled water and filtered into a 50 ml measuring flask, washed three times with hot distilled water until the filtrate is about 50 ml. Then have it diluted up to the mark with distilled water and well shaken for future use. For measurement, dilute the solution 10-fold (blank test is conducted at the same time).

Take 1.00 ml of the sample solution and empty it into a 25 ml measuring flask, adjust it to the neutral with 0.2*M* sodium hydroxide solution and determine its fluorescence intensity IF value using the experiment method. The result is shown in Table 7. Perform the standard addition-recovery test, for the result, see Table 8.

Determination of trace manganese in running water. Get 1.00 ml sample running water (two parallel portions), put it into a 25 ml measuring flask, determine the fluorescence intensity IF value using the experiment method and conduct addition-recovery experiment. The results are shown in Tables 9 and 10.

Table 6. Standard addition recovery experiment on human urine sample

Urine sample	Sample amount ml	Manganese content in the sample ng/25 ml	Added manganese amount ng/25 ml	Measured amount ng/25 ml	Recovery %
I	2.00	4.85	5.03	10.05	103.4
	2.00	4.85	5.03	10.00	102.4
II	2.50	5.32	5.03	10.20	97.0
	2.50	5.32	5.03	10.15	96.0
III	2.50	3.72	5.03	8.68	98.6
	2.50	3.72	5.03	8.33	91.7

Table 7. Measured result of manganese content in skinned fish

Sample weight g	Sample volume ml	Measured manganese content ng/25 ml			Measured value of manganese content in sample fish (ppm)			Average value
2.0019	1.00	1.47	1.47	1.49	1.83	1.83	1.87	1.84

Table 8. Recovery of manganese in skinned fish

Sample weight *g*	Sample volume *ml*	Manganese content in the sample *ng/25 ml*	Added standard manganese amount *ng/25 ml*	Measured amount *ng/25 ml*	Recovery %
2.0019	0.5	7.40	5.03	12.26	96.6
2.0019	0.5	7.40	5.03	12.16	94.6

Table 9. Measured results of trace manganese in running water

Water sample	Sample amount *ml*	Measured manganese amount by regression equation *ng/25 ml*			Measured manganese content in the sample *μg/l*			Average value *μg/l*	RSD %
1	1.00	18.65	18.15	18.15	18.65	18.15	18.15	18.36	1.3
2	1.00	18.40	18.15	18.65	18.40	18.15	18.65		

Table 10. Standard addition-recovery experiment on the running water

Water sample	Sample amount *ml*	Manganese amount of the sample *ng/25 ml*	Added manganese amount *ng/25 ml*	Measured amount *ng/25 ml*	Recovery %
1	0.20	3.67	5.03	8.73	100.6
2	0.20	3.67	5.03	8.97	105.4

Study on kinetic character of the system

Determination of the reaction order. When choosing the best condition for the experiment, we drew Fig. 4 indicating the reaction system, from which it can be seen that when $t = 2$–12 min, ΔIF-t is of linear relation, and within this period the catalytic system can be regarded as pseudo-zero order reaction.

Determination of apparent activation energy of the catalyzed reaction. The determination of apparent activation energy of catalyzed reaction is mainly based on Arrhenius' equation:

$$K_{cat} = K_0 \exp(-E_{cat}/RT).$$

Here, K_{cat}, E_{cat} and K_0 stand for apparent rate constant, apparent activation energy and apparent frequency factor (determiner), respectively. Only when quantity is in direct proportion to the apparent rate constant (or reaction rate) can the above equation be used to determine apparent activation energy of the reaction.

The catalyzed reaction is pseudo-zero order reaction. The quantity in direct proportion to reaction rate is $\Delta IF(\Delta IF = IF_0 - IF_{cat})$. Therefore, there should be a straight line if $\ln \Delta IF$ is used to draw a graph for $1/T$ and from the slope $(-E_{cat}/R)$ of the straight line. The experiment rate and measured results are shown in Table 11.

Table 11. Determination of apparent activation energy

$T(K)$	$\frac{1}{T}(\times 10^3)$	ΔIF	$\ln \Delta$IF
318.15	3.14	4.0	1.39
323.15	3.09	5.4	1.69
328.15	3.05	8.0	2.08
333.15	3.00	10.6	2.36
338.15	2.96	14.6	2.68
343.15	2.91	19.9	2.99

By the data in Table 11, we can get the linear regression equation:

$$-\ln \Delta IF = 7063.6 \times \frac{1}{T} - 23.57,$$

regression coefficient $r = 0.9981$.

Hence, the apparent activation energy of this indicated reaction system:

$$E_{cat} = 7063.6 \times 8.314 \text{ J} \cdot \text{mol}^{-1}$$
$$= 58.73 \text{ KJ} \cdot \text{mol}^{-1}.$$

REFERENCES

1. A. Moreno, M. Silia, D. Perez-Bendito and M. Valcarcel, *Talanta*, 1983, **30**, 107.
2. A. Gomez-Hens and M. Valcarel, *Analyst*, 1984, **109**, 717.
3. A. Navas and F. Sanchez Roias, *Talanta*, 1984, **31**, 437.
4. J. Vazquez Ruiz, A. Garcia de Torres and J. M. Cano-Pavon, *Talanta*, 1984, **31**, 29.
5. A. Moreno, M. Silva and D. Perez-Bendito, *Anal. Chim. Acta*, 1984, **159**, 319.
6. D. Perez-Bendito, J. Peinado and F. Toribio, *Analyst*, 1984, **109**, 1297.
7. F.-J. Lopez Benet, F. Hernandez Hernandee, J. Medina Escriche and R. Marin Saez, *Analyst*, 1986, **111**, 1325.
8. Zhang Zhi qi, Xue Fenghe and Ge xiaodan, *FenXi HuaXue*, 1978, **17**, 753.
9. Zheng Zhao Sheng and Luo Tong, *FenXi HuaXue*, 1990, **18**, 1079.

Talanta, Vol. 40, No. 7, pp. 1049–1057, 1993
Printed in Great Britain.

0039-9140/93 $6.00 + 0.00

SOLVENT AND STERIC EFFECTS ON THE EXTRACTION OF COPPER(II) WITH PIVALIC ACID

HIROMICHI YAMADA* and CHIZUKO KATO†

*Department of Applied Chemistry, Nagoya Institute of Technology, Gokiso-cho, Showa-ku, Nagoya 466, Japan
†Faculty of Engineering, Gifu University, 1-1 Yanagido, Gifu 501-11, Japan

(*Received* 20 *August* 1992. *Revised* 18 *November* 1992. *Accepted* 21 *November* 1992)

Summary—The solvent extraction of copper(II) with trimethylacetic acid using benzene and 1-octanol as solvents was performed at 25°C and 0.1 mole . dm^{-3} ionic strength in the aqueous phase. In contrast to the extraction of copper(II) with a saturated straight-chain carboxylic acid in benzene, the dimeric copper(II) trimethylacetate was observed to dissociate into the monomer, even at a moderately high concentration of copper(II) in the benzene phase. In the system using 1-octanol as a solvent, both the monomeric and dimeric copper(II) species are suggested to be solvated by some 1-octanol molecules. It has been found that the dimerization and adduct formation of copper(II) species in benzene may more effectively enhance the extractability of copper(II) than the solvation by 1-octanol molecules.

In a series of investigations[1–7] on the extraction of copper(II) with various carboxylic acids, the extraction of copper(II) with aromatic carboxylic acids has been found to proceed through a stoichiometry different from that with aliphatic carboxylic acids, by which copper(II) is well known to be extracted into nonsolvating solvents as a dimeric species, $Cu_2A_4(HA)_2$. The presence of a conjugated system in aromatic carboxylic acids can be anticipated to give some negative influence on the formation of the dimeric copper(II) carboxylate, and to result in a lowering of the extractability of copper(II).[4] Further, the extraction of copper(II) with various monosubstituted benzoic acids has been proven to be appreciably influenced by the position and properties of the substituents.[5–7] Also in an aliphatic carboxylic acid, the conjugated system in the carboxylic acid has been reported to inhibit the formation of the dimeric copper(II) carboxylate in the extraction of copper(II) with 2,4-hexadienoic acid.[8] On the other hand, in the extraction systems using an aliphatic carboxylic acid, the difference in carbon-chain length has been revealed not to affect the formation of dimeric copper(II) carboxylate in benzene.[9] Moreover, it has been proven that the formation of dimeric copper(II) carboxylate in benzene is not prevented by the bromine at the α-position in the pentanoic acid.[10] But, in the solvent extraction systems with cyclohexanecarboxylic acid, the adjacent cyclohexane ring to carboxyl group was found to inhibit the formation of the dimeric copper(II) carboxylate, even in benzene.[11] This can be due to the steric hindrance of the cyclohexane group on the formation of the dimeric copper(II) cyclohexane carboxylate. In contrast to nonsolvating solvents such as benzene, the dimeric copper(II) carboxylates were observed to dissociate at a moderately high concentration of copper(II) carboxylate into the monomers in solvating solvents such as alcohols[12] and ketones.[13] This can be attributed to the more extensive solvation of the monomeric copper(II) carboxylate than the dimeric one in these solvating solvents. According to these results, the following three factors can be anticipated to inhibit the dimerization of the monomeric copper(II) carboxylate: (1) the presence of the conjugated system in a carboxylic acid, (2) the solvation of copper(II) carboxylate, and (3) the steric effects of a bulky substituent at the α-position in a carboxylic acid.

In the present paper we report on the extraction of copper(II) with trimethylacetic acid (pivalic acid) by using benzene or 1-octanol as the solvent in view of the steric hindrance and solvent effect on the dimerization of copper(II) pivalate. In the extraction of copper(II) carboxylate, the formation of the dimeric copper(II) species has been found to be more effective than the solvation of the copper(II) species for the enhancement of the extractability of copper(II).

*Author for correspondence.

EXPERIMENTAL

Reagents

Commercial pivalic acid (purity: over 99%) was dissolved in purified benzene and 1-octanol, respectively. Benzene, 1-octanol, and sodium perchlorate were purified by the same methods as employed previously.[8] All other reagents were of reagent grade and used without further purification.

Procedures

Partition was carried out at 5×10^{-5} mole . dm^{-3} initial concentration of copper(II) in the aqueous phase and 0.5–2.0 mole . dm^{-3} pivalic acid in the organic phase for both the systems using benzene and 1-octanol as solvents. Shaking for about 1 hr was performed in a bath thermostatted at 25.0 ± 0.2°C, and was found to be sufficient for complete equilibration. Ionic strength in the aqueous phase was adjusted to 0.1 mole . dm^{-3} by sodium perchlorate. Both the concentrations of copper(II) and hydrogen ions in the aqueous phase after complete equilibration were determined by the same methods as presented previously.[4] The dissociation constant of pivalic acid was potentiometrically determined to be $K_a = [H^+][A^-]/[HA] = 10^{-4.83}$ in the aqueous 0.1 mole . dm^{-3} perchlorate solution at 25°C. In the evaluation of the partition constant of pivalic acid between the aqueous phase and benzene, the concentration of pivalic acid in the aqueous phase was determined by potentiometric titration. While, for that between the aqueous phase and 1-octanol, it was determined by measuring the absorbance at 208 nm, the absorption maximum of the acid.

Apparatus

The apparatus for mechanical shaking in a thermostat, centrifugation, pH measurement, and spectrophotometric determination were the same as employed previously.[4]

RESULTS AND DISCUSSION

Partition of pivalic acid

In the extraction of metal ions with a carboxylic acid, it is important to have information about the partition behavior of the carboxylic acid. The partition ratio of a carboxylic acid between the organic and aqueous phases can be expressed as follows:

$$D = \frac{C_{HA,o}}{C_{HA,w}} = \frac{K_{D,HA} + 2K_{2,HA}K_{D,HA}^2[HA]}{1 + \dfrac{K_a}{[H^+]}}, \quad (1)$$

where K_a, $K_{2,HA}$, $K_{D,HA}$, and [HA] denote the dissociation constant in the aqueous phase, the dimerization constant in the organic phase, the partition constant between the organic and aqueous phases of the carboxylic acid, and the concentration of the monomeric acid in the aqueous phase, respectively. The partition of pivalic acid was carried out between benzene and 0.01 mole . dm^{-3} perchloric acid containing 0.09 mole . dm^{-3} sodium perchlorate which was added to keep the ionic strength in the aqueous phase 0.1 mole . dm^{-3}, and between 1-octanol and 0.1 mole . dm^{-3} perchloric acid, respectively. Under these aqueous conditions, the dissociation of the acid in the aqueous phase can be neglected. In the former case the concentration of pivalic acid in the aqueous phase after the equilibrium was determined titrimetrically with the standard sodium hydroxide. Then, the concentration of perchloric acid coexisted with pivalic acid in the aqueous phase is fixed at 0.01 mole . dm^{-3} in order to make it as low as possible. In this case the partition constant, $K_{D,HA}$ and the dimerization constant, $K_{2,HA}$ in the organic phase were determined by the least-squares method from the linear plots of D against [HA]. The values are summarized in Table 1 together with the other constants. The partition ratio of pivalic acid was constant and independent of the concentration of pivalic acid. And it has been found that the dimerization of pivalic acid in 1-octanol does not occur to any appreciable extent. The distribution ratio of pivalic acid is equal to the partition constant. The value is listed in Table 1.

Extraction of copper(II) with pivalic acid

If a *j*-merized copper(II) pivalate of the composition $Cu_jA_{2j}(HA)_a$ is extracted, the extraction equilibrium using benzene as a solvent can be written as follows:

Table 1. Partition and dimerization constants of pivalic acid and extraction constants of copper(II) pivalates (at 25°C)

Solvent	$\log K_{D,HA}$	$\log K_{2,HA}$	$\log K_{ex(10)}$	$\log K_{ex(11)}$	$\log K_{ex(20)}$	$\log K_{ex(21)}$	$\log K_{ex(22)}$
Benzene	0.02	2.16	−8.39	−7.93			−11.81
1-Octanol	1.42		−8.57	−9.35	−14.13	−14.65	

$$jCu^{2+} + \frac{(2j+a)}{2}(HA)_{2,o} \rightleftharpoons [Cu_jA_{2j}(HA)_a]_o + 2jH^+$$

with

$$K_{ex(ja)} = \frac{[Cu_jA_{2j}(HA)_a]_o[H^+]^{2j}}{[Cu^{2+}]^j[(HA)_2]_o^{(2j+a)/2}}, \quad (2)$$

where $(HA)_{2,o}$ denotes the dimeric pivalic acid in the organic phase, and the subscript "o" refers to the organic phase. Pivalic acid acts primarily as a dimer in benzene through hydrogen bonding.

On the other hand, the extraction equilibrium for 1-octanol can be expressed as follows:

$$iCu^{2+} + (2i + a')(HA)_o \rightleftharpoons [Cu_iA_{2i}(HA)_{a'}]_o + 2iH^+$$

with

$$K_{ex(ia')} = \frac{[Cu_iA_{2i}(HA)_{a'}]_o[H^+]^{2i}}{[Cu^{2+}]^i[HA]_o^{(2i+a')}}, \quad (3)$$

where $(HA)_o$ denotes the monomeric pivalic acid in 1-octanol. The formation of the dimeric pivalic acid in 1-octanol does not occur to any appreciable extent because of solvation of monomeric pivalic acid by 1-octanol molecules.

The concentration of copper(II) in the organic phase is expressed by the following equations, corresponding to equations (2) and (3), respectively.

Using benzene as a solvent,

$$C_{Cu,o} = \sum_j \sum_a jK_{ex(ja)}[Cu^{2+}]^j[(HA)_2]_o^{(2j+a)/2}[H^+]^{-2j}, \quad (4)$$

and using 1-octanol,

$$C_{Cu,o} = \sum_i \sum_{a'} iK_{ex(ia')}[Cu^{2+}]^i[HA]_o^{(2i+a')}[H^+]^{-2i}. \quad (5)$$

Determination of the degree of polymerization of copper(II) pivalates

According to the same plot as employed previously,[2] it was suggested that the monomeric and dimeric copper(II) pivalates are responsible for the extraction of copper(II) with pivalic acid both in benzene and 1-octanol. Then, the following expressions can be derived from equations (4) and (5): for benzene,

$$\log C_{Cu,o} - \log[Cu^{2+}] + 2\log[H^+] = \log K_{ex(1a)} + \frac{(2+a)}{2}\log[(HA)_2]_o + \log\left(1 + \frac{2K_{ex(2b)}}{K_{ex(1a)}}[(HA)_2]_o^{(2+b-a)/2} \times [Cu^{2+}][H^+]^{-2}\right) \quad (6)$$

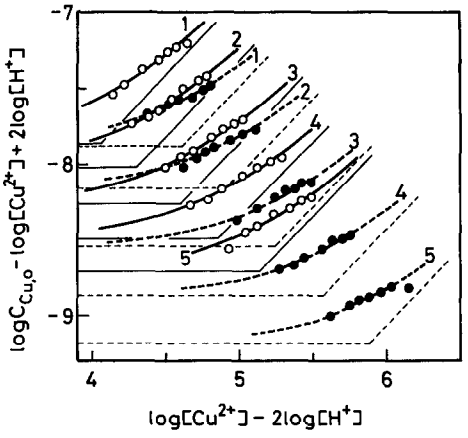

Fig. 1. Determination of the degree of polymerization of copper(II) pivalates. C_{HA}; (1) 2.0, (2) 1.5, (3) 1.0, (4) 0.7, and (5) 0.5 mole . dm^{-3}. Open and closed symbols refer to benzene and 1-octanol, respectively. Solid and dotted curves are the normalized ones, $\log(1+X)$ *vs.* $\log X$. Solid and dotted lines are the straight ones which are the asymptotes of the respective normalized curves.

and for 1-octanol,

$$\log C_{Cu,o} - \log[Cu^{2+}] + 2\log[H^+] = \log K_{ex(1a')} + (2+a')\log[HA]_o + \log\left(1 + \frac{2K_{ex(2b')}}{K_{ex(1a')}}[HA]_o^{(2+b'-a')} \times [Cu^{2+}][H^+]^{-2}\right), \quad (7)$$

respectively.

As described in the previous work,[2] by fitting the plots of $(\log C_{Cu,o} - \log[Cu^{2+}] + 2\log[H^+])$ against $(\log[Cu^{2+}] - 2\log[H^+])$ at constant $[(HA)_2]_o$ for benzene, and $[HA]_o$ for 1-octanol with the normalized curve, $\log(1+X)$ *vs.* $\log X$, it can be confirmed that both the monomeric and dimeric copper(II) species are extracted into both benzene and 1-octanol. The results are shown in Fig. 1. The plots fit well in the normalized curve in the range of the total concentration of pivalic acid from 2.0 to 0.5 mole . dm^{-3} under the extraction systems using either benzene or 1-octanol as a solvent. Therefore, the monomeric and dimeric copper(II) pivalates have been found to be responsible for both the extraction systems.

Determination of the number of pivalic acid molecules involved in the extracted species

In the region where the monomer prevails, the following relations for benzene and 1-octanol can be derived according to the similar manner described in the previous paper:[2]

$$\log C_{Cu,o} - \log[Cu^{2+}] + 2\log[H^+] = \log \sum_a K_{ex(1a)}[(HA)_2]_o^{(2+a)/2}, \quad (8)$$

for benzene, and

$$\log C_{Cu,o} - \log[Cu^{2+}] + 2\log[H^+] = \log \sum_{a'} K_{ex(1a')}[HA]_o^{(2+a')}, \quad (9)$$

for 1-octanol, respectively.

On the other hand, in the region where the main copper(II) species exist as the dimer, the following expressions can be obtained:

$$\log C_{Cu,o} - 2(\log[Cu^{2+}] - 2\log[H^+]) = \log 2 \sum_b K_{ex(2b)}[(HA)_2]_o^{(4+b)/2}, \quad (10)$$

for benzene, and

$$\log C_{Cu,o} - 2(\log[Cu^{2+}] - 2\log[H^+]) = \log 2 \sum_{b'} K_{ex(2b')}[HA]_o^{(4+b')}, \quad (11)$$

for 1-octanol. On the basis of equations (8)–(11), the number of pivalic acid molecules involved in the respective monomeric and dimeric copper(II) species can be estimated from the slope of the plots of $(\log C_{Cu,o} - \log[Cu^{2+}] + 2\log[H^+])$ *vs.* $\log[(HA)_2]_o$ for benzene and *vs.* $\log[HA]_o$ for 1-octanol, and $\log C_{Cu,o} - 2(\log[Cu^{2+}] - 2\log[H^+])$ *vs.* $\log[(HA)_2]_o$ for benzene, and *vs.* $\log[HA]_o$ for 1-octanol, respectively. The results for benzene are shown in Fig. 2. The plots for the dimer fell on the straight line with a slope of 3.0. It has been found that the dimeric species is $Cu_2A_4(HA)_2$. For the monomer the slope of the plots should be 1.0 or 1.5 or 2.0 in the presence of only one type of the monomeric species, since the value of a in equation (8) must be an integer. It is shown in Fig. 2 that the slope of the plots lies between 1.0 and 1.5. This suggests that at least two kinds of the monomeric species are extracted into the benzene phase and one of them is certainly CuA_2. While the results for the extraction using 1-octanol as a solvent are shown in Fig. 3. The plots for both the monomeric and dimeric species fall on the straight lines with slopes of 2.0 and 4.0, respectively, at lower concentration of pivalic acid in the organic phase, but deviate just a little upward from the respective straight lines with increasing $[HA]_o$. Then it has been found that two kinds of both the monomeric and dimeric copper(II) species are at least responsible for the extraction using 1-octanol as a solvent, and one of them is CuA_2 for the monomer, and Cu_2A_4 for the dimer, respectively.

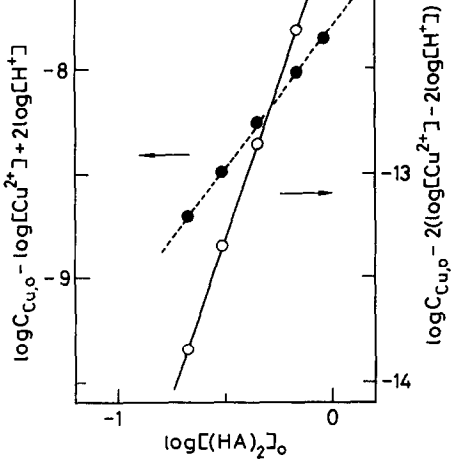

Fig. 2. Determination of the number of pivalic acid molecules involved in the monomeric and dimeric copper(II) species in benzene. Solid and dotted lines are the straight lines with slopes of 3.0 and 1 ~ 1.5, respectively. Open and closed symbols refer to the dimeric and monomeric copper(II) species, respectively.

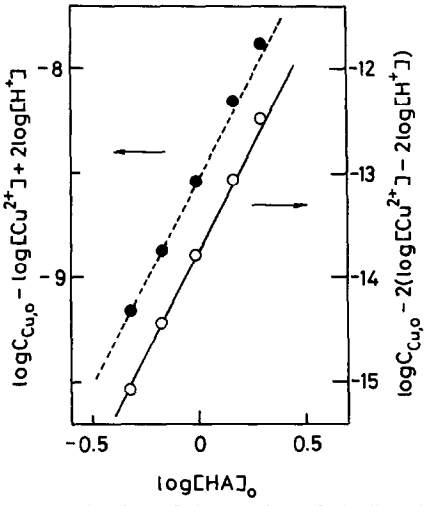

Fig. 3. Determination of the number of pivalic acid molecules involved in the monomeric and dimeric copper(II) species in 1-octanol. Solid and dotted lines are the straight ones with slopes of 4.0 and 2.0, respectively. Open and closed symbols refer to the dimeric and monomeric extracted species, respectively.

The monomeric copper(II) species other than CuA_2, which was recognized from Figs 2 and 3, can be expected to be CuA_2HA and/or $CuA_2(HA)_2$ for both the extraction systems using benzene and 1-octanol as solvents. Similarly for 1-octanol the dimeric ones other than Cu_2A_4, which was suggested from Fig. 3, can be anticipated to be Cu_2A_4HA and/or $Cu_2A_4(HA)_2$. Then,

in the region where the monomer prevails, the total concentration of copper(II) in the organic phase can be presumed as follows:

$$C_{Cu,o} = [CuA_2]_o + [CuA_2HA]_o + [CuA_2(HA)_2]_o. \quad (12)$$

In the region where the dimer prevails, the following expression can be obtained:

$$C_{Cu,o} = 2([Cu_2A_4]_o + [Cu_2A_4HA]_o + [Cu_2A_4(HA)_2]_o). \quad (13)$$

By use of the individual extraction constants these can be rewritten as follows: for benzene,

$$\frac{C_{Cu,o}}{[Cu^{2+}][H^+]^{-2}[(HA)_2]_o} = K_{ex(10)} + K_{ex(11)}[(HA)_2]_o^{1/2} + K_{ex(12)}[(HA)_2]_o, \quad (14)$$

and for 1-octanol,

$$\frac{C_{Cu,o}}{[Cu^{2+}][H^+]^{-2}[HA]_o^2} = K_{ex(10)} + K_{ex(11)}[HA]_o + K_{ex(12)}[HA]_o^2, \quad (15)$$

and

$$\frac{C_{Cu,o}}{2[Cu^{2+}]^2[H^+]^{-4}[HA]_o^4} = K_{ex(20)} + K_{ex(21)}[HA]_o + K_{ex(22)}[HA]_o^2, \quad (16)$$

respectively. From the plots of the values of the left hand side of each equation against $[(HA)_2]_o^{1/2}$ for equation (14), and $[HA]_o$ for equations (15) and (16), the other copper(II) species can be estimated. As shown in Figs 4 and 5, the plots gave a linear relationship in all cases. The plots on the basis of equations (14) and (15) are in good agreement with the straight line calculated by the least-squares method. Although the plots on the basis of equation (16) deviate from the line, a linear relationship between the values of the left hand side of equation (16) and $[HA]_o$ is found. The fluctuation of the plots of the dimeric copper(II) species in Fig. 5 can be due to the amplification of the experimental error on the value of the vertical axis for the plots based on equation (16) compared to that based on equation (15). This amplification of the error results from the fact that each concentration term in the denominator of the left hand side of equation (16) becomes the square of that in equation (15). The resulting information suggests that the third term on the right hand side of equations (14)–(16) can be neglected, that is, $CuA_2(HA)_2$ both in benzene and 1-octanol, and $Cu_2A_4(HA)_2$ in 1-octanol do not exist to any appreciable extent under the present extraction conditions. In addition, the extraction constants for the respective extracted species can be determined from the slope and intercept of the corresponding straight line. The resulting constants are summarized in Table 1. The composition of the dimeric copper(II) species in benzene is consistent with the dimer which has been presented in the extraction of copper(II) with pivalic acid using toluene as a solvent by Haffenden and Lawson.[14] They speculated that the monomeric copper(II) species was also extracted together with the dimeric one. But neither the composition of the monomer nor the extraction constant of the dimeric species were estimated in their work.

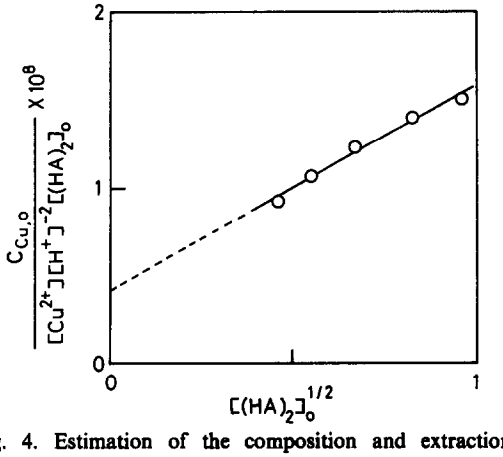

Fig. 4. Estimation of the composition and extraction constants of the monomeric copper(II) species in benzene. The straight line was drawn by the least-squares method.

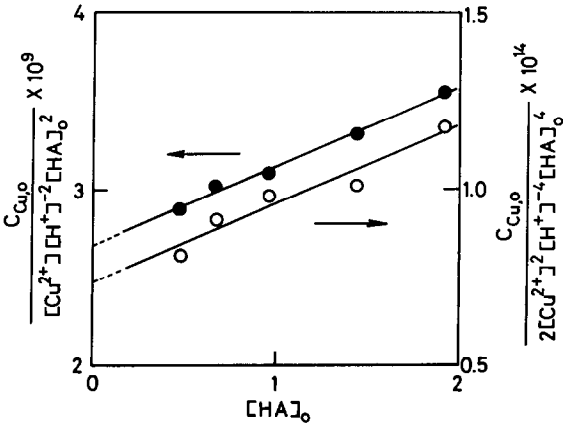

Fig. 5. Estimation of the composition and extraction constants of the monomeric and dimeric copper(II) extracted species for 1-octanol. Straight lines were drawn by the least-squares method. Open and closed symbols refer to the dimeric and monomeric species, respectively.

Consequently, the extraction equilibria for the present extraction systems can be expressed as follows: for benzene,

$$Cu^{2+} + (HA)_{2,o} \overset{K_{ex(10)}}{\rightleftharpoons} (CuA_2)_o + 2H^+$$

$$Cu^{2+} + \tfrac{3}{2}(HA)_{2,o} \overset{K_{ex(11)}}{\rightleftharpoons} (CuA_2HA)_o + 2H^+$$

$$2Cu^{2+} + 3(HA)_{2,o} \overset{K_{ex(22)}}{\rightleftharpoons} [Cu_2A_4(HA)_2]_o + 4H^+,$$

and for 1-octanol,

$$Cu^{2+} + 2(HA)_o \overset{K_{ex(10)}}{\rightleftharpoons} (CuA_2)_o + 2H^+$$

$$Cu^{2+} + 3(HA)_o \overset{K_{ex(11)}}{\rightleftharpoons} (CuA_2HA)_o + 2H^+$$

$$2Cu^{2+} + 4(HA)_o \overset{K_{ex(20)}}{\rightleftharpoons} (Cu_2A_4)_o + 4H^+$$

$$2Cu^{2+} + 5(HA)_o \overset{K_{ex(21)}}{\rightleftharpoons} (Cu_2A_4HA)_o + 4H^+,$$

respectively.

Then the adduct formation and dimerization of copper(II) pivalates in both the benzene and 1-octanol phases can be formulated as follows: for benzene,

$$(CuA_2)_o + \tfrac{1}{2}(HA)_{2,o} \overset{K_{ad,\,ml}}{\rightleftharpoons} (CuA_2HA)_o$$

$$2(CuA_2HA)_o \overset{K_{dim-2}}{\rightleftharpoons} [Cu_2A_4(HA)_2]_o,$$

and for 1-octanol,

$$(CuA_2)_o + (HA)_o \overset{K_{ad,\,ml}}{\rightleftharpoons} (CuA_2HA)_o$$

$$2(CuA_2)_o \overset{K_{dim-1}}{\rightleftharpoons} (Cu_2A_4)_o$$

$$(Cu_2A_4) + (HA)_o \overset{K_{ad,\,dl}}{\rightleftharpoons} (Cu_2A_4HA)_o$$

with the following adduct formation and dimerization constants calculated from the respective extraction constants: $\log K_{ad,\,ml} = 0.46$ and $\log K_{dim-2} = 4.05$ for benzene, and $\log K_{ad,\,ml} = -0.78$, $\log K_{dim-1} = 3.01$, and $\log K_{ad,\,dl} = -0.52$ for 1-octanol, respectively.

The relationship between the distribution ratio of copper(II) and the hydrogen ion concentration in the aqueous phase, which was drawn on the basis of the present results, is shown in Fig. 6. As can be seen from Fig. 6, benzene is more useful as a solvent than 1-octanol for the present extraction systems. That is to say, the dimerization and adduct formation of copper(II) species in benzene may contribute more effectively to the enhancement of the extractability of copper(II) than the solvation of copper(II) species by 1-octanol molecules.

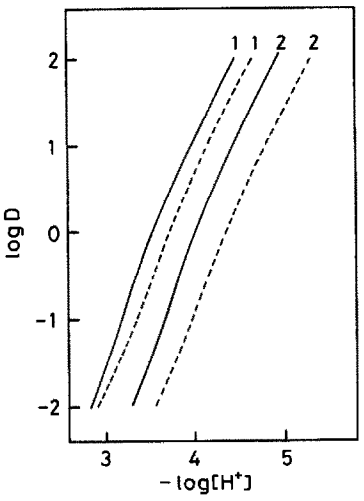

Fig. 6. Relationship between the distribution ratio of copper(II) and the hydrogen ion concentration. Solid and dotted curves, which were drawn on the basis of the results obtained from the present work, refer to benzene and 1-octanol, respectively. Symbols: (1) $C_{HA} = 2.0$, and (2) $C_{HA} = 0.5$ mole . dm^{-3}, respectively.

Distribution diagrams of copper(II) species

The distribution diagram of copper(II) pivalates in the organic phase in the presence of an excess of pivalic acid can be calculated from the results obtained by the present work. It is depicted in Figs 7 and 8. Both the dimerization and adduct formation of copper(II) pivalates are shown to proceed more easily in benzene than in 1-octanol in Figs 7 and 8. At the total copper(II) concentration in the organic phase as high as 10^{-3} mole . dm^{-3}, the dissociation of the dimeric copper(II) pivalate has been found to occur even in benzene. This has never been observed in aliphatic carboxylic acid–benzene systems except for the cyclohexanecarboxylic acid–benzene system.[11]

Solvent effects

The resulting constants suggest that both the adduct formation and dimerization reactions of copper(II) pivalates proceed more easily in benzene than 1-octanol. This can be attributed to stabilization of the monomeric copper(II)

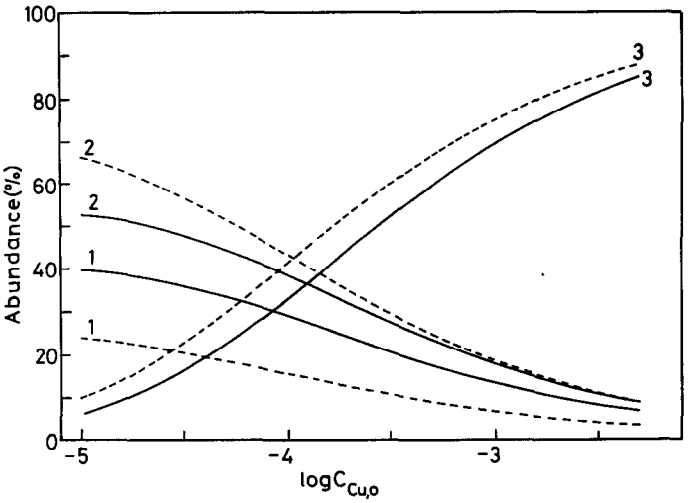

Fig. 7. Distribution diagrams of copper(II) pivalates in benzene. Solid and dotted curves refer to $C_{HA} = 0.5$ and 2.0 mole . dm^{-3}, respectively. Symbols: (1) CuA_2, (2) CuA_2HA, and (3) $Cu_2A_4(HA)_2$, respectively.

species by the solvation with some 1-octanol molecules in 1-octanol phase. The more favorable solvation of the monomeric copper(II) pivalate by 1-octanol molecules can be ascribed in part to the hydrogen bonding ability of 1-octanol as well as in the previous work[13] on the solvent effects on the dimerization of copper(II) decanoate, in which the monomeric copper(II) decanoate was found to be more extensively solvated in alcohol solvents than in ketone ones. On the other hand, in benzene the monomeric species, CuA_2 and CuA_2HA, which do not satisfy the coordination number of copper(II) ion only by pivalic acid, can be expected to be hydrated by two and one water molecules, respectively. This is supported by the fact that in benzene the extraction constant of CuA_2, in which two water molecules are supposed to be involved, is smaller than that of CuA_2HA, in which one water molecule can be involved. Contrary to the case of benzene, in the 1-octanol system, one or two 1-octanol molecules can be anticipated to attach to the coordination-unsaturated sites of copper(II) ion, in order to satisfy the coordination number of copper(II) ion, that is, CuA_2 and Cu_2A_4 can be involved with two 1-octanol molecules, and CuA_2HA and Cu_2A_4HA can be involved with one 1-octanol molecule. The species CuA_2 and Cu_2A_4 solvated by two 1-octanol molecules become more lipophilic than CuA_2HA and Cu_2A_4HA, in which one 1-octanol molecule can be involved, and

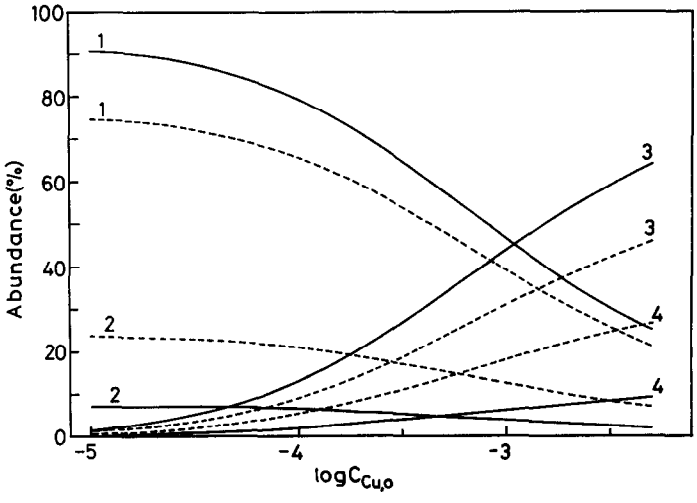

Fig. 8. Distribution diagrams of copper(II) pivalates in 1-octanol. Solid and dotted curves are same as in Fig. 7. Symbols: (1) CuA_2, (2) CuA_2HA, (3) Cu_2A_4, and (4) Cu_2A_4HA, respectively.

the extraction constants of the former species become greater than those of the latter ones as shown in Table 1.

The adduct formation reaction of copper(II) pivalates with pivalic acid molecules can be regarded as the ligand replacement of coordinated water or 1-octanol by pivalic acid. It proceeds more easily in benzene than in 1-octanol, because in the latter the exchange of coordinated 1-octanol with pivalic acid can be inhibited by bulk 1-octanol molecules. The expected results for the respective adduct formation constants have been obtained as described above.

In addition, it can be usually expected that the lower the dielectric constant, the more extensive is the dimerization of copper(II) carboxylate. In the previous paper[1] on the extraction of copper(II) with decanoic acid in various non-solvating solvents ranging in dielectric constant from 1.9 (*n*-hexane) to 10.4 (1,2-dichloroethane), copper(II) was found to be extracted only as the dimeric species $[Cu_2A_4(HA)_2]$ irrespective of the dielectric constant of the solvent used as a solvent. While, in the other paper,[2] we reported that the dissociation of the dimeric copper(II) decanoate to the monomer was observed in the extraction system using 1-octanol whose dielectric constant is similar in magnitude to 1,2-dichloroethane. According to these results, in the present extraction systems the solvation effect of 1-octanol on the dimerization of copper(II) pivalate is much larger than the effect resulted from the difference in the dielectric constant between 1-octanol and benzene.

Steric effect

Steric factors can be also expected to influence the adduct formation and dimerization of copper(II) pivalates in the present extraction systems. In contrast to the extraction with decanoic,[1] α-bromopentanoic,[10] and α-lipoic[3] acids, in which the dissociation of the dimeric copper(II) carboxylates was not observed in benzene in the range of the total concentration of copper(II) in the organic phase from 10^{-4} to 10^{-3} mole . dm^{-3}, the dissociation of the dimeric copper(II) pivalate in the benzene phase has been observed in the similar range as described above. This suggests that the formation of the dimeric copper(II) pivalate can be sterically inhibited by three methyl substituents which are just adjacent to the carboxylic group. Judging from the fact that not only in 1-octanol, but also in benzene, the monomeric copper(II) pivalate, $CuA_2(HA)_2$, could not be recognized to any appreciable extent, three methyl groups can be anticipated to make difficult sterically the arrangement of two pivalic acid molecules around CuA_2 species.

CONCLUSIONS

Consequently, steric hindrance by three methyl substituents at the α-position for the carboxylic group and solvation by 1-octanol and water molecules have been found to influence the adduct formation and dimerization of copper(II) pivalates. And both reactions play an important part on the extraction of copper(II) carboxylates, and can result in an effect similar to the synegistic one. Such steric and solvent effects can be also expected to influence the extractability of a metal ion which is extracted as a polymeric metal carboxylate. Previously, in the extraction of Al(III), Ga(III) and In(III) with decanoic acid, these metal ions have been found to increase the degree of polymerization of metal decanoates in the order, Al > Ga > In, both in benzene and 1-octanol phases.[15] The differences in the degree of polymerization of the extracted species, which will result also in the present extraction systems, can be anticipated to lead to the differences in the extractability of such metal ions as aluminum, gallium and indium.

Then, the present extraction systems can be expected to be also useful for the extraction of other metal ions which can be extracted as polymeric carboxylates with various degrees of polymerization.

Acknowledgement—The authors wish to thank Professor Hiroko Wada of Nagoya Institute of Technology for her valuable discussions.

REFERENCES

1. H. Yamada and M. Tanaka, *J. Inorg. Nucl. Chem.*, 1976, **38**, 1501.
2. H. Yamada, S. Suzuki and M. Tanaka, *J. Inorg. Nucl. Chem.*, 1981, **43**, 1873.
3. H. Yamada, T. Okuda, Y. Fujii, M. Mizuta and M. Tanaka, *Bull. Chem. Soc. Japan*, 1986, **59**, 3855.
4. H. Yamada, K. Adachi, Y. Fujii and M. Mizuta, *Solvent Extr. Ion Exch.*, 1986, **4**, 1109.
5. H. Yamada, S. Horikawa, Y. Fujii and M. Mizuta, *Bull. Chem. Soc. Japan*, 1988, **61**, 835.
6. H. Yamada, S. Horikawa, Y. Fujii and M. Mizuta, *Bull. Chem. Soc. Japan*, 1990, **63**, 3542.
7. H. Yamada and M. Mizuta, *Process Metallurgy (Solvent Extraction*, 1990), **7A**, 1992, 153.

8. H. Yamada, C. Kato and the late M. Mizuta, *Bull. Chem. Soc. Japan*, 1992, **65**, 186.
9. I. Kojima, M. Yoshida and M. Tanaka, *J. Inorg. Nucl. Chem.*, 1970, **32**, 987.
10. Y. Fujii, H. Yamada and M. Mizuta, *Polyhedron*, 1987, **6**, 1203.
11. H. Yamada, M. Ito and M. Mizuta, *Bull. Chem. Soc. Japan*, 1987, **60**, 3557.
12. H. Yamada, R. Kitazaki and I. Kakimi, *Bull. Chem. Soc. Japan*, 1983, **56**, 3302.
13. H. Yamada, K. Takahashi, Y. Fujii and M. Mizuta, *Bull. Chem. Soc. Japan*, 1984, **57**, 2847.
14. W. J. Haffenden and G. J. Lawson, *J. Inorg. Nucl. Chem.*, 1967, **29**, 1133.
15. H. Yamada, H. Hayashi, Y. Fujii and M. Mizuta, *Bull. Chem. Soc. Japan*, 1986, **59**, 789.

Talanta, Vol. 40, No.7, pp. 1059–1066, 1993
Printed in Great Britain.

0039-9140/93 $6.00 + 0.00

DETERMINATION OF TRACES OF ALUMINIUM WITH CHROME AZUROL S BY SOLID-PHASE SPECTROPHOTOMETRY

A. MOLINA-DIAZ,* J. M. HERRADOR-MARISCAL and M. I. PASCUAL-REGUERA
Department of Analytical Chemistry, Faculty of Experimental Sciences, University of Granada, 23071 Jaén, Spain

L. F. CAPITAN-VALLVEY
Department of Analytical Chemistry, Faculty of Sciences, University of Granada, 18071 Granada, Spain

(*Received* 6 *August* 1992. *Revised* 7 *December* 1992. *Accepted* 7 *December* 1992)

Summary—A microdetermination method at sub-μg/l. level for aluminium by solid-phase spectrophotometry has been developed. Chrome azurol S was used as chromogenic reagent to form a blue complex which was easily and strongly sorbed and concentrated on a dextran-type anion-exchange resin. The resin-phase absorbances at 615 and 800 nm were measured directly. Aluminium can be determined in the 0.6–4.0 μg/l. range with a RSD of 2.1%. The method is applied to the determination of aluminium in micaschist, natural and tap water samples.

The potential toxicity of aluminium in man is universally recognized. A series of clinical disorders, including dialysis dementia, has been associated with its accumulation in several tissues (brain and bone principally) in renal-failure patients undergoing regular hemodialysis.[1] It has been suggested[2] that aluminium increases the permeability of the blood–brain barrier which may lead to dementia or other neuronal disorders. Aluminium is present at approximately 1.4 ppm or 100 mg Al/70 kg man and it is ingested with food; the approximate daily dietary intake is 36.4 mg[2] varying with degree of dietary exposure. Aluminium ions in our diet are completely non-bioavailable from the small intestine because the aquated charged ions are not able to penetrate the lipid protein membranes of the duodenal mucosa and thus pass on into the bloodstream.[3] On the other hand, it can be assumed that at least part of human dietary aluminium intake is in the form of chelates with natural food components such as citric, lactic and oxalic acids.[4] In these chemical forms, Slanina *et al.*[4] showed (working with rats) that aluminium is bioavailable. In moderate amounts, aluminium does not exert prejudicial effects in man. It is used in the treatment of tap waters. On the other hand, it has been shown that aluminium is toxic to fish[5]. Hence a great deal of attention to the determination of this element has been paid recently.

Numerous binary complexes of Al(III) with (a) azo reagents, (b) xantene reagents and (c) triphenylmetane reagents [eriochrome cyanine R, pyrocatechol violet and chrome azurol S (CAS)] have been used for spectrophotometric determination of aluminium. They exhibit moderate sensitivity[6] but it can be increased by addition of a cationic surfactant such as cetyltrimethylammonium bromide, cetyltrimethylammonium chloride, cetylpyridinium chloride, cetylpiridinium bromide, tetraphenylphosphonium chloride and zephiramine.[7] However the spectrophotometric determination of aluminium at sub-μg/l. level requires a step of preconcentration. Nevertheless, solid phase spectrophotometry (SPS) enables determining analyte concentrations at this level without requiring an expensive instrumentation combining the measurements of solid-surface absorbance with using a solid support to preconcentrate selectively the analyte and measuring the absorbance directly in the solid phase with the aid of a chromogenic reagent.[8,9,10] Detection limits as low as 0.09 μg/l. have been reported.[11]

The aim of this paper has been to develop a sensitive and selective method for the spectrophotometric determination of aluminium

*Author for correspondence.

with CAS by selective enrichment of the metal as Al(III)–CAS species on a dextrane type resin and measuring of the absorbance in resin phase, *e.g.* by using SPS.

The proposed method has been satisfactorily applied to the determination of aluminium in natural and tap water samples, and other matrices, such as micaschist and enables determining of this element at sub-μg/l. level.

EXPERIMENTAL

Reagents

All reagents were of analytical-reagent grade and the water was doubly distilled.

Ion exchanger, Sephadex QAE A-25 (Aldrich), anion-exchange resin was used in the chloride form in original dry state as obtained from the supplier and without pretreatment.

Aluminium (III) standard solution 1.000 g/l., prepared by dissolving 17.5820 g of aluminium potassium sulfate dodecahydrate $AlK(SO_4)_2 \cdot 12H_2O$ (Merck) in doubly distilled water containing 5 ml of concentrate. H_2SO_4 and diluting the solution with doubly distilled water to 1000 ml. Aluminium (III) working solutions were made *in situ* by dilution with doubly distilled water.

Buffer solution of pH 4.60, was made by dissolving 35.05 g of hexamethylenetetramine (HMTA) and 45 ml of HCl 4*M* in 1000 ml of doubly distilled water and adjusting the pH with a few drops of HCl 4*M* or NaOH 4*M*. This solution was stored under refrigeration.

Chromazurol S solution of various concentrations, prepared by dissolving the necessary amount of the dye in doubly distilled water. This solution was stored under refrigeration. In this conditions the solution is stable for at least one month.

Apparatus

A GBC 911 microcomputer-controlled UV-VIS spectrophotometer with glass cells (1-mm optical path length) was employed for all spectral measurements. The spectrophotometer was controlled by a Bravo AST/80286 microcomputer connected by means of a serial port. A Comx PL80 plotter was used for graphical representations. The pH measurements were made with a Crison Model 2002 pH-meter fitted with a glass-saturated calomel electrode assembly and a temperature probe. An Agitaser 2000 rotating agitator was also used and a centrifuge Selecta model S-240.

Absorbance measurements

The absorbance of the complex species sorbed on the resin was measured in a 1 mm cell at 615 (corresponding to the absorption maximum of the coloured species) and 800 nm (in a region where only the resin absorbs light). The net absorbance (A_c) for the complex was calculated from:[8]

$$A_c = A_{615} - A_{800}, \quad (1)$$

where: $A_{615} = A_{s615} - A_{b615}$ and $A_{800} = A_{s800} - A_{b800}$ and A_{sXXX} and A_{bXXX} are the absorbances of the sample and the blank (cell packed with resin equilibrated with blank solution), respectively at the indicated wavelength. In fact, the observed absorbance, A, at a given wavelength is obtained by:[8]

$$A = A_c + A_{soln} + A_R + A_{RL},$$

where A_c represents the absorbance of the complex species sorbed on the resin, A_{soln} that of the interstitial solution between the resin beads (it can be neglected), A_R that of the resin background ($A_{R800} \simeq 1.000$) and A_{RL} that of the reagent in the solid phase. The packing of the resin in the cell beads affects the values of A_c, A_R and A_{RL}, but when the absorbance is measured at two different wavelengths, one corresponding to the absorption maximum of the coloured species (615 nm) and the other in a region where only the resin absorbs (800 nm), the absorbance difference, $A_{s615} - A_{s800}$, can be assumed to be constant under the similar packing conditions. On the other hand, if the absorbance of a blank resin is measured at the same two wavelengths, the absorbance difference, $A_{b615} - A_{b800}$, allows us to estimate the absorbance of the complex, A_c (that is related with the concentration of analite in the solution as it was shown by Yoshimura)[8] from the equation (1).

Procedures

(I) A 10 ml sample solution containing 20–200 μg/l. (0.74–7.4 μmole/l.) of aluminium was transferred into a 20-ml glass tube with stopper containing 4 ml of 1.5×10^{-4} *M* CAS solution and 1 ml of pH 4.60 HMTA buffer solution (total volume = 15 ml). After 10 min, 30 mg of Sephadex QAE A-25 resin were added. The mixture was shaken mechanically for 5 min after which the resin beads were collected by suction with the aid of a pipette and packed into a 1 mm cell together with a small volume of the aqueous solution. Then, the cell was centrifuged

for 1 min at 5000 rpm. A blank solution containing all reagents except aluminium was prepared and treated in the same way as described for the sample. The absorbances (A_{s615}, A_{s800}, A_{b615} and A_{b800}) were measured as described under "Absorbance measurements" 30 min after collection of resin. The calibration graph was constructed in the same way using aluminium solutions of known concentration.

(II) A 100 ml sample solution containing 2.0–26 μg/l. (0.074–0.96 μmole/l. of aluminium was transferred into a 1-l. polyethylene bottle containing 10 ml of 1.5×10^{-4} *M* CAS solution, 5 ml of pH 4.60 HMTA buffer solution and, after 10 min, 30 mg of Sephadex QAE A-25 resin were added. The mixture was shaken mechanically for 15 min after which the resin beads were collected by filtration and with the aid of a pipette, packed into a 1-mm cell as above procedure, and the absorbance measurement was carried out in the same way.

(III) A 500-ml sample solution containing 0.7–5.0 μg/l. (0.026–0.185 μmole/l.) of aluminium was transferred into a 1-l. polyethylene bottle containing 20 ml of 1.5×10^{-4} *M* CAS solution and 25 ml of pH 4.60 HMTA buffer solution. After 10 min, 30 mg of Sephadex QAE A-25 resin were added. The mixture was shaken mechanically for 110 min. The absorbance of the coloured species was measured as the above procedures.

(IV) A 1000 ml sample solution containing 0.6–4.0 μg/l. (0.022–0.148 μmole/l.) of aluminium was placed in a 2-l. container of polyethylene containing 5 ml of 6.3×10^{-4} *M* CAS solution and 50 ml of pH 4.60 HMTA buffer solution. After 10 min, 30 mg of Sephadex QAE A-25 resin were added. The mixture was shaken mechanically for 125 min and the absorbance measured as described.

Treatment of samples

Analysis of micaschists. A suitable weight of sample (generally 50–100 mg) was treated in a nickel crucible with 2 g NaOH in the usual way. The melt was leached with distilled water with warming and poured into 250 ml HCl 0.44*M* and then distilled water added up to 500 ml (this solution was stored in a polyethylene container carefully cleaned with nitric acid and the samples were stored at 4°C until analysis). For the later process this solution was diluted 1:100 with addition of 0.4 ml NaOH 0.4*M* per ml of initial solution.

Waters. Natural waters were filtered through a filter paper with a pore size of 0.45 μm (Millipore), preserved with concentrate HNO_3 (0.25 ml/l. of water) and stored in a polyethylene container. The samples were stored at 4°C until analysis. Analysis were performed with the least possible delay. The usual general precautions were taken to avoid contamination. The tap water was analysed without pretreatment.

Distribution measurements

CAS, buffer solution and 30 mg of Sephadex QAE A-25 resin were added to an aqueous solution containing 740 nmole of Al(III) and the solution (100 ml) was stirred for 60 min. The equilibrated solution was separated from the resin. Afterwards, the solution was treated in the same way with a further batch of resin (30 mg) and the aluminium left in that was determined as described under "Procedures". The distribution ratio *D* (μmole of aluminium sorbed per gram of resin/μmole of Al(III) per ml of solution) was calculated from the initial and equilibrium concentration in the solution. An average value of $D = 23{,}400$ and S.D. = 600 was obtained from five replicates experiments.

RESULTS AND DISCUSSION

Absorption spectra in resin phase

CAS reacts with Al(III) to originate a blue complex in solution in the pH range 3.5–7.5. Between pH = 2.5 and 8.0 this complex is sorbed on an anion-exchange resin showing the absorption maximum at 615 nm and reaching the absorbance the highest value at pH about 4.6 (Fig. 1a–e). The spectrum of this complex at above pH in aqueous solution shows (Fig. 1f) much lower absorbance than in resin phase: the increasing of sensitivity in resin-phase is self-evident.

Optimization of variables

pH dependence. The optimum pH in the solution phase for the formation of the blue species on the resin falls in the range 3–5. At pH values below 3 and above 5 the absorbance value at 615 nm decreases significantly. We chose pH 4.60 as optimum pH value for the following experiences. The pH can be satisfactorily adjusted by addition of a 0.25*M* HMTA/HCl buffer solution. Other buffers (acetic acid/acetate, formic acid/formiate) decreased the absorbance in respect to

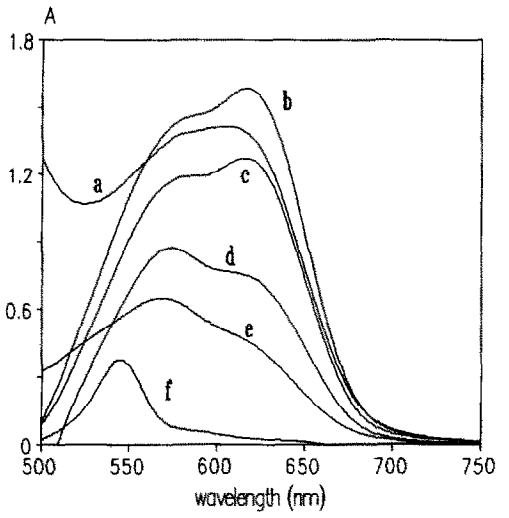

Fig. 1. Net absorption spectra of Al(III)–CAS species: (a)–(e) on the resin (resin as reference). [CAS] = 1.40×10^{-5} *M*, [Al(III)] = 1.48×10^{-6} *M*, 50 mg of resin, 1 mm optical path length, sample volume 100 ml, stirring time 15 min: (a) pH = 4.0; (b) pH = 4.5; (c) pH = 5.0; (d) pH = 5.5; (e) pH = 6.0; (f) in aqueous solution, [CAS] = 9.0×10^{-5} *M*, [AlIII)] = 9.0×10^{-6} *M*, 10 mm optical path length, pH = 5.0.

use HMTA/HCl buffer (80 and 26%, respectively for an aluminium concentration of 40 μg/l. using 50 mg of resin and a final volume of 100 ml).

Reagent concentration. Absorbance increases with an increasing CAS concentration, a plateau occurring from 1.2 to 2.5×10^{-5} (for 100 ml sample). It seems that the excess of free ligand competes with the complex for sorption on the resin phase and it originates these plateaux. The optimum molar [CAS/Al(III)] ratio necessary was 8, 13, 40 and 53 (for 15, 100, 500 and 1000 ml sample volumes, respectively). 4.0×10^{-5}, 1.5×10^{-5}, 6.0×10^{-6} and 3.15×10^{-6}*M* reagent concentration were chosen for 15, 100, 500 and 1000 ml sample volumes, respectively.

Other experimental conditions. The optimum stirring times are 5, 15, 110 and 125 min for 15, 100, 500 and 1000 ml sample volumes, respectively (Fig. 2). The fixed complex is stable for at least 7 hr after equilibration.

The order of addition of the reagents affects significantly the results obtained; the order used was: reagent, buffer, aluminium, resin. The use of a large amount of resin (m_r, g) reduces as usual[9–11] the absorbance values. Absorbance decreases according to the equation: ($r = 0.9987$) $A_c = -0.014 + 0.0224/m_r$ (Fig. 3). 30 mg is in the minimum amount of dry resin that gives the highest absorbance and greatest ease of handling.

Nature of the fixed complex

The composition of the fixed Al(III)-CAS complex on Sephadex was established at the

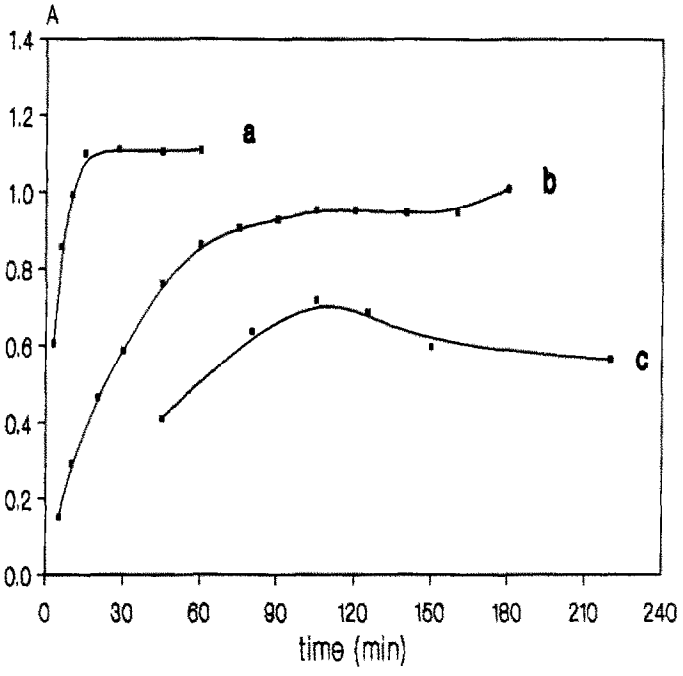

Fig. 2. Stirring time dependence on color development in resin-phase. 30 mg of resin, pH = 4.6, 0.074 μmole of Al(III). (a) 100 ml of sample, [CAS] = 1.5×10^{-5} *M*. (b) 500 ml of sample, [CAS] = 6×10^{-6} *M*. (c) 1000 ml of sample, [CAS] = 3.15×10^{-6} *M*.

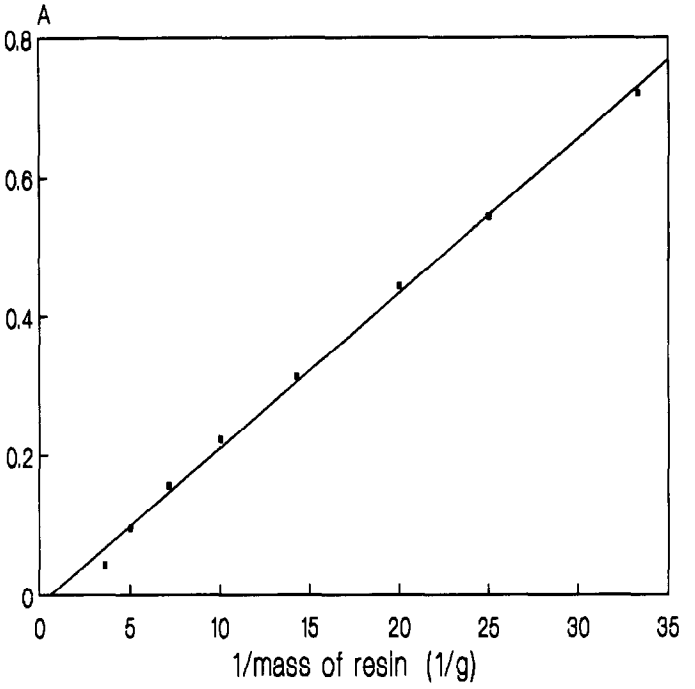

Fig. 3. Resin amount dependence. [CAS] = 1.5×10^{-5} M, [Al(III)] = 3.7×10^{-7}, pH = 4.60, 1 mm optical path length, sample volume 100 ml, stirring time 40 min.

working pH of 4.6 using the Job[12] and the equilibrium shift[13] methods. Job method showed a ratio CAS/Al(III) = 2. Moreover, the graph of log $(A/A_{max} - A)$ *vs.* log [CAS] (equilibrium shift method) gave a slope of 2.087 ($r = 0.9969$). Consequently, results indicated that a 2:1 [CAS:Al(III)] anionic complex is fixed on the anionic resin. These results agree with those found in aqueous solution.[14]

Analytical data

Calibration and precision. The calibration graphs are linear in the concentration ranges: 20–200 g, 2–26 g, 0.7–5.0 and 0.6–4.0 μg for 15, 100, 500 and 1000 ml samples, respectively. The analytical parameters are shown in Table 1.

The reproducibility was established using 15, 100, 500 and 1000 ml sample solutions with a Al(III) concentration of 107.0, 12.5, 4.0 and 2.0 μg/l., respectively. It was possible verifying that the reproducibility is improved when the cells packed with the resin are centrifuged, during 1 min at 5000 rpm, previously the spectrophotometric measurements. The relative standard deviation (RSD) was 4.4% without centrifugation for 100 ml sample and 10 determinations. With centrifugation the absorbance values increase about a 12% and the RSD decreases at 3.0%. For 15 ml sample volume it was studied the effect of adding the resin in a suspension (5 ml) of 3.00 g in 500 ml of distilled water. The RSD increases at 5.3%, but it offers the advantage of a quicker and easier measurement of the amount of resin because it was not necessary weigh it.

Sensitivity and detection limit. In Table 2 the sensitivity, expressed as apparent molar absorptivity, of the proposed procedures is compared with that of spectrophotometric procedures (including extractive procedures and formation

Table 1. Analytical parameters

	Volume sample (ml)			
	15	100	500	1000
Intercept	−0.041	0.025	−0.015	0.025
Slope (l./μg)	0.0108	0.0529	0.1782	0.2528
Linear dynamic range (μg/l.)	20–200	2–26	0.7–5.0	0.6–4.0
Correlation coefficient	0.9962	0.9979	0.9947	0.9984
RSD (%)	2.2	3.0	3.7	2.1
Detection limit ($K = 3$) (μg/l.)	1.11	0.51	0.20	0.14
Quantification limit ($K = 10$) (μg/l.)	3.71	1.70	0.67	0.47

Table 2. Comparison of sensitivity of some aluminium methods

Reagent	Molar absorptivity	Ref.
Chrome azurol S*	5.2×10^4	17,18
Pyrocatechol violet†	6.3×10^4	23
Eriochrome cyanine R*	6.5×10^4	19–22
Eriochrome cyanine R/Cetylpiridinium chloride*‡	1.15×10^5	24
Chrome azurol S/Zephiramine*‡	1.22×10^5	24
Chrome azurol S/Cetylpiridinium chloride*‡	1.22×10^5	24
Eriochrome cyanine R/Zephiramine*‡	1.24×10^5	24
Chrome azurol S (15 ml)§	2.92×10^6‖	This paper
Chrome azurol S (100 ml)§	1.43×10^7‖	This paper
Chrome azurol S (500 ml)§	4.81×10^7‖	This paper
Chrome azurol S (1000 ml)§	6.83×10^7‖	This paper

*Solution methods.
†Extractive procedures.
‡Ternary complexes.
§Solid-phase spectrophotometry.
‖Apparent molar absorptivity: absorbance value of the complex sorbed on the resin from a 1*M* aqueous solution of Al(III) and measured in a 10 mm optical path length cell.

of ternary complexes with surfactants) described in the literature. It is shown that SPS methodology using CAS gives a very noticeable increase in sensibility in relation to the solution and extractive methods.

The effect of volume on sensitivity. In SPS methodology the sensitivity can be enhanced by increasing the sample volume to be analysed. this effect may be calculated by measuring the absorbance of the resin equilibrated with different volumes of solutions containing the same concentrations of Al(III) and optimum established amounts of the other reagents. It is observed that a tendency of absorbance is to be independent of volume at higher volume values as usually in SPS[9–11] (Fig. 4).

The increase of sensitivity using a larger sample volume can be calculated, in practice, form the slope of the calibration graphs. The calculated values of the sensitivity ratio for the samples analysed here are: $S_{1000}/S_{500} = 1.42$, $S_{1000}/S_{100} = 4.79$ and $S_{1000}/S_{15} = 23.45$, where the subscripts represent the sample volume (ml).

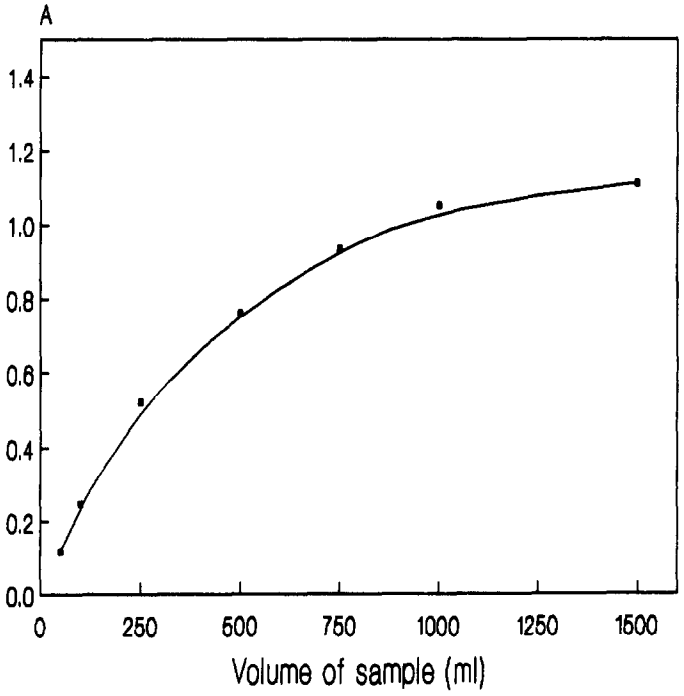

Fig. 4. Effect of volume on sensitivity. [CAS] = 3×10^{-5} *M*–2.5×10^{-6} *M*, [Al(III)] = 1.48×10^{-7} *M*, pH = 4.60, amount of resin = 0.030 g, stirring time = 15–150 min.

The standard deviation of the absorbance of the blank measured for 10 determinations (average values: 0.129, 0.373, 0.761, 0.869) were 0.004, 0.009, 0.012, 0.012 absorbance units for 15, 100, 500 and 1000 ml sample volumes, respectively. The IUPAC detection limit ($K = 3$)[15]and the quantification limit ($K = 10$)[16] were calculated for 15, 100, 500 and 1000 ml sample volumes (Table 1).

On the other hand, the interference level, can be reduced by diluting the samples, taking into account the sensitivity of the method proposed and the dependence of the sensitivity on the sample volume.

Effect of foreign ions

In Table 3 the effect of various potentials interferent species, commonly found in the water, on the determination of 12.5 μg/l. of Al(III) is listed. This effect was investigated by adding a known amount of the test ion to the aluminium solution. First a 20,000 μg/l. level of potentially interfering ions were tested and if the interference occurred, the concentration of interferent was reduced progressively until interference ceased. Higher concentrations were not tested. Tolerance level is defined as the foreign ion concentration that produces not more than ±5% spectrophotometric error in the recovery of Al(III).

The most severe interference is caused by iron. It causes positive error because the iron forms a complex with CAS and this complex absorbs at the wavelength used in the procedures. The use of 1,10-phenanthroline, after reduction with hydrogen in acidic medium, suppresses the iron interference up to 1500 μg/l. [for total Iron: Fe(II) + Fe(III)]. The cationic complex Fe(II)-1,10-phenantroline remained in solution and it was not sorbed on the resin. On the other hand, the high tolerance level for Cu(II) is probably due to the presence of HMTA as buffer. With respect to the interference from anions F^- and EDTA, it can be attributed to the complexation of aluminium. Moreover, in the case of the anions in general, the existence of competition for the anionic sites of the resin is probable.

Table 3. Effect of foreign ions on the determination of 12.5 μg/l. of aluminium

Foreign ion or species	Tolerance level (μg/l.)
Cu(II), Mg(II), CO_3^{-2}, NO_3^-	20,000
Ca(II), Ni(II), Pb(II), Zn(II)	10,000
$S_2O_3^{-2}$	5000
$H_2PO_4^-$	2000
Fe(II), Fe(III)*	1500
SO_4^{-2}	1000
F^-, EDTA	40
Fe(II), Fe(III)	<10

*In the presence of 1,10-phenanthroline, after reduction with hydrogen in acidic medium.

Table 4. Analytical applications

Water†	Added (μg/l.)	Found* (μg/l.)	Average recovery (%)	Found by ICP (μg/l.)
	0.00	3.57	—	3.3
Río Frío	2.22	5.69	98.3	6.0
	4.44	7.94	99.1	8.5
Jaén	0.00	6.86	—	6.5
	4.00	10.66	98.2	11.6
	8.00	14.12	95.0	13.1
Ubeda	0.00	8.96	—	9.5
	4.00	13.10	101.1	12.3
	8.00	16.18	95.4	17.3

Micaschist‡	Found* (%)	Found by AAS (%)
15 ml method	12.59 ± 0.32	12.50

*Average values of three determinations.

†Standard addition calibration graph method, 500 ml sample.

‡Standard calibration graph method. 15 ml sample. Composition of micaschist: 12.50% Al, 4.19% Fe(II), 1.36% Fe(III) and 0.65% Ti.

Analytical applications

The proposed method has been applied to the determination of aluminium content in natural waters (tap waters and raw waters) and a mineral (micaschist).

Natural waters. The method was applied to the determination of aluminium in water samples by standard addition calibration graph method (Table 4).

(a) *Tap water* from Jaén city and Ubeda city (Jaén province);

(b) *raw water* from the spring of Río Frío (Los Villares city, Jaén province).

The loss of sensitivity caused by the matrix effect could be evaluated from the ratio of slopes of the standard addition calibration graph and the standard calibration graph: the ratios were 0.476 (from Jaén), 0.565 (from Ubeda) and 0.555 (from Río Frío). It is seen that the matrix effect in these waters is noticeable. We attribute this strong matrix effect to the high content of, principally, Ca(II), Mg(II) and HCO_3^- in these waters, because they are very hard waters.

Mineral. The method was applied to the determination of aluminium in mineral samples (micaschist) by standard calibration graph method (Table 4).

Acknowledgements—The authors express their thanks to Diputaciónn Provincial de Jaén and to Dirección General de Universidades e Investigación de la Junta de Andalucía (Spain) (Annual Grant No. 1066) for financial support.

REFERENCES

1. M. R. Wills and J. Savory, *Lancet*, 1983, **2**, 29.
2. M. J. Kendrick, M. T. May, M. J. Plishka and K. D. Robinson, *Metals in Biological System*, Ellis Horwood Limited, Chichester, 1992.
3. J. R. Duffield and D. R. Williams, *Aluminium in Food and the Environment*. Royal Society of Chemistry, Cambridge, 1989.
4. P. Slanina, Y. Falkeborn, W. Frech and A. Cedergren, *Fd. Chem. Toxic*, 1984, **22**, 391.
5. J. I. García-Alonso, A. López-García, A. Sanz-Medel, E. Blanco-González, L. Ebdon and P. Jones, *Anal. Chim. Acta*, 1989, **225**, 339.
6. H. Onishi, *Photometric Determination of Traces of Metals*, 4th edn, Part 2A Wiley, New York, 1986.
7. B Bouzid and A. M. G. Macdonald, *Anal. Chim. Acta*, 1988, **207**, 337.
8. K. Yoshimura and H. Waki, *Talanta*, 1985, **32**, 345.
9. A. Molina-Díaz, J. J. Vida-Sagrista, M. I. Pascual-Reguera and L. F. Capitán-Vallvey, *Int. J. Environ. Anal. Chem.*, 1991, **45**, 219.
10. M. I. Pascual-Reguera, A. Molina-Díaz, N. Ramos-Martos and L. F. Capitán-Vallvey, *Anal. Lett.*, 1991, **24**, 2245.
11. M. L. Fernández-de-Córdova, A. Molina-Díaz, M. I. Pascual-Reguera and L. F. Capitán-Vallvey, *Anal. Lett.*, 1992, **25**, 1961.
12. P. Job, *Anal. Chim.* 1927, **9**, 114.
13. H. Dielh and F. Lindstrom, *Anal. Chem.*, 1959, **31**, 414.
14. K. L. Cheng, K. Ueno and T. Imamura, *Handbook of Organic Analytical Reagents*, CRC Press, Boca Raton, Florida, 1982.
15. IUPAC, Nomenclature, Symbols, Units and Their Usage in Spectrometrical Analysis, *Pure Appl. Chem.*, 1976, **105**, 45.
16. Guidelines for Data Acquisition and Data Quality Evaluation in Environmental Chemistry, *Anal. Chem.*, 1980, **52**, 2242.
17. V. N. Tikhonov and T. M. Maksimova, *Zh. Analit. Khim.*, 1976, **31**, 286.
18. A. P. Martynov, V. P. Novak and B. E. Reznik, *Zh. Analit, Khim.*, 1978, **33**, 51.
19. V. N. Tikhonov and T. M. Maksimova, *Zh. Analit. Khim.*, 1975, **30**, 2238.
20. L. H. Jones and D. A. Thurman, *Plant Soil*, 1957, **9**, 131.
21. V. T. Hill, *Anal Chem.*, 1966, **38**, 654.
22. B. F. Reiss, H. Bergamin, E. A. G. Zagatto and F. J. Krug, *Anal. Chim Acta*, 1979, **107**, 309.
23. V. N. Tikhonov and V. V. Bakhtina, *Zh. Analit. Khim.*, 1984, **39**, 2126.
24. Z. Marczenko and M. Jarosz, *Analyst*, 1982, **107**, 1431.

Talanta, Vol. 40, No. 7, pp. 1067–1071, 1993
Printed in Great Britain.

0039-9140/93 $6.00 + 0.00

IMMOBILIZATION OF REAGENTS BY POLYMERIC MATERIALS. DETERMINATION OF METAMIZOL

L. LAHUERTA ZAMORA* and J. MARTINEZ CALATAYUD
Departamento de Química Analítica, Universidad de València, València, Spain

(*Received* 3 *August* 1992. *Revised* 4 *January* 1993. *Accepted* 19 *January* 1993)

Summary—A method for immobilization of inorganic reagents, based on the dispersion of the reagent into an unsaturated polyester solution is applied to immobilization of lead dioxide. The obtained solid is of application in a flow-injection manifold for indirect atomic absorption determination of metamizol in pharmaceutical formulations. The procedure gives a linear calibration graph up to 6 ppm of metamizol with a relative standard deviation of 1.6% (3.0 mg/l) and a sample throughput of 72 hr^{-1}.

Metamizol or dipyrone is a white or yellowish-white odourless crystalline powder, soluble in water and alcohol, slightly soluble in chloroform and practically insoluble in ether. It is the sodium sulphonate of amidopyrine (see formulae); it presents analgesic and antipyretic activities and has been implicated as a causative agent in immune haemalytic anaemia: severe hypothermia might result if it is administered concomitantly with chlorpromazine.[1] The official method (from some pharmacopoeias) for amidopyrine determination is titration against perchloric acid in acetic acid medium using methylrosaniline as an indicator.[2]

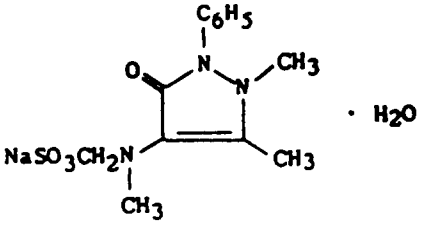

Scheme 1

FORMULAE

The use of insoluble or solid reagents as bed reactors is a consolidated trend in unsegmented continuous-flow methods mainly due to the advantages offered over homogeneous systems, namely simpler manifolds, saving reagents, increased sensitivity and quicker sample passage.[3–6] It is important to point out the number of applications offered by solid-bed reactors like sample or reagent pretreatment, sample-conversion reactions and integrated reaction–detection devices. The use of solid-bed reactors in FIA has been recently reviewed,[6] and also its application to pharmaceutical analysis.[7,8]

The present paper is concerned with the preparation of packed-bed reactors for use in unsegmented continuous-flow analysis. The proposed application is the oxidation of metamizol by means of lead dioxide in perchloric acid media; the drug oxidation yields Pb(II) in the dissolution which is measured by AAS at 217.0 nm. The procedure based on physical entrapment of solid reagents by polymeric resins,[9] is quite simple and fast and it is proposed for the control analysis of the metamizol in a pharmaceutical formulation.

EXPERIMENTAL

Reagents and apparatus

All solutions were prepared with distilled water. Aqueous solutions of metamizol (Guinama, pure), ascorbic acid (Probus, a.r.), thiamine (Acofarma, pure), pirodoxine chlorhydrate (Acofarma, pure), lidocaine chlorhydrate (Guinama, pure), dexamethasone (Guinama, pure), caffeine (Fluka, pure), paracetamol, (Acofarma, pure) and perchloric acid (Panreac, a.r.) were used. Other reagents used were of analytical grade. The packed-bed reactor was prepared with PbO_2 (U.C.B., a.r.) and a polyester resin solution Al-100 (from Reposa) containing low molecular polyester chains and a cobalt compound as activating agent for the reaction; and, methyl ethyl ketone (from Akco) as a catalyst.

*Departamento de Químèca, Colegio Universitario CEU, Moncada (València), Spain.

Flow-injection assembly

Figure 1 shows the continuous-flow manifolds; the sample injector was from Rheodyne, Model 5041; peristaltic pump Minipuls 2, from Gilson; the determination of lead was carried out by means of an AA from Varian, Model SpectrAA-10 at a wavelength of 217.0 nm; internal diameters of the PTFE tubing were of 0.8 and 1.5 mm for the manifold and the reacting column, respectively.

Procedures

Preliminary experiments were carried out by means of the flow assembly depicted in Fig. 1a, in order to test the reactivity in continuous flow of the PbO_2 reactor; 0.2*M* HCl aqueous solution was used for adjusting the acidity of the drug solution, an analyte stream containing 100 ppm

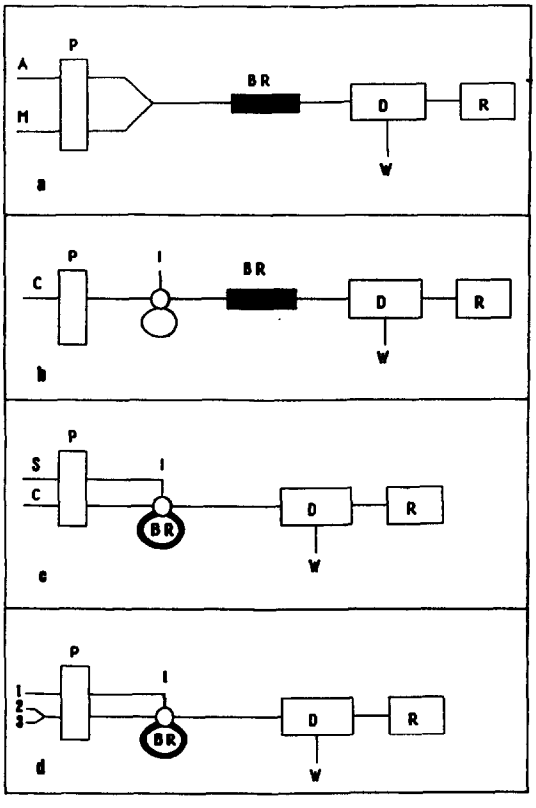

Fig. 1. Flow-injection manifolds. a: Manifold for testing the PbO_2 reactivity with metamizol in different media. b: First manifold proposed for the determination of metamizol. c: Manifold finally proposed for metamizol determination. d: Flow assembly for testing the life-span of the column. A, analyte solution; M, solution for adjusting the medium (acid); P, peristaltic pump; I, injection valve; BR, packed-bed reactor; S, sample; C, carrier; D, detector; and, R, recorder. Channels 2 and 3 (Fig. 1d only) for continuous flowing metamizol and acid, respectively; and 1, for alternative sample injections.

of metamizol, a reagent/polymeric weight ratio of 1/1, and the column was 0.8 i.d. and 15 cm long with 150–250 μm size particles. The procedure consisted of a continuous flow of analyte for 5 min (for column conditioning) and then 10 readings were recorded.

Having established the suitability of the packed-bed reactor, the influence of chemical parameters was sequentially studied: acidity, concentration of the selected acid medium, ionic strength and temperature. The flow manifold configuration was studied on the basis of the chemistry of the system according to the preliminary studies; then the characteristics of the bed reactor and the manifold parameters were established. Finally, the chemical parameters were re-optimized.

Preparation of the bed reactor. Here, 26.40 g of lead dioxide were added to 15.10 g of the polyester resin solution; the mixture was homogeneized by manual stirring and then 0.4 ml of ethyl methyl ketone was added and stirring was continued until the polymer became too rigid. The solid was dried (2–3 hr at room temperature) and then broken with a hammer and ground in a coffee grinder. The selected particles (by sifting) were washed, dried at 80°C, sifted again and stored. The packed-bed was prepared by introducing the particles with the aid of a mini-funnel and continuous stirring into a PTFE tube of 1.5 mm internal diameter.

Preparation of pharmaceutical formulations. The metamizol content was studied in injectables, capsules and solutions. The powder content of three capsules was put in contact with 50 ml of distilled water by magnetic stirring, the resulting mixture was filtered and diluted to 1 l; 1 ml of this solution was levelled to 200 ml. One injection unit was diluted to 1 l and, then, 1 ml of the resulting solution was levelled to 200 ml. The solution was also diluted in two steps: 1 ml to 1 l, and 1 ml to 250 ml.

RESULTS AND DISCUSSION

Preliminary experiments, whose aim was to test the reactivity of the PbO_2 entrapped by the solid polymer, were carried out by means of the manifold depicted in Fig. 1a. The acidified drug solution passing through the reacting column resulted in the oxidation and release of lead from the column; the readings were closely related to the concentration of the drug. Once the suitability of the bed reactor had been established, the flow assembly for the

pre-optimization of the chemical parameters was studied by injecting aqueous sample solutions into the carrier by means of the assembly depicted in Fig. 1b. Different acidic media were tested: hydrochloric, nitric, acetic, phosphoric and perchloric acids (sulphuric acid was excluded in order to avoid lead sulphate precipitation). The acid concentration in the carrier was 0.2*M*; the injected samples contained 50 mg/l of metamizol in 0.2*M* of the same acid as the carrier. Those experiments revealed that the greatest absorbance values were produced by perchloric and phosphoric media. Mean absorbances (5 replicates) were 1.014 HCl; 1.104 HNO_3; 1.122 H_3PO_4; 1.140 $HClO_4$ and 1.068 acetic acid.

Further experiments were carried out with different concentrations of perchloric and phosphoric acids. Both acidic media were studied in three different sets: (a) with a carrier stream of 0.5*M* and varying the acid concentration in the sample solution (50 mg/l of metamizol) over the 0.1–1.0*M* range; (b) aqueous metamizol solutions (50 mg/l) being injected into a carrier stream where acidity varied from 0.1 to 1.0*M*; and, (c) different acidic concentrations containing 50 mg/l of metamizol were injected into a pure distilled water stream. Results are depicted in Fig. 2. The obtained results lead us to select perchloric acid in the carrier and distilled water in the sample. Further work (0, 10^{-4}, 5×10^{-4}, 10^{-3}, 5×10^{-3}, 10^{-2}, 5×10^{-2}, 10^{-1}, 5×10^{-1} and 1*M* perchloric acid) revealed 10^{-1}–1*M* as the best acidic concentration range.

The configuration of the continuous-flow manifold could be important in influencing the degree of reactivity and the dispersion produced. The efficiency of a flow manifold in which the bed reactor is nesting in the sample loop (depicted in Fig. 1c) was tested and results compared with those obtained from the manifold in Fig. 1b. The sample solution was flowing through the sample loop for different time periods, from null to 5 min; best transient signals were obtained for short time intervals and all of them were higher and narrower than those obtained with the manifold in Fig. 1b. The manifold in Fig. 1c with a contact period of 30 sec was selected for further work and the previous results on the influence of acidity were re-optimized by preparing two sets of experiments in which: (a) 20 mg/l of the drug in distilled water were injected into a carrier stream containing different concentrations of perchloric acid, from 0.01 to 1.0*M*; and, (b) 20 mg/l of metamizol in different concentrations of perchloric acid were injected into a carrier 0.1*M* in perchloric acid. The final selected condition from the two sets of experiments was to inject the metamizol dissolved in pure water into a carrier formed by an aqueous solution of 0.1*M* in perchloric acid.

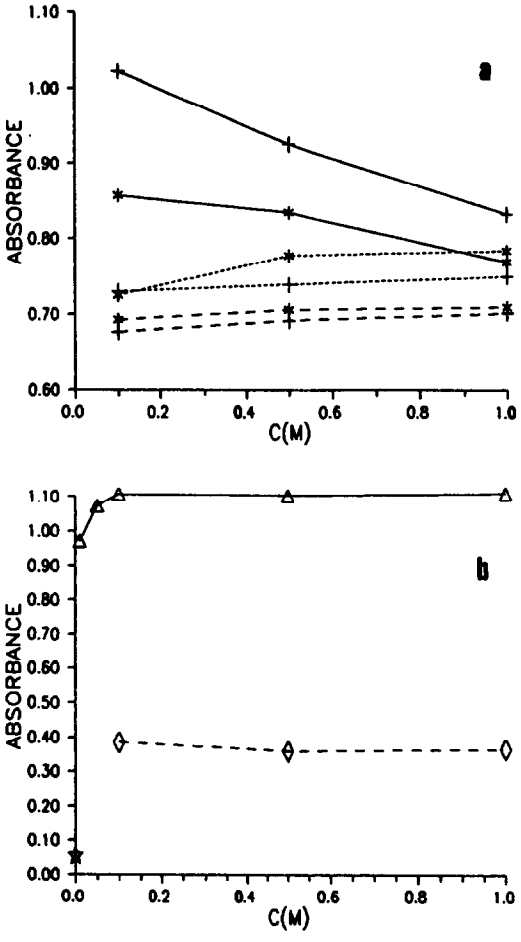

Fig. 2. Influence of acidity on the oxidation of metamizol. a: Influence of acidic media: †perchloric acid; *phosphoric acid solid line, sample in distilled water and perchloric acid solutions as carrier; discontinuous line, carrier stream 0.5*M* in perchloric acid and different acidic concentrations in sample; and, dotted line, different acidic concentrations in sample and distilled water as carrier. For details see text. b: Influence of perchloric concentration. ▲, drug in distilled water and perchloric as carrier; ◇, sample in acidic media and carrier 0.1*M* perchloric; and, ☆, distilled water for sample and carrier.

The influence of ionic strength was tested by preparing different concentrations of KCl in the sample solution; the tested range was 0–2.0*M* in KCl. No relevant influence was observed which lead to the selection of the pure distilled water as the sample and perchloric acid solution as the carrier.

The influence of temperature on the outputs was studied by introducing the carrier container into a water bath at different temperatures; from 20.0 to 78.0°C. Temperature proved not to be a critical parameter; transient signals were slightly increased with temperature. Because of that, room temperature was preferred for further work.

The bed reactor variables are also of relevant importance to the degree of reactivity and the dispersion produced onto the sample, which means a direct influence on the sensitivity and sample throughput. The tested parameters, in the reported order were, internal diameter of the column, size of the bed particles, column length and the weight ratio of entrapped lead dioxide in the resin (milligrams of lead dioxide/milligram of polymeric resin). The first parameter was tested over the range 0.5–1.5 mm at different flow-rates (see Table 1). An internal diameter of 1.5 mm and a flow-rate of 3.00 ml/min were the selected values for further work.

The size of the particles was also tested; selection of the particles was carried out by sifting; the studied range was from 90 to 120 μm up to 300–400 μm. Bearing in mind the peak height and the base width the selected sieve was the one which produced particles over the size 200–300 μm.

The column length was tested from 8.0 to 38.0 cm, with a flow-rate of 3.0 ml/min, particle size of 200–300 μm and 1.5 mm internal diameter, by injecting 20 ppm of that drug in pure water into a carrier containing 0.1M perchloric acid. Results are depicted in Fig. 3 and the selected length was 31 cm. The sample volume of the packed loop, studied by the usual calibration method, was 384.5 μl.

The influence of the weight ratio of immobilized lead dioxide in the resin was studied over the range 0.50–5.00 (g/g); the highest limit of lead dioxide which can be immobilized was limited by the physical consistency of the obtained solid. From the graph of absorbance *vs.* weight ratio, 1.75 was selected for further work.

Table 1. Influence of internal diameter of the column

Internal diameter (*mm*)	*Q*(*ml*/*min*)	Absorbance
0.5	1.1	0.216
0.8	1.1	0.181
	1.5	0.288
	2.3	0.573
1.5	1.1	0.612
	1.5	0.739
	2.3	0.945
	3.0	1.060
	5.5	1.143

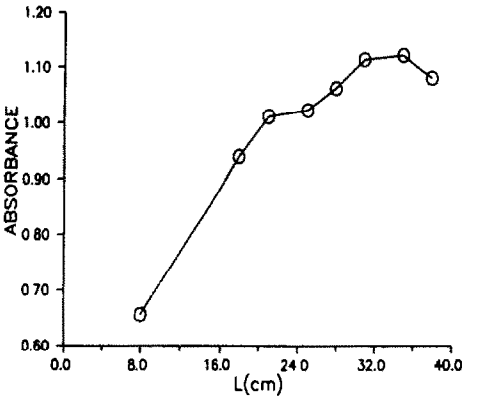

Fig. 3. Influence of column length.

The chemical parameters, concentration of perchloric acid (sample solution and carrier), were re-optimized on the basis of results obtained from the optimization of FIA parameters and by means of the univariate method. No changes are proposed from the above reported values.

After the optimization of chemical and FIA parameters and previous to the study of analytical application, a series of experiments were carried out with the aid of the assembly depicted in Fig. 1d in order to test the life-span of the column. The series of experiments was as follows: (a) the base-line was obtained by passing distilled water (channels 2 and 3), with mean absorbance −0.029; (b) an aqueous solution containing 40 ppm of metamizol was forced through channel 2 and distilled water through channel 3, mean absorbance 0.047; and, (c) as in (b) but the distilled water in channel 3 was replaced by a 0.1M $HClO_4$ stream, mean absorbance 0.615.

Provided the perchloric acid produced the higher degree reaction, (column consumption) the life-span of the column was checked by continuous flow of 40 mg/l of metamizol, channel 2, and 0.1M $HClO_4$, channel 3; after 30 min the column was washed with 0.1M $HClO_4$ and then a set of 10 injections of 5 ppm metamizol were carried out. The experiment was repeated; the average peak-height (in absorbance units) calculated for each set was: 0.735 (3.2%), 0.768 (2.4%), 0.780 (3.2%), 0.780 (3.8%) and 0.732 (4.2%). The readings during the continuous passing of metamizol solution were constant, at 0.645, during the whole experiment. The amount of metamizol forced through the

column by continuous passing was equivalent to 7813 injections of 3 ppm; although the readings remained constant, it was supposed that the life-span of the column did not merit further investigation.

ANALYTICAL APPLICATION

The study of the analytical application of the continuous flow procedures was carried out to establish the application range, reproducibility and sample passage.

The calibration graph was linear over the range 1.0–6.0 ppm of metamizol. The reproducibility of the columns behaviour was tested by preparing three different columns and obtaining the calibration graphs on different days. Table 2 depicts the linear equations and correlation coefficients calculated for the different days tested.

Forty-two different samples containing 3.0 ppm of metamizol were injected into the carrier stream in order to determine the relative standard deviation and sample passage; the results obtained were 1.64% (mean absorbance 0.463) and 72 samples/hr, respectively.

The tolerance of the method to foreign compounds which can be found in typical pharmaceutical samples containing metamizol was investigated by using solutions containing 5.0 mg/l of the drug and adding various concentrations of the interference up to 100 mg/l. The results obtained for various interfering compounds were as follows (concentration in milligrams per litre and relative error, as a percentage): thiamine 100, 1.8; pyridoxin 50, 1.5; lidocaine chlorhydrate 50, 0.6; dexamethasone 100, 1.2; paracetamol 5, 77; caffeine 100, 2.1; ascorbic acid 5, 2.7.

The metamizol content of Nolotil injectables, Nolotil Compositum capsules (from Europharma) and Syntaverin solution (from Igoda) was determined. At least five different preparations were analysed and results were compared with those supplied by the manufacturer. For Nolotil, with given content of 2000 mg/5 ml, the amount found was 2030 mg/5 ml (relative error 1.5%); for Syntaverin, with given content of 500 mg/ml, the amount found was 497.5 (relative error 0.5%) and for Nolotil Compositum, with given content of 300 mg/tablet, the obtained amount was 299.2 (relative error 0.3%).

Table 2. Stability of the column by preparing calibration graphs in different days for three different columns (A, B, C)

Column	Date	Linear equation	Correction coefficient
A	1-VI	$0.140 + 0.100\,X$	0.996
	-VI	$0.114 + 0.105\,X$	0.988
	3-VI	$0.097 + 0.116\,X$	0.992
	4-VI	$0.077 + 0.109\,X$	0.998
	10-VI	$0.043 + 0.093\,X$	0.999
B	1-VI	$0.144 + 0.108\,X$	0.990
	2-VI	$0.126 + 0.102\,X$	0.987
	3-VI	$0.079 + 0.103\,X$	0.996
	4-VI	$0.104 + 0.101\,X$	0.998
C	27-V	$0.135 + 0.118\,X$	0.989
	1-VI	$0.112 + 0.106\,X$	0.992
	2-VI	$0.120 + 0.109\,X$	0.993
	3-VI	$0.093 + 0.100\,X$	0.997
	4-VI	$0.104 + 0.100\,X$	0.998
	8-VI	$0.105 + 0.108\,X$	0.999

REFERENCES

1. A. Wade (ed.), *Martindale, The Extra Pharmacopoeia.* The Pharmaceutical Press, London, 1977.
2. *The Pharmacopoeia of Japan*, 8th ed., p. 52. Society of Japanese Pharmacopoeia, Tokyo, 1973.
3. J. Ruzicka and A. Arndal, *Anal. Chim. Acta*, 1989, **216**, 243.
4. J. Martinez Calatayud and J. V. Garcia Mateo, *Analyst*, 1989, **116**, 327.
5. H. A. Mottola, *Quim. Anal.*, 1989, **8**, 119.
6. J. V. Garcia Mateo and J. Martinez Calatayud, *Chem. Anal.* (Warsaw) in press.
7. J. V. Garcia Mateo and J. Martinez Calatayud, *Pharm. Tech. Int.*, 1992, **4**, 17.
8. *Ibid.*, 1992, **4**, 30.
9. L. Lahuerta Zamora, J. V. Garcia Mateo and J. Martinez Calatayud, *Anal. Chim. Acta*, 1992, **265**, 81.

Talanta, Vol. 40, No. 7, pp. 1073–1075, 1993
Printed in Great Britain.

0039-9140/93 $6.00 + 0.00

STUDY ON THE DETERMINATION OF METRONIDAZOLE IN HUMAN SERUM BY ADSORPTIVE STRIPPING VOLTAMMETRY

ZHENHUI WANG,* HONGXUN ZHOU and SHUPING ZHOU
Department of Chemistry, Henan Normal University, Xinxiang 453002, People's Republic of China

(*Received* 29 *July* 1992. *Revised* 9 *December* 1992. *Accepted* 14 *December* 1992)

Summary—In Britton–Robinson buffer, metronidazole is preconcentrated on a HMDE at 0.0 V (*vs.* Ag–AgCl). An adsorptive stripping peak is observed at −0.62 V. The response is linear from 1×10^{-8} to $1 \times 10^{-6} M$ with 1.5 min accumulation. The method has been successfully applied to the determination of metronidazole in human serum and formulations.

Metronidazole (MTZ)[1-(2-hydroxyethyl)-2-methyl-5-nitroimidazole] is an antimicrobial agent used for the treatment of trichomoniasis and amoebic dysentery. It can kill or inhibit the majority of anaerobic bacteria when its concentration is between 2 and 8 μg/ml in human serum.[1] Therefore, determination of trace levels of MTZ is very important in the prevention of *anaerobic* bacteria infection in clinics.

Various methods have been employed for the determination of MTZ, including spectrophotometry, high-performance liquid chromatography and polarography.[2–4] In this paper, a new method for the determination of trace amounts of MTZ by adsorptive stripping voltammetry has been established. The analyte was preconcentrated by adsorption on the surface of the electrode and the surface-active species was then determined by a voltammetric scan method. As the present study shows, submicromolar MTZ in human serum which has been pretreated can be measured by this method. The sensitivity of this method with 2 min preconcentration is over 50 times higher than that of the pioneer work.[4]

EXPERIMENTAL

Apparatus

A model 79-1 voltammeter (Jinan No.4 Radio Factory) with a Model JM-01 HMDE working electrode (Jiangsu Electroanalytical Instrument Factory), a Ag–AgCl (saturated KCl) reference electrode and a platinum wire auxiliary electrode were used for voltammetric assay. An Orion Research Model SA 720 pH Meter was used for pH determination.

Reagents

Stock solution (4 mg/ml) of MTZ, medical injection, standardized by the standard method.[5] More dilute solutions were prepared daily by dilution with deionized distilled water. The supporting electrolyte was a Britton–Robinson (B.R.) buffer (pH 4.6).[6] All the chemicals were of analytical-reagent grade.

General procedure for adsorptive stripping voltammetry (AdSV)

A 5.0 ml aliquot of B.R. buffer (pH 4.6) solution was placed in the polarographic cell, diluted to 10 ml with de-ionised distilled water, and deaerated by passage of high-purity nitrogen for 5 min. The HMDE was kept at the desired accumulation potential for a given time period, while the solution was stirred at 400 rpm. After a 15 sec rest period, a negative-going scan was initiated, the resulting voltammograms being recorded.

Serum treatment[7]

Pipette 1.00 ml of human serum into a 5-ml centrifugal tube, add 2.0 ml of 0.2 M $Ba(OH)_2$ and 1.0 ml of 5% $ZnSO_4$, mix thoroughly and stand for 2 min. Centrifuge at 2000 rpm in a high speed centrifuge, and then follow the procedure described above. All data were obtained at ambient temperature.

*Author for correspondence.

RESULTS AND DISCUSSION

The derivative technique is an improvement in linear-sweep voltammetry that has been developed for conventional voltammetric measurements. The sensitivity of using second-derivative stripping voltammetry is higher than that of conventional stripping methods.[8,9]

Figure 1 shows the second-derivative cathodic stripping voltammograms for MTZ at the $1 \times 10^{-7}M$ level after 1.5 min preconcentration at 0.0 V from a stirred solution (peak a). With a 4 min accumulation time, a detection limit of $2.5 \times 10^{-9}M$ was obtained. Direct measurement performed under the conditions as mentioned above, but without preconcentration, gave peak b. The stripping peak current b is too small to be useful. It is evident that MTZ can be determined by using AdSV at a mercury electrode.

The effect of pH on the peak potential at a concentration of $1 \times 10^{-7}M$ MTZ was studied over the pH range of 2–8. The peak potential shifts linearly to more negative values with the increase in pH. The peak potential varies with pH according to the following equation: $E_p = -0.24 - -0.08$ pH. Buffer solutions must be used to keep the pH value constant. The peak current was increased at high pH, but the reproducibility was unsatisfactory. The peak form and reproducibility of MTZ were best when pH 4.6 B.R. buffer was used as supporting electrolyte.

The stripping peak current of the MTZ is affected by the preconcentration potential E_a. Experiments showed that the peak current reaches a maximum value at $E_a = 0.0$ V which indicates that this potential is advantageous for the adsorption of the MTZ on the mercury electrode.

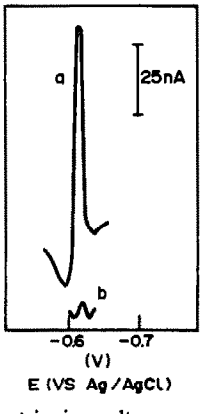

Fig. 1. Adsorptive stripping voltammograms for $1 \times 10^{-7}M$ MTZ in B.R. buffer (pH 4.6). HMDE, scan-rate 100 mV/sec. (a) Preconcentration for 90 sec; (b) without preconcentration.

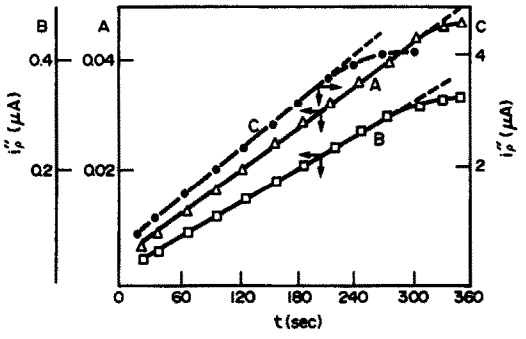

Fig. 2. Effect of preconcentration time on the stripping peak current. (A) [MTZ] = $1 \times 10^{-8}M$; (B) [MTZ] = $1 \times 10^{-7}M$; (C) [MTZ] = $1 \times 10^{-6}M$.

Figure 2 shows the dependence of the adsorptive stripping peak current on the accumulation time at three concentration levels of MTZ. The stripping peak current increased with increasing accumulation time, the corresponding dependence has the nature of an isotherm. At the lower concentration $1 \times 10^{-8}M$, a linear dependence of peak height with accumulation time is observed with a slope of $0.15nA$/sec. The slope is $1.1nA$/sec for $1 \times 10^{-7}M$. But at higher concentration ($1 \times 10^{-6}M$), a linear relation holds up to 200 sec (slope $12.7nA$/sec).

The linear region of the graph depends on the analyte concentration. Thus the choice of optimum accumulation time depends on the range of concentration studied.

The peak current increases linearly with the area of HMDE between 0.02 and 0.04 cm^2, and the latter value was chosen as the optimum.

The presence of other surface-active compounds which might affect the response with competitive adsorption on the mercury surface was investigated, particularly those which might be present in biological samples. The effects of some cations, Cl^- and albumin were examined with a $6 \times 10^{-7}M$ of MTZ solution. The addition of 4 ppm of albumin gives rise to a MTZ peak depression of 35%. It has been proven by our experiments that determination of MTZ has no interference after the human serum is pretreated as mentioned previously. The addition of up to 500 ppm of Na^+, K^+; 430 ppm of Ca^{2+}, Mg^{2+}; 450 ppm of Cl^- and 125 ppm of Cu^{2+}, Pb^{2+}, Cd^{2+} have no interference on the determination of MTZ.

Table 1. Recovery and precision

	MTZ found* (ng/ml)	C.V. (%)	Amount of MTZ added (ng/ml)	Amount of MTZ recovered (ng/ml)	Recovery (%)
Sample					
Human serum	32	4.7	25	55	92
Formulation	120	1.8	70	187	96

*Each value represents the mean of seven analyses.

The preparation of calibration graph in human serum

The serum sample pretreatment step is required owing to high protein content in human serum. The loss of MTZ is unavoidable in the process of serum treatment. For instance, a linear current–concentration relationship in which the slope is $2.9nA$ per $10^{-8}M$ is observed for aqueous standards, the slope is $1.8nA$ per $10^{-8}M$ for serum. Therefore it is necessary to prepare the calibration graph in human serum, and the procedure is as follows.

A 1.00 ml aliquat of human serum not containing MTZ was placed into a 5-ml centrifuge tube. Adding known amounts of MTZ it, and the treatment procedure for serum followed the method given above. The calibration graph passed through the origin and was linear from 1×10^{-8} to $1.6 \times 10^{-7}M$ (a slope of $1.8nA$ per $10^{-8}M$) for 120 sec preconcentration and from 1.8×10^{-7} to $1.6 \times 10^{-6}M$ for 60 sec preconcentration (slope is $2.7nA$ per $10^{-7}M$). The correlation coefficients were 0.9981 and 0.9993, respectively.

Application to determination of MTZ in human serum and in formulation

This determination is feasible for trace amounts of MTZ in human serum with short preconcentration time. The coefficients of variation for the determination of MTZ in human serum and in formulations are 4.7 and 1.8%, respectively, for seven replicate determinations as shown in Table 1.

The recoveries of known amounts of MTZ added to human serum and formulation samples are also given in Table 1. The detection limits have been estimated as 1.7 ng/ml in human serum and 0.63 ng/ml in formulation for 120 sec preconcentration. The results of practical clinical determination are shown in Table 2. This method is suitable for the determination of trace amounts of MTZ in human serum.

The electrochemical behavior of the reductive peak of MTZ was also investigated. The cyclic voltammogram was recorded at HMDE, a reductive peak is observed at −0.62 V, but the oxidative peak is not found on the anodic branch. This result shows that the electrode reaction is irreversible. According to controlled potential coulometry,[10] the number of involved electrons was found to be 4. The total reaction is described as following:

$$[R—NO_2] + 4e + 4H^+ = RNHOH + H_2O$$

This stoichiometry is consistent with the reaction process, in which the nitro group of MTZ is reduced to hydroxylamine in a four-electron process.

Table 2. The concentrations of MTZ in serum following intravenous drips of 0.5 g (drip volume 500 ml)

Time after drip (hr)	MTZ concentration (male serum) (μg/ml)	C.V. %
0	0.00	
1	12.78, 12.29, 11.88, 12.43	3.0
3	16.97, 17.38, 17.63, 17.78, 16.58	2.8
8	8.12, 7.67, 7.74, 8.05, 8.35	3.5

REFERENCES

1. A. Molav, *Med. Clin. North Am.*, 1982, **66**, 12.
2. A. Z. A. Zuhri, S. I. Al-Khalil, M. S. Suleiman, *Anal. Lett.*, 1986, **19**, 453.
3. N. P. Andrew and F. D. Michael, *Anal. Lett.*, 1982, **15**, 739.
4. P. O. Kane, *J. Polarog. Soc.*, 1961, **7(3)**, 58.
5. *Chinese Pharmacopoeia*, 1985, **II**, 96.
6. Department of Chemistry Hangzhou University, *Handbook of Analytical Chemistry* (in Chinese) Book Two, p. 28. Chemical industry press, 1982.
7. W. C. Cai and H. J. Yuan, *Commonly used Analytical Methods for Biological Materials* (in Chinese), p.18. Science Press, 1982.
8. W. Jin and X. Li, *Anal. Chim. Acta.*, 1990, **236**, 453.
9. S. Shi *et al. Fenxi Huaxue*, 1989, **17**, 1085.
10. Zhenhui Wang, Shuping Zhou, *Fenxi Huaxue*, 1989, **17**, 894.

Talanta, Vol. 40, No. 7, pp. 1077–1083, 1993
Printed in Great Britain.

0039-9140/93 $6.00 + 0.00

THE DESIGN OF AN ON-LINE FLOW INJECTION SYSTEM WITH A GRAVITATIONAL PHASE SEPARATOR FOR FLAME ATOMIC ABSORPTION SPECTROMETRY AND ITS ANALYTICAL PERFORMANCE

SOULIN LIN and HWIPING HWANG

Department of Applied Chemistry, China University of Geosciences, Wuhan 430074, People's Republic of China

(*Received* 1 *July* 1992. *Revised* 4 *December* 1992. *Accepted* 28 *December* 1992)

Summary—A liquid–liquid flow extraction system associated with a specifically designed phase separator has been developed. A common trisectional confluence connector was used for segmentation. The system was connected on-line with a flame atomic absorption spectrometer. The performance of the system was studied with respect to determining copper and gold. The detection limits were 1 μg/l. for copper and 1.8 μ/l. for gold, and the precision was 1.8 and 2.5%, respectively, with medium signal enhancement factor 70 for gold, and 78 for copper. Analytical results of real sample analysis were in good agreement with certified values.

Liquid–liquid on-line extraction and preconcentration of trace amounts of heavy metals by flame atomic absorption spectrometry has been found to be very effective and efficient.[1–4] Generic solvent extraction systems with typical segmentors and phase separators were described elsewhere.[5–8] The phase separator is the most critical component of these systems. It seems that the most commonly used phase separators are those constructed using a PTFE membrane sandwiched between two pieces of Perspex. However, these devices are not robust and their use might be restricted, owing to the relatively short life of the membranes. Authors sometimes use a minipore PTFE nylon backed membrane to overcome this difficulty. Backstrom *et al.*[9] described a modified separator using a fluoropore filter supported by a Teflon-coated screen. They used a 1.5 m length of 0.5 mm inner diameter tube as a pressure restrictor to increase the pressure drop across the membrane, which resulted in less loss of organic phase. Sahlestrom and Karlberg[10] developed an unsegmented extraction technique without separation of the two immiscible phases following extraction. Using this technique, they achieved efficiencies typically between 8 and 18% which were far less than routine solvent extraction efficiencies of 60–96%.

The aim of this work is to develop a semi-automated continuous extraction system which is robust and has long-term stability. In this system, the aqueous sample phase and organic solvent were merely segmented by a usual confluence connector. Good regularity of segments was obtained provided that pulse dampers were used to smooth the pulsed streams of the aqueous sample phase and the organic solvent caused by the peristaltic pumps. Copper and gold were used to test the effectiveness and efficiency of the proposed extraction system. Hioki *et al.*[11] reported the liquid–liquid extraction procedure of copper and zinc in 1988. They determined copper and zinc in high purity bismuth by extracting them together as their thiocyanate complexes into methyl isobutyl ketone and followed by atomic absorption spectrometry. In the present work, copper was extracted as its thiocyanate complex into methyl isobutyl ketone (MIBK) and quantified by flame atomic absorption spectrometry. As for gold, the most common method was chosen, which was based on the extraction of the trichloro-complex into MIBK and the gold content was then determined by flame atomic absorption spectrometry. Results obtained in this work demonstrated that the newly designed extraction system and manifold were suitable for routine sample handling and preconcentration of trace metals. This device has made it possible to mechanize the flow system and automate the operation. From the beginning with the aqueous sample to ending with flame atomic absorption measurement, only two manual steps of feeding

the sample and exchanging it with water were needed. A throughput of 28 samples per hour can be achieved with a sample consumption of less than 10 ml per determination.

EXPERIMENTAL

All reagents used were at least of analytical reagent grade. Deionized and distilled water was used throughout. The extraction reagent, NH_4SCN, was made to 15% aqueous solution (w/v) and purified by extraction with MIBK. The extraction was repeated several times until the organic extract was colorless. The purified solution was then diluted successively for use.

The copper standard solution (1000 mg/l. in 2% nitric acid) was prepared from metallic copper. All the standard solutions were prepared by serial dilutions and the standards with concentrations below 0.1 mg/l. were prepared fresh daily.

The gold standard solution (1000 mg/l. in 1% aqua regia) was prepared from metallic gold. All the standard solutions were prepared by serial dilution with 10% hydrochloric acid.

Nitric acid, hydrochloric acid, hydrofluoric acid and ascorbic acid were used in this work.

Equipment and apparatus

A WFX-1A atomic absorption spectrometer (Beijing Second Optical Instrument Factory, China) was used under the operating conditions listed in Table 1.

Table 1. Operating conditions for flame measurements

Wavelength (*nm*)	Au	242.8
	Cu	324.7
Lamp current (*mA*)		4
Slit width (*μm*)		200
Air flow-rate (*l./min*)		6.7
Acetylene flow-rate (*l./min*)		0.67
Optimum burner height (*mm*)		7
Solvent uptake rate (*ml./min*)		10

An IFIS-A intelligent flow-injection sampler (Xian Spring Institute, China) was used for sample handling and preconcentration throughout.

Manifold

The extraction manifold using an eight-channel valve and 1.06 mm inner diameter by 3-m long PTFE tubing as the extraction coil is shown in Fig. 1. The pulses in the sample flow and solvent flow were reduced with the pulse dampeners PD1 and PD2. A trisectional confluence connector with a 1.0 mm inner diameter was used as a segmentor. The flow rates used were 12.6 ml/min for the sample and 0.42 ml/min for MIBK. To facilitate the attainment of the desired flow-rate ratios, the two phases were propelled by separate peristaltic pumps. The sample and MIBK passed the extraction coil, proceeded to segment and finally entered the phase separator. The MIBK was automatically separated from the aqueous phase owing to the difference in specific gravities of the two phases. The solvent extract was then propelled

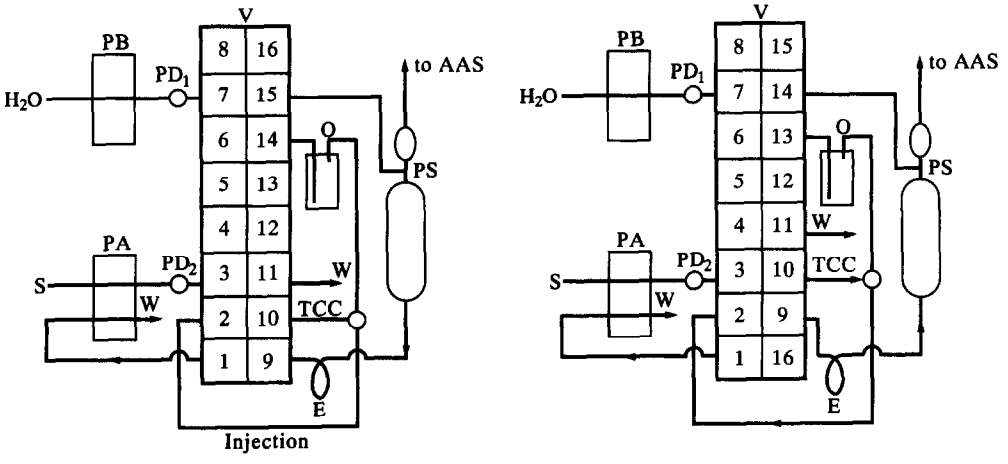

Fig. 1. Extraction manifold: (a) position for injection and washing; (b) position for sample loading. PA—pump A with one silicone rubber pump tube (1.35 mm i.d.) for sampling and a larger one for waste, PB—pump B with one silicone rubber pump tube (1.0 mm i.d.), O—displacement bottle for MIBK, PD1—pulse dampener for MIBK, PD2—pulse dampener for the sample, TCC—trisectional confluence connector, E—extraction coil, 3 m × 1.06 mm i.d. PTFE tubing. V—eight-channel valve, PS—gravitational phase separator, W—wastes.

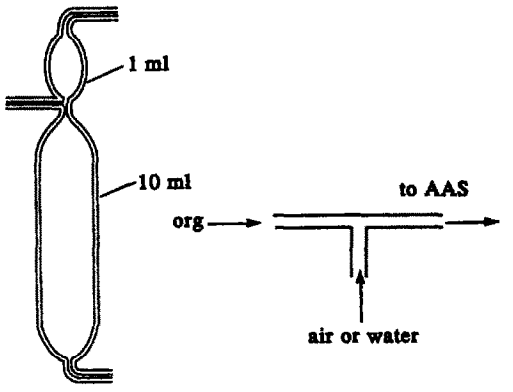

Fig. 2. Construction of the phase separator. (a) Phase separator, (b) compensator.

into the nebulizer of the spectrometer for atomic absorption measurement.

Phase separator

The construction of the phase separator is shown in Fig. 2. The capacity of the bulk of the device was 10 ml with a narrow neck for the separation of MIBK from the aqueous phase. A T-shaped capillary tube was inserted between the phase separator and the spectrometer in order to compensate the difference between the total flow-rate of the manifold and the uptake rate of the spectrometer. Both air and water can be used for compensation.

The capacity of the phase separator was calculated according to the following equation:

$$V_{PS} = Q_w/Q_{org} \times V_{org},$$

where V_{PS} is the capacity of the phase separator, Q_w/Q_{org} is the flow-rate ratio of the aqueous sample phase to the organic solvent, the V_{org} is the volume of organic extract that can give a signal greater than 90% of the equilibrium absorbance. Since an organic extract volume of 200 μl (see Fig. 6) was big enough to meet this requirement and the optimum value of Q_w/Q_{org} for the proposed extraction system was about 30 (see Fig. 5), the capacity of PS must be greater than or equal to 6 ml. In order to provide suitable capacity for extractions which have larger value of Q_w/Q_{org}, V_{PS} was made up to 10 ml. Larger capacity is not suggested, for the larger the capacity is, the longer exhausting time of V_{PS} will be.

The manifold program and time cycle of determinations are shown in Tables 2 and 3.

Segmentor

Several segmentor types of varying efficiency have been described in the literature.[9,12-14] In this work, a usual Teflon trisection confluence connector with 1.0 mm bore size was used as the segmentor instead of a specially designed one, with the three capillaries positioned horizontally. But for segmentation studies, a Perspex connector of the same size was used so that it is possible to follow the segment formation process visually. In these studies, the aqueous phase used was an acidic solution of methyl orange which has a strong red color to permit visual observation of the segments in the PTFE tubing. The organic phase was benzene which does not attack the Perspex connector.

Table 2. Manifold program

Step		1	2	3	4	5	6	7	8
Pump A									
	Time (*sec*)	50	2	1	45	7	9	3	10
	Speed	95	0	90	66	0	92	0	0

Step		1	2	3	4	5	6
Pump B							
	Time (*sec*)	24	7	22	45	17	12
	Speed	0	95	0	4	0	80
Valve position			0			1	0

Valve position 1—loading.
Valve position 0—injection and washing.
Unit of pump speed—rotations per minute.

Flow rate corresponding to the pump speed is as follows:

Speed of pump A	90	80	70	60	50	40
Flow rate (*ml/min*)	17.5	15.5	13.5	11.5	9.5	7.5
Speed of pump B	12	8	4			
Flow rate (*ml/min*)	1.23	0.82	0.42			

Unit of pump speed—rotations per minute.

Table 3. Time cycle of determinations

Time (*sec*)	Function
0–24	Waste in PS is drawn off by PA
25–31	PA stops, PB starts to rinse PS
32–50	PB stops, PA starts again to empty PS
51–52	PA stops. Manually place the sample in position.
53	PA starts, V turns to load position. The sample is allowed to fill up TCC
54–98	PB starts. The two immiscible phases enter TCC at different flow-rates. Segments form in the extraction coil, and then enter PS. The solvent extract is separated from the sample owing to gravitational differences
99–105	PA and PB stop simultaneously. Manually change the sample with water
106–114	PA starts to propel all the segments into PS until the organic extract goes up into the upper bulb of PS
115–117	PA stops, waiting for clear separation. V turns to injection position, waiting for measurement
117–127	PB starts to propel the organic extract to AAS

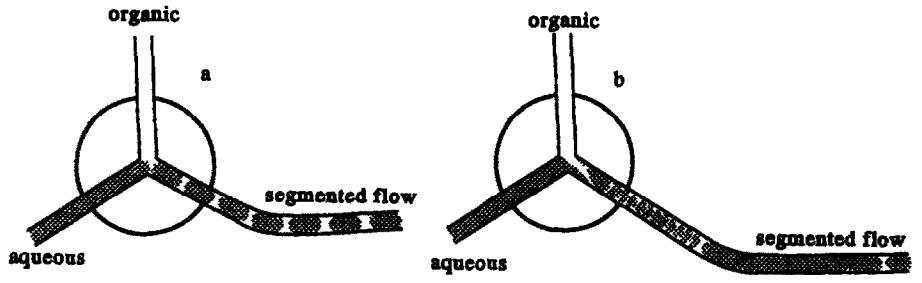

Fig. 3. Process of segment formation (a) at low Q_w/Q_{org} and low total flow rate (< 1 ml/min), (b) at high Q_w/Q_{org} and high total flow rate (10 ml/min). The concentration of Cu is 40 ng/ml.

Pulse dampeners

PD A was an air dampener which had a cylindrical cavity of 200 μl filled with air to smooth the sample flow by the air compressibility. The dampener was initialized 30 sec after starting the pump by introducing air for 4 sec into the sample flow, thus filling the cavity with air at the working pressure.[16] PD B was a glass column 10 cm long and 3 mm inner diameter filled with glass bits.

RESULTS AND DISCUSSION

Segmentation studies

Segments obtained with the trisectional confluence connector had a regular distribution when pulse dampeners for the two phases were incorporated. With the phase flow ratio near to unity, the lengths of the organic and aqueous phase segments were approximately equal. At low phase flow ratio and low total flow rate, droplets or plugs of the organic solvent formed immediately at the confluence point in the continuous flow of the aqueous sample phase, see Fig. 3(a). The segment size mainly depended on the flow rate difference of the two immiscible phases. Segment lengths were short under these flow conditions, e.g. 3 mm for MIBK and 15 mm for the aqueous sample phase. On the other hand, the segmentation mechanism was quite different when the phase flow rate was high. In this circumstance, the process leading to segment formation was attributed to the "ripple process",[15] in which the segment size was determined both by the flow rate difference and the interfacial tension between the two immiscible phases. Firstly, MIBK was drawn into a thin film by the aqueous sample phase. When the tangential force at the interface, which arose from the flow rate difference of the two phases, equalled the interfacial tension, the thin film was broken into very small droplets which wetted the wall of the PTFE tubing, resulting in coalescence so that bigger droplets of MIBK were finally formed at a distance of about 40 mm from the confluence point, see Fig. 3(b). Segmentation remained regular in the extraction coil as long as the inner wall of the tubing was clean and smooth. The segment length of the aqueous phase increased with increasing Q_w/Q_{org}, and in contrast, that of MIBK decreased somewhat when the flow ratio was increased.

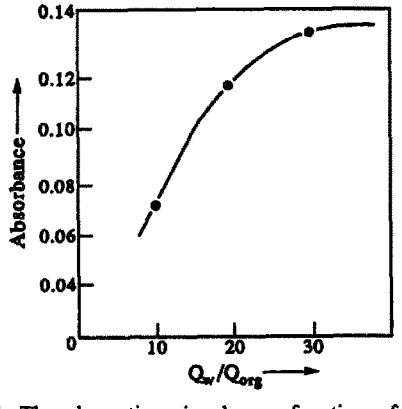

Fig. 4. The absorption signal as a function of Q_w/Q_{org}, varying Q_w at fixed Q_{org}. Length of extraction coil—3 m, Q_{org}—0.42 ml/min, concentration of Cu—40 ng/ml.

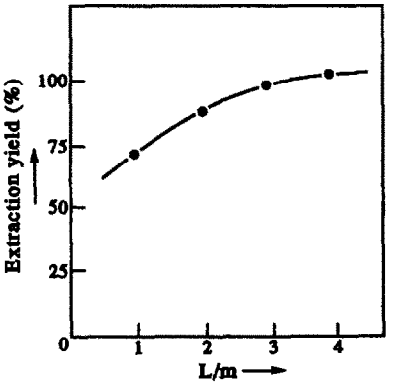

Fig. 5. The extraction yield as a function of extraction coil length.

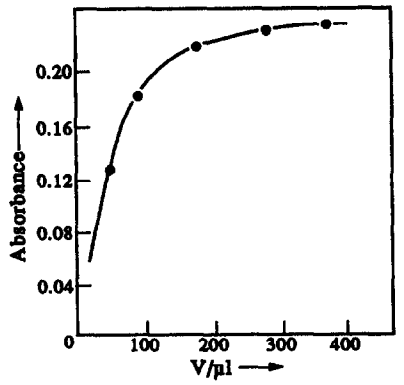

Fig. 6. The absorption signal as a function of the injected volume of the sample.

In the case without a pulse dampener, irregular segmentation may result from the pulse action. The segmentation pattern was complicated with many short segments and a long one sandwiched between them. However, it was found that repeatable patterns can be observed in the extraction coil, though the segment distribution was uneven.

Influence of phase flow ratio

The concentration factor value depends on the flow ratio of the aqueous phase to the organic phase and it would seem that the greater the ratio is the greater the concentration factor will be. However, this is not necessarily always true and there are practical limits to the ratio. Very high phase flow ratio, and thus total flow rate, may cause loss of extraction efficiency. It can be seen from Fig. 4 that the output signal of the spectrometer varies as a function of the phase flow ratio and the curve approaches a maximum plateau at a point corresponding to a flow ratio of 30.

Length of extraction coil

The extraction yields expressed as a percentage of the absorbance at equilibrium at phase flow ratio 30 is given in Fig. 5. It can be seen that the optimum value of tube length was 3 m, corresponding to an extraction time of 12.6 sec at the given pump rates.

Table 4. Extraction efficiencies for the extraction of gold from aqueous phase to MIBK

Coil length (*cm*)	200	200	200
Flow-rate ratio	30	21	10
Total flow rate (*ml/min*)	11.3	10.9	11.3
Extraction efficiencies (%)	94.3	96.8	98.3
Concentration factor	28.3	20.3	9.83

Table 5. Analytical performance of the proposed flow extraction system

	Detection limit (*μg/l*)	Enhancement factor*	Precision (10 *μg/l*)
Au	1.8	70	2.5%
Cu	1.0	78	1.8%
Loading time (*sec*)			30
Sample throughout (*hr*)			28
Sample consumption (*ml*)			7
MIBK consumption (*ml*)			0.22

*Compared with nebulization of aqueous solution.

Injected volume of the organic extract

The effect of injected volume of the organic extract on the absorption peak height was examined. The results are plotted in Fig. 6. In the flow system used in this work for determining Cu and Au, an injected volume of 200 μl was used.

Concentration factor and signal enhancement

The concentration factor, CF, is defined as

$$CF = (Q_w/Q_{org}) \times E \times 100$$

where E is the extraction efficiency given as a percentage of the concentration of the analyte in the organic phase at equilibrium.

The extraction efficiencies for the extraction of gold with different Q_w/Q_{org} are shown in Table 4.

Using the present extraction system, about 70-fold enhancement in sensitivity compared to direct aspiration of aqueous standard was obtained for gold. From Table 4, we may conceive that 2.4-fold enhancement is due to the effect of the organic solvent.

The final manifold

The final manifold shown in Fig. 1 was considered suitable for extractions operating at phase flow ratios of 30 or less. Since much more sample was needed and much larger capacity of the phase separator was required when using higher flow ratios and these would inevitably increase the washing time of the phase separator, a very high phase flow ratio and total flow rate were therefore not preferred. Hysteresis of MIBK in the extraction coil was observed. It was found that MIBK cannot be completely driven out of the extraction coil by water if the resting time in step 5 for pump A in Table 2 was short. This problem was solved by increasing the resting time of pump A, for example 7 sec, allowing coalescence of MIBK which formed thin films on the inner wall of the PTFE tubing,

Table 6. Comparisons of the performance of different phase separators*

	Gravity separator	Membrane separator	Present separator
Construction	Simple	Complex	Simple
Capacity	200 *μl*	150 *μl*	10 *ml*
Sample throughput (*hr*)	20–30	20–30	25–30
Life-time	Long	20 *hr*	Long
Stability	Good	Good	Excellent
Sample consumption (*ml*)	10	16	<10
Solvent consumption (*ml*)	<400	<400	<300
Collection of the organic extract	Differential	Differential	Integral
Separation efficiency (%)	<100	<100	100
Operation	easy	easy	easy

*Values listed are preferred to the average.

leading to the formation of drops and plugs. In order to protect the pump tubing from attack by MIBK, if any, a displacement bottle for MIBK was positioned between the outlet of the injection valve and the pump.

Analytical performance

The analytical performance achieved by the proposed flow extraction system, including detection limits, precision, sensitivity enhancement, sample throughout, sample consumption and MIBK consumption, are listed in Table 5. The sensitivity enhancement factor depends on complex formation, phase flow ratio and loading time, etc. The enhancement factor for a phase flow ratio 30 and a loading time of 30 sec, which is equivalent to a sample volume of 6.8 ml and a MIBK volume of 0.21 ml, is 78 for copper and 70 for gold. The detection limits were calculated on the basis of three times the standard deviation of 11 measurements.

Comparison of the performance of the designed phase separator and that of the existing phase separators are given in Table 6.

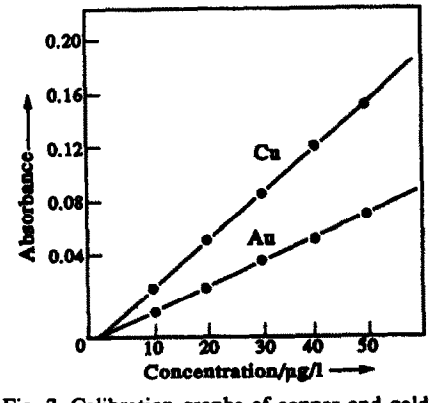

Fig. 7. Calibration graphs of copper and gold.

Real sample analyses

In order to evaluate the figures of merit of the manifold and the accuracy of the procedure, several national and local standard reference rock samples were analyzed. All measurements were performed with the same FI program and using aqueous standard solutions for calibration. As can be seen in Fig. 7, the calibration graphs were linear within the range of interest in this work. It should not be understood that the dynamic range of linearity is much wider. The results presented in Table 7 are in good agreement with the certified values and the precision is acceptable.

Sample preparation

Determination of gold. Weigh out 10 g of the rock sample into a 250 ml conical flask, wet the sample with water. Add 30 ml of hydrochloric acid and heat on a hot-plate for 30 min. Add 10 ml of nitric acid, heat to gently boiling and continue for 2 hr, and then evaporate to a minimum volume. The procedure is repeated one time for complete dissolution of gold and finally evaporate the solution to just dryness. Dissolve the residue with 20 ml of 10% hydrochloric acid, filter through a Bushner funnel

Table 7. Results for copper and gold in standard ore samples

Sample	Au Found	Au Certified value (*ng/g*)	Cu Found	Cu Certified value (*μg/g*)
CSD-1			21.1	21.7 ± 0.2
GSD-2			5.0	4.9 ± 0.2
GSD-3			175.5	177 ± 3
GSD-8				
23CRD-55	940	995 ± 16		
23GRD-56	165	164 ± 2.4		
23GRD-59	4200	4035 ± 23		

using gentle suction. The filtrate is collected in a 100 ml volumetric flask, made up to the mark with 10% hydrochloric acid. The resultant solution is allowed to stand for extraction.

Determination of copper. Weigh out accurately 0.1 g of the rock sample into a PTFE crucible, add 6 ml of hydrochloric acid and heat on a hot-plate for 20 min. Add 2 ml of nitric acid, 5 ml of hydrofluoric acid, followed by several drops of perchloroic acid. Heat gently for 2 hr, and finally evaporate to dryness. Dissolve the residue with 5 ml of hydrochloric acid, dilute with 20 ml of distilled water, filter with a suitable filter paper and collect the filtrate in a 50 ml volumetric flask. Make up to volume with distilled water. Pipette 5 ml of the resultant solution into another 50 ml volumetric flask, add 10 ml of 15% ammonium thiocyanate, 2 ml of 10% ascorbic acid and 1 ml of 5% sodium fluoride, dilute to the mark with distilled water. Shake the solution vigorously and allow to stand for extraction.

CONCLUSION

The results presented in this work demonstrate the applicability of the on-line liquid–liquid extraction system associated with the all-glass gravitational phase separator. This device has a long-term stability and is robust enough for routine analyses.

Acknowledgement—Financial support for this work was provided by Foundation for Developing Geological Sciences and Techniques of China.

REFERENCES

1. L. Nord and B. Karlberg, *Anal. Chim. Acta*, 1980, **118**, 285.
2. M. Varcarcel and M. D. Luque de Castro, *J. Chromatogr.*, 1987, **393**, 3.
3. L. Nord and B. Karlberg, *Anal. Chim. Acta*, 1981, **125**, 199.
4. L. Nord and B. Karlberg, *Anal. Chim. Acta*, 1983, **145**, 151.
5. M. Varcarcel and M. D. Luque de Castro, *Flow Injection Analysis: Principles and Applications*. Ellis Wood, Chichester, 1987.
6. J. Ruzicka and E. Hansen, *Flow Injection Analysis*. John Wiley & Sons, 2nd Edn, New York, 1988.
7. B. Karlberg and S. Thelander, *Anal. Chim. Acta*, 1978, **98**, 1.
8. J. Kawase, *Anal. Chem.*, 1980, **52**, 2124.
9. K. Backstrom, L. Danielson and L. Nord, *Anal. Chim. Acta*, 1985, **169**, 43.
10. Y. Sahlestrom and B. Karlberg, *Anal. Chim. Acta*, 1986, **179**, 315.
11. A. Hioki, Noriko Fudagawa, M. Kubota and A. Kawase, *Anal. Chim. Acta*, 1988, **209**, 281.
12. V. Kuban, L. G. Danielsson and F. Ingman, *Anal. Chem.*, 1990, **62**, 2026.
13. K. Orgata, K. Taguchi and T. Imanari, *Anal. Chem.*, 1982, **54**, 31, 641.
14. M. Bengsson and G. Johansson, *Anal. Chim. Acta*, 1984, **58**, 147.
15. V. Kuban and F. Igman, *Anal. Chem.*, 1991, **22**, 491.
16. K. Backstrom and L. G. Danielsson. *Anal. Chim. Acta*, 1990, **232**, 301.

Talanta, Vol. 40, No. 7, pp. 1085–1090, 1993
Printed in Great Britain.

0039-9140/93 $6.00 + 0.00

SPECTROPHOTOMETRIC DETERMINATION OF TRACE COPPER WITH A Cu-DIETHYLDITHIOCARBAMATE-β-CYCLODEXTRIN COLOUR SYSTEM*

SHIHE LI, SHENGQUAN LI† and ANJIA CHEN
Department of Basic Sciences, Shanxi Agricultural University, Taigu, People's Republic of China

(*Received* 23 *June* 1992. *Revised* 14 *December* 1992. *Accepted* 14 *December* 1992)

Summary—A simple, selective and accurate spectrophotometric method for determination of trace copper with diethyldithiocarbamate(DDTC) in the presence of β-cyclodextrin(β-CD) in ammonia media has been developed. The apparent molar absorptivity of Cu(II)-DDTC-β-CD inclusion complex is 1.3×10^4 $l \cdot mole^{-1} \cdot cm^{-1}$ at 436 nm, and Beer's law is obeyed for copper in the range 0–150 μg/25 ml. The detection limit is $4.38 \times 10^{-7} M (S/N = 3)$. The proposed method has been successfully applied to the determination of copper in aluminium alloys, soils, millet, wheat flour, herbs, vegetables and some traditional Chinese herbal medicines with satisfactory results.

Cyclodextrins are cyclic, non-reducing oligosaccharides containing six, seven or eight glucopyranose units. β-Cyclodextrin(β-CD), the most generally useful member of this group, contains seven glucopyranose units. Cyclodextrins are water-soluble since all of the free hydroxyl group are on the outer surface of the ring. The internal cavity of the doughnut-shaped CD molecule is slightly apolar.[1] The nature and cylindrical structure of cyclodextrin allows it to interact with small molecules having an appropriate size to form inclusion complexes. Qi *et al.*[2,3] have applied β-CD to colour systems for spectrophotometry. The CDs serve to solubilize or sensitize the analytical metal complex system due to the formation of the inclusion complexes.

The reagent diethyldithiocarbamate(DDTC) has been reported as a chromogenic agent for copper.[4–7] However in a great majority of these methods, an extractive procedure is required. Only in a few of these procedures can the determination be carried out directly in aqueous solution due to solubility problems. However upon addition of β-CD, an inclusion complex of Cu(II)-DDTC-β-CD forms in the presence of ammonia. That is, the $[Cu(DDTC)_2]$ complex binds to β-CD and is solubilized in water. The colour reaction of Cu(II) with DDTC can be conducted directly in water in the presence of β-CD. This paper reports on our spectrophotometric studies of Cu(II)-DDTC-CD-β-CD inclusion complex. The use of suitable masking agents ensures that the proposed method for determination of copper(II) is free from interferences from a large number of elements. Moreover, the recommended procedure has been successfully applied to the determination of copper in aluminium alloys, soils, millet, wheat flour, herbs, vegetables and some traditional Chinese herbal medicines with satisfactory results.

*Project supported by the Natural Sciences Foundation of Shanxi Province, China.
†Author for correspondence.

EXPERIMENTAL

Reagents

All chemicals used were of analytical-reagent grade. Demineralized water was used throughout.

Standard copper(II) solution, 0.1 mg/ml. Dissolve 0.0393 g of copper sulphate ($CuSO_4 \cdot 5H_2O$) in ca. 50 ml of water with 0.5 ml of 4*M* sulphuric acid and dilute to the final 100 ml volume with water. This stock solution is further diluted to 20 μg/ml Cu(II) as a working solution.

Sodium diethyldithiocarbamate(DDTC) aqueous solution, 0.011M.

β-CD aqueous solution, $8.8 \times 10^{-3}M$.

Ammonia solution, 7.5M (Ammonia : water = 1:1, v/v).

Ammonium citrate solution, 2M.

1,10-Phenanthroline aqueous solution, 0.01*M.*

Apparatus

Absorption spectra were measured with a Model DU-70 spectrophotometer (Beckman, USA) and the absorbance measurements were performed on a Model 721-100 spectrophotometer (Shanghai).

Procedures

General. To an aliquot containing no more than 150 μg of copper(II) in a 25-ml calibrated flask, add 2.0 ml of 7.5M ammonia solution, 5.0 ml of $8.8 \times 10^{-3}M$ β-CD solution, and 0.5 ml of 0.011M DDTC solution, dilute to the mark with water and shake thoroughly. Measure the absorbance in a 2-cm cell at 436 nm against a reagent blank (or water).

Determination of copper in aluminium alloys. Accurately weigh out 0.1000 g of control aluminium alloy specimen and transfer the specimen to a porcelain evaporating dish. Add 7 ml of 2.5M sodium hydroxide solution, heat, and add about 1 ml of 8.8M hydrogen peroxide after the specimen is decomposed, and continue heating until the bubbles cease. Cool and add 7.9M (1:1, v/v) nitric acid until all salts are dissolved. Transfer the solution to a suitable standard flask (determined by the amount of copper in specimen), add concentrated ammonia-water (about 15M) until the aluminium hydroxide precipitate appears, then add 7.9M nitric acid until the precipitate just dissolves, and dilute to the mark with water. Transfer two aliquots of the specimen solution containing no more than 150 μg of copper to two 25-ml calibrated flasks. Add the following solutions, in order, into both flasks: 5 ml of 2M ammonium citrate solution, 2 ml of 0.01M 1, 10-phenanthroline solution, 2 ml of 7.5M ammonia solution, and 5 ml of $8.8 \times 10^{-3}M$ β-CD solution. Add 0.5 ml of 0.011M DDTC solution to only one of the flasks. Dilute (both flasks) to the mark with water and shake thoroughly. Measure the absorbance of the sample at 436 nm against the solution without DDTC.

Determination of copper in soil. Transfer 1.000 g of the soil to a porcelain crucible and heat to 550°C in a muffle furnace to burn off the organic matter. Transfer the residue to a platinum crucible and dissolve by addition of minimum amount of hydrofluric acid (about 10 ml), heat cautiously, and finally evaporate the solution to dryness. After cooling add 10 drops of 1M sodium hydroxide, evaporate again to dryness, soak the residue with water and transfer the solution to a 50-ml volumetric flask. Next, adjust its pH to around 1 using 1M of sodium hydroxide, dilute to the mark with water, and filter the solution. Transfer two 10 ml portions of the filtrate to two 25-ml calibrated flasks. To both flasks, add ammonia solution (7.5M) until Fe(III) hydroxide precipitate forms completely, and add all 2 ml of 2M ammonium citrate solution (Note 1), 5 ml of $8.8 \times 10^{-3}M$ β-CD solution. Add 0.5 ml of 0.011M DDTC solution to only one of the flasks. Dilute (both flasks) to the mark with water and shake thoroughly. Measure the absorbance of the sample at 436 nm against the solution without DDTC (Note 2).

Notes

1. After adding ammonium citrate, precipitate of Fe(III) hydroxide can dissolve completely for samples that contain a relatively small amount of iron, while for samples that contain a relatively large amount of iron the partial precipitate of Fe(III) hydroxide may still exist in the solution, but with no influence on the determination of copper.

2. The differences between samples may give the following cases. If the diluted solution is clear the determination of copper can be immediately performed. If the solution is slightly turbid, leave it at room temperature for about 10 min, the solution may clear due to solubilization of β-CD. If the solution remains turbid, filtration of the solution is required prior to determination of copper.

Determination of copper in corn and plant samples. Weigh 1.0000 g of sample preliminarily treated (dried, crushed, ground and sifted) and transfer it to a Kjeldahl flask. Moisten the sample using a small amount of water, add 8 ml of concentrated sulphuric acid and leave to set at room temperature for about 12 hr. Boil for 5–10 min, cool, and add several drops of hydrogen peroxide, then continue to boil for about 5 min and follow the same process until the solution appears clear. Boil to remove residual hydrogen peroxide, cool, transfer the solution to a 50-ml volumetric flask. Wash the Kjeldahl flask with concentrated ammonia-water (about 15M) and transfer the washed solution to the 50-ml volumetric flask, adjust the solution so that it is basic with ammonia (add 1–2 ml each time and cool the flask in running tap water), dilute to the mark with water, mix, and then filter the solution. Transfer two 12.5 ml aliquots of filtrate into 25-ml volumetric flasks, add 2 ml

of 2M ammonium citrate, 2 ml of 0.01M 1, 10-phenanthroline, and 5 ml of $8.8 \times 10^{-3}M$ β-CD solution to each flask. Next, add 0.5 ml of 0.011M DDTC solution to the single flask. Dilute (both flasks) to the mark with water and shake thoroughly. Measure the absorbance at 436 nm against the blank solution which contains no DDTC.

RESULTS AND DISCUSSION

Absorption spectra

The absorption spectra of the Cu(II)-DDTC-β-CD inclusion complex and its reagent blank are shown in Fig. 1. The maximum absorption of the inclusion complex is at 436 nm, a wavelength at which the reagent blank does not appreciably absorb. There is essentially no difference between the reagent blank absorbance and that of water.

Effect of acidity

The inclusion complex of Cu(II)-DDTC-β-CD is only formed under basic conditions. The effect of acidity on the absorbance of the complex was studied using 7.5M ammonia. The results obtained are shown in Fig. 2. The recommended amount of 7.5M ammonia is 2.0 ml in the procedures (*i.e.*, the concentration of ammonia is 0.6M).

Effect of β-CD concentration

The effect of β-CD concentration on the absorbance of inclusion complex was examined. The results are shown in Fig. 3. The recommended amount is 5.0 ml of $8.8 \times 10^{-3}M$ β-CD solution in the procedures (*i.e.*, the final concentration of β-CD is $1.76 \times 10^{-3}M$).

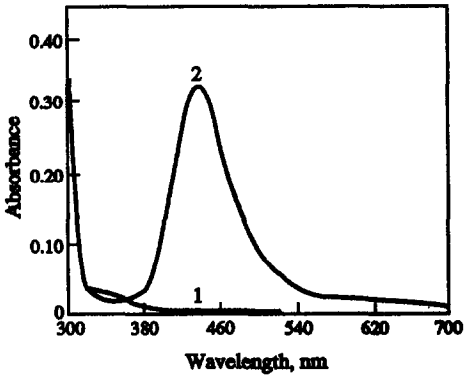

Fig. 1. Absorption spectra. Conditions: the final concentrations of the following reagents and cells are identical for 1 and 2. Ammonia, 0.6M; β-CD, $1.76 \times 10^{-3}M$; DDTC, $2.2 \times 10^{-4}M$; 1-cm cell. 1. DDTC against demineralized water. 2. Inclusion complex against reagent blank, the final concentration of copper(II) is 1.6 μg/ml.

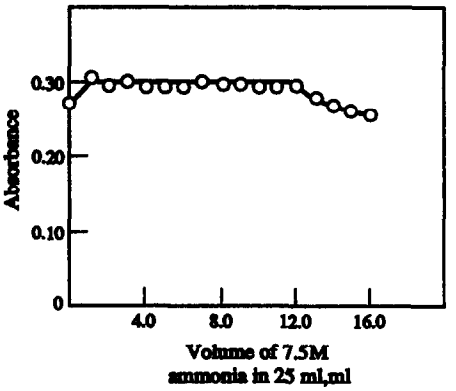

Fig. 2. Variation of the absorbance of the Cu(II)-DDTC-β-CD complex at 436 nm *vs.* the concentration of the ammonia present. Conditions: 1.6 μg Cu(II)/ml; β-CD, $1.76 \times 10^{-3}M$; DDTC, $2.2 \times 10^{-4}M$; 1-cm cell.

Effect of amount of DDTC

The effect of the amount of 0.011M DDTC solution on the absorbance of the inclusion complex was studied. The results obtained indicate that the absorbance is not appreciably affected by changes in the amount of 0.011M DDTC solution used in the procedure between 0.25–10.0 ml (*i.e.*, the final concentration of DDTC solution are between $1.1 \times 10^{-4}M$ and $4.4 \times 10^{-3}M$). The recommended amount of DDTC selected for the subsequent procedures was 0.5 ml (that is, the final concentration is $2.2 \times 10^{-4}M$).

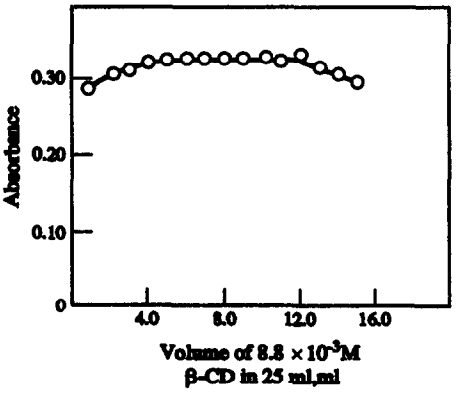

Fig. 3. Variation of the absorbance of the Cu(II)-DDTC-β-CD complex at 436 nm *vs.* the concentration of the β-CD present. Conditions: except ammonia and β-CD, as for Fig. 2. 0.6M ammonia for Fig. 3.

Table 1. Spectrophotometric behaviour of the Cu(II)-DDTC complex in different media

Medium	C	V (*ml*)	λ_{max} (*nm*)	ϵ ($\times 10^4$)	t (*min*)	S.T.
β-CD	1	5	436	1.30	in a tw.	72
Arabic gum	0.5	5	444	0.92	20	480
PVA-124	1	1	444	0.95	in a tw.	72
Emulsifier OP	1	5	450	1.24	in a tw.	15
AEO-9	1	1	450	1.19	in a tw.	3
Tween-80	1	4	454	1.16	in a tw.	240
CTMAB	1	3	450	1.14	5	3
Peregal O	0.5	2	444	1.01	in a tw.	90
β-CD + PVA-124	1,1	5,1	436	1.30	in a tw.	72
β-CD + arabic gum	1,0.5	5,5	436	1.32	5	72

C: Concentration of surfactant, %(w/v); V: Volume of surfactant added; ϵ: Apparent molar absorptivity; t: Time required for colour development; S.T.: Stable time of the complex, hour; in a tw.: in a twinking. The concentrations of DDTC and ammonia are identical with the procedure (general).

Effects of surfactants on the procedure

Spectrophotometric behaviour of the Cu-DDTC complex in the presence of surface-active substances was also studied. The surface-active substances included: arabic gum, polyvinyl alcohol-124 (PVA-124), emulsifier OP-[C_8H_{17}-⬡-$O(CH_2CH_2O)_{9\text{-}10}H$], AEO-9[$C_{12}H_{25}O$-$(CH_2$-$CH_2O)_9H$], Tween-80, cetyltrimethylammonium bromide (CTMAB) and Peregal $O[C_{18}H_{37}O(CH_2CH_2O)_{20}H]$. The test results (shown in Table 1) indicate that the tested surfactants all solubilize the complex and stabilize the colour system to some degree. However, β-CD is the best one, so β-CD was chosen in the procedure.

Effect of temperature

The influence of the temperature on the colour system of Cu(II)-DDTC-β-CD was studied by holding the solution at different temperatures between 20°C and 100°C. The absorbance is not appreciably altered by changes in the temperature between 20°C and 100°C (Fig. 4).

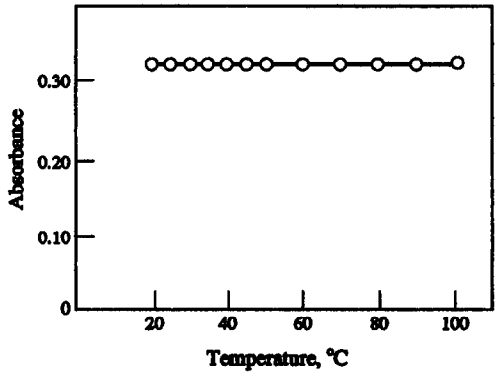

Fig. 4. Effect of temperature. Conditions: 436 nm; 1-cm cell; other conditions as for Fig. 1.

Characteristics of the system

Linear regression of the calibration data (the absorbance at 436 nm *vs.* the concentration of Cu(II), μg/25 ml) yields the equation $A = 0.005 + 0.008c$. The correlation coefficient is 0.9999. Beer's law is obeyed over the range 0–150 μg Cu(II) per 25 ml under the optimum conditions at 436 nm with a molar absorptivity of 1.30×10^4 l · mole^{-1} · cm^{-1}. The standard deviation of separation determination is 1.0×10^{-3} ($n = 10$) and relative standard deviation is 0.3%. The detection limit is $4.38 \times 10^{-7}M$ Cu ($S/N = 3$).

Selectivity

The selectivity was investigated by measurement of 20 μg of Cu(II) (in 25 ml) in the presence of a series of other ions. The results are tabulated in Table 2. The stated levels of the species in Table 2 did not cause an error exceeding 5%.

Masking of interfering ions

Some interfering ions may be masked by using proper masking agents. The tested results are as follows. 5 ml of 2M ammonium citrate can mask 100 mg of Al^{3+}, 7.5 mg of Mg^{2+}, 4 mg of Ti^{4+}, 0.75 mg of Mn^{2+}, 0.4 mg of Cr^{3+}, respectively. After precipitation of iron, 5 ml of 1, 10-phenanthroline (0.01M) can mask 0.3 mg of Ni^{2+}. Iron may be precipitated by adding ammonia-water in a 25-ml volumetric flask and the determination of Cu(II) can be performed directly, without the need for any additional separation steps.

As stated above, the proper masking agent may be added by aiming at different interfering ions according to the actual composition of a sample. For this reason, the selectivity of the proposed method is greatly improved and the

Table 2. Effect of foreign species

Foreign species	Tolerance limit,* *mg*
NO_3^-,ClO_4^-,SO_4^{2-}	1000
Na^+	200
K^+,NH_4^+	100
Ca^{2+},Zn^{2+}	50
Cl^-,CH_3COO^-	10
Li^+,P(V)	5
B(III)	4
Ba^{2+},Cd^{2+},Si(IV),Se(IV),Br^-,I^-	1
V(V)	0.25
Zr^{4+}	0.2
Cs^+,Be^{2+},Mg^{2+},Sr^{2+},Pb^{2+},Sn(II),Al^{3+},Ti^{4+},Ge(IV), As(V),Sb(V),W(VI),Mo(VI),Nd_2O_3,CeO_2,La_2O_3,Y_2O_3	0.1
Fe^{3+},Ni^{2+}	0.05
Fe^{2+},Co^{2+}	0.02
Cr^{3+},Rh(III)	0.01
Ag^+,Hg^{2+},Pd^{2+}	0.002
Ammonium citrate (2*M*)	5 *ml*
Tartaric acid (1*M*)	1 *ml*
Thiocarbamide (0.1*M*)	4 *ml*
Ammonium oxalate (0.1*M*)	5 *ml*
Sodium fluoride (0.5*M*)	5 *ml*
1,10-Phenanthroline (0.01*M*)	5 *ml*

*Maximum values of some species were not determined.

practicality is increased. Particularly, the copper amounts in complex samples may be determined by using the proposed method. Moreover, the tolerance limits of NO_3^-, ClO_4^-, SO_4^{2-} are especially high, which is advantageous with respect to the digestion of samples.

Accuracy and validity

In order to check the accuracy and validity of the proposed method, control aluminium alloy specimens, Chinese herbal medicines and various agricultural samples were analysed using the recommended procedure. The results are shown in Tables 3 and 4.

CONCLUSION

In Marczenko's opinion,[4] the popular spectral methods for copper are mainly the dithizone method, dithiocarbamate methods (*i.e.*, DDTC methods), cuproine methods and cuprizone method. All of these methods, except the cuprizone method, require an extractive procedure, employing organic solvents which are harmful to health and environment, such as carbon tetrachloride, chloroform and isopentanol. Though the proposed system (CU(II)-DDTC-β-CD) uses the old chromogenic agent (DDTC) for copper, it has many advantages over previous DDTC-systems[4-7] and other currently employed spectral methods for copper[4] owing to the presence of β-CD. First, the determination of copper with the proposed colour system can be directly conducted in aqueous solution without the need for any separations. Second, the characteristics of the system have been improved so that the colour development is almost instantaneous and the stability of the inclusion complex is particularly high. In addition, the useful concentration range (0–150 μg/25 ml) for Beer's law is widened. Third, the results obtained in this work show that the proposed method is applicable to a variety of copper containing samples and that the method is simple, selective and accurate.

Table 3. Results of determination of copper in control aluminium alloy specimens

Control specimen	Certified amount of copper, %	Copper found,* %	Relative error, %
ZL_6	0.095	0.096	1.05
LC_4	1.51	1.53	1.32
ZL_3	7.30	7.25	−0.96

*Average of five separate determinations.

Table 4. Results for the determination and recovery of copper in Chinese herbal medicines and agricultural samples*

Sample	Amount determined (μg/g) Initial Cu(II)	Cu(II) added	Final Cu(II)	Recovery, %
Soil sample 25	35.73	20.00	55.04	96.6
Soil sample 26	25.93	20.00	46.13	101
Soil sample 30	35.36	20.00	54.73	96.9
Soil sample 31	39.24	20.00	58.59	96.8
Millet from Taigu	10.60	20.00	30.72	100.6
Wheat flour from Taigu	8.59	20.00	28.24	98.3
Alfalfa from Taiyuan Zoo Garden	16.04	20.00	36.02	99.9
Millet straw from Taigu	18.38	20.00	38.49	100.6
Potato from Taigu	13.80	20.00	33.47	98.4
Carrot from Taigu	17.43	20.00	37.49	100.3
The tuber of multiflower knot weed (Chinese medicine)	9.71	20.00	29.95	101.2
Honeysuckle (Chinese medicine)	15.88	20.00	36.63	103.8

*All determined values given in Table 4 are the averages of three separate determinations.

Acknowledgements—The authors are indebted to Professor Changsong Liu (the Department of Chemistry, Shanxi University, Taiyuan) for his help.

REFERENCES

1. J. Szejtli, *Cyclodextrins and Their Inclusion Complexes*. Akadéiai Kiadó, Budapest, 1982.
2. Lizhong Zhu, Xiaofeng He and Wenbin Qi, *Yankuang Ceshi*, 1990, **9**, 22.
3. Lizhong Zhu and Wenbin Qi, *Huaxue Shiji*, 1991, **13**, 156.
4. Z. Marczenko, *Separation and Spectrophotmetric Determination of Elements*, Horwood, Chichester, 1986.
5. Shaopu Liu, Pengming Zhu, Guoxuan Zhang and Chongde Yang, *Jinshu Huaxue Fenxi Gailun Yu Yingyong (Introduction and Application of Metals Analysis)*. Sichuan Kexue Jishu Chubanshe, Chongqing, 1985.
6. Hao Hu, *Yankuang Ceshi*, 1991, **10**, 114.
7. Huigai Lin, Chenxi Zhao and Guifa Yang, *Lihua Jianyan (Huaxue Fence)*, 1991, **27**, 82.

Talanta, Vol. 40, No. 7, pp. 1091–1095, 1993
Printed in Great Britain.

0039-9140/93 $6.00 + 0.00

THE HYDROLYSIS OF LEAD(II). A POTENTIOMETRIC AND ENTHALPIMETRIC STUDY

J. J. CRUYWAGEN* and R. F. VAN DE WATER
Department of Chemistry, University of Stellenbosch, Republic of South Africa

(*Received* 15 *June* 1992. *Revised* 2 *September* 1992. *Accepted* 20 *October* 1992)

Summary—The hydrolysis of lead(II) has been investigated by potentiometric titrations (ionic medium 1.0*M* $NaClO_4$ and 1.0*M* KNO_3) and enthalpimetric titrations (ionic medium 1.0*M* $NaClO_4$) at 25°. The reaction model that gave the best fit to the data for 1.0*M* $NaClO_4$ comprised the following five ions: $Pb(OH)^+$, $Pb_3(OH)_4^{2+}$, $Pb_3(OH)_5^+$, $Pb_4(OH)_4^{4+}$ and $Pb_6(OH)_8^{4+}$. The formation constants, and enthalpy changes (kJ/mol) for these species, defined according to equation (1), have the values $\log \beta_{11} = -7.8$, $\Delta H^0_{11} = 24$; $\log \beta_{34} = -22.69$, $\Delta H^0_{34} = 112$; $\log \beta_{35} = -30.8$, $\Delta H^0_{35} = 146$; $\log \beta_{44} = -19.58$, $\Delta H^0_{44} = 86$; $\log \beta_{68} = -42.43$, $\Delta H^0_{68} = 215$. Equilibrium constants determined in nitrate medium show good agreement with those pertaining to perchlorate medium if complexation of lead(II) with nitrate is taken into account.

The hydrolysis of lead(II) results in the formation of mono- and polynuclear hydroxo ions; the reaction equilibria can be represented by the general equation

$$p\,Pb^{2+} + q\,H_2O \rightleftharpoons [Pb_p(OH)_q]^{(2p-q)+} + q\,H^+ \quad (1)$$

Complete characterization of these equilibria has been hampered by experimental limitations. For example, to prevent precipitation either the concentration of lead has to be kept rather low or the pH range must be restricted to very narrow limits. Also, carbon dioxide and traces of sodium carbonate must be excluded from test solutions to avoid slow premature precipitation of lead as basic lead carbonate. However, careful experimentation and thorough data analysis have led to agreement among authors about the existence of the following ions: $Pb(OH)^+$, $Pb_3(OH)_4^{2+}$, $Pb_4(OH)_4^{4+}$, and $Pb_6(OH)_8^{4+}$.[1-7] Other species that have been postulated are: $Pb_2(OH)^{3+}$ as a minor component,[3] and more recently $Pb_3(OH)_3^{3+}$, and $Pb_3(OH)_5^+$; the latter ion was proposed as an addition to the model of four species mentioned above,[6] but the $Pb_3(OH)_3^{3+}$ ion was included in the model in the place of the $Pb(OH)^+$ ion.[7] Although medium ions could play a role in stabilizing a particular ion it is evident that the system still needs some clarification. A correct model together with reliable equilibrium constants for the species concerned are prerequisites not only for studies of lead complexation in aqueous solution, but also for the interpretation of calorimetric data. In fact, the calorimetric data collected in two previous investigations have not been interpreted in terms of the same model and appreciable differences occur in the values reported for the thermodynamic quantities of some species,[3,7] notably for the $Pb_3(OH)_4^{2+}$ ion.

In this paper we report the results of a potentiometric investigation of lead(II) in two different ionic media and at an ionic strength not previously studied, namely 1.0*M* $(Na)ClO_4$ and 1.0*M* $(K)NO_3$. Calorimetric data for the hydrolysis reactions were obtained for 1.0*M* $NaClO_4$ and used to calculate the enthalpy and entropy changes for the formation of the various species.

EXPERIMENTAL

Reagents and solutions

All reagents were of analytical grade and solutions were prepared with water obtained from a Millipore Milli-Q system. Carbonate-free sodium hydroxide, prepared from an aged saturated solution,[8] was standardized by titration against potassium hydrogen phthalate. Perchloric acid and nitric acid were standardized against recrystallized borax and the results checked by titration against standard sodium hydroxide. Sodium perchlorate, potassium nitrate, and lead nitrate were purified as follows: a saturated solution was allowed to stand for at least a week and then filtered through a porisity three sintered glass filter. From this solution,

*Author for correspondence.

relatively large crystals were grown by slow evaporation at ~25° in a dust-free environment. These crystals were filtered off, washed with pure water, and used to prepare a stock solution which was standardized by evaporating known volumes to dryness and heating to constant weight at 140°. Lead perchlorate was prepared by treating PbO with standardized perchloric acid.[2] The solid PbO was introduced to a cold acid solution stirred by a stream of purified nitrogen and left to stand overnight. This solution was then filtered through a porosity four sintered glass filter and standardized gravimetrically as lead iodate.[9]

Potentiometric titrations

The hydrolysis was investigated in ionic media, 1.0*M* $(Na)ClO_4$ and 1.0*M* $(K)NO_3$, by titrating an acidified lead solution with sodium hydroxide. The free hydrogen concentration, h was determined by measuring the potential to ±0.1 mV with a Radiometer PHM84 research pH-meter. For the measurements in perchlorate medium a Ross combination electrode (Orion Research) with a 3.0*M* $NaClO_4$ (instead of 3.0*M* KCl) internal salt bridge solution was used. A Radiometer glass electrode (G202C) and calomel reference electrode connected to a Wilhelm type salt bridge with renewable liquid junctions was used for the measurements in nitrate medium;[10] the composition of the salt bridge was: 1.0*M* KNO_3/3.0*M* NaCl/1.0*M* KCl.

The reaction vessel consisted of a double-walled glass vessel and the temperature was kept at 25.0 ± 0.1° by circulating water from a thermostatted bath. Purified nitrogen was passed through the medium solution and then bubbled slowly through the titration solution. The titrant, usually sodium hydroxide solution, was delivered with a Metrohm 665 Dosimat and sufficient time (at least 5 min) was allowed to ensure that equilibrium had been attained. The electrode systems were calibrated by titration of acid with sodium hydroxide in either 1.0*M* $(Na)ClO_4$ or 1.0*M* $(K)NO_3$. The data were treated with the program SUPERQUAD[11] to calculate values for E^0 and s in the Nernst equation

$$E = E^0 + s \log h \qquad (2)$$

The calculations were done on the assumption that a small amount of protolytic impurity was present in the medium salt.[12] For perchlorate medium the value for s obtained was 58.58 compared with the theoretical 59.16 at 25° and the concentration of the impurity (alkaline) was $7 \times 10^{-5}M$. For nitrate medium the impurity was found to be $1.1 \times 10^{-4}M$ and $s = 59.40$. These values were used in calculations of the free hydrogen ion concentration and also when E^0 was determined by titrating excess acid which had been added to the lead(II) solutions. For brevity, $-\log h$ is denoted by pH_c.

The initial concentrations of the lead(II) perchlorate solutions titrated with sodium hydroxide were as follows: 1.0, 1.5, 2.5, 5.0 and 1.0m*M*. The titrations were carried out in duplicate or triplicate, but with different initial acid concentrations in some cases. For the measurements in potassium nitrate medium the titrations were started with the following lead concentrations: 1.0, 2.0, 2.5, 5.0, 7.5, 10.0, 20.0 and 50.0m*M*. Because of the very low solubility of basic lead nitrate species, precipitation begins at lower pH_c values in nitrate medium and fewer data points could therefore be collected at a particular lead concentration.

Enthalpimetric titrations

An isothermal titration calorimeter, Tronac model 550, described elsewhere,[13] was used for the enthalpy measurements. Solutions containing lead perchlorate and some perchloric acid (20.0 cm^3) were titrated with sodium hydroxide from a precision microburette (2.5 cm^3) and the data collected as described previously.[14] The initial concentrations of lead(II) were 5.0, 7.5, 10.0, 25.0 and 50.0m*M* and all solutions were made 1.0*M* with respect to perchlorate. The titrations were carried out in duplicate. The sodium hydroxide was titrated as slowly as possible, typically at speeds varying from 1.25 to 2.50 μl per second, commensurate with the concentrations of the reagents and amount of heat evolved. Blank titrations were carried out which showed that the heat involved in the mixing and dilution of the reagents in 1*M* $(Na)ClO_4$ was negligible.

RESULTS AND DISCUSSION

Potentiometric investigation

Sodium perchlorate medium. The titration data were treated with the computer program SUPERQUAD.[11] Of the various reaction models considered, and taking into account all species previously proposed, the following model resulted in the best fit between calculated and experimental points:

$Pb(OH)^+$, $Pb_3(OH)_4^{2+}$, $Pb_3(OH)_5^+$, $Pb_4(OH)_4^{4+}$, and $Pb_6(OH)_8^{4+}$.

Table 1. Values determined for formation constants $-\log \beta_{pq}$ of species $[Pb_p(OH)_q]^{(2p-q)+}$ in various ionic media

$Pb(OH)^+$	$Pb_2(OH)^{3+}$	$Pb_3(OH)_3^{3+}$	$Pb_3(OH)_4^{2+}$	$Pb_3(OH)_5^+$	$Pb_4(OH)_4^{4+}$	$Pb_6(OH)_8^{4+}$	Medium	Ref.
7.80	—	—	22.69	30.8	19.58	42.43	1*M* $NaClO_4$	*
8.72	6.79	—	24.33	—	21.01	44.91	1*M* KNO_3	*
7.94	—	—	22.83	—	19.01	41.55	1*M* KNO_3	*,†
7.9	6.4	—	22.87	—	19.25	42.12	3*M* $NaClO_4$	3
—	—	15.29	22.78	—	19.42	42.33	3*M* $LiClO_4$	7
7.93	—	—	—	—	19.35	—	2*M* $NaClO_4$	4
8.84	7.11	—	—	—	21.72	—	2*M* $NaNO_3$	4
7.86	—	—	23.91	31.75	20.40	43.38	0.1*M* KNO_3	6

*Results of this investigation.

†Complex formation of Pb^{2+} with NO_3^- taken into account in the calculations.

The value of $s = 0.747$ (sample standard deviation[11]) based on estimated errors of 0.01 cm^3 in the volume and 0.2 mV in the potential implies a very good fit. The formation constants defined by equation (1) are given in Table 1 and the distribution of the various species, as a function of pH_c, is shown in Fig. 1. Also listed in Table 1 are literature values for constants pertaining to different ionic media. It is seen that the present model agrees with that obtained by Sylva and Brown,[6] but differs from the model reported by Ishiguro and Ohtaki[7] which included a $Pb_3(OH)_3^{3+}$ species but excluded both the $Pb(OH)^+$ and $Pb_3(OH)_5^+$ species. When the $Pb_3(OH)_3^{3+}$ ion was included in our model it was rejected by the program. SUPERQUAD automatically rejects species with ill-defined formation constants, *i.e.*, when the standard deviation of the constant is more than 33% of its value, or if its value is negative.[11] Apart from the inclusion of the minor species, $Pb_2(OH)^{3+}$, which occurs only at very high lead concentration (*cf.* next section) the model reported by Carell and Olin[3] differs from the present model only in respect of the $Pb_3(OH)_5^+$ ion. Omission of the $Pb_3(OH)_5^+$ ion from our model resulted in a significantly poorer fit, the value $s = 1.21$ was obtained. The absence in earlier models of the latter ion, first reported by Sylva and Brown,[6] can be ascribed to a lack of data in a small domain defined by relatively low concentration and high pH_c (*cf.* Fig. 1).[6]

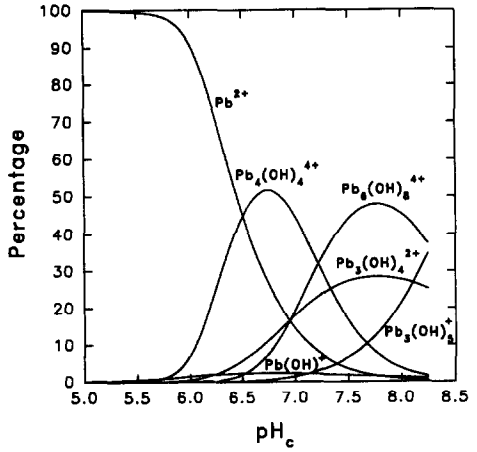

Fig. 1. Distribution of the lead(II) species, expressed as a percentage of the total lead concentration (0.01*M*).

Potassium nitrate medium. For a given lead concentration precipitation begins at much lower pH_c in this medium. Only the titrations at the lowest lead(II) concentrations could proceed to $pH_c \sim 7.5$. Under these conditions the percentage concentration of the $Pb_3(OH)_5^+$ ion is so small that its characterization becomes problematical. At 0.0025*M* Pb^{2+}, for example, the maximum concentration $Pb_3(OH)_5^+$ attained in 1*M* KNO_3 at pH_c 7.2 is only 3.5% of the total lead compared to the 18.2% at pH_c 7.7 in 1.0*M* $NaClO_4$ (*cf.* Fig. 1). Treatment of the data with the program SUPERQUAD resulted in a model comprising the species: $Pb(OH)^+$, $Pb_2(OH)^{3+}$, $Pb_3(OH)_4^{2+}$, $Pb_4(OH)_4^{4+}$, and $Pb_6(OH)_8^{4+}$. Apart from the expected absence of the $Pb_3(OH)_5^+$ ion, the only difference compared to the model obtained for perchlorate medium is the addition of the $Pb_2(OH)^{3+}$ ion. When the values for the stability constants for the two media are compared it is seen that the constants pertaining to the nitrate medium have greater (negative) values. A similar effect is noticeable in the constants reported by Hugel[4,5] for ionic media 2.0*M* $NaClO_4$ and 2.0*M* $NaNO_3$ respectively.

Part of these differences can be explained in terms of lead(II) nitrate complex formation. Introducing the complex ions $PbNO_3^+$ in the treatment of our data resulted in the rejection of the $Pb_2(OH)^{3+}$ species and supplied values for the hydrolysis constants which are very similar to those calculated for perchlorate medium (Table 1). The literature value[15] for the formation constant of $PbNO_3^+$, $\log K_1 = 0.33$, was

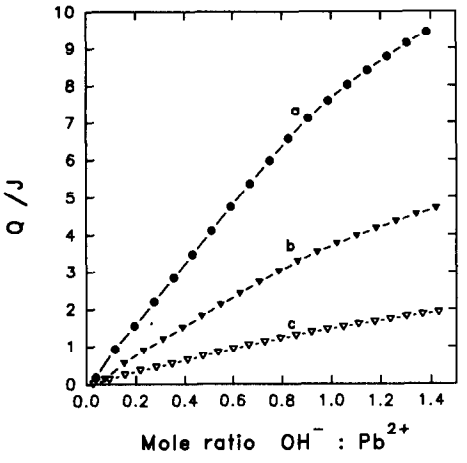

Fig. 2. Measured heat, Q, as a function of the molar ratio of hydroxide to lead(II) for titrations of (a) 0.05, (b) 0.025 and (c) 0.01*M* lead(II) solutions.For the 0.01*M* lead(II) solution $pH_c = 7.1$ at mole ratio 1.0.

treated as a fixed constant. When log K_1 was refined together with the other constants, the value 0.32 ± 0.01 was obtained in good agreement with the literature value.

The $Pb_2(OH)^{3+}$ ion is such a minor species (max. 1% at $pH_c = 6$) that its rejection by the program seems appropriate when NO_3^- complexation (which in effect reduces the free Pb^{2+} considerably at $pH_c < 6.5$) is taken into account. Although Olin and co-workers[3,16] found this species in perchlorate medium also, its maximum concentration under the most favourable conditions, *i.e.*, at lead concentration 1.45*M* and $pH_c = 4.5$, was only 2.1%. For solutions at moderate concentrations and $pH_c > 5.0$, the $Pb_2(OH)^{3+}$ ion can therefore be neglected for most practical purposes.

The reaction model and the values for the formation constants of the species can now be regarded as established with sufficient certainty to be used as basis for a calorimetric investigation, the results of which are described in the following section.

Enthalpimetric titrations

The results of representative titrations of lead (II) with sodium hydroxide are shown in Fig. 2. The total heat measured, Q, is plotted against the molar ratio of base added to lead(II). Depending on the lead concentration, a mole ratio of hydroxide:lead(II) of only about 1.4 could be effected before precipitation started.The measured heat actually represents the enthalpy changes for the following reactions:

$$p\mathrm{Pb}^{2+} + q\mathrm{OH}^- \rightleftharpoons [\mathrm{Pb}_p(\mathrm{OH})_q]^{(2p-q)+} \quad (3)$$

and is given by equation (4)

$$Q = n_w \Delta H^0_w + n_{pq}(\Delta H^0_{pq})' \quad (4)$$

where n_{pq} is the number of moles formed and $(\Delta H^0_{pq})'$ is the molar enthalpy change for the formation of a given species $[p,q]$ at 25°*C* in 1.0*M* $NaClO_4$ medium; n_w is the number of moles of free acid neutralized and ΔH^0_w is the enthalpy change for the formation of water. The contribution of the first term of equation (4) to the total heat measured was quite small because the lead solutions contained very little excess acid, typically $pH_c \sim 4.0$. The literature value[17] 56.1 kJ/mol for ΔH^0_w, pertaining to 1.0*M* $NaClO_4$, was used in the calculations and also to convert $(\Delta H^0_{pq})'$ values to the enthalpy changes for the hydrolysis reactions represented by equation (1). Values for n_{pq} at each titration point were derived from the concentrations of the species by simultaneous solution of the two mass balance equations (5) and (6).

$$B = b + \Sigma p\beta_{pq} b^p h^{-q} \quad (5)$$

$$C_A = h - K_w/h - \Sigma q\beta_{pq} b^p h^{-q} + C_B \quad (6)$$

where B, C_A and C_B are the total analytical concentrations of lead(II), acid and base, respectively; b is the equilibrium Pb^{2+} concentration and log $K_w = -13.71$. The set of linear equations thus obtained from corresponding Q and n_{pq} values were solved for the $(\Delta H^0_{pq})'$ parameters following a least squares procedure. The results are summarized in Table 2. All

Table 2. Values of the equilibrium constants and other thermodynamic quantities (kJ/mol) for the formation of lead(II) hydroxo species in 1.0*M* $(Na)ClO_4$ medium (298 K) according to equation (1). $(\Delta H^0)'$ refers to the reaction: $p\mathrm{Pb}^{2+} + q\mathrm{OH}^- \rightleftharpoons [\mathrm{Pb}_p(\mathrm{OH})_q]^{(2p-q)-}$ and $\Delta H^0 = (\Delta H^0)' - q\Delta H^0_w$ where $\Delta H^0_w = -56.1$ kJ/mol

	log $\beta_{pq} \pm 3\sigma$	ΔG^0	$(\Delta H^0)'$	ΔH^0	$T\Delta S^0$	$\Delta H^0/q$
$Pb(OH)^+$	-7.80 ± 0.06	44.5	-32 ± 10	24 ± 8	-21	24
$Pb_3(OH)_4^{2+}$	-22.69 ± 0.21	129.5	-112 ± 5	112 ± 5	-18	28
$Pb_3(OH)_5^+$	-30.80 ± 0.03	175.8	-135 ± 3	146 ± 3	-30	29
$Pb_4(OH)_4^{4+}$	-19.58 ± 0.02	111.8	-138 ± 1	86 ± 1	-26	22
$Pb_6(OH)_8^{4-}$	-42.43 ± 0.09	242.2	-234 ± 3	215 ± 3	-27	27

Table 3. Summary of thermodynamic data (kJ mol^{-1}) at 25°C for the reaction $pPb^{2+} + qH_2O \rightleftharpoons [Pb_p(OH)_q]^{(2p-q)+} + pH^+$

Species	1*M* (Na)ClO$_4$ ΔG^0	ΔH^0	This work $T\Delta S^0$	3*M* (Na)ClO$_4$ ΔG^0	ΔH^0	Ref. 3 $T\Delta S^0$	3*M* (Li)ClO$_4$ ΔG^0	ΔH^0	Ref. 6 $T\Delta S^0$
$Pb(OH)^+$	44.5	24	−21	45.1	—	—	—	—	—
$Pb_3(OH)_3^{3+}$	—	—	—	—	—	—	87.2	67	−21
$Pb_3(OH)_4^{2+}$	129.5	112	−18	130.5	111	−20	130.0	62	−68
$Pb_3(OH)_5^+$	175.8	146	−30	—	—	—	—	—	—
$Pb_4(OH)_4^{4+}$	111.8	86	−26	109.9	84	−26	110.8	81	−30
$Pb_6(OH)_8^{4+}$	242.2	215	−27	240.4	207	−34	241.6	243	1

species were present in relatively high percentage concentrations (maximum at least 35%) except the $Pb(OH)^+$ ion which attained a maximum concentration of only 4% at the lowest lead concentration (5.00m*M*) titrated. The value obtained for ΔH^0_{11} (24 kJ/mol) is therefore rather uncertain but seems quite reasonable when compared to $\Delta H_{pq}/q$ (~26 kJ/mol) for the polynuclear ions; it has been estimated[3] that ΔH^0_{11} should lie between the limits 20 and 40 kJ/mol. The ΔH^0 values determined for the polynuclear ions $Pb_3(OH)_4^{2+}$, $Pb_4(OH)_4^{2+}$, and $Pb_6(OH)_8^{4+}$ (Table 3) agree very well with those reported by Carell and Olin,[3] while the enthalpy change for the $Pb_3(OH)_5^+$ ion fits well into the pattern set by the other species. The value $\Delta H^0_{34} = 62$ kJ/mol reported by Ishiguro and Ohtaki[7] for the $Pb_3(OH)_4^{2+}$ ion differs greatly from our value (112 kJ/mol) and that of Carell and Olin[3] (111 kJ/mol) and should therefore be questioned. Although the hexanuclear complex is usually formulated as $Pb_6(OH)_8^{4+}$ in potentiometric studies, X-ray diffraction investigations have provided strong evidence[18] for a structure in solution similar to that obtained in the solid state, namely $Pb_6O(OH)_6^{4+}$, which consists of three face-sharing tetrahedra.[19]

CONCLUSION

The results of this investigation confirm the existence of the hydroxo complexes $Pb(OH)^+$, $Pb_3(OH)_4^{3+}$, $Pb_3(OH)_5^+$, $Pb_4(OH)_4^{4+}$ and $Pb_6(OH)_8^{4+}$ in the pH range 5.5–8.5 Hydrolysis constants and other thermodynamic parameters have been determined for these complexes; the enthalpy and entropy changes for $Pb(OH)^+$ and $Pb_3(OH)_5^+$, determined for the first time, are consistent with those of the other species. In view of the very good agreement between the values of thermodynamic quantities determined in this investigation and some values previously reported, the system can now be regarded as fairly well characterized. A comparison of the results for perchlorate and nitrate media shows that the reaction model and equilibrium constants are affected if complexation of lead(II) by nitrate is neglected. Also, due to lower solubility of basic lead nitrate species the range of either pH_c or concentration available for measurements is more limited in nitrate than in perchlorate medium.

Acknowledgements—Financial support by the University of Stellenbosch and the Foundation for Research Development is gratefully acknowledged.

REFERENCES

1. C. F. Bayer Jr. and R. E. Mesmer, *The Hydrolysis of Cations*, Wiley-Interscience, New York, 1976.
2. A. Olin, *Acta Chem. Scand.*, 1960, **14**, 126, and references therein.
3. B. Carell and A. Olin, *ibid.*, 1962, **16**, 2350.
4. R. Hugel, *Bull. Soc. Chim. France*, 1964, 1462.
5. *Idem*, *ibid.*, 1965, 968.
6. R. N. Sylva and P. L. Brown, *J. Chem. Soc. Dalton*, 1980, 1577.
7. S. Ishiguro and H. Ohtaki, *Bull. Chem. Soc. Japan*, 1981, **54**, 335.
8. G. H. Jeffery, J. Bassett, J. Mendham and R. C. Denny, *Vogel's Textbook of Quantitative Chemical Analysis*, 5th Ed., Longman and Wiley, New York, 1989.
9. C. H. R. Gentry and L. G. Sherrington, *Analyst*, 1946, **71**, 31.
10. F. J. C. Rossotti and H. Rossotti, *The Determination of Stability Constants*, McGraw-Hill, London, 1961.
11. P.Gans, A. Sabatini and A. Vacca, *J. Chem. Soc. Dalton Trans.*, 1985, 1195.
12. E. S. Johansen and O. Jons, *Talanta*, 1984, **31**, 743.
13. J. J. Christensen, J. W. Gardner, D. J. Eatough, P. J. Watts and R. M. Hart, *Rev. Sci. Instrum.*, 1973, **44**, 481.
14. J. J. Cruywagen, L. Krüger and E. A. Rohwer, *J. Chem. Soc. Dalton Trans.*, 1991, 1727.
15. R. M. Smith and A. E. Martell, *Critical Stability Constants* Vol. 4, Plenum, New York, 1976.
16. L. Pajdowski and A. Olin, *Acta Chem. Scand.*, 1962, **16**, 983.
17. R. Arnek, *Akiv Kemi*, 1970, **32**, 55.
18. G. Johansson, *Acta Chem. Scand.*, 1989, **43**, 307.
19. T. G. Spiro, D. H. Templeton and A. Zalkin, *Inorg. Chem.*, 1969, **8**, 856.

Talanta, Vol. 40, No. 7, pp. 1097–1105, 1993
Printed in Great Britain.

0039-9140/93 $6.00 + 0.00

PRESERVATION OF SOLID MERCURIC DITHIZONATE SAMPLES WITH POLYVINYL CHLORIDE FOR DETERMINATION OF MERCURY(II) IN ENVIRONMENTAL WATERS BY PHOTOCHROMISM-INDUCED PHOTOACOUSTIC SPECTROMETRY

EDWARD P. C. LAI,* BARBARA WONG and VICTORIA A. VANDERNOOT

Centre for Analytical and Environmental Chemistry, Ottawa-Carleton Chemistry Institute, Department of Chemistry, Carleton University, Ottawa, Ontario, Canada K1S 5B6

(*Received* 24 *April* 1992. *Revised* 11 *September* 1992. *Accepted* 11 *September* 1992)

Summary—A novel sample preparation technique has been developed to preserve solid mercuric dithizonate [$Hg(HDz)_2$] in a matrix of polyvinyl chloride (PVC) for analysis by photochromism-induced photoacoustic spectrometry (PCPAS). This technique, which begins with the extraction of Hg^{2+} from water with dithizone, allows for the determination of Hg^{2+} in environmental samples. Inclusion of $Hg(HDz)_2$ within the polymer matrix enhances the PCPAS signal amplitude over that from the bare $Hg(HDz)_2$ film by almost sixfold. The standard calibration graph of PCPAS signal amplitude as a function of Hg^{2+} concentration is linear in the concentration range of 5–100 μg/ml. A lower detection limit can be achieved by using a laser of higher power tuned to a wavelength closer to the maximum absorptivity of the excited $Hg(HDz)_2$ complex. A study, conducted to monitor the change in PCPAS signal amplitude obtained for the same sample over an extended storage period of 19 days, demonstrates that the PVC protects the integrity of the solid $Hg(HDz)_2$ sample. Hence, it is potentially feasible to collect environmental samples from a remote area for analysis at a later date.

Despite the toxic nature of mercury known since ancient times, the element and its compounds had been used and discarded with little thought to the consequences to human health and to the environment. The seriousness of the problem was first realized in the 1950s among small fishing villages along the shores of Japan's Minamata Bay.[1] The illness, which came to be known as Minamata disease, was caused by methylmercury poisoning as a result of eating contaminated fish. In humans, the initial symptoms include numbness of the lips and limbs. As the sickness progresses, permanent damage is done to the central nervous system, and the victim experiences visual constriction, loss of motor coordination, and, in the final stages prior to death, loss of memory, speech, hearing and taste. The source of the contamination was eventually found at a chemical plant near Minamata Bay. Along with an estimated 220 tons of elemental mercury released into the bay with the plant's waste effluent between 1949 and 1953, traces of methylmercury, produced unintentionally in a side reaction, were discharged. Swedish studies conducted in the 1960s revealed that the inorganic mercuric ion could be methylated by microorganisms in the sediments of waterways.[2] Methylmercury can bioaccumulate in fish as it is at least 1000 times more soluble in lipids than in water and concentrates in muscle tissues, the brain and the central nervous system.[3] Mercury levels as high as 24 ppm were found in the fish in Minamata Bay, which are well above the modern federal guideline of 0.5 ppm of mercury in fish.[4]

The use of mercury in industry and agriculture has decreased dramatically in the developed world since the early 1970s due to legislation regulating the discharge of mercury.[1] Despite efforts to remove the mercury from polluted waterways, mercury contamination of waterways still remains a problem today. Given the recent political changes on the international scene that have brought a new awareness of the environment, one sees the need for sampling at more and increasingly remote sites.[5] Analytical

*Author for correspondence.

methods for environmental specimens often require that samples be transported to sophisticated facilities prior to chemical analysis. As a result, considerable time may elapse between the collection of the samples and the initiation of the analytical procedure, thus potentially compromising the data generated by the analysis. Since many of the analytical methodologies require significant economic expenditures (and potential future clean-up processes even more so), ensuring maximum data reliability is blatantly crucial. Studies which defined the time frame in which samples can be expected to remain stable and recommended storage conditions that maximize this pre-analysis holding time have been reported previously.[6]

Analytical samples are in a chemically dynamic state at the time of collection. At the moment the sample is removed, it is exposed to conditions significantly different from the source conditions and the chemical processes may deviate from those that occur *in situ*. For example, photochemical reactions may take place and the temperature-dependent kinetics of reactions will be altered when the sample is exposed to ambient light and atmospheric temperature. In addition, the dissolved gases will change, air oxygen may initiate oxidation of some chemical species, and the pH of the sample will most likely change.[7] The dynamic process does not end after the sample has been carefully transferred into some vessel for subsequent delivery to an analytical laboratory. The analyte can be lost from samples because of volatilization, absorption, or reaction with container materials.[7] Sample containers may irreversibly adsorb analytes from the sample and act as a negative interference, leading to erroneously low measured values.[7] In fact, the loss of sample integrity is governed by several factors, including photodegradation, chemical action, volatilization, and biological action. Sample containers also represent a major source of sample contamination in environmental measurements; they may introduce extraneous compounds into the sample. Moody and Lindstrom[8] examined 12 different plastic materials including conventional and linear polyethylene, polycarbonate, and several types of Teflon. They found significant levels of leachable trace elements in all of the materials examined. In order to control contamination associated with a particular determination, potential sources of contamination must first be identified for the method employed. Contamination may be introduced either in the field during sample collection, handling, storage, or in transport to the analytical laboratory. Additional contamination may arise during sample preparation or in the analytical process itself.[9]

Significant effort has recently been placed on the development of procedures for the precise fortification and stabilization of collected samples. Preservation techniques are used to minimize changes in samples between collection and analysis; they preserve the integrity of the sample after collection. Physical changes such as volatilization, adsorption, diffusion and precipitation, and chemical changes such as photochemical and microbial degradation are minimized by expeditious, proper preservation of the sample.[7] Aqueous samples collected for soluble metals analysis are typically filtered in the field immediately after collection, and nitric acid is added until the pH is lower than 2. The combination of a low pH and an excess of nitrate ions ensures that the metal ions stay in solution. Since metals can adsorb irreversibly onto glass surfaces, samples are usually collected in plastic or plastic-lined containers to avoid contact with glass. Sample exposure to the ambient environment should also be minimized to avoid airborne contaminants.[9] The choice of storage conditions is dictated by practicality. Aqueous liquid samples probably should not be frozen; the preparation of an extract is expected to substantially increase the holding time.[6]

A new range of applications of polymers in analytical chemistry has recently been developed. Styrene-divinylbenzene copolymer resin (XAD-4) has been used in a sorbent cartridge to extract semivolatile explosive compounds from aqueous environmental samples in order to increase the preanalytical holding time.[6] After extraction of trace metals with diethyl-dithiocarbamate, polystyrene foam has been used for quantitative collection of these metal complexes for neutron activation analysis.[10] Various forms of polymeric substrate have been used for indicator immobilization in the fabrication of fiber-optic chemical sensors.[11–14] Disposable plastic film sheaths have been used over fiber-optic Raman probes to eliminate probe contamination.[15] In surface acoustic wave (SAW) sensors, the piezoelectric crystal has been coated with a polymer that captures the chemical of interest from the gas phase.[16,17] Ion-selective membrane electrodes have been developed based on the incorporation of interactive compounds in polymer membranes.[18,19] A platinized

reticulated vitreous carbon or platinum electrode has been used in the construction of a sensor for the determination of glucose in human serum; this used immobilized glucose oxidase and electropolymerized 1,2-diaminobenzene. The 1,2-diaminobenzene polymer coating drastically reduced the effects of electrochemically active interferents and virtually eliminated electrode fouling by proteins in blood serum. The polymer film also increased the thermal stability of the immobilized glucose oxidase.[20,21] A diffusion-plasticization based electrochemical gas chromatography detector has recently been developed.[22] Most unfortunately, Colombian drug dealers are using a mixture of cocaine and polystyrene plastic in products that can be shipped into the United States of America undetected. Traffickers mix a portion of about 20% cocaine with polystyrene plastic and mold it with heat and chemicals. The unprecedented technology makes it possible to transform the cocaine into a form (*e.g.*, black electrical bushings) undetectable by drug-sniffing dogs or routine visual or chemical tests. The cocaine can be removed later by heating the composition, dissolving the plastic bonds.[23]

In the present study, a sample preparation technique which allows the preservation of a large number of small water samples collected from a remote area was developed. Extraction of Hg^{2+} with dithizone (H_2Dz) was first performed quantitatively. Solid $Hg(HDz)_2$ samples were prepared by placing a given volume of the extract on a glass disk to dry in air. The solid $Hg(HDz)_2$ film, which was susceptible to physical disfiguration and loss, was preserved in a layer of polyvinyl chloride (PVC) until PCPAS measurements could be carried out at a later date.

EXPERIMENTAL

Preparation of solutions

The extraction solution of 0.3–0.4% (w/v) dithizone in CCl_4 was prepared according to Irving's method[24] and stored under 0.5*M* H_2SO_4 in the dark to prevent photodecomposition. The aqueous Hg^{2+} standard solutions were made from the chloride salt. A 0.025-g/ml solution of PVC in tetrahydrofuran (THF) was prepared and molecular sieves were added to keep the solution dry.

Extraction of Hg^{2+} from water (preconcentration)

The extraction was carried out by shaking 50 μl of aqueous Hg^{2+} solution, 30 μl of 1*M* H_2SO_4 and 80 μl of the extraction solution (dithizone in CCl_4) in a small screw-cap vial. After 5 min had passed, 50 μl of the organic extract was placed in another vial and washed with 100 μl of 1:1000 (v/v) aqueous ammonia to remove the excess dithizone.

Sample preparation

Method 1. This method of sample preparation is based on the procedure for making solid films of $Hg(HDz)_2$ described by Chen *et al.*[25] A drop of PVC solution from a pasteur pipette was placed in the center of a small glass disk (18-mm diameter), and the THF solvent was allowed to evaporate. A certain volume of organic extract (*e.g.*, 5 μl) was delivered, drop by drop, from a syringe onto the central area of the PVC, allowing the CCl_4 solvent to evaporate before the next drop was added. The resultant solid film of $Hg(HDz)_2$ was then covered by a drop of PVC solution dispensed from a pasteur pipette.

Method 2. This procedure was similar to method 1 except that the bottom layer of PVC was not used. The top layer of polymer was added by dispensing 1 μl of PVC solution from a micro-pipette.

Method 3. A 25-μl aliquot of the organic extract was placed in a small glass cup. After the CCl_4 solvent had evaporated, the solid $Hg(HDz)_2$ was redissolved by adding 20 μl of the PVC solution. Using a micro-pipette, 1 μl of the resultant solution was placed on the centre of a glass disk. The samples used for the study of PCPAS signal amplitude as a function of Hg^{2+} concentration were prepared in this manner.

Photoacoustic spectroscopy (PAS)

A sample disk was placed in the photoacoustic cell shown in Fig. 1. This special cell was designed so that photochromism could be induced in the sample by a white light source while PAS measurement was being performed. It was then attached to the microphone and placed in the photochromism-induced photoacoustic spectroscopy (PCPAS) set-up as shown in Fig. 2. The mirror was adjusted so that the He–Ne laser beam (spot size = 2 mm in radius), modulated at 200 Hz, passed directly through the sample. Several minutes after the data-collection had begun, a steady PAS signal baseline was observed. At this point, photochromism was induced by using the light from a standard 35-mm slide projector (80 mW). The light was guided by an optical fiber bundle (6-mm diameter) and passed through the sample with the aid

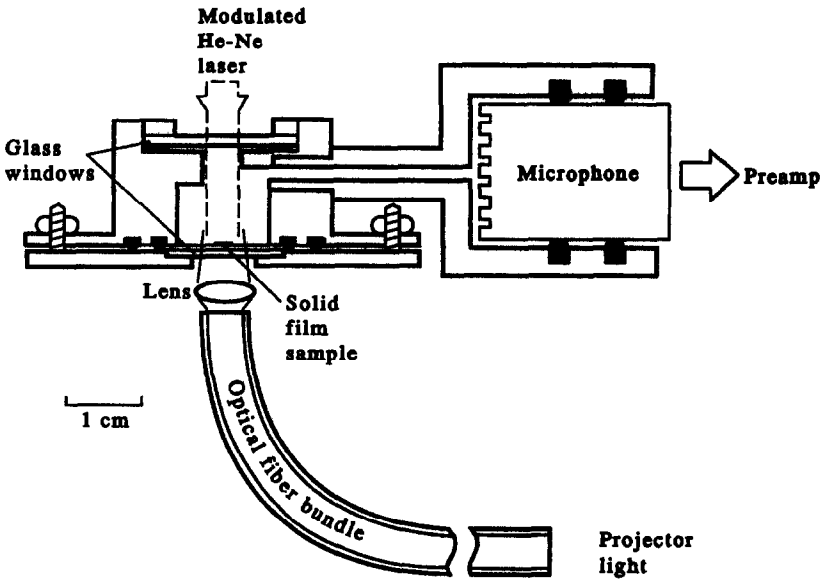

Fig. 1. Sample cell for photochromism-induced photoacoustic spectroscopy of $Hg(HDz)_2$.

of a focusing lens. The projector was left on until the PAS signal stabilized at its new maximum value for the excited state of $Hg(HDz)_2$.

Reproducibility of sample preparation method 3

The precision of the PCPAS measurement was determined by taking triplicate measurements of the same sample. Two sets of measurements were taken in order to find the precision at a high concentration (100 μg/ml) and at a low concentration (12.5 μg/ml). The precision of the solid sample preparation was found by measurement of the PCPAS signals of three samples prepared from a single extraction of a 50-μg/ml Hg^{2+} solution. The precision of the extraction was studied by performing PCPAS on three samples prepared from three different extractions of Hg^{2+} solutions of the same concentration (50 μg/ml).

PCPAS of a $Hg(HDz)_2$ film with and without a PVC cover

A sample was prepared from a 50-μg/ml Hg^{2+} solution as described above in method 2. The volume of organic extract applied to the glass disk was 1.0 μl. PCPAS runs were carried out before and after a top layer of PVC was applied to see how the PVC layer affected the analytical signal.

Changes in the PCPAS signal over time

A sample was prepared from a 100-μg/ml Hg^{2+} solution using method 3. PCPAS measurements of this sample were taken over the course of 19 days in order to study how the sample changed with time.

PCPAS with a laser of higher power

A sample was prepared from a 25-μg/ml Hg^{2+} solution using method 3. In order to study the effect of using a laser of higher power, two PCPAS runs were performed. The first run was carried out using the experimental set-up shown in Fig. 2. The second one was conducted using an Ar^+-pumped dye laser (75 mW, $\lambda = 610$ nm) in place of the He–Ne laser (18 mW, $\lambda = 632.8$ nm). A defocusing lens was used to enlarge the spot size of the dye laser beam so that it was comparable to that of the He–Ne laser beam.

RESULTS AND DISCUSSION

Photochromism

Photochromism literally means a coloration by light. Today the accepted definition of

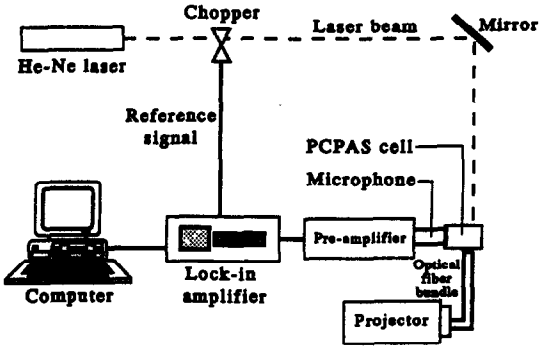

Fig. 2. Experimental set-up for PCPAS measurements.

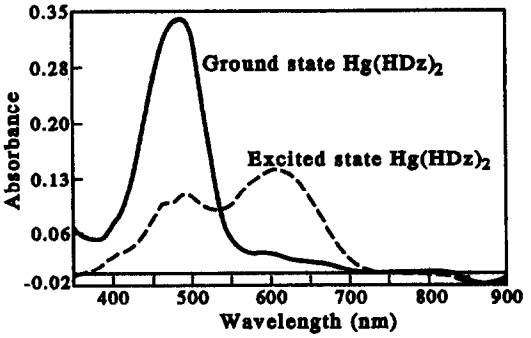

Fig. 3. Visible absorption spectrum of ground and excited state mercuric dithizonate in solution, as measured by a Perkin-Elmer Lambda 4B spectrophotometer. The limited level of projector light irradiation did not produce excited-state $Hg(HDz)_2$ to 100%; some ground-state $Hg(HDz)_2$ remained in the sample.

photochromism is a reversible change of a single chemical species between two states that have distinguishably different absorption spectra. Such a change is induced at least in one direction by the action of electromagnetic radiation.[26] In the mid-1960s, Meriwether *et al.* conducted studies on the photochromic properties of metal dithizonates.[27] Nine of 24 primary dithizonates exhibited photochromism in solution, but only mercuric dithizonate, $Hg(HDz)_2$, was found to be photochromic in the solid state. This complex changes its color from orange to blue upon exposure to bright light, corresponding to a shift of the absorption maximum from 485 to 605 nm (Fig. 3). The structural change that the complex undergoes when going from the normal to the excited state is shown in Fig. 4.[24]

Photoacoustic spectroscopy

In photoacoustic spectroscopy, the sample to be studied is typically placed in a closed cell or chamber. Samples in the gaseous phase usually fill the entire chamber. In the case of liquids or solids, however, only a portion of the cell is occupied by the sample, and the remainder of the cell contains a non-absorbing gas such as air. In addition, the chamber contains a sensitive microphone capable of the detection of minute pressure changes. The sample is illuminated with modulated monochromatic light. If any of the incident photons are absorbed by the sample, the electronic energy levels within the sample are excited. Upon subsequent de-excitation of these energy levels, all or part of the absorbed photon energy is converted to heat energy through non-radiative deexcitation processes. Since the incident radiation is modulated, the internal heating of the sample is also modulated. For solid samples, the periodic heat flow from the sample to the surrounding gas will result in a change of gas pressure within the cell which can be detected by a sensitive microphone. The PAS signal amplitude, S (in mV), can be represented by

$$S = K\,P\,\epsilon(\lambda)\,N \qquad (1)$$

where K is an experimental constant, P is the power of the monochromatic light source (in mW), $\epsilon(\lambda)$ is the optical absorptivity at wavelength λ (in $mole^{-1}\,cm^{-1}$) and N is the amount of solid sample present (in mmoles).[28]

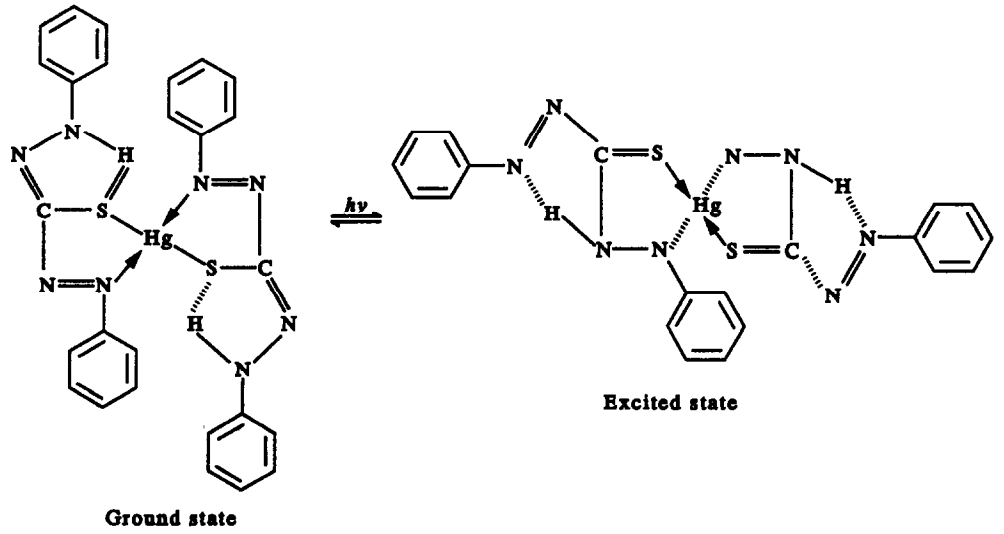

Fig. 4. Structures of normal and excited $Hg(HDz)_2$.

Photochromism-induced photoacoustic spectrometry

By combining the two aforementioned phenomena, Chen *et al.* have developed an analytical technique that allows the determination of Hg^{2+} as its dithizonate in the solid state. A standard calibration curve was obtained in the quantity range from 1.5 to 450 picomoles.[25] A similar experimental arrangement is used in this work (Fig. 2), except that the gas microphone showed signs of performance deterioration in sensitivity due to aging. The modulated light from the He–Ne laser (output wavelength = 632.8 nm) will be absorbed strongly by the excited-state $Hg(HDz)_2$, while the ground-state complex has a negligible absorptivity at this wavelength. Since the He–Ne laser cannot induce photochromism, the PAS signal produced by the ground state will be approximately zero. Upon irradiation by projector light, the excited-state complex is formed and will generate a PAS signal as shown in Fig. 5. The resulting PCPAS signal will be proportional to the change in optical absorptivity, $\Delta\epsilon(\lambda)$, between the ground- and excited-state $Hg(HDz)_2$ and to the amount of solid $Hg(HDz)_2$, thus mercury(II), present. This relationship is only valid when all the $Hg(HDz)_2$ in the sample has undergone photochromism.[25]

Sample preparation

A major problem with sample preparation method 1 was that the dispensed volume of PVC in THF was too large. Thus, the resultant samples were too big to be covered entirely by the laser beam (spot size = 2 mm radius). Precision in measurements of the same sample was poor because the area being sampled might not be the same each time. Also, because the drops dispensed from the pasteur pipette were not always of the same volume, the $Hg(HDz)_2$ was spread over a different area each time. Different volumes of PVC solution thus caused variation in the amounts of the mercury complex in the illuminated polymer matrix even when the original sample solutions contained the same concentration of Hg^{2+}.

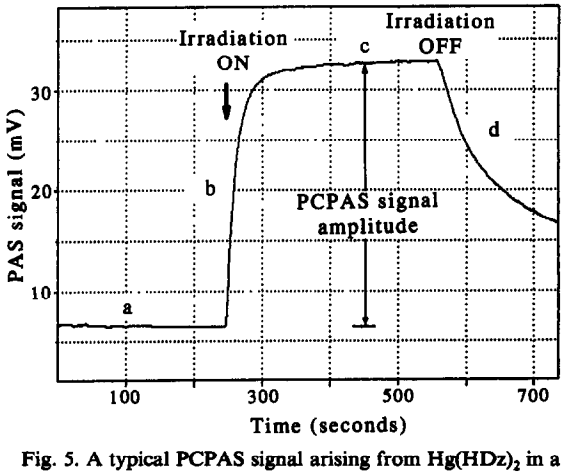

Fig. 5. A typical PCPAS signal arising from $Hg(HDz)_2$ in a PVC matrix. Projector light irradiation started at 245 sec and stopped at 555 sec: (a) ground state without irradiation; (b) forward photochromic reaction; (c) excited state under irradiation; (d) relaxation from excited state to ground state.

Method 2 eliminated the problems discussed above, but difficulty was experienced in trying to cover the entire solid sample film with only one μl of PVC solution. A volume of 2 μl was tried, but the resulting samples became larger than desired. In practice, a defocusing lens could not be used to enlarge the spot size of the laser beam beyond the dimensions of the PAS cell windows.

Another difficulty encountered with the first two methods was that, while dispensing 5 μl of $Hg(HDz)_2$ solution from the syringe, the CCl_4 would sometimes evaporate before the drops could be placed on the glass disk.

Method 3 was designed to achieve reproducible results. The samples were all approximately 2 mm in diameter so that they were easily covered by the laser beam. Using this method of sample preparation, a linear relationship was found between PCPAS signal amplitude and Hg^{2+} concentration in the range 12.5–100 μg/ml. This concentration range is high relative to that which would be useful for certain environmental analyses. The main problem with the present method 3 is the transference of a relatively large volume of the extract to the glass cup and the removal of only a small fraction for analysis. It may be improved by use of a larger fraction of the extract to form the sample. Also, adjustment of the volumes or concentrations of the solutions used in the Hg^{2+} extraction process may help to lower the concentrations that can be determined.

Reproducibility of sample preparation method 3

The variability in the analysis was a combination of the variability associated with the sample preparation technique and the variability of the analytical methodology. The variability of sample preparation method 3 was determined by the repeated preparation and analysis of solid $Hg(HDz)_2$ samples from a given Hg^{2+} solution. Measurements in this study were

carried out in triplicate and the precision of each step was calculated by use of the following equation:

$$P = (S_{extreme} - S_{average})/S_{average} \quad (2)$$

where $(S_{extreme} - S_{average})$ was the greatest deviation from the average and $S_{average}$ was the average of the three PCPAS signal amplitudes. The following precisions were found:

P_1 = precision of the PCPAS measurement (3)

P_2 = [(precision of solid sample preparation technique)$^2 + P_1^2$]$^{\frac{1}{2}}$ (4)

P_3 = [(precision of extraction)$^2 + P_2^2$]$^{\frac{1}{2}}$. (5)

The experimental values of P_1, P_2, and P_3 are listed in Table 1 for easy comparison. These statistical results show that a greatest source of error in sample preparation method 3 lay in the solid sample preparation technique, particularly at high concentrations of Hg^{2+}. Although the micro-pipette was designed to deliver exact volumes of aqueous solutions, the viscous $Hg(HDz)_2$ in PVC solutions could not be delivered as accurately. The precision of the solid sample preparation technique may improve if the PVC solution is delivered from a syringe to the glass disk, as the syringe (calibration = ± 0.05 μl) would transfer a given volume of sample solution more accurately than the micro-pipette (calibration = ± 0.1 μl).

PCPAS of a $Hg(HDz)_2$ film with and without a PVC cover

A solid $Hg(HDz)_2$ sample was prepared from a 50-μg/ml Hg^{2+} solution according to method 2. Before a PVC cover was added, the sample produced a PCPAS signal of 4 mV in amplitude. The same sample, after application of a PVC cover, gave a 23-mV signal amplitude. A possible explanation for this increase in PCPAS signal amplitude is that the bare solid sample scattered incident laser and projector lights, thus decreasing the power of the lights that reached its inside. When the PVC solution was added, the solid complex was redissolved in the THF solvent. Upon evaporation of the solvent, the dispersed film sample became transparent. This allowed the laser and projector lights to reach the $Hg(HDz)_2$ molecules more uniformly than it could in the bare solid sample. The increase in the PCPAS signal amplitude could also be due to a more efficient transfer of heat energy from the dispersed complex to the air in the PAS cell when the PVC cover layer was present. This is, in accordance with the PAS theory, governed by the thermal diffusivity of the material which is typically 10^{-3} cm^2 sec^{-1} for polymers.[29] In comparison, no literature value is available for $Hg(HDz)_2$ and must now be measured in our laboratory using either the conventional calorimetric methodology or the method of Adams and Kirkbright for thin solid films.[30] Another explanation for the increase in PCPAS signal amplitude may be that the polymer matrix was acting as a "solvent" so that excitation of the complex could occur more efficiently. Inclusion of mercury(II) dithizonate within the polymer matrix, whether by entrapment or cross-linking, had a stabilizing effect on the complex. The polymer matrix, like immobilization, increased the rigidity of the complex making it harder to unwind and relax. Similar spectrophotometric determination of tetraphenylporphinecobalt(II) by its catalysis of the photochromic isomerism of norbornadiene immobilized on porous glass beads has recently been reported.[31] Regardless of the nature of the exact mechanism, the addition of a PVC cover did enhance the PCPAS signal amplitude. This lowered the detection limit of 3 pg/ml for the determination of Hg^{2+} in aqueous samples using PCPAS, as reported previously by Chen *et al.*[25] to about 0.5 pg/ml.

Stability study over time

A sample was prepared by extraction of a 100-μg/ml Hg^{2+} solution, and its PCPAS signal was measured over a period of 19 days. A linear signal decrease was observed, at a rate of 1.6%

Table 1. Precisions of PCPAS measurement, solid sample preparation technique and extraction

Concentration of Hg^{2+} solution	Precision of PCPAS measurements*			Precision of solid sample preparation technique	Precision of extraction
(μg/ml)	P_1	P_2	P_3	$[P_2^2 - P_1^2]^{1/2}$	$[P_3^2 - P_2^2]^{1/2}$
100	1.1%	5.5%	7.1%	5.4%	4.4%
12.5	5.2%	7.5%	10.1%	5.4%	4.4%

*See text for definitions of P_1, P_2, and P_3.

per day from the initial amplitude. This loss is possibly ascribed to slow photodissociation of $Hg(HDz)_2$ during projector light irradiation in the PCPAS measurements. Nevertheless, the above results have demonstrated the sample preservation properties of the PVC matrix. The polymer provides the Hg complex with efficient protection from physical disfiguration and loss of sample over an extended period of storage time. It is not difficult to imagine how sample integrity can easily be lost by physical processes, such as scraping and flaking, in the absence of a PVC coating. Any delay in sample analysis would only require a proportional normalization of the PCPAS signal. Extrapolation of the maximum preanalysis holding time allowed for a particular analysis may be statistically possible from the reproducible data. The American Society for Testing and Materials (ASTM) defines the holding time as "the period of time during which a sample can be stored after collection and preservation without significantly affecting the accuracy of analysis".[32] In this case, a month may elapse before the PCPAS signal from a PVC-covered $Hg(HDz)_2$ sample is reduced to one-half of its initial value. The above PCPAS measurement could not be validated for a longer term than 19 days after damage to the gas microphone was accidentally incurred.

PCPAS with a laser of higher power

Vibrations from the surroundings (*i.e.*, ambient noise) caused amplitude fluctuations in the PAS signal. Interference in the PCPAS signal determination by ambient noise, which degraded the analytical detection limit, were overcome by using a high-power, low-noise laser. In one experiment the sample prepared from a 25-μg/ml Hg^{2+} solution gave a PCPAS signal amplitude of 20 mV and a signal-to-noise ratio of 10:1 when the He–Ne laser ($\lambda = 632.8$ nm) was used. Using the Ar^+-pumped dye laser operating at 610 nm, a 94-mV signal amplitude and a signal-to-noise ratio of 47:1 was obtained for the same sample. The enhancement of the PCPAS signal is believed to be the result of two factors: the increase in output power of the dye laser and the use of a wavelength of light which was closer to the maximum absorptivity of the excited-state complex at 605 nm. The output power from the dye laser was measured to be 75 mW which was four times that of the He–Ne laser. Since 94 mV $\gg 4 \times 20$ mV, the $\Delta\lambda$ advantage is clearly evident. No photobleaching of mercury(II) dithizonate and no PAS signal saturation were noticed at this laser power level. Ideally, the dye laser should have been tuned to a wavelength identical with that of the He–Ne laser in order to study the effect of the power of the laser used. Unfortunately, a significant power increase could not be achieved at 632.8 nm for the Rhodamine 6G dye employed.

CONCLUSION

Proper preservation of analytical samples requires planning of critically timed activities performed in both the field by the sampling crew and in the laboratory by the analysis staff. From the results presented in this report, polyvinyl chloride can be used to preserve the integrity of solid $Hg(HDz)_2$ samples prepared by extraction of Hg^{2+} from water with dithizone. The PVC cover provides the $Hg(HDz)_2$ with protection from physical damage (*e.g.*, scraping and flaking) to facilitate easy transport and storage. This allows a longer time period between sampling and analysis. As the polymer also immobilizes the solid complex and may increase its photostability, the maintenance of calibration standards in the laboratory will be easy. In general, equipment used for sample analysis is a common source of sample contamination. Use of PCPAS of solid film samples deposited on disposable glass disks eliminates problems of carry-over and memory effects from consecutive analyses of high- and low-level samples which are common to many types of instrumental methods (viz., carry-over from high-level samples contaminates subsequent low-level samples).

By comparing solid $Hg(HDz)_2$ samples with and without PVC covers, it has been verified that the presence of the polymer matrix enhances the PCPAS signal amplitude obtained. In addition, a greater PCPAS signal amplitude can be obtained with the use of a laser of higher power and an optimum wavelength of the excitation light. Hence, a higher signal-to-noise ratio (and thus a lower detection limit) can be achieved. In view of the promise shown by the preliminary data, the method merits further study and sensitivity enhancement will be pursued in our laboratory.

Finally, the ease of use of this novel sample preservation technique for potential field applications should not be understated. The analysis of standard reference materials, as well as the exchange of samples with laboratories that are skilled in mercury analyses, are underway to

allow further validation of the method. Note that the PCPAS equipment, which measures no more than 70 cm × 85 cm × 25 cm on an optical breadboard, has good potential for use in a mobile laboratory.

Acknowledgements—This work was funded by the Natural Sciences and Engineering Research Council of Canada. A GR-5 grant from the Faculty of Graduate Studies and Research, Carleton University, is gratefully acknowledged. Barbara Wong would like to thank NSERC Canada for an undergraduate student research award for two years.

REFERENCES

1. P. A. D'Itri and F. M. D'Itri, *Mercury Contamination*, Wiley, New York, 1977.
2. S. Jensen and A. Jernelöv, *Nature*, 1969, **223**, 753.
3. W. L. Hughes, *Ann. New York Acad. Sci.*, 1951, **65**, 454.
4. T. C. Hutchinson and K. M. Meena (ed.), *Lead, Mercury, Cadmium, and Arsenic in the Environment*, Wiley, New York, 1987.
5. A. R. Newman, *Anal. Chem.*, 1990, **62**, 847A.
6. M. P. Maskarinec and R. L. Moody, in *Principles of Environmental Sampling*, L. H. Keith (ed.), p. 145. American Chemical Society, Washington, D. C., 1988.
7. J. Parr, M. Bollinger, O. Callaway and K. Carlberg, in *ibid.*, p. 221. American Chemical Society, Washington, D. C., 1988.
8. J. R. Moody and R. M. Lindstrom, *Anal. Chem.*, 1977, **49**, 2264.
9. Lewis, D. L., in *Principles of Environmental Sampling*, L. H. Keith (ed.), p. 119. American Chemical Society, Washington, D. C., 1988.
10. N. Suzuki, Y. Iwata and H. Imura, *Int. J. Environ. Anal. Chem.*, 1987, **30**, 289.
11. L. L. Blyler, J. A. Ferrera and J. B. MacChesney, *Optical Fiber Sensors, 1988 Technical Digest Series*, Vol. 2, Part 2, p. 369. Optical Society of America, Washington, D. C., 1988.
12. Z. Zhang, Y. Zhang, W. Ma, R. Russell, Z. M. Shakhsher, C. L. Grant, W. R. Seitz and D. C. Sundberg, *Anal. Chem.*, 1989, **61**, 202.
13. Y. Kawabata, R. Tahara, T. Kamichika, T. Imasaka and N. Ishibashi, *ibid.*, 1990, **62**, 1528.
14. L. K. Chau and M. D. Porter, *ibid.*, 1990, **62**, 1964.
15. B. Yang and M. D. Morris, *Appl. Spectrosc.*, 1991, **45**, 512–513.
16. S. Kurosawa, N. Kamo, D. Matsui and Y. Kobatake, *Anal. Chem.*, 1990, **62**, 353.
17. D. L. Bartley and D. D. Dominguez, *ibid.*, 1990, **62**, 1649.
18. S. A. Glazier and M. A. Arnold, *ibid.*, 1991, **63**, 754.
19. C. Sanchez-Pedreno, J. A. Ortuno and J. Alvarez, *ibid.*, 1991, **63**, 764.
20. S. V. Sasso, R. J. Pierce, R. Walla and A. M. Yacynych, *ibid.*, 1990, **62**, 1111.
21. C. Malitesta, F. Palmisano, L. Torsi and P. G. Zambonin, *ibid.*, 1990, **62**, 2735.
22. C. J. Barbour, R. W. Murray and J. F. Parcher, *ibid.*, 1991, **63**, 604.
23. The Associated Press, *Cocaine, Plastic Mixed To Avoid Detection*, The Salt Lake Tribune, 1991, June 26, A3.
24. H. M. N. H. Irving, *Dithizone*, The Chemical Society, Burling House, London, 1977.
25. N. Chen, R. Gou and E. P. C. Lai, *Anal. Chem.*, 1988, **21**, 2435.
26. G. H. Brown, G. H. (ed.), *Photochromism, Techniques in Chemistry*, Vol. III. Wiley Interscience, New York, 1971.
27. L. S. Meriwether, E. C. Breitner and C. L. Sloan, *J. Am. Chem. Soc.*, 1965, **87**, 4441.
28. R. Gou, N. Chen, N. and E. P. C. Lai, *Analyst*, 1988, **113**, 595.
29. C. K. N. Patel and A. C. Tam, *Rev. Mod. Phys.*, 1981, **53**, 517.
30. M. J. Adams and G. F. Kirkbright, *Analyst*, 1977, **102**, 678.
31. Y. Kawabata,H. Kumoyama, T. Imasaka and N. Ishibashi, *Anal. Chim. Acta*, 1991, **243**, 97.
32. *Standard Practice for Estimation of Holding Time for Water Samples Containing Organic Constituents*, ASTM D4515–85. American Society for Testing and Materials, Philadelphia, PA, 1987.

Talanta, Vol. 40, No. 7, pp. 1107–1111, 1993
Printed in Great Britain.

0039-9140/93 $6.00 + 0.00

DETERMINATION OF B, Si, Cr, Mo, Th AND Hf IN UF_6 BY END-ON VIEWED ICP-AES

PAN FUXING, TONG DEZHI, REN MING and MA HEYING
P.O. Box 151-21, Lanzhou, Gansu, People's Republic of China

(*Received* 12 *February* 1992. *Revised* 13 *October* 1992. *Accepted* 8 *December* 1992)

Summary—A spectrographic analysis method is described for the determination of B, Si, Cr, Mo, Th and Hf in UF_6 Uranium is separated from UO_2F_2 using a TBP [tributyl phosphate] extraction-elution resin column technique. The six impurity elements, including B and Si, in the fluorine-containing extraction-elution solution are determined by end-on viewed ICP-AES. The method is simple, rapid and suitable for routine analysis.

INTRODUCTION

The ASTM C996-83 (standard specification for UF_6 enriched to less than 5% U-235) requires the determination of impurity elements B, Si, Cr, Mo and Th. However, B and Si in UF_6 are difficult to determine spectrographically among the five elements because they would be lost in large amounts during the conversion of the sample into U_3O_8 if the carrier distillation method is used. Also, Si would be lost completely, and B by large fractions during the driving off of HF by nitric acid if a chemical-spectral analysis method or ordinary ICP-AES is used.

For these reasons, for decades, both the DOE ORO-671-2 method and its replacement ASTM C761-91 method stipulate that UF_6 be hydrolyzed in freshly prepared ammonia water to form NH_4UF_5, NH_4BF_4 and $(NH_4)_2SiF_6$,[1] and that the hydrolyzate be evaporated to dryness below 100°C, charged into a boiler electrode and excited with a dc arc for spectrographic analysis.

However, the development of the modern analytical technique has provided the possibility of determination of B and Si in UF_6 using chemical separation at room temperature.

Our method is as follows: after UF_6 is hydrolyzed in high purity water to form UO_2F_2, an aliquot of it is treated with concentrated nitric acid, and passed through a TBP [tributyl phosphate] extraction-elution resin column for separation. Uranium is absorbed on the column and the impurities remain in the elution solution. Then end-on viewed ICP-AES is used to determine the six impurity elements (B, Si, Cr, Mo, Th and Hf) simultaneously. As both the sample treatment and the separation are performed at room temperature, the loss of volatile fluorides of B and Si does not occur.

The experimental results show that a recovery of 86–114% and a precision (RSD) of less than ±16% are obtained because of the simple operation and the stability of the selected ICP operating conditions and sample inlet system. Analysis of production samples agrees with the analytical results of other methods used for comparison analysis.

EXPERIMENTAL

Instrumentation and ICP operating conditions

As shown in Table 1.[2]

Wavelengths of analysis lines and determination limits

As shown in Table 2.

Preparation of the TBP [tributyl phosphate] extraction-elution resin chromatographic column

A 75–120 mesh TBP extraction-elution resin is put into a glass beaker, rinsed with water, and immersed for over 24 hours after removing the floating material. Then the resin is gently flowed into the column (Fig. 2), stirring the resin frequently with a glass rod so that it can be packed uniformly and no bubbles occur. After packing, the column is eluted with 5% sodium carbonate solution, the volume of which is four times that of the resin, to remove residual butyl and dibutyl, and washed with water to neutrality. To remove the impurities, the column is eluted repeatedly with 1*M* HCl, H_2O and 3*M*

Table 1. Instrumentation and ICP operating conditions

Spectrometer	Medium-size quartz spectrograph, model И С Л- 28; reciprocal linear dispersion: 0.35–11.0 nm/mm; ICP imaged with unit magnification on slit using a single condenser ($f = 75$ *mm*); three-step filter (steps: 10, 50 and 100%) in front of entrance slit.
RF generator	Type GP3.5-D1; anode current: 0.7A, grid current: 110 mA; frequency: 27 MHz.
Load coil	6 mm diameter copper tube, 2 turns, coil diameter 25 mm.
Torch	Fassel torch, positioned horizontally with axis coincident with optical axis.
Air stream for lens protection.	See Fig. 1. Glass device with slit-shaped orifice (0.5 × 25 mm); air gauge pressure: 0.05 MPa; flow rate: 30 l/min.
Gas	Argon
Flow rates:	
Outer	16 l/min
Intermediate	0.75 l/min
Carrier	0.35 l/min
Sample inlet system	Fluorine-resistant aerosol desolvation unit: temperature of heating chamber: 200°C; nebulizer of pneumatic-concentric type, liquid uptake rate: 1.5 ml/min.
Photographic plate	Kodak glass plate No. 1 or TIANJIN u.v. III plate (9 × 6 cm); exposure time 35 s.
Analysis lines	See Table 2.

HNO_3 to an acceptable blank value for routine use.

Preparation and pipetting of standard series solutions

Prepare original solutions with oxides or salts of B, Si, Cr, Mo, Th and Hf, take a portion from each according to the requirements for the analysis of a 300 mg sample, dilute to a standard series (N1-N5) of solutions with certified high purity water, and store in 100 ml plastic containers. Pipet, respectively, 1 ml from each of the standard series solutions, add 1.5 ml of concentrated HNO_3, 3.2 ml high-purity water and 0.3 ml HF to each of them, and mix in PTFE cups (each to a total volume of 6 ml and a total acidity of $4M$ HNO_3–$1.1M$ HF) for future use.

Sample treatment and separation procedure

Hydrolyze UF_6 in high-purity water, and maintain its concentration at 150–300 mg/ml. Pipet a volume of hydrolyzate containing 300 mg of UF_6 into a PTFE cup with a plastic pipet, add first an appropriate amount of high-purity water to give a sample volume of 2 ml and then 1 ml of concentrated HNO_3, and mix thoroughly. Pipet the sample into the column which has been acidified with $4M$ HNO_3, and elute with $4M$ HNO_3 with a flow rate of 0.3 ml/min for separation. Discard the first 4 ml, and collect the last 6 ml effluent solution which contains all the impurities. Uranium absorbed on the column is desorbed with water. Keep one blank of reagent during separation.

Take spectrograms of the effluent solutions and the standard series solutions simultaneously.

Table 2. Wavelengths of analysis lines and determination limits

Spectral lines (*nm*)			Determination limits* (*μg/gU*)
B	I	249.773	0.25
Si	I	251.611	0.1
Cr	II	267.716	0.1
Mo	II	281.615	1.5
Th	II	401.913	1.5
	II	283.730	1.5
Hf	II	264.141	0.5

*Achieved in sampling 300 *mg*.

RESULTS AND DISCUSSION

Interference by fluorine

Since the elutant solution received during separation is an acidic mixture of HNO_3 and HF, the effect of fluorine content on the determination results must be taken into account. Theoretically, 100 mg of UF_6 contains 32.4 mg of fluorine. Our measurement result is 33 ± 2 mg. The fluorine content in 0.1 ml of commercial hydrofluoric acid is 38 mg which is roughly of the same order.

Based on the above consideration and calculation, we studied the addition of 0.1–0.4 ml of hydrofluoric acid (*i.e.*, 38, 76, 114 and 152 mg of fluorine) and the results are listed in Table 3. The increase in the density of the spectral lines due to the gradual addition of the fluorine

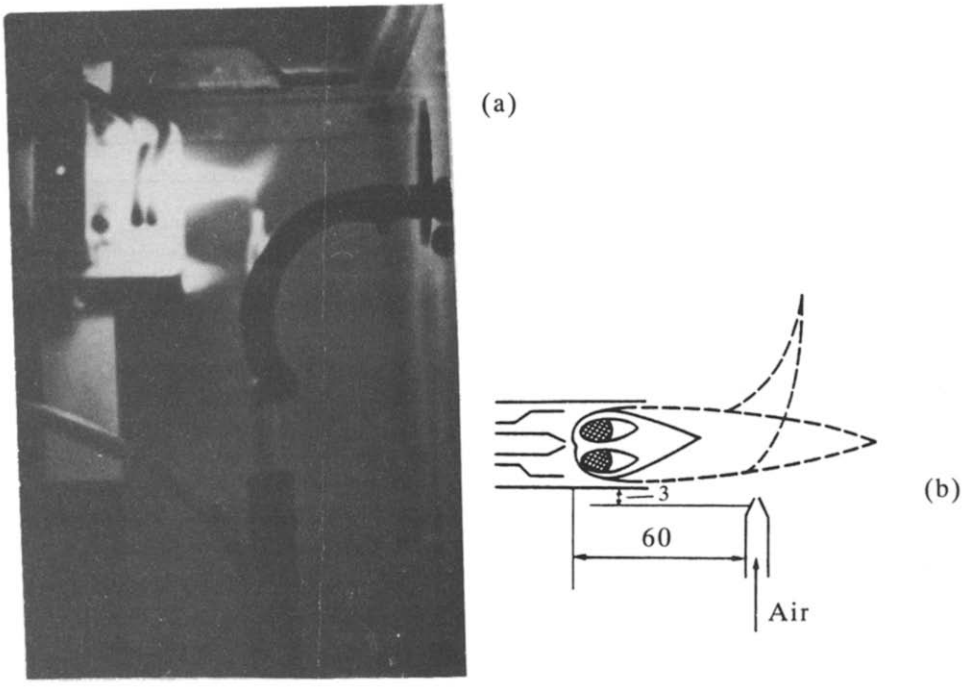

Fig. 1. End-on viewed ICP with a lens protecting unit: (a) photograph; (b) schematic drawing.

content made the corresponding quantitative content of each element tend to increase gradually, notably B. In the range of 114–152 mg of fluorine, the change in determination results of six elements tended toward stabilization. In addition, greater B content may be due to the formation of strongly volatile fluoride in B which increased the flow rate of B into the central channel of ICP; this is also one of the reasons for the lower determination limit of B.

Based on this result, and guided in the principle that the standard solution should correspond with the acidity of the sample solution as closely as possible, for sampling of 300 mg UF_6, we added 0.3 ml of hydrofluoric acid to standard series solution.

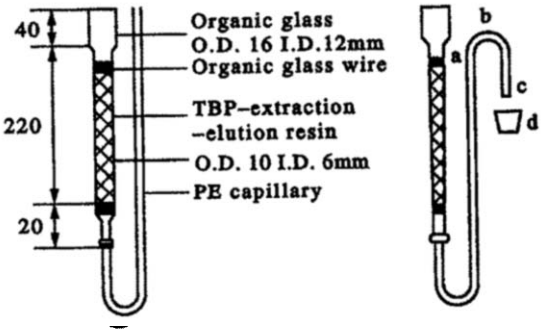

Fig. 2. A TBP-extraction-elution resin chromatographic column.

Spectral interference by CA and Fe

Since our analytical object is high-purity UF_6 with impurity elements at the parts per million level and end-on viewed ICP is used, we studied only Ca which is likely to be a contaminant that may give rise to ionization interference, and Fe which has complicated spectral lines. Since the two elements have similar effects on the determination result, only results of Ca are listed in Table 4.

For samples of 300 mg, Ca with as high as 340 μg/gU (also Fe with 192 μg/gU) has no effect on the results of the six elements. Neither interference of spectral lines nor interference of ionization are apparent.

Interference by U

Since this was our first attempt to separate uranium from HNO_3–HF medium using a chromatographic method, doubt may arise as to whether trace uranium would be lost and thus affect the spectrographic determination. In our practice, within the useful life of a chromatographic column, no noticeable uranium loss occurred, and the separation was complete. But when a column approaches the end of its life, the loss of a small amount of uranium is possible. For this reason and also because uranium is a matrix element with multiple spectral lines, it was necessary to study its interference.

Table 3. Effect of F content in the solution on the determination results (μg/gU)

Fluorine	B	Si	Cr	Mo	Th	Hf
0	0.94	180.0	9.8	10.8	11.5	4.4
38	2.6	220.0*	13.0	13.0	11.5	4.9
76	4.0	190.0	14.0	15.0	12.0	5.0
114	4.8	195.0	15.5	16.0	12.0	5.5
152	5.0	200	15.5	17.0	13.0	5.7

*Possible contamination.

Under the selected ICP conditions we performed an experiment on the interference with 14–110 μg uranium and the result is shown in Fig. 3.

Below 110 μg and within the range of error of the spectrographic method, BI 249.773 nm, SiI 251.611 nm, Cr II 267.716 nm, Th II 401.913 nm and Hf II 264.141 nm experienced only small influences. Only for a larger amount of uranium did the density of Mo II 281. 615 nm tend to decrease. As the residual uranium is generally below 15 μg, no serious interference with the spectrum would occur.

Accuracy and precision

The accuracy and precision of this method were assessed by analyzing a series of laboratory prepared synthetic samples, check samples and several real UF_6 samples following "sample treatment and separation procedures", under the experimental conditions defined in Table 1.

Two synthetic samples were prepared by adding standard solutions to a UO_2F_2 solution. The impurity contents in one sample were at the lower analytical limits of this method, and those in the other sample were at the level of product quality standard. Each of the two synthetic samples was analyzed five times. The mean determination value, average percentage recovery, and relative standard deviation (RSD) after separating with TBP chromatography are listed in Table 5.

To our knowledge, at present there are no certified standard samples for the impurity elements in UF_6. Thus, check samples were used instead. The check samples we used were prepared in the same manner as the reference

Table 4. The effect of Ca content on the determination results (μg/gU)

Ca content	B	Si	Cr	Mo	Th	Hf
0	2.7	180.0	3.6	3.3	3.0	3.4
37	3.0	200.0	3.6	3.2	3.2	3.4
74	3.1	195.0	3.1	3.3	3.2	3.6
170	3.0	190.0	3.2	3.3	3.2	3.4
340	2.9	190.0	3.7	3.5	3.2	3.4

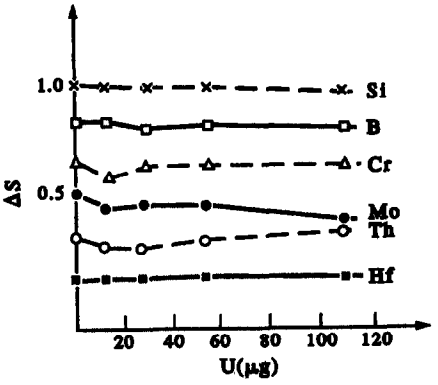

Fig. 3. The effect of uranium on the density (ΔS) of the spectral lines.

solution. The impurity contents in check samples were unknown. Only after the analysis of check samples had been performed, were the impurity contents made known by the checking personnel. Each of the check samples was analyzed five times. The quantitative results obtained and the standard deviation are listed in Table 6.

To demonstrate the effectiveness of this method, several UF_6 samples were analyzed. These samples were taken from an enriched UF_6 product for nuclear reactors. Each of these samples was divided into several aliquots which were subsequently determined by the present method, a chemical method, and TEHP [tri(2-

Table 5. Analysis of laboratory prepared synthetic samples and precision (RSD)*

Element	Addition value (μg/gU)	Blank value of UF_6 matrix (μg/gU)	Determined value (μg/gU)	Recovery (%)	Relative standard deviation (±%)
B	0.5	0.3	0.75	90	15
	2.0		2.3	100	10
Si	20.0	12.5	29.7	86	13
	80.0		104.0	114	9
Cr	3.0	0.54	3.3	92	12
	12.0		11.3	90	7
Mo	3.0	not found	3.4	113	16
	12.0		10.5	88	9
Th	3.0	6.1	9.0	97	11
	12.0		18.2	101	15
Hf	1.5	0.4	2.0	107	16
	6.0		6.0	93	16

*RSD of determination value.

Table 6. Analytical results of check samples (μg/gU)

Element		B	Si	Cr	Mo	Th	Hf
Blank		not found	13.0	2.8	not found	7.8	0.4
Check sample No. 1	A	4.0	25.7	3.5	4.5	3.0	1.5
	D	4.7	33.9	6.9	3.8	11.3	2.0
	S	0.94	4.5	1.6	0.6	2.9	0.2
Check sample No. 2	A	0.6			29.7	24.7	14.8
	D	0.63			28.0	27.1	15.1
	S	0.06			5.3	4.6	1.5
Check sample No. 3	A	17.8	415.0	108.0	2.0	98.6	
	D	16.7	438.0	124.0	1.7	116.0	
	S	2.7	36.0	18.7	0.15	16.2	

Notes: 1. Blank—Blank value of UF_6 matrix.
2. A—Accepted value.
3. D—Determined value.
4. S—Standard deviation.

Table 7. Comparative analysis of production sample of UF_6

Sample	Method	B	Si	Cr	Mo	Th	Hf
No. 1	P*	1.7	76	12.3	7.2	11.5	3.5
	0†	1.9	77	11.4	8.5	8.3	2.3
No. 2	P	0.45	16.0	1.5	1.5	2.3	
	0	0.5	15.0	1.5	1.5	3.0	
No. 3	P			15.0	12.0	13.7	4.8
	0			16.5	12.3	11.0	4.5
No. 4	P	0.35	14.0	1.4	1.5	2.2	
	0	0.4	15.0	1.5	1.5	3	
No. 5	P	6.0	180	38.0	3.4	29.0	13.5
	0	5.1	197	47.0	4.8	26.0	18.0

Notes: Determination results of three separations.
*The present method.
†Chemical method, TEHP separation—ICP-AES[2].

ethyl-hexyl) phosphate] separation—ICP-AES method[2]. The results obtained are listed in Table 7. The results of this method agree with those obtained by other methods.

The data in Tables 5–7 show that TBP chromatographic separation—end-on viewed ICP-AES, is an effective method for the determination of B, Si, Cr, Mo, Th and Hf in UF_6. Its determination limits can satisfy the requirements of UF_6 quality appraisal. The time required for sample preparation and analysis is one working day. This method is simpler and more rapid than the test method for B and Si in UF_6, provided by ASTM C761-91 standard procedure.

Acknowledgements—The assistance of Fan Puren, Sha Shuyan, Feng Ying, Bao Luwei, Wu Zuyong and Li Yongcai is greatly appreciated.

REFERENCES

1. *1980 Annual Book of ASTM Standards*, Part 45, C761, sections 80–87, p. 483. ASTM, PA, 1980.
2. Pan Fuxing, You Suling, He Qinghua, Wang Xiaoping, Ma Heying, Huang Yanmin, Xu Yuxin, Xu Yi and Wu Tingfang, *Spectrochimica Acta*, 1986, **41B**, 1211.

Talanta, Vol. 40, No. 7, pp. 1113–1126, 1993
Printed in Great Britain.

0039-9140/93 $6.00 + 0.00

COMPARISON OF THE SIMPLEX AND POWELL METHODS WITH A WEIGHTED RESPONSE FUNCTION FOR THE OPTIMIZATION OF FIA SYSTEMS

L. M. B. C. ÁLVARES-RIBEIRO and A. A. S. C. MACHADO*
Chemistry Department, Faculty of Science, University of Oporto, P 4000 Porto, Portugal
J. ALONSO, J. BARTROLI and M. DEL VALLE
Department de Química, Universidad Autónoma de Barcelona, E 08193 Bellaterra, Spain

(*Received* 15 *July* 1991. *Revised* 10 *December* 1992. *Accepted* 10 *December* 1992)

Summary—An experimental comparison between the relative performances of the Powell and simplex methods for the optimization of a Flow Injection Analysis (FIA) system for the determination of nitrite in water is reported. An evaluation of the advantages of using a weighted linear combination of two variables (related to sensitivity and sample throughput rate) as the response function in the guidance of the optimization procedures towards different practical requirements is also included.

Both methods proved to be effective for the optimization, none having shown definite advantages over the other. The use of a weighted response function in these optimization methods proved to be useful for assessing the versatility of FIA systems.

The need to optimize the parameters which define FIA systems to improve their response characteristics (usually sensitivity and/or sample throughput rate) is nowadays commonly accepted. For this purpose, due to the complex and strong interdependence which exists between the various parameters (flow rates, lengths and internal diameters of tubes, injection volumes, reagent composition, *etc.*) and performance variables (peak height, residence time, linear working range, *etc.*), methods able to promote their simultaneous optimization in a systematic way are required.

The lack of mathematical models to describe the behaviour of all but the simplest FIA systems prevents the utilization of methods that use derivatives. Among the direct optimization methods, the simplex method,[1–3] devised by Spendley *et al.*,[1] and significantly improved by Nelder and Mead,[2] has been the most commonly used in FIA applications. Its application to analytical chemistry has had a large impetus after the work of Morgan and Deming,[3] and it was first applied in the optimization of FIA systems by Betteridge *et al.*[4] The choice of an adequate response function is a critical step for the optimization procedure,[5–8] and several different kinds of response function have been used for the optimization of FIA systems.[5–16] The automated optimization of FIA systems using simplex procedures has also been reported.[8–10] The utilization of the Powell[17] method has also been proposed for the optimization of FIA systems,[18] and a comparison between the two methods was recently described for a particular FIA system.[19]

This paper reports an evaluation of the relative efficiency of the simplex and Powell methods to promote the optimization of another FIA system and a study of the performance of a particular kind of response function (a weighted linear combination of variables) in the guidance of the optimization procedures towards different compromise requirements between the variables chosen (in this case sensitivity and sample throughput rate).

The response function (*RF*) is a linear combination of two variables,the peak height (*H*), which is to be maximized as it is taken as a measure of sensitivity, and the residence time (*T*), which is to be minimized since it is inversely related to the sample throughput rate. Expressed in terms of the normalized variables (R_H, R_T), *RF* is

$$RF = C_H \cdot R_H + C_T(1\text{-}R_T).$$

*Author for correspondence.

The normalization of variables[3,4] is accomplished through the use of the expression

$$R = (R_{exp} - R_{min})/(R_{max} - R_{min}),$$

where R_{exp} stands for the experimental value of the variable measured and R_{min} and R_{max} for the values of the corresponding minimum and maximum values, found by means of preliminary tests.

Response functions based on independent additive terms can result in unexpected and unwelcome results when one of the terms dominates. In the present case, problems could arise if the residence time coefficient was very large, leading to very fast systems, with small and narrow peaks, thus having low sensitivity and poor repeatability, or if the peak height coefficient was too large, leading to unpractically large systems, with very long residence times and broad peaks. Two possible ways to avoid this problem are the definition of boundaries for the variation of the parameters (to prevent the occurrence of unpractical system) and the use of suitable normalization conditions of the variables (to assure that there is no indirect weighting of them, *i.e.*, when equal coefficients are assigned to both variables, their relative contributions to the response function should be similar).

For this study, the system for the determination of nitrite proposed by Nakashima *et al.*,[20] whose optimization by the simplex method was previously reported,[15] was chosen. The degree of complexity of this system is intermediate and typical of a large number of FIA systems. It involves four hydrodynamic parameters of the manifold (two coil lengths and two flow rates).

Five different sets of the weighting coefficients (C_H, C_T) were used as before[15] to cover systematically their allowed range ($0 \leqslant C_i \leqslant 1$), thus permitting an evaluation of the guidance features of the type of response function used and providing a broader base for the comparison of the simplex and Powell procedures than before.[19]

EXPERIMENTAL

Equipment and reagents

Figure 1 shows the manifold used in the optimization experiments which was fully described in a previous work.[15] Reagents were prepared and stocked as described in the work by Nakashima *et al.*[20]

Algorithms

The program algorithm used for the simplex optimizations has been described in detail before[14] and is based on the modified simplex method of Nelder and Mead,[2] but with some modifications to include boundary conditions, to take into account Aberg's suggestion[21] that the value of *RF* for an expansion should be compared with its reflected point instead of with the best of the simplex values, and to combine the use of massive contraction with the application of "rule 3" from Spendley's original method[1] (this rule states that, if the value of *RF* obtained for the point resulting from the reflection of the worst vertex of the simplex is smaller than the value of *RF* for the worst vertex of the simplex, then the advance in the optimization is achieved through reflection of the next-to-worst vertex).

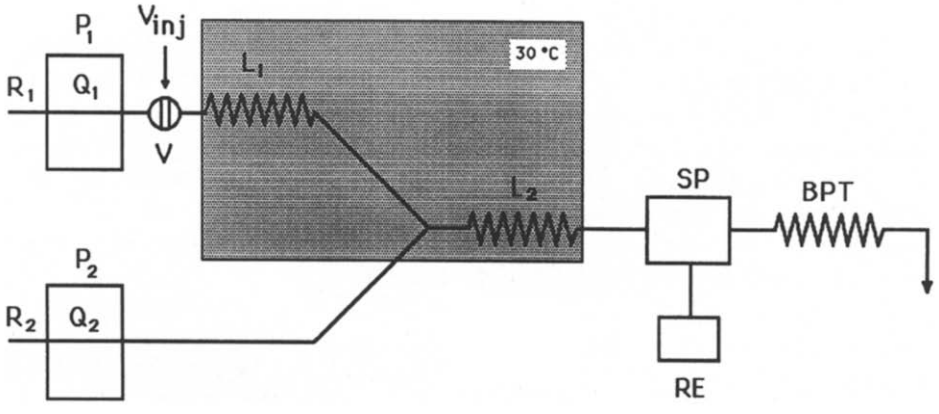

Fig. 1. Flow injection manifold for the optimization experiments: $R_1 = 0.04\%$ (w/v) *p*-aminoacetophenone, pH 1.5; $R_2 = 0.11\%$ (w/v) *m*-phenylenediamine, pH 2.4; P_1 P_2 = peristaltic pumps; V_{inj} = injection valve; SP = spectrophotometer; RE = recorder; BPT = back-pressure tube. The tubing used was made of Teflon with 0.8 mm internal diameter. The tee piece used was made of Perspex and with 120° angles. Parameters allowed to vary: Q_1, Q_2 = flow rates; L_1, L_2 = reaction tube lengths.

The program algorithms used in the Powell optimizations were also previously described in detail,[18] and are based on the original algorithms of Powell.[17]

Both programs were implemented on an Apple IIe microcomputer.

Convergence criteria

The convergence criterion used in the simplex algorithm stated that the sample standard deviation between the values of the response function should be less than a preset value, fixed by the user at the beginning of the optimization procedure. In this study this value was set at 0.5.

In the Powell method a double convergence criterion was used. First, both the coordinate values and the target function increments in two consecutive iterations must be below a present value, in this case 0.5. Second, in each unidirectional search, the interpolated point on the assumed parabolic shape is also checked against the mentioned preset value. This double criterion requires a complete iteration cycle to achieve convergence, which provokes the occurrence of some final points with very similar coordinate values.

Procedure

L_1 and L_2 (see Fig. 1) were allowed to vary from 60 to 400 cm, with 5 cm intervals, and Q_1 and Q_2 were allowed to vary continuously in the range 0.7–4.5 ml/min.

The normalization conditions for peak height (0–0.1 absorbance units) and residence time (0–5 min) and the intial vertices of the simplex were determined in preliminary experiments, using a few systems with extreme values of the variables to be optimized. The coordinates of the initial point used in the Powell method were calculated as the mean value of its corresponding values in the five initial vertices of the simplex (see Table 1).

The values of peak height and residence time were evaluated as averages of the responses to triplicate injections of 500 μl of a 100 ppb(N) nitrite solution.

To study the influence of the relative weights (C_H/C_T) on the optimization results, the optimization experiment was repeated five times, both for the simplex[15] and Powell methods, with different values for the coefficients (C_H/C_T: 0.9/0.1; 0.7/0.3; 0.5/0.5; 0.3/0.7; 0.1/0.9). In each optimization method the same initial values of the parameters (L_1, L_2, Q_1 and Q_2) were used in all experiments.

Table 1. Starting points used for the optimization experiments

	L_1 (cm)	L_2 (cm)	Q_1 (ml/min)	Q_2 (ml/min)
Simplex	300	400	0.94	0.72
	200	400	1.41	0.72
	200	300	1.18	0.72
	300	300	0.94	1.10
	300	200	1.41	0.91
Powell	325	260	1.04	0.96

RESULTS AND DISCUSSION

The five optimization procedures with different combinations of weighting coefficients (C_H/C_T) were carried out in the usual way: the experimental set-up required by the optimization algorithm was assembled, the experimental responses (peak height and residence time) were measured, and all values were interactively introduced into the computer program, in order to calculate the next experimental conditions. Whenever the optimization algorithm proposed points which were too close to their points previously evaluated (*i.e.* when the differences between the values of each of the parameters in the proposed and evaluated points were smaller than 5 cm for tube lengths and 0.02 ml/min for flow-rates), these were not assembled and evaluated. Instead, the characteristics of the previously evaluated point (parameters and variables) were introduced again in the computer program. This decreases the amount of experimental work and is possible in the present case because the system is stable and presents no significant drift.

Figure 2 shows how the response function varies with the number of experiments, both in the simplex and Powell methods, for the five different sets of weighting coefficients used. It should be noticed that, since there are four variables to be optimized, the simplex has five vertices, and so the experimental points before the sixth do not reflect the simplex method's ability to climb the surface but merely the chosen ordering of the points of the initial simplex. This figure, along with the data in Table 2 for the number of experimental points, shows that the Powell method is usually faster in reaching the maximum. This was quickly attained, a few more experiments were made to verify that there was no further improvement in the response function, and in practice the optimization was terminated before meeting the convergence criterion. On the other hand, the convergence criterion was always met on the simplex optimizations. This implied in some

cases a considerable number of complementary experiments, after the maximum response function was attained (see Table 2).

It should be noted that, conceptually, the speed of optimization is associated with the ability of the optimization method to evolve to the maximum after the beginning of the procedure, which is different for the two methods. In fact, the Powell optimization procedure always starts immediately after the first point while for the simplex the begining of the optimization depends on the number of variables considered (in the present case it is after the fifth point). Nevertheless, what is of primordial importance to the analytical chemist is the time spent on and the amount of work required for the optimization. The significance given in this paper to speed of optimization is thus associated with the number of experimental points used, which still has to be discussed in terms of the amount of work required to attain and use each of the experiment points in the optimization procedures used since, as pointed out by Greenfield *et al.*,[23] this increases with the number of variables which change their values in successive experiments.

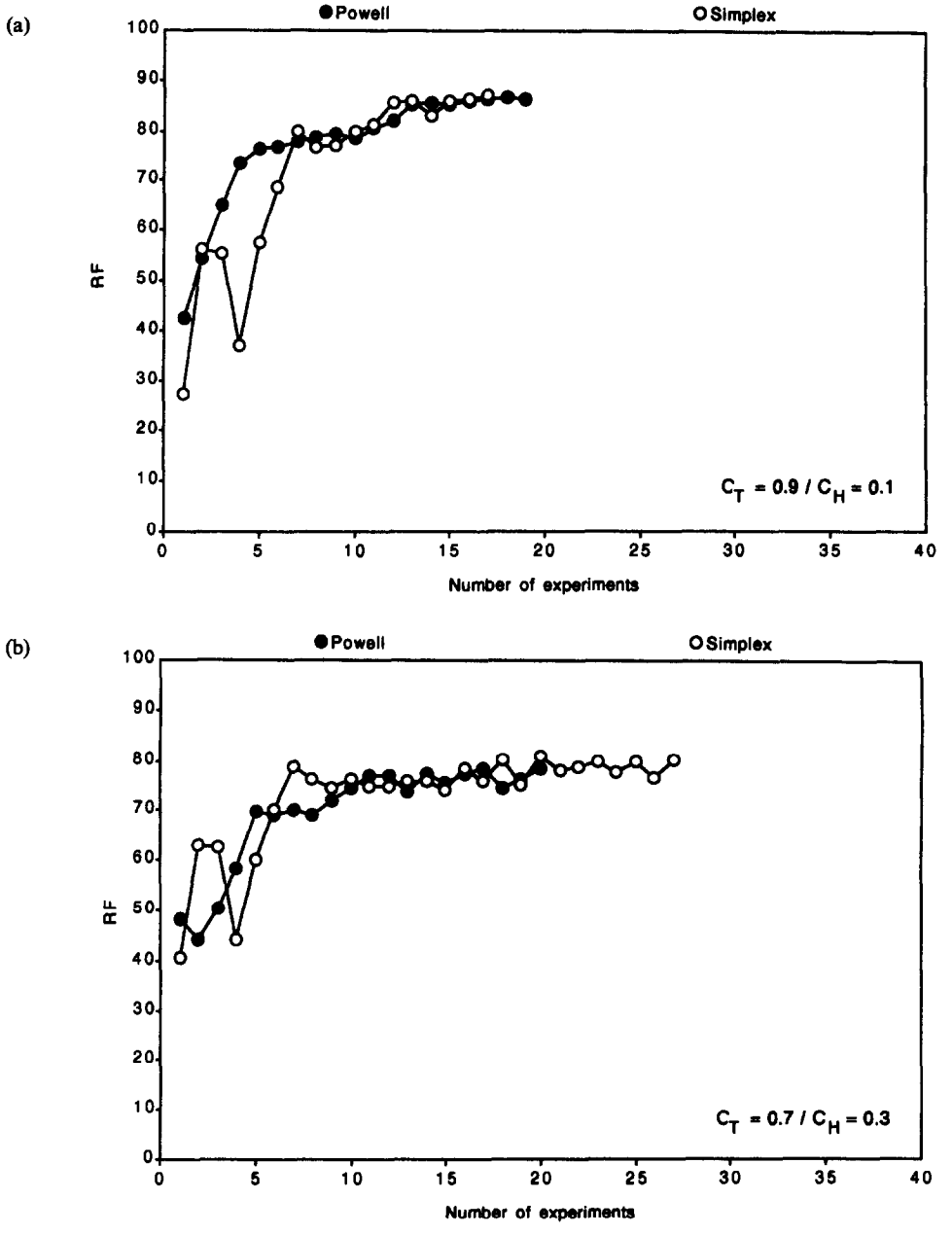

Figs 2(a) and (b).

(c)

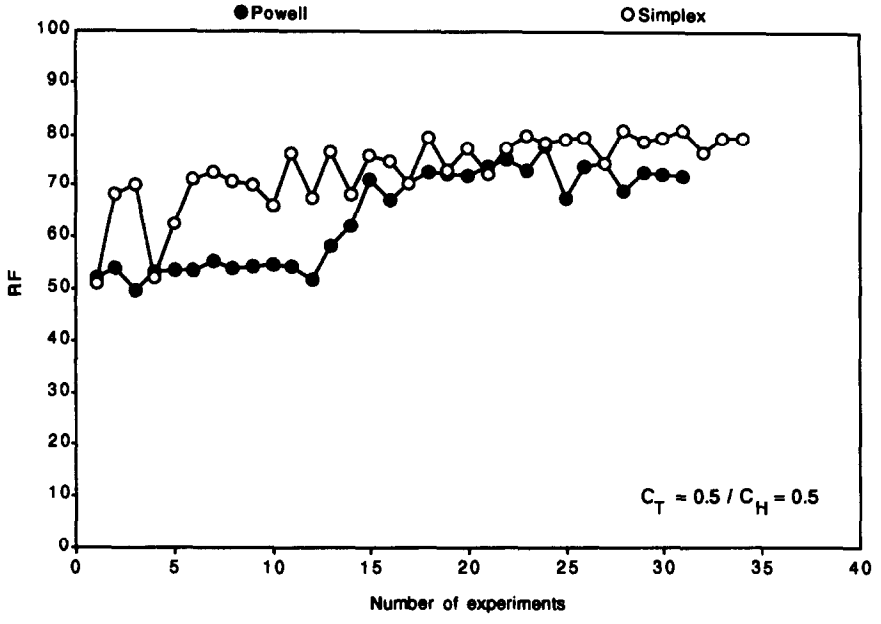

(d)

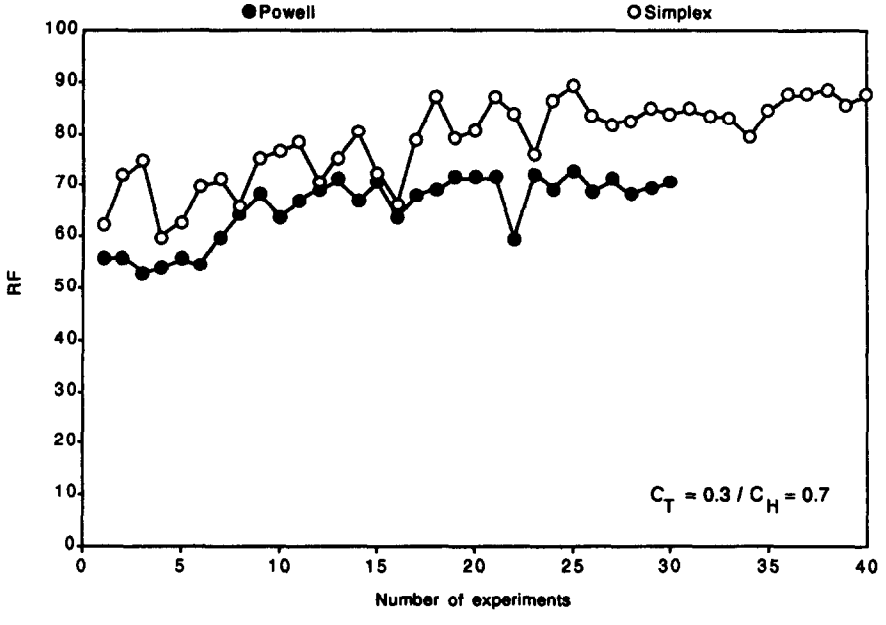

Figs 2(c) and (d).

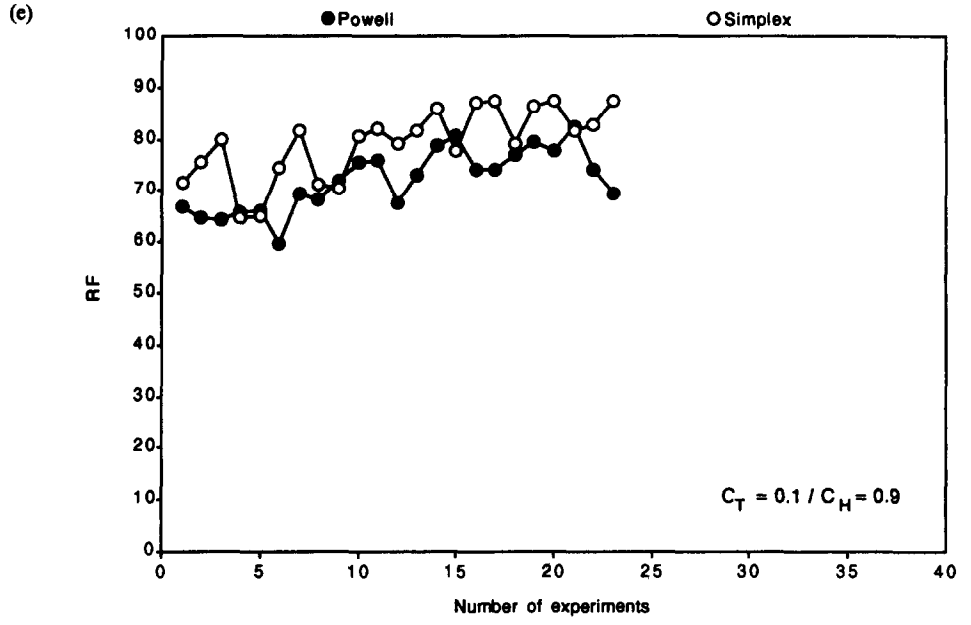

Fig. 2. Variation of *RF* with the number of experiments in the optimization for the five different sets of weighting coefficients in Simplex (○) and Powell (●) methods. C_H/C_T: A. 0.1/0.9; B. 0.3/0.7; C. 0.5/0.5; D. 0.7/0.3; E. 0.9/0.1.

Figure 3 shows the variation of both terms of *RF* ($C_H \cdot R_H$ and $C_T(1-R_T)$) with experiment number, for the five sets of coefficients, both in the simplex and Powell methods. Inspection of these plots shows that when one of the coefficients is set to 0.9 [Figs 3(a) and 3(e)] the corresponding term clearly dominates the value of *RF*, when it is set to 0.7 [Figs 3(b) and 3(d)] the corresponding term is still the most important contribution to *RF* although the contribution from the other one is no longer neglectable, and when both coefficients are set

Table 2. Comparative results of the optimization methods

C_H/C_T		0.1/0.9	0.3/0.7	0.5/0.5	0.7/0.3	0.9/0.1
Q_1 (ml/min)	Simplex†	4.3 ± 0.5	1.9 ± 0.2	1.51 ± 0.05	1.15 ± 0.05	0.99 ± 0.05
	Powell	4.50	1.21	1.42	1.23	1.16
Q_2 (ml/min)	Simplex†	2.5 ± 0.6	1.2 ± 0.1	1.17 ± 0.07	0.90 ± 0.03	0.84 ± 0
	Powell	4.18	0.85	1.25	0.84	0.84
L_1 (cm)	Simplex†	60 ± 0	128 ± 20	132 ± 12	142 ± 5	141 ± 33
	Powell	60	100	110	140	150
L_2 (cm)	Simplex†	60 ± 0	159 ± 31	193 ± 23	161 ± 10	322 ± 26
	Powell	60	100 ± 20*	110	290	290
H (a.u.x 10^3)	Simplex†	12 ± 3	77 ± 6	86 ± 3	96 ± 1	91.2 ± 0.5
	Powell	8	78 ± 3*	76	75.7	84.7
T (s)	Simplex†	15 ± 2	54 ± 6	72 ± 6	114 ± 6	144 ± 18
	Powell	13.4	64 ± 4*	61	102.5	121.5
RF	Simplex†	86.8 ± 0.4	80.2 ± 0.5	80.7 ± 0.5	87.6 ± 0.5	87.3 ± 0.5
	Powell	86.8	78.3	77.8	72.7	82.2
Number of experimental points‡	Simplex	17 (17)	27 (20)	34 (31)	40 (25)	23 (17)
	Powell	19 (18)	20 (17)	31 (24)	30 (25)	23 (21)

*In this case, the same value of response function was obtained for two different experimental points with identical coordinates except L_2. The presented values are the mean values and mean deviations for the two systems.

†The results presented are the mean and its corresponding confidence interval for the five vertices of the final simplex.

‡The number in brackets indicates the point with the highest value of response function. In both cases the experimental point proposed by the algorithm which were equal or too close (see text) to points previously evaluated were not included.

to 0.5 [Fig. 3(c)] the importance of both factors is equally stressed.

Figure 4 shows the variation of values of experimental parameters with experiment number, both for the simplex and Powell methods. The weighting coefficients were set at $C_H = 0.5/C_T = 0.5$ to emphasize equal sensitivity and speed requirements. The experimental responses (H and T) present a very similar variation profile in both methods. On the other hand, the variations of the parameters (L_1, L_2, Q_1 and Q_2) show different profiles, mainly because the unidirectional searches made at the beginning of the Powell method keep three parameters fixed while the fourth varies, but in the simplex method all the parameters change simultaneously.

The effectiveness of the parabolic interpolation in the unidirectional searches of the Powell method can be easily observed from Figs 4(a)–(d), which show that after starting its unidirectional search, each parameter quickly reaches a region close to its optimized value.

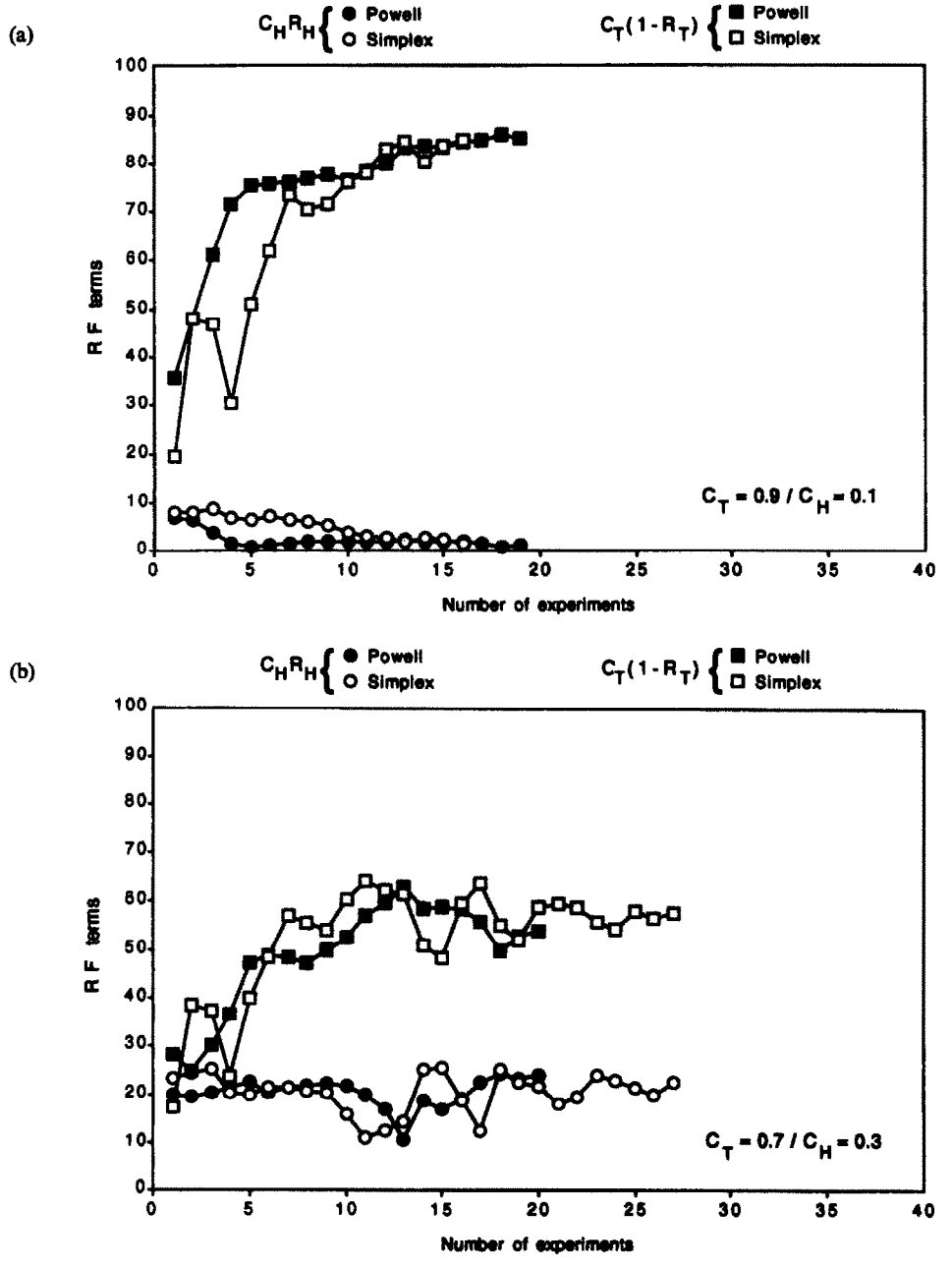

Figs 3(a) and (b).

(c)

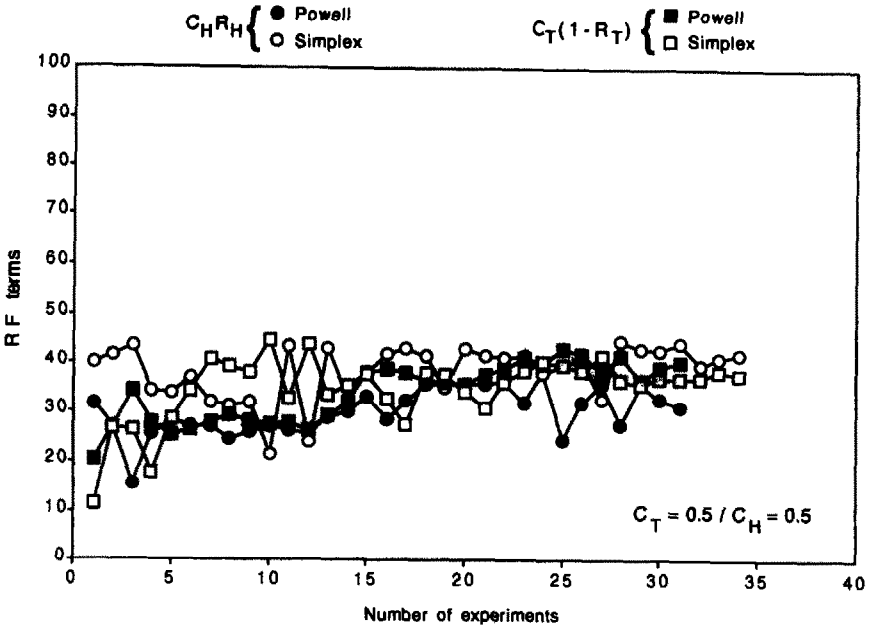

(d)

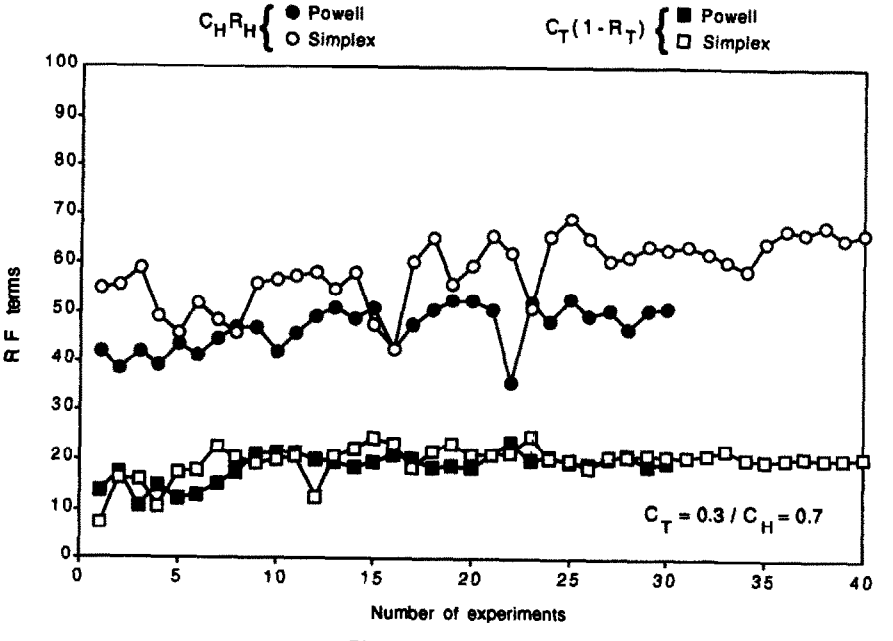

Figs 3(c) and (d).

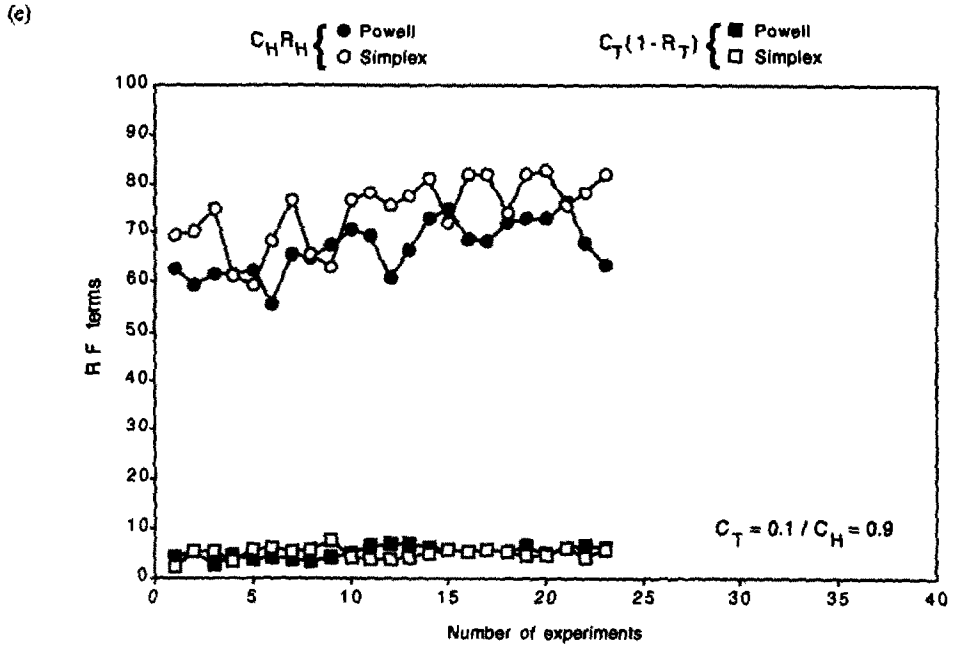

Fig. 3. Variation of the contribution of both terms of RF ($C_H \cdot R_H$ and $C_T(1-R_T)$ with experiment number, for the five different sets of weighting coefficients, in simplex (○, □) and Powell (●, ■) methods. C_H/C_T: A. 0.1/0.9; B. 0.3/0.7; C. 0.5/0.5; D. 0.7/0.3; E. 0.9/0.1.

The final results obtained by both methods are summarized in Table 2. Each of the simplex results presented are the average and the corresponding confidence interval (calculated by the t-function at the 5% significance level)[23] for the set of their respective values in the five vertices of the final simplex. On the other hand, the Powell results are the values corresponding to the point with the highest value of the response function. This is a consequence of the different natures of the convergence criteria used in two methods.

As Table 2 shows, the values of H generally increase with the sensitivity coefficient, C_H, and the sample throughput rate generally increases (*i.e.* the value of T decreases) in the opposite direction, as would be expected from the structure of RF.

For both methods, the marked importance conferred to the sample throughput rate in the optimization experiments with the first set of weighting coefficients, $C_H = 0.1/C_T = 0.9$, leads to very fast systems, whose sensitivity is however very low. It is therefore not surprising that the largest increase in sensitivity and decrease in sample throughput rate between successive sets of weighting coefficients are observed, in both optimization methods, on passing to the following set of coefficients, $C_H = 0.3/C_T = 0.7$. However, some unexpected features are found in the results of the remaining experiments for the two methods. The simplex results proceed its expected trend (increasing the values of peak height and residence time) until the experiment with coefficients $C_H = 0.7/C_T = 0.3$, but on passing to the last, $C_H = 0.1/C_T = 0.9$, the importance of sensitivity cannot be further stressed and no improvement in the resulting systems is obtained, probably due to the fact that the reaction had already almost reached completion and dispersion effects now dominate. A similar situation occurs for the Powell method between the second ($C_H = 0.3/C_T = 0.7$) and third ($C_H = 0.5/C_T = 0.5$) sets of coefficients, from which result systems with very close characteristics. The Powell method was not very successful in optimizing the sensitivity in the central area ($C_H = 0.3/C_T = 0.7$ to $C_H = 0.7/C_T = 0.3$), where the difference in the optimization results are mainly due to the influence of the other term of RF, the sample throughput rate, but a significant increase in sensitivity was obtained in the optimization with the last set of coefficients ($C_H = 0.9/C_T = 0.1$).

The complex interdependence between the parameters and variables of a FIA system leads to the occurrence of points that have the same value of RF (since this is determined by the values of the variables), although they correspond to different sets of parameters (these

points fall on an *RF* surface contour in a *RF vs.* parameters plot). After a surface contour close to the maximum is reached, further iterations provide only small improvements in the value of *RF*, and therefore, to limit the number of experiments, the convergence criteria cannot be too strict. Thus, although the maximum might be unique, it is seldom reached exactly. Therefore, depending on the way the optimization algorithm approaches the maximum, the final value reported as the maximum value of *RF* may correspond to different sets of parameters in the two optimization methods.

For instance, in the experiment with coefficients $C_H = 0.1/C_T = 0.9$, where the importance of analysis time is stressed over sensitivity, a large difference is observed between the values of Q_2 obtained by the two methods. This may be due to an unfavorable simplex orientation with respect to a ridge, while the results from Powell are set on a boundary condition. A few more experimental points confirmed that the simplex would increase Q_2 while maintaining all the

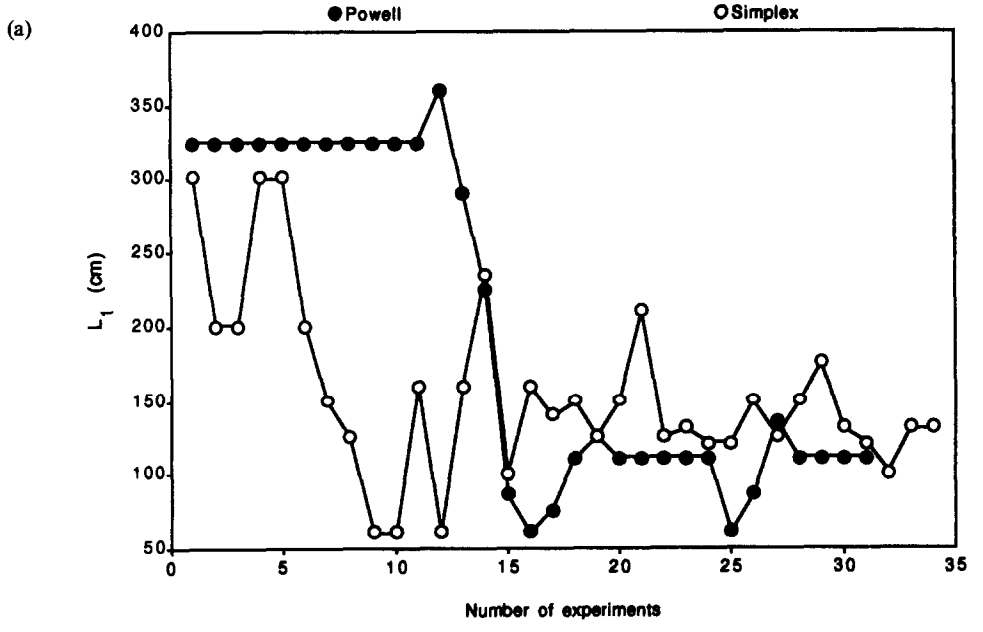

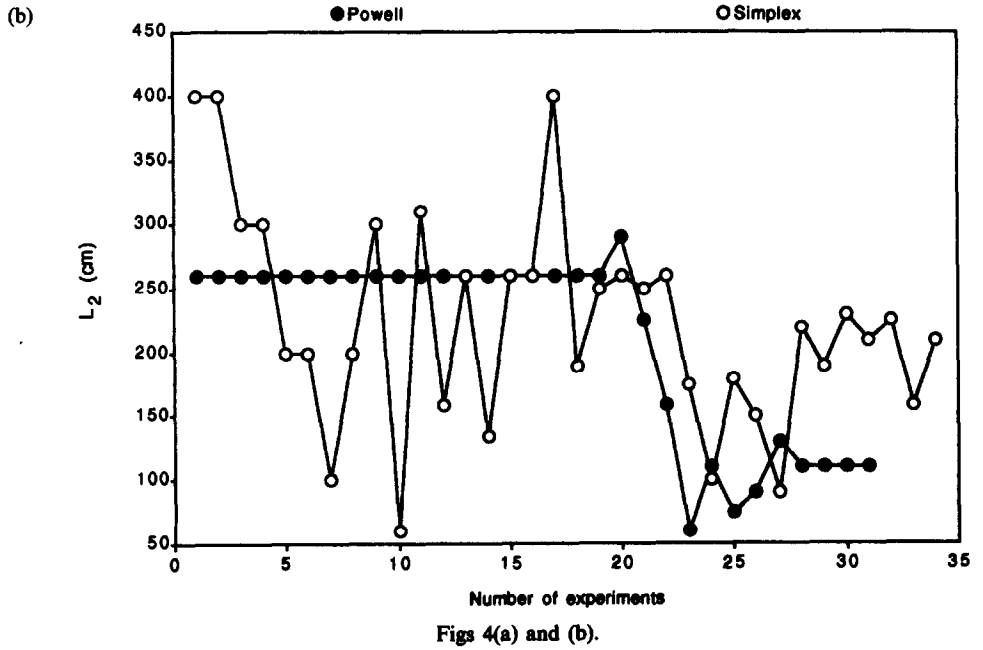

Figs 4(a) and (b).

(c)

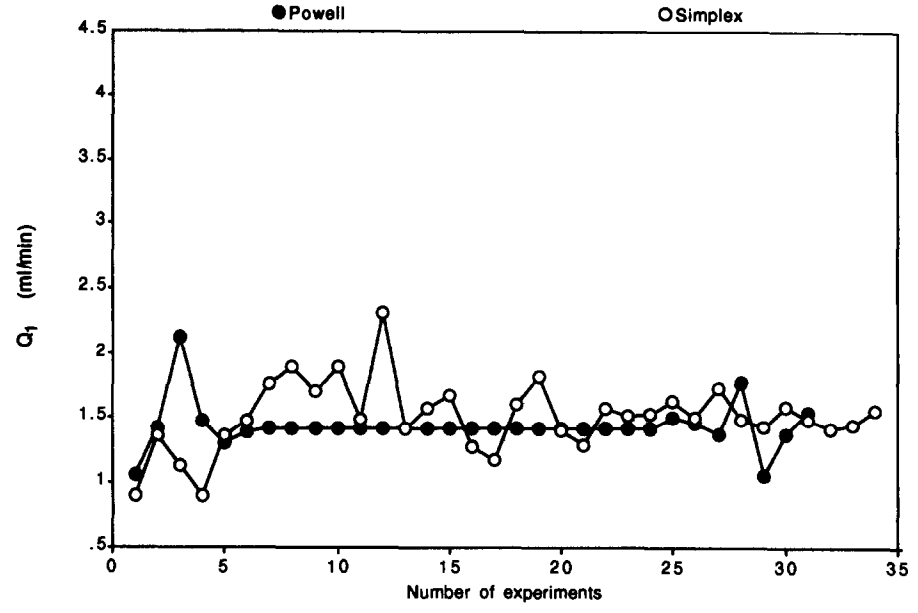

(d)

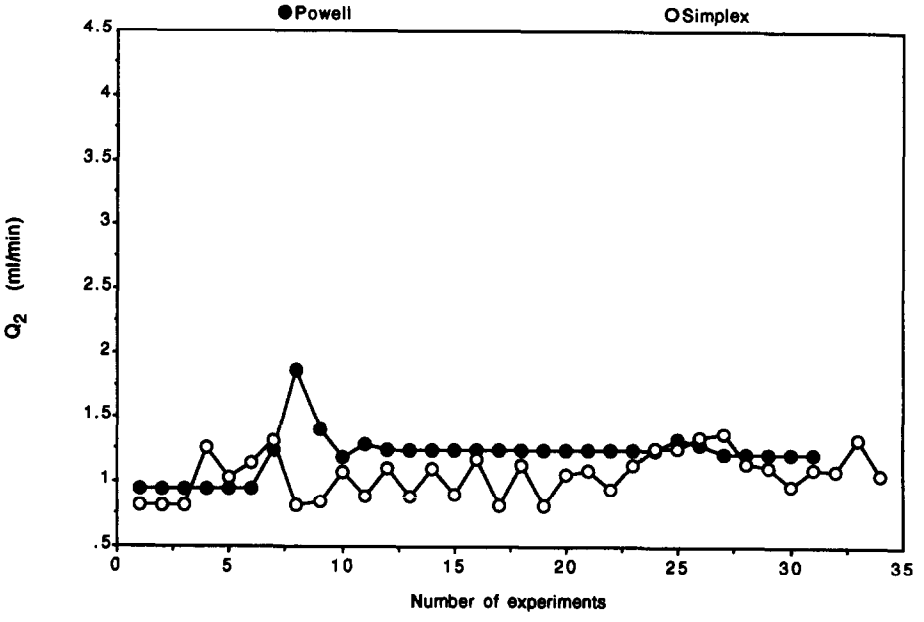

Figs 4(c) and (d).

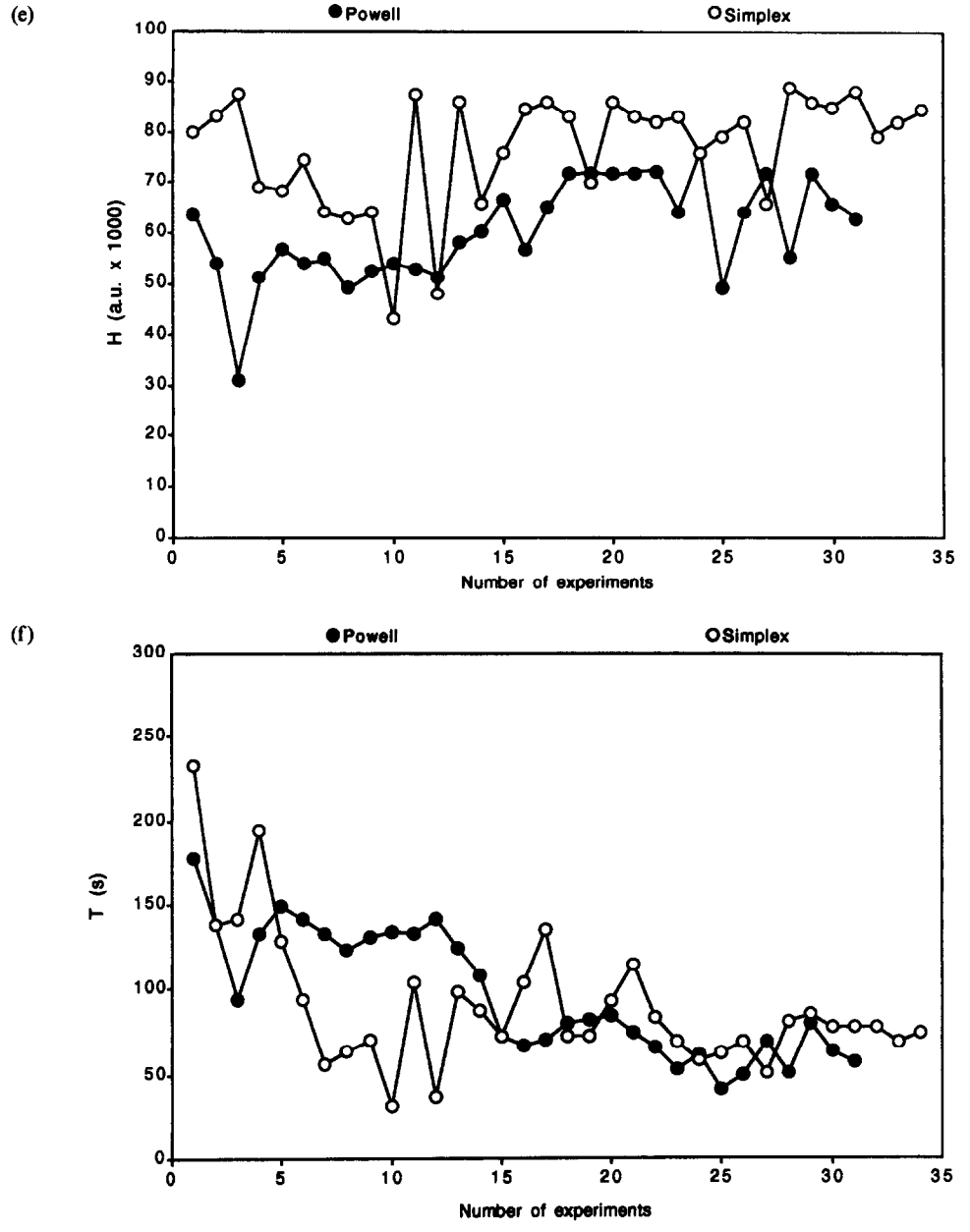

Fig. 4. Variation of parameters and variables with the number of experiments in the optimization experiment with weighting coefficients $C_H = C_T = 0.5$ for simplex (○) and Powell (●) methods. A. L_1; B. L_2; C. Q_1; D. Q_2; E. R_H; F. R_T.

other parameters, which would make closer the final results of both optimization procedures.

In the experiment where sensitivity was given more importance ($C_H = 0.9/C_T = 0.1$), the parameters obtained by both methods were very similar. Some differences were found in the other experiments, which can be explained by the way the variables depend on the parameters.

In the case with $C_H = 0.5/C_T = 0.5$, the only difference found was in the value of the tube length L_2. This is a result of the kind of response function used. Indeed, in the region around the maximum, the alteration of the value of one of the parameters generally provokes variations in the same direction of both variables considered (*i.e.*, if one flow rate is decreased usually both the peak height and the response time increase). Since we intend to maximize the former and minimize the latter, the net consequence in the response function may be very small or even null, and systems with different values of the parameters may have similar values of response

function. The situation for $C_H = 0.7/C_T = 0.3$ is similar, but as there is a certain difference in the values of the response function obtained by the two methods, the comparison may have less relevance.

For the function with $C_H = 0.3/C_T = 0.7$, large differences were found in Q_1 and L_2 (as well as smaller differences in Q_2 and L_1). This results from the fact that variations in the same direction of flow rate and tube length in one channel may produce similar values of peak height and response time. For example, if both tube length and flow rate are increased, the effect in response time will usually be very small, because the distance covered is larger but the speed is also higher, and the same is true for peak height, since the dispersion is higher but so is the extension of the reaction (unless it had already almost reached completion, in which case dispersion effects would dominate).

CONCLUSIONS

The use of a weighted response function in the Powell optimization of FIA systems provides a useful procedure for the characterization of their performances and for stressing the relative importance of sensitivity and sample throughput rate. This fully confirms the conclusion of a previous work with the simplex optimization procedure,[15] showing the usefulness of that type of response function in assessing the versatility of FIA procedures in different practical situations. To guide the optimization procedure to the desired balance requirements between sensitivity and sample throughput rate, it is only necessary to assign adequate values to the wei ghting coefficients and to have determined previously the normalization values of the variables.

The comparison between the simplex and Powell methods demonstrates that both can be useful for the optimization of FIA systems, neither having revealed definite advantages over the other.

In its early stages, at least during the first iteration cycle, the Powell method evolves through univariate searches. These are easier to accomplish experimentally than searches where various parameters have to be changed, thus allowing for savings of time in experimental work. This is particularly important in FIA when tube lengths are to be optimized, since their changes require a complete reset of the system and stabilization of baseline and therefore the savings in time are substantial if the number of alterations of tube length decreases. However, the Powell method requires a deeper knowledge of the system, necessary in order to choose the right order of optimization of the parameters, which is essential to avoid any disorientation of the search path, especially in the early stages of the process.

Although the Powell method was usually faster in searching the maximum, the simplex method provided more consistent results for the optimization, being much more robust. Additionally, the simplex method yields the uncertainty figures of the different parameters upon statistical treatment for the final polyhedron, which provide an indication of the final point precision. In the Powell method, due to the different convergence criterion used, this information cannot be obtained, although as several close points are collected at the final stage of the process, further confidence is also achieved. A more effective convergence criterion would make the Powell method more efficient.

REFERENCES

1. W. Spendley, G. R. Hext and F. R. Himsworth, *Technometrics*, 1962, **4**, 441.
2. J. A. Nelder and R. Mead, *Comput. Jl.*, 1965, **7**, 308.
3. S. L. Morgan and S. N. Demming, *Anal. Chem.*, 1974, **46**, 1170.
4. D. Betteridge, T. J. Sly, A. P. Wade and J. E. W. Tillman, *Anal. Chem.*, 1983, **55**, 1292.
5. A. P. Wade, *Anal. Proc.*, 1983, **20**, 523.
6. D. Betteridge, A. F. Taylor and A. P. Wade, *Anal. Proc.*, 1984, **21**, 373.
7. D. Betteridge, A. P. Wade and A. G. Howard, *Talanta*, 1985, **32**, 709.
8. D. Betteridge, T. J. Sly, A. P. Wade and D. G. Porter, *Anal. Chem.*, 1986, **58**, 2258.
9. C. L. M. Stults, A. P. Wade and S. R. Crouch, *Anal. Chim. Acta*, 1987, **192**, 155.
10. A. P. Wade, P. M. Shiundu and P. D. Wentzell, *Anal. Chim. Acta*, 1990, **237**, 361.
11. T. A. H. M. Janse, P. F. A. Van der Wiel and B. Kateman, *Anal. Chim. Acta*, 1983, **155**, 89.
12. A. Fernandez, M. D. Luque de Castro and M. Valcarel, *Anal. Chem.*, 1984, **56**, 1146.
13. F. Lazaro, M. D. Luque de Castro and M. Valcarel, *Anal. Chim. Acta*, 1985, **169**, 141.
14. J. Alonso, J. Bartroli, J. Coello and M. del Valle, *Anal. Lett.*, 1987, **20**, 1247.
15. J. Alonso, J. Bartroli, M. de Valle, A. A. S. C. Machado and L. M. A. Ribeiro, *J. Chemometrics*, 1988, **3**, 249.
16. S. K. Beh, G. J. Moody and J. D. R. Thomas, *Anal. Proc.*, 1990, **27**, 81.
17. M. J. D. Powell, *Comput. Jl.* 1964, **7**, 155.
18. M. del Valle, J. Alonso, M. Poch and J. Bartroli, *J. Chemometrics*, 1988, **3**, 285.
19. M. del Valle, M. Poch, J. Alonso and J. Bartroli, *Anal. Chim. Acta*, **241**, 31.

20. S. Nakashima, M. Yagi, M. Zenki, A. Takahashi and K. Toei, *Anal. Chim. Acta*, 1974, **155**, 263.
21. E. R. Aberg and G. T. Gustavsson, *Anal. Chim. Acta*, 1982, **144**, 39.
22. S. Greenfield, M. S. Salman, M. Thomsen and J. Tyson, *J. Anal. Atomic Spectrom.*, 1989, **4**, 55.
23. J. C. Miller and J. N. Miller, *Statistics for Analytical Chemistry*, Wiley, Chichester, 1984.

Talanta, Vol. 40, No. 7, pp. 1127–1129, 1993
Printed in Great Britain.

0039-9140/93 $6.00 + 0.00

SHORT COMMUNICATION

SPECTROPHOTOMETRIC DETERMINATION OF Fe(III) IN ALKALINE SOLUTIONS WITHOUT NEUTRALIZATION

LUMINITA VLADESCU and RENATE LERCH-GURGUTA
Department of Analytical Chemistry, Faculty of Chemistry, University of Bucharest, 13, Bv. Carol I, 70346-Bucharest, Romania

(*Received* 25 *July* 1991. *Revised* 15 *December* 1992. *Accepted* 12 *January* 1993)

Summary—Spectrometric study on the complexation of Fe(III) with an organic reagent obtained by coupling 3-methyl-1-phenyl-5-pyrazolone with diazotized 3-hydroxy-4-amino-benzene sulphonic acid was carried out in alkaline solutions.

A 1:2 Fe(III):reagent water soluble complex is formed. The optimum pH is 9.0–11.8. The maximum absorbance of the complex lies at $\lambda = 560$ nm, where the absorbance of the reagent is low. The molar absorptivity is 9000 $l.mole^{-1}.cm^{-1}$ at pH = 11.6. The value of the stability constant determined at $20 \pm 1°C$, pH = 11.6 and $\lambda = 560$ nm is $4 \times 10^5 M$. The Beer–Lambert law is followed for iron concentration in the 0.2–5.0 μg/ml range.

The spectrophotometric method was tested on synthetic solutions and thus applied for determination of traces of Fe(III) in several samples of alkaline hydroxides and carbonates without the neutralization of the solutions.

In a study of the effects of Fe(III) in technical processes and for quality establishment of analytical grade reagent, a simple method for the determination of microgram amount of Fe(III) in commercial 50% solutions and solid NaOH p.a., or other alkaline products p.a., was required. Usually, the amounts of Fe(III) encountered vary between 0.5 and 10 ppm. Other metal ions, such as calcium, magnesium, barium, aluminium, nickel, mercury, manganese and copper may be present in metal/iron ratios varying from 1/2 to 5/1.

All the methods commonly utilized requires that the sample must be first neutralized.[1-9]

In this paper a spectrophotometric investigation of the complexation of Fe(III) with an organic reagent obtained[10] by coupling 3-methyl-1-phenyl-5-pyrazolone with diazotized 3-amine-4-hydroxy-benzenesulphonic acid was carried out. The reagent formula (R) is given in Fig. 1.

The date obtained were used in developing a spectrophotometric method of determining Fe(III) directly in alkaline hydroxides and carbonates without the neutralization of solutions.

EXPERIMENTAL

Reagents and equipment

All chemicals used were analytical reagent grade.

Aqueous solutions of known titre of $10^{-3}M$ and $2 \times 10^{-3}M$ of Fe^{3+} ions were obtained from concentrated stock solution Merck for atomic absorption spectrometry.

$10^{-3}M$ and 2×10^{-3} aqueous solutions of reagent R were prepared starting from the reagent synthesized and characterized by elementary analysis, NMR, IR and UV–VIS technics and by chromatographic methods; on this basis the physical properties, the structure and the purity of the reagent were established.[10]

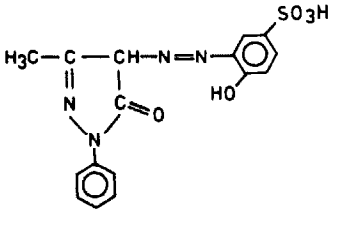

Fig. 1. Formula of reagent R.

1*M* NaOH aqueous solutions were prepared from solid NaOH (Merck), or from alkaline products for analysis and the titre of each solution was determined titrimetrically by 0.1*M* HCl standard solution (Merck); in this way samples with known concentration of NaOH were obtained.

pH buffer NH_3–NH_4Cl and KHphtalate–NaOH solutions.[11]

Absorbance measurements were carried out on a SPECORD UV–VIS Karl Zeiss–Jena spectrometer. The pH of the solutions was measured with a MV-84 (VEB, Pracitrönic Dresden) pH-meter.

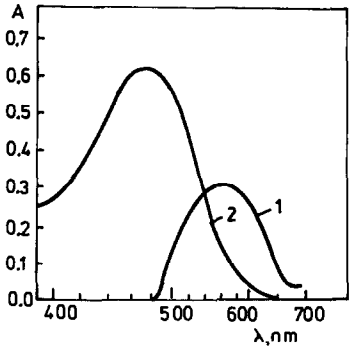

Fig. 2. Absorption spectra of: (1) complex against reagent blank (pH = 11.6); and (2) reagent in buffer solution against buffer solution (pH = 11.6).

PROCEDURE

The solutions to be studied were prepared in 25 ml calibrated flasks where exactly measured volumes of Fe(III) and reagent *R* solutions were introduced; 5 ml of a pH buffer solution, or a calculated volume of 1*M* NaOH solution of known concentration were added to obtain a determined pH. The flasks were filled up to the mark with distilled water. Absorbance of each solution was measured against a corresponding Fe(III) free reagent blank, similarly prepared.

RESULTS AND DISCUSSION

The influence of wavelength, of amount of reagent, of Fe(III) concentration and of pH on the absorbance of Fe(III)-reagent solutions was studied in order to establish the optimal working conditions for the spectrophotometric determination of Fe(III) directly in alkaline hydroxide and carbonate samples without the neutralization of solutions.

The pyrazolonic derivative forms a red complex instantaneously with Fe(III) at room temperature. The absorption spectra of the complex and of the reagent solutions at pH = 11.6 are shown in Fig. 2. The maximum absorbance of the complex is located at $\lambda = 560$ nm, i.e. where the reagent absorbs very little.

The effect of the pH on the absorbance of the solution of the complex at $\lambda = 560$ nm shows that the optimal pH range is 9.0–11.8.

Job's method and the spectrophotometric titration methods were employed for establishing the composition of the complex. The results indicate the formation of a 1:2 complex between Fe(III) and reagent. A 3–4-fold molar excess of the reagent over Fe(III) is required in order to obtain maximum constant absorbance.

The Beer–Lambert law is followed for Fe(III) concentration in the 0.2–5.0 μg/ml range.

The molar absorptivity coefficient is 9000 $l.mole^{-1}.cm^{-1}$ at pH = 11.6. The mean value of the apparent stability constant of the complex calculated from the absorbance data by the mole ratio method at $20 \pm 1°$ and pH = 11.6 was $4 \times 10^5 M$.

The study of the interferences shows that the ions of alkaline, alkaline-earth metals and of Hg(II), Zn(II), Cu(II), Ni(II), Co(II), Al(III), Ti(IV) in a 5-fold molar excess do not interfere in determination of Fe(III).

The method was tested on synthetic solutions containing known amounts of Fe(III) in the presence of 5-times higher amounts of the above-mentioned ions and a volume of 1*M* NaOH standard solution Merck, corresponding at a pH 9.0–11.8 in the total volume of the solution to be analyzed. The results obtained show a good agreement between Fe(III) amount taken in the sample and those determined. Relative standard deviation was $0.5 \pm 0.05\%$.

The method was applied for determining the Fe(III) content in several samples of alkaline hydroxides and carbonates without the neutralization of the solution. The stock sample solution was prepared in a 100 ml calibrated flask and its HO^- concentration was determined titrimetrically with a standard 0.1*M* HCl solution Merck. The solution to be analyzed was prepared and added to a 25 ml calibrated flask containing 5 ml solution $10^{-3}M$ reagent and exactly measured solution of the stock sample solution (calculated to provide a final pH 9.0–11.8). The flasks were filled up to the mark with distilled water. Absorbance of each solution was measured against a corresponding

Table 1. Results of the Fe(III) content determination in alkaline hydroxides and carbonates without the neutralization of solution

Compound analyzed	Fe(III) content %: Spectrophotometric determination with KSCN[7]	with Feron[8]	with *R*	Determination by atomic absorption spectrometry
NaOH 50% solution	—	0.0010	0.0014	0.0012
NaOH p.a.	0.0040	0.0034	0.0038	0.0040
KOH p.a.	—	0.0006	0.0008	0.0005
Na_2CO_3 p.a.	0.4560	0.4655	0.4600	0.4599
K_2CO_3 p.a.	0.0025	0.0030	0.0020	0.0022

Note: Each result is the mean of five determinations.

Fe(III) free reagent blank similarly prepared utilizing a standard 1 *M* NaOH solution Merck. The results in Table 1 show a good agreement between the data obtained by this method and those offered by other methods commonly utilized for the quantitative determination of Fe(III).

CONCLUSIONS

Fe(III) may be determined spectrophotometrically in alkaline hydroxide and carbonate samples without the neutralization of solutions by means of the organic reagent obtained by coupling 3-methyl-1-phenyl-5-pyrazolone with diazotized 3-amine-4-hydroxy-benzenesulphonic acid. This reagent forms with Fe(III) a 1:2 complex with the maximum absorbance at $\lambda = 560$ nm for pH 9.0–11.8.

REFERENCES

1. L. Jones, L. Jerry, E. Raymond and J. Munoz, *Analyt. Chem.*, 1970, **42**, 517.
2. N. M. Kuzmin, T. P. Dubrovina and O. M. Semsuk, *Zavodsk. Lab.*, 1969, **35**, 784.
3. K. Gorczynska and M. Gluzinskaia, *Chem. Anal. (Warsaw)*, 1969, **14**, 318, 591.
4. C. Liteanu, Al. I. Crisan and M. Marian, *Anal. Univ. Babes-Bolyai Cluj*, 1968, **39**, 1.
5. M. M. Gogneva and R. D. Vodianikova, *Zh. analit. Khim.*, 1965, **8**, 831.
6. J. M. Lemus Gallego and J. K. Jimenez, *Analyst*, 1988, **113**, 1341.
7. M. A. Grompone, *J. Chem. Educ.*, 1987, **64**, 1057.
8. L. Vladescu and M. Dumitra, *Rev. Chim. (Bucuresti)*, 1989, **40**, 144 and 350.
9. J. Yang, Yejin Fenxi, 1987, **7**, 48; *Chem. Abstr.*, 1990, **112**, 245,123.
10. N. Dumitrtescu, Thesis, Inst. Politeh. Bucuresti, 1987.
11. E. Banyai, I. Mazor, E. Kocsis and Gy. Rady, *Tabele de Calcul in Chimia Analitica*, p. 314. Tehnica, Bucharest, 1961.

Talanta, Vol. 40, No. 7, pp. 1131–1137, 1993
Printed in Great Britain.

0039-9140/93 $6.00 + 0.00

DEVELOPMENT OF A POLYPYRROLE-BASED AMPEROMETRIC DETECTOR FOR THE DETERMINATION OF CERTAIN ANIONS IN WATER SAMPLES

PEIG WARD and MALCOLM R. SMYTH*
School of Chemical Sciences, Dublin City University, Dublin 9, Ireland

(*Received* 27 *October* 1992. *Revised* 23 *December* 1992. *Accepted* 4 *January* 1993)

Summary—The development of a polypyrrole-based modified electrode for use in the detection of anions in flow-injection analysis and ion chromatography is described. Chloride, nitrate, nitrite, perchlorate, bromide, carbonate, sulphate and phosphate were detected by using flow-injection analysis combined with the polypyrrole-based CME electrochemical detector. All of the anions were detected conveniently and reproducibly over a linear concentration range 1–100 μg/ml. A detection limit of 0.1 μg/ml was obtained for chloride and a limit of 1.0 μg/ml for all of the other anions. Chloride, nitrate, sulphate and phosphate, following separation using ion chromatography, were detected simultaneously by using a conductivity detector and the polypyrrole-based CME electrochemical detector in series. Both methods of detection yielded similar results with comparable sensitivity, linearity and limits of detection. This method was then applied to the analysis of fresh water samples. The electrode was stable over a 2-week period of operation with no evidence of chemical or mechanical deterioration.

Polypyrrole and other conducting polymers have proved very popular in the development of chemically modified electrodes (CMEs) as analytical sensors in recent years. The main advantages of these CMEs lie in improvements in sensitivity and selectivity, as well as the ability to detect electroinactive species.

The ability to deliberately control and manipulate the surface properties can lead to a variety of attractive effects. Such tailoring of the surface can meet the needs of many analytical problems. The incorporation of CMEs into flowing streams or coupled to chromatographic systems has made electrochemical detection a powerful tool for the determination of a wide variety of species.

Many applications of polymer modified electrodes with amperometric detection exist in the recent literature. For example, Ikariyama and Heineman[1] described a flow-injection analysis (FIA) method in which a polypyrrole modified electrode was used as a detector for electroinactive anions based on the repetitive doping–undoping of the polypyrrole layer. They investigated the electrode response for carbonate, phosphate and acetate and found it was linear over the concentration range from 10 μM to 1 mM for each anion. Wallace and co-workers[2–4] have developed polypyrrole and poly(pyrrole-*N*-carbodithionate)-based electrodes incorporating various counterions, for the determination of a variety of cations.

Ye and Baldwin[5] have developed a similar method to that of Ikariyama and Heineman,[1] but used polyaniline as the conducting polymer matrix. They applied the method to a wider range of anions and also looked at the selectivity of the electrode by varying the background electrolyte composition and concentration. Wang and Liu[6] then reported on the use of a polyaniline modified electrode for the detection of anions such as perchlorate, nitrate, sulphate, oxalate and iodate in FIA and ion chromatography (IC). Sung and Huang[7] have also applied a polyaniline–Nafion composite electrode to the determination of alkali and alkaline earth metal ions using FIA and IC. This method involved holding the CME at a potential at which the polymer is reduced, and as the sample plug containing cations arrive at the composite electrode, a transient current signal is obtained which is proportional to the cation concentration.

*Author for correspondence.

This paper reports on the preparation of a polypyrrole CME using a platinum wire (0.5 mm o.d.) as the substrate incorporated into a microelectrochemical flow cell.[8] The aim was to apply this CME as an amperometric electrochemical detector for the detection of a series of electroinactive anions using both FIA and IC. The analysis of river water samples taken from different locations using both IC with conductivity detection and IC using the CME as an amperometric detector was then compared.

EXPERIMENTAL

Reagents

All chemicals used were of Analar grade purity. All standard solutions were prepared using distilled water which was further purified by passing it through a Milli-Q water purification system. Pyrrole was purchased from Riedel-de Haen (Seelze, Germany) and was freshly distilled and stored under nitrogen at 0°C. Platinum wire (0.5 mm o.d.) and silver wire (0.1 mm o.d.) were purchased from Goodfellow Metals (Cambridge, UK). Silver loaded epoxy resin (RS 567-604) was purchased from Radionics (Dublin, Eire). The AG4A guard and AS4A separator ion chromatography columns were purchased from Dionex (Surrey, UK). Polyethylene tubing was purchased from Gallenkamp (Loughborough, UK), and low pressure fittings and peristaltic tubing were purchased from Omnifit (Cambridge, UK).

Instrumentation

The electrochemical system consisted of an EG & G Model 264A potentiostat, a Lloyd PL3 X–Y recorder and a Phillips PM 8251 X-t recorder. The FIA system consisted of a Gilson Minipuls 3 peristaltic pump and a 7125 Rheodyne injection value. The Ion Chromatography system was a Dionex Ion Chromatograph Model 4500 IC system, consisting of a gradient pump (GPM), a conductivity detector (CDM II), an eluant degas module (EDM), a micro membrane suppressor (MMS), a 50 μl fixed loop 6-port pneumatic injection valve and an ACI AI 450 software package (version 2.1). The Dionex columns used were a AG4A guard and a AS4A separator column. The chromatographic conditions used were 1.8 mM Na_2CO_3/1.7 mM $NaHCO_3$ as eluant at a flow rate of 2 ml/min, and the suppressor regenerant used was 12.5 mM H_2SO_4 at a flow rate of 5 ml/min.

Preparation of polypyrrole-based chemically modified electrode

Platinum wire was cleaned by placing a piece of 0.5 mm o.d. platinum wire in chromosulphuric acid for 5 min. It was then removed, and washed thoroughly with deionised water. The wire was then placed in a solution of aqua regia for 5 min, removed, and washed with deionised water. The wire was then polished using alumina powder (0.03 μm) and left to soak in deionised water overnight.

The platinum wire, washed following the above procedure, was then used to construct the working electrode as described in a method previously reported.[9]

Preparation of Ag/AgCl *reference electrode.* Silver chloride was coated onto a silver wire (20 mm length, 0.1 mm o.d.), by connecting the wire to the anode of a 1.5 V battery and connecting a platinum wire to the cathode of the battery. Both wires were then immersed in a solution of 1 mole/dm^3 hydrochloric acid for 2 min. The coated wire was then inserted into a polyethylene tube (30 mm length, 2 mm o.d., 1 mm i.d.). A porous ceramic rod (2 mm length, 1 mm o.d.) was fitted into one end of the tube and was heated sealed into the tube using an electric soldering iron. The tube was filled with an internal reference solution containing 1 mole/dm^3 potassium chloride. Finally, this end of the tube was sealed using an epoxy glue. The electrical connection was made by soldering a copper wire (0.5 mm o.d.) onto the uncoated tip of the Ag/AgCl wire. The auxillary electrode used was a piece of stainless steel tubing (20 mm length, 2 mm o.d., 1 mm i.d.)

The working electrode, reference electrode and auxillary electrode were mounted together in a T-tube (30 mm length, 20 mm height, 2 mm i.d.), the connections being made using silicone tubing (5 mm o.d., 1.5 mm i.d.). The flow cell configuration was as shown in Fig. 1. The cell arrangement is such that the electrolyte first passes the working electrode, then the reference, and finally passes the auxillary electrode to waste.

Modification of the working electrode. The flow cell was connected to a peristaltic pump via a low pressure fitting (Omnifit). The platinum wire and auxillary electrodes were taken through a further cleaning step by pumping a 0.1 mole/dm^3 sulphuric acid solution through the cell at a flow rate of 0.8 ml/min for 1 hr while cycling the potential between -1000 and

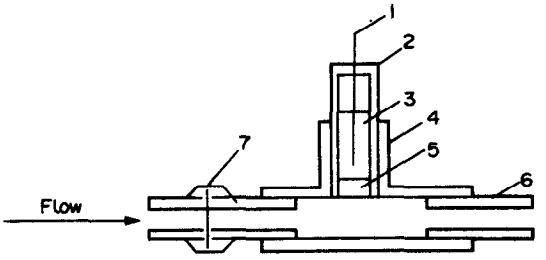

Fig. 1. Structure of polypyrrole-based CME flow cell. 1. Silver wire coated with silver chloride, 2. Reference electrode body, 3. Internal reference solution, 4. T-tube, 5. Ceramic rod, 6. Stainless steel auxillary electrode and 7. Polypyrrole-based CME.

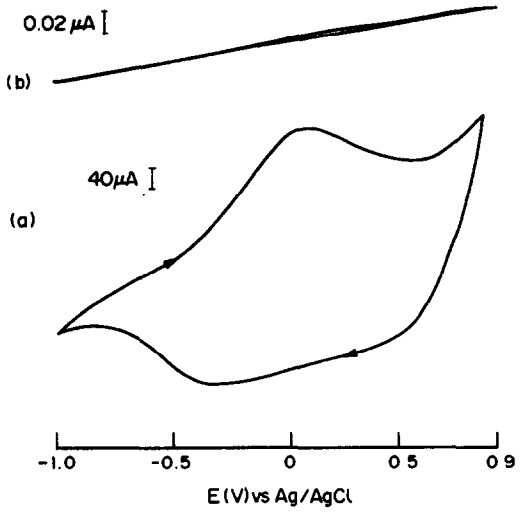

Fig. 2. Cyclic voltammograms of polypyrrole-based CME in (a) 1 mole/dm^3 NaCl and (b) 0.1 mole/dm^3 glycine, scan rate of 50 mV/sec.

+1400 mV at a scan rate of 50 mV/sec. The potential was then held at +400 mV until a steady decay current was obtained. The system was then flushed with deionised water for 10 min.

The electrode was modified by injecting a deoxygenated solution of 0.5 mole/dm^3 pyrrole in 1.0 mole/dm^3 sodium chloride as the electrolyte, into the flow cell using a 2 ml syringe. Electropolymerisation was carried out by slow potential cycling from −1000 mV to +900 mV at a scan rate of 20 mV/sec, for three complete cycles. The polymer film was deposited onto the platinum wire as a purple coloured film.

During the electropolymerisation step, faster scan rates of 100 and 50 mV/sec were investigated, but films produced using these conditions were thin and patchy and not as stable or reproducible as those prepared using the slower scan rate of 20 mV/sec.

RESULTS AND DISCUSSION

Characterisation of polypyrrole-based CMEs

The freshly prepared polypyrrole-based CME was placed in the flow system and using deoxygenated 0.1 mole/dm^3 NaCl as the electrolyte, its cyclic voltammetric behaviour was investigated. The potential was cycled from −1000 to +900 mV at a scan rate of 50 mV/sec. The cyclic voltammogram produced for the electrode shows the classic redox transitions from the neutral to conducting state at potentials similar to those observed by other workers.[4,6]

The cyclic voltammogram (Fig. 2a) shows the anodic current peak at approximately +50 mV (*vs.* Ag/AgCl) which corresponds to the switching of the polymer from its neutral to charged state as well as the counterion incorporation (doping) into the polymer. The reduction response corresponding to the switching of the polymer from its conducting state to its non-conducting state, as well as the non-faradaic current associated with the counterion-exchange (undoping), can be seen at approximately −400 mV (*vs.* Ag/AgCl). On continuous cycling, no noted changes were observed.

A cyclic voltammogram (Fig. 2b) was also recorded in 0.1 *M* glycine as electrolyte. This time no redox waves were observed for the polypyrrole-based CME over a potential range −1000 to +900 mV. The background current observed in this medium was only a fraction of what it was in the sodium chloride electrolyte. This results because of the low conductivity of the glycine zwitterion.

Flow-injection analysis

As described in the previous section, the polypyrrole-based CME did not show any response when cycled in glycine. This was therefore a suitable electrolyte to be used as a mobile phase for flow-injection analysis. A solution of 0.1 mole/dm^3 glycine was deoxygenated using nitrogen and used as mobile phase. The flow rate of mobile phase was set at 0.4 ml/min.

The response of the polypyrrole-based CME was then evaluated using the Cl^- anion. The applied potential was varied to obtain a maximum response. Then, using this potential, the reproducibility of the electrode was investigated. Parameters such as selectivity, linearity, sensitivity and limit of detection (LOD) were then determined. All standard solutions were prepared in 0.1 mole/dm^3 glycine solution and were deoxygenated using nitrogen before

injection. Potentials quoted throughout this section are quoted versus the Ag/AgCl reference electrode.

Effect of applied potential. The applied potential was varied from +200 to +900 mV in 50 mV increments and injections of 20 μl of a 40 μg/ml Cl^- standard solution were made at each potential. The hydrodynamic voltammogram produced showed the response for the Cl^- anion commenced at a low positive potential of +200 mV and increased with increasing applied potential reaching a maximum response at +800 mV.

Reproducibility. To investigate the reproducibility of the response, the applied potential was constantly maintained at +900 mV and a series of 10 injections of 20 μl of a 100 μg/ml Cl^- standard were made, and the anodic peak current recorded each time. The response of the CME was reduced slightly following each injection. This was probably due to the doping of the polymer with the Cl^- anion each time the anion plug passed the electrode surface. An average current response ($n = 10$) of 1.39 μA with a RSD of 1.33% was obtained.

The solution to this doping effect would be to undope the polymer by stepping the applied potential down to a more negative potential, where the polymer is reduced and the dopant anion is released from the polymer, as previously employed by Ikariyama and Heineman.[1] Another solution would be to employ the method reported by Ye and Baldwin,[5] which involved setting the applied potential to a less positive potential where the anion did not fully dope the polymer, but was capable of entering and leaving the polymer as the sample anion plug passed over the electrode surface. The latter method was then investigated where a series of applied potentials were selected and constantly maintained at the working electrode, and the above series of injections repeated at each selected potential. A potential of +500 mV was chosen as the optimum potential as at this potential the response did not vary, an average current response ($n = 10$) of 504 *nA* with an RSD of 0.75% was obtained, and this potential was therefore selected for future studies.

Selectivity. The electrode response to different anions was determined by injecting 20 μl of 100 μg/ml of each of the following anions: chloride, nitrate, nitrite, perchlorate, bromide, carbonate, sulphate and phosphate. The applied potential was constantly maintained at +500 mV and 0.1 mole/dm^3 glycine was used as mobile phase at a flow rate of 0.4 ml/min. The CME showed a response to all of the anions injected, as shown in Fig. 3. The CME exhibits best selectivity for the chloride anion, as this was the counterion used during the electropolymerisation step. Selectivity also seems to depend on anion size, since the response for the smaller anions is much better than that for the bulkier anions. All of the anions investigated produced well defined sharp anodic current peaks, and if a separation step was incorporated into the flow system, the polypyrrole-based CME could be used as an amperometric detector to detect a mixture of the above anions.

Linearity and limit of detection. The linear response of the electrode for all of the anions used in the previous section was investigated over the concentration range $1 \rightarrow 100$ μg/ml. This was done by injecting 20 μl of each standard in the above concentration range for each individual anion and obtaining the response. The mobile phase used was 0.1 mole/dm^3 glycine

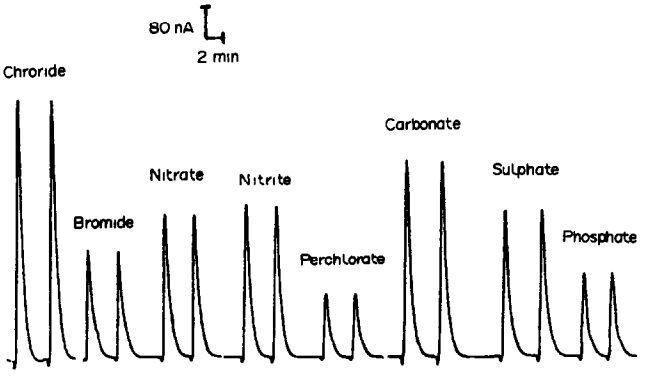

Fig. 3. Selectivity of polypyrrole-based CME for various anions using a 20 μl injection of 100 μg/ml Cl^-, Br^-, NO_3^-, NO_2^-, ClO_4^-, CO_3^{2-}, SO_4^{2-} and PO_4^{3-} standard mixture, a 0.1 mole/dm^3 glycine mobile phase and an $E_{app} = +0.5$ V (*vs.* Ag/AgCl).

at a flow rate of 0.4 ml/min, and a applied potential of +500 mV.

The response produced was linear in this concentration range for all of the anions investigated. The sensitivities for each anion varied, as the CME was found to be more selective for some of the anions. Calibration curves were then constructed by plotting anodic current response (*nA*) versus concentration (μg/ml), and from the graphs obtained the linear correlation coefficients were all better than 0.998 in the concentration range 1–100 μg/ml.

A limit of detection (LOD) of 1 μg/ml was obtained using a S/N ratio of 3/1 or greater for all of the anions investigated, except for the chloride ion. The LOD for the chloride ion was 0.1 μg/ml using a S/N ratio of 3/1.

Effect of flow rate on electrode response. The effect of flow rate on the electrode response was investigated by increasing the mobile phase flow rate in the range 0.2 ml → 2.0 ml/min, while injecting 20 μl of 100 μg/ml Cl^- standard. The response was higher at the lower flow rates, and decreased slightly with increased flow. The peak shape was closer to ideal at faster flow rates, with no major loss in peak height. As the flow rates associated with ion chromatography are in the order of 2–3 ml/min, this result was very promising for the incorporation of the CME as an amperometric detector in an IC system.

Stability. The polypyrrole-based CME was extremely durable. The same CME surface could be used for cyclic voltammetry and flow injection studies for a period of 2 weeks, with no evidence of chemical or mechanical deterioration.

Ion chromatography

In the following section, the polypyrrole-based CME was investigated as an amperometric detector to detect a series of anions, separated using ion chromatography. The results obtained using the CME detector were compared to the results obtained using a conductivity detector. The electrochemical flow cell containing the polypyrrole-based CME was linked in series with the outlet from the conductivity cell on the ion chromatograph system. Using the conditions mentioned under experimental and with an applied potential of +500 mV (*vs.* Ag/AgCl) constantly maintained, the background current obtained for the suppressed eluant carbonic acid, was similar to that previously obtained using glycine as mobile phase in FIA. A stable baseline at similar sensitivities as those used in FIA was also achieved. The CV behavior of the polypyrrole-based CME in this weakly conducting electrolyte was similar to that obtained using glycine as an electrolyte. The response to an injection of 50 μl of a 100 μg/ml standard solution mixture of chloride, nitrate, sulphate and phosphate for both conductivity and amperometric detection is shown in Figs 4 (a) and (b).

Reproducibility. The reproducibility of the both detection methods was tested by repetitive injections ($n = 10$) of a 10 μg/ml standard mixture of chloride, nitrate, sulphate and phosphate. The applied potential of the CME was held constantly at +500 mV throughout.

For the CME, the reproducibility of peak currents for each anion was satisfactory and the RSD varied between 0.53 and 2.14%. Again the CME in this system shows better selectivity for

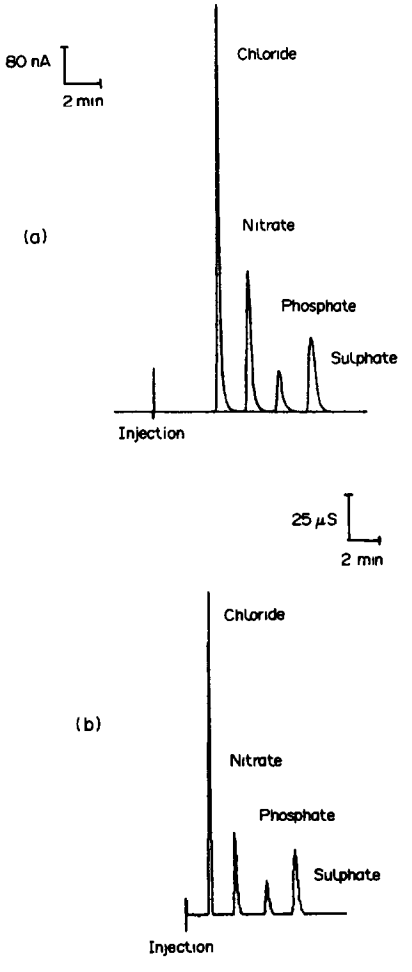

Fig. 4. Signals obtained using (a) a polypyrrole-based CME amperometric detector, $E_{app} = +0.5$ V (*vs.* Ag/AgCl), (b) conductivity detector, for a 50 μl injection of 50 μg ml^{-1} Cl^-, NO_3^-, PO_4^{3-}, and SO_4^{2-} standard mixture with a carbonic acid mobile phase.

the smaller anions, and especially for the chloride ion. The reproducibility using conductivity detection is also very good for all the anions with an RSD varying between 0.7 and 1.38%, except for the Cl^- ion. In this case an RSD of 8.76% was obtained, because the chloride had eluted close to an impurity peak, which could not be eliminated, even using the highest quality salts of both NaCl and KCl. The presence of this impurity obviously affects quantitation of the peak using peak height. Its presence also had a slight effect on reproducibility using the CME as the RSD calculated was higher than that obtained previously in FIA. An RSD of 1.57% was obtained when peak area was used as the quantitation method for the conductivity response. Overall both methods of detection gave comparable results.

Linearity and limit of detection. The linear relationship between the concentration of the solution of anions injected and the corresponding peak currents/conductivity was then examined. The concentration range used was from 1 to 100 μg/ml for each anion. A 50 μl injection of each standard containing chloride, nitrate, phosphate and sulphate at the same concentration level was made, the conditions used being the same as those reported previously.

The linear correlation coefficients obtained using CME as a detector were greater than 0.998 for chloride, nitrate and phosphate and 0.993 for sulphate. Using conductivity detection, correlation coefficients of greater than 0.999 were obtained for nitrate, phosphate and sulphate. A correlation coefficient of 0.952 was obtained for chloride using peak height, whereas a correlation coefficient of 0.999 was obtained when calibration was done using peak area.

The limit of detection for all of the anions investigated using this method was very similar to those limits obtained in the FIA experiment. Again, the LOD for the chloride was 0.1 μg/ml, using a S/N ratio of 3/1. The linearity in this lower range was determined by constructing a calibration curve in the range 0.1–10 μg/ml Cl^-. A 50 μl injection of each standard was injected and the peak current and conductivity obtained. The correlation coefficients obtained using both methods of detection were better than 0.999 in this concentration range.

Application to water analysis

In this section, the polypyrrole-based CME was used as an amperometric detector to detect anions present in fresh water samples, following separation using ion chromatography. The samples were collected from different locations around the country, which had various agricultural and industrial activities nearby. For this reason, quite varied results would be expected. The results obtained using the CME as a detector were compared to those obtained using conductivity detection.

A calibration curve in the range 0.1–50 μg/ml of each of the following anions namely, chloride, nitrate, phosphate and sulphate was constructed. Using the CME as the detector, the linear correlation coefficients were all better than 0.999 except for the chloride anion which had a correlation coefficient of 0.997. Using conductivity detection, linear correlation coefficients obtained using peak area as the calibration method were all better than 0.998.

Each water sample was injected in duplicate and the resulting peak current/conductivity was averaged and the final results reported as the concentration of each anion present in mg/dm^3. Phosphate was not present in any of the water samples analysed. The final results obtained are reported in Table 1.

As can be seen from the final results reported in Table 1, the results obtained using both methods of detection were comparable, and the levels of sensitivity of both methods are similar. Thus in conclusion, the results show that the polypyrrole-based CME is a very promising electrochemical method of detection in ion chromatography.

CONCLUSIONS

A polypyrrole-based CME was incorporated into a flow cell and used as an amperometric

Table 1. Results obtained for various water samples

	Anion concentration determined (mg/dm^3)		
Detector	Chloride	Nitrate	Sulphate
Sample 1			
PpyCME	45.6	7.8	32.4
Conductivity	46.1	7.8	31.4
Sample 2			
PpyCME	33.8	9.8	45.4
Conductivity	33.5	10.4	47.3
Sample 3			
PpyCME	16.7	6.8	18.1
Conductivity	19.0	7.3	17.1
Sample 4			
PpyCME	22.9	5.8	20.2
Conductivity	22.6	5.5	19.2

detector to detect a series of electroinactive anions following their separation using FIA and ion chromatography. The polypyrrole-based CME has been shown to respond to as low as 0.1 μg/ml anion concentration with good reproducibility. The approach is based on the reversible doping–undoping of electroinactive anions within the polymer matrix. At the doping potential, the electroinactive anion causes electron flow from the polymer to the platinum base electrode. This electron flow depends on anion concentration.

At higher anion concentrations it is necessary to undope the electrode. This can be carried out by briefly exposing the CME to a reducing potential (of the order of -300 mV) between successive anion exposures. Holding the electrode potential at a potential lower than its doping potential (of the order of $+500$ mV) has the effect of allowing the anion to enter and leave the polymer matrix, thus improving reproducibility, without having to undope the electrode between each successive anion exposure.

The selectivity of the polypyrrole-based CME was also shown to depend on the size of the dopant anion, with a much greater selectivity for the smaller less bulkier anions. The CME shows best selectivity for the chloride anion, as this was the counterion employed during the electropolymerisation process and this probably has the effect of allowing the chloride ion to dope the polymer matrix more efficiently because of pore size similarity.

The polypyrrole-based CME has similar sensitivity and limits of detection to conductivity detection, was very stable and gave a fast response. The stability of the CME over a 2 week period of operation was observed and the response did not vary during this time period. The CME had a linear range over three orders of magnitude for all of the ions investigated. This range is extended to four orders or magnitude for the chloride ion.

The polypyrrole-based CME flow cell is simple to construct and easy to change without great expense. If the CME stops functioning owing to degradation of the polymer film due to overoxidation or any other reasons, the polymer-coated platinum wire can be removed from the polyethylene tube and the polymer film stripped off by sonication in aqua regia solution.

The low cost, ease of construction of the flow cell and its small size, make this system very suitable as an amperometric detector for use in an ion chromatographic system. In comparison to conductivity detection, both methods produced similar results, proving that the polypyrrole CME could be used as an alternative method of detection.

In the use of conducting polymers electrodes as analytical sensors, careful attention must be paid to the substrate preparation and coating procedures if reproducibility is to be assured.

In studies of the practical application of both conductivity and amperometric detection using the polypyrrole-based CME, the results obtained for the analysis of water samples following separation by ion chromatography were found to be comparable. This proves that the polypyrrole-based CME had a practical application and could be successfully applied to the analysis of real samples.

REFERENCES

1. Y. Ikariyama and W. Heineman, *Anal. Chem.*, 1986, **58**, 1803–1806.
2. G. G. Wallace and Y. P. Lin, *J. Electroanal. Chem.*, 1988, **247**, 145–156.
3. M. D. Imisides and G. G. Wallace, *J. Electroanal. Chem.*, 1988, **246**, 181–191.
4. D. M. T. O'Riordan and G. G. Wallace, *Anal. Chem.* 1986, **58**, 126–131.
5. J. Ye and R. P. Baldwin, *Anal. Chem.*, 1988, **60**, 1979–1982.
6. E. Wang and A. Liu, *Anal. Chim. Acta*, 1991, **252**, 53–57.
7. J.-Y. Sung and H.-J. Huang, *Anal. Chim. Acta*, 1991, **246**, 275–281.
8. C. Hua, K. A. Sagar, K. McLaughlin, M. Jorge, M. P. Meaney and M. R. Smyth, *Analyst*, 1991, **116**, 1117–1120.
9. C. Hua, Y. Wang, T. Zhou and C. Jin, *Anal. Chim. Acta*, 1990, **235**, 273–277.

Talanta, Vol. 40, No. 7, pp. 1139–1145, 1993
Printed in Great Britain.

0039-9140/93 $6.00 + 0.00

ENHANCEMENT OF THE EMISSION INTENSITY OF FLUOROPHORE-LABELED AVIDIN BY BIOTIN AND BIOTIN DERIVATIVES. EVALUATION OF DIFFERENT FLUOROPHORES FOR IMPROVED SENSITIVITY

MINAS S. BARBARAKIS,* TRUIS SMITH-PALMER† and LEONIDAS G. BACHAS‡
Department of Chemistry, University of Kentucky, Lexington, KY 40506-0055, U.S.A.

SUN-YUNG CHEN and B. WIEB VAN DER MEER
Department of Physics and Astronomy, Western Kentucky University, Bowling Green, KY 42101, U.S.A.

(*Received* 1 *July* 1992. *Revised* 21 *October* 1992. *Accepted* 21 *October* 1992)

Summary—Fluorescein, Texas Red, Cascade Blue, 7-amino-4-methylcoumarin-3-acetic acid, and Lucifer Yellow were evaluated as fluorescent labels for homogeneous fluorophore-linked binding assays. Conjugates of avidin with these fluorophores exhibited an enhancement in fluorescence emission in the presence of biotin or biotin derivatives. This property was used in the development of assays for biotin. The biotin-induced fluorescence enhancement of each labeled avidin were compared. Fluorescein led to the most sensitive calibration (dose–response) curve for biotin with a detection limit of $8 \times 10^{-10} M$.

Homogeneous fluorophore-linked assays have gained increasing interest in chemical analysis.[1] Usually in these assays, a fluorescent label is chemically bound to a ligand (analyte) or a ligand-specific binding protein. By monitoring the fluorescence signal, the extent of the binding between the ligand and the binding protein may be determined.[2,3] During the past several years, many different types of homogeneous fluorophore-linked assays have been reported.[4] In one of these approaches, a fluorescent label is attached to a ligand-specific binding protein, and a property of the fluorescence signal (*e.g.*, emission intensity) is altered when a free ligand binds to the labeled protein. This modification of the signal is proportional to the concentration of free ligand present in the sample.[5]

Recently, we proposed the use of homogeneous competitive binding assays for improving the on-line detection of biomolecules separated by HPLC.[6,7] This was accomplished by using a postcolumn reaction detection system that is based on the natural affinity between analytes and the corresponding biological binders (*e.g.*, antibodies, binding proteins, receptors, *etc.*). Because of our interest in designing chromatographic postcolumn reaction detection systems based on homogeneous non-competitive fluorophore-linked assays, a study was undertaken to identify factors that control the detection capabilities of such assays. It should be noted that heterogeneous fluorophore-linked assays typically have better detection limits than homogeneous techniques, however, their use in the development of postcolumn reaction detection systems is not an easy task.

An assay for biotin has been reported that is based on the biotin-induced fluorescence enhancement of fluorescein-labeled avidin.[5] However, there is limited understanding of the variables that control the performance of this assay, including the effect of the nature of the fluorescent label, and of possible interferences by biotin derivatives. Because the proper selection of the fluorophore affects the detection limit and sensitivity of the assay, the applicability of different fluorescent probes in the development of homogeneous fluorophore-linked assays for biotin was evaluated. The fluorescent labels employed in this study were fluorescein, Texas Red, 7-amino-4-methylcoumarin-3-acetic acid (AMCA), Cascade Blue, and Lucifer Yellow. Conjugates of avidin with

*Present address: Ciba Corning Diagnostics Corp., 333 Coney Street, East Walpole, MA 02032, U.S.A.
†On leave from the Department of Chemistry, Saint Francis Xavier University, Antigonish, Nova Scotia, Canada, B2G 1CO.
‡Author for correspondence.

these compounds were used that had a comparable number of fluorescent labels attached to each protein molecule (f/p molar ratio), and the corresponding biotin-induced fluorescence enhancements were compared. Each conjugated avidin was also used in the development of assays for biotin.

EXPERIMENTAL

Reagents

Biotin, biocytin, biotin methyl ester, 2-iminobiotin, fluorescein isothiocyanate (FITC) isomer I (on celite), gelatin, and an avidin-FITC conjugate ($f/p = 3.9$) were purchased from Sigma (St. Louis, MO, U.S.A.). Biotin hydrazide was purchased from Pierce (Rockford, IL, U.S.A.). The conjugates avidin-AMCA ($f/p = 6$), avidin-Cascade Blue ($f/p = 6.5$) and avidin-Lucifer Yellow ($f/p = 4$) were obtained from Molecular Probes (Eugene, OR, U.S.A.). Avidin-Texas Red ($f/p = 3$) was from Vector (Burlingame, CA, U.S.A.). Avidin (egg white, lyophilized) was purchased from Calbiochem (San Diego, CA, U.S.A.). Sephadex G-25 (bead size medium) was obtained from Pharmacia LKB Biotechnology (Piscataway, NJ, U.S.A.). All solutions were prepared by using deionized, distilled water obtained with a Milli-Q Water Purification System (Millipore, Bedford, MA, U.S.A.). The various buffers used in this study were: 0.0500*M* sodium phosphate, pH 8.00 and 0.100*M* sodium bicarbonate, pH 9.10. The sodium phosphate buffer, pH 8.00 was used to prepare a 0.10% (w/v) gelatin solution. Stock solutions (0.10 g/l.) of biotin and biotin derivatives, as well as further dilutions of the stock solutions were prepared with the 0.10% (w/v) gelatin solution. In addition, all the avidin-fluorophore solutions including the stock solutions (0.10 g/l.) were prepared with the 0.10% (w/v) gelatin solution to prevent non-specific binding.

The free fluorophores used to test the validity of the model depicted in Fig. 1 were fluorescein (Matheson Coleman & Bell, Norwood, OH, U.S.A.), 7-amino-4-methylcoumarin (Aldrich Milwaukee, WI, U.S.A.), 1-pyrenebutyric acid (Aldrich), sulforhodamine 101 hydrate (Texas Red) (Aldrich), and *N*-(2-aminoethyl)-4-amino-3,6-disulfo-1,8-naphthal-imide, dipotassium salt (a Lucifer Yellow derivative) (Molecular Probes).

Apparatus

Fluorescence measurements were performed with a Perkin-Elmer (Norwalk, CT, U.S.A.) Model LS 50 luminescence spectrometer that was interfaced with an Epson (equity III+) personal computer (Epson America, Torrance, CA, U.S.A.). Both excitation and emission slits were set at 5 nm. A Perkin-Elmer (Lambda 6) UV/Vis spectrophotometer was employed for all absorbance measurements.

Preparation of avidin–FITC conjugates

Aliquots (500 μl) of a solution of avidin (0.50 g/l.) in sodium bicarbonate buffer were stirred for 4 hr with chosen amounts of a suspension of FITC on celite in buffer.[8] The celite was removed by centrifugation and the avidin-fluorophore conjugate was isolated using

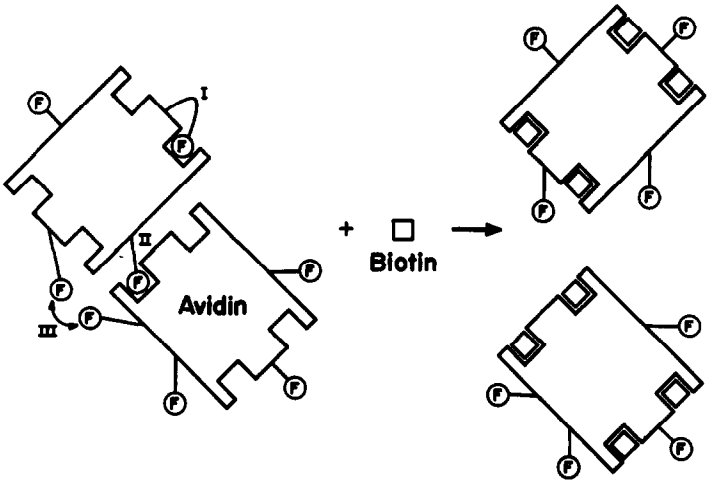

Fig. 1. Model for possible interactions between fluorescent labels and avidin in the presence and absence of biotin.

chromatography on Sephadex G-25 (0.050*M* ammonium bicarbonate as eluent).[9] The conjugate was freeze-dried and stored at −20° in amber vials.

The number of FITC molecules attached to avidin (*f*/*p* ratio) was estimated by measuring the absorbance at 494 nm and by using a molar absorptivity of $7.2 \times 10^4 M^{-1}$ cm^{-1}.[10] The avidin concentration was obtained from the absorbance at 280 nm after correction for the contribution by FITC to the absorbance signal at this wavelength. Molar absorptivities at 280 nm of $2.0 \times 10^4 M^{-1}$ cm^{-1} and $1.5 \times 10^5 M^{-1}$ cm^{-1} were used for FITC and avidin, respectively. This method of estimation of the degree of conjugation was tested on the avidin–FITC conjugate purchased from Sigma. The value obtained was within 5% of the value claimed by the manufacturer. The degree of conjugation for the other avidin–fluorophore conjugates used in this study was provided by the respective manufacturers.

Fluorescence lifetime measurements

All fluorescence lifetime measurements were performed on a frequency-domain cross-correlation fluorometer (ISS, Champaign, IL, U.S.A.). A 300-W Xenon lamp was used as the light source. The excitation monochromator was set at 495 nm. A non-fluorescent glycogen solution was used as a reference sample. A 500-nm lower wavelength cut-off filter (model KV-500, Corning Glass-Works, Corning, NY, U.S.A.) was used to remove the scattering light from the fluorescent signal of the samples and no filter was used for the reference sample. Both the phase delay and modulation ratio were measured at different modulation frequencies ranging from 1 to 200 MHz.

Dose–response curves for biotin

Varying amounts of biotin (or biotin derivative) were dispensed into test tubes to a total volume of 500 μl. A volume of 1.60 ml of the avidin–fluorophore solution was added to each tube. After 15 min incubation, the fluorescence signal was measured. Fifteen minutes was sufficient to reach equilibrium with all concentrations of conjugate and biotin used in this study. Dose–response curves were constructed by plotting the percent enhancement of the fluorescence signal observed versus the concentration of biotin (or biotin derivative) in the assay test tube.

RESULTS AND DISCUSSION

In homogeneous fluorophore-linked assays, the spectral characteristics of the fluorescent label are monitored as a function of the reaction between the ligand and the ligand-specific binding protein. The proper selection of the fluorescent label is critical to the detection limits and sensitivity of these assays. The ideal fluorophore should have high fluorescence intensity, should not interfere with the reaction between the ligand and the binding protein, and the fluorescence signal should be distinguishable from the background.[2,3,11]

In this study, several fluorescent compounds (fluorescein, Texas Red, Cascade Blue, 7-amino-4-methylcoumarin-3-acetic acid and Lucifer Yellow) were evaluated as potential labels for the development of homogeneous fluorophore-linked assays that are based on the use of binding proteins tagged with fluorescent molecules. The avidin–biotin couple was used as a model system in these studies. The only available information on this system is the observation by Al-Hakiem *et al.* that the fluorescence of fluorescein-labeled avidin is enhanced by approximately two-fold upon binding to biotin, a fact that was exploited to develop a fluorometric assay for biotin.[5] In the present study, it was found that conjugates of avidin with fluorophores other than fluorescein also showed fluorescence enhancement upon binding to biotin. The biotin-induced fluorescence enhancement of each labeled avidin is shown in Fig. 2.

Two groups of avidin-fluorophore conjugates were used that had comparable fluorophore/protein molar ratios within each group (Table 1). Because of the noncommercial availability of an avidin–FITC conjugate with an *f*/*p* molar ratio close to 6, several avidin–FITC conjugates were prepared using different initial molar ratios of FITC and avidin. Table 2 summarizes the avidin–FITC conjugates prepared and the *f*/*p* molar ratios obtained. It should be noted that similarity in the *f*/*p* ratio does not necessarily ensure the same degree of self-quenching for each avidin–fluorophore conjugate. Indeed, there is some evidence in the literature that AMCA (an umbelliferone derivative) and Cascade Blue are not as susceptible to concentration-dependent quenching as fluorescein.[12,13] Compared to the other fluorophores, the emission intensity of fluorescein-labeled avidin was enhanced by biotin to the greatest extent (Fig. 2). It should be noted that there is

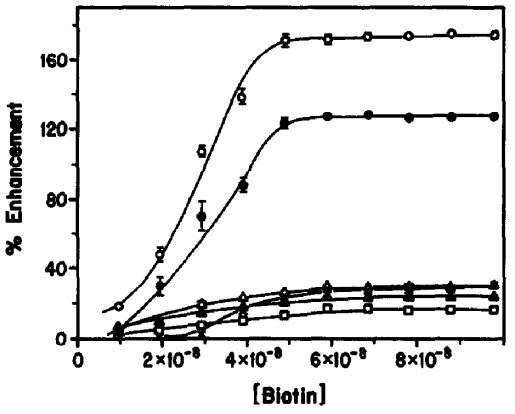

Fig. 2. Dose–response curves that relate the concentration of biotin to the percent enhancement of the fluorescence signal of (○) avidin–FITC-2 ($f/p = 5.9$), (●) avidin–FITC ($f/p = 3.9$), (△) avidin–Cascade Blue ($f/p = 6.5$), (x) avidin–Texas Red ($f/p = 3.0$), (▲) avidin–Lucifer Yellow ($f/p = 4.0$), and (□) avidin–AMCA ($f/p = 6.0$). The concentration of each avidin–fluorophore conjugate in the assay cup was 0.8 mg/l. Error bars indicate ± one standard deviation ($n = 3$). Some error bars are obstructed by the symbol for the point.

no change in the binding capacity of avidin due to fluorescent labeling. Specifically, as it is shown in Fig. 2, the labeled avidin is still capable of binding four biotins per protein molecule (at the break point for all curves the molar ratio biotin/labeled-avidin is *ca.* 4:1).

In order to better understand the variables that control the enhancement of the fluorescence signal, several factors (*i.e.*, local polarity, pH, and the vicinity of quenching groups) that may effect the microenvironment of the fluorophores were considered.[2,12,14,15] Since there is some conformational change in the structure of avidin upon binding to biotin,[16] it is possible that the magnitude of these factors may change in the presence of biotin, thus affecting the intensity of the fluorescence signal. It should be noted that the contribution of each factor to the enhancement of the fluorescence intensity may vary among the various fluorophores employed in this study.

Table 1. Characterization of avidin labeled with different fluorescent moieties

Fluorescent label	f/p	λ_{ex}, nm*	λ_{em}, nm*
AMCA	6.0	390	450
Cascade Blue	6.5	378	418
Fluorescein†	5.9	495	518
Fluorescein	3.9	495	518
Lucifer Yellow	4.0	430	504
Texas Red	3.0	596	614

*λ_{ex} and λ_{em} for the fluorophore while attached to avidin.
†This is avidin–FITC-2 of Table 2.

Table 2. Characterization of the avidin–FITC conjugates

Conjugate	Initial FITC:avidin molar ratio	f/p
Avidin–FITC-1	300:1	3.2
Avidin–FITC-2	600:1	5.9
Avidin–FITC-3	900:1	7.3
Avidin–FITC-4	1800:1	10.9

Spectral changes were used to probe the microenvironment of the fluorophore-avidin conjugates in the absence and presence of biotin. Some of the fluorophores employed in this study can be used as environment-sensitive probes. In particular, it has been reported that the emission maxima of fluorescein[10] and Lucifer Yellow [17] are sensitive to solvent changes, whereas the emission of AMCA exhibits very weak solvent dependence.[18] The emission spectra of the various avidin–fluorophore conjugates in the presence and absence of biotin show that none of the labeled avidins exhibited a shift in its emission maximum that was greater than 1 nm in the presence of biotin. Therefore it may be concluded that there is no significant change in the solvent environment at the sites of immobilized fluorophores on avidin upon binding with biotin.

The high degree of fluorescence enhancement observed when FITC was used as the label can be explained by considering microenvironmental pH changes. The fluorescence spectrum of fluorescein is dependent on pH (the fluorescence intensity is enhanced in more alkaline environments),[19] while for the rest of the fluorophores employed in this study the fluorescence intensity is either pH-independent (Cascade Blue[20] and Lucifer Yellow[21]) or less sensitive to pH changes compared to fluorescein (Texas Red[20] and AMCA[22]). Indeed, of the fluorophores used only avidin–FITC gave a large enhancement in fluorescence in the presence of biotin. These considerations are consistent with a recent report, in which changes in the fluorescence intensity of fluorescein-labeled protein A upon binding to an IgG antibody were attributed to pH changes.[23] Finally, it was found that an excess of biotin does not affect the fluorescence intensity of free fluorescein in solution.

The vicinity of side-chain groups of certain amino acids may also affect the intensity of the

fluorescence signal of the fluorophores attached to avidin. The effectiveness of such a quenching process may vary upon biotin binding, considering that the binding may alter the distance between the interacting groups. This form of dynamic quenching can be verified through fluorescence lifetime measurements. Fluorescence intensity decay measurements of mixtures composed of different ratios of avidin–FITC and biotin were performed at modulation frequencies ranging from 1 to 200 MHz. From the frequency-domain data, it is apparent that the avidin–FITC conjugate ($f/p = 3.9$) has multiple fluorescence lifetimes. By simply fitting the results using a single exponential decay function an effective lifetime of 1.7 nsec was obtained, which is significantly shorter than the lifetime of free fluorescein (3.4 nsec). In contrast, at high biotin concentrations, a single lifetime of 3.3 nsec was measured. At intermediate biotin concentrations effective lifetimes between 1.7 and 3.3 nsec were observed. The lifetime experiments were repeated three times and the standard deviation for each data point was less than 0.1 nsec. These lifetime data suggest that the enhanced fluorescence in the presence of biotin may be due to a different extent of dynamic quenching of the fluorescence signal. However, they do not preclude the existence of additional static quenching that is related to microenvironmental pH changes in the vicinity of the fluorophore.

An alternate explanation for the enhanced fluorescence intensity may be based on the affinity of avidin for certain chromophoric and fluorescent dyes.[24-26] If the fluorophores used in this study behave in a similar manner, then as shown in Fig. 1, avidin may bind fluorophores that are attached to the same (I) or neighboring (II) avidin molecules in the assay mixture. Moreover, type II interactions may also create additional concentration-dependent quenching of the fluorescence intensity (III). The effectiveness of events labeled I–III, in Fig. 1, may vary upon biotin binding, considering that biotin may displace the fluorescent labels from the avidin binding sites. Control experiments were performed to test this hypothesis with unlabeled avidin and free fluorescein. These experiments indicated that the fluorescence intensity of a solution containing avidin and free fluorescein is enhanced on addition of biotin, indicating a possible biotin-induced displacement of the fluorophore from avidin. However, this only happened at high avidin concentrations, which indicates a low binding constant between avidin and fluorescein. Indeed, when this experiment was repeated using a concentration of avidin at the same level as that used for the labeled avidin experiments, no enhancement was observed. Consequently, the mechanism shown in Fig. 1 does not contribute significantly to the observed enhancement in fluorescence emission.

Biocytin, biotin methyl ester, and biotin hydrazide were tested as possible chemical interferents in the assay for biotin. The avidin-fluorophore used was the avidin–FITC-2 conjugate ($f/p = 5.9$). It was revealed (Fig. 3), that the dose–response curves obtained for the several biotin derivatives had worse detection limits in comparison to the dose–response curve obtained for biotin. It should be noted that when 2-iminobiotin was tested as an interferent, the dose–response curve was shifted toward higher concentrations of analyte (in comparison to the other biotin derivatives), and it was out of the concentration range shown in Fig. 3. These observations can be explained by considering the magnitude of the association constants between avidin and the various biotin derivatives. Specifically, the association constant of the avidin–biotin complex has been reported to be in the order of $1 \times 10^{15} M^{-1}$.[27] To the best of our knowledge, the association constants for the rest of the biotin derivatives mentioned above are not known. However, there is some evidence in the literature that the association constant of biocytin with avidin is lower than that of biotin.[7,28] Therefore, it appears that the detection limits of the assays are controlled by the association constants between the labeled avidin and the biotin derivatives, as is expected from

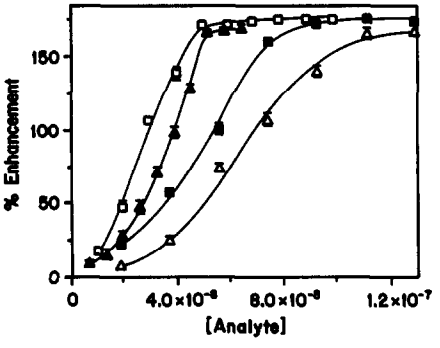

Fig. 3.Dose–response curves that relate the percent enhancement of the fluorescence signal of the avidin–FITC-2 conjugate ($f/p = 5.9$) (0.8 mg/l.) to the concentration of (□) biotin, (▲) biocytin, (□) biotin methyl ester, and (△) biotin hydrazide. Error bars indicate ± one standard deviation ($n = 3$). Some error bars are obstructed by the symbol for the point.

Table 3. Effect of the fluorescent label on the detection limit of the biotin assay

Fluorescent label	f/p	Intensity* arbitrary units	Conjugate concentration,† g/l.	Detection limit, M‡
AMCA	6.0	6.4 ± 0.2	8.0×10^{-4}	2×10^{-8}
Cascade Blue	6.5	216.0 ± 0.4	8.0×10^{-5}	2×10^{-9}
Fluorescein	5.9	59.4 ± 0.5	2.7×10^{-5}	8×10^{-10}
Fluorescein	3.9	35.8 ± 0.5	8.0×10^{-5}	2×10^{-9}
Lucifer Yellow	4.0	12.3 ± 0.5	8.0×10^{-4}	2×10^{-8}
Texas Red	3.0	13.3 ± 0.3	8.0×10^{-4}	3×10^{-8}

*Intensity of the fluorescence signal (in arbitrary units) ±standard deviation ($n = 3$) that corresponds to an avidin–fluorophore concentration of 8.0×10^{-4} g/l. (no biotin present).
†The lowest concentration of avidin–fluorophore (in the assay cup) which gave dose–response curves with a pooled standard deviation for the fluorescence intensity of less than 10%.
‡Detection limit (based on two times the standard deviation of the blank) for the biotin assay using the concentration of avidin–fluorophore in the previous column.

protein binding theory; the higher the association constant between a biotin derivative and avidin, the better the assay detection limits. Furthermore, by keeping the biotin/avidin–FITC-2 concentration ratio constant at a value of 8.4 and varying the amount of avidin–FITC-2 in the assay cup from 8.0×10^{-4} to 2.7×10^{-5} g/l., it was observed that at lower concentrations of avidin–FITC-2 the percent enhancement was lower. The difference in enhancement indicates that at lower avidin–FITC-2 concentrations, a lower percentage of avidin–FITC-2 was complexed with biotin. These data also suggest that binding constants determine the extent of complex formation in the assay, which provides additional evidence in support of the data shown in Fig. 3.

Further, a study was performed to identify the avidin–fluorophore conjugate that gives the best detection limits for assays for biotin. The data given in Table 3 refer to the most diluted solution of the labeled avidin that gave dose–response curves that had a pooled standard deviation for the fluorescence intensity of less than 10%. Note that, although Cascade Blue gives the higher fluorescence intensity, fluorescein allows for the development of assays with better detection limits because it provides a higher percent enhancement. In addition, it was found that the avidin–fluorescein conjugate with the higher f/p ratio (equal to 5.9) gave higher sensitivity for the biotin assay because it provided both high fluorescence intensity and percent enhancement. No further improvement in the detection limits was observed with avidin–FITC conjugates that had higher f/p ratios since, compared to avidin–FITC-2, the conjugates with f/p ratios of 7.3 and 10.9 demonstrated a lower percent enhancement in fluorescence intensity in the presence of biotin.

Development of homogeneous non-competitive fluorophore-linked assays for other analytes is possible as long as the corresponding fluorophore-labeled biological binders undergo spectral changes as a function of the concentration of the analytes. For example, Betts *et al.* developed immunosensors for haptens that were based on the fluorescence enhancement of dansylated Fab antibody fragments upon hapten binding.[29]

CONCLUSIONS

It has been demonstrated that in order to optimize homogeneous fluorophore-linked assays for biotin several factors that may affect the sensitivity and detection limits have to be considered. These factors include the type of fluorescent label used and the association constant of the ligand with the binding protein. These factors should also be important in designing optimization strategies for homogeneous fluorophore-linked binding assays for other analytes.

Acknowledgements—This research was supported by grants from the National Institutes of Health (GM 40510 to LGB), the National Science Foundation (EHR-9108764 to LGB and BWV), and the Natural Sciences and Engineering Research Council (TSP). The authors kindly acknowledge Dr Parkson Chong for allowing us access to his frequency-domain fluorometer.

REFERENCES

1. H. T. Karnes, J. S. O'Neal and S. G. Schulman, in *Molecular Luminescence Spectroscopy: Methods and Applications: Part I*, S. G. Schulman (ed.), p. 717. Wiley, New York, 1985.
2. I. Hemmilä, *Clin. Chem.*, 1985, **31**, 359.

3. E. Soini and I. Hemmilä, *ibid.*, 1979, **25,** 353.
4. R. M. Nakamura, in *Advances in Analytical Fluorescence Immunoassays*, R. M. Nakamura, W. R. Dito and E. S. Tucker III (eds), p. 33. Masson Publishing, New York, 1982.
5. M. H. H. Al-Hakiem, J. Landon, D. S. Smith and R. D. Nargessi, *Anal. Biochem.*, 1981, **116,** 264.
6. A. Przyjazny and L. G. Bachas, *Anal. Chim. Acta*, 1991, **246,** 103.
7. A. Przyjazny, T. L. Kjellström and L. G. Bachas, *Anal. Chem.*, 1990, **62,** 2536.
8. H. Rinderknecht, *Nature*, 1962, **193,** 167.
9. M. S. Barbarakis, *Ph. D. Thesis*, University of Kentucky, Lexington, 1992.
10. R. P. Haugland, *Handbook of Fluorescent Probes and Research Chemicals*, p. 32. Molecular Probes, Eugene, OR, 1989.
11. E. F. Ullman and P. L. Khanna, *Methods Enzymol.*, 1981, **74,** 28.
12. D. S. Smith, M. H. H. Al-Hakiem and J. Landon, *Ann. Clin. Biochem.*, 1981, **18,** 253.
13. Z. Zhujun and W. R. Seitz, *Anal. Chim. Acta*, 1984, **160,** 47.
14. A. J. Pesce, C. G. Rosen and T. L. Pasby, in *Fluorescence Spectroscopy*, A. J. Pesce, C. G. Rosen and T. L. Pasby (eds), p. 65. Marcel Dekker, New York, 1971.
15. G. M. Edelman and W. O. McClure, *Acc. Chem. Res.*, 1968, **1,** 65.
16. A. Pähler, W. A. Hendrickson, M. G. Kolks, C. E. Argaraña and C. R. Cantor, *J. Biol. Chem.*, 1987, **262,** 13,933.
17. J. A. Lee and P. A. G. Fortes, *Biochemistry*, 1985, **24,** 322.
18. W. Retting and A. Klock, *Can. J. Chem.*, 1985, **63,** 1649.
19. M. S. Fuh, L. W. Burgess, T. Hirschfeld, G. D. Christian and F. Wang, *Analyst*, 1987, **112,** 1159.
20. R. P. Haugland, *Handbook of Fluorescent Probes and Research Chemicals*, Molecular Probes, Eugene, OR, 1989.
21. W. W. Stewart, *Cell*, 1978, **15,** 741.
22. H. Khalfan, R. Abuknesha, R. Rand-Weaver, R. G. Price and D. Robinson, *Histochem. J.*, 1986, **18,** 497.
23. C. S. Lee, P. Y. Huang and D. M. Ayres, *Anal. Chem.*, 1991, **63,** 464.
24. D. M. Mock, G. Langford, D. Dubois, N. Criscimagna and P. Horowitz, *Anal. Biochem.*, 1985, **151,** 178.
25. D. M. Mock, G. Langford and P. Horowitz, *Biochim. Biophys. Acta*, 1988, **956,** 23.
26. N. M. Green, *Biochem. J.*, 1965, **94,** 23c.
27. N. M. Green, *Adv. Protein Chem.*, 1975, **29,** 85.
28. T. L. Kjellström, *M. S. Thesis*, University of Kentucky, Lexington, 1989.
29. T. A. Betts, G. C. Catena, J. Huang, K. S. Litwiler, J. Zhang, J. Zagrobelny and F. V. Bright, *Anal. Chim. Acta*, 1991, **246,** 55.

Talanta, Vol. 40, No. 8, pp. 1147–1155, 1993
Printed in Great Britain.

0039-9140/93 $6.00 + 0.00

THE INFLUENCE OF CHELATING REAGENTS ON PLUMBANE GENERATION: DETERMINATION OF LEAD IN THE PRESENCE OF PAN-S

HENGWU CHEN, FULONG TANG and CHANG GU
Department of Chemistry, Hangzhou University, Hangzhou, Zhejiang, P.R. China 310028

IAN D. BRINDLE*
Chemistry Department, Brock University, St Catharines, Ontario, Canada L2S 3A1

(*Received* 23 *December* 1992. *Accepted* 3 *February* 1993)

Summary—A series of 22 chelating reagents were tested for plumbane generation. Besides nitroso R salt, the reagents Bromo Pyrogallol Red, Pyrocatechol Violet, Alizarine Red-S, 5-Br-PADAP and PAN-S could significantly enhance the lead signal. The PAN-S system has been optimized. The characteristic concentration (5 ml sample) is 1.3 ng/ml, and the RSD at the 50 ng/ml level is 3.9%. Lead spiked into tap water and natural water was determined by HG–AAS in the presence of PAN-S. Recoveries of spiked lead were between 90 and 105%. Study of the mechanism suggests that the lead hydride might be directly generated from the chelated Pb(II) instead of the metastable Pb(IV).

Trace amounts of lead, like other hydride forming elements, can be determined by atomic absorption spectrometry in combination with a hydride generation technique (HG–AAS).[1] However, plumbane generation is quite peculiar. In 1974, Thompson and Thomerson first reported that lead(II) could be directly reduced to plumbane in hydrochloric acid, but the sensitivity of AAS determination was very low.[2] Later, Fleming and Ide found that, in the medium of tartaric acid–potassium dichromate, the efficiency of plumbane generation was greatly increased.[3] Since then, various systems with strong oxidizing reagents, such as hydrogen peroxide[4–7] and ammonium peroxodisulphate,[6–8] have been developed for plumbane generation. Recently, a system of lactic acid–potassium dichromate[9] and a system of oxalic acid–ammonium cerium(IV) salt[10] have been developed by a Spanish group and a Chinese group, respectively, and the latter was claimed to be the most sensitive system for HG–AAS determination of lead. It should be noted that, in the latter case, the characteristic concentration of lead was 0.04 ng/ml. The authors did not mention the sample volume; hence the characteristic mass is unknown. Nevertheless, the authors tested various systems, and concluded that the Ce(IV) system is the most sensitive. Vijan *et al.* attributed the increase in the generation efficiency to the conversion of Pb(II) into metastable Pb(IV) before it was reduced to plumbane.[4] Based on the proposed mechanism, Brindle and coworkers improved the generation efficiency of germane with ammonium peroxodisulphate.[11]

Plumbane has also been generated in a non-aqueous medium after solvent extraction of lead(II) with the chelating reagents pyrrolidine-1-carbodithioate or sodium diethyldithiocarbamate.[12] Moreover, Zhang *et al.* reported that lead(II) could be easily reduced to plumbane in aqueous medium in the presence of a chelating reagent, nitroso R salt,[13] and the developed HG–AAS method was successfully applied to the determination of lead in various environmental samples. From the well recognized phenomenon that nitroso R salt reacts with cobalt(II) and forms a cobalt(III) chelate upon air oxidation, the authors assumed that the lead(II) might be similarly oxidized to lead(IV) whilst chelating with nitroso R salt.

To further investigate the influence of chelating reagents on the plumbane generation, 22 chelating reagents with different molecular structures were studied. It was found that some chelating reagents, in addition to nitroso R salt, enhanced the sensitivity of lead determination by the HG–AAS technique. 1-(2-Pyridylazo)-2-naphthol-6-sulphonic acid, (PAN-S), is among

*Author to whom correspondence should be addressed.

the most effective. Thus a method of HG–AAS determination of lead in the presence of PAN-S has been developed, and the mechanism investigated. This paper presents the main results of the investigation.

EXPERIMENTAL

Reagents

Lead(II) standard solution (1.000 mg/ml) was prepared with spectroscopically pure lead oxide (Shanghai, China). Working standard solutions were made daily through appropriate dilutions.

PAN-S solution (1.5%) was prepared by dissolving 1.5 g laboratory made PAN-S in 0.1*M* NaOH solution. The solution was neutralized to pH 3–6 with 0.5*M* HNO_3 before it was diluted to 100 ml. The water soluble PAN-S was made from commercial 1-(2-pyridylazo)-2-naphthol (Shanghai, China) through simple sulphonation of the water insoluble dye with fuming sulphuric acid as described elsewhere.[14]

Sodium tetrahydroborate (III) solution (3%) was prepared from powder (Merck) by dissolution in 0.1*M* sodium hydroxide. The solution was filtered through filter paper before use.

All other reagents used were analytical grade or better. Deionized and distilled water was used throughout the work.

Equipment

An AAS-meter of model WFX-1D (Beijing, China) equipped with a lead hollow cathode lamp (Shanghai, China) and a chart-recorder (Shanghai, China) was used for absorption measurement.

A batch-wise hydride generator, as shown in Fig. 1, was adapted from a 125 ml pear shaped separatory funnel. A "T"-shaped electrically heated quartz cell 10 mm i.d. × 160 mm length was used throughout the experiments. The experimental conditions for AAS measurement and hydride generation are summarized in Table 1.

Procedure

Five millilitres of the test solution, that was made 0.2*M* in HNO_3 or HCl was transferred into the generator. Then 1 ml of 1.5% PAN-S solution was added to make the final reagent concentration 0.25%, and the sample introduction port was closed with a rubber stopper. After the recorder pen moved back to the baseline, 2 ml of 3% sodium tetrahydroborate(III) solution was injected with a syringe. The peak trace was recorded and the peak height measured for calibration.

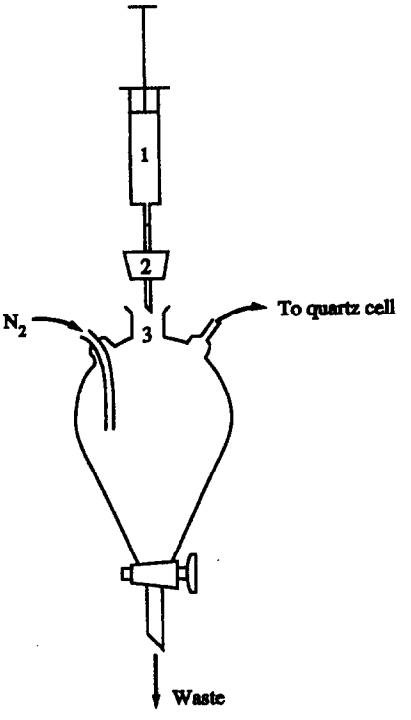

Fig. 1. Hydride generator. (1) Syringe; (2) rubber stopper; (3) sample introduction port.

RESULTS AND DISCUSSION

The influence of various chelating reagents on the plumbane generation

In the preliminary study, 22 kinds of chelating reagent were tested. No attempt was made to optimize the conditions individually for each reagent, yet the comparison serves the purpose of providing a rough guide to the choice of reagent. The results are listed in Table 2. Besides nitroso R salt, the reagents Bromo Pyrogallol

Table 1. Experimental conditions

AAS Measurement		Plumbane generation	
Wavelength	217.0 nm	Sample	5 ml
Band pass	1 nm	Sample acidity	0.2*M* (HNO_3)
Lamp current	5 mA	Volume of PAN-S solution	1 ml (1.5%)
Background correction	No	Volume of $NaBH_4$ solution	2 ml (3%)
Cell temperature	950°	The flow rate of carrier gas	0.8 l/min (N_2)

Red, Pyrocatechol Violet, Alizarine Red-S, 2-(5-bromo-2-pyridylazo)-5-diethylamino-phenol (5-Br-PADAP) and PAN-S significantly enhanced the lead signal. In these systems, lead hydride was generated immediately after the injection of $NaBH_4$, and the reduction was completed in around 30 sec. 8-Hydroxyquinoline-5-sulphonic acid, 4-(2-pyridylazo)-resorcinol (PAR), 2-(o-arsenophenylazo)-1,8-dihydroxynaphthalene-3, 6-disulphonic acid (Arsenazo-I), Acid Chrome Blue K, Tiron and 2-nitroso-1-naphthol have little enhancement effect on the lead signal. The remaining tested reagents were found to be ineffective in the improvement of the plumbane generation efficiency. It appeared that effective reagents belonged mainly to o-nitroso-naphthol, o-hydroxy-phenol and o-hydroxy pyridylazo compounds, and that the compounds containing the chelating functional group of iminodiacetic acid do not enhance the lead signal. Also, it seems that the chelating functional group is not the unique factor affecting the generation effiency. The chelating functional group of 2-nitroso-1-naphthol is similar to that of nitroso R salt, but the former had only a small effect on plumbane generation in comparison with the latter. This might be ascribed to its poor solubility in water. Moreover, surface tension and viscosity of test solution containing organic reagent might also affect the lead signal. Both PAR and PAN-S are water soluble o-hydroxyl pyridylazo compounds. However, the influence of the former on plumbane generation was much less than that of the latter. It is observed that, when sodium tetrahydroborate(III) solution was injected to the acidic test solution containing PAR, a large quantity of fine bubbles (foam) were formed, which were stable over a period of time. In the PAN-S system, the bubbles were relative few and bigger, and they burst quickly. Thus the poor sensitivity of the PAR system could be related to formation of foam which retarded the elimination of plumbane from solution. A similar phenomenon has been reported by Madrid *et al.* in their study on plumbane generation in slurry medium.[15]

The design of the reaction vessel is critical. If a small cylindrical vessel (60 ml) was used as the generator, the bubbles formed on the addition of $NaBH_4$ to the test solution caused some problems even for the PAN-S system. First, the bubbles would rise upwards to reach the gas outlet of the generator. Secondly, when a big bubble burst, a considerable volume of plumbane was released from the bubble, resulting in a small pulse of the signal. Therefore, a 125 ml separatory funnel was used, as shown in Fig. 1. The internal geometry of the generator prevented the risk of any bubbles from being swept into the tube leading to the quartz cell. The generator vessel also acted as a buffer tank to reduce the signal noise. Its use also resulted in some sacrifice of sensitivity in the AAS determination. It would be possible to further improve both sensitivity and precision if an effective and lead-free antifoaming reagent could be found.

Table 2. The influence of chelating reagents on plumbane generation*

Reagent			Absorbance at the acidity of	
Name	Structure	Concentration (% *mV*)	0.075M	0.25M
No chelating reagent	—	—	0	0
Nitroso R salt	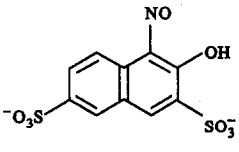	0.13†	0.132	0.054
2-Nitroso-1-naphthol	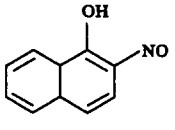	0.13	0	0.045
PAN-S	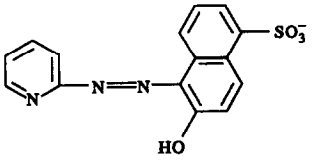	0.13	0.128	0.118

continued overleaf

Table 2.—*continued*

Reagent			Absorbance at the acidity of	
Name	Structure	Concentration (% *mV*)	0.075M	0.25M
PAR	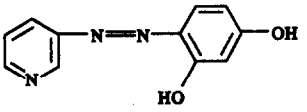	0.13	0	0.03
5-Br-PADPA	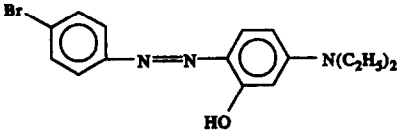	0.10‡	0.100§	0‖
Bromo Pyrogallol Red	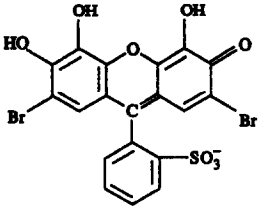	0.13	0.101	0.037
Pyrocatechol Violet	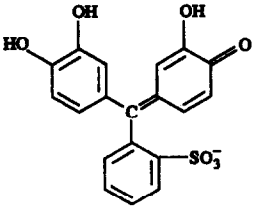	0.13	0.110	0.073
Xylenol Orange	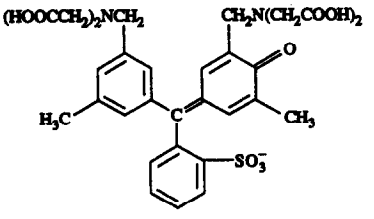	0.13	0	0
Methyl Thymol Blue	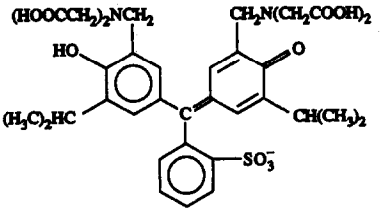	0.13	0	0
EDTA		0.13	0	0
Chromazurol S	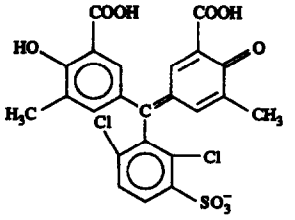	0.13	0	0
Alizarine Red S	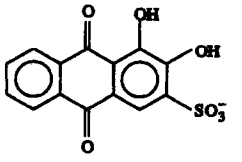	0.13	0.060	0.059

Acid Chrome Blue K	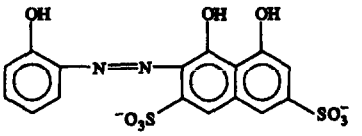	0.13	0.022	0
Eriochrome Black T	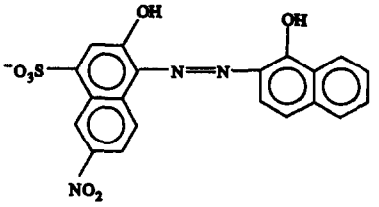	0.13	0	0
Arsenazo I	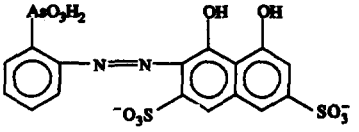	0.13	0.056	0.011
8-Hydroxyquinoline-5-Sulphonic acid	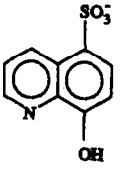	0.13	0.023	0.005
Tiron	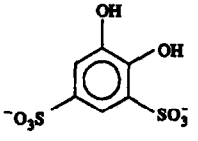	0.33	0.022	0.007
Chromotropic acid	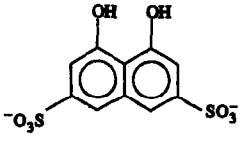	0.13	0	0
Sulfosalicylic acid	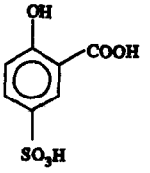	1	—	0
Cupferron	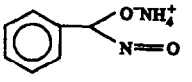	0.13	0	0
1,10-Phenanthroline	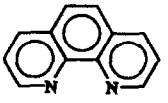	0.05	—	0
Dithizone	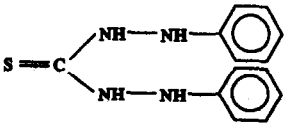	0.13‖	—	0

*1μ g Pb in 6.5–8 ml reagent solution.
†Ethanol solution.
‡40% ethanol solution (water).
§0.18M HNO_3.
‖0.35M HNO_3.

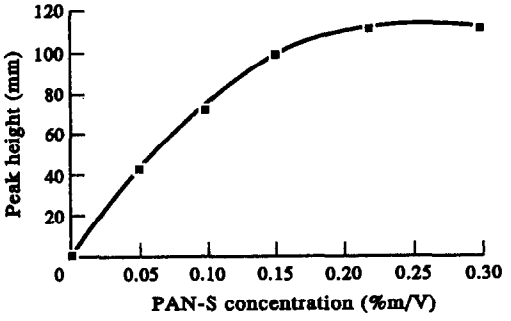

Fig. 2. Effect of PAN-S concentration on lead signal; 5 ml 50 ng/ml Pb(II) in 0.2*M* HCl, 3 ml 3% $NaBH_4$.

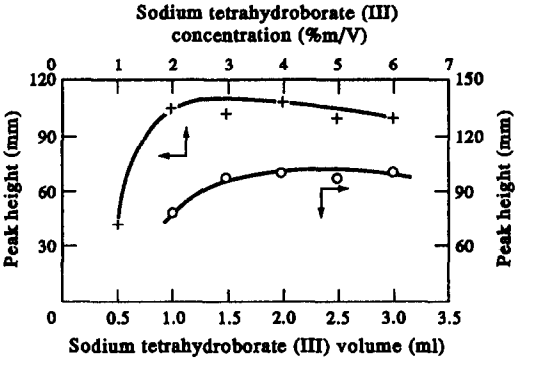

Fig. 4. Effect of $NaBH_4$ concentration and of the injection volume; 5 ml 50 ng/ml Pb(II) in 0.2*M* HCl with 0.25% PAN-S. + Concentration of $NaBH_4$ (3 ml); ○ volume of 3% $NaBH_4$.

Optimization of a PAN-S system

As can be seen from Table 2, although PAN-S is a little inferior to nitroso R salt in the behaviour of enhancing lead signal, it seems to provide a wider acid range in which the generation efficiency is high. Therefore PAN-S was chosen for the further studies.

The enhancement effect of PAN-S on plumbane generation is clearly shown in Fig. 2. Without PAN-S, almost no lead signal could be detected from a 50 ng/ml Pb(II) solution. However, the lead signal increased almost linearly with the increase of PAN-S concentration up to 0.20% (final concentration); where it reached a plateau. Figure 3 shows the influence of the acid concentration. In the concentration range of 0.1–0.3*M*, the lead reached its maximum signal. No significant difference was found between nitric acid and hydrochloric acids. For the PAN-S system, the optimum acid range is wider than other oxidant systems[3,4] and is also wider than the requirements of the nitroso R salt system.[13] Figure 4 shows the influence of sodium tetrahydroborate(III) concentration and of the injection volume of the reductant solution. It is clear that 2 ml of 3% $NaBH_4$ generates the largest signal. Compared with oxidizing reagent systems,[6–10] the PAN-S system consumes less reductant, since the reagent itself does not decompose the reductant. The temperature of the quartz cell, and the flow rate of nitrogen carrier gas have no significant influence over the ranges 800–1000°C and 0.5–1.0 l/min, respectively. Under the optimum conditions shown in Table 1, the characteristic concentration (0.0044 absorbance) was 1.3 ng/ml, and the relative standard deviation for a solution containing 50 ng/ml was 3.9%.

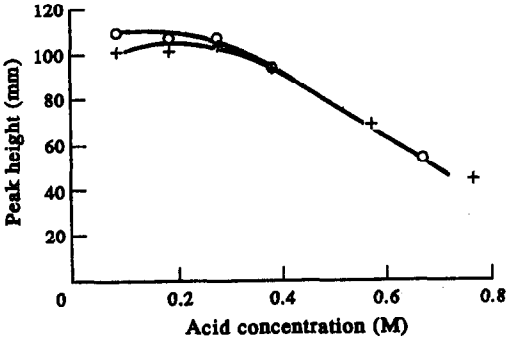

Fig. 3. Effect of acid concentration on lead signal; 5 ml 50 ng/ml Pb(II) with 0.25% PAN-S, 3 ml 3% $NaBH_4$. +Hydrochloric acid; ○ nitric acid.

Interference of foreign ions

When studying interference, amounts of foreign ions, in 0.2*M* HNO_3, were added directly to the generator containing 5 ml of 50 ng/ml lead(II) followed by the addition of 1 ml of PAN-S solution. The signals obtained in this way were compared with those where no interfering ion has been added. As shown in Table 3, among the tested foreign ions, Cu(II), Se(IV), Bi(III), Sn(II) and Sb(II) caused severe interference; while interference free levels of Fe(II), Fe(III), Mn(II), Cr(VI) and Hg(II) were relatively higher.

When no foreign ion was introduced to the test solution, the orange–red coloured test solution became light orange after the injection of $NaBH_4$. In the presence of such foreign ions as Fe(II), Fe(III), Mn(II) and Cd(II), the test solution turned from its original colour (orange–red) to dark red (the colour of the corresponding chelate) upon the injection of $NaBH_4$. Thus, the interference probably resulted from the competition for PAN-S between lead(II) and these foreign ions.

Table 3. Interference of foreign ions on lead signal (50 ng/ml Pb^{2+})

Ions	Concentration ($\mu g/ml$)	Recovery (%)
Cd(II)	1	99
	2	86
Co(II)	2	101
	10	127
Cr(VI)	10	94
	20	86
Cu(II)	0.1	93
	0.2	68
Fe(III)	10	104
	50	95
	100	82
Fe(II)	20	93
	100	77
MN(II)	40	91
	100	86
Mo(IV)	0.4	96
	4	85
Ni(II)	8	94
	10	87
Zn(II)	2	94
	5	75
As(III)	10	94
	20	89
Bi(III)	0.4	91
	1	87
Sb(II)	1	96
	2	83
Se(IV)	0.01	93
	0.02	73
Sn(II)	0.1	99
	2	78
Hg(II)	20	100
	200	102

Recovery of lead spiked into water samples

Although the low level of the lead concentration in the water samples is beyond the quantitative determination limit of the technique, the recoveries of the spiked lead are satisfactory, as shown in Table 4.

Table 4. Recoveries of lead spiked with water samples

Water samples	Lead concentration (ng/ml) Added	Found	Recovery (%)
Surface water from	0	n.d.*	—
West Lake	20	21	105
	30	29	97
Underground	0	n.d.	—
from Xiaoying Well	20	21	105
	30	31	103
Underground water	0	n.d.	—
from Mashi Well	20	19	95
	30	29	97
Tap water	0	2	—
	20	20	90
	30	31	97

*n.d. not detected.

Mechanistic studies

Initially, different emission lines were used to verify that the absorption signal was produced by lead atoms instead of any possible molecular species. When absorption was measured at both lead 217.0 nm and lead 283.3 nm, a sharp signal was recorded; the signal obtained at 217.0 nm was greater than that at 283.3 nm. However, no signal could be detected when zinc, which absorbs at 213.9 nm, close to the lead line at 217.0 nm, was used. Therefore, the absorbing species was atomic lead.

Since PAN-S exerts a great influence on the lead signal, it was felt worthwhile investigating the interaction of PAN-S and lead(II). Spectrophotometric studies reveal that lead(II) can react with PAN-S to form a red chelate whose maximum absorption wavelength is 548 nm at pH 8.6. As shown in Fig. 5, the chelate begins to form at around pH 4, and the best pH range of the colour reaction is between 7 and 9. The pH range does not coincide with the initial acidity of the test solution used for plumbane generation. However, tests showed that the pH of the test solution rose quickly during injection of sodium tetrahydroborate(III) solution. After half of the reductant had been injected, the pH value of the reacting solution went up to around 3, and it was between 5 and 6 at the end of the injection. At this point, the gas was violently released. Usually 15 sec after the injection, the pH value reached 8.0–8.2. With the relatively slow response rate of the glass electrode being considered, the real pH value of the reacting solution might be a little higher than the measured one. Thus, the injection of alkaline $NaBH_4$ solution created a condition under which the PAN-S could react with lead(II).

At this point, we cannot yet exclude the possibility that the lead atomic absorption

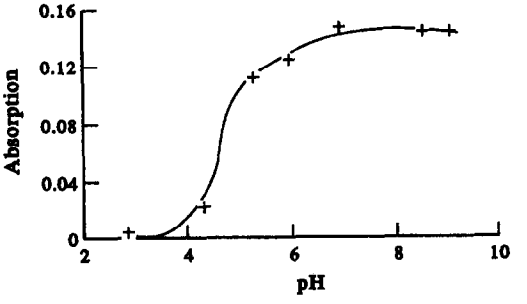

Fig. 5. Effect of acidity on the formation of lead–PAN-S chelate. Test solution was buffered with H_3BO_3–NaOH; absorption was measured at 545 nm against a reagent blank.

might result from the decomposition of the lead-PAN-S chelate that, if it were volatile, was stripped out of the solution by the hydrogen, formed *in situ*, and transported to quartz cell by the carrier gas. To check this, $NaHCO_3$, which has been used to strip $Pb(Et)_4$ from solution,[16] was used to replace $NaBH_4$. When 5 ml of 0.2*M* $NaHCO_3$ solution was injected into the acidic test solution, CO_2 was violently released at the first stage of the injection. At the end of the injection, the pH of the reacted solution reached between 4 and 4.5, while the release of CO_2 diminished. In this way, no lead signal was detected from a 250 ng/ml Pb(II) solution. It appeared that the violent release of the CO_2 formed *in situ*, occurred a little earlier, and, at the first stage of the injection of $NaHCO_3$ solution, the PAN-S-lead(II) chelate might not be formed due to the low pH value of the reacting solution. Therefore, an attempt was made to inject 2 ml of 1*M* HNO_3 solution into 5 ml of 0.5*M* $NaHCO_3$ solution containing both PAN-S and lead(II). In this way, CO_2 was generated violently through the whole course of the injection, while the pH of the test solution decreased from 8.25 to 5.99. Under these conditions, the lead–PAN-S chelate formed before the injection of NHO_3 solution, and it had not totally dissociated by the end of the injection. Once again, no lead signal was observed from a 250 ng/ml solution of lead(II). Therefore, the $NaBH_4$ is essential to the production of lead signal, and the volatile lead species is the reduction product formed by $NaBH_4$, that is, plumbane.

It is well known that the generation efficiency of plumbane is poor if no oxidizing reagent is involved. With respect to the PAN-S system, no other oxidizing reagent was introduced except the dissolved oxygen. Aznarez[12] has reported that plumbane could be generated readily from a solution of chloroform and glacial acetic acid. Zhang *et al.*[17] however, found that a chelating reagent was required to generate plumbane from solutions of chloroform and glacial acetic acid. Thus the chelating agent appears to play a crucial role in the generation of plumbane. If the formation of Pb(IV) is essential to the increase of generation efficiency of plumbane, the air or dissolved oxygen might play the role of an oxidizing reagent which, although it cannot oxidize free Pb(II), may oxidize the chelated lead(II) to lead(IV). If the hypothesis is correct, to purge both the test solution and the reagent solution with nitrogen before they were mixed together in the generator (where the air has been flushed out by carrier gas) will isolate the lead(II) from oxygen and should, in turn, decrease the lead signal. On the other hand, to purge the solution with pure oxygen should further increase the yields of the hydride. However, bubbling the solutions with either nitrogen or oxygen for 10 min produced no change in the lead signal. Thus, the enhancement effect can only be attributed to PAN-S itself. Since o-hydroxyl pyridylazo compounds are not oxidizing reagents, the effect of PAN-S cannot be accounted for in the formation of Pb(IV). Thus it is assumed that the plumbane is generated directly from the PAN-S chelated lead(II). The higher generation efficiency of lead hydride in the PAN-S system is probably chelated lead(II) being kinetically more easily reduced by $NaBH_4$ than free lead(II).

CONCLUSION

This study has shown that some chelating reagents enhance the lead signal obtained by HG–AAS, and that PAN-S is among the most effective. Mechanism studies revealed that in the presence of PAN-S the lead hydride might be generated directly from the chelated lead(II) ions instead of the metastable lead(IV). Though the analytical characteristics of the system are not totally superior to those of the systems with strong oxidizing reagents, it opens a new field for people to search for more effective systems for plumbane generation.

Acknowledgement—The Analysis and Testing Foundation of Zhejiang Province is thanked for funding this work.

REFERENCES

1. T. Nakahara, *Prog. Anal. Atom. Spectrosc.*, 1983, **6**, 163.
2. T. C. Thompson and D. R. Thomerson, *Analyst*, 1974, **99**, 595.
3. H. D. Fleming and R. G. Ide, *Anal. Chim. Acta*, 1976, **83**, 67.
4. P. N. Vijan and G. R. Wood, *Analyst*, 1976, **101**, 966.
5. X. Wang, M. Viczian, A. Lasztity and R. M. Barnes, *J. Anal. Atom. Spectrom.*, 1988, **3**, 821.
6. K. Jin, M. Taga, H. Yoshida and S. Hikime, *Bunseki Kagaku*, 1978, **27**, 759.
7. J. R. Castillo, J. M. Mir, C. Martinez, J. Val and M. P. Colon, *Microchimica Acta*, 1985, **1**, 253.
8. Y. Madrid, M. Bonilla and C. Camara, *J. Anal. Atom. Spectrom.*, 1988, **3**, 1097.
9. Y. Madrid, J. Meseguer, M. Bonilla and C. Camara, *Anal. Chim. Acta*, 1990, **237**, 181.

10. J. Li, Y. Liu and T. Lin, *Anal. Chim. Acta*, 1990, **231**, 151.
11. I. D. Brindle and C. M. Ceccarelli Ponzoni, *Analyst*, 1987, **112**, 1547.
12. J. Aznarez, F. Palacios, J. C. Vidal and J. Galban, *Analyst*, 1984, **109**, 713.
13. S. Zhang, H. Han and Z. Ni, *Anal. Chim. Acta*, 1989, **221**, 85.
14. F. Tang, X. Mao, J. Cheng and J. Zhang, *Fenxi Huaxue*, 1987, **15**, 216 (CA,.107, 167816k).
15. Y. Madrid, M. Bonilla and C. Camara, *J. Anal. Atom. Spectrom.*, 1989, **4**, 167.
16. C. Nerin, S. Olavide and J. Cacho, *Anal. Chem.*, 1987, **59**, 1918.
17. Z. Zhang, X. Zheng and B. Huang, *Fenxi Huaxue*, 1987, **15**, 801.

Talanta, Vol. 40, No. 8, pp. 1157–1162, 1993
Printed in Great Britain.

0039-9140/93 $6.00 + 0.00

CHARACTERIZATION OF MEDIATED AND NON-MEDIATED OXIDASE ENZYME BASED GLASSY CARBON ELECTRODES

A. AMINE, J.-M. KAUFFMANN and G. J. PATRIARCHE✠
Institut de Pharmacie, Universite Libre de Bruxelles, Campus Plaine, CP 205/6, 1050 Bruxelles, Belgium

G. D. CHRISTIAN
Department of Chemistry, University of Washington, Seattle, WA 98195, U.S.A.

(*Received* 14 *December* 1992. *Accepted* 27 *January* 1993)

Summary—The performance and analytical characteristics of a glassy carbon glutaraldehyde immobilized glucose oxidase electrode have been established with regard to the direct detection of hydrogen peroxide produced from the reaction of glucose with oxygen. Measurements were performed at +1.1 V *vs.* SCE, and selectivity was obtained by casting the surface with a cellulose acetate membrane. Results compared favorably with the classical platinum-enzyme probe. The mechanism of ascorbic acid interference in hydrogen peroxide detection is reported. Mediated detection was also investigated for oxidase enzymes (glucose oxidase and xanthine oxidase) immobilized on the bare glassy carbon electrode. The probes were characterized using a specific enzyme mediator in solution (phenazine methosulfate or dichlorophenol-indophenol) plus hexacyanoferrate(III) as an electrochemical mediator. The electrode was poised at +0.36 V *vs.* SCE for the detection of hexacyanoferrate(II). The advantages of this dual mediator configuration include high stability and sensitivity of the electrochemical signal and the ability to use less positive potentials for increased selectivity. Application to other enzymes, such as hydrogenases, using such a binary redox configuration is suggested.

Determination of glucose by direct amperometric measurement of hydrogen peroxide has been reported using immobilized enzyme chemically modified graphite electrodes,[1] adsorbed enzyme on non-porous carbon rod electrodes,[2] covalently attached enzyme on rotating glassy carbon surfaces to produce an extremely thin (*i.e.*, monolayer) with low enzyme activity[3] or by incorporating the enzyme into carbon paste electrodes.[4,5,6] However, in these carbonaceous electrodes, various reducing substances present in biological samples, for instance ascorbic acid or uric acid, may significantly interfere in the oxidation of hydrogen peroxide.

The most frequently used hydrogen peroxide sensor is the platinum electrode[7,8,9] and most commercial glucose analyses are based on the platinum electrode. Recently unmodified glassy carbon, poised at +1.3 V *vs.* SCE, was used to directly monitor the production of hydrogen peroxide produced by choline oxidation in the presence of soluble choline oxidase.[10]

In this work we report a stationary glassy carbon glucose sensor used in two configurations. In the first, the electrode is coated with a cellulose acetate membrane (to protect against electro-oxidation of ascorbic or uric acid), plus glutaraldehyde crosslinked glucose oxidase (to generate hydrogen peroxide), with the electrode poised at +1.1 V *vs.* SCE. In the second, the glutaraldehyde crosslinked enzyme (glucose oxidase or xanthine oxidase) is coated directly on the electrode without cellulose acetate, and an electron mediator (*e.g.*, phenazine methosulfate or dichlorophenolindophenol) in solution is reduced by the enzyme and then reacts with ferricyanide(III) to produce ferrocyanide(II) which is detected at the glassy carbon electrode. The iron(III)-mediator reaction avoids oxygen interference, provides enhanced sensitivity, and allows detection at +0.36 V where interference from other electroactive materials is diminished.

EXPERIMENTAL

Apparatus

Voltammograms were recorded with a BAS CV 27 voltammograph connected to a Hewlett-Packard 7090A X–Y recorder and a three electrode system: a glassy carbon disk (diameter 3 mm) working electrode, a platinum wire counter electrode and a saturated calomel (SCE) reference electrode. Amperometric measurements

were made with a Brucker E-100 potentiostat reference electrode. Amperometric measurements were made with a Brucker E-100 potentiostat polarograph connected to a Servagor X–Y recorder. The 50 ml electrochemical cell used to test the enzyme electrodes was operated in a three electrode configuration. The working electrode was a glassy carbon disk or a platinum disk (3 mm diameter). All experiments were conducted at room temperature and the potentials are referred to the SCE. The pH of the solution was measured with a Tacussel Mini 80 pH meter.

Reagents

All reagents were of analytical grade and supplied by Sigma or Merck. The solutions were prepared with demineralized water. Glucose oxidase, type X-S, activity 150,000 U/g and xanthine oxidase, X3751, from bovine milk, activity 150–300 U/g, were from Sigma. Standard stock solutions of glucose (1*M*) were prepared at least 1 day before use to allow equilibration by dissolution in 0.1*M* phosphate buffer (pH 7.0) and were stored at 4°C for no longer than 1 week. Standard stock solutions of xanthine (10 m*M*) were prepared by dissolution in 0.05*M* NaOH and stored at 4°C for no longer than 1 week. Enzymes were crosslinked on the surface of an Immunodyne membrane (Pall Industrie, Saint-Germain-en-Laye, France) for physical support (BIA002HC5, pore diameter 0.2 μm).

Electrode preparation

To 1 mg of enzyme dissolved in 20 μl 0.02*M* phosphate buffer (pH 7.0), was added 5 μl of 2.5% aqueous glutaraldehyde solution. After 30 sec mixing, the mixture was deposited on a Pall Immunodyne membrane. The crosslinking process proceeded at room temperature for 2 hr. Then the Biodyne membrane was rinsed thoroughly with demineralized water and fixed on the electrode body either with or without a cellulose acetate membrane.

RESULTS AND DISCUSSION

The linear sweep voltammetric behavior of 1 m*M* H_2O_2 at the glassy carbon electrode in solution of varying pH was investigated in the pH range 3.0–10.0 (acetate, phosphate and borax buffers, all 0.1*M*), Fig. 1. Clearly defined diffusion current plateaus were observed in the pH range 4.0–10.0. As expected the plateau range becomes more anodic at lower pH values.[1,7]

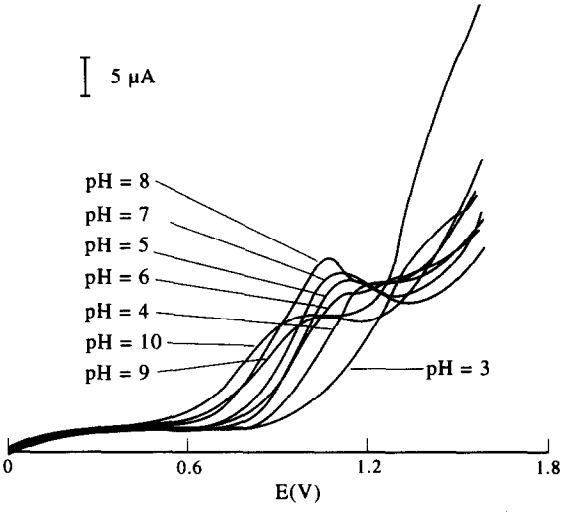

Fig. 1. Linear sweep voltammogram behavior of H_2O_2 at the glassy carbon electrode. $H_2O_2 = 1$ m*M*. Scan rate: 20 mV/sec.

Enzyme immobilized on bare electrode

Figure 2 shows the linear sweep voltammetric behavior of product H_2O_2 at the glassy carbon coated with immobilized glucose oxidase (non-mediated). In these experiments, the electrode was dipped into the solutions of varying pH containing 5 m*M* glucose and a potential of 0.0 V was applied. The current decayed and reached a stable value rapidly (about 1 min) and then the scan was applied. At pH 4.0, the current plateau disappears; this may be attributed to its anodic shift into the region of solvent breakdown and/or low activity of GOX at this pH. At pH 9.0, the enzyme activity decreases, thus a small response was obtained. The glassy carbon enzyme

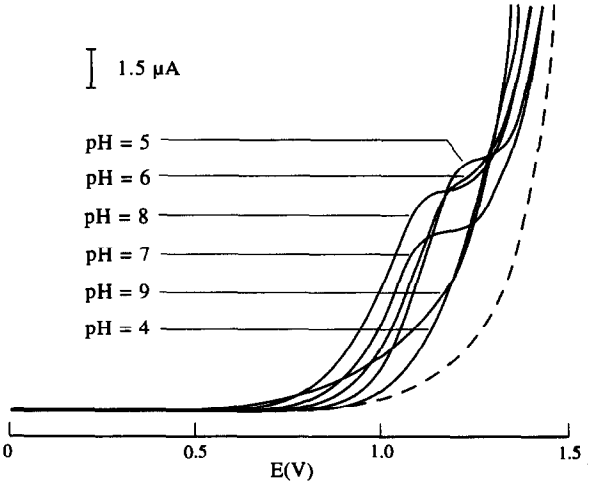

Fig. 2. Linear sweep voltammogram behavior of product H_2O_2 at the glassy carbon enzyme coated electrode. Glucose = 5 m*M*, scan rate: 20 mV/sec (--- background, pH 7.0).

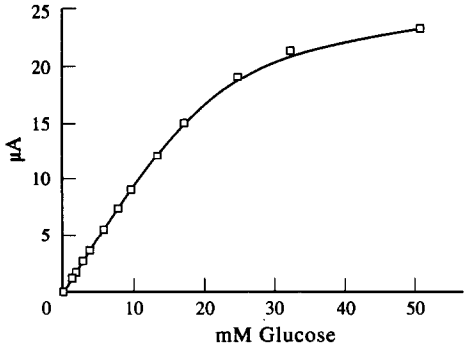

Fig. 3. Calibration curve for glucose coated enzyme electrode. Steady-state current measured at +1.1 V *vs.* SCE, pH 7.0.

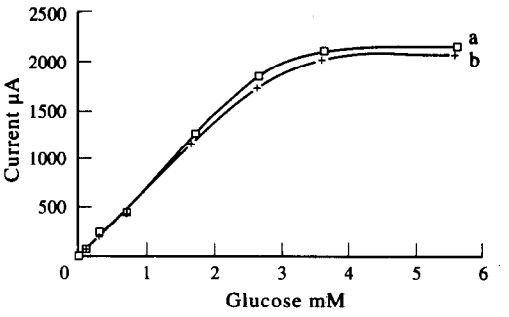

Fig. 5. Calibration curve for glucose (curve a) and after addition of freshly prepared 0.5 m*M* A.A. (curve b). Pt electrode covered with GOX immobilized on Biodyne membrane. Steady-state current measured at +0.65 V *vs.* SCE, pH 7.0.

electrode employed in this study can be used in the pH range 5.0–8.0. It was found that the best signal-to-background and signal-to-noise ratios were obtained around +1.1 V at pH 7.0.

Electrode response as a function of glucose concentration exhibits a Michaelian behavior (Fig. 3). The apparent Michaelis constant (K'_m) calculated from a Lineweaver–Burk plot was 26 m*M*. This value is an order of magnitude greater than some reports for platinum,[7] carbon rod,[2] graphite[1] and powdered graphite carbon[11] electrodes, comparable to a previous report for a monolayer of glucose oxidase covalently attached to glassy carbon[3] and less than the report for glucose oxidase incorporated in a carbon paste electrode.[6] Since the value of the apparent K'_m (26 m*M*) using glassy carbon was higher than the value for GOX in solution ($K_m = 0.2$ m*M*),[12] diffusion resistance of glucose through the enzyme membrane was suspected. Figure 4 shows the Eadie–Hofstee plot of data from Fig. 3. As can be seen, the presence of external diffusional limitations manifests itself by deviation from the straight line, the curve becoming concave towards the origin of the axes.[13] Such shape of deviation was reported with a transaminase bound collagen membrane.[14]

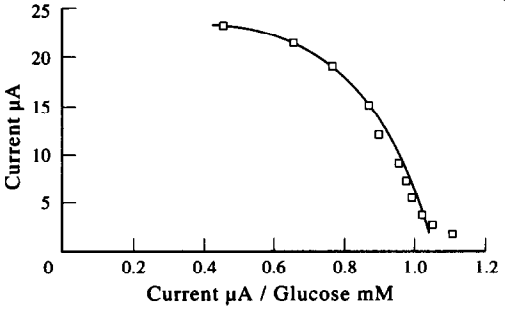

Fig. 4. Eadie–Hofstee plot of data from Fig. 3.

When the Biodyne membrane is assembled with a Pt electrode poised at +0.65 V (Fig. 5 curve a) the apparent K'_m was about 2 m*M*, which is less than the value obtained with a glassy carbon electrode poised at 1.1 V. This is explained by a slight evolution of oxygen at the glassy carbon sensor surface, thus increasing the linear measurement range for glucose.

The response was linear from $5 \times 10^{-7}M$ up to $1.7 \times 10^{-2}M$ (slope 0.9 μA/m*M*, intercept 0.009 μA and linear correlation coefficient 0.999). The anodic oxidation of peroxide and slight evolution of oxygen for water electrolysis at +1.1 V *vs.* SCE results in an increased oxygen concentration at the sensor surface, thus increasing the linear measurement range from glucose. This is reflected by an increased value of the apparent K'_m, as mentioned above. The selected +1.1 V for monitoring reflects a compromise between background current and dynamic range.

Study of interferences: enzyme immobilized on cellulose acetate coated electrode

Electroactive species, *e.g.*, ascorbic acid (A.A.) and uric acid, may oxidize directly on the electrode surface[15] or react with H_2O_2 produced in the enzymatic reaction as reported recently.[16] It is essential to eliminate these effects in the development of a reliable oxidase based sensor. It is known that A.A. is very unstable and breaks down rapidly, and can react easily with dissolved O_2 or with H_2O_2 produced in the enzymatic reaction, as reported in a spectrochemical assay for glucose[17] or an electrochemical assay with GOX immobilized in poly(*o*-phenylendiamine) films.[16] In the latter system, Malitesta *et al.*[18] have also reported a reduction in the current of the H_2O_2 product by A.A., but only at high

glucose concentrations, and attributed this to depletion of dioxygen by A.A.

In order to understand this we performed experiments on hydrogen peroxide with a classical Pt electrode covered with an enzymatic Biodyne membrane and poised at +0.65V, which is less than the potential of water oxidation and thus there was no increase of O_2 at sensor surface. Figure 5, curve a, shows a typical calibration curve for glucose. Curve b shows the calibration curve after addition of freshly prepared 0.5 m*M* A.A. It appears clearly that the sensor response was unaffected by the presence of A.A., except at high glucose concentrations above 1 m*M*. Similar results were obtained with GOX immobilized in poly(*o*-phenylendiamine) films.[18] The decrease in current is ascribed to oxygen depletion, whose effect is particularly pronounced at high substrate concentrations when the reaction rate becomes limited by cosubstrate availability as in concurrence with the GOX ping-pong mechanism.[19] Our results are in agreement with the report of Malitesta *et al.*[18] and in contrast to the recent report[16] which proposed that reduction of the glucose signal is due to the reaction of A.A. with H_2O_2. Normally in the latter hypothesis, we should have a decrease in the glucose signal only at low glucose concentrations, and the glucose concentration calculated should be less than the true glucose concentration by an amount almost exactly equal to the A.A. concentration, as reported in the spectrochemical assay with GOX in solution.[17]

In order to eliminate interference from electroactive chemicals which are directly oxidized on the electrode surface, a cellulose acetate membrane (kindly provided by Prof. M. Mascini, and prepared as previously reported[9]) was first fixed on the glassy carbon surface. Then a Biodyne membrane with immobilized enzyme was layered on top of this and the two membranes were held with an o-ring. Addition of the cellulose acetate membrane resulted in a decrease in the glucose signal about 3-fold, but highly increased the selectivity.[20] A 100 μM solution of A.A. gave no response at all. The signal response of 0.5 m*M* glucose in buffer obtained was exactly equal to the signal of 0.5 m*M* glucose in buffer containing 10 μM A.A., in agreement with the results of Fig. 5, curves a and b (see above for explanation). These concentrations of A.A. and glucose correspond to physiological levels in blood (diluted 10-fold in buffer). The glucose response was

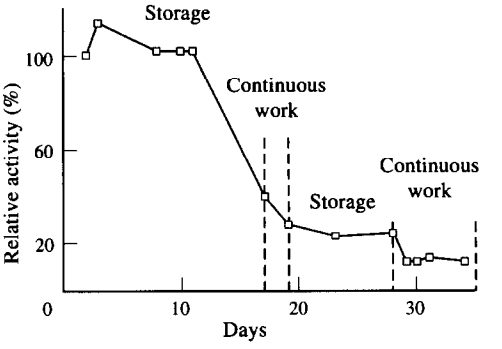

Fig. 6. Long term stability of cellulose acetate coated electrode. Continuous work refers to continuous exposure of the electrode to 1 m*M* of glucose at a permanently poised potential of +1.1 V at pH 7.0. Relative activities were measured at the points indicated.

linear from $1 \times 10^{-6} M$ to $1 \times 10^{-3} M$ glucose (slope 0.34 μA/m*M*, intercept 0.003 μA, linear correlation coefficient 0.999), reaching steady state within 100–120 sec. This measurement range is in approximate agreement with that listed for commercial platinum hydrogen peroxide sensors (Yellow Springs Instrument Co. and Tacussel Electronique).

The stability of the electrode is presented in Fig. 6. There is no significant decrease in activity for 11 days, and from 19 to 28 days the activity of the enzyme remains stable at about 23% of the initial activity. It is important to note that the electrode was stored in phosphate buffer at pH 7.0 and ambient temperature (*ca.* 25°), except under the continuous work conditions when the electrode was permanently poised at +1.1 V *vs.* SCE in 1 m*M* glucose.

Contrary to previous results with a monolayer of covalently linked enzyme[3] there is no large decrease in enzyme activity under working conditions. The apparent continuous decrease during the initial continuous work region is probably just an extension of the original decay, although a relative decrease in enzyme activity under working conditions may be due to inactivation of GOX by H_2O_2.[21] The previous work demonstrated large decreases over a working period of 6 hr.[3] The high ionic strength of the buffer (0.1*M*) and the acetate cellulose membrane interposed between the glassy carbon surface and the enzyme membrane may protect the enzyme from a change in the local pH.

Electron mediated electrode

Table 1 shows that ferricyanide is the best electrochemical mediator in terms of stability. However, in the literature we find that methyl viologen (MV^+) is the best mediator for

Table 1. Electrochemical properties of some mediators

Name	E_0'* (*Volts vs. NHE*)	Oxidizability of reduced form	Other properties	Ref.
Methyl viologen	−0.45	Rapidly oxidized by oxygen	Rapid signal decline attributed to the high instability of reduced form	[22,31]
Phenazine methosulfate	+0.08	Readily oxidized by oxygen	Rapid signal decline attributed to the high instability of reduced form	[23,25,31]
Methylene blue	+0.01	Oxidized by oxygen fairly rapidly at pH 7, only slowly at pH 5	The redox potential is highly dependent on pH	[31]
2,6-Dichlorophenol indophenol	+0.21	Oxidized by oxygen	Risks of surface fouling at high positive potentials	[31,35]
Potassium ferricyanide	+0.36	Quite stable. Only slowly oxidized by oxygen	Stable and large current on glassy carbon. No surface fouling	[23,31]

*E_0' = redox potential at pH 7 at 25°.

hydrogenase enzymes,[22] and phenazine methosulfate (PMS^+) the most effective for NADH,[23] while the list compiled by Dixon[24] shows that the molecules listed in Table 1 are effective mediators for flavoproteins and in general ferricyanide does not react with these enzymes in the presence of O_2.

Kulys and Cenas listed different mediators for GOX.[25] In their report some experiments were carried out anaerobically (undoubtedly because of low stability of the reduced form of the mediator in the presence of dissolved O_2) or in a buffer with 6.6% ethanol (because of low solubility in water of the mediator). Turner and coworkers[26,27] and Thomas and coworkers[28] have reported the use of ferrocene based mediators for electrochemical detection and Bartlett and Whitaker[29] discuss dehydrogenase mediators and TTF·TCNQ mediator for a glucose oxidase electrode.

Owing to these considerations, we chose an effective enzyme mediator at low concentration (0.1 m*M*) in conjunction with ferricyanide at high concentration (10 m*M*) which has a stable reduced form and gives a high oxidation signal on glassy carbon at a relatively low potential, +0.36 V *vs.* SCE (Scheme 1). Recently PMS^+ in conjunction with ferricyanide has been used for regeneration of NAD^+ for glutamate dehydrogenase.[23] Two enzymes were tested, glucose oxidase (GOX) and xanthine oxidase (XOD).

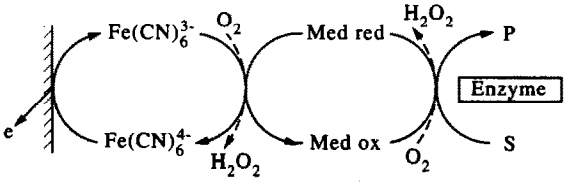

Scheme 1. Reaction sequence for biosensor based on an electron mediator in the presence of ferricyanide for oxidase immobilized glassy carbon electrode.

Neither reacts with ferricyanide in the presence of glucose or xanthine, respectively, at concentrations lower than 1.5 m*M*, due to the competition with O_2 for the cofactor.

PMS^+ is an effective mediator for GOX,[24] but due to the instability of its reduced form, in the presence of oxygen, a steady-state current is not observed[23] even when PMS^+ is adsorbed on graphite electrode surface and thus the reduced form of PMS^+ is in the vicinity of graphite sensor.[30] If we use PMS^+ in conjunction with ferricyanide we obtain a response in the range of 0.1–1.5 m*M* glucose, as presented in Fig. 7. There is no electrochemical response towards the hydrogen peroxide product at the glassy carbon electrode at +0.36 V (according to Fig. 1). The reaction of XOD with 2,6 dichlorophenolindophenol (DCPIP) in conjunction with ferricyanide exhibits a xanthine calibration curve as shown in Fig. 8. The electrochemical response corresponds to oxidation of ferrocyanide and the uric acid product of the enzymatic reaction at +0.36 V *vs.* SCE.

The local oxygen concentration at the surface of the electrode decreases as the substrate (glucose or xanthine) increases, and hence a

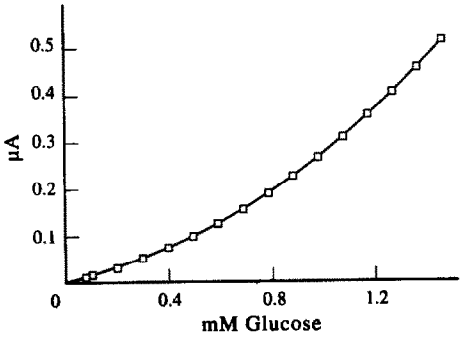

Fig. 7. Calibration curve for electron mediated glucose enzyme electrode in presence of PMS^+ (0.1 m*M*) and ferricyanide (10 m*M*), pH 7.0, +0.36 V *vs.* SCE.

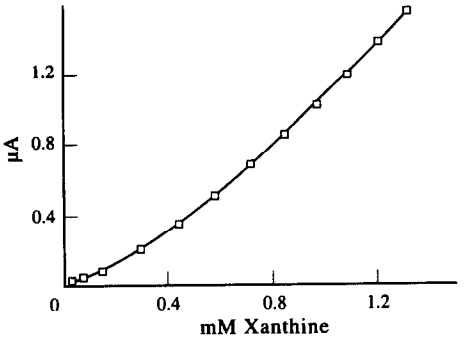

Fig. 8. Calibration curve for electron mediated xanthine enzyme electrode in presence of DCPIP (0.1 m*M*) and ferricyanide (10 m*M*), pH 7.0, +0.36 V *vs.* SCE.

larger fraction of the reduced mediator reacts with ferricyanide owing to the competition of O_2 and the mediator for the enzyme cofactor. The current observed for added standard substrate therefore increases as the total concentration of substrate in solution increases, giving rise to the non-linear calibration graph (Figs 7 and 8).

Compared to the non-mediated cellulose acetate covered glassy carbon electrode, the selectivity of the mediated electrode is lessened, but one aim of this work is to show that this binary redox configuration is easy to prepare and can be generalized for enzymes other than those dependent on O_2. For example, MV^+ is an effective mediator for hydrogenase enzymes[22] but its reduced form, which is readily oxidized,[31] should be successfully coupled with ferricyanide. We should point out that hexacyanoferrate (III) has been successfully used for L-lactate determination in blood plasma[32,33] by measurement of the hexacyanoferrate (II) produced in the reaction (directly at a platinum electrode at +0.35 V *vs.* SCE). The only slight interference was uric acid, and in most cases, this interference was insignificant (maximum 7% at the highest possible uric acid concentration). A bioenzyme electrode for L-carnitine was recently base on hexacyanoferrate (II) detection[34] and an analyzer based on this approach is now commercially available (Microzym-L from SGJ, France).

REFERENCES

1. R. M. Ianniello and A. M. Yacynych, *Anal. Chem.*, 1981, **53**, 2090.
2. L. Gorton, F. Scheller and G. Johansson, *Stud. Biophys.*, 1985, **109**, 199.
3. C. Bourdillon, J. P. Bourgeois and D. Thomas, *J. Am. Chem. Soc.*, 1980, **102**, 4231.
4. W. Matuszewski and N. Trojanowicz, *Analyst*, 1988, **113**, 735.
5. J. Wang, L. H. Wu, Z. W. R. Li and J. Sanchez, *Anal. Chim. Acta*, 1990, **228**, 251.
6. A. Amine, J. M. Kauffmann and G. J. Patriarche, *Talanta*, 1991, **38**, 107.
7. G. G. Guilbault and G. J. Lubrano, *Anal. Chim. Acta*, 1973, **64**, 439.
8. D. R. Trevenot, R. Sternberg, P. R. Coulet, J. Laurent and C. D. Gautheron, *Anal. Chem.*, 1979, **51**, 96.
9. A. Amine, G. J. Patriarche, G. Marrazza and M. Mascini, *Anal. Chim. Acta*, 1991, **262**, 91.
10. J. Z. Stemple, K. M. Rusin and T. L. Fare, *Anal. Chem.*, 1991, **63**, 1050.
11. A. E. G. Carr, G. Davis, G. D. Francis, H. A. O. Hill, W. J. Aston, J. J. Higgins, E. V. Plotkin, L. D. L. Scott and A. P. F. Turner, *Anal. Chem.*, 1984, **56**, 667.
12. H. U. Bergmeyer, M. Grassel and H. E. Walter, in H. U. Bergmeyer (ed.) *Methods of Enzymatic Analysis*, 3rd Ed., Vol. 2, pp. 201–202. VCH, Weinheim, Germany, Deerfield Beach, FL, 1983.
13. J. M. Engasser and C. Horvath, in L. B. Wingard, E. Katchalski and L. Goldstein (eds) *Applied Biochemistry and Bioengineering*, Vol. 1, pp. 127–220. Academic Press, New York, 1976.
14. J. M. Engasser, P. R. Coulet and C. J. Gautheran, *Biol. Chem.*, 1977, **22**, 7919.
15. A. Amine, J.-M. Kauffmann, G. J. Patriarche and G. G. Guilbault, *Anal. Lett.*, 1989, **22**, 2403.
16. J. P. Lowry and R. D. O'Neill, *Anal. Chem.*, 1992, **64**, 453.
17. G. A. Maguire and C. P. Price, *Clin. Chem.*, 1983, **29**, 1810.
18. C. Malitesta, F. Palmisano, L. Torsi and P. Zambanen, *Anal. Chem.*, 1990, **62**, 2735.
19. M. Weibel and H. J. K. Bright, *J. Biol. Chem.*, 1971, **246**, 2734.
20. G. Palleschi, N. Rahni, M. A. Lubrano, J. N. Ngwainbi and G. G. Guilbault, *Anal. Biochem.*, 1986, **159**, 116.
21. P. F. Greenfield, J. R. Kittrel and R. L. Laurence, *Anal. Biochem.*, 1975, **65**, 109.
22. S. D. Yarafolomeev, A. I. Yaropolov, I. V. Berezin, M. R. Tarasevich and V. A. Bogdancrskaya, *Bioelectrochem. Bioenerg.*, 1977, **4**, 314.
23. A. Amine and J. M. Kauffmann, *Bioelectrochem. Bioenerg.*, 1992, **28**, 117.
24. M. Dixon, *Biochim. Biophys. Acta*, 1971, **226**, 269.
25. J. J. Kulys and N. K. Cenas, *Biochem. Biophys. Acta*, 1983, **244**, 57.
26. A. E. G. Cass, G. Davis, G. D. Francis, H. A. O. Hill, W. J. Aston, I. J. Higgins, E. V. Plotkin, L. D. I. Scott and A. P. F. Turner, *Anal. Chem.*, 1984, **56**, 667.
27. E. J. D'Costa, I. J. Higgins and A. P. F. Turner, *Biosensors*, 1986, **2**, 71.
28. S. K. Beh, G. J. Moody and J. D. R. Thomas, *Analyst*, 1991, **116**, 459.
29. P. N. Bartlett and R. G. Whitaker, *Biosensors*, 1987, **3**, 359.
30. G. Jonsson and L. Gorton, *Biosensors*, 1985, **1**, 355.
31. J. L. Peel, in J. R. Norris and D. W. Ribbons (eds) *Methods in Microbiology*, Vol. 6B. Academic Press, London, 1972.
32. J. Racek and J. Musil, *Clin. Chim. Acta*, 1987, **162**, 129.
33. J. Racek and J. Musil, *Clin. Chim. Acta*, 1987, **167**, 59.
34. M. Comtat, M. Galy, P. Goulas and J. Suope, *Anal. Chim. Acta*, 1988, **208**, 295.
35. H. T. Tang, K. Hajizadeh, H. B. Halsall and W. R. Heineman, *Anal. Biochem.*, 1991, **192**, 243.

Talanta, Vol. 40, No. 8, pp. 1163–1165, 1993
Printed in Great Britain.

0039-9140/93 $6.00 + 0.00

DETERMINATION OF L-MALATE IN WINE BY FLOW-INJECTION WITH CO-IMMOBILIZED MALATE DEHYDROGENASE/OXALOACETATE DECARBOXYLASE

NOBUTOSHI KIBA, MIE OGUCHI and MOTOHISA FURUSAWA
Department of Applied Chemistry and Biotechnology, Faculty of Engineering, Yamanashi University, Kofu 400, Japan

(*Received* 14 *December* 1992. *Revised* 29 *January* 1993. *Accepted* 3 *February* 1993)

Summary—A method for determination of L-malate in wine is described. Malate dehydrogenase and oxaloacetate decarboxylase were immobilized on poly (vinyl alcohol) beads and incorporated in a flow-injection system with fluorescence detection. Sample solution (50 μl) was injected into the carrier stream [4*mM* NAD^+ in glycine buffer (pH 10.0)]. The fluorescence based on the NADH formed could be directly related to the amount of malate. The calibration graph was linear over the range 0.4–300μM. The detection limit was 0.2μM. Sampling throughout was 25 samples/hr.

L-Malate affects the taste and flavour of wines. The malate concentration decreases continually during storage due to decomposition by micro-organisms (malo-lactic fermentation). The best time for shipping is decided primarily on the basis of the malate concentration.

Malate in wines has been determined by ion chromatography[1,2] and high-performance liquid chromatography.[3] For the specific determination of malate, batch enzymatic methods have been developed using malate dehydrogenase (EC 1.1.1.37, MDH) and aspartate aminotransferase (EC 2.6.1.1., AAT)[4] (F-kit, No. 139068, Boehringer Mannheim GmbH), and MDH, citrate synthase (EC 4.1.3.7) and phosphate acetyltransferase (EC 2.3.1.8).[5] These methods are unsuitable for the rapid assay of a large number of samples.

MDH reversibly catalyzes the following reaction;

$$\text{malate} + NAD^+ = \text{oxaloacetate} + NADH + H^+$$

The equilibrium strongly favours the formation of malate. Displacement of the equilibrium of the reaction in favour of NADH formation was assisted by increasing the NAD^+ concentration, raising the pH and/or adding a trapping enzyme.[4,5] MDH and AAT were co-immobilized onto controlled-pore glass (CPG) and used in a flow-injection system for the determination of L-malate in wines at pH 9.5.[6] However, CPG is not suitable as the support for the enzymes since CPG is unstable in alkaline solution.[7]

Oxaloacetate decarboxylase (EC 4.1.1.3, OXD) catalyzes the decarboxylation of oxaloacetate to pyrvate and carbon dioxide according to the reaction;

$$\text{oxaloacetate} \rightarrow \text{pyrvate} + CO_2.$$

In this paper, a flow-injection fluorimetric method for the determination of L-malate with co-immobilized MDH/OXD reactor is reported. Here, OXD was used as a trapping enzyme and poly(vinyl alcohol) beads which are relatively stable in alkaline solution were used as support. The enzymes were covalently immobilized with glutaraldehyde on the beads and a fluorimetric procedure was used to monitor the appearance of NADH. The flow-injection method was applied to the determination of free L-malate in wines.

EXPERIMENTAL

Materials

MDH (L-Malate: NAD^+ oxidoreductase, from Thermus sp., type III, 120 U/mg) and OXD (Oxaloacetate carboxy-lyase, from Pseudomonas sp., 350 U/mg) were obtained from Amano Pharmaceutical Co. (Nagoya) and Asahi Chemical Industry (Tokyo), respectively. NAD^+ (free acid, 96%) was from Kohjin (Tokyo). Poly(vinyl alcohol) beads (GS-520, 13 μm diameter) were from Asahi Chemical Industry. A purity of L-(−)-malic acid, obtained from Sigma Chemical Co. (St Louis), was

checked by the enzymatic method.[8] All other chemicals were of analytical-reagent grade.

Glycine buffer (pH 10.0) consisting of 0.1*M* glycine–0.1*M* NaCl–0.1*M* NaOH was prepared. The method for the amination of the beads was similar to that described previously.[9] The aminated beads were packed into a stainless-steel column (5 cm × 4 mm i.d.) by the slurry-packing method. Glutaraldehyde (4%) in 0.1*M* sodium hydrogencarbonate solution was pumped through the column for 2 hr at 0.3 ml/min and the column was washed with deaerated water for 30 min at 0.5 ml/min. Enzymes solution [MDH 3 mg (360 U) and OXD 9 mg (3150 U) in 10 ml of 0.05*M* phosphate buffer (pH 7.0)] was circulated through the column at 0.3 ml/min for 6 hr at 20°. MDH activity in the solution was measured with L-malate as substrate at pH 9.0 at 30°. Also OXD activity was measured with oxaloacetate as substrate and lactate dehydrogenase (EC 1.1.1.28) at pH 8.0 at 30°. MDH and OXD were immobilized on the beads with 69 and 32% yields, respectively.

Apparatus and procedure

The glycine buffer (pH 10.0) containing 0.1*M* $MgCl_2$ and 8*mM* NAD^+ solution were each pumped by a double-plunger pump (KHU-W-52, Kyowa Seimitsu, Japan) at a flow-rate of 0.25 ml/min and mixed before an injector (TVM-6M2, Sanuki, Japan) with a 50 μl loop. The combined solution entered the reactor which was maintained at 30° with a thermostated water bath. Enzymatic reactions took place in the reactor and the NADH produced was monitored at 465 and 340 nm with a spectrofluorimeter (FP-210, Jasco, Japan).

RESULTS AND DISCUSSION

Properties of co-immobilized MDH/OXD reactor

The effect of pH on the activity of the co-immobilized enzymes reactor was studied in the pH range 9.0–11.0 using glycine buffer. The optimum pH was found to be about 10.0. The effect of temperature on the activity of the reactor was studied over the range 20–40°. The reactor exhibited maximum activity at 30°. Compared with the immobilized MDH[10] (optimum pH and temperature are 11.5 and 45°, respectively), the maximum pH and temperature for the co-immobilized enzymes are 1.5 pH units more acidic and 15° lower, respectively.

The optimum NAD^+ concentration in the reactor was investigated in the range 1–10*mM* at the 300μ*M* L-malate level. The peak height increased with increasing concentration. Above 8*mM*, the peak height was constant. A concentration of 8*mM* NAD^+ was chosen; at this concentration, the NAD^+ concentration in the reactor is 4*mM*.

Immobilized OXD was activated by Mg^{2+} in a similar manner as the free OXD.[11] The effect of the $MgCl_2$ concentration on the peak height was investigated in the range of 0.01–0.2*M*. The peak height become constant at 0.03*M*. A solution of 0.1*M* $MgCl_2$ was used; at this concentration, the Mg^{2+} concentration in the reactor is 0.05*M*.

The peak height decreased linearly as the flow-rate of carrier stream increased from 0.3 to 0.8 ml/min. The peak height was strongly influenced by the flow-rate and the peak height at 0.3 ml/min was about 3.4 times that at 0.8 ml/min. A total flow-rate of 0.6 ml/min was selected, as a compromise between sensitivity and sample throughput: at this flow-rate, the sample throughput was 25 hr^{-1}.

Under the conditions described in Apparatus and Procedure, the conversion efficiency of the reactor was 44%. Under the same conditions, the relative activities for L-malate and D-malate were 100 and 9, respectively. Other carboxylic acids such as tartaric acid, citric acid, lactic acid, succinic acid and acetic acid did not interfere at the 2*mM* level. The presence of up to equimolar amounts of pyruvic acid, sulphite or ascorbic acid did not interfere with the measurement of L-malate. In the presence of equimolar oxaloacetate, the peak height decreased to 75% of the standards. However, since the concentrations of the compounds in wines are normally far lower than that of L-malate, this method is not subject to interferences from the compounds.

The operational stability of the reactor was evaluated over 3 weeks. The reactor was used for the analysis of 100 samples (20μ*M* L-malate) during 4 hr/day and stored at 4° in 0.1*M* phosphate buffer (pH 7.0) when not in use. The activity decreased gradually to 80% of the initial value after 3 weeks.

Calibration

The calibration graph of peak height against malate concentration was linear over the range 0.4–300μ*M* with a correlation coefficient of 0.997 ($n = 11$) under the same conditions as described in Apparatus and Procedure. Above a

concentration of 300μM, the graph became curved. The relative standard deviation for 11 replicate injections of 20μM L-malate was 0.95%. The limit of detection (signal-to-noise ratio = 3) was 0.2μM (1.3 ng in a 50 μl injection).

Application

This method was applied to the determination of free L-malate content in wines. White wine (10 μl) was diluted 1000-fold with water because the concentration of free L-malate in white wines is normally in the range from 14mM (2 g/l) to 45mM (6 g/l).[12] Red wines were decolorized by nylon beads (A-1030, 100–150 mesh, Unitika, Osaka) and diluted 500-fold with water because the concentration is in the range from 3mM (0.4 g/l) to 45mM (6 g/l).[12] Diluted sample (50 μl) was injected into the carrier stream.

Red wines with low and high L-malate concentrations were repeatedly analysed during 4 weeks with the reactor. The reactor was used for analyses of 60 samples in a day and standards were measured at 30-sample intervals, in order to correct the variation of the conversion efficiency. The reactor was renewed every 2 weeks. The method gave satisfactorily precise and reproducible results; for wine containing 3.6mM L-malate, the within-day coefficient of variation (CV) was 1.3% and day-to-day CV 1.8%. For wine containing 38mM L-malate, the respective CV values were 0.95 and 1.6%.

A sample of red wine of known L-malate concentration was supplemented with L-malate to give final concentrations of 4.0–41.7mM. The recoveries were in the range 97–102%.

The results (n = 36, 20 red wines, from 3.8 to 42.1mM) were compared with those obtained by F-kit (Boehringer Mannheim) with soluble MDH and AAT. The calculated linear regression and correlation coefficient were $y = 0.979x + 0.03$ and $r = 0.992$, respectively.

CONCLUSION

The flow-injection system with co-immobilized MDH/OXD reactor is useful for the sensitive and reliable measurement of L-malate and can easily be used routinely for the analysis of wines. The method is about twice as sensitive as that with co-immobilized MDH/AAT reactor,[6] conversion efficiencies for MDH/OXD reactor and MDH/AAT reactor are 44 and 25%, respectively. The co-immobilized MDH/OXD reactor is stable enough to permit the measurement of more than 1400 samples.

REFERENCES

1. Y. Suzuki, H. Koizumi, K. Tani and M. Ding, *Bunseki Kagaku*, 1991, **40**, T15.
2. S. A. Kupina, C. A. Pohl and J. L. Gannotti, *Am. J. Enol. Vitic.*, 1991, **42**, 1.
3. K. Yokotsuka, T. Matsudo and T. Kushida, *J. Inst. Vitic. Yamanashi Univ.*, 1983, **18**, 7.
4. H. Mollering, in H. U. Bergmeyer (ed.), *Method in Enzymatic Analysis*, 3rd edn., Vol. 7, p. 39. Verlag Chemie, Weinheim. 1985.
5. W. Schoner, *ibid.*, p. 47.
6. G. C. Chemnitius and R. D. Schmid, *Anal. Lett.*, 1989, **22**, 2897.
7. E. P. Plueddemann, *Silane Coupling Agents*, p. 227. Plenum, New York, 1982.
8. H. O. Beutler and B. Wurst, *Deu. Leb.-Rund.*, 1990, **86**, 341.
9. N. Kiba, Y. Inoue and M. Furusawa, *Anal. Chim. Acta*, 1991, **243**, 183.
10. A. M. Almuiabed and A. Townshend, *Anal. Chim. Acta*, 1989, **221**, 337.
11. A. A. Horton and H. L. Kornberg, *Biochim. Biophys. Acta*, 1964, **89**, 381.
12. K. Yokotsuka, T. Matsuda, K. Nozaki and T. Kushida, *J. Inst. Enol. Vitic. Yamanashi Univ.*, 1983, **18**, 51.

Talanta, Vol. 40, No. 8, pp. 1167–1171, 1993
Printed in Great Britain.

0039-9140/93 $6.00 + 0.00

CATHODIC ADSORPTIVE STRIPPING VOLTAMMETRY OF NICKEL COMPLEXED WITH HYDROXYNAPHTHOL BLUE AT A STATIC MERCURY DROP ELECTRODE

PÉRCIO A. M. FARIAS,* ANIY K. OHARA and IRACEMA TAKASE
Department of Chemistry, Pontificia Universidade Católica, Rua Marqués de São Vicente, 225, CEP 22453-900, Rio de Janeiro, RJ, Brazil

SERGIO L. C. FERREIRA
Institute of Chemistry, Universidade Federal da Bahia, CEP 40210, Salvador, Bahia, Brazil

JON S. GOLD
Department of Chemistry, Santa Clara University, Santa Clara, CA 95053, U.S.A.

(*Received* 25 *November* 1992. *Revised* 16 *February* 1993. *Accepted* 18 *February* 1993)

Summary—A new method is described for the determination of Ni based on the cathodic adsorptive stripping of Ni(II) complexed with hydroxynaphthol blue (HNB) at a static mercury drop electrode. Optimal conditions were found to be: accumulation potential −0.50 V (*vs.* Ag/AgCl); final potential −1.10 V; accumulation time 50 sec; scan rate 200 mV/sec; linear scan mode; filter 0.1 sec; supporting electrolyte acetic acid/acetate (0.25*M*, pH = 6.0) and concentration of HNB $3.3 \times 10^{-5}M$. The response of the system was found to be linear in a range of Ni concentrations from 25 ppb to the detection limit. The detection limit was found to be 1.7 nM (0.10 ppb) with 2 mins of accumulation time. The effect of various potential interferences (including a variety of cations, anions and organic surfactants) were also studied. With the exception of Co, at less than equimolar concentrations no significant interferences were observed. Al was found to interfere at high concentrations with respect to Ni, but Al concentrations up to 1000 ppb may be masked by sodium citrate or sodium fluoride. The utility of the method is demonstrated by the recovery of Ni in a doped sample of commercial mineral water.

Nickel, which is a potentially toxic and carcinogenic metal, has been previously quantitatively determined by adsorptive voltammetric techniques utilizing complexing agents such as dimethylglyoxime,[1] 2-2′-bipyridine[2] and cyclohexane-1,2-dione dioxime.[3] Each technique has its particular sensitivity and is subject to various interferences and limitations. In our laboratory we have been investigating various pre-adsorptive voltammetric techniques utilizing a variety of organic complexing agents for trace and ultratrace metal determinations which both maximize sensitivity and selectivity.[4–7] We report here the trace determination of Ni by cathodic stripping voltammetry using the complexing agent hydroxynaphthol blue (HNB). We have found this technique to be both sensitive (detection limit of 0.10 ppb with a 2-min accumulation time), relatively unaffected by a variety of commonly interfering substances and is performed in an acidic medium (pH ≅ 4.8–6.0). The effect of a number of experimental parameters is presented. The utility of the method is demonstrated by the recovery of nickel in a doped mineral water sample.

EXPERIMENTAL

Apparatus and reagents

The voltammograms were obtained with a PAR 264-A voltammetric analyser interfaced with a PAR 303 static mercury drop electrode which have been described elsewhere.[6,7] A large-sized static mercury drop electrode (SMDE) with a surface area of 0.032 cm^2 was used. A Ag/AgCl (saturated KCl) reference electrode and platinum wire auxiliary electrode were used. All potentials reported are with respect to the Ag/AgCl electrode. Water purified in a Milli-Q water purification system (millipore) was used for all dilutions and sample preparations. All chemicals were of analytical reagent grade. A 2000-ppm stock solution

*Author for correspondence.

(Merck, titrisol) was used to prepare Ni solutions. A $3.3 \times 10^{-3}M$ stock solution of HNB was prepared in water. A stock solution of $1M$ acetate was prepared as supporting electrolyte followed by addition of acetic acid to achieve pH = 6.0. The mineral water subsequently analyzed was obtained commercially.

Procedure

Ten milliliters of a supporting electrolyte solution (7.5 ml of water + 2.5 ml of the stock acetate buffer) containing 100 μl of the $3.3 \times 10^{-3}M$ HNB stock solution were pipetted into the cell and purged with nitrogen for 8 min. The preconcentration potential (−0.5 V *vs.* Ag/AgCl) was applied to a fresh mercury drop while the solution was stirred. Following the accumulation (typically 50 sec) the stirring was stopped and allowed to equilibrate for 30 sec. The voltammogram was recorded by a linear scan of negative-going voltage (scan rate = 200 mV/sec) terminated at −1.10 V. After the background stripping voltammogram has been obtained, aliquots of the nickel standard solution are introduced into the cell while maintaining a stream of nitrogen over the surface. All data were obtained at (23 ± 1)°.

RESULTS AND DISCUSSION

Parameters affecting the adsorptive stripping behaviour

Figure 1 shows the resulting cyclic voltammograms by varying the scan rates from 20 mV/sec up to 500 mV/sec. The ligand peak is seen to become broader with increasing scan rate until at higher scan rates begins to overlap with the complex's peak. A scan rate of 200 mV/sec was found to yield a reasonable sensitivity while retaining resolution. In contrast to some similar systems we have studied, [8] the Ni–HNB complex did not display an adsorptive–accumulative effect with repetitive cyclic voltammetry.

Figure 2(A) shows the effect of pH on the linear scan stripping peak current of the Ni–HNB complex. The current is seen to increase from pH = 4.40 until levelling off at pH = 5.2. It is worth noting that a pH of 6.0 was generally used for subsequent quantitative determinations, as it was later observed that this pH minimized potential interferences by other ions.

The effect of the accumulation potential on the stripping peak's current was evaluated over the range −0.70–0.00 V [Fig. 3(A)]. The largest peak current is obtained using a potential near −0.5 V. A similar dependence of current with accumulation potential was previously observed for the V–TAC system.[9]

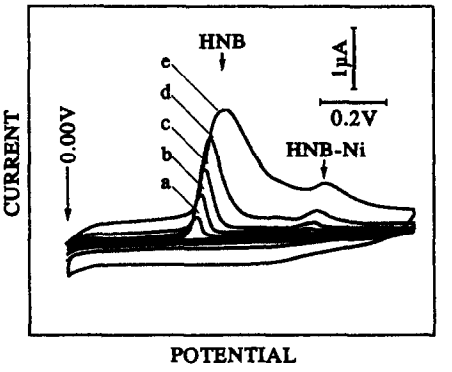

Fig. 1. Effect of scan rate on the cyclic voltammogram of the Ni–HNB system. Experimental conditions: acetic acid/acetate supporting electrolyte, $0.25M$, pH = 6.0; unstirred solution; [HNB] = $3.3 \times 10^{-5}M$; 20 ppb Ni; large size drop; equilibrium time 30 sec and filter 0.1 sec. Curve a = 20; b = 50; c = 100; d = 200; e = 500 mV/sec.

Other experimental variables affecting the adsorptive stripping response were evaluated and optimized. The effect of scan rate on peak potentials and current is shown in Fig. 4(A) and (B), respectively. A similar result was obtained

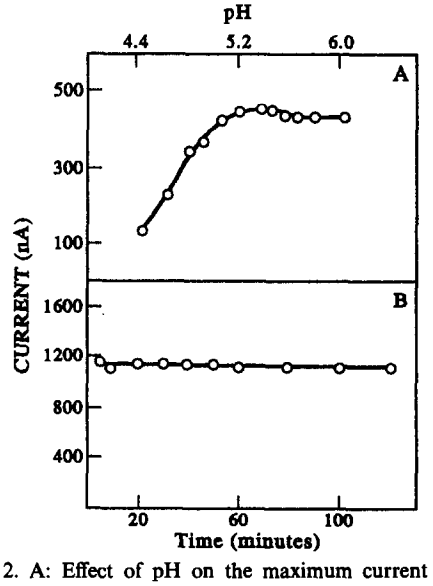

Fig. 2. A: Effect of pH on the maximum current of the stripping peak. Experimental conditions: acetic acid/acetate supporting electrolyte, $0.05M$; large size drop; filter 0.1 sec (linear scan mode); 25 ppb Ni; [HNB] = $3.3 \times 10^{-5}M$; stirred solution; t_{acc} = 30 sec at −0.41 V; t_{equil} = 30 sec; E_{final} = −1.30 V and scan rate 100 mV/sec. B: Repetitive measurements of a single sample of Ni–HNB. Experimental conditions as for A with acetic acid/acetate supporting electrolyte, $0.25M$, pH = 6.0; 20 ppb Ni; t_{acc} = 50 sec at −0.50 V; E_{final} = −1.10 V and scan rate 200 mV/sec.

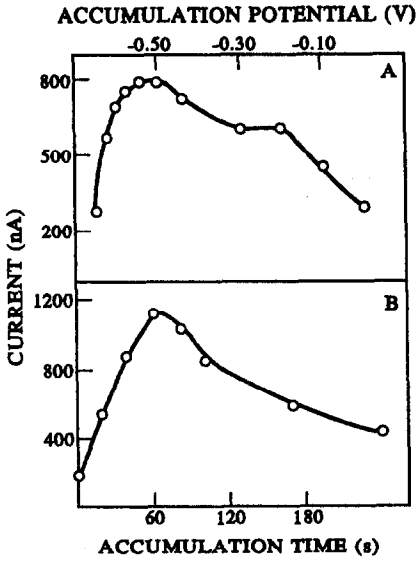

Fig. 3. The effect of accumulation potential (A) and time (B) on the current of the stripping peak for Ni–HNB. Experimental conditions as for Fig. 2(B) with an accumulation time of 30 sec.

by cyclic voltammetry as discussed above. The potential ranges from −0.71 to −0.81 V within the range of scan rates from 10 mV/sec to 500 mV/sec. A plot of current with respect to the scan rate is linear (correlation coefficient of 0.9926 for a scan rate range of 10–200 mV/sec) as expected for the reduction of an adsorbed specie.[10]

The effect of accumulation time is shown in Fig. 3(B) (20 ppb Ni). As can be seen, the current increases linearly until a maximum is obtained at 50 sec of accumulation with a subsequent drop in the peak's current. This is in contrast to the saturation behaviour more commonly observed.[11] Hence to maximize sensitivity, a 50-sec accumulation time was generally used for subsequent quantitative determinations.

The complex was observed to exhibit a high degree of stability. Repeated measurements of a sample over a period of 120 min showed no changes in the stripping peak current [Fig. 2(B)].

A comparison between a linear and differential pulse scan show an eight-fold increase in current for the linear scan mode under the conditions of this study (Fig. 5) and, as the linear scan mode is also faster, it was used for subsequent determinations. It is important to note that the factor of differing scan rates for the two modes plays an important role in this effect, as in order to maintain a similar peak resolution for the differential mode a reduced scan rate was used, which in turn yields a lower observed current.

Quantitative utility

Figure 6 shows the voltammograms obtained by varying the Ni concentration from 0 to 25

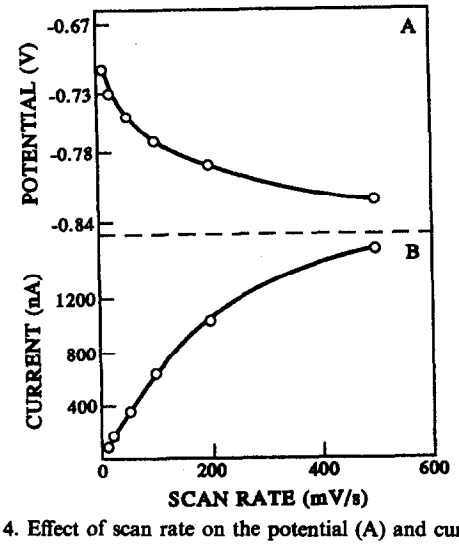

Fig. 4. Effect of scan rate on the potential (A) and current (B) of the Ni–HNB stripping peak. Experimental conditions as for Fig. 2(B).

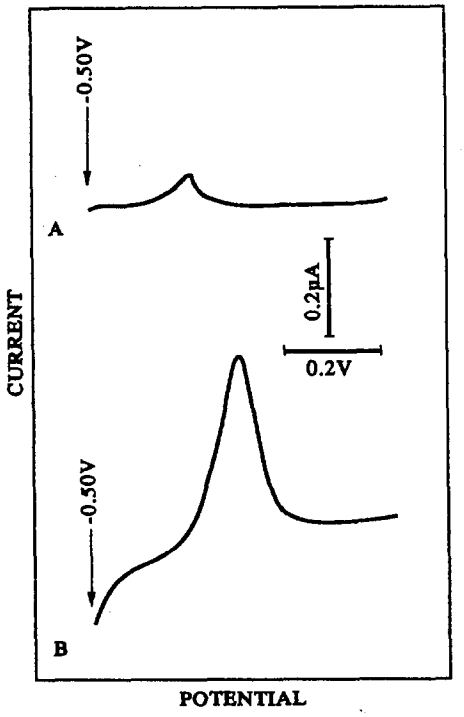

Fig. 5. Comparison between differential pulse (A) and linear scan (B) modes. For differential pulse scan pulse amplitude = 50 mV and scan rate = 10 mV/sec. For linear scan experimental conditions as for Fig. 2(B). Both modes were with a solution of 5 ppb Ni and an accumulation time of 60 sec.

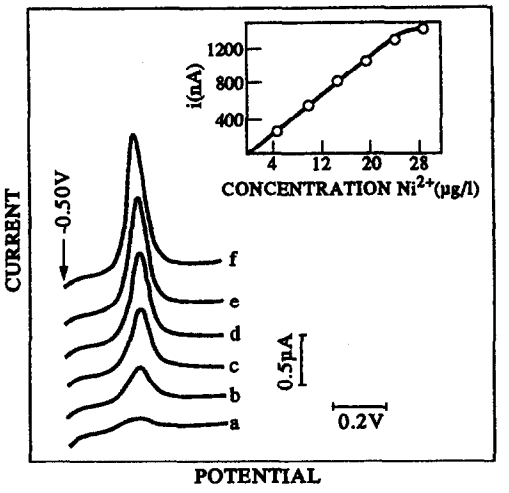

Fig. 6. Voltammograms and resulting calibration curve (inset) obtained by the variation of Ni concentration from 0 (a) to 29.56 ppb (b–f). Experimental conditions as for Fig. 2(B).

ppb (electrolyte acetic acid/acetate, pH = 6.0, accumulation time 50 sec, accumulation potential −0.5 V, final potential −1.10 V, scan rate 200 mV/sec, large drop size, equilibrium time 30 sec). The resulting calibration curve, shown as the inset, is seen to be linear up to 25 ppb (correlation coefficient = 0.999 up to 25 ppb Ni). The detection limit was estimated to be 0.10 ppb (1.7nM) after an accumulation time of 2 mins of $4.3 \times 10^{-8}M$ Ni (S/N = 2). The detection limit was also calculated with an accumulation time of 50 sec (the accumulation time more commonly used in this study) to be 0.14 ppb (2.4nM) using $8.5 \times 10^{-8}M$ Ni.

The major sources of interferences are likely to be coexisting ions and organic surfactants. These species could result in either new reduction peaks or the overlap with the Ni–HNB peak thus obscuring the measurement. The effect of various ions that could yield interferences was studied. The determination of 5 ppb Ni was not affected by the addition of up to 5000 ppb of Ca^{2+}, Ba^{2+}, Mg^{2+}, Sr^{2+}, Cu^{2+}, Zn^{2+}, Mn^{2+}, Th^{4+}, Bi^{9+}, Mo^{6+}, oxalate, carbonate, sulphate, $B_4O_7^{2-}$. tartrate, thiocyanate, chlorate or 4,5-dihydroxy-1,3-benzenedisulphonic acid (tiron). The determination of 5 ppb Ni was not affected by the addition of up to 500 ppb of Ti^{4+}, Al^{3+}, UO_2^{2+}, Br^-, CDTA or cyanide. The interference of Ti^{4+}, is due to a stripping peak near that for the Ni–HNB complex ($E_{Ni} = -0.78$ V, $E_{Ti} = -0.62$ V) which was not masked by fluoride, tiron or oxalate.[12] Figure 7(A) shows the effect of 1 ppm Ti on the stripping voltammogram of 5 ppb Ni–HNB.

The interference by aluminum (due to overlapping peaks) was successfully masked by fluoride or citrate (20 ppm, which were separately observed to not interfere at these concentrations). The determination of 5 ppb Ni was not affected by the addition of up to 50 ppb of Pb^{2+}, Fe^{3+}, V^{5+}, EDTA, triton x-100. The interference by lead is due to the presence of a stripping peak near that for the Ni–HNB complex ($E_{Ni} = -0.78$ V, $E_{Pb} = -0.59$ V). Figure 7(B) shows the effect of 1 ppm Pb on the stripping voltammogram of 5 ppb of the Ni–HNB complex. The determination of 5 ppb Ni was not affected by the presence of up to 5 ppb of Cd^{2+}, at a concentration of 50 ppb Cd^{2+} an increase of 20% of the Ni–HNB peak is observed. The presence of Co(II) was found to interfere at 5 ppb as it displays a strong stripping peak at nearly the same potential as the Ni–HNB complex. An interference by Co(II) was also observed for the determination by adsorptive stripping of the Ni complex of 2,2′-bipyridine (bpy).[2] In that system the presence of Co caused the Ni–bpy complex peak to diminish, whereas in this case (for 1:1 Co/Ni) an augmentation of the stripping peak by 10% was observed.

The method was applied to a sample of commercial mineral water. As it was found that the mineral water contained undetectable quantities of Ni, the sample was "doped" with aliquots of Ni(II) of known concentration. The current of the doped sample was then measured and compared to a previously prepared calibration curve to determine the ability to quantitatively determine the Ni concentration in the sample. For a sample with an added nickel concentration of 0.75 ppb, the analyzed concentration was 0.77 ± 0.19 ppb for three determinations of the sample. For a second sample with

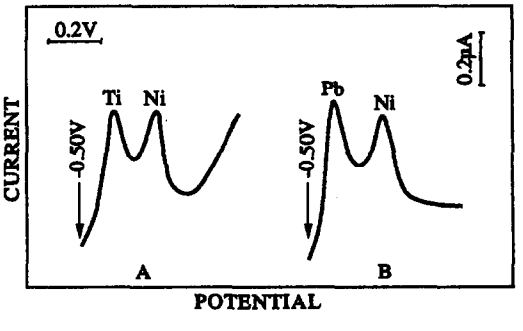

Fig. 7. Effect of the presence of Ti (A) and Pb (B) on the stripping voltammogram of the Ni–HNB complex. Experimental conditions: 5 ppb Ni; 1 ppm Ti (A); 1 ppm Pb (B) and other conditions as in Fig. 2(B).

an added nickel concentration of 10.5 ppb the analyzed concentration was 10.5 ± 0.1 ppb for seven determinations.

CONCLUSIONS

The cathodic stripping of the Ni–HNB complex is seen to be an effective method for the determination of Ni at ppb levels. The possible interference by a very large number of substances was studied and generally the technique was found to be unaffected by a wide variety of materials. In the case of interference by Co, it is worth noting that in natural waters the concentration of Ni is generally much higher than that of Co.[2] For samples with relatively high Co:Ni ratios, the methods of Braun *et al.*[1] or Donat *et al.*[3] are useful as the stripping potentials of the peaks of the Co and Ni complexes are well resolved. However, the technique presented here offers an advantage in those cases where lower pH and shorter accumulation times may be desirable. In addition, the ability to perform successive determinations of other metals which form complexes with HNB (*e.g.*, Pb and Ti), that have stripping peaks well resolved from the Ni–HNB complex, add to the versatility of the technique.

Acknowledgements—The authors gratefully acknowledge the support of the CNPq, SCT-PR of the Government of Brazil and PUC-Rio for support of this research.

REFERENCES

1. H. Braun and M. Metzger, *Z. Anal. Chem.*, 1984, **318**, 321.
2. H. Sawamoto, *J. Electroanal. Chem.*, 1983, **147**, 279.
3. J. R. Donat and K. W. Bruland, *Anal. Chem.*, 1988, **60**, 240.
4. P. A. M. Farias, A. K. Ohara and S. L. C. Ferreira, *Anal. Lett.*, 1992, **25**, 1929.
5. P. A. M. Farias and I. Takase, *Electroanalysis*, 1992, **4**, 823.
6. P. A. M. Farias and A. K. Ohara, *ibid.*, 1991, **3**, 985.
7. P. A. M. Farias and A. K. Ohara, *J. Anal. Chem*, 1992, **342**, 87.
8. P. A. M. Farias, A. K. Ohara and J. S. Gold, *J. Electroanal. Chem.*, submitted for publication.
9. P. A. M. Farias, A. K. Ohara, I. Takase, S. L. C. Ferreira and J. S. Gold, *Anal. Chim. Acta*, 1993, **271**, 209.
10. A. J. Bard and L. R. Faulkner, *Electrochemical Methods—Fundamentals and Applications*, pp. 523. Wiley, New York, 1980.
11. P. A. M. Farias, A. K. Ohara and J. S. Gold, *Electroanalysis*, submitted for publication.
12. D. D. Perrin, in *Chemical Analysis*, Vol. 33, Wiley Interscience, New York, 1970.

Talanta, Vol. 40, No. 8, pp. 1173–1181, 1993
Printed in Great Britain.

0039-9140/93 $6.00 + 0.00

SPECTROPHOTOMETRIC FLOW INJECTION DETERMINATION OF FORMETANATE AND *m*-AMINOPHENOL IN WATER AFTER REACTION WITH *p*-AMINOPHENOL

KARIM D. KHALAF, JOSE SANCENON and MIGUEL DE LA GUARDIA*
Department of Analytical Chemistry, University of València, Dr Moliner 50, 46100 Burjassot, València, Spain

(*Received* 19 *November* 1992. *Revised* 26 *January* 1993. *Accepted* 26 *January* 1993)

Summary—An automated procedure has been developed for the determination of formetanate and its metabolite *m*-aminophenol (MAP) in water samples.

MAP can be selectively determined in the presence of formetanate by direct on-line reaction with *p*-aminophenol and spectrophotometric measurement of the absorbance at 576 nm in the presence of KIO_4, as oxidizing agent. The method has a limit of detection of $5 \times 10^{-7}M$, it provides a recovery percentage from 95 to 104% and permits one to carry out 120 measurements/hr.

The spectrophotometric determination of formetanate must be carried out after a previous hydrolysis to MAP. To determine formetanate in the presence of MAP, two steps are necessary. Firstly, the MAP content is selectively determined as has been mentioned above. After that, the sample is treated with $0.05M$ NaOH at 90°C, to hydrolyze the formetanate to MAP, and then the sum of both is determined spectrophotometrically. The difference between the results obtained in each step gives the formetanate concentration.

The developed procedure for the determination of formetanate provides a sensitivity of 1070 absorbance units mol^{-1} l and a limit of detection of $1.9 \times 10^{-7}M$, which corresponds to 50 μg/l of formetanate hydrochloride.

The method has been applied to the analysis of natural water samples fortified with formetanate and MAP, and formetanate has also been quantitatively recovered in irrigation waters at a concentration level of $1.9 \times 10^{-6}M$ which corresponds to 500 μg/l.

On the other hand, working in the stopped-flow mode, for a reaction time of 100 sec, the sensitivity of the formetanate determination can be increased to 4642 absorbance units mol^{-1} l but the limit of detection remains of the order of 44 μg/l.

Formetanate, [*m*-[[(dimethyl amino) methylene] amino] phenyl] methyl carbamate, is a pesticide which has two active functional groups, dimethyl formamidine and methyl carbamoyl, with potential biological activity.[1-3] Therefore, formetanate is used as an effective acaricide product against the motile stages of fruit tree red spider mites, and glasshouse red spider mite. It is also used as an insecticide and it is effective against several plant bugs, beet fly and thirps. Formetanate has a low stability and because of this, it is formulated as the hydrochloride that is more stable, and highly soluble in water (more than 50%); other formulations, such as "dicarzol 200" and "carzol SP", are prepared from hydrochloride, or as a combined formulation with chlordimeform.[4] The lethal dose LD_{50} of formetanate in mice is 4.5 mg/20 kg.[5]

Few data have been reported about the analysis of formetanate and its residues. However, high performance liquid chromatography (HPLC) has been used in this field.[6-10] Gas chromatography was also employed to determine the pesticide residues by using α-Bromo-2,3,4,5,6-pentafluoro toluene or bromine as derivatization agents.[11-12] However these procedures have a low sensitivity and also, previous preconcentration steps must be employed.

An alkalimetric titration method has been proposed for the indirect determination of formetanate from the presence of hydrochloride, after the identification of the pesticide by thin layer chromatography (TLC)[12] but, this procedure has a poor selectivity.

A spectrophotometric method has been developed to determine formetanate residues. The active principle is separated by TLC, hydrolysed to *m*-aminophenol and this latter coupled with

*Corresponding author.

N-(1-naphthyl)ethylene diamine to form a blue azo dye which absorbs at a wavelength of 555 nm.[12]

m-aminophenol (MAP) is the final major metabolite of formetanate. This compound is soluble in 40 parts cold water and freely soluble in hot water. MAP has a biological effect on the growth of bacteria. However, this product must be handled carefully because it could cause damage to kidneys, eyes and skin, and so, the recommended maximum permissible concentration of MAP in the air is 1 mg/m^3.[13–20]

Many studies and analytical methods have been reported on determining of MAP by HPLC,[21–28] TLC,[29–32] gas chromatography,[33,34] spectrofluorometry[35–38] and spectrophotometry,[39–46] and these methods could also be applied to the determination of formetanate, after a previous hydrolysis to yield MAP. However, we have not found any reference in the literature to the selective determination of formetanate and MAP in the same sample.

Flow injection analysis (FI)[47,48] provides a useful way to automate the analytical determinations and can be very interesting to carry out the control of pesticide residues in environmental water samples, but no data have been reported as yet, on using FI for the determination of formetanate or MAP. However, in a previous work[49] we have found that propoxur, another carbamate pesticide, can be determined by flow injection spectrophotometry at 600 nm after its alkaline hydrolysis and reaction with *p*-aminophenol (PAP), and this reaction could be applied to the direct determination of MAP and to the determination of formetanate after its hydrolysis. So the aim of the present work is to develop an automated spectrophotometric method to determine formetanate and its metabolite MAP.

We have carried out a series of studies on the reaction between MAP and PAP in order to obtain a selective procedure, which can be directly applied in water analysis, and also we have studied the reactivity of formetanate against the PAP, both directly and after alkaline hydrolysis.

EXPERIMENTAL

Apparatus

A Hewlett Packard 8452A diode array spectrophotometer, equipped with HP-89530A MS DOS UV/V software with a response time of 0.1 sec, was used to carry out spectrophotometric determinations. A flow cell of 50 μl internal volume and 1 cm pathlength was used for measurements.

A four channel flow injection manifold [Fig. 1(A)] was employed to carry out the FI–spectrophotometric determination of MAP. A Gilson 2 minipulse peristaltic pump was used to transport the carrier solutions and a Reodhyne 50 valve, with a loop of 100 μl was employed for the injection of samples.

A and B channels were connected by a Y-shaped merging zone, in order to provide a good mixing between PAP and metaperiodate. A similar connection was made between channels C and D and a further connection was made to join the A/B channel and the C/D channel before the measurement zone.

Flexible peristaltic pump tubing of 1.52 mm internal diameter, which provides a carrier flow rate from 2 to 4 ml/min, in each channel, was used.

A 45 cm long coil (LR_1) permits one to obtain the quinoneimine of PAP from the oxidation of PAP by potassium metaperiodate (see the reaction scheme below). The LR_2, 45 cm long coil, provides an adequate alkaline medium for the reaction of samples with PAP. The LR_3 reaction coil, with a length of 800 cm, permits one to obtain a good reaction yield between MAP and the reactive quinoneimine in order to produce the blue dye, which is measured at 576 nm.

All the tubing employed to construct the reaction coils were made of Teflon with an internal diameter of 0.8 mm.

Alternatively to the above described manifold, a three channel assembly [see Fig. 1(B)] was employed in order to avoid an excessive dilution of samples.

On the other hand, some additional experiments were carried out in the stopped-flow mode, using a continuous aspiration of the samples by channel C, as can be seen in Fig. 1(C).

Reagents

All reagents were of analytical grade. Formetanate hydrochloride was supplied by Riedel-de Häen (Germany), *p*-aminophenol (PAP) was supplied by Fluka (Switzerland), *m*-aminophenol (MAP) was supplied by Aldrich (Germany), sodium hydroxide and potassium metaperiodate were supplied by Probus (Spain).

The stock standard solutions were prepared in demineralized distilled water as follows. To

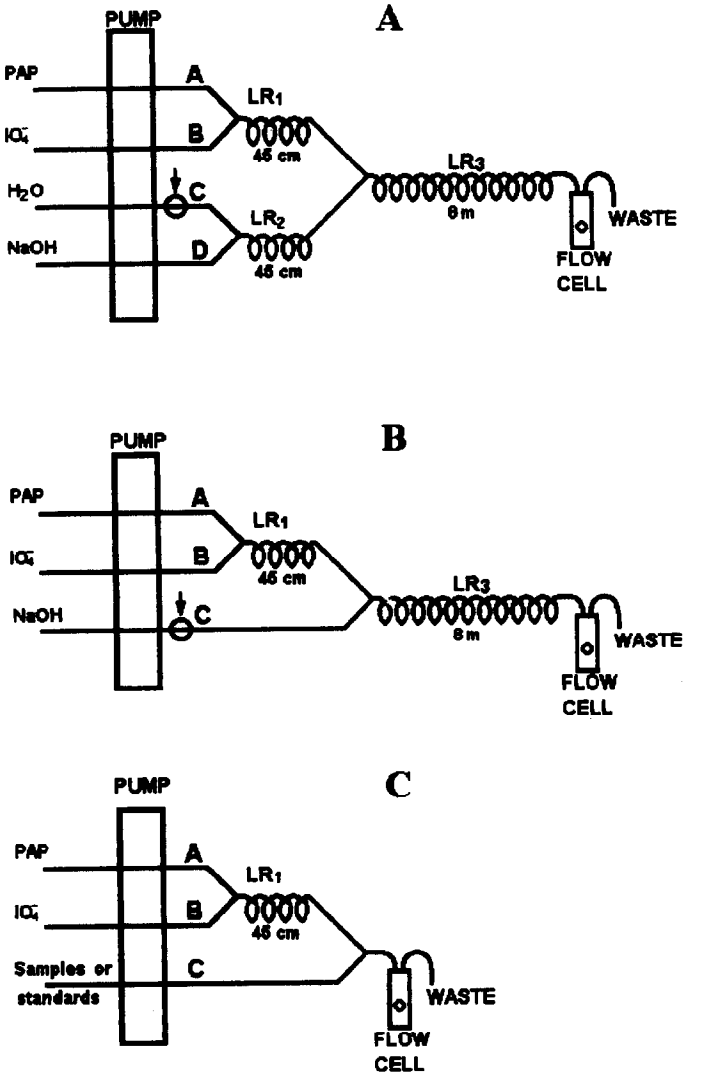

Fig. 1. Manifolds employed for the determination of *m*-aminophenol and formetanate. The length of the reaction coils has been established from experimental studies.

obtain a $3.88 \times 10^{-4}M$ formetanate solution, 10.0 mg of formetanate hydrochloride was dissolved in 100 ml of distilled water; then 50 ml of this solution was diluted to 100 ml with distilled water in order to obtain a $1.94 \times 10^{-4}M$ concentration. In all experiments the standard solution of formetanate was prepared and used the same day, in order to avoid any hydrolysis occurring. A $1.05 \times 10^{-3}M$ PAP solution was prepared by dissolving 0.0287 g in 250 ml of boiled and cooled distilled water (in order to avoid its oxidation by the dissolved oxygen); this solution is stable for more than 8 hr. Standard solution $9.16 \times 10^{-4}M$ MAP was prepared by dissolving 25.0 mg in 250 ml of distilled water. This latter solution is more stable than the PAP solution and does not need special conditions to be prepared.

RESULTS AND DISCUSSION

As previously reported,[50] PAP in alkaline medium and in the presence of a suitable oxidizing agent produces a reactive benzoquinoneimine (I), which can be coupled with MAP through the electrophilic attack on the C_4 of MAP, to give the corresponding diamine (II). (II) undergoes a rapid oxidation to a blue compound (III), as is shown in the following schematic diagram (see over).

Figure 2(A), shows the UV absorption spectra of MAP in distilled water, and in an alkaline medium. As can be seen, the formation of *m*-aminophenolate provides a bathochromic shift of the absorption maximum to 292 nm and it has a hyperchromic effect.

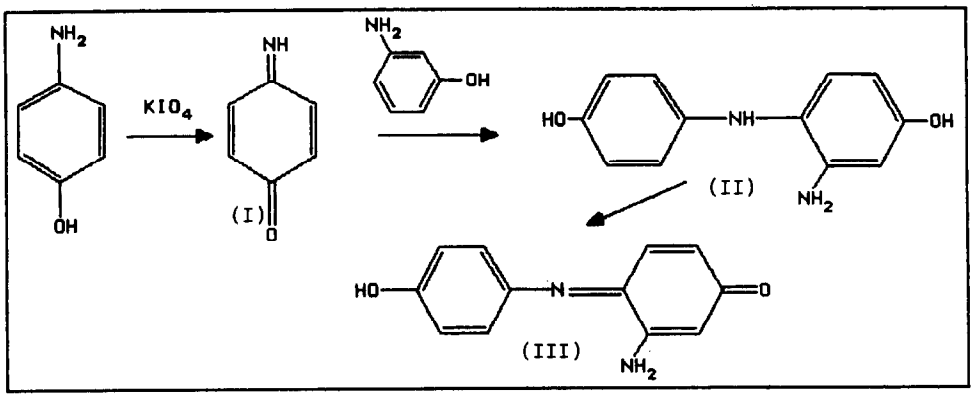

Scheme 1

It can be seen from Fig. 2(B) that the reaction between MAP and PAP provides a very high enhancement of the sensitivity and selectivity of the UV/V determinations of MAP. The reaction product has a maximum of the absorption spectrum at 576 nm.

We have applied the reaction with PAP, from an analytical point of view, to determine MAP in water; therefore, the effects of NaOH, potassium metaperiodate (employed as oxidizing agent), PAP concentrations as well as the reaction time, were studied and monitored by using a diode array spectrophotometer.

Several experiments carried out in batch (results not shown) indicate that $0.02M$ NaOH, $0.004M$ KIO_4 and $2.6 \times 10^{-4}M$ PAP, are the best conditions under which to carry out the reaction between MAP and PAP at room temperature, and so these concentrations were employed in the FI mode.

The variation of the absorbance at 576 nm as a function of time, for a mixture of MAP and PAP, at room temperature and using the oxygen of the air as an oxidizing agent shows that the colour of the reaction product develops gradually during the first 10 min and remains stable for more than 10 min. When potassium metaperiodate ($0.004M$) is used as the oxidizing agent, the reaction rate between MAP and PAP increases rapidly and a reaction time of the order of 120 sec is sufficient to obtain stable absorbance measurements. On the other hand, a typical calibration equation $A = 0.035 + 17{,}100\ C\ (M)$ with a regression coefficient $R = 0.998$ was obtained for MAP concentrations.

An increase in the concentrations of NaOH, KIO_4 and PAP as well as the use of a temperature higher than 90°C, provide an increase in the reaction rate between MAP and PAP. However, the stability of the reaction product is reduced in these conditions and the excess of PAP is decomposed by KIO_4 and NaOH providing an increase in the background. So,

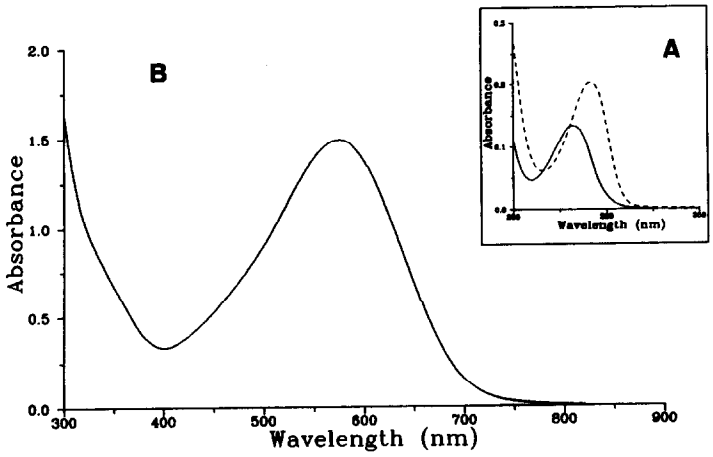

Fig. 2. (A) UV spectra of $7.3 \times 10^{-5}M$ of *m*-aminophenol in distilled water (——) and in $0.2M$ NaOH (– – –). (B) UV/V spectrum of $7.3 \times 10^{-5}M$ of MAP after reaction with $2.6 \times 10^{-4}M$ of PAP in the presence of $0.004M$ of KIO_4. The measurements were taken 2 min after mixing.

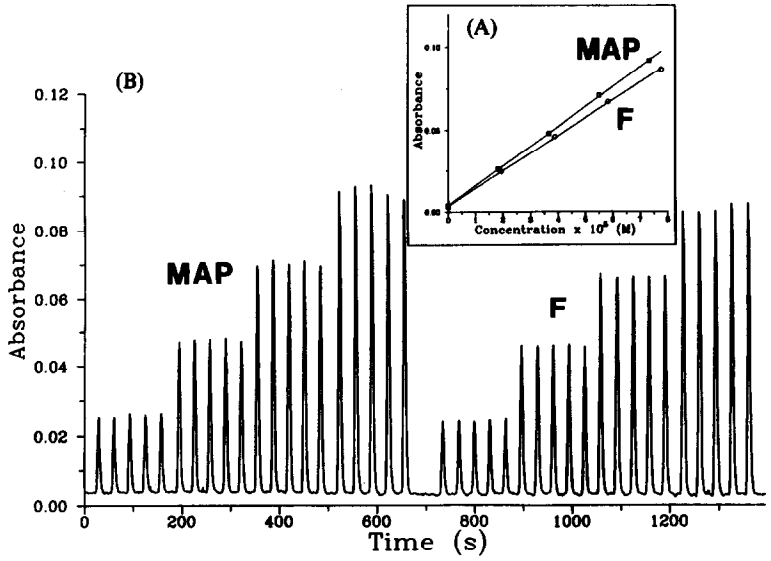

Fig. 3. (A) Calibration graph obtained for the determination of MAP and formetanate (F). (B) FI recording for these calibration graphs.

the use of concentrations higher than those recommended or the use of high temperatures must be avoided.

FI SPECTROPHOTOMETRIC DETERMINATION OF MAP

In order to develop a FI spectrophotometric procedure for the analysis of MAP with PAP, the concentrations of NaOH, KIO_4 and PAP, previously established in batch, were employed. For the above mentioned concentrations of reagents the effect of flow rates of the carrier streams (from 2 to 4 ml/min in each one) and lengths of the reaction coils (LR_1, from 10 cm to 1 m, LR_3 from 1 to 10 m), were studied in a univariate mode. LR_2 was fixed of 45 cm. The obtained results indicate that $LR_1 = 45$ cm, $LR_3 = 8$ m and a flow rate of 2.3 ml/min per channel were the best conditions under which to carry out the reaction between MAP and PAP, providing high absorbance values with low background levels.

A series of standard solutions of MAP were injected in the manifold and the absorbance at 576 nm was monitored as a function of time.

Figure 3 shows the FI-recording profiles and a calibration graph of MAP (from 0 to $7.33 \times 10^{-5}M$) in distilled water, which provides a linear-relationship over the investigated range with the following regression features:

$$A = 0.003 + 1440\ C\ (C \text{ in } M)$$

The regression coefficient, R, for this line was 0.9999. As compared with the regression line found in batch after 120 sec, it can be seen that the FI procedure involves a strong reduction in the analytical sensitivity; however, the FI measurements are carried out in a short period of time and this avoids the PAP decomposition and so, a better intercept value was obtained. The limit of detection in these conditions was $5 \times 10^{-7}M$ of MAP, which is appropriate for the analysis of water samples. The standard deviation of five replicate measurements of a concentration $3.66 \times 10^{-5}M$ of MAP was 1.8%. Using the three channel manifold the sensitivity increases up to 1920 absorbance units mol^{-1} l and the limit of detection reduced to $4 \times 10^{-7}M$. The developed procedure permits one to carry out more than 120 injections/hr, which is an additional advantage of the FI methodology.

DIRECT DETERMINATION OF *m*-AMINOPHENOL IN WATER

To show the applicability of the developed method for the analysis of MAP, three types of natural water, from different sources (tap, irrigation and well water), have been fortified with different concentrations of MAP. The spiked samples were analysed by using the recommended FI procedure. The obtained results, summarized in Table 1, show that the reaction between PAP and MAP is not affected by the sample matrices, and relative errors lower than 8% were found in all cases for MAP concentrations of the order of $10^{-5}M$. On the other hand the relative standard deviation

Table 1. FI spectrophotometric analysis of MAP in spiked water samples

Water	*m*-aminophenol added, *M*	*m*-aminophenol found, *M*	E_r, %
Tap	3.67×10^{-5}	$(3.41 \pm 0.01) \times 10^{-5}$	−7.08
	7.33×10^{-5}	$(7.00 \pm 0.01) \times 10^{-5}$	−4.5
	1.10×10^{-4}	$(1.07 \pm 0.02) \times 10^{-4}$	−2.7
Well	3.67×10^{-5}	$(3.77 \pm 0.03) \times 10^{-5}$	+2.7
	7.33×10^{-5}	$(7.28 \pm 0.01) \times 10^{-5}$	−0.7
	1.10×10^{-4}	$(1.10 \pm 0.05) \times 10^{-4}$	0
Irrigation	3.67×10^{-5}	$(3.64 \pm 0.04) \times 10^{-5}$	−0.8
	7.33×10^{-5}	$(7.7 \pm 0.2) \times 10^{-5}$	+5
	1.10×10^{-4}	$(1.13 \pm 0.03) \times 10^{-4}$	+2.7

Results found are the average of three independent analyses of each sample ± the standard deviation.
E_r (%): relative error in percentage.

obtained for three independent analyses of the same sample was lower than 1%.

HYDROLYSIS OF FORMETANATE

Formetanate does not react with PAP; it must be previously hydrolysed to MAP in order to carry out its spectrophotometric determination by the above mentioned reaction. The alkaline hydrolysis of formetanate, and similar compounds, to phenols has been reported.[12,51–54] All the previous works indicate that the hydrolysis of formetanate is very slow even at 60°C. The effects of sodium hydroxide (from 0.02 to 0.3*M*) and time on the hydrolysis of formetanate were studied at 90°C, for a concentration $7.77 \times 10^{-5}M$ of formetanate, and the absorbance measurements were carried out in batch. The obtained results show that a NaOH concentration of 0.02*M* provides the quantitative hydrolysis of formetanate in 130 min, and 0.1*M* NaOH permits the total hydrolysis in 40 min. A 0.05*M* NaOH concentration provides a 95% hydrolysis yield in 1 hr and this was selected for the formetanate hydrolysis in order to avoid the use of high concentrations of sodium hydroxide, which affects the reaction between PAP and MAP.

On the other hand, it has been noticed that, a heating time for formetanate higher than 1 hr causes a slight degradation of the resulted MAP and so, another absorption maximum could have appeared at 325 nm. The same thing takes place with standard MAP in distilled water heated for long periods of time. However, in the recommended conditions these problems are avoided.

The slow hydrolysis process of formetanate avoids the possibility of carrying out this process on-line and so, for the FI spectrophotometric determinaton of formetanate, the following procedure must be followed. Take the sample, add NaOH to obtain a 0.05*M* NaOH concentration, and allow to stand in a thermostatic water bath at 90°C for 1 hr, then cool at room temperature and after that, take 100 μl of the hydrolyzed sample and inject it in the FI-manifold indicated in Fig. 1. Standard aqueous solutions of formetanate are treated with a NaOH solution in the same conditions as samples.

FI SPECTROPHOTOMETRIC ANALYSIS OF FORMETANATE

The alkaline hydrolysis of formetanate and the injection of the obtained MAP in the FI-manifold provides good analytical signals at 576 nm, which corresponds to the blue form of the reaction product between PAP and MAP.

Figure 3 shows the calibration graph obtained from the injection of standard solutions of formetanate (from 0 to $7.77 \times 10^{-5}M$), previously heated at 90°C for 1 hr and cooled at room temperature. The regression characteristic features of this analytical curve are:

$$A = 0.003 + 1070\ C\ (C \text{ in } M)$$

with a regression coefficient of 0.9998 which provides a detection limit of $1.9 \times 10^{-7}M$ formetanate (which corresponds to 0.05 mg/l). The relative standard deviation of five replicate measurements of a solution with a concentration of $3.9 \times 10^{-5}M$ formetanate was 0.5%.

On comparing this curve with that obtained for MAP in the same work session (see Fig. 3), it can be concluded that the 10% reduction of the analytical sensitivity found for formetanate analysis is due to the non-quantitative hydrolysis of the pesticide in the recommended conditions; so, it is necessary to calibrate the system

with formetanate standard solution treated in the same way as samples.

On the other hand, low levels of formetanate have been determined by the above mentioned procedure in irrigation waters, treated with this pesticide. Results found agree with those previously obtained and, for example, a concentration of $1.7 \pm 0.2 \times 10^{-6}M$ (0.44 ± 0.05 mg/l) of formetanate was found in a sample containing $1.9 \times 10^{-6}M$ (which corresponds to 0.5 mg/l) and $5.3 \pm 0.2 \times 10^{-6}M$ (1.37 ± 0.05 mg/l) was found in another irrigation water containing $5.8 \times 10^{-6}M$ which corresponds to 1.5 mg/l. Note that for these low levels of formetanate concentrations the relative standard deviation of three analyses was 11% and 3.6%, respectively, one order of magnitude higher than those found for the determination of a concentration $10^{-5}M$.

STOPPED-FLOW DETERMINATION OF FORMETANATE

In order to increase the sensitivity of the spectrophotometric determination of both MAP and formetanate, some experiences were carried out in the stopped-flow mode. For this purpose the manifold indicated in Fig. 1(C) was employed.

The use of a three channel manifold reduces the sample dispersion and the stopped-flow avoids the use of a long reaction coil.

Previous experiments, carried out with a 20 mg/l of formetanate previously hydrolyzed, showed that 100 sec is the minimum time required to obtain a maximum sensitivity for the determination of MAP and PAP in the stopped-flow mode and using the KIO_4, NaOH and PAP concentrations previously recommended.

In the above mentioned conditions, a typical calibration line for the determination of formetanate after hydrolysis to MAP corresponds to:

$$A = 0.008 + 4640\ C\ (C \text{ in } M)$$

with a regression coefficient of 0.9998. So, the sensitivity is increased four times, as compared with results found in the flow injection mode. However, the use of high reaction times also increases the degradation of PAP and so, an increase of the blank measurements was found. So, the limit of detection was only 44 μg/l which is comparable to that found in the FI mode.

The standard deviation of three independent measurements of a sample containing $5.8 \times 10^{-5}M$ formetanate was 1.5% and, in summary, it must be accepted that the use of the stopped-flow approach does not improve the limit of detection and reduces the sample throughput.

ANALYSIS OF MIXTURES OF FORMETANATE AND MAP

The fact that formetanate does not react directly with PAP offers the possibility to determine sequentially both formetanate residue and MAP, in the same sample. The procedure involves two steps: a direct determination of MAP in the presence of non-hydrolyzed formetanate, and the determination of the sum of MAP and formetanate after hydrolysis with NaOH and subsequent reaction with PAP.

To obtain an indication about the suitability of the developed procedure to determine MAP in partially hydrolyzed samples, a series of synthetic mixtures of formetanate and MAP were prepared in distilled water. The obtained results for MAP are indicated in Table 2, and it can be seen that a recovery percentage from 101 to 105% was found. The slight increase in the obtained results is due to partial hydrolysis of formetanate by the NaOH solution used in the FI-manifold.

Further evidence was also found about the applicability of the proposed method by analysing a series of synthetic mixtures of formetanate (freshly prepared) and MAP which were prepared in a matrix of irrigation water.

Table 2. FI spectrophotometric determination of MAP in mixtures of formetanate and *m*-aminophenol in distilled water

Formetanate added ($\times 10^{-5}$)	*m*-aminophenol added ($\times 10^{-5}$)	*m*-aminophenol found ($\times 10^{-5}$)	Recovery (%)
1.94	1.83	(1.86 ± 0.04)	101.3
3.89	3.67	(3.73 ± 0.08)	101.8
5.83	5.50	(5.63 ± 0.06)	102.4
7.77	1.83	(1.93 ± 0.02)	105.4

Values found correspond to the average of three independent analyses of each sample $\pm$ the standard deviation.

Table 3. FI spectrophotometric analysis of irrigation water fortified with synthetic mixtures of formetanate and *m*-aminophenol

Formetanate added ($\times 10^{-5}$)	*m*-aminophenol added ($\times 10^{-5}$)	*m*-aminophenol found ($\times 10^{-5}$)	Recovery (%)	Total MAP found	Recovery (%)
1.94	1.83	(1.80 ± 0.06)	98	$(3.85 \pm 0.04) \times 10^{-5}$	103
3.89	3.67	(3.48 ± 0.02)	96	$(8.25 \pm 0.04) \times 10^{-5}$	113
5.83	5.50	(5.22 ± 0.03)	95	$(1.28 \pm 0.07) \times 10^{-4}$	113
7.77	1.83	(1.92 ± 0.02)	104	$(1.044 \pm 0.005) \times 10^{-4}$	108

Total MAP found corresponds to the sum of MAP and formetanate measured after the hydrolysis of the latter.

MAP was directly analysed and after that, samples were hydrolyzed and then analysed using a standard calibration graph of formetanate treated in the same way as the samples. Table 3, indicates that recovery percentages from 95 to 104% were obtained in the analysis of MAP in the presence of formetanate. The recovery percentage of the sum of MAP and formetanate varies from 103 to 113% and so, it can be concluded that the developed methodology permits one to quantitatively recover MAP and the sum of MAP and formetanate in the same sample.

SELECTIVITY OF THE DEVELOPED PROCEDURE

The benzoquinoneimine form of PAP reacts with phenols by an electrophilic attack to produce the corresponding dihydroxyamine. Thus, the determination of MAP by the developed procedure can be affected by any phenolic compound with a free para position; and, on the other hand, after the previous hydrolysis step, any compound which could be hydrolyzed by NaOH to form a para position free phenol, could interfere with the determination of formetanate.

However, the selectivity of the FI spectrophotometric determination of MAP and formetanate with PAP can be due to the differences observed between the maximum wavelength at which the PAP derivatives of different compounds absorb and on the different reaction rates and conditions found for each compound, as for example, the spectrophotometric determination of propoxur by reaction with PAP requires the use of $0.33M$ NaOH, $9 \times 10^{-3}M$ PAP and $0.02M$ KIO_4 as compared with formetanate which requires lower concentrations of each one of these reagents. On the other hand the reaction product of PAP with the hydrolysis product of propoxur absorbs at 600 nm instead of the 576 nm wavelength employed for MAP.

From these comments it can be concluded that the developed procedure is especially interesting for the evaluation of pesticide residues in water samples when crops were treated with formetanate and that, in the analysis of ground water a careful standardization must be carried out.

CONCLUSIONS

The studies carried out show that the reaction of MAP with PAP, in the presence of KIO_4, provides a sensitive and selective way for the determination of MAP in water samples. MAP can be directly analysed in the presence of formetanate and the sum of both MAP and formetanate can be established after the alkaline hydrolysis of formetanate.

The developed method permits one to follow up the degradation of formetanate in environmental waters. Also, it can be successfully used to determine concentrations of the order of $1.8 \times 10^{-6}M$ of *m*-aminophenol or formetanate in real water samples, which correspond to 0.2 and 0.5 mg/l, respectively, with a high sample throughput. The method is very economical and does not need any clean up step, which is an important advantage compared with the previously developed methods for formetanate or MAP determination.

Also, this is the only proposed methodology for the determination of MAP and formetanate in the same sample. The only draw-back of the method is the relatively high limit of detection found, but, the sensitivity of the procedure could be improved by using a preconcentration step based on sorbent or solvent extraction procedures, in order to obtain a better limit of detection.

Acknowledgements—Karim D. Khalaf acknowledges the Spanish Institute of International Cooperation with Arabic World for the financial support towards carrying out his PhD thesis in Spain.

REFERENCES

1. D. Duer, H. Aebi and L. Ebner, *U.S. Pat.* 3284289, 1966.
2. C. J. Counselman, *U.S. Pat.* 3496270, 1967.
3. C. O. Knowles and W. J. Rulston, *J. Econ. Entomol.*, 1973, **66**(6), 1245.
4. H. Martin and C. R. Worthing, *Pesticide Manual*, 5 ed., 1977, British Crop Protection Council.
5. The Merck Index, 10 ed., 1988, Merck & Co. Inc.
6. C. F. Aten and J. B. Bourke, *J. Agric. Food Chem.*, 1977, **25**(6), 1428.
7. T. K. Richard, *J. Chromatogr.*, 1979, **185**, 615.
8. G. Blaicher, W. Pfannhauser and H. Woidich, *Chromatographia*, 1980, **13**(7), 438.
9. J. F. Lawrence, L. G. Panopio, D. A. Lewis and H. A. McLeod, *J. Agric. Food Chem.*, 1981, **29**(4), 722.
10. C. J. Miles and H. A. Moye, *Anal. Chem.*, 1988, **60**(3), 220.
11. M. D. Jackson and S. D. Soileau, *Bull. Environ. Contam. Toxicol.*, 1981, **26**(1), 97.
12. N. A. Jenny and K. Kossmann, *Anal. Method. Pestic. Plant Growth Reg.*, 1978, **12**, 279.
13. S. Kurata Ya, *Nagoya-Shiritsu Daigakkai Zasshi*, 1989, **40**(2), 429.
14. M. Nendza and J. K. Seydel, *Ecotoxicol. Environ. Saf.*, 1990, **19**(2), 288.
15. E. A. Babayan, R. A. Nazaretyan and E. I. Gasparyan, *Zh. Eksp. Klin. Med.*, 1987, **27**(5), 448.
16. K. L. Markaryan and E. A. Babayan, *Gig. TR. Prof. Zabol.*, 1988, **1**, 49.
17. A. M. Richard, J. K. Hongslo, P. F. Boone and J. A. Home, *Chem. Res. Toxicol.*, 1991, **4**(2), 151.
18. A. Rakhamanin Yu, E. V. Shtannikov, I. E. LLin, Y. Eliseev Yu and Y. Lutsevich Ya, *Gig. Sanit.*, 1985, **3**, 4.
19. I. S. LLin, *Gig. Sanit.*, 1986, **6**, 8.
20. Y. Masamoto and Y. Takase, *Shinshu Igaku Zasshi*, 1987, **35**(2), 185.
21. S. H. Lee, T. S. Oh and K. H. Park, *Taehan Hwahakhoe Chi.*, 1990, **34**(1), 44.
22. S. N. Lanin, A. N. Ligaev and Y. Nikitin, *Zh. Anal. Khim.*, 1986, **41**(8), 1411.
23. L. Esclade, D. Guillochon and D. J. Thomas, *J. Chromatogr.*, 1985, **341**(2), 373.
24. M. R. Detaevernier, G. Hoogewijis and D. L. Massart, *J. Pharm. Biomed. Anal.*, 1983, **1**(3), 331.
25. M. T. Bernabei, V. Ferioli, G. Gamberini and R. Cameroni, *Atti. Soc. Nat. Mat. Modena.*, 1980, **111**(1), 35.
26. M. Goto, Y. Koyanagi and D. Ishii, *J. Chromatogr.*, 1981, **208**(2), 261.
27. J. L. Melvin, L. C. Bailey and T. Medwick, *J. Chromatogr.*, 1981, **19**(3), 146.
28. M. Maruyama and M. Kakemoto, *Nippon Kagaku Kaishi.*, 1987, **12**, 1646.
29. R. S. Dhillon, J. Singh, V. K. Gautam and B. R. Chhabra, *J. Chromatogr.*, 1988, **435**(1), 256.
30. M. Blesova, J. Cizmarik and I. Majerikova, *Chem. Pap.*, 1988, **42**(1), 45.
31. M. Petrovic, M. Kastelan-Macan and A. Durrigi, *Prehrambeno-Tehnol. Biotehnol. Rev.*, 1989, **27**(2–3), 141.
32. C. Marutiou, V. Coman, A. Patrut, L. Roman and A. Gansca, *J. Planar Chromatogr-Mod. Tlc.*, 1990, **3**, 435.
33. Y. Osaki and T. Matsueda, *Bunseki Kagaku.*, 1988, **37**(5), 253.
34. Y. Urushigawa, Z. Yonezawa, S. Masunaga, F. Yamaguchi, M. Hirai and M. Tanaka, *Kogai Shigen Kenkyusho Iho.*, 1981, **11**(3), 83.
35. K. W. Street Jr and G. H. Schenk, *J. Pharm. Sci.*, 1979, **68**(10), 1306.
36. P. G. Sennikov, V. A. Kuznetsov, A. N. Egorochkin, M. A. Lopatin and I. Korenman Ya, *Zh. Obshch. Kim.*, 1980, **50**(12), 2761.
37. V. K. Phansalkar, A. V. Khedekar, A. S. Kalgaonkar and R. S. Pande, *Indian J. Phys. B.*, 1984, **58B**(6), 487.
38. C. Gonzalez-Rojas and R. G. E. Morales, *Spectrosc. Lett.*, 1990, **23**(2), 243.
39. K. Nakashima, K. Muraki, S. Nakatsuji, S. Akiyama, T. Kaneda and S. Misumi, *Analyst*, 1989, **114**(4), 501.
40. M. Ansheng and Li Xiulu, *Yaowu Fenxi Zazhi.*, 1989, **9**(5), 294.
41. A. I. Kostromin, D. G. Z. Badret, I. F. Abdullin and T. V. Yakimova, *Zavod Lab.*, 1989, **55**(7), 8.
42. C. Vetuschi and G. Rango, *Spectrosc. Lett.*, 1989, **22**(1), 51.
43. C. Vetuschi and G. Rango, *Pharm. Acta Helv.*, 1988, **63**(11), 290.
44. I. Korenman Ya and N. G. Sotnikova, *Zh. Prikl. Khim. (Leningrad)*, 1983, **55**(10), 2278.
45. R. T. Sane and A. Y. Dhamankar, *Indian Drugs*, 1981, **19**(2), 74.
46. A. Mazzeo-Farina, M. Iorio and A. Laurenzi, *Ann. Chim. (Rome)*, 1981, **71**(3–4), 103.
47. J. Růžika and E. H. Hansen, *Flow Injection Analysis.* John Wiley, New York, 1988.
48. M. Valcarcel and Luque de Castro M.D., *Flow Injection Analysis: Principles and Application.* Ellis Horwood, Chichester, 1987.
49. K. D. Khalaf, J. Sancenón and M. de la Guardia, *Anal. Chim. Acta*, 1992, **266**, 117.
50. K. C. Brown, J. F. Corbett and R. Labinson, *J. Chem. Soc. Perkin Trans.*-2, 1978, **12**, 1292.
51. A. Čegan, J. Šlosar and M. Večeřa, *Czech. Chem. Commun.*, 1980, **45**, 1065.
52. A. Čegan, J. Šlosar and M. Večeřa, *Czech. Chem. Commun.*, 1978, **43**, 134.
53. M. L. Weiner, *J. Organic Chem.*, 1960, **25**, 2245.
54. M. J. Clark, M. W. Brooks, S. A. Woods and W. M. Coli, *J. Amer. Soc. Hort. Sci.*, 1987, **112**(2), 260.

Talanta, Vol. 40, No. 8, pp. 1183–1187, 1993
Printed in Great Britain.

0039-9140/93 $6.00 + 0.00

TRACE MEASUREMENT OF DIPYRIDAMOLE BY ADSORPTIVE STRIPPING VOLTAMMETRY

XIANGQUN ZENG, SHUCHANG LIN and NAIFEI HU*
Department of Chemistry, Beijing Normal University, Beijing 100875, P. R. China

(*Received* 19 *November* 1992. *Revised* 8 *February* 1993. *Accepted* 18 *February* 1993)

Summary—A sensitive adsorptive stripping voltammetric method for trace measurement of dipyridamole in alkaline solution is described. The method is based on the adsorptive accumulation of the drug at the hanging mercury drop electrode, followed by linear sweep voltammetric determination. The response is evaluated with respect to percentage of ethanol, preconcentration time and potential, and concentration of NaOH. The detection limit of $1.0 \times 10^{-9}M$ is obtained under optimized conditions with a 5-min preconcentration. Applicability to injection, tablets and urine analysis is illustrated.

Dipyridamole (DPRM) is known for its effective treatment of heart diseases. Its structure is shown in Fig. 1. The drug can be easily absorbed by the human body and enter into blood. Its effect in the body lasts long and the concentration in urine and blood is low. Highly sensitive methods are thus essential for the determination of dipyridamole. Various chromatographic,[1,2] and spectroscopic[3,4] procedures have been employed for this purpose. However, electrochemistry has not been widely used for measurements of dipyridamole. The drug produces a single 4-electron polarographic reduction wave in alkaline solution.[5] This polarographic method yielded detection limits in the micromolar level that were sufficient only for tablet assay.

The present work reports a sensitive voltammetric procedure for trace measurement of dipyridamole, based on its adsorptive accumulation at a hanging mercury drop electrode. Adsorptive stripping voltammetry has been used for trace measurements of numerous compounds of pharmaceutical significance.[6] As illustrated in this paper, this method yielded detection limits at the subnanomolar levels for measuring dipyridamole. The characteristics of the resulting adsorptive stripping scheme are elucidated and the electrode reaction mechanism is discussed.

EXPERIMENTAL

Apparatus

A model 370 electrochemistry system (EG&G Princeton Applied Research) was used for cyclic voltammetry. The working electrode was a model 303 static mercury drop electrode (SDME). A medium sized drop (surface area 0.0171 cm^2) was employed. The counter electrode was a platinum wire and the reference electrode was a saturated Ag/AgCl electrode.

Chemicals

Dipyridamole was from Beijing Yimin Pharmaceutical Factory. A stock standard solution of dipyridamole in ethanol ($1.00 \times 10^{-2}M$) was prepared and stored in the dark; working standard solutions ($1.00 \times 10^{-4}M$, $1.00 \times 10^{-5}M$ and $1.00 \times 10^{-6}M$) were prepared by dilution with water. All other chemicals were of analytical reagent grade. Triply distilled water was used throughout.

Procedure

A 10-ml volume of $0.05M$ sodium hydroxide containing a specific amount of sample solution and 10%(v/v) ethanol was added to the cell and purged with purified nitrogen to remove oxygen for 4 min. The preconcentration potential (−1.2 V) was applied to a new mercury drop for a selected time while the solution was stirred at 400 rpm. The stirring was then stopped, and after 15 sec the voltamperogram was recorded by applying a linear sweep scan. The scan was terminated at −1.6 V.

RESULTS AND DISCUSSION

Adsorptive properties

Figure 2 is a repetitive cyclic voltamperogram for $5 \times 10^{-7}M$ dipyridamole, recorded after

*Author for correspondence.

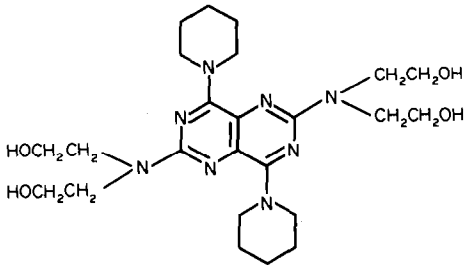

Fig. 1. Structure of dipyridamole.

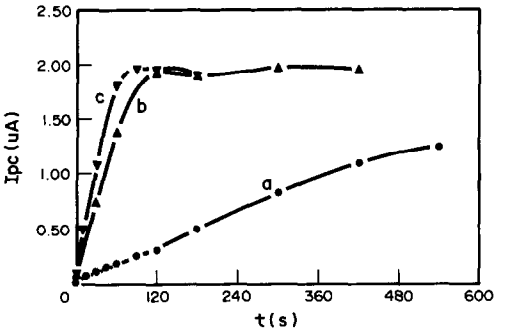

Fig. 3. Effect of preconcentration time on the cathodic voltammetric peak current for $1 \times 10^{-7}M$ (a), $6 \times 10^{-7}M$ (b) and $1 \times 10^{-6}M$ (c) dipyridamole. Other conditions as for Fig. 2.

preconcentration at -1.2 V for 30 sec. A large and well-defined cathodic peak is observed at the first scan (designated as 1) at -1.42 V. Subsequent scans exhibit a dramatic decrease of the peak to a stable value representing the response of solution species. This is an obvious indication that dipyridamole has adsorptive characteristics at a Hg electrode. No peaks are observed in the anodic branch, illustrating that the reduction of dipyridamole at the Hg electrode is irreversible.

Figure 3 shows plots of cathodic peak current (i_{pc}) of linear sweep voltammetry *vs.* preconcentration time (t) for different concentrations of dipyridamole. At first, i_{pc} increased linearly with t at all three levels, indicating that before adsorptive equilibrium is reached, the longer the preconcentration time, the more dipyridamole was adsorbed, and the larger the peak current. However, after a specific period of accumulation time, the peak current at different concentration levels invariably tended to level off, showing that the adsorptive equilibrium of dipyridamole on the Hg electrode surface was achieved.

The adsorption of dipyridamole can be used as an effective preconcentration step before the voltammetric measurement. In this way, highly sensitive adsorptive stripping measurements of the drug can be achieved.

Selection of experimental conditions

Various supporting electrolytes, such as HCl, HOAc–NaAc, NH_3–NH_4Cl, KH_2PO_4–K_2HPO_4, NaOH and Britton-Robinson buffer solution were tested by adsorptive stripping voltammetry, and NaOH was found to be the best because of the well-defined voltamperogram and reasonably high sensitivity.

The amount of ethanol added to the dipyridamole solution strongly affects the adsorptive stripping response (Fig. 4). For example, increasing the percentage of ethanol (v/v) from 0 to 10 resulted in a sharp increase in the peak,

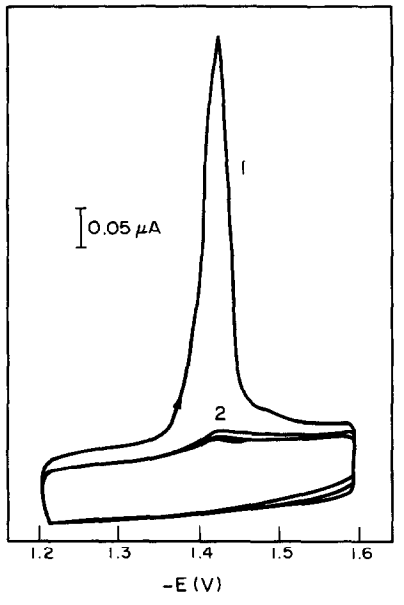

Fig. 2. Repetitive cyclic voltamperograms for $5 \times 10^{-7}M$ dipyridamole after 30 sec accumulation at -1.2 V. Scan rate, 100 mV/sec. Electrolyte, 0.05M NaOH, 10%(v/v) ethanol.

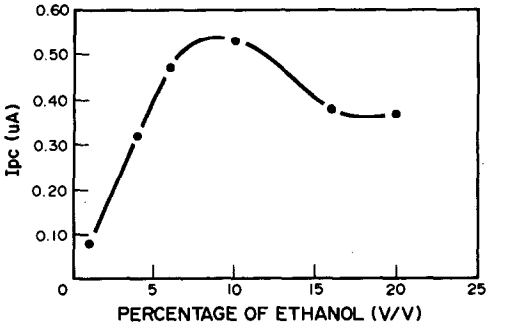

Fig. 4. Effect of the amount of ethanol added to dipyridamole system on the cathodic response. Dipyridamole concentration, $3 \times 10^{-7}M$. Preconcentration time, 60 sec. Other conditions as for Fig. 2.

but a rapid decrease in the response was observed when the percentage of ethanol was larger than 10. The dependence of i_{pc} on the preconcentration potentials was also examined. The results showed that between -0.8 and -1.2 V, i_{pc} kept almost constant at a high level, but above -0.75 V or below -1.25 V it decreased. The concentration of NaOH effects the peak current of dipyridamole, too. The experiments revealed that a concentration of NaOH larger than 0.05M (pH 12.7) offered the best responses.

The adsorptive stripping voltammetric response of dipyridamole was further characterized concerning concentration dependence, detection limit and reproducibility. Under the optimized condition of 10%(v/v) ethanol, 0.05M NaOH and preconcentration potential of -1.2 V, the peak current had a linear relationship with c_{DPRM} over the range from 5.0×10^{-9} to $1.0 \times 10^{-6}M$ when the accumulation time was 60 sec (correlation coefficient 0.9989). The detection limit could reach $1.0 \times 10^{-9}M$ when the preconcentration time was set to 5 min (S/N = 3). The precision was estimated by 12 successive measurements of $5 \times 10^{-7}M$ dipyridamole under the same conditions as above but with accumulation of 15 sec. The average peak current was 0.342 μA, range 0.325–0.370 μA, and relative standard deviation 1.7%.

System weakly adsorbed reactant

Figure 5 indicates the effect of scan rate on i_{pc} at different preconcentration times. When $t = 0$, i_{pc} had a linear relationship with $v^{1/2}$ illustrating the reduction of dipyridamole was diffusion-controlled [curve (a)]. When $t = 10$ sec, the i_{pc} *vs.* $v^{1/2}$ curve showed an upward slope, indicating that the system began to show some adsorptive characteristics [curve (b)]. When

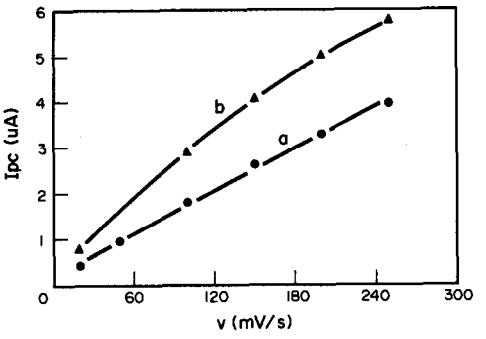

Fig. 6. Influence of scan rate on the cathodic peak current. Dipyridamole concentration, $1 \times 10^{-6}M$ (a) and $2 \times 10^{-5}M$ (b). Preconcentration time, 60 sec. Other conditions as for Fig. 2.

$t = 60$ sec, the upward turning of i_{pc}–$v^{1/2}$ curve was more pronounced [curve (c)] and i_{pc}–v curve became a straight line [Fig. 6, (a)], suggesting the electrode process now was adsorption-controlled.

The effect of c_{DPRM} on i_{pc} at two different accumulation times is shown in Fig. 7. When $t = 0$, the relative peak current expressed as the ratio of i_{pc}/c_{DPRM} was small and kept nearly constant with increasing the concentration of dipyridamole [curve (a)]. This indicates that the reduction of dipyridamole at Hg electrode is almost totally diffusion-controlled. However, when $t = 60$ sec, the values of i_{pc}/c_{DPRM} were much greater than those of curve (a) at lower c_{DPRM} because of the adsorption of dipyridamole on the Hg surface. At higher c_{DPRM}, the adsorption of dipyridamole reached saturation and its contribution to peak current did not increase any more. The ratio then declined very rapidly with increasing concentration of dipyridamole, and eventually tended toward the constant value of curve (a) [curve (b)]. Even with 60 sec of accumulation, the i_{pc} *vs.* v relationship at

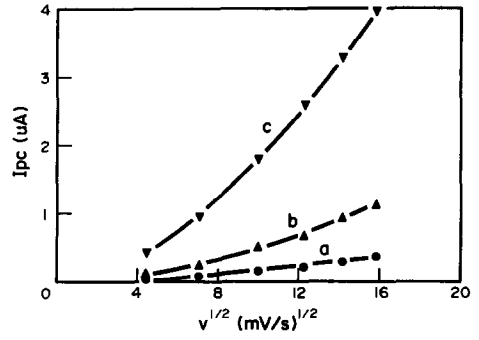

Fig. 5. Influence of square root of scan rate on the cathodic peak current. Preconcentration period, 0 sec (a), 10 sec (b) and 60 sec (c). Dipyridamole concentration, $1 \times 10^{-6}M$. Other conditions as for Fig. 2.

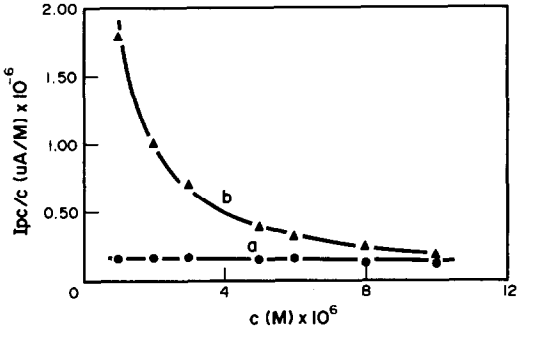

Fig. 7. Effect of concentration of dipyridamole on relative peak current as the ratio of cathodic peak current to dipyridamole concentration. Preconcentration period, 0 sec (a) and 60 sec (b). Other conditions as for Fig. 2.

higher concentration of dipyridamole was not a straight line but a downward bending curve [Fig. 6 (b)]. All of these suggest the gradual transformation of the system from adsorption-controlled to diffusion-controlled when the concentration of dipyridamole grows.

In summary, the reduction of dipyridamole at Hg electrode is contributed to by the reduction of both surface species adsorbed on the electrode surface and solution species diffusing to the electrode surface. However, because the adsorption of dipyridamole is not strong enough, both of the adsorbed and solution species are reduced at the same potential. The cathodic peak current is thus made up of two parts: adsorption current and diffusion current. The preconcentration time, scan rate and concentrations of dipyridamole have different effects on them. Generally, in the condition of smaller c_{DPRM}, faster v and longer t, the system manifests itself mainly with adsorptive properties, but in the condition of larger c_{DPRM}, slower v and shorter t, the system essentially exhibits diffusion properties. This is characteristic of the system when the reactant is weakly adsorbed.[7]

Measurement of the number of electrons transferred

Electrolysis experiments at the potential of -1.6 V with large area of Hg cathode showed that the number of electrons transferred per dipyridamole molecule, n, was 4. This result is in good agreement with that of Boneva.[5] The mechanism of reduction of dipyridamole is not very clear now and the study in our lab is still under way. There are two pyrimidine rings in a dipyridamole molecule. Preliminary UV-visible spectroscopic experiments of dipyridamole system before and after electrolysis indicated that the functional group undergoing reduction was probably the two imines in one of the two pyrimidine rings. Each of the two imines in the same pyrimidine ring may gain 2 electrons and become an amine. The dipyridamole could then retain another pyrimidine ring of conjugate system after electrolysis.

Measurement of the amount of dipyridamole adsorbed

As mentioned above, under the condition of low c_{DPRM}, long t and fast v, the reduction of dipyridamole can be considered to be totally controlled by adsorption of dipyridamole. In this case, the cathodic peak current almost decays to its baseline with little diffusion tail (ref. Fig. 2). Integration of this peak gives a charge Q_a, which represents the reduced charge of surface species of dipyridamole adsorbed at Hg electrode. According to the equation

$$\Gamma = Q_a/(nFA)$$

the surface coverage Γ (mol/cm^2) can then be calculated, where A is the area of electrode (0.0171 cm^2), n is the number of electrons transferred (4) and F is the Faraday constant.

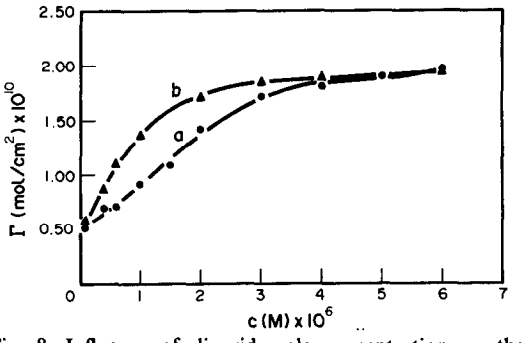

Fig. 8. Influence of dipyridamole concentration on the amount of dipyridamole adsorbed on Hg electrode surface. Preconcentration time, 30 sec (a) and 90 sec (b).

Figure 8 illustrates the relationship between Γ and c_{DPRM} at two different accumulation times. When the concentration of dipyridamole was small, the surface coverage increased linearly with c_{DPRM}. However, at higher concentration of dipyridamole, the curves tended to level off. Γ at two different levels tended to reach the same constant value, which represented full surface coverage of 1.94×10^{-10} mol/cm^2. Each dipyridamole molecule adsorbed thus occupied an area of 0.85 nm^2 if the adsorption of dipyridamole was monolayer adsorption.

Analysis of samples

Measurements of dipyridamole in injection samples were performed by the adsorptive stripping voltammetry. No sample preparation was used other than dilution with the supporting electrolyte. The determination was performed by the standard addition method and the results of a few analyses are given in Table 1.

Table 1. Analytical results of dipyridamole in injection samples

Sample	n	Mean value, mg/injection	S	Recovery of added DPRM,%
1	6	9.54	0.34	88
2	6	9.79	0.34	92

This method was also used to determine dipyridamole in tablets. Before analysis, a sample solution of dipyridamole tablet was prepared by grinding, dissolving and filtering. The excipients in the tablet (starch, talc, *etc.*) did not interfere in the voltamperogram. The results of determination were satisfied. For example, 5 repeated measurements of a tablet showed that the average amount of dipyridamole was 24.6 ± 2.3 mg per tablet with RSD 9.4% and the recovery was 105%.

Determinations of dipyridamole in urine of several patients who took the drug through injection or tablets were also made by the method. Some extraction procedures were required before analysis because of interference by other substances in urine. The results showed that within 24 hr after the patients took the drug, the concentrations of dipyridamole in their urine were in the order of 10^{-5}–$10^{-4}M$.

All of these experiments illustrate the feasibility of measuring dipyridamole in the samples of injection, tablets and urine.

Acknowledgement—This work was financially supported by the National Natural Science Foundation of P. R. China.

REFERENCES

1. I. Jane, A. Mckinnon and R. J. Flanagan, *J. Chromatogr.*, 1985, **323**, 181.
2. C. Deballon and M. Guernet, *J. Pharm. Biomed. Anal.*, 1987, **6**, 1045.
3. A. S. Issa, M. S. Mahrous and M. A. Salam, *Talanta*, 1987, **34**, 670.
4. M. H. Barary, M. A. H. El-Sayed, M. H. Abdel-Hay and S. M. Mohamed, *Anal. Lett.*, 1989, **22**, 1643.
5. A. S. Boneva, N. F. Loginova, V. V. Mishchenko, A. K. Starostina, N. Nino and V. G. Mairanovskii, *Khim-Farm. Zh.*, 1985, **19**, 741.
6. J. Wang, in A. J. Bard (ed.), *Electroanalytical Chemistry*, Vol. 16, pp. 1–89. Dekker, New York, 1989.
7. R. H. Wopschall and I. Shain, *Anal. Chem.*, 1967, **39**, 1514.

Talanta, Vol. 40, No. 8, pp. 1189–1192, 1993
Printed in Great Britain.

0039-9140/93 $6.00 + 0.00

DETERMINATION OF DIBENZO[b,f]-1,4-OXAZEPINE BY DIAZOTIZATION CLEAVAGE OF AZOMETHINE BOND

EMIL HALÁMEK and ZBYNĚK KOBLIHA
Department of Chemistry, Faculty of Arms, Military University, 682 03 Vyškov, Czech Republic

VILIAM FÖLDEŠI
Army Factory VOZ 072, 972 43 Zemianské Kostolany, Slovak Republic

(*Received* 16 *November* 1992. *Revised* 4 *February* 1993. *Accepted* 4 *February* 1993)

Summary—A spectrophotometric determination of dibenzo[b,f]-1,4-oxazepine (CR) has been elaborated, which is based on a diazotation cleavage of azomethine bond followed by a coupling reaction. Twelve coupling agents have been used in the experiments and the following three agents have been recommended for the determination: *N*-(1-naphthyl)ethylenediamine dihydrochloride ($L_Q = 85$ mg/ml), 7-hydroxy-4-methyl coumarin ($L_Q = 105$ mg/ml) and 1-naphthol ($L_Q = 110$ mg/ml). 2-[2-(hydroxy-1-naphthylazo) phenoxy]benzaldehyde has been identified by ^1H and ^{13}C NMR and elementary analysis as the product which results from the diazotization reaction followed by coupling of the CR substance with 2-naphthol. The azo-dye prepared by the described reactions shows azo-hydrazo tautomerism.

Apart from bromobenzyl cyanide (BBC), chloroaceto phenone (CN) and *o*-chlorobenzylidene malononitrile (CS), the dibenzo[b,f]-1,4-oxazepine (CR) is, for the time being, the latest representative of a large group of irritants used in war conflicts and for police purposes.

The tricyclic heterocompounds, among which the CR substance belongs, are used in medicine as antidepressants.

A number of physical methods of determination of the CR substance[1] have been used, apart from the extraction spectrophotometry of ion associates of the proteinized base with some anion active dyes.[2]

Dibenzo[b,f]-1,4-oxazepine is a relatively stable chemical substance. So far, only oxidation[3,4] and chlorination[5] reactions of CR substance have been described.

The purpose of our effort has been to develop a spectrophotometric determination of CR substance based on diazotation cleavage of the azomethine bond and consequent coupling with selected coupling agents, and to identify the product of reaction with 2-naphthol.

EXPERIMENTAL

Chemicals and instruments

Dibenzo[b,f]-1,4-oxazepine (99.5% m/m) was synthesized[6] in the Army Factory VOZ 072, Zemianské Kostolany, Slovak Republic. Its purity was checked by means of extraction spectrophotometry using azodye Orange II ($\lambda_{max} = 480$ nm, $CHCl_3$).[7] The coupling agents *N*-(1-naphthyl)ethylenediamine dihydrochloride (1, *i.e.*, Bratton–Marshall agent), 1-naphthyl amine (2), 8-anilino-1-naphthalene sulphonic acid (3), phloroglucinol dihydrate (4), 1-naphthol (5), resorcinol (6), 7-hydroxy-4-methyl coumarin (7), 4-amino-5-hydroxy-2,7-naphthalene disulphonic acid monosodium salt (8), 3-methyl-1-phenyl-2-pyrazoline-5-one (9), 4,5-dihydroxynaphthalene-2,7-disulphonic acid disodium salt (10) (chromotropic acid disodium salt), 2-naphthol (11) and 4-amino-2,6-dihydroxy pyrimidine (12) (6-amino uracil) were supplied by Merck. The other chemicals were supplied by Lachema, Brno and were of analytical purity.

^1H and ^{13}C NMR spectra were measured by the instrument Bruker AM 400. Elemental analyses were carried out by the Elemental Analyser Model 1102, Carlo Erba. Spectrophotometric determinations were carried out by the spectrophotometer Spekol 11, Zeiss, Jena.

Procedures

(A) Into 5 ml calibrated test tubes were pipetted 10–100 μl of 0.5*mM* solution of the

CR substance in 2*M* HCl, 0.1 ml of mixture (1:1 vol) of dimethyl formamide (DMF) and 2*M* HCl and 0.1 ml of 10*mM* aqueous solution of $NaNO_2$. The test tubes were shaken for 5 min and then 0.1 ml of 0.5*M* aqueous solution of amido sulphuric acid was added. The test tubes were shaken for 3 min. Then 0.1 ml of the coupling agent ($c = 0.1M$) in 2.8*M* NaOH was added. The reaction mixture was allowed to stand for 5 min and then 0.1*M* NaOH was added to make up the final volume of 2 ml. The absorbance was measured at λ_{max} in 1 cm cuvette.

(B) Into 5 ml calibrated test tubes were pipetted 10–100 μl of 0.5*mM* solution of the CR substance in 2*M* HCl, 0.1 ml of mixture (1:1 vol) of dimethyl formamide (DMF) and 2*M* HCl and 0.1 ml of 10*mM* aqueous solution of $NaNO_2$. The test tubes were shaken for 5 min and then 0.1 ml of 0.1*M* aqueous solution of amido sulphuric acid was added. After shaking for 3 min 0.1 ml of the coupling agent was added ($c = 0.1M$) in a mixture of DMF and 2*M* HCl in the ratio 1:1. After 5 min standing the reaction mixture was made up to 2 ml with a mixture of DMF and 2*M* HCl. Absorbance was measured at λ_{max}.

(C) Into 5 ml calibrated test tubes were pipetted 10–100 μl of 0.5*mM* solution of the CR substance in 2*M* HCl and 0.1 ml of 74*mM* aqueous solution of $NaNO_2$. After 5 min shaking, 0.1 ml of 0.5*M* aqueous solution of amido sulphuric acid was added. After 3 min shaking 0.1 ml of aqueous solution of the coupling agent was added ($c = 0.1M$). After an additional 5 min, the reaction mixture was made up to 2 ml with 1*M* HCl and absorbance was measured at λ_{max}.

Preparation and identification of 2-[2-(2-*hydroxy*-1-*naphthylazo*)*phenoxy*]*benzaldehyde*

In a mixture of 16 ml DMF, 8 ml concentrated sulphuric acid and 10 ml water, 0.9761 g of CR substance were dissolved. After cooling to $T = 8°C$, 0.422 g $NaNO_2$ in 10 ml of water were added. The reaction mixture was stirred until all the color disappeared ($t = 30$ min), then 3 ml of aqueous solution of 0.15 g of amido sulphuric acid were added and the mixture was stirred for 10 min. The prepared diazonium compound was gradually poured with vigorous stirring into a solution of 0.721 g of 2-naphthol dissolved in 22.5 ml of 2.8*M* NaOH. The temperature of the reaction mixture did not exceed 10°C. After stirring for 40 min the reaction mixture was filtered. The filtration cake was washed with water and recrystallized from 15 ml of acetic acid. The crystallized product was sucked off and washed by a small amount of ethanol. Melting point of 2-[2-(2-hydroxy-1-naphthylazo) phenoxy]benzaldehyde 152–153°C. Elemental analysis for $C_{23}H_{16}N_2O_3$ ($M_r = 368.4$) was:

calculated: 75% C, 4.4% H, 7.6% N;

found: 74.5% C, 4.4% H, 7.6% N.

^1H NMR spectrum (TMS 400.13 MHz)—($CDCl_3$) δ(ppm): 16.34 (1 H) characteristic shift for azo-hydrazo tautomerism; 10.61 (1 H) corresponds with an aldehydic group; 8.30 (1 H); 7.99 (1 H); 7.33–7.45 (4 H); 7.18–7.22 (2 H); 7.12 (1 H); 7.10 (1 H); 6.88–6.92 (2 H); 6.76 (1 H); 6.54 (1 H).

^{13}C NMR spectrum (TMS 100.61 MHz)—($CDCl_3$) δ(ppm): CH–188.45 a characteristic shift for aldehydic group, 140.62; 135.47; 128.70; 128.43; 126.76; 125.91; 125.35; 125.31; 123.79; 122.40; 121.57; 119.34; 117.71; 116.82.

Quarternary C—174.88 indicates the presence of the hydrazono-formation; 158.72; 146.10; 135.42; 133.12; 130.90; 127.84; 126.88.

RESULTS AND DISCUSSION

Reaction of the CR compound with $NaNO_2$ in acidic environment probably results in *N*-nitrosonium chloride (see I of the outline), a consequence of the addition of the actual diazotization agent—dinitrogen trioxide—on a free electron pair of the nitrogen atom. Intramolecular effect of the oxygen atom of a nitroso group on a strongly electrophilic carbon atom (originally in the azomethine bond) gives rise to a transient quadruple cycle [see II in the outline]. The rearrangement of two electron pairs results in the final product of diazotization, 2-(2-formylphenoxy) benzendiazonium chloride [see III in the outline]. Coupling with 2-naphthol is implemented by a well-known mechanism which results in 2-[2-(2-hydroxy-1-naphthylazo)phenoxy]benzal dehyde [see IV in the outline]. This product exists mainly in the hydrazone formation [see V].

Outline

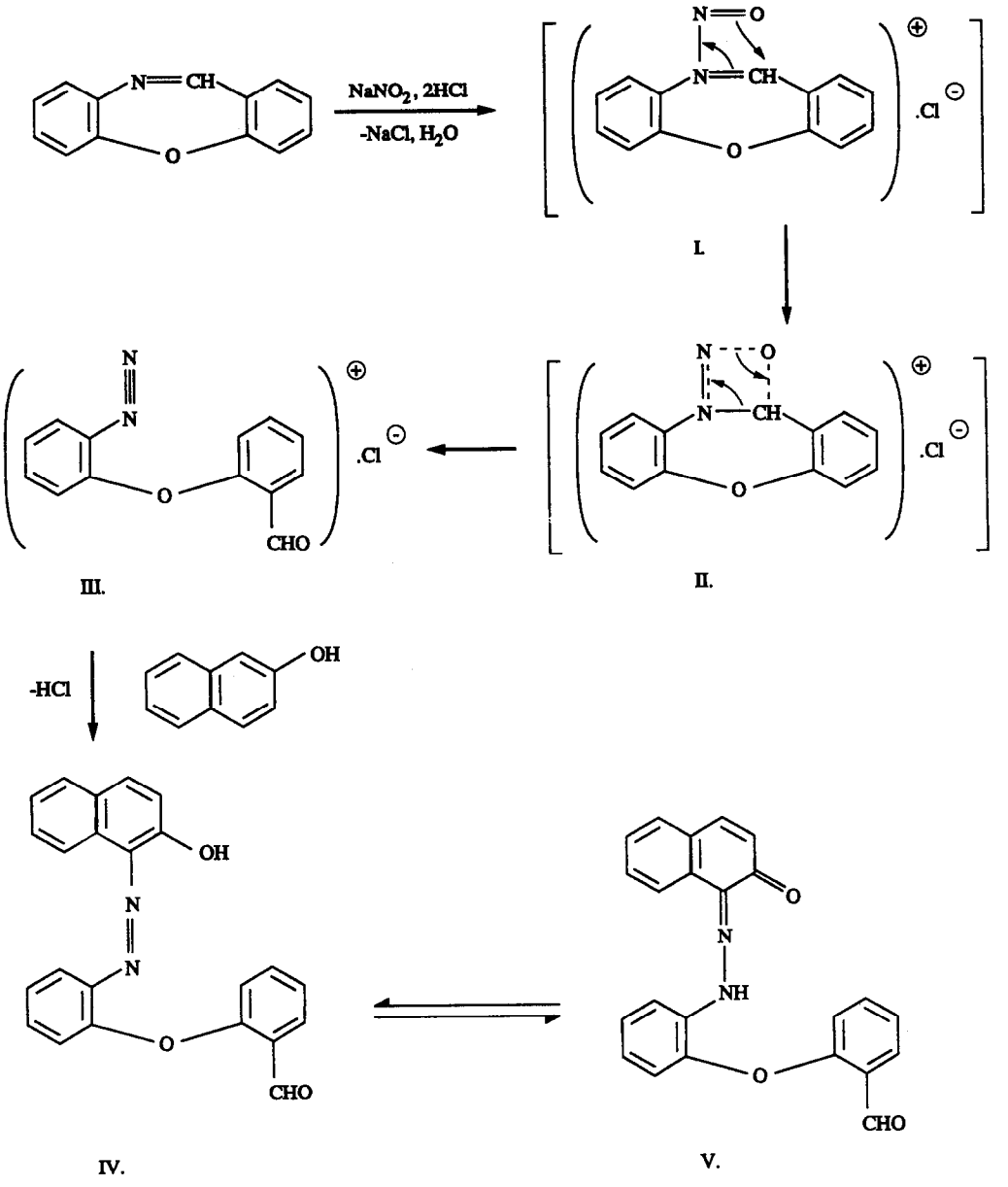

The prepared azo dye shows typical properties of an azo dye, *i.e.*, it is insoluble in alkaline agents. This insolubility comes from the azo-hydrazo tautomerism and from creating stable intramolecular hydrogen bonds.

Absorption maxima (λ_{max}), linear regression parameters, detection limits L_D and determination limits L_Q for spectrophotometric determination of the CR substance are shown in Table 1. All the determinations obey the Lambert–Beer law in the measured concentration range of 2.5–25 μM of the CR substance, as was found from the values of the correlation coefficient r, which is equal to 0.995 in the least favourable case. The prepared solutions of azo dyes are stable. For the spectrophotometric determination of low concentrations of the CR substance in 1 ml sample, first of all *N*-(1-naphthyl)-ethylenediamine dihydrochloride (1), and then 1-naphthol (5) and 7-hydroxy-4-methyl coumarin (7), may be recommended. Our developed method exceeds the extractive spectrophotometry of the ionic pairs[2] in sensitivity and especially in selectivity. Thus, the determination of the CR substance is possible not only in the group of irritants but also in the group of topical warfare chemical agents.

Table 1. Parameters of the spectrophotometric determination of the CR substance by the diazotization and coupling method

Coupling agent	Parameter*						
	μ_{max} *nm*	k (1 *mol*)	q	r	RSD (%)	L_D (*μg ml*)	L_Q (*μg ml*)
1†	554	32 380	0.021	0.999	1.27	0.075	0.085
1‡	554	32 950	0.020	0.998	0.89	0.130	0.160
2†	538	23 100	0.084	0.998	2.27	0.350	0.585
3†	525	22 640	0.058	0.998	1.85	0.555	0.670
4§	415	22 260	0.037	0.998	1.32	0.200	0.245
5§	500	19 740	0.012	0.999	0.99	0.090	0.110
6§	480	19 430	0.014	0.999	1.78	0.175	0.210
7§	490	18 040	0	0.998	1.15	0.080	0.105
8§	538	14 290	0.038	0.999	1.74	0.485	0.510
9§	390	11 330	0.014	0.998	1.57	0.230	0.290
10§	532	10 460	0.010	0.975	3.26	1.774	3.216
11§	503	9 980	−0.006	0.995	2.23	0.927	2.401
12§	380	8 850	0.036	0.997	1.99	1.030	1.100

*λ_{max}—maximum absorbance, k—calibration curve slope ($A = k \cdot c + q$), q—shift on the "Y" axis, r—correlation coefficient, RSD—relative standard deviation, L_D—detection limit, L_Q—determination limit.

†Determination according to procedure B.

‡Determination according to procedure C.

§Determination according to procedure A.

The proposed procedure for the determination of the CR substance may also be used for its potentiometric determination in addition to spectrophotometry.[8]

REFERENCES

1. J. Enqvist *et al.*, *Systematic Identification of Chemical Warfare Agents*, Vol. B.3. The Ministry of Foreign Affairs of Finland, Helsinki, 1982.
2. E. Halámek, Z. Kobliha and J. Souček, *Talanta*, 1992, **40**, 287.
3. J. M. Harrison, K. Brewster and T. D. Inch, *J. Labelled Comp. Radiopharm.*, 1978, **14**, 375.
4. V. N. Aleksandrov and V. I. Emelyanov, *Otravlyaushchie Veshchestva*, p. 210. Voennoe izdatelstvo, Moscow, 1990.
5. I. W. Lawston, J. M. Harrison, T. D. Inch and D. B. Cooper, *J. Chem. Soc.*, 1979, Perkin Trans., **1**, 2642.
6. Pat. CSFR 2677, Army Factory VOZ 072, V. Földeši, E. Halámek and J. Kubuš, The preparation of dibenzo[b,f]-1,4-oxazepine, 1987.
7. Pat. CSFR 2733, Military University, E. Halámek, Z. Kobliha and J. Souče, Extractive spectrophotometric determination of dibenzo[b,f]-1,4-oxazepine by azo dyes, 1988.
8. Pat. CSFR 2641, Army Factory VOZ 072, E. Halámek and V. Földeši, The analysis of dibenzo[b,f]-1,4-oxazepine, 1987.

Talanta, Vol. 40, No. 8, pp. 1193–1200, 1993
Printed in Great Britain.

0039-9140/93 $6.00 + 0.00

A PHOTOMETRIC DETECTOR BASED ON A BLUE LIGHT-EMITTING DIODE

PETER C. HAUSER* and DAVID W. L. CHIANG
The University of Auckland, Department of Chemistry, Private Bag 92019, Auckland, New Zealand

(*Received* 10 *November* 1992. *Revised* 26 *January* 1993. *Accepted* 26 *January* 1993)

Summary—The suitability of blue light-emitting diodes as radiation sources in molecular absorption spectroscopy was evaluated. Electronic as well as spectral considerations are discussed. A transducer based on a blue light-emitting diode and a photodiode is described which yields direct absorbance readings by passing the photocurrent to an integrated circuit logarithmic converter. The performance of this device was tested for commonly used spectrophotometric procedures for Cr, Mn, Zn, Fe and Cl and compared with conventional molecular absorption spectroscopy. Also investigated was the application of the transducer as a detector in flow-injection analysis.

The radiation from light-emitting diodes (LEDs) has limited spectral bandwidths of about 20–70 nm. This imparts a degree of spectral selectivity and often allows the substitution of the commonly used combination of broadband sources and monochromators with these inexpensive devices. Photometric transducers for molecular absorption spectroscopy based on LEDs and photodiodes or phototransistors have been reported repeatedly.[1–14] These have either been dip type probes or more frequently flow-through cells for flow-injection analysis (FIA). The latter application has been reviewed by Trojanowicz *et al.*[15] Devices based on green (565 nm),[1,2,3,5,6,9,11,14] yellow (595 nm),[11,13,14] orange (605–620 nm),[4] red (630–660 nm)[1,3,5,8,11,12,14] and near-infrared (820 nm)[7,10] LEDs have been reported. Blue LEDs however, are not as readily available as those of other colours, because the gallium arsenide or phosphide semiconductor technology normally used in LED manufacture cannot be extended to the production of light of shorter wavelengths. The authors are not aware of any reports on the use of blue LEDs in photometry although they have been employed in passive and active fluorescence based chemical sensors.[16–18] On the other hand, the absorption bands for several commonly employed spectrophotometric procedures lie in the wavelength region of peak emission of blue LEDs. Blue LEDs from two different sources were evaluated for their application in spectrophotometry using a cell with a 1 cm pathlength and a log converter to yield measurements that correspond to absorbance.

*Author for correspondence.

EXPERIMENTAL

Electronic components

Blue LEDs were obtained from Siemens (LB 5410-HO) and Radiospares (RS 589-569). The LEDs of other colours were from Radiospares (Green: RS 585-927; Yellow: 585-933; Orange: RS 578-200 and Red: RS 585-911). The photodiode was from Siemens (SFH 250V), the phototransistors from Siemens (SFH 350-V) and Motorola (MFOD72), the low input bias current operational amplifier (OPA121) and the log converter (LOG 100) from Burr-Brown. The 1 mm plastic optical fibre was purchased from Radiospares.

Intensity measurements

The intensity and stability measurements of the LEDs were carried out by conducting the light from the LEDs through a short length of optical cable to the photodiode which was connected in the photoamperic mode to the operational amplifier. The output voltage from the amplifier in the current follower configuration was passed to a 16 bit analogue-to-digital converter card (NB-MIO-16XH-42 from National Instruments) which was located in a Macintosh IIci computer and controlled by a program written in Lab VIEW (Version 2.1, National Instruments).

Emission spectra of LEDs

These were obtained by positioning the LEDs in the cuvette holder of a Hitachi F-2000 spectrofluorimeter. The spectra were redrawn from the scaled numerical output of the instrument.

Absorbance measurements and spectra

Absorbances were measured with a Shimadzu UV-160A spectrophotometer using 1 cm cuvettes. For the FIA-determinations a Cecil CE 373 spectrophotometer fitted with a Hellma flow-through cuvette with a 1 cm pathlength was used. The blue LED from Radiospares was used for all photometric measurements with the transducer reported here.

Estimated absorbance values

The measured emission intensities for the LED (for 5 nm intervals from 400 to 600 nm) were corrected for the sensitivity of the detector by multiplying with the sensitivity factor for the respective wavelength. The sensitivity factors were taken as 0.327 at 400 nm and to be linearly increasing to 1 at 600 nm. These data were obtained from a plot in Ref. [19]. The resulting values were scaled to a peak intensity of unity. The measured absorbance values for the respective dyes (again at intervals of 5 nm from 400 to 600 nm) were normalized to a peak absorbance of 1. These values were then numerically transformed into transmittance. A numerical estimate of the light intensities measured by the detector was obtained by multiplying the values under both curves, since

$$T = I/I_0 \text{ and } I = T \cdot I_0$$

where T is the measured transmittance, I_0 the original intensity (emission intensities for the LED) and I the intensity after passage through the cell. Adding the results for all wavelength intervals gave an estimate for the total intensity over the wavelength range from 400 to 600 nm. By comparing the total for the individual dyes with the total initial intensity (sum of the values for the normalized LED emission spectrum) an estimate for the integrated overall transmittance was obtained. This value was then transformed back into absorbance according to Lambert–Beer's law.

Solutions

All reagents were of analytical reagent grade. The standard solutions for the chromium calibration curves were prepared by appropriate dilution of a stock solution of potassium dichromate. The reagent for the formaldoxime method was prepared by diluting 7.9 g formaldehyde and 7 g hydroxylamine hydrochloride to 100 ml with water.[20] Then 10 ml of this solution was mixed with an appropriate amount of a stock solution of $1 \times 10^{-5}M$ $MnSO_4$ and 15 ml of $1M$ NaOH, and diluted to 100 ml. The reagent solution for the zinc determination consisted of 100 mg 4-(2-pyridylazo)resorcinol in 100 ml of water. Then, 5 ml of this reagent was mixed with an appropriate amount of $1 \times 10^{-4}M$ $ZnSO_4$ solution and 10 ml of $1 \times 10^{-2}M$ $Na_2B_4O_7$ and made up to 100 ml. The reagent stream for the iron determination in FIA by the phenanthroline method consisted of 1.2 g/l 1,2-phenanthroline, 50 g/l ammonium acetate and 140 ml/l of glacial acetic acid. Standard solutions were made up with an appropriate amount of a stock of $FeNH_4(SO_4)_2$ and 10 ml of a 2% solution of hydroxylamine hydrochloride, and diluted to 100 ml. The reagent stream for the chloride determination consisted of 0.626 g of $Hg(SCN)_2$, 30.3 g of $Fe(NO_3)_3 \cdot 9H_2O$, 4.72 g of concentrated nitric acid and 150 ml of methanol, and was made up to 1 l with water.[21] Standard solutions were made up by appropriate dilution of a stock of a 1000 ppm NaCl solution.

RESULTS AND DISCUSSION

Electronic considerations

Light intensity. The luminous intensities of the two blue LEDs (13 mcd[22] and 2.5 mcd[23]) are very low compared to that of LEDs of other colours which may have intensities 2–3 orders of magnitude higher. Semiconductor detectors based on silicon are most sensitive in the near-infrared and are not very efficient at the lower end of the visible range. The photocurrents obtained by the photodiode irradiated with the blue LEDs were therefore found to be as low as about 50 nA. Phototransistors with their built-in amplification result in significantly higher currents, but the response of two types of phototransistors tested was found not to be linear with light intensity over the relevant range. A photodiode was therefore used. However, the current obtained was too low for direct input to the logarithmic converter (see below) and was therefore amplified by an operational amplifier in the current follower configuration. The input bias current of the operational amplifier used is specified as less than 5 pA[24] and therefore is not a source of error.

Stability. The stability in intensity of the blue LED from Radiospares was tested while operating it with its recommended current of 25 mA. The photocurrent on the detector was acquired in regular intervals over a period of 1 hr. It was found that the intensity was decreasing by 0.06% over this initial period. This corresponds to the same relative error in transmittance measurements and was deemed to be tolerable.

Logarithmic conversion. To obtain an output that corresponds to absorbance, the photocurrent was transformed by a log converter contained in a single integrated circuit package. According to Lambert–Beer's law this leads to calibration curves linear with concentration. Direct analog log or antilog converters are generally useful building blocks for analytical instruments and the use of an antilog converter for example has been reported for the linearization of the response from ion-selective electrodes.[25] The approach has not previously been reported for LED-based photometry, commonly the voltage obtained from a current follower amplifier has been measured directly (this value corresponds to transmittance and in principle yields non-linear calibration curves) or the log conversion has been carried out numerically after the measurements. The complete circuitry is shown in Fig. 1. A provision for an offset adjustment is featured by the log converter which allows the instrument to be zeroed on blank solutions. The output is a potential, with a voltage of zero corresponding to absorbance zero and 1 V being equivalent to an absorbance of 1.

Spectral considerations

The emission spectra of two available blue emitting LEDs (both based on SiN)[23,26] and of typical LEDs for the other colours are shown in Fig. 2. The figure shows the visible range of the spectrum from 400 to 700 nm. As evident, conventional LEDs from green to red cover about half of the range. They show a relatively narrow bandwidth of 20–40 nm (full width at half height) compared to the bandwidths of 65–70 nm for the two blue LEDs. This imparts a higher spectral selectivity for the more conventional colours. A good spectral match should be possible for many absorbing species in the 100 nm span from 565–660 nm because of the availability of the four colours with peak separations of about 15–35 nm. Other LEDs with different peak wavelengths for this region are available. For the lower half of the visible range (from 400 to 565 nm) such a choice is not possible. As can be seen, the emission bands for the two blue LEDs are very similar with peak wavelengths at 460 and 470 nm. However, the fact that the bands from the two blue LEDs encompass a wide region at lower wavelengths may be considered an advantage in the absence of emitters of different wavelengths in that range since a spectral match will always be obtained.

Construction of the cell

A cross-sectional diagram of the cell is shown in Fig. 3. Black perspex was used in order to eliminate the interference from ambient light and internal reflections. The optical path is 1 mm in diameter and the pathlength

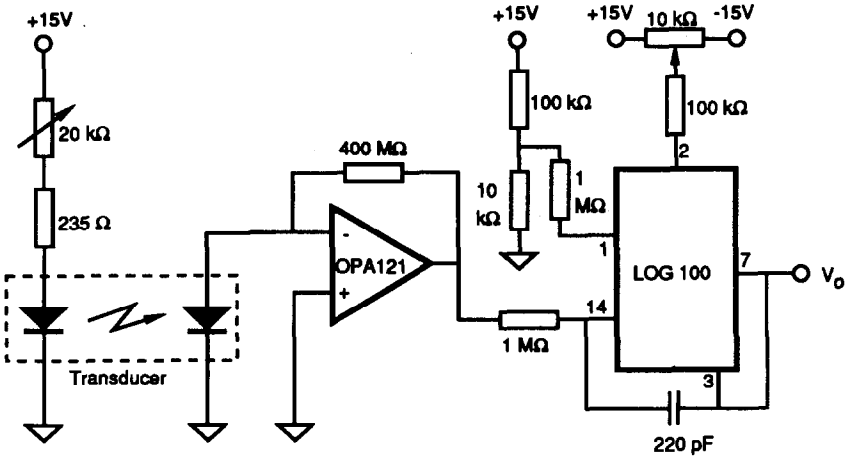

Fig. 1. Electronic circuitry of the transducer.

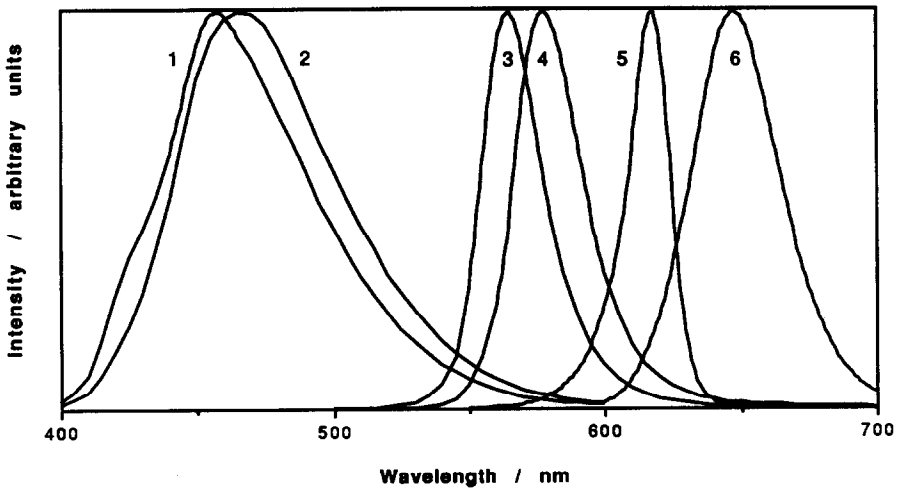

Fig. 2. Emission spectra of typical LEDs: (1) blue (Radiospares), (2) blue (Siemens), (3) green, (4) yellow, (5) orange, (6) red.

1 cm, deliberately chosen to match conventional cuvettes. The cell volume is 8 μl. The solution is passed in and out of the cell through tubing attached with the common 1/4 × 28-type fittings. Light is passed through by the use of 1 mm plastic optical cable. This allowed the location of the opto-electronic components removed from the wet-chemical part. The cell was mounted on a metal housing which contained the electronic circuitry including the emitter and detector. This effectively shielded the detector against electromagnetic noise pick-up. The diameter of the optical cable is ideal for combination with opto-electronic components and specially designed emitters and detectors are available. The photodiode that was used is housed in a package which allows easy screw-on connection to the cable. The plastic bodies of the LEDs used in this project were cut off close to the emitting semiconductor surface and polished so that efficient light coupling into the plastic fibre could be achieved. A specially designed Perspex adaptor was used to facilitate this connection.

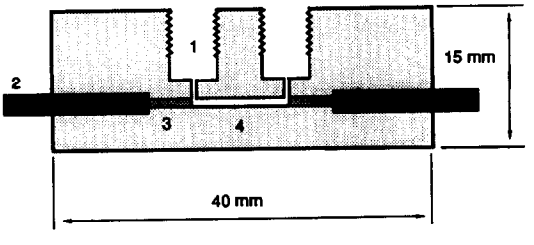

Fig. 3. Cross-sectional view of the transducer cell: (1) inlet/outlet, (2) fibre optic cable, (3) stripped section of the fibre optic cable, (4) optical path.

Equilibrium measurements

The transducer was tested for its use in five common spectrophotometric procedures. The absorption bands for the coloured species detected in these methods all show their highest sensitivity in the emission region of the blue LEDs. The suitability of the LED based transducer was tested with sets of calibration standards. Absorbances at the wavelength of maximum sensitivity were also measured with a conventional spectrophotometer using a cuvette with a 1 cm optical pathlength. Since the transducer has the same pathlength a direct comparison of the two results is possible.

The LED based device was found to be successful for the determination of chromium by oxidation to dichromate with periodate.[20] The two response curves are given in Fig. 4. The response curve for the transducer shows a loss

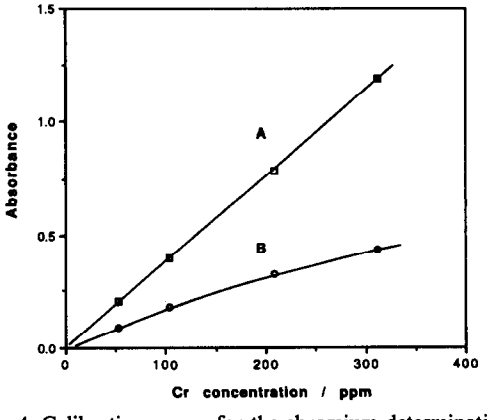

Fig. 4. Calibration curves for the chromium determination by the dichromate method: (A) spectrophotometer (445 nm), (B) LED-based transducer.

of sensitivity and a deviation from Lambert–Beer's law in the form of a curvature. These aspects will be discussed below. Manganese could be determined successfully by the formaldoxime method,[20] as is illustrated by Fig. 5. Here the differences between the two detectors are not very pronounced. Also successful was the determination of zinc by complexation with 4-(2-pyridylazo)resorcinol (PAR) as reagent. Again a somewhat reduced sensitivity was found as illustrated in Fig. 6. This reagent shows a significant background absorption which however did not cause any problems. The detector was zeroed on a blank solution.

The precision of the transducer measurements was found to be excellent, the standard deviation of the absorbance measurements in no case exceeded a value of 0.003 ($n = 5$), which is comparable to the results obtained with the spectrophotometer. The resulting precision in concentration was 1, 0.3 and 0.8% (relative standard deviation, $n = 5$) for the Cr, Mn and Zn methods, respectively. These values were obtained at the high end of the calibration curves and illustrate that the loss of sensitivity observed with the LED-device is not significant in terms of the signal-to-noise ratio. The detection limits (concentration corresponding to a signal three times its standard deviation) were determined as 6, 0.2 and 0.02 ppm for the three analytes, respectively.

The transducer was also tested for its application to the determination of Fe(II) by complexation with 1,10-phenanthroline[20] and of chloride by the thiocyanate method.[27] The results were comparable with the ones obtained for the procedures above and are not shown here because these methods were also adapted

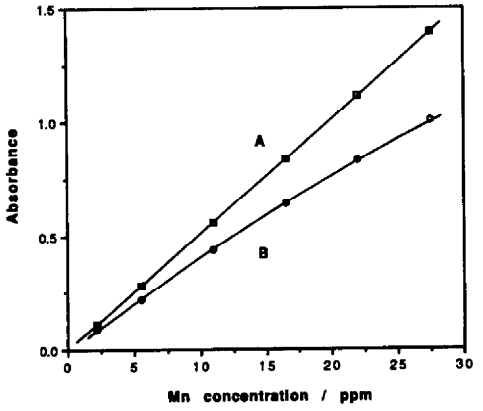

Fig. 5. Calibration curves for the manganese determination by the formaldoxime method: (A) spectrophotometer (451 nm), (B) LED-based transducer.

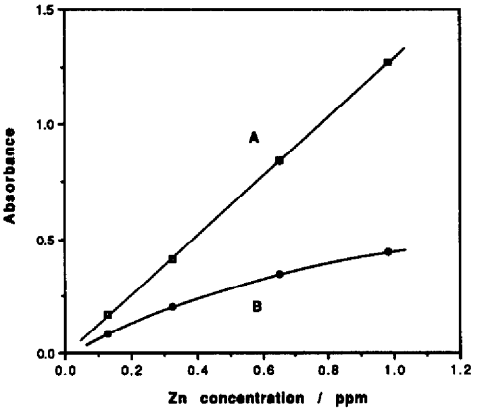

Fig. 6. Calibration curves for the zinc determination by complexation with PAR: (A) spectrophotometer (492 nm), (B) LED-based transducer.

to flow-injection analysis using the detector cell, the results of which are reported below.

FIA measurements

The low internal volume of the transducer makes it well suited as a detector for flow-injection analysis and this aspect was therefore investigated. Measurements were again carried out using both a conventional spectrophotometer and the LED-transducer. A flow through cuvette with a pathlength of 1 cm was used with the spectrophotometer and the manifolds were identical, so that a direct comparison between the two detectors is again possible.

For the determination of Fe(II) by the phenanthroline method in FIA, an aqueous carrier stream at 2 ml/min into which 100 μl sample was injected was used. The reagent solution (2 ml/min) was merged in downstream from the injection valve and the combined streams passed through a 120 cm long mixing coil of 0.5 mm diameter before detection. The results for the Fe(II) determination using the phenanthroline method in the FIA-mode are given in Fig. 7. The detector performs well for this method. The precision in concentration obtained at the high end of the calibration curve for the transducer was 1.3% (r.s.d., $n = 5$). The detection limit was 0.4 ppm. The detector cell showed some tendency to trap gas bubbles from the carrier stream, which was not a problem when the solutions were degassed before use.

It was also found to be possible to successfully carry out chloride determinations by FIA using the thiocyanate method,[21] as the calibration graphs of Fig. 8 illustrate. The precision in concentration obtained at the high end of the calibration curve for the transducer was found

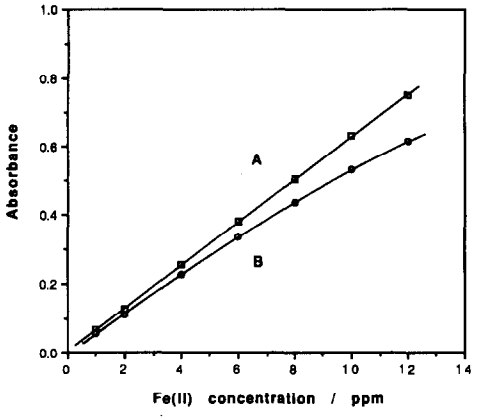

Fig. 7. Calibration curves for the Fe(II) determination by the phenanthroline method in FIA: (A) spectrophotometer (510 nm), (B) LED-based transducer.

to be 0.6% (r.s.d., $n = 5$) and the detection limit as 0.2 ppm. The chloride content of four atmospheric aerosol samples was determined. These had been analysed by ion-chromatography and the agreement between the two methods were found to be good. The following data were obtained: sample (1) LED: 98 ppm; IC: 96 ppm, (2) LED: 90; IC: 82 ppm, (3) LED: 48; IC: 49 ppm, (4) LED: 36; IC: 34 ppm. The correlation coefficient for these data is 0.994.

Sensitivity and shape of calibration curves

The LED-based transducer was always found to show a loss in sensitivity as compared to the conventional spectrophotometer. This behaviour is expected since the light source is not strictly monochromatic and therefore the measured signal contains contributions from wavelengths with lower absorptivities. It was found that it was not possible to estimate the loss of sensitivity from the closeness of the absorbance peak to the emission maximum of the LED. Such a comparison would, for example, predict a high sensitivity for the Cr-determination and a low sensitivity for the Fe-determination when in fact the opposite was observed. The entire spectra have to be considered. The transmittance spectra for the measured species for the Mn-, Cr-, Fe- and Cl-determinations are therefore given in Fig. 9 (the spectrum of the Zn–PAR complex was not included since the blank PAR solution shows a significant absorbance, a fact which complicates the following discussion). These spectra were normalized for an absorbance value of one at the wavelength of peak-sensitivity. Also included in the plot is the emission spectrum for the blue LED. This spectrum has been corrected for the spectral sensitivity of a silicon photodiode as used in this work. Such detectors show their peak at about 900 nm with an almost linear loss of sensitivity from 600 to 400 nm,[19] the wavelength range where emission from the blue LED occurs. The comparison of the emission spectrum of the blue LED and the four transmittance spectra allows a visual estimation of the light intensity observed by the detector after passage through the cell. The larger the area shared by both the LED-spectrum and the respective dye spectrum, the lower the remaining light intensity, and the higher the detected absorbance. Note that all four hypothetical solutions would give identical absorbances of 1 if measured at a monochromatic wavelength at peak sensitivity.

A quantitative estimate of the light intensities measured by the detector was obtained by

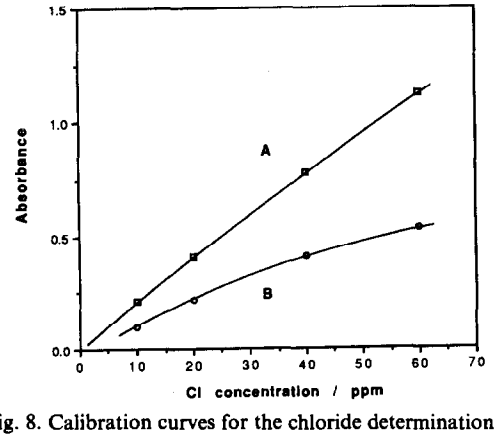

Fig. 8. Calibration curves for the chloride determination by the thiocyanate method in FIA: (A) spectrophotometer (480 nm), (B) LED-based transducer.

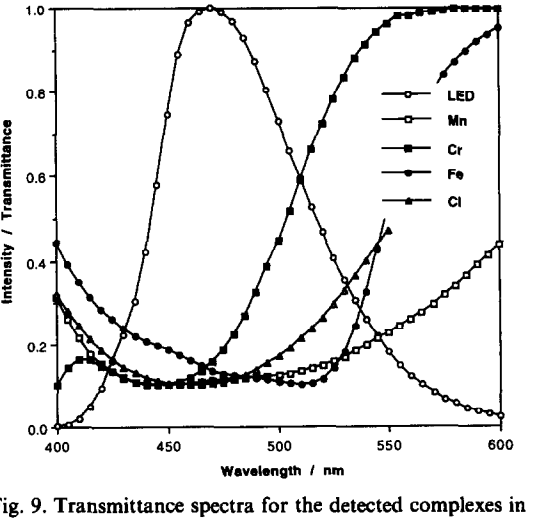

Fig. 9. Transmittance spectra for the detected complexes in comparison with the corrected emission spectrum for the blue LED employed.

multiplying the values under both curves and numerically integrating the result (see the Experimental section for details). This procedure led to estimated absorbance values for the LED-transducer (for an absorbance of 1 at the wavelength of maximum sensitivity) of 0.88, 0.44, 0.74 and 0.70 for the Mn-, Cr-, Fe- and Cl-methods, respectively. The respective experimental data are 0.76, 0.38, 0.73 (estimated) and 0.50. The observed sensitivities can therefore be corroborated reasonably well with the extent of the spectral match between the emission spectrum of the LED and the respective absorbance spectrum.

The calibration curves for the transducer all show a more or less pronounced deviation from the Lambert–Beer law in the form of a curvature. Such a deviation is expected when not strictly monochromatic light sources are employed and the absorptivity and/or the intensity of the incident light varies over the detected wavelength range.[28] As can be seen from Fig. 9 both of these factors are not constant in the case of the LED-transducer. That this indeed causes a non-linearity of the response curve can be demonstrated with the help of Lambert–Beer's law by assuming that the light intensity is measured for two wavelengths simultaneously.[28] The above described modelling procedure for different peak absorbance values can also be applied for a more detailed simulation of a calibration curve for the transducer. As is illustrated by the predicted calibration curve for the chromium method given in Fig. 10, the observed non-linearities can be accounted for by spectroscopic principles.

The loss of sensitivity compared to conventional spectrophotometry is expected to be more significant for the blue LED than for other LEDs, because its wider emission band reduces the probability of a good spectral match. However, there is very little quantitative data available on this aspect for different LEDs, with the exception of the data presented by Trojanowicz *et al.*[15] For peak wavelengths of the absorbing species ranging from 540 to 660 nm, sensitivities of 85–99% of the conventional methods were reported. No information on how these data were obtained was given. Also included were results obtained for the iron determination by the phenanthroline method and for the chloride determination by the thiocyanate method using a green LED at 565 nm. Sensitivities of 21 and 9% of the conventional methods were reported for the two procedures, respectively. This compares to values of 61 and 55% obtained in this work by comparing the measured absorbances in the centre of the calibration curves. Using a blue LED certainly leads to an improvement for these two methods, and the use of the green LED would not be possible or yield very low sensitivities for the other coloured species discussed above.

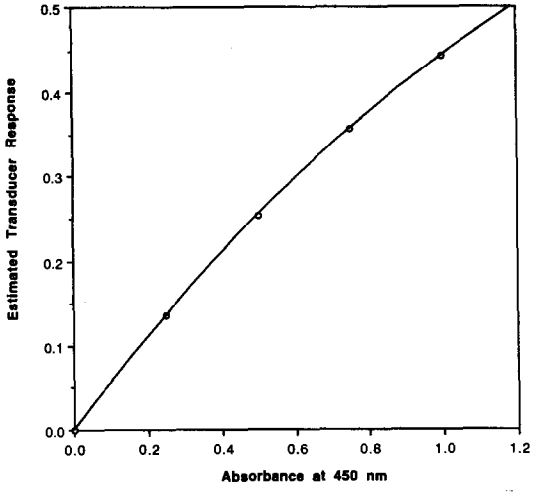

Fig. 10. Correlation of estimated absorbance readings for the chromium determination with the transducer with absorbances for monochromatic determination at 450 nm.

CONCLUSIONS

It was found that the transducer based on a blue LED can be used successfully for quantitative determinations in equilibrium applications as well as flow-injection analysis. The sensitivity is always reduced when compared to the results obtained with conventional instrumentation and perhaps also in comparison to systems employing LEDs of other colours. The calibration graphs tend to show a deviation from Lambert–Beer's law in the form of a downward curvature towards the high end of the calibration curves. This effect is more pronounced for cases of low sensitivity compared to the spectrophotometric measurements and is expected for absorbance measurements with broad-band light sources. The precision of the absorbance measurements however, was found to approach that of conventional double-beam instruments. Therefore the precision in concentration can be expected to be in the order of 1%, even in cases where the sensitivity is strongly degraded. This means that the relatively low sensitivities encountered in some instances with the blue LED do not adversely affect practical applications of this system.

Acknowledgements—The authors thank Dean Clark from Siemens Wellington for providing samples of opto-electronic components, David Wiley for the analysed aerosol samples and Glenn Boyes for preparing solutions. The work was mainly funded by University of Auckland grant number A18/XXXXX/61890/F3391087 and a special Vice Chancellor's grant.

REFERENCES

1. H. Flaschka, C. McKeithan and R. Barnes, *Anal. Lett.*, 1973, **6**, 585.
2. T. Anfält, A. Granéli and M. Strandberg, *Anal. Chem.*, 1976, **48**, 357.
3. D. Betteridge, E. L. Dagless, B. Fields and N. F. Graves, *Analyst*, 1978, **103**, 897.
4. D. J. Hooley and R. E. Dessy, *Anal. Chem.*, 1983, **55**, 313.
5. M. Trojanowicz, W. Augustyniak and A. Hulanicki, *Mikrochim. Acta*, 1984 **II**, 17.
6. G. J. Schmidt and R. P. W. Scott, *Analyst*, 1984, **109**, 997.
7. K. S. Johnson, C. L. Beehler and C. M. Sakamoto-Arnold, *Anal. Chim. Acta*, 1986, **179**, 245.
8. J. R. Clinch, P. J. Worsfold and H. Casey, *Anal. Chim. Acta*, 1987, **197**, 43.
9. J. R. Clinch, P. J. Worsfold and H. Casey, *Anal. Chim. Acta*, 1987, **200**, 523.
10. P. C. Hauser, S. S. Tan, T. J. Cardwell, R. W. Cattrall and I. C. Hamilton, *Analyst*, 1988, **113**, 1551.
11. M. Trojanowicz and J. Szpunar-Lobinska, *Anal. Chim. Acta*, 1990, **230**, 125.
12. P. R. Freeman, I. D. McKelvie, B. T. Hart and T. J. Cardwell, *Anal. Chim. Acta*, 1990, **234**, 409.
13. M. Trojanowicz, J. Szpunar-Lobinska and Z. Michalski, *Mikrochim. Acta*, 1991 **I**, 159.
14. J. Huang, H. Liu, A. Tan, J. Xu and X. Zhao, *Talanta*, 1992, **39**, 589.
15. M. Trojanowicz, P. J. Worsfold and J. R. Clinch, *TrAC*, 1988, **7**, 301.
16. N. Opitz and D. W. Lübbers, in D. Bruley *et al.* (eds), *Oxygen Transport to Tissue*, Vol. 6. Plenum, New York, 1984.
17. O. S. Wolfbeis, B. P. H. Schaffar and E. Kaschnitz, *Analyst*, 1986, **111**, 1331.
18. M. E. Lippitsch, J. Pusterhofer, M. J. Leiner and O. S. Wolfbeis, *Anal. Chim. Acta*, 1988, **205**, 1.
19. J. Wilson and J. F. B. Hawkes, *Optoelectronics*, 2nd Ed. Prentice Hall, New York, 1989.
20. Z. Marczenko, *Separation and Spectrophotometric Determination of Elements*. Ellis Horwood, Chichester, 1986.
21. J. Ruzicka and E. H. Hansen, *Flow Injection Analysis*, Wiley, New York, 1981.
22. Radiospares Components Ltd, Auckland, Catalog, September 1992.
23. *Optoelectronic Semiconductors and Sensors, Short Form Catalog*, Siemens Ltd, 1990.
24. *Integrated Circuits Data Book*, Vol. 33, Burr-Brown, 1989.
25. M. Trojanowicz, T. Krawczynski vel Krawczyk and W. Augustiniak, *Anal. Chim. Acta*, 1988, **207**, 325.
26. Private Correspondence with Michael Hooker, Radiospares Components Ltd. Auckland.
27. J. Bassett, R. C. Denney, G. H. Jeffery and J. Mendham, *Vogels's Textbook of Quantitative Inorganic Analysis*, 4th Ed. Longman, London and New York, 1978.
28. D. A. Skoog, D. M. West and F. J. Holler, *Fundamentals of Analytical Chemistry*, 6th Ed. Saunders College Publishing, Fort Worth, 1992.

Talanta, Vol. 40, No. 8, pp. 1201–1206, 1993
Printed in Great Britain.

0039-9140/93 $6.00 + 0.00

RAPID ASSAY FOR PROCAINE PENICILLIN G IN PHARMACEUTICAL DOSAGES BY SPECTROFLUORIMETRY

J. A. MURILLO PULGARIN and A. ALAÑON MOLINA

Department of Analytical Chemistry and Food Technology, University of Castilla-La Mancha, 13071 Ciudad Real, Spain

(*Received* 5 *November* 1992. *Revised* 2 *February* 1993. *Accepted* 2 *February* 1993)

Summary—A method for the spectrofluorimetric determination of procaine penicillin G is proposed ($\lambda_{ex} = 294$ nm, $\lambda_{em} = 348$ nm) for concentrations between 0.10 and 1.0 ppm. The method was performed in ethanol/water medium (60% V/V), at apparent pH 9.9 provided by adding ammonium/ammonia buffer solution with pH = 10.0.

The effect of other penicillins on the determination of procaine penicillin G was examined over a wide range of concentrations, interferences were not observed in the range of studied concentrations.

The method was successfully applied to assay all Spanish commercialized injections containing procaine penicillin G, penicillin G and/or benzathine penicillin G.

Fifty years after its introduction, penicillin G remains a very useful antibiotic; it is found to be a safe and effective agent. Serious toxic events are rare and dosage flexibility proves to be broad. It is the antibiotic of choice for most infections caused by gram-negative cocci and majority grampositive bacteria.[1]

Penicillin G is available as the sodium or potassium salt in aqueous solutions for intramuscular injection. It is spread all over the organism and is eliminated through urine fundamentally. It reaches the maximum of plasmatic concentration in 15 or 30 min; it has a small half-life. Therefore, the use of the long-acting penicillins like benzathine penicillin G and procaine penicillin G is necessary.

Procaine penicillin G is a result of the combination of 1 mole of penicillin G and 1 mole of procaine. It forms a tissue deposit, from which the drug is slowly absorbed within 12 or 24 h.

The penicillins are not fluorescent compounds because the association of β-lactam and thiazolidine rings does not exhibit native fluorescence.

The penicillins are fluorescent only when the bound group to carboxylate in position 3 (procaine penicillin G) or the group in position 6 (methicillin or nafcillin) are appropriate.

Only one direct fluorimetric assay for penicillins[2] is described but a previous extraction is necessary. The others are based on derivatization reactions.

Jusko *et al.*[3] developed the first fluorimetric determination of penicillins based on the formation of a strongly fluorescent yellow product during acid hydrolysis at elevated temperatures of ampicillin and other α-aminopenicillins.[4–6]

Other described methods involve basic hydrolysis[7] in the presence of 2-methoxyethanol, or acid hydrolysis in the presence of Hg (II).[8–10]

Baker and Havlicek[11] use the fluorescamine derivative of penicillins and Mori *et al.*[12] developed a method of penicillins determination based on quenching reaction.

Procaine penicillin G is one of the few penicillins that shows fluorescence by itself, no existing method of fluorimetric determination is described in the literature.

The purpose of this study is to report the development of a direct and simple fluorimetric method for the estimation of procaine penicillin G in pharmaceutical dosages in the absence and presence of penicillin G and benzathine penicillin G.

REAGENTS AND MATERIALS

Reagents

Stock solution of procaine penicillin G, 250 ppm: prepared by dissolving the standard procaine salt of penicillin G in Milli-Q water.

Stock solution of benzathine penicillin G, 250 ppm: prepared by dissolving the standard benzathine salt of penicillin G in 96% ethanol.

Stock solution of penicillin G, 250 ppm: prepared by dissolving the standard potassium salt of penicillin G in Milli-Q water.

The standard procaine, benzathine and potassium salt of penicillin G were obtained from the Sigma Chemical Products.

Injectable dosage of Farmaproína, Cepacilina 3:2:1, Cepacilina 6:2:1, Cepacilina 6:3:3 (Lab. Cepa), Aquacilina 600, Aquacilina D-A 600, Zoocilina 1000000, Benzetacil 3:2:1, Benzetacil 6:2:1, Benzetacil 6:3:3 (Lab. Antibioticos S.A.), Ortopén 400000 and Ortopén 1000000 (Lab. Fides S.A.) with different nominal contents, were randomly purchased from local pharmacies.

Buffer solution 0.15*M*: buffer solution of pH 10.0 was prepared by mixing adequate amounts of ammonium chloride with sodium hydroxide.

Stock solutions of procaine and potassium salt of penicillin G were stored, protected from light and maintained below 5°C and a stock solution of benzathine penicillin G was stored in the dark and maintained at room temperature. Under these conditions, the solutions of procaine penicillin G and penicillin G were stable for 7 days and the solution of benzathine penicillin G was stable for 3 days.

The working samples of procaine penicillin G were stable at least for 4 hr at room temperature.

Apparatus

All fluorimetric measurements were performed on a Perkin-Elmer LS-50 equipped with a Xenon lamp, connected to an Ataio S 3000 ST 386 computer fitted with the Perkin-Elmer FL Data Manager software (design for handling fluorescence data on a personal computer) and Epson FX-850 printer.

Thermostatic equipment and a Crison, mod. 2001, pH-meter with a glass-saturated calomel combination electrode and centrifuge Selecta mod. Mixtaxel were also used.

CALIBRATION GRAPH, SAMPLE PREPARATION AND PROCEDURE

Calibration graph

A suitable aliquot containing 2.5–25 μg of procaine penicillin G was transferred into a 25 ml volumetric flask, 5.0 ml of buffer solution pH = 10.0 added and enough ethanol to ensure a final ethanol content of 60% V/V to every volumetric flask. This was diluted to the mark with water. The fluorescence intensity was measured at 348 nm, with excitation at 294 nm. Since dissolution prepared in a similar way without procaine penicillin G exhibits negligible fluorescence, a reagent blank is not necessary.

Procedure for injections

To determine procaine penicillin G in the presence of penicillin G, the sample solution was prepared by dissolving the content of the vial in Milli-Q water and diluting to adequate volume with Milli-Q water.

To determine procaine penicillin G in the presence of benzathine penicillin G, which is insoluble in water, a representative amount of aqueous obtained suspension was centrifuged to 2500*g* for 15 min. Five millilitres of clear solution was taken and this was diluted to the mark with Milli-Q water.

In both cases, the assay was completed as described for calibration graph. The percentage recovery of antibiotic is computed from regression equations for pure drugs.

RESULTS AND DISCUSSION

Spectral characteristics

The best characterization of the penicillin fluorescence is achieved by obtaining the tridimensional spectrum with suitable computer program.[13] This spectrum can be obtained and presented as the isometric projection, where the emission spectra at stepped increments of excitation wavelength are recorded and plotted (Fig. 1). A reversed projection of the data can sometime indicate emission peaks hidden by the foreground. Alternatively, the tridimensional

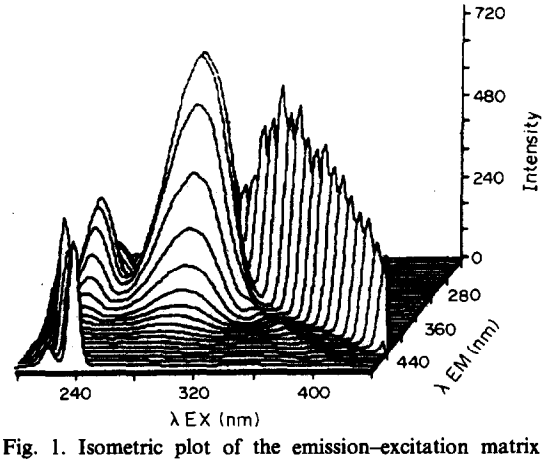

Fig. 1. Isometric plot of the emission–excitation matrix (forward projection) of procaine penicillin G (0.70 ppm). Ethanol–water content 60–40% (V/V), pH = 10.0.

spectra can be effectively transformed to a plot in two dimensions of excitation and emission wavelength by linking points of equal intensity to form contours, as shown in Fig. 2 where Rayleigh scatter has been removed. This contour presentation has generally been found to be more useful than the isometric projection for indicating the presence of hidden emission peaks.

As can be seen, the procaine penicillin G presents three fluorescence maxima, two of them localized at different excitation wavelength (223 and 294 nm) and at the same emission wavelength, 348 nm and the other localized at 220 nm and 295 nm as excitation and emission wavelengths, respectively. The wavelengths chosen were 294 and 348 nm for excitation and emission, respectively, where the higher intensity was obtained.

Factors affecting fluorescence intensity

The effect of changes in solvent composition was investigated using ethanol, methanol, chloroform and aqueous solutions at pH 2.0, 5.0 and 10.0. The highest and the smallest fluorescence intensities were obtained when ethanol and an aqueous solution at pH = 2.0 were used as solvents, respectively. A bathochromic effect was observed in the fluorescent emissions when the solvent polarity increased. Although the intensity of fluorescence in ethanol is higher than in water, we have chosen ethanol–water as the working medium because the aqueous stock solution is more stable than ethanolic stock solution.

The effect of ethanol content in the medium was investigated by preparing samples of penicillin varying only ethanol percentage between 0 and 96% V/V. The results are shown in Fig. 3(a), although the relative intensity of fluorescence increases with the ethanol content in the medium, we have selected a 60% V/V ethanol–water mixture because it provides the maximum intensity with regard to aqueous fraction [Fig. 3(b)].

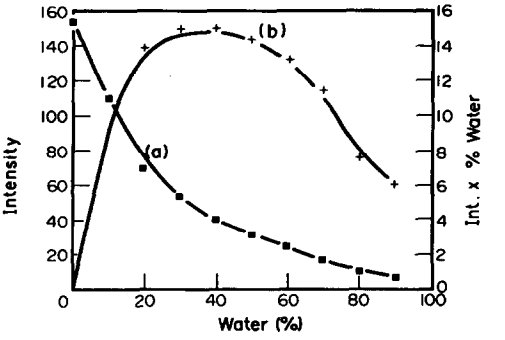

Fig. 3. Influence of the ethanol content. (a). Representation of fluorescence intensity with regard to aqueous fraction. (b). [Procaine penicillin G] = 1.0 ppm, pH = 10.0.

The influence of pH on the fluorescence spectrum was studied in an ethanol–water medium (60–40%) changing the pH by adding $HClO_4$ or NaOH. In Fig. 4 it can be observed that the fluorescence intensity is constant up to apparent pH value 7.0. It vastly increases for pH values between 7.0 and 9.0, the maximum fluorescence intensity is obtained for apparent pH value higher than 9.0. A pH = 9.9 was selected as the optimum apparent pH, which is proportioned by adding ammonium–ammonia buffer solution with pH = 10.0, whose concentration does not affect the fluorescence.

The dependence of the fluorescence intensity on temperature is critical, decreasing the fluorescence emission by 1.1%/°C when the temperature increases from 3 to 70°C. This effect can be explained by the higher internal conversion as temperature increases, facilitating non-radiative

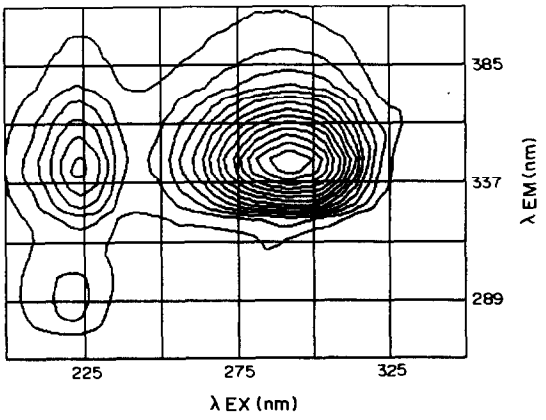

Fig. 2. Contour plot of procaine penicillin G fluorescence (0.70 ppm). Ethanol–water content of 60–40% (V/V), pH = 10.0.

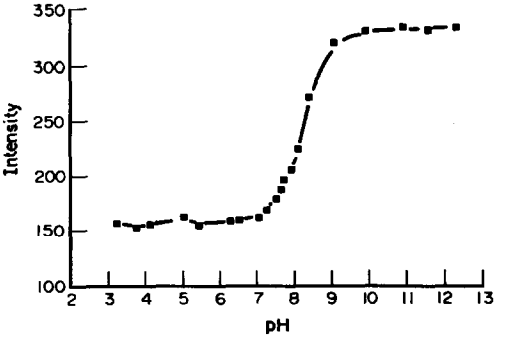

Fig. 4. Influence of the pH. [Procaine penicillin G] = 1.0 ppm. Ethanol–water content 60–40% (V/V), pH = 10.0.

deactivation of the excited singlet state. Thus, it is recommendable to use a thermostat, choosing a measurement of temperature of 20°C, independent of the room temperature.

The influence of the penicillin concentration on the fluorescence intensity was studied. The results show that there is a linear relationship between fluorescence intensity and procaine penicillin G concentration in the range of 0.10–1.0 ppm.

Spectrofluorimetric determination of procaine penicillin G

Under the operating conditions outlined above, we propose a method to determine procaine penicillin G by the direct measurement of fluorescence intensity at 348 nm, with excitation at 294 nm in the range of 0.10–1.0 ppm.

The proposed method was evaluated by a statistical analysis of experimental data by fitting the least squares line according to "$y = a + bx$". The results are presented in Table 1.

To verify if the intercept on the y axis is negligible, its significance was studied by applying the Student's "t" test at 95%[14] of confidence level and nine degrees of freedom. If the intercept on the y axis for the line calculated by the least squares technique is negligible, it is necessary to perform it again according to function "$y = b'x$" and therefore the new value of the slope of graph calibration (b') may be calculated. As can be seen in Table 1, the intercept on the y axis, is negligible, since experimental "t" is smaller than theoretical "t" and therefore the new slope is calculated.

The high value for the correlation coefficient of the regression equation and a negligible value for the intercept on the y axis demonstrate the satisfactory linear relationship between fluorescence intensity and procaine penicillin G concentration.

For a series of 10 standard samples containing 0.48 ppm of procaine penicillin G a relative error of 0.99% and standard deviation of 6.7×10^{-3} ppm were obtained (95% confidence level).

The detection limit is 9.4×10^{-3} ppm when defined as the analyte concentration leading to a luminescence intensity that is three times a blank standard deviation and determination limit is 0.024 ppm when defined as the analyte concentration leading to a luminescence intensity that is 10 times the blank standard deviation.[15,16]

Table 1. Statisticals parameters

Intercept on the y axis	3.30
Standard dev. of intercept	1.89
Slope	484.97
Standard dev. of slope	4.56
Correlation coeffic.	0.9998
Theoretical "t" value	2.262
Experimental "t" value	2.019
New slope	489.67

Interference study

It is easy to find penicillin G, procaine penicillin G and benzathine penicillin G mixtures for combining prompt action with prolonged effects.

For this, the effect of penicillin G and benzathine penicillin G was studied on the determination of 0.70 ppm of procaine penicillin G until a 100:1 ratio of interferent penicillin to procaine penicillin G. No appreciable variation of fluorescence intensity was observed in the value expected when the procaine penicillin G is in its own (all the obtained values are found in the "$\bar{x} \pm ts$' interval, where "x" is the mean of 10 determinations of procaine penicillin G in the absence and presence of penicillin G and benzathine penicillin G, "s" is standard deviation of these determinations and "t" is Student's "t" for nine degrees of freedom and at 95% confidence level).

Applications

The recommended procedure has been applied satisfactorily to the determination of procaine penicillin G in the presence of penicillin G and benzathine penicillin G in all the Spanish commercialized pharmaceutical products that contain these antibiotics in different proportions. Table 2 shows the assay results expressed as a percentage of the nominal contents (%R) resulting from the average of three determinations of three different vials. The recoveries agree well enough with the nominal content and the precision is quite satisfactory.

CONCLUSIONS

A new method for the fluorimetric determination of procaine penicillin G is described. The fluorescence is monitored at 348 nm (wavelength of excitation 294 nm) and the range of application of the method is between 0.10 and 1.0 ppm. Values of 9.4×10^{-3} and 0.024 of the detection and determination limits, respectively are obtained.

Table 2. Results obtained in the determination of procaine penicillin G in commercial pharmaceutical preparations

Commercial preparations	Laboratory	Composition (*mg*) P.P.G	P.G	B.P.B	P.P.G found (*mg*)	Deviation (*mg*)	%R
Farmaproína	Cepa	576.4	—	—	583.9	8.98	101.3
Aqucilina 600	Ant. S.A.	576.4	—	—	598.9	15.16	103.9
Aqucilina D-A	Ant. S.A.	288.2	60.0	—	288.2	1.44	100.0
Aqucilina D-A 600	Ant. S.A.	432.3	90.0	—	437.9	15.18	101.3
Ortopén 400000	Fides S.A.	288.2	60.0	—	284.4	4.86	98.7
Ortopén 1000000	Fides S.A.	576.4	24.0	—	568.9	8.23	98.7
Zoocilina 1000000	Ant. S.A.	864.6	60.0	—	875.8	5.69	101.3
Cepacilina 3:2:1	Cepa	288.2	120.0	76.5	295.4	4.68	102.5
Cepacilina 6:2:1	Cepa	576.4	120.0	76.5	576.4	10.09	100.0
Cepacilina 6:3:3	Cepa	576.4	180.0	229.5	591.4	8.98	102.6
Benzetacil 3:2:1	Ant. S.A.	288.2	120.0	76.5	291.7	5.04	101.2
Benzetacil 6:2:1	Ant. S.A.	576.4	120.0	76.5	569.5	4.07	98.8
Benzetacil 6:3:3	Ant. S.A.	576.4	180.0	229.5	568.9	33.68	98.7

P.P.G = Procaine penicillin G.
P.G = Penicillin G.
B.P.B = Benzathine penicillin G.

The method has been satisfactorily applied to the determination of procaine penicillin G in the presence of other salts of penicillin G.

The proposed method has been compared with spectrophotometric, chromatographic and spectrofluorimetric methods obtaining the following conclusions.

The spectrophotometric methods used to determine penicillins are based on derivatization reactions. The three typical assay are: iodometric,[17] the mercury imidazole[18] and the ferric hydroxamate[19] methods. All of them have a smaller sensitivity than the proposed method. Pillai *et al.*[19] proposed a direct spectrophotometric method to determine procaine penicillin G, obtaining a linear range, a sensitivity and a limit of detection smaller than the proposed method.

Generally the chromatographic methods to determine penicillins include precolumn derivatization or derivatization prior to detection.[20–21] Although the sensitivity is similar, the methods are slower than the proposed method. Procaine penicillin G was determined in pharmaceutical preparation by chromatography[22] without any derivatization with a relative deviation of 2% higher than the value obtained with the method described in this paper (1.4%).

The indirect spectrofluorimetric methods are tedious and high sensitivity is rarely obtained with them.[3–12]

Acknowledgement—The authors gratefully acknowledge financial support from the "Dirección General de Investigación Científica y Técnica" (Project N^0 PB 88-0365).

REFERENCES

1. J. A. Webber and W. J. Wheeler, in R. B. Morin and M. Gorman (eds), *Chemistry and Biology of β-lactam Antibiotic*, Vol. III, p. 288. Academic Press, New York, 1982.
2. D. M. Lichtenwalner, B. Suh, B. Lorber and A. L. Sugar, *Antimicrob. Agents Chemother.*, 1979, **16**, 210.
3. W. J. Jusko, *J. Pharm. Sci.*, 1971, **60**, 728.
4. E. Puigdellivo, G. Obiols and J. Moreno Dalmau, *Afinidad*, 1973, **30**, 749.
5. M. Ortega and B. del Castillo, *Afinidad*, 1973, **30**, 651.
6. F. Belal, A. El-Brashy and F. Ibrahim, *Microchem. J.*, 1989, **39**, 106.
7. R. H. Barbhaiya, P. Turner and E. Saw, *Clin. Chim. Acta*, 1977, **77**, 373.
8. K. Miyazaki, O. Ogino, H. Sato, M. Nakano and T. Arita, *Chem. Pharm. Bull.*, 1977, **25**, 253.
9. T. Tsuji, E. Miyamoto and T. Yamana, *J. Pharm. Pharmacol.*, 1978, **30**, 811.
10. A. B. C. Yu, C. H. Nightingale and D. R. Flanagan, *J. Pharm. Sci.*, 1977, **66**, 213.
11. W. L. Baker and P. J. Havlicek, *J. Gen. Appl. Microbiol.*, 1985, **31**, 107.
12. I. Mori, K. Fujita, K. Ikuta, S. Kitano, H. Kawabe, Y. Nakahashi, K. Kato and Y. Inamori, *Chem. Pharm. Bull.*, 1989, **37**, 1827.
13. J. A. Murillo and A. Alañón, manuscript in preparation.
14. P. K. Lark, B. R. Craven and R. C. L. Bosworth, The relationship between two variables-simple linear relations, in *The Handling of Chemical Data*. Pergamon, Oxford, 1968.
15. "Nomenclature, symbols, units and their usage in spectrochemical analysis, II". *Spectrochim. Acta, B*, 1978, **33B**, 242.
16. Guidelines for data acquisition and data quality evaluation in environmental chemistry, *Anal. Chem.*, 1980, **52**, 2242.
17. M. K. Ray Chowdhurry, R. Goswani and P. Charkrabarti, *Anal. Biochem.*, 1980, **108**, 126.

18. H. Bundgaard and K. Ilver, *J. Pharm. Pharmacol.*, 1972, **24**, 790.
19. E. Avanzini, D. Magnanelli and G. Cerrone, *Ann N.Y. Acad. Sci.*, 1968, **153**, 434.
20. C. B. Pillai and S. J. Rao, *Hind Antibiot. Bull.*, 1984, **26**, 142.
21. A. J. Shah, M. W. Adlard and G. Holt, *Analyst*, 1988, **113**, 1197.
22. D. Westerlund, C. Carlqvist and A. Theodorsen, *Acta Pharm. Suec.*, 1979, **16**, 187.
23. M. Puttemans, M. Lippens, L. Dryon and D. L. Massart, *J. Pharm. Biomed. Anal.*, 1983, **1**, 99.

Talanta, Vol. 40, No. 8, pp. 1207–1211, 1993
Printed in Great Britain.

0039-9140/93 $6.00 + 0.00
Pergamon Press Ltd

A COMPLETE DISSOLUTION PROCEDURE FOR Sn–Pb SOLDERS USING NITRIC AND HYDROCHLORIC ACIDS WITH SIMULTANEOUS DETERMINATION OF MAJOR AND TRACE ELEMENTS BY ICP/OES

D. A. WYNN

Johnson Controls, Inc., Advanced Battery Research, 5757 N. Green Bay Avenue, Milwaukee, WI 53209, U.S.A.

(*Received* 27 *October* 1992. *Revised* 29 *January* 1993. *Accepted* 3 *February* 1993)

Summary—A complete and fast dissolution procedure for tin and lead based solders is described. Trace and major elemental concentrations are determined by inductively coupled argon plasma emission (ICP) spectroscopy. One gram solder samples in the concentration range of 40–63 wt % tin are completely dissolved using nitric and hydrochloric acids. ICP analyses of certified reference materials prepared by this dissolution method are reported and compared to reference values. Based on comparison, the sample preparation method discussed is successful for quantitative analysis of trace and major elements in tin–lead solders.

The purpose of this work is to dissolve solder samples quickly for normal inductively coupled argon plasma emission spectroscopy (ICP) analysis procedures without using any special equipment. Tin and lead based solders are very difficult to dissolve because of metal oxide formation during dissolution. Dissolution is usually accomplished after hours of using nitric and fluoroboric acids. Microwave-oven dissolution procedures have been used to reduce the dissolution time to 4 min for 1 g sample. There is one undesirable problem with fluoroboric acid. It corrodes glass or quartz parts commonly found in analytical instruments and instrument components of special chemically resistant materials must be used.

Other methods for dissolution of solders can be found in the literature. A hydrofluoric acid (HF) and nitric acid mixture[1] is used, but this mixture is also corrosive to glass. A complete dissolution procedure using *aqua regia* is described for 0.1 g of a 50% Sn, 47% Pb and 3% Bi solder.[2] Three other HCl/HNO_3 methods are found in the literature[3,4,5] for determinations of one or two elements, but problems are noted with solution stability. The disadvantages of these procedures are that large dilution volumes must be used to avoid precipitation of the sample, the large dilution factor adversely affects the detectability for most trace elements of interest, the procedures are time consuming, and they have not been validated for multi-element analysis.

Several extraction techniques[6,7,8,9] are reported in the literature with subsequent element determinations by atomic absorption. Extraction techniques are very time consuming which is a major disadvantage.

A novel method for the dissolution of lead and tin based solders has been developed. The procedure requires concentrated nitric (70%) and hydrochloric (37%) acids for complete dissolution of a 1 g solder sample within 15 min. This new method allows multi-element analysis by ICP with no special changes to the ICP instrument (*i.e.*, HF or HBF_4 resistant nebulization systems are not required). Another advantage of ICP analysis is that trace non-metals (< 10 ppm) such as sulfur and phosphorus can be measured. These elements are of interest because of the effect on the quality of wave soldering.[10]

Tin is determined gravimetrically and compared to the ICP results for precision analysis. Reference solder materials are analysed for trace- and major-element concentration comparisons. There is good agreement between the ICP results and reference material values for all elements. This demonstrates that the new dissolution method is complete and is an acceptable alternative method.

EXPERIMENTAL

Apparatus

The ICP instrumentation used was described previously.[11] Modifications of the instrument were made through replacement of the 27 MHz generator with a 40.68 MHz generator (RF Plasma Products) and the Digital computer system with an IBM PS/2 Model 30. Under normal operating conditions, the mini-monochromator was set at 766.490 nm for K and the Hilger–Engis monochromator was set for 588.995 nm for Na. The Hilger–Engis monochromator was also used for element wavelengths which are not available on the polychromator. Off-peak background correction was not available with the two monochromators. Detection limits[11] for this ICP system for water and lead matrixes have been previously reported.

Reagents

House distilled water was purified to 18 MΩ by a MILLI-Q water purification system (Millipore Corp., Bedford, MA). All further references to water implies the use of 18 MΩ water. Reagent grade ("Baker Analyzed"®) nitric acid and purified (Ultrex®) hydrochloric acid were used for sample preparation (J. T. Baker Chemical Co., Phillipsburg, NJ). The nitric acid was further purified by distillation before use.

Dissolution preliminaries

Solder dissolution and dilution of sample solutions were performed in an acid fume hood. Dissolutions were done on Lindberg hot plates (model 53202, Watertown, WI). The surface temperature of the hot plate was measured using a surface thermometer (PTC® model 314F, Pacific Transducer Corp., Los Angeles, CA). All reported temperatures were the measured surface temperature of the hot plate during dissolution. The hot plates were always preheated to the desired temperature before use.

Glassware was soaked in 10% (v/v) hydrochloric acid, followed by 10% (v/v) nitric acid, and finally rinsed with water before use. All solder samples were dissolved in 300 ml tall form beakers (PYREX®, Corning, NY) and the solutions were brought to volume with water in class-A volumetric glassware. During dissolution samples were covered with watch glasses.

The disks of solder alloys used in this study were sampled by using a hard steel saw (nickel chrome alloy steel, model D-23, Disston, Danville, VA). No measurable contamination has been seen from this saw type when used on similar solder alloys. There was a designated saw for each solder alloy group. The saw was not specially cleaned between samples when used only for the designated solder alloy group. Historically this approach has proven satisfactory for sampling lead and its alloys. In this study, cross contamination was not observed between NIST certified and in-house reference materials using this saw.

At least three radial saw cuts towards the center of the sample were made and the chips collected to obtain a representative sample for analysis. Ten to 20 g (dependent on thickness of sample disk) were collected for the analysis. The chips were approximately 0.5 mm in diameter. All sawing chips were then mixed and the appropriate amount was weighed for dissolution.

Solder dissolution

Solder samples were dissolved by adding 1 ml of water and 20 ml of concentrated nitric acid to 1.000 ± 0.001 g of saw chips in a 300 ml tall form beaker. The sample was heated at 150°C for 5 min. Then 5 ml of concentrated hydrochloric acid was added slowly to the hot sample solution and heated for 5 min. Then 30 ml of water was added to the hot sample solution and heating continued for 5–20 min at 150°C until the sample was dissolved. During this time, more water (1 ml at a time) must be added if a white precipitate ($PbCl_2$) forms. The sample solution was cooled and diluted to 100 ml with water. Sample solutions show no visible sign of precipitation after more than 1 month.

Calibration standards

All standard stock solutions were acidic aqueous solutions. The calibration standard solutions were matrix-matched to the sample using the same reagents and acids used in sample dissolution. The appropriate amounts of purified tin (granular, 20 mesh, J. T. Baker Chemical Co., Phillipsburg, NJ) and lead (Doe Run Co., Herculaneum, MO), for the Sn–Pb portion of the calibration standard, were added to 300 ml tall form beakers to matrix-match the samples. The Sn–Pb calibration samples are then treated like samples. Once dissolved, aliquots of multi-element (Inorganic Ventures, Inc., Brick, NJ), single element 10,000 mg/l, and single element 1000 mg/l standard stock

solutions were then added to the Sn–Pb solutions to make complete calibration standards. A sample blank solution containing only 40% Pb and 60% Sn was prepared with the standards to subtract any trace element contamination in the starting materials and reagents.

Major alloy elements (Sn,Pb) contained in the standard stock solutions were compared to appropriate National Institute of Standards and Technology (NIST) standard reference materials (SRM) (Gaithersburg, MD). The SRMs were 10,000 mg/l stock solutions of each analyte.

RESULTS AND DISCUSSION

Preparation procedures

Hydrated tin oxides and/or tin nitrates were formed when nitric acid was added to solder chips. A white–yellow precipitate was suspended in solution. Tin chloride was formed when concentrated hydrochloric acid was added, but dissolution was still not complete until water was added because of the saturated condition of the solution. Some small white particles may still remain after water was added, but continued heating and stirring dissolved them. National Institute of Standards and Technology (NIST) (Gaithersburg, MD) Standard Reference Material (SRM) 127b (40% Sn, 60% Pb) in powder form, NIST SRM 1129 (63% Sn, 37% Pb) in disk form, Alpha (Newark, NJ) reference material TL-62X, lot 101 (60% Sn, 40% Pb) in disk form, and a 50–50 solder sample in disk form were dissolved successfully using the described dissolution method. Other certified solders (*i.e.*, 50–50 type) were not available. The method described should work for all tin–lead solders in the concentration range between the two NIST reference materials.

Matrix-matched calibration solutions were prepared from stock standard solutions containing all elements except Pb and Sn. The aliquots of the stock standard solutions containing all other elements were added to Pb–Sn solutions containing 4000–6300 mg/l Sn and 6000–3700 mg/l Pb. The Pb–Sn solutions were made from granular (20 mesh) purified tin metal and pure lead metal dissolved in the same manner as the samples. In this way, the calibration standard solution acid matrix was the same as that of the sample solution. Adding concentrated hydrochloric and nitric acids directly to purchased Sn and Pb stock standard solutions resulted in problems with precipitation.

Purified tin metal powder (>100 mesh, smaller particles), was first tried for the calibration standards, but resulted in incomplete dissolution. It was not clear why this happened. The incomplete dissolution may be due to the presence of tin oxides in the tin powder because of the higher surface area. Additional tin metal powders (>100 mesh) packaged under argon would need to be investigated to obtain the highest purity tin (oxide free) if >100 mesh powders were used for calibration standard preparation.

Instrumental results

A comparison of tin concentrations (reported in Table 1) as determined by two analytical methods, was done for four reference solder samples. All ICP results were in agreement within the standard deviation of the gravimetric technique. Uncertainty values for the Alpha reference materials and NIST 127b were not available. An estimated uncertainty value was given for the NIST 1129 SRM and agreed with the ICP value within the standard deviation. The gravimetric results were obtained to identify standard deviation values that could be obtained under routine analysis conditions. The standard deviation for Alpha TLS-36X is higher compared to the other standard deviations, in both the ICP and gravimetric methods.

A comparison of ICP results and the certified values of impurities in Alpha TL-62X and NBS 127b was carried out (Table 2). All major-,

Table 1. Tin concentrations (%) in several solders

Sample	Gravimetric*	ICP*	Certified
Alpha TL-62X	62.2 ± 0.4	61.5 ± 0.4	61.9†
Alpha TLS-36X	61.3 ± 0.8	60.7 ± 1.9	59.9‡
NIST SRM 127b	40.2 ± 0.4	38.8 ± 0.4	39.3§
NIST SRM 1129	62.9 ± 0.1	62.4 ± 0.6	62.7 (0.1)‖

*Average and standard deviation for triplicate analyses.
†Lot 101, 1981.
‡Lot A, 1978.
§Provisional, 25 January 1968.
‖NIST estimated uncertainty in parentheses, 8 May 1989.

Table 2. Comparison of ICP and certified reference material concentrations (%)

Element	Wavelengths for ICP (*nm*)	Alpha TL-62X*		Alpha TLS-36X†		NIST SRM 127b‡		NIST SRM 1129§	
		ICP	Certified	ICP	Certified	ICP	Certified	ICP‖	Certified
Al	309.271	0.0002	<0.001	<0.0001		<0.0001		<0.0001	
Sb	206.833	0.0192	0.019	0.520	0.51	0.415	0.43	0.144 ± 0.004†	0.13 (0.01)‡
As	193.696	0.0025	0.003	0.0024		0.0096	0.01	0.0532 ± 0.003	0.055 (0.005)
Bi	306.772	0.0065	0.005	0.0444	0.048	0.0626	0.06	0.149 ± 0.002	0.13 (0.01)
Cd	226.502	0.0008	0.0009	<0.0001		<0.0001		0.0063 ± 0.0002	0.006 (0.001)
Cu	324.754	0.0010	0.001	0.0836	0.073	0.0110	0.011	0.173 ± 0.003	0.16 (0.01)
Au	242.795	0.0102	0.010	<0.001		<0.001		0.0182 ± 0.0002	0.0175 (0.0005)
Fe	238.204	0.0048	0.006	<0.0001		<0.0001		<0.0001	
Pb	373.995	38.1 ± 0.5		35.1 ± 1.1		61.0 ± 0.8		37.2 ± 0.3	
Ni	232.003	0.0011	0.001	<0.0002		0.0113	0.012	0.0118 ± 0.0003	0.010 (0.002)
Ag	328.068	0.0019	0.002	2.66	2.99	0.0123	0.01	0.0668 ± 0.008	0.075 (0.005)
Sn	189.989	61.5 ± 0.4	61.9	60.7 ± 1.9	59.9	38.8 ± 0.1	39.3	62.4 ± 0.6	62.7 (0.1)
Zn	202.548	0.0008	0.002	0.0005		<0.0002		0.0009	
Na	589.000	<0.0008		<0.0008		<0.0008		<0.0008	
P	178.290	<0.001		<0.001		<0.001		<0.001	
S	182.037	<0.001		<0.001		0.002		0.002	

*Lot 101, 1981.

†Lot A, 1978.

‡Provisional, 25 January 1968.

§NIST estimated uncertainty in parentheses, 8 May 1989.

‖Average and standard deviation for triplicate analyses.

minor- and trace-element concentrations were determined simultaneously by ICP in this laboratory. The ICP results were shown to be in reasonable agreement with SRM 1129 results when compared to the estimated uncertainty for SRM 1129. No statistical data were reported for the other reference materials, but ICP results are generally within 10% of the reported values. As previously discussed for lead alloys,[11] slight sample inhomogeneity of the Alpha certified reference materials may be the cause of the larger differences (>10%) between the ICP and the Alpha certified results. Several elements (*i.e.*, Ag, Fe, As, Bi and Zn) fall into the category of differences >10%. The Alpha reference materials were solder disks originally prepared for arc/spark emission instruments. Such disks may be subject to segregation effects if not properly prepared. There did not seem to be any segregation problems with the NIST 1129 SRM disk. No definite conclusions can be made about the larger differences between results without Alpha reference precision data.

The segregation effects observed in lead alloys are based on disk cooling speed. Slower disk cooling times cause less soluble elements to generally form a gradient distribution in the disk. The concentration of the additive elements gradually increases towards the top of the disk. The bottom (surface in contact with the mold) is the surface used for spark emission. There is then a gradual increase in measured concentration as the disk is resurfaced before each spark analysis. A disk with segregration problems in time will become more and more inaccurate. Severe segregation can have more dramatic results. Taking a cross-section of the disk, as done for the ICP determinations, gives an average of the entire disk and different results will be obtained if the sample disk has segregation problems.

Silver analysis was not a problem with the materials analysed. The higher silver sample (Alpha TLS-36X) was cloudy after dissolution and was shaken just before analysis. The precipitation of silver chloride may be more of a problem if the silver concentration increases above 3% by weight.

CONCLUSIONS

Quantitative information for important solder elements can be obtained by using a single dissolution method which eliminates the need for fluoroboric and hydrofluoric acids to dissolve solders in the concentration ranges of 40–63% tin and 63–40% lead. This procedure allows complete dissolution of the solder with nitric and hydrochloric acids with no adverse effects on the elemental determinations by ICP. The detectable limits for all routinely analysed elements are below maximum specification limits.[10] This procedure should be applicable to the majority of solder materials based on the results of the two NIST certified SRMs and the complete dissolution of the two NIST SRMs and the 50–50 solder alloy.

ICP components resistant to fluoroboric and hydrofluoric acid corrosion are thus not required. Simultaneous multi-element determinations of trace impurity and major alloy elements are performed by ICP under normal acidic solution conditions.

Another advantage of ICP determination is that sulfur and phosphorus can be measured. These impurities are of interest because of the undesirable effects of high concentrations (>10 ppm S and >100 ppm P) of these elements on the quality of wave soldering.[10]

More work could be done in the area of improving the precision of the Sn and Pb determinations by using different wavelengths and/or modifying the sample size taken for analysis. Measurement of minor and trace elements by ICP is an ideal situation because of analysis time savings which are realized by simultaneous multi-element analysis.

REFERENCES

1. Standards Association of Australia, *Australian Standard*, Report AS 2292.2:1987, p. 12. Standards House, Australia, 1987.
2. R. Carleer, J. P. Francois and L. C. Van Poucke, *Bull. Soc. Chim. Belg.*, 1981, **90** (4), 357.
3. R. A. Mostyn and A. F. Cunningham, *Anal. Chem.*, 1967, **39**, 433.
4. R. Guerra, *Atomic Absorp. Newsletter*, 1980, **1** (2), 58.
5. A. Vogel, *Quantitative Inorganic Analysis*, 3rd Ed., p. 452. John Wiley, NY, 1961.
6. C. Chow, *Talanta*, 1986, **33** (1), 91.
7. T. Inui, S. Terada, H. Tamura and N. Ichinose, *Fresenius' Z. Anal. Chem.*, 1984, **318** (7), 502.
8. S. Bandyopadhyay and A. K. Das, *J. Ind. Chem. Soc.*, 1986, **63** (6), 623.
9. T. Inui, S. Terada, H. Tamura and N. Ichinose, *Fresenius Z. Anal. Chem.*, 1978, **292** (4), 282.
10. D. F. Bernier, *Electronic Manufact.*, 1988, **34** (8), 35.
11. T. J. Schmitt, J. P. Walters and D. A. Wynn, *Appl. Spectrosc.*, 1989, **43**, 687.

Talanta, Vol. 40, No. 8, pp. 1213–1220, 1993
Printed in Great Britain.

0039-9140/93 $6.00 + 0.00

KINETIC STUDY OF *N*-BROMOSUCCINIMIDE REACTIONS AND KINETIC DETERMINATION OF PYRIDOXINE USING A BROMIDE-SELECTIVE ELECTRODE

STERGIOS A. HALVATZIS, MEROPI M. TIMOTHEOU-POTAMIA* and CONSTANTINOS E. EFSTATHIOU
Laboratory of Analytical Chemistry, University of Athens, Panepistimiopolis, 157 71, Athens, Greece

(*Received* 8 *October* 1992. *Revised* 21 *January* 1993. *Accepted* 26 *January* 1993)

Summary—The bromide released by the alkaline hydrolysis of *N*-bromosuccinimide and its reactions with bromide, pyridoxine and thiamine have been studied potentiometrically using a solid-state bromide-selective electrode to monitor the consumed or produced bromide ion. Potential–time indications are obtained using a microcomputer-controlled potentiometric system. The overall rate constants and the activation energies have been calculated. A kinetic–potentiometric procedure for the determination of pyridoxine in the presence of thiamine in pharmaceutical preparations, based on its reaction with *N*-bromosuccinimide, is presented.

N-Bromosuccinimide (NBS) is probably the most important organic compound used as a source of the strong oxidant Br^+ ("positive bromine"), finding a variety of applications in both chemical synthesis and analysis. NBS is commonly used to bring about specific types of reactions *e.g.*, substitution, bromine addition, oxidation, *etc.* A great number of compounds have been determined using NBS with certain advantages over hypobromites which are usually prepared *in situ* since they disproportionate easily to bromate and bromide ions.[1,2]

Pyridoxine has been determined by many techniques such as spectrophotometry,[3] voltammetry[4] and potentiometric titrimetry with NBS.[5] Thiamine can be determined by spectrofluorimetric measurement of its oxidation product (thiochrome)[6] and by colorimetric[7] and chemiluminometric[8] techniques. Recently, NBS has been proposed for the kinetic–potentiometric determination of these vitamins.[9]

In this paper the bromide-selective electrode is used for the kinetic study of the reactions of NBS with pyridoxine and thiamine by monitoring the produced bromide, over a wide pH range. Since NBS consumes bromide ions generating bromine in acidic solutions and it is also hydrolyzed in alkaline solution generating hypobromite ion which is decomposed yielding bromide ions (the whole sequence hereafter is simply called "alkaline hydrolysis"), it was deemed necessary to study the kinetics of these reactions too. Based on the obtained kinetic data, a kinetic–potentiometric method has been developed for the determination of pyridoxine in the presence of thiamine. The method has been used for the assay of pyridoxine in pharmaceutical preparations containing thiamine.

EXPERIMENTAL

Apparatus

The system for potentiometric rate measurements consisted of a solid-state bromide electrode (Orion Model 94-35-00) in conjunction with a double-junction Ag–AgCl reference electrode (Orion Model 90-02-00), whose outer compartment was filled with a 10% (w/v) KNO_3 solution, and a digital voltmeter (Heath EU-805) interfaced to a microcomputer (Amstrad CPC 6128). The general interface technique and the main features of the control program (KINMOD) have been described elsewhere.[10]

All measurements were carried out in a thermostatted (±0.1°C) double-wall glass cell under constant magnetic stirring. The bromide-selective electrode was stored in 0.0010*M* KBr solution when not in use. pH measurements were carried out with a Metrohm Model E-350B pH-meter equipped with a low alkaline error combination glass electrode.

*To whom correspondence should be addressed.

Reagents

All reagents were of analytical grade and demineralized distilled water was used throughout.

N-Bromosuccinimide solution (0.0200*M*) was prepared by dissolving 0.178 g of NBS (Serva) in water and diluting with water to 50.0 ml. This solution was prepared daily and it was kept in an amber-coloured bottle.

Working standard bromide solutions were prepared by dilution of a 0.100*M* KBr stock solution.

Pyridoxine (Sigma) and thiamine (Serva) hydrochlorides stock solutions (0.0200*M*) were prepared daily by dissolving the appropriate amount of each compound in water and diluting to volume.

The following buffer solutions were used: acetate buffers (pH 3.0–5.0) 0.050*M* in total acetate, phosphate buffers (pH 2.0–4.0 and 5.0–11.0) 0.18 and 0.050*M* in total phosphate, respectively, and bromide containing phosphate buffers (pH 5.0–12.0) $5.0 \times 10^{-6}M$ in KBr and 0.050*M* in total phosphate.

PROCEDURES

General measurement procedure for kinetic studies

The following solutions are transferred into the reaction cell prior to the injection of NBS solution. For the study of the hydrolysis of NBS, 10.00 ml of the mixed bromide–phosphate buffer (pH 10.0–12.0) solution. For the study of the NBS–Br^- reaction, 5.00 ml of the phosphate buffer (pH 2.0–4.0), a 0.200–5.00 ml volume of $1.0 \times 10^{-4}M$ KBr and water to make a total volume of 10.00 ml. For the study of the reactions of NBS with pyridoxine and thiamine, 10.00 ml of the bromide containing buffer (pH 5.0–9.0) and 25–250 μl of the vitamin solution (0.00200*M*).

After transferring the above solutions into the reaction cell the stirrer is started and when the potential has stabilized (after 15–30 sec as shown by the electrometer readings), the reaction is initiated by rapid injection of the appropriate volume of the NBS solution. Potential indications are automatically collected by the microcomputer at constant time intervals. The reaction is followed for about 30–60 sec, its course is shown on the monitor of the microcomputer and the data (potential *vs.* time, *E–t* curve) are stored in magnetic disks for further processing. The cell is then evacuated and washed twice with the same buffer solution, before proceeding to the next measurement.

The data are recalled and the initial slope $(\Delta E/\Delta t)_0$ is measured (in millivolts per second) by interactive selection of the initial linear part, the correlation coefficient (r) of this part being a measure of the linearity (typically: $|r| \geq 0.995$).

The slope (S) of the electrode response, corresponding to the experimental prelogarithmic factor of the Nernst equation (theoretical value: $-RT/F$) and required for the calculation of reaction rate constants, is determined under the same conditions (temperature, pH and ionic medium) by successive additions of small volumes of 0.100*M* KBr stock solution in 10.00 ml of bromide-free buffer solution. An auxiliary computer program is used for the acquisition of potential indications and fast evaluation of S.

Sample preparation

Tablets. At least 20 tablets of the pharmaceutical preparation were weighed and finely powdered. A sample equivalent to approximately 200 mg of analyte was weighed accurately, transferred into a 1 l volumetric flask and diluted to volume with water. The powder was sonicated for 10 min to accelerate the dissolution. Working solutions were prepared from this sample solution by appropriate dilution so that the final analyte concentration was within the linear range of the calibration graph.

Injections. An accurately measured volume of the mixture of five ampules was transferred into a 250 ml volumetric flask and diluted to volume with water. The solution was diluted further so that the final analyte concentrations lay within the linear range of the calibration graph.

Measurement procedure for kinetic determination of pyridoxine

The general procedure, followed for the kinetic study of the reaction of NBS with the vitamins was used: 10.00 ml of bromide containing phosphate buffer of pH 5.0 was transferred into the cell and the reaction starts by adding 100 μl of sample containing pyridoxine in the concentration range 5×10^{-4}–$5 \times 10^{-3}M$. The

analytical signal, $(\Delta E/\Delta t)_0$, is measured as described above. Calibration graphs of $(\Delta E/\Delta t)_0$ *vs.* concentration of the examined reactant are constructed using standard solutions of the latter.

RESULTS AND DISCUSSION

Study of the electrode static and dynamic characteristics

In order to evaluate the operational characteristics of the bromide-electrode at the pH used, calibration graphs were obtained over the concentration range 5.0×10^{-7}–$1.0 \times 10^{-4}M$ at pH range 3.0–11.0 and temperature range 10–35°C. The lower linear concentration limit was $5.0 \times 10^{-6}M$ or less over the temperature and pH range studied.

The dynamic response time of the bromide ion-selective electrode was studied by rapid injections of a bromide solution to cause an increase $\Delta[Br^-]$ of an initial bromide concentration $[Br^-]_0$ and measuring the time required for the stabilization of the potential within 1% of the final potential change. The dynamic response times for the following changes ($[Br^-]_0 + \Delta[Br^-]$, M): $0 + 9.9 \times 10^{-7}$, $9.9 \times 10^{-7} + 4.9 \times 10^{-6}$, and $5.9 \times 10^{-6} + 4.90 \times 10^{-5}$ were found in the range 5.2–17.4, 2.7–9.0 and 0.5–3.6 sec, respectively, over the pH range 3.0–11.0 and temperature range 15–35°C.

From this study, it was concluded that the bromide-selective electrode can be used for the kinetic study, provided that a bromide background concentration not less than $5.0 \times 10^{-6}M$ is present before the initiation of the reaction, when bromide is a reaction product (hydrolysis of NBS and reactions of NBS with vitamins). Similarly, when bromide is consumed (reaction of NBS with Br^-), measurements must be obtained before its concentration becomes lower than $5 \times 10^{-6}M$. A time interval not less than the actual dynamic response time must be allowed before the acquisition of E–t indications for the calculation of $(\Delta E/\Delta t)_0$ to minimize errors due to hysteresis of the electrode response.

Kinetic study of NBS hydrolysis

NBS is relatively unstable in alkaline solutions[1] though no kinetic data of its hydrolysis reaction have appeared in the literature. The hydrolysis can be depicted by the following scheme.

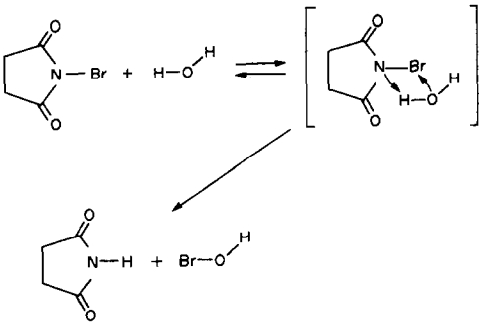

(I)

Hypobromous acid is a rather unstable weak acid ($K_a = 5 \times 10^{-9}$) and its decomposition is influenced by many factors (concentration, pH, temperature, presence of other salts, catalysts, activators, promoters and light).[11] The main competing decomposition reactions are

$$2HBrO \rightarrow 2H^+ + 2Br^- + O_2 \qquad (2)$$

$$3HBrO \rightarrow 3H^+ + 2Br^- + BrO_3^- . \qquad (3)$$

Since, each bromide ion may be the decomposition product of 1–1.5 molecules of NBS, the produced bromide is not expected to correspond stoichiometrically to NBS, nevertheless its production rate is indicative of the overall loss of total Br(+1) activity and indirectly of NBS, as well. Considering that the concentrations of NBS and hydroxide ions influence the overall reaction rate, the bromide formation rate can be generally described by the equation

$$d[Br^-]/dt = k_h[NBS]^x[OH^-]^y \qquad (4)$$

where k_h is the experimental rate constant of the hydrolysis.

By differentiation of the Nernst equation for the bromide-electrode with respect to time, we have

$$dE/dt = S(1/[Br^-])\ (d[Br^-]/dt) \qquad (5)$$

where S is the *experimental value of the* slope of the E *vs.* $\ln[Br^-]$ calibration graph (theoretical value: $-RT/F$).

Combining equations (4) and (5), at the beginning of the reaction where the initial slope $(\Delta E/\Delta t)_0$ is measured and $[Br^-]$ remains practically equal to the initially added (background) bromide concentration $[Br^-]_0$ we have

$$(\Delta E/\Delta t)_0 = (S/[Br^-]_0)\ k_h\ [NBS]_0^x[OH^-]_0^y. \qquad (6)$$

Rate measurements with $[NBS]_0$ in the range 1×10^{-5}–$4 \times 10^{-5}M$, over the pH range 10.0–12.0, and temperature range 10–25°C revealed reaction orders for NBS and OH^- equal to

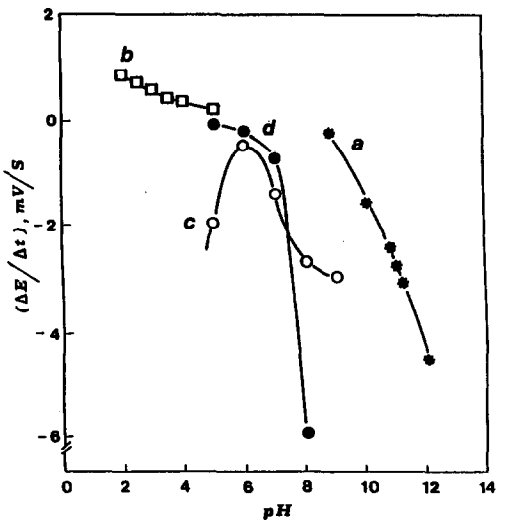

Fig. 1. Effect of pH on the reaction of NBS with reactants: (a) water (alkaline hydrolysis), (b) bromide, (c) pyridoxine and (d) thiamine, at 20°C. [NBS] = $2.0 \times 10^{-4}M$, [Reactant] = $2.0 \times 10^{-5}M$.

1.04 ± 0.08 (range: 0.96–1.18) and 0.23 ± 0.03 (range: 0.20–0.25), respectively.

The effect of pH on the initial rate of the NBS hydrolysis reaction is shown in Fig. 1 [curve (a)].

At pH 10.5 and temperatures of 10, 15, 20 and 25°C, the experimental k_h values were found to be equal to 0.018, 0.026, 0.034 and $0.042M^{-0.23}$/s, respectively and the calculated activation energy was 9.4 ± 0.7 kcal mol.

All data concerning the rate of Br^- production are incorporated in the equation

$$d[Br^-]/dt = 3.6 \times 10^5[NBS][OH^-]^{0.23}\exp[-4753]/(273.15+\theta)] \quad (7)$$

which is valid over the aforementioned ranges of pH, temperature (θ) and NBS concentration.

According to the above results, all kinetic studies of reactions of NBS with other compounds based on monitoring of the produced bromide ions, must take into consideration the parallel hydrolysis of NBS which is particularly pronounced at pH $\geq$ 10.0. This hydrolysis must be considered as a plausible source of blank in kinetic measurement, since part of the intermediately formed hypobromite may escape the primary reaction (in the present case with vitamins) and be decomposed according to reaction (2) and/or (3).

Kinetic study of the NBS–bromide reaction

In acidic solutions NBS reacts with Br^- according to the overall reaction

$$NBS + H^+ + Br^- \rightarrow NHS + Br_2. \quad (8)$$

Considering that the rate of bromide consumption is affected by NBS, bromide and

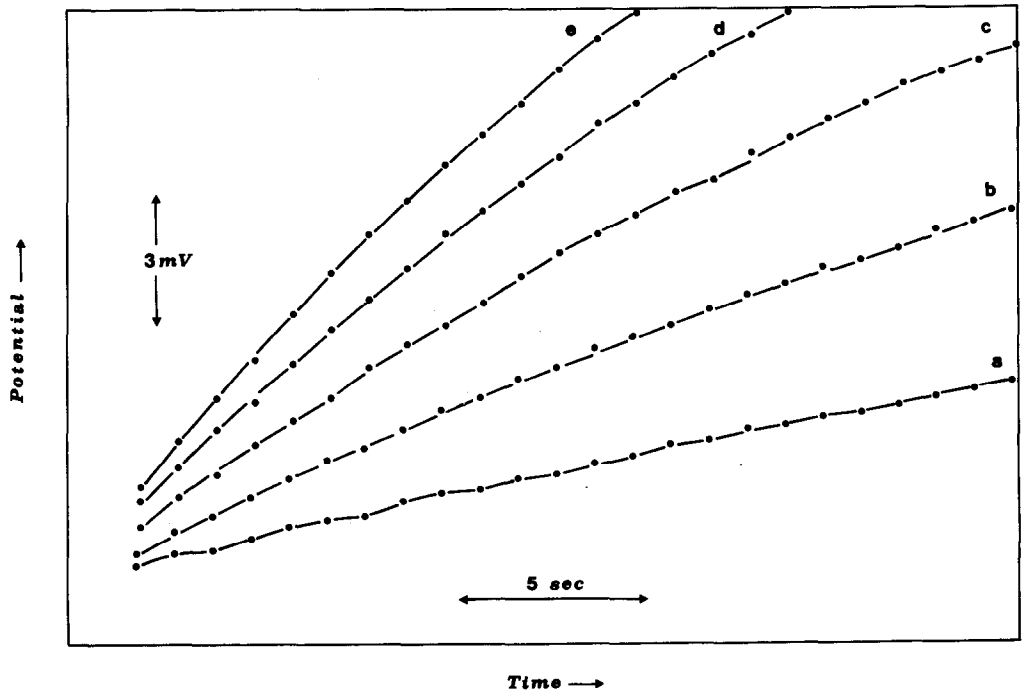

Fig. 2. Typical E–t curves of the NBS–bromide reaction for the calculation of the reaction order with respect to NBS at 25°C and pH 2.5. $[NBS]_0$: (a) 5.0×10^{-5}, (b) 1.0×10^{-4}, (c) 1.5×10^{-4}, (d) 2.0×10^{-4} and (e) $2.5 \times 10^{-4}M$ ($[Br^-]_0 = 5.0 \times 10^{-5}M$).

Table 1. Kinetic data for the kinetic parameters (reaction orders and rate constants) for the reactions of NBS with pyridoxine and thiamine, at a temperature of 20°

	NBS–pyridoxine reaction Reaction order			NBS–thiamine reaction Reaction order		
pH	NBS	Pyridoxine	k_{obs} ($/M\ s$)	NBS	Thiamine	k_{obs} ($/M\ s$)
5.0	0.98 ± 0.03 ($n = 4$)*	1.06 ± 0.04 ($n = 6$)	176 ± 3.7 ($n = 6$)	1.05 ± 0.08 ($n = 4$)	0.99 ± 0.03 ($n = 5$)	0.47 ± 0.00 ($n = 5$)
6.0	1.12 ± 0.10 ($n = 4$)	1.01 ± 0.03 ($n = 6$)	28.4 ± 0.3 ($n = 6$)	1.08 ± 0.07 ($n = 4$)	1.09 ± 0.09 ($n = 4$)	8.3 ± 0.3 ($n = 4$)
7.0	0.98 ± 0.02 ($n = 5$)	1.06 ± 0.06 ($n = 6$)	102 ± 2.6 ($n = 6$)	0.96 ± 0.18 ($n = 3$)	1.05 ± 0.05 ($n = 5$)	33.4 ± 0.8 ($n = 5$)
8.0	0.97 ± 0.06 ($n = 4$)	1.05 ± 0.09 ($n = 4$)	133 ± 3.2 ($n = 4$)	1.06 ± 0.10 ($n = 5$)	1.13 ± 0.08 ($n = 5$)	749 ± 45 ($n = 5$)
8.0	1.02 ± 0.05 ($n = 5$)	1.09 ± 0.11 ($n = 4$)	324 ± 16 ($n = 4$)	1.08 ± 0.10 ($n = 4$)	1.04 ± 0.04 ($n = 5$)	941 ± 24 ($n = 5$)

*n = number of standard solutions, each measured three times.

hydrogen ion concentrations, this rate is described by the overall equation

$$-(\mathrm{d}[Br^-]/\mathrm{d}t) = k_{exp}[Br^-]^x[NBS]^y\ [H^+]^z \quad (9)$$

where k_{exp} is the experimental rate constant of the overall reaction.

Combining equations (5) and (9) at the beginning of the reaction, we have

$$(\Delta E/\Delta t)_0 = Sk_{exp}\ [Br^-]_0^{x-1}[NBS]_0^y[H^+]_0^z. \quad (10)$$

Rate measurements with $[NBS]_0$ and $[Br^-]_0$ in the range 2.5×10^{-5}–$5.0 \times 10^{-5} M$ and 5.0×10^{-6}–$5.0 \times 10^{-5} M$, respectively, over the pH range 2.0–3.5 and the temperature range 10–30°C, revealed reaction orders for NBS, Br^- and H^+ equal to 0.98 ± 0.04 (range: 0.93–1.07), 1.20 ± 0.04 (range: 1.11–1.25) and 0.28 ± 0.06 (range: 0.19–0.32), respectively. Therefore equation (10) can be written

$$(\Delta E/\Delta t)_0 = Sk_{obs,H}[Br^-]_0^{x-1}\ [NBS]_0 \quad (11)$$

and $k_{obs,H}$ expresses the pH dependent overall observed second-order rate constant.

$k_{obs,H}$ values at pH 2.0, 2.5 and 3.0, over the temperature range 15–35°C were calculated in the ranges 1.3×10^3–3.2×10^3, 1.0×10^3–2.4×10^3 and 0.9×10^3–$1.7 \times 10^3/M$ s, respectively. The respective calculated activation energies were 8.1 ± 0.4, 8.4 ± 0.4 and 5.6 ± 0.3 kcal/mol.

Typical E–t curves of the NBS–Br^- reaction, used for the calculation of the reaction order with respect to NBS at pH 2.5 at 25°C are shown in Fig. 2. The effect of pH on the initial rate of the NBS–bromide reaction is included in Fig. 1 [curve (b)].

According to the above results, all kinetic studies of reactions of NBS (in excess) with other compounds based on monitoring of the produced bromide ions, must also take into consideration the parallel consumption of bromide which is particularly pronounced at pH ≤ 4.0.

Kinetic study of NBS reactions with pyrodoxine or thiamine

Recently, potentiometric monitoring of the bromide production rate during the reaction of pyridoxine or thiamine with NBS has been exploited for developing a kinetic–potentiometric procedure for the determination of these vitamins in pharmaceutical preparations. However, no detailed kinetic data were obtained.[9]

Considering that the rate of bromide production is affected by NBS and vitamin (Vit) concentrations, and combining the relevant

Table 2. Kinetic data of the rate constants (k_{obs}) and activation energies (E_a) for the reactions of NBS with pyridoxine and thiamine at various pH

		k_{obs} ($/M\ s$)							
		Temperature (°C)							
Compound	pH	10	15	20	25	30	35	40	E_a (*kcal/mol*)
Pyridoxine	5.0		140	175	194	225	256	278	4.9 ± 0.3
	9.0			433	496	563	633	714	4.6 ± 0.1
Thiamine	6.0	1.56	2.95	4.95	12.5	24.0	37.3	95.0	24.1 ± 1.0
	9.0	314	567	925	1845	3072			19.6 ± 0.6

Table 3. Effect of pH on the pyridoxine and thiamine calibration graphs in the range 5.0×10^{-6}–$5.0 \times 10^{-5} M$

pH	Regression line*	r	n†
Pyridoxine			
5.0	$y = 0.08 + 9.47 \times 10^4 x$	0.999	6
6.0	$y = -0.01 + 2.46 \times 10^4 x$	0.998	6
7.0	$y = 0.18 + 5.43 \times 10^4 x$	0.996	6
8.0	$y = 1.10 + 7.82 \times 10^4 x$	0.994	4
9.0	$y = 0.59 + 11.9 \times 10^4 x$	0.992	4
Thiamine			
5.0	$y = 0.03 + 0.49 \times 10^4 x$	0.997	5
6.0	$y = 0.30 + 1.76 \times 10^4 x$	0.994	4
7.0	$y = 0.17 + 1.90 \times 10^4 x$	0.997	5
8.0	$y = 0.18 + 16.3 \times 10^4 x$	0.997	5
9.0	$y = 0.31 + 56.6 \times 10^4 x$	0.999	5

*$y = (\Delta E/\Delta t)_0$ (mV/s) and $x = C$ (M).
†n = number of samples, each measured three times.

kinetic expression with the Nernst equation we finally obtain the following equation

$$(\Delta E/\Delta t)_0 = (S/[Br^-]_0)\, k_{obs}[NBS]_0^x[Vit]_0^y \quad (12)$$

where k_{obs} is the overall experimental rate constant which is expected to be pH-dependent.

Plots of $(\Delta E/\Delta t)_0$ *vs.* $[Vit]_0$ (for both vitamins) are linear denoting a practically first-order reaction with respect to vitamins ($y \approx 1$), but a positive intercept (blank) is consistently observed probably due to a catalysis of the NBS-hydrolysis reaction by coexisting species or unknown side reactions also producing bromide. Therefore all initial rates $(\Delta E/\Delta t)_0$ used for the subsequent calculations were previously corrected for this blank.

From experiments with various concentrations of vitamin and a constant concentration of NBS, the reaction order with respect to vitamin and k_{obs} can be obtained. From similar experiments, in which NBS concentration is varied with constant vitamin concentration, the reaction order with respect to NBS can also be obtained. The results of this kinetic study at 20°C and at pH range 5.0–9.0 are summarized in Table 1.

The k_{obs} values obtained as described above at pH 5.0 and 9.0 for the NBS–pyridoxine reaction and at pH 6.0 and 9.0 for the NBS–thiamine reaction, at various temperatures (10–40°C) and the calculated activation energies are given in Table 2.

The effect of pH on the NBS–pyridoxine and NBS–thiamine reactions are included and shown comparatively in Fig. 1 [curves (c) and (d), respectively].

Determination of pyridoxine in the presence of thiamine

Equation (12) shows that the initial slope of the reaction curve is linearly related to the

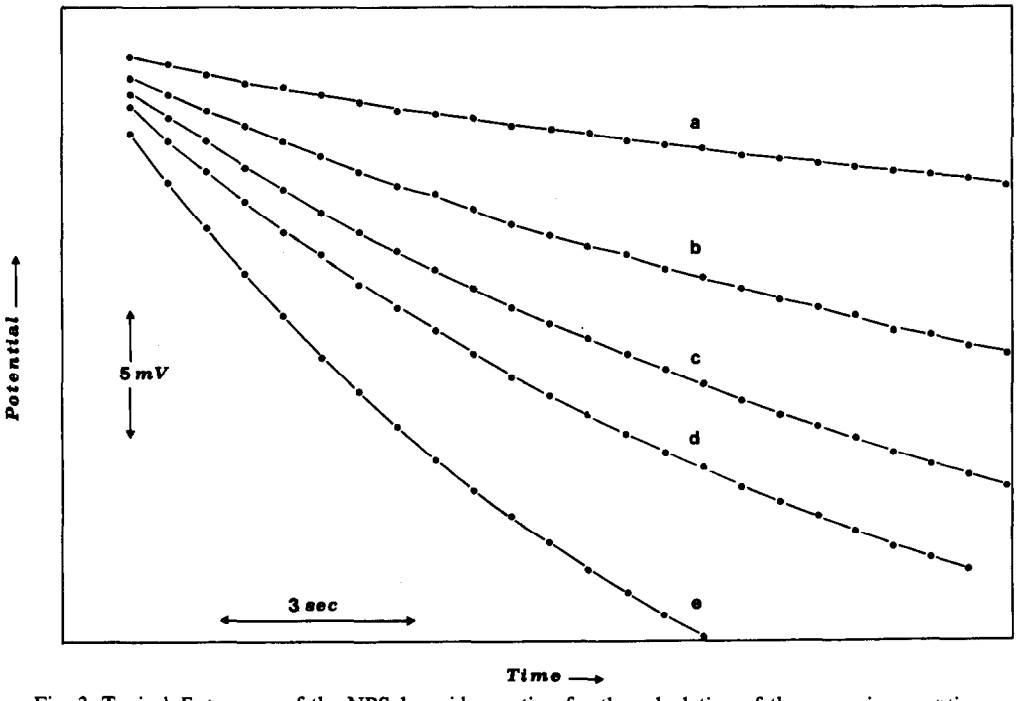

Fig. 3. Typical E–t curves of the NBS–bromide reaction for the calculation of the regression equation for the determination of pyridoxine at 20°C and pH 5.0. $[Pyridoxine]_0$: (a) 5.0×10^{-6}, (b) 1.0×10^{-5}, (c) 1.5×10^{-5}, (d) 2.0×10^{-5} and (e) $3.0 \times 10^{-5} M$ ($[NBS]_0 = 2.0 \times 10^{-4} M$).

Table 4. Determination of pyridoxine in commercial formulations containing thiamine with the proposed method and an official method[12]

Formulation	Pyridoxine content (*mg*/ampule or tablet)			
	Stated composition	Official method	Proposed method ($\pm s$)*	Relative difference (%)
Neurobion (tablet)	200 mg pyridoxine 100 mg thiamine 200 μg cyanocobalamin	192	174 ± 3	−9.4
Neurobion (injection)	100 mg pyridoxine 100 mg thiamine 10 mg cyanocobalamin	104	108 ± 2	+3.8
Vioneurin-6 forte (injection)	250 mg pyridoxine 50 mg thiamine 10 mg cyanocobalamin	251	246 ± 8	−2.0
Triforte (injection)	100 mg pyridoxine 250 mg thiamine 1 mg cyanocobalamin	98	104 ± 2	+6.1

*Each sample measured three times.

vitamin concentration as the reaction is first-order with respect to vitamin (Table 1). The working curves obtained with concentrations of vitamins in the range of 5.0×10^{-6}–$5.0 \times 10^{-5}M$ at various pH values are described by the regression equations shown in Table 3. Maximum reaction initial rates for both reactions are observed at pH 9.0, where thiamine reacts faster than pyridoxine. However, at pH 5.0 the reaction rate of NBS with pyridoxine is about two orders higher than that with thiamine. Therefore the kinetic determination of pyridoxine in the presence of thiamine is feasible when both vitamins are present within the same order of concentration. Typical E–t curves of the NBS–pyridoxine reaction are shown in Fig. 3. Using these curves the regression equation for the determination of pyridoxine at pH 5.0 is obtained.

The method developed was used in the assay of pyridoxine in pharmaceutical preparations containing both vitamins. The mole ratios of thiamine and pyridoxine in all pharmaceutical preparations examined were within the range of 0.2–5.0. Results obtained from determinations of pyridoxine in pharmaceuticals with the proposed method for the determination of pyridoxine are compared very well with those obtained by the US Pharmacopoeia procedure[12] and they are shown in Table 4.

Simultaneous determination of both vitamins by applying differential kinetic analysis[13] and obtaining measurements at *e.g.*, pH 5.0 and 9.0, gave satisfactory results with synthetic mixtures of vitamins, but positive analytical errors were consistently observed with thiamine in real samples.

CONCLUSIONS

N-Bromosuccinimide reactions can be indirectly studied by potentiometric monitoring of the produced bromide with a bromide-selective electrode. This method may be applied for studying reactions of NBS with a number of inorganic and organic compounds (*e.g.*, ammonia, aminoacids, hydrazides). The parallel hydrolysis of NBS, which is particularly fast in the alkaline pH range (pH ≥ 10.0), and the reaction of NBS (when present in excess) with the produced bromide, particularly in acidic pH range (pH ≤ 4.0), must be taken into consideration. The kinetic data presented in this study, concerning these possible parallel reactions of NBS, may prove useful in this case.

It must be stressed that fast NBS reactions *e.g.*, with ascorbic acid, cannot be monitored reliably due to the inherent inability of potentiometric sensors to follow fast reactions.

REFERENCES

1. N. K. Mathour and C. K. Narang (eds), *The Determination of Organic Compounds with N-Bromosuccinimide and Allied Reagents*. Academic Press, London, 1975.
2. R. Filler, *Chem. Rev.*, 1962, **63**, 21.
3. V. Nirmalchandar, R. Viswanathan and N. Balasubramanian, *Analyst*, 1987, **112**, 653.
4. P. Soderhjelm and J. Lindquist, *Analyst*, 1975, **100**, 349.
5. Y. Takeuchi, A. Kawabata and Y. Iwasa, *Nippon Nogei Kagaku Kaishi*, 1968, **42**, 68; *Chem. Abstr.*, 1968, **69**, 38763p.
6. M. Barary, M. Abdel-Hamid, E. Hassan and M. Elsayed, *Pharmazie*, 1986, **41**, 483.
7. R. T. Sane, V. J. Doshi, S. Jukar, S. K. Joshi, S. V. Sawant and U. R. Pandit, *J. Assoc. Off. Anal. Chem.*, 1985, **68**, 83.

8. N. Grekas and A. C. Calokerinos, *Talanta*, 1990, **37**, 1043.
9. S. A. Halvatzis and M. Timotheou-Potamia, *Anal. Chim. Acta*, 1989, **227**, 405.
10. H. A. Archontaki, M. A. Koupparis and C. E. Efstathiou, *Analyst*, 1989, **114**, 591.
11. N. N. Greenwood and A. Earnshaw, *Chemistry of the Elements*, p. 1005. Pergamon Press, Oxford, 1990.
12. United States Pharmacopeial Convention, "*US Pharmacopeia*", XXI. Mack Publishing Co., Easton, P.A., 1985.
13. H. A. Motolla, *Crit. Rev. Anal. Chem.*, 1975, **4**, 229.

Talanta, Vol. 40, No. 8, pp. 1221–1225, 1993
Printed in Great Britain.

0039-9140/93 $6.00 + 0.00

INVESTIGATIONS ON ADSORPTION POTENTIOMETRY—PART VIII. DETERMINATION OF ULTRATRACE COPPER IN FOOD BY DERIVATIVE ADSORPTION CHRONOPOTENTIOMETRY

LI XIAO and WENRUI JIN*
Department of Chemistry, Shandong University, Jinan 250100, Shandong, P.R. China

(*Received* 14 *September* 1992. *Revised* 5 *February* 1993. *Accepted* 18 *February* 1993)

Summary—An electroanalytical method, based on derivative chronopotentiometry of the copper complex with 4-[(4-diethylamino-2-hydroxyphenyl) azo]-5-hydroxy-naphthalene-2,7-disulphonic acid (Beryllon III) accumulated on the surface of a hanging mercury drop electrode, for determining trace copper in food has been developed. The dependence of the peak height of reduction of the copper complex on the preconcentration time and preconcentration potential are discussed. Optimum experimental conditions include 0.01 *M* HOAc, 0.01*M* NaOAc, 1.0×10^{-6} Beryllon III and a preconcentration potential of 0.10 V (*vs.* SCE). Under these conditions the detection limit and the linear range are $4 \times 10^{-11}M$ and 6×10^{-11}–$4 \times 10^{-7}M$, respectively. The method was applied to samples of digested rice.

Of the methods for determination of trace copper by electrochemical analysis, anodic stripping voltammetry is usually used. Since its anodic peak is near the peak of oxidation of the mercury, determining copper is not any more sensitive than other heavy metals, such as zinc, cadmium and lead. Another disadvantage of anodic stripping voltammetry for the determination of copper is interference of metal ions, in particular, Zn(II), due to formation of intermetallic compounds in amalgams. Adsorption voltammetry is well suited to the determination of trace copper ion through its complexes with CNS^-,[1] catechol,[2,3] 8-hydroxyquinoline[4] and thiorea.[5] Usually, the limit of detection of these methods is 10^{-8}–$10^{-9}M$. Of these methods, the adsorption voltammetry of the Cu(II)–catechol system is the most sensitive and the limit of detection is as low as $6 \times 10^{-11}M$. However, the disadvantage of using catechol to determine copper lies in its instability against oxidation by dissolved oxygen.[3] The stock solution needs to be prepared freshly every day.

More recently an ultra-trace electroanalytical method for the determination of inorganic ions, *e.g.*, cobalt,[6] nickel,[8] iron,[7] bismuth[8] and beryllium,[9] called derivative adsorption chronopotentiometry has been proposed. This method is similar to chronopotentiometry stripping analysis, and its theory has been reported.[10] In this method, instead of electrolytic accumulation, inorganic complexes can be accumulated by adsorption like adsorption voltammetry, and the derivative of time with respect to potential is then recorded. The peak height $(dt/dE)_p$ of the curve, adsorption chronopotentiogram, can be written as the following equation[10]

$$(dt/dE)_p = Kt_a c/i_o \quad (1)$$

where K is a constant, t_a is the preconcentration time, i_o is a constant reducing current and c is the concentration of adsorbed complex in the solution which is proportional to the concentration of metal ion.

In this paper the derivative adsorption chronopotentiometry of copper in the presence of 4-[(4-diethylamine-2-hydroxyphenyl)azo]-5-hydroxy-naphthalene-2,7-disulphonic acid (Beryllon III) at a hanging mercury drop electrode (HMDE) was developed. The limit of detection of the method is as low as $4 \times 10^{-11}M$. Except for the lower limit of detection, another advantage of the method is that the ligand (Beryllon III) is stable in the stock solution which can be stored for at least one month at room temperature.

*Author for correspondence.

EXPERIMENTAL

Apparatus

A Model DPSA-3 stripping analyser (Shandong Seventh Electronic Factory, China) for derivative adsorption chronopotentiometry coupled with a Model LZ_3-200 X-Y recorder (Shanghai Dahua Instrument Factory, China) was used in connection with a cell, using potentiostatic control of the electrode potential by means of a three electrode system consisting of a Model SH-84 HMDE (Department of Chemistry, Shandong University, China) as the working electrode, a platinum plate as the counter electrode and a saturated calomel electrode (SCE) as the reference electrode, connected to the analyte via a salt bridge filled with $0.01M$ HOAc + $0.01M$ NaOAc. In the preconcentration step, the solution was stirred with a PTFE-covered stirring bar, rotated by a Model MCP-IT magnetic stirrer (Shandong Seventh Electronic Factory, China).

Reagents and solutions

A $1 \times 10^{-2}M$ stock solution of Cu(II) was prepared by dissolving an appropriate amount of metal copper in 1:1 HNO_3. The solution was then evaporated in a sand-bath until white smoke appeared. The solution was transferred to a 1 l standard flask. The standard solution was obtained by diluting the stock solution with water. A $5 \times 10^{-4}M$ stock standard solution of Beryllon III was prepared by dissolving an appropriate amount of Beryllon III in water. Other reagents were of analytical-reagent grade and all solutions were prepared with triply distilled water.

Procedure

The supporting electrolyte consisted of $0.01M$ HOAc + $0.01M$ NaOAc. The solution was deaerated for 15 min with pure nitrogen. The measurements were carried out after a preconcentration step in which the solution was usually stirred for 60 sec at a preconcentration potential, E_a, of 0.10 V (*vs.* SCE). After a rest period of 30 sec, the potentiostatic circuitry was disconnected and a constant reducing current, i_o, of 1 μA or 0.1 μA was passed through the HMDE and the counter electrode. The plot of dt/dE *vs.* E was stored in the stripping analyser and plotted subsequently. All potentials were measured against the SCE.

RESULTS AND DISCUSSIONS

Derivative adsorption chronopotentiogram of the Cu(II) complex with Beryllon III adsorbed on the HMDE

The structure of Beryllon III, L, is

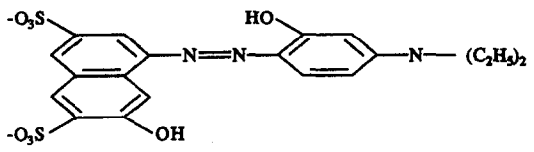

In HOAc + NaOAc solution, it can form a complex with Cu(II), CuL, which is reduced at a mercury electrode[11] according to the following scheme,

$$Cu(II)L + Hg \rightleftharpoons Cu(II)L(ads)(Hg) \quad (1)$$

$$Cu(II)L(ads)(Hg) + 2e^- \rightarrow Cu(O)(Hg) + L(ads) \quad (2)$$

Figure 1 reproduces the derivative chronopotentiogram of Cu(II) (curve 1) and the derivative adsorption chronopotentiograms of Beryllon III (curve 2) and its complex with Cu(II) (curve 3). Cu(II) produces a diffusion-controlled peak at about -0.04 V in the supporting electrolyte. In $1.0 \times 10^{-6}M$ Beryllon III and the supporting electrolyte, one peak appears in the potential range from 0 to -1.0 V, the potential of the peak is -0.26 V. When $5.0 \times 10^{-8}M$ Cu(II) is added into the solution, a new peak appears at a position between the peak of reduction of Cu(II) and that of Beryllon III with the peak potential of -0.13 V and the peak height of reduction of Beryllon III decreases. It is the result of reduction of the Cu(II) complex with Beryllon III adsorbed on the electrode. The relationship between the peak height and the preconcentration time, t_a, is shown in Fig. 2. The peak height increases with increasing t_a, when $t_a > 240$ sec, the straight line begins to deflect, this means that the Cu(II) complex can be adsorbed on the surface of the electrode. The adsorptivity of the complex on the surface of the HMDE is dependent on the preconcentration potential, E_a. The relationship between the peak height, $(dt/dE)_p$, and E_a is shown in Fig. 3. The adsorption is stronger in the potential range 0.15–0 V.

Optimum experimental conditions

Figure 4 shows the dependence of the peak height of reduction, of the Cu(II) complex adsorbed on the electrode, on the concentration of

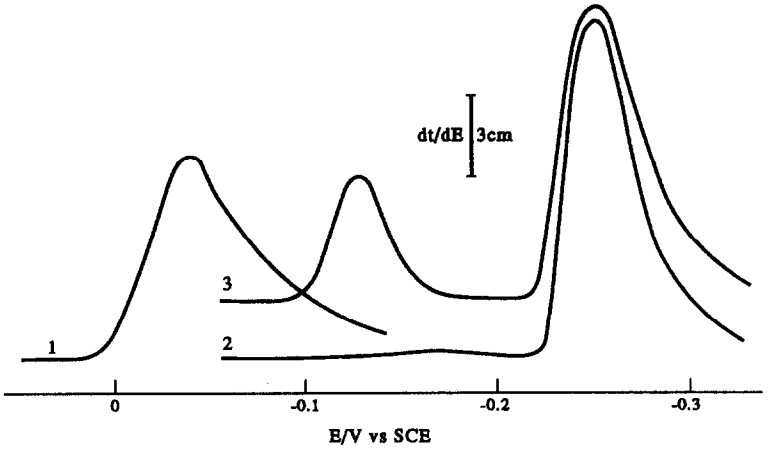

Fig. 1. Derivative chronopotentiogram of Cu(II) and derivative adsorption chronopotentiograms of Beryllon III and its complex with Cu(II). (1) $2.5 \times 10^{-5}M$ Cu(II); (2) $1.0 \times 10^{-6}M$ Beryllon III; (3) (2) + $5.0 \times 10^{-3}M$ Cu(II). $0.01M$ HOAc + $0.01M$ NaOAc. Sensitivity of the analyser is 60; sensitivity of the recorder is 50 mV/cm; $E_a = 0.10$ V; $i_o = 1$ μA; (1), (2) $t_a = 60$ sec, (3) $t_a = 360$ sec.

NaOAc (curve 1) and HOAc (curve 2). NaOAc ($0.01M$) and HOAc ($0.01M$) were chosen in our experiments as supporting electrolytes.

It was found that the optimum concentration of Beryllon III is different for different concentrations of Cu(II), if the concentration of Beryllon III is too high, the peak height of the complex decreases because of the adsorption competition of Beryllon III; if the concentration of Beryllon III is too low, the peak height of the complex decreases too, because not all the Cu(II) can form the complex with Beryllon III. The optimum concentrations of Beryllon III are $2 \times 10^{-8}M$ for $1\text{–}10 \times 10^{-10}M$ Cu(II), $4 \times 10^{-7}M$ for $1\text{–}10 \times 10^{-9}M$ Cu(II) and $1 \times 10^{-6}M$ for $10^{-8}\text{–}4 \times 10^{-7}M$ Cu(II).

Linear range, detection limit and reproducibility

The peak height $(dt/dE)_p$ of the derivative adsorption chronopotentiogram is dependent on the reducing current, i_o. The smaller i_o is, the higher the peak height,[10] so we used $i_o = 0.1$ μA to obtain the linear range and detection limit. The linear range of derivative adsorption chronopotentiometry is $6 \times 10^{-11}\text{–}7 \times 10^{-10}M$ Cu(II) for $2.0 \times 10^{-8}M$ Beryllon III, $1 \times 10^{-9}\text{–}1.8 \times 10^{-8}M$ Cu(II) for $4.0 \times 10^{-7}M$ Beryllon III; $9 \times 10^{-9}\text{–}4 \times 10^{-7}M$ Cu(II) for $1.0 \times 10^{-6}M$ Beryllon III. The detection limit of the method is $4 \times 10^{-11}M$ with a preconcentration time of 200 sec. Figure 5 shows the adsorption chronopotentiograms of the Cu(II) complex with Beryllon III at lower concentrations. For comparing, the derivative anodic stripping chronopotentiogram of Cu(II) at $t_a = 120$ sec and the derivative adsorption chronopotentiogram of Cu(II) complex with Beryllon at $t_a = 60$ sec at the same concentration are plotted in Fig. 6. It is obvious that the present method is more sensitive. The precision, calculated from 10 successive measurements of $5 \times 10^{-8}M$ Cu(II) is 2.6%.

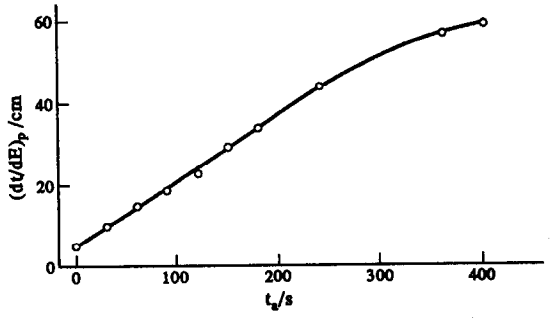

Fig. 2. Relationship between the peak height of the adsorbed complex and the preconcentration time. Sensitivity of the analyser is 5, other conditions as in Fig. 1, curve 3.

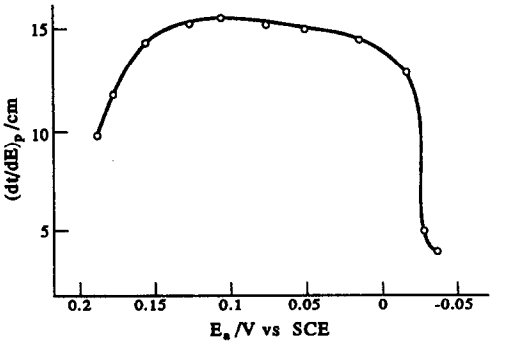

Fig. 3. Dependence of the peak current of reduction of the adsorbed Cu(II)–Beryllon III on the preconcentration potential, $t_a = 60$ sec, other conditions as in Fig. 2 except for E_a.

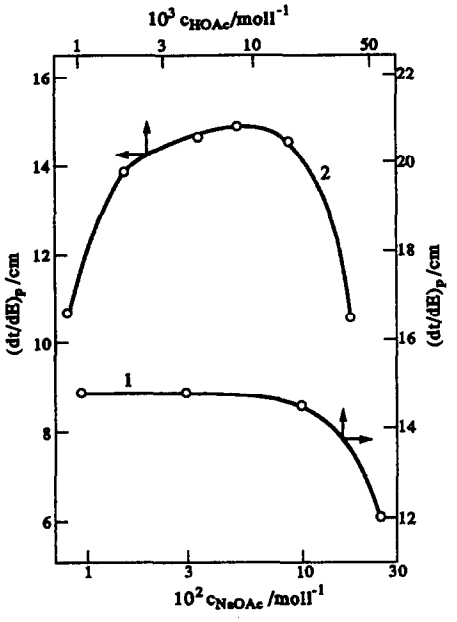

Fig. 4. Relationship between the peak height of the adsorbed complex and the concentration of HOAc and NaOAc, (1) 0.01M HOAc; (2) 0.01M NaOAc, $E_a = 0.10$ V, other conditions as in Fig. 3.

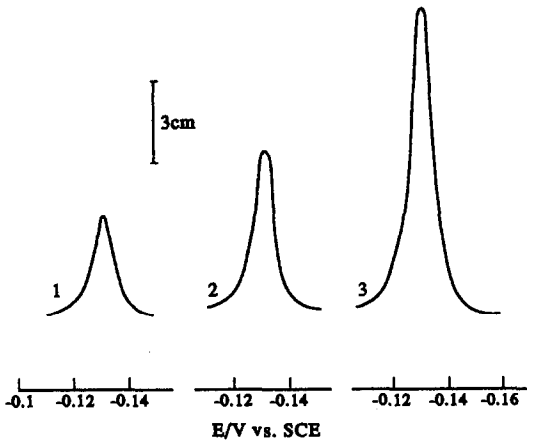

Fig. 5. Derivative adsorption chronopotentiograms of Cu(II) complex with Beryllon III, (1) 6×10^{-11}; (2) 1×10^{-10}; (3) $2 \times 10^{-10}M$ Cu(II). $2 \times 10^{-8}M$ Beryllon III, $E_a = 0.10$ V, $t_a = 200$ sec, $i_o = 0.1$ μA, 0.01M HOAc + 0.01M NaOAc. Sensitivity of the analyser is 5.

Analytical application

The interference of Zn(II) with Cu(II) is a difficult problem in anodic stripping voltammetry due to their intermetallic bonding in amalgam. In the derivative adsorption chronopotentiometry mentioned above, a 200-fold excess of Zn(II) does not interfere with the peak of reduction of the Cu(II) complex with Beryllon III adsorbed on the surface of the HMDE, because the accumulation occurs on the surface of the electrode, not on the inside of the electrode for derivative adsorption chronopotentiometry.

Experimental results show that a 100-fold excess of Ni(II), Bi(III), Co(II) and Mn(II), a 200-fold excess of Zn(II), Cd(II), Sb(II), Pb(II), As(V), Mg(II) and Fe(III) and large amounts of Ca(II), Ba(II), Al(III), Na(I), K(I), SO_4^{2-}, PO_4^{3-}, Cl^- and NO_3^- do not interfere with the determination of Cu(II). For usual biological samples, Cu(II) can be determined directly after digestion.

Samples of rice were digested with an electric oven prior to adsorption chronopotentiometric determination. The procedure is as follows: *ca.* 0.1 g samples of rice were weighed to an accuracy of 0.1 mg in individual 10-ml quartz

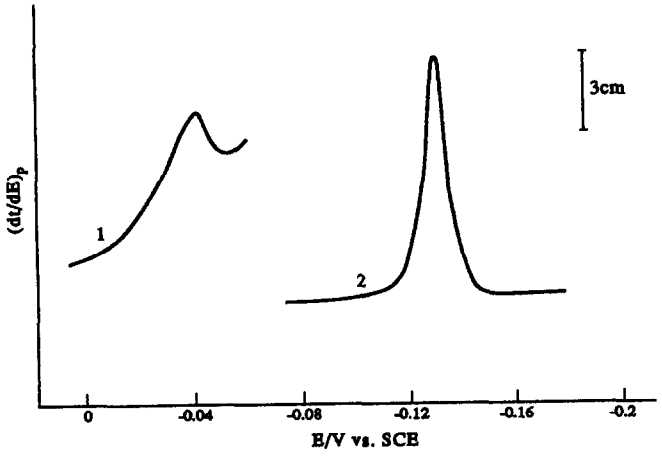

Fig. 6. Comparison between (1) derivative anodic stripping chronopotentiogram of Cu(II) and (2) derivative adsorption chronopotentiogram of Cu(II) complex with Beryllon III. 0.01M HOAc + 0.01M NaOAc, $i_o = 0.1$ μA, sensitivity of the analyser is 30. (1) $1.86 \times 10^{-8}M$ Cu(II), $E_a = -0.60$ V, $t_a = 120$ sec; (2) $1.86 \times 10^{-8}M$ Cu(II) + $1.0 \times 10^{-6}M$ Beryllon III, $E_a = 0.10$ V, $t_a = 60$ sec.

Table 1. Results of the determination of copper in samples of rice

Sample	Content determined by DACP ($\mu g/g$)	Content determined by DASCP ($\mu g/g$)
Rice A	7.28 7.45 7.33	7.37 7.44 7.53
Rice B	7.80 7.88 7.93	7.90 7.87 7.98

crucibles. They were placed on a big clean culture dish to avoid contamination from the electric oven during digestion. Nitric acid (500 μl) was added to each, and then the crucibles were covered overnight. The quartz crucibles on the culture dish were heated slowly for about 5 hr with an electric oven until the yellow smoke disappeared. Then 1 ml of perchloric acid was added to each and the sample solution was digested further until the sample solution was colourless. The solution was cooled, the cover of the crucible was washed with triply distilled water and the sample solution was then evaporated to dryness. The remaining substance should be white. After cooling it to room temperature, water was added and the remaining substance was dissolved. Then the solution was transferred into a 50-ml standard flask and diluted to the mark with water. A 5-ml sample solution was transferred to a 25-ml standard flask containing appropriate amounts of HOAc, NaOAc and Beryllon III. Then the solution was diluted to the mark, which contained 0.01M HOAc, 0.01M NaOAc, $1 \times 10^{-6}M$ Beryllon III and Cu(II).

After the solution was transferred to a cell, the derivative adsorption chronopotentiogram of Cu(II)–Beryllon III was recorded by the method above.

Typical results obtained by derivative adsorption chronopotentiometry with two successive standard additions for samples of rice are summarized in Table 1. The results from the determination of Cu(II) by derivative adsorption chronopotentiometry (DACP) are in agreement with the data obtained by derivative anodic stripping chronopotentiometry (DASCP). The recovery of added copper was 102–106%.

REFERENCES

1. R. Kalvoda, *Anal. Chim. Acta*, 1982, **138**, 11.
2. N. K. Lam, R. Kalvoda and M. Kopanica, *ibid.*, 1983, **154**, 79.
3. C. M. G. van der Berg, *ibid.*, 1984, **164**, 195.
4. *Idem*, *ibid.*, 1986, **215**, 111.
5. Ch. Yarnitzky and R. Schreiber-stanger, *J. Electroanal. Chem.*, 1986, **214**, 65.
6. H. Eskilsson, C. Haraldsson and D. Jagner, *Anal. Chim. Acta*, 1985, **175**, 79.
7. Wenrui Jin and Junying Wang, *ibid.*, 1991, **245**, 77.
8. *Idem*, unpublished work.
9. Wenrui Jin, Xin Zhao and Yuxia Liu, *Anal. Lett.*, 1992, **25**, 1741.
10. Wenrui Jin and Junying Wang, *J. Electroanal. Chem.*, 1991, **306**, 31.

Talanta, Vol. 40, No. 8, pp. 1227–1232, 1993
Printed in Great Britain.

0039-9140/93 $6.00 + 0.00

POTENTIAL OF CHAOTIC CHEMICAL SYSTEMS IN NANOTRACE ANALYSIS BASED ON THE BELOUSOV–ZHABOTINSKII REACTION (BrO_3^-—MALONIC ACID—FERROIN). DETERMINATION OF MANGANESE(II)

KONSTANTIN B. YATSIMIRSKII, PETER E. STRIZHAK* and TATYANA S. IVASCHENKO
Institute of Physical Chemistry, Academy of Sciences of Ukraine, pr. Nauki 31, Kiev, 252028, Ukraine

(*Received* 18 *August* 1992. *Revised* 15 *February* 1993. *Accepted* 15 *February* 1993)

Summary—A new method for the determination of trace amounts of manganese(II) in aqueous solutions by its affect on some types of the chaotic regimes in the Belousov–Zhabotinskii reaction has been proposed. The method is based on the high sensitivity of some types of chaotic regimes of the BZ reaction to small perturbations of initial conditions (*e.g.*, low concentrations of some metal ions). The experimentally obtained detection limit for manganese is 3 pg/ml.

The kinetic methods of analysis are of interest for the determination of trace amounts of different substances and are widely used for quantitative determination of low concentrations of different compounds in solution, among them metal ions.[1–5] The basis of kinetic methods utilizes the ability of a substance to be analysed in order to change the kinetic parameters of a chemical reaction. The choice of such a reaction suitable for the determination of a given compound is determined primarily by picking a regime of chemical process. It was found that chemical reactions can possess different dynamic regimes, for example, monotonic, regular oscillations, quasi-periodicity, chaos *etc.*[6–8] Among them, only monotonic regimes are widely used in kinetic methods for chemical analysis.

The first paper concerning the use of regular chemical oscillations for the determination of trace amounts of ruthenium(III) ions was published in 1978.[9] After this several studies on the possibility of analytical applications of chemical oscillations have been performed.[3,10–12] However, there is no information at the moment on analytical applications of chemical chaos (irregular, unpredictable chemical dynamics) except for some general theoretical discussions.[13–14] A comprehensive discussion on chaotic chemical reactions and proposed models has been published.[6,15–18] The chaotic dynamics are built up by the expanding and folding processes of chaotic orbits, *i.e.*, the path of the chemical system in its phase space with the coordinates represented by chemical species concentrations, and may be described in terms of the local expansion rates of nearby orbits.[18–20] A useful quantity for the description of their structures has recently turned out to be given by the largest Lyapunov characteristic exponent.[18–22] The distinguishing feature of chaotic process is its high sensitivity to initial experimental conditions.[15–22] For example, for the Belousov–Zhabotinskii (BZ) reaction such sensitivity is observed experimentally near the bifurcation point or when the reaction proceeds into chaotic regimes.[17,23–24]

EXPERIMENTAL

Reagents

All reagents were of analytical grade and doubly distilled water was used for dilutions. Aqueous ferroin solution was prepared by the use of the standard method.[25]

Apparatus

Studies were carried out with a 100 ml reactor. The reactor was placed in a constant temperature bath with $T = 21 \pm 0.05$°C, stirring rate was 2000 rpm for a volume of 40 ml in all experiments. The state of the system was followed by measuring the potential of a platinum electrode using a silver–silver chloride electrode

*Author to whom correspondence should be addressed.

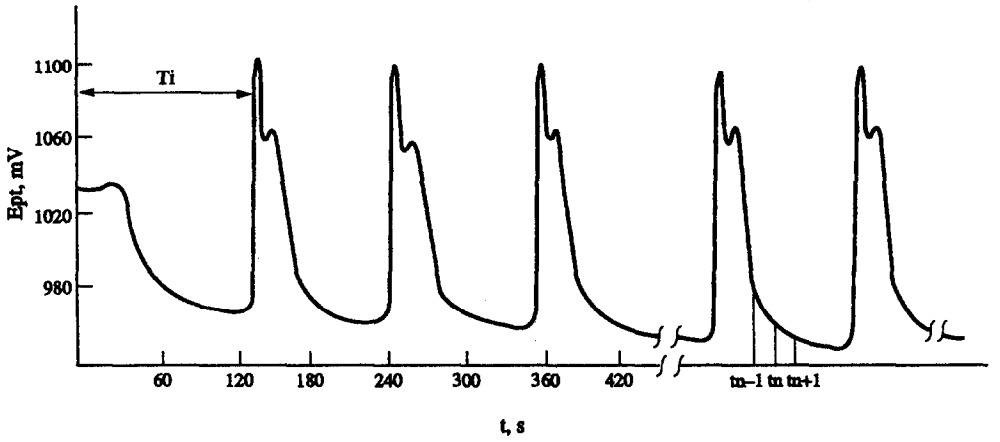

Fig. 1. The Pt-electrode potential–time dependence of the BZ reaction with the following initial concentrations ($T = 294$ K): $[KBrO_3]_0 = 0.115M$: $[H_2SO_4]_0 = 0.32$M; [malonic acid]$_0 = 0.68M$; [ferroin]$_0 = 1.7 \times 10^{-3}M$.

as reference. The potential was recorded as a function of time on Radelkis x–t recorder.

Analyses of the time series obtained were carried out on a IBM PC/AT compatible computer. All programs were written in-house based on the Borland Turbo Pascal system version 3.01A. The reconstruction of phase portraits was adapted from the Packard and Crutchfield algorithm in three-dimensional space, with a time delay of 3 sec from the obtained Pt electrode time series.[26–28] The largest Lyapunov characteristic exponent for each time series was calculated in reconstructed three-dimensional phase space by using the Wolf algorithm with accuracy of approximately 7%.[29]

Procedures

Determination of manganese(II) concentration in aqueous solution was carried out using 0.1 ml of aqueous solution of manganese(II) sulphate added to 39.9 ml of the BZ reaction mixture 30 sec after its preparation. The Pt electrode potential was recorded to the end of the chaotic regime. The mixing solutions were chosen so that in the final solution the reagents were in the following concentrations: $[KBrO_3]_0 = 0.115M$; $[H_2SO_4]_0 = 0.32M$; $[MA]_0 = 0.68M$ (malonic acid); $C_{Fe} = 1.7 \times 10M$ (ferroin). The Lyapunov exponent (λ_L) and time interval from the starting point to the first maximum of potential–time dependent (T_i, see Fig. 1) were calculated from the obtained time series.

The calibration was obtained from the plot $\lambda_L T_i$–Log C_{Mn} of different concentrations of manganese(II).

The determination of manganese(II) trace concentrations can be carried out by using the above method and the obtained calibration.

The concentrations of $KBrO_3$, H_2SO_4 and malonic acid were kept fixed throughout the series of measurements.

The typical view of the Pt electrode potential oscillations is presented in Fig. 1. The Pt electrode potential oscillations have a relaxed character, *i.e.*, they consist of very fast jumps in potential followed by a slower decrease. However, in spite of the regular and pseudoregular oscillations, its amplitudes and "periods" (*i.e.*, the times between maxima) were not constant. These oscillations are not periodic but chaotic.[16] Certainly, the behaviour of the chaotic chemical system is not reproducible, but, in contrast to

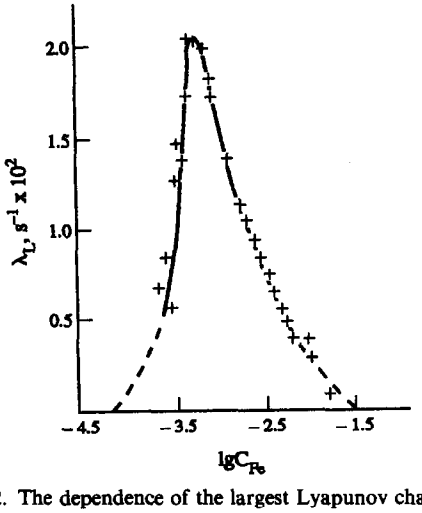

Fig. 2. The dependence of the largest Lyapunov characteristic exponent with respect to the initial ferroin concentration for the BZ reaction (other experimental conditions are as in Fig 1).

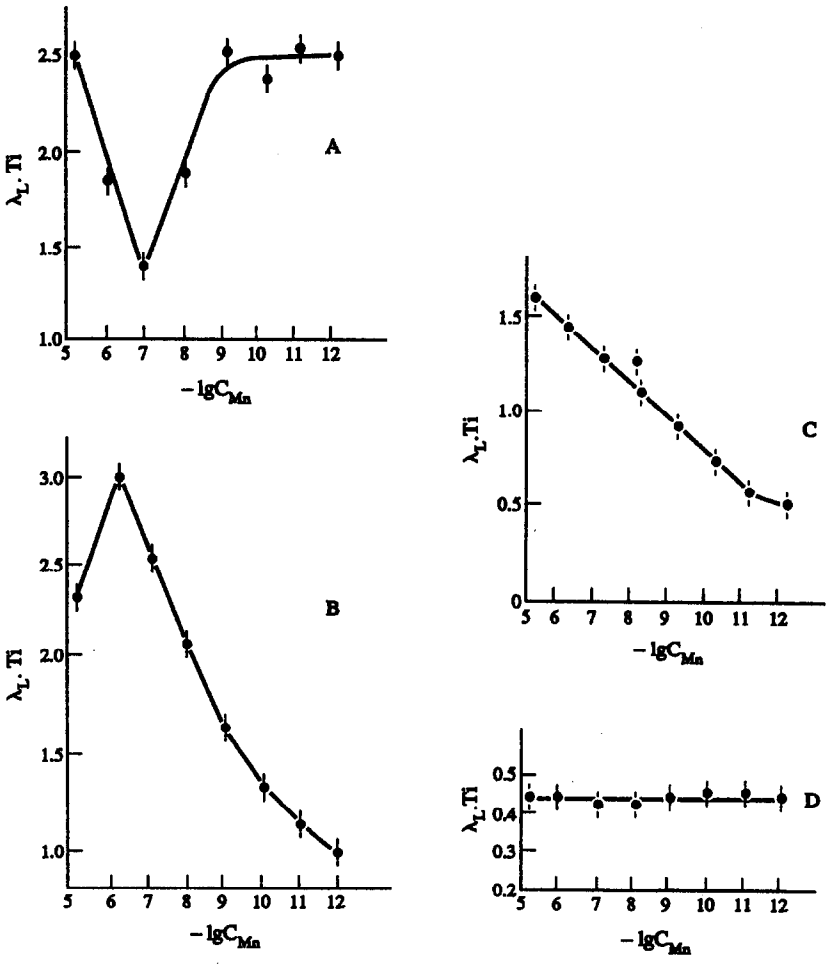

Fig. 3. The dependence of values of $\lambda_L T_i$ with respect to changes in initial time concentration of manganese(II) for BZ chaotic reaction with the following initial ferroin concentrations (other experimental conditions are analogous to Fig. 1): A—[ferroin]$_0 = 8.7 \times 10^{-4} M$; B—[ferroin]$_0 = 1.25 \times 10^{-3} M$; C—[ferroin]$_0 = 1.7 \times 10^{-3} M$; D—[ferroin]$_0 = 5 \times 10^{-3} M$.

the Pt-electrode potential time dependence, the statistical characteristics (for example, the probability density, and fractal dimension) of chaotic motion are reproducible.

RESULTS AND DISCUSSION

The possibility of an analytical application of chemical chaos may be based on the definition of the largest Lyapunov characteristic exponent which can be represented by the following expression:[15-22,29-31]

$$\lambda_L = \lim_{t \to \infty} 1/t \ \mathrm{Log} \ |\delta X(t)/\delta X(0)| \qquad (1)$$

where $\delta X(0)$ is almost any initial perturbation of the starting point $X(0)$ in the phase space of the chemical system, and $\delta X(t)$ describes its evolution in time. In general, the complex chaotic chemical reaction is characterized by a great number of chemical species. So we have no practical possibility for constructing a chaotic attractor from experimental data by using the values of concentrations of all chemical species, but we may construct this attractor from the values of a single variable (in our case, the Pt-electrode potential) at different times, $E(t)$, $E(t + \Delta t)$, $E(t + 2\Delta t)$, ..., *i.e.*, from the experimentally obtained time series.[26-28] For the deter-

Table 1. Determination of manganese(II) in aqueous solutions by the use of the calibration represented in Fig. 3(C)

Amount of manganese (*g/ml*)	Added	7.5×10^{-3}	1.1×10^{-5}	4.3×10^{-6}	3×10^{-7}
	Found	$(7.5 \pm 1) \times 10^{-3}$	$(9 \pm 2) \times 10^{-5}$	$(4 \pm 2) \times 10^{-6}$	$(5 \pm 4) \times 10^{-7}$

Table 2. The values of determined parameters for chaotic BZ reaction for different experiments with initial conditions as in Fig. 1

λ_L (sec^{-1})	T_i (sec)	$\lambda_L T_i$
0.010	165	1.65
0.008	208	1.66
0.012	142	1.70
0.008	197	1.58
0.006	266	1.60
0.014	113	1.58

mination of the largest Lyapunov characteristic exponent the following expression was used[29]

$$\lambda_L = 1/(t_M - t_0) \sum_{i=1}^{M} \mathrm{Log}(L'(t_i)/L(t_{i-1})) \quad (2)$$

where $L(t)$ is a distance (in the Euclidian sense) between two nearest points in constructed phase space and $L'(t)$ is its evolution after the time interval Δt. Three-dimensional phase space is required for the determination of λ_L for the BZ reaction.[15-18] Notice that the largest Lyapunov characteristic exponent is positive only for chaotic regimes.[18]

Let us consider the case of small perturbation of the initial conditions of a chemical system by the addition of a trace amount of a given compound (with concentration C in the system). In this case the chemical system is perturbed by the variation in the initial conditions, *i.e.*, in (1) we can make the substitution of C for $\delta X(0)$ and obtain the following expression

$$\lambda_L \sim \frac{1}{T} \mathrm{Log} \frac{\bar{X}}{C}$$

where T is a suitable chosen characteristic time of the chemical system, and $\bar{X}$ is an average value of $\delta X(t)$, which depends on the value of T. This relation gives the following expression for the correlation between C and

$$\mathrm{Log}\, C \sim \gamma - \lambda_L T \quad (3)$$

where the constant γ is dependent on $\bar{X}$.

The possibility of the analytical application of chemical chaos on the basis of the expression (3) was verified by the investigation of the influence of trace amounts of manganese(II) on the transient chaotic dynamics in a BZ reaction (L^1S^1 regime). It was estimated that the existence of the linear $\lambda_L T - \mathrm{Log}\, C_{Mn}$ plot occurs only if the characteristic time interval (T) is the time interval from the starting point to the first maximum of the time-dependent potential (T_i, see Fig. 1).

It is necessary to know the largest Lyapunov characteristic exponent for such an investigation. Figure 2 shows the plot of λ_L *vs.* the log of the concentration of the catalyst (ferroin) in the BZ reaction. The typical feature of this dependence lies in the large changes of λ_L values caused by the small changes in ferroin concentrations. This is a result of the high sensitivity of quantitative parameters of the chaotic process to small variations in the experimental conditions. It follows from Fig. 2 that it is possible to vary the value of λ_L (*i.e.*, the sensitivity of the chemical system) through the variation of the ferroin initial concentration in the BZ reaction.

The plots of $\lambda_L T_i$ values *vs.* the log of the manganese(II) concentrations are shown in Fig. 3. It follows from the data presented in Figs 2 and 3 (A) that the dependence observed is not linear in the case of large values of λ_L. So the relationship (3) is not valid and linear calibration can not be obtained in the range of the maximal sensitivity of chaotic process.

Figures 3(B) and 3(C) show the possibility of obtaining the linear calibration. It follows from

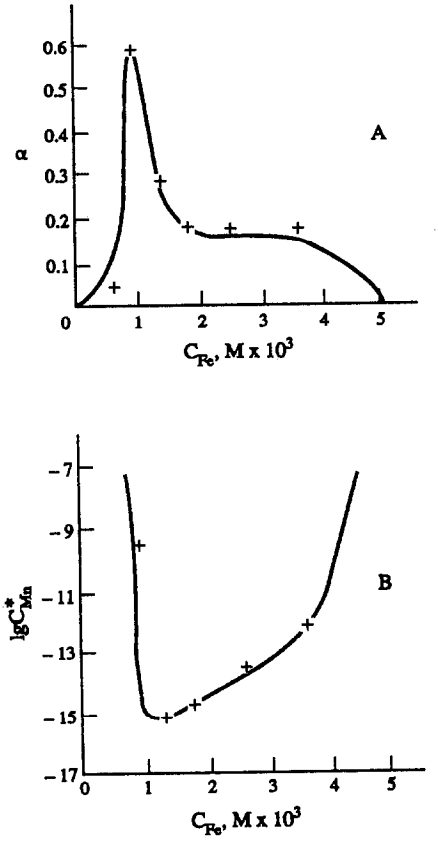

Fig. 4. The dependence of a sensitivity (A) and theoretically attainable detection limit (B) with respect to initial ferroin concentration for BZ reaction (experimental conditions are as in Fig. 1).

Fig. 2 that the expression (3) is valid in the case of intermediate values of λ_L. The chaotic system loses its sensitivity when the largest Lyapunov characteristic exponent decreases to zero. This is illustrated by the data represented in Fig. 3(D). Hence the analytical application of chemical chaos is possible only in the case of intermediate sensitivity. This holds for investigated chaotic reaction at $C_{Fe} = (1-2) \times 10^{-3} M$.

It follows from Fig. 2 that the optimal conditions for the linear $\lambda_L T_i - \text{Log } C_{Mn}$ plot can exist also in the case where $C_{Fe} \sim 3.2 \times 10^{-4} M$. However, linear correlation was not found in this region. Maybe it is due to the short time when the chaotic process exists for such ferroin concentrations.

It follows from data presented in Fig. 3 that the $\lambda_L T_i - \text{Log } C_{Mn}$ is linear in a narrow region of the initial ferroin concentration. This creates the possibility of an analytical application of the method developed for the determination of trace amounts of manganese(II). The results of such a determination are shown in Table 1.

The question about the reproducibility of data obtained, appears to be due to high sensitivity of chaotic regimes and their irreproducibility. It follows from our experiments that small accidental variations of the experimental conditions may cause great variations of the values of λ_L and T_i, but its product is practically constant (Table 2).

The results obtained allow the discussion of the principal possibility of the chemical chaos analytical application on the basis of expression (3). In general, the existence of the chaotic strange attractor (SA) for a chemical system is a condition of the existence of regions with $\lambda_L > 0$ in the phase space. The variations of the initial conditions in a given chemical system [in our case, by the addition of trace amounts of manganese(II)] give rise to the displacement of the starting point in phase space. Hence the possibility of the existence of the linear $\lambda_L T_i$–Log C plot is determined by the relative positions of the starting point, regions where $\lambda_L > 0$, and SA in the phase space of an oscillating chemical system. In general, such a possibility cannot be predicted because the regions $\lambda_L > 0$ and SA are not continuous and are characterized by a fractal structure. So the trajectories of evolution of the system flow alternatively diverging and converging.[18–22]

Let us consider the sensitivity and the detection limit of the manganese determination by proposed method. It follows from data represented in Fig. 3 that linear portions of the $\lambda_L T_i$–Log C_{Mn} plots can be described by the following expression

$$\lambda_L T_i = \alpha \text{ Log}(C_{Mn}/C^*_{Mn}). \quad (4)$$

The calculation of the parameters α and C^*_{Mn} was performed by using the extrapolation of the linear portions of the $\lambda_L T_i$–Log C_{Mn} plots in Fig. 3.

The parameters α and C^*_{Mn} characterize the sensitivity and theoretical attainable detection limit, respectively. This is, of course, a tentative estimation of the values for $C_{Fe} < 10^{-3} M$ because in this case only initial portions of plots were chosen. The influence of the starting ferroin concentration (bifurcation parameter that determines the value of λ_L) on the sensitivity and the detection limit is illustrated by Fig. 4. These plots show that the sensitivity and the value of Log C^*_{Mn} vary qualitatively in a similar manner according to the bifurcation parameter. The maximum sensitivity and the minimum detection limit are reached in the case of $C_{Fe} = 1.25 \times 10^{-3} M$. Notice that it follows from the general run of the curve represented in Fig. 4(B) that the value of the theoretical attainable detection limit is approximately $10^{-15} M$.

CONCLUSIONS

On the basis of results obtained we may formulate some conditions for the realization of the analytical application of chemical chaos.

(1) A substance to be determined must be involved in the chemical reactions with the components of the chaotic chemical system and must cause a change in the rates of their accumulation or degradation.

(2) The addition to chaotic chemical system of a substance to be determined must not lead to any bifurcations of the regimes observed.

(3) The optimal conditions for the existence of a suitable linear calibration are determined by the existence of a lower limit of λ_L, beyond which the system loses its sensitivity, and by the existence of a higher limit of λ_L above which the behaviour of the system is irreproducible.

(4) The parameters (in our case, characteristic time of the evolution of system and largest Lyapunov characteristic exponents) may be irreproducible but some combinations of them (for example, their product) must be reproducible.

Hence, in this work we developed a method for the determination of trace amounts of manganese(II) that is rather complicated and cumbersome. However, the principal significance of such an approach is the illustration of the possibility

of analytical applications of some types of chemical chaos. Such an application enables the determination of trace amounts of manganese(II) due to the high sensitivity of chaotic regimes to initial conditions. We found experimentally that the detection limit is approximately 3 pg/ml for the determination of manganese(II). There does not appear to be a lower limit for this method. We emphasize that the detection limit, obtained by using the traditional kinetic methods, is approximately 100 pg/ml.

In addition, the approach developed in this work can be used for the determination of trace amounts, not only of manganese, but of other metal ions as well. Such a possibility remains to be verified.

REFERENCES

1. K. B. Yatsimirskii, *Kinetic Methods of Analysis*, Pergamon Press, Oxford, 1965.
2. H. A. Mottola, *Kinetic Aspects of Analytical Chemistry*, John Wiley and Sons, New York, 1988.
3. D. Perez-Bendito and M. Silva, *Kinetic Methods in Analytical Chemistry*, Ellis Horwood, New York, 1988.
4. S. U. Kreingold, *Kinetic Methods for the Analysis of Compounds and Substances with High Purity*, Chemistry, Moscow, 1983 (Rus.).
5. K. B. Yatsimirskii and L. P. Tichonova, *Talanta*, 1987, **34**, 69.
6. D. Gurel and O. Gurel, *Oscillations in Chemical Reactions*, Springer, Berlin, 1983.
7. R. J. Noyes and M. Burger (eds.), *Oscillations and Traveling Waves in Chemical Systems*, Wiley, New York, 1985.
8. R. J. Field, *J. Chem. Educ.*, 1989, **66**, N3.
9. L. P. Tichonova, L. N. Zakrevskaya and K. B. Yatsimirskii, *J. Anal. Chem. (Rus.)*, 1978, **33**, 1991.
10. K. B. Yatsimirskii, *J. Anal. Chem. (Rus.)*, 1987, **42**, 1743.
11. Z. Varadi and M. T. Beck, *Reaction Kinet. Catal. Lett.*, 1982, **21**, 527.
12. S. Takehisa, H. Kazuo and U. Nobuyuki, *J. Coll. Eng. Nihon Univ. A.*, 1990, **31**, 105.
13. I. R. Epstein, *Chem. Industry*, 1991, 4 March, 157.
14. S. Oishi and T. Koga, *Trans. IEICE*, 1990, **73**, 759.
15. F. Argoul, A. Arneodo, P. Richetti, J. C. Roux and H. L. Swinney, *Acc. Chem. Res.*, 1987, **20**, 436.
16. F. W. Schneider and A. F. Munster, *J. Phys. Chem.*, 1991, **95**, 2130.
17. C. Vidal, *Ann. Telecommun.*, 1987, **42**, 334.
18. G. Nicolis, *J. Phys.: Condens. Matter*, 1990, **2**, SA47.
19. B. Peng, V. Petrov and K. Showalter, *J. Phys. Chem.*, 1991, **95**, 4957.
20. R. Larter, C. L. Bush, T. R. Lonis and B. D. Aguda, *J. Chem. Phys.*, 1987, **87**, 5765.
21. D. P. Lathrop and E. J. Kostelich, *Phys. Rev. A.*, 1989, **40**, 4028.
22. J. L. Hudson, *Z. Phys. Chem. (DDR)*, 1989, **270**, 497.
23. Z. Noszticzius, W. D. McCormic and H. L. Swinney, *J. Phys. Chem.*, 1987, **91**, 5129.
24. J. Finkeova, M. Dolnik, B. Hrudka and M. Marek, *J. Phys. Chem.*, 1990, **94**, 4110.
25. B. Z. Shakhashir and J. Jordon, *Inorg. Chem.*, 1968, **7**, 2454.
26. N. H. Packard, J. P. Crutchfield, J. D. Farmer and R. S. Shaw, *Phys. Rev. Lett.*, 1980, **45**, 712.
27. J. C. Roux, R. H. Simoyi and H. L. Swinney, *Physica D*, 1983, **8**, 257.
28. A. M. Fraser, *Physica D*, 1989, **34**, 391.
29. A. Wolf, J. B. Swift, H. L. Swinney and J. A. Vastano, *Physica D*, 1985, **16**, 285.
30. P. E. Strizhak, T. S. Ivashchenko and K. B. Yatsimirskii, *Dokl. Ac. Sci. U.S.S.R. (Rus.)*, 1991, **322**, 107.
31. A. Wolf and J. A. Vastano, in *Dimensions and Entropies in Chaotic Systems: Proc. Int. Workshop*, p. 94, Springer, Berlin, 1986.

Talanta, Vol. 40, No. 8, pp. 1233–1243, 1993
Printed in Great Britain.

0039-9140/93 $6.00 + 0.00

STRUCTURAL CHARACTERIZATION AND SEQUENCE DISTRIBUTIONS OF POLYSILOXANES USING PYROLYSIS MS/MS

ASOKA RANASINGHE, LING LU, TAPAN K. MAJUMDAR and R. GRAHAM COOKS*
Department of Chemistry, Purdue University, West Lafayette, IN 47906, U.S.A.

WILMER K. FIFE, SLAWOMIR RUBINSZTAJN and MARTEL ZELDIN
Department of Chemistry, Purdue University, Indianapolis, IN 46205, U.S.A.

(*Received* 17 *August* 1992. *Revised* 26 *October* 1992. *Accepted* 27 *October* 1992)

Summary—Novel polysiloxanes, with 4-(dialkylamino)pyridine substituents, are characterized by pyrolysis tandem mass spectrometry. These polymers form abundant cyclic oligomeric ions under both desorption electron ionization (DEI) and desorption chemical ionization (DCI) conditions. Product MS/MS spectra of the cyclic ions reveal characteristic fragmentations under low energy collision activated dissociation. Protonated cyclic oligomers higher than the pentamer are mainly due to the proton bound dimers of lower oligomeric units. The cyclic oligomers are shown to have proton affinities greater than 1000 kJ/mole. It is proposed that thermal depolymerization occurs through an intramolecular siloxane bond rearrangement, which is in agreement with a previously proposed "loop mechanism". Markovian statistical calculations are applied to the DCI mass spectral data in order to determine the sequence distribution of siloxane copolymers. Application of this method show that the monomers in the copolymers examined are non-randomly distributed.

Mass spectrometry is widely used for direct analysis of polymers.[1–9] Increasingly, the combination of tandem mass spectrometry (MS/MS)[10,11] and desorption ionization techniques[12] has been used in the characterization of polymers, including biopolymers present in mixtures.[13–20] Some of these MS/MS studies involve chemical degradation[16–18] but most utilize thermolysis in conjunction with ionization in the mass spectrometer. The advantages of pyrolysis/tandem mass spectrometry include speed, sample economy and simplicity.

The importance of determining monomer distributions in copolymers, together with recent successes achieved in characterizing alkylisocyanates[13] by a combination of pyrolysis tandem mass spectrometry and DCI, encourage further application of this method to other types of copolymers. An important question is whether a copolymer has a random or a non-random arrangement of monomers. The data from such experiments were compared with statistical (Bernoullian) calculations in a previous pyrolysis DCI study on alkylisocyanate copolymers.[13] The monomer distribution in random co-polymers has also been calculated by a simple method due to Price[21] and compared with chemical degradation and FAB–MS data to describe the sequence distribution of co-polyesters[22] and poly(β-hydroxybutyrate-*co*-β-hydroxyvalerate).[23] In both cases the polymers gave results which were consistent with a random distribution of monomers.

Polysiloxanes are well recognized for their useful physical and chemical characteristics, *viz.*, good chain flexibility, low-temperature elasticity, low viscosity, permeability, hydrophobicity, low entropies of dilution, thermal stability and stability towards thermal oxidation. Owing to these useful properties, polysiloxanes are of commercial importance as synthetic polymers.[24–30] Some of their common uses are as membranes, electrical insulators, high performance-elastomers, synthetic lubricants, coolants, plastics, brake fluids, sealants, surfactants, water repellents, adhesives, dielectric fluids, artificial organs and contact lenses.

This study includes structural and sequence analysis of a new class of polysiloxanes functionalized with 4-(dialkylamino)pyridines.

*Author for correspondence.

4-(Dialkylamino)pyridines are well known as highly active nucleophilic catalysts for a variety of reactions, *viz.*, alkylation, acylation, phosphorylation, silylation, esterification, polymerization and redox reactions.[31,32] The polymers used in this study retain the desirable properties of polysiloxanes as well as the catalytic properties of 4-(dialkylamino)pyridines. Their structures are shown below.

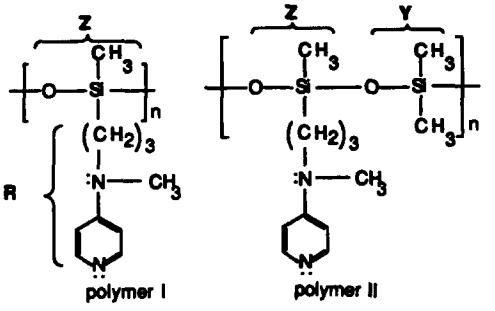

Unit	m/z
Y	74
Z	208
R	149

Polymer-I is a homopolymer containing methyl 3-[*N*-methyl-*N*-(4-pyridinyl)amino] propylsiloxane monomer (Z) units and was synthesized by hydrolytic polycondensation of 4-[*N*-(3-diethoxymethylsilyl)propyl]-*N*-methylamino]pyridine with a strongly basic catalyst.[31,32] Polymer II is a copolymer containing dimethyl siloxane (Y) and Z monomer units and was synthesized by polymerization of octamethylcyclotetrapolysiloxane (tetramer) and 4-[*N*-(3-diethoxymethylsilyl)propyl]-*N*-methylamino]pyridine in a molar ratio of 1:4, respectively. The sequence distribution of these copolymers prepared by such polymerization methods can be predicted based on the concentration and the functionality of the different pre-polymeric units. For example, ring opening copolymerization of octamethylcyclotetrasiloxane (1 mole) with 4-[*N*-(3-diethoxymethylsilyl)propyl]-*N*-methylaminopyridine (1 mole) should yield a copolymer with a block of four Y units along with randomly distributed Z single units along the polymer chain. However, redistribution reactions occurring under equilibrium conditions might change the expected sequence.

It is well known that siloxane polymers equilibrate under the influence of a catalyst or heat to produce a thermodynamically controlled distribution of ring and chain molecules.[33,34] Furthermore, these polymers, upon heating in a vacuum, depolymerize to smaller cyclic molecules of varying sizes. Ballistreri and coworkers[35] have studied the thermal decomposition mechanism of polydimethylsiloxane (PDMS) using pyrolysis mass spectrometry. Although no intact cyclic ions were observed in the mass spectrum, they interpreted the fragment ions as originating from the cyclic neutral molecules. The very rapid heating employed in the DCI technique is known to yield higher mass molecular ions in other classes of compounds without causing significant fragmentation.[36] The redistribution of monomer units during mass analysis is also highly improbable under these non-equilibrium conditions. Therefore, DCI mass spectral data, with the help of statistical methods, are expected to provide information on the sequence distribution of copolymers. The polymers investigated are potentially useful as artificial enzymes,[37] and their catalytic properties depend on the polymer micro-environment at the reactive sites which, in turn, depend on their structural arrangements.[31,32,37] Thus, structure elucidation and sequence distributions of these macromolecules have direct significance.

The specific objectives of this study are to (i) characterize polymers I and II using DEI, DCI and MS/MS, (ii) study the ion chemistry of these novel siloxanes, and (iii) develop a general mass spectrometric method for sequence distribution of siloxane copolymers.

EXPERIMENTAL

Experiments were performed using the Finnigan TSQ 700 mass spectrometer. All samples were dissolved in methanol or methylene chloride, transferred to the loop of rhenium wire filament of the direct insertion probe, and dried before introduction into the ion source. The amount of sample on the probe tip was approximately 0.5 μg. Samples were pyrolyzed by heating the probe from 30 to 800° at a rate of 170°C/sec. At this heating rate, desorption of the sample starts when the temperature of the filament is approximately 200° and continues until the temperature is 700°. The filament was held at 800° for 5 sec and then at 1200° for another 5 sec at the end of each ramp. These times had no effect on the spectra because the sample completely desorbs before it reaches

800°. However, over the temperature range 30–800°, the heating rate should be sufficiently high (100°C/sec and above) to minimize thermally induced decompositions. At lower rates, the DCI ion abundances of lower protonated oligomers increase at the expense of higher oligomers, indicating that thermal decompositions of higher oligomers occur. The scan speed of the quadrupole was typically 1000 amu/sec. This allows the data system to average 3–4 scans covering a range of 1000 amu during sample desorption. The signal-to-noise ratio can be improved by narrowing the mass range and keeping the scan speed constant. Temperatures of the ion source and the manifold were 150 and 70°C, respectively. Electron energy was 20 eV during DEI and 70 eV during DCI. The filament emission current was 0.2 mA. Isobutane was used as the reagent gas for chemical ionization at a pressure of 0.5 torr. Argon was used as collision gas for MS/MS experiments at a pressure of 2.0×10^{-3} torr measured using an ion gauge connected to the collision cell. Polydimethylsiloxane (PDMS; average molecular weight distribution, 11400) was obtained from Hüls America, Inc. Bristol, PN.

RESULTS AND DISCUSSION

The 20 eV DEI mass spectra of polymer I and II are shown in Fig. 1. Note that in all the figures only the $^{12}C^{1}H$ isotopic peaks are indicated. Ions corresponding to the intact cyclic oligomers, the trimer (m/z 624) and tetramer (m/z 832), occur in both spectra. The base peak in Fig. 1(a) is due to the ion, m/z 121, which is assigned the structure $CH_2 = N^+(CH_3)C_5H_4N$. The other major peaks, m/z 503 and 711, are fragments originating from the cyclic oligomeric ions, m/z 624 and 832, respectively, by loss of a neutral radical $CH_2(CH_3)NC_5H_4N$ (mass 121). For example, the molecular ion of the tetramer,

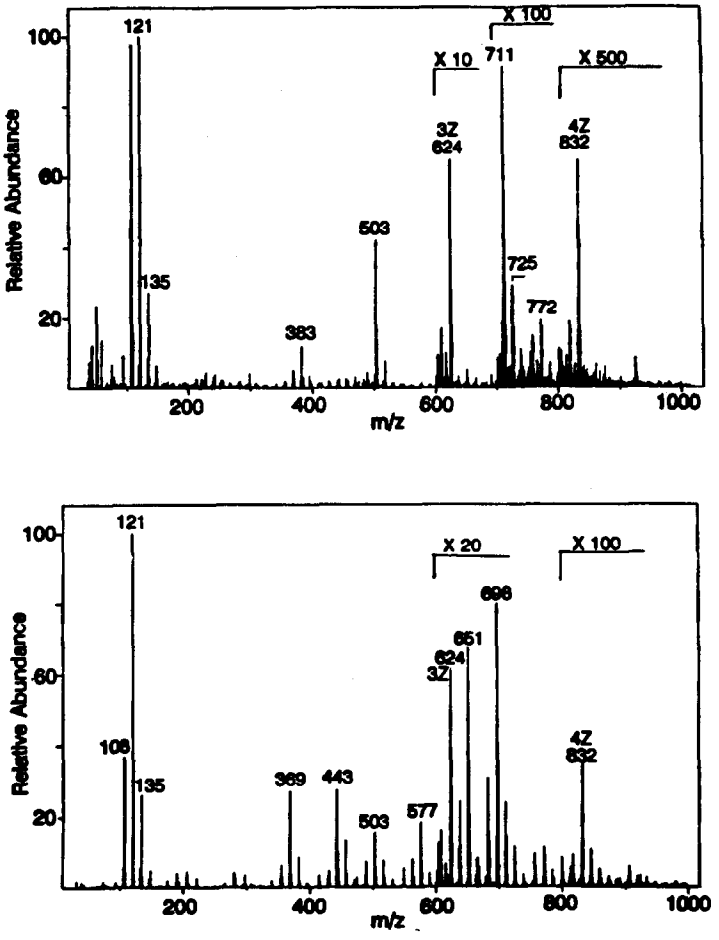

Fig. 1. 20 eV DEI mass spectra of siloxane polymers. (a) Polymer I, containing Z units. The nomenclature nZ refers to the molecular ion of cyclic oligomer containing n number of Z units. (b) Polymer II, containing both Z and Y units. Mass assignments refer to the $^{12}C,^{1}H$-isotope.

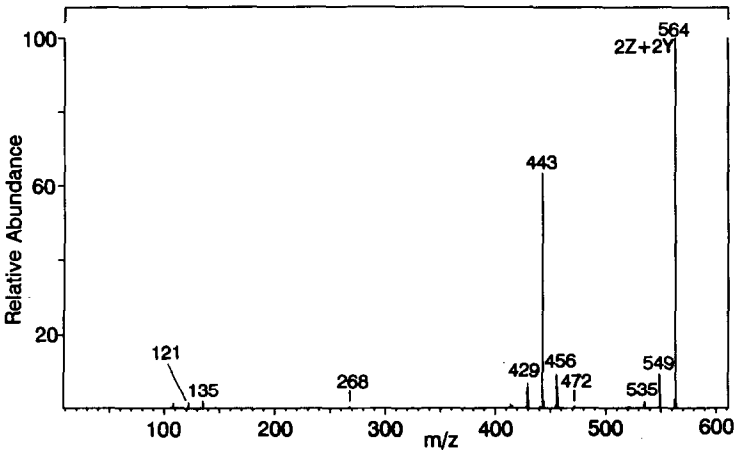

Fig. 2. MS/MS product spectrum of the molecular ion of mixed-oligomer, 2Z + 2Y, generated from polymer II, collision energy 50 eV.

m/z 832, fragments to yield the ion, m/z 711, losing the neutral radical. The copolymer [Fig. 1(b)] shows fragment ions resulting from both the mixed-oligomers and homo-oligomers. For example, m/z 369, 443, 577 and 651 are formed as a result of losing the neutral amino radical (mass 121) from the corresponding mixed-oligomer units, 2Z + Y (m/z 490), 2Z + 2Y (m/z 564), 3Z + Y (m/z 698) and 3Z + 2Y (m/z 772), respectively. These observations were confirmed by recording the product ion MS/MS spectra of individual cyclic oligomeric ions mass selected from polymer II. Figure 2 shows a typical MS/MS product spectrum, that of m/z 564, which corresponds to the cyclic mixed-tetrameric ion (2Z + 2Y). EI fragmentation mechanisms of cyclic polysiloxanes with various substituents have been studied in detail.[38–40] The loss of the whole substituent as a neutral radical forming an even electron cyclic ion is the major fragmentation path for cyclic siloxanes under EI conditions. Furthermore, when the silicon substituents have different chain lengths, the loss of the larger alkyl group is favored. This is in agreement with many other observations on competitive radical losses.[41] When a substituent containing a π bond (*e.g.*, a phenyl group) is present, extra stabilization occurs as a result of the bonding between the *d* orbitals of silicon and the π bond and the other silicon substituent is lost preferentially. In contrast to the behavior of these simple systems, for polymers I and II major fragmentation is the C–C bond cleavage with the loss of $CH_2(CH_3)NC_5H_4N$ group. Loss of the whole substituent (mass 149) is a minor path. For example, co-tetramer, 2Z + 2Y (Fig. 2), shows an abundant ion, m/z 443 (2Z + 2Y − 121), while showing low abundance signals for the ions, m/z 549, m/z 415 and 429 resulting from the loss of CH_3, $CH_2CH_2CH_2(CH_3)NC_5H_4N$ and $CH_2CH_2(CH_3)NC_5H_4N$, respectively.

The DCI mass spectrum of homopolymer I (Fig. 3) is dominated by abundant oligomeric

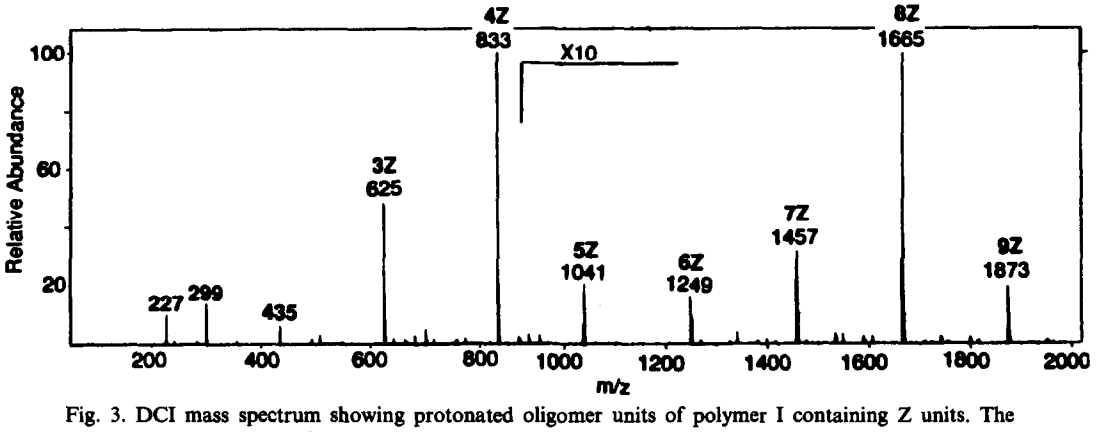

Fig. 3. DCI mass spectrum showing protonated oligomer units of polymer I containing Z units. The nomenclature *n*Z refers to the protonated cyclic oligomer containing *n* number of Z units.

ions assigned as the protonated cyclic oligomers. The most abundant ions are the protonated trimer (m/z 625) and the protonated tetramer (m/z 833), assigned as 6-membered and 8-membered cyclic structures, respectively. The protonated cyclic dimer (m/z 417) is not observed, as expected, because of the instability of the 4-membered ring. However, the corresponding protonated open chain disiloxanodiol (m/z 435) and the silanodiol monomer (m/z 227) are seen. Their structures and the associated fragmentation paths are confirmed by product ion MS/MS spectra. For example, protonated silanodiol monomer undergoes fragmentation upon CAD to yield m/z 77(100%), 109(97%), and 209(17%).

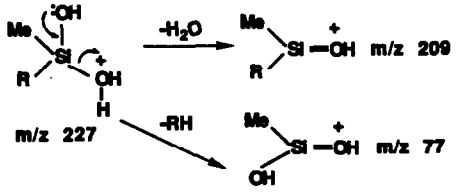

The DCI mass spectrum of polymer II (Fig. 4) is similar to that of polymer I, except that protonated mixed-oligomers are present as well as the protonated homo-oligomers. The DCI mass spectrum of polydimethylsiloxane (PDMS) also shows analogous behavior, giving abundant protonated cyclic oligomers. These simple DCI mass spectra, consisting mainly of protonated cyclic oligomers, are noteworthy because earlier reports[42,43] of the mass spectral behavior of PDMS under conventional CI and EI conditions showed only fragment ions arising from the cyclic oligomers, but not the cyclic oligomeric ions themselves. The ions present in the EI and CI mass spectra of PDMS are remarkably similar and only the relative ion abundances are different in the two experiments. Since the CI spectrum of PDMS gives abundant high mass ions, it is used as a mass reference for calibrating mass spectrometers in the higher mass range.[44,45] The protonated cyclic ions formed under DCI conditions are very stable and they require a relatively high collision energy (100 eV) to cause fragmentation upon collision with Ar (2.0 mtorr). These observations suggest that DCI imparts very little internal energy to the neutral cyclic oligomers and they make DCI/MS/MS a very promising technique for the sequence distribution and structural characterization of these polymers. A characteristic feature of the protonated cyclic oligomers of polymers I and II is the sequential loss of the neutral radical (mass 121) upon CAD. This is illustrated in the MS/MS product spectrum of the protonated trimer, m/z 625, (Fig. 5) which shows fragment ions m/z 504 and 383 which are formed by the loss of one and two radicals, respectively. This is noteworthy because it violates the odd–even electron rule of fragmentation, which states that the dissociation of even-electron-ion to yield a radical ion and a neutral radical is energetically unfavorable. The more favored path of decomposition of an even-electron-ion is to yield an even-electron-ion and a closed shell neutral molecule. The corresponding protonated trimer with all methyl substituents (m/z 223) does not lose a radical neutral under the same conditions. The major fragmentation path in this latter ion upon CAD is the sequential loss

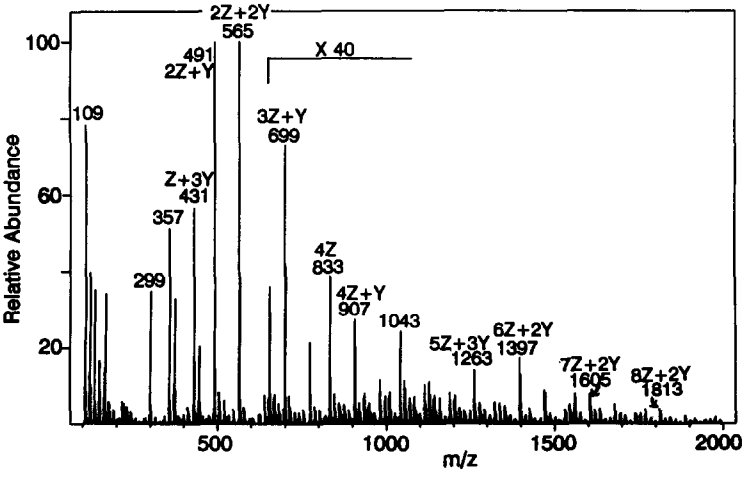

Fig. 4. DCI mass spectrum showing protonated co-oligomer units of polymer II containing Z and Y units.

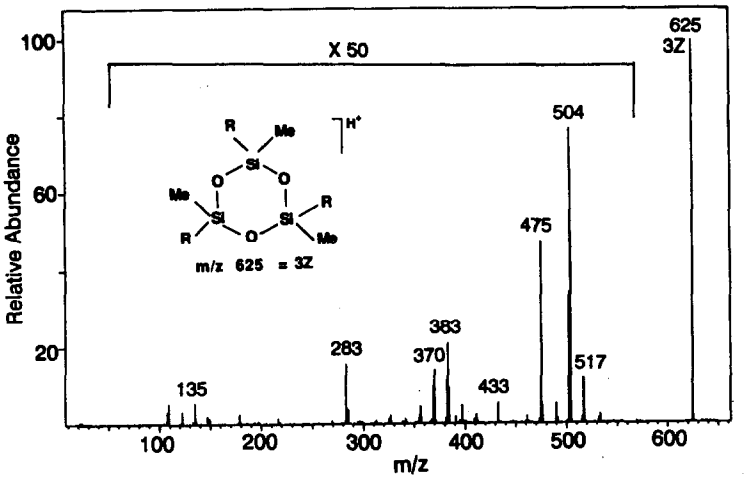

Fig. 5. MS/MS product spectrum of the protonated trimer (3 Z units) from polymer I, collision energy 50 eV.

of neutral methane molecules to yield even-electron ions, m/z 207 and m/z 191. Elimination of the closed shell neutral molecule, $[CH_3,CH_2CH_2(CH_3)NC_5H_4N]$, from the protonated trimer (Fig. 5), to form an even-electron ion, m/z 475, is also observed.

Proton bound dimers

The protonated oligomers higher than the pentamer show strikingly different behavior when compared to the lower members of the series. Figure 6 shows the MS/MS product spectrum of the protonated heptamer, m/z 1457, derived from polymer I. Unlike the oligomers up to the pentamer, this ion undergoes CAD readily, yielding the protonated tetramer at very low collision energy (8 eV). Also note that no other product ions are generated, even though some, including the trimer, are very stable. The EI mass spectra of higher cyclic polydimethylsiloxanes are known to produce lower ring structures through a ring contraction mechanism.[39] However, the corresponding protonated heptamer generated from PDMS (m/z 519) does not produce significant fragmentation under the same CAD conditions (Ar pressure 2.0 mtorr, collision energy 8 eV). These observations lead us to believe that these protonated ions of higher oligomers are mainly comprised of the proton bound dimers of the lower ones. Proton bound dimers have weak interactions through hydrogen bonds, and they undergo CAD fairly easily at low collision energies, giving the corresponding protonated monomers. The fragmentation of proton bound dimers has been used[46] to estimate relative gas phase basicities of the constituent monomers. The product ion abundances are very sensitive to the proton

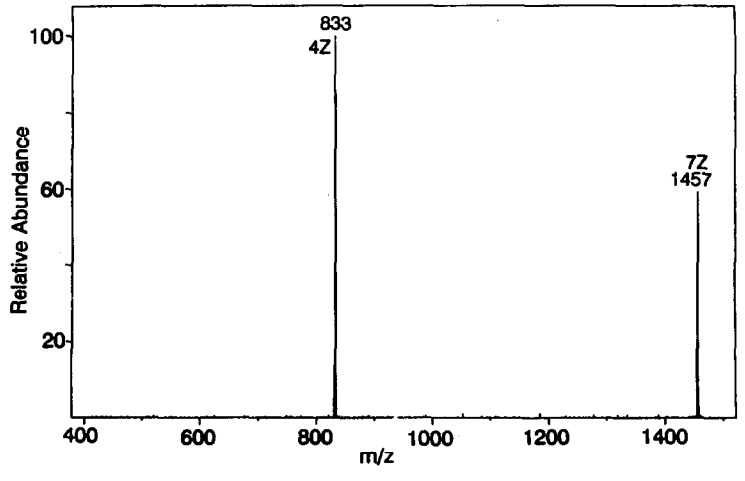

Fig. 6. MS/MS product spectrum of the protonated heptamer (7 Z units) from polymer I, collision energy 8 eV.

affinity difference between the different monomers comprising the proton bound dimer, and under typical conditions, only one protonated monomer is formed when the PA difference is greater than 2 kJ/mole.[47] This explains the formation of the protonated tetramer, and not the protonated trimer, from the heptamer upon CAD, since the tetramer has four *N*-methylalkylpyridyl units compared to three in the trimer. Other higher protonated oligomers showed similar behavior, producing only a single product ion upon CAD. For example, CAD of the hexamer (6Z), the octamer (8Z) and the nonamer (9Z) yielded the trimer (3Z), the tetramer (4Z) and the pentamer (5Z), respectively.

Product ion MS/MS spectra recorded at 8 eV collision energy for the copolymer, polymer II, are summarized in Table 1. Note that polymer II shows abundant protonated mixed-oligomer units in the product spectra. As seen from the results, the product distributions are consistent with the expectation that they are governed by the proton affinity difference between the individual oligomer units; the most abundant product ion, formed from a particular dimer, in a particular product spectrum is the one expected to have the highest proton affinity. Because several combinations of oligomer units can form a particular dimer, the product distribution does not directly reflect the proton affinity of individual oligomers. For example, the ion, *m/z* 1055 (4Z + 3Y), yields four product ions, with different relative abundances (see Table 1). Although the proton affinity of 3Z + Y is expected to be higher than that of 2Z + Y, the former has the lower relative abundance of the two. However, the parent ion population of 4Z + 3Y is not expected to contain proton bound dimers formed between 2Z + Y and 3Z + Y. Therefore, one has to consider the proton affinity difference between certain pairs in order to apply the proton affinity rule. In this example, 2Z + 2Y *vs.* 2Z + Y, 3Z + Y *vs.* Z + 2Y, 3Z *vs.* Z + 3Y and 4Z *vs.* 3Y are the combinations which are expected to form the parent dimer, 4Z + 3Y. The product 3Z is formed upon CAD of 4Z + 3Y whereas the corresponding partner, Z + 3Y, is not formed, indicating that the proton affinity of the former is the higher of the two. Another important parameter, which affects the relative abundances of the product ions originating from a particular parent ion (protonated dimer), is the concentration of the individual oligomer units which make up the parent ion population. Although 4Z has the highest proton affinity of all the oligomer units which make up the parent dimer, 4Z + 3Y, the probability of combining 4Z and 3Y units is very low because of the low abundance of those units in the polymer chain. Note that the abundance of 4Z and 3Y units are much lower than the mixed-oligomer units, 2Z + 2Y and 2Z + Y, in the DCI mass spectrum of polymer II (Fig. 4). Therefore, 4Z is not seen in the product MS/MS spectrum of the ion 4Z + 3Y.

In an attempt to evaluate the proton affinity of the cyclic oligomers using the kinetic method,[46,47] polymer II was pyrolyzed in the presence of standard compounds with known proton affinities. Although the exact proton affinities of these cyclic oligomers were not determined, the results show that these oligomers have very high proton affinities, above 1000 kJ/mole. For example, the proton bound dimer formed between the mixed-trimer, Z + 2Y, and 4-dimethylaminopyridine (PA = 990 kJ/mole[48]) yields, upon CAD, only the protonated trimer (Fig. 7). With another standard with higher PA, tetramethylethylenediamine (PA = 1003 kJ/mole[47]), it again yields only the trimer (spectrum not shown), suggesting that the PA of the trimer is even higher than 1003 kJ/mole. These results further

Table 1. Product MS/MS spectral data for protonated mixed-oligomers, collision energy 8 eV

Parent ion		Product ions				
m/z	Composition	Composition (normalized abundances)				
787	2Z + 5Y	Z + 3Y (100)	Z + 2Y (44)			
847	3Z + 3Y	2Z + Y (100)	Z + 2Y (13)			
921	3Z + 4Y	2Z + Y (100)	2Z + 2Y (46)	Z + 2Y (6)		
995	3Z + 5Y	2Z + 2Y (100)	2Z + Y (65)	2Z + 3Y (17)		
1055	4Z + 3Y	2Z + 2Y (100)	2Z + Y (36)	3Z + Y (7)	3Z (6)	
1129	4Z + 4Y	2Z + 2Y (100)	2Z + Y (50)	2Z + 3Y (30)		
1163	5Z + 3Y	3Z + Y (100)	2Z + 2Y (10)	3Z + 2Y (7)	2Z + Y (2)	
1189	5Z + 2Y	3Z + Y (100)	3Z (50)	2Z + 2Y (13)	2Z + Y (5)	
1203	4Z + 5Y	2Z + 3Y (100)	2Z + 2Y (57)	3Z (15)	2Z + 4Y (12)	2Z + Y (6)
1277	4Z + 6Y	2Z + 3Y (100)	2Z + 4Y (78)	2Z + 2Y (51)		
1337	5Z + 4Y	3Z + Y (100)	2Z + 3Y (81)	3Z + 2Y (73)	2Z + 2Y (16)	

confirm that the higher ionic-oligomers are mainly comprised of proton bound dimers of lower oligomers.

Mechanism of thermal depolymerization

Two major mechanisms have been proposed for the thermal depolymerization of polysiloxanes.[33] One is based upon siloxane bond rearrangement which is thought to occur via an intramolecular, four-center cyclic transition state (loop mechanism).[49] Zeldin *et al.* suggested[50] that depolymerization through the loop mechanism involves the random cleavage of siloxane bonds followed by a rapid and complete unzipping of the kinetically active fragments. The other mechanism involves intermolecular siloxane bond interchange reactions occurring via a cyclic transition state (bond scission mechanism).[51] It is important to elucidate the mechanism of depolymerization operating under the present experimental conditions of rapid heating (DCI) and non-equilibrium processes because the bond scission mechanism allows redistribution of monomers to occur during the heating process in the mass spectrometer, whereas the loop mechanism does not. Therefore, sequence distribution of the copolymer becomes impossible if the bond scission mechanism is operative. To test which mechanism best represents the thermal depolymerization of polysiloxanes under DCI conditions, a physical mixture of the two homopolymers, polymer I and PDMS was deposited on to the rhenium filament and heated under the same DCI conditions. The mass spectrum of the physical mixture revealed no new ions besides those originating from individual homopolymers. In other words, there were no protonated co-oligomers present. These observations eliminate the bond scission mechanism for explaining depolymerization in our experiments. Therefore, we can confidently use the mass spectral data of polymer II to obtain monomer sequence distribution as discussed below.

Sequence distribution of copolymers

The first-order Markovian statistics have been used in ^{13}C-NMR to determine the sequence distribution of copolymers.[52] In previous studies,[13] we have implemented a Bernoullian model (zero-order Markovian) to determine the sequence distribution of synthetic polymers using pyrolysis DCI mass spectral data. However, the Bernoullian model is insufficient to discriminate between block, alternating random ordering of monomers. For a Markovian distribution of a two component copolymer (components A and B), six parameters are needed to calculate the intensities of MS peaks of the different oligomers. They are S_a, S_b, P_{aa}, P_{ab}, P_{bb} and P_{ba} (P_{ij} in general) where, S_a (or S_b) is the probability that an oligomer starts with A (or B), P_{ij} is the probability of finding the component j after the component i. If these parameters are known, the normalized peak intensity, $I_{a,b}^{\text{calc}}$, of any oligomer can be calculated. For example, $I_{a,b}^{\text{calc}}$ of a sequence $AABBA$ is equal to $S_aP_{aa}P_{ab}P_{bb}P_{ba}$. We have the following four independent equations to solve for the six parameters:

$$S_a + S_b = 1 \quad (1)$$

$$P_{aa} + P_{ab} = 1 \quad (2)$$

$$P_{bb} + P_{ba} = 1 \quad (3)$$

$$S_aP_{aa} + S_bP_{ba} = S_a \quad (4)$$

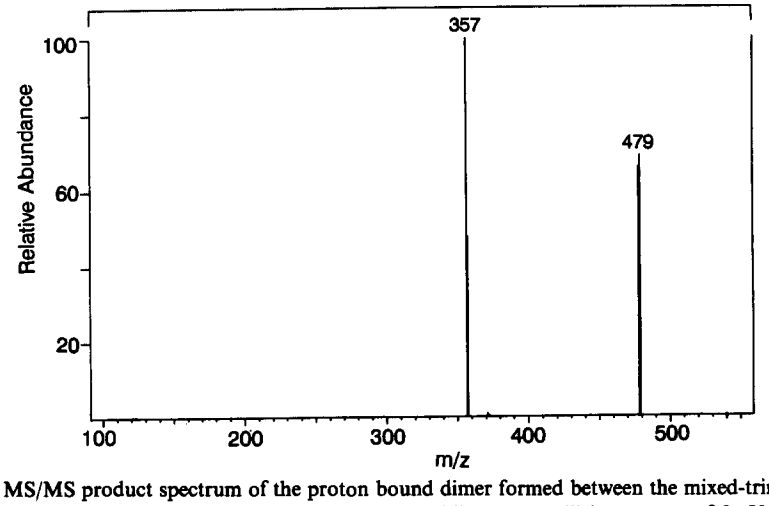

Fig. 7. MS/MS product spectrum of the proton bound dimer formed between the mixed-trimer (Z + 2Y) from polymer II and 4-dimethylaminopyridine, at a collision energy of 8 eV.

Because there are two independent variables, if we have more than two sets of experimental data, this system of equations is sufficiently over-determined to test for first-order Markovian behavior. The Bernoullian distribution is a special case of Markovian distribution, where, $S_a = P_{ba} = P_{aa} = M(A)$ and $S_b = P_{ab} = P_{bb} = M(B)$. $M(A)$ and $M(B)$ are mole fractions of monomers A and B used during polymerization.

A computer program has been written to search for those independent variables from which the peak intensities are calculated. By comparing $I_{a,b}^{calc}$ with the experimental intensity, $I_{a,b}^{exp}$ from the DCI mass spectrum, the program adjusts these variables to minimize the agreement factor χ^2 in order to determine the best fit with the experimental data. The Nedler and Mead[53] algorithm is used for χ^2 minimization.

Agreement Factor

$$X^2 = \frac{\sum_i \left(I_{y,z}^{exp} - I_{y,z}^{calc}\right)^2}{\sum_i \left(I_{y,z}^{exp}\right)^2}$$

The information obtained from the calculated parameters is important to understand the properties of the polymer. Two-component copolymers, when P_{aa} is equal to P_{ba}, represent a random distribution. When $P_{aa} = 0$, $P_{bb} = 0$ and $P_{ab} = P_{ba}$, the system has an alternating distribution. The number-average lengths of like monomers, n, *viz.* the degree of "blockness", can also be calculated as $n_a = 1/P_{ab}$ and $n_b = 1/P_{ba}$.

DCI data of the siloxane copolymer with Z and Y units (*i.e.*, $A = Z$; $a = z$; $B = Y$; $b = y$) were treated in this way. The calculated intensities based on zero-order Markovian (Bernoullian) and first-order Markovian statistics along with the experimental intensities are shown in Table 2. Both trimer and tetramer data correspond to non-random distributions. The agreement factors, χ^2, for a random distribution were 0.16 and 0.21, for the trimer and tetramer, respectively. The best-fit calculation showed that the trimer had $S_z = 0.39$, $P_{zz} = 0.12$, $P_{yy} = 0.44$ with χ^2 of 0.001 and the tetramer had $S_z = 0.40$, $P_{zz} = 0.12$ and $P_{yy} = 0.42$ with χ^2 of 0.001. The results, obtained from data for open-chain oligomers, are also in agreement with the results obtained from the protonated cyclic oligomers. For example, open-chain dimer (Table 2) data show $S_z = 0.43$, $P_{zz} = 0.17$, $P_{yy} = 0.39$ at χ^2 of 0.0001. These parameters suggest that the larger monomer unit Z, prefers to react with the smaller monomer unit Y, therefore, the probability P_{zz} is small and P_{zy} is large (0.91). On the other hand, P_{yy} and P_{yz} are both close to 0.5, suggesting that Y does not have a preference during polymerization and

Table 2. Calculated and experimental monomer distributions

Composition of oligomer (Y_nZ_m)*	Observed intensities†	Calculated intensities from monomer mole ratio (Y/Z) assuming random polymer‡	Calculated intensities from best-fit parameters	Best-fit parameters for Markov distribution(%)
Y_4	11.6	16.7	8.9	$S_y = 60.6$ $S_z = 39.4$
Y_3Z	75.6	66.7	75.6	$P_{yy} = 42.3$
Y_2Z_2	100	100	100	$P_{yz} = 57.7$
YZ_3	10.9	66.7	10.7	$P_{zz} = 11.7$
Z_4	1.2	16.7	0.1	$P_{zy} = 88.3$
		$\chi^2 = 0.21$	$\chi^2 = 0.001$	
Y_3	20.9	33.3	20.0	$S_y = 61.1$ $S_z = 38.9$
Y_2Z	100	100	100	$P_{yy} = 44.3$
YZ_2	45.3	100	45.8	$P_{yz} = 55.7$
Z_3	3.2	33.3	1.0	$P_{zz} = 12.3$
		$\chi^2 = 0.16$	$\chi^2 = 0.001$	$P_{zy} = 87.7$
Y_2	30.8	50	32.0	$S_y = 57.5$ $S_z = 42.5$
YZ	100	100	100	$P_{yy} = 39.0$
Z_2	10.7	50	10.6	$P_{yz} = 61.0$
				$P_{zz} = 17.0$
		$\chi^2 = 0.13$	$\chi^2 = 0.0001$	$P_{zy} = 83$

*Y and Z are used as symbols for methyl and pendant group substituted siloxanes.
†Average of 6 sets of data with average deviation of ± 15%.
‡Y/Z = 50/50.

thus reacts with Y or Z randomly. This preferential reaction of a Z unit with a Y unit may be perhaps due to the steric interference from the large Z unit during the equilibration process occurring in the solution. The blockness of like monomers, n_z and n_y, are approximately 1 and 2, showing that the dimethylsiloxyl units (Y) have a tendency to aggregate in blocks of two units.

CONCLUSIONS

This study clearly demonstrates the strengths of DCI/MS/MS in characterization and sequence distribution of siloxane polymers. The polymers used in this work yield abundant protonated cyclic oligomers upon thermolysis. These neutral cyclic oligomers undergo two processes under DCI conditions. The primary process is simple protonation, as indicated by the lower series of protonated oligomers (dimers, trimers, tetramers and pentamers) in the DCI mass spectra. These oligomers, up to the pentamer, directly represent the original polymers. Markovian statistical calculations applied to DCI mass spectral abundances of protonated oligomers up to the tetramer reveal that the monomer distribution in the copolymer II is non-random. The second process yields the proton-bound dimers comprised of the protonated oligomers and the neutral oligomers, which are held together by weak hydrogen bonds. The formation and dissociation of these higher oligomers, which represent a low percentage compared to the overall ion abundance, are governed by several factors including proton affinities.

Acknowledgements—This work was supported by the National Science Foundation (CHE 87-21768). WKF, MZ and SR gratefully appreciate support from the Office of Naval Research.

REFERENCES

1. J. A. Moore, in *The Analytical Chemistry of Silicones*, A. L. Smith (ed.), Chap. 13, p. 421. Wiley, New York, 1991.
2. H.-R. Schulten and R. P. Lattimer, *Mass Spectrom. Rev.*, 1984, **3**, 231.
3. I. V. Bletsos, D. M. Hercules, V. D. Leyen, B. Hagenhoff, E. Niehuis and A. Benninghoven, *Anal. Chem.*, 1991, **63**, 1953.
4. G. Montaudo, E. Scamporrino and D. Vitalini, *Macromolecules*, 1989, **122**, 623.
5. B. Durairaj, A. W. Dimock, E. T. Samulski and M. T. Shaw, *J. Polym. Sci., Part A: Polymer Chemistry*, 1989, **27**, 3211.
6. H. Feld, A. Leute, R. Zurmühlen and A. Benninghoven, *Anal. Chem.*, 1991, **63**, 903.
7. L. M. Nuwaysir, C. L. Wilkins and W. J. Simonsick, Jr, *J. Am. Soc. Mass Spectrum*, 1990, **1**, 66.
8. J. T. Brenna and W. R. Creasy, *Applied Spec.*, 1991, **45**, 80.
9. S. Fujimoto, H. Ohtani and S. Tsuge, *Z. Anal. Chem.*, 1988, **331**, 342.
10. K. L. Busch and R. G. Cooks, in *Tandem Mass Spectrometry*, F. W. McLafferty (ed.), Chap. 2, Wiley, New York, 1983.
11. K. L. Busch, G. L. Glish and S. A. McLuckey, *Mass Spectrometry/Mass Spectrometry: Techniques and Applications of Tandem Mass Spectrometry*, VCH Publishers, Inc., New York, 1988.
12. S. J. Pachuta and R. G. Cooks, *Chem. Rev.*, 1987, **87**, 647.
13. T. K. Majumdar, M. N. Eberlin, R. G. Cooks, M. M. Green, B. Muñoz and M. P. Reidy. *J. Am. Soc. Mass Spectrom.*, 1991, **2**, 130.
14. J. M. Richards, W. H. McClennen and H. L. C. Meuzelaar, *J. Appl. Polym. Sci.*, 1990, **40**, 1.
15. R. P. Lattimer, H. Münster and H. Budzikiewicz, *Int. J. Mass Spectrom. Ion Processes*, 1989, **90**, 119.
16. G. Montaudo, E. Scamporrino and D. Vitalini, *Macromolecules*, 1989, **22**, 623.
17. G. Montaudo, E. Scamporrino, G. Puglisi and D. Vitalini, *J. Polym. Sci. Polym. Chem. Ed.*, 1987, **25**, 475.
18. G. Montaudo, E. Scamporrino and D. Vitalini, *Macromolecules*, 1989, **22**, 627.
19. H. R. Morris, A. Dell, M. Panico, J. Thomasoates, M. Rogers, R. McDowel and A. Chatterjee, in *Mass Spectrometry of Biological Materials*, Practical Spectroscopy Series, Vol. 8, C. N. McEwen and B. S. Larsen (eds), p. 137. Marcel Dekker, New York, 1990.
20. D. L. Lippstreu-Fisher and D. L. Gross, *Anal. Chem.*, 1985, **57**, 1174.
21. F. P. Price, *J. Chem. Phys.*, 1962, **36**, 209.
22. A. Ballistreri, G. Montaudo, G. Impallomeni, R. W. Lenz, B. Y. Kim and R. C. Fuller, *Macromolecules*, 1990, **23**, 5059.
23. A. Ballistreri, D. Garozzo, M. Giuffrida, G. Impallomeni and G. Montaudo, *ibid.*, 1989, **22**, 2107.
24. J. E. Mark, in *Silicon-Based Polymer Science, A Comprehensive Resource, Advances in Chemistry Series 224*, J. M. Zeigler and F. W. G. Fearon (eds), Chap. 2, p. 47. American Chemical Society, Washington, DC, 1990.
25. M.Zeldin, K. J. Wynne and H. R. Allcock, *Inorganic and Organometallic Polymers*, Am. Chem. Soc. Symp. Series 360, American Chemical Society: Washington, DC, 1988.
26. D. R. Weyenberg, in *Silicon Chemistry*, E. R. Corey, J. Y. Corey and P. P. Gaspar (eds), Ellis Horwood Ltd, 1988.
27. A. L. Smith, *Analysis of Silicones*, Krieger Publishing Co., Malabar, Florida, 1983.
28. E. L. Warrick, O. R. Pierce, K. E. Polmanteer and J. C. Saam, *Rubber Chem. Technol.*, 1979, **52**, 437.
29. R. W. West, *J. Organomet. Chem.*, 1986, **300**, 327.
30. S. Patai and Z. Rappoport, *The Chemistry of Organic Silicon Compounds*, Vols. I and II, Wiley, 1989.
31. S. Rubinsztajn, M. Zeldin and W. K. Fife, *Macromolecules*, 1990, **23**, 4026.
32. S. Rubinsztajn, M. Zeldin and W. K. Fife, *Macromolecules*, 1991, **24**, 2682.

33. T. C. Kendrick, B. Parbhoo and J. W. White, in *The Chemistry of Organic Silicon Compounds*, Part 2; S. Patai and Z. Rappoport, Chap. 21, p. 1289. Wiley, 1989.
34. J. A. Semlyen, *Adv. Polym. Sci.*, 1976, **21**, 41.
35. A. Ballistreri, D. Garozzo and G. Montaudo, *Macromolecules*, 1984, **10**, 1312.
36. A. Guarini, G. Guglielmetti, N. Andriollo and M. Vincenti, *Anal. Chem.*, 1992, **64**, 204.
37. W. K. Fife, S. Rubinsztajn and M. Zeldin, *J. Am. Chem. Soc.*, 1991, **113**, 8535.
38. H. Schwarz, in *The Chemistry of Organic Silicon Compounds*, S. Patai and Z. Rappoport, Vol. 1, Chap. 7, p. 445. Wiley, 1989.
39. G. R. Pickering, C. J. Olliff and K. J. Rutt, *Organic Mass Spec.*, 1975, **10**, 1035.
40. E. Pelletier and J. F. Harrod, *Can. J. Chem.*, 1983, **61**, 762.
41. I. Howe, D. H. Williams and R. D. Bowen, *Mass Spectrometry: Principles and Applications*, 2nd Ed., McGraw-Hill, 1981.
42. M. J. Bertrand, L. Maltais and M. J. Evans, *Anal. Chem.*, 1987, **59**, 194.
43. M. McCamish, A. R. Allan and J. Roboz, *Rapid Comm. Mass Spec.*, 1987, **1**, 124.
44. J. D. Pinkston, G. D. Owens, L. J. Burkes, T. E. Delaney, D. S. Millington and D. A. Maltby, *Anal. Chem.*, 1988, **60**, 962.
45. J. D. Pinkston, G. D. Owens and E. J. Petit, *Anal. Chem.*, 1989, **61**, 775.
46. R. G. Cooks and J. Kruger, *J. Am. Chem. Soc.*, 1977, **99**, 1279.
47. B. Nourse and R. G. Cooks, *Int. J. Mass Spec. Ion Proc.*, 1991, **106**, 249.
48. S. G. Lias, J. E. Bartmess, J. F. Liebman, J. L. Holmes, R. D. Levin and W. G. Mallard, *J. Phys. Chem. Ref. Data*, 1988, **17**, Suppl. 1.
49. T. M. Thomas and T. C. Kendrick, *J. Polym. Sci.*, 1969, **A2 7**, 537.
50. M. Zeldin, B. R. Qian and S. J. Choi, *J. Polym. Sci., Polym. Chem. Ed.*, 1983, **21**, 1361.
51. N. Grassie, K. F. Francey and I. G. MacFarlane, *Polym. Degrad. Stab.*, 1980, **2**, 67.
52. J. C. Randall, *Polymer Sequence Determination*, Academic Press, New York, 1977.
53. J. A. Nedler and R. Mead, *Computer J.*, 1965, **7**, 308.

Talanta, Vol. 40, No. 8, pp. 1245–1254, 1993
Printed in Great Britain.

0039-9140/93 $6.00 + 0.00

CONTINUOUS-FLOW CHEMILUMINOMETRIC DETERMINATION OF AMMONIUM ION IN FERTILIZERS

STERGIOS A. HALVATZIS and MEROPI M. TIMOTHEOU-POTAMIA*
Laboratory of Analytical Chemistry, University of Athens, Panepistimiopolis, 157 71 Athens, Greece

(*Received* 3 *August* 1992. *Revised* 8 *January* 1993. *Accepted* 25 *January* 1993)

Summary—A simple continuous-flow chemiluminometric method for the determination of 0.0540–5.40 μg/ml of ammonium ion is described. The method is based on the chemiluminescence generated during the oxidation of ammonium ion by *N*-bromosuccinimide in alkaline medium. The emission intensity is greatly enhanced if dichlorofluorescein is also present in the reaction solution. The analysis is automated, requires no sample pre-treatment and solutions can be analysed at a rate of 106 solutions/hr with a relative error of about 2.5%. The method was applied satisfactorily to the determination of ammonium ion in solid and liquid fertilizers.

A wide variety of methods and techniques are available for the determination of ammonium ion. Spectrofluorimetry,[1,2] molecular emission cavity analysis,[3] gas phase molecular absorption spectrometry,[4] capillary isotachophoresis,[5] ion-selective electrodes,[6] conductometry,[7,8] and thermometric titrimetry[9] are only some examples of the techniques available for the determination of ammonia and ammonium ions. Flow injection systems with gas diffusion or ion exchange modules and spectrophotometric detection are described in the literature.[10–12] The spectrophotometric determination of ammonia can be carried out either by the Nessler[12] or the Berthelot reaction,[13] or by using pH indicators.[11] However, special precautions must be taken when these methods are applied to coloured or turbid sample solutions.

Few chemiluminometric methods have been established for the determination of ammonia. Ammonia reacts with hypochlorite to form monochloramine in alkaline solution. Thus, the intensity of chemiluminescence (CL) generated during the reaction of luminol with hypochlorite decreases.[14] Ammonia has also been determined by oxidative pyrolysis and subsequent measurement of the CL intensity of excited NO_2.[15] However, a direct CL method for the determination of ammonia or ammonium ion has not been traced in the literature.

This work involves the development and optimization of a method for the analysis of ammonium ion in fertilizers, based on a new CL reaction between *N*-bromosuccinimide (NBS) and ammonium ion in alkaline medium. During the development of the method, it was found that a number of fluorescent compounds enhance the CL emission intensity if present in the reaction medium. The effect of these compounds on the emission intensity is investigated. Reduction of interferences by cations on the emission intensity is also reported in this paper.

EXPERIMENTAL

Apparatus

A schematic diagram of the continuous-flow CL analyser is shown in Fig. 1. It consisted of two basic units, the detector housing and the flow-through system.

The detector housing included a coiled glass flow cell situated in front of the photomultiplier tube (PMT). The cell consisted of 3.5 turns of glass tubing (i.d. 2 mm) and its total height was 22 mm. The coil volume was 300 μl. The distance of the coil from the PMT was 2 mm for greatest sensitivity. The coil was backed by a mirror for maximum light collection by the PMT. High voltage (−720 V) was supplied to the PMT (EMI 9783R, S-5 response) by two Heath Universal Power Supplies (0–500 V) connected in series. The output of the PMT was connected to an operational amplifier (RCA CA 3140) which served as a current-to-voltage converter (I–V). Damping was provided

*To whom correspondence should be addressed.

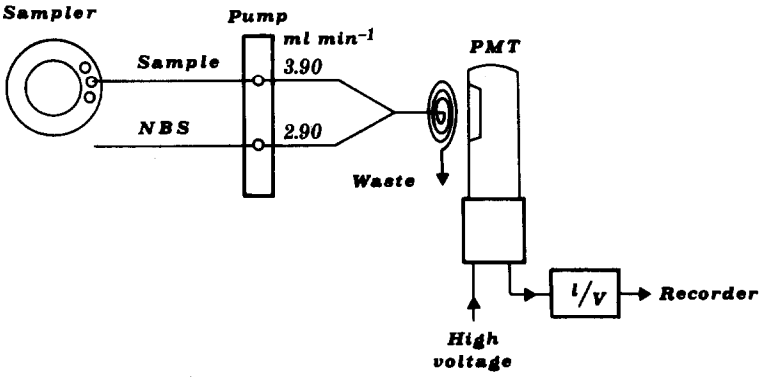

Fig. 1. Schematic diagram of the continuous-flow CL analyser (not to scale).

by inserting an RC circuit between the output of the I–V converter and the recorder. The output of the CL analyser was recorded with a Knauer (Model 73341) recorder.

The solutions of reactants were supplied by a Technicon Proportioning Pump III and were mixed at a Y-junction, 20 mm before entering the flow cell. The final solution was carried into the flow cell by a Tygon tube with an i.d. of 2 mm. Samples were supplied to the manifold by a Technicon Sampler II with a 40-sample capacity.

Reagents

All solutions were prepared from analytical-reagent grade materials with de-ionized, distilled water.

N-Bromosuccinimide stock solution (0.0500*M*) was prepared daily by dissolving 2.225 g of NBS (Serva) in water, transferring the solution into a volumetric flask and diluting to 250 ml with water.

Dichlorofluorescein stock solution (0.0010*M*) was prepared daily by dissolving 0.200 g of dichlorofluorescein (Fluka) in 0.10*M* sodium hydroxide solution, transferring the solution into a volumetric flask and diluting to 500 ml with the same alkaline solution.

Ammonium chloride stock solution (0.100*M*) (1800 μg/ml of ammonium ion) was prepared by dissolving 2.675 g of ammonium chloride (Merck) in water, transferring the solution into a calibrated flask and diluting to 500 ml with water.

More dilute solutions were prepared daily by the minimum number of dilution steps possible.

All other common laboratory chemicals were of the best grade available and were used without further purification.

PROCEDURES

Measurement procedure

The instrument was set at the optimized conditions shown in Fig. 1, but the sampling needle was kept in the "wash" position until the baseline on the recorder had been established. The sampler was adjusted to allow analyte or standard solution and washing water to enter the manifold at equal time intervals and at a rate of 106 solutions/hr. The sampler was then activated and the analysis proceeded automatically. A calibration graph was constructed by plotting the emission intensity [I(mV)] vs. concentration of ammonium ion [C(μg/ml)] in standard solutions and the ammonium content of the sample solution was determined. A standard solution after every 12 sample solutions was included.

Sample preparation

Ten millilitres of 1.0*M* sodium hydroxide solution and 10.00 ml of 0.0010*M* dichlorofluorescein solution were transferred into a 100 ml volumetric flask with the appropriate volume of stock ammonium ion solution and were diluted to volume with water.

For the preparation of fertilizer stock solutions, an amount about 10 g of fertilizer was weighed accurately, transferred into a 1 l volumetric flask and diluted to volume with water. The mixture was sonicated for 10 min to aid dissolution and then filtered. An appropriate volume of the filtrate was diluted further with water so that the concentration of ammonium ion in the final solution was within the working range (0.0540–5.40 μg/ml). The final solution should also contain 0.10*M* sodium hydroxide and $1.0 \times 10^{-4}M$ dichlorofluorescein.

RESULTS AND DISCUSSION

Chemiluminescent reactions that occur by the action of oxidants containing positively charged bromine atoms are restricted to hypobromite[16] and 1,3-dibromo-5,5-dimethyl-hydantoin.[17] *N*-Bromosuccinimide belongs to the same group of compounds, it is more stable than hypobromite and has been used extensively as a brominating and oxidizing agent.[18] Recently, the CL intensity generated during the oxidation of isoniazid by NBS has been found to increase when ammonia is present.[19] This observation was attributed to the CL oxidation of ammonia to nitrogen by NBS. The reaction which occurs is:[20]

$$NH_4^+ + OH^- \rightarrow NH_3 + H_2O$$

$$3NBS + 2NH_3 + 3OH^- \rightarrow 3NHS + N_2 + 3Br^- + 3H_2O$$

NHS: succinimide.

The reaction probably belongs to the group of CL redox reactions which generate nitrogen.[21] Nitrogen is probably produced in an excited state,[22] and has the ability to chemi-excite coexisting fluorophores, like dichlorofluorescein.

A series of experiments were conducted to establish the optimum analytical conditions for the CL oxidation of ammonium ions by NBS.

Effect of flow-rate

Figure 2 shows the effect of flow-rate of NBS on the emission intensity from 18.0 and 54.0 μg/ml of ammonium ion. At flow-rates of oxidant ⩾2.90 ml/min, the emission intensity is independent of NBS flow-rate. This was expected since the concentration of NBS is at least four times higher than the stoichiometric and the reaction is therefore, pseudofirst-order with respect to ammonium ions.

The chosen values for reagent and sample flow-rates were 2.90 and 3.90 ml/min, respectively. The manifold configuration and the optimized flow-rates allow the constituents of the final solution to react for about 0.6 sec before entering into the cell. The sampling and wash times of the sampler were chosen to give sharp and smooth peaks. Under these experimental conditions, the response

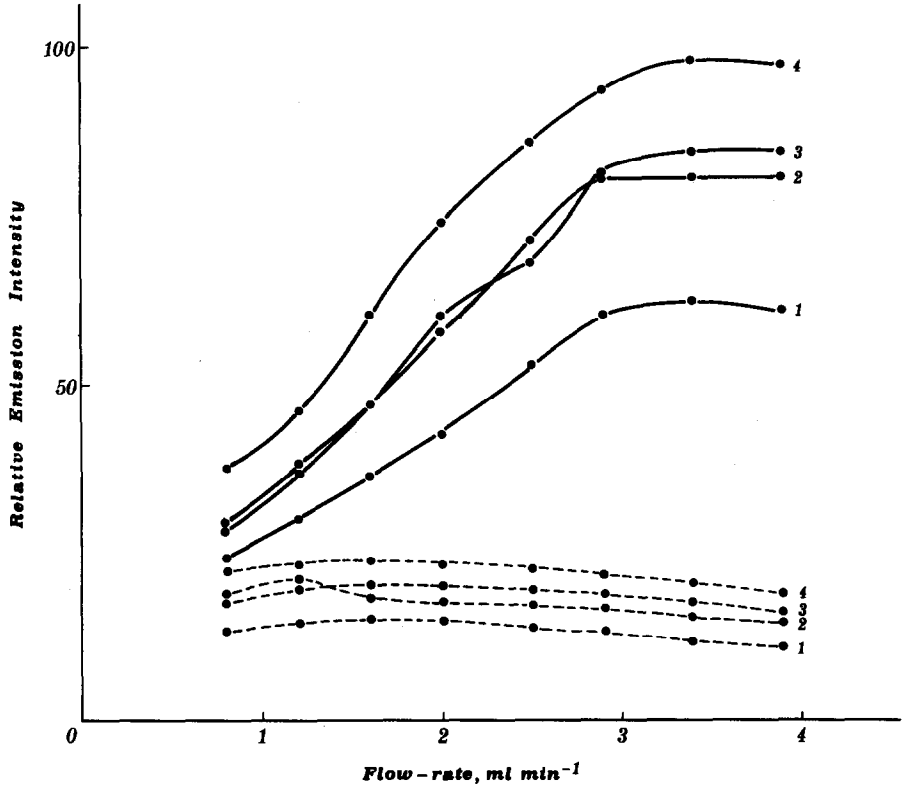

Fig. 2. Effect of the flow-rate of 0.150*M* NBS in 0.50*M* sodium hydroxide on the CL intensity, from 18.0 (broken line) and 54.0 (solid line) μg/ml of ammonium ion supplied to the manifold at (1) 2.50, (2) 2.90, (3) 3.40 and (4) 3.90 ml/min.

was equivalent to 95% of that from the steady state.

Effect of NBS and alkali concentrations

The oxidation of ammonium ions by NBS is accompanied by radiation only when the reaction is carried out in alkaline medium. The effect of NBS concentration on 18.0 and 54.0 μg/ml of ammonium ions at various sodium hydroxide concentrations (range 0.010–2.0 M) is shown in Fig. 3. Concentrations of 0.0150M for NBS and 0.30M for sodium hydroxide were determined to be optimal. A decrease in light intensity at higher concentrations of NBS was observed probably due to kinetic reasons. The rate increases and the reaction proceeds to completion before entrance of the solution into the measuring cell. The same reason explains the decrease of the signal at concentrations of sodium hydroxide > 0.5M.

Effect of surfactants and fluorescent compounds

The efficiency of some CL reactions increases by using surfactants.[23] Their action alters favourably chemical pathways and reaction rates[24] and, therefore, the sensitivity of the analytical measurement is greatly improved. However, typical surfactants did not show such an effect on the CL reaction examined. Each surfactant tested, when present in concentrations higher than the critical micellar concentration (CMC), caused severe reduction in response due to suppression of the CL reaction and quenching of the emission. The effect of 3-cyclohexylamino-propanesulphonic acid (CAPS), a well known CL sensitizer,[25] on the emission intensity, was also investigated. Concentrations of CAPS $\geq 1.0 \times 10^{-4}M$ reduce severely the emission intensity from ammonium ion.

Fluorescent compounds, such as rhodamine B,[26] fluorescein[27] and riboflavin,[28] have been used as sensitizers in CL procedures. Their action is mainly due to energy transfer.[29] In this work, fluorescent compounds which belong to the triphenylmethane dyes containing an "oxo bridge" were examined. The oxidation of these dyes was accompanied by light emission.[30] The chemiluminescence is due to the emission from singlet oxygen and intermolecular energy transfer.[31] However, a mixed solution of ammonium ion and a fluorescent compound generates emission with intensity higher than the sum of the intensities from each component of the mixture. This observation is due to energy transfer from the excited states of nitrogen (produced by the

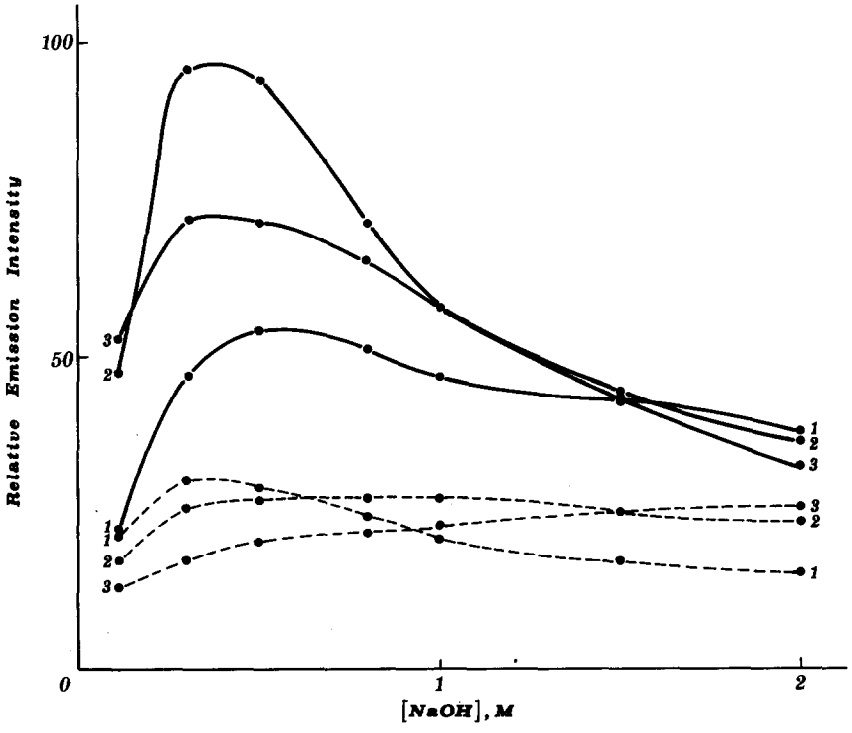

Fig. 3. Effect of concentration of sodium hydroxide on the CL intensity from 18.0 (broken line) and 54.0 (solid line) μg/ml of ammonium ion with (1) 0.0050, (2) 0.0150 and (3) 0.050M NBS.

Table 1. Effect of fluorescent compounds on the CL emission from 18.0 μg/ml of ammonium ion

Compound	Concentration (M)	Ammonium ion ($\mu g/ml$) 0	18.0
		Emission intensity (mV)	
None		*	17.2
Rhodamine B	1.0×10^{-6}	*	17.2
	1.0×10^{-5}	*	20.5
	1.0×10^{-4}	*	38.4
	1.0×10^{-3}	1.2	45.9
Fluorescein	1.0×10^{-6}	2.3	20.6
	1.0×10^{-5}	5.5	47.3
	1.0×10^{-4}	10.8	206
	1.0×10^{-3}	21.2	411
Dichlorofluorescein	1.0×10^{-6}	2.6	34.7
	1.0×10^{-5}	8.0	224
	1.0×10^{-4}	18.4	1420
	1.0×10^{-3}	59.0	624

*Not detectable.

reaction of ammonium ion with NBS) to the emitting species produced by the reaction of fluorescent compound with NBS which caused an increase in the CL efficiency. Table 1 shows that the most enhanced emission was obtained when $1.0 \times 10^{-4}M$ dichlorofluorescein was present in the analyte solution. As the addition of dichlorofluorescein allows the determination of very low concentrations of ammonium ions, the effect of sodium hydroxide on the emission intensity was re-investigated (Fig. 4). When dichlorofluorescein was also added to the ammonium ion solution the optimum was $0.10M$ sodium hydroxide, while the optimum values of NBS concentration and flow rates of reagents remain unaffected.

Analytical parameters

A typical recording for a series of ammonium ion standards obtained by the proposed method is shown in Fig. 5. The calibration graph [I(mV) vs. concentration, C (μg/ml)] was linear in the range 0.0540–0.540 μg/ml of ammonium ion

$$I = (11.9 \pm 0.38) + (75.4 \pm 1.3)C;$$

$$r = 0.9992, \quad (n = 7)$$

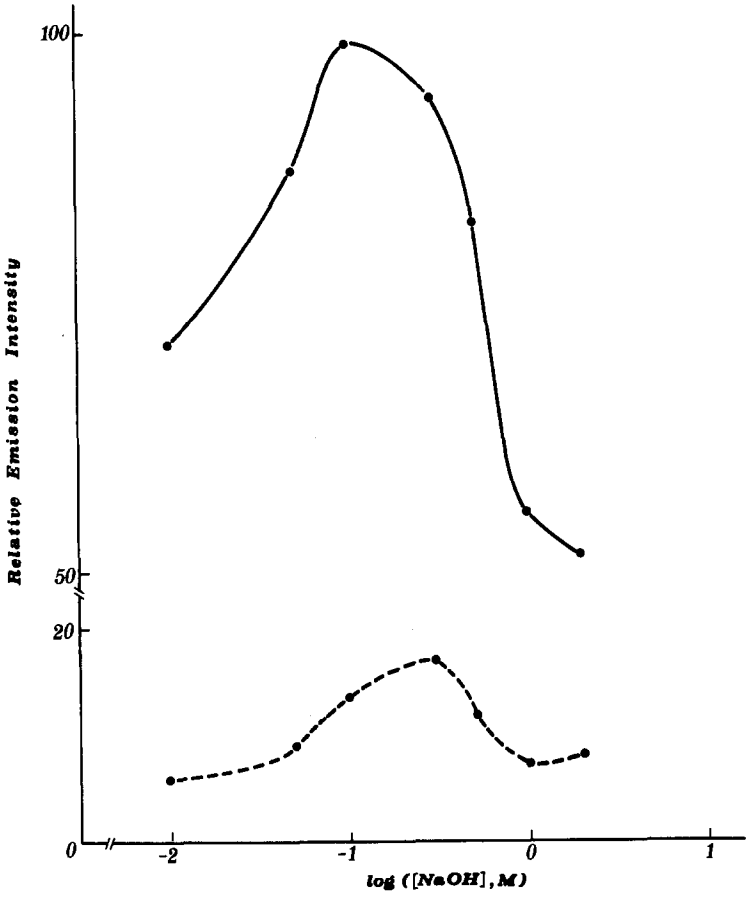

Fig. 4. Effect of concentration of sodium hydroxide on the CL intensity from 0.180 (broken line) and 0.900 (solid line) μg/ml of ammonium ion ([Dichlorofluorescein] = $1.0 \times 10^{-4}M$ and [NBS] = $0.0150M$).

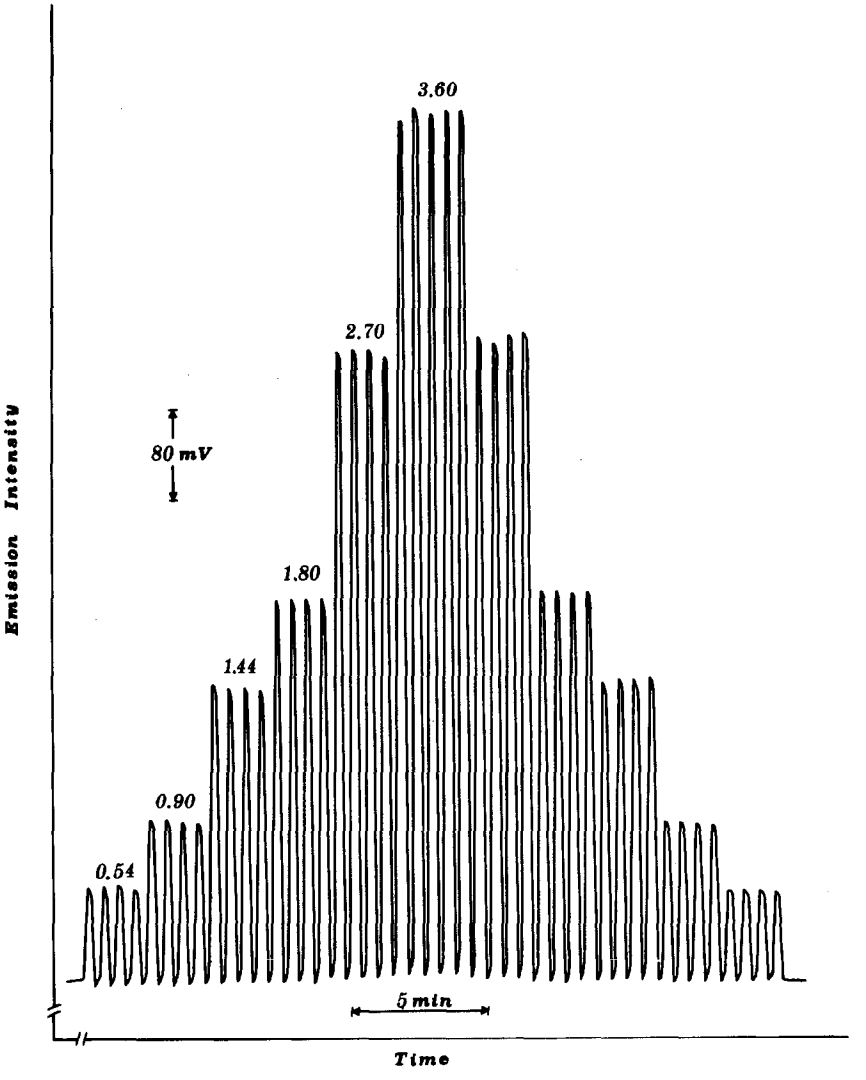

Fig. 5. Typical recording output for the NBS–ammonium ion reaction under the recommended conditions (the numbers above each set of peaks are micrograms per millilitre of ammonium ion).

and in the range 0.540–5.40 μg/ml of ammonium ion

$$I = (-49.6 \pm 11) + (225 \pm 3.7)C;$$

$$r = 0.999, \quad (n = 11).$$

The change of slope of the calibration graph was attributed to the increase of energy transfer yield from the lower to the higher ammonium ion concentration range.

The detection limit (blank + three times its standard deviation[32]) was 0.032 μg/ml of ammonium ion. Repeatability was measured with standard solutions. The relative standard deviations for 10 measurements were 1.6 and 0.4% for 0.540 and 3.60 μg/ml, respectively. Aqueous solutions of ammonium ion (0.0900–5.40 μg/ml) were analysed as samples of unknown concentration with a mean relative error of 1.3% (range 0–3.5%).

Interference studies

Interferences from anions were investigated by recovering 1.80 μg/ml of ammonium ions in the presence of 180.0, 18.0 and 1.80 μg/ml of anion. The results are shown in Table 2. No CL emission was observed from pure solutions of the anions except sulphide, which therefore interferes severely. No effect was observed from nitrate and phosphate which are major constituents of solid fertilizers. Hexacyanoferrate(II), arsenite, nitrite and sulphide interfere since they react with NBS and reduce its concentration.

Interferences from cations were investigated by the same procedure followed for anions.

Table 2. Analytical recovery of 1.80 μg/ml of ammonium ion from solutions which contain various anions

Anion	Concentration ratio (anion:ammonium ion)	Recovery (%) ($n = 3$)
PO_4^{3-}	100	100.4
NO_3^-	100	100.6
CO_3^{2-}	100	99.6
SO_4^{2-}	100	100.1
Cl^-	100	100.8
Br^-	100	101.6
I^-	100	96.5
$C_2O_4^{2-}$	100	103.3
AsO_2^-	100	88.4
	10	96.6
NO_2^-	100	45.6
	10	75.6
	1	90.3
$[Fe(CN)_6]^{4-}$	100	0
	10	16.0
	1	19.8
S^{2-}	100	34.2
	10	76.7
	1	100.3

However, most cations form insoluble compounds in alkaline medium. Formation of precipitates can be avoided by using complexing agents. Common complexing agents were found to decrease the emission intensity from ammonium ions due to quenching effect (Table 3). The least severe reduction in response is caused by citrate which was used at 0.010*M*. This concentration is in adequate excess for complexing the cations tested. The equation of the calibration graph, using citrate in standard solutions, obtained in the range 0.540–5.40 μg/ml of ammonium ion was:

$$I = (-102 \pm 12) + (227 \pm 4.0)C;$$

$$r = 0.999, \quad (n = 9).$$

Table 3. Effect of some common complexing agents on the CL emission from 1.80 μg/ml of ammonium ion (emission intensity from pure ammonium ion = 100)

Compound	Concentration (*M*)	Relative emission intensity (%)
EGTA*	0.0010	37.5
	0.0100	3.5
DCTA†	0.0010	59.7
	0.0100	8.5
EDTA‡	0.0010	59.7
	0.0100	9.0
Citrate	0.0010	97.2
	0.0100	91.7
	0.1000	50.7

*Ethyleneglycol-bis(2-aminoethylether)-*N,N,N′,N′*-tetraacetic acid.

†1,2-Diaminocyclohexane-*N,N,N′,N′*-tetraacetic acid.

‡Ethylenediamino-*N,N,N′,N′*-tetraacetic acid.

When citrate was present in the analyte solution, the detection limit was 0.450 μg/ml of ammonium ion and the relative standard deviations for 10 measurements were 1.8 and 0.5% for 0.600 and 4.50 μg/ml, respectively.

The results of the recovery studies for cations are shown in Table 4. Manganese(II) was the most severe interferant of all the cations examined. Cobalt(II) and chromium(III) increase the intensity, probably due to a catalytic effect.[33,34] The unusual effect of copper(II) is probably due to the absorption of radiation by the coloured solution and the catalytic effect of cation on the CL reaction.

Since many fertilizers contain urea, the effect of this compound on the emission intensity was also investigated. The recovery results of 1.80 μg/ml of ammonium ions from solutions with 18.0, 1.80 and 0.180 μg/ml of urea were 153.1, 110.4 and 100.3% ($n = 3$), respectively. The increase in the CL intensity is attributed to

Table 4. Analytical recovery of 1.80 μg/ml of ammonium ion from solutions which contain various cations and 0.010*M* sodium citrate

Cation	Concentration ratio (cation:ammonium)	Recovery (%) ($n = 3$)
Mg^{2+}	100	104.0
Ni^{2+}	100	80.4
	10	103.6
Cu^{2+}	100	90.0
	10	114.4
	1	123.2
Cr^{3+}	100	390.5
	10	227.3
	1	210.1
Mn^{2+}	100, 10	*
	1	92.1
Fe^{3+}	100	*
	10	96.8
Al^{3+}	100	91.5
	10	96.7
Pb^{2+}	100	83.5
	10	93.5
	1	99.3
Zn^{2+}	100	93.8
	10	104.3
Ca^{2+}	100	110.5
	10	100.5
Ba^{2+}	100	102.0
Co^{2+}	100	229.3
	10	128.1
	1	103.4
Cd^{2+}	100	*
	10	100.1

*Precipitate formed after mixing of ammonium and metal ion solution.

ammonia produced by hydrolysis of urea in alkaline medium. The method can only be applied to samples that also contain urea at concentrations lower than that of ammonium ion.

Accuracy

The accuracy of the proposed continuous-flow CL method was examined by performing recovery experiments on solutions prepared from commercial solid and liquid fertilizers. Table 5 summarizes the results of these studies. 0.010*M* sodium citrate was added to all solutions used in the analysis of samples which contained cations, in order to avoid formation of precipitates. Average recoveries were 100.6% (97.0–106.1%) and 110.9% (104.6–119.7%) for solid and liquid samples, respectively. High recoveries of ammonium ion from liquid samples might be related to the effect of cations, such as copper(II). The proposed method was also evaluated by analysing commercial samples and the results are compared with the values determined by the standard method.[35] A satisfactory agreement between the results was obtained (Table 6), with a mean relative difference of 1.3 and 4.2% for solid and liquid samples, respectively.

CONCLUSIONS

The proposed automated method is the first direct chemiluminometric method developed for ammonium ions. Dilution is the only sample pre-treatment required and the detection limit, sensitivity and selectivity compare very well with existing analytical methods for ammonium ion. The results are repeatable and show that the method can be applied to the determination of ammonium ion in fertilizers. Urea is the only severe interferent when present at concentration ratios $\geqslant 1$. The method has no interferences

Table 5. Recovery experiments for ammonium ion added to sample solution of commercial fertilizers

	Ammonium ion ($\mu g/ml$)			
Sample	Initially present	Added	Recovered	Recovery, (%) ($n = 3$)
Solid fertilizer				
No 1	0.875	0.810	0.834	103.0
		1.800	1.746	97.0
		2.700	2.658	98.4
No 6	0.854	0.810	0.823	101.6
		1.800	1.800	100.0
		2.700	2.701	100.0
No 13	0.910	0.810	0.826	102.0
		1.800	1.791	99.5
		2.700	2.654	98.3
No 21	0.907	0.810	0.852	103.1
		1.800	1.790	99.4
		2.700	2.704	100.1
No 22	0.904	0.810	0.838	103.5
		1.800	1.738	99.1
		2.700	2.708	100.3
Fleran*	1.012	0.540	0.526	97.4
		0.900	0.923	102.6
		1.800	1.909	106.1
			Mean:	100.6
Liquid fertilizer				
Viofyt*	1.045	0.540	0.611	113.1
		0.900	1.077	119.7
		1.800	2.112	117.3
Algoflash*	1.052	0.540	0.569	105.4
		0.900	0.947	105.2
		1.800	1.893	105.2
Anthin*	1.212	0.540	0.565	104.6
		0.900	0.982	109.1
		1.800	2.125	118.1
			Mean:	110.9

*The solutions contain 0.010*M* sodium citrate.

Table 6. Determination of ammonium–nitrogen in commercial fertilizers with the proposed method and the standard method[35]

Sample	Composition (%N–%P_2O_5–%K_2O)	Ammonium–nitrogen (%) Proposed method (±SD)*	Standard method	Relative difference (%)
Solid				
No 1	20–10–0	18.85 ± 0.08	18.94	−0.5
No 2		18.74 ± 0.16	19.07	−1.7
No 3		18.90 ± 0.02	19.04	−0.7
No 4		19.08 ± 0.08	19.18	−0.5
No 5		18.72 ± 0.10	19.05	−1.7
No 6	16–20–0	15.48 ± 0.05	15.57	−0.6
No 7		15.47 ± 0	15.92	−2.8
No 8		15.56 ± 0.19	15.48	+0.5
No 9		15.63 ± 0.05	15.53	+0.6
No 10		15.53 ± 0.04	15.46	+0.5
No 11		15.44 ± 0.06	15.50	−0.4
No 12		15.22 ± 0.03	15.57	−2.2
No 13	11–15–15	11.32 ± 0	11.21	+1.0
No 14		10.78 ± 0.10	10.93	−1.4
No 15		11.33 ± 0.04	11.00	+3.0
No 16		11.01 ± 0.06	11.04	−0.3
No 17		11.05 ± 0.02	10.79	+2.4
No 18		11.14 ± 0.07	11.15	−0.1
No 19		10.98 ± 0.06	10.89	+0.8
No 20		11.03 ± 0.02	10.79	+2.2
No 21	8–20–20	8.58 ± 0.02	8.52	+0.7
No 22	5–0–0	4.65 ± 0.04	4.63	+0.4
Fleran†[a]	21–30–15	19.67 ± 0.25	20.46	−3.9
			Mean:	1.3
Liquid				
Viofyt†[b]	5–10–5	5.08 ± 0.03	4.83	+5.2
Algoflash†[c]	6–6–6	2.05 ± 0.01	1.98	+3.5
Anthin†[d]	14–4–6	15.70 ± 0	15.12	+3.8
			Mean:	4.2

*Standard deviation ($n = 3$).

†The standard and sample solutions contain 0.010*M* sodium citrate because these samples contain (a) Mg, Mn, B, Pb; (b) Fe, Cu, Zn, Mg, B, Mn, Ca, S; (c) Fe, Cu, Zn, Pb, B; (d) Fe, Cu, Mn, Mg, B.

from common anions, such as nitrate and phosphate and the interferences from cations have been significantly reduced or eliminated.

Acknowledgements—The authors are grateful to Prof. A. C. Calokerinos for helpful discussions. One of the authors (S. A. H.) thanks the University of Athens for financial support.

REFERENCES

1. T. Aoki, S. Uemura and M. Munemori, *Anal. Chem.*, 1983, **55**, 1620.
2. Z. Genfa and P. K. Dasgupta, *Anal. Chem.*, 1989, **61**, 408.
3. R. Belcher, S. L. Bogdanski, A. C. Calokerinos and A. Townshend, *Analyst*, 1981, **106**, 625.
4. V. C. Anigbogu, M. L. Dietz and A. Syty, *Anal. Chem.*, 1983, **55**, 535.
5. K. Fukushi and K. Hiiro, *Talanta*, 1988, **35**, 799.
6. S. Alegret, J. Alonso, J. Bartroli and E. Martinez-Fabregas, *Analyst*, 1989, **114**, 1443.
7. F. E. Friedl, *Anal. Biochem.*, 1972, **48**, 300.
8. C. Pasquini and Lourival Cardoso De Faria, *Anal. Chim. Acta*, 1987, **193**, 19.
9. I. Sajo and B. Sipos, *Talanta*, 1972, **19**, 669.
10. W. E. Van Der Linden, *Anal. Chim. Acta*, 1983, **151**, 359.
11. R. Nakata, T. Kawamura, H. Sakashita and A. Nitta, *Anal. Chim. Acta*, 1988, **208**, 81.
12. H. Bergamin, B. F. Reis, A. O. Jacintho and E. A. G. Zagatto, *Anal. Chim. Acta*, 1980, **117**, 81.
13. C. Pasquini and W. A. Oliviera, *Anal. Chem.*, 1985, **57**, 2575.
14. P. R. Kraus and S. R. Crouch, *Anal. Lett.*, 1987, **20**, 183.
15. K. Gerth, *Anal. Biochem.*, 1985, **144**, 432.
16. J. Teckentrup and D. Klockow, *Talanta*, 1981, **28**, 653.
17. A. T. Pilipenlo, O. V. Zui and A. V. Terletskaya, *J. Anal. Chem., U.S.S.R.*, 1986, **41**, 560.
18. N. K. Mathour and C. K. Narang, *The Determination of Organic Compounds with N-Bromosuccinimide and Allied Reagents*. Academic Press, London, 1975.
19. S. A. Halvatzis, M. M. Timotheou-Potamia and A. C. Calokerinos, *Analyst*, 1990, **115**, 1229.

20. G. W. Stevenson and J. M. Luck, *J. Biol. Chem.*, 1961, **236,** 715.
21. F. McCapra, *Prog. Org. Chem.*, 1973, **8,** 231.
22. H. Jurgensen and J. D. Winefordner, *Talanta*, 1984, **31,** 777.
23. T. E. Riehl, C. L. Malehorn and W. L. Hinze, *Analyst*, 1986, **111,** 931.
24. E. Pelizzetti and E. Pramauro, *Anal. Chim. Acta*, 1985, **169,** 1.
25. I. I. Koukli, E. G. Sarantonis and A. C. Calokerinos, *Anal. Lett.*, 1990, **23,** 1167.
26. J. S. Lancaster, P. J. Worsfold and A. Lynes, *Analyst*, 1989, **114,** 1659.
27. M. Yamada and S. Suzuki, *Anal. Chim. Acta*, 1987, **193,** 337.
28. S. A. Al-Tamrah, A. Townshend and A. R. Wheatley, *Analyst*, 1987, **112,** 883.
29. M. Yamada, T. Nakada and S. Suzuki, *Anal. Chim. Acta*, 1983, **147,** 401.
30. G. N. Chen and C. S. Huang, *Talanta*, 1988, **35,** 625.
31. D. Slawinska and J. Slawinski, *Anal. Chem.*, 1975, **47,** 2101.
32. J. C. Miller and J. N. Miller, *Statistics for Analytical Chemistry*. Horwood, Chichester, 1986.
33. I. M. A. Shakir and A. T. Faizullah, *Analyst*, 1989, **114,** 951.
34. V. I. Rigin and A. I. Blokhin, *J. Anal. Chem. U.S.S.R.*, 1977, **32,** 246.
35. International Organization for Standardization, International Standard ISO 5314-1981.

Talanta, Vol. 40, No. 8, pp. 1255–1259, 1993
Printed in Great Britain.

0039-9140/93 $6.00 + 0.00

CHEMICALLY MODIFIED ELECTRODE BASED ON POLY[TETRA(4-AMINOPHENYL)PORPHYRIN] AS A pH SENSOR

RUO YUAN, YA-QIN CHAI, GUO-LI SHEN and RU-QIN YU*
Department of Chemistry and Chemical Engineering, Hunan University, Changsha, 410082, People's Republic of China

(*Received* 29 *July* 1992. *Revised* 19 *October* 1992. *Accepted* 26 *October* 1992)

Summary—A chemically modified platinum electrode with coated poly[tetra(4-aminophenyl)porphyrin] has been used as a potentiometric pH sensor. It gives a linear response over the pH range 1.5–13.7 with a slope of 55 mV/pH (at 20°). The sensor has fair resistance to erosion of hydrofluoric acid and to interference of a coexisting redox couple. The sensor can be used for pH determination and end-point indication for potentiometric titration of hydrofluoric acid with sodium hydroxide. The a.c. impedance of the polymer membrane has also been studied.

Although the glass membrane pH sensor is the most widely used device for determination of pH, there are limitations to its use due to its high resistance, fragility, erosion by hydrofluoric acid, "sodium error" and "acid error". There has been a considerable interest in designing non-glass sensors for pH measurements. One direction for non-glass pH electrodes using neutral ionophores.[1–4] These electrodes have relatively low impedance and are easier to miniaturize than glass pH sensors. For the purpose of miniaturization, an even more convenient version of the non-glass pH sensor has been the coated-wire type chemically modified electrode (CME). Several papers reported the use of chemically modified electrodes as potentiometric sensors, especially as pH sensors.[5–9] Recently, a pH-sensor based on electrochemical polymerization of amino derivatives on platinum wires was investigated in this laboratory.[10] However, these chemically modified pH sensors reported so far showed rather poor potentiometric response characteristics in solutions of pH below 3 or above 11. Searching for new monomers to prepare polymer film coated electrodes with potentiometric response characteristics similar to those of a glass electrode is of considerable interest. In the present paper, tetra(4-aminophenyl)porphyrin (TAPP) was used as the monomer for a CME pH sensor preparation. Poly(cobalt(II)tetrakis(2-aminophenyl)porphyrin) film was reported as a potentiometric anion sensor.[11] A poly[tetra-(2-aminophenyl)porphyrin] film can easily be formed on a platinum surface by electropolymerization.[12] We use the 4-amino derivative to prepare a similar polymer film and CME. The resulting polymer film coated electrode has fair pH response characteristics and can be used for the potentiometric determination of pH and end-point indication of acid–base titrations.

*Author for correspondence.

EXPERIMENTAL

Apparatus and reagents

Electropolymerization was carried out with an EG & G Princeton Applied Research Potentiostat galvanostat (Model 270) in conjunction with an X-Y recorder (Houston Instrument, Model 200). A conventional three-electrode cell was used with a platinum wire as the working electrode, and a saturated calomel electrode (SCE) and a platinum electrode as reference and counter electrodes, respectively. Potentiometric and pH measurements were made with a Microprocessor Ionalyzer (Orion Research, Model 901) or PHS-3 pH meter (Shanghai Rex Instrument Factory). The a.c. impedance was recorded with a Potentiostat galvanostat (PAR 368). IR spectra were recorded with a Nicolet FT-IR spectrometer (Model 740).

Samples of TAPP were purchased from Dahua Chem. Co. (Sichuan) as well as being synthesized according to Collman *et al.*,[13] and the product was identified by elemental analysis. Tetrabutylammonium perchlorate (TBAP) was

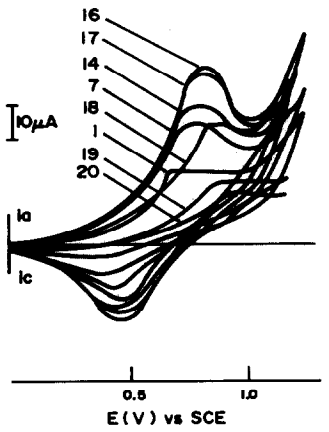

Fig. 1. Cyclic voltammetric scans at Pt electrode: 5m*M* TAPP in CH_3CN (0.1*M* in TBAP) at 100 mV/sec. The scan number is indicated above the voltammograms.

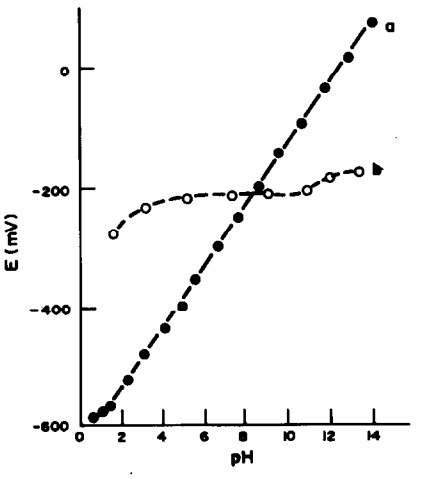

Fig. 2. pH response of PTAPP coated Pt electrode(a) and solvent polymeric membrane containing TAPP coated Pt electrode(b) as pH sensors.

prepared by the reaction of tetrabutylammonium bromide with sodium perchlorate. Redistilled demineralized water and analytical grade reagents were used throughout all experiments.

Electropolymerization

The solution used to prepare the electropolymerized film was 10.0 ml of 5.0m*M* TAPP in acetonitrile (0.10*M* in TBAP). The electrolytic solution was deoxygenated by bubbling nitrogen through the solution for approximately 10 min and then allowing the N_2 to flow over the solution during the experiment. TAPP was polymerized onto the platinum electrodes from the electrolytic solution by cycling the working electrode potential repetitively between 0 and 1.2 V (*vs.* SCE) at a scan rate of 100 mV/sec for 20 complete cycles (Fig. 1). The newly formed brown poly[tetra(4-aminophenyl)-porphyrin] (PTAPP)-coated electrodes were thoroughly washed with acetone and water.

RESULTS AND DISCUSSION

pH response of the PTAPP-coated electrode

The PTAPP-coated electrode performance was examined in a 69.0m*M* solution in Na^+, 11.4m*M* in BO_3^{3-}, 10.0m*M* in PO_4^{3-} and 6.7m*M* in citrate. The PTAPP electrode and a glass electrode together with the SCE reference were dipped into the solution and 2*M* orthophosphoric acid (or 4*M* sodium hydroxide) was added dropwise with simultaneous recording of the emf of the PTAPP-SCE pair and the solution pH given by the glass electrode. As shown in Fig. 2(a), the response was linear from pH 1.5 to 13.7 with a slope of 55 mV/pH (at 20°, correlation coefficient 0.998). The response time was less than min. The electrode has a lifetime of at least 3 weeks. The d.c. resistance of the electrode was 310 ± 0.3 kΩ which was much lower than that of a glass membrane pH electrode. The standard deviation of the electrode potential readings over a period of 2 hr in a *tris*-buffered solution of pH 7.3 was

Table 1. pH measurements on serum samples

Serum sample	pH measured by PTAPP coated electrode	pH measured by glass electrode
A	7.40	7.43
B	7.36	7.38
C	7.37	7.41
D	7.72	7.79
E	7.75	7.82
F	7.74	7.82
G	7.78	7.85

A, B, C: fresh serum samples; D, E, F, G: samples exposed to the air for 2 days.

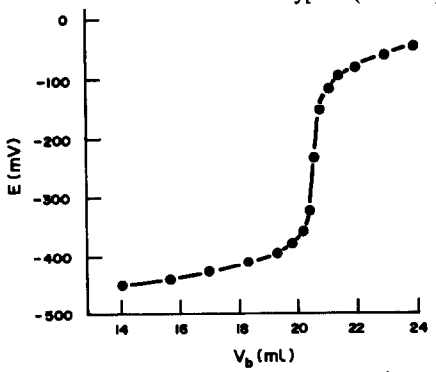

Fig. 3. E–V curve for titration of HF with NaOH (V_b: volume of base added).

0.7 mV ($n = 24$) and potential readings for the electrode dipped alternatively into stirred solutions of pH 7.0 and 7.6 showed a standard deviation of 0.6 mV over 2 hr ($n = 12$). The potentiometric selectivity coefficient with respect to some clinically important ions such as Na^+, K^+, Li^+, Ca^{2+} were determined by the fixed interference method, the values obtained for log $K^{pot}_{H^+,M^{n+}}$ for different M^{n+} were: -13.6 for Na^+; -13.5 for K^+; < -12.0 for Li^+; < -11.4 for Ca^{2+}. The interferent concentration was kept at the level of 1M.

Preliminary applications

Clinical chemistry. The PTAPP coated electrode has fair response characteristics in the pH range 6.5–8.5 which is of interest for biological studies. Seven serum samples were chosen for pH measurements using the PTAPP electrode as the pH sensor. A glass-membrane pH electrode was also used for comparison (Table 1). The PTAPP electrode gave acceptable results, though these results tended to be slightly lower than the glass electrode readings and the reason was not uncovered.

End-point indication in titrations of hydrofluoric acid with sodium hydroxide. There is no erosion effect for the PTAPP coated electrode as a pH sensor in hydrofluoric acid. The electrode can be used for end-point indication in titrations of hydrofluoric acid with sodium hydroxide. Figure 3 shows an E–V curve for this type of titration using a sample of 20 ml of 0.0514M HF titrated with 0.0504M NaOH. The HF concentration found was 0.0517 with a standard derivation of 0.0003 ($n = 3$).

Mechanism of PTAPP-coated electrode toward hydrogen ion

Figure 1 shows a typical cyclic voltamperogram for the oxidation of TAPP. As the number of cycles increased, the anodic peak shifted toward more positive potentials and the cathodic peak shifted in the reverse direction. This was probably due to the iR drop of the growing PTAPP film. The anodic peak current for the oxidation of TAPP increased with increasing numbers of cycles, n, until reaching 16, and then decreased. It was thought that the amount of TAPP monomer diffusing from bulk solution to Pt working electrode increased initially with each successive potential scan, the electrochemical oxidation of TAPP then produced the insulating PTAPP film which was adhesively coated on the platinum electrode surface. The insulating PTAPP film blocked the access of the TAPP monomer to the Pt working electrode surface. The initial electrochemical oxidation of TAPP produced a cation radical, followed by chemical reactions such as hydrolysis or polymerization to form an amine-linked polymer or at least some amine linkages. The same phenomenon was observed in the case of the electrochemical oxidation of amino derivatives.[5,8,14–15] The PTAPP film was chemically inactive and it showed no electronic conductivity in dry conditions. However, when a PTAPP film was immersed in a supporting solution, swelling of the polymer films occurred. Electrolyte ions could penetrate selectively into the swollen polymer films. The hydrogen ions seemed preferable to other ions to penetrate through the swollen polymer films. Similar results were observed with polyphenol, polyaniline and poly(1,2-diaminobenze)films.[6]

Figure 4 shows the effect of the redox couple Ce^{4+}/Ce^{3+} on the electrode potential. It is well known that the emf of a bare platinum electrode is affected by the presence of oxidation–reduction agents. To show whether the coated

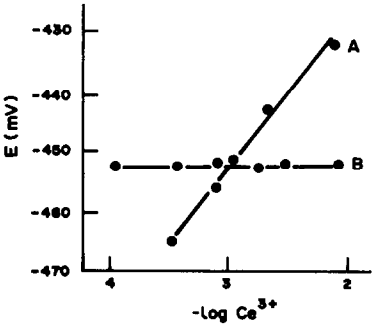

Fig. 4. Effect of concentration ratio, Ce^{4+}/Ce^{3+} on electrode potential measured *vs.* SCE: (A) uncoated Pt electrode; (B) PTAPP coated electrode.

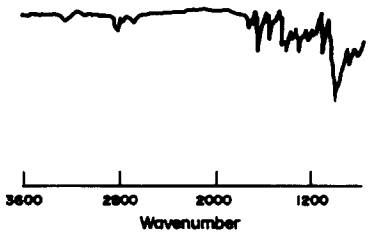

Fig. 5. The IR spectrum of PTAPP film.

platinum electrode has the same effect, different amounts of Ce^{3+} were added into a pH 5.2 buffer which was 0.01*M* in Ce^{4+}, and the bare platinum electrode and PTAPP coated electrode showed potential change as measured against the SCE reference as shown in Fig 4. It can be seen that the effect of the redox couple on the potential of the bare platinum electrode was eliminated by coating PTAPP on the electrode surface. The slope of the bare electrode response toward the cerium redox couple was about 1/3 of that expected from the Nernst equation. The result obtained was similar to that of poly(4,4′-diaminobiphenyl)polymer film.[9] This seemed to be related to the hydrolysis of Ce^{4+} and Ce^{3+} ions in the pH 5.2 aqueous solution. The quinone/hydroquinone redox couple in a concentration of 0.02*M* also did not affect the potential of PTAPP coated electrode (not shown in Fig. 4). This indicated that Ce^{4+} ions, Ce^{3+} ions, quinone and hydroquinone cannot penetrate into the PTAPP film.

White *et al.*[12] reported the preparation of polymer film of tetra(2-aminophenyl)porphyrin using electropolymerization. Their experiments showed the electrochemical and spectral similarities of the monomer to the electropolymerized porphyrin film. From this fact the authors claimed that the monomer porphyrin π-system had remained intact upon electropolymerization. We tried to examine the IR spectra and a.c. impedence of PTAPP obtained from the 2-amino derivative as the monomer to obtain some information about the mechanism of the pH response of the PTAPP-coated electrode. The IR spectrum (Fig. 5) showed one wide peak at 3330 cm^{-1}, which presumably represented a combination peak of both symmetric and unsymmetric stretching vibrations of the N—H bond due to the TAPP π-system. Other IR absorption peaks observed seemed to originate from the stretching vibration of the ArC=N double bond, the skeletal vibration of the benzene ring and the characteristic peaks for 1,4-substituted benzenes. Figure 2(b) shows the pH response of a solvent polymeric membrane electrode with TAPP monomer as the ionophore toward hydrogen ion. The solvent polymeric membrane electrodes was prepared as follows: an uncoated Pt electrode was soaked repeatedly in the mixture containing 10 mg of TAPP, 4 mg of potassium tetrakis(*m*-chlorophenyl)borate, 200 mg of poly(vinyl chloride), 80 mg of *o*-nitrophenyl ether, and 10 ml of tetrahydrofuran and dried after each dipping. The Pt electrode coated with a solvent polymeric membrane containing TAPP did not have normal potentiometric response towards hydrogen ion. This indicated that the monomeric TAPP probably entrapped in the film during the electropolymerization made no contribution to the hydrogen ion response. The rate of diffusion of hydrogen ion within the film varied with the kind of the polymer films.[6] The hydrogen ion response functional group of the PTAPP film was probably the nitrogen atoms in PTAPP which could pump hydrogen ion into the polymer film. The pH response of a hydrogen ion sensor based on neutral ionophores depended on the acidity constant (p*K*) and the net surplus charge in the vicinity of nitrogen atom of incorporated ionophores.[2,4] The basicity of the nitrogen atom in the porphyrin ring was different from that of nitrogen atoms in the phenyl ring. It seems that different nitrogen atoms of the PTAPP were responsible for the different pH range functions of the PTAPP-coated electrode. The equilibrium could be described by the following equation:

$$\text{PTAPP(m)} + \text{H}^+\text{ (aq)} + \text{X}^-\text{ (aq)} \rightleftharpoons \text{PTAPP}\cdot\text{H}^+\text{ (m)} + \text{X}^-\text{ (m)}$$

This explanation is in accordance with the a.c. impedance of the PTAPP film. The PTAPP-coated electrode conditioned in phosphoric acid–*tris* buffer solutions of different pH for 4 hr displayed well-resolved bulk

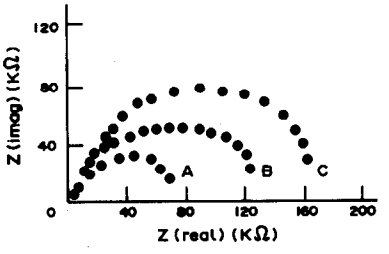

Fig. 6. Impedance plots of PTAPP-coated electrodes bathed in (A) pH 3.0, (B) pH 5.0 and (C) pH 9.0 H_3PO_4-*tris* buffered solutions for 4 hr (frequency: 10^5–10^{-3} Hz, 26°).

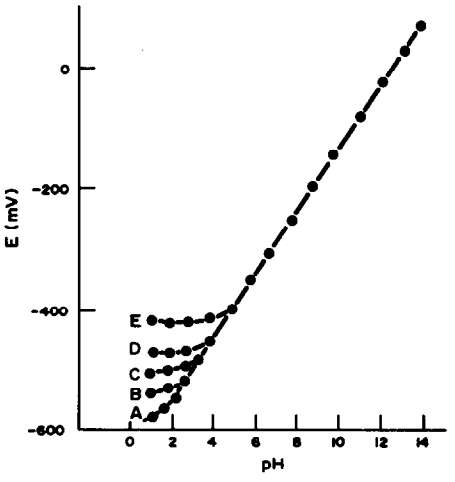

Fig. 7. Influence of the anion contained in solutions ((A) 0.1*M* NO_3^-; (B) 0.1*M* Cl^-; (C) 0.1*M* Br^-; (D) 0.1*M* SCN^-; (E) 0.1*M* I^-).

impedance semicircles. The bulk resistances increased with increasing pH values (Fig. 6). It is proposed that the energy of transfer of the hydrogen ion across the polymer membrane increased with increasing pH values. The effect of anions on the pH response can be seen from the left ends of the response curves shown in Fig. 7. The following sequence of anion interference was observed: $I^- > SCN^- > Br^- > Cl^- > NO_3^-$. The iodide was actually an interfering ion. As Karagozler *et al.*[16] reported, an electrode based on a poly(3-methylthiophene) films doped with iodine by electrochemical oxidation of iodide showed Nernstian response towards iodide at pH 2–10. The PTAPP coated electrode dipped in aqueous solution of pH below 5.5 displayed a Nernstian response toward iodide. The linear response ranges toward iodide increased with decreasing pH values of the solution. Work is in progress to study the response mechanism of the PTAPP film toward iodide.

Acknowledgements—This work was supported by the National Natural Science Foundation of China and partially by Laboratory of Electroanalytical Chemistry, Changchun Institute of Applied Chemistry, Chinese Academy of Sciences.

REFERENCES

1. P. Schulthess, Y. Shijo, H. V. Pham, E. Pretsch and W. Simon, *Anal. Chim. Acta*, 1981, **131**, 111.
2. U. Oesch, Z. Brzozka, A. P. Xu, B. Rusterholz, G. Suter, H. V. Pham, D. H. Welti, D. Ammann, E. Pretsch and W. Simon, *Anal. Chem.*, 1986, **58**, 2285.
3. H. L. Wu and R. Q. Yu, *Talanta*, 1987, **34**, 577.
4. R. Yuan, H. L. Wu and R. Q. Yu, *Science in China (Series B)*, 1992, No. **5**, 455.
5. W. R. Heineman, H. J. Wieck and A. M. Yacynych, *Anal. Chem.*, 1980, **52**, 345.
6. Y. Ohnukl, H. Matsuda, T. Ohsaka and N. Oyama, *J. Electroanal. Chem. Interfacial Electrochem.*, 1983, **158**, 55.
7. G. Cheek, C. P. Wales and R. J. Nowak, *Anal. Chem.*, 1983, **55**, 380.
8. N. Oyama and T. Hirokawa, *ibid.*, 1987, **59**, 258.
9. L. Jin, Z. Shi, J. Ye, J. Qian and Y. Fang, *Anal. Chim. Acta*, 1991, **244**, 165.
10. S. S. Huang, X. H. Song, H. G. Lin and R. Q. Yu, *Mikrochim. Acta*, 1992, **107**, 27.
11. S. Daunert, S. Wallace, A. Florido and L. G. Bachas, *Anal. Chem.*, 1991, **63**, 1676.
12. B. A. White and R. W. Murray, *J. Electroanal. Chem.*, 1985, **189**, 345.
13. J. P. Collman, M. Marrocco, P. Denisevich, C. Koval and F. C. Anson, *ibid.*, 1979, **101**, 117.
14. R. N. Adams, *Electrochemistry at Solid Electrodes*, p. 305. Marcel Dekker, New York, 1969.
15. H. Y. Lee and R. N. Adams, *Anal. Chem.*, 1962, **34**, 1587.
16. A. E. Karagozler, O. Y. Ataman, A. Galal, Z. L. Xue, H. Zimmer and H. B. Mark, *Anal. Chim. Acta*, 1991, **248**, 163.

Talanta, Vol. 40, No. 8, pp. 1261–1266, 1993
Printed in Great Britain.

0039-9140/93 $6.00 + 0.00
Pergamon Press Ltd

SOLVENT EXTRACTION OF URANIUM(VI) INTO TOLUENE BY DICYCLOHEXANO-18-CROWN-6 FROM MIXED AQUEOUS-ORGANIC SOLUTIONS

J. P. SHUKLA, ANIL KUMAR* and R. K. SINGH*
Radiochemistry Division, Bhabha Atomic Research Centre, Trombay, Bombay-400085, India

(*Received* 22 *July* 1992. *Revised* 18 *November* 1992. *Accepted* 23 *November* 1992)

Summary—Extraction behaviour of uranium(VI) from mixed organo-aqueous solutions containing water-miscible protic aliphatic alcohols and several aprotic solvents was investigated by using dicyclohexano-18-crown-6(DC18C6) as an extractant. The organic phase was a binary solution of DC18C6 and toluene while the polar phase was a three component solution of uranyl nitrate, polar additive and aqueous nitric acid. Methanol, ethanol, isobutanol, dioxane, acetone, propylene carbonate and acetonitrile were used as the organic components of the mixed (polar) phase. Propylene carbonate, acetone, acetonitrile and dioxane increased the extractability of U(VI), whereas alcoholic additives showed only an antagonistic effect. The relative increase in extraction was found to be more at lower nitric acid concentrations. Possible reasons for such behaviour are briefly discussed. Recovery of U(VI) from loaded organic phase was easily accomplished using dilute perchloric acid and sulphuric acid. A sample method was standardized for the separation of plutonium(IV) from uranium(VI) based on its reductive stripping.

Liquid–liquid extraction has been commercially exploited, particularly for the separation and purification of both rare earths and actinides such as thorium, uranium and plutonium. The separation of the metals is difficult, however, if their chemical properties are similar. To this end, several techniques have been suggested to improve the separation factors between such metals, such as: (i) introducing an auxiliary extractant with the main extractant, generally called a "synergic" extraction;[1] (ii) adding a complexing agent such as EDTA, acetylacetone, *etc.*, to an aqueous phase,[2,3] and (iii) incorporating a polar water-miscible organic additive such as acetone, dioxane, dimethyl sulfoxide, acetonitrile, *etc.*, to an aqueous phase.[4,5] Among these, solvent extraction of metals from mixed aqueous–organic solutions has especially drawn attention recently owing to several practical advantages and ease of manipulations. To date, most of the effort in this field has been restricted to extractions with amines and tributyl phosphate,[6,7] whereas use of mixed solvents with macrocyclic crown compounds has not been significant so far. Macrocycles are novel cyclic liposoluble organic molecules which contain hetero atoms, *e.g.* O, N, S and P, capable of forming electron-rich interior cavities and possess the ability to complex ions or molecules via ion–dipole or dipole–dipole stereo-selective interactions. Among several 18-crown-6 derivatives, dicyclohexano-18-crown-6 (DC18C6) has already been shown to have potential for uranium(VI) and plutonium(IV) extraction[8] from aqueous nitric acid media.

As part of comprehensive studies on the extraction of actinides with polydentate macrocycles, we have recently reported on the extraction behaviour of plutonium(IV) from several hydro-organic solutions using DC18C6 as the extractant.[9] This paper now reports data on the extraction characteristics of uranium(VI) under similar conditions for which no data are available for the extraction from acidic nitrate solutions in the presence of protic as well as aprotic common organic solvents.

EXPERIMENTAL

All the chemicals used were "analytical reagent".

Reagents

Aliphatic alcohols (methanol, ethanol and isobutanol), dioxane, propylene carbonate (PC), acetone and acetonitrile (AN) used were all G.R. grade. The organic and the aqueous phase were saturated with each other prior to their use in order to prevent any volume change during

*Power reactor fuel reprocessing plant, BARC.

extraction. DC18C6, obtained from Aldrich, USA, was of high purity grade.

Tracer

U-233 used was purified by tributyl phosphate (TBP) extraction and checked for its radiochemical purity. U-233 radiotracer (10^{-6}–$10^{-4}M$) was used throughout this study and assayed radiometrically by alpha scintillation counting.

Distribution ratio (D_U) measurements

Equal volumes (1 ml) of U-233 tracer containing an organic additive in the desired nitric acid molarity and DC18C6 dissolved in toluene, were pipetted into a 15-ml glass-stoppered equilibration tube and stirred mechanically for about 40 min at room temperature (23–25°C). Preliminary experiments had shown that equilibrium was established in about 25 min. After settling for half an hour, and centrifuging if necessary, suitable aliquots from both the phases were withdrawn for radioassay. The distribution ratio (D_U) of uranium, defined as: D_U = total concentration of uranium in the organic phase/total concentration of uranium in the aqueous phase, was thus calculated.

From a knowledge of D_U, the volume of the aqueous phase (V_w) and the volume of the organic phase (V_o), the percentage extraction (%E) was then evaluated:

$$\%E = 100\ D_U/[D_U + (V_w/V_o)].$$

All the measurements were done at least in duplicate and the agreement in D_U values obtained was within ±2% with good material balance (>95%).

In evaluating the effect of various organic additives such as alcohols, acetone, acetonitrile, dioxane and propylene carbonate on D_U, the procedure adopted was essentially the same except that the aqueous phase contained the appropriate proportion of an organic additive. The relative permittivity of the mixed aquo-organic media, D, was calculated from the equation (10).

$$D = (V/100)D_1 + (100 - V/100)D_2,$$

where D_1 and V are the relative permittivity and percentage organic additive present, respectively, and D_2 is the dilectric constant of pure water.

For studying the back extraction, suitable aliquots from the loaded organic phase were withdrawn into an equilibration tube and subsequently back extracted for about 10 min with similar volumes of the strippant.

Absorption spectra

Uranium(VI) was extracted from 7M HNO_3 containing 20% AN and 0.2M DC18C6/toluene and the spectra of the organic extracts thus separated were recorded on a Shimadzu, model UV-160, UV-visible spectrophotometer.

RESULTS AND DISCUSSION

Liquid–liquid extraction of U(VI) into toluene by DC18C6 from mixed aquo-organic solutions is strongly influenced by the addition of certain organic additives to the aqueous acidic phase. Distribution ratios attained were quite high and quantitative extraction was even possible at the lower nitric acid concentrations admixed with suitable non-aqueous solvents. Values of D_U were virtually independent of the initial metal concentration employed (10^{-6}–$10^{-4}M$), indicating the absence of polynuclear species in the extraction systems. Detailed study on mutual solubility of the various components and on the swelling of the organic phase was not attempted. Generally, however, it is known that at concentrations of alcohols of about 30% or less in the polar phase, the change in the volume of phases is of the same order as in the case of pure aqueous mineral acid solutions. Higher proportions of organic additives than 30% were therefore not employed to avoid such complications. Also, the presence of a high concentration of the alcohols in the polar phase results in a decrease in the specific gravity of the latter, resulting in the reversal of the extraction phases. Owing to its reversal, separation of the phases becomes difficult. Sometimes only one phase is formed when the percentage of organic additive is increased beyond a certain limit.

Dependence of D_U on nitric acid concentration

To assess the dependence of the extraction capacity on the polar phase acidity, the extraction behaviour of uranium(VI) from increasing nitric acid molarity into toluene by DC18C6 was systematically examined. Representative data for only acetonitrile and propylene carbonate are shown in Fig. 1. The upper two curves show that the values of D_U were considerably enhanced by addition of these organic solvents. Maximum extractability is slightly shifted towards lower acidity in the presence of such additives, though the general pattern of acid

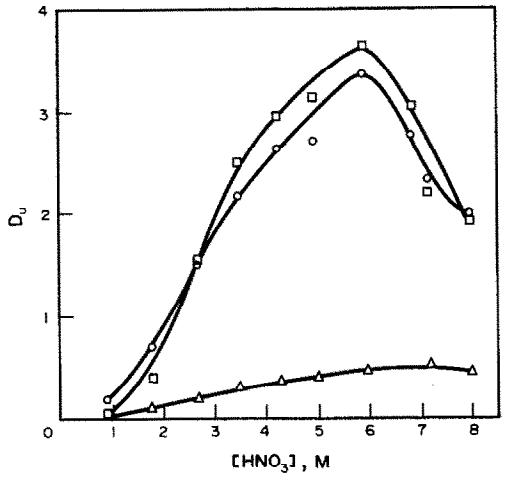

Fig. 1. Effect of nitric acid concentration on the extraction of U(VI) with 0.2*M* DC18C6/toluene from pure nitric acid solution (—△—); solution containing 20% (v/v) propylene carbonate (—○—); solution containing 20% (v/v) acetonitrile (—□—).

dependence is essentially similar to that with no additive. Maximum extraction of uranium took place at around 6–7*M* HNO_3 and the same trend was followed in the presence of 20% AN or PC in the polar phase with significant increase in D_U values. Similarly maximum enhancement in Pu(IV) extraction by this macrocycle took place at acidity around 5–6*M* HNO_3 in the presence of 20% PC.[9] After the maximum, values of D_U decreased with further increase in polar phase acidity. The initial growth in the extraction was probably caused by the salting out effect of the nitric acid in the presence of the water-miscible organic solvents, the further increase in the content of which decreased the concentration of free extractant as a result of coextraction of nitric acid which is attributed to the competitive formation of CE.*m* HNO_3 ($m = 1,2$) complex in the organic phase[11] and incomplete dissociation of HNO_3 in the polar phase. It is evident that at the same acidity, extraction was generally higher in the presence of acetonitrile than propylene carbonate in the polar phase (Table 1). At higher acid concentrations (>5*M*), extraction of U(VI) was relatively less influenced by introducing organic component in the polar phase, whereas comparatively higher D_U values were obtained by adding organic solvents at lower acid concentrations (<3–4*M* HNO_3). This phenomenon has been previously observed for extraction from mixed media.[12]

Table 1. Extraction of U(VI) into toluene by DC18C6 from acidic solutions containing an organic additive as a function of nitric acid concentration (organic phase: 0.2*M* DC18C6/toluene; volume ratio, O/A: 1)

HNO_3 (M)	D_U*	Distribution ratio (D_U) (in 20%) 20% AN	20% AF	20% PC	20% AF
0.9	0.01	0.04	4.0	0.18	18.0
1.8	0.10	0.40	4.0	0.68	6.8
2.7	0.19	1.56	8.2	1.55	8.2
3.5	0.28	2.53	9.0	2.17	7.8
4.3	0.35	2.93	8.4	2.64	7.5
5.0	0.40	3.14	7.9	2.70	6.8
6.0	0.47	3.65	7.8	3.37	7.2
7.2	0.52	2.20	4.2	2.32	4.5
8.0	0.44	1.92	4.4	1.98	4.5

*Extraction without organic additive.

Dependence of D_U *on DC18C6 concentration*

The concentration of the crown ether, DC18C6, in the organic phase strongly influenced the extraction of uranium from polar media. To examine this, extraction of uranium with 0.05–0.5*M* DC18C6 from aqueous–organic media (HNO_3 + AN) with varying acetonitrile concentration was investigated. From the results summarized in Table 2, it is quite evident that metal extractability was markedly enhanced by increasing the concentrations of both DC18C6 and acetonitrile up to 30 vol. (%). The height of synergic maximum followed the trend: 0.5 > 0.2 > 0.1 > 0.05*M* DC18C6. Thus the synergic effect was more pronounced at higher crown ether concentrations. Extraction of U(VI) exceeding 90% could be readily achieved in a single equal-volume contact by 0.5*M* DC18C6 from 4*M* HNO_3 solutions containing 30% (v/v) acetonitrile (Table 2). A similar behaviour was also noted with propylene carbonate as the organic component.

In order to study the extraction mechanism, the dependence of D_U on crown ether

Table 2. Effect of DC18C6 concentration on uranium(VI) extraction into toluene from aqueous-acetonitrile polar phase*

Acetonitrile (%)	Distribution ratio (D_U) DC18C6† (*M*) 0.05	0.1	0.2	0.5
0	—	0.17	0.31	—
10	0.17	0.93	1.69	3.29
20	0.29	1.19	2.78	5.28
30	0.52	1.46	3.15	7.12
40	0.39	1.21	2.26	4.78

*Initial concentration of acidity in the polar phase was 4*M* HNO_3.
†Dissolved in toluene.

concentration was examined at $HNO_3 = 4M$. The extraction of U(VI) is represented by,

$$UO^{2+}_{2(a)} + 2\ NO^{-}_{3(a)} + nCE_{(o)} \rightleftharpoons UO_2(NO_3)_2 \cdot nCE_{(o)}, \quad (1)$$

where subscripts a and o refer to the species present in aqueous and organic phases, respectively, for which the equilibrium constant, K_{ex}, is

$$K_{ex} = \frac{[UO_2(NO_3)_2 \cdot nCE]_{(o)}}{[UO_2^{2+}]_{(a)}[NO_3^-]^2_{(a)}[CE]^n_{(o)}}. \quad (2)$$

Introducing the distribution ratio,

$$D_U = [UO_2(NO_3)_2 \cdot nCE]_{(o)}/[UO_2^{2+}]_{(a)},$$

one obtains

$$\log D_U = \log K_{ex} + 2 \log[NO_3^-]_{(a)} + n \log [CE]_{(o)}. \quad (3)$$

Since U(VI) is at the tracer level and the partition of free DC18C6(CE) in the aqueous phase is negligible, particularly with toluene, the equilibrium concentration, $[CE]_o$, is equal to $[CE]_{initial}$. The plot of log D_U *vs.* log $[CE]_o$ in the organic phase is depicted in Fig. 2. The line drawn through the experimental points yielded a slope, n of 1.1 which indicated that the extracted species in the macrocycle–diluent phase is predominantly of the type $UO_2(NO_3)_2$.CE. Contrary to this, PU^{4+} forms an 1:2 ion pair complex of the type, $Pu(NO_3)_4$.2CE, as studied recently under similar conditions.[9] With acetonitrile the slope is nearly +1, showing that this additive, and presumably also most of the others, does not change the type of the extracted species. Values of log K_{ex} with DC18C6/toluene for $4M$ HNO_3 + 20% AN, $4M$ HNO_3 + 20% PC and pure $4M$ HNO_3 are 0.66, 0.63 and −0.20, respectively, which reflects the relatively high extractability of U(VI) from mixed media (Table 1). Visible absorption spectra of the U(VI) complex extracted with DC18C6 from $7M$ HNO_3 aqueous solution and that from $7M$ HNO_3 admixed with 20% AN were essentially alike which indicated the similarity of the species involved in the extraction process.

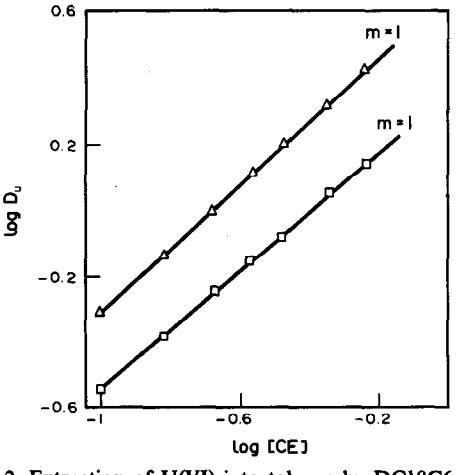

Fig. 2. Extraction of U(VI) into toluene by DC18C6 as a function of extractant concentration from pure $4M$ HNO_3 solutions (—□—); solutions containing $4M$ HNO_3 + 20% (v/v) acetonitrile (—△—).

Dependence of D_U *on the concentration of organic additives*

Preliminary experiments indicated that the organic additives generally exerted a pronounced effect on uranium extraction. Table 3 presents data on its extraction into toluene by $0.2M$ DC18C6 from $4M$ HNO_3 containing varying amounts of methanol, ethanol, isobutanol, acetone, dioxane, propylene carbonate and acetonitrile. It is evident that the values of D_U are significantly enhanced by introduction of some of these polar organic additives to the aqueous phase, except alcohols. When protic solvents such as methanol, ethanol and higher alcohols like isobutanol were used as additives, a remarkable depression in the metal extraction was observed as compared with the extraction using aprotic components, *e.g.* acetone, acetonitrile, dioxane and propylene carbonate. Such an inhibitory effect is presumably caused by the interaction of alcoholic solvents with DC18C6/toluene in the organic phase and to the decrease in the partition coefficient of the macrocycle caused by the swelling of the organic phase. In general, the addition of both types of such organic substances brings about a considerable decrease of relative permittivity (D) of the

Table 3. Effect of organic additives on the extraction of U(VI) into toluene by DC18C6 from aqueous nitric acid media (organic phase: $0.2M$ DC18C6/toluene; aqueous phase: $4M$ HNO_3 + organic additive; volume ratio (O/A): 1)

Organic additive	Distribution ratio* (D_U) (%) 10	20	30	40
Dioxane	0.92	1.36	1.86	1.25
Acetone	1.75	2.01	2.75	1.60
Acetonitrile	1.69	2.78	3.15	2.26
Propylene carbonate	1.58	2.47	2.95	2.18
Methanol	0.17	0.18	0.20	0.15
Ethanol	0.24	0.34	0.42	0.30
Isobutanol	0.19	0.27	0.30	0.20

*Mean value of D_U obtained from pure $4M$ HNO_3 medium is 0.31.

aqueous phase. Maximum enhancement in extraction was accomplished in the presence of both acetonitrile as well as propylene carbonate. Thus their additions to the aqueous phase may prove helpful in uranium recovery. To illustrate the advantage obtained by using these additives, the D_U values and the advantage factor (AF), defined as,

$$AF = D_U \text{ in mixed medium}/D_U \text{ in pure aqueous medium}$$

for 20 vol. (%) PC and AN are presented in Table 1. These results indicate that for most of the nitric acid concentrations ranging from 0.9 to 8*M* HNO_3, high D_U values (AF: 4–9) could be easily realized for uranium extraction. At the same additive percentage, the values of distribution ratio follow the sequence: methanol < isobutanol < ethanol < dioxane < acetone < propylene carbonate < acetonitrile (Fig. 3). Extraction of uranium had maxima at about 30% (v/v) additive concentration and then it steadily decreased with further proportions. Such behaviour has also been observed earlier[9] while studying Pu^{4+} as well as Am^{3+} extractions.[13] It merits mention that these substances did not pass into the nonpolar phase (the volume of the latter phase remained nearly constant after reaching equilibrium except when it contained about 30 vol. % or more of higher alcohols) and hence their effects can be explained by interaction in the aqueous phase only. Such organic liquids, being less polar than water, favour the formation of the neutral adduct, $UO_2(NO_3)_2.CE$, which ultimately brings about a substantial increase in extraction. At low additive concentrations, the dehydration effect[14] due to their presence facilitates interaction with the NO_3^- anion to form the extractable nitrate complex, and should lead to an increase in the metal extraction.

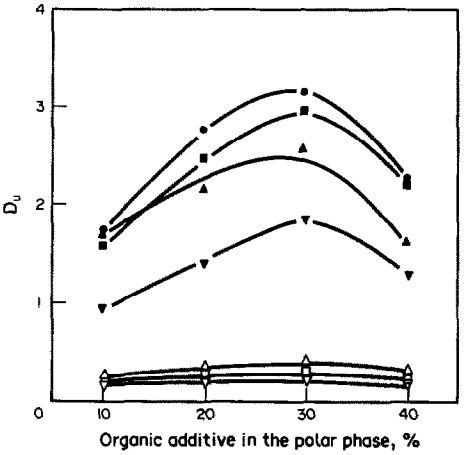

Fig. 3. Effect of organic additives on the extraction of U(VI) into toluene by 0.2*M* DC18C6 as a function of initial concentration of the organic solvents in the polar phase; initial acidity of polar phase: 4*M* HNO_3. Methanol (—▽—); isobutanol (—□—); ethanol (—△—); dioxane (—▼—); acetone (—▲—); propylene carbonate (—■—); acetonitrile (—●—).

Back extraction of uranium

Several aqueous solutions were evaluated as strippants for uranium from loaded toluene solutions of DC18C6 extracted from a polar phase containing 4*M* HNO_3 + 20% AN. From Table 4, it is evident that the strippants like $HClO_4$ as well as H_2SO_4 could strip uranium from DC18C6/toluene solutions almost quantitatively (>95%) in a single step. Sodium carbonate and oxalic acid were also tested for back extraction, and could only recover around 87 and 40%, respectively.

Separations of plutonium from uranium when extracted together

Since both U(VI) and Pu(IV) at mg/ml levels could be efficiently extracted (>95%) with 0.2*M* DC18C6/toluene from a polar phase containing 4*M* HNO_3 + 20% (v/v) CH_3CN, reductive stripping with 0.2*M* ascorbic acid or 0.2*M* $NH_2OH.HCl$ was attempted to separate them when present together. Both these strippants could recover plutonium around 95% in a single equal volume contact, while back extraction of uranium was negligibly small (<1%). Uranium

Table 4. Back extraction (stripping) of U(VI) from loaded DC18C6/toluene phase* (extractant: 0.2*M* DC18C6/toluene; volume ratio (O/A): 1)

Strippant†	D_U	U stripped (%)
Ascorbic acid (0.2*M*)	14.5	6
$NH_2OH.HCl$ (0.2*M*)	12.5	7
Na_2CO_3 (0.5*M*)	1.5	40
Oxalic acid‡ (1.0*M*)	0.15	87
H_2SO_4 (2.0*M*)	0.10	91
$HClO_4$ (1.0*M*)	Negligible	>99

*U(VI) was extracted from a polar phase containing 4*M* HNO_3 + 20% (v/v) AN.

†Aqueous solutions of strippants were made by directly weighing or measuring the volumes approximately; concentrations (*M*) are given in brackets.

‡Dissolved in 0.5*M* HNO_3.

was subsequently back extracted (>98%) with 1*M* $HClO_4$ from loaded organic extracts. Applicability of this method was successfully tested in the analysis of several low/medium level fuel reprocessing waste solutions containing large amounts of uranium (mg/ml) and trace concentrations (μg/ml) of plutonium. Recovery of uranium from triplicate experiments exceeded $98 \pm 1\%$ under the standardized conditions.

CONCLUSIONS

Extraction of uranyl ions with DC18C6 from the mixed aqueous–organic solution has been examined in order to evaluate the synergistic effect of several common polar water-miscible organic solvents. Its extraction is strongly affected by the addition of some of these components. Acetonitrile and propylene carbonate prove to be most efficient for this purpose. Slope analyses and spectral studies of the uranyl complex extracted from pure nitric solutions and those admixed with organic additives have shown the similarity of the species involved in both the systems. Separation of Pu(IV) and U(VI) is easily accomplished using reductive strippants.

Acknowledgements—The authors thank Dr R. H. Iyer, Head, Radiochemistry Division, Shri M. K. Rao, Associate Director, FRD and Shri D. D. Bajpai, PREFRE for their keen interests in this work.

REFERENCES

1. J. S. Preston, *Hydrometallurgy*, 1982, **9**, 115.
2. Q. Zheng and H. Fan, *Hydrometallurgy*, 1986, **16**, 263.
3. R. Harder and S. Chaberek, *J. Inorg. Nucl. Chem.*, 1959, **11**, 197.
4. J. P. Shukla and M. S. Subramanian, *J. Radioanal. Chem.*, 1980, **60**, 403.
5. J. Hala, in *Ion Exchange and Solvent Extraction*, J. A. Marinsky and Y. Marcus (eds), Vol. 8, p. 369. Marcel Dekker, New York, 1981.
6. J. Hala, *Chem. Listy*, 1977, **71**, 113.
7. J. Hala and J. Boleslav, *Sol. Extr. Ion Exch.*, 1986, **4**, 949.
8. J. P. Shukla, R. K. Singh and A. Kumar, *Radiochim. Acta*, 1991, **54**, 73–77.
9. J. P. Shukla, A. Kumar and R. K. Singh, *Radiochim. Acta*, in press.
10. A. K. Babko, *Analiza Fizykochemiczna Zwiazkow Kompleksowydv Ztworach.* PWN, Warsaw, 1959.
11. V. V. Yakshin, V. M. Abashkin, N. G. Zhukova, N. A. Tsarenko and B. N. Laskorin, *Dokl. Akad. Nauk SSSR*, 1979, **247**, 1938.
12. N. Souka, R. Shabana and F. Hafez, *Microchem. J.*, 1976, **21**, 515.
13. J. P. Shukla, M. S. Nagar and M. S. Subramanian, *Sepn. Sci. Tech.*, 1982–83, **17**, 1577.
14. B. Kingston and M. C. R. Symons, *J. Chem. Soc., Farad. Trans.*, 1973, **69**, 978.

Talanta, Vol. 40, No. 8, pp. 1267–1271, 1993
Printed in Great Britain.

0039-9140/93 $6.00 + 0.00

SIMULTANEOUS SPECTROPHOTOMETRIC DETERMINATION OF NICKEL AND IRON IN COPPER-BASE ALLOY WITH BROMO–PADAP

A. C. SPINOLA COSTA, SÉRGIO L. C. FERREIRA, MARIA G. M. ANDRADE and IVON P. LOBO
Instituto de Química, Universidade Federal da Bahia, Campus Universitário da Federação-40210, Brazil

(*Received* 22 *May* 1992. *Revised* 29 *December* 1992. *Accepted* 5 *January* 1993)

Summary—The reaction of nickel (II) with Br–PADAP, in the presence of tergitol NPX surfactant, forms a complex with absorption peaks at 520 and 560 nm. The iron(II)–Br–PADAP system at the same conditions forms a chelate with absorption peaks at 560 and 748 nm. This allows the simultaneous spectrophotometric determination of nickel and iron by measuring the absorbance at 560 and 748 nm. The proposed method, at pH 4.0–5.7, shows a molar absorptivity of 1.22×10^5 l · mole^{-1} · cm^{-1} for nickel at 560 nm and 8.20×10^4 l · mole^{-1} · cm^{-1} at 560 nm and 3.35×10^4 l · mole^{-1} · cm^{-1} at 748 nm for iron(II). Beer's law is obeyed up to 0.40 μ/ml of nickel(II) and up to 0.65 μg/ml of iron(II). Thiosulphate as masking agent allows the simultaneous determination of iron and nickel in the presence of high concentrations of copper. The ethylene glycol 2-(2-amino-ethyl) tetracetic acid provides the elimination of many other interferences. The method has been applied successfully to the simultaneous determination of nickel and iron in reference samples.

The reagent 2-(5-bromo–2-pyridylazo)-5-diethylaminophenol (Br–PADAP) has been frequently used as a spectrophotometric reagent, because of its sensitivity for metallic cations. As it has low solubility in water, the reagent cannot be used in aqueous media. Proposed methods include extractions using organic solvents in the presence of surfactants or in aqueous-ethanol systems. The main applications of Br–PADAP as a colorimetric reagent are for the determination of uranium(VI),[1] palladium,[2] thorium,[3] cadmium[4] and nickel.[5,6] The first study of the reaction of Br–PADAP with nickel(II) was made by Fu-Sheng and co-workers.[5] In it, nickel(II) reacts with Br–PADAP in aqueous-ethanol media, forming a complex with a composition of 1:2, cation:reagent, which has two absorption maxima at 520 and 560 nm.

The use of Br–PADAP as reagent for spectrophotometric determination iron was described several times. It reacts with iron(II) and iron(III). Its reaction with iron(II) forms a stable complex that has been applied for the analysis of iron in several materials.[7–11]

The iron(III)–Br–PADAP system was used for iron determination in irrigation water.[12] Wang and Song[13] used Br–PADAP for simultaneous determination of iron(III) and iron(II). Bursik *et al.*[14] proposed a simultaneous method for determination of iron(III) and copper(II).

Table 1 shows the characteristics of systems used during the proposed methods for the determination of nickel and iron with Br–PADAP. The reaction of nickel with Br–PADAP in the presence of tergitol NPX surfactant provides the formation of a complex with absorption peaks at 530 and 560 nm, while the reaction of iron(II)–Br–PADAP under the same conditions, forms a complex with absorption peaks at 560 and 748 nm. Considering these facts, a method has been proposed for the simultaneous determination of nickel and iron, by measuring the absorbances at 560 and 748 nm, based on the additive property of the absorbance.

EXPERIMENTAL

Apparatus

Spectrophotometric measurements were made a VARIAN DMS-100 spectrophotometer with matched 1.00-cm quartz cells. A FISHER-600 pH meter was used to measure the pH values of the solutions.

Reagents

All reagents were of analytical reagent grade unless otherwise stated.

Br–PADAP (MERCK) solution. 0.10 g in 100 ml of ethanol.

Table 1. Determination of nickel and iron using Br–PADAP

Cation	Media	pH	$\lambda_{work}^{(nm)}$	$\epsilon \cdot 10^4$	Masking	Application	Ref.
Ni(II)	Ethanol	5–10	560	12.6	—	Al alloys	5
Ni(II)	Ethanol	4–10	558	12.6	—	—	6
Ni(II)	Tergitol NPX	4–5.7	560	12.2	EGTA $S_2O_3^{-2}$	Cu alloys	*
Fe(II)	Ethanol	5–7	555	7.2	EDTA	Fe in copper Al Mg alloys	7
Fe(II)	Ethanol	3–10	753	3.4	—	Al alloys	8
Fe(II)	Ethanol	4	552	4.5	—	—	9
Fe(II)	Ethanol + OP	5.5	600	13.0	EDTA	Zn and its alloys	10
Fe(II)	DMF†	4.7	756	3.35	—	$BaCO_3$ and urea	11
Fe(II)	Tergitol NPX	4–5.7	560	8.20	EGTA	Cu alloys	*
			748	3.35	$S_2O_3^{-2}$		
Fe(II)	Ethanol	2.5–3.5	557	8.4			13
Fe(III)			592	8.98			
Fe(III)	Ethanol	—	600	7.6	—	water	12
Fe(III)	Triton-X100	—	535				14

*This work.

†DMF: Dimethylformamide; OP emulsifier: polyoxyethylene glycol octylphenyl ether; ϵ: molar absorptivity ($l \cdot mole^{-1} \cdot cm^{-1}$).

Standard nickel(II) solution (100 μg/ml). Prepared by dissolving pure nickel in diluted hydrochloric acid and dissolution up to 1 l. demineralized water.

Standard iron(II) solution (100 μg/ml). Prepared by dissolving iron(II) ammonium sulphate in sulphuric acid (0.50%).

Working solutions of nickel(II) and iron(II). Prepared by dilution of the standard solution in demineralized water.

Buffer solution. Prepared by mixing 2.0*M* sodium acetate and 2.0*M* acetic acid in appropriate ratios.

EGTA solution (0.40 mg/ml $\simeq 1.05 \times 10^{-3}M$/l). Prepared by dissolving ethylene glycol 2-(2-amino-ethyl) tetracetic acid (Merck) in water.

Tergitol NPX (J. T. Baker Chem. Co.) solution. 10.0 g in demineralized water (100 ml).

Thiosulphate solution (10.0%). Prepared by dissolving sodium thiosulphate in water.

Reducing solution (5.0%). Prepared by dissolving hydroxylammonium chloride in water.

General procedure

Transfer a portion of solution containing 5.00 μg of nickel and/or 10.0 μg of iron, into a 25 ml volumetric flask, add 2.0 ml of a 5% solution of hydroxylammonium chloride, 2.0 ml of tergitol NPX (10%), 2.0 ml of EGTA (0.40 mg/ml), 5.0 ml of acetate buffer (pH 4.5) and 1.0 ml of a 0.10% ethanolic solution of Br–PADAP. Dilute to the mark with water, mix, and after 50 min, measure the absorbances at 560 and 748 nm *vs.* an approximately prepared blank.

RESULTS AND DISCUSSION

Characteristics of the complexes

The reaction of Br–PADAP with iron(II) in presence of Tergitol NPX forms a coloured complex with absorption peaks at 560 and 748 nm. The absorbance of the complex reaches a maximum after 2 min of mixing the reagents and it is stable for at least 6 hr. Br–PADAP reacts with nickel(II) in presence of Tergitol NPX forming a red complex with absorption peaks at 520 and 560 nm. The colour developed within 40 min and is then stable for at least 6 hr. Therefore, measurement of the absorbances by the proposed method must be made after 50 min.

Effect of Tergitol NPX surfactant on the system N:(II)–Br–PADAP and iron(II)–Br–PADAP

The reagent and its complex have a low solubility in water, but the use of Tergitol NPX solves this inconvenience. The solubilization of 1000 μg of reagent is obtained with 50 mg of Tergitol NPX per 25 ml. Thus, 200 mg was selected as optimal. The study of the effect of the amount of Tergitol NPX on the iron(II)–Br–PADAP system revealed that it does not affect the absorbance signal of the iron(II)–Br–PADAP system when the Tergitol NPX is in the concentration range of 2.00–12.00 mg/ml. However, it was observed that, with the increase

Table 2. Effect of Tergitol NPX on the system

Concentration (*mg/ml*)	Ni(II)–Br–PADAP	Fe(II)–Br–PADAP
	Absorbance at 560 nm	
0.00	—	—
2.00	0.488	0.601
4.00	0.477	0.603
6.00	0.452	0.602
8.00	0.439	0.601
10.00	0.419	0.606
12.00	0.399	0.598

Fe(II): 0.40 μg/ml; Ni(II): 0.20 μg/ml.

Table 3. Effect of pH

pH	Ni(II)–Br–PADAP	Fe(II)–Br–PADAP	
	Absorbance		
	560 nm	560 nm	748 nm
3.75	0.403	0.576	0.241
4.00	0.414	0.614	0.246
4.40	0.437	0.611	0.247
4.90	0.439	0.612	0.249
5.20	0.433	0.611	0.251
5.70	0.438	0.615	0.250
6.00	0.435	0.589	0.253

Fe(II): 0.40 μg/ml; Ni(II): 0.20 μg/ml.

of the amount of Tergitol NPX, the absorbance signal of the nickel(II)–Br–PADAP system is reduced (Table 2).

Effect of the pH

The effect of the pH on the nickel(II)–Br–PADAP system was studied and the results demonstrated that the absorbance signal is maximum and constant in a pH range of 4.0–6.0 (Table 3). The same study for the iron(II)–Br–PADAP revealed that the optimum range is 4.0–5.7. Then, the pH range indicated for the method is 4.0–5.7. The general procedure was developed with an acetate buffer at pH 4.50, because in this pH the effect of the EGTA on the nickel(II) reaction was lower and the buffer-index of the acetate buffer was higher.

Effect of the EGTA

EDTA has been used as masking agent during iron[7,10] determination with Br–PADAP, but it cannot be used in nickel determination because its complex formation constant is too high. However, the EGTA can be used because its complex formation constant is lower.

$$\log \beta_{\text{NI(II)-EDTA}} = 18.6 \quad \log \beta_{\text{NI(II)-EGTA}} = 12.0.$$

The study of the masking agent EGTA on the iron(II)–Br–PADAP system revealed that it does not affect the absorbance signal of the system when the masking agent EGTA is in the concentration range of $0.0–1.6810^{-4}M$. However, it was observed that, with the increase of the concentration of EGTA, the absorbance signal of the nickel(II)–Br–PADAP is reduced (Table 4).

Effect of the amount of acetate buffer solution

The effect of the buffer concentration on the nickel(II)–Br–PADAP and iron(II)–Br–PADAP systems was studied and the results demonstrated that it does not affect the absorbance signal of the system when the buffer is in the concentration range of $0.04–0.20M$ in acetate.

Interference

The selectivity of the Br–PADAP during the simultaneous determination of iron and nickel was investigated by determining of 5 μg iron(II) and 5 μg of nickel(II) in the presence of various amounts of other ions. The interference limit of an ion was attributed as the proportion in which a change of ±2% in absorbances of the chelates were observed. The results are shown in Table 5.

Calibration curve

Ni(II)–Br–PADAP system. The calibration curve for the determination of nickel(II) was determined using the optimum experimental conditions. The straight line calibration curve indicated that Beer's Law is obeyed up to 0.40 μg/ml.

The equation found for the calibration curve was:

$$A = 2.075 \cdot \text{Conc} \cdot \text{Ni(II)} + 0.003, \quad r = 0.9998 \quad (\mu\text{g/ml}).$$

Table 4. Effect of EGTA on the system

Concentration (*M*)	Ni(II)–5-Br–PADAP	Fe(II)–5-Br–PADAP
	Absorbance at 560 nm	
0.0	0.430	0.605
4.20×10^{-5}	0.420	0.606
8.41×10^{-5}	0.409	0.607
1.26×10^{-4}	0.396	0.600
1.68×10^{-4}	0.376	0.601

Fe(II): 0.40 μg/ml; Ni(II): 0.20 μg/ml.

Table 5. Simultaneous determination of iron and nickel in the presence of various ions

Ion	Reagent used	Proportion of ion:metal 100:1	10:1	1:1
Cu^{+2}	$CuSO_4 \cdot 5H_2O$	N	N	N
Zn^{+2}	$ZnSO_4 \cdot 7H_2O$	N	N	N
Hg^{+2}	$Hg(NO_3)_2/HNO_3$	N	N	N
Cd^{+2}	$Cd(CH_3COO)_2 \cdot 2H_2O$	N	N	N
Mg^{+2}	$Mg(NO_3)_2$	N	N	N
Ca^{+2}	$Ca(NO_3)_2$	N	N	N
Bi^{+3}	$Ni(NO_3)_3/HCl$	Y	N	N
Pb^{+2}	$Pb(NO_3)_2$	Y	N	N
Al^{+3}	$KAl(SO_4)_2 \cdot 7H_2O$	Y	N	N
Mn^{+2}	$MnSO_4$	Y	N	N
Co^{+2}	$CoSO_4 \cdot 7H_2O$	Y	Y	Y
SO_4^{-2}	Na_2SO_4	N	N	N
Cl^-	NaCl	N	N	N
CO_3^{-2}	Na_2CO_3	Y	N	N
PO_4^{-3}	Na_3PO_4	Y	Y	N

N = Does not interfere; Y = interferes.
Fe(II): 0.20 μg/ml; Ni(II): 0.20 μg/ml.

The apparent molar absorptivity (at 560 nm) calculated from the slope of the regression line is 1.22×10^5 l · mole^{-1} · cm^{-1}.

Fe(II)–Br–PADAP system. Beer's Law is obeyed up to 0.65 μg/ml; molar absorptivities were determined as being 8.20×10^4 and 3.35×10^4 l · mole^{-1} · cm^{-1} at 560 and 748 nm, respectively.

The equations found for the calibration curves were:

$A = 1.474 \cdot \text{Conc} \cdot \text{Fe(II)} - 0.002$, $r = 0.9997$ (at 560 nm) μg/ml:

$A = 0.606 \cdot \text{Conc} \cdot \text{Fe(II)} + 0.001$, $r = 1.0000$ (at 748 nm) μg/ml.

Thiosulphate as masking agent for copper (II)

The effect of the masking agent thiosulphate on the iron(II)–Br–PADAP and nickel(II)–Br–PADAP systems was studied. The results showed that thiosulphate does not affect the absorbance signal of the systems when it is in the concentration range of 0.016–0.065*M*.

Addition of 400 mg of sodium thiosulphate is enough to mask 2500 μg of copper(II) when 4 μg of iron(II) and 4 μg of nickel(II) are simultaneously determined.

Simultaneous determination of nickel and iron in copper-base alloys

The present work has as an objective for the simultaneous determination of nickel and iron in copper-base alloys. These elements are normally present in copper-base alloy. The copper(II) is a serious interferent, but the reaction in the presence of thiosulphate solves this inconvenience.

The proposed procedure (in the Experimental section) was applied for the simultaneous determination of iron and nickel in copper-base alloys standards of compositions given in Table 7. The results are shown in Table 6.

CONCLUSIONS

Br–PADAP has high sensitivity for the simultaneous determination of iron and nickel. The use of EGTA as masking agent decrease the signal absorbance of the nickel(II)–Br–PADAP,

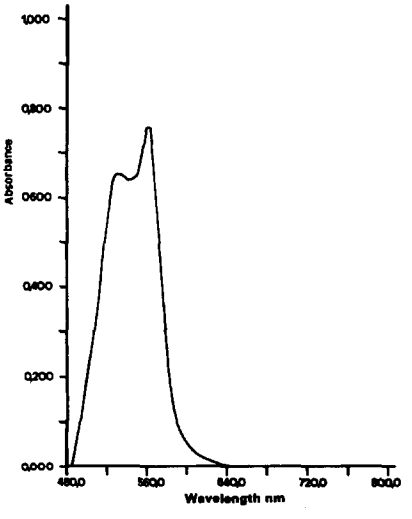

Fig. 1. Absorption spectra system nickel(II)–Br–PADAP.

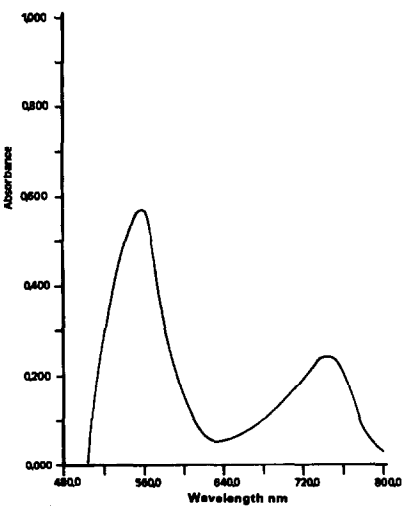

Fig. 2. Absorption spectra system iron(II)–Br–PADAP.

Table 6. Simultaneous determination of nickel and iron in copper-base alloys

Metal	Standard sample	Brass 10a-IPT,SP	Brass 486-CEPED,Ba
	N	10	10
Nickel	Present(%)	0.33	0.29
	Found(%)*	0.34 ± 0.01	0.30 ± 0.01
	S.D.	0.0092	0.0099
Iron	Present(%)	0.21	0.21
	Found(%)*	0.21 ± 0.01	0.20 ± 0.01
	S.D.	0.0084	0.0074

N = determination number; S.D. = standard deviation.
*Confidence level (95%).

Table 7. Composition of standard samples

Standard sample	Cu	Zn	Fe	Ni	Al	Pb
			(%)			
Brass 486-CEPED,Ba	85.13	4.71	0.21	0.33	4.58	4.72
Brass 10a-IPT,SP	85.86	2.87	0.21	0.29	0.05	5.32

IPT—Instituto de Pesquisas Tecnológicas do Estado de São Paulo, Brazil.
CEPED—Centro de Pesquisa e Desenvolvimento do Estado da Bahia, Brazil.

but this effect is constant and the calibration curve has a good correlation coefficient.

Cobalt(II) is the main interferent in the simultaneous determination of iron and nickel, however it is not a usual constituent of copper-base alloys.

The application of the proposed method indicated that it has very good accuracy and precision. Synthetic samples analysed showed that this method under the proposed conditions can deal with samples with iron/nickel ratio in the range of 10:1–1:10. As a result, the proposed method is perfectly useful for routine analysis due to its simplicity and possibility of determining simultaneously iron and nickel in aqueous solutions.

Acknowledgements—The authors acknowledge the financial support of the CNPq and CAPES (Brazil).

REFERENCES

1. D. A. Johnson and T. M. Florence, *Anal. Chim. Acta*, 1971, **53**, 73.
2. C. Y. Po and Z. Nan, *Talanta*, 1986, **33**, 939.
3. R. Liu and J. Ruan, *Fenxi Shiyanshi*, 1987, **6**, 32; *Anal. Abstr.*, 1988, 3B118.
4. M. Jarosz, *Chem. Anal. (Warsaw)*, 1986, **31**, 713; *Anal. Abstr.* 1987, 11B87.
5. W. Fu-Sheng, Q. Pei-Hua, S. Nai-Kui and Y. Fang, *Talanta*, 1981, **28**, 189.
6. M. Jarosz, *Chem. Anal. (Warsaw)*, 1986, **31**, 719; *Anal. Abstr.*, 1987; 11B266.
7. O. Rong, H. Li, L. Lin and M. Li, *Fenxi Huaxue*, 1982, **10**, 224; *Chem. Abstr.*, 1983, **98**, 82936v.
8. F. Wei, Q. Song, F. Yin and N. Shen, *Mikrochim. Acta*, 1983, **II(1-2)**, 17, *Anal. Abstr.*, 1984, 1B45.
9. A. Z. Abu-Zuhri, *Indian J. Chem.* 1983, **22A**, 909; *Anal. Abstr.*, 1985, 3B115.
10. X. Wu, *Lihua Jianyan, Huaxue Fence*, 1987, **23**, 95; *Anal. Abstr.*, 1988; 1B227.
11. G. Yan, *Fenxi Shiyanshi*, 1988, **7**, 61; *Anal. Abstr.*, 1988; 8B77.
12. X. Qiu and Y. Zhu, *Int. J. Environ. Anal. Chem.* 1986, **26**, 19; *Anal. Abstr.*, 1987, 4B144.
13. B. Wang and N. Song, *Fenxi Huaxue*, 1988, **16**, 402; *Anal. Abstr.*, 1989, 1B158.
14. V. Bursik, V. Kuban and L. Sommer, *Collect. Czech. Chem. Commun.*, 1988, **53**, 3040; *Anal. Abstr.*, 1989, 6B182.

Talanta, Vol. 40, No. 8, pp. 1273–1281, 1993
Printed in Great Britain.

0039-9140/93 $6.00 + 0.00

DETERMINATION OF GALLIUM BY SQUARE-WAVE VOLTAMMETRY ANODIC STRIPPING, BASED ON THE ELECTROCATALYTIC ACTION OF 2,2′-BIPYRIDINE IN DIMETHYLSULPHOXIDE: COMPARISON WITH AN AQUEOUS NaSCN/$NaClO_4$ ELECTROLYTE

GASTON EAST* and PABLO COFRE†

Facultad de Química, Pontificia Universidad Católica de Chile, Vicuña Mackenna 4860, Santiago, Chile

(*Received* 23 *March* 1992. *Revised* 1 *February* 1993. *Accepted* 10 *February* 1993)

Summary—Deposition potential, deposition time, square-wave frequency, 2,2′-bipyridine concentration, and gallium concentration have been studied in detail, for the determination of trace concentration levels of the metal by square-wave voltammetry anodic stripping analysis, in dimethylsulphoxide. Optimum conditions have been found for gallium(III) determination and results compared to those obtained in $0.5M$ NaSCN + $4.2M$ $NaClO_4$ aqueous electrolyte by obtaining calibration graphs for the range $1 \times 10^{-8}M$–$1 \times 10^{-5}M$ gallium. Accuracy (±3%) and precision (4–6% SD) of this method were assessed with both $4 \times 10^{-8}M$ and $4 \times 10^{-7}M$ gallium solutions used as synthetic samples. The efficiency of solvent extraction of gallium with di-isopropyl ether was found to be 99.98% at a $4 \times 10^{-7}M$ gallium concentration. The proposed method was applied to the determination of the gallium content in rock mineral samples (using the above mentioned solvent extraction procedure), and results compared to those obtained with the NaSCN–$NaClO_4$ based electrolyte. No statistically significant difference was observed. Analytical procedures followed are given in detail.

The need for sensitive and reliable methods for the determination of trace concentrations of gallium has been recognized in different fields. The special affinity of sarcomatous tissues for this element has led to studies of its tissue retention and cytotoxicity and motivated previous analytical works.[1,2]

From an environmental point of view, the increasing importance and use of compounds such as gallium arsenide in the semiconductor industry, has posed the question of its toxicity and potential hazard when suspended in the industrial atmosphere.[3] As a doping element, it has to be determined in microscopic weighed samples in minute amounts.[4] On the other hand, surveys in the mining industry require the determination of trace concentrations of gallium in samples of different mineral compositions.

Our attention in the past has been focused on the use of anodic stripping combined with square-wave voltammetry in a $0.5M$ NaSCN + $4.2M$ $NaClO_4$ electrolyte.[5] This electrolyte has proven to be effective in transforming an inherently irreversible electrochemical reduction of gallium(III)[6] into a reversible process,[7,8] a condition which is required for electroanalytical methods. However, the high concentration of electrolyte required is a disadvantage, because of the metal impurities introduced by the reagents, and this has led us to initiate studies in the search for alternative systems.

In previous work[9] we explored the possibility of changing from aqueous to non-aqueous media (acetonitrile and dimethylsulphoxide) and the use of 2,2′-bipyridine (DIPY) as electrocatalyst[10] to transform the irreversible reduction of aquo-gallium(III) to a more facile process. We succeeded in obtaining a catalytic wave in dimethylsulphoxide (DMSO), corresponding to the reduction of gallium(III) to gallium metal which deposits in the mercury drop electrode, with catalyst concentrations between 10^{-3} and $10^{-2}M$, only.

In this work we extend our study to the application of this electrocatalytic reduction to the determination of trace concentrations of gallium, by means of anodic stripping combined with square-wave voltammetry. A comparison

*On sabbatical leave from Departamento de Química, Universidade de Brasilia, Brazil.
†Author for correspondence.

with the previous NaSCN–$NaClO_4$ aqueous electrolyte is carried out. Our results show how well this new system works, with some sacrifice in sensitivity.

EXPERIMENTAL

Instrumentation

The anodic stripping experiments were run with an EG & G Princeton Applied Research polarographic analyzer model 384B in its square-wave voltammetry mode. This was connected to the PAR 303A static mercury drop electrode (HMDE), which contains a silver–silver chloride reference electrode. The filling solution was substituted with an aqueous tetramethyl ammonium chloride (TMACl) solution. Its concentration was adjusted so that the electrode potential was coincident with that of a saturated calomel electrode (SCE).

Curves were plotted on a Houston Instrument model DMP-40 plotter. A cell design with a side tube at the bottom for collection of mercury drops[11] was modified to contain 5 ml of solution. Solutions were degassed with high purity argon presaturated with DMSO and stirred with a 305 EG & G magnetic stirrer in its slow speed setting (nominally 400 rpm).

Gallium(III) stock solution volumes were measured with Gilson Pipetman micropipettes.

A 600 W SAMSUNG microwave oven model RE-610TC, provided with an acrylic plastic box and fume exhaust tube, was used for rock mineral sample digestion.

The samples plus digesting acids were placed into Parr microwave acid digestion bombs model 4781 (23 ml capacity).

Test tubes used in solvent extraction were shaken with an HEIDOLPH vortex shaker model REAX 2000.

Reagents

Supporting electrolytes were made with sodium thiocyanate (Fluka purum p.a.) and sodium perchlorate, obtained by neutralization of sodium carbonate (Merck p.a.) with 70% perchloric acid (Baker analysed) in aqueous media. Tetraethylammonium perchlorate (TEAP), made by neutralization of 20% (w/w) aqueous tetraethylammonium hydroxide (Aldrich) with 70% perchloric acid (Baker analysed) and recrystallization from absolute ethanol (Merck p.a.), was used in non-aqueous media. Solvents used were dimethylsulphoxide (DMSO) with 0.03% water (Merck p.a.), or >99% purity from Aldrich and distilled water, obtained from a high performance automatic self-flushing still.[12]

Gallium(III) perchlorate [$Ga(ClO_4)_3 \cdot 6H_2O$] was prepared by dissolving 6N grade gallium metal (Strem Chemicals) in 70% perchloric acid (Merck, Suprapur) following a known procedure.[13] The electrocatalyst used was 2,2′-bipyridine (DIPY) from Aldrich (dissolved in the corresponding solvent). Antimony(III) chloride (Merck p.a.) was used to prevent the formation of a Ga–Zn intermetallic compound which raises the detection limit.[5]

Gallium primary standard solutions were made by dissolution of Strem Chemicals 99.999% pure gallium(III) oxide in the smallest amount of Merck Suprapur concentrated hydrochloric acid.

Solvent extraction of gallium(III) was made with di-isopropyl ether (Merck p.a.). Digestion of rock mineral samples was made with a mixture of 30% hydrochloric acid, 65% nitric acid and 40% hydrofluoric acid (all Merck Suprapur).

The rock mineral samples were provided by Laboratorio de Química Analítica y Electroquímica, PUC. Composition was mainly feldspar with gallium content between 5 and 30 ppm.

Procedures

Voltammetric measurements. The required amount of dry TEAP was weighed directly in the cell and dissolved by the addition of 5 ml of DMSO. The required gallium(III), antimony(III), perchloric acid and DIPY concentrations were obtained by spiking the solution in the cell with the appropriate stock solutions. Solutions were degassed for 300 sec and then preconcentration of gallium on a small size (0.13 mm^3) mercury drop was conducted at the specified deposition potential (E_d) and deposition time (t_d) with constant speed stirring (~400 rpm). This was followed by a 15 sec rest period before stripping. The gallium stripping was performed by square-wave voltammetry with 120 Hz frequency, 2 mV step height and 20 mV amplitude. Peak stripping currents ($I_{p,a}$) were automatically measured by a tangent fit programme, together with the measurement of peak potentials (E_p), which are referred to the SCE.

Experiments in aqueous 0.5*M* NaSCN + 4.2*M* $NaClO_4$ or 4.2*M* $NaClO_4$ were carried out after adjustment to pH 2.0.

Synthetic gallium samples. The synthetic gallium samples were prepared as follows: a $2 \times 10^{-2}M$ stock solution was made by dissolving the required amount of 99.999% Ga_2O_3 in 3 ml of 30% HCl in a digestion bomb, which was heated for 5 min at 300 W in the microwave oven. It was cooled to room temperature and the excess HCl evaporated on a hot plate. The resulting solution was transferred to a 25 ml volumetric flask and made up to volume with DMSO. Then fresh $1 \times 10^{-4}M$ and $2 \times 10^{-5}M$ gallium solutions in DMSO were made daily from the $2 \times 10^{-2}M$ stock solution. The synthetic sample concentrations were obtained by spiking the cell with 20 μl of the $1 \times 10^{-4}M$ solution to provide a $4 \times 10^{-7}M$ sample or with 10 μl of the $2 \times 10^{-5}M$ solution to provide a $4 \times 10^{-8}M$ sample.

The gallium determination was made as follows: 115 mg of TEAP was weighed directly in the cell. Then 5 μl of a $10^{-2}M$ Sb(III) stock solution were added plus 100 μl of a $0.15M$ DIPY stock solution in DMSO, and 5 ml of DMSO which was transferred, through a PTFE tube by pressurizing the solvent bottle with argon, into a measuring cylinder and then into the cell. The resulting solution was then spiked with the corresponding gallium stock solution to obtain the desired concentration. After degassing, preconcentration in the mercury drop was performed at $E_d = -1.3$ V, $t_d = 180$ or 300 sec. This was followed by the rest period and stripping step.

Solvent extraction experiments. The gallium solvent extraction experiments were performed as follows: 5 ml of a $10^{-4}M$ gallium solution were prepared daily from a $2 \times 10^{-2}M$ stock solution (aqueous and non-aqueous $10^{-4}M$ gallium solutions were prepared and when an aqueous solution was made, 50 μl $7M$ HCl was first added to the 5 ml volumetric flask to prevent hydrolysis). To a 15 ml stoppered test tube, 40 μl of the $10^{-4}M$ gallium solution were transferred, followed by 4 ml of $7M$ HCl and 4 ml of di-isopropyl ether. The tube was shaken for 5 min with the vortex shaker and allowed to stand until phase separation ($\sim$5 min). After decantation, 2 ml of the organic phase were transferred to a 20 ml beaker and the organic solvent was evaporated to dryness with an air blower. This was followed by the addition of 115 mg of TEAP, 5 ml DMSO, 100 μl of $0.15M$ DIPY and 5 μl of $10^{-2}M$ Sb(III) solution. This solution was transferred, after mixing, to the polarographic cell.

The gallium content was determined by means of a standard addition method (one or three additions) by spiking the solution with a $10^{-4}M$ gallium solution in DMSO. The experimental parameters for deposition and stripping were the same as before.

Rock mineral samples. The determination of gallium in rock mineral samples was performed as follows: the sample was ground and sieved to a particle size below 350 μm and dried at 100°C overnight. Then ca. 0.2000 g of the sample were weighed out in the PTFE vessel (which is part of the digestion bomb), 1 ml of HNO_3, 3 ml of HCl and 2 ml of HF were added, and after assembling the digestion bomb, it was heated in the microwave oven for 3 min at 600 W. It was cooled to room temperature, disassembled and after collecting all the droplets from the vessel lid with water, the solution was evaporated to dryness on a hot plate. Then 1 ml of HCl was added and the solution was evaporated to dryness again. This step was repeated once more. The solid residue was dissolved with 1 ml HCl and transferred into a ground glass stoppered test tube. The vessel was washed twice with 1 ml HCl portions and once with 1 ml H_2O and transferred into the test tube. This results in a $7M$ HCl solution. Then 0.2–0.4 ml of Hg were added to reduce the iron(III) to iron(II) and the air in the test tube was displaced with argon before replacing the stopper. The test tube was shaken for 3 min. and after solution decolouration, 4 ml of di-isopropyl ether was added and the tube was shaken again for another 5 min. Phase separation was allowed and after decantation 2 ml of the organic phase were taken and transferred into a 20 ml beaker. The solvent was evaporated with an air blower. Then, 115 mg TEAP, 5 ml DMSO and 5 μl of $0.15M$ DIPY solution were added and after dissolution transferred into the polarographic cell. The gallium determination was made by a standard addition method (spiking with 50–100 μl of a fresh $4 \times 10^{-4}M$ solution in DMSO). The experimental parameters for deposition and stripping were the same as before except that a shorter deposition time ($t_d = 30$ sec) was required.

RESULTS AND DISCUSSION

Effect of deposition potential

The effect of deposition potential (E_d) on the gallium stripping peak current was studied to compare the catalytic action of SCN^- in

water [Fig. 1(a)] with that of DIPY in DMSO [Fig. 1(b)].

In the absence of SCN^- [Fig. 1(a)], a peak-shaped curve (●), which suddenly drops to zero at −1.75 V, is obtained. This shape is consistent with an irreversible reduction of gallium(III) that approaches a diffusion controlled current at −1.7 V, but which gradually overlaps with the proton and solvent reduction at more negative potentials. The reduction and consumption of protons at the electrode–solution interface raises the local pH so that the gallium(III) diffusing towards the electrode precipitates before it can be reduced.

In the presence of SCN^- [Fig. 1(a)], gallium deposition is obtained at more positive potentials and higher stripping currents are observed (×). A current plateau appears around −1.0 V and two maxima at −1.25 and −1.55 V are found before the current drops to zero at −1.85 V.

The electrocatalytic effect of SCN^- which makes the gallium(III) reduction a more reversible process, explains the lower deposition potentials required and also the higher stripping currents observed. The existence of the current plateau around −1.0 V, with a height equal to that of the current peak at −1.25 V, suggests that two different processes involving two different species, that are reduced to gallium metal at different electrode potentials, are present.

This was confirmed by cyclic voltammetry (cyclic voltammogram not shown) in which two cathodic peaks appeared at −0.9 and −1.2 V. The current drop at −1.4 V is the result of proton reduction, with the consequent precipitation and loss of gallium(III) at the electrode–solution interface. The following current increase, that reaches a maximum at −1.55 V, is due to the overlapping of the irreversible reduction of gallium(III), as described by Fig. 1(a) curve (●), which adds to the reduction of gallium(III) catalyzed by $SCN,^-$ and counteracts the previous process. At deposition potentials more negative than −1.55 V, the current drop observed is the result of the solvent reduction which produces a gallium(III) loss due to the pH increase at the electrode–solution interface[14] as for Fig. 1(a) curve (●).

When DMSO is substituted for water [Fig. 1(b)], the reduction of gallium(III) in the absence of DIPY (○) takes place at less negative potentials, but the stripping currents found are lower and decrease at potentials more negative than −2.0 V. The fact that deposition of gallium is obtained at a lower E_d indicates that more labile (easily desolvated) species are present in this solvent, probably due to a much lower water activity. On the other hand, the more bulky solvated species, assumed to have smaller diffusion coefficients as compared to the aquo gallium(III) ions, produce lower deposition currents. The current drop observed at sufficiently negative potentials can be ascribed to changes in the local pH and gallium(III) loss at the electrode–solution interface, because of the reduction of protons. The gallium(III) loss is observed in this solvent at more negative

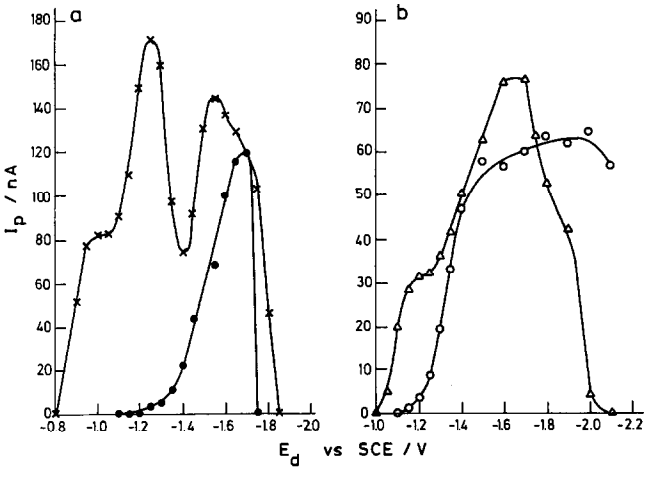

Fig. 1. Effect of deposition potential (E_d) (deposition time t_d = 180 sec) on the gallium stripping current ($I_{p,a}$) for a $10^{-7}M$ gallium(III) perchlorate plus $2 \times 10^{-5}M$ antimony(III) solution in: (a) 4.2M $NaClO_4$ (●) and 0.5M NaSCN + 4.2M $NaClO_4$ (×), both of pH = 2.0. (b) 0.1M TEAP (DMSO) in the presence (△) and in the absence (○) of $2 \times 10^{-3}M$ DIPY, both containing $10^{-3}M$ $HClO_4$.

deposition potentials than in aqueous media due to the lower water activity.

In the presence of DIPY (△), a catalyzed reduction of gallium(III) is observed at less negative deposition potentials and higher stripping currents are obtained. A slight shoulder appears around −1.2 V and a current maximum at −1.65 V. For potentials more negative than −1.7 V the current drops and reaches zero at −2.1 V. The shoulder at −1.2 V is a consequence of the existence of different catalytic waves at different electrode potentials as described in our previous report.[9] The current drop at the negative end in the presence of DIPY is observed at more positive potentials as a result of the catalytic action of this compound on the proton reduction. Now, only one maximum at −1.65 V is observed due to a greater degree of overlapping between the catalyzed (△) and non-catalyzed (○) reduction of gallium(III).

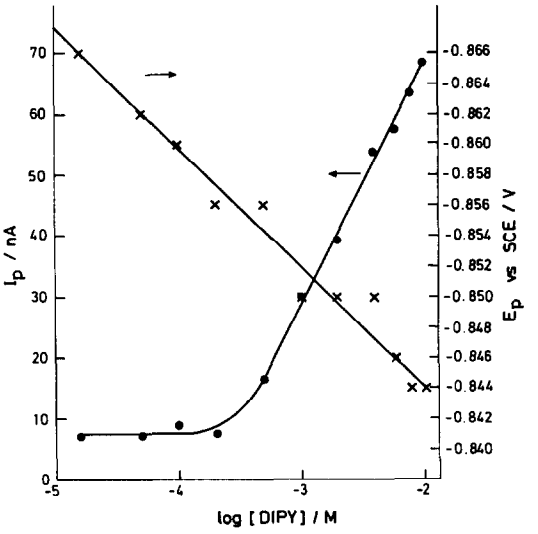

Fig. 3. Effect of DIPY concentration on the gallium stripping current ($I_{p,a}$) for $10^{-7}M$ gallium perchlorate plus $2 \times 10^{-5}M$ Sb(III) and $0.1M$ TEAP (DMSO). Deposition potential $E_d = -1.25$ V; deposition time $t_d = 180$ sec.

Effect of square-wave frequency

A linear dependence of gallium stripping peak current with the square root of the frequency (f) (Fig. 2) is observed in the NaSCN (●) as well as in the DIPY (○) based electrolytes (currents for frequencies below those shown were not detected). While a straight line which goes through the origin is obtained in the first case, as one would expect for a diffusion controlled process, in the second case the straight line gives a negative intercept. If we consider that the only common process to both systems is the diffusion of the deposited gallium in the mercury drop towards the electrode surface during the stripping step, to give a soluble species after charge transfer, the difference observed has to be due to a difference in the following steps. The smaller slope obtained with the DIPY based electrolyte can be interpreted as a consequence of a lower diffusion coefficient of the more bulky gallium–DIPY as compared to the gallium–SCN^- species in solution during the deposition step, so that a smaller amount of gallium metal is deposited for the same deposition time.

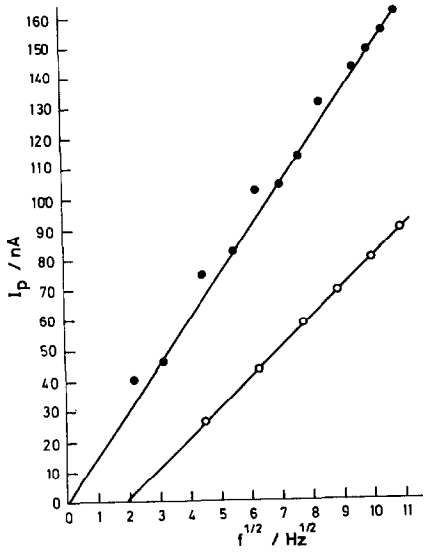

Fig. 2. Effect of square-wave frequency (f) on the gallium stripping peak current ($I_{p,a}$) after a deposition time $t_d = 180$ sec, for a solution containing $[Ga^{III}] = 1 \times 10^{-7}M$ + $[Sb^{III}] = 2 \times 10^{-5}M$ in: $0.5M$ NaSCN + $4.2M$ $NaClO_4$ (pH = 2.0; $E_d = -1.05$ V) (●) and $0.1M$ TEAP + $2 \times 10^{-3}M$ DIPY in DMSO ($E_d = -1.25$ V) (○).

Effect of DIPY concentration

The effect of DIPY concentration on the gallium stripping current, Fig. 3 (●), was explored within the range 1.5×10^{-5}–$1.0 \times 10^{-2}M$. No gallium stripping current increase is observed when DIPY concentrations up to $2.8 \times 10^{-4}M$ are used. For concentrations over this point a linear increase of stripping current with log[DIPY] is observed. This is an indication that there is a DIPY consumption by coordination to the different metal ions present in the electrolyte, which precludes its catalytic action on the gallium discharge. Only when excess DIPY is added, to complex first all these metal ions, the catalytic action of the ligand appears. Figure 3 also depicts the effect of DIPY concentration on

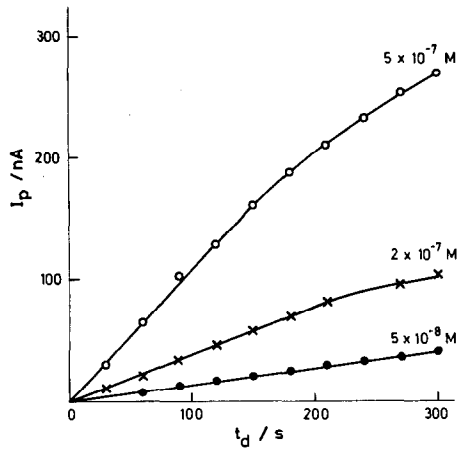

Fig. 4. Effect of deposition time (t_d), on the gallium stripping current ($I_{p,a}$) for $5 \times 10^{-8}M$ (●), $2 \times 10^{-7}M$ (×) and $5 \times 10^{-7}M$ (○) gallium perchlorate, plus $2 \times 10^{-5}M$ Sb(III), $3 \times 10^{-3}M$ DIPY and $0.1M$ TEAP in DMSO. Deposition potential $E_d = -1.25$ V.

the stripping peak potential (×). There is a linear positive shift of peak potential with log[DIPY]. This potential shift is in the opposite direction to that predicted by a Nernstian effect. Therefore, the linear dependence of the stripping current with log[DIPY] cannot be attributed to the effect of DIPY on the equilibrium potential, but rather to an adsorption of DIPY on the electrode surface, which follows a logarithmic Temkin isotherm.[15] The electrocatalytic action of DIPY on the gallium(III) discharge prevails over a possible Nernstian effect.

Effect of deposition time

The effect of deposition time (t_d) on the gallium stripping current was explored for three different gallium concentrations in the range 5×10^{-8}–$5 \times 10^{-7}M$. Results in Fig. 4 show a linear dependence for the lowest concentration as one would expect for an ideal system. However, negative deviations to linearity are soon seen for higher concentrations. This is a consequence of gallium loss due to diffusion towards the mercury thread in the capillary. The longer the deposition time, the greater the loss. An equilibrium could eventually be attained, between the amount of gallium being deposited into the mercury drop and the amount of gallium loss per unit time. At this point, the stripping current becomes independent of deposition time. Also, the greater the gallium concentration the shorter the deposition time required to observe this deviation.

A similar deviation was previously observed for zinc and gallium in an aqueous $NaSCN/NaClO_4$ electrolyte, and a detailed study was carried out.[5] This problem, also known as backdiffusion, is a disadvantage of the Kemula-type HMDE. We have found with our PAR 303A electrode, that this phenomenon can seriously affect sensitivity, detection limit and reproducibility unless a preconditioning to obtain electrode stabilization is performed before the set of measurements. This means that several deposition-stripping cycles have to be run or alternatively, a long deposition time run has to be carried out previously, to get a stable electrode; this creates an amount of residual gallium along the mercury thread, which minimizes the concentration gradient between the mercury drop and the mercury thread, and thus, hinders the gallium backdiffusion.

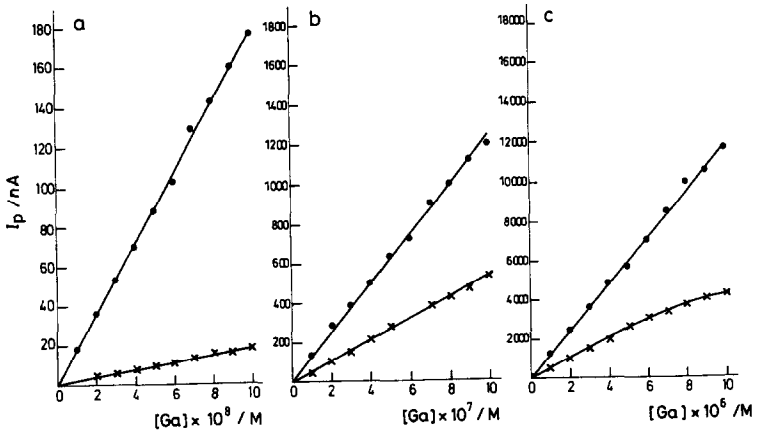

Fig. 5. Effect of gallium concentration on the gallium stripping currents in an aqueous $0.5M$ $NaSCN + 4.2M$ $NaClO_4$, pH 2.0 ($E_d = -1.15$ V; $[Sb^{III}] = 1 \times 10^{-5}M$) (●) and in $3 \times 10^{-3}M$ DIPY + $0.1M$ TEAP, DMSO ($E_d = -1.30$ V; $[Sb^{III}] = 2 \times 10^{-5}M$) (×). $E_d = 180$ sec.

Calibration graphs

Figure 5 shows calibration plots obtained in aqueous $NaSCN + NaClO_4$ (●) and non-aqueous DIPY + TEAP (×) electrolytes. Linear relationships between peak current and gallium concentration are found in both cases for all the ranges under survey, except for a slight negative deviation observed in DMSO for concentrations over $6 \times 10^{-6}M$. Blank substraction was applied when necessary but no peak current normalization using the zinc stripping peak current was required for the 10^{-8}–$10^{-7}M$ range as used previously,[5] since good linear correlations were always obtained. As a rule, higher slopes are observed in aqueous solutions than in DMSO, *e.g.*, the slope in DMSO is about one half of the slope in water for the 10^{-7}–$10^{-5}M$ range [Fig. 5(a)]. This loss in sensitivity when DIPY is substituted for NaSCN as electrocatalyst, is counterbalanced by the much lower concentrations of DIPY, one hundredth of the NaSCN, and TEAP, one fortieth of the $NaClO_4$, required. This is a clear advantage when trace levels of gallium are determined since much smaller amounts of metal contaminants are introduced by the reagents.

The DIPY concentration required is not very stringent provided that an excess is used. In fact, in the 10^{-8}–$10^{-7}M$ gallium range we could use lower values (1.5×10^{-3} and $3 \times 10^{-4}M$ DIPY) with no significant loss in sensitivity while preserving the linear dependence of the peak currents with gallium concentration.

The lower electrocatalyst concentration required was interpreted as a consequence of a greater DIPY adsorption compared to SCN^- However, the loss in sensitivity can be attributed to lower diffusion coefficients of the Ga–DIPY species in DMSO, to a higher solvent viscosity and also to a slower charge transfer rate, which would result in smaller amounts of gallium deposited and lower stripping currents.

The use of a shorter deposition time, 180 sec instead of the 360 sec employed in the previous work,[5] decreases the method sensitivity but, linearity of $I_{p,a}$ *vs.* [Ga] is preserved up to higher concentrations.

Some benefit could be gained in both electrolytes, if a more negative deposition potential was used, as one can infer from Fig. 1. For instance, sensitivity was doubled when a calibration plot for the 10^{-8}–$10^{-7}M$ range was obtained in DMSO with $E_d = -1.8$ V. The disadvantage of applying such a negative deposition potential is the likely codeposition with gallium of other interfering metals at the mercury drop electrode.

The order of addition of DIPY and gallium (III) into the cell proved to be important. When DIPY was added prior to gallium(III), a drastic sensitivity drop was observed and no stripping peak was obtained for gallium(III) concentration below $4 \times 10^{-8}M$. We have no clear explanation to this fact, but it deserves further study.

We also observed that upon mixing of the reagents in the cell, the peak currents are rather low at the start, but if several consecutive runs are performed with the same solution, an increase of the peak height is observed from one scan to the next. This behaviour could be ascribed to a slow rate of formation of the Ga–DIPY species [from Ga(III) and adsorbed DIPY] responsible for the Ga deposition at the mercury drop and also to the backdiffusion of Ga into the mercury thread as described in the previous work.[5]

Determinations in synthetic samples

The accuracy and precision of the method were assessed by analysing synthetic samples of gallium(III) solutions in DMSO at two different concentration levels. Single and multiple standard addition methods were employed. The 384B built-in standard addition programme was found to give erroneous results and was thus abandoned. Table 1 shows the results obtained, after rejection of all those values with a relative error $\pm > 10\%$. The relative mean error in all cases is exceptionally low for both concentration levels. However, the multiple standard

Table 1. Determination of gallium(III) in synthetic sample solutions in DMSO

Amount taken	Amount found							
	Single std. add.				Multiple std. add.			
	n	X	% SD	mean error (%)	n	X	% SD	mean error (%)
$4.00 \times 10^{-8}M$	23	$4.00 \times 10^{-8}M$	4.3	0	17	$3.87 \times 10^{-8}M$	5.5	−3.2
$4.00 \times 10^{-7}M$	13	$4.07 \times 10^{-7}M$	6.1	+1.8	12	$3.91 \times 10^{-7}M$	5.8	−2.1

n: Number of determinations.
X: Mean gallium concentration.
% SD: Percent standard deviation.

addition method is biased to lower results. It was found that the plot of stripping current *vs.* standard concentration always showed a slight positive deviation from linearity, so that the extrapolated intercept value on the concentration axis was lower than expected. This curvature is again a consequence of gallium backdiffusion towards the mercury thread, which gradually decreases after each standard addition, so that the first few measurements of stripping current are in fact lower than they should be. Therefore a single standard addition method should be preferred with the Kemula-type HMDE.

The precision obtained at both concentration levels is between 4 and 6% SD which is very good for trace analysis.

Solvent extraction of gallium(III)

The determination of gallium in DMSO imposes the need of transferring the metal in a quantitative way from an aqueous medium, after a mineral sample digestion, to the organic solvent. Solvent extraction of gallium(III) as a gallium–chloride complex species with di-isopropyl ether[1] has been used down to only 9.04 ppm ($\sim 1.3 \times 10^{-4} M$). It is therefore necessary to evaluate the percentage of extraction at lower concentration levels. For this purpose, a $4 \times 10^{-7} M$ aqueous gallium solution in $7 M$ HCl was used, following the procedure previously described.

Table 2 shows the results obtained. The precision of 11 determinations is of the same order of that reported on Table 1 and the average percent of extraction (99.98%) is quite satisfactory at this low concentration level.

Table 2. Extraction of gallium(III) with di-isopropyl ether from a $4.00 \times 10^{-7} M$ aqueous solution in $7 M$ HCl

Trial number	Amount found (X $10^{7} M$)
1*	3.80
2*	3.90
3*	3.70
4*	3.85
5†	4.03
6†	4.30
7†	4.26
8†	3.77
9†	4.33
10†	4.10
11†	3.95

$X = 3.999 \times 10^{-7} M$;
% SD = 5.55;
% Extraction = 99.98%.
*Aliquot of a gallium(III) stock solution in DMSO evaporated to dryness.
†Aliquot of a gallium(III) stock solution in $H_2O + HCl$ evaporated to dryness.

Table 3. Determination of gallium(III) in a rock mineral sample.* Comparison between the DIPY and NaSCN–$NaClO_4$ based methods†

Sample no.	NaSCN–$NaClO_4$ method‡	Sample no.	DIPY–DMSO method§
1	12.5 ppm	7	11.7 ppm
2	11.0 ppm	8	11.9 ppm
3	11.8 ppm	9	14.1 ppm
4	12.2 ppm	10	12.1 ppm
5	12.7 ppm	11	10.0 ppm
6‖	10.4 ppm	12‖	10.4 ppm
		13	10.7 ppm

$X = 11.77$ ppm $X = 11.55$ ppm
% SD = 7.65 % SD = 11.9
*Sample digested in a microwave oven.
†After a Q-test was used to reject results.
‡$E_d = -1.05$; $t_d = 30$ sec.
§$E_d = -1.30$; $t_d = 30$ sec.
‖Sample digested on a hot plate.

Determinations in a rock mineral sample

The gallium content of a rock mineral sample was determined with this new method and results were compared to those obtained with the NaSCN–$NaClO_4$ method.[9]

The solvent extraction with di-isopropyl ether was used after iron(III) reduction with mercury metal, as described previously.

Results in Table 3 show that the DIPY–DMSO method gives a mean value which is 1.8% lower than the mean value obtained with the NaSCN–$NaClO_4$ method. This difference is not significant at this concentration level. However, the precision of both methods, when applied to a solid sample, is lower than that reported in Table 1. This is a consequence of a greater number of operations involved in the sample handling. If an F-test with a 95% confidence level[16] is applied to both sets of data, one can conclude that there is no statistically significant difference between both methods (calculated $F = 2.42 < 4.95$ tabulated value for 95% confidence level).

CONCLUSIONS

Gallium(III) concentrations down to $2 \times 10^{-8} M$ can be determined with the DIPY–DMSO method, Fig. 5(a), as opposed to 1×10^{-8} M previously reported with the NaSCN–$NaClO_4$ method.[9] The new method requires a somewhat more negative deposition potential ($E_d = -1.3$ V) as compared to the thiocyanate based method ($E_d = -1.05$ V). Stripping current *vs.* square root of frequency is linear in the range studied (Fig. 2) with both

DIPY and SCN^- electrocatalysts, which is an indication that diffusion of gallium metal in the mercury drop is the rate determining step during stripping in both cases.

The electrocatalyst required is [DIPY] at only $1.5 \times 10^{-3}M$, as opposed to [NaSCN] at $0.5M$, and the supporting electrolyte concentration $[TEAP] = 0.1M$ is also much lower than $[NaClO_4] = 4.2M$ required previously. The use of Sb(III) to suppress the formation of a Ga–Zn intermetallic compound is still recommended, as traces of zinc can also be found in high purity organic solvents and/or reagents.

Separation of gallium(III) from its mineral matrix can be successfully achieved by solvent extraction with di-isopropyl ether from a $4 \times 10^{-7}M$ (or stronger) gallium aqueous solution in $7M$ HCl.

An accuracy of $\pm 3\%$ was obtained with a precision between 4 and 6% SD at $4 \times 10^{-8}M$ and $4 \times 10^{-7}M$ gallium concentrations (Table 1).

Comparison with the NaSCN based method proved that equally good results can be obtained with the DIPY–DMSO method (Table 3), when applied to rock mineral samples, but with the great advantage of introducing much less impurities from reagents since the supporting electrolyte and electrocatalyst concentrations are much lower.

REFERENCES

1. P. H. Davis and E. D. Moorhead, *Anal. Lett.*, 1975, **8**(6), 387.
2. E. D. Moorhead and W. H. Doub, Jr., *ibid.*, 1977, **10**(9), 673.
3. N. Scott, D. E. Carter and Q. Fernando, *Anal. Chem.*, 1987, **59**, 888.
4. A. A. Kaplin and N. T. Rud, *J. Anal. Chem. U.S.S.R.*, 1980, **35**, 730.
5. P. Cofré and K. Brinck, *Talanta*, 1992, **39**, 127.
6. K. Asada, P. Delahay and A. K. Sundaram, *J. Am. Chem. Soc.*, 1961, **83**, 3396.
7. E. D. Moorhead and P. H. Davis, *Anal. Lett.*, 1974, **7**, 781.
8. E. D. Moorhead and G. A. Forsberg, *Anal. Chem.*, 1975, **47**, 231.
9. P. Cofré, G. East and C. Aguirre, *Talanta*, 1992, **39**, 621.
10. O. E. Ruvinskii and Ya. I. Tur'yan. *Zh. Anal. Khim.* 1976, **31**, 543.
11. J. Wang and T. Peng, *Anal. Chem.*, 1987, **59**, 2014.
12. E. Bishop and R. B. Sutton, *Anal. Chim. Acta*, 1960, **22**, 592.
13. L. S. Foster, *J. Am. Chem. Soc.*, 1939, **61**, 3122.
14. E. D. Moorhead and G. M. Frame, II, *Anal. Chem.*, 1968, **40**, 280.
15. A. J. Bard and L. R. Faulkner, *Electrochemical Methods: Fundamentals and Applications*, p. 517, John Wiley and Sons, New York, 1980.
16. G. D. Christian, *Analytical Chemistry*, 2nd edition, John Wiley, New York, 1977.

Talanta, Vol. 40, No. 8, pp. 1283–1287, 1993
Printed in Great Britain.

0039-9140/93 $6.00 + 0.00

INDIRECT DETERMINATION OF TETRAHYDROBORATE (BH_4^-) BY GAS-DIFFUSION FLOW INJECTION ANALYSIS WITH AMPEROMETRIC DETECTION

SNEŽANA D. NIKOLIĆ and EMIL B. MILOSAVLJEVIĆ*
Faculty of Chemistry, University of Belgrade, P.O. Box 550, 11001 Belgrade, Yugoslavia

JAMES L. HENDRIX and JOHN H. NELSON
Departments of Chemistry and Chemical and Metallurgical Engineering, Mackay School of Mines, University of Nevada, Reno, NV 89557, U.S.A.

(*Received* 26 *December* 1991. *Revised* 22 *April* 1992. *Accepted* 22 *April* 1992)

Summary—A rapid, indirect gas-diffusion flow injection analysis (FIA) method with amperometric detection has been developed for the selective and sensitive determination of tetrahydroborate (BH_4^-). The injected analyte reduces arsenic(III) to arsine. The arsine formed diffuses through the PTFE (polytetrafluoroethylene) membrane and is quantified amperometrically at a platinum working electrode. The precision of the technique was better than a relative standard deviation of 2.1% at 60 μM levels and better than 0.5% at 0.1 mM, with a throughput of 60 samples/hr. The detection limit of the method was found to be 1 μM (1.5 ng BH_4^-) with a linear range up to 1 mM. The dynamic range extends over five orders of magnitude in BH_4^- concentration. The effects of working potential, concentration of As(III) and HCl in the reagent stream, type and flow rate of the acceptor solution, temperature and interferents on the FIA signals were studied.

Tetrahydroborate (borohydride) salts have been extensively utilized in inorganic and organic syntheses.[1,2] As was pointed out recently,[3] for carrying out these syntheses and in studies of the methods for the synthesis of borohydride, rapid, selective and accurate analytical methods to control its concentration in solution are needed.

To the best of our knowledge, there are no FIA methods reported for tetrahydroborate analysis, even though FIA methods are well suited for studying and/or continuously monitoring processes of importance to the chemical and metallurgical industries.[4–7]

On the other hand, there are only a few FIA publications[8–13] that combine separation based on membrane diffusion with amperometric detection, which is surprising considering that the selectivity of the diffusion process and inherent sensitivity of the amperometric detection makes this combination a powerful analytical tool. Extensive discussions of the merits of gas-diffusion FIA methods may be found elsewhere.[14–16]

The present paper describes a novel approach to the use of gas-diffusion in combination with amperometric detection for the indirect determination of BH_4^-. In the FIA manifold developed, the injected analyte reduces on-line arsenic(III) to arsine. The arsine formed diffuses from the donor stream through the hydrophobic PTFE membrane into the acidic acceptor solution. The latter carries arsine to the flow-through amperometric detector, where it is oxidized at a platinum working electrode. The anodic current measured is proportional to the concentration of BH_4^- in the sample or standard injected.

It is interesting to note that, to the best of our knowledge, this is the first time FIA amperometry is utilized in an analytical procedure based on the hydride generation principle. This opens up the possibility of utilizing similar FIA schemes for determining the elements which form volatile hydrides, as well as mercury.

EXPERIMENTAL

Reagents

All chemicals were of analytical-reagent grade. The aqueous reagent and standard solutions

*Author for correspondence.

were stored in glass containers. Demineralized water was used throughout. A stock solution of 0.01*M* BH_4^- was made from sodium borohydride (Fisher Scientific, Fair Lawn, NJ, U.S.A.) and checked using the published procedure.[17] Standard BH_4^- solutions, which were stabilized with 1% (w/v) sodium hydroxide, were prepared by diluting aliquots of the stock solution to the appropriate volume. The As^{3+} solutions were made by dissolving reagent-grade sodium arsenite (Carlo Erba, Milan, Italy) in reagent-grade hydrochloric acid and diluting to the appropriate volume.

Apparatus

The FIA manifold is illustrated in Fig. 1. Two peristaltic pumps were used. One was a Model Mini S-840 (Ismatec, Zurich, Switzerland) and the other was a Model MS-4-REGLO 100 (Ismatec). The injection valve was a Model 5020 (Rheodyne, Cotati, CA, U.S.A.) equipped with a 100-μl sample loop. The gas-diffusion unit, which was obtained from Shenyang Film-Projector Reflector Factory (Shenyang, China), is similar in construction to the Tecator (Högänas, Sweden) Chemifold V gas diffusion cell. The PTFE membrane used was supplied with the unit. All connections were made with 0.5 mm i.d. tubing.

A thin layer flow-through amperometric cell was part of a LC-17A package (BAS, West Lafayette, IN, U.S.A.) and was equipped with a Model MF-1012 dual platinum working electrode (BAS) and a Model MW-2021 Ag/AgCl reference electrode (BAS). A 0.13 mm thick MF-1047 PTFE gasket (BAS) was used to separate the working electrode from the cell body. The working electrode was polished daily with CF-1050 polishing alumina (BAS). The potential was applied to the flow-through amperometric cell and currents were measured with a Model MA 5450 polarograph (Iskra, Kranj, Yugoslavia); the resulting FIA signals were recorded on a Servograph Model 61 strip-chart recorder (Radiometer, Copenhagen, Denmark) equipped with a REA 110 unit. The measurements were made with both donor and acceptor streams flowing continuously and concurrently. Temperature regulation was achieved with a constant temperature bath, type VEB MLW (Prüfgeräte, Medingen, Germany).

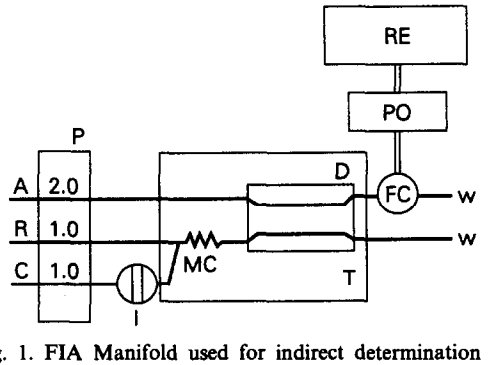

Fig. 1. FIA Manifold used for indirect determination of BH_4^-: C, carrier; R, reagent (25 m*M* As^{3+} in 1.0*M* HCl); A, acceptor solution (0.01*M* H_2SO_4); P, peristaltic pump; I, injection valve; MC, mixing coil (30 cm × 0.5 mm i.d.); D, diffusion cell; T, constant temperature bath; FC, amperometric flow-through cell; PO, potentiostat; RE, recorder; W, waste. Flow rates are given in ml/min.

RESULTS AND DISCUSSION

The indirect gas-diffusion flow injection amperometric determination of BH_4^- was performed with the manifold illustrated in Fig. 1. The alkaline (1% w/v sodium hydroxide) BH_4^- standard or sample, after injection (I), is washed by the water carrier (C) to a mixing point with a reagent (R) (0.025*M* As^{3+} in 1*M* hydrochloric acid). The mixing coil (MC), positioned downstream ensures thorough reduction of As^{3+} to arsine by the injected analyte, according to the following reaction:

$$H_3AsO_3 + NaBH_4 + HCl \Rightarrow AsH_3 + B(OH)_3 + NaCl + H_2.$$

The arsine formed on-line in the FIA manifold diffuses from the donor stream through the hydrophobic PTFE membrane into the acidic (0.01*M* sulphuric acid) acceptor solution. The latter carries arsine to the flow-through amperometric detector (FC), where it is oxidized at a platinum working electrode. The anodic current measured is proportional to the BH_4^- concentration in the injected standard or sample.

The main reason for choosing hydride generation of arsine *vs.* some other volatile hydride was based on the fact that the number of publications dealing with hydride generation of arsine is larger than for any other volatile hydride, which facilitates comparisons with the present work.

The effects of several parameters on the performance of the FIA system were studied. The effect of the applied potential at the working Pt electrode, shown in Fig. 2, was investigated in the range 0.4–1.0 V *vs.* the Ag/AgCl reference electrode. Taking into account the signal-to-noise ratio achieved, the

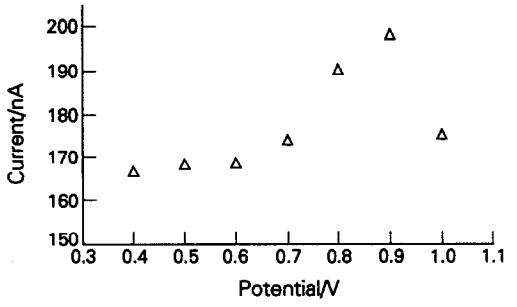

Fig. 2. Hydrodynamic voltamperogram for a 100 μl injection of a 1.00 mM sodium borohydride standard.

optimum potential was found to be 0.8 V. A possible reason for the current decrease at potentials greater than 0.9 V is the enhanced anodic formation of thin oxide films at the Pt-working electrode.[18] Of the three acceptor solutions tested (0.01M sodium hydroxide, potassium nitrate and sulphuric acid), the best results were obtained with the latter. For example, when sulphuric acid was used as the acceptor stream, the peak current for a 1.00 mM BH_4^- standard was over eight times greater than with sodium hydroxide as the acceptor solution. Even though no tendency to form "onium" (MH_4^+) ions for arsenic has been established, it is plausible that sulphuric acid in the acceptor solution might show a slight trapping effect (small AsH_3 and relatively large hydronium ion concentrations). Also the highest FIA signals were achieved with the shortest mixing coil utilized. Hence, for most of the subsequent experiments, a potential of 0.80 V *vs.* Ag/AgCl reference electrode, a 0.01M sulphuric acid acceptor solution and a 30 cm × 0.5 mm i.d. mixing coil were used.

The effect of arsenic(III) concentration in the reagent stream, illustrated in Fig. 3, was studied by injecting the same BH_4^- standard, while varying the concentration of As^{3+} in the reagent from 2.5 mM to 0.15M. In this series of experiments the concentration of hydrochloric acid in the reagent solution was kept constant at a 1.0M level. It should be pointed out that no statistically significant change in the blank signal was observed as As(III) concentration in the donor stream increased. As a compromise between reagent consumption and sensitivity, the concentration of As^{3+} used for most of the subsequent experiments was 25 mM. The concentration of hydrochloric acid in the reagent solution chosen was 1.0M since an increase in its concentration causes a slow but steady decrease in sensitivity. At this point in time we do not have a definitive explanation for the observed phenomenon. A possible reason for the decrease observed could be that the concurrent reaction of BH_4^- with H_3O^+ to form hydrogen is more pronounced at higher hydrochloric acid levels. It was suggested in the review process that formation of volatile $AsCl_3$ and its effects on the membrane pores due to possible hydrolysis at the interface might play a role. However, in a recent study of utilizing polymer-bound tetrahydroborate for arsine generation in a FIA system, Tesfalidet and Irgum[19] found similar hydrochloric acid concentration effects on the sensitivity of the system, even though they employed a "classical" gas–liquid separator for hydride generation atomic spectroscopy and not a microporous membrane. This observation coupled with what we have seen probably rules out the notion that, under our particular experimental conditions, hydrolysis reactions at the membrane surface play an important role.

The effect of acceptor flow rate was investigated by injecting a 1.00 mM sodium borohydride standard, while varying the flow rate in the range 0.5–2.5 ml/min (Fig. 4). As may be seen, the highest peak current was obtained when the acceptor flow rate was 2.0 ml/

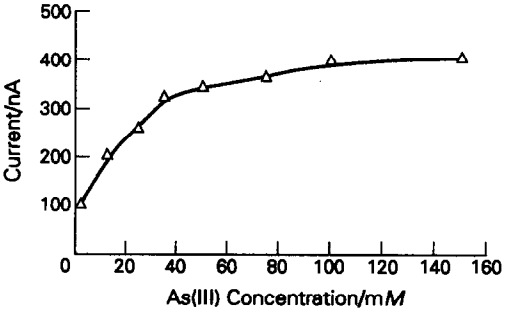

Fig. 3. Variation of the peak current as a function of As^{3+} concentration in the reagent stream.

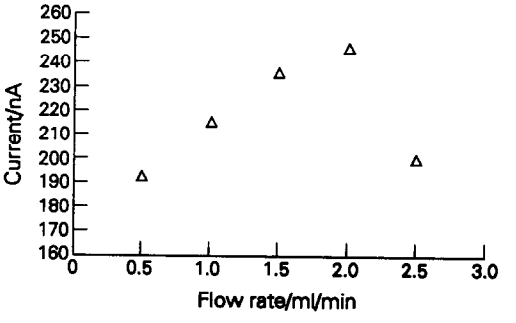

Fig. 4. Variation of the peak current as a function of the acceptor flow rate.

min. Bearing in mind that the total donor stream flow rate was also 2.0 ml/min, this finding is in agreement with the previously reported observation[16] that the optimum FIA signals were obtained when the donor and acceptor flow rates were equal.

Temperature effects were studied by injecting the same sodium borohydride standard, while varying the temperature in the interval 20–50°. No increase in the sensitivity with increase in temperature was observed. This is contrary to previously described indirect gas-diffusion amperometric FIA methods.[11,13] A plausible explanation for the observed phenomenon could be based on the much lower solubility of the diffusing species; arsine in comparison to chlorine[11] or bromine.[13] Also, it is obvious that the reduction of As(III) to arsine is fast on the FIA time scale (longer mixing coils decreased the peak currents), which was not the case with the permanganate oxidation of chloride[11] and bromide.[13]

Linearity studies were conducted by injecting in triplicate a total of 12 BH_4^- standards between 8.00 μM and 1.00 mM stabilized with 1% (w/v) sodium hydroxide. The linear calibration equation for a typical calibration run was: $i = (-5.38 \pm 1.42) + (196.0 \pm 7.3) \times C$ (i is the peak current expressed in nA and C is the millimolar concentration of BH_4^-) with a correlation coefficient of 0.9986 (all the statistics were calculated for a 95% confidence level). The relative standard deviations were found to be 2.01% ($n = 5$) at 60 μM levels and only 0.45% ($n = 5$) at 0.10 mM. The detection limit, calculated according to the recommended procedure,[20] was 1 μM which corresponds to only 1.5 ng BH_4^- (the sample loop volume was 100 μl). Figure 5 illustrates the dynamic range for the method obtained at two different As(III) concentrations in the reagent stream. As may be seen, the dynamic range (defined as that range of concentrations of the test substance, over which a change in concentration produces a change in detector signal)[21] extends over five orders of magnitude in BH_4^- concentration.

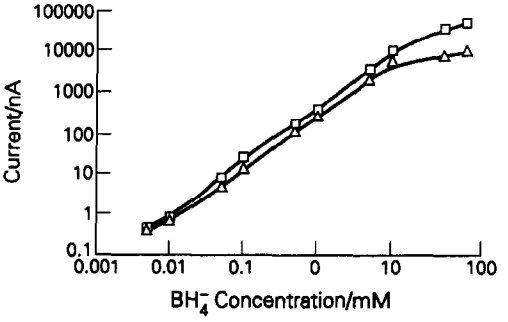

Fig. 5. Logarithmic calibration graphs illustrating the dynamic range of the method developed; As(III) concentration in the reagent stream: 25 mM (△△△) and 100 mM (□□□).

Table 1. Solutions tested for their possible interference*

Compound	Conc./M	Compound	Conc./M
NH_4NO_3	0.1	Na_2EDTA†	0.1
KCl	0.1	Na-citrate	0.1
Na_2SO_3	2×10^{-6}	CH_3COONa	0.1
$KBrO_3$	0.01	NaF	0.1
$Na_2S_2O_3$	0.001	KH_2PO_4	0.1
KCN	0.04	KBr	0.1
$Na_2C_2O_4$	0.1	$NaNO_2$	0.002
Na_2CO_3	0.1	KI	0.1
Na_2S	1×10^{-5}	L-cysteine	0.1

*All samples contained 1% (w/v) NaOH. The response of the amperometric detector to 100 μl injections of the solutions tested could not be distinguished from the base line. The maximum concentrations tested were 0.1M.

†Na_2EDTA = Disodium ethylenediaminetetraacetate.

Table 1 summarizes the study of possible interferents. It has been established previously that the PTFE membranes used in the FIA gas-diffusion studies are effective barriers for ionic species.[22,23] Hence, in order for a particular species to interfere in the determination of BH_4^- with the manifold described, it has to satisfy two conditions. It has to form a gas or a molecular species with a high vapor pressure when acidified (the donor stream of the FIA manifold contains hydrochloric acid) and the gas or molecular species formed has to be electroactive (oxidizable) at the potential applied to the platinum working electrode. As can be seen from Table 1, the only serious interferents found were the sulphite and sulphide ions.

This work demonstrates that it is possible to use gas-diffusion FIA amperometry for the development of novel analytical procedures based on a hydride generation principle.

Acknowledgements—The authors acknowledge the financial support of the U.S. Bureau of Mines under the Mining and Mineral Resources Institute Generic Center program (Grant number G1125132-3205, Mineral Industry Waste Treatment and Recovery Generic Center) and the Serbian Republic Research Fund.

REFERENCES

1. H. C. Brown, *Organic Synthesis via Boranes*, Wiley, New York, 1975.
2. A. Petler, K. Smith and H. C. Brown, *Borane Reagents*, Academic Press, London, 1988.

3. M. V. Mirkin and A. J. Bard, *Anal. Chem.*, 1991, **63,** 532.
4. J. Růžička and E. H. Hansen, *Flow Injection Analysis*, 2nd Ed., pp. 372–376. Wiley, New York, 1988.
5. N. P. Gallagher, J. L. Hendrix, E. B. Milosavlević and J. H. Nelson, *J. Electrochem. Soc.*, 1989, **136,** 2546.
6. N. P. Gallagher, J. L. Hendrix, E. B. Milosavljević, J. H. Nelson and Lj. Solujić, *Hydrometallurgy*, 1990, **25,** 305.
7. C. C. Nesbitt, E. B. Milosavljević and J. L. Hendrix, *Ind. Eng. Chem. Res.*, 1990, **29,** 1698.
8. M. Granados, S. Maspoch and M. Blanco, *Anal. Chim. Acta*, 1986, **179,** 445.
9. E. B. Milosavljević, Lj. Solujić, J. L. Hendrix and J. H. Nelson, *Anal. Chem.*, 1988, **60,** 2791.
10. D. Utley, *Analyst*, 1990, **115,** 1239.
11. S. D. Nikolić, E. B. Milosavljević, J. L. Hendrix and J. H. Nelson, *Analyst*, 1991, **116,** 49.
12. M. Novič and B. Pihlar, *Anal. Chim. Acta*, 1991, **251,** 261.
13. S. D. Nikolić, T. D. Janković, E. B. Milosavljević, J. L. Hendrix and J. H. Nelson, *Fresenius J. Anal. Chem.*, 1992, **342,** 98.
14. G. E. Pacey, D. A. Hollowell, K. G. Miller, M. R. Straka and G. Gordon, *Anal. Chim. Acta*, 1986, **179,** 259.
15. J. Růžička and E. H. Hansen, *Flow Injection Analysis*, 2nd Ed., pp. 192–200. Wiley, New York, 1988.
16. B. Karlberg and G. E. Pacey, *Flow Injection Analysis—A Practical Guide*, pp. 111–118. Elsevier, Amsterdam, 1989.
17. J. M. Kolthoff and P. J. Elving, *Treatise on Analytical Chemistry*, Part II, Vol. 12, p. 213. Wiley, New York, 1965.
18. D. S. Austin, J. A. Polta, T. Z. Polta, A. P. -C. Tang, T. D. Cabelka and D. C. Johnson, *J. Electroanal. Chem.*, 1984, **168,** 227.
19. S. Tesfalidet and K. Irgum, *Anal. Chem.*, 1989, **61,** 2079.
20. Analytical Methods Committee, *Analyst*, 1987, **112,** 199.
21. C. A. Dorshel, J. L. Ekmanis, J. E. Oberholtzer F. V. Warren, Jr. and B. A. Bidlingmeyer, *Anal. Chem.*, 1989, **61,** 951A.
22. W. E. Van der Linden, *Anal. Chim. Acta*, 1983, **151,** 359.
23. D. A. Hollowell, G. E. Pacey and G. Gordon, *Anal. Chem.*, 1985, **57,** 2851.

Talanta, Vol. 40, No. 8, pp. 1289–1294, 1993
Printed in Great Britain.

0039-9140/93 $6.00 + 0.00

SPECTROPHOTOMETRIC DETERMINATION OF CLOTRIMAZOLE IN BULK DRUG AND DOSAGE FORMS

OSAMA H. ABDELMAGEED and PAKINAZ Y. KHASHABA
University of Assiut, Department of Analytical Pharmaceutical Chemistry, Faculty of Pharmacy, Assiut, Egypt

(*Received* 22 *December* 1992. *Received* 10 *February* 1993. *Accepted* 11 *February* 1993)

Summary—A simple, specific, rapid and sensitive spectrophotometric method has been developed for the assay of clotrimazole, in bulk drug and its pharmaceutical preparations. This method is based on the ion-pair complex reaction of clotrimazole and methyl orange in aqueous methanol, and in the presence of citric acid. The chromogen, being extractable with chloroform, could be measured quantitatively at 422 nm. All variables were studied to optimize the reaction conditions. Regression analysis of Beer's plot showed good correlation in a general concentration range of 2–14 μg/ml. The proposed method has been successfully applied for the analysis of the bulk drug and its dosage forms such as powder, vaginal tablets, topical solution and creams. No interference was observed from betamethasone dipropionate (Lotriderm cream) or dexamethasone acetate and azidamphenicol (Baycuten cream) or other common pharmaceutical adjuvants. In addition, this method was also found to be specific for the analysis of clotrimazole in the presence of its hydrolytic products as well as imidazole, as a possible impurity.

Clotrimazole, 1-[(2-chlorophenyl) diphenyl methyl]-1H-imidazole (pKa: 4.7), is a broad spectrum antifungal agent[1] which is available in different pharmaceutical formulations such as creams, topical solutions, vaginal tablets and pessaries. Several methods have been reported for the quantitative determination of clotrimazole in pure form or in its dosage forms, including titrimetry,[2–5] TLC,[6] GC,[7] HPLC,[8,9] derivative spectrophotometry[10,11] and colorimetry.[12–14] The reported methods required high concentration of the drug,[2–5,12] or sophisticated equipment and were time consuming.[6–9] In addition, UV spectrophotometric analysis of clotrimazole has been limited due to its low absorptivity and absence of characteristic bands.[15] Some of the colorimetric methods required heating for a long time with the reagent under investigation and sensitivity is low.[13,14] Therefore the aim of this work is to develop an accurate, simple, sensitive, inexpensive and specific colorimetric method for the estimation of clotrimazole either in pure form and single dosage forms, or in the presence of other drugs such as betamethasone dipropionate (Lotriderm cream) and azidamphenicol, dexamethasone acetate (Baycuten cream). This method depends on the formation of an ion-pair complex between clotrimazole, in methanol, and 0.1% W/V methyl orange (M.O.) (in 40% aqueous methanol), in the presence of 0.1*M* citric acid solution. The formed complex was found to be extractable with chloroform as a yellow colored product which could be measured quantitatively at $\lambda_{max} = 422$ nm. In addition, the specificity of our proposed method for the estimation of clotrimazole in the presence of imidazole, as a possible impurity, and its hydrolytic products was also studied.

EXPERIMENTAL

Apparatus

Perkin-Elmer model Lambda 3B UV–Vis spectrophotometer and chart recorder model 561 were used.

Chemicals and reagents

All chemicals and reagents were of analytical grade. Clotrimazole (the Arab Drug Co., Cairo, Egypt), betamethasone dipropionate (Memphis

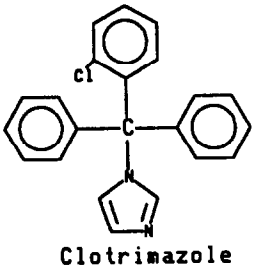

Clotrimazole

Scheme 1

Chemical Co., Egypt), dexamethasone acetate and azidamphenicol (Alex. Co., Egypt), imidazole (Merck product) were used as working standards. The methyl orange solution was 0.1% W/V (M.O.) in 40% aqueous methanol. The citric acid solution was 0.1*M* solution in distilled water, and the sulphuric acid solution was 1*M* solution in distilled water. The ammonia solution was 2*M* solution in distilled water, with the sodium hydroxide solution being 20% W/V solution, in distilled water.

Dosage forms used in this investigation were: Canesten powder, Canesten vaginal tablets, Canesten topical solution and Canesten cream (Alex. Co., Egypt, and Bayer, GFR) labeled to contain clotrimazole as 10 mg/g, 100 mg/tablet, 10 mg/ml and 10 mg/g, respectively. Lotriderm cream (Medical Union Pharm. Co., Egypt and Schering Co., U.S.A.) was labeled as containing 10 mg clotrimazole and 0.6 mg betamethasone dipropionate per each gram of cream. Baycuten cream (Alex. Co., Egypt, and Bayer, GFR) was labeled to contain 10 mg clotrimazole, 10 mg azidamphenicol and 0.443 mg dexamethasone acetate per each gram of cream.

Preparation of standards

Twenty five milligrams of clotrimazole, accurately weighed, were transferred into a 10 ml volumetric flask, dissolved in methanol and completed to volume with the same solvent. From this solution, a series of dilutions were prepared in methanol so as to obtain a range of 50–350 μg clotrimazole/ml.

Preparation of samples

Canesten powder. A portion of the powder equivalent to 25 mg clotrimazole was accurately weighed and transferred into a 100 ml volumetric flask. It was then shaken with about 50 ml of methanol and completed to volume with the same solvent. The resulting solution was filtered and the first portion of the filtrate rejected.

Vaginal tablets. Twenty tablets were weighed and finely powdered, and then completed as indicated above.

Topical solution. Into a 100 ml volumetric flask an aliquot of the solution equivalent to 25 mg of clotrimazole was accurately pipetted. This was then diluted to the mark with methanol.

Creams. An accurately weighed portion of cream, equivalent to 25 mg of clotrimazole, was placed in a 20 ml beaker. Then 12 ml of a mixture of 1*M* sulphuric acid and methanol (1:4) was added and melted in a water bath at ~50°C for 5 min, then sonicated for another 5 min. The mixture was transferred quantitatively to a 100 ml separating funnel, then shaken with three, 10 ml quantities of carbon tetrachloride, discarding the organic layers. This was made alkaline with 2*M* ammonia, then a further 2.5 ml was added. Extraction with three, 10 ml quantities of chloroform was carried out. Combination of the chloroform extracts into 100 ml volumetric flask was carried out and the samples were evaporated to dryness. The residue was dissolved in 100 ml methanol.

Preparation of hydrolyzed sample of clotrimazole

Twenty five milligrams of clotrimazole powder was accurately weighed into a 10 ml volumetric flask. Then 1 ml of 1*M* HCl was added, and the solution heated in a water bath at 90°C for about 2 hr and cooled to room temperature (25°C). This was neutralized with 20% sodium hydroxide solution, filtered if necessary, then diluted to volume with methanol.

General procedure for the assay method

One millilitre of the standard or sample solution of clotrimazole was pipetted into a 100 ml separating funnel containing 3 ml 0.1*M* citric acid solution. Then 2 ml of 0.1% W/V M.O. in 40% aqueous methanol was added. This was mixed well and three 8 ml quantities of chloroform extracted. The extracts were collected in a 25 ml volumetric flask and diluted to volume with chloroform. Approximately 0.1 g anhydrous sodium sulphate was added, shaken for about 1 min, filtered and the first portion of the filtrate rejected. The absorbance of the resulting solution at 422 nm against a similarly treated reagent blank was measured.

Assay of clotrimazole in the presence of its hydrolytic products

A certain volume from a standard solution of clotrimazole was pipetted into an accurately measured volume of the hydrolyzed sample and mixed. Methanol was used to dilute the solution so as to obtain final dilutions of 125 μg/ml of pure clotrimazole plus a hydrolyzed sample equivalent to 75, 150 and 225 μg/ml of clotrimazole. The method described under general procedure was then followed.

Stoichiometric relationship

According to Job's method[16] of continuous variation, an equimolar solution of clotrimazole and M.O. ($14.5 \times 10^{-5}M$) were prepared. A

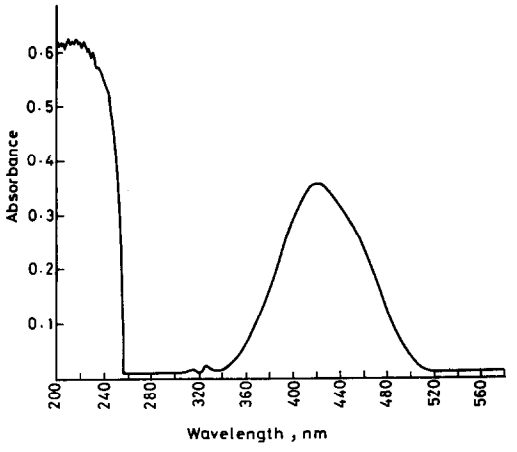

Fig. 1

Table 2. Effect of different acidic pH values on the formation of the ion-pair complex

Buffer* pH	Absorbance at 422 *nm*†
2	0.384
2.3	0.429
2.4	0.426
2.5	0.416
3.0	0.277
3.5	0.197
5‡	0.000
0.1*M* citric acid	0.432

*Torell and Stenhagen buffer.
†Final concentration of clotrimazole is 6 μg/ml.
‡No color was observed in the organic layer at pH 5.

series of extraction experiments were carried out using 10 ml portions of the solutions in different complementary proportions (from 0 + 10 to 10 + 0 inclusive) using 3 ml of buffer in all cases.

RESULTS AND DISCUSSION

Ion-pair extraction spectrophotometry has received considerable attention for quantitative estimation of many pharmaceutical compounds.[17–19] Clotrimazole was previously determined through colorimetric methods based on measuring the yellow color of the complex formed, using buffered bromothymol blue (pH 3.4), at 410 nm.

In this study M.O., being an anionic dye, forms with clotrimazole, in acidic pH, a yellow colored ion-pair complex which is soluble in chloroform and can be measured at λ_{max} 422 nm (Fig. 1). Applying Job's method of continuous variation the reaction stoichiometry of this associated ion-pair proved to be 1:1. A number of immiscible organic solvents were tested so as to provide an applicable extraction procedure. Table 1 shows that the yellow colored product is extractable only with methylene chloride and chloroform. Although methylene chloride was found to be slightly better, owing to its high volatility chloroform was used throughout this work.

The optimum conditions for the quantitative estimation of the associated ion-pair formed were established by a number of preliminary experiments. The effect of pH was studied by extracting the colored complex formed in the presence of Teorell and Stenhagen buffer[20] of different acidic pH values. Accordingly, Table 2 shows that a pH below 3 is recommended, and best results were found at pH 2.3. This result is more or less comparable with that obtained using 0.1*M* citric acid. Stability of color in both cases was studied. Figure 2 shows that the colored product in the case of citric acid is more stable for about 3 hr even when kept overnight. Therefore, 0.1*M* citric acid was selected. The optimum volume of citric acid was found to be 3 ml as indicated in Fig. 3. The significant decrease in absorbance at little or excess volume of citric acid may be explained on the basis of the change of the overall pH and incorrect ratio between methanol and water which may lead to the incomplete extraction of the complex by chloroform.

Table 1. Effect of different solvent on the extraction efficiency of the ion-pair complex

Solvent	Color of organic layer	Absorbance*
Benzene	No color	—
Toluene	No color	—
Cyclohexane	No color	—
Carbon tetrachloride	No color	—
Chloroform	Yellow color	0.430
Methylene chloride	Yellow color	0.464

*Final concentration of clotrimazole is 6 μg/ml.

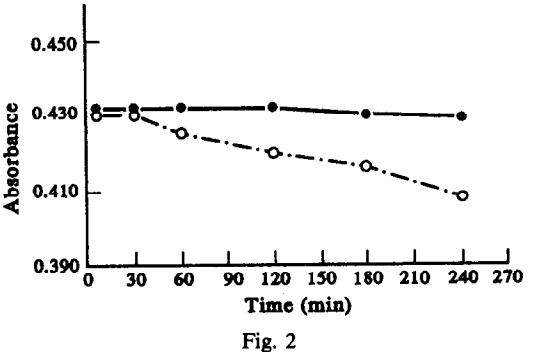

Fig. 2

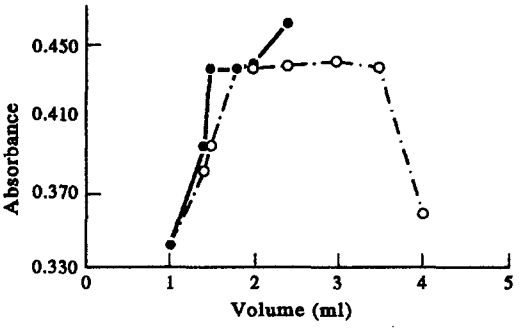

Fig. 3

The optimum volume of the dye used was also studied. Figure 3 revealed an increase in the absorbance readings with the increase of volume of M.O. used up to 3.0 ml. However, a significant increase in the absorbance value of the blank was observed at volumes larger than 2.2 ml. Therefore, 2 ml of 0.1% W/V M.O. was found to be quite enough.

Quantification

A linear correlation was found between absorbance and concentration of clotrimazole in the range 2–14 μg/ml (where the Y intercept = 0.019 ± 0.013, slope = 0.066 ± 0.002, and $r = 0.999 \pm 0.0002$; $n = 3$). Regression analysis of Beer's plot gave the following linear regression equation:

$$A_{422} = 0.019 + 0.066\ C,$$

Table 3. Analysis of clotrimazole, in bulk drug, by the proposed and the official methods

Amount taken (*mg*)	Proposed method Recovery† (%)	Official method* Recovery† (%)
200	99.40	98.83
225	99.62	99.24
250	98.93	99.00
275	99.16	99.56
300	99.77	99.30
	Mean 99.4	99.2
	S.D. ± 0.34	0.28
	CV (%) 0.34	0.28

*Reference 2.
†Average of three determinations.

where A_{422} is the absorbance at 422 nm and C is the concentration in micrograms per milliliter. The calculated molar absorptivity ϵ is 2.37×10^4 l moles^{-1} cm^{-1}.

The detection limit of the studied drug was calculated according to a reported method[21] and was found to be 0.05.

Precision of the proposed method was excellent as indicated from the relative standard deviation (0.37%) calculated from eight replicate analyses of 10 μg/ml of pure clotrimazole.

The proposed method was applied for the determination of clotrimazole in bulk drug as well as in various pharmaceutical formulations. Tables 3 and 4 show that average recoveries range from 97.7–99.4% indicating efficiency, accuracy and reproducibility of the method.

Table 4. Determination of clotrimazole in different pharmaceutical formulations by the proposed and the official methods

Formulation	Label claim (*mg*)	% Found ± SD* Proposed method	% Found ± SD* Official† method	Amount added‡ (*mg*)	% Recovery ± SD* Proposed method
Canesten powder	10/*g*	99.1 ± 0.34	—	10	99.9 ± 1.19
Canesten tablets	100/*tab*	99.0 ± 0.47 *t*§ = 1.39 *F*‖ = 1.45	99.4 ± 0.39	10	99.6 ± 0.60
Canesten drops	10/*ml*	98.8 ± 0.59 *t* = 0.38 *F* = 2.80	99.1 ± 0.35	10	99.8 ± 0.75
Canesten cream	10/*g*	97.7 ± 0.48 *t* = 0.97 *F* = 1.34	97.9 ± 0.42	10	99.0 ± 0.75
Lotriderm cream	10/*g*	98.2 ± 0.39	—	10	99.2 ± 0.43
Baycuten cream	10/*g*	97.8 ± 0.31	—	10	99.0 ± 0.92

*Average of five determinations.
†Reference 4.
‡Pure clotrimazole added to each formulation.
§t-test at $P = 0.05$ is 3.83.
‖F-test at $P = 0.05$ is 6.39.

Table 5. Analysis of clotrimazole in the presence of betamethasone dipropionate, azidamphenicol and dexamethasone acetate by the proposed method

Synthetic mixture* No.	mg taken Bet.	Az.	Dex.	Final dilution (μg/ml)	% Recovery† ± SD
1	0.06	—	—	6	98.0 ± 0.69
				8	99.2 ± 1.86
				12	98.9 ± 1.69
2	—	1	0.04	6	98.6 ± 1.51
				8	97.7 ± 1.00
				12	98.1 ± 1.17

*Each mixture contains 1 mg of clotrimazole.
†Average of three determinations.

Absence of interferences from frequently encountered common excipients and additives was proved by the resulting high percentage recoveries of the add method (99.0–99.9%; Table 4).

Formation of the associated ion-pair complex with the anionic dye needs a basic drug; therefore any possible interference from other common active ingredients combined with the studied drug such as betamethasone dipropionate (in Lotriderm cream) and azidamphenicol and dexamethasone acetate (in Baycuten cream), during analysis by the proposed method, is not expected at all due to lack of any basic center in these drugs. This was proved by the analysis of clotrimazole in two laboratory synthetic mixtures, constituting these common drugs, where no interference is observed (Table 5). The same fact was also confirmed, first from the high recoveries obtained after analysis of clotrimazole in Lotriderm and Baycuten creams (Table 4) and second from the spectra of these drugs when each one was analysed by the proposed method (Fig. 4).

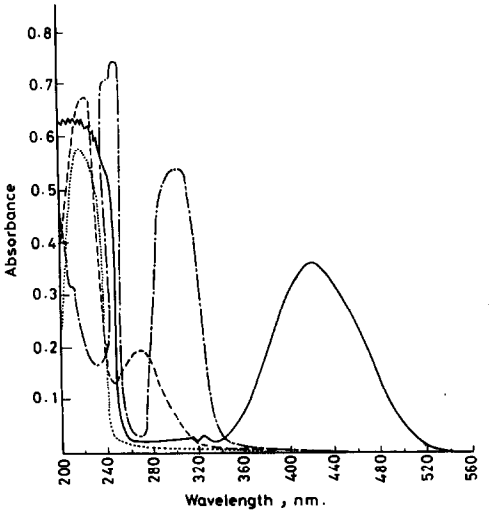

Fig. 4

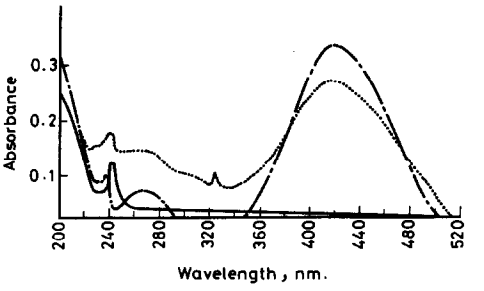

Fig. 5

Results of analysis show good agreement with those obtained by the official methods[2,4] (Tables 3 and 4). No significant differences were found between calculated and theoretical values of the t and F tests (95% confidence) which indicates high accuracy and precision. Furthermore, the proposed method appears superior to current official methods owing to its simplicity, sensitivity and selectivity.

In addition, it is possible that imidazole, which is well known as a weak base and is used in the synthesis of clotrimazole as described,[22] is present as a common impurity in clotrimazole bulk drug. Therefore attention was focused to investigate if there is any interference from imidazole upon the analysis of clotrimazole by the proposed method. This was done by analysis of authentic imidazole samples (containing initial concentrations of 50–2500 μg imidazole/ml methanol) by the proposed method. As shown in Fig. 5 no chromogen could be detected at 422 nm in a concentration range of 5–30 μg/ml (final dilution). However at concentrations ⩾40 μg/ml, a yellow chromogen was being formed at λ_{max} 422 nm, but no accuracy, precision or even reproducibility was observed. This finding seems obvious owing to the fact that imidazole—unlike clotrimazole—is freely soluble in water as well as in chloroform.[23] Accordingly the complex of imidazole: M.O—being formed—might be soluble in an aqueous as well

Table 6. Analysis of clotrimazole in presence of imidazole by the proposed method

Synthetic mixture* No.	Conc. of imidazole added (μg/ml)	% Recovery ± SD
1	2	97.8 ± 0.52
2	5	98.3 ± 0.93
3	10	98.0 ± 1.00
4	15	98.1 ± 0.51
5	20	97.5 ± 0.62
6	30	98.3 ± 0.72

*Each mixture contains 10 μg/ml clotrimazole (final dilution).
†Average of three determinations.

Table 7. Analysis of clotrimazole in the presence of its hydrolytic products by the proposed method

Synthetic mixture* No.	Conc. taken ($\mu g/ml$)†	% Recovery‡
1	3	98.84
2	6	99.00
3	9	99.27
		Mean 99.0
		S.D. ± 0.22

*Each mixture contains 5 μg/ml clotrimazole (final dilution).

†Final dilution of hydrolytic products equivalent to pure clotrimazole.

‡Average of three determinations.

as in an organic layer. At concentrations $\leqslant 30$ μg/ml the absence of chromogen at 422 nm is probably due to low sensitivity, under the established experimental conditions. In the case of a concentrated sample ($\geqslant 40$ μg/ml), the complex started to partitionate between the aqueous and organic layer where a volume of chloroform more than 25 ml was found to be needed for full extraction. Consequently no correlation was found between absorbance and concentration as shown in Fig. 5. By comparison with the specified concentration of clotrimazole (2–14 μg/ml) imidazole should never interfere with its analysis by the proposed method as long as sample concentration is kept within the specified limit. This was further confirmed by analysis of synthetic mixtures containing fixed amount of clotrimazole with increasing concentration of imidazole. Results of these analyses (Table 6) revealed that no interference from imidazole as proved by reproducible recoveries in all cases.

Analysis of clotrimazole in the presence of its acid hydrolytic products

It is well known that stability of clotrimazole in solution is pH dependent. Only in acid medium is it hydrolyzed to O-chlorophenyl-diphenyl methanol and imidazole.[24] Hydrolysis has been carried out using different concentrations of hydrochloric acid (0.1, 0.5, 1, 2, 5 and 10*M* HCl). This study revealed that 0.1*M* HCl is not enough for complete hydrolysis, as proved by the UV spectrum of the resulting hydrolytic sample which indicates the presence of clotrimazole, as well as the formation of a yellow chromogen under the condition of the assay method. However, concentrations $\geqslant 0.5M$ HCl were found to be good enough for hydrolysis. Therefore 1*M* HCl was used throughout this study. Neutralization was carried out, before dilution with methanol, using 20% sodium hydroxide to pH 7. High percentage recovery (99.0 ± 0.22%, Table 7) of an added known concentration of the studied drug to the hydrolytic sample indicates the absence of interferences. Accordingly, the proposed method is considered not only specific for analysis of clotrimazole in the presence of its hydrolytic products but also may be applied as a stability indicating assay, under acidic condition, and detailed studies will be described in the next paper.

REFERENCES

1. Herausgegeben von-Redige par Ernst Jucker (ed.), *Progress in Drug Research*, Vol. 22, p. 117, Basel, 1978.
2. *B.P. Pharmacopoeia* Vol. I, Her Majesty's Stationery Office, London, p. 148, 1988.
3. M. Massaccesi, *Analyst*, 1986, **111**, 987.
4. *U.S. Pharmacopoeia* 21 St. Rev., US Pharmacopoeial Convention, Rockville, M.D., p. 236, 1985.
5. D. Volkmann, *G.I.T. Fachz. Lab.* **27**, 524; *Chem. Abstr.* 1983, **99**, 58985 K.
6. W. Ritter, M. Plempel and J. Puetter, *Arzneim. Forsch.*, 1974, **24**, 521.
7. S. M. Wallace, V. P. Shah, S. Reigelman and W. L. Epstein, *Anal. Lett.*, 1978, **B.11**, 461.
8. J. G. Hoogerheide, S. H. Strusiak, C. R. Taddel, E. R. Townley and B. E. Wyka, *J. Assoc. Off. Anal. Chem.*, 1981, **64**, 864.
9. V. Cavrini, A. M. Di Pietra and M. A. Raggi, *Int. J. Pharm.*, 1982, **10**, 119.
10. M. M. Bedair, M. A. Korany, M. A. Elsayed and O. T. Fahmy, *J. Assoc. Off. Anal. Chem.*, 1989, **72**, 432.
11. Y. Zhou, *Yaowu Fenxi Zazhi* 1986, **6**, 359; *Anal. Abstr.*, 1987, **9**, E71.
12. D. M. Shingbal and H. S. Kudchadkar, *Indian Drugs*, 1987, **24**, 408; *Anal. Abstr.*, 1987, **12**, E83.
13. M. L. Chianani, L. S. Rao and S. J. Chavda, *Indian Drugs*, 1981, **18**, 405; *Anal. Abstr.*, 1982, **10**, 4E83.
14. K. Florey (ed.), *Analytical Profiles of Drug Substances*, Vol. 11, p. 247, Academic Press, New York, 1982.
15. A. C. Moffat, J. V. Jackson, M. S. Moss and B. Widdop (eds) *Clarke's Isolation and Identification of Drugs* p. 487, the Pharmaceutical Press, London, 1986.
16. T. Rose, *Advanced Physico-Chemical Experiments*, p. 45, Pitman, London, 1964.
17. Y. M. Dessouky, B. A. Mousa and H. M. Nour El-Din, *Pharmazie*, 1974, **29**, 577.
18. S. Tosunglu and S. Atmaca, *ibid.*, 1989, **44**, 498.
19. M. H. Barary and A. M. Wahbi, *Drug Development and Industrial Pharmacy*, 1991, **17**, 457.
20. M. Pesez and J. Bartos (eds), *Colorimetric and Fluorimetric Analysis of Organic Compounds and Drugs*, p. 628, Marcel Dekker, Inc., New York, 1974.
21. Analytical Methods Committee, *Analyst*, 1987, **112**, 199.
22. K. H. Buechel, W. Draber, E. Regel and M. Plempel, *Arzneim. Forsch.*, 1972, **22**, 1260; *Analytical Profiles of Drug Substances*, Vol. 11, p. 242, 1982.
23. S. Budavari (ed.), *The Merck Index*, p. 779, Merck & Co., Inc. Rahway, N.J., U.S.A., 1989.
24. K. H. Buechel, M. Plempel and K. Bartmann, *Ther. Ber.*, 1973, **39**; *Analytical Profiles of Drug Substances*, Vol. 11, p. 242, 1982.

Talanta, Vol. 40, No. 8, pp. 1295–1299, 1993
Printed in Great Britain.

0039-9140/93 $6.00 + 0.00

SHORT COMMUNICATION

MATRIX EFFECT OF BARIUM ON SPECTRAL LINE INTENSITIES AND DETECTION LIMITS IN INDUCTIVELY COUPLED PLASMA ATOMIC EMISSION SPECTROSCOPY

ZOJA ILIĆ*
The Institute of Nuclear Sciences—VINČA, Chemical Dynamics Laboratory, P.O. Box 522, 11001 Belgrade, Yugoslavia

JULIJANA GEORGIJEVIĆ
Faculty of Technology and Metallurgy, University of Belgrade, P.O. Box 494, Belgrade, Yugoslavia

VELJKO GEORGIJEVIĆ
Faculty of Civil Engineering, University of Belgrade, Yugoslavia

(*Received* 3 *February* 1992. *Revised* 11 *May* 1992. *Accepted* 11 *May* 1992)

Summary—The effect of four concentrations of Ba (as nitrate) on emission intensities of La(II) 337.7, Mg(I) 285.2, Mg(II) 279.1, Cd(I) 228.8, Cd(II) 226.5, Zn(I) 213.8 and Zn(II) 206.2 nm as a function of power and height above the load coil is studied. The detection limits of atomic and ionic lines of La, Mg, Zn and Cd with/without addition of Ba are reported. Low Ba concentration (0.001M) decreases the detection limit of the element of low ionization energy (La) while high Ba concentration (0.3M) decreases detection limits of the elements of high ionization energies (Cd and Zn) and increases the detection limit of the element of medium ionization energy (Mg).

Effect of an excess of easily ionizable elements (EIE) on atomic and ionic emission intensity in ICP–AES is a problem numerous investigators have already been faced with. This effect has been considered, in a number of papers, as a serious obstacle to quantitative spectrochemical analyses. Solution of the problem lies in determination of suitable operation conditions under which these interferences can be reduced or even eliminated. Since the operating conditions are always connected to a particular ICP instrument and a specific type of sample, it is difficult to draw a general conclusion on the changes in the excitation mechanism caused by the presence of an excess of EIEs.

In the first detailed study of the effect, Larson *et al.*[1] have investigated the effect of different Na concentrations on atomic and ionic emission intensity from Ca, Cr and Cd at various heights above the load coil (ALC). They have found that an increase in Na concentration from 100 to 1000 μg/ml depresses the intensity of Ca(II), Cr(II), Cd(II) and Cd(I), and enhances the intensity of Ca(I), while the intensity of Cr(I) is depressed at a height of 15 mm but increased at heights from 20 to 25 mm. Due to depression of all ionic lines, the authors suggested an ionization suppression mechanism, including also some other factors, since the behaviour of some atomic lines was in conflict with the interpretation given. However, axially and radially-resolved measurements of excitation temperatures, electron number densities, *etc.* revealed that several excitation mechanisms must be considered and that the predominance depends on the location in the ICP.[2–13]

The aim of this paper was to investigate the influence of Ba addition on the detection limits of elements of different ionization energies.

EXPERIMENTAL

Details of instrumentation and operating conditions are given in Table 1.

Low in the plasma, in the Initial Radiation Zone, excitation of both atoms and ions is

*Author for correspondence.

Table 1. Plasma equipment and operating conditions

Apparatus	Perkin–Elmer ICP 6500, 27.12 MHz operating frequency and cross-flow nebulizer
Operating Conditions:	
Ar gas flow	Outer 15 l./min Intermediate 0.5 l./min Central 0.9, 1.0, 1.1 l./min
Liquid sample uptake	1.0 ml/min controlled by peristaltic pump
Height above the load coil (ALC)	8, 10, 13, 18 and 20 mm
RF power	1.0, 1.2, 1.5 and 1.75 kW
Emission lines	La(II) 333.75 nm, E_{ion} 5.59 (eV) Mg(I) 285.21 nm Mg(II) 279.53 nm, E_{ion} 7.64 (eV) Cd(I) 228.80 nm Cd(II) 226.50 nm, E_{ion} 8.99 (eV) Zn(I) 213.86 nm Zn(II) 206.19, E_{ion} 9.39 (eV)

Table 2. Effect of central gas flow rate (Q) and RF power on relative standard deviation of background $(RSD)_B$

RF power (kW)	Q (l./min)	$(RSD)_B$ % Zn(II) 206.19	Cd(I) 228.80	Mg(II) 279.55	La(II) 333.75
	0.9	1.12	1.20	1.30	1.26
1.0	1.0	1.05	1.10	1.25	1.18
	1.1	1.15	1.23	1.42	1.35
	0.9	0.84	0.92	1.23	1.15
1.75	1.0	0.81	0.85	1.12	0.92
	1.1	0.93	1.05	1.34	1.25

usually enhanced. This effect is generally greater on ion than on neutral atom.[14] However, analytical measurements are generally made in the plasma region termed the Normal Analytical Zone,[9] within which EIEs usually depress the atomic and ionic excitation.[15] In this paper, ALCs in both zones were selected. Choice of elements (from easily to hardly ionizable) was made on the basis of the ionization energies of their atoms.

All reagents were of analytical grade. Solutions were prepared in doubly distilled water. Concentration of Mg was 0.5 mg/l., Cd and Zn 1.0 mg/l., and La 2.0 mg/l.

RESULTS AND DISCUSSION

Detection limits are calculated using the relation[16]

$$C_L = \frac{3 \cdot (RSD)_B C}{I_n/I_B}$$

where:

- I_n is the net line intensity for an analyte concentration,
- I_B is the background intensity,
- $(RSD)_B$ is the relative standard deviation of the background
- C is the analyte concentration.

According to the relation, low detection limits are obtained with as high as possible signal-to-background ratio (I_n/I_B) and as low as possible relative standard deviation of the background $(RSD)_B$.

Optimization of the central gas flow rate was carried out by determining the minimum relative standard deviation of the background $(RSD)_B$. The reason for such an approach was to establish a plasma discharge, as stable as possible, at introduction of samples in the plasma. $(RSD)_B$ was determined for Zn(II) 206.19, Cd(I) 228.80, Mg(II) 279.55, and La(II) 333.75 at an observation height of 15 mm, RF powers of 1.0 and 1.75 kW, and central gas flow rates of 0.9, 1.0 and 1.1 l./min. The results (an average value of 10 measurements) are given in Table 2.

As $(RSD)_B$ is minimum for the central gas flow rate of 1.0 l./min, both RF powers, and for all four wavelengths, this central gas flow rate was selected as optimum.

To achieve a maximum signal-to-background ratio, optimization of ALC (8–20 mm) for four RF powers (1.0, 1.2, 1.5, and 1.75 kW) has been performed. Results are summarized in Table 3.

Table 3. Influence of RF power on signal-to-background ratio for optimum ALC

	RF power							
	1.0 kW		1.2 kW		1.5 kW		1.75 kW	
Element	ALC mm	I_n/I_B	ALC mm	I_n/I_B	ALC mm	I_n/I_B	ALC mm	I_n/I_B
La(II)	13	6.23	15	5.07	18	3.69	18	2.76
Mg(I)	10	1.90	13	1.56	13–15	1.33	13–15	1.19
Mg(II)	10	7.59	13	6.91	13	6.05	13	4.35
Cd(I)	10	2.12	13	1.92	13	1.72	15	1.50
Cd(II)	10	2.47	10	2.17	13	2.28	13	1.98
Zn(I)	10	3.08	10	1.67	13	1.03	13–15	1.61
Zn(II)	8	1.95	8	2.10	10	2.05	13	1.81

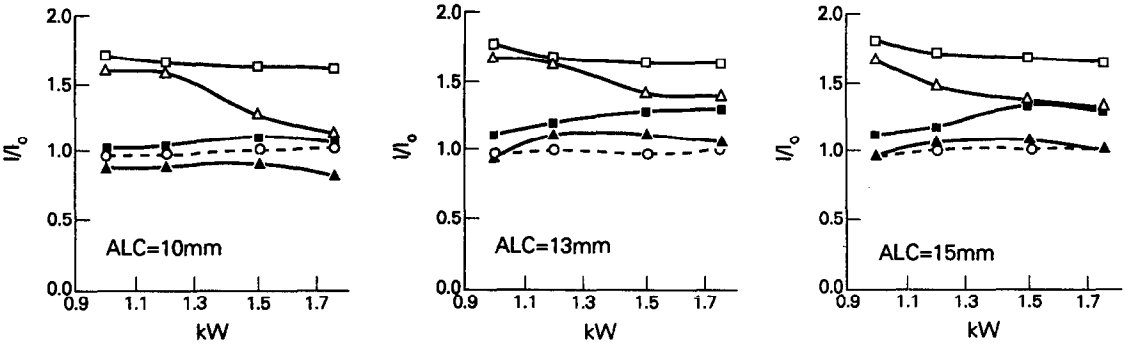

Fig. 1. Effect of different concentrations of Ba on La(II) 337.7 nm line as a function of RF power and ALC. I/I_0 is the ratio of the relative intensities with/without Ba added; □ 0.001M; △ 0.01M; ■ 0.1M; and ▲ 0.3M Ba. —— is the ratio of the background intensity with 0.3M Ba/without Ba added.

The effect of barium (as nitrate) of four different concentrations (0.001, 0.01, 0.1 and 0.3M) on the atomic and ionic emission intensity from the selected elements was investigated. Spectral line intensities were measured at the following powers: 1.0, 1.2, 1.5 and 1.75 kW. Investigations were carried out at ALCs of 8, 10 and 13 mm line intensities were measured at the following powers: 1.0, 1.2, 1.5 and 1.75 kW. Investigations were carried out at ALCs of 8, 10 and 13 mm for Zn and Cd, 10 and 13 mm for Mg, and 10, 13 and 15 mm for La. Selection of ALC was based on the values from Table 3 and the fact that the EIE effect is more pronounced in lower regions of the plasma. Measurements of the background intensity at wavelengths for all investigated lines in the presence of 0.3M Ba were performed. A slight change in the background intensity, regardless of the applied power, was found compared to the sample without Ba (Figs 1 and 2).

The ion emission intensity of La(II) is presented in Fig. 1, where I/I_0 is the ratio of

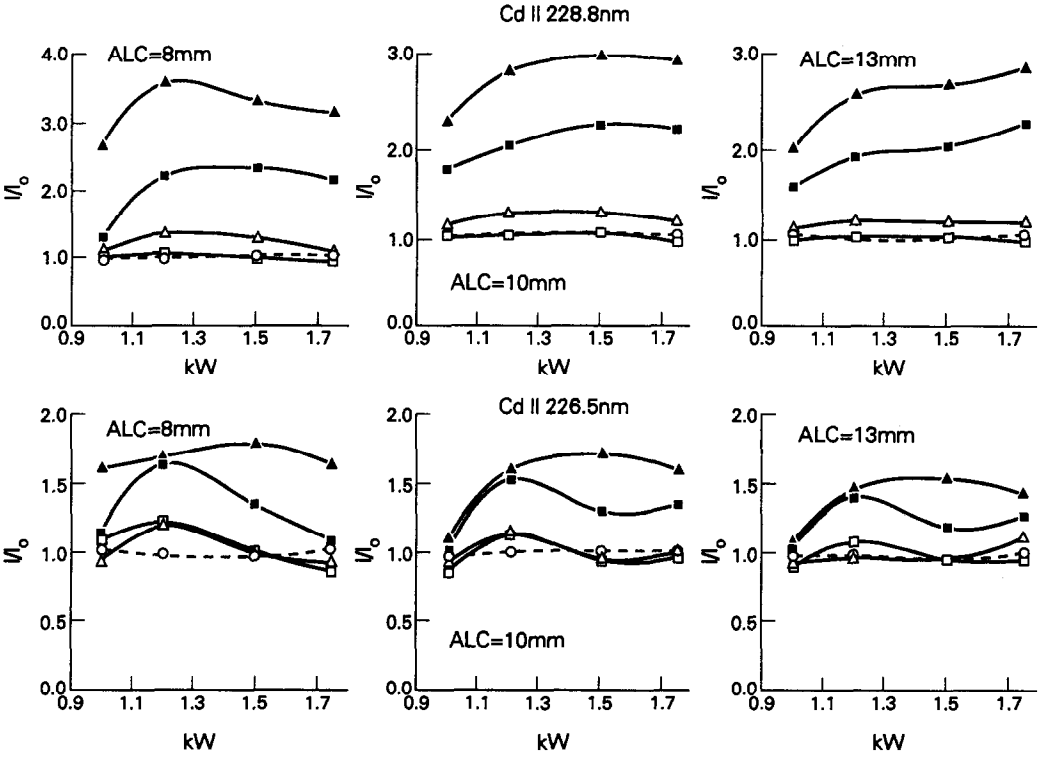

Fig. 2. Effect of different concentrations of Ba on Cd(I) 228.8 and Cd(II) 226.5 nm lines as a function of power and ALC. I/I_0 is the ratio of the relative intensities with/without Ba added; □ 0.001M; △ 0.01M; ■ 0.1M; and ▲ 0.3M Ba. —— is the ratio of the background intensity with 0.3M Ba/without Ba added.

Table 4. Cd(II)/Cd(I) relative intensity ratio in the presence of different Ba concentrations

Ba (M)	RF power (kW) 1.00	1.20	1.50	1.75
		Z = 8 mm		
0.001	1.44	1.74	2.12	1.85
0.01	1.15	1.31	1.61	1.57
0.1	1.08	1.12	1.19	1.20
0.3	0.78	0.85	1.07	1.11
		Z = 10 mm		
0.001	1.29	1.55	1.77	1.91
0.01	1.00	1.25	1.47	1.60
0.1	0.85	1.02	1.13	1.19
0.3	0.75	0.82	1.03	1.08
		Z = 13 mm		
0.001	1.22	1.51	1.68	1.79
0.01	0.89	1.12	1.45	1.65
0.1	0.80	0.95	1.05	1.08
0.3	0.50	0.80	0.95	0.95

the relative intensities with/without Ba added. When the sample contains 0.001M Ba, the La(II) intensity in the plasma is the highest at all RF powers. As can be seen this ratio is insensitive to changes in RF power. When the sample contains 0.01 and 0.1M Ba the position of the La(II) emission intensity maximum depends on the height above the load coil. For 0.3M Ba concentration, the intensity is close to that of the sample without Ba added. Effects of different Ba concentrations on the increase of the relative intensity of atomic and ionic lines of Mg are negligible. On the contrary, a certain depression trend (up to 50%) is noticeable at higher Ba concentrations.

Effect of different Ba concentrations on the relative intensities of atomic and ionic lines of Cd is presented in Fig. 2. Similar curves were obtained for Zn(I) and Zn(II).

Changes in Cd(I) and Zn(I) atomic line intensities lead to a conclusion that there is a similarity in their behaviour. Irrespective of applied RF power or observation height, the lower concentrations of Ba gave no measurable effect. An increase in Ba concentration causes an increase in the intensity. Thus, for 0.3M Ba this increase is by a factor of between 2 and 3. The emission intensity in both cases is higher at lower observation heights. Similar behaviour was observed for Cd(II) and Zn(II) ionic lines except that the enhancement factor is somewhat lower, about 1.5.

Behaviour of the relative intensities of the investigated lines proved a complexity of the processes is taking place in the excitation mechanism with addition of Ba.

The fact that an increase in the Ba concentration results in an increase in the relative intensity of atomic and ionic lines of Zn and Cd, the effect being higher for atomic lines, suggests a simultaneous action of collisional excitation and ionization depression processes. Justification of such a suggestion is confirmed by the effect of Ba concentration on the relative intensity ratio of ionic to atomic lines of Cd (Table 4).

Results in Table 4 illustrate not only the presence of shifts in ionization equilibrium, but a participation of this process in different zones of the plasma as well. This is obvious from the data showing that:

(a) an increase in Ba concentration decreases the I_{CdII}/I_{CdI} ratio at all powers and observation heights;

(b) the I_{CdII}/I_{CdI} ratio, at a given Ba concentration and constant RF power, decreases with increasing height above the load coil.

Table 5. Detection limits of investigated elements with and without Ba at different ALC and optimum RF powers

Elements	ALC, *mm*	Detection limits, *ng/ml* Without Ba	0.001M Ba	0.3M Ba
		1.0 kW	1.0 kW	1.0 kW
La(II)	10	11.4	6.3	11.6
	13	9.6	5.4	10.1
	15	10.1	5.9	11.5
	Ref. 17	6.5	—	—
		1.0 kW	1.0 kW	1.0 kW
Mg(I)	10	7.9	8.3	9.1
	13	8.1	8.3	11.4
	Ref. 17	1.1	—	—
		1.0 kW	1.0 kW	1.0 kW
Mg(II)	10	2.0	2.1	3.2
	13	2.5	2.6	4.6
	Ref. 17	0.1	—	—
		1.0 kW	1.0 kW	1.2 kW
Cd(I)	8	15.1	15.2	5.1
	10	14.1	14.1	5.8
	13	13.3	13.7	6.1
	Ref. 17	1.8	—	—
		1.0 kW	1.0 kW	1.5 kW
Cd(II)	8	12.7	11.6	8.0
	10	12.1	14.1	7.8
	13	13.3	14.4	9.6
	Ref. 17	2.5	—	—
		1.0 kW	1.0 kW	1.5 kW
Zn(I)	8	9.9	9.7	6.4
	10	9.7	10.1	5.7
	13	11.2	11.7	8.5
	Ref. 17	1.2	—	—
		1.2 kW	1.5 kW	1.75 kW
Zn(II)	8	14.3	15.1	12.2
	10	14.6	14.9	12.3
	13	15.9	14.8	13.3
	Ref. 17	4.0	—	—

In general, according to the above comments, an increase in height lowers the collisional excitation effect making the influence of shift in ionization equilibrium more pronounced.

Table 5 lists the calculated detection limits for the La ionic line, Mg, Zn and Cd atomic and ionic lines with (0.001M and 0.3M) and without Ba at different ALC and optimum RF powers.

As can be seen from Table 5, small Ba concentration (0.001M) decreases detection limit of the element of low ionization energy (La), while high Ba concentration (0.3M) decreases detection limits of the elements of high ionization energies (Cd and Zn), and increases detection limit of the element of medium ionization energy (Mg).

REFERENCES

1. G. F. Larson, V. A. Fassel, R. H. Scott and R. N. Kniseley, *Anal. Chem.*, 1975, **47**, 242.
2. D. J. Kalnicky, V. A. Fassel and R. H. Kniseley, *Appl. Spectrosc.*, 1977, **31**, 137.
3. H. Kawaguchi, T. Ito and A. Mizuike, *Spectrochim. Acta*, 1981, **36B**, 615.
4. P. W. J. M. Boumans and F. J. de Boer, *ibid.*, 1977, **32B**, 371.
5. M. W. Blades and G. H. Horlick, *ibid.*, 1981, **36B**, 879.
6. R. N. Savage and G. M. Hieftje, *Anal. Chem.*, 1980, **52**, 1267.
7. G. R. Kornblum and L. de Galan, *Spectrochim. Acta*, 1977, **32B**, 71.
8. G. H. Horlick and M. W. Blades, *Appl. Spectrosc.*, 1980, **34B**, 229.
9. S. R. Koirtyohann, J. S. Jones, C. P. Jester and D. A. Yates, *Spectrochim. Acta*, 1981, **36B**, 49.
10. W. Gunter, K. Visser and P. B. Zeeman, *Spectrochim. Acta*, 1985, **40B**, 617.
11. S. R. Koirtyohann, J. S. Jones and D. A. Yates, *Anal. Chem.*, 1980, **52**, 1965.
12. L. J. Prell, C. Monning, R. E. Harris and S. R. Koirtyohann, *Spectrochim. Acta*, 1985, **40B**, 1401.
13. B. L. Caughlin and M. W. Blades, *ibid.*, 1985, **40B**, 987.
14. J. P. Rybarczyk, C. P. Jester, D. A. Yates and S. R. Koirtyohann, *Anal. Chem.*, 1982, **54**, 2162.
15. M. W. Blades and G. Horlick, *Spectrochim. Acta*, 1981, **36B**, 881.
16. H. Kaiser, *Anal. Chem.*, 1970, **26A**, 42.
17. P. W. J. M. Boumans, *Inductively Coupled Plasma Atomic Emission Spectroscopy*, Vol. I. Wiley, New York, 1987.

Talanta, Vol. 40, No. 8, pp. 1301–1306, 1993
Printed in Great Britain.

0039-9140/93 $6.00 + 0.00

AMPEROMETRIC LYSINE BIOPROBES ANALYSIS IN FEEDS

M. G. LAVAGNINI, D. MOSCONE and G. PALLESCHI*
Dipartimento di Scienze e Tecnologie Chimiche Universita' di Roma Tor Vergata Via della Ricerca Scientifica 00133 Rome, Italy

D. COMPAGNONE
Dipartimento di Biologia Universita' di Roma Tor Vergata Via della Ricerca Scientifica 00133 Rome, Italy

C. CREMISINI°°
ENEA Environmental Chemistry Division Casaccia Via Anguillarese 301, 00060 Rome Italy

(*Received* 14 *December* 1992. *Revised* 12 *January* 1993. *Accepted* 13 *January* 1993)

Summary—Amperometric enzyme electrode probes have been constructed for the specific determination of *L*-lysine and used in batch and flow analysis. The enzyme lysine oxidase was immobilized on a preactivated polymer support which was placed on a platinum electrode. Additional blocking membranes conferred high stability, reproducibility and avoided electrochemical and enzyme interferences. Parameters including pH, temperature, storage and operational times were optimized. Lysine was determined in the range 10^{-6}–$2.10^{-3}M$ with a detection limit of $5 \times 10^{-7}M$. The Michaelis constant was $2 \times 10^{-3}M$. This value was approximately two order of magnitudes higher than that reported in literature for the free enzyme. The response time of the probe was about 2 min in batch and flow analysis and 30 sec in flow injection analysis (FIA). The resulting probes were stable for more than three months with more than 300 analyses performed. The determination of lysine was carried out by both flow-through analysis and FIA. Analysis in feeds was carried out by acid hydrolysis to liberate lysine; then the solution was analyzed by the bioprobe and HPLC procedures. Results by the two methods correlated well.

The increasing demand in many countries for regulatory rules on the nutritional values for proteins has led scientists to develop new, rapid and specific methods for the determination of essential aminoacids in food and feeds. In this context, *L*-lysine, an essential amino acid is an important indicator of the nutritional quality of food.[1,2]

Several analytical methods for quantitative determination of lysine have been proposed, including reverse-phase liquid chromatography with precolumn derivatization,[3] liquid chromatography with fluorescence detection via precolumn dansylation,[4] aminoacid analysis[5] and paper electrophoresis.[6] These methods often do not satisfy the requirement for fast, accurate and specific analysis. Moreover they require expensive instrumentation and reagents. Electroanalytical methods based on the use of a CO_2 electrode and the enzyme lysine decarboxylase,[7] or using a platinum electrode coupled to *L*-lysine dehydrogenase have been reported.[8]

The first electrode, however, suffers from interference by atmospheric CO_2 and has a high detection limit ($10^{-4}M$). The second requires the cofactor NAD^+ and the mediator ferricyanide ion in solution. This makes the analysis more complicated with the potential problem of collateral reactions when the probe is used in a real matrix.

Recently a flow-through analyzer was described for lysine analysis using a Clark-type oxygen electrode and *L*-lysine-2-monooxygenase immobilized on silica gel.[9]

Romette *et al.*[10] used a Clark O_2 electrode coupled with *L*-lysine oxidase Li *et al.* used an optical sensor for determining lysine.[11]

Our system is based on an amperometric H_2O_2 electrode assembled with the enzyme, *L*-lysine oxidase, immobilized on a polymer support placed in intimate contact with the platinum electrode.

The reaction is as follows:

$$L\text{-lysine} + O_2 + H_2O \rightarrow \alpha\text{-keto-}\mathcal{E}\text{-aminocaproate} + NH_3 + H_2O_2$$

*Author for correspondence.

The production of H_2O_2 is detected by the platinum electrode held at 650 mV applied potential *vs.* a silver/silver chloride cathode. The output current is correlated to the concentration of lysine in the sample. The use of blocking membranes eliminated all electrochemical and enzymatic interferences. The detection limit ($5 \times 10^{-7} M$) was two orders of magnitude lower than the O_2 probe used in previous work.[10]

EXPERIMENTAL

Reagents and materials

L-lysine α-oxidase from *Trichoderma viride* (EC 1.4.3.14) lyophilized powder, 45 U/mg, was obtained from Yamasa Shoyu Co. Tokyo, Japan.

L-lysine monohydrochloride (*puriss. p.a.*) was from Fluka (Germany). Other amino acids tested were from Sigma Chemical Co. (St Louis, MO). All other reagents of pure grade were from Farmitalia C. Erba (Milan, Italy).

Five samples of feed (dietetic preparations for laboratory animals) were a gift from ENEA, two samples of feed for rabbits were obtained from a local grocery store.

The Immobilon-AV affinity membrane, 0.65-μ pore size, 125 μm thick was from Millipore (Bedford, MA).

Cellulose acetate membrane, with an approximate molecular weight cut-off of 100, was prepared in our laboratory. The procedure is reported in the literature.[12]

Polycarbonate membrane (0.03-μm pore size) 6 μm thick was from Nucleopore, Pleasanton, CA.

Apparatus

For batch analysis the probe used was a hydrogen peroxide sensor from Universal Sensors Inc. Metaire, LA.

For FIA and flow through analysis we used a wall-jet cell model 656 electrochemical detector from Metrohm, Herisau, Switzerland. This cell was assembled with a platinum working electrode (1.6 mm diameter) (Model MF 2013) from BAS, Lafayette, IN.

Steady state and transient currents were measured with an Amperometric Biosensor Detector ABD from Universal Sensor, Metaire, LA and recorded with an AMEL model 868 recorder, Milan, Italy.

The peristaltic pump was a Minipuls 3 from Gilson, France. For the FIA technique a HPLC Rheodyne valve model 7125 with a closed loop of 20 μl was used.

Electrochemical biosensor and biocell assembling

The biosensor probe consists of a platinum electrode polarized at +650 mV *vs.* a built in silver/silver chloride reference electrode. This probe was assembled by placing on an inverted electrode jacket in the given order the following membranes: cellulose acetate which protects the platinum electrode from electrochemical interferences, [13] the enzyme membrane and a polycarbonate membrane which protects the enzyme from proteins or bacteria. These membranes were then secured with an O-ring. The electrode jacket was filled with a solution of potassium chloride 0.1*M*, then the electrode was inserted into the jacket and screwed down until the tip of the platinum was firmly in contact with the membranes.

The wall jet cell was assembled covering the working electrode with the same membranes. Then the electrode was firmly secured into the cell which was connected to the flow system.

Procedures

Lysine oxidase was immobilized on the Immobilon membrane according to the following procedure: for a single membrane of 1 cm diameter, 200 μg of dry enzyme were placed on the Immobilon membrane, 20 μl of 0.1*M* phosphate buffer pH 7.0 were added, the resulting mixture was homogeneously spread-out on the membrane with a glass stick. The membrane was air-dried for about 1 hr and then kept immersed in the same buffer until ready to use. When the bovine serum albumine (BSA)/glutaraldehyde immobilization on Immobilon was performed we used the procedure described by Villarta *et al.*[14]

Batch procedure

The lysine probe was immersed in 10 ml of stirred phosphate buffer solution (PBS) and then allowed to equilibrate. Aliquots of standard *L*-lysine solutions were then injected into the buffer and the current change recorded.

Flow through procedure

The assembled probe was inserted in the electrochemical wall-jet cell. The buffer was passed through the flow system and a current baseline recorded.

Then lysine standard solutions prepared in the same buffer were introduced into the cell and the current change recorded.

FIA

A closed 20-μl loop of a HPLC valve previously connected in series to the flow system was filled with the analyzing solution, then after the initial steady-state current was recorded, the solution was injected into the flow stream and a transient current variation recorded.

Feeds

When feeds were analyzed, samples were first ground to pass through 0.75-mm diameter openings and then mixed thoroughly by tumbling. Then 300-mg samples were weighed and transferred into test tubes. Then 10 ml of 6*N* HCl was added and heated at 120 ± 5° for 24 hr. The hydrolyzate was filtered and adjusted with dry NaOH and 1*M* NaOH to pH values between 6 and 7.5. The solution was then centrifuged, and appropriately diluted with buffer in order to have a response which fits within the calibration curve.

Analysis of lysine by HPLC was carried out using a C 18 reversed phase column and a solvent mixture consisting of acetonitrile and 100 m*M* sodium acetate pH 7.2 pumped at 0.8 ml/min.

RESULTS AND DISCUSSION

The lysine probe was first used in batch analysis. To select the best immobilization procedure and the optimum response, we assembled our probe using different protective membranes and different immobilization procedures. In previous work[14] it has been demonstrated that an enzyme immobilized on an Immobilon pre-activated membrane has higher specific activity if the immobilization is carried out by adding BSA and glutaraldehyde on the Immobilon membrane.

The same approach has been used in this work. Figure 1 shows calibration curves obtained using the enzyme lysine oxidase immobilized on Immobilon in the presence and absence of BSA and glutaraldehyde, and using polycarbonate membranes of different porosity.

The best response was attained using the BSA/glutaraldehyde procedure on Immobilon and a 0.8-μm polycarbonate membrane. This result was expected because the polycarbonate membrane has the highest porosity and the

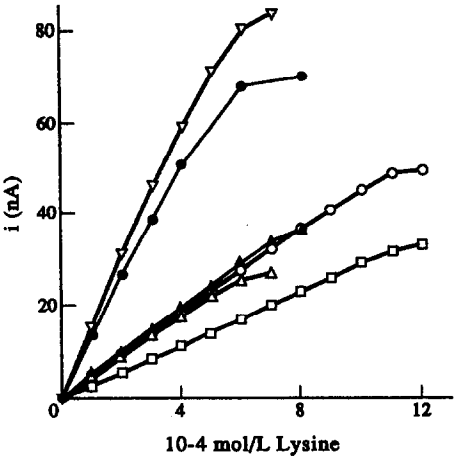

Fig. 1. Lysine calibration curves using two different immobilization procedures and protective polycarbonate membranes with different porosity. ▽ BSA/glutaraldehyde on Immobilon and 0.8-μm polycarbonate; ● Immobilon only and 0.8-μm polycarbonate; ○ BSA/glutaraldehyde on Immobilon and 0.03-μm polycarbonate; ▲ BSA/glutaraldehyde on Immobilon and 0.05-μm polycarbonate; △ Immobilon only and 0.05-μm polycarbonate; □ Immobilon only and 0.03-μm polycarbonate. Buffer phosphate 0.1*M* pH 7.0 $T = 25°$.

immobilization procedure was optimized to have a higher amount of enzyme. However the linearity reached for this immobilization was up to $5 \times 10^{-4}M$ lysine. Using a 0.03-μm polycarbonate membrane the sensitivity of the probe decreased because of slower diffusion of the substrate through the membrane pores but better linearity was attained. This phenomenon, already observed for other substrates in previous work,[15] allowed us to detect lysine up to $10^{-3}M$.

The enzyme immobilized on Immobilon without BSA/glutaraldehyde gave the same linearity but less sensitivity.

Since our goal was to use this sensor for the analysis of lysine in feeds, we selected the probe assembled with the enzyme immobilized on Immobilon with BSA/glutaraldehyde procedure and with the 0.03-μm polycarbonate. The last membrane was used to protect the enzyme from possible interferences in the hydrolized matrix, and to obtain an extended linear range of the probe to allow the analysis of a wider range of concentrations. Calibration curves for Fig. 1 were obtained in pH 7.0 phosphate buffer. This pH was previously selected by studying the probe response *vs.* pH with lysine injections of $10^{-4}M$ in a solution containing an appropriate buffer.

Figure 2 shows the current response of our probe used in different buffers for different pHs.

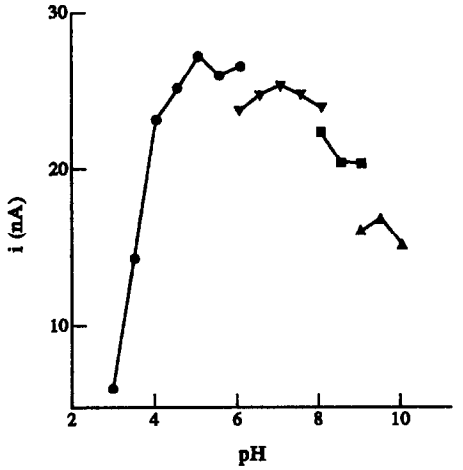

Fig. 2. Effect of pH on lysine oxidase activity. The enzyme activity was measured in the following buffers: ● citrate; ▼ phosphate; ■ tris; ▲ borax, $T = 25°$.

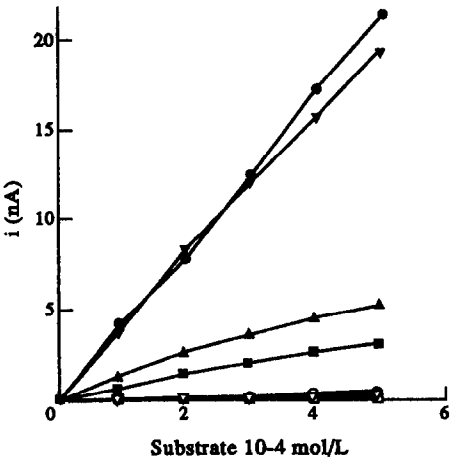

Fig. 4. Relative lysine oxidase activity toward some substrates pH 7.0 phosphate buffer $T = 25°$. ● lysine; ▼ lysine after the analysis of other aminoacids. ▲ ornithine; ■ arginine; ○ tyrosine; □ phenylalanine; ▽ histidine.

The best response was obtained between 5 and 7.5 which enabled use of our probe over a large pH range and in different buffers. For our study, phosphate buffer pH 7.0.

Temperature studies were carried out in the range 15–40°. By increasing the temperature, an increase in the probe response was observed. This effect is due to two factors; the increase in enzyme activity and the increased rate of diffusion substrates through the membrane pores. However, for temperatures up to 30° the current noise also increased, resulting in a lower current/noise signal output.

The best compromise was reached at 25° and this temperature was selected for further experiments.

A calibration curve for lysine after these parameters had been optimized is shown in Fig. 3. The detection limit was $5 \times 10^{-7}M$ with a linearity up to $10^{-3}M$. The apparent Michaelis Constant (Km) was 2×10^{-3} which is almost 2 orders of magnitude higher than that reported in the literature for the free enzyme (0.04 mM).[16]

The reproducibility of our probe was tested by running several calibration curves.

Five consecutive calibration curves gave a maximum variation of 5% over the lysine concentration range 10^{-5}–$10^{-3}M$.

The catalysis of this immobilized enzyme to oxidize various L-aminoacids as L-lysine derivatives and amines was investigated. Figure 4 shows calibration curves of lysine, and other aminoacids which gave a detectable response. The major interferent was ornithine followed by

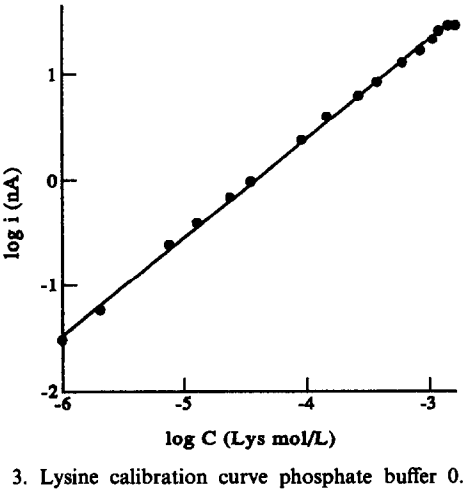

Fig. 3. Lysine calibration curve phosphate buffer 0.1M; $T = 25°$; immobilization: BSA/GLU on Immobilon.

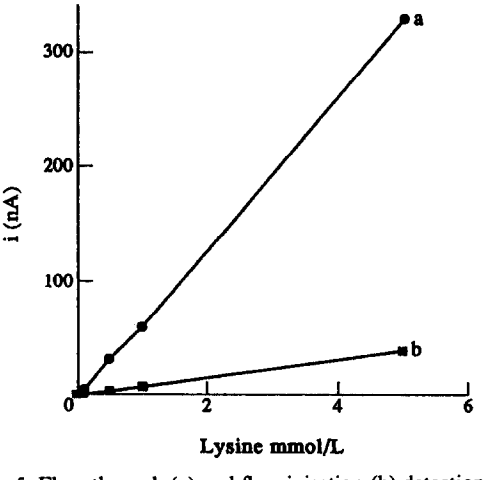

Fig. 5. Flow-through (a) and flow injection (b) detection of lysine. Sample carrier phosphate buffer 0.1M pH 7.0 $T = 25°$.

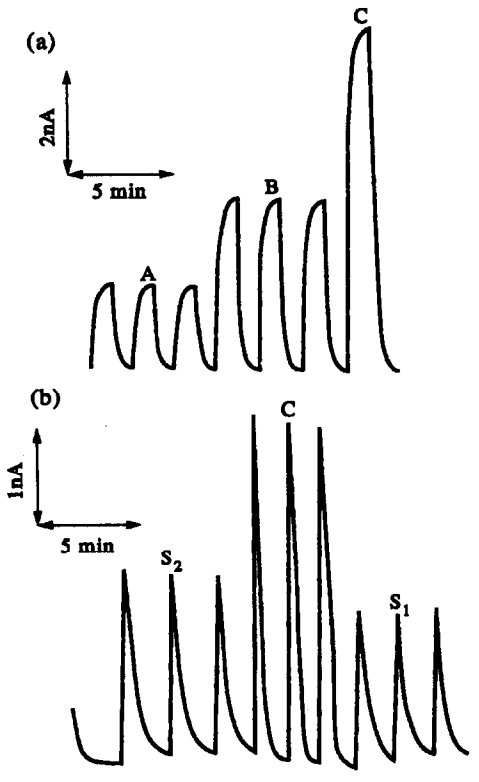

Fig. 6. Reproducibility and response time of the bioprobe in flow through analysis and FIA a = flow through: lysine concentration in standard solution. A = $5 \times 10^{-5}M$; B = $10^{-4}M$; C = $2 \times 10^{-4}M$; b = FIA; S_1 and S_2 foodstuff samples. C = lysine standard $5 \times 10^{-4}M$.

arginine. The effects of tyrosine, phenylalanine and histidine were negligible. Other aminoacids did not give any appreciable response. A calibration curve for lysine was run after measurements of all interferences were studied. Complete signal recovery was attained.

The lifetime of our sensor was investigated by studying the decrease of the enzyme activity with time.

The probe lost 70% of its original activity in 10 days, then it remained constant for more than 90 days. This decrease in enzyme activity did not pose any particular problem to probe performance. In fact analyses of lysine could be performed in the range 10^{-5}–$10^{-3}M$ with a detection limit of $5 \times 10^{-6}M$. These concentrations largely cover the range for feed analyses.

The operational time of our probe was more than 300 analyses of lysine. The response time was 2 min with 90% response in less than 1 min.

In order to make this method suitable for continuous flow analysis we used a wall-jet electrochemical cell with a lysine probe, assembled as previously described, inserted into the cell. Calibration curves of lysine were optimized by varying the flow rate to select the best linear range and the lower and upper detection limits of the analysis. The best results were attained at a flow rate of 0.2 ml/min, compromise between the probe sensitivity and stability and the time of analysis.

Analysis of lysine by FIA was carried out at the same flow rate used for continuous flow analysis. In this case an injection valve with a closed loop of a 20-μl sample was placed between the peristaltic pump and the electrochemical cell. Results are reported in Fig. 5. As is shown in this figure, the flow analysis is much more sensitive than FIA but despite this, the response time of FIA is less than 30 sec and the reproducibility is higher. However the sensitivity of the two methods was good enough to carry out analysis of lysine in foodstuff.

Figure 6 shows the reproducibility of the sensor both in flow analysis and FIA.

Feed analysis

Table 1 reports the determination of lysine in some products used to feed animals. The analysis was carried out by continuous flow and by FIA. Both flow-through and FIA methods correlated well with the HPLC procedure with a relative error varying between 1 and 12%. Only one sample gave an error of 17% in flow/HPLC correlation and 13% in FIA/HPLC correlation but gave only 3% when both the amperometric

Table 1. Lysine concentration (% w/w) in foodstuff determined with the biosensor method (continuous flow and FIA) and by HPLC

Sample	Flow	FIA	HPLC	Relative error (E%)		
				Flow/HPLC	FIA/HPLC	Flow/FIA
1	0.171	0.164	0.167	2.4	1.8	4.1
2	0.198	0.189	0.191	3.7	1.0	4.6
3	0.128	0.115	0.127	0.8	9.4	10.2
4	0.089	0.086	0.076	17.2	13.2	3.4
5	0.123	0.112	0.110	11.8	1.8	8.9
6	0.074	0.071	0.066	12.1	7.6	4.1
7	0.061	0.055	0.058	5.2	5.2	9.8

procedures were compared. Values obtained with the three methods were the mean of three determinations. Each sample was determined within 2 min, in flow, and 30 sec in FIA.

During the analysis of feeds the required washing time was longer than that measured during calibration with the buffer solution. This is probably due to the effect of some compounds present in the matrix which adhere to the polycarbonate membrane and require a longer washing time. Using the buffer solution as a washing solution between foodstuff samples, the time required to recover the initial current background was 3 min for flow through analysis and 2 min for FIA.

This allows a sampling rate of 12 samples/hr in flow through analysis and 20 samples/hr in FIA.

Acknowledgements—The authors wish to thank the Italian National Research Council (CNR) Target Project RAISA SUB-PROJECT 4, PAPER No. 905 for financial support.

REFERENCES

1. S. Davidson and R. Passmore, *Human Nutrition and Dietetics*, pp. 61–88. Williams and Wilkens, Baltimore, U.S.A., 1969.
2. J. P. Greenstein and M. Winitz, *Chemistry of the Amino Acids*, Vol. 1, pp. 245–432. Wiley, New York, 1961.
3. A. Cubedo Fernandez-Trapiella, *J. Assoc. Off. Anal. Chem.*, 1990, 73, **6**, 935.
4. A. P. Thio and D. H. Tompkins, *ibid.*, 1989, **72**, 4, 609.
5. B. N. Jones and J. P. Gilligan, *J. Chromatogr.*, 1983, **266**, 471.
6. B. S. Hartleys, *Biochem. J.*, 1970, **119**, 805.
7. W. C. White and G. G. Guilbault, *Anal. Chem.*, 1978, **50**, 11, 1481.
8. E. Dempsey, J. Wang, V. Wollenberger, M. Ozsoz and M. R. Smyth, *Biosensor and Bioelectronics*, 1992, **7**, 323.
9. A. L. Simonian, G. E. Khachatrian, S. Sh. Tatikian, Ts. M. Avakian and I. E. Badalian, *ibid.*, 1991, **6**, 93.
10. J. L. Romette, J. S. Yang, H. Kusakabe and D. Thomas, *Biotechnology and Bioengineering*, 1983, Vol. XXV, 2557–66.
11. H. Li, H. He and O. S. Wolfbeis, *Biosensors 92 Proceedings*, p. 234. 20–22 May 1992, Geneva, Switzerland.
12. M. Mascini, F. Mazzei, D. Moscone, G. Calabrese and M. Massi, Benedetti, *Clin Chem.*, 1987, **33**, 591.
13. G. Palleschi, M. A. Nabi Ranhi, G. J. Lubrano, J. Ngeh Ngwainbi and G. G. Guilbault, *Anal. Biochem.*, 1986, **159**, 114.
14. R. L. Villarta, G. Palleschi, G. L. Lubrano, A. A. Suleiman and G. G. Guilbault, *Anal. Chim. Acta*, 1991, **245**, 63.
15. G. Palleschi, M. H. Faridnia, G. J. Lubrano and G. G. Guilbault, *Applied Biochem. Biotechn.*, 1991, **31**, 21.
16. H. Kusakabe, K. Kodama, A. Kuninaka, H. Yoshino H. Misono and K. Soda, *J. Biol. Chem.* 1980, **255**, 3, 976.

Talanta, Vol. 40, No. 9, pp. 1307–1311, 1993
Printed in Great Britain.

0039-9140/93 $6.00 + 0.00
Pergamon Press Ltd

OBITUARY

Professor Dr.Dr.h.c. Wilhelm Simon (1929–1992)

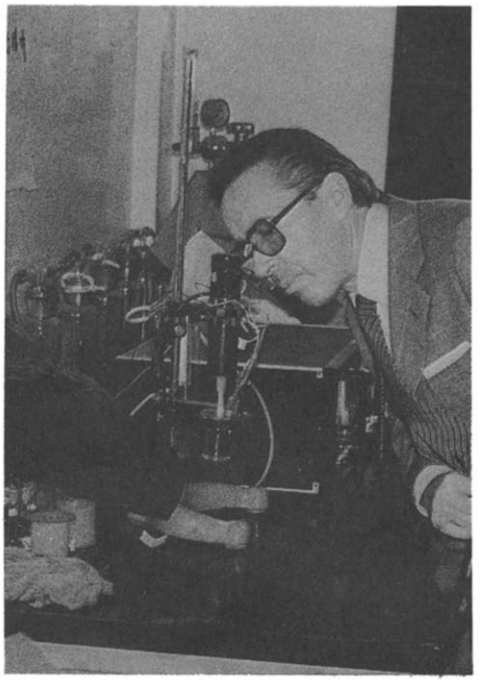

Wilhelm Simon had scarcely arrived in New Orleans for the 1992 Pittsburgh conference on 7 March when he was admitted to hospital. Colleagues and friends from all over the world were shocked by the news. On 17 November he passed away, released from 8 months of weakness and disability. He had not feared anything so much as being physically and mentally disabled in his old age. Consequently, during his illness, he retrained his memory by remembering the names of related persons, doctoral students, postdocs and collaborators all over the world, One day, when he realized his condition, he said to me: "I will tell you some day if it was a 'highlight' to save me from death!" However, in spite of this doubt, he fought optimistically for his recovery.

Wilhelm Simon was born in Fahrwangen on 26 September 1929, a small village in the canton of Berne in Switzerland. He grew up in a family of social modesty which was an attitude he never lost. He worked hard for his education and training, he cultured his language and created his own very effective, exquisite and appropriate vocabulary. Every letter was examined several times. Every lecture was prepared to highlight the relevant and fundamental points, and was enlivened with spontaneous inspiration.

He graduated in chemistry from the Swiss Federal Institute of Technology in 1953 and in the same year married his wife Agnes. He completed his diploma work although he was suffering from severe tuberculosis and was ill for several months during his studies. His enthusiasm for chemistry was supported by his teacher and Mentor Prof. Leopold Ruzicka (retired 1957) who visited him in the clinic in Leysin (Wallis) and encouraged him to stay at the ETH for his Ph.D. He received the latter in 1956 at the Department of Organic Chemistry of the Swiss Federal Institute of Technology in Zűrich (ETH). The doctoral thesis has the ETH – number 2590 and is entitled "Über die Mikrobestimmung scheinbarer Dissoziationskonstanten in nichtwässrigen Medien". At this time he regularly used his bicycle for transport and later he urged his students "I prefer to teach racers, not common cyclists!" During this period he was already teaching analytical chemistry and the application of spectroscopic techniques in organic chemistry and was developing

analytical instruments. His creativity was promoted by Prof. V. Prelog his "doctor father" and his Mentor Prof. E. Heilbronner, who was much more than an authority to him. He remembered many exciting moments when turning over the pages of fascinating books and discussing papers of well-known foreign authors.

During his studies in chemistry he strongly inclined to medicine and was registered at the University of Zürich for basic medical lectures. He was especially fascinated by the lectures in pathophysiology of Prof. W. Siegenthaler, the so called "Sigirama" where real "cases" were discussed and demonstrated. This medical interest structured his research projects throughout.

In 1965 he became an assistant professor in instrumental methods for chemical analysis at the ETH. Since 1970 he had been a full professor in organic chemistry. His instrumental developments, during this first period of research, initialized a typical field of analytical science. Swiss Industries did not utilize the chance. Though a chemist at heart he was, however, very grateful to belong to the field of organic chemistry, especially later in his career when he had the idea to imitate nature, without using complicated enzymes, to recognize compounds by synthetic molecules for analytical use. Thus he had the opportunity to synthesize the compounds planned by himself: "imitate nature, but do it better!"

Four years ago in 1989 the celebration of his 60th birthday was an unforgettable event, assembling all his doctoral students, 115 to date, as well as his promotors at the ETH, Prof. V. Prelog and Prof. E. Heilbronner. Plenty of typical daily events were remembered: the aversion to ferrets in the laboratory ("a pain in the neck!"), the fight against reading the daily press in the lab and many further events showing his enthusiasm and spontaneity. However, the last period of his life in the clinic in "Zihlschlacht" (SG) revealed his strong love of nature, especially of birds and their song.

ACHIEVEMENTS

To date his name is mainly connected to the development of optical and potentiometric sensors as well as potentiometric microdetectors. However, a list of more than 450 papers and 500 talks shows the spectrum of his productivity and opus. Some of his earliest accomplishments are less known. His earliest contribution derives from the title of his thesis. The scope was the development of the instrumentation for the micro-determination of the dissociation constant of organic compounds using glass electrodes and the interpretation of the results related to the constitution by the Hammett acidity function.[1-3] Microtitrations gave input in clinical chemistry in 1961 for the titration of free fatty acids in body fluids.[4] His glass electrodes were based on a broad collection of glasses of different compositions such as germanium dioxide[5] which were processed to electrodes by his friend Willy Möller, who still cultivates the art of manufacturing glasses for various different applications.

The automation of elemental analysis of organic compounds (C, H, N) resulted in a large space-filling instrument, which had a strong input in the industrial evolution of elemental analysis.[6,7] Further accomplishments were made in gas chromatography[8] and Currie-point pyrolysis gas chromatography.[9,10] The instrumental analysis of organic compounds was one of his main fields of research which he followed up for the whole period of his creative work.[11-13] He recognized the gain in information by combined analytical techniques. In 1964 he presented the first papers on combined spectroscopic techniques for the analysis of the structure of organic compounds[12] and presented the coupled GC–MS technique in 1966.[14] In 1967 the accessory to the polarimeter for magneto-optic rotation dispersion (MORD) was published and added to the coupled techniques.[15]

The development of the instrumentation for vapor phase osmometry resulted in a commercially successful product.[16-18] In a subsequent period Willy Simon was mainly concerned with the interpretation of spectra.[19-22]

Few scientists have the vision of a building before it is completed, he was such a visionary. He always realized his plans and concepts in a very early, but final, way. In most cases a commercial instrument was the product of his creative activity in analytical sciences. One of the most convincing examples for his purposeful, systematic procedure is the development of the magnesium-selective carriers over about 20 years.[23] This purposeful behaviour even assisted in opening the doors of industrial sponsorship. With the financial support of companies and different funds it was possible for him to employ assistants for his lectures and students for his research group. His achievements, in many cases, did not hit the headlines, but they were

valued much later; he was honored by awards of four medals and five honorary professorships.

The valinomycin based potassium-selective electrode, for example, is widely used all over the world and in various types of instruments. Willy Simon estimated sales of 64 million potassium sensors worldwide for 1990. The history of this accomplishment sounds close to the story of the recovery of penicillin by Alexander Fleming published in 1929. Valinomycin and rat liver mitochondria were used as tools for metabolic studies.[24] It was suggested that the oxidative phosphorylation of these cells is decoupled by cation transport through the membranes. Cation carriers were suspected of being responsible for this transport by Moore and Pressmann.[25] Experiments *in vitro* were started. Working with buffered solutions of valinomycin a precipitation occurred and was assumed to be due to a complexation of potassium by valinomycin. The first data based on X-ray structure analysis of valinomycin-potassium complexes were published stimulated by Willy Simon.[26] The cation specificity of valinomycin was shown earlier by Shemyakin *et al.*[27] In 1966 the *in vitro* behaviour of macrotetrolides as ion-selective compounds and of valinomycin, especially, as a potassium-selective compound was confirmed potentiometrically by use of artificial membranes.[28–30] In 1969 these sensors were listed under the heading "miscellaneous" and denoted as "even more exotic systems!" The potassium-selective electrode was published and applied to blood serum measurements in 1970.[31,32] At this time I had the chance to contribute to the success by first measurements of the potassium selectivity in serum and by comparison to FAES. I was then employed in my first position in clinical chemistry at the University Hospital Zürich. Much later I noticed the great success but also the trouble created by the ion-selective electrodes and undertook comparisons between electrolyte measurements by ISEs and FAES. I had just evaluated the first potassium-selective optical test by solid state, or so-called "dry chemistry" assays in 1985. It was at this time, nearly 20 years later, that I first met with Prof. Willy Simon personally at a meeting where I presented my results. He was fascinated by the results of these test strips and initialized the optode programme.

The design of ion-selective carriers was accelerated in the subsequent period. Many successful synthetic carriers were evaluated for monovalent and divalent cations, as well as anions. The tailoring of carriers lastly resulted in carriers for neutral compounds coupled to optical transduction as well. Even the sodium-selective glass electrode was born in his kitchen.[33] Also in the field of ion-selective electrodes, research and development were permanently followed up by the industrial contacts. In 1972 the first clinical analyser, using a valinomycin based sensor, was commercialized (STAT-ION, Technicon/Photovolt Corp., USA). The potentiometric as well as optical ion-selective principle of chemical sensors were treated theoretically over all the years.[34–37]

PERSONALITY

For lunch with guests a special place was selected, very frequently on top of a building. One of his favourite places was the "Dozenten-Foyer" at ETH where I remember fascinating discussions with guests from all over the world. As important as the meal, however, was the view of the mountains. On such an occasion he instructed me on the theories of Manfred Eigen, whose papers on thermodynamical properties of electrolyte solutions fascinated him. I was instructed on the dependence of the rate of substitution of solvent molecules in the inner coordination sphere of a metal ion related to the charge and the radius of an ion. I was confronted with ion hydration theories during my studies in the field of plant physiology, taught by Prof. A. Frey-Wyssling at the ETH-Zürich, related to ion uptake by roots. In 1971 and the following years W. Simon presented some papers on calculations of free enthalpies of hydration of ions related to the stability constants and the influence of the medium on the complexation of ions.[38,39] Based on these early thermodynamic calculations Clementi stimulated the calculations of interaction energies and early programs for molecular modelling calculations were written in his laboratory.[40] After teaching me, Willy Simon shifted to the educational and social situation in South Africa. Such appointments were completely dedicated to exciting discussions, more commonly than enjoyment of the meal.

In his heart Willy Simon felt a deep affinity with Japan. Beside his travels for teaching, he had strong respect for some famous chemists as H. Kobayashi, K. Kimura, S. Kamata, T. Shono and others. He considered moving to Japan after his retirement for part of the year. He was learning the Japanese language and

could converse. However he always felt a deep responsibility for his own country, the Swiss products as well as the chemical industry and the education of chemists in Switzerland. His trip around the chemical companies in Switzerland, his talks collecting and presenting the news of Pittsburgh Conference each year, were a main event for all his colleagues and students. Also in our laboratory at the ETH we looked forward to these reports as out of the ordinary and I never learned as much analytical chemistry in a shorter time.

He opened his laboratory to guests from Eastern Europe during a period of a general intensive inclination of science in Europe to the USA. At this time a visit to the Shemyakin Institute of Technology in Moskow was regarded by some as tantamount to being a traitor to his country. The strong relations with Hungary and a deep friendship with Prof. Ernö Pungor and his group, paved the way for him to relax and enjoy his success. Some publications derived from joint projects. Willy Simon was able to accept and enjoy the achievements of his colleagues as well, and was stimulated by these sound relationships which flourished with forward-looking scientific discussions that appealed so much to his temperament.

He opened his laboratory to Chinese researchers, whose intensive and productive attitude I seriously learnt to respect during the last years. Many other coworkers, more than 72 all over the world, have taken the opportunity to share experiences, moments of recognition and fascinating discussions in Willy Simon's elegant office or the "documentation" reserved for internal meetings. In these sessions we got to the bottom of the projects with fundamental considerations and questions. Occasionally young outsiders and shy, sensible newcomers lost the thread, startled by his flow of ideas and his delicate humour. His critical mind and the broad field of his experiences made him a member, advisory and honorary editor of in total 18 editorial boards, 26 scientific committees and a demanded, but occasionally inconvenient, member of different societies.

His responsibility for the technical development and future of Switzerland was his main motivation to activate the last, strongest, efforts for the realization of the "Swiss Centre of Chemical Sensors" in the area of Technopark Zürich. This idea was based on his belief that his country should invest manpower as well as ideas for developments in the field of high technology. He formulated a speech for ILMAC'90: "Es müsste aber das Ziel sein, selbst wieder durch eine Vorwärtsstrategie die Speerspitze des Fortschrittes zu bilden und die Spielregeln selbst zu bestimmen, statt sie aufgezwungen zu bekommen".[41] It happened during the last years that he felt afraid of his own courage and became tired: "Was bringt's?" Nevertheless the phrase above probably puts in words his last will concerning his research area and country.

A great scientist has left the arena leaving behind 20 doctoral students, his coworkers and plenty of plans and projects. In Switzerland his loss is followed by a tragic loss of position in education, training and research in analytical chemistry. Even when he stayed in Switzerland he was mentally participating in projects globally. All over the world colleagues, friends, scientists and analysts will mourn the loss of his strong and fair personality. All over the world his friends and colleagues will miss his humorous, stimulating and sensitive friendship and his compassion, he was a hard working analyst as well as a serious and fascinating teacher.

REFERENCES

(A series of publications is given in the following list by the first paper or a very representative paper.)

1. W. Simon, E. Kováts, L. H. Chopard-dit-Jean and E. Heilbronner, *Helv. Chim. Acta*, 1954, **37**, 1872.
2. A. Mörikofer, W. Simon and E. Heilbronner, *ibid.*, 1959, **42**, 1737.
3. W. Simon, *Angew. Chem. Int. Ed. Engl.*, 1964, **3**, 661.
4. P. Bally, W. Simon, P. F. Sommer and E. Ramseier, *Proc. of the 4th Int. Congress on Clinical Chemistry*, Edinburgh, 1960, Edinburgh and London, 1961, 189.
5. W. Simon and D. Wegmann, *Helv. Chim. Acta*, 1958, **41**, 2099.
6. P. F. Sommer, W. Sauter, J. T. Clerc and W. Simon, *Helv. Chim. Acta*, 1962, **45**, 595.
7. W. Simon and J. T. Clerc, *14th Pittsburgh Conf. on Analytical Chemistry and Applied Spectroscopy*, Pittsburgh, 1963, Abstract No. 137.
8. E. Heilbronner, E. Kováts and W. Simon, *Helv. Chim. Acta*, 1957, **40**, 2410.
9. H. Giacobbo and W. Simon, *Pharm. Acta Helv.*, 1964, **39**, 162.
10. W. Simon and H. Giacobbo, *Chem.-Ing.-Tech.*, 1965, **37**, 709.
11. W. Simon, *Chimia*, 1962, 312.
12. C., Pascual, D. Wegmann, U. Graf, R. Scheffold, P. F. Sommer and W. Simon, *Helv. Chim. Acta*, 1964, **47**, 213.
13. C. Pascual, J. Meier and W. Simon, *Helv. Chim. Acta*, 1966, **49**, 164.
14. J. A. Völlmin, I. Omura, J. Seibl, K. Grob and W. Simon, *ibid*, 1966, **49**, 1468.
15. J. T. Clerc, H.-K. Wipf and W. Simon, *Helv. Chim. Acta*, 1967, **50**, 1794.

16. W. Simon and C. Tomlinson, *Chimia*, 1960, **14**, 301.
17. Ch. Chylewski and W. Simon, *Helv. Chim. Acta*, 1964, **47**, 515.
18. R. E. Dohner, A. H. Wachter and W. Simon, *ibid.*, 1967, **50**, 2193.
19. W. Simon, *Cron. Chim.*, 1967, **16**, 17.
20. E. Pretsch, H. Immer, C. Pascual, K. Schaffner and W. Simon, *Helv. Chim. Acta*, 1967, **50**, 105.
21. F. W. Wehrli, E. Pretsch and W. Simon, *ibid.*, 1967, **50**, 2189.
22. E. Pretsch, J. T. Clerc, J. Seibl and W. Simon, *Strukturaufklärung Organischer Verbindungen*, 3rd ed. Springer-Verlag, Berlin, 1986.
23. U. E. Spichiger, *Electroanalysis*, 1993 (submitted).
24. L. Pioda, *Zur Ionenspezifität von Antibiotika*, Swiss Federal Institute of Technology, Thesis Nr. 4368, 1969.
25. C. Moore and B. C. Pressman, *Biochem Biophys. Res. Commun.*, 1964, **15**, 562.
26. B. T. Kilbourn, J. T. Dunitz, L. A. R. Pioda and W. Simon, *J. Mol. Biol.*, 1967, **30**, 559.
27. M. M. Shemyakin, N. A. Aldanova, E. I. Vinogradova and M. Yu. Feigina, *Tetrahedron Letters*, 1963, **28**, 1921.
28. Z. Stefanac and W. Simon, *Chimia*, 1966, **20**, 436.
29. Z. Stefanac and W. Simon, *Microchem. J.*, 1967, **12**, 125.
30. L. A. R. Pioda, A. H. Wachter, R. E. Dohner and W. Simon, *Helv. Chim. Acta*, 1967, **50**, 1373.
31. L. R. A. Pioda, H.-K. Wipf and W. Simon, *Chimia*, 1968, **22**, 189.
32. L. R. A. Pioda, W. Simon, H.-R. Bosshard and H. Ch. Curtius, *Clin. Chim. Acta*, 1970, **29**, 289.
33. Z. Stefanac and W. Simon, *Anal. Lett.*, 1967, **1**, 1.
34. H. R. Wuhrmann, *Zur Theorie von Ionenselektiven Sensoren*, Swiss Federal Institute of Technology (ETH), Zürich, Switzerland, Thesis Nr. 4805, 1972.
35. W. E. Morf and W. Simon, *Helv. Chim. Acta*, 1971, **54**, 794.
36. W. E. Morf, *The Principles of Ion-selective Electrodes and of Membrane Transport*. Elsevier, Amsterdam, 1981.
37. W. E. Morf, K. Seiler, B. Lehmann, Ch. Behringer, K. Hartman and W. Simon, *Pure & Appl. Chem.*, 1989, **61**, 1613.
38. W. E. Morf and W. Simon, *Helv. Chim. Acta*, 1971, **54**, 794.
39. W. Simon, in M. Eigen and L. De Maeyer (eds), *Carriers and Specificity in Membranes. A Report Based on an NRP Work Session, Neurosciences Res. Prog. Bull.*, 1971, **9**, 308.
40. G. Corongiu, E. Clementi, E. Pretsch and W. Simon, *J. Chem. Phys.*, 1979, **70**, 1266.
41. W. Simon, *Chimia*, 1990, **44**, 395.

U. E. SPICHIGER

Talanta, Vol. 40, No. 9, pp. 1313–1324, 1993
Printed in Great Britain.

0039-9140/93 $6.00 + 0.00

DOUBLE ARMED CROWN ETHERS AND ARMED MACROCYCLES AS A NEW SERIES OF METAL-SELECTIVE REAGENTS: A REVIEW

HIROSHI TSUKUBE

Department of Chemistry, College of Liberal Arts & Science, Okayama University, Okayama 700, Japan

(*Received* 10 *December* 1992. *Accepted* 9 *February* 1993)

Summary—Various double armed crown ethers and related macrocycles are presented as metal-selective reagents characterized by macrocyclic ligands and metal-ligating sidearms. They exhibit unique metal binding and recognition functions via macroring-sidearm cooperative action. Since they form three dimensional complexes suitable for metal-sensing and separation, we can develop a new series of metal-selective reagents via armed macrocycle strategy. Polymerization and immobilization of the armed macrocycles further enhance the usefulness in analytical science. This review focuses primarily on the molecular design, host–guest chemistry, and analytical applications of the armed macrocycles, and clearly indicates that these macrocycles provide new options in designing a metal-selective reagent.

Because crown ethers and other macrocyclic reagents are known to selectively bind metal cations, they have considerable potential as metal-selective reagents in sensing and separation science.[1,2] They are employed as the carriers in metal-selective extraction, phase transfer catalyses, membrane transport, and related processes. Literally thousands of macrocyclic reagents have been prepared which provide a variety of donor atoms, ring sizes, and ligand geometries.[3] Crown ethers and cryptands were particularly well-recognized as useful metal-selective reagents. Recently, "armed macrocycles" were developed as a new type of metal-selective reagent which are characterized by a parent macrocyclic ligand and a cation-ligating sidearm.[4,5] They topologically lie between crown ethers and cryptands and exhibit both the kinetically fast complexation properties of crown ethers and the three dimensional binding characteristics of cryptands. These metal binding features are similar to those of naturally occurring ionophores which effectively and selectively transport several metal cations across a biomembrane.[6] Because of their great advantages of facile synthesis and versatile molecular structures, a variety of metal-selective reagents were designed along this line and successfully employed in analytical science.

This review describes: (1) strategy for molecular design, (2) recognition of metal cations, and (3) analytical applications of the double armed crown ethers and other armed macrocycles. Their carrier activities in membrane systems are particularly detailed, because there is a wealth of valuable and interesting chemistry to be understood and applied to practical separation problems. We deal here with only a limited number of armed macrocycles; other types of metal-selective reagents have been reviewed elsewhere.[7]

STRATEGY FOR MOLECULAR DESIGN OF ARMED MACROCYCLES

Armed crown ether strategy

Double armed crown ethers[8] are typical examples of the armed macrocycles which are composed of two flexible cation-ligating arms and a parent crown ring. In this class of compounds, the donor group on the flexible sidearm provides further coordination of a guest cation trapped in the crown ring. The crown ring enforces a rudimentary "hole size" selectivity on the complexation, while sidearm donor provides three dimensional solvation. Their complexation behaviors are schematically shown in Fig. 1. We can design a metal-selective reagent of this type by choosing a combination of parent crown ring structure and functionalized sidearm.

Double armed crown ethers occupy an intermediate position between crown ethers and cryptands. The former affects rapid and circular coordination for guest cations, while the latter forms rigid and encapsulated complexes. Since

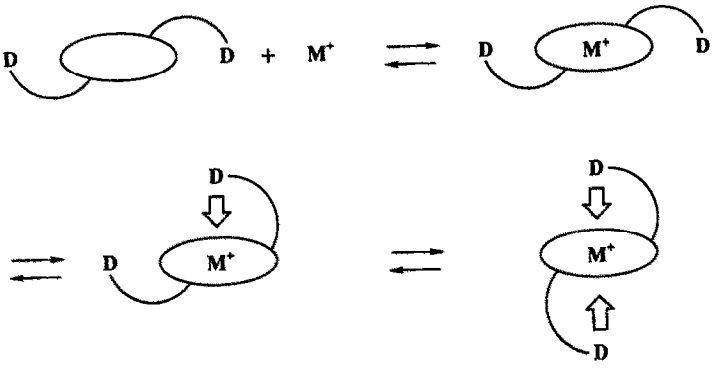

Fig. 1. Cation binding of double armed crown ether.

double armed crown ethers are stronger cation binders than the crown ethers and more flexible than the cryptands, they offer great promise in broad areas of metal-sensing and separation processes. A typical example is the facilitated transport of metal cation.[6] The rates of the carrier-mediated transport, in graphic terms, generally display a bell-shaped dependence on extraction or stability constants: the rate decreases when there is either too little extraction at the entry or too much extraction at the exit of the membrane.[9-11] Both crown ethers and cryptands are excellent cation binders but inadequate as membrane carriers. The monocyclic crown ethers are two dimensional and flexible binders, while the bicyclic cryptands form three dimensional and rigid complexes. Since an effective carrier is required to offer kinetically fast and three dimensional complexation, the double armed crown ether is most suitable and promising for this purpose. This has a flexible molecular structure to wrap a guest metal cation completely. Several kinds of armed crown ethers have already been demonstrated to mediate specific membrane transport of various metal cations.

Structural variation of the sidearm functionalities have been made to enhance usefulness in analytical applications. Introduction of an anionic metal-chelating group on the sidearm generally increases metal extraction activity of a macrocycle, because of the lack of requirement for a lipophilic counter-anion.[12] Addition of a chromophore on the sidearm makes possible colorimetric metal detection,[13] while addition of a signal-responsive group allows the use of signal-switching to control the solvent extraction and membrane transport.[14] Double armed crown ethers, therefore, provide a wide variety of possible uses in metal-sensing and separation processes. Their interesting metal binding and recognition behaviours have been illustrated on a molecular basis in solution and in solid state and are discussed below.

Armed macrocycles

In addition to the crown ethers, other kinds of macrocyclic ligands are available as parent macro-rings. Macrocyclic polyamines, polysulphides, cyclic peptides, calixarenes, cyclophanes, and cyclodextrins are potential candidates. Basic host–guest chemistry and

Table 1. Basic host–guest chemistry of parent macrocycle

Macrocycle	Major guest	Structural diversity*	Guest selectivity*
Crown ether	Na^+, K^+, Ca^{2+} Ba^{2+}, Ag^+, Pb^{2+} NH_4^+, RNH_3^+	A	A
Macrocyclic polyamine	Cu^{2+}, Ni^{2+}, Co^{2+} Polyanion	A	B
Macrocyclic polysulfide	Ag^+, Pb^{2+}	C	A
Cyclic peptide	Ca^{2+}, Ba^{2+} Cu^{2+}, Zn^{2+}	C	B
Calixarene	Na^+, K^+, Cs^+ Organic substrate	A	B
Cyclophane	Organic substrate	C	C
Cyclodextrin	Organic substrate	B	C

*A: excellent, B: fair, C: not good.

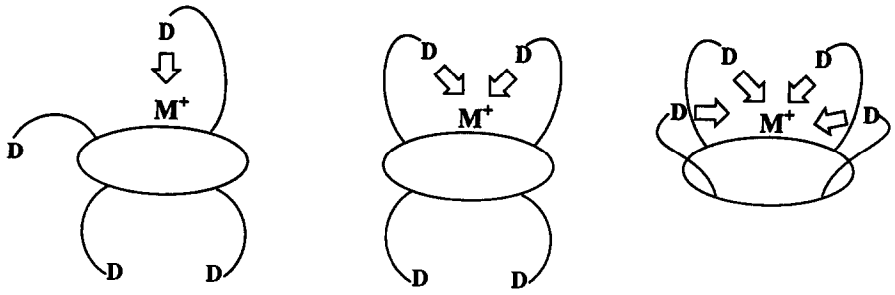

Fig. 2. Cation binding of armed macrocycle.

other characteristics of these macrocycles are summarized in Table 1. Polyamines and polysulphides have soft donor atoms effective for binding of soft metal cations, though crown ethers favour hard metal cations. Cyclic peptides complex with various metal cations, while calixarenes, cyclophanes, and cyclodextrins bind organic substrates. Many attempts have been made to attach the ligating sidearm groups to various macrocyclic ligands.[15] Several examples exhibited different guest selectivity from the armed crown ethers. Their target guest species included alkali, alkaline earth, heavy, and transition metal cations as well as organic substrates.[16] Such armed macrocycles often used a varying number of ligating sidearms for cation binding as schematically shown in Fig. 2, and offered various kinds of host–guest complexations. Since the nature of the parent macroring greatly influences the guest recognition profile of the armed macrocycle, we have many options in designing metal-selective reagents of these types.

HOST–GUEST COMPLEXATION OF ARMED MACROCYCLE

Solid-state structure of metal complex with armed crown ether

Three dimensional complex structures of the armed crown ethers have been demonstrated in the crystal state. Gokel *et al.* reported crystal structures of K^+ complexes with diaza-18-crown-6 **1**, lariat ether **2**, and double armed crown ether **3** (Fig. 3).[17] In the complex of lariat ether **2**, the guest K^+ cation is coordinated to donor atoms of both crown ring and sidearm. The crown ring donor atoms are disposed in a chair conformation with K^+ ion distinctly above the plane of four ether oxygen atoms. Its sidearm oxygen is located underneath the plane in an apical position. Since counter-anion

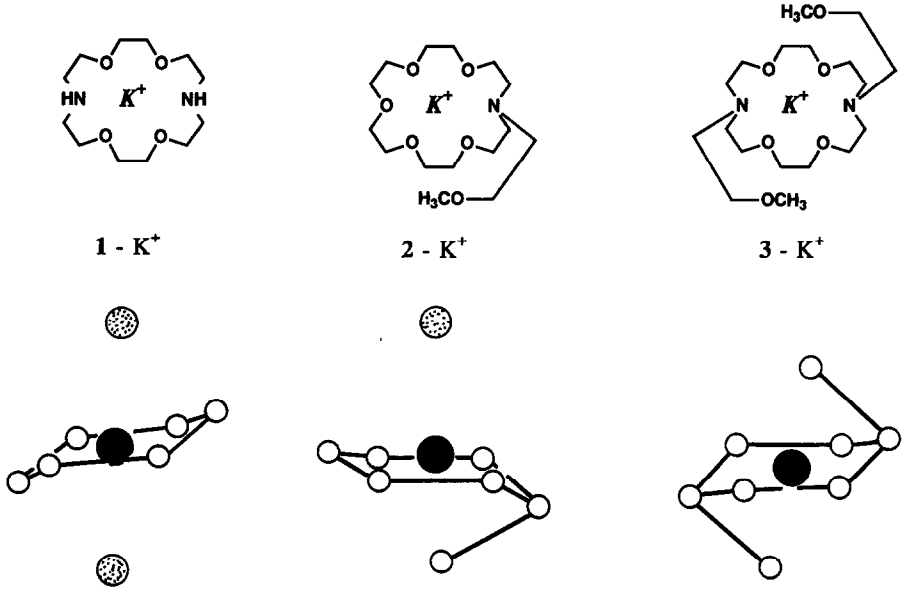

Fig. 3. Crystal structures of KI complexes with diaza-crown ether **1**, lariat ether **2**, and double armed crown ether **3**.

occupies the opposite apical position, the coordination number of the K^+ cation increases to eight. The K^+ ion is also octacoordinated in the double armed crown ether **3** complex, though anion does not contact the K^+ ion. The donor atoms of the crown ring adopt the chair conformation, but oxygen atoms of the sidearms are located above and below the mean plane of the crown ring. The K^+ ion is completely accommodated in a three dimensional cavity, which is topologically similar to those of cryptands. In contrast, the parent diaza-18-crown-6 **1** accommodates K^+ ion in a circular cavity and its encapsulation is not as complete as those with the lariat ether and the double armed crown ether. The solid-state structures of these complexes confirm the "armed crown ether strategy" described above, and suggest promising uses of the armed crown ethers in the metal-sensing and separation processes.

Armed crown ether–metal ion interaction in solution

The effect of functionalized sidearm on the complex stability was clearly demonstrated by comparing double armed crown ether with parent diaza-crown ether. Tsukube *et al.* found that attachment of pyridine-functionalized arms to the diaza-crown ring significantly increased binding constants for Ca^{2+} and Cu^{2+} ions.[18] As shown in Table 2, the stability constant of pyridine-armed diaza-18-crown-6 **4** for Cu^{2+} ion was an order of magnitude greater than that of the unsubstituted diaza-18-crown-6 **1**. Since only slight enhancement was observed for binding of Na^+ ion, the pyridine nitrogen atoms of the double armed crown ether **4** provided more effective coordination with divalent Ca^{2+} and Cu^{2+} ions than with monovalent Na^+ ion. Pyridine-armed crown ether **5**, which has all the structural elements present in the rest of the series, nonetheless behaved differently, because its pyridine nitrogen atoms are too remote to interact with the crown-bound metal cations. Pyridine-armed diaza-15-crown-5 and diaza-21-crown-7 derivatives similarly exhibited large enhancements for binding of several divalent metal cations. One precondition for cation binding enhancement is that the potential donor groups must be appropriately situated on the sidearms to provide effective coordination with the guest cation trapped in the parent crown ring.

Table 2. Stability constants of double armed crown ethers

	Log K in H_2O		
	Na^+	Ca^{2+}	Cu^{2+}
4	2.64	4.01	8.98
5	2.55	3.09	*
diaza-18-crown-6 **1**	2.44	3.43	7.59

*This compound forms an insoluble complex.

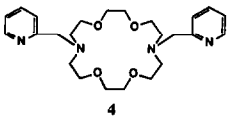

4

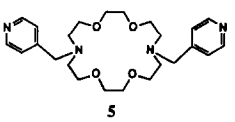

5

Cation inclusion behaviour of the pyridine-armed crown ether **4** was characterized by a ^{13}C NMR titration experiment.[18,19] Addition of $Ca(ClO_4)_2$ salt to a solution of pyridine-armed crown ether **4** caused significant and continuous shifts of the signals for both pyridine and crown ring carbons, indicating that the pyridine nitrogen atom on the sidearm effectively coordinated with Ca^{2+} ion trapped in the diaza-crown ring. This armed crown ether offered three dimensional but kinetically slow complexation with Zn^{2+} ion. When 0.5 equiv. of Zn^{2+} ion was present, each carbon exhibited two split signals corresponding to the free and complexed forms. This did, however, affect circular coordination for Na^+ cation in the same way as did simple crown ethers, because only the signals for crown ring carbons were shifted in the presence of Na^+ cation. Thus, the pyridine-armed diaza-crown ether **4** provides different coordination characteristics toward Na^+, Ca^{2+} and Zn^{2+} cations, which may explain the enhanced binding for Ca^{2+} and Zn^{2+} cations.

Cation binding of armed macrocycles

Armed aza- and thia-macrocycles form encapsulated complexes with the guest cations in different coordination modes. Dale *et al.* demonstrated that cyclen **6** having four hydroxyethyl-functionalized arms formed three dimensional complexes with Li^+, Na^+ and K^+ cations.[20] This used a varying number of ligating sidearms and accommodated its molecular cavity to the size and shape of the guest metal cation. Macrocyclic polyamines are not good ligands for these hard metal cations, but cooperative binding of the sidearm and the polyamine ring offered effective inclusion of the uncommon metal cations. Kaden *et al.* prepared transition metal complexes with the armed polyamine **7**, in which amide-functionalized sidearm was significantly involved in the metal encapsulation.[21] Since ring-size and donor atom of parent macrocyclic ligand, number and nature of arm donor group,

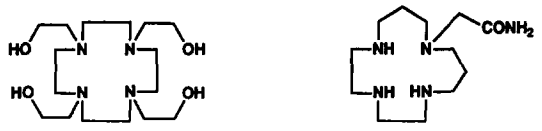

6 7

Fig. 4.

and shape of molecular cavity are variable factors, a large number of metal-selective reagents can be derived from various macrocycles.

Double armed crown ethers and related armed macrocycles have great advantages of facile synthesis and versatile molecular structures. We can tune the metal selectivity of these compounds by considering a combination of parent macroring and ligating sidearm. Their specific complexation behaviours satisfactorily meet the level required of metal-selective reagents available for multi-purposes. Their promising uses are discussed below from the viewpoint of analytical science.

ANALYTICAL APPLICATIONS

Depending on the structural characteristics, armed macrocycles bind several metal cations with varying strength. Since their metal selectivity is easily controlled through molecular architecture, they can be used to enrich, separate, mask and determine the concentration of metal cations. Their analytical applications include membrane transport, extraction separation, spectroscopic determination, electrochemical sensing, and chromatographic analysis as well as biomembrane mimetic processes. Typical examples of the armed macrocycles exhibiting characteristic metal-selectivity are described below.

Carrier in liquid membrane

Liquid membrane transport is a useful process for metal separation and enrichment, because there is no necessity for the separation of carrier and guest metal salt.[22] In principle, metal cation is moved from one aqueous phase through a lipophilic liquid membrane into a second aqueous phase. Selective transport of the metal cation is effected by a metal-selective reagent embedded in the membrane phase. Several useful carriers were designed by considering:

1. size and shape of cavity for guest encapsulation
2. nature of guest binding force
3. coordination geometry
4. solubility and stability of carrier and complex
5. molecular flexibility and binding dynamics.

Membrane transport produces different requirements for the carrier to be used from those of extraction and other metal separation processes. The effective carrier should not form too strong a complex with a transported metal ion. Double armed crown ethers and armed macrocycles are recognized as the most suitable candidates for effective carriers.[6] They have intermediate stability constants between crown ethers and cryptands and offer very high transport rates. Their three dimensional ligand topology provides highly lipophilic complexes with specific metal cations, while the high mobility of ligating sidearm promises fast kinetics of complexation. These binding features are common to several naturally occurring ionophores which specifically transport metal cations across a biomembrane. Thus, by careful selection of parent macrocycle and functionalized sidearm, we can prepare an armed macrocycle specific for encapsulation and transportation of metal cation.

Tsukube *et al.* first presented systematic studies on cation transport properties of double armed crown ethers.[23,24] They attached benzene, furan (oxygen atom), and thiophene (sulphur atom) rings to the diaza-18-crown-6 system as well as pyridine (nitrogen atom) ring. Interestingly, furan-armed crown ether **9** showed much larger transport rates for K^+, Ba^{2+}, NH_4^+ and Pb^{2+} ions than simple crown ether **8**, though other alkali and alkaline earth metal cations were only slightly transported. In contrast, thiophene- and pyridine-armed crown ethers **12** and **4** offered enhanced transport rates for heavy and transition metal cations such as Pb^{2+}, Cu^{2+} and Zn^{2+} ions.[18] Arm-functionalization of crown ether largely increased transport efficiencies especially for complementary guest cations. Transport selectivity was modified by varying ring-size of the parent crown structure: furan-armed 15-crown-5 **10** effectively mediated Na^+ ion transport, while a 21-crown-7 **11** was a good carrier of K^+ and Cs^+ ions. Therefore, double armed crown ethers have a "tunable" guest-selectivity both in complexation and transportation processes. By considering ring-size of the parent crown ring and coordinating character of donor arm groups, we can easily draw the molecular structure of a carrier specific for a target guest cation.

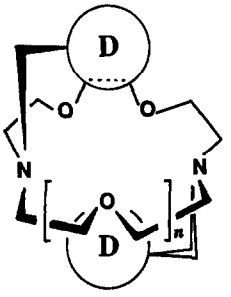

	n	D
8:	2	
9:	2	
10:	1	
11:	3	
12:	2	

Fig. 5.

Other examples of metal-selective armed crown ethers **13–15** are shown, together with their favourite metal cations.[9,25,26] Among them, thiazole-armed diaza-crown ether **14**, recently prepared via high pressure SNAr reaction, is notable.[26] This specifically formed a binuclear complex with Ag^+ ion. In this complex, two Ag^+ ions were cooperatively coordinated by thiazole-functionalized sidearms and parent diaza-crown ring, and the Ag....Ag' separation was shorter than the intermetallic distance.[27] Such a unique metal complexation attained a high Ag^+ ion-specificity in extraction and transport processes.

Attachment of an ionizable sidearm to the crown skeleton offers other possibilities in the design of useful carriers. Kimura *et al.* reported that phenoxide anion-armed 14-crown-4 derivative **16** was a specific carrier of Li^+ ion; this recorded an extremely high Li^+/Na^+ selectivity.[28] When the anion-armed crown ether is employed as a carrier, transfer of the metal cation into an organic medium does not require concomitant transfer of a counter-anion. Thus, crown ether ring and anion-charged sidearm act as cooperative complexing functions. Crown ethers having acidic functionalities such as **17** are effective for proton-driven active transport ("uphill transport") whenever guest ion is pumped against a concentration gradient.[29] The carrier shuttles back and forth between the metal-rich and the proton-rich aqueous phases, coupled with proton-transport. A similar coupled cation transport is often observed in the biomembrane processes. Nakatsuji *et al.* prepared crown ether **18** having $-NH_2$ group on the sidearm and demonstrated active transport of K^+ ion.[30] Since the $-NH_2$ group is readily protonated, this crown ether forms intramolecular "tail-biting" complexation of the crown ring with $-NH_3^+$ moiety under acidic conditions. This means that it strongly binds the K^+ cation under basic conditions and rapidly releases under acidic conditions. Such a unique binding realized uphill transport of the K^+ cation.

More interesting for practical applications and theoretical investigations are switchable transport processes, which can be turned on and off by photochemical, electrical, or other energy. Armed crown ethers such as **19**[31] and **20**[32] were designed so that they could be activated either electrochemically or photochemically and thus induce a change in the carrier activity. By

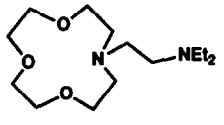

13

Li^+

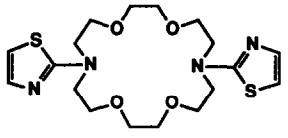

14

Ag^+

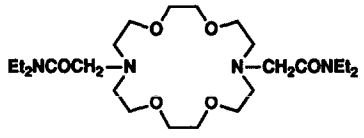

15

Ba^{2+}

Fig. 6.

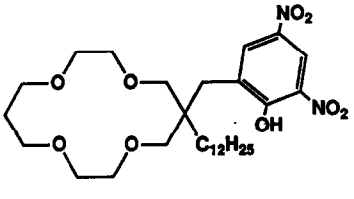

16

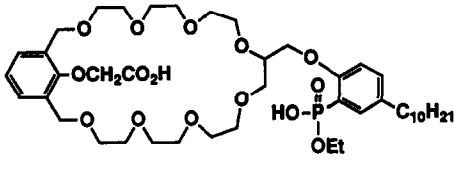

17

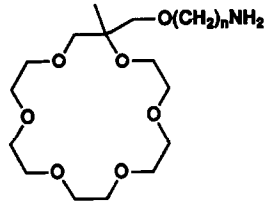

18

Fig. 7.

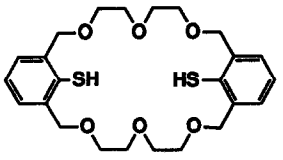

19

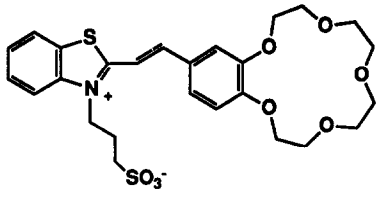

20

Fig. 8.

triggering a switch at the membrane interface, the membrane transport of the metal cation can be increased, changed to another ion or interrupted.[33]

Armed macrocycles have characteristically shaped-cavities for effective metal encapsulation. Tsukube *et al.* demonstrated that cyclams **21** bearing amide-functionalized sidearms had unique transport ability for Ba^{2+} ion, though the parent 1,4,8,11-tetraazacyclotetradecane ring favoured soft transition metal cations.[34] This formed a three dimensional, 1:1 complex with the hard Ba^{2+} ion, which was located on the polyamine ring and effectively coordinated both amide and macroring nitrogen groups. On the other hand, pyridine-armed cyclam **22** accommodated a hard Na^+ ion nicely in its molecular cavity and effectively transported it.[35] Since selective binding and transport of Ba^{2+} and Na^+ ions over K^+ ion are not attained by common crown ether-type carriers, unique donor combination and ligand geometry led to the new carrier functions. Furthermore, thiophene-armed thia-macrocycle **23** exhibited specific carrier activity for Ag^+ ion, while Na^+, K^+ and NH_4^+ cations of similar ion-sizes were rarely transported.[36] Although selective transport of Ag^+ ion was observed with the parent thia-macrocycle, its transport efficiency was much lower. Arm-functionalization greatly modified metal recognition profiles of the parent macrocycles and enhanced their carrier performances.

McKervey and Chang chose calixarenes as the parent macro-rings for a new series of metal-selective carriers.[37,38] Calixarenes are cyclic oligomers from *p*-tert-butylphenol and easily prepared in good yields. Chemical functionalization of intraannular OH groups of the calixarene is apparently effective in constructing a locked molecular cavity suitable for specific metal accommodation and transportation.[39] For example, ester derivative **24** from calix[4]arene existed in any one of four conformations: cone, partial cone, 1, 2-alternate, or 1, 3-alternate. Its moderately rigid skeleton allowed satisfactorily high Na^+ cation selectivity, but its conformational freedom assured high binding dynamics.

Ionophore in sensory system

The chemistry of double armed crown ether and armed macrocycle also provides the basis for constructing new spectroscopic and electrochemical sensory systems. When a chromophore is introduced to the armed macrocycle in a proper position, selective inclusion of metal cation greatly influences the spectral characteristics of the chromophore. Thus, detection and determination of a target metal cation are monitored visually or spectrophotometrically. Takagi *et al.* presented a pioneering work on this subject. They prepared a series of proton-dissociable crown ethers in which various chromophores were introduced on the sidearms.[13] When the anion produced upon deprotonation/complexation was singly charged, the resulting armed crown ether formed a neutral complex with a monovalent metal ion to be extracted from aqueous to water-immiscible organic

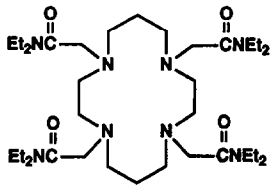

21

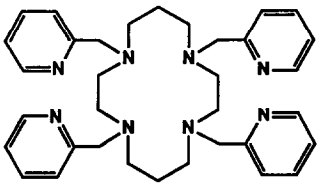

22

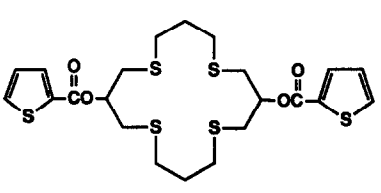

23

Fig. 9.

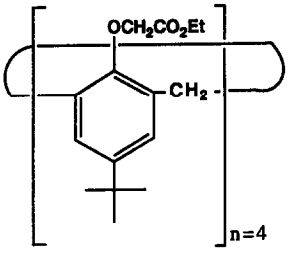

24

Fig. 10.

solvent. The introduction of two anionic sidearms allowed efficient extraction of divalent metal cations. These armed crown ethers were called "chromoionophores"[40,41] and were employed in selective extraction photometry of alkali and alkaline earth metal cations. Typically, armed crown ethers **25** and **26** exhibited high Na^+ cation selectivities for practical use. Their guest selectivities were significantly determined by the structures of crown ring and sidearm as described above.

Fluorimetric methods are useful for the assay of metal ions, especially in medicinal analysis, and several types of armed macrocycles were designed for this purpose. Double armed crown ether **27** is a commercially available reagent for determination of K^+ cation in the biocell.[42] Its principle is similar to that of Takagi's chromoionophore. Armed macrocycles **28**[43] and **29**[44] were recently developed as new metal-specific fluorescent probes, in which cation binding was coupled to emission changes of covalently anthracene fluorophores. Another example is Eu^{3+} or Tb^{3+} complex with bipyridine-armed macrocycle **30**.[45] Three dimensional topology of this macrocycle provided excellent protection against the deactivating action and offered high luminescence quantum yields of lanthanide cations even in water.

Armed macrocycles exhibited excellent performances, especially in the electrochemical sensory systems. An ion-selective electrode is a typical example and is of high analytical interest for selective determination of metal concentrations. The electrode membrane contains a lipophilic metal-selective reagent and responds to a specific metal ion. In such a system, a metal-selective reagent should have similar properties to those required for membrane carriers:[46] (1) high complexation or extraction selectivity for a given metal cation; (2) enough conformational flexibility for rapid ion exchange; (3) high lipophilicity to remain in the membrane; and (4) moderate molecular weight to allow high mobility. Many armed macrocycles have these features and are recognized as useful.

Kimura *et al.* reported that armed 14-crown-4 derivative **31** exhibited high Li^+ ion selectivity in the PVC membrane electrode.[47] Introduction of dodecyl sidearm prevents a sandwich type 2:1 complexation (crown:metal) due to the steric hindrance, and further coordination of the amide group attached enhances Li^+ cation binding. Actually, the electrochemical selectivity (K_{LiNa} value) was observed as 4.4×10^{-3}. Armed calix[4]arene **32** was also reported to be a potential carrier for Na^+ ion selective electrode.[48] Incorporation of cation-ligating ester group into the calixarene backbone enhanced Na^+ ion selectivity as described above, K_{NaK} value being 4.0×10^{-3}. A similar approach was used in the design of armed oligopeptide carrier **33** of Ca^{2+} ion.[49] These have practical applicability.

Polymeric "armed crown ethers" as metal-selective reagents

There is great expectation that the incorporation of an armed macrocycle into a polymer system may enhance its usefulness, and several attempts to polymerize and/or immobilize the armed macrocycles have been reported.

Tsukube *et al.* prepared poly(double armed crown ether) **34** and characterized its carrier profile for alkali metal cations in the liquid membrane system.[50] Transport ability of poly(diaza-crown ether) was clearly enhanced by attaching hydroxyethyl sidearms. Since the guest selectivity of the polymeric carrier was significantly controlled by the host–guest chemistry of the monomeric unit, a variety of polymeric armed macrocycles can be derived

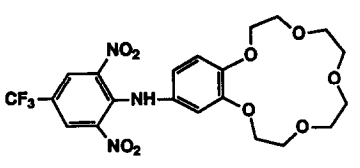

25

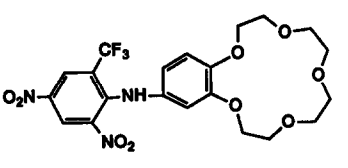

26

Fig. 11.

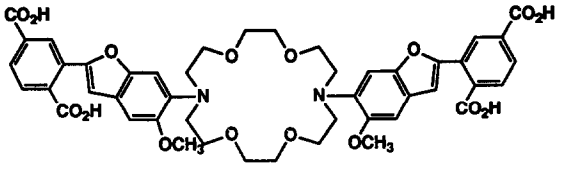

27

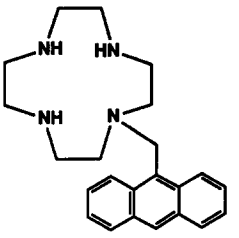

28

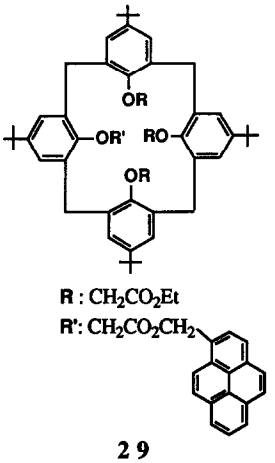

29

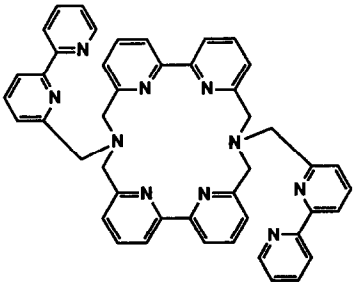

30

Fig. 12.

from well-characterized armed macrocycles. Cast film of this polymer also showed an interesting metal-selectivity.[51] The response in conductivity to the alkali metal cations was specific and further application is envisaged.

Bartsch *et al.* applied poly(crown ether) **35** bearing carboxylic acid-functionalized sidearm to the column concentration of Na^+ cation.[52] Column concentration is based on a single-stage sorption and requires strong binding of a specific metal cation. The proton-dissociable crown ether polymer fitted these requirements well. The participation of carboxylate anion on the sidearm significantly increased the binding ability and enhanced the guest selectivity. Since the polymer-bound metal cation was easily stripped with aqueous HCl, this type of polymer became a good stationary phase for selective metal concentration.

Polymer resin **36** was readily made from armed cyclam.[53] Its adsorption ability of Cu^{2+} and other transition metal cations from aqueous solution was much higher than those with common polyamine resins. A further combination of macrocyclic structure, functionalized sidearm, and polymeric backbone may offer other excellent polymeric reagents for metal-sensing and separation.

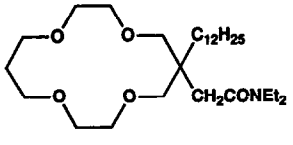

31

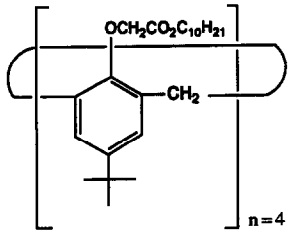

32

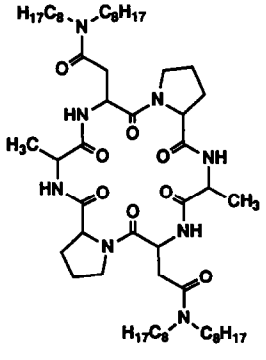

33

Fig. 13.

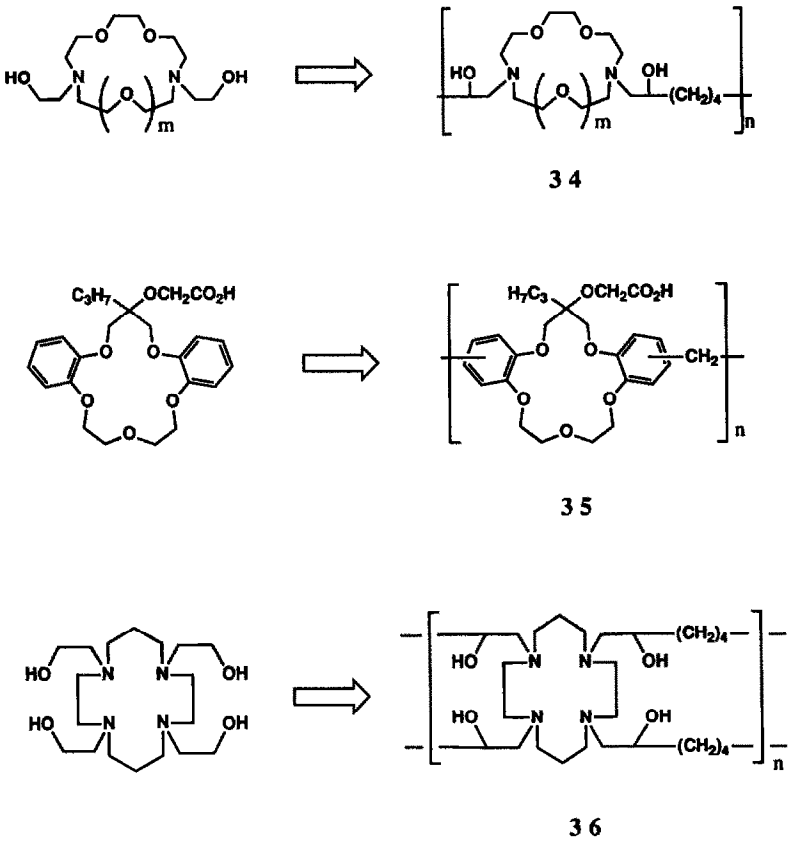

34

35

36

Fig. 14.

Armed macrocycles in membrane assembly

Lipid-like membrane assembly is formed from a variety of surfactants and possesses interesting properties similar to those of biological lipid membranes.[54] This acts as a useful vehicle for the ordering of metal-specific reagents and provides a variety of structurally organized and functionally integrated molecular systems. In particular, a specific

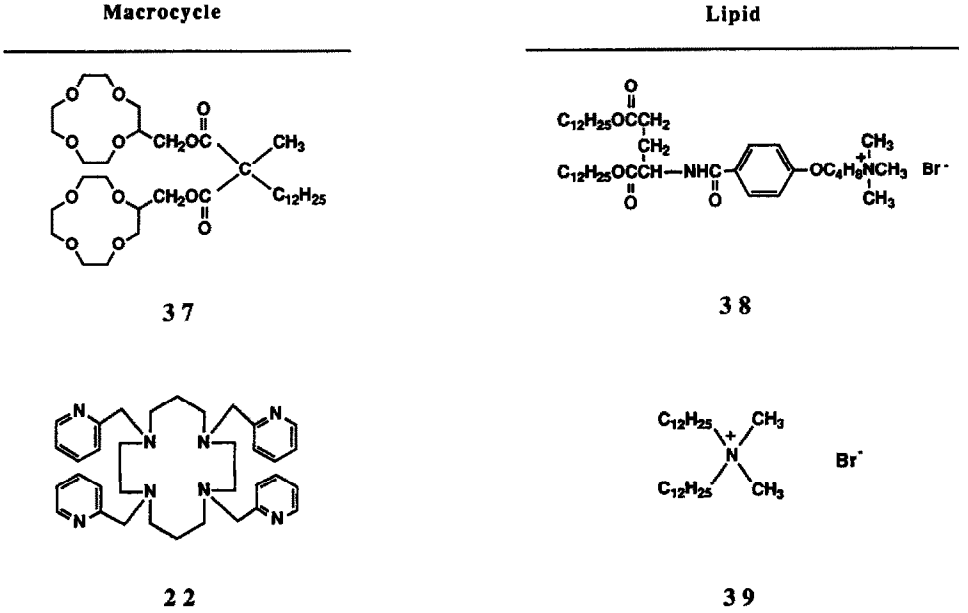

37 38

22 39

Fig. 15.

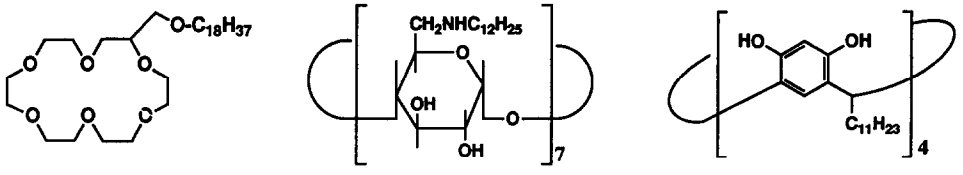

40 41 42

Fig. 16.

metal complexation on the membrane assembly is important for developing a new application in analytical science,[55] because remarkable amplification and modification of metal-sensing are realized in the biomembrane assemblies.

Nakashima *et al.* developed a highly Na^+ ion-selective membrane assembly which was composed of lipophilic bis-12-crown-4 **37** and chiral lipid **38**.[56] Its cation recognition process was monitored by circular dichroism spectroscopy. They noted that Na^+ ion-selectivity of the bis-12-crown-4 was remarkably amplified in such a bilayer-type membrane assembly.

Tsukube *et al.* reported that a lipid-bound armed macrocycle exhibited different metal selectivity from that observed in the usual liquid/liquid extraction system.[57] This membrane assembly was simply prepared by dispersing an aqueous solution of a lipophilic armed cyclam **22** and a quaternary ammonium surfactant **39**. It extracted Cu^{2+} ion very effectively from a bulk aqueous phase into the lipid-like membrane, while Ni^{2+}, Co^{2+}, and Zn^{2+} ions were rarely extracted. The resulting Cu^{2+} complex was immediately precipitated with lipid-aggregate by addition of $Mg(ClO_4)_2$ salt and easily separated from the aqueous solution by filtration. Since the armed macrocycle employed bound various transition metal cations in the solution systems, the membrane assembly may provide a unique microenvironment for specific metal extraction and recognition.

A variety of membrane assemblies was formed by crown ethers,[58] cyclodextrins,[59] calix arenes,[60] and related surfactants.[61] Some of them **40–42** were reported to show specific guest responses at the air–water and water–electrode interfaces. Since armed macrocycles recognize the guest species in various membrane assemblies, a wide variety of applications may be envisaged.

CONCLUSIONS

Double armed crown ethers and armed macrocycles are of particular interest because they generate many opportunities for analytical science. Since the synthetic strategies for this class of compounds have been presented, a variety of new metal-selective reagents has been designed for membrane transport, liquid–liquid extraction, spectroscopic determination, electrochemical sensing, chromatographic analysis, and so on. These offered good examples of metal-sensing and separation based on molecular recognition. Combinations of armed macrocycle chemistry with membrane chemistry, supramolecular chemistry, and related knowledge provided further possibilities in building up new sensing and separation systems. Development of this magnitude allows us to see a new horizon of metal-sensing and separation science.

Acknowledgements—The author is grateful to Professors Tadashi Iwachido of Okayama University, Lars Kryger of Nanyang Technological University, and Gary D. Christian of the University of Washington for their encouragement. He also thanks the American Chemical Society for granting permission to reproduce Fig. 3. This work was supported by grants from the Ministry of Education, Science, and Culture, Japan (No. 04804037) and from the Salt Science Research Foundation (No. 92002).

REFERENCES

1. G. W. Gokel, *Crown Ethers and Cryptands*, p. 1. The Royal Society of Chemistry, Cambridge, 1991.
2. M. Hiraoka (ed.), *Crown Ethers and Analogous Compounds*, p. 1. Elsevier, Amsterdam, 1992.
3. R. M. Izatt, K. Pawlak, J. S. Bradshaw and R. L. Bruening, *Chem. Rev.*, 1991, **91**, 1721.
4. G. W. Gokel and J. E. Trafton, *Cation Binding by Macrocycles*, Y. Inoue and G. W. Gokel (eds), p. 253. Marcel Dekker, New York, 1990.
5. E. Weber, *Crown Ethers and Analogs*, S. Patai and Z. Rappoport (eds), p. 305. Wiley, New York, 1989.
6. H. Tsukube, *Liquid Membranes: Chemical Applications*, T. Araki and H. Tsukube (eds), p. 51. CRC Press, Boca Raton, 1990.
7. W. L. Hinze, *Ordered Media in Chemical Separations*, W. L. Hinze and D. W. Armstrong (eds), p. 1. American Chemical Society, Washington, 1987.
8. A. Nickon and E. F. Silversmith, *Organic Chemistry: The Name Game*, p. 25. Pergamon Press, New York, 1987.
9. H. Tsukube, H. Adachi and S. Morosawa, *J. Chem. Soc., Perkin Trans. 1*, 1989, 89.

10. J. P. Behr, M. Kirch and J. M. Lehn, *J. Am. Chem. Soc.*, 1985, **107**, 241.
11. S. Yoshida and S. Hayano, *ibid*, 1986, **108**, 3903.
12. P. R. Brown and R. A. Bartsch, *Inclusion Aspects of Membrane Chemistry*, T. Osa and J. L. Atwood (eds), p. 1. Kluwer Academic Pub., Dordrecht, 1991.
13. M. Takagi and K. Ueno, *Topics in Current Chemistry*, Vol. **121**, p. 39. Springer-Verlag, Berlin, 1984.
14. S. Shinkai and O. Manabe, *Topics in Current Chemistry*, Vol. **121**, p. 67. Springer-Verlag, Berlin, 1984.
15. H. Tsukube, *J. Coord. Chem.*, 1987, **B-16**, 101.
16. L. F. Lindoy, *The Chemistry of Macrocyclic Ligand Complexes*, p. 51. Cambridge University Press, Cambridge, 1989.
17. R. D. Gandour, F. R. Fronczek, V. J. Gatto, C. Minganti, R. A. Schultz, B. D. White, K. A. Arnold, D. Mazzocchi, S. R. Miller and G. W. Gokel, *J. Am. Chem. Soc.*, 1986, **108**, 4078.
18. H. Tsukube, K. Yamashita, T. Iwachido and M. Zenki, *J. Org. Chem.*, 1991, **51**, 268.
19. H. Tsukube, K. Yamashita, T. Iwachido and M. Zenki, *Tetrahedron Lett.*, 1988, **29**, 569.
20. S. Buoen, J. Dale, P. Groth and J. Krane, *J. Chem. Soc., Chem. Commun.*, 1982, 1172.
21. Th. A. Kaden, *Topics in Current Chemistry*, Vol. **121**, p. 157. Springer-Verlag, Berlin, 1984.
22. R. D. Noble and J. D. Way, *Liquid Membranes: Theory and Applications*, R. D. Noble and J. D. Way (eds), p. 1. American Chemical Society, Washington, 1987.
23. H. Tsukube, K. Takagi, T. Higashiyama, T. Iwachido and N. Hayama, *J. Chem. Soc., Perkin Trans. 1*, 1986, 1033.
24. H. Tsukube, K. Takagi, T. Higashiyama, T. Iwachido and N. Hayama, *J. Inclusion Phenomena*, 1984, **2**, 103.
25. H. Tsukube, K. Hori, and T. Inoue, unpublished results.
26. H. Tsukube, H. Minatogawa, M. Munakata, M. Toda and K. Matsumoto, *J. Org. Chem.*, 1992, **57**, 542.
27. K. Hirotsu, I. Miyahara, T. Higuchi, M. Toda, H. Tsukube and K. Matsumoto, *Chem. Lett.*, 1992, 699.
28. K. Kimura, M. Tanaka, S. Iketani and T. Shono, *J. Org. Chem.*, 1987, **52**, 836.
29. B. P. Czech, H. Huh and R. A. Bartsch, *ibid.*, 1992, **57**, 725.
30. Y. Nakatsuji, H. Kobayashi and M. Okahara, *J. Chem. Soc., Chem. Commun.*, 1983, 800.
31. T. Nabeshima, H. Furusawa and Y. Yano, *7th International Symposium on Molecular Recognition and Inclusion*, PA23, Kyoto, Japan, 1992.
32. A. V. Barzykin, M. A. Fox, E. N. Ushakov, O. B. Stanislavsky, S. P. Gromov, O. A. Fedorova and M. V. Alfimov, *J. Am. Chem. Soc.*, 1992, **114**, 6381.
33. S. Shinkai and T. Matsuda, *Liquid Membranes: Chemical Applications*, T. Araki and H. Tsukube (eds), p. 161. CRC Press, Boca Raton, 1990.
34. H. Tsukube, H. Adachi and S. Morosawa, *J. Org. Chem.*, 1991, **56**, 7102.
35. H. Tsukube, K. Yamashita, T. Iwachido and M. Zenki, *J. Chem. Soc., Perkin Trans. 1*, 1991, 1661.
36. H. Tsukube, K. Takagi, T. Higashiyama, T. Iwachido and N. Hayama, *Tetrahedron Lett.*, 1985, **26**, 881.
37. M. A. McKervey, E. M. Seward, G. Ferguson, B. Ruhl and S. J. Harris, *J. Chem. Soc., Chem. Commun.*, 1985, 388.
38. S. K. Chang and I. Cho, *J. Chem. Soc., Perkin Trans. 1*, 1986, 211.
39. C. D. Gutsche, *Calixarenes*, p.105. The Royal Society of Chemistry, Cambridge, 1989.
40. F. Voegtle, *Pure Appl. Chem.*, 1980, **52**, 2405.
41. M. Takagi, *Cation Binding by Macrocycles*, Y. Inoue and G. W. Gokel (eds), p. 465. Marcel Dekker, New York, 1990.
42. A. Minta and R. Y. Tsien, *J. Biol. Chem.*, 1989, **264**, 19449.
43. E. U. Akkaya, M. E. Huston and A. W. Czarnik, *J. Am. Chem. Soc.*, 1990, **112**, 3590.
44. T. Jin, K. Ichikawa and T. Koyama, *J. Chem. Soc., Chem. Commun.*, 1992, 499.
45. V. Balzani and J. M. Lehn, *Angew. Chem. Int. Ed. Engl.*, 1991, **30**, 190.
46. K. Kimura and T. Shono, *Crown Ethers and Analogous Compounds*, M. Hiraoka (ed.), p. 198. Elsevier, Amsterdam, 1992.
47. K. Kimura, H. Yano, S. Kitazawa and T. Shono, *J. Chem. Soc., Perkin Trans. 2*, 1986, 1945.
48. K. Kimura, M. Matsuo and T. Shono, *Chem. Lett.*, 1988, 615.
49. N. Nishino, T. Kamizuru, Y. Sano, T. Nakashima, H. Karakawa and T. Fujimoto, *Peptide Chem.*, 1989, 365.
50. H. Tsukube, T. Iwachido, T. Shimotani, T. Dando and M. Zenki, *Bull. Chem. Soc. Jpn.*, in press.
51. H. Ohno, H. Yamazaki and H. Tsukube, *Polymer Commun.*, in press.
52. T. Hayashita, J. H. Lee, S. Chen and R. A. Bartsch, *Anal. Chem.*, 1991, **63**, 1844.
53. H. Tsukube, unpublished results.
54. J. H. Fendler, *Membrane Mimetic Chemistry*, p. 223. Wiley, New York, 1982.
55. K. Odashima, M. Sugawara and Y. Umezawa, *Trends in Anal. Chem.*, 1991, **10**, 207.
56. N. Nakashima, I. Moriguchi, K. Nakano, and M. Takagi, *J. Chem. Soc., Chem. Commun.*, 1987, 617.
57. H. Tsukube, T. Yoden, T. Iwachido and M. Zenki, *ibid.*, 1991, 1069.
58. S. Yoshida, Y. Okawa, T. Watanabe, S. Inokuma and T. Kuwamura, *Chem. Lett.*, 1989, 243.
59. M. Tanaka, Y. Ishizuka, M. Matsumoto, T. Nakamura, A. Yabe, H. Nakanishi, Y. Kawabata, H. Takahashi, S. Tamura, W. Tagaki, H. Nakahara and K. Fukuda, *Chem. Lett.*, 1987, 1307.
60. M. A. Markowitz, V. Janout, D. G. Castner and S. L. Regen, *J. Am. Chem. Soc.*, 1989, **111**, 8192.
61. K. Kurihara, K. Ohta, Y. Tanaka, Y. Aoyama and T. Kunitake, *ibid.*, 1991, **113**, 444.

Talanta, Vol. 40, No. 9, pp. 1325–1330, 1993
Printed in Great Britain.

0039-9140/93 $6.00 + 0.00

SUPERCRITICAL FLUID EXTRACTION OF ORGANIC AND INORGANIC MERCURY FROM SOLID MATERIALS

C. M. WAI,* YUEHE LIN, RUSSELL BRAUER and SHAOFEN WANG
Department of Chemistry, University of Idaho, Moscow, ID 83843, U.S.A.

WERNER F. BECKERT
EPA, Environmental Monitoring Systems Laboratory, Las Vegas, NV 89119, U.S.A.

(*Received* 21 *April* 1993. *Accepted* 23 *April* 1993)

Summary—Mercuric ions (Hg^{2+}) can be extracted from solid samples (cellulose matrix) using methanol modified supercritical CO_2 containing the fluorinated chelating agent lithium bis(trifluoroethyl)dithiocarbamate (LiFDDC). Methylmercuric chloride (CH_3HgCl) and dimethylmercury [$(CH_3)_2Hg$] can be extracted by supercritical CO_2 without chelating agent and modifier. The solubility of $Hg(FDDC)_2$ in supercritical CO_2 has been determined to be $5 \times 10^{-3}M$ at 50°C and 150 atm, which is about 3 orders of magnitude greater than that of the non-fluorinated analogue $Hg(DDC)_2$. Use of methanol (5%)-modified CO_2 further enhances the solubility of $Hg(FDDC)_2$ by a factor of 2.4. A small amount of water added to the sample matrix tends to facilitate the extraction of $Hg(FDDC)_2$ and CH_3HgCl. Potential applications of this *in situ* chelation-supercritical fluid extraction method for the preconcentration of mercury species and treatment of mercury contaminated wastes are discussed.

Supercritical fluid extraction (SFE) has become an attractive alternative to conventional solvent extraction for the recovery of organic compounds from environmental and biological samples because of several advantages, including increased speed, better recovery, and the reduction in both solvent usage and solvent waste generation.[1–4] To date, most of the published SFE work has focused on organic compounds, and few reports have dealt with SFE of metal ions and organometallic compounds. Wai and coworkers first reported the extraction of Cu^{2+} from liquid and solid materials using supercritical carbon dioxide containing lithium bis(trifluoroethyl)dithiocarbamate (LiFDDC) as an extractant.[5] These authors also showed that the solubilities in supercritical CO_2 of some metal–FDDC complexes, including those of Cu^{2+}, Ni^{2+}, Co^{3+}, and Bi^{3+}, are 2–3 orders of magnitude greater than those of the non-fluorinated analogues.[6] The use of fluorinated ligands for SFE of metal ions appears necessary in order to achieve significant recoveries of metals from liquid and solid materials. Addition of a modifier such as methanol to supercritical CO_2 alters the polarity of the fluid phase which may also enhance the extraction of metal chelates. However, no quantitative information regarding the effect of modifiers on the SFE of metal chelates is available in the literature. This paper reports an *in situ* chelation method for the extraction of Hg^{2+} from solid materials with supercritical CO_2 and methanol-modified CO_2, both containing LiFDDC as a chelating agent. The extraction of CH_3HgCl and $(CH_3)_2Hg$ from solid materials by supercritical CO_2 is also described.

*Author for correspondence.

EXPERIMENTAL

Reagents and materials

Lithium bis(trifluoroethyl)dithiocarbamate was synthesized according to a procedure outlined in the literature.[7] The starting material, bis(trifluoroethyl)amine, was obtained from PCR Chemicals (Gainesville, FL). Other chemicals used in the synthesis, including *n*-butyllithium (2.5*M* in hexane), carbon disulfide, and isopentane were obtained from Aldrich Chemical Co. (Milwaukee, WI). Sodium diethyldithiocarbamate, NaDDC, was purchased from Fisher Scientific Company (Pittsburgh, PA). The $Hg(FDDC)_2$ and $Hg(DDC)_2$ were prepared by mixing LiFDDC or Na(DDC) with an excess amount of Hg^{2+} in a buffered aqueous solution at pH 3. The resulting precipitate was extracted with chloroform, and the organic phase was washed with deionized water after phase

separation. Purification of $Hg(FDDC)_2$ and $Hg(DDC)_2$ was achieved by recrystallization from chloroform/ethanol (1:1 v/v) at 60°C. After evaporation of the chloroform, the crystals of mercury chelates were collected by filtration. An aqueous Hg^{2+} solution was prepared by dissolving a known amount of solid $Hg(NO_3)_2$ in deionized water.

Methylmercuric chloride standard solution and dimethylmercury (Alfa Chemical Co., Ward Hill, MA) were used as received. For the extraction of mercury compounds from the solid matrix, a known amount (usually 10 μg) of Hg^{2+}, CH_3HgCl or $(CH_3)_2Hg$ was spiked onto a cellulose-based filter paper (Whatman 42, 0.5 × 2 cm in size). For the preparation of standard samples of mercury for neutron activation analysis, we found it necessary to add a small amount of LiFDDC solution to the sample spiked with the Hg^{2+} compound in order to stabilize the Hg^{2+}. Otherwise, loss of mercury might occur during neutron irradiation and analysis.

Apparatus

All experiments were performed with a laboratory-built supercritical fluid extraction apparatus. SFC-grade CO_2 or CO_2 with 5% methanol (Scott Specialty Gases, Plumsteadville, PA) was delivered to the system using a microprocessor-controlled high-pressure pump (Haskel Inc., Burbank, CA). The pressure of the system was monitored to ±5 psi using a Setra Systems (Acton, MA) pressure transducer. The extractor consisted of an inlet valve (SUPELCO, Bellefonte, PA) and an outlet valve connected to a 3.5 mL commercial extraction cell (Dionex, Sunnyvale, CA). The extraction cell was placed in an oven that was temperature controlled by a thermostat. Fused-silica tubing (Dionex, 50 μm i.d. and 20 cm in length) was used as the pressure restrictor for the exit gas. The SFE system allows static and dynamic extractions to be performed by use of the outlet and inlet valves.

Extraction procedures

A glass tube plugged at the forward end with a piece of glass wool was used as a sample holder. Into the rear end of the glass tube, a filter paper spiked with 10 μg of Hg^{2+} was inserted, and 10 mg of solid LiFDDC was added. The rear end was plugged with glass wool and the sample tube was placed in the extraction cell. The extraction cell was immediately installed in the oven, heated to 50°C, and pressurized to 100 atm. After 20 min of static extraction, the exit valve was opened and the sample was extracted dynamically for 10 min. The tube was removed from the extraction cell and the filter paper was placed into a polyethylene vial which was then heat sealed for neutron irradiation. A standard consisting of a filter paper spiked with 10 μg of Hg^{2+} was also sealed in a polyethylene vial and irradiated together with the samples under identical conditions. The extraction efficiencies, as reported here, are the activities of ^{197}Hg found in the extracted samples times 100, divided by the activity of ^{197}Hg found in the standard. The SFE conditions for CH_3HgCl and $(CH_3)_2Hg$ were the same as in the Hg^{2+} experiments, except no LiFDDC was added to the sample.

Solubility measurements

A weighed amount (around 100 mg) of $Hg(FDDC)_2$ or $Hg(DDC)_2$ was placed in a glass sample tube. The sample tube was then plugged with glass wool at both ends and inserted into an extraction cell of known volume (0.57 mL). The sample was extracted at 50°C under 150 atm of CO_2 for 30 min. After this static extraction, the fluid phase was vented into a collection vial containing 4 mL of chloroform. The sample tube was removed from the cell and the empty cell was reinstalled into the oven. The system was then flushed with CO_2 for 20 min to collect any mercury complex that had precipitated within the system during depressurization. The total amount of the mercury complex collected in the chloroform solution was back-extracted with 2 mL of 50% Ultrex HNO_3. Aliquots of 0.5 mL of the acid solution were sealed in polyethylene vials for neutron activation analysis. The solubility was calculated from the amount of mercury collected in the chloroform divided by the volume of the extraction cell.

Neutron activation analysis (NAA)

All samples and standards were irradiated for 1 h in a 1 MW TRIGA nuclear reactor at a steady flux of 6×10^{12} n cm^{-2} s^{-1}. After irradiation, the samples were cooled for 24 h before counting. Each sample was counted for 200 s in a large-volume ORTEC Ge(Li) detector with a resolution (FWHM) of about 2.3 keV at the 1332 keV ^{60}Co peak. The 77.6 keV gamma peak from ^{197}Hg ($t_{\frac{1}{2}} = 65$ h) was used for the detection of mercury. The detector output was fed to a Nuclear Data 4096-channel pulse-height

analyser. The details of the NAA procedures are given elsewhere.[8]

RESULTS AND DISCUSSION

Solubilities of Hg(FDDC)$_2$ in supercritical CO$_2$ with and without modifier

Supercritical fluid extraction of metal chelates in CO_2 has received little attention in the literature. This is believed to be caused by the low solubilities of these compounds in supercritical fluids. Several studies have been reported on the separation of metal chelates by supercritical fluid chromatography using CO_2 as a mobile phase, but no solubility data were given.[9,10] In a recent study, we observed that a number of metaldiethyldithiocarbamates (DDC) exhibited limited solubilities in supercritical CO_2.[11,12] It was also found that if fluorine was substituted for hydrogen in the ligand, as in the case of bis(trifluoroethyl)dithiocarbamate (FDDC), the solubilities of the fluorinated metal chelates of Cu, Co, Ni, and Bi in supercritical CO_2 at 50°C and 100 atm were increased by 2–3 orders of magnitude. The solubilities of these metal–FDDC complexes were measured by their absorption in the UV–Vis region using a high-pressure view-cell described previously.[6] The spectroscopic analysis method can not be applied to Hg(FDDC)$_2$ because it does not have characteristic absorption peaks in the UV–Vis region. Therefore, we measured in this study the solubility of Hg(FDDC)$_2$ by NAA as the amount of the metal chelate dissolved in a known volume of CO_2 in an extractor at fixed T and P. The procedure described in the experimental section for the solubility measurement was tested with Cu(FDDC)$_2$ whose solubility in supercritical CO_2 had previously been determined by the spectroscopic method.[6] The chemical analysis method gave a solubility value for Cu(FDDC)$_2$ within 5% of that determined by the UV–Vis spectroscopic method, thus proving the reliability of the method used in this study. The solubilities of Hg(DDC)$_2$ and Hg(FDDC)$_2$ determined at 50°C and 150 atm are $(8.2 \pm 0.6) \times 10^{-6} M$ and $(5.0 \pm 0.4) \times 10^{-3} M$, respectively. Thus, the solubility of the fluorinated complex Hg(FDDC)$_2$ in supercritical CO_2 is about three orders of magnitude greater than that of the nonfluorinated analogue Hg(DDC)$_2$ under the conditions used.

Another factor that affects the solubility of metal chelates in supercritical CO_2 is the presence of a polar modifier such as methanol. The solubilities of Hg(FDDC)$_2$ and Hg(DDC)$_2$ increased by a factor of 2.4 and 3.6, respectively, when 5% methanol was added to CO_2 (Table 1). The critical temperature and pressure for the methanol (5%) modified CO_2 are known in the literature ($T_c = 41.8$°C and $P_c = 73.6$ atm).[13] Our experimental T and P were kept significantly higher than the T_c and P_c of the modified fluid phase to ensure that the extraction occurred in the supercritical fluid region. The strong solubility increase when methanol is added as a modifier is a useful feature for the SFE of metal-chelates.

Effects of methanol modifier on the extraction of mercury

The efficiency of the SFE of solutes from solid matrices generally depends on at least the following three factors: (1) the analyte solubility in the supercritical fluid, (2) the interactions between the substrate and the analytes, and (3) the kinetics of the fluid to transport analytes from active sites on the matrix. In this study, a cellulose-based filter paper was used as a solid support where both strong chemical and physical interactions between solute and matrix can lead to slow extraction of ionic analytes. In our initial SFE experiments with mercury compounds, we used 10 μg Hg^{2+} (about 5×10^{-8} moles) spikes on 2 × 0.5 cm filter paper and 10 mg LiFDDC (3.8×10^{-6} moles) as the chelating agent. The ligand was in large excess relative to the mercury ions in these experiments. A static extraction time of 20 min at 50°C and 100 atm, followed by a dynamic extraction for 10 min at the same T and P was chosen for extraction efficiency studies. The results of the SFE of Hg^{2+} with CO_2 under these conditions are summarized in Table 2. The extraction efficiency of Hg^{2+} from filter paper with pure CO_2 in the absence of LiFDDC was insignificant (<2%). With the addition of LiFDDC, some Hg^{2+} was extracted by CO_2, but the extraction efficiency was low (8–12%) for dry samples. This could

Table 1. Solubility of Hg(FDDC)$_2$ and Hg(DDC)$_2$ in pure and modified CO_2 at 150 atm and 50°C

Metal chelate	Solubility (*mol/L*)	Ratio (*FDDC/DDC*)
	Carbon dioxide	
Hg(FDDC)$_2$	$(5.0 \pm 0.4) \times 10^{-3}$	610
Hg(DDC)$_2$	$(8.2 \pm 0.6) \times 10^{-6}$	
	Carbon dioxide with 5% methanol	
Hg(FDDC)$_2$	$(1.2 \pm 0.4) \times 10^{-2}$	400
Hg(DDC)$_2$	$(3.0 \pm 0.5) \times 10^{-5}$	

Table 2. Extraction efficiencies of Hg^{2+} from Whatman 42 filter paper by pure and modified CO_2 at 100 atm and 50°C

Fluid phase	Ligand amount Li(*FDDC*)	Matrix condition	Extraction efficiency (%)*
CO_2	0	Wet	1.2 ± 0.5
CO_2	10 *mg*	Dry	10.3 ± 2.0
CO_2	10 *mg*	Wet	84.5 ± 3.0
CO_2 + 5%MeOH	10 *mg*	Dry	92.5 ± 2.5
CO_2 + 5%MeOH	10 *mg*	Wet	99.5 ± 2.0

*Average value of three runs.

not have been caused by a solubility limitation because the Hg^{2+} spike amounted to less than 1% of the solubility limit of $Hg(FDDC)_2$ in the fluid phase. This low extraction efficiency is probably due to strong interactions between Hg^{2+} and the cellulose matrix.

The extraction efficiency for Hg^{2+} increased from 10 to 84% when a small amount of water (10 μL) was added to the filter paper. The presence of water probably facilitates the chelation and transport of $Hg(FDDC)_2$ from the cellulose matrix to the fluid phase. The water may also serve as a matrix modifier by blocking active sites of the matrix and thus reducing sorption of the solute on the active sites of the polar matrix. Similar observations were reported in the literature for the extraction of polar compounds from polar matrices by supercritical CO_2.[14]

The efficiency of extracting Hg^{2+} can be further enhanced when methanol is added to the fluid phase. The results of extracting Hg^{2+} using a commercially available SFC grade CO_2 containing 5% methanol are also summarized in Table 2. The methanol-modified CO_2 increases the extraction efficiency of Hg^{2+} from 10% to 92% under dry conditions and from 84 to >99% under wet conditions. The large increase in SFE efficiency is most likely due to enhanced interactions between the solute and the modified solvent. Thus, quantitative extraction of Hg^{2+} directly by supercritical CO_2 from a cellulose matrix becomes possible with methanol as a solvent modifier and water as a matrix modifier.

The rate of extraction of Hg^{2+} from the filter paper using this *in situ* chelation/SFE approach was measured using CO_2 modified with 5% methanol and 10 μL water deposited into the matrix. The extraction process consisted of a 20 min static extraction step, followed by a dynamic extraction step of varying time lengths. The experimental results show that quantitative extraction of Hg^{2+} was virtually achieved after 5 min of dynamic extraction. Variations of the static extraction time as shown in Fig. 1 (with a constant dynamic extraction time of 5 min) indicate that the efficiency increases rapidly in the first 10 min of extraction, with over 80% of Hg^{2+} removed after 5 min and about 90% of Hg^{2+} removed at the end of 10 min. After 20 min of static extraction and 5 min of dynamic extraction, over 97% of the spiked Hg^{2+} was removed. The standard extraction times we decided to use were therefore 20 min of static extraction followed by 10 min of dynamic extraction.

Extraction of methylmercury and dimethylmercury with supercritical CO_2

Interest in the speciation of mercury in environmental analysis stems from the marked

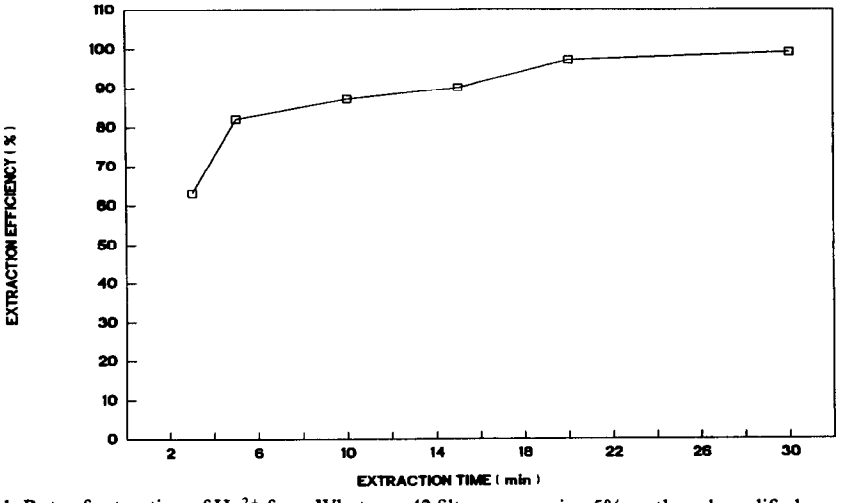

Fig. 1. Rate of extraction of Hg^{2+} from Whatman 42 filter paper using 5% methanol-modified supercritical CO_2 containing LiFDDC at 50°C and 100 atm. Extraction conditions: 10 μg Hg^{2+}, 10 mg LiFDDC, 10 μL H_2O, and 5 min of dynamic flushing following each of the specified static extraction times.

difference in toxicity between Hg^{2+} and organomercurial compounds.[15-17] The methylmercury compounds have been implicated in a number of mercury poisoning episodes.[18] Supercritical fluid extraction of CH_3HgCl and $(CH_3)_2Hg$ was investigated in this study by spiking each methylmercury compound separately on the cellulose based filter papers. The extraction efficiencies for CH_3HgCl and $(CH_3)_2Hg$ from the filter paper by supercritical CO_2 at 100 atm and 50°C are given in Table 3. The samples were prepared by spiking 10 μg of CH_3HgCl or $(CH_3)_2Hg$ on the filter paper similar to that described for the Hg^{2+} experiments. Methylmercuric chloride was spiked with the standard CH_3HgCl solution obtained from Alfa Chemical Company. Dimethylmercury (boiling point 93°C at 1 atm) is a liquid at room temperature, therefore it was introduced directly onto the filter paper in its pure liquid form. The samples were extracted under the same conditions (20 min static followed by 10 min dynamic extraction) as the Hg^{2+} experiments except no LiFDDC was added. The results indicate that methylmercury can be quantitatively extracted from the filter paper by pure CO_2 when 10 μL of water is used as a matrix modifier. Apparently, CH_3HgCl is soluble in supercritical CO_2 and no ligand is needed for its extraction from the filter paper. For dimethylmercury, quantitative extraction from the filter paper by supercritical CO_2 can be achieved even without the presence of water. In this study, the extraction efficiencies were determined by comparing the extracted sample with a standard filter paper treated by the same analytical procedures. The filter papers were sealed separately in polyethylene vials during irradiation and counted without opening the container to avoid volatilization of the mercury compounds. Since monomethylmercury and dimethylmercury can be extracted directly by supercritical CO_2 without the use of a ligand, this method may be used to separate the methylmercury compounds from Hg^{2+} in environmental samples.

Table 3. Extraction efficiency of CH_3HgCl and $(CH_3)_2Hg$ from the filter paper with supercritical CO_2 at 100 atm and 50°C

Sample No.	Matrix condition	Extraction efficiency (%)
	CH_3HgCl	
#1	Dry	16.3 ± 2.0
#2	Dry	14.5 ± 2.0
#3	Wet	99.2 ± 1.0
#4	Wet	100.0 ± 1.0
	CH_3HgCH_3	
#1		99.2 ± 1.0
#2		99.0 ± 1.0

CONCLUSIONS

Methylmercuric chloride and dimethylmercury can be extracted directly from cellulose based filter paper with neat supercritical CO_2. Mercuric ions (Hg^{2+}) adsorbed on the filter paper can be effectively extracted by an *in situ* chelation/SFE technique using LiFDDC as a chelating agent. Water and methanol can significantly improve the extraction efficiency of Hg^{2+} from the polar matrix. The solubility of $Hg(FDDC)_2$ in supercritical CO_2 at 50°C and 150 atm is about three orders of magnitude greater than the non-fluorinated analogue $Hg(DDC)_2$. The choice of ligand is important for this *in situ* chelation/SFE technique. LiFDDC happens to be moderately soluble in supercritical CO_2 and complexes effectively with Hg^{2+} to form a stable chelate which also has a sufficient solubility in the fluid phase. The polar cellulose matrix used in this study should resemble other polar matrices in biological samples such as plant and animal tissue. The SFE technique described in this paper thus offers a potential new approach for the preconcentration of mercury ions (Hg^{2+}) and methylmercury compounds from environmental samples for analytical purposes and for treatment of mercury contaminated wastes.

Acknowledgements—This material is based upon work supported by the Center for Hazardous Waste Remediation Research of the University of Idaho and by the U.S. Environmental Protection Agency, Environmental Monitoring Systems Laboratory, Las Vegas, Nevada. Neutron irradiation was performed at the Nuclear Radiation Center, Washington State University, under a Reactor Sharing Program supported by DOE. The information contained in this paper does not necessarily reflect the views of the funding agencies.

REFERENCES

1. S. B. Hawthorne, *Anal. Chem.*, 1990, **62**, 633A.
2. L. J. Mulcahey and L. T. Taylor, *Anal. Chem.*, 1992, **64**, 981.
3. J. W. Hills and H. H. Hill Jr., *Anal. Chem.*, 1991, **63**, 2152.
4. S. B. Hawthorne, D. J. Miller, D. E. Nivens and D. C. White, *Anal. Chem.*, 1992, **64**, 405.
5. K. E. Laintz, C. M. Wai, C. R. Yonker and R. D. Smith, *Anal. Chem.*, 1992, **64**, 2875.
6. K. E. Laintz, C. M. Wai, C. R. Yonker and R. D. Smith, *J. Supercritical Fluids*, 1991, **4**, 194.

7. A. Tavlaridis and R. Neeb, *Fresenius Z.Anal. Chem.*, 1978, **242,** 135.
8. W. M. Mok and C. M. Wai, *Anal. Chem.*, 1987, **59,** 233.
9. M. Ashraf-Khorassani, J. W. Hellgeth and L. T. Taylor, *Anal. Chem.*, 1987, **59,** 2077.
10. F. Brickmann and B. Wenclawial, *Fresenius Z. Anal. Chem.*, 1984, **319,** 305.
11. K. E. Laintz, G. M. Shieh and C. M. Wai, *J. Chromatogr. Sci.*, 1992, **30,** 120.
12. K. E. Laintz, J. J. Yu and C. M. Wai, *Anal. Chem.*, 1992, **64,** 311.
13. B. I. Lee and M. G. Kessler, *AIChE J.*, 1975, **21,** 510.
14. C. R. Knipe, R. D. Gere and M. E. P. McNally, in *Supercritical Fluid Technology—Theoretical and Applied Approaches to Analytical Chemistry*, F. V. Bright and M. E. McNally (Eds); *ACS Symposium Series* 488; *Amer. Chem. Soc.*, Washington D. C., 1991, pp. 251–265.
15. K. Irukayama, *Adv. Water Poll. Res.*, 1967, **3,** 153.
16. K. Burg, H. Wanntorp, K. Erne and E. Hanko, *J. Appl. Ecol.*, 1971, **3,** 171.
17. J. M. Wood, *Adv. Environ. Sci. Technol.*, 1971, **2,** 39.
18. L. J. Goldwater, *Methyl Mercury in Fish.* Nordisk Hygienisk Tidskrift, Supplementum 4, Stockholm, 1976.

Talanta, Vol. 40, No. 9, pp. 1331–1338, 1993
Printed in Great Britain.

0039-9140/93 $6.00 + 0.00

HIGH PERFORMANCE OPTICAL ABSORBANCE DETECTORS BASED ON LOW NOISE SWITCHED INTEGRATORS

HANGHUI LIU, PURNENDU K. DASGUPTA* and HONG J. ZHENG
Department of Chemistry and Biochemistry Texas Tech University, Lubbock, TX 79409-1061, U.S.A.

(*Received* 11 *February* 1993. *Revised* 17 *March* 1993. *Accepted* 18 *March* 1993)

Summary—Optical absorption detection is the most common analytical measurement principle in liquid phase analysis. The current state-of-the-art of commercially available detectors exhibit peak-to-peak (p–p) noise levels in the range of 1×10^{-5}–2×10^{-5} absorbance units (10–20 μAU). Using circuitry based on newly available switched integrator integrated circuit (IC) packages, it is possible to construct inexpensive absorbance detectors with p–p noise levels as low as 3 μAU under actual use conditions. The necessary electronics are described and performance data are reported with light emitting diodes (LEDs) as light sources. Even in the capillary format with a rectangular capillary (50 × 1000 μm cross section) with a slitwidth < 50 μm and with the 1000 μm dimension as the nominal pathlength, p–p noise levels of 10 μAU are observed, from which a concentration limit of detection (LOD) of 10 n*M* for bromothymol blue (BTB) can be estimated with a 660 nm light source.

The wide use of colorimetric methods for analysis first came into vogue in the 1940s. Snell and Snell[1] report that 23% of all articles on analytical chemistry published in 1946 utilized colorimetry. Even today the measurement of optical absorbance (typically following separation, selective reaction, *etc.*) is the most common principle used for quantification in liquid phase analysis. Current practice commonly involves absorbance measurement in a flowing stream, *e.g.* in flow injection analysis (FIA) or high performance liquid chromatography. Relative to static measurements, the detection of a transient signal due to the analyte over a continuously measured background is not only more convenient and more easily automated, significant improvement in limits of detection results. Assuming that flow-induced noise of the background absorbance is not the limiting factor, the intrinsic detector noise becomes the parameter that determines LOD. A survey of specifications of flow-through optical absorbance detectors available from major manufacturers (Applied Biosystems, Beckman Instruments, Dionex Corp., Perkin-Elmer Corp., Shimadzu Scientific, Spectra-Physics Analytical, Varian Associates, Waters Associates) available at the time of this writing indicate that p–p noise levels with integration time ≤ 1 sec are 10–20 μAU. This is equivalent to a change in light intensity of 2–3 parts in 10^5 and is particularly striking when one considers that at the transducer level what is being monitored is a small decrease in a large standing current. Using an 814 nm LED with an output of 35 mW, voltage–frequency conversion and measurements in a static solution, Imasaka *et al.*[2] were able to achieve a record low noise level of 0.75 μAU. This used an integration time of 50 sec, however, unacceptably large for flow-through applications. Further, to eliminate power supply noise, it was necessary to operate the system with batteries; which was not always practical.

When absorbance detection must be accomplished in the capillary format, *e.g.*, for micro-column liquid chromatography or capillary electrophoresis, very narrow slit widths must be used to minimize stray light. The resulting decrease in light throughput further degrades S/N performance. Thermo-optical absorbance detection methods with a laser source are capable of very low noise levels.[3] These methods do not involve a simple measurement of the change in transmission of a probe beam of the desired wavelength. For the same absorbance change, the change in the signal is much greater at the transducer level in such measurements relative to that in conventional measurements of

*Author for correspondence.

transmission intensity. Unfortunately, practical affordable variable wavelength absorbance detectors based on the thermo-optical principles are not on the horizon.

All high sensitivity absorbance detectors use a reference measurement of the incident light (or some portion thereof) and a log ratio circuit then produces the absorbance output from the reference photodetector and transmission photodetector current inputs. It is desirable to keep these photocurrents at a relatively high level (*i.e.* use a bright light source) to minimize the relative contributions of noise picked up from a multitude of sources. It has recently been shown that sufficiently high light intensities can be obtained by operating LEDs in a pulsed mode (these sources are essentially monochromatic) and it is possible to reach very low noise levels using high speed personal computer based data acquisition and digital integration.[4] In this study, it was shown that at a sampling rate of 22 kHz, the standard deviation of the measured absorbance decreases linearly with the square root of the integration period, reaching 2 μAU at an integration period of 0.5 sec. No further improvement was observed at longer integration periods, presumably other sources of noise, that are not adequately compensated for by this type of integration, become the limiting factor.

Precise measurement of low levels of current is also important in many other fields. A pressing need, for example, was perceived for the improvement of precision in the measurement of pA level X-ray induced photocurrents in computerized tomography scanners. In this case, any increase in measurement precision translates into a reduction of the necessary exposure of the patient to ionizing radiation. A low noise (10 μV rms), wide dynamic range (120 dB) low bias current (100 fA) switched integrator was expressly developed for this purpose.[5] These relatively inexpensive IC packages are also ideal for photocurrent measurements in optical absorbance detectors. Each package contains two independent integrators, one can be devoted to the reference and the other to the transmission photodetector and the respective integrator outputs are then processed by the log ratio converter. In this note, we describe an

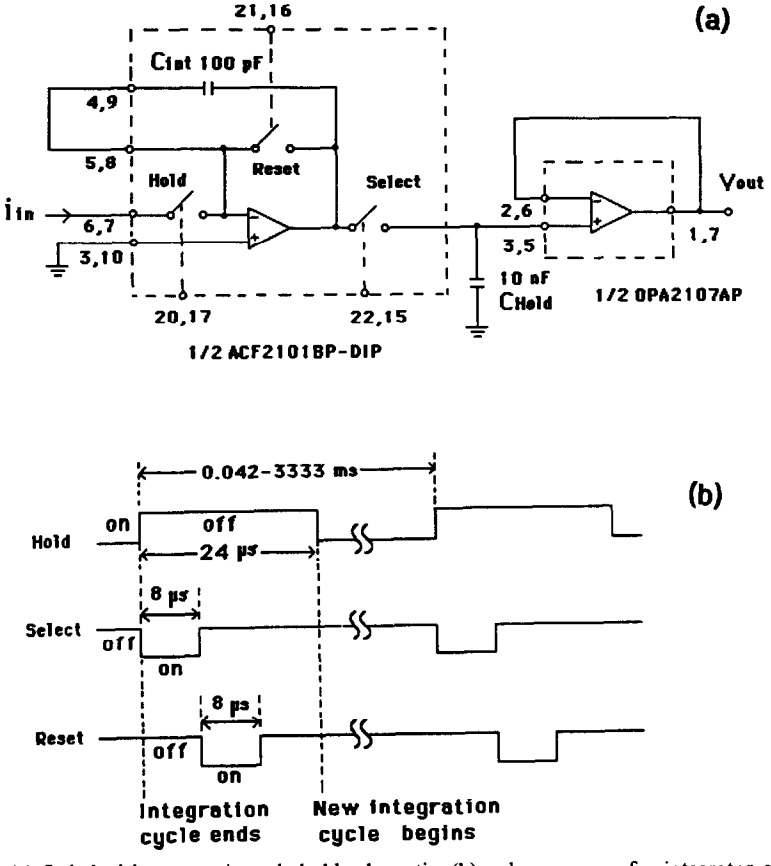

Fig. 1. (a) Switched integrator/sample-hold schematic; (b) pulse sequence for integrator operation.

absorbance detector based on the switched integrator and evaluate its performance.

EXPERIMENTAL

Detector electronics

The dual in-line package version of the ACF2101 IC (ACF2101BP-DIP, Burr-Brown, Tucson, AZ) was used. The block diagram of half of a ACF2101 device with its output processed by a high input impedance operational amplifier ($\frac{1}{2}$ OPA2107) is shown in Fig. 1a. The designation of the pinouts indicate individual halves of each device, *i.e.*, pin 21 is the reset input for one half of the integrator and pin 16 is that for the other half, *etc.* Each integrator has three logic operated switches: hold, reset and select. With the hold switch on and the reset switch off, the device is in the "integrate mode". Under this condition, the integrator output slews to the maximum permissible negative voltage (~ -10 V) at a rate depending on the input current and the integration capacitance. The IC contains an on-board 100 pF integration capacitor, this can be augmented by external capacitors if desired; additional capacitance was not used in the present design. When the hold and reset switches are both off, the device is in the hold mode, the output of the integrator remains constant (except for droop). When the reset switch is enabled, the integration capacitor is discharged and the integrator output drops to zero. The hold switch, the hold capacitor and the sample and hold amplifier (OPA2107) together effectively constitute a low noise (the integration process is very effective at sampling frequencies greater than 60 Hz for rejecting power line noise), high gain current–voltage converter without the use of high value feedback resistors and conventional transimpedance amplifier designs that are prone to leakage current errors and noise pickup. Figure 1b shows the pulse sequence. At the end of an integration cycle, the hold switch is opened to hold the output of the integrator constant. This value is transferred to the 10 nF hold capacitor by closing the select switch. The select switch then opens and the output of the OPA2107 remains constant during the next integration cycle; in effect the select switch, the hold capacitor and OPA2107 form a sample/hold circuit. After the select switch is opened, the integrator is reset by a brief pulse and the hold switch then closes to begin integration. The integration cycle repeats with a frequency of 0.3–24,000 Hz, the value is chosen depending on the input current level (*vide infra*). A longer integration period is chosen for low currents; using overly long integration periods at higher current levels can saturate the integrator output. The integration period is typically in the millisecond time scale whereas the hold, select and reset pulses are, respectively 24, 8 and 8 μS wide. Except at the higher end of the sampling frequency range used, each integration cycle is dominated by the integration period.

The general functional diagram is shown in Figure 2. Figure 3 shows the actual implementation of each functional component. The fundamental clock frequency of 24 MHz is generated by a crystal oscillator (U1, Bomar Crystal oscillator). A series of 10 decade counters (U2–U6, 74LS390) then reduce the initial clock frequency in steps all the way to 0.3 Hz. The range of 0.3–12 Hz sampling frequency is necessary only for very low levels of photocurrent and when pulses of these low frequencies are generated on-board, the noise in the overall instrument output is dominated by noise pickup from this source unless precautions are taken. In normal operation, we therefore use switch S1 to bypass U2 unless sampling frequencies in the range of 0.3–12 Hz are of interest—thus the lowest frequency available in this mode is 30 Hz.

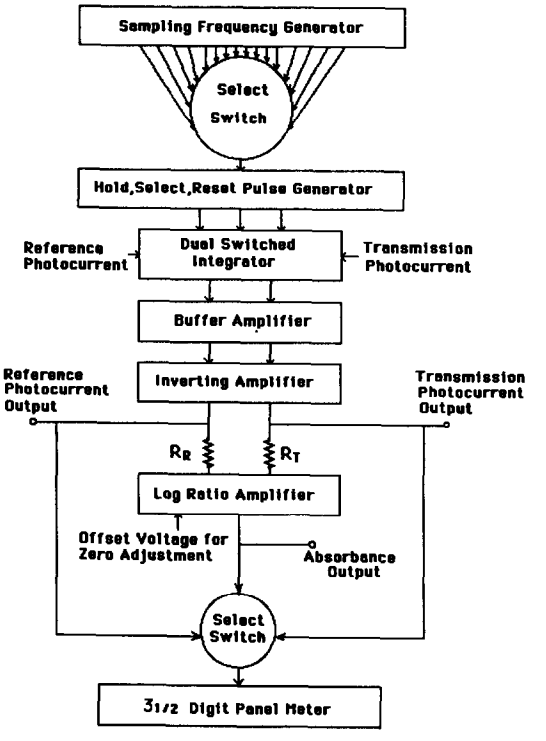

Fig. 2. Block diagram of instrument.

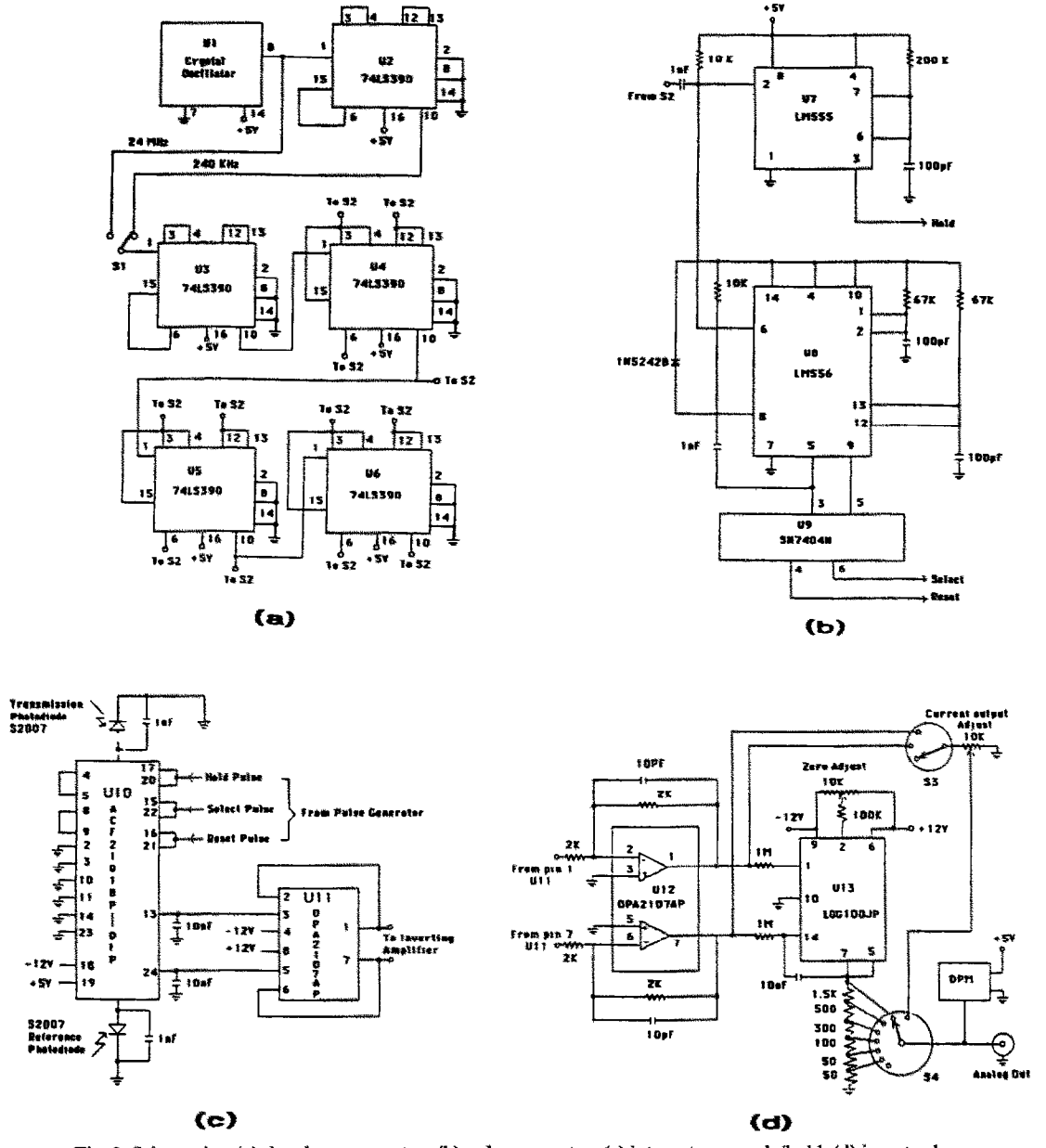

Fig. 3. Schematics: (a) time base generator; (b) pulse generator; (c) integrator-sample/hold; (d) inverter-log ratio amplifier-display.

Further, we isolate the entire frequency generator and selector switch portion (Fig. 3a) in a separate board and a small grounded metallic enclosure which is put inside the main enclosure housing other components. Note that frequencies above 24 KHz are not used at all. For those interested in building such a device it may be preferable to use a lower frequency time base and fewer decade counters.

Indicated frequency outputs are connected to switch S2 (not shown in Fig. 3, a 12-position rotary switch) that connects any one selected frequency to the pulse generator circuit utilizing a 555 timer and a 556 dual timer as shown in Fig. 3b. The desired pulse trains shown in Fig. 1b are generated by this circuit, the reset and select pulses need to be inverted with a inverter (SN7404N) before transmission to the integrator. Note that the hold, select and reset pulses are connected in common to both halves of the integrator.

Photodiode inputs are connected to the integrator (U10, Fig. 3c) using 1 nF input capacitors. In our specific detector, there are provisions for providing either fiber optic or photocurrent inputs (through shielded leads

terminating in BNC connectors) to the front panel. This input is selected by a DIP switch. When fiber optic inputs are connected (SMA connectors), photodiodes mounted inside the instrument and sealed from extraneous light provide the photocurrents to U10. The printed circuit board housing U10 contained imprinted guard loops to protect critical pins from noise pickup as suggested by the manufacturer. The U10 output is processed by U11, operating with unity gain as a sample/hold amplifier. The output of U11 is negative and it is necessary to invert this before processing by the log ratio amplifier that accepts only positive inputs. This task is accomplished by U12 (Fig. 3d). The log ratio amplifier (U13) accepts current inputs. Voltage outputs from U12 are converted to current by reference resistor R_R and transmittance resistor R_T. Both were 1MΩ in this application but if reference and transmittance currents are vastly different (this is dependent on the flow cell design), R_R and R_T should be so chosen as to have essentially equal current inputs into pins 1 and 14 of U13. U12 outputs are also sent to switch S3. Either one (or none) of these photocurrent outputs may be selected by this switch and the value can be scaled by a 10 kΩ potentiometer, displayed and output at analog output terminals if so selected by switch S4 (switch S4 and S3 are actually separate decks of a multi-tier switch). A 10 kΩ potentiometer provides the zero adjust control for U13 which is configured to have an output of 5 V/AU (DIP switch selectable to 1 and 3 V/AU as well). If selected by S4, the absorbance is scaled by a voltage divider, output to the digital display (0.04–1.999 AUFS, readability 0.05% of FS) and to the analog output socket.

Power to the electronics is provided by a wall-mounted power supply (±12 V, +5 V). The instrument is enclosed in a metallic enclosure (30 × 17.5 × 10 cm). The component cost for fabrication of the detector electronics is under $350. A commercial version of this detector is available from Bern Tech-Lite Corp. (Lubbock, TX).

Flow cell designs

The detector electronics was tested with several different flow cell designs previously described[4] and the modified sandwich cell.[6,7] The absorbance noise levels appeared independent of cell design. No difference was perceived between the results when the cell was dry and with water flowing under gravity through the cell.

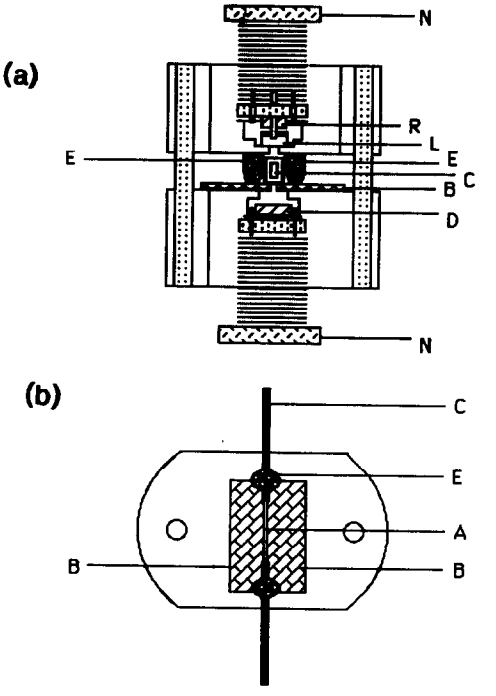

Fig. 4. Design of the capillary flow cell. (a) Horizontal cross section, N: hollow holding nuts, R: reference detector, L: LED, C: capillary, E: epoxy adhesive/spacer, B: razor blades, D: detector photodiode; (b) vertical cross section of bottom block, B: Razor blades, A: optical aperture (approximately 1 mm long).

Except as stated, the reported data were obtained with a 605 nm LED as the light source in demountable Z-path flow cell as shown in Fig. 9 of Ref. 4.

An LED-based detector design using the present electronics was also tested for use with rectangular capillaries used for capillary electrophoresis.[8] The design is shown in Fig. 4. First, the relevant area of the glass capillary is

Table 1. Recommended sampling frequency as a function on input photocurrent

Input photocurrent range (*nA*)	Recommended sampling frequency (*Hz*)
<0.25	0.3
0.25–0.50	0.6
0.50–1.25	1.5
1.25–2.50	3.0
2.50–5.00	6.0
5.00–10.0	12
10.0–25.0	30
25.0–50.0	60
50.0–125	150
125–250	300
250–500	600
500–1000	1200
1000–2500	3000
2500–5000	6000
5000–10,000	12,000
10,000–20,000	24,000

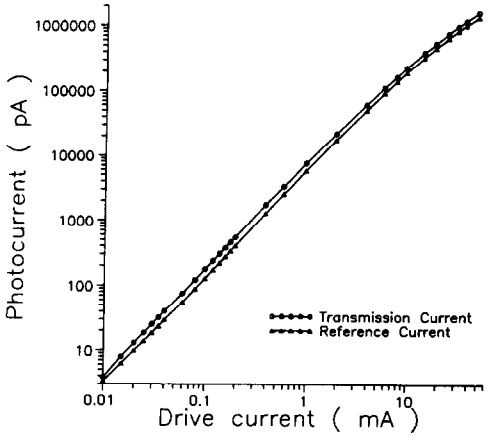

Fig. 5. Transmission and reference photodiode photocurrents as a function of LED drive current (605 nm).

completely covered with opaque epoxy adhesive (made by mixing a generous amount of activated carbon with epoxy adhesive). After curing, a small area of the epoxy is removed with a sharp scalpel blade from opposing sides of the capillary to create optical slits on the narrow edge. This is then mounted in the cell arrangement shown in horizontal cross section in Fig. 4a. The cell is composed of two aluminum blocks held together by screws. On one side, LED L (660 nm, H-1000-L, I.I. Stanley Co., Battle Creek, MI) sits over the reference photodetector R (which makes use of the light retroreflected from the front dome of the LED). In the second block is mounted detector D (R and D are both polymer encapsulated silicon photodiodes, S2007, Electronic Goldmine, Phoenix, AZ). Rectangular capillary C passes between the two blocks (through the plane of the paper). An excess amount of epoxy E both holds the capillary in place and acts as a spacer to keep the capillary from being crushed by the two blocks. Components are held in place by, and necessary cables exit through, hollow knurled fittings N on either side. The slit and affixing arrangements on the second block are shown in vertical cross section in Fig. 4b. An initial slit of 100–150 μm is created by two razor blades B. The epoxy covered capillary, with the optical slit already created on it, is now appropriately positioned, oriented and then cemented on the gap between the two razor blades. More opaque glue is now applied to eliminate stray light. The two blobs of adhesive E act as the spacer. After the cell is fully assembled, all exposed areas are covered up by opaque tape to eliminate extraneous light.

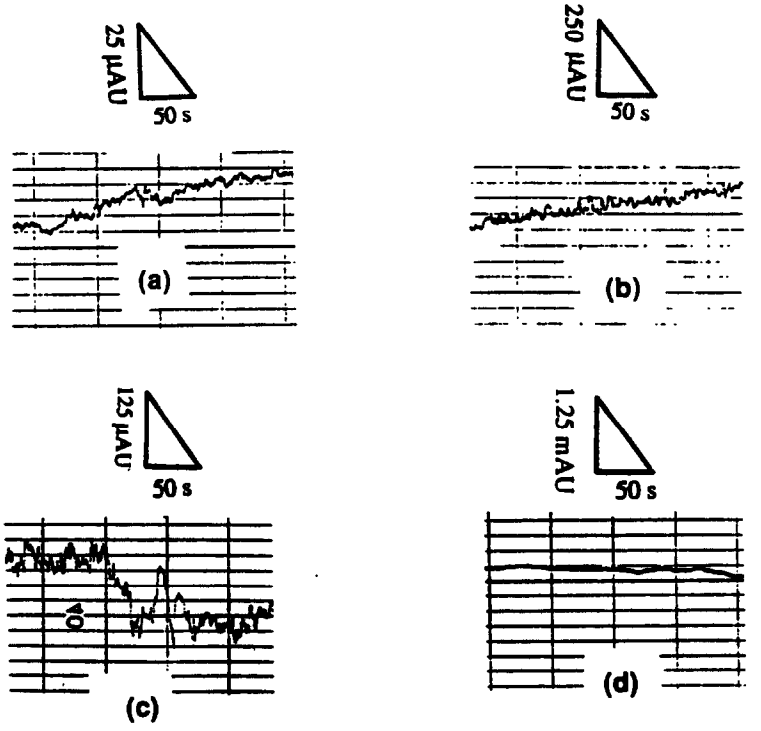

Fig. 6. Noise levels as a function of photocurrent and detector electronics, 605 nm LED source. (a) $I_{ref} = 890$ nA, $I_{transm} = 660$ nA, present electronics; (b) as in (a), old electronics design (photocurrent–voltage conversion, log ratio amplifier, see Ref. 4); (c) $I_{ref} = 4.2$ nA, $I_{transm} = 3.0$ nA, present electronic design; (d) as in (c), old electronic design.

Table 2. Noise levels as a function of photocurrent*

Emitter wavelength (*nm*)	I_{ref} (*nA*)	I_{transm} (*nA*)	Absorbance noise (p–p, μAU)
605	0.18	0.18	100
605	0.88	0.88	50
605	4.15	4.18	40
605	21	21	20
605	90	89	10
605	341	341	5
605	708	709	3–5
560	112	155	10
660	8750	14,530	2–3

*Dry cell test conditions.

Approximately 1 mm length of the capillary is illuminated, constituting the optical aperture A.

The LEDs were operated in the DC mode (continuously on) from a constant current power supply. No efforts were made to use a battery operated power source to further reduce noise and drift originating in the power supply. The drive current was changed to simulate different light levels so that the performance could be evaluated at different light levels.

Identical experiments were performed with a tungsten lamp filtered with a 590 nm interference filter (half bandwidth 15 nm) for purposes of comparison.

RESULTS AND DISCUSSION

The sampling frequency chosen is based on the photocurrent level and the ranges used are shown in Table 1. The performance of the instrument even as a picoammeter is attractive. Figure 5 depicts the reference and transmittance photodiode currents measured as a 605 nm LED was driven over a current range of 5μA–50 mA. Note that at the low end, essentially no emission is visible to the naked eye. Table 2 contains the important noise specifications. It will be apparent that the observed noise levels are essentially independent of the specific wavelengths of the LED and are dependent on the absolute level of the photocurrents, reaching a noise level of 2–3 μAU when the photocurrent levels reach several μA. Figure 6 shows the noise levels observed with photocurrent levels of several nA to several hundred nA, respectively. Performance data for both the new design and the older design involving direct photocurrent to voltage conversion and processing by a log ratio amplifier are shown for comparison.

High intensity continuum sources coupled to high throughput low-resolution monochromators are typically used in commercial detectors; microampere levels of detector photocurrent are typical in such instruments. What is striking is that even at sub-nA photocurrents, the present electronics still provides very usable noise levels (10^{-4} AU). This would allow the use of both sources and detectors well beyond ranges within which they, respectively emit and respond optimally.

The improved performance of the present design is not dependent on the use of an LED as the light source. Figure 7 shows that at comparable photocurrent levels, noise levels obtained with an LED and a tungsten lamp source are essentially the same, albeit admittedly the baseline drift is greater with the latter source.

Actual outputs from the detector, both with a cell of conventional dimensions (path length 6 mm) and with the rectangular capillary are shown in Figs 8a and b, respectively. The noise level in the capillary cell is 10 μAU under dry

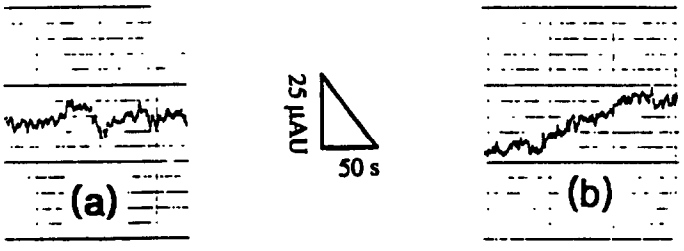

Fig. 7. Noise levels. (a) 605 nm LED: $I_{ref} = 310$ nA, $I_{transm} = 250$ nA; (b) W-lamp, 590 nm interference filter: $I_{ref} = 260$ nA, $I_{transm} = 255$ nA.

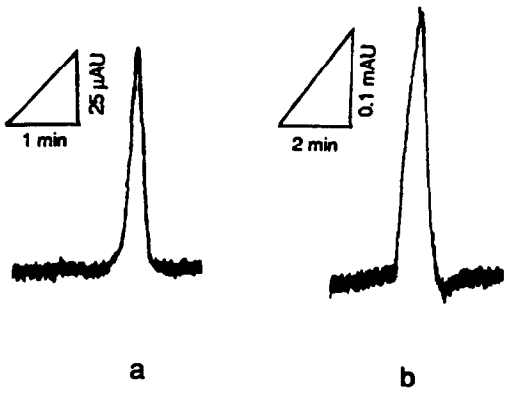

Fig. 8. Detector performance: (a) conventional flow cell (6 mm pathlength), 4.8 n*M* bromothymol blue injected, estimated dilution factor at peak maximum is 2. Carrier is dilute NaOH flowing under gravity. (b) Rectangular capillary flow cell (1 mm path length), 95 n*M* bromothymol blue injected, sample is essentially undiluted at peak maximum.

cell test conditions. With liquid flow in the cell this noise increases marginally but still permits an LOD of 10 n*M* for BTB even though the absorption of BTB ($\lambda_{max} = 615$ nm) is not well matched to the emission of the 660 nm emitter used. This performance exceeds that of any commercially available detector available for use with capillaries. For the conventional cell, the noise level is even lower, 3 μAU. We feel therefore that the dual switched integrator based absorbance measurement approach is a particularly attractive and simple technique that can provide performance levels surpassing those of current commercially available detectors.

Acknowledgement—This research was supported by the U.S. Department of Energy, Office of Basic Energy Sciences through DE-FG05-84ER-13281. However, this report has not been subject to review by the DOE and no endorsement should be inferred.

REFERENCES

1. F. D. Snell and C. T. Snell, *Colorimetric Methods of Analysis*, 3rd ed. Van Nostrand, New York. Vol. II, 1949.
2. T. Imasaka, T. Kamikubo, Y. Kawabata and N. Isibashi, *Anal. Chim. Acta*, 1983, **153**, 261.
3. C. E. Burnett and M. D. Morris, *Anal. Chem.*, 1982, **54**, 1824.
4. P. K. Dasgupta, H. S. Bellamy, H. Liu, J. L. Lopez, E. L. Loree, K. Morris, K. Petersen and K. A. Mir, *Talanta*, 1993, **40**, 53–74.
5. Burr-Brown Corp., Tucson, AZ. ACF2101 Low noise dual switched integrator. Product announcement, 1990.
6. J. L. P. Pavon, E. R. Gonzalo, G. D. Christian and J. Ruzicka, *Anal. Chem.*, 1992, **64**, 923.
7. P. K. Dasgupta, H. S. Bellamy and H. Liu, *Talanta*, 1993, **40**, 341–345.
8. T. Tsuda, J. V. Sweedler and R. N. Zare, *Anal. Chem.*, 1990, **62**, 2149.

Talanta, Vol. 40, No. 9, pp. 1339–1343, 1993
Printed in Great Britain.

0039-9140/93 $6.00 + 0.00

DISSOCIATION CONSTANTS OF ORGANOPHOSPHINIC ACID COMPOUNDS

M. MARTINEZ, N. MIRALLES and A. SASTRE
Chemical Engineering Department, Universitat Politècnica de Catalunya, E.T.S.E.I.B., Avda. Diagonal 647, E-08028 Barcelona, Spain

E. BOSCH
Department of Analytical Chemistry, Universitat de Barcelona, Martí i Franqués 1, E-08028 Barcelona, Spain

(*Received* 5 *February* 1993. *Revised* 22 *March* 1993. *Accepted* 22 *March* 1993)

Summary—The dissociation equilibria of di(2,4,4-trimethylpentyl) phosphinic acid, mono(2,4,4-trimethylpentyl)phosphinic acid, di(*n*-octyl)phosphinic acid and mono(*n*-octyl)phosphinic acid have been studied in ethanol–water mixtures by potentiometric titration at 25°C. These data have been analysed both graphically and numerically using the program LETAGROP-ZETA.

The obtained pK_a values have been correlated with the corresponding values in water, determined both indirectly by means of extraction measurements and by estimation using the suitable Hammett equation.

Organophosphorus acid compounds have attained importance in recent years in the separation by solvent extraction of many metal ions on a commercial scale.[1–3] Among these, alkylphosphinic acids have been reported to possess higher separation factors for successive members of chemically similar groups such as lanthanides[4,5] actinides,[6] cobalt and nickel[7,8] and other metal ions.[9,10,11]

In solvent extraction chemistry the knowledge of the acidity constants as well as the interaction constants between the components of an extracting system is essential in order to clarify the processes that take place in solution and to ascertain the stoichiometry of the extracted species. With such knowledge it is possible to design optimal conditions for separation or purification steps in various technical applications.

However, the low water solubility of long-chain organophosphorus acid compounds prevent the determination of pK_a values in water. Nevertheless, it is possible to evaluate the extracting behaviour of an organophosphorus acid compound towards a particular metal[12] from the pK_a in 75% (v:v) ethanol–water. For this purpose, the following empirical relationship has been proposed:

$$pH_{0.5} = A\,pK_a + B\nu_{P=O} - C$$

where $pH_{0.5}$ is the pH at 50% of extraction of a given metal, pK_a and $\nu_{P=O}$ are the acidic dissociation constant in 75% (v:v) ethanol–water and the characteristic frequency of infrared absorption for P=O group, respectively. A, B and C are constants which depend on the extracted metal.

In the present work the acidity constants of some alkylphosphinic acids in mixtures of ethanol–water have been determined potentiometrically. These constants have been correlated with the pK_a values in water, determined indirectly by distribution measurements and, alternatively, with the values estimated by means of the Hammett equation.

EXPERIMENTAL

Reagents and solutions

Mono(2,4,4-trimethylpentyl)phosphinic acid (H[(TMP)(H)P]), mono(*n*-octyl)phosphinic acid (H[(O)(H)P]) and di(*n*-octyl)phosphinic acid (H[DOP]) were synthesized and purified as described elsewhere.[13]

Bis(2,4,4-trimethylpentyl)phosphinic acid (H[DTMPP]) were supplied by Cyanamid as Cyanex-272 and purified as described in the literature.[14]

Sodium hydroxide solution (Merck p.a.) were prepared in ethanol–water mixture and was standardized against perchloric acid.

Procedure

Potentiometric measurements. The acidity constants of different organophosphinic acid compounds were determined by potentiometric titration of an ethanol–water solution of the corresponding acid with 0.1 mol/dm^3 NaOH at 25°C.

The mef measurements were determined in the range $3 < pH < 7$ using a CRISON Digilab 517 pH meter equipped with a Metrohm AG 9100 combined glass electrode. The concentration of acids HA was varied from 0.006 mol/dm^3 to 0.050 mol/dm^3. Previously the electrode was standardized using Gran plots.[15]

Extraction measurements. The distribution experiments were carried out by shaking mechanically, in special stoppered glass tubes, 10 cm^3 of organic phase (toluene) containing C mol/dm^3 of an organophosphinic acid, with an equal volume of an aqueous phase having composition 0.05 mol/dm^3 (Na^+, H^+) NO_3^-, until the equilibrium was achieved. The concentration of the organophosphinic compound was determined in the aqueous phase, analysing the phosphorus concentration by ICP spectrometer, and the pK_a was determined as described in the literature.[16]

TREATMENT OF DATA

From the experimental values of emf (E) and volume V_T, values of z and $-\log[H^+]$ were determined for each initial concentration of acid C_A, where z is the formation degree[17] defined as:

$$z = \frac{H_{TOT} - [H^+]}{C_A} \quad (1)$$

where $[H^+]$ is the hydrogen concentration calculated with the equation

$$E = E_0 + g \log[H^+],$$

$$g = 59.15 \text{ mV at } 25°C \quad (2)$$

and H_{TOT} is the hydrogen concentration calculated as:

$$H_{TOT} = \frac{V_0 H_0 + V_A C_A - V_T C_T}{V_0 + V_A + V_T} \quad (3)$$

where V_0, V_A and V_T are the initial, acid, and NaOH volumes, respectively, C_T is the NaOH concentration and H_0 is the initial concentration determined previously using Gran plots.

An example of z *vs.* pH plot is given in Fig. 1.

The experimental data obtained have been treated graphically by using normalized curves.[18] Afterwards, a numerical treatment by means of the program LETAGROP-ZETA[19] has been performed in order to confirm the proposed model and refine the values of the constants obtained graphically.

As $z \leqslant 1$ and polynuclear complexes have been excluded because plots of z *vs.* $-\log[H^+]$ are independent of the total concentration of organophosphorus compound, it can be assumed that only HA and A^- species of organophosphinic acids are in solution and the dissociation equilibria can be written as:

$$HA = A^- + H^+ \quad (4)$$

and K_a is the dissociation constant defined as

$$K_a = \frac{[A^-][H^+]}{[HA]}. \quad (5)$$

Taking into account the mass balance equations

$$H_{TOT} = [H^+] + [HA], \quad (6)$$

$$C_A = [A^-] + [HA], \quad (7)$$

and substituting equations (5), (6) and (7) in equation (1) the following expression can be written:

$$z = \frac{[HA]}{[HA] + [A^-]} = \frac{[H^+]K_a^{-1}}{1 + K_a^{-1}[H^+]}. \quad (8)$$

Defining a normalized variable $u = [H^+]\,K_a^{-1}$ and substituting, the expression (8) can be written as:

$$z = \frac{u}{1+u}. \quad (9)$$

Comparing the experimental curves z *vs.* $-\log[H^+]$ with the theoretical curves z *vs.* $\log u$, from the position of best fit the value of K_a can be determined as the difference:

$$-\log K_a = -\log[H^+] + \log u.$$

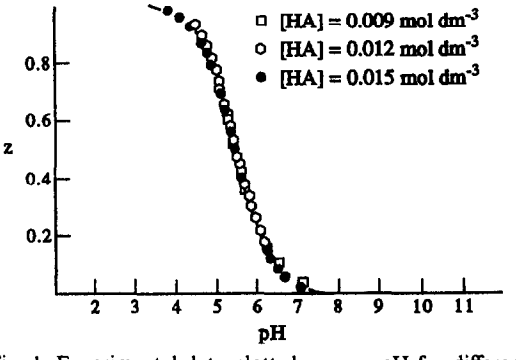

Fig. 1. Experimental data plotted as z *vs.* pH for different concentrations of bis(2,4,4-trimethylpentyl)phosphinic acid in 75% (v:v) ethanol–water.

Table 1. Acidity constants of some organophosphinic acid compounds determined in ethanol–water mixtures at 25°C

Acid	Method of calculation	pK_a	Ethanol–water ($v:v$)
H[(O)(H)P]	Graphical	3.60	75:25
	LETAGROP-ZETA	3.62 ± 0.05	
H[DOP]	Graphical	5.01	75:25
	LETAGROP-ZETA	5.03 ± 0.05	
H[(TMP)(H)P]	Graphical	3.77	75:25
	LETAGROP-ZETA	3.66 ± 0.03	
H[DTMP]	Graphical	5.42	75:25
	LETAGROP-ZETA	5.44 ± 0.02	
H[(O)(H)P]	Graphical	4.11	90:10
	LETAGROP-ZETA	4.06 ± 0.03	
H[DOP]	Graphical	5.42	90:10
	LETAGROP-ZETA	5.43 ± 0.06	

Once the estimated values of the constants were obtained graphically for each acid, the experimental data were treated numerically using the program LETAGROP-ZETA in order to confirm the proposed model and refine the graphical values.

In this program the computer searches for the best set of constants that minimizes the sum of squares errors, defined by

$$U = \Sigma(z_{exp} - z_{calc})^2 \qquad (10)$$

where z_{exp} is the value obtained experimentally and z_{calc} is the calculated value obtained by solving the mass balance equation. The program also calculates the standard deviation

$$\sigma(Z) = (U/N_p - 1)^{1/2}$$

where N_p is the total number of experimental points.

RESULTS AND DISCUSSION

The obtained experimental results in hydroalcoholic solvents are given in Table 1. The two calculation methods used show a very good agreement and the standard deviation values are satisfactory. All the obtained pK_a values are in the range 3.6–5.5. Although Danesi *et al.*[20] point out approximate pK_a values of 6 for phosphinic acids in alcohol–water mixtures (75% v:v), these values are not directly comparable with those obtained here because it is not clear what alcohol has been used in their work. Dialkylphosphinic acids show pK_a values 1.4–1.8 units higher than those of the corresponding monoalkylphosphinic acids. This fact can be explained by means of the higher electron-donor capacity of the alkyl group with respect to the hydrogen, that destabilizes the anionic species. In the same way, the higher electron-donor ability of the branched substituents, compared to their linear homologous, explains why the pK_a value increase with the substituent steric complexity. Consequently, the acid strength of organophosphinic acids decreases in the order: linear monoalkylphosphinic > branched monoalkylphosphinic > linear dialkylphosphinic > branched dialkylphosphinic.

Although the dissociation constants of these acids in water are very important parameters to elucidate the metallic complex extraction processes when these acids are used as ligands, it is not possible to determine them by means of common potentiometric or spectrophotometric methods because of their very low solubility in water. Therefore, two different methods have been used in order to estimate these constants. The first one is an indirect experimental approach based on distribution measurements that leads to the values shown in Table 2. The second one is the estimation of the pK_a values in aqueous solution using the Hammett equation for substituted phosphorus acids of type

Table 2. Acidity constants in water of some organophosphinic acids

Acid	pK_a*	pK_a†	Ref.†
H[(O)(H)P]	2.10	2.72 ± 0.03	16
H[DOP]	3.20	3.40 ± 0.04	16
H[(TMP)(H)P]	2.19	2.67 ± 0.04	16
H[DTMP]	3.38	3.51 ± 0.05	21

*Estimated by means of the Hammett equation.
†Determined from distribution measurements.

XYPOOH using the suitable tabulated constants.[22,23] The obtained values are given in Table 2. As expected, the experimental values are always slightly higher than the estimated ones, because the extraction diluent, toluene, is water-saturated (solubility of water in toluene at 25°C is 0.072% wt or 0.040 mol/dm^3) and here the water shows basic behaviour. In fact, the value of the Kamlet–Taft basicity parameter, β, is 0.11 for toluene and 0.18 for monomeric water.[24] Since for pure water, with polimeric structure, a revised value of 0.47 has been proposed,[25] an intermediate value slightly higher than 0.18 may be assumed for the very dilute solution of water in toluene used as the extractant solvent.

Both the estimated and experimental values are linearly correlated and show that the estimation of dialkyl-derivative dissociation constants leads to a better agreement with the experimental values.

Because the pK_a of *n*-octyl phosphinic acids have been determined in two different ethanol–water mixtures with very different molar fraction values, the Born equation[26] has been tested by plotting the pK_a values in different ethanol–water mixtures as a function of the reciprocal of the relative permittivity, $1/\epsilon$ using both estimated and experimental values in aqueous solutions. Good correlations have been obtained for the two acids from the values in Table 3, as can be seen in Fig. 2.

In fact, the standard free energy of dissociation is made up of two terms, an electrostatic one, which includes specific solute–solvent interactions, and solvation phenomena. When the electrostatic effects predominate, a straight line should be obtained in the plot of pK_a *vs.* the reciprocal relative permittivity as it occurs with the studied *n*-octyl phosphinic acids.

The pK_a values of the four studied phosphinic acids in ethanol–water mixtures (75% v:v) have been plotted *vs.* the pK_a in water both, experimental and calculated, and good correlations have been obtained. As expected, the slope is slightly higher than unity (1.4) showing a better resolution for these acids in the hydroalcoholic solvent, which shows a relative permittivity value approximately half that of water, and a wider pH scale.[28] Finally, the pK_a of the mono and di *n*-octyl derivatives have been plotted *vs.* the polarity parameter[29] $E^N_{T(30)}$ of the solvent and a straight line has been obtained for both acids using the values in Table 3. The literature shows only a theoretical attempt to relate the electrolyte pK_a variation with the variation of solvent polarity $E^N_{T(30)}$ in binary solvents, and a linear equation with the change of solvent composition was proposed.[30] But, unfortunately, the experimental work covers the variation only until about 20% of water added to isopropyl alcohol. In fact, linear correlations have been obtained using both experimental and calculated values. Because only three experimental points can be used, the difference in the obtained regression coefficients $r = 0.969$ and $r = 0.995$ for experimental and calculated pK_a values in water, respectively, are not significant.

As a conclusion, the Hammett equation developed for phosphorus acids allows a very good estimation of pK_a in water of octyl, both linear and branched octyl derivatives of phosphinic acids and can be used for pK_a estimation for this kind of non water-soluble acids. Nevertheless, if experimental pK_a values (such as those given in Table 2) are available, they should be chosen for solvent extraction uses because they show the acid behaviour in solvent extraction processes better than the estimated

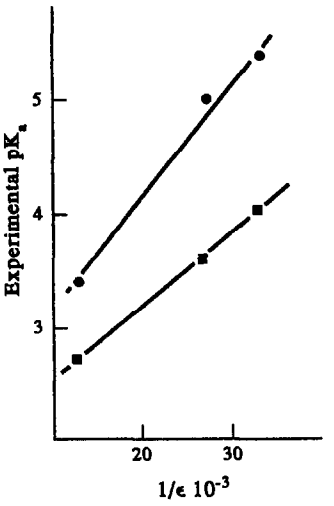

Fig. 2. Experimental pK_a values of mono(*n*-octyl)-phosphinic acid (■) and di(*n*-octyl)phosphinic acid (●) *vs.* the reciprocal of permittivity.

Table 3. Values of % ethanol–water (v:v) $\phi_{ethanol}$, molar fraction $X_{ethanol}$, reciprocal of permittivity $1/\epsilon$ and polarity parameter $E^N_{T(30)}$

$\phi_{ethanol}$	$X_{ethanol}$	$1/\epsilon$*	$E^N_{T(30)}$†
0.00	0.00	12.8×10^{-3}	1.000
0.75	0.48	26.7×10^{-3}	0.706
0.90	0.73	32.8×10^{-3}	0.667

*Values from Ref. 27.

†Values calculated by means of ethanol–water equation from Ref. 31.

values. In addition, the linear relationship between pK_a values in ethanol–water (75% v:v) and in water can also be used successfully to estimate the pK_a in water of new members of this series of phosphinic acids.

Acknowledgements—The authors wish to thank CYANAMID Canada for kindly donating CYANEX-272. This work has been supported by CICYT (Ministerio de Educación y Ciencia, Spain).

REFERENCES

1. C. M. Ritcey and A. W. Ashbrook, *Solvent Extraction: Principle and Application to Process Metallurgy*, Part II. Elsevier Scientific Publishing Co., Amsterdam, 1979.
2. H. Reinhart, H. Ottertun and T. Troeng, *Inst. Chem. Eng. Sym. Ser.*, 1975, **41**, W1.
3. E. D. Nogueira, J. M. Regife and P. M. Blythe, *Chem. Ind.*, 1980, 63.
4. T. Cecconie and H. Freiser, *Solvent Extr. Ion Exch.*, 1989, **7**, 15.
5. K. Li and H. Freiser, *Solvent Extr. Ion Exch.*, 1986, **4**, 739.
6. Y. Komatsu and H. Freiser, *Anal. Chim. Acta*, 1989, **227**, 397.
7. F. Xun and J. A. Golding, *Solvent Extr. Ion Exch.*, 1987, **5**, 205.
8. W. A. Rickelton, D. S. Flett and D. W. West, *Solvent Extr. Ion Exch.*, 1984, **2**, 815.
9. A. M. Sastre, N. Miralles and E. Figuerola, *Solvent Extr. Ion Exch.*, 1990, **8**, 597.
10. N. Miralles, A. Sastre, E. Figuerola and M. Martinez, *Hydrometallurgy*, 1992, **31**, 1.
11. M. Martinez, N. Miralles, A. Sastre and C. Herranz, *Hydrometallurgy*, 1993, **32**, (in press).
12. Q. Dianyun, Z. Longao and H. Rongjun, *Solvent Extr. Ion Exch.*, 1989, **7**, 937.
13. C. Herranz and M. Martínez, *J. Dispersion Sci. Technol.*, 1988, **3**, 209.
14. J. S. Preston and A. C. Du Preez, *The Solvent Extraction of Cobalt, Nickel, Zinc, Copper, Calcium, Magnesium and Rare-Earth Metals by Organophosphorus Acids*, Council for mineral technology, report M 378, 1988.
15. G. Gran, *Analyst*, 1952, **77**, 661.
16. M. Martinez, N. Miralles, A. Sastre and C. Herranz, *Anal. Sciences*, 1992, **8**, 613.
17. J. Bjerrum, *Metal Amine Formation in Aqueous Solution*. P. Haase, Copenhagen, 1941.
18. L. G. Sillén, *Acta Chem. Scand.*, 1956, **10**, 803.
19. N. Ingri and L. G. Sillén, *Arkiv Kemi*, 1965, **23**, 97.
20. P. R. Danesi, L. Reichley-Yinger, G. Mason, L. Kaplan, E. P. Horwitz and H. Diamond, *Solv. Extr. Ion Exch.*, 1985, **3**, 435.
21. J. L. Cortina, N. Miralles, A. Sastre, M. Aguilar, A. Profumo and M. Pesavento, *Reactive Polymers*, 1993, in press.
22. D. D. Perrin, B. Dempsey and E. P. Serjeant, *pK_a Prediction for Organic Acids and Bases*. Chapman and Hall, London, 1981.
23. T. A. Mastrynkova and M. I. Kabachnik, *J. Org. Chem.*, 1971, **36**, 1201.
24. M. J. Kamlet, J. L. M. Abboud, M. H. Abraham and R. W. Taft, *J. Org. Chem.*, 1983, **48**, 2877.
25. Y. Marcus, *J. Phys. Chem.*, 1987, **91**, 4422.
26. M. Born, *J. Phys. Chem.*, 1920, **1**, 45.
27. Y. Marcus, *Ion Solvation*. Wiley, Chichester, 1985.
28. S. Rondinini, P. Longhi, P. R. Mussini and T. Mussini, *Pure and Appl. Chem.*, 1987, **59**, 1693.
29. C. Reichardt, *Solvents and Solvent Effects in Organic Chemistry*. VCH, Weinheim, 2nd ed., 1988.
30. E. Bosch and M. Rosés, *Anal. Chem.*, 1990, **62**, 102.
31. E. Bosch and M. Rosés, *J. Soc. Faraday Trans.*, 1992, **88**, 3541.

Talanta, Vol. 40, No. 9, pp. 1345–1352, 1993
Printed in Great Britain.

0039-9140/93 $6.00 + 0.00

THE SEPARATION OF TELLURIUM AND SELENIUM BY POLYURETHANE FOAM SORBENTS

I. I. STEWART and A. CHOW*
Department of Chemistry, University of Manitoba, Winnipeg, MB, Canada R3T 2N2

(*Received* 14 *January* 1993. *Revised* 1 *March* 1993. *Accepted* 3 *March* 1993)

Summary—Tellurium and selenium can be sorbed from hydrochloric acid and hydrobromic acid solution by both polyether and polyester-based polyurethane foam. Although some acid is needed, the substitution of sodium chloride or sodium bromide increases the extraction significantly. Tellurium is extracted rapidly with > 99% sorbed in 2 min from 1.0/5.0*M* and 2.0/4.0*M* hydrochloric acid/sodium bromide. Selenium can also be sorbed quantitatively but much more slowly so that a separation is possible based on the relative rates of extraction. The capacity of polyether foam is 3% by weight of tellurium.

The use of polyurethane foam as an extractant for organic and inorganic compounds has been developed over 20 years through the publications of H. Bowen in the U.K., T. Braun in Hungary, and workers at the University of Manitoba. Polyurethane has been shown to be a very versatile material for analytical purposes acting as a solid "solvent extractor" in some instances and by a more complex sorption mechanism for the extraction of anionic species. Two books[1,2] and several reviews[3–8] of this field give an excellent overview of the development of this area.

The two general types of polyurethane foam material available are a polyether-based and a polyester-based polyurethane. Each of these has been used as a sorbent for compounds from aqueous solution, although several differences between the polyurethane types have been noted and related to the structure of the polymer. In particular, the polyester-based material acts through a solvent extraction type of mechanism, while the polyether-based material indicates a more complicated process. In some circumstances the polyether-based polymer indicates a solvent extraction mechanism; in others, a cation chelation mechanism predominates as evidenced by the effect of alkali metal ions on the extraction which mimics a crown ether extraction process.

Selenium and tellurium are of analytical interest because of the difficulty in their separation. One element can be determined in the presence of the other by spectrometric methods although large ratios may present some difficulties in analysis. Preconcentration of these elements would be of interest because of the concern of very low concentrations of selenium in the environment, however there is very little recently published literature in this area.[9–10]

In this paper the extraction of tellurium and selenium by both polyether- and polyester-based polyurethane foam is reported and the separation of the two elements is evaluated. The effects of varying concentrations of different acids and salts, concentration of element and length of extraction time are surveyed.

EXPERIMENTAL

Apparatus

All analytical data were obtained with a Varian Spectra AA-20 atomic absorption spectrophotometer equipped with Hamamatsu hollow cathode lamps. The sample solutions were shaken with a modified Burrell wrist-action shaker, where the clamping arms were removed and replaced with baskets to hold the sample containers.

Reagents

All of the chemicals used in these experiments were of reagent grade. The water used in the preparation of all solutions was purified by reverse osmosis and then circulated through a Barnsted Nanopure II™ system. The stock solutions were prepared from; Se powder 99.9% (Alfa Products), SeO_2 99.4% (Alfa Products), TeO_2 99.995% (Aldrich), and Te powder 99.5% (Matheson, Coleman and Bell). The halide salts

*Author to whom correspondence should be addressed.

Table 1. Percentage extraction of tellurium as a function of HCl concentration

Time/concentration	0.0*M*	2.0*M*	3.0*M*	4.0*M*	5.0*M*	6.0*M*	7.0*M*
Polyether foam							
2 min	0.0	4.2	24.0	43.3	42.8	42.5	55.0
5 min	0.0	3.7	28.2	47.2	42.5	47.2	59.8
10 min	0.0	4.2	30.3	49.5	44.5	46.8	58.8
15 min	0.0	4.2	33.3	51.7	45.3	48.2	59.2
30 min	0.0	4.3	34.0	49.0	43.8	48.3	60.5
60 min	2.3	3.5	35.5	50.0	43.3	49.2	57.8
120 min	4.0	2.8	34.3	50.5	45.0	49.3	60.0
180 min	5.8	2.7	33.7	51.5	44.3	48.5	58.5
Polyester foam							
2 min	3.5	2.3	8.7	33.2	47.7	53.0	68.0
5 min	0.7	2.0	12.8	46.2	57.5	70.2	74.2
10 min	0.7	1.5	15.2	53.2	67.7	75.8	72.2
15 min	1.8	2.2	16.5	57.7	73.0	75.2	68.5
30 min	2.8	1.7	18.3	60.3	76.2	76.2	54.3
60 min	0.7	2.0	19.5	61.3	75.3	70.0	45.2
120 min	1.7	2.8	20.2	60.5	63.8	46.2	35.0
180 min	5.2	2.5	20.2	57.5	53.7	38.8	32.2

Foam weight 1.00 ± 0.05 g; samples were 50.0 ml of 60 ppm tellurium solution.

used were; NaCl (Mallinckrodt), NaBr (Shawinigan), NaI (Fisher), and KCl (Mallinckrodt).

There were two types of polyurethane foams used, a polyether-type, primarily an 80% PEO/PPO polyol, 20% polystyrene/acrylonitrile copolymer + TDI 105 index (5000 m.n.) and a polyester-type obtained from Canlab, Winnipeg, Canada, in the form of diSPo™ plugs.

Procedure

Two 1000 ppm tellurium stock solutions were prepared from tellurium powder and tellurium oxide. For one solution 1.0001 g of tellurium powder was dissolved in 60 ml of a 1:1:1 mixture of $HCl/HNO_3/H_2O$ on a hot plate. The cooled mixture was then diluted to 1000 ml with water. The stock solution made from tellurium oxide was prepared by dissolving 1.2548 g in 100 ml of HCl and then diluting to 1000 ml with water. The selenium stock solutions were prepared similarly except that 1.0119 g of selenium powder and 1.4264 g of the oxide were used.

The sample solutions were prepared from combinations of stock acid and salt solutions. The various matrix combinations were normally prepared by mixing the appropriate amount of acid and salt solutions, before addition to the samples. When preparing the standards and samples for the experiments, a volume of stock solution was placed in a 50 ml volumetric flask and diluted with a solution of the appropriate matrix.

The two types of foam were washed individually. The foam was first placed into 1*M* HCl, squeezed regularly for 2 hr and then rinsed and squeezed repeatedly with water to remove all of the residual acid. After thoroughly squeezing to remove all excess water, the foam was placed in a Soxhlet extraction apparatus and was refluxed in acetone for 6 hr. The foam was squeezed gently to remove the bulk of the acetone and then ground in a stainless steel container on a Waring™ blender. The foam was then air dried and stored out of the light in a covered plastic beaker.

Table 2. Double extraction of tellurium

	Original concentration (*ppm*)	Final concentration (*ppm*)	% Total extraction
Polyether	30.0	—	—
	—	4.6	84.7
	60.0	—	—
	—	10.9	81.8
	90.0	—	—
	—	15.8	82.4
	120	—	—
	—	23.9	80.1
	150	—	—
	—	34.5	77.0
Polyester	30.0	—	—
	—	2.2	96.7
	60.0	—	—
	—	4.8	92.0
	90.0	—	—
	—	8.8	90.2
	120	—	—
	—	16.8	86.0
	150	—	—
	—	24.4	83.7

Two consecutive 2 min extractions with 1.05 ± 0.05 g foam from 50.0 ml of 7.0*M* HCl.

Table 3. Capacity of polyether and polyester foams for tellurium

	Mass (g)	Time (min)	Original concentration (ppm)	Final concentration (ppm)	% Extraction	% Weight on foam
Polyether	0.545	30	30	13.4	55.3	0.15
	0.542	30	60	31.3	47.8	0.26
	0.510	30	90	52.3	41.9	0.37
	0.525	30	120	77.2	35.7	0.41
	0.513	30	150	95.2	36.5	0.53
Polyester	0.534	10	30	10.9	63.7	0.18
	0.527	10	60	23.1	61.5	0.35
	0.531	10	90	37.9	57.9	0.49
	0.529	10	120	58.4	50.9	0.58
	0.494	10	150	84.9	43.4	0.66

Solution volume 50.0 ml.

Both the sample and standard solutions were prepared in identical matrices at the same time in all cases. The extraction experiment was carried out by placing a measured quantity of foam into a 50 ml plastic bottle with screw cap and then adding the 50 ml sample solution. The bottles were then placed in the baskets of the wrist-action shaker and shaken for the appropriate time. The sample was then removed and the liquid and foam components separated by filtering the solution through Whatman No. 541 paper prior to analysis. The foam was normally discarded except for a few experiments where it was collected quantitatively and the recovery experiments attempted.

The analysis of tellurium was carried out by atomic absorption spectroscopy with the lamp at 10 mA, a slit width of 0.2 nm, and a wavelength of 214.3 nm. For selenium analysis the lamp was operated at 10 mA, a slit width of 1nm, and at a wavelength of 196.0 nm. Where solutions were low in salt concentration, five replicates were performed and where there was a high salt concentration four replicates were used. In all cases the measurement time was 4 sec, with a time constant of 0.05 sec. An air–acetylene flame was used with a Varian Mark VI™ burner head. Depending on the viscosity of the solutions the sample uptake pressure was adjusted to ensure a smooth aspiration. The instrument was zeroed with water, and the particular blank was based on the type of matrix used for the set of samples. Background correction was used for all samples.

The efficiency of a system may be calculated either as the percent extraction of the species ($\%E$), or the distribution coefficient (D):

$$\%E = 100(C_0 - C_{eq})/C_0;\ D = (VE)/W(100\text{-}E)$$

where C_0 is the initial species concentration in ppm before extraction, C_{eq} is the species concentration after the extraction period, V is the volume of solution in ml, and W is the mass of the foam sample in grams.

The distribution coefficient expressed in ml/g (or alternately in l/kg) is a ratio of the species concentration in the foam to the concentration of the sample solution. This ratio should become a constant when the extraction process has attained equilibrium. The distribution coefficient is not always useful, especially with very high or very low percent extractions, because the coefficients may become extremely large or small with only a slight incremental change. Because the foam samples used were about 1.0 g, the distribution coefficient for samples having greater than 95.0% extraction, or less

Table 4. The separation of tellurium from selenium

Time (min)	Original concentration (ppm)		Final concentration (ppm)		% Extraction	
	Te	Se	Te	Se	Te	Se
2	60	60	34.1	60	43.2	0.0
5	60	60	31.2	60	48.0	0.0
10	60	60	31.5	60	47.5	0.0
15	60	60	31.5	60	47.5	0.0
30	60	60	32.5	60	45.8	0.0
60	60	60	31.7	60	47.2	0.0
120	60	60	32.6	60	45.7	0.0
180	60	60	31.8	60	47.0	0.0

Extraction from 50.0 ml of 6.0M HCl by 1.05 ± 0.05 g of polyether foam.

Table 5. The double extraction of tellurium in the presence of selenium

	Original concentration (*ppm*)		Final concentration (*ppm*)		% Extraction	
	Te	Se	Te	Se	Te	Se
6.0*M* HCl	60	60	—	—	—	—
	—	—	9.9	60	83.5	0.0
	60	60	—	—	—	—
	—	—	11.6	60	80.7	0.0
	60	60	—	—	—	—
	—	—	12.4	60	79.3	0.0
4.0*M* HCl	60	60	—	—	—	—
	—	—	25.1	60	58.2	0.0
	60	60	—	—	—	—
	—	—	24.4	60	59.3	0.0
	60	60	—	—	—	—
	—	—	24.4	60	59.3	0.0

Extraction from 50.0 ml solution with two consecutive 1.05 ± 0.05 g samples of polyether foam for 10 min each.

than 5.0% extraction become less significant due to inherent errors.

Although this study primarily focuses on the extraction of tellurium–halide species, selenium–halide species were also examined to a lesser extent, as well as the separation of these two species from solution.

The first system examined was the tellurium–chloride system in matrices of varying HCl concentrations from $\sim 0.1M$ to $7M$. Preliminary experiments showed that the extraction was very rapid so the extraction time periods were varied from about 2 min up to 3 hr as shown in Table 1.

The results with polyether foam show that there is essentially no extraction until reaching an acidity of $\sim 3.0M$, and then there was increasing extraction up to $7.0M$, with a secondary maximum at $4.0M$. The experiments at $4.0M$ HCl and $5.0M$ HCl were repeated to confirm this. It was expected from results with other elements that the extraction would increase with acidity. It should also be noted that for $0.0M$, and $2.0M$ HCl there was some small, irregular extraction.

The polyester foam also shows some interesting properties with the extraction increasing with increased acidity as expected. However increasing the acidity also has a negative effect because it degrades the foam. For polyester foam a maximum is achieved before 180 min, but for samples in greater than the $3.0M$ HCl degradation of the foam caused a decrease in the extraction. This effect is especially severe in the $7.0M$ system where the effects of degradation were seen in as little as 5min.

A double extraction of tellurium (30–150 ppm), was carried out using 50 ml solutions, which were shaken for about 2 min with two different samples of foam in succession. The

Table 6. Percentage extraction of tellurium from HCl/NaCl matrices

	HCl/NaCl Time (*min*)	6.0/0	5.0/1.0	4.0/2.0	3.0/3.0	2.0/4.0	0/6.0
Polyether	2	42.5	54.2	56.2	63.7	34.2	0.0
	5	47.2	60.2	60.8	68.8	29.0	0.0
	10	46.8	61.5	64.5	73.8	40.7	0.0
	15	48.2	64.0	71.0	77.5	43.5	0.0
	30	48.3	63.3	71.7	80.0	45.7	0.0
	60	49.2	64.2	71.7	80.7	45.3	0.0
	120	49.3	62.8	74.0	81.7	47.2	0.0
	180	48.5	63.0	74.0	82.8	45.2	0.0
Polyester	2	53.0	48.5	42.8	32.3	8.0	0.0
	5	70.2	64.7	50.5	38.8	10.3	0.0
	10	75.8	70.7	62.7	48.8	19.0	0.0
	15	75.2	75.7	69.5	54.3	17.2	0.0
	30	76.2	79.2	77.8	59.2	23.3	0.0
	60	70.0	79.2	80.0	64.8	25.2	0.0
	120	46.2	71.0	76.5	65.5	28.5	0.0
	180	38.8	59.5	76.3	64.3	27.2	0.0

Foam weight 1.05 ± 0.05 g; samples were 50.0 ml of 60 ppm tellurium solution; HCl/NaCl ratio is the ratio of molar concentrations.

Table 7. Percentage extraction of tellurium from HBr/NaBr matrices

HBr/NaBr	6.0/0	3.0/0	4.0/2.0	3.0/3.0	2.0/4.0	0/6.0
Time (*min*)						
2	88.3	93.8	95.2	n.d.*	98.0	19.0
5	90.2	95.5	96.3	97.2	98.8	26.5
10	91.3	96.7	97.2	98.0	99.0	29.5
15	91.7	96.7	97.8	98.2	99.3	29.2
30	92.2	97.0	98.0	98.3	99.3	35.2
60	92.0	97.0	98.0	98.3	99.3	57.2
120	92.2	97.3	98.3	98.5	99.7	73.8
180	92.7	97.5	98.7	98.7	99.8	76.7

Foam weight 1.05 ± 0.05 g polyether foam; samples were 50.0 ml of 60 ppm tellurium solution; HBr/NaBr ratio is the ratio of molar concentrations.
*n.d. = not determined.

results shown in Table 2 indicate that the extraction process resembles a solvent extraction, where the same percentage of the species is extracted with each separation step. From the data for tellurium in 7*M* HCl (Table 1), the extraction of the 60 ppm solution is 55% after 2 min for the polyether foam. If under these conditions the extraction is repeated where 55% is extracted each time, approximately 48 ppm total will be extracted, and an 80% extraction is obtained. This value agrees quite well with sample 2 from Table 2, which is 82%. Similarly for polyester we obtain 90% upon calculation, which also agrees with the 92% obtained in sample 7, as shown in Table 2. From these data we may conclude that to obtain a near quantitative extraction at least three extractions would have to be performed under these conditions.

The capacity of polyether and polyester foam was evaluated by varying the tellurium concentration in 7*M* HCl solutions and the data are given in Table 3. The data were extrapolated and it was found that the capacity for tellurium was approximately 0.70% by weight for polyether foam and 0.85% by weight for the polyester foam. Although the polyester foam has a greater capacity for tellurium than does the polyether foam under these conditions, it is not as useful as the polyester degrades.

Studies on analogous selenium systems yielded negligible extraction from solutions containing 0–7*M* HCl. This system was then studied in order to see if separation could be achieved.

The results in Table 4 demonstrate that the two elements may be separated. The effect of large concentrations of selenium on the extraction of tellurium was studied and it was found that there was no appreciable effect. Under these conditions it would require multiple extractions to obtain a quantitative separation. The data from Table 5 show that as expected, at least three extractions would be required for the 6*M* HCl solutions and at least four for the 4*M* HCl solutions. The separation could be done quantitatively in either case, although inconveniently.

As the extraction process resembles a solvent extraction the effect of salting out the tellurium species was studied. As shown in Table 6 it was found that the presence of sodium chloride in the system enhanced the extraction of the tellurium species significantly.

The data from Table 6 show that the salting-out effect is significant in the extraction of the tellurium species, increasing the extraction in comparison with acid alone. However, some acid must be present for the extraction to be effective. This was further investigated.

Table 8. Percentage extraction of tellurium from HCl/NaBr matrices

HCl/NaBr	0/6.0	0.1/5.9	0.5/5.5	1.0/5.0	2.0/4.0	3.0/3.0	4.0/2.0	6.0/0
Time (*min*)								
2	19.0	72.0	92.2	99.3	99.0	97.5	95.7	42.5
5	26.5	83.5	97.2	99.5	99.7	98.3	96.7	47.2
10	29.5	90.7	98.5	99.7	100	98.7	97.8	46.8
15	29.2	92.2	98.5	99.7	100	98.8	97.8	48.2
30	35.2	94.5	98.8	99.8	100	99.0	98.2	48.3
60	57.2	96.2	99.7	100	100	99.0	98.2	49.2
120	73.8	97.2	99.7	100	100	99.2	98.3	49.3
180	76.7	97.7	99.8	100	100	99.3	98.7	48.5

Foam weight 1.05 ± 0.05 g polyether foam; samples were 50.0 ml of 60.0 ppm tellurium solution; HCl/NaBr ratio is the ratio of molar concentrations.

Table 9. Capacity of polyether foam for tellurium species in 2.0*M* HCl/4.0*M* NaBr matrix

Mass (*g*)	Original concentration (*ppm*)	Final concentration (*ppm*)	% Extraction	% Te on Foam
0.227	10	0.60	94.0	—
0.220	30	0.70	97.7	—
0.204	60	1.60	97.3	—
0.218	90	2.40	97.3	2.01
0.216	120	8.30	93.8	2.59
0.210	150	31.8	78.8	2.82
0.205	175	55.0	68.6	2.94
0.209	200	76.2	61.9	2.96

Solution volumes 50.0 ml; extraction time 15 min.

As chloride is a good extraction matrix, the effect of bromide on the extraction of tellurium was similarly investigated. It can be seen from the data in Table 7 that the extraction is quantitative in most cases. The 0*M* HBr/6*M* NaBr system is not entirely free of hydrochloric acid since there is about 0.1*M* HCl, from the acid in the original stock solution. These results suggest that a minimum acidity is required for the extraction to proceed. The rapid increase to essentially 100% extraction in the 2*M* HBr/4*M* NaBr system would indicate that an acidity somewhere between 0 and 2*M*, might give a rapid and complete extraction of the tellurium species. The above data also suggest that the extraction is independent of the acid type, but proceeds quite well with the sodium bromide salt. The study of a mixed HCl/NaBr system was then examined and the results are listed in Table 8.

The above data indicate that for rapid, complete extraction a minimum acidity of between 0.5*M* and 1.0*M* HCl is required. Other trials have shown that quantitative extraction may be achieved in systems with lower than 6*M* balance of halide. In a 1*M* HCl/2*M* NaBr system 75% extraction (45 ppm) was obtained in 2 hr.

A capacity study was then performed on the 2*M* HCl/4*M* NaBr system where the most rapid extraction was obtained and the results given in Table 9. These data show that the polyether foam has a high capacity for tellurium species from this matrix. When the data are extrapolated the capacity was determined to be approximately 3.00% by weight of foam. If this is compared with the data obtained from polyether foam in HCl it can be seen to be approximately four times as great. This system would seem ideal for the extraction of larger amounts of tellurium from solution.

The extraction of selenium was observed in analogous systems and the data are listed in Table 10. From these data, it is observed that the extraction of selenium still goes to completion under the same conditions although more slowly than for tellurium. It is interesting to note that the extraction seems slower in the lower acid matrix and that after 2 min there is only 11% extracted (6.60 ppm). With this in mind a separation of tellurium from selenium

Table 10. Extraction of selenium from HCl/NaBr solution

HCl	NaBr	Time (*min*)	Original concentration (*ppm*)	Final concentration (*ppm*)	% Extraction
4.0*M*	2.0*M*	2	60	48.2	19.7
4.0*M*	2.0*M*	5	60	34.0	43.3
4.0*M*	2.0*M*	10	60	21.7	63.8
4.0*M*	2.0*M*	15	60	11.9	80.2
4.0*M*	2.0*M*	30	60	2.2	96.3
4.0*M*	2.0*M*	60	60	0.3	99.5
4.0*M*	2.0*M*	120	60	0.0	100
4.0*M*	2.0*M*	180	60	0.0	100
2.0*M*	4.0*M*	2	60	53.4	11.0
2.0*M*	4.0*M*	5	60	46.6	22.3
2.0*M*	4.0*M*	10	60	40.8	32.0
2.0*M*	4.0*M*	15	60	31.3	47.8
2.0*M*	4.0*M*	30	60	18.3	69.5
2.0*M*	4.0*M*	60	60	5.8	90.3
2.0*M*	4.0*M*	120	60	0.0	100
2.0*M*	4.0*M*	180	60	0.0	100

Solution volumes 50.0 ml; foam weight 1.05 ± 0.05 g polyether foam; matrices are nitric acid-free.

Table 11. Separation of tellurium and selenium

	Time (*min*)	Final concentration (*ppm*)		% Extraction	
		Te	Se	Te	Se
4.0*M* HCl/2.0*M* NaBr	10	0.0	35.8	100	40.3
	10	0.0	35.3	100	41.2
	10	0.0	35.0	100	41.7
	10	0.0	36.5	100	39.2
2.0*M* HCl/4.0*M* NaBr	2	0.8	57.1	98.7	4.8
	2	0.6	56.7	99.0	5.5
	2	0.5	56.9	99.2	5.2
	10	0.5	47.7	99.2	12.4
	10	0.3	48.0	99.5	12.1
	10	n.d.*	n.d.	n.d.	n.d.
0.5*M* HCl/5.5*M* NaBr	2	6.0	57.8	90.0	3.7
	2	5.3	57.3	91.2	4.5
	5	2.6	55.4	95.7	7.7
	5	3.1	57.0	94.8	5.0
	10	1.9	56.0	96.8	6.7
	10	2.0	56.8	96.7	5.3

Solution volume 50.0 ml, nitric acid-free; original tellurium and selenium concentrations 60.0 ppm; foam weight 1.05 ± 0.05 g polyether foam.
*n.d. = not determined.

was performed under these matrices and the results listed in Table 11.

It can be seen that the separation is not complete in 4*M* HCl/2*M* NaBr but one species is extracted completely and the other partially. This system would seem inefficient for the quantitative separation of these elements. A more quantitative separation is achieved in a lower acid matrix, and for a 2 min rapid extraction, it is possible to extract the tellurium species quantitatively in the presence of selenium with minimal extraction of the other. The extraction of selenium is reduced in the lower acid matrix, however the extraction of tellurium is slowed and becomes less quantitative.

As chloride and bromide both provided suitable extraction matrices, we investigated iodide. The results for tellurium were essentially 100% extraction for a 2*M* HCl/4*M* NaI matrix in 5 min and 100% extraction for a straight 0*M* HCl/6*M* NaI matrix in 10 min, (there was 0.1*M* residual HCl from the stock solution present). When selenium was investigated under similar conditions a precipitate formed, presumably Se_2I_2. Therefore a separation of these two elements in this matrix could be done by filtering the sample solution to collect the precipitate and then running the extraction with the polyether foam to collect the tellurium.

Table 12. Effect of nitric acid on selenium extraction

Time (*min*)	% Extraction from HNO_3	% Extraction from "clean" system
2	4.5; 5.8	11.0
5	9.3; 9.0	22.3
10	10.7	32.0
15	14.3	47.8

Solutions were 50.0 ml of 60 ppm selenium in 2.0*M* HCl/4.0*M* NaBr; extraction with 1.05 ± 0.05 g polyether foam; acid samples were digested for 1 hr in 0.30 ml HNO_3/50 ml sample prior to extraction; "clean" data from Table 10.

In previous studies both tellurium and selenium metals were dissolved in a HCl/HNO_3 mixture, to prepare their respective stock solutions. When this was done it was noticed that there seemed to be negligible extraction of selenium in the HCl/NaBr matrices before 1 hr. However when the extraction was performed in similar matrices with nitric acid-free stock solutions, prepared from dissolving the oxide in HCl there was a much greater and consistent extraction over 3 hr, as shown in Table 10. With this in mind a series of experiments were performed where a volume of HNO_3 was introduced to the nitric acid free selenium stock and the solutions was then left to sit before the matrix was added. Once the matrix solution was added, the extraction was carried out immediately.

From Table 12 it can be seen that there is a marked difference in the extraction of the Se in the presence of HNO_3. A more extended investigation into this effect and its kinetics might lead to a more quantitative separation of the elements.

The reverse extraction of tellurium was investigated and it was found that if the foam was left to sit for a period of greater than 3 hr water with gentle, periodic squeezing the tellurium could be removed quantitatively from the foam. Other investigations also showed that acetone and 1% sodium hydroxide solutions could also be used

to recover completely, the sorbed tellurium species.

CONCLUSIONS

The sorption of tellurium from hydrochloric acid solutions as concentrated as 7*M*, is not quantitative and there is no extraction below 3*M* with polyurethane foam. Although a multiple step procedure or a larger amount of foam would provide a more quantitative sorption, this would be somewhat inconvenient. Under these conditions polyester foam shows a higher extraction than polyether and the capacities are 0.85% and 0.70%, respectively; under similar conditions, selenium is not sorbed so a reasonable separation of the two elements is possible with little contamination of the tellurium on foam by selenium.

The addition of sodium chloride to the hydrochloric acid solutions increases the sorption of tellurium to a maximum of about 80% when both are 3*M*. The use of hydrobromic acid and sodium bromide increases the sorption even more with >95% sorbed by polyether foam in 10 min or more over a range of acid and salt concentrations. Similarly, a mixture of hydrochloric acid and sodium bromide gave excellent and rapid extraction of tellurium with >99% sorbed in 2 min from 1.0/5.0*M* and 2.0/4.0*M*. Under these conditions the capacity of polyether foam is about 3% by weight of tellurium.

The sorption of selenium from 2.0/4.0*M* and 4.0/2.0*M* HCl/NaBr solutions is also quantitative by polyether foam but requires 2 hr for complete extraction. The sorption of both elements under similar conditions prevents a "clean" separation. However by varying the conditions to less than ideal for tellurium, it is possible to take advantage of the difference in the rates of sorption of the two species; in this situation an extraction of >95% of tellurium is obtained with about 6% co-extraction of selenium. The presence of nitric acid has a considerable effect on the rate and percentage extraction of selenium. A more detailed study of the nitric acid system will be undertaken in the future.

Overall it is apparent that polyurethane foam can be used to sorb selenium and tellurium from halo-acid solutions. The presence of some acid is required with higher concentrations more effective, but the presence of larger concentrations of sodium halide salts facilitates a quantitative extraction. A reasonable separation of tellurium from selenium is possible and this method is rapid, efficient and inexpensive.

Further investigations in this area would focus on the separation of selenium and tellurium using polyurethane foam sorbents in columns, the sorption and separation of trace levels of the metals from more complex matrices and a more extensive study of the effects of different acids on the separation process.

Acknowledgement—This work was supported by the Natural Sciences and Engineering Research Council of Canada.

REFERENCES

1. G. J. Moody and J. D. R. Thomas, *Chromatographic Separation and Extraction with Foamed Plastics and Rubbers*. Dekker, New York, 1982.
2. T. Braun, J. D. Navratil and A. B. Farag, *Polyurethane Foam Sorbents in Separation Science*. CRC Press, Boca Raton, 1985.
3. T. Braun and A. B. Farag, *Anal. Chim. Acta*, **99**, 1, 1978.
4. G. J. Moody and J. D. R. Thomas, *Analyst*, **104**, 1, 1979.
5. T. Braun, *Z. Anal. Chem.*, **314**, 652, 1983.
6. T. Braun, *Cellular Polymers*, **3**, 81, 1984.
7. T. Braun, *Z. Anal. Chem.*, **333**, 785, 1989.
8. S. Palagyi and T. Braun, in Z. B. Alfassi and C. M. Wai, *Preconcentration Techniques for Trace Elements*. CRC Press, Boca Raton, 1992.
9. W. C. Cooper, *Tellurium*. Van Nostrand Reinhold, New York, 1971.
10. I. I. Nazarenko and A. N. Ermakov, *Analytical Chemistry of Selenium and Tellurium*, (translated by R. Kondor, Israel Program for Sc. Trans.). Halsted Press, New York, 1972.
11. J. Korkisch, *Modern Methods for the Separation of Rarer Metal Ions*. Pergamon Press, Oxford, 1969.

Talanta, Vol. 40, No. 9, pp. 1353–1356, 1993
Printed in Great Britain.

0039-9140/93 $6.00 + 0.00

SPECTROFLUOROMETRIC STUDY OF THALLIUM (I) COMPLEXES WITH SEVERAL MACROCYCLIC LIGANDS IN METHANOL SOLUTION

HOOSHANG PARHAM and MOJTABA SHAMSIPUR*
Department of Chemistry, Shiraz University, Shiraz, Iran

(*Received* 12 *January* 1993. *Revised* 1 *March* 1993. *Accepted* 1 *March* 1993)

Summary—The fluorescent signal of Tl^+ was employed as a sensitive probe to study the complexation reactions between this cation and several macrocyclic ligands in methanol solution at 20°C. The stability constants of the resulting 1:1 complexes were determined and found to vary in the order C222 > C221 > 18C6 > DC18C6 > DB30C10 > DB18C6 > 15C5 > DA18C6 > B15C5 > DA15C5. The influence of a number of members in the macrocycle, the nature of substituents on the polyether ring and of the dimensionality of the ligands on the stability and selectivity of the complexes is discussed.

The monovalent thallium ion has been suggested as a probe for potassium ion in biological systems.[1,2] It can substitute for K^+ in activation of some important enzymes such as ATPase[3] and pyruvate kinase.[4] Thus, the stability and selectivity of Tl^+ complexes with macrocyclic ligands are of special interest with this respect. Among different spectroscopic and electroanalytical methods used for the study of Tl^+ complexes,[5] the fluorescent properties of the cation, well characterized by Steffen and Sommermeyer in aqueous solution,[6] possess some promising features for such studies in both aqueous and nonaqueous media.

We have been currently involved in the study of the thermodynamics[7–11] and kinetics[12–14] of metal ion complexes with macrocyclic ligands in nonaqueous and mixed solvents. In this paper we report the use of the fluorescent signal of Tl^+ ion as a very sensitive probe to study its complexes with crown ethers 15-crown-5 (15C5), benzo-15-crown-5 (B15C5), 1,7-diaza-15-crown-5 (DA15C5), 18-crown-6 (18C6), dibenzo-18-crown-6 (DB18C6), dicyclohexyl-18-crown-6 (DC18C6), 1,10-diaza-18-crown-6 (DA18C6) and dibenzo-30-crown-10 (DB30C10) and cryptands C221 and C222 in methanol solution at 20°C.

EXPERIMENTAL

Reagent grade thallium nitrate (BDH) was of the highest purity available and used without any further purification except for vacuum drying over P_2O_5. Macrocyclic ligands B15C5, 18C6, DB18C6, DA18C6 (all from Merck) and DB30C10 (Parish) were purified and dried using the previously reported methods.[7,9,10] Macrocycles 15C5, DA15C5, C221 and C222 (all from Merck) were used after vacuum drying over P_2O_5. Spectroscopic grade methanol (MeOH, Merck) was used as received. Fluorometric measurements were made using a Shimadzu RF-5000 spectrofluorometer at 20 ± 1°C.

The formation constants of 1:1 complexes between Tl^+ ion and macrocyclic ligands used were determined by the fluorescence intensity measurements, at the maximum emission wavelength of 354 nm, of solutions in which varying concentration of ligand (1.6×10^{-6}–$2.1 \times 10^{-4} M$) were added to a fixed concentration of thallium ion ($3.2 \times 10^{-5} M$) in MeOH. Attainment of equilibrium was checked by the observation of no change in the spectra after several hours.

When Tl^+ ion reacts with a macrocyclic ligand, L, to form a 1:1 complex, the formation constant is given as

$$K_f = \frac{[TlL^+]}{[Tl^+][L]}. \quad (1)$$

The mass balance equations and the observed fluorescence intensity, $(F1)_{obs}$, are given by

$$C_{Tl^+} = [Tl^+] + [TlL^+] \quad (2)$$

$$C_L = [L] + [TlL^+] \quad (3)$$

$$(F1)_{obs} = K'_{Tl} + [Tl^+] + K'_{TlL} + [TlL^+] \quad (4)$$

*Author for correspondence.

where C and K' values are the analytical concentration and fluorescence constant of the species indicated, respectively. The mass balance equations can be solved in order to obtain an equation for the free metal ion concentration, $[Tl^+]$ as

$$K_f[Tl^+]^2 + (1 + K_f(C_L - C_{Tl^+}))[Tl^+] - C_{Tl^+} = 0. \quad (5)$$

For the evaluation of the formation constants from fluorescence intensity *vs.* mole ratio data (7–14 points), a non-linear least-squares curve fitting program KINFIT was used.[15] The program is based on the iterative adjustment of the calculated values of the fluorescence intensities to the observed values by using either the Wentworth matrix technique[16] or the Pawell procedure.[17] Adjustable parameters are K_f and K'_{TlL^+}.

The free Tl^+ concentration was calculated from equation (5) by means of a Newton–Raphson procedure. Once the value of $[Tl^+]$ had been obtained, the concentration of all other species involved were calculated from the mass balance equations (2) and (3), by using the estimated values of the formation constant at the current iteration step of the program. Refinement of the parameters is continued until the sum-of-squares of the residuals between calculated and observed values of the fluorescence intensity for all experimental points is minimized. The output of the program KINFIT is comprised of refined parameters, the sum-of-squares and the standard deviation of the data.

RESULTS AND DISCUSSION

The present study showed that the fluorescent signal of Tl^+ ion in methanol solution can be used as a convenient and very sensitive probe for macrocyclic complexation of the cation. The fluorescence spectra of Tl^+ ion at different excitation wavelengths were obtained and a wavelength of 232 nm was selected as the most convenient excitation wavelength for further studies. Maximum fluorescence emission occurs at 354 nm. The fluorescence intensity of Tl^+ ion in methanol solution was found to be independent of the nature of the anion, which indicates that an ion pair formation would be negligible in the concentration range studied.

The formation constants of different Tl^+-macrocycle complexes were determined as described in the Experimental section. A sample spectrum is shown in Fig. 1. As is seen, increasing the macrocycle concentration results in a decrease in the fluorescence intensity at 354 nm and appearance of a fluorescence signal at 308 nm, indicating the formation of a new Tl^+ species. It should be noted that, only in the cases of 18C6 and DC18C6 the 308 nm band was so intense and comparable with the 354 nm band. In all other cases, however, the intensity of this signal was about 1/10th of the original Tl^+ band at 354 nm. In all cases studied, the resulting fluorescence intensity–mole ratio data showed the best computer fitting to the 1:1 Tl^+-macrocycle stoichiometry. A sample computer fit of the data is shown in Fig. 2. Moreover, the existence of a well defined isosbestic

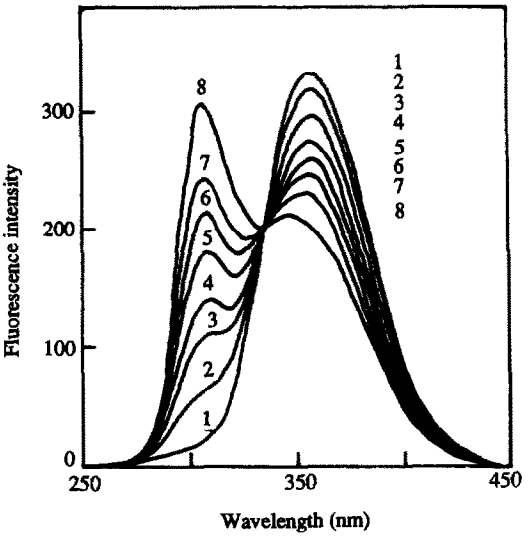

Fig. 1. Fluorescence spectra of Tl^+ ($3.2 \times 10^{-5}M$) upon titration with DC18C6 in MeOH at 20°C. [DC18C6] is: 1, 0.0; 2, $4.1 \times 10^{-6}M$; 3, $8.3 \times 10^{-6}M$; 4, $1.2 \times 10^{-5}M$; 5, $1.7 \times 10^{-5}M$; 6, $2.1 \times 10^{-5}M$; 7, $2.5 \times 10^{-5}M$; 8, $3.3 \times 10^{-5}M$.

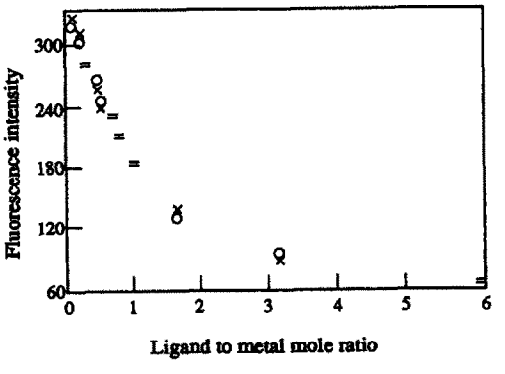

Fig. 2. Computer fit fluorescence intensity–mole ratio data for complexation of Tl^+ with DC18C6 in MeOH at 25°C: (x) experimental point; (o) calculated point; (=) experimental and calculated points are the same within the resolution of the plot.

Table 1. Stability constants of Tl^+ complexes with different macrocyclic ligands in methanol solution at 25°C

Ligand	Cavity size (Å)	Log K_f
15C5	1.7–2.2*	3.91 ± 0.06
B15C5		3.65 ± 0.08
DA15C5‡		3.56 ± 0.05
18C6	2.6–3.2*	4.95 ± 0.05
DC18C6		4.67 ± 0.06
DB18C6		4.42 ± 0.06
DA18C6‡		3.69 ± 0.04
DB30C10	—	4.53 ± 0.06
C221	2.2†	>6
C222	2.8†	>7

*Ref. 19. †Ref. 20. ‡The corresponding solution was neutral and the protonation constants were not taken into account in the process of determining the stability constant.

point in the fluorescence spectra of Tl^+ upon titration with ligand is further evidence for a simple complexation equilibrium.

All the calculated formation constants for different TL^+-macrocycle complexes in MeOH at 20°C are summarized in Table 1. As can be seen, in the cases of C221 and C222 cryptates, the formation constants were greater than 10^6 and their precise values could not be determined by our technique. It is obvious that, the relative size of Tl^+ ion (3.0 Å)[18] and the cavity of polyether rings,[19,20] as well as the nature of substituents on the macrocyclic ring, plays an important role in the complexation reactions. Among different crown ethers used, 18-crowns form the most stable complexes with thallium ion, most probably because of the suitable fitting of Tl^+ ion inside the cavity of these ligands. However, among 18-crowns used, the stability of the resulting Tl^+ complexes vary in the order 18C6 > DC18C6 > DB18C6 > DA18C6.

The presence of two cyclohexyl groups in DC18C6 would cause some reduced stability, in comparison with 18C6, probably because of the reduced flexibility of the ligand. On the other hand, the addition of the two benzo groups to 18C6 lowers the stability of Tl^+ complex markedly. This behaviour may be attributed to some combination of the electron withdrawing property of the benzo groups which weakens the electron donor ability of the oxygen atoms of the ring, and reduced flexibility of the ligand which prevents the macrocyclic molecule from 'wrapping itself' around the cation. Finally, despite the soft character of the two nitrogen atoms of DA18C6 ring which is expected to favor its interaction with Tl^+ ion as a soft acid,[21] this ligand forms the least stable complex in the series. A possible cause of this unexpected behavior would be the existence of a specific interaction between protic solvents such as water and methanol and macrocyclic ligands containing nitrogen atoms, via hydrogen bonding of the solvent with >N–H groups of the ring.[22,23]

It is interesting to note that in the case of 15-crowns used, where the resulting Tl^+ complexes are less stable than those with 18-crowns because of the too small cavity size of the macrocyclic rings for the metal ion, the same trend of stability can also be observed (i.e. 15C5 > B15C5 > DA15C5).

On the other hand, although the cavity of DB30C10 seems too large for Tl^+ ion, it forms a stable 1:1 complex with cation (i.e. in the order of DC18C6). This result is not surprising, since it has been shown that large crown ethers such as DB30C10 can easily twist around a cation of suitable size (such as K^+ ion, ionic size 2.86 Å)[18] to form a stable three-dimensional "wrap-around" complex in which all oxygen atoms of the ring participate in the bond formation with the central cation.[9,10,13,24]

From the stability constant listed in Table 1, it is obvious that the macrobicyclic ligands C222 and C221, despite their small cavity sizes for the complete accommodation of the cation,[20] form more than their corresponding macrocyclic ligands DA18C6 and DA15C5. This rapid increase in stability, obtained by connecting another $-CH_2CH_2-O-CH_2CH_2-O-CH_2CH_2-$ bridge onto the macrocyclic ligands DA18C6 and DA15C5 (to form the corresponding macrobicyclic ligands C222 and C221), is well known as the "cryptate effect".[11,24]

Acknowledgement—We gratefully acknowledge the support of this work by the Shiraz University Research Council.

REFERENCES

1. F. J. Kayne and J. Ruben, *J. Am. Chem. Soc.*, 1970, **92**, 220.
2. R. J. F. Williams, *Quart. Rev. Chem. Soc.*, 1970, 331.
3. J. S. Britten and M. Blank, *Biochim. Biophys. Acta*, 1968, **159**, 160.
4. F. J. Kayne, *Arch. Biochem. Biophys.*, 1971, **143**, 232.
5. R. M. Izatt, K. Pawlak, J. S. Bradshaw and R. L. Bruening, *Chem. Rev.*, 991, **91**, 1721.
6. G. Steffen and K. Sommermeyer, *Biophysik*, 1968, **5**, 192.
7. S. Kashanian and M. Shamsipur, *Inorg. Chim. Acta*, 1989, **155**, 203.
8. H. Parham and M. Shamsipur, *J. Electroanal. Chem.*, 1991, **314**, 71.

9. A. Semnani and M. Shamsipur, *J. Electroanal. Chem.*, 1991, **315**, 95.
10. M. K. Amini and M. Shamsipur, *Inorg. Chim. Acta*, 1991, **183**, 65.
11. H. Parham and M. Shamsipur, *Polyhedron*, 1992, **11**, 987.
12. M. Shamsipur and A. I. Popov, *J. Phys. Chem.*, 1987, **91**, 447.
13. M. Shamsipur and A. I. Popov, *J. Phys. Chem.*, 1988, **92**, 147.
14. M. K. Amini and M. Shamsipur, *J. Phys. Chem.*, 1991, **95**, 9601.
15. V. A. Nicely and J. L. Dye, *J. Chem. Educ.*, 1971, **48**, 443.
16. W. E. Wentworth, *J. Chem. Educ.*, 1962, **42**, 96.
17. M. J. D. Pawell, *Comput. J.*, 1964, **7**, 155.
18. R. D. Shannon, *Acta Cryst.*, 1976, **32A**, 751.
19. H. K. Frensdorff, *J. Am. Chem. Soc.*, 1971, **93**, 600.
20. J. M. Lehn, *Pure Appl. Chem.*, 1977, **49**, 857.
21. J. E. Huheey, *Inorganic Chemistry*, 3rd Ed., p. 312. Harper and Row, New York, 1983.
22. L. P. Golovkova, A. I. Telyatnik, V. A. Bidzilya, N. E. Akhmetova and V. I. Konovalova, *Ther. Exp. Chem.* (Engl. Transl.), 1985, **21**, 238.
23. R. M. Izatt, J. S. Bradshaw, K. Pawlak, R. L. Breuning and B. L. Tarbet, *Chem. Rev.*, 1992, **92**, 1261.
24. M. A. Bush and M. R. Truter, *J. Chem. Soc., Perkin Trans.*, 1975, **2**, 345.

Talanta, Vol. 40, No. 9, pp. 1357–1360, 1993
Printed in Great Britain.

0039-9140/93 $6.00 + 0.00

EVALUATION OF ASTEMIZOLE PURITY BY HPLC

M. V. SURYANARAYANA,* S. VENKATARAMAN, M. SATYANARAYANA REDDY and B. PARTHASARADHI REDDY

Dr. Reddy's Laboratories Ltd., Research and Development Division, 7-1-27, Ameerpet, Hyderabad 500 016, India

C. S. P. SASTRY

School of Chemistry, Andhra University, Visakhapatnam 530 003, India

G. L. DAVID KRUPADANAM

Department of Chemistry, Osmania University, Hyderabad 500 007, India

(*Received* 24 *December* 1992. *Revised* 16 *March* 1993. *Accepted* 22 *March* 1993)

Summary—A liquid chromatographic method is described for the evaluation of Astemizole purity. The method is also applicable for the analysis of pharmaceutical dosage forms of Astemizole using indole as internal standard. Separation was achieved with a μ bondapak C_{18} column and phosphate buffer (pH 6.0):acetonitrile (50:50 v/v) as eluent, at a flow rate of 1.5 ml/min with UV detection at 280 nm. The method is suitable for estimating the possible impurities if any present in Astemizole up to 0.05% for 1a and 0.25% for 1b. The method is simple, rapid and accurate for the analysis of Astemizole.

Astemizole [1-[(4-fluoro phenyl)methyl]-*N*-[1-[2-(4-methoxy phenyl)ethyl]-4-piperidinyl]-1H-benzimidazol-2-amine; 1, Fig. 1] is a new antihistamine of current interest that differs structurally from other antihistamines. Astemizole was found to be a long-acting non-sedating antihistamine with major clinical implications for the treatment of allergic diseases.

Currently Astemizole and its pharmaceutical dosage forms are not found in any pharmacopoeia. However an analytical profile[1] was found in a survey of the literature which include elemental analysis, radioimmunoassays and HPLC.

The synthetic route to Astemizole was described in two patents[2,3] where in both 2-chloro-1-[(4-fluoro-phenyl)methyl]-1H benzimidazole (1a, Fig. 1) and 1-(2-(4-methoxy phenyl)ethyl)-4-aminopiperidine (1b, Fig. 1) were allowed to react to give the expected product (1). Our investigation examined the product for the presence of both reactants as potential impurities. As the quantitative analysis[1] of Astemizole was already published, our aim was to develop an HPLC procedure suitable for detecting these impurities in Astemizole and to apply the same procedure for the analysis of this drug at various stages in the production of Astemizole. Also we want to apply these parameters for the assay of pharmaceutical dosage forms of Astemizole.

A study of several combinations of different solvents and buffer systems, different types of stationary phases and suitable internal standards for proper quantification, led to the described analytical conditions giving sharp and well resolved peaks.

EXPERIMENTAL

Apparatus

The HPLC (Waters Associates) instrument was equipped with a model 501 pump, U6K injector, model 481 variable wavelength UV detector. Separations were performed on a μ bondapak C_{18}, 10 microns stainless steel column (Waters USA) 300 × 3.9 mm at ambient temperature. The flow rate of the system was maintained at 1.5 ml/min with UV detection at 280 nm. The attenuation was set at 2.0 AUFS (Absorbance units full scale) with a chart speed of 0.25 cm/min. Chromatographic peaks were electronically integrated and recorded with a model 745 (Waters Associates) computing integrator.

*Author for correspondence.

Reagents

Chromatographic grade acetonitrile, analytical reagent grade Potassium dihydrogen orthophosphate, dipotassium hydrogen orthophosphate, perchloric acid, and indole and Milli Q water were used throughout these experiments.

Mobile phase

The mobile phase was composed of 50:50 v/v phosphate buffer pH 6.0 and acetonitrile.

Buffer solution was prepared by mixing the solutions of 0.022*M* potassium dihydrogen orthophosphate and 0.003*M* dipotassium hydrogen orthophosphate, and the pH of the solution adjusted to 6.0 with 0.01*M* perchloric acid.

Indole standard solution

A 0.5-mg/ml mobile phase solution of Indole was used as the internal standard.

Astemizole standard solution

A 1.0-mg/ml mobile phase solution of Astemizole was used as the drug standard.

Mixed indole and astemizole standard solution

Four millilitres of Astemizole solution and 1.0 ml of Indole solution were transferred to a 10-ml standard flask and diluted to the mark with mobile phase.

Sample preparation

A mass of powdered tablets equivalent to 25 mg of Astemizole was suspended in 25 ml of mobile phase and vortexed for 10 min. The insoluble portion, if any, was removed by filtration and the filtrate analysed after 4.0 ml of this solution was added to 1.0 ml of Indole standard.

Procedure

Five microlitres of the mixed standard or sample were injected into a universal injector using a 10-μl Hamilton Syringe. Each injection was done at an interval of 15 min to ensure complete elution of the previously injected material. Sample and mixed standard solutions were injected in triplicate. Quantitative determinations were made by comparison of the peak area ratio of Astemizole and Indole (Internal standard) for a sample injection to the

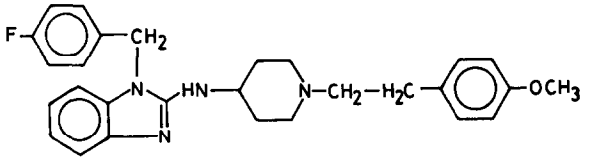

[ASTEMIZOLE, 1]

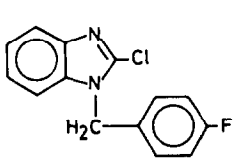

[2-CHLORO-1-[(4-FLUOROPHENYL)METHYL]-1H BENZIMIDAZOLE, 1a]

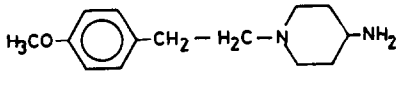

[1-(2-(4-METHOXY PHENYL) ETHYL)-4-AMINOPIPERIDINE, 1b]

Fig. 1.

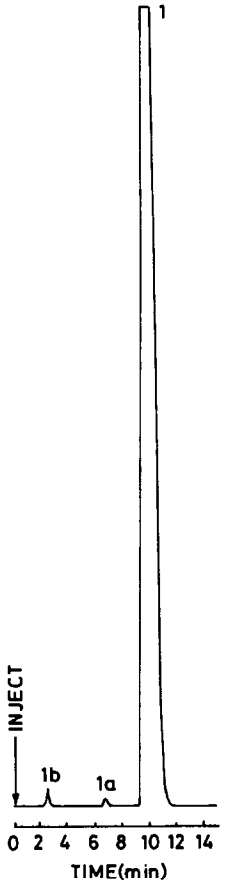

Fig. 2. HPLC separation of astemizole (1), 1(a) and 1(b).

corresponding area ratio for a mixed standard injection. Blank samples showed no interfering peaks.

Impurity analysis of Astemizole

To demonstrate HPLC resolution of Astemizole, 1(a), and 1(b), mobile phase solutions were prepared by adding known amounts of 1(a) and 1(b), 0.05 to 1.0%, to Astemizole. The impurity levels were also determined by comparison of peak area ratios for solutions of 1(a) and 1(b) at the levels up to 0.05 and 0.25%, respectively.

RESULTS AND DISCUSSION

The systematic study of the operating parameters that would optimize the HPLC resolution of chemical compounds involved in the synthesis of Astemizole led to the procedure.

As shown in Fig. 3, Astemizole and Indole (Internal standard) are distinctly eluted having retention times of 10.76 and 4.88 min, respectively. The ratios of peak area of Astemizole to that of Indole (Internal standard) were plotted against concentrations of Astemizole. The plot

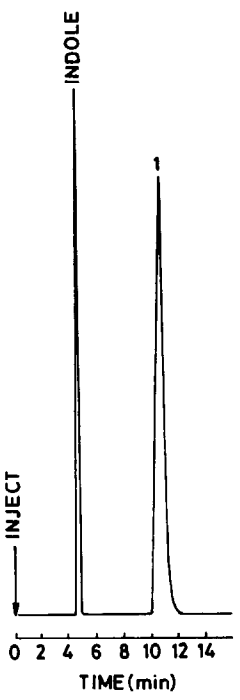

Fig. 3. Separation of indole and astemizole (1) by HPLC on μ bondapak C_{18} column.

was linear over the range 0.125–3.0 μg with a standard deviation of 0.137.

As shown in Fig. 2, Astemizole, 1(a) and 1(b) were distinctly eluted having retention times of 10.76, 7.80 or 2.78 min, respectively, with detection limits of 0.05% for 1(a) and 0.25% for 1(b).

Tablets of Astemizole were analysed by the proposed and reference HPLC methods and the results are tabulated in Table 1. The accuracy of the method was further ascertained through recovery studies by adding known amounts of Astemizole to placebo tablet powder and analysed by HPLC. Recovery was found to be 99.4–99.8%. These values indicate a lack of interference by the tablet diluents and lubricants. The precision of the method was found to

Table 1. Assay of Astemizole in pharmaceutical dosage forms by the proposed method

Sample No.	Sample	Content (*mg*)	% Label claim: Proposed HPLC method	% Label claim: Reference method*
1	Tablet	10	99.4	99.3
2	Tablet	10	99.8	99.8
3	Tablet	10	99.6	99.5
4	Tablet	10	99.8	99.8
5	Tablet	10	99.6	99.6

*HPLC method reported for pharmaceutical dosage forms in the analytical profile of Astemizole.

be 99.4–99.7% with a standard deviation of 0.04, giving evidence of excellent precision.

In conclusion, the proposed HPLC method allows rapid separation and determination of starting materials 1(a) and 1(b), which may be present in crude Astemizole. The method is also useful for the determination of Astemizole and its pharmaceutical dosage forms and results are comparable with the reported HPLC method.[1]

Acknowledgement—The authors are grateful to Dr. B. Saida Reddy of Dr Reddy's group for providing samples of Astemizole and its intermediates.

REFERENCES

1. Abdulrahman M. Al-Obaid and Mohammad Saleem Main, in *Analytical Profiles of Drug Substances*, Klaus Florey (ed.), Vol. 20, p. 173. Academic Press, New York, 1991.
2. Laboratorio Fides S.A. *Span. ES 533, 613* (Cl. C07D235/30), 16 Jun 1985, Appl 22 Jun 1984, 7 pp.
3. Montserrat Faba, Eusebio (Inke S.A.) *Span. ES 542, 807* (Cl. C07D401/12), 16 Dec. 1985, Appl. 03 May 1985.

Talanta, Vol. 40, No. 9, pp. 1361–1365, 1993
Printed in Great Britain.

0039-9140/93 $6.00 + 0.00

FLOW-INJECTION FLUORIMETRIC DETERMINATION OF TRIMEPRAZINE AND TRIFLUOPERAZINE IN PHARMACEUTICAL PREPARATIONS

T. PÉREZ-RUIZ,* C. MARTÍNEZ-LOZANO, V. TOMÁS and C. SIDRACH DE CARDONA
Department of Analytical Chemistry, University of Murcia, Murcia, Spain

(*Received* 15 *December* 1992. *Revised* 22 *February* 1993. *Accepted* 19 *March* 1993)

Summary—A flow-injection configuration for the fluorimetric determination of trimeprazine and trifluoperazine is proposed. The procedure is based on oxidation of the drugs by cerium(IV). The fluorescence of cerium(III) formed in the oxidation of trimeprazine or trifluoperazine is monitored. Lineal calibration graphs were obtained between 2×10^{-7} and $1 \times 10^{-5} M$ for both trimeprazine and trifluoperazine with a sampling rate of 60 samples/hr. The relative standard deviations were over the ranges 0.78–1.16 and 0.84–0.97% for trimeprazine and trifluoperazine, respectively. The applicability of the method to determination of trimeprazine and trifluoperazine was demonstrated by investigating the effect of potential interferences and by analysis of commercial pharmaceutical preparations.

Trimeprazine (*N*,*N*,*β*-trimethyl-10-H-phenothiazine-10-propanamine) and trifluoperazine (10[3-(4-methyl-1-piperazinyl)propyl]-2-(trifluoromethyl)-10-H-phenothiazine) are phenothiazines derivatives. These compounds have a profound psychotherapeutic activity,[1] trimeprazine being widely used as an antipruritic agent and trifluoperazine for the treatment of various mental illnesses. The importance of phenothiazine tranquilizers has prompted many investigators to look for methods for their rapid determination. The use of such drugs in chemotherapy and methods for their determination have been revised.[2–4] Titrimetric,[4] spectrophotometric,[5–9] chromatographic[3,10–12] and kinetic[13,14] methods have been used. A variety of methods based on the fluorescence of both unoxidized and oxidized compounds have also been used and cover a wide range of concentrations. Oxidation of phenothiazine drugs has been carried out with chemical reagents (H_2O_2, MnO_4^-, etc.) and photochemical decomposition.[15–18] Despite the large number of manual methods available, there are very few automated procedures. In recent years, flow-injection analysis (FIA) has found wide application in the determination of phenothiazines. Flow-injection procedures generally involve the use of chemical[19–22] or photochemical[23–26] oxidation of phenothiazines and use photometric and fluorimetric detection of their oxidized form. Other procedures using amperometric detection[27] and pseudo-titration in a non-aqueous medium[28] have also been reported.

Cerium(IV) has been used as an oxidizing agent for the determination of trimeprazine[20] and prometazine[21,22] in flow-injection systems. The red colour produced by the oxidized species of these drugs has been monitored spectrophotometrically. However, no method has been found dealing with the indirect determination of phenothiazines by measuring the fluorescence of cerium(III) formed.

In this paper the development of a spectrofluorimetric flow-injection method for the determination of trimeprazine and trifluoperazine and its application to routine are presented. The determination is based on the oxidation of these drugs by cerium(IV) and the parameter measured is the fluorescence of the Ce(III) formed during the reaction. The procedure is very simple, inexpensive and fast and allows the determination of these two drugs in pharmaceutical formulations.

EXPERIMENTAL

Apparatus and manifold

A Hitachi F-3010 spectrofluorometer equipped with a plotter unit and 1 × 1 cm quartz cell was used for recording spectra; excitation and emission spectra were corrected.

The flow-injection system consisted of a Tecator FIAstar 5020 flow-injection analyser

*Author for correspondence.

equipped with an injection valve and a peristaltic pump (40 r.p.p.). A Hitachi F-3010 spectrofluorometer connected to a plotter unit was used as a detector with a Hellma 176.052 QS flow cell (inner volume 25 μl). The manifold used is diagrammed in Fig. 1.

The cerium(IV) solution, $10^{-3}M$ (1M in H_2SO_4) was pumped at a flow rate of 0.8 ml/min. Trimeprazine, or trifluoperazine, covering the range of 2×10^{-7}–$1 \times 10^{-5}M$, were prepared by dilution of stock solutions and injected (158 μl) into the manifold; the peak heights were measured and recorded at 355 nm with excitation at 255 nm. The spectrofluorometer was set with excitation and emission slits at 10 nm.

Reagents

All reagents were of analytical reagent grade and were used as received. Doubly distilled water was used throughout. Aqueous $10^{-2}M$ trimeprazine and trifluoperazine stock solutions were prepared from the pure products (Sigma). Cerium(IV) solutions, $10^{-2}M$, were prepared by dissolving $Ce(SO_4)_2 . H_2O$ (Merck) in 1M sulphuric acid. Sodium bismuthate was added when Ce(IV) solutions were prepared in order to oxidize any Ce(III) present in the Ce(IV). The excess of sodium bismuthate was eliminated by filtering.

All phenothiazine and cerium(IV) solutions were stored in amber-coloured bottles. The drugs solutions were kept refrigerated to ensure stability. Working solutions were freshly prepared from stock solutions by suitable dilution.

Determination of trimeprazine and trifluoperazine in pharmaceutical formulations

Tablets of the pharmaceuticals were ground in an agate mortar to a fine powder and dissolved in water with the help of ultrasonic mixing and filtrated through Whatman No. 42 filter paper. The filtrate was diluted in a standard flask and an aliquot (158 μl) was injected into the flow-system.

For analysis of pharmaceuticals in solution the requisite volume of the solution was transferred to a 100-ml standard flask and diluted to the mark with doubly-distilled water.

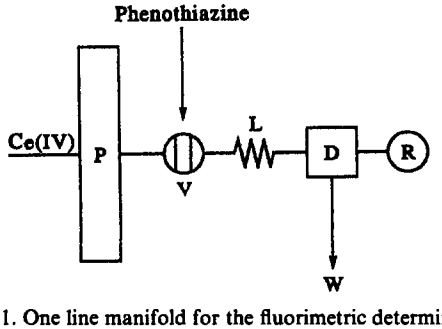

Fig. 1. One line manifold for the fluorimetric determination of phenothiazines.

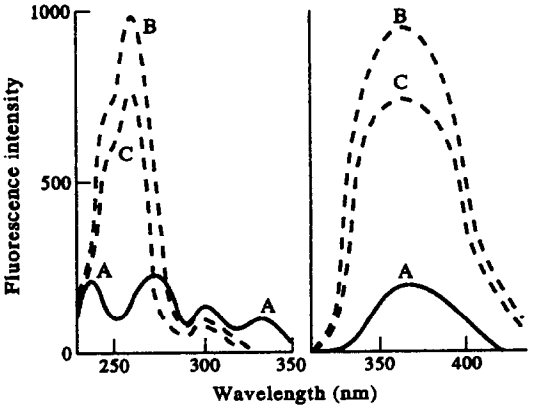

Fig. 2. Excitation and emission spectra of (A) Trimeprazine, $10^{-5}M$; $KMnO_4$, $2 \times 10^{-5}M$ and H_2SO_4, 1M. (B) Trimeprazine, $10^{-5}M$; Ce(IV), $10^{-4}M$ and H_2SO_4, 1M. (C) Ce(III), $10^{-5}M$; Ce(IV), $10^{-4}M$ and H_2SO_4, 1M.

RESULTS AND DISCUSSION

The oxidation of phenothiazines by Ce(IV) occurs in two steps and has already been described as an example of transient redox effects.[13] In excess of Ce(IV), the redox reaction is very fast and phenothiazines are completely oxidized to their sulphoxide form. The development of the reaction can be monitored by fluorescence of the Ce(III) or the sulphoxide formed. However, Ce(III) is more than 4 times as fluorescent as the oxidized phenothiazines, and so the measurement of its fluorescence can be used as a very sensitive indirect fluorimetric method for the determination of phenothiazines.

In addition, some oxidized phenothiazines also show excitation and emission maxima in the same spectral region where Ce(III) fluoresces; in such cases, an additional enhancement of the fluorescence readings is achieved. The excitation and emission spectra of oxidized trimeprazine (Fig. 2) clearly demonstrate this.

On the other hand, trimeprazine and trifluoperazine can be easily oxidized in a flow system by injecting the drugs, which react with the Ce(IV) solution flowing on line. A single-line FIA manifold with fluorimetric detection is suitable for the determination of both drugs.

The manifold schematized in Fig. 1 was used to investigate the effect of chemical and FIA variables on the peak height (fluorescence signal at λ_{em} 355 nm with a λ_{exc} 255 nm). The studies were performed by altering each variable in turn while keeping the others constant.

Chemical variables

The composition of the Ce(IV) stream had strong influence on the peak height. Three different acids (HNO_3, HCl and H_2SO_4) were tested to determine which was the most suitable for optimum reaction development. The nitric acid could not be used owing to the inhibitory effect of nitrate ions of the fluorescence of Ce(III).[29] In the presence of hydrochloric or sulphuric acid the reaction rate and the fluorescence of Ce(III) were high. Since cereus ions were always present to some extent in the Ce(IV) solutions, the fluorescence intensities of cerium(IV) solution were also measured to obtain appropriate blank corrections. In this study, sulphuric acid was selected because the baseline was less in this medium than in hydrochloric acid.

The influence of sulphuric acid concentration is shown in Fig. 3. The recommended concentration was 1*M*, because the fluorescence intensities obtained for trimeprazine and trifluoperazine remained virtually constant with slight changes in the concentration of sulphuric acid.

The effect of the concentration of the cerium(IV) stream was studied in the range 1×10^{-4}–$1.5 \times 10^{-3}M$. As can be seen from Fig. 4, the analytical signal increased with increasing reagent concentration up to $9 \times 10^{-4}M$ above which it remained virtually constant. The concentration selected was $1 \times 10^{-3}M$.

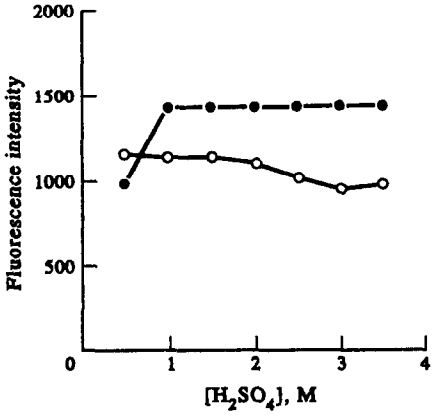

Fig. 3. Influence of sulphuric acid concentration on fluorescence intensity. Curves: (1) trimeprazine; (2) trifluoperazine. Sample injected = 158 μl of $10^{-5}M$.

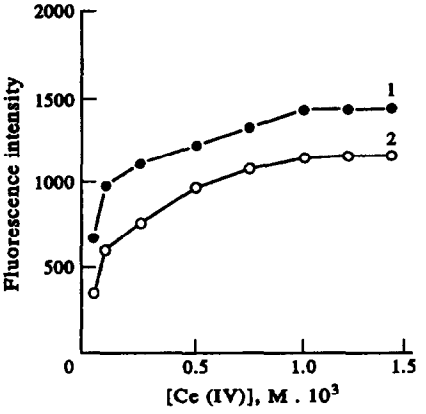

Fig. 4. Influence of Ce(IV) concentration on fluorescence intensity. Curves: (1) trimeprazine; (2) trifluoperazine. Sample injected = 158 μl of $10^{-5}M$.

The influence of temperature on the peak height was studied over the range 25–45°. The signal decreased slightly with an increase in temperature. In the FIA procedure this variable was controlled at 30°.

Optimization of the FIA variables

Because the oxidation of trimeprazine and trifluoperazine by Ce(IV), under the recommended conditions is very fast, a simple manifold using cerium(IV) sulphate solution in 1*M* sulphuric acid as carrier was found to be the most suitable. Optimization of the different variables influencing the FIA system was carried out. Figure 5 shows the effect of the pumping

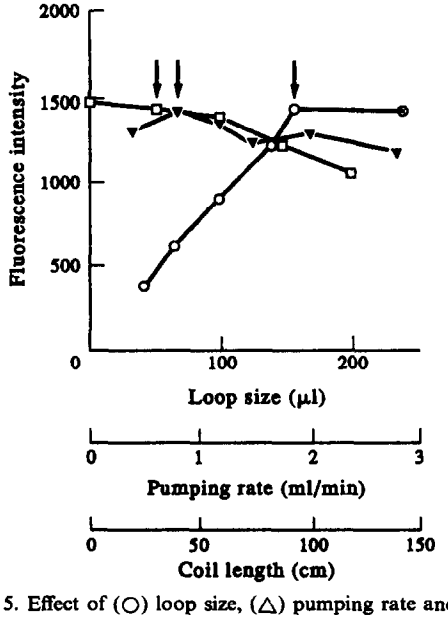

Fig. 5. Effect of (○) loop size, (△) pumping rate and (□) coil length on fluorescence intensity. Sample injected = $10^{-5}M$ trimeprazine. The arrows mark the values of the parameters selected.

Table 1. Features of the calibration graphs for the determination of trimeprazine and trifluoperazine

Parameter	Trimeprazine	Trifluoperazine
Determination range	2×10^{-7}–$1 \times 10^{-5} M$	2×10^{-7}–$1 \times 10^{-5} M$
Slope/I_F, M^{-1}	7.2×10^7	7.6×10^7
Intercept/I_F (%)	159	185
Correlation coefficient*	0.9967	0.9989
RSD%†	±1.16; ±0.78	±0.976; ±0.84

*The correlation coefficients were calculated using 11 different concentrations of each analyte.

†Relative standard deviations ($n = 10$), [phenotiazine] = $2 \times 10^{-6} M$ and $1 \times 10^{-5} M$.

rate, loop size and length of coil. The selected values of the FIA variables are: flow rate, 0.8 ml/min; injection volume, 158 μl and reactor length, 30 cm. The inner diameter of the coil was 0.5 mm. These values allow the phenothiazine drugs to be oxidized by the time the sample plug passes through.

Determination of trimeprazine and trifluoperazine

A series of standard solutions of trimeprazine or trifluoperazine were pumped in triplicate to test the linearity of the calibration graphs. The calibration graphs have a linear range (Table 1), from which the excellent sensitivity of the proposed method is evident. A statistical study was performed on 10 samples ($P = 0.05$) by triplicate injections of 2×10^{-6} and $1 \times 10^{-5} M$ levels of each analyte. The sampling rate was 60 samples/hr.

Table 2. Tolerance of the proposed method to interferences*

Substance	Tolerance molar ratio Interferent: Trimeprazine or Trifluoperazine
Glucose, saccharine, D-mannose, sucrose	100†
Lactose, galactose, ethanol, sodium benzoate	50
EDTA, starch†	10
Citric acid	6
Gelatin‡	5
Propyleneglycol	1

*$1 \times 10^{-5} M$ phenothiazine added.

†Maximum tested.

‡Tolerable W/W ratio.

Interferences

An interference study aimed at the determination of trimeprazine and trifluoperazine in pharmaceutical preparations was performed. Samples containing a fixed concentration of each phenothiazine, $10^{-5} M$, and various concentrations of foreign substances were injected into the FIA system. A substance was considered not to interfere if the variation in the peak height of the phenothiazine was less than ±3% in its presence. The results are shown in Table 2.

The foreign substances tested were substances and excipient generally present in pharmaceutical preparations. Under the reaction conditions used most of them do not interfere. However ascorbic acid, acetylsalicylic acid and sodium sulphite interfere and must therefore be eliminated.

Table 3. Determination of trimeprazine and trifluoperazine in pharmaceuticals

Sample*	Source	Nominal value/*mg*		Found/*mg*	
		Trimeprazine	Trifluoperazine	Reference method‡	FIA method§
Efralen† (syrup)	Italfarmaco	25.0	—	25.54	25.75 ± 0.32
Variargil alimemazine (drops)	Italfarmaco	40.0	—	39.20	39.06 ± 0.81
Eskazine (sugar-coated pill)	Beecham	—	5	5.12	5.09 ± 0.12

*Mean of four determinations ± SD.

†Composition of samples: Efralen: trimeprazine tartrate, 0.025 g; ammonium acetate 2.500 g; sodium benzoate 0.240 g; magnesium sulphate 0.200 g; sodium saccharin 0.025 g; surcrose 70.642 g and sulphite and ethanol as excipient (100 ml). Variargil alimemazine: trimeprazine tartrate, 40 mg; surcrose, 192 mg and ethanol as excipient (1 ml). Eskazine: trifluoperazine dihydrochloride, 5 mg in a sugar-coated pill.

‡Sulphite was previously eliminated by passing the solution through a strongly basic anion-exchanger (chloride form) column.

§Average of three determinations obtained by the manual spectrophotometric method using molybdophosphoric acid (30).

Table 4. Recovery of trimeprazine and trifluoperazine from pharmaceutical preparations

Sample*	Added, mg/ml	Found,† mg/ml	Recovery, %
Efralen	0.50	0.52 ± 0.03	104.0
	1.00	1.02 ± 0.05	102.0
	1.50	1.46 ± 0.06	97.0
Variargil	0.50	0.51 ± 0.04	102.0
	1.00	0.99 ± 0.03	99.0
	1.50	1.45 ± 0.06	96.7
Eskazine	0.50	0.49 ± 0.03	98.0
	1.00	1.01 ± 0.06	101.0
	1.50	1.47 ± 0.05	98.0

*See Table 3.
†Average of three determinations ± SD.

Applications

The proposed methods were applied satisfactorily to the determination of trimeprazine and trifluoperazine in pharmaceutical preparations. Table 3 summarizes the data obtained.

The recovery was determined by adding various amounts of trimeprazine or trifluoperazine to pharmaceutical preparations and subtracting the results obtained for pharmaceuticals prepared in a similar manner but to which no phenothiazine has been added. The results are shown in Table 4.

CONCLUSIONS

The results obtained clearly demonstrate the suitability of monitoring the fluorescence of Ce(III) liberated during the oxidation of trimeprazine and trifluoperazine by Ce(IV). The high tolerance level for foreign species can be ascribed to the kinetic aspect of the flow-injection methods; as a consequence, unwanted reactions do not develop to any significant extent in the short measurement period.

The versatility and simplicity of this method allows its adaption to the type of analysis in which a large number of samples of very similar composition have to be analysed, *e.g.*, testing the uniformity of pharmaceutical preparations (required for all solid formulation with < 50 mg of drug).

When this method is compared with other methods that measure the fluorescence of phenothiazines, it can be seen that its sensitivity is as good as those methods which use photochemical oxidation[23–26] but much greater than those based on chemical oxidation.

The method has been successfully applied to the determination of trimeprazine and trifluoperazine in pharmaceutical preparations.

Acknowledgements—The authors express their gratitude for the financial support from Spanish DGICYT (Project PB90-008).

REFERENCES

1. A. G. Gilman, L. S. Goodman, T. W. Rall, and F. Murad, *Las Bases Farmacológicas de la Terapeutica*, Panamericana, Madrid, 1989.
2. J. E. Fairbrother, *Pharm. J.*, 1979, **222**, 271.
3. G. Cimbura, *J. Chromatogr. Sci.*, 1972, **10**, 287.
4. U.S.P., 22nd Revision, 1990.
5. H. S. Gowda, P. G. Ramappa and A. N. Nayak, *Anal. Chim. Acta*, 1979, **108**, 277.
6. P. G. Ramappa, H. S. Gowda and A. N. Nayak, *Microchem. J.*, 1983, **28**, 586.
7. M. S. Mahrous and A. A. Abdel-Khalek, *Talanta*, 1984, **31**, 289.
8. M. Rizk, N. A. Zakhari, F. Ibrahim and M. I. Walash, *ibid.*, 1986, **33**, 111.
9. M. Gayarama, M. D'Souza, H. S. Yathirajan and Y. Ragaswam, *ibid.*, 1986, **33**, 352.
10. N. E. Larsen, L. B. Mansen and P. Kraudsen, *J. Chromatog. Biomed. Appl.*, 1985, **42**, 244.
11. I. R. Tebbett, *J. Chromatog.*, 1986, **356**, 227.
12. U. A. Th. Brikman, P. L. M. Welling, G. de Vries, A. H. M. T. Scholten and R. W. Frei, *ibid.*, 1981, **217**, 463.
13. H. A. Mottola and A. Hanna, *Anal. Chim. Acta*, 1978, **100**, 167.
14. M. C. Gutierrez, A. Gomez-Hens and D. Perez-Bendito, *Anal. Lett.*, 1987, **20**, 1847.
15. J. B. Ragland and V. J. Kinross-Wright, *Anal. Chem.*, 1964, **36**, 1356.
16. F. J. Mellinger and C. E. Keeler, *Ibid.*, 1963, **35**, 554.
17. *Idem*, *ibid.*, 1964, **36**, 1840.
18. V. R. White, C. S. Frings, J. E. Villafranca and J. M. Fritzgerald, *ibid.*, 1976, **48**, 1314.
19. M. A. Koupparis and A. Barcuchova, *Analyst*, 1986, **111**, 313.
20. S. M. Sultan, *Microchem. J.*, 1991, **44**, 304.
21. J. Martínez Calatayud and V. García Mateo, *Anal. Chim. Acta*, 1992, **264**, 283.
22. J. Martínez Calatayud and T. García Sancho, *J. Pharm. Biomed. Anal.*, 1992, **10**, 37.
23. D. Chen, A. Rios, M. D. Luque de Castro and M. Valcarcel, *Analyst*, 1991, **116**, 171.
24. J. Martinez Calatayud and C. Gomez Benito, *Anal. Chim. Acta*, 1992, **256**, 105.
25. M. T. Tena, M. D. Luque de Castro and M. Valcarcel, *J. Automat. Chem.*, 1991, **13**, 11.
26. D. Chen, A. Rios, M. D. Luque de Castro and M. Valcarcel, *Talanta*, 1991, **11**, 1227.
27. J. Wang and H. D. Dewald, *Anal. Chim. Acta*, 1983, **153**, 325.
28. C. A. Georgiou and M. A. Koupparis, *Analyst*, 1988, **113**, 755.
29. P. Cukor and R. P. Weberling, *Anal. Chim. Acta*, 1968, **41**, 401.
30. H. Sanke Gowda, P. G. Ramappa and A. N. Nayak, *ibid.*, 1979, **108**, 277.

Talanta, Vol. 40, No. 9, pp. 1367–1373, 1993
Printed in Great Britain.

0039-9140/93 $6.00 + 0.00

β-CYCLODEXTRIN CHIRAL STATIONARY PHASES FOR LIQUID CHROMATOGRAPHY. EFFECT OF THE SPACER ARM ON CHIRAL RECOGNITION

ALAIN BERTHOD

Laboratoire des Sciences Analytiques, UA C.N.R.S. 435 (J. M. Mermet) Université de Lyon 1, 69622 Villeurbanne cedex, France

CHAU-DUNG CHANG and DANIEL W. ARMSTRONG

Department of Chemistry, University of Missouri-Rolla, Rolla, MO 65401, U.S.A.

(*Received* 15 *December* 1992. *Revised* 10 *February* 1993. *Accepted* 18 *March* 1993)

Summary—Cyclodextrins (CDs) can be bound on silica to prepare chiral stationary phases (CSPs) for liquid chromatography. The cyclodextrin ring is connected to a spacer previously bonded on the silica surface. Three different CD-CSPs were prepared with three different spacers. (i) A dimethylethoxysilane with a linear 6 carbon chain produced a monomeric layer. The bonded CD units can move and rotate freely. (ii) The corresponding trimethoxysilane produced a polymeric layer. The bonded CD units were not located at the same distance of the silica surface, but they could still move and rotate freely. (iii) The third spacer contained a cyclohexyl ring that may introduce some conformational rigidity in the CD connection to silica. The three CSPs prepared contained a CD surface coverage of about 0.3 μmol/m^2 which is approximately half of the maximum theoretical CD coverage. The first spacer was the most efficient to bond CDs with an average value of 1.7 spacers per CD ring, whereas 5.5 spacers per CD ring were needed with the two other spacers. The chiral recognition capabilities of the three phases were compared using 14 racemic compounds. No pronounced differences were noted, but the CSP prepared with the dimethylethoxysilane monomeric spacer seems to be the most efficient for chiral recognition.

Stereoisomeric or chiral separations are a very challenging analytical problem. Liquid chromatography (LC) and gas chromatography (GC) are the most powerful techniques in enantiomer separations.[1,2] A chiral stationary phase (CSP) is most often used together with a classical achiral mobile phase. Among the available CSPs for LC are the polymeric chiral phases, the crown ether phases, the protein phases,[3] the π-complex, hydrogen bond phases (Pirkle type),[4] and the cyclodextrin (CD) bonded phases.[1,5] The latter type of CSPs were introduced and developed by Armstrong and DeMond in 1984.[6] To date, three underivatized or native CD–CSPs and nine derivatized CD–CSPs have been marketed. Some derivatized CD–CSPs are multimodal: they can work with non-polar (normal mode) mobile phases and polar (methanol–water or acetonitrile–water) mobile phases which is known as reversed phase mode.[1] The underivatized CD–CSPs can work with reversed mobile phases and with polar but purely organic mobile phases (acetonitrile–methanol phases). The latter mobile phases used together with native CD stationary phases are very effective for chiral separations.[7]

Cyclodextrins have an internal toroidal and relatively non-polar cavity. It can easily accommodate molecules or parts of molecules having the size of an aromatic ring. The secondary 2- or 3-hydroxyl groups of each glucopyranoside ring in the CD are located axially at the mouth of the cavity. They form a polar crown that is most important for chiral recognition. CD rings are not bonded directly on the silica surface to prepare a CD–CSP. Rather, a primary hydroxyl group of the CD is used to graft it on a spacer which was first attached on the silica surface.[5] The aim of this work is to prepare different CSPs with β-CD and different spacer molecules and to investigate the effect of the spacer on the chiral recognition ability of the CSPs. Three β-CD–CSPs were prepared with three different spacers bonded on the same silica base. They were tested with a variety of chiral compounds to determine which spacer gives the best chromatographic performance.

EXPERIMENTAL

Chemicals

The silica base used to prepare the three CSPs was Spherisorb silica from Phase Separations Inc. (Norwalk, CT, U.S.A.). It is a 5-μm spherical bare silica, 220 m^2/g surface area, 8 nm pore diameter and 0.44 cm^3/g pore volume.[8] The three silanizing reagents were three epoxydized methoxysilanes whose full structures and names are presented in Fig. 1. They were obtained from Petrarch Systems as viscous liquids of ~93% purity (Bristol, PA, U.S.A.) and used as received. Toluene, methanol and other usual solvents were obtained from Aldrich (Milwaukee, WI), Sigma (Saint Louis, MO) and Fisher (Pittsburgh, PA, U.S.A.). Water was demineralized and filtered on a Barnstead D8922 system. The chiral solutes were obtained from Sigma as racemates. Fluoxetine is a drug under pharmaceutical investigation at Eli Lilly (Indianapolis, IN). It was kindly supplied by Thomas L. Jeatran.

Bonding procedure

Spacer bonding. Four grams of Spherisorb silica were dried overnight at 110° in a drying gun under vacuum. The dried silica was placed in a flask with approximately 100 ml of anhydrous toluene. Water was further removed at 84° as an azeotrope by distillation of 25 ml into a Dean-Stark trap. Next, 10 ml of the appropriate epoxysilane was added and the solution was maintained at 90–95° for 4 hr. The bonded sorbent was collected on a fritted glass filter and washed with dry toluene followed by methanol and air-dried.

Cyclodextrin bonding. The epoxy bonded sorbent was dried overnight at 60° in a drying gun under vacuum. Four grams of β-CD (3.5 mmoles) were similarly dried in another drying gun. The dried CD was dissolved in approximately 100 ml of anhydrous dimethylformamide (DMF) and 1 g of sodium hydride (NaH, 42 mmoles), as an 80% suspension in paraffin oil, was carefully added. After 15 min at room temperature, the hydrogen gas release stopped. The solid (excess NaH or sodium hydroxide) was filtered off and the solution was added to a round bottom flask containing the dried epoxy bonded sorbent in DMF. The mixture was refluxed for 4 hr. The cyclodextrin bonded sorbent was filtered on a fritted glass filter and washed with the sequence DMF, toluene, methanol, water, methanol again and air-dried.

The silane A (Fig. 1) can only produce a monomeric bonded layer. The two other silanes, B and C, could produce a polymeric layer if some water was introduced at the end of the spacer bonding reaction. Water molecules hydrolyze methoxysilane groups to generate methanol and silanol groups which can further

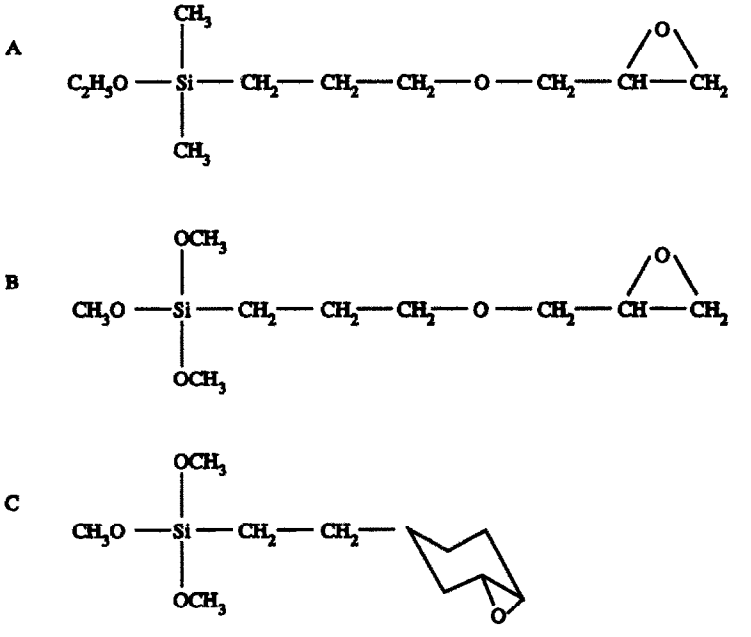

Fig. 1. Structure of the three silanizing reagents. A—3-glycidoxy-propyldimethylethoxysilane. B—3-glycidoxypropyltrimethoxy silane. C—2-(3,4-epoxycyclohexyl)ethyltrimethoxysilane.

Table 1. Characteristics of the chiral phases prepared

Phase type	Bonding agent (Fig. 1)	Spacer bonding		CD bonding		Aver. spacer per CD
		%C	μmol/m²	%C	μmol/m²	
Monomeric	A	1.26	0.6	4.87	0.35	1.7
Polymeric	B	2.59	1.7	5.83	0.32	5.5
Cyclohexyl	C	2.81	1.4	5.47	0.26	5.5

react with the original silane reagent. The reaction with Spacer C was done without any trace of water. At the end of the reaction, water was used in the washing sequence. The residual methoxysilane groups may then be hydrolyzed. Thus, the monomeric bonded spacer C probably bears two silanol groups close to the silica surface. A polymeric CD–CSP was prepared using Spacer B by Tom Beesley at Astec (Advanced Separation Technologies, Whippany, NJ, U.S.A.). The first step was identical to the Spacer C bonding procedure. Next, trace amounts of water were added to hydrolyse some methoxysilane groups and to create silanol groups. Then, more fresh Spacers B were introduced to react with the newly created silanol groups. These steps were repeated four times.

The carbon elemental analysis were done by Galbraith Laboratories Inc, Knoxville, TN, U.S.A.

Chromatographic system

The CD–CSPs were slurry packed in three 25 cm × 4.6 mm i.d. stainless steel columns. A Shimadzu chromatographic system was used with a LC-6A pump, a SPD-6A UV detector, a SCL-6B controller and a CR5A integrator.

RESULTS AND DISCUSSION

The stationary phases

The β-CD ring is more likely attached to the epoxy end group by one of its seven primary hydroxyl groups. These seven more acidic groups protrude on the external side of the CD ring when the less acidic secondary hydroxyl groups are all 21 gathered at the CD mouth. Linkage could occur through secondary hydroxyl groups, but primary hydroxyl groups are less sterically hindered. Table 1 lists the carbon analysis of the three stationary phases after the spacer grafting and after CD addition. The corresponding organic coverage was calculated using

$$\frac{\dfrac{\%C}{12n_c \times 100}}{S\left(1 - \dfrac{\%C}{12n_c \times 100} \times M\right)}$$

in which %C is the carbon mass percentage in bonded sorbent, obtained by elemental analysis, n_c is the number of carbon atoms in the bonded moiety ($n_c = 8$, 6, 8, 42 for Spacers A, B, C and CD, respectively), M is the molecular weight of the bonded moiety ($M = 173$, 175, 187 and 1135 for Spacers A, B, C and CD, respectively) and S is the bare silica surface (220 m²/g).

The bonding density for Spacer B, which produces a polymeric layer, is indicated for comparison and corresponds to an average of 1.7 μmol/m² of 3-glycidoxypropylsilane. From a chemical point of view, Spacer A is the most efficient to link a CD unit to the silica surface. An average value of 1.7 Spacer A units was needed to bond one CD ring. An average value of 5.5 Spacers B and C were necessary to link one CD unit. However, the CD surface concentration was 0.3 μmol/m² for approximately the three phases prepared.

The 0.3 μmol/m² CD surface concentration is more than 10 times lower than the usual surface concentration, in the 3 μmol/m² range,[8] proposed by the manufacturers of classical C18, C8 and C1 LC column packings. The maximum bonding density for linear alkyl chains is close to 5 μmol/m².[9] The height of a CD ring is 0.79 nm and the external diameter of the β-CD ring is 1.53 nm, corresponding to a 1.84×10^{-18} m² area. If the CD ring stands flat on the silica surface, it occupies a square area of about 2.34×10^{-18} m². On a square meter, 4.27×10^{17} CD rings could be packed, which corresponds to 0.7 μmol/m². If the CD ring is placed sideways on the silica surface, the area occupied is about 1.21×10^{-18} m², corresponding to a maximum theoretical bonding coverage value of 1.37 μmol/m². With these data, the 0.3 μmol/m² CD coverage that we obtained experimentally corresponds to

approximately 50% of the maximum CD flat coverage and 22% of the maximum CD sideways coverage. The 220 m^2/g surface area given by the manufacturer includes the surface area of small pores that are not accessible to β-CD rings. This means that it may be very difficult to increase substantially the 0.3 $\mu mol/m^2$ CD bonding coverage obtained using the procedure described in the Experimental section.

Chiral separations

Table 2 lists the results of the separation of 14 compounds already separated by a β-CD phase in a recent study.[10] All drugs were separated on the three stationary phases, adjusting the mobile phase composition (acetonitrile–water + 0.1% triethylammonium acetate) so that the k' values were similar.

Table 2. Chromatographic parameters of the chiral separations performed on the three CD-CSPs

Compound structure	spacer	mobile phase buffer/acetonitrile	pH	k'	α	Rs	N
Aminoglutethimide 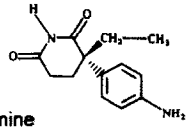	A	70/30	7.1	3.91	1.04	0.47	3700
	B	80/20	7.1	3.5	1.02	0.2	2700
	C	70/30	7.1	3.48	1	0	2200
Chlorpheniramine 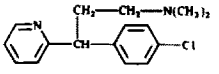	A	60/40	7.1	10.3	1.05	0.68	3900
	B	70/30	7.1	4.22	1.03	0.31	2800
	C	60/40	7.1	7.96	1.03	0.17	700
Chlorthalidone 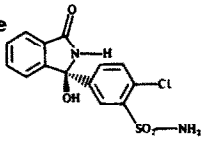	A	80/20	4.1	0.63	1.19	0.84	3000
	B	80/20	4.1	0.85	1.25	1.21	2800
	C	80/20	4.1	1.29	1.15	0.92	2500
Dansyl Leucine 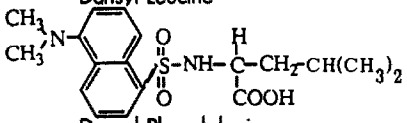	A	70/30	4.1	1.5	1.13	0.9	2700
	B	50/50	4.1	3.42	1.19	1.38	2000
	C	60/40	4.1	3.23	1.14	1.03	1900
Dansyl Phenylalanine 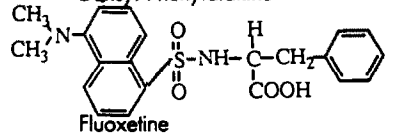	A	70/30	4.1	1.76	1.14	0.8	1700
	B	50/50	4.1	4	1.13	1.39	3600
	C	60/40	4.1	4.15	1.11	0.95	2300
Fluoxetine 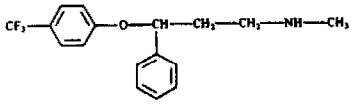	A	60/40	7.1	5.94	1.07	1.16	7000
	B	70/30	7.1	3.59	1.06	0.81	5300
	C	60/40	7.1	5.52	1.06	0.41	1200
	A	70/30	4.1	1.54	1.11	0.94	4000
	B	85/15	4.1	1.66	1.11	0.55	1300
	C	70/30	4.1	1.16	1.09	0.4	1300
Ibuprophen 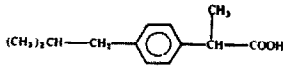	A	70/30	4.1	10.8	1.05	0.62	3200
	B	50/50	4.1	9.17	1.06	0.96	5700
	C	60/40	4.1	6.75	1.04	0.47	3200
Ketoprofen 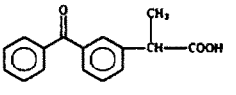	A	80/20	4.1	6.55	1.04	0.48	3300
	B	70/30	4.1	8.27	1.03	0.27	1700
	C	80/20	4.1	15	1	0	1600
Mephenytoin 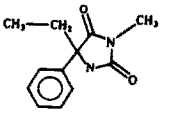	A	80/20	4.1	1.54	1.42	4.7	11000
	B	80/20	4.1	0.93	1.31	2.05	5100
	C	80/20	4.1	1.64	1.22	2.4	7300

Table 2—*continued*

Compound structure	spacer	mobile phase buffer/acetonitrile	pH	k′	α	Rs	N
Methylphenidate 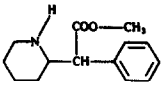	A	60/40	7.1	4.62	1.03	0.6	10000
	B	80/20	7.1	1.93	1.07	0.76	5000
	C	70/30	7.1	3.67	1.04	0.5	4400
Metoprolol 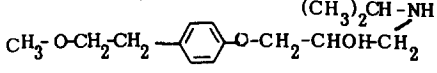	A	70/30	7.1	6.81	1.02	0.31	5300
	B	80/20	7.1	3,5	1	0	5000
	C	70/30	7.1	4.46	1.01	0.15	5500
Phensuximide 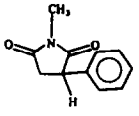	A	80/20	4.1	1.27	1.12	1	4400
	B	80/20	4.1	0.68	1.09	0.7	7000
	C	80/20	4.1	1.38	1.09	0.62	2700
Propranolol 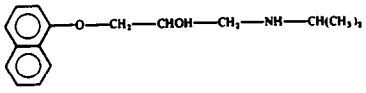	A	70/30	7.1	5.79	1.02	0.4	9200
	B	80/20	7.1	4.36	1.02	0.2	2500
	C	70/30	7.1	5.42	1.01	0.17	6600
Suprofen 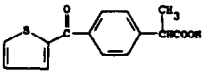	A	83/17	7.1	2.69	1.05	0.28	1000
	B	70/30	7.1	1.59	1.05	0.49	4500
	C	83/17	7.1	7.93	1.04	0.27	1000

The chiral recognition by CD cavities depends on the sp^2 hybridization of the groups attached to the chiral center.[11,12] If the chiral center is part of a ring structure, the chiral recognition by CDs is enhanced.[10,11] The effect of the solvent, the pH and the solute substituents are also very important, as described in other works.[13,14] The highest enantioselectivity factors were obtained with the solutes mephenytoin ($\alpha = 1.42$) and chlorthalidone ($\alpha = 1.19$) in which the chiral center is part of a ring and bears two sp^2 hybridized carbons. The lowest enantio-selectivity factors were obtained with the solutes propranolol ($\alpha = 1.02$) and metoprolol ($\alpha = 1.01$), in both compounds the chiral center is not part of a ring and not connected to sp^2 hybridized carbons. Note that aminoglutethimide has a chiral center in a ring structure with two sp^2 hybridized carbons; however its chiral recognition is very low ($\alpha = 1.02$). Table 2 shows some differences in the enantioselectivity factor of a given compound on the three different phases as discussed below.

Spacer influence

Spacer A is the linear monofunctional spacer of the patented procedure used to prepare the commercialized β-CD-CSP.[5] Spacer B was chosen to obtain a polymeric bonded layer with spacer arms similar to A. Both spacers A and B do not hold the CD ring tightly. They allow some motion that may orientate the CD cavity in any direction. Spacer C contains a cyclohexyl unit that renders the structure more rigid. The CD ring orientation may be limited with this spacer.

Table 2 shows that the enantioselectivity factors for a given compound are not drastically different on the three β-CD CSPs. However, there are some differences. For 10 compounds α is slightly (~0.02 unit) higher on the Spacer A β-CD phase while four compounds have their highest α value on the Spacer B β-CD phase. The chiral recognition seems somewhat more limited on the Spacer C β-CD phase. Figure 2 shows the separation of *N*-dansyl phenylalanine on the three different β-CD CSPs. The racemate is almost baseline resolved on the Spacer B β-CD phase. These small differences in chiral recognition may be due to the difference in CD coverage listed in Table 1.

Table 2 also lists *R*s, the resolution factor between the two enantiomers. The resolution factor combines k', the capacity factor, α, the enantioselectivity factor, and N, the peak efficiency (in plate number). The efficiency was measured by hand using $W_{0.6H}$, the peak width at 60% of the peak height and computed as $N = 4(t_r/W_{0.6H})^2$. Again, the efficiency obtained on the Spacer A β-CD phase is higher, in general,

than the one obtained on the two other phases. Only four compounds showed the highest efficiency on the Spacer B β-CD phase (Table 2). The low efficiency observed with the Spacer C β-CD phase may be due to the silanol groups present at the foot of the spacer after hydrolysis of the two remaining methoxy groups (Fig. 1). The efficiency is especially low with the solutes chlorpheniramine (700 plates) and fluoxetine (1200 plates) which both contain an amino group, but it is equally low (1000 plates) with suprofen, which does not. The fluoxetine separation on the three CSPs is shown in Fig. 3. The selectivity factor is similar on the three phases ($\alpha = 1.06$). The resolution is almost baseline with the Spacer A phase ($Rs = 1.16$ with 7000 plates) and it is very weak with the Spacer C phase ($Rs = 0.41$ with 1200 plates) due to peak broadening. It is known that basic compounds are sensitive to residual silanol groups and produce broad peaks. However, also metoprolol and propranolol have a secondary amino group in their molecule and the observed efficiencies are good (5500 and 6600 plates, respectively). The mobile phase pH was adjusted by triethylamine (0.1% v/v) and acetic acid. Triethylamine was used to shield possible residual silanols.

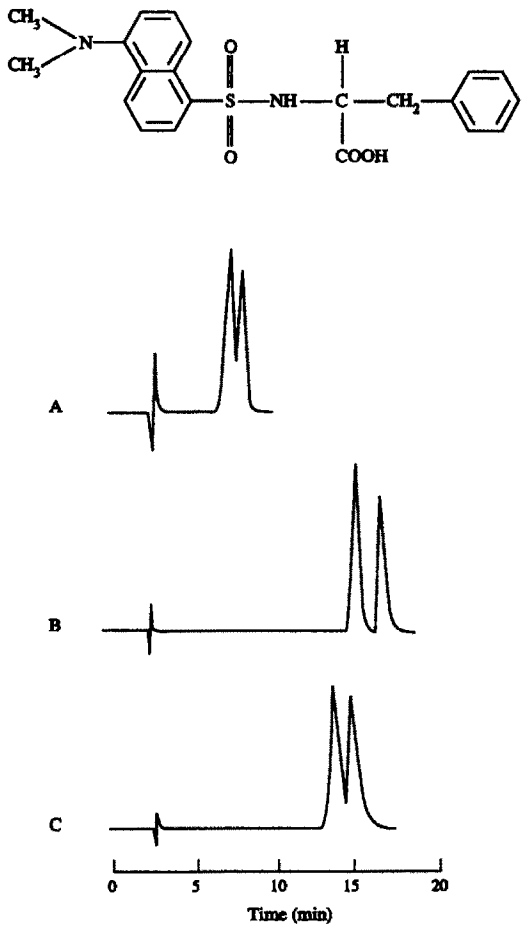

Fig. 2. Enantiomer resolution of *N*-dansyl phenylalanine on the three stationary phases prepared. Mobile phase: 0.1% v/v triethylamine, pH adjusted to 4.1 with acetic acid, water–acetonitrile. A—buffer 70%–ACN 30% v/v; B—buffer 50%–ACN 50% v/v; C—buffer 60%–ACN 40% v/v. Flow rate 1 ml/min. Detection UV = 254 nm.

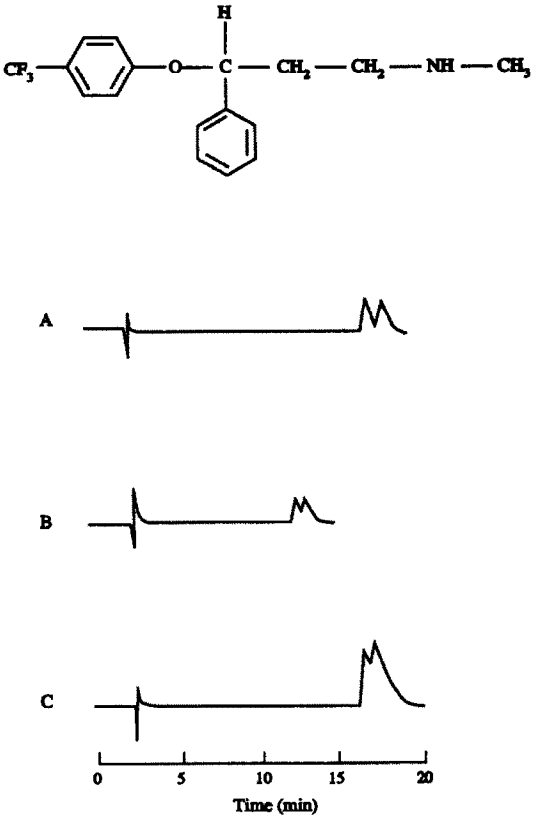

Fig. 3. Enantiomer resolution of fluoxetine on the three stationary phases prepared. Mobile phase: 0.1% v/v triethylamine, pH adjusted to 7.1 with acetic acid, water–acetonitrile. A—buffer 60%–ACN 40% v/v; B—buffer 70%–ACN 30% v/v; C—buffer 60%–ACN 40% v/v. Flow rate 1 ml/min. Detection UV = 254 nm.

CONCLUSIONS

Spacer A produces a monomeric layer. An average value of 1.7 Spacer A molecule is needed to bond one cyclodextrin rings on the surface of silica against 5.5 molecules for the two other spacer studied. From an economical point of view, Spacer A seems the most appropriate to prepare a chiral stationary phase for liquid chromatography. The CD coverage obtained (0.35 μmol/m^2) is close to 50% of the maximum theoretical coverage. The CD coverage obtained with the two other spacers

is similar. However, the Spacer B bonding procedure, that produces a polymeric bonded layer, is more difficult than the two others. The Spacer C phase bears residual silanol groups that may be a problem in a number of chiral separations.

From a mechanistic point of view, this study does not give conclusive advice on the accessibility of the CD rings and on the rigidity of CD bonding to silica. The Spacer A and Spacer B phases join the CD ring to the silica surface with a flexible arm. The CD ring can rotate and take any orientation in the three dimensions. With the Spacer A monolayer bonding, all CD rings may be located at the same distance from the silica surface. With the Spacer B polymeric bonding, the CD rings may be more or less buried in the bonded layer. No significant difference in chiral recognition capabilities were noted with these two phases. The cyclohexyl group in the Spacer C molecule makes the link between the CD ring and the silica surface more rigid. The chiral recognition by the Spacer C phase was somewhat lower than the one obtained with the two other phases. An end-capping treatment would reduce the number of residual silanol groups and may balance the chiral recognition capability of the three phases.

REFERENCES

1. D. W. Armstrong and S. M. Han, *CRC Crit. Rev. Anal. Chem.*, 1988, **19**, 175.
2. M. Zief and L. J. Crane (eds), *Chromatographic Chiral Separations, Chromatogr. Sci. Series*, Vol. 40, Dekker, New York, 1988.
3. L. Dalgaard, J. J. Hansen and J. L. Pedersen, *J. Pharm. Biomed. Anal.*, 1989, **7**, 361.
4. P. Macaudière, M. Lienne, A. Tambute and M. Caude, in *Chiral Separations by HPLC*, A. M. Krstulovic (ed.), p. 399–445. Wiley, New York, 1989.
5. D. W. Armstrong, *US Patent No.* 4,539,399, 1985.
6. D. W. Armstrong and W. DeMond, *J. Chromatogr. Sci.*, 1984, **22**, 411.
7. T. E. Beesley, *Chiral Separations*, Paper No. 5, Eastern Analytical Symp., Sommerset, NJ, U.S.A., Nov. 16–20 1992.
8. A. Berthod, *J. Chromatogr.*, 1991, **549**, 1.
9. K. K. Unger, F. E. Regnier and R. E. Majors (eds), *Liquid Chromatography Packings, J. Chromatogr.*, Vol. 544, 1991.
10. A. Berthod, H. L. Jin, T. E. Beesley, J. D. Duncan and D. W. Armstrong, *J. Pharm. Biomed. Anal.*, 1990, **8**, 123.
11. S. M. Han, Y. I. Han and D. W. Armstrong, *J. Chromatogr.*, 1988, **441**, 376.
12. A. Berthod, S. C. Chang and D. W. Armstrong, *Anal. Chem.*, 1992, **64**, 395.
13. S. H. Lee, A. Berthod and D. W. Armstrong, *J. Chromatogr.*, 1992, **603**, 83.
14. D. W. Armstrong, *New Mechanisms for Chiral Recognition on Cyclodextrin Chiral Stationary Phases*, Paper No. 118, Eastern Analytical Symp., Sommerset, NJ, U.S.A., Nov. 16 1992.

Talanta, Vol. 40, No. 9, pp. 1375–1378, 1993
Printed in Great Britain.

0039-9140/93 $6.00 + 0.00

KINETIC SPECTROPHOTOMETRIC DETERMINATION OF LOW LEVELS OF NITRITE BY CATALYTIC REACTION BETWEEN PYROGALLOL RED AND BROMATE

ALI A. ENSAFI* and M. SAMIMIFAR
College of Chemistry, Isfahan University of Technology, Isfahan, Iran

(*Received* 4 *December* 1992. *Revised* 19 *March* 1993. *Accepted* 22 *March* 1993)

Summary—A kinetic spectrophotometric method for the determination of trace nitrite (0.003–1.000 μg/ml) based on its catalytic effect on the reaction between potassium bromate and pyrogallol red in acidic media is described. The reaction is monitored spectrophotometrically by measuring the decreasing colour of pyrogallol red at 467 nm by the fixed-time method. At a given time of 3.0 min at 30°, the detection limit is 0.001 μg/ml and the relative standard deviation for 0.010 μg/ml nitrite is 1.8% ($n = 8$). The method is free from most interferences, especially from large amounts of nitrate and ammonium. The procedure was successfully applied to the determination of trace nitrite in natural water without preconcentration.

In recent years, there has been growing concern about the role of the nitrite ion as an important precursor in the formation of *N*-nitrosamines, many of which have been shown to be carcinogens.[1] The occurrence of nitrite salt in the environment and their use as food preservatives is widespread. Thus there has been an increasing need for a highly sensitive and relatively selective method for the determination of trace nitrite in different natural and artificial samples.

Recent developments in the determination of trace nitrite have been reviewed,[2–4] but not all are suitable for routine trace determination. A spectrophotometric method based in the formation of azo dyes has been investigated.[5–7] These methods suffer from poor sensitivity, interference from other substances, and they typically involve long reaction time and toxic reagents. Other methods such as pulse polarography,[8–10] chromatography[11,12] and spectrofluorometry[13] are also used but suffer from more or less time-consuming procedures and complicated instrumentation. The catalytic kinetic methods[14,15] are one of the most attractive methods for the ultra trace determination of nitrite. Its advantantage is that only a spectrophotometer is required as the main instrumentation.

Few methods for nitrite based on kinetic procedures have been published.[16–18] The bromate oxidation of pyrogallol red (PGR) has been used for the kinetic determination of vanadium[19] and osmium.[20] The present work describes the application of a catalytic method based on the indicator reaction between PGR and potassium bromate in the determination of nitrite. The reaction is monitored spectrophotometrically. The method has been applied satisfactorily to the determination of nitrite in water.

EXPERIMENTAL

Reagents

All chemicals used were of analytical-reagent grade and were used without further purification. Doubly distilled water was used for the experiments.

Potassium bromate solution ($7.5 \times 10^{-3}M$) was prepared by dissolving 0.313 g of $KBrO_3$ in doubly distilled water in a 250-ml standard flask.

Sodium nitrite was dried at 110° for 4 hr. A 1000-μg/ml nitrite solution was prepared by dissolving 0.375 g of $NaNO_2$ in water in a 250-ml standard flask. A few milligrams (50–100) of sodium hydroxide were added to prevent its decomposition and 0.1 ml of chloroform was also added to prevent bacterial growth. The stock solution was kept in a refrigerator and diluted as required.

PGR solution ($2.50 \times 10^{-4}M$) was prepared by directly dissolving 0.0100 g of PGR (Merck) in methanol in a 100-ml standard flask. The solution is stable for at least 1 month.

Sulphuric acid ($1.35M$) was prepared from concentrated H_2SO_4 (98%, Merck).

*Author for correspondence.

Apparatus

A UV-240 spectrophotometer (Shimadzu) was used for measurements of absorption spectra. A model 35 spectrophotometer (Perkin-Elmer) with 1.0-cm glass cuvettes was used to measure the absorbance at a fixed wavelength (467 nm).

A thermostat (Gallenkamp Griffin, BJ-420-V) was used to keep the reaction temperature at 30°. A stop-watch was used for recording the reaction time.

General procedure

Into a 10-ml standard flask, introduce an aliquot of sample containing 0.03–10 μg of nitrite, 1.0 ml of 1.35M sulphuric acid and 2.0 ml of $2.5 \times 10^{-4}M$ PGR. Dilute the mixture to *ca.* 7 ml. Add 2.0 ml of $7.5 \times 10^{-3}M$ bromate solution, and dilute to the mark with distilled water. Time was measured from just after the addition of the bromate solution. The blank solution was prepared by the same procedure. Keep the sample and blank tube at $30 \pm 0.1°$ in a thermostat bath. After 3.0 min, add 0.1–0.2 g of solid urea to the solution to stop the catalyzed reaction. Transfer the solutions into 1.0-cm glass cuvettes and measure the absorbance of the solutions against water. Label the absorbance of the sample and blank A and A_0, respectively. Then determine the amount of nitrite from a calibration graph.

RESULTS AND DISCUSSION

It was found that some oxidants such as bromate could oxidize PGR in acidic media at a very slow rate.[17,20] On the other hand, the oxidation of PGR by bromate in acidic media is increased in the presence of ultra-trace amounts of nitrite. This reaction can be followed spectrophotometrically by monitoring the change in absorbance at 467.0 nm. Figure 1 shows the absorption spectra of PGR at different times.

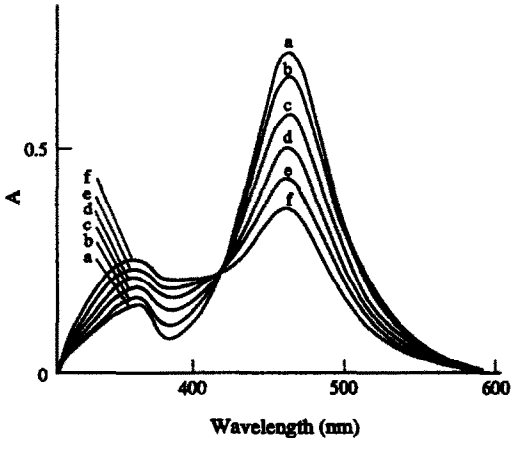

Fig. 1. Variation of PGR–BrO_3^- oxidation system with time in the presence of nitrite; at the optimum conditions with 0.10 μg/ml of nitrite after a. 30 sec; b. 130 sec; c. 230 sec; d. 330 sec; and f. 430 sec, from initiation of the reaction.

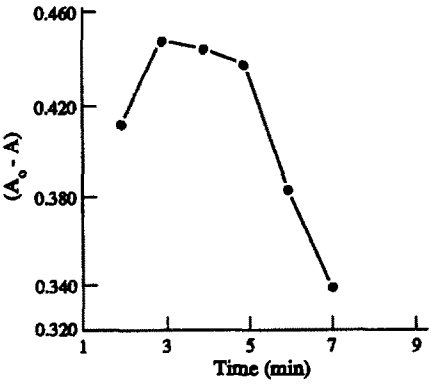

Fig. 2. Effect of time on the reaction rate; conditions: H_2SO_4, 0.0135M; PGR, $4.8 \times 10^{-5}M$; BrO_3^-, $1.5 \times 10^{-3}M$; nitrite, 0.400 μg/ml.

There are many methods such as fixed-time, initial rate and rate constant method for measuring the catalytic species. Among these, the fixed-time method is the most conventional and simple, involving the measurement of A_0 and A at 467.0 nm. Figure 2 shows the relationship between A_0–A and reaction time for the reaction. From the results, 3.0 min was chosen as the optimum interval reaction time.

Effect of variables on the rate of reaction

Experimental results showed that the catalytic reaction can proceed only in strongly acidic media (pH < 3). Among sulphuric, hydrochloric

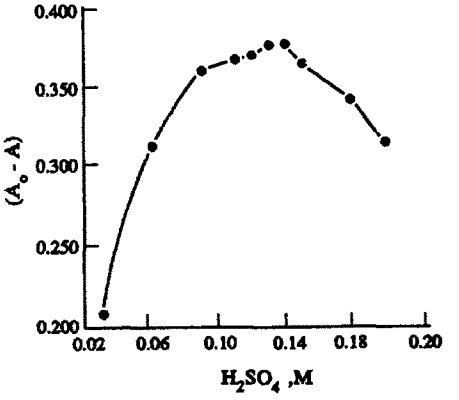

Fig. 3. Effect of sulphuric acid concentration on the reaction rate; conditions: PGR, $7.5 \times 10^{-5}M$; BrO_3^-, 0.001M; nitrite, 0.400 μg/ml and reaction time, 3.0 min.

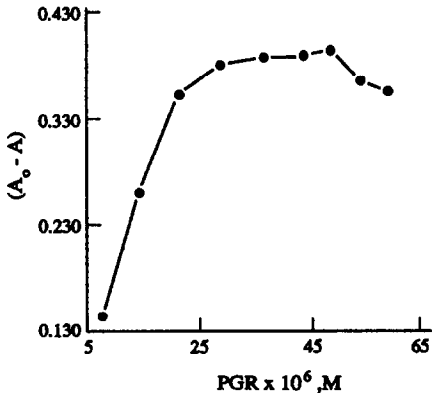

Fig. 4. Effect of BrO_3^- concentration on the rate of reaction; conditions: H_2SO_4, 0.135M; PGR, $5 \times 10^{-5}M$; nitrite, 0.400 μg/ml and reaction time, 3.0 min.

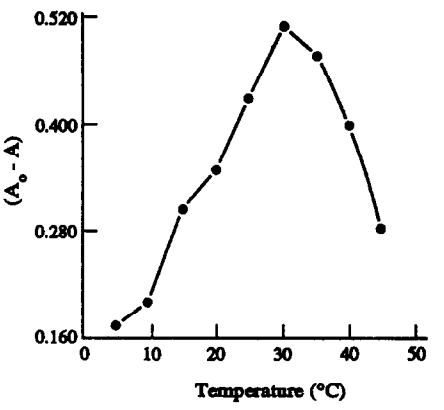

Fig. 6. Effect of temperature on the rate of reaction; conditions: H_2SO_4, 0.135M; PGR, $5 \times 10^{-5}M$; BrO_3^-, $1.5 \times 10^{-3}M$; nitrite, 0.400 μg/ml and reaction time, 3.0 min.

and phosphoric acid, 0.135M sulphuric acid was the optimum as shown in Fig. 3.

The effect of $KBrO_3$ concentration on obtaining maximum sensitivity was investigated. Figure 4 shows that the optimum concentration of $KBrO_3$ is $1.5 \times 10^{-3}M$. Thus $1.5 \times 10^{-3}M$ $KBrO_3$ was used for the study.

The effect of PGR concentration on the rate of catalyzed and uncatalyzed reaction was studied. Figure 5 shows that the A_0–A increases with increasing PGR concentration, thus $5.0 \times 10^{-5}M$ PGR was adopted.

The effect of reaction temperature was studied in the range 5–45°. Figure 6 shows that below 30°, A_0–A increases with temperature, but at higher temperatures it decreases, owing to the decrease in A_0; this means that the rate of the uncatalyzed reaction increases with temperature to a greater extent than the catalyzed reaction and the difference between the rate of the catalyzed and uncatalyzed reaction (equivalent to A_0–A) diminishes at high temperature. The drop in absorbance difference (A_0–A) could also be due to a change in reaction mechanism. The optimum reaction temperature was fixed at 30°.

Rapid cooling, or the use of a chemical inhibitor, can be used to stop the catalytic reaction, which may be required in the fixed-time method in practical applications. It was found that urea is a very good inhibitor which decomposes nitrite rapidly. Addition of 0.1–0.2 g of urea quenches the catalyzed reaction almost completely and very rapidly dissolves in 10 ml of the solution. The absorbance of the solution remains constant for at least 5 min in the presence of urea.

The effect of ionic strength on the rate of reaction was studied by using $NaNO_3$ (3M). The results indicate that, the rate of reaction increases very slightly when ionic strength increases from 0.01 to 1.0M (Fig. 7).

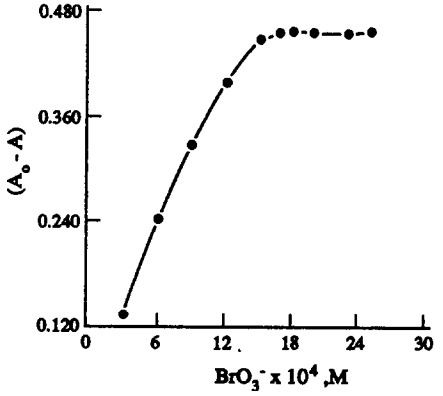

Fig. 5. Effect of PGR concentration on the rate of reaction; conditions: H_2SO_4, 0.135M; BrO_3^-, $1 \times 10^{-3}M$; nitrite, 0.400 μg/ml and reaction time, 3.0 min.

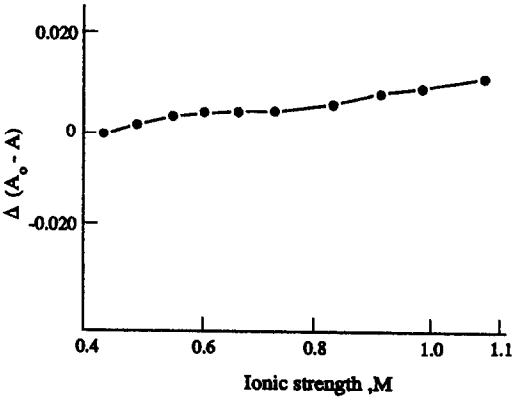

Fig. 7. Effect of ionic strength on the rate of reaction (at the optimum conditions with 0.400 μg/ml nitrite).

Table 1. Determination of nitrite in water ($n = 6$)

Sample	Amount of nitrite found ($\mu g/ml$)		
	This method	Reference value	RSD%*
River Water	0.020	0.022	1.2
Lake Water	0.110	0.105	1.3
Tap Water	0.035	0.034	1.0
Waste Water	0.250	0.258	1.4

*For the proposed method.

Calibration

Under the optimum conditions described above, and the concentration range 0.003–1.000 μg/ml the following regression equation was obtained:

$\log(A_0/A) = -4.116 \times 10^{-3} + 0.934C$ ($n = 5$ and $r = 0.9993$), where C is the concentration (μg/ml) of nitrite.

The experimental limit of detection is 0.001 μg/ml. The relative standard deviation is 1.8 and 1.2% for 0.010 and 0.500 μg/ml nitrite, respectively.

Interferences

More than 50 ions were tested for their possible interference with the determination of nitrite. The results showed that at least 10,000-fold alkali and alkaline earth metal ions and Al(III), Zn(II), Cu(II), U(VI), La(III), Th(IV), Co(II), Cd(II), Mn(II), Zr(IV), Ni(II), acetate, citrate, $B_4O_7^{2-}$, tartarate, CO_3^{2-}, F^-, ClO_4^-, CN^-, $C_2O_4^{2-}$, 1000-fold Cl^-, $S_2O_5^{2-}$, Ir(III) do not interfere, but more than 30-fold Mo(VI), Bi(III), Ce(III), Ag(I), Cr(III), Fe(III), SCN^-, I^-, Br^-, S^{2-}, Hg(II), and 5-fold V(V), V(III), Ce(IV), As(III), IO_4^- interfere. It is important to note that up to 10^6-fold nitrate has little effect, making possible the determination of trace amounts of nitrite in nitrate. The interference of ions may be due to the complex formation of PGR with metal ion or due to the catalytic effects of metal ion (such as V(V) and Ce(IV)) on the reaction.

Determination of nitrite in real samples

Four samples of water were analyzed by the above procedure.

For analysis of real samples some pretreatment is necessary. All suspended particles should be removed by suitable procedures. For tap water analysis, chlorine should also be removed to prevent oxidation of PGR.

For waste water samples, precentrifugation was used. For river water samples, 1 ml of a saturated solution of aluminum hydroxide was added to precipitate the suspended particles, then a mixed solution was filtered and the filtrate used for analysis. The results agreed well with those given by the standard method,[21] and the recovery was also good enough for practical use, as shown in Table 1.

Acknowledgements—The authors are grateful to the Isfahan University of Technology Research Council for the support of this work.

REFERENCES

1. U. Lijinsky and S. S. Epstein, *Nature*, 1970, **223**, 21.
2. W. J. Williams, *Handbook of Anion Determination*, p. 143. Butterwords, London, 1979.
3. W. Fiddler, R. C. Doerr, R. A. Gates and J. B. Fox, *J. Assoc. Off. Anal. Chem.*, 1984, **67**, 525.
4. J. B. Fox, *CRC Crit. Rev. Anal. Chem.*, 1985, **15**, 283.
5. S. Flamers and W. A. Bashir, *Analyst*, 1985, **110**, 1513.
6. G. Norwitz and P. N. Keliher, *ibid.*, 1985, **110**, 689.
7. P. K. Tarafder and D. P. S. Rathor, *ibid.*, 1988, **113**, 1073.
8. A. G. Fogg and R. M. Alonso, *ibid.*, 1988, **113**, 1337.
9. Z. Gao, G. Wang and Z. Zhao, *Anal. Chim. Acta*, 1990, **230**, 105.
10. S. Sabharwal, *Analyst*, 1990, **115**, 1305.
11. S. H. Lee and L. R. Field, *Anal. Chem.*, 1984, **56**, 2647.
12. W. Zhai and N. Cao, *Fenxi Huaxue*, 1985, **13**, 708.
13. A. Y. Chamsi and A. G. Fogg, *Analyst*, 1988, **113**, 1723.
14. H. L. Pardue, *Anal. Chim. Acta*, 1989, **216**, 69.
15. M. A. Koupparis, K. M. Walczak and H. V. Malmstadt, *Analyst*, 1982, **107**, 1309.
16. C. Sanchenz-Pedreno, M. T. Sierra, M. I. Serra and A. Sanz, *ibid.*, 1987, **112**, 837.
17. R. Montes and J. J. Laserna, *Talanta*, 1987, **34**, 1021.
18. Z. Zhang, *Fenxi Huaxue*, 1989, **17**, 122.
19. A. S. Cabeza, J. M. Escriche and F. B. Reing, *Analyst*, 1984, **109**, 1559.
20. A. A. Ensafi and A. Safavi, *Anal. Chim. Acta*, 1991, **244**, 231.
21. W. Horwitz (ed.), *Official Methods of Analysis of the Association of Official Analytical Chemists*. 13th Ed., p. 381. Association of Official Analytical Chemists, Washington, 1980.

Talanta, Vol. 40, No. 9, pp. 1379–1384, 1993
Printed in Great Britain.

0039-9140/93 $6.00 + 0.00

ELECTROCHEMICAL OXIDATION OF METHYLENEDIOXYAMPHETAMINES

J. A. SQUELLA,[1] B. K. CASSELS,[2] M. ARATA,[3] M. P. BAVESTRELLO[3] and LUIS J. NUÑEZ-VERGARA[3]

[1]Electrochemistry Laboratory, University of Chile, P.O. Box 233, Santiago, Chile
[2]Department of Chemistry, University of Chile, P.O. Box 653, Santiago, Chile
[3]Pharmacology Laboratory, University of Chile, P.O. Box 233, Santiago, Chile

(*Received* 2 *December* 1992. *Revised* 22 *March* 1993. *Accepted* 23 *March* 1993)

Summary—Four amphetamine derivatives bearing a methylenedioxy group at positions 3 and 4 of the benzene ring and differing in their substitution at C(6) were studied by differential pulse voltammetry in aqueous media. These experiments showed a single oxidation peak for the C(6)-H, -Br and -Cl compounds, while the C(6)-NO_2 analogue was not oxidized. The oxidation peak is interpreted as due to the removal of one electron from the aromatic electrophore with formation of a radical cation stabilized by the dioxole ring. The linear relationship between the peak current and the concentration of the derivatives is appropriate for development of a quantitative method for their determination. pK′ values were determined using both electrochemical and spectrophotometric methods.

The last few years have seen a renewal of interest in the psychotropic drugs 1-(3,4-methylenedioxyphenyl)-2-aminopropane or 3,4-methylenedioxyamphetamine (MDA) and its *N*-methyl and *N*-ethyl analogues (MDMA, "XTC", or "Adam", and MDEA or "Eve", respectively), owing to their disputed use in psychotherapy and to their neurotoxicity.[1,2] MDMA may be regarded as the prototype of a new class of drugs called "entactogens"[3,4] whose mechanism of action and structural requirements are almost totally unknown. It is only clear at this time that their subjective effects differ from those of the structurally similar phenylalkylamine hallucinogens, and that these effects are mainly due to their (S) isomers while the more potent hallucinogens possess the (R) configuration. Thus far, the exploration of this group of compounds has been limited to variations of the amine chain keeping the 1-(3,4-methylenedioxyphenyl) moiety intact and devoid of additional substitution, and has only very recently been extended to include the aminotetralin and aminoindan analogues.[3–5] Nevertheless, it is known that the bromination of MDA to afford 1-(6-bromo-3,4-methylenedioxyphenyl)-2-aminopropane leads to a non-hallucinogenic compound whose subjective effect was interpreted almost twenty years ago as "amphetamine-like" although this was only observed in the rather high dose range which is also required for MDA, MDMA and MDEA.[6,7]

As part of a synthetic program related to the known "entactogens", MDA and the above mentioned bromo derivative were prepared once more, as well as another two compounds substituted at C(6) of the benzene ring with a chlorine atom or a nitro group, respectively. In order to round out our vision of substituent effects on the electrochemistry of amphetamine analogues, obtained with a series of 1-(2,5-dimethoxyphenyl)-2-aminopropane derivatives substituted at C(4),[8] we have now studied the voltammetric behavior of MDA and its congeners.

The electrochemistry of amphetamine derivatives is an unexplored field of research. There are only three published papers related to: the nitro-reduction of 2,5-dimethoxy-4-nitroamphetamine (DON)[9] and 4,5,-dimethoxy-2-nitroamphetamine,[10] and the electrochemical behavior of several 4-substituted 2,5-dimethoxy-amphetamine derivatives.[8] From this latter work it is possible to conclude the existence of a correlation between the ring substitution and the oxidation potential. As the ring substitution in the amphetamine derivatives play an important role in their pharmacological activity, it may be possible to find empirical relationships between oxidation potentials and pharmacological activities.

EXPERIMENTAL

Reagents

MDA and its C(6)-bromo analogue were synthesized following published procedures.[6,7] Melting points are uncorrected. ^{1}H NMR spectra were recorded at 60 MHz in D_2O unless stated otherwise (chemical shifts in ppm from TMSPA-d_4).

1-(3,4-methylenedioxyphenyl)-2-aminopropane. (3,4-MDA)hydrochloride. M.p. 193.5–194.5° (i-PrOH-EtO); ^{1}H NMR (TFA) δ (from TMS) 1.53 (3H, d J = 6.4 Hz, C-CH3), 3.0 (2H, m, CH2), 3.8 (1H, m, CH), 6.02 (2H, s, OCH2O), 6.85 (3H, br s, ArH).

1-(3,4-methylenedioxyphenyl-6-nitrophenyl)-2-aminopropane. (3,4-MD-6-NA) nitrate. 1-(3,4-methylenedioxyphenyl)-2-aminopropane (2.00 g) was dissolved in 2*N* HNO_3 (5.5 ml) and treated dropwise, with efficient stirring and cooling, with 65% HNO_3 (6 ml). After several minutes the product separated out as a thick creamy precipitate which was diluted with water (18 ml), collected by filtration, resuspended in water, filtered again and dried. The yield was practically quantitative, m.p. 171° (decomp.) (EtOH); ^{1}H NMR δ (DMSO-d6) 1.19 (3H, d J = 6 Hz, C-CH3), 3.10 (2H, d J = 6 Hz, CH2), 3.5 (1H, m, CH), 6.27 (2H, s, OCH2O), 7.10 (1H, s, ArH), 7.67 (1H, s, ArH). Anal. C, 41.94; H, 4.59; N, 14.49%; calc. C10H13N207; C, 41.82; H, 4.56; N, 14.63%.

1-(6-bromo-3,4-methylenedioxyphenyl)-2-aminopropane(6-Br-3,4-MDA) hydrochloride. M.p. 221–222° (i-PrOH-acetone); ^{1}H NMR δ 1.32 (3H, d J = 6.5 Hz, C-CH3), 3.00 (2H, app. d Japp = 7 Hz, CH2), 3.7 (1H, m, CH), 6.00 (2H, s, OCH2O), 6.85 (1H, s, ArH), 7.12 (1H, s, ArH). Anal. C, 40.73; H, 4.49; N, 4.40%; calc. C10H13BrClNO2; C, 40, 76; H, 4.45; N, 4.75%.

1-(6-chloro-3,4-methylenedioxyphenyl)-2-aminopropane (6-Cl-3,4-MDA) hydrochloride. Prepared by LiAlH4 reduction of 1-(6-chloro-3,4-methylenedioxyphenyl)-2-nitropropene in Et_2O and precipitation of the salt; m.p. 222.5–223.5° (i-PrOH); ^{1}H NMR δ 1.33 (3H, d J = 6.4 Hz, C-CH3), 2.97 (2H, app. d Japp = 7 Hz, CH2), 3.7 (1H, m, CH), 6.01 (2H, s. OCH2O), 6.87 (1H, s, ArH), 7.00 (1H, s, ArH). Anal. C, 47.85; H, 5.28; N, 5.28%; calc. C10H13Cl2NO2: C, 48.02; H, 5.24; N, 5.60%.

Voltammetric experiments were carried out in buffered aqueous solutions containing 0.02*M* phosphoric acid with 0.02*M* acetic acid for pH 1–8.5 or 0.02*M* Na_2CO_3 for pH 8.5–12. The ionic strength was raised to 0.3*M* with $NaNO_3$.

For spectrophotometric experiments the Universal UV Spectroscopy buffer containing 0.1*M* in citric acid, potassium monophosphate, sodium tetraborate, TRIS and potassium chloride was used.

For both buffers, the pH was adjusted using HCl or NaOH. All reagents were p.a. grade.

The solid electrodes were routinely cleaned with chromic acid solution for 10 sec. This procedure permit to increase the reproducibility considerably.

Apparatus

A Tacussel CPRA thermostatic cell with three different working electrodes (platinum, glassy carbon and carbon paste) was employed. A platinum wire and a saturated calomel electrode were used as auxiliary and reference electrodes. A TACUSSEL model EDI rotating electrode assembly was used with platinum and glassy carbon electrodes. A METROHM carbon paste electrode with a geometric area of 38.5 mm^2 was also used.

Electrochemical data were obtained from an Inelecsa assembly equipped with the following elements:

(a) a generator–potentiostat type PDC-210.

(b) an interface containing 12-bit A/D and D/A converters, connected to a microprocessor with suitable software for fully automated control of the experiments and data acquisition. A Multitech, Apple II Plus-compatible microcomputer was used for data control, acquisition and treatment.

UV-Vis spectra were recorded using a SHIMADZU UV-160A spectrophotometer with 1 cm quartz cells.

A VARIAN Anaspect EM-360 (60 mHz) NMR spectrometer for NMR measurements was used.

RESULTS AND DISCUSSION

The present paper deals with the study of the voltammetric behavior of 3,4-methylenedioxyamphetamine (MDA) and its 6-chloro, 6-nitro and 6-bromo derivatives (Fig. 1).

In aqueous solution, using platinum, glassy carbon and carbon paste electrodes as working electrodes, MDA and the 6-chloro and 6-bromo derivatives produce an anodic peak which is

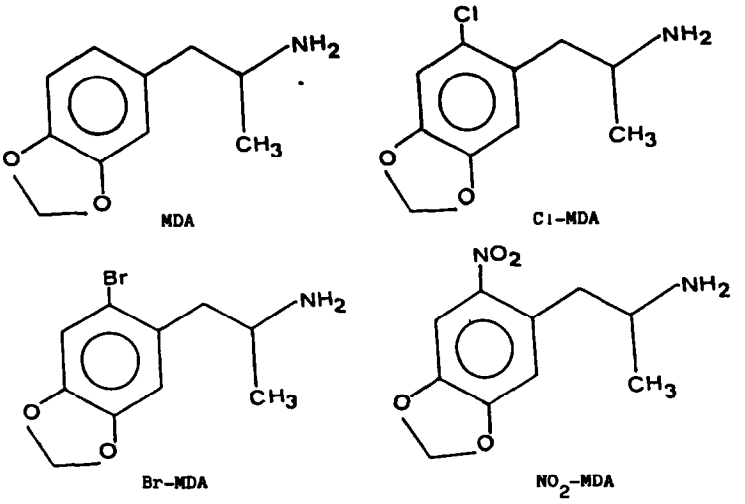

Fig. 1. Molecular structures of 3,4-methylenedioxyamphetamine (MDA) and its 6-chloro (Cl–MDA), 6-nitro (NO_2–MDA) and 6-bromo (Br–MDA) derivatives.

best resolved using differential pulse voltammetry. Unlike these compounds, the 6-nitro derivative of MDA did not reveal any anodic peak under these conditions. For comparative purposes, we also examined the electrochemical behavior of unsubstituted amphetamine and 2-methoxy amphetamine. No oxidation peaks were obtained for these compounds, suggesting that the anodic process observed with the other analogues does not involve the amine-substituted side chain but rather the 3,4-methylenedioxy-substituted benzene ring. In earlier work,[8] similar behaviour was observed for the 2,5-dimethoxyamphetamine derivatives.

The MDA and its chloro and bromo derivatives exhibited a single voltametric peak over the entire pH range studied, extending from pH 1 to 12. The peak potential (E_p)–pH plots (Fig. 2) show two linear segments for each compound, indicating that the electrode process is pH-dependent over the whole range. E_p decreases linearly with increasing pH; therefore, these compounds are oxidized more easily in more alkaline solutions as expected for common oxidative behavior. Moreover, the breaks in the E_p–pH plots can be ascribed to the voltammetric pK' values, showing that, when $pH < pK'$ the dominant chemical species is the protonated amine and when $pH > pK'$ the free base is more abundant. In order to confirm the above assumption we also studied the pH influence on the UV absorption spectra of the derivatives. In Fig. 3 we can observe the UV spectra of the amphetamine derivatives at two different pHs, displaying the strong pH-dependence of their UV band at approximately 210 nm. In the Fig. 4 plots of the absorptivity as a function of pH for the band at 210 nm are shown. From these curves we estimate the UV spectrophotometric pK_a values, which can be found in Table 1. The

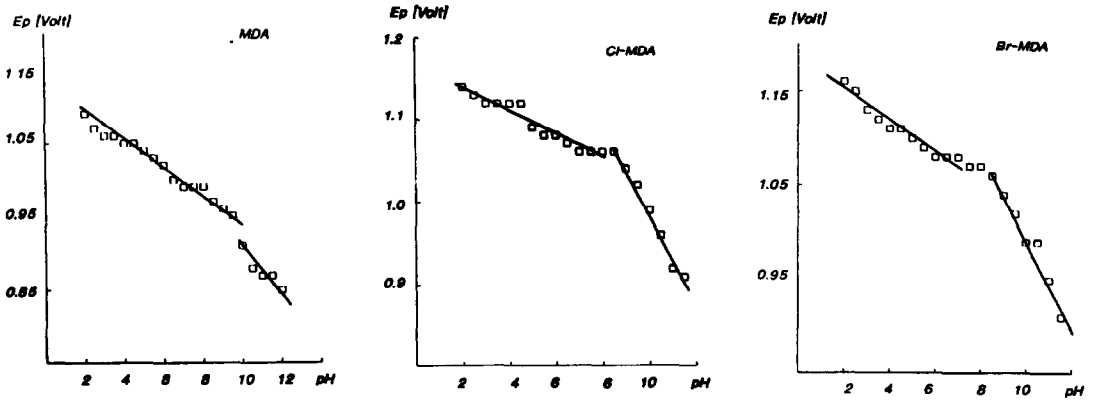

Fig. 2. Variation of the peak potential (E_p) with pH for the differential pulse voltammetric oxidation of the 3,4-methylenedioxyamphetamine derivatives. Voltammograms obtained on glassy carbon electrode.

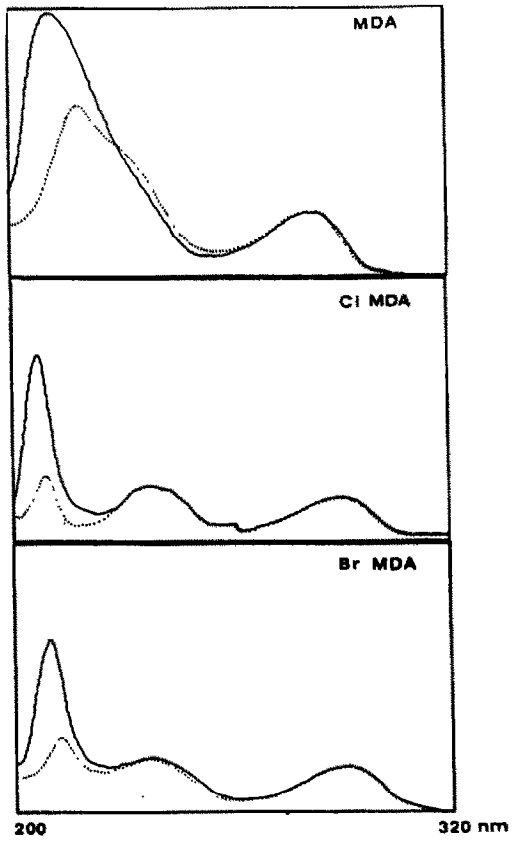

Fig. 3. UV spectra for the 3,4-methylenedioxyamphetamine derivatives. Solid line, pH = 2. Dashed line, pH = 10.

agreement between the voltammetric and the UV values supports the validity of the above assumption.

Examination of the peak current (i_p) values indicates that these fall (Fig. 5), and the peak broadens, as the pH rises. This may be due to a decrease in the heterogeneous rate constant affected by proton transfer.[11]

We also studied the electrochemical behavior of all derivatives under two different experimental conditions: a) variation of the temperature using a glassy carbon electrode as a working electrode, b) the effect of a platinum rotating disk electrode as a working electrode, maintaining a constant temperature (25°). From these experiments it was concluded that I_p does not exhibit variation with temperature or the rate of rotation, indicating that the oxidation rate is controlled by charge transfer without participation of the diffusion of the electroactive species to the electrode surface.

Table 1. pK' values obtained by voltammetric (glassy carbon and carbon paste electrodes) and spectrophotometric methods

Drug	Voltammetric C.P.E.	Voltammetric G.C.E.	Spectrophotometric
MDA	9.15	9.20	9.21
Cl–MDA	9.10	9.30	9.02
Br–MDA	8.75	8.80	9.12

One of the goals of this work was to evaluate the incidence of the C-6 substituent on the electrochemistry of these drugs. The experimental evidence here shown indicates that the electron acceptor or donor character of this substituent is directly related to the greater or lesser ability of oxidation. A simple explanation is that the electron-donating substituent increases the electron density of the aromatic ring π system, making it easier to remove an electron, thus producing a cation radical which is stabilized by the methylenedioxy group at C-3 and C-4. Consistent with this latter interpretation, the lowest E_p value was found for MDA itself, which lacks any substituent at C-6. Conversely, the chloro- and bromo-derivatives present higher E_p values. In these cases, the oxidation of the ring system is presumably more difficult due to the decreased stability of the resulting cation radical. In Fig. 2 we can see that

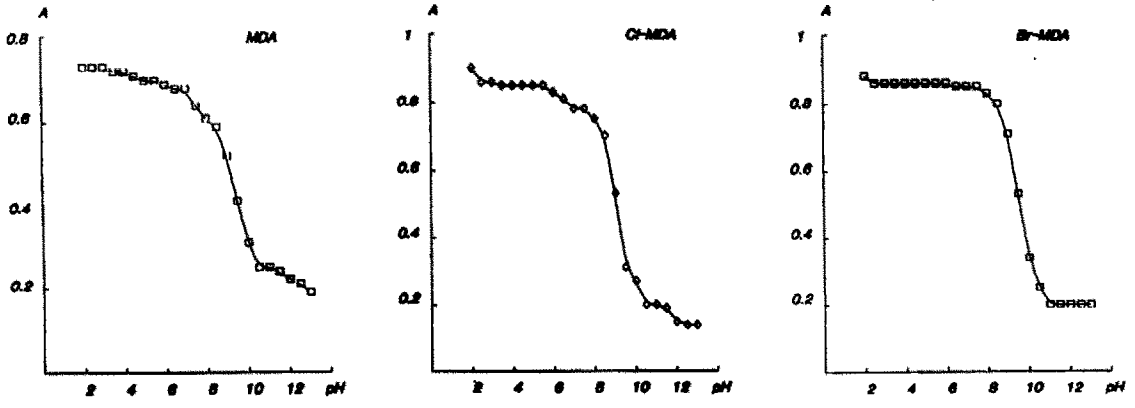

Fig. 4. Absorbance–pH plots for the band at 210 nm for the 3,4-methylenedioxyamphetamine derivatives.

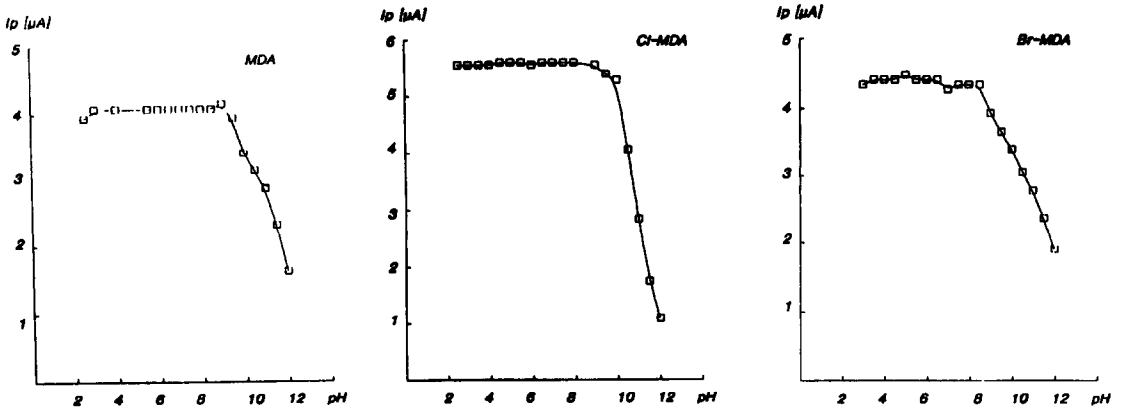

Fig. 5. Peak current–pH dependence for the amphetamine derivatives. Glassy carbon electrode, 25°.

in all the pH range the E_ps follow the order: MDA < Cl MDA < Br MDA. From the above results, it seems obvious that direct oxidation of the aromatic ring, influenced by the C-6 substituent, is occurring. Although, the suggestion that a carbocation is formed in an aqueous medium is arguable, it is quite justified in this case due to the stabilizing effect of the methylenedioxy group. This effect is well documented for a similar substituent, the methoxyl group.[12]

Linear sweep cyclic voltammetric experiments showed a single oxidation peak for all drugs, recording the voltammograms at sweep rates between 50 mV/sec and 5 V/sec at pH 7. From this study it can be seen that the potential peak shifts anodically by about 30 mV for each 10-fold increase in sweep rate. These results agree with an EC mechanism[13] with a one-electron transfer in the electrochemical step and a subsequent chemical reaction, *e.g.*, the electrochemical formation of a cation radical with a subsequent chemical reaction of this species. The chemical reaction of the cation radical is fast enough for the reduction of the cation radical not to occur in the time scale of the experiment.

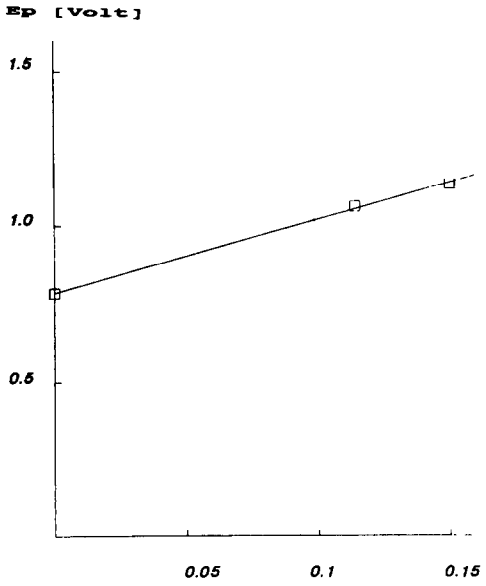

Fig. 6. Linear relationship between the extra-thermodynamic parameter, σ_p^+, and the peak potential of the amphetamine derivatives. pH 7 on glassy carbon electrode.

In order to confirm the relationship between E_p and the effect of the C-6 substituent on the oxidizable moiety, we consider σ_p^+ as an extra-thermodynamic parameter which combines the inductive and resonant effects of the substituents on the benzene ring. This factor can be applied to oxidation reactions involving resonance stabilization of a positive charge in an aromatic ring.[14] As can be seen in Fig. 7, there is a linear relationship between the σ_p^+ factor of the C-6 substituents and the E_ps experimentally obtained by differential pulse voltammetry. From the above behavior it is possible to extrapolate an E_p value for the 6-nitro derivative. The extrapolated value was 1460 mV, which is located in the discharge zone of the support electrolyte, explaining the absence of any oxidation peak for this derivative.

The voltammetric technique also can be used as an analytical tool to quantify these derivatives in aqueous solution. For this purpose we studied the dependence of the voltammetric peak on the concentration of the amphetamine derivatives. A linear relationship between the peak current and the concentration of the derivatives for 0.01 m*M* and 0.1 m*M* solutions at pH 7 were found (Table 2).

Peak potentials were independent of the concentration indicating that no adsorption or second order processes are involved. Reproducibility studies were carried out with the carbon

Table 2. Linear relations between peak current and concentrations of the drugs for 10 points between 0.01 m*M* and 0.1 m*M*. pH = 7.0, 25° and CPE as the working electrode.
i_p (μA) = slope × C (*M*) + intercept

Drugs	Intercept	Slope × 10^{-5}	Correlation
MDA	1.306	1.668	0.996
Br–MDA	−0.168	1.625	0.994
Cl–MDA	−0.938	1.386	0.995

paste and glassy carbon electrodes, obtaining an average CV = 0.5 and 0.4% for the peak potentials and a CV = 3.8 and 3.4% for the peak currents, respectively. These results indicate good reproducibility and accuracy to develop a quantitative voltammetric assay for these derivatives. Furthermore, the behavior presented here would be useful for developing a method of HPLC with electrochemical detection. On the other hand, stability assays allow us to conclude that aqueous solutions of these compounds remain unchanged after 30 days at room temperature under normal room light.

Acknowledgements—This work was supported in part by FONDECYT grants N° 915-89, 1120-92 and DTI Universidad de Chile grant N° 3121-9223. The authors also express their gratitude to the Pharmacology Department of the Medicine Faculty, University of Chile for its hospitality to our group.

REFERENCES

1. C. J. Schmidt and V. L. Taylor, *Biochem. Pharmacol.*, 1987, **36**, 4095.
2. M. A. Nader, S. M. Hoffmann and J. E. Barret, *Phychopharmacology*, 1989, **98**, 183.
3. D. E. Nichols, A. J. Hoffman, R. A. Oberlender, P. Jacob and A. T. Shulgin, *J. Med. Chem.*, 1986, **29**, 2009.
4. D. E. Nichols, in *MDMA Conference Proceedings*, *J. Psychoactive Drugs*, 1986, **18**, 305.
5. D. E. Nichols, W. K. Brewster, M. P. Johnson, R. Oberlender and R. M. Riggs, *J. Med. Chem.* 1990, **33**, 703.
6. S. Sepúlveda, R. Valenzuela and B. K. Cassels, *J. Med. Chem.*, 1972, **15**, 413.
7. A. T. Shulgin and A. Shulgin, *PIHKAL-Phenethylamines I Have Known and Loved.* Transform Press, Berkeley, California, 1991.
8. J. A.Squella, M. A. Berguecio, A. Hernández, B. K. Cassels and L. J. Núñez-Vergara, *J. Chim. Phys.*, 1992, **89**, 669.
9. P. Richter, A. Morales, J. S. Gómez-Jeria and D. Morales, *Analyst*, 1988, **113**, 5351.
10. J. A. Squella, M. Pezzani, M. Aillon-Torres, M. C. Rezende, B. K. Cassels and L. J. Nuñez-Vergara, *Electroanalysis*, 1992, **4**, 555.
11. I. Navarro, D. Gonzalez, E. Roldan and M. Rueda, *J. Pharm. Biomed. Analysis*, 1988, **6**, 969.
12. R. N. Adams, *Electrochemistry at Solid Electrodes.* Marcel Dekker, New York, 1969.
13. G. Bomtempelli, F. Magno, G. Mazzochim and R. Seeber, *Annali Chim.*, 1989, **79**, 103.
14. J. E. Leffer, *Rates and Equilibrium of Organic Reactions.* Wiley, New York, 1963.

Talanta, Vol. 40, No. 9, pp. 1385–1390, 1993
Printed in Great Britain.

0039-9140/93 $6.00 + 0.00

SCREENING OF URINARY COPROPORPHYRIN USING CLOUD POINT EXTRACTION AND CHEMILUMINESCENCE DETECTION

WILLIAM J. HORVATH and CARMEN W. HUIE

Department of Chemistry, State University of New York at Binghamton. P.O. Box 6000, Binghamton, NY 13902-6000, U.S.A.

(*Received* 23 *November* 1992. *Revised* 2 *March* 1993. *Accepted* 3 *March* 1993)

Summary—A simple screening test was developed for the sensitive and selective measurement of urinary coproporphyrin. In this screening test, efficient and selective extraction/pre-concentration of coproporphyrin from the aqueous medium(urine) into a much smaller volume phase containing a common non-ionic surfactant (Triton X-100) and ethyl acetate was accomplished by the addition of a relatively large amount of a cloud point depressing electrolyte (K_3PO_4) into the sample solution to effect cloud point separation. Sensitive and selective detection of coproporphyrin in the mixed Triton X-100 and ethyl acetate phase was performed via chemical excitation using the peroxyoxalate chemiluminescence reaction. The effects of surfactant and cations (from the cloud point depressing electrolyte) on the chemiluminescence intensity of coproporphyrin were briefly investigated. Furthermore, the spectrum of urinary coproporphyrin obtained using the present chemiluminescence method was briefly compared with that obtained from fluorescence method.

Measurement of porphyrins present in biological materials is important for the diagnosis of a group of disorders known as porphyrias.[1–5] These diseases can be inherited or acquired and are usually linked to a deficiency in enzyme activities associated with the heme bio-synthetic pathway. In most clinical laboratories determination of elevated levels of porphyrins in biological fluids such as urine usually involves simple screening tests. Most of these tests consist of an extraction procedure involving the use of talc[5] or organic solvents,[6] *e.g.* ethyl acetate, followed by visual observation of the fluorescent color of the extract under ultraviolet (UV) light. Recently a sensitive and selective method based on the use of flow injection analysis and visible laser fluorimetry has been developed for the rapid screening of a large number of untreated urine samples.[7]

A major limitation of conventional screening tests lies in their inability to estimate the individual concentrations of the two major urinary porphyrin components, *i.e.* coproporphyrin and uroporphyrin. This is an important problem because it is often necessary to distinguish coproporphyrinuria from uroporphyrinuria; the former is more common and its occurrence usually signifies a number of significant diseases such as malignancies, alcohol cirrhosis, infectious hepatitis, lead poisoning, hereditary coproporphyria and variegate porphyria.[1–5] Relatively simple chromatographic procedures have been employed to separate urinary coproporphyrin from uroporphyrin;[8] however, these procedures add extra complexities, costs and time to the screening tests. A possible solution to this problem involves the use of ether to extract coproporphyrin but not uroporphyrin from urine, followed by fluorimetric excitation of the ether layer using UV light.[9] However, this method lacks sensitivity, and perhaps more importantly, efficient and selective extraction of coproporphyrin into the ether layer is highly sensitive to pH and matrix effects. Moreover, ether presents a fire hazard in clinical laboratories.

In recent years analytical methods based on chemiluminescence(CL) have been shown to be highly sensitive and selective for the determination of a large number of biologically important molecules.[10,11] In particular CL based methods are especially well suited for routine analyses in clinical laboratories due to their simplicity and low cost. Albrecht *et al.*[12,13] have recently exploited the advantages of CL and developed a sensitive and highly selective screening test for urinary porphyrins based on the peroxyoxalate CL reaction. When compared to one of the most commonly used screening tests, *i.e.* talc test, the sensitivity of the

porphyrin-sensitized peroxyoxalate CL test was quite similar (visual detection limit ~250 μg/l. of porphyrins in urine). Unfortunately, as in the talc test, this particular CL-based screening test was not selective for coproporphyrin. Positive CL results (orange or red CL emission) can arise from elevated levels of coproporphyrin and/or uroporphyrin due to chemical excitation involving the oxidation of bis(2,4-dinitrophenol) oxalate (DNPO).

In this paper a simple screening test capable of highly sensitive and selective detection of urinary coproporphyrin based on the use of cloud point extraction and peroxyoxalate CL reaction is reported. The use of a relatively stable peroxyoxalate CL reagent—bis(2,4, trichlorophenyl) oxalate (TCPO)—to generate relatively strong and long lasting CL emission from urinary coproporphyrin was made possible by extracting and pre-concentrating the coproporphyrin from urine into a smaller volume phase containing a common non-ionic surfactant (Triton X-100) and ethyl acetate.

EXPERIMENTAL

Reagents

Coproporphyrin, pentacarboxylporphyrin, hexacarboxylporphyrin, heptacarboxylporphyrin and uroporphyrin were all obtained from Porphyrin Products (Logan, UT, U.S.A.). Analytical grade Triton X-100 and imidazole were obtained from Sigma (St Louis, MO, U.S.A.). Acetonitrile(HPLC grade), tri-potassium phosphate, sodium and potassium monohydrogen phosphate, 30% hydrogen peroxide, ethyl acetate, magnesium sulfate, ammonium sulfate, and zinc sulfate were obtained from Fischer Scientific (Fairlawn, NJ, U.S.A.). Di-sodium sulfate was obtained from Baker (Phillipsburg, NJ, U.S.A.). DNPO was obtained from Fluka (Lake Ronkonkoma, NY, U.S.A.). All water used was doubly distilled and deionized.

TCPO was prepared by the method of Mohan and Turro[14] and recrystallized from benzene to ensure purity. TCPO solutions ($1.3 \times 10^{-3} M$) were prepared by dissolving appropriate amounts of TCPO in ethyl acetate. H_2O_2 solutions ($1 \times 10^{-2} M$) were prepared by diluting 30% hydrogen peroxide with acetonitrile. The chemiluminescence reagent solution was prepared by combining equal volumes of both TCPO and H_2O_2 solutions. This solution is unstable and should be used within 15 min of mixing. Surfactant solutions (1% Triton X-100 v/v) were prepared by dissolving appropriate amounts of Triton X-100 in doubly distilled deionized water. Stock solutions of porphyrin standards were prepared by dissolving in acidified (pH 1) doubly distilled deionized water and then stored at 5° in the dark.

Urine samples were collected from a healthy male over a 24 h period and were preserved with sodium carbonate (5 g/l. urine) and ethylenediaminetetraacetate (3 g/l. urine) and stored under refrigeration in the dark at 5°. To prepare urine samples spiked with various known concentrations of porphyrin standards naturally occurring porphyrin was removed by employing the talc extraction procedure described in literature.[15] Urine was readjusted to its previous pH after porphyrin removal.

Apparatus

Fluorescence measurements used to determine extraction efficiencies ($E\%$) were taken with a SLM 8000 photon-counting spectrofluorometer (Amico, Urbana, IL, U.S.A.) The bandwidths of the emission and excitation monochromator were set at 16 nm. The excitation wavelength of all the measurements was set at the Soret band at ~400 nm. The sample solutions were placed in a 1-cm pathlength quartz cell.

CL spectra were obtained using a home-made fiber optic device connected to a Perkin-Elmer fluorescence spectrometer (model 650-10M, Norwalk, CT, U.S.A.) with the light source turned off; for purposes of comparison, fluorescence spectra were obtained using the same spectrometer with the light source turned on. CL was initiated in the test tubes by the addition of CL reagent solution using a syringe. One end of the fiber optic was placed next to the meniscus of the solution on the outside of test tube. The other end of the fiber optic was connected to a monochromator that was interfaced to a photomultiplier tube. To acquire CL and fluorescence spectra scan speed and bandwidth of the monochromator were set at 480 nm/min and 16 nm, respectively.

Procedure

A 10 ml urine sample spiked with porphyrin standards was placed into a test tube and diluted with an equal volume of surfactant solution (Triton X-100, 1% v/v). A small amount of ethyl acetate (~0.5 ml) was then poured into the tube so that a small layer of ethyl acetate just covers the meniscus of the sample solution

(alternatively, the ethyl acetate can be added to the top surfactant layer after phase separation has occurred). To maximize the solubility of the salting-out agent the tube was warmed in a beaker of hot water. After a few minutes the tube was removed from the water bath and 9 g of K_3PO_4 (4*M*) was added. The solution was thoroughly mixed to completely dissolve all of the salt. The tube was then left to stand for 5 min or more. Centrifugation may be required depending on the conditions of the experiment. Centrifugation for 10 min at 4000 rpm (2500 G) was more than adequate to effect phase separation. Afterward 2–3 ml of the chemiluminescence solution was added with a pipet to the top layer of the tube. The chemiluminescence signal varied from a very pale pink to a bright red depending on the concentrations of coproporphyrin.

RESULTS AND DISCUSSION

In our previous paper[16] it was reported that both the hydroxide and phosphate anions can be used as salting-out agents to effect separation of the non-ionic surfactant (Triton X-100) from the aqueous medium based upon the cloud point phenomenon. Highly efficient extractions ($E\% > 95\%$) of a number of hydrophobic porphyrins (hematoporphyrin, protoporphyrin and coproporphyrin) from the aqueous into the surfactant phase were obtained once a certain threshold concentration of the cloud point depressing electrolyte was added to the aqueous non-ionic surfactant solutions. On the other hand the $E\%$ was found to be dramatically lower ($< 3\%$) for the extraction of a hydrophilic porphyrin, *i.e.* uroporphyrin. These findings indicated that the use of hydroxide or phosphate anion as the salting out agent could provide a means by which coproporphyrin could be extracted from urine samples and pre-concentrated into the smaller volume surfactant phase with good efficiency and selectivity, while the majority of the uroporphyrin fraction would remain in the aqueous urine medium.

Table 1 shows the $E\%$ values for coproporphyrin and uroporphyrin in spiked human urine using the phosphate anion as the salting-out agent. The high $E\%$ values for coproporphyrin (and low $E\%$ for uroporphyrin) were obtained immediately after the samples were centrifuged at 4000 rpm for about 10 min (2500 G). These results indicate that the phosphate anion is useful as a salting-out agent for the cloud point extraction and preconcentration of coproporphyrin from real biological matrices. In addition to the two major urinary porphyrin components, Table 1 shows that $E\%$ of the three minor urinary porphyrin components: penta-, hexa-, and heptacarboxylporphyrins.

Table 1. Extraction efficiencies of major and minor porphyrin components (400 μg/l. each) by Triton X-100 (1% v/v) in spiked urine samples using 4*M* K_3PO_4 as the salting-out agent

copro-	penta-	hexa-	hepta-	uro-
93.9%	82.4%	61.2%	22.1%	3.7%

Although the concentrations of the minor urinary porphyrin components in normal urine are negligible when compared to coproporphyrin and uroporphyrin, significant amounts of the minor components, in particular penta- and heptacarboxylporphyrins, can be found in urine samples from patients suffering from different types of porphyrias.[1–5] Since relatively high $E\%$ were obtained for the extraction of pentacarboxylporphyrin into the surfactant phase as shown in Table 1, one would expect that this minor urinary porphyrin component could represent an interferent for the measurement of coproporphyrin when present in high concentrations as occurs in some forms of coproporphyrinuria. Fortunately the increase in urinary pentacarboxylporphyrin level is usually accompanied by a significantly higher levels of coproporphyrin in almost all cases of coproporphyrinuria.[5] This suggests that false positive results originating from signals obtained from pentacarboxylporphyrin in the screening of coproporphyrinuria would be unlikely. On the other hand, significant amounts of heptacarboxylporphyrin can be found in some forms of uroporphyrinuria. Although the $E\%$ of heptacarboxylporphyrin was found to be much lower than that of pentacarboxylporphyrin as shown in Table 1, the existence of elevated levels of heptacarboxylporphyrin in urine, *e.g.* 1000 μg/l., could represent a major interference problem for the screening of coproporphyrinuria. The rise in heptacarboxylporphyrin concentration is usually correlated with that of uroporphyrin, which is the major marker for uroporphyrinuria.

In the present method, potential interference problems for the selective measurement of coproporphyrin in urine due to the presence of elevated levels of minor urinary porphyrin components, in particular from heptacarboxylporphyrin, was minimized by employing a two

step extraction procedure as follows: using 10 ml of urine containing Triton-X-100 (1% v/v), selective extraction of coproporphyrin from uroporphyrin into a very thin surfactant layer (~0.1 ml) sitting on top of the higher density urine medium can be achieved with good $E\%$ using phosphate anion as the salting out agent as shown in Table 1. To achieve selective extraction of coproporphyrin from the minor urinary porphyrin components, a few drops of ethyl acetate (~0.5 ml) was added to the sample solution. The ethyl acetate serves to loosen the viscous surfactant layer, which allows for better mixing with the peroxyoxalate CL reagents and, more importantly, it allows for the major hydrophobic porphyrin component, *i.e.* coproporphyrin, to partition into the mixed organic and surfactant layer (top layer) with good efficiency.[1] The majority of the minor porphyrin components, *e.g.* heptacarboxylporphyrin, remain at the interface of the two layers and/or in the aqueous medium and are not amenable to chemical excitation by the peroxyoxalate CL reagents (*vide infra*).

The present experimental conditions are designed to give rise to a net pre-concentration factor of ~15 for the porphyrins extracted into the top layer and to provide a just barely detectable CL emission at the average normal concentration of coproporphyrin in urine, *i.e.* ~50 μg/l. At this concentration of coproporphyrin in urine, which corresponds to ~750 μg/l. in the top layer, the CL emission from coproporphyrin appeared pale orange in color (negative result). When urinary coproporphyrin concentrations were adjusted to the range of 100–200 μg/l. and 200–400 μg/l., the CL emission becomes light orange and orange-red (positive results), respectively. At concentrations of 400 μg/l. and higher, the top layer appeared intensely red. The color of this visible emission corresponds to the characteristic spectral region of porphyrins ($\lambda_{max} = 610$–650 nm) and the duration of the emission lasted for about 30 sec. To evaluate the effectiveness of the present method in minimizing interference signal due to the presence of abnormal concentrations of heptacarboxylporphyrin, large amounts of heptacarboxylporphyrin (~1000 μg/l.) was spiked into urine and the characteristics of CL emission from the top layer was examined. Importantly, it was found that even at this excessive level of heptacarboxylporphyrin, no discernable CL emission from porphyrins was observed, suggesting that abnormal concentrations of heptacarboxylporphyrin found in most cases of uroporphyrinuria would not give rise to significant numbers of false positive results.

For purposes of comparison, the peroxyoxalate CL reaction involving the oxidation of DNPO was used for the chemical excitation of urine spiked with coproporphyrin. As expected DNPO yielded a relatively strong CL signal (orange) from the top layer even at a coproporphyrin concentrations of ~50 μg/l. At concentrations lower than 50 μg/l. of coproporphyrin, the CL emission appeared slightly greenish-yellow in color. Similar emission has also been reported by Albrecht *et al.*[12] in the use of the DNPO-based peroxyoxalate system for the screening of urinary porphyrins. They postulated that this signal arose from bilirubin and/or other related species in urine. Fortunately, this greenish-yellow is relatively weak and spectrally far away from the orange–red emission of coproporphyrin, such that it does not present an interference problem especially when using TCPO-based systems. As reported by Albrecht *et al.*[12] in the investigation of 1000 serum samples (500 controls and 500 pathological samples) using their porphyrin-sensitized peroxyoxalate CL test, other pathological or physiological components of urine did not show any CL emission in the characteristic spectral region of porphyrins. These results indicated that peroxyoxalate CL reaction is not only sensitive but highly selective for the detection of urinary porphyrins.

Some major difficulties encountered in the analytical applications of the peroxyoxalate CL reaction are directly related to the insolubility and instability of TCPO or DNPO in aqueous solutions.[10,11] In the present method these particular problems are minimized as a result of the extraction of the fluorophore(porphyrins) from urine into the surfactant-rich phase, thus allowing for enhanced CL signal (high intensity and longer lifetime) due to the more reproducible and efficient mixing of the CL reagents and the porphyrins, and to less TCPO hydrolysis. Figures 1(a) and (b) show that when compared to ethyl acetate alone, which is the solvent of choice for most analyses involving the peroxyoxalate CL reaction, the CL intensity of coproporphyrin dissolved in ethyl acetate containing 10% Triton X-100 (resembles the chemical composition of the top layer) is even slightly higher. Moreover, Fig. 1(c) shows that with the use of small amounts of imidazole as a catalyst,[17] the

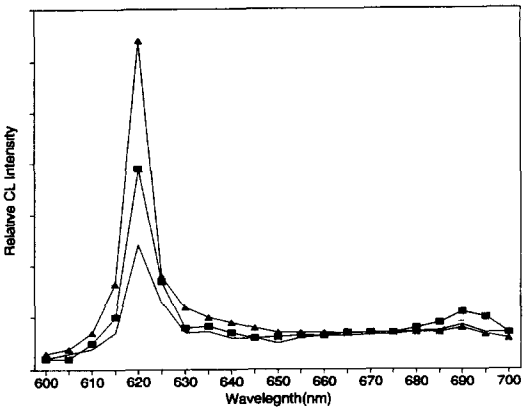

Fig. 1. Relative CL intensity of 400 μg/l. coproporphyrin dissolved in (a) ethyl acetate (□), (b) ethyl acetate and 10% Triton X-100 (■) and (c) ethyl acetate and 10% Triton X-100 in the presence of imidazole (▲). TCPO, H_2O_2 and imidazole concentrations were $1.3 \times 10^{-3}M$, $1 \times 10^{-2}M$ and $3 \times 10^{-2}M$, respectively.

CL intensity of the coproporphyrin dissolved in ethyl acetate containing 10% Triton X-100 was further increased.

It should be noted that addition of non-ionic surfactant at concentrations above those of the critical micelle concentration (CMC) into aqueous solutions (resulting in the formation of normal micelles) have been shown to enhance the CL intensity of certain fluorophores.[18] However, under the experimental conditions described in Fig. 1(b), the non-ionic surfactants probably form dynamic aggregates of reversed micelles in which the hydrophobic portion (alkyl group) of the Triton X-100 extended into the bulk non-polar solvent (ethyl acetate), whereas the polyoxyethylene functional groups formed the hydrophilic core of these aggregates.[19] It is important to note that the observed enhancement of CL as shown in Fig. 1(a) and (b) was accompanied by an increase in the fluorescence intensity of coproporphyrin. This suggests that the coproporphyrin molecules were somehow associated with the micellar assemblies, resulting in a change in their micro-environments, *e.g.*, micro-viscosity, local pH, polarity *etc*, and an increase in the fluorescent quantum yield. However, an enhancement in the CL intensity of coproporphyrin due to increases in the chemical excitation efficiency and rate of reaction are also possible. Finally, it should be noted that the use of reversed micelles to prolong the duration of the light emission generated from the peroxyoxalate CL reaction has been reported.[19]

Table 2 shows the effects of different sulfate and phosphate salts on the relative CL intensity of coproporphyrin. It can be seen that for identical concentrations of sulfate salts ($2.5M$), the salts containing Na^+ yielded the greatest CL intensity while those containing NH_4^+, Zn^{2+} and Mg^{2+} provided lesser CL intensity. It should be noted that although the sulfate anion concentrations were identical the concentrations of the cations were different for singly and doubly charged cations. Similarly for identical concentrations of various phosphate salts ($3.5M$), it was found that the relative CL intensity obtained from using the monohydrogen phosphate salt containing Na^+ was slightly higher than that containing K^+ However, K_3PO_4 yielded the highest relative CL intensity at identical salt concentration and was used as salting-out agent in most of the experiments in this work due to its ease of dissolution in the sample solutions.

The effect of different cations (from the salting-out agents) on the relative CL intensity could be explained in part by their influence on the E% of coproporphyrin. It has been postulated in our previous work[16] that a doughnut-like complex may form between the porphyrin and Triton X-100 molecules. This complex may be stabilized by the chelation of the cation with the oxygen atoms of the polyoxyethylene functional groups (cation chelation mechanism) and could result in the concomitant interaction of this moiety with the porphyrin nucleus and in differing degrees of E% for different cations.

Table 2. Effects of different cations from different sulfate and phosphate salts on the relative CL intensity of coproporphyrin extracted from spiked urine samples (urinary coproporphyrin concentration: 75 μg/l.). TCPO and H_2O_2 concentrations were $1.3 \times 10^{-3}M$ and $1 \times 10^{-2}M$, respectively

Sulfate Salts ($2.5M$)	Relative CL intensity	Phosphate Salts ($3.5M$)	Relative CL intensity
Na_2SO_4	100.0	K_3PO_4	100.0
$(NH_4)_2SO_4$	65.1	Na_2HPO_4	89.2
$ZnSO_4$	47.3	K_2HPO_4	73.5
$MgSO_4$	36.6		

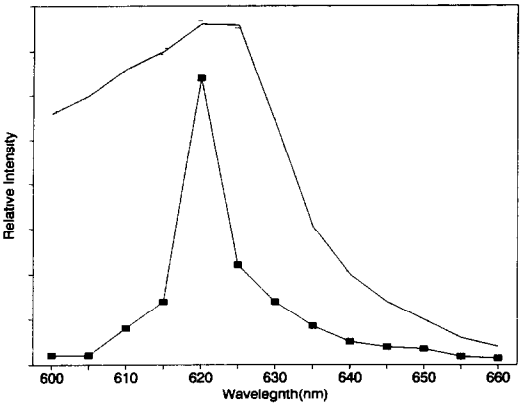

Fig. 2. Comparison of (a) chemiluminescence (■) and (b) fluorescence (□) spectra of coproporphyrin extracted from spiked urine samples. (Urinary coproporphyrin concentration: 75 μg/l.) TCPO and H_2O_2 concentrations were $1.3 \times 10^{-3}M$ and $1 \times 10^{-2}M$, respectively.

Another possibility is that the cation coordinated to the polyoxyethylene groups may provide an electrostatic attraction for the peroxyoxalate reaction species to penetrate the micelles more efficiently,[18] thus allowing for enhancement in CL intensity. More detailed and systematic investigations are necessary to provide insight into the effects of cations on the E%, chemical excitation efficiency, and kinetics of the peroxyoxalate CL reaction in aqueous and non-aqueous solutions.

Figure 2 compares the fluorescence and CL spectra of coproporphyrin extracted from spiked urine samples. It is clear that the intensity of fluorescence signal was slightly higher than that of the CL at the peak maximum (at ~620 nm); however the band-width of the fluorescence spectrum was broader than that of the CL spectrum. It is important to note that the CL spectrum of coproporphyrin extracted from urine samples is very similar to that obtained from coproporphyrin dissolved in ethyl acetate and 10% Triton X-100 as shown in Fig. 1(b). This observation suggests that the broadening effect of fluorescence measurement could arise from fluorescent interferent species present in the urine samples such as riboflavin and/or bilirubin-related compounds[20] and that CL is a more selective method for the detection of urinary coproporphyrin.

In summary, this work demonstrates that cloud point extraction coupled with peroxyoxalate CL reaction provides a highly sensitive and selective method for the detection of urinary coproporphyrin. With the rise in the number of cases of porphyrin related diseases this simple and inexpensive method may prove valuable for the rapid screening of elevated levels of urinary coproporphyrin in clinical laboratories.

REFERENCES

1. S. Schwartz, M. H. Berg, I. Bossenmaier and H. Densmore, in D. Glick (ed.), *Methods of Biochemical Analysis*, Vol. VIII, p. 221. Interscience Publishers, NY, 1960.
2. M. Doss, *Diagnosis and Therapy of Porphyria and Lead Poisoning*. Springer-Verlag, Berlin, 1978.
3. G. H. Elder, *Clin. Haemetal.*, 1980, **9**, 371.
4. A. A. Lamola, *J. Invest. Dermatol.*, 1981, **31**, 114.
5. M. O. Doss, in H. G. Curtious and M. Roth (eds), *Clinical Biochemistry—Principles and Methods*, Vol. 2, p. 1323. DeGruyter, New York, 1974.
6. R. G. Haining, T. Huse and R. F. Labbe, *Clin. Chem.*, 1969, **15**, 460.
7. C. W. Huie, J. H. Aiken and W. R. Williams, *Anal. Chim. Acta.*, 1991, **254**, 189.
8. J. Nutter and R. F. Labbe, *Clin. Chem.*, 1972, **18**, 739.
9. F. K. Herbert, *Clin. Chem. Acta*, 1966, **13**, 31.
10. K. Rohards and P. J. Worsfold, *Anal. Chim. Acta.*, 1992, **266**, 147.
11. P. J. M. Kwakman and U. A. Th. Brinkmen, *Anal. Chim. Acta.*, 1992, **266**, 175.
12. S. Albrecht, H. Brandl and E. Kostler, *Z. Klin. Med.*, 1989, **44**, 2071.
13. S. Albrecht, H. Brandl, W. D. Bohm, R. Bechart, H. Knoschwitz and V. Neumeister, *Anal. Chim. Acta*, 1991, **255**, 413.
14. A. G. Mohan, N. J. Turro, *J. Chem. Ed.*, 1974, **51**, 528.
15. Z. J. Petryka and C. J. Watson, *J. Chromatogr.*, 1979, **179**, 143.
16. W. J. Horvath and C. W. Huie, *Talanta*, 1992, **39**, 487.
17. N. Hanaoke, R. S. Givens, R. L. Schowen and T. Kuwana, *Anal. Chem.*, 1988, **60**, 2193.
18. N. Dan, M. L. Lan and M. L. Grayeski, *Anal. Chem.*, 1991, **63**, 1766.
19. H. Hoshino and W. L. Hinze, *Anal. Chem.*, 1987, **59**, 496.
20. O. S. Wolfbeis, in S. G. Scherlman (ed.), *The Fluorescence of Organic Natural Products, Molecular Luminescence Spectroscopy, Method and Application*, Vol. 1, pp. 167–370. Wiley, New York, 1985.

Talanta, Vol. 40, No. 9, pp. 1391–1396, 1993
Printed in Great Britain.

0039-9140/93 $6.00 + 0.00

SIMULTANEOUS DETERMINATION OF TARTRAZINE AND SUNSET YELLOW BY DERIVATIVE SPECTROPHOTOMETRY AND RATIO SPECTRA DERIVATIVE

J. J. BERZAS NEVADO,* J. RODRIGUEZ FLORES and M. J. VILLASEÑOR LLERENA
Department of Analytical Chemistry and Foods Technology, University of Castilla-La Mancha, 13071 Ciudad Real, Spain

(*Received* 16 *November* 1992. *Revised* 28 *January* 1993. *Accepted* 2 *February* 1993)

Summary—Two methods for determining Tartrazine and Sunset Yellow in mixtures by first derivative spectrophotometry and by first derivative of the ratio spectra are described. The procedures do not require any separation step. By the first method, the measurements are obtained in the zero-crossing wavelengths and the calibration graphs are linear up to 20 μg/ml of Tartrazine and up to 40 μg/ml of Sunset Yellow. The determinations of Tartrazine and Sunset Yellow are also done by the first derivative of the ratio spectra. The methods are applied for determining both compounds in four commercial food products.

Tartrazine (T) is an azo dye available as yellow powder. This colorant must be named in a list of ingredients after an extensive study[1] of the genotoxicity of food, drug and cosmetic color. Sunset Yellow (S), the other determined colorant, is a synthetic azo dye. Derivative spectrophotometry, particularly with digital processing,[2] is an analytical technique of great utility for resolving some mixtures with overlapping spectra. The fundamental principles have been described in the pioneering work of O'Haver and Green,[3] Fell *et al.*[4-6] and others.[7]

Recently, Salinas *et al.*[8] developed a new method for resolving mixtures of chromophores with overlapped spectra. This method is based on the use of the first derivative of the ratio of the spectra. The absorption spectrum of the mixture is divided by the absorption spectrum of a standard solution of one of the chromophores (amplitude by amplitude at each wavelength) and the first derivative of the ratio spectrum is obtained. The concentration of the other component is then determined from a calibration graph previously obtained.

The aim of this work was to demonstrate the ease in which the derivative methods (first and ratio spectra) circumvent the problem of overlapping spectral bands, allowing the simultaneous determination of these two colorants (Tartrazine and Sunset Yellow) without prior separation. The two methods yield accurate and reproducible results in different commercial products.

EXPERIMENTAL

Apparatus

A Beckman Instruments DU-70 spectrophotometer connected to an IBM PS/2 fitted with Beckman Data Leader Software[9] and an Epson FX-850 printer were used for all the measurements and treatment of data.

Solutions

All solvents and reagents were of analytical reagent grade. Tartrazine (T) and Sunset Yellow (S) aqueous solutions were prepared from Sigma products. Their Sigma numbers are T 0388 and O 1625, respectively. T and S solution stocks have a concentration of 200 μg/ml. Acetic acid/sodium acetate buffer solution (0.5*M* and pH = 4.5) was made of analytical reagent grade.

Procedures

(a) First derivative spectrophotometry. Samples were prepared in 25 ml calibrated flasks containing 2–20 μg/ml of T or 4–40 μg/ml of S or their binary mixtures, 5 ml of pH 4.5 buffer solution, and were diluted with water to the mark. The absorption spectra of the samples thus prepared were recorded, and by measuring the signal of their first derivative spectra (obtained with $\Delta\lambda = 8$ nm) at 481.6 ($^1D_{481.6}$),†

*Author for correspondence.
†$^{\text{order derivative}}\text{Derivative}_{\text{wavelength measure}}$.

Tartrazine (E-102)

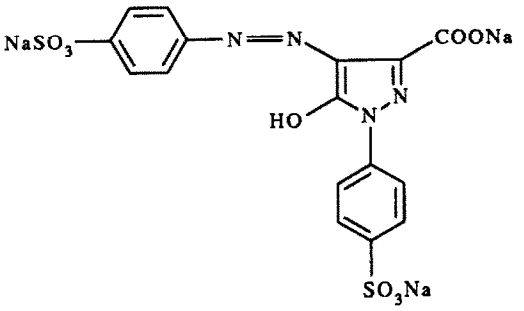

Sunset Yellow (E-110)

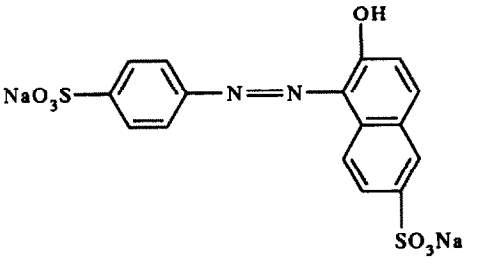

Scheme 1

(zero-crossing point for Sunset Yellow) and by using an appropriate calibration graph, their concentration could be determined. These calibrations were done by varying the concentration of a colorant, without the presence of the other colorant. The S content was also determined by measuring the signal at 426.5 nm ($^1D_{426.5}$) or 538.0 ($^1D_{538.0}$) (zero-crossing points for Tartrazine). Eventually, these spectra were treated with a smoothing of 11 experimental points. (All the spectra have been multiplied by 100 in order to obtain an increase in the accuracy measure.)

(b) First derivative of the ratio spectra. By this method for determining T, the stored spectra were divided by a standard spectrum of S of 16.0 μg/ml. From the ratio spectra thus obtained, first derivatives were calculated with $\Delta\lambda = 6$ nm. The concentration of T was proportional to the amplitude of the maximum at 445.0 nm ($^1DD_{445.0}$)* or at the minimum at 397.0 nm ($^1DD_{397.0}$). For the determination of S, the stored spectra were divided by a standard spectrum of T of 8.8 μg/ml. From the ratio spectra thus obtained, first derivatives were calculated with $\Delta\lambda$ of 8 nm. The concentration of S was proportional to the amplitude of the maximum at 528.0 nm ($^1DD_{528.0}$) or at the minimum at 503.0 nm ($^1DD_{503.0}$) and to the addition of these two signals ($^1DD_{528.0+503.0}$).† All these spectra were smoothed with different experimental points for each of the two dyes.

RESULTS AND DISCUSSION

Method development

The influence of pH on the absorption spectra of T and S was studied. The best results for analytical purposes were obtained at pH = 4.5 (acetic acid/sodium acetate buffer solution) because the T and S absorption spectra were stable in the range pH 4.0–7.0.

Samples were prepared in aqueous solution at pH = 4.5. Under these conditions diluted solutions of T and S were stable for 12 hr at least.

Derivative spectrophotometry

In Fig. 1 the zero order spectra of T and S in the 350–600 nm wavelength range are shown. It can be seen that the absorption spectra of T and S are very overlapped and as a result, the determination of the two colorants cannot be possible for reliable direct absorbance measurements. Derivative spectrophotometry can be suitable to obviate this problem. The "zero-crossing method" is the most common procedure for the preparation of analytical calibration graphs.

In practice, the measurement selected is that which exhibits the best linear response, gives a zero or near zero intercept on the ordinate of the calibration graph, and is less affected by the concentration of any other component. The

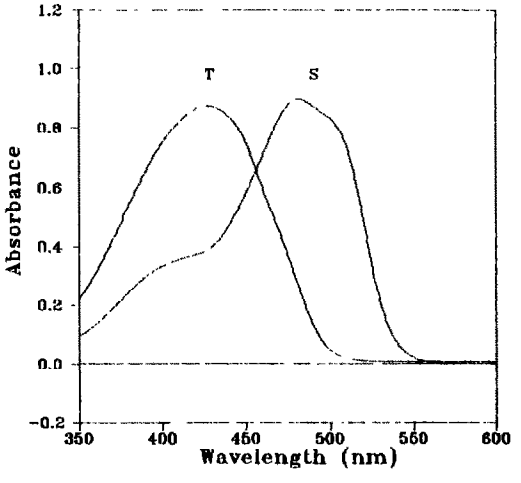

Fig. 1. Absorption spectrum of 18.4 μg/ml of Tartrazine (T) and 20.0 μg/ml of Sunset Yellow (S).

*order derivative Derivative Divided$_{\text{wavelength measure}}$.
†order derivative Derivative Divided$_{\text{w m (peak to peak)}}$.

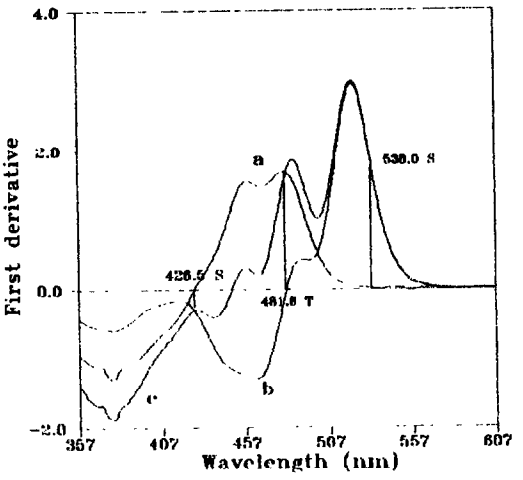

Fig. 2. a. First derivative spectrum of 18.4 μg/ml of T. b. First derivative spectrum of 20.0 μg/ml of S. c. First derivative spectrum of a mixture of 18.4 μg/ml of T and 20.0 μg/ml of S.

shape of the first derivative spectra is adequate for determining T in the presence of S and vice versa. Figure 2 shows the first derivative absorption spectra, respectively, of a solution of T, a solution of S and their mixture. (These spectra are multiplied by 100 as we mentioned in the Experimental section.)

It can be seen that due to the overlapping spectra of these compounds in a determined region, the zero-crossing method is the most appropriate for resolving mixtures of these compounds and it was used in this work with satisfactory results.

Preliminary experiments showed that the signals of the first derivative at 481.6 nm (working zero-crossing wavelength of S) are proportional to the T concentration and the signals of the first derivative at 426.5 and 538.0 nm (working zero-crossing wavelengths of T) are proportional to the S concentration.

Selection of optimal instrumental conditions

The main instrumental parameters that affect the shape of the derivative spectra are the wavelength scanning speed, the wavelength increment over which the derivative is obtained ($\Delta\lambda$) and the smoothing. These parameters need to be optimized to give a well resolved large peak *i.e.*, to give good selectivity and larger sensitivity in the determination. Generally, the noise level decreases with an increase in $\Delta\lambda$ thus decreasing the fluctuations in the derivative spectrum. However, if the value of $\Delta\lambda$ is too large, the spectral resolution is very poor.

Therefore, the optimum value of $\Delta\lambda$ should be determined by taking into account the noise level, the resolution of the spectrum and the sample concentration. Some values of $\Delta\lambda$ were tested. By first derivative 8.0 nm was selected as the optimum in order to give a satisfactory signal-to-noise ratio. In this way, a smoothing of 11 experimental points function was used.

Having established the experimental conditions, the calibration graphs were tested between 2.0 and 20.0 μg/ml of the T concentration at 481.6 nm for the first derivative spectra, without the presence of S (Fig. 3). Equally, the calibration graphs were tested between 4.0 and 40 μg/ml of the S concentration, in the absence of T, at 426.5 and 538.0 nm for the first derivative spectra (as can be seen in Fig. 4). Good linearities were observed in all cases.

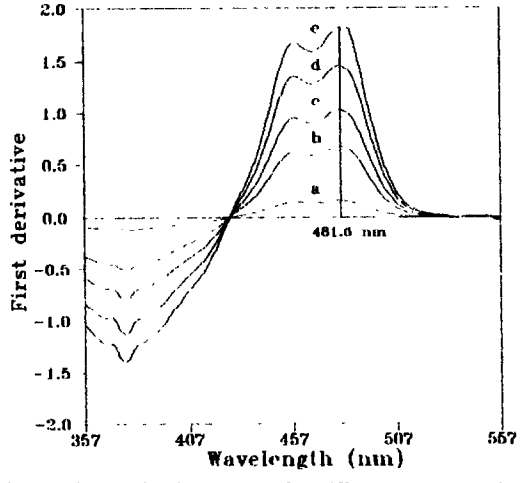

Fig. 3. First derivative spectra for different concentrations of T, in the absence of S. a. 2.0 μg/ml; b. 7.2 μg/ml; c. 11.2 μg/ml; d. 16.0 μg/ml; e. 20.0 μg/ml.

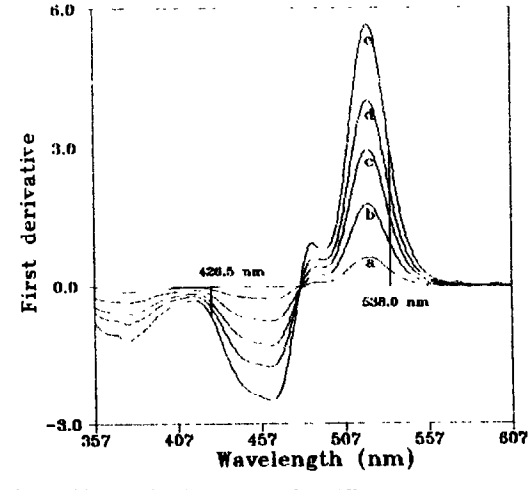

Fig. 4. First derivative spectra for different concentrations of S, in the absence of T. a. 4.0 μg/ml; b. 12.0 μg/ml; c. 20.0 μg/ml; d. 28.0 μg/ml; e. 40.0 μg/ml.

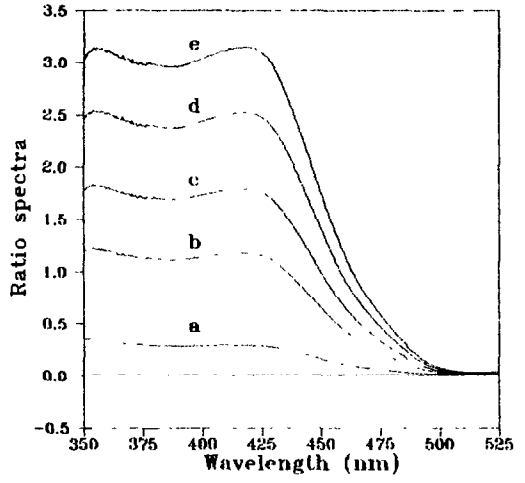

Fig. 5A. Ratio spectra for different concentrations of T when S divisor was 16.0 μg/ml. a. 2.0 μg/ml; b. 7.2 μg/ml; c. 11.2 μg/ml; d. 16.0 μg/ml; e. 20.0 μg/ml.

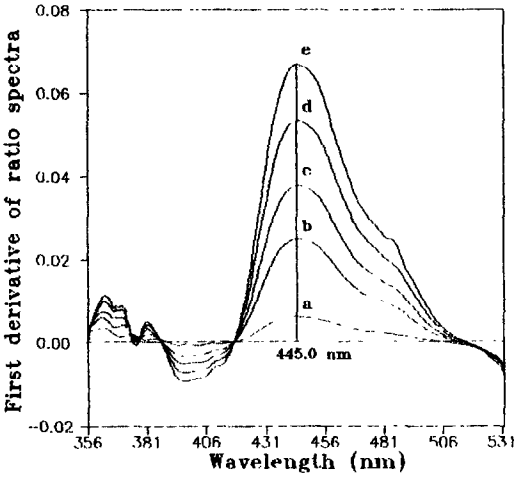

Fig. 5B. First derivatives of ratio spectra for different concentrations of T when S divisor was 16.0 μg/ml. a. 2.0 μg/ml; b. 7.2 μg/ml; c. 11.2 μg/ml; d. 16.0 μg/ml; e. 20.0 μg/ml.

First derivative of the ratio spectra

The use of the "zero-crossing" method in derivative spectrophotometry for resolving a mixture of chromophores with overlapped spectra produces a considerable loss of accuracy and sensitivity. This problem is due to the fact that the measurements are taken at a very critical wavelength, the localization of which is sometimes very difficult and whose value is sometimes very small for obtaining a good analysis.

The named "ratio spectra derivative" permits the determination of a component in their mixture at the wavelengths corresponding to a maximum or minimum and, also, the use of the peak to peak between consecutive maximum and minimum. The values of absorbance in these points permit one, in some cases, to reach a better sensitivity.

The influence of the $\Delta\lambda$ for obtaining the first derivative was tested and an $\Delta\lambda$ of 6 nm was considered as suitable for the T determination and a value of 8 nm for the S determination. The concentration of the S solution used as divisor could be modified and different calibration graphs were obtained. A standard spectrum of 16 μg/ml of S was considered as suitable for the T determination and a standard spectrum of 8.8 μg/ml of T as divisor was considered as suitable for the S determination.

In Fig. 5A a calibration graph of T when the divisor is a spectrum of 16 μg/ml of S, in the

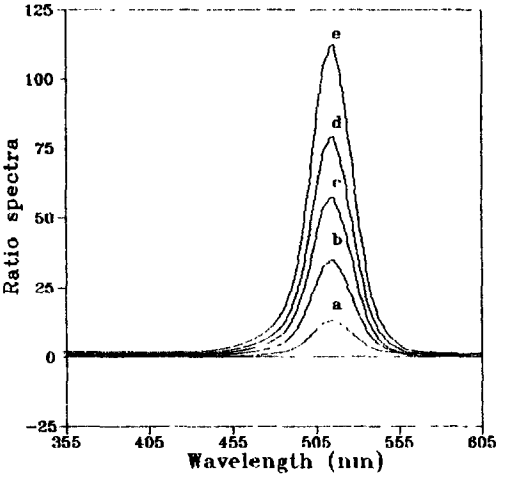

Fig. 6A. Ratio spectra for different concentrations of S when T divisor was 8.8 μg/ml. a. 4.0 μg/ml; b. 12.0 μg/ml; c. 20.0 μg/ml; d. 28.0 μg/ml; e. 40.0 μg/ml.

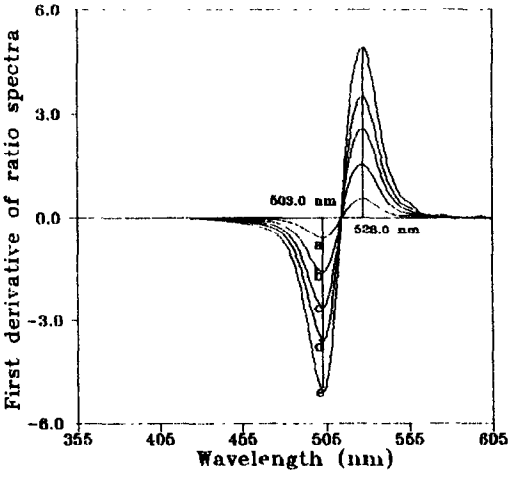

Fig. 6B. First derivatives of ratio spectra for different concentrations of S when T divisor was 8.8 μg/ml. a. 4.0 μg/ml; b. 12.0 μg/ml; c. 20.0 μg/ml; d. 28.0 μg/ml; e. 40.0 μg/ml.

Table 1. Statistical data

Equation		Regression coefficient	Linearity range ($\mu g/ml$)	Detection limit* ($\mu g/ml$)
$^1D_{481\,6}$	$= 0.0190 + 0.0890\ C_T$	1.0000	2.0–20.0	0.053
$^1D_{426\,5}$	$= 0.0026 + 0.0153\ C_S$	0.9995	4.0–40.0	0.220
$^1D_{538\,0}$	$= 0.0200 + 0.0515\ C_S$	1.0000	4.0–40.0	0.060
$^1DD_{445\,0}$	$= 0.0010 + 0.0033\ C_T$	1.0000	2.0–20.0	0.126
$^1DD_{528\,0}$	$= 0.0466 + 0.1240\ C_S$	0.9998	4.0–40.0	0.021
$^1DD_{503\,0}$	$= 0.0849 + 0.1257\ C_S$	1.0000	4.0–40.0	0.099
$^1DD_{528+503}$	$= 0.1550 + 0.248\ C_S$	0.9999	4.0–40.0	0.060

C_T = micrograms per millilitre of Tartrazine.
C_S = micrograms per millilitre of Sunset Yellow.
*$C_L = 3S_B/m$; C_L = detection limit; S_B = standard deviation of blank; m = slope of calibration.

Table 2. Resolution of T and S mixture by first-derivative spectrophotometry

Ratio T/S	T ($\mu g/ml$)	S ($\mu g/ml$)	% Recovery T	% Recovery S	
			$^1D_{481\,6}$	$^1D_{426\,5}$	$^1D_{538\,0}$
0.13	4.8	36.0	124.5	96.1	101.1
0.31	8.8	28.0	104.0	98.0	99.9
0.64	12.8	20.0	101.3	98.5	100.9
1.30	16.0	12.0	99.4	100.9	100.8
5.00	20.0	4.0	100.0	105.1	96.8

absence of Sunset Yellow, is shown. These spectra were derived and the $\Delta\lambda$ used was 6 nm. Eventually, all the spectra were smoothed with a value of 13 experimental points. In Fig. 5B a calibration graph of ratio spectra derivative of T is shown.

Figure 6A shows the ratio spectra of different S standards (spectra divided by the spectrum of a 8.8 μg/ml T solution) in acid medium and in Fig. 6B their first derivatives are calculated, without the presence of T. The first derivative amplitudes at a given wavelength are proportional to the S concentration. Due to the noise levels, a smoothing of 23 experimental points function is used.

A calibration graph was established at a wavelength of 445.0 nm, corresponding to a maximum. Straight lines up to 20.0 μg/ml were obtained for the Tartrazine determination. Calibration graphs were established at wavelengths 528.0 and 503.0 nm, corresponding to a maximum and minimum, and also at the addition of these two signals for the Sunset Yellow determination. Straight lines up to 40.0 μg/ml were obtained for this colorant.

STATISTICAL COMPARATIVE STUDY

In Table 1 summary of the most characteristic statistical data obtained from the different calibration graphs and from the reproducibility of the reagent-blank and a standard by eight successive scans are shown. In all cases good results were obtained.

The best detection limits were obtained from the first derivative at 481.6 nm for T determination and at 528.0 nm for S determination. Nevertheless, in general, the method that used the first derivative of the ratio spectra shows better accuracy and comparable limit detections.

APPLICATIONS

The proposed methods were applied for resolving the determination of T and S, in

Table 3. Resolution of T and S mixtures by ratio spectra derivative

Ratio T/S	T ($\mu g/ml$)	S ($\mu g/ml$)	% Recovery T	% Recovery S		
			$^1DD_{445\,0}$	$^1DD_{528\,0}$	$^1DD_{503\,0}$	$^1DD_{528+503}$
0.13	4.8	36.0	104.7	99.1	99.4	99.7
0.31	8.8	28.0	100.6	99.0	98.4	99.1
0.64	12.8	20.0	100.9	100.9	99.2	100.3
1.30	16.0	12.0	100.0	100.7	97.9	99.2
5.00	20.0	4.0	100.1	97.1	84.8	89.4

Table 4. Percentages of T and S in commercial products

(%)	Standard addition*		Zero-crossing		Ratio spectra derivative	
	T	S	T	S	T	S
Food dye	11.8	0.12	12.6	0.17	12.5	0.14
Lemon gelatin	0.020	1.5×10^{-3}	0.019	1.4×10^{-3}	0.019	1.3×10^{-3}
Orange gelatin	0.053	0.023	0.055	0.023	0.055	0.022
Light custards	0.090	0.033	0.083	0.031	0.081	0.030

*With measurements at the "zero-crossing".

artificial mixtures. The results corresponding to these determinations are summarized in Tables 2 and 3. The obtained recoveries were very good in general. The recoveries (%) by the first derivative spectrophotometry were of the order of 99% except when the ratio T:S was 5:1 and 1:7.5 (0.13). In this case the recovery was poorer, due to the low concentration of one of the colorants in the presence of high concentrations of the second colorant. Similar results were obtained by the first derivative of the ratio spectra method as can be seen in Table 3. The recoveries for the determination of S were in the same range. In conclusion, the first and the ratio spectra derivative methods gave good results for the simultaneous determination of Tartrazine and Sunset Yellow.

The proposed methods were also applied for the determination of T and S in four different food commercial products. These were a **spice** named *Colorante Alimentario* from Granja San Francisco (Spain), two different **gelatin desserts**: orange and lemon flavours, and in **light custards** from Royal Brands S.A.

The percentage of these two dyes can be seen in Table 4 and they were calculated by the method of standard addition, with measuring at "zero-crossing" and by the methods mentioned in this paper.

In all cases, these determinations were made with good recoveries, which were higher than 90% with regard to the data supplied by the companies aforementioned.

REFERENCES

1. R. Combes and R. Haveland-Smith, *Mutat. Res.*, 1982, **98**, 101.
2. A. Savitzky and M. J. E. Golay, *Anal. Chem.*, 1964, **36**, 1627.
3. T. C. O'Haver and G. L. Green, *Anal. Chem.*, 1976, **48**, 312.
4. A. F. Fell, *Proc. Anal. Div. Chem. Soc.*, 1978, **15**, 260.
5. A. F. Fell, D. R. Jarvie and M. J. Stewart, *Clin. Chem.*, (Winston-Salem, NC), 1981, **27**, 286.
6. A. A. Fasanmade and A. F. Fell, *Analyst*, 1985, **110**, 1307.
7. B. Morelli, *Analyst*, 1983, **108**, 870.
8. F. Salinas, J. J. Berzas Nevado and A. Espinosa Mansilla, *Talanta*, 1990, **37**, 347.
9. Beckman Instruments, Inc., *Spectroscopy*, 1987, **2**, 16.

Talanta, Vol. 40, No. 9, pp. 1397–1403, 1993
Printed in Great Britain.

0039-9140/93 $6.00 + 0.00

VOLATILIZATION OF METHYL BORATE IN IRON MATRIX. DETERMINATION OF BORON IN STEEL BY ICP ATOMIC EMISSION SPECTROMETRY

A. LOPEZ MOLINERO,* A. FERRER and J. R. CASTILLO

Department of Analytical Chemistry, Sciences Faculty, University of Zaragoza, 50009 Zaragoza, Spain

(*Received* 27 *October* 1992. *Revised* 29 *January* 1993. *Accepted* 29 *January* 1993)

Summary—A rapid and reliable method for the determination of boron by ICP–AES in steels is described. The procedure is based on a discontinuous generation of methyl borate, in concentrated sulphuric acid and phosphoric acid medium, after injecting 45 μl of methanol in 20 μl of sample. The gaseous methyl borate and excess methanol are fed into the ICP torch via the intermediate tube by a flow of 430 ml/min Ar carrier gas, without disturbing the discharge. This work simplifies drastically the existing methodology of boron analysis in steels. Acid-soluble boron has been determined, but acid-insoluble boron can also be determined. The determination is carried out without iron interferences, with a reproducibility of 1.90% r.s.d. for a concentration of 20 μg/ml, and an absolute detection limit of 20 ng of total boron, working with a solution volume of 20 μl.

The microdetermination of boron is especially important in steels, where the addition of small amounts of the element, in the order of the micrograms per gram noticeably improves their hardness and toughness.

Even though the analysis of boron can be undertaken by techniques such as Molecular Absorption Spectrophotometry,[1] Atomic Absorption Spectrometry[2] or Flame Atomic Emission Spectrometry[3,4] the Atomic Emission Spectrometry with an inductively Coupled Plasma (ICP–AES) technique yields adequate[5] detection limits (L.D.) (4.8 ng/ml) to approach this problem.

The limitation for the boron determination by ICP–AES in ferric matrix lies in the fact that iron has emission lines at 249.77 nm Fe(II), 249.65 and 249.70 nm Fe(I), which produce spectral interferences for the more sensitive lines of boron at 249.77 and 249.67 nm.

The microdetermination of boron in ferric alloys relies on avoiding the iron interference. This has been carried out by means of:

(a) Fe elimination; through: (a.i) Fe extraction;[6] (a.ii) precipitation[7] and electrodeposition,[8]
(b) Boron extraction,[9,10]
(c) Boron volatilization or distillation mainly through the methyl borate,[11] although there are other boron volatile phases.[12]

Utilizing the last methodology (c), the boron distillation from a ferric matrix of steel[11] has been applied as a preconcentration method and thus it is possible to reach an L.D. of 0.0036 μg/ml when the absorption aqueous solution containing the boron distillate is analysed by ICP–AES. However, to perform this, a considerable experimental manipulation is necessary. In a more simplified method, Novozamsky *et al.*[13] have described a continuous-flow technique for generation and separation of methyl borate with subsequent determination of boron by ICP–AES. An L.D. of 0.05 μg/ml was obtained, but with this assembly serious difficulties prevent practical work. So the excess of methanol must be removed to prevent quenching of the plasma and experimental difficulties of working with a continuous flow of concentrated sulphuric acid are found.

In the present paper, the discontinuous introduction of methyl borate into an ICP spectrometer through its intermediate tube is proposed, enabling a great stabilization of the discharge in spite of the injection of relatively high amounts of methanol. The methodology has been applied to the boron volatilization in an iron matrix (steel).

EXPERIMENTAL

Apparatus

A Perkin-Elmer model Plasma 40 ICP–AES system equipped with an IBM XT Data station

*Author to whom correspondence should be addressed.

Table 1. Characteristic of the Perkin-Elmer P40 atomic emission spectrometer, and optimized operating conditions

Radio-frequency generator	40 MHz "Free running" type
Radio-frequency power	1 kW
Monochromator	Czerny–Turner assembly
Focal length 408 nm	
Two holographic gratings:	
—UV 4200 lines/mm, 160–460 nm	
—visible 1800 lin./mm, 460–800 nm	
Slit width 25 μm	
Computer	IBM PC XT. 10 Mb hard disk
	P40 software
Torch	De-mountable P.E.
Nebulizer	Ryton, cross-flow
Nebulization chamber	Scott, dual pass
Gas flow rates (Ar, 99.995%)	
External	12 l/min
Intermediate	0.6 l/min

was used. Operating conditions are given in Table 1.

Methyl borate generation assembly

The flow chart for generation of the methyl borate is shown in Fig. 1. The apparatus consists of a 3 ml reaction vessel made of PTFE. A rubber stopper, pierced with two stainless steel needles and fitted to the reaction vessel, is used. Methanol is injected with an FIA injection valve (Omnifit) equipped with a loop of 45 μl. A two-way valve is utilized to lead the Ar carrier gas either to the reaction vessel or to the plasma. Nylon tubes of 2 mm O i.d. are used and are joined with quick connectors (Clifco series PM).

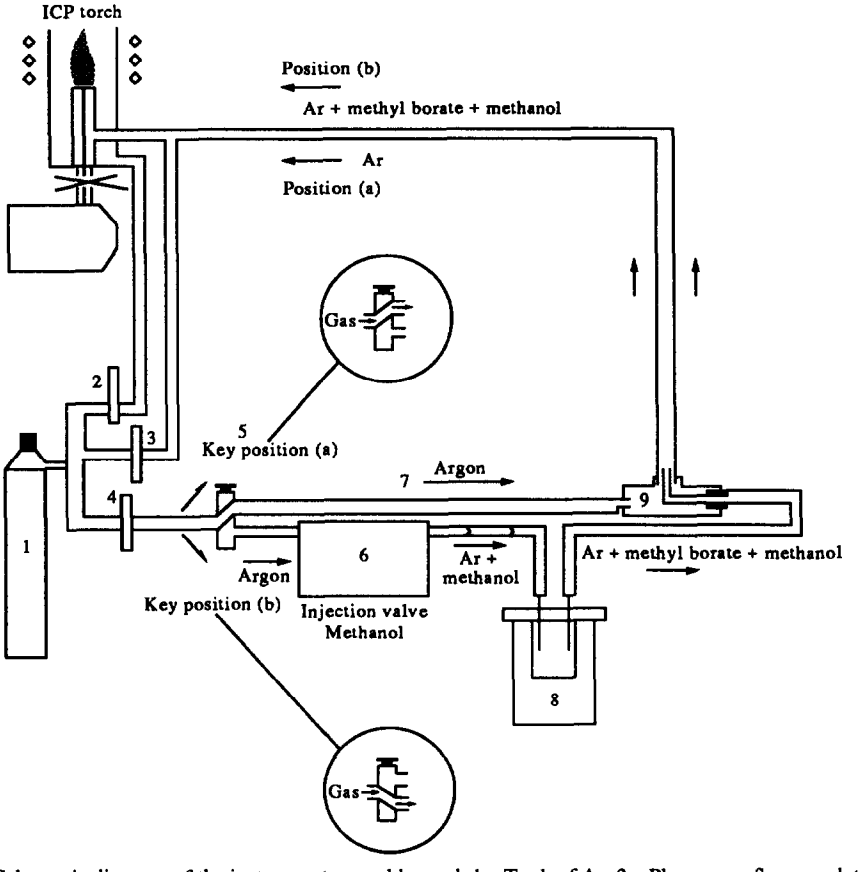

Fig. 1. Schematic diagram of the instrument assembly used. 1—Tank of Ar. 2—Plasma gas flow regulator. 3—Intermediate gas flow regulator. 4—Injector or carrier gas flow regulator. 5—Two-way key. 6—Injection valve for methanol. 7—Nylon tube. 8—Reaction chamber. 9—Three-port quick connector.

Procedure of methyl borate generation

Concentrated sulphuric acid (200 μl) and the sample solution containing boron (20 μl) are placed in the reaction vessel. After stoppering the vessel, the Ar carrier gas (a steady flow of 450 ml/min is maintained) is channelled throughout it, and passed to the top of the liquid surface. By setting the key (5) to position (b) (see Fig. 1) the gas is first passed through the FIA valve, then through the reaction vessel and finally directed to the torch. A brief period of time is needed to stabilize the plasma (30 sec) prior to the injection of methanol (45 μl) via the FIA valve.

The atomic line of boron at 249.773 nm is chosen to measure the emission intensity, which is continuously recorded and thus transient peaks are obtained. Once the recording of boron emission has finished, the flow of Ar carrier gas through the FIA valve and the reaction vessel is interrupted utilizing the key (5), which is rotated to its position (a), re-directing the flow of gas to the torch. With this last configuration, a stable plasma is maintained during the time a new sample is being prepared for analysis. In all instances, Ar flow is fixed and controlled by a flow regulator (see its position on Fig. 1).

Procedure for steel dissolution

Two grams of steel were dissolved in a similar way to the literature[14] and subsequently diluted to 20 ml in a volumetric flask. Using this procedure only acid-soluble boron can be determined.

Procedure for boron determination in steels

Boron in steels is determined according to the following procedure: 200 μl of concentrated sulphuric acid and 20 μl of concentrated phosphoric acid followed by 20 μl of the steel solution are placed in the reaction vessel. The mixture is shaken until homogenized and methanol (45 μl) is injected. The gaseous methyl borate is carried into the plasma torch.

Reagents

All chemicals used were of analytical grade. Deionized water, quality Milli Q, was utilized in all dilutions. A standard solution of boron (1000 μg/ml), made from boric acid was prepared and stored in a polyethylene bottle. Methanol, concentrated sulphuric acid, phosphoric acid and iron nitrate were used.

Standard reference steels from BCS No. 458 and 459 were utilized.

RESULTS

Experiment assembly

The introduction of gaseous methyl borate into an ICP spectrometer, generated by reaction of borate with methanol in concentrated sulphuric acid, presents considerable experimental difficulties.[13] In our paper a new method for gas introduction (methyl borate and methanol in excess) has been accomplished, through the intermediate tube of an ICP torch. It allows one to work with a stable discharge and at the same time, good analytical values are obtained.

In ICP measurements it has been demonstrated that the excess of methanol injected must be removed to prevent quenching of the plasma. We have verified that plasma is able to accept a higher amount of methanol if it comes through the intermediate gas instead of being introduced through the central channel. Up to 90 μl of pure methanol have been injected in this way, against a maximum volume allowed of 20 μl if fed through the central axial channel of the discharge. According to our configuration, a green aureole is produced in the plasma, from its periphery, surrounding and compressing the plasma.

In our assembly (see the scheme of Fig. 1) the nebulizer gas acts as carrier gas and it is channelled directly to the torch via the intermediate tube, using key (5) in position (a), or else it can be passed through the FIA valve and the reaction vessel using key (5) in position (b).

Our proposed method introduces a considerable advantage by being able to maintain stable plasma with a relatively simple gas switching strategy.

We have studied the instability of the discharge during the change which must be fast. This has been carried out by measuring the carbon emission (present in the Ar gas), at its 193.091 nm line, before and after the change of the gas. The signal stability is reached 30 sec after the production of that change. In consequence all analytical measurements have a waiting time of 30 sec, prior to the methanol injection.

Conditions for ester generation: water, methanol, sulphuric acid

The optimum ratios of water, methanol and sulphuric acid for methyl borate generation, have been studied as seen in the bibliography.[2,4] In these works, it is postulated that the exothermic reaction between methanol and sulphuric

acid generates considerable heat. So the temperature of the reaction medium rises, even over the boiling temperature of the methyl borate (b.p. 68°C). However, we have worked with very small volumes of reagents and consequently the thermal effect is limited. So we have tried to evaluate the temperature in the reaction mixture.

A theoretical calculation of the temperature increase (ΔT) generated under the optimum reaction conditions provides a value of $\Delta T = 9$°C. This value was obtained by calculation for dilution of 200 μl of concentrated sulphuric acid (36M) with 20 μl of water (dilution heat 0.146 kcal/mol[15] and for a density of 1.8 kg/l and a specific heat of 0.33 cal/g for the concentrated sulphuric acid).[16] Therefore the reaction mixture is far from reaching the methyl borate b.p. temperature.

This value has been checked experimentally, determining the temperatures in the reaction vessel by means of a Thermistor Thermometer-Digitec model 5831 (type 704 YSI) thermic sounding line. In this way a temperature value for sulphuric acid prior to the reaction of 26.07°C is obtained and after the addition of water (waiting for 30 sec corresponding to the plasma stabilization), a temperature of 36.0°C is measured.

At these temperatures the vapour pressures of methanol (b.p. = 65°C) and of methyl borate ester (b.p. = 68°C) are 220.1 and 222.4 torr, respectively.[17] It has been proved that, under these conditions, boiling point of the methyl borate is not reached but high volatilization of the methyl borate is observed. It can be said that temperature is not the only effect that facilitates the methyl borate volatilization.

However because temperature effects have been profusely argued as being responsible for methyl borate volatilization we have experimented with higher temperatures of both the reaction mixture (an isothermic bath was used at 50 and 60°C) and the carrier gas. In these experiments improvement in sensitivity was not obtained.

On the other hand, boric acid esterification in the presence of phosphoric acid (its dilution heats are lower than those of sulphuric acid) also leads to boron emission. However, the peak signals are less pronounced and wider, and they show lower sensitivity (based on peak height) than those produced in sulphuric medium.

It can be concluded that the high sensitivity obtained in methyl borate volatilization with our set up, depends on the temperature effect and on a very important "sweep effect" produced by the carrier Ar flow.

Optimization of variables

The variables studied can be classified as two types.

—Variables of the reaction. That is: concentrated sulphuric acid volume, water volume, methanol volume.
—Instrumental parametres of detection. That is: injection gas flow (carrier gas), observation height, photomultiplier voltage.

These variables were optimized by means of the Simplex, MSM method,[18] and the following optimum values were adopted: 45 μl of methanol were injected into a solution of 200 μl of sulphuric acid and 20 μl of water. The Ar carrier gas was set at 430 ml/min, the observation height of 20 mm above the coil selected and the PM voltage adjusted to 450 V.

In the same way, the effect of other variables was studied, and they are discussed below.

Firstly, a cylindrical shape for the reaction chamber was chosen and different sizes were tested (varying in section and height). The optimum vessel is shown in Fig. 2.

The effect of the transport length between the reaction vessel and the ICP torch was studied. In our assembly we have worked with a

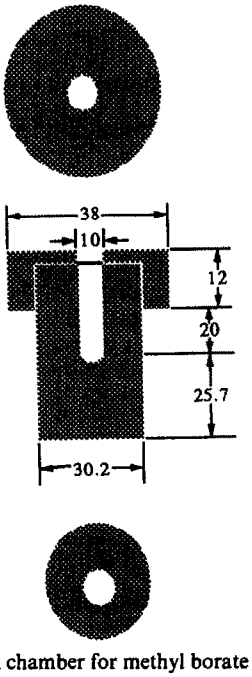

Fig. 2. Reaction chamber for methyl borate generation. The dimensions are given in millimetres.

Table 2. Variables for the experimental assembly and response range of the parameters of the FIA peak

Hydrodynamic variables	
Conduction length—L	= 15.0–30.0 cm
Conduction diameter—d	= 0.2–0.3 cm i.d.
Carrier gas flow—q	= 300 ml/min (5 ml/sec)–530 ml/min (8.8 ml/sec)
FIA peak parameters	
Appearance time—t_a	= 1–7 sec
Baseline-base line time—Δt	= 20–50 sec
Residence time—T	= 2–8 sec
Peak height—H	= 1–12 cm

minimum distance of 15 cm. For a distance of 25 cm, a signal loss of 17% with respect to the one obtained at 15 cm was observed. In the same way the reproducibility decreased (10.3% r.s.d., for 20 μg/ml of boron).

Methanol injection by means of a microsyringe was tested and its results compared to FIA injection. The first method of injection presents high irreproducibility (up to 20% r.s.d.) and so FIA injection was chosen.

The effect of surface-active agents, as favouring the methanol transport and injection (Triton × 100 at 0.1% in methanol), as well as the presence of sodium bicarbonate as favouring a greater gaseous emission (methanol saturated with sodium bicarbonate) showed very little modification in the ICP signal of methyl borate, but increased its irreproducibility.

The method of methyl borate introduction into the ICP torch has been studied. Firstly, the vapour stream was fed into the ICP at the torch entrance normally used for the nebulizer gas (the injector tube), but using the nebulizer gas as carrier gas, and secondly, according to an experimental arrangement used by us previously in the study of hydrides.[19] The results obtained with these two approaches showed a low tolerance to methanol, and the injection of 20 μl of pure methanol produced quenching of the plasma.

Characterization of boron emission signal

The flow conditions through our assembly can be characterized by the following data: working pressure of gases (Ar) of 5.5 atm; carrier gas flow average of 430 ml/min through a section of 2 mm i.d.; values of the Reynolds number of the order of 1800. With these values we are under conditions of laminar flow, and the signal obtained by the measurement of the emission intensity of boron at 249.773 nm *vs.* time, shows a profile which has been defined by the parameters of a FIA peak. That is to say: t_a (appearance time), Δt (base line–base line time), H (peak height), T (residence time).

Valcarcel[20] has proposed a characterization of the parameters of a FIA peak from a multiple regression, among the logarithmic values of the manifold hydrodynamic variables [length (L), diameter (d) of conduction and carrier gas flow (q)] and parameters of FIA peak [t_a, Δt,H,T].

The application of the model in our experience (after experimental measurements carried out with the variable ranges shown in Table 2), allows us to characterize and define the signals obtained by the following mathematical expressions:

$$\log t_a = 2.446 + (0.603 \log L) - (0.140 \log d) - (3.253 \log q)$$

$$\log \Delta t = 1.351 + (0.546 \log L) + (0.095 \log d) - (0.450 \log q)$$

$$\log H = -3.229 + (1.248 \log L) + (3.411 \log d) + (0.828 \log q)$$

$$\log T = 2.639 + (0.539 \log L) + (0.263 \log d) - (2.937 \log q).$$

Iron interference

Before beginning the boron determinations on practical samples of steels, boron was determined in a synthetic solution whose Fe and B content was similar to a standard steel. So a simple method (method (a), see Table 3) based on the addition of sulphuric acid and methanol was applied to the boron determination. In these experiments, it was observed that the addition of concentrated sulphuric acid to the steel solution produces precipitation of iron (III) sulphate (by supersaturation) with boron adsorption on precipitate preventing a later reaction of it with methanol. Thus, boron was not detected when analysed.

The addition of phosphoric acid (this is method (b), until the dissolution of the iron (III) sulphate precipitate, obtains the recovery of the

Table 3. Recovery of boron from synthetic iron solution

Analysis method	[Fe] present (μg/ml)	[B] present (μg/ml)	[B] found (μg/ml)	% r.s.d.
Method (a)	100,000	20.00	not found	—
Method (b)*	100,000	20.00	20.82	1.68
Method (b)*	100,000	40.00	42.32	1.18

*In method (b) 20 μl phosphoric acid is added to sulphuric acid medium. Results are expressed as the average of four determinations.

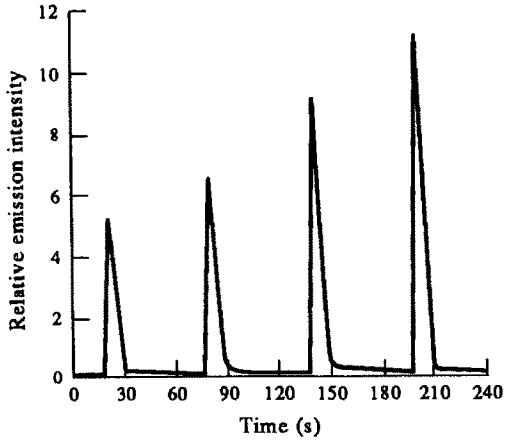

Fig. 3. Emission peak shapes. Signals produced by 0, 10, 30 and 40 μg/ml of boron.

boron signal. According to the results obtained by the two methods ((a), (b)) (see Table 3), the addition of phosphoric acid is proposed to complex iron and to eliminate its interference.

Performance of the method

A linear calibration graph $Y = 5.05 + 0.145X$ between 5 and 1000 μg/ml of boron was found with a regression coefficient of 0.996. Y is the intensity of the boron emission in relative units and X is the concentration of boron in solution in micrograms per millilitre. Typical peak shapes obtained in this experiment are shown in Fig. 3. From this experiment, instrumental detection limit (D.L.) of 1.0 μg/ml can be derived considering that the D.L. is the concentration at which the analyte signal is equal to the mean blank signal plus three times the standard deviation of the blank solution. The standard deviation of the background has been approximated by $(3 \times 0.01 \times I_B)$[21] ($I_B$, being the emission signal corresponding to the blank solution, with a value of 5.05 from the above equation). Sensitivity of the analytical procedure expressed as the slope of the calibration graph of 0.145 was used in this calculation.

This detection limit, obtained with 20 μl of sample, corresponds to an absolute limit of detection of 20 ng. This value is excellent and significantly lower than the detection limit reported so far.[11,13] The reproducibility of the method is 1.90% r.s.d. based on six measurements of 20 μg/ml B.

Using our proposed technique, analysis time for boron is shortened considerably. The signal evolution is not time consuming, and its shape can be seen in Fig. 3. The "limiting step" in the analytical measurement (without decomposition step) is determined by the plasma stabilization between measurements and this only takes 30 sec. All of these factors as well as the simplicity of the experimental device yield a method that can be advantageously applied to the boron determination in steel.

In the work described here, analytical grade reagents were used (Merck). However boron is a common contaminant and for this reason a high content of boron was found in the blank solution (35.7 μg/ml). Considerable effort has been made to reduce this signal and to reproduce it. The best results have been obtained working always with the same batch of reagents.

Application

To test the reliability of the proposed method, the analysis of two certified BCS steel samples, Nos 458 and 459, was carried out by both direct interpolation in a calibration graph, and standard addition methods. In these tests only acid-soluble boron was determined. The results are given in Tables 4–5. In Table 4 it is observed

Table 4. Determination of boron in BCS steels

Sample	Amount dissolved (g)	Dilution (ml)	Boron found* in solution (μg/ml)	Boron found in solid (w/w)%	Boron certified (w/w)%
BCS 458	4.0138	20	9.83 ± 0.10	0.0049 ± 2e-4	0.006
BCS 459	2.0065	20	11.55 ± 0.70	0.011 ± 7e-4	0.010

*Results are expressed as the average of four determinations ± standard deviation.

Table 5. Recovery of boron added to BCS steel solution

Sample	Boron in solution (μg/ml)	Boron added (μg/ml)	Boron found* (μg/ml)	Recovery (%)
BCS 458	9.83	19.6	29.21 ± 0.26	98.88
BCS 459	11.55	19.6	30.76 ± 0.00	98.01

*Results are expressed as the average of four determinations ± standard deviation.

that for steel BCS No. 458 there is a significant difference between the certified and the found boron content. This discrepancy can be explained by a boron loss in the process of steel dissolution. That is, boron is not completely dissolved in the acid attack, in agreement with what other authors have published about this steel.[6,22] However, on the other hand, standard addition of boron to the steel solution previously analysed, reveals a high level of recovery of boron added.

Steel BCS 459 shows a good agreement between the values found and the certified ones. In the same way the standard addition test confirms the results already obtained.

A t-test applied to compare the experimental mean found in BCS steel No. 459, with its certified value revealed no significant difference at $P = 0.05$. That is the "null hypothesis" can be retained: there is no evidence of systematic error in our new analysis method.

Acknowledgement—This work has been financed by project PB 88/0385 of DIGICYT (Spanish Education and Science Department).

REFERENCES

1. Z. Marczenko (ed.), *Spectrophotometric Determination of Elements*. Ellis Horwood, Chichester, 1976.
2. J. R. Castillo, J. M. Mir, C. Bendicho and C. Martinez, *Atom. Spectrosc.*, 1985, **6**, 152.
3. J. R. Castillo, J. M. Mir, C. Martinez and C. Bendicho, *Analyst*, 1985, **110**, 1435.
4. J. Sanz, R. Lopez Martin, J. Galban and J. R. Castillo, *Analusis*, 1990, **18**, 279.
5. R. K. Winge, V. J. Peterson and V. A. Fassel, *Appl. Spectrosc.*, 1979, **33**, 206.
6. A. Gomez Coedo and M. T. Dorado Lopez, *Rev. Metal. Madrid*, 1985, **21**, 87.
7. M. Takeuchi and S. Takeyama, *Bunseki Kagaku*, 1983, **32** (6), T66.
8. J. Minczewski, J. Chwastowska and R. Dybzynski, *Separation and Preconcentration Methods in Inorganic Trace Analysis*. Ellis Horwood, Chichester, 1982.
9. E. M. Donaldson, *Talanta*, 1981, **28**, 825.
10. J. Aznarez and J. M. Mir, *Analyst*, 1984, **109**, 183.
11. M. Hosoya, K. Tozawa and K. Takada, *Talanta*, 1986, **33**, 691.
12. A. A. Nemodruk and Z. K. Karalova (eds) *Analytical Chemistry of the Elements; Analytical Chemistry of Boron*. Ann Arbor, London, 1969.
13. I. Novozamsky, R. van Eck, J. J. van der Lee, V. J. G. Houba and G. O. Ayaga, *Atom. Spectrosc.*, 1988, **9**, 97.
14. T. S. Harrison, *Handbook of Analytical Control of Iron and Steel Production*. Ellis Horwood, NY, 1979.
15. W. D. Ross, *Chem. Engng Prog.*, 1952, **48**, 314.
16. *Handbook of Chemistry and Physics*, 65th ed., CRC Press, Florida, 1985.
17. TRC data bases for Chemistry and Engineering, Thermodynamics Research Center of the Texas Engineering Experiment Station, Texas A&M University, 1989.
18. J. A. Nelder and R. Mead, *Computer Jl*, 1965, **7**, 308.
19. A. Lopez Molinero, O. Barriovero, J. M. Lechon and J. R. Castillo, *ICP Inf. Newsletter*, 1992, **17** (9), 557.
20. M. Valcarcel and M. D. Luque de Castro, *Flow Injection Analysis*. Caja de Ahorros de Cordoba, Cordoba, 1984.
21. R. K. Winge, V. J. Peterson and V. A. Fassel, *Appl. Spectrosc.*, 1979, **33**, 206.
22. E. M. Donaldson, *Talanta*, 1981, **28**, 825.

Talanta, Vol. 40, No. 9, pp. 1405–1409, 1993
Printed in Great Britain.

0039-9140/93 $6.00 + 0.00

DETERMINATION OF TRACE AMOUNTS OF COBALT BY SOLVENT EXTRACTION—SECOND DERIVATIVE SPECTROPHOTOMETRY*

M. INÉS TORAL,† PABLO RICHTER and LORENA SILVA

Department of Chemistry, Faculty of Sciences, University of Chile, Las Palmeras 3425, P.O. Box 653, Santiago, Chile

(*Received* 19 *October* 1992. *Revised* 21 *January* 1993. *Accepted* 3 *February* 1993)

Summary—A sensitive derivative spectrophotometric method is described for the determination of microamounts of cobalt based on the integration of liquid–liquid separation and reaction, in dichloroethane, of the analyte with 3-(4-phenyl-2-pyridinyl)-5-phenyl-1,2,4-triazine (PPT) and 2,4,6-trinitro-phenol (picric acid). Cobalt was thus determined in the range 7.2–500 ng/ml. The method has a high selectivity with a detection limit of 2.2 ng/ml. The relative standard deviations were 3.2 and 1.5% for 20 and 100 ng/ml cobalt, respectively. The proposed method was applied to the determination of the analyte in vitamins.

The analytical chemistry of cobalt has been developed considerably in recent years, which is indicated by the large number of studies reported in the literature. Cobalt is not only of interest in the environment but also in human bio-chemical metabolism,[1] because it is present in the essential vitamin B_{12}. This vitamin is concerned with a wide variety of metabolic processes which include factors affecting growth, hemopoiesis and the maintenance of the integrity of nerve cells.

On the other hand, it is known that some metals that are essential nutrients, can also exert a toxic action, depending on their concentration levels. For these metals a narrow concentration difference exists between the toxic and the essential levels. As a result, knowledge of the metal content in various matrices, together with the development of reliable analytical methods for determination at trace levels are mandatory.

A number of analytical techniques have been used to determine cobalt in different types of samples at ultratrace[2–3] and trace[4–15] levels. Direct batch spectrophotometric methods,[11–15] using organic chelates, have shown some drawbacks as regards sensitivity, selectivity or simplicity. On the other hand, the use of derivative spectrophotometry offers a useful means for enhancing sensitivity and selectivity.[16] However, while derivative methods reported for the determination of cobalt are more selective than those using classical spectrophotometry, these show serious interferences principally from iron, copper and nickel when no masking agents are used.[6,9]

In this context, the purpose of this work was to develop a reliable, inexpensive and selective derivative spectrophotometric method for the determination of cobalt which is based on the integration of liquid–liquid separation and reaction in 1,2-dichloroethane of the analyte with PPT and picric acid, and on the subsequent derivative spectrophotometric measurement.

EXPERIMENTAL

Apparatus

A Shimadzu UV-160 spectrophotometer with 10 mm cells was used for measurements of the absorbance and derivative absorption spectra. An Orion Research Digital Ion-Analyzer 701 with glass and satured calomel electrodes was used for pH determinations.

Reagents

All reagents were of analytical reagent grade and the solutions were prepared with high-purity water from a Millipore Milli-Q Water Purification system device.

Standard cobalt (II) *solution (Titrisol Merck*, 1000 μg/ml. A 10 μg/ml working solution was prepared by diluting standard solution and other cobalt concentrations were prepared by appropriate dilution.

*In memory of Professor Alfonso Morales.
†To whom correspondence should be addressed.

3-(4-phenyl-2-pyridinyl)-1,2,4-triazine (PPT) solution. A 1×10^{-3} *M* solution was prepared by dissolving 0.3104 g of the compound (Merck) in 100 ml of DCE.

Picric acid solution. A 0.01 *M* solution was prepared by dissolving 2.291 g of picric acid in 1000 ml of water. Picric acid was previously purified by recrystallization.

Sodium acetate–acetic acid buffer solution ($pH = 5$). Prepared by adding acetic acid to 2.0 *M* sodium acetate solution until pH 5 was reached.

Foreign ion solutions. Solutions of diverse ions for the interference studies were prepared by dissolving the calculated amount of each compound in order to give 10–1000 μg/ml solutions of each species.

All these solutions were stored in polyethylene containers.

1,2-Dichloroethane (DCE) extrapure (sp. gr. 1.25).

Procedure

Ordinary spectrophotometry. To an aliquot of sample solution containing less than 50 μg of cobalt in a 250 ml separating funnel, 1 ml of the buffer solution and 4 ml of picric acid solution were added and the total volume adjusted to 100 ml. This was mixed and set aside for 2 min. Then 5 ml of 1×10^{-3} *M* PPT solution in dichloroethane was added and the funnel shaken for 2 min. The phases were allowed to separate and the organic layer run into a dry flask. The spectra of the brown DCE extract were recorded over the range from 700 to 350 nm against a reagent blank prepared under the same experimental conditions, using 10 mm cells.

Derivative spectrophotometry. The extract was prepared as above and the second derivative spectra recorded over the range from 700 to 350 nm against a reagent blank at a scan speed of 480 nm/min with $\Delta\lambda 5$.

RESULTS AND DISCUSSION

Spectral characteristics

The absorption spectra of the ion-association complex cobalt(II)–PPT–picrate, of the binary combinations cobalt(II)–PPT, cobalt(II)–picrate, PPT–picrate extracted into DCE and of the PPT solution in DCE were measured against DCE (Fig. 1). It can be observed in Fig. 1 that the spectrum of the PPT solution shows one band at 380 nm. This spectrum was not altered

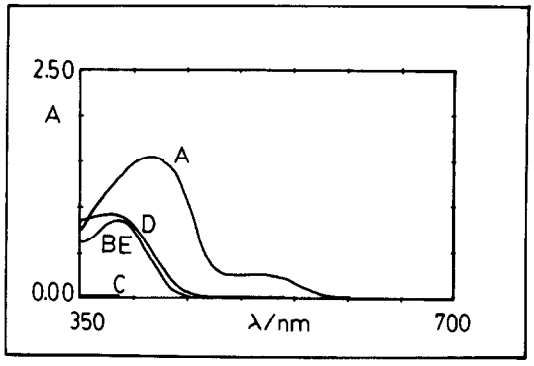

Fig. 1. Absorption spectra of DCE extract of the Co(II)–PPT–pic complex, the binary combinations of reactants and the PPT solution in DCE, measured against DCE. (A) Co–PPT–pic; (B) Co–PPT; (C) Co(II)–pic; (D) PPT–pic and (E) PPT.

when cobalt was added in aqueous phase, which indicates that cobalt remained in aqueous phase and the cobalt(II)–PPT binary complex was not extracted into DCE.

The introduction of a third component, picric acid, leads to the formation of an ion-association complex. The absorption spectrum of the extract of Co(II)–PPT–picrate ternary complex showed two bands at 350–480 nm and 500–600 nm. Based on the spectroscopic behavior of other metal–ferroine–picrate complexes[17–21] the first band can be assigned to the absorption of picrate and PPT and the second to the absorption of the chromophore Co–PPT. However, significant changes in both bands were observed when the concentration of cobalt was increased (Fig. 2), indicating that probably Co–PPT presents not only absorption at 500–600 nm but also another band which is overlapped with the absorption of PPT and mainly of picrate. In order to obtain more information, derivative spectrophotometry,

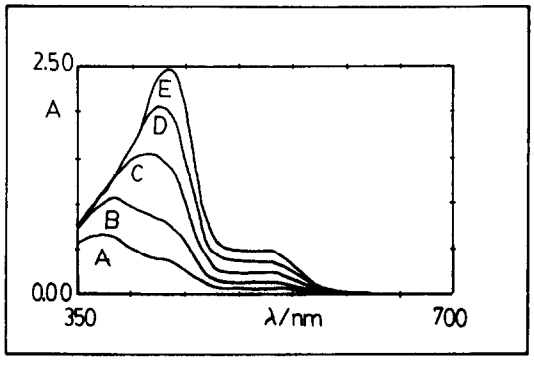

Fig. 2. Effect of cobalt concentration on absorption spectrum of DCE extract of Co(II)–PPT–pic, measured against a reagent blank. Aqueous phase cobalt concentrations (ng/ml) (A) 50; (B) 100; (C) 200; (D) 300; (E) 400. All other conditions as in the text.

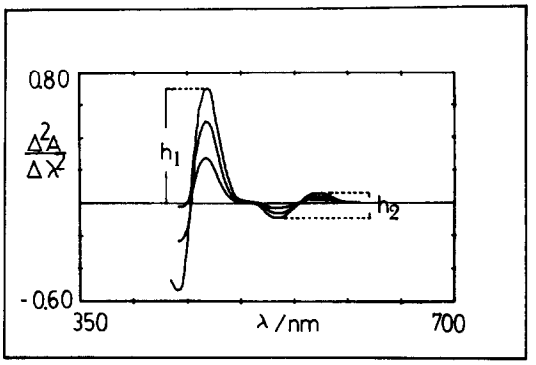

Fig. 3. Second-derivative spectra of DCE extract of the Co–PPT–pic complex measured against a reagent blank. Aqueous phase cobalt concentrations (ng/ml) (A) 100; (B) 200; (C) 300. All other conditions as in the text.

which provides higher spectral resolution, was used. The second-order spectrum shows that the absorption at 350–480 nm is split into two contributions and the portions of the derivative spectrum between 430 and 480 nm and between 500 and 600 nm could be used to measure the cobalt concentration (Fig. 3). On the other hand, if perchlorate is used instead of picrate, the second derivative spectrum of the Co–PPT–perchlorate complex showed similar, but less sensitive, absorptions at 430–480 nm and 500–600 nm, which indicates that both correspond to the absorption of the chromophore Co–PPT.

In order to make the determination more sensitive and reproducible, second-derivative spectrophotometry was adopted and the value of the vertical distance from the base line to peak values at 470 nm or from trough to peak values between 500 and 600 nm can be used for analytical purposes (Fig. 3).

Optimization of variables

Variables were optimized by the univariate method. Table 1 shows the optimum values found for the chemical and spectral variables and the range over which they were studied. The signal increased with the concentration of PPT and picrate to reach a maximum and constant value over 6.2×10^{-4} *M* PPT and 1.6 ml of 1×10^{-2} *M* picric acid in the aqueous phase. An increase in the concentration of both reagents had no influence in the blank and in the analytical signal, and the optimum values were selected by taking into account that foreign cations can be present in the samples with the evident consumption of both reagents. Similarly, the signal was at a maximum at pH = 2.5–9.0. At pH <2.5, formation of the ion pair was incomplete owing to protonation of the picrate ($pK_a = 1.6$). In all subsequent experiments a buffer system of acetic acid–acetate pH 5 was used.

Table 1. Optimization of variables

Variable	Range studied	Optimum value
Chemical		
pH	1.0–12.0	5.0
PPT solution (10^{-4} *M*)	0.6–12.0	10.0
1×10^{-2} Picric acid solution (*ml*)	0.2–6.0	4.0
Aqueous/organic phase ratio	2–24	20
Spectral		
Derivative order	0–4	2
$\Delta\lambda$	1–9	5
Analytical wavelength (*nm*)	700–350	470

It was found that the liquid–liquid separation and reaction of the analyte with PPT and picric acid can be carried out in 1,2-dichloroethane, chloroform and dichloromethane (DCM). The signal values for DCE and DCM solutions were higher than those for chloroform solutions. DCE was selected because it is less volatile than DCM.

The aqueous–organic phase ratio was chosen in order to obtain the maximum enrichment factor. A value of 20 was selected as optimum because miscibility occurred when higher ratios were selected.

The main spectral variable affecting the shape of the spectra was the order of the derivative value. Zero and first order did not resolve the large overlap between absorption of the reagents and complex at 350–480 nm (Fig. 1). However, when the second derivative is used the spectrum is sufficiently resolved for analytical purposes (Fig. 3) and both h1 and h2 signals can be used for measurement. In our spectrophotometer $\Delta\lambda$ values can be selected between 1 and 9. Generally the noise level decreases with an increase of $\Delta\lambda$, thus decreasing the fluctuation in the derivative spectrum. However, if the $\Delta\lambda$ value is too high, the spectral resolution is deteriorated. Therefore, the optimum value of $\Delta\lambda$ should be selected by taking into account the signal-to-noise ratio and the resolution of the spectrum. A $\Delta\lambda$ value of 5 was selected as optimum in order to give the best resolution and signal-to-noise ratio. The wavelength scanning speed has no influence on the signal, because the differentiation is obtained digitally. Hence, a fast value of 480 nm/min was selected.

Calibration graph, sensitivity and precision

Two calibration graphs were obtained by plotting the second-derivative value (h1 or h2, Fig. 3), with $\Delta\lambda = 5$ nm, *vs* the cobalt concentration. The equations for the lines using the least squares method were found to be:

$$h1 = 2.35 \times 10^{-3} (Co)_{ppb} + 0.010 \quad (r = 0.9998)$$

$$h2 = 5.33 \times 10^{-4} (Co)_{ppb} + 0.001 \quad (r = 0.9989)$$

where h is the second derivative value in derivative units.

The precision of the method was tested with solutions of 20 and 100 ng/ml cobalt and the relative standard deviations were found to be 3.2 and 1.5%, respectively.

By using the first equation, the determination range was over 7.2–500 ng/ml and the limit of detection (3σ) was found to be 2.2 ng/ml.

Interference studies

In order to investigate the analytical applications of this method, the effect of several foreign ions that are usually present with cobalt in real samples were examined. The tolerance limits for various species are shown in Table 2. A deviation of more than 5% of the signal was taken as a sign of interference. The results indicate the good selectivity achieved. The most serious cationic interference is from iron which interferes at concentrations twice those of cobalt. However, this problem can be resolved if both ions are determined simultaneously by using an equation system at two wavelengths, taking into account that cobalt does not interfere in the determination of iron with PPT and picrate.

Application of the method: determination of cobalt in vitamins

The content of 2 ml ampoules of vitamin injection were decomposed in a Kjeldahl flask by heating with a mixture of concentrated nitric and sulphuric acids (10 + 1), first at low temperature to avoid violent reaction, then more strongly until the acids were evaporated. Dropwise addition of concentrated nitric acid and boiling were continued until either a colorless or pale yellow residue was obtained. The residue was diluted and heated gently in water, and then was diluted to an appropriate volume (100 ml). The cobalt content of this solution was determined by the recommended procedure, using 5 ml of aliquot solution. The results are presented in Table 3.

Table 3. Determination of cobalt in vitamin B_{12}

	Cobalt content* (*ng/ml*)		Cobalt		
Sample	Stated	Found† (RSD)%	Added (*ng/ml*)	Found (*ng/ml*)	Recovery (%)
1‡	144.5	145.0 (2.0)	100.0	99.0	99.0
			120.0	121.2	101.0
			140.0	138.2	98.7
2§	72.3	73.0 (2.3)	74.0	75.8	102.4
			90.0	88.1	97.9
			110.0	111.9	101.7
3‖	14.45	15.0 (3.0)	30.0	30.5	101.7
			45.0	46.5	103.3
			80.0	79.1	98.8

*Concentration in aqueous phase.
†Average of eight determinations.
‡Neurobionta Forte (Merck). Vitamin B_{12}, equivalent to 0.4347 mg of cobalt, vitamin B_6 (100 mg), vitamin B_1 (200 mg); excipient up to 3 ml.
§Tol-12 (Saval). Vitamin B_{12}, equivalent to 0.2174 mg of cobalt, vitamin B_6 (100 mg), vitamin B_1 (200 mg); excipient up to 3 ml.
‖Complejo Vitaminico (Chile). Vitamin B_{12}, equivalent to 0.0435 mg of cobalt, vitamin B_6 (100 mg), vitamin B_1 (200 mg); excipient up to 3 ml.

CONCLUSIONS

A relatively simple and inexpensive extraction–derivative–spectrophotometric method for the determination of cobalt has been developed. It provides a high sensitivity with a determination limit of 7.2 ng/ml. Compared with previous direct and derivative spectrophotometric methods, the proposed approach is more

Table 2. Effect of foreign ions. Concentration of cobalt 100 *ng/ml*

Foreign species	Tolerance limit (*ng/ml*)	Foreign species	Tolerance limit (*ng/ml*)
Al^{+++}, Mg^{++}, Na^{+}		Cl^-, SO_4^{2-}, SO_3^{2-}	
Ca^{++}, Sr^{++}, K^{+}		NO_3^-, CH_3COO^-, SCN^-,	
Mn^{++}, Zn^{++}, Hg^{++}		NO_2^-, $S_2O_3^{2-}$, tartrate,	
Cd^{++}, Cu^{++}, Bi^{+++}	10,000*	F,Br,PO_4^{-3}	10^6*
Ni^{++}	1000	Oxalate, citrate	10^5
Fe^{++}	200	CN^-	200
		EDTA	10

*Maximum tested.

selective and simpler because it requires neither separation nor masking of foreign species. Compared with continuous flow injection–chemiluminescence methods,[2,3] which are highly sensitive (limit of detection 0.00006 ng/ml), this method is less sensitive but cheaper and less complicated in terms of assay procedure and equipment used. Finally the method was successfully applied to the determination of cobalt in vitamin.

Acknowledgements—The authors are grateful to the Department of Investigation (DTI) of the University of Chile (Project Q-3285) for financial support.

REFERENCES

1. E. J. Underwood, *Trace Elements in Human and Animal Nutrition*. Fourth Edition, Academic Press, New York, 1977.
2. M. Yamada, T. Komatsu, S. Nakahara and S. Suzuki, *Anal. Chim. Acta.*, 1983, **155**, 259.
3. T. Komatsu, M. Ohira, M. Yamada and S. Suzuki, *Bull. Chem. Soc. Jpn*, 1986, **59**, 1849.
4. R. K. Sharma and S. K. Sindhwani, *Talanta*, 1988, **35**, 661.
5. M. Llobat-Estelles, A. Sevillano Cabeza and J. Medina-Escriche, *Analyst*, 1986, **111**, 193.
6. Ana I. Jimenez, F. Jiménez and J. J. Arias, *Analyst*, 1989, **114**, 93.
7. H. Zhang, R. Wollast, J.-C. Vire and G. J. Patriarche, *Analyst*, 1989, **114**, 1597.
8. J. C. Thompsen and A. B. Carel, *Analyst*, 1989, **114**, 1197.
9. T. Odashima, T. Kikuchi, W. Ohtani and H. Ishii, *Analyst*, 1986, **111**, 1383.
10. M. C. Mehra and R. Daigle, *Analyst*, 1989, **114**, 979.
11. D. M. Rao, K. H. Reddy and D. V. Reddy, *Mikrochim. Acta*, 1987, **II**, 57.
12. K. C. Bayan and H. K. Das, *J. Indian Chem. Soc.*, 1987, **64**, 357.
13. D. Cheng, Y. Ma and Z. Li, *Huaxue Shiji*, 1988, **10**, 42; *Anal. Abstr.*, 1988, 8B195.
14. H. Shen and J. Li, *Fenxi Huaxue*, 1988, **16**, 301; *Anal. Abstr.*, 1988, 10B228.
15. A. G. Asuero, M. L. Marques and M. J. Navas, *Int. J. Pharm.*, 1987, **40**, 43.
16. P. Levillain and D. Fompeydie, *Analusis*, 1986, **14**, 1.
17. A. Morales and M. I. Toral, *Analyst*, 1985, **110**, 1447.
18. M. I. Toral and A. Bermejo, *Talanta*, 1989, **36**, 1069.
19. M. I. Toral and C. Almendares, *Anal. Lett.*, 1991, **24**, 2063.
20. A. Morales, M. I. Toral, P. Richter and M. Silva, *Anal. Lett.*, 1992, **25**, 1765.
21. M. I. Toral, C. Viollo and A. Albornoz, *Bol. Soc. Chil. Quim.*, 1992, **37**, 1644.

Talanta, Vol. 40, No. 9, pp. 1411–1417, 1993
Printed in Great Britain.

0039-9140/93 $6.00 + 0.00

MIXED LIGAND COMPLEXES INVOLVING SULPHUR CONTAINING LIGANDS—PART II.* TERNARY COMPLEXES OF Zn(II) INVOLVING *L*-CYSTEINE/*D*-PENICILLAMINE/*L*-CYSTEIC ACID AND IMIDAZOLES

M. SIVASANKARAN NAIR† and P. THILLAI ARASU

Department of Chemistry, Manonmaniam Sundaranar University, Schaffter Hall, St. Mark's Road, Palayamkottai-627 002, Tamil Nadu, India

M. SANKARANARAYANA PILLAI

Department of Chemistry, S.T. Hindu College, Nagercoil-629 002, Tamil Nadu, India

C. NATARAJAN

Department of Inorganic Chemistry, Madurai Kamaraj University, Madurai 625 021, Tamil Nadu, India

(*Received* 9 *October* 1992. *Revised* 12 *March* 1993. *Accepted* 21 *March* 1993)

Summary—The chemical equilibria involved in nine mixed ligand systems Zn(II)–*L*-cysteine (Cys)/*D*-penicillamine(Pen)/*L*-cysteic acid(Cya)(A)–imidazole(Him), histamine(Hist) and *L*-histidine(His)(B) have been investigated in aqueous perchlorate medium by pH titrimetry at 37° and ionic strength, $I = 0.15M$ ($NaClO_4$). The mixed ligand complex species of the types $ZnABH_2$, ZnABH, ZnAB or $ZnAB_2$ have been detected in addition to various binary species due to ligands A and B. The results obtained for the ZnABH type of species indicate that the site of protonation is the amino group of Cys/Pen ligands in the Zn(II)–Cys/Pen(A)–Him, Hist and His(B) systems, and the amino group of Hist/His secondary ligands in the Zn(II)–Cya(A)–Hist and His(B) systems. In the $ZnABH_2$ type of species, one proton is attached with the primary ligand (A) and the other with the secondary ligand(B). In both ZnAB and $ZnAB_2$ type ternary species in all the systems, the primary ligand binds the metal in a bidentate manner and the secondary ligands Him, Hist and His bind the metal, respectively in a uni, bi and terdentate manner.

The studies on the interaction of sulphur containing amino acids such as cysteine, penicillamine and cysteic acid with zinc(II) are important both from the chemical and biological points of view.[1] This point becomes more clear, if one considers the fact that the zinc core consisting of Zn(II) cysteine–histidine residue has an important biochemical role[2,3] in the stabilization of the 'zinc fingers' that bind to DNA. The ligands *L*-cysteine and *D*-penicillamine increase their complex forming tendency via the soft mercapto sulphur atoms. These soft ligands generally form thermodynamically more stable complexes with transition metal ions such as Ni(II) and Zn(II). However, copper(II) complexes with cysteine and penicillamine are readily oxidised. The oxidative product of *L*-cysteine is *L*-cysteic acid. The Zn(II)–cysteic acid complexes are very useful in the field of pharmaceutical chemistry. Considerable attention has been paid in recent years to the studies of Zn(II) complexes with cysteine and its derivatives.[1–6] In continuation of our research work on sulphur containing amino acids,[7] the present paper deals with the systematic equilibrium studies on Zn(II)–*L*-cysteine(Cys)/*D*-penicillamine(Pen)/*L*-cysteic acid(Cya) (A)–imidazole (Him), histamine(Hist) and *L*-histidine(His)(B) mixed ligand systems by pH titrimetry at 37° and $I = 0.15M$ ($NaClO_4$). The Zn(II)–Cys, Pen and Cya(A) binary systems have also been investigated under the present experimental conditions.

EXPERIMENTAL

All the ligands, used were obtained from Fluka. The stock solution of zinc(II)

*Part I: *J. Chem. Soc. Dalton Trans.*, 1993, 917.
†Author for correspondence.

perchlorate and other reagents were prepared and estimated as described earlier.[8] All the measurements were carried out as described elsewhere.[7] The electrode system was calibrated by the method of Irving *et al.*[9] For the ternary systems, the pH titrations have been carried out using 50-ml solutions containing low concentrations of $Zn(ClO_4)_2$, ligand A and ligand B in 1:1:1, 1:2:1 or 1:1:2 ratios with known volumes of standard carbonate free NaOH. Nitrogen was used throughout the titrations to maintain an oxygen-free atmosphere. The stability constants of the various binary and ternary complex species were derived from the pH titration data by the MINIQUAD-75 computer program[10] on a CYBER 180/830A computer. The binary stability constants for the Zn(II)–Cys, Pen and Cya(A) systems have been re-estimated under the present experimental conditions and reported in Table 1. The titrations for the binary systems were carried out on 50-ml solutions containing the metal perchlorate and the ligand in 1:1, 1:2 and 1:5 ratios. The binary stability constant data of Zn(II)–Him, Hist and His(B) systems have been reported previously.[8] The results obtained for the mixed ligand systems are given in Table 2. The charges of all the complex species reported in this paper are omitted for clarity.

RESULTS AND DISCUSSIONS

Zn(II)–Cys, Pen and Cya(A) binary systems

The formation of different types of complex species in solution depends upon the experimental conditions used. Thus, though in the Zn(II)–Cys and Pen(A) systems the polynuclear binary complexes in addition to the ZnA, ZnA_2 and their corresponding protonated complex species have been reported,[6,11,12] in the present experimental conditions the Zn(II)–Cys(A) system showed the presence of ZnA, ZnA_2H_2, ZnA_2H and ZnA_2 types of binary complex species, while in the Zn(II)–Pen(A) system the binary complexes of stoichiometry ZnAH, ZnA, ZnA_2H_2, ZnA_2H and ZnA_2 have been found to be present. The Zn(II)–Cya(A) system showed only ZnA and ZnA_2 types of binary species to be important.

As reported earlier[1,13] the $\log \beta_{ZnA}$ values obtained in the present study in the Zn(II)–Cys and Pen(A) systems (Table 1) correspond to the bidentate binding of these ligands through the mercapto and primary amino groups. In the Cr(III)–Cys system also, where the metal prefers to have a stable coordination number of six, Cys binds the metal through the sulphur and nitrogen atoms.[14] Since $\log K_1/\log K_2$ values obtained in both the above systems approaches unity, it can be inferred that in the ZnA_2 species also, Cys/Pen ligands bind the metal in a bidentate manner as in the case of ZnA Cys/Pen species. Of course, the 1:2 species will be more stabilized due to the ability of sulphur to accept electrons from the metal ion by π-bonding, thereby facilitating the addition of a second sulphur atom to the metal. The protonated species of the types ZnAH, ZnA_2H_2 or ZnA_2H in the Zn(II)–Cys/Pen(A) systems have been found to be favoured at low pH values. Hence, as

Table 1. Stability constants for the proton and Zn(II) complexes of Cys, Pen, Cya, Him, Hist and His binary systems ($T = 37°$; and $I = 0.15M$ $NaClO_4$)

	Ligands					
Parameters	Cys	Pen	Cya	Him*	Hist*	His*
$\log \beta_{HB}$	10.31 (2)	10.89 (1)	8.41 (1)	6.55 (2)	9.39 (8)	8.96 (3)
$\log \beta_{H_2B}$	18.53 (7)	18.89 (5)	10.56 (4)	—	15.34 (1)	14.96 (5)
$\log \beta_{H_3B}$	19.93 (8)	20.80 (9)	—	—	—	17.37 (9)
$\log \beta_{ZnBH}$	—	14.93 (9)	—	—	11.91 (5)	—
$\log \beta_{ZnB}$	9.64 (9)	10.33 (3)	3.77 (9)	2.55 (9)	5.39 (3)	6.41 (2)
$\log \beta_{ZnB_2H_2}$	29.93 (5)	31.31 (3)	—	—	—	22.80 (12)
$\log \beta_{ZnB_2H}$	24.63 (9)	25.99 (3)	—	—	—	17.47 (9)
$\log \beta_{ZnB_2}$	17.81 (9)	20.19 (1)	6.02 (8)	4.98 (8)	10.45 (4)	11.74 (2)
$\log \beta_{ZnB_3}$	—	—	—	7.40 (10)	—	—
$\log \beta_{ZnB_4}$	—	—	—	9.59 (11)	—	—
pK^{H}_{ZnBH}	—	4.60	—	—	6.52	—
$pK^{H}_{ZnB_2H_2}$	5.30	5.32	—	—	—	5.33
$pK^{H}_{ZnB_2H}$	6.82	5.80	—	—	—	5.73
$\log K^{ZnB}_{ZnB_2}$	8.17	9.86	2.25	2.43	5.06	5.33
$\log K^{ZnBH}_{ZnB_2H}$	—	11.06	—	—	—	—

*Ref. 8: The ligands Cys, Pen and Cya become the primary ligand A in the ternary systems.

Table 2. Stability constants of Zn(II)–Cys/Pen/Cya(A)–Him, Hist and His(B) mixed ligand systems. ($T = 37°$; $I = 0.15M$ ($NaClO_4$))

	Zn(II)–Cys(A)–B systems			Zn(II)–Pen(A)–B systems			Zn(II)–Cya(A)–B systems		
	Ligands B			Ligands B			Ligands B		
Parameters	Him	Hist	His	Him	Hist	His	Him	Hist	His
$\log \beta_{ZnABH_2}$	—	—	27.42 (9)	—	27.62 (9)	27.83 (9)	—	—	—
$\log \beta_{ZnABH}$	18.76 (9)	21.63 (4)	22.07 (6)	19.82 (9)	21.93 (9)	22.66 (8)	—	16.65 (5)	17.63 (5)
$\log \beta_{ZnAB}$	12.22 (9)	14.91 (4)	15.97 (5)	13.32 (9)	15.56 (8)	16.66 (5)	7.89 (7)	9.68 (3)	11.15 (5)
$\log \beta_{ZnAB_2}$	15.55 (9)	—	—	16.13 (9)	—	—	10.15 (8)	—	—
$pK^{H}_{ZnABH_2}$	—	—	5.35	—	5.69	5.17	—	—	—
pK^{H}_{ZnABH}	6.54	6.72	6.10	6.50	6.37	6.00	—	6.97	6.48
$\log K^{ZnA}_{ZnAB}$	2.58	5.27	6.33	2.99	5.23	6.33	4.12	5.91	7.38
$\log K^{ZnB}_{ZnAB}$	9.67	9.52	9.56	10.77	10.17	10.25	5.34	4.29	4.74
$\log K^{ZnAB}_{ZnAB_2}$	3.33	—	—	2.81	—	—	2.26	—	—
$\Delta \log K_{ZnABH_2}$	—	—	—	—	0.78	—	—	—	—
$\Delta \log K_{ZnABH}$	—	—	—	2.34	1.61	1.32	—	—	—
$\Delta \log K_{ZnAB}$	0.03	−0.12	−0.08	0.44	−0.16	−0.08	—	—	—
$\Delta \log K_{ZnAB_2}$	0.93	—	—	0.82	—	—	—	—	—
$\log X_{ZnAB}$	1.65	1.56	2.39	1.47	0.48	1.39	—	—	—
$\log X_{ZnAB_2}$	3.70	—	—	2.48	—	—	—	—	—

described elsewhere[15,16] it can be concluded that the S,O coordination plays an important role in the lower pH range, with the extra proton residing with the primary amino group of the coordinated ligand. Thus, in the ZnAH species in the Zn(II)–Pen(A) system, Zn(II) binds the ligand through the mercapto and carboxylato groups and the proton occurs with the primary amino group of the ligand. In the $Zn(AH)_2$ species type in the Zn(II)–Cys/Pen(A) systems, both the ligands should bind the metal through the mercapto and carboxylato groups and the primary amino group of both the ligands will be

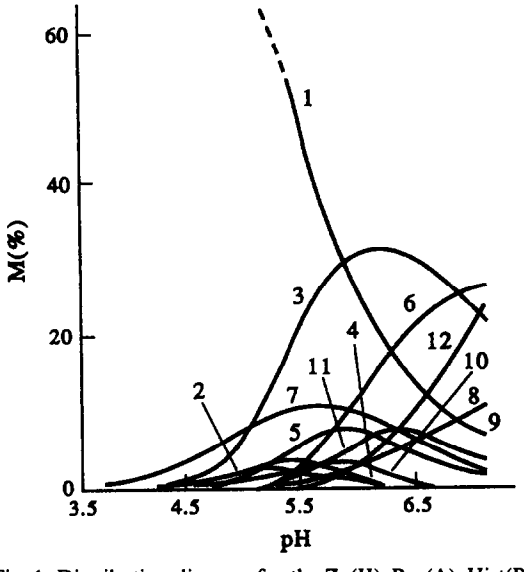

Fig. 1. Distribution diagram for the Zn(II)–Pen(A)–Hist(B) system ($C_{Zn} = 3.062 \times 10^{-3}$, $C_A = 3.042 \times 10^{-3}$, $C_B = 3.045 \times 10^{-3} M$). 1) Unbound Zn(II), 2) ZnAH, 3) ZnA, 4) ZnA_2H_2, 5) ZnA_2H, 6) ZnA_2, 7) ZnBH, 8) ZnB, 9) ZnB_2, 10) $ZnABH_2$, 11) ZnABH, 12) ZnAB.

protonated. In the Zn(AH)A type of species in the above two systems, one ligand will bind the metal through the mercapto and primary amino groups and the other ligand with the protonated amino group binds the metal through mercapto and carboxylato groups. Thus the ambidentate behaviour of Cys and Pen ligands are well demonstrated by the results obtained for Zn(AH)A species in the Zn(II)–Cys/Pen(A) systems. The same type of protonation sites have been suggested for the Ni(CysH)(Cys), $Cd(CysH)_2$ and $Cd(PenH)_2$ complexes.[7,17,18]

The stability constant studies on the Zn(II)–Cya(A) system appear to be more interesting. In this system, ZnA and ZnA_2 types of species with respective $\log K_1$ and $\log K_2$ values of 3.77 and 2.25 have been detected in the present study. The stepwise stability constant values for the formation of ZnA and ZnA_2 types of species in the Zn(II)–glycine system[11,12] are, respectively 5.3 and 4.2. The $\log K_1$ value obtained in the Zn(II)–Cya(A) system is *ca.* 1.6 log units lesser than that expected for the glycine-like mode of binding of Cya with Zn(II). This shows that in the ZnA Cya species no chelate is formed, *i.e.*, the metal should bind any one of the three donor groups, *viz.*, sulphonic acid, primary amino or carboxylato groups. In case it binds through sulphonic acid or carboxylato groups, the $\log K_1$ value should be in the range of two. But the value obtained here is 3.77. This indicates that the metal should bind the ligand through the primary amino group. In the ZnA_2 Cya species also, both Cya ligands should bind the metal through the two primary amino nitrogen atoms. This is supported by the fact that

the $\log \beta_{ZnA_2}$ value of 6.02 obtained in the Zn(II)–Cya(A) system bears favourable comparison with the $\log \beta_{ZnA_2}$ value of 6.3 reported[19] in the Zn(II)–methylamine system, where the metal binds the ligands through the primary amino nitrogen atoms.

Zn(II)–Cys/Pen/Cya(A)–Him, Hist and His(B) ternary systems

The various types of ternary species detected in the title systems are indicated in Table 2. Sovago *et al.*[16] in their studies on Zn(II)–Cys/Pen(A)–Hist and His(B) systems at 25° and 0.2*M* (KCl) could detect only the ZnAB type of species. Kayali and Berthon[20] studied Zn(II)–Cys(A)–Hist and His(B) systems and reported the formation of ZnABH and ZnAB types of species. Reddy *et al.*[3] reported the stability constants of ZnAB and $ZnAB_2$ types of species in the Zn(II)–Cys(A)–Him(B) system, ZnAB type of species in the Zn(II)–Cys(A)–Hist(B) system and ZnAB and ZnA_2B_2 types of species in the Zn(II)–Cys(A)–His(B) system. The types of ternary species reported above under different experimental conditions differ from the results obtained in the present study. Thus, in the Zn(II)–Cys(A)–Him(B) system, the formation of ZnABH ternary species in addition to ZnAB and $ZnAB_2$ species could also be detected. The present results in the Zn(II)–Cys(A)–Hist(B) system agree well with Kayali and Berthon.[20] In the Zn(II)–Cys(A)–His(B) system, the presence of $ZnABH_2$ type of ternary species also in addition to ZnABH and ZnAB species could be detected in the present study. In the Zn(II)–Pen(A)–Hist and His(B) systems, we could detect the presence of $ZnABH_2$ and ZnABH species in addition to ZnAB species reported by Sovago *et al.*[16] The stability constant data reported by these groups of workers bear favourable comparison with the present results after giving due allowance for the change in the experimental conditions.

Stability and structure of ZnAB and $ZnAB_2$ types of species

In the ZnA binary species in the Zn(II)–Cys/Pen(A) binary systems, the ligands bind the metal through the mercapto and amino groups. Hence, it may be expected that in the ZnAB species in the Zn(II)–Cys/Pen(A)–Him, Hist and His(B) systems, Cys/Pen primary ligand would bind the metal in a bidentate manner through its mercapto and amino groups. This becomes clearer by noting that the $\log K^{ZnB}_{ZnAB}$ values obtained in these systems (Table 2) compare favourably with the respective $\log \beta_{ZnA}$ values obtained in the Zn(II)–Cys/Pen(A) systems (Table 1). In the Zn(II)–Cya(A)–Him, Hist and His(B) systems, the $\log K^{ZnB}_{ZnAB}$ values obtained (Table 2) are higher than the $\log K^{Zn}_{ZnA}$ value of 3.77 obtained in the Zn(II)–Cya(A) binary system by ~ 1.5 log units, where Cya binds the metal only through its primary amino group. This probably suggests that in Zn(II)–Cya(A)–Him, Hist and His(B) ternary systems, Cya primary ligand binds the metal in a glycine-like mode. The higher $\log \beta_{ZnAB}$ values obtained in the Hist secondary ligand systems compared to that in the Him secondary ligand systems suggest that Hist in its ZnAB species in the Zn(II)–Cys/Pen/Cya(A)–Hist(B) systems bind the metal in a bidentate manner through its imidazole and amino nitrogen atoms. Thus, ZnAB species in the Hist secondary ligand systems would have a coordination number of four. The $\log \beta_{ZnAB}$ values obtained in the Zn(II)–Cys/Pen/Cya(A)–His(B) systems are higher than those values obtained in the corresponding Hist secondary ligand systems. This indicates that His in its ZnAB species in the above systems binds the metal in a terdentate manner. However, the difference in the $\log \beta_{ZnAB}$ value between those obtained in the His and Hist secondary ligand systems in the range of ~ 1 log unit suggests that the binding of the carboxylato group in the His secondary ligand systems is very weak.

In the $ZnAB_2$ type of species in the Zn(II)–Cys/Pen/Cya(A) Him(B) systems, the coordination number of the metal ion would be four due to the bidentate binding of Cys/Pen/Cya primary ligands and the involvement of two imidazole nitrogen atoms in the two Him secondary ligands. The $\log \beta_{ZnAB_2}$ values in the Zn(II)–Cys/Pen/Cya(A)–Him(B) systems and $\log \beta_{ZnAB}$ values in the Zn(II)–Cys/Pen/Cya(A)–Hist(B) systems, where both the species have tetrahedral geometry, can now be compared. Owing to the chelate effect and higher basicity of the Hist ligand, one would expect higher $\log \beta_{ZnAB}$ values in the later systems compared to the $\log \beta_{ZnAB_2}$ values in the former systems, where the binding of two imidazoles does not result in the formation of a chelate ring. Actually this is the trend in the corresponding binary systems where the $\log \beta_{ZnB}$ value is 5.39 in the Zn(II)–Hist(B) system and $\log \beta_{ZnB_2}$ value is 4.98 in the Zn(II)–Him(B)

system (Table 1). Due to the chelate effect and higher basicity of Hist, one can expect still higher differences between the above $\log \beta_{ZnB}$ and $\log \beta_{ZnB_2}$ values. The lesser difference of ~ 0.4 log units between the above two parameters suggests that the π-acceptor property of the two imidazole ligands in the ZnB_2 imidazole species makes this species have higher stability than those expected. This trend is even higher in the ternary systems involving Cys/Pen/Cya primary ligands and Him and Hist secondary ligands, *i.e.*, the higher $\log \beta_{ZnAB_2}$ value in the Zn(II)–Cys/Pen/Cya(A)–Him(B) systems compared to the $\log \beta_{ZnAB}$ value in the Zn(II)–Cys/Pen/Cya(A)–Hist(B) systems can be due to the fact that π-acceptor property of two imidazole ligands in the $ZnAB_2$ species overcomes the chelate effect and the basicity of Hist ligand in the ZnAB species in presence of Cys, Pen and Cya primary ligands.

$$ZnA + ZnB_2 \rightleftharpoons ZnAB_2 + Zn \quad (1)$$

$$\Delta \log K_{ZnAB_2} = \log \beta_{ZnAB_2} - (\log \beta_{ZnA} + \log \beta_{ZnB_2}) \quad (2)$$

$$ZnA_2 + ZnB_4 \rightleftharpoons 2ZnAB_2;$$

$$X_{ZnAB_2} = [ZnAB_2]^2/([ZnA_2][ZnB_4]) \quad (3)$$

$$\log X_{ZnAB_2} = 2 \log \beta_{ZnAB_2} - (\log \beta_{ZnA_2} + \log \beta_{ZnB_4}) \quad (4)$$

$$ZnA + ZnB \rightleftharpoons ZnAB + Zn \quad (5)$$

$$\Delta \log K_{ZnAB} = \log \beta_{ZnAB} - (\log \beta_{ZnA} + \log \beta_{ZnB}) \quad (6)$$

$$ZnA_2 + ZnB_2 \rightleftharpoons 2ZnAB;$$

$$X_{ZnAB} = [ZnAB]^2/([ZnA_2][ZnB_2]) \quad (7)$$

$$\log X_{ZnAB} = 2 \log \beta_{ZnAB} - (\log \beta_{ZnA_2} + \log \beta_{ZnB_2}). \quad (8)$$

Now, if one compares the $\Delta \log K$ and $\log X$ values obtained for the $ZnAB_2$ species [equations (1)–(4)] with those values of ZnAB species [equations (5)–(8)] in the Zn(II)–Cys/Pen(A)–Him(B) systems, it may be noted that these parameters are more positive for the $ZnAB_2$ species compared to those for the ZnAB species (Table 2) demonstrating that $ZnAB_2$ species are having higher stability compared to ZnAB species. This can probably be accounted for by considering the fact that the primary ligand in each of the above systems results in the formation of the five membered chelate ring and hence the formation of $ZnAB_2$ species is not sterically unfavourable as in the case of Cu(II) ternary complex systems.[23]

The $\Delta \log K$ values [equations (5) and (6)] obtained for the ZnAB type of species in the Zn(II)–Cys/Pen(A)–Him, Hist and His(B) systems are more positive compared to their statistical values[21,22] showing preference for the formation of ternary complexes compared to the binary analogues. The positive values obtained for this parameter in some of the systems show that the secondary ligand prefers to add on to the ZnA complex rather than the aquated metal ion. The $\log X_{ZnAB}$ values [equations (7) and (8)] obtained in these systems (Table 2) also follow these trends. The $\Delta \log K$ and $\log X$ values for the ZnAB species in the Zn(II)–Cya(A)–Him, Hist and His(B) systems could not be computed because only stability constant data for the monodentate binding of Cya with Zn(II) is available both in the ZnA and ZnA_2 type of species (Table 2) while it is bidentate in the ternary species.

Stability and structure of ZnABH and $ZnABH_2$ species

As indicated initially, the protonated ternary species of the type ZnABH has been found to be present in the Zn(II)–Cys/Pen(A)–Him, Hist and His(B) and Zn(II)–Cya(A)–Hist and His(B) systems under study in the lower pH ranges. The protonated binary species have been detected in the Zn(II)–Cys/Pen(A) systems but not in the Zn(II)–Him(B) system (Table 1). Hence, in the ZnABH species in the Zn(II)–Cys/Pen(A)–Him(B) systems, it can be expected that the proton resides with the Cys/Pen primary ligand, possibly with its amino group as is the case with the ZnA_2H_2 and ZnA_2H Cys/Pen species as described in the beginning. The pK^{H}_{ZnABH} values (Table 2) obtained in the Zn(II)–Cys(A)–Him, Hist and His(B) systems are comparable to each other indicating the same protonation site in the ZnABH species in all these three systems, *i.e.*, as is the case for the ZnABH species in the Zn(II)–Cys-Him(B) system, in the corresponding Hist and His secondary ligand systems, the extra proton in the ZnABH species is attached with the Cys primary ligand, possibly by its primary amino group. This argument appears to be more reasonable because when the extra proton in the ZnABH species in the Zn(II)–Cys(A)–Hist(B) system is attached to the Hist secondary ligand, the binding of the Hist ligand would not result in the formation of any chelate ring and hence would lead to lower

stability. Conversely, the Cys ligand with the protonated amino group can bind the metal through the mercapto and carboxylato groups resulting in a six-membered chelate ring. From similar arguments for the Zn(II)–Pen(A)–Him, Hist and His(B) systems, it can be concluded that the extra proton in the ZnABH species in the above systems resides with the Pen primary ligand.

Of the ternary systems containing Cya primary ligands, the Zn(II)–Cya(A)–Hist and His(B) systems gave rise to the formation of ZnABH type of species. Of the Zn(II)–Cya(A) and Zn(II)–Hist and His(B) binary systems, the protonated binary species have only been detected in the latter. Hence, it may be inferred that in the ZnABH type of species in the Zn(II)–Cya(A)–Hist and His(B) systems, the possibilities are more for the attachment of the extra proton with the Hist/His secondary ligand possibly to their primary amino group. Since the $\log \beta_{ZnABH}$ values obtained in the Zn(II)–Cys/Pen/Cya(A)–His(B) systems are higher by about one log unit compared to those in the Zn(II)–Cys/Pen/Cya(A)–Hist(B) systems (Table 2), it may be concluded that in the ZnABH species in the His secondary ligand systems the carboxylato group is also involved in the metal-ligand binding.

$$ZnAH + ZnB \rightleftharpoons ZnABH + Zn \qquad (9)$$

$$\Delta \log K_{ZnABH} = \log \beta_{ZnABH} - (\log \beta_{ZnAH} + \log \beta_{ZnB}) \qquad (10)$$

The $\Delta \log K_{ZnABH}$ [equations (9) and (10)] values obtained (Table 2) in the Zn(II)–Pen(A)–Him, Hist and His(B) systems are more positive compared to the statistical values,[21,22] indicating higher stability for the ZnABH species. Again the $\Delta \log K_{ZnABH}$ values in the Zn(II)–Cya(A)–Hist(B) system has not been calculated because of the reasons outlined in the case of ZnAB species in the above system.

The $ZnABH_2$ type of species has been detected in the Zn(II)–Cys(A)–His(B) and Zn(II)–Pen(A)–Hist and His(B) systems. In this species it may be expected that the two protons should reside, respectively with the primary and secondary ligands possibly with their amino groups. The $\log \beta_{ZnABH_2}$ values in these two systems differ only by *ca.* 0.20 log units, showing that the binding of the carboxylato group in the His secondary ligand system is very weak.

Species distribution plots

The distribution of various binary and ternary complexes (in terms of the percentage bound total metal ion as a function of pH) has been calculated for all the mixed ligand systems under study. The concentration of the $ZnABH_2$ ternary species never exceeded 10% of the total metal ion. About 30% of the total metal ion has been found to be present in the form of ZnABH species. In all the title ternary systems the ZnAB type of species occurs in higher concentrations than the binary analogues, indicating the preference for the formation of ternary species, which is in agreement with the predictions made from the $\Delta \log K$ values. The formation of $ZnAB_2$ species in the Zn(II)–Cys/Pen/Cya(A)–Him(B) systems has been found to be maximum in a 1:1:2 solution of metal, ligand A and Him. The diagram obtained for the Zn(II)–Pen(A)–Hist(B) system at a metal, ligand A and ligand B ratio of 1:1:1 is given in Fig. 1.

REFERENCES

1. A. Gergely and I. Sovago, in *Metal Ions in Biological Systems*, H. Sigel (ed.), Vol. 9, pp. 77–102. Marcel Dekker, New York, 1979.
2. B. A. Krizek and J. M. Berg, *Inorg. Chem.*, 1992, **31**, 2984.
3. P. R. Reddy, K. Sudhakar and T. K. Adharani, *Indian J. Chem.*, 1991, **30A**, 522.
4. A. Avdeef, F. Hartenstein, A. R. Chemotti, Jr. and J. A. Brown, *Inorg. Chem.*, 1992, **31**, 3701.
5. I. Sovago, T. Kiss, K. Varnagy and B. D. Reverend, *Polyhedron*, 1988, **7**, 1089.
6. D. D. Perrin and I. Sayce, *J. Chem. Soc. A*, 1968, 53.
7. M. S. Nair, P. T. Arasu, M. S. Pillai and C. Natarajan, *J. Chem. Soc. Dalton Trans.*, 1993, 917.
8. M. S. Nair, K. V. Chalapathy and M. Santappa, *ibid.*, 1982, 555.
9. H. Irving, M. G. Miles and L. D. Pettit, *Anal. Chim. Acta*, 1967, **38**, 475.
10. P. Gans, A. Vacca and A. Sabatini, *Inorg. Chim. Acta*, 1976, **18**, 237.
11. L. G. Sillen and A. E. Martell, *Stability constants of Metal—Ion Complexes*, The Chemical Society, London, 1964, No. 17, Suppl. 1, 1971, No. 25.
12. A. E. Martell and R. M. Smith, *Critical Stability Constants*, Vols 1–6, Plenum Press, New York, 1974–1989.
13. C. A. McAuliffe and S. G. Murray, *Inorg. Chim. Acta Rev.*, 1972, **6**, 103.
14. K. V. Chalapathy, M. S. Nair, D. Ramaswamy and M. Santappa, *J. Chem. Soc. Dalton Trans.*, 1982, 291.
15. C. R. Cothern, W. E. Moddeman, R. G. Albridge, W. J. Sanders, P. L. Kelly, W. S. Hanly and L. Field, *Anal. Chem.*, 1976, **48**, 162.
16. I. Sovago, A. Gergely, B. Harman and T. Kiss, *J. Inorg. Nucl. Chem.*, 1979, **41**, 1629.

17. G. D. Zhegzda, V. N. Kabahova and F. M. Tulupa, *Zh. Neorg. Khim.*, 1975, **20**, 2325.
18. A. J. Carty and N. J. Taylor, *Inorg. Chem.*, 1977, **16**, 177.
19. A. Tamister, *Bull. Soc. Chim. France*, 1933, **53**, 157.
20. A. Kayali and G. Berthon, *J. Chem. Soc. Dalton Trans.*, 1980, 2374.
21. H. Sigel, *Angew, Chem., Int. Ed. Engl.*, 1975, **14**, 394.
22. H. Sigel, in *IUPAC Coordination Chemistry-20*, D. Banerjea (ed.), p. 27. Pergamon Press, Oxford, 1980.
23. M. S. Nair, M. Santappa and P. K. Murugan, *Inorg. Chem.*, 1982, **21**, 142.

Talanta, Vol. 40, No. 9, pp. 1419–1423, 1993
Printed in Great Britain.

0039-9140/93 $6.00 + 0.00

FLUORIMETRIC DETERMINATION OF DIACETYL AND 2,3-PENTANEDIONE WITH ISONIAZIDE AND A ZIRCONIUM SALT

RAFAEL J. GARCÍA-VILLANOVA* and ROSA M. GARCÍA ESTEPA
Departamento de Nutrición y Bromatologia, Facultad de Farmacia. Universidad de Granada, 18012 Granada, Spain

(*Received* 3 *August* 1992. *Revised* 25 *March* 1993. *Accepted* 26 *March* 1993)

Summary—Diacetyl and 2,3-pentanedione react with isoniazide in acidified solutions to give the corresponding hydrazones which, by reacting with a zirconium (IV) salt, form fluorescent complexes. Both reactions have been studied separately. Variables such as pH, heating time, and excess of reactives are discussed. The method may be used for the determination of these compounds in foods.

INTRODUCTION

Diacetyl was the first α-diketone to be reported as an important agent responsible for flavour in many foods[1] with 2,3-pentanedione and pyruvic aldehyde being reported subsequently (in fact, one of the functions of the latter is aldehyde). Awareness and, above all, control of the levels of these compounds in foods are of considerable interest since their occurrence determines the quality of many foods; in some cases they may be considered as indicators of optimum maturation, while in others they may be indicators of spoilage. Diacetyl is normally a major compound, with methyl glyoxal appearing in much lower amounts and is rarely a matter for determination. Few references may be found in the literature on this subject and many authors who proposed methods for the determination of α-diketones were probably unaware of its occurrence.

The first colorimetric method[2] to appear was a modification of the well-known Voges–Proskauer reaction, with creatinine and α-naftol in potassium hydroxide; this was followed by many modifications on that method. Other methods include those derived from the reaction with hydroxylamine: UV or visible spectrophotometry[3] after forming complexes with Ni(II)[4] or Fe(II)[5] (the latter procedure being the most common)[6] usually after distillation. Gas chromatography has been used to quantify both diacetyl and 2,3-pentanedione separately using either flame ionization[7–9] or an electron-capture detector.[10–12] The latter has proved to be 1200-fold more sensitive.[13] The head-space technique is the most commonly applied to differentiation in beers.[14,15] Only one fluorimetric method, based on the reaction of diacetyl with 3,4-diaminoanysol to yield a fluorescent quinoxaline, has been reported;[16] nothing has been found on 2,3-pentanedione.

The method reported in the present work is based on the previous synthesis of diacetyldiisonicotinoyl hydrazone (dDIH) and a study of its complexes with Sn(II) and (IV), Y(III), Sc(III), and Zr(IV).[17] The complex/complexes formed with excess Zr(IV) is/are fluorescent and we conclude that the structure in Fig. 1 is the most likely for it/them.

Although we suspect the coexistence of several stoichiometries in aqueous solution, the prevailing one is most likely 1 : 1 [dDIH : Zr(IV)]. 2,3-pentanedione yields a product with very similar features, suggesting that the two reactions are alike. Figure 2 shows the reaction leading to the formation of these complexes.

EXPERIMENTAL

Reagents

0.06*M* zirconyl chloride A.G. (Merck) was prepared by adding hydrochloride acid (viable for no longer than 20 days). A 0.035*M* isoniazide (Sigma) solution was freshly prepared. Solutions of Diacetyl (Merck) and 2,3-pentanedione (Fluka) were prepared from freshly

*Departamento de Química Analítica, Nutrición y Bromatología, Facultad de Farmacia, Universidad de Salamanca, 37007 Salamanca, Spain.

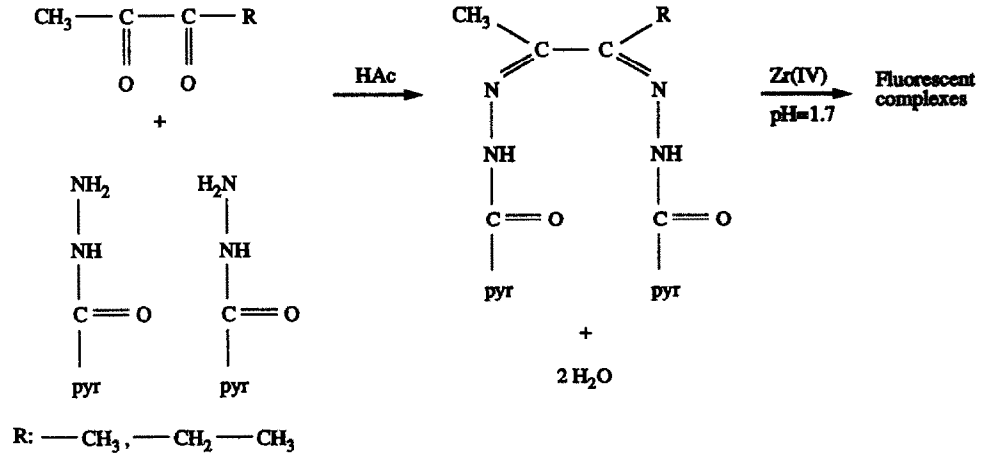

Fig. 1.

rectified reagents. Acetic acid, 4*M* sodium hydroxide, and 3*M* hydrochloric acid solutions were also employed. Other reagents used in this work, but not necessary for the analytical procedure, are noted in the text.

Apparatus

A Radiometer 26 pH-meter and a Perkin-Elmer mod. 204 Spectrofluorimeter with a xenon lamp, 10 nm slit width and 10 × 10 mm quartz cells at room temperature were used. Except where indicated, all measurements were performed with both "0" and "100" knobs turned top right. Just before measurements, air was removed from the reaction mixtures by bubbling nitrogen for a few seconds.

Glass distillation apparatus: 250–500 ml (Ø = 14/23) boiling flask; distillation tube with a vertical-delivery recovery bend; Liebig condenser, connected vertically (effective length = 150 mm); tapered water-tube adapter to dip below the liquid level contained in a 100 ml beaker receiver.

Procedure

$1.0 \times 10^{-5}M$ diacetyl (or 2,3-pentanedione) was added to 10 ml of 0.035*M* isoniazide solution, acidified with a few drops of acetic acid. After several minutes, 5 ml of 0.06*M* Zr(IV) salt was added; the pH was adjusted to 1.7 ± 0.1 with 3*M* HCl and 4*M* NaOH. The solution was transferred to a 50 ml volumetric flask and diluted with water. After approximately 30 min, fluorescence was measured against a blank prepared under similar conditions using excitation and emission wavelengths of 410 and 510 nm, respectively. Calibration curve: A curve was plotted with final diacetyl concentrations between 20 and 200 ppb. The "0" knob was adjusted with a blank and the "100" knob with the higher-concentration solution.

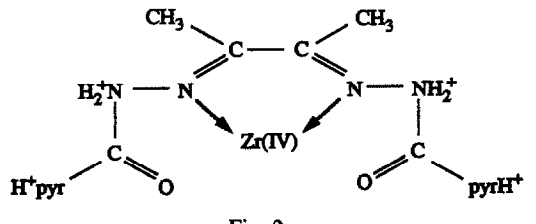

Fig. 2.

RESULTS AND DISCUSSION

Fluorescence spectra

Uncorrected excitation and emission spectra of the complexes were obtained with final concentrations of 0.0023 m*M* diacetyl and 0.0010 m*M* 2,3-pentanedione. In both cases, 10 ml of 0.0523*M* isoniazide, a few drops of acetic acid, and 5 ml of 0.025*M* Zr(IV) were added. pH was adjusted to 1.7 ± 0.1 with HCl and NaOH solutions and both reaction mixtures were diluted to 50 ml in a volumetric flask. After about 30 min, excitation and emission spectra were recorded (Fig. 3). Bands with maximum at 410 and 510 nm, respectively, were observed. Optimization of each reaction was based on the measurement performed at these wavelengths.

Optimum pH value

Following the same protocol, different pH values were studied for the formation of the complexes. A value of 1.7 ± 0.1 was confirmed

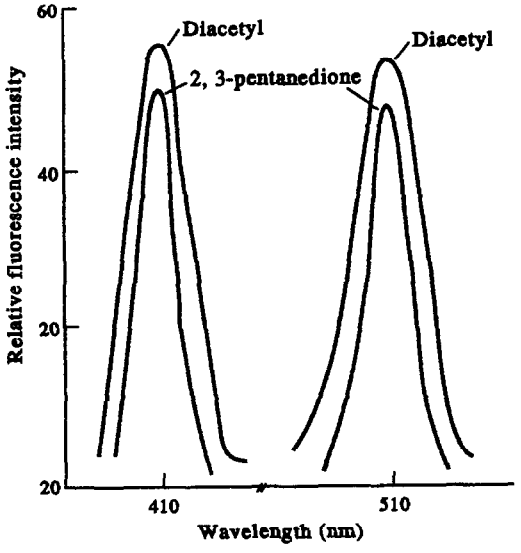

Fig. 3. Uncorrected excitation and emission spectra of both final-reaction mixtures: 0.0023 m*M* diacetyl and 0.0010 m*M* 2,3-pentanedione.

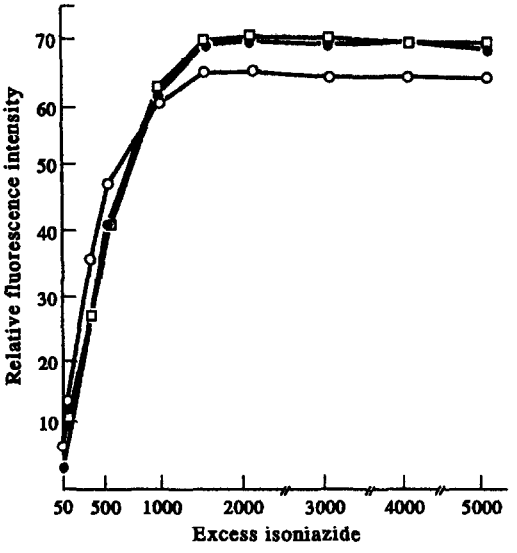

Fig. 4. Excess of isoniazide and time required for formation of diacetyl hydrazone (● just prepared, □ 15 min, ○ 30 min).

as optimum for both reactions, that being the equilibrium state with the maximum complexes formation and the minimum protonation of azomethynic nitrogen atoms and the minimum formation of Zr(IV) hydrocomplex species.

Excess of isoniazide and time for the formation of hydrazones

A preliminary experiment was carried out to establish the amount of Zr(IV) necessary to form the dDIH:Zr(IV) complex. Increasing amounts of Zr(IV) salt were added to a synthesized dDIH solution until a constant value of relative fluorescence intensity was reached. This corresponds to a 2500-fold excess of Zr(IV) in relation to the molar amount of α-diketone. This experiment is necessary to fix the Zr(IV) variable so that the study on excess isoniazide can be accurate. We later fixed the optimum excess of Zr(IV) salt for the determination of vicinal diketones.

The excesses of isoniazide indicated in Figs 4 and 5 in relation to the stoichiometry (2:1) were added to solutions of diacetyl (0.0052 m*M* final concentration) and 2,3-pentanedione (0.005 m*M* final concentration) plus a few drops of acetic acid. After the indicated time, 2500-fold excesses of Zr(IV) were added; pH was adjusted to 1.7 ± 0.1, and measurements were performed 30 min later. Minimum isoniazide excesses of 1500-fold for diacetyl and 4000-fold for 2,3-pentanedione were found to be optimum, and these amounts also resulted in an almost instantaneous formation of hydrazones.

Zirconium (IV) excess, time and temperature for the formation of complexes

Excesses of Zr(IV) ranging from 500- to 5000-fold were added to solutions of diacetyl (0.0052 m*M* final concentration) and 2,3-pentanedione (0.0050 m*M* final concentration). After addition of excess isoniazide (1500- and 4000-fold, respectively), a few drops of acetic acid and adjustment of pH to 1.7 ± 0.1, the reaction mixtures were either let to stand at room temperature or heated to 70–75°C for 15, 30, 45, or 60 min. In Fig. 6 only those experiments providing optimum results are reported, which were 30 min at room temperature for diacetyl, and the same time and heating for 2,3-pentanedione. For both compounds, the optimum amount of Zr(IV) was found to be in excess of 2500-fold.

Analytical features of the reactions

These are reported in Table 1. The calibration range is taken from the detection limit to the

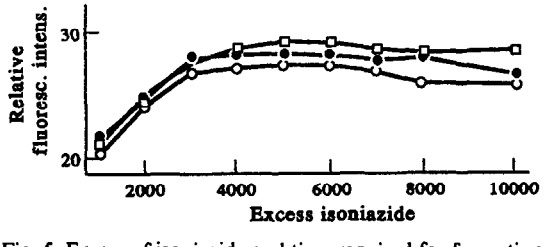

Fig. 5. Excess of isoniazide and time required for formation of 2,3-pentanedione hydrazone (● just prepared, □ 15 min, ○ 30 min).

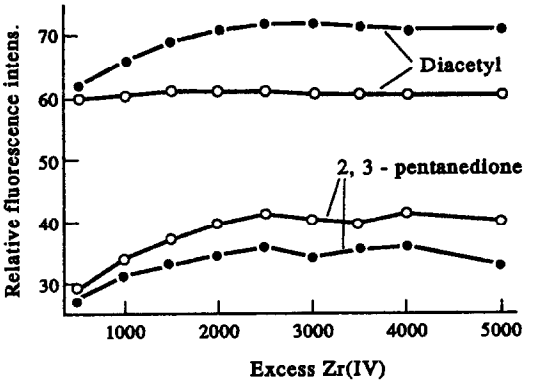

Fig. 6. Excess of Zr(IV) required for formation of complexes with diacetyl and 2,3-pentanedione when measurements were performed after 30 min either at (●) room temperature or (○) 70–75°C.

beginning of fluorescence quenching. There is no way of distinguishing between the factors responsible for the quenching. It was possible to ascertain that Zr(IV) is not the cause, but it was not possible to determine the concentrations at which either the fluorophore or the excess isoniazide are responsible.

Precision was determined at four levels of concentration for both diacetyl and 2,3-pentanedione. The results are shown in Table 2.

Recovery

In separate aliquots, 5 ml of $1.0 \times 10^{-5}M$ diacetyl and 5 ml of $1.0 \times 10^{-5}M$ 2,3-pentanedione were diluted to 50 ml and then distilled to about 30 ml. Six similar distillations were performed for each sample. Three of the distillates were collected into water, and the other three into an excess of isoniazide and acetic acid and compared with three non-distilled controls. All the samples were analysed according to the method outlined in the Procedures section. In the first case, recovery for diacetyl was $81.0 \pm 1.0\%$, while in the second $98.6 \pm 0.3\%$. For 2,3-pentanedione, recovery with water was $87.9 \pm 1.0\%$, while with isoniazide it was $99.6 \pm 0.4\%$.

Table 1. Analytical features of reactions with diacetyl and 2,3-pentanedione

Characteristics	Diacetyl	2,3-pentanedione
Linear range,* ($\mu g/l$)	4.0–860	20–1200
Detection limit,† ($\mu g/l$)	4.3	20
Sensitivity,† ($\mu g/l$)	2.0	8.0

*$r = 0.9998$ (diacetyl) and $r = 0.9999$ (2,3-pentanedione).
†*IUPAC Anal. Chem. Div.*[18].

Table 2.Precision study

Compound	Concentration ($\times 10^{-7}M$)	C.V.* (%)
Diacetyl	4.64	1.95
	9.28	0.86
	13.92	0.87
	18.56	0.74
2,3-pentanedione	4.00	2.66
	8.00	1.39
	12.00	0.86
	16.00	0.70

*Mean $n = 10$ determinations.

Recoveries were also studied in a vinegar model system. Two solutions of vinegar were prepared as follows:

Diacetyl or 2,3-pentanedione = 5.0 mg;
Acetoin = 250 mg;
2,3-butanediol = 300 mg;
Tartaric acid = 2.5 g;
Acetic acid = 40 g;
Ethanol 96°C = 12.5 ml;
Water = up to 1000 ml.

Ten millilitre solutions of vinegar were diluted to 100 ml with water. Three 10 ml aliquots of each solution were neutralized with NaOH, diluted to 50 ml, and distilled to about 30 ml. The distillates were collected into solutions of isoniazide acidified with acetic acid (see Procedures). Recoveries of $98.0 \pm 0.0\%$ and $98.3 \pm 0.6\%$ were obtained for solutions with diacetyl and 2,3-pentanedione, respectively.

Application: determination of vicinal diketones

Any colorimetric method for determining diacetyl based on condensation reactions with diacetyl's carbonyl groups inevitably also determines 2,3-pentanedione since it reacts in exactly the same manner. What is thus being measured are vicinal diketones.

We therefore propose a method for the determination of vicinal diketones according to the reaction conditions reported for diacetyl. Although the method chosen does not give the best results for 2,3-pentanedione, we have nevertheless chosen it for the following reasons: (1) diacetyl is almost always the major (if not the only) vicinal diketone present. (2) Flavourwise, the 2,3-pentanedione taste-threshold is some 10-fold higher than that of diacetyl[19] (the same sensory response requires a 10-fold higher concentration of 2,3-pentanedione) and hence diacetyl is of major analytical interest.

Results are therefore expressed as diacetyl and plotted on a calibration curve ($r = 0.9998$).

Table 3. Recovery of diacetyl from store-bought vinegar

Diacetyl added (μg)	Diacetyl found (μg)	Recovery* (%)
1.000	0.985	98.5
2.000	1.998	99.9
3.000	2.988	99.6

*Mean of three determinations.

In order to confirm its effectiveness, the method was applied to determine the α-diketones in store-bought vinegar.

The vinegar was diluted to 10%, from which 10 ml were taken. Known quantities of diacetyl were added to the 10 ml sample, and the whole was then further diluted to 50 ml. After this, the sample was distilled until around 30 ml of distillate was collected into a solution of isoniazide acidified with acetic acid (see Procedures). Untreated samples were taken as references. The results are given in Table 3.

By the present method it is possible to estimate values as low as 0.02 mg/ml.

The major advantage of using this spectrofluorimetric method, as opposed to other colorimetric methods is therefore the former's greater sensitivity, thus allowing the determinations to be carried out with a very small sample.

REFERENCES

1. C. B. Van Niel, A. J. Kluyver and H. G. Derx, *Biochem. Z.*, 1929, **210**, 234.
2. W. W. Westerfeld, *J. Biol. Chem.*, 1945 **161**, 495.
3. A. M. Canales and N. Martínez, *Am. Brewer*, 1962, **95**, 10.
4. D. B. West, A. L. Lautenbach and K. Becker, *Amer. Soc. Brew. Chem. Proc.*, 1952, **81**.
5. E. A. Prill and B. W. Hammer, *Iowa State College J. Sci.*, 1938, **12**, 385.
6. B. Walsh and T. M. Cogan, *J. Dairy Res.*, 1974, **41**, 25.
7. G. Mizuno, E. McMeans and J. R. Chiplault, *Anal. Chem.*, 1965, **37**, 151.
8. V. Palo and H. Ilkova, *J. Chromatogr.*, 1970, **53**, 367.
9. E. M. Skibina, P. A. Artamonov and E. I. Gorshkova, *Zh. Anal. Khim.*, 1975, **30**, 1839.
10. G. A. F. Harrison, W. J. Byrne and E. Collins, *J. Inst. Brew.*, 1965, **71**, 336.
11. W. Postel and U. Guveng, *Z. Lebensm.-Unsters. Forsch.*, 1976, **161**, 35.
12. W. Postel and B. Meier, *Z. Lebensm.-Unsters. Forsch.*, 1981, **173**, 85.
13. A. Shilman and L. W. Schaper, *J. Gas Chromatogr.*, 1966, **4**, 486.
14. F. H. White and T. Wainwright, *J. Inst. Brew.*, 1975, **81**, 37.
15. I. Lange, *Brauwelt*, 1984, **124**, 1367.
16. A. J. Maroulis, A. M. Voulgaropoulos and C. P. Hadjiantonion-Maroulis, *Talanta*, 1985, **32**, 504.
17. R. J. García-Villanova, R. García-Villanova and R. García Estepa, *An. Quím.*, 1983, **79B**, 593.
18. IUPAC analytical chemistry division, *Spectrochim. Acta (B)*, 1978, **33B**, 242.
19. T. Wainwright, *J. Inst. Brew.*, 1973, **76**, 486.

Talanta, Vol. 40, No. 9, pp. 1425–1432, 1993
Printed in Great Britain.

0039-9140/93 $6.00 + 0.00

THE BINDING OF STRONTIUM AND EUROPIUM BY AN AQUATIC FULVIC ACID—ION EXCHANGE DISTRIBUTION AND ULTRAFILTRATION STUDIES

MARIA NORDÉN, JAMES H. EPHRAIM and BERT ALLARD
Department of Water and Environmental Studies, Linköping University, S-581 83 Linköping, Sweden

(*Received* 20 *July* 1992. *Revised* 15 *February* 1993. *Accepted* 8 *March* 1993)

Summary—The complexation of an aquatic fulvic acid, FA, with Sr^{2+} and Eu^{3+} was studied at 0.10 and 0.01*M* $NaClO_4$ using trace levels of metal ($[Sr^{2+}] = 10^{-9}M$ and $[Eu^{3+}] = 10^{-11}M$) and a constant FA concentration (0.12 g/l) by an ultrafiltration technique (UF) and an ion exchange distribution method (IEDS). The overall complex formation function, β_{ov}, for the two metals was calculated and its dependence on pH, ionic strength and method was investigated. The absolute value of log β_{ov}, the pH dependence and the influence of the ionic strength on the complexation differed depending on the metal ion and experimental technique employed. By considering the functional group heterogeneity of the FA molecule, it was possible to predict the most predominantly bound site (keto–enol) and resolve the complex formation function for this site and Eu^{3+} (IEDS: 9.43 ± 0.29 l/eq at 0.10*M* and 10.58 ± 0.72 l/eq at 0.01*M*; UF: 7.19 ± 1.51 l/eq at 0.10*M* and 6.88 ± 0.91 l/eq at 0.01*M*). The results are discussed in the light of possible intrinsic problems of the two experimental methods.

The need to describe the dispersion of radionuclides from waste repositories due to possible leakage has mandated the study of typical radioisotopes and their interaction with natural organic acids. Earlier simulations of metal dispersion/speciation have normally left out the role of natural organic acids in this important exercise. However, in recent studies[1] it has been shown that small amounts of these ubiquitous natural organic acids have strong affinities for metal ions, thus their contribution to the mobility of radioisotopes cannot be neglected. Attempts to incorporate the role of these organic acids, have been stymied by a lack of a conceptual interpretation of their solution chemistry.

To describe metal ion binding by humic substances, complex formation functions (β) have been widely applied.[2] These functions are highly conditional, *i.e.* dependent on the ratio of metal ion to humic substance, ionic strength, pH and method of study.[3,4,5] In broad terms, models that have been proposed to describe metal–humate interactions may be categorized as the discrete ligand and the continuous distribution model.[6] Our approach may be categorized as a discrete ligand approach but emphasizes the need to incorporate contributions due to ionic strength effects and functional site heterogeneity.

This paper has been written to satisfy three objectives. The first is to address the role of natural organic acids in the mobility of radionuclides. The elements Sr and Eu were chosen as model elements for the study because as fission products in spent uranium, they also have properties similar to other long-lived radionuclides, *e.g.* Ra(II), Pu(III), and Am(III). The second objective is to compare results, expressed as overall complex formation functions at two ionic strengths and varying pH values, obtained by two different methods. The third objective is to describe the metal–fulvate interaction by considering the functional group heterogeneity of the fulvic acid. The complex formation function for the interaction between Eu and the acid site presumed to be the strongest, was determined. Comparison of this value with the literature-reported value[7,8] for the interaction between Eu and the functional group closely resembling the strongest site is made to justify the assignment of functionality to this site. In this exercise Sr was neglected because of its low binding affinity for fulvic acid.

EXPERIMENTAL

Chemicals and equipment

A well-characterized aquatic fulvic acid isolated from surface water in a bog area

(Bersbo, about 200 km south of Stockholm) was used.[9,10] In the ion exchange distribution studies, the sodium form of a Dowex 50 WX8 (mesh 50–100) was employed as the cation exchanger. The isotopes, ^{85}Sr (in aqueous solution) and ^{152}Eu (in 0.10M HCl), were purchased from Amersham. Milli-Q water was used in preparing all solutions. Analytical grade chemicals were employed. An Amicon ultrafiltration cell, 8050, was used in conjunction with a YM2 (1000 cut-off) Diaflo membrane. Radioactivity measurements were carried out using a LKB (Wallac) 1282 Compugamma counter. A radiometer pHM 85 precision pH-meter and a pH-combination glass electrode, GK 2402B, were employed for pH determinations. The experiments were performed at two ionic strengths (0.10M and 0.01M $NaClO_4$), a fixed total concentration of FA (0.12 g/l, corresponding to a total capacity of 5.6×10^{-4} eq/l), and initial metal ion concentrations of $[Sr^{2+}] = 10^{-9}M$ and $[Eu^{3+}] = 10^{-11}M$. The pH-adjustments were effected with $HClO_4$ or NaOH without the use of buffering agents. All experiments were performed at an ambient temperature of 22°C.

Procedure

The ion exchange distribution method has previously been developed for the determination of overall complex formation functions of metal–ligand systems.[11] In a typical IEDS experiment, 5 ml of the metal or fulvic acid–metal solution was added to a carefully weighed amount of the cation exchanger (0.005–0.100 g) in polyethylene tubes. The pH was adjusted with $HClO_4$ or NaOH and after equilibration on a shaking-table for approximately 24 h the pH was determined and aliquots were taken out for radioactivity measurements. To separate the solid from the liquid phase adequately the solutions were centrifuged for about 10 min at an appropriate speed.

The ultrafiltration experiments were performed following the procedure outlined previously.[12] The performance of the membrane, YM2, was checked by ascertaining that the rejection coefficient of the fulvic acid was unity, whereas that of the metal ion was zero.[13] A detailed description of the ultrafiltration method may be found elsewhere.[12,13]

MODE OF COMPUTATION

The classical expression for the conditional stability constant[14] has been the basis for the calculation of the overall complex formation function, β_{ov} as follows:

$$\beta_{ov} = \frac{\Sigma M_b}{M_f \Sigma A^-} \quad (1)$$

where ΣM_b is total metal bound, M_f is metal free in solution and ΣA^- is the summation of ionized acidic species.

In the IEDS the quotient $\Sigma M_b / M_f$ is calculated according to equation (2):

$$\frac{\Sigma M_b}{M_f} = \frac{D_0 - D}{D} \quad (2)$$

where D_0 and D are the respective distribution coefficient of the metal in absence and presence of FA. The D_0 was obtained from a linear regression analysis performed on the results of an experiment where D_0 was investigated as a function of the concentration of bulk electrolyte ($NaClO_4$), Table 1.

$$D = \frac{(wt_s A_c) - ((wt_s + wt_{NaOH} + wt_{HClO_4})A_s)}{(A_s wt_{sp})} \quad (3)$$

where wt_s is weight of solution, A_c is specific activity of the control solution (cpm/g), wt_{NaOH} is weight of added base, wt_{HClO_4} is weight of added acid, A_s is specific activity of the reaction solution (cpm/g) and wt_{sp} is weight of solid phase.

ΣA^- has been defined as:

$$\Sigma A^- = \alpha_{ov} HA_T - \Sigma M_b \quad (4)$$

where α_{ov} is overall degree of neutralization (dissociation) of the fulvic acid molecule and HA_T is total titratable acid in aqueous medium at the ionic strength of study. HA_T is derived at by multiplying the acid capacity (4.65 meq/g FA) with the amount of FA used (0.12 g/l). In these experiments only trace quantities of metal ions have been used and therefore $\Sigma M_b \ll \alpha_{ov} HA_T$ and equation (4) reduces to:

$$\Sigma A^- = \alpha_{ov} HA_T. \quad (5)$$

Table 1. The distribution coefficient of the metal in absence of fulvic acid, D_0, derived from linear regression analysis

Linear relationship: $y = mx + c$ where $y = \log D_0$ and $x = \log\{NaClO_4\}$.*
r = correlation coefficient and n = number of points.

Metal	m	c	r	n
Eu^{3+}	−2.974	2.071	0.9993	5
Sr^{2+}	−2.058	1.716	0.9955	7

*Kielland's (1937)[15] individual ion activity coefficients, γ, have been used for the conversion of concentration to activity.

For the two ionic strengths α_{ov} was calculated using third degree polynomials derived from potentiometric titrations.[16]

$$\alpha_{ov} = 1.035 - 0.644\text{pH} + 0.177(\text{pH})^2 - 0.0125(\text{pH})^3, \quad I = 0.10M \text{ NaClO}_4 \tag{6}$$

$$\alpha_{ov} = 0.4020 - 0.2461\text{pH} + 0.0874(\text{pH})^2 - 0.0060(\text{pH})^3, \quad I = 0.01M \text{ NaClO}_4. \tag{7}$$

In the ultrafiltration experiments $\Sigma M_b/M_f$ is calculated according to equation (8):

$$\frac{\Sigma M_b}{M_f} = \frac{A_o - A_f}{A_f} \tag{8}$$

where A_o is specific activity of the original (unfiltered) solution (cpm/g) and A_f is specific activity of the filtered solution (cpm/g).

Heterogeneity considerations

The description of the interaction between europium and fulvic acid may, however, be achieved by considering the various acidic moieties of the fulvic acid molecule. The fulvic acid employed has been characterized via the comprehensive physicochemical approach outlined by Marinsky.[17,18] In this approach, the fulvic acid is conceptualized as an assemblage of relatively small hydrophobic moieties that are slightly different, but composed of four to five predominant separate acidic sites with each site characterized by a distribution of acid strengths which may be averaged. The characteristics of Bersbo fulvic acid are summarized in Table 2.

Following an earlier treatment of the interaction between Eu^{3+} and a soil fulvic acid and reconciling with the envisaged acid spectrum in Bersbo fulvic acid (Table 2) it has been postulated that Eu^{3+} is predominantly sequestered by the keto–enol-like site.[20] Consequently, the complex formation function for this interaction has been computed by first subtracting the contributions of metal bound by the other acidic functionalities from the experimental value of metal bound. The contribution of the acidic functionalities has been estimated using literature values of stability constants[7,8] describing the interaction between Eu^{3+} and the acidic functional group that resembles the active sites in the fulvic acid molecule (Table 2).

Table 2. The characteristics of Bersbo aquatic fulvic acid.[9,19]

Elemental Analysis (%)	C	H	N	O	S	Ash
	52.5	3.6	1.1	38.8	1.0	3.0
Acidity (meq/g FA)	Aqueous			Non-Aqueous		
				-COOH	-OH	Total
	4.65			4.78	1.35	6.13
Extra acidity due to chelation (% of aqueous capacity)	Cu^{2+}			La^{3+}		
	65-70			25-30		
Molecular weight (Gel Permeation Chromatography)	M_n	M_w	M_w / M_n			
	1750	2650	1.51			
Site Characterization	Acid Site	pK_a	Abundance	Functionality		
	1	1.7	0.20	unidentate -COOH		
	2	3.3	0.25			
	3	5.0	0.30	unidentate -COOH		
	4	6.5	0.20			
	5	7.0	0.05			

The unidentate complexation between the metal ion and the acid site with a pK_a of 1.7 has been described as follows:

$$-R\text{–}COO^- + Eu^{3+} \rightleftharpoons -R\text{–}COOEu^{2+}. \quad (9)$$

The (M_b/M_f) due to this site is estimated from the mass action relationship as follows:

$$\left(\frac{M_b}{M_f}\right)_I = \beta_I(R\text{–}COO^-) \quad (10)$$

where $\beta_I = 10^{2.13}$ and $(R\text{–}COO^-)$ is the concentration of the ionized form of the acid site obtained by the following:

$$R\text{–}COO^- = \alpha_i Ab_i HA_T \quad (11)$$

where α_i is equal to the degree of neutralization for a specific site and might be expressed as in equation (12). The abundance of a specific site is in equation (11) written as Ab_i.

$$\alpha_i = \frac{1}{1 + 10^{pK_a - pH}} \quad (12)$$

Since the acid site with pK_a 1.7 is considered adjacent to the $-R\text{–}COO^-$ site with pK_a of 5.0, an additional mode of interaction is anticipated by envisaging a chelation as follows:

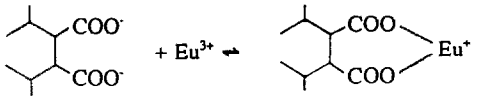

(13)

from which $(M_b/M_f)_{II}$ is computed by the relationship:

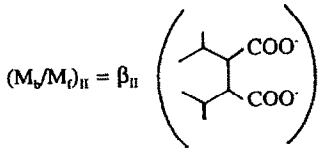

(14)

where $\beta_{II} = 10^{3.70}$ and the concentration term is obtained by considering the ionization of the second –COOH ($pK_a = 5.0$) as the limiting factor. The extra 10% of the acid site with pK_a of 5.0 is considered to complex the Eu^{3+} ion in an unidentate fashion and its contribution was estimated as:

$$\left(\frac{M_b}{M_f}\right)_{III} = \beta_{III}(R'\text{–}COO^-). \quad (15)$$

The acid site with a pK_a of 3.3 and an abundance of 0.25 which was considered to mimic a salicylic acid like site where a very weak –OH ($pK_a = 13.4$) is adjacent to a weak –COOH ($pK_a = 3.3$) was considered to bind the Eu^{3+} in two fashions. The first involved the unidentate complexation between the –COOH and the Eu^{3+} ion, as follows:

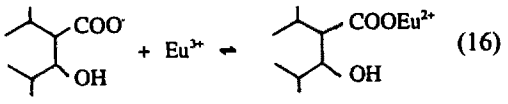

(16)

$(M_b/M_f)_{IV}$ is thus estimated from the mass relationship as follows:

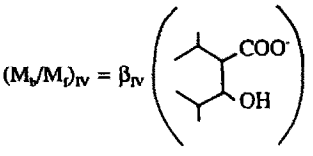

(17)

The other envisaged possible reaction is the chelation involving the $-COO^-$ and the –OH with the subsequent removal of a proton as follows:

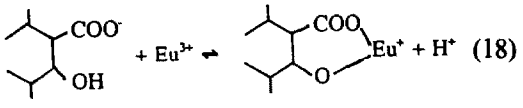

(18)

The $(M_b/M_f)_V$ computed from the mass action relationship as follows:

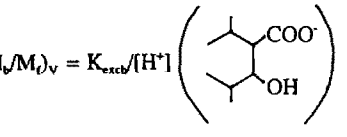

(19)

indicates the small contribution of such an envisaged mode of complexation.[21] The K_{exch} is β for Eu^{3+}–salicylic acid ($10^{4.44}$) multiplied with K_a for the –OH group in this site ($10^{-13.4}$).

The complex formation function for the keto–enol site has been calculated according to equation (20):

$$\beta_{k-e} = \frac{\left(\frac{\Sigma M_b}{M_f}\right)_{exp} - \left(\frac{\Sigma M_b}{M_f}\right)_{i,cal}}{A^-_{k_e}} \quad (20)$$

where A^-_{k-e} is the ionized form of the keto–enol site given by:

$$A^-_{k-e} = \frac{HA_T Ab_{k-e}}{1 + 10^{pK_a - pH}} \quad (21)$$

HA_T is the total titratable acid and Ab_{k-e} is the abundance of the keto–enol site in the fulvic acid molecule. $(\Sigma M_b/M_f)_{exp}$ is experimentally

derived (according to the above) and $(\Sigma M_b/M_f)_{i,cal}$ is obtained as follows:

$$\left(\frac{\Sigma M_b}{M_f}\right)_{i,cal} = \left(\frac{M_b}{M_f}\right)_I + \left(\frac{M_b}{M_f}\right)_{II} + \left(\frac{M_b}{M_f}\right)_{III} + \left(\frac{M_b}{M_f}\right)_{IV} + \left(\frac{M_b}{M_f}\right)_V. \quad (22)$$

RESULTS AND DISCUSSION

Ion exchange distribution studies

The results of the IEDS for the interaction between Sr and Eu and aquatic FA shown in Fig. 1 indicate that Eu binds more strongly to FA than Sr. Whereas the log β_{ov} for the Eu is dependent on pH (in the pH range 3–6.5 (0.10M) and 3.5–5 (0.01M)) the values for Sr are pH-independent. The log β_{ov} for the Eu–FA system at 0.10M may be described by an equation obtained by linear regression analysis. A similar relationship between pH and log β_{ov} for the Eu–FA system at $I = 0.01M$ can be used (Table 3). A constant value of 9.16 ± 0.02 is obtained after pH of 5.5 in the 0.01M system whereas a no clear cut average could be obtained for the 0.10M system. The corresponding values for the Sr–FA system are also reported in Table 3. The dependence of log β_{ov} on the ionic strength is greater in the case of Sr–FA than Eu–FA (Δ log $\beta_{ov,Sr(0.10-0.010M)} \approx 2.0$ while Δlog $\beta_{ov,Eu(0.10-0.010M)} \approx 1.5$).

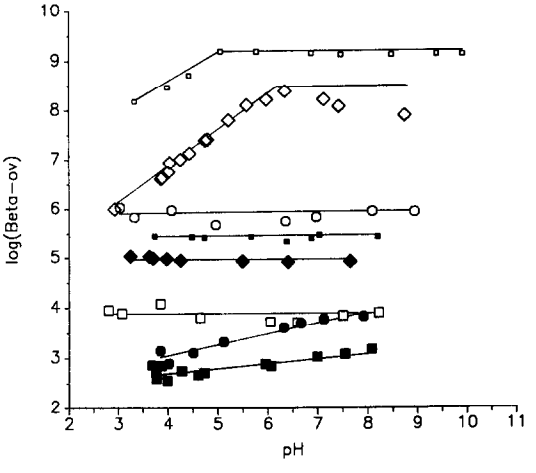

Fig. 1. The effect of pH and ionic strength (0.10 and 0.01M $NaClO_4$) on the overall complex formation function, β_{ov} for Eu^{3+} and Sr^{2+} and Bersbo aquatic fulvic acid investigated by ion exchange distribution studies (IEDS) and ultrafiltration (UF). Note that for IEDS, Eu^{3+} in 0.10M $NaClO_4$, the line has been drawn as above to conform with results in 0.01M $NaClO_4$ because a similar pattern of interaction is expected. IEDS: □ Sr^{2+} in 0.10M, ○ Sr^{2+} in 0.01M, ◇ Eu^{3+} in 0.10M, □ Eu^{3+} in 0.01M; UF: ■ Sr^{2+} in 0.10M, ● Sr^{2+} in 0.01M, ◆ Eu^{3+} in 0.10M, ■ Eu^{3+} in 0.01M.

Ultrafiltration

The UF results also attest to the fact that Eu is more strongly bound by the FA than Sr. The log β_{ov} values for the Eu–FA system showed an insensitivity to pH whereas the Sr–FA system yielded values slightly dependent on pH. The log β_{ov} values obtained for the Eu–FA system at 0.10M and 0.01M $NaClO_4$ maybe averaged to give 4.97 ± 0.04 and 5.44 ± 0.04, respectively. For the Sr–FA system at 0.10M and 0.01M $NaClO_4$ the log β_{ov} may be described by equations obtained by linear regression analysis (Table 3). The effect of ionic strength on the log β_{ov} seems the same for the two metal–humate systems (Δlog $\beta_{ov,Sr(0.10-0.010M)} \approx 0.6$ while Δlog $\beta_{ov,Eu(0.10-0.010M)} \approx 0.5$).

Comparison of methods

The comparison of results obtained from the two methods shows interesting discrepancies. The values of log β_{ov} for both metals obtained by the ion exchange method are invariably higher than those obtained by the ultrafiltration method (Fig. 1). For the two metals this discrepancy in absolute value is more pronounced at the lower ionic strength, 0.01M than at 0.10M $NaClO_4$. The interesting observation, however, is that the effect of method on the behaviour of the resolved log β_{ov} is reversed for the two metals. Whereas for the Eu the log β_{ov} obtained by the IEDS was dependent on pH that obtained by the UF was not. On the other hand the log β_{ov} obtained for the Sr–FA system by the IEDS showed no dependence on pH but those resolved from the UF showed a pH dependence. This discrepancy is not completely understood but similar observations have been made by earlier researchers.[3,22] In addition, the ionic strength effect on log β_{ov} is more enhanced in the IEDS than in the UF and this behaviour is the same for both metals. Sources of error in the IEDS are the accuracy of the determination of D_0 and the possible ion–dipole interactions between the ion exchange resin and the fulvic acid molecule.[20]

An explanation for the low log β_{ov} values obtained in the UF method as compared to the IEDS is the hypothesis of possible fragmentation of the fulvic acid molecule in the presence of the metal ion. These "small" fragments which might pass through the membrane with some

Table 3. Overall complex formation functions for Eu^{3+} and Sr^{2+} binding to Bersbo aquatic fulvic acid. Ionic medium $NaClO_4$. r = correlation coefficient and n = number of points

System	pH range	log β_{ov}–pH relationship (l/eq)	r	n
IEDS, Eu^{3+}, $I = 0.10M$	2.93–6.35	log $\beta_{ov} = 3.84 + 0.74$ pH	0.99	13
IEDS, Eu^{3+}, $I = 0.01M$	3.33–5.06	log $\beta_{ov} = 6.17 + 0.59$ pH	0.98	4
IEDS, Eu^{3+}, $I = 0.01M$	5.78–9.92	log $\beta_{ov} = 9.16 \pm 0.02$	—	6
IEDS, Sr^{2+}, $I = 0.10M$	2.80–8.22	log $\beta_{ov} = 3.87 \pm 0.12$	—	8
IEDS, Sr^{2+}, $I = 0.01M$	3.04–8.94	log $\beta_{ov} = 5.88 \pm 0.12$	—	8
UF, Eu^{3+}, $I = 0.10M$	3.25–7.65	log $\beta_{ov} = 4.97 \pm 0.04$	—	8
UF, Eu^{3+}, $I = 0.01M$	3.74–8.20	log $\beta_{ov} = 5.44 \pm 0.04$	—	8
UF, Sr^{2+}, $I = 0.10M$	3.69–8.08	log $\beta_{ov} = 2.30 + 0.10$ pH	0.72	13
UF, Sr^{2+}, $I = 0.01M$	3.85–7.92	log $\beta_{ov} = 2.17 + 0.22$ pH	0.93	8

metal ions would bring about an over-estimation of the free metal ion concentration which will translate into a reduced estimate of bound metal and thus a smaller log β_{ov}. It has been observed for an Al^{3+}–FA system investigated with a dialysis technique that an increase in metal load caused an increase in fulvic acid concentration outside the dialysis membrane.[23] In a calculation, based on UV–visible spectroscopy experiments, of the over-estimation of the free metal ion concentration it was found that less than 10% of the fulvic acid has to bind 64% of the Sr^{2+} ions and 98% of the Eu^{3+} ions to achieve log β_{ov} values of the same order as the IEDS. This exercise appears to indicate that smaller fragments of fulvic acid predominantly bind the metal ion at the expense of the larger fragments, a conclusion that is contrary to observed results.[24]

The difference in ionic strength effects in the two methods may be attributed to the effect of bulk electrolyte concentration on the measured parameters (*i.e.* D_0 for IEDS and M_f for UF). While the effect of bulk electrolyte concentration on D_o is very pronounced (Table 1) its effect on the estimated M_f is negligible. The parameter M_f is apparently not affected as much by the ionic strength of the system as D_0 and this situation is postulated to account for the decrease in ionic strength effects in the UF method.[25]

The results from two recent studies[25,26] indicate that overall complex formation functions can be both dependent and independent on changes in pH. In one of the studies[25] two methods were employed, IEDS and UF, and log β_{ov} exhibited a dependence on pH for IEDS but not for UF (IEDS: log $\beta_{ov} = 6.65$ l/eq (pH = 4), log $\beta_{ov} = 7.40$ l/eq (pH = 5), log $\beta_{ov} = 8.15$ l/eq (pH = 6), log $\beta_{ov} = 8.95$ l/eq (pH = 7); UF: log $\beta_{ov} = 5.10$ l/eq (pH = 4–7); $I = 0.10M$ $NaClO_4$ for both methods). In the other study[26] using the same FA (Bersbo FA)[25] and laser induced fluorescence, LIF, as a method, no significant variations of log β_{ov} (6.34 ± 0.16 l/eq) was observed in a pH range of 2.7–6.5 and ionic strength of $0.1M$ $NaClO_4$. The results from this study agree with previously reported values.[25] Very few studies of Sr–FA systems with calculated log β_{ov} values are reported in the literature. However, one reported log β_{ov} of 4.53 l/eq for a Sr–HA system at a pH = 5 and $I = 0.1M$[27] is higher than values obtained in this study using both methods.

Heterogeneity considerations

The binding of Eu^{3+} and Sr^{2+} ions by the fulvic acid molecule has additionally been explained by considering the interactions between the metal ions and the various discrete acid sites that have been employed to describe the acid–base properties of the fulvic acid molecule.[9] The Eu^{3+} is considered to be mainly sequestered by the keto–enol-like site[9,25] and the complex formation function for this reaction has been computed. The results of this exercise (Table 4) show the influence of ionic strength effect, which is only significant in the ion exchange distribution studies, and the

Table 4. Complex formation functions for the selective binding of Eu^{3+} by the keto–enol site of the Bersbo aquatic fulvic acid. Employed methods are Ion Exchange Distribution Studies, IEDS and Ultrafiltration, UF

Metal ion	Bersbo fulvic acid (g/l)	Ionic strength, $NaClO_4$ (M)	Method	pH range	log β (1/eq)
Eu^{3+}	0.12	0.10	IEDS	3.87–7.43	9.43 ± 0.29
Eu^{3+}	0.12	0.01	IEDS	3.33–8.48	10.58 ± 0.72
Eu^{3+}	0.12	0.10	UF	3.25–7.65	7.19 ± 1.15
Eu^{3+}	0.12	0.01	UF	3.74–8.2	6.88 ± 0.91

difference between the methods. The values of log $\beta_{\text{keto-enol}}$ obtained in the ion exchange distribution studies agree with earlier results where a similar mode of analysis was employed.[20] The values of complex formation function obtained in this exercise compare well with literature values for the interaction between Eu^{3+} and the probable functionalities, *e.g.* log $\beta_{\text{Eu-catechol}} = 11.17$ l/eq and the log $\beta_{\text{Eu-kojic acid}} = 6.14 \pm 0.02$ l/eq (both measured at $I = 0.1M$ and at 25°C).[7] That the values are not exactly the same as those published in the literature may be explained by considering that the extent of complexation of the envisaged sites might be perturbed by adjacent functional groups.[28]

CONCLUSIONS

The results of this study, though confirming the fact that Eu^{3+} is more strongly bound by fulvic acid than Sr^{2+}, indicate that the overall complex formation functions obtained by the different methods are different both in absolute values, behaviour with respect to pH changes and ionic strength. The influence of method on the overall complex formation function is additionally illustrated by the results of a study where the Bersbo fulvic acid–Eu system studied with LIF[26] yielded values different from UF and IEDS.

In an exercise to determine the speciation of the Eu–FA system using an arbitrary concentration of $10^{-8}M$ (a typical trace metal ion concentration) for the initial total free metal ion, varying concentrations of FA (1, 50, 120 mg/l), log $\beta_{\text{Eu-carbonate}} = 5.93$ l/eq[29] and log $\beta_{\text{Eu-hydroxy}} = 7.45$ l/eq determined from our own data by considering the relationship between D_0 and pH[30], it was shown that with as little as 1 mg/l of FA in the Eu–FA system, the metal ion was predominantly sequestered by the FA ($\geqslant 90\%$ in the pH range of 3–7.5). In the above-mentioned exercise, log β_{ov} values from the IEDS were employed (*i.e.* the highest log β_{ov} values of the two methods were selected). This exercise shows that very small amounts of natural organic acids can have significant effects on the mobility/speciation of trace metals in the environment.

By considering the functional group heterogeneity of the fulvic acid molecule the site which predominantly binds Eu^{3+} has been computed. Comparison of this value with the literature value gave credence to the functionality assigned to the most active site.

The approach outlined in this paper is yet another testimony emphasizing the need for a thorough characterization of the fulvic acid as a ligand in order to facilitate a comprehensive description of metal–fulvate interactions.

Acknowledgements—Financial support from the Swedish Nuclear Fuel and Waste Management Company and the Swedish Natural Science Research Council is gratefully acknowledged. Additionally acknowledged is the technical assistance from Mr Lars Wigforss.

REFERENCES

1. G. R. Choppin and B. Allard, in *Handbook on the Physics and Chemistry of the Actinides*, A. J. Freeman and C. Keller (eds), p. 407. Elsevier, Amsterdam, 1985.
2. S. Boggs Jr., D. Livermoor and M. G. Seitz, *Humic Substances in Natural Waters and their Complexation with Trace Metals and Radionuclides: A Review*, ANL-84-78, 1985.
3. E. L. Bertha and G. R. Choppin, *J. Inorg. Nucl. Chem.*, 1978, **40**, 655.
4. R. A. Torres and G. R. Choppin, *Radiochim. Acta*, 1984, **34**, 143.
5. L. Carlsen, *European Appl. Res. Rept.—Nucl. Sci. Technol.*, 1985, **6**, 1419.
6. D. A. Dzombak, W. Fish and F. M. M. Morel, *Environ. Sci. Technol.*, 1986, **20**, 669.
7. A. E. Martell and R. M. Smith, *Critical Stability Constants, Vol. 3: Other Organic Ligands*. Plenum Press, New York, 1977.
8. L. G. Sillén and A. E. Martell, *Stability Constants of Metal Ion Complexes*. The Chemical Society, Burlington House, London, 1964.
9. J. H. Ephraim, H. Borén, C. Pettersson, I. Arsenie and B. Allard, *Environ. Sci. Technol.*, 1989, **23**, 356.
10. C. Pettersson, I. Arsenie, J. H. Ephraim, H. Borén and B. Allard, *Sci. Tot. Environ.*, 1989, **81/82**, 287.
11. J. J. Schubert, *Phys. Colloid. Chem.*, 1948, **52**, 340.
12. J. H. Ephraim and H. Xu, *Sci. Tot. Environ.*, 1989, **81/82**, 625.
13. J. H. Ephraim and J. A. Marinsky, *Anal. Chim. Acta*, 1990, **232**, 171.
14. F. J. C. Rossotti and H. Rossotti, *The Determination of Stability Constants*. McGraw-Hill, New York, 1961.
15. J. Kielland, *J. Am. Chem. Soc.*, 1937, **59**, 1675.
16. J. H. Ephraim, H. Borén, I. Arsenie, C. Pettersson and B. Allard, *Sci. Tot. Environ.*, 1989, **81/82**, 615.
17. J. A. Marinsky, *J. Phys. Chem.*, 1985, **89**, 5294.
18. J. A. Marinsky and J. Ephraim, *Environ. Sci. Technol.*, 1986, **20**, 349.
19. C. Pettersson and B. Allard, in *Humic Substances in the Aquatic and Terrestrial Environment*, B. Allard, H. Borén and A. Grimvall (eds), p. 135. Springer-Verlag, Heidelberg, 1991.
20. J. H. Ephraim, J. A. Marinsky and S. J. Cramer, *Talanta*, 1989, **36**, 437.
21. J. Ephraim, S. Alegret, A. Mathuthu, M. Bicking, R. L. Malcolm and J. A. Marinsky, *Environ. Sci. Technol.*, 1986, **20**, 354.
22. M. S. Caceci, *Radiochim. Acta*, 1985, **39**, 51.
23. D. Berggren, *Int. J. Environ. Anal. Chem.*, 1989, **35**, 1.

24. S. A. Green, F. M. M. Morel and N. V. Blough, *Environ. Sci. Technol.*, 1992, **26**, 294.
25. J. H. Ephraim, *Sci. Tot. Environ.*, 1991, **108**, 261.
26. G. Bidoglio, I. Grenthe, P. Qu, P. Robouch and N. Omenetto, *Talanta*, 1991, **38**, 999.
27. J. V. Ibarra, J. Osacar and J. M. A. Gavilan, *Ann. Quim.*, 1981, **77**, 224.
28. E. M. Perdue, *Humic Substances in Soil, Sediment and Water*, p. 493. John Wiley & Sons, New York, 1985.
29. R. Lundqvist, *Acta Chem. Scand.*, 1982, **A36**, 741.
30. M. Nordén, J. H. Ephraim and B. Allard, in *Humic Substances in the Aquatic and Terrestrial Environment*, B. Allard, H. Borén and A. Grimvall (eds), p. 297. Springer-Verlag, Heidelberg, 1991.

Talanta, Vol. 40, No. 9, pp. 1433–1435, 1993
Printed in Great Britain.

0039-9140/93 $6.00 + 0.00

SUITABILITY OF NITRIC–SULPHURIC ACID DECOMPOSITION FOR THE DETERMINATION OF TUNGSTEN AND MOLYBDENUM IN GEOCHEMICAL EXPLORATION

G. S. REDDI, C. R. M. RAO and H. S. MURALIDHAR
Chemical Laboratory, Geological Survey of India, Madras-600 032, India

(*Received* 29 *May* 1992. *Revised* 17 *December* 1992. *Accepted* 28 *December* 1992)

Summary—A mixture of nitric and sulphuric acids is used for the decomposition of geochemical samples for the estimation of tungsten. In the resulting sample solution tungsten is determined colorimetrically by the dithiol method. The decomposition procedure suggested works well for scheelite mineral. However wolframite is only partially decomposed. The same sample solution is used for estimation of molybdenum by the thiocyanate method. The method is suitable for batch analysis and results in a high throughput.

Tungsten estimation in geological materials is usually accomplished by fusing the sample with the alkali mixture (Na_2CO_3, NaCl, KNO_3),[1,2] by fusion with pyrosulphate,[3] or by acid decomposition using HF and $HClO_4$[4,5] and the final determination is achieved by colorimetric methods involving thiocyanate or dithiol. A review on the colorimetric method involving thiocyanate has been published.[6] Tungsten in higher quantities is generally determined by the gravimetric method using cinchonine.[7] Tungsten is less sensitive than other elements by the atomic absorption method and is normally not included in the suite of elements determined by the AAS method. Tungsten has also been determined by an energy dispersive X-ray determination method in a suite of nine elements.[8]

Visual colorimetric methods, with detection limits in the same range as the crustal abundance levels, are utilized in many geochemical laboratories around the world, especially since, with many of these methods, the per-man-day output is high.

Many geochemical exploration programmes require the determination of both tungsten and molybdenum. These two elements have been determined after a pyrosulphate fusion with different hydrochloric acid aliquots.[9] Pyrosulphate fusion process has been reported to cause problems in the molybdenum estimation[10] and it also does not suit organic or sulphide rich samples as there is no oxidizing agent in the fusion process.[11]

A sulphuric and nitric acid mixture has been suggested as a suitable decomposition medium for the estimation of molybdenum.[12] In this communication we report the appropriateness of the same decomposition for the determination of tungsten thereby facilitating the determination of both tungsten and molybdenum after a single decomposition step.

EXPERIMENTAL

Apparatus

Spectrophotometer Model No. GS8660 ECIL, India.

Reagents

Analytical Reagent Grade (BDH) H_2SO_4, HNO_3, HCl, $SnCl_2$, NaOH, ethyl alcohol, thioglycollic acid, sodium tungstate and reagent grade zinc dithiol (BDH) are used.

Zinc dithiol solution. 0.3 g of zinc dithiol is dissolved in 2 ml of ethyl alcohol followed by five pellets of sodium hydroxide and 1 ml of thioglycollic acid. The solution is made to 100 ml with distilled water and filtered using Whatman No. 41 paper.

Stannous chloride solution. 15 g of stannous chloride is dissolved in 100 ml of concentrated hydrochloric acid.

Standard tungsten solution. 0.1794 g of sodium tungstate is dissolved in 100 ml of water to obtain 1000 μg/ml of W solution. From this necessary dilutions are made to obtain 5.0 μg/ml working solution.

Table 1. Comparison of values obtained by the proposed method with pyrosulphate fusion method

Sample		Values obtained in ppm (RSD %) Present method W	Mo	Pyrosulphate method* W	Mo
1	Test sample 1 (scheelite-bearing calcgranulite)	10 (4)	<2	10 (6)	<2
2	Test sample 2 (scheelite-bearing calcgranulite)	50 (4)	20 (6)	52 (3)	18 (4)
3	Internal standard, W-01 (wolframite in quartz vein)	21 (2)	<2	25 (2)	<2
4	Internal standard, W-04 (scheelite-bearing calcgranulite)	200 (5)	30 (2)	200 (6)	26 (1)

*Ref. 5.

Table 2. Values of standard samples obtained by the proposed method

Sample	Values obtained in ppm (RSD%) Mo	W	Certified values in ppm Mo	W
Flue dust (AMDEL-24610)	360 (3)	55 (6)	370	50
Granite (AMDEL-BH1)	330 (3)	0.432% (3)	330	0.422%
Low grade tungsten ore (AMDEL-3131)	307 (5)	1.038% (6)	300	1.042%

PROCEDURE

Up to 0.5 g of the sample is weighed into borosilicate beakers (50 ml capacity with marking at 20 ml). Ten millilitres of concentrated nitric acid and 5 ml of 1:1 sulphuric acid are added from an automatic dispenser. The beakers are heated on an electric hot plate to strong fumes of sulphuric acid and then to a syrupy stage. Ten millilitres of concentrated hydrochloric acid are added to the cooled contents and digested for half an hour at low heat. The remains are then made up to 20 ml with concentrated hydrochloric acid. From the solution above the settled constituents of the beaker a 5 ml aliquot is transferred into a borosilicate tube with ground glass stopper. A 4 ml portion of stannous chloride solution is added and the contents are mixed. The tubes are then placed in boiling water for 20 min. To the warm contents of the tube, 1 ml of dithiol solution is added. The contents are mixed well. A 0.3 ml volume of benzene is added and the stoppered tubes are thoroughly shaken. The colour of the organic layer is visually compared against standards.

Preparation of standards

To five different borosilicate test tubes containing 4 ml portions of pure hydrochloric acid, 0.25, 0.5, 0.1, and 3.0 μg of tungsten is transferred using the 5 μg/ml standard working solution. Four millilitres of stannous chloride solution is added to each of the test tubes and the procedure continued as described above.

For a 0.5 g sample made to 20 ml, when 5 ml aliquot is taken for analysis, a minimum value of 2 ppm is obtained. When the colour of the organic layer exceeds that of the highest standard the procedure is repeated with a smaller aliquot. For samples with W content exceeding 250 ppm, the spectrophotometric method is adopted measuring the absorbance at 640 nm.

For the molybdenum estimation 2 ml aliquot of the sample solution is transferred in to a borosilicate tube containing 4 ml of distilled water. One millilitre of 10% potassium nitrate solution in water and 1 ml of 25% sodium tartrate solution in water are added and the thiocyanate complex developed, after a stannous chloride reduction step. A visual comparative method is adopted as per the recommended procedure.[12]

RESULTS AND DISCUSSION

The results obtained for some of the test samples and laboratory standards are given in Table 1. Good agreement is seen between the values obtained by the proposed method as compared to the pyrosulphate method. Good precision figures are obtained. Accurate values

Table 3. Results of tungsten in mineralized samples

Sample	W values obtained by the pyrosulphate method in % (RSD%)	W values obtained by the suggested method in % (RSD%)
Test sample 1 (scheelite)	0.329 (5)	0.325 (3)
Test sample 2 (wolframite)	0.430 (7)	0.239 (16)
Test sample 3 (wolframite)	0.971 (2)	0.623 (20)

were obtained for the three reference samples analysed (Table 2).

Applying the suggested decomposition technique to high mineralized samples it was found that while scheelite ($CaWO_4$) is attacked fully, wolframite ($FeMnWO_4$) is only partially attacked (Table 3).

The method is adaptable for batch analysis and especially suits exploration programmes where both tungsten (occurring as scheelite) and molybdenum are required to be analysed.

Acknowledgements—The authors wish to thank Shri C. R. Narayanan, Deputy Director General (Geochemistry), Geological Survey of India, for his keen interest and support in the project and to two unknown referees whose critical comments have greatly improved the manuscript.

REFERENCES

1. F. N. Ward, H. W. Lakin and F. C. Canney, Analytical methods used in geochemical exploration by the U.S. Geol. Survey. *U.S. Geol. Surv., Bull. 1963, No. 1152.*
2. R. E. Stanton, *Rapid Methods of Trace Analysis for Geochemical Applications*, p. 86. Edward Arnold, London, 1966.
3. B. F. Quin and R. R. Brooks, *Anal. Chim. Acta*, 1972, **58**, 301.
4. P. J. Aruscavage and E. Y. Campbell, *U.S. Geol. Survey J. Res.*, 1978, **6**, 697.
5. K. M. Chan and J. P. Riley, *Anal. Chim. Acta*, 1967, **39**, 103.
6. A. G. Fogg, D. R. Marriot and D. Thorburn-Burns, *Analyst*, 1970, **95**, 848.
7. W. W. Scott, *Standard Methods of Chemical Analysis*, Vol. 1, p. 1005. Van Nostrand, New Jersey, 1939.
8. J. M. Hansel and L. J. Martel, Los Alamos Science Lab, Informal Report, LA-6869-MS, 1977.
9. R. E. Stanton, *Analytical Methods for Use in Geochemical Exploration*, p. 19. Edward Arnold, London, 1976.
10. E. Upor, M. Mohai and G. Y. Novak, Photometric methods in inorganic trace analysis, Vol. 20, in *Comprehensive Analytical Chemistry*, G. Swehla (Ed.), p. 254. Elsevier, Amsterdam, 1985.
11. W. K. Fletcher, Analytical methods in geochemical prospecting, Vol. 1, in *Handbook of Exploration Geochemistry*, G. J. S. Govett (Ed.), p. 66. Elsevier, Amsterdam, 1981.
12. G. S. Reddi and C. R. M. Rao, *Anal. Chim. Acta*, 1991, **244**, 245.

Talanta, Vol. 40, No. 9, pp. 1437–1444, 1993
Printed in Great Britain.

0039-9140/93 $6.00 + 0.00

POTENTIOMETRIC RESPONSE OF POLY(3-OCTYLTHIOPHENE), POLY(3-METHYLTHIOPHENE) AND POLYTHIOPHENE IN AQUEOUS SOLUTIONS

JOHAN BOBACKA, ANDRZEJ LEWENSTAM and ARI IVASKA*
Laboratory of Analytical Chemistry, Åbo Akademi University, SF-20500 Turku-Åbo, Finland

(*Received* 29 *January* 1993. *Revised* 1 *March* 1993. *Accepted* 1 *March* 1993)

Summary—The potentiometric response of some polythiophenes in aqueous solutions has been investigated. Polythiophene (PT), poly(2,2′-bithiophene) (PBT), poly(3-methylthiophene) (PMT), poly(3-octylthiophene) (POT) and poly(4,4′-dioctyl2,2′-bithiophene) (POTd) were electrochemically deposited on platinum in 0.1*M* $LiBF_4$-propylene carbonate solution containing the corresponding monomer or dimer. Polymer electrodes were also prepared by solution casting of chemically synthesized poly(3-octylthiophene) (POTc) dissolved in chloroform. After film deposition (electrochemical or chemical) the polymer coated electrodes were used as indicator electrodes in potentiometric measurements. The open-circuit potential of the polymer electrodes was measured in aqueous solutions containing inorganic salts (10^{-1}–$10^{-4}M$). Interestingly, all the polythiophenes studied were found to give a cationic response to monovalent cations such as H^+, Li^+, Na^+, K^+ and NH_4^+ (Cl^- salts). The slope, calculated from the linear part of the response curve, was found to depend on the polythiophene used but always remained lower than that predicted for a Nernstian response. The polythiophenes also showed some sensitivity to divalent cations such as Mg^{2+} and Ca^{2+} (Cl^--salts). POT was used as the polymer to study the influence of the polymerization conditions on the potentiometric response. By investigating different polymers from the polythiophene family it was possible to evaluate how the starting material (monomer or dimer) and the presence of alkyl side-chains influence the potentiometric response of the polymer membranes.

INTRODUCTION

Polythiophene (PT) and poly(3-methylthiophene) (PMT) belong to the group of conducting polymers that are environmentally stable both in their doped (electrically conducting) and undoped states.[1] Furthermore, poly(3-alkylthiophenes) containing relatively long alkyl chains (PATs) are processable, which makes them particularly attractive for technological applications.[2–5] One possible application is in the field of electrochemical sensors.[6] Considering the possible use of polythiophene and its derivatives as sensors their electrochemical behaviour in aqueous solutions is of interest.

A number of investigations concerning the electroactivity of polythiophenes in aqueous solutions has been reported.[7–10] Tourillon *et al.*[7] have demonstrated that PT and PMT can be reversibly doped in aqueous solutions. The doping level and conductivity were similar to those obtained in acetonitrile. More recently, Sunde *et al.*[8,9] found that the electrochemical doping process of PT and PMT is sensitive to the anion in aqueous electrolyte solutions, which also is of interest in sensor applications.

Although PT and PMT can reversibly be doped in aqueous solutions, this is not the case of PATs.[9,10] No current response was observed for poly(3-octylthiophene) (POT) in aqueous solutions when studied by cyclic voltammetry in the potential range 0–2 V.[9] The POT film remained red in colour, indicating that the oxidation (doping) process was inhibited.[9] This behaviour is in contrast to that observed in organic solutions where the PATs can be reversibly oxidized.[3,11–18] Roncali *et al.*[10] suggested that the increased hydrophobicity, due to the long alkyl chains, is responsible for the low electroactivity of PATs in aqueous media. It is likely that the hydrophobic PATs are poorly swollen in water, which obviously has an inhibiting influence on the doping process. The apparent electroinactivity of PATs in aqueous solutions may be considered as a limitation for these materials, especially in applications based on the reversible doping reaction. It will be shown below that, in spite of its low voltammet-

*Author for correspondence.

ric activity in aqueous media, POT nevertheless gives a fast and reproducible potentiometric response towards several monovalent and divalent cations in aqueous solutions.

The present work is an extension to our previous studies on the electrochemical characteristics of poly(3-octylthiophene) film electrodes in organic solutions.[14-17] The main objective of the present work is to study the potentiometric response of poly(3-octylthiophene) and some other polythiophene derivatives in aqueous solutions of inorganic salts. The chemical structure of the polythiophenes investigated are schematically shown in Fig. 1. Our preliminary investigations indicated that poly(3-octylthiophene) is sensitive to cations. To the best of our knowledge, this is a new feature of polythiophenes and has not been considered earlier. Therefore we decided to study this behaviour more thoroughly. Anion sensitivity of polypyrrole (PPy), another conducting polymer, is, however, well documented.[19,20] The response mechanism for the polythiophenes will be discussed. Finally, some conclusions will be drawn regarding the potential usefulness of the polythiophenes from an analytical point of view.

EXPERIMENTAL

Chemicals

Thiophene, 3-methylthiophene (Aldrich, 99 + %) and 2,2′-bithiophene (Aldrich, 97%) were used as received. Chemically synthesized poly(3-octylthiophene) (POTc) and 3-octylthiophene were used as received from Neste Oy (Research Centre, SF-06850 Kulloo, Finland). The 4,4′-dioctyl-2,2′-bithiophene was synthesized from 3-octylthiophene as described elsewhere.[14] Propylene carbonate (Aldrich, anhydrous), $LiBF_4$ (Fluka, pract.), $NaBF_4$ (Fluka, purum), $NaClO_4$ (Aldrich, 99 + %), HCl, LiCl, NaCl, $NaNO_3$, KCl, NH_4Cl, $K_3[Fe(CN)_6]$ and $K_4[Fe(CN)_6] \cdot 3H_2O$ (Merck, p.a.), $CaCl_2 \cdot 4H_2O$ (Merck, suprapur) and $MgCl_2 \cdot 6H_2O$ (Merck, p.a.) were used as received. Distilled deionized water was used to prepare the solutions for potentiometric measurements.

Electrode preparation

Electrochemical polymerization was performed by using a one-compartment and three-electrode electrochemical cell (Metrohm 663 VA Stand). The working electrode was a Pt disc (area = 0.07 cm^2) and a glassy carbon (GC) rod was used as the auxiliary electrode. For comparison, Au and GC discs were also used as working electrodes in some cases. The reference electrode was an aqueous Ag/AgCl/KCl(3*M*) electrode that was connected to the cell via a bridge filled with 0.1*M* $LiBF_4$-propylene carbonate ($LiBF_4$-PC). Prior to the polymer deposition, the electrode surface was polished with 0.3 μm alumina and rinsed with water and chloroform.

PT, PBT, PMT, POT and POTd (Fig. 1) were deposited by galvanostatic polymerization of thiophene (0.1*M*), 2,2′-bithiophene (0.1*M*), 3-methylthiophene (0.1*M*), 3-octylthiophene (0.1*M*), and 4,4′-dioctyl-2,2′-bithiophene (0.005*M*), respectively, in 0.1*M* $LiBF_4$-PC. The galvanostatic polymerization was performed by

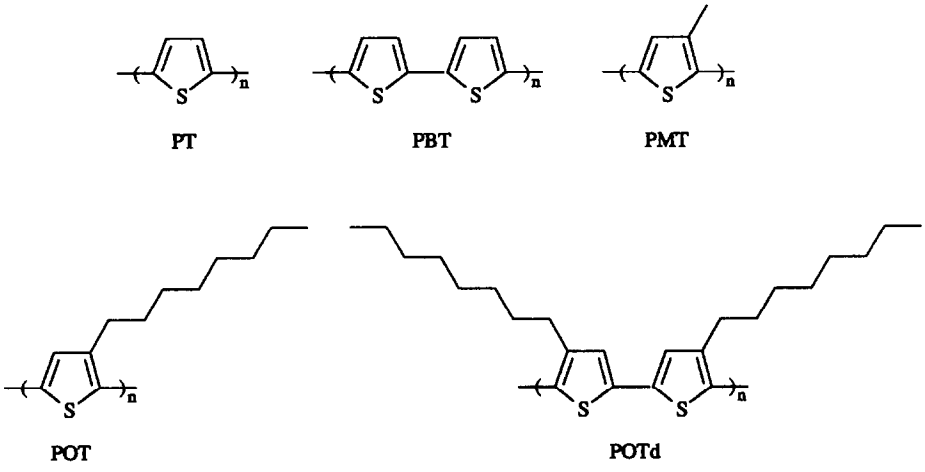

Fig. 1. Chemical structure of the polythiophenes studied. PT = polythiophene, PBT = poly(2,2′-bithiophene), PMT = poly(3-methylthiophene), POT = poly(3-octylthiophene), POTd = poly(4,4′-dioctyl-2,2′-bithiophene).

using a Metrohm type E211 coulometer supplying a constant current of 0.1 mA (1.43 mA/cm^2). The amount of charge passed during polymerization of PT, PMT and POT was 8 mC. The film thickness for POT prepared under these conditions has been estimated to 0.25 ± 0.1 μm by using a Sloan Dektak II profilometer.[17] This gives an indication of the film thicknesses also for the other polythiophenes prepared by using the same polymerization charge. In the case of PBT and POTd only 4 mC was used since the starting materials were dimers. The cell solution was purged with nitrogen and the working electrode was rotated at about 1500 rpm during polymerization which was performed at room temperature (23 ± 2°C).

After polymerization the potential of the polymer electrodes were kept at 0 V for 1 min in the polymerization solution in order to reduce (undope) the polymer films. After undoping, the electrodes were rinsed with PC and water and stored in an aqueous solution ($10^{-1}M$ KCl) for at least two days prior to the potentiometric measurements.

Chemically prepared poly(3-octylthiophene) (POTc) was dissolved in chloroform (0.475 mg/ml) and films of POTc were prepared by solution casting. The average film thickness was estimated to 3 μm by using a density of 0.9 g/cm^3 for POTc.[15]

Potentiometric measurements

Potentiometric measurements were done by using an Orion Research Expandable Ion Analyzer EA 940. The polymer electrodes were used as indicator electrodes in conjunction with the Ag/AgCl/KCl($3M$) reference electrode, connected to the cell via a bridge filled with the test solution ($10^{-1}M$). The liquid junction potential arising from the concentration difference between the reference bridge ($10^{-1}M$) and the test solution (10^{-1}–$10^{-4}M$) were taken into account and the potential values reported in this work have been corrected by using the Henderson equation.[21] Due to the low selectivity of the polythiophenes studied, the measurements were performed in unbuffered solutions.

Prior to the measurements the polymer electrodes were conditioned in $10^{-1}M$ solution of the salt to be tested. The measurements were performed in the concentration range 10^{-1}–$10^{-4}M$, and the polymer electrodes were equilibrated for 2 min in each solution in order to ensure the equilibrium conditions. The electrode was rotated (500 rpm) during the 1st min in order to speed up the equilibration and the potential was read 1 min after the rotation was stopped. The response time of the POT electrode was in the order of a few seconds in the concentration range studied. Film conditioning and potentiometric measurements were performed at room temperature (23 ± 2°C) in open air. The slopes that will be presented in this work have been calculated by linear regression using three points spanning a concentration range of 2 decades (usually 10^{-1}–$10^{-3}M$). The correlation coefficient (r) will be given together with the slopes.

RESULTS AND DISCUSSION

Effects of polymerization conditions on the potentiometric response of POT

Electrode rotation. When POT was electrochemically deposited on the Pt disc without rotation, the outmost layers of the polymer formed were loosely bound to the rest of the film and were removed during rinsing of the electrode in PC after polymerization. The polymer remaining on the electrode after rinsing gave a cationic response to K^+, but the slope was only 23.4 mV/decade ($r = 0.956$). When the Pt disc was rotated at 1500 rpm during deposition of POT, the polymer film was strongly attached to the substrate and no dissolution of the film was observed when rinsing in PC. The potentiometric response of six POT electrodes prepared under the same experimental conditions (rotation rate = 1500 rpm) on different platinum substrates gave a potentiometric response with a slope of 49.7 ± 2.5 mV/decade ($r = 0.999$) during measurements in KCl solutions. It has been observed previously that the yield of POT on the electrode is lower when the electrode is rotated during polymerization.[15] Due to convection at the rotating electrode, oligomers of POT are obviously swept away before they are attached to the Pt or to the growing polymer. Not only the yield but also the morphology of the polymer formed at the rotating electrode may therefore be different from that prepared in a quiescent solution. Since rotation seems to be advantageous for the cationic response of Pt/POT, the electrode is rotated at 1500 rpm during all electrochemical polymerizations in the rest of this work.

Substrate material. In order to study the influence of the substrate material, POT was electrochemically deposited on Pt, Au and GC. The slopes of the potentiometric response

Table 1. Slopes of the potentiometric response curves for POT in KCl solution as function of current density (and potential) used during galvanostatic polymerization. The correlation coefficient $r \approx 0.999$

Current density (mA/cm^2)	Potential (V)	Slope ($mv/decade$)
0.43	1.4	36.1
1.43	1.5	47.4
4.29	1.7	52.1
14.3	2.4	22.9*

*$r = 0.964$.

measured in KCl solutions were 50.3 and 52.6 mV/decade ($r \geq 0.9997$) for Au/POT and GC/POT, respectively. These slopes are similar to those observed for Pt/POT (49.7 ± 2.5 mV/decade, $n = 6$) indicating that the substrate material has only a little influence on the slope. This also confirms that the cationic response is due to the polymer and not due to the substrate, since the slopes observed for the bare electrodes in KCl solutions were -15.1, 26.0 and 31.9 mV/decade ($r \geq 0.995$) for Pt, Au and GC, respectively. Also in the case of polypyrrole (PPy) electrodes, the ionic response is attributed to the PPy layer and not to the Pt substrate.[22] In the following of this work, Pt is used as the substrate material for all the polythiophenes studied.

Current density. POT was polymerized on the rotating Pt disc by using four different current densities but keeping the polymerization charge constant at 8 mC. The potentiometric slopes of the four POT electrodes were then measured in KCl solutions and the results are summarized in Table 1. The results show that the potentiometric slopes increase with increasing current density in the range 0.43–4.29 mA/cm^2. The highest current density used (14.3 mA/cm^2) is obtained at such a high potential (2.4 V) that side-reactions and overoxidation may take place during polymerization.[15] This may be the reason for the low value of the potentiometric slope (22.9 mV/decade) observed for this electrode. Our results can be compared with those obtained by Roncali *et al.* using visible absorption spectroscopy.[11] Their results indicate that the conjugation length and yield of PATs increase with increasing current density (0.5–10 mA/cm^2) during electropolymerization on indium–tin oxide electrodes. It is thus possible that the slope of the cationic response observed for POT increases due to the increasing conjugation length and/or yield of POT, keeping in mind that also other effects may be involved. It will be shown below that the slope depends on the film thickness and this may explain why the slope increases with increasing current density during electropolymerization. One additional effect of the increasing current density might be the increasing degree of crosslinking between polymer chains, and this is regarded as the reason for the low solubility of electrochemically prepared POT.[11,14] A current density of 1.43 mA/cm^2 is used throughout the remaining experiments in this paper, since this value gives a reasonably big slope and since this current density has been used also in our previous works on POT.[14–17]

Film thickness. The effect of film thickness was studied by varying the charge used in polymerization of POT on the rotating Pt disc at the current density of 1.43 mA/cm^2. The results are shown in Fig. 2. It is assumed that the film thickness increases linearly with the amount of charge passed during electropolymerization.[15] By measuring the potentiometric response for the POT electrodes in KCl solutions the slopes can be plotted as function of charge, as shown in Fig. 2. The results indicate that the slope increases sharply with increasing film thickness up to a polymerization charge of about 8 mC and then gradually decreases. In the remaining part of this paper, a polymerization charge of 8 mC (114 mC/cm^2) is used (4 mC when starting from the dimer) for all the polythiophenes studied.

Stability and redox sensitivity of POT

The same POT electrode was used for potentiometric measurements in various aqueous solutions (HCl, LiCl, $LiBF_4$, NaCl, $NaBF_4$, KCl, NH_4Cl, $MgCl_2$, $CaCl_2$) during a time period of 5 weeks. Thereafter the POT electrode was conditioned for about 5 weeks in 0.1M KCl and the potentiometric response to K^+ was then

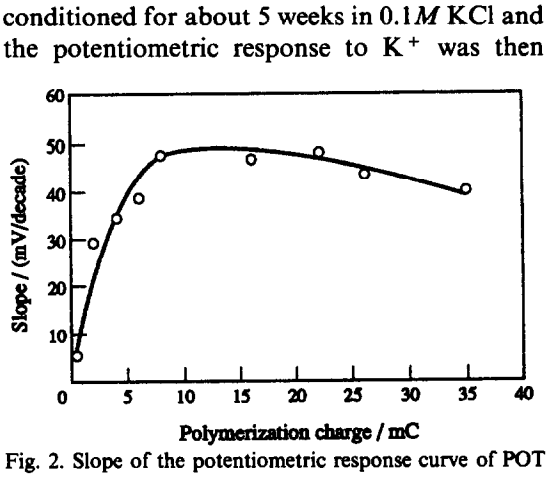

Fig. 2. Slope of the potentiometric response curve of POT in KCl solutions as function of the polymerization charge.

measured again. The slope observed was 46.7 mV/decade ($r = 0.9995$) which is comparable to the slope observed for the freshly prepared polymer electrode (47.4 mV/decade, $r = 0.999$). These results indicate that the POT film is stable and remains attached to the Pt substrate for at least 10 weeks in aqueous solutions although the thickness of the film is only about 0.25 μm. During potentiometric measurements, the potential of the POT electrode is in the range where POT is in its undoped, semiconducting state,[15-17] and therefore one can expect that there is no risk for overoxidation.[15] Furthermore, the polythiophenes are relatively stable to O_2 also in their undoped state, in contrast to PPy.[1] These factors certainly contribute to the good stability of POT observed in our experiments.

The redox sensitivity of POT was studied by measuring the potentiometric response to K^+ in solutions containing different total concentrations of the redox couple, $Fe(CN)_6^{3-}/Fe(CN)_6^{4-}$. The concentration ratio, $[Fe(CN)_6^{3-}]/[Fe(CN)_6^{4-}]$, was kept constant = 1/1. The potassium concentration was varied by using KCl and the contribution originating from the redox couple was considered when calculating the final potassium concentrations. The following slopes in mV/decade ($r \approx 0.999$) were obtained for the different total concentrations of redox couple (C_{Fe}): 49.0 ($C_{Fe} = 0$ mM), 48.3 ($C_{Fe} = 0.01$ mM), 49.1 ($C_{Fe} = 0.1$ mM), 40.2 ($C_{Fe} = 1$ mM). It can be seen that the redox couple does not interfere at $C_{Fe} \leqslant 0.1$ mM, but at $C_{Fe} = 1$ mM the slope is reduced. This may be due to electron transfer between POT and the redox couple in solution, giving rise to a mixed ionic and redox sensitivity in analogy to that observed for PPy.[23,24] It can be mentioned, however, that POT seems to be less redox sensitive than PPy.[24] This can be related to the difference in the oxidation potential between these two polymers, i.e. PPy is in its doped (conducting) state,[1] while POT is in its undoped (semiconducting) state,[15-17] at the redox potential of the $Fe(CN)_6^{3-}/Fe(CN)_6^{4-}$ couple. Therefore the electron transfer between the polymer and the redox couple in solution is faster for PPy than for POT.

Potentiometric response of some polythiophenes

Cation sensitivity. The potentiometric response of PT, PBT, PMT, POT, POTd and POTc to several cations were investigated and the results are summarized in Table 2. Interestingly, all polymer electrodes give a cationic response to the monovalent cations studied but the slopes are always lower than the theoretical value of 58.7 mV/decade (23°C) as expected for a Nernstian response. Also for the divalent cations, the slopes are smaller than the theoretical (29.4 mV/decade) and for PMT even a slight anionic response to Cl^- is observed in $MgCl_2$ solutions. It can be seen in Table 2 that each polymer responds to several cations, i.e. the selectivity is poor, although small differences in slopes can be observed. In general the polythiophenes, especially PMT, are less sensitive to divalent cations than to monovalent cations. Among the polythiophenes studied, POTc gives the biggest sensitivities to Na^+, K^+, NH_4^+, Mg^{2+} and Ca^{2+}, while PT and POT are most sensitive to H^+ and Li^+, respectively. It is remarkable that POT gives very similar slopes (44.4–47.4 mV/decade, $r \approx 0.999$) for all the monovalent cations studied. On the other hand, the slopes for PT, PBT, PMT, POTd and POTc increase in the following order: $Li^+ < Na^+ < K^+$, i.e. with increasing crystal ionic radii and decreasing hydrated ionic radii for these cations.[25] The slopes as a function of the hydrated ionic radii are shown in Fig. 3. These results indicate that the potentiometric response of the polythiophenes studied (except POT) is influenced also by the size of the cation.

Table 2. Slopes of the potentiometric response curves for some polythiophenes deposited on platinum in Cl^- solutions of different cations. The correlation coefficient $r \geqslant 0.994$

Polymer	Slope (*mV/decade*)						
	H^+	Li^+	Na^+	K^+	NH_4^+	Mg^{2+}	Ca^{2+}
PT	48.2	39.4	41.8	42.4	44.9	13.6	13.7
PBT	10.6	29.6	34.9	38.5	40.8	5.3*	6.0*
PMT	22.3	30.7	37.4	38.1	38.8	−2.0	3.5
POT	44.4	46.6	46.2	47.4	45.0	17.5	11.7
POTd	42.8	35.5	39.1	43.5	46.2	12.3	12.6
POTc	41.3	45.6	50.4	51.4	50.1	20.6	18.2

*$r = 0.976$.

Anion influence. In the experiments described above, Cl^- was the anion of the salts. When BF_4^- was used as the anion, the slopes observed for POT were only 20.5 and 14.3 mV/decade ($r \geqslant 0.998$) for Na^+ and Li^+, respectively. This

It should be mentioned that the measured potential values for all polymer electrodes in 0.1M HCl solution were in the range 0.47–0.61 V, which is significantly higher than the potential values (0.22–0.46 V) in the other solutions used (0.1M). These results show that H^+ shifts the standard potential of the polythiophene electrodes in the positive direction.

clearly indicates that also the anion influences the potentiometric response and this may contribute to the sub-Nernstian response found in Cl^- solutions. The BF_4^- anion, however, seems to cause more interference than Cl^-. For POTc, the slopes for Li^+ and Na^+ were 2.3 mV/decade ($r = 0.445$) and 12.2 mV/decade ($r = 0.944$), respectively, when BF_4^- was used as the anion. This anion effect cannot only be related to the fact that BF_4^- was used as the doping anion during electrosynthesis of POT, since both POT and POTc give smaller slopes in the presence of the BF_4^- anion.

The measured potential values for POT and POTc were found to be significantly higher in the BF_4^- solutions than in the corresponding Cl^- solutions. This was investigated further by measuring the equilibrium potential for the POT electrode in 0.1*M* NaCl, $NaNO_3$, $NaClO_4$ and $NaBF_4$. In Cl^-, NO_3^- and ClO_4^- solutions, the equilibrium potential (0.26 V) was reached immediately. In BF_4^- solution, however, the potential continuously increased for several hours and finally stabilized at 0.55 V. When the electrode, after measurements in BF_4^- solution, was transferred to 0.1*M* NaCl the potential started to decrease and finally stabilized at 0.42 V. This indicates that an irreversible chemical transformation (doping) of POT occurred when the electrode was exposed to BF_4^- in solution. Hotta *et al.*[26] have also observed that BF_4^- behaves differently from ClO_4^- when used as dopant for PMT in nitrobenzene.

Response mechanism. An examination of the results presented in Table 2, allows some conclusions to be drawn regarding the mechanism of the potentiometric response. A cationic response is observed for both electrochemically prepared POT and chemically prepared POTc. Therefore the cationic response seems to be an inherent property of poly(3-octylthiophene) and not as the result of, e.g. residual doping anions (BF_4^-) or solvent (PC) originating from the electrochemical polymerization step. Polymerization of 4,4′-dioctyl-2,2′-bithiophene takes place at a relatively low potential (1.1 V) compared to 3-octylthiophene (1.5 V). Therefore one can expect POTd to be less overoxidized than POT.[14] Furthermore, due to the symmetrically substituted dimer (4,4′-dioctyl-2,2′-bithiophene), POTd is expected to be more stereoregular than POT.[27,28] Nevertheless POTd gives smaller slopes than POT towards most of the cations studied. This indicates that a regular polymer structure does not improve the potentiometric response. Due to the high polymerization potential of thiophene (1.7 V) in comparison to 2,2′-bithiophene (1.2 V), PT is expected to be more overoxidized than PBT.[29] The bigger slopes observed for PT thus indicate that overoxidation may even be beneficial to the cationic response. PMT gives smaller slopes than PT, especially towards the divalent cations, while POT and POTd give slightly bigger slopes than PT and PBT, respectively. This indicates that the presence of octyl groups (in contrast to methyl groups) slightly improves the cationic response, but the effect is small. These observations lead to the conclusion that the cationic response may be attributed mainly to the interaction between the cations and the polythiophene backbone. Therefore the oxidation level of the polymer is expected to influence the potentiometric response.

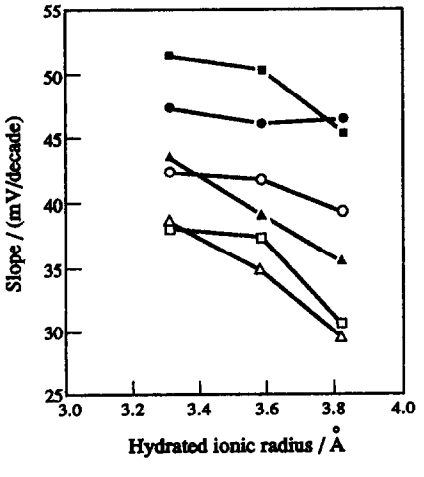

Fig. 3. Slope of the potentiometric response curves of PT (○), PBT (△), PMT (□), POT (●), POTd (▲) and POTc (■) as function of the hydrated ionic radii of the cations: K^+ (3.31 Å), Na^+ (3.58 Å) and Li^+ (3.82 Å).

The oxidation potentials for the polythiophenes studied have been determined by cyclic voltammetry in organic electrolyte solutions.[14,30,31] The oxidation potential of PT, POT, POTd and POTc are very similar (1.1 V) and higher than those of PBT and PMT (0.7 V). In the potentiometric measurements in this work, potentials of the polymer electrodes were in the range of 0.1–0.6 V. The upper limit, 0.6 V, is well below the oxidation potential of PT, POT, POTd and POTc, and therefore these polymers are believed to remain in their undoped state during the potentiometric measurements in the Cl^- solutions. Furthermore, cyclic voltammetry have shown that POT cannot be electrochemically oxidized even at 2 V in

aqueous solutions.[9] In presence of the BF_4^- anion, however, chemical oxidation may influence the potentiometric response characteristics.

For PBT and PMT the upper potential limit in the measurements was rather close to their oxidation potential. Therefore it is possible that PBT and PMT are partly oxidized during the potentiometric measurements. This would mean that there are some positive charges (polarons, bipolarons) on the PBT and PMT backbones decreasing interaction with cations and increasing interaction with anions. Although the slopes were slightly smaller for PBT and PMT, in comparison to the other polythiophenes studied (Table 2), both PBT and PMT give a definite cationic response. It can thus be suggested that the electrostatic repulsion is sufficiently small to still allow interaction between the polythiophene backbones and the cations. The sulphur atoms of the thiophene rings may act as electron donors and thereby increase interactions with cations.[32]

According to this reasoning, an anionic response can be predicted for PPy when used in its oxidized state, in agreement with experimental results.[19] However, in the case of PPy, the anionic response was found to be influenced also by the cation.[20] Incomplete discrimination between anions and cations thus seems to be quite general for conducting polymers, resulting in a mixed ionic response.[23,24] Furthermore, the low selectivity of the polythiophenes studied in this work and of PPy in Ref. 20, indicates that the binding sites in these polymers, e.g. polarons and bipolarons for anions and electron donating S atoms for cations, are rather non-specific.

CONCLUSIONS

The polythiophene electrodes were found to give a fast but non-selective cationic response to several cations in aqueous solutions. This cation sensitivity is unique for the polythiophenes and different from the anion sensitivity observed for, e.g. polypyrrole.[19,20] The polythiophenes showed excellent stability, since they were used in their undoped, semiconducting states. It was suggested that the cationic response may originate from interactions between the cations and the electron donating sulphur atoms of the thiophene rings. The low selectivity will naturally limit the use of polythiophenes (as such) as specific cation sensors. On the contrary, the electronic conductivity and non-selective cation sensitivity of polythiophenes may be useful in combination with traditional ion-selective materials. Following the idea presented by Cadogan *et al.*[33] one may suggest that the polythiophenes can be suitable as the intermediate layer connecting the ion-selective membrane to the metal substrate in solid-state cation-selective electrodes. This kind of electrode has several advantages, compared to traditional ion-selective electrodes with the internal filling solution, e.g. simplicity of design, lower costs and possibility of miniaturization.[33] Furthermore, the interface between the ion selective membrane and the metal will not be blocked, which is an advantage compared to coated-wire electrodes.[33] In view of such applications, the potentiometric response of polythiophene and its derivatives may be of interest to researchers in the field of analytical chemistry.

REFERENCES

1. G. Tourillon and F. Garnier, *J. Electrochem. Soc.*, 1983, **130**, 2042.
2. R. L. Elsenbaumer, K. Y. Jen and R. Oboodi, *Synth. Met.*, 1986, **15**, 169.
3. M. Sato, S. Tanaka and K. Kaeriyama, *J. Chem. Soc., Chem. Commun.*, 1986, 873.
4. K.Y. Jen, G. G. Miller and R. L. Elsenbaumer, *J. Chem. Soc., Chem. Commun.*, 1986, 1346.
5. S. D. D. V. Rughooputh, M. Nowak, S. Hotta, A. J. Heeger and F. Wudl, *Synth. Met.*, 1987, **21**, 41.
6. A. Ivaska, *Electroanalysis*, 1991, **3**, 247.
7. G. Tourillon and F. Garnier, *J. Electroanal. Chem.*, 1984, **161**, 407.
8. S. Sunde, G. Hagen and R. Ødegård, *J. Electrochem. Soc.*, 1991, **138**, 2561.
9. S. Sunde, G. Hagen and R. Ødegård, *Synth. Met.*, 1991, **41–43**, 2983.
10. J. Roncali, L. H. Shi, R. Garreau, F. Garnier and M. Lemaire, *Synth. Met.*, 1990, **36**, 267.
11. J. Roncali, R. Garreau, A. Yassar, P. Marque, F. Garnier and M. Lemaire, *J. Phys. Chem.*, 1987, **91**, 6706.
12. M. Onoda, Y. Manda, S. Morita and K. Yoshino, *J. Phys. Soc. Jpn.*, 1989, **58**, 1895.
13. T. Kawai, T. Kuwabara and K. Yoshino, *Synth. Met.*, 1991, **41–43**, 2907.
14. J. Bobacka and A. Ivaska, *Synth. Met.*, 1991, **41–43**, 3053.
15. J. Bobacka, A. Ivaska and M. Grzeszczuk, *Synth. Met.*, 1991, **44**, 9.
16. J. Bobacka, A. Ivaska and M. Grzeszczuk, *Synth. Met.*, 1991, **44**, 21.
17. J. Bobacka, M. Grzeszczuk and A. Ivaska, *Electrochimica Acta*, 1992, **37**, 1759.
18. J. Tanguy, A. Proń, M. Zagórska and I. Kulszewicz-Bajer, *Synth. Met.*, 1991, **45**, 81.
19. S. Dong, Z. Sun and Z. Lu, *Analyst*, 1988, **113**, 1525.
20. A. Cadogan, A. Lewenstam and A. Ivaska, *Talanta*, 1992, **39**, 617.

21. A. J. Bard and L. R. Faulkner, *Electrochemical Methods*, p. 71. Wiley, New York, 1980.
22. Q. Pei and R. Qian, *Electrochimica Acta*, 1992, **37**, 1075.
23. A. Lewenstam, J. Bobacka and A. Ivaska, *J. Electroanal. Chem.*, submitted.
24. J. Bobacka, Z. Gao, A. Ivaska and A. Lewenstam, *J. Electroanal. Chem.*, submitted.
25. A. L. Horvath, *Handbook of Aqueous Electrolyte Solutions*, p. 344. Ellis Horwood, Chichester, 1986.
26. S. Hotta, W. Shimotsuma, M. Taketani and S. Kohiki, *Synth. Met.*, 1985, **11**, 139.
27. M. Zagórska and B. Krische, *Polymer*, 1990, **31**, 1379.
28. R. M. Souto Maior, K. Hinkelmann, H. Eckert and F. Wudl, *Macromolecules*, 1990, **23**, 1268.
29. B. Krische and M. Zagórska, *Synth. Met.*, 1989, **28**, C263.
30. J. Bobacka, M. Grzeszczuk and A. Ivaska, unpublished results.
31. G. Tourillon and F. Garnier, *J. Electroanal. Chem.*, 1984, **161**, 51.
32. P. D. Beer, in *Chemical Sensors*, T. E. Edmonds (ed.), p. 17. Blackie, New York, 1988.
33. A. Cadogan, Z. Gao, A. Lewenstam, A. Ivaska and D. Diamond, *Anal. Chem.*, 1992, **64**, 2496.

Talanta, Vol. 40, No. 9, pp. 1445–1448, 1993
Printed in Great Britain.

0039-9140/93 $6.00 + 0.00

ATROPINIUM SCOPOLAMINUM INTEGRATED MICROCONDUITS IN A POTENTIOMETRIC ANALYTICAL SYSTEM

CUI HONGBO
Institute of Applied Ecology, Academia Sinica, Shenyang, People's Republic of China

(*Received* 28 *December* 1992. *Revised* 26 *January* 1993. *Accepted* 4 *March* 1993)

Summary—The preparation of the flow-through tubular atropinium and scopolaminum electrodes and assemblage of the integrated microconduit potentiometric analytical system with tubular ISEs, microvalve, chemfold, electrostatic and pulse inhibitors are described. Electrochemical characteristics of new atropinium scopolaminum integrated microconduit FIA–ISEs were studied. The contents of atropine and scopolamine in drugs could be determined at almost equilibrium state at sampling rates of 120/hr. The standard deviation over the linear range was about 0.1 mV (N = 11).

Atropinium and scopolaminum in drugs are routinely determined by the extraction–spectrophotometric method which are complicated, overloaded, consuming and require considerable organic reagent consumption. We have constructed a novel integrated microconduit system with tubular electrodes, microvalve, coil, inhibitors for flow injection potentiometric determinations of atropine and scopolamine in drugs. The proposed method has a high sampling rate (120/hr), good precision (±0.1 mV) and low sample and reagent consumption. Meanwhile, the overall volume of the FIA system was extremely reduced by integration of the flow parts. The detection can be executed exactly within a tubular electrode integrated into the FIA channel, where the dispersion, flow rate and other conditions of an individual assay are optimal.[2]

In this work, the preparation of the flow-through tubular atropinium and scopolaminum electrodes and assemblage of the integrated microconduit potentiometric analytical system are described. The performance characteristics of the electrodes in different experimental conditions were studied. The contents of atropine and scopolamine in drug were determined using the micro device. The analytical results agreed well with those obtained by the extraction–spectrophotometric method.

EXPERIMENTAL

Apparatus

A schematic diagram of the FIA–ISE manifold used in this study is shown in Fig. 1(a). An Orion Research 901 microprocessor ion analyzer connected to a Dahua recorder is used. The home-made peristaltic pump with Tygon pump tubes was used to propel the carrier and to aspirate the sample solution. The integrated microconduit analytical system was used to precise sampling volume, reproducible transport, detection on line.

Tubular flow-through electrodes

Composition. The electrodes consisted of 1.0% atropinium–tetraphenylboron or scopolaminum–tetraphenylboron, 68.0% dibutyl phthalate, 31.0% PVC w/w.

Preparation of the atropinium tetraphenylboron. Pipette 1 ml of 0.1 *M* atropine sulphate solution and 1 ml of 0.1 *M* sodium tetraphenylboron. Extract the precipitate with 10 ml of 2-nitrotoluene. Wash organic phase twice with water and dry thoroughly with anhydrous sodium sulphate.[3]

Preparation of the scopolamine tetraphenylboron. Weigh 0.22 g of scopolamine and add 25 ml of water. Heat to 50°, add 45 ml of 0.6% sodium tetraphenyl boron solution (50°) very slowly and leave to stand overnight. Then, filter through a G-5 glass crucible and wash 3 times with water and alcohol successively. Dry for 6 hr at 50° and store in a dryer.[4]

Construction. The basic cell design and construction were the same as those described previously.[5] Atropinium and scopolaminum tubular electrodes were prepared by replacing part of the wall of a small piece of PVC tubing (1.5 cm long, 0.5 mm i.d., 1.5 mm o.d.) with the

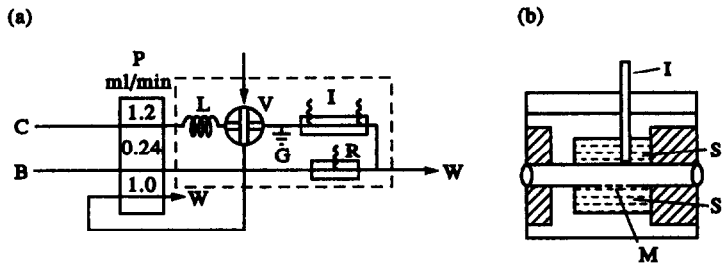

Fig. 1. (a). Integrated microconduit FIA manifold for potentiometric measurement. C, carrier stream; B, solution for the reference electrode; P, pump; V, injection valve; I, indicator electrode; R, reference electrode; L, pulse inhibitor; G, ground; W, waste. (b) Expanded view of tubular flow-through cell. I, Ag/AgCl inner reference electrode; M, sensitive membrane; S, internal reference solution.

conforming sensing membrane (0.25 mm^2). They were then placed into the Perspex housing as shown in Fig. 1(b). The housing was filled with 0.1 *M* NaCl–10^{-2} *M* atropinium or 0.1 *M* NaCl–10^{-2} *M* scopolaminum inner solution with saturated AgCl into which a Ag/AgCl wire was inserted to serve as the inner reference system. This piece tubing acts as potentiometric flow-through detector with zero dead volume.

Assemblage of the integrated microconduit system

Atropinium electrode (i_1) and scopolaminum electrode (i_2) are placed in a single-channel of the integrated microconduit Perspex block ($10 \times 30 \times 50$ mm) and very close to the injection position in order to minimize sample dispersions (Fig. 2). A common Ag/AgCl reference electrode is placed in a side channel fed by stream B, and the combined streams are ultimately led to waste, W. The microvalve with two channels is placed into microconduit right and fixed with small screw. The connection between the microvalve and the electrode was made with a 0.5-cm length stainless steel tube which was grounded to prevent interference from static electricity earthed by the pump roller.[5]

Reagents

Analytical reagent grade organic and inorganic chemicals were used without further purification. Doubly distilled water was used throughout. The standard 0.1000 *M* solution of atropine and scopolamine were prepared by dissolving the appropriate amount of substance in 0.05 *M* $Mg(CH_3COO)_2$. Working solutions were prepared by appropriate dilutions with 0.05 *M* $Mg(CH_3COO)_2$. Carrier solution was 0.05 *M* $Mg(CH_3COO)_2$.

RESULTS AND DISCUSSION

Sample preparation

Pipette 0.1, 0.2, 0.4, 0.6, 0.8 and 1.0-ml scopolamine injections into 50-ml flasks and dilute with 0.05 *M* $Mg(CH_3COO)_2$ to 50 ml.

Grind 10 tablets of atropine sulphate into powder. Thoroughly mix and accurately weigh 50, 100, 150, 200, 250 and 300 mg of the powder into 50-ml flasks and dilute with 0.05 *M* $Mg(CH_3COO)_2$ to 50 ml.

Electrode characteristics

In order to study the response characteristics of atropinium and scopolaminum electrodes in different experimental conditions, a rod electrode and a tubular flow-through electrode integrated microconduits with the same sensing membrane were made and tested separately in the static state and in the flow state at 25°. These results are summarized in Table 1. The results show that the characteristics of a tubular electrode under hydrodynamic flow conditions differ from those observed under static conditions. Rapid response (5–10 sec), high reproducibility (±0.1 mV) and good stability (overall EMF drift of 0.2 mV/hr over at least 8 hr) were obtained by the microdevice under flow conditions. This is due to the stable experimental conditions for precise sampling volume,

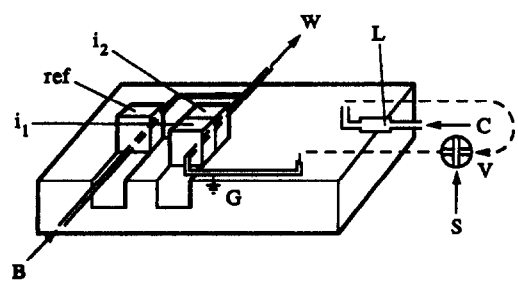

Fig. 2. Details of the integrated microconduit; shown within the dotted lines in Fig. 1(a).

Table 1. Electrode response characteristics (25°)

Type	Condition	Linear range (M)	Response time (sec)	Repeatability ($N = 11$) (mV)	Detection limit (M)	Slope (mV/pX)	Selectivity coefficient (separate solution method)		
							K^{AH^+,K^+}	$K^{AH^+,Ca^{++}}$	$K^{AH^+,Mg^{++}}$
Atropine (AH^+)	Static	10^{-1}–10^{-5}	10–30	±0.5	10^{-6}	59.2	3.6×10^{-4}	2.3×10^{-3}	9.0×10^{-5}	9.5×10^{-5}
	Flow	10^{-1}–2×10^{-5}	5–10	±0.1	2×10^{-6}	58.8	3.4×10^{-4}	1.4×10^{-3}	1.0×10^{-4}	1.1×10^{-6}
Scopolamine (SH)	Static	10^{-1}–10^{-5}	10–40	±0.4	2×10^{-6}	58.0	6.2×10^{-3}	1.5×10^{-2}	4.6×10^{-4}	4.9×10^{-4}
	Flow	10^{-1}–2×10^{-5}	5–15	±0.1	4×10^{-6}	57.3	1.2×10^{-2}	1.8×10^{-2}	1.2×10^{-4}	4.7×10^{-4}

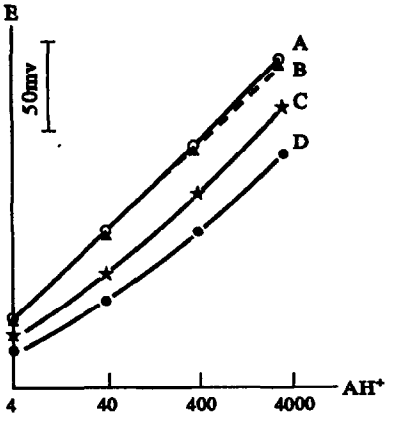

Fig. 3. Calibration curves for the atropinium electrode. A. Steady state measurement; B. response by injecting 120 μl sample volume; C. response by injecting 80 μl sample volume; D. response by injecting 30 μl sample volume.

reproducible transport, constant flow in the system were obtained. Meanwhile, the possibility of preventing the periodical exposure of the electrode to ambient atmosphere which could cause error due to temperature changes, variation in dry and wet conditions at the surface of the electrode, changing solutions, chemical and physical effect was reduced.

Selectivity coefficient values of the electrode under flow conditions differ slightly from those obtained under static conditions. A plausible

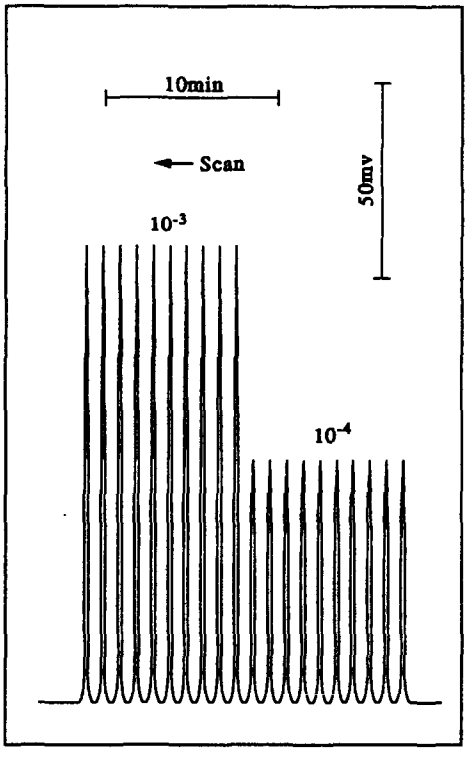

Fig. 4. Repeated determinations of two atropinium standard solution with the system depicted in Fig. 1.

explanation is that the contact time between the interference solution and the membrane is much shorter under dynamic conditions than in static measurement. It is shown that adsorption, desorption and response speed on the sensing membrane may be different. By adjusting experimental conditions, changing carrier components or using FIA treatment on line, the effect of interference ions on the results may be decreased.

Calibration curves of atropinium electrode obtained by injecting sample volumes of $S_v = 120$ μl, $S_v = 60$ μl, $S_v = 30$ μl and static state measurement are shown in Fig. 3. For the lower sample volume, the maximum potentials (peak heights) are lower than those obtained by static state measurement, revealing the influence of the sample dispersion and response time on the readout. The slope value of calibration curve B (58.8 mV/pAH$^+$ differs slightly from the slope value of curve A (59.2 mV/pAH$^+$) from that based on static state measurements. For $S_v = 30$ μl (curve D), a markedly lower slope is observed.

Standard and sample measurement

The integrated microconduits manifold was connected according to Fig. 1(a). The conditions selected were; the sampling volume $S_v = 120$ μl, the pumping rate for the indicator electrodes $Q = 1.2$ ml/min and for the reference electrode $Q = 0.24$ ml/min. The system was calibrated with a series of standard solutions. The results show excellent agreement between the proposed method and extract spectrophotometric method. The accuracy of the proposed method was also tested by the standard additions method. Known amounts of atropinium or scopolaminum were added to samples which were processed before and after the additions. Integrated microconduit FIA–ISEs system gave recoveries of 98–102%.

Typical outputs for reproducibility measurement of two standard solutions are shown in Fig. 4, which represents a sampling rate of about 120/hr. The standard deviation over the linear range with tubular electrodes was about 0.1 mV ($N = 11$).

REFERENCES

1. The People's Republic of China, *Pharmacopoeia*, 1977, **2**, 372.
2. J. Ruzicka and E. H. Hansen, *Anal. Chim. Acta*, 1984, **161**, 1.
3. E. P. Diamandis, E. Athanasion-Malaki, D. S. Papastathopoulos and T. P.Hadjiioannou, *ibid*, 1981, **128**, 239.
4. Cui Hongbo, Sun Junyan and Li Bingyin, *Physical Testing and Chemical Analysis (Chinese)*, 1990, **5**, 296.
5. Cui Hongbo and Sun Junyan, *Talanta*, 1991, **38**, 989.

Talanta, Vol. 40, No. 9, pp. 1449–1459, 1993
Printed in Great Britain.

0039-9140/93 $6.00 + 0.00

POTENTIOMETRIC MONITORING OF PROTEINS—PART 6. INDIRECT POTENTIOMETRY

MICHAEL L. HITCHMAN and FRAZIER W. M. NYASULU*
Department of Pure and Applied Chemistry, University of Strathclyde, 295, Cathedral Street, Glasgow G1 1XL, U.K.

(*Received* 28 *December* 1992. *Revised* 26 *January* 1993. *Accepted* 4 *March* 1993)

Summary—In a study of the indirect potentiometry of amino acids and proteins with metal ions it has been discovered that electrode potential responses to organic ligand concentrations can be linear over a range of tens of millivolts. In this paper the reasons for this are considered and a general model is presented in terms of an electrode of the second kind. Experimental results for the indirect potentiometry of a number of amino acids and proteins are then presented and are discussed in the context of the model derived. Applications to flow injection analysis and to the determination and identification of proteins eluting from a gel chromatography column are also considered.

Proteins have a high affinity for some metal cations and this feature is the basis of several methods for protein determination. Metal ions which have proved most useful are copper(II) and silver(I). The use of Cu^{2+}, for example, in the biuret[1] and Lowry *et al.*[2] determinations is well known. Direct and indirect potentiometric determinations of amino acids with copper electrodes have been described,[3,4] and we have reported on the extension of copper based potentiometry to the determination of proteins.[5–8] Copper based potentiometric detection has in addition been used for monitoring in both liquid chromatography[4] and flow injection analysis.[5] Determinations based on silver[9–12] have also been examined, but have received rather less attention from the point of view of applications, probably because only thiol containing proteins give a satisfactory response.[13–16]

Direct potentiometry enjoys the advantage of being a non-destructive technique, but the inherent insensitivity of a semi-logarithmic relationship between potential and concentration leads to poor precision. Indirect potentiometry, which uses an excess of a reagent with the analyte, still, in principle, relies on a Nernstian relationship but it has an advantage in that electrode potentials measured before and after addition of the analyte to the reagent are usually with respect to relatively simple cations or anions and so problems of slow electrode response and irreproducibility often associated with complex analyte molecules[8,11] are minimised. In a previous paper[5] we reported on the application of indirect potentiometry to protein monitoring and we showed that a sufficient level of precision was attainable for quantitative analysis. However, we have also discovered that for indirect potentiometric determination of proteins and amino acids at low concentrations that electrode responses are linear in ligand concentration and that this linearity can extend over a potential range of as much as ~60 mV. This is to be welcomed for it further assists in improving sensitivity, but it is rather surprising that a potentiometric response can be linear for such a large potential range. In this paper the reasons for this are considered.

We also report on results for indirect potentiometry of amino acids and proteins and discuss the experimental data in the context of the model derived. Application to flow injection analysis and to the determination of proteins eluting from a gel chromatography column are considered, and, in particular, the ratio of the responses for copper based and silver based potentiometry is shown to be useful for the identification of proteins eluting from the column.

THEORY

Model based on electrode of the first kind

For a metal electrode in contact with ions of the metal in a solution of concentration C_{mi}, the

*Present address: Department of Chemistry, University of Washington, Seattle, WA 98196, U.S.A.

electrode potential (E_i) is given by the very simple form of the Nernst equation:

$$E_i = E^0 + k \ln C_{mi} \quad (1)$$

where $k = RT/nF$. On adding a complexing species such as a protein or amino acid to the solution the potential (E_e) corresponding to the equilibrium concentration (C_{me}) of metal ions after reaction with the ligand can be represented by

$$E_e = E^0 + k \ln C_{me} \quad (2)$$

If y cations are bound per ligand molecule (Pr) according to

$$\mathrm{Pr} + y\mathrm{M}^{n+} \overset{K}{\rightleftharpoons} \mathrm{M}_y\mathrm{Pr}^{n+} \quad (R1)$$

the metal ion mass balance is

$$C_{mi} = C_{me} + yC_{mpe} \quad (3)$$

where C_{mpe} is the equilibrium concentration of the metal–ligand complex. Using the above equations equation (2) becomes

$$E_e = E^0 + k \ln\{C_{mi}[1 - yC_{mpe}C_{mi}^{-1}]\} \quad (4)$$

If experimental measurements are taken as the difference between a blank solution and that with added ligand then

$$\Delta E = E_e - E_i = k \ln[1 - yC_{mpe}C_{mi}^{-1}] \quad (5)$$

From the metal–ligand equilibrium (R1)

$$C_{mpe} = KC_{pe}C_{me}^{y} \quad (6)$$

The ligand mass balance is

$$C_{pi} = C_{pe} + C_{mpe} \quad (7)$$

where C_{pi} is the ligand concentration before reaction. Expressing metal ion and ligand mass balances in terms of C_{me} and C_{pe} and substituting into equation (6) leads to

$$C_{mpe} = K(C_{pi} - C_{mpe})(C_{mi} - yC_{mpe})^{y} \quad (8)$$

Expansion yields

$$C_{mpe} = \mathrm{K}C_{mi}^{y}(C_{pi} - C_{mpe})[1 - y^2C_{mpe}/C_{mi} + y^3(y-1)C_{mpe}^2/2!C_{mi}^2 - \ldots..] \quad (9)$$

The maximum value of $C_{mpe} = C_{pi}$, *i.e.*, 100% conversion of the ligand to metal–ligand complex. Normally for indirect potentiometry one would have $C_{mi} \gg C_{pi}$ and so $C_{mpe} \ll C_{mi}$. Now provided that y is not too large, and this is usually the case for metal–protein and metal–amino acid complexes,[17] then equation (9) can be approximated by

$$C_{mpe} \simeq C_{pi}C_{mi}^{y}(K^{-1} + C_{mi}^{y})^{-1} \quad (10)$$

Thus

$$\Delta E \simeq k \ln[1 - yC_{pi}C_{mi}^{y-1}(K^{-1} + C_{mi}^{y})^{-1}] \quad (11)$$

The formation constants for silver and copper with proteins are usually large. For example, it has been reported[18] that the equilibrium constant for the reaction between Cu^{2+} and human serum albumin is 1.6×10^{16}, and we have recently determined[17] that for Ag^+ complexation with protein stability constants are equally large. With $K \gg 1$ and then expressing the logarithmic term in equation (11) as a power series and simplifying leads to

$$\Delta E \simeq -kyC_{pi}/C_{mi} \quad (12)$$

This equation predicts that for an initial metal ion concentration much greater than the initial ligand concentration and for a large formation constant for the metal–ligand complex then for a given initial metal ion concentration the potential difference before and after complexation will be linearly dependent on the initial ligand concentration.

Let us consider, though, the potential range over which we would expect equation (12) to be valid. If a discrepancy of up to 10% between a logarithmic expression of the form $\ln(1-x)$ and the linear approximation of $-x$ is taken as being acceptable then it is required that $x \leqslant 0.2$. For the case above this means $yC_{pi}/C_{mi} \leqslant 0.2$ and equation (12) will be valid for $\Delta E \leqslant 5.1/n$ mV where n is the charge on the metal ion. Thus for complexation with Ag^+ linearity between the observed potential difference and initial ligand concentration will only be linear over a range of ~ 5 mV whilst for complexation with Cu^{2+} it will only hold for ~ 2.5 mV. In practice, as mentioned above, we find linearity over a potential range up to ~ 60 mV. Furthermore, we have also found that for linearity it is not essential that the condition assumed above of $C_{mi} \gg C_{pi}$ holds. For example, we have obtained the surprising result that linearity for indirect potentiometry of bovine serum albumin (BSA) with $0 \leqslant [\mathrm{BSA}] \leqslant 0.08\mathrm{m}M$ and $[Cu^{2+}] = 0.1\mathrm{m}M$ (*i.e.*, a value of C_{pi}/C_{mi} up to 0.8) extends over a range of ~ 30 mV [see Fig. 5(a)]. Even more surprising is the result for complexing of *L*-histidine (*L*-hist) with $0 \leqslant [L\text{-hist}] \leqslant 0.45\mathrm{m}M$ and again with $[Cu^{2+}] = 0.1\mathrm{m}M$ (*i.e.* a ratio of ligand to metal ion concentration of up to 4.5) of a linear potential plot over a range of 56 mV (see Fig. 4). Clearly the simple metal electrode model

considered above is inadequate to explain the experimental observations. The linear response in the presence of excess ligand in the case of *L*-histidine together with our earlier results for the direct potentiometry of proteins with copper electrodes would suggest that we might have an electrode of the second kind. This electrode at low concentrations of ligand responds to the excess metal ions, the concentration of which is a measure of the ligand concentration, but it then responds to the ligand itself at higher concentrations. Such a model which takes into account both indirect and direct potentiometry is now discussed.

Model based on electrode of the second kind

The half cell for the metal ligand system can be represented as

$$\begin{array}{cccccc} \alpha' & & \lambda & \delta & \beta & \alpha \end{array}$$

$$\mathrm{Pt|Reference\ electrode\|M^{n+},Pr|M_{y}Pr^{n+}|M|Pt}$$

where the Greek symbols are used to distinguish the different phases. The potential difference (U) between the two platinum wires is given by

$$FU = \mu_{e^-}(\alpha') - \mu_{e^-}(\alpha) \qquad (13)$$

At equilibrium for the chemical potentials of the metal ions (μ_m) and ligands (μ_p) one has

$$\mu_m(\delta) = \mu_m(\lambda) \qquad (14)$$

and

$$\mu_p(\delta) = \mu_p(\lambda) \qquad (15)$$

Combining equations (13)–(15) and using the classical expression for chemical potential gives

$$\bar{\mu}^0_{mp} - \mu^0_{mp} = RT\ \ln(K_{sp,mp}/\bar{a}_{mp}) \qquad (16)$$

where $\bar{\mu}^0_{mp}$ and μ^0_{mp} are the standard chemical potentials for the metal–ligand complex in the solid phase δ and in the solution phase λ, respectively. The solubility product ($K_{sp,mp}$) is for the equilibrium (R1) and is given by

$$K_{sp,mp} = a^{y}_{m} a_p \qquad (17)$$

and the activity ($\bar{a}_{mp}$) of the complex in the solid phase is related to the activities of the individual species by

$$\bar{a}_{mp} = \bar{a}^{y}_{m} \bar{a}_p \qquad (18)$$

Now for an electrode/solution interface not just the chemical potential has to be considered but also the electrochemical potential. If this is done and at the same time account is taken of the asymmetric coupling between the metal and the ligand [cf. equation (R1)] then an equation for the interfacial potential difference is obtained:

$$\bar{\phi}_m - \phi_m = \Delta\phi_m = y(RT/nF) \times \ln(K^{1/y}_{exm} a_m/\bar{a}_m) \qquad (19)$$

where K_{exm} is the extraction coefficient for metal ions and is related to the chemical potentials of the metal ions by

$$K_{exm} = \exp[\mu^0_m - \bar{\mu}^0_m)/RT] \qquad (20)$$

K_{exm} is essentially a traditional partition coefficient modified by the effect of an electric field at the interface [cf. the exponential form of equation (19)] and is a measure of the standard electrochemical potential for the metal ions [cf. equations (19) and (20)].

What determines the activity of metal ions in solution is now considered. This activity (a_m) will be made up of contributions from the excess metal ions left over after the addition of the ligand and from the dissolution of the complex M_yPr^{n+}. If these two contributions are denoted by a_{mx} and a_{md} then

$$a_m = a_{mx} + a_{md} \qquad (21)$$

and equation (17) for the solubility product becomes

$$K_{sp,mp} = (a_{mx} + a_{md})^{y} a_{pd} \qquad (22)$$

where a_{pd} is the ligand activity arising from dissolution of the complex. In terms of concentrations equation (22) can be written as

$$K_{sp,mp} = \gamma^{1+y}_{\pm}(C_{mx} + C_{md})^{y} C_{pd} \qquad (23)$$

where $\gamma_{\pm}$ is the mean ionic activity coefficient for M_yPr^{n+}. Implicit in equation (22) is the assumption that all the ligand is complexed and so $a_{pd} = a_{md}$ and equation (23) becomes

$$K_{sp,mp} = \gamma^{1+y}_{\pm} C_{md} C^{y}_{mx}[1 + (C_{md}/C_{mx})]^{y} \qquad (24)$$

If the binomial expansion is now used and powers greater than unity are neglected then equation (24) for C_{md} can be readily solved:

$$C_{md} \simeq [-C^{y}_{mx} \pm (C^{2y}_{mx} + 4yC^{y-1}_{mx} K_{sp,mp}/\gamma^{1+y}_{\pm})^{1/2}]/2yC^{y-1}_{mx} \qquad (25)$$

The approximation of neglecting higher powers of C_{md}/C_{mx} assumes that the metal–ligand complex has a low solubility, but this is probably not unreasonable in view of the fact that an electrode of the second kind is being considered.

The total activity of the metal ions is given by equation (21) which in terms of concentrations is

$$a_m \simeq (\gamma_+/2y)[C_{mx}(2y-1) + (C_{mx}^2 + 4yK_{sp,mp}C_{mx}^{1-y}/\gamma_\pm^{1+y})^{1/2}] \quad (26)$$

Note that only the value of C_{md} with the square root added to $-C_{mx}$ is used since it is obvious that only this solution can give a positive value for C_{md}.

Substituting back into equation (19) gives

$$\Delta\phi_m \simeq y(RT/nF)\ln\{\gamma_+ K_{exm}^{1/y}/2y\bar{a}_m][C_{mx}(2y-1) + (C_{mx}^2 + 4yK_{sp,mp}C_{mx}^{1-y}/\gamma_\pm^{1+y})^{1/2}]\} \quad (27)$$

With $y = 1$ this equation corresponds to a symmetric 1:1 complex. A simple, common example would be for the formation of AgCl. In this case equation (27) is identical in form to that derived by Buck[19] for the potential of a solid state silver halide membrane electrode in contact with excess silver ions.

Of course, equation (27) is for the interfacial potential difference when the electrode responds to metal ions. In practice in indirect potentiometry what one measures is the difference in electrode potential (ΔE) before and after addition of the complexing agent [cf. equation (5)]. Replacing the subscript x on C_m by a subscript i to represent the initial conditions and subtracting the resulting equation from equation (27) leads to the expression for ΔE. Equation (28) gives this with C_{mx} replaced by $(C_{mi} - yC_{pi})$ to emphasise that it is the relationship between electrode potential and ligand concentration that is of interest.

Before these rather cumbersome equations are examined further let us obtain the corresponding equations for when the electrode responds directly to the added ligand; *i.e.*, once all the metal ions have been complexed.

The analogous equation to equation (19) is

$$\bar{\phi}_p - \phi_p = \Delta\phi_p = -(RT/nF)\ln(K_{exp}a_p/\bar{a}_p) \quad (30)$$

K_{exp} is the extraction coefficient for ligand. Using equation (16) for $K_{sp,mp}$, equation (20) for K_{exm} and the corresponding equation for K_{exp} the following relationship is obtained

$$K_{exp} = \bar{a}_m^y \bar{a}_p / K_{sp,mp} K_{exm}^y \quad (31)$$

Therefore equation (30) becomes

$$\Delta\phi_p = -(RT/nF)\ln(\bar{a}_m^y a_p / K_{sp,mp} K_{exm}^y) \quad (32)$$

Now, as in the case of excess metal ions one has to consider what determines the activity (a_p) of the electroactive species. Again it will be made up from contributions of excess unreacted species, such as protein, and from the dissolution of the complex $M_y Pr^{n+}$; *i.e.*,

$$a_p = a_{px} + a_{pd} \quad (33)$$

The solubility product is now given by

$$K_{sp,mp} = \gamma_\pm^{1+y}(C_{px} + C_{pd})C_{md}^y \quad (34)$$

Following a similar line of argument to that used for the cation case the expression for the interfacial potential difference is arrived at:

$$\Delta\phi_p \simeq -(RT/nF)\ln\{[\gamma_- \bar{a}_m^y / 2K_{sp,mp}K_{exm}^y] \times [C_{px} + (C_{px}^2 + 4K_{sp,mp}C_p^{1-y}/\gamma_\pm^{1+y})^{1/2}]\} \quad (35)$$

For the case of a 1:1 complex this equation reduces to that given by Buck[19] for the anion response. The difference in electrode potential between the point when just enough ligand has

$$\Delta E_m \simeq \frac{yRT}{nF}\ln\left\{\frac{(2y-1)(C_{mi}-yC_{pi}) + \left[(C_{mi}-yC_{pi})^2 + \dfrac{y(4K_{sp,mp}/\gamma_\pm^{1+y})}{(C_{mi}-yC_{pi})^{y-1}}\right]^{1/2}}{(2y-1)C_{mi} + \left[C_{mi}^2 + \dfrac{y(4K_{sp,mp}/\gamma_\pm^{1+y})}{C_{mi}^{y-1}}\right]^{1/2}}\right\} \quad (28)$$

If the ligand concentration added is a fraction $0 \leqslant \alpha \leqslant 1$ of the initial metal ion concentration then $C_{pi} = \alpha C_{mi}$ and equation (28) becomes

$$\Delta E_m \simeq \frac{yRT}{nF}\ln\left\{\frac{(2y-1)C_{mi}(1-y\alpha) + \left[(C_{mi}^2(1-y\alpha)^2 + \dfrac{y(4K_{sp,mp}/\gamma_\pm^{1+y})}{C_{mi}^{y-1}(1-y\alpha)^{y-1}}\right]^{1/2}}{(2y-1)C_{mi} + \left[C_{mi}^2 + \dfrac{y(4K_{sp,mp}/\gamma_\pm^{1+y})}{C_{mi}^{y-1}}\right]}\right\} \quad (29)$$

been added to complex with all the metal ions and for subsequent additions of ligand is given by

$$\Delta E_p \simeq -(RT/nF)\ln\{(C_{px} + [C_{px}^2 + (4K_{sp,mp}C_{pd}^{1-y}/\gamma_{\pm}^{1+y})]^{1/2}/(4K_{sp,mp} \times C_{pd}^{1-y}/\gamma_{\pm}^{1+y})^{1/2}\} \quad (36)$$

In order to examine further the dependence of potential on the ligand solution concentration it is convenient to take a simpler form. This is obtained for the case when $y = 1$ (*i.e.*, a symmetric complex), the activity coefficients are unity and the ionic charge $n = \pm 1$. First equation (27) is considered where some of the constants are lumped together to give

$$\Delta\phi_m \simeq (RT/nF)\ln\{A[C_{mx} + (C_{mx}^2 + 4K_{sp,mp})^{1/2}]\} \quad (37)$$

The constant A will have an effect on the absolute value of $\Delta\phi_m$, but will not affect the general shape of a plot of potential *vs.* concentration. If the simplification is now continued by taking a specific value for 4 $K_{sp,mp}$ (*e.g.*, 10^{-10}) then a plot of $\Delta\phi$ *vs.* concentration is readily made. This is shown in Fig. 1. The classical Nernstian region is obvious for $C_{mx} > \sim 2 \times 10^{-5}M$ but for concentrations below this curvature sets in, not because the Nernstian response breaks down, but rather because the concentration of electroactive species is not solely determined by that deliberately added to the solution. The dissolution of the metal complex gives additional metal ions in the solution and so the potential is less than that expected on the basis of the added ions. At very low concentrations of added ions ($\sim 10^{-7}M$) the dissolution of the complex is the major source of ions and so the potential becomes independent of the added ion concentration.

In general one may readily show that for, say, a 5% deviation from Nernstian linearity it is necessary that $C_{mx}^2 > 40K_{sp,mp}$. For the case considered here with $4K_{sp,mp} = 10^{-10}$ then it is required that $C_{mx} \geqslant \sim 3 \times 10^{-5}M$ and this is what is found on closer inspection of the plot in Fig. 1. For the potential to become within 5% of being independent of C_{mx} the condition is $C_{mx}^2 < 10^{-2}K_{sp,mp}$. For $4K_{sp,mp} = 10^{-10}$ this means $C_{mx} \leqslant 5 \times 10^{-7}M$. Again the plot of Fig. 1 verifies this.

If one now takes the potentials calculated from equation (37) for the curved region of Fig. 1 (*i.e.*, for $0.1 \times 10^{-6}M \leqslant C_{mx} \leqslant 30 \times 10^{-6}M$) and plots them as a linear function of C_{mx} then Fig. 2 is obtained. The result is a gentle curve, but it can be seen that at low values of C_{mx} (*i.e.*, $C_{mx} < \sim 14 \times 10^{-6}M$) the curve can be approximated by a straight line with all points within 5% of the curve over a total potential range of ~ 30 mV. Thus experimental data which may often be no more precise than a few percent, especially in the case of complex species, could well appear to show potential linearity over a range of up to 30 mV. This can be shown in a different manner by using equations (29) and (36). Again a simplified version is taken with y, n and $\gamma_{\pm}$ all equal to unity and with $4K_{sp,mp} = 10^{-10}$. In addition a fixed value for the initial metal ion concentration is taken; *e.g.*, $10^{-5}M$. Equation (29) then becomes

$$\Delta E_m \simeq (RT/F)\ln\{0.414(1-\alpha + [1 + (1-\alpha)^2]^{1/2})\} \quad (38)$$

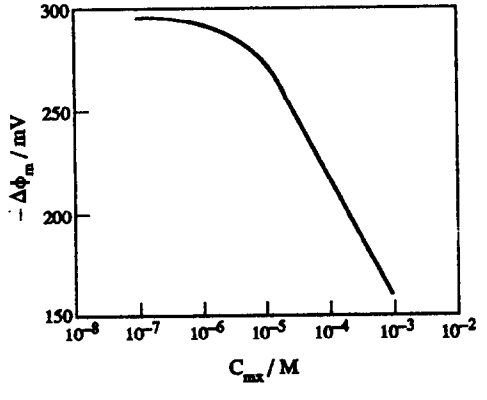

Fig. 1. Plot of equation (37) with $4K_{sp,mp} = 10^{-10}$.

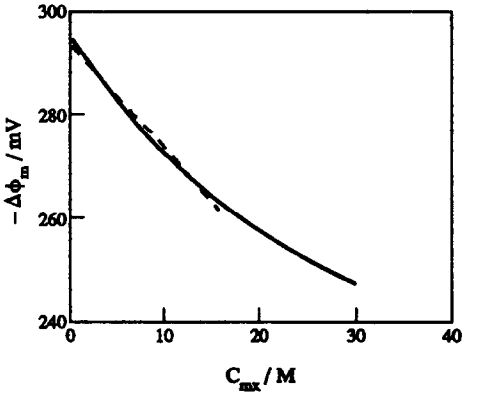

Fig. 2. Plot of potentials from Fig. 1 for $0.1 \times 10^{-6}M \leqslant C_{mx} \leqslant 30 \times 10^{-6}M$ as a linear function of C_{mx}

——— Values taken from Fig. 1.

– – – – – Linear plot through the values from Fig. 1.

Equation (36) simplifies to

$$\Delta E_p \simeq (-RT/F)\ln\{(C_{px} + [C_{px}^2 + 10^{-10}]^{1/2})/10^{-5}\} \quad (39)$$

Or if C_{px} is related to the concentration of ligand (C_{pi}) when it is equal to the initial metal ion concentration by $C_{px} = \beta C_{pi}$ with $\beta \geq 0$ then

$$\Delta E_p \simeq (-RT/F)\ln\{\beta + [\beta^2 + 1]^{1/2}\} \quad (40)$$

Figure 3 shows the plots for these two equations. For $C_{pi} \leqslant 10^{-5}M$ (*i.e.*, $\alpha \leqslant 1$) the response of the electrode is to the metal ions; the plot analogous to that in Fig. 2 for $0 \leqslant C_{mx} \leqslant 10^{-5}M$. For ligand added in excess of $10^{-5}M$ (*i.e.*, $\beta > 0$) the electrode response is for ligand and the potentials are additive to those calculated up to that point. Following on from the analysis of Fig. 2, each mode will show approximate linearity over a potential range of ~ 30 mV thus giving a total linear range ~ 60 mV, as is shown by the dashed line.

The analysis given above is quite general for potentiometric systems involving cations and anions or ligands which constitute the components of an electrode of the second kind. In order to illustrate the effect the cumbersome equations have been simplified and only the 1:1 symmetric case has been considered. To try and illustrate the effect with very general equations [*e.g.*, equations (29) and (36)] would be complicated and probably not very helpful. Results will now be considered for the indirect potentiometry of some amino acids and proteins.

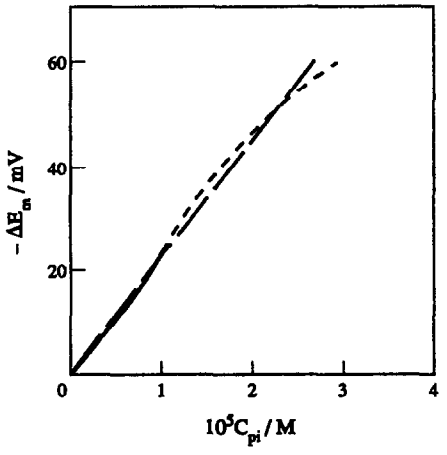

Fig. 3. Plots of equations (38) and (40).
——— Calculated from equation (38) with $0 \leqslant \alpha \leqslant 1$.
– – – – – Calculated from equation (40) with $0 \leqslant \beta \leqslant 1$.
— — — Linear plot through the calculated values.

EXPERIMENTAL

The flow injection system, the potentiometric detection cell and the potential measuring equipment used in this work have all been described in detail previously.[5] Briefly, the flow injection system consisted of a reservoir of reagent, a peristaltic pump, a pulse damping system, an injection valve and the detector cell all in series. They were all connected together with silicone rubber tubing. For indirect potentiometry it is clearly necessary that enough time is allowed for adequate mixing of the sample and the reagent and yet not to have too long a time which would allow excessive dispersion of the injected sample. It was found that both these conditions could be met with a short distance (3 cm) between the injection valve and mixing junction and a longer distance (20 cm) from the junction to the detector. Depending on the sample injection volumes (V_i) typical values of the dispersion (D_t) were found to lie in the range 2.5–9.7 for $300 \times 10^{-6} \geqslant V_i \geqslant 50 \times 10^{-6}$ dm^3. In order to maximise sensitivity all determinations were done with the highest sample injection volume. This was found to give a baseline to baseline time of 30 sec which would thus allow a sampling rate of ~ 120/hr. The detector cell consisted[5] of a small beaker with an inlet and overflow outlet. In the cell were three electrodes. The working or indicator electrode was a high purity copper or silver wire and the reference electrode was a double junction Ag/AgCl electrode. The third electrode was a platinum wire coiled around, but insulated from, the indicator electrode. This platinum coil was used for the electrochemical cleaning procedure (see below). Potential measurements were made simply with a high impedance digital voltmeter.

The flow system for indirect potentiometric detection with a chromatography column was essentially the same as that used for flow injection analysis. The column (Pharmacia LKB C10/40) had a packing of Sephacryl S300. The mobile phase was a buffer solution (pH 7) with, in addition, $0.5M$ sodium nitrate. A high level of inert electrolyte reduces the ionic interactions between proteins and the stationary phase and this enhances separations.[20] It also keeps the ionic strength of the eluting solution effectively constant which is necessary for potentiometric detection. The recommended[20,21] inert electrolyte is $0.5M$ sodium chloride, but since it has been shown that[5,16] chloride ions in excess of $\sim 10^{-1}M$ can interfere with protein

potentiometry using Cu and Ag electrodes the chloride anion was replaced by nitrate: no deleterious effect on the separation of the proteins was observed. The output from the detector cell was recorded as a function of time with a chart recorder.

The amino acids and proteins used in this study were all obtained from Sigma Chemical Company and were used without further purification. They were *L*-histidine, *L*-cysteine, ribonuclease A, phosvitin, ovalbumin, bovine serum albumin, human serum albumin, lysozyme and γ-globulin.

The effect of pH on potential response has been reported earlier.[5] It was shown that the optimum value of pH was ~7 and so all solutions were buffered to this value. The electrochemical cleaning of the electrodes was done as has been described before.[5-8,10,12] Essentially the cleaning consisted of a cathodic current pulse applied to the indicator electrode. The purpose of this electrochemical treatment was to remove excess oxide from the surface of the indicator electrode.[6,8] This technique has been shown to lead to significantly improved reproducibility and response for metallic electrodes when monitoring proteins and amino acids.

RESULTS AND DISCUSSION

Figure 4 shows the dependence of electrode potential on amino acid concentrations for *L*-histidine and *L*-cysteine as measured using the flow injection system and with an initial Cu^{2+} concentration of $10^{-4}M$. The reason for choosing these two particular amino acids initially was that it had been previously shown[3,22] that *L*-histidine gave consistent and reproducible results with a copper electrode, whilst *L*-cysteine had been found by some workers[3] to give less successful results. They thus represented two extreme possibilities of electrode reference. With the cathodic cleaning technique which we have developed[1,5-8,10,12] the problem of reproducibility of electrode response is significantly diminished.

It can be seen that for both amino acids the data points lie approximately on straight lines with zero intercepts. For *L*-histidine the linearity extends up to ~0.07 mg/cm³ corresponding to a concentration of $\sim 4.5 \times 10^{-4}M$. For *L*-cysteine the plot is linear up to 0.10 mg/cm³ or $8.3 \times 10^{-4}M$. Thus the linear relationships hold for amino acid to metal ion ratios of 4.5 for *L*-histidine and 8.3 for *L*-cysteine. The dotted

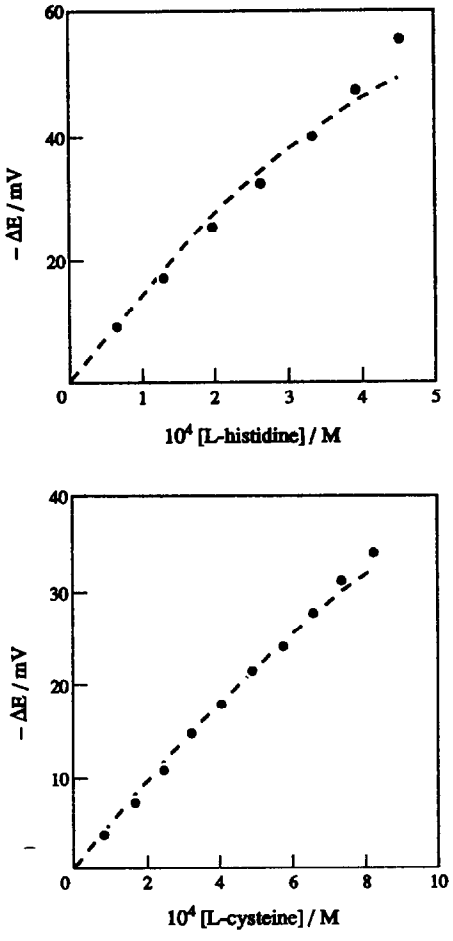

Fig. 4. Dependence of electrode potential on added amino acid concentration
(a) *L*-histidine data points
(b) *L*-cysteine data points
– – – – – Curves calculated from equations (29) and (36)—see text.
$[Cu^{2+}] = 10^{-4}M$; flow rate = 60 cm³/hr.

lines in each case have been calculated using the formulae derived above for the electrode response with equation (29) being used for $C_{pi} < 10^{-4}M$ and equation (36) for $C_{pi} > 10^{-4}M$. In using these formulae there is the question of which species the electrode responds to. For low concentrations of added ligand there will be excess metal ions and one might expect a simple metal/metal ion electrode. However, as the ligand concentration increases then for strong complexation the potential of the metal electrode could also depend on equilibria between the metal electrode and the metal complex. For both *L*-histidine and *L*-cysteine we have recently obtained[8] good evidence that there is strong complexing between the amino acids and copper and that the potential of a copper electrode in the presence of the complexes will

depend on the equilibrium between the soluble complexes in solution and the copper surface. This type of mechanism has also been suggested by Alexander *et al.* for the response of a copper electrode to complexing inorganic ions[13] and for the potentiometric monitoring of α amino acids with copper wire and tubular electrodes.[3] If the metal–ligand complex is very insoluble then there will be a transition from an electrode of the first kind to one of the second kind, as has been discussed above in the Theory section. For the two amino acids used it has been reported[23] that, indeed, the complexes with Cu(II) are rather insoluble so such a transition might be expected to be observed. However, the situation could be complicated even further if at the same time there is a changeover in the number of electrons involved in the electrochemical couples. At low ligand concentrations with Cu^{2+} in solution then the simple couple

$$Cu^{2+}(aq) + 2e^- \leftrightharpoons Cu(s) \qquad (R2)$$

could operate. As the ligand concentration increases and an insoluble complex is formed then the electrochemical equilibrium might be

$$CuL(s) + H^+(aq) + e^- \leftrightharpoons Cu(s) + HL(aq) \qquad (R3)$$

Such a couple also gives a 1:1 complex which will allow the use of simpler forms of equations (29) and (36). For the interaction of the amino acids with a copper surface 1:2 complexes have been suggested,[6] but when interaction can take place in solution there will be less steric constraints and a higher ratio of copper to ligand may be possible; there is certainly good evidence for 1:1 complexes in solution in the case of *L*-histidine.[24] Thus in applying the derived equation we have taken $y = 1$ in all cases and $n = 2$ when $C_{pi} < C_{mi}$ and $n = 1$ when $C_{pi} > C_{mi}$. There will clearly not necessarily be a sharp changeover, but in the absence of more detailed investigations we make this simplifying assumption. It has also been assumed that activity coefficients are always unity. This then leaves in the equation a choice of values for the solubility product $K_{sp,mp}$ for the complexes. For the case of *L*-histidine and $[Cu^{2+}] = 10^{-4}M$ a value of $K_{sp,mp}$ of 8×10^{-9} gives the best fit while for the same value of C_{mi} for *L*-cysteine a value of 8×10^{-8} is chosen. The fits are quite good over the whole range of values of amino acid concentrations which correspond to amino acid to metal ratios of greater than unity. Thus in spite of the various approximations and assumptions made the concept of an electrode of the second kind responding to both metal ions and the ligand is seen to be consistent with the data. The relatively low values of the solubility products for the two amino acid complexes are consistent with the observed[23] low solubilities and with the strong complexing[8] already mentioned.

If the initial copper ion concentration is changed to $9.5 \times 10^{-4}M$ linear plots of potential *vs.* amino acid concentration are obtained over the same concentration range as before but the slopes are reduced in both cases by a factor of about 9.5. Calculating the expected dependence of potential on concentration with the same values of $K_{sp,mp}$ as used above gives a plot for *L*-histidine with a slope of ~ 8 less than that of $[Cu^{2+}] = 10^{-4}$. This is in reasonable accord with

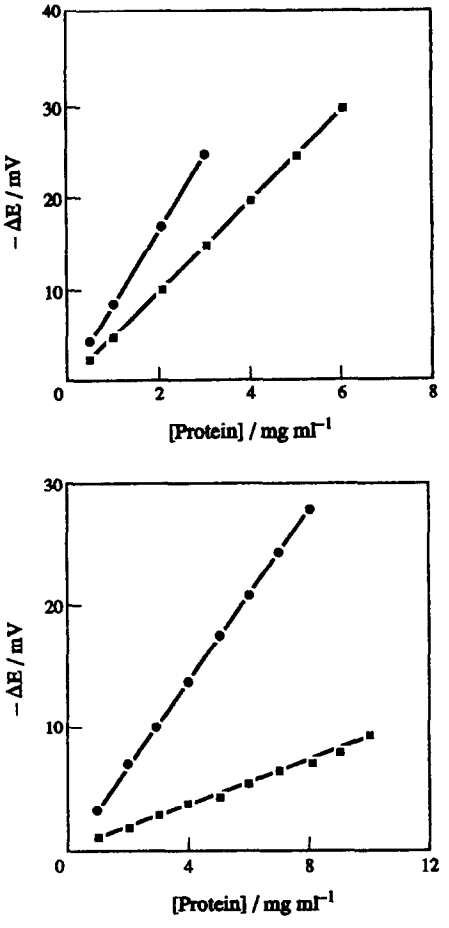

Fig. 5. Dependence of electrode potential on added protein concentrations
(a) ● human serum albumin
■ bovine serum albumin
(b) ● ribonuclease A
■ γ-globulin
$[Cu^{2+}] = 10^{-4}$ M; flow rate = 60 cm³/hr.

Table 1. Response indices and detection limits for potentiometric determination of proteins with Cu^{2+}

Protein	$[Cu^{2+}]$,*M*	Flow rate cm^3/hr	Response index $mV(mg/cm^3)^{-1}$	Detection limits *M*
	10^{-4}	60		
Human albumin			8.74	1.4×10^{-6}
Bovine albumin			5.21	2.8×10^{-6}
Ribonuclease A			3.50	2.0×10^{-5}
γ-Globulin			0.95	2.8×10^{-5}
	10^{-4}	23		
Phosvitin			14.2	1.0×10^{-6}
Human albumin			12.9	5.0×10^{-7}
Bovine albumin			7.8	9.3×10^{-7}
Ovalbumin			4.1	2.7×10^{-6}
γ-Globulin			1.4	2.5×10^{-6}
	10^{-5}	23		
Phosvitin			138.3	1.0×10^{-7}
Human albumin			131.3	5.5×10^{-8}
Bovine albumin			76.7	9.3×10^{-8}
Ovalbumin			41.8	2.4×10^{-7}
γ-Globulin			13.2	2.6×10^{-7}

experiment. For *L*-cysteine the calculated plot gives a slope which is only reduced by a factor of ~ 3. This may be due to the fact that the experimental data corresponds to a more complicated changeover in electrochemical couples, as mentioned above; this discrepancy is being investigated further.

Notwithstanding the lack of a complete quantitative agreement between the model and experiment, the concept of an electrode of the second kind responding to either the metal ions or the ligand does offer a semi-quantitative explanation for a linear relationship over several decades of millivolts between electrode potential and ligand concentration. We now consider the case of proteins complexing with copper ions.

Figure 5 shows results comparable to those given in Fig. 4 but for four different proteins. The situation here, though, will be even more complicated than in the case of the amino acids. This is illustrated by the different results obtained for human and bovine serum albumin. These two proteins are very similar in structure, size and amino acid sequence[25] and for direct potentiometry with a copper electrode we have, in fact, obtained[6] very similar responses. Here, however, if one takes the slope of the plots as indicative of the number of binding sites [cf. equation (29)] then bovine serum albumin would appear to bind only $\sim 60\%$ of the copper that human serum albumin binds. This also highlights the fact that proteins have multiple binding sites[27] and thus y may be >1 in equations (29) and (36). So that although the maximum protein concentrations added to the Cu^{2+} solution give, except for ribonuclease A, values of $\alpha < 1$($\alpha \sim 0.4$ for human serum albumin, ~ 0.8 for bovine serum albumin and ~ 0.1 for γ globulin) this does not necessarily mean that the electrode is primarily functioning as a Cu^{2+}/Cu couple, as postulated for the amino acids when $\alpha < 1$. The multiple binding sites of proteins give a further complication in that the sites are not necessarily equivalent,[26] and so the model on which the theory is based of one type of metal complexation is probably oversimplistic. Complexation between metals and proteins is clearly far from straightforward and for this and the various reasons mentioned above it is difficult to interpret the data of Fig. 5 in terms of the derived equations. Nevertheless, the different responses of the various proteins, particularly for ribonuclease A where the maximum concentration used corresponds to $\alpha \sim 6.3$, together with the range of up to 30 mV over which direct linearity between electrode potential and protein concentration is observed, suggest that a mechanism based on an electrode of the second kind is operating.

Table 1 summarises the response indices in terms of mV $(mg/cm^3)^{-1}$ for the data in Fig. 5 and also, from similar plots, for other proteins with either different initial concentrations of Cu^{2+} and/or flow rate. For the results from Fig. 5 it is clear that, maybe apart from γ globulin, the technique is suited for flow injection analysis determination at the mg/cm^3 level; *i.e.*, for concentrations as low as 10^{-4}–$10^{-5}M$. The sensitivity can be improved by lowering the flow rate to reduce the dispersion of the injected samples and by reducing the initial copper ion concentration. With the last set of conditions given in Table 1 a sensitivity of ~ 0.1 mg/cm^3 is readily achievable.

Table 2. Measurements of precision at the 95% confidence level

Concentration mg/ml	$\Delta E \pm$ error mV	
	Human albumin	Phosvitin
0.2	2.61 ± 0.08	2.85 ± 0.07
0.3	3.85 ± 0.09	4.30 ± 0.07
0.4	5.21 ± 0.07	5.71 ± 0.09
0.5	6.44 ± 0.05	7.13 ± 0.08

Note: $[Cu^{2+}] = 10^{-4}M$; Flow rate = 23 cm³/hr.

Table 2 shows examples of the precision attainable with the technique. Ten measurements were made randomly with respect to concentration and each protein. In all cases the error is less than 3% of the average value. For direct potentiometry of albumins a precision of ± 0.4 mV at the 95% confidence level was found[6] for $\Delta E \sim 20$ mV. So the two techniques give comparable levels of precision in terms of potential measurements; this is prehaps not too surprising since if the technique described here is relying upon the interaction between the protein ligand and an electrode of the second kind then it is exactly equivalent to the direct potentiometric measurements reported earlier. However, in terms of concentration measurements the precision of the "indirect" method is higher because of the linear dependence of concentration on potential. A given error in mV will be less critical than if there is an exponential dependence of concentration on potential, as is the case of the classical Nernstian response.

A summary of the detection limits computed on the basis of Midgley's statistical definitions[27] are also shown in Table 1. The limit corresponds to a 5% chance of failing to detect the determinand. The limits are generally one to two orders of magnitude lower than those found with direct potentiometry,[6] and this is because we are making use of the non-linear part of the classical Nernstian plot (cf. Fig. 1).

Similar results to those obtained with flow injection analysis for amino acids and proteins with Cu(II) in solution and with a copper electrode have also been found with Ag(I) in solution and a silver electrode. Table 3

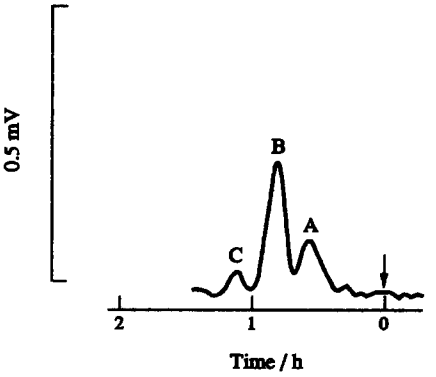

Fig. 6. Typical chromatogram obtained with a potentiometric detector
A catalase
B bovine serum albumin
C lysozyme

[Protein] = 20 μg/cm⁻³;$[Cu^{2+}] = 10^{-5}M$; Flow rate = 23 cm³/hr.

summarises some typical results for the response indices and the detection limits. The response indices are higher and the detection limits are lower than those for the corresponding proteins with Cu(II), which could indicate more binding by Ag^+ than with Cu^{2+}; this is being investigated further.[17]

The technique described for the determination of proteins with Ag^+ and Cu^{2+} has been used for the detection of proteins eluting from a gel chromatography column. An example of a typical chromatogram for an artifical mixture of catalase, bovine albumin and lysozyme is shown in Fig. 6; it was found that the lowest level of the signals which could be readily discerned from the background noise were 10 μg/cm³, 5 μg/cm³ and 20 μg/cm³ for the three proteins, respectively. In accordance with the data in Table 3, limits of detection about one order of magnitude lower were generally attainable when using the Ag^+/Ag systems. The background noise mainly arose from the pulsating action of the peristaltic pump, and a pulse free pump together with signal amplification would probably allow determination at the sub μg/cm³ to be made. A comparison with chromatograms recorded with a UV detector showed that the

Table 3. Response indices and detection limits for potentiometric determination of proteins with Ag^+

Protein	Response Index $mV(\mu g/cm^{-3})^{-1}$	Detection limits M
Human albumin	1.4	1.0×10^{-8}
Ovalbumin	1.2	1.0×10^{-8}
γ-Globulin	0.6	8.0×10^{-9}

Note: $[Ag^+] = 10^{-5}M$; Flow rate = 23 cm³/hr.

Table 4. Ratio of silver:copper response indices

Protein	Response index ratio
γ-Globulin	45
Ovalbumin	29
Bovine albumin	19
Human albumin	11

Note: $[Cu^{2+}] = [Ag^+] = 10^{-5}M$; Flow rate = 23 cm³/hr.

potentiometric method was more sensitive for the proteins with molecular weights less than 50 kamu (*e.g.*, ribonuclease A), but that otherwise results from both techniques were comparable. An advantage of the potentiometric technique over UV detection is that by carrying out simultaneous determinations with both the Ag^+/Ag and Cu^{2+}/Cu systems protein identification could be achieved. Table 4 gives the ratio of the Ag:Cu response indices and it is seen that these are unique for each protein. This procedure for identifying proteins worked well, as long as the proteins were well separated in the chromatogram. A disadvantage of the potentiometric technique compared with UV analysis is the need for post column addition of reagents, which may lead to band broadening. However, this problem could be avoided by chronocoulometric generation of the Cu^{2+} and Ag^+.

Acknowledgements—We thank the British Council for a training award for FWMN and Pharmacia LKB AB, Uppsala, for financial and material support.

REFERENCES

1. R. H. Haschemeyer and A. E. V. Haschemeyer, *Proteins: A Guide to Study by Physical and Chemical Methods*. Wiley-Interscience, New York, 1973.
2. O. H. Lowry, N. J. Roseborough, A. L. Farr and R. J. Randall, *J. Biol. Chem.*, 1951, **193,** 265.
3. P. W. Alexander and C. Maitra, *Anal. Chem.*, 1981, **53,** 1590.
4. P. W. Alexander, P. R. Haddad, G. K. C. Law and C. Maitra, *J. Chromatog.*, 1981, **209,** 29.
5. M. L. Hitchman and F. W. M. Nyasulu, *Anal. Chim. Acta*, 1985, **173,** 337.
6. *Idem, J. Chem. Soc. Farad. Trans. I*, 1986, **82,** 1223.
7. M. L. Hitchman, J. M. Fisher and F. W. M. Nyasulu, *Analyst*, 1988, **113,** 875.
8. M. L. Hitchman and M. Trojanowicz, *Electroanalysis*, 1992, **4,** 941.
9. T. Y. Toribara and L. Koval, *Talanta*, 1970, **17,** 1003.
10. M. L. Hitchman, F. W. M. Nyasulu, A. Aziz and D. D. K. Chingakule, *Anal. Chim. Acta*, 1983, **155,** 219.
11. M. L. Hitchman, *ibid.*, 1985, **171,** 131.
12. M. L. Hitchman, A. Aziz, D. D. K. Chingakule and F. W. M. Nyasulu, *ibid.*, 1985, **171,** 141.
13. P. W. Alexander, P. R. Haddad and M. Trojanowicz, *Anal. Chem.*, 1984, **56,** 2417.
14. P. D'Orazio and G. A. Rechnitz, *ibid.*, 1977, **49,** 41.
15. K. Kentaro, Y. Tetsutaro and T. Toshifumi, *Buneki Kagaka*, 1983, **32,** 308.
16. F. W. M. Nyasulu, PhD Thesis, University of Salford, 1985.
17. M. L. Hitchman and C. Zhang, in preparation.
18. S. Lau, T. P. A. Kruck and B. Sarkar, *J. Biological Chem.*, 1974, **249,** 5878.
19. R. P. Buck, *Anal. Chem.*, 1968, **40,** 1432.
20. *Gel Filtration—Theory and Practice*, p. 42. Pharmacia Fine Chemicals, Uppsala, 1982.
21. R. E. Pfeifer, W. M. Skea and J. Waraska, *Chromatog. Sci.*, 1982, **20,** 43.
22. P. W. Alexander, P. R. Haddad and M. Trojanowicz, *Anal. Chim. Acta.*, 1985, **171,** 151.
23. E. M. Athanasiou-Malaki and M. A. Koupparis, *ibid.*, 1984, **161,** 349.
24. D. R. Williams, *J. Chem. Soc., Dalton Trans.*, 1972, 790.
25. T. Peters, *Adv. in Clin. Chem.*, 1970, **13,** 51.
26. R. A. Bradshaw, W. T. Shearer and F. R. N. Gurd, *J. Biol. Chem.*, 1968, **243,** 3817.
27. D. Midgley, *Analyst*, 1979, **104,** 248.

Talanta, Vol. 40, No. 9, pp. 1461–1464, 1993
Printed in Great Britain.

0039-9140/93 $6.00 + 0.00

A DOUBLE-MEMBRANE EPHEDRINE SELECTIVE ELECTRODE BASED ON EPHEDRINE-TETRAPHENYLBORATE IN POLY (VINYL CHLORIDE) RESIN

PILAR R. CHAMORRO
Department of Experimental Didactic Sciences, University of Zaragoza, 22003 Huesca, Spain

RAFAEL CARMELO DÍAZ*
Department of Analytical Chemistry, Polytechnical University School, 22071 Huesca, Spain

(*Received* 13 *November* 1992. *Revised* 1 *March* 1993. *Accepted* 1 *March* 1993)

Summary—The construction and performance characteristics of a double-membrane ephedrine selective electrode are described. The electrode is based on the use of an internal conducting membrane made of tetrabutylammonium bromide and another external electroactive membrane containing the ionic pair ephedrine-tetraphenylborate in a poly (vinyl chloride) resin (with some plasticizers incorporated) as an inert matrix. The ephedrine electrode exhibits linear Nernstian response within the range 10^{-2}–$5 \times 10^{-5}M$ of ephedrine, with a slope of 58.2 ± 0.5 mV decade^{-1} at $25 \pm 0.2°$. The detection limit is $10^{-4.5}M$. The reproducibility (coefficient of variation) was 0.54% ($n = 10$ determinations) and the stability of its potential is 2.3 mV/24 h. The selectivity coefficients for 15 ions were calculated. The electrode was applied to the determination of ephedrine in some pharmaceutical preparations with satisfactory results.

Ephedrine is a drug that stimulates both α- and β-adrenergic receptors. It is used in therapeutic doses at the level of 15–60 mg to produce pheripheral vasoconstriction, to raise blood pressure, to prevent hypotension and treat allergic states, catalepsy and myasthenia gravis. It is also utilized as an antidote for poisoning by the central nervous system.

Ephedrine (EPH) has been determined by some instrumental methods[1] like spectrophotometry, polarography and potentiometry.

We have described a double-membrane ion-selective electrodes based on the coated-wire technique (CWEs) for the determination of nitrate,[2] potassium[3] and metoclopramide[4]. This paper proposes the preparation of a double-membrane ephedrine selective electrode that improves the reproducibility and stability of measured potentials.[5] The internal membrane contains a conducting substance, tetrabutylammonium bromide (BrTBA) over an inert matrix of a poly (vinyl chloride) resin (VCR). The outer selective membrane contains ephedrine ion as ion pair complex ephedrine-tetraphenylborate (TPB). The active external membrane composition is a determinant for obtaining a Nernstian slope. The electrode has been applied to the determination of ephedrine in some pharmaceutical preparations.

EXPERIMENTAL

Reagents

Ephedrine clorhidrate, sodium tetraphenylborate (NaTPB), tetrabutylammonium bromide, pH solution buffers, potassium nitrate, potassium chloride and tetrahydrofuran (THF) were all provided by Merck. The poly (vinyl chloride) resin used as inert matrix was provided by FAL S.A. Industries (Zaragoza, Spain) and had the following composition (% (w/w)); poly(vinyl chloride) resin (FAL S.A. Industries) (40.3), Chemigun resin (FAL S.A. Industries) (20.2), stabilizer H-260 (FAL S.A. Industries) (1.2), $CaCO_3$ (4.0), primary plasticizer (dioctylphtalate) (20,2), secondary plasticizer (epoxidaded oleum soha) (FAL S.A. Industries) (2.0) and polymer plasticizer (paramoll) (FAL S.A. Industries) (12.1).

The pharmaceutical products containing ephedrine were obtained from local drug stores.

Stock interference ion solutions were prepared at $1M$ concentrations

*To whom correspondence should be addressed.

Solutions of 0.1M ephedrine as standard stock solution, 2M KCl for studying the influence of ionic strength on the electrode response and 10% (w/v) KNO_3 for filling the outer chamber of the reference electrode were also prepared.

The ephedrine-TPB ion pair precipitate was prepared by mixing 50 ml of a $10^{-3}M$ aqueous solution of ephedrine with a $10^{-3}M$ solution of NaTPB. The precipitate was then filtered, washed with high purity water and finally left to dry at room temperature.

High purity water was obtained from a Millipore Milli-Q Water System.

Apparatus

The determination was carried out at $25 \pm 0.2°$ in a double-walled vessel with a circulating Haake thermostat bath, using a Crison Model 2002 pH-millivolt meter. The standard and test solutions were stirred magnetically (30 r.p.m.) with a Teflon bar for 1 min.

A Commercial Instruments Cedar Grove Industrial Instruments INC. electrolyte conductivity meter was used for the determination of the electrode resistance.

A double junction Ingold Model 31451 was used as external reference electrode, with aqueous 4M KCl and 10% (w/v) KNO_3 as internal and external filling solutions. The membranes were coated on an Ingold Pt cylindrical ring electrode (with a flat surface with a diameter of about 5 mm). So the electrode cell is: Pt | internal membrane | external membrane | sample solution || 10% (w/v) KNO_3 | 4M KCl | AgCl, Ag.

Procedure

The Pt electrode, washed with THF and left to dry, it was dipped in a mixture of BrTBA and a 10% (w/v) solution of poly (vinyl chloride) resin in THF. The optimum composition of internal membrane was BrTBA:resin/THF in weight proportions of 5:95. The thickness of the resulting membrane is about 0.1 mm.

After being left to dry for 12 h, the internal membrane was coated with the active membrane by dipping in a mixture of EPH^+ TPB^- and a 10% (w/v) solution of poly (vinyl chloride) resin in THF. The optimum composition of the external membrane was in weight proportions of 40:60. The total thickness is about 0.3 mm. Once dry, the electrode was conditioned for 1 h in a $10^{-4}M$ EPH solution.

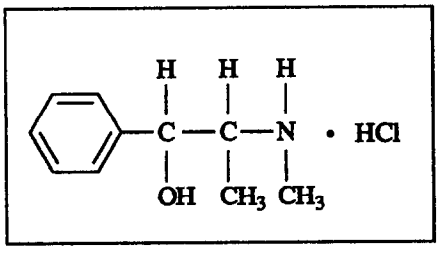

Fig. 1. The formula of ephedrine clorhidrate.

RESULTS AND DISCUSSION

Construction of the EPH electrode

The conducting properties and response time of the electrode seem to depend on the mobility of TBA^+ in the poly(vinylchloride) matrix.[6] The absence of this internal membrane gives rise to bad reproducibility and time-stability.

The principal electrode characteristics (slope, linear response and detection limit) depend on the composition and thickness of the active external membrane. Figure 2 shows the variation in the calibration graph slope as a function of the active membrane composition. A membrane made with a mixture of EPH^+–TPB^- and poly(vinyl chloride) resin in weight proportions of 40:60 exhibits the best results, with a slope of 58.2 ± 0.5 mV decade^{-1}.

It is important when preparing the EPH electrode to control the thickness of both internal and external membranes. If the thickness of the internal membrane is maintained constant, between 0.1 and 0.2 mm, the electrode response depends on the thickness (δ) of the external active membrane. The best results were obtained with $\delta = 0.1$ mm. For values above 0.1 mm the electrode behaviour is subNernstian and the linear response is shorter.

Response characteristics of the electrode

The effect of ionic strength on the electrode response was studied to determine the optimum parameters for the principal electrode characteristics. The calibration graphs were plotted using EPH solutions and dilute solutions of KCl for ionic strength adjustment (ISA). The results are given in Table 1. The ionic strength used was $\leq 0.01M$, where the electrode had a Nernstian slope.

The selectivity coefficients ($K_{EPH,M}^{POT}$) of the EPH electrode were calculated graphically by the mixed solutions method from potential measurements on 20 ml of a solution containing

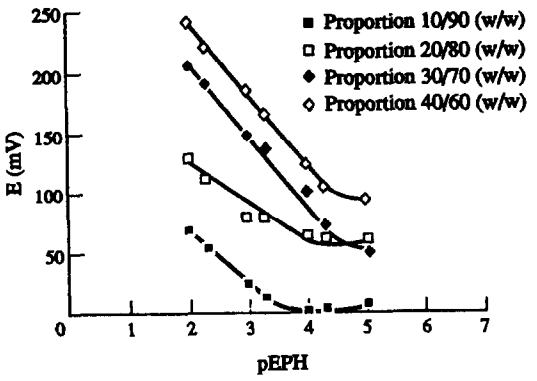

Fig. 2. Effect of the active membrane composition on the double-membrane ephedrine-selective electrode response. The proportion of EPH^+ TPB^-–VCR/THF in%(w/w).

Table 2. Selectivity coefficients for the EPH electrode

Ion (M)	$K^{POT}_{EPH,M}$
Na^+	7.5×10^{-3}
K^+	1.5×10^{-2}
NH_4^+	1.1×10^{-2}
Mg^{++}	5.9×10^{-3}
Ca^{++}	6.7×10^{-3}
Dextrometorphane bromhidrate	0.9
Alanine	2.7×10^{-3}
Acetamide	3.5×10^{-3}
Aminobenzoic acid	1.2×10^{-2}
Nicotinic acid	1.4×10^{-2}
Caffeine	1.0
Sucrose	6.4×10^{-3}
Tetrabutylammonium bromide	1.7×10^{-2}
Oxalic acid	3.3×10^{-3}
Citric acid	6.7×10^{-3}

a fixed ephedrine concentration ($10^{-4}M$) (C_{EPH}) and varying the interfering ion concentration by adding small volumes (0, 0.5, 1.0, 1.5 and 2.0 ml) (V) of $1M(C_M)$ solution of interfering ion.

The selectivity coefficients for 15 ions were calculated. The values obtained with $C_{EPH} = 10^{-4}M$ and $C_M = 1M$ are shown in Table 2. Dextrometorphane bromhidrate and caffeine appear to be the principal interferences.

The effect of the pH on the potential response was studied. To 10 ml of $10^{-2}M$ ephedrine solution, equal volumes of different buffer solutions were added up to 100 ml with distilled water. Values lower than 4 or higher than 8 produce a sharp drop in electrode potential. Results are shown in Fig. 3.

Analytical performance of the electrode

Stability of electrode potential with time was studied ([EPH] = $10^{-4}M$). A drift of 2.3 mV was formed in 24 hr and it is mainly due to the temperature changes.

The response time of electrode (t_R) depends on EPH activity, ranging from 1 min (for [EPH] $\geq 10^{-3}M$) to 5 min (for [EPH] $< 10^{-3}M$). Influences on the electrode response are time and speed of stirring before potential measurement, ionic strength, air bubbles in the membrane of the EPH electrode or reference electrodes, etc. The appropriate control of these variables shortens the response time of the electrode.

The reproducibility (10 replicate determinations) in the determination of $10^{-3}M$ EPH was also studied. The coefficient of variation was 0.54%.

The electrode was stored dry if not in use. Otherwise it deteriorates and its performance impaired. Kept dry, electrode life time was about 21 days. Nevertheless, conditioning of electrode before use for 1 h in a solution $10^{-3}M$ of EPH is essential. Otherwise, the response time is long and the reproducibility is poor.

The electrical resistance of the electrode was measured. The total resistance of the EPH electrode was approximately 10 MW.

The principal analytical characteristics of the EPH electrode were calculated. Employing an ionic strength $\leq 0.01M$ as ionic strength adjustment, the sensitivity (determined by the slope of the calibration graph) was 58.2 ± 0.5 mV (10 different electrodes made) within the concentration range 10^{-2}–$5 \times 10^{-5}M$ and the detection limit calculated according to the IUPAC

Table 1. Effect of ionic strength on the response of the EPH electrode

Ionic strength (M)	Slope ($mV\ decade^{-1}$)	Linear range ($pEPH$)	Detection limit ($pEPH$)
<0.01	59.9	2–4.3	4.5
0.01	58.4	2–4.3	4.5
0.05	52.5	2–4.0	3.7
0.10	44.8	2–3.3	3.7

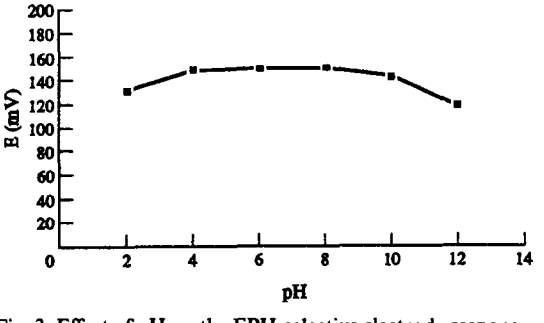

Fig. 3. Effect of pH on the EPH-selective electrode response.

Table 3. Results obtained in the determination of ephedrine in some pharmaceutical preparations

Drug	Certified value (*mg*)	Calibration graph		Standard addition	
		EPH calculated	Standard deviation (%)	EPH calculated	Standard deviation (%)
Tedral	48.0	49.3	2.7	48.9	1.8
Amidrín	8.0	7.6	1.4	7.9	1.3
Toscal	12.5	12.7	1.5	12.7	1.7
Fluidín	1.0	1.0	4.0	1.0	1.5
Bisolvón	1.5	1.6	3.3	1.5	1.3

recommendation[9] is $10^{-4.5}M$ of EPH. The least-squares equation obtained from the calibration data is $E(\text{mV}) = 58.2\ \text{pEPH} + 2.4$ (coefficient of correlation, $R = 0.9999$).

The electrode was applied to the determination of ephedrine in some pharmaceutical preparations by its interpolation on the calibration graph and standard addition methods. In the case of Tedral (solid drug), a pill weighing approximately 0.46 g with 48 mg of EPH was weighed, ground in a mortar and dissolved directly with high purity water to 0.5 l in a volumetric flask. For the other pharmaceutical products (liquid drugs), high purity water of up to 100 ml was added to a volume of 10 ml of drug. The results obtained are given in Table 3 (mean of five determinations) and show a good agreement with the certified EPH concentrations.

REFERENCES

1. S. S. M. Hassan and M. M. Saoudi, *Analyst*, 1986, **111**, 1367.
2. C. Díaz, J. C. Vidal, J. Galbán, M. A. Navas and J. Lanaja, *Fresenius' Z. Anal. Chem.*, 1989, **333**, 619.
3. C. Díaz, J. C. Vidal, J. Galbán, M. L. Urarte and J. Lanaja, *Microchem. J.*, 1989, **39**, 289.
4. C. Díaz, J. C. Vidal and J. Galbán, *J. Electroanal. Chem. and Interfacial Electrochem.*, 1989, **258**, 295.
5. M. A. Arnold and M. E. Meyerhoff, *Anal. Chem.*, 1984, **56**, 20 R.
6. J. H. Crawford and L. M. Slifkin, *Point Defects in Solids, Vol.* I. *General* and *Ionic Crystals*. Plenum Press, New York, 1972.
7. K. Srinivasan and G. A. Rechnitz, *Anal. Chem.*, 1969, **41**, 1203.
8. C. Maccà and M. Cakrt, *Anal. Chim. Acta*, 1983, **154**, 51.
9. IUPAC analytical chemistry division, commission on analytical nomenclature: recommendations for nomenclature of ion selective electrodes, *Int. Union Pure and Appl. Chem.*, 1976, **48**, 127.

Talanta, Vol. 40, No. 9, pp. 1465–1471, 1993
Printed in Great Britain.

0039-9140/93 $6.00 + 0.00

POTENTIOMETRIC DETERMINATION OF CHLORIDES WITH AN "AIR-GAP" CYANIDE SENSOR

RYSZARD BARANOWSKI and TOMASZ KUBIK
Department of Analytical and General Chemistry, Silesian Technical University, PL 44-101 Gliwice, Poland

(*Received* 4 *October* 1991. *Revised* 19 *November* 1991. *Accepted* 9 *March* 1993)

Summary—A new electroanalytical method for determining chloride ions with an Air-Gap cyanide sensor system is described. The method is based on the reaction of chloride with mercury(II) cyanide in dilute sulphuric acid. This reaction leads to hydrogen cyanide which can be determined with an Air-Gap cyanide sensor. Optimum concentrations of mercury(II) cyanide and sulphuric acid were established and an analytical curve was prepared for 1×10^{-1}–$1 \times 10^{-5} M$ Cl^-. The slope of the calibration curve was equal to 62.8 mV/log C. The correlation coefficient (R) was equal to 0.9992. The method can determine chloride with good results in high saline solutions and in the presence of surfactants, which is in contrast to direct potentiometry with a chloride electrode. The method was applied for chloride determination in fuses used for initiating explosions. The chlorides were determined both in the raw materials used to prepare the fuse braids and in the other fuse components. Chloride was also determined in drinking water and river water. In dependence of source, chloride amount analyzed in drinking water was in the range 2.18–182.6 mg/l. and 25.8 mg/l. in river water. A comparative analysis was carried out. In the first case, chloride was determined by a turbidimetric method, whereas in the second one by potentiometric titration against a chloride–ISE.

The chloride anion occurs widely in nature. Small quantities of chloride present in natural water and soils are necessary for plants and animals to function correctly. Chlorides participate in oxygen release in photosynthesis, increase hydration of colloids, and influence water balance in plants. They act as a stimulant on plants by influencing the swelling of plasma colloids. The plants absorb chloride from a soil solution through their root system. Chloride anion content in plants is variable and depends on the plant species and organs.

Mechanical processing of plant raw materials such as flax and hemp used in the textile industry removes only adsorbed chlorides. Chlorides as components in cellular plasma and combined in organic compounds are not removed during processing. Flax and cotton fibres are contained in fuses used to initiate explosion, when construction elements in high pressure industrial boilers for the nuclear power industry are connected. Due to the corrosive action on construction materials, the fuse components contain as little chloride as possible.

For a number of plants, high concentrations of chlorides in soil are toxic. Potassic fertilizers, used for soil manuring, usually contain some of chlorides ballast. These excessive chloride concentrations can penetrate natural watercourses and reservoirs, considerably increasing their salination.

The natural environment, rivers and water underflows are permanently contaminated with some surfactants, coming from municipal and food industry wastes, which unfortunately are not completely biodegradable. The possibility of ion determinations in the presence of surface active agents has been considered in other works.[1–5]

The concentrations of the contaminants in the present work was selected based on actual amounts in environmental samples from Upper Silesia. Two potentiometric sensors, for chloride determination, were applied (an Ag_2S/AgCl cell and an Air-Gap cyanide sensor).

Many industrial electrochemical processes, *e.g.*, copper plating, nickel plating, metals electropurification, aluminum electropassivation, require constant chloride concentration. An excess of chloride leads to irregular build-ups on the electroplating surface (fir-tree crystal formation) so the quality of coppering surfaces gets worse. The presence of chloride causes the anodic dissolution velocity to increase. This way an increasing cathodic current density is possible while electroplating. The oxygen evolution

from the electrolyte solution and the passivation process of the anode is observed while the concentration of chlorides is too small. One method of aluminum electropassivation requires the Cl^- level to be less than 20 mg/l.[6] If Fe^{3+} is present, then Cl^- amounts as low as 4 mg/l. lead to formation of pits on the electropassivated aluminum surface.[6] Chloride determination in these baths was made with two ion-selective electrodes: $Ag_2S/AgCl$ cell and the Air-Gap cyanide sensor.

The method described in this paper consists of potentiometric determination of chlorides by applying an Air-Gap cyanide sensor system. Our studies were based on the reaction of mercury cyanide with chloride anions in sulphuric acid, described in the literature[7]

$$Hg(CN)_2 + 2H^+ + 2X^- = HgX_2 + 2HCN$$

where

$$X^- = Cl^-, Br^-, I^-, SCN^-.$$

Hydrogen cyanide is formed in this reaction. As a weak acid it diffuses from acid solution to the gaseous phase. We proposed to determine the evolving hydrogen cyanide by means of the Air-Gap cyanide sensor system. Therefore, studies have been carried out to determine the analytical parameters such as the concentrations of reagents taking part in the above reaction and the response time of the cyanide sensor.

Mercury(II) cyanide has a high stability constant $10^{34.7}$,[8] which is exploited in this method. In the literature, it is stated that this complex undergoes decomposition in sulphuric acid solution whose concentration exceeds $0.56M$.[9] The studies performed by other authors prove that a mercury(II) cyanide does not undergo decomposition in diluted acid solution even at an elevated temperature.[10] Besides sulphuric acid, other acids like tartaric, nitric, phosphoric were examined. It was found that they do not cause mercury(II) cyanide to decompose, but that the complex decomposes in diluted hydrochloric acid solution. Adding chloride, bromide, iodide or thiocyanate to $Hg(CN)_2$ solution in diluted sulphuric acid also caused decomposition of mercury(II) cyanide with hydrogen cyanide evolution.[10]

The design and principle of operation of the Air-Gap cyanide sensor system has been described in the literature.[11] The cyanide sensor has previously been used to determine cyanides at low concentrations and mercury.[9]

EXPERIMENTAL

Reagents

Analytical grade reagents and reagents and redistilled water were used in the studies. Mercury(II) cyanide was synthesized by a literature method.[12] From weighed samples of mercury cyanide, solutions with concentrations from 0.1 to 2.0% were prepared. Solutions of 0.1 and $0.3M$ sulphuric acid, $0.1M$ nitric acid, $0.01M$ silver nitrate and $0.1M$ sodium chloride were prepared. Sodium chloride solutions in concentrations from 0.01 to $10^{-5}M$ were obtained by successive dilutions from $0.1M$ stock sodium chloride solution. The electrolyte, $0.01M$ potassium dicyanoargentate in 1% methylcellulose, was buffered by addition of borax to pH 9.3.

The following reagents were used for investigating the influence of surfactants on chloride analysis:

—an anionic SULFAPOL (sodium alkylbenzosulphonate)

—a weak anionic ROKSOL (block copolymer made from ethylene oxide, propylene and polyoxyethylated alcohols phosphoric acid ester)

—a nonionic ROKANOL K-20 (made from addition of ethylene oxide to unsaturated fat alcohols)

—a cationic KAMINOX L-11 (alkylpolyoxyethylenemethylammonium sulphate).

Apparatus

The Air-Gap OCN-01 METRON cyanide sensor system and type CT1 ELFA-JOT magnetic stirrer with CP-311 ELMETRON microcomputer pH/mV meter were used. For turbidimetric determination of chlorides, a Spekol spectrophotometer with a TK Carl Zeiss Jena attachment was used. Chlorides were also determined by a potentiometric method using a CRYTUR chloride ISE or RADELKIS chloride ISE or Polish private manufacture chloride ISE and a Ag/AgCl reference electrode with electrolytic nitrate bridge.

Mineralization of the examined samples

The raw materials used to manufacture fuse braids and its components were mineralized in an oxygen-bomb calorimeter. Approximately 0.5 g samples were placed in a quartz crucible containing wire coil resistors. Wire ends were attached to electrodes. Redistilled water (5 ml), in which combustion products were absorbed, was placed in the bomb calorimeter. The bomb

calorimeter was filled with oxygen up to 2.5 MPa. After combusting the sample and cooling the bomb, the solution containing the mineralization products was quantitatively transferred to a 25-ml measuring flask.

Procedures

About 5 μl of electrolyte (potassium dicyanoargentate, see Reagents) was placed between an Ag/AgCl reference electrode and a silver electrode of the Air-Gap cyanide sensor system. Next, 1 ml of mercury(II) cyanide solution, 1 ml of standard sodium chloride solution or sample and 1 ml of sulphuric acid solution were pipetted into a 5-ml sample cell. The sample cell was then closed with a ground-in stopper. A magnetic stirrer was started. After 2 min, the stopper was replaced with the cyanide sensor connected to a millivoltmeter. The response time of the sensor was recorded, *i.e.*, the time elapsed from sensor insertion to the moment when the potential was constant for 1 min. The potential was read with a precision of 1 mV. Each measurement was repeated five times and the average value was calculated. After each measurement, the sensor was taken out of the sample cell, the electrode was rinsed with redistilled water, dried with filter paper and a new electrolyte portion was poured in. The sensor was kept in a vertical position in the neck of a 100-ml measuring flask containing about 50 ml of distilled water. After each measurement, the test solution was poured out of the sample cell. The cell was flushed with redistilled water, and then rinsed with methanol and thoroughly dried.

Turbidimetric determination of chlorides

Turbidimetry was applied to determine chlorides in raw materials for manufacturing the fuse braids and other fuse components after mineralization of the samples in a bomb calorimeter. The solutions were filtered by hard filters free of chlorides, and then chlorides were determined as AgCl using the Spekol spectrophotometer with TK attachment.[13]

Potentiometric titration of chlorides

Potentiometric titration was applied to determine chlorides in drinking and river water. The interfering species were removed from water samples,[14] and then the chlorides were titrated with 0.01M silver nitrate solution until the largest difference in potential was reached at a constant insignificant increase of the added titrant.

Preparation of investigation baths for analysis

The samples of copperizing and aluminum electropassivation baths were neutralized with 1M sodium hydroxide and then diluted 10-fold with distilled water. The sample of nickel electroplating baths was also diluted 10-fold, then an additional 100-fold with distilled water.

RESULTS AND DISCUSSION

The effect of mercury(II) cyanide concentration at constant concentration of sulphuric acid and chloride ions on the potential and response time of the Air-Gap cyanide sensor system was studied. Mercury(II) cyanide solutions with concentrations from 0.1 to 2.0%, 0.3M sulphuric acid and standard 0.1–10^{-5}M sodium chloride solutions were used in the studies. Figure 1 presents the relationship of sensor potential *vs.* mercury(II) cyanide solution concentration at a constant sulphuric acid concentration in standard chloride solutions from pCl = 1–5. For pCl = 1 to 3, the cyanide sensor potential decreases with increasing mercury(II) cyanide concentration from 0.1 to 0.5%. However, for mercury(II) cyanide solutions from 0.5 to 2.0% concentration, the cyanide sensor potential is constant. Hence, there is no need to use a mercury(II) cyanide solution, whose concentration exceeds 0.5%. It can be, therefore, expected that mercury(II) cyanide reacts quantitatively with chloride ions. When the effect of

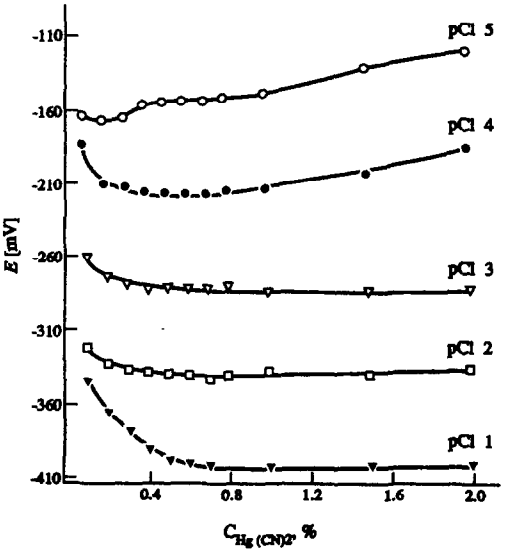

Fig. 1. The effect of mercury(II) cyanide concentration on the potential of the Air-Gap cyanide sensor.

$Hg(CN)_2$ concentration on a cyanide sensor response for chloride solutions of pCl = 4 and 5 was examined, a stable potential was observed in the more narrow concentration range of 0.4–0.8%. Due to these facts, a 0.5% $Hg(CN)_2$ solution was used in further studies. The effect of $Hg(CN)_2$ concentrations on the response time of the cyanide sensor was examined. Also in this case, 0.1–2.0% $Hg(CN)_2$ solutions, 0.3*M* sulphuric acid solution and chloride solutions from pCl = 1 to 5 were used. This relationship is illustrated in Fig. 2. For chlorides of pCl = 1 and 2, the increasing $Hg(CN)_2$ concentration did not cause any change in response time of the cyanide sensor. In each case, the response time was 2 min. The effect of $Hg(CN)_2$ solution concentration on the response time of the cyanide sensor for chloride solutions from pCl = 3 to 5 is more important. The shortest response times were recorded for $Hg(CN)_2$ solutions from 0.3 to 0.5% concentration. For higher concentrations, the response time was doubled. This study proved that the 0.5% $Hg(CN)_2$ solution is suitable for determination of chlorides.

The effect of sulphuric acid solution concentration on the replacement of cyanide ion by chloride ion with simultaneous evolution of hydrogen cyanide from a liquid phase to a gaseous one was investigated. The cyanide sensor potential was recorded *vs.* mercury(II) cyanide concentration at pCl = 3, for 0.3 and 0.1*M* sulphuric acid. The relationship is illustrated in Fig. 3. In case of 0.1*M* sulphuric acid, the measured cyanide sensor potentials dropped

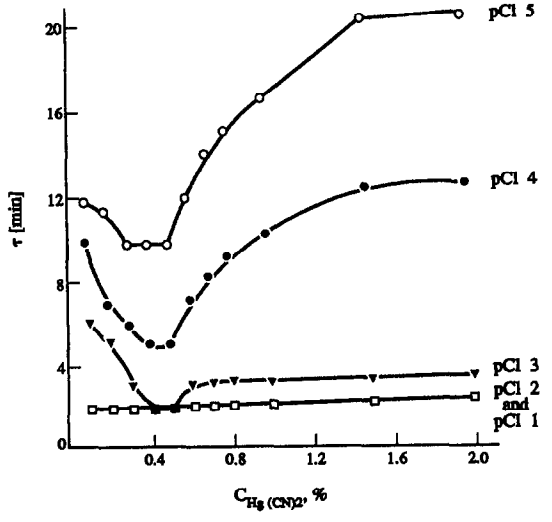

Fig. 2. The effect of mercury(II) cyanide concentration on the time response of the Air-Gap cyanide sensor.

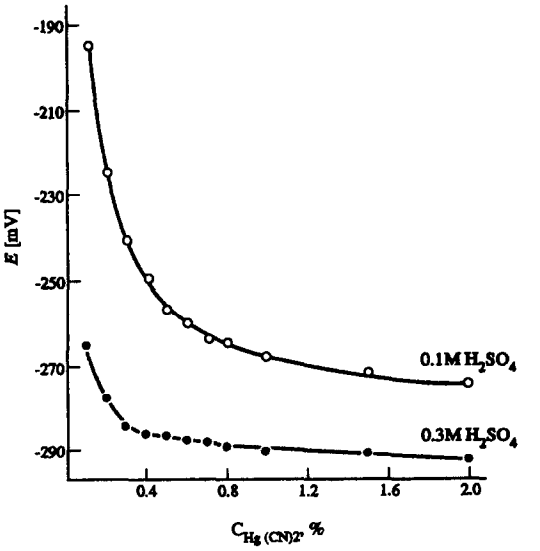

Fig. 3. The effect of mercury(II) cyanide concentration on the potential of the Air-Gap cyanide sensor in various sulphuric acid concentrations.

sharply with increasing mercury(II) cyanide concentrations. This potential became stable at a concentration above 1.6%, but with a prolonged response time. When a 0.3*M* H_2SO_4 solution was used, the potentials underwent slight variations within a wide range of concentrations from 0.4 to 2.0%.

As in this case, the application of >0.8% mercury(II) cyanide causes a considerable extension of sensor response time. The 0.5% solution is considered to be optimum.

The analytical curve for determining the chlorides within a concentration range of $0.1–10^{-5}M$ was plotted for a 0.5% mercury(II) cyanide solution. Its equation is $E = 62.8 \cdot pCl - 467.5$. A correlation coefficient of 0.9992 enables us to determine chlorides within a specified concentration range with high precision.

Studies were performed to define the effect of other ions on the determination of chloride. The results are collected in Table 1. Each ion was introduced to 35.5 μg/ml chloride solution at molar ratios of 1:1, 1:10 and 1:100.

The anions recorded in the table do not significantly affect the determination of chloride even at 100-fold excess. However, interferences are observed in the presence of halides and pseudohalides.

The suitability of the Air-Gap cyanide sensor system for determining chlorides is evaluated in Table 2 by comparing the results with a standard method. When chlorides are determined in raw materials for fuse braids and other

Table 1. Interferences from various anions [A^-] in determination of chloride anion (35.5 μg/ml)

Anion	SO_4^{2-}	NO_3^-	BO_3^{3-}	$H_2PO_4^-$	HPO_4^{2-}
$[A^-]/[Cl^-]$	1–100	1–100	1–100	1–100	1–100
Cl^- determined (μg/ml)	36.3–39.6	34.7–42.2	34.2–29.3	36.8–37.2	35.8–31.8

components, the best conformity of the test results was achieved for chlorides in braid 2. This braid was cleaned before determination many times by repeated boiling in distilled water to remove chlorides adsorbed on the surface. Similarly, satisfactory agreement of the test results was achieved, when chlorides were determined in braid 3 by the two methods. In the remaining case, slight differences in determinations were found to be due to a distinct inhomogeneity of the tested materials.

Chloride was also determined in river and drinking water by the Air-Gap cyanide sensor and by potentiometric titration. The results in Table 3 show good agreement. Small differences lie within experimental error. A low chloride amount in water samples taken from a deep well, required, that titration with an ISE be carried out in a mixed solvent system whereas the newly developed method determine chlorides in aqueous medium with good accuracy, without additions.

The possibility of applying the Air-Gap cyanide sensor to chloride analysis in the presence of surfactants was studied. The analysis of chloride with widely available ISE ($Ag_2S/AgCl$) was made to compare the results obtained. Four surfactants were used for these studies: anionic, weak anionic, cationic and nonionic. The 0.1, 0.01 and 0.005% solutions of these agents of 35.5 mg/l. each, were investigated. Results are compiled in Table 4. The surfactants added to the analysed solutions considerably disturbs the results of chloride determination when the ISE was used, because of the influence of the surfactant on the membrane material. Only the nonionic surface active agent did not cause a negative interference. Chloride analysis with an

Table 2. A comparison of chloride determinations in materials used for fuse preparation performed by the described and comparative methods

	Found Cl^-, % . 10^2					
Sample	n	Air-Gap	s	n	Turbidymetric	s
Raw-material no. 1	5	5.06 ± 0.41*	0.33	—	—	—
	5	5.45 ± 0.35	0.28			
Raw-material no. 2	5	3.09 ± 0.15	0.12	—	—	—
	5	3.15 ± 0.12	0.10			
Raw-material no. 3	5	4.86 ± 0.10	0.08	5	4.22 ± 0.53	0.42
	5	3.90 ± 0.18	0.14			
Fuse Braid no. 1	5	7.50 ± 0.69	0.55	—	—	—
	5	6.95 ± 0.35	0.28			
Fuse Braid no. 2	5	4.88 ± 0.32	2.63	5	2.75 ± 0.23	0.19
	5	3.07 ± 0.08	0.06			
Fuse Braid no. 2 (purified)	5	1.48 ± 0.32	0.09	5	1.48 ± 0.14	0.11
	5	1.41 ± 0.09	0.07			
Fuse Braid no. 3	5	2.30 ± 0.13	0.10	5	2.43 ± 0.22	0.18
	5	2.96 ± 0.11	0.09			

n = number of measurements.
* = confidence interval, probability, $P = 0.95$.
s = standard deviation.

Table 3. A comparison of chloride determination in selected water samples performed by the described and comparative methods

Water sample	Found Cl^-, *mg/l.*					
	n	Air-Gap	*s*	*n*	Potentiometric titration with ISE	*s*
Well water from Myszków	5	22.4 ± 1.20*	1.0	3	21.6 ± 0.6	0.2
Deep-well water from Myszków	5	2.18 ± 0.15	0.12	3	2.05 ± 0.29	0.12
Water from Czarna Struga River	5	25.8 ± 1.00	0.08	3	20.8 ± 0.4	0.1
Drinking water from Gliwice	5	182.6 ± 6.4	5.1	3	190.6 ± 4.3	1.7

n = number of measurements.
* = confidence interval, probability, $P = 0.95$.
s = standard deviation.

Air-Gap cyanide sensor in solutions containing surfactants was not subject to significant error. Good results are obtained because the Air-Gap electrode is not in contact with the solution.

The possibility of applying the Air-Gap cyanide sensor to chloride determination in copperizing, nickel electroplating and aluminum electropassivation was also studied. The results of chloride analysis with the Air-Gap cyanide sensor and an ISE in three of the electrolytic baths are shown in Table 5. These baths are equivalent to those applied in industry. Those baths contain high metal concentration, *e.g.*, copperizing baths contain 170–200 g of $CuSO_4 . 5H_2O$ in 1 l. and the nickel plating bath contained 250 g of $NiSO_4 . 7H_2O$ and 30 g of $NiCl_2 . 6H_2O$ in 1 l. In spite of 10-fold dilution, or 100-fold dilution in the case of the nickel bath, the concentration of anions and cations was so large that chloride analysis with ISE was impossible. A very large error was observed because of interaction between dissolved ions and the ion selective electrode membrane material. In the case of the Air-Gap cyanide sensor application, the chlorides were determined in solutions 1–3, with a relative error not higher than 5.6%. The other anions and cations present in the solution did not interfere because the sensor was not directly connected to the solution.

In an acidic (pH 1) solution of mercury(II) cyanide, when hydrogen cyanide was generated as a result of the reaction with chloride, the cyanide complexes of other metals cannot be formed, so measurements by the Air-Gap cyanide sensor were correct.

The above results show the advantage of the developed chloride method in high saline

Table 4. Comparison of results of chloride analysis made with Air-Gap cyanide sensor and ISE in solution of surface active agents

Surfactant	Taken 35.5 *mg* Cl^-/*l.*	Found Cl^- *mg/l.*					
	C, % (w/w)	ISE (Polish)	RE %	ISE (RADELKIS)	RE %	Air-Gap	RE %
Anionic SULFAPOL	0.005	37.2	4.8	32.7	7.9	36.4	2.5
	0.01	38.2	7.6	30.9	13.0	37.1	4.5
	0.1	25.5	28.2	21.2	40.3	37.6	5.5
Weak Anionic ROKSOL	0.005	40.3	13.5	36.9	3.9	35.9	1.1
	0.01	45.0	26.8	38.2	7.6	36.9	3.9
	0.1	55.0	54.9	42.8	20.6	37.2	4.8
Nonionic ROKANOL K-20	0.005	36.4	2.5	33.9	4.5	34.5	2.8
	0.01	36.4	2.5	32.7	7.9	36.9	3.9
	0.1	37.0	4.2	32.7	7.9	37.2	4.8
Kationic KAMINOX L-11	0.005	56.2	58.3	41.6	17.2	35.9	1.1
	0.01	65.3	83.9	57.1	60.8	35.9	1.1
	0.01	72.8	105.1	61.2	72.4	37.3	5.1

RE = relative error.

Table 5. Comparison of results of chloride analysis made with Air-Gap cyanide sensor and ISE in selected electrolytical baths

Electrolytic bath	Taken, Cl^-	Found, Cl^- ISE (Polish)	RE %	ISE (RADELKIS)	RE %	Air-Gap	RE %
Copperizing bath	70.9 *mg/l.*	27.6 *mg/l.*	61.1	61.9 *mg/l.*	12.7	74.8 *mg/l.*	5.5
Nickel plating bath	8.90 *mg/ml*	10.9 *mg/ml*	22.5	10.1 *mg/ml*	13.5	8.4 *mg/ml*	5.6
Aluminium electropassivation	20.0 *mg/l.*	50.4 *mg/l.*	152.0	33.5 *mg/l.*	67.5	19.8 *mg/l.*	1.1

RE = relative error.

solution as compared to direct potentiometry. Our investigations show that an Air-Gap cyanide sensor could be applied to chloride ion determination in such systems where the classical ion selective electrode action is disturbed by some active agents, *e.g.*, surfactants or highly concentrated electrolytes.

CONCLUSIONS

A new indirect electroanalytical method for determining the chlorides using the Air-Gap cyanide sensor system has been developed. It has a number of advantages. The method is quick, not requiring the expensive analytical equipment. Owing to simple construction, the cyanide sensor can be made at low expense, even in laboratories that are not equipped for regular manufacture of such equipment. The small dimensions of the sensor, measuring cell and magnetic stirrer permit analysis of trace chlorides in small volume solutions. The use of a milli-voltmeter and battery supplied magnetic stirrer enables the method to be performed in the field. This new method makes it possible to determine chlorides over a wide concentrations range *i.e.*, $0.1–10^{-5}M$.

The suitability of the Air-Gap cyanide sensor for chloride analysis in high saline solutions and surfactant-containing solutions was demonstrated in comparison to the direct method with ISE. The advantages of this method make it more competitive than other well-known methods. Furthermore, it extends the applicability of the Air-Gap cyanide sensor system used until now solely in the analysis of cyanides and mercury, to trace chlorides.

REFERENCES

1. P. Pakalns and Y. J. Farrar, *Water Res.*, 1976, **10**, 1087.
2. A. Hulanicki, M. Trojanowicz and E. Pobozy, *Analyst*, 1982, **107**, 1356.
3. A. Craggs, G. J. Moody, J. D. R. Thomas and B. J. Birch, *ibid.*, 1980, **105**, 426.
4. A. J. Frend, G. J. Moody, J. D. R. Thomas and B. J. Birch, *ibid.*, 1983, **108**, 1072.
5. H. Hara and S. Okazaki, *ibid.*, 1985, **110**, 11.
6. Multi-author work. *Poradnik Galwanotechnika*, WNT, Warszawa 1985.
7. M. K. Bathy and P. C. Uden, *Talanta*, 1971, **8**, 799.
8. J. Ciba *et al. Poradnik Chemika Analityka*, Vol. 1, p. 123. WNT, Warszawa, 1989.
9. P. Czichoń, J. Fligier and Z. Gregorowicz, *Anal. Chim. Acta*, 1981, **126**, 221.
10. F. Feigl and F. L. Chan, *Mikrochim. Acta*, 1967, **2**, 339.
11. J. Fligier, P. Czichoń and Z. Gregorowicz, *Anal. Chim. Acta*, 1980, **118**, 145.
12. J. Supniewski, *Preparatyka Nieorganiczna*, 1st Ed., p. 675. PWN, Warszawa, 1958.
13. Z. Marczenko, *Spectrophotometric Determination of Elements*, 2nd Ed., Ellis Horwood, New York, 1976.
14. W. Hermanowicz, *Fizyczno-chemiczne Badanie Wody I Ścieków*, 1st Ed., p. 504. Arkady, Warszawa, 1976.

Talanta, Vol. 40, No. 9, pp. 1473–1476, 1993
Printed in Great Britain
Pergamon Press Ltd.

BOOK REVIEWS

Anionic Surfactants—Biochemistry, Toxicology, Dermatology: Second Edition, C. GLOXHUBER and K. KÜNSTLER (editors), Dekker, New York, 1992. Pages ix + 471. $160.00. ISBN 0-8247-8621-1.

This second edition includes significant amounts of new data and reflects the current thinking in the many areas which have been included. The material has been well structured into nine chapters with some major topics such as dermatological considerations appearing in many of these.

The first chapter covers the interaction of the anionic surfactants with proteins and their effect on enzymes and membranes is also discussed with numerous references being provided for further reading. The following three chapters include details of absorption, excretion, toxicity and tolerance studies again providing experimental techniques along with data and references for further reading. The fifth chapter which comprises a third of the total text gives extensive coverage of local tolerance in animal tests. It provides many tables of data for a large number of surfactants from different manufacturers, although there are others which are not covered.

Dermatological observations in humans is well presented in the next chapter with permeation and irritation being discussed in some detail. The number of references from the late 1980s indicates the current interest in this particular field. A review of test procedures and data for carcinogenic, mutagenic and teratogenic properties are then presented in Chapter 7. Again a tremendous amount of information is presented here in the appendices but the text does try to highlight the difficulties involved in the interpretation of such data in many cases. The final chapter on pharmacological properties presents some good examples but is rather brief and could have been expanded.

This is a rather specialized text and although certain areas may be of interest to many scientists the vast majority of the data presented will only be of real interest to those working or researching in this particular field. To these researchers however it may well prove to be a valuable reference source.

K. I. CUMMING

Voltammetric Determination of Molecules of Biological Significance: W. F. SMYTH, Wiley, Chichester, 1992. Pages x + 133. £35.00. ISBN 0-471-93345-7.

This short monograph offers a critical review of recent applications of electrochemical methods for determination of traces of organic, organometallic and inorganic molecules, mainly, but not exclusively, of biological interest. The main techniques included are differential-pulse polarography (DPP), square-wave voltammetry (SWV), anodic, cathodic and adsorptive stripping voltammetry (ASV, CSV and AdSV), electrochemical detection coupled with flow-injection analysis (FIA-ED), ion chromatography (IC-ED), and high-performance liquid chromatography (HPLC-ED), electrochemical immunoassay, and amperometric biosensors. The molecules are considered according to the hetero atom or functional groups they contain, namely, nitrogen, sulphur, oxygen, C—C multiple bonds, halogens, phosphorus, mercury, tin, lead and arsenic. Some inorganic molecules are also included. The critical assessment of methods includes comparisons with competing methods.

MARY MASSON

Successful Management of the Analytical Laboratory: O. I. MILNER, Lewis Publishers (Division of CRC), Boca Raton, Florida, 1992. Pages 162. £35.00. ISBN 0-87371-438-5.

According to the preface, the book " ... reviews the operation of an analytical laboratory from the standpoint of the manager's responsibilities ... and should be particularly helpful to relatively new and potential managers by defining problems they are likely to encounter and offering possible solutions to them".

There are 12 chapters. The first two deal, respectively with the functions and organization of a typical industrial analytical laboratory. Succeeding chapters deal with managerial problems related to staffing, management and development of personnel, communication (oral and written), employee safety and environmental concerns, sample handling, workload management, quality performance, budgeting the cost control, capital investments, and information management (LIMS).

There are three chapters which form the backbone of the book. The first two are, quite rightly, those devoted to staffing the laboratory, and managing laboratory personnel. In the former, the author writes at length on the process of recruitment, from advertisement of the post, through reviewing job applications, the interview and decision, to orientation of the new employee. In the latter, he concentrates on the motivation of employees, delegation of responsibility, communicating with employees, handling personnel problems, managerial power and control, performance evaluations, handling "marginal" employees (i.e., those who are willing but unable, those who are able but unwilling, and those who are in a rut) training and continuing education, and promotion of a subordinate. This chapter also contains seven of 17 short case histories, included to illustrate practical solutions to the kind of personnel and technical problems encountered in a laboratory.

The third main chapter is on quality performance. It is defined as " ... the generation of required information as accurately, rapidly, and inexpensively *as warranted by its intended use* ..." (*Sic*). The latter qualification is sometimes disregarded by chemists, whose scientific training has usually stressed the need always to be as accurate as possible. To

Talanta, Vol. 40, No. 9, pp. 1473–1476, 1993
Printed in Great Britain
Pergamon Press Ltd.

BOOK REVIEWS

Anionic Surfactants—Biochemistry, Toxicology, Dermatology: Second Edition, C. GLOXHUBER and K. KÜNSTLER (editors), Dekker, New York, 1992. Pages ix + 471. $160.00. ISBN 0-8247-8621-1.

This second edition includes significant amounts of new data and reflects the current thinking in the many areas which have been included. The material has been well structured into nine chapters with some major topics such as dermatological considerations appearing in many of these.

The first chapter covers the interaction of the anionic surfactants with proteins and their effect on enzymes and membranes is also discussed with numerous references being provided for further reading. The following three chapters include details of absorption, excretion, toxicity and tolerance studies again providing experimental techniques along with data and references for further reading. The fifth chapter which comprises a third of the total text gives extensive coverage of local tolerance in animal tests. It provides many tables of data for a large number of surfactants from different manufacturers, although there are others which are not covered.

Dermatological observations in humans is well presented in the next chapter with permeation and irritation being discussed in some detail. The number of references from the late 1980s indicates the current interest in this particular field. A review of test procedures and data for carcinogenic, mutagenic and teratogenic properties are then presented in Chapter 7. Again a tremendous amount of information is presented here in the appendices but the text does try to highlight the difficulties involved in the interpretation of such data in many cases. The final chapter on pharmacological properties presents some good examples but is rather brief and could have been expanded.

This is a rather specialized text and although certain areas may be of interest to many scientists the vast majority of the data presented will only be of real interest to those working or researching in this particular field. To these researchers however it may well prove to be a valuable reference source.

K. I. CUMMING

Voltammetric Determination of Molecules of Biological Significance: W. F. SMYTH, Wiley, Chichester, 1992. Pages x + 133. £35.00. ISBN 0-471-93345-7.

This short monograph offers a critical review of recent applications of electrochemical methods for determination of traces of organic, organometallic and inorganic molecules, mainly, but not exclusively, of biological interest. The main techniques included are differential-pulse polarography (DPP), square-wave voltammetry (SWV), anodic, cathodic and adsorptive stripping voltammetry (ASV, CSV and AdSV), electrochemical detection coupled with flow-injection analysis (FIA-ED), ion chromatography (IC-ED), and high-performance liquid chromatography (HPLC-ED), electrochemical immunoassay, and amperometric biosensors. The molecules are considered according to the hetero atom or functional groups they contain, namely, nitrogen, sulphur, oxygen, C—C multiple bonds, halogens, phosphorus, mercury, tin, lead and arsenic. Some inorganic molecules are also included. The critical assessment of methods includes comparisons with competing methods.

MARY MASSON

Successful Management of the Analytical Laboratory: O. I. MILNER, Lewis Publishers (Division of CRC), Boca Raton, Florida, 1992. Pages 162. £35.00. ISBN 0-87371-438-5.

According to the preface, the book " ... reviews the operation of an analytical laboratory from the standpoint of the manager's responsibilities ... and should be particularly helpful to relatively new and potential managers by defining problems they are likely to encounter and offering possible solutions to them".

There are 12 chapters. The first two deal, respectively with the functions and organization of a typical industrial analytical laboratory. Succeeding chapters deal with managerial problems related to staffing, management and development of personnel, communication (oral and written), employee safety and environmental concerns, sample handling, workload management, quality performance, budgeting the cost control, capital investments, and information management (LIMS).

There are three chapters which form the backbone of the book. The first two are, quite rightly, those devoted to staffing the laboratory, and managing laboratory personnel. In the former, the author writes at length on the process of recruitment, from advertisement of the post, through reviewing job applications, the interview and decision, to orientation of the new employee. In the latter, he concentrates on the motivation of employees, delegation of responsibility, communicating with employees, handling personnel problems, managerial power and control, performance evaluations, handling "marginal" employees (i.e., those who are willing but unable, those who are able but unwilling, and those who are in a rut) training and continuing education, and promotion of a subordinate. This chapter also contains seven of 17 short case histories, included to illustrate practical solutions to the kind of personnel and technical problems encountered in a laboratory.

The third main chapter is on quality performance. It is defined as " ... the generation of required information as accurately, rapidly, and inexpensively *as warranted by its intended use* ..." (*Sic*). The latter qualification is sometimes disregarded by chemists, whose scientific training has usually stressed the need always to be as accurate as possible. To

some, the quote will be passed off as common sense, but I suspect to the majority of trainee and new managers, in particular those making the transition from bench science to the ranks of management, the voice of experience will come as a breath of fresh air.

This book is relatively short, but it is short and to the point. It is very well written indeed, interesting and easy to read, and pitched at the correct level for its intended readership. References at the end of each chapter are largely American in origin, but their U.K. or European equivalent should be quite obvious.

D. F. RENDLE

Emerging Strategies for Pesticide Analysis: T. CAIRNS and J. SHERMA (editors), CRC Press, Boca Raton, Florida, 1992. Pages 352. $74.95 (U.S.A.), $90.00 (elsewhere). ISBN 0-8493-7991-1.

This volume comes as part of a series on 'Modern Methods for Pesticide Analysis' and contains 16 chapters in three sections. The first section (Chapters 1–3) covers extraction and clean-up, the second section (Chapters 4–9) covers multi-residue analysis and the third section (Chapters 10–16) covers emerging techniques.

The 'Development of Microextraction Methods in Residue Analysis' covers an old subject in a fresh and enlightening way. Analysts rarely refer to the extraction theory to predict the efficiency of the method. This chapter redresses that balance by giving clear guidelines on the microextraction techniques that can be used for a wide range of polarity of solute and solvent mixtures. The chapter on solid-phase partition is only an overview and is rather limited in detailed information. Likewise Chapter 3 on 'Supercritical Fluid Extraction' is a useful overview, but, in a book on emerging strategies, more space could have been devoted to the very important area.

Chapters 4–7 and Chapter 9 cover specific multiresidue methods for specific groups of pesticides in foodstuffs and environmental matrices. They are primarily a review of current practices rather than 'emerging techniques', but nevertheless are a valuable contribution to our knowledge on the current state of the art. The 'Multi-residue Analysis of Fruit and Vegetables' (Chapter 4) covers the basic requirement in a method to comply with monitoring and regulatory requirements. Chapters 5 and 9 cover more specific areas of carbamate analysis in foodstuffs and headspace analysis for dithiocarbamates, while Chapters 6 and 7 include methods for the determination of organophosphorus pesticides in water, soil, sediment and biological samples, and the multiresidue methods for organonitrogen pesticides. Each of these chapters are well written and, collectively, are useful overviews of present methodology.

Chapter 8 on two-dimensional gas chromatography should, in my view, be placed in the section on emerging techniques, but this should in no way detract from the value of this contribution. It reports the recent developments well and gives a broad spectrum of examples in an area where this technique has been invaluable in the identification or confirmation of the determinand. It does not, however, discuss the difficulties associated with obtaining good quantitative data, particularly with the use of internal or surrogate standards, in the 'heart-cut' mode.

Chapter 10 covers 'Fibre Optic Spectroscopy', Chapter 11 'Enzyme Linked Competitive Immunoassay' and Chapter 12 Ion-Trap Mass Spectrometry'. Each of these contribution are short overviews which perhaps do not do justice to the extensive literature on these subjects, and I missed any attempt to evaluate the use of these techniques in the future. Chapters 13 and 14 cover 'Hyphenated Methods' and 'Liquid Chromatography–Mass Spectrometry' which gave an alternative approach to much of the information given in the previous 'compound orientated' chapters. Chapter 15 gave an overview on 'Immunochemical Methods' and contained a small section on 'Emerging Concepts'.

The book is well written by many of the relevant authorities in their field with good examples of recent work; however, I think that some of the chapters appear in the wrong place. It is a valuable reference for anyone wishing to grasp the present state-of-the-art in pesticide analysis, but the title of 'Emerging Strategies' and the actual content of the book do not altogether lie well with each other.

D. E. WELLS

Basic Solid State Chemistry: A. R. WEST, Wiley, Chichester, 1988 (reprinted 1991). Pages x + 415. £17.50 (softcover). ISBN 0-471-91798-2.

Professor Tony West has produced a succinct text covering the basics of solid state chemistry which is suitable for students, teachers and practitioners. It is clear that this book has been written by an author with great enthusiasm for his subject area.

As expected the emphasis throughout is on inorganic structures and explanations are generally descriptive rather than rigorously mathematical. As molecular structures are three-dimensional, numerous figures are used to aid the concepts of crystal packing arrangements. I believe computer programs and hand held models are very useful in this context and the author has included templates for the tetrahedral and octahedral structures in the Appendices along with details of constructing packing arrangements with polystyrene balls.

There are eight chapters which cover topics that might well be incorporated into eight separate books! The first three chapters cover crystal structures, bonding in solids, and crystallography and diffraction techniques. Other techniques are then explained; microscopy, spectroscopy and thermal analysis. Crystal defects, non-stoichiometry and solid solutions are introduced from both theoretical and practical viewpoints. Interpretation of phase diagrams are restricted to one- and two-component systems.

The final two chapters cover electrical properties, and magnetic and optical properties. Here the explanations of observed phenomena are supplemented with details of the relevance of properties such as superconductivity to current and future technology.

some, the quote will be passed off as common sense, but I suspect to the majority of trainee and new managers, in particular those making the transition from bench science to the ranks of management, the voice of experience will come as a breath of fresh air.

This book is relatively short, but it is short and to the point. It is very well written indeed, interesting and easy to read, and pitched at the correct level for its intended readership. References at the end of each chapter are largely American in origin, but their U.K. or European equivalent should be quite obvious.

D. F. RENDLE

Emerging Strategies for Pesticide Analysis: T. CAIRNS and J. SHERMA (editors), CRC Press, Boca Raton, Florida, 1992. Pages 352. $74.95 (U.S.A.), $90.00 (elsewhere). ISBN 0-8493-7991-1.

This volume comes as part of a series on 'Modern Methods for Pesticide Analysis' and contains 16 chapters in three sections. The first section (Chapters 1–3) covers extraction and clean-up, the second section (Chapters 4–9) covers multi-residue analysis and the third section (Chapters 10–16) covers emerging techniques.

The 'Development of Microextraction Methods in Residue Analysis' covers an old subject in a fresh and enlightening way. Analysts rarely refer to the extraction theory to predict the efficiency of the method. This chapter redresses that balance by giving clear guidelines on the microextraction techniques that can be used for a wide range of polarity of solute and solvent mixtures. The chapter on solid-phase partition is only an overview and is rather limited in detailed information. Likewise Chapter 3 on 'Supercritical Fluid Extraction' is a useful overview, but, in a book on emerging strategies, more space could have been devoted to the very important area.

Chapters 4–7 and Chapter 9 cover specific multiresidue methods for specific groups of pesticides in foodstuffs and environmental matrices. They are primarily a review of current practices rather than 'emerging techniques', but nevertheless are a valuable contribution to our knowledge on the current state of the art. The 'Multi-residue Analysis of Fruit and Vegetables' (Chapter 4) covers the basic requirement in a method to comply with monitoring and regulatory requirements. Chapters 5 and 9 cover more specific areas of carbamate analysis in foodstuffs and headspace analysis for dithiocarbamates, while Chapters 6 and 7 include methods for the determination of organophosphorus pesticides in water, soil, sediment and biological samples, and the multiresidue methods for organonitrogen pesticides. Each of these chapters are well written and, collectively, are useful overviews of present methodology.

Chapter 8 on two-dimensional gas chromatography should, in my view, be placed in the section on emerging techniques, but this should in no way detract from the value of this contribution. It reports the recent developments well and gives a broad spectrum of examples in an area where this technique has been invaluable in the identification or confirmation of the determinand. It does not, however, discuss the difficulties associated with obtaining good quantitative data, particularly with the use of internal or surrogate standards, in the 'heart-cut' mode.

Chapter 10 covers 'Fibre Optic Spectroscopy', Chapter 11 'Enzyme Linked Competitive Immunoassay' and Chapter 12 Ion-Trap Mass Spectrometry'. Each of these contribution are short overviews which perhaps do not do justice to the extensive literature on these subjects, and I missed any attempt to evaluate the use of these techniques in the future. Chapters 13 and 14 cover 'Hyphenated Methods' and 'Liquid Chromatography–Mass Spectrometry' which gave an alternative approach to much of the information given in the previous 'compound orientated' chapters. Chapter 15 gave an overview on 'Immunochemical Methods' and contained a small section on 'Emerging Concepts'.

The book is well written by many of the relevant authorities in their field with good examples of recent work; however, I think that some of the chapters appear in the wrong place. It is a valuable reference for anyone wishing to grasp the present state-of-the-art in pesticide analysis, but the title of 'Emerging Strategies' and the actual content of the book do not altogether lie well with each other.

D. E. WELLS

Basic Solid State Chemistry: A. R. WEST, Wiley, Chichester, 1988 (reprinted 1991). Pages x + 415. £17.50 (softcover). ISBN 0-471-91798-2.

Professor Tony West has produced a succinct text covering the basics of solid state chemistry which is suitable for students, teachers and practitioners. It is clear that this book has been written by an author with great enthusiasm for his subject area.

As expected the emphasis throughout is on inorganic structures and explanations are generally descriptive rather than rigorously mathematical. As molecular structures are three-dimensional, numerous figures are used to aid the concepts of crystal packing arrangements. I believe computer programs and hand held models are very useful in this context and the author has included templates for the tetrahedral and octahedral structures in the Appendices along with details of constructing packing arrangements with polystyrene balls.

There are eight chapters which cover topics that might well be incorporated into eight separate books! The first three chapters cover crystal structures, bonding in solids, and crystallography and diffraction techniques. Other techniques are then explained; microscopy, spectroscopy and thermal analysis. Crystal defects, non-stoichiometry and solid solutions are introduced from both theoretical and practical viewpoints. Interpretation of phase diagrams are restricted to one- and two-component systems.

The final two chapters cover electrical properties, and magnetic and optical properties. Here the explanations of observed phenomena are supplemented with details of the relevance of properties such as superconductivity to current and future technology.

some, the quote will be passed off as common sense, but I suspect to the majority of trainee and new managers, in particular those making the transition from bench science to the ranks of management, the voice of experience will come as a breath of fresh air.

This book is relatively short, but it is short and to the point. It is very well written indeed, interesting and easy to read, and pitched at the correct level for its intended readership. References at the end of each chapter are largely American in origin, but their U.K. or European equivalent should be quite obvious.

D. F. RENDLE

Emerging Strategies for Pesticide Analysis: T. CAIRNS and J. SHERMA (editors), CRC Press, Boca Raton, Florida, 1992. Pages 352. $74.95 (U.S.A.), $90.00 (elsewhere). ISBN 0-8493-7991-1.

This volume comes as part of a series on 'Modern Methods for Pesticide Analysis' and contains 16 chapters in three sections. The first section (Chapters 1–3) covers extraction and clean-up, the second section (Chapters 4–9) covers multi-residue analysis and the third section (Chapters 10–16) covers emerging techniques.

The 'Development of Microextraction Methods in Residue Analysis' covers an old subject in a fresh and enlightening way. Analysts rarely refer to the extraction theory to predict the efficiency of the method. This chapter redresses that balance by giving clear guidelines on the microextraction techniques that can be used for a wide range of polarity of solute and solvent mixtures. The chapter on solid-phase partition is only an overview and is rather limited in detailed information. Likewise Chapter 3 on 'Supercritical Fluid Extraction' is a useful overview, but, in a book on emerging strategies, more space could have been devoted to the very important area.

Chapters 4–7 and Chapter 9 cover specific multiresidue methods for specific groups of pesticides in foodstuffs and environmental matrices. They are primarily a review of current practices rather than 'emerging techniques', but nevertheless are a valuable contribution to our knowledge on the current state of the art. The 'Multi-residue Analysis of Fruit and Vegetables' (Chapter 4) covers the basic requirement in a method to comply with monitoring and regulatory requirements. Chapters 5 and 9 cover more specific areas of carbamate analysis in foodstuffs and headspace analysis for dithiocarbamates, while Chapters 6 and 7 include methods for the determination of organophosphorus pesticides in water, soil, sediment and biological samples, and the multiresidue methods for organonitrogen pesticides. Each of these chapters are well written and, collectively, are useful overviews of present methodology.

Chapter 8 on two-dimensional gas chromatography should, in my view, be placed in the section on emerging techniques, but this should in no way detract from the value of this contribution. It reports the recent developments well and gives a broad spectrum of examples in an area where this technique has been invaluable in the identification or confirmation of the determinand. It does not, however, discuss the difficulties associated with obtaining good quantitative data, particularly with the use of internal or surrogate standards, in the 'heart-cut' mode.

Chapter 10 covers 'Fibre Optic Spectroscopy', Chapter 11 'Enzyme Linked Competitive Immunoassay' and Chapter 12 Ion-Trap Mass Spectrometry'. Each of these contribution are short overviews which perhaps do not do justice to the extensive literature on these subjects, and I missed any attempt to evaluate the use of these techniques in the future. Chapters 13 and 14 cover 'Hyphenated Methods' and 'Liquid Chromatography–Mass Spectrometry' which gave an alternative approach to much of the information given in the previous 'compound orientated' chapters. Chapter 15 gave an overview on 'Immunochemical Methods' and contained a small section on 'Emerging Concepts'.

The book is well written by many of the relevant authorities in their field with good examples of recent work; however, I think that some of the chapters appear in the wrong place. It is a valuable reference for anyone wishing to grasp the present state-of-the-art in pesticide analysis, but the title of 'Emerging Strategies' and the actual content of the book do not altogether lie well with each other.

D. E. WELLS

Basic Solid State Chemistry: A. R. WEST, Wiley, Chichester, 1988 (reprinted 1991). Pages x + 415. £17.50 (softcover). ISBN 0-471-91798-2.

Professor Tony West has produced a succinct text covering the basics of solid state chemistry which is suitable for students, teachers and practitioners. It is clear that this book has been written by an author with great enthusiasm for his subject area.

As expected the emphasis throughout is on inorganic structures and explanations are generally descriptive rather than rigorously mathematical. As molecular structures are three-dimensional, numerous figures are used to aid the concepts of crystal packing arrangements. I believe computer programs and hand held models are very useful in this context and the author has included templates for the tetrahedral and octahedral structures in the Appendices along with details of constructing packing arrangements with polystyrene balls.

There are eight chapters which cover topics that might well be incorporated into eight separate books! The first three chapters cover crystal structures, bonding in solids, and crystallography and diffraction techniques. Other techniques are then explained; microscopy, spectroscopy and thermal analysis. Crystal defects, non-stoichiometry and solid solutions are introduced from both theoretical and practical viewpoints. Interpretation of phase diagrams are restricted to one- and two-component systems.

The final two chapters cover electrical properties, and magnetic and optical properties. Here the explanations of observed phenomena are supplemented with details of the relevance of properties such as superconductivity to current and future technology.

Details of further reading, restricted to text books, is given for each chapter and numerous questions (without answers) are included at the end of the book. An extensive index is included. The book is keenly priced and is an excellent introduction to solid state chemistry.

P. J. Cox

Electrochemical Oxygen Technology: Kim Kinoshita, Wiley, Chichester, 1992. Pages ix + 431. £105.00. ISBN 0-471-570-435.

The author has harvested most or all of the published information on the electrochemical reactions of oxygen and distilled it into a very useful, comprehensive, reference book. After a brief chapter on the physicochemical properties (solubility, diffusion, etc.) of oxygen species, the author discusses the reaction rates and mechanisms of oxygen reduction, at low and high temperatures, and of oxygen evolution, paying particular attention to the role of electrocatalysts. The third chapter deals with the types and structures of oxygen electrodes. The remaining chapters deal with the many applications of oxygen in electrochemical processes, such as those in fuel cells, metal/air and rechargeable batteries, and in industrial electrochemical processes.

The book is well constructed, comprehensive, up-to-date, and maintains the tradition of quality of the former books sponsored by the (American) Electrochemical Society. I recommend this book to all those, academic and industrial, involved in oxygen electrochemistry.

J. B. Craig

Preparative and Production Scale Chromatography: G. Ganetsos and P. E. Barker (editors), Dekker, New York, 1993. Pages xiv + 786. $195.00. ISBN 0-8247-8738-2.

Sometimes, when you ask a number of scientists to write chapters for a book on their own specialist subject, the total result can be very fragmented and a poor book may be produced. In this book, however, the editors, have carefully added introductions to most of the sections, which bind together the contributions from each individual author and make this a very practical, informative book that will be of great interest to anyone involved in separation science—from engineers to graduates.

The book covers all aspects of preparative chromatography from packed columns (with all the different separation processes of normal phase), reverse phase, size exclusion and ion exchange. Counter current and moving bed reaction chromatography are also covered. With the methods, real examples are given on separations and then further detailed studies are given on the separation of proteins, amino-acids and hydrocarbons.

The book, however, covers far more areas than the title would suggest by including sections on the theory of the chromatographic process, and extending this in other chapters to the modelling of the process. A very informative view is provided of the problems involved in taking a procedure from the analytical separation stage to both pilot scale and process scale separation. This makes the book an excellent practical reference guide that is suitable for the practitioner involved in analytical through to process scale chromatography. It will be welcomed in all disciplines from pharmacy to bioprocessing technology.

P. Myers

Spectroscopy of Advanced Materials: R.J.H. Clark and R.E. Hester (editors), Wiley, Chichester, 1991. Pages xix + 405. £133.00. ISBN 0-471-929-816.

The 19th volume of the *Advances in Spectroscopy* series by Clark and Hester is dedicated to the use of spectroscopic methods in the rapidly growing research field of advanced materials. A total of six chapters, by an international team of authors, review a wide field of advanced materials including charge transfer crystals, molecular conductors, non-linear optical polymers, thin film semi-conductors and polyconjugated materials. The battery of techniques, including vibrational, pulsed neutron, photoluminescence and photoexcitation spectroscopies, used to study these materials is discussed in depth. All chapters include references up to 1990 and most quote references up to 1991.

The use of infrared and Raman spectroscopy in materials science is discussed in Chapters 1 and 5, the former concentrating on strong charge transfer crystals and organic molecular conductors and the latter on investigating electrical phenomena in polyconjugated polymers, with particular attention given to the theoretical basis underlying the interpretation of data.

Non-linear spectroscopy of conjugated polymers is dealt with in Chapter 2, with detailed discussions on the effect of excited state structure on NLO spectra, third harmonic generation and the interpretation of two photon absorption spectra. Chapter 3 reviews the applicability of pulsed neutron spectroscopy to study advanced materials. The authors provide details on the experimental aspects of the technique before describing new work on magnetic transitions in rare-earth, actinide and 3*d* transition-metal systems and in following proton dynamics in molecular spectroscopy and tunnelling spectroscopy.

The characterization of thin-film semiconductors using photoluminescence spectroscopy is reviewed in Chapter 4, and covers the basic theory of the technique and its application to thin-film semiconductor systems based on GaAs, InP and ZnSe. Finally, Chapter 6 is devoted to the spectroscopy and photoexcitation spectroscopy of polyaninlines and related polymers, and provides a fundamental understanding of why these materials exhibit different behaviour compared to other polymers.

Overall, this is a well-written book and provides valuable information to researchers on the application of advanced techniques to investigate new materials.

R. Raval

Details of further reading, restricted to text books, is given for each chapter and numerous questions (without answers) are included at the end of the book. An extensive index is included. The book is keenly priced and is an excellent introduction to solid state chemistry.

P. J. Cox

Electrochemical Oxygen Technology: Kim Kinoshita, Wiley, Chichester, 1992. Pages ix + 431. £105.00. ISBN 0-471-570-435.

The author has harvested most or all of the published information on the electrochemical reactions of oxygen and distilled it into a very useful, comprehensive, reference book. After a brief chapter on the physicochemical properties (solubility, diffusion, etc.) of oxygen species, the author discusses the reaction rates and mechanisms of oxygen reduction, at low and high temperatures, and of oxygen evolution, paying particular attention to the role of electrocatalysts. The third chapter deals with the types and structures of oxygen electrodes. The remaining chapters deal with the many applications of oxygen in electrochemical processes, such as those in fuel cells, metal/air and rechargeable batteries, and in industrial electrochemical processes.

The book is well constructed, comprehensive, up-to-date, and maintains the tradition of quality of the former books sponsored by the (American) Electrochemical Society. I recommend this book to all those, academic and industrial, involved in oxygen electrochemistry.

J. B. Craig

Preparative and Production Scale Chromatography: G. Ganetsos and P. E. Barker (editors), Dekker, New York, 1993. Pages xiv + 786. $195.00. ISBN 0-8247-8738-2.

Sometimes, when you ask a number of scientists to write chapters for a book on their own specialist subject, the total result can be very fragmented and a poor book may be produced. In this book, however, the editors, have carefully added introductions to most of the sections, which bind together the contributions from each individual author and make this a very practical, informative book that will be of great interest to anyone involved in separation science—from engineers to graduates.

The book covers all aspects of preparative chromatography from packed columns (with all the different separation processes of normal phase), reverse phase, size exclusion and ion exchange. Counter current and moving bed reaction chromatography are also covered. With the methods, real examples are given on separations and then further detailed studies are given on the separation of proteins, amino-acids and hydrocarbons.

The book, however, covers far more areas than the title would suggest by including sections on the theory of the chromatographic process, and extending this in other chapters to the modelling of the process. A very informative view is provided of the problems involved in taking a procedure from the analytical separation stage to both pilot scale and process scale separation. This makes the book an excellent practical reference guide that is suitable for the practitioner involved in analytical through to process scale chromatography. It will be welcomed in all disciplines from pharmacy to bioprocessing technology.

P. Myers

Spectroscopy of Advanced Materials: R.J.H. Clark and R.E. Hester (editors), Wiley, Chichester, 1991. Pages xix + 405. £133.00. ISBN 0-471-929-816.

The 19th volume of the *Advances in Spectroscopy* series by Clark and Hester is dedicated to the use of spectroscopic methods in the rapidly growing research field of advanced materials. A total of six chapters, by an international team of authors, review a wide field of advanced materials including charge transfer crystals, molecular conductors, non-linear optical polymers, thin film semi-conductors and polyconjugated materials. The battery of techniques, including vibrational, pulsed neutron, photoluminescence and photoexcitation spectroscopies, used to study these materials is discussed in depth. All chapters include references up to 1990 and most quote references up to 1991.

The use of infrared and Raman spectroscopy in materials science is discussed in Chapters 1 and 5, the former concentrating on strong charge transfer crystals and organic molecular conductors and the latter on investigating electrical phenomena in polyconjugated polymers, with particular attention given to the theoretical basis underlying the interpretation of data.

Non-linear spectroscopy of conjugated polymers is dealt with in Chapter 2, with detailed discussions on the effect of excited state structure on NLO spectra, third harmonic generation and the interpretation of two photon absorption spectra. Chapter 3 reviews the applicability of pulsed neutron spectroscopy to study advanced materials. The authors provide details on the experimental aspects of the technique before describing new work on magnetic transitions in rare-earth, actinide and 3*d* transition-metal systems and in following proton dynamics in molecular spectroscopy and tunnelling spectroscopy.

The characterization of thin-film semiconductors using photoluminescence spectroscopy is reviewed in Chapter 4, and covers the basic theory of the technique and its application to thin-film semiconductor systems based on GaAs, InP and ZnSe. Finally, Chapter 6 is devoted to the spectroscopy and photoexcitation spectroscopy of polyaninlines and related polymers, and provides a fundamental understanding of why these materials exhibit different behaviour compared to other polymers.

Overall, this is a well-written book and provides valuable information to researchers on the application of advanced techniques to investigate new materials.

R. Raval

Luminescence Spectroscopy of Proteins: E. A. PERMYAKOV, CRC Press, Boca Raton, 1993. Pages iv + 164. $79.95 (U.S.A.), $95.00 (elsewhere). ISBN 0-8493-4553-7.

The book by Permyakov is an excellent, *brief* summary of luminescence spectroscopy. For example, in 29 pages, the author covers an Introduction (Chapter 1—four pages), and fundamentals of luminescence including an introduction to quantum mechanics (Chapter 2—25 pages). The instrumentation is discussed in about four pages and is therefore extremely weak. The majority of the book is devoted to the spectroscopic properties of isolated protein chromophores (tryptophan, tyrosine and phenyl alanine) in Chapter 3 (20 pages) and to protein luminescence in Chapter 4 (130 pages) (position and shape of spectra, quantum efficiencies, fluorescence decay of proteins fluorescence parameters, intermediate states, the effect of temperature, pH, ionic strength and denaturants on protein fluorescence, the interaction of protein with low mass compounds, selective fluorescence quenching and low temperature luminescence). Chapter 4 is well-written with considerable useful information, concepts, and procedures and certainly makes buying the book worth while. The references seem incomplete; for example, there are only 31 references for Chapter 4 of which the majority of references refer to Burstein and/or Permyakov. Overall, the book is worth while, especially Chapters 3 and 4, reads well, and is worth purchasing despite its high price.

J. D. WINEFORDNER

Talanta, Vol. 40, No. 10, pp. 1477–1480, 1993
Printed in Great Britain.

0039-9140/93 $6.00 + 0.00
Pergamon Press Ltd

DETERMINATION OF MERCURY IN ZINC ORE CONCENTRATE REFERENCE MATERIALS USING FLOW INJECTION AND COLD-VAPOR ATOMIC ABSORPTION SPECTROMETRY

RAJANANDA SARASWATI,* CHARLES M. BECK and MICHAEL S. EPSTEIN†
Inorganic Analytical Research Division, Chemical Science and Technology Laboratory, National Institute of Standards and Technology, Gaithersburg, MD 20899, U.S.A.

(*Received* 22 *March* 1993. *Accepted* 21 *April* 1993)

Summary—A flow-injection, cold-vapor atomic absorption spectrophotometric method was developed for the determination of trace amounts of mercury in a proposed zinc ore concentrate Standard Reference Material (SRM 113b). The samples were digested with nitric and hydrochloric acids in closed Teflon digestion vessels. The experimental details for sample preparation and the flow injection method are discussed. The effect of matrix and various acid concentrations on the extraction and subsequent analysis of mercury were also studied. The method has a detection limit of 0.08 μg Hg/g in the sample. A certified reference material (CZN-1) was analyzed and the results obtained agreed well with the certified value.

Of the various techniques that have been developed for the determination of low mercury levels in geological and metallurgical samples, such as radiochemical neutron activation analysis, fluorescence spectrometry and cold-vapor mercury generation atomic absorption spectroscopy (CVAAS),[1-3] the latter is the most cost-effective and popular. Flow injection analysis (FIA) methodologies can be combined with CVAAS to improve the speed, precision, and sensitivity of that method even further. The concept behind FIA is to both miniaturize and automate large-scale and manual analytical procedures. FIA has been applied in many fields,[4-8] and its use is rapidly increasing because of the simplicity of the method.

The aim of the present work was to develop a rapid and accurate analytical method for the determination of mercury in a proposed Standard Reference Material (SRM) zinc ore concentrate (SRM 113b) by FIA and CVAAS. The method is based on the reduction of mercury ions by tin(II) followed by sweeping the free mercury atoms into an absorption cell and detection at 253.7 nm. FIA has recently been shown to be an efficient way to apply CVAAS to the determination of mercury.[9]

EXPERIMENTAL

Instrumentation

Absorption measurements were made using a commercial FIA system interfaced to an atomic absorption spectrometer. Specific information about the instrumentation and operating parameters is presented in Table 1. The FIA is computer-controlled with two peristaltic pumps, four switching valves, a sample injection loop, a mixing coil, and a liquid–gas separator. Dilute hydrochloric acid, 3% (v/v), is used in the carrier stream to sweep the sample from the injection loop to the mixing coil where it reacts with a solution of 1.1% (w/v) stannous chloride. The reaction produces free mercury atoms which are separated from the solution phase (in the liquid–gas separator) as an atomic vapor carried by argon gas. The argon gas stream sweeps the mercury vapor to a heated (200°C) quartz absorption cell mounted in the light path of a mercury electrodeless discharge lamp in the atomic absorption spectrometer. Because of the short residence time of the mercury atoms in the absorption cell, peak height measurements can be accurately used for quantification.

Reagents

High-purity acids obtained by a sub-boiling distillation process at NIST and high-purity de-ionized water (18 MΩ/cm) were used for preparing solutions. All glassware used for the

*On leave from the Defense Metallurgical Research Laboratory, Hyderabad, India.

†Author to whom correspondence should be addressed.

preparation and storage of solutions was precleaned by soaking in 20% nitric acid for 1 hr followed by a rinse with high-purity de-ionized water. Standard solutions of mercury were prepared by serial dilution of SRM 3133 (Mercury Spectrometric Standard Solution) to the required levels (1–10 ng Hg/g). The reductant solution was prepared by dissolving 11 g reagent grade stannous chloride ($SnCl_2 . H_2O$) in 30 ml of concentrated hydrochloric acid and subsequent dilution to 1 l by the addition of de-ionized water. Some batches of stannous chloride required filtering after dilution to obtain a particle-free solution. This was done using vacuum filtration through a 0.45 μm Millipore filter. Fresh reagent solutions were prepared daily.

Sample preparation

Two accurately weighed samples of approximately 0.25 g, were taken from each of four bottles of the zinc ore concentrate. Two samples of the control material, Certified Reference Material (CRM) CZN-1 were also taken. Samples of the zinc ore concentrate were dried at 105°C for 1 hr, and CRM CZN-1 was dried for 2 hr. Undried samples of the zinc ore concentrate were also analyzed to confirm that no mercury loss occurred during the drying procedure. Samples were placed in Teflon microwave digestion vessels, 2.5 ml of nitric acid and 2.5 ml of hydrochloric acid were added, and the vessels were capped to prevent vapor loss. The vessels were heated in a water bath at 60°C for 3 hr and then cooled to room temperature. The contents were then transferred to 250-ml volumetric flasks with the addition of 0.75 ml of 1% potassium dichromate solution as an oxidative stabilizing agent.

Analysis

Sample solution concentrations were determined by: (a) direct comparison to a calibration curve prepared using solutions from 1 to 10 ng Hg/ml that were matched in acid and stabilizer concentration to the samples and (b) the method of standard addition, in which a sample is diluted 1:1 with either a blank or a standard of known mercury concentration, and the recovery of the standard mercury concentration in the sample matrix is used to calculate the sample mercury concentration. Method (b) was repeated on three separate days for the results to be used for certification.

RESULTS AND DISCUSSION

Because of the extremely low mercury concentrations involved in these analyses, sample handling procedures were optimized to avoid mercury contamination. The closed digestion conditions used in this experiment not only reduced possible loss of mercury, but also dissolved the ore concentrate sample more rapidly than under the open digestion conditions used for a previous determination of zinc using an EDTA titration.

In order to determine the optimum acid concentration for the digestion and analysis, both the effect of acid concentration on (a) the FIA-CVAAS determination of mercury and (b) the extraction of mercury from the ore concentrate during the digestion had to be considered. The former would be correctable by the method of standard addition, although severe suppression of the mercury signal could drastically reduce the measurement precision. The latter was critical to the success of the experiment, since incomplete extraction of mercury from the matrix could not be tolerated.

The effect of acid concentration on the recovery of mercury in standards was first determined by varying one of the two acid concentrations while holding the other constant at 1% (v/v). The effects of varying either the nitric acid or the hydrochloric acid concentration are shown in Fig. 1. The acid concentrations shown on the x-axis are the percentage of acid in the final sample volume of 250 ml. The optimum concentrations of both acids appear to be in the 2%–3% range, with the hydrochloric acid concentration being the more critical. An excessive amount of hydrochloric acid is known to generate chlorine, which leads to the loss of volatile

Table 1. Instrumentation used for FIA-CVAAS determination of Hg

Spectrometer	Perkin-Elmer model 5000 AAS
Flow injection system	Perkin-Elmer FIAS-200
Computer	386SX running MS-DOS 5.0
Wavelength	253.7 *nm*
Source	Perkin-Elmer electrodeless discharge lamp at 5 *W*
Injection loop volume	500 *µl*

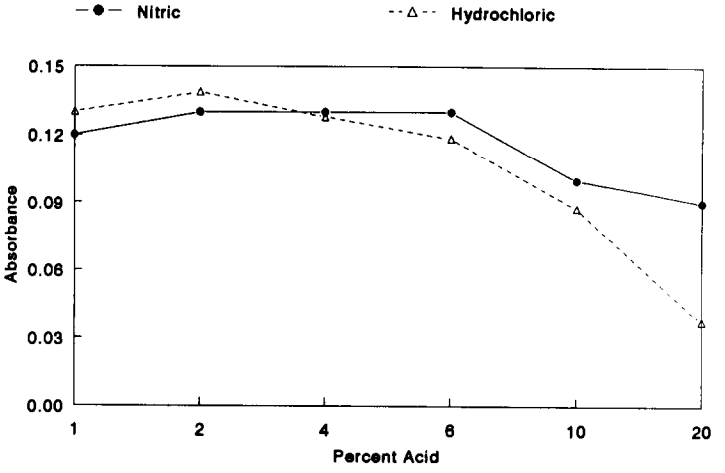

Fig. 1. Effect of varying either nitric (–●–) or hydrochloric acid (–△–) concentration in a mercury standard of 10 ng Hg/ml while the other acid concentration is held constant at 1% (v/v).

mercury chlorides.[10,11] The effect of varying the concentration of a 1:1 mixture of the acids is shown in Fig. 2, with an optimum again around 2%.

The effect of acid concentration on extraction of mercury from the samples was then examined by digesting identical ore concentrate samples with varying concentrations of a 1:1 acid mixture. The results are also plotted in Fig. 2 to allow comparison to the effect of the acid concentration (described in the previous paragraph) on the generation of the mercury vapor using the FIA. The maximum mercury absorption signal was obtained when the acid mixture concentration was approximately 2–3% (corresponding to 5–7.5 ml of acid mixture and a sample weight of 250 mg in the digestion vessel). The lower recovery of mercury at acid concentrations less than 2% is likely to be caused by inefficient extraction during digestion. At higher concentrations of acid, the decreased signal is an interference on the generation of mercury using the FIA cold-vapor system. Apparently, the combination of sample matrix with the higher acid concentrations reduces the efficiency of mercury release. The optimum digestion time using a 1:1 mixture of acids at a concentration of 2% was found to be 3 hr, as shown in Fig. 3. A period of at least 3 hr of digestion at 60°C was required to extract all the mercury from the sample using a combined acid concentration of 2%.

The calibration curve prepared in the range 1–10 ng Hg/ml was linear. However, the method

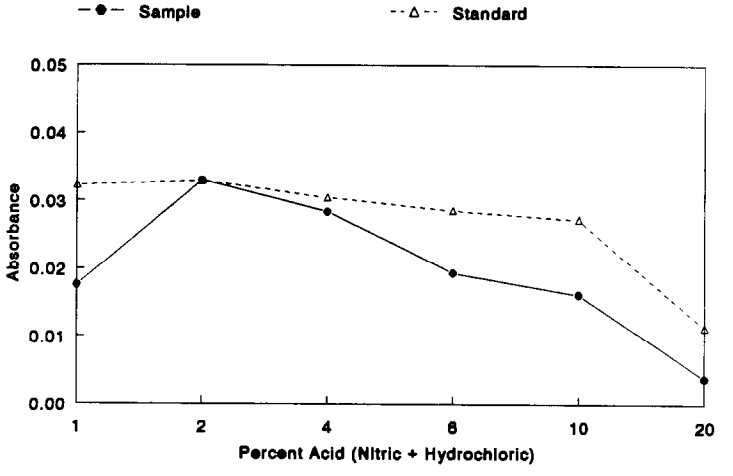

Fig. 2. Effect of (a) varying the concentration of a 1:1 mixture of nitric and hydrochloric acids on a 10 ng Hg/ml standard (–△–) and (b) varying the acid mixture concentration in the digestion procedure for certified reference material CZN-1 (–●–). The curves are normalized to the maximum signal for comparison.

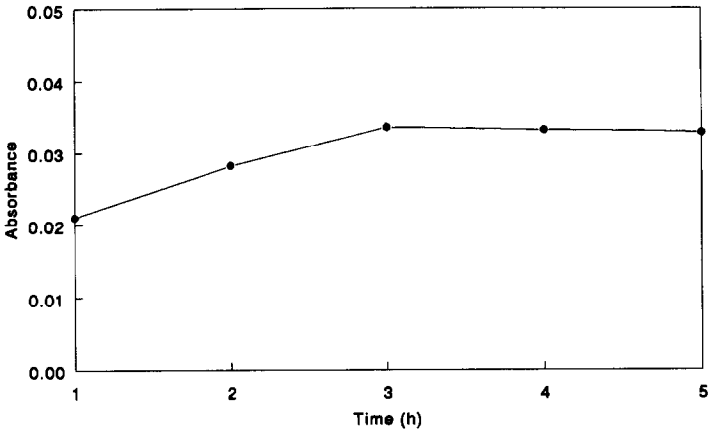

Fig. 3. Effect of digestion time on the signal for Hg in SRM 113b.

of standard addition revealed a suppression of the mercury signal of approximately 10% in the presence of the sample matrix. Therefore, all results are corrected for spike recovery. For the instrumental conditions used in this analysis, the detection limit, defined as the mercury concentration corresponding to three times the standard deviation of the blank, is 0.08 ng Hg/ml, corresponding to a detection limit in the sample of 0.08 μg Hg/g.

The accuracy of this method was tested by the determination of mercury in a certified zinc ore concentrate reference material (CRM CZN-1) produced by the Canada Center for Mineral and Energy Technology.[12] The analysis of this material yielded a value of 44.7 ± 0.1 μg Hg/g (95% confidence interval), in excellent agreement with the certified concentration of 43 ± 4 μg Hg/g. Analysis of the proposed NIST SRM zinc ore concentrate yielded a value of 0.55 ± 0.06 μg Hg/g (95% confidence interval).

Samples of both the zinc ore concentrate and CRM CZN-1 were analyzed with, and without, oven drying at 105°C. Weight loss on drying was 0.21% for CZN-1 and 0.06% for the zinc ore concentrate. No significant difference was observed in the mercury concentrations of dried and undried samples.

CONCLUSION

The high accuracy, precision, and sensitivity of the FIA-CVAAS system when combined with an optimized sample preparation method is apparent from the results obtained in this study. Acid concentration and digestion time are critical for efficient extraction of mercury from the ore concentrate or minimum matrix interference in the generation of mercury using FIA-CVAAS.

Acknowledgements—One author (RS) acknowledges the support of the Department of Science and Technology, New Delhi, India and NIST. To describe experimental procedures adequately, it was occasionally necessary to identify commercial products by manufacturer's name or label. In no instance does such identification imply endorsement by NIST nor does it imply that the particular product or equipment is necessarily the best available for that purpose.

REFERENCES

1. M. Zmijeska, *J. Radioanal. Chem.*, 1977, **35**, 389.
2. M. Shull and J. D. Winefordner, *Anal. Chem.*, 1971, **43**, 799.
3. W. R. Hatch and W. L. Ott, *Anal. Chem.*, 1968, **40**, 2085.
4. G. D. Christian and J. Ruzicka, *Anal. Chim. Acta*, 1992, **261**, 11.
5. R. Kuroda, K. Oguma, K. Kitada and S. Kozuka, *Talanta*, 1991, **38**, 1119.
6. C. G. Maria and A. Townshend, *Anal. Chim. Acta*, 1992, **261**, 137.
7. J. Ruzicka and E. H. Hansen, *Flow-injection Analysis*, 2nd Ed. John Wiley, New York, 1988.
8. M. Valcarcel and M. D. L. de Castro, *Flow-injection Analysis: Principles and Applications*. Ellis Horwood, Chichester, 1987.
9. C. P. Hanna, J. F. Tyson and S. McIntosh, *Anal. Chem.*, 1993, **65**, 653.
10. J. J. Lingane, *Analytical Chemistry of Selected Metallic Elements*. Reinhold, New York, 1966.
11. H. Agemian, K. I. Aspila and A. S. V. Chau, *Analyst*, 1975, **100**, 253.
12. Certificate of Analysis, Reference Zinc Ore Concentrate CZN-1, Canada Centre for Mineral and Energy Technology, Ottawa, Canada.

Talanta, Vol. 40, No. 10, pp. 1481–1488, 1993
Printed in Great Britain.

0039-9140/93 $6.00 + 0.00

DIFFERENTIAL PULSE CATHODIC STRIPPING VOLTAMMETRY OF THE COPPER COMPLEXES OF GLYCYL–L-HISTIDYL–GLYCINE AT A HANGING MERCURY DROP ELECTRODE

F. NIL ERTAS, ARNOLD G. FOGG* and JOSINO C. MOREIRA†
Department of Chemistry, Loughborough University of Technology, Loughborough, Leicestershire LE11 3TU, U.K.

JIRI BAREK
UNESCO Laboratory for Environmental Electrochemistry, Department of Analytical Chemistry, Charles University, Prague, Czechoslovakia

(*Received* 12 *February* 1993. *Revised* 30 *April* 1993. *Accepted* 30 *April* 1993)

Summary—The behaviour of the copper complexes of glycyl–L-histidyl–glycine (GHG) was investigated using cyclic voltammetry and differential pulse voltammetry after their adsorptive accumulation on the surface of a hanging mercury drop electrode (HMDE). The nature of the observed cathodic and anodic peaks was established and optimum conditions were found for the differential pulse cathodic stripping voltammetric determination of GHG at the $1 \times 10^{-8} M$ concentration level using adsorptive accumulation at −0.20 V *vs.* Ag/AgCl reference electrode and the cathodic stripping peak around −0.4 V (pH 8.3). This peak corresponds to the reduction of the Cu(I)–GHG complex formed at the HMDE surface as an intermediate in the reduction of Cu(II)–GHG to Cu(O)amalgam.

The electrochemical behaviour of copper(II) complexes with various oligopeptides is of current interest since these substances mimic the specific Cu(II) transport site of several proteins. Using a small molecule, which represents a simplification of the natural binding site sequence of a larger molecule, it is possible to carry out many important studies which are not feasible with a protein molecule. It is well known that the stabilities of the copper(II) complexes of oligopeptides are considerably enhanced by the presence of a histidyl residue in position three[1–4] from the end of the peptide because of the formation of a very strong tetradentate chelate. In our previous paper[5] this fact was utilized in developing an extremely sensitive cathodic stripping voltammetric method for determining glycylglycyl–L-histidine. Similarly, the presence of the histidyl residue in the second position from the end of the peptide produces a strong tridentate chelate as is demonstrated in the case of glycyl–L-histidylglycine.[4] This tripeptide, because of its histidyl residue within the chain, is also important as a model for further studies of the basic interactions between proteins and copper ions.[4] For this reason the Cu(II)–GHG complexes have been investigated as useful models of copper–protein interaction both in solution[2–7] and in the solid phase[8] and it has been proved that copper(II) is coordinated via the 1-nitrogen of the imidazole ring and the nitrogen atoms of the peptide and amide groups.

Therefore, it is quite clear that the position of the histidyl residue in oligopeptide molecules may cause remarkable differences in both the modes of their complex formation and in their polarographic and voltammetric behaviour. There are relatively few papers on the polarographic behaviour of Cu(II)-oligopeptides.[8–12] The appearance of one predominant cathodic peak, which corresponds to the reduction of the Cu(II) complex to Cu(O)amalgam, has been reported for complexes with glycylglycylglycine,[10] glycyl–L-histidyl–L-lysine and glycyl–L-histidyl–glycine,[11] and glycylglycyl–L-histidine.[5,12] This is in agreement with the well known fact[10] that the electrochemical reduction of copper(II) preferentially occurs by two electrons to form Cu(O)amalgam. When

*Author for correspondence.
†Present address: Departamento de Quimica da UFRRJ, Antiga Rio SP Km 47, Itaguai, Brazil.

complexation stabilizes copper(I), however, this can give rise to a one-electron reduction of copper(II) occurring more readily than the two-electron reduction. This results in two successive and distinct single electron transfer steps being obtained, as has been reported for copper(II) complexes of histidine and β-alanyl–L-histidine.[13] Our previous studies on the cathodic stripping behaviour of copper(II) complexes of imidazole,[14] histidine[15] and glycylglycyl–L-histidine[5] have led to extremely sensitive methods for the determination of copper(II) and the latter two biologically significant organic substances.

So far, no detailed study of the cathodic stripping behaviour of the copper complexes of glycyl–L-histidylglycine (GHG) has been reported. For this reason the present study was carried out and its results are reported with the aim of increasing the understanding of the electrochemical behaviour of these biologically interesting systems and of developing a sensitive method for the cathodic stripping voltammetric determination of GHG which is itself polarographically inactive.

EXPERIMENTAL

Apparatus and reagents

Cathodic stripping voltammetry was carried out with a Metrohm 626 Polarecord and a 663 VA-Stand, or with a Metrohm 646/647 VA Processor, using a multi-mode electrode in the HMDE mode. The three-electrode system was completed by means of a glassy carbon auxiliary electrode and an Ag/AgCl (3*M* KCl) reference electrode. All potentials given are relative to this Ag/AgCl electrode. The cyclic voltammetric experiments were carried out by connecting the electrodes on the Metrohm 663 VA-Stand to a PAR 174A polarographic analyser (Princeton Applied Research); the multimode-electrode (HMDE) was still activated by means of the Metrohm 626 Polarecord.

Supporting electrolytes and buffers were prepared using analytical grade reagents supplied by BDH. A $1 \times 10^{-2}M$ solution of glycyl–L-histidylglycine was prepared by dissolving precisely weighed amounts of pure substance supplied by Sigma in 5 ml of 0.2*M* HCl using sonication. It was kept in a refrigerator and prepared freshly each day. Standard solutions of copper(II) were prepared by diluting SpectrosoL atomic absorption standard solution (BDH). Stock solutions of copper(I) were prepared by dissolving copper(I) chloride in hydrochloric acid according to Svehla.[16] Hydrogencarbonate supporting electrolyte solution (0.1*M*) was used for voltammetric measurements at pH 8.3.

Procedures

The general procedure used to obtain cathodic stripping voltammograms was as follows. A 20 ml aliquot of 0.1*M* hydrogencarbonate supporting electrolyte solution was placed in a voltammetric cell and the required amounts of standard GHG and copper(II) solutions were added. The stirrer was switched on and the solution was purged with nitrogen for 5 min. After forming a new HMDE, accumulation was effected for the required time at the appropriate potential while stirring the solution. Maximum drop size and stirrer speed were used throughout with the Metrohm 626 (medium drop size—nominally 0.40 mm^2—with the 646). At the end of the accumulation period the stirrer was switched off, and, after 20 sec had elapsed to allow the solution to become quiescent, a negative potential scan was initiated between the accumulation potential and −0.8 V. When the adsorptive accumulation was carried out at more negative potentials, the potential was changed immediately to −0.1 V from where a negative potential scan was initiated.

Cyclic voltammetry was carried out either immediately after forming a new HMDE or after preceding accumulations at different potentials for different times while stirring the solution. Either negative or positive scans were initiated after accumulation depending on the potential of accumulation. Sampled direct current polarography was performed using the static mercury drop electrode (SMDE) mode with drop time 1 sec and scan rate of 5 mV/sec.

In carrying out medium exchange experiments the PAR 174A instrument was switched to 'off' on the front control panel whilst the solution was being changed: this puts the cell onto open circuit. The cell was reconnected with the accumulation potential being applied.

RESULTS AND DISCUSSION

GHG was found to be electroinactive over the pH range of 5–12 in which range the 1:1 complex is known to be formed.[1-7,17] Sampled DC polarography of a solution containing $1 \times 10^{-4}M$ copper(II) and a five-fold excess of GHG gave two waves which are not well separated at higher pH. Takehari and Ide[11] reported

only a single two-electron reduction process for copper(II)–GHG on the basis of orientative cyclic voltammetry measurements. However, they used equimolar solutions of copper(II) and GHG with relatively high net concentrations of the complex. Under these conditions the two steps mentioned above probably coalesce into one two-electron step. In a $0.1M$ $NaHCO_3$ solution containing $1M$ KCl, which stabilizes Cu(I), the second wave increased after addition of Cu(I) chloride solution prepared according to Svehla,[16] thus confirming that it corresponds to the reduction of the Cu(I)–GHG complex to Cu(O)amalgam. Two main peaks were observed in differential pulse polarograms of a solution containing $1 \times 10^{-4}M$ Cu(II) and $5 \times 10^{-4}M$ GHG, their peak potentials shifting in this pH range from -0.15 to -0.20 V and from -0.36 to -0.47 V. These potentials correspond to the half wave potentials of the above mentioned DC polarographic waves. At a lower pH, a peak at -0.07 V corresponding to reduction of uncomplexed copper(II) was also observed. A polarographic maximum appeared around neutral pH: this was easily removed by the addition of Triton X-100. The best developed, and highest, peaks were observed at pH values of approximately 8. Therefore, further studies were carried out using $0.1M$ hydrogencarbonate supporting electrolyte (pH 8.3). The formation of the 1:1 Cu(II):GHG complex at pH 8.3 was confirmed by the fact that the height of the polarographic wave of a $1 \times 10^{-5}M$ solution of uncomplexed copper(II) decreased to one half of its original value in the presence of $0.5 \times 10^{-5}M$ GHG and disappeared completely in the presence of $1 \times 10^{-5}M$ GHG.

Cyclic voltammetric behaviour of copper complexes of glycyl–L-histidyl–glycine

The effect of GHG concentration on the cyclic voltammograms of Cu–GHG complexes after preceding accumulation at -0.6 V in a pH 8.3 hydrogencarbonate supporting electrolyte, is shown in Fig. 1. Three cathodic and three anodic peaks are observed, the exact position and heights of which depend on both the GHG and Cu(II) concentrations, the accumulation potential and the accumulation time, and on the scan rate, direction and switching potentials of subsequent cyclic voltammetric scans. On the basis of the cyclic voltammetric behaviour of free copper(II) (in the absence of GHG) under these conditions, the first cathodic peak at -0.12 V can be assigned to the reduction of free copper(II) to copper(O)amalgam, while the most positive anodic re-oxidation peak at -0.07 V can be assigned to re-oxidation of Cu(O)amalgam back to free copper(II). On the basis of the DC and DP polarographic behaviour of the Cu(II)–GHG complex, the second cathodic peak around -0.2 V and the third cathodic peak around -0.4 V can be assigned to a stepwise one electron reduction of the Cu(II)–GHG complex to the Cu(I)–GHG complex (peak around -0.2 V), followed by the reduction of the Cu(I)–GHG complex to Cu(O)amalgam (peak around -0.4 V). The morphology of the observed peaks and their dependence on the scan rate suggest that the first cathodic and the most positive anodic peak correspond to diffusion-controlled processes, while the second and third cathodic peaks and

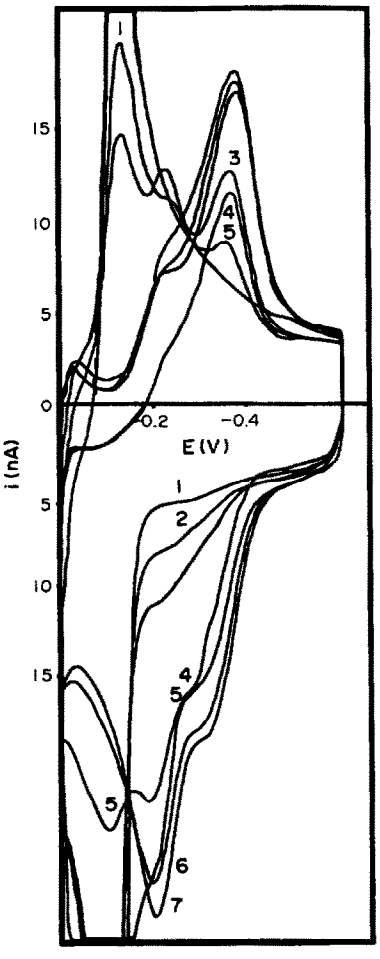

Fig. 1. Effect of GHG concentration on the cyclic voltammograms of Cu–GHG complexes: $1 \times 10^{-6}M$ Cu(II); pH 8.3; scan rate 50 mV/sec; accumulation potential -0.6 V; accumulation time 2 min in stirred solution; [GHG]: (1) 0; (2) 2.5×10^{-6}; (3) 5×10^{-6}; (4) 1×10^{-5}; (5) 2×10^{-5}; (6) 3×10^{-5}; (7) 4×10^{-5}.

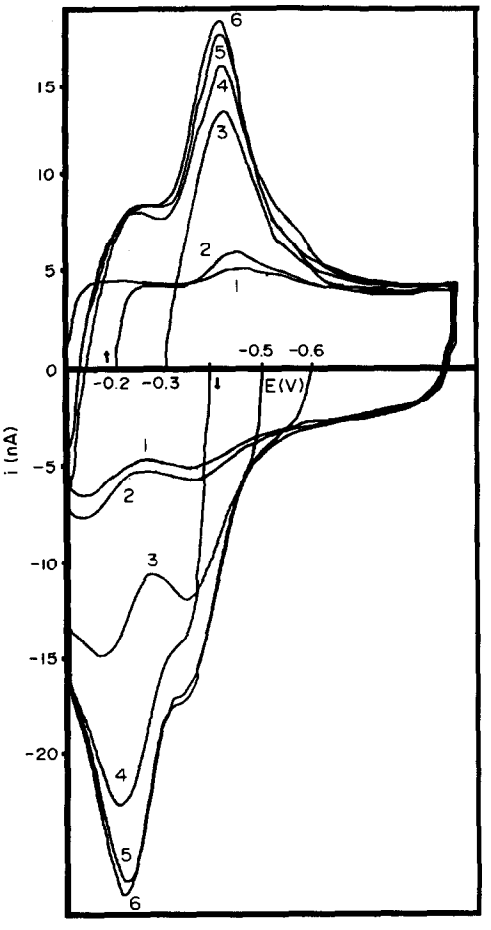

Fig. 2. Effect of accumulation potential: $1 \times 10^{-6}M$ Cu(II); $1 \times 10^{-5}M$ GHG; pH 8.3; scan rate 50 mV/sec; accumulation time 2 min in stirred solution; accumulation potential: (1) −0.1 V; (2) −0.2 V; (3) −0.3 V; (4) −0.4 V; (5) −0.5 V; (6) −0.6 V. The arrows show the direction of the scan initiated after the accumulation step.

the remaining anodic peaks correspond to the reduction and oxidation of adsorbed species.

The above assignment of the observed cathodic peaks is in agreement with the reported electrochemical evidence for the formation of the copper(I) complexes as intermediates in the reduction of Cu(II) complexes of glycine[18] and of histidine and carnosine[13] and with the polarographic behaviour of the copper(I)–histidine complex.[19]

The effect of accumulation potential on the cyclic voltammograms obtained is shown in Fig. 2. The third peak around −0.4 V was very small at accumulation potentials more positive than −0.3 V, which supports the assumption that it corresponds to a species formed at the electrode surface at potentials between −0.2 and −0.3 V (increasingly near −0.3 V). Furthermore, it is clear that during accumulation at −0.1 and −0.2 V no Cu(O)amalgam is formed as the anodic peak at −0.07 V is absent during the subsequent anodic scan. This is not apparent from Fig. 2 as the potential −0.07 V is out of the range shown. Therefore, the product of the reduction of Cu(II)–GHG complex at −0.2 V is not Cu(O)amalgam, and this was further proved by an experiment with medium exchange. In this experiment, after accumulation at −0.25 V in a solution containing $1 \times 10^{-5}M$ GHG and $1 \times 10^{-6}M$ Cu(II), the HMDE was transferred to a solution containing only $0.1M$ $NaHCO_3$ supporting electrolyte and an anodic scan was initiated. No anodic peak that would have indicated the dissolution of Cu(O)amalgam could be detected. However, the peak around −0.4 V is clearly seen after accumulation at −0.25 V. This means that the species formed at −0.25 V is further reduced which supports our assumption that the second and third peaks correspond to stepwise one-electron reductions of the Cu(II)–GHG complex.

To establish the nature of the anodic peaks, a medium exchange experiment was carried out using an accumulation potential of −0.7 V. After accumulating in the presence of excess of GHG and transferring the HMDE into a solution containing only hydrogencarbonate supporting electrolyte solution, only the peak at −0.07 V corresponding to the re-oxidation of Cu(O)amalgam was observed during the subsequent anodic scan. Therefore, it can be assumed that Cu(O)amalgam is formed at −0.7 V, and that GHG is not adsorbed sufficiently strongly at this potential—repulsion of the negatively charged GHG molecule by the negatively charged HMDE surface would be expected—and is removed during medium exchange. This medium exchange experiment confirms that the third cathodic peak around −0.4 V can be assigned to the reduction of the Cu(I)–GHG complex to copper(O)amalgam in accordance with our previous finding. A similar medium exchange experiment using Cu(O)amalgam accumulated at −0.7 V in the absence of GHG followed by an anodic scan after addition of GHG clearly showed that the anodic peaks around −0.2 and −0.3 V can be assigned to a stepwise oxidation of Cu(O)amalgam to the Cu(II)–GHG complex via the Cu(I)–GHG complex.

The cyclic voltammograms in Fig. 3 show that accumulation at −0.7 V in a solution containing a 1:10 metal ion to ligand concentration ratio yields two reduction peaks at

−0.24 and −0.42 V and two related anodic peaks at about −0.19 and −0.36 V, which increase in height with collection time from 0 to 120 sec. The relative position of these cathodic and anodic peaks indicate a degree of irreversibility for both the Cu(II)–GHG/Cu(I)–GHG and the Cu(I)–GHG/Cu(O)-amalgam systems. A small shift in the more positive anodic peak from −0.16 to −0.22 V with increasing accumulation time can be explained by the increase of concentration of GHG at the HMDE surface. When the accumulation was performed at 0 V, only very small cathodic and anodic peaks were observed. The height of these peaks did not increase with increasing accumulation time thus confirming our findings on the nature of these peaks.

Multiple scan cyclic voltammograms after accumulation at −0.1 and −0.7 V are shown in Fig. 4. After accumulation at −0.1 V, only very small cathodic peaks were observed during the first cathodic scan (see Fig. 4(a)). The anodic peaks obtained during the first anodic scan were much higher than the cathodic peaks thus confirming our assumption that copper(O)-amalgam is accumulated during the scans at potentials more negative than that of the cathodic peak around −0.4 V. This assumption is further confirmed by the observed increase of all cathodic and anodic peaks with subsequent scans. It is possible that the Cu(I)–GHG complex can be formed at the HMDE surface not only as an intermediate in the reduction of the Cu(II)–GHG complex to Cu(O)amalgam but also via the reaction of Cu(O)amalgam with the Cu(II)–GHG complex. The decreasing height of all observed cathodic and anodic peaks with subsequent scans after accumulation at −0.7 V (see Fig. 4(b)) can be explained by the desorption of the accumulated species at the switching potentials which are sufficiently far away from the potential of the electrocapillary zero where maximum adsorption of the metal–peptide complexes would be expected to occur.

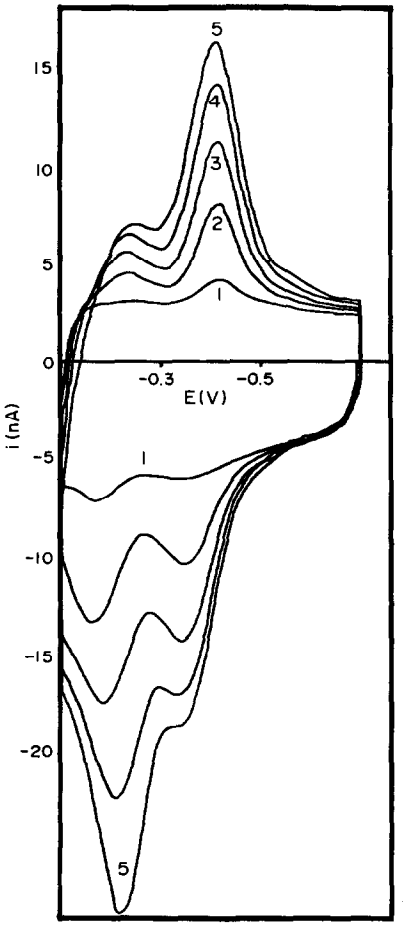

Fig. 3. Effect of accumulation time: $1 \times 10^{-6}M$ Cu(II); $1 \times 10^{-5}M$ GHG; pH 8.3; scan rate 50 mV/sec; accumulation potential −0.7 V; accumulation time: (1) 0; (2) 30; (3) 60; (4) 90; (5) 120 sec.

Differential pulse cathodic stripping voltammetric determination of glycyl–L-histidyl–glycine

Hydrogencarbonate supporting electrolyte solution (pH 8.3) was used for this determination as it gives a smaller background current in the presence of excess of copper(II). In a solution containing $1 \times 10^{-6}M$ Cu(II) and $1 \times 10^{-7}M$ GHG and using an accumulation potential of −0.2 V, the height of the peak around −0.3 V increases rectilinearly with accumulation time up to 3 min; the peak potential shifts from −0.27 to −0.31 V with increasing accumulation time. It should be noted that in the presence of $1 \times 10^{-6}M$ Cu(II) and an equal amount of GHG under otherwise identical conditions, the height of the peak around −0.32 V is not a linear function of accumulation time thus indicating that the HMDE surface is becoming saturated. Under these conditions, the peak potential shifts from −0.24 to −0.27 V for accumulation times increasing from 15 sec to 2 min. Note that the differential pulse voltammetric peaks are shifted towards more positive potentials compared with the cyclic voltammetric peaks in agreement with theory.[20]

On the basis of the above results, the following optimum conditions were chosen for the determination of GHG in the concentration region $(1 - 12) \times 10^{-8}M$: $0.1M$ $NaHCO_3$ (pH 8.3) as a base electrolyte, concentration of

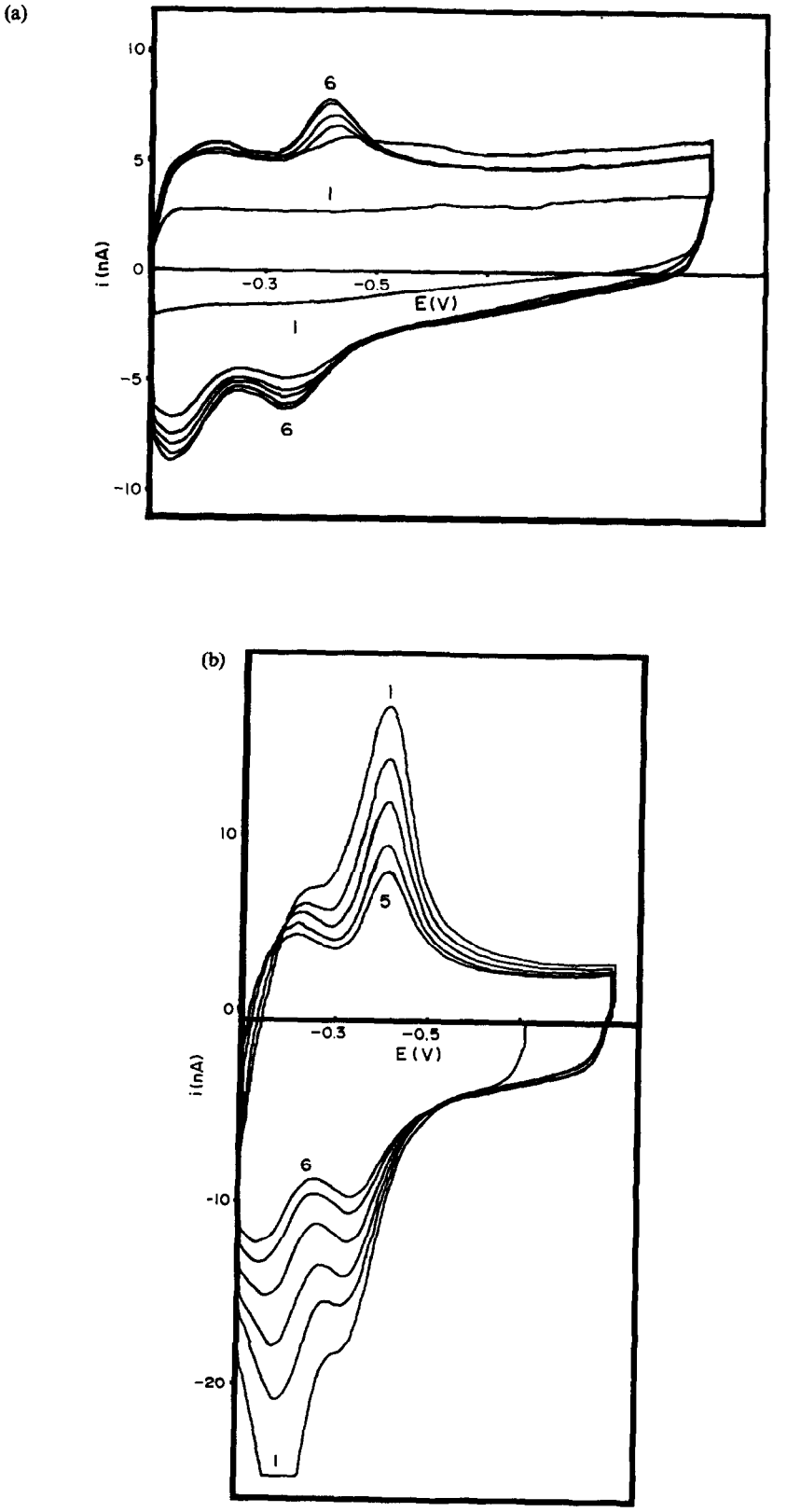

Fig. 4. Effect of accumulation potential on multiple scan cyclic voltammograms of the Cu(II)–GHG complexes: $1 \times 10^{-6}M$ Cu(II); $1 \times 10^{-5}M$ GHG; pH 8.3; scan rate 50 mV/sec; accumulation time 2 min in stirred solutions; accumulation potential -0.1 V (a) and -0.7 V (b). The numbers on the plots indicate the sequence of the scans.

copper(II) = $5 \times 10^{-6}M$, accumulation potential = -0.2 V *vs.* Ag/AgCl reference electrode, accumulation time = 2 min in stirred solution. The height of the peak at -0.37 V, which corresponds to the reduction of Cu(I)–GHG complex to Cu(O)amalgam, was measured. Calibration graphs obtained in this way after subtraction of the blank were rectilinear with a slope of 0.10 A/M and an intercept of 0.2 nA. Coefficients of variation at the $2 \times 10^{-8}M$ level were typically <3% (five determinations). The limit of detection calculated as three times the standard deviation of the determination of GHG at the $2 \times 10^{-8}M$ level was about $0.5 \times 10^{-8}M$. Typical differential pulse cathodic stripping voltammograms for obtaining a calibration graph for the determination of GHG are shown in Fig. 5. It should be noted that this method of determining GHG is not as satisfactory as that for determining GGH, which was described previously.[5] The peak currents obtained in the determination of GHG using the present method are much lower than those obtained for an equivalent amount of GGH, and the peak potential is at a less negative potential. Therefore in the present method at the $10^{-8}M$ level blank peaks can be quite high relative to the sample peaks. The blanks appear to be caused by traces of a complexable material in the buffers used. UV irradiation of suitable buffers to remove organic material might be tried to improve this situation.

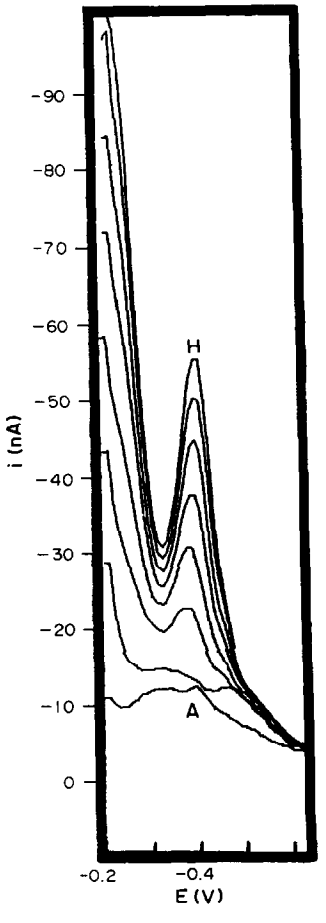

Fig. 5. Differential pulse cathodic stripping voltammograms obtained for preparing a calibration graph for the determination of GHG. Accumulation potential: -0.2 V; scan rate: 10 mV/sec; accumulation time: 2 min; A–I. 0.1M pH 8.2 hydrogen carbonate supporting electrolyte. B–I. $[Cu^{2+}] = 5 \times 10^{-6}M$. GHG concentration = C. $1 \times 10^{-7}M$, D. $2 \times 10^{-7}M$, E. $3 \times 10^{-7}M$, F. $4 \times 10^{-7}M$, G. $5 \times 10^{-7}M$, H. $6 \times 10^{-7}M$.

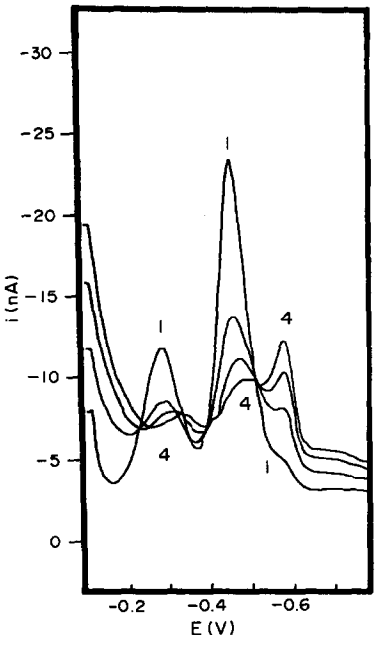

Fig. 6. Differential pulse cathodic stripping voltammograms of the Cu–GHG complexes at pH 10.5: $1 \times 10^{-6}M$ Cu(II); $1 \times 10^{-4}M$ GHG; 0.1M borate supporting electrolyte (pH 10.5); scan rate 50 mV/sec; modulation amplitude 50 mV; accumulation potential -0.1 V; accumulation time: (1) 0; (2) 15; (3) 30; (4) 45; (5) 60; (6) 75; (7) 90 sec.

Considerably different cathodic stripping voltammetric behaviour of the Cu–GHG complexes was observed at pH 10.5 (Fig. 6). Two peaks, at -0.29 and -0.46 V were observed without accumulation. However with increasing accumulation time these two peaks gradually disappeared as a third peak, at about -0.6 V, appeared. This mechanism has not been studied here, but clearly some change in the composition of the complex is occurring on the electrode surface. The presence of isosbestic points seems to indicate a conversion of one species into another single species.

CONCLUSIONS

The sampled DC polarographic, cyclic voltammetric and cathodic stripping voltammetric characteristics of the Cu–GGH complexes described above have some significant differences from those of the Cu–GHG complex investigated in our previous communication[5] in terms of the peak potentials and the relative position of the copper(I) and copper(II) peaks. Nevertheless, use of the peak around −0.4 V (copper(I) → copper(O)) provides a very sensitive method for the differential pulse cathodic stripping voltammetric determination of polarographically inactive GHG. The selectivity of this determination is limited by the interference of surface active substances, by polarographically active substances reducible around −0.3 V, and by substances which can form complexes either with copper (such as some amino acids[13,15] or peptides[10–12]) or with GHG (such as some other bivalent cations[1,17]). A preliminary separation step would be required in the presence of these interferents. Many model biological studies, however, are carried out in a simple matrix, and the voltammetric method developed here can provide a very sensitive tool for determining trace amounts of the GHG. Furthermore, it was confirmed by the present study, that cathodic stripping voltammetry can give us a useful insight into the redox behaviour of biologically interesting complexes of copper with various oligopeptides, when these are adsorbed on the surface of the HMDE. The HMDE can be considered to mimic a hydrophobic physiological redox site. It can be expected that further relevant information, clarifying the role of Cu(II)–peptides complexes in redox processes in biological systems, can be obtained in this way.

REFERENCES

1. R. J. Sundberg and R. B. Martin, *Chem. Rev.*, 1974, **74**, 471.
2. E. Farkas, I. Sovago, T. Kiss and A. Gergely, *J. Chem. Soc. Dalton. Trans.*, 1984, 611.
3. R. P. Agarwal and D. D. Perrin, *J. Chem. Soc. Dalton. Trans.*, 1975, 268.
4. R. Osterberg and B. Sjoberg, *J. Inorg. Nucl. Chem.*, 1975, **37**, 815.
5. A. G. Fogg, F. N. Ertas, J. C. Moreira and J. Barek, *Anal. Chim. Acta*, 1993, **278**, 41.
6. H. Aiba, A. Yokohama and H. Tanaka, *Bull. Chem. Soc. Jpn.*, 1974, **47**, 1437.
7. R. Osterberg and B. Sjoberg, *Acta Chem. Scand.*, 1968, **22**, 639.
8. R. Osterberg, B. Sjoberg and R. Soderquist, *Acta Chem. Scand.*, 1972, **26**, 4184.
9. M. Aihara, Y. Nakamura, Y. Nishida and K. Noda, *Inorg. Chim. Acta*, 1968, **124**, 169.
10. M. P. Youngblood and D. W. Margerum, *J. Coord. Chem.*, 1981, **11**, 103.
11. K. Takehara and Y. Ide, *Inorg. Chim. Acta*, 1991, **183**, 195.
12. K. Takehara and Y. Ide, *Inorg. Chim. Acta*, 1991, **186**, 73.
13. R. Bilewicz, *J. Electroanal. Chem. Interfacial. Electrochem.*, 1989, **267**, 231.
14. F. N. Ertas, J. C. Moreira and A. G. Fogg, *Analyst*, 1991, **116**, 369.
15. J. C. Moreira and A. G. Fogg, *Analyst*, 1990, **115**, 41.
16. G. Svehla, *Vogel's Qualitative Inorganic Analysis*, 6th Ed., p. 288. Longmans, Singapore, 1979.
17. A. H. Sigel and R. B. Martin, *Chem. Rev.*, 1982, **82**, 385.
18. G. Thomas and P. S. Zacharias, *Polyhedron*, 1985, **4**, 811.
19. D. C. Davis and W. R. Bordelon, *Anal. Letters*, 1970, **3**, 449.
20. A. J. Bard and L. R. Faulkner, *Electrochemical Methods*. Wiley, New York, 1980.

Talanta, Vol. 40, No. 10, pp. 1489–1498, 1993
Printed in Great Britain.

0039-9140/93 $6.00 + 0.00

WATER–ORGANIC SOLVENT SYSTEMS IN COUNTERCURRENT CHROMATOGRAPHY: LIQUID STATIONARY PHASE RETENTION AND SOLVENT POLARITY

ALAIN BERTHOD* and NATHALIE SCHMITT
Laboratoire des Sciences Analytiques, UA CNRS 435, Université de Lyon 1, 69622 Villeurbanne cedex, France

(*Received* 11 *February* 1993. *Revised* 26 *March* 1993. *Accepted* 26 *March* 1993)

Summary—Countercurrent chromatography (CCC) is a separation technique in which the stationary phase is a liquid. The liquid stationary phase retention is a critical problem in CCC. The retention of 18 organic solvents in a hydrodynamic CCC apparatus was measured with an aqueous mobile phase, the centrifuge spin rate and the mobile phase flow rate being constant, 800 rpm and 2 ml/min, respectively. Conversely, water retention was measured when the 18 solvents were the mobile phases. A direct relationship between the liquid stationary phase retention and the phase density difference was found. The liquid phase density difference is the most important parameter for stationary phase retention in a hydrodynamic CCC apparatus with coiled tubes. The chromatographic retention of formanilide was measured in biphasic systems and expressed as the formanilide partition coefficient. It is shown that the partition coefficient correlates with the Reichardt polarity index of the organic solvent when the liquid stationary phase retention volume does not.

Countercurrent chromatography (CCC) is an emerging technique for preparative purification and extraction of a wide variety of solutes.[1–5] CCC is a technique in which the stationary phase is a liquid. The mobile phase is also a liquid.

The main advantages of CCC are (i) high loadability, (ii) unique selectivities and (iii) robustness. In classical liquid chromatography, the injected solutes can access only the surface of the solid stationary phase. In CCC, the whole volume of the liquid stationary phase is used for solute partitioning. Tannins (4.3 g) were separated in one run with a 180 ml CCC apparatus.[6] The chromatographic selectivity is due to solute partition between the two immiscible liquid phases. The combination of solvents that produces two-phase systems is almost infinite. It is possible to use two, three or more solvents, which means that it is possible to adjust the selectivity by additions of a solvent that has some affinity for the two phases of a biphasic system.[7] The robustness of CCC is due to the liquid character of the stationary phase. Overload and irreversible adsorption problems are common in preparative liquid chromatography. Irreversible adsorption cannot occur in CCC. If a solute is retained too long, it is possible to switch the phase role: the mobile phase becomes stationary and the liquid stationary phase is pushed out of the CCC apparatus with the solute.

Liquid stationary phase retention by the CCC "column" is the most important problem in CCC. The liquid stationary phase should be retained while the mobile phase is pushed through. Many CCC apparatuses contain a continuous open tube coiled on one or several spools which are rotated in a centrifuge. The centrifugal field holds the liquid stationary phase tightly so that the liquid mobile phase can be pumped through it. Stationary phase retention depends on the CCC apparatus design, the operating conditions and the liquid system used. More than 20 different CCC apparatuses were designed by Ito.[1–3,5,8] Most of them contain coiled Teflon tubing. The liquid stationary phase retention capabilities of these apparatuses are difficult to compare. A constant observation with different CCC apparatuses is that liquid stationary phase retention increases with the centrifuge rotation speed and decreases with the flow rate.[7] Liquid stationary phase retention also depends on the liquid system used. Ito and

*Author for correspondence.

co-workers studied the CCC retention behaviour of several liquid systems.[9-12]

This work presents the behaviour of water–organic solvent biphasic liquid systems. In CCC, the liquid stationary phase should be retained somewhat to obtain solute retentions and separations. First, a systematic study of liquid stationary phase retention was done by limiting the numerous parameters as follows: (i) only one CCC apparatus with coiled Teflon tubes was used; (ii) the spin rate was kept constant at 800 rpm; (iii) the mobile phase flow rate was 2 ml/min in all experiments; (iv) the biphasic liquid systems studied were made with two pure solvents only; and (v) one of the two pure solvents was water. In such conditions, the retention of 18 organic solvent stationary phases was measured with the aqueous phase being the mobile phase. The retention of the aqueous phase was also measured when the 18 different organic phases were the mobile phases. The collected data were compared to different physico-chemical properties of the binary liquid systems. Second, the retention of a solute, formanilide, expressed as the liquid–liquid partition coefficient, was studied and related to the organic solvent polarity.

EXPERIMENTAL

Chromatographic system

The CCC apparatus was the Model CPHV 2000 from Société Française de Chromato Colonne (SFCC, 95610 Eragny, France), which is a coil planet centrifuge apparatus first designed by Mandava and Ito.[2] It contains three multilayer coils connected in series spinning with a planetary motion around a central axis. A special gear arrangement is designed to avoid any rotary seal. The apparatus was described in a recent publication.[13] Each spool was filled with 133 turns of PTFE tubing, i.d. 1/16 in. (1.6 mm), length 26 m, coiled in seven layers of 19 turns. The Ito β value is the ratio of the coil radius, r, to the spool revolution radius, R. The β ratio was 0.37 for the first inner layer with $r = 2.2$ cm and $R = 6$ cm. It was 0.75 for the outermost visible layer with $r = 4.5$ cm and $R = 6$ cm. The average β value for this CCC apparatus was 0.56. The internal volume of one coiled spool was 52 ml. The three-coil apparatus had a total internal volume, V_T, of 158 ml. The whole system was housed in an air-thermostatted box. The temperature was regulated to 22 ± 0.5°C.

A Shimadzu LC6A pump was used to fill the CCC apparatus with the stationary phase and to push the mobile phase at a flow rate of 2 ml/min. A Shimadzu SPD-6A UV detector was used at 254 nm with a CR5-A recorder integrator.

Chemicals

The 18 solvents are listed in Table 1. They were obtained from Merck (Darmstadt, Germany), Fluka (Saint Quentin Fallavier, France), Prolabo (Paris, France) and Laurylab (Chassieu, France). Methyl-2-cyclohexanol acetate and trimethylbenzene (TMB or mesitylene, trimethyl-1,3,5-benzene) were industrial solvents (80% average purity) supplied by ELF-Atochem (Vernaison, France). Ethane trichloro-1,1,2-trifluoro-1,1,2 is also called Freon 113. Formanilide was used as a test solute of intermediate polarity and was soluble in many of the 18 solvents tested. It was supplied by MTM (Lancaster Synthesis, Strasbourg, France). Reichardt's dye, 2,6-diphenyl-4-[2,4,6-triphenylpyridinio]-phenolate inner salt, was obtained from Sigma (St Louis, MO, U.S.A.).

Physico-chemical measurements

Densities were estimated simply by weighing a known volume of the liquid phase. Surface tension and interfacial tension were measured using a Du Nouy Tensiometer (Krüss, Hamburg, Germany) with a 15 mm diameter platinum ring. The measurements were performed at 21 ± 0.5°C. The physico-chemical data of the pure liquids are listed in Table 1.

Method

The water–organic solvent was equilibrated overnight to obtain an aqueous phase saturated in organic solvent and a water-saturated organic phase. The apparatus was first filled with the liquid chosen to be the stationary phase. This took about 25 min at 8 ml/min flow rate. Next, the centrifuge was turned on up to a stable rotation speed of 800 rpm. The pump was rinsed with the mobile phase. The mobile phase was pushed into the apparatus at 2 ml/min. The mobile phase entered through the tail of the apparatus if it was lighter than the liquid stationary phase and vice versa. As long as the apparatus was not equilibrated, the stationary phase was pushed off the apparatus and collected in a graduated cylinder. Once the immiscible mobile phase appeared at the exit of the apparatus, two liquid layers were seen in the

Table 1. Physico-chemical parameters of the solvents used

Solvent	*M* (Daltons)	b.p. (°C)	m.p. (°C)	vap. P. (mbar)	*d* (g/ml)	Viscosity (cP)	Surf. t. (dyne/cm)	Dielec. const.	Dip. mom. (Debye)
Butane dichloro-1,4	127.0	153.9	−37.3	—	1.140	—	34.6	—	—
Butanol	74.12	117.7	−88.6	6.83	0.806	2.571	24.67	17.51	1.75
Chloroform	119.3	61.17	−63.5	194.8	1.485	0.55	26.5	4.806	1.15
Dibutylphthalate	278.3	340	−35	0.1	1.043	15.4	33.4	6.44	2.82
Dichloromethane	84.93	39.64	−94.9	435.8	1.317	0.393	27.89	8.9	1.14
Ethane trichloro-1,1,2-trifluoro-1,2,2	187.3	47.63	−36.4	363.6	1.563	0.711	17.75	2.41	—
Ethane-1,1,1-trichloro	133.4	74.08	−30.4	123.7	1.330	0.795	25.56	7.252	1.7
Ethane dichloro-1,2	98.96	83.48	−35.6	83.35	1.246	0.83	31	10.37	1.83
Ethyl acetate	88.10	77.11	−83.5	94.51	0.895	0.426	23.1	6.02	1.82
Furfural	92.08	161.8	−36.5	2.5	1.154	1.49	41.1	38	3.54
Heptane	100.2	98.42	−90.5	45.7	0.679	0.3967	19.7	1.92	0
Methylethylketone	72.10	79.58	−86.6	90.6	0.780	0.378	24.6	18.51	2.76
Methyl tert-butyl ether	88.14	55.2	−108	313	0.741	0.27	19.4	4.5	1.32
Octanol	130.2	195.1	−14.9	0.075	0.822	7.363	26.92	10.34	1.76
Methyl-2-cyclohexanol acet.	156.2	193	—	0.5	0.936	—	28.5	—	—
Trimethylbenzene	120.1	164.7	−44.7	2.5	0.861	1.15	28.3	2.27	0
Toluene	92.14	110.6	−94.9	28.53	0.862	0.552	27.92	2.38	0.31
Tributylphosphate	266.3	289	−80	0	0.973	3.39	27.5	8.91	3.07
Water	18.01	100	0	23.75	0.997	0.8902	71.81	78.3	1.82

M, molecular weight; b.p., boiling point; m.p., melting point; vap. P., vapour pressure; *d*, density; surf. t., surface tension; dielectric constant is dimensionless; dip. mom., dipole moment, at 20°C.

Data from C. Reichardt, *Solvents and Solvent Effects in Organic Chemistry*. VCH, Weinheim, Germany, 1988, and from R. Weast, *Handbook of Chemistry and Physics*, 67th edn. CRC Press, Boca Raton, FL, 1987.

graduated cylinder, and equilibrium was reached. The CCC "column" was then ready and the displaced liquid stationary phase volume was measured. This volume, V_0, corresponds to the mobile phase volume inside the apparatus. The stationary phase volume inside the apparatus, V_s, is:

$$V_s = V_T - V_0.$$

The stationary phase retention is quantified by:

$$\%\text{ret} = V_s/V_T \times 100.$$

The test solute, formanilide, was injected in aqueous solution. Its retention volume, V_r, is linked to its liquid–liquid partition coefficient, P, by:

$$V_r = V_0 + PV_s = V_T + (P-1)V_s.$$

The peak efficiency was roughly estimated using:

$$N = 4(V_r/W_{0.6h})^2,$$

in which N is the peak efficiency expressed in plate number and $W_{0.6h}$ is the peak width at 60% of the peak height.

RESULTS AND DISCUSSION

Table 2 lists the stationary phase retention for the two sets of experiments: water mobile phase, organic stationary phase and vice versa. The driving pressure indicated corresponds to the equilibrated CCC "column", *i.e.* mobile phase leaving the apparatus. The partition coefficient and peak efficiency of formanilide are also listed in Table 2. They will be used in the solvent polarity discussion.

Solvent stationary phase retention

The first set of experiments was to push the water phase through the different organic stationary phases. The solvent miscibility in water was low enough so that the aqueous phase density and viscosity were close to 1 g/cm^3 (Table 3) and 0.9 cP (not measured), respectively. The interfacial tension varied from 1.3 (butanol) to 44.8 dyne/cm (heptane, Table 3).

The highest retention percentage, 82%, was obtained with the chloroform stationary phase. Similarly high retention percentages, 81%, were obtained with methyl tert-butyl ether and Freon 113 liquid stationary phases. The lowest retention percentages, 12% and 16%, were obtained with tributylphosphate and dibutylphthalate. Table 1 shows that chloroform and Freon 113 have the highest densities; tributylphosphate and dibutylphthalate have density values close to unity. The density difference between the organic stationary phase and the aqueous mobile phase seems to be an important parameter for CCC liquid stationary phase retention. To calculate exactly the phase density difference,

Table 2. Experimental CCC data obtained with 18 organic solvents

	Water mobile phase			Solvent mobile phase				
System: water with	P (bar)	V_s (ml)	%ret	P (bar)	V_s (ml)	%ret	K_{fo}	N_{fo} (plates)
Butane dichloro-1,4	0.8	55	34	0.9	68	42	0.5	400
Butanol	1.9	61	38	3.8	58	36	4.66	260
Chloroform	0.6	130	82	1.6	130	82	1.24	400
Dibutylphthalate	0.8	26	16	4	2	1	UV absorbing solvent	
Dichloromethane	0.7	122	76	2	125	78	1.83	370
Ethane dichloro-1,2	0.5	112	64	0.8	40	23	0.973	600
Ethane trichloro-1,1,1	0.8	129	81	2.4	108	67	0.64	380
Ethane trichloro-1,1,2-trifluoro-1,2,2	0.4	126	79	4.1	128	80	0	—
Ethyl acetate	1.4	89	51	0.4	99	57	1.58	700
Furfural	2	52	33	2	34	21	UV absorbing solvent	
Heptane	2.5	138	79	0.4	158	90	0.013	780
Methylethylketone	1.9	67.4	42	0.3	104	65	1.97	530
Methyl tert-butyl ether	3	141	81	0.2	164	94	0.51	500
Octanol	3	93	53	2.9	42	26	2.19	200
Methyl-2-cyclohexanol acetate	0.8	37	21	1.2	7	4	0.5	850
Trimethyl benzene	1.2	73	42	0.7	102	58	0.2	3250
Toluene	1.3	91	52	0.3	91	52	0.134	660
Tributylphosphate	0.6	21	12	2	0	0	2.43	400

The water mobile phase is pumped in the head to tail direction with light ($d < 1$) organic solvents and in the tail to head direction with heavy ($d > 1$) organic solvents, and vice versa with the organic mobile phase. P, experimental pressure in bar (=0.1 MPa); V_s, stationary phase volume retained; K_{fo}, formanilide partition coefficient, accuracy 10%; N_{fo}, formanilide peak efficiency in theoretical plates, accuracy 20%.

Table 3. Solvent polarity, mutual solubility, phase density, interfacial tension and capillary wavelength

Biphasic system: water with	Delta	E_0	E_T dry	Reichardt index water weighted	Solubility (% w/w)		Interfacial tension	Density (g/ml)			Capillary wavelength
					solv. in water	water in solv.		solvent	water	Δd	
Butane dichloro-1,4	20.5	3	34	34	—	—	21.22	1.14	0.998	0.142	0.390
Butanol	17.8	3.9	60.2	64.2	7.45	20.5	1.27	0.845	0.983	0.138	0.096
Chloroform	18.9	4.1	25.9	30.7	0.815	0.056	18.26	1.484	1.001	0.482	0.196
Dibutylphthalate	17.4	4.6	20	33	0.01	0.46	15.50	1.042	0.998	0.044	0.596
Dichloromethane	20.1	3.1	30.9	37	1.3	0.198	26.84	1.316	1.002	0.314	0.295
Ethane dichloro-1,2	18.6	3.2	32.7	38.1	0.81	0.187	20.39	1.245	1.000	0.245	0.290
Ethane trichloro-1,1,1	17.9	3.2	26.9	30.7	0.132	0.034	23.36	1.329	0.998	0.331	0.268
Ethane trichloro-1,1,2-trifluoro-1,2,2	14.5	0	0.1	8.6	0.017	0.011	27.01	1.562	0.998	0.564	0.220
Ethyl acetate	17.1	4.4	22.8	48.4	8.08	2.94	3.02	0.897	0.989	0.092	0.182
Furfural	23.6	3.8	50	61.2	8.2	6.3	3.63	1.144	1.010	0.133	0.166
Heptane	14.7	0.1	1.2	9	0.00035	0.0091	44.77	0.679	0.997	0.318	0.378
Methylethylketone	17.8	4.7	32.7	61.3	24	10	0.56	0.801	0.945	0.143	0.062
Methyl tert-butyl ether	15.1	2.5	14.8	33.3	4.8	1.5	6.78	0.744	0.985	0.240	0.169
Octanol	17.0	3.4	54.3	61.2	0.0538	4.1	4.14	0.828	0.997	0.169	0.157
Methyl-2-cyclohexanol acetate	17.4	4.2	20	20	—	—	12.30	0.936	0.998	0.062	0.449
Trimethyl benzene	17.8	2.2	6.8	15.6	0.0048	0.029	9.95	0.861	0.997	0.136	0.272
Toluene	18.5	2.4	9.9	18.1	0.0515	0.0334	23.69	0.862	0.997	0.135	0.422
Tributylphosphate	15.7	4.6	27.5	50.7	0.039	4.67	4.01	0.974	0.997	0.023	0.414
Water	48.6	10.2	100	100	—	—	—	—	0.998	—	—

Delta, Hildebrand solubility parameter in $J^{1/2}cm^{-3/2}$; E_0, solvent strength parameter according to Snyder; E_T, solvent polarity index according to Reichardt; interfacial tension measured in dyne/cm; density of the organic phase saturated in water and the aqueous phase saturated in solvent, accuracy 4%; capillary wavelength in cm, see text.

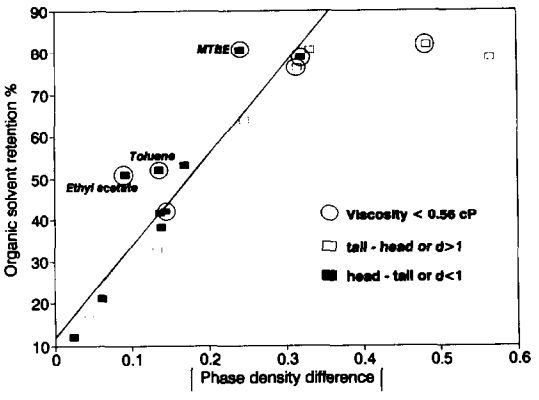

Fig. 1. Organic stationary phase retention percentage *vs.* the phase density difference. Flow rate: 2 ml/min; rotation speed: 800 rpm. Data listed in Tables 2 and 3. Closed squares: $d < 1$ solvents, the aqueous phase enters through the head of the CCC apparatus. Open squares: $d > 1$ solvents, see text. The circled points correspond to low-viscosity pure solvents (Table 1). The regression line equation is given in the text.

Δd, the density of both phases saturated in the other were measured (Table 3). The difference between pure solvent density and water-saturated solvent density is due to mutual solubility. If the water solubility in a given solvent is low, the saturated solvent density is very close to the pure solvent density (Table 3).

Figure 1 shows a plot of the organic solvent retention percentage, %ret, *vs.* the absolute value of the phase density difference, Δd. For absolute Δd values lower than 0.35, there is a linear increase of the retention percentage with Δd. The regression equation is:

$$\%\text{ret} = 222\Delta d + 11$$
$$(\pm 20)\,(\pm 8)$$
$$n = 16,\ r^2 = 0.876.$$

The retention percentage reaches a maximum of about 85% for Δd values higher than 0.40.

The circled points of Fig. 1 correspond to pure organic solvents with a viscosity lower than 0.56 cP (Table 1). The retention percentage of the stationary phase could be inversely related to the stationary phase viscosity. Multiple linear regression analysis of the data set was performed. However, it was not possible to establish a clear relationship between viscosity, density and stationary phase retention. Only the linear relationship density difference *vs.* percentage retention was confirmed. Three low-viscosity solvents, ethyl acetate, toluene and MTBE, have retention percentages higher than the regression line (Fig. 1). Four other low-viscosity solvents, chloroform, dichloromethane, heptane and MEK, are well fitted by the regression line (Fig. 1). A high viscosity of the stationary phase does not affect the retention percentage as illustrated by octanol and tributylphosphate, 7.4 and 3.4 cP, respectively, whose retention percentages are well located on the regression line.

The open squares of Fig. 1 correspond to solvents with a density higher than 1 g/cm^3. In a test tube, these solvents are the lower liquid phase. When the organic solvent is used as the stationary phase in CCC, water, the mobile phase, should enter through the tail side of the apparatus. The three low-viscosity solvents already mentioned and pointed out in Fig. 1 were also low-density solvents. This parameter may partly explain their higher than average retention percentages.

Water stationary phase retention

The next step was to push the organic phases through a water stationary phase. In this way, the mobile phase viscosity and density changed as listed in Tables 1 and 3. Figure 2 shows the plot of water retention percentage, %ret, *vs.* the phase density difference. The trend noticed in Fig. 2 is similar to that in Fig. 1: the water stationary phase retention percentage increases with phase density difference up to $|\Delta d| = 0.35$, where a plateau at percentage retention $\sim$85% is reached. However, the scattering of the data in Fig. 2 is much higher than that in Fig. 1. The

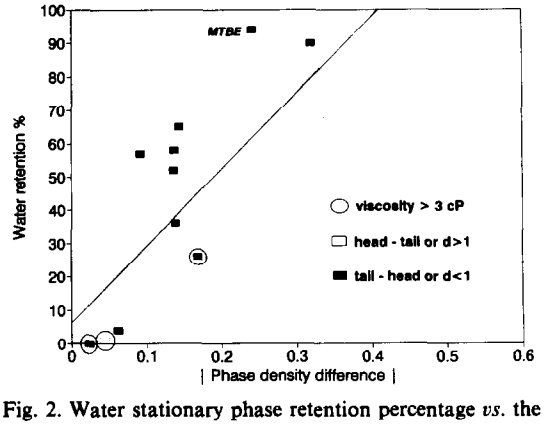

Fig. 2. Water stationary phase retention percentage *vs.* the phase density difference. Flow rate: 2 ml/min; rotation speed: 800 rpm. Data listed in Tables 2 and 3. Closed squares: $d < 1$ solvents, the organic phase enters through the tail of the CCC apparatus. Open squares: $d > 1$ solvents, see text. The circled points correspond to high-viscosity pure solvents (Table 1). The regression line equation is given in the text.

regression line was computed for $|\Delta d|$ values lower than 0.35:

$$\%\text{ret} = 230\Delta d + 6$$
$$(\pm 60)\,(\pm 20)$$
$$n = 16,\ r^2 = 0.540.$$

If the slope and intercept values are similar, the standard errors are too high and the regression coefficient is too low to be acceptable. With organic mobile phases and a water stationary phase, the stationary phase viscosity is almost constant. The circled points in Fig. 2 correspond to highly viscous (>3 cP) mobile phases. The corresponding water retention percentages seem to be below the regression line. For low-viscosity solvents, higher water retention percentages were obtained, *e.g.* methyl tert-butyl ether (MTBE, 0.27 cP) with a 94% water retention percentage. A viscous solvent seems to push more aqueous stationary phase out of the CCC apparatus than a low-viscosity solvent. As already noted, a low-viscosity liquid stationary phase is favourable for retention, although no direct relationship can be defined.

The same notation as in Fig. 1 was used. The open squares correspond to organic solvents denser than water. If water is the stationary phase, a denser liquid must enter the CCC apparatus through the head; a lighter liquid ($d < 1$) must enter the apparatus through the tail and leave it exiting out of the head. Ito has shown that the rotation of a coiled tube filled by a liquid produced a pressure difference between the two ends of the tube due to a "screw effect".[2,3] When two immiscible liquids are loaded in a coiled tube, the rotation also produces a pressure difference. For most binary liquid systems, the lighter liquid accumulates on the high pressure side of the rotating coil, called "head". The denser liquid is located on the low pressure side of the coil, called "tail", where it pushes the lighter liquid towards the head.[1-3] Table 2 lists the experimental pressures. For all solvents denser than water ($d > 1$ g/cm^3), the pressure is lower with the water mobile phase than with the corresponding organic mobile phase. With $d > 1$ organic phases, the water mobile phase entered the CCC apparatus through the tail, the lower pressure side. The corresponding organic phase entered through the head, the high pressure side. Head entering $d > 1$ organic solvents, the open squares of Fig. 2, produced a low aqueous phase retention compared to tail entering $d < 1$ organic solvents (closed squares, Fig. 2). Although the regression line shown in Fig. 2 is not really significant, the open squares ($d > 1$ solvents) are all located below the line and most of the closed squares ($d < 1$ solvents) are above. There was not such a difference when water was the mobile phase. Head or tail entering water phase had little effect on the organic solvent retention (open and closed squares, Fig. 1).

Capillary wavelength

The capillary wavelength, L_c, was recently introduced in CCC by Menet *et al.*[14] as a parameter related to solvent behaviour in coil planet centrifuge CCC apparatus as the one we used. The capillary wavelength is a relation between the interfacial tension, $\Delta\gamma$, and the density difference, Δd, of a biphasic liquid system:

$$L_c = \sqrt{\frac{\Delta\gamma}{\Delta d \times g}}.$$

L_c is expressed in cm, Δd in g/cm^3, and g, the gravity field, in cm/sec^2. In Table 3, the capillary wavelengths were calculated with $g = 981$ cm/sec^2 although the actual field at 800 rpm inside the centrifuge is higher. There is no direct relationship between the capillary wavelength and the phase retention percentage. A slight trend to a decrease of phase retention with L_c increases is due to Δd, as shown by Figs 1 and 2. There is no obvious relationship between interfacial tension (Table 3) and stationary phase retention (Table 2). It may be interesting to relate the capillary wavelength to solvent polarity.

Solvent polarity

The characterization of a solvent by means of its polarity is an unsolved problem, since the term "polarity" itself has, until now, not been precisely defined. Solvent polarity was linked to the permanent dipole moment of solvent molecules, the dielectric constant and/or the sum of selected molecular properties responsible for interaction forces between solvent molecules (*e.g.* coulombic, inductive, hydrogen bonding, electron pair donor/acceptor interaction forces).[15] Different polarity scales were established. Hildebrand linked solvent polarity to its solubilization capability defining the solubility

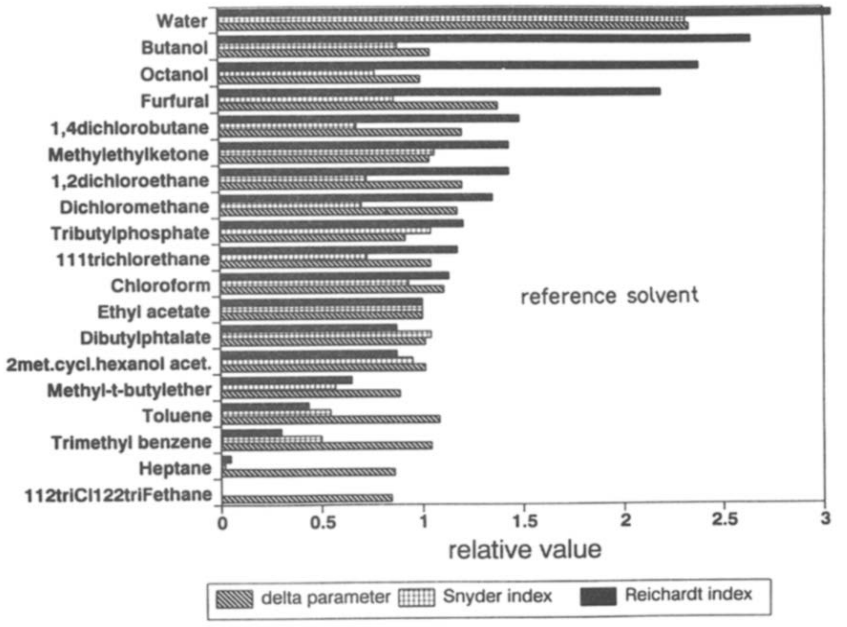

Fig. 3. The comparison of three polarity scales: the Hildebrand δ parameter (hatched bars), the Snyder E_0 index (dotted bars) and the Reichardt E_T index (closed bars). The relative values refer to the ethyl acetate values. The exact values are listed in Table 3.

parameter, δ, as the work necessary to separate two solvent molecules:[16]

$$\delta = \sqrt{\frac{\Delta H_v - RT}{V_m}}$$

in which ΔH_v is the solvent molar heat of vaporization and V_m is its molar volume. In this work, the δ parameter was computed using the Beerboweer approximation:[17]

$$\delta = 3.74 \sqrt{\frac{\gamma}{\sqrt[3]{V_m}}},$$

in which γ is the solvent surface tension.

The idea to link the polarity of a solvent to its overall solvation ability led to the definition of polarity scales in terms of experimental parameters. Snyder defined an eluant strength parameter, E_0, based on the eluting power of the solvent when used as a mobile phase in thin layer chromatography on silica or alumina plates.[18] Reichardt proposed a solvent polarity parameter, E_T, based on the transition energy for the longest wavelength solvatochromic absorption band of a pyridinium-*N*-phenoxide betaine dye. The E_T parameter was normalized using water ($E_T = 100$) and tetramethylsilane ($E_T = 0$) as extreme reference solvents.[15] Table 3 lists the δ parameter in $J^{1/2}cm^{-3/2}$ and the dimensionless Snyder and Reichardt polarity indexes. Figure 3 compares the three polarity indexes in a relative scale with ethyl acetate as the reference solvent. The three polarity indexes of all solvents were divided by the corresponding ethyl acetate value, $\delta = 17.1$ $J^{1/2}cm^{-3/2}$, $E_0 = 4.4$ and $E_T = 22.8$. The solvents were sorted by decreasing Reichardt values. Figure 3 shows that there is only approximate correspondence between the three polarity scales. For example, the butanol E_T value is 60.2 and the δ value is 17.8. The furfural E_T value is lower, 50, and its δ value is higher, 23.6. In liquid chromatography, the E_T index was elected as the best representation of solvent polarity.[19]

Obviously, the mixing of two solvents changes their polarity. An organic solvent saturated in water has a higher polarity than the dry solvent. The E_T values of water-saturated butanol, MEK, MTBE and ethyl acetate were measured using the visible spectrum (750–400 nm) of the Reichardt dye freshly dissolved in each solvent.[15] These four solvents were selected because they have a relatively high mutual solubility with water. Furfural was brown coloured and could not be used. With the measured water-saturated E_T values, all other dry solvent E_T values were weighted using their water content and water polarity. The measured and weighted E_T values are listed in Table 3.

Figure 4 shows the plot of the capillary wavelength, L_c, *vs.* the water-weighted Reichardt polarity index, E_T, of the solvents. In

this scattered point plot, short L_c values seem to correspond to high E_T indexes. However, there is no direct relationship; for information, the regression line shown in Fig. 4 is:

$$L_c = -0.004E_T + 0.42$$

$$(\pm 0.002)\,(\pm 0.12)$$

$$n = 18,\ r^2 = 0.270.$$

For example, dibutylphthalate (DBP) has a low mutual solubility with water and a high L_c value, 0.6, far from the other solvents. L_c is high because the density of DBP is very close to the density of water. It seems to be difficult to connect solvent density to solvent polarity.

Solute partition coefficient

In classical liquid chromatography, solute retention depends on numerous parameters: solute partition with an organic layer bonded on the solid stationary phase, adsorption on active sites of the surface, ion-exchange, size exclusion or binding with specific sites on the stationary phase. In CCC, the sole parameter responsible for solute retention is the liquid–liquid partition coefficient. CCC allows accurate determination of liquid–liquid partition coefficients.[20–22] These coefficients are dependent on solvent polarity. Table 2 lists the partition coefficient for formanilide, K_{fo}, used as a test solute. It was not possible to use the UV detector with furfural and DBP. Both solvents strongly absorb UV light. Figure 5 shows a plot of the K_{fo} partition coefficient *vs.* the water content-weighted E_T polarity index. The full line is the regression line obtained using all points:

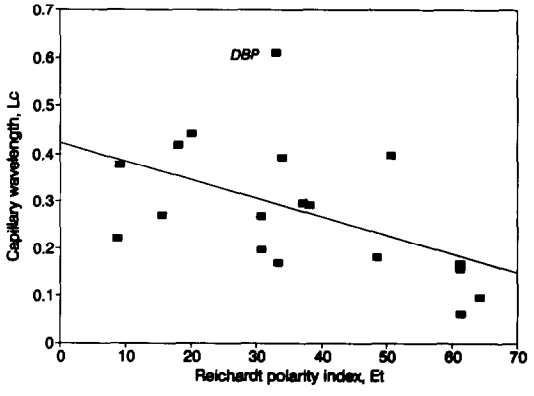

Fig. 4. The capillary wavelength L_c *vs.* the water-weighted E_T polarity index. The regression line is shown for convenience (regression parameter $r^2 = 0.27$, see text).

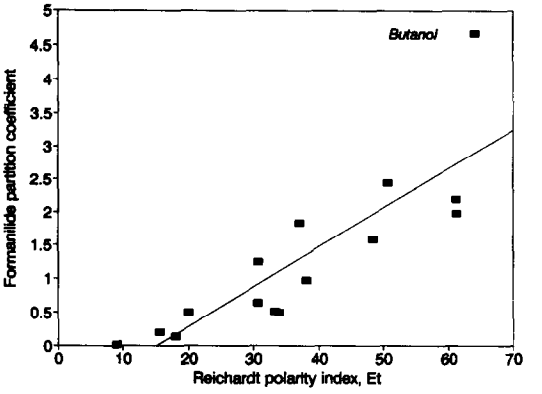

Fig. 5. Formanilide partition coefficient, K_{fo}, *vs.* the water-weighted E_T polarity index for the 15 solvents with which UV detection was possible. The full line corresponds to the regression line, whose equation is given in text.

$$K_{fo} = 0.060E_T - 0.91$$

$$(\pm 0.010)\,(\pm 0.66)$$

$$n = 15,\ r^2 = 0.725.$$

The representative point of butanol is posted on Fig. 5. With $K_{fo} = 4.66$, it is far from the regression line. We note that butanol has the highest mutual solubility with water (20.5% w/w water dissolves in butanol and 7.5% w/w butanol dissolves in water). Anyway, it can be concluded that the partition coefficient of a given solute is strongly linked to the polarity difference between the two liquid phases. For years, the octanol–water partition coefficient has been used as a hydrophobic scale in biochemistry, pharmaceutical and environmental studies.[23]

CONCLUSIONS

Separation using CCC is impossible if there is no liquid stationary phase retention. The liquid stationary phase retention percentage in a hydrodynamic countercurrent chromatograph is directly proportional to the density difference between the two liquid phases. The mutual solubility between phases increases as the polarity difference decreases and the density difference decreases if the two solvents used have a high mutual solubility. That is why the liquid stationary phase retention in a CCC apparatus is related to the polarity difference between the two liquid phases used. The retention of a solute depends on its partition coefficient in the biphasic liquid system used. This

coefficient is directly related to the phase polarity difference. This shows that the choice of the biphasic liquid system is essential to adjust selectivity in CCC.

From a practical point of view, this work demonstrates that the density difference between phases is the first parameter to be considered when dealing with liquid stationary phase retention in CCC hydrodynamic apparatuses. To obtain a high liquid stationary phase retention in coiled tubes, the two liquid phases used must have a high density difference whatever phase is used as the stationary phase. The chloroform–methanol–water and chloroform–acetic acid–water systems are very popular in CCC separations.[1-3] The density of chloroform, 1.5 g/cm^3, produces a high density difference with the $\sim$0.8 g cm^{-3} density of the methanol or acetic acid phases. The phase retention in CCC apparatuses is good. Also, these two liquid systems have very low viscosities.

Acknowledgements—This work was made possible by the grant 91/41 CNRS 820501 from ELF-Atochem and by the continuous support of CNRS, UA 435, which are gratefully acknowledged.

REFERENCES

1. W. D. Conway, *Countercurrent Chromatography, Apparatus, Theory and Applications*. VCH Publishers, Weinheim, 1990.
2. N. B. Mandava and Y. Ito, *Countercurrent Chromatography*, Chromatographic Science Series, Vol. 44. Marcel Dekker, New York, 1988.
3. Y. Ito, in *Advances in Chromatography*, J. C. Giddings, E. Grushka and J. Cazes (eds), Vol. 24, Ch. 6, p. 181. Marcel Dekker, New York, 1984.
4. A. Berthod, *Eur. Chromatogr. Anal.*, 1991, February, 13.
5. A. Foucault, *Anal. Chem.*, 1991, **63**, 569A.
6. T. Okuda, T. Yoshida, T. Hatano, R. Kira and Y. Ikeda, *J. Chromatogr.*, 1986, **362**, 375.
7. A. Berthod, *J. Chromatogr.*, 1991, **550**, 677.
8. Y. Ito, in *Chromatography*, 5th edn, E. Heftman (ed.), J. Chromatogr. Library, Ch. 2, p. A69, Vol. 51A. Elsevier, Amsterdam, 1992.
9. Y. Ito, *J. Chromatogr.*, 1984, **301**, 377.
10. Y. Ito, *J. Chromatogr.*, 1984, **301**, 387.
11. Y. Ito and W. D. Conway, *J. Chromatogr.*, 1984, **301**, 405.
12. Y. Ito, *J. Liq. Chromatogr.*, 1992, **15**, 2639.
13. A. Berthod and M. Bully, *Anal. Chem.*, 1991, **63**, 2508.
14. J. M. Menet, D. Thiebaut, R. Rosset, J. E. Wesfred and M. Martin, Poster 2P18, *19th Int. Symp. Chromatogr.*, Aix en Provence, France, 13–18 Sept., 1992.
15. C. Reichardt, *Solvents and Solvent Effects in Organic Chemistry*. VCH Publishers, Weinheim, 1988.
16. J. H. Hildebrand, J. M. Prausnitz and R. L. Scott, *Regular and Related Solutions*. Van Nostrand-Reinhold, Princeton, NJ, 1970.
17. A. Beerbower, *J. Colloid Interface Sci.*, 1971, **35**, 46.
18. L. R. Snyder, *Principles of Adsorption Chromatography*. Marcel Dekker, New York, 1968.
19. B. P. Johnson, M. G. Khaledi and J. G. Dorsey, *J. Chromatogr.*, 1987, **384**, 221.
20. A. Berthod and V. Dalaine, *Analysis*, 1992, **20**, 325.
21. A. Berthod, Y. I. Han and D. W. Armstrong, *J. Liq. Chromatogr.*, 1988, **11**, 1441.
22. A. Berthod, R. A. Menges and D. W. Armstrong, *J. Liq. Chromatogr.*, 1982, **15**, 2769.
23. J. A. Riddick, W. B. Bunger and T. K. Sakano, *Organic Solvents*, 4th edn, *Techniques of Chemistry*, Vol. II. Wiley-Interscience, New York, 1986.

Talanta, Vol. 40, No. 10, pp. 1499–1503, 1993
Printed in Great Britain.

0039-9140/93 $6.00 + 0.00

EXTRACTION OF MANGANESE(II) WITH DITHIZONE AND POTASSIUM THIOCYANATE ON FOAM SORBENTS FOR SPECTROPHOTOMETRIC DETERMINATION IN SILICATES

NIBEDITA CHAKRABORTI and S. K. ROY
Analytical Chemistry Division, Central Glass and Ceramic Research Institute, Calcutta 700 032, India

(*Received* 10 *February* 1993. *Revised* 16 *April* 1993. *Accepted* 18 *April* 1993)

Summary—A method for selective extraction of Mn(II) with dithizone and potassium thiocyanate has been described. The method involves formation of a Mn(II)–thiocyanate–dithizone complex in a hexamine medium containing potassium thiocyanate (2.8*M*), dithizone (5.5–6.5 × 10^{-5}*M*) and hydroxylamine hydrochloride (0.25%) at pH ~6 followed by extraction of the complex on polyurethane foam using batch squeezing mode within 1 hr. The sorbed Mn–thiocyanate–dithizone complex is eluted with acetone and made alkaline with 0.5 ml of a stabilizer solution (19 ml 2*M* NH_3 solution + 1 ml 5% hydroxylamine hydrochloride). The absorbance of the solution is measured at 506 nm. The adverse effect due to Pb may be obviated by separating the Pb as the sulphate during decomposition of sample and that due to iron may be removed before extraction of Mn by any suitable method. The other interfering elements (Cd, Zn, Ni, Co, Cu, *etc.*) are masked with KCN (6 × 10^{-3}*M* optimum) solution. The method obeys Beer's Law from 0.1 to 2.0 μg Mn/ml. The method has been applied to various silicates, carbonates and glasses.

Diethyl dithiocarbazone (dithizone) reacts with various metal ions to produce coloured complexes[1] which have been utilized for their spectrophotometric determination for a long time. Numerous spectrophotometric methods involving solvent extraction with dithizone have been reported for determination of various elements.[2] Reaction of manganese(II) with dithizone,[1,3] is known to produce a violet coloured primary dithizonate, $Mn(HDz)_2$, in alkaline solution (pH 10–11) which can be extracted with chloroform or carbon tetrachloride. But $Mn(HDz)_2$ in alkaline medium is unstable and thus could not be utilized for the spectrophotometric determination. Akaiwa *et al.*[4] on further studies observed a change in the absorption curve of Mn-dithizonate produced in the presence of pyridine. This change was explained as pyridine forming an adduct with dithizonate (or the formation of an adduct by pyridine with dithizonate). Later Akaiwa and Kawamoto[5] extracted the Mn(II) complex produced by dithizone and pyridine reproducibly with CCl_4 at pH 9.5 in the presence of hydroxylamine hydrochloride which stabilized the lower oxidation state of manganese which can be determined spectrophotometrically at 530 nm. But the working range was established between 0.4 and 4 μg Mn/ml. Marczenko and Mojski[6] reported in another study that Mn(II)-dithizonate adduct with pyridine has the composition $Mn(HDz)_2/(Pyridine)_2$ developed a practical method for the determination of Mn(II). Later, in 1979 Akaiwa *et al.*[7] observed that Mn(II) forms a mixed ligand complex with dithizone (H_2DZ) and 1,10-phenanthroline (phen) and that can also be extracted into chloroform in the pH range 8–9. Further, they observed that the absorbance of the complex in chloroform solution is higher and more stable than the complex obtained by using pyridine or bipyridyl. The method was applied to carbonate rock and hot spring water. However, the present authors could not obtain satisfactory results during extraction of Mn(II) in the presence of phenanthroline and dithizone on polyurethane foam in the same pH range. But it has been reported that polyurethane foam (PUF) sorbents have been used in the separation and preconcentration of various elements by sorbing their dithizonate complexes from aqueous solutions.[8,9] It was reported in a study[10] where Mn(II) was extracted on PUF from a thiocyanate solution by a batch technique for understanding the reaction mechanism of thiocyanate complexes from aqueous solution. α-Dinonylphthalate (DNP)

plasticized 1,(2-pyridylazo)-2-naphthol (PAN) loaded foam has also been reported[11] for the extraction of Mn(II) at pH ~9 by a batch and column technique, and determined radiometrically. Furthermore, foam loaded with Kelex-100 has been reported for the extraction of Mn(II) by a column and batch technique and determined by AAS.[12] But sorption characteristics of Mn(II)-dithizonate in the presence of KSCN on unloaded polyurethane foam is yet to be studied.

The present paper describes a study in which manganese was extracted on PUF in the presence of dithizone and potassium thiocyanate from hexamine solution containing hydroxylamine hydrochloride. Based on these studies, a method was established for the spectrophotometric determination of manganese in silicates, carbonates and glasses. The method enables us to determine Mn down to the concentration of existing level (0.4 μg/ml Mn) reliably in a matrix free system using 1 cm cell.

EXPERIMENTAL

Apparatus—UV-VIS Spectrophotometer, Spectromom Model 361.

Reagents—A.R. grade. Double distilled water was used throughout the experiment. Potassium cyanide solution (1%, w/v), hydroxylamine hydrochloride solution (5%, w/v, neutralized with dilute ammonia solution), sodium fluoride (2%, w/v), hexamine solution (10%, w/v, purified by shaking with dithizone loaded polyurethane foam), dithizone (0.03% in methanol), potassium thiocyanate solution 8*M*, MIBK.

Standard Mn-solution—1000 μg/ml

Mn(II) solution was prepared by dissolving (99.9%) electrolytic manganese metal in dilute nitric acid (10 ml). Then, the volume was made up in a 1000 ml volumetric flask.

A working solution (5.1 μg/ml) was prepared by proper dilution of the stock solution with water and acidified with 2 drops of HNO_3.

Preparation of foam

The polyurethane foam (commercial U-foam) was cut into regular shapes and sizes with a cork borer. Each piece was about 2 cm in length and 0.5 cm in diameter and weighed about 0.01 gm. The pieces of foam were soaked in 4*M* hydrochloric acid in a beaker for 4 hr with squeezing at 15 min interval, then washed thoroughly in a 50 ml glass syringe and finally by refluxing with acetone for 6 hr in a Soxhlet apparatus. The washed foam pieces were dried in a desiccator and stored in a plastic container in the dark.

Procedure

Calibration. Manganese solutions (1–4 ml) containing 1–20 μg of Mn were pipetted into 50 ml glass beakers and evaporated to almost dryness on a water bath and the residue dissolved in 2 ml water. To that solution 6 ml of 10% hexamine, 1 ml hydroxylamine hydrochloride, 1 ml NaF, 1 ml KCN, 8 ml 8*M* potassium thiocyanate and 1 ml dithizone were added sequentially and kept for 5 min. Five pieces of foam chip were put into each solution and squeezed at 5 min intervals with the help of a flat ended glass plunger to facilitate the aqueous solution to flow freely through the foam cell for a period of 60 min. The chips were then transferred to a 5 ml glass syringe and washed thoroughly four times with a stabilizer solution (19 ml 2*M* NH_3 solution + 1 ml 5% hydroxylamine hydrochloride) and subsequently washed with water four times. Sorbed Mn-thiocyanate–dithizone complex was then eluted with acetone using four 2 ml volumes into a 10 ml volumetric flask and made alkaline with 0.5 ml stabilizer solution. The volume was finally made up with acetone and the absorbance was measured at 506 nm against a reference blank prepared in the same way as above. The calibration curve (absorbance *vs* μg of Mn) was plotted.

Analysis of samples. A 0.2 g sample (dried at 110°C) was digested with 5 ml H_2SO_4 (1 + 1) and 5 ml HF in a PTFE basin on a sand bath and digested until SO_3 fumes evolved, cooled and diluted with 10 ml water and filtered (if necessary for separation of $PbSO_4$) into a 100 ml beaker. The residue was washed four times with 1% H_2SO_4 solution (total 10 ml). A 20 ml volume of hydrochloric acid was added to the filtrate and was transferred to a 10 ml separating funnel. A 10 ml volume of methyl isobutyl ketone (MIBK) was added to the solution and the mixture was shaken to extract iron (if present). The process was repeated till the solvent layer became colourless. The aqueous layer was transferred to a 100 ml volumetric flask and diluted with water to make the volume.

Five milliliters of this solution was taken into a 50 ml beaker and evaporated to dryness on a water bath, 2 ml of water was added to dissolve the residue and the determination procedure

was applied. The MnO content was calculated from

$$\%MnO = 2.58 \times 10^{-2} A/W$$

where A is the number of μg of Mn corresponding to the absorbance measured and the sample weight is W in grams.

RESULTS AND DISCUSSION

It has been observed that Mn(II) reacts with dithizone to form a coloured complex in the presence of hydroxylamine hydrochloride in hexamine medium, but its extraction on polyurethane foam is incomplete and the colour of the eluted complex in acetone medium showed maximum absorbance at 490 nm. However, on further studies it was observed that if potassium thiocyanate was added to the solution before reaction with dithizone (in the presence of hydroxylamine hydrochloride and hexamine) the colour of the complex was notably changed to a stable pink colour and could be extracted on foam within 1 hr. The extracted complex could also be eluted with acetone and showed maximum absorption at 506 nm. This observation indicates a similarity in nature with that observed with pyridine and dithizone by earlier workers.[6,7] The shift of the absorption maxima from 490 to 506 nm suggests that Mn(II)-thiocyanate forms first and this reacts with dithizone probably to form a ternary complex like Mn(SCN)(HDz) although the nature of the complex has not been studied and established here. It has been reported that polyether type polyurethane foam is regarded to be analogous to oxygenated solvents. Therefore, sorption of Mn-thiocyanate–dithizone can be accounted for by a solvent extraction mechanism.[13,14]

However, quantitative formation of the probable complex Mn(SCN)(HDz) in hexamine medium at pH = 6 and its sorption on PUF is dependent upon the concentration of KSCN, dithizone, and equilibration time.

In the present study it has been observed that Mn(SCN)(HDz) complex can be well formed in hemamine medium at pH = 6 and the complex can be stabilized with hydroxylamine hydrochloride for a considerable period for its sorption on PUF and therefore for subsequent experiments, the hexamine medium (*i.e.* pH = 6) was chosen.

The effect of thiocyanate concentration was studied by taking 20 μg of Mn(II) in a 50 ml beaker containing 1 ml of 5% hydroxylamine hydrochloride, 1 ml dithizone, 6 ml hexamine solution, and varying only the concentrations of thiocyanate (from 2 to 3.2M) in a total volume of 20 ml. The solution was equilibrated for 1 hr and the absorption of the complex is measured at 506 nm after stripping the complex with acetone. It can be seen from Fig. 1 that formation and maximum extraction can be obtained only at, and above, 2.8M KSCN concentration.

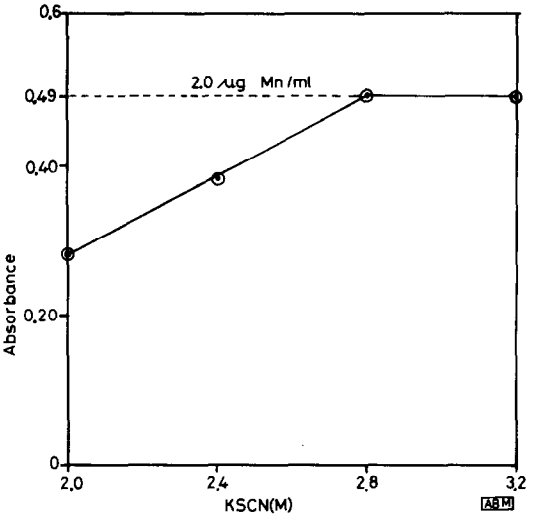

Fig. 1. Effect of potassium thiocyanate concentration on the extraction of Mn(SCN)(HDz): $[H_2Dz] = 5.85 \times 10^{-5}M$, [Hexamine] = $2.1 \times 10^{-4}M$.

Effect of dithizone concentration on the formation and extraction of Mn(II) was studied as above and by varying the concentration of

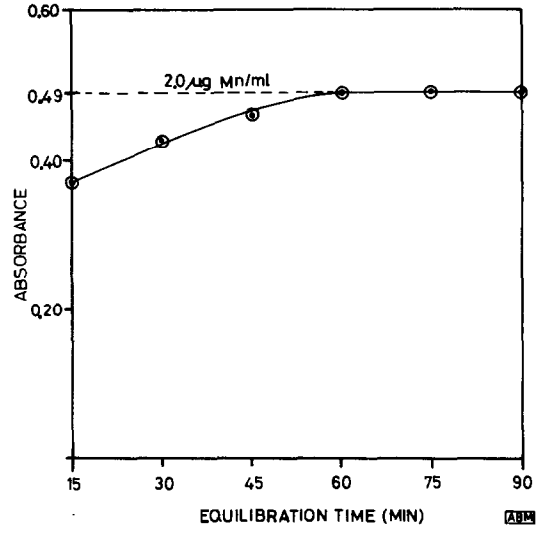

Fig. 2. Effect of equilibration time on the extraction of Mn(SCN)(HDz): $[H_2Dz] = 5.85 \times 10^{-5}M$; [KSCN] = 2.8$M$, [Hexamine] = $2.1 \times 10^{-4}M$.

Table 1. Determination of MnO in different materials

Nature of sample	% of MnO obtained	Mean MnO	Values obtained by other method*
1. Lime Stone NBS-1a	0.040 0.039 0.039	0.039	0.038†
2. Silicate rock	0.110 0.120 0.114	0.114	0.110
3. Amber glass	0.035 0.034 0.036	0.036	0.036
4. Clay I	0.204 0.210 0.211	0.208	0.200
5. Clay II	0.108 0.114 0.116	0.112	0.110
6. Clay III	0.059 0.063 0.062	0.061	0.058

*Periodate method.
†National Bureau of Standards certified value.
Mean standard deviation = ±0.0028.

dithizone ($3.0 \times 10M$–$12.0 \times 10^{-5}M$). It has been observed that the formation of Mn(SCN)(HDz) as well as quantitative extraction of the complex is possible only at, or above, $5.5 \times 10^{-5}M$ dithizone concentration. Below this concentration, the extraction efficiency was found to be less due to the formation of an unextractable species. Yet, at a concentration greater than $6.5 \times 10^{-5}M$ dithizone, a high blank value was obtained. Therefore, in further studies the dithizone concentration was kept between 5.5×10^{-5} and $6.5 \times 10^{-5}M$.

Equilibration time was studied by taking 20 μg of Mn(II) solution as mentioned above and the solution was equilibrated with foam chips by varying the time up to 90 min. After each time interval, foam pieces were washed and eluted as described. Absorbance of each solution was measured. The study indicated that maximum extraction was possible only after 1 hr of equilibration and no further extraction took place beyond that period. Acetone has been found to be suitable for the elution of Mn(SCN)(HDz) complex from polyurethane foam. It has been observed that the complex after elution with acetone was found to be unstable when made alkaline with only ammonia solution (0.5 ml of $2.0M$ NH_3 solution in 10 ml volume) probably due to oxidation of Mn(II) to Mn(III). Therefore, a stabilizer solution containing hydroxylamine hydrochloride (19 ml $2M$ NH_3 solution + 1 ml 5% hydroxylamine hydrochloride) was prepared for its addition to the acetone elute. It was found that the addition of such a stabilizer solution (0.05 ml) stabilizes the complex Mn(SCN)(HDz) for at least 5 hr before measuring its absorbance.

The effect of Mn concentration was studied by the following the procedure and observed that Beer's law is obeyed from 0.1 to 2.0 μg Mn/ml. From the regression analysis of the calibration curve, the correlation coefficient was calculated to be 0.99.

Dithizone forms coloured complexes with many other metal ions such as Cd, Zn, Ni, Co, Cu, and others which interfere seriously with the determination of Mn. To overcome these adverse effects, KCN solution was used for masking all such interfering cations. However, the effect of KCN on the formation and extraction of Mn(SCN)(HDz) complex on PUF was carried out as it has been reported[15] that KCN forms a complex with Mn(II) at higher pH. It was found that KCN at a concentration of $6 \times 10^{-3}M$ has no effect on the formation and extraction of the Mn(SCN)(HDz) complex. Moreover, $6 \times 10^{-3}M$ KCN is sufficient for masking interfering cations up to 10-fold the amount of Mn. It was further observed that an appreciable amount of fluoride ion has no effect on the extraction of Mn(II).

In conclusion it can be stated that manganese(II), stabilized with hydroxylamine hydrochloride (0.025%) in hexamine medium forms a ternary complex with thiocyanate ($2.8M$) and dithizone (5.5–$6.5 \times 10^{-5}M$) at pH = 6. The complex is extracted on PUF, eluted with acetone and made alkaline with 0.5 ml of a stabilizer solution (19 ml $2M$ NH_3 + 1 ml 5% hydroxylamine hydrochloride) and the absorbance is measured at 506 nm for the determination of manganese. The advantage of the method lies in the fact that manganese reliably and comfortably can be separated out from a complex system to a pure one so that the determination level can be four times lower than the existing level. The method has been standardized against standard lime stone NBS-1a and applied to the determination of manganese present in glass, silicate and carbonate samples. The results are presented in Table 1. It can be seen from Table 1 that results obtained are slightly higher than the values obtained by

the other method in some cases but within a maximum error of 5.1%.

Acknowledgement—The authors are thankful to Dr B. K. Sarkar, Director, Central Glass and Ceramic Research Institute, Calcutta 700 032, for his kind permission to publish the paper.

REFERENCES

1. E. B. Sandell and H. Onishi, *Photometric Determinations of Traces of Metals*, Part 1, p. 789. Wiley, New York, 1978.
2. H. M. N. H. Irving, *CRC Crit. Rev. Anal. Chem.*, 1980, **8**(4), 321.
3. B. Chiswell and G. Rauchle, *Talanta*, 1990, **37**, 237.
4. K. Akaiwa, H. Kawamoto and M. Hara, *J. Chem. Soc. Japan Pure Chem. Sec.*, 1966, **90**, 186.
5. K. Akaiwa and H. Kawamoto, *Anal. Chim. Acta.*, 1968, **40**, 407.
6. Z. Marczenko and M. Mojski, *Anal. Chim. Acta.*, 1971, **54**, 469.
7. H. Akaiwa, H. Kawamoto and S. Kogure, *Buneski Kagaku*, 1979, **28**(8), 498; *Chem. Abstr.*, 1979, **91**, 203736W.
8. D. Kundu and S. K. Roy, *Anal. Letters*, 1991, **24**(i), 139.
9. D. Kundu and S. K. Roy, *Talanta*, 1992, **39**, 415.
10. G. J. Moody, J. D. R. Thomas and M. A. Yarmo, *Anal. Proc.*, 1983, **20**, 132.
11. T. Braun, A. B. Farag and M. P. Maloney, *Anal. Chim. Acta.*, 1979, **93**, 191.
12. F. Vernon, *Sep. Sci. Technol.*, 1978, **13**, 587.
13. T. Braun, J. D. Navratril and A. B. Farag, *Polyurethane Foam Sorbents in Separation Science*. CRC, Boca Raton, Fl, 1985, p. 44.
14. R. F. Hamon, A. S. Khan and A. Chow, *Talanta*, 1982, **29**, 313.
15. J. W. Mellor, *A Comprehensive Treatise on Inorganic and Theoretical Chemistry*. Longman, Green and Co., 1947, Vol. XII, p. 190.

Talanta, Vol. 40, No. 10, pp. 1505–1510, 1993
Printed in Great Britain.

0039-9140/93 $6.00 + 0.00

SIMULTANEOUS KINETIC DETERMINATION OF PHENOLS BY USE OF THE KALMAN FILTER

ANTONIO VELASCO, XIONG RUI,* MANUEL SILVA and DOLORES PÉREZ-BENDITO
Department of Analytical Chemistry, Faculty of Sciences, University of Córdoba, E-14004 Cordoba, Spain

(*Received* 29 *January* 1993. *Revised* 29 *April* 1993. *Accepted* 30 *April* 1993)

Summary—A multicomponent analysis method based on the Kalman filter algorithm is proposed for the determination of phenolic compounds. The method relies on the oxidative coupling of phenols (phenol, 2-chlorophenol and 3-chlorophenol) to *N,N*-diethyl-*p*-phenylenediamine in the presence of hexacyanoferrate(III), the reaction being monitored via changes in the absorbance at 660 nm of the dye formed. Phenols can be determined individually over the concentration range 1.25–25 μM with a relative standard deviation of *ca* 0.6–0.8%. Differences in the kinetic behaviour of the three species were exploited by using the linear Kalman filter to resolve mixtures of the phenols at the μM level in a widely variable concentration ratios with errors less than 10%.

Phenols are of a high significance to environmental studies since they are present in many organic pollutants, of which chlorophenols, widely used in pesticide production, are particularly hazardous owing to their highly toxic character. Several procedures have been developed for the determination of phenols at trace concentration levels. Both high-performance liquid chromatographic[1–4] and gas chromatographic[5–9] techniques, are widely used for this purpose; however, they are even employed for the determination of a single phenol (*e.g.* phenol in plasma,[10] urea,[11] industrial products[12]) or two compounds in mixtures (*e.g.* phenol and *p*-cresol in urine[13]). The sensitivity typically afforded by these methods is of a few micrograms per millilitre. In this context, it is interesting to note the development of new analytical methods for the resolution of mixtures of these compounds with adequate sensitivity by using simpler, faster instrumentation. Kinetic methods of analysis are powerful tools for this purpose, especially those based in new multipoint approaches which allow the resolution of closely related species.

In this work we developed simple, rapid simultaneous kinetic determination for phenol and chlorophenols using the Kalman filter algorithm. The method is based on the well-known oxidative coupling reactions of these compounds in a weakly basic medium. The singular features of the Kalman filter[14–17] allow these mixtures to be resolved over wide concentration ranges with a high accuracy even at low rate constant ratios.

Kinetic methods have rarely been applied to the individual or simultaneous determination of phenolic compounds;[18–20] in fact, the proposed method is the first attempt at the kinetic resolution of chlorophenol mixtures. Thus, metaperiodate is a common oxidant for hydroxyl compounds, which are individually determined by using a fixed-time method[18,19] based on absorbance measurements at the wavelength of maximum absorption of the resulting quinols and quinones. The determination range covered is *ca* 50–1000 μg/ml. The only reference to a simultaneous kinetic determination of phenol mixtures was concerned with cresol mixtures that were resolved by using the oxidative coupling reactions of the phenols with *N,N*-diethyl-*p*-phenylenediamine in the presence of potassium hexacyanoferrate(III). The quinonedi-imine formed reacts with the cresol to form a dye in a reaction that is monitored photometrically by using the stopped-flow technique.[20]

EXPERIMENTAL

Reagents

All solvents and reagents were of analytical-reagent grade and purified water was obtained from a Milli-Q apparatus. Stock solutions of $3 \times 10^{-2} M$ phenol, 2-chlorophenol and 3-

*Beijing Institute of Telemetry, Ministry of National Aerospace, Box 9200-74, Beijing, China.

chlorophenol (Merck) were prepared in ethanol and diluted 1:250 for use in the experiments as follows: 1.0 ml of the stock solution was mixed with 10.0 ml of 0.5*M* phosphate buffer of pH 8.0 and diluted to 250 ml with purified water. A $6 \times 10^{-3}M$ stock solution of *N,N*-diethyl-*p*-phenylenediamine (Merck) was prepared by dissolving 98.6 mg of the chemical in ethanol in a 100-ml volumetric flask. This stock solution was stored in a refrigerator to minimize degradation. A $2.4 \times 10^{-2}M$ stock solution of potassium hexacyanoferrate(III) (Merck) was prepared by dissolving 790 mg of the chemical in 100 ml of purified water. The 0.5*M* phosphate buffer (pH 8.0) was prepared by dissolving 87.1 g of di-potassium hydrogen phosphate (Merck) in *ca* 850 ml of purified water, adjusting the pH to 8.0 with hydrochloric acid and diluting to 1 l with purified water.

Apparatus

Spectrophotometric measurements were made on a Metrohm 662 spectrophotometer equipped with an immersion probe that was furnished with a Metrohm Dosimat 665 autoburette to dispense a small volume of reagent in order to start the reaction, as well as a data acquisition system consisting of a Mitac PC-AT 12-MHz compatible computer equipped with a PC-Multilab PCL-812PG 12 bit analog-to-digital converter. Data acquisition were synchronized with the start of the reaction by using a trigger that actuated the autoburette and computer simultaneously. The software required for application of the Kalman filter method was developed by the authors.

Procedure

In an 80-ml reaction vessel were placed a solution containing 0.12–1.08 μmol of each phenol (binary mixtures), plus 2.0 ml of $6 \times 10^{-3}M$ *N,N*-diethyl-*p*-phenylenediamine solution, 5.0 ml of 0.5*M* phosphate buffer (pH 8.0) and purified water up to a final volume of 60 ml. The reaction was started by adding 1.0 ml of $2.4 \times 10^{-2}M$ potassium hexacyanoferrate(III) solution from the autoburette at a rate of 60 ml/min (addition time, 1 sec). Data were acquired at a rate of 1.5 sec per point and a wavelength of 660 nm for 5 min in both instances.

RESULTS AND DISCUSSION

Oxidative coupling reactions of *p*-phenylenediamines with amines and phenolic compounds are widely known by analytical chemists.[21–29] The kinetics and mechanism of these reactions were widely investigated in the late 1960s due to the great relevance of the dye formed to the photographic industry. The proposed method for the resolution of mixtures of phenolic compounds (phenol and chlorophenols) relies on this type of reaction, in which *N,N*-diethyl-*p*-phenylenediamine (PPD) is oxidized to its quinonedi-imine (QDI) by potassium hexacyanoferrate(III) in weakly basic medium. In the rate-limiting step, QDI reacts with the phenolic compound to give leucoindophenols, which are rapidly oxidized to coloured indophenols with the aid of a QDI[24] molecule, these last absorb maximally and with high molar absorptivities at *ca* 660 nm (see Scheme 1).

Preliminary studies on the kinetic behaviour of these phenolic compounds showed differences in their reactivity. The reaction rate for phenol, 2- and 3-chlorophenol was similar (the three reactions develop to completion within a few minutes) whereas that for 4-chlorophenol was very low, which is consistent with Scheme 1. Therefore, the last phenol can be determined in the presence of the others by using a simple sequential method (whether kinetic or equilibrium). This was not assayed in this work, even though it can be resorted to whenever this compound is present in the unknown mixture. The major problem arises from the resolution of mixtures of the other phenolic compounds owing to their similar kinetic behaviour (their pseudo-first rate constant ratios are *ca* 2.0, which precludes usage of classical differential reaction-rate methods). We chose to use the powerful Kalman filter algorithm to address this problem. This algorithm allows the reliable calculation of the concentrations of mixture components from the net signal changes for each (linear Kalman filter), as well as the determination of their pseudo-first rate constants (extended Kalman filter).

Figure 1 shows typical absorbance *vs* time curves for the three phenolic compounds, which were processed by the data acquisition system. As can be seen, the reaction was somewhat faster for 2-chlorophenol and very similarly rapid for phenol and 3-chlorophenol; therefore, the effect of the reaction variables was subsequently investigated in order to establish the experimental conditions resulting in the greatest possible discrimination between the kinetic behaviour of 2-chlorophenol and one of the other two phenols (phenol was selected because

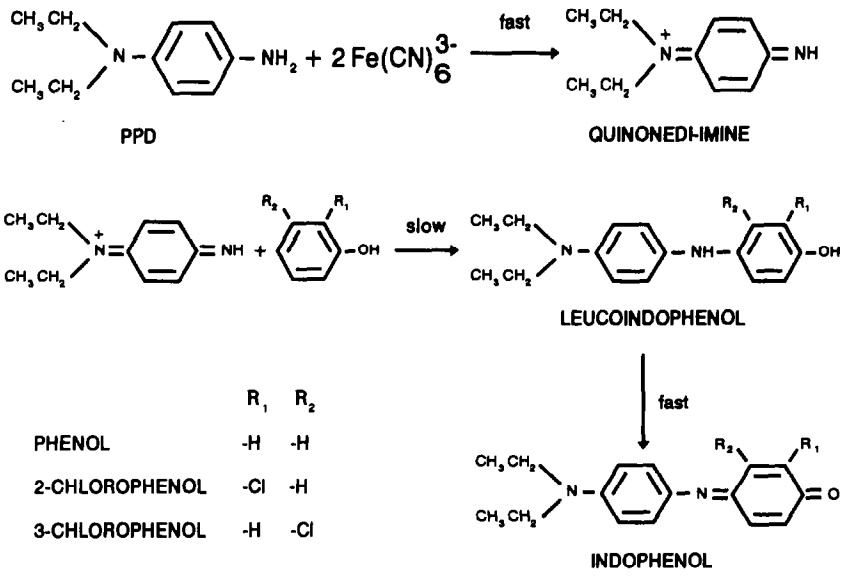

Scheme 1

of its smaller reaction rate and greater practical relevance).

Influence of variables

In order to establish the most suitable conditions, several variables potentially affecting the oxidative coupling reaction were investigated. Their influence was studied individually for each phenolic compound and the selected value for each was determined as that resulting in the maximum ratio between the pseudo-first rate constant *vs* concentration plots for the two compounds concerned.

The influence of pH on the rate constants was studied over the range 7.7–10.3 (Fig. 2). The plot of the logarithm of the rate constant for each phenolic compound against pH was linear, whereas the rate constant ratio ($k_{2\text{-ClPh}}/k_{\text{Ph}}$) decreased with increase in pH; above pH 10, k_{Ph} became larger than $k_{2\text{-ClPh}}$. This relationship can be accounted for on the basis of the pK_a values of the two phenolic compounds, viz. 10.0 and 8.48 for phenol and 2-chlorophenol, respectively, and available knowledge on the influence of chlorine substituents on the reaction rate. In fact, according to Corbett,[28] the reactivity of phenoxide ion is decreased on chlorination. Thus, at pH $\simeq$ 8.0, 2-chlorophenol is in ionized form ($\simeq$25%) whereas phenol remains protonated, so this effect offsets that of chlorination. As the pH is raised (and phenol ionization increased), the two rate constants approach; above pH 10, where both species occur as phenoxide ions, phenol being more reactive according to Corbett. Taking into account the above kinetic relationships, pH 8.0, at which $k_{2\text{-ClPh}}/k_{\text{Ph}} = 2.3$, was selected for the simultaneous kinetic determination of these compounds. Even though this rate constant ratio was higher at lower pH values, the reactions were very slow and of no practical analytical

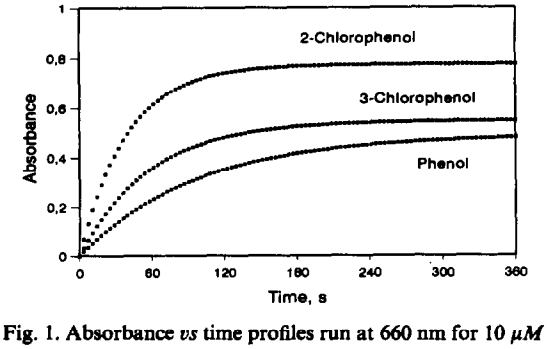

Fig. 1. Absorbance *vs* time profiles run at 660 nm for 10 μM of each phenolic compound. Conditions as described under procedure.

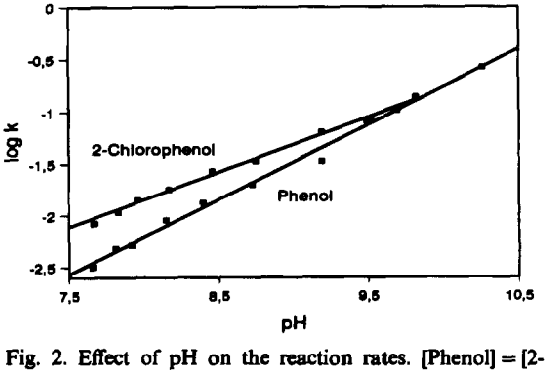

Fig. 2. Effect of pH on the reaction rates. [Phenol] = [2-chlorophenol] = 10 μM. Other experimental conditions as described under the procedure.

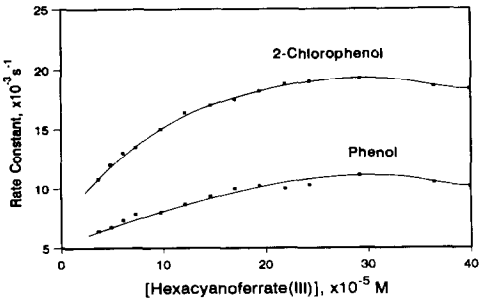

Fig. 3. Influence of the oxidant concentration on the rate constants. [Phenol] = [2-chlorophenol] = 10 μM. Other experimental conditions as described under the procedure.

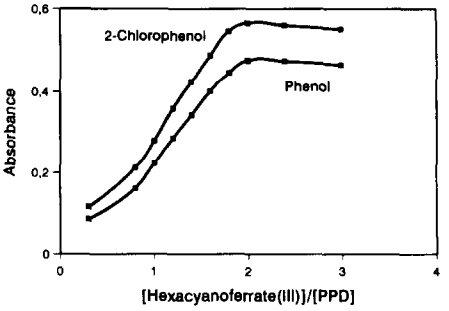

Fig. 4. Determination of the stoichiometric ratio for the oxidation of PPD by potassium hexacyanoferrate(III) using an equilibrium method. Experimental conditions as described under the procedure.

interest. In order to adjust the pH, 5 ml of 0.5M phosphate buffer (pH 8.0) was added to the reaction vessel as part of the procedure. Borate buffer was not used owing to its smaller buffering capacity and poorer solubility (concentrations above 0.1M are impossible to obtain).

The concentration of potassium hexacyanoferrate(III) was varied over the range 3.6×10^{-5}–$4.0 \times 10^{-4}M$ in order to investigate its effect on the rate constants (Fig. 3). In both cases, the pseudo-first rate constants increased with increasing oxidant concentration up to $2.4 \times 10^{-4}M$, above which they were virtually independent on such a concentration. In order to select the most suitable potassium hexacyanoferrate(III) concentration, another experiment was carried out as follows: the influence of the signal increments resulting from full conversion of phenol and 2-chlorophenol into their corresponding indophenols on the [oxidant]/[PPD] ratio was studied; *i.e.* the reaction stoichiometry was determined. As can be seen in Fig. 4, the ratio was 2 for both phenolic compounds, which is consistent with Scheme 1 and the exchange of two electrons in the reaction. A concentration of $4 \times 10^{-4}M$ (1.0 ml of a $2.4 \times 10^{-2}M$ solution) was thus selected for the simultaneous kinetic determination of these compounds.

The effect of the concentration of *N,N*-diethyl-*p*-phenylenediamine (PPD) was examined in the range 1.0–$4.0 \times 10^{-4}M$, the [oxidant]/[PPD] ratio being kept constant at the stoichiometric value. Both rate constants remained virtually constant throughout the assayed interval, whereas signal increments increased linearly with increase in the reagent concentration. A $2.0 \times 10^{-4}M$ PPD concentration (2.0 ml of a $6 \times 10^{-3}M$ ethanolic solution) was chosen as optimal.

Individual determination of phenols

Absorbance *vs* time graphs were plotted for solutions containing various concentrations of the phenolic compounds under the selected working conditions. The figures of merit of the individual determinations of these compounds are summarized in Table 1. The analytical sensitivity was taken as the slope of the calibration plot and the detection limit was calculated according to the IUPAC's recommendations.[30] The precision (expressed as the relative standard deviation) was determined by analysing 11 samples containing 10 μM of phenolic compound each, and the pseudo-first rate constants were calculated by applying the extended Kalman filter.[16]

Simultaneous kinetic determination of phenols

According to the reported pseudo-first rate constant values, the constant ratios between these phenolic compounds were $k_{2\text{-ClPh}}/k_{\text{Ph}} = 2.29$, $k_{3\text{-ClPh}}/k_{\text{Ph}} = 1.66$ and $k_{2\text{-ClPh}}/k_{3\text{-ClPh}} = 1.37$. The simultaneous kinetic determination of these phenols by traditional

Table 1. Analytical features of the individual determination of phenols

Analytical features	Phenol	2-Chlorophenol	3-Chlorophenol
Linear dynamic range (μM)	2.5–25	1.25–12.5	1.25–17.5
Sensitivity ($\times 10^{-2}$ A/μM)	4.68 ± 0.05	7.26 ± 0.02	5.39 ± 0.06
Detection limit (μM)	0.45	0.25	0.30
Precision (RSD) (%)	0.8	0.6	0.8
Rate constant ($\times 10^{-2}$/sec)	1.06 ± 0.04	2.43 ± 0.02	1.77 ± 0.02

Table 2. Model information used by the program

$\mathbf{X}(j)$	$\begin{bmatrix} S_1 \\ S_2 \\ S_B \end{bmatrix}$
$\mathbf{H}^T(j)$	$[1-\exp(-k_1 t_j)\ 1-\exp(-k_2 t_j)\ 1]$
$Z(j)$	$S(t_j)$
$R(j)$	10^{-6}
$\mathbf{X}(0,0)$	$\begin{bmatrix} 0.5 \\ 0.5 \\ 0 \end{bmatrix}$
$\mathbf{P}(0,0)$	$\begin{bmatrix} 0.5 & 0 & 0 \\ 0 & 0.5 & 0 \\ 0 & 0 & 0.5 \end{bmatrix}$

$R(j)$, variance of noise; $\mathbf{X}(0,0)$, initial guesses for state vector; $\mathbf{P}(0,0)$, initial guesses for error variance–covariance matrix.

differential reaction-rate methods is impossible as they require higher rate constant ratios for application. We thus chose to use the linear Kalman filter, a mathematical approach that is arousing growing interest for the resolution of mixtures by kinetic analysis.[14–16] Thus, we assayed the 2-chlorophenol/phenol and 2-chlorophenol/3-chlorophenol mixtures, which offer the maximum and minimum rate constant ratios, respectively. The resolution of ternary mixtures was impossible (high relative errors) owing to an inadequate difference between the fastest component (2-chlorophenol) and the slowest (phenol).

Provided that the signal increments are proportional to the initial analyte concentration, the signal measured at time t_j, $S(t_j)$, can be expressed by

$$S(t_j) = S_1[1-\exp(-k_1 t_j)] + S_2[1-\exp(-k_2 t_j)] + S_B + \text{Noise} \quad (1)$$

where S_1 and S_2 are the signal increments resulting from full conversion of compounds 1 and 2 in the mixture; S_B the background contribution; and k_1 and k_2 the pseudo-first rate constants of components 1 and 2, respectively. The measurement of N signals ($j = 1, 2, 3, \ldots N$) allows the establishment of a system of N linear equations in S_1, S_2 and S_B, which can be recursively solved by means of the Kalman filter algorithm. Equation (1) can be written according to the Kalman notation as

$$Z(j) = \mathbf{H}^T(j)\,\mathbf{X}(j) + v(j), \quad (2)$$

where $Z(j)$ denotes the absorbance measurement of the mixture sample; $\mathbf{H}^T(j)$ the measurement function vector; $\mathbf{X}(j)$ the state vector; and $v(j)$ the measurement noise. The actual values of these parameters as well as of the others required for the implementation of the filter are listed in Table 2. By applying the filter to the samples, the estimated net signal increments, S_1 and S_2 were determined, and subsequently interpolated in the corresponding calibration graphs in order to obtain the respective concentrations.

The results obtained for various binary synthetic mixtures containing different amounts of phenol, 2-chlorophenol and 3-chlorophenol are given in Tables 3 and 4; 2-chlorophenol/phenol mixtures in ratios from 7:1 to 1:5 can be satisfactorily resolved. These limits correspond to a relative error less than 7.5%. The precision of the method, expressed as the relative standard deviation (RSD), was also determined for mixtures containing 10 μM of each compound (11 samples), and turned out to be 1.8% and 2.5% for 2-chlorophenol and phenol, respectively. The 2-chlorophenol/3-chlorophenol mixtures in ratios from 4:1 to 1:4 were also successfully analysed. These limits correspond to a relative error less than 10%. The precision of the method was also determined for a mixture containing 10 μM of each phenol and was found to be 2.7% and 3.2% for 2-chlorophenol and 3-chlorophenol, respectively ($P = 0.05$, $n = 11$).

These results are quite satisfactory and testify to the good performance of the linear Kalman filter in the simultaneous kinetic determination of the phenols, even though the rate constant ratio is very low (only 1.3 for the 2-chlorophenol/3-chlorophenol mixture). On the other

Table 3. Analysis of 2-chlorophenol/phenol mixtures

Compound taken (μM)		2-Chlorophenol		Phenol	
2-Chlorophenol	Phenol	Found (μM)	Error (%)	Found (μM)	Error (%)
17.50	2.50	16.63	−4.97	2.46	−1.60
16.70	3.30	15.46	−7.42	3.46	+4.85
14.30	5.70	14.00	−2.10	5.35	−6.14
10.00	10.00	9.60	−4.00	9.87	−1.30
5.70	14.30	5.82	+2.10	13.71	−4.12
3.30	16.70	3.21	−2.73	16.25	−2.69
2.50	17.50	3.77	+50.8	16.22	−7.31

Table 4. Analysis of 2-chlorophenol/3-chlorophenol mixtures

Compound taken (μM)		2-Chlorophenol		3-Chlorophenol	
2-Chlorophenol	3-Chlorophenol	Found (μM)	Error (%)	Found (μM)	Error (%)
18.00	2.00	17.55	−2.50	2.79	+39.5
16.00	4.00	15.48	−3.25	4.52	+13.0
14.00	6.00	14.28	+2.00	5.59	−6.83
12.00	8.00	12.00	0.00	7.90	−1.25
10.00	10.00	9.80	−2.00	9.60	−4.00
8.00	12.00	8.19	+2.37	11.58	−3.50
6.00	14.00	6.52	+8.66	12.63	−9.78
4.00	16.00	4.35	+8.75	15.03	−6.06
2.00	18.00	2.43	+21.5	16.98	−5.66

hand, concentration ratios are quite acceptable (somewhat lower for 2-chlorophenol/3-chlorophenol mixtures owing to the lower rate constant ratio between the two) and the precision is good (the RSD is usually less than 3%). From a practical point of view, the method is simple and rapid and features modest requirements in terms of instrumentation and computational power. In addition, the proposed method affords higher concentration ratios and is more accurate than the stopped-flow method for the resolution of *o*- and *m*-cresol mixtures,[20] where the rate constant ratio is 1.54 (similar to that for the 2-chlorophenol/3-chlorophenol mixture).

Acknowledgements—The authors gratefully acknowledge financial support from the Dirección General Interministerial de Ciencia y Tecnología (DIGICyT) for the realization of this work as part of Project PB91-0840.

REFERENCES

1. O. Busto, J. C. Olucha and F. Borrull, *Chromatographia*, 1991, **32**, 423.
2. E. Delage, G. Bohuon, A. Baron and J. F. Drilleau, *J. Chromatogr.*, 1991, **555**, 125.
3. T. A. Berger and J. F. Deye, *J. Chromatogr. Sci.*, 1991, **29**, 54.
4. C. Brage and K. Sjoostrom, *J. Chromatogr.*, 1991, **538**, 303.
5. E. S. Brodskii, N. A. Klyyuev, V. G. Zhil'nikov, N. V. Murenets, A. K. Prokof'ev and B. V. Bocharov, *Zh. Anal. Khim.*, 1991, **46**, 2027.
6. A. J. Sequeira and L. T. Taylor, *Chromatogr. Sci.*, 1991, **29**, 351.
7. R. Herterich, *J. Chromatogr.*, 1991, **549**, 313.
8. D. T. Williams, Q. Tran, P. Fellin and K. A. Brice, *J. Chromatogr.*, 1991, **549**, 297.
9. M. Abdel-Rehim, M. Hassan and H. Ehrsson, *J. High-resolut. Chromatogr.*, 1991, **14**, 284.
10. L. H. Harrison, J. E. Morrison and P. V. Fennessey, *Clin. Chem.*, 1991, **37**, 1739.
11. M. T. Dmitriev and Yu. B. Suvorova, *Gig. Sanit.*, 1991, 85.
12. Z. Huangfu, *Sepu*, 1991, **9**, 137.
13. W. Tashkov, I. Benchev, N. Rizov, M. Kafedzhieva and A. Kolarska, *Chromatographia*, 1991, **32**, 466.
14. S. D. Brown, *Anal. Chim. Acta*, 1986, **181**, 1.
15. S. C. Rutan, *J. Chemometr.*, 1987, **1**, 7.
16. R. Xiong, A. Velasco, M. Silva and D. Pérez-Bendito, *Anal. Chim. Acta*, 1991, **251**, 313.
17. G. Gauglitz, M. Mettler and S. Weiss, *Trends in Anal. Chem.*, 1992, **11**, 203.
18. L. R. Sherman, V. L. Trust and H. Hoang, *Talanta*, 1981, **28**, 408.
19. N. G. Buckman, R. J. Magee and J. O. Hill, *Anal. Chim. Acta*, 1983, **153**, 285.
20. E. Pelizzetti, G. Giraudi and E. Mentasti, *Anal. Chim. Acta*, 1977, **94**, 479.
21. L. K. J. Tong and C. M. Glesmann, *J. Amer. Chem. Soc*, 1968, **90**, 5164.
22. J. F. Corbett, *J. Chem. Soc. B*, 1969, **(3)**, 207.
23. J. F. Corbett, *J. Chem. Soc. B*, 1969, **(3)**, 213.
24. J. F. Corbett, *J. Chem. Soc. B*, 1969, **(7)**, 818.
25. J. F. Corbett, *J. Chem. Soc. B*, 1969, **(7)**, 823.
26. J. F. Corbett, *J. Chem. Soc. B*, 1969, **(7)**, 827.
27. J. F. Corbett, *J. Soc. Dyers Colour*, 1969, **85**, 71.
28. J. F. Corbett, *J. Chem. Soc. B*, 1970, **(7)**, 1418.
29. E. Pellizzetti and G. Saini, *J. Photogr. Sci.*, 1974, **22**, 49.
30. G. L. Long and J. D. Winefordner, *Anal. Chem.*, 1983, **55**, 712A.

Talanta, Vol. 40, No. 10, pp. 1511–1518, 1993
Printed in Great Britain.

0039-9140/93 $6.00 + 0.00

COLUMN CHROMATOGRAPHIC SEPARATION OF MOLYBDENUM (VI) FROM ALLOYS WITH POLY-(DIBENZO-18-CROWN-6) FROM A HYDROCHLORIC ACID MEDIUM

B. S. MOHITE,* J. M. PATIL and D. N. ZAMBARE
Environmental Analytical Chemistry Laboratory, Department of Chemistry, Shivaji University, Kolhapur-416 004, India

(*Received* 4 *January* 1993. *Revised* 14 *April* 1993. *Accepted* 19 *April* 1993)

Summary—A very simple column chromatographic separation method has been developed for molybdenum (VI) using poly-(dibenzo-18-crown-6). The separations are carried out from hydrochloric acid medium. The adsorption of molybdenum (VI) on a poly-(DB-18-C-6) was quantitative from 2.5 to 10.0*M* HCl. Amongst the various eluents tested, 0.5*M* ammonium hydroxide was found to be an efficient eluent. Molybdenum (VI) was separated from a large number of elements in binary form, as well as from multicomponent mixtures. The method was applied for the analysis of molybdenum from various alloy samples. The method is very simple, rapid, selective and reproducible. The reproducibility of the procedure is ±2%.

Molybdenum has a large number of applications in various fields. It is used in radios, wireless sets, anticathodes of X-ray tubes and in the production of special steels. Along with tungsten, it is used in thermocouples for high temperature measurements. Molybdenum occurs in water, soil, plants and animals at trace level. Molybdenum is one of the seven micronutrients required for the growth and development of plants. It is required to change nitrogen into other forms the plant can use. Thus nitrogen-fixing-bacteria employ enzymes containing both molybdenum and iron.

The separation of molybdenum from other elements was carried out using various chelating resins. Chelex-100 was used for trace element analysis, in which, molybdenum along with other elements was determined from natural water samples using neutron activation analysis,[1] a significant increase in time and effort was required. The chelating resins containing amidoxime groups[2] such as Duolite ES-346, Duolite CS-346 and Chelite-N, *etc.* formed strong complexes with a number of metal ions including molybdenum (VI). Resin having an active oxime group was used for the extractive separation of molybdenum from aqueous sulfuric acid.[3] The molybdenum was then recovered by eluting with alkaline solutions. A chelating resin was prepared[4] by loading pyrogallolsulfonic acid on to Seralite SRA-400, it showed high selectivity towards Mo(VI), V(V) and Fe(III). Various amphoteric ion exchangers were tested for the recovery of molybdenum from sulfuric acid leaching liquors of molybdenum calcines,[5] the maximum sorption capacity for molybdenum was shown by the exchanger ANKB-7 and VP-14K, the elution of molybdenum was carried out with 7.5% NH_4OH.

Crown ethers have been extensively used in extraction analysis studies of various metal ions and those methods have been reviewed,[6] but the use of crown ethers for the extractive separation analysis of Mo(VI) is limited. DB-18-crown-6 was used for the solvent extraction of technetium from ascorbic acid medium, Mo(VI) showed very poor extraction.[7] DC-18-crown-6 was used in presence of polyurethane foam for the extractive separation of molybdenum from a thiocyanate–hydrochloric acid medium[8] but the separation of molybdenum from other elements was not achieved. Mo(VI) was quantitatively extracted from 7 to 10*M* hydrochloric acid with 0.01*M* DB-18-crown-6 in nitrobenzene.[9] Mo(VI) from the organic phase was then stripped with 2*M* nitric acid. It was possible to separate Mo(VI) from a large number of elements in binary as well as in multicomponent mixtures. The selective extraction of molybdenum permits its separation from a number of elements which are usually associated with it.

*Author for correspondence.

From the literature survey it is clear that no attempts have been made for the use of crown ethers or crown polymers in the column chromatographic separation studies of molybdenum (VI). This paper presents a systematic investigation of the column chromatographic separation studies of molybdenum (VI) from associated elements in hydrochloric acid medium using poly-dibenzo-18-crown-6. The method has been extended to the separation of molybdenum (VI) from a large number of other elements and also from a number of various alloy samples.

EXPERIMENTAL

Apparatus and reagents

A Zeiss spectrophotometer (German), a digital pH meter (Model LI-120 ELICO, India) with glass and calomel electrodes, a digital flame photometer (PEI, Model No. 041, India) and a Pyrex glass chromatographic column (20 × 0.8 cm i.d.) with a glass wool plug at the bottom were used.

A crown ether polymer (poly-(DB-18-C-6) Merck (German)) was used after screening with 100–200 mesh; 0.8 gm of poly-(DB-18-C-6) was slurried with distilled deionized water and poured into a Pyrex glass chromatographic column. The column was used after preconditioning with hydrochloric acid.

A stock molybdenum (VI) solution was prepared by dissolving 4.60 g of ammonium molybdate tetrahydrate (AnalaR) in 500 ml distilled deionized water and standardized gravimetrically.[10] A working standard solution (molybdenum 500 μg/ml) was prepared by appropriate dilution of the standard stock solution.

Procedure

An aliquot of solution containing 500 μg of molybdenum (VI) was mixed with hydrochloric acid in the concentration range of 0.5–10.0M in a total volume of 10 ml. The solution was then passed through the column, preconditioned with hydrochloric acid of the same acidity as that of the sample solution at a flow rate of 0.5 ml/min. The column was subsequently washed with hydrochloric acid of the same acidity and then with water. The adsorbed molybdenum (VI) was eluted with different eluting agents (described later) at a flow rate of 0.5 ml/min. Five millilitre fractions were collected and after evaporating the acid it was extracted with water and the molybdenum (VI) content was determined spectrophotometrically with Tiron[11] at 390 nm. The concentration of molybdenum (VI) was calculated from the calibration curve.

RESULTS AND DISCUSSION

Adsorption of molybdenum (VI) as a function of hydrochloric acid concentration on poly-(DB-18-crown-6)

In order to ascertain the optimum concentration of hydrochloric acid for the quantitative adsorption of molybdenum (VI) on poly-(DB-18-C-6) various studies were conducted by varying the concentration of hydrochloric acid from 0.5 to 10.0M. It was found that there was 75% adsorption of molybdenum (VI) at 0.5M hydrochloric acid, it was 90% at 1.5M, 98% at 2.5M and was quantitative from 3.0 to 10M hydrochloric acid (Table 1). Further adsorption studies of molybdenum (VI) were carried out at 5.0M hydrochloric acid concentration.

Elution studies of molybdenum (VI)

Molybdenum (VI) was adsorbed on poly-(DB-18-C-6) resin column at 5M hydrochloric acid concentration. After adsorption, molybdenum (VI) was eluted with various eluents such as ammonium hydroxide, hydrobromic acid, perchloric acid, sulfuric acid, acetic acid in the concentration range of 0.5–8.0M. Except for ammonium hydroxide and sulfuric acid other eluents were found to be inefficient for the

Table 1. Adsorption of molybdenum (VI) as a function of hydrochloric acid concentration on poly-(debenzo-18-crown-6). Mo(VI) 500 μg; eluent 0.5M ammonium hydroxide

Hydrochloric acid concentration (M)	Adsorption (%)
0.5	75
1.0	84
1.5	90
2.0	94
2.5	98
3.0	100
3.5	100
4.0	100
4.5	100
5.0	100
5.5	100
6.0	100
6.5	100
7.0	100
7.5	100
8.0	100
8.5	100
9.0	100
9.5	100
10.0	100

elution of molybdenum (VI). With 0.1*M* ammonium hydroxide there was 77% elution, with 0.5*M* ammonium hydroxide there was quantitative elution of molybdenum (VI). With 1*M* ammonium hydroxide there was 83% elution and subsequently elution of molybdenum (VI) decreased from 2.0 to 7.0*M* ammonium hydroxide, for 7*M* ammonium hydroxide the elution of molybdenum (VI) was 58%. There was no quantitative elution of molybdenum (VI) with perchloric and hydrobromic acid in the concentration range of 0.5–8.0*M* with 6.0–8.0*M* sulfuric acid there was quantitative elution of molybdenum (VI). The acetic acid in the concentration range of 0.5–8.0*M* was found to be an inefficient eluent for the elution of molybdenum (VI). The elution profiles of molybdenum (VI) with ammonium hydroxide are shown in Fig. 1. Further, elution studies of molybdenum (VI) were carried out with 0.5*M* ammonium hydroxide.

Effect of varying concentration of molybdenum (VI)

In order to ascertain quantitative adsorption of molybdenum (VI) on 1 gm of poly-(DB-18-C-6) resin column, various adsorption studies were carried out for the 5*M* hydrochloric acid concentration, by varying the concentration of molybdenum (VI) in the concentration range of 10–100 mg/l (Table 2). Ten millilitre solutions of the above concentration range were employed. After adsorption, molybdenum (VI) was eluted with 0.5*M* ammonium hydroxide. From Table 2 it is clear that there was quantitative adsorption of molybdenum (VI) up to 70 mg/l. The extent

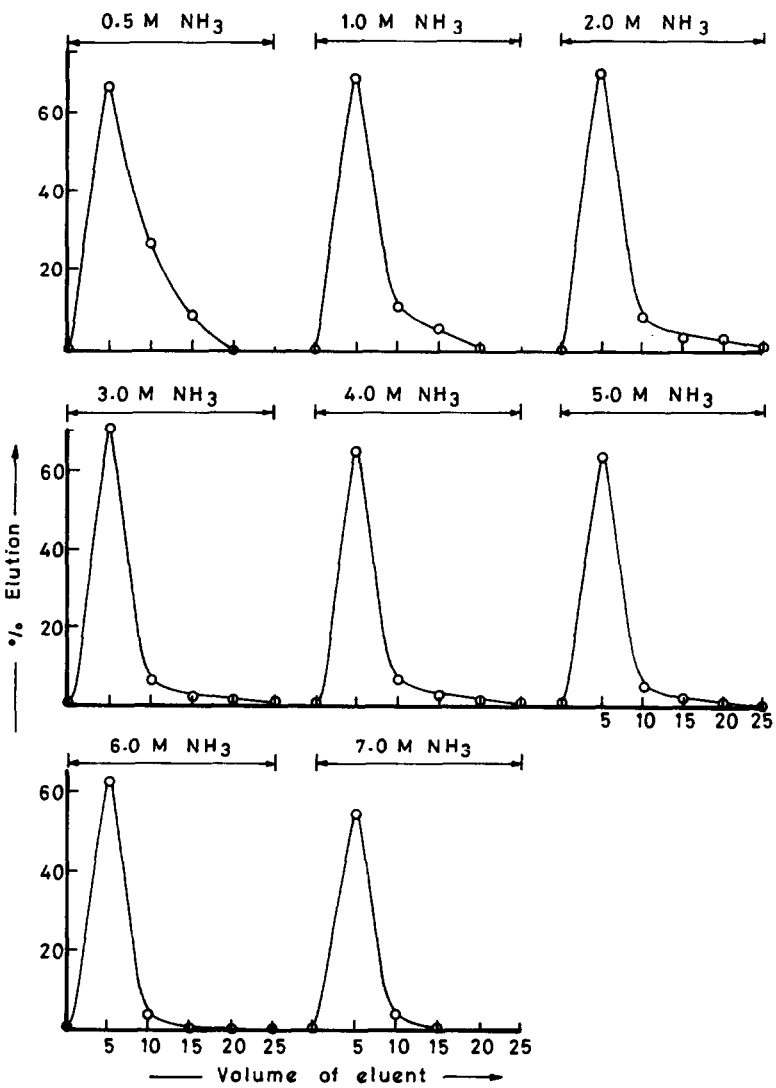

Fig. 1. Elution studies of molybdenum (VI) with ammonia.

Table 2. Effect of varying concentration of molybdenum (VI). Vol. of soln. used 10 ml, adsorbing conditions 5*M* HCl, Eluent 0.5*M* ammonium hydroxide

Amount of molybdenum (VI) (*mg/l*)	Adsorption (%)
10	100
20	100
30	100
40	100
50	100
60	100
70	100
80	95
90	87
100	80

of adsorption decreased with an increase in the concentration of molybdenum (VI).

Adsorption isotherm of molybdenum (VI) on poly-(DB-18-C-6)

The adsorption studies of molybdenum (VI) were carried out for 5*M* hydrochloric acid by varying the concentration of molybdenum (VI) in solution. The results are shown in Table 3. The capacity of poly-(DB-18-C-6) for molybdenum (VI) was found to be 7.81 mmol/gm of crown polymer.

Separation of molybdenum (VI) from a binary mixture

An aliquot of solution containing molybdenum (VI) and the foreign ions to be tested was taken and hydrochloric acid was added so that its concentration was 5*M* in a total volume of 10 ml. The tolerance limit of foreign ion was set as the amount of foreign ions required to cause ±2% error in the recovery of molybdenum (VI). The solution was then passed through the column preconditioned with 5*M* hydrochloric acid at a flow rate of 0.5 ml/min. Subsequently the column was washed with 5*M* hydrochloric acid and then with water. Those foreign ions which were not adsorbed on poly-(DB-18-C-6), passed through the column. Most of the foreign ions were not adsorbed (Table 4). Amongst the alkali metals, sodium was adsorbed to the extent of 70%, potassium 80% and rubidium 90%. From the alkaline earths only strontium and barium were adsorbed quantitatively. From the nontransition metals gallium (III) and thallium (III) were adsorbed quantitatively, whereas of the inner transition series, uranium (VI) was adsorbed to the extent of 94%. Iron (III) was

Table 3. Adsorption isotherm of molybdenum (VI) on poly-(DB-18-crown-6). Vol. of soln. used 10 ml, adsorbing condition 5*M* HCl, eluent 0.5*M* ammonium hydroxide

Concentration of molybdenum (VI) in solution (*mg/l*)	Concentration of molybdenum (VI) on poly-(DB-18-C-6) ($\times 10^{-2}$ *mg/gm*)
10	10
20	20
30	30
40	40
50	50
60	60
70	70
80	76
90	78.3
100	80.0

Table 4. Separation of molybdenum (VI) from binary mixtures. Mo 500 μg, poly-(DB-18-C-6), 6*M* HCl (adsorption), 0.5*M* ammonium hydroxide (elution)

Ions	Added as	Tolerance limit (*mg*)
Li^+	LiCl	4.50
*Na^+	NaCl	6.00
*K^+	KCl	6.50
*Rb^+	RbCl	7.00
Cs^+	CsCl	5.00
NH_4^+	NH_4Cl	6.50
Be^{2+}	$Be(NO_3)_2 . 4\ H_2O$	5.50
Mg^{2+}	$MgCl_2 . 6\ H_2O$	7.00
Ca^{2+}	$CaCl_2$	6.50
*Sr^{2+}	$Sr(NO_3)_2$	4.00
*Ba^{2+}	$Ba(NO_3)_2$	3.50
Co^{2+}	$CoCl_2 . 6\ H_2O$	1.50
Ni^{2+}	$NiCl_2 . 6\ H_2O$	2.50
Cu^{2+}	$CuCl_2 . 2\ H_2O$	1.50
Zn^{2+}	$ZnCl_2$	2.50
Mn^{2+}	$MnCl_2 . 4\ H_2O$	2.50
Sn^{2+}	$SnCl_2 . 2\ H_2O$	2.00
Pb^{2+}	$Pb(NO_3)_2$	1.00
Cr^{3+}	$Cr(NO_3)_3 . 9\ H_2O$	5.50
Fe^{3+}	$FeCl_3 . 6\ H_2O$	0.20
Al^{3+}	$Al(NO_3)_3 . 9\ H_2O$	2.50
La^{3+}	$La(NO_3)_3 . 6\ H_2O$	7.50
Ce^{3+}	$CeCl_3 . 6\ H_2O$	5.00
Bi^{3+}	$Bi(NO_3)_3 . 5\ H_2O$	1.00
*Ga^{3+}	$GaCl_3$	3.50
In^{3+}	$InCl_3 . 4\ H_2O$	3.50
*Tl^{3+}	$Tl(NO_3)_3 . 3\ H_2O$	0.50
Sb^{3+}	$SbCl_3$	3.00
Ge^{4+}	Na_2GeO_3	2.00
Th^{4+}	$Th(NO_3)_4$	4.50
V^{5+}	NH_4VO_3	4.00
*U^{6+}	$UO_2(NO_3)_2 . 6\ H_2O$	4.00
W^{6+}	$Na_2WO_4 . 2\ H_2O$	2.00
Br^-	HBr	8.00
I^-	HI	10.00
NO_3^-	HNO_3	9.00
SCN^-	NaSCN	7.00
ClO_4^-	$HClO_4$	6.00
CH_3COO^-	CH_3COOH	12.00
$C_2O_4^{2-}$	$H_2C_2O_4$	5.00
PO_4^{3-}	H_3PO_4	8.00
BO_3^{3-}	H_3BO_3	4.00
Ascorbate	Ascorbic acid	6.50
Tartarate	Tartaric acid	4.50
Citrate	Citric acid	6.00
EDTA	EDTA	7.00

*Adsorption.

adsorbed partially which was eluted with 2.5*M* hydrochloric acid. Most of the non-transition and transition metals showed a higher tolerance limit. Similarly most of the anions were tolerated in higher ratios. The adsorbed sodium, potassium, rubidium, similarly strontium, barium and gallium were eluted by washing the column with water whereas molybdenum (VI) was eluted with 0.5*M* ammonium hydroxide. This condition was exploited for the separation of molybdenum in multicomponent mixtures.

Separation of molybdenum (VI) from multicomponent mixtures

Molybdenum (VI) was separated from various multicomponent mixtures, when a mixture of Pb, Sr/Ba/Ga and Mo(VI) was passed through the column at 6*M* hydrochloric acid concentration, lead was not adsorbed (hence passed through the column) whereas other elements were adsorbed on the column. The adsorbed Sr/Ba/Ga were eluted by washing the column with water and finally molybdenum was eluted with 0.5*M* ammonium hydroxide.

When a mixture of Th, Sr/Ba/Ga and Mo was passed through the column at 5*M* hydrochloric acid, thorium was not adsorbed (hence passed through the column). The adsorbed Sr/Ba/Ga was eluted with water and then molybdenum with 0.5*M* ammonium hydroxide. The separation of molybdenum from other multicomponent mixtures was accomplished similarly (Table 5).

The separation of molybdenum (VI) from other elements in multicomponent mixture are shown in Figs 2(a) and (b).

Application to analysis of molybdenum from various alloys and steel

The method was applied for the analysis of molybdenum from nickel base alloy (BCS-CRM No. 345), alloy steel (BCS-CRM 401/1), low alloy steel (SS-407/1) and high speed tool steel (SS-486/1), 0.1 gm of the alloy sample was dissolved in *aqua regia*, after evaporation of the acid it was extracted with water and diluted to 10 ml. An aliquot of this sample solution was mixed with hydrochloric acid so as to have its concentration of 5*M* in a total volume of 10 ml. The solution was passed through the column preconditioned at 5*M* hydrochloric acid. The column was subsequently washed with 5*M* hydrochloric acid to remove most of the unadsorbed elements. Then it was eluted with 2.5*M* hydrochloric acid to remove partially adsorbed iron. At this stage only molybdenum remained on the column. The column was then washed with water and molybdenum (VI) was eluted with 0.5*M* ammonium hydroxide and was determined spectrophotometrically with Tiron. The

Table 5. Separation of molybdenum (VI) from multicomponent mixtures

No.	Mixture	Taken (*mg*)	Found (*mg*)	Recovery (%)	Adsorbing condition	Eluent
1	Pb	0.05	0.05	100	6*M* HCl, NAPC†	—
	Sr/Ba*/Ga	0.10	0.10	100	6*M* HCl	H_2O
	Mo(VI)	0.50	0.49	98	6*M* HCl	0.5*M* NH_4OH
2	Th	0.10	0.10	100	5*M* HCl, NAPC	—
	Sr/Ba*/Ga	0.10	0.10	100	5*M* HCl	H_2O
	Mo(VI)	0.50	0.50	100	5*M* HCl	0.5*M* NH_4OH
3	Ce(III)	0.10	0.098	98	5*M* HCl, NAPC	—
	Sr/Ba*/Ga	0.10	0.10	100	5*M* HCl	H_2O
	Mo(VI)	0.50	0.49	98	5*M* HCl	0.5*M* NH_4OH
4	La	0.10	0.10	100	5*M* HCl, NAPC	—
	Sr/Ba*/Ga	0.10	0.10	100	5*M* HCl	H_2O
	Mo(VI)	0.50	0.50	100	5*M* HCl	0.5*M* NH_4OH
5	Cr(III)	1.0	0.99	99	5*M* HCl, NAPC	—
	Sr/Ba*/Ga	0.10	0.10	100	5*M* HCl	H_2O
	Mo(VI)	0.50	0.50	100	5*M* HCl	0.5*M* NH_4OH
6	V(V)	0.10	0.098	98	5*M* HCl, NAPC	—
	Sr/Ba*/Ga	0.10	0.10	100	5*M* HCl	H_2O
	Mo(VI)	0.50	0.49	98	5*M* HCl	0.5*M* NH_4OH
7	Cs	0.10	0.10	100	5*M* HCl, NAPC	—
	Sr/Ba*/Ga	0.10	0.10	100	5*M* HCl,	H_2O
	Mo(VI)	0.50	0.50	100	5*M* HCl	0.5*M* NH_4OH
8	Co(II)	0.10	0.10	100	5*M* HCl, NAPC	—
	Sr/Ba*/Ga	0.10	0.10	100	5*M* HCl	H_2O
	Mo(VI)	0.50	0.49	98	5*M* HCl	0.5*M* NH_4OH

*0.5 mg.

†NAPC—No Adsorption Passing through the Column.

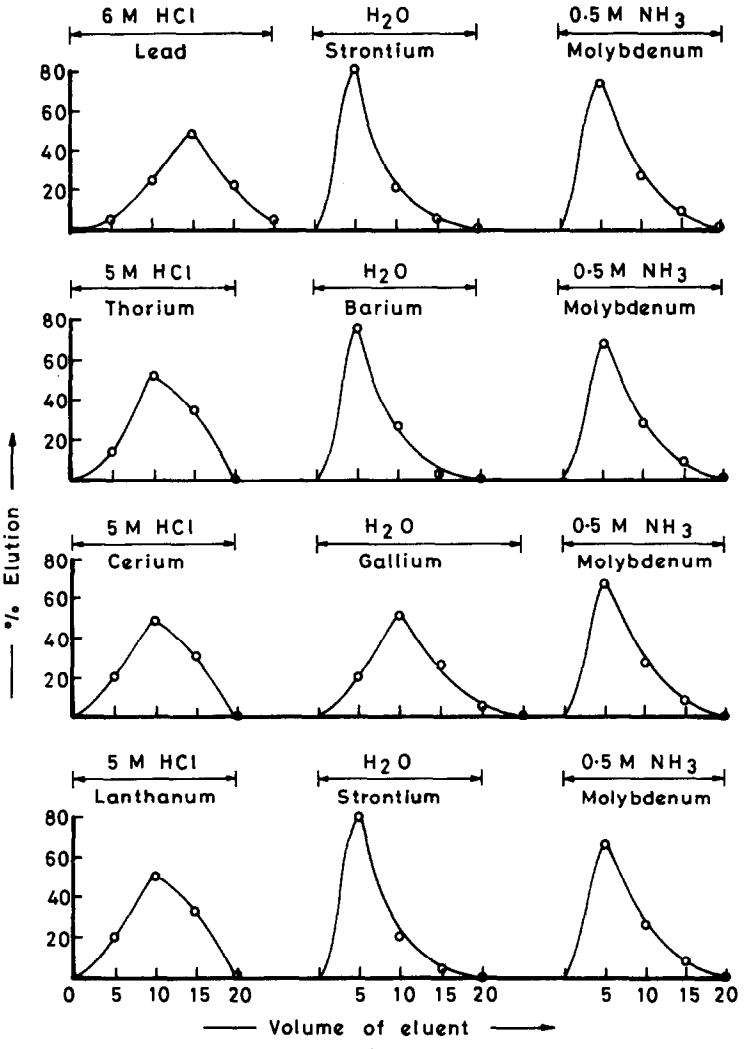

Fig. 2. (a) Separation of molybdenum (VI) from other elements.

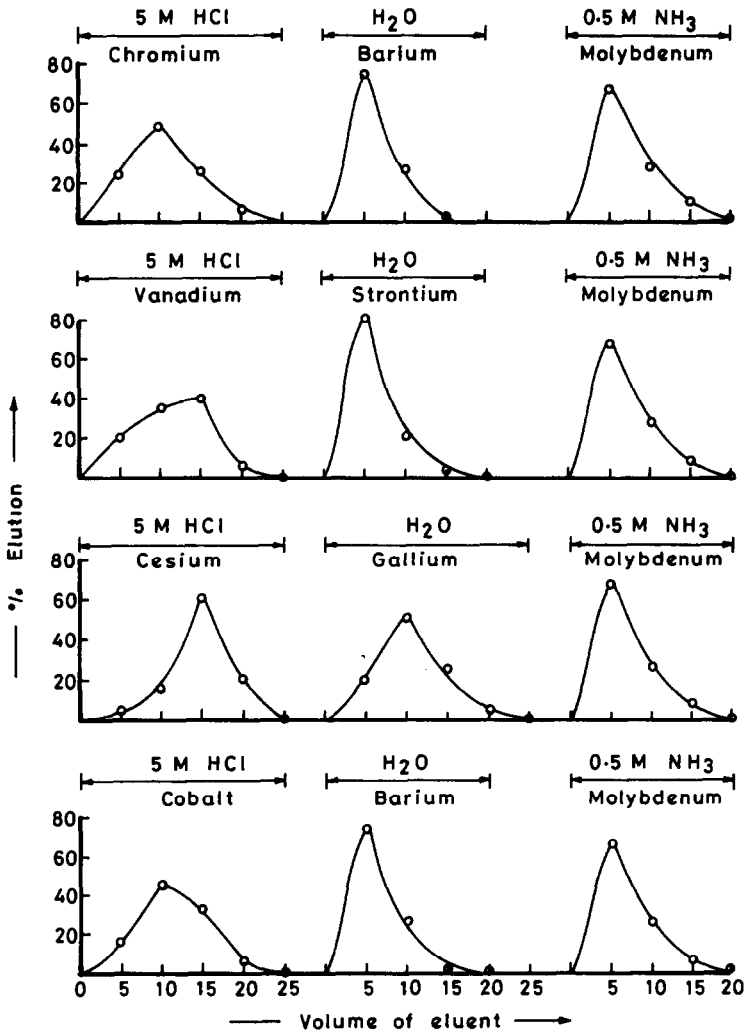

Fig. 2. (b) Separation of molybdenum (VI) from other elements.

results in triplicate analysis are shown in Table 6.

The strong binding of poly-(dibenzo-18-crown-6) for molybdenum (VI) can be explained on the following grounds. According to Pedersen[12] the selectivity of crown ether for a cation is based on (i) the relative size of ion and cavity of polyether, (ii) the number of oxygen atoms, (iii) the basicity of oxygen atom, (iv) the steric hindrance in a polyether ring, and (v) the tendency of the ion to associate with the solvent. Especially the relationship between the ion size and crown ether cavity has been extensively investigated and established as the primary principle for the cation selectivity. For the selectivity of crown ether polymer for a cation there is a simple rule. The polymer prefers[13] the cation for which the ratio of the diameter of cation to the diameter of polyether ring is 0.8. However, this relationship is not absolute. It was recently found[14] that the electrostatic interaction between lone pair orbitals of cyclic polyether and cation is the dominant part of the interaction energy. The stabilization energy which is accompanying the complex formation is divided into

Table 6. Determination of molybdenum (VI) in alloy sample

No.	Sample	Molybdenum (%) Present	Found
1	Nickel base alloy (BCS-CRM No. 345)	3.01	3.00
2	Alloy steel (BCS-CRM No. 401/1)	0.47	0.48
3	Low alloy steel (SS-407/1)	0.78	0.77
4	High speed tool steel (SS-486/1)	5.20	5.16

energies due to charge transfer interaction, electrostatic interaction, exchange interaction and polarization interaction. The strong binding of poly-(dibenzo-18-crown-6) for molybdenum (VI) may be due to the presence of electrostatic field in the crown ether cavity and high charge on molybdenum (VI) which results in the stabilization of the electrostatic and charge transfer interactions.

CONCLUSIONS

The important feature of this method is that it permits the separation of molybdenum from lead, strontium, barium, lanthanum, chromium, vanadium, iron, cesium and cobalt. The method was applied to the analysis of molybdenum from various alloy samples. The proposed method is very simple, rapid, selective and reproducible. The recovery of molybdenum in all instances from duplicate determinations is $100 \pm 2\%$.

Acknowledgement—We are thankful to the Board of Research in Nuclear Sciences, Department of Atomic Energy, Government of India, for sponsoring the project (No. 37/12/88-G) and awarding a Junior Research Fellowship to one of us (J.M.P.).

REFERENCES

1. R. R. Greenberg and H. M. Kingstone, *Anal. Chem.*, 1983, **55**, 1160.
2. Diamond Sharmrock, Duolite CS-346, Technical Sheet, OH, U.S.A. (*Talanta*, 1990, **37**, 491).
3. D. Beutier and Q. Y. Le, *Appl.*, **108**, 98477 x.
4. J. Lucy, P. Vaddsseril and N. Shivashankara, *Analyst*, 1989, **114**, 439.
5. M. M. Bogomolova, E. G. Tarasova and A. Yu. Dadabae, *Kompleksn. Ispol. Miner. Syrya*, 1988(5) 40, **111**, 10,574.
6. B. S. Mohite, Ph.D. Thesis, Indian Institute of Technology, Bombay, 1986.
7. Le Toung Minh and T. Lengyel, *J. Radioanal. Nucl. Chem.*, 1989, **135**, 403.
8. R. Caletka, R. Hausbeck and V. Kirvan, *Talanta*, 1986, **33**, 315.
9. B. S. Mohite and J. M. Patil, *J. Radioanal. and Nucl. Chem. Articles.*, 1991, **150**, 207.
10. A. I. Vogel, *A Text Book of Quantitative Inorganic Analysis*, p. 509. Longmans, Green, London, 1968.
11. F. Wills and J. H. Yoe, *Anal. Chim. Acta*, 1953, **8**, 546.
12. C. J. Pedersen, *J. Am. Chem. Soc.*, 1967, **89**, 7017.
13. E. Blasius and K. P. Janzen, *Pure & Appl. Chem.*, 1982, **54**, 2115.
14. K. Hori, H. Yamada and T. Yamabe, *Tetrahedron*, 1983, **39**, 67.

Talanta, Vol. 40, No. 10, pp. 1519–1524, 1993
Printed in Great Britain.

0039-9140/93 $6.00 + 0.00

FIRST DERIVATIVE SPECTROPHOTOMETRY FOR INDIVIDUAL AND SIMULTANEOUS DETERMINATION OF MAGNESIUM(II) AND COPPER(II) USING EMODIN(1,3,8-TRIHYDROXY-6-METHYLANTHRAQUINONE) AS REAGENT

TARASANKAR PAL and NIKHIL R. JANA
Department of Chemistry, Indian Institute of Technology, Kharagpur 721 302, India

(*Received* 15 *December* 1992. *Revised* 14 *April* 1993. *Accepted* 20 *April* 1993)

Summary—First derivative spectrophotometry are presented in comparison with simple spectrophotometric method for Cu(II) and Mg(II) determination with emodin in alkaline pH range. The molar absorptivity at the λ_{max} of 572 nm and 553 nm for Cu(II) and Mg(II) are 5.5×10^3 and 3.9×10^3 lit/mol/cm, respectively. Zero crossing measurement technique is found suitable for the simultaneous determination of the metal ions. The interference effects, statistical analyses and limits of detection are also reported.

Emodin, a polyphenolic anthraquinone, is a biochemically active[1,2] natural product and has been isolated from several plants as plant pigments.[3,4] It reacts with Cu(II) and Mg(II) ions in an alkaline medium to form coloured complexes. Recently, we reported its importance as photometric reagent.[5] It has been reported that Cu(II) interferes strongly in the determination of Mg(II) and both the complexes of Cu(II) and Mg(II) of emodin showed similar absorption profiles. This made the determination of Mg(II) impossible if present in a mixture with Cu(II) in the straight cut spectrophotometric process.

Recent development of the derivative spectrophotometry is now being used for eliminating the background interference and also for resolving the overlapping absorption bands.[6] It has been widely used in pharmaceutical analysis, amino-acid and protein analysis, clinical chemistry and environmental analysis.[7] The derivative method is being intensively used for the simultaneous determination of inorganic ions through the formation of complexes with the same organic ligands.[8–17] This advancement has led to the development of first derivative spectrophotometry for Cu(II) and Mg(II) for their quick determination without any separation if present singly or in mixtures and a comparison has also been made between normal and first derivative spectrophotometric determination of Cu(II) and Mg(II) to indicate the improved sensitivities.

The cations which interfere strongly in the determination of Cu(II) and Mg(II) includes Ni(II), Co(II), Mn(II), Cd(II), Cr(III), Fe(II) and Fe(III). The last three metal ions quench the absorbance values of Cu(II) and Mg(II) complexes of emodin. However, the remaining metal ions showed positive interference and because of their low molar absorptivities ($\sim 10^2$ lit/mol/cm), analytical procedure for their sensitive determination could not be developed. Moreover, these complexes have similar absorption profile and very close λ_{max} values. Hence simultaneous determination could not be achieved.

EXPERIMENTAL

Apparatus

All absorbance measurements were made with a Shimadzu UV-160 digital spectrophotometer with 1 cm quartz cells.

A digital (ECIL, Hyderabad, Govt. of India Enterprise) pH meter was used for pH measurements.

Reagents

All materials were of analytical reagent grade. Double distilled deionized water was used in all preparations.

A stock solution of emodin ($10^{-3}M$) was prepared by dissolving 67.5 mg of emodin (Aldrich Chemical Company, U.S.A.) in 250 ml volumetric flask using methanol as solvent. Fresh stock solutions of $Cu(NO_3)_2$ and $Mg(NO_3)_2$ were prepared using double distilled

water. The solutions were standardized[18] by using iodometric method for Cu(II) and complexometric method for Mg(II) and diluted to the range of $10^{-3}M$. Borate buffer with pH ranging from 8.0 to 9.2 were prepared with $0.2M$ boric acid and $0.05M$ borax solution. Buffer solutions with pH ranging between 9.2 and 11.0 were prepared with $0.05M$ borax and $0.2M$ sodium hydroxide solution. The pH was finally adjusted using a pH meter.

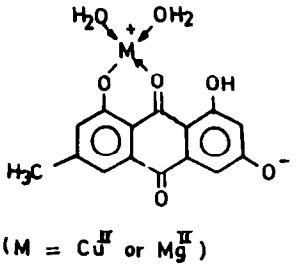

Fig. 2. Metal chelates at pH 9.8.

Procedure

In a 10 ml calibrated flask, 2.5 ml of the stock solution of emodin was mixed with varying amounts of Cu(II) and/or Mg(II) at a constant pH of 9.8, adjusted with 2.5 ml of the buffer solution. After 10 min the solution was diluted to the mark with methanol and the final methanol concentration in the solution was almost 75%.

For normal spectrophotometry of Cu(II), the absorbance values against reagent blank (emodin–methanol in alkaline buffer) were recorded at 572 nm.

The first derivative spectrum against reagent blank in all cases were recorded at a scan speed of 1500 nm/min and $\Delta\lambda = 11.2$ nm. The amplitudes were measured at 600 nm and 580 nm for Cu(II) and Mg(II), respectively when they were present alone, but in mixture the amplitudes used were 553 nm for Cu(II) and 572 nm for Mg(II).

RESULTS AND DISCUSSION

Effect of pH on complex formation

The effect of pH on the formation of Cu(II) and Mg(II) complexes with emodin were studied over the pH range of 2.0–12.0 at room temperature (25°C) and at 75% methanol–water mixture.

Cu(II) forms three types of complex in presence of emodin depending on the pH of the solution. In the pH range of 6.0–7.0 yellow coloured complex was formed which was insoluble in methanol, ethanol and water. In the pH range of 8.0–11.0, a pink coloured complex was formed having λ_{max} at 572 nm. The complex was soluble in both methanol and water. In the pH range of 11.0–12.2, another complex having λ_{max} of 585 nm with comparatively lower molar absorptivity than the second complex was formed. In each case emodin was in excess in comparison to Cu(II) and the complex formation was reversible and interconvertible depending on the pH condition of the medium.

Unlike Cu(II), Mg(II) forms two types of complex with emodin depending upon pH.

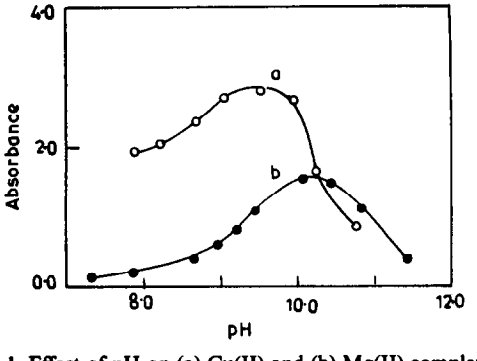

Fig. 1. Effect of pH on (a) Cu(II) and (b) Mg(II) complexes of emodin in 67% methanol at 572 nm and 553 nm, respectively.

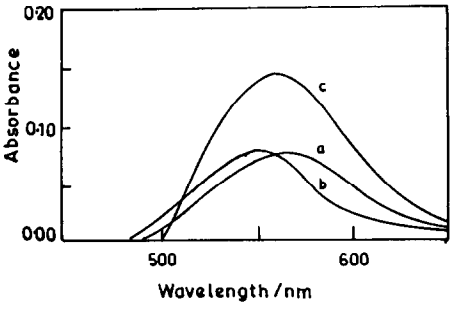

Fig. 3(a). Absorption spectra of emodin complexes of Cu(II) and Mg(II) against reagent blank at pH 9.8.

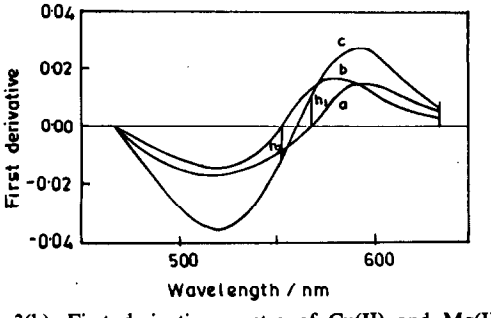

Fig. 3(b). First derivative spectra of Cu(II) and Mg(II) complexes of emodin at pH = 9.8.

Table 1. Statistical analyses of the determination of Cu(II) and Mg(II) from zeroth and 1st order derivative spectrophotometry

Element determined	Order of the derivative	Slope	Intercept	Correlation coefficient	LOD (*ppb*)
Cu(II)	Zeroth	0.087	4.5×10^{-4}	0.997	40
	First	0.017	5.8×10^{-4}	0.997	25
Mg(II)	Zeroth	0.162	-1.24×10^{-4}	0.995	20
	First	0.032	4.0×10^{-4}	0.994	10

When excess emodin was used, Mg(II) forms a coloured complex having λ_{max} at 553 nm, soluble in methanol and water in the pH range of 8.0–11.5, which was shown in our previous study.[5] In the pH range of 11.5–12.2 another complex having $\lambda_{max} = 575$ nm with comparatively lower molar absorptivity, was identified. These complex formations were also reversible and by changing pH one complex could be converted to the other. Detailed structural studies of all the complexes are in progress.

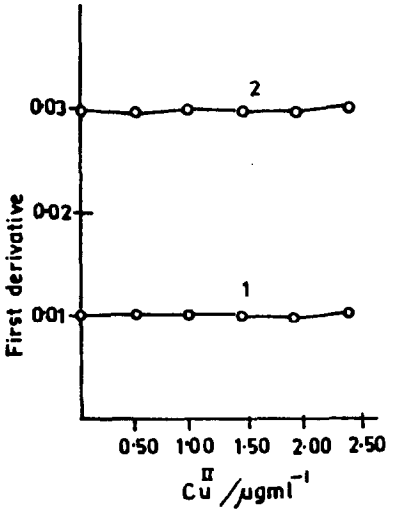

Fig. 4(a). Amplitude of the first derivative for Mg(II) = 0.36 μg/ml (1) and 0.97 μg/ml (2) at 572 nm in the presence of variable amounts of Cu(II).

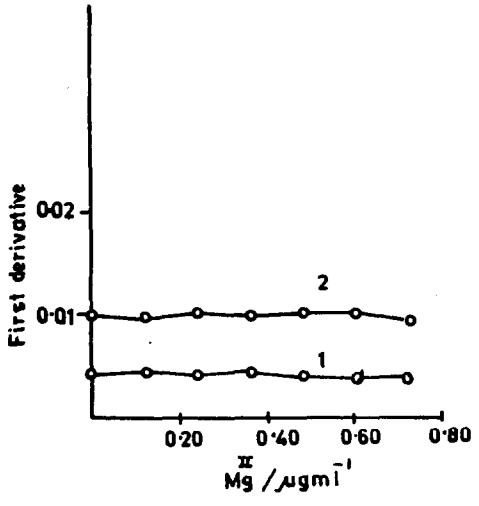

Fig. 4(b). Amplitude of the first derivative for Cu(II) = 0.32 μg/ml (1) and 0.79 μg/ml (2) at 553 nm in the presence of variable amounts of Mg(II).

Selection of optimum pH

In the pH range of 9.0–10.0 the absorbance of Cu(II)–emodin complex appeared to be constant and maximum (Fig. 1(a)). However, for Mg(II)–emodin complex, the constant and maximum absorbance was in the pH range of 9.7–10.0 (Fig. 1(b)). Considering the solubilities, maximum absorbance of both the complexes and quantitative complexation with the reagent, we developed the analytical method at 9.8 pH condition.

Effect of excess metal ions

When large excess of Cu(II) was used, a coloured precipitate was formed in the pH range of 8.0–12.1 and the solution becomes colourless. The precipitate was insoluble in DMF, chloroform, methanol, water, acetone but slightly soluble in DMSO when heated but it dissociates to release free emodin in acid medium.

Mg(II) forms a similar type of coloured precipitate, but at a higher pH range of 11.0–12.1. A large excess of metal ions precipitates both the reagent and the complex which may be due to flocculation. Therefore, in all measurements we have used large excess of emodin to inhibit the precipitation.

Effect of methanol concentration

The pK values of emodin in methanol–water system varies with the change in methanol concentration. This fact may be explained by the interaction of the solvent with >C=O group of the reagent.[19] It was observed that in the pH range of 8.0–11.0 Cu(II) forms a pink coloured soluble complex ($\lambda_{max} = 572$ nm) with emodin while the methanol concentration is >50%. Another yellow coloured Cu(II)–emodin complex may be obtained from the medium with

Table 2. Statistical analyses for simultaneous determination of Cu(II) and Mg(II) by first derivative spectrophotometry

Element determined	Other element present: Element	Concentration ($\mu g/ml$)	Slope	Intercept	Correlation coefficient
Cu(II)	Mg(II)	0.00	0.013	1.0×10^{-4}	0.995
		0.36	0.013	1.8×10^{-4}	0.992
		0.97	0.013	9.2×10^{-5}	0.993
Mg(II)	Cu(II)	0.00	0.030	2.0×10^{-4}	0.989
		0.32	0.029	3.3×10^{-4}	0.988
		0.79	0.030	6.0×10^{-4}	0.991

lower (<50%) methanol concentration and its λ_{max} is blue shifted from 572 nm. We developed the method for Cu(II) determination with the pink coloured complex ($\lambda_{max} = 572$ nm) only because the absorbance value of it remained constant for days together unlike the yellow complex.

On the contrary, Mg(II) formed only one type of complex with emodin unlike Cu(II) which was indicated by the unaltered λ_{max} value for varied methanol concentrations of the medium at a pH range of 8.0–11.5.

Stoichiometry and nature of the chelates

The stoichiometry and the nature of the complexes formed at pH 8.0–11.0 for Cu(II) and 8.0–11.5 for Mg(II) were studied. Cu(II)–emodin complex studied by continuous variation method at a pH of 9.8 showed that the metal–ligand ratio was 1:1 which was similar to Mg(II)–emodin stoichiometry.[5] The rate of complex formation with emodin was slower in case of Cu(II) than with Mg(II). The Cu(II)–emodin complex remained stable for 72 hr. In addition, non-extractability of the complexes in common organic solvents like chloroform, carbon tetrachloride and ethylacetate and fixation of the chelates as a counter ion in both cation and anion exchange resin, indicated the presence of cationic and anionic part in the complexes, and the following structures (Fig. 2) have been proposed. As the complex could not be isolated, the conductometric studies were not possible.

Optimum $\Delta\lambda$ and scan speed

The characteristic of derivative spectra depends on the choice of instrumental parameters. These were optimized with respect to reduction of noise levels and sensitivity. The best results were obtained at a scan speed of 1500 nm/min over the wavelength range of 450–650 nm, with a wavelength interval of 11.2 nm for the first derivative spectrophotometry.

Spectrophotometric measurements

Figure 3(a) shows zero order absorption spectra of (a) Cu(II)–emodin complex (0.95 μg/ml of Cu(II), (b) Mg(II)–emodin complex (0.49 μg/ml of Mg(II)), and (c) the mixture of Cu(II) and Mg(II) complexes (0.95 and 0.49 μg/ml of Cu(II) and Mg(II), respectively).

Figure 3(b) shows the first derivative spectra of the complexes showed in Fig. 3(a). The wavelengths corresponding to the maximum amplitude for the first derivative spectrum of Cu(II)–emodin complex are 522 nm and 600 nm, while those for Mg(II)–emodin complex are 530 nm and 580 nm. The zero point wavelength for Cu(II)–complex is 572 nm and that for Mg(II) complex is 553 nm.

Due to the closeness of the two overlapping spectra, the first derivative of their mixtures were not sufficiently resolved to generate two

Table 3. Determination of Mg(II) in rock samples by normal and first derivative spectrophotometry

Sample	Mg (%) Present*	Found: normal	Found: 1st D	Relative % error: normal	Relative % error: 1st D
Charnockite	0.14	0.14	0.14	0.0	0.0
Amorthosite	0.74	0.78	0.77	+5.4	−4.1
Charnockite	0.41	0.39	0.40	−4.9	−2.4
Charnockite	0.25	0.25	0.26	0.0	+4.0

*Analysed by AAS.

distinct peaks. So we used the zero crossing measurement technique,[20] for the preparation of the calibration curves for mixtures. Amplitude h_1 and h_2 in the first derivative spectra of the mixture at wavelengths 572 nm and 553 nm were proportional to Mg(II) and Cu(II) concentration, respectively.

Determination of Cu(II)

A number of solutions of Cu(II)–emodin complexes were prepared at a variety of Cu(II) concentrations and at constant pH of 9.8. After 10 min the absorbance values corresponding to 572 nm were recorded. The plot of concentration of Cu(II) *vs* absorbance was a straight line while the Cu(II) concentration varies from 0.5 to 2.5 ppm, (Table 1).

Two wavelengths (522 nm and 600 nm) of maximum amplitude in first derivative spectrum for Cu(II) complex were noted. There was a shift in wavelength corresponding to maximum negative amplitude with varied Cu(II) concentrations. So we prepared the calibration curve by measuring amplitudes of first derivatives at 600 nm for different concentrations of Cu(II) ions. A linear relationship was obtained for 0.15–2.38 μg/ml of Cu(II) (Table 1).

Determination of Mg(II)

Use of first derivative method has improved the sensitivities in comparison to normal spectrophotometric methods reported earlier.[5]

The first derivative spectrum of Mg(II)–emodin complex had two wavelengths (530 and 580 nm) of maximum amplitude, but there was a small shift in wavelength of 530 nm, corresponding to maximum negative amplitude with the change of Mg(II) concentration. So we have used 580 nm for amplitude measurement to prepare calibration curves for Mg(II) and the linear relationship was obtained for 0.06–1.46 μg/ml of Mg(II) (Table 1).

Determination of Cu(II) and Mg(II) in mixtures

We have seen that a fixed concentration of Mg(II)–emodin complex has a sufficient and constant amplitude at 572 nm (the Cu(II)–emodin complex zero point wavelength) in the presence of various amounts of Cu(II) concentration (Fig. 4(a)). Similarly, the amplitude at 553 nm (the Mg(II)–emodin complex zero point wavelength) for Cu(II)–emodin complex was independent of Mg(II) concentration (Fig. 4(b)).

Two calibration curves were obtained for standards containing 0.12–0.73 μg/ml of Mg(II) in the presence of 0.32 μg/ml and 0.79 μg/ml of Cu(II). Similarly, curves for standards containing 0.48–2.38 μg/ml of Cu(II), in the presence of 0.36 μg/ml and 0.97 μg/ml of Mg(II) were prepared. Slope, intercepts, correlation coefficients are summarized in Table 2.

Precision and accuracy

In order to test the accuracy and precision of the method, eight successive measurements were done with stock solutions containing 1.91 μg/ml of Cu(II) and 0.49 μg/ml of Mg(II). Relative standard deviations for zeroth order and first order derivative method of Cu(II) were 2 and 1%, respectively and those for Mg(II) were 1.8% and 0.8%, respectively.

For simultaneous determination of Cu(II) (0.95 μg/ml) and Mg(II) (0.49 μg/ml), the relative standard deviations were 1.1 and 1.2%, respectively.

Effect of foreign substances

Investigations were carried out to examine the influence of common ions for the determination of Cu(II) and Mg(II),[5] when they were present separately in solution. Both the metal ions can be determined in presence of Sr(II), Ba(II), Na(I), K(I) ions. Cu(II) can be determined in the presence of equal amount of Ni(II), Cd(II), Pb(II) and two-fold excess of Co(II), Zn(II), Ag(I) and Mn(II) ions. Common anions NO_3^-, NO_2^-, $CH_3CO_2^-$, Cl^-, Br^- can also be tolerated if they are present in 1000-fold excess.

Application

Magnesium was successfully determined in several rock samples, following HF digestion method. The base metals were separated out at a pH of 6.0 as their hydroxides using NaOH solution. The process was repeated four times and peptization of the base metal precipitate was avoided using NH_4NO_3 solution to collect all the Mg(II) ions in the filtrate. Determination of Cu(II) was not possible as the percentage of Cu(II) in those samples were very low (<50 ppm) in comparison to Mg(II). However, the results were satisfactory for copper–magnesium synthetic mixtures.

Acknowledgement—The authors thank Dr T. Vo-Dinh, ORNL, U.S.A. for his invaluable suggestions for the completion of this work.

REFERENCES

1. J. V. Supniewski, J. Hano and E. Taschner, *Berges. Physiol. Expt. Pharmakol.*, 1936, **95**, 516.
2. H. Anke, I. Kolthoum and H. Laatsch, *Arch. Microbiol.*, 1980, **126**, 231.
3. P. P. Rai and M. Shok, *Indian J. Pharm. Sci.*, 1983, **45**, 87.
4. T. R. Kelly, N. S. Chandrakumar, N. Walters and J. Blancaflor, *J. Org. Chem.*, 1983, **48**, 3573.
5. T. Pal, N. R. Jana and P. K. Das, *Analyst*, 1992, **117**, 791.
6. T. Nowicka-Jankowska, K. Gorczyńska, A. Michalik and E. Wieteska, *Comprehensive Analytical Chemistry*, Vol. XIX, p. 356. Elsevier, Amsterdam, 1986.
7. F. Sanchez Rojas, C. Bosch Ojeda and J. M. Cano Pavón, *Talanta*, 1988, **35**, 753.
8. B. Morelli, *Analyst*, 1983, **108**, 1506.
9. B. Morelli, *Analyst*, 1982, **107**, 282.
10. B. Morelli, *Analyst*, 1983, **108**, 870.
11. B. Morelli, *Anal. Lett.*, 1985, **18**, 2453.
12. F. Salinas, A. Muñoz de la Peña and J. A. Murillo, *Analyst*, 1987, **112**, 1391.
13. R. Kuroda, M. Kurosaki, Y. Hayashibe and S. Ishimaru, *Talanta*, 1990, **37**, 619.
14. A. R. Farnández-Alba, J. L. Martínez-Vidal, P. Aguilera, F. Freniche and A. Agüera, *Anal. Lett.*, 1992, **25**, 1581.
15. F. Salinas, J. J. Berzas Nevado and E. Espinosa Mansilla, *Talanta*, 1990, **37**, 347.
16. A. I. Jiménez, F. Jiménez and J. J. Arias, *Analyst*, 1989, **114**, 93.
17. J. A. Murillo, J. M. Lemus, A. Muñoz de la Peña and F. Salinas, *Analyst*, 1988, **113**, 1439.
18. A. I. Vogel, *A Textbook of Quantitative Inorganic Analysis*, 4th Ed. Longman, London, 1978.
19. I. M. Issa, R. M. Issa, K. A. Idriss and A. M. Hammam, *Ind. J. Chem.*, 1976, **14B**, 117.
20. T. C. O'Haver and G. L. Green, *Anal Chem.*, 1976, **48**, 312.

Talanta, Vol. 40, No. 10, pp. 1525–1528, 1993
Printed in Great Britain.

0039-9140/93 $6.00 + 0.00

EXTRACTIVE SPECTROPHOTOMETRIC DETERMINATIONS OF SOME PHENOTHIAZINE DERIVATIVES IN PHARMACEUTICAL PREPARATIONS

S. L. BHONGADE and A. V. KASTURE

Dept. of Pharmaceutical Sciences, Nagpur University, University Campus, Nagpur 440 010, India

(*Received* 11 *December* 1992. *Revised* 24 *March* 1993. *Accepted* 18 *April* 1993)

Summary—Two sensitive methods for the determination of phenothiazine derivatives based on the formation of coloured salts of these drugs formed with Brilliant Blue or Orange-II in the presence of 0.1*M* HCl are described. The ion pair salts formed are quantitatively extracted into chloroform and the dried chloroform solutions analyzed using spectrophotometry.

Phenothiazine derivatives are widely used as antipsychotropic, anticholinergic and antihistaminic drugs.[1] In view of the importance of phenothiazines, considerable work has been done for their detection and quantification.[2,3,4] Many phenothiazine derivatives and their formulations are official in British Pharmacopoeia[5] and Indian Pharmacopoeia.[6] The methods used for their determination include spectrophotometry,[7] spectrofluorimetry,[8] conductometry[9] and chromatography.[10,11] The aim of the present work is to provide a simple and sensitive method for the estimation of phenothiazine in formulations. While the acid–dye method has been employed so far for the estimation of a single basic drug at suitable pH, the present method facilitates the analysis of the foresaid drugs in combination without buffer solutions.

The proposed extractive spectrophotometric methods are based on the formation of ion pair complexes with Brilliant Blue ($\lambda_{max} = 620$ nm) or Orange-II ($\lambda_{max} = 495$ nm) and their complexes are quantitatively extracted into chloroform.

Structures of Brilliant Blue and Orange-II and their chloroform soluble complexes with a phenothiazine (Promethazine hydrochloride) are shown in Fig. 1.

EXPERIMENTAL

Apparatus

Shimadzu UV-150 spectrophotometer with 1 cm matched quartz cells was used.

Reagents and solutions

The chemicals of analytical grade were used. Aqueous solutions (0.5%) of Brilliant Blue and Orange-II and 0.1*M* HCl were employed.

Standard solutions

Commercially available phenothiazines of I.P. or B.P. grade were used. Stock solutions of phenothiazine derivatives (1 mg/ml) were prepared in distilled water. Insoluble compounds were initially dissolved in a minimum amount of dilute hydrochloric acid. Working solutions were prepared by appropriate dilution of the stock solution with the same solvent.

Assay procedures

Method A. Aqueous aliquots containing 15–150 μg of standard drug were transferred into a series of separatory funnels, 1 ml of Brilliant Blue was added to each and the total volume of the aqueous phase was adjusted to 10 ml with distilled water. Fifteen millilitres of chloroform were added and the contents were shaken for 2 min. The two phases were allowed to separate and the chloroform layer passed through anhydrous sodium sulphate. Absorbance was measured at 620 nm against a reagent blank and the amount of drug was computed from a Beer–Lambert plot.

Method B. Aqueous aliquots containing 45–375 μg of standard drug were transferred into a series of separatory funnels. Two millilitres of 0.1*M* HCl and 2 ml of Orange-II solutions were added to each and the total volume of the aqueous phase was adjusted to 10 ml with distilled water. Fifteen millilitres of

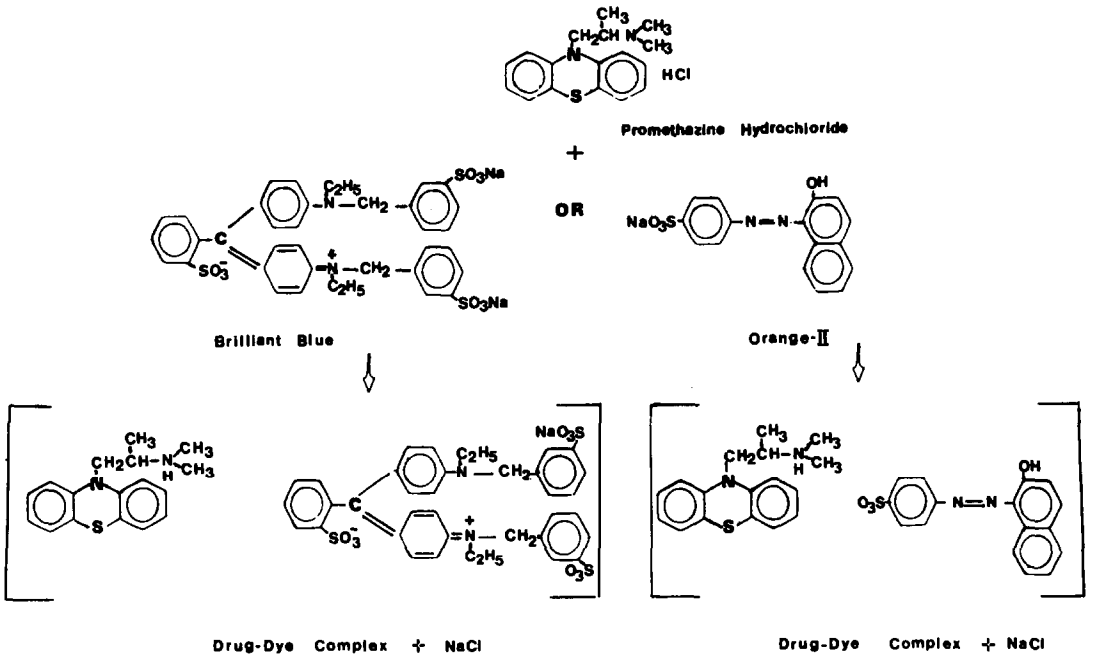

Fig. 1. Structure of Brilliant Blue and Orange-II and their respective complexes with promethazine hydrochloride.

chloroform was added and the contents were shaken for 2 min. The two phases were allowed to separate and the chloroform layer passed through anhydrous sodium sulphate. Absorbance was measured at 495 nm against a reagent blank and the amount of drug was computed from a Beer–Lambert plot.

In each case the absorbance value was plotted against the corresponding concentration of drug in μg/ml. These plots were linear through the limiting concentration as shown in Table 1.

British Pharmacopoeia methods include extraction followed by non-aqueous titration or spectrophotometric determination for individual phenothiazine drug.

Estimation from tablets. Twenty tablets were massed and powdered. The powder equivalent to 50 mg of active ingredient was transferred to a 100 ml volumetric flask and dissolved in 100 ml of distilled water (for dissolving Prochlorperazine maleate, minimum amount of dilute hydrochloric acid was used) and filtered. Ten millilitres of filtrate was further diluted to 100 ml with distilled water. Two millilitres of the resulting solution was used for determination by the Brilliant Blue and Orange-II methods. The amount of drug in these tablets was calculated using the observed absorbance, the mass of powdered sample and dilution factor. Results are given in Table 2.

For the determination of drug in a syrup or injectable dosage form, the mass of drug per ml

Table 1. Optical characteristics of drug dye complexes in chloroform. A—Brilliant Blue, B—Orange-II

Compound	Beer–Lambert limits ($\mu g/ml$) A	B	Molar absorptivity* A	B	Sandell's sensitivity† A	B	RSD (≤) A	B
Promethazine HCl	1–10	3–25	22.1	5.4	0.014	0.058	1.75	1.36
Chlorpromazine HCl	1–10	3–30	22.3	5.8	0.016	0.061	1.09	1.01
Prochlorperazine maleate	2–10	3–25	18.1	9.2	0.033	0.065	1.19	1.46
Thioridazine HCl	1–10	3–25	24.0	8.2	0.017	0.049	1.78	2.07
Trifluoperazine HCl	1–10	3–25	27.8	7.5	0.017	0.063	1.40	1.02
Trimeprazine tartrate	3–25	3–25	15.1	11.4	0.049	0.065	1.58	1.60
Fluophenazine HCl	2–10	5–20	10.2	3.2	0.050	0.150	2.04	1.82

*Molar absorptivity (L/mole/cm $\times 10^{-3}$).

†Sandell's sensitivity (μg/cm/0.001 absorbance unit).

Table 2. Analysis of phenothiazine derivations in various formulations

Sample	*mg/tab* or *mg/ml*	Found *mg/tab* or *mg/ml* by method Proposed† A	B	B.P.*	% Recovery A	B
Promethazine HCl						
tablet	25	24.79	24.71	24.68	99.18	100.24
injection	25	24.60	24.78	24.60	98.72	97.84
syrup	0.5	0.50	0.49	0.51	98.17	97.76
elixir	1	0.98	0.98	0.99	98.70	101.04
Chlorpromazine HCl						
tablet	25	24.87	24.90	24.75	99.36	98.84
tablet	100	99.04	99.17	99.00	99.00	97.86
injection	25	24.81	24.47	24.72	99.19	100.01
syrup	5	4.91	4.87	4.90	98.68	98.39
Thioridazine HCl						
tablet	25	24.78	24.69	24.71	99.70	98.55
tablet	100	98.87	98.92	98.86	98.42	99.08
Trifluoperazine HCl						
tablet	5	4.91	5.00	5.02	98.56	100.39
tablet	10	10.07	9.97	9.92	99.70	99.17
Fluophenazine HCl						
tablet	1	0.98	0.99	1.05	98.16	98.91
Prochlorperazine maleate						
tablet	5	4.88	4.86	4.77	99.75	99.17
Trimeprazine tartrate						
tablet	10	9.77	10.02	9.98	99.16	98.84
syrup	6	5.92	5.97	5.90	98.95	100.65

*—British Pharmacopoeia.
†A—Brilliant Blue; B—Orange-II.

was determined. A quantity of syrup or injectable dosage form equivalent to 50 mg of drug was transferred to a 100 ml volumetric flask and diluted to 100 ml with distilled water. This solution was further diluted with water so that the final solution contained about 50 μg/ml, before analysis by the Brilliant Blue and Orange-II method.

Recovery experiment

To determine the precision and accuracy of the above methods, recovery experiments were performed using the method of additions. A fixed volume sample of solution was added to one of three different concentrations of the standard drug solution. The total amount of drug was then determined using Brilliant Blue and Orange-II and the amount of added drug found by difference.

Results obtained by the Brilliant Blue and Orange-II and the British Pharmacopoeia methods for the various dosage forms are compared in Table 2.

RESULTS AND DISCUSSION

These drugs form salts that exhibit absorption maxima at 620 nm with Brilliant Blue and 495 nm with Orange-II. Beer–Lambert law limits, molar absorptivity and Sandell's sensitivity values found for various phenothiazines are shown in Table 1. The mole ratio of drug to dye was found to be 1:1 for Brilliant Blue and Orange-II. To test the reproducibility and accuracy of these methods, six replicate determinations were made with each drug and the relative standard deviation from the mean are presented in Table 1.

A significant advantage of an extractive spectrophotometric determination is that it can be applied to the determination of individual compounds in a multicomponent mixture. This aspect of spectrophotometric analysis is of major interest in analytical pharmacy since it offers distinct possibilities in the assay of a particular component in a complex dosage formulation. In the present study, a number of phenothiazines were determined successfully as

pure compounds as well as components in representative dosage formulation.

Results of proposed methods show good agreement when compared with the official method (Table 2). Additives used in the formulation do not interfere with the proposed methods. These results indicate that the proposed methods are simple, rapid and accurate and offer advantage in that only a small amount of drug or dosage formulation is required for analysis.

REFERENCES

1. R. Cass and T. L. B. Spring, *Br. J. Pharmac. Chemother.* 1961, **17**, 442.
2. J. E. Fairbrother, *J. Pharm.*, 1979, **222**, 1771.
3. J. Blazek, A. Dymes and Z. Stejskal, *Pharmazie*, 1976, **31**, 10.
4. V. N. Pathak and I. C. Shukla, *Talanta*, 1982, **29**, 58.
5. British Pharmacopoeia, HM Stationery Office, London, 1988.
6. Pharmacopoeia of India, Ministry of Health and Family Welfare, Govt. of India, New Delhi, 1985.
7. P. G. Ramappa and K. Basavaiah, *The Eastern Pharmacist*, 1984, **27**(315), 131.
8. J. J. Menninger and C. E. Keeler, *Anal. Chem.*, 1964, **36**, 1840.
9. F. Dima, M. Stan and C. Ghimecescu, *Farmacia*, 1977, **25**, 47.
10. L. Laitem, I. Bella and P. Gaspar, *J. Chromatogr.*, 1978, **156**, 327.
11. A. C. Mehta, *Analyst*, 1981, **106**, 1119.

Talanta, Vol. 40, No. 10, pp. 1529–1534, 1993
Printed in Great Britain.

0039-9140/93 $6.00 + 0.00

SULPHATE PRECONCENTRATION BY ANION EXCHANGE RESIN IN FLOW INJECTION AND ITS TURBIDIMETRIC DETERMINATION IN WATER

MARINA M. SANTOS FILHA
Departmento de Química, Universidade Federal de Sergipe, 49000 Aracajú SE, Brazil

BOAVENTURA F. REIS and FRANCISCO J. KRUG
Centro de Energia Nuclear na Agricultura, Universidade de São Paulo, Caixa Postal 96, 13400 Piracicaba SP, Brazil

CAROL H. COLLINS and NIVALDO BACCAN
Instituto de Química, Universidade Estadual de Campinas, 13081 Campinas SP, Brazil

(*Received* 3 *November* 1992. *Revised* 22 *March* 1993. *Accepted* 22 *March* 1993)

Summary—A preconcentration procedure was established for sulphate determination in rain waters at the mg/l level, employing a small column packed with the AG1-X8 (200–400 mesh) anionic resin inserted into a flow injection system. Sulphate determination was performed by using the turbidimetric method based on reaction with barium. For concentrations within 0.10 and 2.0 mgSO_4^{2-}/l, a throughput of 50 determinations/hr was achieved, and the relative standard deviation of results was better than 2%.

Research programmes in environmental science have caused a continuous increase in the demand for determinations of several analytes in a large number of water samples from dams, rivers or rain. Although some analytic methodologies are available for cations, only a few well-established ones have been reported for anions. Sulphate is one of the anions with less options, particularly for concentrations at low mg/l levels.

Flow injection analysis (FIA) is an attractive approach for automation when a large number of samples are to be processed, and has often been implemented with low cost instrumentation.[1] A few photometric FIA procedures for the determination of sulphate in water samples were proposed[2,3] and that based on barium sulphate turbidimetry[2] presents good characteristics, such as high sample throughput, low reagent consumption, high precision and accuracy. However, its detection limit of about 2 mg/l is not enough for some water samples.

This paper reports the development of a sulphate preconcentration procedure by anion exchange resin in order to improve the detection limit of the turbidimetric FIA method.

EXPERIMENTAL

Apparatus

A Micronal B342 II spectrophotometer equipped with a tubular flow cell (12 mm optical path, 200 μl inner volume) and coupled to a Radiometer REC 61 strip chart recorder was used. The Ismatec mp13GJ4 peristaltic pump was furnished with Tygon tubing.

A sliding bar automatic injector with three commutation sections[4] was used. It was controlled by a laboratory-made microcomputer based on the Intel 8085 microprocessor.[5] A software written in Assembly language run by the microcomputer provides facilities to program different time delays for both resin loading and elution steps.

Reagents

All chemicals were of analytical grade quality and freshly distilled and deionized water was used throughout.

The standard stock solution of sulphate 1000 mg/l was prepared by dissolving ammonium sulphate in water. Working standards within the 0.00–2.00 mg/l range were prepared daily. Sulphate solutions (50 and 100 mg/l) used as spike

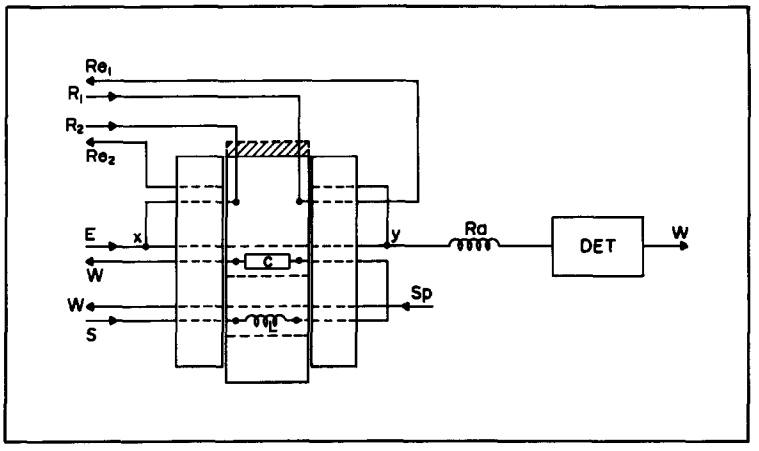

Fig. 1. Flow diagram of the system for on-line preconcentration of sulphate and its turbidimetric determination. The three rectangular pieces represent an overview of the sliding bar injector; C = resin column (15 × 6 mm i.d.); S = sample; W = waste; E = eluent solution; Sp = spike sulphate solution at 1 ml/min; R_1 = barium chloride solution at 1 ml/min; R_2 = washing solution, 0.5*M* sodium nitrate at 5 ml/min; Re_1 and Re_2 = recovery for reagents R_1 and R_2, respectively; x and y = confluence points; Ra = tubular helical reactor (100 cm long, 0.8 mm i.d.); DET = spectrophotometer at 410 nm; L = loop (20 cm long, 0.8 mm i.d.). Broken lines indicate inner holes and hatched portion the injector at the elution position. Arrows indicate flow directions.

were prepared by appropriated water dilutions of the stock solution.

A 20% w/v barium chloride dihydrate solution in 0.05% w/v polyvinyl alcohol (PVA-Du Pont Elvanol 71-30) was prepared by first producing a slurry of PVA in 100 ml of water and, while stirring, slowly adding 300 ml of boiling water. Thereafter, barium chloride was dissolved, the solution was cooled and the volume made up to 1000 ml with water.

Eluent solutions were prepared in the 0.1–2.0*M* range as sodium chloride or sodium nitrate by dissolving appropriate amounts of the respective salts in water.

Preparation of the resin column

The resin column (8 × 5 mm) was machined in a Perspex block as described elsewhere.[6] The AG1-X8 anion exchange resin 200–400 mesh (Bio-Rad Labs) was employed. The column was filled with a slurry of the resin up to its volume by using a syringe, the excess of water being drained. The resin, initially in chloride form, was converted to nitrate by pumping a 1.0*M* sodium nitrate solution through it at 3 ml/min, until the effluent showed no turbidity after addition of a few drops of 0.1*M* silver nitrate solution. Before use, the resin column was equilibrated with nitrate ions by pumping 0.5*M* sodium nitrate for about 20 min at 3 ml/min.

Experimental variables

To simplify the investigations of the variables involved in the preconcentration step, the resin column was coupled to the injector sliding bar. The amount of sulphate ions adsorbed by the resin is dependent on both, the sample flow-rate through the resin and the column loading time. These two parameters were investigated with the FIA network outlined in Fig. 1. In the specified position, the sample (S) is pumped through both loop (L) (previously loaded with a sulphate spike solution) and the resin column (C). The

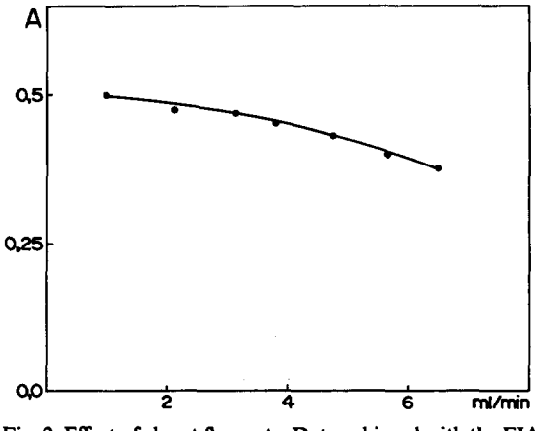

Fig. 2. Effect of eluent flow rate. Data achieved with the FIA manifold of Fig. 1. Preconcentration with 4.0 mg/l sulphate flowing at 6 ml/min sample during 30 sec column loading time, elution with 1.0*M* sodium nitrate over 20 sec, and spiked with 100 mg/l sulphate; *A* = absorbance.

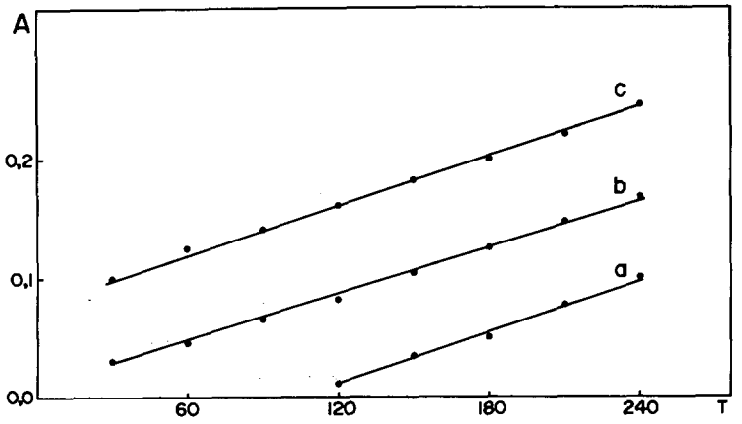

Fig. 3. Effect of sulphate spike solution. Preconcentration with 0.20 mg/l sulphate flowing at 7 ml/min, elution with 0.25*M* sodium nitrate solution at 3.1 ml/min. *T* is the column loading time in seconds, and *A* denotes absorbance values. Curves a, b and c correspond to 0, 50 and 100 mg/l sulphate spike solutions.

outlet flow depleted of sulphate ions is directed towards waste (W), while the barium chloride solution (R_1) is recovered and the washing solution (R_2) is added at confluence point x to clean the analytical path. When the injector is switched to the other position, the resin column is inserted into the analytical path and the eluent solution (E) is pumped through it. Reagent R_1 is added to the eluted sample zone at confluence point y and precipitation reaction takes place inside the reactor (Ra). The turbidity is monitored at 410 nm, yielding a transient signal proportional to analyte concentration in the sample which is traced by the stripchart recorder. At the same time the spike solution (Sp) is pumped to fill again the loop L. The spike solution was used to improve barium sulphate nucleation.[2] By moving the sliding bar back to position specified in Fig. 1 another preconcentration step is initialized.

Effects of both eluent flow-rate and concentrations were investigated with a 4.0 mg/l sulphate standard. Sample flow-rate was maintained at 6 ml/min and time delays for column load and elution were both 30 sec. When the injector was switched to the elution position the speed of peristaltic pump was changed accordingly at the same time. Experiments were carried out with flow-rates ranging from 1 to 7 ml/min. As eluent, 0.10, 0.15, 0.50 and 1.0*M* aqueous sodium nitrate or sodium chloride solutions were tested.

Influence of column loading time was investigated by maintaining a constant sample flow-rate of 7 ml/min and programming the microcomputer to increase the loading time from 30 to 240 sec in 30 sec steps. Effects of sample flow-rate were investigated in the range 2–15 ml/min by keeping the column loading time at 60 sec.

In order to evaluate the system performance, two sets of rain water samples were analysed. The first group was used to check the accuracy by analyte additions and the other one to verify the long term stability.

The analyte additions were performed manually by delivering aliquots of 100 μl (Finnpipette) from a 250 mg/l sulphate standard to 100 ml sample volume.

RESULTS AND DISCUSSION

Elution

The increase of the ions average velocity through the column can affect both the kinetic of ion exchange in the resin and the nucleation process in the analytical path, which could explain the signal diminution with the increase in flow-rate shown in Fig. 2. Better elution results were obtained with a 0.25*M* sodium nitrate solution. Lower nitrate concentrations

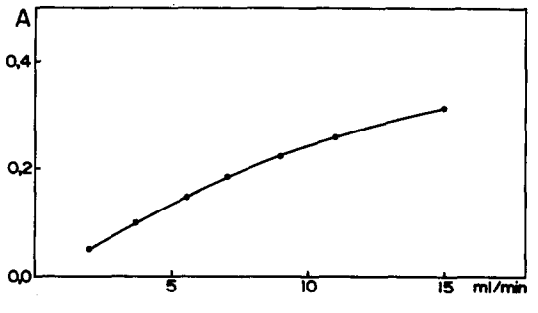

Fig. 4. Effect of sample flow-rate through the resin column. Preconcentration with 1.00 mg/l sulphate flowing at 7 ml/min during 60 sec, elution with 0.25*M* sodium nitrate solution at 3.1 ml/min, and spike with 50 mg/l sulphate solution. *A* = absorbance.

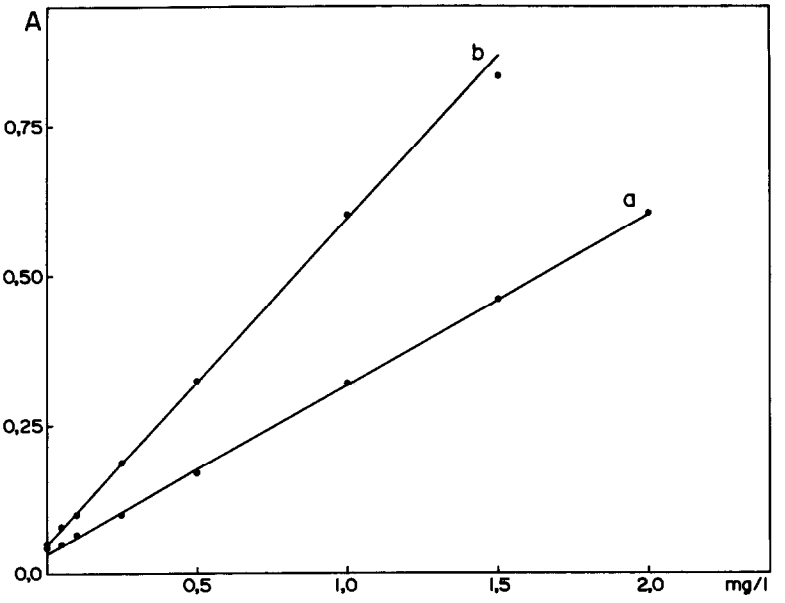

Fig. 5. Effect of column loading time. Sample flow-rate 7 ml/min, elution with 0.25*M* sodium nitrate solution flowing at 3.1 ml/min. Curves a and b refer to 120 and 240 sec column loading times, respectively. *A* = absorbance.

yielded lower measurements, and higher caused disturbance in baseline due to the "Schlieren" effect.[7] It should be pointed out that this effect in the refraction index was also caused by the added washing solution.

Preconcentration

As expected, an increase in the analytical signal with the column loading time was obtained, as shown in Fig. 3. Also, it can be seen that the sulphate spiking solution had an enhancement effect due to its influence on the barium sulphate nucleation, resulting in a remarkable improvement on detection limit. The 50 mg/l sulphate solution was the threshold concentration for this improvement and it was used in the subsequent experiments.

Figure 4 shows that absorbance also increased with the sample flow-rate, a linear response being obtained up to 7 ml/min. Beyond this value, a asymptotic behavior was observed. In this case, the analyte ions went through the resin column more quickly, impairing the kinetic of exchange. On the other hand, similar results would occur when the resin column capacity to exchange anions would tend to

Table 1. Effects of potential interfering anions

Sulphate (*mg/l*)	Nitrate added (*mg/l*)	Carbonate added (*mg/l*)	Chloride added (*mg/l*)	Phosphate added (*mg/l*)	$\frac{h}{h_0} \times 100$*
2.5	30	0.0	0.0	0.0	100
0.5	30	0.0	0.0	0.0	100
0.05	30	0.0	0.0	0.0	100
2.5	0.0	30	0.0	0.0	99.2
0.5	0.0	30	0.0	0.0	100
0.05	0.0	30	0.0	0.0	98
2.5	0.0	0.0	30	0.0	98.5
0.5	0.0	0.0	30	0.0	101
0.05	0.0	0.0	30	0.0	97.3
2.5	0.0	0.0	0.0	30	96.5
0.5	0.0	0.0	0.0	30	91.5
0.05	0.0	0.0	0.0	30	88
2.5	30	30	30	30	97.1
0.5	30	30	30	30	91.5
0.05	30	30	30	30	88

*h and h_0 are peak heights obtained for the sulphate standards with and without the specified anion.

Table 2. Analyte additions to rain water samples

Rain water	Concentration* (mg/l)	Addition (mg/l)	Recovery (%)
1	0.52	0.25	104
2	0.74	0.25	100
3	0.28	0.25	103
4	0.93	0.25	99
5	0.13	0.25	108
6	0.93	0.25	96
7	1.75	0.25	97
8	0.52	0.25	105
9	0.49	0.25	96
10	0.48	0.25	102
11	1.07	0.25	103
12	0.19	0.25	104
13	0.23	0.25	105
14	0.35	0.25	95
15	1.40	0.25	101
16	1.25	0.25	103
17	1.55	0.25	99

*Average concentrations ($n = 3$). Recovery 101.1 ± 3.7.

saturation. In order to ascertain this assumption other experiments were carried out yielding the results shown in Fig. 5. It can be seen that the amount of sulphate ions adsorbed by the resin were directly proportional to the column loading time, the same signal being obtained for 0.50 and 1.00 mg/l sulphate standards flowing at 7.0 ml/min during 120–240 sec loading times, respectively. It can also be deduced that the ratio between the slopes of curves a and b is exactly 1:2. Thus, it can be ascribed that the main reason for the signal behaviour observed in Fig. 4 for sample flowing at values higher than 7 ml/min was associated to column efficiency. Although 7 ml/min seemed the threshold value for maximum resin efficiency, there is no practical restriction to work at 15 ml/min sample flow-rate. To get a better efficiency of preconcentration and also to avoid fluid leakage caused by hydrodynamic over pressure, a sample flow-rate of 7 ml/min was chosen for the remaining experiments.

The ability of the resin for complete sulphate ions removal from sample bulk solution was verified by using a 0.50 mg/l sulphate standard solution. The resin column effluent was collected during several column loading steps, and analyzed in the same way as the standard. Results were practically identical to those of the blank, indicating a high efficiency of the resin column for adsorbing sulphate.

Interference

Anions usually present in natural waters, such as orthophosphate, chloride, nitrate and carbonate, are also adsorbed by the resin and may cause its saturation. To evaluate the column exchange capacity, experiments were carried out, by using standard solutions containing 0.05, 0.50 and 2.50 mg/l sulphate plus 30 mg/l of each chloride, nitrate, carbonate and orthophosphate (sodium salts). Results summarized in the Table 1 show that, in general, negligible variations in the measured signal were observed, except for orthophosphate, where a 12% decrease in absorbance was noted for 0.05 mg/l sulphate. As this effect was less pronounced for higher sulphate concentrations, the effect cannot be attributed to the resin saturation. Identical results were obtained for a mixed solution containing 30 mg/l of chloride, nitrate, carbonate and orthophosphate. In this sense, the interference caused by orthophosphate ions was probably associated to its effect on the barium sulphate nucleation process. This assumption can be corroborated if one considers that the resin affinity for sulphate is 13 times higher than that for orthophosphate.[8]

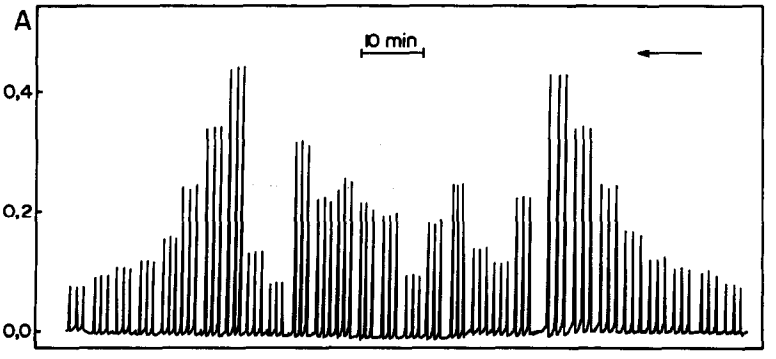

Fig. 6. Recorder tracing of a routine water analysis. From left to right, eight standard solutions (0.00, 0.05, 0.10, 0.25, 0.50, 1.00, 1.50, 2.00 mg/l), 13 samples and the standards again, always in triplicate. Arrow indicates the displacement of recorder chart. A = absorbance.

It should be pointed out that the concentrations of these anions in waters are quite variable depending on the origin of the sample, but they are generally much lower than the maximum levels tested, particularly orthophosphate. It should also be mentioned that the orthophosphate interference observed here was lower than that reported in the methylthymol blue method.[9]

Routine analysis

The working conditions for using the FIA network of Fig. 1 in routine scale were set up considering the results presented in the last section, *i.e.* preconcentration was done after pumping 7.0 ml/min of sample for 60 sec, and elution carried out with 0.25*M* $NaNO_3$ solution flowing at 3.2 ml/min for 15 sec. The 50 mg/l sulphate spike solution was introduced by a 20 cm loop L.

Table 2 shows the results obtained with 17 samples of rain water. The relative standard deviations of measurements ($n = 10$) for all samples were always lower than 2%, which can be considered very good for sulphate in the 0.50–2.00 mg/l range. The long term stability can be ascertained with the help of Fig. 6. An acceptable baseline drift, which was indeed insignificant, is observed. Also, it can be deduced from the same figure that a throughput of 48 samples/hr can be obtained with precision. In addition, it should be mentioned that this FIA system has proven to be analytically robust in the large scale routine programme at the author's laboratory, after processing more than 10,000 samples.

Acknowledgements—The authors are grateful to Cláudia M. F. Corrêa for typing assistance, to FAPESP (Fundação de Amparo à Pesquisa do Estado de São Paulo, processo no. 89/0488-0) and FINEP (Financiadora de Estudos e Projetos—PADCT II, processo 65.91.0324.00) for financial support, to CAPES (Coordenadoria de Aperfeiçoamento de Pessoal de Nível Superior) for M.M.S.F. grant, to CNPq (Conselho Nacional de Desenvolvimento Científico e Tecnológico) for fellowships, and to Elias A. G. Zagatto for critical comments.

REFERENCES

1. J. Ruzicka and E. H. Hansen, *Flow Injection Analysis*, 2nd ed. John Wiley, New York, 1988.
2. F. J. Krug, E. A. G. Zagatto, B. F. Reis, O. Bahia Fo., A. O. Jacintho and S. S. Jørgensen, *Anal. Chim. Acta*, 1983, **145**, 179.
3. B. F. Band, P. Linares, M. D. L. Castro and M. Valcarcel, *Analyst*, 1991, **116**, 305.
4. B. F. Reis, M. F. Giné and E. A. M. Kronka, *Quím. Nova*, 1989, **12**, 82.
5. B. F. Reis, M. F. Giné and E. A. M. Kronka, *Quím. Nova*, 1992 **15**, 231.
6. M. M. Santos Filha, B. F. Reis, H. Benjamin Fo and N. Baccan, *Anal. Chim. Acta*, 1992, **261**, 339.
7. E. A. G. Zagatto, M. A. Z. Arruda, A. O. Jacintho and I. L. Mattos, *Anal. Chim. Acta*, 1990, **234**, 153.
8. Strong anion exchange resin instruction manual, Bio-Rad Laboratories, 1414 Harbour Way South, Richmond, CA 94804.
9. M. Karlsson, J. A. Persson and J. Möller, *Anal. Chim. Acta*, 1991, **244**, 109.

Talanta, Vol. 40, No. 10, pp. 1535–1539, 1993
Printed in Great Britain.

0039-9140/93 $6.00 + 0.00

SOLVENT EXTRACTION SEPARATION OF COBALT(II) FROM NICKEL AND OTHER METALS WITH CYANEX 272

M. N. GANDHI,* N. V. DEORKAR† and S. M. KHOPKAR‡
Department of Chemistry, Indian Institute of Technology, Bombay-400 076, India

(*Received* 15 *October* 1992. *Revised* 1 *March* 1993. *Accepted* 10 *March* 1993)

Summary—Cobalt(II) was quantitatively extracted at pH 8.0 with $5 \times 10^{-3}M$ Cyanex 272 [Bis(2,4,4 trimethyl pentyl) phosphoric acid] in chloroform. Cobalt(II) was stripped with $0.5M$ nitric acid and was determined by atomic absorption spectrometry as well as by spectrophotometry of the complex with nitroso R salt. Cobalt(II) was separated from vanadium, chromium, nickel, manganese, iron and zinc. Mixtures having different ratios of iron, cobalt and nickel were separated by proposed method.

Oxygen containing extractants have proven to be poor extractants for cobalt as well as for nickel.[1] The extraction of cobalt was effective with tributylphosphate (TBP) in the presence of salting out agents. It was quantitative from 10–12M hydrochloric acid.[2] This result facilitated the separation of cobalt and nickel as nickel was poorly extracted with TBP,[3] cobalt was extracted with MIBK from 4M ammonium thiocyanate.[4] Extraction with liquid anion and liquid cation exchangers was generally poor.[5] However, bis(diethyl hexyl phosphoric acid) (HDEHP)[6,7,8] was successfully used for extraction of cobalt. The extraction of nickel was poorer than that of cobalt, with most of the oxygen containing extractants like ethers and alcohols with TBP, extraction was not quantitative.[9] The separation factor for separating cobalt from nickel in TBP—10M hydrochloric acid system was 1700. The extraction with octyl alcohol[10] from bromide media was satisfactory.

The suitable extractants for separation were chelating extractants *e.g.* 1-nitroso-2-naphthol[11] or dimethylglyoxime.[12] Such chelating extractants were effective for the individual separation of nickel or cobalt from other elements but were not useful for mutual separations of cobalt and nickel.

Cyanex reagents[13] have come to the forefront in recent years. Of these, Cyanex 272, *i.e.* bis (2,4,4 trimethyl pentyl) phosphoric acid, Cyanex 301 and Cyanex 302 are versatile as the extractants. The last two are thio substituted derivatives of Cyanex 272. However, systematic studies with Cyanex 272 for cobalt are lacking. Therefore it was thought worthwhile to undertake the solvent extraction separation studies of cobalt and nickel with Cyanex 272. Both atomic absorption spectroscopy as well as spectrophotometric determination of cobalt with Nitroso R salt were carried out.

EXPERIMENTAL

Apparatus and reagents

GBC 902 Atomic absorption spectrometer (GBC Australia), ECIL Spectrophotometer Model as 866C; Orion microprocessor ion analyser model 901 (Orion, USA), wrist action flask shaker (Toshniwal Ltd, India).

A stock solution of cobalt(II) was prepared by dissolving 4.037 gm of cobalt chloride in 1 l of distilled water containing 0.5% of concentrated hydrochloric acid. The solution was standardized complexometrically.[14] It contained 1.009 gm/ml cobalt(II). The diluted solution containing 5 μg/ml of cobalt(II) was prepared by appropriate dilution. Cyanex 272, bis(2,4,4 trimethyl pentyl) phosphoric acid (American Cyanamid Co., USA), was used directly without further purification.

*Regional Sophisticated Instrumentation Centre, Indian Institute of Technology, Bombay 400 076, India.
†Department of Chemical Engineering and Materials Science, Syracuse University, Syracuse, U.S.A.
‡Present address: Chemical Engineering Division, Department of Chemical Technology, Bombay University, Bombay 400 019, India.

GENERAL PROCEDURE

An aliquot of solution containing cobalt(II) was taken and its pH was adjusted to 8.0 with 0.1*M* sulphuric acid or ammonium hydroxide. The total volume was made to 10 ml. The solution was then transferred into a separatory funnel, 10 ml of $5 \times 10^{-3}M$ Cyanex 272 in chloroform was added to it, and the mixture was shaken on a wrist action flask shaker for 5 min. The two phases were allowed to settle and separate. The concentration of cobalt from the aqueous phase after phase separation was determined by atomic absorption spectrometry. From the organic phase cobalt(II) was back extracted with 10 ml of 0.5*M* nitric acid and cobalt was determined either by atomic absorption spectrometry at 240.7 nm with an air acetylene flame or spectrophotometrically. From these data the distribution ratio (*D*) was evaluated. The results of the extraction were further confirmed by spectrophotometric determination of cobalt with Nitroso R salt in both phases.

During systematic investigation of various parameters influencing the process of extraction, cobalt from both phases was determined by atomic absorption spectrometry as multiple samples were involved. However during separation of cobalt from binary and multicomponent mixtures, cobalt was determined spectrophotometrically at 500 nm as the complex with Nitroso R salt. This also facilitated identifying the coextraction of certain ions during separations.

RESULTS AND DISCUSSION

Extraction as a function of pH

Cobalt(II) was extracted in the pH range of 2.0–10.0 with $5 \times 10^{-3}M$ Cyanex 272 in chloroform. The high pH was adjusted using ammonium phosphate and borax buffer. The extraction was quantitative between pH 8.0 and 9.5, hence all extractions were carried out at pH 8.0 (Fig. 1).

Extraction as a function of Cyanex 272 concentration

Cobalt(II) was extracted with varying concentrations of Cyanex 272 ($0.25–50 \times 10^{-3}M$). The extraction was quantitative with $5 \times 10^{-3}M$ of Cyanex (Table 1).

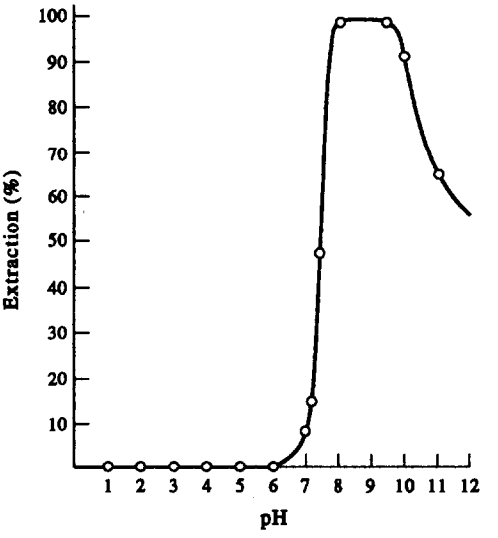

Fig. 1. Extraction as a function of pH with Cyanex 272.

Extraction with various diluents

Cobalt(II) was extracted with $5 \times 10^{-3}M$ Cyanex 272 in different solvents. The extraction was quantitative with benzene, toluene, xylene, carbon tetrachloride, and chloroform as the diluent, while with dichloromethane, 1,2 dichloroethane, *n*-hexane, cyclohexane and nitrobenzene the extraction was not quantitative (Table 2). Chloroform was preferred as the diluent since it provided better phase separation and ease of removal.

Effect of various stripping agents

Cobalt(II) was stripped with various mineral acids after extraction. Cobalt was quantitatively stripped with 0.5–5*M* hydrochloric, nitric, sulphuric and perchloric acids while with 2–6*M* acetic acids, it was complete. A solution of 0.5*M* nitric acid was used as the stripping agent (Table 3).

Table 1. Extraction as a function of Cyanex 272 concentration Co(II) = 25 μg, pH 8.0

Cyanex 272 conc. ($1 \times 10^{-3}M$)	% extraction (*E*)	Distribution ratio (*D*)
0.25	4.6	0.04
0.40	9.8	0.10
0.50	14.0	0.16
0.60	20.2	0.25
0.80	29.3	0.41
0.90	37.6	0.60
1.0	49.5	0.98
2.0	66.6	1.99
2.5	81.8	4.49
3.0	91.8	11.2
3.5	93.0	13.2
4.0–50.0	99.9	999

Table 2. Effect of solvents on extraction of cobalt(II) Co(II) = 25 μg, Cyanex 272 = $5 \times 10^{-3}M$, pH = 8.0

Diluents	Dielectric constant (ε)	% extraction
n-hexane	1.90	60.8
Carbon tetrachloride	2.00	99.9
Cyclohexane	2.02	20.0
Benzene	2.20	99.9
Toluene	2.23	99.9
Xylene	2.28	99.9
Chloroform	4.80	99.9
Dichloromethane	9.50	98.3
1,2 dichloroethane	10.2	77.5
Nitrobenzene	34.5	56.5

Extraction with varying metal ion concentration

Cobalt(II) was extracted with cobalt concentrations ranging from 25 to 250 μg/10 ml, *i.e.* 0.424–4.244*M*. The extraction was quantitative from 25 to 170 μg/10 ml, *i.e.* 0.424–2.886*M*. For complete extraction the molar ratio between metal and Cyanex should be $2.886:5 \times 10^{-3}$, *i.e.* 576:1.

Period of equilibration

The solution was shaken on a wrist action flask shaker for periods ranging from 1 to 20 min. The extraction was quantitative with 5 min or less of shaking. Therefore, a 5 min period of equilibrium was used.

Nature of the extracted species

It was necessary to evaluate *D* while varying extractant concentration, to ascertain the nature of the extracted species. The composition of the extracted species was ascertained from the graph of log [*D*] *vs.* log [Cyanex 272] at fixed pH of 8.0. The slope was 1.72 (Table 1). Therefore the Cyanex concentration range used was from 0.25 to $4 \times 10^{-3}M$ and the probable composition of the extractable species is 1:2 or Co(Cyanex 272)$_2$. Usually for extractions with Cyanex as extractant, the effective pH range for quantitative extraction is narrow.

Table 4. Tolerance limit

<0.5 *mg*	<1 *mg*	<5 *mg*	<10 *mg*	Interference by coextraction
Ca^{2+}	Mg^{2+}	Rb^{+}	Li^{+}	None
Al^{3+}	Ga^{3+}	Cs^{+}	Na^{+}	Zr^{4+}
VO_2^{+}	In^{3+}	Be^{2+}	K^{+}	Hf^{4+}
Cr^{3+}	Sn^{4+}	Sr^{2+}		Pb^{2+}
Mn^{2+}	Sb^{3+}	Tl^{3+}		Mn^{2+}
Fe^{3+}	Sc^{3+}	Bi^{3+}		Cd^{2+}
Fe^{2+}	Y^{3+}	MoO_4^{2-}		Fe^{3+}
Cu^{2+}	Tl^{4+}			Fe^{2+}
Zn^{2+}	CrO_4^{2-}			
	Ni^{+2}			
	Ce^{4+}			
	UO_2^{2+}			
	Th^{4+}			

Separation of Cobalt(II) from binary mixtures

Cobalt(II) was extracted in the presence of a large number of elements. The tolerance limit was set as the amount of foreign ion causing interference of 1% in the extraction of cobalt. The alkali metals were tolerated at a ratio of 1:150. Magnesium, strontium, gallium, thallium(III), antimony, bismuth, scandium, molybdenum, chromium(VI), nickel, cerium(IV) and uranium were tolerated at a ratio of 1:40. Aluminium, indium, tin(IV), yttrium, vanadium(IV), titanium(IV), chromium(III), copper and thorium, were tolerated at a ratio of 1:20. Calcium, lead, zirconium, hafnium, manganese, iron(II), iron(III), zinc and cadmium were tolerated at a smaller ratio (*i.e.* 1:4). Anions like chloride, nitrate and perchlorate were tolerated at a ratio of 1:20, but acetate, citrate and malonate (Table 4) showed lower tolerance limits.

Separation of multicomponent mixture

Various metals showed different extents of extraction at different pH and varying concentration of Cyanex 272. Such differences were fully exploited to devise a different separation by resorting to a technique selective to extraction at different pH with varying concentration of Cyanex 272. However difference in stripping power was not much use for devising a novel separation.

Table 3. Effect of stripping agents on back extraction of cobalt

Stripping agent (*M*)	% recovery 0.01	0.05	0.1	0.5	1–5	6.0	7.0	8.0
HCl	57.0	71.0	91.3	999	99.9	96.0	87.6	80.0
HNO_3	47.1	67.3	99.2	99.9	99.9	99.9	99.9	99.9
H_2SO_4	71.4	87.6	96.9	99.9	99.9	99.9	99.9	99.9
$HClO_4$	73.1	86.0	98.0	99.9	99.9	99.9	99.9	99.9
CH_3COOH	18.4	55.1	66.1	96.0	99.9	99.9	—	—

Table 5. Distribution ratio of various metals at different pH values

	Distribution ratio (D)			Separation factor* $\alpha = (Dw/Dm)$		
pH	3.0	6.0	8.0	3.0	6.0	8.0
Fe	999	3.6	0.70	0	0	1427
Ni	0	0	0	—	—	—
Mn	0	2.4	999	—	0	1.0
Cu	0	0.10	0.30	—	0	3330
Zn	0	2.2	999	—	0	1.0
Cd	0	0.20	0.90	—	0	1110
Pb	0	0.15	999	—	0	1.0
Co	0	0	999	—	—	—

*Dw for cobalt; Dm for metal.

Table 6. Separation from multicomponent mixtures

Sr. No.	Mixture	Amt. taken (μg)	pH	Extractant	Stripping agent	% recovery
1	Fe(III)	25	3.0	Cyanex 272 (0.005M)	1M HCl	99.8
	Zn(II)	25	6.7	Cyanex 272 (0.005M)	0.5M $HClO_4$	98.7
	Co(II)	25	8.0	Cyanex 272 (0.005M)	0.5M HNO_3	99.0
2	Fe(III)	25	3.0	Cyanex 272 (0.005M)	1M HCl	99.6
	Co(II)	25	8.0	Cyanex 272 (0.005M)	0.5M HNO_3	99.8
	Cr(III)	25	8.0	Unextracted	aq. phase	99.9
3	Mn(II)	25	6.5	Cyanex 272 (0.008M)	0.1M H_2SO_4	98.7
	Co(II)	25	8.0	Cyanex 272 (0.005M)	0.5M HNO_3	99.1
	Ni(II)	50	8.0	Unextracted	aq. phase	99.9
4	Mn	25	6.5	Cyanex 272 (0.008M)	0.1M H_2SO_4	98.7
	Co(II)	25	8.0	Cyanex 272 (0.005M)	0.5M HNO_3	99.1
	V(IV)	50	8.0	Unextracted	aq. phase	99.9

The mixture of iron(III), zinc, cobalt(II) and molybdenum(VI) was resolved by first extracting iron(III) at pH 3.0 with $5 \times 10^{-3}M$ Cyanex 272, then extracting zinc at pH 6.7 with $5 \times 10^{-3}M$ Cyanex 272 and then cobalt(II) at pH 8.0 with $5 \times 10^{-3}M$ Cyanex 272 during which molybdenum(VI) was not extracted. From the organic phase iron(III) was stripped with 1M hydrochloric acid as usual, zinc, with 0.5M perchloric acid and cobalt(II), with 0.5M nitric acid. The metals were determined by atomic absorption spectrometry.

The separation of cobalt from binary (Table 4) as well as a tertiary mixture (Table 6) was determined using more or less the same methodology. All of these separations are based upon the magnitude of the separation factor (α) (Table 5). Only those separations indicating a large separation factor ($\alpha = \infty$) was preferred while selecting optimum conditions for separation.

Sequential separation of iron(III), cobalt(II) and nickel(II)

This separation is interesting because these metals belong to the same group of the periodic table. It was possible to separate such mixtures by utilizing the differences in response of the extractions to pH. Iron was selectively extracted at pH 3.0 with $5 \times 10^{-3}M$ Cyanex 272 while cobalt(II) was extracted at pH 8.0 with $5 \times 10^{-3}M$ Cyanex 272. Nickel was not extracted under these conditions. It was possible to separate such mixtures in ratios ranging from 1:1:10 to 1:10:1.

The proposed method is simple, rapid and selective. It permits separation of cobalt from commonly associated elements like manganese, zinc, molybdenum, chromium and vanadium. The method permits the cleancut sequential separation of iron, cobalt and nickel. The results are reproducible with a relative standard deviation of $\pm 1.2\%$.

Acknowledgements—We are grateful to Council of Scientific and Industrial Research for sponsoring the project and awarding a Senior Research Fellowship to one of the authors (NVD). Thanks are due to American Cyanamid Co NY, for gift samples of Cyanex extractants

REFERENCES

1. A. K. De, S. M. Khopkar and R. A. Chalmers, *Solvent Extraction of Metals*. Van Nostrand Reinhold, New York (1970).
2. T. Sekine and Y. Hasegawa, *Solvent Extraction Chemistry*. Marcel Dekker, New York (1972).
3. H. Specker and G. Warding, *Z. Anal. Chem.*, **200**, 337 (1964).

4. H. Goto, Y. Kakita and M. Wamiki, *J. Chem. Soc. Jap.*, **92,** 580 (1961).
5. K. G. Nakagawa, *J. Chem. Soc. Jap.*, **81,** 44 (1960).
6. L. F. Cook and W. W. Szmakaluk, *Solvent Extraction Proceeding of International Solvent Extraction Conference*, 1451 (1971).
7. Yu. B. Klatenik and I. A. Bykhovskaye, *Zhur. Anal. Khim.*, **20,** 567 (1965).
8. M. Goricon and D. Grelenic, *Proc. Chem. Soc.*, 288 (1960).
9. T. E. Moore, R. W. Goodrich, E. A. Gootman, B. S. Slezak and P. C. Yates, *J. Phy. Chem.* **60,** 564 (1956).
10. J. Aggett, J. E. Clark and R. A. Richardson, *J. Inorg. Nucl. Chem.*, **31,** 2919 (1969).
11. J. O. Hibbits, W. F. Davis and M. R. Menke, U.S. atomic energy comm. APEX 519 (1959) (C.A. **54,** 136969).
12. N. Suzuki and H. Yoshida, *J. Chem. Soc. Jap.*, **80,** 1008 (1959).
13. Cyanex 272 extractant: solvent extraction reagent cyanamid, American Cyanamid Co., New Jersey (1985).
14. A. I. Vogel, *Quantitative Inorganic Analysis*, 3rd Ed. p. 443 (1962).

Talanta, Vol. 40, No. 10, pp. 1541–1549, 1993
Printed in Great Britain.

0039-9140/93 $6.00 + 0.00

THE GAS–LIQUID CHROMATOGRAPHIC STATIONARY PHASE PROPERTIES OF LIQUID ORGANIC SALTS: ANOMALOUS SELECTIVITY VARIATION WHEN EMPLOYING THE ROHRSCHNEIDER/McREYNOLDS SYSTEM

RAUL MORALES,* CARLOS BLANCO† and KENNETH G. FURTON‡
Department of Chemistry, Florida International University, University Park, Miami, FL 33199, U.S.A.

(*Received* 14 *July* 1992. *Revised* 14 *April* 1993. *Accepted* 20 *April* 1993)

Summary—The liquid organic salts studied here have wide stable liquid temperature ranges and act as efficient, highly selective gas–liquid chromatographic stationary phases. The effect of carbon number on the gas–liquid chromatographic stationary phase properties of this series of tetra-*n*-butylammonium *n*-alkylsulfonate salts was evaluated by the well-known Rohrschneider/McReynolds system. Several problems arose when attempting to characterize these polar liquid organic salts employing this system. The specific retention volumes for the polar selectivity probes were generally not affected by an increase in the carbon number for the series studied here. However, the specific retention volumes for the *n*-alkane retention index markers increased dramatically as the anion carbon number was increased. The overall effect was a net decrease in the calculated McReynolds constants with increasing carbon number, although the true selectivity of the different stationary phases remained constant. Additionally, the specific retention volumes of the basic test probe, pyridine, showed large erratic variations and, in some cases, was not recovered from the columns. The results suggest the possibility of on-column chemical reactions occurring with some of these salts, and an alternative test probe, 2,6-dimethylpyridine (lutidine) is proposed to eliminate this problem. As McReynolds constants are presently the most commonly used parameters for predicting retention and gas chromatographic stationary phase selection, it is important that workers are aware of the inherent limitations of this scheme.

Organic molten salts (OMS), also referred to as liquid organic salts (LOS) are a unique class of highly polar, selective solvents which make efficient, thermally stable gas chromatographic stationary phases.[1] Liquid organic salts exhibit unique selectivity compared to conventional polymeric nonionic liquid phases presently used. These salts exhibit unusually strong orientation and proton donor/acceptor intermolecular interactions, and also possess interionic forces, such as ion–dipole interactions, absent in molecular liquids. Retention of a solute in gas–liquid chromatography (GLC) is determined from the sum total of all interactions in the liquid stationary phase. The magnitude of individual intermolecular interactions is commonly described as the stationary phase selectivity; whereas, the extent of all possible intermolecular interactions for the stationary phase represents the stationary phase polarity. Therein lies the problem with conventional polarity/selectivity schemes. There are few test solutes (also called probes) which exhibit, and, therefore, test for, only one intermolecular interaction. Likewise, it is impossible to devise a single test probe which can test for all possible intermolecular interactions.

Generally, polarity/selectivity schemes are based on a relative measure of retention for several solutes which test for the dominant intermolecular interactions and a sum of all of the probes acts as an estimate of the stationary phase polarity. Although there are obvious deficiencies with such an empirical approach, contemporary knowledge of solution interactions is inadequate to calculate all forces involved for complex molecules. There have been numerous approaches to estimating the polarity/selectivity of stationary phases including the calculation of the reluctance of a stationary phase to retain non-polar solutes such as hydrocarbons, as

*United States Drug Enforcement Administration, Southeast Laboratory, 5205 NW 84th Avenue, Miami, FL 33166, U.S.A.
†Konik Instruments, 6065 NW 167 Street STE B-20, Miami, FL 33015-9969, U.S.A.
‡Author to whom correspondence should be addressed.

fundamental thermodynamic parameters of test solutes, as solubility parameters, and, recently, several solvation models have emerged. Critical reviews of conventional schemes as well as recent advances in solvation models have recently appeared.[2,3] These more rigorous solvation models should emerge pre-eminent as they are further refined and more evidence emerges, such as that presented here, which illustrates the inadequacies of current selectivity schemes.

In this paper, we discuss the various intermolecular forces which may contribute to GLC retention and the difficulty in devising a polarity/selectivity scheme to evaluate the magnitude of all of these forces. In particular, the inadequacies of the Rohrschneider/McReynolds scheme will be demonstrated for a series of tetrabutylammonium *n*-alkylsulfonate salts. Two significant limitations of the Rohrschneider/McReynolds system are discussed presently. First is the fact that the role of the *n*-alkane retention index standards in determining the magnitude of stationary phase constants is not accounted for. Secondly, questions regarding the type and number of test solutes appropriate for stationary phase characterization are discussed. Additionally, results presented here demonstrate a hereto unreported reactivity of the common test probe, pyridine, with these salts, which was eliminated by employing the sterically hindered pyridine analogues (2,6-di-tert-butylpyridine and 2,6-dimethylpyridine).

EXPERIMENTAL

Tetra-*n*-butylammonium ethane-, propane-, butane-, pentane-, and hexanesulfonate were synthesized as previously described.[4] The column support material, Chromosorb W-AW, was washed with deionized water several times until clear to remove the fines present in the commercially obtained support. After overnight drying at 110°C, the support was sieved to 40–60 mesh. Column packings containing 7–15% (w/w) of salt on the support were prepared using the rotary evaporator technique with methylene chloride as the slurry solvent. After coating, the packings were dried in a fluidized bed drier and packed into nickel columns (3 m × 2 mm I.D.) with the aid of suction and gentle vibration. Individual phase loadings were determined by initial weighings and by overnight Soxhlet extraction of the column packing with methanol after chromatographic measurements. No significant discrepancy was seen between these two measurements. Previous experimental tests have established that any contribution to retention due to solid or liquid surface adsorption is negligible.[4]

Chromatographic separations were performed on a Hewlett-Packard 5890 Series II Gas Chromatograph (Palo Alto, CA, U.S.A.) with a heated on-column injector and a flame ionization detector. The column temperature was determined with a digital platinum RTD thermometer checked against a NIST certified mercury thermometer and was stabilized at 120.1°C (±0.1°C). Helium carrier gas flow rates were determined with a thermostatted soap-film meter making the appropriate corrections for the saturation vapor pressure of the water. The column pressure drop was determined with a mercury manometer (±1 mm Hg). Solutions of the test solutes in hexane were injected to approximate the infinite dilution condition in the linear portion of the sorption isotherm. The symmetrical (Gaussian) peaks and retention volumes independent of sample size suggested that the condition of effective infinite dilution was attained.

RESULTS AND DISCUSSION

Stationary phase properties of the salts

The tetra-*n*-butylammonium *n*-alkanesulfonates studied here had low melting points and were easy to synthesize in high yield and purity. These salts were very hygroscopic and deliquescent under normal laboratory conditions. Even small amounts of hydration caused marked melting point depressions, and, therefore, all handling was performed in a glove bag and melting points were determined chromatographically. The phase transition corresponding to the melting point of a salt is often determined from plots of the logarithm of the specific retention volume for test solutes *vs* the reciprocal column temperature when the salt is used as the stationary phase.[1,4] Alternatively, a more straightforward approach is to plot the logarithm of the adjusted retention time ($\log t'_R$) or the number of effective theoretical plates (N) for solutes directly against the column temperature. The melting point is indicated by a sharp increase in $\log t'_R$ or N. A plot of this type is illustrated in Fig. 1 for tetrabutylammonium *n*-pentanesulfonate. Melting points determined

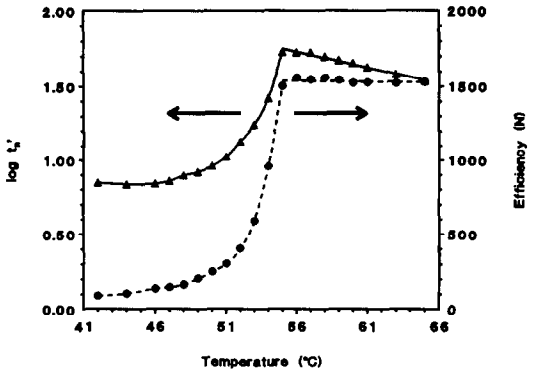

Fig. 1. Plot of the logarithm of the adjusted retention times (▲) and the number of effective theoretical plates (●) for dodecane on tetra-*n*-butylammonium *n*-pentane sulfonate at various temperatures.

by this method as well as some typical column operating conditions for the salts are summarized in Table 1. Most of the salts studied had wide useful liquid temperature ranges (several more than 100°C) and average column efficiencies either comparable to or higher than those observed for several common nonionic phases prepared from the same batch of support. Overall, these salts had desirable chromatographic stationary phase properties including stability, high purity (and therefore column reproducibility), high efficiency and good solute peak shape. However, characterization of the chromatographic polarity and selectivity of these salts by classical means proved problematic. Problems experienced when applying the well-known Rohrschneider/McReynolds system to these salts are also manifest with conventional phases and an explanation requires a thorough understanding of the components of this established method.

Possible intermolecular and interionic forces

Classical gas–liquid stationary phase polarity/selectivity schemes are designed to evaluate the various intermolecular forces which can occur between the chromatographic phase and various test solutes. Additionally, interionic forces may be important for the liquid organic salts studied here. Table 2 summarizes the various interactions which can possibly contribute to solute retention in gas–liquid chromatography. Of the 10 interactions listed, the first three are generally the most significant and are evaluated in the major polarity/selectivity schemes including the Rohrschneider/McReynolds system as well as in the Snyder selectivity triangle system, discussed below. The first two interactions listed are among the strongest intermolecular interactions exhibited by stationary phases, namely proton donor (acidity) and proton acceptor (basicity) complexation. The third interaction listed (dipole–dipole) can also be quite strong and any selectivity scheme must therefore test these first three interactions. The next three interactions listed (dipole–induced dipole, instantaneous dipole–induced dipole, and quadrupole) are non-specific and have varying strengths of interaction. Although London forces are often the dominant interaction in many liquids, they are non-polar in nature and are not generally evaluated in conventional selectivity schemes.

The last four interactions listed are highly-specific and generally present only in selective phases chosen for particular applications. These

Table 1. Column operating conditions for tetra-*n*-butylammonium *n*-alkanesulfonate salts

Salt	Melting point (°C)*	Decompositioin temperature (°C)	Maximum operating temperature (°C)†	Liquid temperature range (°C)‡	Average column efficiency (N)§
Methanesulfonate	79	220	170	93	2200
Ethanesulfonate	120	225	170	51	2400
Propanesulfonate	121	215	160	39	2600
Butanesulfonate	51	215	160	110	2100
Pentanesulfonate	56	200	160	105	1700
Hexanesulfonate	Gel	200	150	(150)	2600

*Determined from plots of efficiency and log t'_R *vs* temperature.

†Defined as the highest temperature that the column could be maintained at overnight without change in retention or peak shape in a test chromatogram obtained at a lower temperature before and after the conditioning period.

‡Value in parentheses assumes a minimum operating temperature of room temperature (20°C) although the salt remains usable below room temperature.

§Approximate values for a variety of test solutes on 3 m × 2 mm column with a 10% salt loading (w/w) on Chromosorb W-AW (40/60 mesh).

Table 2. Classification of some possible intermolecular and interionic forces in GLC systems

#	Solute–stationary phase interactions	Common name (Investigator)
1	Proton donor complexation	Hydrogen bonding
2	Proton acceptor complexation	Hydrogen bonding
3	Dipole–dipole forces	Orientation (Keesom)
4	Dipole-induced dipole forces	Induction (Debye)
5	Instantaneous dipole–induced dipole forces	Dispersion (London)
6	Quadrupole–dipole forces	Quadrupole
7	Electron pair donor–acceptor (EPD–EPA)	Charge-transfer complex
8	Solvophobic interactions	Hydrophobic in aqueous systems
9	Isomer recognition	Unique to chiral and liquid–crystal phases
10	Ion–dipole forces	Ionic interaction, unique to LOS

include electron pair donor–electron pair acceptor (EPD–EPA), or charge-transfer interactions and solvophobic interactions. Although specific forces such as isomer recognition and solvophobic interactions are not technically interactions, but rather the sum of interactions, they can contribute significantly to GLC retention and are included in this table for completeness. For example, solvophobic interactions are really the consequence of interactions, both attractive and repulsive (overlap of hard cores) but are, nonetheless, still commonly referred to as interactions.[5] Since the electron pair donor/acceptors may involve n-, σ-, or π-electrons, there are actually nine different possible types of EPD–EPA complexes, although π-EPD–π-EPA and π-EPD–σ-EPA have been studied in the greatest detail.[5] Hydrophobic interactions are well known in aqueous systems when apolar molecules or apolar groups in large molecules aggregate with expulsion of water molecules from the hydration shells. Similar interactions may be present in solvents resembling water including some liquid organic salts studied, and, the more general term, solvophobic interactions may be used. Such interactions have been reported in solvents including glycerol and ethanol.[5] Selective stationary phases can resolve enantiomers, as well as close-boiling positional and geometric isomers. Enantiomorphic resolution is the result of interactions between the enantiomers and the stationary phase, which form a transient diastereomeric association complex with a different sorption enthalpy and, therefore, different retention characteristics. Liquid–crystalline phases exhibit liquid mechanical properties while maintaining some of the anisotropic properties of the solid allowing close-boiling positional and geometric isomers of rigid molecules to be resolved.[6] Additionally, the liquid organic salts investigated here also exhibit ion–dipole forces which involve the Coulomb forces between ions and electrically neutral dipolar molecules.

Conventional polarity/selectivity schemes for stationary phase characterization

Of the scores of polarity/selectivity schemes proposed over the years, two major schemes have stood the test of time. Namely, the Snyder selectivity triangle,[7,8] which is the most common solvent classification method used in liquid chromatography, and McReynolds constants, which are widely used for evaluating gas chromatographic polarity and selectivity. The Snyder selectivity triangle has recently been re-evaluated by Rutan *et al.*[9] using new experimental measurements of the gas–liquid partition coefficients of Rohrschneider probe solutes and a set of normal alkanes. Although the Snyder selectivity scheme has been mainly applied in liquid chromatography, it can be applied with equal success to gas–liquid chromatographic system. Its application to the characterization of liquid organic salts is discussed elsewhere.[10]

McReynolds constants are based on theoretical considerations originally proposed by Rohrschneider which utilize retention indices. The retention index, originally proposed by Kovats in 1958 in the first of a series of papers[11–13] is widely used in studies of stationary phase characterization. The retention index uses the linear relationship that exists between the logarithm of retention parameters and the number of carbon atoms within a homologous series. Refinements of the retention index have been made since its introduction.[14] Retention behavior is most commonly expressed on a uniform scale of homologous n-alkanes. The retention index of a substance is equal to 100 times the carbon number of a hypothetical n-alkane with the same retention parameter (time, volume, *etc.*). The retention index scale is made up of the n-alkanes with retention index

values equal to 100 times the carbon number of the *n*-alkane. The retention index of a substance X is typically calculated by coinjection of bracketing *n*-alkanes differing by one carbon number, and using equation (1):

$$I = 100n + 100\frac{\log R_X - \log R_n}{\log R_{n+1} - \log R_n} \quad (1)$$

where R is the retention parameter (adjusted retention time, adjusted retention volume, specific retention volume, partition coefficient, *etc.*) n is the carbon number of the *n*-alkane eluting before substance x, and $n+1$ is the carbon number of the *n*-alkane eluting directly after substance x. One of the most commonly used parameters, due to its simplicity, is the adjusted retention time. In theory, the retention index of a substance should depend only on the stationary phase and the column temperature and should be independent of the other column variables (chromatographic support material, flow rate, column efficiency, *etc*). In fact, the retention index is only independent of column variables when the *n*-alkanes and the substance are retained by a single retention mechanism, namely partitioning. This is not true in many cases and the retention index may be subject to systematic errors.

The most widely used method for retention prediction and for characterizing gas chromatographic stationary phase polarity and selectivity is based on the retention index system and was introduced by Rohrschneider[15–17] and modified by McReynolds.[18] Rohrschneider proposed a scheme based on the principle that intermolecular forces are additive and can be evaluated from differences in the retention of test solutes (as Kovat's retention indices) on the phase being studied and on a nonpolar standard reference phase (such as squalane). In principle, for each type of intermolecular interaction, the interaction energy is proportional to a value (a, b, ...) characteristic of a particular test solute, and to a value (x, y, ...) characteristic of the stationary phase. The index difference can therefore be described as:

$$\Delta I = ax + by + cz. \quad (2)$$

Rohrschneider first tried to characterize ΔI with three terms, namely, benzene, ethanol, and methyl ethyl ketone. Subsequently, he found it necessary to add two additional terms (symbolized du and es).

"McReynolds Constants" are phase specific constants calculated by subtracting the retention index values measured on a non-polar reference phase, squalane (2,6,10,15,19,23-hexamethyltetracosane), from that measured on the phase to be characterized as indicated by the following equation:

$$C' = I^{\text{phase}}_{(\text{probe})} - I^{\text{squalane}}_{(\text{probe})} \quad (3)$$

where C' is the McReynolds constant, $I^{\text{phase}}_{(\text{probe})}$ is the Kovats retention index for the test probe on the stationary phase of interest and $I^{\text{squalane}}_{(\text{probe})}$ is the Kovats retention index for the test probe on squalane. The values for the retention indices of the test probes on squalane can be taken from McReynolds original work[19] as follows: $I_{(\text{benzene})} = 653$; $I_{(n\text{-butanol})} = 590$; $I_{(2\text{-pentanone})} = 627$; $I_{(1\text{-nitropropane})} = 652$; $I_{(\text{pyridine})} = 699$.

The calculation is repeated for each probe generally using a phase loading of 10% and a column temperature of 120°C. McReynolds chose some higher molecular weight homologues of Rohrschneider's original probes and added five additional probes in an attempt to more completely characterize stationary phase selectivity. The number of terms needed to adequately characterize GLC stationary phase selectivity and the test solutes most appropriate for this purpose continues to be a matter of debate.[20,21] The McReynolds probes and the key interactions they measure are listed in Table 3.

Table 3. Intermolecular interactions exhibited by common test probes

Snyder probe (symbol)	Rohrschneider probe (symbol)	McReynolds probe (symbol)	Principle interactions exhibited by probe (Secondary interactions exhibited by probe)
	Benzene (X_p)	Benzene (X′)	Dispersive (inductive, EPD–EPA, quadrupole)
Ethanol (x_e)	Ethanol (Y_p)	1-butanol (Y′)	Proton donor (orientative, proton acceptor)
	2-butanone (Z_p)	2-pentanone (Z′)	Weak proton acceptor (orientative)
Nitromethane (x_n)	Nitromethane (U_p)	Nitropropane (U′)	Orientative (weak proton acceptor)
	Pyridine (S_p)	Pyridine (S′)	Proton acceptor (orientative, EPD–EPA)
		2-methyl-2-pentanol (H′)	Proton donor (orientative, proton acceptor)
		1-iodobutane (J′)	Orientative (weak proton acceptor)
		2-octyne (K′)	Dispersive (EPD–EPA)
1,4-dioxane (x_d)		1,4-dioxane (L′)	Orientative (proton acceptor, EPD–EPA)
		cis-hydrindane (M′)	Dispersive

Table 4. Specific retention volumes for test solutes on a series of tetra-*n*-butylammonium *n*-alkanesulfonate salts at 120.1°C

Test solute	Sulfonate anion					
	Methane	Ethane	Propane	Butane	Pentane	Hexane
Octane	9.5	10.0	11.3	13.6	14.9	16.1
Nonane	16.1	17.1	19.5	23.0	25.9	28.4
Decane	26.8	28.9	33.1	38.5	44.6	49.3
Undecane	44.3	48.1	55.5	64.6	76.0	84.9
Dodecane	72.7	79.5	92.5	107.4	128.8	145.2
Tridecane	118.6	130.8	153.1	178.7	217.0	247.0
Tetradecane	192.8	214.3	252.5	296.7	364.3	418.7
Pentadecane	312.4	349.9	414.9	491.2	609.7	707.1
Hexadecane	504.8	569.6	679.6	811.0	1017.6	1191.0
Benzene	26.2	24.3	24.4	25.3	26.2	26.0
1-Butanol	373.2	341.9	343.2	388.2	360.7	350.4
2-Pentanone	37.9	36.4	36.7	37.5	38.7	38.0
1-Nitropropane	174.3	159.7	156.9	153.3	158.2	151.6
Pyridine	126.6	1950.2*	939.7*	1267.3*	142.7	322.2*
Ethanol	122.4	110.3	108.3	106.2	111.2	107.2
Nitromethane	127.7	110.7	106.7	104.2	107.6	103.2
Dioxane	44.3	41.2	40.6	41.4	42.1	41.5

*Broad, tailing peak (values may be unreliable).

For comparison, the selectivity probes originally proposed by Rohrschneider are also listed in Table 3, as well as the three Snyder selectivity probes. McReynolds published phase constants for some 200 common liquid phases which led to the discontinuation of many phases with duplicate separation properties. Over the years, McReynolds constants have become the most quoted indicator of chromatographic selectivity. Column manufacturers customarily quote McReynolds constants for each stationary phase marketed to aid in the selection of phases for particular applications. Additionally, researchers normally determine the same constants for new phases as proof of the uniqueness of new phases. Finally, McReynolds constants are used "as an aid to the accurate prediction of chromatographic behavior".[22] It is this later application, particularly, where McReynolds constants can yield erroneous results, as demonstrated in the present study.

Limitations of retention index based schemes

The inherent limitation of any selectivity scheme based on retention indices is that any derived constants will be a composite of the index standards as well as the polarity probes used to evaluate specific interactions. For example, Kovats' retention indices calculated via equation (1) measure a stationary phases' retention of a selectivity probe, X, relative to the non-polar *n*-alkanes bracketing that probe. Therefore, Kovats' retention indices are a composite measure of how strongly a phase retains a polar solute relative to a non polar solute. So, ambiguous McReynolds constants due to the hydrocarbon index standards are inherent in the system, and must be considered whenever a stationary phase is chosen for a particular application. For the series of tetrabutylammonium *n*-alkanesulfonate stationary phases investigated here, we have observed that their McReynolds constants vary substantially, although they have very similar chromatographic retention properties for the McReynolds probes. Any apparent differences in polarity and selectivity for these stationary phases are entirely due to the variations in retention times of the alkane standards, rather than variations in the retention of the selectivity probes. Specific retention volumes for McReynolds and Snyder selectivity probes as well as the bracketing *n*-alkanes standards are listed in Table 4.

Figure 2 illustrates that while there was either no increase or, in fact, a small decrease in specific retention volumes for the major polarity probes for the series of liquid organic salts studied here, the retention of the *n*-alkane standards increases substantially. The resulting McReynolds constants calculated via equation (3) are given in Table 5. The net effect of the increase in retention of the *n*-alkanes is a substantial decrease in the calculated McReynolds constants for the polar probes with an average decrease of more than one third (*ca.* 36%) from methane to hexane sulfonate. The apparent observed differences in selectivities are entirely attributable to the hydrocarbon index standard, rather than the polar test probes. These data

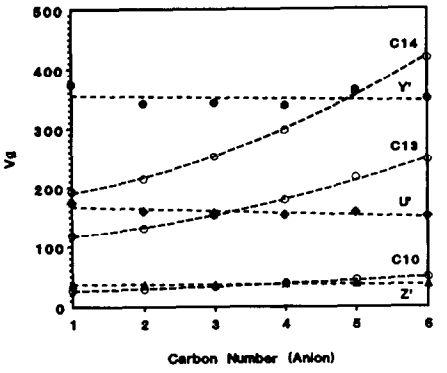

Fig. 2. Plot of the specific retention volume *vs* the carbon number of the anion for tetra-*n*-butylammonium *n*-alkanesulfonates at 120°C. Probe identification: Y′ = *n*-butanol (●); U′ = 1-nitropropane (◆); Z′ = 2-pentanone (▲); C14 = *n*-tetradecane (○); C13 = *n*-tridecane (○); C10 = *n*-decane (○).

support those previously published for very polar conventional non-ionic liquid phases;[23] namely, that the magnitude of McReynolds constants is determined primarily by a lack of solute–solvent interactions with the hydrocarbon index standards and, to a lesser extent, from specific solute–solvent interactions with the polar selectivity probes.

Limitation of using a single solute to evaluate a specific interaction

The earlier discussion of the multitude of possible intermolecular and interionic forces within the phases illustrates the inherent problem associated with assigning a single test probe for a single interaction. With the exception of the non-polar alkanes, any chosen test probe will necessarily exhibit multiple intermolecular interactions and thus serves as a composite measure of polar interactions. For example, Rohrschneider and McReynolds chose pyridine as their probe for stationary phase proton–donor interaction, when, in fact, pyridine may also exhibit orientative interactions and EPD–EPA complexation. Additionally, we have encountered what appear to be on-column reactions of pyridine with some of the phases studied. Possible on-column reactions were indicated by very broad, tailing peaks whose peak area was not representative of the amount of test solute injected and whose retention times were unpredictable. One possible explanation for such behavior is the possibility of a nucleophilic displacement reaction occurring with the liquid organic salts studied. Two sterically hindered bases, namely, 2,6-di-tert-butylpyridine and 2,6-dimethylpyridine were chosen to investigate this possible on-column chemical reaction. A higher temperature was chosen in an attempt to improve the excessively broad chromatographic peaks for pyridine at 120°C. Specific retention volumes for McReynolds and Snyder selectivity probes as well as the bracketing *n*-alkanes standards and 2,6-di-tert-butylpyridine and 2,6-dimethylpyridine at 140°C are listed in Table 6. Even at higher temperatures, the excessive tailing and peak breadth precluded the use of pyridine for characterizing the acidity of these phases. However, the two sterically-hindered (more weakly nucleophilic) bases, 2,6-di-tert-butylpyridine and 2,6-dimethylpyridine, exhibited expected peak symmetry, efficiency, and relative retention for the phases studied.

Table 5. McReynolds constants calculated for tetra-*n*-butylammonium *n*-alkanesulfonates at 120°C

Tetra-*n*-butylammonium	Test solute X′	Y′	Z′	U′	L′
Methanesulfonate	345	944	446	728	450
Ethanesulfonate	316	903	422	690	420
Propanesulfonate	290	871	396	656	389
Butanesulfonate	266	836	369	619	361
Pentanesulfonate	249	809	349	591	337
Hexanesulfonate	230	778	327	560	316

The absolute values of the retention indices for squalane were taken from McReynolds original work[19] as follows: $I_{(benzene)} = 653$; $I_{(n\text{-butanol})} = 590$; $I_{(2\text{-pentanone})} = 627$; $I_{(1\text{-nitropropane})} = 652$; $I_{(pyridine)} = 699$. Identification of symbols for McReynolds probes are given in Table 3.

The specific retention volumes for traditional basic probes, including 2-pentanone and pyridine, as well as for 2,6-di-tert-butylpyridine and 2,6-dimethylpyridine are shown in Fig. 3. Pyridine demonstrates erratic behavior for the phases studied. Whereas, the polar selectivity probes generally exhibited no significant change in V_g as the carbon number of the anion was increased, and the non-polar *n*-alkane index standards exhibited a substantial increase as a function of the carbon number, there is no systematic behavior for pyridine. The behavior of the two alternative bases investigated, 2,6-di-tert-butylpyridine and 2,6-dimethylpyridine, were more in keeping with the results for the other test solutes. However, the highly lipophilic 2,6-di-tert-butylpyridine displayed chromatographic retention behavior approaching that observed for the *n*-alkanes, and therefore, could also yield erroneous results if used as a test probe for bases. For example, the percentage of the slopes relative to the average V_g values (slope/Ave. $V_g \times 100$) for the plots in Fig. 3

Table 6. Specific retention volumes for test solutes on a series of tetra-*n*-butylammonium *n*-alkanesulfonate salts at 140.3°C

Test solute	Sulfonate anion					
	Methane	Ethane	Propane	Butane	Pentane	Hexane
Decane	14.9	16.0	18.4	20.5	24.3	26.7
Undecane	23.4	25.4	29.4	32.9	39.5	43.7
Dodecane	36.4	40.0	46.5	52.4	63.7	71.0
Tridecane	56.3	62.6	73.0	83.1	101.9	114.6
Tetradecane	86.9	97.4	114.4	131.0	162.4	184.2
Pentadecane	133.5	151.1	178.4	206.0	257.8	295.0
Hexadecane	204.8	233.6	277.4	322.9	407.9	471.0
Benzene	16.3	15.6	15.7	15.8	16.7	16.6
1-Butanol	176.5	164.4	164.4	164.4	173.8	168.4
2-Pentanone	22.89	22.5	22.6	22.6	23.9	23.3
1-Nitropropane	96.9	90.6	89.2	87.3	90.7	86.1
Pyridine	70.9	552.2*	341.2*	595.7*	79.3	145.3*
Ethanol	66.9	59.5	58.6	57.6	60.8	58.2
Nitromethane	75.5	66.8	64.5	61.4	65.1	60.7
Dioxane	27.2	25.1	24.9	24.6	25.8	25.5
2,6-di-t-butylpyridine	99.4	102.2	112.0	122.4	140.3	148.3
2,6-Dimethylpyridine	54.5	53.1	—	—	58.3	63.5

*Broad, tailing peak (values may be unreliable).

shows a marked difference between the polar probe pentanone and the alkane standard *n*-tridecane. The slope for pentanone is just 0.8% of the average value for pentanone; whereas, the slope for *n*-tridecane is 14.6% of its average value for the six salts studied. In contrast, the slope for 2,6-dimethylpyridine is 3.1% and that for 2,6-di-tert-butylpyridine is 8.7%. Not surprisingly, the more aliphatic a selectivity probe is, the more its chromatographic behavior will mimic that of the alkane markers. Of the limited number of basic test probes studied here, 2,6-dimethylpyridine was the best compromise between acceptable chromatographic behavior (peak symmetry, *etc.*) and minimal aliphatic character.

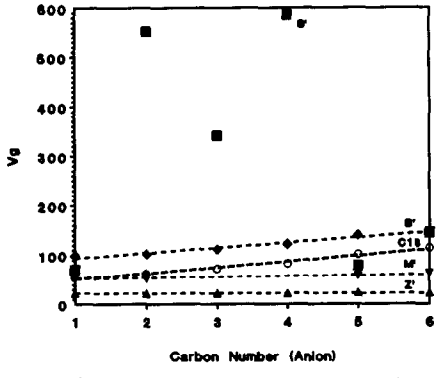

Fig. 3. Plot of the specific retention volume *vs* the carbon number of the anion for tetra-*n*-butylammonium *n*-alkanesulfonates at 140°C. Probe identification: S′ = pyridine (■); B′ = di-tert-butyl-pyridine (◆); M′ = dimethylpyridine (▼); C13 = *n*-tridecane (○); Z′ = 2-pentanone (▲).

These results support previous studies[24] illustrating that McReynolds constants can be an unreliable measure of selective solute-stationary phase interactions for stationary phases. McReynolds constants are a composite indicator of the strength of specific solute–solvent interactions for polar test probes, as well as a measure of the weakness of non-specific solute–solvent interactions for the *n*-alkane retention index markers. A large McReynolds constant may indicate a strong specific interaction between the stationary phase and the test probe and/or it may indicate generally weak interactions with *n*-alkanes. Additionally, the choice of single solutes to probe for specific interactions, and in particular basic interactions, is a difficult, if not impossible, task. Therefore, before selecting a stationary phase for a particular application, additional measures of stationary phase selectivity, including specific retention volumes, thermodynamic values, *etc.* for similar solutes as those to be separated should be sought. Ultimately, it is desirable that a more complete, and, subsequently, a slightly more complex, system of stationary phase characterization be adopted. Such systems are currently under development[2,3] and adoption of any new system by the community of practising chromatographers will require a thorough knowledge of the limitations of our current system as well as the attributes of any new scheme to be adopted.

Acknowledgement—Acknowledgement is made to the donors of the Petroleum Research Fund, administered by the American Chemical Society, for support of this research.

REFERENCES

1. C. F. Poole, K. G. Furton, R. M. Pomaville, S. K. Poole and B. R. Kersten, in R. J. Gale and D. G. Lovering (eds), *Molten Salt Techniques*, Vol. 4. Plenum, New York, 1991.
2. C. F. Poole and S. K. Poole, *Chem. Rev.*, 1989, **89**, 377.
3. C. F. Poole, T. O. Kollie and S. K. Poole, *Chromatographia*, 1992, **34**, 281.
4. K. G. Furton and R. Morales, *Anal. Chim. Acta*, 1991, **246**, 171.
5. C. Reichard, *Solvent Effects in Organic Chemistry*. Verlag Chemie, New York, 1979.
6. C. F. Poole and S. K. Poole, in E. Heftman (ed.), pp. 14–20. *Chromatography*, 5th Ed. Elsevier, Amsterdam, 1992, A407.
7. L. R. Snyder, *J. Chromatogr.*, 1974, **92**, 223.
8. L. R. Snyder, *J. Chromatogr. Sci.*, 1978, **16**, 223.
9. S. C. Rutan, P. W. Carr, W. J. Cheong, J. H. Park and L. R. Snyder, *J. Chromatogr.*, 1989, **463**, 21.
10. B. R. Kersten and C. F. Poole, *J. Chromatogr.*, 1988, **452**, 191.
11. E. Kovats, *Helv. Chim. Acta*, 1958, **41**, 1915.
12. E. Kovats, *Z. Anal. Chem.*, 1961, **181**, 351.
13. E. Kovats, *Helv. Chim. Acta*, 1963, **46**, 2705.
14. L. S. Ettre, *Chromatographia*, 1974, **7**, 261.
15. L. Rohrschneider, *J. Chromatogr.*, 1965, **17**, 1.
16. L. Rohrschneider, *J. Chromatogr.*, 1966, **22**, 6.
17. L. Rohrschneider, *J. Chromatogr.*, 1969, **39**, 383.
18. W. O. McReynolds, *J. Chromatogr. Sci.*, 1970, **8**, 685.
19. W. O. McReynolds, *Gas Chromatographic Retention Data*, Preston Technical Abstract Co., Evanston, IL, 1966.
20. A. Hartkopf, *J. Chromatogr. Sci.*, 1974, **12**, 113.
21. C. F. Poole and T. O. Kollie, *J. Chromatogr.*, 1991, **556**, 457.
22. P. Overaa, *Lab. Practice*, 1990, **39**, 17.
23. W. A. Aue and V. Paramasigamani, *J. Chromatogr.*, 1978, **166**, 253.
24. B. R. Kersten, C. F. Poole and K. G. Furton, *J. Chromatogr.*, 1987, **411**, 43.

Talanta, Vol. 40, No. 10, pp. 1551–1555, 1993
Printed in Great Britain.

0039-9140/93 $6.00 + 0.00

VOLTAMMETRIC DETERMINATION OF BUSPIRONE

SHENG-ZONG CHEN, FENG XU, HONG ZHANG and ZHENG-QI ZHANG*
Department of Chemistry and Chemical Engineering, Hunan University, Changsha, People's Republic of China

(*Received* 18 *June* 1992. *Revised* 25 *September* 1992. *Accepted* 25 *September* 1992)

Summary—The electroanalytical chemical properties of buspirone are reported in this paper. A sensitive single sweep voltammetric procedure for trace buspirone determination was developed. The detection limit is $5.0 \times 10^{-9} M$. The method has been applied to the determination of buspirone in blood serum by simple dilution in a buffer.

Polarography and voltammetry are widely applied to the determination of drugs. Several reviews have appeared covering the voltammetric determination of drugs.[1-4] Volke[5] reviewed the development of polarographic and voltammetric assay of drugs, and investigated the relation between the polarographic data and the physiological action of drugs. The polarographic and voltammetric techniques applied in the assay of drugs include d.c. polarography, a.c. polarography, pulse polarography, cyclic voltammetry, linear sweep voltammetry and adsorptive stripping voltammetry. Differential pulse polarography (DPP) possesses higher sensitivity and better selectivity among these, so its application to the determination of drugs is the widest. The adsorptive stripping voltammetry has a lower detection limit, which has frequently prompted its use for the determination of drugs. Recently, Peng[6-8] used adsorptive voltammetry to determine chlorprothixene and haloperidol.

Buspirone (I, 8-(4-(4-(2-pyrimidinyl)-1-piperazinyl)butyl)-8-azaspiro(4,5)decane-7,9-dione) is an antidepressant which was synthesized in the 1970s. Its analytical methods, such as high-performance liquid chromatography[9] and DPP,[10] have been reported. However, other electroanalytical methods have not been reported yet. This paper describes the application of adsorptive voltammetry to the determination of trace amounts of buspirone. The drug can be adsorbed and reduced at the dropping mercury electrode. The cyclic voltammetric data show that the surfactants can promote the adsorption of buspirone at the mercury electrode. In the presence of Triton X-100 the limit of detection for buspirone was $5.0 \times 10^{9} M$.

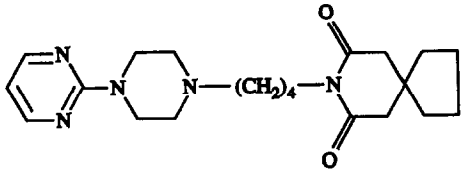

I, Buspirone

*Author for correspondence.

EXPERIMENTAL

Apparatus

The single-sweep polarograms were recorded on a JP-1A polarograph. The polarographic cell has the three electrode system: a dropping mercury electrode (DME) as working electrode, a silver/silver chloride (saturated potassium chloride) reference electrode and a platinum wire auxiliary electrode. (A drop time of 7 sec was selected using a knocker, with a rest time of 5 sec and a scan time of 2 sec/250° mv/sec.) An XJP-821 neopolarograph in connection with an LZ3-100 X–Y recorder and a JM-01 (manual micro-metric screw delivery) hanging mercury drop electrode (HMDE) were used for linear scan voltammetry and cyclic voltammetry measurements.

Reagents

Standard buspirone solution. A stock solution ($1.0 \times 10^{-3} M$) of buspirone was prepared by dissolving the drug in ethanol.

Triton X-100 solution, 0.020%. Dissolve 0.10 g of Triton X-100 in 50 ml of water, and dilute to 500 ml.

The buffer solution was 0.20*M* sodium dihydrogenphosphate solution, adjusted to pH 5.80 with 2*M* sodium hydroxide.

Other reagents were of suprapure or analytical-reagent grade. Demineralized water was used throughout.

Procedure

Polarography of pure buspirone solution. Mix 2.0 ml of buffer solution (pH 5.80), 0.70 ml of 0.020% Triton X-100 solution and various amounts of standard buspirone solution. Dilute to 10 ml with water. The solution was transferred to the voltammetric cell, and purged with oxygen-free nitrogen for 10 min. A flow of nitrogen was maintained over the cell throughout the analysis to prevent interference from oxygen. Record the derivative polarogram, starting the potential scan at −1.0 V. The peak potential is −1.35 V.

Analysis of samples. Blood serum was prepared for centrifuging blood samples three times. Transfer 1–3 ml of the blood serum into a 10-ml standard flask, and continue as above.

Recovery experiment. Add the amounts of buspirone shown in Table 1 into a 50-ml beaker containing the serum samples and treat as described above.

RESULTS AND DISCUSSION

Single-sweep polarography

In a pH 3.0–10.0 buffer solution buspirone yields a sensitive polaragraphic wave, the peak potential shifting in the negative direction with increasing pH value of test solutions. In a pH 5.80 buffer solution the peak potential of the drug is −1.35 V [Fig. 1(b)]. In the presence of 0.0014% Triton X-100 the peak potential does not shift, but the peak height increases two-fold [Fig. 1(c)]. Over the range 3.0×10^{-8}–$5.0 \times 10^{-6}M$, the peak currents are linearly proportional to the concentration of the drug. The detection limit is $5.0 \times 10^{-9}M$, which was taken as the concentration that gave a signal equal to three times the standard deviation of the blank signal, calculated from the calibration slopes. The reproducibility was evaluated by 15 repetitive experiments on a $5.0 \times 10^{-7}M$ buspirone solution. The relative standard deviation was 1.5%.

Effect of pH and buffer concentration

Figure 2(a) shows the influence of the acidity of the test solution on peak current. A very low response to buspirone was observed in solutions more acidic than pH 4.0. Increasing the pH from 4.0 to 5.5 led to a rapid increase in the peak height. The increase in the pH beyond 6.0 caused the peak current to decrease. Over the pH range 5.5–6.0 the peak currents are very close. Accordingly, a pH of 5.8 was used throughout for maximum sensitivity. Various buffers such as 0.05*M* ammonium acetate, 0.05*M* sodium acetate and 0.05*M* NaH_2PO_4 were examined in $5.0 \times 10^{-7}M$ busiprone. The best results were obtained with NaH_2PO_4 buffer. Figure 2(b) shows the influence of the added amounts of the buffer on peak height. The peak current increases with increasing buffer concentration from 0.010 to 0.040*M* and decreases slightly when the buffer concentration exceeds 0.045*M*. In this paper the buffer concentration is 0.040*M*.

Effect of surfactants

In order to choose the most suitable surfactant, various cationic, anionic and non-ionic surfactants, all of them highly soluble in water, were tested. The surfactants were cetyl trimethyl ammonium bromide (CTMAB), sodium lauryl sulphate (SLS), *p*-octyl

Table 1. Determination of buspirone in serum samples

Samples	Buspirone added, μg/ml	Buspirone found, μg/ml	Recovery* %	Content† μg/ml
	0	0	—	0
	0.0800	0.0720	90.0	
	0.200	0.216	108	
	0.400	0.430	108	
	1.20	1.24	103	
No. 1	2.00	1.98	99.0	
	0	1.60	—	1.63
No. 2	0.400	2.04	110	
	0	7.62	—	7.50
No. 3	4.00	12.1	112	

*Mean of three parallel determinations.
†Determined by HPLC.

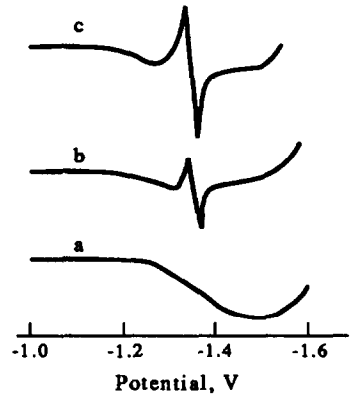

Fig. 1. Derivative single-sweep polarograms of buspirone (a) pH 5.80, 0.0014% Triton X-100; (b) pH 5.80, $1.0 \times 10^{-6}M$ buspirone; (c) pH 5.80, 0.0014% Triton X-100, $1.0 \times 10^{-6}M$ buspirone.

polyethylene glycol phenylether(OP), Tween-80 and Triton X-100. The results obtained are shown in Table 2. Obviously, cationic, anionic and non-ionic surfactants can all increase the peak current of the drug. Triton X-100 is the best and so we used it as a sensitizer. The influence of its concentration on the peak height is shown in Fig. 2(c). The peak current increases rapidly with increasing Triton X-100 concentration from 0.0006 to 0.0013% and decreases greatly when the concentration of Triton X-100 exceeds 0.0016%. A percentage of 0.0014% for the surfactant was chosen for subsequent studies.

Adsorptive characters of buspirone

The adsorption of buspirone at the dropping mercury electrode was demonstrated by constructing electrocapillary curves and by carrying out medium-exchange experiments.

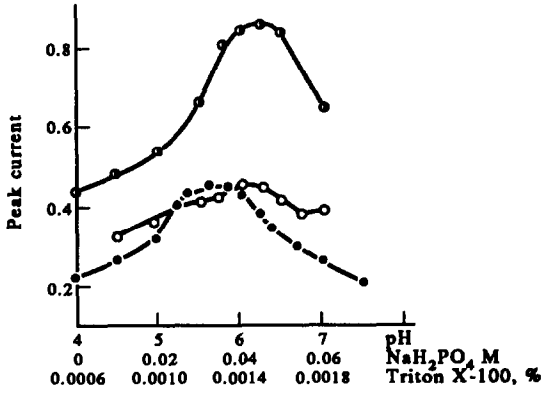

Fig. 2. Effect of the solution conditions $1.0 \times 10^{-6}M$ buspirone; (a) effect of pH: 0.0006% Triton X-100, $0.020M$ NaH_2PO_4; (b) effect of NaH_2PO_4 concentration: pH 5.80, 0.0006% Triton X-100; (c) effect of Triton X-100 concentration: pH 5.80, $0.040M$ NaH_2PO_4.

Table 2. The effect of surfactants*

Surfactants	Peak height, μA
—	0.38
CTMAB	0.63
SLS	0.48
OP	0.55
Tween-80	0.50
Triton X-100	0.75

*pH 5.80, $5.0 \times 10^{-7}M$ buspirone, 0.0010% each of surfactant.

The electrocapillary curves of the buspirone–Triton X-100 system are shown in Fig. 3. The electrocapillary curve of a solution containing buspirone [Fig. 3(b)] is lower than that of the pure buffer [Fig. 3(a)], indicating that buspirone is adsorbed at the dropping mercury electrode. The electrocapillary curve of the solution containing buspirone and Triton X-100 [Fig. 3(d)] is lower still than that of the buspirone solution, indicating that Triton X-100 promotes the adsorption of the drug at the mercury electrode.

For medium-exchange studies, the static mercury drop electrode (SMDE), J-shaped capillary, used as a working electrode, was kept in contact with a solution containing buspirone and Triton X-100 for 180 sec with stirring. Following this, the electrode was cleaned in water for 15 sec while stirring and transferred into another cell containing the background solution only. The reduction process shown in the voltamperogram obtained in the new cell closely resembled that in the original cell.

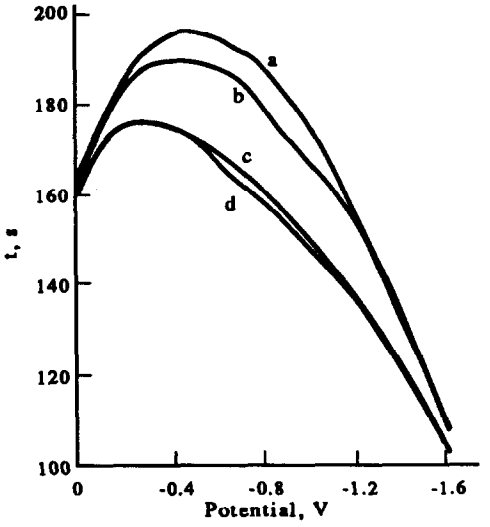

Fig. 3. Electrocapillary curves of the buspirone–Triton X-100 system (a) pH 5.80 ($0.040M$ NaH_2PO_4); (b) pH 5.80, $5.0 \times 10^{-7}M$ buspirone; (c) pH 5.80, 0.0014% Triton X-100; (d) pH 5.80, 0.0014% Triton X-100, $5.0 \times 10^{-7}M$ buspirone.

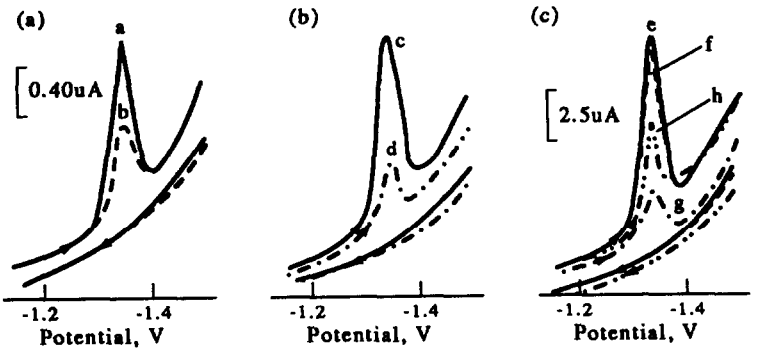

Fig. 4. The cyclic voltamperograms of buspirone system A: pH 5.80, 0.0014% Triton X-100, $5.0 \times 10^{-7}M$ buspirone, $V = 100$ mV/sec, $t = 15$ sec, electrode area of 0.012 cm^2, (a)—first scan, (b)—second scan; B: (c)—in the presence of Triton X-100, (d)—in the absence of Triton X-100, other conditions as same as A; C: $5.0 \times 10^{-6}M$ buspirone, (e) and (f) in the presence of Triton X-100, $t = 15$ sec, (e)—first scan, (f)—second scan, (g) and (h)—in the absence of Triton X-100, $t = 45$ sec for (g), $t = 180$ sec for (h), other conditions are same as for A.

Cyclic voltammetry

The redox and interfacial behaviour of the drug can be evaluated by using cyclic voltammetry. Figure 4 shows the cyclic voltamperogram for the buspirone–Triton X-100 system. From Fig. 4 the following information can be obtained.

In Fig. 4(a) subsequent repetitive scans yielded significantly smaller (but stable) cathodic peaks corresponding to the reduction of dissolved species. This behaviour indicates that the adsorption of the drug at the mercury electrode is reactant adsorption.[11] Buspirone shows cathodic peak at about -1.35 V due to its reduction, and no peak was observed on the anodic branch, indicating that the reduction of the drug is irreversible. The width at the mid-peak of buspirone was determined (curve a) and found to be 65 mV; the αn_α value can be calculated and found to be 0.96.[12] Squella[10] reported that the number of electrons involved in the buspirone reduction process is two, so the α value is 0.48.

In Fig. 4(b) the curve c is the cyclic voltamperogram in the presence of Triton X-100, and curve d, one in the absence of the surfactant. From curve d the width at half-peak of buspirone was determined and found to be 65 mV, so the αn_α value is 0.96, which indicates that Triton X-100 does not improve the reversibility of the reduction process of the drug. However, the peak height in curve c is two times that in curve d, which shows that the surfactant promotes the adsorption of buspirone at the mercury electrode.

Figure 4(c) shows the cyclic voltamperograms for $5.0 \times 10^{-6}M$ buspirone. Curves e and f are the cyclic voltamperograms in the presence of the surfactant for an accumulation time of 15 sec. The peak height during the first scan (curve e) is close to that during the second (curve f), indicating that for the buspirone concentration larger than $5.0 \times 10^{-6}M$ the adsorption of the drug at the mercury electrode achieves likely saturation adsorption. The curves g and h are the cyclic voltamperograms in the absence of Triton X-100 for an accumulation time of 45 and 180 sec, respectively. The adsorption time in the absence of the surfactant is longer than that in the presence of the surfactant, but the peak height of the former is smaller than that of the latter, demonstrating that the Triton X-100 promotes the adsorption of the drug at the mercury electrode.

Application

Serum samples are generally pretreated because the proteins interfere in the determination of drugs in serum. Using the single-sweep polarographic procedure proposed in this paper to determine the buspirone in serum, no sample pretreatment was required, other than a dilution with the supporting electrolyte.

Calibration graphs. Treat the standard buspirone solutions used for the preparation of the calibration line in the procedure as described in the section on analysis of samples. The regression equation of the calibration line has the form:

$$Y = 0.0145X + 0.0003 \quad (1)$$

where Y is the peak current in μA and X is the buspirone concentration in μg/ml. The correlation coefficient was 0.999. The results

of the determination of the buspirone in the serum samples and recovery of added buspirone by using the recommended method are summarized in Table 1. Samples 2 and 3 were from rabbits used in toxiological test for buspirone.

REFERENCES

1. A. J. Bard, *Electroanalytical Chemistry*, Vol. 11, pp. 141–343. Marcel Dekker, New York, 1979.
2. P. T. Kissinger and W. R. Heineman, *Laboratory Techniques in Electroanalytical Chemistry*, pp. 569–609. Marcel Dekker, New York, 1983.
3. G. J. Patriarche and J.-C. Vire, *Anal. Chim. Acta*, 1987, **196**, 193.
4. X. K. Kong and J. H. Pang, *Yaoxue Xuebao*, 1991, **26**, 627; *Chem. Abstr.*, 116, 28247y.
5. J. Volke, *Bioelectrochem. Bioenerg.*, 1983, **10**, 7.
6. Peng Tuzhi, Yang Zhongping and Li Huiping, *Analyst*, 1991, **116**, 727.
7. Peng Tuzhi and Lu Rongshan, *Talanta*, 1991, **38**, 741.
8. Peng Tuzhi, Yang Zhongping and Li Huiping, *Yaoxue Xuebao*, 1990, **25**, 936.
9. F. Kristjansson, *J. Chromatogr.*, 1991, **566**, 250; *Chem Abstr.*, 114, 239814c.
10. J. A. Squella, Y. Borges, L. Bobadilla and J. Nunez-Vergara, *Electroanalysis*, 1990, **2**, 333.
11. S. Dong, *Fenxi Yiqi*, 1984, **1**, 1.
12. E. Laviron, J. *Electroanal. Chem.*, 1974, **52**, 355.

Talanta, Vol. 40, No. 10, pp. 1557–1561, 1993
Printed in Great Britain.

0039-9140/93 $6.00 + 0.00
Pergamon Press Ltd

A NEW CHEMILUMINESCENCE SYSTEM: MnO_4^-–Na_2CO_3–KOH AND ITS APPLICATION IN THE DETERMINATION OF MANGANESE

ZHANG FAN and LIN QINGXIONG*
Department of Chemistry, Fuzhou University, Fuzhou, Fujian 350002, People's Republic of China

(*Received* 29 *March* 1992. *Revised* 24 *September* 1992. *Accepted* 6 *October* 1992)

Summary—A new, fast and simple inorganic chemiluminescence method for the determination of trace amounts of manganese is described. When MnO_4^- is injected into 0.40*M* Na_2CO_3–0.70*M* KOH mixed solution in a reaction cell, the strong chemiluminescence occurs and is recorded. The detection limit is 0.1 ppb Mn and the linear range extends from 0.1 to 10 ppb Mn. A 5-ppb Mn concentration can be determined with a relative standard deviation of 5.6% (15 replicates). The commonly encountered cations do not interfere with the determinations. This method has been successfully applied to the direct determination of manganese in bauxite. The reaction mechanism is also briefly discussed.

The use of chemiluminescence (CL) in analysis for organic and inorganic species at trace levels has received attention mainly because of the simplicity of the instrumentation, the low detection limits and the wide dynamic range. Chemiluminescence reactions based on reagents such as luminol, lucigenin, lophine and some oxalate esters[1] are most common. Many trace metals, including manganese, have been determined by their catalysis of CL reaction.[2,3] There are also some inorganic CL systems,[4–8] without organic CL reagents but generally containing some oxidants such as H_2O_2 and O_3, in the application of analytical chemistry. However, the lack of selectivity of these CL systems limits their direct application to analysis of complex, real samples.

Determination of manganese based on CL has been reported. Kalinichenko[9,10] determined 0.05–5 ng of manganese using luminol, but many other transition metals interfered. Dubovenko and Tovmasyan[11] reported a similar system for determining 0.1–1 μg/ml manganese with photographic rather than photoelectric detection. Seitz and Hercules[12] used ion-exchange to remove interferences for the determination of manganese, with a detection limit of 10^{-8}M manganese. Burguera and Townshend[13] re-investigated the determination of manganese with luminol, but no application was reported. Zheng *et al.*[14] obtained a detection limit of 8×10^{-6} μg/ml manganese using a luminol–KIO_4 system, but Co(II) and Cr(III) interfered. Lucigenin can be used in place of luminol, and Dubovenko *et al.*[15,16] used this system to determine 1–3 μg/ml manganese, but many metal ions interfered. Another CL reaction[17,18] between permanganate and siloxene has been reported for the determination of 0.1–10 μg of manganese. Yamada *et al.*[19] also described a new CL system to determine 0.01–10 ng manganese, but Fe(III) and Mg(II) interfered.

In this study we investigate a new, simple, sensitive and selective inorganic CL system–MnO_4^-–Na_2CO_3–KOH for the determination of manganese. The reaction of decomposition of MnO_4^- to MnO_4^{2-} and O_2 in alkaline medium is a common reaction, but no one has reported its CL behaviour in the past. We found that strong CL occurred when MnO_4^- was injected into Na_2CO_3–KOH mixed solution, but CL was hardly observed without Na_2CO_3. Because of the specificity of the reaction, the commonly encountered cations did not interfere with the determinations.

EXPERIMENTAL

Apparatus

An FG83-1 CL Photometer (made in our laboratory) and a XWT-104 Recorder (Shanghai) were used.

*Present address: Departamento de Química Analítica, Facultad de Química, Universidad de Sevilla, 41012-Seville, Spain.

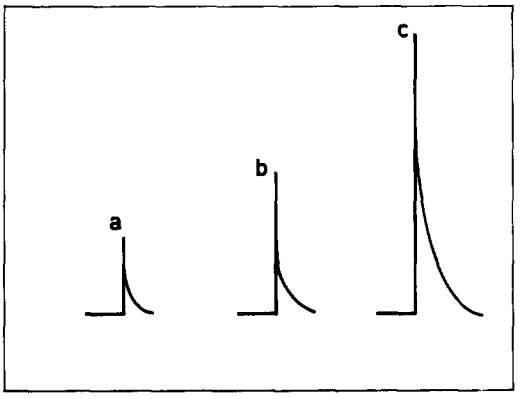

Fig. 1. Typical CL signals. (a) 0.5 ppb; (b) 1 ppb; (c) 2 ppb.

Reagents

Mn(II) standard solution (1 mg/ml). Dissolve 500.0 mg of high-purity manganese metal (cleaning the metal surface with diluting sulphuric acid before weighing) with 10 ml of 1:4 sulphuric acid, transfer the solution into a 500-ml standard flask and dilute to volume with water. Mn(II) standard solution (0.01 mg/ml) is prepared by dilution of this standard solution with water.

MnO_4^- standard solution (100 ppb Mn).[20] Add 0.5 ml of 0.01 mg/ml Mn(II) standard solution, 1.0 ml of concentrated nitric acid, 2.0 ml of 1:1 sulphuric acid by pipette to a 100-ml beaker and evaporate the smoke throughout. Then add 10 ml of water, 2.5 ml of 1:1 sulphuric acid to the beaker and heat to dissolve the salts. Also add 1.0 ml of phosphoric acid and 0.30 g of potassium periodate to the beaker, then heat the solution to produce a reddish colour, transfer the solution to a 50-ml standard flask, and preserve the solution in boiling water for 40 min. Cool and dilute to volume with water. Working standard solutions are prepared by dilution of the standard solution with water.

Na_2CO_3(0.40M)–KOH(0.70M) mixed solution. A 21.20-g portion of Na_2CO_3 and 19.64 g of KOH are dissolved in water. Dilute to volume in a 500-ml standard flask with water, mix and then transfer to a plastic bottle.

All reagents are analytical grade or better and water is doubly distilled in a fused-silica apparatus.

Procedures

Pipette 1.00 ml of Na_2CO_3–KOH mixed solution to a reaction cell. The cell is then put into the cassette of FG83-1 photometer, close the cassette with a cover, then open a shutter in the photometer and start the recorder. The standard solution of MnO_4^- (or sample solution) is rapidly injected into the reaction cell through a fill orifice by an injector and the CL signal is recorded by the recorder (the signals are shown in Fig. 1).

RESULTS AND DISCUSSION

Possible mechanism of chemiluminescence reaction

The CL spectra, the products and their absorption spectra from the CL reaction are investigated. The CL spectra show three spectrum peaks at 420, 480 and 580 nm, which coincides with the emitting wavelength (480 and 580 nm) of excited double molecular oxygen $(O_4)^*$ reported by Khan *et al.*[21] except that at 420 nm, and it is proposed that $(O_4)^*$ is the main luminous species in this system. When we substitute 0.1*M* H_3BO_3 for 0.40*M* Na_2CO_3, the CL intensity becomes very low, only two spectrum peaks occur at 480 and 580 nm. It is evident that Na_2CO_3 is another luminous species in this system.

Wierzchowski *et al.*[22] studied the CO_3^{2-}–H_2O_2–$Fe(SCN)_6^{3-}$ CL system, and it was suggested that $^{\cdot}OH$, $^{\cdot}O_2^-$ and $^{\cdot}HCO_3$ radicals may be generated with one of the possible modes of recombination of the $^{\cdot}HCO_3^-$ radical and its decomposition being:

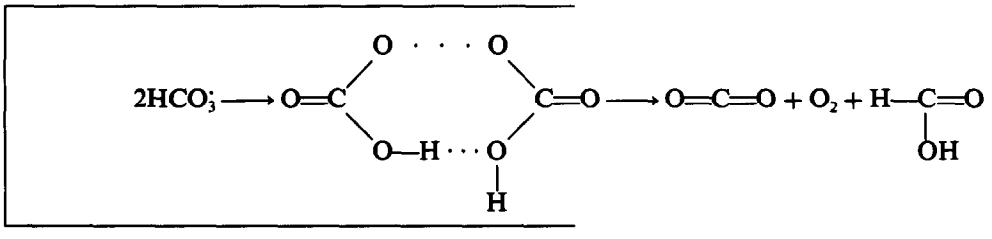

For this mode the energy difference is $\Delta E = E_{c=o} + E_{c=o} + E_{C-H} - (E_{2C-O} + E_{O-H}) =$ 305 kJ/mol that approximately corresponds to the spectrum peak at 420 nm.

The study of the reaction products shows that the absorption peaks of the solution of the reaction products are similar to that of MnO_4^{2-} solution at 600, 500 and 369 nm,[23] and $BaMnO_4$

(blue solid) is obtained when saturated $Ba(OH)_2$ solution is added to the solution of the reaction products. It is evident that one of the products is MnO_4^{2-}.

On the basis of these investigations, a possible mechanism of the CL reaction is proposed, and several conclusions can be drawn as follows.

(1) The main CL reaction is the decomposition of MnO_4^- to MnO_4^{2-} and O_2 accompanying CL, and the reaction is a free radical reaction. The possible mechanism of the reaction, in which reactions (1)–(5) have been reported by Symons,[24,25] is proposed as follows:

$$MnO_4^- + OH^- = MnO_4^{=} + {}^{\cdot}OH \quad (1)$$

$${}^{\cdot}OH + OH^- = {}^{\cdot}O^- + H_2O \quad (2)$$

$$MnO_4^- + OH^- + {}^{\cdot}O^- = MnO_4^{=} + HO_2^- \quad (3)$$

$$MnO_4^- + HO_2^- = MnO_4^{=} + HO_2^{\cdot} \quad (4)$$

$$HO_2^{\cdot} + OH^- = O_2^- + H_2O \quad (5)$$

$$MnO_4^- + O_2^- = MnO_4^{=} + O_2^{\cdot} \quad (6)$$

$$O_2^{\cdot} + O_2^{\cdot} = (O_4)^* \quad (7)$$

$$(O_4)^* \rightarrow 2O_2 + h\nu \quad (8)$$

$$4MnO_4^- + 4OH^- = 4MnO_4^{=} + O_2 + 2H_2O + h\nu \quad (9)$$

It is suggested that reaction (6) generates $O_2^{\cdot}$ radicals and their recombination may generate energy-rich precursors of excited molecules $(O_4)^*$, which decompose to O_2 accompanying CL with two spectrum peaks at 480 and 580 nm.

(2) It is suggested that CO_3^{2-}/HCO_3^- is another luminous species in this system. The CL spectrum peak at 420 nm possibly results from the decomposition of the complex in reaction (12):[22]

$${}^{\cdot}OH + HCO_3^- \rightarrow OH^- + HCO_3^{\cdot} \quad (10)$$

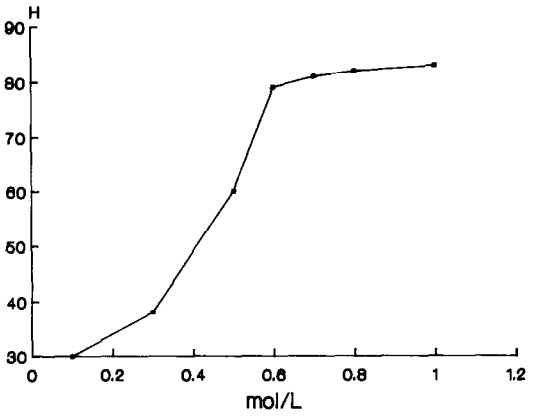

Fig. 2. Effect of KOH concentration, $[Na_2CO_3] = 0.4M$, 5 ppb Mn.

However, the contribution of reaction (12) cannot entirely account for the strong enhancement of CL by the presence of sodium carbonate. It is suggested that CO_3^{2-} or HCO_3^- can also catalyze the decomposition of MnO_4^-,[26] or that the radical reactions of CO_3^{2-}/HCO_3^- as reactions (10)–(12) induce the decomposition of MnO_4^-, which dramatically increase the intensity of CL.

Optimization of experimental conditions

The CL intensity is dependent on the concentrations of sodium carbonate and potassium hydroxide. If potassium hydroxide solution is freshly prepared and without addition of sodium carbonate, CL can hardly be observed, which indicates that CO_3^{2-}/HCO_3^- is as important as OH^- in this system. It is found out that $0.70M$ potassium hydroxide and $0.40M$ sodium carbonate are optimized conditions for this system, as shown in Figs 2 and 3. It is also found out that the Na_2CO_3–KOH system is the most sensitive system of those shown in Table 1. Under the optimized conditions, the relative standard

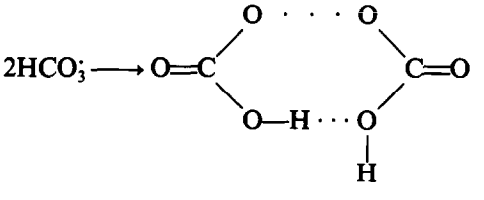

(11)

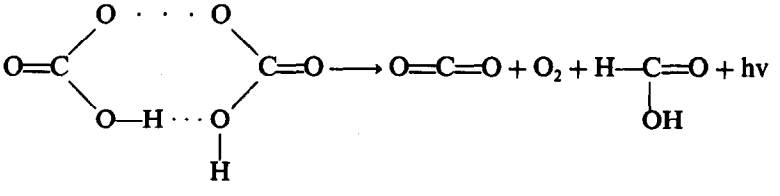

(12)

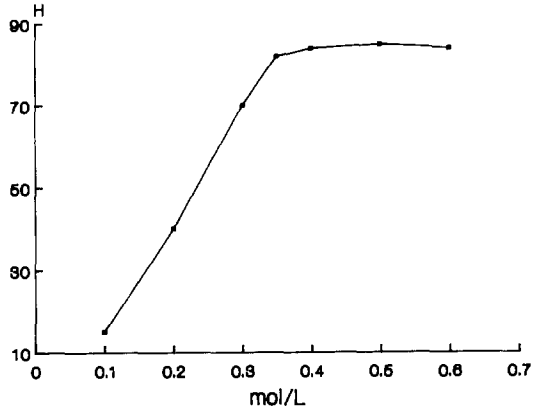

Fig. 3. Effect of Na_2CO_3 concentration, [KOH] = 0.7*M*, 5 ppb Mn.

Table 1. Comparison of CL intensity among various systems

System	Relative peak height
0.4*M* $(NH_4)_2CO_3$/0.7*M* KOH	0
0.4*M* Na_2CO_3/0.7*M* NaOH	1
Li_2CO_3 (saturated)/0.7*M* KOH	6
0.4*M* K_2CO_3/0.7*M* KOH	27
0.4*M* Na_2CO_3/0.7*M* KOH	43

deviation found (15 replicates) for 5 ppb Mn is 5.6%, the linear range extends from 0.1 to 10 ppb Mn (Fig. 4).

An investigation of interference in the determination of 5 ppb Mn shows that the following commonly encountered cations do not interfere with the determinations: Ca(II), Al(III), Pb(II), Mg(II), Fe(III), B(III), Cd(II), Ba(II), Zn(II) (>0.1 mg/ml); Co(II), Cr(III), Cu(II), Tl(III), Pd(II), Ga(III), Ge(IV), Te(IV), Ni(II), Ti(IV) (>0.01 mg/ml); La(III), Be(II), Sr(II) (>0.001 mg/ml). It is evident that the selectivity of this system is very good. However, some organic compounds, such as alcohol, acetone, mannitol,

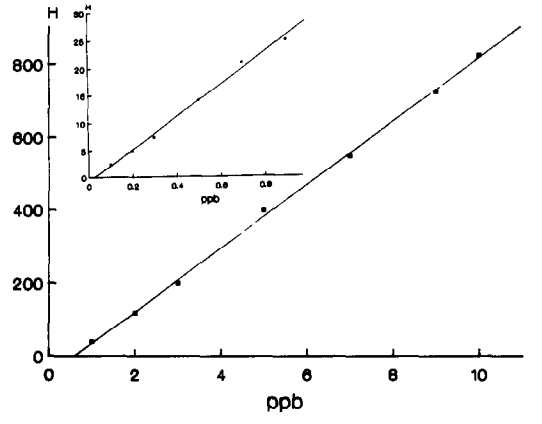

Fig. 4. Calibration curve for the determination of manganese.

Table 2. Results of the determination of manganese in bauxite

Sample	Reported value (%)	Determined value (%) 1	2	3	Average
8820015	0.223	0.25	0.25	0.24	0.25
8820024	0.1	0.14	0.14	0.14	0.14
8820025	0.11	0.14	0.14	0.13	0.14

*All the samples with the reported values were provided by The Research Centre of Geology of Fujian.

ascorbic acid, sodium acetate, added into Na_2CO_3–KOH mixed solution, decrease the CL intensity, and some cations such as V(V) (>0.4 ppm), Ta(V) (>1 ppm) and In(III) (>2 ppm), like MnO_4^-, can generate CL in this system.

Application in analytical chemistry

The proposed method can be used to determine manganese in bauxite, without any preliminary separation, and good results are obtained, as shown in Table 2.

Acknowledgements—The authors would like to express their gratitude to Drs F. F. de la Rosa and R. Escobar from the University of Seville (Spain) for helpful discussions during the preparation of this manuscript.

REFERENCES

1. L. J. Kricka and G. H. G. Thorpe, *Analyst*, 1983, **108**, 1274.
2. U. Isacsson and C. Wettermark, *Anal. Chim. Acta*, 1976, **83**, 277.
3. D. B. Paul, *Talanta*, 1978, **25**, 377.
4. A. K. Shtol's, V. K. Slepukhin, Yu. A. Kovyazin, R. D. Okunev and A. N. Sol'manov, *Tr. Ural. Politekh. Inst.*, 1971, **193**, 61; *Chem. Abstr.*, 1974, **80**, 65137w.
5. V. P. Kazakov, G. S. Parshin, R. G. Bulgakov, L. A. Khamidullina and D. D. Afonichev, *Tezisy Dokl.-knof. Anal. Khim. Radioakt. Elem.*, (B. F. Myasoedov and A. V. Davydov (eds), p.45. Ind. Nauka, Moscow, 1977; *Chem. Abstr.*, 1979, **91**, 48872s.
6. A. B. Yusov, G. S. Parshin, A. V. Mamykin, V. P. Kazakov and N. N. Krot, *Radiokhimiya*, 1983, **25**, 779; *Chem. Abstr.*, 1984, **100**, 162577d.
7. Koji Takeuchi and Takashi Ibusuki, *Kogai*, 1984, **19**, 239; *Chem. Abstr.*, 1985, **102**, 119245y.
8. D. F. Marino and J. D. Ingle Jr., *Anal. Chim. Acta*, 1981, **123**, 247.
9. I. E. Kalinichenko, *Ukr. Khim. Zh.*, 1969, **35**, 755.
10. *Idem*, *Russ. Pat.*, 252, 712, Sept. 22, 1969.
11. L. I. Dubovenko and A. P. Tovmasyan, *Ukr. Khim. Zh.*, 1971, **37**, 943.
12. W. R. Seitz and D. M. Hercules, *Intern. J. Env. Anal. Chem.*, 1973, **2**, 273.
13. J. L. Burguera and A. Townshend, *Talanta*, 1981, **28**, 731.
14. G. Zheng, Zh. Zhiqui and B. Lujiao, *Gaodeng Xuexiao Huaxue Xuebao*, 1988, **9**, 1114.
15. L. I. Dubovenko and A. P. Tovmasyan, *Zh. Analit. Khim.*, 1970, **25**, 940.

16. *Idem, Arm. Khim. Zh.*, 1970, **23**, 690.
17. A. K. Babko, L. I. Dubovenko and L. S. Mikhailova, *Sov. Prog. Chem.*, 1966, **32**, 471.
18. *Idem, Ukr. Khim. Zh.*, 1966, **32**, 614.
19. M. Yamada, S. Kamiyama and S. Suzuki, *Chem. Lett.*, 1985, **10**, 1597.
20. *Analysis of Minerals*, Laboratory of Geology of Henan, p. 122. China, 1974.
21. A. U. Khan and M. Kasha, *J. Amer. Chem. Soc.*, 1966, **88**, 1574.
22. J. Wierzchowski, D. Slawinsika and J. Slawinsiki, *Z. Phys. Chem. Neue Folge*, 1986, **148**, S 197.
23. *Gmelin Handbook of Inorganic Chemistry*, p. 17. Mangan, Teil C1, 1975.
24. M. C. R. Symons, *J. Chem. Soc.*, 1953, 3956.
25. *Idem, ibid.*, 1954, 36760.
26. *Gmelin Handbook of Inorganic Chemistry*, p. 53. Mangan, Teil C2, 1975.

Talanta, Vol. 40, No. 10, pp. 1563–1568, 1993
Printed in Great Britain.

0039-9140/93 $6.00 + 0.00
Pergamon Press Ltd

DEVELOPMENT OF A TUBULAR PERIODATE ELECTRODE FOR FLOW-INJECTION DETERMINATION OF GLYCEROL

M. CONCEIÇÃO B. S. M. MONTENEGRO and JOSÉ LUIS F. COSTA LIMA
Departamento de Química-Física, Faculdade de Farmácia, Universidade do Porto, 4000 Porto, Portugal

IVANILDO L. MATTOS, GRACILIANO OLIVEIRA NETO,* JOSÉ A. GOMES NETO and ELIAS A. G. ZAGATTO
Centro de Energia Nuclear na Agricultura, Universidade de São Paulo, 13416-000 Piracicaba SP, Brazil

(*Received* 8 *February* 1993. *Revised* 15 *April* 1993. *Accepted* 15 *April* 1993)

Summary—Periodate electrodes without inner reference solution based on tetraoctylammonium periodate plus solvent mediator (dibutyl phthalate or 2-nitrophenyl octylether) were constructed. Linear dynamic range, practical detection limit, slope, stability, selectivity coefficients, pH dependence, response time and lifetime were evaluated. A tubular version was further developed and coupled to a flow-injection system for glycerol determination in samples relevant to the industrial production of soaps, detergents and similar.

The method involves glycerol oxidation by periodate with potentiometric evaluation of its consumption. The influence of oxidizing agent concentration (10^{-5}–$10^{-2}M$ $NaIO_4$), ionic strength (0.0–1.0M Na_2SO_4) and mean resident time were investigated and the feasibility of using a single-line manifold was discussed.

The proposed system handles about 40 samples/hr, is very stable and suitable to industrial control. Results within the 1000 and 5000 mg/l range glycerol are precise (r.s.d. <0.005) and in fair agreement with conventional procedures. Baseline drift or noise is not observed and a thermostat water bath is not required. A noteworthy feature is the almost linear relationship between glycerol concentration and recorded peak height which is a consequence of combined effects of reaction kinetics and electrode Nernstian response.

Quaternary ammonium salts are frequently used as ion-exchangers in mobile carrier membrane electrodes.[1] Like these salts,[2–4] other ion-exchangers[5–8] have been reported for the preparation of periodate electrodes. As mediator solvents, nitrobenzene,[3,5] o-nitrotoluene[6] or decanol[2] have been used in conventional-shaped electrodes with internal reference solution. Elimination of the inner reference solution by direct application of the selective membrane on a conductive surface,[9] associated with the use of long-chain quaternary ammonium compounds and suitable plasticizers result in electrodes with good reproducibility, stability and response time.[10–13] Additionally, lifetimes are longer when compared with conventional electrodes.[14]

This construction process opens also the possibility of designing special devices such as microelectrodes,[15] low-volume potentiometric cells,[16] and sandwich[17] or tubular potentiometric detectors[10–12] for FIA systems. This justified the construction and evaluation of a periodate electrode without inner reference solution to be used as a flow-injection detector. Tetraoctylammonium periodate plus dibutyl phthalate or 2-nitrophenyl octylether were used as ionophore.

Oxidation by periodate is widely used in carbohydrate chemistry. The reaction proceeds at room temperature and usually takes place under mild conditions.[18] It has often been automated for sugar and glycerol determinations[18–20] and is the basis of the official method for free glycerol determination in soaps, detergents and similar.[21] Periodate consumption after glycerol oxidation has been usually estimated by titrimetry, spectrophotometry or potentiometry.[19]

For industrial control, flow analysis is worthwhile. In this context, flow injection systems become particularly attractive in view of its versatility, simplicity and suitability for large scale analyses.

The aim of this work was the development of a periodate tubular electrode and its use for the flow-injection determination of glycerol in

*Instituto de Química, Universidade Estadual de Campinas, Campinas SP, Brazil.

samples relevant to the industrial production of soaps, detergents and similar.

EXPERIMENTAL

Solutions

All solutions were prepared with de-ionized water (specific conductivity <0.1 μS/cm) and *pro analisi* reagents. Tetraoctylammonium bromide was purified by recrystalization in ethyl acetate.

Periodate solutions were freshly prepared by water dilutions of a $0.1M$ $NaIO_4$ solution which was protected from light. The glycerol stock (10.00 g/l) was iodometrically standardized[21] and the working standards within 1000 and 5000 mg/l were daily prepared in water.

Samples (bottom lixivia, industrial brine, washing solutions, and waters from evaporator/condensators) were collected in 250-ml bottles. Before dilution, they were heated (50–60°C) until clear solutions were obtained. Initial dilution was accomplished by accurately weighing 100 g of the clear solution and mixing with 500 ml water. Whenever needed, further water dilutions were performed immediately before sample injection into the flow system.

Apparatus

For performance evaluation of the conventional-shaped electrodes, a Crison 2002 potentiometer with an electrode switch and a double junction Orion 900200 reference electrode ($0.033M$ Na_2SO_4 external solution) were used.

The flow-injection system consisted of an Ismatec mp13 GJ4 peristaltic pump with Tygon pumping tubes, a home-made injector,[22] a manifold built-up with 0.8 mm (i.d.) polyethylene tubing, and a Micronal B352 potentiometer connected to a REC 61 Radiometer recorder. Alternatively, a six-port Reodyne 5020 rotary valve was used. Work and reference electrodes were assembled by means of a Perspex device.[23] The system was grounded as in early work.[24]

Electrode preparation

The ionic sensors were prepared as previously described[10–12] by adding 0.36 g tetraoctylammonium bromide plus 9.75 g dibutyl phthalate (Type I) or 4.71 g 2-nitrophenyl octylether (Type II) into 5 ml chloroform. The final mixture was shaken with six 15-ml aliquots of a $0.1M$ $NaIO_4$ solution. The aqueous phase was discarded and the chloroform was evaporated slowly in order to obtain the liquid ionophore.

For the membrane preparations, 0.18 g PVC, 6 ml tetrahydrofuran and 0.4 ml of the ionophore solution were mixed. The resulting solution was applied dropwise on the conductive surface of the conventional electrode[25] or inside the hole drilled in the conductive material of the tubular detector.[23] Drying was accomplished by leaving the electrodes at room temperature for one day. Thereafter, the electrodes were placed in contact with $0.01M$ $NaIO_4$ for at least three days, in order to achieve equilibrium of the inner reference system.

Evaluation of conventional-shaped and tubular electrodes

The conventional-shaped electrodes (Types I and II) were evaluated by using 10^{-1}–$10^{-7}M$ $NaIO_4$ solutions with ionic strength adjusted to $0.1M$ with sodium sulphate. A single line flow-injection system (Fig. 1(a)) with very low sample dispersion (volumetric fraction >0.95) was used to evaluate the response behavior of the tubular electrodes.[10–12] A 150-μl volume was injected into C carrier stream and the reaction coil was only 25 cm long.

Influence of pH between 2 and 13 was investigated for 10^{-1}, 10^{-3} and $10^{-5}M$ $NaIO_4$ by

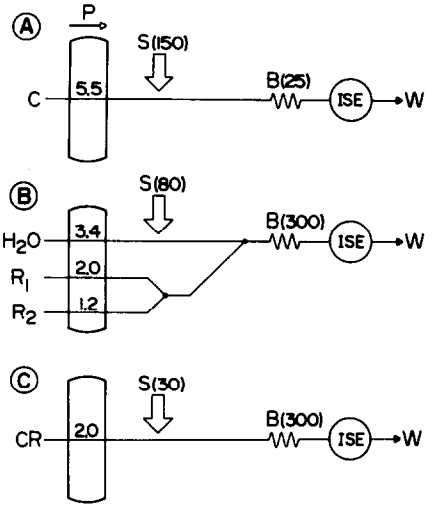

Fig. 1. Flow diagrams of the systems for evaluation of tubular electrodes (a), study of glycerol oxidation (b), and determination of glycerol (c). C = sample carrier stream with identical matrix as the injected solution; H_2O = water carrier stream; CR = combined reagent; R_1 = acetic acid/sodium acetate plus Na_2SO_4 reagent; R_2 = periodate reagent; P = peristaltic pump with flow rates in ml/min; S = sample with specifications of injected volumes, in μl; B = reactor, with specification of coil length, in cm; ISE = detector; W = waste.

Table 1. Potentiometric selectivity coefficients, log K^{Pot}. Data with standard deviations in brackets, are with reference to batch measurements carried out with periodate electrodes using dibutyl phthalate (I) or 2-nitrophenyl octylether (II) as mediator solvents

	Concentration, (M)					
	0.01		0.001		0.0001	
Interferent	I	II	I	II	I	II
Chloride	−3.97 (0.02)	−3.06 (0.04)	−2.97 (0.04)	−2.09 (0.08)	−1.90 (0.01)	−1.10 (0.10)
Nitrate	−2.63 (0.04)	−2.75 (0.03)	−2.33 (0.03)	−1.65 (0.03)	−1.75 (0.02)	−0.98 (0.05)
Bromide	−3.23 (0.05)	−2.62 (0.03)	−2.80 (0.01)	−1.94 (0.01)	−2.16 (0.04)	−1.06 (0.02)
Perchlorate	−0.20 (0.03)	+0.014 (0.003)	−0.41 (0.02)	+0.009 (0.008)	−0.23 (0.01)	+0.03 (0.02)
Iodide	−0.08 (0.02)	−3.08 (0.01)	−0.25 (0.01)	−1.67 (0.01)	+0.34 (0.02)	−0.54 (0.01)
Sulphate	−4.89 (0.03)	−5.19 (0.17)	−5.15 (0.04)	−5.28 (0.09)	−5.14 (0.04)	+5.32 (0.13)

simultaneously recording potential and pH variations after dropwise additions of sulfuric acid or sodium hydroxide solutions.

Interferences due to foreign ions (Table 1) were evaluated with the method of separated solutions[26] for 10^{-2}, 10^{-3} and $10^{-4}M$ in both periodate and interfering ions. Since iodate was formed after glycerol oxidation, its interference was also evaluated by injecting different iodate solutions (10^{-3}–$10^{-1}M$) into the 1(a) flow-injection system furnished with Type I tubular electrode. In this experiment, a slow confluent stream (0.4 ml min^{-1}) was used to add different periodate (10^{-6}–$10^{-4}M$) and sodium sulphate ($0.33M$) concentrations. The possibility of injecting concentrated glycerol was investigated within the 10^{-3}–$10^{-1}M$ range.

Determination of glycerol

The system of Fig. 1(b) with a Type I flow-through electrode was used to investigate the main parameters involved in the automated determination of glycerol. Glycerol standards within the 100.0–500.0 mg/l range were used. After sample injection, buffer and periodate reagents were added, allowing glycerol oxidation to proceed in the main reactor under buffered conditions and constant ionic strength. The passage of the sample zone through the detector resulted in a transient increase in measured potential recorded as a peak proportional to the glycerol content in the sample.

Influence of periodate concentration (10^{-5}–$10^{-2}M$), pumping speed (25, 50, 75 and 100% flow rates relative to Fig. 1(b)), ionic strength (0.0–1.0M Na_2SO_4 in R_1) and pH for glycerol oxidation were studied.

Subsequently, the system was simplified to a single line configuration (Fig. 1(c)). The sample volume was reduced to about 30 μl (6-cm sampling loop), the carrier stream was a combined reagent ($0.003M$ $NaIO_4$ plus $0.5M$ Na_2SO_4 plus $0.1M$ acetic acid $+0.1M$ sodium acetate) and the reactor length was selected as 300 cm. With this simplified system, the samples were run and the analytical characteristics evaluated.

RESULTS AND DISCUSSION

Response behavior of conventional-shaped and tubular electrodes to periodate

Regardless of the electrode configuration, the lower limit of linear response was always about $5.10^{-5}M$ periodate. During an 8 hr working period, variations of potential observed for 10^{-4}–$10^{-1}M$ IO_4^- were less than 0.2 mV. This means a baseline without any significant drift in the flow-injection systems.

Within this concentration range, the response of the conventional-shaped electrode was very fast: after doubling periodate concentration, equilibrium was attained in less than 2 sec. The dynamic response of the tubular electrode based on 2-nitrophenyl octylether was checked by using 10^{-1} and $10^{-3}M$ IO_4^- (also $0.1M$ Na_2SO_4) intermittent streams at 2.0 ml min^{-1} merging 10 cm from the detector. After switching the injector, the intermittent streams were interchanged.[22] Transition time between recorded steady state signals was about 2 sec, emphasizing the feasibility of this tubular electrode as a flow-injection detector. Studies concerning the use of this detector as a relocating sensor[27] are presently in progress.

Nernstian response (60.5 ± 0.2 mV/decade—Type I; 57.4 ± 0.3 mV/decade—Type II) was observed for both electrodes. Because of the low response times, similar slopes were calculated for tubular and conventional-shaped electrodes.

For $3.0 < pH < 7.5$, pH has no pronounced influence on electrode potential (Fig. 2) regardless of the electrode configuration. This is in

close agreement with predicted values based on calculations including periodate speciation.[2] This pH range is broad enough for analytical applications of this electrode, and permits measurements to be performed under good conditions at pH = 4.7, the recommended acidity for the present procedure.[19,20,28]

Selectivity data related to conventional-shaped electrodes are shown in Table 1. Data gathered in batch conditions were similar to those obtained in a flow-injection system with limited dispersion, emphasizing that the concentration reaching the detector was practically that of the injected solution and kinetic aspects were not relevant. Table 1 is globally better when compared to already reported values,[2,3,5,6,8] especially with regard to sulphate. Sodium sulphate was then elected to provide ionic strength adjustment in the experiments for electrode evaluation and further analytical application. Although periodate electrodes suffer from severe perchlorate interference, selectivity coefficients towards perchlorate were lower than the reported values.

The electrodes can be used for periodate monitoring in the presence of iodate formed after the glycerol oxidation since pK^{Pot} was determined as *ca.* $^{-4}$. Higher glycerol concentrations should be avoided, if higher than $0.1M$, membrane deterioration was observed, probably due to reduction of periodate ion constituents of the membrane. Since the drawback was not observed for glycerol concentrations $<0.01M$ under flow conditions, the flow-injection system was designed with large dispersion.

Determination of glycerol

The acetic/acetate buffer system was elected after considering the electrode operating plateau (Fig. 2) and the faster glycerol oxidation at pH about 4.7. No alterations in the behavior of the Type I tubular electrode in the presence of this buffer system were observed. As a consequence, the lower limit of linear response was maintained.

Periodate concentration was an important parameter in the procedure for glycerol determination. With a concentration lower than $10^{-5}M$ in the 1(b) flow system, the baseline was noisy and recorded peak heights were not measurable because the remaining periodate concentration approached the practical limit of detection. The time interval between peak maximum and baseline restoration was unacceptably high (>20 sec). For periodate concentrations within the 10^{-4}–$10^{-1}M$ range, baseline noise was about ± 0.2 mV (exception for $IO_4^- = 10^{-4}M$, see Fig. 3), washing time reached a constant value of 11 sec, and the tendency for linearization of the relation between glycerol concentration and recorded peak height was observed (Fig. 3). This was due to the combination of Nernstian response of the electrode and kinetics of glycerol oxidation which, in the initial development steps, tends to be of first order relatively to periodate.[19] Better linearity ($r > 0.99$) was observed for $IO_4^- = 3.0 \times 10^{-3}M$. For periodate concentrations higher than $10^{-2}M$, linearity decreased and lower peaks were recorded (Fig. 3). In this situation, glycerol concentrations were very low relative to periodate, so that the relative oxidant consumption underwent a pronounced reduction. Also, an oscillating baseline was observed, probably due to inefficient mixing conditions associated with the fast electrode response.

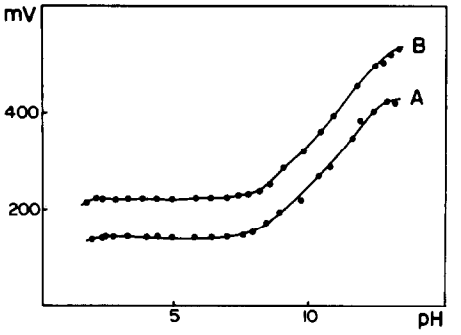

Fig. 2. Influence of pH on electrode potential. Reilley diagrams refer to Type I (a) and Type II (b) conventionally-shaped electrodes on a $10^{-3}M$ $NaIO_4$ solution.

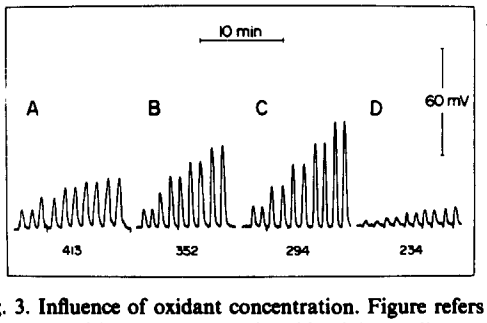

Fig. 3. Influence of oxidant concentration. Figure refers to (b) system with $R_1 = 0.1M$ acetic acid + $0.1M$ sodium acetate plus $0.1M$ sodium sulfate. A, B, C and D correspond to periodate concentrations of 10^{-4}, 10^{-3}, 10^{-2} and $10^{-1}M$ in R_2. From left, recorded peaks correspond to 100.0, 200.0, 300.0, 400.0 and 500.0 mg glycerol/l. Numbers refer to baseline potentials, in mV.

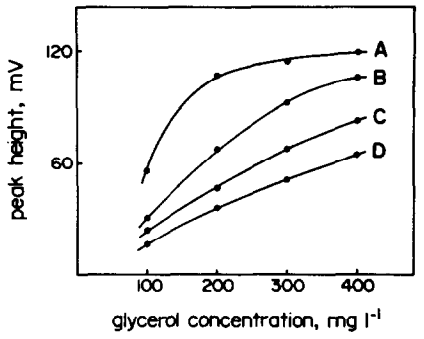

Fig. 4. Influence of pump speed. A, B, C and D correspond to 25, 50, 75 and 100% of flow rates specified in Fig. 1(b).

Sensitivity was very dependent on peristaltic pump speed which was proportional to the mean sample residence time (Fig. 4). However, this parameter could not be selected at will since linearity of the calibration curve was also affected by variations in mean available time for glycerol oxidation. The flow rates for the 1(b) system were then selected as a compromise between sensitivity, sampling rate and linearity of the calibration plot.

The 1(b) system is remarkably stable and suitable for glycerol determination in lixivia and similar up to 500.0 mg/l. As large dispersion is involved, variations in ionic strength of the injected solution within 0.0 and 0.5*M* are not relevant. Also, when sample alkalinity varied within the 0.1–0.5*M* NaOH range, slight variations (<5%) in peak heights were observed. When placed under a climatized ambient with temperature variations lower than about 5°C per day, a thermostat water bath is not required. The system can then be applied to soap analysis without restrictions.

After defining reagent concentrations, and studying the relevance of the main parameters and involved dispersions, a single-line system was designed. With this system (Fig. 1(c)), 40 samples are run/hr, corresponding to a consumption of 1.8 mg $NaIO_4$ per determination. Reproducible results (s.d. <0.2 mV) were achieved and baseline drift was not observed (see also Fig. 5) which in turn also confirms the stability of the periodate reagent. Accuracy can be assessed from Table 2.

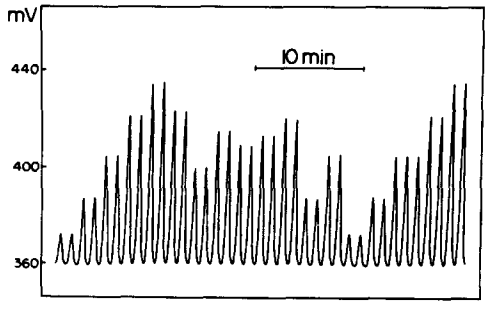

Fig. 5. Recorder output of a routine run carried out with the 1(c) system. From left, duplicate measurements of five glycerol standard solutions (1000, 2000, 3000, 4000 and 5000 mg/l), eight lixivia and the standards again.

Table 2. Comparative results. Glycerol contents in lixivia (in % w/v) as determined by the proposed system of Fig. 1(c) (FIA) and by iodometric titration[21] (AOCS). Standard deviations related to FIA values are always lower than 0.5% (see also Fig. 5) and related to AOCS are usually *ca.* 1%

Sample	FIA	AOCS
1	34.1	32.3
2	26.0	27.0
3	34.3	*
4	31.5	31.2
5	26.2	27.4
6	37.8	35.4
7	29.0	32.7
8	29.4	29.6

*Unavailable data.

The tubular electrode is being used for routine purposes in the last three months, with no pronounced variations in slope, baseline potential or response time.

Acknowledgements—This work was linked to a Luso-Brazilian Collaborative Project involving Junta Nacional de Investigação Científica e Tecnológica (JNICT), Conselho Nacional de Desenvolvimento Científico e Tecnológico (CNPq) and Commission of the European Communities (contract CI1*–CT92-0052). Authors thank the STRIDE program. Belmira Pereira is thanked for laboratorial support, and Gessy Lever Co, Valinhos SP (Brazil) for supplying analyzed samples.

REFERENCES

1. R.-Q. Yu, *Ion-Selective Electrode Rev.*, 1986, **8**, 153.
2. J. L. F. C. Lima and A. A. S. C. Machado, *Rev. Port. Quim.*, 1978, **20**, 70.
3. M. Kudoh, M. Kataoka and T. Kambara, *Talanta*, 1980, **27**, 495.
4. R.-Q. Yu, Y.-P. Feng, W.-W. Huang and Z.-Y. Guo, *Chem. J. Chin. Univ.*, 1984, **5**, 169.
5. S. S. M. Hassan and M. M. Elsaied, *Analyst*, 1987, **112**, 545.
6. A. K. Jain, M. Jahan and V. Tyagi, *Analyst*, 1989, **114**, 1155.
7. J. Pan, F. Hao, *Fenxi Huaxue*, 1982, **10**, 469.
8. M. A. F. Elmosalmy, G. J. Moody and J. D. R. Thomas, *Anal. Lett.*, 1987, **20**, 1541.
9. J. L. F. C. Lima and A. A. S. C. Machado, *Analyst*, 1986, **111**, 799.

10. J. L. F. C. Lima, M. C. B. S. M. Montenegro, J. Alonso, J. Bartroli and J. G. Raurich, *J. Pharm. Biom. Anal.*, 1989, **7**, 1499.
11. J. L. F. C. Lima, M. C. B. S. M. Montenegro, J. Alonso, J. Bartroli and J. G. Raurich, *Anal. Chim. Acta*, 1990, **234**, 221.
12. J. L. F. C. Lima, M. C. B. S. M. Montenegro and A. M. R. Silva, *J. Pharm. Biom. Anal.*, 1991, **9**, 1041.
13. R. C. Pereira, L. M. Aleixo, O. E. S. Godinho and G. Oliveira No, *Quim. Nova*, 1990, **13**, 202.
14. G. J. Moody, J. D. R. Thomas, J. L. F. C. Lima and A. A. S. C. Machado, *Analyst*, 1988, **113**, 1023.
15. S. A. H. Khalil, G. J. Moody, J. D. R. Thomas and J. L. F. C. Lima, *Analyst*, 1986, **111**, 611.
16. J. L. F. C. Lima and A. A. S. C. Machado, *Quim. Nova*, 1987, **10**, 137.
17. S. Alegret, J. Alonso, J. Bartroli, J. L. F. C. Lima, A. A. S. C. Machado and J. M. Paulis, *Anal. Lett.*, 1985, **18**, 2291.
18. J. M. Bobbitt, *Adv. Carbohydr. Chem.*, 1956, **11**, 1.
19. E. A. G. Zagatto, I. L. Mattos and A. O. Jacintho, *Anal. Chim. Acta*, 1988, **204**, 259.
20. J. J. B. Nevado and P. V. González, *Analyst*, 1989, **114**, 989.
21. A. O. C. S. *Tentative Method Da 23–56* (amended 1959).
22. F. J. Krug, E. A. G. Zagatto and H. Bergamin Fº, *Anal. Chim. Acta*, 1986, **179**, 103.
23. J. L. F. C. Lima, M. C. B. S. M. Montenegro and A. M. R. Silva, *J. Flow Injection Anal.*, 1990, **7**, 19.
24. S. Alegret, J. Alonso, J. Bartroli, A. A. S. C. Machado, J. L. F. C. Lima and J. M. Paulis, *Quim. Anal.*, 1987, **6**, 278.
25. R. A. S. Lapa, J. L. F. C. Lima and A. M. R. Silva, *Il Farmaco*, 1990, **45**, 901.
26. Commission on analytical nomenclature, recommendations for nomenclature of ion-selective electrodes, *Pure Appl. Chem.*, 1976, **48**, 129.
27. E. A. G. Zagatto, H. Bergamin Fº, S. M. B. Brienza, M. A. Z. Arruda, A. R. A. Nogueira and J. L. F. C. Lima, *Anal. Chim. Acta*, 1992, **261**, 59.
28. I. L. Mattos and E. A. G. Zagatto, *Quim. Anal.*, in press.

Talanta, Vol. 40, No. 10, pp. 1569–1573, 1993
Printed in Great Britain.

0039-9140/93 $6.00 + 0.00

A REVERSIBLE OPTODE MEMBRANE FOR PICRIC ACID BASED ON THE FLUORESCENCE QUENCHING OF PYRENE

HUI-HUI ZENG, KE-MIN WANG, CHENG-LIN LIU and RU-QIN YU*
Department of Chemistry and Chemical Engineering, Hunan University, Changsha, 410082, People's Republic of China

(*Received* 8 *February* 1993. *Accepted* 23 *March* 1993)

Summary—Pyrene immobilized in plasticized poly(vinyl chloride) (PVC) membrane is able to extract selectively picric acid from the sample solution into the organic membrane phase. Since this extraction equilibrium is accompanied by a change in the fluorescence spectrum of pyrene, the chemical recognition process can be directly translated into an optical signal. With the optode membrane described, picric acid in sample solutions from 8.7×10^{-6} to $4.3 \times 10^{-3} M$ can be determined. The calibration curve of the optode membrane for picric acid shows a good correlation with the mathematically derived formalism and thus confirms the theoretically expected behaviour. Besides a high reproducibility of the optical signals, the very short response times less than 35 sec are realized. The optode membrane presented exhibits good selectivity for picric acid over many other usual hydrophobic anions.

Picric acid, 2,4,6-trinitrophenol, is an important organic acid. The classical chemical method,[1] ultra-visible spectrophotometry,[2] gas chromatography methods[3] have been used for picric acid determination. These methods demand a cumbersome pretreatment of the sample solution and require expensive instrumentation. Potentiometry with ion-selective electrodes (ISEs)[4–7] has been applied and shows some remarkable advantages over other methods in the area of pharmaceutical analysis[8,9] and biological chemical determination.[10,11] Since picric acid ion-selective electrodes are generally based on classical ion-exchangers, their inherent selectivity pattern may cause interference problems. The selectivity of classical anion exchangers is governed by lipophilicity of the anions. It is a function of hydration energies of these anions and follows the Hofmeister sequence.[12,13] Careful consideration has to be given to potential interferences from SCN^- and ClO_4^-. Recently, the optical chemical sensor (optodes or optrodes) has become a rapidly expanding area of analytical chemistry.[14] Optodes for a variety of analytes have been reported.[15,16] Jian and Seitz have developed a fluorescent membrane for detection of organic nitro compounds,[17] in which pyrenebutyric acid is incorporated into a plasticized cellulose triacetate matrix. In this paper, a new optode membrane for the determination of picric acid is described. The optode membrane incorporates a polycyclic aromatic compound pyrene in a plasticized PVC matrix. Because the interaction between pyrene and picric acid is not controlled by the Hofmeister sequence, the interference of lipophilic anions such as SCN^- and ClO_4^- can be largely overcome.

*Author for correspondence.

THEORY

Pyrene is one of the polycyclic aromatic hydrocarbons which can emit strong fluorescence. After being immobilized in a plasticized PVC membrane, pyrene can selectively extract picric acid from the aqueous phase into the organic membrane phase to form the non-fluorescence ground state complex.[20] Figure 3 shows the fluorescence spectra of the optode membrane incorporating pyrene exposed to $1.9 M$ sulphuric acid solution containing different concentrations of picric acid. Fluorescence intensity measurements of the optode membranes were made at an excitation wavelength of 338 nm and an emission wavelength from 350 to 550 nm. The fluorescence intensity of the membrane decreased while the concentration of picric acid increased. It illustrates that the optode membrane can indeed be used to sense picric acid in sample solutions.

If the complex equilibrium between pyrene in the plasticized PVC membrane phase (org) and picric acid in the aqueous sample solution (aq) will form $m:n$ ground state complex, the overall equilibrium is described as follows:

$$m\mathrm{P(aq)} + n\mathrm{A(org)} = \mathrm{P}m\,.\,\mathrm{A}n\,\mathrm{(org)} \quad (1)$$

where P represents picric acid and A represents pyrene. The corresponding equilibrium constant K depends on the law of mass action:

$$K = \frac{{}^{a}\mathrm{P}_m\,.\,\mathrm{A}_n\mathrm{(org)}}{a^{m}_{\mathrm{P(aq)}} \times a^{n}_{\mathrm{A(org)}}} \quad (2)$$

where ${}^{a}\mathrm{P}_m\,.\,\mathrm{A}_n, a_{\mathrm{P}}, a_{\mathrm{A}}$ are the activities of respective species.

The following equilibrium was involved between the membrane and aqueous phases:

$$m\mathrm{P(aq)} = m\mathrm{P(org)} \quad (3)$$

$$m\mathrm{P(org)} + n\mathrm{A(org)} = \mathrm{P}m\,.\,\mathrm{A}n\,\mathrm{(org)} \quad (4)$$

$$k_{\mathrm{d}} = \frac{{}^{a}\mathrm{P(org)}}{{}^{a}\mathrm{P(aq)}} \quad (5)$$

$$\beta = \frac{{}^{a}\mathrm{P}_m\,.\,\mathrm{A}_n\mathrm{(org)}}{a^{m}_{\mathrm{P(org)}} \times a^{n}_{\mathrm{A(org)}}} \quad (6)$$

where k_{d}, β are the distribution coefficient and complex formation constant, respectively. If the difference between the activities and concentrations is neglected, one can write:

$$K = \frac{[\mathrm{P}_m\,.\,\mathrm{A}_n]_{\mathrm{(org)}}}{[\mathrm{P}]^{m}_{\mathrm{(aq)}} \times [\mathrm{A}]^{n}_{\mathrm{(org)}}} = k_{\mathrm{d}} \times \beta \quad (7)$$

where $[\mathrm{P}_m\,.\,\mathrm{A}_m]$, [P], [A] are the concentrations of the respective species. As the concentration of the undissociated picric acid is pH dependent, the acidity of the test solution should be kept constant.

The relative fluorescence value α (*vide infra*) equals the ratio of the concentration of free pyrene, [A], to the total amount of pyrene, C_{A}:

$$\alpha = [\mathrm{A}]/C_{\mathrm{A}} \quad (8)$$

α is shown to depend on the concentration of picric acid in aqueous sample solution, [P], as follows:

$$\frac{\alpha^{n}}{1-\alpha} = \frac{1}{(nKC_{\mathrm{A}}^{n-1}[\mathrm{P}]^{m})} \quad (9)$$

The relationship between α and [P] as expressed by equation (9) is the basis of quantitative determination of picric acid using this optode membrane.

EXPERIMENTAL

Apparatus

Fluorescence was measured using a Hitachi M-850 fluorescence spectrometer with a specially designed flow-through measuring cell similar to the device described elsewhere (*vide infra*).[18] Data processing were carried out on a Macintosh II computer.

Reagents

Pyrene (A.R; Aldrich), poly(vinyl chloride) (high molecular weight; Fluka Selectophore), bis(2-ethylhexyl)sebacate (C.P; Shanghai Chemical Reagent Corporation) and tetrahydrofuran (A.R; Shanghai Chemical Reagent Corporation) were used for membrane preparation.

The $1 \times 10^{-2}M$ stock solution of picric acid was prepared by dissolving 11.45 g of picric acid (recrystallized twice) in 500 ml of distilled water. The actual concentration of picric acid was determined by titration with sodium hydroxide standard solution. The picric acid solution of other concentrations were obtained from the stock solution by dilution with $1.9M$ sulphuric acid.

Membrane preparation

The optode membranes were prepared from a mixture of 2 mg of pyrene, 50 mg of PVC and 100 mg of bis(2-ethylhexyl)sebacate. The membrane components were dissolved in 2 ml of freshly distilled THF. A circular 35-mm diameter quartz plate was mounted on the end of an aluminum alloy rod which was rotating at high constant speed. From a syringe, 0.2 ml of the THF solution was injected to the central point of the plate. After a spinning time of only about 4 sec (rotating frequency, 600 rpm) two membranes of approximately 4-μm thickness were cast onto two 35-mm diameter quartz plates.[19]

Procedure

Two identical membranes on their respective plates were mounted in the special flow-through measuring cell (Fig. 1). The volume capacity of the cell was *ca.* 3.4 ml. The cell was introduced into the fluorescence spectrometer in an appropriate position (Fig. 2) to guarantee the detection of the intensity of fluorescence emission without interference from the excitation source.

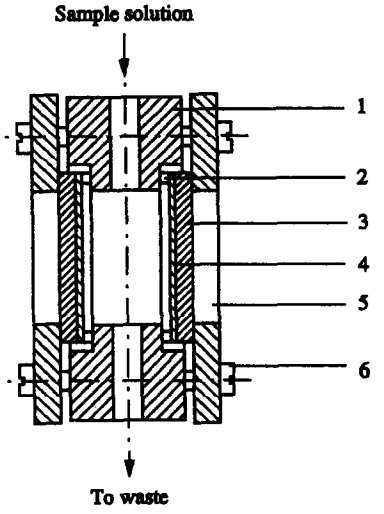

Fig. 1. Schematic representation of the flow-through cell.
1. Poly(propylene) support with sample inlet and outlet.
2. O-ring seal.
3. Quartz glass support.
4. Optode membrane.
5. Plexiglas cell wall.
6. Screw for fixation.

About 3 ml of sample solution was introduced and the fluorescence intensity F was measured. The membrane was washed with the blank solution not containing picric acid until the fluorescence intensity (F_1) was stabilized. The limiting fluorescence intensity (F_0) for the case of complete complexation of pyrene in the membrane with picric acid was taken as zero. The relative fluorescence value α was calculated according to following formula:

$$\alpha = \frac{(F - F_0)}{(F_1 - F_0)} = \frac{F}{F_1} \qquad (10)$$

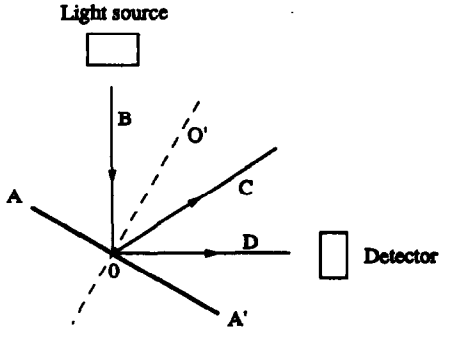

Fig. 2. Position of the optode membrane on the fluorescence spectrophotometer.
AA, Quartz glass plates with optode membranes
BO, Excitation beam from light source
OC, Normal beam
OD, Emission beam to light detector.

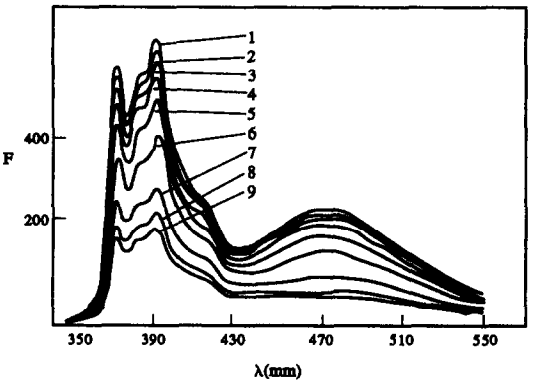

Fig. 3. Effect of picric acid on the extent of quenching.
1. blank solution
2. 2.14×10^{-6}
3. 8.54×10^{-6}
4. 2.14×10^{-5}
5. 4.27×10^{-5}
6. 8.54×10^{-5}
7. 2.14×10^{-4}
8. 3.42×10^{-4}
9. $4.27 \times 10^{-4} M$ picric acid.

RESULTS AND DISCUSSION

Composition of the ground state complex

From equation (9), it is known that when the stoichiometric ratio of the ground state-complex changes, the relative fluorescence valued α has different functional relation with the concentration of picric acid. The experimental data were fitted to equation (9) by changing the ratio of m to n and adjusting the overall equilibrium constant K. The result showed that the curve (4) was the best one to represent the experimental data (Fig. 4). In other words, the complex ratio of picric acid to pyrene in the optode membrane should be 1:2. The actual

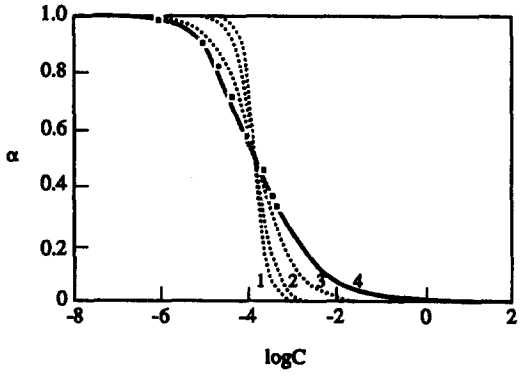

Fig. 4. Fitting the experimental data to equation (9).
$C_A = 5.3 \times 10^{-2} M$
1. $m:n = 3:1$, $K = 3.31 \times 10^{11}$
2. $m:n = 2:1$, $K = 4.78 \times 10^{7}$
3. $m:n = 1:1$, $K = 6.9 \times 10^{3}$
4. $m:n = 1:2$, $K = 1.3 \times 10^{5}$ (best fit).

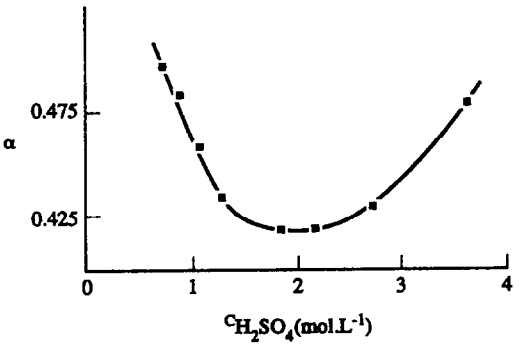

Fig. 5. Effect of acidity.

ratio of picric acid to pyrene was determined independently with molar ratio method in solutions by using dichloromethane as solvent. The results showed the ratio of picric acid to pyrene was 1:2, in exact agreement with the ratio obtained by curve fitting of the membrane fluorescence data. The curve (4) can serve as the calibration curve to determine the concentration of picric acid. It is clear that a sufficient response to picric acid is obtained from 8.7×10^{-6} to $4.3 \times 10^{-3}M$.

Effect of the acidity

Figure 5 shows the effect of acidity on the relative fluorescence value α of the optode membrane. The fluoresence intensity measurements were made for $3.6 \times 10^{-4}M$ picric acid in sulphuric acid solutions of different concentrations. With the increase of the concentration of sulphuric acid, the extent of picric acid ionization is reduced to increase the concentration of picric acid in the membrane. And therefore the ratio of the concentration of free pyrene to the total amount of pyrene, α, will be decreased. After the acidity reaches a relative high value, the ionization of picric acid will be completely inhibited so that the α value remains constant. On the other hand, too high acidity seems unfavourable to the extraction of picric acid from aqueous solution into the membrane phase, the α value will decrease with further increase of the acidity. It has been shown that the optode membrane has a better and constant response to picric acid in sulphuric acid solutions from 1.8 to $2.2M$.

Reproducibility and response time

Figure 6 shows the fluorescence intensity response *vs* time recordings for the picric acid optode membrane when it was exposed to repeated concentration step changes between 8.5×10^{-6} and $8.5 \times 10^{-5}M$ picric acid in $1.9M$ sulphuric acid solution. The results show a remarkably high reproducibility of the optical signals. The mean fluorescence intensity values with standard deviations were found to be 313.9 ± 1.2 ($n = 5$, $8.5 \times 10^{-6}M$ picric acid) and 206.4 ± 0.4 ($n = 5$, $8.5 \times 10^{-5}M$ picric acid). From this figure, it can also be seen that the response times of the optode membrane are less than 35 sec.

Lifetime

The fluorescence signal at a wavelength of 394 nm for the optode membrane in contact with a $4.3 \times 10^{-4}M$ picric acid in $1.9M$ sulphuric acid solution was recorded over a period of 6 hr. From fluorescence intensity values taken every 30 min ($n = 12$) a mean value of 110.0 and a standard deviation of ± 0.4 were obtained. It is shown that pyrene is not washed out significantly during this period of time. The fluorescence signal of the optode membrane at 394 nm dropped by 4% during the measurement of sample solutions over a week.

Selectivity

With the concentration of picric acid fixed at $3.6 \times 10^{-4}M$, there is no influence on the fluorescence signal of the optode membrane when less than $10^{-2}M$ potassium perchlorate and sodium thiocyanate exist. This shows the sensing device has much better selectivity over hydrophobic anions compared with picric acid ion-selective electrodes. Organic acids and inorganic salts, such as *o*-phthalic acid, benzonic acid, phenol, *o*-chlorophenol, sodium fluoride and mercury dichloride, at concentrations less than $10^{-1}M$ do not interfere with the determi-

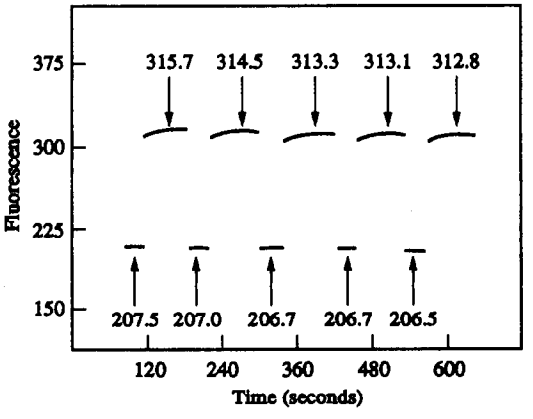

Fig. 6. Fluorescence intensity response *vs* time at 349 nm after several repeated concentration step changes.

nation. But when the concentrations of the nitrophenols, whose structures are similar to picric acid, at concentration levels one order of magnitude higher than the concentration of picric acid in sample solution, will quench the fluorescence signal of the optode membrane to some degree. The sequence of selectivity is picric acid > 2,4-dinitrophenol > *p*-nitrophenol > *o*-nitrophenol > *m*-nitrophenol.

Application

Since picric acid can react quantitatively with some drugs such as cinchonine and quinine to form insoluble precipitates, the optode membrane can be applied to the indirect determination of these drugs. The determination of cinchonine in drug samples, for example, was carried out by following the procedure. About 4 g of sample was dissolved in $0.014M$ sulphuric acid to make a 500-ml solution. To this solution, 100 ml of $4.27 \times 10^{-2}M$ picric acid was added while stirring. The solution was filtered and the filtrate was diluted to appropriate concentration. The picric acid content in filtrate was determined by using the fluorescent membrane. For $2.14 \times 10^{-2}M$ cinchonine, the measured mean concentration was $2.16 \times 10^{-2}M$. Seven repeated measurements for different aliquots from the sample solution gave a standard deviation of $2 \times 10^{-4}M$. A similar procedure was applied to the determination of quinine. For $1.08 \times 10^{-2}M$ quinine, the measured concentration was $(1.07 \pm 0.02) \times 10^{-2}M$ (seven measurements).

Acknowledgements—The work described in this paper was supported by the National Science Foundation of China and the Chinese National Educational Committee Science Foundation for Excellent Young Teachers.

REFERENCES

1. P. R. W. Baker, *Analyst*, 1954, **79**, 289.
2. M. Tarasiewiccz and H. Basinska, *Talanta*, 1974, **21**, 425.
3. S. S. Cheng and J. X. Wang, *Environ. Sci.*, 1985, **6**, 71.
4. T. P. Hadjiioannou and E. P. Diamandis, *Anal. Chim. Acta*, 1977, **94**, 443.
5. E. P. Diamandis and T. P. Hadjiioannou, *ibid.*, 1981, **123**, 143.
6. J. H. Pan, M. W. He and Y. M. Liu, *Chinese Journal of Analytical Chemistry*, 1983, **11**, 518.
7. Z. Y. Hu, X. X. Qian, J. Z. Chen, X. L. Yang and Q. Yuan, *Acta Chim. Sin.*, 1981, **39**, 719.
8. E. P. Diamandis and T. P. Hadjiioannou, *Anal. Chim. Acta*, 1981, **123**, 341.
9. Z. W. Zeng and Y. L. Tian, *Chinese Journal of Analytical Chemistry*, 1988, **16**, 743.
10. E. P. Diamandis, D. S. Papastathopoulos and T. P. Hadjiioannou, *Clin. Chem.*, 1981, **27**, 427.
11. E. P. Diamandis, M. A. Koupparis and T. P. Hadjiioannou, *Microchem. J.*, 1977, **22**, 498.
12. F. Hofmeister, *Arch. Exp. Pathol. Pharmacol.*, 1888, **24**, 247.
13. K. M. Wang and Y. Q. Yu, *Acta Chim. Sin.*, 1988, **46**, 1087.
14. W. R. Seitz, *CRC Crit. Revs. in Anal. Chem.*, 1989, **19**, 135.
15. H. H. Zeng, K. M. Wang, Z. Qin and Y. Q. Yu, *Chemical Journal of Chinese Universities*, 1993, **14**, 180.
16. W. E. Morf, K. Seiler, B. Rusterholz and W. Simon, *Anal. Chem.*, 1990, **62**, 738.
17. C. Jian and W. R. Seitz, *Anal. Chim. Acta*, 1990, **273**, 265.
18. K. M. Wang, K. Seiler, B. Rusterholz and W. Simon, *Analyst*, 1992, **117**, 57.
19. K. Seiler and W. Simon, *Anal. Chim. Acta*, 1992, **266**, 73.
20. J. R. Lakowicz, *Principles of Fluorescence Spectroscopy*, p. 265. Plenum Press, New York, 1983.

Talanta, Vol. 40, No. 10, pp. 1575–1581, 1993
Printed in Great Britain.

0039-9140/93 $6.00 + 0.00

DETERMINATION OF NH_3 IN PYROLYSIS GASES BY AMMONIA SELECTIVE ELECTRODE

J. P. HÄMÄLÄINEN,* J. L. TUMMAVUORI† and M. J. AHO*

*Technical Research Centre of Finland, P.O. Box 221 40101 Jyväskylä, Finland
†Department of Chemistry, University of Jyväskylä, SF-40100 Jyväskylä, Finland

(*Received* 1 *December* 1992. *Revised* 29 *March* 1993. *Accepted* 22 *April* 1993)

Summary—The suitability of ion-selective electrode for the determination of ammonia in pyrolysis gases of fossil fuels was studied. The ammonia was absorbed into acidic solution and two kinds of determination methods were carried out. The ammonia was either measured directly from the acid solution, or ammonia was first released into the gas phase and then determined (air gap method) by the ammonia selective electrode. The electrode functioned well in both cases, but the linear calibration range was rather narrow, slightly more than one tenfold. The quantitative detection limit in the water phase was $5 \times 10^{-6}M$ (0.085 ppm) NH_3 and in gas phase operation solutions above $5 \times 10^{-4}M$ (8.5 ppm) NH_3 it was possible to measure quantitatively. The applications were carried out with Finnish energy peat samples and a coal sample.

The combustion of fossil fuels has a number of associated environmental consequences. One of the major problems is the formation of nitrogen oxides (N_xO_y). The two major routes for the formation of N_xO_y are the fixation of atmospheric nitrogen and the conversion of fuel nitrogen itself.[1,2]

The fixation of atmospheric nitrogen goes by radical reactions:

$$O^{\cdot} + N_2 \rightarrow NO + N^{\cdot} \quad (1)$$

$$N^{\cdot} + O_2 \rightarrow NO - O^{\cdot} \quad (2)$$

These reactions are sensitive to temperature, and therefore important at higher temperatures (>1300°C). However, in modern combustion furnaces, the formation of nitrogen oxides, originating from the air, are effectively controlled by air staging, or by using lower combustion temperatures. Thus the major source of N_xO_y in flue gases is usually fuel nitrogen.

Typically fossil fuels contain ≈0.5–3 wt % nitrogen, unfortunately the distribution of nitrogen containing functional groups in fuels is not accurately known. Recent X-ray photoelectron spectroscopy (XPS) studies have shown that in high rank fuels, like coal, the nitrogen occurs principally in pyrrolic and pyridinic type heterocyclic ring moieties that constitute the organic matter. In low rank fuels, like peat, other functional groups such as amines may also be important.[3,4]

The mechanism of the formation of N_xO_y from fuel is particularly complex and still not completely understood. A simple view of the process (Fig. 1) is that the volatile nitrogeneous fragments are initially converted into compounds such as HCN and NH_3 (the most important intermediates) which can subsequently react either with oxygen to generate NO, or combine with NO itself to produce nitrogen. The reactions involving the oxidation of char-nitrogen are similar to those for volatile-nitrogen although the direct reduction of NO by carbon and the char-catalysed reduction by CO may also be important.[5]

Several new and efficient techniques exist for sampling and determination of ammonia. Diffusion scrubbers have been used for the sampling of atmospheric gases[6] such as ammonia[7] and sulfur dioxide,[8] and for the collection of gaseous hydrogen peroxide.[9] A newly developed photoacoustic spectrometer method is now available for the determination of NH_3 with a detection limit below 1 ppm.[10,11] In this study the conversion of fuel nitrogen to NH_3 and HCN was measured for several fuels. Thus simultaneous sampling of both intermediates was needed and the classical wet-chemical approach, where the sample gas is passed through absorption solution, was selected. Therefore the ammonium selective electrode was used for determination of NH_3.

The collection solution used was dilute ($0.01M$) HNO_3. Besides ammonia, many other

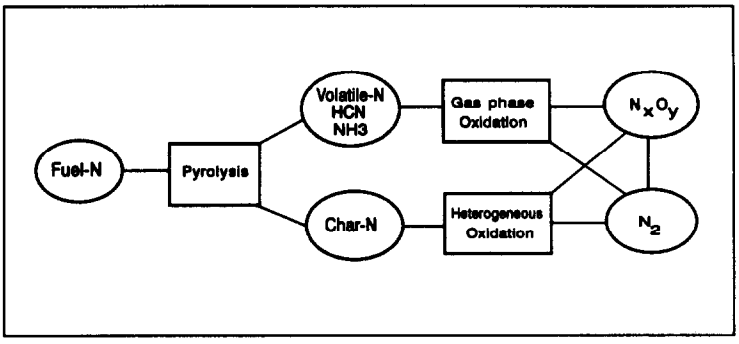

Fig. 1. Conversion of fuel nitrogen in combustion.

pyrolysis products will simultaneously be absorbed in the acidic solution, changing the composition and colour of the solution. Thus, there are only a few methods available for determining ammonia from the water phase. One possibility is the Kjeldahl method, but it is more complicated and slower than the potentiometric method. The colour of the water phase, on the other hand, is the main reason for rejecting the ordinary spectroscopic methods.

EXPERIMENTAL

NH_3-measurements

An Orion Ammonia Electrode Model 95-12 was used with an Orion mv/pH meter Model EA 920. The electrode consists of a hydrophobic gas-permeable membrane which separates the alkaline test solution from an internal solution 0.1*M* in ammonium chloride. A glass pH electrode and a silver–silver chloride reference electrode are immersed in the internal solution.[12] Electromotive force (e.m.f.) of the electrode obeys ammonia concentrations both in liquid and gas phases according to the Nernstian equation

$$E = E' + 2.3RT/F \log([NH_3]/[NH_4^+]), \quad (3)$$

where E' = standard potential, R = gas constant, T = temperature and F = Faraday constant.

The $pK_{NH_4^+}$ is 9.25. Thus the ammonia measurement must be performed in alkaline solutions at pH > 11. In gas phase operations one has to ensure that the pH is high enough for NH_3 liberation into gas phase. A 0.100*M* stock solution of ammonium chloride was made from p.a. reagent (Merck). The buffer solution (ISA) for pH adjustment contained 5*M* NaOH and 0.05*M* EDTA in 10% (v/v) methanol–water solution. Measurements were performed in a titration vessel (150 cm^3) with an air-tight cover. The electrodes and burette were also led air-tightly through the cover. In the tests with standard solution we had electrodes in each phase simultaneously. Thus it was possible to use the same test solution for simultaneous measurements of ammonia in both phases. The volume of the studied solution was 100 cm^3, so the volume of the gas phase was about 50 cm^3, 2 cm^3 ISA solution and a magnetic stirrer were used in the measurements.

Samples for application experiments

Four fuel peat samples, originally from Central and Northern Finland, and one coal sample were used. The peats were medium humified (H3–H8 by von Post) and represented the main peat constituents of Scandinavian peats: B, C and S-peats. The subsamples for pyrolysis experiments were dried, milled and sieved to a particle size of <63 μm before analysis. The main composition of samples is represented in Table 1.

Table 1. Fuel analysis (wt%)

Sample*	Ash (%)	Vol (%)	C (%)	H (%)	N (%)	O (%)	S (%)	O/N	N/C
ColCoal	7.3	40.0	81.3	5.3	1.5	11.4	0.50	7.5	0.018
CB-peat	10.6	75.0	50.8	5.4	3.2	29.8	0.22	9.0	0.063
C-peak	7.5	71.6	54.4	5.6	2.4	29.9	0.18	12.5	0.044
S-peat	4.6	72.1	55.9	5.6	1.8	31.9	0.16	17.5	0.032
LS-peat	5.9	69.0	55.6	5.4	1.6	31.2	0.35	19.5	0.028

*Coal from Colombia. Peats: C = *Carex*; B = *Bryales*; S = *Sphagnum*; L = *Woody*.

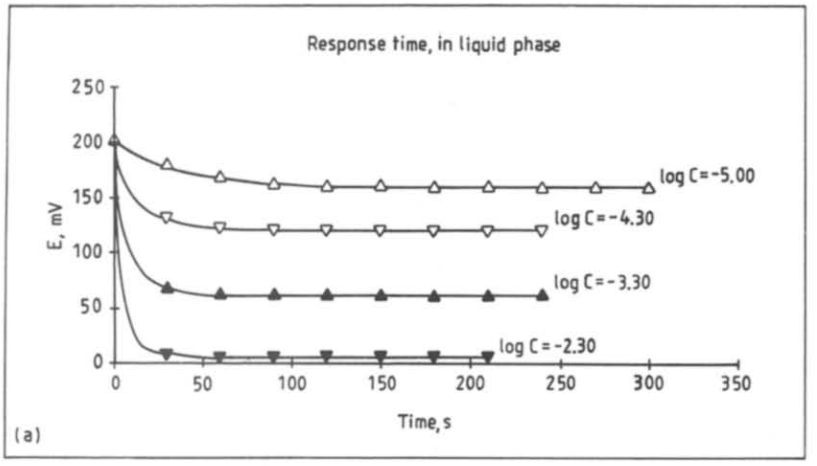

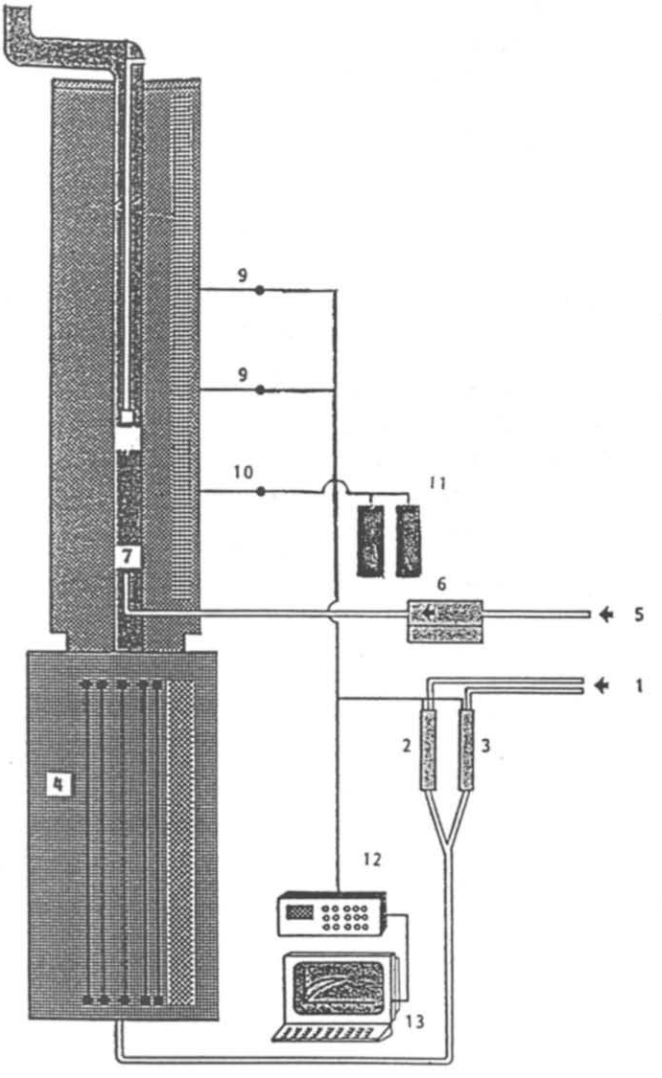

Fig. 2. Schematic diagram of entrained flow reactor: 1, source of reaction gases; 2,3, mass flow meters for air and nitrogen; 4, preheater 0–1200°C, 25 kW; 5, N_2 for fuel feeding; 6, fuel feeder; 7, quartz reactor tube ($L = 2$ m, $D = 0.1$ m); 8, insulation with observation window; 9, small suction pyrometers; 10, mobile probe for pyrolysis gas; 11, data-logger HP 3497; 12, computer HP 9845.

Reactor design and pyrolysis experiments

The fuels were pyrolysed in an entrained flow reactor. The detailed structure of the reactor has been described in Fig. 2. The incoming gas (reaction gas) was heated to the desired temperature by a preheater and the flow rate and oxygen content in the reactor were adjusted by two mass flow controllers connected to a computer. The fuel feeding rate is higher in this reactor as is the case in drop tube furnaces which makes it possible to study the formation and emissions of flue gas components.

The conversion of fuel nitrogen to ammonia was studied at 800°C. At the beginning of the reaction there was a trace of oxygen in the reaction gas but the fuel consumed the oxygen rapidly as the fuel feeding rate was quite high for this reactor (0.2 g/s). Because N_xO_y was not observed in the pyrolysis gas (measured by F.T.-ir[13]), it is evident, that the pyrolysis of the sample took place in an inert atmosphere. The pyrolysis gas sample was taken with a short mobile probe after pyrolysis. The sample line was connected with a gas washing bottle (500 cm^3), and the NH_3 was absorbed in the 300 cm^3 of 0.01M HNO_3 solution. The sampling rate was 10 dm^3/min. Because the fuel feeding rate was adjusted to be constant and the pyrolysis conditions were also unchanged it was possible to use the not continuous determination of conversion of fuel nitrogen to ammonia.

RESULTS AND DISCUSSION

The linear range of the ammonia electrode was reported to be from 1M to $5 \times 10^{-7}M$ (0.01 ppm to 17,000 ppm) NH_3.[12] Because of the low amounts of nitrogen in fuels, the ammonia concentration in the gas phase remained low. Thus a careful study of the function of the electrode both in liquid and gas phases was first required.

Response time

The response time of the electrode was studied in both phases by using several concentration levels. The results are presented in Figs 3(a) and (b). The response time was generally a function of the concentration, and the time was usually longer in the gas phase than in the liquid phase. For instance, at the concentration level of about $10^{-5}M$ of NH_3 the response time in the water phase was about 2 min and in the gas phase operation about 4 min. At high concentrations ($10^{-2}M$), the response time had a minimum value of 1.5 min in both cases.

Calibration

We calculated the concentration of ammonia according to the equation (3) and fitted the experimental results into a linear or quadratic equation using the least square calculation method:

$$E = E' + S \times pC_{NH_3}, \quad (4)$$

$$E = B + A \times pC_{NH_3} + C \times (pC_{NH_3})^2, \quad (5)$$

where E = measured e.m.f.; E' = standard e.m.f. of the studied system; S = the Nernstian slope; A,B,C = parameters of the quadratic equation; $pC_{NH_3} = -\log C_{NH_3}$.

Water phase. The values of the parameters together with the results of the statistical calculations are in Table 2. The results of equation (4) in the water phase show that E' is roughly constant, and the value of S is constant but below the theoretical value of 59.1 mV. The r-values are excellent and the values of s_A and s_B are acceptable. The value of $s_B = 0.6$ causes an error of $<3\%$ at the midpoint of the regression line. The standard error estimate (s.e.e.) shows, however, that the more narrow the range the more accurate are the results. The experimental results fitted excellently to the quadratic equation. From a statistical point of view the results are good, but there is some fluctuation in the values of the parameters between different measurements.

Concluding the measurements of ammonia in the water phase showed some curvature in calibration line over a large concentration range. Within a narrower range (about two decades) we can use linear calibration line for measurements. The use of quadratic equation for calibration is not recommendable. The quantitative detection limit is about $5 \times 10^{-6}M$ (0.085 ppm) NH_3 in the water phase.

Gas phase. The measurements of the standard curves in the gas phase were made using an air gap technique. The values of the parameters for equation (4) (in Table 2) show that neither E' nor S are constants in the series of measurements performed although the statistical values for the curves are acceptable. As in the water phase, the measured data fitted better to the quadratic equation. The variation of the slope, especially in weak solutions, might be due to the

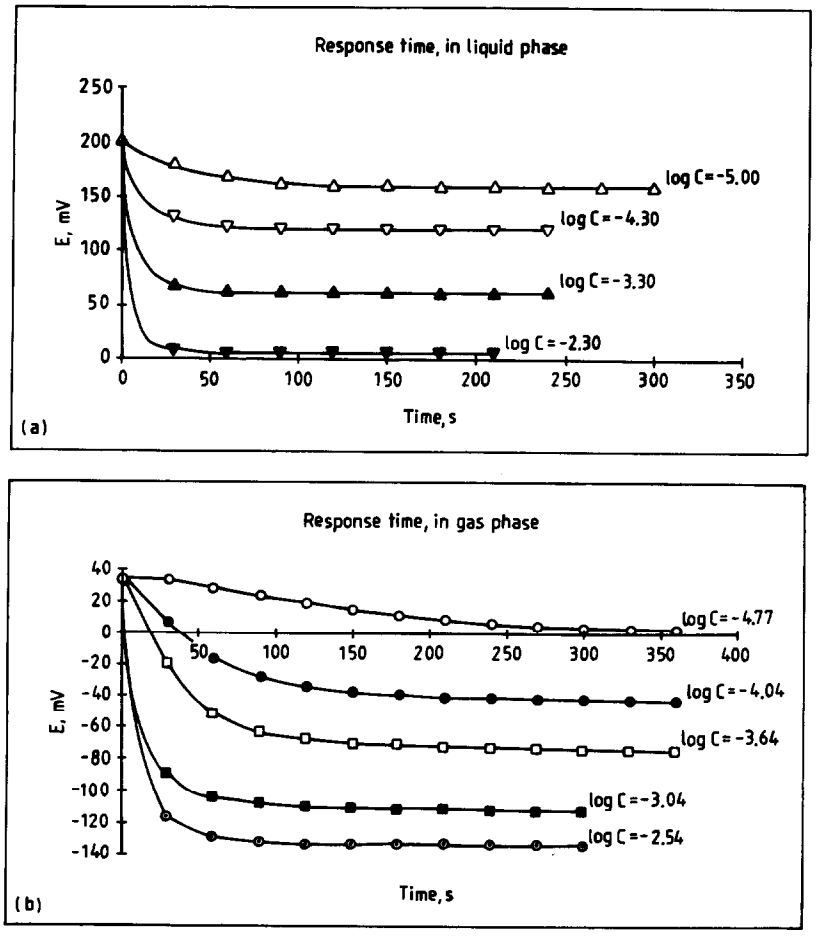

Fig. 3. Response time of the ammonia electrode in different concentrations. (a) In liquid phase; and (b) in gas phase.

fact that the ammonia concentration is low in the gas phase and the equilibrium between the electrode and the gas phase is difficult to reach in a moderate time. Because of a fluctuation in the values of the parameters between the different measurement series, a known addition technique should be used in air gap measurements. In the gas phase operation the quantitative detection limit of the electrode extends to $5 \times 10^{-4}M$ (8.5 ppm) NH_3.

Simultaneous measurements in liquid and gas phases

In these measurements two ammonium electrodes were used simultaneously: one in the liquid and the other in the gas phase. In this way random errors in the results could be minimized. The e.m.f. of the electrode was measured in both phases. Then a known amount of standard solution was added to the

Table 2. Calculated calibration curves in liquid and gas phases. Form of the equations are $E = E' + S \times pC_{NH_3}$ and the quadratic equation $E = B + A*pC_{NH_3} + C*pC_{NH_3})^2$. s_E and s_s are the standard deviations of intercept (E') and slope (S). A,B and C are parameters of quadratic equation.

Code	$-\log C_{NH_3}$	C	S	E'	$s_{E'}$	s_s	Est.error	r	n
Liq.	5.52 – 3.88	—	56.65	−137.5	3.17	0.65	0.796	0.9997	7
Liq.	5.30 – 4.32	—	56.95	−138.6	2.81	0.58	0.373	0.9998	5
Gas	3.30 – 1.70	—	64.32	−265.5	0.47	0.19	0.174	~1.000	7
Gas	5.00 – 3.70	—	57.61	−272.3	12.0	2.75	2.49	0.9955	6
Code	$-\log C_{NH_3}$	C	A	B	$s_{E'}$	s_s	est.error	r	n
Liq.	5.52 – 3.88	−2.73	82.32	−197.5	—	—	0.262	0.9999	7
Gas	5.30 – 3.70	−15.3	189.7	−554.7	—	—	0.005	0.9999	7

Table 3. Simultaneous determination of ammonia in liquid (A) and in gas phase (B)

$-\log C_{liq.}$	$-\log C_{gas}$	diff.A-B
4.060	4.033	0.027
4.041	4.020	0.021
4.021	4.040	−0.019
4.000	3.964	0.036
3.777	3.771	0.006
3.602	3.611	−0.009
3.523	3.540	−0.017
3.478	3.506	−0.028
3.301	3.315	−0.014
2.613	2.752	−0.139
2.252	2.284	−0.032

vessel and the concentrations were calculated after the change of the e.m.f. The response time used was in accordance with the gas phase. The results have been collected in Table 3.

Statistical methods were used in analysing the experimental data. Linear regression analysis showed very high regression between the liquid and gas phase operation methods: the equation being $Y = 0.132 + 0.929\ X$ with the value of $r \approx 1.000$. The slope of the equation was 0.929, which means that the air gap method gives slightly lower concentrations than direct determination from the water phase. This indicates that the slope of the electrode is higher in the gas phase than the theoretical value, and the real slope is quite difficult to measure precisely because of its fluctuation.

Generally, the statistically acceptable confidence level is $P = 0.05$ in analytical chemistry. We used the results in Table 3 to compare the accuracy of the results of the two phases by some statistical methods: The paired t-test gave $t_{calc.} = 1.39$ (critical value $t_{0.05} = 2.23$), the paired t-test for the means $t_{calc.} = 0.073$ ($t_{0.05} = 2.09$) and F-test for variances $F_{calc.} = 1.16$ ($F_{a,b} = 2.98$). All tests fulfilled the criteria above, which means that the results obtained from the different phases are the same at significance level $P = 0.05$.[14]

APPLICATION

In application experiments the conversion of fuel nitrogen into NH_3 was determined during pyrolysis at 800°C (see Fig. 1) for five fuels by using an indirect method described above. The concentrations of the sample solutions varied between $C = 5 \times 10^{-5}$–$4 \times 10^{-4} M$ (0.85–6.8 ppm) NH_3 with the peat and 1×10^{-5}–$1 \times 10^{-4} M$ (0.17–1.7 ppm) NH_3 with the coal sample. According to these results the concentration of NH_3 in the pyrolysis gas varied between 8 and 90 ppm depending on the fuel sample. The measurements were carried out using the air gap method, because peat samples have high volatile content and the water phase may thus contain interfering compounds. Ammonia was also measured directly from the sample solution in samples of low NH_3 content (coal, low volatile). The results show that there are differences in fuel nitrogen conversions between different fuels.[15]

The data can be used when studying the mechanisms of N_xO_y formation from fuel nitrogen through NH_3. Using experimental data as basic information it is possible to create kinetic models for combustion with greater accuracy. It is also possible to find evidence for existing combustion models on the basis of the experimental results.

CONCLUSIONS

In this study, the ammonia selective electrode was applied in a determination of NH_3 in pyrolysis gases. It is possible to accurately analyse dilute solutions of NH_3 with the electrode. By extending the sampling time, the sensitivity of the electrode can be increased. In addition, the electrode is available at a low price and is easy to use. The above benefits ensure that many application fields exist for NH_3 selective electrode. If the time cycle is long enough continuous detection of NH_3 is also possible. In our study the experiments did not take long and so the electrode was not suitable for ON-LINE detection because of the long response time.

REFERENCES

1. P. F. Nelson, M. D. Kelly and M. J. Wornat, *Fuel*, 1991, **70**, 403.
2. S. Wallace, K. D. Bartle and D. L. Perry, *Fuel*, 1989, **68**, 1450.
3. M. D. Kelly, A. N. Buckley and P. F. Nelson, *Int. Conf. on Coal Science*, p. 356. Butterworth-Heinemann, London, 1991.
4. M. J. Aho, J. P. Hämäläinen and J. L. Tummavuori, *Combustion and Flame* (accepted).
5. N. A. Burdett and J. W. Pye, 1987 *Int. Conf. on Coal Science*, J. A. Moulijn *et al.* (eds), p. 845. Elsevier Science Publishers B. V., Amsterdam, 1987.
6. P. K. Dasgupta, W. L. McDowell and J-S. Rhee, *Analyst*, 1986, **111**, 87.
7. Z. Genfa, P. K. Dasgupta and S. Dong, *Environ. Sci. Technol.*, 1989, **23**, 1467.
8. P. F. Lindberg and P. K. Dasgupta, *Anal. Chem.*, 1989, **61**, 19.
9. G. Zhang and P. K. Dasgupta, *Anal. Chim. Acta*. 1992, **260**, 57.

10. A. Olafsson, M. Hammerich, J. Bulow and J. Henningsen, *Appl. Phys. B.*, 1989, **B49**, 91.
11. R. Wessel, T. Theiler and F. Keilmann, *J. Quantum Electron.*, 1987, **QE-23**, 385.
12. Instruction manual for ammonia electrode, Orion Research Inc., Cambridge, 1987.
13. M. J. Aho and J. Rantanen, *Fuel*, 1989, **68**, 585.
14. J. C. Miller and J. N. Miller, in R. A. Chambers and H. Masson (eds), *Statistics for Analytical Chemistry*, Vol. 1., p. 56. John Wiley & Sons, Chichester, 1984.
15. M. J. Aho, J. P. Hämäläinen and J. L. Tummavuori, in *Fuel* (accepted).

Talanta, Vol. 40, No. 10, pp. 1583–1585, 1993
Printed in Great Britain.

0039-9140/93 $6.00 + 0.00
Pergamon Press Ltd

BOOK REVIEWS

Vibrational Spectroscopy—Methods and Applications: A. FADINI and F.-M. SCHNEPEL, Ellis Horwood, Chichester, 1989. Pages 205. £50.00, US$85.00.

This book of 205 pages is a translation from German. It consists of five parts comprised of 24 short chapters (some very short) and aims to describe the theoretical background for the interpretation of vibrational spectra. According to the Introduction it is a textbook for undergraduate and postgraduate students and it attempts to give an overview of applications and "an understanding of some problem-oriented approaches".

Chapter 1 which is also part 1 contains some irritating errors in the units which are to be used. It states, for example that 1 nm = 10^{-3} mm instead of 10^{-3} μm. Also the standard abbreviation for seconds in SI units is s not sec. One needs to be circumspect in insisting on SI units since cm^{-1}, beloved of spectroscopists, for very good reasons, is not an SI unit. Nevertheless, the relation between wave number in cm^{-1} and wavelength λ in μm is $\nu(cm^{-1}) = 10^{+4}/\lambda$ (μm) not $10^{-4}/\lambda$ (μm). Theoretical results, concerning the mechanism by which IR and Raman spectra are obtained, are stated without proof and little explanation. The illustration (Fig. 1.6) of the IR spectrum and the Raman spectrum of CS_2 is in principle a good one and the diagrams to demonstrate them are potentially useful but they in no way indicate why the polarizability changes in either the asymmetric vibration or the degenerate bending vibrations. The text referring to the diagram is no help either and it is unfortunately separated from the picture by text.

Part II of the book contains three chapters on the non-mathematical interpretation of vibrational spectra. Most of the first of these chapters is an adequate description of "fingerprinting". The section on the use of vibrational spectroscopy for following the course of reactions is marred by some unfortunate misprints; the formula of N-pentafluoroethyltetrafluoro-sulphurimide is $C_2F_5—N{=}SF_4$ and the captions for Figs 2 and 3 have formulae where B has mysteriously replaced N. The third chapter of this part concerns the interpretation of the vibrational spectra of organic compounds and contains quite a useful reference list of group frequencies and also some useful rules of thumb about the intensities of IR and Raman bands.

Chapter 4 describes the quantitative analytical use of vibrational spectroscopy with some instructive examples.

Part III of the book develops the use of group theory in interpreting vibrational spectra. The description of point groups is accurate but the representation of groups is presented without any derivation and will be very puzzling to beginners. The diagram illustrating a table of group characters is fine but there is a misprint in one of the formulae concerning the orthogonality of irreducible representations. The selection rules are stated without proper explanation. Students will be able to get the right answer without any insight as to why it is correct. The small section on the extension of symmetry concepts to the solid state is very short and incomplete although the concepts are to be used later. Chapter 6 describes some applications, considering the vibrational spectra of AsF_6^-, the changes which occur when this ion behaves as a ligand and the use of vibrational spectroscopy to distinguish between conformational isomers. This useful chapter concludes with a short discussion of molecules in the solid state.

Part IV considers the interpretation of molecular spectra using mathematical tools and makes reference to a number of other books which contain the detailed development of the ideas. There then follows a chapter on elementary matrix algebra which stops short of the diagonalization of matrices; just the material necessary for a proper understanding of the use of F and G matrices which are considered in the next chapter. This may be useful to experienced users but is likely to be confusing to students. Then follows a number of such short chapters that one wonders whether this is a translation of the original book or a precis of it. Without seeing the original German edition it is not possible to decide this. There are a number of places where one line has been partially printed over another but this may just be the copy which I have.

Part V continues with a discussion of the vibrational spectroscopy of solids and again results are stated without derivation or reference.

Parts of this book may be a useful aide-memoire to experienced practitioners but students new to the field will not be helped to any great extent. I suspect that the price of the book will deter even those who would be able to follow it easily.

J. H. BINKS

The Kirk–Othmer Encyclopedia of Chemical Technology: Volume 5, Fourth Edition. Carbon and Graphite Fibers to Chlorocarbons and Chlorohydrocarbons-C_1. J. I. KROSCHWITZ and M. HOWE-GRANT (editors), Wiley–Interscience, Chichester, 1992. Pages: xxviii + 1072. £150.00. ISBN 0-471-52673-8 (v. 5).

Volumes in the new edition of this encyclopedia now extend, alphabetically, to the topic of chlorocarbons and chlorohydrocarbons. An excellent softback index covering the first four volumes is also included with volume five.

Almost 70 authors have contributed to this volume which is divided into 31 topics. The main areas covered are: ceramics (129 pages), cardiovascular agents (95 pages), cellulose—esters and ethers (88 pages), chlorine oxygen acids and salts (86 pages), catalysts (79 pages) and catalysis (64 pages), and carboxylic acids (61 pages). The final topic—chlorocarbons and chlorohydrocarbons—is also extensive and continues into volume six of the encyclopedia.

Talanta, Vol. 40, No. 10, pp. 1583–1585, 1993
Printed in Great Britain.

0039-9140/93 $6.00 + 0.00
Pergamon Press Ltd

BOOK REVIEWS

Vibrational Spectroscopy—Methods and Applications: A. FADINI and F.-M. SCHNEPEL, Ellis Horwood, Chichester, 1989. Pages 205. £50.00, US$85.00.

This book of 205 pages is a translation from German. It consists of five parts comprised of 24 short chapters (some very short) and aims to describe the theoretical background for the interpretation of vibrational spectra. According to the Introduction it is a textbook for undergraduate and postgraduate students and it attempts to give an overview of applications and "an understanding of some problem-oriented approaches".

Chapter 1 which is also part 1 contains some irritating errors in the units which are to be used. It states, for example that 1 nm = 10^{-3} mm instead of 10^{-3} μm. Also the standard abbreviation for seconds in SI units is s not sec. One needs to be circumspect in insisting on SI units since cm^{-1}, beloved of spectroscopists, for very good reasons, is not an SI unit. Nevertheless, the relation between wave number in cm^{-1} and wavelength λ in μm is $\nu(cm^{-1}) = 10^{+4}/\lambda$ (μm) not $10^{-4}/\lambda$ (μm). Theoretical results, concerning the mechanism by which IR and Raman spectra are obtained, are stated without proof and little explanation. The illustration (Fig. 1.6) of the IR spectrum and the Raman spectrum of CS_2 is in principle a good one and the diagrams to demonstrate them are potentially useful but they in no way indicate why the polarizability changes in either the asymmetric vibration or the degenerate bending vibrations. The text referring to the diagram is no help either and it is unfortunately separated from the picture by text.

Part II of the book contains three chapters on the non-mathematical interpretation of vibrational spectra. Most of the first of these chapters is an adequate description of "fingerprinting". The section on the use of vibrational spectroscopy for following the course of reactions is marred by some unfortunate misprints; the formula of N-pentafluoroethyltetrafluoro-sulphurimide is $C_2F_5—N{=}SF_4$ and the captions for Figs 2 and 3 have formulae where B has mysteriously replaced N. The third chapter of this part concerns the interpretation of the vibrational spectra of organic compounds and contains quite a useful reference list of group frequencies and also some useful rules of thumb about the intensities of IR and Raman bands.

Chapter 4 describes the quantitative analytical use of vibrational spectroscopy with some instructive examples.

Part III of the book develops the use of group theory in interpreting vibrational spectra. The description of point groups is accurate but the representation of groups is presented without any derivation and will be very puzzling to beginners. The diagram illustrating a table of group characters is fine but there is a misprint in one of the formulae concerning the orthogonality of irreducible representations. The selection rules are stated without proper explanation. Students will be able to get the right answer without any insight as to why it is correct. The small section on the extension of symmetry concepts to the solid state is very short and incomplete although the concepts are to be used later. Chapter 6 describes some applications, considering the vibrational spectra of AsF_6^-, the changes which occur when this ion behaves as a ligand and the use of vibrational spectroscopy to distinguish between conformational isomers. This useful chapter concludes with a short discussion of molecules in the solid state.

Part IV considers the interpretation of molecular spectra using mathematical tools and makes reference to a number of other books which contain the detailed development of the ideas. There then follows a chapter on elementary matrix algebra which stops short of the diagonalization of matrices; just the material necessary for a proper understanding of the use of F and G matrices which are considered in the next chapter. This may be useful to experienced users but is likely to be confusing to students. Then follows a number of such short chapters that one wonders whether this is a translation of the original book or a precis of it. Without seeing the original German edition it is not possible to decide this. There are a number of places where one line has been partially printed over another but this may just be the copy which I have.

Part V continues with a discussion of the vibrational spectroscopy of solids and again results are stated without derivation or reference.

Parts of this book may be a useful aide-memoire to experienced practitioners but students new to the field will not be helped to any great extent. I suspect that the price of the book will deter even those who would be able to follow it easily.

J. H. BINKS

The Kirk–Othmer Encyclopedia of Chemical Technology: Volume 5, Fourth Edition. Carbon and Graphite Fibers to Chlorocarbons and Chlorohydrocarbons-C_1. J. I. KROSCHWITZ and M. HOWE-GRANT (editors), Wiley–Interscience, Chichester, 1992. Pages: xxviii + 1072. £150.00. ISBN 0-471-52673-8 (v. 5).

Volumes in the new edition of this encyclopedia now extend, alphabetically, to the topic of chlorocarbons and chlorohydrocarbons. An excellent softback index covering the first four volumes is also included with volume five.

Almost 70 authors have contributed to this volume which is divided into 31 topics. The main areas covered are: ceramics (129 pages), cardiovascular agents (95 pages), cellulose—esters and ethers (88 pages), chlorine oxygen acids and salts (86 pages), catalysts (79 pages) and catalysis (64 pages), and carboxylic acids (61 pages). The final topic—chlorocarbons and chlorohydrocarbons—is also extensive and continues into volume six of the encyclopedia.

Topics covered in less detail include carbon dioxide, carbon monoxide, castor oil, cement and chemicals from brine. The elements surveyed in this volume are cerium and cesium. Other topics which I found to be of particular interest—from an intellectual as well as professional viewpoint—include carbonated beverages, chelating agents, chemicals in war, chemometrics and chemurgy. I would liked to have seen a little more on chemometrics but the extent to which a reader thinks a topic should be covered is related to personal interest as well as to the overall importance of the topic.

As usual, extensive bibliographies (including books, journals and patents) are included after each topic and the presentation is of a high standard. Highly recommended reading and a worthy purchase for all science libraries.

P. J. Cox

Soil Analysis—Modern Instrumental Techniques: Second Edition. K. A. Smith, Dekker, New York, 1991. Pages viii + 659. $150.00 (US and Canada), $180.00 (elsewhere). ISBN 0-8247-8355-7.

The second edition of Keith Smith's *Soil Analysis—Modern Instrumental Techniques* is a timely and very welcome addition to the literature of environmental, and especially soil, analysis. The new edition is substantially enlarged to reflect developments over the seven years since the first edition was published, and now, very appropriately, includes chapters on ion chromatography, ICP atomic emission spectrometry, and NMR spectrometry for functional group analysis. As in the first edition, the authors selected for each topic write from the viewpoint of extensive first hand experience, which contributes both to the reliability of the information and to the book's success in achieving its goals, namely to bridge the gap between excessively detailed monographs on individual techniques and the occasional superficiality of all-embracing general analytical texts. For those not familiar with the earlier addition, other topics covered include: atomic absorption and flame emission spectrometry, ion-selective electrodes, automated colorimetric analysis, automated C, N and S determination, nuclear and radiochemical methods, XRF, INAA, isotope ratio measurements for C, N and O, soil atmosphere analysis and pesticide analysis. The quality and style of presentation is commendably uniform and high for such a multi-author text, and the original literature is thoroughly referenced. The book will not date rapidly, and will remain an asset to researchers and higher education teachers in soil science, environmental science and analytical chemistry for years to come.

M. Cresser

Macmillan's Chemical and Physical Data: A. M. James and M. P. Lord, Macmillan, London, 1992. Pages xxv + 565. £35.00. ISBN 0-333-51167-0.

Though we live in an age of information technology it can still be a painful and time-consuming experience to track down a particular fact, especially so if it relates to an unfamiliar field. This book attempts to address such problems by assembling a mass of diverse information—the density of the planet Mars, the melting point of calcium iodide, the half-life of ^{126}Sn, the volume of the Royal Opera House—but is yet sufficiently compact to drop into a briefcase. It ranges over many fields: properties of molecules, electrochemistry, kinetics, health and safety, optics, acoustics, astronomy and geophysics. About two thirds of the compilation is devoted to three topics: atomic and nuclear physics (102 pages), physical properties of compounds (146 pages) and thermodynamic properties of compounds (56 pages). The compilers have assumed that readers are familiar with underlying theory or have access to appropriate textbooks. Most of the tables indicate the sources from which they have been compiled and some give references to more specialist texts.

As a structural chemist I was disappointed in the fairly brief section on molecular structure. The existence of comprehensive structural databases is not mentioned and bond length compilations seem to be mainly based on Special Publication No. 18 of the Chemical Society (1965) rather than on recent average values from the Cambridge Structural Database (*J.C.S. Perkin II*, 1987, S1; *J.C.S. Dalton*, 1989, S1) which allow distances in most organic compounds to be estimated with fair reliability. Page 53 gives the benzene C–C distance as 139.5 pm whereas two pages later it has lengthened to 142.10 pm.

Nevertheless I consider that this is a helpful addition to the bookshelf of a working scientist. Coverage is wider and generally more authoritative than many of the paperback data books available. And, though the book is not as comprehensive as the Chemical Rubber Company Handbook, neither is it as bulky or expensive.

K. W. Muir

UltraFit—version 2.1: non-linear curve-fitter for the Apple Macintosh. Biosoft, Cambridge, U.K., £149.00, US $ 299.00.

UltraFit is a non-linear curve-fitter for the Apple Macintosh family of computers. Two versions of the program are supplied and this ensures that the program can be used on the whole Macintosh range provided that at least 1MB of RAM is present. The program also supports a maths' coprocessor, it is claimed to be fully compatible with systems 6 and 7 and this does indeed appear to be the case. The manual is clearly written in a style that most Macintosh users will instantly recognize. Although, on opening the manual it is surprising not to find an introductory chapter describing the installation of the program. However, this omission will inconvenience only the most inexperienced of Macintosh users. Chapter 1 of the manual guides the user through a series of tutorials which cover the main features of UltraFit. These include data entry, creating new graphs, adding plots to graphs, fitting curves to data and customizing plots. The following chapters provide detailed accounts of each feature illustrated in the tutorials. Chapter 2 introduces worksheets which allow for the entry and manipulation of data. The program allows data entry directly from the keyboard or to be imported from other

Topics covered in less detail include carbon dioxide, carbon monoxide, castor oil, cement and chemicals from brine. The elements surveyed in this volume are cerium and cesium. Other topics which I found to be of particular interest—from an intellectual as well as professional viewpoint—include carbonated beverages, chelating agents, chemicals in war, chemometrics and chemurgy. I would liked to have seen a little more on chemometrics but the extent to which a reader thinks a topic should be covered is related to personal interest as well as to the overall importance of the topic.

As usual, extensive bibliographies (including books, journals and patents) are included after each topic and the presentation is of a high standard. Highly recommended reading and a worthy purchase for all science libraries.

P. J. Cox

Soil Analysis—Modern Instrumental Techniques: Second Edition. K. A. Smith, Dekker, New York, 1991. Pages viii + 659. $150.00 (US and Canada), $180.00 (elsewhere). ISBN 0-8247-8355-7.

The second edition of Keith Smith's *Soil Analysis—Modern Instrumental Techniques* is a timely and very welcome addition to the literature of environmental, and especially soil, analysis. The new edition is substantially enlarged to reflect developments over the seven years since the first edition was published, and now, very appropriately, includes chapters on ion chromatography, ICP atomic emission spectrometry, and NMR spectrometry for functional group analysis. As in the first edition, the authors selected for each topic write from the viewpoint of extensive first hand experience, which contributes both to the reliability of the information and to the book's success in achieving its goals, namely to bridge the gap between excessively detailed monographs on individual techniques and the occasional superficiality of all-embracing general analytical texts. For those not familiar with the earlier addition, other topics covered include: atomic absorption and flame emission spectrometry, ion-selective electrodes, automated colorimetric analysis, automated C, N and S determination, nuclear and radiochemical methods, XRF, INAA, isotope ratio measurements for C, N and O, soil atmosphere analysis and pesticide analysis. The quality and style of presentation is commendably uniform and high for such a multi-author text, and the original literature is thoroughly referenced. The book will not date rapidly, and will remain an asset to researchers and higher education teachers in soil science, environmental science and analytical chemistry for years to come.

M. Cresser

Macmillan's Chemical and Physical Data: A. M. James and M. P. Lord, Macmillan, London, 1992. Pages xxv + 565. £35.00. ISBN 0-333-51167-0.

Though we live in an age of information technology it can still be a painful and time-consuming experience to track down a particular fact, especially so if it relates to an unfamiliar field. This book attempts to address such problems by assembling a mass of diverse information—the density of the planet Mars, the melting point of calcium iodide, the half-life of ^{126}Sn, the volume of the Royal Opera House—but is yet sufficiently compact to drop into a briefcase. It ranges over many fields: properties of molecules, electrochemistry, kinetics, health and safety, optics, acoustics, astronomy and geophysics. About two thirds of the compilation is devoted to three topics: atomic and nuclear physics (102 pages), physical properties of compounds (146 pages) and thermodynamic properties of compounds (56 pages). The compilers have assumed that readers are familiar with underlying theory or have access to appropriate textbooks. Most of the tables indicate the sources from which they have been compiled and some give references to more specialist texts.

As a structural chemist I was disappointed in the fairly brief section on molecular structure. The existence of comprehensive structural databases is not mentioned and bond length compilations seem to be mainly based on Special Publication No. 18 of the Chemical Society (1965) rather than on recent average values from the Cambridge Structural Database (*J.C.S. Perkin II*, 1987, S1; *J.C.S. Dalton*, 1989, S1) which allow distances in most organic compounds to be estimated with fair reliability. Page 53 gives the benzene C–C distance as 139.5 pm whereas two pages later it has lengthened to 142.10 pm.

Nevertheless I consider that this is a helpful addition to the bookshelf of a working scientist. Coverage is wider and generally more authoritative than many of the paperback data books available. And, though the book is not as comprehensive as the Chemical Rubber Company Handbook, neither is it as bulky or expensive.

K. W. Muir

UltraFit—version 2.1: non-linear curve-fitter for the Apple Macintosh. Biosoft, Cambridge, U.K., £149.00, US $ 299.00.

UltraFit is a non-linear curve-fitter for the Apple Macintosh family of computers. Two versions of the program are supplied and this ensures that the program can be used on the whole Macintosh range provided that at least 1MB of RAM is present. The program also supports a maths' coprocessor, it is claimed to be fully compatible with systems 6 and 7 and this does indeed appear to be the case. The manual is clearly written in a style that most Macintosh users will instantly recognize. Although, on opening the manual it is surprising not to find an introductory chapter describing the installation of the program. However, this omission will inconvenience only the most inexperienced of Macintosh users. Chapter 1 of the manual guides the user through a series of tutorials which cover the main features of UltraFit. These include data entry, creating new graphs, adding plots to graphs, fitting curves to data and customizing plots. The following chapters provide detailed accounts of each feature illustrated in the tutorials. Chapter 2 introduces worksheets which allow for the entry and manipulation of data. The program allows data entry directly from the keyboard or to be imported from other

Topics covered in less detail include carbon dioxide, carbon monoxide, castor oil, cement and chemicals from brine. The elements surveyed in this volume are cerium and cesium. Other topics which I found to be of particular interest—from an intellectual as well as professional viewpoint—include carbonated beverages, chelating agents, chemicals in war, chemometrics and chemurgy. I would liked to have seen a little more on chemometrics but the extent to which a reader thinks a topic should be covered is related to personal interest as well as to the overall importance of the topic.

As usual, extensive bibliographies (including books, journals and patents) are included after each topic and the presentation is of a high standard. Highly recommended reading and a worthy purchase for all science libraries.

P. J. Cox

Soil Analysis—Modern Instrumental Techniques: Second Edition. K. A. Smith, Dekker, New York, 1991. Pages viii + 659. $150.00 (US and Canada), $180.00 (elsewhere). ISBN 0-8247-8355-7.

The second edition of Keith Smith's *Soil Analysis—Modern Instrumental Techniques* is a timely and very welcome addition to the literature of environmental, and especially soil, analysis. The new edition is substantially enlarged to reflect developments over the seven years since the first edition was published, and now, very appropriately, includes chapters on ion chromatography, ICP atomic emission spectrometry, and NMR spectrometry for functional group analysis. As in the first edition, the authors selected for each topic write from the viewpoint of extensive first hand experience, which contributes both to the reliability of the information and to the book's success in achieving its goals, namely to bridge the gap between excessively detailed monographs on individual techniques and the occasional superficiality of all-embracing general analytical texts. For those not familiar with the earlier addition, other topics covered include: atomic absorption and flame emission spectrometry, ion-selective electrodes, automated colorimetric analysis, automated C, N and S determination, nuclear and radiochemical methods, XRF, INAA, isotope ratio measurements for C, N and O, soil atmosphere analysis and pesticide analysis. The quality and style of presentation is commendably uniform and high for such a multi-author text, and the original literature is thoroughly referenced. The book will not date rapidly, and will remain an asset to researchers and higher education teachers in soil science, environmental science and analytical chemistry for years to come.

M. Cresser

Macmillan's Chemical and Physical Data: A. M. James and M. P. Lord, Macmillan, London, 1992. Pages xxv + 565. £35.00. ISBN 0-333-51167-0.

Though we live in an age of information technology it can still be a painful and time-consuming experience to track down a particular fact, especially so if it relates to an unfamiliar field. This book attempts to address such problems by assembling a mass of diverse information—the density of the planet Mars, the melting point of calcium iodide, the half-life of ^{126}Sn, the volume of the Royal Opera House—but is yet sufficiently compact to drop into a briefcase. It ranges over many fields: properties of molecules, electrochemistry, kinetics, health and safety, optics, acoustics, astronomy and geophysics. About two thirds of the compilation is devoted to three topics: atomic and nuclear physics (102 pages), physical properties of compounds (146 pages) and thermodynamic properties of compounds (56 pages). The compilers have assumed that readers are familiar with underlying theory or have access to appropriate textbooks. Most of the tables indicate the sources from which they have been compiled and some give references to more specialist texts.

As a structural chemist I was disappointed in the fairly brief section on molecular structure. The existence of comprehensive structural databases is not mentioned and bond length compilations seem to be mainly based on Special Publication No. 18 of the Chemical Society (1965) rather than on recent average values from the Cambridge Structural Database (*J.C.S. Perkin II*, 1987, S1; *J.C.S. Dalton*, 1989, S1) which allow distances in most organic compounds to be estimated with fair reliability. Page 53 gives the benzene C–C distance as 139.5 pm whereas two pages later it has lengthened to 142.10 pm.

Nevertheless I consider that this is a helpful addition to the bookshelf of a working scientist. Coverage is wider and generally more authoritative than many of the paperback data books available. And, though the book is not as comprehensive as the Chemical Rubber Company Handbook, neither is it as bulky or expensive.

K. W. Muir

UltraFit—version 2.1: non-linear curve-fitter for the Apple Macintosh. Biosoft, Cambridge, U.K., £149.00, US $ 299.00.

UltraFit is a non-linear curve-fitter for the Apple Macintosh family of computers. Two versions of the program are supplied and this ensures that the program can be used on the whole Macintosh range provided that at least 1MB of RAM is present. The program also supports a maths' coprocessor, it is claimed to be fully compatible with systems 6 and 7 and this does indeed appear to be the case. The manual is clearly written in a style that most Macintosh users will instantly recognize. Although, on opening the manual it is surprising not to find an introductory chapter describing the installation of the program. However, this omission will inconvenience only the most inexperienced of Macintosh users. Chapter 1 of the manual guides the user through a series of tutorials which cover the main features of UltraFit. These include data entry, creating new graphs, adding plots to graphs, fitting curves to data and customizing plots. The following chapters provide detailed accounts of each feature illustrated in the tutorials. Chapter 2 introduces worksheets which allow for the entry and manipulation of data. The program allows data entry directly from the keyboard or to be imported from other

programs. The data may be manipulated either by using a range of predefined transformations, for example, simple arithmetic functions, conversion to reciprocals or logs, or by using user-defined transformations. Chapter 3 describes the use of graphics in UltraFit. Graphic objects are created and edited using tools from a toolbox which includes a drawing line and ellipse, and a text editor. These tools and their use will be very familiar to all Macintosh users. The creation of graphs is somewhat different to the method used by the majority of plotting programs in that a blank graph is created using the graphing tool and then the data are plotted onto the graph. These data may be in the form of a worksheet or alternatively, UltraFit can use an equation to create a line. This equation may either be one of the 26 predefined equations supplied with the package or be user-defined. Graphs are plotted and manipulated in a very straightforward manner and the user quickly adapts to the program. The formats of the axes are user-defined and the control over the appearance of the plot is far greater than that normally found in similarly priced plotting packages. Graphs can be further customized using the toolbox. Chapter 4 introduces the use of equation documents in just two sides but this is then expanded in Chapter 5 which provides a nice account of the language used to enter equations. However, the strength of UltraFit rests largely with its ability to fit experimental data and this is described in the final chapter of the manual. An equation is chosen or is user-defined to fit the experimental data. Before the data are fitted one of four different weighting methods is used. The default is the simple method in which all residuals, *i.e.*, the difference between the fitted value and observed value, are weighted equally. The other three methods are: the statistical method which is suitable for handling data such as radioactivity counts, the proportional method for use if each point has the same proportional error and the explicit method. A further type of weighting, robust weighting, is also available and this allows for the suppression of data points that contain errors which deviate significantly from the overall error distribution. The residuals or weighted residuals can be added to a worksheet. The output from the fitting process is recorded in a log book and this contains such information as the type of weighting used, estimates of variable parameters and the goodness-of-fit index. UltraFit offers a choice of two fitting algorithms, the Marquardt or the Deming algorithm and there is a very brief description of these given as an Appendix. The manual also has Appendices describing fitting statistics, a particularly useful section on common errors and a list of the predefined equations. The program appears to be robust and the manual is well written. In addition, considering its functionality, the package is priced very reasonably. In consequence, UltraFit can be strongly recommended not only as a general plotting package but in particular, for the fitting of experimental data.

C. T. IMRIE

Talanta, Vol. 40, No. 11, pp. 1587–1588, 1993
Printed in Great Britain.

0039-9140/93 $6.00 + 0.00
Pergamon Press Ltd

FOREWORD

While scientific and technological development in Spain rose dramatically in the past decade, Spanish analytical chemistry grew well above average in qualitative and quantitative terms, so much so that it makes an atypical scientometric model. This has been acknowledged by the analytical community worldwide but not so by domestic professionals, some of whom have been compelled to share or even yield ground to others as a result. Thus, we decided to accept the assignment of compiling a special issue for *Talanta* devoted to Spain as it not only reflected the interest in the late growth of Spanish analytical chemistry, but also might help in placing this discipline in its rightful place within the Spanish scientific and technological system. The 25 groups invited in mutual agreement with the journal editor gave a warm welcome to the proposal and contributed 25 papers of a high quality on a variety of topics which are a good reflection of Spanish analytical chemistry in the 1990s.

Two recently published complementary papers on analytical chemistry in Spain[1,2] showed the dramatic increase in the proportion of Spanish papers published in international analytical journals and their increasingly higher quality—particularly in the late 1980s—as well as a change from essentially inorganic analyses to a variety of other analyses in better accordance with worldwide practice in this respect.

Spanish contributions to *Talanta* have evolved very similarly to Spanish analytical chemistry in general (see Fig. 1). The earliest Spanish paper ever appearing in *Talanta* was contributed by Professor Lucena, of the University of Salamanca,[3] in the first year *Talanta* was released (1958). Up until 1979, Spanish papers never exceeded 2% of all contributions. However, in the 1980s, Spanish contributions grew in an almost exponential fashion though they had levelled off by the end of the decade. It is interesting to note the unusually high proportion of Spanish papers published in *Talanta* in 1986 (*ca.* 18%), which can probably be ascribed to the extra pressure placed on Spanish university researchers, who were compelled to pass some tests where their research curriculum was decisive. This was also the case with other scientific–technical disciplines. Spanish analytical chemists have contributed an average 4.4% of all papers published in the 35 years of *Talanta*; however, Spanish contributions between 1983 and 1992 accounted for more than twice that percentage, *ca.* 11.5%. This is quite a remarkable figure taking into account that *Talanta* publishes papers from a large number of countries. Hence it was logical to devote a special issue to this country, in the wake of those previously published in the U.S.A. and the former Soviet Union.

Finally, we wish to thank Professors Winefordner and Hansen for their initiative and the assignment they gave us in the course of Pitcon '92, held in Atlanta in February 1992. On accepting the assignment, we could hardly envisage such a warm welcome by Spanish analytical chemists, who have contributed their best. All of them deserve our earnest acknowledgement. We should also like to thank the 50 referees who acted as reviewers for their constructive criticisms. We believe our endeavour as guest editors was worth the while and hope this feeling will be shared by the readers of this special issue.

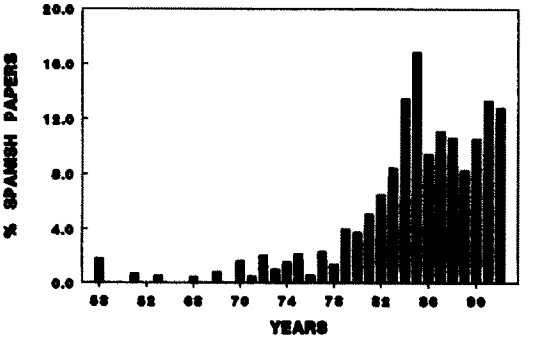

Fig. 1. Relative contribution of Spanish analytical chemists to *Talanta* (from the Teledocumentation Service, University of Extremadura, Spain).

REFERENCES

1. M. Valcárcel, *Trends Anal. Chem.*, 1993, **12**, IX.
2. A. Muñoz de la Peña and A. Pulgarín, *Anal. Proc.*, 1992, **29**, 517.
3. F. Lucena-Conde and I. Sánchez-Bellido, *Talanta*, 1958, **1**, 305.

M. Valcárcel
M. D. Luque de Castro
Guest Editors
Córdoba, March 1993

Talanta, Vol. 40, No. 11, pp. 1589–1593, 1993
Printed in Great Britain.

0039-9140/93 $6.00 + 0.00

CRYSTALLIZATION OF ORGANIC CRYSTALS WITH "TAILOR-MADE" INHIBITORS. DETERMINATION OF *L*-LYSINE USING *L*-GLUTAMIC ACID AS SUBSTRATE

F. GRASES and C. GENESTAR

Department of Chemistry, University of Balearic Islands, 07071 Palma de Mallorca, Spain

Summary—A very simple turbidimetric procedure is used for determination of *L*-lysine, based on its inhibitory action on the crystallization of *L*-glutamic acid. The obtention of supersaturated solutions of *L*-glutamic acid was accomplished by means of the change in the solvent composition. Thus, the addition of ethanol to stable aqueous solutions of this amino acid allows the obtainment of unstable supersaturated solutions. The method suffers from very few interferences and permits the development of an analytical procedure to determine *L*-lysine in the presence of *D*-lysine. The method was also applied to the determination of *L*-lysine in pharmaceutical products.

The analytical determination of chiral molecules has aroused notable interest due to their different behaviour, thus the biological activity of a chiral molecule can be different between the two configurations, *i.e.*, the efficacy of some therapeutic drugs or pesticides is a function of definite configurations of chiral structures, *etc.* The analytical resolution of racemic mixtures is nevertheless very difficult due to the practically identical chemical behaviour of the chiral substances. This usually implies the use of complex chromatographic procedures.[1]

The most common methods for determination of *L*-lysine implies enzymatic procedures.[2,3] Other general methods include the use of high performance liquid chromatography.[4–6]

We report a very simple procedure for *L*-lysine determination based on the interaction between a crystallizing substrate and a stereospecific "tailor-made" growth inhibitor. This permits the development of a specific analytical procedure to determine *L*-lysine in the presence of *D*-lysine. The application of crystallization inhibitory processes in analytical chemistry has been discussed previously.[7]

EXPERIMENTAL

Reagents and apparatus

L-glutamic acid and *L*-lysine, as all reagents used, were purchased from Sigma. The solvents (ethanol, methanol and acetone) were supplied by Merck. Solutions of *L*-lysine ($4.38 \times 10^{-3}M$) and glutamic acid ($5.85 \times 10^{-2}M$) were prepared in doubly distilled, deionized water and filtered through a disposable 0.45-μm filter membrane. These solutions were stable for a week.

Turbidimetric measurements were taken by means of a single-beam spectrophotometer (Bausch and Lomb Spectronic-21) at 550 nm. The usual cell compartment was replaced by a spiral copper tube surrounding a cylindric glass vial of 2.3 cm in diameter and 22 ml in volume. The suspension (solution) contained in the glass vial was stirred by a magnetic bar and a rotatory external magnetic field, placed under the photometer. The transmittance was continuously measured by a pen recorder.

A Hitachi S-530 scanning electron microscope was used to obtain the scanning electron micrographs.

Procedure

To a glass vial placed in the photometer containing 13.5 ml of ethanol (84.4%) were added the necessary volume of *L*-lysine solution to give a final concentration of 2.5–25 μg/ml (the pH of this sample solution was 4.5), water to achieve a final volume of 16 ml and 2 ml of $5.85 \times 10^{-2}M$ *L*-glutamic acid, while stirring. All solutions were filtered through a disposable 0.45-μm filter membrane before use. After addition of *L*-glutamic acid, the transmittance–time curves were recorded at a wavelength of 550 nm. From the resulting curve, the time elapsed before precipitation was detected (see

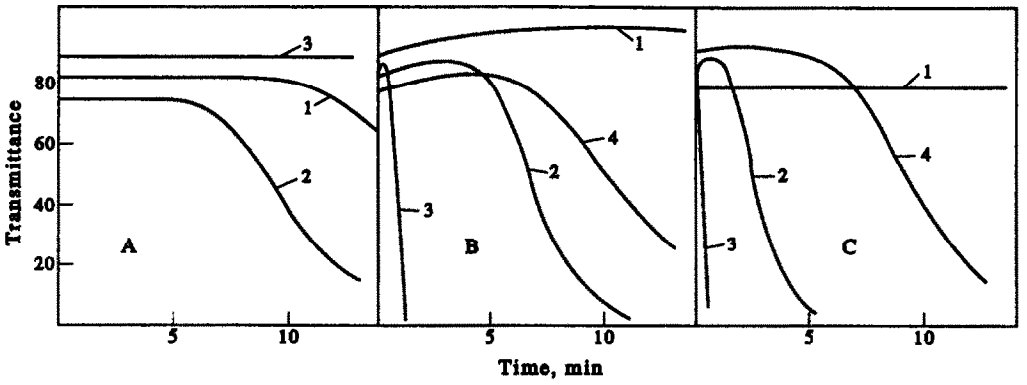

Fig. 1. Influence of the solvent on the crystallization of *L*-glutamic acid, in the absence and presence of *L*-lysine. [*L*-glutamic acid] = $7.31 \times 10^{-3}M$, temperature 26°. A (1) 84.4% of methanol, (2) 87.5% of methanol, (3) 84.4% of methanol and [*L*-lysine] = 10 μg/ml; B (1) 62.5% of ethanol, (2) 81.2% of ethanol, (3) 87.5% of ethanol, (4) 81.2% of ethanol and [*L*-lysine] = 10 μg/ml; C (1) 50% of acetone, (2) 75% of acetone, (3) 84.3% of acetone, (4) 75% of acetone and [*L*-lysine] = 10 μg/ml.

Fig. 4) and was used to prepare the calibration graph (Fig. 5). The duration of each measurement was *ca.* 10 min. The system was kept at constant temperature by circulating water at $26 \pm 0.2°$.

RESULTS AND DISCUSSION

Many crystal properties such as shape, size, stabilization of one or another polymorph, *etc.*, depend on the interactions between crystals and the environment in which the crystal grows. This influence can be non-specific, such as in solvent polarity or solubility effects, or highly specific as in the stereochemical correlation between growing crystals and crystal growth inhibitors as the "tailor-made" additives.[8,9] These substances are organic molecules whose chemical structure is only slightly modified with respect to the bulk component of the molecular crystal. As a consequence, this molecule can selectively absorb on to specific crystal surfaces and this causes dramatic changes in the growth rates. In the present study the effects of *L*-lysine as "tailor-made" inhibitor in the crystallization of *L*-glutamic acid has been studied with analytical purposes. The obtention of supersaturated solutions of *L*-glutamic acid was accomplished by means of the change in the solvent composition. Thus, the addition of an organic solvent to stable aqueous solutions of this aminoacid, allows us to obtain unstable supersaturated solutions. The results of several experiments using methanol, ethanol and acetone as organic solvents, in the presence and absence of *L*-lysine are shown in Fig. 1. The experiments were followed by turbidimetry. When the experiments were finished, a sample of the suspension was taken and examined by SEM. Optimum results are considered those

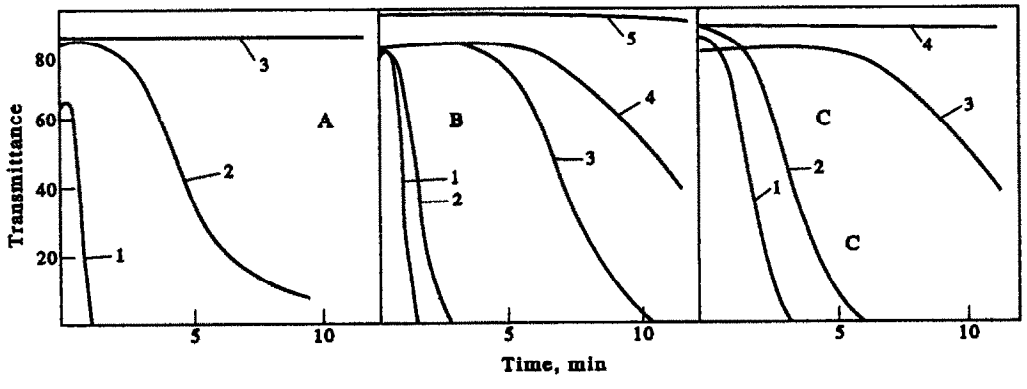

Fig. 2. Crystallization of *L*-glutamic acid in ethanol at different supersaturations. Temperature 26°. A [*L*-glutamic acid] = $3.66 \times 10^{-3}M$, (1) 93.8% of ethanol, (2) 87.5% of ethanol, (3) 81.3% of ethanol; B [*L*-glutamic acid] = $7.31 \times 10^{-3}M$, (1) 87.5% of ethanol, (2) 84.4% of ethanol, (3) 81.3% of ethanol, (4) 78.1% of ethanol, (5) 75% of ethanol; C [*L*-glutamic acid] = $1.46 \times 10^{-2}M$, (1) 75% of ethanol, (2) 71.9% of ethanol, (3) 68.8% of ethanol, (4) 62.5% of ethanol.

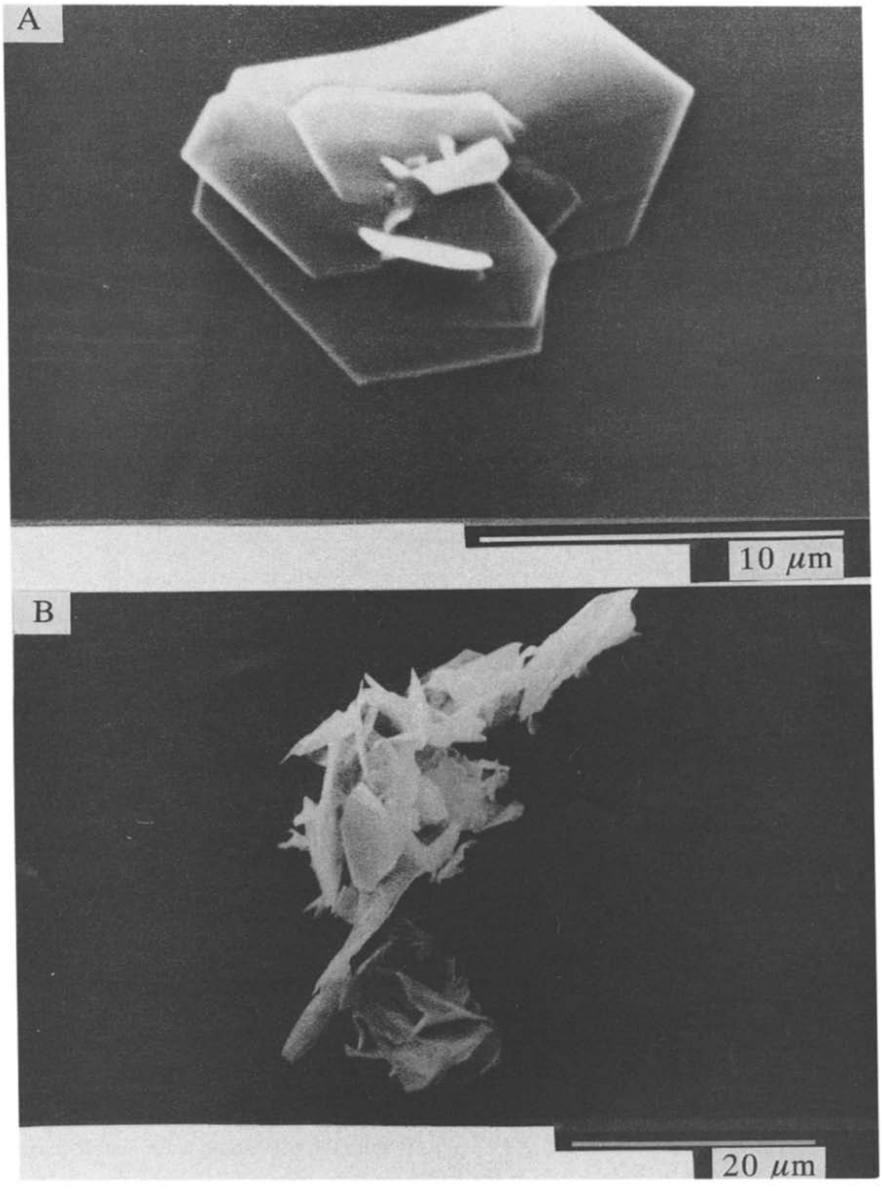

Fig. 3. Scanning electron micrographs (SEM) of *L*-glutamic acid crystallization. [Glutamic acid] = $7.31 \times 10^{-3}M$, 84.4% of ethanol, temperature 26°. (A) Without *L*-lysine. (B) In presence of 10 μg/ml of *L*-lysine.

that correspond to maximum reproducibility and sensitivity and this coincided with the experiments performed with ethanol. Consequently this solvent was selected in further experiments. Analogous criteria was used to select the optimum ethanol and *L*-glutamic acid concentrations. The results obtained appear in Fig. 2. Optimum results were obtained with 84.4% ethanol and in the presence of $7.31 \times 10^{-3}M$ *L*-glutamic acid. Such conditions were chosen to prepare the calibration graph. As can be seen in Fig. 3, when applying the above conditions, a clear inhibition of the hexagonal *L*-glutamic acid crystals formation was observed.

Characteristics of the analytical methods

The transmittance–time curves (Fig. 4) recorded in the presence of different amounts of *L*-lysine under selected conditions were used in order to obtain the calibration graph. The time necessary to initiate the crystallization, the induction period and the relation between the time required to initiate the crystallization in the presence and absence of *L*-lysine were the methods applied. A linear calibration graph was

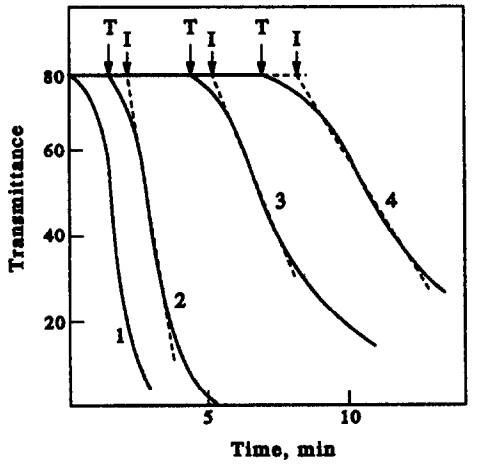

Fig. 4. *L*-glutamic acid crystallization runs in the absence and presence of *L*-lysine. [*L*-glutamic acid] = $7.3 \times 10^{-3}M$, 84.4% of ethanol, temperature 26°. (1) Without *L*-lysine, (2) [*L*-lysine] = 5 μg/ml, (3) [*L*-lysine] = 15 μg/ml, (4) [*L*-lysine] = 25 μg/ml.

obtained between 2.5 and 25 μg/ml in all methods applied. The calibration graphs obtained in the proposed methods by least-squares treatments are described by

$$T = 0.3942 + 0.2496[L] \quad (r = 0.997;\ n = 5)$$

$$I = 0.7410 + 0.2989[L] \quad (r = 0.991;\ n = 5)$$

$$R = 0.4126 + 0.5203[L] \quad (r = 0.996;\ n = 5)$$

where T is the time necessary to initiate the crystallization (time necessary for transmittance starts decreasing, Fig. 4), I the induction period (Fig. 4), R the relation between the time necessary to initiate the crystallization in presence and absence of analite, L the *L*-lysine concentration and r the correlation coefficient.

The three proposed methods exhibited good analytical characteristics, but due to their simplicity, the time necessary to initiate the crystallization was chosen for further experiments.

Reproducibility was measured on 11 replicates of *L*-lysine at 10 μg/ml (RSD = 3.15%) and on 11 replicates of a reference sample (without *L*-lysine) (RSD = 4.17%). These results were obtained when the time necessary to initiate the crystallization was applied to prepare the calibration graph.

Interferences

To evaluate the selectivity of the proposed method, the effect of other aminoacids on the crystallization of *L*-glutamic acid was studied. The aminoacids selected were those currently included in formulations together with *L*-lysine. Various volumes of stock solutions of

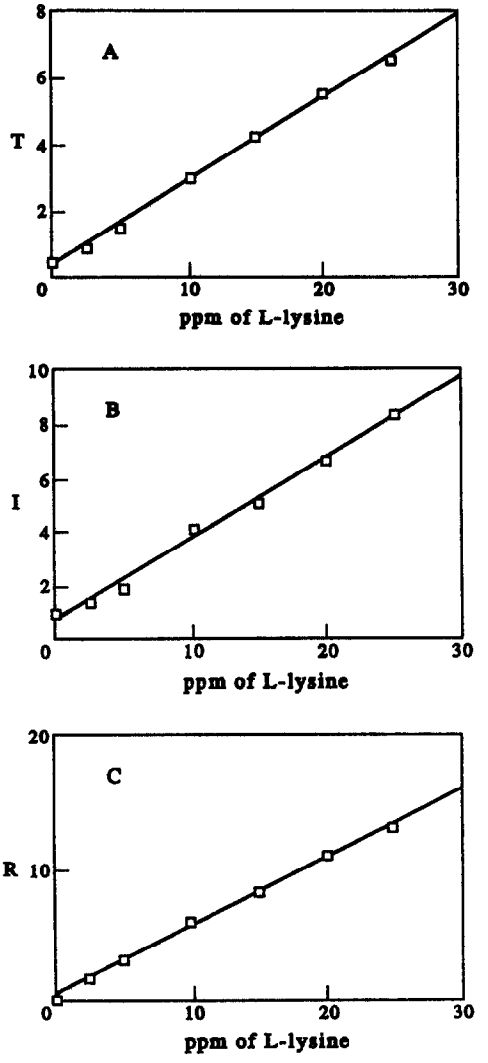

Fig. 5. Calibration graphs for *L*-lysine. (A) T: Time necessary to initiate the crystallization. (B) I: Induction period. (C) R: Relation between the time necessary to initiate the crystallization in the presence and absence of *L*-lysine.

Table 1. Tolerance levels (μg/ml) for several aminoacids in the determination of 10 μg/ml *L*-lysine

Aminoacids	Maximum tolerated amount* (μg/ml)
L-leucine, *L*-tyrosine, *L*-aspartic acid	
L-glutamine, *L*-phenylalanine, *L*-threonine	
L-serine, *L*-asparagine, *L*-isoleucine	
L-methionine, *L*-valine	>50
D-lysine	500†
L-histidine‡	15
L-ornithine‡	3

*The obtained results in the determination of *L*-lysine were identical to those obtained in absence of the checked aminoacid.

†Higher concentration assayed.

‡Higher concentrations inhibited the glutamic acid crystallization.

Table 2. Determination of *L*-lysine in the presence of *D*-lysine in synthetic samples

Composition (μg/ml)	Found (μg/ml)	Recovery (%)
10 *L*-lysine + 50 *D*-lysine	9.82	98.2
10 *L*-lysine + 250 *D*-lysine	9.94	99.4
10 *L*-lysine + 500 *D*-lysine	9.86	98.6

Table 3. Determination of *L*-lysine in pharmaceutical products

Sample No.	Found*	Value certified by the manufacturer
1§	39.7 ± 0.57†	40†
2‖	11.99 ± 0.317‡	11.03‡

*Average of 5 determinations.
†As *g/l*.
‡As percentage *w/w*.
§Pharmaceutical product: Acticinco, supplied by Pierre Fabre S.A.E.
‖Pharmaceutical product: Aminoácidos esenciales, supplied by Nutri Sport.

the different potential interferences were added to *L*-glutamic acid in order to know the tolerance levels. The results summarized in Table 1 show that only the assayed diaminocarboxylic acids such as *L*-lysine (*L*-histidine and *L*-ornithine) caused some disturbance. It is interesting to point out that the presence of *D*-lysine causes no important interference on the crystallization of *L*-glutamic acid. Scanning electron micrographs show no difference between samples obtained in presence of *D*-lysine and samples of the crystallization of *L*-glutamic acid, without additives, at the same percentage of ethanol.

Application

The resolution of racemic mixtures is an important and very difficult analytical problem. Due to the slight effects that the presence of *D*-lysine caused on the crystallization of *L*-glutamic acid, as it was commented above, the proposed method was applied to the determination of *L*-lysine in the presence of *D*-lysine in synthetic samples (Table 2).

To test the applicability of the proposed method, this was applied to the determination of *L*-lysine in pharmaceutical products. *L*-lysine constitutes a common constituent in pharmaceutical products to promote the muscular and osseous growth. The determination of *L*-lysine in one of these pharmaceutical products (sample No. 1, Table 3) was carried out without any previous treatment of the sample (except appropriate dilution).

On the other hand, *L*-lysine is one of those labelled essential amino acids and for this reason is included in pharmaceutical preparations of dietetic supplements. The proposed method allows the determination of *L*-lysine in the presence of other aminoacids (*L*-leucine, *L*-phenylalanine, *L*-threonine, *etc.*) without previous separation. The results obtained are shown in Table 3 (sample No. 2).

As can be seen, the results for *L*-lysine analysis in samples of pharmaceutical products using the proposed method are in good agreement with the certified values. The proposed procedure cannot be applied to the determination of *L*-lysine in pharmaceutical products that also contain quantities of *L*-histidine and/or *L*-ornithine similar to the former, due to their important inhibitory effects on the crystallization of *L*-glutamic acid.

Acknowledgement—Financial support by the Dirección General de Investigación Científica y Técnica (Grant PB 89-0423) is gratefully acknowledged.

REFERENCES

1. N. Bargmann, A. Tambuté and M. Caude, *Analusis*, 1992, **20**, 189.
2. N. D. Tran, J. L. Romette and D. Thomas, *Biotechnol. Bioeng.*, 1983, **25**, 329.
3. J. L. Romette, J. S. Yang, H. Kusakabe and D. Thomas, *ibid.*, 1983, **25**, 2557.
4. B. A. Bidlingmeyer, S. A. Cohen and T. L. Tarvin, *J. Chromatogr.*, 1984, **336**, 93.
5. M. Alaiz, J. L. Navarro, J. Giron and E. Vioque, *ibid.*, 1992, **591**, 181.
6. H. Brueckner and C. Gah, *ibid.*, 1991, **555**, 81.
7. F. Grases and J. G. March, *Trends in Anal. Chem.*, 1991, **10**, 190.
8. L. Addadi, S. Weinstein, E. Gati, I. Weissbuch and M. Lahav, *J. Am. Chem. Soc.*, 1982, **104**, 4610.
9. L. Addadi, Z. Berkovitch-Yellin, I. Weissbuch, J. Mil, L. J. W. Shimon, M. Lahav and L. Leiserowitz, *Angew. Chem. Int. Ed. Engl.*, 1985, **24**, 466.

Talanta, Vol. 40, No. 11, pp. 1595–1600, 1993
Printed in Great Britain.

0039-9140/93 $6.00 + 0.00

DETERMINATION OF THE OXIDATIVE STABILITY OF OLIVE OIL BY USE OF A ROBOTIC STATION

JOSÉ A. GARCÍA MESA, M. D. LUQUE DE CASTRO and MIGUEL VALCÁRCEL
Department of Analytical Chemistry, Faculty of Sciences, University of Córdoba, E-14004 Córdoba, Spain

Summary—A gravimetric method for the determination of the oxidative stability of olive oil based on the use of a robotic station for the monitoring of the oxygen absorbed by a sample subjected to heating under controlled working conditions is proposed. The method was developed in order to relieve the typically heavy work load of olive oil laboratories in winter. The results obtained were consistent with those provided by a well-established method (Rancimat), which the proposed method clearly surpasses in sample throughput (6 samples/batch *vs* 150 samples/batch).

The number of samples to be analysed by some laboratories varies enormously from season to season, particularly for agricultural products and their derivatives. The seasonal factor compels laboratories to deal with large numbers of sample during the harvest period and remain virtually inactive the rest of the year. Laboratory automation has solved this problem in some cases[1] by means of analysers with high sample throughputs; however, the scarce flexibility of this type of instrument poses an additional shortcoming: such powerful, expensive tools must be kept inactive for rather long periods (8–10 months/year).

The potential final solution to this problem may lie in accomplishing flexible automation in order to meet the great demand for analyses of the harvest period and provide for other tasks during the rest of the year, thus maximizing the profitability of the initial costly investment. Such is the case with the use of robots.[2]

Olive oil industry laboratories are ideal targets for the proposed solution. The aim of this work was to show how robots can solve such problems; in particular the determination of the oxidative stability of oils. Resistance to oxidation is a measure of oil quality and dictates storage and usage stability. Such stability, the interval until the oil becomes rancid, depends both on intrinsic features (*viz*, type of olive in olive oils, and fatty acid and natural antioxidant—tocopherols and polyphenols—contents) and on environmental conditions (temperature, light, air exposure, type and material of the container, metal trace content, *etc.*).

Oil rancidity is assessed either by sensory or by laboratory procedures.[3,4] Because olive oils are stable for a few months under their usual storage conditions, oxidation is accelerated in laboratory tests by increasing the temperature and, occasionally, also by increasing exposure to oxygen. This "forced" side of the study conditions may distort the results compared with real conditions; notwithstanding this shortcoming, the long experience in accelerated stability assays has fostered usage of this type of analysis.

In previous work[5] the deficiencies of the methods used so far for studying the stability to oxidation of virgin olive oils were discussed and an alternative method based on the gravimetric monitoring of the oxygen absorbed by a sample subjected to heating under controlled working conditions was developed. This method features a much higher sample throughput than its earlier counterparts. The manual determination as performed by using this method is rather tedious because the experimental procedure involves an endless series of weighings which are prone to personal errors. This makes the method a good candidate for implementation by a robotic station.

EXPERIMENTAL

Instrument and apparatus

Analyses were performed by a Zymark Co. robotic station consisting of the following elements (Fig. 1). A Zymate II plus robot, a System V controller, a Printer, a Power, an

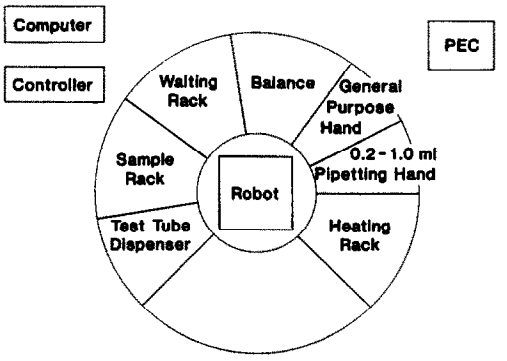

Fig. 1. Bench layout of the robotic station for the determination of oxidative stability of olive oil.

Event controller, a General purpose hand (with a disposable pipet tip rack), a 0.2–1.0 ml Syringe hand, a test-tube dispenser and racks for 16 × 100 mm tubes. A Mettler AE 200 balance, a Plactronic (P-Selecta) heating-plate and a Netset AT PC compatible computer were used. A lab-built aluminium bore heating block was also employed.

Gravimetric determination of the oxidative stability of olive oil

After the operator enters the number and identification of samples, the robot performs the following operations: weighing test-tubes equal to the number of samples to be processed, which are placed in the waiting rack; weighing 1 g of sample in its test-tube; transferring each sample to the heating rack; heating at 98° for 5 hr; transferral of all the samples to the waiting rack; pause for cooling (20 min); weighing the samples and final transferral to the waiting rack, the weights being stored in a disk in the controller device for subsequent treatment. The cycle is repeated as many times as required depending on the stability of the sample concerned, until the weight gain of all the samples has reached 9 mg (Fig. 2).

RESULTS AND DISCUSSION

Optimization of variables

On the basis of preliminary results, the manual method was adapted for implementation of the robotic station by establishing the most suitable conditions for the assay (a fast oxidation kinetics no detracting from the discriminating power of the method; minimal space occupancy per sample in order to maximize throughput; robot-friendliness; and results consistent with those provided by other methods. These requisites were met as follows:

(a) Working temperature. The temperature selected for sample heating was 98° in order to operate under thermal conditions similar to those of well-established methods since temperature was a key to the process rate.[5]

(b) Compatibility between the robot, heating system and productivity. A heating-plate was used to heat samples since ovens are not robot-friendly. The heating-plate provided uneven heating of the different samples (especially when small vessels were used), possibly because of the non-flat bottom of the containers. This shortcoming was circumvented by constructing a bore aluminium block that was used to hold the vessels (test-tubes), thus facilitating the robot operation. The block was placed on the heating-plate. Its dimensions and the position of the holes were adjusted to those of the rack from Zymark so as to take advantage of PyTechnology. A fairly small amount of sample was used to avoid filling the test tube (16 mm diameter) with sample to an excessive height which would delay the oxidation process through hindered access of oxygen to the sample. On the other hand, handling very small amounts of sample would give rise to small changes in

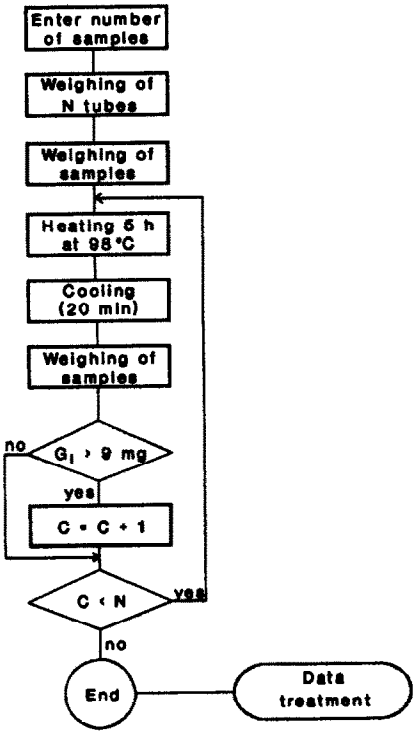

Fig. 2. Flow chart of the method.

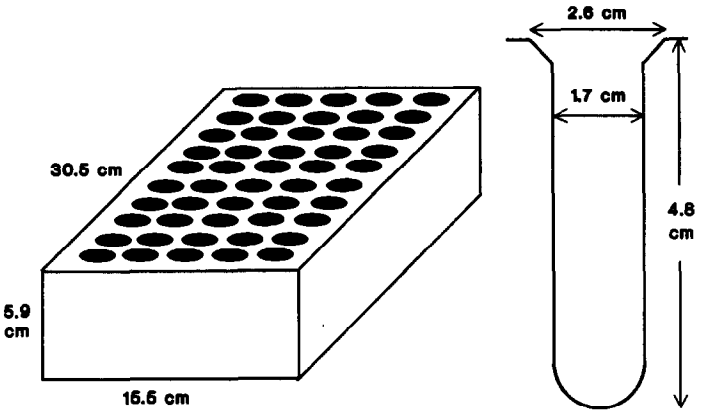

Fig. 3. Scheme of the heating block.

the weight to be monitored, which in turn would result in increased relative weighing errors. A 1-g sample was selected as it provided acceptable performance of the proposed method (see below) with less sample than other methods (2–3 g for Rancimat[6] and 10 g for AOM[7]) and a maximum sample thickness of 9 mm in the test-tube. This amount of sample is critical, as has been demonstrated[5] in order to achieve comparable results between laboratories.

(c) Cautions and peculiarities of the system. Special caution was exercised to avoid errors in the method arising from several potential sources, namely light, dust, electrostatic charges and delivery system.

(1) The heating block was protected by an opaque cover which did not hinder motion of the robot arm, but prevented light from directly impinging on the sample (which accelerated the oxidation process) and dust to settle (which would affect weighings). The use of a heating-plate instead of an oven had other additional advantages related to the robot safety: thus, the robot hand was not exposed to the typically high temperatures of ovens (*ca.* 100°) and the fingers were kept from contact with very hot vessels as the upper part of the test-tube was at a considerably lower temperature than the heated zone.

(2) Figure 4 shows how the test-tube underwent a weight loss between successive weighings under no heating. This arose from friction with the plastic material which caused electrostatic charges to build up; such charges could not be eliminated as all materials in contact with the test-tube (robot fingers included) were of insulator materials. This shortcoming, which has probably so far been overlooked in robotic methodologies was satisfactorily solved by having a small aluminium sheet establish electrical contact between the inside of the balance tube holder and the balance pant and drive the accumulated electrical charge to earth.

(3) Sample dispensing was different from that of PyTechnology owing to the high viscosity of oil. Zymate robots usually dispense liquids through a pipeting hand by twisting the wrist and leaning the pipette tip on the inner wall of the vessel. In this way, the liquid trickles down the tube wall, thus ensuring maximum accuracy. With oil samples and taking into account the subsequent heating steps, this dispensing procedure was inappropriate as the oil drops which remained randomly in the inner wall of the tube offered a large oxidation surface compared with the whole sample, so they were a source of high

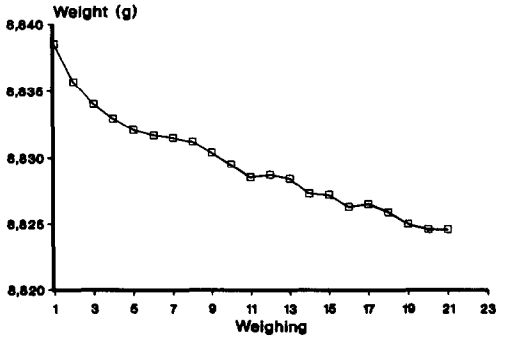

Fig. 4. Weight loss of a test-tube between successive weighings under no heating conditions.

irreproducibility. For this reason, the computer software was modified and the oil sample was dropped directly to the bottom of the test-tube without twisting the wrist of the robot at a small rate in order to avoid drops splashing on to the tube-walls.

(d) Temporal variables. The optimal heating, cooling and weighing times were also established. Inasmuch as the method is based on discrete exposure to the oxidation-promoting factor (a high temperature), each step must be precisely timed for every sample and any differences in this respect arising from the position of the tube in the batch be avoided as far as possible.

(1) Figure 5 shows the cooling weight change curves for a test-tube containing 1 g of oil after the heating block was removed. Although complete cooling required *ca.* 25 min, the weight remained stable after 15 min. However, a cooling time of 20 min was selected in order to increase the confidence level of the weighings.

(2) The heating time was chosen as a compromise since short heating times and high weighing frequency resulted in near-continuous monitoring of the oxidation curves, but detracted from evenness of the heating process and slowed down analyses as the heating time relative to the total analysis time was shorter. In addition, small weigh changes were more markedly affected by weighing errors. Figure 6 shows the real working times of the system for the analysis of a 100-sample batch heated for different times. It follows from the figure that too short heating times are inadvisable. On the other hand, too long heating times would provide insufficient

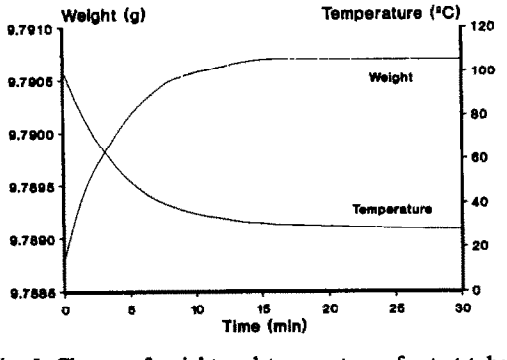

Fig. 5. Change of weight and temperature of a test-tube.

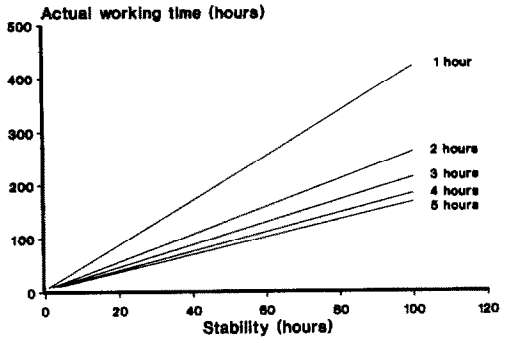

Fig. 6. Actual working time of the robot for analysis of 100 samples/batch by using different heating times.

information about the process, and hence give rise to errors, especially for unstable samples. A heating time of 5 hr was finally selected.

(3) The influence of the heating time on the overall kinetics was also investigated by heating a sample for different times (2.5, 5 and 10 hr). No differences between the oxidation curves were observed.

Processing of the chemical information

The results obtained by the robotic station were delivered as kinetic curves showing the weight changes with time. This information can be processed in different ways depending on how the time required for oil to become rancid is defined.

Some possible ways of defining the stability of oil are described in Fig. 7.

(1) The induction period (I), defined as the intercept of the tangent to the curve in the quasi linear portion of maximum slope (see Fig. 7).

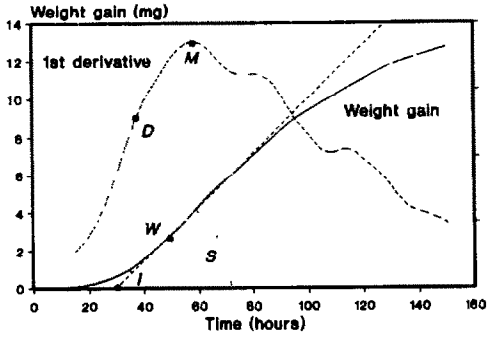

Fig. 7. Different ways of processing the experimental curves. *I*, induction; *W*, gain of a present weight; *S*, slope of the rising portion of the curve; *M*, and *D*, maximum and preset value, respectively, of the first derivative of the experimental curve.

(2) The slope of the above quasi linear portion of the curve (S).
(3) The time elapsed until the weight of the sample reaches a preset value (W).
(4) The time elapsed until the slope reaches a preset value (D) or the maximum value (M).

The use of one or another definition provides different results. Thus, one can: a) use one (or several) definitions to obtain characteristic results, or, b) use that (or those) definitions which provide results consistent with those obtained by other common methods (Rancimat and AOM). Since the final aim of this work was to solve the problems of the manual method (*viz* a low sample-throughput), option b) was the clear choice.

Among the above four definitions of stability, the fourth is the least precise as minimal changes in the kinetic curve give rise to great changes in its slope. In addition, there is no interval of maximum slope in many cases, but a plateau with a linear weight change. This definition was thus avoided.

Twenty virgin olive oil samples whose stability (between 25 and 170 hr) had been previously calculated by the Rancimat method were used for comparing with the proposal method. Only the heating time was considered here for greater consistency with the results provided by the Rancimat method.

The different correlations obtained between the selected parameter in the proposed method and the Rancimat stability are listed in Table 1. There was excellent correlation between the induction period of the robotic method and the Rancimat stability (also based on the induction period). The calculated correlation coefficient (0.9957) was similar to that obtained by Gutiérrez *et al.*[8] (0.9962) for comparison of Rancimat and AOM methods. Using other parameters resulted in lower correlations.

Table 1. Correlation between the Rancimat stability and several parameters of the curves of the robotic method†

y	x	a	b	r
Rancimat stability (hr)	Induction period (I) (hr)	−0.102	0.986	0.9957
Slope (S)	Rancimat stability (hr)	0.175	-5×10^{-4}	0.7502
W_2*	"	1.111	0.101	0.9893
W_4	"	2.110	0.111	0.9877
W_6	"	3.147	0.118	0.9871
W_8	"	4.259	0.128	0.9788
W_{10}	"	6.276	0.129	0.9733

*W_i: Elapsed time for a gain of i mg.
†General equation: $y = a + bx$. For more details, see text.

It is worth noting that the data from two samples in the batch (those corresponding to 148 and 179 hr of Rancimat stability) were discarded as the results provided by the robotic method were inconsistent with the rest and lower than those provided by the Rancimat method. This discrepancy could have arisen from the Rancimat method giving rise to changes in the concentration of the solution in the conductivity cell due to water evaporation in the long heating period required with very stable oils,[7] and therefore, there is uncertainty in the validity of these results. The robotic method does not have this drawback; this makes the proposed method especially suitable for olive oil, whose longer stability is well-known.

A BASIC program for data treatment was written in the dedicated PC. After all the samples have been oxidized, this program read the weights stored in the controller disk and calculated the induction period of every sample.

Features of the method

The reproducibility of the proposed method, calculated as the relative standard deviation of the results for 11 samples of the same oil, was evaluated with two samples of low (12 hr) and high stability (100 hr). The RSDs obtained were 8.7 and 2.6%, respectively. These results show that the precision of the proposed method is not good for unstable oils (less than 15–20 hours), which is not usual in virgin olive oil.

The throughput of the proposed method as implemented in the design station is 50 samples/batch. However, the throughput can be increased to 150 samples/batch by taking advantage of the free space around the robot arm, where other racks can be placed. This requires only minimal changes in the computer program, but always using Zymark's PyTechnology.

Comparison of the results

Table 2 shows the induction periods obtained by analysing the same batch of 20 samples of virgin olive oil by using both the Rancimat and the robotic method. There is a clear difference between the Rancimat stabilities for samples of 148 and 170 hr, which can be explained for the reasons cited above.

Table 2. Comparison of results of Rancimat and automated method

Rancimat (hr)	Robot (hr)
58	56
107	108
29	31
89	93
48	51
170	153
69	69
125	133
141	141
112	116
92	97
25	30
148	123
66	61
47	36
62	56
85	90
28	28
48	52
29	28

CONCLUSIONS

A robotic station was designed for the determination of the oxidative stability of virgin olive oil by using a fully automated method based on monitoring the weight changes of heated samples.

The different analysis steps are described in detail in order to facilitate implementation of the proposed method at other laboratories.

The main advantages of the proposed method compared to its well-established counterparts are full automation of the process and a much higher sample throughput (150 samples/batch), which amply offsets the higher initial cost of the equipment required.

Acknowledgements—Comisión Interministerial de Ciencia y Technologia (CICyT) is thanked for financial support (Grant No. PTR 89-0113).

REFERENCES

1. M. Valcárcel and M. D. Luque de Castro, *Automatic Methods of Analysis*. Elsevier, Amsterdam, 1988.
2. F. H. Zenie, *J. Autom. Chem.*, 1991, **13**, 39.
3. K. Robards, A. F. Kerr and E. Patsalides, *Analyst*, 1988, **113**, 213.
4. J. I. Gray, in *Flavor Chemistry of Fats and Oils*, Min & Smouse (ed.), p. 223. American Oil Chemist's Society, 1985.
5. J. A. García-Mesa, M. D. Luque de Castro and M. Valcárcel, *J. Am. Oil Chem. Soc.*, in press.
6. J. Frank, J. V. Geil and R. Feeaso, *Food Technol.*, 1982, **36**, 71.
7. *Official and Tentative Methods of the American Oil Chemist's Society*, Vol. 1, AOCS Champaign IL 1980, Method Cd 8-53.
8. F. Gutiérrez-Rosales, *Grasas y Aceites*, 1989, **40**, 1.
9. G. Reynhout, *J. Am. Oil Chem. Soc.*, 1991, **68**, 983.

Talanta, Vol. 40, No. 11, pp. 1601–1607, 1993
Printed in Great Britain.

0039-9140/93 $6.00 + 0.00

MULTIDATA TREATMENT APPLIED TO THE SIMULTANEOUS RESOLUTION OF CATECHOL–RESORCINOL MIXTURES BY KINETIC ENZYMATIC PROCESSES

E. GÓMEZ, A. CLADERA, J. M. ESTELA and V. CERDA*
Departament de Química, Universitat de les Illes Balears, 07071 Palma de Mallorca, Spain

Summary—This paper reports a multicomponent least-squares regression method based on the use of multiple standards for the simultaneous resolution of substrates involved in kinetic enzymatic processes. The proposed method was applied to the determination of catechol–resorcinol mixtures by oxidation with hydrogen peroxide in the presence of the enzyme peroxidase (EC 1.11.1.7) in a stopped-flow reversed flow injection system. The mathematical algorithm used is superior to other alternatives as it is not affected by side reactions between the oxidation products. The proposed method allows the simultaneous resolution of 50–150μM catechol and 30–180μM resorcinol over the wavelength range 340–500 nm. The concentration ranges can be modified by varying the injected amount of enzyme. The mathematical treatment is applied to the spectra of several standards and those of the samples, which are recorded 6 sec after the flow is stopped. This redounds to a high sampling frequency (up to 60/hr).

Multicomponent analysis methods have aroused increasing interest in the last few years on account of their ability to simultaneously resolve systems of two or more components by use of a variety of analytical techniques. However, because of the large number of data involved in the process, extensive development was only possible lately thanks to the advent of powerful computers in terms of processing capacity and data storage. Thus, a number of mathematical procedures including linear regression,[1] partial least-squares,[2] iterative methods[3] and factor analysis[4] currently allow mixtures to be resolved in very short times.

Multicomponent methods usually rely on the use of multichannel detectors to obtain a data set that is processed mathematically in order to determine the individual contribution of each analyte in a mixture. They simplify the analytical procedures required to a great extent as they allow several analytes to be determined without a previous separation step. UV–visible spectrophotometry has so far been the most frequently used technique in connection with multicomponent analysis.[5] The most commonly used kinetic enzymatic procedures use this technique and the initial slope or fixed time kinetic method, which have so far been applied to the determination of a wide variety of substances including metal ions and organic and biological substrates. As a rule, these determinations are highly selective thanks to the peculiar properties of the enzymes used. Alternative mathematical models such as the Kalman filter have been used in recent years to determine the rate constant and concentration of the substrate involved in this type of reaction. Thus, Rutan and Brown[6] addressed the kinetics of hydrolysis of *p*-nitrophenyl phosphate to *p*-nitrophenol by using the enzyme alkaline phosphatase.

Kinetic determinations of very similar substrates (*e.g.*, isomers), however are hindered by mutual interferences that cannot be overcome by the selective features of enzymes. Multicomponent determination techniques based on spectral differences between the analytes to be determined may come to the rescue in such cases. Also, unlike equilibrium methods, these techniques are in no way affected by the occurrence of background signals—provided they do not contribute to the kinetics of the process—as they will not vary over time. This type of determination has been addressed by some authors. Thus, Pardue *et al.*[7,8] accomplished simultaneous determinations by using real and simulated multipoint data, and a non-linear regression method. They also reviewed different aspects of kinetic methods in this context.[9] However, they did not use or even mention the possibility of using spectra for resolving simultaneous kinetic processes.

*Author for correspondence.

In continuation of previous research into the development of multicomponent analysis techniques[10–13] in this work we address the simultaneous resolution of kinetic enzymatic processes by applying a multistandard linear regression method to the kinetics of oxidation of various substrates by hydrogen peroxide, catalysed by the enzyme peroxidase (EC 1.11.1.7). We applied the method thus developed to the resolution of mixtures of catechol and resorcinol traces by using an automated FIA system and the stopped-flow mode for data acquisition.

EXPERIMENTAL

Reagents

A 0.1*M* phosphate buffer of pH 7.0 ± 0.1 was prepared from its monopotassium salt (Probus, PA, U.S.A.).

A peroxidase solution was made by dissolving 0.512 g of lyophilized enzyme (EC 1.1.11.7, purified from Grade II horseradish peroxidase, Boehringer Manheim, Germany) in 4 ml of 3.2*M* ammonium sulphate (Fluka, PA). The suspension thus obtained (D_1) was stored at 4° in a refrigerator and remained stable for at least 2 months. It was used weekly to prepare solution sets (D_2) by diluting 100 μl of D_1 in 25 ml of 3.2*M* ammonium sulphate which were subsequently refrigerated as well. Working strength solutions were made daily by dissolving 150 μl of D_2 in 10 ml of phosphate buffer. The working solutions thus contained 7.68 μg peroxidase/ml (1.5 U/ml, 25°, and guaiacol-hydrogen peroxide as substrate).

Individual standards of catechol and resorcinol of concentration $9.0 \times 10^{-3}M$ were prepared from PA-grade Sigma and Panreac chemicals, respectively.

Finally, a 0.030% hydrogen peroxide solution was made by dilution of 30% Panreac PA reagent.

Apparatus

The experimental set-up used for the automatic determinations is depicted in Fig. 1. It consisted of the following components:

A PC compatible computer for instrumental control and data acquisition and processing that was equipped with an HP-IB interface and a PC8255 I/O card from Flytech Technology.

Two laboratory-assembled valve electromechanical actuators that were commanded by the computer via the PC8255 card. One of them was used to effect enzyme injections and the other to divert the flow to the spectrophotometer inlet and enable stopped-flow readings.

A Hewlett-Packard HP-8452A diode array spectrophotometer furnished with a flow-cell of 18 μl void volume and 1-cm pathlength, and connected to the computer via the HP-IB interface.

An FIA manifold (Fig. 2) consisting of a Gilson Miniplus peristaltic pump, two valves (a Rheodyne injection valve and a Rheodyne six-way valve) that were switched by the mechanical actuator; PTFE tubing of 0.5 mm i.d. for reactors and the injection loop; a thermostatic bath and an automatic burette furnished with a 0.5 ml syringe intended to load the injection loop with the minimum possible consumption of enzyme.

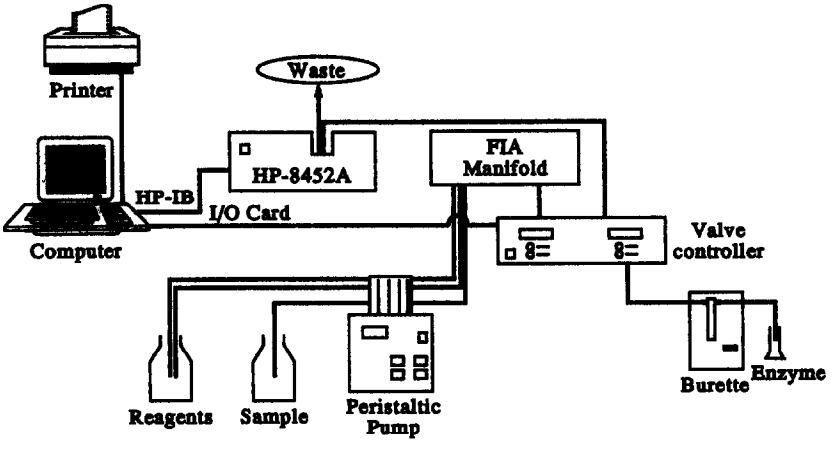

Fig. 1. Experimental set-up used for the simultaneous automatic determination of substrates involved in enzymatic kinetics.

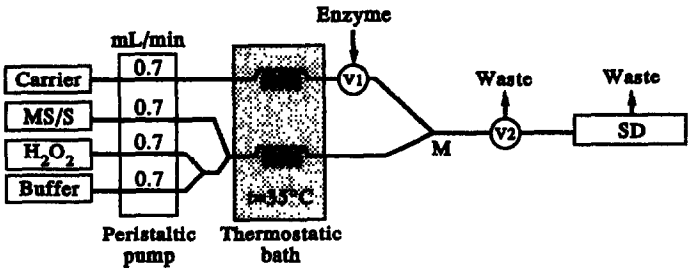

Fig. 2. FIA manifold used. Carrier and buffer: 0.1*M* phosphate, pH 7.0 MS/S: multiple standard/sample. V_1: enzyme injection valve. V_2: 6-way valve for stopping the flow. SD: spectrophotometric detector.

*Software**

We used essentially two programmes: DARRAY[14] and MULT13[15]. This latter was used in the multistandard mode: on the assumption that Beer's law is obeyed, the molar absorptivity of each component i at each wavelength j, ϵ_{ij}, is calculated by regression from mixtures of standards of each component at different concentrations. This requires solving an equation system at each wavelength given by

$$A_{jk} = z_j + \sum_{i=1}^{N} \epsilon_{ij} b c_{ik}; \quad k = 1 \ldots K \qquad (1)$$

where A_{jk} is the absorbance of standard k at wavelength j, z_j is the independent fitting term, b is the pathlength and c_{ik} is the concentration of component i in standard k. The above equation system can be solved by multiple linear regression provided the number of standards used (K) is greater than that of components. Solving the system will provide the ϵ_{ij} and z_j values, as well as the deviation of the fitting at each wavelength (D_j). The analyte concentrations in the samples can then be calculated by solving the overdimensioned equation system obtained by applying Beer's law to the mixture concerned at each working wavelength.

Procedure

Recording of the stopped-flow kinetic curves of the standards and sample. The process is started by setting reagents and a mixture of standards in motion along the manifold depicted in Fig. 2 and waiting for the system to stabilize. Then, an injection of 100 μl of the working solution of peroxidase is commanded and, 15 sec later—the time required for the maximum of the FIA peak to be reached—the flow is halted automatically in order to monitor the kinetic process. Subsequently, the computer commands loading of the injection coil with the enzyme solution and resumption of the flow. This cycle can be repeated as many time as required depending on the number of standards and replicates used.

Analytical data are acquired at 2-nm intervals over the wavelength range 250–550 nm and the absorbance corresponding to the 550 nm reading is subtracted. We used a data acquisition rate of 1 reading per second, even though this can be adjusted to the kinetic process concerned.

The same computer file where the kinetic curves of the multiple standards are stored can be used to save the kinetic data of the samples to be resolved. In this manner a single file can contain the data of all the standards required for calibration and sample analysis.

The above process is entirely carried out by the programme DARRAY.

Processing of data

Once the above computer file has been obtained, DARRAY saves the spectra of the different standards of the mixtures obtained at the preset time for data processing ($t = 6$ sec). These spectra are subsequently captured as multiple standards by the programme MULTI3 in order to perform calibration over the optimal wavelength range (340–500 nm in our case). Finally, the spectrum of the mixture to be resolved, recorded at the same time as those of the standards, is processed and the concentration of each analyte calculated.

RESULTS AND DISCUSSION

Optimization of experimental variables

The manifold employed is depicted in Fig. 2 and it was selected for the following reasons.

Reversed FIA manifolds use up very little reagent, which ensured minimal consumption of the enzyme.

*The software used in this work can be obtained on request from SCIWARE, Banco de Programas, Departament de Química, Universitat de les Illes Balears, 07071 Palma de Mallorca, Spain.

The enzyme was injected via V_1, which was placed as close as possible to the six-way valve V_2 in order to delay the start of the kinetic process as far as possible while allowing for efficient mixing with all other reactants.

The loops (0.5 m) that were immersed in the thermostatic bath (35°) were only intended to thermostat the stream containing the sample and carrier.

The injected volume used, 100 μl, was chosen as a compromise between a high sample throughput and low dispersion in order to achieve wide enough peaks to monitor the kinetics at their maxima.

The time elapsed between injection and the appearance of the maximum of the FIA peak was calculated previously (by using a dye) and was found to be 15 sec. The time elapsed between passage by the merging point (M) and stopping of the flow was also calculated (5 sec).

The oxidation reaction taking place up on injection of peroxidase (POD) can be represented by[16]

$$\text{Donor}(DH_2) + H_2O_2 \xrightarrow{\text{POD}} 2H_2O + \text{Oxidized donor}$$

where Donor denotes catechol and resorcinol in our case. The oxidized donor consists of several intermediate species presumably including semiquinone substances. The occurrence of radical intermediates from both catechol and resorcinol in their mixtures may account for the appearance of mixed coupling intermediates whose spectra would be different from those obtained in the presence of one component only. Under the working conditions used, this reaction only took place in the presence of the catalyst.

The absorption spectra of the oxidized forms of catechol and resorcinol, the maxima of which lie at 388 and 402 nm, respectively, are extensively overlapped.

However, we found the absorbance maximum of the two diphenol compounds to shift to shorter wavelengths with time, probably as a result of the occurrence of side reactions between intermediate radicals to yield other, new forms.

Thus, the kinetics of the mixtures were monitored by recording their absorption spectra over a given wavelength range (*e.g.*, 250–550 nm) at regular intervals (1 sec) by means of the diode array spectrophotometer. Each point of the kinetic curve was obtained by subtracting the absorbance measured at 550 nm from that obtained at a wavelength (*e.g.*, 388 nm) in order to offset the change in the refractive index arising from injection of the enzyme, thereby avoiding negative absorbance values.

The phosphate buffer and working temperature used were selected according to literature recommendations for similar processes.

With regard to the influence of the concentration of the different substances involved in the enzymatic reaction, we found H_2O_2 concentrations between 0.015 and 0.060% to have no effect on the initial reaction rate. We thus chose 0.030% as the working concentration. However, a linear dependence of the signals on the enzyme concentration throughout the range studied (2.56–7.68 μg peroxidase/ml) was obtained. We chose a concentration of 7.68 μg/ml as optimal—this can obviously be adjusted to the working concentrations of the substrates to be used.

Once the optimal working conditions were established, we calculated the linear determination ranges of the initial reaction rate *vs.* concentration plot and obtained 50–150μM for catechol and 30–180μM for resorcinol. The reproducibility in the initial rate for a mixture of the two diphenols was 3.4% ($n = 6$).

Resolution of catechol–resorcinol mixtures

A preliminary survey of the kinetic curves for the enzymatic action of peroxidase on the oxidation of the two substrates revealed both to conform to the Michaelis–Menten equation. Therefore, at initial substrate concentrations $[S]_0$ much smaller than the Michaelis constant, K_m, one can establish a linear relation between initial rate values and $[S]_0$—this is the typical working region for most enzymatic applications, even though some authors used alternative methodologies to extend the linear range beyond K_m.[17]

On the other hand, when the overall absorbance signal of the kinetic process arises from more than one substrate, the general procedure obviously cannot be used. Multicomponent analysis methods do allow mixtures to be resolved under these conditions. Among the various available options, that of multiple least-squares regression involves a fairly simple mathematical treatment that makes it advisable whenever the spectrum of each component to be determined or its oxidation product is known.

Table 1. Results and confidence intervals (95%) obtained in the resolution of catechol–resorcinol mixtures by using the multiple standard method

	[Catechol] (μM)		[Resorcinol] (μM)	
	Added	Found	Added	Found
S_1	100	107 ± 2	60	57 ± 2
S_2	100	93 ± 2	100	103 ± 2
S_3	50	50 ± 2	150	150 ± 3

Table 2. Catechol and resorcinol concentrations (μM) in the multiple standards used to resolve the mixtures in Table 1

	MS_1	MS_2	MS_3	MS_4	MS_5
Catechol	50	100	50	150	50
Resorcinol	50	50	100	50	150

However, the resolution of mixtures such as those of catechol and resorcinol poses some problems arising from side reactions between the oxidation products. Inasmuch as the oxidation products could not be readily identified, the customary regression procedure based on the use of individual standards of each of the substances significantly contributing to the overall signal was useless. Also, using the spectra of the two substrates was inadvisable as they would be fully overlapped and lie in an unsuitable region (274 nm). For the same reason, and due to the small absorbance values involved (a few milliunits), attempts at resolving the system by using an optimization method (*viz.* that of Gauss–Newton) for the kinetic curves of the samples from individual standards were also unsuccessful.

The above shortcomings can be circumvented by applying the multiple standard regression method[15] to the spectra of the oxidized forms. In this way, using mixtures of the two components in different proportions as standards will reproduce the same side reactions taking place in the sample. In practice, the regression procedure is applied to spectra recorded at the same time t as for the sample so that the results obtained may accurately reflect the concentration of each analyte.

Table 1 lists the results obtained in the resolution of three samples containing different proportions of the analytes. We used five mixtures of catechol and resorcinol at the concentrations given in Table 2, which provided significant information about their relative proportions. Even though, in mathematical terms, the system could be resolved with only four multiple standards, the deviations thus obtained were somewhat high, so we opted for using five standards. In resolving the mixtures at different times after halting the flow we found the results obtained to improve substantially within a few seconds of the start of the kinetic process.

Table 3 lists the concentrations obtained for each substrate in the three mixtures analyzed (S_1, S_2 and S_3) at times 0, 2, 4, 6 and 8 sec, as well as at saturation of the kinetic curve (120 sec). It follows from these results that both the concentrations and the confidence intervals obtained after 6 sec were quite reliable. On the other hand, the concentrations obtained at the saturation time were somewhat worse whereas the confidence intervals were slightly better. This can be ascribed to more reproducible spectra—absorbance values are greater than those measured at the beginning of the kinetic process—which, however, are also less accurate because of the side reactions involved. We thus chose to resolve the system with data from the initial kinetic segment, using a time of 6 sec following halting of the flow.

Figure 3 shows the kinetic curves yielded by two replicates of each of the three samples assayed (S_1, S_2 and S_3). The enzyme injection and flow stopping instants (the latter was

Table 3. Results and confidence intervals (95%) obtained in the resolution of catechol–resorcinol mixtures as a function of the time elapsed from halting of the flow

	S_1		S_2		S_3	
t (sec)	[Catechol] (μM)	[Resorcinol] (μM)	[Catechol] (μM)	[Resorcinol] (μM)	[Catechol] (μM)	[Resorcinol] (μM)
0	76 ± 3	71 ± 3	124 ± 3	89 ± 3	36 ± 3	151 ± 3
2	78 ± 5	75 ± 3	122 ± 5	85 ± 3	14 ± 5	170 ± 3
4	93 ± 5	61 ± 5	107 ± 5	99 ± 5	32 ± 6	156 ± 5
6	107 ± 2	57 ± 2	93 ± 2	103 ± 2	50 ± 2	150 ± 3
8	109 ± 3	57 ± 2	91 ± 3	102 ± 2	54 ± 2	149 ± 2
120	81 ± 1	66 ± 1	119 ± 1	94 ± 1	48 ± 1	149 ± 1

The catechol and resorcinol concentrations in S_1, S_2 and S_3 are given in Table 1.

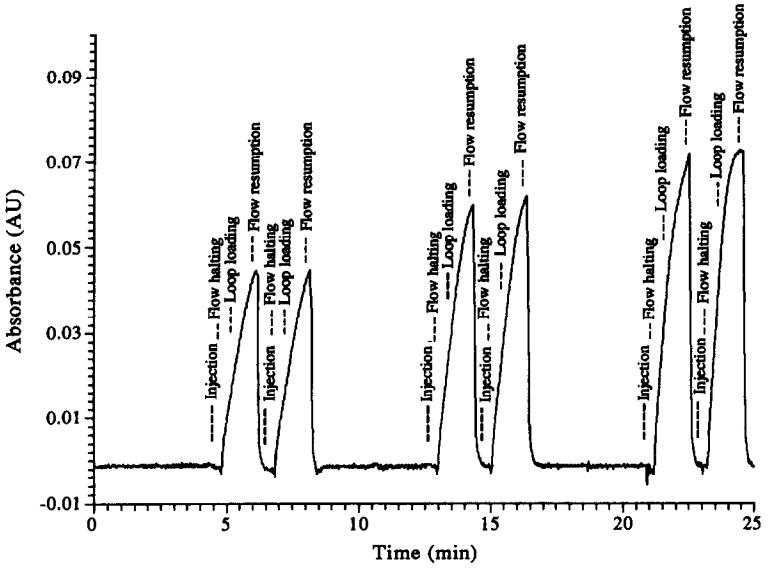

Fig. 3. FIA recording obtained on duplicate stopped-flow processing of samples S_1, S_2 and S_3. Enzyme injection, flow halting, the start of the loop loading for the next injection and resumption of the flow are signalled for each kinetics.

arbitrarily assigned $t = 0$), as well as the start of the loop loading process for the following injection ($t = 30$ sec) and flow resumption ($t = 120$ sec) are shown in the figure.

CONCLUSIONS

The results obtained testify to the usefulness of the multiple standard linear regression procedure for simultaneously resolving substrates on the basis of enzymatic reaction kinetics. Its advantages and disadvantages were clearly shown above.

The proposed method was automated by using an FIA system which allows the resolution of catechol–resorcinol mixtures within a few seconds of the start of the kinetic process by performing injections of the enzyme peroxidase. We found a set of five multiple standards to be more than adequate to ensure accurate resolution in spite of the very small absorbance values obtained as a result of working in the initial kinetic region.

The results were quite satisfactory in terms of accuracy, sensitivity and reproducibility, particularly taking into account that the chemical model used involved side reactions that would render resolution by any ordinary analytical method quite difficult.

In this work we resolved fixed-time kinetic enzymatic processes involving catechol and resorcinol only owing to the problems posed by the occurrence of side reactions between the oxidation products. However, the proposed procedure should be readily applicable to systems of more than two components provided they involve none of these undesirable side reactions.

Acknowledgements—The authors wish to express their gratitude of the DGICyT (the Spanish Council for Scientific and Technological Research) for funding this work as a part of Project PB 90–0359.

REFERENCES

1. G. Sala, S. Maspoch, H. Iturriaga, M. Blanco and V. Cerdà, *J. Pharm. Biomed. Anal.*, 1988, **6**, 765.
2. I. Lukkari and W. Lindberg, *Anal. Chim. Acta*, 1988, **211**, 1.
3. S. D. Brown, *ibid.*, 1986, **181**, 1.
4. B. Vandeginste, R. Essers, T. Bosman, J. Reijnen and G. Kateman, *Anal. Chem.*, 1985, **57**, 971.
5. B. Bermúdez, F. Lázaro, M. D. Luque de Castro and M. Valcárcel, *Analyst*, 1987, **112**, 535.
6. S. C. Rutan and S. D. Brown, *Anal. Chim. Acta*, 1985, **175**, 219.
7. W. E. Weiser and H. L. Pardue, *Anal. Chem.*, 1986, **58**, 2523.
8. C. P. Fitzpatrick and H. L. Pardue, *ibid.*, 1989, **61**, 2551.
9. H. L. Pardue, *Anal. Chim. Acta*, 1989, **216**, 69.
10. E. Gómez, J. M. Estela, V. Cerdà and M. Blanco, *J. Anal. Chem.*, 1992, **342**, 318.
11. A. Cladera, E. Gómez, J. M. Estela and V. Cerdà, *Intern. J. Environ. Anal. Chem.*, 1991, **45**, 143.
12. G. Turnes, A. Cladera, E. Gómez, J. M. Estela and V. Cerdà, *J. Electroanal. Chem.*, 1992, **338**, 49.

13. A. Cladera, A. Caro, E. Gómez, J. M. Estela and V. Cerdà, *Talanta*, 1992, **39**, 887.
14. A. Cladera, E. Gómez, J. M. Estela and V. Cerdà, *Analyst*, 1991, **116**, 913.
15. *Idem*, *Anal. Chim. Acta*, 1992, **267**, 95.
16. H. U. Bergmeyer, *Methods of Enzymatic Analysis*, Vol. II, 3rd Ed. Verlag Chemie, Germany, 1983.
17. M. P. Goren and J. E. Davis, *Clin. Chem.*, 1986, **32**, 2021.

Talanta, Vol. 40, No. 11, pp. 1609–1617, 1993
Printed in Great Britain.

0039-9140/93 $6.00 + 0.00

ON-LINE MICROWAVE-ASSISTED DIGESTION OF SOLID SAMPLES FOR THEIR FLAME ATOMIC SPECTROMETRIC ANALYSIS

M. DE LA GUARDIA*, V. CARBONELL, A. MORALES-RUBIO and A. SALVADOR

Department of Analytical Chemistry, University of Valencia, 50 Dr. Moliner St., 46100 Burjassot, Valencia, Spain

Summary—A new procedure has been developed for the on-line digestion of solids in a microwave oven. The direct injection in a water carrier flow of dispersions of solid samples in concentrated nitric acid, the merging of these slurries with 30% (v/v) H_2O_2 and the microwave-assisted digestion in a Teflon coil of 100 cm permit a fast and quantitative extraction of Cu and Mn from different solid matrices, such as vegetables, powdered dietary products and sewage sludges. The development of an appropriate interphase, in which digested samples are cooled and degassified, previous to their introduction into the nebulizer of a flame atomic absorption spectrometer, makes possible the full automatization of the digestion and measurement steps of the elemental analysis of solids and it provides a sample frequency of 180 injections per hour. The developed procedure has also been applied for Pb and Zn determination in certified sewage sludge samples, with accurate results obtained for Pb but low results found for Zn.

The use of microwave ovens improves the acid digestion[1–4] and the dry ashing of solids,[5] and it provides an alternative to the preparation of samples for their analysis by atomic spectrometry.

Microwave-assisted decomposition methods are less time consuming than traditional ones and they reduce the digestion step from several hours to a few minutes; thus, they have opened up new possibilities to the full automatization of the analysis of samples including not only the measurement step but also the sample preparation.

The on-line digestion of liquid samples, such as serum or blood samples, can be carried out without difficulty by using a quartz digestion coil introduced into a microwave oven.[6]

The digestion of solids in flow injection (FI) analysis usually requires a higher irradiation time than that reported for liquids and it supposes a more sophisticated manifold.[7]

Slurries, obtained by dispersion of solids in water, have been used for the direct introduction of samples in atomic spectrometry.[8–11] Also, slurries have been introduced directly into the atomization systems by flow injection.[12,13] However, in several cases, elements to be determined are not easily atomized from dispersed solids and they need previous treatment in order to dissolve or to extract them from the solid to the aqueous phase by leaching. This treatment can be carried out using closed flow systems.[14,15] Other approaches, based on the digestion of slurries, employ stopped-flow systems[16] or very long digestion coils (20 m), and in-line filters,[17] in order to obtain a solids-free acid solution.

The aim of the present work is to develop a simple and inexpensive system for the on-line digestion of solid samples based on: (i) the direct injection of acid slurries in an FI manifold, (ii) the use of a domestic microwave oven, without any modification, to improve the sample digestion and (iii) the development of an adequate interphase to couple the FI manifold and the nebulizer of a flame atomic absorption spectrometer, which permits the cooling and degassing of the digested samples, in order to perform a fast analysis of the samples with a high sample frequency.

EXPERIMENTAL

Apparatus

A Perkin–Elmer 5000 atomic absorption spectrometer, equipped with a multielemental hollow cathode lamp of Cr, Co, Cu, Fe, Mn and Ni and monoelemental lamps of Pb and Zn, was used to carry out absorbance measurements in the instrumental conditions, reported in Table 1.

*Author for correspondence.

Table 1. Instrumental conditions employed for the determination of Cu, Mn, Pb and Zn

Parameter	Cu	Mn	Pb	Zn
Wavelength (*nm*)	324.7	279.5	283.3	213.9
Lamp current (*mA*)	12	12	10	8
Slit (*nm*)	0.7	0.2	0.7	0.7
Burner height (*cm*)*	1.3	1.3	1.3	1.3
Acetylene flow (*l./min*)	1.3	1.3	1.2	1.2
Air flow (*l./min*)	12.1	12.1	12.1	12.1

*The burner height is the distance below the focal point of the optical system.

A domestic microwave oven (Balay Bahm 100) equipped with a 2450 MHz magnetron and with a nominal exit power of 650 W was employed for the digestion of samples, without any modification.

The manifold employed for the on-line digestion of slurries of solid samples is shown in Fig. 1. This manifold is a double channel assembly that includes two Rheodyne RS50 rotatory valves, which are operated at the same time in order to inject simultaneously the same volume of an acid slurry of the sample and a hydrogen peroxide solution. The two channels join in a Y-shaped merging zone and then the mixture passes through a Teflon digestion coil, located inside the microwave oven. This coil was introduced by making use of the vent holes of the oven and therefore no additional holes are required; thus there is no radiation leakage from the oven.

A Gilson P-2 Minipuls peristaltic pump, equipped with two vinyl chloride flexible tubes of 2.79 mm internal diameter, was employed for sample transport. All the parts of the manifold are made of Teflon and have 0.8 mm internal diameter.

A special interphase was designed to couple the FI manifold with the nebulizer of the atomic spectrometer (see Fig. 2). It consists of a 70 mm long glass tube (of 5 mm internal diameter) with an upper part 50 mm long (with an internal diameter of 26 mm). This form permits the degassing of the samples at the exit of the microwave oven, because, during the microwave irradiation of acid slurries in the presence of H_2O_2, a high amount of gases is produced. To avoid sample ejections, the end of the Teflon tubing, proceeding from the oven, is introduced into a fine glass tubing of 3 mm internal diameter. A waste vent, located 25 mm above the base of the interphase, avoids the excessive dispersion of samples when the aspiration flow (of the nebulizer) and the carrier flow (provided by the FI system) are not of the same order. An ice water cooling bath permits the cooling of the water carrier flow and condenses the sample plug before its introduction into the atomic spectrometer. The aspiration tubing of the nebulizer is introduced until the end of the interphase in order to carry out continuous aspiration of the solution coming from the microwave oven.

Reagents

A standard stock solution of Cu (1000 μm/g) was prepared from 1.0000 g of copper metal dissolved in a minimum volume of (1 + 1) HNO_3 and diluted to 1 l. with 1% (v/v) HNO_3. A stock solution of Mn was prepared from

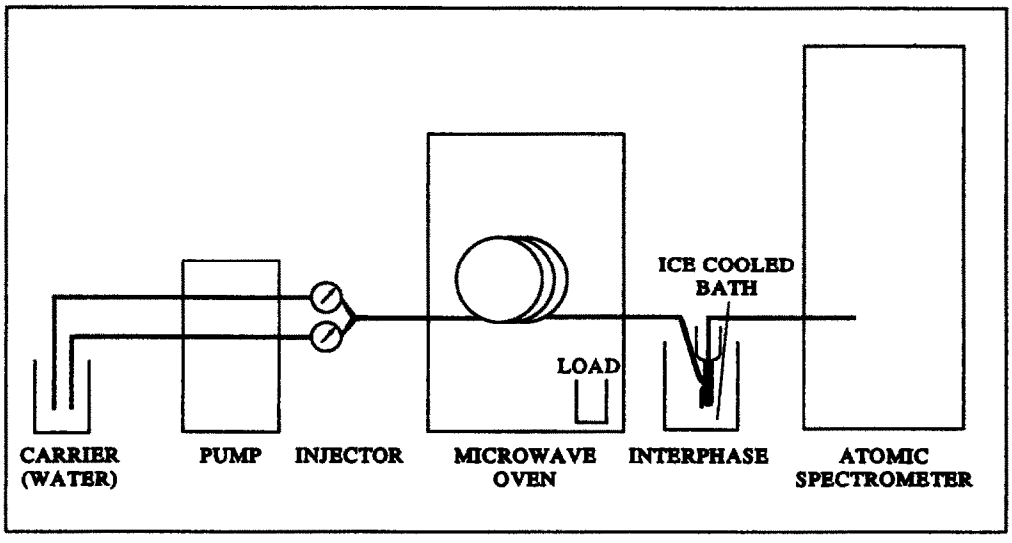

Fig. 1. FI manifold employed for the on-line digestion of solid samples.

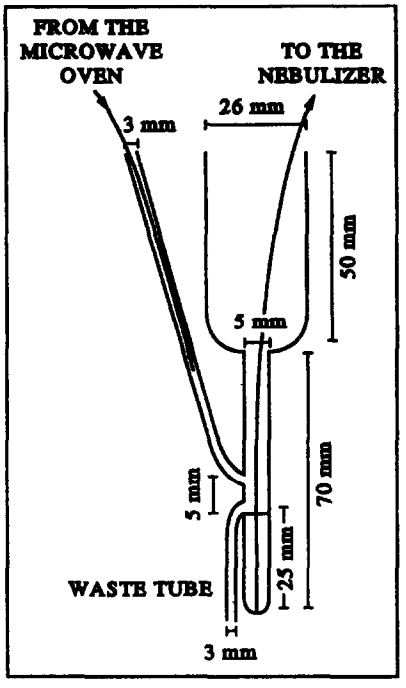

Fig. 2. Interphase employed to couple the FI manifold with the nebulizer of the atomic spectrometer.

1.0000 g of manganese metal dissolved in a minimum volume of HNO_3 (1 + 1) and diluted to 1 l. with 1%(v/v) HCl. A stock solution of 1000 μg/g of lead was prepared from 1.5980 g of analytical reagent grade $Pb(NO_3)_2$ dissolved in 1 l. distilled water and, a stock solution of 1000 μg/g of zinc was prepared from 1.0000 g of zinc metal dissolved in 30 ml of 5*M* HCl and diluted to 1 l. with distilled water. Working standards were prepared by diluting the stock solution with analytical grade concentrated HNO_3 (Panreac, Barcelona, Spain).

A hydrogen peroxide solution (30% v/v; Probus, Barcelona, Spain) was employed to improve the digestion of the nitric acid slurries of samples.

Samples

Real artichoke samples were supplied by the Instituto Valenciano de Investigaciones Agrarias (IVIA, Montcada, Spain). Full artichokes were dried in a thermal oven at 80° for several days, until a constant weight was obtained. They were then pulverized in a vegetable processor IKA model M-20, until a particle size lower than 100 μm was obtained.

Fine dry powder of dietary product samples (particle size lower than 100 μm) was provided by PENSA laboratories (Valencia, Spain).

Real sewage sludge samples were supplied from the water treatment plant of Pinedo (Spain). The sample was dried, in a thermal oven at 80°, and then pulverized in an agate ball mill until a fine powder with a particle size lower than 200μm was obtained.

Certified samples of tomato leaves (SRM 1573) and sewage sludges samples (CRM 144 and CRM 146) were employed to check the accuracy of the developed procedure.

General procedure

In order to study the effect of the experimental parameters on the on-line treatment of samples, 100 μl of dietary product slurries in concentrated nitric acid, containing 20 mg/ml of dispersed solids, were injected in a water carrier flow by using the previously described manifold, at the same time as 100 μl of H_2O_2 of different concentrations. Then, the mixture of both channels was passed through a reaction coil of 100 cm length, introduced into a microwave oven.

The aspiration flow rate of the nebulizer in these experiments was 8 ml/min and the total carrier flow rate was between 7 and 8 ml/min.

In the above mentioned conditions, the effect of H_2O_2 on the digestion of acid slurries and the influence of the parameters which control the digestion time were studied.

Recommended procedure

Between 20 and 250 mg of a solid sample were weighed in a glass beaker, 10 ml of concentrated nitric acid added and the mixture shaken vigorously to obtain a homogeneous dispersion. One hundred microlitres of this slurry were injected in the double channel manifold indicated in Fig. 1 at the same time as 100 μl of a 30% (v/v) H_2O_2 solution. Both carrier streams merge in a Y-shaped merging zone and then pass through a Teflon coil of 100 cm located inside a microwave oven. They were worked at 100% power level of the microwave oven and an additional load of 100 ml of distilled water was introduced into the oven, as a safety measure.

To obtain accurate results the total carrier flow in the FI system must be equal, or a little higher, than the aspiration flow of the nebulizer, and a value of the order of 8 ml/min of the latter is recommended.

Standard calibration curves can be established from the injection of different concentrations of conventional standards in concentrated nitric acid, treated in the same way as the samples.

RESULTS AND DISCUSSION

Stability of acid slurries

Solid dispersions, containing between 20 and 250 mg of sample in 10 ml of concentrated nitric acid, are stable for several minutes, after manual shaking, and the addition of surfactant agents is not required in order to improve their stability.

Figure 3 shows the variation of the absorbance at 500 nm, obtained using a UV–vis spectrophotometer, for an acid slurry containing 100 mg of a powdered dietary product dispersed in 10 ml of HNO_3 and then diluted 1:10 (in order to achieve absorbance values in the minor photometric error range). The continuous recording of absorbance as a function of time shows that, during the first 20 min, the change in the turbidity of the sample dispersion is lower than 10%. So, for the preparation of samples it is sufficient to obtain a fine particle size of the solid and to disperse these particles in HNO_3. After the homogenization of this dispersion, 100 μl of the slurry are injected in the FI manifold of Fig. 1.

Digestion of acid slurries

As was previously confirmed by using a closed FI manifold, the microwave-assisted digestion of vegetable and sewage sludge samples provides a quantitative recovery of inorganic elements in a few minutes when mixtures of nitric acid and hydrogen peroxide are employed.[15] So, for on-line digestion, solid samples were dispersed in concentrated nitric acid and then mixed with the same volume of H_2O_2 solution.

The on-line treatment of samples supposes a very low digestion time; so, the effect of digestion parameters such as digestion mixture and time of microwave irradiation were studied carefully in order to obtain the total recovery of the elements to be determined in a minimum time. The influence of the injection volume and solid content of the sample slurries was also studied.

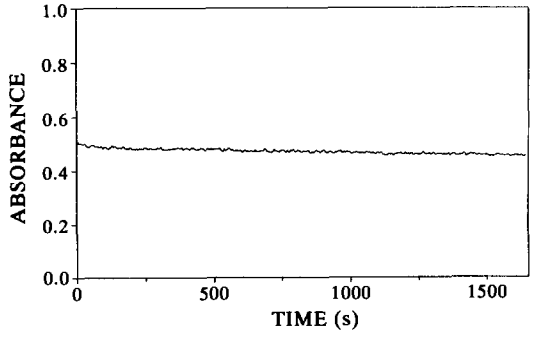

Fig. 3. Variation, as a function of time, of the absorbance at 500 nm of 10 mg of a dietary product dispersed in 10 ml HNO_3.

Table 2. Effect of H_2O_2 concentration on the determination of Cu and Mn in a dietary solid sample by on-line digestion

H_2O_2 (*v*/*v*) (%)	Cu ($\mu g/g$)	Mn ($\mu g/g$)
0	44 ± 4	11 ± 3
6	40 ± 2	43 ± 5
12	37 ± 3	47 ± 2
21	36 ± 2	50 ± 5
30	36 ± 2	45 ± 4
Actual concentration	41 ± 2	52 ± 2

Values of real concentration were established from the batch analysis of samples after a conventional wet ashing digestion. The total carrier flow employed was 7.8 ml/min and the content of solids in the slurries was 20 mg/ml. Results indicated are the mean of three independent analyses ± their relative standard deviation.

Digestion mixture

To improve the microwave-assisted digestion of acid slurries of solid samples, an H_2O_2 solution was added to increase the oxidizing power of HNO_3.

In the experimental conditions indicated in the general procedure, the effect of different H_2O_2 concentrations on the recovery of Cu and Mn was studied.

Table 2 summarizes the results found in the analysis of a real sample for the determination of Cu and Mn, and, as can be seen, the addition of H_2O_2 is necessary to obtain accurate concentration values of the same order as those found by a conventional wet ashing digestion procedure (real concentration) for Mn; however, a simple treatment with HNO_3 seems to be enough to obtain total recovery of Cu.

Digestion time

The digestion time of samples in the manifold employed, for a fixed internal diameter of manifold tubing, depends on the reaction coil length and the carrier flow rate. Therefore, we studied the effect of these two parameters on the determination of Cu and Mn in a sewage sludge sample, in order to obtain a good recovery and to take the shortest time possible.

A 0.8 mm internal diameter Teflon tubing was used, because tubing with diameters lower than this could be blocked easily with slurries and the use of tubing with a diameter higher than 0.8 mm could cause an excessive dispersion of samples (results not shown).

Table 3. Effect of digestion coil length on the recovery of Cu and Mn from slurries of sewage sludge

Coil length (*cm*)	Carrier 6.2 *ml/min* Cu ($\mu g/g$)	Carrier 8.8 *ml/min* Cu ($\mu g/g$)
50	720 ± 30	830 ± 50
100	890 ± 50	780 ± 20
200	780 ± 90	360 ± 30
250	860 ± 70	600 ± 60
Actual concentration of Cu	820 ± 2 $\mu g/g$	
Coil length (*cm*)	Carrier 6.2 *ml/min* Mn ($\mu g/g$)	Carrier 8.8 *ml/min* Mn ($\mu g/g$)
50	111 ± 7	145 ± 5
100	131 ± 8	87 ± 3
200	120 ± 10	50 ± 6
250	120 ± 10	54 ± 5
Actual concentration of Mn	141 ± 2 $\mu g/g$	

Note: aspiration flow was 8.4 ml/min. Data are the average of three independent analyses $\pm$ the standard deviation, for different slurries of the same solid sample.

Reaction coil length

Table 3 summarizes the results found for the digestion of a real sewage sludge sample by using different digestion coil lengths (from 50 to 250 cm) at two different carrier flow rates (6.2 and 8.4 ml/min) and for a fixed nebulizer aspiration flow of 8.4 ml/min. The comparison between the concentration values found for Cu and Mn with the actual concentration values, determined previously by flame absorption analysis after pressurized total acid digestion of these samples, provides information about the effect of the digestion time on the accuracy of the developed procedure.

The data on Table 3 indicate that in only few cases were accurate results found. These data show that the use of high length values of the reaction coil did not provide any enhancement of the digestion of samples, especially when a carrier flow of 8.8 ml/min was employed. An increase in the reaction coil length increases the residence time of the sample in the oven; however, we have observed that an increase in the digestion time provide an excessive amount of gases, which modifies the flow at the exit of the microwave oven and causes the gas segmentation of the sample plug. This latter effect can cause losses in the interphase, especially when high carrier flows are employed, and this could explain the bad precision values and the low recoveries obtained when long digestion coils were used. From these preliminary experiments, we selected a length of 100 cm for the digestion coil and then studied carefully the effect of the carrier flow for different values of the nebulizer aspiration flow.

Aspiration and carrier flow rates

The coupling between the FI manifold and the nebulizer makes necessary an adequate equilibrium between the carrier and the aspiration flows. The interphase mentioned above was developed in order to compensate the differences between these two flows, because the use of carrier flow values lower than the aspiration flow could cause instability of the measurements, due to the segmentation of the flow. On the other hand, the use of a carrier flow higher than the aspiration flow causes losses of the sample in the interphase.

The volume of the interphase, under the waste vent, was approximately 500 μl to assure a low dispersion of the digested samples and a sufficient amount to avoid the hold-up of the aspiration flow.

A series of experiments for the digestion of real dietary product samples was carried out in order to check the most appropriate flow values.

Table 4 summarizes the sensitivity and accuracy values found for the determination of Cu and Mn using different aspiration and carrier flows. It can be seen that the use of an aspiration flow of 7.7 ml/min provides more sensitive results than the use of a flow of 5.4 ml/min. On the other hand, carrier flow values lower than the aspiration flow provide inaccurate results. An aspiration flow of 7.7 ml/min and a carrier flow of 8.8 ml/min seem to be the most adequate conditions for the determination of both Cu and Mn in dietary samples. For these two carrier flows and for a digestion coil of 100 cm, the residence time of the samples in the microwave oven is of the order of 5 sec. However, in this

Table 4. Effect of the carrier flow and aspiration flow on the concentration fond for Cu and Mn in the analysis of dietary samples

Carrier flow	Aspiration flow	Slope	Cu ($\mu g/g$)	Error (%)	Slope	Mn ($\mu g/g$)	Error (%)
3.6	5.4	0.007	34.8 ± 0.1	−15	0.004	60 ± 14	+15
5.3	5.4	0.008	37.6 ± 0.1	−8	0.007	48.7 ± 0.1	−6
7.0	5.4	0.007	44 ± 7	+7	0.005	43.5 ± 0.1	−16
5.3	7.7	0.009	40 ± 5	−2	0.009	34 ± 3	−35
7.0	7.7	0.01	39 ± 4	−5	0.011	46 ± 5	−12
8.8	7.7	0.009	44 ± 3	+7	0.008	54 ± 6	+4
Actual concentration			41 ± 2			52 ± 2	

Note: The slope values of the calibration curves obtained in each set of experimental conditions are expressed in absorbance units per mg/l. The carrier flow and the aspiration flow are expressed in ml/min. In all cases a digestion coil length of 100 cm was employed. ± the standard deviation. The relative errors, expressed as percentages, were calculated from the difference between results found in the FI mode and actual values.

short period of time Cu and Mn are quantitatively extracted from the solid matrix.

In the above conditions, the dispersion coefficient of the manifold is equal to 15, taking into account that samples are diluted 1:2 with H_2O_2 and that the interphase also causes additional dispersion.

On the other hand, when acid slurries of real samples were injected in the FI manifold, at the same time as H_2O_2, carrying out the transport of samples without irradiation, the recovery of Cu was 91% in the sewage sludge sample and 66% in the dietary product sample, and for Mn, only a 79% recovery was found for sewage sludge and 33% for the dietary product. Thus, the microwave irradiation of samples is absolutely necessary in order to obtain accurate results in the determination of the elements studied.

An important aspect of the continuous on-line digestion of slurries is that the microwave irradiation of a sample plug, containing HNO_3 and H_2O_2, provides a high amount of gases, which improves the sample digestion, but can also cause problems of drawing back the carrier flow. So, the use of high values of this latter parameter is necessary. In the recommended conditions we have not encountered flow problems during working sessions of 1 or 2 hr and using a conventional peristaltic pump.

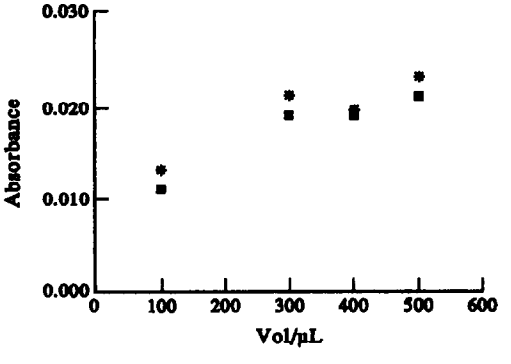

Fig. 4. Effect of the injection volume on the sensitivity of the determination of Cu in a dietary product sample by on-line digestion and FI atomic spectrometry. Absorbance values correspond to a standard solution of 1 mg/l (*) and a dietary product sample slurry with a similar content of Cu (■).

Effect of the injection volume

Figure 4 shows, as an example, the effect of the volume injected on the absorbance of Cu; it can be seen that the absorbance values increase when the sample volume increases, this effect being similar for standards and samples.

In these experiments, a standard acid solution of 1 mg/l and slurries of 500 mg of a dietary product sample (containing 41 ± 2 $\mu g/g$ of Cu) dispersed in 25 ml of HNO_3 (which corresponds to a Cu concentration of the order of 1 mg/l) were employed.

From the comparison between results found by on-line digestion in FI atomic spectrometry and those obtained in batch analysis (results not shown), it can be concluded that the injection of slurry volumes greater than 100 μl does not improve the accuracy of the developed procedure, but the use of high sample volumes reduces the sample frequency and could cause damage in the nebulizer due to the introduction of high amounts of acid. So, an injection volume of 100 μl was selected for the determination of elements which does not require a high sensitivity.

Effect of solid content

The direct injection of slurries in an FI system could cause clogging problems in different parts of the manifold and so it is important to establish the amount of dispersed solids that can be processed without problems.

Table 5. Effect of solid content of slurries on the determination of Cu and Mn in a dietary sample

Sample mass (*g*/10 *ml*)	Cu (*μg/g*)	Mn (*μg/g*)
0.1242	49 ± 6	56 ± 4
0.1705	41 ± 7	57 ± 5
0.2308	44 ± 3	57 ± 4
0.2620	50 ± 4	53 ± 5
0.2797	45 ± 4	47 ± 2
Actual concentration	41 ± 2	52 ± 2

Table 5 summarizes the results found in the determination of Cu and Mn in a dietary product sample for different amounts of sample, dispersed in a total volume of 10 ml of concentrated nitric acid. It can be seen that the content of solids does not seem to be a critical parameter on the accuracy and reproducibility of the analytical results, because in most cases values of the same order as the actual ones were found in FI atomic spectrometry.

To obtain a better representation of the solid samples the sample amount taken must be greater than or equal to 20–30 mg/ml.

Another way to increase the repeatability of the analysis of solids could be the use of higher sample amounts dispersed in higher acid volumes. However, the results in Table 6 show that, for a content of dispersed solid of the order of 20–25 mg/ml, the repeatability of the results found for the determination of Cu and Mn is similar for the different sample masses assayed.

Analysis of real and certified samples

In order to check the applicability of the developed procedure, three real samples of different nature, artichoke, dietary and sewage sludge, and three certified samples were analysed by the proposed method. The results found were compared with those certified or obtained by continuous aspiration after a traditional pressurized wet ashing digestion. Table 7 summarizes the results found for the proposed method, which have been tested by comparing them with those obtained by using the reference method. The *F*-test has been applied in order to check if the two methods provide standard deviations which are not significantly different and the *t*-test has been used to verify whether the difference between the means obtained by both methods differs significantly from zero. The critical values for *F* and *t*, for a confidence level of 95% and $n_1 + n_2 - 2$ degrees of freedom, are 19.16 and 2.78, respectively.[18]

In the Cu determination there is no significant difference between the two variances, except in the case of the real sewage sludge sample. The obtained values of *t*, for all the samples, are lower than the critical value; so, it can be assumed that the means of the results given by the two methods are equal.

In the Mn determination there is no significant difference between the two variances of each sample. Using the *t*-test, it can be assumed that the means of the results given by the two methods are equal except in the case of the certified CRM-144 sample, a domestic origin sewage sludge, probably due to the presence of very stable chemical forms of Mn.

Analytical features of the developed procedure

The FI flame atomic absorption procedure developed for the determination of Cu and Mn in solid samples permits a fast analysis.

Figure 5 shows, as an example, the typical FI recording obtained for the determination of Mn in certified samples. The time scale shows that more than 180 injections per hour can be carried out.

The high dispersion of slurries into the FI manifold reduces the analytical sensitivity of the flame atomic spectrometric measurements and so the limit of detection found for Cu determination is 0.033 μg/ml (for a probability level of 95%) which is equivalent to 1.2 μg/g of the dispersed solid. For Mn the obtained limit of detection is 0.037 μg/ml; thus, a minimum con-

Table 6. Effect of the dispersed sample mass on the determination of Cu and Mn in a dietary sample

Sample mass (*g*)	Dilution volume (*ml*)	Cu (*μg/g*)	RSD (%)	Mn (*μg/g*)	RSD (%)
0.2620	10	50 ± 4	8	53 ± 5	9
0.5239	25	47 ± 3	6	65 ± 2	3
1.0018	50	45 ± 3	7	62 ± 3	6
2.5955	100	45 ± 4	9	67 ± 6	9
Actual concentration		41 ± 2		52 ± 2	

Note: all the results are the average of five independent analyses of the same sample ± their standard deviation. RSD, relative standard deviation.

Table 7. Analysis of real and certified samples

Sample	Cu (μg/g)				Mn (μg/g)			
	Method 1 (reference)	Method 2 (proposed)	F	t	Method 1 (reference)	Method 2 (proposed)	F	t
Artichoke	—	—	—	—	54 ± 1	55 ± 4	16	0.42
Dietary	41 ± 2	41 ± 2	1	0	52 ± 2	50 ± 6	9	0.55
Sewage sludge	820 ± 3	826 ± 22	53	0.47	140 ± 2	144 ± 4	4	1.55
SRM 1573	—	—	—	—	238 ± 7	238 ± 7	1	0
CRM 146	713 ± 26	704 ± 13	4	0.38	449 ± 13	440 ± 20	2.37	0.65
CRM 144	934 ± 24	960 ± 10	2.25	1.73	588 ± 24	480 ± 20	1.44	5.99

F was calculated from the quotient between the variances of both methods, this quotient always being ≥ 1.

$$t = \left| \frac{\bar{x}_1 - \bar{x}_2}{\sqrt{s^2\left(\frac{1}{n_1} \frac{1}{n_2}\right)}} \right|$$

X_1 and X_2 being the average concentration obtained by each method, n_1 and n_2 the number of analyses and S^2 a pooled estimate of variance,

$$S^2 = \frac{[(n_1 - 1)S_1^2 + (n_2 - 1)S_2^2]}{n_1 + n_2 - 2}.$$

centration of 1.3 μg/g in the solid sample is required.

The relative standard deviation obtained from five independent analyses of the same sample varies from 1 to 5% for Cu determination and from 2.7 to 12% for Mn, as a function of the different nature of the sample and the different concentration of the elements to be determined.

The above mentioned features show that the developed method can be applied for the accurate determination of Cu and Mn in a wide variety of solid samples, but it cannot be applied for the determination of very low concentrations.

Determination of Pb and Zn in sewage sludges by the recommended procedure

In order to demonstrate the applicability of the developed methodology for the analysis of solids, elements other than those studied were determined in slurries of certified sewage sludge samples. Table 8 shows that Pb can be accurately determined using the recommended procedure, but for the determination of Zn inaccurate results were found for the analysis of a domestic origin sewage sludge and, in summary, results found evidence that some samples need a stronger treatment to quantitatively leach the elements to be determined.

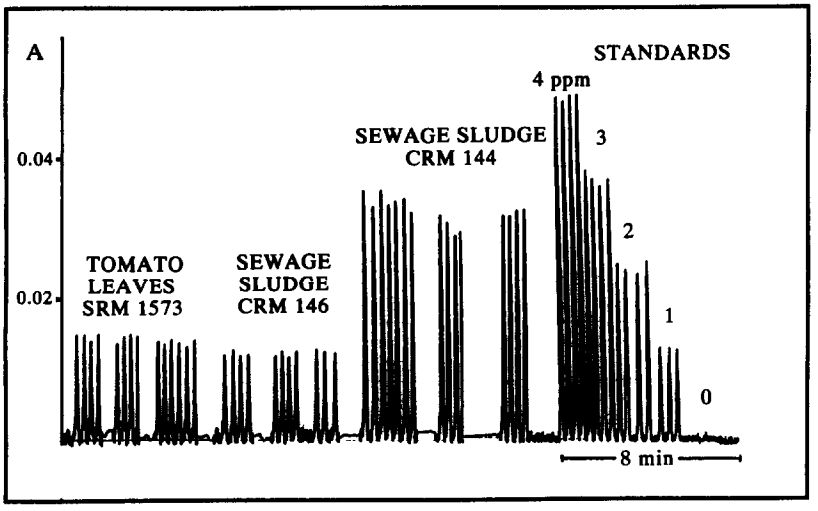

Fig. 5. FI recording obtained for the determination of Mn in certified samples. Records correspond to the injection of different acid standards and a series of injections of acid slurries of samples. In all cases, samples and standards were irradiated on-line following the proposed procedure.

Table 8. Determination of Pb and Zn in certified sewage sludge samples by on-line digestion and FI atomic spectrometry

	Pb (μg/g)			Zn (μg/g)		
Sample	Certified	Found	Error (%)	Certified	Found	Error (%)
CRM 146	1270 ± 28	1270 ± 80	—	4059 ± 90	3800 ± 150	−6
CRM 144	495 ± 19	505 ± 8	+2	3143 ± 103	2500 ± 100	−20

Safety considerations

The modification of a domestic microwave oven in order to be used in FI analysis can cause safety problems related to radiation leakage, which can be found when systems have been modified by drilling holes in the walls of the oven. In our case, we have employed the vent holes of the oven to introduce the Teflon tubing and so radiation leakage does not occur.

The introduction of an additional load of water into the oven is recommended in order to avoid magnetron damage if the oven operates with little or no load.

The use of a Teflon tubing of 0.8 mm internal diameter as digestion coil has provided good results; we have found no liquid or fume losses, nor coil damage, during 4 months working with the same coil.

The glass interphase is essential in avoiding acid leakages and it can be adapted without special safety precautions. It provides a cooling system in which acid vapours are condensed and its special design avoids acid ejections when samples are irradiated.

The only safety conditions required by the proposed method are related to the handling of sample slurries in concentrated acid, which must be treated carefully in order to avoid operator damage.

CONCLUSIONS

The developed procedure provides automation of the sample digestion and measurements steps of the determination of Cu and Mn in different types of solid samples. The method is six times quicker than those previously reported for the on-line digestion of solids and does not require the use of a closed flow system nor to work in the stopped flow mode. This method can also be applied to the determination of Pb and Zn in sewage sludges.

Acknowledgements—This work has been carried out with the financial support of the Spanish CICYT Project PB 88-0351. A. Morales-Rubio acknowledges the FPI grant from Ministerio de Educación y Ciencia.

REFERENCES

1. H. M. Kingston and L. B. Jassie (eds), *Introduction to Microwave Sample Preparation: Theory and Practice*. American Chemical Soc., Washington, DC, 1988.
2. M. de la Guardia, A. Salvador, J. L. Burguera and M. Burguera, *J. Flow Injection Anal.*, 1988, **5**, 121.
3. H. Matusiewicz and R. E. Sturgeon, *Prog. Anal. Spectrosc.*, 1989, **12**, 21.
4. A. Morales, F. Pomares, M. de la Guardia and A. Salvador, *J. Anal. At. Spectrom.*, 1989, **4**, 329.
5. A. Morales-Rubio, A. Salvador and M. de la Guardia, *Fresenius' J. Anal. Chem.*, 1992, **342**, 452.
6. M. Burguera, J. L. Burguera and O. M. Alarcón, *Anal. Chim. Acta*, 1986, **179**, 351.
7. M. Burguera, J. L. Burguera and O. M. Alarcón, *Anal. Chim. Acta*, 1988, **214**, 421.
8. F. J. Langmyhr and G. Wibetoe, *Prog. Anal. At. Spectrosc.*, 1985, **8**, 193.
9. L. Ebdon and A. Lechotycki, *Microchem. J.*, 1986, **34**, 340.
10. N. J. Miller-Ihli, *J. Anal. At. Spectrom.*, 1988, **3**, 73.
11. Z. A. Benzo, M. Velosa, C. Ceccarelli, M. de la Guardia and A. Salvador, *Fresenius' Z. Anal. Chem.*, 1991, **339**, 235.
12. R. Martinez-Avila, V. Carbonell, M. de la Guardia and A. Salvador, *J. Assoc. Off. Anal. Chem.*, 1990, **73**, 389.
13. R. Martinez-Avila, V. Carbonell, A. Salvador and M. de la Guardia, *Talanta* 1993, **40**, 107.
14. V. Carbonell, M. de la Guardia, A. Salvador, J. L. Burguera and M. Burguera, *Anal. Chim. Acta*, 1990, **238**, 417.
15. V. Carbonell, A. Morales-Rubio, A. Salvador, M. de la Guardia, J. L. Burguera and M. Burguera, *J. Anal. At. Spectrom.* 1992, **7**, 1085.
16. V. Karanassios, F. H. Li, B. Liu and E. D. Salin, *J. Anal. At. Spectrom.*, 1991, **6**, 457.
17. S. J. Haswell and D. Barclay, *Analyst*, 1992, **117**, 117.
18. J. C. Miller and J. N. Miller, *Statistics for Analytical Chemistry*. Ellis Horwood, Chichester, 1984.

Talanta, Vol. 40, No. 11, pp. 1619–1623, 1993
Printed in Great Britain.

0039-9140/93 $6.00 + 0.00

A BIOSENSOR FOR FERRIC ION

J. M. BARRERO, M. C. MORENO-BONDI, M. C. PÉREZ-CONDE and C. CÁMARA
Department of Analytical Chemistry, Faculty of Chemistry, Complutense University, 28040 Madrid, Spain

Summary—A new biosensor for monitoring iron has been developed. The active solid phase is pyoverdin, a natural fluorescent pigment biosynthesized by *Pseudomonas fluorescens* immobilized on controlled pore glass (CPG) and packed in a quartz flow-through cell. The biosensor is very selective for iron(III) and can be easily regenerated in about 2 min by passing 1*M* HCl through the cell. The optimum conditions and analytical characteristics (detection limit, precision and linear range) for the new sensor in solution (DL = 10 ng/ml) and in immobilized form (DL = 3 ng/ml) are reported. The biosensor has good stability and can be used continuously over a period for at least 3 months (over 1000 determinations). The sensor was successfully applied to determine iron in different water samples. There were no significant differences between the new method and the Inductively Coupled Plasma Atomic Emission Spectroscopy (ICP–AES) reference method at the 95% confidence level.

Under iron deficiency conditions, most microorganisms synthesize iron carrier molecules called siderophores, which solubilize iron and transport it into the cell, and are considered a high specific transport system.[1] The bacterium *Pseudomonas fluorescens* is characterized by the excretion of pyoverdin, a yellow–green water soluble fluorescent siderophore. The structure of many pyoverdins has been elucidated by high field nuclear magnetic resonance (NMR) spectroscopy.[2] They consist of a peptide and, bound to it, a chromophore derived from 2,3-diamino-6,7-dihydroxyquinoline common to all pyoverdins. Each pyoverdin contains 3 bidentate chelating groups: a catechol group located on the chromophore and either two hydroxamates (as *N*-hydroxyornithines acylated on the nitrogen atom, or cyclic) or one hydroxamate and one hydroxyaspartic acid, belonging to the peptide portion. Each strain of *Pseudomonas fluorescens* produces several pyoverdins possessing the same peptide and differing only in the side chain bound to the chromophore. From strain to strain, the peptide can vary considerably.

Siderophores in general are characterized by the following properties: (1) they specifically complex Fe(III) and have a weak or negligible affinity for Fe(II), and (2) the Fe(III) complexes have very high stability constants[3] (about 10^{32}). These properties make pyoverdin a promising agent for iron determination and for the construction of an optical biosensor.

The development of chemical optical sensing of chemical species using an immobilized reagent[4,5] has provided a novel technique for "*in situ*" analyte monitoring without reagent consumption.

The most common analytical techniques for iron determination are flame atomic absorption and Vis–UV spectrophotometry, although the former is not sensitive enough to determine concentrations at the ng/ml level and the latter is not sensitive or selective enough for many purposes. A coulometric method has also been employed for seric iron determinations, although the colorimetric methods are considered more accurate for this type of measurements.[6] An optical fiber Fe(III) sensor using Chromazurol S immobilized on an ionic exchanger[7] has been described in the literature. This reflectance sensor showed a linear response range between 0.2 and 2.5 ppm but the measuring procedure was not appropriate for continuous determinations. This lack of suitable sensors prompted us to develop a biosensor for iron(III) measurements using the highly selective pyoverdin pigment. This paper describes the conditions for pyoverdin immobilization on CPG as well as the optimum chemical and physical variables for the fluorimetric determination of Fe(III) in a continuous flow-system.

EXPERIMENTAL

Apparatus

Fluorescence intensity measurements were made on a Perkin-Elmer LS-50 spectrofluorometer, equipped with a xenon-lamp as light source and an IBM Model 55 SX computer. This set up

Table 1. Optimum conditions to iron determination using pyoverdin immobilized and in aqueous solution

Parameters	Aqueous solution	Immobilized Pyoverdin
Maximum of excitation	390 nm	500 nm
Maximum of emission	465 nm	552 nm
pH	6.5	4.5
Buffer	0.05 *M* MES	0.01 *M* Biphtalate/Phtalate
Regeneration	—	1*M* HCl
Flow rate	—	5 ml/min

was used in combination with a Hellma flow quartz cell (3 mm light path). All measurements were made with 5 nm band widths for the emission and excitation monochromators. All spectra were uncorrected. A simultaneous ICP–AES Jobin Yvon JY-48 spectrometer was used as reference technique. Absorbance readings were made on a Hewlett Packard 8452-A diode array spectrophotometer. Readings of pH were made on a Crison 2001 pH-meter and temperature control was effected by means of a thermostated bath. A Gilson Minipuls 2 pump was used to pump all the solutions.

Reagents

Analytical reagent-grade chemicals were employed for the preparation of all solutions. Freshly prepared Milli-Q (Millipore) ultrapure water was used in all experiments. A 1000 μg/ml Fe stock solution was prepared by dissolving $Fe(NO_3)_3 \cdot 9H_2O$ in 1%HNO_3 and titrating it with potassium permanganate.

Pyoverdin was biosynthesized and purified from *Pseudomonas fluorescens*, strain AR-11, by a modified version of the method described by Meyer and Abdallah.[8] *P. fluorescens* was grown in a PMS_7Ca iron-deficient culture medium consisting of *N,N*-bis-[2-hydroxyethyl]-2-aminomethane sulphonic acid, sodium pyruvate, magnesium sulphate, ammonium chloride, dipotassium phosphate and calcium chloride. The pigment was isolated from the supernatant by centrifugation and passed through a G-25 Sephadex column. The eluate fractions were analyzed spectrophotometrically and only those with a peak in the visible region ($\lambda = 460$ nm) and an absorbance above 0.2 were used and treated with an excess of 8-hydroxyquinoline to remove traces of iron.

Controlled pore glass with different pore size (237 and 460 Å, particle size 37–74 microns was obtained from Pierce).

Buffer solutions like 2[*N*-morpholino]-ethanesulphonic acid (MES), tris[hydroxymethyl]aminomethane hydrochloride (TRIS), imidazole, phthalic acid, acetic acid, were used.

Procedure

Pyoverdin immobilization. About 0.2 g of CPG (460 Å) were cleaned with HNO_3, rinsed with distilled water, and activated with an aminoalkyl agent by the method described by León-González.[9] Four millilitres of $6.5 \times 10^{-5}M$ pyoverdin in biphthalate (0.01*M*, pH 6) were added to the activated glass (0.123 g), and immobilization was allowed to proceed at 4° for 2.5 hr in the absence of oxygen. The glass beads were rinsed afterwards to remove the excess of unlinked siderophore. Different fractions of the rinsings were analyzed by Vis–UV spectrometry at 460 nm to quantify the amount of siderophore linked to the CPG.

Iron determination. Buffer solutions containing a given iron concentration from 10 to 200 ng/ml and containing no iron were alternatively pumped at a flow rate of 5 ml/min through the flow cell, where pyoverdin immobilized on CPG was packed. Emission signal intensity *vs* time was measured at 552 nm upon excitation at 500 nm. Fluorescence intensity decreased when Fe(III) was passed through the cell. Once the signal had been recorded the pyoverdin reactor was regenerated by pumping 1*M* HCl for 2 min through the cell. This sequence was repeated several times to obtain a

Table 2. Analytical characteristics of immobilized pyoverdin–Fe(III) and pyoverdin–Fe(III) in aqueous solution

Parameters	Aqueous solution	Immobilized Pyoverdin
Linear range	10–180 ng/ml	3–200 ng/ml
Detection limit	10 ng/ml	3 ng/ml
Precision	4%($n = 9$, 50 ng/ml)	3%($n = 10$, 60 ng/ml)

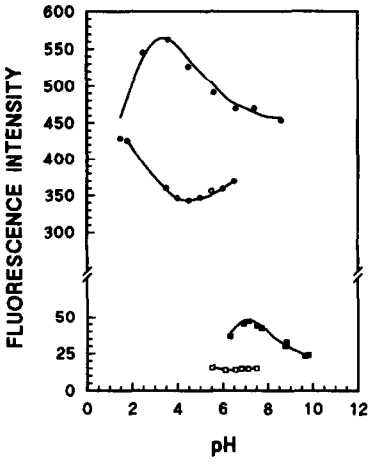

Fig. 1. Effect of pH on fluorescence intensity: -■- 6.6 μM pyoverdine aqueous solution; -□- Fe(III)–pyoverdin complex, 6.6 μM pyoverdine aqueous solution and 200 ng/ml Fe(III); -●- 0.001 mmol/g immobilized pyoverdin on CPG; -○- Fe(III)–pyoverdin complex on CPG Fe(III) 60 ng/ml.

Table 3. Study of interferences

Ion	Ion/Fe(III) Ratio*	Relative sensitivity (%)†
Na	500/1	100
Ca	100/1	100
Mg	500/1	98
Zn	100/1	97
Ni	100/1	100
Pb	100/1	100
Be	10/1	100
Mn	10/1	100
Mo	10/1	100
Al	50/1	98
Cr	100/1	90
	10/1	100
Cu	50/1	97
Cl^-	1000/1	100
F^-	100/1	100
SO_4^{2-}	1000/1	100

All experiments were carried out at 60 ppb Fe(III) at pH 4.5.
*Maximum ratio tested.
†Expressed as the ratio of the signal of Fe(III) in presence of interferent to that of Fe(III) alone.

calibration graph, slope of decrease of fluorescence intensity for 2 min *vs* iron concentration. The same procedure was followed for water analyses.

RESULTS AND DISCUSSION

Because of its natural procedure the selectivity of a siderophore for iron(III) determinations is advantageous over the use of artificial compounds for this analyte. On the other hand, fluorescence measurements are usually considered more sensitive than spectrophotometric ones for analytical purposes. In this sense, pyoverdin immobilization would allow the development of a highly selective and sensitive biosensor for continuous Fe(III) measurements.

Controlled pore glass has been widely used as solid support for enzymes and other reagents immobilization because it is fairly inert and therefore not subject to microbial degradation or swelling due to varying ionic strength. In this work two different CPG pore size (460 and 237 Å) have been tested. The emitted fluorescence of CPG immobilized pigment was significantly higher on the 460 Å CPG than on 237 Å CPG in agreement with Kurtz[10] observations that CPG yields higher enzyme immobilization efficiencies when higher porous size is used, so the 460 Å CPG was chosen for further experiments.

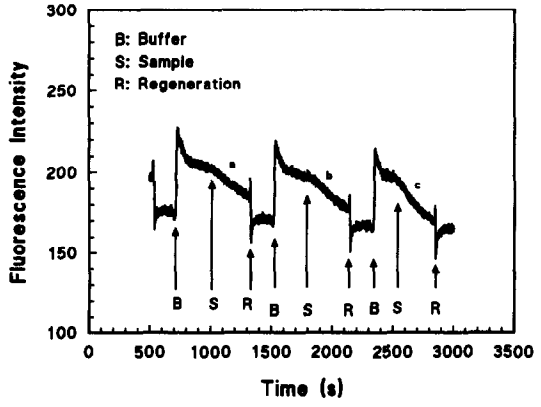

Fig. 2. Response curve at different concentrations of iron(III) -a- 50 ng/ml, -b- 70 ng/ml and -c- 100 ng/ml. Flurorescence intensity *vs* time.

In order to select the most suitable concentration of CPG immobilized pyoverdin, three different pyoverdin concentrations ($6.65 \times 10^{-5} M$, $1.33 \times 10^{-4} M$, $6.65 \times 10^{-4} M$) were tested using the same amount of CPG. The pyoverdin remaining in solution was monitored by Vis–UV spectrophotometry. In all cases the same concentration of the pigment (0.001 mmole/g) became attached to the CPG. The optimized parameters for iron(III) determination using aqueous and immobilized pyoverdin are summarized in Table 1.

In aqueous solution, pyoverdin has an emission maximum at 465 nm when excited at 390 nm, whereas if it is immobilized the emission maximum is shifted to 552 nm and the excitation to 500 nm. This shift could be attributed to a drastic change in the luminophore environment and/or electronic structure upon covalent bonding between the siderophore and the solid support. Another important feature of this indicator is that its high emission fluorescence pro-

portionately decreased with the ferric ion concentration. In aqueous solution the pyoverdin–Fe(III) system exhibits a linear range of 10–180 ng/ml Fe(III), with a detection limit of 10 ng/ml and precision of 4% ($n = 9$, 50 ppb) (Table 2).

The fluorescence emission intensity of pyoverdin and pyoverdin–Fe(III) complex formation are significantly affected by the pH of the solutions. The strength of this pH effect depends on whether the pigment is in solution or immobilized on CPG (Fig. 1). The largest differences between the fluorescence intensity of pyoverdin and pyoverdin–Fe(III) were in aqueous solution at pH 6.5 and at pH 4.5 in the immobilized system.

The nature of the buffer significantly affected reactivity in both the aqueous and immobilized systems. MES, TRIS, phosphate, imidazole and bipthalate buffers were tested and 0.01*M* biphthalate provided the greatest sensitivity in the solid system, whereas 0.05*M* MES was the optimum buffer in aqueous solution. However, the MES buffer produced considerable base line drifts in the immobilized system.

Electrolytes (NaCl, $KClO_4$) at concentrations 0.1–1*M* were used to evaluate the effect of ionic strength. No significant effect was observed below 0.5*M* electrolyte, while sensitivity decreased at concentrations above 0.5*M* (the fluorescence intensity of pyoverdin decreased less in the presence of Fe(III)). Temperature showed no significant influence on the sensor response when tested between 5 and 40°.

The flow-rate was varied from 0.5 to 5.0 ml/min to evaluate its effect on response time. The optimum flow selected was a compromise between time of pyoverdin Fe(III) contact and amount of iron passing through the cell. The reaction rate is extremely fast, as shown in Fig. 2. Thus, faster flow rates result in a greater slope because the effect of delivering more analyte overrides the effect of reduced contact time. An optimum flow of 5.0 ml/min was selected for further studies.

The bead surface is the active phase of our sensor and it must be periodically regenerated to regain the free pyoverdin. Different iron complexing agents, such as EDTA and 8-hydroxyquinoline and pH modifiers were tested for their regeneration efficiency, the regeneration effect of these complexing agents was slow because of the high formation constant of the pyoverdin–Fe(III) complex. In contrast, a low pH gave more promising results, 1*M* HCl was chosen as the optimum medium for regeneration since the analytical signal returned rapidly to the base line when it was used (Fig. 2).

The lifetime of the biosensor was at least three months, which was equivalent to about 1000 iron determinations. The analytical characteristics of the biosensor are shown in Table 2. The linear range, expressed as the slope of the response curve *vs* concentration, allows the determination of 10–200 ng/ml of Fe(III) with a coefficient of correlation of 0.997, the detection limit is 3 ng/ml and the relative standard deviation is about 3% for 10 determinations of 60 ng/ml of Fe(III). The interference study (Table 3) showed that none of the ions tested interferes seriously, which signifies that the biosensor is highly selective for iron(III). Notably, fluoride, a well-known complexing agent for iron, does not interfere at a concentration 100 times that of the iron.

Sample analysis

The proposed method using immobilized pyoverdin was applied to the determination of iron in tap and mineral water. Samples were analyzed without any special treatment; 1 ml of buffer was simply added to 5 ml of the water sample and was made up to 50 ml with deionized water. Determination was made as described in the "Procedure" section above.

The results obtained were compared with those provided by the ICP–AES reference technique (Table 4) and there were no

Table 4. Application of the biosensor to determine Fe(III) in different waters

Sample	Fluorimetric	ICP
Tap Water 1	0.36 ± 0.03 mg/ml	0.33 ± 0.04 mg/ml
Tap Water 2	0.26 ± 0.02 mg/ml	0.25 ± 0.03 mg/ml
Tap Water 3	0.22 ± 0.02 mg/ml	0.24 ± 0.03 mg/ml
Mineral water	0.08 ± 0.01 mg/ml	Below detection limit

significant differences at the 95% confidence level.

CONCLUSIONS

The proposed biosensor is sensitive and selective for iron and it has considerable advantages over methods based on pigment in solution; namely that a small amount of immobilized pyoverdin is sufficient for 1000 or more iron determinations and that the detection limit is three times smaller.

Acknowledgements—The authors wish to thank the CICYT for the financial support under project N. PB 88-0094 and to the Complutense University of Madrid under project 1990 N. 640.1, to Dr Carmen San José for providing the strain of *Pseudomonas fluorescens* and the procedure for purification of pyoverdin. J. M. Barrero thanks the Complutense University of Madrid for a Ph.D. grant.

REFERENCES

1. J. B. Neilands, *Inorganic Biochemistry*, G. Eichorn (ed.), Vol. 1, pp. 167–202. Elsevier, Amsterdam, 1973.
2. P. Demange, S. Wendenbaum, A. Bateman, A. Dell and M. A. Abdallah, *Iron Transport in Microbes, Plants and Animals*, G. Winkelmann, D. Van der Helm and J. B. Neilands (eds), pp 167–187. VCH, Weinheim, F.R.G., 1987.
3. G. Anderegg, F. L'Eplattenier and G. Schwartzenbach, *Helv. Chim. Acta*, 1963, **46**, 1409.
4. W. R. Seitz, *CRC Crit. Rev. Anal. Chem* 1988, **19**, 135.
5. C. Cámara, M. C. Moreno, G. Orellana, *Biosensors with Fiberoptics*, D. L. Wise and L. B. Wingard Jr. (Eds). The Humana Press, Clifton, NJ, pp 29–84, 1991.
6. A. J. Pesce and L. A. Kaplan, *Métodos Química Clínica. MédicaPanamericana Ed.* Buenos Aires, pp. 1266–1269, 1990.
7. C. Cámara, M. C. Moreno and M. C. Faraldos, *Analusis*, 1988, **16**, 87.
8. J. M. Meyer and M. A. Abdallah, *Journal of General Microbiology*, 1978, **107**, 319.
9. M. E. León-González and A. Townshend, *Anal. Chim. Acta.*, 1990, **236**, 267.
10. K. S. Kurtz and S. R. Crouch, *ibid.*, 1991, **254**, 201.

Talanta, Vol. 40, No. 11, pp. 1625–1630, 1993
Printed in Great Britain.

0039-9140/93 $6.00 + 0.00

APPLICATION OF PHOTOCHEMICAL INHIBITION IN FLOW INJECTION SYSTEMS: DETERMINATION OF EPINEPHRINE AND *L*-DOPA

T. PÉREZ-RUÍZ, C. MARTÍNEZ-LOZANO, V. TOMÁS and O. VAL
Department of Analytical Chemistry, Faculty of Chemistry, University of Murcia, Murcia, Spain

Summary—An automated procedure for the photochemical determination of epinephrine and *L*-dopa has been developed. It is based on the strong inhibition by these catecholamines on the photochemical reaction between phloxin and ethylenediaminetetraacetic. The proposed flow-injection method allows the fluorimetric determination of epinephrine in the range 1.9–26.4 μg/ml and of *L*-dopa in the range of 1.5–12.7 μg/ml, with a sampling frequency of 35 samples/hr. The method was applied successfully to the determination of body catecholamines in pharmaceutical preparations.

Catecholamines are compounds with amines attached to a benzene ring bearing two hydroxy groups. The main sites of production of the catecholamines are the brain, chromaffin cells of the adrenal medulla and the sympathetic neurons. Epinephrine is the principal sympathomimetic hormone produced by the adrenal medulla in most species and occurs as the *L*-form in animals and man.

The determination of catecholamines in biological specimens normally requires the use of trace analysis techniques, mainly chromatography with fluorimetric or electrochemical detection.[1] In contrast, catecholamines in pharmaceutical preparations are present in relatively large amounts, and increasing efforts have been directed towards the development of simple and reliable analytical methods. Recently, spectrophotometric, fluorimetric, titrimetric, kinetic and photokinetic methods[2–9] have been widely used for the determination of catecholamines in pharmaceuticals. Some of these methods have been adapted to the stopped-flow technique and flow injection analysis.[10–13]

The last few years have seen a tremendous growth in the amount of research and the number of publications on the use of photochemical reactions in chemical analysis. This is not surprising if it is remembered that photochemical reactions have a number of favourable features not possessed by ordinary chemical reactions. For example, the reagent in photochemical reactions, the photon, can readily be changed by modifying the wavelength of the light used for irradiation, and by this means the selectivity of a reaction can be increased. The rate of a photochemical reaction can be influenced by regulating the intensity of the photon current. A further substantial advantage results from the fact that photochemical reactions are in general fairly sensitive and accordingly permit the determination of microcomponents.

Photochemical reactions have been applied to the determination of a large number of species using different approaches (kinetic methods, photochemical titrations, gravimetry, *etc.*) and reviews have already appeared on the results to date.[14–16] Many of the photochemical methods developed for batch analysis can be adapted to flow systems such as high performance liquid chromatography or flow injection analysis.[17]

The leuco-forms of thionine blue and thionine, generated through the photochemical reaction between these dyes and ethylenediaminetetraacetic acid, have been applied as reductive and chromogenic reagents for the determination of various oxidants using flow injection systems.[18,19] The amperometric determination of oxalate by the photochemical decomposition of ferrioxalate in the reaction coil or in the flow cell of the flow system has been reported.[20,21] Photochemical reactions coupled with flow injection systems have also been described for individual[22–24] and simultaneous[25] determinations of phenothiazine compounds, nitrite,[26] hydrogen peroxide,[27] organoarseni-

cals[28] and of the organic phosphorus in natural waters.[29]

The purpose of the present investigation was to develop a simple, sensitive and rapid assay for catecholamines (epinephrine and *L*-dopa) using a flow injection system coupled to a photochemical reaction. The method is based on the strong inhibition by catecholamines on the photoreduction of phloxin by EDTA, which is monitored by the fluorescence intensity of the dye.

EXPERIMENTAL

Reagents

All chemicals were of analytical-reagent grade and were used as received. Doubly distilled water was used throughout. Epinephrine and *L*-dopa stock solutions (1 mg/ml) were prepared from the Sigma product in 0.01*M* hydrochloric acid and stored frozen in a dark bottle before use. Working solutions were prepared daily from these solutions by diluting with doubly distilled water. Phloxin (tetrachlorotetrabromofluorescein, C.I. 45410) solutions were prepared by appropriate dilution of the stock solution (447 mg in 250 ml of distilled water) buffered at the desired pH with 0.10*M* phosphate buffer. EDTA solution, was prepared from Merck product (disodium salt) and adjusted to pH 6 with 0.2*M* sodium hydroxide.

Apparatus

A Hitachi F 3010 spectrofluorimeter equipped with a plotter unit was used for recording spectra and a Perkin-Elmer 3000 spectrofluorimeter connected to a Linseis 6512 recorder was used as the detector with a Hellma 176.052 QS flow cell (inner volume 25 μl). The irradiation was performed with an Olimpus Europe illumination device, which was equipped with a halogen quartzline lamp (General Electric, 20 V, 150 W) and optical fibers to guide the light from the lamp to the reaction coil (PTFE tubing, 0.5 mm i.d.).

The spectrofluorimeter parameters were: $\lambda_{ex} = 530$ nm, $\lambda_{em} = 543$ nm, excitation slit = 5 nm and emission slit = 5 nm.

RESULTS AND DISCUSSION

Basis of the method

When a solution containing phloxin (Ph) and EDTA in the absence of oxygen is irradiated with white light at a suitable pH, photoreduction of the dye occurs and the pink colour disappears:[30]

$$Ph_{ox} + EDTA \xrightarrow{h\nu} Ph_{red} + \text{EDTA oxidation products}$$

In the presence of epinephrine or *L*-dopa the rate of the photochemical reaction is strongly decreased, and this change can be measured by the fluorescence of phloxin. Figure 1 illustrates the excitation and emission spectra for a sample without irradiation (curve 1) and another irradiated for one minute in the presence (curve 2) and absence (curve 3) of epinephrine. The fact that epinephrine inhibits the photoreduction of phloxin by EDTA is shown by the fact that the change in the fluorescence intensity is much smaller in its presence.

At a fixed irradiation time, there was a linear relationship between epinephrine or *L*-dopa concentration and the fluorescence intensity of the photolyzed solution. This is the basis of the proposed method for the determination of these catecholamines.

Configuration designs

The flow injection configuration used for the determination of epinephrine and *L*-dopa was so designed to provide different reaction conditions for magnifying the inhibition effect of these two analytes on the photochemical reaction between phloxin and EDTA. Three different configurations were tested for this purpose (Fig. 2).

In configuration I, the sample and phloxin

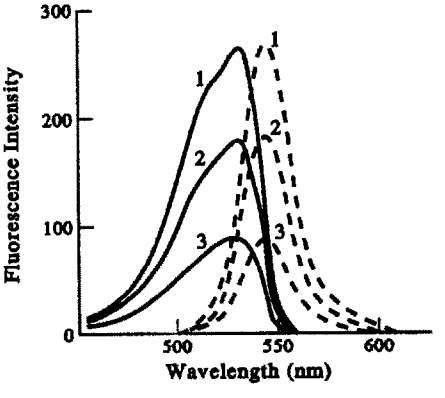

Fig. 1. Inhibiting effect of epinephrine of the photoreduction of phloxin by EDTA. Excitation spectra (solid line); emission spectra (broken line). Phloxin, $6 \times 10^{-6}M$; EDTA, 0.05*M*; phosphate buffer (pH 6.0), 0.01*M*. 1 = Without irradiation. 2 = Irradiation time, 1 min; epinephrine, 6.6 μg/ml. 3 = Irradiation time, 1 min; without epinephrine.

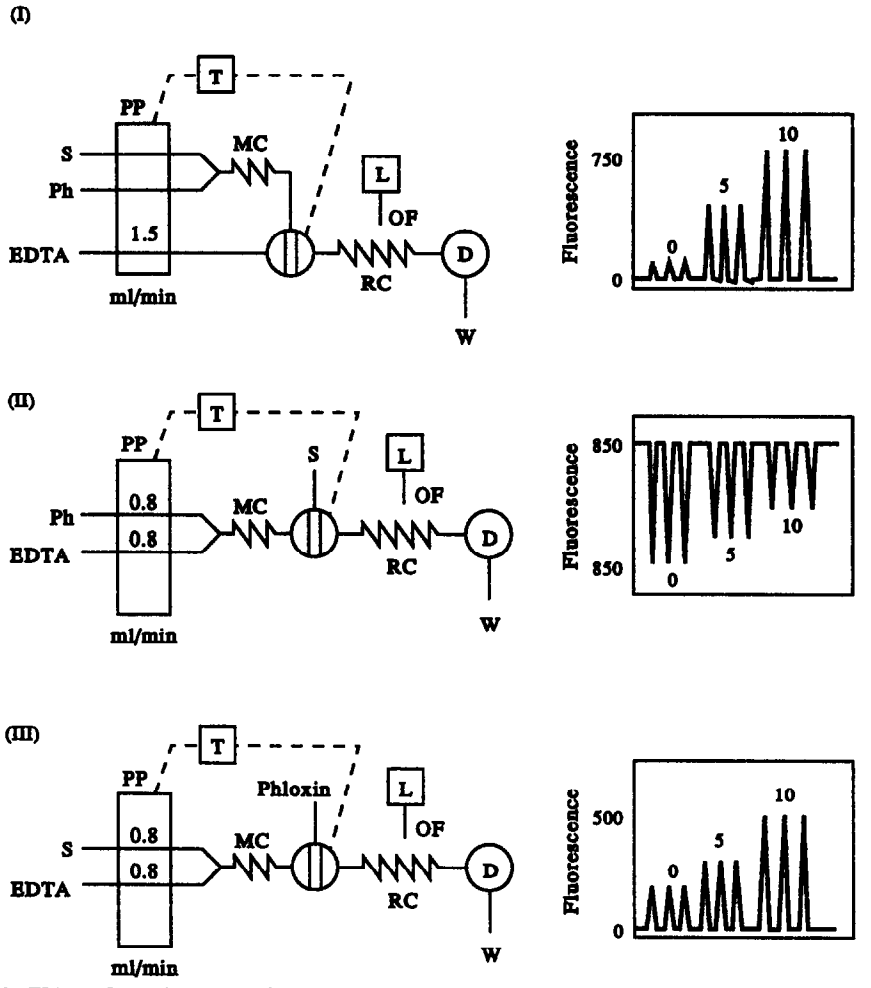

Fig. 2. FIA configurations tested for the determination of epinephrine and *L*-dopa. PP = peristaltic pump (with flow-rates given in ml/min); MC = mixing coil; RC = reaction coil; L = light source; OF = optical fibre; D = detector; W = waste; S = sample. Dashed lines represent synchronous control line. The values on the peaks are concentrations of epinephrine in μg/ml.

solutions were mixed before injection into the EDTA stream.

In configuration II, the reagents (Ph and EDTA) were propelled by two separate lines and mixed within the flow system prior to sample injection.

Configuration III was a reverse mode, the sample and EDTA streams being mixed before the injection of phloxin.

In all configurations, the sample and reagent solutions were de-aerated by bubbling argon through them, in order to minimize the presence of oxygen in the systems.

A laboratory-built timer was used in all cases to control the pump and the injection valve. The timer was programmed so that after 15 sec, when the sample zone was in the reaction coil (PTFE tube, 0.5 mm i.d.), the flow was stopped. The sample plug was then irradiated by the halogen lamp, after 25 sec of irradiation the pump was triggered by the timer and the sample zone was directed towards the detector.

Configuration I was finally chosen as it provided the greatest sensitivity and the fastest restoration of the baseline.

Optimization of manifold parameters

The variables studied were volume injected, length of the reactor, flow-rate and time of irradiation. The concentrations used in these experiments were as follows: EDTA line, 0.1*M*; phloxin line, $5 \times 10^{-5}M$ Ph and 0.1*M* phosphate buffer pH 6; sample solution $3 \times 10^{-5}M$. The mixing ratio between phloxin line and sample line was always 1:1. The manifold parameters used in the optimization procedure were a reactor of 150 cm × 0.5 mm i.d. and an irradiation time of 30 sec.

The volume injected was varied between 35 and 250 μl. The difference in peak heights between the sample and blank increased with increasing volumes injected up to 185 μl, above which it remained virtually constant. The volume chosen was 185 μl.

The reactor length selected was 200 cm; 100 cm of which was irradiated. To obtain as high a sensitivity as possible, the reactor was coiled around a glass tube (1 cm of diameter) and placed over a mirror; the end of the optical fibre was situated at a distance of 0.3 cm from the reactor.

Although the light source generated very little heat, a fan was used so that the temperature of the reactor was constant.

Flow-rates over the range 0.8–2.5 ml/min did not affect the analytical signal. A flow-rate of 1.5 ml/min was chosen.

Special attention was paid to the influence of the irradiation time on the analytical signal. Different irradiation times were achieved in two ways: (a) by using different length for the PTFE tube irradiated with an extended light source; (b) by stopping the peristaltic pump when the sample was located in the reaction coil and irradiating with a quasi-point light source. The last arrangement provided the best sensitivity and speed and was chosen for further experiments.

Figure 3 shows the influence of the irradiation time on the development of the photochemical reaction in the absence and presence of epinephrine. An exposure time of 25 sec was sufficient to obtain the maximum difference in peak height between the sample and blank (without catecholamine).

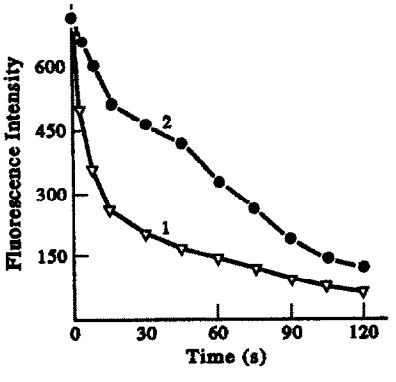

Fig. 3. Influence of irradiation time. Curve 1: Without epinephrine. Curve 2: [epinephrine] = 6.6 μg/ml.

Optimization of reagent concentration

The rate of photoreduction of Ph by EDTA and the inhibition by epinephrine and *L*-dopa on this photochemical reaction are very much pH-dependent.[30] A pH value of 6.0 gives a high degree of inhibition and a fast photochemical reaction.

The effect of EDTA concentration was studied in the range 0.04–0.2*M*. The rate of the photochemical reaction in the absence and presence of catecholamine increased with increasing EDTA concentrations up to 0.09*M*, above which it remained virtually constant. A 0.1*M* EDTA solution adjusted to pH 6.0 with 0.2*M* sodium hydroxide was used as carrier.

The peak height obviously increased with increasing pH concentration for the blank solution and analyte. However, the difference between them was found to increase with floxin concentration up to $4 \times 10^{-5}M$ and to be constant at higher concentrations. A $6 \times 10^{-5}M$ solution buffered at pH 6.0 with 0.1*M* phosphate buffer was selected in order to obtain a wide concentration range in the determination of the analyte.

Calibration graph and reproducibility

A series of standard solutions were pumped in triplicate to test the linearity of the calibration graph. The calibration graph was linear from 1.9 to 26.4 μg/ml with a correlation coefficient of 0.9998 for epinephrine and from 1.5 to 12.7 μg/ml with a correlation coefficient of 0.9989 for *L*-dopa. The sample rate was about 35 samples/hr. The statistical study performed on 10 samples of triplicate pumping of 3.3 μg/ml of epinephrine and of 1.9 μg/ml of *L*-dopa yielded relative standard deviations of 0.96% and 0.59%, respectively.

Interferences

The influence of foreign compounds that commonly accompany epinephrine and *L*-dopa in pharmaceutical preparations was studied by preparing solutions containing 3.0 μg/ml of the catecholamine and increasing concentrations of the potential interferent up to 300 μg/ml or by adding an amount to give an error of $\pm 3\%$. The errors were determined by comparing the peaks given by a solution of analyte containing no foreign substance. Glucose, sucrose, lactose, citrate and tartrate were tolerated in large amounts (100-fold excesses were the maximum ratio tested) and 50-fold excesses of antipyrine,

Table 1. Determination of epinephrine and L-dopa in pharmaceutical preparations

Sample*	Catecholamine	Nominal value, mg/ml	Trihydroxyindol method found,† mg/ml	FIA method found,‡ mg/ml
Epistaxol	Epinephrine	0.5	0.48 ± 0.026	0.49 ± 0.005
Adrenalina	Epinephrine	1.0	1.01 ± 0.01	0.99 ± 0.004
Oculos epilo	Epinephrine	10.0	10.02 ± 0.02	10.07 ± 0.09
Maipedopa§	L-dopa	10.0	9.82 ± 0.19	10.08 ± 0.09

*Composition of samples. Epistaxol: epinephrine hydrochloride, 0.5 mg; vitamin P(rutin), 0.2 mg; naphazoline hydrochloride, 0.5 mg; antipyrine, 30 mg; and water 1 g. Adrenalina: epinephrine hydrochloride, 1 mg; and water, 1 g. Oculos epilo: epinephrine hydrogen tartrate, 10 mg; pilocarpine hydrochloride, 40 mg; and water, 1 g. Maipedopa: L-dopa, 250 mg capsule.

†Average of three determinations ± standard deviation.

‡Average of four determinations ± standard deviation.

§Prepared by dissolving the capsule in 25 ml of distilled water.

pilocarpine and hydrogen sulphite were also tolerated in the determination of epinephrine and L-dopa.

Analysis of pharmaceutical preparations

The proposed method was applied satisfactorily to the determination of epinephrine and L-dopa in pharmaceutical preparations. Commercially available formulations were analysed and the results obtained are summarized in Table 1. As can be seen, for all the formulations the assay results were in good agreement with values for the nominal contents and with those obtained using the fluorimetric method based on the formation of the hydroxyindol derivatives.[1,31] The recoveries obtained to add epinephrine or L-dopa to each pharmaceutical formulation are shown in Table 2.

CONCLUSIONS

The results presented in this work clearly demonstrate that the inhibition of a photochemical reaction which takes place in a flow-injection assembly has great analytical potential for the determination of the inhibitor. The main advantages of this procedure are: on the one hand, the selectivity and sensitivity brought about by the photochemical reaction and on the other the rapidity, ease of automation and low sample and reagent consumption resulting from the flow injection system.

The phloxin–EDTA system was used to check the viability of the proposed method in the determination of epinephrine and L-dopa using fluorimetric detection.

Acknowledgements—The authors express their gratitude to Dirección General de Investigación Científica y Técnica (DGICYT) for financial support (grant No. PB90-0008).

Table 2. Recovery of epinephrine and L-dopa from pharmaceutical preparation

Sample*	Catecholamine	Added, mg/ml	Found,† mg/ml	Recovery (%)
Epistaxol	Epinephrine	3.40	3.36	98.8
		10.20	10.16	99.6
Adrenalina	Epinephrine	3.40	3.43	100.9
		10.20	10.18	99.8
Oculos epilo	Epinephrine	3.40	3.43	100.9
		10.20	9.98	97.7
Maipedopa	L-dopa	1.0	1.04	104.4
		2.0	1.98	99.0

*See Table 1.

†Average of three determinations.

The recovery was determined by adding two amounts of epinephrine or L-dopa to each sample and subtracting the results obtained for the pharmaceutical formulations prepared in a similar manner but to which no catecholamine had been added.

REFERENCES

1. A. J. Pesce and L. A. Kaplan, in *Methods in Clinical Chemistry*, S. Bircher (ed.), pp. 944–963. The C.V. Mosby Company, St. Louis, MO, 1987.
2. D. G. Sankar, C. S. Sastry, M. N. Reddy and S. N. Pradad, *Indian J. Pharm. Sci.*, 1987, **49**, 69.
3. Y. Fujita, I. Mori, K. Fijita and T. Takana, *Chem. Pharm. Bull*, 1985, **38**, 5385.
4. F. B. Salem, *Talanta*, 1987, **34**, 810.
5. R. C. Canson and M. J. Brown, *Ann. Clin. Biochem.*, 1982, **19**, 396.
6. W. I. Mohamed and F. B. Salem, *Anal. Lett.*, 1984, **17**, 191.
7. D. Amin, *Analyst*, 1986, **111**, 255.
8. M. J. Rodríguez-Dopazo, M. Silva and D. Pérez-Bendito, *Microchem. J.*, 1989, **39**, 235.
9. T. Perez-Ruíz, C. Martínez-Lozano, V. Tomás and O. Val, *Analyst*, 1991, **116**, 857.
10. E. Plizzeti, E. Mentasti, E. Premanro and G. Ginandi, *Anal. Chim. Acta*, 1976, **85**, 161.
11. M. P. Llavero, S. Rubio, A. Gómez-Hens and D. Pérez-Bendito, *ibid.*, 1990, **229**, 27.
12. A. Kojlo and J. Martínez-Calatayud, *J. Pharm. Biomed. Anal.*, 1990, **8**, 663.
13. M. Herrera, L. Kao, D. J. Curran and E. W. Westhead, *Anal. Biochem.*, 1985, **144**, 218.
14. J. M. Fitzgerald, *Analytical Photochemistry and Photochemical Analysis*, pp. 128–141, 157–163. Marcel Dekker, New York, 1971.
15. A. Péter and J. Csányi, *Acta Phys. Chem.*, 1975, **21**, 37.
16. T. Pérez-Ruíz, C. Martínez-Lozano and V. Tomás, *Quim. Anal*, 1987, **6**, 119.
17. J. W. Birks, *Chemiluminescence and Photochemical Reaction Detection in Chromatography*, pp. 151. VCH, New York, 1989.
18. T. Pérez-Ruíz, C. Martínez-Lozano, V. Tomás and E. Yagüe, *Analyst*, 1988, **113**, 1057.
19. H. Müller and E. H. Hansen, *Chem. Techn*, 1992, **42**, 304.
20. L. E. Leon, A. Ríos, M. D. Luque and M. Valcárcel, *Anal. Chim. Acta*, 1990, **234**, 227.
21. *Idem*, *Analyst*, 1990, **115**, 1549.
22. D. Chen, A. Ríos, M. D. Luque and M. Valcárcel, *ibid.*, 1991, **116**, 171.
23. M. T. Tena, M. D. Luque and M. Valcárcel, *J. Autom. Chem.*, 91, **13**, 111.
24. J. Martínez-Calatayud and C. Gómez, *Anal. Chim. Acta*, 1992, **256**, 105.
25. D. Chen, A. Ríos, M. D. Luque and M. Valcárcel, *Talanta*, 1991, **38**, 1227.
26. R. Liu and D. Liu, *Analyst*, 1991, **116**, 497.
27. Z. Genfa, P. Dasgupta, W. S. Edgemond and J. H. Marx, *Anal. Chim. Acta*, 1991, **243**, 207.
28. R. H. Atalian and D. A. Kalman, *Talanta*, 1991, **38**, 167.
29. I. D. McKelvie, B. T. Hart, T. J. Cardwell and R. W. Cattrall, *Analyst*, 1989, **114**, 1549.
30. T. Pérez-Ruíz, C. Martínez-Lozano, V. Tomás and C. López-Balsera, *J. Pharm. Biom. Anal.*, 1991, **9**, 123.
31. R. A. Heacock, *Chem. Rev.*, 1959, **59**, 181.

Talanta, Vol. 40, No. 11, pp. 1631–1636, 1993
Printed in Great Britain.

0039-9140/93 $6.00 + 0.00

SPECIATION OF ORGANOMERCURIALS IN MARINE SAMPLES USING CAPILLARY ELECTROPHORESIS

I. MEDINA
Institute of Marine Research, C.S.I.C., Vigo, Spain

E. RUBÍ, M. C. MEJUTO and R. CELA*
Department of Analytical Chemistry, Faculty of Chemistry, University of Santiago de Compostela, Santiago, Spain

Summary—A rapid method for speciation and determination of organomercury compounds in biological samples of marine origin using Capillary Electrophoresis (CE) is reported. Organomercurials were extracted from the samples by means of the classical Westöö procedure thus giving organomercury–cysteine complexes which can be separated from each other by means of CE resulting in effective speciation. Electrophoretic separation was achieved in an open silica capillary tube at 15–18 kV using a 100m*M* sodium borate buffer (pH 8.35). All mercury species were distinctively separated within 12 min. Results are presented for the analysis of real marine samples and reference materials, and compared with those obtained by the GC commonly accepted procedure.

Many studies[1] have reported that organic mercury forms, especially the methylated forms, are considerably more toxic than the inorganic ones. In fact, methylmercury is considered to be one of the most dangerous chemical species in the environment because of its intrinsic toxicity and availability to living organisms. However, the analytical measurement and speciation of organomercurials in complex natural world samples remains a very difficult problem with two main requirements: high selectivity and very low detection limits. Moreover, since high levels of methylmercury have been found in various marine organisms, especially in large predators (tuna, swordfish, *etc.*) analytical methodology for methylmercury must be at the same time fast, low in cost and reliable for use in the routine analysis of biological and environmental samples.

During the last few decades several procedures have been proposed for these purposes[2–15] but the most frequently used approach is the gas chromatography separation of the halogen derivatives of organomercurials with electron capture detection[4,16–20] based on the classical Westöö's method[4]. On the other hand, several papers[17,21–23] have focused on the drawbacks of these gas chromatographic procedures. In fact, the lack of consistent reproducibility, the tailing of peaks, the absorption of variable amounts of the organomercurial compounds in the GC-system and the need of special column conditioning or priming with inorganic mercury salts and related consequences in the analysis of real samples (dead times of operation, doubts about the real nature of the compound detected after the priming, frequent drop-out of the peaks, *etc.*) as well as in the life of the columns and detector itself, has led to search for alternative procedures to carry out the organomercurials analysis on a more reliable basis. Recently[24] some of these drawbacks have been overcome by means of the use of special narrow bore chromatographic columns.

Capillary electrophoresis has demonstrated in recent years powerful capabilities for the resolution and analysis of very complex samples.[25] Although several papers[26] were dealing with the separation of inorganic ions and neutral or charged complexes of metals, this technique had so far limited application for speciation studies.[27] The high resolution and peak capacity characteristics of this technique could be used favourably in speciation studies for very complex samples. However, since the time needed for separation is usually very short in this technique, having full possibilities in automation, it can be easily used for routine analysis.

In this paper, a procedure is presented for speciation of organomercurials and the quantitative determination of methylmercury in

*Author for correspondence.

marine samples by means of capillary electrophoresis. Cysteine has been used to complex organomercurials according to the classical extraction method of Westöö.[4] The resulting cysteine-organomercury complexes were well separated in an electric charge density, using an alkaline buffer. Parameters affecting the separation have been optimized and the results for some types of marine samples as well as for an existing reference material has been compared with those obtained by the usual gas chromatographic method.[19]

EXPERIMENTAL

Reagents

All reagents used were HPLC or analytical grade. Ultrapure water was obtained by means of a MilliQ system (Millipore Co.). Mercury(II) chloride, methyl, phenyl and ethyl-mercury chlorides (Merck) were used as calibrants. A stock solution (1.00 g/l.) in methanol was used to obtain weekly standards by suitable dilution with methanol:water (1:1). All the organomercury solutions were protected against light and stored at 4° in the dark when not in use.

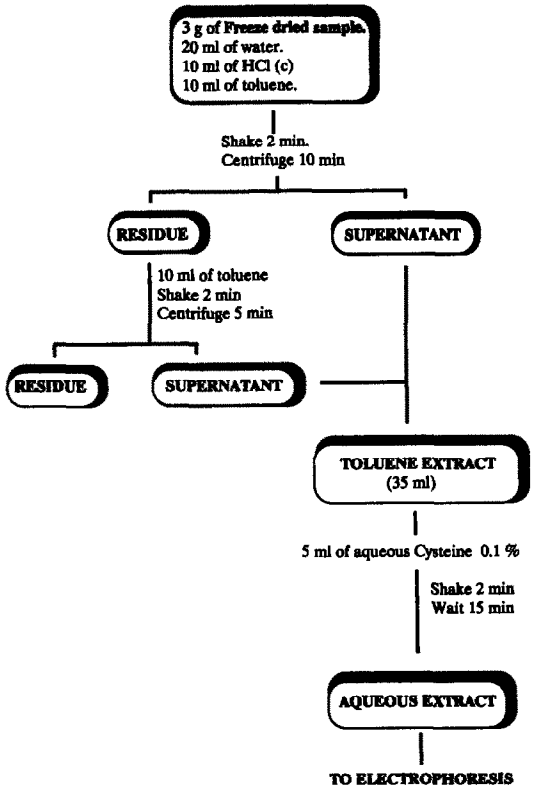

Fig. 1. Sample preparation scheme for methylmercury determination.

Aqueous cysteine chlorhydrate was used instead of cysteine acetate solution recommended by Westöö.[4] Buffers were prepared with boric acid and sodium hydroxide to pH 8.35. Aqueous cysteine and the buffer containing sodium dodecyl sulfate were prepared weekly and stored at 4° when not in use.

Standards

Standards for injection containing one or more organomercurials were prepared by mixing 400 μl of the appropriate standard solution of each organomercurial and 100 μl of 1% aqueous cysteine solution.

Preparation of samples

Samples were prepared in the way outlined in the scheme of Fig. 1 which essentially agrees with the Westöö procedure.[4] Final aqueous extracts were subjected to capillary electrophoresis separation.

Capillary electrophoresis

High performance capillary electrophoresis was carried out at 30° in a 75-μm (i.d.) 50-cm long fused silica capillary (window at 5 cm) using a PACE system 2050 (Beckman). Samples were introduced into the capillary by pressure injection over 8.6 sec (corresponding to a volume of 77.4 nl). Electroendosmosis was toward the cathode at 18 kV in a 100mM sodium Borate buffer (pH 8.35) during 12 min. UV detection at 200 nm and a System Gold (Beckman) equipment were used for detection, data acquisition and processing.

The capillary was daily prepared by flushing with 0.5M sodium hydroxide for 10 min, followed by a 10-min rinse with ultrapure water. A typical run consisted of a 2-min washing period with ultrapure water, followed by 3 min of capillary reconditioning with the selected buffer.

RESULTS AND DISCUSSION

Buffer selection

The pH of the buffer used to carry out the electrophoregram, was usually the most important operational parameter. For cysteine, the isoelectric point was 6.24 thus, in alkaline media, complexes formed by cysteine with organomercurials were charged negatively. As can be seen in Fig 2(a), using a 100mM borate buffer (pH 8.35) it was possible to separate the cysteine–methylmercury complex from the excess of ligand. Also a small peak having a

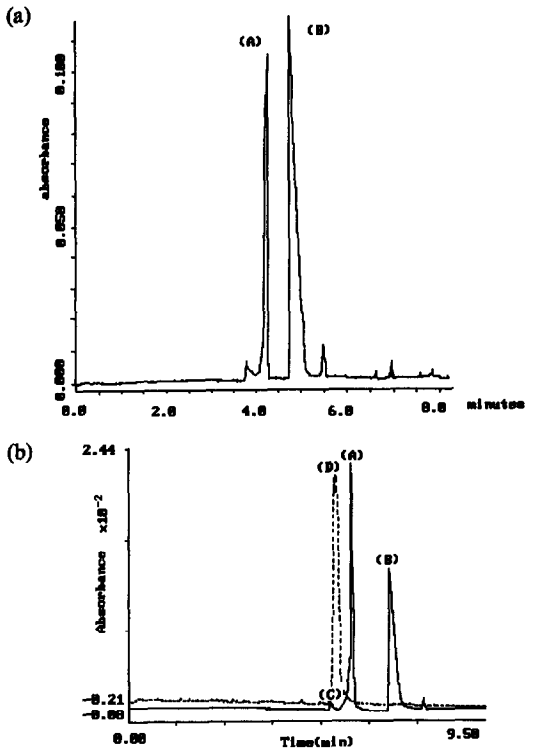

Fig. 2. Separation of cysteine complexed methylmercury and the cysteine excess by CE. a) Applied potential 20 kV, 100m*M* borate buffer (pH 8.35), 10% methanol. 13.5 μg of methylmercury chloride mixed with 1% aqueous cysteine, 27 nl injected. b) Same conditions as for a) but an injection of 27 nl of methylmercury chloride standard have been superimposed (dotted line). Key for peaks: (A) methylmercury–cysteine complex; (B) excess cysteine; (C) unknown; (D) uncomplexed methylmercury.

retention time lower than the one of the complex was observed. Since the standards for injection were prepared simply by mixing adequate solutions of methylmercury and cysteine just before the injection it was possible that this small peak would correspond to the not complexed form neutral methylmercuury. This hypothesis was confirmed by comparison with the behaviour of methylmercury alone (no cysteine added) as shown in Fig. 2(b). These data were in accordance with the electroendosmosis theory for alkaline media. In the same way the elution order of the complex and the free ligand form were according to the number of negative charges corresponding to the molecules:

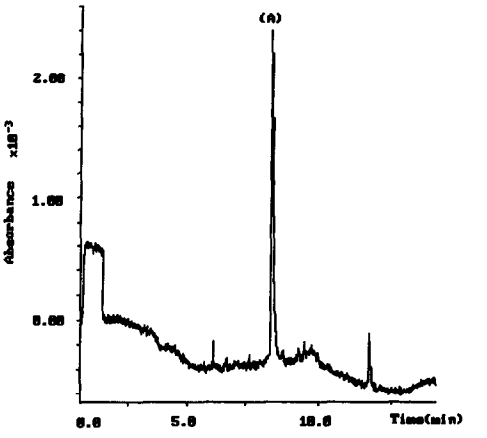

Fig. 3. Separation of cysteine complexed methylmercury in acidic buffer (100m*M* phosphate buffer pH 2.5, 10% methanol). Applied potential 20 kV, 13.5 μg of methylmercury chloride mixed with 1% aqueous cysteine. (A) methylmercury peak.

It was possible to obtain separations using media of pH lower than the isoelectric point. Experiments were carried out using a phosphate buffer (pH 2.5). However, as shown in Fig. 3, the peaks obtained were much less intense. In fact, the electrophoregram in Fig. 3 corresponds to the same standard solution as the one in Fig. 2 but the absorbance scale is 20 times greater. In this case the use of acidic buffers resulted in poor sensitivity.

The use of the borate buffer (pH 8.35) enabled the separation of the three organomercurials to be achieved as shown in Fig. 4. In alkaline media the (1:2) mercury(II)–cysteine complex had two negative charges which meant that inorganic mercury appeared to the right of the free cysteine peak in the electrophoregram. The order of elution was ethyl, methyl and phenylmercury. Decreasing the applied potential (up to 10 kV) did not improve the resolution of ethyl–methyl mercury pair. For phenylmercury, the contribution of the aromatic ring to the absorbance led to a greater sensitivity as compared to the others.

The influence of variable concentrations of a micellar agent [sodium dodecyl sulphate (SDS)] in the borate buffer was also studied, trying to

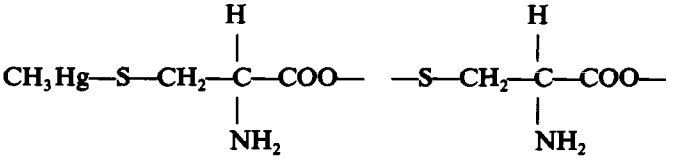

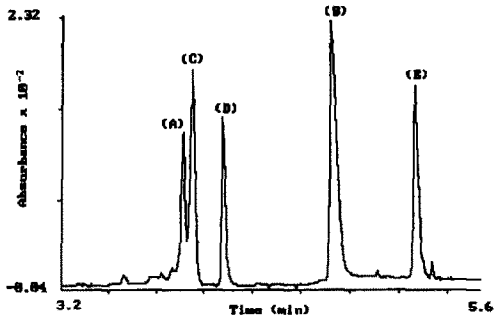

Fig. 4. Speciation of mercury forms complexed with cysteine, 1.5 μg methylmercury, 1.5 μg ethylmercury, 0.4 μg phenylmercury and 0.3 μg mercury(II) mixed in proportion 1:4 with 0.1% aqueous cysteine; 27 nl injected. Applied potential 15 kV, 100m*M* borate buffer (pH 8.35), 10% methanol. (A) ethylmercury; (B) excess cysteine; (C) methylmercury; (D) phenylmercury and (E) inorganic mercury.

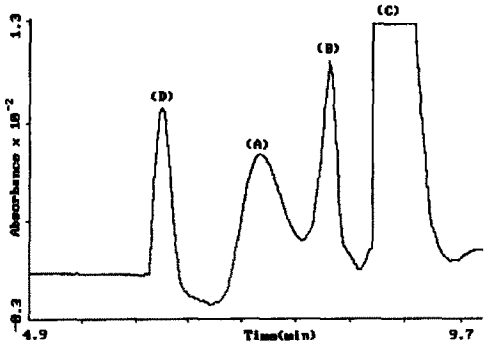

Fig. 5. Speciation of organomercurials in alkaline buffer containing SDS. Applied potential 15 kV, 100m*M* borate buffer (pH 8.35), 10% methanol, 25m*M* SDS. (A) methylmercury; (B) phenylmercury; (C) cysteine excess and (D) ethylmercury.

improve the resolution of the ethyl–methylmercury pair. However this possibility was discarded owing to the fact that the peaks appeared broader and with lower area values while no significant improvement in overall resolution was achieved. In Fig. 5 it can be seen that the methyl–ethyl pair was somewhat better resolved but in this case a significant overlap between methyl and phenyl peaks took place. Moreover, from a practical point of view, the inclusion of SDS into the buffer meant that it could not be used for more than 2–3 days. On the contrary a simple borate buffer remained usable during weeks.

Signal linearity

The relationship between the amount of methylmercury injected and peak area in the electrophoregram showed good linearity (correlation coefficient 0.9974, R-squared = 99.48% with a standard error of estimate of 4.39×10^{-3}) in the range 12–300 pg. The detection limit was 10 pg in the conditions described in the Experimental section for a signal to noise ratio of 10:1. Data for repeatability (retention times and peak areas) for five successive injections of a methylmercury standard (11.2 ng injected) were: average retention time = 4.28 ± 0.01 seconds; variation coefficient = 0.3% and, average peak area (arbitrary units) = 4.76 ± 0.10; variation coefficient = 2.1%. These data also indicated that the procedure sequence (programmed prerinse, *etc.*) were adequate for practical purposes. In Table 1 some data of reproducibility for several standard solutions of methylmercury determined in different days (one measurement each day) are listed. It is observed that variation coefficients were very similar with those of repeated injections, hence the ruggedness of the procedure was considered to be good.

Analyte recovery

Table 2 summarizes the results for recovery of methylmercury along the proposed procedure. For these experiments a freeze dried mussel tissue sample was used. This sample did not give any detectable signals for methylmercury nor for inorganic mercury so, it was considered as a matrix-blank sample. A 1.00-g sample of this material was used in the experiments adding variable amounts of a methylmercury standard in water. Once homogenized and dried, the resulting material was analyzed by means of the proposed procedure. Simultaneously the same

Table 1. Reproducibility of peak area counts (injections carried out in five different days)

Methylmercury amount (*pg*)	Injection number						Variation Coefficient
	1	2	3	4	5	Average	
193.5	0.1808	0.1674	0.1830	0.1712	0.1725	0.1750	3.8
96.7	0.0970	0.0907	0.0930	0.0941	0.0959	0.0941	3.0
38.7	0.0390	0.0400	0.0410	0.0408	0.0404	0.0403	2.0
30.9	0.0260	0.0248	0.0260	0.0266	0.0260	0.0260	2.8
15.5	0.0152	0.0157	0.0142	0.0139	0.0150	0.0148	5.0
7.7	0.0082	0.0081	0.0085	0.0077	0.0073	0.0079	5.9

Table 2. Influence of the matrix in the recovery of methylmercury

Material*	Methylmercury added (*pg*)		Methymercury found (*pg*)		Average (*pg*)	Standard deviation	Variation coefficient	Recovery, %
Mussel	309.6	206.6	192.3	205.0	201.3	7.8	3.9	65.0 ± 2.5
Mussel	154.8	102.0	107.3	102.2	103.8	3.0	2.9	67.1 ± 1.9
Mussel	61.9	39.9	36.2	39.0	38.4	1.9	4.9	62.0 ± 3.1
Blank	309.6	231.8	220.2	206.3	219.4	12.7	5.8	70.8 ± 4.3
Blank	154.8	118.1	117.3	118.3	117.9	0.5	0.5	76.1 ± 0.3
Blank	61.9	43.5	42.0	44.5	43.3	1.2	2.8	70.0 ± 2.0

*Mussel means a freeze-dried mussel tissue sample having a non-detectable level of mercury; blank means the absence of biological material in the experiments.

standard solutions used for spiking the mussel sample were extracted and analyzed. Thus the only difference between the rows in Table 2 labelled as "sample" and those labelled as "blank" is the presence or absence of the biological matrix. The results in Table 2 indicate that important losses took place during the extraction process. Only 72% of the methylmercury initially present is extracted. Furthermore, the results of a two-way ANOVA carried out on the data in Table 2 indicated a significant effect of the matrix in the methylmercury recovery. This effect can be explained by considering the formation of persistent scums in the extraction stages which hampered correct phase separation. Taking this into account, the recovery for methylmercury in real samples by the proposed procedure was 64.7 ± 3.1%.

Analysis of real samples

The initial experiments with real samples were carried out using a 1% cysteine acetate solution as back-extractant, because this is the usual concentration used in the gas chromatographic method.[4] Soon, it was observed that this excess of cysteine hampered the effective separation of the methylmercury complex from the free ligand when methylmercury concentration in the samples was low. This effect was provocated not only by the relative size of both peaks but it is believed that the excess of free ligand blocked-out or saturated the walls of the capillary tube giving poor separations. After a series of experiments, it was demonstrated that the use of a 0.1% solution of cysteine chlorhydrate allowed to complexation of all the organomercurials in the samples without impairing the peak separation.

It was noted that one artifact occurred when analyzing real samples. This consisted of a gross peak at a retention time lower than the corresponding one for methylmercury. As shown in Figs 6 and 7, this peak did not overlap with that of methylmercury, so in most cases it was not necessary to take any special precaution. In any case, this unknown compound has a lifetime of about 10 hr, so, if the extracts were left to stand for some hours in a dark cool place before the analysis, the artifact peak almost disappeared (see Fig. 7) enabling a more easy and accurate integration of the methylmercury peak which area did not change in this time. Although we have observed this artifact in all the real samples analyzed, we are not sure that it was present in other types of samples. Table 3 summarizes some of the results obtained for real samples

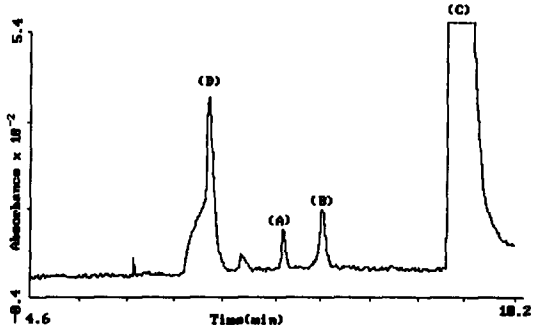

Fig. 6. Analysis of a blank mussel sample spiked with methyl and phenylmercury. Applied potential 15 kV, 100m*M* borate buffer, 10% methanol. (A) methylmercury; (B) phenylmercury; (C) cysteine excess; (D) unknown.

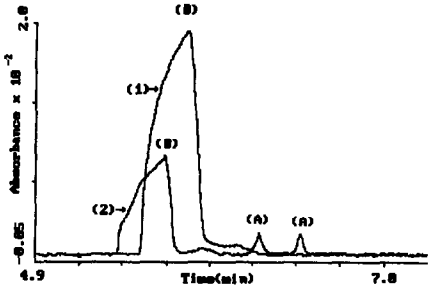

Fig. 7. Analysis of a blank mussel sample spiked with methylmercury (1) injected immediately after extraction and (2) injected after 10 hr. Both graphs have been delayed in the time axis to provide a more easy comparison. (A) methylmercury; (B) unknown. Same experimental conditions as for Fig. 6.

Table 3. Determination of methylmercury in real samples (all results expressed in mercury)

Sample material	Methylmercury content ($\mu g/g$)		Sample Weight (g)	Methylmercury Injected‡ (pg)	Methylmercury found by CE¶ (pg)	Methylmercury content, corrected for losses§¶	
	Certified*	Known†				(pg)	($\mu g/g$)
DORM-1	0.731 ± 0.060	–	6.0298	56.29	34.80	53.78	0.698 ± 0.025
DORM-1	0.731 ± 0.060	–	4.0056	37.39	23.09	35.68	0.697 ± 0.033
MUSSEL	–	2.142 ± 0.092	1.0075	29.60	19.64	30.35	2.224 ± 0.084
COCKLE	–	1.703 ± 0.151	1.5441	33.59	20.88	32.27	1.636 ± 0.060
CLAM	–	1.585 ± 0.050	1.4645	31.41	20.41	31.54	1.590 ± 0.081
TUNA	–	3.662 ± 0.355	0.9102	38.70	24.42	37.75	3.534 ± 0.344

*DORM-1 is a Dogfish muscle Certified Reference Material distributed by the National Research Council of Canada.
†Methymercury concentration values obtained by means of the Hight's gas chromatographic method[19] in our laboratory.
‡All the samples were extracted with 40 ml of toluene and backextracted into 5 ml of 0.1% cysteine colution. Injection volume in all cases were 77.4 nl.
§Assuming a 64.7% of average recovery in the whole process.
¶Average of three indepenedent analyses.

using the proposed procedure. These results are compared in this table with the ones obtained by means of the usual gas chromatographic procedure[19] for the same samples. It can be seen that the results for CE analyses were systematically lower than those obtained by gas chromatography for which no cysteine back-extraction was carried out. This is because of the aforementioned losses in the back-extraction stage with cysteine. When the results for CE analyses were corrected for these losses (last column in Table 3) the obtained data were in good agreement with the gas chromatographic ones as well as with certified values for the reference material analysed.

CONCLUSIONS

Up to this date, capillary electrophoresis has been only used in a very limited extent in speciation studies. The presented results shows that this technique could be used as a powerful tool in the separation of several organometallic forms in biological and environmental samples. Even more, separations could be understood on the basis of a well-established background without the need for special or sophisticated separation schemes. In the particular case of organomercurials speciation, the use of capillary electrophoresis avoids the drawbacks associated with gas chromatographic procedures and is rapid, and simple enough to be used on a routine basis.

Acknowledgements—A part of this work has been supported by the Spanish Interministerial Commission for Science and Technology (CICYT) under the project ALI-0773.

REFERENCES

1. IPCS, *Environmental Health Criteria 101: Methylmercury*, World Health Organization, Geneva, 1990.
2. J. F. Uthe and F. A. J. Armstrong, in L. Frieberg and J. Vostal (eds), *Mercury in the Environment*, pp. 21–53. CRC Press, Cleveland, OH, 1972.
3. J. C. Cage, *Analyst*, 1961, **86**, 457.
4. G. Westöo, *Acta Chem Scand.*, 1966, **20**, 2131; 1967, **21**, 1790; 1968, **22**, 2277.
5. D. Beauchemin, K. W. M. Siu and S. S. Berman, *Anal. Chem.*, 1988, **60**, 2587.
6. S. S. Berman, K. W. M. Siu, P. S. Maxwell, D. Beauchemin and V. P. Clancy, *Z. Anal Chem.*, 1989, **333**, 641.
7. L. Magos, *Analyst*, 1971, **96**, 847.
8. I. M. Davies, *Anal. Chim. Acta*, 1978, **102**, 189.
9. M. Fujita and E. Takabatake, *Anal Chem.*, 1983, **55**, 454.
10. N. Bloom and W. F. Fitzgerald, *Anal. Chim. Acta*, 1988, **208**, 151.
11. N. Bloom, *Can. J. Fish. Aquat. Sci.*, 1989, **46**, 1131.
12. G. Decadt, W. Baeyens, D. Bradley and L. Goeyens, *Anal. Chem.*, 1985, **57**, 2788.
13. P. Lansens and W. Baeyens, *Anal. Chim. Acta.*, 1990, **228**, 93.
14. W. A. McCreham, *Anal. Chem.*, 1981, **53**, 74.
15. O. Evans and G. D. McKee, *Analyst*, 1987, **112**, 983.
16. K. Sumino, *Kobe J. Med. Sci.*, 1968, **14**, 115; 1968, **14**, 131.
17. S. C. Hight and S. G. Capar, *J. Assoc. Off. Anal. Chem.*, 1983, **66**, 1121.
18. G. H. Alvarez, S. C. Hight and S. G. Capar, *J. Assoc. Off. Anal. Chem.*, 1984, **67**, 715.
19. S. C. Hight and M. T. Corcoran, *ibid.*, 1987, **70**, 24.
20. Mercury(Methyl) in Fish and Shellfish. Rapid Gas Chromatographic Method. First Action., *J. Assoc. Off. Anal. Chem.*, 1988, **71**, 210.
21. J. E. O'Reilly, *J. Chromatogr.*, 1982, **238**, 433.
22. E. Nulska, D. C. Baxter and W. Frech, *Anal. Chim. Acta*, 1991, **249**, 5454.
23. E. Rubí, R. A. Lorenzo, C. Casais, A. M. Carro and R. Cela, *J. Chromatogr.*, 1992, **605**, 69.
24. R. A. Lorenzo, A. Carro, E. Rubí, C. Casais and R. Cela, *J. of AOAC Internat.*, in press.
25. W. G. Kuhr, *Anal. Chem.*, 1990, **62**, R403.
26. W. G. Kuhr and C. A. Monning, *ibid.*, 1992, **64**, 389R.
27. M. Albert, C. Demesnay, M. Porthault and J. L. Roca, *Analusis*, 1992, **20**, 383.

Talanta, Vol. 40, No. 11, pp. 1637–1642, 1993
Printed in Great Britain.

0039-9140/93 $6.00 + 0.00

VOLTAMMETRIC DETERMINATION OF PIROXICAM IN MICELLAR MEDIA BY USING CONVENTIONAL AND SURFACTANT CHEMICALLY MODIFIED CARBON PASTE ELECTRODES

J. A. ACUÑA, C. DE LA FUENTE, M. D. VÁZQUEZ, M. L. TASCÓN and P. SÁNCHEZ-BATANERO
Department of Analytical Chemistry, Faculty of Sciences, University of Valladolid, Valladolid, Spain

Summary—A method for piroxicam determination based on adsorptive stripping voltammetric techniques, using conventional and chemically modified carbon paste electrodes in micellar media, is described. The employed surfactants were sodium dodecyl sulfate (SDS), Triton X-100, Triton X-405, Tween 80 and Brij 30. However, the purpose of this paper is, at present, to research the use of surfactants as carbon paste modifier because one of the mechanisms of hydrophobic drugs ad-accumulation on the carbon paste electrode is based on the chemical affinity. Besides, because of the water piroxicam insolubility, a special aqueous medium, such as a surfactant solution above its c.m.c. was used, this micellar media being very advantageous in relation to the use of organic or aqueous-organic media, in order to dissolve the studied drug and to remove the problems derived from the organic solvents use. In addition, a piroxicam ad-accumulation increase, on surfactant modified carbon paste electrode, with the surfactant mass incorporated into the electrode, was observed.

Piroxicam is a new non steroidian anti-inflammatory drug of the oxicam family that are carboxamic *N*-heterocycles derived from the benzothiazin-1,2-dioxyde-1,1. This drug acts as anti-inflammatory mainly by prostaglandin synthesis inhibition, as well as by leucocyte migration and phagocyte activity inhibition.[1]

Due to its hydrophobic properties, piroxicam molecule is quite insoluble in water, but soluble enough in organic and aqueous-organic media[1] as well as in micellar media.[2]

Regarding the electrochemical properties, piroxicam is polarographically reducible[1] and voltammetrically oxidizable.[1,2] Both processes have been sufficiently studied.[1,3–5]

On the other hand, regarding piroxicam determination methods, we can consider the spectrometric ones,[6,7] with detection limits of several ppm, the chromatographic ones,[8–14] with detection limits of several ppb and finally the electrochemical ones[15,16] with detection limits of several ppt.

All piroxicam electroanalytical methods require the presence of organic solvents because of its insolubility in water. The use of non-aqueous solvents in electrochemistry presents different problems, mainly derived from their toxicity, as well as from the necessary use of special reference electrodes. However, surfactant solutions with concentrations above a critical value (CMC), are able to dissolve hydrophobic substances, remaining in this these media their aqueous nature, therefore, we can employ the classical reference electrodes, such as Hg_2Cl_2/Hg, KCl or AgCl/Ag, KCl.

Use of surfactants in electrochemistry is well known, mainly by their polarographic maxima suppressor properties.[17,18] Nevertheless, when surfactant concentrations are above the c.m.c., we must consider this type of solution belongs to a new type of media, organized media, about which many reviews and books have appeared some years ago in the literature.[19–23]

The most important effects of micellar media in relation to electrochemistry are based on the following aspects[23]: (a) the presence of surfactant molecules in an aqueous solution modifies the double layer structure, the electrokinetic potential, and the charge transfer rate constant, and as an example we can mention the Iwunze *et al.* paper,[24] in which a very important potential shift of the medium oxidation is described; (b) surfactants can stabilize radicals or intermediate reaction products; (c) surfactants easily dissolve hydrophobic substances. Thus, the electrochemical spectra of an analyte in two different media, one fully aqueous and the other of micellar nature, can be completely different.

In our paper, several experiments about the piroxicam electrochemical behaviour study in micellar media, formed by an anionic surfactant, such as sodium sulfate dodecyl (SDS), or by non-ionic ones, such as Triton X-100, Triton X-405, Tween 80 or Brij 30, were carried out, in order to contribute to the best knowledge of surfactant-drug interactions, this knowledge being of great interest, because, actually, in human biological fluids, hydrophobic substances, as for example, cholesterol bonded to lipoproteins in the blood, are carried in the same manner.

Finally, we can consider that, according to the literature checked by us, the use of surfactants as carbon paste modifier has not been very general. Kalcher[25] and Albahadily and Mottola,[26] observed an uncompensed cell resistance decrease after the carbon paste electrode was treated with a 10% (w/v) aqueous surfactant solution, although in this case surfactants were not incorporated at the carbon paste formation step, but after the paste was prepared. We can also mention the papers of the Patriarche's group about the carbon paste modification by chemical substances like the surfactants, such as phospholipids and others.[27,28]

EXPERIMENTAL

To obtain the current–potential curves, an Amel 553 Potentiostat, an Amel 568 Function Generator and a Philips-PM 8271 XYt recorder were employed. A carbon paste working electrode, a saturated calomel reference electrode and a Pt wire as auxiliary electrode, were used. To obtain rapidly suitable micellar media, a Selecta Ultrasonic bath was also used. To control the temperature and the pH, a Tamson TC-3 Thermostat and a Crison pH-meter respectively, were employed.

All used surfactants, such as Triton X-100, Triton X-405, Tween 80, Brij 30 and SDS were supplied by Serva Feinbiochemica GMBH & Co., D-6900 Heidelberg, Germany, and used without purification. Piroxicam was supplied by Pfizer (Spain). All these reagents, buffers, supporting electrolytes, *etc.*, were of analytical grade. The employed water was deionized up to Nanopure II grade by the Barnstead system. The graphite powder, spectroscopically pure and particle size corresponding to 200 mesh, was supplied by Johnson Matthey S.A., Rue de la Perdrix, BP 50240, Paris, France.

Conventional carbon paste (without modification) was classically prepared, but surfactant modified carbon paste was prepared as follows: 500 mg of graphite were mixed with 250 or 300 μl of Nujol oil. To this mixture, 25 mg (or 50 mg) of surfactant dissolved in chloroform were added and mixed with the paste in an agate mortar, when an electrode modification was required.

With a conventional carbon paste electrode, two types of experiments were carried out: (1) direct voltammetry of piroxicam solutions; (2) adsorptive stripping voltammetry of piroxicam solutions. In all adsorptive experiments we must cut a paste disk about 1 mm thick to obtain a fresh and reproducible electrode surface.

With the surfactant modified carbon paste electrode only adsorptive stripping voltammetric measurements were carried out.

For the first type of experiments, the following solution was prepared: 10 ml of 0.1M $HClO_4$ (to obtain a pH 2), 1 ml of 0.1M $LiNO_3$, 1.54 g of SDS, 16.6 mg of piroxicam and deionized water to make 100 ml. This solution was $5 \times 10^{-4}M$ in piroxicam and $4 \times 10^{-2}M$ in SDS.

For the second type of experiments, the following solutions were prepared: (1) 25 ml of 0.1M $HClO_4$, 2.163 g of SDS, 8.3 mg of piroxicam and deionized water to make 250 ml. This solution, named "adsorption solution" was $3 \times 10^{-2}M$ in SDS and $10^{-4}M$ in piroxicam; (2) 3 ml of 0.1M $HClO_4$, 0.3 ml of 0.1M $LiNO_3$ and deionized water to make 30 ml. This solution was named "stripping solution".

RESULTS AND DISCUSSION

Direct voltammetry of piroxicam solutions

With the $5 \times 10^{-4}M$ piroxicam solution, the potential was cyclically scanned between 0 and 800 mV (*vs* SCE) at different scan rates, the optimal one being 100 mV/sec, as a result of a choice of residual current, peak height and recorder sensitivity values. Peak potentials of the voltammograms obtained were developed between 650 and 660 mV, as can be seen in Fig. 1, in which a well-defined piroxicam oxidation peak is shown.

In order to evaluate our method, several voltammograms of piroxicam solutions at different concentrations were obtained. By plotting i_p *vs* concentration, a straight line was also obtained, with equation:

$$i_p = 0.067 + 3612.67\ C$$

where i_p denotes the peak heights in μA and C denotes the molar piroxicam concentration. The correlation coefficient was 0.9981 and the detection limit 6.14 ppm. A linear variation of i_p *vs* piroxicam concentration was obtained, the sensitivity of the determination was acceptable but the detection limit, calculated by Miller and Miller's method,[29] was mediocre.

Adsorptive stripping voltammetry of piroxicam solutions

A previous adsorption process of piroxicam was carried out. For this, a new experimental parameter, ad-accumulation time, needed to be studied. For this, we introduced the carbon paste electrode, at open circuit, in a $10^{-4}M$ piroxicam solution (adsorption solution), at pH 2 and $3 \times 10^{-2}M$ SDS, over different times, while stirring. After a fixed ad-accumulation time, we introduced the electrode, washed with deionised water, in the stripping solution and scanned the potential at a scan rate of 100 mV/sec. The results obtained with the same paste, but different surfaces (cutting discs 1 mm thick), were practically the same, and very similar between different paste batches. Figure 2 shows an example of a peak obtained.

By plotting the peak heights *vs* ad-accumulation time, a straight line was obtained, in which i_p increased with the ad-accumulation time up to 11 min, and then decreased with time, as shown in Fig. 3.

Although the optimal value should be achieved in 10 min according to Fig. 3, the employed ad-accumulation time was only 7 min to save time in our experiments.

In order to evaluate the sensitivity of our adsorptive stripping method, by plotting i_p *vs*

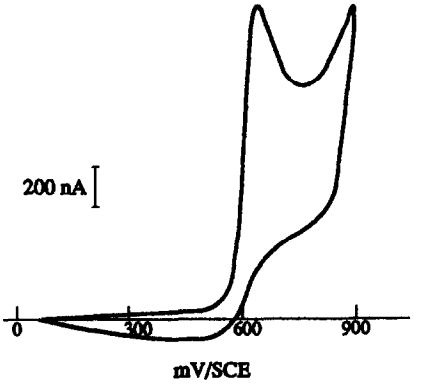

Fig. 1. Voltammogram of $5 \times 10^{-4}M$ piroxicam obtained at a conventional carbon paste electrode; V = 100 mV/sec; pH 2; $0.01M$ $LiNO_3 + 4.10^{-2}M$ SDS.

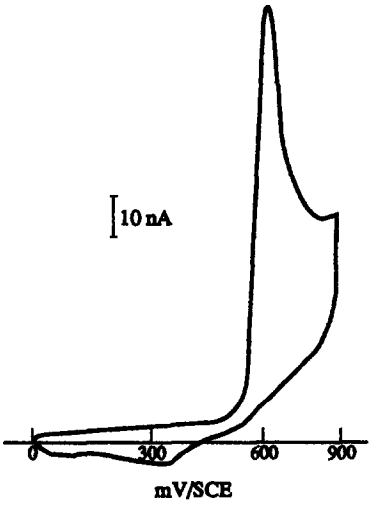

Fig. 2. Adsorptive stripping voltammogram of $10^{-4}M$ piroxicam at a conventional carbon paste electrode; V = 100 mV/sec; t_{ad} = 6 min; pH 2.

piroxicam concentration, a straight line was obtained, with equation:

$$i_p = 0.00346 + 1791.51\ C$$

where i_p denotes the peak heights in μA and C the molar piroxicam concentration. The correlation coefficient was 0.9993 and the detection limit 0.127 ppm, calculated by the method mentioned above.

Comparing Figs 1 and 2, taking into account the recorder sensitivity and the piroxicam concentration, we can deduce that i_p in Fig. 2 is lower, even though accumulation was used. This apparent anomaly can be explained by remembering that the experiment corresponding to

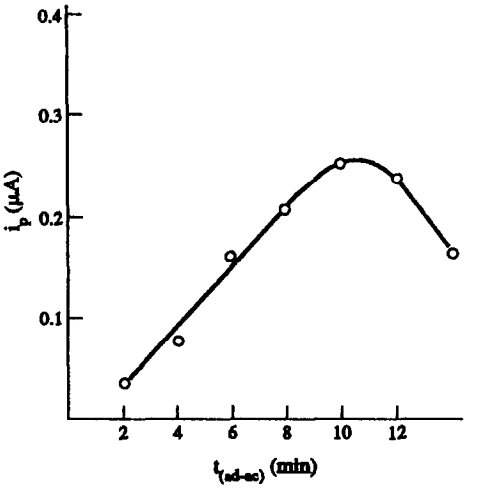

Fig. 3. Influence of ad-accumulation time on piroxicam adsorptive stripping peaks at a conventional carbon paste electrode; $10^{-4}M$ piroxicam; V = 100 mV/sec; pH 2.

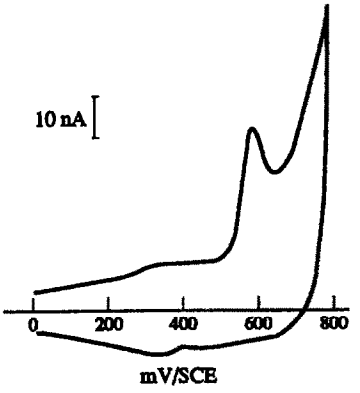

Fig. 4. Adsorptive stripping voltammogram of $10^{-5}M$ piroxicam solution at a conventional carbon paste electrode; $t_{ad} = 7$ min; pH 2; V = 100 mV/sec.

Fig. 2 was carried out to give an example, showing that a piroxicam preconcentration phenomenon can be produced on a conventional carbon paste electrode. Also, the voltammetric peaks in Figs 1 and 2 correspond to very different mechanisms, the first one diffusion and the second adsorption, which also has a lower slope than the first. The adsorption process has the advantage of giving lower detection limits. However, improved detection limits have not been obtained because piroxicam, at lower concentrations, does not readily adsorb on conventional carbon paste electrodes.

The voltammogram of $10^{-5}M$ piroxicam solution is shown in Fig. 4.

Adsorptive stripping voltammetry of piroxicam on surfactant modified carbon paste electrodes

In this case, the carbon paste electrode was previously modified by a surfactant, such as SDS, Triton X-100, Triton X-405, Tween 80 or Brij 30, in order to obtain an electrode surface with hydrophobic properties, so as to improve the piroxicam preconcentration. So, if the electrode surface contain a chemical modifier with the same chemical character than the analyte molecules, an attraction by chemical affinity is created between the two types of molecules, according to the literature.[27,28] Moreover, the electrochemical reactions were carried out in micellar media at a suitable pH, in order to dissolve the piroxicam and to improve its preconcentration on the electrode surface. In addition, the presence of surfactants could improve the selectivity of these preconcentrations, although, in our case, this point has not been studied, because only one drug was considered in this paper.

Our experiments have been carried out as follows.

Voltammetric study on carbon paste electrode modified with sodium dodecyl sulphate

A 500-mg sample of graphite powder was well mixed with 300 μl of Nujol oil in an agate mortar. To this mixture, 25 mg of SDS as modifier, solved in chloroform, were added and mixed up to evaporate the solvent, to obtain a paste with 5% concentration (surfactant/carbon).

The ad-accumulation time and potential scan steps were carried out as above.

In order to estimate the sensitivity of our adsorptive stripping method, i_p *vs* piroxicam concentration was plotted, obtaining a straight line whose equation was the following:

$$i_p = 0.0018 + 1640\ C$$

where i_p denotes the molar piroxicam concentration. The correlation coefficient and detection limit (calculated as above) were 0.9934 and 0.66 ppm, respectively.

Voltammetric study on carbon paste electrode modified with Triton X-100

This carbon paste electrode was prepared as follows: 500 mg of graphite powder were mixed with 250 μl of Nujol oil in an agate mortar. To this mixture, 25 mg of Triton X-100 solved in chloroform were added, giving a paste where the surfactant was 5% (surfactant/carbon).

By plotting voltammetric peaks heights *vs* piroxicam concentration, the following equation was obtained:

$$i_p = -0.002 + 604\ C$$

where i_p denotes the peak heights in μA and C the molar piroxicam concentration. The correlation coefficient was 0.9980, and the detection limit, obtained according to Miller and Miller,[29] was 2 ppm. By comparing these results with those obtained with SDS, we deduce that the determination sensitivity, using Triton X-100 as modifier, is lower, because of the lower calibration graph slope. The detection limit was also lower.

Increasing the Triton X-100 amount in the carbon paste electrode up to 10% (surfactant/carbon), that is to say, 0.300 g of graphite powder, 150 μl of Nujol oil and 30 mg of Triton X-100 solved in chloroform, a similar voltammetric study gave the following equation:

Table 1. Experimental adsorptive i_p values obtained for different electrodes, composition and surfactants

Conc. M ($\times 10^{-5}$)	Peak (μA) CPE without modification	Peak (μA) Modified CPE		
		5% SDS	5% Triton X-100	10% Triton X-100
1.0	0.0215	0.020	0.0040	0.025
0.8	0.0175	0.015	0.0030	0.021
0.6	0.0104	0.012	0.0015	0.019
0.4	0.0052	0.007	0.0004	0.015

$$i_p = 0.014 + 8900\ C$$

where i_p and C have the same significance as above, and whose correlation coefficient and detection limit, were 0.9985 and 1.3 ppm, respectively. In this case, an increase of the method sensitivity (higher slope), according to the slope increase, and a detection limit decrease (lower detected mass) were obtained.

In order to compare the influence of % Triton X-100 on peak heights, the corresponding voltammograms are plotted in Fig. 5, in which we can see that piroxicam peak height increases with the % surfactant. However, the most important result is the fact that with the % (surfactant/carbon) increase, both detection limit and sensitivity of the piroxicam determination method were improved, thus in order to have a comparative view about these improvements, obtained results are summarised in Table 1.

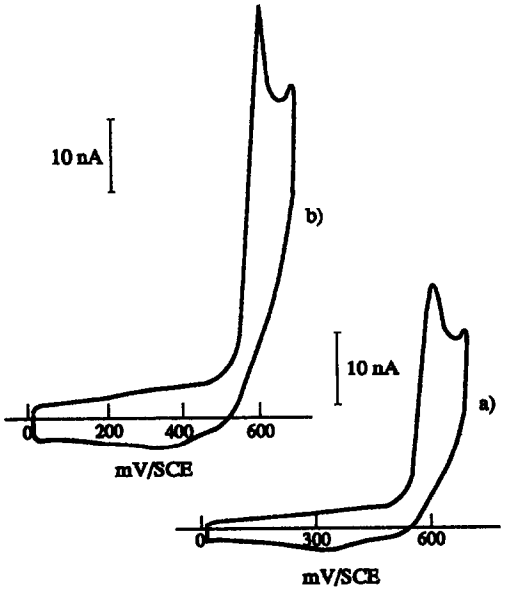

Fig. 5. Adsorptive stripping voltammograms of piroxicam on surfactant modified carbon paste electrode. Influence of % (Triton X-100/Carbon) into the electrode on peak heights: (a) $6.10^{-5}M$ piroxicam, pH 2, V = 100 mV/sec, t_{ad} = 8 min, 5% (Triton X-100/Carbon); (b) as (a) but with 10% (Triton X-100/Carbon).

We have used other surfactants, such as the non-ionic Triton X-405, Tween 80, and Brij 30; the first of which supplied the same results as Triton X-100, the second gave a very important residual current, and with the third, Nujol oil loses its properties as a binder, therefore these surfactants were not used as carbon paste modifiers in our experiments.

CONCLUSIONS

As we have mentioned above, the main purpose of this paper is to research the use of surfactants as carbon paste modifiers, in order to improve the sensitivity of drug determination by using electroanalytical methods. Because of the surfactant presence between the carbon particles on the electrode, a suitable lipoaffinity to preconcentrate hydrophobic substances, such as piroxicam molecules, is created, giving an increase of the piroxicam amount ad-accumulation, showing that the higher was the % surfactant on carbon paste and the higher was the piroxicam accumulation. However, this cannot be the only preconcentration mechanism on this type of electrode, because the Nujol oil can also preconcentrate hydrophobic substances by an extractive mechanism into the paste, as can be seen in the literature.[27,28,30,31] So, due to the extractive properties of Nujol oil, hydrophobic substances, such as promethazine, for example, can be extracted by this pasting, whereas celiptium, is adsorbed on carbon particles at the same electrode.[31] In this sense, we deduced, from our experimental results, that carbon paste electrodes without modification are also suitable in relation to the glassy carbon electrode to improve electroanalytical piroxicam determinations, probably due to an extractive process by the Nujol oil of the paste. Furthermore, according to our results, the use of surfactants as modifier carbon paste electrode have a promising future in studies of the carbon paste

modification because of the preconcentration increase, at least for hydrophobic drug determination whose solutions can be easily prepared without organic solvent addition.

Acknowledgements—This work has been supported by the DGICYT, Project PB 89-0361-CO3-01, of the Ministerio de Educación y Ciencia of Spain. The authors thank Dr E. Velasco of the University Clinic Hospital of Valladolid (Spain) as well as the commercial firm Pfizer (Spain) who kindly provided the studied drug.

REFERENCES

1. J. C. Viré, J. M. Kauffmann, J. Braun and G. J. Patriarche, *Analusis*, 1985, **13**, 38, 134.
2. J. A. Acuña Bruña, *Tesis de Licenciatura*, Universidad de Valladolid, November, 1991.
3. J. M. Kauffmann, A. Laudet, G. J. Patriarche and D. G. Christian, *Anal. Chim. Acta*, 1982, **135**, 153.
4. J. M. Kauffmann, A. Laudet, G. J. Patriarche and D. G. Christian, *Talanta*, 1982, **29**, 1077.
5. J. M. Kaufmann, A. Laudet, J. C. Viré, G. J. Patriarche and D. G. Christian, *Microchem. J.*, 1983, **28**, 357.
6. C. S. Sastry and A. R. M. Rao, *Anal. Lett.*, 1984, **20**, 349.
7. X. Hu and X. Zhou, *Youri Fenxi Zazhi*, 1986, **6**, 30.
8. I. Kochevar, W. L. Mousom, J. L. Lamm, D. J. McAuliffe, A. Western and A. F. Hood, *Arch. Dermatol.*, 1986, **122**, 34.
9. Y. H. Tsai, L. R. Hsu and S. Naito, *Kaohnsiung. Int. J. Pharm.*, 1985, **24**, 101.
10. H. M. Stevens and R. Gill, *J. Chromatogr.*, 1986, **370**, 39.
11. X. Chen, N. Xi and S. Ghe, *Yaoxue Xuebao*, 1986, **21**, 629.
12. K. D. Riedel and H. Lauyen, *J. Chromatogr.*, 1983, **276**, 242.
13. U. Knie, *J. Chromatog.*, 1983, **275**(2); *Biomed. Appl.*, **26**(2), 463.
14. C. J. Richardson, S. G. Ross, K. Blocka and R. Verbeek, *J. Chromatogr.*, 1986, **382**, 382.
15. El-Maali, N. Abo, J. C. Viré, G. J. Patriarche, M. A. Ghandour and G. D. Christian, *Anal. Sci.*, 1990, **6**, 245.
16. M. González, M. D. Vázquez, M. L. Tascón and P. Sánchez-Batanero, *Electroanalysis*, in press.
17. I. M. Kolthoff and J. J. Lingane, *Polarography*, Vol. 1, p. 160. Interscience Publishers, New York, London, 1952.
18. D. R. Crow and J. V. Westwood, *Polarographie*, C. Armand (ed.), p. 43. Paris, 1971.
19. C. Tanford, *The Hydrophobic Effect, Formation of Micelles and Biological Membranes*. Wiley, New York, 1973.
20. W. L. Hinze, *Use of Surfactant and Micellar Systems in Analytical Chemistry*, in *Solution Chemistry of Surfactants*, K. L. Mittal (ed.), Vol. 1, pp. 78–127. Plenum Press, New York, 1979.
21. K. L. Mittal and E. J. Fendler, *Solution Behaviour of Surfactants, Theoretical and Applied Aspects*, Vol. 1 and 2. Plenum Press, New York, 1982.
22. A. Berthod, *J. Chim. Phys.*, 1983, **80**, 5, 407.
23. L. J. Cline Love, J. G. Habarta and J. G. Dorsey, *Anal. Chem.*, 1984, **56**, 11, 1133A.
24. T. C. Franklin and M. Iwunze, *ibid.*, 1980, **52**, 973.
25. K. Kalcher, *Electroanalysis*, 1990, **2**, 419.
26. F. N. Albahadily and Horacio A. Mottola, *Anal. Chem.*, 1987, **59**, 7, 958.
27. O. Chastel, J. M. Kauffmann and G. J. Patriarche, *ibid.*, 1989, **61**, 170.
28. M. Khodari, J. M. Kauffmann, G. J. Patriarche and M. Ghandour, *Electroanalysis* 1989, **1**, 501.
29. J. C. Miller and J. N. Miller, *Statistics for Analytical Chemistry*, p. 96. Ellis Horwood, New York, 1984.
30. J. Wang and B. A. Freiha, *Anal. Chem.*, 1984, **56**, 849.
31. J. Arcos, J. M. Kauffmann, G. J. Patriarche and P. Sánchez-Batanero, *Anal. Chim. Acta*, 1990, **236**, 299.

Talanta, Vol. 40, No. 11, pp. 1643–1648, 1993
Printed in Great Britain.

0039-9140/93 $6.00 + 0.00

SOLVENT EXTRACTION OF CADMIUM AS A PREVIOUS STEP FOR ITS DETERMINATION IN BIOLOGICAL SAMPLES BY ELECTROTHERMAL ATOMIZATION ATOMIC ABSORPTION SPECTROMETRY

J. M. ESPINOSA ALMENDRO, C. BOSCH OJEDA, A. GARCIA DE TORRES and J. M. CANO PAVON
Department of Analytical Chemistry, Faculty of Sciences, University of Málaga, 29071 Málaga, Spain

Summary—A method is proposed for the solvent extraction of cadmium using 1,5-bis(di-2-pyridylmethylene)thiocarbohydrazide (DPTH) as extractant. The optimum extraction conditions were evaluated from a critical study of the effect of pH, concentration of extractant, shaking time and ionic strength. The maximum volume ratio of the aqueous to organic phase was 30:1 for a single-stage extraction of 99–100% of the metal ion. The detection limit is 0.01 ng/ml cadmium, and the calibration is linear from 0.1 to 5 ng/ml. The relative standard deviation for 10 replicate measurements is 1.8% for 2 ng/ml cadmium. The extraction method was applied to the determination of cadmium in some biological materials using graphite furnace atomic absorption spectrometry.

The toxic effects of cadmium are now well recognized and many researchers have reported the determination of cadmium in biological materials by Electrothermal Atomization Atomic Absorption Spectrometry (ETA-AAS).[1–6] However, in most cases there is the problem of matrix interference. The application of the standard additions method increases the probability of correct results, but cannot guarantee them.[7] This problem can be overcome by diverse procedures: introduction of an active gas during the ashing step,[8] use of matrix modifiers,[9–11] use of an effective background correction system (Zeeman, habitually),[1,12] or separation of the cadmium from the matrix using electrodeposition,[13] ion-exchange[14] or, more frequently, liquid–liquid extraction.

Liquid–liquid extraction provides an easy method of reducing the interference of the matrix, and improving the sensitivity by concentrating the metal in a small volume of an organic solvent. Cadmium has been extracted by means of different extracting systems: ammonium pyrrolidine dithiocarbamate into methyl isobutyl ketone (MIBK),[15] hexamethylene ammonium hexamethyleneditiocarbamate into xylene[16] and tetrahexylammonium iodide into MIBK from a hydrochloric acid medium.[17] All these procedures have been used as a preconcentration step for the determination of cadmium by ETA-AAS.

In this work, a systematic study was made to determine the optimum conditions for cadmium determination in biological samples by ETA-AAS after extraction of the metal into MIBK containing 1,5-bis(di-2-pyridylmethylene)thiocarbohydrazide (DPTH). The proposed extraction method has some advantages. The complex formed is quite soluble in MIBK, so much so that it allows the use of aqueous-to-organic phase volume ratios up to 30 (*i.e.* much higher than those typically afforded by other extractants) and hence the determination of concentrations down to 30 times lower than those afforded by the direct non-extractive method.

The microwave digestion procedure was used for sample preparation. Microwave heating in sealed Teflon containers was applied with only one treatment. The advantages of this procedure include faster reaction rates which result from the high temperatures and pressures attained inside the sealed containers. The use of closed vessels makes it possible to eliminate uncontrolled trace element losses of volatile molecular species that are present in a sample. Another advantage of microwave dissolution is a decrease in blank values as compared to open-beaker work, both because contamination from the laboratory environment is much lower and because closed vessels make it possible to use smaller quantities of reagent.[18,19] In this work, due to the limited volume of the Teflon vessels, conventional digestion procedures were also used for sample preparation when the

concentration of cadmium in the sample analysed was too small, so that a great amount of sample should be dissolved.

EXPERIMENTAL

Apparatus

Atomic absorption measurements were made with a Varian 475 atomic absorption spectrophotometer with a standard air–acetylene burner, and a Perkin–Elmer Zeeman electrothermal atomic absorption spectrometer model 4100ZI equipped with an automatic sampling system model AS-70, a Zeeman background correction system and a PC-ICL computer. Pyrolytically coated graphite tubes, L'vov-type graphite platforms and a cadmium hollow cathode lamp were used. Argon was used as the purge gas. A cadmium hollow cathode lamp was used for atomic absorption measurement at 228.8 nm.

A Panasonic (National) microwave oven model NN-8507 and a Parr Microwave Acid Digestion Bomb, model 4782, were used for sample digestion. The bombs were cleaned before use with 10% nitric acid for 1 day followed by repeated rinsing with water.

pH measurements were made with a Crison Digit 501 pH-meter (combined electrode). A variable rate, time-programmable Gallenkamp mechanical flask agitator was used for sample agitation.

Reagents

All chemicals were of analytical reagent grade. Distilled and deionized water was used throughout.

The ligand for the DPTH solution was synthesized as described elsewhere.[20] A stock solution in MIBK was prepared by dissolving 0.1 g of DPTH in 9 ml of *N,N*-dimethylformamide and diluting to 100 ml with MIBK. The solution was found to remain stable for over a week.

A stock solution of Cd(II) was prepared from the nitrate (Merck P. A.) and standardized complexometrically. Standards of working strength were made by appropriate dilution as required.

An acetic acid–acetate buffer of pH 5.6 was prepared by mixing 4.8 ml of 0.2*M* HOAC and 45.2 ml of 0.2*M* NaOAc in a 100-ml volumetric flask and making to the mark with distilled water.

A 1*M* solution of $NaClO_4$ was also used.

Samples

The certified reference materials analysed to determine the accuracy of the proposed procedure were: Community Bureau of Reference (BCR), Certified Reference Materials (CRMs); 060 Lagarosiphon Major (Aquatic Plant); 061 Platihypnidium Ripariodides/Aquatic Plant); 150 Milk powder; 151 Milk powder; 184 Bovine Muscle; 186 Pig Kidney; National Research Council Canada (NRCC), CRMs DORM-1 Dogfish Muscle; DOLT-1 Dogfish Liver; TORT-1 Lobster Hepatopancreas; National Institute of Standards and Technology (NIST), Standard Reference Materials (SRMs) 2670 Freeze-Dried Urine (Toxic Metals at Normal and Elevated Levels); 1577a Bovine Liver.

Procedures

All glassware and plasticware were acid cleaned (25% v/v nitric acid) prior to use.

Choice of optimum extraction conditions. The metal ion was extracted as follows. In 500 ml separatory funnels was placed 20 μg of cadmium with variable volumes of HCl, NaOH and $NaClO_4$ solutions and the mixture was diluted to an overall volume of 20 ml in the aqueous phase. Then, variable volumes of DPTH solution in MIBK at different concentrations were added and the mixture was shaken vigorously on the mechanical agitator for different periods of time. Once both phases had been separated, the content of cadmium of the aqueous phase was determined by flame absorption spectrometry, using appropriate calibration graphs. From the concentration found, the fraction of metal extracted was calculated. Appropriate blanks were prepared and were run in the same manner.

Sample preparation. The samples of the various types of material considered were first dried in accordance with the norms of the respective analysis certificates. Each dried sample (with the exception of human urine) was mineralized according to one of the following two procedures.

(1) Microwave mineralization. An amount of 0.200–0.600 g of powdered sample (NBS 1577a, BCR 186, DOLT-1, TORT-1, CRM 060 and CRM 061) was placed in the reaction bomb together with 4 ml of 65% nitric acid. Then, after 30 min, 2 ml of 37% HCl was added and the digestion bomb was shut and placed in the microwave oven, where it was kept at 360 W for 4.0 min, followed by 10.0 min at 180 W. The oven was allowed to cool for 14 min (the same

time as the programme duration) after it was opened. After digestion, the solutions were evaporated to a small volume by heating in a hot plate to remove the nitric acid, neutralized with sodium hydroxide, and finally diluted with deionized water to 50 ml in a standard flask.

(2) Reflux mineralization with nitric acid and hydrogen peroxide. In a reaction flask were placed 2.000–4.000 g of weighed sample (BCR 184, DORM-1, CRM 150 and CRM 151) and 15 ml of concentrated nitric acid, and the mixture was heated under reflux up to the disappearance of nitrous fumes. Then, 3 ml of hydrogen peroxide were added and the mixture was evaporated to a small volume by heating in a hot plate to remove the nitric acid. Next, the mixture was neutralized with NaOH and made to 25 or 50 ml with deionized water.

Procedure 1 is quicker, but cannot be applied to a sample amount greater than 1 g, due to the small capacity of the digestion bomb. For this reason, if it is necessary to take a sample amount greater than 1 g (when the concentration of cadmium in the samples is very small), procedure 2 must be used.

The human urine SRM 2670 does not require mineralization; the sample was prepared from concentrates according to the directions supplied.

Aliquots of these sample solutions containing 0.015–0.75 μg of cadmium were placed in 250-ml separating funnels. The analysis of each sample, in triplicate, was completed as described in the Recommended Procedure.

Recommended analytical procedure. In separatory funnels were placed aliquots of samples or standards solutions containing 0.015–0.75 μg of cadmium, 0.5 ml of 1*M* $NaClO_4$ and 5 ml of acetic acid–acetate buffer, pH 5.6. Then, 5 ml of 0.1% DPTH in MIBK were added (the maximum volume ratio of the aqueous to organic phase was 30:1 for a single-stage extraction of 99–100%). The mixture was shaken vigorously at 3000 rpm for 5 min, after which the phases were allowed to separate and the solvent layer was transferred into a polypropylene centrifugate tube (some samples may need centrifugation for up to 5–20 min to improve separation between the layers). Aliquots (20 μl) of organic phase were injected, in triplicate, into the graphite furnace and the absorbance was measured at the wavelength of 228.8 nm using the instrumental conditions shown in Table 1. Triplicate determinations of each sample were made and the cadmium concentration was evaluated from the calibration graph; alternatively, the standard-addition method was also satisfactorily applied.

RESULTS AND DISCUSSION

Optimization of extraction conditions

Extraction of metal ions by organic reagent is known to depend on several factors such as type and amount of reagent, organic solvent, chemical form of metal ion, pH of solution, shaking time, etc. We have investigated the extraction process in order to obtain optimum conditions. MIBK has a significant solubility in water but was chosen as the organic solvent because of its high extraction efficiency for the Cd(II)–DPTH complex.

The effects of pH on the extraction of cadmium with DPTH into MIBK are shown in Fig. 1. As can be seen, the optimum pH range for quantitative extraction is around 4.0–10.7. All subsequent studies were carried out at pH 5.6; this pH was adjusted using an acetic acid–acetate buffer solution. The volume of this buffer added (3–8 ml) had no effect. The

Table 1. Instrumental conditions for the Zeeman electrothermal atomic absorption spectrometer

Lamp current	4 *mA*					
Slit width	0.7 *nm*					
Wavelength	228.8 *nm*					
Injection volume	20 *µl*					
Operating mode	Peak height					
Integration time	5 *sec*					
Furnace programme: Perkin–Elmer 4100ZI						
	Dry	Ash	Atomize		Clean	
Temperature (°)	110	130	400	650	2000	2400
Ramp (*sec*)	1	5	3	7	1	1
Hold (*sec*)	20	30	20	20	4	2
Argon flow rate (*ml/min*)	250		250		0	250

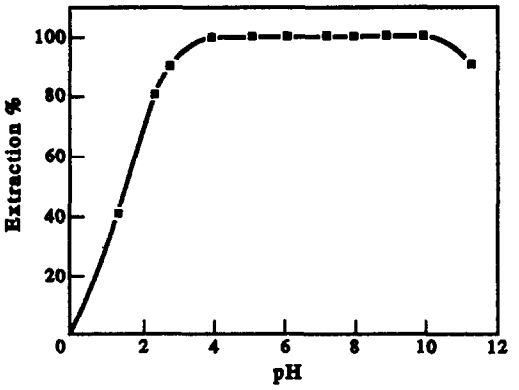

Fig. 1. Effect of pH on the extraction of Cd(II) with DPTH in MIBK in the presence of perchlorate. $[Cd(II)]_{initial} = 0.60$ μg/ml,[A] $[DPTH]_0 = 2.3 \times 10,^{-3}M$, $[ClO_4] = 0.75M$; shaking time: 10 min.

presence of $NaClO_4$ makes feasible a good separation of the phases, although it produces no significant changes in the extraction; for this reason, a concentration of $3.3 \times 10^{-3}M$ $NaClO_4$ was used in all experiments.

The minimum shaking time was determined by varying the shaking time from 1 to 7 min; 5 min was sufficient (Fig. 2a) and was selected in all subsequent work. However, prolonged shaking had no adverse effect on the extraction.

The extraction behaviour of Cd(II) was examined by the single extraction of a fixed amount of cadmium (1 μg/ml), varying the concentration of DPTH in the organic phase while keeping its final volume at 5 ml. The results obtained showed (Fig. 2b) that the extracted fraction remained constant for DPTH concentrations equal or greater than $2.3 \times 10^{-3}M$ (0.1%) for a Cd(II) concentration of 1 μg/ml. For a smaller concentration of cadmium, smaller concentrations of DPTH can be used. A molar ratio of 1:250 [Cd(II):DPTH] was used for subsequent experiments in order to ensure the presence of reagent excess.

The volume of the aqueous phase was varied between 10 and 200 ml while keeping that of the organic phase constant at 5 ml (0.1% m/v of DPTH); hence, the phase volume ratios have been varied between 2 and 40. For a ratio greater than 30, the phase separations were unsatisfactory and the procedure was thus inapplicable. Such a high phase ratio results in a sensitivity higher than that of the direct non-extractive method.

Under these optimum conditions, the recovery factors for the extraction of cadmium were calculated by means of a series of experiments in which the atomic absorption of cadmium in the organic phase was compared with that of a standard prepared in water-saturated MIBK. In all instances, cadmium in the range 0.015–150 μg was extracted completely from the aqueous solution by a single extraction with $2.3 \times 10^{-3}M$ DPTH solution in MIBK.

On the other hand, prior to the analysis of real samples it was necessary to optimize the instrumental conditions for the determination of cadmium by ETA-AAS. The complete programme developed as a result of the normal optimization procedure is as described in Table 1.

Analytical performance. Under the optimum conditions used, a linear calibration graph was obtained for 0.1–5 μg/l of cadmium in the aqueous phase. Ten determinations of standard

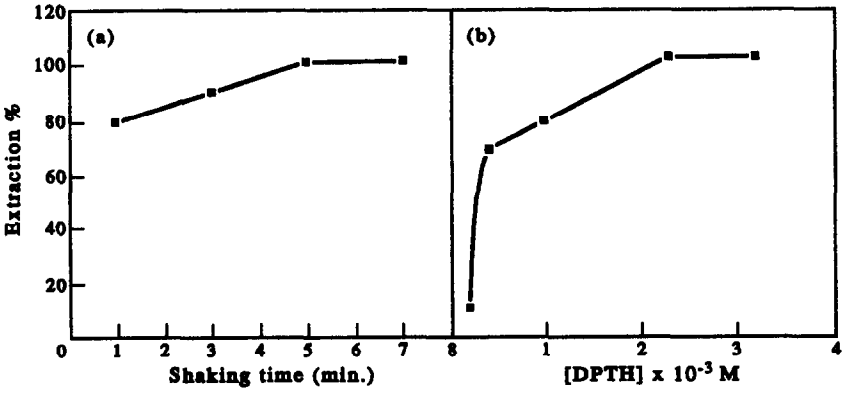

Fig. 2. (a) Influence of shaking time on the extraction. Concentration of cadmium in the aqueous phase: 1 μg/ml. Concentration of DPTH in the organic phase: $2.3 \times 10^{-3}M$. (b) Influence of the concentration of DPTH on the extraction. Concentration of cadmium in the aqueous phase: 1 μg/ml. Shaking time: 6 min.

Table 2. Tolerance to foreign ions in the determination of 1 μ/l. of Cd (in the aqueous phase) by the proposed method; $[DPTH]_0 = 1.15 \times 10^{-3} M$

Tolerated ratio	Ion
>5000	K(I), Tl(I), V(V), Se(IV), W(VI), F^- Br^-, I^-, SO_4^{2-}, CO_3^{2-}, SCN^- Cl^-, Al(III), Fe(II), Fe(III), Zn(II), Bi(III), Cu(II), Co(II), Ni(II), Ga(III)
4000	Cr(III), pB(II), Mn(II), Ba(II), Mo(VI), Li(I), Mg(II), Rb(I), Ca(II)
3000	U(VI), Sr(II), Sb(III), Ag(I), Hg(I), Hg(II)
1000	Y(III)

Table 3. Determination of cadmium in biological samples

	Amount of cadmium ($\mu g/g$)	
Sample	Found	Certified
Olive leaves, CRM 060	1.85 ± 0.14	2.20 ± 0.10
Olive leaves, CRM 061	0.92 ± 0.04	1.07 ± 0.08
Milk powder, CRM 150	18.0 ± 1.0*	21.8 ± 1.4*
Milk powder, CRM 151	112.5 ± 17.7*	101.0 ± 8.0*
Pig kidney, BCR-186	2.48 ± 0.11	2.71 ± 0.15
Bovine muscle, BCR-184	17.4 ± 0.9*	13.0 ± 2*
Dogfish liver, DOLT-1	3.65 ± 0.21	4.18 ± 0.28
Lobster hepatopancreas, TORT-1	26.0 ± 2.1	26.3 ± 2.1
Dogfish muscle, DORM-1	0.094 ± 0.010	0.086 ± 0.012
Bovine liver, NBS 1577a	0.47 ± 0.05	0.44 ± 0.06
Human urine, SRM 2670	0.102 ± 0.009†	0.088 ± 0.003†

*In ng/g.
†In $\mu g/ml$.

solutions containing 2 μg/l gave a relative standard deviation of 1.8% ($P = 0.05$).

The detection limit was calculated as the concentration of analyte giving an atomic absorption signal equal to three times the standard deviation of the blank plus the net blank intensity, under optimum operating conditions. The detection limit was found to be 0.01 μg/l of cadmium in the aqueous phase for an aqueous-to-organic phase ratio of 30.

Study of interferences. The effect of diverse ions on the determination of cadmium was examined under the optimum conditions of the procedure. The tolerance limit was taken as that concentration which does not cause more than a 5% change in the atomic absorption. For these studies different amounts of ionic species were added to a solution of 1 μg/l of cadmium. The starting point was a 5000-fold m/m ratio of interferent to cadmium, and if interference occurred the ratio was progressively reduced until interference ceased. The solutions were analysed three times on different days and the average result was calculated. The interference effects are shown in Table 2, which shows that cadmium can be determined in the presence of a large number of diverse ions. Interferences due to ETA-AAS detection were: Cr(III), Pb(II), Mn(II), Sb(III), Mg(II), Ca(II), Li(I) and Rb(I); the other interferences are due to the extraction step.

Analysis of samples. In order to test the accuracy and applicability of the proposed method to the analysis of real samples, several certified reference materials were analysed. Matrix interferences were verified by comparison of the slopes of the calibration graphs with those using the standard additions method. Only for SRM 2670 were matrix effects apparent for the ICP measurements and quantification was performed with the standard additions methods. The results are given in Table 3 as the average of three replicates. As can be seen, the cadmium concentrations determined by the proposed method are in close agreement with the certified values.

Acknowledgements—The authors are grateful to the Spanish Comisión Interministerial de Ciencia y Tecnología (CICYT; Project PB 90–0809) and also the Regional Government of Andalucia for financial support.

REFERENCES

1. P. Dube, C. Krause and L. Windmuller, *Analyst*, 1989, **114**, 1249.
2. K. Akatsuka and I. Atsuya, *Anal. Chem.*, 1989, **61**, 216.
3. Z. A. De Benzo and R. Fraile, *Anal. Chim. Acta.*, 1990, **231**, 283.

4. D. L. Tsalev, T. A. Dimitrov and P. B. Mandzhukov, *J. Anal. At. Spectrom.*, 1990, **5**, 189.
5. J. Smeyers-Verbeke, Q. Yang, W. Pennick and F. Vendervoot, *J. Anal. At. Spectrom.*, 1990, **5**, 393.
6. S. J. Haswell (ed.), *Atomic Absorption Spectrometry*. Elsevier, Amsterdam, 1992.
7. K. Dung and B. Neidhart, *Analyst*, 1984, **109**, 877.
8. T. Maeda, M. Nakateni and Y. Tanimoto, *Bunseki Kagaku*, 1989, **38**, 734.
9. X. Yin, G. Schlemmer and B. Welz, *Anal. Chem.*, 1987, **59**, 1462.
10. M. Patriarca, E. Petrozzi and G. Morisi, *G Ital. Chim. Clin.*, 1988, **13**, 111.
11. Lucinda, M. Voth. Beach and D. E. Shrader, *J. Anal. At. Spectrom.*, 1987, **2**, 45.
12. U. Voelkopf and Z. Grobenski, *At. Spectrosc.*, 1984, **5**, 115.
13. G. E. Bately, *Anal. Chim. Acta*, 1981, **124**, 121.
14. L. Rasmussen, *Anal. Chim. Acta*, 1981, **125**, 117.
15. P. Allain and Y. Mauras, *Clin. Chim. Acta*, 1979, **91**, 41.
16. R. Heinrich and J. Angerer, *Fresenius' Z. Anal. Chem.*, 1983, **315**, 528.
17. M. Jawaid, B. Lind and G. G. Elinder, *Talanta*, 1983, **30**, 509.
18. H. M. Kingston and L. B. Jassie (eds), *Introduction to Microwave Sample Preparation*. ACS, Washington, DC, 1988.
19. R. Jaffe, C. A. Fernandez and J. Alvarado, *Talanta*, 1992, **39**, 113.
20. J. R. Bonilla Abascal, A. Garcia de Torres and J. M. Cano Pavón, *Microchem. J.*, 1983, **28**, 132.

Talanta, Vol. 40, No. 11, pp. 1649–1656, 1993
Printed in Great Britain.

0039-9140/93 $6.00 + 0.00

VOLTAMMETRIC STUDIES OF A PSYCHOTROPIC DRUG WITH NITRO GROUPS. DETERMINATION OF FLUNITRAZEPAM IN URINE USING HMDE

E. BERMEJO, A. ZAPARDIEL, J. A. PÉREZ, A. HUERTA and L. HERNÁNDEZ*
Department of Analytical Chemistry and Instrumental Analysis, Autonoma University, 28049 Madrid, Spain

Summary—The adsorption behaviour of flunitrazepam at the hanging mercury drop electrode was studied by staircase voltammetry and by adsorptive stripping differential pulse voltammetry. Flunitrazepam is adsorbed in the whole potential range, from the most positive values up to the reduction potential. Flunitrazepam reduction product is also adsorbed. The time dependence of the voltammetric response proves that a diffusion-controlled adsorption takes place. Flunitrazepam can be determined (down to nanomolar levels) by using adsorptive preconcentration prior to the differential pulse voltammetric scan. An application of such a method to flunitrazepam determination in human urine is described. The detection limit was 30 ng per milliliter of urine with a 20-sec accumulation time; the mean relative standard deviation was lower than 3.2% and the mean recovery 97.8%.

Flunitrazepam [5-(2-fluorophenyl)-1,3-dihydro-1-methyl-7-nitro-2H-1,4-benzodiazepin-2-one], a compound with interesting pharmacological applications marketed as the active ingredient in the commercial preparation Rohipnol-Roche, is a member of the 1,4-benzodiazepine group, undoubtedly the most important chemicals of those with ansyolitic properties. It is used as a sleep-inducing drug in all kinds of insomnia, as premedication prior to anesthesia and in cases where a preparation with anti-anxiety, antidepressive and relaxant properties is required.

As a direct result of its ansyolitic properties, flunitrazepam has become a much overused drug, to the point of being classified among the drugs of abuse. For this reason, the bibliography on different methods for its detection and determination[1] is extensive.

Several analytical data of the drug are described,[2–6] as well as the results of the different studies carried out: pharmacokinetic,[7–10] pharmacodynamic[11] and photochemical,[12–13] and dealkylation and diazotization studies.[14] Some flunitrazepam hydrolysis products (aminobenzophenones) have also been studied.[15–17]

Among the methods applied to flunitrazepam detection are gas chromatography,[2,18–27] thin-layer chromatography,[2,17,23,27–36] high-performance liquid chromatography,[37–43] infrared spectroscopy[44,45] and electrochemical methods.[46] Among those used for its determination are gas chromatography (usually with electron capture detection[47–54] coupled with mass spectrometry[55–57] or with Fourier transform I.R. detection[58]), high-performance liquid chromatography (with ultraviolet detection,[23,24,59–63] immunoassay[64,65] and radioimmunoassay.[66–69] Many of them can be used to determine flunitrazepam in different biological fluids.

As far as the electrochemical reduction studies are concerned, Smyth *et al.*,[46] Oelschlaeger[70] and Sengun and Calishan[71] studied the feasibility of identifying and determining flunitrazepam polarographically over a wide range of pH values. The studies conducted with differential pulse polarography[46] established that flunitrazepam reduction peaks appear at −0.16 V and −0.73 V (*vs* SCE) in Britton-Robinson buffer of pH 4.0, and at −0.61 V and −1.20 V in the same buffer when the pH is 12.0. The mechanism of the reduction has been discussed at mercury[70–73] and glassy carbon[72,73] electrodes. In acidic solution, the first is a four electron wave corresponding to reduction of the 7-nitro group to the hydroxilamine derivative and the second was due to the consumption of four electrons in the simultaneous reduction of 4,5-azomethine and the hydroxilamine (formed as an intermediate of the nitro group reduction). However, under alkaline conditions the second

*Author for correspondence.

process was only to the two-electron 4,5-azomethine reduction. Differential pulse polarography has been used to determine flunitrazepam in pharmaceutical preparations,[71] serum and plasma.[74] Moreover, flunitrazepam has been determined in pharmaceutical preparations by flow injection analysis with amperometric detection;[75] in serum and urine by stripping voltammetry using clay-modified carbon paste electrodes,[76,77] it has been applied to samples containing 1.5 μg of flunitrazepam per milliliter of urine.[76]

Electrochemical oxidation studies[78,79] using a glassy carbon electrode show that flunitrazepam is not electro-oxidable.

So far, none of the studies published have taken into consideration the fact that flunitrazepam is adsorbed at the mercury electrode. And that is the aim of the present work: to explore the properties of the adsorption process of flunitrazepam at the mercury electrode and see if such a phenomenon can be taken advantage of in order to be used as a preconcentration step prior to the voltammetric measurement of surface-bound species. The voltammetric measurement has been carried out on the reduction peak of the nitro group with the aim of determining the drug at nanomolar level using adsorptive stripping voltammetry. We have sought to develop a method for determination of the drug in urine that is at the same time sensitive, accurate, quick and easy to use.

Adsorptive stripping voltammetry has already been used in our laboratories to determine several benzodiazepines that can be adsorbed at the mercury electrode.[80-86]

The work presents a study of all the factors that may influence both the accumulation process and the voltammetric response; it also takes into account the influence exerted by the different urine components, develops a process for extraction of flunitrazepam from urine and gives interfacial and redox data that can help to achieve a better understanding of flunitrazepam activity.

EXPERIMENTAL

Apparatus

The experiments of adsorptive stripping voltammetry were performed using a Metrohm 646 VA processor in conjunction with a 647 VA stand. A three-electrode system was used made up of Ag/AgCl/3*M* KCl reference electrode, a glassy carbon auxiliary electrode and a multimode mercury drop electrode (Metrohm 6.1246.020) that served as the working electrode in the hanging MDE mode with a medium surface of 0.0060 cm^2.

The electrocapillary curves were carried out with a 564 Amel polarograph. A mercury drop working electrode, a platinum auxiliary electrode and a saturated calomel reference-electrode was used.

The cyclic staircase voltammetric measurements were carried out using a 384B PAR polarographic analyzer together with a 303A PAR static mercury drop electrode (GO 199 capillary) with a surface of 1.01 mm^2; the reference electrode was a Ag/AgCl/3*M* KCl and the auxiliary a platinum electrode. The polarograph was coupled to an AMETEK DMP-40 series digital plotter.

All measurements were performed at room temperature and all potentials are referred to the Ag/AgCl/3*M* KCl electrode unless other conditions are expressed in the text.

Reagents

Pure flunitrazepam was kindly supplied by Roche S.A., Spain. The compound and the electrolytes (Merck P.A.) were used without further purification. Stock solutions ($8.0 \times 10^{-4}M$) of flunitrazepam, prepared by dissolving the compound in methanol, were stored in the dark under refrigeration to minimize decomposition. The supporting electrolytes were Britton-Robinson, acetate, ammonium, carbonate and borate buffer of different pH and ionic strengths.

Aqueous solutions were prepared in purified water (Milli-Q and Milli-Ro, Millipore). Human urine samples were pooled from five subjects.

Procedures

Cyclic staircase voltammetry. A 10.0-ml flunitrazepam solution was put in the voltammetric cell and deoxygenated with nitrogen (99.999%) for 10 min. After a mercury drop had formed on the working electrode and was maintained at a potential of -0.350 V for the duration of the adsorption time, which is performed in still solutions, a cyclic potential scan (scan rate 500 mV/sec, step height of 4 mV and step width of 0.008 sec) was applied, beginning with the reduction scan.

Adsorptive stripping differential pulse voltammetry. A 25.0-ml flunitrazepam solution was used with an accumulation potential of −0.350 V. The solution was stirred at 1920 rpm throughout the accumulation time. After a 30-sec rest, a differential pulse scan towards more negative potential values (scan rate 30 mV/sec and pulse amplitude 75 mV) was employed to obtain the stripping voltammograms.

Treatment of urine samples. A 2.0-ml sample of urine containing from 100 to 500 ng of flunitrazepam per milliliter of urine were placed in an extraction funnel and 1 ml of 0.04*M* borate buffer at pH 9.2 was added. The drug was extracted by adding 3 ml of diethyl ether, shaking the funnel for one minute and letting it rest for 5 min. The organic layer was transferred to a conical centrifuge tube and evaporated under a nitrogen stream; the residue was reconstituted with 200 μl of methanol and diluted to 25.0 ml using 0.02*M* Britton-Robinson buffer of pH 10.0. The accumulation time was 20 sec and the stripping adsorptive voltammogram was recorded under the optimum instrumental conditions.

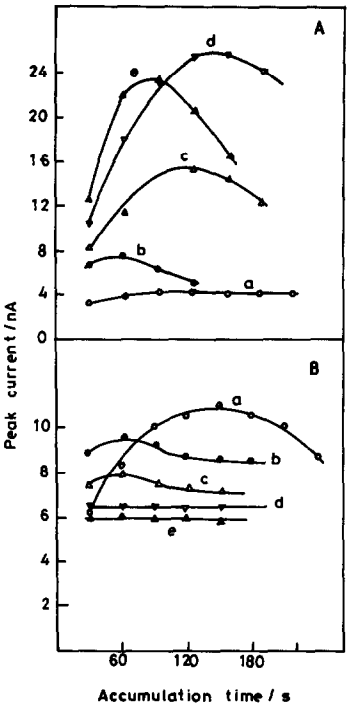

Fig. 1. Dependence of stripping peak current with accumulation time for $1.1 \times 10^{-7}M$ flunitrazepam (A) nitro group reduction peak, (B) azometine group reduction peak. Britton-Robinson buffers (0.04*M*) at pH (a) 5.0, (b) 8.0, (c) 9.0, (d) 10.0 and (e) 10.5. Scan rate 20 mV/sec, pulse amplitude 50 mV and electrode surface 0.0060 cm². The accumulation potential was optimized in every case.

RESULTS AND DISCUSSION

Influence of electrolyte and pH

Both the redox and interfacial behaviour of flunitrazepam are affected by the pH and supporting electrolyte of the solutions, an effect that is even greater in the peak current of the voltammetric response. Acetate, phosphate, carbonate, ammoniacal and Britton-Robinson buffers were used as electrolytes, with pH values between 5.0 and 11.0. The optimum accumulation potential was chosen first in every case. The differential pulse mode was employed for detection of the stripping voltammetry on the two reduction peaks of flunitrazepam.

Figure 1(A) shows the plots of peak current *vs* accumulation time for the nitro group response; Fig. 1(B) does the same for the second wave, which corresponds to the azomethine group reduction. Britton-Robinson buffers were used as electrolytes in both cases. The results obtained prove that the voltammetric response gives a higher peak current if the nitro group reduction wave is used in Britton-Robinson buffer of pH 10.0.

In both cases peak potentials move towards more negative values as pH increases. In the case of the nitro group peak, the variation in potential is expressed by the equation

$$E_p(V) = -0.011 - 0.0499\ \text{pH}\ (r = 0.995)$$

valid for pH between 5.0 and 10.5. The accumulation potential is approximately 150 mV (for the nitro group response) and 350 mV (for the azomethine group one) more positive than the potential of the reduction peak. Table 1 shows some significant data of the voltammetric responses. The study of the influence exerted by electrolyte concentration on the voltammetric response proved that the most sensitive response was obtained in 0.02*M* Britton-Robinson buffer of pH 10.0, which was thereafter used for the rest of the experiment.

Adsorptive behaviour of flunitrazepam

When measurements of drop time were carried out at the mercury drop electrode [Fig. 2(A)

Table 1. Stripping voltammetry data

	E_p (V)	t_a (sec)	E_p (V)	I_p (nA)
First reduction peak	−0.350	110	−0.490	26.0
Second reduction peak	−0.750	80	−1.100	6.5

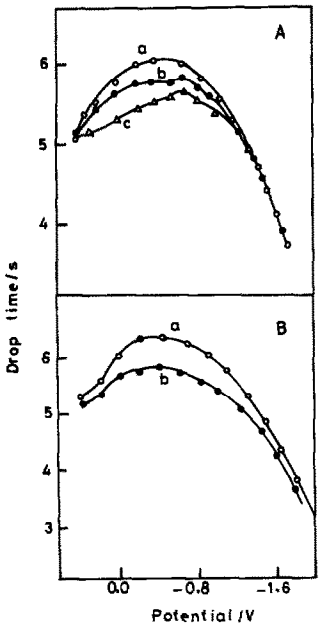

Fig. 2. Electrocapillary curves in 0.04*M*. Britton-Robinson buffer. (A) pH 5.0 in the (a) absence and (b) presence of $2.3 \times 10^{-4}M$ and (c) $4.8 \times 10^{-4}M$ of flunitrazepam. (B) pH 10.0 in the (a) absence and (b) presence of $2.3 \times 10^{-4}M$ flunitrazepam.

and (B)] in the presence and absence of flunitrazepam, it was observed that drop time shortens in the presence of the drug. This fact indicates that flunitrazepam is adsorbed at the electrode in the whole potential range; it is also adsorbed in the whole pH range studied (5.0–10.5). A decrease in drop time was also recorded after flunitrazepam had been completely reduced, indicating that the product is also adsorbed.

Adsorption of the compound was confirmed by the results obtained with cyclic staircase voltammetry, which was used because, under the conditions used in this work, it was virtually identical to cyclic voltammetry.[87] The response obtained using staircase voltammetry for flunitrazepam first reduction wave at the hanging mercury drop electrode is shown in Fig. 3. When the initial potential (−0.350 V) is maintained for 100 sec before beginning the cyclic scan, an irreversible, well-defined cathodic peak is observed whose peak current is nine times higher than the current obtained when the initial potential is applied for 2 sec only.

The morphology of this peak indicates that it is basically due to the reduction of the drug adsorbed. It has a potential that varies between −0.560 and −0.770 V depending on scan rate and concentration. The fact that peak potential moves towards more negative values as scan rate increases proves an irreversible electrode reaction.

Dependence of charge on concentration of flunitrazepam and on time. The adsorption of reducible substances can be adequately followed by measuring the cyclic or single-sweep voltammetric response at the HMDE.[88–91] And, since it is preferable, the charge (Q) transferred through the interface in the course of reduction was calculated. It is essential that the voltammetric response corresponds only to the reduction of the adsorbed substance, that is to say, contribution to the response due to reduction of the species that diffuses toward the electrode must be kept negligible at the working scan rate. A study of the influence of scan rate on the transferred charge (Q) (for $9.5 \times 10^{-5}M$ flunitrazepam in 0.02*M* Britton-Robinson buffer of pH 10.0 at a 110 sec adsorption time) proved the transferred charge to be constant between 160 and 800 mV, giving a value of 0.65 μQ with a relative standard deviation of 2.3% that demonstrates that, within that range, contribution due to the reduction response of the species diffusing toward the electrode is insignificant. A scan rate of 500 mV/sec was chosen for the rest of the study.

The influence of adsorption time on the charge transferred was studied using flunitrazepam solutions between 1.4×10^{-5} and $9.5 \times 10^{-5}M$. Figure 4 shows the results obtained. It can be observed that initially the charge rises linearly with the square root of the adsorption time, pointing to a diffusion-controlled adsorption of flunitrazepam before its reduction. Later on the charge reaches its highest value, this is indicating the total

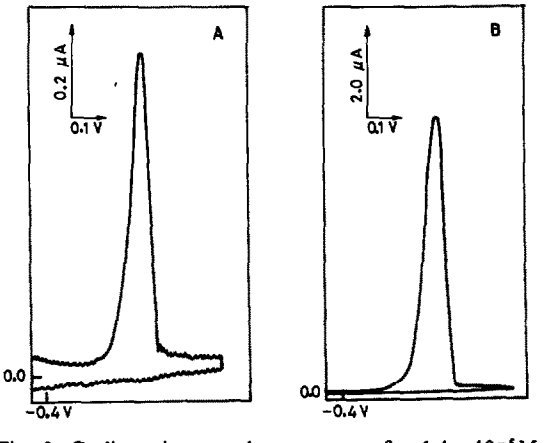

Fig. 3. Cyclic staircase voltammograms for $1.4 \times 10^{-5}M$ flunitrazepam in 0.02*M*. Britton-Robinson buffer of pH 10.0. Adsorption time (A) 2 sec and (B) 100 sec. Initial potential −0.35 V; scan rate 500 mV/sec.

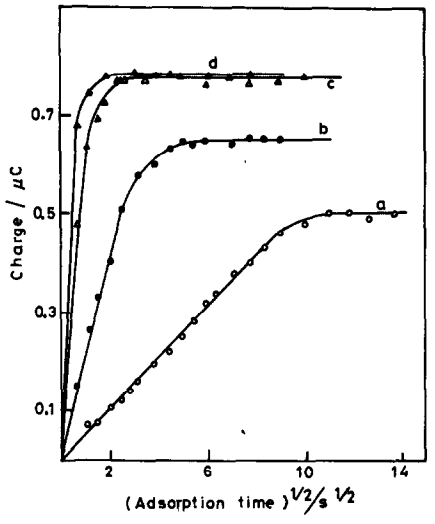

Fig. 4. Dependence of the reduction response (charge Q) on the adsorption time at adsorption potential −0.350 V. Britton-Robinson buffer pH 10.0, at different concentrations of flunitrazepam: (A) 1.4×10^{-5}M, (B) $2.4 \times 10^{-5}M$, (C) $4.8 \times 10^{-5}M$ and (D) $9.5 \times 10^{-5}M$.

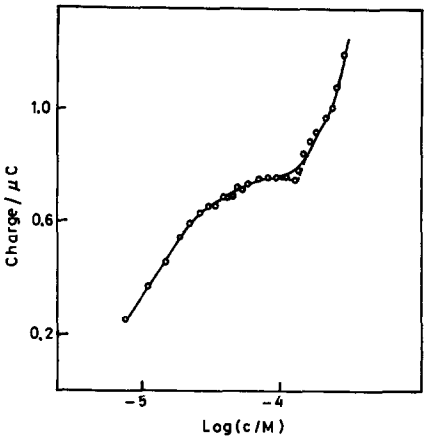

Fig. 5. Half logarithmic plot of flunitrazepam adsorption isotherm in 0.02M Britton-Robinson buffer pH 10.0. Adsorption potential −0.350 V, scan rate 550 mV/sec, adsorption time 60 sec.

covering of the electrode. The time elapsed until the electrode has been completely covered decreases when flunitrazepam concentration increases.

Adsorption isotherms. When the voltammetric response corresponds only to the reduction of the matter adsorbed, charge density (Q/A) is proportional to the surface concentration (Γ) of the matter adsorbed at the initial scan potential: $Q/A = nF\Gamma$, where $n = 4$, the number of electrons consumed in the reduction of the nitro group. The coverage θ is Γ/Γ_m, where Γ_m is the maximum surface concentration for full coverage with a monolayer. Since the electrodic reaction is known, the values of Γ and its maximum value Γ_m can be easily determined. Figure 5 shows the adsorption isotherm obtained; it is double-step adsorption isotherm. The second step of the adsorption isotherm does not appear at all, probably because, at this concentration range (2.0×10^{-4}–$1.00 \times 10^{-3}M$), contribution to the response coming from diffusion of the substance has not been totally eliminated at the working scan rates.

Figure 6(A) plots the variation in charge density (Q/A) as a function of concentration for the first step of the adsorption isotherm. The fraction of covered surface (θ) can be calculated from the Q/Q_m relationship.

The type of adsorption isotherm was assigned starting from the plots of log $[\theta(1-\theta)^{-1}C^{-1}]$ as a function of θ [Fig. 6(B)]. A straight line was obtained up to $3.4 \times 10^{-5}M$ flunitrazepam concentration (with a slope of 0.94, an intercept of 4.46 and a correlation coefficient of 0.994), indicating that flunitrazepam adjusts to a Frumkin-type isotherm $[\beta C = \theta(1-\theta)^{-1}\exp(-2\gamma\theta)]$. Starting from this plot, an adsorption coefficient (β) of 2.8×10^4 l./mole and an attraction factor (γ) of 1.08 were estimated. Starting from the value of the adsorption coefficient, the value of the free energy of adsorption ($-\Delta G°$) could be deduced,[88] giving a value of 35.4 kJ/mole.

Adsorptive stripping differential pulse voltammetry

For analytical purposes, the adsorption process of the drug can be used to increase the sensitivity of the voltammetric procedures. In the case under discussion, the accumulation step was carried out in stirred solutions and the

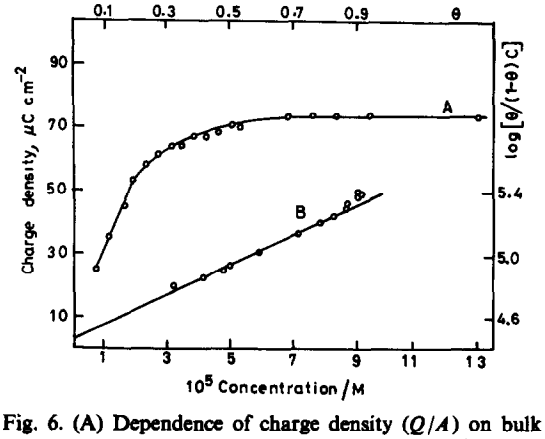

Fig. 6. (A) Dependence of charge density (Q/A) on bulk concentration and (B) dependence of $\log[\theta(1-\theta)^{-1}C^{-1}]$ on surface coverage (θ) for the first step of the adsorption isotherm. Conditions as in Fig. 5.

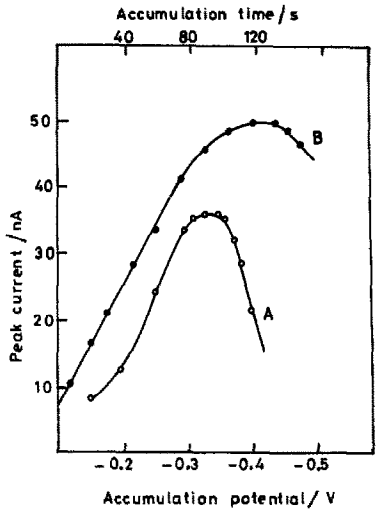

Fig. 7. Variation of stripping peak current with (A) accumulation potential at 60 sec accumulation time; (B) accumulation time at −0.350 V accumulation potential. $1.1 \times 10^{-7}M$ flunitrazepam in $0.02M$ Britton-Robinson buffer pH 10.0. Stirring rate 1920 rpm, scan rate 20 mV/sec, pulse amplitude 75 mV and drop size 0.60 mm².

stripping step quantified by differential pulse mode, since the response obtained is approximately five times higher than the one obtained by linear scan mode at scan rates in the same order of magnitude.

Factors influencing the accumulation step. The value of the potential at which the accumulation process takes place strongly affects the voltammetric response (see Fig. 7). The maximum values in peak current were obtained at values of potential between −0.31 and −0.36 V, therefore a value of −0.35 V was chosen for the analytical process.

For accumulation times shorter than 80 sec, peak current increases linearly with increasing accumulation time [see Fig. 6(B)] for a drug concentration in the $10^{-7}M$ range. In such a case, surface saturation is reached after 100 sec. The ultimate choice of accumulation time should depend on the concentration range studied.

Variations in stripping peak current with drop size, in mm² [I_p(nA) = −2.2 + 99.9A, $r = 0.994$] and with stirring rate between 1220 and 2620 rpm, for $1.1 \times 10^{-7}M$ flunitrazepam solutions, and a 60 sec accumulation time proved that a satisfactory voltammetric response was obtained with the maximum drop size (0.60 mm²) at a 1920 rpm stirring rate.

None of the factors studied affect peak potential values.

A rest time of between 10 and 30 sec does not affect the analytic signal either in its value or its reproducibility.

Factors controlling the stripping step. Peak current varies linearly with pulse amplitude between 30 and 80 mV [I_p(nA) = −7.14 + 0.47ΔE, $r = 0.9998$]; the half-peak width remained constant at 55 mV. Amplitudes wider than 80 mV not only do not increase sensitivity but slightly lower resolution. A pulse amplitude of 75 mV was chosen for further analytical work.

A rise in the scan rate of the potential causes an increase in the stripping peak current [I_p(nA) = 4.54 + 2.66 V (mV/sec), $r = 0.998$]. A rate of 30 mV/sec affords maximum sensitivity.

Influence of concentration. The influence of flunitrazepam concentration was studied at various accumulation times: 30, 60, 80, 110 and 180 sec. Linear variations were obtained with concentrations from 0.6×10^{-8} to $3.1 \times 10^{-7}M$, depending on the linearity range of the accumulation time used. Sensitivity varies from 0.78×10^8 nA l./mole (with 0 sec accumulation time) to 7.65×10^8 nA l./mole (with 180 sec). An accumulation time of 110 sec gives a peak current dependence on concentration that adjusts to the equation I_p(nA) = 2.3 + 6.58 × 10^8C(mole/l.), $r = 0.9996$.

Precision was determined by five successive measurements of 1.2×10^{-8}, 5.1×10^{-8} and $1.3 \times 10^{-7}M$ flunitrazepam solutions; the relative standard deviation was found to be lower than 2.7% and the relative error lower than 1.0%. A detection limit (3σ) of $9.0 \times 10^{-10}M$ and a determination limit (10σ) of $3.1 \times 10^{-9}M$ was calculated.

Table 2. Variation in the slope (in nA L mole^{-1}) of flunitrazepam calibration plot in the range of 1.0×10^{-8} to $2.0 \times 10^{-7}M$ in the presence of urine components

Accumulation time, sec	Without interferent	Albumin 6.4 ppm	Uric acid	Glucose, 8 ppm	Creatinine, 120 ppm	Urea, 2400 ppm
30	2.93 ± 10^8	4.62×10^7	*	2.76×10^8	2.95×10^8	2.45×10^8
60	4.67×10^8	1.64×10^8	*	4.77×10^8	4.32×10^8	3.83×10^8
110	6.58×10^8	—	*	5.60×10^8	4.05×10^8	4.47×10^8

*Flunitrazepam reduction peak not observed.

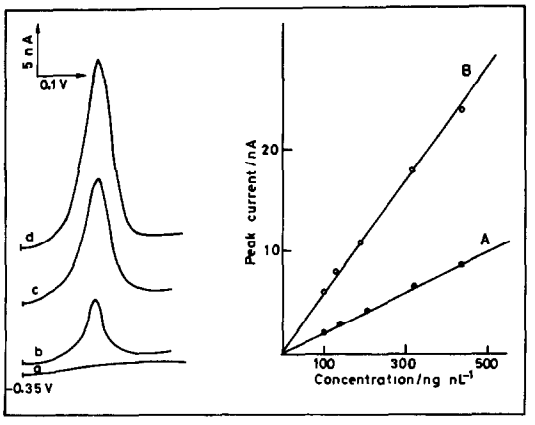

Fig. 8. Differential pulse stripping peaks for different concentrations of flunitrazepam in urine, (a) 0, (b) 100, (c) 190 and (d) 315 ng of flunitrazepam per milliliter of urine. Accumulation time 20 sec. Calibration plots of flunitrazepam in urine (A) 0, and (B) 20 sec of accumulation time. Other conditions were as in Fig. 7.

Interferences study

To study the effect of urine components on the analytical signal of flunitrazepam, calibration plots of flunitrazepam in the range 1.0×10^{-8}–$2.0 \times 10^{-7} M$ were obtained in the presence of albumin (6.4 ppm), uric acid (64 ppm), glucose (8 ppm), creatinine (120 ppm) and urea (2400 ppm) with different accumulation times (30, 60 and 110 sec). The values in parentheses correspond to the normal values of the compounds in the urine of healthy subjects, calculated taking into the account that 2 ml of urine is diluted to 25 ml for the analysis, as is the norm throughout this work.

Table 2 shows the slopes of the calibration plots in the absence and presence of the urine components studied. As can be seen, sensitivity is not affected by the presence of glucose, creatinine or urea as long as short accumulation times are used. The presence of uric acid, however, causes the signal to disappear entirely, while the presence of albumin greatly lowers sensitivity, down to 16% of the initial signal, even when working with short accumulation times.

Flunitrazepam determination in urine samples

The facts described above made it necessary to use an extraction procedure (described in the Experimental) in order to eliminate the aforementioned interferences.

Figure 8 is an example of the stripping peaks obtained and the resulting mean calibration graphs after analyzing five series of solutions of different concentration at zero and 20 sec accumulation times.

For the 20-sec accumulation time the determination of flunitrazepam in urine was possible in the range of 100–500 ng/ml with a sensitivity of 0.052 nA ml ng^{-1} (correlation coefficient 0.9991) and a mean relative error lower than 5.0%; the detection limit (estimated as the concentration corresponding to a signal-to-noise ratio of 3) was 30 ng/ml and the mean recovery 97.8% in the range mentioned above. Precision, expressed in terms of the relative standard deviations, was 3.2%.

REFERENCES

1. H. Schütz, *Benzodiazepines, A Handbook*. Verlag, Heidelberg, 1982.
2. S. Ebel and H. Schütz, *Z. Rechtsmed.*, 1978, **81**, 107.
3. B. Unterhalt, *Arch. Pharm.*, 1981, **314**, 733.
4. M. Giusiani, G. Poggi, G. Martinelli, U. Palagi and M. A. Lombardi, *Riv. Ital. Ig.*, 1981, **41**, 258.
5. O. Otura, T. Takahashi and T. Tomiyama, *Kagaku Keisatsu Keukyushu Hokuku Heu*, 1983, **36**, 98.
6. J.Vasiliades, *J. Toxicol. Clim. Toxicol.*, 1983, **20**, 23.
7. H. Fukazawa, H. Ichishita, M. Honda and H. Schimizu, *Rinsho Yakuri*, 1978, **9**, 251.
8. H. G. Boxembaum, H. N. Posmanter, T. Macasieb, D. A. Geitner, L. Weissman and S. A. Kaplan, *J. Pharmacokinet. Biopharm.*, 1978, **6**, 283.
9. P. M. Lauren, H. Stoeckel, H. Schwilden and J. Schueler, *Anaesth. Intensivther. Notfallmed.*, 1981, **16**, 135.
10. D. Greenblatt, R. Ochs Hermann, A. Lacniskar and M. P. Lauren, *Pharmacology*, 1982, **24**, 82.
11. P. Jacquin and M. Lesne, *Arch. Int. Pharmacodyn. Ther.*, 1982, **259**, 333.
12. R. S. Given, J. Gringrich and S. Hecklenburg, *Int. J. Pharm.*, 1986, **29**, 67.
13. P. J. G. Cornelissen and G. M. J. Beijersbergen Van Henegouwen, *Pharm. Weekbl. Sci.*, 1981, **3**, 800.
14. H. Schültz, *Aertz. Lab.*, 1982, **28**, 117.
15. *Idem., J. Anal. Toxicol.*, 1978, **2**, 147.
16. M. M. A. De Bruyne, A. Sinnema and M. A. Verweij, *Forensic. Sci. Int.*, 1984, **24**, 125.
17. R. Slechova and B. Chundela, *Beitr. Diagn. Ther Akuter Intox Vortr. Symp., 4th*, 1982, 113.
18. A. W. Missen, *J. Anal. Toxicol.*, 1977, **1**, 224.
19. T. B. Vree, B. Lenselik, E. Van der Kleijn and G. M. M. Nijhuis, *J. Chromatogr.*, 1977, **143**, 530.
20. R. C. Pedroso and E. Moraes, *Rev. Farm. Bioquim. Univ. Sao Paulo*, 1987, **18**, 183.
21. A. W. Missen, *Chem. Div.*, 1979, C.D. 2282.
22. R. Jochemeusen and D. D. Greimer, *J. Chromatogr.*, 1982, **227**, 199.
23. T. Daldrup, E. Susauto and P. Michalke, *Z Anal. Chem.*, 1981, **308**, 413.
24. M.Ch. Dutt, *J. Chromatogr.*, 1982, **248**, 115.
25. G. W. Hime, K. Bednarcz and R. Leonard, *J. Anal. Toxicol.*, 1982, **6**, 247.
26. C. Lora-Tamayo, M. A. Rams and J. M. R. Chacón, *J. Chromatogr.*, 1986, **374**, 73.
27. H. Schütz, *Z. Anal. Chem.*, 1979, **294**, 135.

28. P. Haefelfinger, *J. High Resolut. Chromatogr. Commun.*, 1979, **2**, 394.
29. E. Stahl and J. Mueller, *J. Chromatogr.*, 1981, **209**, 484.
30. I. Wouter, E. Roets and H. Hoogmartens, *ibid.*, 1979, **179**, 381.
31. H. H. Van Rooij, A. Fakiera, R. Verrijk, W. Soudijn and J. P. Weijers-Everjard, *Anal. Chim. Acta*, 1985, **1**, 22.
32. M. Bakavdi, V. Navaratnam and N. K. Nair, *J. Chromatogr.*, 1984, **229**, 465.
33. G. Musumarra, G. Scarlata, G. Cirma, G. Romano, S. Palazzo, S. Clemente and G. Giulietti, *ibid.*, 1985, **350**, 151.
34. P. Corti, G. Murratzu, A. Caricctria and G. Corbini, *Boll. Chim. Farm.*, 1987, **126**, 376.
35. G. Musumarra, G. Scarlata, G. Romano, G. Cappello, S. Clementi and G. Giulietti, *J. Anal. Toxicol.*, 1987, **11**, 154.
36. G. Musumarra, G. Scarlata, G. Romano, G. Clemente and S. Wold, *J. Chromatogr. Sci.*, 1984, **22**, 538.
37. R. Gill, B. Law and J. P. Gibbs, *J. Chromatogr.*, 1986, **356**, 37.
38. P. Mura, A. Piriu, P. Fraillon, Y. Papet and D. Reiss, *ibid.*, 1987, **416**, 303.
39. T. Daldrap, P. Michaele and W. Boechme, *ibid.*, 1982, **244**, 115.
40. K. Jinno, M. Kuwajima, M. Mayashida, T. Watanabe and T. Hondo, *ibid.*, 1988, **436**, 11.
41. N. De Giovanni and M. Chiarotti, *ibid.*, 1988, **428**, 321.
42. H. Kaeferstein and G. Sticht, *Beirt. Grichtl. Med.*, 1986, **44**, 253.
43. E. Minder, R. Schaubhut, C. E. Minder and D. S. Vonderschmitt, *J. Chromatogr.*, 1987, **419**, 153.
44. S. I. Magalani and F. Pala, *Hum. Toxicol.*, 1983, **2**, 395.
45. F. Pala, G. De Cosmo, A. F. Sabato and A. Bondoli, *Resuscitation*, 1981, **9**, 125.
46. W. F. Smyth, M. R. Smyth, J. A. Groves and S. B. Tan, *Analyst*, 1978, **103**, 497.
47. J. P. Cano, J. Guintrand, C. Aubert and A. Viala, *Arzneim-Forsch.*, 1977, **27**, 338.
48. J. A. F. De Silva and I. Berkesky, *J. Chromatogr.*, 1974, **99**, 447.
49. J. A. F. De Silva, C. V. Puglisi and N. Munno, *J. Pharm. Sci.*, 1974, **63**, 520.
50. D. B. Faber, R. M. Kok and E. M. Dijk, *J. Chromatogr.*, 1977, **133**, 319.
51. T. Kaniewska and W. Wejman, *ibid.*, 1980, **182**, 81.
52. R. Jochemeusen and D. D. Greimer, *ibid.*, 1982, **227**, 199.
53. X. C. Sumirtapura, C. Aubert and J. P. Cano, *Arznein-Forsch.*, 1982, **32**, 252.
54. J. M. F. Douse, *J. Chromatogr.*, 1984, **301**, 135.
55. A. Gailleux, A. Turcaut, A. Gabic and P. Allain, *J. Chromatogr. Sci.*, 1981, **19**, 163.
56. H. Maurer and K. Pfleger, *J. Chromatogr.*, 1987, **422**, 85.
57. *Idem, ibid.*, 1981, **222**, 409.
58. B. Rollmann and B. Tilquin, *J. Pharm. Belg.*, 1991, **46**, 357.
59. C. Vislon and A. Vercruysse, *J. Chromatogr.*, 1980, **189**, 94.
60. F. Barbato, C. Filipo and A. Vittorio, *Soc. Ital. Biol. Sper.*, 1980, **56**, 879.
61. M. Phulich, M. Boubakeur and G. Le Moan, *Ann. Falsif. Exper. Chim. Toxicol.*, 1982, **75**, 387.
62. G. Violon, L. Pessemier and A. Vercruysse, *J. Chromatogr.*, 1982, **235**, 157.
63. A. Boukhabza, A. A. J. Lugnier, P. Kintz and P. Mangin, *J. Anal. Toxicol.*, 1991, **15**, 319.
64. Y. Pegon, E. Poucher and J. J. Vallon, *ibid.*, 1982, **6**, 1.
65. J. A. Sise and J. R. Sharman, *N.Z.J. Med. Lab. Technol.*, 1988, **42**, 46.
66. K. Robinson, M. G. Rutterfor and R. N. Smith, *J. Pharm. Pharmacol.*, 1980, **32**, 773.
67. N. Rutnaraj, V. Goldberg and P. T. Lascelles, *Hum. Toxicol.*, 1983, **2**, 395.
68. M. Manchon, M. F. Jerdier, P. Pallud, A. Vialle, F. Besaue and I. Bienvenu, *J. Anal. Toxicol.*, 1985, **9**, 209.
69. M. A. Peritto, I. A. Marianacci, L. del Valle Ruiz and A. Arce, *Acta Bioquim. Clin. Latinoam.*, 1986, **20**, 559.
70. H. Oelschlaeger, *Bioelectrchem. Bioenerg.*, 1983, **10**, 25.
71. F. Sengun and Z. Caliskan, *Sci. Pharm.*, 1983, **51**, 297.
72. P. Richter, A. Morales and J. Lahsen, *Analyst*, 1990, **115**, 409.
73. A. Morales, P. Richter and M. I. Roral, *ibid.*, 1987, **112**, 965.
74. F. Sengun, A. Ari-Ulubelen, K. Ulas and I. Fedai, *Sci. Pharm.*, 1984, **52**, 66.
75. W. F. Smyth, J. S. Burmicz and A. Ivaska, *Analyst*, 1982, **107**, 1019.
76. W. F. Smyth and A. Ivaska, *ibid.*, 1985, **110**, 1377.
77. E. Ruiz, M. Hernández, E. Lorenzo and L. Hernández, *Analyst*, 1987, **112**, 697.
78. L. Hernández, P. Hernández, M. H. Blanco, E. Lorenzo and E. Alda, *ibid.*, 1988, **113**, 1719.
79. L. Hernández, P. Hernández and E. Lorenzo, in A. Ivaska, A. Lewenstam and R. Sara (eds), *Contemp. Electroanal. Chem.*, pp. 205–211. Plenum, New York, 1990.
80. L. Hernández, A. Zapardiel, J. A. Pérez López and E. Bermejo, *J. Electroanal. Chem.*, 1988, **255**, 85.
81. A. Zapardiel, J. A. Pérez López, E. Bermejo and L. Hernández, *Z Anal. Chem.*, 1988, **330**, 707.
82. L. Hernández, A. Zapardiel, J. A. Pérez López and E. Bermejo, *Talanta*, 1988, **35**, 287.
83. *Idem, Analyst*, 1987, **112**, 1149.
84. A. Zapardiel, J. A. Pérez López, E. Bermejo and L. Hernández, *J. Electroanal. Chem.*, 1990, **289**, 143.
85. A. Zapardiel, J. A. Pérez López, E. Bermejo, L. Hernández and M. J. Valenciano, *Microchem. J.*, 1990, **41**, 10.
86. A. Zapardiel, J. A. Pérez López, E. Bermejo, L. Hernández and A. G. Espartero, *Anal. Lett.*, 1991, **24**, 233.
87. A. Webber and J. Osteryoung, *Anal. Chim. Acta*, 1984, **157**, 17.
88. D. Krznazic, P. Valenta, H. W. Nurnberg and M. Branica, *J. Electroanal. Chem.*, 1978, **93**, 41.
89. Y. M. Temerk, P. Valenta and H. W. Nurnberg, *Bioelectrochem. Bioenerg.*, 1980, **7**, 705.
90. Y. M. Temerk and P. Valenta, *J. Electroanal. Chem.*, 1986, **214**, 391.
91. A. Webber, M. Shah and J. Osteryoung, *Anal. Chim. Acta*, 1984, **157**, 1.

Talanta, Vol. 40, No. 11, pp. 1657–1664, 1993
Printed in Great Britain.

0039-9140/93 $6.00 + 0.00

HOST–GUEST STABILIZED ROOM TEMPERATURE PHOSPHORESCENCE IN β-CYCLODEXTRIN/ BROMOALCOHOL SOLUTIONS FROM 2-NAPHTHYL-OXY-ACETIC ACID AND 1-NAPHTHYL-ACETIC ACID

A. MUNOZ DE LA PENA,* F. SALINAS, M. J. GOMEZ, M. SANCHEZ-PENA and I. DURAN-MERAS
Department of Analytical Chemistry, University of Extremadura, 06071, Badajoz, Spain

Summary—Room temperature phosphorescence (RTP) from 2-naphthyl-oxy-acetic acid (NOA) and 1-naphthyl-acetic acid (NAA), with stabilization by use of β-cyclodextrin (β-CD) as a host system, has been examined. 2-Bromoethanol and 2,3-dibromopropanol have been evaluated as external heavy atom perturbers to enhance the rate of intersystem crossing and, consequently, populating the triplet state for phosphorescence emission. The deoxygenation of the solutions was achieved chemically by use of sodium sulphite. The spectral characteristics of the phosphorescence emission from these relatively polar compounds and the optimization of the chemical variables involved are reported. The role of the bulkiness of the bromoalcohol employed, in comparison with the unoccupied space of the interior of the cyclodextrin cavity by the guest, is an important factor in the attainment of an effective RTP emission, and should be taken into account in the selection of the appropriate external heavy atom for the observation of RTP from other organic molecules of interest by this approach. 2,3-Dibromopropanol seems a more adequate bromoalcohol than 2-bromoethanol for the observation of RTP emission in the systems investigated.

Apart from sensitized room temperature phosphorescence (RTP),[1] all the methods proposed for the observation of RTP in fluid solution involve the use of some kind of organization. This approach is particularly attractive as a potential detection method in dynamic methodologies. The first reported observation of RTP, by microscopically organized media stabilization, was made using sodium dodecyl sulphate (SDS) micelles in the presence of thallium.[2] Since then, several media have been investigated to stabilize the triplet state in fluid solution at room temperature. Both micelles and host molecules have been found to be useful media for achieving triplet-state emission at room temperature.[3]

Normal micelles, mainly SDS[4,5] and cetyltrimethylammonium bromide (CTB) micelles,[6,7] have been used in RTP analysis. Microemulsions, formed in heptane–SDS–1-pentanol, have also been evaluated as an alternative to normal micelles for RTP obtention.[8] A recent communication[9] claims the use of water-soluble co-polymers of 1-vinylnaphthalene and metacrylic acid as a new class of medium for RTP analysis in aqueous systems.

Among the host molecules, cyclodextrins (CDs) are by far the most common media for host–guest stabilized RTP. CDs are molecules formed from different numbers of α(1,4)-linked D(+)-glucopyranose units: α-, β- and γ-CDs comprise 6, 7 and 8 units, respectively. CD-stabilized RTP is a recently observed phenomenon, which was initially reported by Turro *et al.*[10–12] for halonaphthalenes and several 4-bromo-1-naphthoyl-alquyl surfactant probes. The β- and γ-CDs have been proposed as appropriate hosts to form inclusion complexes with various phosphor guest molecules, where the guest is embedded totally or partially in the CD cavity.[13–19] Another study uses CDs to enhance sensitized RTP emission from biacetyl.[20]

A new kind of host, the synthetic macrocyclic azaparacyclophanes, in mixtures with SDS, has recently been reported as capable of inducing RTP from several compounds.[21] Mixed organized media of β-CD and SDS have also been evaluated as organized assemblies for RTP stabilization.[21,22]

Apart from compounds including a heavy atom in their structure, the observation of RTP,

*Author for correspondence.

in the different organized media described, needs to fulfil two main conditions. Firstly, the use of external heavy atom compounds is required. By increasing the rate of the intersystem crossing process, the presence of heavy atoms in the environment of the potential phosphor usually enhances the phosphorescence of the phosphor. In addition, phosphorescence signals are only obtainable if quenching of the emitting triplet state, by small amounts of dissolved oxygen, is prevented.

The two conditions are common to micelles and cyclodextrins but, to obtain significant CD-stabilized RTP emission, the hydrophobic CD cavities need to allow sufficient interaction between the analyte and the heavy atom compound to produce effective population of the triplet states of the analyte. For this, both the lumiphor and the heavy atom need to be in close proximity at the same time, *i.e.* inside the CD cavity.[15]

Only a few compounds, mainly non-polar substances, have been found to phosphoresce when included in CDs. Cline Love's group reported on CD-stabilized RTP from polynuclear aromatic hydrocarbons (PAHs),[13] two- and three-nitrogen heterocycles,[14] biphenyl and the bridged biphenyls fluorene, benzofuran, dibenzotiophene and carbazole,[14] and the more polar drug naproxen,[15] in the presence of 1,2-dibromoethane. It was established that the observed phosphorescence emission resulted from the formation of a ternary association between the phosphor, the CD and the external heavy atom compound employed. Similarly, using two haloalkanes, 1,2-dibromoethane and 1,2-dibromopropane, Zhang *et al.*[16,17] reported on RTP emission from 1-naphthyl-acetic acid (NAA), included in β-CD.

As an alternative to the use of haloalkanes, Hamai[18] and Muñoz de la Peña *et al.*[19] proposed the use of bromoalcohols as heavy atom perturbers, and demonstrated the feasibility of using sodium sulphite for chemical deoxygenation in CD studies,[19] in a similar way to the approach used for micelle-stabilized RTP.[23]

The purpose of this work is to advance understanding of CD-stabilized RTP emission, in order to investigate the possibilities of expanding its applications and, eventually, to apply it to the detection of organic species of analytical interest. We report upon the observation of phosphorescence from two pesticides that are naphthalene derivatives. The stabilized RTP emission has been attained in β-CD, in the presence of 2-bromoethanol (2-BE) and 2,3-dibromopropanol (2,3-DBP) as external heavy atom perturbers. The relatively polar character of the compounds investigated is considered in order to evaluate the potential applications of this technique for the analytical determination of relatively polar compounds.

EXPERIMENTAL

Apparatus

Steady-state fluorescence and phosphorescence measurements were made on a Perkin–Elmer Model LS 50 luminescence spectrometer equipped with a xenon discharge lamp equivalent to 20 kW for 8 μsec duration. The instrument is connected via RS-232 with an IBM PS/2 80386-SX microcomputer. Data acquisition and data analysis were performed by use of the Perkin–Elmer Fluorescence Data Manager Software, version 2.70. Solutions were excited at 274 nm, the maximum excitation wavelength of 2-naphthyl-oxy-acetic acid (NOA), or at 284 nm, the maximum excitation wavelength of NAA. Fluorescence measurements were made with excitation and emission band widths of 5 nm and phosphorescence measurements with excitation and emission bands of 15 and 20 nm, respectively. The delay time and the gate time were typically maintained at 1.0 and 5.0 msec, respectively. The scan rate of the monochromators was maintained at 240 nm/min. All measurements were made at $20 \pm 0.1°$ by use of a thermostatic cell holder and a thermostatic bath Selecta Model 382.

Reagents

All experiments were performed with analytical grade chemicals. Purified LC-grade water (Millipore Milli-Q-system) was used. NOA (97%) was obtained from Chem Service (West Chester, PA), NAA (97%) was obtained from Aldrich-Chemie and β-CD was obtained from Sigma and used as received.

2-BE (95%) and 2,3-DBP (96%) were obtained from Aldrich-Chemie and used as received. Anhydrous sodium sulphite (>98%) was obtained from Merck. Sodium sulphite solutions were prepared daily and kept in tightly stoppered containers.

Methods and sample preparation

A $10^{-2}M$ stock solution of NOA or NAA was prepared in absolute ethanol. Aqueous $10^{-4}M$ NOA or NAA solutions were prepared

by pipetting an aliquot of the stock solution into a 250 ml volumetric flask. The ethanol was evaporated by use of dry nitrogen, deionized water was added and, after sonication, was diluted to the mark. Solutions of lower concentrations were prepared by appropriate dilution of the stock aqueous solutions.

General procedure for phosphorescence measurements

An aliquot of the NOA or NAA solution was transferred to a 10-ml volumetric flask and the appropriate amount of β-CD to give a $10^{-2}M$ final concentration was added. After dilution with water, the solution was mixed at the ultrasonic bath to dissolve the cyclodextrin and 1.0 ml of $0.3M$ Na_2SO_3 and 0.4% 2,3-DBP or 1.0% 2-BE were added. After dilution to the mark with water, the sample was introduced into the cell compartment and continuously irradiated with the xenon lamp at 274 nm for NOA or 284 nm for NAA. The RTP signal was monitored and measured at 504 nm for NOA and 494 nm for NAA, when it was stable for at least 5 min.

RESULTS AND DISCUSSION

The inclusion complexes between NOA or NAA and β-CD have been investigated previously in aqueous solution by absorption and fluorescence measurements.[24] At neutral pH, NOA and NAA are dissociated, as the respective carboxylic groups have acidic character. It was demonstrated that the naphthalene derivatives from 1:1 complexes when included in the CD in pure aqueous solutions. A possible structure with an axial inclusion of the naphthalene derivatives was proposed. In the case of the β-CD:NOA complex, the naphthyl moiety is practically included in the CD and the acetic acid group protrudes from the cavity, while NAA is only partially included because of the steric effect of the substituted group at position 1. Association constants of $560M^{-1}$ and $100M^{-1}$ were calculated for the β-CD:NOA and β-CD:NAA binary complexes, respectively.

Influence of bromoalcohols on the fluorescence of β-CD:NOA and β-CD:NAA

The only two classes of heavy atom perturbers reported to date, for CD RTP stabilization, are bromoalkanes and bromoalcohols. The use of a bromoalcohol for phosphorescence enhancement was suggested as a possibility[19] after the detailed study of the strong ternary complexes formed between pyrene, as a model compound, CDs and alcohols of different size and polarity.[25–27]

To investigate the possibility of RTP obtention from NOA and NAA, the influence of different bromoalcohols on the fluorescence emission of the binary complexes between the naphthalene derivatives and β-CD was evaluated. For this, several additions of bromoalcohols were made to an aqueous solution of NOA or NAA in β-CD. The final concentrations of NOA or NAA and β-CD were $1 \times 10^{-5}M$ and $1 \times 10^{-2}M$, respectively.

The results obtained for the β-CD:NOA complex in the presence of 2-BE and 2,3-DBP are plotted in Fig. 1. The concentrations of 2-BE and 2,3-DBP were varied between 0.1% and 3%. The fluorescence emission was monitored at 350 nm. The addition of the bromoalcohols produces a decrease of the fluorescence emission of the β-CD:NOA inclusion complex. In the case of 2-BE, the remaining fluorescence is around 20% of the initial emission, while in the case of 2,3-DBP, the decrease is more pronounced, leading to less than 10% of the initial fluorescence in 3% 2,3-DBP. The maximum decrease of the fluorescence was attained for bromoalcohol concentrations higher than 2%.

Similarly, the effect of the presence of 2-BE and 2,3-DBP on the fluorescence intensity of the binary complex formed between NAA and β-CD is shown in Fig. 2. The concentrations of 2-BE and 2,3-DBP were varied between 0.1% and 3%. The fluorescence intensity was monitored at 336 nm. As in the case of the NOA complex, it can be observed that an effective quenching of the fluorescence emission is produced in the presence of both bromoalcohols,

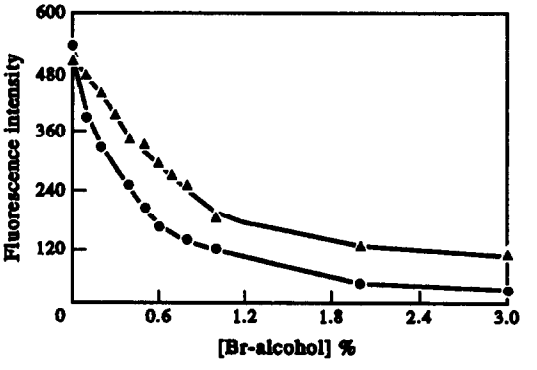

Fig. 1. Effect of 2-BE (▲) and 2,3-DBP (●) on the fluorescence intensity of the complex β-CD:NOA. $\lambda_{ex} = 274$ nm, $\lambda_{em} = 350$ nm. [NOA] = $1 \times 10^{-5}M$, [β-CD] = $1 \times 10^{-2}M$.

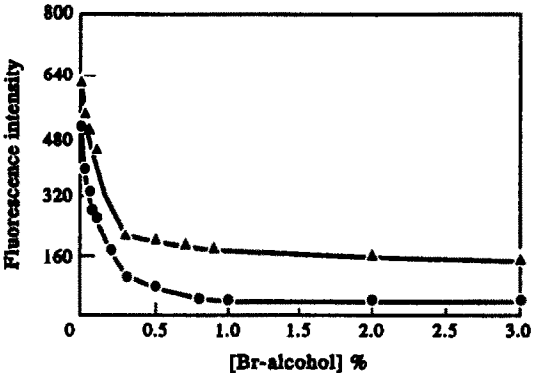

Fig. 2. Effect of 2-BE (▲) and 2,3-DBP (●) on the fluorescence intensity of the complex β-CD:NAA. $\lambda_{ex} = 284$ nm, $\lambda_{em} = 336$ nm. [NAA] = $1 \times 10^{-5}M$, [β-CD] = $1 \times 10^{-2}M$.

but the attenuation of the fluorescence is more effective in the presence of 2,3-DBP than in the presence of 2-BE. In this case, concentrations of bromoalcohol higher than 0.5% are enough for a maximum decrease of fluorescence. It is interesting to note that the quenching effect is more pronounced for the β-CD:NAA than for the β-CD:NOA complex. Smaller amounts are needed to obtain the maximum attenuation of the fluorescence.

The observed quenching can be explained as the result of an effective interaction between NOA or NAA and the bromoalcohols inside the CD cavity. The hydroxylic group of the bromoalcohol may interact at the hydroxyl edge of the CD, via hydrogen bonding, while the brominated part of the alcohol is facing and is totally or partially included in the cyclodextrin.

Obtention of RTP in the presence of bromoalcohols

RTP emission has been obtained from NOA and NAA in aqueous solutions of β-CD in the presence of both bromoalcohols and sodium sulphite. The addition of sodium sulphite is necessary in order to minimize the quenching effect of dissolved oxygen. This technique of chemical deoxygenation is an alternative to the classical pass of nitrogen and has been used for phosphorescence studies by other authors in different micellar and host systems.[6-8,19,21,23,28-33] Upon deaeration of NOA or NAA solutions containing both β-CD and 2-BE or 2,3-DBP, a new emission appears at longer wavelength regions than the fluorescence.

According to the literature, the low temperature phosphorescence (77 K) emission of NOA in ethanol–water (1:9, v/v) appears at 503 and 530 nm, and the room temperature phosphorescence in filter paper appears at 504 nm,[34] while it is reported to appear at 499 and 529 nm in filter paper treated with $1M$ NaI.[35] For NAA, the low temperature phosphorescence emission appears at 484 and 514 nm and the room temperature phosphorescence in filter paper at 494 and 516 nm.[34] When the filter paper is treated with NaI, the maxima reported appeared at 489 and 519 nm.[35]

In Fig. 3, the RTP spectra of NAA in $10^{-2}M$ β-CD, in the presence of 0.5% 2-BE and 0.5% 2,3-DBP, are shown. In the absence of bromoalcohol no phosphorescence signal appears. In contrast, an appreciable RTP emission is evident in the presence of the bromoalcohols. The phosphorescence bands for NOA in our experimental conditions appeared at 504 and 525 nm and for NAA at 494 and 521 nm, in close agreement with the reported literature values. In view of this, the longer wavelength emission observed can be assigned to the RTP of NOA or NAA.

In order to record the RTP spectra, temporal discrimination has been employed, as the fluorescence emission is not totally quenched and still remains in these conditions.

Although the RTP emission observed is much weaker than the fluorescence presented by these compounds, the results indicate a favourable microenvironment that stabilizes the triplet state of the NOA or NAA molecules. It is evident that the presence of the halogen atom of the brominated alcohol enhances the rate of emission of the phosphorescence via heavy atom spin–orbit coupling, although the intersystem

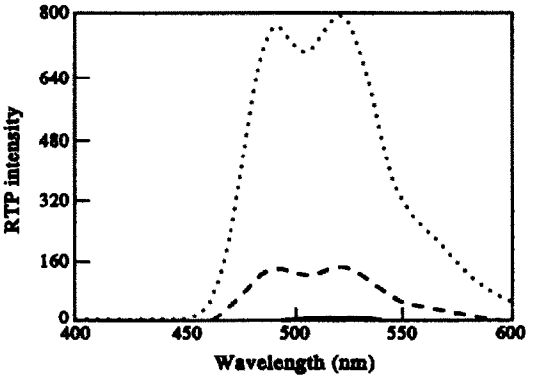

Fig. 3. RTP spectra of the complex β-CD:NAA in the absence of bromoalcohol (—), in the presence of 0.5%2-BE (– – –), and in the presence of 0.5% 2,3-DBP (..).

crossing process is not totally effective, as an appreciable fluorescence remains.

It is also evident that 2,3-DBP is more effective as a heavy atom perturber than 2-BE. This fact can be explained taking into account the following considerations.

The assignation of the phosphorescence emission to a ternary association has been suggested by various authors. Turro *et al.*[10] observed an increase in phosphorescence and lifetime when adding acetonitrile to a β-CD solution containing 1-bromonaphthalene, suggesting the formation of a complex composed of β-CD, 1-bromonaphthalene and acetonitrile. Scypinsky and Cline Love[13,14] attributed the RTP emission of selected analytes in CDs, in the presence of 1,2-dibromoethane, to the formation of a trimolecular complex.

The ternary complexes formed between pyrene, β-CD and alcohols of different size and polarity have been studied previously.[26] It was demonstrated that the stability of the ternary complexes was directly related to the proper geometry and volume of the alcohol to fill the residual void space of the interior of the CD unoccupied by the guest. For example, the ternary complexes formed in the presence of tert-butanol or cyclopentanol presented higher association constants than the complexes formed in the presence of *n*-propanol or ethanol.

From the data presented here, it can be inferred that 2,3-DBP, which is a bulkier molecule than 2-BE, is of a size that is more compatible with the remaining space of the interior of the CD cavity. Consequently, the interaction of the naphthalene derivatives and the heavy atom is more effective with 2,3-DBP than with 2-BE.

On the other hand, higher signals have been obtained, in the same experimental conditions, for the NAA complex than for the NOA complex. The fact that the quenching is more effective in the case of the NAA complex than in the NOA complex, and that the RTP emission obtained is higher, can be attributed to the more effective interaction of NAA with the bromoalcohol in the interior of the CD. The reason lies in that more void space remains in the interior of the CD in the case of the NAA complex than in the case of the NOA complex for the co-inclusion of the bromoalcohol.

An axial inclusion of both naphthalene derivatives in β-CD has been demonstrated previously,[24] and the inclusion of the NAA in the interior of the CD is only partial, because of the steric impediment of the substituted group in position 1, while NOA is almost totally included in the cavity.

In consequence, the bromoalcohol can enter more deeply into the CD cavity in the β-CD:NAA complex than in the β-CD:NOA complex, allowing a closer interaction between the heavy atom of the bromoalcohol and the guest.

The observed behaviour is similar to the effect reported by Turro *et al.*[10] with 1-bromonaphthalene and 2-bromonaphthalane included in β-CD. The addition of acetonitrile increased the phosphorescence intensity and the phosphorescence lifetime of 1-bromonaphthalene. Similar behaviour was observed for 1-chloronaphthalene. However, for 2-bromonaphthalene no appreciable effect of acetonitrile was observed. Similarly to our case, the 1-halonaphthalenes must be only partially included in β-CD, with more void space remaining for the third component to be included inside the cavity, while 2-bromonaphthalene is included more deeply in the cavity and the remaining space for the co-inclusion of acetonitrile is smaller.

Kinetics of the reaction. Optimization of chemical variables

The phosphorescence emission signal is not obtained instantly, but develops with time. The development of RTP emission with time suggests consumption of oxygen in the sample solution by sulphite, as already reported for a similar system.[19] It was also noted that higher signals were obtained when the sample was continuously irradiated at the excitation wavelength with the pulsed xenon lamp than without irradiation. The need for sample irradiation appears to be related to the oxygen consumption in the system. Similar irradiation effects have been reported for other systems and the effect was rationalized in terms of a photochemical catalysis of the reaction.[6,19]

The concentrations of 2-BE,2,3-DBP, Na_2SO_3 and β-CD were optimized by monitoring the phosphorescence emission from NOA and NAA in the presence of several concentrations of these compounds. The study was performed following the kinetics of development of the RTP emission with time under continuous irradiation of the samples with the pulsed xenon lamp.

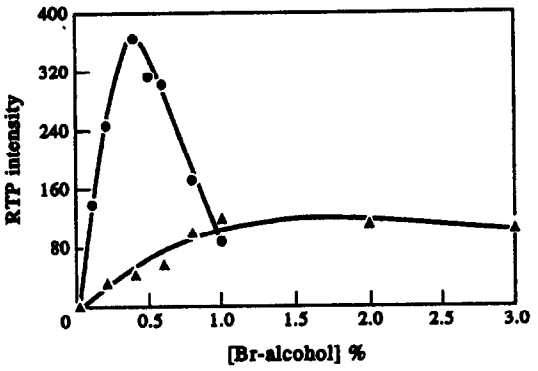

Fig. 4. Influence of the concentration of 2-BE (▲) and 2,3-DBP (●) on the RTP emission from β-CD:NOA:bromoalcohol. [NOA] = $3 \times 10^{-5}M$, [β-CD] = $10^{-2}M$, [Na_2SO_3] = $0.03M$, λ_{ex} = 274 nm, λ_{em} = 504 nm.

Influence of the bromoalcohols in CD-stabilized RTP

The influence of the concentrations of 2-BE and 2,3-DBP on the RTP emission from β-CD:NOA is represented in Fig. 4. Concentrations of 1% 2-BE and 0.4% 2,3-DBP were found as optima for both bromoalcohols, producing the maximum intensities without presenting turbidity.

It is interesting to note that the phosphorescence signals obtained in the presence of 2,3-DBP are always more intense than those in the presence of 2-BE. In addition, it has been observed that the deoxygenation reaction is slower when using 2-BE than when using 2,3-DBP. In consequence, for these particular systems, 2,3-DBP appears to be a more suitable heavy atom perturber than 2-BE for RTP obtention.

Influence of sodium sulphite and β-CD concentrations

Apart from the simplicity, one of the advantages of using sodium sulphite as deoxygenant is a more permanent protection of the solution against contamination with oxygen.[8] However, as stated above, the consumption of oxygen is not immediate, and a photo-induced catalysis of the reaction has been reported for an effective deoxygenation in some cases.[6,19]

The study has been performed by monitoring the signal as a function of time until the RTP signal was stabilized for at least 5 min. The deoxygenation kinetic is a complex process depending on various variables such as irradiation time, naphthalene derivative, and β-CD, bromoalcohol and sodium sulphite concentrations.

To find the optimum concentration of sodium sulphite, various amounts were added to a solution with a fixed amount of NOA ($3 \times 10^{-5}M$), β-CD and bromoalcohol. The concentration of β-CD was $1 \times 10^{-2}M$, and the concentrations of 2,3-DBP or 2-BE were 0.4% and 1.0%, respectively. The development of the RTP emission was followed kinetically by monitoring at 504 nm.

Figure 5 shows the influence of sodium sulphite concentration on the RTP emission from the β-CD:NOA inclusion complex in the presence of 2,3-DBP or 2-BE. The [Na_2SO_3] influences the intensity of phosphorescence and also the time of appearance of the emission. An increment of the concentration of sodium sulphite produces a more rapid obtention of the phosphorescence, because of a more effective deoxygenation. A $0.03M$ sodium sulphite concentration was selected as optimum.

An increment on the phosphorescence intensity has been found in both systems with the increment of β-CD concentration. [β-CD] = $1 \times 10^{-2}M$ has been selected as optimum because higher concentrations of the CD produced turbidity in the samples.

Analytical figures of merit

The phosphorescence intensities of solutions containing NOA in the concentration interval between $1 \times 10^{-5}M$ and $7 \times 10^{-5}M$ were recorded, in the presence of [β-CD] = $1 \times 10^{-2}M$, [Na_2SO_3] = $0.03M$ and 0.4% 2,3-DBP. Each of the samples was continuously irradiated with the pulsed xenon lamp at 274 nm. The phosphorescence was measured at 504 nm (Fig. 6). The results obtained show that a linear

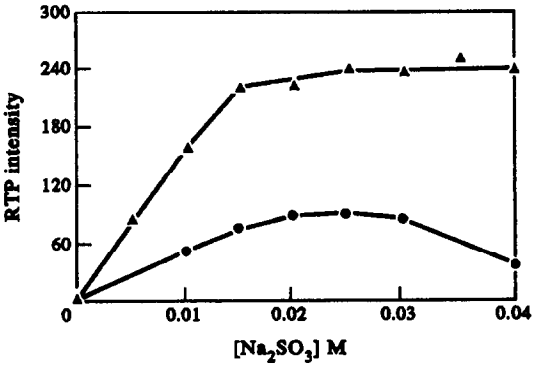

Fig. 5. Influence of sodium sulphite concentration on the RTP emission from β-CD:NOA:2,3-DBP. [NOA] = $3 \times 10^{-5}M$, [β-CD] = $10^{-2}M$, λ_{ex} = 274 nm, λ_{em} = 504 nm. (▲) [2-BE] = 1.0%; (●) [2,3-DBP] = 0.4%.

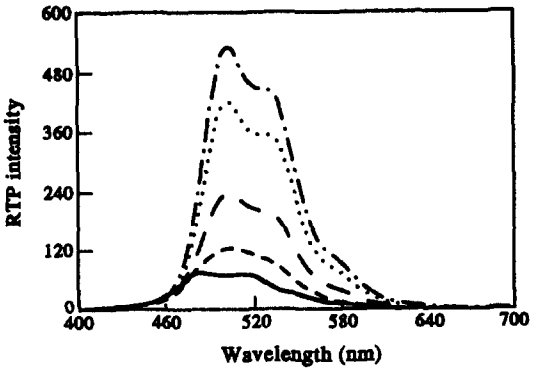

Fig. 6. RTP spectra of β-CD:NOA;2,3-DBP at different NOA concentrations: (a) 0; (b) $1 \times 10^{-5}M$;(c) $3 \times 10^{-5}M$; (d)$5 \times 10^{-5}M$; (e) $7 \times 10^{-5}M$.

relationship exists between the phosphorescence intensity and NOA in the concentration interval assayed.

In the same experimental conditions, exciting at 284 nm and measuring at 494 nm, the RTP emission obtained was linearly related to NAA concentration in the interval between $5 \times 10^{-6}M$ and $5 \times 10^{-5}M$.

The reproducibility of the assay was investigated by measuring the RTP signal of 11 replicated samples. Relative standard deviation values around 10% were obtained in both systems. Sample preparation is one of the critical aspects that must be carefully taken in consideration, as kinetic aspects are involved in the approach. Also, a recent article[36] reports on the use of commercially available β-CD, with respect to some absorption in the UV–visible region and solubility problems because of the lack of purity, which may contribute to the reproducibility problems encountered.

An emission signal from the blank, composed of β-CD and 2,3-DBP, is also evident. This fact has been observed previously by other authors,[37] who found phosphorescence signals from a blank of β-CD in the presence of 1,2-dibromopropane, attributing such emission to the low solubility of the inclusion complex β-CD:1,2-dibromopropane, which produces turbidity in the medium and a dispersion peak in the phosphorescence spectrum.

CONCLUSIONS

It has been shown that potential excited phosphorescent compounds of relatively polar character, such as NOA and NAA, when included in β-CD, in the presence of bromoalcohols, are partially deactivated in deaerated fluid solution at room temperature by triplet state emission. The photophysical characteristics of the triplet state emission for these naphthalene derivatives have been evaluated. 2,3-DBP has been found to be a more adequate external heavy atom perturber than 2-BE for RTP observation in the systems investigated, because of a better size compatibility with the void space of the interior of the CD. Such compatibility should be taken into account in the selection of the appropriate external heavy atom perturber for the observation of RTP emission from other organic molecules of interest.

It is interesting to note that, to date, the obtention of RTP in aqueous CD solutions has only been reported from a few compounds, mainly PHAs and some other compounds of non-polar character.[13,14] Naproxen[15] and NAA[16,17] were the only two compounds of relatively polar character that had been reported to produce RTP in the presence of bromoalkanes. In this work, the approach has been extended to the observation of RTP from NOA and NAA in the presence of bromoalcohols instead of bromoalkanes as external heavy atom perturbers.

A deeper understanding of the systems investigated should lead to a better optimization of the factors involved in the process and, consequently, to a better analytical exploitation of the phenomenon.

Acknowledgements—The authors acknowledge the D.G.I.C.Y.T. of the Ministry of Education and Science of Spain (Project PB91-0856) for financial support of this work.

REFERENCES

1. J. J. Donkerbroek, J. J. Elzas, C. Gooijer, R. W. Frei and N. H. Velthorst, *Talanta*, 1981, **28**, 717.
2. K. Kalyanasundaram, F. Grieser and J. K. Thomas, *Chem. Phys. Lett.*, 1977, **51**, 501.
3. A. Muñoz de la Peña, T. T. Ndou and I. M. Warner, Spectroscopic studies in organized media. An overview, in *Advances in Multidimensional Luminiscence*, I. M. Warner and L. B. McGown (eds), Vol. II. JAI Press, Greenwich, in press.
4. L. J. Cline Love, M. Skrilec and J. G. Habarta, *Anal. Chem.*, 1980, **52**, 754.
5. M. Skrilec and L. J. Cline Love, *J. Phys. Chem.*, 1981, **85**, 2047.
6. A. Sanz-Medel, P. L. Martinez García and M. E. Díaz García, *Anal. Chem.*, 1987, **59**, 774.
7. M. R. Fernandez de la Campa, M. E. Díaz García and A. Sanz-Medel, *Anal. Chim. Acta*, 1988, **212**, 235.
8. G. Ramis Ramos, I. M. Khasawneh, M. C. García-Alvarez-Coque and J. D. Winefordner, *Talanta*, 1988, **35**, 41.
9. I. Soutar and L. Swanson, *Analyst*, 1991, **116**, 671.

10. N. J. Turro, J. D. Bolt, Y. Kuroda and I. Tabushi, *Photochem. Photobiol.*, 1982, **35**, 69.
11. N. J. Turro, T. Okubo and C.-J. Chung, *J. Am. Chem. Soc.*, 1982, **104**, 1789.
12. N. J. Turro, G. S. Cox and X. Li, *Photochem. Photobiol.*, 1983, **37**, 149.
13. S. Scypinsky and L. J. Cline Love, *Anal. Chem.*, 1984, **56**, 322.
14. S. Scypinski and L. J. Cline Love, *Anal. Chem.*, 1984, **56**, 331.
15. L. J. Cline Love, M. L. Grayeski and J. Noroski, *Anal. Chim. Acta*, 1985, **170**, 3.
16. S. Zhang, C. Liu and Y. Bu, *Fenxi Huaxue*, 1988, **16**, 494.
17. S. Zhang, C. Liu and Y. Bu, *Fenxi Huaxue*, 1988, **16**, 682.
18. S. Hamai, *J. Am. Chem. Soc.*, 1989, **111**, 3954.
19. A. Muñoz de la Peña, I. Durán-Merás, F. Salinas, I. M. Warner and T. T. Ndou, *Anal. Chim. Acta*, 1991, **255**, 351.
20. F. J. DeLuccia and L. J. Cline Love, *Talanta*, 1985, **32**, 665.
21. H. Kim, S. R. Crouch and M. J. Zabik, *Anal. Chem.*, 1989, **61**, 2475.
22. R. A. Femia and L. J. Cline Love, *J. Coll. Interf. Sci.*, 1985, **108**, 271.
23. M. E. Díaz García and A. Sanz-Medel, *Anal. Chem.*, 1986, **58**, 1436.
24. A. Muñoz de la Peña, F. Salinas, M. J. Gómez and M. Sánchez Peña, *J. Incl. Phenom. Mol. Recog. Chem.*, in press.
25. A. Muñoz de la Peña, T. T. Ndou, J. B. Zung and I. M. Warner, *J. Phys. Chem.*, 1991, **95**, 3330.
26. A. Muñoz de la Peña, T. T. Ndou, J. B. Zung, K. L. Greene, D. H. Live and I. M. Warner, *J. Am. Chem. Soc.*, 1991, **113**, 1513.
27. J. B. Zung, A. Muñoz de la Peña, T. T. Ndou and I. M. Warner, *J. Phys. Chem.*, 1991, **95**, 6701.
28. M. E. Díaz García, M. R. Fernández de la Campa, W. L. Hinze and A. Sanz-Medel, *Mikrochim. Acta (Wien)*, 1988, **III**, 269.
29. N. E. Nugara and A. D. King, Jr., *Anal. Chem.*, 1989, **61**, 1431.
30. Yi-M. Liu, M. R. Fernández de la Campa, M. E. Díaz García and A. Sanz Medel, *Anal. Chim. Acta*, 1990, **234**, 233.
31. H. Kim, S. R. Crouch, M. J. Zabik and S. A. Selim, *Anal. Chem.*, 1990, **62**, 2365.
32. N. E. Nugara and A. D. King, Jr., *Anal. Chem.*, 1989, **61**, 1431.
33. Y. Wei, C. Liu and S. Zhang, *Fenxi Huaxue*, 1990, **13**, 1001.
34. J. J. Aaron, E. M. Kaleel and J. D. Winefordner, *J. Agric. Food Chem.*, 1979, **27**, 1233.
35. J. J. Aaron and J. D. Winefordner, *Analusis*, 1979, **7**, 168.
36. A. J. Sophianopoulos and I. M. Warner, *Anal. Chem.*, 1992, **64**, 2652.
37. R. A. Femia and L. J. Cline Love, *Spectrochim. Acta*, 1986, **42A**, 1239.

Talanta, Vol. 40, No. 11, pp. 1665–1670, 1993
Printed in Great Britain.

0039-9140/93 $6.00 + 0.00

SOLID-PHASE EXTRACTION USING C_{18} BONDED SILICA DISKS: INTERFERENCES AND ANALYSIS OF CHLOROTRIAZINES IN SEAWATER SAMPLES

GAEL DURAND and DAMIA BARCELO*

Environmental Chemistry Dept., CID-CSIC, c/Jordi Girona, 18–26, 08034 Barcelona, Spain

Summary—The interferences in C_{18} Empore extraction disks were obtained by processing 5 l. of HPLC water with average blanks of 1 ng/l. A C_{19} alkane, plasticizers and the antioxidant Nonox A were identified in the blanks as possible interferences. The extraction of the components of the disks was carried out with methanol, acetonitrile and/or ethyl acetate with subsequent analysis by gas chromatography–mass spectrometry (GC–MS). The identification of interferences was a requirement for the determination of the chlorotriazine herbicides atrazine and simazine, and of a transformation product, de-ethylatrazine, at concentration levels varying between 2 and 140 ng/l. Seawater samples of 3–28 parts-per-thousand were pre-filtered through a 47-mm diameter of 0.7 μm and subsequently with 0.45 μm glass-fibre filters to trap particulate matter, followed by Empore extraction disks of 500 mg C_{18} bonded silica. Water volumes of 5 l. could be processed within 150 min. The disks were extracted with methanol, the extract was blown down under nitrogen, and the analytes were quantified by GC with nitrogen–phosphorus detection (NPD) with further confirmation using GC–MS in the selected ion monitoring (SIM) mode. The proposed method has been applied to the determination of the environmental levels of atrazine and simazine in seawater samples of varying salinity. The recovery of de-ethylatrazine was 10%, so the method was not appropriate for this compound. The concentration of the herbicides has been plotted against the salinity values, showing a decrease in the levels as the salinity increases, with two inflexion points that indicate a non-conservative mixing with loss of the herbicides in the mixing zone of the estuary.

Several hundred pesticides of different chemical nature are currently used for agricultural and non-agricultural purposes throughout Europe and the U.S.A. Pesticides applied to crops are eventually transported to surface waters by various mechanisms, such as non-point source run-off, groundwater discharge or atmospheric deposition. It has been estimated that pesticide losses are generally less than 0.5% of the amount applied.[1–3] Their residues are currently detected by gas chromatography with nitrogen–phosphorus and mass spectrometric detection (GC–NPD and GC–MS, respectively) in various environmental matrices, such as soil, water and air.[3–7] Atrazine, one of the herbicides most widely used in the U.S.A. and European countries over the last 30 years,[8,9] is employed for both pre- and post-emergency weed control among crops of corn, wheat, barley and sorghum, and also along railways and roadside verges. It has been detected in some U.S. groundwaters at concentrations in the range of 100 ng/l,[10] in the Mississippi river,[1] in Canadian rivers,[2] in the Po river and its effluents[11] and in the waters of various other European countries.[3,9] Recently we reported results on the monitoring of several herbicides in estuarine areas of the Rhône and the Ebro delta,[12,13] where levels varied from 10 to 30 ng/l. This monitoring is particularly important since the estimated annual use of atrazine and simazine in France alone is *ca* 7000 tonnes.[12] The transport of atrazine within river waters occurs through dissolved river matter[1,8] and as a consequence residues of chlorotriazines can easily reach the sea through estuarine areas. Recently, residue levels have been detected in estuarine samples from the U.K. and their concentration levels decreased with increasing salinity.[14]

In the last 2 years, alternative trace enrichment techniques for organic compounds, including pesticides, from water samples have become available. They are based on the solid phase extraction (SPE) principle and use membrane extraction disks, of similar diameter and size to liquid chromatographic (LC) solvent filters. Their main advantage over the conventional SPE cartridges is the high sampling flow

*Author for correspondence.

rate, which is more convenient for sampling in the field. At present, such disks have been tested for different groups of compounds, including pesticides, organotins and phthalates.[15–18]

One of the disadvantages of using SPE techniques, either with cartridges[19] or disks,[16,17] is the impurities which are present in the surface and which, when eluted during the analysis, can interfere with the final measurements. Although a detailed study has been published for C_{18} bonded silica cartridges,[19] only very general statements have been made concerning the interferences in the Empore disks, without giving a detailed description of the various interfering components.[16,17]

The purpose of the present research was to evaluate the presence of extraneous peaks from the Empore extraction disks that can interfere with low level determination of chlorotriazine pesticides in seawater samples. Real seawater samples of varying salinity have been determined by GC–NPD with further confirmation by GC–MS in the selected ion monitoring mode (SIM). The concentrations of chlorotriazines have been plotted against salinity values.

EXPERIMENTAL

Chemicals

HPLC grade water, methanol, acetonitrile and pesticide grade ethyl acetate from Merck (Darmstadt, Germany) were passed through a 0.45 μm filter before use. Simazine was obtained through Polyscience (Miles, IL, U.S.A.); atrazine was purchased from Promochem (Wesel, Germany). De-ethylatrazine was a gift from Ciba-Geigy (Basel, Switzerland).

Sample preparation

HPLC water (5 l.) was used for the blanks study, whereas 5 l. of seawater samples were collected with different salinity values of 0–34‰. The seawater samples were first filtered through fibre-glass filters (Millipore Corp. Bedford, MA, U.S.A.) of 0.70 μm and subsequently with filters of 0.45 μm. The SPE method used a standard Millipore 47-mm filtration apparatus. The membrane extraction disks were manufactured by 3 M (St. Paul, MN, U.S.A.) under the trademark Empore and are distributed by J. T. Baker and Analytichem International. The disks used in these experiments were 47 mm in diameter and 0.5 mm thick. Each disk contains about 500 mg of C_{18} bonded silica material.

The extraction procedure used was as follows: the HPLC blank water samples were passed directly through the Empore extraction disks, whereas the seawater sample solutions were prefiltered to eliminate particulate matter. The disk, placed in the conventional Millipore apparatus, was washed with 2 × 10 ml of methanol under vacuum. The disk was not allowed to become dry and 5 l. of water were immediately extracted with the vacuum adjusted to yield 2 hr 30 min extraction time. After this operation, the pesticides trapped in the disk were collected in 20 ml of methanol, acetronitrile or ethyl acetate (for the blank study) or in 20 ml of methanol for the real seawater samples. After careful evaporation of the methanol to dryness the samples were re-dissolved in 50 μl of ethyl acetate for determination by GC–MS.

In a previous paper,[18] recovery values for atrazine and simazine were, respectively, 100 and 85 with a coefficient of variation (CV) of 5–10%, whereas for de-ethylatrazine the recovery was 10% with a CV of 15%, when spiking the various pesticides at low μg/l levels in artificial seawater samples. The low recovery level of de-ethylatrazine was attributed to a surpass of the breakthrough volume and for this reason the values given in this paper for this particular compound are tentative, since the use of another adsorbent instead of C_{18} is recommended.

GC–NPD and GC–MS analysis

Following SPE, the extracts were injected onto the column of a gas chromatograph (GC 5300 Mega series, Carlo Erba, Milan, Italy) equipped with an NPD. A 15 m × 0.25 mm i.d. fused silica capillary column coated with chemically bonded 50% cyanopropylphenyl–50% methyl polysiloxane DB 225 (film thickness: 0.15 μm) and a 30 m × 0.25 mm capillary column coated with chemically bonded 5% phenyl–95% methyl polysiloxane DB-5 (film thickness: 0.25 μm) (J and W Scientific, Folsom, CA, U.S.A.) were used. Hydrogen was used as carrier gas at 60 kPa and helium as make-up gas at 110 kPa. The temperatures of injector and detector were held at 270°. Both columns were programmed from 60 to 90° at 10°/min and from 90 to 220° at 6°/min.

A Hewlett–Packard 5995 instrument (Palo Alto, CA, U.S.A.) interfaced to a 59970C data system was used. The fused silica column described above was used and was introduced directly into the ion source. Helium was used as the carrier gas (30 cm/sec). The temperature of

the injector was 250°. The ion source and the analyser were held at 200 and 230°, respectively. EI spectra were obtained at 70 eV. Identification of an analyte was from the signals of two ions and their proper ratio, and correct retention time. Ions used for identification were at m/z values of 173 and 215 (atrazine), 172 and 187 (de-ethylatrazine) and 173 and 201 (simazine).

RESULTS AND DISCUSSION

General considerations

The main advantage of using SPE membrane disks such as Empore, instead of SPE cartridges, is the increase in sample throughput as a result of the relatively high flow rates. In this study, only 2 hr 30 min sampling time was needed for the pre-concentration of 5 l. water samples, whereas SPE cartridges would have taken at least 5 hr for the same samples. These results were in good agreement with other studies using disks.[15,17] Pre-filtration of (sea) water samples through 0.45 μm PTFE filters has been recommended before when C_8[20] or C_{18}[14] cartridges, or Empore extraction disks,[15,17] were used. Pre-filtration[21] is extremely important when using membrane extraction disks. So, when using 1 μm over 0.45 μm, the filtration time was reduced by half and effectively removed the particles. When non-pre-filtering was used, the filtration time for 2 l. of natural water was 7 hr,[21] whereas 1.8 hr were needed when using 1 μm pre-filter.

Pre-filtering does not affect the determination of polar pesticides since they exhibit log K_{oc} (partition coefficient between soil organic carbon and water) values of 2, and consequently remain in the dissolved phase and not on the suspended particulates, according to Ref. 1 with a proportion of 99.5% *vs* 0.5%, respectively. In contrast, performing the same experiments with hydrophobic organochlorine pesticides (log K_{oc} of *ca* 6), when there is a strong tendency to adsorb onto the particulate matter on the filter,[22] the same pre-filtering would give much lower recoveries.

Blank levels

In a previous paper,[18] we examined the use of extraction disks for isolation of various pesticides from artificial seawater samples in combination with liquid chromatography–diode array detection (LC–DAD). In this case, blank levels of the cartridges were briefly examined by the use of DAD at 220 and 205 nm. Interferences were noticed in the range of a few μg/l (or ng/l) when isolating pesticides from 4 l. of artificial seawater (or surface water) samples. In the present paper, we have decided to undertake a more in-depth study of the interferences extracted from the SPE disks, since our purpose was to determine chlorotriazine pesticides in water at low ng/l levels. Three different eluting solvents were used: methanol, acetonitrile and ethyl acetate. The blanks obtained when isolating 5 l. of HPLC water samples are shown in Fig. 1. The different compounds identified in the extracts are shown in Table 1. Some of the compounds identified were similar to those found in C_{18} bonded silica cartridges, such as phthalates. The different plasticizers are added

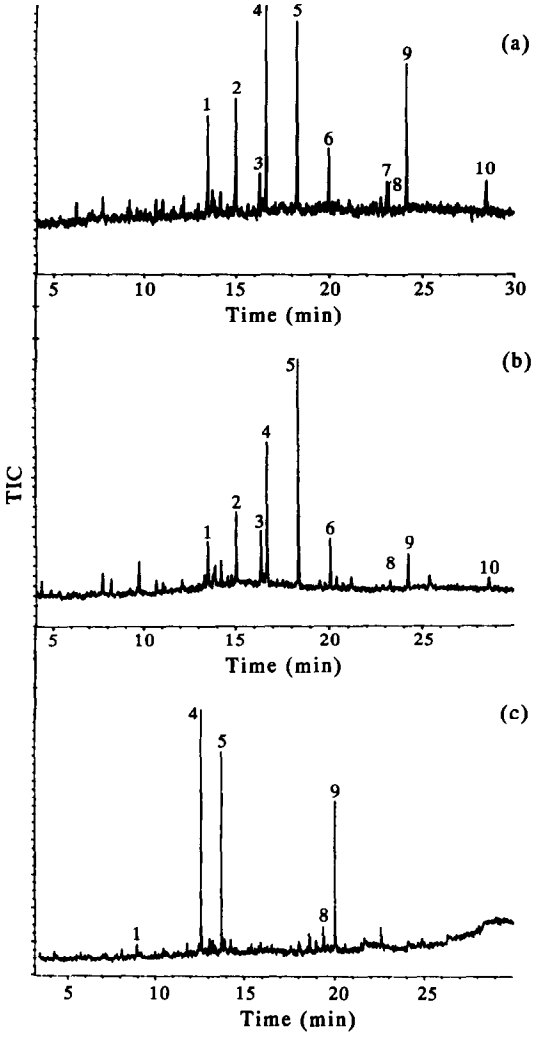

Fig. 1. GC–MS traces obtained on the extract of 5 l. of HPLC water after eluting with methanol (A), acetonitrile (B) and ethyl acetate (C). For compound numbers, see Table 1. For chromatographic conditions, see Experimental section. Two capillary GC columns, DB-225 (A and B) and DB-5 (C), were used.

Table 1. Compounds eluted from C_{18} Empore extraction disks using 5 l. of HPLC water. Unknown compounds are indicated by their m/z values and relative abundance (in parentheses)

Peak no.	Compound	Eluting solvent		
		Methanol	Acetonitrile	Ethyl acetate
1	Diethyl phthalate	+	+	+
2	$C_{19}H_{40}$ (alkane)	+	+	−
3	Dimethyl polysiloxane	+	+	−
4	Dibutyl phthalate	+	+	+
5	Butyl-2-ethylhexyl phthalate	+	+	+
6	Unknown			
	m/z 119 (70%), 213, 215 (100%)	+	+	−
7	Nonox A (antioxidant)	+	−	−
8	Unknown			
	m/z 57 (100%), 171 (50%)	+	+	+
9	Di-(2-ethylhexyl) phthalate	+	+	+
10	Unknown			
	m/z 91 (100%), 290 (30%)	+	+	−

either during manufacture or are present as contaminants in the polymer components. This is due to the polymeric housing used to house the bonded phase materials, in both cartridges[19] and disks.[17] The alkane C_{19} H_{40} was also found as an interference in the disks, as well as in the cartridges, although other alkanes and alkenes were also reported in the latter case.[19] In the case of cartridges, the antioxidant butahydroxytoluene (BHT) was reported,[19] whereas for the disks the antioxidant Nonox A has been found. One of the most relevant differences found between interferences in the use of C_{18} bonded silica cartridges and disks is that no dimethyloctadecylsilanol was found in the case of the disks. This was checked by using the m/z 89 ion corresponding to $[(CH_3O)Si(CH_3)_2]^+$. The absence of this particular ion, which caused great interference in a previous work using cartridges,[19] indicates that a better bonding is achieved in the Empore extraction disks, thus avoiding hydrolysis of the C_{18} bonded porous silica material. Consequently, no silanols are released from cartridges. Another compound, peak no. 3 (Fig. 1) corresponds to the dimethyl polysiloxane phase, which corresponds to the bleeding from the GC column used, DB-225, in Figs 1A and B, whereas in Fig. 1C a DB-5 column was used and this particular peak is not present.

Two previous papers on the use of disks reported a very vague indication of interferences.[16,17] Since interferences depend on the final analytical method of determination used, the GC–ECD traces showed higher background peaks compared to our experiments, but they were lower than when commercial C_{18} bonded porous silica columns were used.[16] This could be caused by the high sensitivity of the phthalates in the GC–ECD determinations. A second paper indicated that phthalate esters and similar plasticizers were probably present in the disks, causing systematic errors when using EPA method 525, with recoveries up to 149% for compounds such as diethyl phthalate.[17] This paper presents the first detailed description of the interferences present in C_{18} Empore extraction disks.

The interference in the blanks has been estimated to be in the range of 0.1–1 ng/l, when filtering 5 l. of water samples. When comparing the three eluting solvents used (see Fig. 1 and Table 1), we noticed that phthalates (compounds 4, 5 and 9) gave somewhat higher background levels when using ethyl acetate. This agrees with previous results when optimizing EPA method 506 for the isolation of phthalates from water samples with C_{18} extraction disks.[23] The percentage recovery for these compounds using ethyl acetate was higher than with the other solvents, with values up to 150%, thus indicating that this eluting solvent has the capacity of removing the phthalates from the C_{18} bonded silica disk more efficiently. The higher recoveries for phthalates match earlier results for the same disks.[17] When ethyl acetate is used as eluting solvent, higher amounts of phthalates are eluted, the polymer housing is wetted more extensively and emulsions are easily formed, causing practical difficulties. Therefore, methanol was preferred for the isolation of the different chlorotriazine pesticides from seawater samples since it is less toxic for routine work.

Environmental levels

The environmental degradation of atrazine has been studied in many agricultural environments, where rates are affected by factors such as pH, the amount of organic matter, soil type and temperature.[9,14,24,25] For example, in Chesapeake Bay, degradation studies indicated that sediments in the bay could easily degrade these contaminants at an accelarated grade compared to inland agricultural environments.[25]

In our experiments, we have studied the variation in concentration of atrazine according to salinity. To achieve this point, we have analysed real seawater samples ($n = 3$ at each sampling point, with a CV of 7% for atrazine and simazine) of different salinities. Typical total ion current GC–MS chromatograms of low and high salinity samples are shown in Fig. 2. Comparing both chromatograms of Fig. 2, it can be noticed that the GC–MS chromatogram obtained at 3 parts-per-thousand salinity has less noise level and is much cleaner than the one obtained at 28 parts-per-thousand salinity. This is due to two reasons: the lower levels of herbicide obtained at higher salinity values and, as consequence, the interferences in the GC–MS traces reach higher values when analysing the samples of high salinity. The different ions used for the identification of the various pesticides have been reported in the Experimental section.

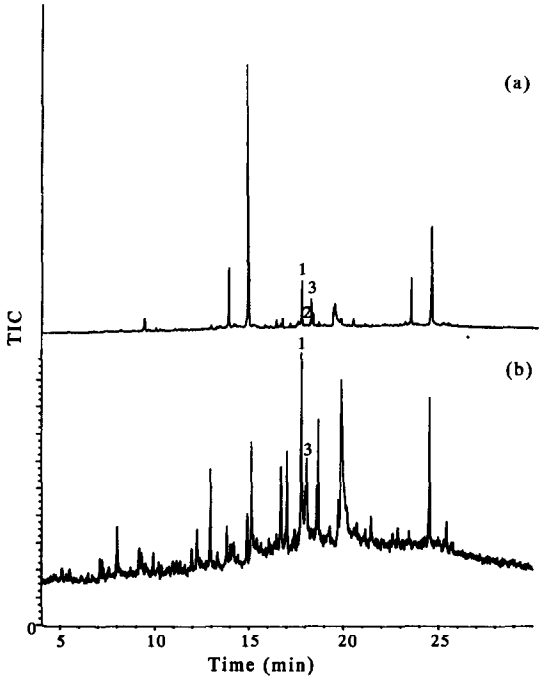

Fig. 2. GC–MS traces obtained on the extract of two estuarine waters of 3 parts-per-thousand (A) and 28 parts-per-thousand (B) salinity. Compounds identified were: (1) atrazine, (2) de-ethylatrazine and (3) simazine.

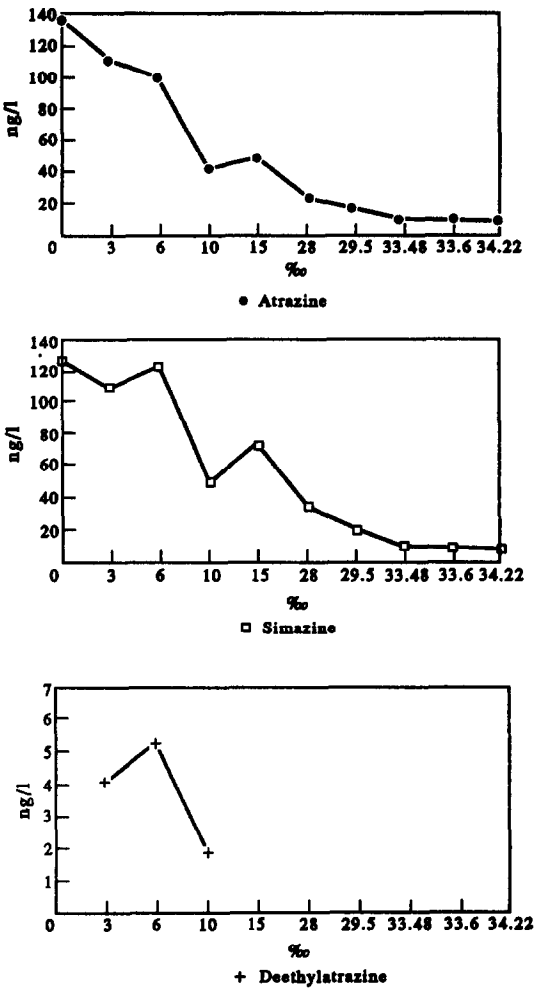

Fig. 3. Concentrations of atrazine, simazine and de-ethylatrazine *vs* salinity values of real seawater samples.

To distinguish between the influence of salinity in the concentration levels of the herbicides in the estuarine waters, in Fig. 3 the concentrations of the different herbicides were plotted against the difference in salinity. In principle, if there were no significant losses in the water column, relatively herbicide-free ocean waters would be expected to mix conservatively with fresh waters, producing a steady decline of the different herbicide concentrations as it progresses from low to high salinity values. A negative, in all three cases, with two inflexion points at the values of 3 and 10 parts-per-thousand salinity, indicates a non-conservative mixing with loss of the herbicides occurring in the mixing zone of the estuary. This behaviour, in the case of atrazine, agrees with that reported in Chakespeare Bay.[8,25] The concentration levels of simazine follow a similar degradation pattern in the estuarine waters. The values of

de-ethylatrazine exhibit poor recoveries (in the range of 10%) with the method used. The values of de-ethylatrazine obtained were in the range of 2–7 ng/l (without correction for the recovery) and are given as an indication. A second point to consider is that its value should always be lower than atrazine and simazine, since it is a compound formed mainly by microbial degradation of atrazine and depends on the application time of atrazine. Its content usually corresponds to *ca* 10–20% of the atrazine level in soil samples.[24]

CONCLUSIONS

The list of the different interferences obtained when using C_{18} bonded silica Empore extraction disks is reported for the first time, phthalates being the main interferences identified in the GC–MS traces. No silanol interference compounds were detected, thus indicating a better bonding of the C_{18} material in the case of these disks in comparison with conventional C_{18} bonded silica cartridges. One main advantage of the Empore disks over C_{18} cartridges is the shorter extraction time (5 l. of water are extracted in 2 hr 30 min, whereas the cartridges require 5 hr). It has been shown for seawater samples that pre-filtration is very important in order to remove the particulate material present in these samples. This operation will not affect the determination of chlorotriazine pesticides, since they are transported into the dissolved phase of the water. GC–MS allows the identification of atrazine, simazine and de-ethylatrazine from interferences and it is of help in avoiding false positives.

The use of SPE with Empore disks described here is recommended for screening chlorotriazine pesticides in real seawater samples at levels as low as 1 ng/l, with different salinity values. A limit of detection of 0.02 ng/l (at a signal-to-noise ratio of 3) has been estimated using GC–NPD or GC–MS with SIM detection. Since interfering compounds are present in real seawater samples, GC–MS is needed for confirmation of the triazines at levels as low as 10 ng/l.

The method proposed in this work can be used in remote places and it is an adequate method for carrying out monitoring studies with large amounts of water to be processed. This is much more convenient since smaller amounts of toxic solvents are used and it avoids the difficulties of handling 5 l. of seawater samples under liquid–liquid extraction procedures.

Acknowledgements—This work was supported by the Environment R & D Programme 1991–94 (Commission of the European Communities) on the Analysis and Fate of Organic Pollutants in Water (EV5V-CT92-0105). R. Alonso is thanked for laboratory assistance in the GC–MS. L. Beumer from J. T. Baker (Deventer, NL) is thanked for kindly supplying the Empore disks.

REFERENCES

1. W. E. Pereira and C. E. Rostad, *Environ. Sci. Technol.*, 1990, **24**, 1400.
2. R. Frank and Ll. Logan, *Arch. Environ. Contam. Toxicol.*, 1988, **17**, 741.
3. H.-R. Buser, *Environ. Sci. Technol.*, 1990, **24**, 1049.
4. G. Durand, R. Forteza and D. Barceló, *Chromatographia*, 1989, **28**, 597.
5. G. Durand and D. Barceló, *Anal. Chim. Acta*, 1991, **243**, 259.
6. W. E. Pereira, C. E. Rostad and Th. J. Leiker, *Anal. Chim. Acta*, 1990, **228**, 69.
7. H. Stan and A. Bockhorn, *Fresenius' J. Anal. Chem.*, 1991, **339**, 158.
8. J. C. Stevenson, T. W. Jones, W. M. Kemp, W. R. Boynton and J. C. Means, An overview of atrazine dynamics in estuarine systems, *Proc. Workshop on Agrichemicals and Estuarine Productivity*, Duke University Marine Laboratory, Beaufort, NC, 18–19 Sept., 1980. U.S. Department of Commerce, National Technical Information Service, pp. 71–94, 1982.
9. D. Barceló, *Analyst (London)*, 1991, **116**, 681.
10. N. Aharonson, *Pure Appl. Chem.*, 1987, **59**, 1419.
11. S. Galassi, L. Guzzella, M. Mingazzini, L. Viganó, S. Capri and S. Sora, *Water Res.* 1992, **26**, 19.
12. J. Tronczynski, C. Munschy, G. Durand and D. Barceló, *Sci. Total Environ.*, 1993 **132**, 327.
13. G. Durand, V, Bouvot and D. Barceló, *J. Chromatogr.*, 1992, **607**, 319.
14. M. Ahel, K. M. Evans, T. W. Fileman and R. F. C. Mantoura, *Anal. Chim. Acta*, 1992, **268**, 195.
15. D. F. Hagen, C. G. Markell, G. A. Schmitt and D. D. Blevins, *Anal. Chim. Acta*, 1990, **236**, 157.
16. O. Evans, B. J. Jacobs and A. L. Cohen, *Analyst (London)*, 1991, **116**, 15.
17. A. Kraut-Vass and J. Thoma, *J. Chromatogr.*, 1991, **538**, 233.
18. D. Barceló, G. Durand, V. Bouvot and M. Nielen, *Environ. Sci. Technol.*, 1993, **27**, 271.
19. G. A. Junk, M. J. Avery and J. J. Richard, *Anal. Chem.*, 1988, **60**, 1347.
20. D. A. Hinckley and T. F. Bidleman, *Environ. Sci. Technol.*, 1989, **23**, 995.
21. Th. McDonnell, J. Rosenfeld and A. Raiz-Farouz, Paper presented at the Division of the Environmental Chemistry, American Chemical Society, San Francisco, CA, pp. 358–361, 5–10, April, 1992.
22. M. Valls, J. M. Bayona and J. Albaigés, *Int. J. Environ. Anal. Chem.*, 1990, **39**, 329.
23. A. Alvarado, Paper presented at the Division of the Environmental Chemistry, American Chemical Society, San Francisco, CA, pp. 355–357, 5–10 April, 1992.
24. G. Durand and D. Barceló, *Toxicol. Environ. Chem.*, 1992, **36**, 225.
25. J. C. Means, R. D. Wijayaratne and W. R. Boynton, *Can. J. Fish Aquat. Sci.*, 1983, **40** (suppl. 2), 337.

Talanta, Vol. 40, No. 11, pp. 1671–1676, 1993
Printed in Great Britain.

0039-9140/93 $6.00 + 0.00

DETERMINATION OF ASCORBIC ACID IN PHARMACEUTICAL PREPARATIONS BY NEAR INFRARED REFLECTANCE SPECTROSCOPY

M. BLANCO, J. COELLO, H. ITURRIAGA, S. MASPOCH and C. DE LA PEZUELA
Departamento de Química, Unidad de Química Analítica, Universidad Autónoma de Barcelona, E-08193 Bellaterra, Barcelona, Spain

Summary—We developed a method for determination of ascorbic acid in pharmaceutical preparations containing various excipients by using near infrared diffuse reflectance spectroscopy and two different calibration methods, *viz.* stepwise multiple linear regression (SMLR) and partial least-squares (PLS) regression, which provided comparable results and resulted in prediction errors of 1–2%. However, the PLS method provided somewhat better results with the more complex samples.

Near infrared reflectance spectroscopy (NIRRS) has experienced great developments in the last two decades, during which it has been increasingly used in the field of food analysis.[1,2]

However, the appearance of commercially available instruments that allow fast recording of full NIR spectra (basically between 1100 and 2500 nm) and there use for implementation of modern chemometric methods for processing complex signals has extended their scope of application to include all types of solid samples. Control analyses by pharmaceutical industries, where the dependence of the NIRRS signal on both the chemical and the physical properties of the sample, and the accuracy and expeditiousness of this technique offer a great potential, has so far been one the chief applications of this technique.[3]

While early pharmaceutical applications of NIRRS relied essentially on the determination of moisture contents,[4,5] most published work in this respect is concerned with the characterization of compounds (*e.g.*, qualitative identification of pure substances,[6–8] determination of mixture homogeneity,[9,10] particle size,[11] enantiomeric purity,[12] *etc.*). In fact, there are relatively few references to the use of NIRRS for quantitative determination of compounds in end-products.[13,14]

Ascorbic acid (vitamin C) is a frequent occurrence in pharmaceutical preparations, where it is often the principal active component. Most of the host of methods developed for its determination are based on its redox properties;[15] the most commonly used of such methods involves titration[16] with iodine or Ce(IV). All these methods entail prior dissolution of the sample, which is time-consuming and a source of potential error arising from the instability of ascorbic acid solutions. In this work we develop a determination for ascorbic acid in solid pharmaceutical preparations by using the NIRRS technique. Calibration was performed by using two different multivariate procedures: inverse stepwise multiple linear regression (SMLR) and partial least-squares (PLS) regression. The results provided by each are compared below.

Calculation procedures

The SMLR method[17] is a least-squares approach based on the inverse of Beer's law; the concentration is modelled as a linear combination of absorbances in order to obtain the best possible correlation $[C = k_0 + k_1 A_1 + k_2 A_2 + \cdots]$ by using a small number of wavelengths.

The PLS method[17] is a factor-based procedure which can process full spectra. It factors the spectral data calibration matrix into the product of two smaller matrices. This involves a data compression step where the intensities measured at all the wavelengths used in the analysis are compressed to a small number of intensities in a new full-spectrum coordinate system which is composed of loading vectors that can be used to represent the original spectral data. A model is then applied to the intensities in the new full-spectrum coordinate system, called scores, that assumes the concentration to be a linear function of such intensities. The PLS method performs spectral factoring in order to account for the spectral variation while assuring that the

new basis vectors relate to the calibration concentrations:

$$Y = F_y L_y + E_y$$

$$X = F_x L_x + E_x$$

where Y is the concentration matrix, X the analytical data matrix, F_x and F_y the score matrices, L_x and L_y the loading matrices, and E_x and E_y the residual matrices. The score matrices are related by

$$F_y = F_x V + E_c$$

where V is the internal relationship and E_c the residual matrix.

The unknown sample is quantified by determining x_0 and y_0 from

$$y_0 = x_0 (F_y' X)' V L_y.$$

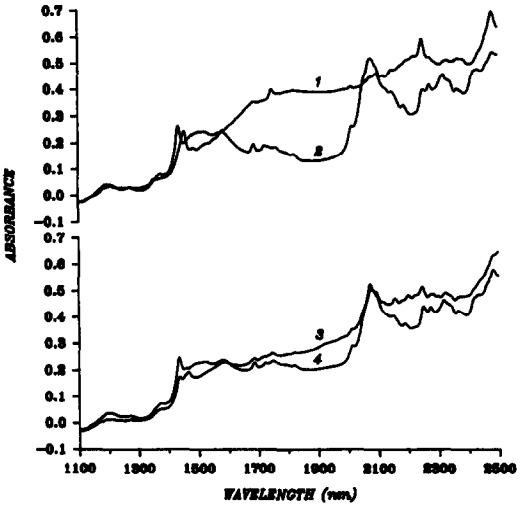

Fig. 1. Spectra of (1) ascorbic acid, (2) sugar, (3) Redoxón and (4) 1-g Cebión.

EXPERIMENTAL

Samples and reagents

We assayed two different commercial preparations, namely: Cebión® (Merck), which is commercialized in bags containing 1 or 2 g of ascorbic acid in granules, and Redoxón® (Roche), which is available as effervescent tablets. Ascorbic acid was the active principle in all three products, which contained various excipients (sweeteners, flavourings, *etc.*). The samples used were selected from five different batches of Redoxón, 11 of 1-g Cebión and 8 of 2-g Cebión.

The reagents used in this work included ascorbic acid, sodium bicarbonate, sugar and 0.1*M* KIO_3, 1*M* HCl and 0.5*M* KI solutions. All reagents and solutions were supplied by Merck or prepared from RA grade chemicals from this firm with the exception of sugar, which was for nutritional use. Figure 1 shows the NIRRS spectra of ascorbic acid, 1-g Cebión and Redoxón, while Fig. 2 shows their corresponding first derivatives.

Instrumentation and software

The experimental set-up used consisted basically of the following elements:

A NIRSystems 6500 near infrared spectrophotometer equipped with a reflectance detector and a Spinning Module for sample delivery. The instrument was controlled by the software package NSAS v. 3.20.

A dead-stop detection system composed of a Radiometer pHM29b potentiometer furnished with a Radiometer PP1311 platinum dual electrode, an adapter for connection of a Holder H22 electrode and a polarizer wire of 1 MΩ.

A set of sieves (C.I.S.A.).

Samples were handled and quantified by using the spectrophotometer's bundled software (NSAS), which included both the SMLR and the PLS algorithm. On the other hand, optimization of the PLS procedure and implementation of the multiplicative scatter correction (MSC) method were performed with the aid of UNSCRAMBLER v. 3.54, which required modifying the spectral format by using JCAMP.

Procedure

Laboratory procedure. The laboratory procedure used to determine ascorbic acid involved

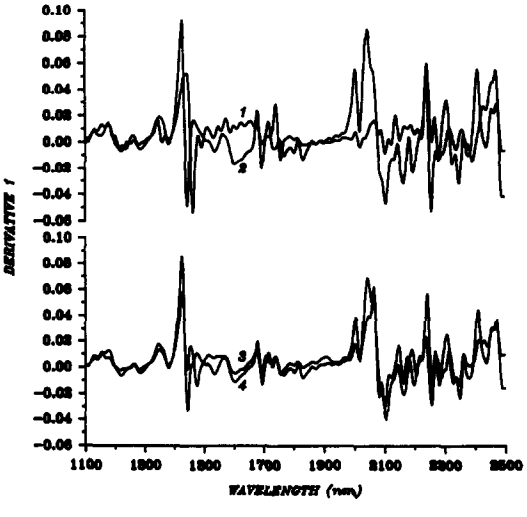

Fig. 2. First-derivative spectra of (1) ascorbic acid, (2) sugar, (3) Redoxón and (4) 1-g Cebión.

titration with potassium iodate[18] and biamperometric dead-stop detection. For this purpose, an amount of 0.3–1.1 g of sample was added to 25 ml of distilled water, 10 ml of 0.5*M* KI and 3 ml of 1*M* HCl, and the resulting solution was titrated with a KIO_3 standard. The ascorbic acid content in each sample was determined as the average of three replicates.

NIRRS procedure. Samples were ground and sifted through 250 μm (1-g Cebión and Redoxón) or 100 μm mesh (2-g Cebión). Each sample was used to record three spectra; the cuvette content was homogenized after each run in order to minimize errors arising from differences between sample fractions. The spectra thus obtained were averaged and the resulting spectrum was used to determine the ascorbic acid content by using the above-described procedures.

Overdosing procedures. In order to expand the calibration range, some samples were overdosed as follows: a known amount of sample was added to a known amount of ascorbic acid or the major excipient (sugar for Cebión and sodium bicarbonate for Redoxón). The mixture was then ground, sifted through 250 or 100 μm mesh and homogenized. Finally, the ascorbic acid content was determined by using the above-described laboratory procedure.

RESULTS AND DISCUSSION

An NIRRS signal is a complex function that depends both on the physical (grain size, crystal structure, *etc.*) and on the chemical properties of the sample. Its mathematical relationship to the concentration can be expressed as follows:

$$\log \frac{1}{R} = a\frac{C}{s} \qquad (1)$$

where R denotes reflectance, a absorptivity, C the concentration and s the scattering coefficient.

One of the factors most markedly influencing the scattering coefficient is the particle size and its distribution. In order to minimize its effect on a quantitative chemical analysis one should process the signal obtained by using a mathematical procedure before the calibration proper is started.[19] There are basically three such types of mathematical treatments, namely: multiplicative scatter correction (MSC), the use of derivative spectra, and signal scaling. We found neither MSC nor scaling to affect result quality, whereas quantification on first-derivative spectra provided substantially improved results. Consequently, all results given below were obtained from unscaled first-derivative spectra.

Table 1. Nominal ascorbic acid content (%) and calibration ranges

	Nominal content (%)	Comercial samples (%)	Overdosed samples (%)
1-g Cebión	16.67	16.33–18.68	14.88–19.16
2-g Cebión	40.0	38.69–45.09	36.60–51.08
1000-mg Redoxón	22.88	22.25–23.16	19.92–25.22

Sample overdosing

The intrinsic complexity of NIRRS signals requires calibration samples to be analogous to the unknown samples and, ideally, the calibration set to consist of samples whose content has previously been determined by a reference analytical method. However, constructing the calibration matrix for pharmaceutical analyses poses special problems. In fact, an appropriate quality control method must be able to accurately quantify both central values and the accepted pharmacopoeial limits. However, only real samples with near-nominal contents are normally available, which compels sample overdosing (*i.e.*, adding a given amount of analyte or excipient in order to expand the concentration range). This is a complicated process that calls for strict control in order to avoid altering the physical properties of the samples and hence the risk of spurious results. To check that the proposed overdosing procedure (*viz.* substance addition, grinding, sifting and homogenizing) did not alter the results at all, a set of real samples was chosen and quantified by using calibration matrices containing increasing numbers of overdosed samples and the sum of the squared differences $[\Sigma(C_{LAB} - C_{NIR})^2]$ calculated and compared. No significant differences were found in any case. The chief drawback of this

Table 2. Results obtained in the quantification of samples by SMLR

	C.E. (%)	V.E. (%)	Wavelength (nm)
1-g Cebión	0.67	0.72	1756, 1650, 2184
2-g Cebión	0.59	0.98	1756, 1646
1-g and 2-g Cebión	1.82	1.98	1756, 1582, 1454
1000-mg Redoxón	1.18	2.34	1462, 2318, 1492, 2372

C.E.: Calibration error, V.E.: Validation error.

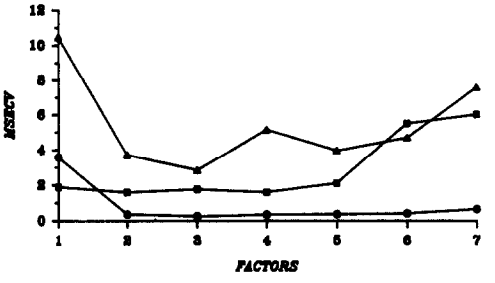

Fig. 3. Plot of the prediction error (MSECV) against the number of factors. (▲) Redoxón, (■) 2-g Cebión, (●) 1-g Cebión.

procedure is the need to subsequently grind and sift the samples to the same particle size as those used for calibration. Table 1 lists the concentration ranges encompassed by the samples and those used in this work.

The initial set of samples (unaltered and overdosed) was divided into two groups. The larger group was used for calibration while the smaller was employed as an external validation set. The accuracy of the analytical procedure was assured by having the validation set contain samples from batches that were not used for the calibration samples.

Quantification of samples by SMLR

One key to obtaining quality results was appropriate choice of the small set of wavelengths to be used. Ideally, one should test all possible combinations; however, this is quite impractical when a large number of wavelengths are involved, so one must use a stepwise selection procedure[20] even though the chosen set may not be the optimal. We choose the first wavelength of the model to be one that: (*a*) belonged to a region of the first-derivative spectrum in which the sample signal were mainly due to ascorbic acid; (*b*) belonged to a broad, non-jagged zone of the plot of the correlation coefficient against the wavelength; and (*c*) possessed a high correlation coefficient. The classical stepwise procedure was used to select a further three wavelengths at the most until the multiple correlation coefficient did not vary significantly. We found this procedure to provide better results than those achieved by having the NSAS algorithm automatically select the wavelengths to be used.

We assayed four calibration models for the quantification of the three commercial preparations and that of 1-g and 2-g Cebión jointly. In order to assess the quality of the results obtained we calculate the errors made in quantifying the mixtures used to construct the calibration matrix (CE) and validation matrix (VE) by using the following expression:

$$\text{Error}(\%) = \sqrt{\frac{\sum_{i=1}^{n} (C_{\text{LAB}} - C_{\text{NIR}})^2}{\sum_{i=1}^{n} C_{\text{LAB}}^2}} \times 100 \quad (2)$$

where C_{LAB} and C_{NIR} denote the ascorbic acid concentration determined by redox titration and spectroscopic quantitation, respectively, and n denotes the number of calibration or validation samples.

Table 2 lists the errors found and the corresponding wavelengths. It should be emphasized that the selection of the first wavelength is not independent of the composition of the sample. Thus, Cebión samples provided good results with 1756 nm as the first wavelength, which however, resulted in relatively large error (VE = 4.0%) for Redoxón samples.

In all cases, both calibration and validation, the intercept and slope of the plots NIR-values *vs.* Laboratory-values close to 0 and 1, respectively, and a regression coefficient $r \geqslant 0.99$, indicate that the NIRRS procedure is subject to no systematic errors relative to the laboratory procedure.

Quantification of samples by PLS regression

The PLS model was constructed by cross-validation; the number of factors to be used was calculated by plotting the prediction

Table 3. Results obtained in the quantification of samples by PLS regression

	C.E. (%)	V.E. (%)	Wavelength range (*nm*)	No. Factors
1-g Cebión	1.04	1.43	1100–2500	3
	1.04	0.89	1300–1800	2
2-g Cebión	0.69	1.30	1100–2500	2
1-g and 2-g Cebión	1.73	1.62	1100–2500	5
1000-mg Redoxón	2.46	2.85	1100–2500	2
	1.93	2.08	1300–1800	3

C.E.: Calibration error, V.E.: Validation error.

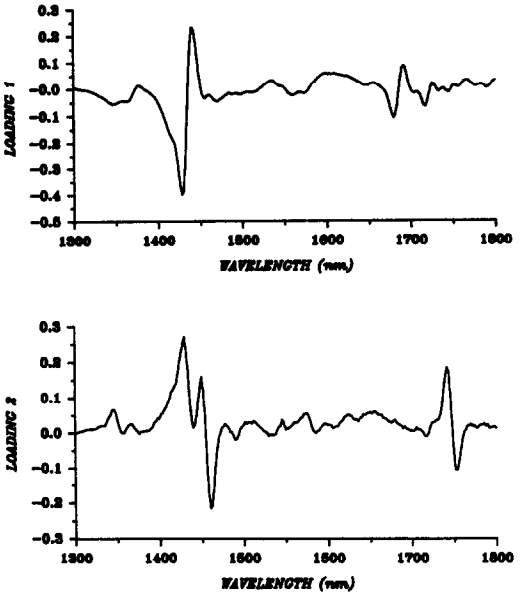

Fig. 4. Plot of the first (*a*) and second (*b*) loading of 1-g Cebión.

error (MSECV) against the number of factors (Fig. 3).

Even though PLS regression is a full-spectrum procedure, selecting the wavelengths to be used for quantification may be of aid, particularly if the calibration matrix is composed of a fairly small number of samples.[17] Such a selection was done by eliminating those wavelengths that either provide no information on the ascorbic acid content or resulted in an anomalously high residual. These two criteria coincided essentially with the two ends of the spectrum (the results were substantially better in the range 1300–1800 nm).

Table 3 compares the results obtained by applying the PLS procedure to the full spectrum and the above reduced wavelength range. As can be seen, the reduced range only improved on the results obtained for 1-g Cebión and Redoxón, which were sifted through 250 μm mesh; on the other hand, those obtained for 2-g Cebión, which was sifted through 100 μm, were virtually the same, which can be ascribed to the increased noise arising from the larger grain size, particularly high in the nearer end of the spectrum.

We used two factors for 1-g and 2-g Cebión separate determination. The corresponding loadings show that the first factor coincided essentially with the spectrum of sugar whereas the second corresponded to ascorbic acid minus the contribution of sugar at some wavelengths [Figs 4(a) and 4(b)]. The larger number of factors used in the joint determination was a result of the need to model the differences between the two types of sample. Redoxón was quantified from three factors, the loadings of which were linear combinations of the spectra of sugar, ascorbic acid and sodium bicarbonate.

CONCLUSIONS

We should emphasize that both the SMLR and the PLS results were very good. Validation errors were always less than 2.5%. Also, the SMLR results were more accurate for the simpler samples (Cebión), while the opposite was true for the more complex sample (Redoxón).

Even though the SMLR procedure is seemingly simpler to implement, it actually involves considerable work in selecting the wavelength set to be used, work which is difficult to systemize. In this respect, the PLS procedure is a much more powerful alternative that allows resolution of more complex samples and systematic optimization.

Finally, we should underscore that the NIRRS technique is accurate enough to ensure that the active principle content is within pharmacopoeial limits. In addition, its expeditiousness make it an appealing alternative to classical analytical control procedures.

Acknowledgements—The authors are grateful to the Spanish DGICyT for financial support granted for the realization of this work as part of Project PB90-0722 and to Laboratorios Igoda-Merck and Laboratorios Roche for kindly supplying the pharmaceutical samples.

REFERENCES

1. B. G. Osborne and T. Fearn, *Near Infrared Spectroscopy in Food Analysis*. Wiley, New York, 1986.
2. P. Williams and K. Norris, *Near-Infrared Technology in the Agricultural and Food Industries*, American Association of Cereal Chemists, St. Paul, Minnesota, 1987.
3. E. W. Ciurczak, *Appl. Spec. Rev.*, 1987, **23**, 147.
4. J. E. Sinsheimer and N. M. Poswalk, *J. Pharm. Sci.*, 1968, **57**, 2007.
5. R. J. Warren, J. E. Zarembo, C. W. Chong and M. J. Robinson, *ibid.*, 1970, **59**, 109.
6. E. W. Ciurczak and T. A. Maldacker, *Spectrosc.*, 1986, **1**, 36.
7. H. L. Mark and D. Tunnell, *Anal. Chem.*, 1985, **57**, 1449.
8. P. A. Salamin, Y. Cornelis and H. Bartels, *Chem. Intel. Lab. Sys.*, 1988, **3**, 329.
9. E. W. Ciurczak, *Pharm. Tech.*, 1991, **15**, 87.
10. P. Corti, E. Dreassi, G. Corbini, S. Lonardi and S. Gravina, *Analusis*, 1990, **18**, 112.
11. E. W. Ciurczak, R. P. Torlini and P. M. Demkowicz, *Spectrosc.*, 1986, **1**, 36.

12. B. R. Buchanan, E. W. Ciurczak, A. Q. Grunke and D. E. Honigs, *ibid.*, 1988, **3**, 54.
13. A. F. Zappala and A. Post, *J. Pharm. Sci.*, 1977, **66**, 292.
14. E. W. Ciurczak and R. P. Torlini, *Spectrosc.*, 1987, **2**, 41.
15. N. K. Pandeg, *Anal. Chem.*, 1982, **54**, 793.
16. *Pharmacopeia Britannica*, 1988, 47 and 901.
17. H. Martens and T. Naes, *Multivariate Calibration.* Wiley, New York, 1991.
18. F. J. Welcher, *Standard Methods of Chemical Analysis.* van Nostrand-Reinhold Co., New York, 1968.
19. L. S. Aucott, P. H. Garthwaite and S. T. Buckland, *Analyst*, 1988, **113**, 1849.
20. E. V. Thomas and D. M. Haaland, *Anal. Chem.*, 1990, **62**, 1091.

Talanta, Vol. 40, No. 11, pp. 1677–1685, 1993
Printed in Great Britain.

0039-9140/93 $6.00 + 0.00

FLOW INJECTION FLAME ATOMIC ABSORPTION SPECTROMETRY FOR SLURRY ATOMIZATION. DETERMINATION OF IRON, CALCIUM AND MAGNESIUM IN SAMPLES WITH HIGH SILICA CONTENT

IGNACIO LÓPEZ GARCÍA, JESUS ARROYO CORTÉZ and MANUEL HERNÁNDEZ CÓRDOBA*
Department of Analytical Chemistry, Faculty of Chemistry, University of Murcia, 30071 Murcia, Spain

Summary—A study on the use of slurries in flame atomic absorption spectrometry is reported. Samples with a very high silica content are ground and then slurried in a solution containing 2% hydrochloric and 3% v/v hydrofluoric acids. The suspensions are prepared in the 0.01–1% m/v range and introduced into the flame by means of a simple flow injection manifold. Relative standard deviations for the measurements of iron, calcium and magnesium in diatomaceous earth samples are in the 1.5–2.8, 2.2–5.3 and 2.8–5.0% ranges, respectively. To avoid the use of suspensions prepared with a very low percentage of solid sample and to improve the reproducibility, an on-line dilution manifold is tried. The use of an easy-to-construct variable volume dilution chamber allows the on-line dilution of the slurries, thus permitting the determination of calcium and magnesium over a wide range of concentrations. Calibration is performed using aqueous standards. The experimental conditions, optimized for the determination of iron, calcium and magnesium in diatomaceous earth samples, can also be applied to other silica-based materials, as is shown by the analysis of several standard reference materials.

Conventional sample introduction in flame atomic absorption spectrometry (FAAS) requires that solid samples be dissolved to obtain suitable solutions for measurement. In some instances, this involves a straightforward, easy-to-perform step but, in many other practical situations, the stage is time-consuming, involving tedious digestion or fusion procedures and the risk of contamination or analyte loss due to prolonged sample manipulation. If the dissolution step can be avoided and the solid sample is directly introduced into the atomizer, these drawbacks are overcome and the time needed to perform the determination is considerably shortened. For this, interest has focused on slurry-based methodology, in which, instead of a solution, a suspension prepared from fine particles of the sample is introduced into the atomizer. This is a recognized approach when electrothermal atomization is used,[1] but severe problems restrict its application with a flame. Firstly, there are transport efficiency problems through the spray chamber, which are strongly affected by the particle size and the density of the particles. As is to be expected, the greater the particle size and density, the lower the analytical signal and reproducibility obtained. A low particle size is also needed to minimize the risk of the nebulizer clogging when the suspension is being continuously aspirated. On the other hand, although the finest particles can reach the flame, atomization is hindered by the relatively low temperature of the flame and the short residence time. Thus, a sufficiently low particle size appears to be a pre-condition for the slurry–FAAS approach to be successful. How low the particle size must be for a good analytical signal to be obtained is related to the characteristics of the sample and the analyte. Predictably, a suspension prepared from biological material is easier to atomize than one prepared from a refractory material.

Despite the above difficulties, following the work of Willis,[2] a number of researchers have reported successful results in the flame atomization of slurries. O'Reilly and Hicks[3] carried out a detailed study of the direct analysis of coal samples. Fagioli *et al.* have also reported FAAS procedures for vegetables[4,5] after a partial wet-ashing with concentrated sulphuric acid. Other workers have also developed procedures for the determination of several elements in soils,[6] sewage sludges[7] and biological materials.[8,9]

As Fuller suggested many years ago,[10] the risk of nebulizer clogging when aspirating suspensions is greatly minimized if discrete

*Author for correspondence.

nebulization, instead of continuous aspiration, is used. This problem can also be overcome by using Babington nebulizers.[8] Flow injection (FI) methodology also appears to be a suitable method of avoiding clogging problems when introducing a suspension into the flame,[11] because this approach is similar to the one in which FI is used for the introduction of liquid samples with high concentrations of dissolved solids.[12] The FI–FAAS–slurry approach has been reported for the determination of several analytes in sewage sludges,[13] iron oxide pigments[11,14] and foods.[15–17] From our previous experience on this topic, the inclusion in the FI manifold of a simple three-way connector with a tip open to the air aids the fragmentation of the plug. This system of air compensation of the difference between the nebulizer uptake rate and the peristaltic pump flow rate, which is based on an idea from Yoza *et al.*,[18] and discussed by others,[19–21] is a simple, inexpensive way of improving nebulization, the T-piece acting as a pre-nebulizer. However, this approach does not improve slurry volatilization in the flame.

It has been shown that, when dealing with some slurries, a considerable fraction of the analyte is in the supernatant,[22,23] as a consequence of ultrasonic treatment or of the solubilizing action of the suspension media. For this reason, if the samples are pre-digested[4,5,7,13,17] or submitted to cold acid extraction processes,[24] a low particle size is not so critical, as most of the analyte is brought into solution.

On the other hand, the linear response range of FAAS is narrow. When dealing with suspensions from samples with high contents of the analyte, very dilute suspensions need to be prepared, which can generate reproducibility problems due to the low amount of sample to be weighed and to the errors associated with the sampling of slurries.[25] FI methodology can help solve this problem, as a variety of manifolds have been described which permit the on-line dilution of the sample.[26–35]

In this paper, we report the determination of iron, calcium and magnesium by direct introduction into the flame of slurries prepared from samples with a high silica content. The study was mainly performed using diatomaceous earth (DE) samples, a commercial product with very high silica content. The conclusions can be extended to other silica-based materials, as is shown by analysing several standard reference materials.

EXPERIMENTAL

Apparatus

Most of the measurements were obtained using a Pye Unicam Model SP1900 atomic absorption spectrometer. The analogical output of the instrument was connected to a personal computer via a PCLab 818PG data acquisition card. Home-made software written in C language together with a commercial package for the plotting of scientific data were used for the direct plotting of the absorbance–time relationship. The software also permitted the measurement of the area (integrated absorbance). Some experiments were performed using a Perkin–Elmer Model 1100B atomic absorption spectrometer equipped with deuterium-arc background correction. The measurements were made at 248.3, 422.7 and 285.2 nm for iron, calcium and magnesium, respectively. Air–acetylene flames were used exclusively. X-ray fluorescence measurements were made, for comparison purposes, with a Philips PW1400 wavelength dispersive X-ray spectrometer.

The two FI manifolds used are shown in Fig. 1. The simplest one (a) consisted of a Gilson Minipuls HP4 peristaltic pump with an Omnifit injection valve. Sample loops, as well as all connecting lines, were made of 0.8 mm i.d. polytetrafluoroethylene. For both manifolds, a three-way connector with a tip open to the air was included immediately before the spectrometer. The entry of air through this T-piece as a consequence of the difference between the nebulizer uptake rate and the pumping flow rate aids the fragmentation of the sample plug.[19] Manifold (b), which uses two injection valves, has recently been reported[35] and is shown here in a simplified manner. This manifold permits the on-line dilution of the suspensions. S_1 is a common plastic syringe used to inject a plug of air. S_2 is another similar syringe adapted as a variable volume dilution chamber.[34] V_3 is a two-way valve to switch between the upper and lower outlets of S_2. To obtain the on-line dilution, a plug of suspension and a plug of air, with a volume higher than that of the dilution chamber, are simultaneously injected into the manifold. When the sample plug reaches the dilution chamber, it is rapidly mixed with the carrier filling it. In this way, the diluted suspension leaving the chamber, pushed by the plug of air, has a constant concentration and a plateau is obtained for the absorbance–time

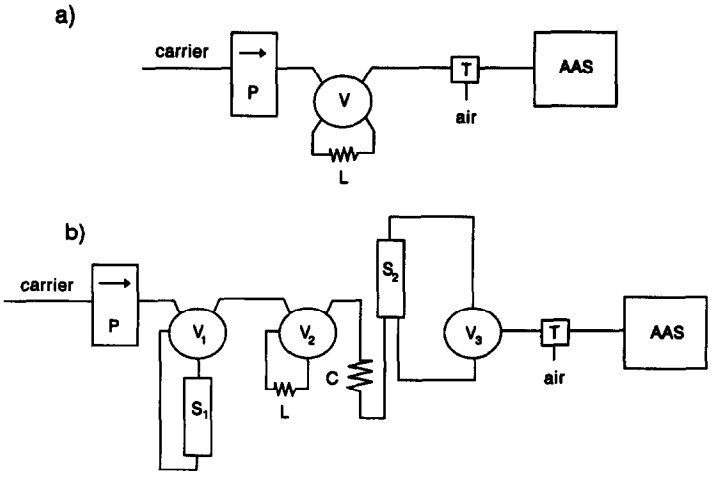

Fig. 1.(a) FI manifold for the direct introduction of the slurries. P, peristaltic pump; V, injection valve; L, sample loop; T, T-piece for air compensation. (b) FI on-line dilution manifold used for calcium and magnesium determinations (see text for details).

relationship. A detailed description of the manifold, its performances and its limitations is given elsewhere.[35]

Slurry procedures

DE samples were ground for 20 min using an agate ball mill. For the determination of calcium and magnesium, slurries were prepared in the range 0.01–0.05% by weighing the samples in 100 ml plastic containers and then adding 50 ml of a 2% v/v hydrochloric acid and 1% v/v hydrofluoric acid solution. For the determination of iron, the slurries were prepared in the 0.1–1% range and the hydrofluoric acid concentration increased up to 3%. The suspensions were submitted to ultrasounds for 10 min and then 0.5 g of solid lanthanum nitrate were added. After the slurries were magnetically stirred for another 10 min, and while they were being continuously stirred, a 150 μl volume was injected into the FI manifold reported in Fig. 1a. Bidistilled water was used as the carrier at a flow rate of 2.5 ml/min.

When the on-line dilution device was used, 0.1–0.8% suspensions were prepared in a similar way. For this case, the hydrofluoric acid percentage was increased up to 3% and no lanthanum was added to the slurries. A 2% v/v hydrochloric acid and 1% m/v lanthanum nitrate solution was used as the carrier at pumping rates ranging between 1 and 4 ml/min. The size of the sample loop as well as the internal volume of the dilution chamber were adjusted so that the response was in the linear range of the instrument. Typical values used for a representative DE sample were 50 μl for the injected volume and 4 ml for the dilution chamber, thus providing a dilution degree of about 80. In all cases calibration was performed using aqueous standard solutions.

For the analysis of standard reference materials, the same methodology was followed, the grinding time being increased up to 30 min.

Reference procedures

For comparison purposes, ground DE samples (0.1 g) were accurately weighed into a platinum crucible and 0.9 g of boric acid and 0.6 g of lithium carbonate were added. The powders were mixed carefully using a platinum rod and then fused (1000° for 30 min). The melt was treated with 10 ml of a 3*M* hydrochloric acid solution by heating until total dissolution. The solution was finally diluted up to 100 ml.

The samples were also analysed by using an acid dissolution procedure. For this, using a platinum crucible, 5 ml of a 1:4 sulphuric acid solution and 5 ml of concentrated hydrofluoric acid were added to 0.2 g samples. The crucible was heated until sulphur trioxide fumes were seen and, once cooled, 5 ml of a 1:1 hydrofluoric acid solution were added, and the final volume adjusted to 100 ml with water. The calcium content was also obtained using X-ray fluorescence spectrometry and the standard additions technique.

RESULTS AND DISCUSSION

A considerable number of previous experiments were devoted to studying the stability of suspensions prepared from ground DE samples.

Sodium hexametaphosphate, polyvinylalcohol and Triton X-100 provided only partial stabilization. A number of detergents of the Span and Tween series,[36] covering a wide range of hydrophilic/lipophilic ratios, were also tried. Partial stabilization was achieved using Tween 20 in a high percentage (10%) or 20% glycerol as the suspension media. However, the severe change in the physical properties of the suspensions led to low atomic absorption signals. For this reason, the use of stabilizing agents was discarded and the sample loops were filled while the suspensions were being continuously stirred.

Recovery

The difficulties in transporting the sample to the atomizer can be greatly alleviated if the samples are introduced by means of the simple FI manifold shown in Fig. 1a, as the discrete nature of the sample introduction mode and the continuous rinsing action of the carrier minimizes the risk of the system clogging. However, the problem of partial atomization remains, since this is more severely affected by particle size and the short residence time inside the flame. It is apparent that, in general, better performances should be obtained if plasma techniques are used, instead of FAAS, due to the higher temperature of plasma, which facilitates atomization and permits successful results.[37–39] In spite of these considerations, our efforts were directed at obtaining atomization efficiencies close to those obtained using aqueous solutions, which would enable the simplest calibration with aqueous standards. The quality of the approach can be followed by means of the recovery value. It can be defined as the ratio, expressed as a percentage, between the apparent concentration of the analyte obtained when atomizing the slurry and the true concentration obtained using a reference method. If the recovery is close to 100%, direct calibration with aqueous standards is valid, whereas if it is less, slurries prepared from previously analysed similar samples must be used for calibration or empirical correction factors are needed. Recovery values reported in the literature are in the 20–100% range, depending on the type of sample. As the particle size severely affects the recovery, previous experiments were devoted to studying the sample comminution. DE samples of several batches were submitted to grinding during different intervals of time; 0.1% suspensions were prepared in water and 150 μl aliquots injected into

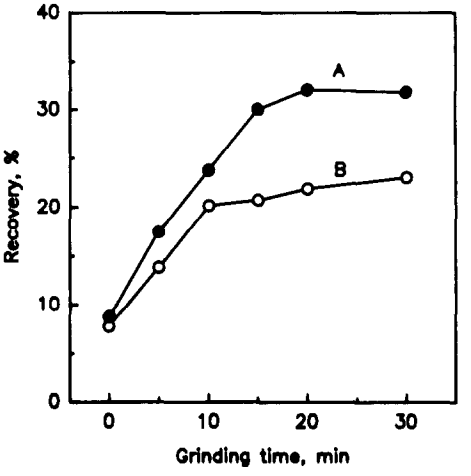

Fig. 2. Recovery of iron from 0.1% DE suspensions using water as the suspending medium. (A) A sample with high content of tridymite. (B) A sample with high content of cristobalite.

the simple FI manifold shown in Fig. 1a using water as the carrier. As can be seen in Fig. 2, where the recovery values for iron are plotted against the grinding time, 20 min was sufficient to obtain the maximum analytical signal, though the recovery was far from 100%. It was noted that the recovery values varied slightly among different batches of DE samples, and this was shown by X-ray diffractometry to be related to the mineralogical composition of the samples. Those containing higher amounts of tridymite provided higher signals than those in which cristobalite was the predominant crystallographic phase.

Previous experiments using the visual observation of electron micrographs indicated that, after a 20 min grinding time, the bulk of the particles was below 5 μm. However, this estimation was considered to be prone to error and not sufficiently accurate for FAAS purposes, and other approaches were considered. Since no instrumental facilities were available to measure particle size, 1% slurries were prepared in water using a DE sample which had been submitted to different grinding times. Next, aliquots were taken at different times and the mass of solid contained in each aliquot weighed. In this way, the application of Stokes' law allowed an estimation of the particle size distribution. The results, summarized in Fig. 3, indicated that grinding considerably decreased mean particle size, although not to the high degree that visual observation of electron micrographs suggested. It is clear that this particle size is not sufficiently low to allow complete atomization, which

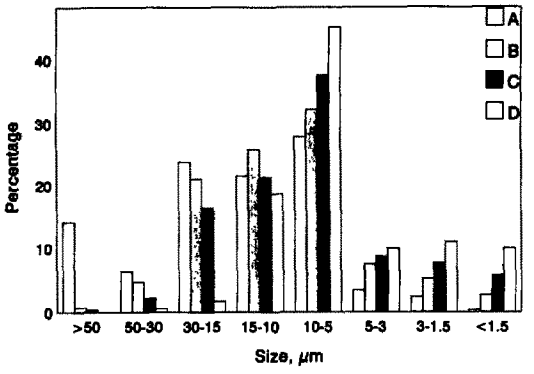

Fig. 3. Particle size distribution of a DE sample. A, B, C and D indicate 0, 5, 10 and 20 min of grinding time, respectively.

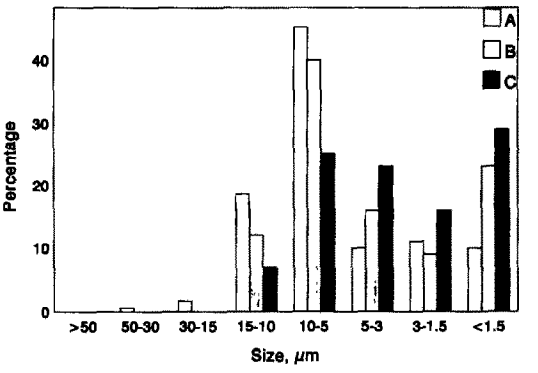

Fig. 4. Particle size distributions for a sample ground during 20 min and slurried using different media: (A) water; (B) 2% hydrochloric acid; (C) 2% hydrochloric acid and 3% hydrofluoric acid.

explains the low recovery values shown in Fig. 2. Thus, in addition to grinding, a modification of the procedure is needed to increase the recovery values.

It has been proved[22,23] that when dealing with slurries, in many instances, a considerable fraction of the analyte is extracted into the liquid phase of the suspension, as a consequence of the solubilizing action of the suspending media. If this occurs, a very low particle size is not so critical. With this in mind, diluted solutions of hydrochloric acid and mixtures of hydrochloric and hydrofluoric acids were assayed as the suspension media. Suspensions were prepared, in triplicate, from 14 DE samples and submitted to stirring for 20 min before injecting into the manifold; each slurry was injected three times. As is shown in Table 1, the use of a mixture of hydrochloric and hydrofluoric acids allowed recovery values very close to 100%. This approach of using dilute solutions of hydrofluoric acid as the suspending media has already been reported as a means to extract analytes into the aqueous phase and to increase the lifetime of the graphite material when slurries of samples of high silica content are introduced into electrothermal atomizers.[40-42]

The successful results obtained are mainly due to the extracting effect which brings to solution a considerable fraction of the analytes and, to a lesser extent, to the decrease in particle size as a consequence of partial solubilization. Figure 4 shows data obtained using Stokes' law for the particle size distribution when suspensions were prepared using different suspension media. From the experimental data it was calculated that when using water as the suspending medium, 90% of the particles were below 11 μm and 50% below 7 μm (these are the d_{90} and d_{50} values, respectively, as defined in the literature[43]). These values decreased to 9 and 3 μm, respectively, when the mixture of hydrochloric and hydrofluoric acids was used. The extracting effect is shown in Fig. 5a, in which the extraction percentage, obtained by analysing the supernatant after the suspensions were filtered through a 0.45 μm chromatographic membrane filter, is plotted against the time of contact between the solid sample and the suspending solution. As Fig. 5b shows, when using a 1% v/v hydrofluoric acid and 2% hydrochloric acid solution as the suspension medium, recoveries for iron were complete after the suspensions

Table 1. Recovery values for different suspending media

	Recovery* (%)		
Suspending medium	Iron	Calcium	Magnesium
Water	31 ± 9	23 ± 6	17 ± 5
2% hydrochloric acid	64 ± 5	71 ± 8	45 ± 6
2% hydrochloric acid and 1% lanthanum nitrate	65 ± 5	79 ± 3	57 ± 3
2% hydrochloric acid and 1% hydrofluoric acid	99 ± 2	92 ± 10	87 ± 8
2% hydrochloric acid, 1% hydrofluoric acid and 1% lanthanum nitrate	99 ± 2	101 ± 2	100 ± 3

*Mean value ± standard deviation for 14 DE samples.

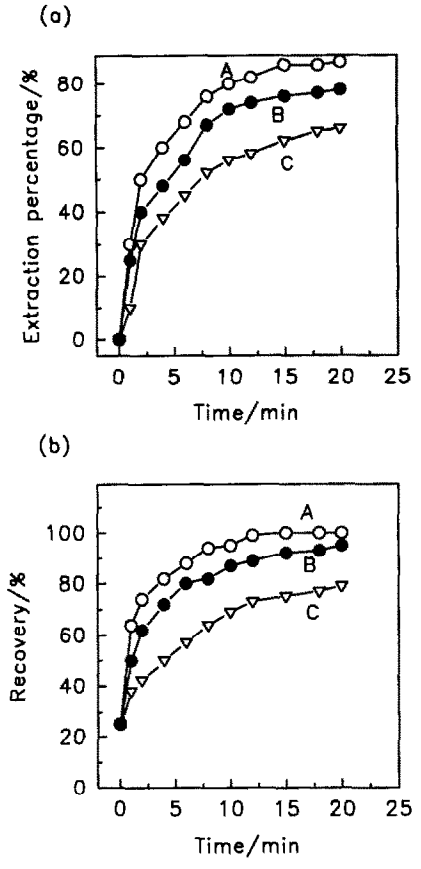

Fig. 5. Effect of hydrofluoric acid. (a) Percentage of iron extracted into the supernatant at different times after the addition of hydrofluoric acid. (b) Recovery of iron at different times. In all cases 0.1% suspensions and 2% hydrochloric acid were used. Curves A, B and C were obtained using 1, 0.1 and 0.05% hydrofluoric acid.

were stirred for a minimum of 15 min. Similar results were obtained for calcium and magnesium when lanthanum nitrate was added to the suspension medium (Table 1).

The effects of the sample loop and the flow rate were studied in the 26–350 μl and 0.5–4.5 ml/min ranges, respectively. Maximum and constant peak heights were obtained when the sample loop was above 130 μl. An injection volume of 150 μl and a flow rate of 2.5 ml/min are recommended.

It should be noted that in order to obtain the highest recovery values for calcium and magnesium, lanthanum nitrate was added to the suspending media. No practical problems related to calcium fluoride or lanthanum fluoride precipitates were encountered. On the other hand, in spite of the very high number of injections performed to carry out this work, clogging problems were only occasional, and were more frequent when dealing with slurries containing more than 1% of solid sample. When this occurred, clogging was invariably located at an FI connection.

Slurry percentage

A number of suspensions with different percentages of DE were prepared and the peak heights for the three analytes obtained (10 measurements in each case). In all cases, the percentages of the suspensions were chosen in such a way that the analytical signals were in the linear response range of the spectrometer. A linear relationship was verified between the percentage and the peak height in the 0.1–1% m/v range for iron and in the 0.01–0.05% m/v for calcium and magnesium for a DE sample containing 0.18, 2.4 and 0.12% m/m of iron, calcium and magnesium, respectively. The relative standard deviations (RSDs) of the measurements were 1.5–2.8, 2.2–5.3 and 2.8–5.0%, respectively.

When possible, the use of suspensions with a very low percentage of solid sample should be avoided because it is prone to poor reproducibility caused by weighing errors and problems of heterogeneity. To avoid this, the manifold shown in Fig. 1b was used to obtain the on-line dilution of the slurries. In such a way, in spite of the high calcium and magnesium content of the samples, suspensions more concentrated than 0.1% could be analysed. The manifold uses an easy-to-construct variable volume chamber[34,35] as an on-line dilution device. If a volume V_i of suspension is injected, the slurry inside the chamber suffers a degree of dilution, which is given by the V_c/V_i ratio[35] where V_c is the internal volume of the dilution device. The suspension leaving the chamber has a constant percentage, thus providing a plateau for the absorbance–time relationship. The height of the plateau or, better still, its area, can be used as the analytical signal.[35] One problem when suspensions are injected into such a dilution device is the risk of a partial sedimentation of the particles inside the chamber, which requires the use of a stabilizing agent. However, this was not observed for DE suspensions, which can be attributed to the low particle size and the low density of the sample, as well as to the short time the suspension remains inside the chamber.

In this case, due to the high degree of dilution suffered by the sample plug, lanthanum was added to the carrier instead of to the suspension media. The main FI conditions were again studied and the best results were found when a

1% lanthanum nitrate and 2% hydrochloric acid solution was used as the carrier and the slurries were prepared using a 2% hydrochloric and 3% hydrofluoric solution as the suspending medium. The manifold permits a wide range of degrees of dilution simply by moving the piston of the syringe used as the dilution chamber. In such a way, the suspensions can be prepared with percentages higher than 0.1% and the internal volume, V_c, can easily be adjusted, depending on the content of analyte in the sample, to provide a response in the linear response range of the instrument. It should be noted that it is not necessary to know the exact position of the piston and the consequent value of V_c, provided that samples and standards are injected under the same conditions, since they suffer an identical degree of dilution.

To check the behaviour of the device, a number of suspensions were prepared using a DE sample containing 6.3% of calcium. When these slurries were injected into the manifold, using a flow rate of 3.5 ml/min and a degree of dilution of about 80, a linear relationship was verified between the analytical signal (height or integrated absorbance of the plateau) and the slurry percentage in the 0.1–0.8% range. Values of RSD were in the range 2.3–3.6% (10 measurements). Similar experiments were carried out for magnesium as the analyte and using different DE samples. In all cases, excellent agreement was found between the experimental results and those expected.

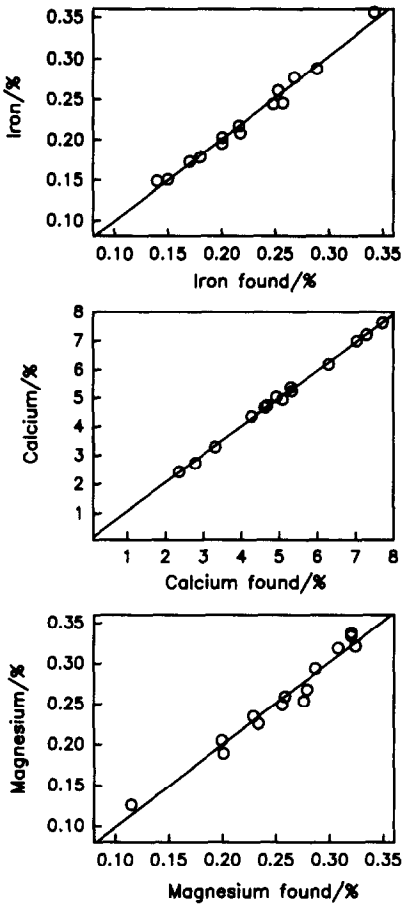

Fig. 6. Comparison of results for 14 DE samples. Values on the abscissae were obtained using the slurry procedure. Values on the ordinates were obtained using reference procedures.

Comparison of results

Taking into account all the above, direct calibration with aqueous standards is valid. To assess this, a considerable number of DE suspensions were prepared and standard addition calibration graphs for iron, calcium and magnesium were obtained using the simplest FI manifold. As can be seen from Table 2, the slopes of these lines agreed (95% confidence level) with those of calibration graphs obtained for aqueous standards, which are included for comparison.

Table 2. Slopes of standard addition calibration graphs

	Slope ± standard deviation (A *ml*/*μg*)	
Analyte	Aqueous standards*	DE slurries†
Iron	0.0182 ± 0.0002	0.0178 ± 0.0005
Calcium	0.0334 ± 0.0004	0.0336 ± 0.0008
Magnesium	0.256 ± 0.003	0.259 ± 0.004

*Values obtained from five calibration graphs. Each graph was constructed from four points and each point was measured three times.

†Values obtained from 14 DE samples. Three slurries were prepared from each sample. Each graph was constructed from four points and each point was measured three times.

To assess the reliability of the approach, the contents of iron, calcium and magnesium in 14 DE samples were obtained using alternative methods and the results compared with those found by means of the procedure discussed here. Three different procedures were used for comparison, two of them using AAS measurements after the samples were dissolved with a mixture of hydrofluoric and sulphuric acids or by means of a fusion with lithium carbonate and boric acid, as indicated in the Experimental. In the third procedure, calcium content was also obtained using X-ray fluorescence spectrometry. Figure 6 shows the correlation between the data obtained using the reference procedures and those found by the slurry procedure discussed

Table 3. Results for certified reference materials

	Element* (%)					
	Iron		Calcium		Magnesium	
Sample	Certified	Found	Certified	Found	Certified	Found
NBS 1633a coal fly ash	9.4 ± 0.1	9.2 ± 0.3	1.11 ± 0.01	1.07 ± 0.02	0.455 ± 0.01	0.464 ± 0.01
SARM 1 granite	1.4	1.26 ± 0.08	0.557	0.590 ± 0.02	0.036†	0.038 ± 0.002
NBS 688 basalt rock	7.23 ± 0.03	7.5 ± 0.2	8.69†	9.11 ± 0.03	5.03†	5.07 ± 0.02
BCS-CRM 348 ball clay	0.73 ± 0.02	0.75 ± 0.02	0.123 ± 0.006	0.130 ± 0.004	0.184 ± 0.006	0.194 ± 0.005
BCS-376 potash feldspar	0.07	0.068 ± 0.003	0.380 ± 0.02	0.408 ± 0.02	0.023†	0.027 ± 0.003
BCS-375 soda feldspar	0.084 ± 0.007	0.077 ± 0.002	0.630 ± 0.03	0.640 ± 0.01	0.028 ± 0.012	0.032 ± 0.002
China clay III	0.769	0.81 ± 0.03	—	—	0.307	0.32 ± 0.02
Slate VI	7.31	6.7 ± 0.1	0.136	0.142 ± 0.006	1.69	1.65 ± 0.03

*Mean ± SD ($n = 5$).
†Not certified values.

here. Data on the ordinate axis are the mean values obtained by the reference procedures. Data for calcium and magnesium on the abscissa axis are the mean of the values obtained using the simple FI manifold and the on-line dilution device.

To check that the experimental conditions studied for DE samples can also be applied to other silica-based samples, a number of reference standard materials were submitted to the discussed procedure and the results are summarized in Table 3. It is important to indicate that when these materials were analysed, the results were lower than those certified and problems due to a partial sedimentation of the solid particles inside the dilution device were encountered when this manifold was used to determine calcium and magnesium. The problems were overcome and the results agreed with those certified when the samples were previously submitted to grinding for 30 min.

Acknowledgements—The authors are grateful to the Spanish DGICYT (Project 90-0302) for financial support. J. A. C. thanks the Venezuelan Foundation Gran Mariscal de Ayacucho for scholarship. Technical support of Dr R. Ortiz (Instrumentation Department) and Dr C. Pérez (Department of Geology) in the X-ray experiments is also gratefully acknowledged.

REFERENCES

1. C. Bendicho and M. T. C. de Loos-Vollebregt, *J. Anal. At. Spectrom.*, 1991, **6**, 353.
2. J. B. Willis, *Anal. Chem.*, 1975, **47**, 1752.
3. J. E. O'Reilly and D. G. Hicks, *Anal. Chem.*, 1979, **51**, 1905.
4. F. Fagioli, S. Landi, C. Locatelli and C. Bighi, *Anal. Lett.*, 1983, **16**, 275.
5. F. Fagioli and S. Landi, *Anal. Lett.*, 1983, **16**, 1435.
6. J. Stupar and R. Ajlec, *Analyst*, 1982, **107**, 144.
7. A. Morales, F. Pomares, M. de la Guardia and A. Salvador, *J. Anal. At. Spectrom.*, 1989, **4**, 329.
8. N. Mohamed and R. C. Fry, *Anal. Chem.*, 1981, **53**, 450.
9. N. Carrión, Z. A. de Benzo, E. J. Elguri, F. Ippoliti and D. Flores, *J. Anal. At. Spectrom.*, 1987, **2**, 813.
10. C. W. Fuller, *Analyst*, 1976, **101**, 961.
11. I. López Garcia, F. Ortiz Sobejano and M. Hernández Córdoba, *Analyst*, 1991, **116**, 517.
12. Z. Fang, B. Welz and G. Schlemmer, *J. Anal. At. Spectrom.*, 1989, **4**, 91.
13. R. Martinez Avila, V. Carbonell, M. de la Guardia and A. Salvador, *J. Assoc. Off. Anal. Chem.*, 1990, **73**, 389.
14. I. López Garcia, F. Ortiz Sobejano and M. Hernández Córdoba, *Analyst*, 1991, **116**, 831.
15. J. C. de Andrade, F. C. Strong and N. J. Martin, *Talanta*, 1990, **37**, 711.
16. P. Viñas, N. Campillo, I. López Garcia and M. Hernández Córdoba, *Food Chem.*, 1993, **46**, 307.
17. P. Viñas, N. Campillo, I. López Garcia and M. Hernández Córdoba, *Anal. Chim. Acta* (in press).
18. N. Yoza, Y. Aoyogi and S. Ohashi, *Anal. Chim. Acta*, 1979, **111**, 163.
19. I. López Garcia, M. Hernández Córdoba and C. Sánchez-Pedreño, *Analyst*, 1987, **112**, 271.
20. J. F. Tyson, *Anal. Chim. Acta*, 1988, **214**, 57.
21. Z. Fang and B. Welz, *J. Anal. At. Spectrom.*, 1989, **4**, 83.
22. N. J. Miller-Ihli, *J. Anal. At. Spectrom.*, 1988, **3**, 75.
23. D. Bradshaw and W. Slavin, *Spectrochim. Acta*, 1989, **44B**, 1245.
24. S. J. Haswell, J. Mendham, M. J. Butler and D. C. Smith, *J. Anal. At. Spectrom.*, 1988, **3**, 371.
25. J. A. Holcombe and V. Majidi, *J. Anal. At. Spectrom.*, 1989, **4**, 423.

26. J. L. Burguera (ed.), *Flow Injection Atomic Spectroscopy*. Dekker, New York, 1989.
27. J. F. Tyson, J. R. Mariara and J. M. H. Appleton, *J. Anal. At. Spectrom.*, 1986, **1**, 273.
28. J. F. Tyson and S. R. Bysouth, *J. Anal. At. Spectrom.*, 1988, **3**, 211.
29. G. D. Clark, J. Ruzicka and G. D. Christian, *Anal. Chem.*, 1989, **61**, 1773.
30. D. A. Whitman and G. D. Christian, *Talanta*, 1989, **36**, 205.
31. M. de la Guardia, V. Carbonell, A. Morales and A. Salvador, *Fresenius' Z. Anal. Chem.*, 1989, **335**, 975.
32. Y. Israel and R. M. Barnes, *Analyst*, 1991, **116**, 489.
33. V. Carbonell, A. Sanz, A. Salvador and M. de la Guardia, *J. Anal. At. Spectrom.*, 1991, **6**, 233.
34. E. Beinrohr, P. Csémi and J. F. Tyson, *J. Anal. At. Spectrom.*, 1991, **6**, 307.
35. I. López Garcia, J. Arroyo Cortez and M. Hernández Córdoba, *J. Anal. At. Spectrom.* (in press).
36. S. Budavari (ed.), *The Merck Index*, 11th edn, p. 8691. Merck, Rahway, 1989.
37. A. J. Ambrose, L. Ebdon, M. E. Foulkes and P. Jones, *J. Anal. At. Spectrom.*, 1989, **4**, 219.
38. L. Ebdon, M. E. Foulkes and S. Hill, *J. Anal. At. Spectrom.*, 1990, **5**, 67.
39. M. L. Fernández Sánchez, B. Fairman and A. Sanz-Medel, *J. Anal. At. Spectrom.*, 1991, **6**, 397.
40. C. Bendicho and M. T. C. de Loos-Vollebregt, *Spectrochim. Acta*, 1990, **45B**, 679.
41. C. Bendicho and M. T. C. de Loos-Vollebregt, *Spectrochim. Acta*, 1990, **45B**, 695.
42. I. López Garcia, J. Arroyo Cortéz and M. Hernández Córdoba, *J. Anal. At. Spectrom.* (in press).
43. J. Sneddon (ed.), *Sample Introduction in Atomic Spectroscopy*. Elsevier, Amsterdam, 1990.

Talanta, Vol. 40, No. 11, pp. 1687–1694, 1993
Printed in Great Britain.

0039-9140/93 $6.00 + 0.00

MULTICOMPONENT ANALYSIS: COMPARISON OF VARIOUS GRAPHICAL AND NUMERICAL METHODS

R. D. BAUTISTA, F. JIMENEZ, A. I. JIMENEZ and J. J. ARIAS*

Departamento de Química Analítica, Bromatología y Toxicología, Facultad de Química, Universidad de La Laguna, E-38204 La Laguna, Tenerife, Spain

Summary—The performance of several graphical (zero-crossing and derivative quotient spectra with standardized divisor) and numerical methods (MULTIC and PLS) for the resolution of binary and ternary mixtures of species is compared. Numerical methods were found to be specially suited to multicomponent analysis, particularly for mixtures containing more than two analytes with highly overlapped spectra. The results obtained by using the compared methods to analyse various synthetic mixtures of acetylsalicylic acid, caffeine and thiamine were quite consistent and errors in the simultaneous quantification of the analytes amounted to less than 5% in all instances.

Resolving complex multicomponent systems with no prior separation of the constituent analytes is rather a difficult task. As a rule, the problem is worsened when two or more of the analytes involved interact with one another, as is often the case with biochemical and clinical samples. In the last few years, development of methods for the resolution of such systems has grown dramatically, probably as a result of the increasing affordability of powerful instrumentation and the availability of robust numerical methods.

Thus, the inception of derivative spectrophotometric techniques has brought about significant gains in spectral resolving power: changes in ordinary absorbance spectra can be detected more readily, which allows many complex mixtures to be assessed both qualitatively and quantitatively. The zero-crossing method, developed by O'Haver,[1] and that of derivative quotient spectra, designed by Salinas *et al.*,[2] are the most frequently used for this purpose.[3–6] In recent work we developed a modified version of the latter.[7]

On the other hand, the inception of computers in the analytical laboratory has fostered the development of a large number of mathematical treatments (*e.g.* Simplex, Multiple Linear Regression, Principal Component Regression, Partial Least Squares)[8] which facilitate the analysis of mixtures yielding highly overlapped peaks. By using a multiple linear regression procedure, these methods determine the concentration that best fits an over-dimensioned equation system that is, in turn, established by measuring the absorbance of a given sample at a larger number of wavelengths than that of analytes to be determined.

In this work we compare the performance of various graphical and numerical methods in the resolution of several binary and one ternary mixture of caffeine, thiamine and acetylsalicylic acid. All three are of pharmacological interest and had previously been determined individually,[9] but never in mixtures.

THEORY

Zero-crossing method

The method is based on the measurement of the absolute value of the derivative spectrum of the mixture at an abscissa value (wavelength) where the intensity of one of the components of the mixture goes to zero. At this wavelength the intensity is directly proportional to the other component.

Derivative quotient spectra method

The quotient spectrum method was originally developed by Blanco *et al.*[10] and subsequently modified by Salinas *et al.*,[11] who calculated the derivative of the spectrum obtained by dividing the Beer law expression as applied to a binary mixture into a standard spectrum recorded for

*Author for correspondence.

a solution containing a known amount of either component. Thus,

$$\frac{\mathrm{d}}{\mathrm{d}\lambda}\left(\frac{A_{\mathrm{M},\lambda_i}}{\epsilon_{\mathrm{A},\lambda_i}C_{\mathrm{A}}^0}\right)=\frac{C_{\mathrm{B}}}{C_{\mathrm{A}}^0}\frac{\mathrm{d}}{\mathrm{d}\lambda}\left(\frac{\epsilon_{\mathrm{B},\lambda_i}}{\epsilon_{\mathrm{A},\lambda_i}}\right), \quad (1)$$

where A_{M} is the absorbance of the mixture at wavelength λ_i and C_{A}^0 is the concentration of A in the dividing spectrum. From the above equation, it follows that the quotient spectrum of a mixture depends solely on C_{B} and C_{A}^0, so the former concentration can readily be calculated similarly; dividing equation (1) into C_{B}^0 provides an analogous expression for calculating C_{A}.

The chief shortcoming of this method lies in the need to empirically determine which standard spectrum is to be used as divisor. However, by dividing into an αC_{A}^0 spectrum (α = constant), one obtains

$$\frac{1}{\alpha}\frac{\mathrm{d}}{\mathrm{d}\lambda}\left(\frac{A_{\mathrm{M},\lambda_i}}{\epsilon_{\mathrm{A},\lambda_i}C_{\mathrm{A}}^0}\right)=\frac{1}{\alpha}\frac{C_{\mathrm{B}}}{C_{\mathrm{A}}^0}\frac{\mathrm{d}}{\mathrm{d}\lambda}\left(\frac{\epsilon_{\mathrm{B},\lambda_i}}{\epsilon_{\mathrm{A},\lambda_i}}\right), \quad (2)$$

which coincides with the expression obtained by multiplying equation (1) by $1/\alpha$, *i.e.* decreasing the concentration at which the dividing spectrum is recorded has the same effect as diminishing α (namely increasing the signal). Therefore, calibration curves obtained at higher analyte concentrations have greater slopes, even though they do not provide increased sensitivity since background noise also rises concomitantly.

The goodness of the results obtained in resolving the mixtures is thus dependent on the experimental or instrumental errors made in recording the standard spectra, and is independent of the divisor concentration in any case. Thus, in order to minimize errors and expedite the process, we chose to use the normalized spectrum of each substance as divisor.[7] This variant of the derivative quotient spectrum method was thus applied to the resolution of the binary mixtures addressed in this work.

Use of the programme MULTIC for resolving binary and ternary mixtures

Application of MULTIC relies on the assumption that the analytes obey Beer's law and their absorbances are additive, and involves solving the matrix constructed from a mixture of N components at j wavelengths by using the expression

$$A_j=\sum_{i=1}^{i=N}\epsilon_{ij}bc_i+k_0,$$

where k_0 is the independent term corresponding to the experimental error, A_j and ϵ_{ij} denote the absorbances of the mixture components and their molar absorptivities at various wavelengths within the working range, and c_i is the concentration of each species.

ϵ_{ij} values can be obtained from standard solutions of the pure components (i), which are related to one another by the ($i \times j$) matrix. The equation thus formed is resolved by using a multiple regression procedure.

Use of the programme PLS for resolving binary and ternary mixtures

The PLS method[12,13] breaks down the absorbance matrix A obtained from absorbance measurements on N_s solutions at the selected wavelengths and the concentration matrix C constructed from the corresponding caffeine, thiamine and acetylsalicylic acid concentrations into two latent variable matrices:

$$A=F_{\mathrm{A}}L_{\mathrm{A}}+E_{\mathrm{A}},$$

$$C=F_{\mathrm{C}}L_{\mathrm{C}}+E_{\mathrm{C}},$$

where F_{C} and F_{A} are the latent concentration and absorbance matrices, L_{C} and L_{A} are the concentration and absorbance loading matrices, and E_{A} and E_{C} are the error matrices.

The latent variable matrices can be related by a diagonal regression matrix V such that

$$F_{\mathrm{C}}=F_{\mathrm{A}}V+E_{\mathrm{D}},$$

where E_{D} is an error matrix. Matrix V is used to estimate the concentrations from the absorbance spectrum a_0 for an unknown mixture by using the equation

$$C_0=a_0(F_{\mathrm{C}}^{\mathrm{T}}A)^{\mathrm{T}}VL_{\mathrm{C}},$$

where matrices F_{C}, L_{C} and A can be obtained by calibration.

EXPERIMENTAL

Apparatus

We used a Hewlett–Packard HP8452A diode array spectrophotometer furnished with quartz cuvettes of 1 cm light path and interfaced to a Vectra ES computer and a Think Jet printer, also from Hewlett–Packard.

Absorption and derivative spectra were acquired and processed with the aid of the spectrophotometer's bundled software.

A Radiometer PHM84 digital pH-meter furnished with a dual glass-saturated calomel electrode was used for pH measurements.

Reagents

Standard solutions containing 100 μg/ml of either acetylsalicylic acid, caffeine or thiamine were prepared by direct weighing of the required amount of commercially available chemical (Sigma) and dissolution in bidistilled water. An acetic acid–sodium acetate buffer (pH 5) and $C_t = 1.0M$ was also utilized. All reagents and solvents used were of analytical grade, and bidistilled water obtained from a quartz still was employed throughout.

Software

Multicomponent analysis was carried out by using the programme MULTIC[14] and a PLS version[15] for IBM PC XT/AT computers.

Procedure

Binary and ternary mixtures were prepared in triplicate by placing in a 25-ml volumetric flask 5 ml of HAcO–NaAcO buffer (pH 5.0), a volume containing 3.2–36.4 μg/ml of acetylsalicylic acid and another containing between 1.6 and 16 μg/ml of caffeine and/or thiamine, and the volume of ethanol required to obtain a 20% content in the alcohol after making to the mark with bidistilled water.

The spectra of the above mixtures were recorded between 190 and 350 nm against a blank prepared under the same conditions but containing none of the analytes. The integration time was set to 1 sec in all experiments.

Binary mixtures. (A) *Zero-crossing method.*

(1) Caffeine–thiamine mixtures were analysed by recording their first-derivative spectra and measuring signals at 266 and 286 nm for caffeine and thiamine, respectively. Finally, the contribution from caffeine was subtracted from the latter signal.

(2) Acetylsalicylic acid–thiamine mixtures were quantified by recording their first- and second-derivative spectra and determining the thiamine concentration by measuring the signal at 296 nm in the latter. On the other hand, the signal at 282 nm in the first-derivative spectra was used to determine acetylsalicylic acid by subtracting the signal from thiamine at such a wavelength.

(3) Acetylsalicylic acid–caffeine mixtures were analysed by recording their first-derivative spectra and measuring the signals at 266 and 236 nm for caffeine and acetylsalicylic acid, respectively. The contribution from caffeine was subtracted from the latter signal.

(B) *Quotient spectrum method (normalized divisor).* The spectra yielded by the mixtures were divided into the normalized spectrum of each component and the resulting spectrum was derived in order to determine the component that was not used as divisor. Thus:

(1) In caffeine–thiamine mixtures, caffeine was determined from the derivative of the quotient spectrum (using the thiamine spectrum as divisor) by measuring the signal at 266 nm, while thiamine was quantified from the derivative of the quotient spectrum (using the caffeine spectrum as divisor) at 250 nm.

(2) Acetylsalicylic acid–thiamine mixtures were analysed by measuring the signals at 230 and 292 nm on the derivatives of the quotient spectrum of the mixture using thiamine and acetylsalicylic acid, respectively, as divisor.

(3) Acetylsalicylic acid–caffeine mixtures were quantified by measuring the signals at 248 and 290 nm on the derivatives, respectively, of the quotient spectra.

In both methods, zero-crossing and derivative quotient spectra, the two components were finally quantified by comparing the measured signal with the corresponding calibration curves run.

RESULTS AND DISCUSSION

The simultaneous determination of acetylsalicylic acid, caffeine and thiamine in binary and ternary mixtures was tackled by first checking the temporal pH stability of the products.

The absorbance of caffeine and thiamine solutions over the wavelength range 230–350 nm did not change appreciably during the first 48 hr after they were made. On the other hand, the absorbance of acetylsalicylic acid solutions was somewhat different after only 12 hr, probably as a result of hydrolysis into salicylic and acetic acids, as supported by the presence in the recorded spectrum of the characteristic peak of the former at 296 nm.

The pH was found to scarcely influence the stability of caffeine solutions over the range 1–12. On the other hand, thiamine and acetylsalicylic acid provided the greatest signals at pH 5 (HOAc–NaOAc buffer), which was thus chosen as the optimum. In order to prevent the hydrolysis of the products, all the subsequent experiments were made using fresh solutions.

Figure 1 shows the individual spectra of the three analytes, as well as their first and second derivatives, obtained in a 1:4 ethanol–water

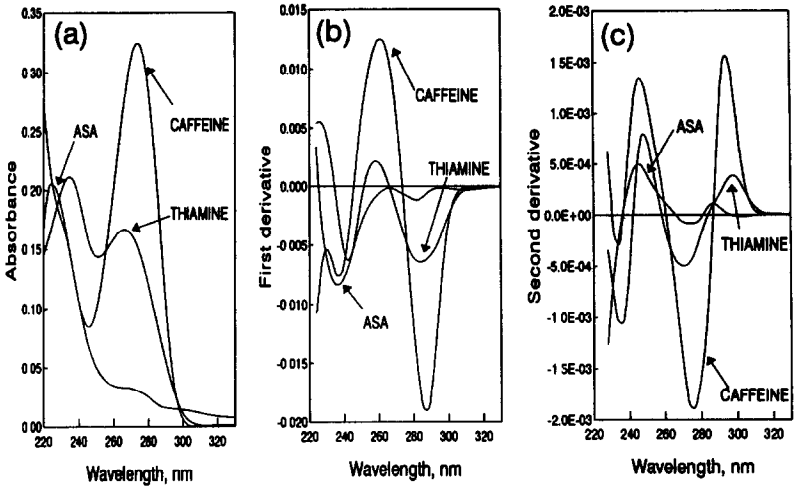

Fig. 1. Absortion (a), first- (b) and second-derivative (c) spectra of acetylsalicylic acid (6.5 μg/ml), caffeine (6.5 μg/ml) and thiamine (6.5 μg/ml) at pH 5.0.

medium at pH 5. As can be seen, the spectra were strongly overlapped.

Graphical methods

Zero-crossing method. Figure 2a shows the first-derivative spectra for caffeine–thiamine mixtures containing a fixed amount of the former and variable concentrations of the latter. As can be seen, the signal at 266 nm does not depend on the thiamine concentration.

Figure 2b shows the second-derivative spectra of the acetylsalicylic acid–thiamine mixtures obtained at a constant concentration of thiamine and various concentrations of acetylsalicylic acid. As can be seen, the signal at 296 nm depends on the concentration of thiamine alone.

Figure 2c shows the first-derivative spectra of acetylsalicylic acid–caffeine mixtures containing the same amount of the latter and a variable amount of the former. Note that the signal at 266 nm depends only on the caffeine concentration.

Table 1 shows the results obtained by analysing various synthetic mixtures using the zero-crossing method. Errors were less than 5% in all cases, even for analyte ratios of up to 10:1.

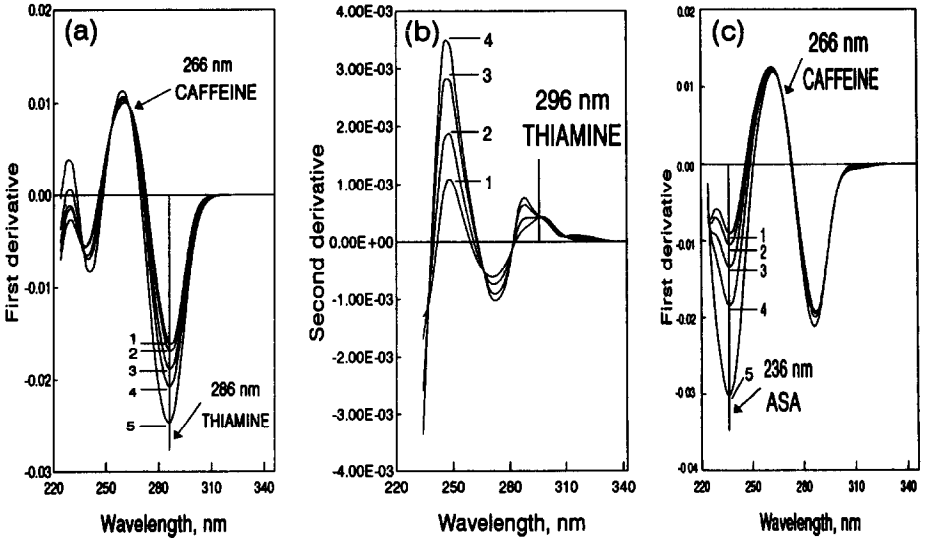

Fig. 2. (a) First-derivative spectra of $C_{Caf} = 5$ μg/ml = cte, $C_{Th} = 2$ μg/ml (1); 4 μg/ml (2); 6 μg/ml (3); 8 μg/ml (4); 10 μg/ml (5). (b) Second-derivative spectra, $C_{Thi} = 5$ μg/ml = cte, $C_{ASA} = 6.5$μg/ml (1); 13 μg/ml (2); 19.5 μg/ml (3); 26 μg/ml (4). (c) First-derivative spectra, $C_{Caf} = 5$ μg/ml = cte, $C_{ASA} = 3.2$ μg/ml (1); 6.5 μg/ml (2); 13 μg/ml (3); 19.5 μg/ml (4); 26 μg/ml (5).

Table 1. Results obtained for different binary mixtures of two components by use of the zero-crossing method*

Amount added (μg/ml)		Amount found (μg/ml)		Relative error (%)	
CAF	THIA	CAF	THIA	CAF	THIA
1.648	1.616	1.635	1.646	−0.79	+1.85
1.648	8.080	1.587	8.227	−3.70	+1.82
9.888	9.696	9.832	9.969	−0.52	+2.82
13.184	7.488	13.512	7.237	+0.24	−3.47
16.480	16.160	16.030	16.030	−2.73	−1.66
ASA	CAF	ASA	CAF	ASA	CAF
3.288	16.480	3.195	17.090	−2.83	+3.57
3.483	6.976	3.540	7.158	−3.81	+2.60
6.966	10.464	6.881	10.636	−1.23	+1.62
13.932	1.744	13.976	1.662	+0.31	−4.93
34.830	3.488	34.286	3.375	−1.59	−3.35
ASA	THIA	ASA	THIA	ASA	THIA
3.633	5.616	3.698	5.549	+1.79	−1.20
10.899	1.872	10.545	1.849	−3.36	−1.74
14.532	1.872	14.339	1.924	−1.35	+2.70
19.728	4.848	19.965	4.638	+1.19	−4.63
36.330	7.488	36.040	7.743	−0.80	+3.29

*CAF, caffeine; THIA, thiamine; ASA, acetylsalicylic acid.

Derivative quotient spectra method. Figure 3a shows the derivative quotient spectra of thiamine obtained by dividing its absorbance spectrum into the standardized spectrum of caffeine and obtaining the first derivative of the resulting spectrum. The best wavelength for determining the concentration was 250 nm; in fact, other regions provided greater signals, but the noise arising from dividing the spectrum into the very small absorbances of the caffeine spectrum caused serious interference.

Figures 3b and c illustrate the determination of acetylsalicylic acid at 230 nm and of caffeine at 290 nm in mixtures with thiamine in both cases. Table 2 shows the results obtained by analysing various synthetic binary mixtures using this method. In any case, errors were less than 5% in all cases, even for analyte ratios of up to 10:1. Statistical analysis of the regression equations is reported in Table 3.

Numerical methods

Use of the programme MULTIC for resolving binary and ternary mixtures. In view of the results obtained and bearing in mind that, with few exceptions,[11] derivative methods cannot be applied to mixtures of more than two components, we addressed the resolution of the above-mentioned binary mixtures and that

Table 2. Results obtained for different binary mixtures of two components by use of the derivative quotient spectra (normalized divisor)*

Amount added (μg/ml)		Amount found (μg/ml)		Relative error (%)	
CAF	THIA	CAF	THIA	CAF	CAF
1.648	1.616	1.626	1.642	−1.35	+1.58
1.648	8.080	1.603	8.037	−2.81	−0.53
9.888	9.696	9.779	9.962	−1.11	+2.74
13.184	7.488	13.410	7.246	+1.68	−3.34
16.480	16.160	16.069	16.050	−2.56	−0.68
ASA	CAF	ASA	CAF	ASA	CAF
3.288	16.480	3.273	17.170	−0.46	+4.02
3.483	6.976	3.359	7.158	−3.69	+2.61
6.966	10.464	6.936	10.718	−0.43	+2.37
13.932	1.744	13.414	1.687	−3.86	−3.38
34.830	3.488	33.932	3.625	−2.58	+3.93
ASA	THIA	ASA	THIA	ASA	THIA
3.633	5.616	3.698	5.402	+1.76	−3.96
7.266	3.744	7.283	3.615	+0.23	−3.57
10.899	1.872	10.893	1.858	−0.05	−0.75
14.532	1.872	14.256	1.859	−1.90	−0.69
19.728	4.848	20.263	4.849	+2.71	+0.02

*Abbreviations as in Table 1.

Table 3. Statistical analysis of the determination of caffeine, thiamine and acetylsalicylic acid in mixtures by derivative spectrophotometry

Analyte	Wavelength (nm)	Regression equation*	Correlation coefficient	Variance (s^2)	Detection limit (μg/ml)
ZERO-CROSSING METHOD					
Caffeine	266	$D_1 = 5.878E\text{-}5 + 1.593E\text{-}3c$	0.9999	1.369E-8	0.089
Thiamine	286	$D_1 = 1.209E\text{-}5 + 9.860E\text{-}4c$	0.9988	2.710E-7	0.647
Thiamine	296	$D_2 = 4.689E\text{-}8 + 5.730E\text{-}5c$	0.9999	2.756E-11	0.112
ASA†	282	$D_1 = 8.610E\text{-}5 + 1.675E\text{-}4c$	0.9990	2.335E-8	1.224
ASA	236	$D_1 = 3.194E\text{-}4 + 1.246E\text{-}3c$	0.9996	4.918E-7	0.755
DERIVATIVE QUOTIENT SPECTRA METHOD					
Thiamine	250	$D_1 = -2.169E\text{-}3 + 1.020E\text{-}1c$	0.9991	2.236E-3	0.567
Thiamine	292	$D_1 = -1.989E\text{-}2 + 3.800E\text{-}1c$	0.9993	2.156E-2	0.473
Caffeine	266	$D_1 = 2.260E\text{-}3 + 6.240E\text{-}2c$	0.9999	2.362E-5	0.095
Caffeine	290	$D_1 = 4.948E\text{-}2 + 1.091c$	0.9999	8.463E-3	0.103
ASA	230	$D_1 = 4.968E\text{-}2 + 4.524E\text{-}2c$	0.9952	8.252E-3	2.694
ASA	248	$D_1 = 3.348E\text{-}2 + 6.019E\text{-}2c$	0.9998	4.600E-4	0.478

*Where c is the concentration of the analyte (μg/ml); number of standard solutions, $n = 8$.
†Abbreviation as in Table 1.

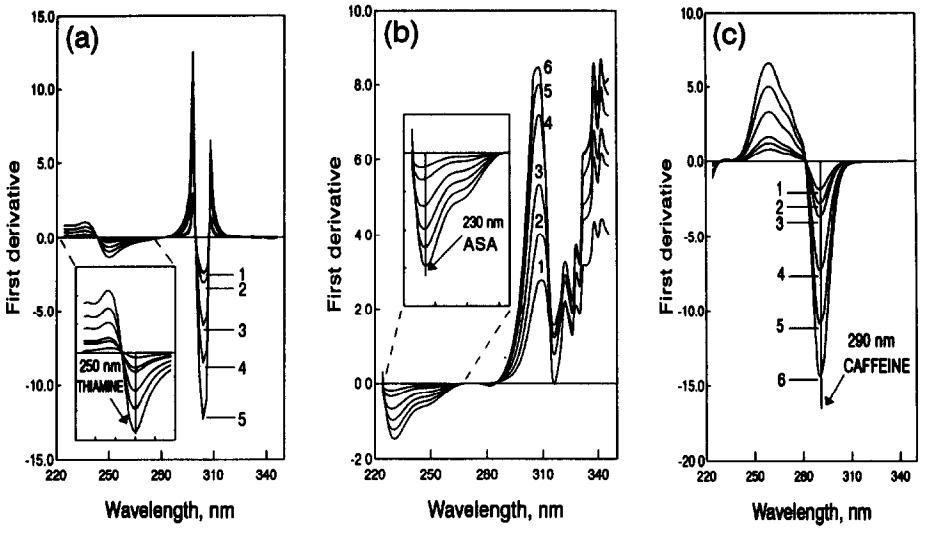

Fig. 3. First-derivative of quotient spectra when divisor was normalized. (a) Thiamine: (1) 1.6 μg/ml; (2) 3.2 μg/ml; (3) 5 μg/ml; (4) 9.7 μg/ml; (5) 13 μg/ml; (6) 16.1 μg/ml caffeine divisor. (b) Acetylsalicylic acid: (1) 1.6 μg/ml; (2) 3.2 μg/ml; (3) 6.5 μg/ml; (4) 19.5 μg/ml; (5) 26 μg/ml; (6) 32.5 μg/ml thiamine divisor. (c) Caffeine: (1) 1.6 μg/ml; (2) 3.2 μg/ml; (3) 5 μg/ml; (4) 9.7 μg/ml; (5) 13.2 μg/ml; (6) 16.5 μg/ml acetylsalicylic acid divisor.

of the three components jointly by using the programmes MULTIC and PLS.

We chose the wavelength ranges 228–350, 230–296, 236–330 and 246–296 nm as optimal for the resolution of the caffeine–thiamine, acetylsalicylic acid–caffeine, acetylsalicylic acid–thiamine and acetylsalicylic acid–caffeine–thiamine mixtures, respectively. The results obtained are listed in Table 4.

Use of the programme PLS for resolving binary and ternary mixtures. The experimental results were processed by using the PLS calibration method. The calibration matrix was designed at two factor levels. We thus used five and nine solutions, respectively, in addition to a central point, in order to design the model for the binary and ternary mixtures.

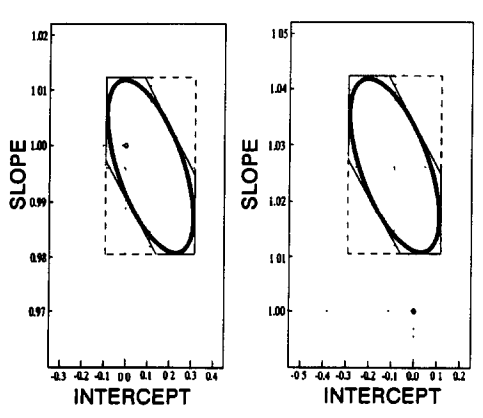

Fig. 4. Illustrative joint confidence region at the $p = 0.05$ level of significance for slope and intercept. Determination of one analyte in a binary mixture with good accuracy and with systematic error.

The lowest and highest concentrations used were 3.20 and 38.0 μg/ml for acetylsalicylic acid, 1.8 and 18 μg/ml for caffeine, and 1.6 and 18 μg/ml for thiamine, respectively.

The results obtained by analysing the different synthetic binary mixtures and the ternary one using the two above-described methods are summarized in Tables 4 and 5. As can be seen, added and found concentrations were quite consistent. However, the PLS method resulted in slightly larger errors with the binary mixtures. On the other hand, it provided better results for the ternary mixture and for binary mixtures with high analyte ratios than did the MULTIC method.

The determination of these three analytes in pharmaceutical preparations is currently under way at our laboratory.

ACCURACY AND PRECISION

The values obtained have been compared with the added value in each sample to quantitatively evaluate the accuracy. When the test on the joint confidence region for slope and intercept, given by Mandel and Lining,[16] is applied to all the binary samples solved by the four methods (24 possibilities), a systematic error appears only for a level of $\alpha = 0.05$ ($F = 9.55$) in the following cases: caffeine in the presence of acetylsalicylic acid determined by

Table 4. Simultaneous determination of the components of binary and ternary mixtures of caffeine, thiamine and acetylsalicylic acid by MULTIC*

Amount added (μg/ml)		Amount found (μg/ml)		Relative error (%)		
CAF	THIA	CAF	THIA	CAF	THIA	$s \times 10^3$†
1.648	1.616	1.645	1.637	−0.18	+1.30	0.121
9.888	9.696	9.817	9.931	−0.72	+2.42	1.406
1.648	8.080	1.624	8.150	−1.46	+0.87	0.657
13.184	7.488	13.184	6.975	0.00	−6.85	3.015
16.48	16.16	15.96	16.37	−3.16	−1.30	2.548
ASA	CAF	ASA	CAF	ASA	CAF	$s \times 10^3$†
3.483	5.232	3.575	5.366	+2.64	+2.56	0.181
3.288	16.488	3.376	17.17	+2.68	+4.14	3.270
3.483	17.440	3.702	17.77	+6.29	+1.89	2.063
10.449	1.744	10.07	1.790	−3.63	+2.64	1.169
20.898	10.464	20.13	10.70	−3.67	+2.26	1.889
ASA	THIA	ASA	THIA	ASA	THIA	$s \times 10^3$†
3.633	5.616	3.613	5.740	−0.55	+2.21	1.889
7.266	3.744	7.189	3.766	−1.06	+0.59	0.9
7.266	11.232	7.278	11.66	+0.17	+3.81	2.817
25.431	9.360	24.39	9.432	−4.09	+0.77	1.885
36.33	7.488	35.16	7.561	−3.22	+0.97	1.365
ASA	CAF	THIA	ASA	CAF	THIA	ASA	CAF	THIA	$s \times 10^5$†
3.294	1.840	1.696	3.149	1.816	1.672	−4.40	−1.30	−1.42	6.056
6.588	1.840	1.696	6.455	1.829	1.803	−2.02	−0.60	+6.31	7.654
9.882	1.840	1.696	9.625	1.813	1.764	−2.60	−1.47	+4.01	6.451
9.882	3.680	3.392	9.467	3.574	3.603	−4.20	−2.88	+6.22	14.95
13.176	3.680	3.392	12.78	3.596	3.596	−3.01	−2.28	+6.01	1.657

*Abbreviations as in Table 1.

†s = standard deviation of the fit.

Table 5. Results obtained for different binary and ternary mixtures of acetylsalicylic acid, caffeine and thiamine by use of PLS*

Amount added (μg/ml)		Amount found (μg/ml)		Relative error (%)	
CAF	THIA	CAF	THIA	CAF	THIA
1.648	1.616	1.567	1.658	−4.91	+2.60
1.648	8.080	1.583	8.233	−3.94	+1.89
9.888	9.696	9.830	10.130	−0.59	+4.47
13.184	7.488	13.306	7.398	+0.92	−1.20
16.480	16.160	16.170	16.308	−1.88	+0.91
ASA	CAF	ASA	CAF	ASA	CAF
3.288	16.480	3.380	16.694	+2.80	+1.30
3.483	6.976	3.527	7.099	+1.26	+1.76
6.966	10.464	7.017	10.436	+0.73	−0.27
13.932	1.744	13.507	1.805	−3.05	+3.50
34.830	3.488	35.067	3.435	+0.68	−1.52
ASA	THIA	ASA	THIA	ASA	THIA
3.633	5.616	3.764	5.598	+3.60	−0.32
10.899	1.872	11.341	1.812	+4.05	−3.20
14.532	1.872	14.950	1.801	+2.88	−3.79
19.728	4.848	20.720	4.679	+5.03	−3.49
36.330	7.488	36.526	7.555	+0.65	+0.89
ASA	CAF	THIA	ASA	CAF	THIA	ASA	CAF	THIA
3.294	1.840	1.696	3.272	1.807	1.620	−0.67	−1.79	−4.48
9.882	1.840	1.696	9.871	1.836	1.637	−0.11	−0.22	−3.47
13.176	3.680	3.392	13.182	3.702	3.431	+0.46	+0.60	+1.15
16.470	3.680	3.392	16.466	3.680	3.410	−0.02	0.00	+0.53
16.470	9.200	8.480	16.587	9.152	8.530	+0.71	−2.24	+0.59

*Abbreviations as in Table 1.

Abstract components 3 and 5 for binary and ternary mixtures, respectively; number of wavelengths = 26 in all cases; calibration solutions 5 and 9 for binary and ternary mixtures, respectively.

the zero-crossing method and the quotient spectra, acetylsalicylic acid with caffeine by quotient spectra and MULTIC, and acetylsalicylic acid with thiamine by MULTIC.

The other 19 possibilities of comparison between added amounts and the values found give good results because the point of slope one and the zero intersection are inside the joint confidence region (Fig. 4). The ternary mixture is solved by PLS without systematic errors.

We have also applied a one-way ANOVA test with six replies during 3 days, and for all the cases an F-Snedecor value lower than the tabulated value is obtained ($F = 3.68$; $n_1 = 2$, $n_2 = 15$) for all the proposed models.

When we applied Bartlett's test for the four methods and the three binary mixtures, we found values for the M[8] parameter between 0.02 and 4.11, always lower than the tabulated value ($\chi^2_3 = 7.81$).

CONCLUSIONS

Both graphical and numerical methods were found to provide good results in the resolution of various synthetic binary and ternary mixtures of acetylsalicylic acid, caffeine and thiamine, whose spectra are strongly overlapped.

From the results obtained we can conclude that all the methods are precise although the graphical and MULTIC present systematic errors in some cases. The PLS is the method which offers better results relative to the accuracy and precision due to the elimination of the errors produced when the matrix effect is taken into consideration in the calibration.

On the other hand, the MULTIC bases the calibration on the standard spectra of the pure analytes without considering the possible interaction between them.

The numerical methods are much more expeditious and can be applied to a larger number of analytes in the same sample, although they need a specific software. On the other hand, graphical methods are much easier to implement and have a lower cost.

Acknowledgement—The authors wish to acknowledge the financial support of this work by the Canary Autonomic Government, grant no. 13/31.07.89.

REFERENCES

1. T. C. O'Haver, *Anal. Chem.*, 1979, **51**, 91A.
2. F. Salinas, J. J. Berzas and A. Espinosa, *Talanta*, 1990, **37**, 347.
3. F. A. El-Yazbi, M. A. Korany, O. Abdel-Razak and M. A. Elsayed, *J. Assoc. Off. Anal. Chem.*, 1986, **69**, 614.
4. F. García, J. C. Márquez and M. Hernández, *Analyst*, 1987, **112**, 649.
5. J. J. Berzas, J. Rodríguez and M. L. de la Morena, *Talanta*, 1991, **38**, 1261.
6. J. Soriano, F. Jiménez, A. I. Jiménez and J. J. Arias, *Spectrosc. Lett.*, 1992, **25**, 257.
7. J. M. García, A. I. Jiménez, F. Jiménez and J. J. Arias, *1st Spanish Congress on Analytical Spectrophotometry* (S.E.Q.A.), Costa Brava, Spain, 13–15 May, 1992.
8. D. L. Massart *et al.* (Eds), *Chemometrics: A Textbook*. Elsevier, Amsterdam, 1988.
9. M. S. Karawya, A. M. Diab and N. Z. Swelem, *Anal. Lett.*, 1984, **17**, 77.
10. M. Blanco, J. Gene, H. Iturriaga, S. Maspoch and J. Riba, *Talanta*, 1987, **34**, 987.
11. J. J. Berzas, C. Guibertean and F. Salinas, *Talanta*, 1992, **39**, 547.
12. M. Otto and W. Wegscheider, *Anal. Chem.*, 1985, **57**, 63.
13. A. Lorber, L. E. Wagen and B. R. Kowalski, *J. Chemometrics*, 1987, **1**, 19.
14. G. Sala, S. Maspoch, H. Iturriaga, M. Blanco and V. Cerda, *J. Pharm. Biomed. Anal.*, 1988, **6**, 765.
15. J. Havel, in *Proc. Chemometrics II, 2nd Czech. Chemometrics Conf.*, J. Havel and M. Holík (Ed.), Brno, Czech Republic, 3–6 Sept. 1990.
16. J. Mandel and F. J. Lining, *Anal. Chem.*, 1957, **29**, 743.

Talanta, Vol. 40, No. 11, pp. 1695–1701, 1993
Printed in Great Britain.

0039-9140/93 $6.00 + 0.00

SIMULTANEOUS DETERMINATION OF CARBARYL AND *o*-PHENYLPHENOL RESIDUES IN WATERS BY FIRST-DERIVATIVE SYNCHRONOUS SOLID-PHASE SPECTROFLUORIMETRY

LUIS FERMIN CAPITÁN-VALLVEY, JAMAL ROHAND, ALBERTO NAVALÓN, RAMIRO AVIDAD and JOSÉ LUIS VILCHEZ

Department of Analytical Chemistry, University of Granada, E-18071 Granada, Spain

Summary—A spectrofluorimetric method for the simultaneous determination of carbaryl (CBL) and *o*-phenylphenol (OPP) residue mixtures in waters has been developed. Carbaryl was hydrolysed in alkaline medium to give 1-naphthol. This compound and *o*-phenylphenol were fixed on QAE Sephadex A-25 gel at pH 10.75. The fluorescence of the gel, packed in a 1-mm silica cell, was measured directly with a solid-surface attachment. Overlapping of conventional fluorescence spectra is resolved by using first-derivative synchronous spectrofluorimetry and allows for the complete resolution of the mixture. The range of application is between 0.4 and 25.0 ng/ml for OPP and 0.8 and 25.0 ng/ml for CBL. The detection limits for *o*-phenylphenol and carbaryl were 0.1 and 0.2 ng/ml, respectively. The accuracy and precision of the method are reported. The method is suitable for determination of carbaryl and *o*-phenylphenol residues in natural waters. Recoveries from 95 to 105% have been obtained for natural waters spiked with CBL and OPP.

(1-Naphthyl-*N*-methylcarbamate) and (1-1-biphenyl)-2-ol commonly named carbaryl (CBL) and *o*-phenylphenol (OPP), are two powerful pesticides used today as the active ingredients of several commercial formulations. OPP is a disinfectant and fungicide used in post-harvest applications.[1] CBL is an insecticide, used to control pests on more than 100 different crops, with a relatively short half-life, the final product by alkaline hydrolysis being 1-naphthol. CBL and 1-naphthol may cause toxic effect[2–4] and therefore determination of CBL (or 1-naphthol) and OPP residues in natural waters is clearly important.

OPP and CBL show native fluorescence enabling its determination in soils, waters, crops and commercial formulations.[5–9] On the other hand fluorimetric detection has been used in TLC[10–11] and HPLC.[12–18]

However, methods for determination of CBL or OPP, separately, in waters are frequent[19–21] and we are not aware of any methods so far for the simultaneous determination of the two compounds mixed without previous separation.

As fluorescent spectra of OPP and CBL overlap considerably, conventional fluorimetric methods do not allow simultaneous determination of these compounds. However, we have found[22–26] that synchronous spectrofluorimetry in combination with derivative techniques minimize overlapping effects and can be used for the analysis of mixtures involved in clinical and pharmacological preparations.

Solid-phase spectrofluorimetry (SPF) is a technique that combines preconcentration on a solid-phase, *e.g.*, an ion exchange and direct measurement of fluorescence.[27–34]. Use of conventional instrumentation, simplicity, high selectivity and low detection limits, are some of the advantages associated to SPF.

Here we propose a simple and sensitive method for simultaneous determination of OPP and CBL in waters by the use of SPF combined with derivative techniques. The method can be used at low concentrations of the mixtures without previous separation of the components.

EXPERIMENTAL

Apparatus

All the spectrofluorimetric measurements were conducted with a Perkin-Elmer LS 5 luminescence spectrometer as described earlier.[32] A STARNA standard rectangular silica cell (type 1,Q,1,6) with 1-mm path length and external dimensions 12.5 × 3.5 × 46.0 mm, was used.

The LS 5 spectrometer was interfaced to an IBM PS/2 30-286 microcomputer using RS 232C connections for spectral acquisition

and subsequent calculation of the excitation-emission matrices and of the derivative spectra.[35] Smoothed and derivative spectra were calculated by the Savitzky and Golay method[36,37] and contour plots in the excitation-emission plane were produced linking points of equal fluorescence intensity. A Cannon BJ-300 printer was used for graphical representations.

Further, we used a Braun Melsungen Thermomix 1441 thermostatic water-bath circulator for temperature control, a Crison 501 digital pH-meter with a combined glass-saturated calomel electrode and an Agitaser 2000 rotating bottles agitator.

Reagents

All reagents were of analytical-reagent grade unless stated otherwise. Reverse osmosis quality water was used throughout.

CBL stock solution (0.1 mg/ml) (Riedel-de Haën). Prepared by exact weighing and dissolution in absolute ethanol. This solution is stable for at least two weeks. Working solutions were prepared by appropriate dilutions with water maintaining a 1% (v/v) of ethanol.

1-Naphthol stock solution (0.1 mg/ml) (Merck). Prepared in the same way as described above for CBL stock solution.

OPP stock solution (0.1 mg/ml) (Laboratory Dr Ehrenstorfer). Prepared by exact weighing and dissolution in absolute ethanol. This solution is stable for at least one month. Solutions of lower concentration were obtained by dilution with water maintaining a 1% (v/v) of ethanol.

QAE Sephadex A-25 dextran type anion-exchange gel (Sigma). Used in the chloride form and without pre-treatment in order to avoid contamination.

Fluorescence measurements

The measured relative fluorescence intensity (RFI) of the gel beads containing the fluorescent analytes fixed and packed in a 1-mm silica cell, was the diffuse transmitted fluorescence emitted from the gel at the unirradiated face of the cell. The optimum angle formed between the cell plane and the excitation beam was 45° in all instances.[38]

Procedures

Basic procedure. A 500-ml water sample containing between 0.2 and 12.5 μg of OPP and between 0.4 and 12.5 μg of CBL was transferred into a one-litre glass bottle and 5 ml of 0.1*M* NaOH solution and 100 mg of QAE Sephadex A-25 gel were added. The mixture was shaken mechanically for 10 min. Afterwards, the gel beads were collected by filtration under suction and packed in a 1-mm silica cell together with a small volume (around 0.2 ml) of the filtrate with the aid of a pipette. A blank solution containing all the reagents except both OPP and CBL was prepared and treated in the same way as described for the sample.

The synchronous spectra were recorded (at $20.0 \pm 0.5°$) with the following fixed instrumental parameters: $\Delta\lambda = \lambda_{em} - \lambda_{ex} = 105$ nm, scan speed 240 nm/min, and spectrometer response time of 1 sec. The spectra were then stored on a disk file, corrected for the blank signal and the first derivative spectra were calculated using 25-nm intervals for this purpose.

Measurements on the first-derivative synchronous spectrum were made for OPP from the point located at $\lambda_{ex}/\lambda_{em} = 338/443$ to the baseline while for CBL the point chosen was located at $\lambda_{ex}/\lambda_{em} = 318/423$.

Calibration graphs were constructed in the same way with OPP and CBL solutions of known concentrations.

Procedure for natural waters. A volume of natural water sample containing an adequate amount of CBL and OPP was levelled off to 500-ml with water, placed in a one-litre glass bottle and additions of 5 ml of 0.1*M* NaOH solution, an amount of EDTA necessary to eliminate the interferences from metallic ions and 100 mg of QAE Sephadex A-25 gel. The mixture was shaken mechanically for 10 min and then treated as described under *Basic procedure*. The standard additions method was used for calibration.

Treatment of the sample. Natural waters were filtered through a filter-paper with a 0.45-μm size pore (Millipore) and collected in a glass container that had been cleaned carefully with nitric acid. The samples were stored at 4° until analysis and the usual precautions were taken to avoid contamination.[39] Analyses were performed with the least possible delay.

Distribution measurements. A 500-ml water sample containing 3.5 μg of pesticide was transferred into a one-litre glass bottle. Then the required amounts of QAE Sephadex A-25 gel and NaOH solution were added. Next, the mixture was treated in the same way as described under *Basic procedure*. The analyte concentration fixed in the gel was determined as

described above. The resulting aqueous phase was then treated in the same manner with a further batch of gel, and the analyte remaining in the aqueous phase was measured as before.

The distribution ratio was calculated in the usual way from the initial and equilibrium concentrations in the solution, according to the equation:

$$D = \frac{\text{mmol of analyte fixed gel}}{\text{kg of dry gel}} \Big/ \frac{\text{mmole of analyte solution}}{\text{dm}^3 \text{ of solution}}.$$

The following results were obtained: $D_{OPP} = 2054$ at 7.0 ng/ml of initial concentration of OPP and $D_{CBL} = 4520$ at 7.0 ng/ml of initial concentration of CBL.

RESULTS AND DISCUSSION

Spectral characteristics and effect of experimental variables

In neutral and acid media CBL in solution shows native fluorescence with excitation and emission maxima at 279 nm and 333 nm, respectively. While for its hydrolysis product, 1-naphthol, native fluorescence is limited to basic media, the maxima now being 332 and 460 nm, respectively. Although CBL is not fixed in QAE Sephadex A-25 gel, it shows fluorescence at pH > 8 due to the fixation of its hydrolysis product, 1-naphthol, the fluorescence maxima then being 332 and 450 nm, respectively. The hydrolysis of CBL in the presence of QAE Sephadex A-25 gel start at pH 8.0 and is complete at pH 11.0, occurring quickly. We have taken advantage of this fact previously[49] to evaluate CBL.

On the other hand, OPP is fixed on gel from an aqueous solution at alkaline media. The peak wavelengths of excitation and emission spectra in the gel phase are 320 and 414 nm, respectively.[41]

Figure 1 shows the pH dependence on the fluorescence for the fixation of CBL (obviously 1-naphthol) and OPP. OPP presents a maximum RFI for pH 10.2 while CBL requires a pH of 11.2. In order to obtain a fluorescence signal for both compounds simultaneously a pH value of 10.75 was selected, *i.e.*, the point where the value of fluorescence is identical for both samples.

The dependence of the fluorescence of the gel fixed compounds on temperature is small

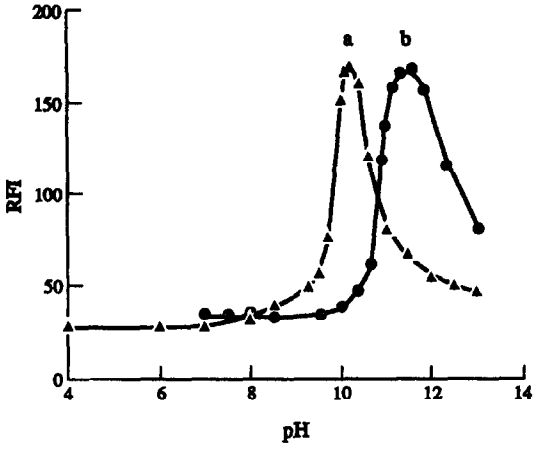

Fig. 1. Influence of pH on RFI in gel phase. (a) OPP, and (b) CBL; [OPP] = 8.0 ng/ml, [CBL] = 8.0 ng/ml, 500 ml of sample, 100 mg of QAE Sephadex A-25.

(−0.3%/°C for OPP and −0.25%/°C for CBL between 5 and 60°). The RFI decrease with temperature was totally reversible for both compounds. Nevertheless all RFI measurements reported here were made at 20.0 ± 0.5°, *i.e.*, about room temperature.

The retention of both analytes was carried out at room temperature, because the ion-exchange process was independent of temperature in the range 0–60° for both compounds.

The equilibration time necessary for maximum RFI development was 10 min for both compounds. RFI remains unaltered for equilibration times longer than 10 min. Fluorescence for both compounds remains constant for at least 3 hr after equilibration.

Variation in the order of addition of reactants was shown to have no effect on the emission intensity.

As the use of a large amount of the gel lowered the RFI, only the amount required to fill the cell (100 mg) was used in all instances.

Selection of the optimum $\Delta\lambda$ for synchronous scanning

The extent of the spectral overlap of these compounds has been examined by obtaining total fluorimetric information available in the excitation–emission matrix. Suitable plots of excitation *vs.* emission wavelengths have been drawn from the three-dimensional spectra. This allows us to examine the most suitable trajectory in the excitation–emission matrix to obtain synchronous fluorescence spectra for the total resolution of overlapping component peaks. The optimum scan path for determining OPP and CBL in mixtures seems to be a $\Delta\lambda = 105$

nm, because it passes near the maximum of both compounds, allowing the determination without a considerable loss of sensitivity.

Figure 2 shows synchronous spectra of CBL and OPP fixed on QAE Sephadex A-25 and of a mixture of both compounds, corrected for the blank signal, and maintaining 105 nm as constant interval between the emission and excitation wavelengths.

Because of the large overlap of the spectra, the determination of OPP and CBL by synchronous spectrofluorimetry is subject to considerable difficulties. This problem has been resolved by taking the first-derivative of the spectrum as shown in Fig. 3.

The technique used to choose suitable wavelengths to take measurements proportional to OPP and CBL concentrations for the preparation of calibration graphs was the "zero-crossing" method. Assuming that the derivative of a spectral band is equivalent to the sum of the derivatives of its individual bands, it is obvious that the total derivative spectrum is only a function of the concentration of the other component, and *vice versa* when the first-derivative spectrum of one of two components is zero. Thus, the height h_1 ($\lambda_{ex}/\lambda_{em} = 338/443$ nm) is proportional to the OPP concentration and h_2 ($\lambda_{ex}/\lambda_{em} = 318/423$ nm) is proportional to the CBL concentration (Fig. 3).

Instrumental parameters

We selected the most adequate parameters to register synchronous spectra in order to obtain good estimates of the derivatives, aiming to find a compromise between reasonable speed and reasonable time for the practical analysis. Therefore a scan speed of 240 nm/min and a luminescence spectrometer response time of one second were selected after verifying that these parameters hardly affect the signal obtained. Intervals of 25 nm for wavelength sampling were chosen as well in order to obtain numerically reasonable estimates of the first-derivative spectra by the Savitzky and Golay method.

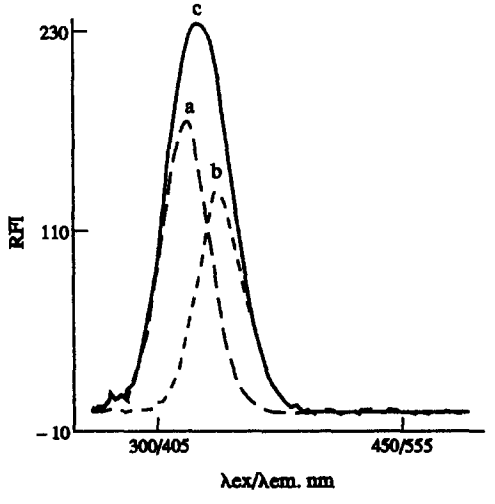

Fig. 2. Synchronrous fluorescence spectra of (a) OPP-QAE Sephadex A-25, (b) CBL-QAE Sephadex A-25 and (c) a mixture of both compounds-QAE Sephadex A-25. ($\Delta\lambda$ = 105 nm, [OPP] = 10 ng/ml, [CBL] = 10 ng/ml).

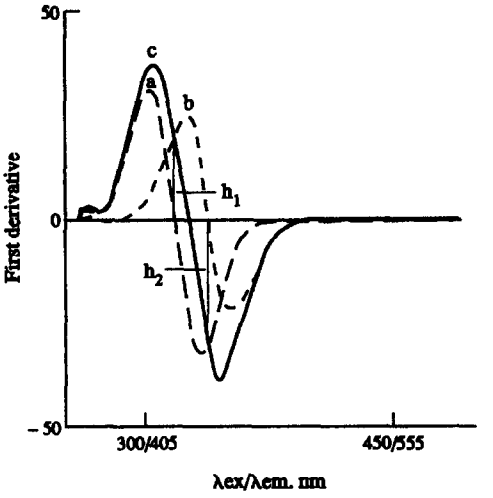

Fig. 3. First-derivative synchronous spectrum of (a) OPP-QAE Sephadex A-25, (b) CBL-QAE Sephadex A-25 and (c) a mixture of both compounds-QAE Sephadex A-25. ($\Delta\lambda$ = 105 nm, [OPP] = 10 ng/ml, [CBL] = 10 ng/ml).

Analytical parameters

In order to test the mutual independence of the analytical signals selected for OPP and CBL, showing that h_1 and h_2 are independent of CBL and OPP concentrations, four calibration graphs were obtained using the measurement height (h) for standard containing between 0.4 and 25.0 ng/ml OPP, in the absence of CBL and in the presence of 2.5, 5.0 and 8.0 ng/ml CBL, respectively.

Following the same procedure, four calibration graphs were prepared for standards containing between 0.8 and 25.0 ng/ml CBL, in the absence of OPP and in the presence of 2.5, 5.0 and 8.0 ng/ml OPP, respectively.

As Table 1 shows, the amplitude of the derivative signal of the mixture in the gel measured at the zero-crossing point of the derivative spectrum of one of two components, is a function of only the concentration of the other component, in accordance with theoretical predictions. Also, the values of the

Table 1. Statistical analysis of the determination of OPP (0.4–25.0 ng/ml) and CBL (0.8–25.0 ng/ml) in mixtures by first-derivative synchronous SPF

Compound determined	Other compound present	ng/ml	Slope ng/ml	Intercept	Correlation coefficient
CBL	OPP	0.0	1.62	0.05	0.998
		2.5	1.61	0.90	0.999
		5.0	1.66	−0.25	0.999
		8.0	1.57	0.10	0.997
OPP	CBL	0.0	2.28	−0.24	0.999
		2.5	2.24	−0.40	0.999
		5.0	2.21	0.07	0.999
		8.0	2.20	−0.06	0.998

Table 2. Methods for determination of OPP and/or CBL in waters

Sample	OPP/CBL	Technique	D.L.*	Reference
River water	CBL	Stopped-flow Spectrophoto.	170	43
Drinking water	CBL	Derivative Spectrophoto.	4	44
Ground-water	CBL	Solid-phase extr. N-P det.	1	45
River water	CBL	HPLC-fluoresc.	0.1	46
Natural water	OPP	HPLC-electro-chem. detect.	0.1	47
Waters	OPP	MHPLC	—	48
Natural water	OPP	LC-electro-chem. detect.	—	19
Natural water	OPP	LC-electro-chem. detect.	1	21
This paper	OPP/CBL	Solid-phase spectrofluor.	0.1/0.2	—

*D.L. Detection limit (ng/ml).

correlation coefficients and the low values for the intercepts indicate good linearity for all the calibration graphs obtained from the first-derivative measurements.

The IUPAC detection limits ($k = 3$)[42] found were 0.1 ng/ml for OPP and 0.2 ng/ml for CBL and the quantification limits ($k = 10$)[43] were 0.4 ng/ml and 0.8 ng/ml for OPP and CBL, respectively. The relative standard deviation (RSD%) ($P = 0.05$, $n = 10$) were 0.9% for 8.0 ng/ml OPP and 0.9% for 10.0 ng/ml CBL.

For the sake of comparison and/or choice of method when other instruments are only available or to choose a measuring strategy for a given problem Table 2 provides information on each of the methods here compared.

The proposed method, compared with others described in the literature for water[19,21,44–49], shows two advantages: simultaneous determination of OPP and CBL in waters and an improvement of about one order of magnitude against other methods except HPLC.

The precision (RSD) of the packing operation, calculated for 10 measurements, was 0.8% for the gel with OPP and CBL fixed, 0.8% for the gel blank (gel with 0.1 *M* NaOH solution) and 0.8% for the gel alone.

Effect of foreign species

The effect of ions commonly found in water and other pesticides fluorescents and

Table 3. Effect of foreign ion or species on the simultaneous determination of 8 ng/ml OPP and 8 ng/ml CBL

Foreign ion or species	Tolerance level (μg/ml) OPP	CBL
Alkaline ions, Cl^-, NH_4^+	40.0	40.0
EDTA	12.0	6.0
F^-, Cl^-, Ca^{2+}, Mg^{2+}	10.0	10.0
NO_3^-	2.0	1.0
SO_4^{2-}	1.0	1.2
Al^{3+}	1.0	1.0
CO_3^{2-}	1.0	4.0
Cu^{2+}	0.2	0.2
Fe^{3+}	0.02	0.03
Dichlone	8.0	8.0
Lindane	2.2	1.2
Captan	1.1	1.1
Humic acid	1.06	1.06
Thiabendazole	0.07	0.08

Table 4. Recovery study of OPP and CBL in natural waters

Sample	OPP, ng/ml			CBL, ng/ml		
	Taken	Found*	% Recovery	Taken	Found*	% Recovery
Raw water(1)	20.0	19.8	99.0	4.0	4.1	102.5
	20.0	19.7	98.5	5.0	4.8	96.0
	1.0	1.0	100.0	1.0	1.0	100.0
	5.0	5.2	104.0	20.0	20.0	100.0
	2.0	1.9	95.0	10.0	10.1	101.0
Raw water(2)	20.0	19.8	99.0	4.0	3.9	97.5
	20.0	19.9	99.5	5.0	4.9	98.0
	1.0	1.0	100.0	1.0	1.0	100.0
	5.0	5.1	102.0	20.0	20.1	100.5
	2.0	2.0	100.0	10.0	9.9	99.0
Tap water(3)	20.0	20.2	101.0	4.0	3.8	95.0
	20.0	20.3	101.5	5.0	4.9	98.0
	2.0	1.9	95.0	2.0	2.0	100.0
	5.0	5.1	102.0	20.0	20.3	101.5
	2.0	1.9	95.0	10.0	10.1	101.0

*Data are the average value of three determinations.
(1)From Genil River.
(2)From Quentar Dam.
(3)From Granada City.

not fluorescents and species as potential interferents was studied on determinations involving mixtures of 8 ng/ml OPP and 8 ng/ml CBL. A 50 μg/ml level of each potentially interfering species was tested first. If interference occurred, the ratio was reduced until it ceased. The tolerance level was defined as the amount of foreign species producing an error not exceeding $\pm 5.0\%$ in the determination of the analyte. The results obtained are summarized in Table 3.

The most serious interference was from Fe(III), owing to the absorption of ferric hydroxide on the gel surface. This negative interference can be eliminated by addition of appropriate amounts of EDTA. In this work the EDTA amount used was 1.0 μg/ml.

Determination of OPP and CBL in natural waters

The method was applied to the determination of both pesticides in natural water samples by the standard additions method in order to minimize the matrix effect observed. As representative samples we selected tap water and raw water from Granada City supplies. The volume of water used for the determination was 500 ml in all instances.

The levels found for both pesticides in all waters studied were lower than the detection limits of the proposed method.

To check the accuracy of the proposed method, a recovery study was carried out on the above waters. Various amounts of both OPP and CBL were added to 500-ml water samples and the percentage recovery was determined. The results obtained, summarized in Table 4, indicated that the proposed method can be applied satisfactorily to determination of both OPP and CBL in waters when they are present at levels at or above the detection limits. According to Table 4 the OPP/CBL ratio range over which the proposed method can be applied within an error limit, say $\leqslant 5\%$ goes from 5:1 to 1:5.

CONCLUSION

This paper provides a practical application of derivative synchronous spectrofluorimetry in combination with the solid-phase spectrofluorimetry to multi-component pesticide analysis at low levels without previous preconcentration nor separation.

Acknowledgements—This research was supported by the Dirección General de Investigación Científica y Técnica (DGICYT) del Ministerio de Educación y Ciencia of Spain (Project No. PS88-0101).

REFERENCES

1. Charles R. Worthing, *The Pesticide Manual*, 1983, 7th Ed., The British Crop Protection Council.
2. R. Elespuru, W. Lijinsky and J. K. Setlow, *Nature*, 1974, **247**, 386.
3. M. Uchiyama, *Bull. Envirom. Contam. Toxicol.*, 1975, **14**, 589.
4. J. Seifert and J. E. Casida, *Biochem. Pharmacol.*, 1978; **27**, 2611.
5. T. M. Bridges, P. T. Creaven and R. T. Wiliams, *Biochem. J.*, 1965, **96**, 872.
6. R. J. Argauer and W. Bontoyan, *J. Assoc. Off. Anal. Chem.*, 1970, **53**, 1166.

7. J. J. Aaron and N. Some, *Analusis*, 1982, **10**, 481.
8. M. J. Larkin and M. J. Day, *Anal. Chim. Acta*, 1979, **108**, 425.
9. F. García-Sánchez and C. Cruces, *Talanta*, 1990, **37**, 573.
10. M. Chiba and H. V. Morley, *J. Assoc. Off. Agr. Chem.*, 1964, **47**, 667.
11. G. F. Ernst, S. J. Roder, G. H. Tjan and J. T. A. Jansen, *ibid.*, 1975; **58**, 1015.
12. B. J. Duck and M. Woolias, *J. Anal. Toxicol.*, 1985, **9**, 177.
13. M. C. Pietrogrande, G. Blo and C. Bighi, *J. Chromatog.*, 1985, **349**, 63.
14. T. D. Spitler, R. A. Marafioti, G. W. Helfman and R. A. Morse, *ibid.*, 1986, **352**, 439.
15. S. Kawai, *Bunseki Kagaku*, 1987, **36**, 574.
16. R. T. Krause, *J. Assoc. Off. Anal. Chem.*, 1980, **63**, 1114.
17. R. T. Krause and E. M. August, *ibid.*, 1983, **66**, 234.
18. M. de Berardinis Jr. and W. A. Wargin, *J. Chromatog.*, 1982, **246**, 89.
19. T. J. Cardwell, I. C. Hamilton, M. J. McCormick and R. K. Symons, *Int. J. Environ. Anal. Chem.*, 1988, **34**, 167.
20. B. Roessner and G. Schwedt, *Z. Anal. Chem.*, 1983, **315**, 610.
21. D. N. Armentrout, J. D. McLean and M. W. Long, *Anal. Chem.*, 1979, **51**, 1039.
22. J. N. Miller, T. A. Ahmad and A. F. Fell, *Proc. Anal. Div. Chem. Soc.*, 1982, **19**, 37.
23. M. C. Ortega, A. Reyes, M. Morell and J. J. Laserna, *Anal. Lett.*, 1986, **19**, 1097.
24. M. C. Gutierrez, S. Rubio, A. Gómez-Hens and M. Valcárcel, *Talanta*, 1987, **34**, 325.
25. F. García-Sánchez and C. Cruces Blanco, *Anal. Chem.*, 1988, **60**, 323.
26. F. Salinas, A. Muñoz de la Peña and M. S. Durán, *Analyst*, 1991, **116**, 291.
27. F. Capitán, A. Navalón, J. L. Vilchez and L. F. Capitán-Vallvey, *Talanta*, 1990, **37**, 193.
28. F. Capitán, E. Manzano, J. L. Vilchez and L. F. Capitán-Vallvey, *Anal. Sci.*, 1989, **5**, 549.
29. F. Capitán, J. P. de Gracia, A. Navalón, L. F. Capitán-Vallvey and J. L. Vilchez, *Analyst*, 1990, **115**, 849.
30. F. Capitán, A. Navalón, E. Manzano, J. P. de Gracia, L. F. Capitán-Vallvey and J. L. Vilchez, *Analusis*, 1991, **19**, 132.
31. F. Capitán, E. Manzano, A. Navalón, J. L. Vilchez and L. F. Capitán-Vallvey, *Analyst*, 1989, **114**, 969.
32. *Idem*, *Talanta*, 1992, **39**, 21.
33. F. Capitán, G. Sánchez-Palencia, A. Navalón, L. F. Capitán-Vallvey and J. L. Vilchez, *Anal. Chim. Acta*, 1992, **259**, 345.
34. F. Capitán, E. Alonso, R. Avidad, L. F. Capitán-Vallvey and J. L. Vilchez, *Anal. Chem.*, in press.
35. M. T. Oms, V. Cerdá, F. García-Sánchez and A. L. Ramos, *Talanta*, 1988, **35**, 671.
36. A. Savitzky and M. J. E. Golay, *Anal. Chem.*, 1964, **36**, 1627.
37. J. Steinier, Y. Termonia and J. Deltour, *ibid.*, 1972, **44**, 1906.
38. J. P. de Gracia, *Tesis de Licenciatura*, 1989, University of Granada, Spain.
39. American Public Health Authority, American Water Works Association and Water Pollution Control Federation, *Standard Methods for Examination of Water and Waste Water, APHA*, 15th Ed., Washington, D.C., 1980.
40. J. L. Vilchez, R. Avidad, A. Navalón, J. Rohand and L. F. Capitán-Vallvey, *Int. J. Environ. Anal. Chem.*, in press.
41. *Idem*, *Z. J. Anal. Chem.*, 1993, **345**, 716.
42. IUPAC, *Nomenclature, Symbols, Units and Their Usages in Spectrochemical Analysis*, *Pure Appl. Chem.*, 1976, **45**, 105.
43. Guidelines for Data Acquisition and Data Quality Evaluation in Environmental Chemistry, *Anal. Chem.*, 1980, **52**, 2242.
44. M. C. Quintero, M. Silva and D. Perez-Bendito, *Talanta*, 1988, **35**, 943.
45. A. Salvador, Z. A. De Benzo and M. De la Guardia, *Microchem. J.*, 1990, **42**, 187.
46. M. W. Brooks, D. Tessier, D. Soderstrom, J. Jenkins and C. J. Marshall, *J. Chromatogr. Sci.*, 1990, **28**, 487.
47. Y. Yasuda, N. Watanabe, T. Hayakawa, M. Yamada, K. Yamazaki and R. Funasaka, *Suishitsu Odaku Kenkyu*, 1990, **13**, 189.
48. M. Sonneborn, E. Pabel and R. Schwabe, *Comm. Eur. Communities Anal. Org. Micropollut. Water*, 1982, EUR 7623, 335.
49. H. Z. Pei, T. Takeuchi and D. Ishii, *J. High Resolut. Chromatogr. Chromatogr. Commun*, 1982, **5**, 434.

Talanta, Vol. 40, No. 11, pp. 1703–1710, 1993
Printed in Great Britain.

0039-9140/93 $6.00 + 0.00

CLOUD POINT METHODOLOGY: A NEW APPROACH FOR PRECONCENTRATION AND SEPARATION IN HYDRODYNAMIC SYSTEMS OF ANALYSIS

BERNARDO MORENO CORDERO,* JOSÉ LUIS PÉREZ PAVÓN, CARMELO GARCÍA PINTO and Mª ESTHER FERNÁNDEZ LAESPADA

Departamento de Química Analítica, Nutrición y Bromatología, Facultad de Química, Universidad de Salamanca, 37008 Salamanca, Spain

Summary—The analytical potential shown by the cloud point phenomenon for the separation and preconcentration of different analytes as an alternative method to other separation techniques is studied. We offer and discuss several examples that can be applied in flow injection analysis and high performance liquid chromatography with both optical (UV and fluorescence) and electrochemical detection.

The possibilities of micellar systems and of other organized molecular assemblies (vesicles, microemulsions, cyclodextrines, liposomes, *etc.*) were recognized many years ago and have been exploited in almost all fields of analytical chemistry with a view to improving or proposing new methods of analysis. This is currently a research area in constant development.[1–15]

These new microheterogeneous structures can interact—sometimes in a selective fashion—with molecules of a very different nature by drastically modifying solubility, reaction rates, the equilibrium position, the products obtained and spectral or analytical parameters, thus permitting, on one hand their use in reactions hitherto unexploited and on the other, the possibility of modifying the sensitivity and selectivity of determinations.

In addition, one of the most characteristic properties of micellar systems is their capacity to dissolve species that are rather water-insoluble; that is, the correct choice of a micellar solution permits direct insertion of insoluble analytes into both FIA and HPLC analytical systems. Other advantages have been described by different authors.[9–13]

The separation and/or preconcentration of an analyte in a sample before its quantification continues to be a stage that in some cases is indispensable; over the past few years many analytical schemes of preconcentration and/or separation have been proposed as alternatives to the use of organic solvents, mediated by surfactants;[16–26] these have opened new possibilities in research areas that are closely linked with analytical chemistry (clinical chemistry, biotechnology or environmental analysis).

In this work, an overview of the analytical possibilities of the cloud-point phenomenon is presented, considering these as alternatives to other techniques of separation and/or preconcentration. Different examples of their analytical potential in flow injection analysis and high performance liquid chromatography are discussed.

The cloud point phenomenon: analytical potential

Aqueous solutions of some surfactants, both non-ionic and zwitterionic, display the so-called cloud point or turbidity point phenomenon; that is, when an isotropic micellar solution is heated above a certain temperature (the cloud point temperature) it suddenly becomes turbid owing to the decrease in the solubility of the surfactant in water. The mechanism by which this separation occurs is still not very clear and continues to be a source of controversy among different researchers.[27–31]

After the two phases have formed, and after a given time (a stage that can be accelerated by centrifugation), two transparent liquid phases are obtained: one rich in surfactant; and the other aqueous, containing a concentration of surfactant close to the critical micellar concentration (cmc).

*Author for correspondence.

Table 1 shows the cloud points displayed by some surfactants. It should be stressed that both the presence of additives (organic or inorganic) and the surfactant concentration may change these values.

From an analytical point of view, the surfactant-rich phase can be used to separate and/or preconcentrate different analytes before their injection into any hydrodynamic analytical system (FIA or HPLC).

The use of micellar systems as an alternative to other techniques of separation has the following characteristics:

1. A high capacity to concentrate a wide variety of analytes of widely varying nature with high recoveries and very high concentration factors since the analytes can be collected in very small volumes (0.2–0.4 ml) of surfactant-rich phase; this allows one to obtain preconcentration factors identical to those of other techniques.

2. The separation yield depends on the greater or lesser hydrophobicity of the analyte under study, thus permitting one to use the same strategies as in liquid–liquid extractions. The preconcentration factor can readily be modified merely by changing the amount of surfactant since, on varying the volume of the surfactant-rich phase obtained, this allows one to design analytical schemes with a given separation factor as a function of the amount of analyte to be determined, of the volume of sample available and of the analytical technique to be used.

3. The surfactants used are not toxic and are less dangerous than the organic solvents habitually used in liquid–liquid extraction because they are neither volatile nor inflammable; additionally, the amount of surfactant required (generally a few milligrams) and the price of commercially available surfactants means that the use of these media is also cheaper.

4. The surfactant-rich phase is compatible with the carrier solutions used in FIA and with both micellar and hydro-organic mobile phases, thus enabling their later use in HPLC.

5. The low temperature of the cloud point of certain surfactants (see Table 2) allows one to design schemes for the separation or preconcentration of temperature-sensitive molecules of biological or environmental interest.

6. The experimental way of performing the process of separation and/or preconcentration is very simple and has been described by different authors.[7–13]

7. The phase separation phenomenon is reversible; this allows one to rapidly obtain one or two phases simply by varying the temperature of the solution.

8. Finally, it should be stressed that as well as commercially available surfactants, the possible synthesis of other types of more specific nature[23,32] and the mixing of several of them[22] confers this methodology great versatility, although more basic studies should be conducted to elucidate the phenomenon and its analytical applications.

Table 1. Cloud point values for some nonionic and zwitterionic surfactants

Surfactant	Concentration, %	Cloud point, °C	Ref.
Polyoxyethylene (7.5) nonyl phenyl ether (PONPE-7.5)			16
(PONPE-7.5)	0.1	1	
(PONPE-7.5)	5.0	6	
(PONPE-7.5)	10.0	11	
(PONPE-7.5)	30.0	30	
in 1.0 M KSCN	3	43	39
(PONPE-7.5)	10	48	
(PONPE-7.5)	15	53	
Triton X-100	1	65	41
Triton X-114	0.1	23.6	25
Triton X-114	1.0	24	
Triton X-114	5.0	25	
	10	30	
n-alkyl-polyoxyethylene ether			
C_6E_3	3	46	28
C_6E_3	11	45.5	
C_6E_3	20	44.8	
$C_{12}E_8$	2	71.1	29
$C_{12}E_8$	10	72	
$C_{14}E_7$	1	57.7	28
$C_{14}E_7$	5	58.6	
3-(nonyldimethylammonium) propylsulfate (C_9-APSO$_4$)			23
	2	19	
	5	52	
	10	64	
3-(decyldimethylammonium) propyl sulfate (C_{10}-APSO$_4$)			23
	2	62	
	5	77	
	10	85	
Tetrabutylammonium tetradecylsulfate			40
	3	37	
	10	31	
	20	25	

EXPERIMENTAL

Reagents

The surfactants Triton X-114 and Brij 30 were obtained from Fluka and used without further purification. The pesticides parathion

and fenitrothion were purchased from Riedel-de Haen (Seelze-Hannover, Germany). Vitamins A and E were obtained from Fluka and vitamin K from Sigma. Dansyl aminoacids were obtained from Sigma and benzo(a)pyrene was purchased from Sugelabor Chemical Service. Stock solutions of $2.0 \times 10^{-3}M$ uranium were prepared by dissolving appropriate amounts of uranyl nitrate hexahydrate (Merck). Methanolic solutions of PAN (1-(2-pyridylazo)-2-naphthol) were obtained from the solid product (Merck).

Other reagents were of analytical grade; all solvents and analytes were filtered through 0.45-μm nylon membranes filters (Milipore); ultra-high-quality water obtained from a Elgastat UHQ water purification system was used.

Apparatus

The flow system consisted of a peristaltic pump (Gilson Minipuls 2 HP4) and a Rheodine 5020 six-port injection valve; all connections were 0.5 mm i.d. Teflon tubing. Other experimental details have been described elsewhere.[14]

A modular component liquid chromatographic system was used consisting of a Spectra Physics SP 8800 ternary pump, an SP 8450 UV detector, a Spectra FL 2000 fluorescence detector, an EG&G PARC 400 electrochemical detector and an SP 4290 integrator; the electrodes employed for electrochemical detection, their pretreatment and other additional details have already been described.[24,33,34]

Easyspin, Sorval Instruments, Du Pont (Giralt) and Beckman, Model J2-21M centrifuges were also used.

Procedures

Cloud point determination and ratio phases. The cloud point for TX-114 was determined by observing the appearance of the two phases on heating different previously cooled aqueous solutions of surfactant in a bath kept at constant temperature.

The ratio of phases was obtained by measuring the volumes of the respective phases in tubes calibrated for different amounts of surfactant under the same experimental conditions as those used for phase separation (heating at 40° and centrifuging at 3500 rpm).

Cloud point preconcentration. Aliquots of cold solutions containing the analyte and a given amount of surfactant were kept for 15 min in a thermostatted bath at 40°; the two phases were separated by centrifugation for 5 min at 3500 rpm. Sixty microlitres of the surfactant-rich phase were collected with a Hamilton syringe; 10 μl of these were injected in a chromatography system. Following this, elution was made with a suitable mobile phase for each analyte studied.

For injection in the FIA system, the aqueous phase was separated by inverting the tubes once the solution had been chilled in an ice-bath; before being injected the surfactant-rich phase was placed in 1 ml of $3.6M$ HCl medium in order to destroy the PAN–U(VI) chelate, to provide the appropriate medium for uranium reduction and diminish the viscosity of the sample; 100 μl of the mixture were injected into the carrier stream.

The detection of uranium was performed spectrophotometrically, employing a flow injection system previously developed by us.[14]

RESULTS AND DISCUSSION

Figure 1 shows the corresponding diagram of temperature–concentration phases for Triton X-114 (L means single isotropic solution and 2L indicates that two isotropic phases coexist); it may be seen that for surfactant concentration values ranging between 0.5 and 4% the temperature of the cloud point remains almost constant and equal to 25°, thus facilitating experimentation.

Figure 2 shows the percentage of surfactant-rich phase obtained and the theoretical preconcentration factor as a function of the concentration of Triton X-114. The percentage of surfactant-rich phase was calculated as the ratio of its volume to the volume of solution used for the cloud point separation. The theoretical preconcentration factor (maximum attainable value for 100% recovery) was calculated as

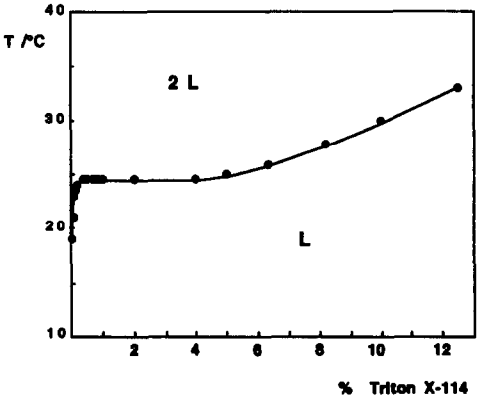

Fig. 1. Phase diagram of Triton X-114 in aqueous solution. L: single isotropic phase region, 2L: two isotropic phase region.

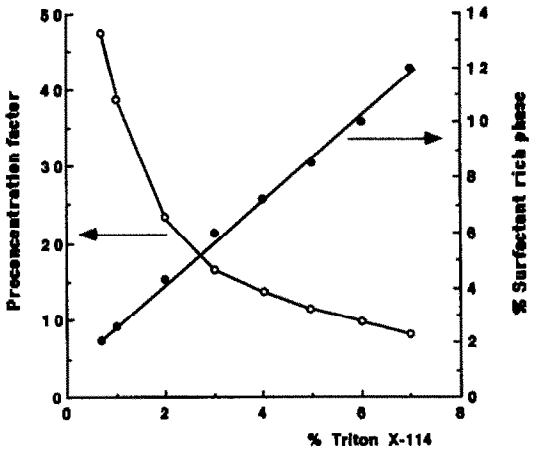

Fig. 2. Variation of the preconcentration factor and the % of surfactant rich phase obtained as a function of Triton X-114 concentration.

the ratio of the volume of solution used to the surfactant-rich phase volume.

Cloud point methodology prior to flow injection analysis

Flow injection analysis can be considered a new concept in continuous flow techniques and is currently used routinely in many laboratories both in chemical analysis and in research, owing to its versatility, simplicity and low instrumental costs.[35,36] However, as in many other analytical techniques, some of the proposed procedures lack the sensitivity and selectivity required for the analysis of trace amounts of substances, which makes it necessary to separate and/or preconcentrate the analyte of interest prior to injection into the FIA system.[35,38]

Although the literature reports some procedures that use micellar media in FIA[12,14] none of them has exploited the cloud point methodology for the preconcentration and/or separation of analytes.

Recently, with a view to checking the feasibility of this method in FIA determination, we have studied the separation and preconcentration of traces of uranium using the U(VI)–PAN–Triton X-114 system before inserting the samples in the analysis system;[25,26] the experimental results showed that it is possible to detect an amount of uranium close to $10^{-8}M$ starting out from only 10 ml of sample and using 0.2% of surfactant.

Watanabe[16,18,19,21] and Pramauro[20,22] have developed several procedures for the preconcentration of certain metal ions by the formation of a hydrophobic chelate using as non-ionic surfactants polyoxyethylene-7,5-nonylphenyl ether (PONPE 7.5) and a mixture of Triton X-100 and polyoxyethylene (4,2) dodecanol, respectively. In both cases the system could be readily adapted to the FIA technique with the advantages of simplicity and speed in the analysis.

Cloud point methodology prior to high performance liquid chromatography analysis

Having subjected a sample to phase separation, the surfactant-rich phase which will contain the compounds of hydrophobic nature can be injected directly into a liquid chromatograph since it is compatible with the mobile phases customarily used in this technique.

UV detection

When cloud-point preconcentration is used prior to HPLC analysis it should be taken into account that the time of elution of the surfactant injected depends on the composition of the mobile phase used for the elution of the different analytes being studied.

Figure 3 shows the blank signals obtained with a UV detector at 254 nm when 10 μl of a surfactant-rich phase containing only Triton X-114 or Brij 30 is injected after cloud point separation. Figure 3(a) corresponds to a mobile phase of 100% MetOH and Fig. 3(b) to 70:30 MetOH:H_2O.

When the mobile phase contains an amount of MetOH close to 100%, quantification of analytes would be possible as long as their elution times are above 8 min. However, for lower organic modifier contents, the peaks due to the surfactant [see chromatograms in Fig. 3(b)] would avoid any quantification of analytes and hence the methodology is unsuitable; this has already been reported by other authors.[23,24]

Figure 4 shows comparatively the chromatograms obtained when 10 μl of a solution containing 0.70 ppm of vitamin K are injected with UV detection at 254 nm; in the right part of Fig. 4 the signal for the injection of the cloud-point preconcentrated solution is shown.

Fluorescence detection

The high background absorbance displayed by non-ionic surfactants at the wavelengths usually used in UV detection[254-260] can be avoided using a fluorescence detector.

Figure 5 shows the chromatograms obtained when 10 μl of a solution containing 0.08 ppm of vitamin A are injected, with fluorescence detection ($\lambda_{ex} = 330$ nm and $\lambda_{em} = 480$ nm) and 0.01

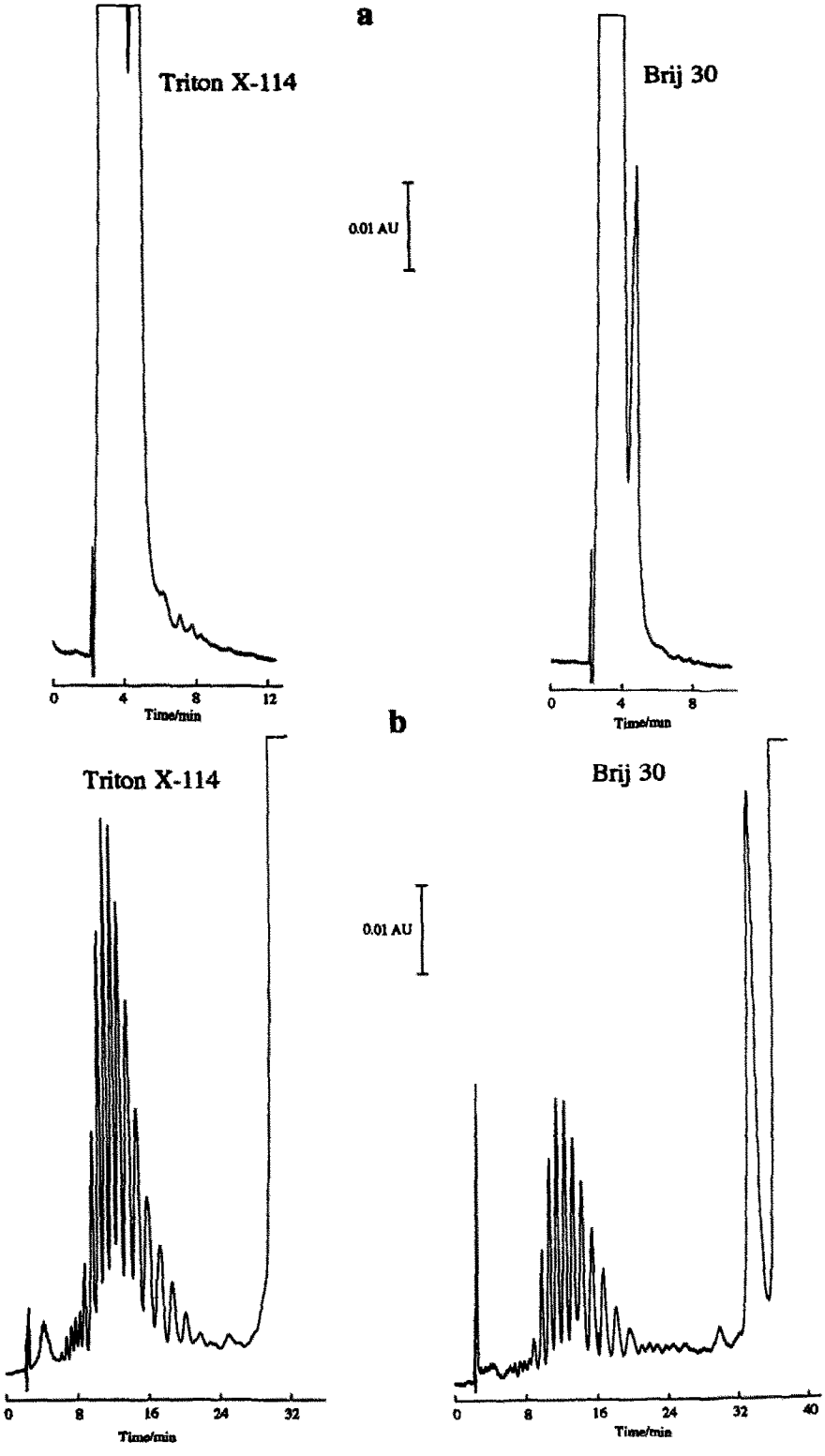

Fig. 3. Blank chromatograms obtained for the injection (10 μl injected) of a surfactant-rich phase of Triton X-114 and Brij 30 after cloud point preconcentration with UV detection at 254 nm. Mobile phases: (a) 100% MetOH (Q = 1.00 ml/min); (b) 70:30 MetOH/H_2O (Q = 1.00 ml/min).

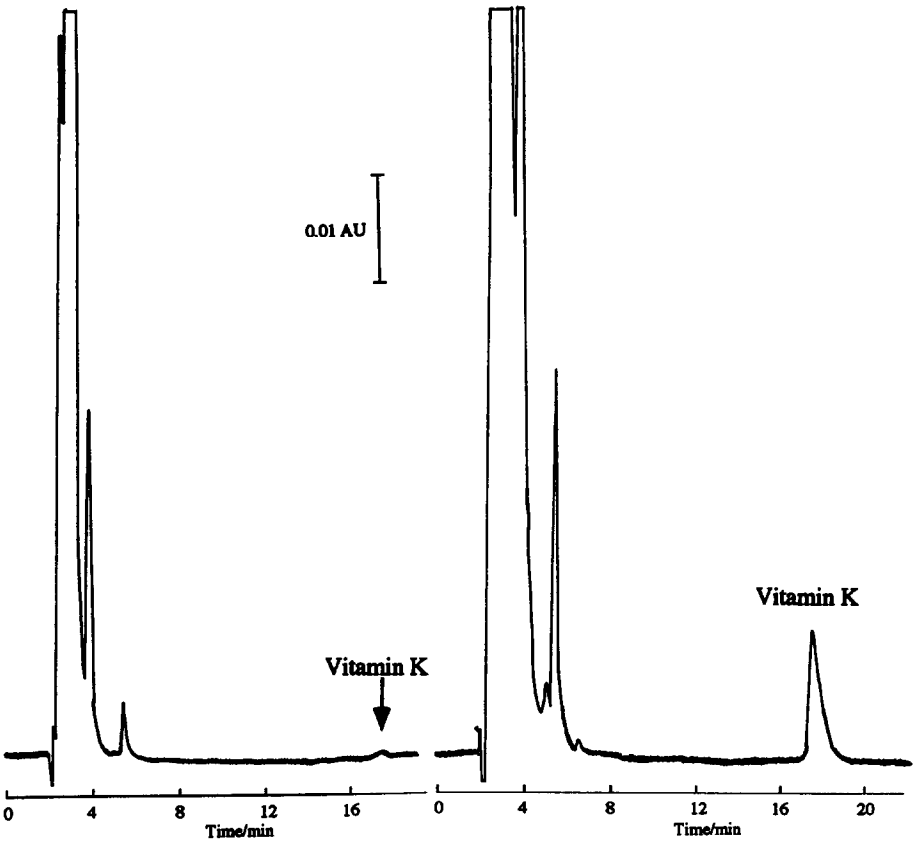

Fig. 4. Chromatograms obtained for the injection of 0.70 ppm (left) of vitamin K (10 μl injected) and of the surfactant-rich phase obtained after the cloud point preconcentration of 15 ml of the sample (right) with UV detection at 260 nm. Chromatographic conditions as described in the text.

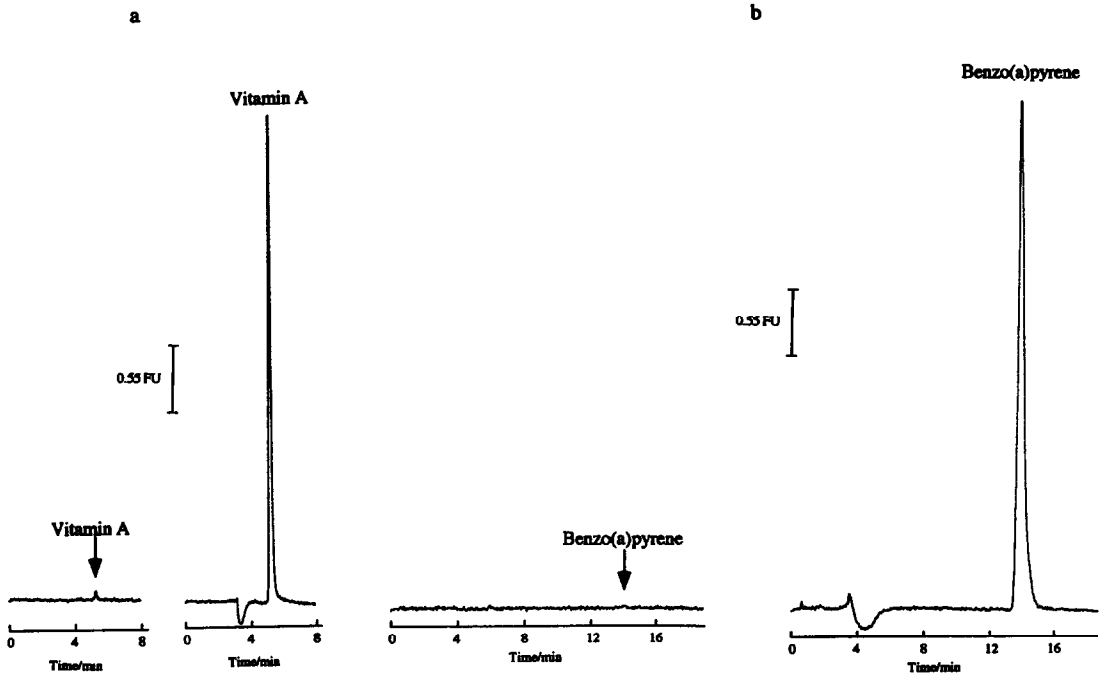

Fig. 5. Chromatograms obtained for the injection (10 μl injected) of (a) 0.08 ppm of vitamin A (λ_{ex} = 330 nm, λ_{em} = 480 nm) and (b) 0.01 ppm of benzo(a)pyrene (λ_{ex} = 300 nm, λ_{em} = 430 nm) before (left) and after (right) cloud point preconcentration of 15 ml of the sample. Chromatographic conditions as described in the text.

ppm of benzo(a)pyrene ($\lambda_{ex} = 300$ nm and $\lambda_{em} = 430$ nm) before and after cloud-point preconcentration, eluting with 95:5 MetOH/H_2O (Q = 1 ml/min) and 75:25 A CN/H_2O (Q = 2 ml/min), respectively.

The signals obtained show that for both mobile phases and under the experimental conditions used for detection, the surfactant (Triton X-114) does not show a blank signal that will prevent measurement and quantification of the analytes; secondly, it should be noted that the amounts of analyte injected, without the cloud-point preconcentration, would be very difficult to quantify.

Electrochemical detection

Bearing in mind that many commercially available surfactants do not contain any functional group subject to electrodic reaction, another feasible alternative for resolving the high background absorbance would be the use of electrochemical detectors, which would provide the additional advantage of a greater sensitivity (50–100-fold) and selectivity.

Recently[24] we have shown that under certain experimental conditions it is possible to use electrochemical detection without obtaining any background signal, making cloud-point preconcentration useful for the determination of important molecules that could not be measured if UV detection were employed.

Table 2 shows the relative increases in signal obtained for certain vitamins, dansyl aminoacids, pesticides and PAHs as representative analytes of biological and environmental interest dealt with by the cloud-point preconcentration method with different forms of detection. The relative standard deviation obtained for sets of replicates (8–10 samples) in which the procedures were applied (including the cloud point separation step and the chromatographic separation or the flow injection measurement) was below 5% in all cases; as this value includes the instrumental errors, it can be concluded that the reproducibility of the cloud point preconcentration is quite good (<5%).

The behaviour of other surfactants for use in the cloud-point methodology and its application to the preconcentration of different analytes is currently under study.

Table 2. Relative signal enhancement for different analytes after cloud point preconcentration in HPLC analysis

Analyte	*Vs*	Detection	*R*	Enhancement factor
Vitamin K	15	UV	40	40
Vitamin E	15	UV	40	40
Vitamin A[a]	25	F	75	76
Vitamin A[b]	15	EC	40	32
Dansyl-L-Alanine[c]	15	F	40	10
Dansyl-L-Serine[c]	15	F	40	24
Dansyl-L-Leucine[c]	15	F	40	40
Anthracene[d]	15	F	40	35
Benzo(a)pyrene[e]	15	F	30	60
Parathion[f]	25	EC	75	71
Fenitrothion[f]	200	EC	200	196

Mobile phases and HPLC conditions: (a) 95:5 MetOH/H_2O (Q = 1.00 ml/min), $\lambda_{ex} = 330$ nm, $\lambda_{em} = 480$ nm; (b) 99:1 MetOH/H_2O and 0.1 M $LiClO_4$ (Q = 1.00 ml/min), E = +800 mV; (c) 40:60 MetOH/H_2O (0.01 M Na_2HPO_4 Q = 2 ml/min), $\lambda_{ex} = 330$ nm, $\lambda_{em} = 510$ nm; (d) 95:5 MetOH/H_2O (Q = 1.00 ml/min), $\lambda_{ex} = 350$ nm, $\lambda_{em} = 410$ nm (e) 75:25 Acetonitrile/H_2O (Q = 2 ml/min), $\lambda_{ex} = 300$ nm, $\lambda_{em} = 430$ nm; (f) 70:30 MetOH/H_2O (0.0025 M AcOH/AcO^- Q = 1.25 ml/min), $E_1 = -1500$ mV (generating electrode), $E_2 = +400$ mV.
Detection: UV, ultraviolet; F, fluorimetric; EC, electrochemical *R* is the volume ratio of phases; *Vs* is the sample volume used.

CONCLUSION

The present work shows that the cloud point methodology has great analytical potential yet to be exploited that may also offer a feasible alternative to other techniques of separation and/or preconcentration with good recoveries and similar standard deviation.

Cloud point preconcentration can be used as a sample preparation step prior chromatographic analysis or flow injection systems, specially for fluorimetric or electrochemical detection due to the low background signal of the surfactant.

So far this technique has been used for the preconcentration of hydrophobic and ionic analytes in samples of analytical interest.

Acknowledgements—This work was supported by DGICYT (project no. PB91-0185). C. G. P. acknowledges the financial support by the Spanish Government (PFPI). M.E.F.L. wishes to express her gratitude to the Junta de Castilla y León for the awarded grant through the Consejería de Cultura y Turismo.

REFERENCES

1. B. Chernova, *J. Anal. Chem. U.S.S.R.*, 1977, **32**, 1171.
2. W. L. Hinze, in K. L. Mittal, (ed.) *Solution Chemistry of Surfactants*, Vol. I. Plenum Press, New York, 1979.
3. J. H. Fendler, *Membrane Mimetic Chemistry*. Wiley-Interscience, New York, 1982.
4. W. L. Hinze, H. N. Singh, Y. Baba and N. G. Harvey, *Trends Anal. Chem.*, 1984, **3**, 193.
5. L. Cline Love, J. G. Habarta and J. G. Dorsey, *Anal. Chem.*, 1984, **56**, 1132A.
6. E. Pelizzetti and E. Pramauro, *Anal. Chim. Acta*, 1985, **69**, 1.

7. D. W. Armstrong, *Separation and Purification Methods*, 1985, **14**, 213.
8. J. H. Fendler, *Chem. Rev.*, 1987, **87**, 877.
9. W. L. Hinze, *Anali di Chimica*, 1987, **77**, 167.
10. W. L. Hinze, in *Ordered Media in Chemical Separations*, W. L. Hinze and D. Armtromg (eds), ACS 342, American Chemical Society, Washington, DC, 1987.
11. S. Rubio and D. Pérez Bendito, *Anal. Chim. Acta*, 1989, **224**, 185.
12. B. Moreno Cordero, J. L. Pérez Pavón and J. Hernández Méndez, *Quim. Anal.*, 1989, **8**, 231.
13. G. L. MacIntire, *Crit. Rev. Anal. Chem.*, 1990, **4**, 257.
14. B. Moreno Cordero and J. L. Pérez Pavón, *Anal. Chim. Acta*, 1990, **217**, 230.
15. J. L. Pérez Pavón and B. Moreno Cordero, *Analyst*, 1992, **117**, 215.
16. H. Watanabe and H. Tanaka, *Talanta*, 1978, **25**, 585.
17. C. Bordier, *J. Biol. Chem.*, 1981, **256**, 1604.
18. H. Watanabe, in *Solution Behaviour of Surfactants*, K. L. Mittal and E. F. Fendler (eds), Vol. 2. Plenum Press, New York, 1982.
19. S. Kwamorita, H. Watanabe and K. Haraguchi, *Anal. Sci.*, 1985, **1**, 41.
20. E. Pramauro, C. Minero and E. Pelizzeti, in *Ordered Media in Chemical Separations*, W. L. Hinze and D. Armstrong (eds), ACS 342, American Chemical Society, Chap. 7, Washington DC, 1987.
21. T. Saitoh, Y. Kimura, T. Kamidate, H. Watanabe and K. Haragucki, *Anal. Sci.* 1989, **5**, 577.
22. E. Pramauro, *Anali di Chimica*, 1990, **80**, 101.
23. T. Saitoh and W. L. Hinze, *Anal. Chem.*, 1991, **63**, 2520.
24. C. Garcia Pinto, J. L. Peréz Pavón and B. Moreno Cordero, *Anal. Chem.*, 1992, **64**, 2335.
25. M. E. Fernánde Laespada, J. L. Pérez Pavón and B. Moreno Cordero, Communication presented to the 12th International Symposium on Microchemical Techniques, Córdoba 1992.
26. M. E. Fernández Laespada, J. L. Pérez Pavón and B. Moreno Cordero, *Analyst*, 1993, **118**, 209.
27. R. J. Kjellander, *Chem. Soc. Faraday Trans*, 1982, **2**, 78.
28. M. Corti, C. Minero and V. Degiorgio, *J. Phys. Chem.*, 1984, **88**, 309.
29. V. Degiorgio, R. Piazza, M. Corti and C. Minero, *J. Chem. Phys.*, 1985, **82**, 1025.
30. V. Degiorgio, in *Physics of Amphiphilic Micelles, Vesicles, and Microemulsions*, V. Degiorgio and M. Corti (eds). North-Holland, Amsterdam, 1985.
31. R. E. Goldstein, *J. Phys. Chem.*, 1986, **84**, 3367.
32. P. G. Nilsson, B. Lindman and R. G. Laughlin, *J. Phys. Chem.*, 1984, **88**, 6357.
33. J. Hernández Méndez, R. Carabias Martínez, E. Rodriguez Gonzalo and F. Garay García, Presented at the Symposium on Fungicides, Herbicides and Insecticides, London, 1992.
34. M. M. Delgado Zamarreño, A. Sánchez Pérez, C. Gómez Pérez and J. Hernández Méndez, *J. Chromatogr.*, 1992, **623**, 69.
35. M. Valcárcel and M. D. Luque de Castro, *Flow Injection Analysis. Principles and Applications*. Ellis Horwood, Chichester, 1987.
36. J. Ruzicka and E. H. Hansen, *Flow Injection Analysis*, 2nd Ed. John Wiley and Sons, New York, 1988.
37. V. Kuban, *Crit. Rev. Anal. Chem.*, 1991, **22**, 477.
38. M. Valcárcel and M. D. Luque de Castro, *Non-Chromatographic Continuous Separation Techniques*. Royal Society of Chemistry, London, 1991.
39. T. Okada, *Anal. Chem.*, 1992, **64**, 2138.
40. Z. J. Yu and G. Xu, *J. Phys. Chem.*, 1989, **93**, 7441.
41. S. Kawamorita, H. Watanabe and K. Haraguchi, *Anal. Sci.*, 1985, **1**, 41.

Talanta, Vol. 40, No. 11, pp. 1711–1718, 1993
Printed in Great Britain.

0039-9140/93 $6.00 + 0.00

CONVENTIONAL AND THERMAL LENS SPECTROPHOTOMETRIC DETERMINATION OF *p*-AMINOBENZOIC ACID AND ARYLAMINE DIURETICS PREVIOUS AZODYE FORMATION IN A MICELLAR MEDIUM

J. S. ESTEVE-ROMERO,† E. F. SIMO-ALFONSO,‡ M. C. GARCIA-ALVAREZ-COQUE‡ and G. RAMIS-RAMOS*‡

†Escola Superior de Tecnologia i Ciències Experimentals, Universitat Jaume I, 12006 Castelló, Spain
‡Departament de Química Analítica, Facultat de Química, Universitat de València, 46100 Burjassot (València) Spain

Summary—The determination of the diuretics hydrochlorothiazide, bendroflumethiazide and furosemide by both conventional and thermal lens spectrophotometry (TLS, 100 mW of pump power at 514.5 nm) following previous hydrolysis, diazotization and coupling with *N*-(naphthyl)ethylenediamine (NED) in a sodium dodecyl sulphate (SDS) micellar medium of pH ≈ 1 was studied. *p*-Aminobenzoic acid (PABA) was used as a model compound to optimize the derivatization procedures. 3-Substituted indoles, such as 5-hydroxyindole-3-acetic acid and tryptophan, gave *N*-nitroso derivatives which interfered with the determination of the diuretics in urine. The derivatized diuretics in urine were separated using HPLC with a Spherisorb ODS-2 C_{18} column, and a 0.1*M* SDS mobile phase containing 5% *n*-propanol and 0.01*M* sodium dihydrogen phosphate (pH 3). The diuretics gave limits of detection (LODs) of *ca.* $5 \times 10^{-9}M$ for the TLS procedure. The LODs were 20–50-fold higher for the corresponding spectrophotometric procedure.

Diazotization and coupling of primary arylamines to form intensely coloured azodyes are highly sensitive and widely applicable chromogenic reactions. The amines are diazotized with nitrous acid in an HCl medium, the nitrite excess is eliminated with sulphamic acid and the diazonium ions are coupled with *N*-(naphthyl)ethylene-diamine (NED). In conventional procedures, coupling of most diazonium ions is too slow at low pH values, and a buffer is used to increase the pH. Usually, after coupling, excess HCl is also added, since the protonated azodyes give higher molar absorptivities at longer wavelengths than the corresponding conjugated bases.

The use of a micellar medium of sodium dodecyl sulphate (SDS) has improved the colorimetric determination of arylamines and sulphonamides.[1–4] In this medium, the coupling rate increases greatly and the protonation constants of the azodyes are larger than in water. In an SDS micellar medium, the diazotization, coupling and measurement of the absorbance of the protonated azodye are thus possible at pH ≈ 1 for a large number of diazotizable substances. In a non-micellar medium, the pH should be modified twice during the procedure to form the chromophore.

Thermal lens spectrophotometry (TLS) allows the measurement of extremely low absorbances, often with dynamic ranges over two orders of magnitude.[5] Requirements of an advantageous TLS procedure are: (a) the absorptivity of the analyte should be large; (b) the absorbance of the blank should be negligible, otherwise the background noise and limit of detection increase, and the dynamic range is reduced; (c) the conditional constant of the chromogenic reaction should be very large. In addition, the use of a selective reaction, or the combination of the TLS determination with a separation technique to improve selectivity and to reduce the blank signal, has been recommended.[6]

The diazotization and coupling reactions fulfil these requirements and should lead to advantageous TLS procedures for the determination of many drugs. The azodyes formed with NED by most diazotizable substances of interest show absorption maxima in the 540–560 nm range, with $\varepsilon = 20{,}000$ $mol^{-1}l.$ cm^{-1} or

*Author for correspondence.

higher. Therefore, NED azodyes absorb the intense Ar^+ laser line at 514.5 nm which is most frequently used for pumping in TLS experiments. The determination of inorganic nitrite by azodye formation with NED and TLS has been described.[7]

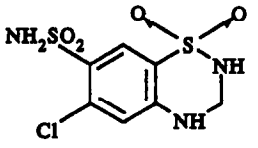

I

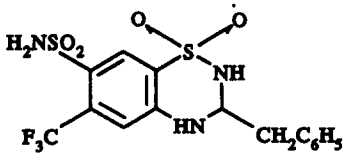

II

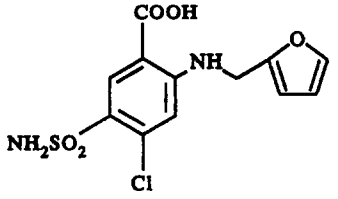

III

In this work, the diazotization and coupling of the diuretics hydrochlorothiazide (I), bendroflumethiazide (II) and furosemide (III) with NED in an SDS micellar medium is described. These diuretics are secondary arylamines and, therefore, hydrolysis to give the primary arylamines was required before diazotization. The corresponding spectrophotometric and TLS procedures were optimized using *p*-aminobenzoic acid (PABA) as a model compound. A comparative study of the spectrophotometric and TLS procedures was performed. 5-Hydroxyindole-3-acetic acid (5-HIAA) and tryptophan also gave a chromogenic reaction with the reagents; therefore, 3-substituted indoles interfered in the determination of the diuretics in urine. Thus, an HPLC procedure with precolumn derivatization was tried.

During the last few years micellar liquid chromatography with UV absorptiometric detection has been studied as an alternative means of determining drugs in urine, including banned drugs in sports competitions.[8–13] However, in the corresponding procedures urine gives a high background during the first minutes of the chromatograms, thus hindering the detection of many drugs. As shown in this work, precolumn derivatization and absorptiometric detection in the visible can be an excellent auxiliary tool in micellar liquid chromatography of physiological samples, since the chances of interference are dramatically reduced.

An SDS mobile phase containing *n*-propanol, and conventional and TLS spectrophotometric detection at 514.5 nm was used. Urine samples were spiked with arylamine diuretics. After hydrolysis, diazotization and coupling in the micellar medium, the samples were injected in the chromatograph. The diuretics were well separated by this chromatographic system. The urine blanks gave almost flat chromatograms, with a single small peak which did not interfere with the determination of the diuretics.

EXPERIMENTAL

Reagents

Analytical grade PABA (Scharlau, Barcelona, Spain), sodium nitrite, sulphamic acid (Fluka, Buchs, Switzerland), NED dihydrochloride, SDS (Merck, Darmstadt, Germany), *n*-propanol, methanol, sodium dihydrogen phosphate and HCl (Panreac, Barcelona, Spain) were used.

Hydrochlorothiazide (Galloso Wellcome, Madrid, Spain), bendroflumethiazide (Davur, Madrid, Spain) and furosemide (Lasa, Barcelona, Spain) were kindly donated by the pharmaceutical laboratories. A $10^{-3}M$ stock solution of the diuretics in $0.15M$ HCl and $0.043M$ SDS was prepared. A small volume of methanol was initially added to facilitate dissolution of the drugs. The purity of the diuretics was checked using HPLC with UV absorptiometric detection at 254 nm, and was found to be *ca.* 100%.[14,15] The stock solutions of hydrochlorothiazide and furosemide are stable, but bendroflumethiazide solutions are not stable and, therefore, they were prepared daily. Distilled and nanopure deionized water (Barnstead deionizer, Sybron, Boston, MA, U.S.A.) was used.

Solid-phase extractions were performed with Bond-Elut SCX (strong cationic exchange) columns using a Vac-Elut SPS 24 vacuum station (Analytichem International, Harbor City, CA, U.S.A.).

Apparatus

The thermal lens set-up with an Ar^+/He–Ne coaxial pump-probe configuration has been described elsewhere.[16,17] The 514.5 nm line of the Ar^+ laser with 100 mW of pump power, modulated at 4 Hz, was used. A Hewlett–Packard 8452A spectrophotometer (Palo Alto, CA, U.S.A.) and 1 cm optical path cells were also used.

The HPLC system consisted of a Hewlett–Packard HP 1050 chromatograph with an isocratic pump, a programmable UV–vis detector and an integrator HP 3396A, connected to a compatible computer (μP 386SX) provided with the HP Peak-96 program package. When working with TLS detection, data acquisition and peak integration were performed using the TRAD-2 program.[18] Samples were injected with a Rheodyne valve (Berkeley, CA, U.S.A.) with a 20 μl loop. A Spherisorb ODS-2 C_{18} column (5 μm particle size, 12 cm × 4.6 mm i.d.) and a C_{18} precolumn of similar characteristics (3.5 cm × 4.6 mm i.d.) from Scharlau (Barcelona, Spain) were used.

Procedures

The solution containing PABA or the diuretics was made 0.15M in HCl (pH ≈ 0.8) and 0.043M in SDS (1.25%). The diuretics were hydrolysed in a water bath at 100° for 10 min. A 10 ml aliquot was introduced into a 25 ml volumetric flask and, for the spectrophotometric determinations, was mixed with 2 ml of $1.8 \times 10^{-2}M$ sodium nitrite. After 10 min, 2 ml of $7.5 \times 10^{-2}M$ sulphamic acid was added and the mixture was allowed to react for an additional 10 min. Finally, 2 ml of $7.5 \times 10^{-3}M$ NED was added, the volume was completed up to the mark with water and the absorbance was measured at 556 nm for PABA and at 530 nm for the diuretics. For the TLS determinations, $2.5 \times 10^{-3}M$ nitrite, $2.5 \times 10^{-2}M$ sulphamic acid and $2.5 \times 10^{-3}M$ NED solutions were used.

Only preliminary results are given in this work for the HPLC separation of the derivatized diuretics. The following non-optimized HPLC procedure was used: a 0.1M SDS mobile phase containing 5% n-propanol and 0.01M sodium dihydrogen phosphate (pH 3) was used, and the flow rate was 1 ml/min. Urine samples taken from healthy volunteers were spiked with the diuretics when necessary, and were forced through 0.45 μm pore size filters (Analytichem International). The procedure given above was used, but 8 and 3 ml urine were initially taken to obtain the UV–vis and TLS chromatograms, respectively. After derivatization, 20 μl of the sample was injected in the chromatograph through 0.22 μm pore size filters (Analytichem International). The UV–vis detector was set at 514 nm. With TLS, the standard cell of the HP UV–vis detector was located in the beam path, and 100 mW of pump power at 514.5 nm was used.

RESULTS AND DISCUSSION

Optimization of the reagent concentrations

Physico-chemical requirements of similar nature should be met for a chromogenic reaction to be successfully exploited in both conventional and thermal lens spectrophotometry; however, and as a consequence of the lower concentrations used, for TLS procedures those requirements are much more demanding.[6] Thus, for instance, in TLS the concentrations of the competing ligands should be frequently reduced, to increase the conditional stability constants of the chromogenic reactions. It may also be necessary to increase the concentration of the chromogenic reagents to displace the reactions to the right, or to increase reaction rates. Therefore, the simultaneous optimization of both the conventional and the corresponding TLS procedures can be of interest.

The HCl (pH) and SDS concentrations were optimized elsewhere for the spectrophotometric determination of a large number of diazotizable substances with NED.[4] Final HCl and SDS concentrations (0.06M and 0.017M, respectively) assure an optimal pH ($1 < pH < 1.5$), as well as formation of micelles. Therefore, these concentrations were also assumed to be optimal for the spectrophotometric and TLS determination of the diuretics. Optimization of the concentration of sodium nitrite, sulphamic acid and NED was performed using constant PABA concentrations, *i.e.* $8 \times 10^{-5}M$ and $8 \times 10^{-7}M$ PABA for the spectrophotometric and TLS experiments, respectively.

In Fig. 1, the absorbance and TLS signals obtained are represented against the log of nitrite/PABA molar ratio. The absorbance of the blanks was negligible and, similarly, the TLS

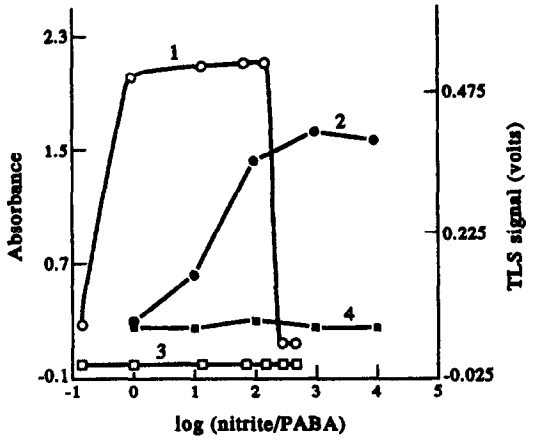

Fig. 1. Influence of sodium nitrite; 1) absorbance, series of single experiments; 2) TLS signal, means of series of duplicated experiments; 3), absorbance blanks; 4) TLS blanks. The logarithms of the nitrite/PABA molar ratios are represented on the X-axis. Final concentrations: $8 \times 10^{-5}M$ and $8 \times 10^{-7}M$ PABA for the spectrophotometric and TLS experiments, respectively; $6 \times 10^{-3}M$ sulphamic acid and $6 \times 10^{-4}M$ NED.

blanks gave a low and constant signal. A maximum and constant value of the absorbance was obtained for nitrite/PABA molar ratios between 1:1 and 200:1, but no dye formation was observed at higher ratios. Instead, the nitrite/PABA molar ratio had to be increased up to 1000:1 to achieve a reasonably constant value of the TLS signal. In comparison to spectrophotometry, the diazotization yield probably decreased at the much lower PABA concentration used in TLS.

Figure 2 shows the absorbance and TLS signal against the log of sulphamic acid/nitrite molar ratio. In TLS high blanks were obtained at sulphamic acid/nitrite ratios lower than 1:1, due to the incomplete destruction of nitrite (sulphamic acid eliminates nitrite following a 1:1 reaction). The use of sulphamic acid/nitrite ratios larger than 1:1 had a negligible influence on sensitivity. For the spectrophotometric and TLS experiments given below, 4:1 and 10:1 sulphamic acid/nitrite molar ratios were used, respectively.

The results obtained using different NED/PABA molar ratios are shown in Fig. 3. The values of the TLS blanks were low and constant, except at NED concentrations larger than $10^{-3}M$. In both spectrophotometric and TLS experiments, an NED/PABA molar ratio over the stoichiometric value (1:1) was enough to assure quantitative coupling, and no significant sensitivity changes were observed at the larger ratios studied. The following experiments were performed using the optimized procedure given above. The excess of NED assured quantitative reaction at relatively large analyte concentrations.

Optimization of the reaction time periods

The results obtained by varying the diazotization time are shown in Fig. 4. The blanks gave negligible absorbances and very low and constant TLS signals in all cases. Using $8 \times 10^{-5}M$ PABA, the absorbance was the

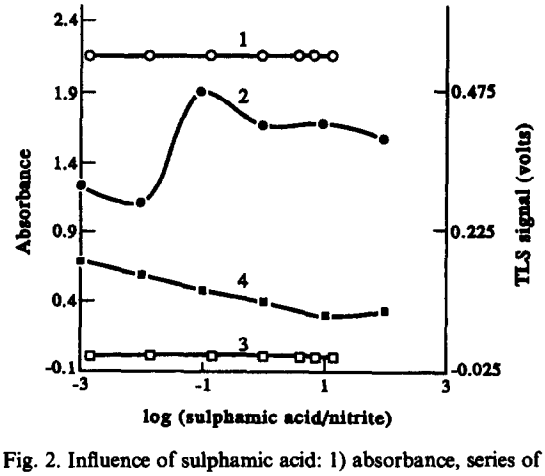

Fig. 2. Influence of sulphamic acid: 1) absorbance, series of single experiments; 2), TLS signal, means of series of duplicated experiments; 3) absorbance blanks; 4) TLS blanks. The logarithms of the sulphamic acid/nitrite molar ratios are represented on the X-axis. Final concentrations: PABA and NED as in Fig. 1; nitrite was $1.4 \times 10^{-3}M$ and $2 \times 10^{-4}M$ for the spectrophotometric and TLS experiments, respectively.

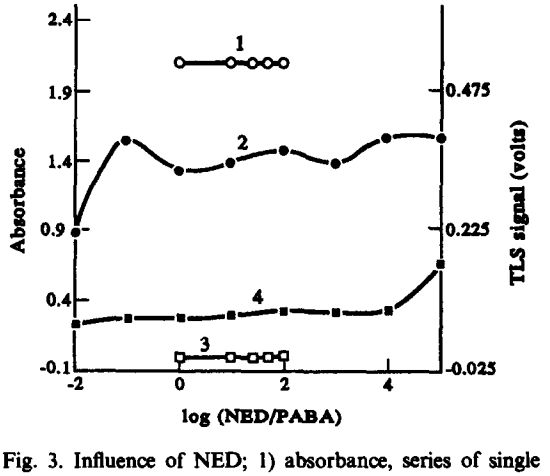

Fig. 3. Influence of NED; 1) absorbance, series of single experiments; 2) TLS signal, means of series of duplicated experiments; 3) absorbance blanks; 4) TLS blanks. The logarithms of the NED/PABA molar ratios are represented on the X-axis. Final concentrations: PABA as in Fig. 1; nitrite as in Fig. 2; sulphamic acid was $6 \times 10^{-3}M$ and $2 \times 10^{-3}M$ for the spectrophotometric and TLS experiments, respectively.

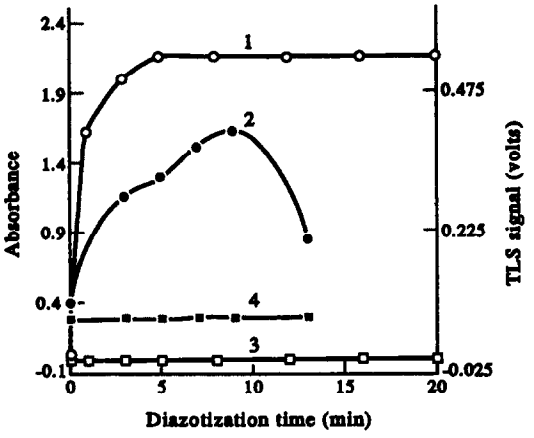

Fig. 4. Influence of diazotization time; 1) absorbance, series of single experiments; 2) TLS signal, means of series of duplicated experiments; curves 3 and 4 are the corresponding blanks. Concentrations are those given in the Procedures section.

same for diazotization times between 4 and 20 min. However, for $8 \times 10^{-7}M$ PABA, the TLS experiments showed a continuous sensitivity increase, followed by a decrease at diazotization times larger than 10 min. Therefore, at the low concentrations used in TLS, diazotization is slower but the decomposition of the diazonium ion in the presence of excess nitrite is more rapid than in the spectrophotometric experiments. The diazotization time was set at 10 min in the recommended procedure.

After addition of sulphamic acid, 2 min were enough to assure quantitative nitrite excess elimination in all cases, and no significant variations of the blank and PABA signals were observed for reaction times between 1 and 20 min. Finally, no sensitivity changes were observed when the absorbance and TLS signals were measured immediately after the addition of NED and 20 min later; therefore, coupling with NED was very rapid in the SDS micellar medium, and the azodye was stable.

Hydrolysis and azodye formation of the diuretics

The diuretics studied here are secondary arylamines and, therefore, diazotization required previous hydrolysis of the α N—C bond. However, some colour appeared when the procedure was applied directly to the diuretics. This was attributed to partial hydrolysis produced by the acid medium of the diazotization reaction. The yield of azodye formation increased largely when the solutions containing the diuretic, $0.15M$ HCl and $0.043M$ SDS, were put in a water bath at 100° for a few minutes. Brown precipitates were formed using hydrolysis times longer than 10 min for hydrochlorothiazide and bendroflumethiazide, and longer than 20 min for furosemide. The precipitates appeared in less than 1 min when hydrolysis was performed in a $1M$ HCl medium. The results shown in Fig. 5 suggested that hydrolysis was complete after 5 min for bendroflumethiazide and furosemide, and was about 50% for hydrochlorothiazide at 10 min.

The hydrolysis time was also optimized using $3 \times 10^{-7}M$ hydrochlorothiazide and TLS detection. Figure 5 also shows the TLS signal obtained for hydrolysis times between 1 and 15 min. Formation of a precipitate was observed for more than 15 min of hydrolysis.

Interference of 3-substituted indoles in urine

Application of an absorptiometric procedure to urine samples requires efficient separation of the analytes from the coloured substances of the urine matrix, or urochromes; otherwise, high blanks are obtained.[19,20] First, low blanks and isolation of the diuretics was attempted using SCX solid-phase extraction columns. Urine samples, taken from two different healthy volunteers, were centrifuged, passed through 0.45 μm pore filters, and made $0.043M$ in SDS to avoid protein precipitation.

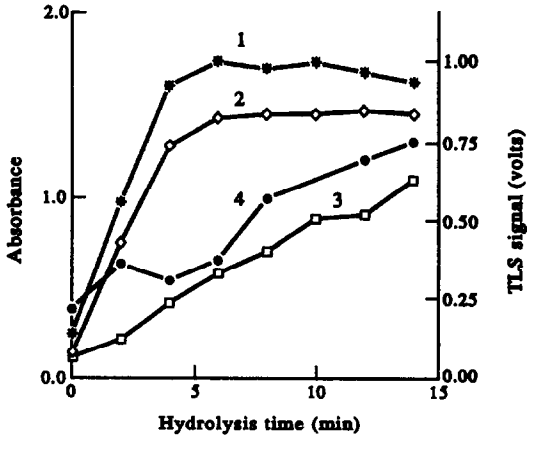

Fig. 5. Influence of hydrolysis time: spectrophotometric determination of $6 \times 10^{-5}M$ bendroflumethiazide (1), furosemide (2) and hydrochlorothiazide (3), and TLS determination of $2.5 \times 10^{-7}M$ hydrochlorothiazide (4). Series of single experiments.

The SCX columns were equilibrated with a solution of 0.2*M* acetic acid and 0.043*M* SDS. A 0.5 ml sample of the $10^{-3}M$ solutions of the diuretics, as well as 2 ml aliquots of urine in the same medium, were passed through the columns. Elution was performed by washing three times with 0.5 ml of 0.1*M* HCl. Recovery of the diuretics was not quantitative, *i.e.* $70 \pm 5\%$ and $50 \pm 5\%$ for hydrochlorothiazide and bendroflumethiazide, respectively (series of eight extractions). Urine samples gave transparent eluates which showed negligible absorbance at 514.5 nm, and a very low TLS signal. However, the slow formation of a red–blue colour was observed when the derivatization procedure was applied to the urine eluates. Absorbance increased slowly for 2 hr, a maximum being formed at 560 nm. The concentration of arylamines in urine (*e.g.* folic acid) is too low (nanomolar level) to explain colour formation upon diazotization and coupling.

Urine contains 3-substituted indoles, *e.g.* 5-HIAA, tryptophan, serotonine and other metabolites, at the millimolar level. When treated with nitrite, 3-substituted indoles give *N*-nitroso derivatives.[21] The derivatization procedure was applied to 0.5 ml of 0.01*M* 5-HIAA and tryptophan solutions (final volume was 10 ml). When nitrite was added, tryptophan gave a yellow colour. Further addition of sulphamic acid and NED slowly produced dark yellow and red–blue colours with 5-HIAA and tryptophan, respectively. No references about the possible reactions involved were found.

The apparent molar absorptivity of the colour developed by tryptophan was low ($\epsilon = 135\ \mathrm{cm^{-1}mol^{-1}\,l}$ at 560 nm), but the colour given by several urine samples in the same wavelength region was intense; thus, 3-substituted indoles seriously interfered in the determination of the diuretics in urine owing to their large concentration. The position of the maximum (560 nm) and colour intensity did not vary when the tryptophan solutions were previously made 0.15*M* and 1*M* in HCl, or 1*M* in NaOH, and were treated at 100° for 30 min.

HPLC preliminary results

Owing to the presence of these spectral interferences in urine, and to the lack of an adequate solid-phase extraction procedure, HPLC was tried. A micellar mobile phase of SDS was chosen. Using this phase, direct injection of the urine samples (without deproteinization or extraction) is possible, and the samples are ready to be injected immediately after derivatization in the same micellar medium.

A series of chromatograms, including unmodified and spiked urine samples, with both conventional and thermal lens spectrophotometric detection, are given in Fig. 6. Using both conventional and thermal lens detection, changes of the refractive index produced deformations of the background, beginning at 0.8 ml (0.8 min), *i.e.* at the dead volume. The same value was obtained by injecting an aqueous potassium iodide solution. The narrow isolated peak at 3.7 min was also produced by changes of the refractive index, and should be attributed to the mismatch of sodium concentrations between the mobile phase and the injected solution.[22] Sodium was retained by this chromatographic system owing to the ion-exchange processes on the negatively charged stationary phase.

The urine blanks gave a single small peak at 5 min which did not interfere. This peak was not present in the corresponding chromatograms performed with the reagents in the absence of urine. The peaks of hydrochlorothiazide, bendroflumethiazide and furosemide were observed at 6.5, 8.2 and more than 20 min, respectively. No significant modifications of the chromatograms were observed by spiking the samples with up to $1 \times 10^{-4}M$ 5-HIAA and tryptophan.

Analytical figures of merit

The limits of detection (LODs) were calculated as three times the standard deviation of the blanks (eight measurements), divided by the slope of the calibration curves (six points per curve). Spectral characteristics of the dyes, LODs and coefficients of variation of the batch procedures are given in Table 1 for PABA and the diuretics. The TLS procedures gave limits of detection 20–50-fold smaller than the corresponding conventional spectrophotometric procedures. Dynamic ranges were over two orders of magnitude for the TLS procedures; furthermore, in TLS the upper limit of the dynamic range can be extended up to high absorbance values by decreasing the pump beam power, as long as the probe beam is not significantly absorbed.

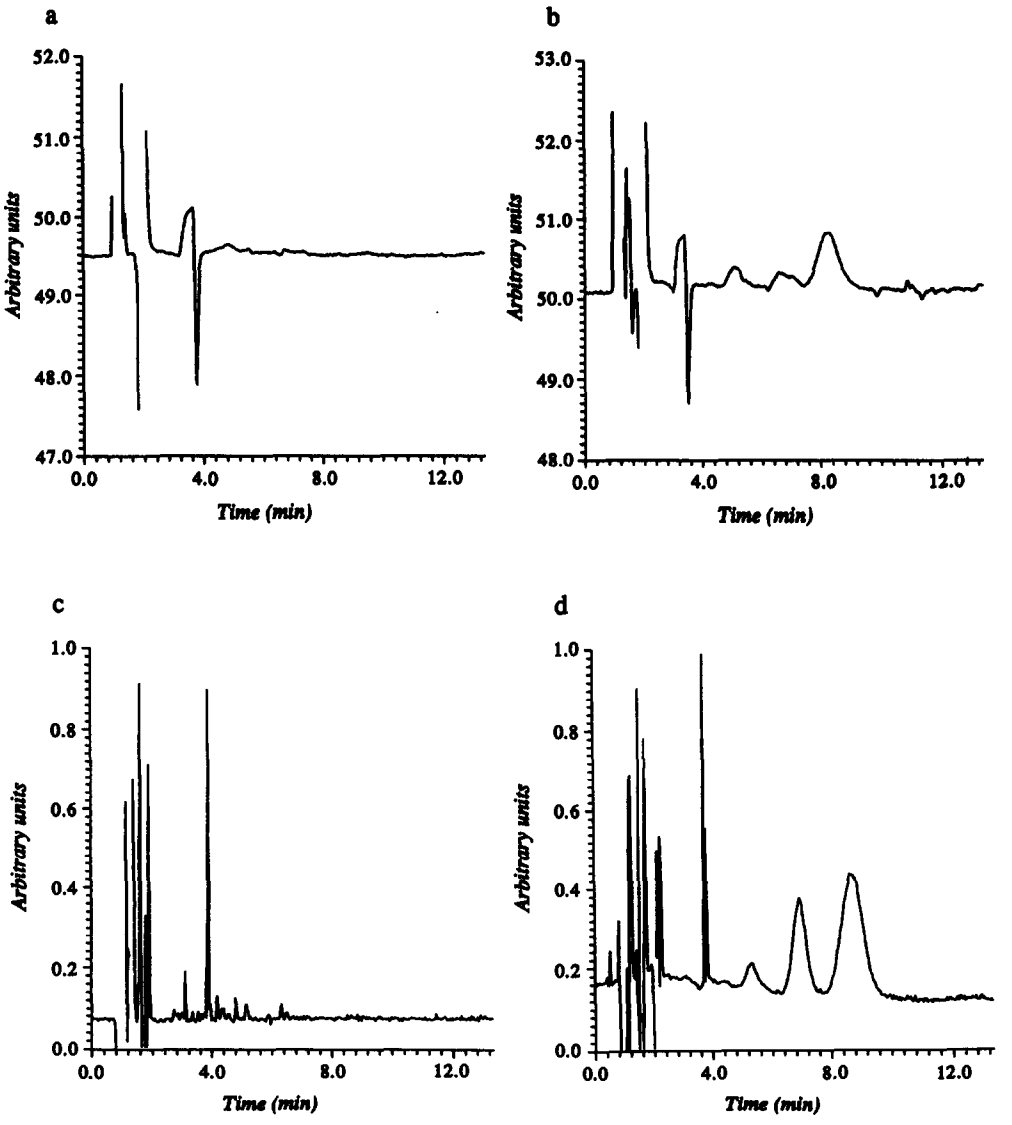

Fig. 6. Chromatograms obtained after derivatization of: (a) urine matrix, UV–vis detection; (b) urine spiked with 20 μg/ml hydrochlorothiazide and 28 μg/ml bendroflumethiazide, UV–vis detection; (c) urine matrix, TLS detection; (d) urine spiked with 15 μg/ml hydrochlorothiazide and 21 μg/ml bendroflumethiazide, TLS detection. Mobile phase: 0.1*M* SDS + 5% *n*-propanol at pH 3 (phosphate buffer).

Table 1. Spectral characteristics and figures of merit for the conventional spectrophotometric (sp) and thermal lens (TLS) determination of diazotizable substances with NED

Compound	λ_{max} (log ϵ_{max})	$\frac{\epsilon_{514}}{\epsilon_{max}}$	LOD $M \times 10^9$ sp	LOD $M \times 10^9$ TLS	Coefficient of variation,%* (conc., *M*) sp	Coefficient of variation,%* (conc., *M*) TLS
PABA	556 (4.34)	0.57	160	4	4 (2×10^{-6})	4 (1×10^{-7})
Hydrochloro thiazide	532 (4.12)	0.91	300	7	12 (3×10^{-5})	11 (2×10^{-7})
Bendroflume thiazide	526 (4.50)	0.95	120	5	5 (3×10^{-5})	3 (2×10^{-7})
Furosemide	538 (4.32)	0.92	190	4	4 (3×10^{-5})	5 (2×10^{-7})

*Calculated from a series of eight independent solutions at the concentration levels indicated in parentheses.

CONCLUSIONS

The results have shown that the diazotization and coupling reactions were adequate to be exploited for the derivatization of arylamines in TLS determination procedures. The reactions were sufficiently quantitative and rapid at the low concentrations used, and the blanks gave negligible signals. In the batch procedures, the LODs were more than one decade lower than the corresponding values obtained with conventional spectrophotometry.

In addition, several new approaches which may be useful to determine drugs in physiological samples have been successfully tried in this work, *i.e.* it has been shown that arylamine diuretics can be determined in urine after hydrolysis, diazotization and coupling in a micellar medium, and micellar liquid chromatography of the corresponding azodyes. Both conventional and thermal lens spectrophotometric detection were possible, TLS giving lower LODs. Furthermore, the problem of the high background observed at the beginning of the chromatograms when micellar liquid chromatography of physiological samples is performed in the UV is overcome by using detection of the derivatized drugs in the visible region.

Acknowledgements—Thanks are due to the DGICYT (Projects PB90/425 and PB91/629) and the CICYT (Project DEP89/429) of Spain for financial support. E. F. Simó-Alfonso thanks the MEC of Spain for the FPI grant.

REFERENCES

1. G. Ramis Ramos, J. S. Esteve-Romero and M. C. García Alvarez-Coque, *Anal. Chim. Acta*, 1989, **223**, 327.
2. J. S. Esteve-Romero, E. F. Simó Alfonso, M. C. García Alvarez-Coque and G. Ramis Ramos, *Anal. Chim. Acta*, 1990, **235**, 317.
3. J. S. Esteve-Romero, M. C. García Alvarez-Coque and G. Ramis Ramos, *J. Coll. Interface Sci.*, 1991, **141**, 44.
4. J. S. Esteve-Romero, M. C. García Alvarez-Coque and G. Ramis Ramos, *Talanta*, 1991, **38**, 1285.
5. N. J. Dovichi, *CRC Crit. Rev. Anal. Chem.*, 1987, **17**, 357.
6. G. Ramis-Ramos, *Anal. Chim. Acta* (in press).
7. K. Fujiwara, H. Uchiki, F. Shimokoshi, K. I. Tsuonda, K. Fuwa and T. Kobayashi, *Appl. Spectrosc.*, 1982, **36**, 157.
8. G. Khaledi, *Trends Anal. Chem. (Pers. Ed.)*, 1988, **7**, 293.
9. J. Haginaka, J. Wakai and H. Yasuda, *J. Chromatogr.*, 1989, **488**, 341.
10. M. J. Koenigbauer, *J. Chromatogr., Biomed. Applic.*, 1990, **96**, 79.
11. L. J. Cline Love and J. J. Fett, *J. Pharm. Biomed. Anal.*, 1991, **9**, 323.
12. I. Carretero, M. Maldonado, J. J. Laserna, E. Bonet and G. Ramis-Ramos, *Anal. Chim. Acta*, 1992, **259**, 203.
13. E. Bonet Domingo, M. J. Medina Hernández, G. Ramis Ramos and M. C. García Alvarez-Coque, *J. Chromatogr., Biomed. Applic.* 1992, **582**, 189.
14. E. Bonet Domingo, M. J. Medina Hernández, G. Ramis Ramos and M. C. García Alvarez-Coque, *Analyst*, 1992, **117**, 843.
15. E. Bonet Domingo, M. J. Medina Hernández and M. C. García Alvarez-Coque *J. Pharm. Biomed. anal.* (in press).
16. E. F. Simó Alfonso, M. A. Rius Revert, M. C. García Alvarez-Coque and G. Ramis Ramos, *Appl. Spectrosc.*, 1990, **44**, 1501.
17. E. F. Simó Alfonso, M. C. García Alvarez-Coque, G. Ramis Ramos, A. Cladera Forteza, M. Estela Ripoll and V. Cerdá Martín, *Anal. Lett.*, 1992, **25**, 573.
18. J. R. Torres-Lapasió, J. J. Baeza-Baeza and G. Ramis-Ramos (awaiting publication).
19. R. M. Villanueva-Camañas, J. M. Sanchis-Mallols, E. F. Simó-Alfonso and G. Ramis-Ramos, *Anal. Lett.*, 1992, **25**, 1425.
20. J. M. Sanchis-Mallols, R. M. Villanueva-Camañas and G. Ramis-Ramos, *Analyst*, 1992, **117**, 1367.
21. D. Barton and W. D. Ollis (eds), *Comprehensive Organic Chemistry*, Vol. 4, *Heterocyclic Compounds*, p. 422. Pergamon, Oxford, 1979.
22. J. M. Sanchis-Mallols, R. M. Villaneuva-Camañas and G. Ramis-Ramos (submitted).

Talanta, Vol. 40, No. 11, pp. 1719–1723, 1993
Printed in Great Britain.

0039-9140/93 $6.00 + 0.00

13-HYDROXYACENAPHTO[1,2-b]QUINOLIZINIUM BROMIDE AS A NEW FLUORESCENCE INDICATOR

M. A. MARTIN, B. DEL CASTILLO* and P. PRADOS

Laboratorio de Técnicas Instrumentales, Facultad de Farmacia, Universidad Complutense de Madrid, 28040-Madrid, Spain

Summary—13-Hydroxyacenaphtho[1,2-b]quinolizinium bromide (13-HQBr) was selected as a fluorescence indicator to determine basic compounds in non-aqueous media. This compound possesses an acidic phenolic hydroxyl group. It presents varying absorption (R—OH, 408, 430 nm; R—O^- 456, 478 nm) and excitation spectra (R—OH, 425 nm; R—O^-, 471 nm) depending on the pH of the media, but the same emission fluorescence spectrum (R—OH = R—O^-, 526 nm) at different pH in buffered aqueous solutions. However, in acidic non-aqueous media (acetic, formic and trifluoroacetic acids), it can be observed that the fluorescence emission spectra differ for the ionized (λ_{em} = 530 nm) and non-ionized (λ_{em} = 440, 470 nm) forms. The fluorescence intensity at the characteristic peaks depends on the acid–base equilibria in the ground and excited states. Therefore, this property could be used to evaluate the concentration of basic compounds, showing a good linearity range between fluorescence intensity and basic sample concentration.

Fluorescence sensors are devices able to indicate, continuously and reversibly, changes in either the concentration of the analyte or in the physico-chemical behaviour of a medium. Thus, the variation of the analyte concentration causes changes in the fluorescent properties of the sensor, such as spectral shifts, increase or decrease in the fluorescent intensity, quantum yield and fluorescence lifetime. In most cases, an indicator is included or immobilized onto the optical fibre and reacts with the analyte; the reaction produces a variation in the fluorescent properties which can be measured and related to the analyte concentration. Extensive reviews have been dedicated to this subject.[1-3] It is necessary to search for adequate fluorescent compounds sensitive to analyte concentration variations. Fluorescence pH indicators are very sensitive to pH variation and detect changes in the pH value of 0.01 units.[4] Bromothymol blue[5] and 7-hydroxycoumarine-3-carboxylic acid[6] have been immobilized onto optical fiber and used as fluorescence pH sensors. In the same way, NH_3 can be sensitively determined using an oxazine derivative[7] or *p*-nitrophenol[8] as fluorescent pH sensors.

There are many compounds which can behave as fluorescent sensors which can be incorporated on an optical fiber and thus allow the detection of non-fluorescent compounds. Quinolizinium salts show interesting chemical and spectroscopic properties, including the fluorescent intensity changes related to solvent polarity,[9] and can also be considered as good fluorescent probes for micellar media[10] as well as fluorescent reagents for nucleophiles.[11] We propose here 13-hydroxyacenaphtho[1,2-b]-quinolizinium bromide (13-HQBr) as a fluorescence pH indicator. This compound also shows changes in the fluorescent excitation and emission spectra in the presence of basic compounds in non-aqueous media and consequently it can be considered as a potential fluorescent sensor for amine determination.

EXPERIMENTAL

Apparatus and reagents

UV–visible spectra of 13-HQBr were obtained with an automatic, double beam Kontron Uvikon 810 spectrophotometer. Uncorrected excitation and fluorescence emission spectra and measurements at fixed wavelength were carried out with a Perkin–Elmer LS-3 spectrofluorimeter (Xenon lamp 150 W) commanded from a personal computer. A Radiometer Copenhagen PHM 72 MKZ pH meter was used to measure the pH values.

All the reagents and solvents were analytical grade. 13-HQBr was synthesized at the

*Author for correspondence.

Department of Organic Chemistry of the University of Alcalá de Henares.

Procedures

General procedure. In all of the experiments, a stock $1.0 \times 10^{-4}M$ ethanolic solution of 13-HQBr was prepared. Aliquots of 1 ml taken from this solution were evaporated to dryness under reduced pressure and redissolved in 10 ml of the desired solvent (buffered aqueous solutions or acetic, formic or trifluoroacetic acids). From this solution aliquots were taken in order to obtain final concentrations of $1.0 \times 10^{-8}M$ and $1.0 \times 10^{-7}M$ of the quinolizinium derivative.

Determination of the pK_a *and* pK_a^*. The pK_a and pK_a^* values of 13-HQBr were determined spectrophotometrically and spectrofluorimetrically. Measurements at specific pH values involved the use of McIlvaine buffers (0.1*M* citric acid–0.2*M* sodium biphosphate; enough potassium chloride for adjusting the ionic strength to 1.0*M*). Britton–Robinson titrated solutions (1.0*M* orthophosphoric acid,1.0*N* acetic acid, 1.0*N* boric acid, titrated with 0.2*N* sodium hydroxide solution) were also used, and in both cases two extreme values of pH were achieved by using 1.0*M* sulphuric acid and 1.0*M* sodium hydroxide solutions. The quinolizinium salt concentration was $1.0 \times 10^{-5}M$ for spectrophotometric measurements and $1.0 \times 10^{-6}M$ for spectrofluorimetric measurements.

The determination of pK_a^* was performed by adding 10 μl aliquots of triethylamine, corresponding to concentrations of $2.88 \times 10^{-6}M$ to $5.76 \times 10^{-3}M$, to a $1.0 \times 10^{-7}M$ solution of the quinolizinium salt in formic acid. The pH values varied from -2.21 to -1.10.

Assay of basic compounds. 13-HQBr behaves as a fluorescent indicator for amines and basic compounds. In order to prove this behaviour, $1.0 \times 10^{-6}M$ solutions of the quinolizinium derivative in acetic acid, prepared according to the general procedure, were treated with increasing concentrations of each basic compound. In the case of pharmacologically active compounds (benzocaine and phenylephrine hydrochlorides), they were treated with mercury acetate in order to obtain the free base. UV–visible and excitation and fluorescent emission spectra were obtained from these solutions and measurements of fluorescence intensity at fixed wavelength were also performed for the linear regression analysis.

Assay of humidity. Solutions ($1.0 \times 10^{-6}M$) of the quinolizinium derivative were prepared in acetic and formic acids according to the general procedure. Aliquots of 1 ml were taken from these solutions, to which increasing amounts of water were added; the final volume of 10 ml was then completed with acetic or formic acid. The final concentration of the quinolizinium was $1.0 \times 10^{-7}M$ and that of water covered the values from 0% to 5% (v/v).

RESULTS AND DISCUSSION

The presence of a phenolic hydroxyl group attached to the quinolizinium ring gives an acidic character to the compound. Its acid–base ionization equilibrium is presented in Fig. 1.

The acid (R—OH) and the ionized ($R—O^-$) forms present different absorption spectra, as can be observed in Fig. 2. Thus, the non-ionized form exhibits two absorption maxima in the visible region at 408 and 430 nm, while the ionized form absorbs at 456 and 478 nm, as well as having a molar absorption coefficient lower than the R—OH species. The existence of an isosbestic point at 370 nm shows that there are only two forms in the equilibrium.

These changes in the absorption spectra imply similar behaviour in the excitation and emission properties of 13-HQBr. Thus, the excitation maxima are 425 and 471 nm for the R—OH and $R—O^-$ species, respectively. In aqueous buffered solutions, only an emission maximum at 526 nm was observed for both forms. Similarly, the emission intensity for the phenolate anion is lower than that observed for the phenolic non-ionized form, as can be seen in Fig. 3. Therefore, we can propose the use of 13-HQBr as a sensitive fluorescence and absorbance pH indicator due to the pH-associated spectral changes observed in the positions and intensity of the

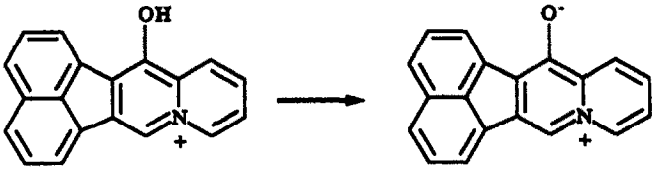

Fig. 1. Acid–base ionization equilibrium for 13-HQBr.

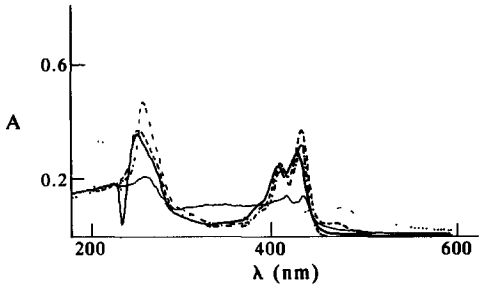

Fig. 2. UV–visible spectra of 13-HQBr ($c = 1.0 \times 10^{-5} M$) in different solvents: buffered aqueous solutions. (——) pH 2; (·····) pH 8; (– – –) acetic acid; (–·–·–) formic acid; (——) trifluoroacetic acid. A, absorbance; λ, wavelength.

absorption, excitation and fluorescence emission spectra.

Figures 4 and 5 show the pK_a value (3.7) calculated for this compound on the basis of the spectrophotometric and spectrofluorimetric values. This strongly acidic character can be explained by the electron-withdrawing ability of the azonia nitrogen atom and the acenaphtho moiety. Similar effects explain the very low pK_a values of phenolic compounds such as picric acid.

In buffered aqueous solutions, the phenolic and phenolate forms exhibit different excitation spectra depending on pH. However, the emission maximum is the same and the fluorescent intensity decreases when the pH is increased (Fig. 3). This means that in the excited state, the ionized and non-ionized forms present the same fluorescence. Deactivation of excited state and acid–base equilbria are two competitive processes that take place in solution. If it is assumed that the proton transfer process is slower than deactivation of the excited state, the existence of only one fluorescent species in the pH range from 1 to 12 can be explained.[12,13] In

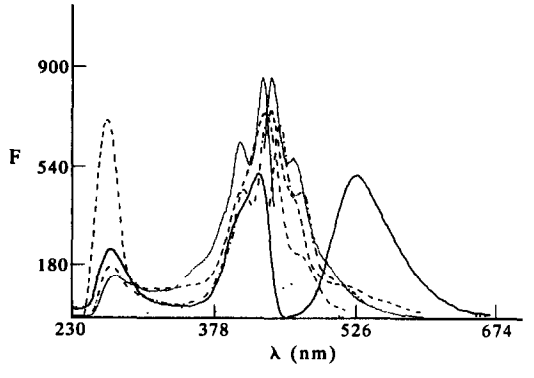

Fig. 3. Excitation and fluorescence emission spectra of 13-HQBr ($c = 1.0 \times 10^{-6} M$) in different solvents: buffered aqueous solutions. (——) pH 2; (·····) pH 8; (– – –) acetic acid; (–·–·–) formic acid; (——) trifluoroacetic acid. F, fluorescence intensity in arbitrary units; λ, wavelength.

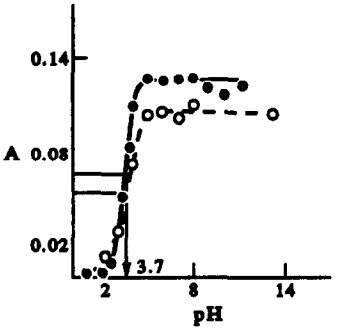

Fig. 4. Spectrophotometric determination of pK_a of 13-HQBr: (●) in titrated solution of Britton–Robinson; (○) in McIlvaine buffer. Absorbance (A) at 478 nm against pH.

order to confirm this hypothesis, the fluorescence emission intensity was measured at the wavelength of the isosbestic point (370 nm) at different pH values; no significant differences in the fluorescence emission were found. In these conditions the fluorescence intensity should have changed if different excited species (R—OH*, R—O$^-$*) had existed.

However, the ionization rate for many ionizable compounds is very high compared to the deactivation rate of the excited state. In such cases, the fluorescence emission spectrum changes with pH, the pK_a* value (pK_a for the compound in the excited state) can be obtained and the ionization equilibrium can be observed in the excited state and therefore detected by changes in the fluorescence emission spectrum or fluorescent intensity. For such compounds, the pK_a* value is extremely different from the pK_a value and the ionization process corresponding to the excited state can be detected in strongly acidic or basic media.[14] This particular behaviour was observed for 13-HQBr in acetic, trifluoroacetic and formic acid solutions. In the last two solvents, whose pK_a values are lower

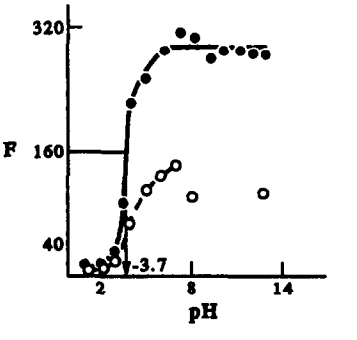

Fig. 5. Spectrofluorimetric determination of pK_a of 13-HQBr: (●) in titrated solution of Britton–Robinson; (○) in McIlvaine buffer. Fluorescence intensity (F) in arbitrary units ($\lambda_{ex} = 471$ nm, $\lambda_{em} = 526$ nm) against pH.

than that of the quinolizinium derivative in the ground state, excitation maxima are seen at 408 and 438 nm (formic acid), or 405 and 428 nm (trifluoroacetic acid). In formic and trifluoroacetic acids, the emission maximum at 520–530 nm cannot be observed because these solvents present pK_a values lower than those of the fluorescent compound; therefore, 13-HQBr is only present as the R—OH form, which emits at 442 and 467 nm; the R—O^- species does not exist. In the case of acetic acid ($pK_a = 4.75$), a solvent slightly less acidic than the quinolizinum derivative, both forms (R—OH and R—O^-) will exist and the maxima are located at 445 (excitation), and 467 and 534 nm (emission), as can be seen in Fig. 3. The different positions of the maxima, depending on the acidity of the solvent, allowed the calculation of pK_a^*, since addition of small amounts of base (triethylamine or water; see Figs 7 and 8) caused a decrease in the fluorescence intensity of the shorter emission maxima and an increase in the intensity of the maximum at 530 nm. The pK_a^* value thus calculated was -1.84 (Fig. 6). This value proves that the excited state is several orders of magnitude more acidic than the ground state, in agreement with previous observations on other compounds where an acid–base equilibrium has been observed in the excited state.[15]

The behaviour of 13-HQBr in solution is defined by the acid–base equilibrium, as well as the solvatochromic effects. The presence of small amounts of water causes significant differences in the emission spectra. However, high amounts of water originate the excitation and emission spectra of 13-HQBr dissolved in buffered aqueous solutions and the spectral resolution characteristic of acidic non-aqueous media is lost. Thus, solutions of the quinolizinium derivative in $10M$ trifluoroacetic, formic and acetic acids do not exhibit emission maxima in the vicinity of 440 and 470 nm and only the emission maximum at 520–530 nm is present. Therefore, this compound is very sensitive to changes in the polarity and pH of the media, and consequently it can be considered as an indicator for testing the pH of the media. In non-aqueous media (acetic acid), 13-HQBr shows emission spectra corresponding to the ionized and non-ionized forms, as can be seen in the following equation:

$$R—OH + BH \rightarrow R—O^-\cdot BH_2^+$$

$$\lambda_{ex} = 410 \text{ nm } \lambda_{ex} = 467 \text{ nm}$$

$$\lambda_{em} = 445 \text{ nm } \lambda_{em} = 530 \text{ nm.}$$

In such media, the indicator behaves as a strong acid and reacts with bases. The increase

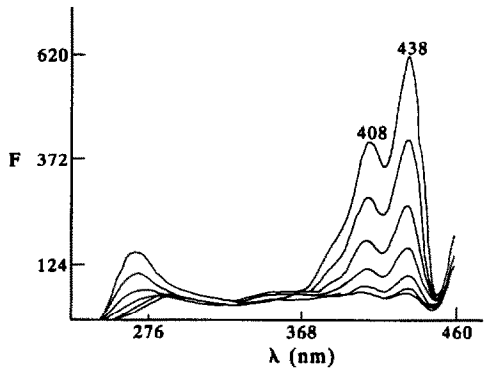

Fig. 7. Effect of the addition of increasing amounts of water on the excitation spectra of 13-HQBr dissolved in formic acid. F, fluorescence in arbitrary units, $\lambda_{em} = 467$ nm; λ, wavelength.

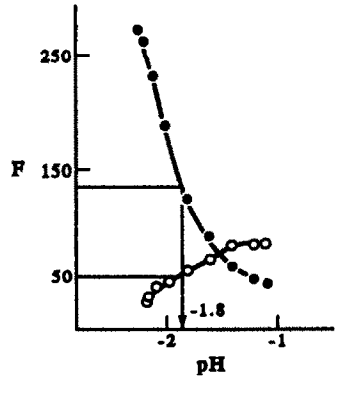

Fig. 6. Spectrofluorimetric determination of pK_a from the excited state (pK_a^*) of 13-HQBr in formic acid. Fluorescence intensity (F) in arbitrary units against pH. (●) $\lambda_{ex} = 408$ nm, $\lambda_{em} = 443$ nm (R—OH). (○) $\lambda_{ex} = 408$ nm, $\lambda_{em} = 519$ nm (R—O^-).

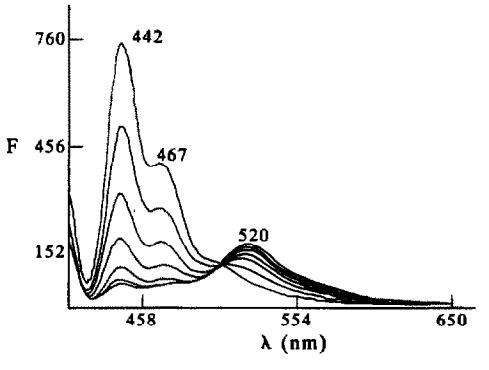

Fig. 8. Effect of the addition of increasing amounts of water on the emission spectra of 13-HQBr dissolved in formic acid. F, Fluorescence intensity in arbitrary units, $\lambda_{ex} = 408$ nm; λ, wavelength.

Table 1. Linear regression parameters and linear range obtained in the quantitation of different basic compounds using 13-HQBr as fluorescent indicator in non-aqueous solvents

Compound	Linear range	Correlation coefficient	Slope	Ordinate
Triethylamine	9.0×10^{-8}–$7.2 \times 10^{-7}M$	0.9515	921×10^{7}	91.3*
	1.4×10^{-7}–$2.9 \times 10^{-5}M$	0.9999	-2.9×10^{6}	270.0†
Pyridine	1.0×10^{-6}–$1.0 \times 10^{-4}M$	0.9794	8.3×10^{4}	40.5*
Piperidine	1.0×10^{-6}–$5.0 \times 10^{-5}M$	0.9996	4.1×10^{5}	34.99*
Benzocaine	1.0×10^{-6}–$1.0 \times 10^{-3}M$	0.9998	1.1×10^{4}	49.3*
Phenylephrine	1.0×10^{-6}–$5.0 \times 10^{-5}M$	0.9938	-3.3×10^{6}	432.7‡
Glycine	5.0×10^{-7}–$1.0 \times 10^{-5}M$	0.9962	4.8×10^{5}	95.3*
Water	0–1%	0.9921	−17.8	77.6‡
	0–5%	0.9987	−28.8	391.6†

*Acetic acid at $\lambda_{ex} = 467$ nm, $\lambda_{em} = 534$ nm.
†Formic acid at $\lambda_{ex} = 408$ nm, $\lambda_{em} = 442$ nm.
‡Acetic acid at $\lambda_{ex} = 410$ nm, $\lambda_{em} = 445$ nm.

or decrease in the emission intensity after addition of small amounts of a base allows the quantitation of basic compounds. The changes in the excitation and emission spectra of 13-HQBr in acidic solvents due to the presence of very low concentrations of water can be observed in Figs 7 and 8.

Table 1 shows the linear range obtained in the linear regression analysis for the indicator dissolved in acidic media and at different concentrations of basic compounds.

Low concentrations of water cause significant changes in the excitation and emission fluorescence spectra (Figs 7 and 8), which allows their quantitation. However, water at concentrations higher than 10% (v/v) produced an emission spectrum with only one maximum, at 526 nm, which precluded quantitation. This behaviour can be explained by the solvatochromic effect, as detailed elsewhere.[16]

This indicator is not specific because it allows quantitation based on the acid–base characteristics of the compounds; however, the good correlation coefficients proved the utility of 13-HQBr as a potential fluorescence indicator to detect basic compounds at low concentrations. Consequently, the use of 13-HQBr supported on an optical fiber allows its use as a potential fluorescence sensor for the sensitive and easy detection of amines with a good linear response.

REFERENCES

1. O. S. Wolfbeis, Fiber optical fluorosensors in analytical and clinical chemistry, in *Molecular Luminescence Spectroscopy*, S. G. Schulman (ed.), Vol. 2. John Wiley, New York, 1988.
2. O. S. Wolfbeis, *Chem. Anal.*, 1988, **77**, 129.
3. O. S. Wolfbeis, *Appl. Fluoresc. Technol.*, 1989, **1**, 1.
4. O. S. Wolfbeis and H. Marhold, *Fresenius' Z. Anal. Chem.*, 1987, **327**, 347.
5. M. J. Goldfich and C. R. Lowe, *Anal. Biochem.*, 1984, **138**, 430.
6. H. Offenbacher, O. S. Wolfbeis and E. Fürhger, *Sens. Actuators*, 1986, **9**, 73.
7. J. F. Giuhani, H. Wohltjen and N. L. Jarvis, *Opt. Lett.*, 1983, **8**, 54.
8. M. A. Arnold and T. J. Ostler, *Anal. Chem.*, 1986, **58**, 1137.
9. M. A. Martín, M. Ballesteros and B. del Castillo, *Anal. Chim. Acta*, 1985, **170**, 95.
10. M. A. Martín, D. A. Lerner, J. Ezquerra, J. Alvarez-Builla and B. del Castillo, *Anal. Chim. Acta*, 1988, **205**, 117.
11. M. A. Martín and B. del Castillo, *Anal. Chim. Acta*, 1991, **245**, 217.
12. H. Shikuza, T. Ogiwara and E. Kimura, *J. Phys. Chem.*, 1985, **89**, 4302.
13. S. G. Schulman, R. M. Threatte, A. C. Campomechne and W. L. Paul, *J. Pharm. Sci.*, 1974, **63**, 876.
14. S. G. Schulman, in *Modern Fluorescence Spectroscopy*, E. L. Whery (ed.), Vol. 2. Plenum Press, New York, 1976.
15. S. G. Schulman, *Fluorescence and Phosphorescence Spectroscopy: Physicochemical Principles and Practice*, pp. 69–92. Pergamon Press, Oxford, 1977.
16. P. Prados, Unpublished results.

Talanta, Vol. 40, No. 11, pp. 1725–1729, 1993
Printed in Great Britain.

0039-9140/93 $6.00 + 0.00

A COATED PIEZOELECTRIC CRYSTAL SENSOR FOR ACETIC ACID VAPOUR DETERMINATION

J. A. MUNOZ LEYVA,* J. L. HIDALGO HIDALGO DE CISNEROS and D. GARCIA GOMEZ DE BARREDA

Department of Analytical Chemistry, Apdo, 40, 11510 Puerto Real, Cádiz, University of Cádiz, Spain

Summary—A novel sensor for acetic acid vapour determination is proposed. This sensor is based on a piezoelectric crystal covered with a film of diethylenetriamine. For the sensor development a system of our own design—consisting of testing chamber, oscillator circuit and measure instruments—has been employed. The sensor shows its activity to the acetic acid vapours for more than 60 days. The selectivity is adequate although some vapours interfere: hydrochloric acid, formic acid, formaldehyde, tributyl phosphate, chloroform, chlorobenzene, acetone and isobutylmethylketone. The sensor described can be applied to detect acetic acid vapours in the presence of other vapours: acetonitrile, acrolein, benzene, *n*-hexane, ethanol, propanol, *n*-butyl acetate, isopropyl ether, isoamyl alcohol, ethyl ether, methylene chloride, carbon tetrachloride and toluene. The major advantages of the proposed sensor over other existing techniques are its simplicity, reduced cost and capacity for use *in situ*.

Piezoelectric crystals, due to their special characteristics,[1] are very appropriate for the construction of portable, simple and cheap detection units. In recent years coated piezoelectric crystal sensors have attracted increasing interest for monitoring traces of toxic gases in the atmosphere as well as in the air of working environments.[2–15]

Acetic acid is a corrosive acid which has numerous industrial applications and hence it is present, mainly as vapour, in some industrial atmospheres. On the other hand, it is the principal constituent of the volatile acidity of wines[16] and its content in vinegars is not smaller than 50–60 g/l.[17] The Threshold Limit Value - Time Weighted Average (TLV-TWA) for the acetic vapours is 10 ppm (25 mg/m^3).[18] So for all these reasons, it is very important to have sensor systems to detect acetic acid.

The existing methods for detecting acetic acid vapours use gas chromatography with a preconcentration stage on a column with adsorbent;[19,20] determination has also been described using pulsed UV photoacoustic spectroscopy.[21] With these techniques a high level of sensitivity is achieved, but they involve the use of sophisticated instruments.

As for using sensors to detect acetic acid, only one process has been described and it is used to detect the acid in solution. The sensor described in the literature is based on the property of certain bacteria which produce oxygen from acetic acid, so the acid can be detected using immobilized *Trichosporon brassicae* on a Teflon membrane electrode and an amperometric oxygen electrode. The minimum concentration for determination is 5 mg/l.[22]

In the literature which we reviewed, we found no sensors for the determination of acetic acid in its vapour form. This paper describes for the first time one sensor for acetic acid vapours, based on AT-cut piezoelectric crystals coated with diethylenetriamine films. This sensor combines a good selectivity and an acceptable sensitivity.

For studying and perfecting the new sensor we used our own design system,[23] which is capable of working statically, and is thus easily adaptable to measurement *in situ*, unlike other techniques proposed with other sensors, which work dynamically.

EXPERIMENTAL

Reagents

All reagents, those used as coatings and those used in the interference study, were of analytical reagent grade. The nitrogen was type N-50 from S.E.O. (Spanish Oxygen Company).

Materials and equipment

The 8.9 MHz At-cut PZ crystals (Universal Sensors) were mounted on HC-25/U type bear-

*Author for correspondence.

ings. The oscillator circuits employed were made of common commercial electronic components (resistors, capacitors, transistors). The sensor unit was placed inside a testing chamber which was capable of reproducing atmospheric conditions. The rest of the equipment consisted of control and measurement instruments. The complete installation, of our own design, has been reported elsewhere.[23]

Procedures

Preparation of the coated crystal. The crystal, cleaned with ethanol, was dried in warm air and placed in the testing chamber under vacuum for 5 min, whereupon dry nitrogen was injected. After 30 min, the frequency was measured and noted, the crystal removed from the chamber and then coated by immersion for 5 sec or more (or by several immersions)—according to the amount of coating desired—in a solution of 0.100 g of diethylenetriamine in 10 ml of ethanol. The crystal was dried again and the frequency measured and noted. For storage the coated crystals were each protected with a metallic capsule and introduced in a vacuum dessicator.

Measurement of the response to acetic acid. The stabilized frequency of the coated crystals in an air or nitrogen atmosphere (in the testing chamber) was measured and noted. The chamber was evacuated and the acetic acid injected. The initial conditions (pressure and temperature) were re-established and the frequency again measured and noted, calculating the difference, Δf, between this measurement and the previous one. The sensor was restored to its original condition by vacuum and nitrogen after this second measurement. The time necessary for this restoration is defined as recovery time (T_R). In this manner, the measurements are all independent.

The concentration of acetic acid vapours was calculated from the previously constructed calibration graphs.

RESULTS AND DISCUSSION

Selection of coatings

The acidic nature of the sample for analysis led us to select basic coatings. With all the coatings tested, a reduction in frequency was noted in the coated crystal, but the magnitudes of variation were very different. For a fixed amount of 4.33 mg/l. of acetic acid in the chamber, the differences in frequency in Hz, Δf, of the crystal, in the absence and presence of the sample being analysed, were as follows:

Diphenylamine, 6 Hz
Thiosemicarbazide, 9 Hz
Diethylenetriamine, 32 Hz
Phenylhydrazine, 10 Hz
2,4-dinitrophenylhydrazine, 8 Hz
1,10-phenanthroline, 19-Hz
2,2′-bipyridine, 5 Hz
4-ethyl-3-thiosemicarbazide, 16 Hz
4-phenylthiosemicarbazide, 1 Hz
2,6-diacetylpyridine, 20 Hz.

On the basis of these results, diethylenetriamine was chosen as the coating. The fact that the aliphatic amine responds most sensitively to acetic acid suggests that interaction between the ethyl group of the acetic acid and the amine could help to attract acetic acid into the coating.

Variation of response with the amount of coating and with time

The decrease in the frequency of the coated crystal with respect to that of the non-coated crystal, Δf_O, is dependent on the coating amount: the greater the coating the greater the Δf_O value. We prepared coated crystals with two different quantities of diethylenetriamine, obtaining the decreasing frequencies (Δf_O) shown in Table 1.

On the other hand, we found that the frequencies of the coated crystals shift with time. Using the above mentioned crystals, we measured Δf_O of the coated crystals over 60 days and the results are also shown in Table 1.

The Δf_O values first decrease quickly and then slowly, indicating a loss of coating. After 19 days, Δf_O begins to increase slowly, probably

Table 1. Variation of Δf_O with time

Time elapsed (days)	Δf_O(Hz)	Δf_O(Hz)
1*	5786	2242
2	2589	1368
3	1292	432
4	1217	—
5	—	322
8	1204	—
9	1151	—
11	1382	266
15	1416	235
20	1440	266
25	1512	275
35	1559	278
40	1687	280
50	1720	—
60	1764	—

*Coated crystals only.

Table 2. Influence of pressure

Pressure (*mm Hg*)	Δf_0(Hz)*	Δf_0)Hz)†	Δf_0(Hz)
720	8,995,877	8,995,848	29
747	8,995,876	8,995,847	29
775	8,995,875	8,995,846	29
802	8,995,874	8,995,845	29
829	8,995,873	8,995,844	29

*In the absence of acetic acid.
†In the presence of acetic acid.

owing to progressive contamination of the crystals. Nevertheless, after 60 days the crystals are even sensitive to acetic acid vapours.

The frequency variations we observed have been borne in mind when realizing the experiments measuring Δf_0 at that time.

Variation in the measuring conditions

In order to study the alterations when the operating conditions are modified, we utilized a testing chamber which reproduces environmental conditions and enables us to study the influence on the sensor response to acetic acid vapours in several atmospheric conditions (pressure, temperature or relative humidity). For each value studied we measured the frequencies of the coated crystals (for a given Δf_0) first in the absence and then in the presence of a definite quantity of acetic acid, calculating the difference between them (Δf). Subsequently, the magnitude should be varied in both cases in the same way.

The influence of pressure

Experiments were carried out at a constant temperature of 27°, making a vacuum in the chamber and injecting dry nitrogen at different pressures with a fixed amount (10 μl) of acetic acid each time. The variation of frequency in the range from 720 to 829 mm Hg—in the absence as well as in the presence of acetic acid—is only 4 Hz, whereas Δf for crystals with and without acetic acid at the same pressure is constant in the range studied (Table 2).

The crystal response in a dry air atmosphere (obtained by passing laboratory air through silica gel) has also been studied, and was the same as in the case of a nitrogen atmosphere.

The influence of temperature

Experiments were carried out in a nitrogen atmosphere at a constant pressure of 787 mm Hg (crystal with $\Delta f_0 = 1435$ Hz), injecting in each case a volume of 10 μl of acetic acid (4.33 mg/l.), and measuring the Δf and the recovering times of the sensor. The results are shown in Fig. 1. An increase of 0.33 Hz/° is observed within the range 15–30°, and a decrease of 0.2 Hz/° between 30 and 35°.

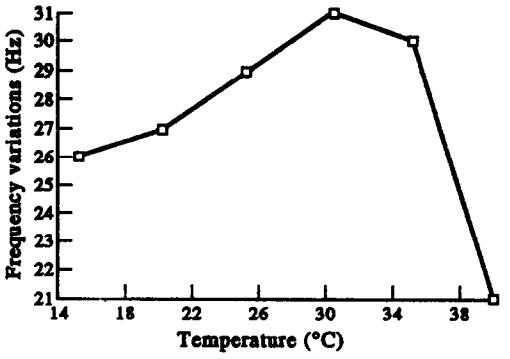

Fig. 1. Effect of temperature on the sensor frequencies.

The influence of humidity

Since the presence of water had a great influence on the frequency of some coated crystals,[23] we carried out a study on the effect of relative humidity (RH) on the oscillation frequency of the sensors tested (crystal with $\Delta f_0 = 1375$ Hz). To do this, we used a test chamber temperature of 25°, with a vacuum to cause the water to evaporate, and injected 5, 10 and 50 μl of water (equivalent respectively, to 10, 20 and 100% RH) and 10 μl of acetic acid each time. Then we injected dry nitrogen into the chamber until a pressure of 750 mm Hz was reached, measuring the oscillation frequencies of the crystal at that time, and comparing these with those measured in the absence of acetic acid.

The frequency of the PZ crystal with a diethylenetriamine coating shows a reduction of 2.8 Hz/% RH between 0 and 10% RH, whereas it is only 0.28 Hz/% RH between 10 and 100% RH (Fig. 2). The difference in frequencies in-

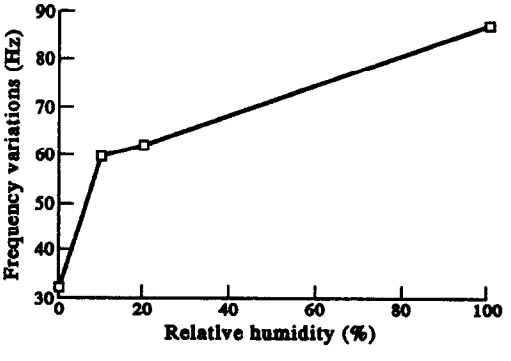

Fig. 2. Effect of relative humidity on the sensor frequencies.

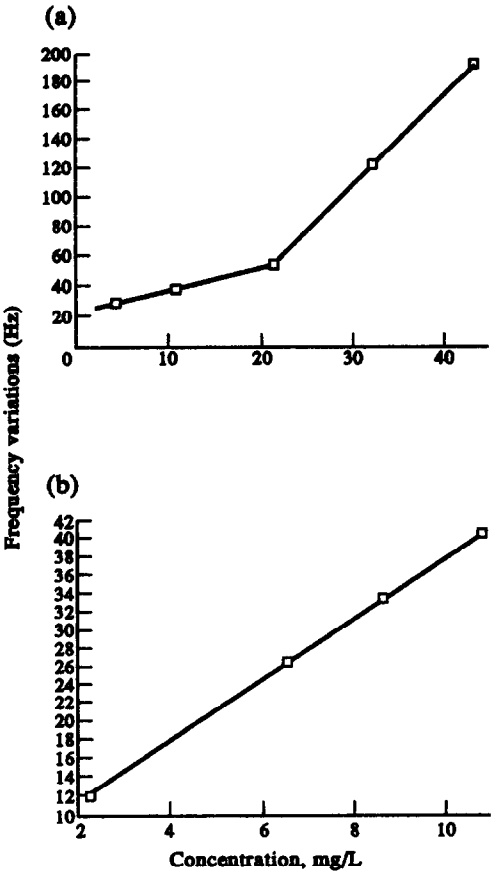

Fig. 3. Influence of acetic acid concentration: (a) $\Delta f_0 = 1490$ Hz; (b) $\Delta f_0 = 652$ Hz.

creases over the complete range, so we have to conclude that the humidity content interferes in the determination of acetic acid, but this interference is eliminated by passing the sample through silica gel.

Influence of acetic acid concentration

The calibration of the sensors in the presence of acetic acid was done in a dry air atmosphere (0% RH) at 25° and a pressure of 760 mm Hg. For each concentration of acetic acid we measured the frequencies, both in the presence and the absence of the acid, and calculated the difference between them (Δf).

We tested two crystals with different quantities of coating and with values of Δf_0 at the time of the experiments of 1490 and 652 Hz for the larger and smaller quantities of diethylenetriamine, respectively.

Figure 3 shows the results obtained for the coated crystals. The calibration equations for the crystals coated with diethylenetriamine were as follows:

($\Delta f_0 = 1490$ Hz) $\Delta f = 1.63$ [CH_3COOH] + 22.3, $r = 0.9981$ (4.33–21.7 mg/l.)

($\Delta f_0 = 1490$ Hz) $\Delta f = 6.28$ [CH_3COOH] – 79.0, $r = 0.9997$ (21.65–43.3 mg/l.)

($\Delta f_0 = 652$ Hz) $\Delta f = 1.31$ [CH_3COOH] + 8.00, $r = 0.9944$ (0.43–32.5 mg/l.).

Greater sensitivity was obtained for $\Delta f_0 = 1490$ Hz, *i.e.*6.3 Hz/mg/l. The detection limit—defined as the concentration of sample for analysis which produces a three-fold greater variation than the sensor in the absence of the sample—was 0.22 mg/l.

When we used coated crystals alone the sensitivity was much greater than that above (Δf_0: 5786 Hz; sensitivity: 46.9 Hz/mg/l.); nevertheless, it varies quickly with time. For this reason in this paper coated crystals alone are not used.

Recovery time (T_R and variation of response with time

Once the sensor had been exposed to the action of acetic acid, we studied the time it took to recover its original frequency for a content of acetic acid in the chamber of 4.33 mg/l. The average recovery time was found to be 14 min. Nevertheless, the recovery time is dependent on the acetic acid concentration.

Repeatability

In order to determine the repeatability, we carried out 11 measurements in the optimized conditions, in each case by injecting acetic acid

Table 3. Study of interferences

Interferences	Conc. (*mg/l.*)	Δf
Carbon tetrachloride	63	3
Acetonitrile	31	0
Ethanol	32	0
2-Propanol	32	0
n-Hexane	27	0
Benzene	36	0
Isopropyl ether	29	0
Isoamyl alcohol	50	1
Ethyl ether	29	2
n-Butyl acetate	35	0
Methylene chloride	54	3
Toluene		0
Chlorobenzene	45	14
Isobutylmethylketone	32	9
Acrolein	34	0
Acetone	32	60
Chloroform	61	147
Tributyl phosphate	40	220
Hydrochloric acid	17	952
Formaldehyde	16	94
Formic acid	33	499

Acetic acid concentration = 4.33 mg/l.

into the chamber so that its concentration was 4.33 mg/l. Statistical treatments (95% probability level) for the greater amount of coatings used gave us the following data:

PZ coated with diethylenetriamine

$$(\Delta f_O = 1440 \text{ Hz}),$$

$$\Delta f_m = 29.63 \text{ Hz}, \ \delta_{\Delta f} = 1.43, \ (\delta_{\Delta f})_m = 0.45,$$

$$\Delta f = 29.63 \pm 1.01, \ \epsilon = \pm 5.4\%,$$

$$T_R = 14.36 \pm 1.48 \text{ min}.$$

Study of interferences

First, we measured the frequency with a given amount of acetic acid (10 μl, equivalent to 4.33 mg/l. within the chamber) and then the frequency with the same amount of acetic acid and a volume of the interfering substance 5–20 times greater.

We studied the responses of crystals coated with diethylenetriamine to 21 interfering species. In each case we worked under conditions of constant pressure (750 mm Hg) and temperature (25°). Table 3 shows the concentration of the interferents (mg/l.) and the decrease in frequency Δf.

From the results it can be concluded that the greatest interferences are caused by species of an acidic nature (hydrochloric acid, formic acid), with the effect of tributyl phosphate, chloroform, formaldehyde and acetone being significant as well.

The following do not have any effect on the sensors: acetonitrile, ethanol, 2-propanol, toluene, acrolein, *n*-hexane, benzene, isopropyl ether and *n*-butyl acetate. The rest of the specimens studied interfere to a lesser extent.

Acknowledgements—The authors wish to acknowledge their gratitude to CICYT (Project ABM92-0863) for their financial support.

REFERENCES

1. G. Sauerbrey, *Z. Phys.*, 1959, **155**, 206.
2. W. H. King Jr, *Environ Sci. Technol.*, 1970, **4**, 1136.
3. E. P. Scheide and J. K. Taylor, *Am. Ind. Hyg. Assoc. J.*, 1975, **36**, 897.
4. K. H. Karmarkar and G. G. Guilbault, *Anal. Chim. Acta.*, 1974, **71**, 419.
5. Idem, *Environ. Lett.*, 1975, **10**, 237.
6. J. Hlavay and G. G. Guilbault, *Anal. Chem.*, 1978, **50**, 1044.
7. M. H. Ho, G. G. Guilbault and B. Reitz, *Anal. Chem.*, 1983, **55**, 1830.
8. A. Mierzwinski and Z. Witkiewicz, *Uchr. Powietrza*, 1984, **18**, 73; *Chem. Abstr.*, 1985, **102**, 66570s.
9. H. M. Fog and B. Rietz, *Anal. Chem.*, 1985, **57**, 2634.
10. J. F. Alder, A. E. Bentley and P. K. Drew, *Anal. Chim. Acta*, 1986, **182**, 123.
11. J. J. McCallum, *Analyst*, 1989, **114**, 1173.
12. J. A. Muñoz, J. L. Hidalgo, D. García and A. Fraidías, *Analyst*, 1993, **118**, 175.
13. C. S. I. Lai, G. J. Moody and J. D. R. Thomas, *Analyst*, 1986, **111**, 511.
14. C. S. I. Lai, G. J. Moody, J. D. R. Thomas, D. C. Mulligan, J. F. Stoddart and R. J. Zarzycki, *J. Chem. Soc., Perkin Trans.*, 1980, **2**, 319.
15. M. A. F. Elmosalamy, G. J. Moody, J. D. R. Thomas, F. A. Kohnke and J. F. Stoddart, *Anal. Proc.*, 1989, **26**, 12.
16. P. Dubois and C. Jouret, *C. R. Acad. Agric.*, 1965, **51**, 595.
17. H. Ebner and H. Follman, *Biotechnology*, XV, H. J. Rehm and G. Reed (ed.) Weinheim, 1983.
18. American Industrial Hygiene Association (Spanish section), 1990–1991 TLVs—Valores Límites e Indices Biológicos de la ACGIH, Generalitat de Valençia, Valencia, Spain, 1990.
19. A. I. Parimskii, *Otkrytiya, Izobret., Prom. Obraztsy, Tavarnye Znaki*, 1981, **13**, 192; *Chem. Abstr.*, **95**, 17728c.
20. S. Nishiriura and S. Esaka, *Kyoto-fu Eisei Kogai Kenkyusho Nempo*, 1983, **28**, 92; *Chem. Abstr.*, **103**, 41701t.
21. P. V. Cvijin, D. A. Gilmore and G. H. Atkinson, *Appl. Spectrosc.*, 1988, **42**,(5), 770.
22. M. Hikuma, T. Kubo, T. Ysauda, I. Karube and S. Suzuki, *Anal. Chim. Acta*, 1979, **109**, 33.
23. J. A. Muñoz, J. L. Hidalgo, A. Fraidías and D. García, *Talanta* (submitted).

Talanta, Vol. 40, No. 11, pp. 1731–1739, 1993
Printed in Great Britain.

0039-9140/93 $6.00 + 0.00

KALMAN FILTERING OF DATA FROM FIRST- AND SECOND-ORDER KINETICS

R. JIMENEZ-PRIETO, A. VELASCO, M. SILVA and D. PEREZ-BENDITO
Department of Analytical Chemistry, Faculty of Sciences, University of Córdoba, E-14004 Córdoba, Spain

Summary—The Kalman filter algorithm was used to process data obtained in the simultaneous determination of species following first- and second-order kinetics. The performance of the algorithm in the quantification of chemical components from simulated data was assessed, and the influence of various parameters involved was estimated. The algorithm was applied to the resolution of cysteine–ascorbic acid and glutathione–ascorbic acid mixtures where the ascorbic acid followed pseudo first-order kinetics and the amino acids second-order kinetics in the reaction with the copper(II)–neocuproine system. Some features of the determinations (namely, afforded concentration ratios, accuracy and precision) are discussed.

The Kalman filter[1] is a mathematical algorithm which has aroused growing interest from analytical chemists in recent years.[2–7] In its various versions (linear, extended and adaptive), the algorithm has been used to address troublesome analyses in different areas. Thus, the basic principles of Kalman filtering have been widely used in high performance liquid chromatography[6] to resolve overlapped peaks[8–15] and optimize the chromatographic conditions,[16–18] as well as for quantitative multicomponent analysis in spectrophotometric applications.[7,19–25] Other uses of the Kalman filter include the resolution of fluorescence responses and background correction in thin-layer chromatography,[26–29] the resolution of overlapping lines in inductively coupled plasma atomic emission spectra,[30,31] that of strongly overlapped square wave voltammetric signals,[32,33] background correction and interference removal in first-derivative fluorimetry,[34] and a variety of applications to titrimetric methods.[35–38]

In addition, the Kalman filter is an interesting approach to reaction-rate analytical methods. In this context, the algorithm has been primarily used to develop error-compensated and multicomponent kinetic methods. With the former, the extended Kalman filter provides a powerful tool for offsetting changes in the variables influencing a kinetic process such as between-sample rate constant variations[4,39,40] and within-run temperature variations—the latter are offset by using a combined approach involving an integrated first-order rate expression and an Arrhenius equation as a model for the filter.[41,42] Because the algorithm is used in its non-linear form, its performance relies heavily on the initial parameters chosen and the number of iterations carried out. In multicomponent kinetic analysis, the linear form of the filter is also a suitable approach[43,44] to obtain accurate results in the resolution of mixtures of components in quite small rate constant ratios (even less than 2) as an alternative to classical differential reaction-rate methods.[44] The uses of this methodology include the resolution of mixtures of amino acids,[43] corticosteroids,[44] isoenzymes[45] and lower straight-chain alcohols.[46] The most recently reported application of this algorithm to multicomponent analysis involves using its extended form in combination with multiwavelength photometric detection.[47] This makes for accurate determinations under conditions where equilibrium methods based solely on spectral differences or kinetic methods relying only on rate constant differences typically fail.

In this work we extend the scope of application of the Kalman filter to the resolution of mixtures of species following different kinetics (pseudo first- and pseudo second-order) by using the algorithm both on simulated data and real data obtained in the simultaneous resolution of cysteine–ascorbic acid and glutathione–ascorbic acid mixtures by having these species react with the Cu(II)–neocuproine system, with which they form a coloured Cu(I) complex. The algorithm allows the accurate, precise resolution of the above mixtures in

widely different ratios over broad concentration ranges. Although the Kalman filter has previously been used to estimate initial reactant concentrations and rate constants for rate-based chemical assays employing a second-order chemical reaction,[48] the research reported in this work is the first attempt to apply this filter to the resolution of mixtures of species following different kinetics.

THEORETICAL BACKGROUND

Consider the following chemical system:

$$A + R \xrightarrow{k_A^*} P \qquad (I)$$

$$B + R \xrightarrow{k_B^*} P, \qquad (II)$$

the rate equations of which are:

$$d[P]/dt = k_A^*[A][R] \qquad (III)$$

$$d[P]/dt = k_B^*[B]^2[R]. \qquad (IV)$$

If $[R]_0 \gg [A]_0$ and $[R]_0 \gg [B]_0$, then, provided the analytical signal is proportional to the amount of product formed, the integrated equation for the above system can be expressed as

$$S(t) = S_0 + S_A[1 - \exp(-k_A t)] + S_B\left(1 + \frac{1}{k_B[B]_0 t}\right)^{-1}, \qquad (1)$$

where $S(t)$ denotes the signal measured at time t; S_0 the initial signal; S_A and S_B the signal increments resulting from full conversion of A and B; and k_A and k_B the pseudo first-order and pseudo second-order rate constants of A and B, respectively.

Application of the Kalman filter to the resolution of this binary mixture entails defining the state vector, $\mathbf{X}(j)$, which is what one wishes to determine: S_A, S_B and S_0, and the measurement function vector, $\mathbf{H}^T(j)$, which describes the dependence of the measurement on the states. The form of the vector for first-order kinetics is quite well known; however, that of the vector for pseudo second-order kinetics remains unknown as, to date, no reactions of this order have been studied in this context. Specifically, a measurement function vector for (II) is given by

$$\mathbf{H}^T(j) = \left[\left(1 + \frac{1}{k_B[B]_0 t}\right)^{-1} 1\right], \qquad (2)$$

which, unlike a first-order reaction, depends on the initial concentration of analyte. The algorithm was expanded by using an apparent first-order constant for this component, defined as

$$k_B^1 = k_B[B]_0, \qquad (3)$$

which is dimensionally analogous to the first-order constant. In addition, this constant allows one to compare the kinetic curves of the two species.

Under these conditions, the measurement function vector can be expressed as

$$\mathbf{H}^T(j) = \left[\left(1 + \frac{1}{k_B^1 t}\right)^{-1} 1\right], \qquad (4)$$

so the Kalman filter for this component is used to calculate k_B^1 recursively from k_B—known beforehand—and $[B]_0$, determined by the algorithm.

The procedure used involves the prior estimation of S_B at point j from its value at point $j-1$ by using the Kalman filter; the estimated S_B value allows vector $\mathbf{H}^T$ to be updated and used by the filter to update S_B. In summary, the Kalman gain and state estimation update in the linear Kalman filter are used twice: once to update $\mathbf{H}^T$ and also to update S_B from its initial value (*i.e.* S_B at point $j-1$). The linearization procedure used (one of several possibilities) largely obviates reliance of the filter on initial guesses for the parameter concerned. Specifically, if the reaction is monitored photometrically, the apparent constant k_B^1 is calculated recursively by substituting the estimated S_B values into the following expression:

$$k_B^1 = \frac{k_B}{\epsilon_B l} S_B, \qquad (5)$$

where $\epsilon_B l$ is the slope of the calibration curve.

In this work we deal with the kinetic determination of A and B in samples containing either and the simultaneous determination of both in mixtures containing them in various ratios by using the Kalman filter in three different versions, namely K_FIRST (A alone), K_SECOND (B alone) and K_MIX (mixtures of A and B).

The practical procedure involves the following steps: (a) construction of two calibration graphs relating S_A and S_B with their respective concentrations; (b) determination of the rate constants (the first-order constant k_A is obtained from the slope of a plot of $\ln[(S_A/(S_A - S_t + S_0)]$ against time, whereas the apparent first-order constant k_B^1 is calculated from the slope of a plot of $(S_t - S_0)/(S_B + S_0 - S_t)$ *vs.* time); (c) application of the pertinent filter to the samples in

order to obtain the estimated S_A and S_B; (d) interpolation of the previous values on the corresponding calibration graphs in order to obtain the respective concentrations.

The net absorbance increments—provided the reaction is monitored photometrically—required to determine the concentrations by interpolation on the pertinent calibration curves are obtained by applying the Kalman algorithm using the three BASIC programmes whose essential features are described in Table 1. The measurement noise variance, $\mathbf{R}(j)$, is taken to be $10^{-6} \times 10^{2\text{Abs}}$, which is quite realistic as it is equivalent to assuming that the standard deviation for the transmittance is 0.002 units. However, such a value must be increased when using K_SECOND and K_MIX in order to ensure that the filter eventually converges.[49] Taking into account that

$$\mathbf{K}(j) = \mathbf{P}(j/j)\mathbf{H}^{\mathrm{T}}(j)/R(j),$$

where $\mathbf{K}(j)$ is the Kalman gain vector and $\mathbf{P}(j/j)$ the error covariance matrix, the more $R(j)$ increases, the more slowly will the filter converge. Consequently, in using the programme K_MIX for the resolution of the mixtures, one must perform three iterations and use $R(j)$ values equal to one-half and one-quarter those listed in Table 1 in the second and third iterations, respectively. On the other hand, the elements of the principal diagonal of the matrix $\mathbf{P}(0/0)$ are assumed to be 0.5 in using all three programmes. Also, the state transition matrix is taken as the identity matrix and the system noise vector is assumed to be zero.

Simulated experiments

We simulated a set of kinetic curves for samples containing A (first-order) or B alone (second-order), and for others containing mixtures of both species. The signal recorded in each case was assumed to be due to a single reaction product and Beer's law was assumed to be obeyed. The results obtained for single component samples show determination errors to be less than 0.5% in all instances. We shall thus concentrate on the results obtained for simulated mixtures. The overall signal for a mixture of A and B will be given by

$$S(t) = S_0 + S_A[1 - \exp(-k_A t)] + S_B\left(1 + \frac{1}{k_B^1 t}\right)^{-1} + N(t), \quad (6)$$

where $N(t)$ denotes pseudo random noise, whose variance is taken to be $10^{-6} \times 10^{2S(t)}$. By using the programme K_MIX we calculated the errors made in estimating A and B as a function of two major parameters: (a) the constant ratio (k_B^1/k_A), which is directly proportional to the concentration of the second-order component in the mixture; (b) the signal ratio (S_A/S_B), *i.e.* the ratio of contributions to the end product formed. Since the degree of conversion is independent of the analyte concentration in first-order reactions, we chose to use a data acquisition time equal to the half-life of the first-order component (k_A^{-1}). From the results shown in Fig. 1, it follows that:

(a) The error made in the determination of component A (first-order kinetics) were less than 1% except for a k_B^1/k_A ratio of 4 or when this component contributed only moderately (*ca.* 30%) to the overall signal. If the constant ratio is unfavourable, then the accuracy in the determination of component A in a mixture increases with an increase in its concentration.

(b) The error in the determination of component B increases slightly with increasing k_B^1/k_A ratios of up to about 4, as well as with an increase in the concentration of the other component. Figure 1 does not include the curve corresponding to $k_B^1/k_A = 4$ because it oscillated

Table 1. Model information used by the programmes

Programme	$\mathbf{H}^{\mathrm{T}}(j)$	$R(j)/10^{2Z(j)}$	$\mathbf{X}(j)$	$\mathbf{X}(0/0)$	$\mathbf{P}(0/0)$
K_FIRST	$[1 - \exp(-k_A t) \quad 1]$	10^{-6}	$\begin{bmatrix} S_A \\ S_0 \end{bmatrix}$	$\begin{bmatrix} 0.5 \\ 0 \end{bmatrix}$	$\begin{bmatrix} 0.5 & 0 \\ 0 & 0.5 \end{bmatrix}$
K_SECOND	$[[1 + (k_B^1 t)^{-1}]^{-1} \quad 1]$	10^{-5}	$\begin{bmatrix} S_B \\ S_0 \end{bmatrix}$	$\begin{bmatrix} 0.5 \\ 0 \end{bmatrix}$	$\begin{bmatrix} 0.5 & 0 \\ 0 & 0.5 \end{bmatrix}$
K_MIX	$[1 - \exp(-k_A t)[1 + (k_B^1 t)^{-1}]^{-1} \quad 1]$	10^{-3}	$\begin{bmatrix} S_A \\ S_B \\ S_0 \end{bmatrix}$	$\begin{bmatrix} 0.5 \\ 0.5 \\ 0 \end{bmatrix}$	$\begin{bmatrix} 0.5 & 0 & 0 \\ 0 & 0.5 & 0 \\ 0 & 0 & 0.5 \end{bmatrix}$

$\mathbf{H}^{\mathrm{T}}(j)$, measurement function vector; $R(j)$, measurement noise variance; $Z(j)$, measurement; $\mathbf{X}(j)$, state vector; $\mathbf{X}(0/0)$ and $\mathbf{P}(0/0)$, initial guesses for state vector and error covariance matrix, respectively.

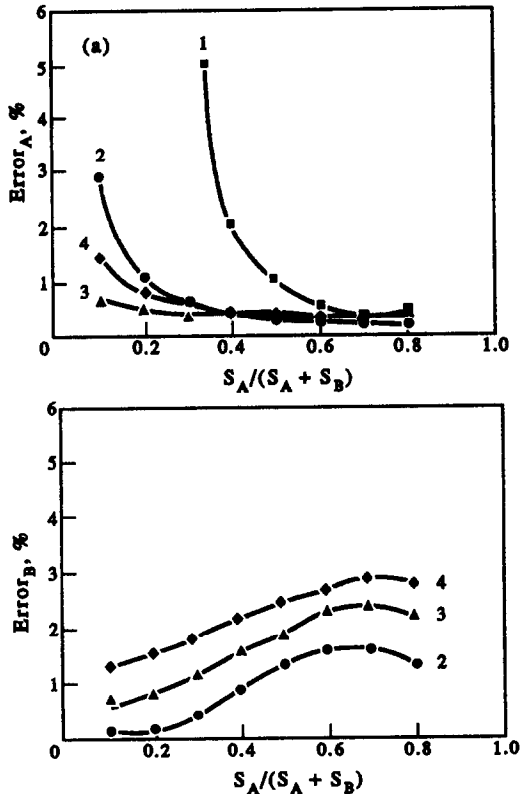

Fig. 1. Variation of the relative error in the determination of: (a) reactant A in a mixture with B and (b) reactant B in a mixture with A, as a function of S_A (contribution of A to the end product). Curves 1–4 correspond to k_B^1/k_A ratio of 4, 6, 8, and 10 h, respectively. $k_A = 10^{-2}$ sec^{-1}; $S_B = 0.250$.

somewhat, even though it gave rise to errors of less than 4% in all cases.

The filter used requires the rate constants for both reactions (k_A and k_B) to be accurately known, so errors in these constants arising from changes in the reaction conditions or inherent in their determination will detract from the accuracy of the results. We then investigated the effect of over- or underestimating such constants on the estimated concentrations of A and B in the mixtures. For this purpose we assumed a maximum variation of 5–10% in the rate constants. Figure 2 shows the results obtained at a fixed concentration of the second-order component, *i.e.* a constant k_B^1/k_A ratio (10 in this case), and three different concentrations of the first-order component. The symbols +, − and 0 in the figure denote positive, negative and nil errors in the rate constants of the two components. The results obtained allow one to draw the following conclusions:

(a) The largest errors in the determination of A (first-order kinetics) are made when those of the two constants are of opposite sign. In such cases, the errors in A are of the opposite sign to those in k_A.

(b) The errors in the determination of B are positive unless both rate constants are overestimated.

(c) The percent errors made in the determination of both A and B are much lower than those in the rate constants in most cases.

EXPERIMENTAL

Apparatus

Kinetic runs were carried out on a Metrohm 662 spectrophotometer equipped with an immersion probe and a Metrohm Dosimat 665 autoburette for dispensing a small volume of reagent in order to start the reaction. Data acquisition was done by means of a Mitac PC-AT 12-MHz compatible computer equipped with a PC-Multilab PCL-812PG AD converter and an HADC574Z industrial standard successive approximation converter featuring a conversion speed of 30 MHz. Acquisition of data was synchronized with the start of the reaction by using a trigger that acted simultaneously on the autoburette and the computer.

Reagents

We use the following solutions, all of which were made in distilled water: $10^{-3}M$ cysteine (Merck), $10^{-3}M$ ascorbic acid (Merck), $10^{-3}M$ glutathione (Sigma), $2.15 \times 10^{-2}M$ neocuproine hydrochloride, $3.15 \times 10^{-2}M$ $Cu(NO_3)_2$, $10^{-1}M$ sodium oxalate and $1M$ sodium acetate–acetic acid buffer (pH 4.8).

Procedure

In an 80-ml reaction vessel were placed an appropriate volume of an aqueous solution containing 0.06–7.0 μmoles of cysteine, 0.1–5.0 μmoles of ascorbic acid, 0.1–9.0 μmoles of glutathione or a mixture of these species (see Tables 3 and 4), plus 6.0 ml of $1M$ sodium acetate–acetic acid buffer (pH 4.8), 3.0 ml of $2.15 \times 10^{-2}M$ neocuproine hydrochloride, 15.0 ml of $10^{-1}M$ sodium oxalate and distilled water up to a final volume of 60 ml. The reaction was started by adding 1.5 ml of $3.15 \times 10^{-2}M$ $Cu(NO_3)_2$ from the autoburette at a rate of 30 ml/min (addition time, 3 sec). The addition half-interval (*i.e.* 1.5 sec) was taken as time zero. Data were acquired at a wavelength of 455 nm for 30, 40 and 180 sec for cysteine, ascorbic acid and glutathione, respectively, and for 40 and

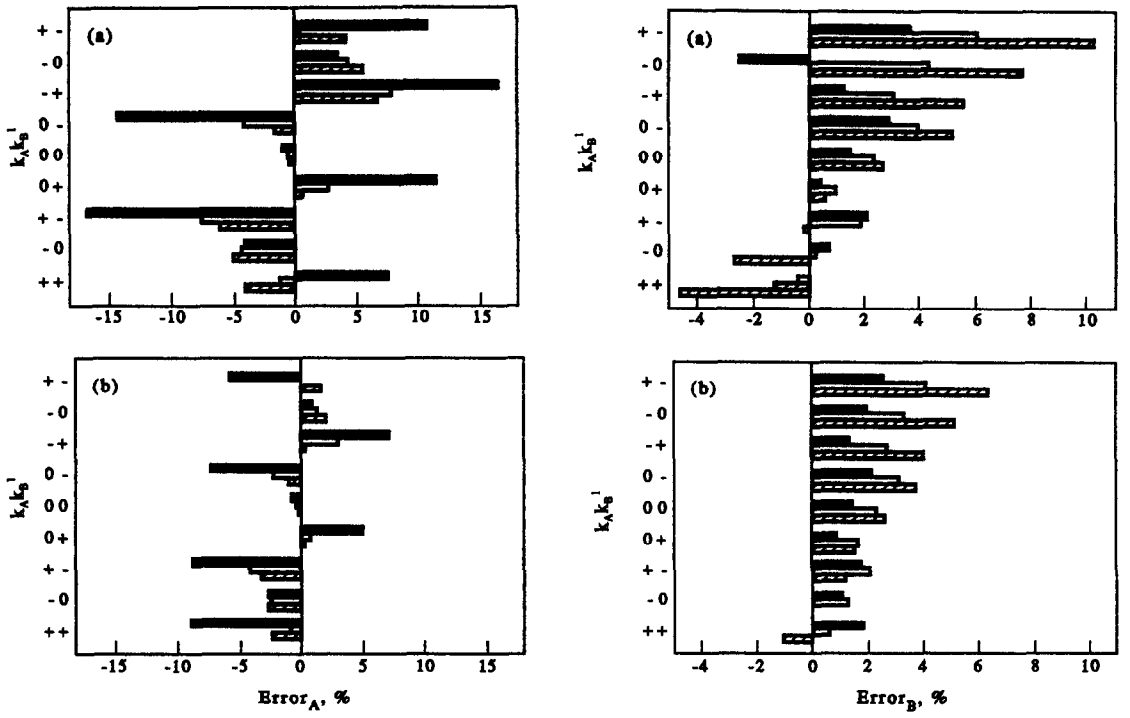

Fig. 2. Effect of: (a) a 10% error and (b) a 5% error in the determination of the rate constants on the determination of reactant A in a mixture with B and vice versa by using the Kalman filter. $k_A = 10^{-2}$ sec^{-1}; $k_B^1 = 10^{-1}$ sec^{-1}; $S_B = 0.25$; $S_A =$ 1.0 (▨), 0.25 (□) and 0.0625 (■).

180 sec in the resolution of the cysteine–ascorbic acid and glutathione–ascorbic acid mixtures, respectively.

RESULTS AND DISCUSSION

The chief aim of this work was to assess the potential of the proposed approach by applying it to the resolution of mixtures of species following different kinetics (namely first- and second-order). For this purpose, we chose the reduction of copper(II) by ascorbic acid, cysteine and glutathione in the presence of neocuproine, which yields the well-known Cu(I)–neocuproine orange complex. This system was previously employed by us for the kinetic determination of glutathione in blood serum using the continuous-addition-of-reagent technique.[50]

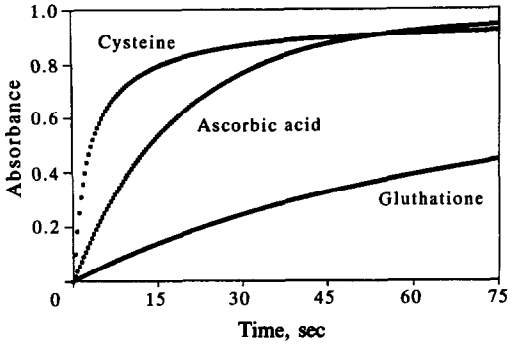

Fig. 3. Typical absorbance *vs.* time curve for cysteine (4.0 μmoles), ascorbic acid (2.0 μmoles) and glutathione (4.0 μmoles), each measured at 455 nm. For details, see Procedure.

Figure 3 shows the kinetic curves provided by the photometer as processed by the data acquisition system. As can be seen, the reaction rate for ascorbic acid (the component following pseudo first-order kinetics) lies between those of the two amino acids, which follow second-order kinetics. Consequently, we chose to use mixtures of ascorbic acid and either cysteine or glutathione to assess the performance of the proposed algorithm.

Effects of experimental variables

Given the aim of this work, the experimental conditions to be optimized were obviously those which resulted in the best possible accuracy and precision in the resolution of the mixtures. Thus, the following criteria were adopted for the reactions concerned to be usable for our purpose:

(a) They should allow precise recording of their kinetic curves by conventional means (*i.e.* they should not be too fast);

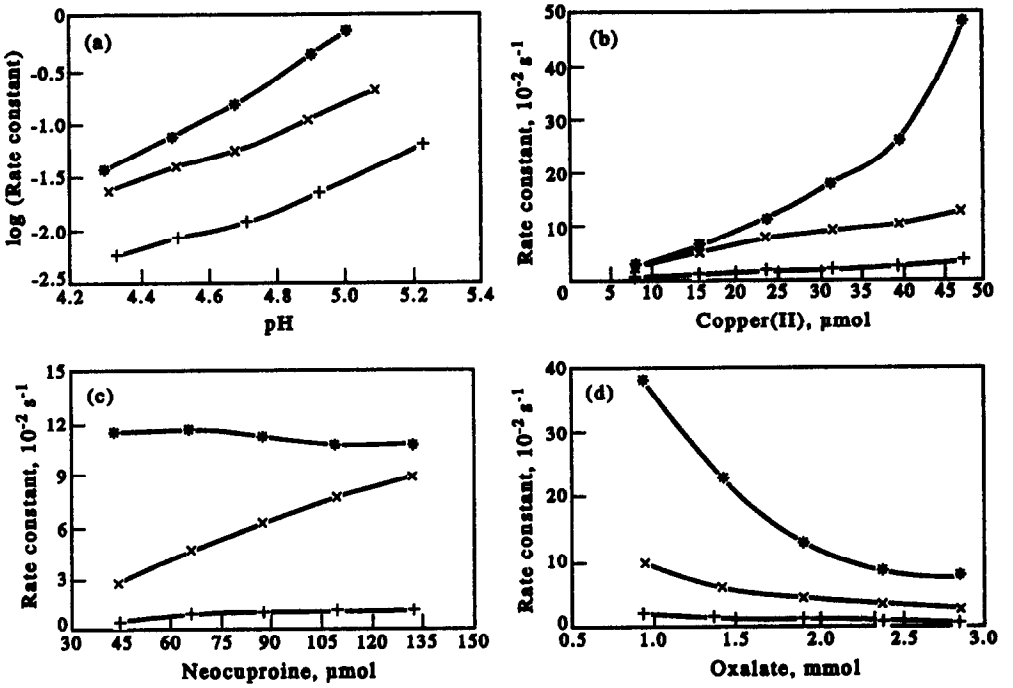

Fig. 4. Influence of chemical variables on the rate constant of ascorbic acid (X), cysteine (*) and glutathione (+). Conditions: [ascorbic acid] = 2 μmoles, [cysteine] = [glutathione] = 4 μmoles. (a) [Copper(II)] = 47 μmoles, [neocuproine] = 86 μmoles and [sodium oxalate] = 1.5 mmoles; (b) [neocuproine] = 86 μmoles and [sodium oxalate] = 1.5 mmoles; (c) [copper (II)] = 47 μmoles and [sodium oxalate] = 1.5 mmoles; and (d) [copper(II)] = 47 μmoles and [neocuproine] = 65 μmoles.

(b) they should conform to the kinetic model used, which is indispensable for correct application of the Kalman filter; and

(c) both the rate constants and their ratios should allow for kinetic resolution. Thus, if $k_A/k_B^1 \gg 1$, then either the first reaction would be too fast and hence difficult to record a kinetic curve or the second would be too slow, so the determination would have to be sequential rather than simultaneous. If, on the other hand, $k_A/k_B^1 \simeq 1$, then the mixture resolution would be subject to major errors arising from the similarity between the two kinetic curves.

Based on the above considerations, the initial chemical systems was modified slightly by introducing oxalate ion, which was chosen among a few tested copper(II) chelating agents. In fact, complexing Cu(II) ion slowed down its reduction to Cu(I), which in turn allowed us to select an appropriate reaction rate—and hence precisely record the kinetic curves—and achieve a more suitable rate constant ratio.

We thus chose to use the rate constants k_A and k_B^1 instead of the corresponding reaction rates—which are typically employed in kinetic methods—as measurement parameters.

In order to investigate the influence of pH on the development of the two reactions we added various small amounts of NaOH or HCl to the reaction vessel so as to keep the ionic strength constant throughout the process. The pH range studied was close to the initial pH of the buffer used, since more acidic media resulted in virtually no reaction development, whereas more basic media gave rise to too fast a reaction for

Table 2. Analytical figures of merit of the methods

Feature	Ascorbic acid	Cysteine	Glutathione
Linear dynamic range (*μmoles*)	0.1–5.0	0.06–7.0	0.1–9.0
Analytical sensitivity (*A/μmole*)	0.430 ± 0.06	0.225 ± 0.003	0.220 ± 0.001
Precision, RSD (%)	0.45	0.31	0.40
Rate constant (sec^{-1})	5.4×10^{-2}	1.7×10^{-1}*	8.4×10^{-3}†

*For 2.0 μmoles of cysteine.
†For 2.8 μmoles of glutathione.

Table 3. Resolution of synthetic cysteine–ascorbic acid mixtures

Micromoles added		Found			
Cysteine	Ascorbic acid	Cysteine (*μmoles*)	Error (%)	Ascorbic acid (*μmoles*)	Error (%)
3.67	0.50	3.31	−9.8	0.52	+4.0
3.14	0.75	3.05	−2.9	0.74	−1.3
2.62	1.00	2.67	+1.9	1.07	+7.0
2.10	1.25	2.10	0.0	1.41	+12.8
1.57	1.50	1.23	−21.6	1.86	+24.0

precise recording. As can be seen in Fig. 4a, the rate constants increased sharply with increase in the pH. Also, the k_{AA}/k^1_{GLU} ratio was almost constant over the pH range studied, whereas the k^1_{CYS}/k_{AA} ratio increased sharply (*e.g.* from 1.6 at pH 4.4 to 4.6 at pH 5.0). We chose the pH value directly provided by the buffer (pH 4.8) since it resulted in rates that allowed precise recording of the kinetic curves and acceptable rate constants; in addition, it was the pH where the buffering capacity was optimal.

Figure 4b shows the marked influence of the Cu(II) concentration on the rate constants, particularly on that of cysteine. Thus, the k^1_{CYS}/k_{AA} ratio increased linearly from 0.80 for 1.57 μmoles of copper to 3.87 for 110.2 μmoles of copper, and so did the k_{AA}/k^1_{GLU} ratio, though in a more gradual fashion. Bearing in mind the above prerequisites, we chose an amount of copper of 47.2 μmoles, which corresponded to 1.5 ml of a $3.15 \times 10^{-2}M$ solution.

Figure 4c shows the effect of the neocuproine concentration on the rate constants. As can be seen, that of ascorbic acid—the sole component following pseudo first-order kinetics—behaved differently in response to changes in the concentration of this reagent. Thus, k_{AA} increased sharply with increase in neocuproine concentration, whereas k^1_{CYS} and k^1_{GLU} hardly varied under the same conditions. An amount of neocuproine of 43 μmoles (2.0 ml of a $2.15 \times 10^{-2}M$ solution) provided the best possible k^1_{CYS}/k_{AA} ratio and quite an acceptable k_{AA}/k^1_{GLU} ratio.

The concentration of oxalate ion, which was added to the mixtures to slow down the reactions, had a similar effect on all three (Fig. 4d). Low concentrations of $C_2O_4^{2-}$ gave rise to favourable kinetic constant ratios; however, the reactions were too fast for precise recording with the instrumentation used. On the other hand, high oxalate concentrations resulted in poor rate constant ratios. We thus chose an amount of 1 mmole of oxalate (10 ml of a $10^{-1}M$ solution) as a compromise.

Individual kinetic determinations

The absorbance *vs.* time graphs constructed from different concentrations of ascorbic acid, cysteine and glutathione under the selected working conditions were analysed by using the programmes K_FIRST and K_SECOND. The figures of merit of the determinations are summarized in Table 2. The analytical sensitivity was taken as the slope of each calibration plot; as can be seen, the increased sensitivity of ascorbic acid relative to cysteine and glutathione arises since the former involves the loss of two electrons whereas that of the latter two involves S—S binding and the loss of a single electron. The precision, expressed as RSD, was determined by analysing 11 samples containing 1.0, 2.0 or 2.8 μmoles of ascorbic acid, cysteine or glutathione each.

Table 4. Resolution of synthetic glutathione–ascorbic acid mixtures

Micromoles added		Found			
Glutathione	Ascorbic acid	Glutathione (*μmoles*)	Error (%)	Ascorbic acid (*μmoles*)	Error (%)
3.43	0.25	3.39	−1.1	0.24	−4.0
2.94	0.50	2.87	−2.4	0.50	0.0
2.45	0.75	2.37	−3.3	0.75	0.0
1.96	1.00	1.94	−1.0	0.98	−2.0
1.47	1.26	1.52	+3.4	1.23	−2.4
0.98	1.51	1.20	+22.4	1.48	−2.0

Analysis of cysteine–ascorbic acid mixtures

Table 3 summarizes the results obtained by analysing several synthetic mixtures of ascorbic acid and cysteine. From the results given in the table it follows that:

(a) The error in the determination of the two components was acceptable (less than 10%) above a cysteine–ascorbic acid concentration ratio of 2, where the k^1_{CYS}/k_{AA} ratio was much greater than unity.

(b) Below a concentration ratio of 2, the k^1_{CYS}/k_{AA} ratio was close to unity and the errors increased sharply with decreasing ratios.

(c) The fact that the errors made in the determination of mixtures containing lower proportions of cysteine were larger can be ascribed to a decrease in the apparent pseudo first-order constant, k^1_{CYS}, which was thus similar to that of ascorbic acid, as well as to the lower efficiency of the Kalman filter with components following kinetics of orders other than unity. One should bear in mind that k^1_{CYS} was unknown, so the filter had to calculate it iteratively in addition to the net signal increment.

In summary, the determination of cysteine–ascorbic acid mixtures was feasible over a molar ratio range of *ca.* 7.5:1 to 1.5:1 with accuracy better than ±10%. Application of the proposed algorithm to 11 samples containing 2.9 μmoles cysteine and 1.0 μmole ascorbic acid yielded an RSD of 1.6% for the former and 2.1% for the latter.

Analysis of glutathione–ascorbic acid mixtures

Table 4 lists the results obtained in the analysis of several synthetic mixtures containing various amounts of glutathione and ascorbic acid. As can be seen, the results were quite satisfactory (errors smaller than ±4%) for glutathione to ascorbic acid concentration ratios between 13.7:1 and 1.2:1. The k^1_{GLU}/k_{AA} ratios in the mixtures varied from 0.22 to 0.09. Mixtures with smaller amounts of glutathione still allowed ascorbic acid, though not glutathione itself, to be accurately determined. This is seemingly paradoxical since the k_{AA}/k^1_{GLU} ratios in the mixtures were quite high (above 10); however, one should take into account the potential effect of one other significant factor, namely the contribution of each component to the overall signal of the mixture. As one descends in Table 4, the relative contribution of glutathione to the signal not only decreases through its smaller concentration fraction but also through its smaller apparent first-order constant, k^1_{GLU}, which accounts for the increased errors made in the resolution of these mixtures.

Based on the above results, mixtures of these compounds can be accurately resolved (errors less than ±4%) in glutathione to ascorbic acid ratios between *ca.* 14:1 and 1:1. The precision of the determination was calculated by analysing 11 mixtures containing 2.0 μmoles of glutathione and 1.0 μmole of ascorbic acid and was found to be 0.63% and 0.76%, respectively.

CONCLUSIONS

The simulated and experimental results obtained in this work show that the Kalman filter allows one to distinguish between pseudo first- and second-order kinetics. In all the mixtures studied, the best features (wide concentration ratios and high accuracy and precision) were obtained when the rate constant ratio (k_A/k^1_B) was greater than unity (*i.e.* the first-order reaction was faster than the second-order reaction), even though this was dependent on the concentration of the component following second-order kinetics, which affected k^1_B. Consequently, unlike the resolution of mixtures of species following first-order kinetics, no generalizations can be made as regards the rate constant ratio. The performance of the Kalman filter is somewhat less reliable for ratios below 1, even though the results are still acceptable. Also, as in any other mixture resolution, the errors made in the determination of one component increase as its contribution to the overall signal decreases. This approach is of both theoretical and practical interest, since applying a mathematical treatment to a binary mixture on the assumption that both species react with pseudo first-order kinetics when one of them actually follows pseudo first-order kinetics occasionally results in inexplicable errors. In such a case, the proposed approach provides a correct treatment and minimizes errors.

Acknowledgement—The authors gratefully acknowledge financial support from the Dirección General Interministerial de Ciencia y Tecnología (DIGICyT) for the realization of this work as part of Project PB91-0840.

REFERENCES

1. R. E. Kalman, *J. Basic Engng*, 1960, **82**, 34.
2. S. D. Brown, *Anal. Chim. Acta*, 1986, **181**, 1.
3. S. C. Rutan, *J. Chemometrics*, 1987, **1**, 7.
4. P. D. Wentzell, *Anal. Proc.* (*London*), 1989, **26**, 128.

5. R. L. Tranter, *Anal. Proc. (London)*, 1990, **27**, 134.
6. P. Wu, Y. Tan and M. Lou, *Sepu*, 1991, **9**, 166.
7. G. Gauglitz, M. Mettler and S. Weiss, *Trends Anal. Chem.*, 1992, **11**, 203.
8. Y. Hayashi, T. Shibazaki and M. Uchiyama, *J. Chromatogr.*, 1987, **411**, 95.
9. Y. Hayashi, T. Shibazaki and M. Uchiyama, *Anal. Chim. Acta*, 1987, **201**, 185.
10. Y. Hayashi, T. Shibazaki, R. Matsuda and M. Uchiyama, *Anal. Chim. Acta*, 1987, **202**, 187.
11. R. Matsuda, Y. Hayashi, M. Ishibashi and Y. Takeda, *J. Chromatogr.*, 1988, **438**, 319.
12. Y. Hayashi, S. Yoshioka and Y. Takeda, *Anal. Chim. Acta*, 1988, **212**, 81.
13. M. Redmond, S. D. Brown and H. R. Wilk, *Anal. Lett.*, 1989, **22**, 963.
14. T. Barker and S. D. Brown, *Anal. Chim. Acta*, 1989, **225**, 53.
15. T. Rotunno, F. Palmisano, G. Tiravanti and P. G. Zambonin, *Chromatographia*, 1990, **29**, 269.
16. R. Matsuda, Y. Hayashi, M. Ishibashi and Y. Takeda, *Anal. Chim. Acta*, 1989, **222**, 301.
17. Y. Hayashi and R. Matsuda, *Anal. Chim. Acta*, 1989, **222**, 313.
18. Y. Hayashi and R. Matsuda, *Anal. Sci.*, 1989, **5**, 459.
19. G. Luo and Y. Wang, *Yaowu Fenxi Zazhi*, 1986, **6**, 316.
20. S. Hartwell, *Int. Lab.*, 1988, **18**, 42.
21. G. Luo, J. Qui, Y. Wang and Z. Yu, *J. Pharm. Biomed. Anal.*, 1989, **7**, 507.
22. Z. Li, M. Li, R. Luo, L. Shi and R. Yu, *Yankuang Ceshi*, 1989, **8**, 241.
23. Z. Li, P. Peng and J. Li, *Fenxi Huaxue*, 1989, **17**, 1134.
24. L. Shi, Z. Xu, Z. Pan, X. Liu, Y. Gao, F. Qian, S. Nie and Z. Li, *J. Micronutr. Anal.*, 1990, **8**, 1.
25. Z. Zhang, W. Tao, Z. Zhang, Y. Su and S. Zhang, *Yaowu Fenxi Zazhi*, 1991, **11**, 100.
26. D. D. Gerow and S. C. Rutan, *Anal. Chim. Acta*, 1986, **184**, 53.
27. S. C. Rutan and C. B. Motley, *Anal. Chem.*, 1987, **59**, 2045.
28. S. C. Rutan, D. D. Gerow and G. Hartmann, *Chemom. Intell. Lab. Syst.*, 1988, **3**, 61.
29. D. D. Gerow and S. C. Rutan, *Anal. Chem.*, 1988, **60**, 847.
30. E. H. Van-Veen and M. T. C. De Loss-Vollebregt, *Sprectrochim. Acta*, 1990, **45B**, 313.
31. E. H. Van-Veen and M. T. C. De Loss-Vollebregt, *Anal. Chem.*, 1991, **63**, 1441.
32. C. A. Scolari and S. D. Brown, *Anal. Chim. Acta*, 1984, **166**, 253.
33. C. A. Scolari and S. D. Brown, *Anal. Chim. Acta*, 1985, **178**, 239.
34. J. Li, Y. Zeng and G. Chen, *Talanta*, 1990, **37**, 809.
35. P. C. Thijssen, N. H. M. De Jong, G. Kateman and H. C. Smit, *Anal. Chim. Acta*, 1985, **170**, 265.
36. P. C. Thijssen, N. J. M. L. Janssen, G. Kateman and H. C. Smit, *Anal. Chim. Acta*, 1985, **177**, 57.
37. I. Lavagnini, P. Pastore and F. Magno, *Anal. Chim. Acta*, 1990, **239**, 95.
38. Z. Li, M. Li, L. Shi and R. Yu, *Fenxi Huaxue*, 1990, **18**, 1044.
39. S. C. Rutan and S. D. Brown, *Anal. Chim. Acta*, 1985, **167**, 23.
40. S. C. Rutan and S. D. Brown, *Anal. Chim. Acta*, 1985, **175**, 219.
41. C. A. Corcoran and S. C. Rutan, *Anal. Chem.*, 1988, **60**, 1146.
42. C. A. Corcoran and S. C. Rutan, *Anal. Chem.*, 1988, **60**, 2450.
43. P. D. Wentzell, M. I. Karayannis and S. R. Crouch, *Anal. Chim. Acta*, 1989, **224**, 263.
44. R. Xiong, A. Velasco, M. Silva and D. Pérez-Bendito, *Anal. Chim. Acta*, 1991, **251**, 313.
45. W. H. Lewis, Jr. and S. C. Rutan, *Anal. Chem.*, 1991, **63**, 627.
46. E. Förster, M. Otto, M. Silva and D. Pérez-Bendito, *Anal. Chim. Acta*, 1993, **274**, 109.
47. S. R. Crouch and B. M. Quencer, *Fourth International Symposium on Kinetics in Analytical Chemistry*, Erlangen (Germany), Sept., 1992.
48. T. Q. Barker and S. D. Brown, *J. Chemometrics*, 1988, **2**, 137.
49. H. W. Sorenson, *IEEE Spectrum*, 1970, **7**, 63.
50. R. Jiménez-Prieto, A. Velasco, M. Silva and D. Pérez-Bendito, *Anal. Chim. Acta*, 1992, **269**, 273.

Talanta, Vol. 40, No. 11, pp. 1741–1747, 1993
Printed in Great Britain.

0039-9140/93 $6.00 + 0.00
Pergamon Press Ltd

SURFACE-ENHANCED RAMAN SPECTROMETRY FOR DETECTION IN LIQUID CHROMATOGRAPHY USING A WINDOWLESS FLOW CELL

L. M. CABALIN,* A. RUPEREZ† and J. J. LASERNA*‡

*Department of Analytical Chemistry and †Department of Physical Chemistry, Faculty of Sciences, University of Málaga, 29071 Málaga, Spain

Summary—A windowless flow cell has been developed for surface-enhanced Raman (SER) detection in liquid chromatography. Using colloidal silver as an active substrate, SER spectrometry of banned drugs in sport is presented. The experimental factors of primary influence on the analytical performance of the cell have been studied. The results of SER detection with the proposed cell have been compared to UV detection.

Surface-enhanced Raman spectrometry (SERS) on colloidal systems is a sensitive, selective and fairly simple method for the analysis of a variety of compounds of technical, environmental, biomedical and pharmaceutical interest. The requirement for analyte-induced aggregation of the colloidal system introduces a range of experimental variables that are difficult to control. Driven by the excellent separative and sample handling performance of modern analytical flowing systems, colloid SERS systems have been adapted for detection in flowing streams [flow injection analysis (FIA) and high performance liquid chromatography (HPLC)]. In the earliest configuration,[1,2] a relative standard deviation of 3% was reported for replicate injection of *p*-aminobenzoic acid on a stream of colloidal silver prepared on-line at room temperature. After these reports, other applications of colloid SERS on flowing streams were described.[3–7] The separation and determination of four purine bases (adenine, guanine, hypoxanthine and xanthine) by reverse-phase HPLC in combination with real-time SERS have been demonstrated.[8] Limits of detection in the nanomolar range were reported. In spite of these advantages, SERS detectors using conventional, closed flow cells have several drawbacks. Tailing in the chromatographic peaks results from memory effects caused by deposition of Ag sol and adsorbed compounds on the inner wall of the cell.[8] To eliminate the memory effect, it is often necessary to change the flow cell or to rinse it with nitric acid after each chromatographic run. Adsorption on the cell walls also results in baseline drifts, contamination problems and mixing of the spectra of the previously separated compounds.

The need for a reliable but simple analytical device for detection in HPLC remains an important goal in SERS. Open flow cells have been proposed for detection in HPLC under a variety of analytical principles. A windowless cell was first proposed for laser-induced fluorescence detection.[9] Using the 325-nm modulated output of a He–Cd laser and phase-sensitive detection, carcinogenic aflatoxins were linearly quantitated to 7.5×10^{-13} g. Later, the fluorescence and photoacoustic characteristics of an open flow cell intended for liquid chromatographic applications were compared with the respective characteristics of a static cuvette cell.[10] The advantage of such a detector is that photoacoustic detection is complementary to fluorescence detection and may be useful in quantitating substances which do not appreciably luminesce. A laser two-photon ionization technique was applied for the trace determination of pyrene using a windowless cell made of two stainless steel electrodes.[11] With 300-μl dead volume, the cell, in combination with a pulsed nitrogen laser, allowed the detection of 100 ng/ml pyrene in *n*-heptane. An open cell was developed that had simultaneous detection capabilities by molecular fluorescence, photoacoustic effect and two-photon photoionization processes. The cell was evaluated for drugs,[12] aromatic compounds[13] and polycyclic aromatic hydrocarbons.[14] In the present paper we discuss the utility of SERS detection in HPLC using an

‡Author for correspondence.

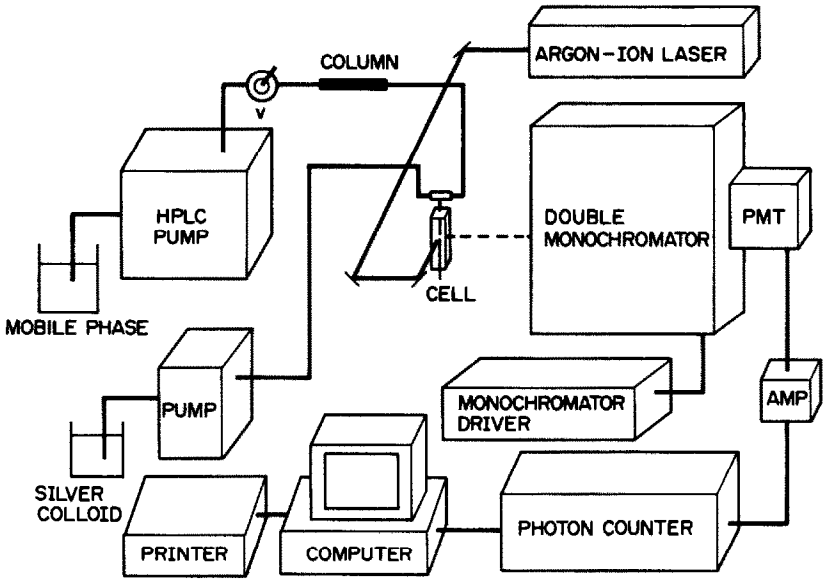

Fig. 1. Schematic diagram of the HPLC–SERS system. PMT, photomultiplier tube and cooled housing; AMP, fast preamplifier; V, injection valve.

open flow cell. The operating performance of the cell is illustrated for banned drugs in sport. The results of SER detection with the proposed cell have been compared to UV detection.

EXPERIMENTAL

Instrumentation

A schematic diagram of a coupled HPLC–SERS system is shown in Fig. 1. Spectra were obtained with a 0.22-m double-grating spectrometer (Spex Industries, model 1680B) with a 1200 grooves/mm classically ruled grating. The Raman scattering was collected at right-angles and detected with a cooled photomultiplier tube (Hamamatsu, model R-928), a fast preamplifier (Stanford Research Systems, model SR440) and a two-channel gated photon counter (Stanford Research Systems, model SR400). Operation of the photon counter was controlled by an AT personal computer with Stanford Research SR465 software. Spectral data were generated in binary code and converted to ASCII for processing in standard graphics software. The 488-nm line of an argon-ion laser (Coherent, model Innova 70-5) was used, and the laser power at the windowless flow cell was approximately 400 mW. A 25-cm focal length glass lens focused the laser beam onto the cell.

The liquid chromatography system consisted of an isocratic pump (Shimadzu model LC-6A) with a Rheodyne injection valve using a 20-μl sample loop. The analytical column was a 5-μm OD-MP Spheri-5 RP-18 (10 cm × 4.6 mm i.d.; Brownlee Labs). A model SPD-6A variable-wavelength UV–visible detector and a Chromatopac integrator, both from Shimadzu, were also used. The wavelength for UV detection was 254 nm. The mobile phase was methanol–water (1:1, v/v). Prior to use, the mobile phase was vigorously degassed and particulate matter was removed by passage through a 0.45-μm nylon membrane filter under vacuum. The flow rate was 0.2 ml/min. For flow injection analysis the Ag sol and drug solutions were pumped by two peristaltic pumps (Heidelberg model 131900 and Gilson model M312, respectively). The flow rate was 1.5 ml/min for silver hydrosol and 0.075 ml/min for the analyte sample.

The windowless flow cell was designed and constructed in our laboratory and consisted of two chromatographic stainless steel tubes of $\frac{1}{16}$ inch i.d. and 1.4 mm external diameter mounted on an aluminium frame. The dimensions of the cell are shown in Fig. 2. The eluent from the chromatographic column and the silver hydrosol are mixed on a chromatographic tee and then flow to the windowless cell. The draining liquid is supported by surface tension between the two tubes. The column of liquid is approximately cylindrical with a diameter of 1.4 mm and height of 1.6 mm. The dead volume of the cell is roughly 2.5 μl. The flowing liquid exits the flow cell through the stainless steel tubing to a waste beaker.

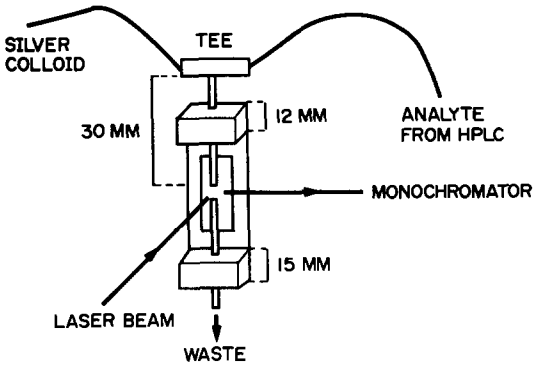

Fig. 2. Schematic diagram of the windowless flow cell.

Chemicals and procedure

All chemicals used were of analytical reagent grade or equivalent. Demineralized water was used throughout. Amiloride, amiphenazole, caffeine, chlorthalidone, hydrochlorothiazide, 2-mercaptopyridine, pemoline and triamterene were purchased from Sigma. They were used without further purification. Stock solutions (100 μg/ml) of the drugs were prepared in methanol–water (1:1, v/v). Silver hydrosols were prepared with fresh aqueous solutions of $1 \times 10^{-3}M$ silver nitrate and $2 \times 10^{-3}M$ sodium tetrahydroborate. Fifty millilitres of the silver nitrate solution were added dropwise to 150 ml of vigorously stirred, ice-cooled sodium tetrahydroborate solution. After mixing, the resulting colloid was maintained in an ice bath for 2 hr with constant stirring. With this procedure, the aggregation process of hydrosol has been stopped and the hydrosol remained stable for several days. Silver hydrosols were used at room temperature. Urine samples were obtained from healthy human volunteers not receiving any medical treatment and were filtered through a 0.45-μm membrane filter prior to injection.

RESULTS AND DISCUSSION

For SERS to be used as a detector for HPLC and FIA it is necessary that the analyte-induced aggregation kinetics of the colloid be rapid and that the solvent employed be adequate. Montes *et al.*[15] demonstrated that the kinetics of aggregation depend on the chemical structure of the analyte studied. On the other hand, it is also known[16] that the adsorptive behaviour of the analyte on the Ag surface can change when different types of mobile phase are used. One effect is the direct adsorption of the mobile phase onto the active sites of the colloidal particles, which diminishes the analyte's affinity

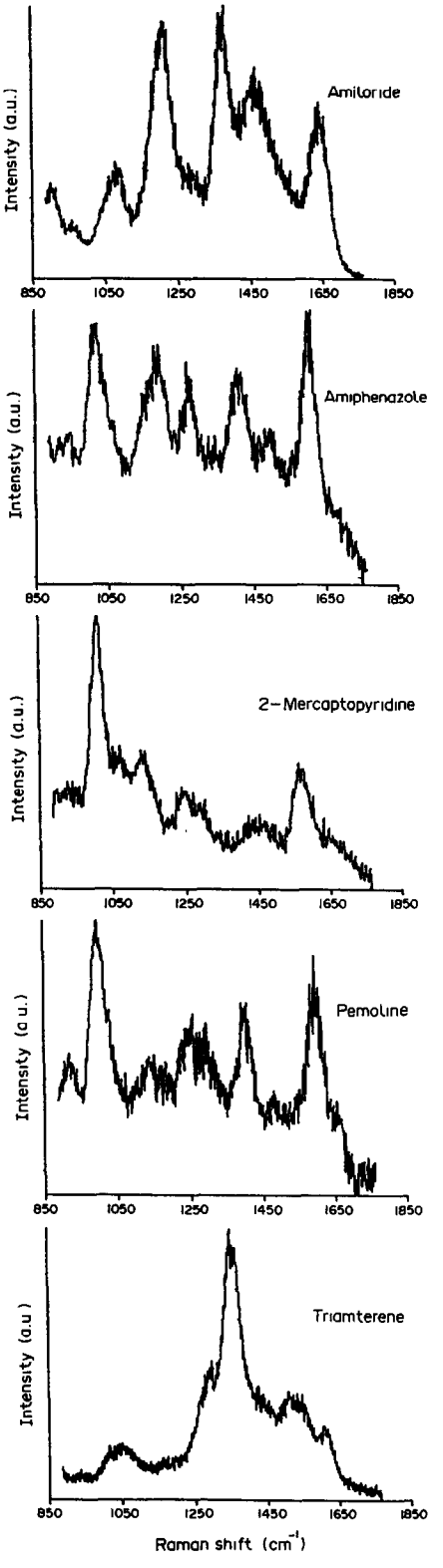

Fig. 3. Surface-enhanced Raman spectra of drugs in FIA system. Drug concentration, 100 μg/ml. The flow rates of silver hydrosol and drug solution were 1.5 and 0.075 ml/min, respectively.

Table 1. Surface-enhanced Raman bands of drugs on colloidal silver. Band positions are given in cm^{-1}. The values of parentheses represent the relative intensities of the bands on a semi-quantitative scale from 1 to 10

Amiloride	Amiphenazole	2-Mercaptopyridine	Pemoline	Triamterene
1082 (3)	1013 (8)	1010 (10)	918 (2)	1040 (1)
1209 (9)	1187 (6)	1134 (4)	998 (10)	1294 (5)
1375 (10)	1272 (5)	1246 (3)	1146 (3)	1357 (10)
1466 (8)	1404 (5)	1448 (2)	1246 (5)	1426 (5)
1645 (7)	1495 (2)	1570 (4)	1294 (5)	1516 (4)
	1606 (10)		1407 (6)	1606 (3)
			1484 (1)	
			1602 (8)	

for the Ag surface or affects the aggregation behaviour of the Ag colloid. In the present paper, a methanol–water (1:1, v/v) mobile phase proved adequate for the drugs of interest. On the other hand, the good optical alignment of the laser beam onto the SERS cell is a critical parameter for obtaining high-quality SERS data, because the optical path length has been shown to significantly affect the SERS measurements.[17]

In a previous work, we have studied the SERS activity on colloidal silver of a variety of drugs.[18] Five drugs have been chosen to evaluate the windowless flow cell, which provides aggregation kinetics fast enough to be processed in flow systems. Figure 3 illustrates the SER spectra of five drugs (amiloride, amiphenazole, 2-mercaptopyridine, pemoline and triamterene) obtained at room temperature by continuously flowing the analyte solution and the silver colloid through the windowless cell. The flow rates were optimized in order to maximize the signal intensity. The optimal flow rates of silver hydrosol and analyte were 1.5 and 0.075 ml/min, respectively. Few authors have reported SER spectra under flowing conditions.[1,8,19] The SER spectra in Fig. 3 demonstrate that the Raman bands are easily discernible, and each individual SER

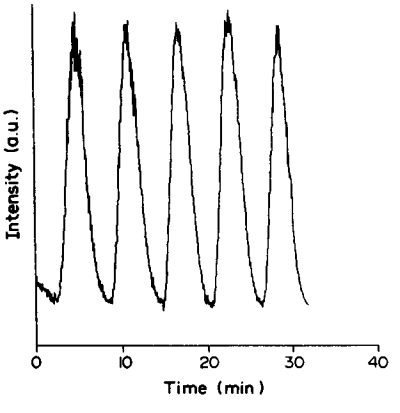

Fig. 4. Reproducibility of the FIA–SERS system for amiloride. Five successive injections of 625 ng of amiloride monitored at a Raman shift of 1375 cm^{-1}. The flow rates of silver hydrosol and amiloride were 1.5 and 0.075 ml/min, respectively.

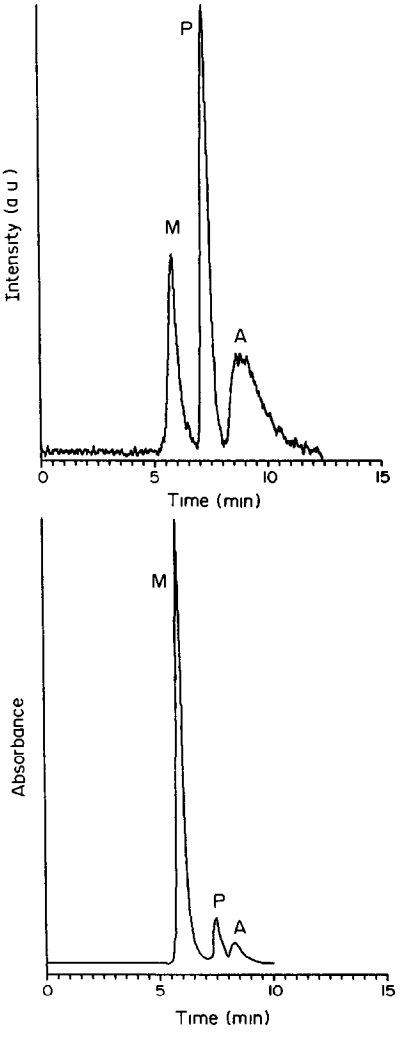

Fig. 5. (Top) SERS chromatogram of a mixture of amiloride (A), 2-mercaptopyridine (M) and pemoline (P) obtained by monitoring the intensities of the peak at 1407 cm^{-1}. (Bottom) UV chromatogram of the same mixture monitored at 254 nm. The mobile phase was methanol–water (1:1, v/v), flow rate 0.2 ml/min. The flow rate of silver colloid was 1.5 ml/min.

Table 2. Chromatographic parameters and analytical figures of merit obtained for 2-mercaptopyridine and pemoline by UV and SERS detection

	UV detection					SERS detection				
Analyte	t_r* (min)	N†	LR‡ (μg/ml)	RSD§ (%)	LOD‖ (ng)	t_r* (min)	N†	LR‡ (μg/ml)	RSD§ (%)	LOD‖ (ng)
Mercaptopyridine	5.81	2800	100	1.9	0.12	5.60	860	25	2.5	100
Pemoline	7.47	3730	100	2.5	1.00	7.25	2000	25	1.6	32

*Retention time obtained at a flow rate of 0.2 ml/min.

†Efficiencies in theoretical plates calculated using $N = 4\,(t_r/W_{0.6H})^2$ where $W_{0.6H}$ is the peak width at 60% of the peak height expressed in time units.

‡Limit for the range of linear response of peak height with concentration.

§Relative standard deviation for five replicate measurements at 25 μg/ml.

‖Limit of detection calculated for a signal equivalent to twice the baseline noise, expressed in ng injected.

spectrum can serve as a fingerprint for each compound. Table 1 summarizes the SER band positions of the drugs.

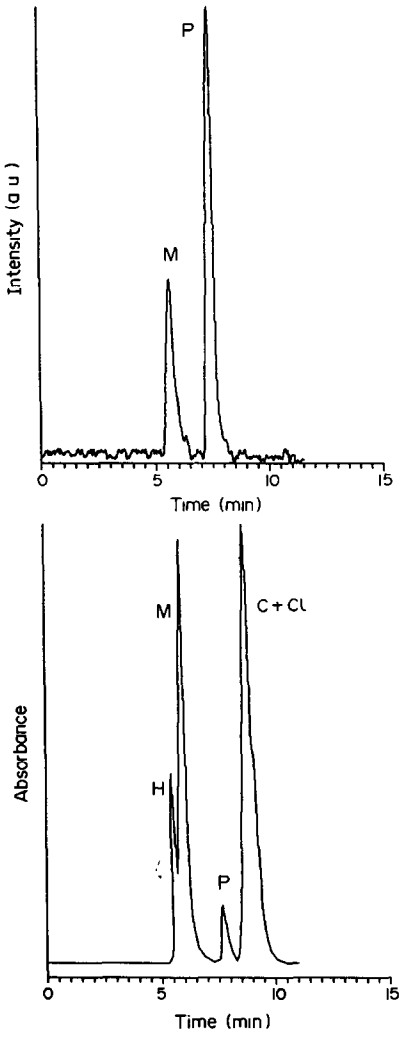

Fig. 6. Comparison of SERS and UV chromatograms for five drugs [caffeine (C), chlorthalidone (Cl.), hydrochlorothiazide (H), 2-mercaptopyridine (M) and pemoline (P)]. Other conditions as in Fig. 5.

It is important to note that the preparation of silver hydrosol affects the state of aggregation and consequently the reproducibility of results and signal stability. To eliminate this problem, silver hydrosols have to be prepared using consistent laboratory practices, as described in the Experimental section. With the procedure used, the aggregation process prior to analyte injection can be controlled. Figure 4 shows the signal reproducibility for five consecutive injections of amiloride. The absolute amount in each injection was 625 ng amiloride and the samples were injected at 6 min intervals. A band at 1375 cm^{-1} in amiloride was used to monitor the signal. The measured reproducibility was 1% (relative standard deviation). Similar reproducibility was reported by Freeman *et al.*,[5] for pararosaniline hydrochloride. Figure 4 also shows the rapid baseline restoration after each injection and the absence of memory effects.

The use of the windowless flow cell for SERS detection in HPLC is illustrated in Fig. 5. An SERS-detected chromatogram of a mixture of amiloride, 2-mercaptopyridine and pemoline and a UV chromatogram of the same mixture are shown. The HPLC flow rate was 0.2 ml/min. However, the mixing of the silver sol with the column eluent just prior to the SERS detector causes the retention time to be shifted to shorter times by about 20 sec over the UV chromatogram. The relative peak areas differ on going the SERS to the UV detection modes. For instance, pemoline is the largest peak in the SERS chromatogram while 2-mercaptopyridine is the largest peak in the UV chromatogram.

A comparison of efficiency, linear range, precision and detection power for 2-mercaptopyridine and pemoline using UV detection and SERS detection is summarized in Table 2. The lower efficiency of the SERS detection results from the mixing of the eluent with the silver sol.

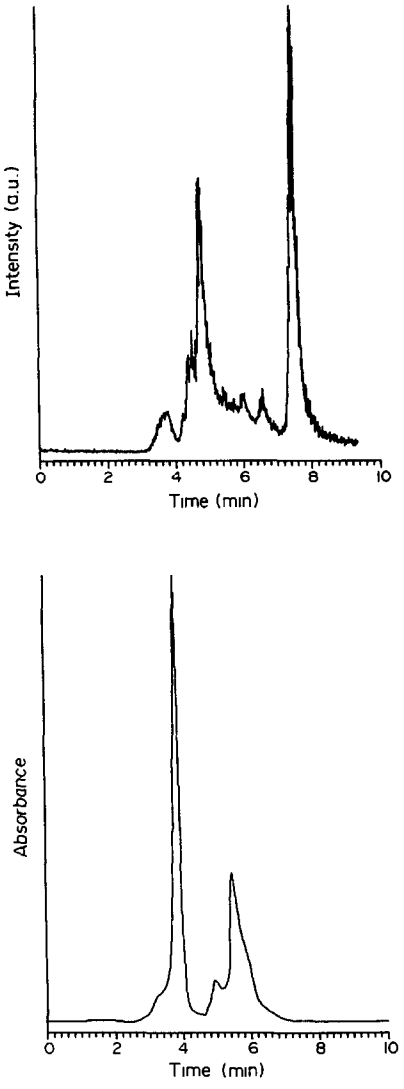

Fig. 7. Comparison of human urine chromatograms. (Top) SERS chromatogram. (Bottom) UV chromatogram. Other conditions as in Fig. 5.

The precision of SERS intensities has been one of the weakest points of this technique. Remarkably, with the windowless flow cell used here, RSD values for the SERS detection mode are comparable to those found by UV detection. On the other hand, the SERS mode provides higher limits of detection. The main reason for this effect is the dilution of the analyte resulting from mixing the chromatographic eluent with the silver colloid. At the flow rates used, the dilution factor is about 20-fold. The unique selectivity provided by the SERS detector can be illustrated by comparison of chromatograms of a mixture of caffeine, chlorthalidone, hydrochlorothiazide, 2-mercaptopyridine and pemoline. Figure 6 shows the UV and SERS chromatograms of the mixture monitored at 254 nm and at 1407 $cm,^{-1}$ respectively. Caffeine and chlorthalidone co-elute and appear as a single peak in the UV chromatogram ($t_r = 8.6$ min), while hydrochlorothiazide ($t_r = 5.42$ min) overlaps the peak of 2-mercaptopyridine ($t_r = 5.85$ min). The SERS-detected chromatogram presents only two peaks, at 5.6 and 7.25 min, corresponding to 2-mercaptopyridine and pemoline, respectively. Caffeine, chlorthalidone and hydrochlorothiazide are not detected since these drugs are not SERS active under the present conditions. No peak tailing or memory effets in the cell are observed. To further evaluate the selectivity of the SERS detector, an SERS chromatogram of human urine is compared with a UV chromatogram in Fig. 7. The peaks observed correspond to proteinaceous and other endogenous urine components. As shown, the peak at 7.5 min in the SERS chromatogram does not appear in the UV chromatogram. This fact indicates that there are urine components that can only be detected by SERS. On the other hand, the relative peak areas are also different in both chromatograms. For instance, the peak at 3.8 min is much higher in area in UV than SERS. The opposite is seen for the peak at 4.5 min.

CONCLUSIONS

There are advantages in using the windowless flow cell for SERS detection in HPLC. First, the open character of the cell provides continuous renewal of the aggregated colloid in the cell. This helps to remedy a recurring problem in conventional flow cell experiments, which is adsorption of aggregated silver on the cell walls resulting in undesirable memory effects. Also, baseline drifts and peak tailing are circumvented using this approach. The LODs achievable are within the limits reported for conventional batch systems, although they are much higher than in UV for two drugs studied. The unique band position and shape of spectral features in the SER spectra of the drugs could be beneficial in the dope analysis of these and similar compounds. This information could complement or supplement general gas chromatography–mass spectrometry data in confirmatory analysis. Presently, we cannot fully exploit the spectral selectivity of the SERS–HPLC approach because a monochannel detector is used to disperse the Raman scatter. Detection based on

charge-coupled devices or diode arrays will allow further refinement and evaluation of the technique. These modifications have been initiated.

Acknowledgements—This research was supported by Dirección General de Investigación Científica y Técnica (Ministerio de Educación y Ciencia, Madrid, PB87-0729 and PB90-0814) and Dirección General de Universidades e Investigación (Junta de Andalucía, Sevilla), Spain.

REFERENCES

1. J. J. Laserna, A. Berthod and J. D. Winefordner, *Talanta*, 1987, **34**, 745.
2. A. Berthod, J. J. Laserna and J. D. Winefordner, *Appl. Spectrosc.*, 1987, **41**, 1137.
3. F. Ni, R. Sheng and T. M. Cotton, *Anal. Chem.*, 1990, **62**, 1958.
4. J. J. Laserna, A. Berthod and J. D. Winefordner, *Microchem. J.*, 1988, **38**, 125.
5. R. D. Freeman, R. M. Hammaker, C. E. Meloan and W. G. Fateley, *Appl. Spectrosc.*, 1988, **42**, 456.
6. G. T. Taylor, S. K. Sharma and K. Mohanan, *Appl. Spectrosc.*, 1990, **44**, 635.
7. V. L. Schlegel and T. M. Cotton, *Anal. Chem.*, 1991, **63**, 241.
8. R. Sheng, F. Ni and T. M. Cotton, *Anal. Chem.*, 1991, **63**, 437.
9. G. J. Diebold and R. N. Zare, *Science*, 1977, **196**, 1439.
10. E. Voigtman, A. Jurgensen and J. D. Winefordner, *Anal. Chem.*, 1981, **53**, 1921.
11. S. Yamada, K. Kano and T. Ogawa, *Bunseki Kagaku*, 1982, **31**, E247.
12. E. Voigtman and J. D. Winefordner, *Anal. Chem.*, 1982, **54**, 1834.
13. E. Voigtman and J. D. Winefordner, *J. Liq. Chromatogr.*, 1982, **5**, 2113.
14. A. Berthod, T. Mellone, E. Voigtman and J. D. Winefordner, *Anal. Sci.*, 1987, **3**, 405.
15. R. Montes, C. Contreras, A. Rupérez and J. J. Laserna, *Anal. Chem.*, 1992, **64**, 2715.
16. S. A. Soper, K. L. Ratzlaff and T. Kuwana, *Anal. Chem.*, 1990, **62**, 1438.
17. J. J. Laserna, L. M. Cabalín and R. Montes, *Anal. Chem.*, 1992, **64**, 2006.
18. A. Ruperez, L. M. Cabalín and J. J. Laserna, *Council of Scientific Research Integration*, J. Menon (ed.), Trivandrum, India (in press).
19. N. J. Pothier and R. K. Forcé, *Anal. Chem.*, 1990, **62**, 678.

Talanta, Vol. 40, No. 11, pp. 1749–1757, 1993
Printed in Great Britain.

0039-9140/93 $6.00 + 0.00
Pergamon Press Ltd

CHEMOMETRIC CHARACTERIZATION OF 5TH CENTURY A.D. AMPHORA-PRODUCING CENTRES IN THE MEDITERRANEAN

J. A. REMOLÀ
CODEX SCCL-ARCHAEOLOGY & HERITAGE, 43003 Tarragona, Spain

M. S. LARRECHI and F. X. RIUS
Chemistry Dept. University of Tarragona, 43005 Tarragona, Spain

Summary—The application of two chemometric techniques for data structure analysis (Ward's hierarchical clustering and Principal Components Analysis) has permitted the characterization of 5th century A.D. amphora-producing centres in the Mediterranean on the basis of X-ray fluorescence data on 66 amphora fragments. The chemometric study complements and reinforces the conclusions drawn from typological and archaeological analysis. Nineteen samples of unknown origin have been classified (using the SIMCA method) into the eight proposed classes of amphora production.

Amphorae are a type of ceramic container used in antiquity for transporting liquid and semi-liquid foodstuffs (pickled, salted and other forms of preserved food) by sea. Because of their nature, the contents have rarely withstood the passage of time. Amphorae thus provide indirect evidence on these products as well as the commercial ties linking geographically separated regions. However, in order to establish this connection, it is essential to know the origin of the amphora itself and to be aware of the contents transported in it.

The traditional method used for identifying the place of origin of both amphorae and other pottery has a largely archaeological and typological basis. It was not until the 1970s that chemical information started to be used as a means of relating the composition of ceramic materials to their area of origin. To be more precise, in the case of amphorae, the most widely-used method to date is that known as petrological analysis, which consists of the identification of the mineral inclusions in the fabric, their physical characteristics and their rate of frequency. The results obtained from these analyses are compared with those obtained from samples taken from the waste materials of the amphora-manufacturing centres themselves or from the sources of raw material used in the production of a particular type of amphora. At present this method of relating the product's origin to the manufactured product itself has one serious drawback, namely the lack of a detailed register of reference material.

A second widely-used method for relating products to their origins is the chemometric analysis of chemical composition data; this technique enables groups of geo-chemically homogeneous samples to be established. After a seminal work by Kowalski *et al.*,[1] numerous applications have been published, many of them related to ceramic materials.[2–5] Nevertheless, amphorae which show a similar chemical composition may well come from geographically differing areas, and, in contrast, samples whose composition in geochemical terms is quite different may come from a zone which formed a historical unit in the past.

It is thus clear that only by combining all the possible means of analysis (typological, chemical, physical, *etc.*) that a suitable solution can be found for the problems raised in the identification of centres that produced amphorae (and other pottery).

In the present paper a chemometric characterization of 5th century A.D. amphora-producing centres in the Mediterranean is proposed on the basis of the data derived from X-ray fluorescence analysis on 85 amphorae fragments found in a waste dump at Tarragona (Imperial Tarraco, Hispania). This study complements the typological characterization of over 350

fragment samples and sets up an objective chemical foundation for the overall archaeological study.

In the first instance, our aim was to identify the groups that were established naturally, taking into account only the 66 samples of certain and doubtful provenance. This study made it possible to compare these groupings with those established through purely archaeological and typological considerations. Thereafter, we decided to use classification techniques to enable the association of the 19 pieces of unknown origin with their production area.

EXPERIMENTAL

Samples: the waste dump at Vila-roma

This waste dump, dated to between A.D. 425 and 450, is a site of exceptional significance in view of the fact that more than 30,000 fragments have been found, of which approximately 28,000 come from amphorae.[6]

Late Roman amphorae[7] are classified into three principal groups according to their area of origin: North Africa, Southern Hispania (Baetica and Lusitania) and Eastern Mediterranean (Fig. 1). In the case of the waste dump

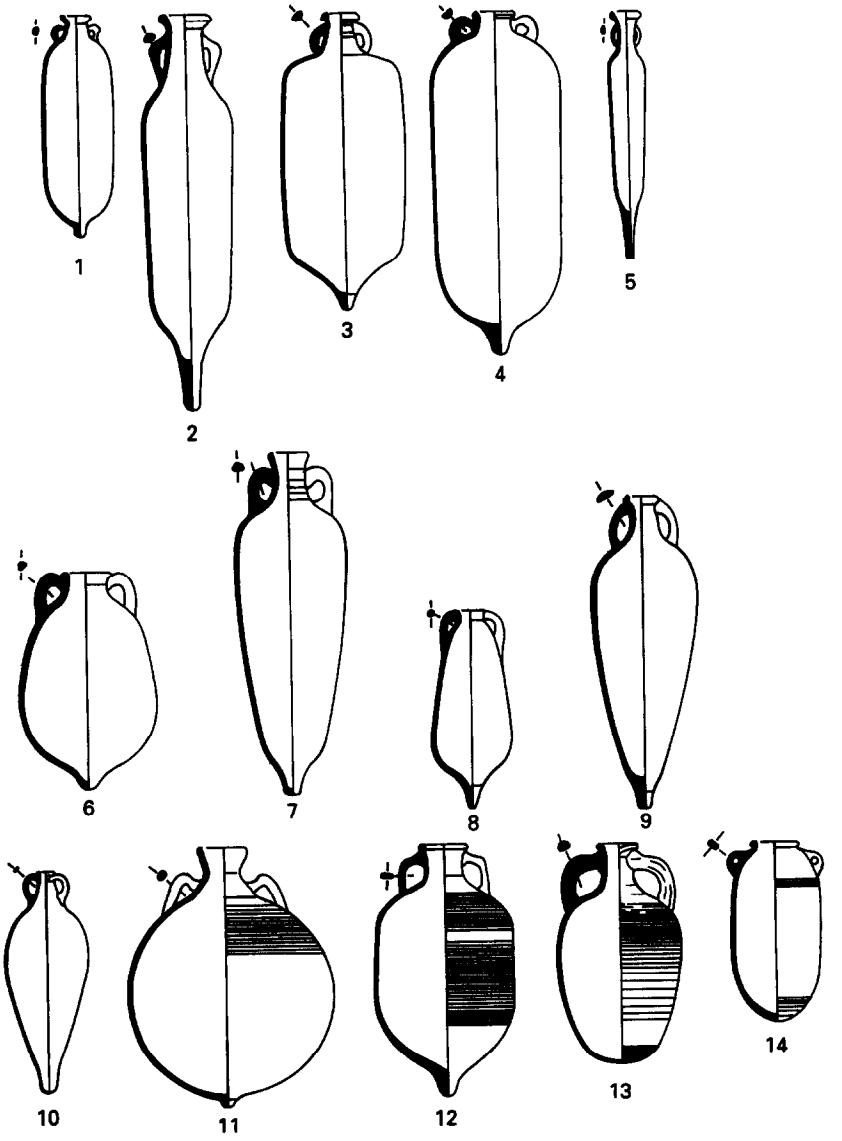

Fig. 1. Objects 1–5: main amphora types of North African origin (1: evoluted African group 1, 2: cylindrical containers of medium size, 3–4: cylindrical containers of considerable size, 5: spatheia). Objects 6–9: main amphora types of South Hispania origin (6: Keay 13a/c, 7: Keay 19a/b, 8: Keay 16, 9: Keay 23). Objects 10–14: main amphora types of Oriental origin (10: Keay 54 bis, 11: Keay 65, 12: Agora od Athens M.273, 13: Keay 53, 14: Keay 54.

at Vila-roma, of the estimated 400 or so examples of amphorae, 100 (25%) have their origins in the south of Hispania, 98 (24.4%) come from North Africa, while 102 (25.5%) were manufactured in the eastern Mediterranean.[8] To these should be added 79 examples of as yet uncertain provenance. The classification of samples to the above mentioned zones was carried out strictly on the basis of archaeological and typological criteria and the geographical names used do not necessarily imply the geo-chemical or typological homogeneity of the products. Table 1 presents a list of the 85 samples from this waste tip that are the subject of the present study, together with their type and their inventory number. Of these 85 samples, 57 are well identified according to archaeological criteria, 9 are of doubtful attribution, and 19 belong to the group of unknown provenance.

X-ray fluorescence analysis

Iron, manganese, titanium, calcium, potassium, silicon, aluminium, phosphorus and magnesium content, expressed as percentages of their respective oxides, were determined by X-ray fluorescence analysis. The samples were prepared by the fusion technique in a Perlex X2 oven. X-ray fluorescence intensities were measured on a computer controlled Philips PW/1400 dispersive wave length X-ray spectrometer equipped with rhodium and scandium sources.

The samples were prepared by weighing one gram of crushed sample of pottery and four

Table 1. Sample sherds from Vila-roma grouped according to their typological characteristics

North Africa

1. Evoluted African Group I

N°	Type	N° Inventory
20	K.3b	2236
29	K.3a	2235
36	K.3a	2227
61	K.3a	2271

2. Cylindrical containers of medium size

N°	Type	N° Inventory
17	K.25p	2268
18	K.25p	2269
21	K.27b	2281
23	K.25y	2264
27	K.25g/h	2242
40	K.27b	2282

3. Cylindrical containers of considerable size

N°	Type	N° Inventory
25	K.41	2305
26	K.35	2303
28	K.41	2312
30	K.41	2310
31	K.35b	2300
32	K.35b	2302
35	K.62	2948
37	K.57	2966
38	K.61a	2944
39	K.59	2963
41	K.35b	2301

4. "Spatheia"

33	K.26	2255
85	K.26	2255

5. Other African types

24	K.77	2964
34	K.86	2965
42	VLR 8.58	3215

Southern Hispania

1. Keay 13a (Betica)

44	K.13a	2144
45	K.13a	2149
60	K.13a	2164

2. Keay 13c (Betica)

43	K.13c	2100
47	K.13c	2103
48	K.13c	2097
50	K.13c	2143
65	K.13c	2101

3. Keay 19a/b (Betica)

52	K.19a/b	2169
55	K.19a/b	2200
57	K.19a/b	2180
62	K.19a/b	2175

4. Keay 16 (Lusitania)

46	K.16	2225
59	K.16	2226
63	K.16	2223

5. Keay 23 (Lusitania)

49	K.23	2209
53	K.23	2222
78	K.23	3307

Table 2. X-ray fluorescence analysis results (%)

N°	Fe_2O_3	MnO	TiO_2	CaO	K_2O	SiO_2	Al_2O_3	P_2O_5	MgO
01	5.82	0.12	1.14	9.83	1.78	57.44	10.14	0.18	2.26
02	5.61	0.09	0.69	11.35	2.45	49.45	13.23	0.16	1.57
03	5.52	0.11	0.62	17.10	2.23	45.74	12.35	0.22	3.32
04	5.55	0.12	0.54	19.29	2.59	40.67	10.99	0.25	3.53
05	5.59	0.12	0.53	17.74	2.45	39.69	10.45	0.22	4.91
06	5.56	0.08	0.77	8.89	2.82	48.22	13.60	0.18	2.59
07	4.97	0.10	0.97	12.33	1.41	56.29	9.02	0.21	2.07
08	6.11	0.13	1.22	8.16	2.09	54.89	10.56	0.24	2.14
09	5.58	0.10	0.69	11.81	2.54	50.29	12.97	0.16	1.36
10	10.98	0.09	0.85	1.80	3.45	48.17	20.85	0.42	3.24
11	4.90	0.09	0.99	12.38	1.51	53.96	8.52	0.11	1.89
12	5.72	0.11	1.13	10.02	2.03	53.11	10.24	0.21	2.28
13	4.99	0.09	0.54	16.70	2.29	43.62	9.17	0.15	3.63
14	5.94	0.10	0.64	17.89	2.21	45.35	10.20	0.18	3.97
15	5.18	0.09	0.68	11.36	2.70	47.34	12.78	0.15	1.45
16	5.41	0.08	0.72	9.67	2.66	50.69	13.73	0.16	1.47
17	4.90	0.09	0.64	6.87	1.90	58.72	11.49	0.35	1.56
18	5.40	0.03	0.64	12.68	2.06	49.06	12.02	0.37	1.53
19	4.79	0.02	0.72	8.47	1.20	57.19	14.93	0.24	1.37
20	5.04	0.05	0.71	6.89	1.81	63.00	11.52	0.16	1.06
21	4.47	0.05	0.68	11.96	1.75	54.04	11.74	0.19	1.04
22	4.88	0.02	0.75	8.76	1.21	56.94	16.45	0.20	1.53
23	5.09	0.07	0.69	7.05	2.36	59.56	12.57	0.28	1.72
24	5.36	0.05	0.63	10.62	2.30	50.90	12.37	0.34	1.51
25	5.22	0.05	0.62	13.08	2.05	49.28	12.37	0.27	1.49
26	4.80	0.03	0.74	6.12	2.36	61.08	11.33	0.15	2.62
27	4.83	0.03	0.79	3.34	2.46	61.63	11.71	0.14	1.46
28	5.85	0.05	0.69	11.97	2.03	49.48	13.42	0.22	1.63
29	4.60	0.04	0.72	7.79	1.74	58.75	11.82	0.15	1.01
30	5.12	0.05	0.62	10.68	2.48	50.52	12.16	0.42	1.56
31	6.26	0.04	0.84	3.26	2.19	64.46	14.22	0.16	1.41
32	5.37	0.03	0.84	4.62	2.56	64.39	13.25	0.19	1.78
33	5.16	0.05	0.71	7.36	2.23	64.49	12.48	0.21	1.67
34	5.15	0.07	0.71	7.07	2.32	61.31	12.45	0.23	1.86
35	6.12	0.04	0.82	6.64	2.22	60.86	14.14	0.17	1.83
36	4.36	0.04	0.71	11.51	1.76	58.18	11.84	0.25	1.19
37	5.29	0.04	0.87	3.58	2.59	65.94	13.06	0.15	1.68
38	4.23	0.04	0.64	14.75	2.36	55.24	11.33	0.14	1.68
39	4.88	0.03	0.86	8.10	3.46	55.62	13.81	0.20	1.90
40	5.07	0.04	0.77	7.92	1.93	64.28	12.96	0.19	1.23
41	5.23	0.03	0.84	4.21	2.66	64.92	13.28	0.15	1.58
42	5.22	0.05	0.71	12.34	1.74	56.94	12.27	0.15	1.69
43	5.40	0.07	0.69	11.10	2.76	55.37	13.08	0.24	2.26
44	5.39	0.05	0.68	13.42	2.14	53.13	12.20	0.30	2.09
45	5.36	0.05	0.69	11.51	2.24	53.31	12.21	0.25	2.13
46	4.69	0.03	0.73	0.64	3.04	67.21	13.91	0.07	0.96
47	5.18	0.07	0.68	10.18	2.79	55.92	12.55	0.36	2.07

grammes of lithium tetraborate, mixing it and melting it in a platinum crucible. The instrument was calibrated with 20 international standard rock samples prepared by means of the glass bead technique. The effects of different types of potential interference were considered and the alpha correction factors were calculated to compensate. The results obtained are shown in Table 2. A summary of the raw data distribution is given in Fig. 2.

Chemometric techniques

Two unsupervised methods of analysis available in the pattern recognition packages CLUSTAN[9] and ARTHUR[10] were applied in order to show the overall structure of the 66 amphora samples of known origin in the multidimensional space. These methods are respectively, a hierarchical cluster analysis (the Ward method) and a representation method, Principal Components Analysis (PCA). Subsequently, the SIMCA classification method[11] from the statistical package SIMCA[12] was used in order to evaluate whether any of the amphora of unknown origin might belong to any of the previously established areas of origin.

RESULTS AND DISCUSSION

Figure 3 shows the dendogram obtained as a result of the application of the Ward clustering

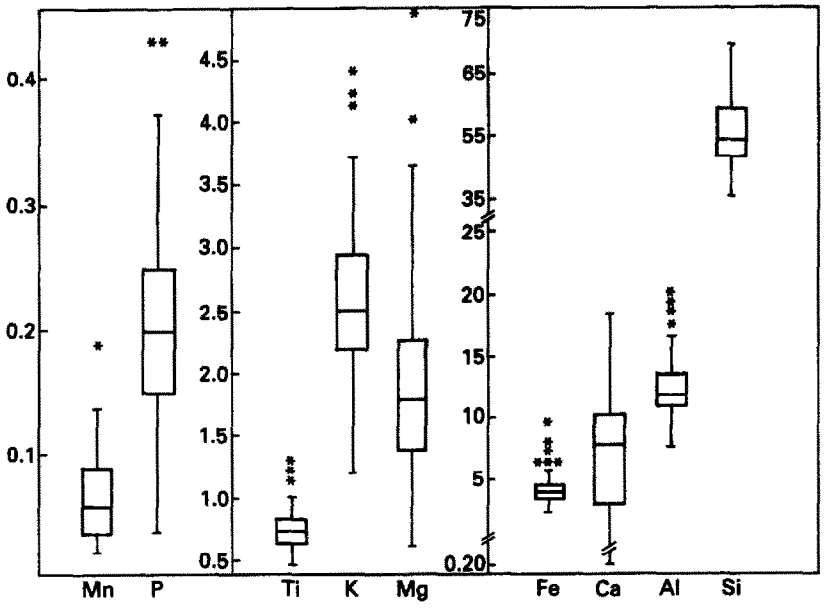

Fig. 2. Box and whisker plots of the raw data listed in Table 2.

method on the 66 samples characterised according to typological and archaeological criteria. The projection of the samples into the space defined by the first two principal components is displayed in Fig. 4. The results obtained from both the dendogram and the PCA plot indicate that even though the natural grouping according to chemical compositional data does not always agree with the three principal zones defined (northern Africa, the south of Hispania, and the eastern Mediterranean), aspects which had been evident on the grounds of purely archaeological evidence are confirmed. Thus, sample 10 (Keay type 54 bis), from Sardis, shows a considerable similarity, in the Ward diagram (Fig. 3), to samples 66 and 76

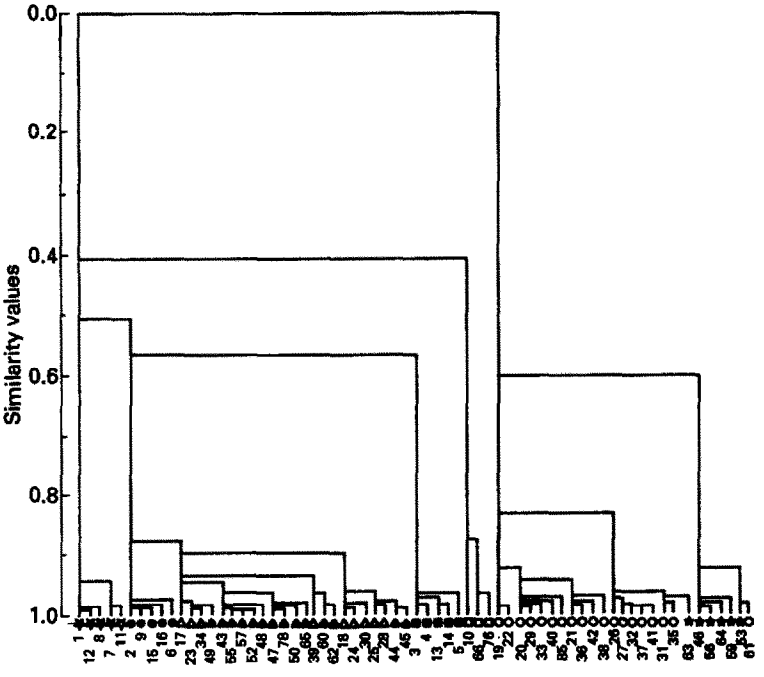

Fig. 3. Dendogram of the 66 objects in the 9th-dimensional space of the variables obtained by Ward's hierarchical clustering method. (☆) class 1, (★) class 2, (●) class 3, (○) class 4, (□) class 5, (■) class 6, (▲) class 7, (△) class 8.

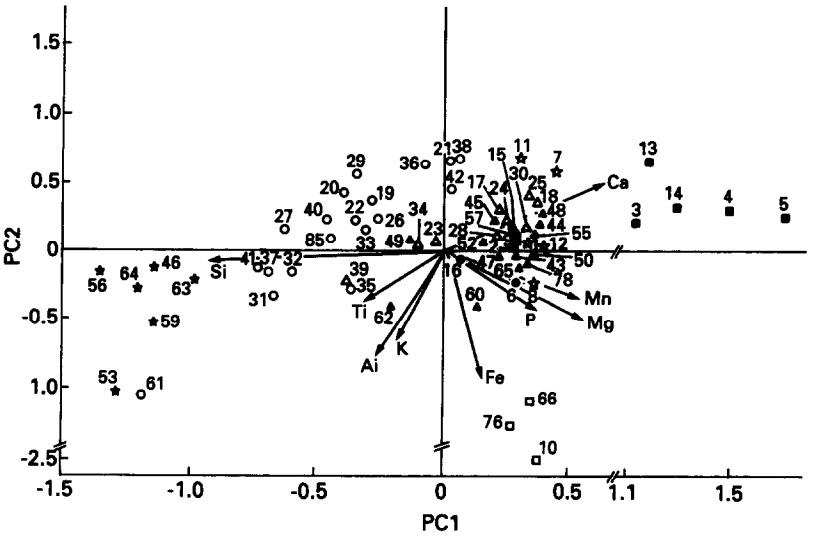

Fig. 4. Projection of the 66 archaeological samples described by the original 9 variables into the plot defined by the first two principal components. (62.1% of the total variance retained). The symbols are the same as in Fig. 3.

(Athenian Agora type M.273), possibly from the western and northern Aegean. These samples, classified into the small class 5 in Table 3, appear in the PCA plot (Fig. 4) displaying a very different performance from the rest, on the variables analyzed, which may suggest an identical production area for both types, situated in an area of similar geo-chemical characteristics.

Samples included in the eastern Mediterranean group can be easily detected. Thus, a small class made up of pieces 3, 4 and 5, coming from the Black Sea/northern Aegean, and by samples 13 and 14, from the Antioch area, can be observed both in the dendogram and the PCA plot. It should be pointed out that in this class, numbered 6 in Table 3, samples of very different types (Keay 65 and Keay 53), which as far as can be seen were produced in very different areas, have been included. Principal Components Analysis (Fig. 4), supplies useful information on the variables that are responsible for the disposition of the eastern Mediterranean samples, the high Mn, Ca and Mg content of these samples in comparison with the others being particularly noticeable, which may indicate that the clays used in Antioch and in an area situated somewhat imprecisely on the Black Sea/northern Aegean coastline were very similar as regards their chemical composition, since the widely-differing typology of this set of pieces makes it unlikely that all of them came from a single production centre.

The presence of the elements in classes 5 and 6, well separated from the rest, leads to a bunching together of all other samples in the PCA plot, so a new PCA was carried out without considering these objects. After attempting several preprocessing data techniques to obtain better results, a principal components analysis of the logarithmically transformed reduced data set is shown in Fig. 5.

In this three-dimensional plot and the dendogram of Fig. 3 a small set (class 1) formed by pieces 1, 12, 8, 7 and 11 (examples of Keay type 54) can be easily detected; these come from the eastern Mediterranean, to be more precise from

Table 3. Classes of samples established on the basis of the Ward hierarchical clustering and Principal Components Analysis techniques

Class 1 (☆):	1-12-8-7-11 (Type K. 54, zone of Gaza)
Class 2 (★):	46-59-63-53 (Type K. 16. Lusitania) 56-64 (Type K. 21, unknown)
Class 3 (●):	2-9-15-16-6 (Type VLR 8.198, unknown)
Class 4 (○):	19-22 (Type K.24, probably from North-Africa) 61-20-29-36-21-40-27-26-31-32-35-37-38-41-33-85-42 (North-Africa)
Class 5 (□):	10 (Type K.54 bis, zone of Sardis) 66-76 (Agora of Athens M.273, Aegean zone)
Class 6 (■):	3-4-5 (Type K.65, North Aegean) 13-14 (Type K.53, zone of Antioch)
Class 7 (▲):	44-45-60-43-47-48-50-65-52-55-57-62- (Betica) 49 (Lusitania)
Class 8 (△):	17-18-23-25-28-30-39-24-34 (North Africa)

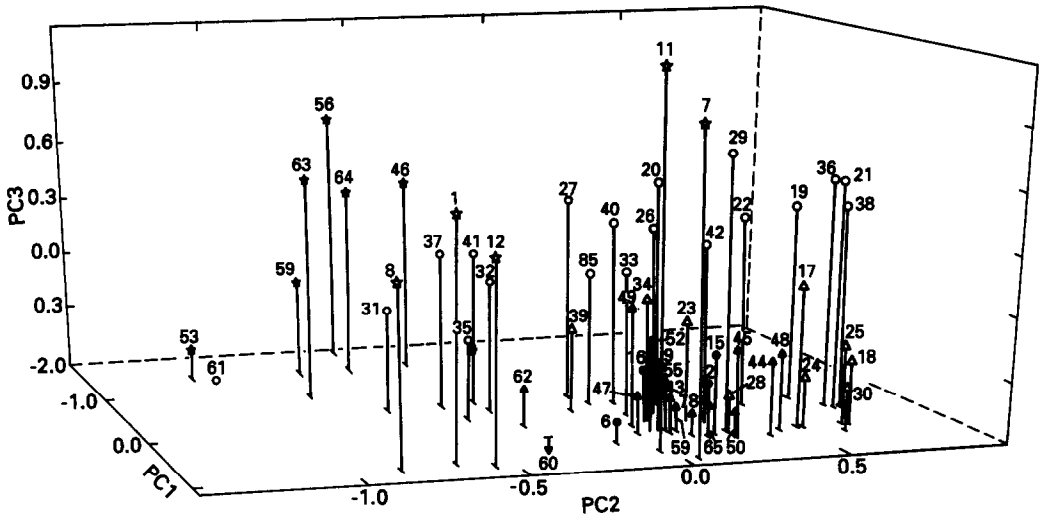

Fig. 5. Three-dimensional projection of 58 archaeological samples, data have been log transformed, into the plot defined by the first three principal components. (75.5% of the total variance retained). Same symbols as in Fig. 3.

the Gaza area, and have little connection with the North Aegean samples in class 6.

The Ward diagram and the 3d PCA plot also corroborate the idea of considering samples 2, 6, 9, 15 and 16 as a homogeneous class. These samples might have their origin at some unknown point in the eastern Mediterranean. They appear as a group of high internal consistency, which is in accordance with the typological classification given, but, in chemical terms however, show a stronger tendency towards joining those samples from the south of Hispania and some from north Africa. In spite of this, these pieces have been considered members of a new class (class 3 in Table 3) quite different from all other classes.

Nevertheless, samples 19 and 22, corresponding to Keay type 24, which are morphologically related to the large north African containers, but which, because of the visual characteristics of their fabric had not been included within this geographical group, can be chemically grouped with the set of samples from this zone (class 4), and thus supply objective reasons for including them in it. The same does not occur with fragments 56 and 64 of Keay type 21, the technical (but not typological) characteristics of which point to a north African origin, but which, however, on the basis of the chemical evidence in the Ward diagram and the PCA plot, appear to be closer to numbers 46, 59 and 53, from the south of Hispania (class 2), more exactly Lusitania, and sample 61 of north African origin. Bearing in mind the clear separation in chemical terms of these fragments from the south of Hispania, more precisely Lusitania, from the remainder of the southern Spanish pieces from Baetica, it seems reasonable to consider that samples 63, 46, 56, 64, 59 and 53 form the large class 2. It should be pointed out that piece number 49, also from Lusitania, has been excluded from this group, for it is chemically included with those from Baetica. This is only to be expected since the same form may have been produced in different areas in the past.

Finally, by means of both the Ward diagram and principal component analysis, it can be seen that the samples from Baetica cluster together and display chemical characteristics similar, as far as the variables analyzed are concerned, to samples 17, 23, 34, 39, 24 and 42, which correspond to various forms of north African origin (class 8). Given that there exist typological

Table 4. Number of Principal Components and typical standard deviation for each group modeled with SIMCA method

Group	No. of PCs considered (Aq)	Typical standard deviation (s_0)
1	2	0.49
2	2	0.68
3	2	0.17
4	2	0.72
5	1	0.74
6	2	0.75
7	1	0.84
8	2	0.36

*The number of variables, M, in all groups is 9.

Table 5. Results of the SIMCA method. Standard deviation (s_i) for the 19 unknown samples to every established class

Sample	Gr.1	Gr.2	Gr.3	Gr.4	Gr.5	Gr.6	Gr.7	Gr.8
51	6.50	0.83	4.21	1.85	11.81	8.45	3.87	4.14
54	5.39	7.95	2.10	6.95	2.70	9.56	6.99	6.17
58	5.79	1.64	3.77	1.85	11.09	6.93	3.20	3.74
67	4.40	9.05	1.27	6.86	2.09	5.21	5.23	5.59
68	4.52	4.41	1.81	3.42	3.58	7.16	4.08	4.06
69	3.83	3.17	4.14	1.84	4.15	6.22	2.68	1.67
70	2.60	6.15	2.63	2.19	2.45	2.82	1.63	2.49
71	3.13	8.03	1.52	2.03	4.18	3.11	1.88	2.45
72	4.53	3.54	1.64	3.25	9.16	7.38	3.38	3.57
73	4.80	5.51	1.29	1.41	10.41	4.71	3.25	2.87
74	5.43	0.93	4.92	1.30	10.73	7.54	3.54	3.01
75	2.90	6.54	2.44	0.88	7.32	2.91	1.78	0.72
77	3.67	3.76	1.52	3.14	5.61	6.83	2.64	2.26
79	4.89	3.39	2.71	3.36	8.46	7.78	3.91	3.98
80	5.12	8.40	1.18	2.31	11.61	3.31	3.54	1.79
81	2.95	5.15	0.83	1.93	4.46	3.92	1.10	1.32
82	3.42	4.71	1.98	4.28	5.78	6.60	3.00	2.55
83	3.32	5.29	2.71	2.66	1.99	4.83	2.16	2.88
84	5.48	1.22	4.40	1.61	9.91	7.69	3.26	3.34

and archaeological reasons for not considering them all as coming from a single manufacturing centre, they have been taken to be different groups.

By means of the combination of typological, archaeological and chemometrical criteria described, the existence of the eight classes summarized in Table 3 can be considered to be accepted. On the basis of these classes an attempt was made to classify the 19 remaining pieces, considered to be of uncertain origin, through the application of the SIMCA method. In this method, a Principal Components model is calculated for each class under consideration. Once the model is validated by means of the cross-validation technique, the prediction step is carried out by calculating the standard deviation of each of the pieces considered to be of unknown origin, s_i, which is compared to that of the model s_0 by means of a suitable F-test, in accordance with the expression:

$$F = s_i^2/s_0^2$$

for (M-Aq) and (Nq-Aq-1)(M-Aq) degrees of freedom, M being the number of variables, Aq the number of principal components calculated for each class, and Nq the number of objects. The full results are listed in Table 4.

The results of the SIMCA technique for the 19 samples of unknown origin are shown in Table 5. When their variance values (s_i^2) were statistically compared to that of the model (s_0^2) by means of the F-test, it was found that fragments 51 and 74 were able to be assigned to class 2, which, as has already been indicated, covers types of Lusitanian provenance; fragment 75 was assigned to the north African groups and 81 to the Baetican one. Nothing can be rigorously stated about the remaining pieces on valid statistical criteria, for, on the basis of the chemical variables analyzed, they present analogies with none of the established classes.

CONCLUSIONS

The usefulness of chemical and chemometric analysis in the characterization of amphora-producing centres in the Mediterranean basin has been shown. It is valuable in archeometry to spot the weakness of conclusions derived solely from the application of multivariate analysis to chemical composition data of materials such as ceramics or glass. Due to the composition of the raw material and the variations introduced during the manufacturing process, amphora having a similar chemical composition may come from different zones and, conversely, samples whose elemental composition is different may come from zones considered to be a historical unit in the past. However, this study shows the value of chemometrical techniques as complementary tools of typological and archaeological analysis in the characterization of samples. Moreover, pattern recognition techniques are very effective in establishing classes and classifying fragments whose origin cannot be assigned by means of any other technique.

Acknowledgements—We would like to thank the Spanish Ministerio de Educación Ciencia (DGICYT project no. PB90-0453) for their financial support.

REFERENCES

1. B. R. Kowalski, T. F. Schatzki and F. H. Stross, *Anal. Chem.*, 1972, **44**, 2176.
2. D. L. Massart and L. Kaufman, *The Interpretation of Analytical Chemical Data by the Use of Cluster Analysis*. Wiley, New York, 1983.
3. E. W. H. Hayek, P. Krenmayr, H. Lohninger, U. Jordis, W. Moche and F. Sauter, *Anal. Chem.*, 1990, **62**, 2038.
4. P. Mirti, R. Aruga, V. Zelano, L. Appolonia and M. Aceto, *J. Anal. Chem.*, 1990, **336**, 215.
5. K. Heydorn and I. Thuesen, *Chem. and Intell. Lab. System*, 1989, **7**, 181.
6. TED'A, Un abocador del segle V d.C en el forum provincial de Tàrraco. Memòries d'Excavació, núm 2, Taller Escola d'Arqueologia, Tarragona, 1989.
7. S. J. Keay, 1984. *Late Roman Amphora in the Western Mediterranean. A Tipology and Economic Study: The Catalan Evidence*. BAR International Series 196, Oxford, 1984.
8. J. A. Remolà and A. Abelló in Un abocador del segle V D.C. en el fòrum provincial de Tàrraco. Memòries d'Excavació, núm 2, Taller Escola dArqueologia, Tarragona, 1989.
9. D. Wishart in Clustan User Manual, Program Library Unit, Edimburg University, 1982.
10. ARTHUR81 User's Manual, Informetrix, Inc., Seattle, WA 1981.
11. S. Wold, C. Albano, K. Dunn III, W. J. Esbensen, S. Helberg, E. Johansson and M. Sjöström, in *Pattern Recognition: Finding and Using Regularities in Multivariate Data, Proc.* IUFOST Conf. on Food Research and Data Analysis, ed. by Martens H. and Russwurm H. Jr., Applied Science Publishers, London, 1983.
12. SIMCA-3B package. SEPANOVA AB, Oshandsvägen 14, S-12243 Enskede, Sweden.

Talanta, Vol. 40, No. 11, pp. 1759–1768, 1993
Printed in Great Britain.

0039-9140/93 $6.00 + 0.00

SURFACTANT-BASED ORDERED MEDIA IN ANALYTICAL ATOMIC SPECTROMETRY*

A. SANZ-MEDEL,† M. R. FERNANDEZ DE LA CAMPA, M. C. VALDES-HEVIA Y TEMPRANO, B. AIZPUN FERNANDEZ and Y. M. LIU

Department of Physical and Analytical Chemistry, Faculty of Chemistry, University of Oviedo, Julián Clavería 8, 33007 Oviedo, Spain

Summary—During the last 10 years or so we have witnessed an enormous growth of interest and applications of surfactant-based ordered media in analytical chemistry. However, their use in analytical atomic spectroscopy (AAS) has been rather scarce and often controversial. The utilization of surfactants in this latter field is discussed here along two main lines: one refers to the favourable manipulation of physical properties of the sample solutions (Part A) while the other, demonstrated very recently, refers to the adequate manipulation of chemical reactions and/or interactions of analytes in solution by resorting to surfactants use (Part B). The control of physical properties of sample solutions, *e.g.* manipulation of the surface tension, allows three main applications of surfactants in atomic methods: possible increases of nebulization/atomization efficiencies in flame-AAS, improvement of aqueous/organic solvent compatibility (emulsification applications) and enhancement of the wettability of graphitic solid surfaces. The facts and controversies existing today on this method of utilization of surfactants to enhance atomic methodologies is critically discussed. The ability of surfactant-based "ordered media" to organize reactants at the molecular level has also been applied to enhance chemical generation of volatile species (*e.g.* hydride generation or cold Hg vapour generation) used in atomic methods. The analytical potential and usefulness of micelles and vesicles to improve the detection power of hydride generation ICP-AES methodologies are summarized for the determination of arsenic, lead and cadmium by plasma emission. Increases up to two-fold in the sensitivity of As and Pb have been observed by addition of organized media. A volatile Cd species is formed very easily in cationic vesicles with $NaBH_4$. This Cd species can be used to increase by five times the detectability of Cd by ICP-AES. Moreover, synergic combinations of liquid chromatography separations/atomic detection are possible by resorting to the use of micellar or vesicular mobile phases. The successful application of this principle to the modern problem of toxic arsenic HPLC speciation by using a vesicular solution [as mobile phase for the HPLC separation of As(III), As(V), monomethylarsonic and dimethylarsinic acids] and "on-line" surfactant-enhanced arsine generation is also described in detail and completes the whole picture of the present interface between analytical atomic spectroscopy and surfactant assemblies.

During the last 10 years or so we have witnessed an enormous growth of interest and applications of micelles, and other not so well known "organized" media, in analytical chemistry. It has been conclusively demonstrated that surfactant-based organized assemblies formed in solution (also referred to as "organized" or "ordered" media) may provide a peculiar type of reaction medium able to solubilize reagents, change equilibria and kinetics of reactions in solution or change the spectral characteristics of coloured/fluorescent compounds.

In brief, surfactants have become a special type of "analytical reagent" able to improve analytical reactions and performance of analytical methods in nearly all fields of modern analytical chemistry.[1–3] The favourable spectroscopic interactions of surfactants and their assemblies with absorptiometric dyes,[4] fluorescent[5] and phosphorescent[2] reagents and metal complexes[6] determined their wide utilization in the field of molecular UV–vis spectroscopy to improve absorptiometric,[1] fluorimetric[5] and phosphorimetric[2,6] analytical methods. This initial impetus of surfactants in molecular spectroscopy has moved slowly to other fields, such as electrochemistry[7,8] and separation science.[9–13]

Topics of particular analytical interest in the latter field are the use of mobile phases containing surfactants at concentrations above the CMC (critical micellar concentration), as is the case for micellar liquid chromatography[9]

*Invited Lecture presented at the "XIIIth National Meeting on Spectroscopy", Gandía, Spain, 1992.
†Author for correspondence.

and micellar electrokinetic capillary chromatography.[10] The use of surfactant-improved approaches for non-chromatographic new separation/preconcentration techniques, such as ion-pair liquid–liquid extraction,[11] flotation[12] or micellar "cloud-point" separations,[13] have also aroused considerable interest in the last few years.

It is noteworthy, however, that the use of surfactant-mediated methodologies in analytical atomic spectrometry is rather scarce and often controversial. The more popular application of surfactants in this field is probably their utilization to manipulate the surface tension of sample solutions. The changes observed in the physical properties of solutions by adding surfactants have been used to improve nebulization efficiency,[14–18] to achieve compatibility of aqueous phases with organic solvents allowing for emulsification[19–21] and to improve wettability of a graphitic solid surface.[22,23] Thus, in the light of presently available experimental evidence, in Part A we will critically review to what extent addition of surfactant organized assemblies, to manipulate the physical properties of dissolved samples, constitutes an effective method for enhancing analytical signals in atomic methods.

Very recently the ability of micelles, and other ordered media, to organize reactants at the molecular level (and thus to favourably modify equilibria or kinetic constants) has been utilized in atomic spectroscopy[24–26] to enhance chemical generation processes of volatile species (*e.g.* hydride generation) and this favourable effect can be combined with the potential of organized media as mobile phases in liquid chromatography[9] in order to pursue a possible synergic surfactant-mediated coupling of separation/detection. In fact, the favourable effect utilization of a vesicular solution as mobile phase for HPLC separation and "on-line" arsine generation has been demonstrated very recently.[27] The application of such a concept to the modern problem of arsenic analytical speciation[28,29] has also been addressed.[27] The utilization of surfactant assemblies to manipulate chemical interactions for atomic analytical methods is revised in Part B.

This paper intends to be a critical account of the interface surfactant assemblies/analytical atomic spectroscopy (see Fig. 1). Therefore, the potential and realized analytical applications of organized media in atomic spectroscopy will be systematically revised and critically discussed.

PART A. SURFACTANTS ENHANCING THE PHYSICAL PROPERTIES OF SAMPLE SOLUTIONS

1. Improving nebulization efficiency

The addition of surfactants to the sample solution in flame/atomic absorption spectroscopy (AAS) has been extensively studied as a means of enhancing the analytical sensitivity and of getting rid of some interferences.[14–18] Depending on the surfactant and system studied, the AAS signal increases, decreases or remains unchanged. Positive effects of surfactants

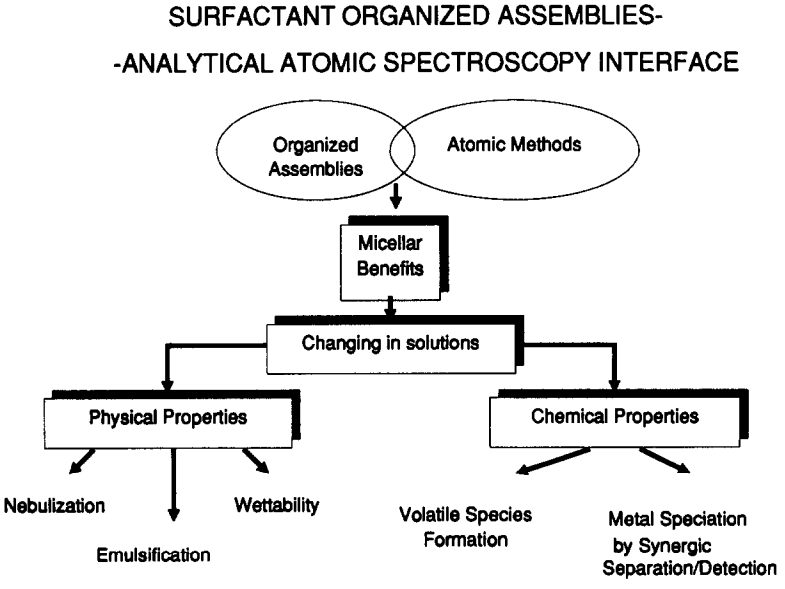

Fig. 1. The interface surfactant assemblies/analytical atomic spectroscopy.

on AAS signals have been attributed mostly to their effects on the nebulization process: the decrease in surface tension brought about by the surfactant should originate a finer aerosol and, hence, transport efficiency and/or atomization efficiency should be enhanced.[14] However, this explanation is questioned today by several authors because the surface tension values for aqueous solutions of surfactants are usually equilibrium values which might not apply in fast processes such as pneumatic nebulization. Surface tension is a property which requires a certain period of time to stabilize, the time required by the monomers of the surfactant to migrate from the bulk of the liquid or other surfaces to the surface which is being generated in the new drops. They also need time to redistribute and reorientate there (sodium laurilsulphate, SLS, requires about 10 msec for such processes). Thus, the actual surface tension ("dynamic σ") governing the drop formation in a nebulizer may not be different from that existing in the absence of the surfactant.[18]

The theory[15,30] of "aerosol ionic redistribution" (AIR) again suggests a selective enrichment of the analyte in the aerosol reaching the flame during the nebulization process if a surfactant (micelles) is present in the sample solution.

Recent work, however, tend to negate AIR's validity. Mora *et al.*[18] have shown that long-chain surfactants do not modify the basic features of the primary aerosol formed, nor the transport efficiency of the analyte to the atomizer. Yin Yan and Zhang[17] compared two atomizers, flame and ICP-AES, and concluded that enhancements are not related to nebulization/transport processes, but to a chemical effect in the atomizer. According to Yin Yan, inverted or "reversed micelles" would form around the analyte and this environment would benefit its atomization efficiency in flames. On the contrary, in ICP-AES no micellar enhancement effect was observed and this was attributed to the higher temperature in the plasma.[17]

Our experience on the determination of aluminium by conventional nebulization ICP-AES in the presence of surfactants of different charge and type tends to confirm the idea that in high temperature atomizers (plasmas) the micellar effect detected in flames, if any, is analytically unimportant.[31]

Summarizing, the enhancement of the nebulization characteristics of sample solutions for AAS by surfactants is not clear. It appears that the surfactant effect in flame-AAS is more related to atomization changes than to nebulization or analyte transport enhancement in the primary aerosol.[17,18] Much more work is needed to unveil such mechanisms of surfactant signal enhancement or surfactant interference elimination in flames. Meanwhile, trial and error techniques are mandatory to use surfactants in flame-AAS because the signals depend on experimental set-up, instrumental conditions, analyte and type of surfactant used, *etc.*

*2. Enhancing wettability of solid surfaces (*e.g. *graphite)*

A most useful alternative to conventional continuous sample introduction/atomization with nebulizer/flames or plasmas is discontinuous electrothermal atomization with graphite furnaces. There, a liquid microsample is deposited onto the surface of the usually graphite atomizer and therefore a reproducible spreading of the microsample drop over the surface is mandatory for good analytical precision. However, water has rather unfavourable surface properties to spread over graphite (surface tension, contact angle and film pressure are not as suitable as in an organic solvents/graphite system). Water/graphite systems can be made more suitable by adding surfactants. The resulting surfactant solution will have a lower surface tension, a much lower contact angle on graphite and will wet the surface in a more profound and stable manner. In this way, the formation of a thin liquid film over, *e.g.* the L'vov platform, becomes instantaneous, more stable and reproducible. Especially in connection with the use of autosamplers, the use of surfactants to decrease the surface tension, as with serum samples,[23] is most advisable in order to avoid splitting of the microdrop, sticking to the tip of the autosampler tubing, *etc*, which would bring about unreliability, lack of precision and eventually poor detection limits (by worsening the reproducibility of the measurements).

The present trend to use atomic emission techniques (AES) in connection with the graphite furnace (FAPES = furnace atomization plasma excitation[32]) should also consider this important use of surfactants when tested for real sample analysis (*e.g.* biological and other acuo-organic samples).

Lakatos *et al.*[22] have also reported on the use of surfactants to enhance conventional spark-atomic emission (AES) for the analysis of aqueous solutions with the rotrode technique.

Detection limits observed in aqueous solution were poorer than those in organic solvents. However, addition of surfactants to the aqueous phase improved the situation, even if the improvements were rather modest. In any case, the surfactant should be properly selected and applied at low concentration.[22]

3. Enhancing aqueous compatibility of organic solvents (emulsifiers)

Dispersion of an aqueous phase in an organic phase, or vice versa, increases the interfacial free energy of the system and, hence, decreases the thermodynamic stability of the liquid solution. Addition of a surfactant stabilizes the emulsion because it accumulates in the interphases forming an oriented interfacial film. This interphase reduces the surface thermodynamic instability of the system and the coalescence of drops in the dispersed phase, ensuring emulsion homogeneity.

The appropriate surfactant must be chosen to obtain stable emulsions for atomic spectroscopy. Unfortunately, this selection is generally done by trial and error. There are several factors to be considered: the nature of the phases and the type of emulsion (oil-in-water or water-in-oil), the structure of the surfactant amphiphatic groups (which should be akin to the solvent molecules), and the solubility of the surfactant (it must be very soluble and chemically similar to the continuous phase).

Oil-in-water (o/w) emulsions have been employed in AAS much more frequently than water-in-oil (w/o) ones, because of the lower viscosity and better transport behaviour of the former type. For the analysis of oil samples, however, it should always be borne in mind that the emulsification step is really a sample dilution of the oil in water and so o/w emulsification techniques could bring about an unacceptable worsening of the required detection limits. The vast majority of papers published on the use of emulsions in atomic spectroscopy techniques refer to flame-AAS analysis,[19] although a few papers on flame[21] and plasma[33,34] atomic emission, spectroscopy have appeared. The improvements observed in plasma work using emulsions are rather modest and very few papers have been published on this topic, in spite of the fact that it has been claimed that the use of emulsions in ICP-AES provides more stable emissions and lower background than pure organic solutions, while lower RF powers can be used. According to the literature, emulsion formation can be a useful alternative to organic solvent dilution in order to tackle the problem of analysing metallic elements in oils and other liposoluble matrices.

Recent developments on emulsions refer to the combination of an "on-line" treatment of solids in a flow system using a microwave oven and final dispersion of partially dissolved solids with a carrier flow containing a surfactant. The resulting suspension/emulsion feeds the nebulizer of the AAS instrument. Future work on the use of emulsions in atomic spectrometry, suggested by de la Guardia *et al.*,[19] should focus on their utilization for ICP-AES methodologies and, combined with flow injection analysis (FIA) technology, for improved on-line sample pretreatments before final atomic spectroscopic detection.

PART B. ANALYTICAL APPLICATIONS OF SURFACTANTS BASED ON THEIR ABILITY TO ENHANCE CHEMICAL REACTIONS

It is widely recognized today that the major limitation in atomic spectroscopy is the sample introduction system,[35,36] because conventional nebulizers provide a comparatively poor efficiency for the nebulization process (5–10% in AAS and 1–2% in ICP-AES and ICP-MS). Among the different approaches suggested to improve such limitations, and thus to enhance the analytical sensitivity achievable, some workers have proposed the addition of surfactants to aqueous solutions of the sample.[14–16] As discussed, in Part A, recent evidence[17,18] points to possible improvements in atomization processes taking place in flames, while addition of surfactant to samples to be analysed in high temperature atomizers (such as plasmas) might not provide significant enhancements.

A more effective approach to increase the efficiency of conventional sample introduction systems (nebulizers) is to resort to volatile species formation. Hydride generation (HG) in particular has proved to be a most adequate and sensitive technique for the determination of very low levels of hydride-forming elements by AAS,[37] ICP-AES[37,38] or ICP-MS[39] detection modes.

When one considers that the generation of volatile species for atomic spectrometry methods is a chemical reaction and that organized media exhibit unique properties in solution to enhance reactions, it seems likely that some improvement in HG by adding surfactants to the liquid samples is to be expected. Analyti-

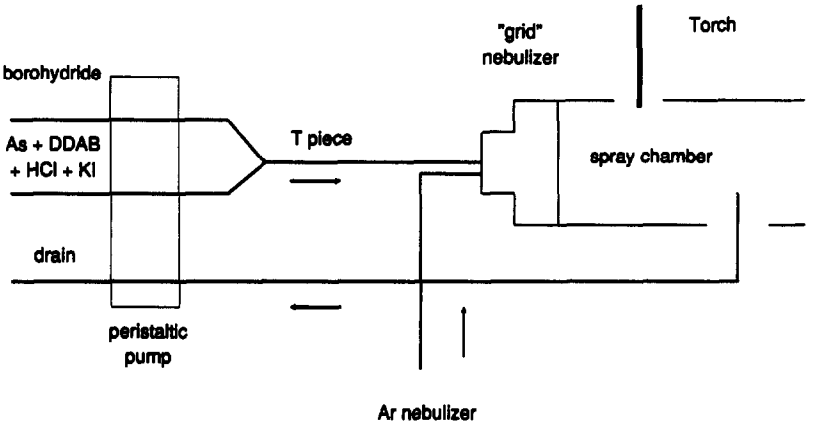

Fig. 2. The continuous HG flow system.

cal sensitivity and selectivity achieved with hydride generation/atomic detection could be improved with surfactants because: (a) they may concentrate reactants at a molecular level and so change thermodynamic and kinetic reaction constants. Thus, the analytical sensitivity can be substantially changed and improved in an adequate medium. (b) Surfactants may solubilize, in a selective manner, analytes and reactants (*e.g.* sodium borohydride) in organized "aggregates". Thus, the special microenvironment existing in/on these aggregates may change the reactions (interferences) observed in the bulk aqueous phase. In other words, analytical selectivity could be favourably changed in adequate organized media.

In fact, the analytical potential of using micelles and vesicles to improve volatile species chemical generation has already been realized, and demonstrated, in our laboratory.[24] In the following, a brief account of the progress on this topic is given.

1. Improving detection capabilities of hydride generation ICP-AES

Arsine generation in organized media. After a preliminary study on the effect of different organized media (including normal micelles with positive, negative or zwitterionic charge, non-ionic micelles and vesicles), positively charged vesicles of didodecyldimethylammonium bromide (DDAB) were selected as the most adequate medium for arsine generation using $NaBH_4$ (and iodide as the prereduction agent). As shown in Fig. 2, a commercially available continuous hydride generation system based on a de-tuned Hildebrand nebulizer was used in these studies[24] to introduce the hydride formed into the ICP (PU7000-Philips Instrument). The ICP operating experimental conditions and optimum chemical and flow conditions for HG from vesicles were first worked out. Using such optimal conditions, the analytical performance characteristics observed for HG-ICP-AES determination of arsenic from aqueous and vesicular media were evaluated for comparative purposes. Calibration graphs obtained in both media demonstrated that the sensitivity was improved by a factor of 2 using vesicles. The corresponding detection limits were 0.6 ng/ml of As for DDAB and 1.3 ng/ml in conventional aqueous medium. A significant improvement in the precision of the ICP emissions and greater tolerance to matrix interferences were also observed by using DDAB vesicles for HG. As a result of such basic studies, a new HG-ICP-AES method of As analysis has been proposed which was tested successfully for the determination of μg/g levels of As in real samples without preconcentration.[24]

Plumbane generation improvement in organized media. With a similar methodological approach, the effect of various organized media (see Table 1) on the HG-AAS signal of lead using the most commonly used mixture, $K_2S_2O_8$ and nitric acid, for the preoxidation to Pb (IV)[40] and using $NaBH_4$ for final reduction was thoroughly studied. As shown in Table 1, positively charged surfactants, cetyltrimethylammonium (CTAB) and DDAB, produced an important increase in the lead signal. This increase was dependent upon the final concentration of surfactant in a rather critical manner, particularly with CTAB (see Fig. 3). Kinetic studies using a batch hydride generator (discon-

Table 1. Comparison of lead hydride generation with ersulphate–nitric acid from water and organized molecular assemblies using AAS detection

Media	Surfactant conc.	Slope*	$A_B \pm \sigma_B$†	DL‡	Micellar factor§
Water	—	2.2×10^{-3}	0.039 ± 0.005	7	1.0
DDAB	$2 \times 10^{-3}M$	3.6×10^{-3}	0.05 ± 0.07	6	1.7
TX-100	0.02%	3.4×10^{-3}	0.029 ± 0.006	5	1.6
ZW-3.16	$10^{-3}M$	2.0×10^{-4}	0.012 ± 0.009	135	0.1
SLS	$10^{-3}M$	9.0×10^{-4}	0.050 ± 0.03	99	0.4
CTAB	$10^{-4}M$	5.8×10^{-3}	0.026 ± 0.002	1	2.6

*Slope of the calibration line: $A = A_B +$ slope·[ppb of Pb].
†A blank (mean value of absorbance for 10 blanks).
‡DL (detection limit, ng/ml) = $3\sigma_B$/slope (σ_B, standard deviation of the blank).
§Micellar enhancement factor = organized media slope/water slope.
Total sample volume used in the batch procedure = 5 ml.

tinuous device MHS-10 system from Perkin–Elmer) indicated that the observed increases were due to faster volatile species generation/transport processes in the presence of organized media, as shown in Fig. 4.

Using optimized chemical and flow conditions for HG from the different media (conventional aqueous medium, micelles of CTAB and vesicles of DDAB) and optimum instrumental parameters in the ICP, positively charged micelles of CTAB proved to provide a better reaction medium for plumbane generation and final determination of lead by continuous HG-ICP-AES.

These basic results have also been applied to develop a new HG-ICP-AES method for the determination of low levels of lead,[25] using CTAB micelles.

Cadmium volatile species generation in organized media. Generation of volatile CdH_2 in aqueous solutions at room temperature for analytical purposes is a rather difficult task due to the instability of this hydride at temperatures above liquid nitrogen.[41] In spite of such instability, CdH_2 has been proposed as the volatile species of Cd formed, and detected by AAS, when treating Cd^{2+}solutions with $NaBH_4$ in an organic medium of dimethylformamide.[42] It has to be stressed, however, that no conclusive evidence of the hydride nature, or otherwise, of such detected cadmium volatile species formed with borohydride from organic solvents has yet been provided.

In the light of the special aquo-organic microenvironment provided by surfactant-based organized assemblies, the formation of such volatile Cd species could be favoured in the presence of surfactants. Therefore, we have investigated the effect of micelles and vesicles on the HG-ICP-AES signals of Cd at 228.80 and 214.44 nm using the continuous HG system previously described for arsenic (Fig. 2).

Several types of organized assemblies were assayed, including cationic (CTAB), anionic (SLS), zwitterionic (ZW-3.16) and non-ionic (Triton X-100) micelles and also cationic ves-

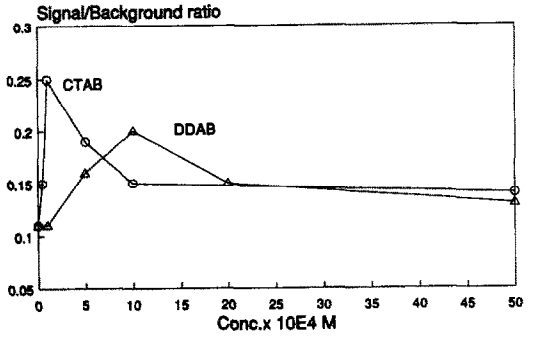

Fig. 3. Effect of organized media concentration on the HG-ICP-AES Pb signal using ammonium persulphate–nitric acid. [Pb] = 50 ng/ml.

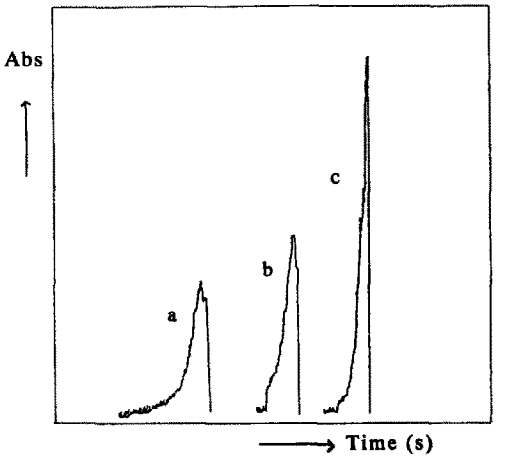

Fig. 4. Effect of the different organized media on the lead AAS peak profile. (a) Water. (b) DDAB, $2 \times 10,^{-3}M$. (c) CTAB,$10^{-4}M$.

Table 2. Comparison of cadmium volatile species from water and organized molecular assemblies using ICP-AES detection

	Surfactant	Detection limit*	Slope	Precision (%)†
Conventional nebulization	—	5	2.66×10^5	1.3
Hydride generation:				
Water	—	—	—	—
CTAB	Cationic micelles	7	3.83×10^5	2.7
TX-100	Non-ionic micelles	3	6.81×10^5	2.8
ZW-3.16	Zwiterionic micelles	2	8.59×10^5	2.6
SLS	anionic micelles	2	9.18×10^5	2.3
DHDF	Anionic vesicles	3	7.69×10^5	2.2
DDAB	Cationic vesicles	1	1.55×10^6	2.1

*Detection limit (ng/ml) = $3\sigma_b$/slope.
†Precision (RSD,%) = relative standard deviation on 50 ng/ml ($n = 10$).

icles (DDAB). Presence of cadmium in the plasma was always checked at both Cd emission lines given previously. The observed effect of the surfactants on the HG-ICP-AES cadmium signal intensities, on the background of the ICP and on the precision of the recorded Cd signals, have been summarized in Table 2.

As can be seen, results showed that the most promising analytical results were obtained using vesicles of DDAB. The importance of vesicle formation in order to obtain good ICP-AES Cd signals was tested with sonication experiments, which showed that when both the analyte, Cd^{2+} and the reducing agent, BH_4^-,were in the vesicles (that is, when both of them were present in the DDAB solution before the required sonication to form individual vesicles was carried out) maximum signals were observed for Cd. In order to verify if the analyte was actually in the vesicles, ultrafiltration experiments were performed: solutions of Cd^{2+}added to already sonicated DDAB and, alternatively, of $Cd^{2+}$and BH_4^- sonicated at the same time as the surfactant solution (in order to form the vesicles), were ultrafiltrated and the Cd^{2+}in the ultrafiltrate was determined by ICP-AES. The results observed are shown in Table 3. These results demonstrate that when sonication of DDAB solution is carried out with Cd^{2+}present, around 50% of the total Cd^{2+}added remains in the vesicles (which do not pass the ultrafiltration membrane). Maximum HG-ICP-AES signals for Cd are then obtained. If $Cd^{2+}$is added to DDAB vesicles, virtually all added Cd^{2+}seems to remain outside the vesicles in the bulk aqueous solution, because it passes quantitatively in the ultrafiltrable fraction, as seen in the results of Table 3.

On the other hand, our efforts to characterize the nature of the observed volatile species of Cd measured in the ICP (formed when the analyte and $NaBH_4$ vesicular solutions merge in the continuous HG system of Fig. 2) have failed so far. Attempts to "trap" the possible "hydride" (by passing the gases resulting from HG through a liquid N_2 cryogenic trap) and its eventual release by warming in the injection port of a GC-MS instrument (for elemental identification) have been unsuccessful so far.

In any case, this "vesicular hydride" generation technique offers five times better detection limits for Cd than conventional nebulization ICP-AES. Thus, it is presently being assessed as a new technique for determination of the metal in environment samples.[26]

A recent alternative for volatile species for-

Table 3. Ultrafiltration studies of cadmium in vesicles

	% Cd ultrafiltrated*	I_{ICP} (relative emission)
Cd in aqueous solution	100.0 ± 2.0	0
BDDA + Cd without ultrasonication	93.0 ± 2.0	300
Cd + BDDA simultaneously sonicated	46.7 ± 1.3	700

*Studies realized on 30 ng/ml Cd ($n = 7$).

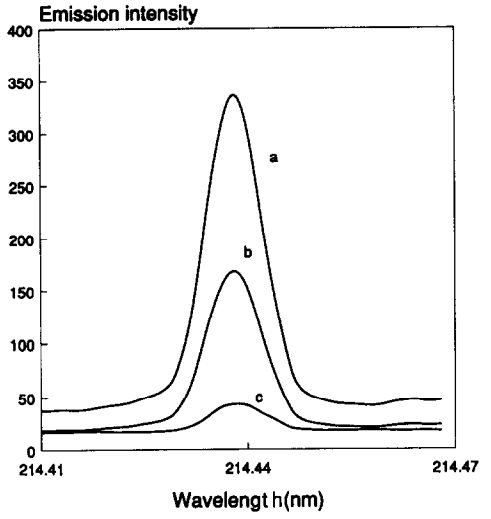

Fig. 5. Emission spectra of 100 ng/ml of cadmium. (a) Generation of $CdEt_2$ from water. (b) Generation of CdH_2 from DDAB. (c) Conventional nebulization.

mation is alkylcadmium generation using alkylboranes for alkylation. Honeycutt and Riddle[43] first reported the use of sodium tetraethylborate, $NaBEt_4$, in aqueous solutions to produce volatile organometallic species of lead and mercury from their inorganic salts, and this approach has already been applied to lead[44] and mercury.[45] D'Ulivo and Chen[46] have recently reported the use of such alkylation reactions for the atomic fluorescence determination of very low amounts of Cd. However, no conclusive identification of the exact cadmium species formed could be achieved.[46] Our preliminary results using alkylcadmium generation point to an even more efficient approach to increase the sensitivity of the ICP-AES determination of cadmium, as is needed in biological and environment samples today (see Fig. 5 for a comparison of the relative strength of the corresponding ICP signals observed). It is expected that the use of organized media may favour the efficiency of these alkylation reactions in aqueous solutions. Thus, alkylations in ordered media could offer a most exciting field of research, particularly in connection with speciation studies, where extremely high sensitivity for detection is required.

2. Improving separation/detection capabilities simultaneously

Adequate analytical technologies to tackle the present problem of element speciation are increasingly required in agricultural, environmental and clinical fields and also in the pharmaceutical and biotechnological industries.[47] It is accepted today that the most reliable approaches for speciation are tandem techniques, that is hybrid analytical methods involving interfaced chromatographic/atomic spectroscopic methods. The ICP-AES has been frequently used as a "specific" detector coupled to a liquid chromatograph for metal speciation.[48]

Unfortunately, common mobile phases for high performance liquid chromatography (HPLC) utilize organic solvents, which may be detrimental to the ICP's analytical performance (*e.g.* bringing about higher plasma background, increased instability and noise and even eventual extinction of the plasma due to excessive solvent loading). Therefore, the search for alternative mobile phases is worthwhile because it could result in better performance of HPLC-ICP-AES hybrid methods used for speciation purposes. In fact, micellar mobile phases have already been proposed for HPLC-ICP-MS speciation of alkyltin compounds.[49]

On the other hand, as we described before for the vesicle-enhanced HG-ICP-AES determination of arsenic,[24] the ability of "ordered media" to organize reactants at the molecular level can be utilized to improve the generation of volatile species (to enhance the detection power of the ICP-AES techniques). This favourable effect on detection could be combined with the potential of "ordered media" in HPLC separations.[9] That is, a synergic combination of HPLC separation/atomic detection can be achieved by resorting to the use of ordered media as mobile phases.

In fact, we have already developed such a new strategy for solving the problem of arsenic speciation[27] using synthetic vesicles of DDAB as the mobile phase. Toxic arsenic species, *e.g.* arseneous, arsenic, monomethylarsonic and dimethylarsinic acids, can be separated and determined by this HPLC-HG-ICP-AES coupling, enhanced by vesicles, within about 10 min, as shown in Fig. 6. The column is a typical C_{18} bonded silica column, modified previously by passing DDAB, while the mobile phase is phosphate buffer of pH 5.7 containing vesicles of DDAB at a surfactant concentration of $10^{-5}M$.

The detection limits observed for the different toxic species of As were found to be down to the sub-nanogram level, while the precision achieved, at the 10 ng As level, was always better than $\pm$ 5%. Thus, the synergic exploitation of beneficial effects of vesicles for both

HPLC separation and ICP-AES detection is demonstrated for the first time.[27]

CONCLUSIONS

The widespread variety of applications possible when using surfactants in analytical chemistry can be extended, as illustrated here, to the field of AAS. Two main lines of surfactant-enhanced progress can be envisaged: one refers to the favourable manipulation of physical properties of the sample solutions (*e.g.* surface tension), while the other is the intelligent manipulation of chemical reactions and/or interactions of analytes in the sample solution.

Important advantages of adding surfactants to control the physical properties of solutions include: possible increase of nebulization/atomization efficiencies in AAS, improvement of aqueous/organic solvents compatibility (emulsification purposes) and enhancement of the wettability of graphitic solid surfaces, particularly in graphite furnace techniques.

Substantial advantages of adding surfactants to manipulate reactions include the possible increase of kinetic reaction rates of volatile species formation and transport to the atomizer. By now, enhancements of about two-fold of the HG-atomic spectroscopy signals have been observed for various elements and in the cold vapour generation of Hg. Moreover, synergic combinations of the HPLC/atomic detector type are possible by resorting to micellar–vesicular mobile phases.

Summarizing, we can conclude that the advantages encountered so far by using surfactants in atomic spectroscopy methods are more modest than the enhancements observed when used in other detection techniques, *e.g.* fluorimetry.[5] However, the interface surfactant assemblies/analytical atomic spectroscopy (see Fig. 1) still holds a great potential for innovative applications, particularly so in the area of developing hybrid chromatography/atomic detector techniques, a combination which has proved extremely valuable for solving modern speciation problems.

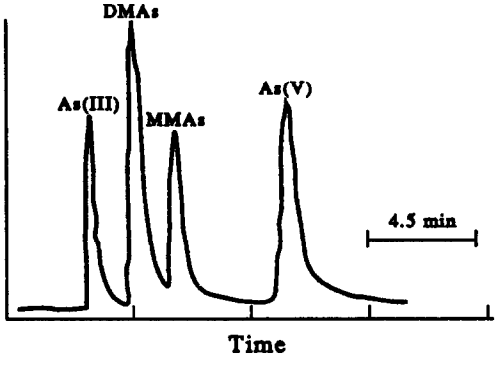

Fig. 6. Arsenic speciation by vesicle-mediated-HPLC coupled to ICP-AES. DMAs, dimethylarsinic acid; MMAs, monomethylarsonic acid; DDAB, didodecyldimethylammonium bromide.

REFERENCES

1. W. L. Hinze, Use of surfactant and micellar systems in analytical chemistry, in *Solution Chemistry of Surfactants*, K. L. Mittal (ed.), Vol. 1, p.79. Plenum Press, New York, 1979.
2. L. J. Cline Love, J. G. Habarta and J. G. Dorsey, *Anal. Chem.*, 1984, **56**, 1132A.
3. E. Pelizzetti and E. Pramauro, *Anal. Chim. Acta*, 1985, **169**, 1.
4. M. E. Diaz García and A. Sanz-Medel, *Talanta*, 1986, **33**, 255.
5. J. Georges, *Analusis*, 1989, **17**, 231.
6. A. Sanz-Medel, P. L. Martinez and M. E. Diaz García, *Anal. Chem.*, 1987, **59**, 774.
7. T. C. Franklin and M. Iwunze, *Anal. Chem.*, 1980, **52**, 973.
8. M. D. Ryan and T. Q. Chambers, *Anal. Chem.*, 1992, **64**, 99R.
9. W. L. Hinze and D. W. Armstrong (eds), *Ordered Media in Chemical Separations*, ACS Symposium Series, 342. ACS, Washington, DC, 1987.
10. S. Terabe, K. Otsuka and T. Ando, *Anal. Chem.*, 1989, **61**, 261.
11. S. Igarashi and T. Yotsuyanagi, *Mikrochim. Acta*, 1992, **106**, 37.
12. M. Uygur-Garip and M. Thompson, *Anal. Proc. R. S. C.*, 1991, **28**, 2.
13. H. Watanabe, T. Saitoh, T. Kamidate and K. Haraguchi, *Mikrochim. Acta*, 1992, **106**, 83.
14. M. Kodama and S. Miyagawa, *Anal. Chem.*, 1980, **52**, 2358.
15. J. A. Borowiec, A. W. Boorn, J. R. Dillard, M. Cresser and R. F. Browner, *Anal. Chem.*, 1980, **52**, 1054.
16. M. Tang, Y. Takabatake and H. Yoshida, *Bunseki Kagaku*, 1984, **33**, 439.
17. Z. Yin Yan and W. Zhang, *J. Anal. At. Spectrom.*, 1989, **4**, 797.
18. J. Mora, A. Canals and V. Hernandis, *J. Anal. At. Spectrom.*, 1991, **6**, 139.
19. M. de la Guardia and A. Salvador, *Analusis*, 1991, **19**, m 52.
20. V. Berenguer and J. Hernández, *Quim. Anal.*, 1977, **31**, 81.
21. M. de la Guardia, A. Salvador and V. Berenguer, *Ann. Quim.* 1982, **78B**, 321.
22. I. Lakatos, J. Lakatos and Gy Bagdi, *Proc. Third Italo-Hungarian Symp. on Spectrochemistry*, p. 43, Ispra, Italy, 1987.
23. K. S. Subramanian, *Prog. Anal. Spectrosc.*, 1986, **9**, 237.
24. B. Aizpún Fernández, M. C. Valdés-Hevia y Temprano, M. R. Fernández de la Campa and A. Sanz-Medel, *Talanta*, T. S. West special issue, 1992.

25. M. C. Valdés-Hevia y Temprano, B. Aizpún Fernández, M. R. Fernández de la Campa and A. Sanz-Medel, *Anal. Chim. Acta.* (submitted for publication).
26. M. C. Valdés-Hevia y Temprano, M. R. Fernández de la Campa and A. Sanz-Medel, Generación de especies volátiles de Cadmio desde medios organizados. Abstracts of XII Reunión Nacional de Espectroscopía, Gandía, España, 1992.
27. Y. Liu, M. L. Fernández, E. Blanco and A. Sanz-Medel, Book of abstracts of the *1993 Winter Conf. on Plasma Spectrochemistry*, Oral Session, Granada, Spain, 1993.
28. J. S. Blais, G. M. Momplaisir and W. D. Marshall, *Anal. Chem.*, 1990, **62**, 1161.
29. J. C. Van Loon and R. R. Barefoot, *Analyst*, 1992, **117**, 563.
30. H. Kornahrens, K. D. Cook and D. W. Armstrong, *Anal. Chem.* 1982, **54**, 1325.
31. R. M. Rodriguez Roza, Ph. D. Thesis, Oviedo University, 1989.
32. B. L. Sharp, R. Jowitt, S. T. Sparkes, A. P. Thorne and S. J. Walton, *J. Anal. At. Spectrom.*, 1992, **7**, 160R.
33. M. de la Guardia, A. Salvador and V. Berenguer, *Analusis*, 1981, **9**, 74.
34. M. de la Guardia, G. Legrand, M. Druon and J. L. Louvrier, *Analusis*, 1982, **10**, 476.
35. R. F. Browner and A. W. Boorn, *Anal. Chem.*, 1984, **56**, 786A.
36. J. Sneddon (ed.), *Sample Introduction in Atomic Spectroscopy*. Elsevier, Amsterdam, 1990.
37. T. Nakahara, *Prog. Anal. At. Spectrosc.*, 1983, **6**, 163.
38. M. Thompson, B. Pahlavanpour, S. J. Walton and G. F. Kirkbright, *Analyst*, 1978, **103**, 568.
39. J. Akagi, T. Hirata and A. Masuda, *Anal. Sci.*, 1990, **6**, 397.
40. I. D. Brindle and X. Le, *Anal. Chem.*, 1989, **61**, 1175.
41. G. D. Barbaras, C. Dillard, A. E. Finholt, T. Wartik, K. E. Wilzbach and H. I. Schlesinger, *J. Am. Chem. Soc.*, 1951, **73**, 4585.
42. J. Cacho, I. Beltrán and C. Nerín, *J. Anal. At. Spectrom.*, 1989, **4**, 661.
43. J. B. Honeycutt and J. M. Riddle, *J. Am. Chem. Soc.*, 1961, **83**, 369.
44. S. Rapsomanikis, O. F. X. Donard and J. H. Weber, *Anal. Chem.*, 1986, **58**, 35.
45. N. Bloom, *Can. J. Fish Aquat. Sci.*, 1989, **46**, 1131.
46. A. D'Ulivo and Y. Chen, *J. Anal. At. Spectrom.*, 1989, **4**, 319.
47. A. M. Ure, in *Heavy Metals in Soils*, B. J. Alloway (ed.). Blackie and Sons, Glasgow, 1990.
48. L. Ebdon, S. Hill and R. W. Ward, *Analyst*, 1987, **112**, 1.
49. H. Suyani, D. Heitkemper and J. Creed, *J. Caruso. Appl. Spectrosc.*, 1989, **43**, 962.

Talanta, Vol. 40, No. 11, pp. 1769–1774, 1993
Printed in Great Britain.

0039-9140/93 $6.00 + 0.00

BEHAVIOUR OF SOLID ADSORBENTS FOR THE SAMPLING OF ATMOSPHERIC ORGANOCHLORINE COMPOUNDS

C. NERIN, M. MARTINEZ, B. PONS and J. CACHO

Dept. Química Analítica, Centro Politécnico Superior de Ingenieros, Universidad de Zaragoza, Zaragoza, Spain

Summary—The behaviour of Tenax® GC, Polyurethane foam (density 0.022 g/cm^3), Amberlite® XAD-2 and Amberlite® XAD-4 alone or in combination has been studied. Standard atmospheres containing different concentration levels of hexachlorocyclohexane and chlorobenzene isomers were generated and trapped in adsorbent cartridges. The generation of the atmosphere, the adsorption by the cartridges, the extraction of the compounds, the evaporation of the final solution and the analysis of GC/ECD have been studied. The most efficient system for trapping the test gases is the use of two cartridges connected in series, one containing Polyurethane foam and the second one containing Tenax GC. Recovery values ranging from 72% for 1,3-dichlorobenzene to 98% for gamma-hexachlorocyclohexane are obtained, most of them >90%. The SD values for all the compounds under study are around 4% for a total sampled amount of 0.5 μg of each compound.

The environmental distribution of organochlorine compounds in water, sediments, fish, *etc*, has been studied.[1–13] There are many papers about their distribution in these different media. However, very few papers address the atmospheric distribution of these compounds even though they are used as pesticides and appear in the atmosphere around industrial waste dumps, *e.g.*, from Lindane factories. These emissions contain hexachlorocyclohexane and chlorobenzene isomers. Nevertheless, the atmospheric distribution of these compounds and the typical concentration level is not well known. Due to their relatively higher vapour pressure, the presence of these species in the atmosphere may be important.[1–3]

The classical methods of sampling organochlorine compounds in the atmosphere consist of trapping them in an organic solvent, usually iso-octane. Due to the evaporation of the solvent during sampling and the consequent difficulty of long term sampling, this is not very practical. Also, the use of an organic solvent in the impinger demands attention. To avoid these disadvantages, relatively few studies have been conducted to determine trapping efficiencies of adsorbents to airborne pesticides.[14–16] Polyurethane foams, Porapak® N and R, Tenax® GC and Chromosorb® 102 have been used for trapping several pesticides or related compounds; only hexachlorocyclohexanes, chlordane and heptachlor have been studied.[17] Their ability to trap more volatile compounds such as chlorobenzenes has not previously been checked.[16]

This paper describes the results of studies carried out with Polyurethane foam, Tenax® Amberlite® XAD-4 and Amberlite® XAD-2 in order to establish the optimum procedure for sampling organochlorine compounds, such as hexachlorocyclohexanes (HCHs) and chlorobenzenes, in the atmosphere.

EXPERIMENTAL

Apparatus

A Varian (Palo Alto, CA) Aerograph Gas Chromatograph and a silanized hollow glass column were used to generate the standard atmosphere. A Hewlett–Packard (Palo Alto, CA) Gas Chromatograph 5890 equipped with an Electronic Capture Detector (ECD) and automatic injector was used to analyse the samples. A capillary column DB-1701, 60 m × 0.25 mm × 0.25 μm film thickness, was used under the following conditions: inj. temperature: 250°; detector temperature: 350°. Split ratio 1:10. Initial temperature 50° for 5 min, 7°/min up to 250° and then held at 250° for 9.5

min. Column head pressure: 95 kPa; carrier H_2; make up gas N_2.

Reagents

Alpha-, beta-, gamma- and delta-hexachlorocyclohexane, 1,2-dichlorobenzene, 1,3-dichlorobenzene, 1,4-dichlorobenzene, 1,2,3-trichlorobenzene, 1,2,4-trichlorobenzene, 1,2,5-trichlorobenzene, 1,3,5-trichlorobenzene, 1,2,3,4-tetrachlorobenzene and 1,2,4,5-tetrachlorobenzene were obtained from Chem Service (West Chester, PA). Nitrobenzene standard was from Fluka (Buchs, Switzerland) and methyl chlorpyriphos was from Riedel-de Haën (Seelze, Germany).

Polyurethane foam (PUF) of 0.022 g/cm^3 density was specially produced by Pikolin (Zaragoza, Spain); Tenax GC, Amberlite XAD-2 and Amberlite XAD-4 were supplied by Supelco (Bellefonte, PA) and Florisil was from Fluka.

All glassware was cleaned using an ultrasonic bath with distilled water and neutral soap for 6 hr, after which it was washed sequentially with distilled water, acetone and hexane.

PUF cartridges of 100 mm length and 20 mm diameter were cleaned before using a hexane–diethylether mixture (19:1, v/v) for 12 hr in a Soxhlet extractor. After this treatment the cartridges were dried under a nitrogen current and stored in a clean glass container in the dark in a nitrogen atmosphere. Tenax was heated at 250° under N_2 current for 2 hr, in order to clean the adsorbent before using it. Amberlite XAD-2 and XAD-4 were extracted with a hexane–diethyl ether (19:1, v/v) mixture before use. Figure 1 shows the chromatogram of a blank of each adsorbent used after the mentioned clean-up.

Procedure

A hexane solution (0.5 ml) containing about 1 μg/g of the compounds mentioned was injected in an empty silanized glass column ($\frac{1}{4}$″ × 2 m, i.d.) placed in a GC at 60°, using synthetic air as carrier. The carrier flow is set at 0.8 l./min. In the GC outlet a glass cartridge containing a solid adsorbent is placed. After 1 hr the solid adsorbent sampling cartridge was introduced in a Soxhlet and a 12 hr extraction with the hexane–diethyl ether (19:1, v/v) mixture carried out. The extract obtained was concentrated under N_2 current up to 2 ml. This extract was transferred to a volumetric flask with a suitable amount of the internal standard, and then analysed by GC/ECD.

RESULTS AND DISCUSSION

Generation of standard atmosphere

Figure 2 depicts the scheme of the system employed. A GC with a hollow silanized glass column was used to evaporate a solution of known concentration of the compounds to be

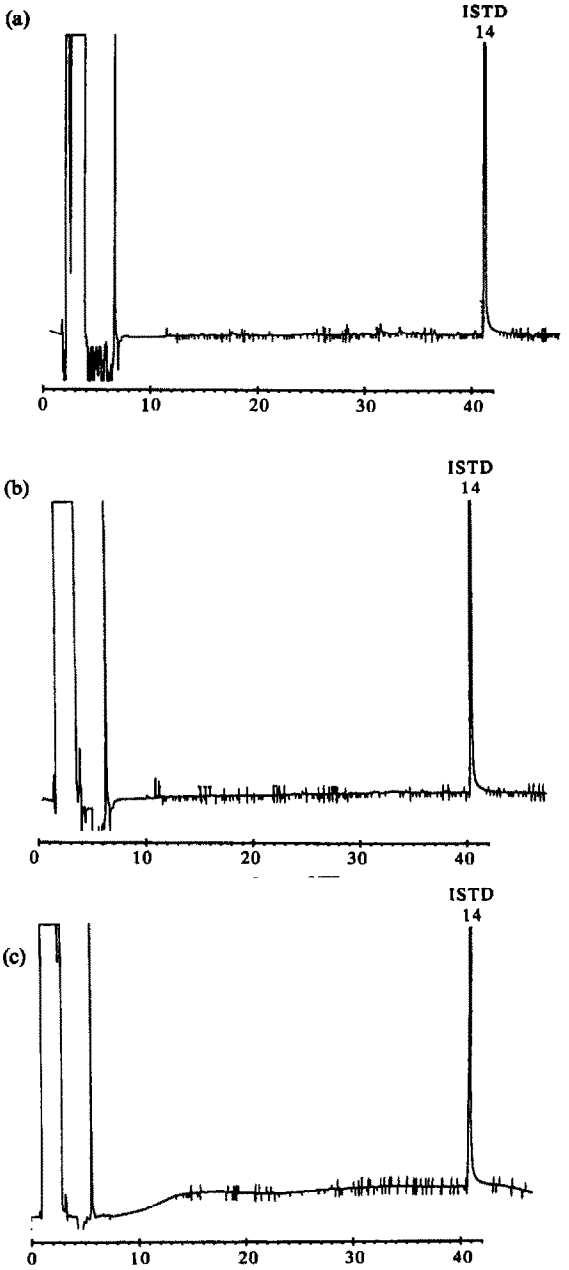

Fig. 1. (a) Chromatogram of a blank of PUF. (b) Chromatogram of a blank of Tenax GC. (c) Chromatogram of a blank of Amberlite XAD-2.

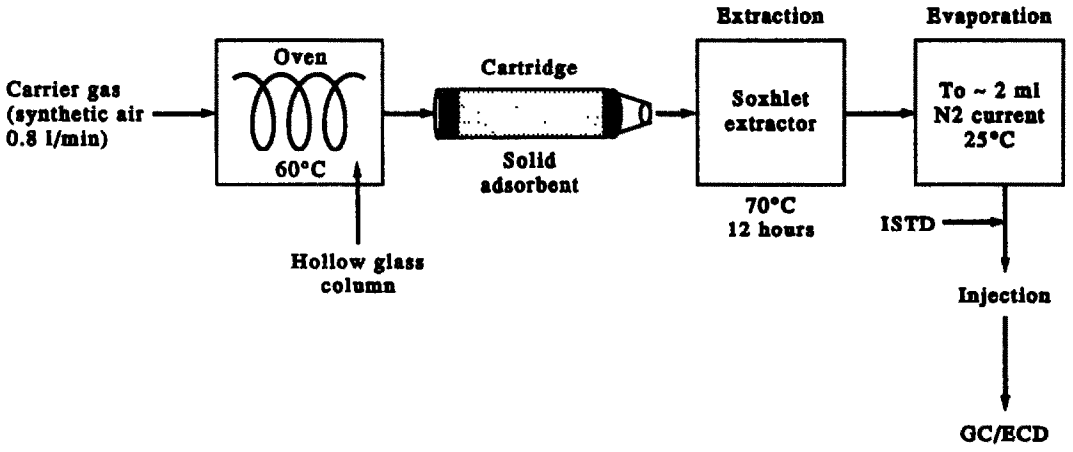

Fig. 2. Scheme of the system used to generate the standard atmosphere and to study the behaviour of solid adsorbents.

studied. To stimulate the real sampling conditions, the injection port was heated at 90°, whereas the empty column was kept at 60°, under the boiling point of the solvent used in the injected solution. In the first part of the glass column a small amount of glass wool was placed to give more homogeneity to the evaporation process. In these conditions the compounds were evaporated slowly and because of the low oven temperature, the adsorption occurred essentially at room temperature. One or more glass cartridges containing the solid adsorbents were placed at the column outlet to trap the compounds. Fifty minutes after injecting the solution in the glass column, the temperature of the oven was increased to 100° and all the exhaust from the column was trapped in the same cartridge. Synthetic air (0.8 l./min) was used as carrier gas for the evaporation of the compounds. After each injection, 0.5 ml of hexane was injected into the system and the exhaust was trapped in another cartridge; this was used as a blank. No analyte compounds were observed in this blank. Figure 3 shows a

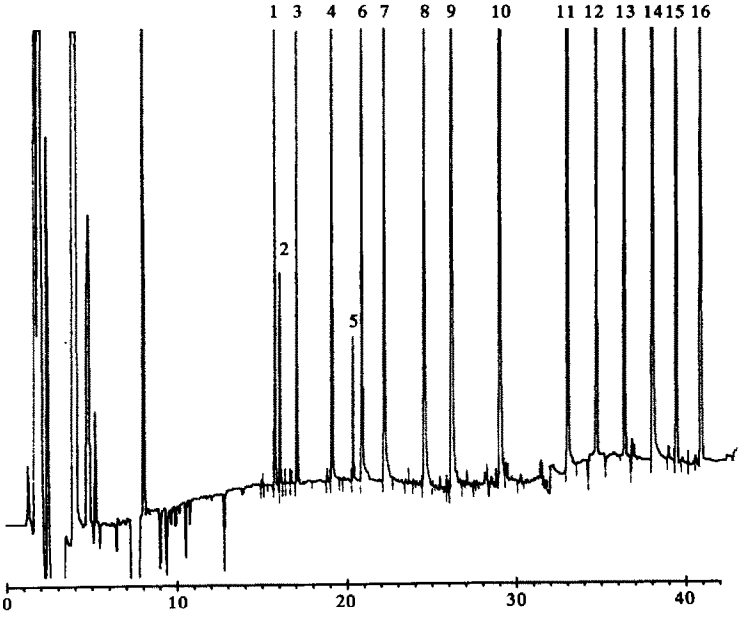

Fig. 3. Chromatogram of a standard solution. **1**: 1,3-dichlorobenzene; **2**: 1,4-dichlorobenzene; **3**: 1,2-dichlorobenzene; **4**: 1,3,5-trichlorobenzene; **5**: nitrobenzene (1st ISTD); **6**: 1,2,4-trichlorobenzene; **7**: 1,2,3-trichlorobenzene; **8**: 1,2,4,5-tetrachlorobenzene; **9**: 1,2,3,4-tetrachlorobenzene; **10**: pentachlorobenzene; **11**: hexachlorobenzene; **12**: alpha-HCH; **13**: gamma-HCH; **14**: methyl chlorpyriphos (2nd ISTD); **15**: beta-HCH; **16**: delta-HCH.

Table 1. Percentage recoveries of hexachlorocyclohexanes and chlorobenzenes from spiked polyurethane foam samples after extraction and evaporation steps

Compound	Mean	SD	n
1,3-Dichlorobenzene	88.04	5.07	5
1,4-Dichlorobenzene	68.06	5.02	5
1,2-Dichlorobenzene	77.45	6.82	6
1,3,5-Trichlorobenzene	88.87	5.26	6
1,2,4-Trichlorobenzene	94.63	6.93	5
1,2,3-Trichlorobenzene	97.70	5.93	5
1,2,4,5-Trichlorobenzene	100.70	6.75	5
1,2,3,4-Trichlorobenzene	98.56	4.80	5
Pentachlorobenzene	95.57	4.17	5
Hexachlorobenzene	94.17	7.74	4
Alpha-HCH	99.63	8.19	4
Gamma-HCH	102.19	3.19	5
Beta-HCH	88.89	13.10	4
Delta-HCH	104.05	7.12	4

chromatogram of the compounds studied under the conditions mentioned above.

Extraction study

Once the compounds were trapped on the solid sorbents it was necessary to extract them. A study was carried out to optimize the extraction procedure. A 50 ml Soxhlet extractor was used with a hexane–diethyl ether (19:1, v/v) mixture during 12 hr. Several spiked samples were prepared by adding 0.5 ml of a solution containing 2 μg/ml to a cartridge of PUF. After drying the PUF well, it was extracted in the Soxhlet extractor under the conditions mentioned above.

According to previous studies, one of the major sources of error in the analysis of volatile compounds is due to the loss of compounds during the concentration/evaporation step. Among evaporation methods reported in the literature,[18] the use of N_2 current at constant temperature was selected as the most appropriate. The extracts obtained from the spiked samples were evaporated and analysed. The results are shown in Table 1. No losses are apparent from the extraction and evaporation steps.

Behaviour of solid adsorbents

Some organic compounds cannot be sampled on charcoal owing to decomposition reactions, irreversible adsorption, or due to the adsorption of other compounds which can interfere in the analysis. In such cases adsorbents of the porous polymer type may be useful alternatives. Previous work[16] on PUF showed that this can be a good adsorbent for HCHs, but its applicability to the sampling of chlorobenzenes was unknown. Therefore, the first adsorbent checked was PUF. Tenax, Amberlite XAD-4 and Amberlite XAD-2 are mentioned in the literature as very efficient adsorbents of volatile compounds.[16,19–22] A second cartridge containing one of these adsorbents was connected serially after the cartridge containing PUF. Several standard atmospheres as calibrants were generated and these were sampled in the cartridges. In order to compare the trapping efficiency, when more than one cartridge was sequentially employed, the solid adsorbents from each cartridge were extracted together in the same Soxhlet. Table 2 shows the results obtained as an average of five independent determinations. These values include the recoveries obtained in the overall process, which includes the steps of generation, adsorption, extraction, concentration and analysis.

Two different aspects can be emphasized. The first is the different trapping efficiency of PUF

Table 2. Trapping efficiency of different solid adsorbents and combinations expressed as percentage recoveries

	PUF alone			PUF–TENAX			PUF–XAD2			PUF–XAD4		
Compound	Mean	SD	n	Mean	SD	n	Mean	SD	n	Mean	SD	n
1,3-Dichlorobenzene	63.84	17.59	4	72.41	6.09	5	69.89	4.43	5	86.28	4.37	5
1,4-Dichlorobenzene	94.31	5.29	4	96.81	8.47	5	94.20	4.44	5	106.05	5.42	5
1,2-Dichlorobenzene	88.23	0.05	4	81.70	1.98	5	87.78	5.36	5	103.29	7.61	5
1,3,5-Trichlorobenzene	83.69	6.04	4	81.59	5.24	5	73.24	3.67	5	81.73	2.24	5
1,2,4-Trichlorobenzene	79.42	4.72	4	78.27	7.47	5	88.08	3.81	5	109.17	3.45	5
1,2,3-Trichlorobenzene	77.00	5.21	4	75.22	7.00	5	79.18	3.43	5	83.18	4.61	5
1,2,4,5-Trichlorobenzene	78.38	3.65	4	79.96	7.44	5	84.46	3.34	5	141.87	6.00	5
1,2,3,4-Trichlorobenzene	60.65	24.64	4	89.35	4.82	5	87.03	4.08	5	105.70	4.31	5
Pentachlorobenzene	101.41	5.46	4	66.45	4.97	5	115.53	4.71	5	106.98	2.95	5
Hexachlorobenzene	72.13	3.78	4	79.45	4.83	5	81.20	0.16	5	76.42	1.39	5
Alpha-HCH	81.04	6.02	4	86.27	5.72	5	95.46	0.87	5	144.20	18.23	5
Gamma-HCH	59.51	5.40	4	63.85	4.19	5	74.56	0.59	5	72.06	7.23	5
Beta-HCH	61.77	1.41	4	66.12	6.65	5	84.13	1.05	5	64.03	2.41	5
Delta-HCH	48.27	1.35	4	53.43	6.98	5	71.77	4.41	5	56.16	4.12	5

for chlorobenzene isomers compared to that for HCHs. The recovery of chlorobenzene is quite low. According to the literature,[14] the recoveries of volatile compounds from PUF are very low. As chlorobenzenes are quite volatile, especially dichlorobenzenes and trichlorobenzenes, PUF does not seem to be appropriate to trap them in the atmosphere. On the other hand, volumes of air around 1 m^3 have to be sampled in order to measure the low concentration of such compounds commonly found in the atmosphere. Obviously, in these conditions the breakthrough volumes for these volatile compounds on PUF are surpassed, which means that this adsorbent is not efficient enough to sample these compounds. It can be further observed that the higher the boiling point of the compound, the higher is the recovery. The second aspect is that when two cartridges are combined in series, one of them serves mainly to trap the more volatile compounds and the other to capture the HCHs. No differences were found in the behaviour of Tenax and the Amberlite adsorbents, except that the standard deviation was slightly higher for the PUF + Amberlite combination. Taking into account these considerations, the PUF + Tenax combination in series was selected for trapping atmospheric HCHs and chlorobenzenes.

Clean-up of the PUF cartridges

The typical atmospheric concentration of the compounds of interest is usually very low. Consequently, it is necessary to improve the sensitivity of the procedure. This can be achieved through the concentration step. However, in this way, other compounds present in the PUF which can also be extracted are concentrated as well and some interferences appear. On the other hand, it was observed experimentally that when PUF was recently prepared no interferences appeared from other compounds present in the PUF, even after this concentration step. This fact can be seen in Fig. 1a, in which a chromatogram of a new PUF cleaned with hexane–diethyl ether (19:1, v/v) as mentioned above is shown.

Nevertheless, as soon as the PUF became older, which happens after approximately 2 months of being produced, new interferences from the PUF appeared in the concentration step, as shown in Fig. 3a. Figure 4a shows a chromatogram of an extract of an old PUF before the clean-up step. It is obvious that a clean-up step is necessary in such a case.

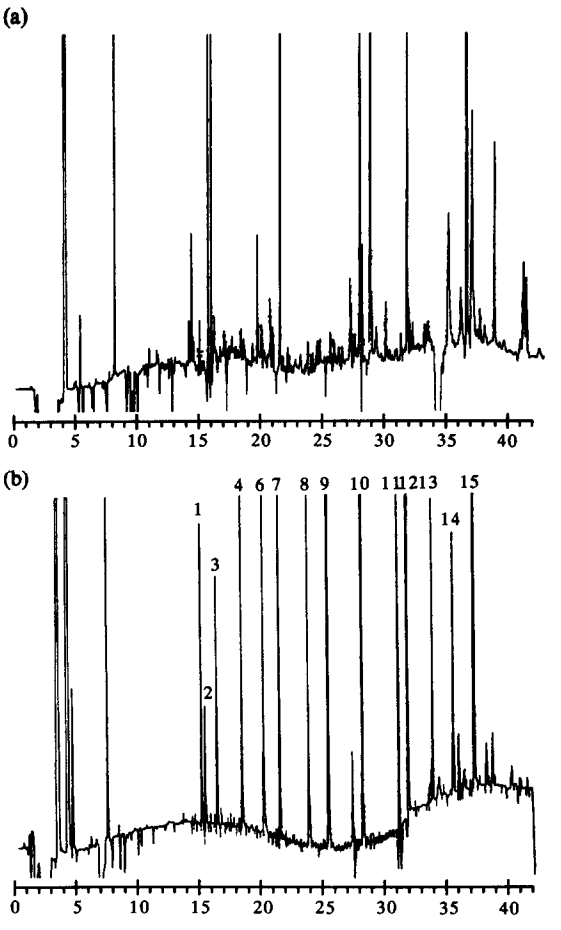

Fig. 4. (a) Chromatogram of an old PUF before clean-up. (b) Chromatogram of a spiked old PUF after clean-up with 10% Florisil. The peak identifications are the same as in Fig. 3.

It is well known that both Florisil® and silica are good adsorbents for the clean-up of different matrices.[23–25] Although in this particular case the interferences to be removed are not major components, several experiments were carried out using 10% deactivated Florisil. The columns used were of 20 mm internal diameter, filled with about 7 g of Florisil and topped with 1 g of anhydrous sodium sulphate. The Soxhlet extract, about 70 ml, was added to the column and the compounds were eluted with 15 ml of hexane. The final solution obtained was evaporated to 2 ml and analysed. Figure 4b shows the chromatogram of a spiked PUF obtained after the clean-up step. The results obtained show that the use of Florisil in the conditions mentioned is adequate to remove the interferences from the old PUF. Furthermore, no losses of the OCPs occur in this clean-up step. This is detailed in the data presented in Table 3.

Table 3. Percentage recoveries of spiked polyurethane foams after clean-up on Florisil

Compound	Amount added (μg)	Percent recovered	CV	n
1,3-Dichlorobenzene	1.14	74.1	5.06	4
1,4-Dichlorobenzene	0.75	79.9	5.02	4
1,2-Dichlorobenzene	1.06	79.3	6.82	4
1,3,5-Trichlorobenzene	0.37	83.2	5.27	4
1,2,4-Trichlorobenzene	0.39	89.5	6.93	4
1,2,3-Trichlorobenzene	0.32	91.1	5.94	4
1,2,4,5-Trichlorobenzene	0.32	88.3	6.75	4
1,2,3,4-Trichlorobenzene	0.49	86.4	4.80	4
Pentachlorobenzene	0.37	85.9	4.17	4
Hexachlorobenzene	0.34	78.1	8.19	4
Alpha-HCH	0.40	87.2	7.74	4
Gamma-HCH	0.36	84.5	8.11	4
Beta-HCH	0.34	83.3	3.19	4
Delta-HCH	0.39	54.0	7.12	4

CONCLUSIONS

The system used here to generate standard calibrant gases is efficient and lets the user obtain a great variety of contaminated atmospheres at different concentration levels.

Among the solid adsorbents checked, the use of two cartridges connected in series, one containing polyurethane foam (PUF) and the other Tenax GC, is the most efficient trap for HCHs and chlorobenzenes in the atmosphere. This system has the advantage over other combinations that PUF is quite rigid and porous and the structure facilitates the handling of the cartridge. On the other hand, as two cartridges are independent, each cartridge can be recycled after use. Furthermore, in a real atmosphere, the PUF is not clogged by humidity from the air, and for this reason it is more convenient to place PUF in the first cartridge. As was shown in previous work,[16] humidity does not influence the efficiency of PUF to trap HCHs; this is a significant advantage over particulate polymeric adsorbents.

Acknowledgements—This paper was financially supported by the Project "Estudio de Accidentes Mayores en la Industria Quiímica y sus consecuencias Medioambientales" de la Diputación General de Aragón.

REFERENCES

1. S. Tanabe, R. Tatsukawa, M. Kawano and H. Hidaka, *J. Ocean. Soc. Japan*, 1982, **38**, 137.
2. R. Wittlinger and K. Ballschmiter, *Chemosphere*, 1987, **16**, 2497.
3. K. Ballschmiter and R. Wittlinger, *Environ. Sci. Technol.*, 1991, **25**, 1103.
4. C. Nerín, M. Martínez and J. Cacho, *Toxicol. Environ. Chem.*, 1992, **35**, 125.
5. R. C. Fischer, W. Kramer and K. Ballschmiter, *Chemosphere*, 1991, **23**, 889.
6. C. Ang, K. Meleady and L. Wallace, *Bull. Environ. Contam. Toxicol.*, 1989, **42**, 595.
7. D. M. Lockerbie and T. A. Clair, *Bull. Environ. Contam. Toxicol.*, 1988, **41**, 625.
8. C. Nerín, I. Echarri and J. Cacho, *Z. Anal. Chem.*, 1991, **339**, 684.
9. K. W. McDougall, G. Singh, C. R. Harris and F. R. Higginson, *Bull. Environ. Contam. Toxicol.*, 1987, **39**, 286.
10. T. Samuel, H. C. Agarwal and M. K. K. Pillai, *Pestic. Sci.*, 1988, **22**, 1.
11. S. Panda, M. Sharmila, K. Ramanand, D. Panda and N. Sethunathan, *Pestic. Sci.*, 1988, **23**, 199.
12. L. Granier, M. Chevreuil, A. M. Carru and R. Lètolle, *Chemosphere*, 1990, **21**, 1101.
13. L. M. Hernandez, M. A. Fernandez and M. J. Gonzalez, *Bull. Environ. Contam. Toxicol.*, 1991, **46**, 9.
14. R. G. Lewis and K. E. MacLeod, *Anal. Chem.*, 1982, **54**, 310.
15. R. G. Lewis and M. D. Jackson, *Anal. Chem.*, 1982, **54**, 592.
16. R. B. Leidy and C. G. Wright, *J. Environ. Sci. Health*, 1991, **4**, 367.
17. C. Nerín, S. Ballestar, J. Cacho and V. Ferreira, *Man and his Ecosystem (Proc. 8th World Clean Air Congress)*, 1989, **3**, 701.
18. V. Ferreira, Ph.D., University of Zaragoza, 1992.
19. H. Rothweiler, R. T. Wager and C. Schlatter, *Atm. Environ.*, 1991, **25**, 231.
20. Y. Yokouchi and M. Sano, *J. Chromatogr.*, 1991, **555**, 297.
21. J. O. Levin and L. C. Carleborg, *Ann. Occup.*, 1987, Hyg., **31**, 31.
22. P. Ciccoli, E. Brancaleoni and A. Ceniuato, *J. Chromatogr.*, 1986, **35**, 433.
23. I. Levi and T. W. Nowicki, *J. AOAC*, 1974, **57**, 924.
24. M. J. Chessells, D. W. Hawker, D. W. Connell and I. A. Papajcsik, *Chemosphere*, 1988, **17**, 1741.
25. T. S. S. Dikshith, S. N. Kumar and G. S. Tandon, *Bull. Environ. Contam. Toxicol.*, 1989, **42**, 50.

Talanta, Vol. 40, No. 12, pp. 1775–1779, 1993
Printed in Great Britain.

0039-9140/93 $6.00 + 0.00

EXTRACTION AND ELECTROCHEMICAL QUANTIFICATION OF THE ACTIVE INGREDIENT (DIAZEPAM) IN PHARMACEUTICAL PRODUCTS

M. GUADALUPE GARCÍA,[1] ALVARO GARCÍA[1] and IGNACIO GONZÁLEZ[2]*

[1]Instituto de Investigaciones Científicas, Universidad de Guanajuato, Cerro de la Venada s/n, Pueblo de Rocha, 3600 Guanajuato, GTO, Mexico

[2]Universidad Autónoma Metropolitana-Iztapalapa, Departamento de Química, Apartado Postal 55-534, 09340 México, D.F., Mexico

(*Received* 10 *May* 1993)

Summary—A method for the extraction and separation of the active ingredient diazepam (7-chloro-dihydro-1-methyl-5-phenyl-2H, -1,4-benzodiazepam-2-one) in pharmaceutical tablets is discussed. This method avoids the hydrolysis of diazepam. Polarographic studies with direct current (DCP), alternating current (ACP) and differential pulse polarography (DPP) were used under different sets of conditions. The pH value most suitable for these studies was found to be 4.6. The detection range for ACP was found to be from 17.4 to 167 μM, whereas for DPP, the range was 4.8–96 μM.

Commercial tablets of diazepam labelled to contain 10 mg per tablet were assayed. For five replicate samples, the relative standard deviations were lower than 1% and the contents were determined with errors lower than 4%.

Diazepam (7-chloro-dihydro-1-methyl-5-phenyl-2H,-1,4-benzodiazepam-2-one) belongs to the group of 1,4-benzodiazepines (see Fig. 1), commonly used as tranquilizers and ansiolytics. Their use has great therapeutic importance for the treatment of diseases of the central nervous system. For this reason, the quality control of these substances is rather important as well as the concentrations of their metabolites in biological fluids. These benzodiazepines possess both electroactive and chromophoric groups[1] that allow for their polarographic and spectrophotometric determination.[1,2] In fact, a flow injection analysis system (FIA) equipped with a polarographic and a spectrophotometric detector has been used in the analysis of clotiazepan.[1]

The official pharmacopeias[3,4] describe spectrophotometric assays for measuring diazepam and oxazepam in dosage forms. These methods require a previous dissolution in sulfuric and hydrochloric media. Like other benzodiazepines, these drugs are susceptible to acid hydrolysis with subsequent ring opening.[5] The kinetics of the hydrolysis of such compounds have been extensively studied.[6,7] Abdel-Hamid and Abuirjeie[8] have reported that the spectrophotometric methods produce variable and non-significant results, indicating that the official procedures are not specific for the intact drug and do not reveal the presence of the degradation products. For these reasons, it is necessary to develop procedures in order to solve these problems.

The HPLC procedure and the fourth-derivative spectrophotometry have been proposed for these purposes.[8] Brooks[9] reports a general review of the application of electrochemistry in pharmaceutical analysis, where the 1,4-benzodiazepines determination is extensively described, however the problems related to the drug extraction from the pharmaceutical products are not deeply discussed.

Kalvoda[10] has studied polarographically active ingredients such as diazepam, nitrazepam, papaverine and other nitroaromatic compounds. Jacobsen and Jacobsen[11,12] have measured with this technique the concentration of diazepam in pharmaceutical products as well as in biological samples (with a previous extraction). However, they used electrolytes that tend to hydrolyze diazepam. This hydrolysis may affect the accuracy of the polarographic analysis.

In this work, the extraction and identification of diazepam in pharmaceutical tablets is presented as well as its quantification with electroanalytical techniques. The aim is to design an

*Author to whom the correspondence should be addressed.

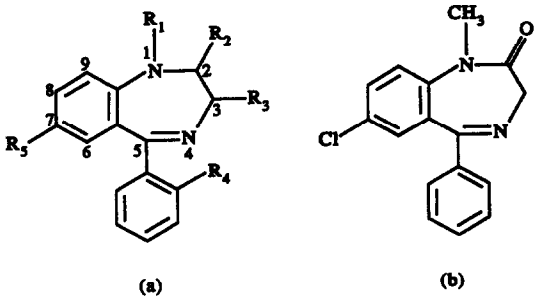

(a) (b)

Fig. 1. (a) General formula of 1,4-benzodiazepines, (b) diazepam formula.

exact and reproducible method that may be used for similar compounds in pharmaceutical products.

Experimental

The polarographic studies were performed with home-made polarographs. Direct current (DCP), alternating current (ACP) and differential pulse polarography (DPP) were performed. The electrochemical cell was a three-electrode cell with a dropping mercury electrode (working electrode), an Ag/AgCl reference electrode and a platinum wire as the auxiliary electrode.

The potential intervals where the polarographic studies were performed are: for DCP from -0.45 to -1.5 V, and for ACP from -0.4 to -1.2 V. The scan rate for both DCP and ACP was 5 mV/sec with a drop time of 1 sec. The spectrometric determinations were performed with a Perkin-Elmer 4 V spectrophotometer and a FTIR. The pH determinations were done with a Corning Ion Analyzer model 250.

The reagents used for the preparation of the solutions were of reagent grade; the buffer solutions were prepared with sodium phosphates 0.033*M*, sodium acetate 2*M*, sodium tetraborate 0.033*M*, acetic acid and KOH 2*M*, HCl for pH adjustment. DMF, methanol, sulfuric acid, ether and formaldehyde were also used. The active ingredient was extracted from a batch of 10 mg Valium tablets. The standard used was diazepam (Aldrich 99.31% purity).

RESULTS AND DISCUSSION

Extraction solvent selection

Ethyl ether, methanol, dimethyl formamide and a formaldehyde/H_2SO_4 mixture were tested as solvents for the extraction of diazepam from Valium tablets. Of these solvents, only ether facilitated the separation of the active ingredient from the filler; this led to the production of crystals. The infrared spectra of such crystals (Fig. 2) displays features that are characteristic of the groups corresponding to the structure of the diazepam molecule.[13] In addition, the melting point of the crystals was found to be 132°C which agrees well with that reported elsewhere.[13] These results indicate that the active ingredient does not undergo chemical changes in the extraction process with ether.

For the polarographic determination, a 2*M* solution of acetic acid/sodium acetate (pH = 4.6) was used as supporting electrolyte (see below). The diazepam crystals are not soluble in such an electrolyte. For this reason they were previously dissolved. The polarograms, shown in Fig. 3, were obtained after the addition of aliquots of diazepam, dissolved previously either in DMF (Fig. 3(a)) or else in H_2SO_4/formaldehyde solution (Fig. 3(b)), to the supporting electrolyte.

The well-defined reduction wave at -0.82 V in Fig. 3(a) is characteristic of diazepam.[10] Conversely, the polarogram in Fig. 3(b) shows two waves which indicate that the active ingredient is undergoing a hydrolysis reaction in an acidic medium, as previously reported.[14]

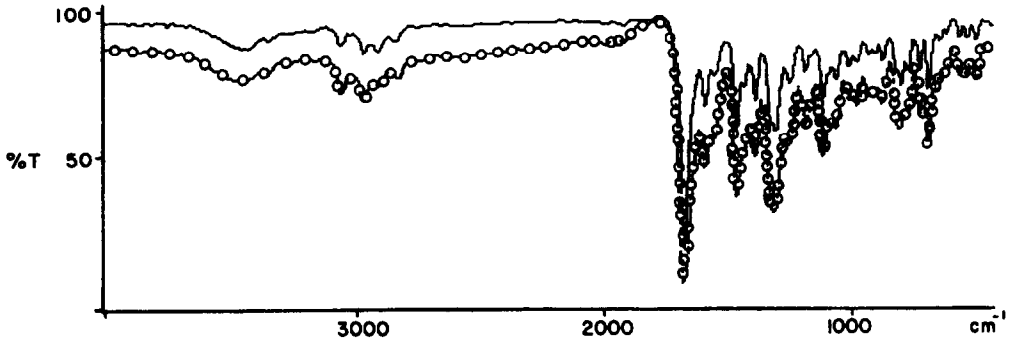

Fig. 2. Infrared spectra of pure diazepam crystals (– – –) and of the crystals from ether extraction of Valium tablets (00000).

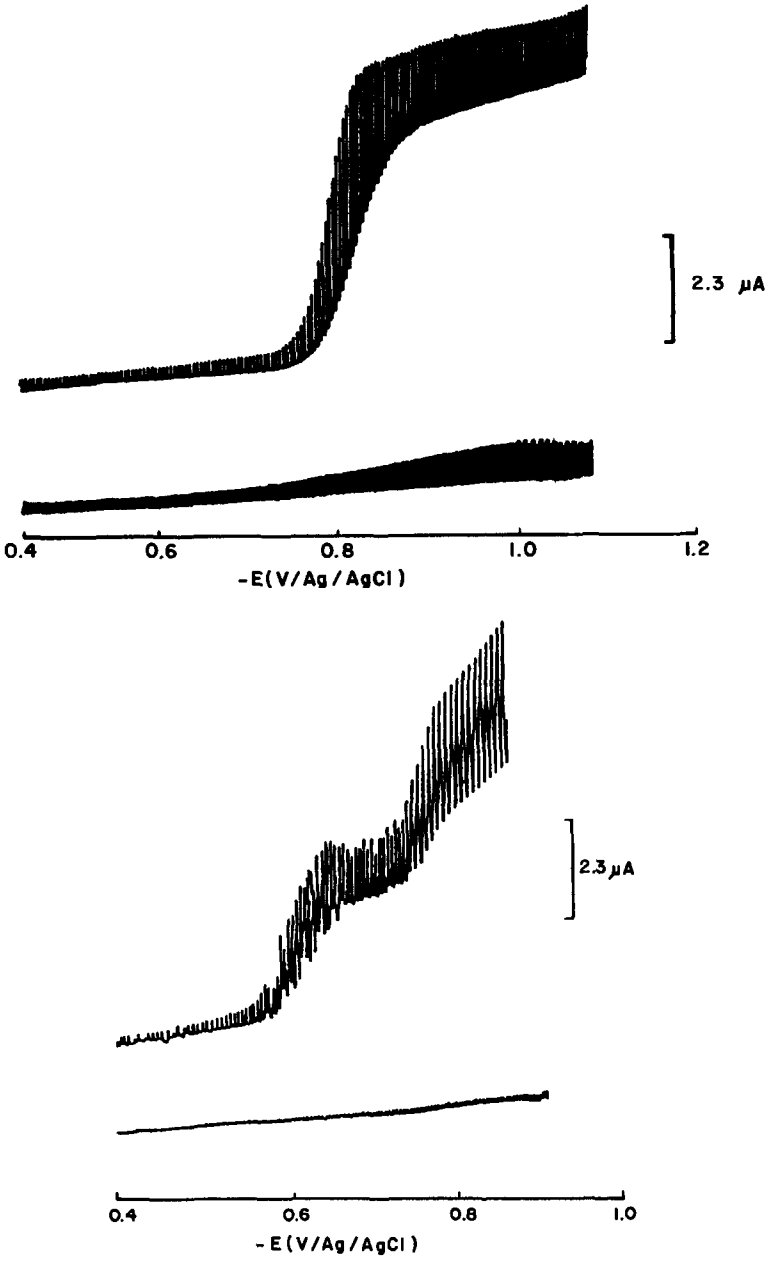

Fig. 3. DC polarograms in a 2M solution of acetic acid/sodium acetate (pH = 4.6) of diazepam extracted from Valium and previously dissolved in: (a) DMF, (b) H_2SO_4/formaldehyde. DC polarogram of support electrolyte is showed in both cases.

Figure 4 shows the spectrophotometric behavior of diazepam, previously dissolved in DMF or in a H_2SO_4/formaldehyde solution, in a 2*M* buffer solution, of acetic acid/sodium acetate. The diazepam band becomes wider if it is previously dissolved in H_2SO_4/formaldehyde, thus providing further evidence of its hydrolysis. The extraction and determination of diazepam is commonly carried out in H_2SO_4/formaldehyde media;[11,12] this may lead to a decreased precision in its quantification, by spectrophotometric methods, when the hydrolysis products are present. For this reason, the active ingredient is first dissolved in DMF.

The study of the hydrolysis of diazepam is not the objective of this paper. The kinetics of the hydrolysis of 1,4-benzodiazepines to benzophenones have been extensively studied.[6,7] This reaction is catalysed by the bisulfate anions.[15] Alonso *et al.*[1] have chosen acetate buffer, with pH that would prevent hydrolysis (pH > 3) and avoid the use of potentials so negative that

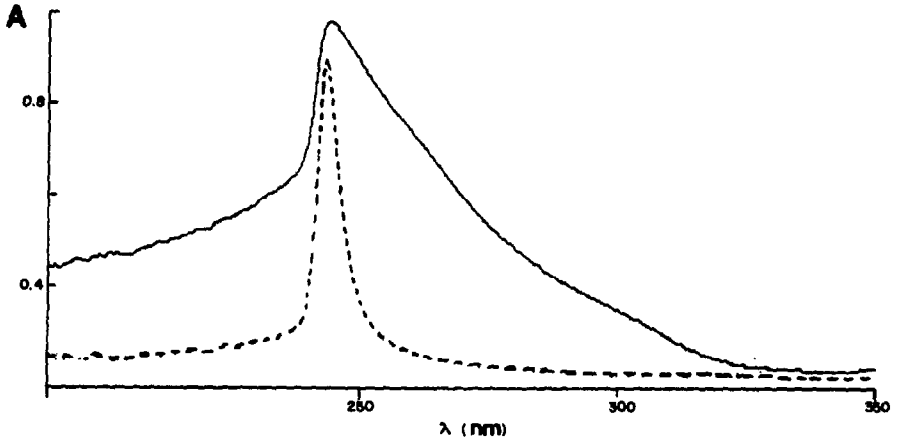

Fig. 4. Spectrophotometric behavior of diazepam (0.5 mg/l) in a 2*M* acetic acid/sodium acetate buffer solution (pH = 4.6). The diazepam was previously dissolved in: (a) DMF (– – –), (b) H_2SO_4/formaldehyde (– – – – – –).

problems would arise with mercury drop electrode. For this reason, we have selected the acetate buffer pH = 4.6 as supporting electrolyte.

Polarographic determination

The effect of pH upon the diazepam reduction peaks in DPP is shown in Fig. 5, at a constant diazepam concentration and a pH interval of 1–13. It can be noted that at intermediate pH values (pH 8–9) the peaks are wide, whereas they become sharper at either high or low pH values. This is an indication of a complication in the electron exchange process at intermediate pH values as compared to more extreme values; it is likely that the electron transfer occurs in two steps as has been suggested earlier.[16]

The peak potential is cathodically displaced with an increase in pH at a rate of −0.070 V per pH unit. The reduction of the azomethine group

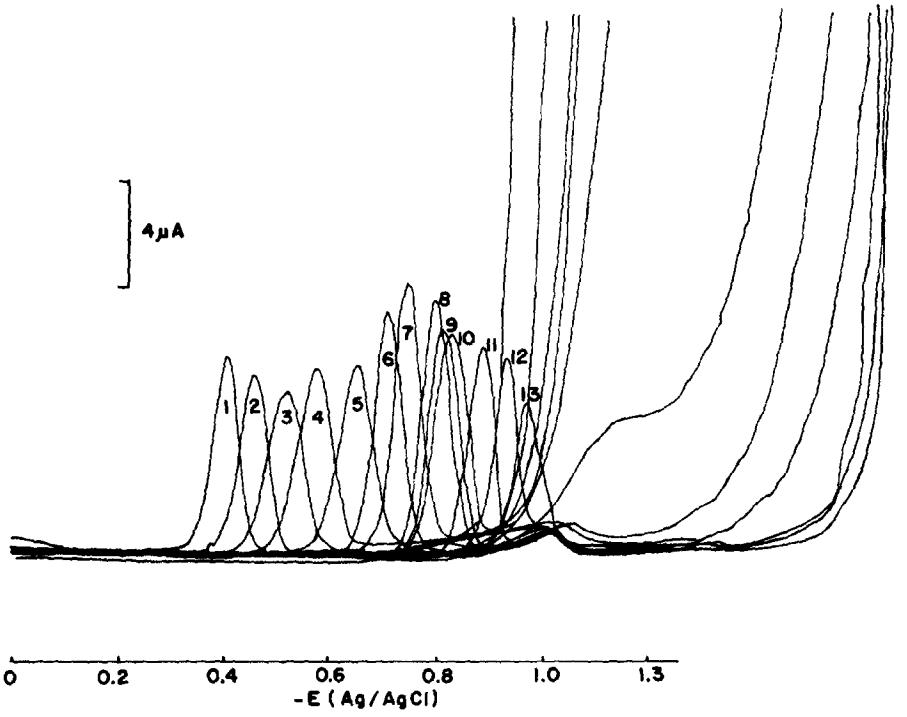

Fig. 5. Differential pulse polarogram in a 2*M* solution of acetic acid/solution acetate of diazepam previously dissolved in DMF. The pH values are individually shown.

Table 1. Determination of diazepam from commercial tablets, labelled to contain 10 mg, using DPP and spectrophotometric (UV) methods

Sample No.* (diazepam) Valium tablets (Roche—10 *mg*)	DPP	UV
1	9.97 ± 0.64	9.33
2	9.79 ± 0.24	9.06
3	10.31 ± 0.58	9.16
4	10.05 ± 0.05	9.45
5	10.40 ± 0.28	9.55
6	9.81 ± 0.40	9.41
7	10.61 ± 0.68	10.01
8	10.11 ± 0.27	9.50

*Each sample was realized five times.

involves two electrons and two protons,[16] which should yield a slope of −0.056 V per pH unit; this indicates that the observed process is kinetically limited.

The variation of i_p for the reduction of diazepam is linear with concentration both in ACP and in DPP; this permits the drawing of calibration curves for diazepam. Linear correlations over the concentration ranges 4.8–96 μM (DPP) and 17.4–167 μM (ACP) were obtained. Representative calibration graphs for diazepam resulted in the following linear regression equations:

$$y = 0.02017 + 0.01165x, \quad (r = 0.9975) \text{ (DPP)}$$

$$y = -0.00727 + 0.01261x, \quad (r = 0.9934) \text{ (ACP)}$$

where y, x and r correspond, respectively, to current peak (μA), drug concentration (μM) and linear correlation coefficient.

Commercial tablets of diazepam (Roche) labelled to contain 10 mg per tablet were assayed, using the extraction procedure proposed here. Table 1 reports the quantities obtained by DPP and spectrophotometric method (UV) (the adsorption lectures were performed at 266 nm). The precision of the polarographic technique was confirmed by analysing five replicate samples. The relative standard deviations are lower than 1% (Table 1), indicating good precision. The diazepam formulation can be detected by DPP with errors (<4%) lower than those obtained by the spectrophotometric method.

Acknowledgements—Funding from DIGICSA, SEP (C89-01-0153-A5) is gratefully acknowledged. We thank Dr Roberto Contreas Z. for his collaboration in this project and Dr Jorge G. Ibáñez for the English translation.

REFERENCES

1. R. M. Alonso, R. M. Jiménez, A. Carvajal, J. García, F. Vicente and L. Hernández, *Talanta*, 1989, **36**, 761.
2. R. M. Alonso-Rojas, L. Hernánez-Hernández and M. A. Fernández-Arcienega, *Quim. Anal.*, 1987, **6**, 215.
3. British Pharmacopoeia 1980, HM Stationery Office. London, 1980, p. 758.
4. United States Pharmaceopoeia XXI, United States Pharmacopeial Convention, Rockville, MD, 1985, pp. 762 and 308.
5. Florey, K., *Analytical Profiles of Drug Substances*. **1**, **3**. Academic Press, New York, 1972.
6. W. W. Han, J. G. Yakatan and D. D. Maness, *J. Pharm. Sci.*, 1976, **65**, 1198.
7. W. W. Han, J. G. Yakatan and D. D. Maness, *J. Pharm. Sci.*, 1977, **66**, 573.
8. M. E. Adbel-Hamid and M. A. Abuirjeie, *Analyst*, 1988, **113**, 1443.
9. M. A. Brooks, *Laboratory Techniques in Electroanalytical Chemistry*, in P. Kissinger and W. Heineman (eds). M. Dekker, New York, 1984.
10. R. Kalvoda, *Anal. Chim. Acta*, 1989, **162**, 197.
11. E. Jacobsen and T. Jacobsen, *Anal. Chim. Acta*, 1972, **60**, 472.
12. E. Jacobsen and T. Jacobsen, *Anal. Chim. Acta*, 1973, **64**, 473.
13. Clarke, *Isolation and Identification of Drugs*. pp. 526–696. The Pharmaceutical Press, London, 1986.
14. W. F. Smyth and J. A. Groves, *Anal. Chim. Acta*, 1982, **134**, 227.
15. L. B. Pfendt and T. J. Janjic, *Analyst*, 1990, **115**, 1457.
16. J. Volke, M. M. Ellaith and O. Manousek, *Talanta*, 1978, **125**, 209.

Talanta, Vol. 40, No. 12, pp. 1781–1788, 1993
Printed in Great Britain.

0039-9140/93 $6.00 + 0.00

CHARACTERIZATION OF THE IONIZATION AND SPECTRAL PROPERTIES OF SULFONEPHTHALEIN INDICATORS. CORRELATION WITH SUBSTITUENT EFFECTS AND STRUCTURAL FEATURES

RITA CASULA, GUIDO CRISPONI,* FRANCO CRISTIANI and VALERIA NURCHI
Dipartimento di Chimica e Tecnologie Inorganiche e Metallorganiche, Via Ospedale 72, 09124 Cagliari, Italy

MARIANO CASU and ADOLFO LAI
Dipartimento di Scienze Chimiche, Via Ospedale 72, 09124 Cagliari, Italy

(*Received* 1 *April* 1993. *Revised* 18 *May* 1993. *Accepted* 18 *May* 1993)

Summary—The pK values of the second ionization of a set of substituted sulfonephthaleins are studied by spectrophotometry and ^{13}C NMR spectroscopy. A study of the correlation between equilibrium and spectral data on the one hand and the substituent effects on the other is presented, using the dual substituent analysis of Swain and Lupton. This shows a complete dependence of pK values on the $\mathcal{F}$ field variable, and of the wavelengths of the bands of basic forms on the $\mathcal{R}$ resonance variable.

The study of the ionization of indicators dates back 70 years, when Kolthoff[1–5] published his first fundamental works on the subject. Since then the studies on this subject have been sporadic and unsystematic and unfortunately a classification of accurate data on indicators is lacking despite the widespread use of these substances, the upgrading of spectrophotometric methods, the availability of computing facilities and calculation techniques and IUPAC proposals.[6] In this work we present a spectrophotometric and ^{13}C NMR analysis of a class of indicators, the sulfonephthaleins, aimed at classifying in the first place their ionization and spectral features and secondly at accounting for the mechanism by which various substituents affect these properties. With a such knowledge the design and synthesis of indicators which satisfy user expectations will then be possible. In fact, because of their large and specialized use, indicators should be available with the greatest flexibility of colour and pK properties.

EXPERIMENTAL

Materials

The studied sulfonephthaleins, of the general formula here reported, were the 15 products shown in Table 1.

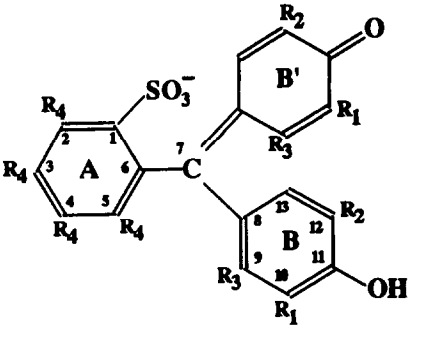

All these indicators were Aldrich products used without further purification.

Spectrophotometric measurements

Absorption spectra were recorded on a Hewlett-Packard 8452 diode array spectrophotometer; a flow cell was used joined to a titration vessel by a peristaltic pump; all the apparatus was thermostated at 25°C.

In order to make a reliable spectrophotometric determination of the ionization constant, 15–20 spectra (as those presented in Fig. 1) were collected at pH values equally spaced in a range ± 2 pH units around the pK value to be determined. This was achieved by titrating a weak non-absorbing $\cong 10^{-3}M$ acid, with a pK similar to that to be determined, using a $10^{-1}M$ base; in this way the concentration of the indicator undergoes only a very small dilution.

*Author for correspondence.

Table 1. Substituents R_1, R_2, R_3 and R_4 of the 15 studied sulfonephthaleins

Compound	Name	R_1	R_2	R_3	R_4
1	Cresol red	H	CH_3	H	H
2	Phenol red	H	H	H	H
2Br	3,4,5,6-Tetrabromophenolsulfonephthalein	H	H	H	Br
3	Bromocresol purple	Br	CH_3	H	H
4	Chlorophenol red	H	Cl	H	H
5	Bromochlorophenol blue	Br	Cl	H	H
6	Bromophenol blue	Br	Br	H	H
6Br	Tetrabromophenol blue	Br	Br	H	Br
7	3′,3″,5′,5″-Tetraiodophenolsulfonephthalein	I	I	H	H
$1CH_3$	Xylenol blue	H	CH_3	CH_3	H
$1'CH_3$	Thymol blue	H	$CH(CH_3)_2$	CH_3	H
$2CH_3$	Cresol purple	H	H	CH_3	H
$3CH_3$	Bromoxylenol blue	Br	CH_3	CH_3	H
$3'CH_3$	Bromothymol blue	Br	$CH(CH_3)_2$	CH_3	H
$6CH_3$	Bromocresol green	Br	Br	CH_3	H

In order to measure the 15 studied indicators (pK values 3.5–8.5) in the same medium, a mixture of seven acids (Table 2) with regularly increasing pK values was used.

The titration plot of such a mixture exhibits a typical trend in the 3–9 pH range (Fig. 2), which allows us to explore the neighbouring values of the pK of each studied indicator.

It was therefore possible to examine and record the spectra of the indicator at variable $[H^+]$ by titrating the mixture, containing the $\cong 10^{-5}M$ sulfonephthalein with KOH at an ionic strength of $0.1M$ KNO_3 and moving a portion of the solution to the flux cell after each KOH addition.

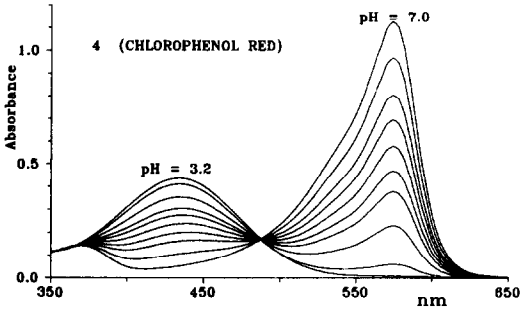

Fig. 1. Ten spectra of compound 4 (chlorophenol red) at a concentration of $2.8 \times 10^{-5}M$, collected in the 3.2–7.0 pH range are presented.

Table 2. Composition of the acid medium used for the spectrophotometric titration of the sulfonephthaleins. Refs 8–12 report the pK values for the above substances

Compound	Conc. $\times 10^3M$	pK_{exp}
Hydrochloric acid	8.000	—
Dichloroacetic acid[7]	0.6006	—
Monochloroacetic acid[8]	0.5250	2.837 ± 0.003
Acetic acid[9]	0.7725	4.629 ± 0.001
Pyridine[10]	0.7778	5.363 ± 0.002
2′-Aminopyridine[11]	1.001	6.812 ± 0.002
Ammonium hydroxide[12]	1.593	9.322 ± 0.001

Potentiometric studies

Titrations were performed on a Dosimat 655 Metrohm automatic titrator equipped with a Metrohm 654 pH meter, using a Metrohm combined pH electrode for highly alkaline solutions, at an ionic strength of $0.1M$ KNO_3. The solutions (25 cm^3) were titrated with KOH ($0.1M$) at 25°C under a nitrogen atmosphere and at the same conditions reported in a previous paper.[13]

Potentiometric data for the electrode standardization were analyzed with the Gran method[14] using our BASIC program GRANPLOT. The titrations for the potentiometric determination of the pK values reported in Table 2 were run under the same conditions and the concentration are $2 \times 10^{-3}M$. The ionization constants were calculated by a slightly modified version of the PSEQUAD program.[15]

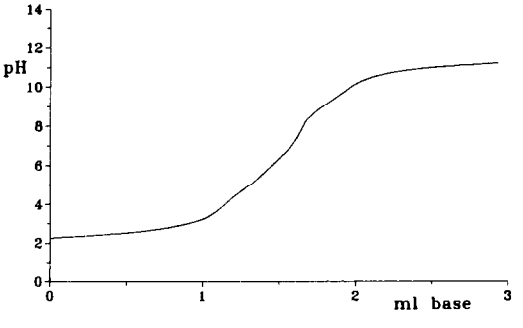

Fig. 2. Titration curve of the mixture of acids presented in Table 2. Absence of any net inflexion in the 2–10 pH range can be observed. Therefore also a region limited to two pH units can be thoroughly explored by proper titrant additions.

NMR measurement

Natural abundance ^{13}C NMR spectra were recorded on a Varian VXR-300 spectrometer at 75.43 MHz, using 10 mm diameter tubes. The ^{13}C spectra were ^{1}H decoupled by means of square wave modulation of the decoupler carrier, centred on the proton field. Solutions at pH > 8 were prepared in D_2O by adding NaOD. The carbon chemical shifts were measured at 25°C from the dioxane used as internal standard and the values so estimated were referred to TMS. Spectra were collected with a number of transients up to 10,000, depending on the aqueous solubility of the compounds.

Calculation of ionization constants of sulfonephthaleins

Matrix A of absorbance data for each sulfonephthalein, collected at N_w wavelength on N_s solutions of different pH, was analyzed with the program SPECFIT[16] which allows us to perform an Evolving Factor Analysis. EFA is a new powerful mathematical method for a model-free analysis of an ordered set of multi-wavelength data. When applied to spectrophotometric titration it allows to calculate both the concentration profiles and the spectra of all absorbing species, without using the law of mass action or defining the stoichiometric composition of the species. As a second step, SPECFIT allows the usual least-squares analysis of spectral data for calculating the equilibrium constants and spectra of all absorbing species.

RESULTS AND DISCUSSION

^{13}C NMR analysis

The NMR study has been limited to compounds exhibiting a sufficient solubility in water. The assignment of natural abundance ^{13}C spectra has been performed by comparing the NMR spectra with complete noise decoupling of the protons and the corresponding ^{1}H coupled spectra performed with gated decoupling.

It can be seen that the chemical shifts change significantly as the substituent group in the phenolic ring is changed, since they are induced by the usual inductive and mesomeric effects.

Particularly, we note that, unlike the remaining compounds, those with the methyl substituent in the *meta* position to the OH group give rise to two well distinct resonances for each carbon atom of the phenolic rings B and B′. This finding clearly shows that a hindered rotation of the phenolic rings around the C(7)–C(8) and C(7)–C(8′) bonds occurs, due to mutual steric interaction of the methyl substituents. This effect induces different average orientation of the two phenolic rings B and B′, which therefore experience different anisotropic shielding especially as far as the *meta* carbon atoms are concerned.

From these findings and considering that the chemical shifts of carbon atoms are in general affected by the substituent groups through a number of effects, such as electron densities, bond orders, orbital energies and

Table 3. ^{13}C NMR chemical shift assignments of the 15 studied sulfonephthaleins

Compound	C(1)	C(2)	*C(3)	C(4)	*C(5)	C(6)	C(7)	C(8)	C(9)	C(10)	C(11)	(12)	C(13)
1	143.1	128.6	131.5	133.1	130.8	139.1	171.1	127.1	140.4	131.5	181.5	122.3	140.2
2	143.1	128.7	131.7	133.1	131.1	138.7	173.3	126.9	142.0	123.0	182.8	123.0	142.0
2Br	144.6					140.7	171.0	125.0	141.1	123.7	182.5	123.7	141.1
3	143.4	128.9	131.5	132.9	131.2	138.0	167.6	128.1	138.5	132.0	174.3	118.9	140.8
4	143.3	129.1	133.2	134.5	131.7	138.0	172.2	128.7	140.6	123.3	176.8	121.1	139.4
5	143.8	129.0	132.0	134.5	131.7	137.2	170.5	128.0	141.5	126.2	171.8	119.5	138.4
6	143.8	129.1	132.1	133.1	131.7	137.1	169.5	127.2	141.7	118.8	171.7	118.8	141.7
6Br	145.1					138.9	167.3	126.0	140.9	119.5	171.1	119.5	140.9
7	145.2	130.7	133.6	134.3	133.0	138.4	176.5	130.4	150.4	95.9	168.3	95.9	150.4
$1CH_3$	143.7	129.3	131.8	134.1	131.4	141.7	171.9	129.3	148.1	119.9	181.6	125.8	143.0
								128.7	147.4	116.0	180.0	125.2	141.0
$1'CH_3$	143.9	129.4	131.6	133.8	131.4	141.7	172.5	130.7	140.1	139.3	180.0	126.2	147.1
									138.0	138.7	179.4	126.0	146.9
$2CH_3$	143.7	129.3	131.8	134.1	131.7	141.4	174.2	131.4	144.7	126.3	182.5	120.8	149.8
									142.6	125.6	180.8	120.2	149.1
$3CH_3$	144.1	129.4	131.7	134.6	131.7	141.2	170.2	129.5	140.8	132.4	176.4	126.1	146.8
								128.4	138.8	131.4	174.5	124.9	145.7
$3'CH_3$	144.3	129.5	131.7	134.2	131.6	141.3	170.6	131.5	138.0	139.0	174.8	126.8	145.6
									135.8	138.3	174.0	126.0	
$6CH_3$	144.5	129.9	132.7	134.8	131.9	140.0	171.2	132.2	143.3	125.6	171.6	115.9	147.4
								131.6	141.7	124.7	170.4	115.0	146.9

*No distinction can be made between C(3) and C(5) signals; the higher was therefore conventionally attributed to C(3).

local polarizations, which only rarely can be factored out, we estimated the substituent effects for the reported chemical shifts on a purely empirical basis. Subsequently the Grant and Paul[17] rules were also used to assign and/or substantiate the carbon resonances of the aromatic rings. The resulting assignments are reported in Table 3.

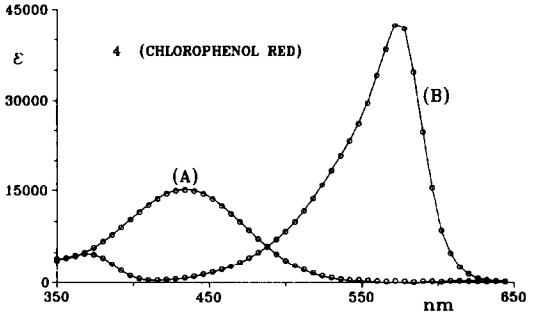

Fig. 4. The absorptivity spectra of the acid (A) and basic form (B) of chlorophenol red obtained by EFA are reported as continuous curves, while those obtained by least-squares calculations are reported as point.

Equilibrium data

The dissociation scheme proposed by Kolthoff for this class of indicators takes into account two successive steps.

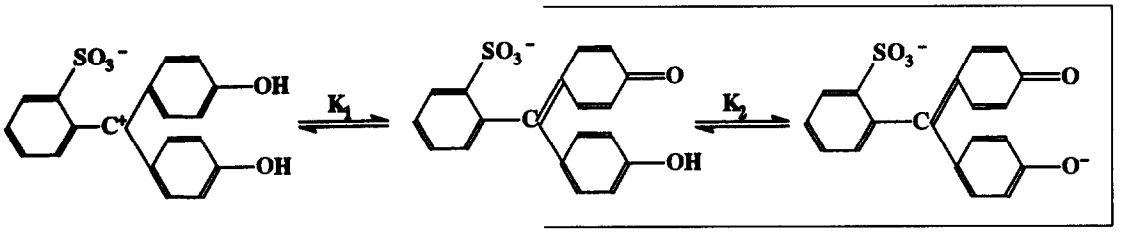

The structures of the neutral biprotonated form may also be represented as follows.

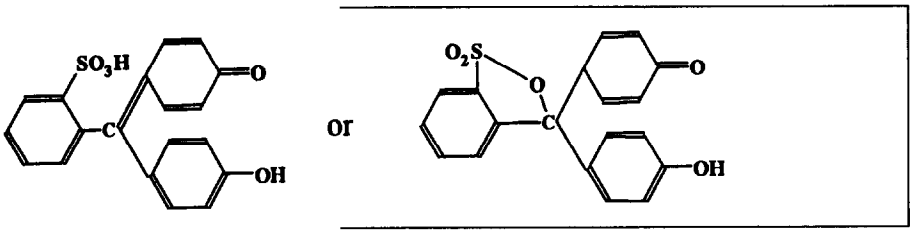

The pK_1 generally presents values below 2, while pK_2 ranges from 3.5 to 8.5 according to the substituents in the phenolic rings. In this work only the second ionization was taken into account. In Fig. 1 the experimental spectra of chlorophenol red in the 3.2–7 pH range are presented as an example. These data were analyzed by Evolving Factor Analysis (EFA): the factor analysis indicates the presence of only two absorbing species in the examined pH ranges. Without any model assumption, EFA has lead to the distribution curves in Fig. 3 and to the spectra in Fig. 4 reported as continuous lines.

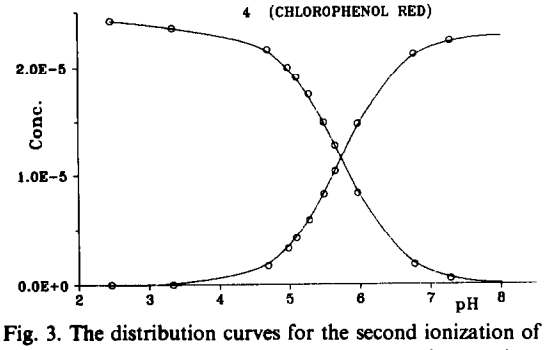

Fig. 3. The distribution curves for the second ionization of chlorophenol red obtained by EFA are reported as continuous curves, while those calculated with the pK 5.74 estimated by least-squares calculations are reported as points.

Still with the SPECFIT program, assuming a simple model of a single ionization and a guess of $pK_2 = 5.8$ obtained from the distribution curves in Fig. 3, it was possible to optimize both the pK value (5.74) and the spectra of the two species with a least squares procedure. The distribution curves and the spectra obtained with the optimized pK are reported as points in Figs 3 and 4, respectively. The very good agreement between the values obtained by EFA and those by the conventional least-squares method with model assumption can be clearly observed. This is not surprising in view of the very simple system studied and the high precision of the experimental measurements.

With an analogous procedure the pK values for all the studied indicators were calculated and are reported as pK_{exp} in Table 4.

The trend of pK values as a function of the substituents is shown in Fig. 5.

Using the unsubstituted indicator 2 as a basis for comparison, these data can be totally explained by assuming a proper ΔpK value for each kind of substituent. The $pK_{calc} = pK(2) + \Sigma\Delta pK$ calculated in this way are reported in the third column of Table 4. The Br substituents in the A ring seem to play no role in determining pKs.

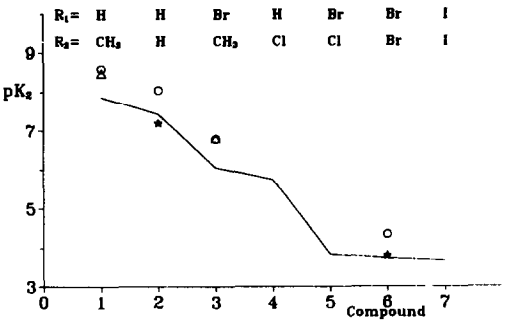

Fig. 5. The pK values of compounds 1–7 are reported as a continuous line; those of $1CH_3$, $2CH_3$, $3CH_3$ and $6CH_3$ as o, those of $1'CH_3$ and $3'CH_3$ as Δ and those of 2Br and 6Br as *.

UV–visible spectra

The spectra of the 15 indicators were also collected both in HCl and NaOH $10^{-2}M$ in the 250–700 nm spectral range, whereas in the equilibrium study it was not possible to collect data below 380 nm for the absorption of the buffer solution. The spectra of basic forms coincide with those obtained by SPECFIT least-squares calculations in the 400–700 nm range. In acidic medium, instead, a marked difference was observed in six cases. This is due to the high values of pK_1, and therefore to the existence of the completely protonated form in large amounts, since pH = 2. In these cases the spectra from SPECFIT, attributable to a single absorbing species, were therefore examined.

Some qualitative considerations can be made on the most intense band of the basic form:

(a) the absorptivity spectra of compounds 1–7 with only R_1 and R_2 substituents show a comparable intensity and reveal a shift from ≅560 nm for unsubstituted compound 2 to ≅575 nm for the monosubstituted compounds 1 and 4, to ≅595 nm for the disubstituted 3, 5 and 6 and to ≅600 nm for the disubstituted compound 7. The general pattern of the seven spectra is very similar;
(b) when R_4 = Br, a red shift of the spectra of about 30 nm is observed;
(c) the $R_3 = CH_3$ substituent causes a red shift of ≅25 nm of the band, accompanied by a drastic increase in halfbandwidth and a decrease in maximum absorptivity.

A very similar trend is also presented by the two bands of basic form at ≅300 and 380 nm, respectively, while the acid band at ≅450 nm does not show a sensible variation as a function of the substituents.

Table 4. pK values of the 15 studied sulfonephthaleins

Compound	pK_{exp}*	pK_{calc}†
1	7.87 ± 0.01	7.87
2	7.42 ± 0.01	7.42
2Br	7.19 ± 0.01	7.42
3	6.05 ± 0.01	6.03
4	5.74 ± 0.01	5.74
5	3.85 ± 0.01	3.90
6	3.76 ± 0.01	3.75
6Br	3.81 ± 0.01	3.75
7	3.70 ± 0.01	3.70
$1CH_3$	8.59 ± 0.01	8.53
$1'CH_3$	8.47 ± 0.01	8.53
$2CH_3$	8.04 ± 0.01	8.09
$3CH_3$	6.78 ± 0.01	6.72
$3'CH_3$	6.80 ± 0.01	6.72
$6CH_3$	4.35 ± 0.01	4.42

*The references for the literature pK values of the more common sulfonephthaleins can be found in Beukenkamp and Rieman.[18]

†The pK_{calc} values were calculated with ΔpK values reported in Table 5.

Conclusive remarks

The good agreement between pK_{calc} and pK_{exp} values reported in Table 4 indicates that the effects of R_1 and R_2 substituents can be considered additive. An analysis of the substituent effects was therefore accomplished. The Swain and Lupton[19] dual substituent analysis, in the form $y = r_1\mathcal{F} + r_2\mathcal{R} + y_0$ was made on pK values, on wavelengths of maxima of basic forms and on NMR chemical shifts. On the basis of completely additive effects of substituents in

Table 5.

R_1, R_2	ΔpK	R_3	ΔpK
CH_3	0.45	CH_3	0.66
$CH(CH_3)_2$	0.45		
Br	−1.84		
Cl	−1.69		
I	−1.53		

Table 6. Results of the Swain–Lupton dual substituent analysis*

		y_0	r_1	r_2	$\Sigma_{i=1}^{N} r_i^2$	Corr. coeff.
pK	set 1	7.52	−2.97	−1.24	0.156	0.9955
	set 2	8.00	−3.09	−2.49	0.034	0.9987
λ_{max}	set 1	559.3	−2.01	−109.2	19.2	0.9926
	set 2	584.4	−5.22	−116.8	0.71	0.9996
$\delta_{C(11)}$	set 1	183.3	−3.95	19.8	6.59	0.9806
	set 2	182.4	−4.14	13.3	3.25	0.9824
	†set 2bis	180.9	−4.50	11.4	0.57	0.9967
pK *vs* $\mathcal{F}$	set 1	7.63	−2.72		0.21	−0.9944
	set 2	8.31	−2.61		0.21	−0.9917
λ_{max} *vs* $\mathcal{R}$	set 1	559.7		−101.3	22.0	−0.9917
	set 2	586.2		−97.7	15.4	−0.9917

*For the $CH(CH_3)_2$ group the values $\mathcal{F} = -0.086$ and $\mathcal{R} = -0.139$, evaluated from the values for CH_3 and $C(CH_3)_3$, are used.

†C(11) exhibits two distinct NMR signals in the compounds of set 2, analyzed as set 2 and set 2*bis*, respectively.

R_1 and R_2, parameters $\mathcal{F}$ and $\mathcal{R}$ were taken as the sum of the tabulated values[19] for the various substituents. The data for the two sets of seven (1–7) and six ($1CH_3$–$6CH_3$) compounds, reported as set 1 and set 2, respectively, were analyzed, and the calculated r_1, r_2 and y_0 values are reported in Table 6.

A clear explanation of the dependence of the measured chemical properties of this class of indicators on the R_1 and R_2 substituents can be inferred on the basis of these results: 89% of variability of the pK values, for set 1, from the reference pK_0 value is explained by the $\mathcal{F}$ field variable; furthermore, if a linear regression of pK is calculated on the $\mathcal{F}$ field variable alone, as shown in Fig. 6, the value $\Sigma_{i=1}^{N} r_i^2$ of square residuals for this regression is greater than that reported in Table 6, for the dual substituent regression; nevertheless this difference is not significant at the confidence level 0.05, as can be calculated with an F test. Similar consideration can be made for the set of compounds with the CH_3 substituent on the C(9) carbon atom; the only observable difference is a shift of 0.6 pK units of the pK_0 values, while the slope is almost equal to that calculated for the first set. A purely inductive effect exerted by the R_1 and R_2 *ortho* substituents on the ionizable OH group is therefore evident, not perturbed by the CH_3 substituent in *meta*. The latter affects the pK values in the same direction as *ortho* CH_3; but its effect, which is greater than that of *ortho* CH_3, cannot be explained as only inductive; on the other hand no serious discrimination between inductive, resonance or steric contributions can be made on the basis of data for a single *meta* substituent. Steric contributions are certainly important according to NMR results.

The spectra of basic forms, which are the only ones to be affected by ring substituents, were decomposed in various components bands. The most important of these bands are reported in Table 7. The maximum wavelength of each band in the various compounds is strictly correlated with that of the other bands (except for band III, but this depends on the poor precision of its evaluation, connected to its low weight). Therefore any consideration made on the principal band can be generalized without loss of significance to the remaining bands. As for the pK values the Swain–Lupton analysis of the

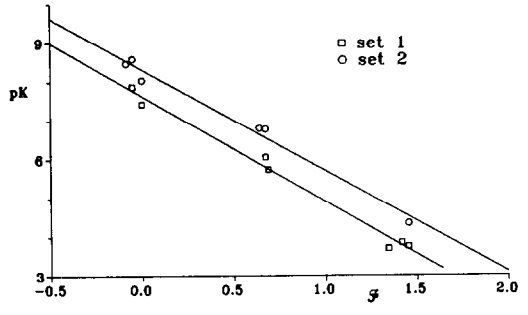

Fig. 6. The pK values of compounds 1–7 (set 1) and those of $1CH_3$, $3CH_3$, $2CH_3$, $6CH_3$, $1'CH_3$ and $3'CH_3$ (set 2) are reported as a function of the $\mathcal{F}$ variable of Swain–Lupton.

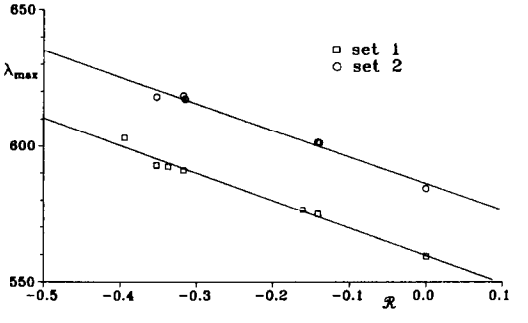

Fig. 7. The λ_{max} values of compounds 1–7 (set 1) and those of $1CH_3$, $2CH_3$, $3CH_3$, $6CH_3$, $1'CH_3$ and $3'CH_3$ (set 2) are reported as a function of the $\mathcal{R}$ variable of Swain–Lupton.

Table 7. Parameters (λ_{max} = wavelength of the maximum, W = halfbandwidth and H = height of the band) of the most intense Gaussian peaks. The bands are ordered from higher to lower wavelengths

Compound	Band I			Band II			Band IV			Band VI		
	λ_{max}	W	$H \times 10^{-3}$	λ_{max}	W	$H \times 10^{-3}$	λ_{max}	W	$H \times 10^{-3}$	λ_{max}	W	$H \times 10^{-3}$
1	574.9	31.4	35.4	550.3	67.3	30.0	368.9	37.4	6.0	298.9	27.0	5.3
2	559.4	33.6	36.0	532.7	66.5	27.5	361.5	34.1	6.9	299.5	19.9	3.2
3	591.0	33.5	40.7	568.1	67.4	31.5	378.0	37.4	7.4	304.2	27.5	10.9
4	576.4	30.7	35.2	552.9	67.1	28.5	372.2	37.1	6.1	299.4	27.0	12.5
5	592.4	33.0	41.9	569.7	67.1	29.4	381.7	37.0	6.3	308.4	26.2	10.7
6	592.9	35.6	41.1	568.8	65.6	28.0	383.8	37.5	7.8	310.1	27.3	12.3
7	603.0	34.2	35.0	578.9	71.8	30.7	393.3	42.9	6.6	317.8	31.2	9.8
1_{CH_3}	601.3	51.8	15.1	576.5	91.7	27.2	380.2	63.0	10.5	301.2	31.4	12.1
2_{CH_3}	584.4	46.4	17.8	556.7	88.7	23.7	375.8	56.2	9.3	296.5	30.6	9.6
3_{CH_3}	618.5	52.0	13.8	595.3	96.1	24.4	391.6	61.9	8.5	305.8	31.3	10.9
6_{CH_3}	618.0	57.0	21.3	594.0	99.0	24.4	401.0	56.3	9.2	312.5	22.4	5.9
$1'_{CH_3}$	601.1	59.4	20.4	580.2	89.4	16.7	381.0	62.3	8.4	303.7	31.3	10.0
$3'_{CH_3}$	617.2	58.0	19.7	592.7	111.1	22.3	393.9	61.5	8.9	307.7	31.2	12.9
2_{Br}	578.2	30.5	36.6	553.0	69.4	35.0						
6_{Br}	613.6	33.3	40.2	589.2	69.7	32.0						

band positions for the set of compounds 1–7 shows that the effect of substituents can be explained by only one independent variable; in this case, however, it isresonance parameter $\mathscr{R}$ that accounts for 94% of the variability around the reference value of the unsubstituted compound 2 as can be observed clearly in Fig. 7.

This total dependence on the resonance parameter is reasonable, since the spectra is due to a system of conjugated double bonds extended to the whole molecule. An analogous behaviour is observed for the set of the six *meta* substituted compounds, but two different behaviours are to be pointed out:

(i) a red shift of about 25 nm with respect to the analogous compounds without the *meta* CH_3 substituent;
(ii) a decrease of the intensities and an increase of half bandwidths.

These findings can be tentatively explained considering the non-equivalence of the two rings deduced from the NMR findings, upon R_3 substitution. Each of the two rings in this case should give a distinct single contribution to the electronic spectra, which therefore appear broader and lower.

As regards the swain and Lupton analysis of NMR chemical shifts, the C(11) carbon atom was examined, both because it is bonded to the studied acid group and because it does not feel vicinal effects, since it is the only carbon atom not in direct contact with any substituents. In this case both field and resonance variables $\mathscr{F}$ and $\mathscr{R}$ account for the chemical shift variations. The two examined sets do not depend on the two variables in the same way and this can be explained with steric effects of the CH_3 substituents, which play a further role in determining the $\delta_{C(11)}$ value: in fact in both sets 2 and 2*bis*, the contribution of the inductive effect with respect to the resonance effect is increased. This can be explained by a reduced resonance transmission in the hindered positions of rings B and B′ due to the CH_3 substituents.

Some considerations should be made on the two compounds with R_4 = Br: the pK values of these two compounds are not affected by the Br substituents and are equal to those of the parent compounds 2 and 6, respectively, as expected if one considers the behaviour of the other indicators. On the other hand, the spectra are affected to a great extent by the substituent Br group and show a red shift of about 30 nm. This confirms a resonance extended to the whole molecule, since C(7) is definitely not a carbocation, as demonstrated by its chemical shift.

To sum up, even though extended to a limited set of functional groups, the analysis of the mechanism of action of the various substituents can be considered reliable thanks to the additivity of the R_1 and R_2 effects, which expands the ranges of the independent variables. New indicators with particular features both of pK and colour can now be designed on the basis of the achieved knowledge.

REFERENCES

1. I. M. Kolthoff, *Rec. Trav. Chim.*, 1921, **40**, 775; *ibid*, 1923, **42**, 251; *J. Am. Chem. Soc.*, 1924, **46**, 2009; *ibid.*, 1926, **48**, 1453; *J. Phys. Chem.*, 1928, **32**, 1820; *ibid.*, 1930, **34**, 1466; *ibid.*, 1931, **35**, 1433.
2. I. M. Kolthoff and L. S. Guss, *J. Am. Chem. Soc.*, 1938, **60**, 2516.
3. I. M. Kolthoff and T. B. Reddy, *Inorg. Chem.*, 1962, **1**, 189.

4. I. M. Kolthoff and M. K. Jr. Chantooni, *J. Phys. Chem.*, 1966, **70**, 856; *J. Am. Chem. Soc.*, 1965, **87**, 4428.
5. I. M. Kolthoff, M. K. Jr. Chantooni and S. Bhowmik, *J. Am. Chem. Soc.*, 1966, **88**, 5430; *ibid.*, 1968, **90**, 23; *Anal. Chem.*, 1967, **39**, 315.
6. I.U.P.A.C. analytical chemistry division commission on analytical reactions and reagents, *Pure Appl. Chem.*, 1979, **51(b)**, 1357–1365.
7. J. A. M. Ahmad and W. C. E. Higginson, *J. Chem. Soc., Dalton*, 1983, 1449.
8. P. G. Daniele, A. DeRobertis, C. DeStefano, S. Sammartano and C. Rigano, *J. Chem. Soc., Dalton*, 1985, 2353.
9. D. D. Ensor and G. R. Choppin, *J. Inorg. Nucl. Chem.*, 1980, **42**, 1477.
10. E. Casassas and R. Tauler, *J. Chem. Phys.*, 1985, **82**, 1067.
11. J. Kulig, B. Lenarcik and M. Rzepka, *Polish J. Chem.*, 1985, **59**, 1029.
12. F. Mulla, F. Marsicano, B. S. Nakani and R. D. Hancock, *Inorg. Chem.*, 1985, **24**, 3076.
13. M. L. Ganadu, V. Leoni, G. Crisponi and V. Nurchi, *Polyhedron*, 1991, **10**, 333.
14. G. Gran, *Analyst*, 1952, **77**, 661.
15. L. Zekany and I. Nagypal, *Computational Methods for the Determination of Formation Constants*, D. J. Leggett (ed.), Ch. 8. Plenum Press, New York (1985).
16. H. Gampp, M. Maeder, Ch. J. Meyer and A. D. Zuberbuhler, *Talanta* 1985, **32**, 1133; *ibid.*, 1986, **33**, 943; *Anal. Chim. Acta*, 1987, **193**, 287.
17. D. M. Grant and E. G. Paul, *J. Am. Chem. Soc.*, 1964, **86**, 2984.
18. J. Beukenkamp and W. Rieman III, *Treatise on Analytical Chemistry*, I. M. Kolthoff and P. J. Elving (eds), Vol. 11, Ch. 115. John Wiley, New York (1975).
19. C. G. Swain and E. C. Lupton, Jr. *J. Am. Chem. Soc.*, 1968, **90**, 4328

Talanta, Vol. 40, No. 12, pp. 1789–1798, 1993
Printed in Great Britain.

0039-9140/93 $6.00 + 0.00

THE ELECTROCHEMICAL OXIDATION OF 2,6-DICHLORO-1,4-PHENYLENEDIAMINE

TH. WANDLOWSKI,[1] D. GOSSER Jr.,[2] E. AKINELE,[1] R. DE LEVIE[1] and V. HORAK[1]

[1]Chemistry Department, Georgetown University, Washington, DC 20057, U.S.A.
[2]Chemistry Department, City College, City University of New York, NY 10031, U.S.A.

(*Received* 4 *February* 1993. *Accepted* 9 *April* 1993)

Summary—The electrochemical oxidation of 2,6-dichloro-1,4-phenylenediamine was studied at a glassy carbon electrode in a 50 vol% methanol–water mixture containing 0.1*M* $HClO_4$. Single sweep voltammograms are compared with curves obtained by digital simulation. Characteristic reaction parameters, such as formal potentials, charge transfer coefficients, rate constants of the electrochemical and the chemical steps, and diffusion coefficients, were determined from potential-step experiments in combination with a simulation–curvefitting routine.

The pioneering work of Adams *et al.*[1,2] on the anodic oxidation of *p*-phenylenediamine (PPD) and on several of its derivatives in aqueous media illustrates the complex coupling between electron transfer and chemical reactions.

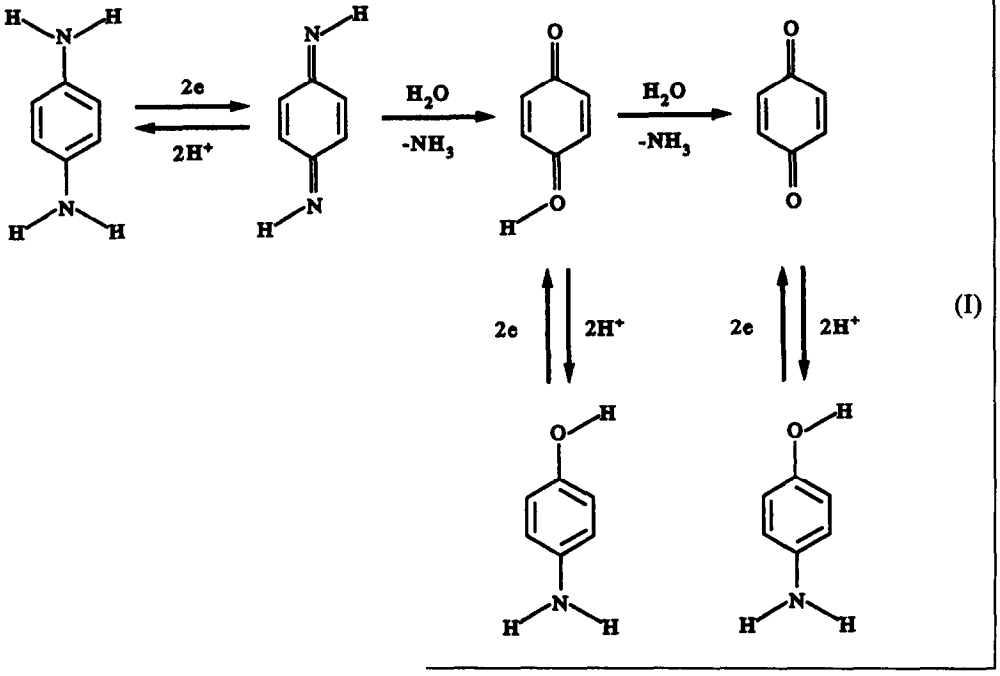

(I)

Detailed investigations of electrode mechanisms require sophisticated electrochemical techniques, often combined with spectroelectrochemical experiments.[3–5] As pointed out by Heinze[6] and Gosser,[7] linear sweep (LSV) and cyclic voltammetry (CV) are among the most universal electrochemical techniques for qualitative and quantitative studies of complex electrode processes.

Based on the numerical solution of the corresponding integral equations for the LSV-and/or CV-response, Nicholson and Shain derived diagnostic criteria for various electrode mechanisms.[8–10] Their work was extended by contributions by Savéant *et al.* who introduced the concept of kinetic zones, defined via dimensionless rate constants for charge transfer and chemical steps, respectively.[11] The semi-integral technique, developed by Oldham *et al.*,[12,13] and

the equivalent convolution sweep voltammetry,[14] provide excellent tools to utilize all experimental data for analysis and parametrization of electrode reactions. Its application to nontrivial ECE-mechanisms was recently discussed by Neudeck and Dittrich.[15]

The concept of digital simulation developed by Feldberg[16] provides a powerful, independent route to the interpretation of linear and cyclic voltammograms. Model curves can be calculated for a multitude of electrode mechanisms and for various electrode geometries.[7,17,18] The original technique, based on an explicit approximation of the partial differential equations, has been complemented by two other methods. One is based on the implicit Crank–Nicholson technique to approximate the second derivatives of the digital concentration profiles.[19] The other uses orthogonal polynomials.[20]

The comparison between experimental and simulated linear sweep and cyclic voltammograms can provide qualitative information on the actual electrode mechanisms, as well as quantitative information on reaction parameters. Recent attempts have shown that the analysis of experimental data might be improved by combining digital simulation and/or semi-integration/semi-differentiation with multiple regression techniques.[21–24]

We have chosen to study the oxidation, at a glassy carbon electrode, of 2,6-dichloro-1,4-phenylenediamine (DCDP) in a 50 vol% water–methanol mixture containing 0.1*M* $HClO_4$. In view of the mechanism proposed for the oxidation of 1,4-phenylenediamine (Scheme 1), we have investigated the reduction of 2,6-dichloro-1,4-benzoquinone (DCQ), the oxidation of 2,6-dichloro-1,4-aminophenol (DAP) and DCDP at comparable experimental conditions by cyclic voltammetry and double potential step chrono-amperometry. The reaction parameters are determined (or, in some cases, optimized) by analyzing the cyclic voltammetric response in the slow scan regime with the simulation-fitting program CVFIT, described in[23]. In order to diminish the effect of adsorption, all quantitative experiments will be restricted to low scan rates and relatively high reactant concentrations (usually 1 m*M*).[25] Furthermore, we will assume that all protonations are at equilibrium.[26] The substitutions in the 2 and 6 positions prevent mechanistic complications due to the Michael reaction.

EXPERIMENTAL

All measurements were carried out at 298.2 K using a glassy carbon working electrode (Bio-Analytical Systems), a silver/silver chloride reference electrode connected via a liquid junction with the cell, and a platinum auxiliary electrode. The electrochemically active area was estimated from the analysis of the limiting diffusion current in cyclic voltammograms and single potential step transients[5] for aqueous solutions containing known concentrations $Fe(CN)_6^{3-}$ or $Fe(CN)_6^{4-}$. Using the literature values for the corresponding diffusion coefficients ($D = 7.6 \times 10^{-6}$ cm^2/sec and $D = 6.3 \times 10^{-6}$ cm^2/sec, respectively,[2] we calculated the electrode area A as 0.074 ($\pm$ 0.005) cm^2. The glassy carbon electrode was polished with Buehler 0.05 μm Micropolish alumina powder, and subsequently sonicated and rinsed with the base electrolyte solution before each measurement.

The electrochemical experiments were carried out with a home-built potentiostat, interfaced via a 12 bit ADC and a 12 bit DAC with a 80286-based computer. Positive feedback just short of oscillatory instability was used for compensation of the solution resistance. Generation of the excitation waveforms and data acquisition of the electrode response were controlled by commercially available software.[27]

The solutions were made from pyrodistilled water and from reagent grade (Baker "analyzed") methanol and $HClO_4$. All supporting electrolyte solutions were treated with activated charcoal and carefully deaerated before use. All solutions were freshly prepared and kept in an inert nitrogen atmosphere.

The 2,6-dichloro-1,4-phenylenediamine (DCDP) was synthesized[28] from 2,6-dichloro-1,4-nitroaniline (Aldrich) and recrystallized from ethanolic solutions. 2,6-dichloro-4-aminophenol (DCAP) was purchased from Aldrich and was recrystallized several times from ethanol before use. The 2,6-dichloro-1,4-benzoquinone (DCQ) was obtained from DCAP by oxidation and recrystallization,[29] 2,6-dichloro-hydroquinone (DCQH2) was synthesized from DCQ following Vogel's procedure,[30] and 2,6-dichloro-4-hydroxyaniline was prepared following the procedure described in Ref. 31.

DATA ANALYSIS

The cyclic voltammograms were recorded with a resolution of 1 mV per point, both for the

pure supporting electrolyte solution and in the presence of DCQ (reduction), DCAP (oxidation) or DCDP (oxidation). The charging current contribution of the base electrolyte was subtracted digitally, implying the assumption of a simple additivity of Faradaic and non-Faradaic currents. The scan rate varied between 5 mV/sec and 2 V/sec. The digital simulation and multiple regression were carried out with the program CVFIT,[23] which utilizes the modified simplex minimization procedure of Nelder and Mead to find the best fit between experimental and simulated results. The errors are estimated by unweighted summation of the squares of the differences between experimental currents i_{ex} and simulated currents i_{th} at the same potentials.

Fixed input parameters of the simulation were usually the electrode area A and the diffusion coefficients D_i of the individual species. The latter were determined from voltage step measurements under diffusion-controlled conditions according to

$$i = nFAc_i\sqrt{(D_i/\pi t)} \qquad (1)$$

where n is the number of electrons involved in the charge transfer, F, the Faraday constant, and c_i the bulk concentration of the electroactive species.

Initial parameter estimates for the simulation-fitting routine were provided for the formal potentials E_i, the standard heterogeneous charge transfer rate constants k_i, the transfer coefficients α_i and, in some cases, for the chemical rate constants k_{ci}. We note that the chemical rate constants have been determined independently from double potential step experiments $E_1 \rightarrow E_2(\tau) \rightarrow E_1$ and comparison with model curves of $i_c(t)/i_a(t-\tau)$ *vs* $k_{ci}\tau$ published by Schwarz and Shain.[32] Here τ is the time interval between the application of the two successive voltage steps.

In order to describe in a quantitative way the cyclic voltammograms of DCDP obtained at slow scan rates, we have assumed a mechanism similar to Scheme I. First we have analyzed the reduction of DCQ. Using the parameters so obtained for E_i, k_i and α_i as fixed input data, we have applied CVFIT to optimize simulated voltammograms for the oxidation of DCAP. Based on these results, we have tried to fit the experimentally obtained CV of the oxidation of DCDP with simulated curves. This approach decreases the number of freely adjustable input parameters.

RESULTS AND DISCUSSION

Reduction of 2,6-dichloro-1,4-benzoquinone

Figure 1 illustrates cyclic voltammograms at three different scan rates obtained for the

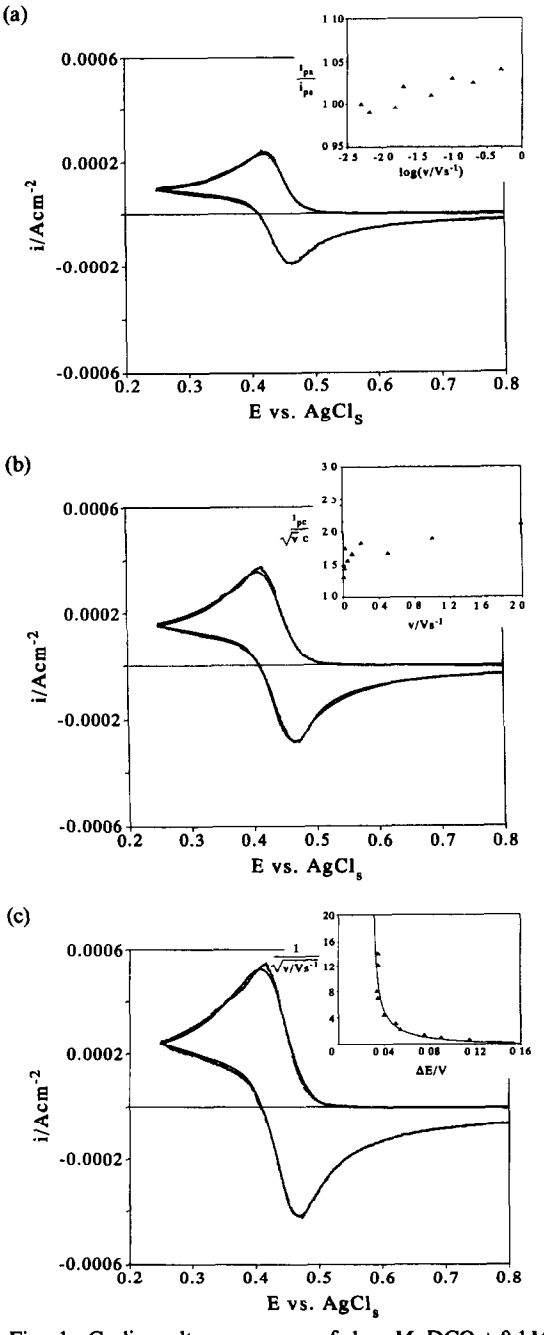

Fig. 1. Cyclic voltammograms of 1 mM DCQ + 0.1M $HClO_4$ in a 50 vol% methanol–water mixture at a glassy carbon electrode. The dotted lines are the experimental data, the solid lines are the result of the fitting routine, see Table 1. Scan rates: (a) 20 mV/sec; (b) 50 mV/sec; (c) 100 mV/sec. The insets illustrate (a) the ratio of the peak currents, (b) the normalized cathodic peak potential *vs* a scan rate function, and (c) $1/\sqrt{v}$ *vs* the peak-to-peak separation ΔE. The solid curve in Fig. 1(c) has been calculated with equation (3) using $k_{III} = 9.4 \times 10^{-3}$ cm/sec.

Table 1. Fitting parameters for DCQ. χ^2 is the sum of the squares of the differences between experimental and simulated values of the current density

v (mV/sec)	E_5 (V)	k_5 (cm/sec)	α_5	E_6 (V)	k_6 (cm/sec)	α_6	χ^2 (μA/cm^2)
20	0.414	0.010	0.49	0.467	0.110	0.41	0.00105
50	0.407	0.011	0.57	0.472	0.07	0.45	0.00241
100	0.419	0.0098	0.52	0.461	0.179	0.58	0.00724
av.	0.413	0.010	0.53	0.467	0.120	0.48	—

oxidation of 1 m*M* DCQ + 0.1 *M* $HClO_4$ in a 50 vol% methanol–water mixture at a glassy carbon electrode. We note that the peak current ratio i_{pa}/i_{pc} estimated from equation (2) is approximately 1 for scan rates between 5 mV/sec and 2 V/sec, see the inset in Fig. 1(a).

$$\frac{i_{pc}}{i_{pa}} = \frac{i_a(0)}{i_{pa}} + \frac{0.485 * i_s(0)}{i_{pa}} + 0.086 \qquad (2)$$

where $i_a(0)$ is the uncorrected anodic peak current, and $i_s(0)$ the uncorrected current at the switching potential E, both measured with respect to the zero-current base line[10].

Laviron[26] showed, on the basis of model calculations with $\alpha_i = 0.5$, that all protonations may be considered to be in equilibrium. Under those conditions, and at pH < 2, the complicated nine-membered square scheme reduces to a simpler CECE sequence:

$$Q \overset{H^+}{\rightleftharpoons} QH^+ \overset{e^-}{\rightleftharpoons} QH^\cdot \overset{H^+}{\rightleftharpoons} QH_2^+ \overset{e^-}{\rightleftharpoons} QH_2 \quad \text{(II)}$$

We have applied a similar approach to the reduction of DCQ under our experimental conditions. Assuming fast protonation reactions we formulate

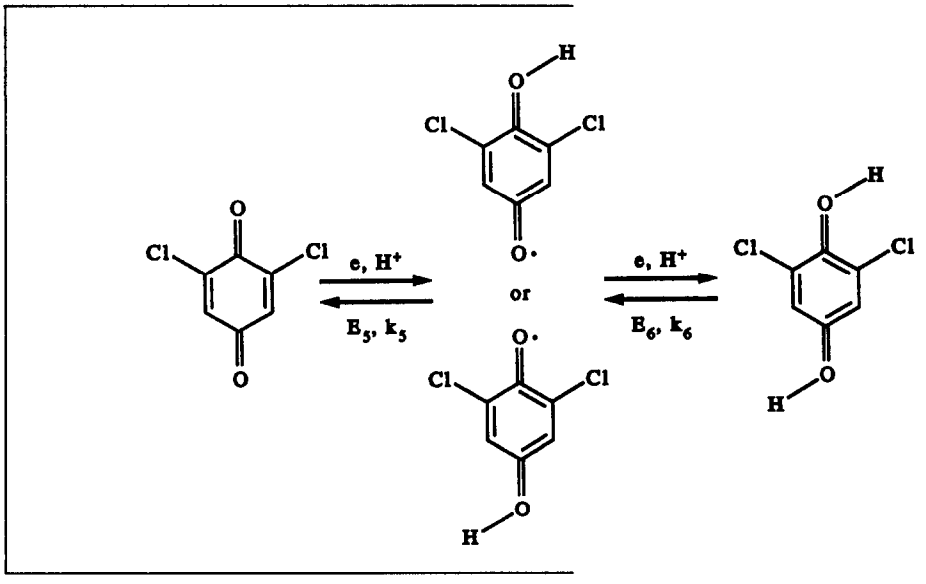

(III)

Furthermore, the current function $i_{pa}/\sqrt{(vc)}$ increases with scan rate while i_{pa}/vc remains essentially constant, cf. the inset of Fig. 1(b). Both criteria point to weak adsorption of reactants and products.[25] At scan rates larger than 20 mV/sec the peak separation exceeds 30 mV and increases significantly with v, as shown in the inset of Fig. 1(c).

The more detailed analysis of our experimental voltammograms was based on results reported for the oxidation of the unsubstituted 1,4-benzoquinone (Q), at mercury[33] and platinum working electrodes.[34] Using those data, where E_5, E_6, k_5 and k_6 are apparent formal potentials and apparent rate constants of reactions 5 and 6, respectively. As shown by Laviron,[26] they reflect the coupling between charge transfer and protonation steps. In our case, the quasireversible electrochemical reaction should predominantly determine the values of k_5 and k_6. Finally, $E(\text{III})^\circ = \frac{1}{2}(E_5 + E_6)$ may be considered as the equilibrium potential for the reaction

$$DCQ + 2e^- + 2H^+ \rightleftharpoons DCQH_2 \qquad \text{(IIIa)}$$

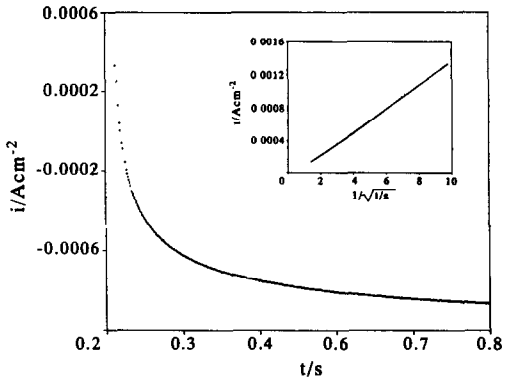

Fig. 2. Current response to a single potential step experiment $E_1 \rightarrow E_2$ with $E_1 = 0.800$ V, $E_2 = 0.200$ V and [DCQ] = $5.0 \times 10^{-4} M$. All other conditions were the same as in Fig. 1. The inset shows the experimental current i as a function of $1/\sqrt{t}$. The solid line was obtained from a linear regression analysis using $t > 0.016$ sec.

The application of Scheme III, with two subsequent one-electron reactions, to the description of our experimental data, was tested with the simulating-fitting routine CVFIT. In order to reduce as much as possible the contributions from adsorption, we have confined ourselves to low scan rates and to relatively high DCQ concentrations. Table 1 summarizes the parameters obtained, and Figs 1(a)–(c) illustrate the agreement between experimental and calculated voltammograms. The diffusion coefficients of DCQ and $DCQH_2$, under our experimental conditions, were determined with voltage step experiments $E_1 \rightarrow E_2$ where $E_1 = 0.800$ V and $E_2 = 0.200$ or 0.250 V, or with $E_1 = 0.250$ V and $E_2 = 0.700$ or 0.750 V, see Fig. 2. With the help of equation (1) we determined D_{DCQ} as $(7.0 \pm 0.3) \times 10^{-6}$ cm^2/sec and D^2_{DCQH} as $(7.0 \pm 0.2) \times 10^{-6}$ cm^2/sec. The diffusion coefficient D_{DCQH} was assumed to be equal to 7.0×10^{-6} cm^2/sec for the purpose of the simulation. The average value of the apparent formal potential E_6 is 54 mV more positive than E_5, which implies that the second one-electron step is thermodynamically more favored. The equilibrium potential E(III)° is estimated as (0.440 ± 0.005) V. The apparent rate constants k_5 and k_6, which primarily reflect the charge transfer step, differ by one order of magnitude, with k_5 being the smaller. A similar sequence was experimentally obtained for the reduction of 1,4-benzoquinone on platinum,[33] and was predicted on the basis of Laviron's theoretical analysis.[26] Both comparisons support the application of Scheme III to describe the reduction of DCQ from acidic media at low scan rates.

Furthermore, analysis of the peak separation as a function of scan rate,[15] using

$$k_{III} = 0.4325 \frac{nFDv}{RT} \times \{\sinh(9.428\ V^{-1}(nE - 0.05666))\}^{-1.044} \quad (3)$$

yields an overall rate constant of reaction III, $k_{III} = (9.4 \pm 0.9) \times 10^{-3}$ cm/sec. Equation (3) is

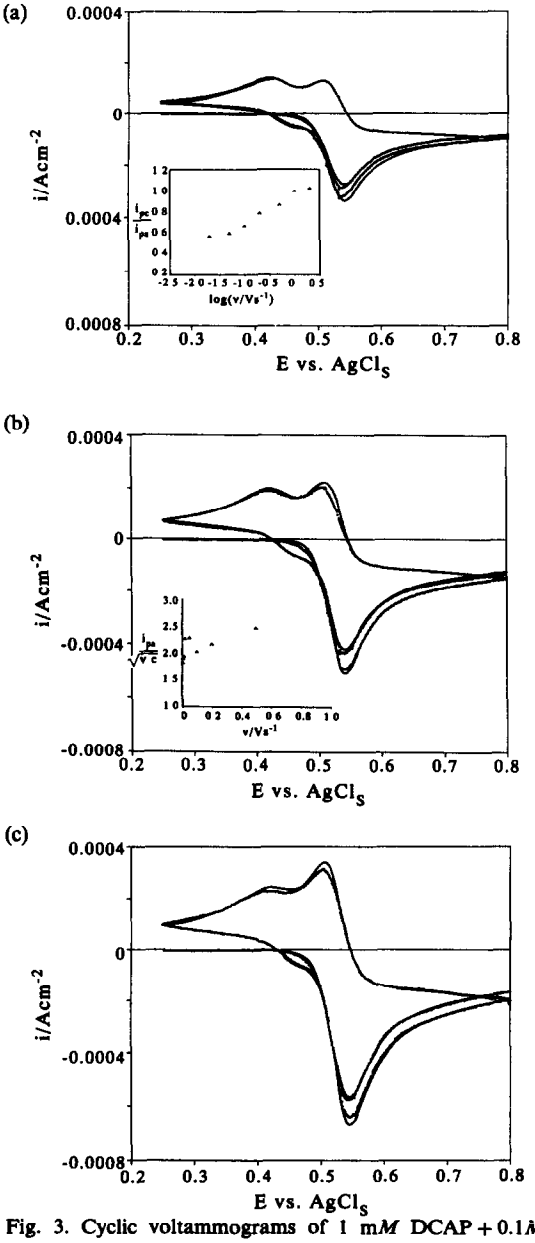

Fig. 3. Cyclic voltammograms of 1 mM DCAP + 0.1M $HClO_4$ in 50 vol% methanol–water at a glassy carbon electrode. The dotted lines show the experimental data, while the solid lines depict the results of the data fitting, see Table 2. Scan rates: (a) 20 mV/sec; (b) 50 mV/sec; (c) 100 mV/sec. The insets illustrate (a) the ratio of the peak currents corresponding to DCAP and (b) the normalized cathodic peak potential *vs* a scan rate function.

an analytical expression based on the parametrization of the kinetic parameters for quasi-reversible charge transfer reactions, as introduced by Nicholson and Shain.[8] The result is in agreement with the rate determining step obtained with CVFIT, see Table 1.

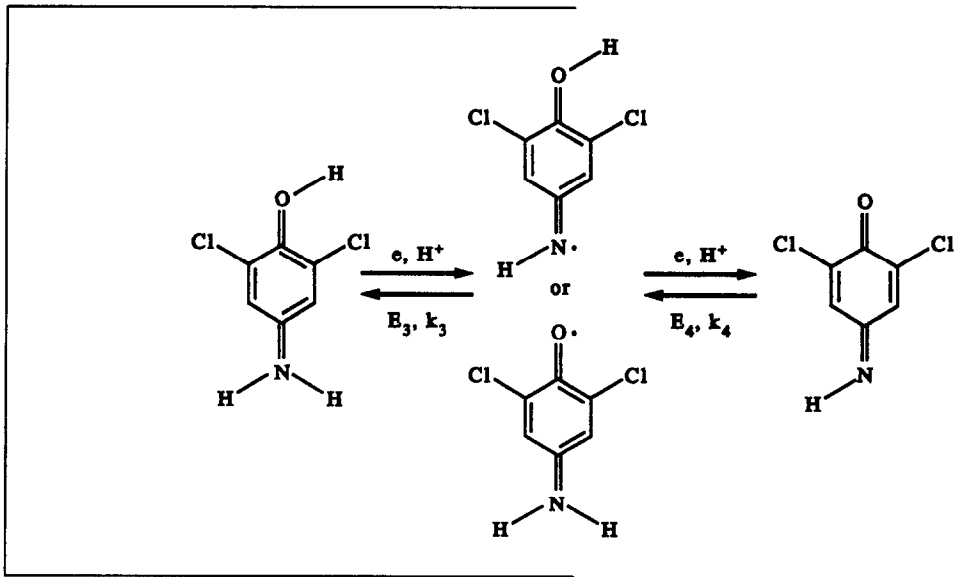

(IV)

We note that the values of the individual rate constants for the reduction of the unsubstituted quinone determined at mercury[32] and platinum electrodes[33] are lower than our results. This is likely to be caused by substituent effects, and possibly may also reflect the less pronounced interference from adsorption under our experimental conditions.

Oxidation of 2,6-dichloro-4-aminophenol (DCAP)

Figures 3(a)–(c) show typical cyclic voltammograms for the oxidation of DCAP at low scan rates and pH < 2. We observe one major anodic peak and two well developed cathodic waves. In view of Scheme I and the parameters obtained for the reduction of DCQ, we associate the more negative peak with the DCQ/DCQH$_2$-redox couple.

During the course of our further phenomenological analysis we will first focus on the processes responsible for the dominant anodic and cathodic peaks. The ratio of the peak currents i_{pc}/i_{pa}, estimated from equation (2), increases with scan rate, see the inset of Fig. 3(a). Furthermore, $i_{pa}/\sqrt{vc}$ increases slightly with v, cf. the inset in Fig. 3(b). The peak potentials E_{pa} and E_{pc} are not significantly influenced by the scan rate, provided that 0.005 V/sec < v < 2 V/sec.

Assuming fast protonation equilibria as in Scheme III we propose the following oxidation pathway:

The substituted quinone imine is unstable, and undergoes hydrolysis to the corresponding quinone:

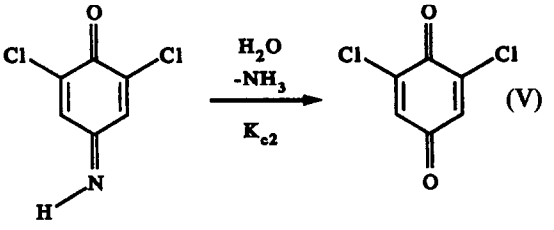

(V)

The rate constant k_{c2} was obtained from double potential step experiments $E_1 \rightarrow E_2 \rightarrow E_1$, with $E_1 = 0.250$ V, $E_2 = 0.600$ V and $\tau_2 = 2.0$, 3.0, 4.0 or 5.0 sec, following the procedure described by Schwarz and Shain.[31] Figure 4 shows a typical transient as well as the ratio $i_c(t)/i_a(t-\tau)$ obtained for different times t. These experiments yield an average value for k_{c2} of (0.23 ± 0.04)/sec. The diffusion coefficient of DCAP in 50 vol% methanol–water mixture + 0.1M $HClO_4$ was obtained, according to equation (2), from the first part of the transient as $D_{DCAP} = (9.2 \pm 0.4) \times 10^{-6}$ cm^2/sec. For the purpose of the simulation, the diffusion coefficients of DCAP, of both semiquinoid species and of the corresponding quinone imines were considered to be identical.

The experimental voltammograms for the oxidation of DCAP were fitted to the

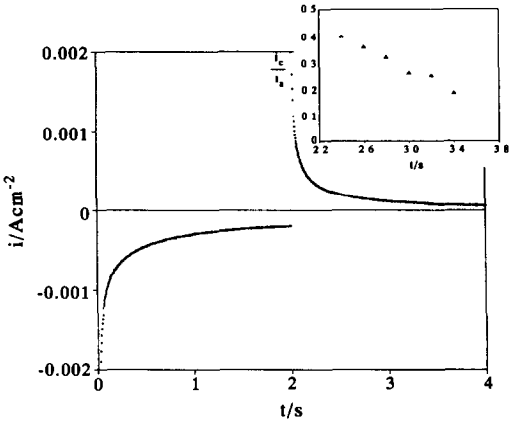

Fig. 4. Current response to a double potential step experiment $E_1 \rightarrow E_2 \rightarrow E_1$ with $E_1 = 0.250$ V, $E_2 = 0.600$ V, and $\tau_2 = 2.0$ sec. All other conditions were the same as in Fig. 3. The inset shows the ratio $i_c(t)/i_a(t-\tau)$ obtained for different times.

mechanism described by the combination of Schemes III–V. The DCQ data have been considered as fixed input data. The results are summarized in Table 2 and are plotted in Figs 3(a)–(c). We note that an alternative route to obtain DCQ from DCDP at our reaction conditions is via the second possible quinone imine formed by the oxidation of 2,6-dichloro-4-hydroxyaniline (DCHA).

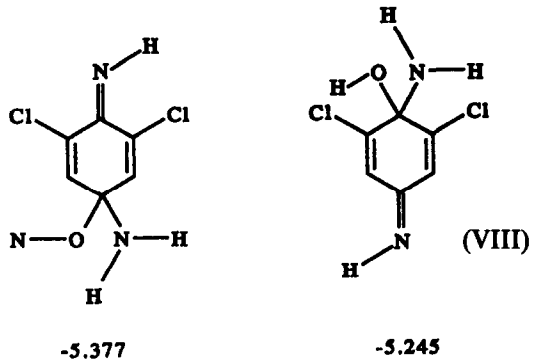

(VIII)

Our cyclic voltammetric and transient studies provided no distinguishable features on which to base a choice between the pathways represented by Schemes IV and V, or VI and VII, respectively. The parameter set compiled in Table 2 therefore represents both possible pathways. This approach is supported by the very similar values of the heats of formation of the two possible intermediates obtained from 2,6-dichloro-*p*-phenylenediimine, estimated with MNDO/2 calculations, Scheme VIII. The hydrolysis of 2,6-dichloro-*p*-phenylenediimine is initiated by the addition of water in either

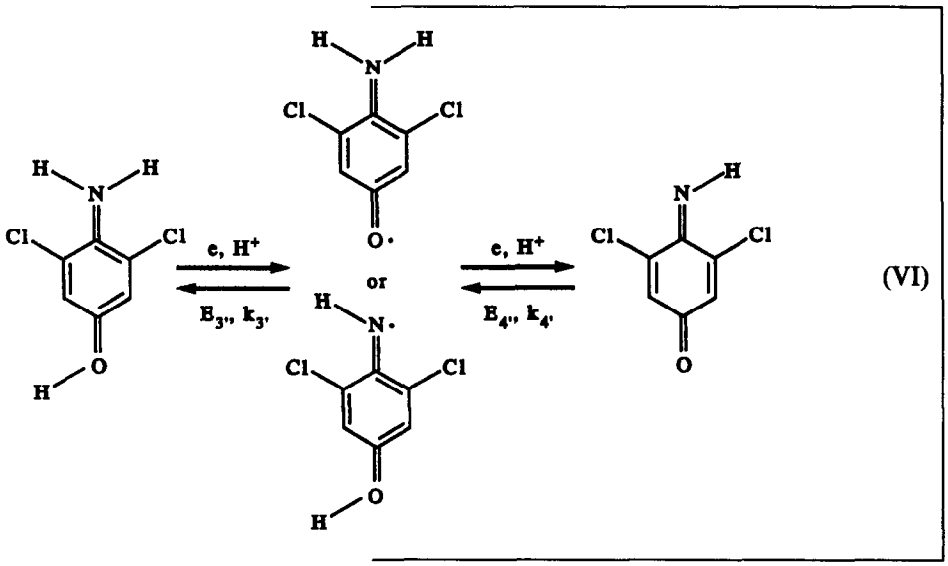

(VI)

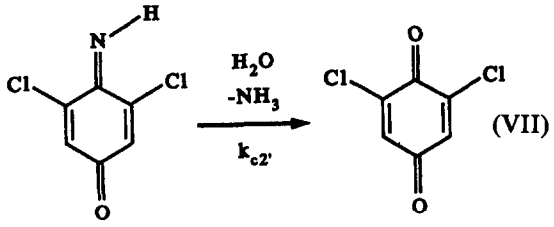

(VII)

position 1 or 4. The elimination of ammonia then yields DCAP and/or DCHA.

Our results are close to those obtained by Adams *et al.* for the oxidation of DCAP at carbon paste electrodes from 0.05*M* H_2SO_4.[1] Comparison with the unsubstituted *p*-benzoquinoneimine shows that the presence of −I

and +M substituents such as chlorine increase the rate of hydrolysis.

Oxidation of 2,6-dichloro-1,4-phenylenediamine

Representative voltammograms are shown in Figs 5(a)–(c). In view of our previous results, we associate the major anodic wave with the formulation of the 2,6-dichloro-1,4-quinonediimine according to:

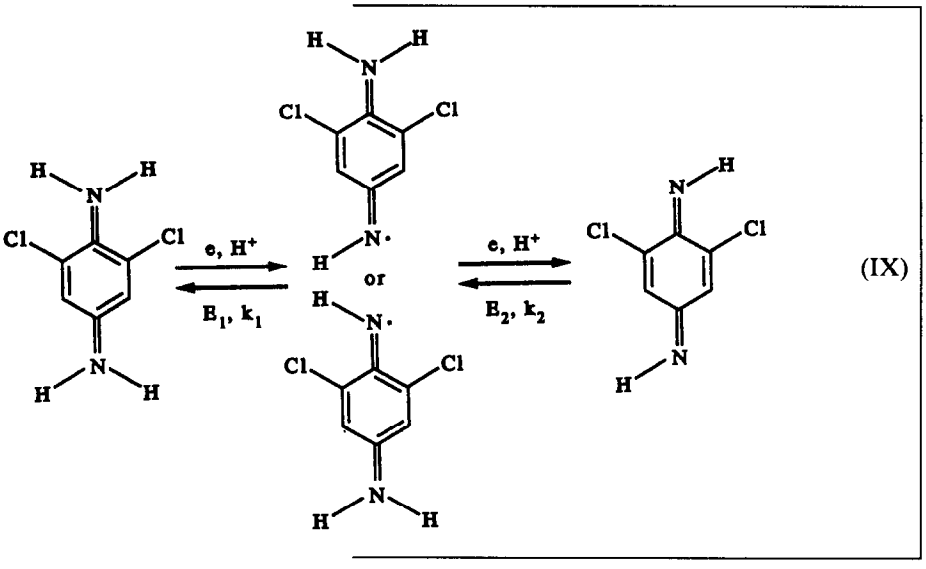

(IX)

The latter is chemically unstable in acidic medium and, in a subsequent step, undergoes hydrolysis to one or both of the possible 2,6-dichloro-1,4-quinoneimines:

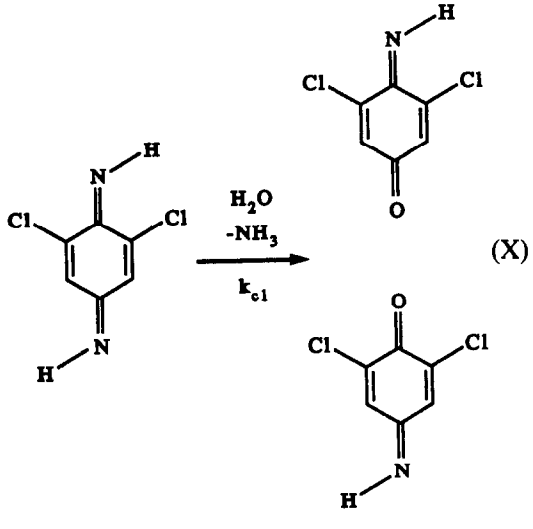

(X)

The peak ratio i_{pc}/i_{pa} of the major redox couple increases with increasing scan rate, which reflects the subsequent reaction X, see the inset of Fig. 5(a). As illustrated by the plot of $i_{pa}/\sqrt{(vc)}$ *vs* v, adsorption effects are not completely negligible cf. the inset of Fig. 5(b). The positions of the peak potentials are independent of the scan rate in the range 0.005 V/sec $< v <$ 2 V/sec. Diffusion coefficients and the rate of the chemical reaction shown in Scheme X were estimated from single and/or double potential step measurements along the lines described earlier. A typical experimental transient is shown in Fig. 6. The analysis of current transients in response to voltage step experiments yielded $D_{DCDP} = (9.2 \pm 0.6) \times 10^{-6}$ cm^2/sec. The value of k_{cl} amounts to (0.29 ± 0.05)/sec, determined from various double potential step measurements $E_1 \rightarrow E_2 \rightarrow E_1$ with $E_1 = 0.250$ V, $E_2 = 0.750$ V and $\tau_2 = 1.0$, 2.5 or 5 sec. Our experimental approach allowed no conclusive distinction between the two possible pathways of the hydrolysis of the quinonediimine as depicted in Scheme X.

Attempts to apply the simulation-fitting routine CVFIT to the theoretical description of the oxidation of DCDP, using the parameters determined for DCQ and DCAP, showed that a chemical rate constant $k_{cl} = (0.34 \pm 0.03)$/sec suffices to describe our experimental results. This is in reasonable agreement with the value obtained from current transients following voltage step experiments (Fig. 5, Table 3).

CONCLUSIONS

The anodic oxidation of 2,6-dichloro-1,4-phenylenediamine at a glassy carbon electrode can be described by the mechanisms II to

Table 2. Adjustable fitting parameters of DCAP

v (mV/sec)	E_4 (V)	k_4 (cm/sec)	α_4	E_3 (V)	k_3 (cm/sec)	α_3	k_{c2} (/sec)	χ^2 (μA/cm^2)
20	0.440	1.00	0.51	0.613	1.02	0.47	0.23	0.02580
50	0.430	1.20	0.42	0.625	0.72	0.53	0.237	0.00922
100	0.398	0.86	0.41	0.655	1.06	0.24	0.23	0.01110
av.	0.423	1.020	0.45	0.630	0.93	0.41	0.23	—

Table 3. Adjustable fitting parameters of DCDP

v (mV/sec)	E_2	k_2 (V)	α_2 (cm/sec)	E_1	k_1 (V)	α_1 (cm/sec)	k_{c1} (/sec)	χ^2 (μA/cm)
50	0.581	0.70	0.50	0.610	0.65	0.52	0.306	0.26701
100	0.579	0.50	0.49	0.618	0.52	0.58	0.340	0.01250
200	0.587	0.43	0.59	0.616	0.58	0.57	0.306	0.02390
av.	0.582	0.54	0.53	0.615	0.58	0.56	0.327	—

X, fully in accordance with the model originally proposed by Adams *et al.*[1,2] for the oxidation of *p*-phenylenediamine. The over-all fit shows considerable deviations at scan rates larger than 0.2 V/sec, due to adsorption effects, which are more pronounced at higher sweep rates.

Because of the complexity of the mechanism, independent control experiments were required in order to reduce the number of freely adjustable parameters to be used in the simulation routine. We believe that our results illustrate both the power and some of the inherent limitations of combining digital simulation with non-linear regression in the kinetic analysis of experimentally observed electrode processes.

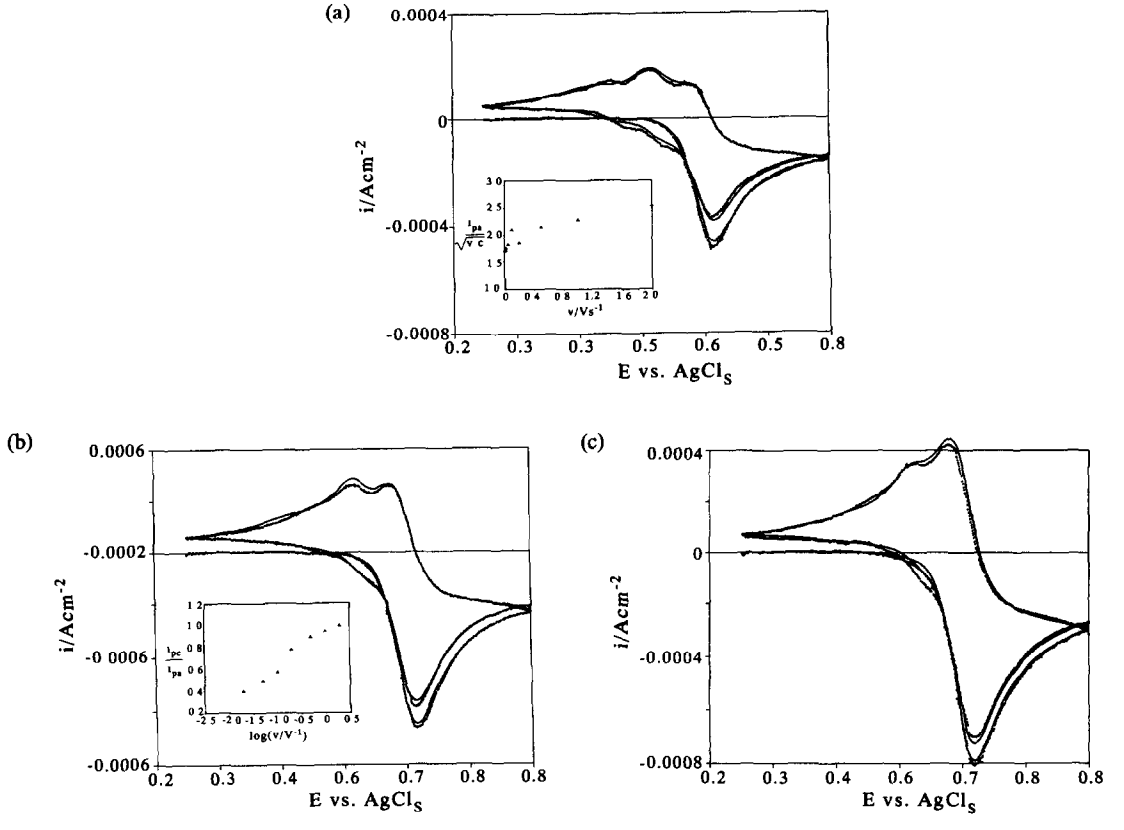

Fig. 5. Cyclic voltammograms of 1 m*M* DCDP + 0.1*M* $HClO_4$ in 50 vol% methanol–water at a glassy carbon electrode. Dotted lines: experimental data; solid lines: results of fitting routine, see Table 3. Scan rates: (a) 50 mV/sec; (b) 100 mV/sec; (c) 200 mV/sec. The insets illustrate (a) the ratio of the peak currents corresponding to DCDP, and (b) the normalized cathodic peak potential *vs* a scan rate function.

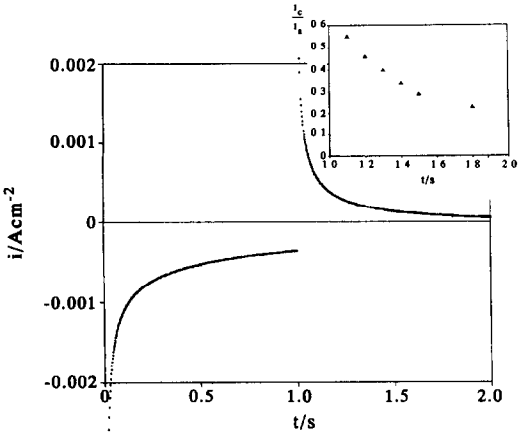

Fig. 6. Current response to a double potential step experiment $E_1 \rightarrow E_2 \rightarrow E_1$ with $E_1 = 0.250$ V, $E_2 = 0.750$ V, and $\tau_2 = 1.0$ sec. All other conditions were the same as in Fig. 5. The inset shows the ratio $i_c(t)/i_a(t-\tau)$ obtained as a function of time t.

Acknowledgements—We gratefully acknowledge financial support from the Educational Foundation of the American Association for University Women (E.A.) and from the National Science Foundation under grant CHE-8921563 (Th. W. and R. de L.).

REFERENCES

1. Z. Galus and R. N. Adams, *J. Am. Chem. Soc.*, 1962, **84**, 2061; D. Hawley and R. N. Adams, *J. Electroanal. Chem.*, 1965, **10**, 376.
2. R. N. Adams, *Electrochemistry at Solid Electrodes*. Dekker, New York, 1971; R. N. Adams, *Acc. Chem. Res.*, 1969, **2**, 175.
3. M.-A. Fox in, *Organic Electrochemistry*, H. Lund, M. Baizer (eds). Dekker, New York, 1991.
4. B. Rossiter and J. F. Hamilton (eds). *Physical Methods of Chemistry*, Vol. 2. John Wiley, New York, 1986.
5. A. J. Bard and L. Faulkner, *Electrochem. Methods—Fundamentals and Applications*. Wiley, New York, 1980; P. Kissinger and W. R. Heineman, (eds), *Laboratory Techniques in Electroanalytical Chemistry*. Dekker, New York, 1984.
6. J. Heinze, *Angew. Chem.*, 1984, **96**, 823.
7. D. Gosser Jr., *Cyclic Voltammetry*. VCH, New York, 1993.
8. R. S. Nicholson and I. Shain, *Anal. Chem.*, 1964, **36**, 706; 1965, **37**, 178, 190.
9. R. S. Nicholson, *Anal Chem.*, 1965, **37**, 1351.
10. R. S. Nicholson, J. M. Wilson and M. L. Olmstedt, *Anal. Chem.*, 1966, **38**, 542; M. L. Olmstedt, R. G. Hamilton and R. S. Nicholson, *J. Electroanal. Chem.*, 1969, **41**, 260.
11. J. M. Savéant and E. Vianello, *Electrochim. Acta*, 1967, **12**, 629; J. M. Savéant, *Electrochim. Acta*, 1967, **12**, 753; C. P. Andrieux, L. Nadjo and J. M. Savéant, *J. Electroanal. Chem.*, 1970, **26**, 147; J. M. Savéant and F. Xu, *J. Electroanal. Chem.*, 1986, **208**, 197.
12. K. B. Oldham, *Anal Chem.*, 1969, **41**, 1904; 1972, **44**, 196.
13. K. B. Oldham and J. Spanier, *J. Electroanal. Chem.*, 1970, **26**, 331.
14. J. C. Inbeaux and J. M. Savéant, *J. Electroanal. Chem.*, 1973, **44**, 169; J. M. Savéant and D. Tessier, *J. Electroanal. Chem.*, 1975, **65**, 57; *Faraday Disc. Chem. Soc.*, 1982, **74**, 7.
15. A. Neudeck and J. Dittrich, *J. Electroanal. Chem.*, 1989, **264**, 91.
16. S. W. Feldberg in, *Electroanalytical Chemistry*, A. J. Bard (ed.), Vol. 3. Dekker, New York, 1969.
17. S. W. Feldberg in, *Electrochemistry*, J. S. Mattson, H. B. Mark and H. C. McDonald (eds). Dekker, New York, 1972.
18. D. H. Evans, *Chem. Rev.*, 1990, **90**, 1972; D. H. Evans, K. M. Connel in, *Electroanalytical Chemistry*, A. J. Bard (ed.), Vol. 14. Dekker, New York, 1986.
19. S. W. Feldberg, *J. Electroanal. Chem.*, 1981, **127**, 1; A. Lasia, *J. Electroanal. Chem.*, 1983, **146**, 397.
20. S. Pons in, *Electroanalytical Chemistry*, A. J. Bard (ed.), Vol. 14. Dekker, New York, 1986; B. Speiser, S. Pons and A. Riecker, *Electrochim. Acta*, 1982, **27**, 1171; B. Speiser, *J. Electroanal. Chem.*, 1980, **110**, 69; 1984, **170**, 95; P. Hertl and B. Speiser, *J. Electroanal. Chem.*, 1987, **217**, 225.
21. J. V. Arena and J. F. Rusling, *Anal. Chem.*, 1986, **58**, 1481.
22. T. F. Brown, D. M. Caster and D. Brown, *Anal. Chem.*, 1984, **56**, 1214.
23. D. K. Gosser Jr. and F. Zheng, *Talanta*, 1991, **38**, 715.
24. Q. Huaong and D. K. Gosser Jr., *Talanta*, 1992, **39**, 1155.
25. R. Wopschall and I. Shain, *Anal. Chem.*, 1967, **39**, 1515, 1527, 1535.
26. E. Laviron, *J. Electroanal. Chem.*, 1983, **146**, 15; 1984, **164**, 213.
27. pClamp, Axon Instruments Inc., Foster City, CA.
28. *Organic Synthesis*, Vol. I, p. 455. Wiley, New York, 1948.
29. *Organic Synthesis*, Vol. IV, p. 148. Wiley, New York, 1963.
30. *Vogel's Practical Organic Chemistry*, B. S. Furniss, A. J. Hannaford, P. W. Smith and A. R. Tachell (eds), p. 1261. Wiley, New York, 1989.
31. W. Hodgen, *J. Chem. Soc.*, 1927, 2218.
32. W. M. Schwarz and I. Shain, *Anal. Chem.*, 1965, **69**, 30.
33. J. M. Hale and R. Parsons, *Faraday Soc. Trans.*, 1963, **59**, 1429.
34. K. J. Vetter, *Z. Elektrochem.*, 1952, **56**, 797.

Talanta, Vol. 40, No. 12, pp. 1799–1807, 1993
Printed in Great Britain.

0039-9140/93 $6.00 + 0.00

SIMULTANEOUS DETERMINATION OF ACETYLSALICYLIC ACID AND CAFFEINE IN PHARMACEUTICALS BY FLOW INJECTION WITH FOURIER TRANSFORM INFRARED DETECTION

SALVADOR GARRIGUES, MÁXIMO GALLIGNANI and MIGUEL DE LA GUARDIA*

Department of Analytical Chemistry, University of Valencia, 50 Dr. Moliner St. 46100, Burjassot, Valencia, Spain

(*Received* 20 *January* 1993. *Revised* 7 *May* 1993. *Accepted* 21 *May* 1993)

Summary—A fast quality control methodology has been developed for the simultaneous determination of acetylsalicylic acid (ASA) and caffeine in pharmaceuticals by flow injection–Fourier Transform Infrared Spectrometry. The method is based on the solubilization of ASA and caffeine in CH_2Cl_2 and the use of a flow system to introduce samples and standards in the spectrometer. Two solutions, containing 90 and 110% of the reported concentration of the two active principles in the sample, were employed in order to control the extreme tolerance levels accepted by the International Pharmacopeia for the composition of formulations. A 300 μl volume of each solution was injected in turn, into a carrier stream of the sample, and their absorbances were measured at wavenumbers of 1770 and 1661/cm for ASA and caffeine, respectively. The absorbance values obtained for the carrier, at the same wavenumbers, were interpolated between those obtained for the standards. This rapid methodology provides a simultaneous quantitative evaluation of the concentration of ASA and caffeine in pharmaceuticals. The method permits us to carry out 53 injections/hr and provides a sensitivity of 0.231 absorbance units/mg ml/mm for ASA and 1.065 for caffeine. Accurate results were obtained for the analysis of different samples containing one or both compounds in the presence of excipients which are insoluble in CH_2Cl_2 and also in the presence of other active principles, such as acetaminophen or ergotamine tartrate.

Flow-injection (FI) is a well established sample handling methodology, based on the injection of samples or standards in a continuous flow carrier stream, which provides the automatization of different steps in the quantitative analysis.[1–3]

The use of FI in Infrared Spectrometric analysis (FI–IR) provides a simple and reproducible means of filling and cleaning the measurement cells[4] and offers important advantages in terms of reproducibility and saving of time and consumables. Moreover, the use of the Fourier Transform permits continuous monitoring of the spectral baseline[5] and simultaneous analysis of different components of the same sample.[6–8]

The few papers published until now on the use of FI–IR[4] and FI–FT–IR[5–13] have shown some of the possibilities offered by the synergistic combination of FI and infrared spectrometry. Some of these papers have been focused on the study of IR detectors in flow systems by means of the use of test molecules[4,10,11] and others have provided alternative methods for the analysis of paint solvents,[5,7,8] gasolines,[13] pesticides[14] and pharmaceuticals.[6,9,12] In this latter case several products, such as choline compounds,[6] aliphatic esters[9] and Ibuprofen[12] were determined in real samples.

In the analysis of pharmaceutical products, infrared spectrometry provides a suitable method for the identification[15] of drugs and also for their quantitative determination.[16,17] However, active principles in pharmaceuticals are usually determined by other spectrometric techniques, such as ultraviolet–visible spectrophotometry,[18] or by chromatographic methods,[19] specially when a multicomponent analysis must be made.

There are various reasons why IR quantitative analysis procedures have not been extensively developed for quality control of pharmaceuticals: (i) the excessive sample handling and time required for the traditional IR techniques, such as the use of alkali halide disks, mulls or thin films, (ii) the poor reproducibility of absorbance values obtained with liquid cells filled manually, (iii) the difficulty of establishing and controlling an appropriate baseline,

*Corresponding author.

especially when dispersive instrumentation is used, and (iv) the interferences among some active principles and also those due to the excipients commonly employed. However, most of these difficulties can be avoided by the hyphenation between FI and FT–IR and so, one of the objectives of the present paper is to evidence that FI–FT–IR can be a good choice for the simultaneous control analysis of different active principles in the same pharmaceutical product. Acetylsalicylic acid (ASA) and caffeine have been used as test molecules to prove the applicability of the FI–FT–IR for this purpose and so, a new analytical procedure has been developed for the simultaneous determination of these two compounds in pharmaceuticals.

Traditionally, ASA and caffeine are determined by volumetric procedures in non-aqueous media[18] or by ultraviolet–visible spectrometry.[20–23] Recently a series of chromatographic methods, based on the use of gas chromatography,[24] high performance thin layer chromatography (HPTLC)[25,26] or high performance liquid chromatography (HPLC), has been developed. This latter technique has been applied for the determination of ASA,[27] caffeine[28,29] or both[30–32] using ultraviolet detection.

FT–IR has been also employed as the detector for the analysis of mixtures of caffeine and ASA by HPLC[33,34] and by TLC.[35] Near infrared has been employed for the quantitative determination of caffeine[36] and mixtures of caffeine and ASA[37] and also FT–IR in the medium range, has been used for the quantitative determination of caffeine in pharmaceuticals[38–40] and for the determination of ASA.[41] However, to the best of our knowledge, no paper has been published on the simultaneous determination of caffeine and ASA by FT–IR either in batch or the flow analysis mode.

Direct injection of samples in a FI manifold is a convenient procedure to obtain a fast analysis but it provides, in general, an excessive dispersion of samples. In the present study, taking into account the reduced sensitivity of the infrared techniques, we have employed two alternative strategies in order to reduce the sample dispersion in the flow injection system: (i) the stopped-flow mode,[7,14] which enhances the limit of detection of the analytical measurements, by improving the signal to noise ratio in a series of accumulated scans, and (ii) the reversed mode flow injection, which was first suggested by Johnson and Petty[42] and has been extensively employed in ultraviolet–visible spectrometric analysis by the Valcárcel group.[43–45] This consists of injecting standards in a carrier stream of samples. In the case of analysis of pharmaceuticals, this opens up new possibilities in order to develop fast analytical procedures for the quality control of these materials.

EXPERIMENTAL

Apparatus

A Perkin-Elmer Fourier Transform Infrared spectrometer, model 1750, with a temperature stabilized DTGS detector and equipped with a 7700 data station, was used to carry out infrared measurements, both in the stopped-flow and in the reversed flow mode. In all cases a micro-flow cell SPECAC (Orpington, U.K.) with KBr windows, with a 5 μl volume, for a 0.117 mm Pb spacer, was employed. To carry out the simultaneous FT–IR measurements in the reversed flow mode, a series of computer programs, developed by us and previously described,[5,8] were employed.

The manifolds indicated in Fig. 1 permit a fast and reproducible filling and cleaning of the micro-flow cell for the stopped-flow measurements (1A) and the reversed FT–IR flow analysis of pharmaceuticals (1B).

Two Gilson P-2 Minipuls peristaltic pumps with Viton (iso-versinic) flexible tubes of 0.15 cm internal diameter were used to transport CH_2Cl_2 or the corresponding carrier solutions and to introduce samples and standards into the flow cell. The use of a second pump to fill the injection valve, or to introduce the sample into the cell, avoids bubble formation, contamination and memory effects. The presence of

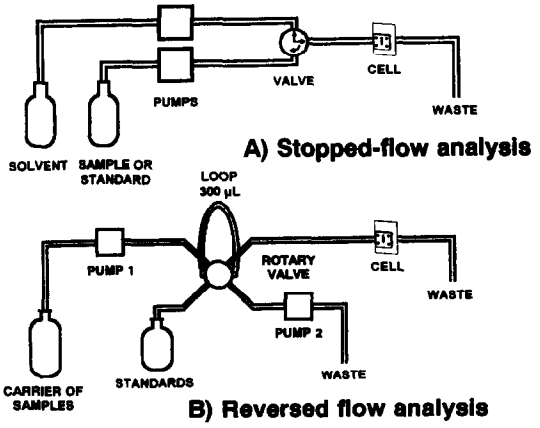

Fig. 1. Manifolds employed for: (A) stopped-flow FT–IR measurement, and (B) reversed flow analysis.

bubbles, observed when only one pump was employed in a single channel manifold, can be attributed to the low boiling point of CH_2Cl_2 which causes gas (vapour phase) formation in the coils when injected samples remain stopped inside flexible tubes during a period of time. So, the use of a second channel, employed for the continuous transport of samples is very convenient and avoids the formation of bubbles. On the other hand the use of a second pump permits reduction of the consumption of reagents because it is not necessary to operate continuously as when a second channel of the same pump is employed. A rheodyne 50 injection valve, with a fixed volume loop of 300 μl, was employed for the standard injection in the reversed flow mode, but, in the stopped-flow procedure, only a three way directional valve is required to select the solvent or the sample flow alternately.

All the tubes to connect the different parts of the two manifolds are made in Teflon[tm] and they have a 0.8 mm internal diameter.

Reagents

Acetylsalicylic acid and caffeine standards were obtained from FLUKA (Switzerland). Analytical grade dichlormethane (Panreac, Barcelona, Spain) was dried by using 4 Å molecular sieves obtained from SDS (France) and employed for the preparation of standards and samples. The choice of CH_2Cl_2 is due to the fact that it is very transparent to infrared radiation and it completely solubilizes ASA and caffeine but, in the samples excipients remain undissolved and so it avoids some matrix effects. Other solvents more commonly employed in IR analysis, such as CCl_4 and hexane, were not employed because they do not solubilize ASA.

The six following analgesic formulations were analyzed by FI–FT–IR: ASPIRINA® (from Bayer) tablets containing 500 mg of ASA per unit; CAFIASPIRINA® (from Bayer) tablets containing 500 mg of ASA and 50 mg of caffeine per unit; MEJORAL® (from Bayer) tablets containing 500 mg of ASA and 30 mg of caffeine per unit; CAFERGOT® (from Sandoz) sugar coated pills containing 100 mg of caffeine and 1 mg of ergotamine tartrate per unit; FIORINAL® (from Sandoz) capsules containing 200 mg of ASA, 40 mg of caffeine and 300 mg of acetaminophen per unit; NEOCIBALENA® (from Ciba-Geigy) tablets containing 200 mg of ASA, 50 mg of caffeine and 150 mg of acetaminophen per unit.

[*] All the names of the analgesic formulations analyzed are trade names registered in Spain by the Pharmaceutical Laboratories.

GENERAL PROCEDURE

FI–FT–IR determination of ASA and caffeine

To determine ASA and caffeine in a pharmaceutical preparation, an appropriate amount of sample must be accurately weighed and dissolved with CH_2Cl_2 in order to obtain an ASA concentration of approximately 10 mg/ml and a caffeine concentration of 1 mg/ml. Both compounds are highly soluble in CH_2Cl_2, but excipients in general and other active principles cannot be dissolved and thus, after manually shaking for a few seconds, the samples can be filtered or centrifuged to separate the undissolved part. After that, sample solutions are continuously introduced as the carrier in the manifold in Fig. 1(b) using a constant flow of 0.81 ml/min, and the absorbance peak height is measured at 1770/cm for ASA and 1661/cm for caffeine, using a common baseline established between 1900 and 1537/cm. 300 μl of a CH_2Cl_2 standard solution, containing ASA and caffeine in a concentration equal to 90% of the theoretical concentration of the sample to be analyzed, is injected in the above-mentioned sample carrier flow. After that, the same volume of another standard solution, containing 110% of the theoretical concentration of ASA and caffeine in the sample, is injected, and the absorbance measurements are carried out for both standard solutions in the same conditions employed for the samples. The two standards injected correspond to the lower and upper level permitted by the Pharmacopoeia for the specifications of pharmaceuticals. So, the absorbance values for the sample carrier must be between those found for the standards. To determine the ASA and caffeine concentrations, the absorbance peak height values of the sample are interpolated between the two points of the calibration line established for the two standard solutions injected. For the analysis of each sample, the carrier and the concentrations of the standard solutions must be changed according to the pharmaceutical to be analyzed.

RESULTS AND DISCUSSION

FT–IR spectra of ASA and caffeine

The FT–IR absorbance spectra of ASA and caffeine, obtained in CH_2Cl_2 solutions, present

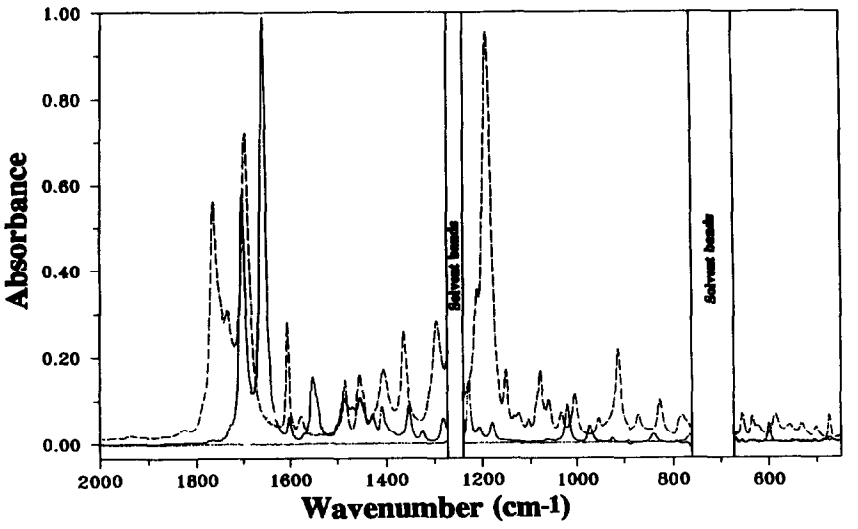

Fig. 2. FT–IR spectra of pure solutions of acetylsalicylic acid 20 mg/ml (– – –) and caffeine 8 mg/ml (——) in CH_2Cl_2.

well defined and very intense bands in the wavenumber range between 1800 and 1200/cm, being those at 1198/cm for ASA and 1661/cm for caffeine the most sensitive (see Fig. 2).

The ASA band at 1198/cm is too close to the non-transparent range of the CH_2Cl_2 and it is overlapped with small bands of caffeine. In the range between 1800 and 1675/cm ASA presents a series of intense bands. However, as it can be seen in Fig. 3, an increase in the concentration of ASA in the range between 0.2 and 20 mg/ml, modifies the relative intensity of these bands, being that at 1703/cm the most sensitive only for concentrations higher than 5 mg/ml. The band of ASA at 1770/cm is the only one which obeys Beer's law, as it can be seen in Fig. 3(c) and which is not overlapped with those of caffeine, and so it seems the most appropriate for the ASA determination.

Caffeine has been determined by IR spec-

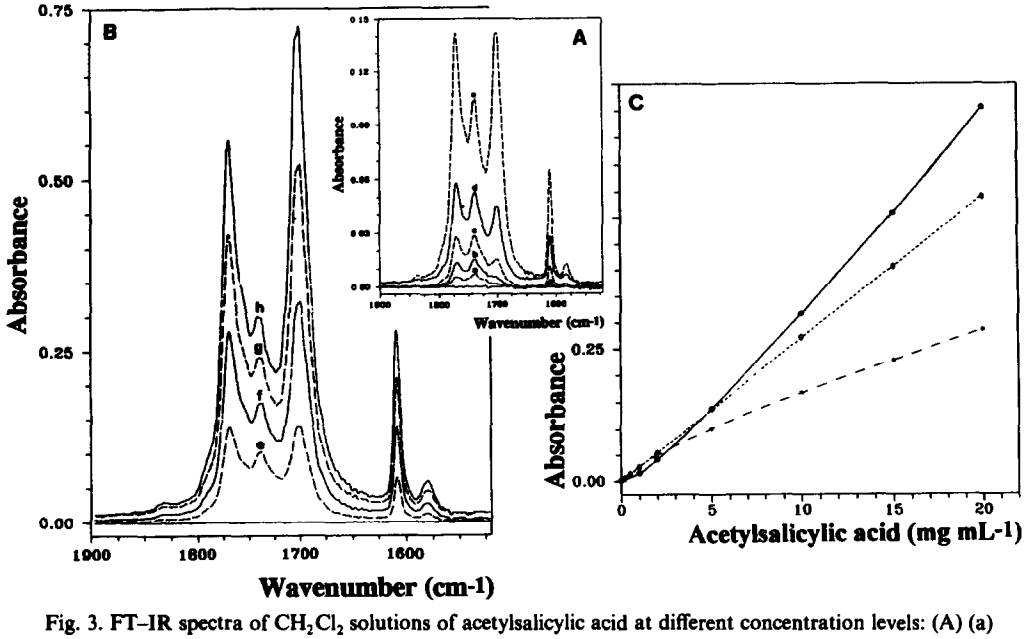

Fig. 3. FT–IR spectra of CH_2Cl_2 solutions of acetylsalicylic acid at different concentration levels: (A) (a) 0.2 mg/ml, (b) 0.5 mg/ml, (c) 1 mg/ml, (d) 2 mg/ml, (e) 5 mg/ml. (B) (f) 10 mg/ml, (g) 15 mg/ml, (h) 20 mg/ml. (C) calibration lines obtained for pure acetylsalicylic acid solutions in CH_2Cl_2, measured at different wavenumbers: (○) 1703/cm, (◇) 1770/cm and (*) 1738/cm.

troscopy in the region between 650 and 400/cm.[40] However, caffeine bands in this range are less sensitive than that at 1661/cm. Thus this latter band represents the best potential wavenumber for the determination of caffeine in the presence of ASA.

A common baseline between 1900 and 1520 or between 1900 and 1537/cm can be established for bands considered for the determination of ASA and caffeine. In standard solutions, both baselines provide comparable results, but in complex samples, which include other active principles, the base-line between 1900 and 1537/cm avoids interferences and provides the most accurate results.

Direct determination of ASA

Stopped-flow measurements, carried out in the above mentioned conditions, provides a typical calibration line for ASA (in the concentration range between 1 and 20 mg/ml) which corresponds to $A = 0.000_6(\pm 0.0006) + 0.0270_5(\pm 0.00006)C_{(\text{in mg/ml})}$ with a regression coefficient, R, of 0.99998. This equation is close similar to that obtained for another series of standards in the presence of a 1:10 caffeine: ASA proportion, which corresponds to an equation $A = 0.000_9(\pm 0.0005) + 0.0270_1(\pm 0.00005)C_{(\text{in mg/ml})}$ with $R = 0.99998$. So, a calibration line, defined from pure solutions of ASA in CH_2Cl_2, can be used for the direct determination of ASA in pharmaceuticals containing also caffeine. Accurate results can be also obtained in the presence of other compounds, such as acetaminophen, which do not interfere with the 1770/cm bands of ASA.

Interference of ASA in the FT–IR determination of caffeine

ASA interferes on the FT–IR determination of caffeine as it can be seen in Fig. 4. For a fixed concentration of 1 mg/ml of caffeine, ASA concentrations lower than 8 mg/ml cause a little negative interference in the absorbance of caffeine which provides a maximum interference of the order of −5% in relative absorbance. Higher concentrations of ASA cause a positive interference in the caffeine absorbance measurements; for an ASA:caffeine proportion higher than 20:1, the relative error of the absorbance is higher than +10%.

The interference of ASA on the caffeine determination by FT–IR can be attributed to the proximity between the absorbance bands of

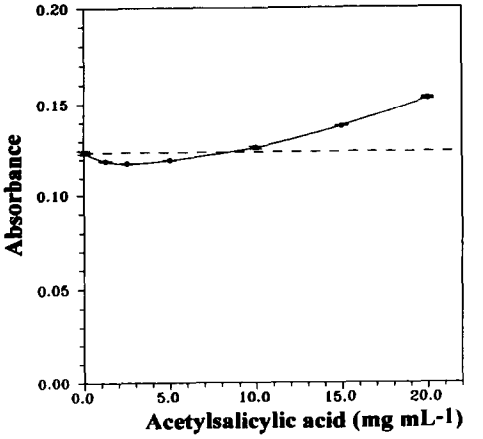

Fig. 4. Effect of the ASA concentration on the absorbance values of caffeine at 1661/cm for a fixed concentration of caffeine of 1 mg/ml.

these compounds and this is aggravated by the high concentration of ASA in pharmaceuticals containing caffeine. For low ASA concentrations this interference is very little and the small errors caused are due to changes in the baseline which reduces the peak height of the caffeine absorbance at 1661/cm. In this case caffeine concentrations lower than real ones were obtained due to the variation of the absorbance of ASA at 1703/cm as indicated in Fig. 3. The positive interference found at high ASA concentration levels must be attributed to the contribution of the intense band of ASA at 1703/cm which increases with the ASA concentration and overlaps with the 1661/cm band of caffeine.

The change in the relative absorbance of ASA at 1703/cm, as a function of the ASA concentration (Fig. 3), hinders the possibility of correcting its interference in the caffeine determination by means of the use of derivative measurements.

FT–IR determination of caffeine

A typical calibration line obtained from pure standards of caffeine in CH_2Cl_2, in a concentration range between 0.1 and 2 mg/ml, corresponds to an equation $A = 0.0008(\pm 0.0004) + 0.1246(\pm 0.0004)C_{(\text{in mg/ml})}$ with $R = 0.99997$. This equation has a slope of the same order than that obtained from standard solutions containing ASA and caffeine in a 10:1 proportion, which is $A = 0.003(\pm 0.001) + 0.123(\pm 0.001)C_{(\text{in mg/ml})}$ with $R = 0.9998$. For this proportion, the interference of ASA has a minimum value (see Fig. 4); however, the high value of the

intercept in this latter equation, evidences the overlapping with the band of ASA.

From these experiments it can be recommended to prepare standard solutions for the determination of caffeine with a similar content of ASA than that of the samples to be analyzed.

Some indications about the order of magnitude of the error which can be found by using standards of pure caffeine for the analysis of samples containing ASA and caffeine can be obtained from the following examples. A caffeine amount of 33.4 mg per tablet was obtained for a sample with 30 mg of caffeine and 500 mg of ASA and a value of 50.1 mg of caffeine per tablet was found for a sample containing 50 mg of caffeine and 500 mg of ASA. Using a calibration line in which ASA was added to the caffeine standards, the above mentioned samples provide values of 29.6 mg per tablet and 49.6 mg, respectively.

Effect of the sample weight

The high dynamic range provided by the FT–IR determination of ASA and caffeine, in the above mentioned conditions, makes possible to work at different dilution levels of the sample, and accurate and precise results were found for a sample amount from 50 to 750 mg dissolved in 25 ml of CH_2Cl_2.

Figures of merit of the FT–IR determination of ASA and caffeine

In the above mentioned conditions, the main figures of merit of the FT–IR determination of ASA and caffeine have been established from the characteristics of the analytical lines and also from a series of analysis carried out at different concentration levels. Table 1 summarizes the values found for the dynamic range, sensitivity, limit of detection and repeatability obtained for each compound considered.

Table 1. Figures of merit of the FT–IR determination of ASA and caffeine in CH_2Cl_2 solutions

Parameter	ASA	Caffeine
Dynamic range *mg/ml*	0–20	0–4
Sensitivity *au/mg ml/mm*	0.231	1.065
Limit of detection *μg/ml* (3σ)	22	5.8
Repeatability *RSD% $n^* = 5$	0.14	0.16
Precision RSD% $n^{**} = 3$	0.5	1.1

*RSD: relative standard deviation. $n^* = 5$ measurements of a sample containing 12 *mg/ml* ASA and 1.2 *mg/ml* caffeine, $n^{**} = 3$ independent analysis of the same sample.

The sensitivity was obtained from the slope of the calibration line and taking into account the bandpass of the cell employed for measurements.

The limit of detection was established for a probability level of 99.6% ($k = 3$), from the standard deviation of 10 independent measurements of a blank solution (3σ) and from the corresponding sensitivity for each compound.

The repeatability was calculated in terms of the variation coefficient (relative standard deviation expressed in percentage) obtained for five absorbance measurements of a same solution containing 12 mg/ml of ASA and 1.2 mg/ml of caffeine and the precision from the variation coefficient for three independent analysis of the same sample.

From results obtained, it can be concluded that FT–IR provides an adequate sensitivity and reproducibility for the determination of ASA and caffeine in pharmaceuticals; the sensitivity for this latter compound at 1661/cm in CH_2Cl_2 solutions being five times higher than that obtained for ASA at 1770/cm.

Analysis of real samples

Samples described in the Experimental section were analyzed in the stopped-flow mode by using a common calibration line obtained with standards containing ASA and caffeine in a 10:1 proportion. Results obtained are summarized in Table 2 and, although all the values found are in the range tolerated by the Pharmacopoeia, it could be convenient to use appropriate sets of standards for each kind of samples.

Reversed flow-injection–FT–IR simultaneous determination of ASA and caffeine

As has been previously indicated, FI–FT–IR can provide simultaneous information about different components of the same sample[6–8] and, as can be seen in Fig. 5, which shows the spectra of three solutions with different concentrations of ASA and caffeine, it is possible to obtain, from the same spectrum, absorbance peak values from which both ASA and caffeine can be simultaneously determined. Arrows in this figure indicate the ASA and caffeine peaks obtained for each solution. Bold lines show the maximum absorbance values reached for ASA and dotted lines evidences that the carrier

Table 2. Analysis of real samples by FI–FT–IR spectrometry

Pharmaceutical	Active principle	Theoretical content (mg per tablet)	Results found (mg per tablet) Stopped-flow	Reversed-FI
Aspirina	ASA	500	509	501
Cafiaspirina	ASA	500	504	501
	Caffeine	50	49.6	50.0
Mejoral	ASA	500	497	495
	Caffeine	30	34.1	29.6
Fiorinal	ASA	200	186	198
	Caffeine	40	38.6	43.2
Neocibalena	ASA	200	182	187
	Caffeine	50	43.6	47
Cafergot	Caffeine	100	94	101

solution of the sample to be analyzed (B) provides an absorbance peak value between those found for the two standard solutions injected (A and C). The sample effect can be also observed for caffeine by measuring the peak height at 1661/cm.

The use of reversed-flow injection FT–IR permits rapid determination of ASA and caffeine in pharmaceuticals. As has been described in the Experimental Part, the injection of standard solutions containing ASA and caffeine (in the same relative proportion as the samples) in a carrier stream of a CH_2Cl_2 solution of each sample provides reference values which can be used for the quantitative analysis of these two compounds. This basic idea, taken from the principles of reversed flow analysis[42–45] and on-line standard additions,[46,47] offers new possibilities in fast quality control of pharmaceuticals by providing a comparison of the samples with the extreme values permitted by the Pharmacopoeia for the content of active principles in pharmaceutical preparations (from 90 to 110% of the reported value).

Figure 6 shows the FI recording established at 1770 and 1661/cm, for the injection of two standard solutions containing 9 mg/ml ASA and 0.9 mg/ml caffeine and 11 mg/ml ASA and 1.1 mg/ml caffeine, respectively in a carrier of a sample of ASA and caffeine. As can be seen the carrier solution provides absorbance values between those obtained for the injected standards

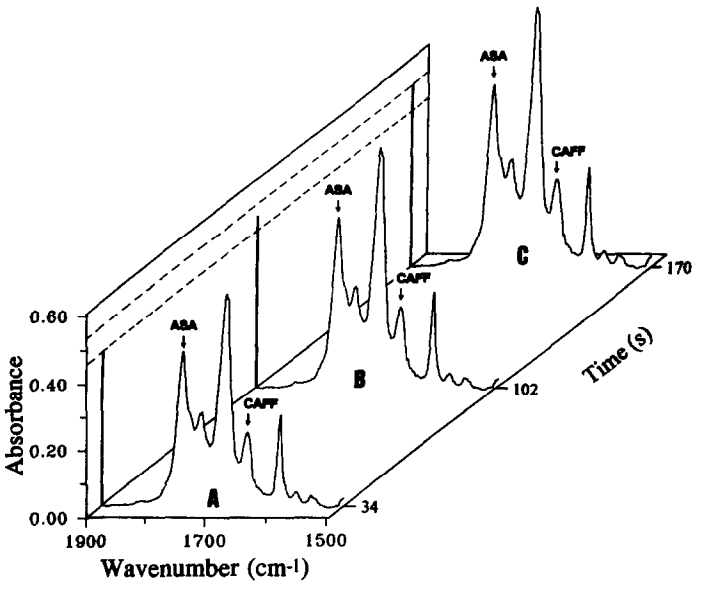

Fig. 5. FT–IR spectra obtained, as a function of time, for: (A) the injection of a standard solution of ASA and caffeine in CH_2Cl_2 containing 9 mg/ml ASA and 0.9 mg/ml caffeine, (B) a carrier solution of a sample with a theoretical content of 10 mg/ml ASA and 1 mg/ml caffeine and (C) the injection of a standard solution containing 11 mg/ml ASA and 1.1 mg/ml caffeine. These figures show only the maximum absorbance values reached for each one of the three solutions considered; intermediate values have been deleted in order to present the spectra from which the flow injection peak height values can be established.

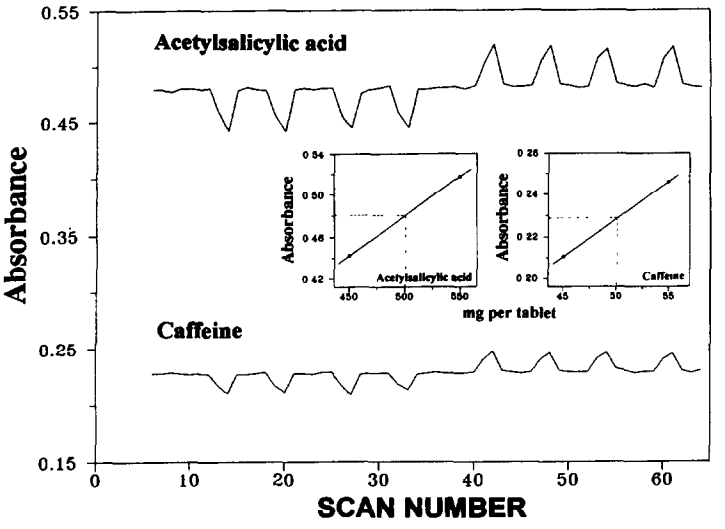

Fig. 6. Flow injection recording obtained by the reversed mode for the simultaneous determination of acetylsalicylic acid and caffeine in a pharmaceutical preparation. Inset: calibration lines obtained for the determination of ASA and caffeine from the injection of the two standard solutions in the sample carrier stream.

and it evidences that the concentration of the active principles in the sample agree with the reported value. Moreover, the content of ASA and caffeine in the sample can be determined from the peak height values found for sample and standards, by interpolation as described in the insets of this figure.

Following this procedure (described in the Experimental section) a series of real samples were analyzed and results found are summarized in Table 2. Results found evidence that the developed procedure is very accurate and permits a fast quality control of pharmaceuticals.

The FI–FT–IR procedure permits us to carry out 53 injections/hr (taking into account that the use of the 7700 Data Station requires more than 17 sec to obtain and store a full interferogram, working with a nominal resolution of 4/cm). However, this sample frequency can be increased by working with a faster instrumentation and software.

The quantitative analysis of a sample, by using the on-line injection of two reference standards in a sample carrier solution, takes less than 15 min to obtain results for both compounds from four repetitive injections of each standard solution.

CONCLUSIONS

ASA can be directly analyzed in pharmaceuticals by FT–IR at 1770/cm; caffeine, acetaminophen and ergotamine tartrate do not interfere with this determination.

The interference of ASA on the FT–IR determination of caffeine at 1661/cm can be avoided by using a baseline established between 1900 and 1537/cm and standard solutions with an ASA:caffeine proportion similar than that expected for samples.

The reversed FI–FT–IR procedure developed for the determination of ASA and caffeine in pharmaceuticals is very accurate and precise and permits us a fast quality control of these two active principles in formulations. This basic strategy could be applied for the simultaneous determination of several compounds in other pharmaceuticals and opens up new possibilities for on-line control analysis.

Acknowledgements—Salvador Garrigues acknowledges the grant of the Conselleria de Cultura, Educació i Ciència de la Generalitat Valenciana to carry out Ph.D. studies, and Máximo Gallignani acknowledges the grant of the Agencia Española de Cooperación Internacional to carry out Ph.D. studies and the financial support of Los Andes University and CONICIT (Venezuela).

REFERENCES

1. J. Ruzicka and E. H. Hansen, *Flow Injection Analysis*, 2nd Ed. John Wiley, New York, 1988.
2. M. Valcarcel and M. D. Luque de Castro, *Flow Injection Analysis. Principles and Applications*. Ellis Horwood, Chichester, 1987.
3. B. Karlberg and G. E. Pacey, *Flow Injection Analysis. A Practical Guide*. Elsevier, Oxford, 1989.

4. D. J. Curran and W. G. Collier, *Anal. Chim. Acta*, 1985, **177**, 259.
5. M. de la Guardia, S. Garrigues, M. Gallignani, J. L. Burguera and M. Burguera, *Anal. Chim. Acta*, 1992, **261**, 53.
6. B. E. Miller, N. D. Danielson and J. E. Katon, *Appl. Spectrosc.*, 1988, **42**, 401.
7. M. Guzman, J. Ruzicka, G. D. Christian and P. Shelley, *Vib. Spectrosc.*, 1991, **2(1)**, 1.
8. S. Garrigues, M. Gallignani and M. de la Guardia, *Analyst*, 1992, **117**, 1849.
9. D. K. Morgan, N. D. Danielson and J. E. Katon, *Anal. Lett.*, 1988, **18**, 1979.
10. S. V. Olesick, S. B. French and M. Novotny, *Anal. Chem.*, 1986, **58**, 2256.
11. P. T. McKittrick, N. D. Danielson and J. E. Katon, *Microchem. J.*, 1991, **44**, 105.
12. S. Garrigues, M. Gallignani and M. de la Guardia, *Talanta*, 1993, **40**, 89.
13. M. Gallignani, S. Garrigues and M. de la Guardia, *Anal. Chim. Acta*, 1993, **274**, 267.
14. M. Gallignani, S. Garrigues, A. Martínez-Vado and M. de la Guardia, *Analyst*, 1993, in press.
15. A. C. Moffat (Ed.), *Clarke's Isolation and Identification of Drugs*, 2nd Ed. The Pharmaceutical Society of Great Britain, London, 1986.
16. M. J. de Faubert Maunder, *Practical Hints on Infrared Spectrometry with Particular Reference to Forensic Analysis*. Adam Hilger, London, 1971.
17. R. G. J. Miller and B. B. Stace, *Laboratory Methods in Infra-red Spectrometry*. Heyden, Chichester, 1972.
18. *United States Pharmacopeia*, 22nd revision, 1989 USP Convention Inc, Rockville MD, USA.
19. R. K. Gilpin and L. A. Pachla, *Anal. Chem.*, 1991, **63**, 130R.
20. G. Sala, S. Maspoch, H. Iturriaga, M. Blanco and V. Cerdá, *J. Pharm. Biomed. Anal.*, 1988, **6**, 765.
21. B. Webb, *Lab. Pract.*, 1990, **39**, 85.
22. K. K. Verma and A. Jain, *Anal. Chem.*, 1986, **58**, 821.
23. M. S. Karawya, A. M. Diab and N. Z. Swelem, *Anal. Lett.*, 1984, **17**, 77.
24. S. Markovic and Z. Kusec, *Pharmazie*, 1990, **45**, 935.
25. J. Sherma, S. Stellmacher and T. J. White, *J. Liq. Chromatogr.*, 1985, **8**, 2961.
26. M. El-Sadek, A. El-Shanawany, A. Aboul-khier and G. Ruecker, *Analyst*, 1990, **115**, 1181.
27. A. Verstraeten, E. Roets and J. Hoogmartens, *J. Chromatogr.*, 1987, **388**, 201.
28. I. Sakano and S. Kokubo, *Anal. Sci.*, 1989, **5**, 623.
29. M. E. El-Kommos and K. M. Emara, *Talanta*, 1989, **36**, 678.
30. P. Cockaerts, E. Roets and J. Hoogmartens, *J. Pharm. Biomed. Anal.*, 1986, **4**, 367.
31. K. K. Verma, S. K. Sanghi, A. Jain and D. Gupta, *J. Pharm. Sci.*, 1987, **76**, 551.
32. I. M. Jalal and S. I. Sa Sa, *Talanta*, 1984, **31**, 1015.
33. J. J. Gagel and K. Biemann, *Mikrochim Acta*, 1988, **II**, 185.
34. S. Shah and L. T. Taylor, *LC-GC*, 1989, **7**, 340.
35. R. L. White, *Anal. Chem.*, 1985, **57**, 1819.
36. E. W. Ciurczak and R. P. Torlini, *Spectroscopy (Springfield, Oreg.)*, 1987, **2**, 41.
37. E. W. Ciurczak and T. A. Maldacker, *Spectroscopy (Springfield, Oreg.)*, 1986, **1**, 36.
38. L. Yin and Y. Liu, *Fenxi Huaxue*, 1986, **14**, 307; *Anal. Abstr.* 4901E005.
39. L. Yin and Y. Liu, *Yaowu Fenxi Zazhi*, 1986, **6**, 139; *Anal. Abstr.* 4903A029.
40. M. Baucells, N. Ferrer, G. Lacort and M. Roura, *Quim. Anal.*, 1991, **10**, 211.
41. A. S. R. Krishnamurthy, R. Shailaja and S. Husain, *Indian Drugs*, 1986, **23**, 513.
42. K. S. Johnson and R. L. Petty, *Anal. Chem.*, 1982, **54**, 1185.
43. M. D. Luque de Castro and M. Valcárcel, *Analyst*, 1984, **109**, 413.
44. A. Rius, M. D. Luque de Castro and M. Valcárcel, *Analyst*, 1984, **109**, 1487.
45. M. D. Luque de Castro and M. Valcárcel, *Trends Anal. Chem.*, 1986, **5**, 71.
46. J. F. Tyson and A. B. Idris, *Analyst*, 1984, **109**, 23.
47. V. Carbonell, A. R. Mauri, A. Salvador and M. de la Guardia, *J. Anal. Atom. Spectrom.*, 1991, **6**, 581.

Talanta, Vol. 40, No. 12, pp. 1809–1814, 1993
Printed in Great Britain.

0039-9140/93 $6.00 + 0.00

EVALUATION OF COLOUR QUALITY OF COMPLEXOMETRIC INDICATORS IN THE TITRATION OF NICKEL(II) WITH EDTA BY TRISTIMULUS COLORIMETRY

S. RAHEEM and K. M. M. KRISHNA PRASAD
School of Chemistry, Andhra University, Visakhapatnam 530 003, India

(*Received* 19 *January* 1993. *Revised* 15 *April* 1993. *Accepted* 20 *April* 1993)

Summary—Trichromatic colorimetry was applied to the specification of colour changes of metallochromic indicators viz., murexide, pyrocatechol violet, bromopyrogallol red, pyrogallol red and chromazurol S in the complexometric titration of Nickel(II) with ethylene-diaminetetraacetic acid (EDTA), in order to assess the quality of colour change at the equivalence point with the help of CIE $L^*a^*b^*$ 1976 system and the values of SCD (Specific Colour Discrimination) parameter. A screened indicator, a mixture of murexide and methylene blue in the ratio 10:1 (m/m), is proposed as an ideal indicator in this titration as evidenced by the plots of a^* *vs.* b^* and from the numerical values of standard deviation for a large number of visual titrations.

In spite of a large number of indicators available for the visual titrimetric determinations, it is difficult to choose the best indicator with a good quality of colour change. Tristimulus colorimetry is an important tool to study the quality of colour changes of the indicators.[1] Principles of tristimulus colorimetry have been applied for the evaluation of colour transition in acid–base indicators.[2–4] As per the recommendations of IUPAC, Analytical Chemistry division,[5] tristimulus coordinates were utilized for the specification of the colour changes of metallochromic indicators.[6–10]

Since the colour diagram is non-uniform, a more uniform colour space defined by CIE $L^*a^*b^*$ 1976[11] has been proposed by using the following expressions.

$$L^* = 116\,(Y/Y_o)^{1/3} - 16,$$

$$a^* = 500\,[(X/X_o)^{1/3} - (Y/Y_o)^{1/3}],$$

$$b^* = 200\,[(Y/Y_o)^{1/3} - (Z/Z_o)^{1/3}],$$

where X, Y and Z are tristimulus values of the solution and $X_o = 98{,}041$, $Y_o = 100{,}000$, $Z_o = 118{,}103$.

In the present study five metallochromic indicators, murexide, pyrocatechol violet, bromopyrogallol red, pyrogallol red and chromazurol S were used to assess the quality of their colour changes, by using tristimulus colorimetry, in the titration of nickel(II) with EDTA.

The accuracy of the titrimetric method depends upon the quality of colour change at the equivalence point, which in turn depends upon the nature of the colours before and after the end point and the rapidity with which the colour transition is occurring. The best colour transition involves a colour change between two complementary colours through greyness (colourlessness). Such a best colour change for the visual indicators can be obtained by screening it with an appropriate inert dye.[12–14] In this study a screened indicator murexide + methylene blue, was developed and the superiority of its quality of colour change over the unscreened indicator was verified utilising the parameter 'standard deviation'.

EXPERIMENTAL

Apparatus

A Shimadzu (U.V. 260) U.V./visible double-beam recording spectrophotometer with temperature control attachment was used for recording spectra. An 'Elico' digital pH meter and OMC Omega 58000 mini-computer were used for pH measurements and for the calculation of chromatic parameters, respectively.

Reagents

A $2 \times 10^{-2}M$ solution of nickel(II) sulphate (E. Merck GR) and a $2 \times 10^{-2}M$ solution of

ethylenediaminetetraacetic acid (EDTA) (BDH AnalaR) were prepared and standardized.

Some $1.0 \times 10^{-4}M$ solutions of the indicators, murexide (BDH AnalaR), pyrocatechol violet (Sigma) chromazurol S (E. Merck GR) in water and bromopyrogallol red (Sigma), pyrogallol red (Sigma) in 50% ethanol were prepared. 1.0×10^{-4} solution of methylene blue (BDH AnalaR) was prepared in triply distilled water.

Determination of chromatic parameters

A 10 ml portion of $0.01M$ solution of nickel(II) and 1 ml of indicator solution were taken in a clean, dry 100 ml beaker. After adjusting pH with appropriate buffer, the total volume of the titrand solution was made up to 50 ml by adding a requisite volume of EDTA and triply distilled water. The absorbance and transmittance values were recorded at different values of C_L/C_M (ratio of concentration of ligand to that of metal ion) in the wavelength range 380–770 nm with an interval of 10 nm. A computer program written in FORTRAN 77, was used for the calculation of chromatic parameters. The algorithm adapted is the weighted ordinate method with the coefficients of standard illuminant C.[15]

RESULTS AND DISCUSSION

The values of tristimulus coordinates (x, y) and complementary colour coordinates (Q_x, Q_y) for all the studied indicators, are determined at different values of C_L/C_M.

The colour transition curves drawn on the complementary colour diagram by using the complementary colour coordinates (Q_x, Q_y), are represented in Fig. 1. This diagram unequivocally indicates that the quality of colour change at the end point is much superior when murexide is used as the indicator in this titration because of long distance between the colour points at the end point and the relative position of colour transition curve. The colour transition curves of pyrocatechol violet, bromopyrogallol

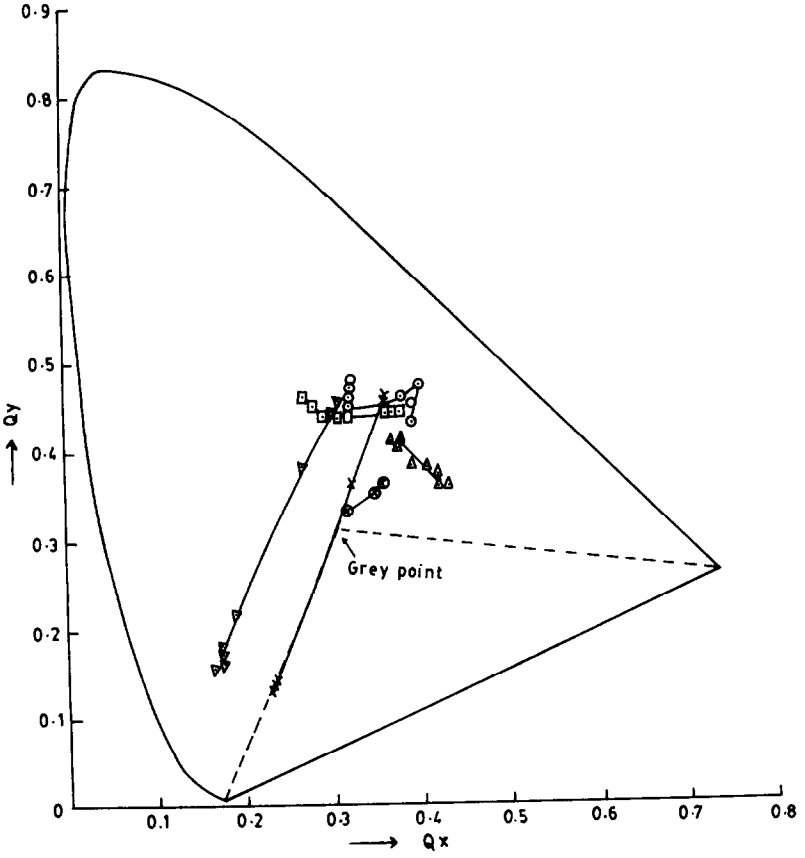

Fig. 1. Colour transition curves of the indicators on the complementary colour diagram: ▽–▽ murexide; △–△ pyrocatechol violet; ○–○ bromopyrogallol red; ◙–◙ pyrogallol red; ⊙–⊙ chromazurol S; x–x screened indicator.

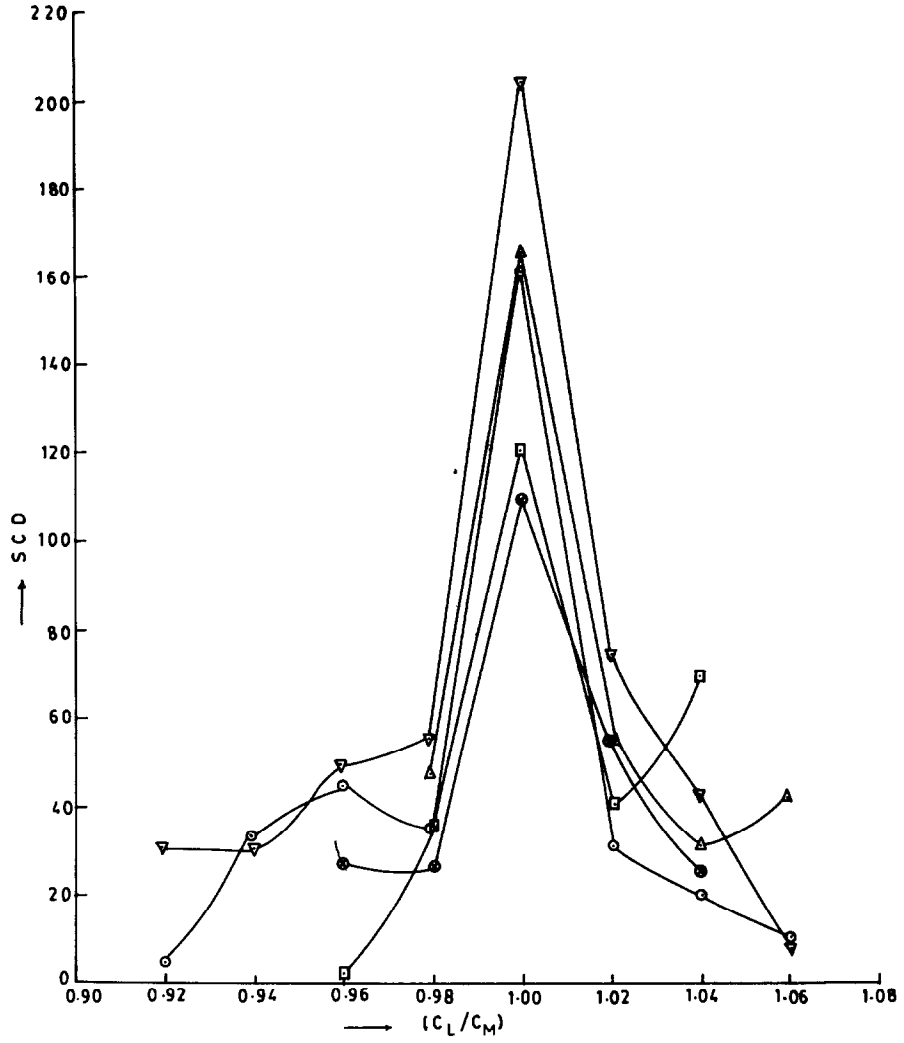

Fig. 2. Specific colour discrimination, SCD *vs.* C_L/C_M (index as in Fig. 1).

red and pyrogallol red are comparable in length whereas the colour transition curve of chromazurol S is short in length.

The values of Specific Colour Discrimination (SCD) are determined in each case in accordance with the method of Bhuchar,[16] for a quantitative measure of quality of colour change. The SCD *vs.* C_L/C_M curves are presented in Fig. 2. The greatest SCD peak exhibited by the indicator, murexide at $C_L/C_M = 1$, indicates that it exhibits a better quality of colour change at the end point, over the other studied indicators. From this graph the following order of quality of colour change of the indicators is concluded, based on the numerical value of SCD at $C_L/C_M = 1$.

Murexide > pyrocatechol violet > bromopyrogallol red > pyrogallol red > chromazurol S.

Figure 3 shows the colour transition curves of the indicators on a^* *vs.* b^* colour space from which it is observed that the colour transition curve of murexide passes very nearer to the origin (grey point). The colour transition curves of bromopyrogallol red and pyrogallol red are present in a single quadrant indicating that a decrease in saturation as the color change at the equivalence point.

The total colour difference, ΔE^* (CIE $L^*a^*b^*$ 1976) for all the studied indicators at different values of C_L/C_M are determined by using the equation

$$\Delta E^*[(\Delta L^*)^2 + (\Delta a^*)^2 + (\Delta b^*)^2]^{\frac{1}{2}}.$$

The highest peak exhibited by murexide in the graph ΔE^* *vs.* C_L/C_M (Fig. 4) revealed that this indicator shows the best quality of colour change at $C_L/C_M = 1$. From this graph the

quality of colour changes of the indicators are arranged in the following order which is similar to the one observed in the case of SCD parameter.

Murexide > Pyrocatechol violet > bromopyrogallol red > pyrogallol red > chromazurol S.

Screening

In a visual titration a sharp endpoint can be achieved by using a screened indicator. In the present study to improve the quality of colour change of the indicator, (murexide) a screened indicator is developed by mixing murexide with an inert colorant, methylene blue. Different proportions of murexide and methylene blue are prepared and their chromaticity parameters are determined at different values of C_L/C_M to arrive at the suitable composition of screened indicator. The colour transition curve of the screened indicator having a composition of 10:1 (murexide:methylene blue), is passing through the origin (Fig. 3) indicating that the colour transition at the end point involves a colour change through colourlessness. The colour transition curve of the screened indicator (Fig. 1) also passes through the illuminant point. A number of visual titrations are carried out by using the screened indicator as well as the unscreened (murexide) indicator and the results obtained are presented in Table 1. The numerical values of the standard deviation for replicate titrimetric determinations, showed that the precision achievable while using the screened indicator is higher than that observed in the case of unscreened indicator.

CONCLUSIONS

A study on the quantitative measure of the quality of colour change of metallochromic indicators with the help of tristimulus parameters viz., SCD (Specific Colour Discrimination) and CIE $L^*a^*b^*$ 1976, revealed the following order of decreasing quality of

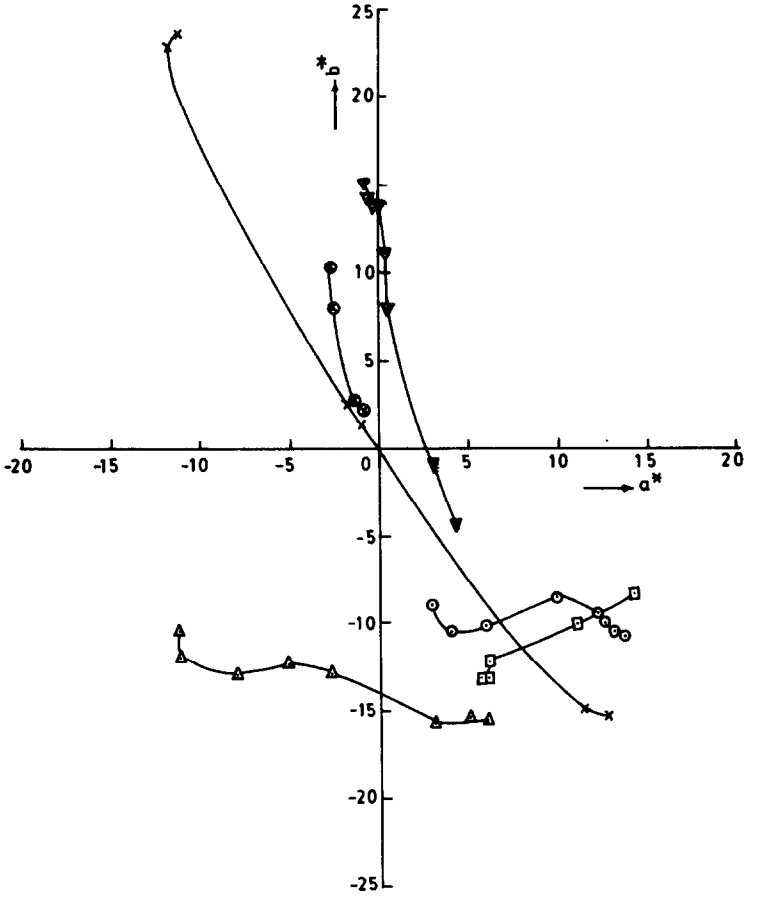

Fig. 3. Colour transition curves on CIE (a^*, b^*) colour space (index as in Fig. 1).

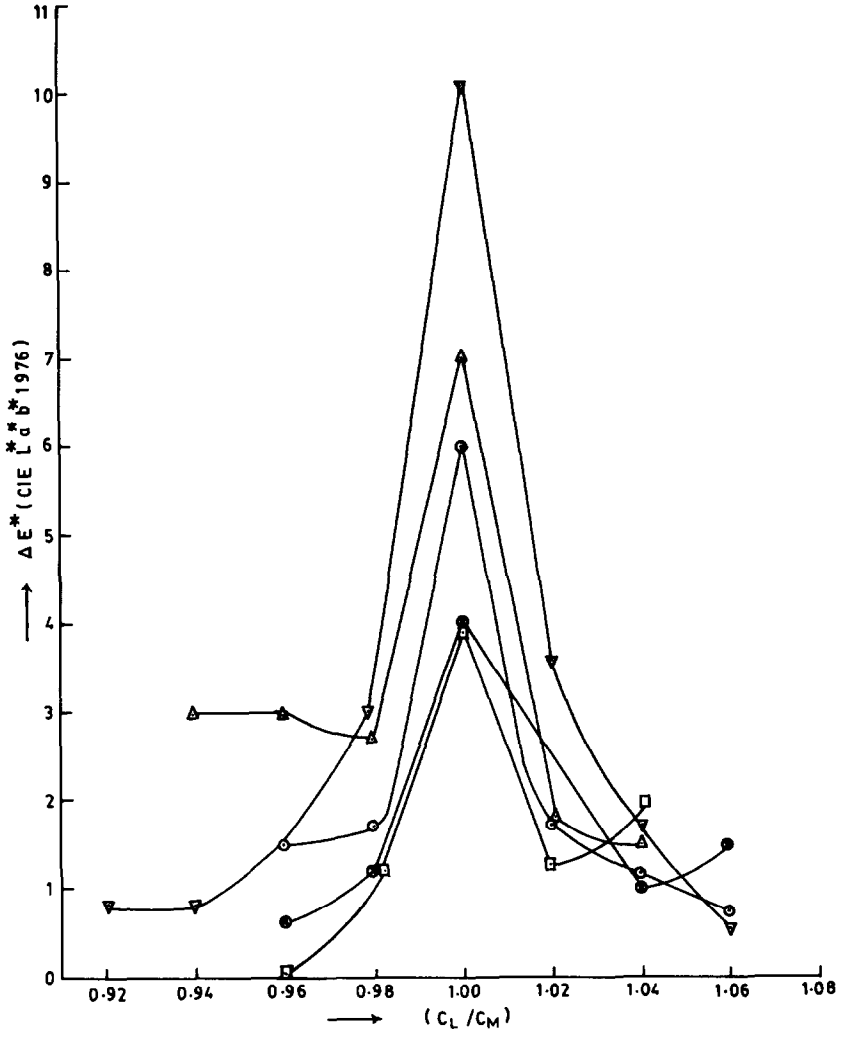

Fig. 4. Total colour difference, ΔE^* (CIE $L^*a^*b^*$ 1976) *vs.* C_L/C_M (index as in Fig. 1).

Table 1. Results obtained with murexide (single) as indicator and murexide + methylene blue (10:1), screened indicator

Indicator	Ni(II) taken (*mg*)	Ni(II) found* (*mg*)	Relative standard deviation (%)	Relative error (%)
Single	0.587	0.595	1.01	1.33
screened		0.589	0.81	0.33
Single	1.761	1.773	0.41	0.68
screened		1.767	0.36	0.35
Single	2.348	2.360	0.31	0.51
screened		2.352	0.25	0.18
Single	4.109	4.120	0.21	0.25
screened		4.113	0.14	0.11
Single	5.871	5.880	0.15	0.16
screened		5.873	0.08	0.03
Single	8.806	8.814	0.10	0.09
screened		8.808	0.05	0.03

*Each value is an average of six determinations.

colour change in the titration of nickel(II) with EDTA.

murexide > pyrocatechol violet > bromopyrogallol red > pyrogallol red > chromazurol S.

The indicator murexide is screened with methylene blue (10:1) to enhance its quality of colour change and thereby the accuracy of the determination.

REFERENCES

1. C. N. Reilley, H. A. Flaschka, S. Laurent and B. Laurent, *Anal. Chem.*, 1960, **32**, 1218.

2. J. Barbosa, E. Bosch and R. Carrera, *Talanta*, 1985, **32**, 1077.
3. A. Izquierdo, E. Bosch and V. Rodrigo, *Talanta*, 1982, **29**, 1125.
4. J. Barbosa, E. Bosch and F. Saurez, *Analyst*, 1985, **110**, 1473.
5. IUPAC analytical chemistry division commission on analytical reactions and reagents, *Pure Appl. Chem.*, 1979, **51**, 1357.
6. K. M. M. Krishna Prasad and S. Raheem, *Asian J. of Chemistry*, 1992, **4**, 726.
7. J. Martinez Calatayud, M. C. Pascual Marti and S. Sagrado Vives, *Analusis*, 1985, **13**, 87.
8. K. M. M. Krishna Prasad and S. Raheem, *Talanta*, 1991, **38**, 793.
9. K. M. M. Krishna Prasad and Syed Raheem, *Anal. Chim. Acta*, 1992, **264**, 137.
10. K. M. M. K. Prasad and S. Raheem, *Analusis*, 1992, **20**, 401.
11. H. Pauli, *J. Opt. Soc. Am.*, 1976, **66**, 866.
12. J. Martinez Calatayud, M. C. Pascual Marti and S. Sagrado Vives, *Analyst*, 1985, **110**, 837.
13. J. Martinez Calatayud and M. C. Pascual Marti, *Analusis*, 1984, **12**, 409.
14. J. Cacho, C. Nerin and M. J. Torres, *Microchem. J.*, 1990, **41**, 227.
15. D. B. Judd, *J. Opt. Soc. Am.*, 1933, **23**, 359.
16. V. M. Bhuchar, V. P. Kikreja and S. R. Das, *Anal. Chem.*, 1971, **43**, 1847.

Talanta, Vol. 40, No. 12, pp. 1815–1822, 1993
Printed in Great Britain.

0039-9140/93 $6.00 + 0.00

DETERMINATION OF Sb, Ni AND V IN SLURRY FROM AIRBORNE PARTICULATE MATERIAL COLLECTED ON FILTER BY GRAPHITE FURNACE ATOMIC ABSORPTION SPECTROMETRY

MANUEL C. CARNEIRO,[1] REINALDO C. CAMPOS[1,2] and ADILSON J. CURTIUS[1,2]

[1]Departamento de Química, Pontifícia Universidade Católica do Rio de Janeiro, 22453-900, Rio de Janeiro, RJ, Brazil

[2]Departamento de Química, Universidade Federal Rural do Rio de Janeiro, 23460-000, Itaguai, RJ, Brazil

(*Received* 11 *January* 1993. *Revised* 10 *May* 1993. *Accepted* 11 *May* 1993)

Summary—A microdigestion procedure performed directly in the autosampler cup is proposed. Small quartz filter pieces loaded with the particulate material are transferred to the cup. The sample is digested by a mixture of nitric, sulfuric and hydrofluoric acid (1:1:1) under sonication. After the addition of a boric acid solution the elements are determined by graphite furnace atomic absorption spectrometry using the autosampler to deliver the slurry into the furnace. A mixture of palladium and magnesium nitrates was used as a modifier for Sb. Spiking studies showed recoveries close to 100% using aqueous analytical curves for Ni and Sb. For V, an analytical curve in the blank slurry, obtained by submitting an unloaded filter to the same procedure, was used. The method was applied to two standard reference materials, Coal Fly Ash (NIST 1633a) and Urban Particulate (NIST 1648) and the concentrations showed good agreement with the certified or recommended values using aqueous analytical solutions.

The analysis of airborne particulate material collected on filters is generally performed using a digestion step. For the analysis of quartz filters, acid mixtures, such as HNO_3–$HClO_4$[1] or HNO_3–H_2SO_4–HCl[2] have been proposed. In this case the quartz filter is not dissolved, and the bulk elements of its matrix are not completely released to the solution. However, acid mixtures containing HF were also suggested.[3,4] An alternative to the acid digestion is the direct analysis of the filter by GFAAS.[5,6] The direct analysis of solids avoids the chemical pre-treatment of the sample, reduces the risks of contamination or losses, and saves time. The full detection power of the instrument can also be used, as the dilution generally associated with chemical pre-treatment is avoided. Nevertheless problems involving high background, calibration difficulties, microweighing errors, sample representativity, *etc.* must also be considered.

A possibility that combines the advantages of the solid and liquid sampling is the analysis of slurried samples.[7–12] Slurry sampling can use the normal autosampler system of the equipment. This overcomes the intensive manual work of the direct analysis of solids related to weighing small sample amounts. The mass to volume ratio of the slurry can also be controlled, in order to extend the dynamic range of the analysis. Difficulties such as bringing the sample to a fine powder or sampling errors may still remain.[13,14] Sedimentation during the analysis is also a problem. Some authors suggest the use of stabilizing agents.[8,9] Mechanical agitation[15] or sonication[16,17] have also been proposed. More recently, an ultrasonic probe attached to the autosampler has become commercially available.[18]

In this work an alternative procedure for the determination of Sb, Ni and V in airborne particulate material collected on quartz filters (HI-vol) is proposed. Small filter pieces are partially digested by an acid mixture in the autosampler cup, using sonication. The resulting slurry is then introduced in the graphite tube via the autosampler.

The interest on Ni and V came from the possibility of using these elements as tracers for oil burning stationary sources. Sb can be used as a tracer to study the environmental impact of oil refineries since it is used as a catalyst during the cracking process.

EXPERIMENTAL

Instrumental

The Sb measurements were carried out on a Perkin-Elmer Zeeman 3030 atomic absorption spectrometer equipped with an HGA-600 graphite furnace and an AS-60 autosampler. For Ni and V the measurements were also carried out on a Model 1100 atomic absorption spectrometer (D_2 background correction), equipped with an HGA-300 graphite furnace and an AS-40 autosampler, all Perkin-Elmer. The light sources were an electrodeless discharge lamp for Sb and hollow cathode lamps for Ni and V. Pyrolytically graphite coated tubes (Perkin-Elmer no. B 0091 504) were used for V. For Sb and Ni, pyrolytically graphite coated tubes (Perkin-Elmer no. B 0109 322) with totally pyrolytic graphite platforms (Perkin-Elmer no. B 0109 324) were used. The microweighings were proceeded on a Perkin-Elmer AD-4 microbalance. For Ni and V a volume of 20 μl was pipetted in the furnace. For Sb, 10 μl of the sample solution and 10 μl of the modifier were used.

Reagents and solutions

The acids HNO_3 and HF were purified by subboiling distillation of the analytical grade reagents in a quartz (HNO_3) or Teflon (HF) subboiling apparatus (Hans Kürner). Analytical grade H_2SO_4 and H_3BO_3 were used. The water was purified by the Milli-Q process. The acid extraction solution (FNS) was prepared by mixing the same volume of HF, HNO_3 and H_2SO_4. The modifier for the Sb determination was a 0.2% m/v Pd and 0.5% m/v Mg, as nitrates, solution. The analytical solutions were prepared after convenient dilutions of 1000 mg/l stock solutions obtained from Titrisol ampoules (Merck) diluted to 1 l with 0.2% v/v HNO_3.

Samples

The airborne particulate material was collected with a Hi-vol sampler, on a 20 × 25 cm quartz filter (Pallflex). Only the particles with a diameter larger than 50 μm were retained. Also two reference materials from the National Institute of Standards and Technology, NIST were used: Coal Fly Ash (SRM NIST 1633a) and Urban Particulate (SRM NIST 1648).

Procedure

Proposed microdigestion procedure: small filter discs (d = 6.0 mm; surface area, 28 mm^2) were cut with a stainless steel cutting tool, from different parts of the filter. Four to eight pieces were placed in a polyethylene autosampler cup (Perkin-Elmer no. B 008 7056) and 150 μl of the acid extraction mixture were added. After placing the cup in an ultrasonic bath for 6 min, 750 μl of water and 150 μl of a saturated boric acid solution were added. After homogenization by manually stirring the slurry with a glass rod, the sample solution was measured for Sb. For V and Ni the sample slurry was diluted 10 times before being measured. In the analysis of the standard reference materials 5 mg aliquots, accurately weighed, instead of the filter pieces, were used.

Table 1. Maximum pyrolysis temperatures (°C) for Sb, Ni, V in different matrices. Atomization temperatures: 2200°C (Sb), 2500°C (Ni) and 2650°C (V)

Matrix	Elements		
	Sb	Ni	V
0.2% HNO_3	1600	1400	1600
Unloaded filter	1600	1300	1400
Loaded filter	1300	1500	1600
NIST 1633a	1300	1200	1600

RESULTS AND DISCUSSION

Temperature programs

Table 1 shows the maximum pyrolysis temperatures for the three studied elements in 0.2 HNO_3 and in different media resulting from the application of the procedure to different samples. These temperatures were derived from pyrolysis temperature curves. Some effects of the matrix on the optimum pyrolysis temperature are shown in Table 1 confirming that pyrolysis temperatures obtained from aqueous solutions cannot be acritically used in any matrix, even using a modifier as in the case of Sb. The temperature programs are shown in Table 2.

Optimization of the microdigestion procedure

Acid mixture volume. Figure 1 shows the effect of the acid mixture volume added to the

Table 2. Temperature programmes for Sb, Ni and V (a: Sb, b: Ni, c: V)

Step	Temperature (°C)	Ramp (s)	Hold (s)	Argon flow (*ml min*)
1	90	1	10	300
2	20	5	10	300
3	1300[a]; 1200[b]; 1400[c]	10	20[a]; 10[b]; 10[c]	300
4	600	1	20	300
5	2200[a]; 2500[b]; 2600[c]	0	3[a]; 5[b]; 7[c]	0
6	2650	1	5	300
7	20	1	20	300

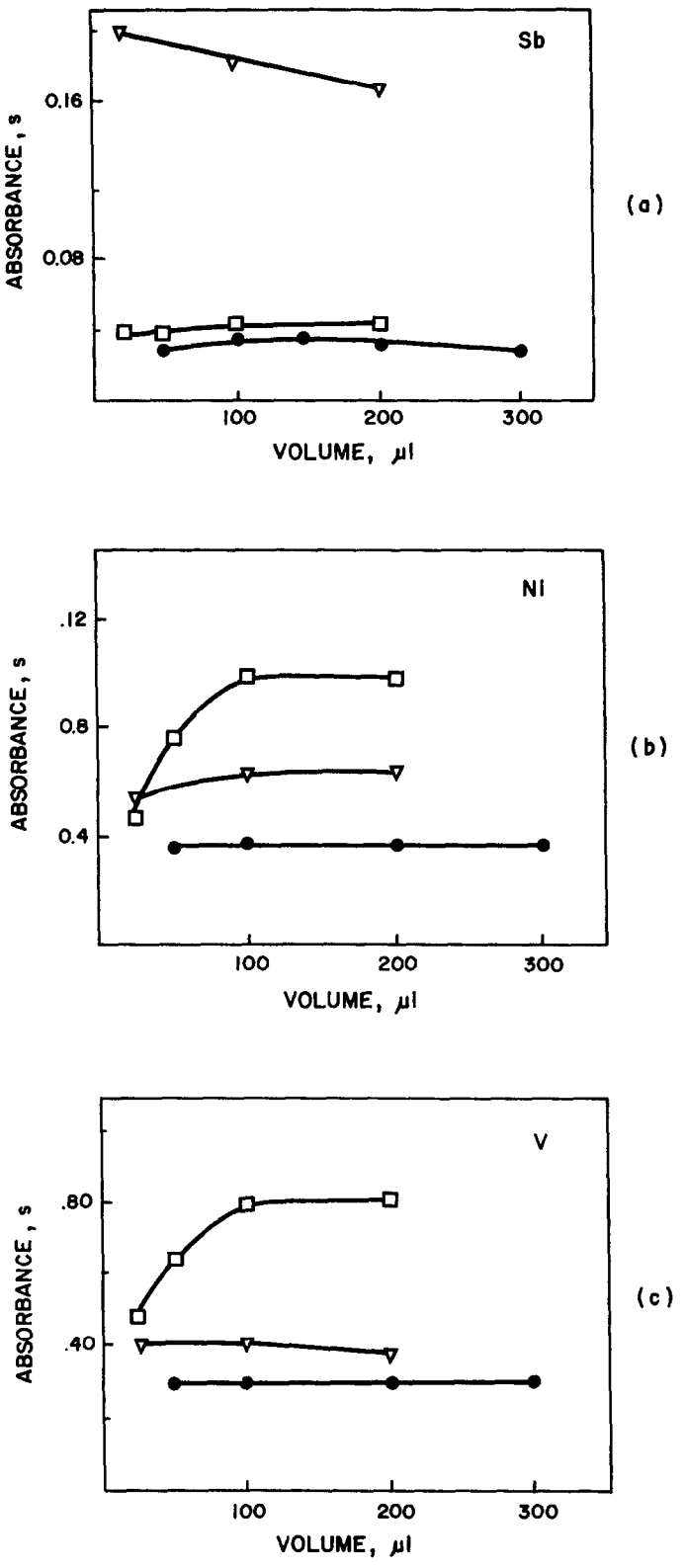

Fig. 1. Effect of the acid mixture volume on the peak area of Sb(a), Ni(b) and V(c) applying the proposed procedure to different materials: (□) SRM NIST 1633a, Coal Fly Ash; (▽) SRM NIST 1648, Urban Particulate and (○) loaded filter.

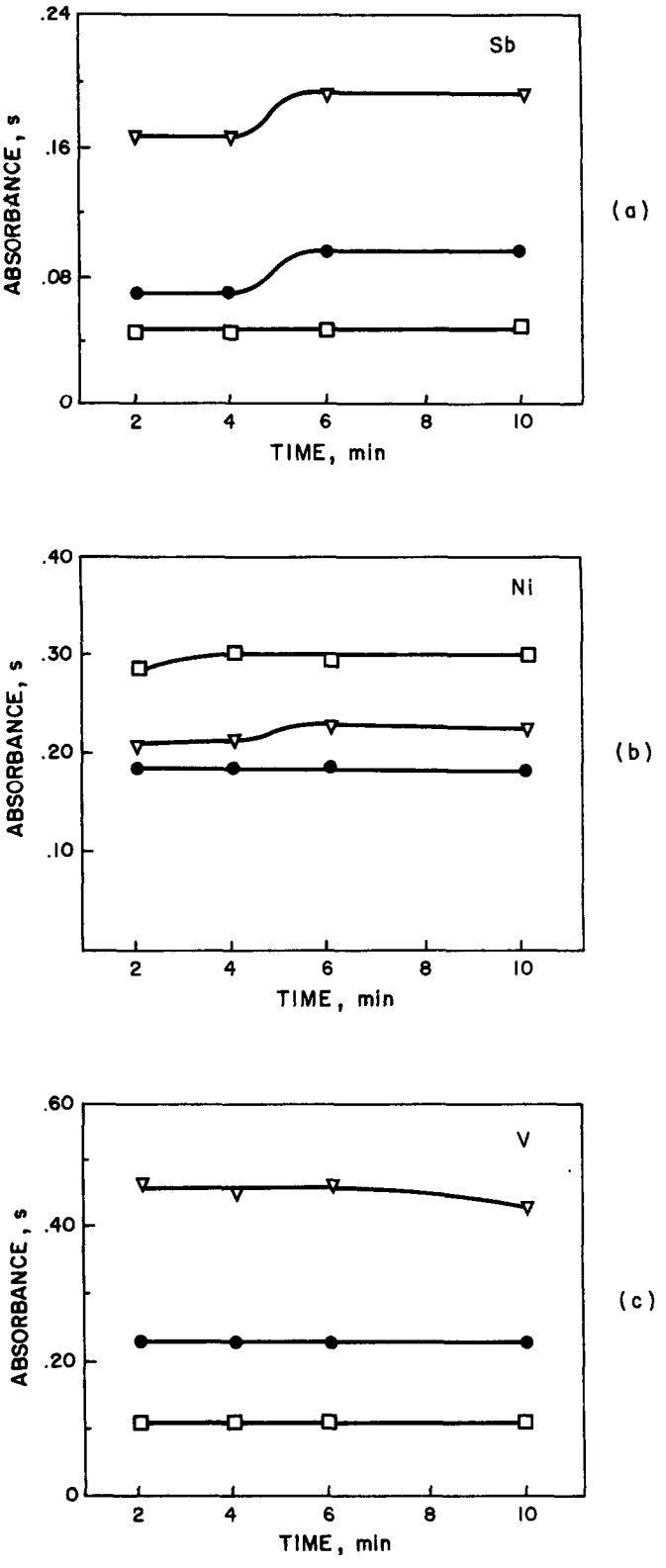

Fig. 2. Effect of the sonication time on the peak area of Sb(a), Ni(b) and V(c) in the final suspension resulting from the analysis of different materials by the proposed procedure: (□) SRM NIST 1633a, Coal Fly Ash; (▽) SRM NIST 1648, Urban Particulate and (○) airborne particulate material collected on a quartz filter. Acid mixture volume, 150 μl.

autosampler cup prior to the sonication on the Sb, Ni and V recovery from standard reference materials (SRM) and airborne particulate material collected on quartz filter. Five milligrams of SRM or four 28 mm^2 filter discs were used. The saturated H_3BO_3 solution volume was always the same as that of the acid mixture and the final volume was 1.0 ml. The drop in the Sb signal (Fig. 1(a)) for SRM 1648 could result from the effect of the higher acid concentration in the Sb signal. However this effect was not found for the other two samples. The volume of 150 μl was chosen as the best compromise for the observed tendencies.

Sonication time. Figure 2 shows the effect of the sonication time on the recovery of Sb, Ni and V from two SRMs and from an airborne particulate material collected on a quartz filter. Five milligrams of SRM or four 28 mm^2 filter pieces were used. The volume of the saturated H_3BO_3 solution was 150 μl and the final volume was made up to 1.0 ml with purified water. There was no significant influence of the sonication time for the studied range, except for the determination of Sb in the particulate material. This indicates that Sb is partially associated with larger particles and it is only partially leached, as it will be discussed later under Stability of the slurries. A sonication time of 6 min was chosen.

Filter homogeneity. As the filter part taken for analysis was small compared to the total filter area, two studies of representativity were performed. In the first one, a filter was divided in four quadrants and from each quadrant, two sets of four 28 mm^2 pieces were taken. The relative standard deviations were calculated for the eight samples. In the other one, 10 sets of four 28 mm^2 pieces were taken at random. For the first study the relative standard deviations were 10%, 6% and 5% for Sb, Ni and V, respectively. In the second experiment, the relative standard deviations were 29% (Sb), 11% (Ni) and 6% (V). Such results demonstrate that in spite of the small sampled filter area (4×28 mm^2) in comparison with the total filter area (50.10^3 mm^2), the distribution of Ni and V on the filter surface was homogeneous enough to permit a representative sampling. For Sb, the distribution was less homogeneous certainly due to its origin. To reduce the relative deviations the first procedure is recommended, specially for Sb.

Accuracy and precision

Table 3 shows the concentration of Sb, Ni and V in two SRMs (NIST 1633a, Coal Fly Ash and NIST 1648, Urban Particulate) obtained using the proposed procedure. The matrices of these materials are expected to have a composition similar to that of the intended samples. The masses taken ranged from 0.94 to 1.89 mg for the NIST 1648 and from 1.86 to 15.68 mg for the NIST 1633a. Aqueous analytical curves were used. There was a good agreement between the found and the certified or recommended values. The reproducibility was typically better than 8% (relative standard deviation) except for Ni in Urban Particulate. A significant part of this variation must be due to the sample inhomogeneity, a major source of uncertainty when such small masses are taken for analysis.

Matrix interferences

Possible matrix interference effects were verified submitting real samples (loaded filters) to the analyte addition technique and comparing the obtained slopes with that of an aqueous (0.2% HNO_3) analytical curve. The analyte addition curves were obtained spiking the suspension resulting from the proposed digestion procedure with known amounts of the analyte, directly in the furnace. The effect of the filter matrix alone was also investigated. In this case, 28 mm^2 discs of an unloaded filter were submitted to the proposed procedure and the resulting suspension was spiked in the same way. The results are summarized in Table 4. The comparison of the slopes shows that there is no significant matrix effect in the Sb and Ni determination in real samples. However, such effects are evident for V. The slopes in the presence of the matrix (loaded or unloaded filter) are significantly larger (57%) than the slope resulting from the aqueous (0.2% HNO_3) analytical curve. This enhancement is the same

Table 3. Concentrations, μg/g ($\pm$standard deviations) for Sb, Ni and V in the standard reference materials by the proposed procedure. Values between parentheses are recommended only

	Sb		Ni		V		
SRM	Certified	Found	Certified	Found	Certified	Found	n
NIST 1633a	(7)	7.0 ± 0.5	127 ± 4	120 ± 8	289 ± 7	325 ± 21	10
NIST 1648	(45)	42 ± 3	82 ± 3	83 ± 14	(130)	128 ± 10	22

Table 4. Linear regression parameters for Sb, Ni and V, resulting from analyte addition curves (number of additions: 3)

Analyte	Matrix	Slope ($s \cdot ml/ng \cdot 10^3$)	Slope standard deviation	Correlation coefficient
Sb	0.2% HNO_3	1.40	0.06	0.9999
	unloaded filter	1.43	0.07	0.9965
	loaded filter	1.39	0.03	0.9989
Ni	0.2% HNO_3	3.10	0.02	0.9996
	unloaded filter	3.25	0.06	0.9998
	loaded filter	3.18	0.07	0.9994
V	0.2% HNO_3	1.40	0.05	0.9980
	unloaded filter	2.20	0.09	0.9993
	loaded filter	2.21	0.06	0.9997

for loaded or unloaded filters. In a previous experiment, it was observed that the acids alone did not interfere in the V sensitivity. Also the analysis of the standard reference material showed no interferences. Therefore the observed slope enhancement can only be due to the quartz matrix. According to Matousek and Powell,[19] the atomization of V proceeds through the formation of vanadium carbide. Since Si also forms carbide,[20] it could be that in the presence of this element another atomization mechanism takes place. For other elements in slurries of glass materials, Bendicho and de Loos–Vollebregt[21] found that the silica matrix behaves as a chemical modifier, producing a retention of the analyte, which is released later in the atomization step. So this retention and also the reduction of the formation of vanadium carbide, could explain the improvement in the *V* signal produced by the silica matrix.

Recovery studies

Known amounts of the analyte were delivered to the cups containing four 28 mm^2 filter discs, before the digestion. The slopes of the curves and the recoveries are displayed in Table 5. For Sb and Ni, the recoveries were calculated from the ratio between the slope of the recovery curve and that of the aqueous analytical curve. For V, instead of the slope of the aqueous analytical curve, the slope of a spiked blank (unloaded filter) was used.

Detection limits

As it was not possible to obtain a "field blank",[22] the detection limits were estimated from the analysis of then unloaded filters. Four 28 mm^2 discs were used. The detection limits obtained ($k = 3$) were 15, 36 and 38 ng/cm^2 for Sb, Ni and V, respectively.

Stability of the slurries

Figure 3 shows the average of five consecutive measurements as function of the number of firings. Each cycle takes about 2 min, depending on the temperature program. For Sb a drop in the signal was observed if the suspension was standing for more than 20 min. For more than 40 min the signal was again stable, indicating that this element could be partially associated with larger particles, which are sedimented earlier. The Ni signal drops continuously after about 20 min, suggesting that this element was

Table 5. Recovery of Sb, Ni and V using the proposed procedure

Analyte	Matrix	Slope ($s \cdot ml/ng \cdot 10^3$)	Slope standard deviation	Correlation coefficient	Recovery (%)
Sb	0.2% HNO_3	1.40	0.06	0.9999	
	unloaded filter	1.43	0.06	0.9965	102
	loaded filter	1.39	0.03	0.9992	93
Ni	0.2% HNO_3	2.62	0.02	0.9996	
	unloaded filter	2.53	0.07	0.9993	97
	loaded filter	2.46	0.08	0.9945	94
V	0.2% HNO_3	1.52	0.05	0.9859	
	unloaded filter	2.20	0.06	0.9980	
	loaded filter	2.22	0.04	0.9963	101

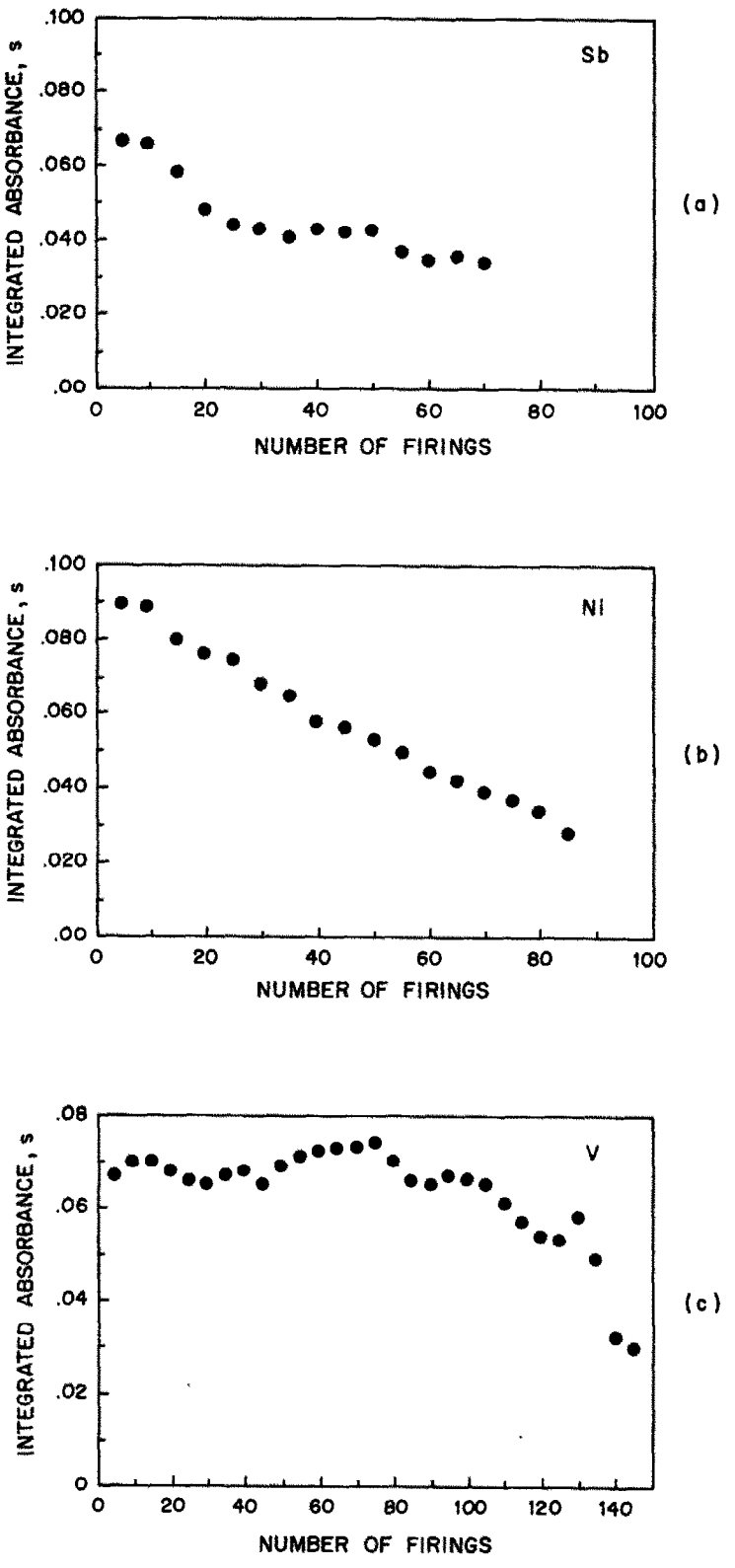

Fig. 3. Average peak area of five measurements for Sb(a), Ni(b) and V(c) in the slurry of a loaded quartz filter as a function of the number of firings.

not leached by the acid mixture, but remained in the particles. For V the signal is rather stable for very long period of time, indicating that this element is released to the solution or associated with very small particles. The drop for V after more than 100 firings is probably related to the end of the tube lifetime. In conclusion, the obtained slurry is stable enough to allow the analysis, but the determination should be performed just after the homogenization. The solution to be measured should not stand for more than 20 min, specially for the determination of Sb and Ni. Probably continuous sonication or agitation would allow longer standing times, but this procedure was not tested.

CONCLUSION

The proposed procedure is very rapid, taking about 15 min for the digestion and the determination. Also small quantities of reagents are used, making the analysis very economical.

Using the recommended background correctors, no interferences were detected for Sb and Ni, making the use of aqueous analytical solutions in the calibration possible. For V, the enhancement in the signal detected in the presence of the partially digested quartz filter, requires the use of analytical solutions prepared from a blank slurry resulting from the application of the procedure to an unloaded filter or the use of the analyte addition method. For the analysed standard reference materials, no interference was detected, not even for V, and aqueous analytical curves can be used.

REFERENCES

1. A. H. Trindade, W. C. Pfeiffer, H. Londres and C. L. Costa-Ribeiro, *Environ. Sci. Technol.*, 1980, **4**, 84.
2. J. Hrsak and M. Fugas, *Mikrochim. Acta*, 1981, **II**, 111.
3. IUPAC, *Pure Appl. Chem.*, 1974, **40**, 37; J. Sneddon, *Talanta*, 1983, **30**, 631.
4. T. Yamshige, M. Yamamoto and H. Sunahara, *Analyst*, 1989, **114**, 1071.
5. M. J. M. P. Moura, M. T. S. D. Vasconcelclos and A. A. S. C. Machado, *J. of Anal. At. Spectrom.*, 1987, **2**, 451.
6. M. Yamamuchi, N. Okubo, H. Yokoyama, T. Mi and E. Asada, *Bunseki Kagaku*, 1982, **31**, 561. C. Bendicho and M. T. C. de Loos-Vollebregt, *J. Anal. At. Spectrom.*, 1991, **6**, 353.
7. N. Miller-Ihli, *J. Anal. At. Spectrom.*, 1988, **3**, 73.
8. L. Ebdon and H. G. M. Parry, *J. Anal. At. Spectrom.*, 1987, **2**, 131.
9. L. Ebdon and H. G. M. Parry, *J. Anal. At. Spectrom.*, 1988, **3**, 131.
10. M. W. Hinds and K. W. Jackson, *J. Anal. At. Spectrom.*, 1988, **3**, 997.
11. M. Hoenig, P. Regnier and R. Wollast, *J. Anal. At. Spectrom.*, 1989, **4**, 631.
12. C. A. Fernandez, R. Fernandez, N. Carrion, D. Loreto, Z. Benzo and R. Fraile, *At. Spectrosc.*, 1991, **12**, 111.
13. D. Bradshaw and W. Slavin, *Spectrochim. Acta*, 1989, **44B**, 1245.
14. J. A. Holcombe and V. Majidi, *J. Anal. At. Spectrom.*, 1989, **4**, 423.
15. L. Haraldsen and B. M. A. Pougnet, *Analyst*, 1989, **114**, 1331.
16. M. S. Epstein, G. R. Carnrick and W. Slavin, *Anal. Chem.*, 1989, **61**, 1414.
17. N. J. Miller-Ihli, *J. Anal. At. Spectrom.*, 1989, **4**, 295.
18. G. R. Carnrick, G. Daley and A. Fotinopoulos, *At. Spectrosc.*, 1989, **10**, 170.
19. J. P. Matousek and H. K. J. Powell, *Spectrochim. Acta*, 1988, **43B**, 167.
20. W. Wendl and G. Müller-Vogt, *Spectrochim. Acta*, 1984, **39B**, 237.
21. C. Bendicho and M. T. C. de Loos-Vollebregt, *Spectrochim. Acta*, 1990, **45B**, 679.
22. Analytical Methods Committee, *Analyst*, 1987, **112**, 199.

Talanta, Vol. 40, No. 12, pp. 1823–1827, 1993
Printed in Great Britain.

0039-9140/93 $6.00 + 0.00

A NOVEL AND HIGHLY SENSITIVE CATALYTIC METHOD FOR THE DETERMINATION OF ULTRATRACE AMOUNTS OF GOLD IN ORES WITH LINEAR SCAN VOLTAMMETRY AT A DME

ZHI-LIANG JIANG
Department of Chemistry, Guangxi Normal University, Guilin 541004 People's Republic of China

(*Received* 6 *January* 1993. *Revised* 29 *April* 1993. *Accepted* 5 *May* 1993)

Summary—Gold(III) has a strong catalytic effect on the slow redox reaction between Ce(IV) and Hg(I) in a sulphuric acid medium at 90°C, and the Ce(IV) unreacted in the catalytic reaction reacts with benzilic acid to form benzophenone that exhibits a sensitive linear scan voltammetric wave at −0.78 V *vs.* SCE. This provides the basis for a novel and highly sensitive and selective catalytic method with linear scan voltammetry at a DME for gold. Both reactions of Ce(IV)–Hg(I)–Au(III) and Ce(IV)–benzilic acid are investigated by means of linear scan voltammetry. The detection limit is 0.05 ng/ml with a fixed-reaction time of 15 min. A linear calibration graph from 0.15 to 5 ng/ml is obtained. Possible influences by co-existing ions are examined. Gold in ore samples is analysed by this catalytic method with satisfactory results.

Because gold(III) has a high redox potential, there are no good polarographic methods for gold. Several oscillopolarographic methods for the determination of gold have been reported.[1–4] A single sweep oscillopolarographic method for gold from 5×10^{-8} to $3 \times 10^{-6}M$ has been proposed, based on Au(III) oxidation of phenylthiourea to form symdiphenyldithioformamidine that exhibits a polarographic wave at −0.30 V.[1] Gao *et al.*[3] have reported a voltammetric method for determination of gold in the range 3×10^{-8}–$1 \times 10^{-6}M$ with a carbon paste electrode modified with chelating resin. The above polarographic methods for gold are not completely satisfactory, especially with respect to the detection limit.

Catalytic method with oscillopolarographic (linear scan voltammetry at a DME) detection is a sensitive means of catalytic kinetic analysis.[5–9] Catalytic methods for silver,[10] osmium,[11] ruthenium,[12] iridium,[13] rhodium[14] and palladium[15,16] with oscillopolarographic detection have been developed. However, a catalytic method for gold with oscillopolarographic detection does not seem to have been reported to date. Gold(III)–Ce(IV)–Hg(I) catalytic reaction has been applied to determining gold at ng/ml level by spectrophotometry.[17,18] Our experiments demonstrate that benzilic acid can be oxidized by Ce(IV) to form benzophenone that exhibits a sensitive oscillopolarographic wave at −0.78 V. In the present work, we first studied the coupled reaction of Au(III)–Hg(I)–Ce(IV)–benzilic acid by single sweep oscillopolarographic detection. A novel catalytic method with oscillopolarographic detection was proposed for the determination of ultratrace amounts of gold, with a detection limit of 0.05 ng/ml and a determination range of 0.15–5 ng/ml.

EXPERIMENTAL

Apparatus

A model JP-2 single sweep oscillopolarograph (Chendu Instrumental Factory) was used for the polarographic measurements. The settings on the JP-2 single sweep oscillopolarograph were: dropping mercury period 7 sec; scanning rate 250 mV/sec; scanning potential range of 500 mV in the negative direction; initial scanning potential −400 mV; I''_p (second derivative wave); and a three-electrode system-DME, SCE, and platinum electrode. A model JY-501B thermostatted water bath was used to control the reaction temperature.

Reagents

A 0.0020M ammonium ceric nitrate (containing 0.040M sulphuric acid) and a 0.020M $HgNO_3$ (containing 0.07M nitric acid) and a 0.0030M benzilic acid solution were used.

Standard solutions of Au(III) were prepared according to the following procedure: weigh out 10 mg pure gold and place in a 100-ml beaker. Add about 3 ml of concentrated hydrochloric acid and 1 ml of concentrated nitric acid, heat to dissolve, cool, then transfer to a 100-ml standard flask, add 20 ml of concentrated hydrochloric acid and dilute to the mark with doubly distilled water. The stock solution of Au(III) is 100 μg/ml. Take 25 ml of 100 μg/ml Au(III) solution to a 50-ml beaker, add about 0.2 ml of 10% NaCl solution, evaporate to dryness over a boiling water bath, add 2 ml of concentrated nitric acid and evaporate to dryness, repeat again to expel Cl^-, cool, add 0.0020M Ce(IV) solution to dissolve the salt, then transfer to a 250-ml standard flask and dilute to the mark with 0.0020M Ce(IV) solution. The standard solution of gold is 10 μg/ml. A working solution was prepared by dilution with 0.0020M Ce(IV) solution shortly before use.

Procedure

Into a 25-ml graduated test-tube fitted with a glass stopper, place 0.02–0.65 ml of 100 ng/ml Au(III) solution (containing 0.0020M Ce(IV)), and add 0.0020M Ce(IV) solution to 1 ml of the total volume. Add 2.5 ml of 5.0M sulphuric acid, dilute to 10-ml mark with water, mix well. Add 1.0 ml of 0.02M Hg(I) solution, mix vigorously, and place in a water bath at 90°C to start the reaction. After 15 min the reaction was quenched by addition of 1.0 ml of 0.0030M benzilic acid solution and cooled with tap-water. The second derivative peak current $(I''_p)_{c,t}$ was measured. The $(I''_p)_{u,t}$ for the uncatalysed reaction was measured in a similar manner.

The log $((I''_p)_{u,t}/(I''_p)_{c,t})$ values for a range of gold concentrations were plotted as a function of gold concentration to prepare a calibration graph.

RESULTS AND DISCUSSION

Study of the reaction of Ce(IV) and benzilic acid

The reaction of Ce(IV) and benzilic acid was investigated spectrophotometrically and oscillopolarographically. The results show that the reaction is slow at room temperature when Ce(IV) concentration is less than $4 \times 10^{-4}M$. It is fast when the reaction temperature is higher than 60°C. Several reaction media including sulphuric acid, perchloric acid and hydrochloric acid were tested. Sulphuric acid is best, and was chosen for use. In 1.0M sulphuric acid medium at 90°C, Ce(IV) reacts with benzilic acid to form an electroactive species which exhibits a sensitive single sweep oscillopolarographic wave at −0.78 V. The electroactive species was identified by a chemical method and oscillopolarography.[19] Figure 1 indicates that the second derivative peak current is most sensitive, and was selected for use. The experiment shows that I''_p is proportional to Ce(IV) concentration in the range 1×10^{-6}–$3 \times 10^{-4}M$. The oscillopolarographic behaviour of benzophenone has been studied.[19] The influence of Hg(I), Hg(II), and Ce(III) on the oscillopolarographic measurement of benzophenone was examined. No effect was observed.

Principle for the catalytic determination of gold with oscillopolarographic detection

Our experiments show that Ce(IV), Ce(III), Hg(I) and Hg(II) in the catalytic system of Ce(IV)–Hg(I)–Au(III)–H_2SO_4 have no oscillopolarographic wave. And the indicator reaction for gold can not be applied to the catalytic determination of gold with oscillopolarographic detection. We tried to utilize the Ce(IV)–Hg(I)–Au(III) system for catalytic determination of gold with oscillopolarographic detection by addition of an organic reagent that reacts with Ce(IV) to form an electroactive species.

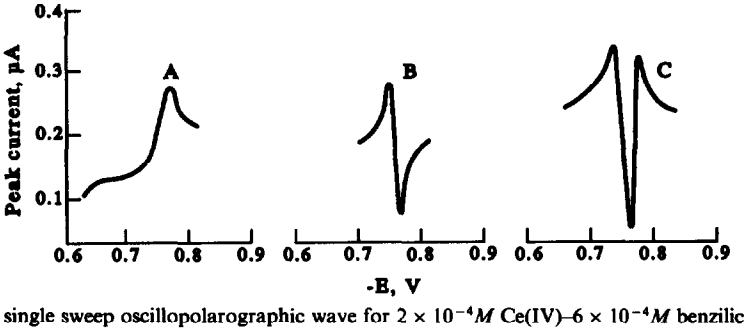

Fig. 1. The single sweep oscillopolarographic wave for $2 \times 10^{-4}M$ Ce(IV)–$6 \times 10^{-4}M$ benzilic acid, 90°C for about 1 min. (A) Normal wave; (B) first derivative wave; (C) second derivative wave.

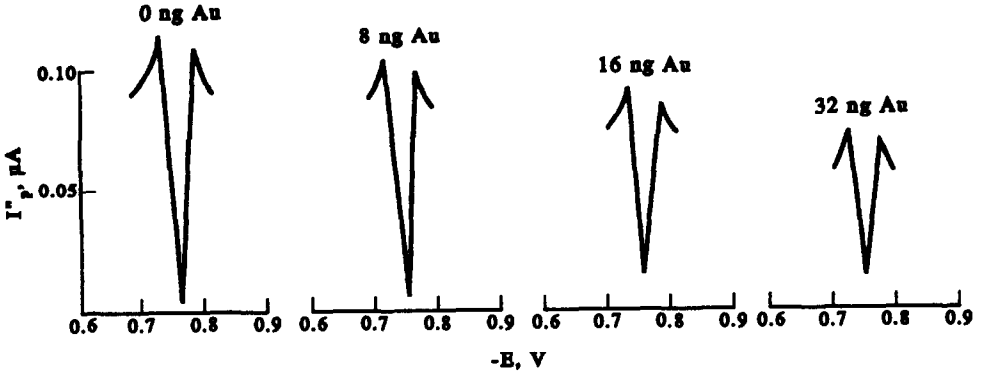

Fig. 2. The relationship of the I''_p and Au concentration.

Several organic reagents have been examined. The results show that benzilic acid can satisfy the need. Two millilitres of $3.0 \times 10^{-3}M$ benzilic acid were selected. On these grounds, we studied the coupled reaction of Au(III)–Hg(I)–Ce(IV)-benzilic acid by oscillopolarography. Figure 2 shows the relationship between I''_p and gold concentration.

In the catalytic reaction solution, both of the following reactions occur simultaneously

$$\mathrm{Ce(IV) + Hg(I) \xrightarrow[\text{fast}]{\text{Au(III) cat.}} Ce(III) + Hg(II)} \quad (1)$$

$$\mathrm{Ce(IV) + Hg(I) \xrightarrow{\text{slow}} Ce(III) + Hg(II)} \quad (2)$$

Refer to Ref. 20 and deduce the following equation

$$\log(C_{u,t}/C_{c,t}) = k \cdot C_{Au} \cdot t \quad (3)$$

where $C_{u,t}$ and $C_{c,t}$ are the concentrations of Ce(IV) in the uncatalysed reaction and catalysed reactions at reaction time t, respectively, C_{Au} is the concentration of gold, and k is a constant. Addition of benzilic acid when the indicator reaction is at time t, the following reaction takes place

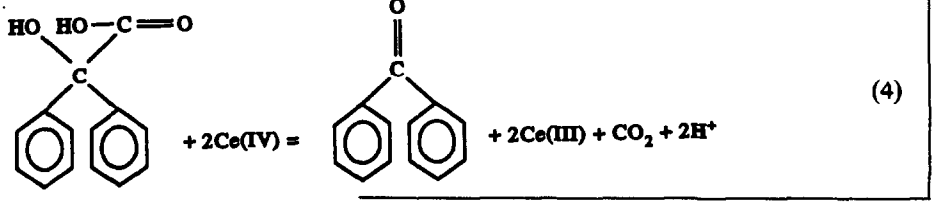

(4)

According to the reaction, $C_{Ce(IV)} = 2 \times C$, where C is benzophenone concentration. Since $I''_p = k'C$, where k' is a constant, the equation may be rewritten as

$$C_{Ce(IV)} = 2k' \cdot I''_p. \quad (5)$$

Combining (3) and (5), we obtain

$$\log((I''_p)_{u,t}/(I''_p)_{c,t}) = k \cdot C_{Au} \cdot t. \quad (6)$$

Equation (6) shows that the logarithmic term is proportional to gold concentration, with the other variables held constant for the given system. This is in agreement with the experimental results.

Effect of variables

The effects of the concentrations of sulphuric acid, Ce(IV) and Hg(I), reaction temperature and reaction time on $\log((I''_p)_{u,t}/(I''_p)_{c,t})$ were investigated by the fixed-reaction time procedure. In general the effect of each variable leads to higher $\log((I''_p)_{u,t}/(I''_p)_{c,t})$ and larger $(I''_p)_{u,t}$ which is expected.

The reaction media tested were sulphuric acid, perchloric acid and hydrochloric acid. The results show that $1.0M$ sulphuric acid medium gives larger $\log((I''_p)_{u,t}/(I''_p)_{c,t})$ and $(I''_p)_{u,t}$ values than the others and was chosen.

The effect of variation of Hg(I) concentration on $\log((I''_p)_{u,t}/(I''_p)_{c,t})$ is shown in Fig. 3. When the concentration of Hg(I) is higher than $1.1 \times 10^{-3}M$, the $\log((I''_p)_{u,t}/(I''_p)_{c,t})$ values are constant. A concentration of $1.54 \times 10^{-3}M$ Hg(I) was selected. Figure 4 indicates the relationship between $\log((I''_p)_{u,t}/(I''_p)_{c,t})$ and Ce(IV) concentration. A concentration of $1.54 \times 10^{-4}M$ Ce(IV) was chosen, giving a good

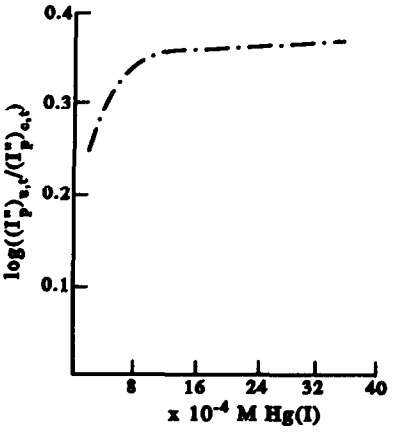

Fig. 3. The effect of Hg(I) concentration on $\log((I''_p)_{u,t}/(I''_p)_{c,t})$. Conditions as in the procedure.

compromise between high $\log((I''_p)_{u,t}/(I''_p)_{c,t})$ and high $(I''_p)_{u,t}$ values.

The influence of reaction temperature in the range 60–95°C on the $\log((I''_p)_{u,t}/(I''_p)_{c,t})$ was studied. The logarithmic terms increase with reaction temperature. A reaction temperature of 90°C was used, giving high sensitivity, and the reaction temperature can be easily controlled by the thermostatted water bath. A fixed-reaction time of 15 min was chosen, giving a good compromise between high sensitivity and short analysis time.

Effect of foreign ions

The effect of 34 foreign ions on the catalytic determination of 1 ng/ml Au was examined. The results are summarized in Table 1. The tolerance limit is that giving not more than ±5% error. Most common ions do not interfere with the catalytic determination of gold.

Calibration graph

Under the conditions as in the Procedure, the logarithmic terms are proportional to the concentration of Au in the range of 0.15–5.0 ng/ml (Fig. 5). The detection limit is 0.05 ng/ml. The relative standard deviation for 0.5, 1.0 and 4.0 ng/ml Au was 4.0, 3.3 and 2.8%, respectively (10 determinations).

Table 1. Influence of foreign ions

Tolerance limit (Ion)/(Au)	Ion added
3×10^4	Ca(II), Mg(II), Sr(II), SiO_3^{2-}
1×10^4	Cu(II), Zn(II), Cd(II), Ba(II), Mo(VI)
5×10^3	Pb(II), F^-, PO_4^{3-}
4×10^3	Al(III), Ag(I), La(III), Mn(II)
2×10^3	Fe(III), Co(II), Ni(II), Cr(III), Hg(II)
1×10^3	W(VI), Ti(IV), Br^-
4×10^2	Os(IV), As(III)
1×10^2	Sb(III), Ru(III), Se(IV), Tl(I)
50	Pd(II), Pt(IV)
20	Rh(III)
10	Ir(IV)

Analysis of ore samples

Weigh out 1–10 g ore sample and place in a 30-ml porcelain crucible, set in a Muffle Furnace at 500°C for about 1 hr, then increase the temperature to 700°C for 1 hr. Cool, transfer into a 250-ml beaker, add 20–100 ml of the acid mixture ($V_{HNO_3}:V_{HCl}:V_{H_2O} = 1:4:2.5$), cover for about 1.5 hr, and shake. After the sample dissolved the solution was evaporated to a paste state. Add 10 ml concentrated sulphuric acid and evaporate again. After cooling add 50 ml of 2.5*M* hydrochloric acid, heat to boiling for several minutes, cool, transfer to a 250-ml separate funnel. Accurately add 10 ml of methyl isobutyl ketone (MIBK) that was balanced by 2.5*M* HCl, shake vigorously for about 1 min. After separation discard the water layer, add 15 ml of 0.1*M* HCl solution that was balanced by MIBK, shake for 15 sec. After separation

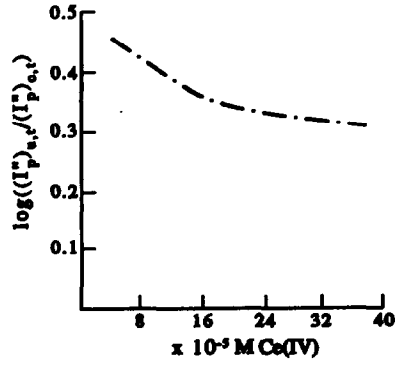

Fig. 4. Effect of Ce(IV) concentration on $\log((I''_p)_{u,t}/(I''_p)_{c,t})$.

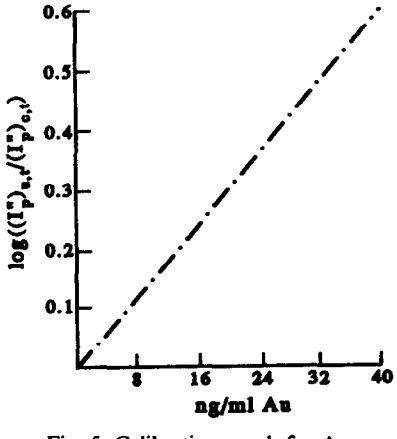

Fig. 5. Calibration graph for Au.

Table 2. Results and recovery

Sample	Added Au (g/t)	Found Au (g/t)	Recover (%)	Content (g/t)	
				This method	AAS
Ore I	0	2.25	—	2.25	2.35
	2.00	4.20	97.5		
Ore II	0	1.60	—	1.60	1.73
	1.00	2.58	98		
Ore III	0	0.84	—	0.84	0.83
	0.80	1.63	98.8		

discard the water layer. Pipet 4–10 ml of the organic layer into a porcelain crucible, add about 0.1 ml of 0.1M KCl solution, evaporate to dryness at low temperature. Add 3 ml concentrated nitric acid and 1 ml concentrated hydrochloric acid, cover and destroy the organic compound by heating, then evaporate to near dryness. Add 1–2 ml nitric acid, evaporate to dryness over a water bath, repeat again to expel Cl^-. After cooling, accurately add 10 ml of 0.1M H_2SO_4, and stir. Pipet a portion of the sample solution into a 25-ml graduated test tube, and follow as for the Procedure. The results are summarized in Table 2, which is in agreement with the results of AAS.

REFERENCES

1. Zhang Zhenzhen, Qiang Xiaolin and Xie Ziwen, *Fenxi Shiyanshi*, 1985, **11**(4), 30.
2. Cao Guangzhou and Zhao Zaofan, *Chem. J. of Chinese University*, 1985, **6**, 211.
3. Gao Zhiqiang, Li Peibiao, Dong Shihua and Zhao Zaofan, *Anal. Chim. Acta.*, 1990, **232**(2), 367.
4. Zhao Zaofan, Jiang Mian and Liu Qiang, *Electroanal.*, 1990, **2**(1), 51.
5. Jiang Zhiliang, *Xiyou Jinshu*, 1988, **12**, 310.
6. Jiang Zhiliang, Liang Aihui and Dai Guazhong, *Chem. J. of Chinese University*, 1992, **13**, 749.
7. Jiang Zhiliang, Li Xiaojin, Wu Daqiang and Dai Guozhong, *Fenxi Shiyanshi*, 1992, **11**(5), 4.
8. Jiang Zhiliang, *Acta. Chimica Sinica*, 1992, **50**, 483.
9. Idem, *Anal. Chim. Acta.*, 1992, **250**(1), 45.
10. Idem, *Precious Metals*, 1991, **12**(2), 34.
11. Jiang Zhiliang and Liang Aihui, *Talanta*, 1990, **37**, 1077.
12. Jiang Zhiliang, *ibid*, 1991, **38**, 641.
13. Idem, *ibid*, 1992, **39**, 1317.
14. Wang Lisheng and Jiang Zhiliang, *Electroanal.*, 1993, **5**.
15. Jiang Zhiliang, Wang Lisheng and Qin Chenzhen, *The 34th IUPAC Congress*. Beijing, 1993, 20,056.
16. Jiang Zhiliang and Wang Lisheng, *Precious Metals*, 1993, **14**(2).
17. B. G. Jeliazkova, P. R. Bontchev and A. A. Alexiev, *Mikrochim. Acta.*, 1972, **6**, 896.
18. Zhang Zhaohong, Li Zirong, Gan Weitang and Liu Liuzhan, *Fenxi Huaxue*, 1984, **12**, 435.
19. Jiang Zhiliang and Lu Ba, *ibid*, 1991, **19**, 111.
20. Jiang Zhiliang, *Xiyou Jinshu*, 1992, **16**, 35.

Talanta, Vol. 40, No. 12, pp. 1829–1831, 1993
Printed in Great Britain.

0039-9140/93 $6.00 + 0.00

ANALYTE PRECONCENTRATION AND SEPARATION FROM SMALL VOLUMES BY ELECTRODEPOSITION FOR ELECTROTHERMAL ATOMIC ABSORPTION SPECTROSCOPY

JAROSLAV P. MATOUSEK* and H. KIPTON J. POWELL
Department of Chemistry, University of Canterbury, Private Bag 4800, Christchurch, New Zealand

(*Received* 23 *December* 1992. *Revised* 23 *April* 1993. *Accepted* 17 *May* 1993)

Summary—Electrodeposition of Pb from 50 μl volumes of 0.1*M* KCl solution was studied by electrolysis at uncontrolled potentials of 4.0–6.0 V on a pyrolytic graphite platform cathode. Deposition efficiency was evaluated as a function of time by ASV measurements on aliquots of the electrolysed solution. Quantitative separation of the analyte from the matrix was achieved in a relatively short time, aided by convective stirring of the sample achieved through gas evolution. Thus, the feasibility of rapid electrodeposition directly in a pyrolytic graphite-coated furnace has been demonstrated, allowing construction of an automated electrodeposition-electrothermal atomic absorption spectroscopic system.

Electrolysis in an attractive method for both preconcentration and separation of analyte from interfering matrix prior to electrothermal atomic absorption spectroscopy (ETAAS). While alkali metal halides cause most serious interferences in ETAAS, they are ideal media for electrochemical techniques. For this reason, a number of studies and systems have been reported which advantageously combine the ability of both techniques. These have included (i) electrodeposition onto Hg-coated graphite furnaces from a circulating solution,[1–3] (ii) electrodeposition (at 3–5 V)[4] or adsorption[5] on a tungsten wire followed by its insertion into a cold furnace (or a pre-heated furnace[6]), (iii) electrodeposition in a well in a porous carbon rod[7] and (iv) electrodeposition onto a Hg-coated pyrolytic graphite platform.[8] Circuitry has involved three-electrode systems[1,3,7] and simple two-electrode constant potential systems.[8]

The electrolytic method can achieve useful improvements in sensitivity, compared with conventional ETAAS, such as a 15-fold enhancement by 300 sec electrolytic deposition on a tungsten wire from an unstirred solution[4] and a 20- to 50-fold enhancement by 60 sec adsorption from a stirred solution.[5] More importantly it also achieves separation of analyte from a matrix which may be difficult to remove by thermal pretreatment and may be a source of both chemical and spectral interferences in ETAAS, *e.g.* NaCl in seawater or blood digests. In addition, controlled potential electrolysis may achieve speciation by plating only the labile species of a metal.[1,3] When coupled with ETAAS the electrode position technique is also applicable to metals which have low sensitivity by ASV (such as Ni, Mn, Cr and Co) due to their irreversible reduction.[1]

However, despite these advantages, the recovery of the analyte from the sample is generally low and slow. If quantitative deposition is required, prohibitively long electrolysis times are involved.[7] If, on the other hand, short deposition times are used only a small fraction of the analyte is recovered. For example, Fairless and Bard[7] reported an efficiency of 1% in plating Cu from 5 μl stationary solution on a porous carbon rod (60 sec at 0.18 V).

In addition to slow analyte accumulation all of the above approaches suffer from common problems that include contamination, complicated apparatus (especially for the recirculating technique) and invariably poor reproducibility. A possible solution to such problems is automation of the combined electrodeposition–ETAAS technique. *In situ* deposition as performed by Fairless and Bard[7] with subsequent removal of the exhausted electrolyte and washing of the deposit would lend itself well

*Author for correspondence. On leave from Department of Analytical Chemistry, University of New South Wales, P.O. Box 1, Kensington, NSW 2033, Australia.

to automated electrodeposition–ETAAS performed inside a conventional graphite furnace. However, the very inefficient analyte recovery which results from use of controlled potential electrolysis makes this approach unattractive for practical use.

Invariably, controlled potential deposition has been used when combining electrochemical separation and preconcentration with atomic spectroscopic techniques. Even for stirred electrolyte the deposition times are inordinately long.[9] This rather rigid adherence to controlled potential electrolysis (which is probably perceived as a well proven electrochemical approach) is not justified for techniques having the selectivity of ETAAS. Unless speciation is an objective, there is no need for controlled potential work.

A necessary prerequisite for automation of the electrodeposition–ETAAS technique is fast and efficient separation and preconcentration of the analyte elements from volumes compatible with the capacity of conventional graphite furnaces (usually in the range 20–100 μl). In order to evaluate if this can be achieved on the time scale similar to conventional graphite furnace analysis, we have studied electrodeposition from 50 μl volumes by applying relatively high voltages to sustain high electrolysis currents and to enhance the deposition rate further by convection created by gas evolution at both electrodes.

EXPERIMENTAL

To establish conditions for quantitative deposition, electrolysis was effected on samples deposited in the well of a Perkin-Elmer "V' pyrolytic graphite platform.[10] The platform with the "V"-shaped well 0.7 mm deep was 15 mm long, 4 mm wide and 1 mm thick. It served as a cathode, with a 0.5 mm dia. Pt wire anode mounted centrally 1 mm above the platform surface. In later experiments, the Pt anode was mounted on a micrometer attachment to allow accurate setting of the anode–cathode separation and a 0.5 mm dia. Ag/AgCl reference electrode was added to monitor the cathode potential.

The electrolyte used consisted of 0.1*M* KCl and 0.02*M* acetate buffer (pH 4.7) containing 0.02, 0.10 or 0.50 mg/l Pb. Each electrolysis was effected on a 50 μl sample for a fixed time using a constant potential power supply (4.0, 5.0 or 6.0 V). To determine concentration of the analyte element remaining in the electrolysed solution, a 25 μl aliquot was taken using a micropipette and transferred from the platform to a PAR 303 polarographic cell containing 5 ml Milli-Q water and 20 μl Aristar HNO_3. The solution was analysed by differential pulse ASV using a PAR 174A polarograph. ASV conditions were: N_2 flush, 9 min; stir, fast; drop size, medium; deposition time, 6 min; $E_d = -0.7$ V; scan rate = 5 mV/sec; modulation, 25 mV. After washing with 3% HNO_3 (electrodeposited Pb is dissolved readily by dilute HNO_3)[8] and drying the pyrolytic graphite platform was ready for a new electrolysis.

Since measurements of Pb concentrations down to sub-ppb levels were involved in the solutions remaining after electrolysis (and dilution in the polarographic cell), all experiments were performed in a class 100 clean room.

RESULTS AND DISCUSSION

In this study, we have simulated the problem of *in situ* deposition inside a graphite furnace by using a pyrolytic graphite platform and depositing from small volumes compatible with the size of the graphite furnace in ETAAS. Electrolysis was effected with uncontrolled potential set at 4.0, 5.0 or 6.0 V.

The efficiency of the deposition was evaluated as a function of time from the analyte concentration remaining after electrolysis. This was determined by differential pulse ASV measurements on aliquots of the electrolysed solution. The results presented in Fig. 1 show that the deposition efficiency increases significantly with the applied voltage. The increase in the depo-

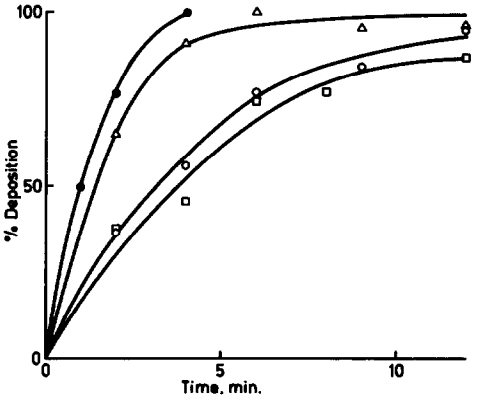

Fig. 1. The effect of applied voltage on efficiency of electrodeposition of 0.1 mg/l Pb from 0.1*M* KCl. Applied voltages used: (□) 4, (○) 4 with Hg co-deposition, (△) 5 and (●) 6 V.

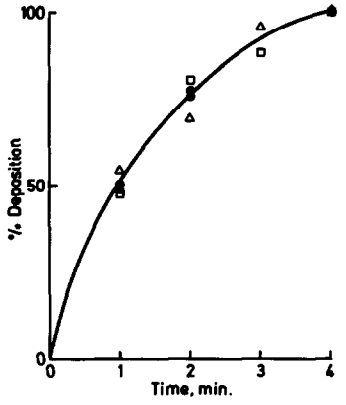

Fig. 2. The effect of Pb concentration on efficiency of electrodeposition from 0.1*M* KCl electrolysed at 6 V. Pb concentrations used: (□) 0.02, (●) 0.10 and (△) 0.50 mg/l.

sition rate with applied voltage is related to convective stirring of the sample which is achieved through adequate evolution of Cl_2, O_2 and H_2; gas evolution is apparent once the current exceeds 5 mA. Thus, deposition was complete in 4 min at 6.0 V and 90% complete in 12 min at 4.0 V. Co-deposition of Pb with Hg (from 0.0002*M* Hg^{2+}) did not significantly increase plating efficiency (Fig. 1). Our experiments further confirmed that the deposition rate was independent of the Pb concentration as shown in Fig. 2 for 0.02, 0.1 and 0.5 mg/l Pb. This indicates that the rate of deposition is controlled by the degree of convection achieved through the liberation of H_2, O_2 and Cl_2.

In order to characterize the pyrolytic graphite platform electrodeposition system, separate experiments were performed in which cathode potentials were measured relative to a Ag/AgCl reference electrode. With the anode–cathode separation set at 0.63 mm by a micrometer attachment, the cathode potential was established as −1.23, −1.52 and −1.87 V at $E_{applied} = 4.0$, 5.0 and 6.0 V, respectively. The current depended on the anode–cathode separation but was approximately 0.3, 2.0 and 4.5–6.0 mA at 4.0, 5.0 and 6.0 V, respectively.

The pyrolytic graphite platforms used in these experiments showed only limited lifetime. Exfoliation of pyrolytic graphite layers was observed to increase gradually with number of electrolyses performed, however this did not appear to affect the deposition rate for the first 50 electrolyses. The problem appears to be directly related to the number of pyrolytic graphite layers exposed in the manufacture of the platform used.[10] The electrolyte gradually forces its way between the layers, causing exfoliation, especially at higher electrolysis currents. It should be noted that similar problems, interpreted as being caused by intercalation, have been experienced when pyrolytic graphite platforms are used in ETAAS.[10]

CONCLUSIONS

The present report establishes that a batch electrolysis from 50 μl solution volumes can achieve quantitative deposition of the analyte element in relatively short times when conducted at a potential which can effect convective mixing by evolution of H_2, O_2 and Cl_2.

In recent publications, Sioda *et al.*[11,12] have suggested and experimentally verified that there are limits to electrolytic preconcentration caused by equilibrium concentrations of cations remaining in solution. It is possible to conclude that even though such limits apply to controlled potential work, they do not measurably affect the outcome of electrolyses performed under the conditions of our experiments.

Based on the principles established here, a recent paper by Matousek and Grey[13] has described instrumental modifications to allow automated *in situ* electrodeposition of analytes in the conventional pyrolytic graphite-coated furnace. The modified system consists of a GBC GF 2000 graphite furnace system equipped with a PAL autosampler and is capable of performing automated sample loading, electrolysis, withdrawal of the electrolyte, washing and chemical pretreatment of the electrodeposited metal.

REFERENCES

1. G. E. Batley and J. P. Matousek, *Anal. Chem.*, 1977, **49**, 2031.
2. G. Vollard, P. Tschöpel and G. Tölg, *Anal. Chim. Acta*, 1977, **90**, 15.
3. G. E. Batley and J. P. Matousek, *Anal. Chem.*, 1980, **52**, 1570.
4. E. J. Czobik and J. P. Matousek, *Spectrochim. Acta*, 1980, **35B**, 741.
5. Y. Hoshino, T. Utsunomiya and K. Fukui, *Chem. Lett.*, 1976, **9**, 947.
6. J. P. Matousek, Ph.D. Thesis, The University of New South Wales, 1978.
7. C. Fairless and A. J. Bard, *Anal. Lett.*, 1972, **5**, 433.
8. J. Shiowatana and J. P. Matousek, *Talanta*, 1991, **38**, 375.
9. H. Matusiewicz, J. Fish and T. Malinski, *Anal. Chem.*, 1987, **59**, 2264.
10. G. R. Carnrick and B. K. Lumas, *Atom. Spectrosc.*, 1984, **5**, 135.
11. R. E. Sioda, *Anal. Chem.*, 1988, **60**, 1177.
12. A. Ciszewski, J. R. Fish, T. Malinski and R. E. Sioda, *ibid.*, 1989, **61**, 856.
13. J. P. Matousek and R. Grey, *Proc. 27th Coll. Spectrosc. Int.*, Paper No. B-6.4, Bergen, 1991.

Talanta, Vol. 40, No. 12, pp. 1833–1838, 1993
Printed in Great Britain.

0039-9140/93 $6.00 + 0.00

ELECTROREDUCTION AND DETERMINATION OF PIPRIL (PIPERACILLIN) IN BOTH AQUEOUS AND BIOLOGICAL SAMPLES

N. ABO EL-MAALI* and M. A. GHANDOUR
Chemistry Department, Faculty of Science, Assiut University, Assiut 71516, Egypt

M. KHODARI
Chemistry Department, Faculty of Science Assiut University, Qena branch, Qena, Egypt

(*Received* 15 *December* 1992. *Revised* 15 *April* 1993. *Accepted* 15 *April* 1993)

Summary—The electrochemical behavior of the relatively new antibacterial antibiotic Pipril (Piperacillin) at the dropping mercury electrode is investigated using both direct current polarography (DCP) and differential pulse polarography (DPP). At the hanging mercury electrode (HMDE), the reduction mechanism has been elucidated using cyclic voltammetric technique in the pH range from 2 to 10. The effect of some metal ions, *e.g.* Cu(II) and Pb(II) has been also tested. Determination of the drug using adsorptive stripping analysis was assessed in both aqueous and urine samples. The effect of the different experimental parameters affecting the drug determination, *e.g.* pH, supporting electrolyte nature, accumulation potential, accumulation time and other operational parameters are also mentioned. Detection limits of 5×10^{-9} and $1 \times 10^{-8} M$ Pipril in aqueous and urine samples, respectively, are achieved.

Pipril (Piperacillin) is a relatively new bactericidal semisynthetic penicillin with a broad spectrum of activity, encompassing both gram-negative and gram-positive anaerobic and aerobic organisms. The activities of Pipril was found to be more efficient than many other penicillins such as ticarcillin and carbenicillin.[1] The activity of piperacillin against pseudomonas may create a unique place for piperacillin amongst penicillins.[2] Piperacillin was shown to have considerable antibacterial activity against a wide range of 485 bacterial pathogens including anaerobic species which was generally superior to other beta-lactam antibiotics such as ampicillin, carbenicillin and cephalosporins.[3–6] Piperacillin has a potent bactericidal action since the ratio between the minimum bactericidal concentration (MBC) and the minimum inhibitory concentration (MIC) for it, was found to be equal to, or no more than twice.[7,8] Pipril has also a very high affinity for penicillin-binding proteins (PBPs).[9]

To date, no metabolites of Piperacillin have been found. In patients with normal renal function, Pipril is eliminated primarily (80%) by glomerular filtration and tubular secretion.[10,11] Its concentration in the urine is in excess of 10,000 μg/ml after a single 2 g intramuscular dose.[12] About 20% Pipril is excreted through the biliary tract.[10,13]

From the analytical point of view, Piperacillin have been determined using high-performance liquid chromatography.[14,15] It has been also determined using pulse polarographic technique by Schroeder *et al.*[16] They could determine the drug in both urine and serum samples but they could only reach a detection limit of 1 μg/ml. The aim of the present work is to elucidate the electrochemical reduction behavior of the drug and owing to the sensitivity of the adsorptive stripping methods of analysis,[16–19] we try to determine the drug in both aqueous and urine samples.

EXPERIMENTAL

Instrumentation

Direct current polarograms were obtained with a Tacussel (France) type PRG 5 in conjunction with a TV II GD built-in potentiometer and an EPL 1 B recorder. The capillary of the dropping mercury electrode has the following characteristics: $m = 2.10$ mg/sec, $t = 4.11$ sec (open circuit) and $m^{2/3}\, t^{1/6} = 2.07$ mg$^{2/3}$/sec$^{1/2}$.

*Author to whom correspondence should be addressed.

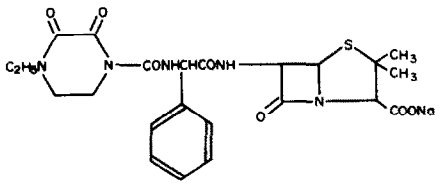

Fig. 1. Chemical structure of Piperacillin (Pipril).

Stripping and cyclic voltammograms were measured with an EG & G Princeton Applied Research Corp. microprocessor-controlled: (PAR) Model 264 A stripping analyzer, coupled with a PAR 303 A static mercury drop electrode SMDE (drop size; medium, area of the drop: 0.014 cm^2). The polarographic cell bottom (PAR model K 0060) was fitted with an AG/AgCl reference electrode, and a platinum wire was used as a counter electrode. A PAR 305 stirrer was connected to the 303 SMDE. For the collection of experimental data, a PAR Model RE 0089 X–Y recorder was used.

Reagents

Stock solutions ($1 \times 10^{-3} M$) of Pipril as Piperacillin sodium (CID Laboratories, Egypt) were prepared daily by dissolving the appropriate amounts in bidistilled water. Supporting electrolytes were analytical grade reagents and prepared also in bidistilled water.

Urine samples (from healthy people) were used in the analyses by spiking the drug under investigation in these samples, after dilution, 10 times with the supporting electrolyte.

Procedure

An aliquot of 10 or 50 ml of the supporting electrolyte was deareated with nitrogen for 12 or 20 min for differential pulse (DPP) and cyclic voltammetric (CV) or direct current (DC) measurements, respectively. The drug was then spiked and then polarograms or voltammograms were recorded.

For stripping voltammetric measurements, the accumulation potential was applied to a new mercury drop then the solution was stirred at 400 rpm. A negative-going scan was performed after the equilibration period (15 sec) when needed. Unless otherwise stated, the following parameters were used: accumulation potential (and initial potential) of -0.5 V *vs.* Ag/AgCl/$KCl_{(s)}$, equilibrium time 15 sec; scan rate 5 m V/sec, pulse amplitude 50 mV. The same procedure was repeated after spiking the solution with the analyte. Quantitative analysis was then performed by the standard addition method using different spikes. Quantitative measurements of the drug in urine samples were carried out by replacing the supporting electrolyte blank solution with another containing a urine sample diluted 10 times with the same supporting electrolyte and then repeating the foregoing steps under the same experimental conditions. All data were obtained at room temperature (25 ± 1°C).

RESULTS AND DISCUSSION

The structure of the drug under investigation is shown in Fig. 1.

Polarographic measurements

Preliminary investigation of the DC polarography of $2 \times 10^{-4} M$ Pipril (PIP) in $0.1 M$ phosphate buffer gives rise to only one reduction wave shifted to more electronegative potentials as the pH increases. Figure 2 shows these reduction waves; as the pH increases, the

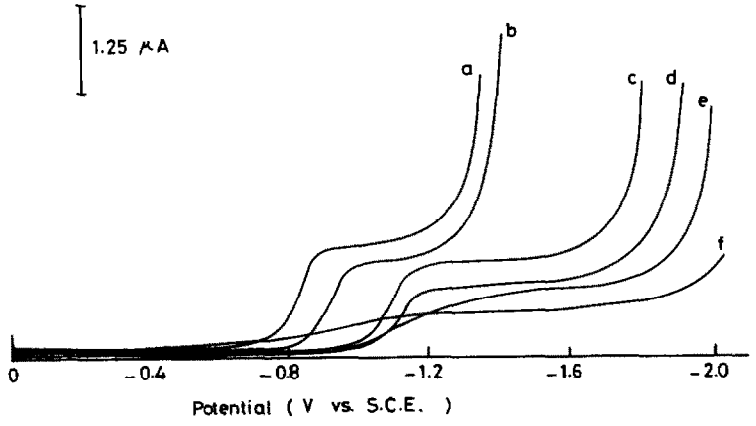

Fig. 2. Effect of the pH on $2 \times 10^{-4} M$ Pipril, $0.1 M$ phosphate buffer, pH: (a) 2.0, (b) 3.0, (c) 4.0, (d) 5.2, (e) 6.6, (f) 8.8. DC mode, 240 mV/min.

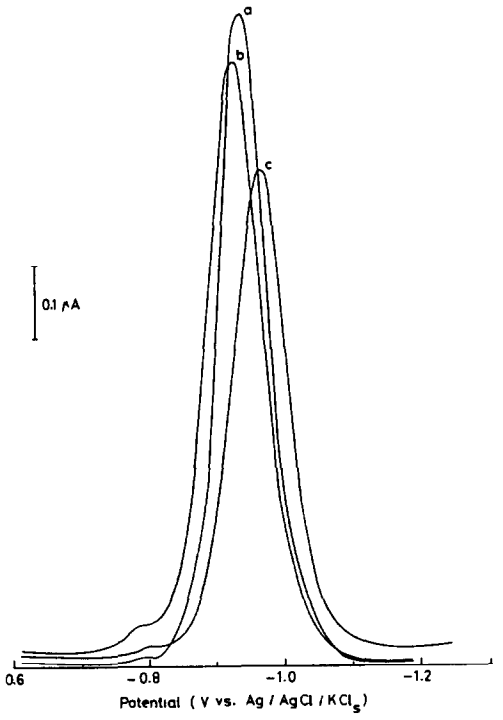

Fig. 3. Differential pulse polarography of $1 \times 10^{-5}M$ Pipril in different media, pH 1.5, $0.1M$ supporting electrolyte: (a) perchloric acid, (b) phosphate buffer, (c) acetate buffer. Pulse amplitude 50 mV, scan rate 5 mV/sec.

morphology of the wave changes until it disappears at about pH 9.0 probably due to hydrolysis of the drug in alkaline medium. By analyzing these polarographic waves, irreversibility of the reduction process have been elucidated; α is calculated to be 0.33 as the number of electrons consumed during this process was found to be two using coulometry. The shift of the half-wave potentials is drawn against the pH using the following equation:[20]

$$\frac{\Delta E_{\frac{1}{2}}}{\Delta pH} = -\frac{2.3\,PRT}{2\alpha F}.$$

A straight line is obtained, and as the value of α being 0.33, the number of protons consumed in the reduction process is calculated to be 2. Therefore, the reduction mechanism involves two electrons and two protons/mole of the drug. The logarithms of the limiting currents of these waves are drawn against the logarithms of the corrected mercury height, slopes ranged from 0.47 to 0.53 are obtained indicating that the reduction is under diffusion—controlled in the pH range from 2 to 7, while it was difficult to test it in alkaline media as the morphology of the peak becomes distorted.

On applying the differential pulse mode on $1 \times 10^{-5}M$ PIP in perchloric acid, acetate buffer and phosphate buffer, one peak is obtained having a half-peak width of about 80 mV corresponding to irreversible two-electron process. It is obvious from Fig. 3 that both perchloric acid and phosphate buffer gave almost the same sensitivity while it decreases in presence of acetate buffer as supporting electrolyte. For this reason, further investigation of the drug have been carried out in phosphate buffer medium. It is worthwhile mentioning that a pre-peak always appears in acidic media, indicating that adsorption of the oxidized form may occur.

Voltammetric measurements

Cyclic voltammetric measurements of $1 \times 10^{-5}M$ PIP show one irreversible, cathodic peak. The effect of the scan rate on the cyclic voltammogram of $1 \times 10^{-4}M$ PIP is shown in Fig. 4. When the peak current is drawn as a function of the square root of the scan rate $v^{\frac{1}{2}}$, in the pH range from 1.5 to 7, diffusion-controlled process is elucidated as a linear plot is obtained.

From the DC, DPP and CV measurements, it could be concluded that the following reduction mechanism may occur:

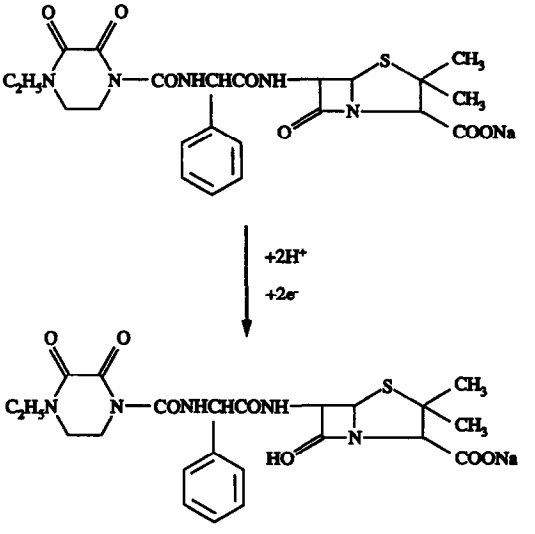

On scanning multiple cycles on the same drop (Fig. 5) for $1 \times 10^{-4}M$ PIP over all the investigated pH values, fast desorption behavior of the drug is noticeable as a marked decrease in the peak current is measured on scanning the second, third, ... cycles on the same drop. It should be noted that this desorption is strong in relatively high pH (3–6) while in strong acidic

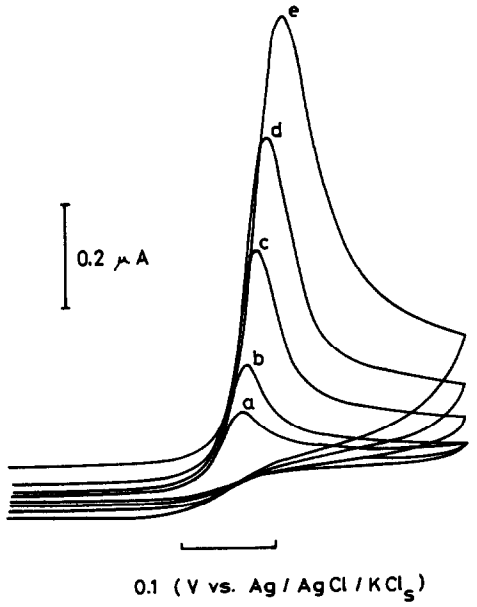

Fig. 4. Cyclic voltammograms of $1 \times 10^{-4}M$ PIP in $0.1M$ phosphate buffer, pH 5.8, scan rate: (a) 10, (b) 20, (c) 50, (d) 100, (e) 200 mV/sec. Starting potential -0.9 V *vs.* Ag/AgCl/KCl$_s$.

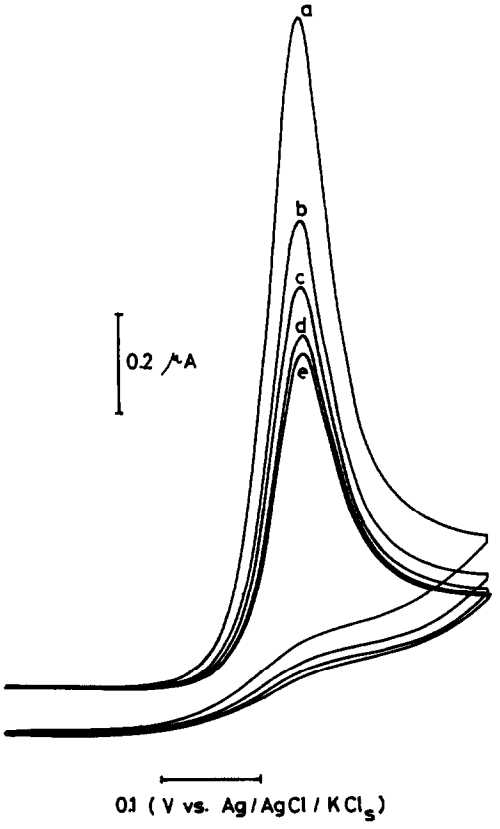

Fig. 5. Multiple cyclic voltammograms of $1 \times 10^{-4}M$ PIP in $0.1M$ phosphate buffer, pH 3.5, scan rate 200 mV/sec. Starting potential -0.8 V *vs.* Ag/AgCl/KCl$_s$. (a) First, (b) second, (c) third, (d) fourth, (e) fifth cycle.

media (pH < 3), it is relatively weak. This fact will be useful for the accumulation of the drug in strong acidic medic (pH $\leqslant$ 2) as will be mentioned later in this paper.

Effect of possible interfering metal ions

The effect of the possible interfering metal ions on the peak shape and height of Pipril has been also tested. We choose two metals, one essential non-toxic metal ion viz. Cu(II) and the other is non-essential, toxic metal ion viz. Pb(II).[21] On applying cyclic voltammetry on $1 \times 10^{-5}M$ Pipril in presence of up to $4 \times 10^{-4}M$ Cu(II), no noticeable change in either the Pipril peak height or potential is observed. The same behavior is also obtained in presence of up to $6 \times 10^{-4}M$ Pb(II). However, there is an observed shift in the peak potential of these metals indicating that a complexation reaction takes place. From the biological point of view, this interaction is useful as human fluid always contains Cu(II) because it is an essential metal ion while Pb(II) is a toxic non-essential-metal ion.[22] These facts are useful in the analysis of the drug itself in presence of either of these metals, as will be stated later.

Analytical application in aqueous and urine samples

Preliminary investigation on $1 \times 10^{-6}M$ Pipril showed that the drug has a tendency to be adsorbed and accumulated at the hanging mercury drop electrode (HMDE). However, on applying accumulation times of more than 15 sec, it begins to be desorbed again from the HMDE indicating that fast desorption behavior is almost finished. This fact has also been elucidated by applying multiple cycles (CV) on the same drop (HMDE) after the accumulation of the drug for a certain time, as on the second cycle the adsorptive peak begins to decrease and almost disappear.

The adsorptive behavior of the drug under investigation is studied by comparing two different techniques, direct current stripping voltam metry (DCSV) and differential pulse stripping

Table 1. Characteristics of Pipril, peak current–accumulation time plots ($0.1M$ phosphate buffer), pH 2.0

Concentration, (M)	Linearity range (*sec*)	Equation*	Correlation coefficient
5×10^{-8}	0–25	$Y = 0.042x + 0.003$	0.9973
1×10^{-7}	0–20	$Y = 0.002x + 0.070$	0.9969
5×10^{-7}	0–15	$Y = 0.011x + 0.120$	0.9961
1×10^{-6}	0–10	$Y = 0.008x + 0.180$	0.9971

*Y in μA, x in sec, slope in μA/sec, intercept in μA.

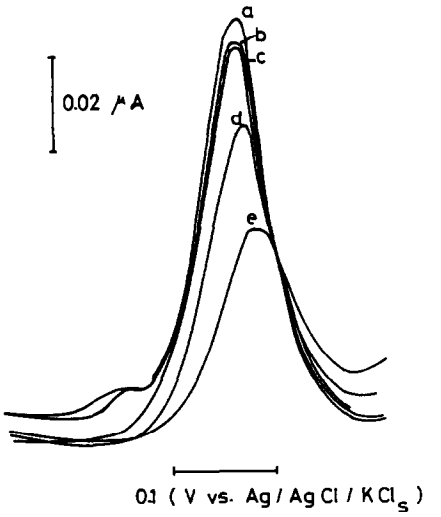

Fig. 6. Differential pulse cathodic stripping voltammograms of $1 \times 10^{-6}M$ Pipril in urine sample diluted 10 times with $0.1M$ phosphate buffer, pH = 2.0 $E_{acc} = -0.5$ V, $E_{initial} = -0.7$ V *vs.* Ag/AgCl.KCl$_{(s)}$, t_{acc}: (a) 0, (b) 5, (c) 10, (d) 30, (e) 60 sec.

voltammetry (DPSV). Although using the DCSV mode we can apply high scan rates to avoid desorption of the drug in measuring the adsorptive peak current I_{ps}, DPSV mode was found to be more sensitive. The effect of the different experimental parameters on the DPSV, *e.g.* pulse amplitude, scan rate, accumulation potential, supporting electrolytes and accumulation time has been tested. The optimum conditions to increase the sensitivity for the determination of the drug at the (HMDE) were found to be 50 mV pulse amplitude, 5 mV/sec scan rate, accumulation potential of -0.5 V *vs.* Ag/AgCl/KCl(s) and among four tested supporting electrolytes viz. perchloric acid, sulfuric acid, acetate buffer and phosphate buffer, the last one gives rise to more sensitive peak height and also to a more defined peak form.

The effect of the pH on the adsorptive behavior of $5 \times 10^{-7}M$ Pipril has been examined, the sensitivity was found to be more pronounced in acidic medium. Phosphoric acid adjusted to pH 2.0 gives rise to a good signal. It should be mentioned that almost the same sensitivity is obtained in weakly acidic solutions but with lower reproducibility. For this reason phosphoric acid (pH 2) was utilized for further investigations.

The influence of the accumulation time on the adsorptive behavior of Pipril has been tested using four different concentrations viz.; $5 \times 10^{-8}M$, $1 \times 10^{-7}M$, $5 \times 10^{-7}M$ and $1 \times 10^{-6}M$ Pipril. Table 1 summarizes the results obtained, the limit of linearity and their correlation coefficients. It is obvious from the data listed in the table that as Pipril concentration increases, the limit of linearity (expressed by the accumulation time) decreases.

Reproducibility was evaluated by performing 10 measurements on a $5 \times 10^{-8}M$ solution after a 10 sec accumulation, with stirring. A mean value of 0.065 μA was found, with a range of 0.06–0.07 μA and a relative standard deviation of 2.5%.

Calibration curves have been established with different accumulation times viz. 5, 10, 15 and 20 sec. In spite of desorption behavior described above, linearity could be obtained for a constant preconcentration time in the concentration range from 5×10^{-8} to $1 \times 10^{-6}M$.

Detection limit of $5 \times 10^{-9}M$ Pipril in 10 ml has been established considering the signal-to-noise ratio of 3. This means that 0.27 ng Pipril are detectable in 10 ml solution.

Urine analysis

Figure 6 shows the cathodic stripping voltammograms of spiked $1 \times 10^{-6}M$ Pipril in urine samples diluted 10 times with the supporting electrolytes. As seen from these voltammograms, applying accumulation times of more than 5 sec. the peak begins to decrease, part of this phenomenon is (as previously mentioned in this work) due to fast desorption of the drug and the other part may be attributed to the interference of the unknown potentially interfering urine constituents. Therefore, direct current measurements, *i.e.* DPP without preconcentration were preferable in such analysis. Linear relationships were obtained when the peak current is drawn as a function of Pipril concentration in the range from 5×10^{-7} to $5 \times 10^{-5}M$. However, as the concentration range found in human urine after a single 2 g intramuscular exceeds 10,000 μg/ml,[12] corresponding to $0.018M$ Pipril, our linearity range is very sensitive compared with the dose originally found.

Detection limit of $1 \times 10^{-8}M$ Pipril could easily be achieved based on the signal-to-noise ratio of 3.

REFERENCES

1. A. L. Barry, *Cleveland Clin. Quart.*, 1980, **47**, 311.
2. I. Roy, *Curr. Ther. Res*, 1978, **23**, 200.
3. D. A. Leigh and K. T. Simmons, *Drugs Expti. Clin. Res.*, 1979, **5**, 99.

4. N. A. Kuck and G. S. Redin, *J. Antibiot.*, 1978, **31**, 1175.
5. R. J. Fass and J. Barnishan, *Rev., Infect. Dis.*, 1980, **2**, 841.
6. R. J. Fass, *Antimicrob. Ag. Chemother.*, 1982, **21**, 1003.
7. N. O. Agudelo and H. S. Trujillo, *Invest. Med. Int.*, 1979, **6**, 264.
8. N. A. Kuck, *Antimicrob. Ag. Chemother.*, 1981, **19**, 634.
9. G. A. Botta and J. T. Park, *J. Bact.*, 1981, **145**, 333.
10. P. J. DeSchepper, *Proc. Italian Congr. Clin. Pharm. Taormina* (Italy), 1978.
11. M. A. Evans, *J. Antimicrob. Chemother.*, 1978, **4**, 255.
12. B. R. Meyers, *Antimicrob. Agents Chemother.*, 1980, **17**, 608.
13. J. A. Morrison and V. K. Batra, *Drugs Exptl. Clin. Res.*, 1979, **5**, 105.
14. S. Qiu and J. Liu, *Yaowu Fenxi Zazhim Jan*, 1989, **9**(1), 27.
15. A. P. Ocampa, K. D. Hoyt, N. Wadgaonkar, A. H. Carver and C. V. Puglisi, *J. Chromatogr., Biomed. Appl.*, 1989, **88**, 167.
16. S. Schroeder, R. Voigt, G. Horn, I. Sestakova and P. Skarka, *Pharmazie*, 1985, **40**(5), 333.
17. J.-C. Vire, N. Abo El-Maali, G. J. Patriarche and G. D. Christian, *Talanta*, 1988, **35**, 997.
18. N. Abo El-Maali, A. M. M. Ai, M. Khodari and M. A. Ghandour, *Bioelectrochem. Bioenerg.*, 1991, **26**, 485.
19. A. M. M. Ali, N. Abo El-Maali and M. A. Ghandour, *Electroanalysis*, 1993, **5**, 85.
20. J. Heyrovsky, *Principles of Polarography*, Chapter XIV, p. 257. Academic Press New York, 1966.
21. N. Abo El-Maali and H. Berg, *J. Electroanal. Chem.* 1993, accepted for publication.
22. J. Wang, *Stripping Analysis, Principles, Instrumentation and Application*. Verlag Chemie, Deerfield Beach, FL, 1985.

Talanta, Vol. 40, No. 12, pp. 1839–1846, 1993
Printed in Great Britain.

0039-9140/93 $6.00 + 0.00

KINETICS OF INDIUM ATOMIZATION FROM DIFFERENT ATOMIZER SURFACES IN ELECTROTHERMAL ATOMIC ABSORPTION SPECTROMETRY (ETAAS)

XIU-PING YAN and ZHE-MING NI*
Research Center for Eco-Environmental Sciences, Academia Sinica, P.O. Box 2871, Beijing, China 100085

XIAO-TAO YANG
Institute of Rock and Mineral Analysis, Beijing, China

GUO-QIANG HONG
Factory of Geological Instrument, Beijing, China

(*Received* 3 *December* 1992. *Revised* 18 *May* 1993. *Accepted* 20 *May* 1993)

Summary—The kinetic parameters of indium atomization in electrothermal atomic absorption spectrometry (ETAAS) have been determined by a newly proposed method. Effect of the atomizer surface and the palladium modifier on the kinetics of indium atomization has been investigated. The mechanisms of indium atomization seem to be identical for the pyrolytically coated graphite and the uncoated graphite tubes, *i.e.* the rate-limiting step for the atomization changes from a first order kinetics at lower temperatures into a nearly 1/3 order kinetics at higher temperatures, which may suggest that the analyte moves from a dispersed state to agglomates with increasing temperature. However, for the zirconium coated graphite tube, the atomization of indium is controlled by a single mechanism with the kinetic order of near 2/3 and the activation energy of 186 ± 13 kJ/mol. Relatively weak indium–zirconium carbide interactions and the release of indium from the sphere of molten indium metal on the zirconium coated surface are suggested. In the presence of palladium, a simple mechanism, *i.e.* the release of indium from the solid solution of the In and the Pd on the pyrolytically coated graphite surface, is proposed to account for the observed first order kinetics and the activation energy of 421 ± 27 kJ/mol.

The atomization of analytes in electrothermal atomic absorption spectrometry (ETAAS) has been studied by many researchers based on kinetic,[1–5] thermodynamic[6–10] and combined kinetic–thermodynamic considerations.[11–15] Usually, most of these reports focused on the atomization mechanisms of analytes without matrices nor modifiers from one type of graphite surface. However, it is more important to elucidate the mechanisms of analyte released in the presence of matrices or modifiers from different atomizer surfaces since normal analysis is often carried out under such conditions. Thus far, there have been a few papers appearing to deal with the atomization mechanisms of the analyte from various atomizer surfaces. Aggett and Sprott[16] compared the appearance temperatures for the atomization of various analytes from both graphite and tantalum surfaces, and concluded that the most possible mechanism for the analyte atomization from a tantalum surface was the thermal decomposition of the oxide. Gregoire *et al.*[17] studied the atomization mechanisms of U, V, Mo, Ni, Mn, Cu and Mg from pyrolytic graphite and tantalum surfaces. The atomization mechanisms of various analytes from molybdenum[18] and tungsten[19] surfaces were compared with those from the graphite surface. Gao and Ni[20] suggested that the atomization mechanism of germanium in the zirconium coated graphite tube was the vaporization of germanium following the reduction of GeO_2 or GeO by zirconium carbide, which was different from the thermal decomposition mechanism of the oxide in the uncoated graphite tube. Recently, Chakrabarti and Cathum[21] investigated the mechanism of cobalt atomization from different atomizer surfaces in ETAAS, and suggested that the atomization mechanism of

*Author for correspondence.

cobalt seemed to be the same for the pyrolytically coated graphite and the uncoated electrographite surfaces, but different for the glassy carbon furnace. Fonseca *et al.*[22] studied the vaporization/atomization characteristics of Cu sample from graphite and Ta-lined tubes using both Ta and graphite platforms and found first order release of Cu from both Ta and graphite surfaces.

Much less attention has been paid to the behavior of indium in the graphite furnace compared with other analytes. Grinshtein *et al.*[23] studied the interaction between indium and the graphite surface at various temperatures by using a tube-in-tube, spatially isothermal furnace. At temperatures less than 1900 K, indium adsorbed to the graphite surface and the effective residence time of this element was greater than theoretically predicted residence time. However, at temperatures greater than 1900 K, no significant adsorption of In occurred. In an earlier study, Katskov *et al.*[24] determined an activation energy of 234 kJ/mol at lower temperatures followed by 134 kJ/mol at higher temperatures for the atomization of In. Recently, McNally and Holcombe[25] studied the topology and vaporization characteristics of indium in a CRA- 90 min. Massmann furnace. Two activation energies of 238 ± 29 and 138 ± 21 kJ/mol were obtained over the course of release from In using manual pipetting. An appearance order of greater than one was suggested for indium release from the concentration study, and the aggregate surface was proposed as one of the generation mechanisms for indium. They also observed the relatively weak interaction between indium and graphite.

The purpose of this work is to study the atomization kinetics of indium from different atomizer surfaces, *i.e.* pyrolytically coated, uncoated and zirconium coated graphite surfaces, and the effect of the palladium modifier on the kinetics of indium atomization from the pyrolytically coated graphite surface by using a newly proposed method.[26]

THEORY

In a previous report,[26] a method was developed for the simultaneous determination of the kinetic parameters of atom formation from a single absorbance signal profile under normal analytical conditions in electrothermal atomic absorption spectrometry (ETAAS). The change of the absorbance, A, with time, t, was given by the following equation:

$$dA/dt = P^{x-1}k_1\left(\int_t^\infty k_2 A\,dt - A\right)^x - k_2 A \quad (1)$$

where k_1 and k_2 are the temperature and subsequently time dependent rate constants for the formation and dissipation of gaseous atoms, respectively; P a proportionality factor, x the kinetic order of the atom formation reaction. According to the Arrhenius' law, the temperature dependence of k_1 can be expressed as follows:

$$k_1 = k_0 . \exp(-E_a/RT) \quad (2)$$

where k_0 and E_a are the frequency factor and activation energy for atom formation, respectively; R the gas constant and T the absolute temperature at time t. Substituting equation (2) into equation (1) and rearranging yields:

$$dA/dt + k_2 A = k_0 P^{x-1} \times\left(\int_t^\infty k_2 A\,dt - A\right)^x . \exp(-E_a/RT) \quad (3)$$

Taking logarithm of equation (3), differentiating and rearranging give

$$\Delta \ln(dA/dt + k_2 A)/\Delta \ln\left(\int_t^\infty k_2 A dt - A\right) = x - (E_a/R)\Delta(1/T)/\Delta \ln\left(\int_t^\infty k_2 A\,dt - A\right). \quad (4)$$

Equation (4) shows that if the atomization of the analyte from the atomizer surface is governed by a single kinetic mechanism, a plot of $\Delta \ln(dA/dt + k_2 A)/\Delta \ln(\int_t^\infty k_2 A\,dt - A)$ *vs* $\Delta(1/T)/\Delta \ln(\int_t^\infty k_2 A\,dt - A)$ should be a straight line. From the slope of such a plot, the activation energy (E_a) can be calculated, while the kinetic order (x) can be obtained from the intercept. The validity of equation (4) has been confirmed both by computer simulation study[26,27] and the ETAAS experiments.[26]

To obtain the kinetic order and activation energy by using equation (4), the temperature dependence of k_2 should be known. In this study, the gas-stop mode is used in the atomization step and the dissipation of the analyte by convection is distinctly negligible. Therefore, k_2 is the total rate constant for the dissipation of the analyte by diffusion and thermal expansion only, *i.e.*

$$k_2 = k_d + k_e \quad (5)$$

where k_d and k_e are the constants for atom dissipation by diffusion and thermal expansion at any time, respectively; K_d is defined as[28]

$$k_d = k_d^0 (T/T_0)^y \quad (6)$$

where k_a and k_d^0 are diffusional rate constants at temperature T and T_0, respectively; y varies between 1.5 and 2.0,[28] K_e is given by[29]

$$k_e = (dT/dt)/T \quad (7)$$

where dT/dt is the heating rate at any temperature T.

For determining the temperature dependence of k_2, the values of k_d^0 and y should be obtained. For indium, the y value of 1.84 can be found from Ref. 30. The value of k_d^0 can be determined from the decay portion of the absorbance signal profile based on the method proposed by Akman *et al.*[29]

To determine E_a and x based on equation (4), the terms of dA/dt and $\int_t^\infty k_2 A\, dt$ should be calculated. To this end, mathematical expressions of $A = f_1(t)$ and $k_2 A = f_2(t)$ are obtained by polynomial regressions. Thus, the functions of $dA/dt = f'_1(t)$ and $\int_t^\infty k_2 A\, dt = F_2(t)$ can be obtained by differentiating the expression of $A = f_1(t)$, and integrating $k_2 A = f_2(t)$, respectively.

Data from the appearance to the maximum in the absorbance signal can be used to construct the plot based on equation (4) for determination of the kinetic order and activation energy since the amount of the analyte unatomized on the tube surface at time t, $P(\int_t^\infty k_2 A\, dt - A)$, is greater than zero from the beginning at least to the maximum in the signal. In addition, special conditions to isolate the supply and removal function, and linear temperature ramp are indeed not required with the use of equation (4) because of no such assumptions made during the derivation of equation (4).

EXPERIMENTAL

Apparatus

A Perkin-Elmer model 4000 atomic absorption spectrometer, equipped with a deuterium background corrector and a model HGA-400 graphite furnace was used for the measurement of the atomic absorption in the gas-stop mode. An indium hollow-cathode lamp (Shanghai Tienkuang Scientific Instruments Works, Shanghai, China) was employed at a lamp current of 5 mA. The 303.9 nm line of indium was used as the analysis line, with a spectral bandpass of 0.7 nm. High purity argon gas was used as both sheath and purge gas. The furnace programme is given in Table 1.

Table 1. Furnace programme

	Dry	Ash	Atomize	Clean
Ramp time (*sec*)	20	5	1	1
Hold time (*sec*)	50	30	5	2
Temperature (°C)	130	Various	Various	2650
Int. gas flow (*ml/min*)	300	300	0	300

The graphite tube wall temperature was obtained from the output of a germanium phototransistor (B 1918-01, Hamamatsu), which was calibrated by focusing a disappearing filament optical pyrometer (Ircon Inc., UX-10, USA) through the sample injection hole in the graphite tube. The absorbance and temperature signal were synchronously acquired by a microcomputer-based data acquisition system at 20-msec intervals.[26] The signals could be subsequently stored on a diskette for further use.

Three different atomizer surfaces were used for the atomization of indium: Pyrolytically coated (PG), uncoated graphite tubes (UG) and the zirconium coated PG (ZrPG). The ZrPG were prepared according to Ref. 31.

Reagents

The stock solution containing 1000 mg/ml In was prepared by dissolving In_2O_3 in an adequate volume of diluted nitric acid and subsequently diluting with deionized water. Working standards of the element were prepared daily from this stock solution with deionized water just before use. Indium working solutions were manually introduced into the furnace in 20-μl volumes using an Eppendorf pipette.

A 5% m/v of $ZrO(NO_3)_2 . 2H_2O$ solution was prepared by dissolving $ZrO(NO_3)_2 . 2H_2O$ in diluted nitric acid and then diluting with deionized water.

All chemicals were of analytical-reagent grade.

RESULTS AND DISCUSSION

Atomization from the pyrolytically coated graphite tube (PG)

The concentration study, which is illustrated in Fig. 1, contains absorbance–time plots for various initial masses of In deposited on the

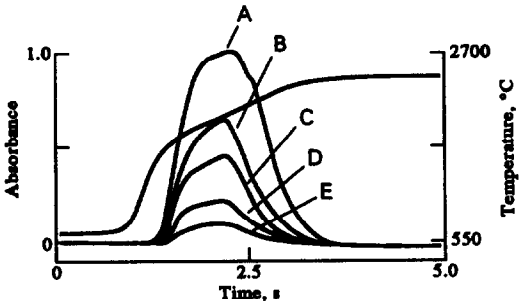

Fig. 1. Absorbance signal profiles for various masses of In from the pyrolytically coated graphite tube: (a) 5 (b) 3 (c) 2 (d) 1 (e) 0.5 ng. Ashing temperature: 500°C, atomization temperature: 2600°C, other conditions as listed in Table 1.

bottom of the PG. As the initial amount of In deposited on the surface of the PG is increased, peak times are similar and there is a slight shift to earlier appearance times. Thus, the apparent kinetic order for indium atomization from the PG appears to be unity.[25] To obtain the kinetic order of indium atomization accurately, the plot of $\Delta \ln(dA/dt + k_2 A)/\Delta \ln(\int_t^\infty k_2 A \, dt - A)$ *vs* $\Delta(1/T)/\Delta \ln(\int_t^\infty k_2 A \, dt - A)$ is constructed from the absorbance signal profile. Figure 2 shows such a plot obtained from Fig. 1(c). As can be seen, the plot exhibits curvature, and so assignment of a single straight line from this plot is difficult, which may, in fact, reflect a continuous varying slope. This could imply gas-phase dissociation as step governing atom formation or a temperature dependence of activation energy (E_a) and kinetic order (x) on surface coverage. Figure 3 shows the decomposition (curve A) and atomization (curve B) curves for indium from the PG. As can be seen, there is a gap between the temperature in the decomposition curve at which the absorbance begins to decrease (the maximum tolerant ashing temperature), and the appearance temperature in the atomization

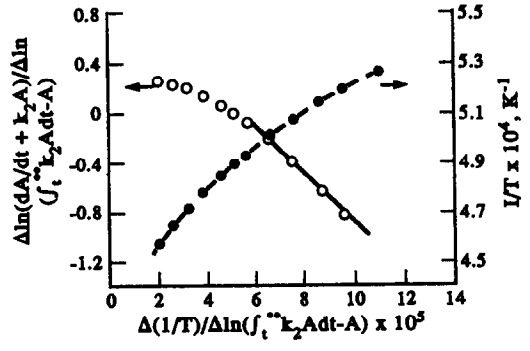

Fig. 2. Plot obtained from Fig. 1(c) based on equation (4) for 2 ng of In from the pyrolytically coated graphite tube.

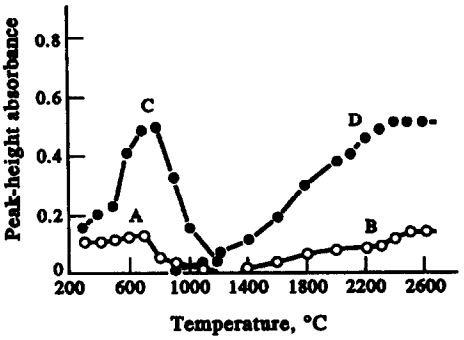

Fig. 3. Decomposition and atomization curves for 0.5 ng of In by atomization from the pyrolytically coated graphite tube; (a) decomposition curve, at the atomization temperature of 2600°C (b) atomization curve, at the ashing temperature of 500°C, and from the zirconium coated graphite tube; (c) decomposition curve, at the atomization temperature of 2400°C and (d) atomization curve, at the ashing temperature of 800°C.

curve. This means that the decrease in the absorbance is not only due to loss of $In_{(g)}$ but also to the formation of other gaseous species at temperatures above 700°C. Calculations of thermodynamic equilibrium in the In–O–C system over the temperature range of 500–2000 K have shown that $In_2O_{(g)}$ is likely to be formed at either high ashing or lower atomization temperatures, but that $InO_{(g)}$ should not play a significant role in the atomization of In.[32] This has been confirmed by means of graphite furnace-mass spectrometry (GFMS) experiment.[32] However, it is not easy to discuss the formation of free indium via gas-phase dissociation of an oxide in terms of kinetics since one must take into account the change in partial pressure of oxygen as well as the generation function of the indium oxide from the surface and the generation of the metal from the gas.[33]

An alternative explanation for the curvature observed in Fig. 2 may be that multiple release mechanisms contribute to the atomization of indium from the PG surface. If two straight lines are used to fit the plot in Fig. 2, then the activation energy (E_a) and kinetic order (x) could be found to be 134 kJ/mol and 0.97 at lower temperatures, 63 kJ/mol and 0.37 at higher temperatures, respectively. This probably indicates that the rate-limiting step for the atomization of indium changes from a nearly first order kinetics with larger E_a value at lower temperatures into the kinetics of $x = 0.37$ with lower E_a value at higher temperatures.

If we assume that either two straight lines or a continuous curve exists in Fig. 2 and that the

intercept of any portion of the curve (*i.e.* the kinetic order x) would represent the state of the morphology of the analyte on the surface at that time, then one could conclude that the material moves from a dispersed state of $x = 1$ to agglomerates (*i.e.* $x = 0.37$). This suggests that the analyte begins as dispersed atoms or molecules containing indium and then forms droplets with increasing temperature. Although indium metal indeed exhibits weak interactions at the graphite observed by McNally and Holcombe,[25] some indium molecular species may have a strong interaction which causes it to be dispersed on the surface and exhibited nearly first order release at lower temperatures. The obtained larger E_a value (134 kJ/mol) could represent indium molecular species-graphite interaction energy. Furthermore, the weak indium metal–graphite interactions would foster the formation of droplets which is consistent with the higher temperature order of release ($x = 0.37$). The observed lower E_a value may represent the energy required for indium release at the edge of the metal–graphite interface.[25,34] It is possible that indium metal would be formed either through carbon reduction of the oxide or the thermal decomposition of the oxide at higher temperatures. In addition, no significant influence of the initial injected mass of indium studied on the indium atomization from the PG is observed, as shown in Table 2.

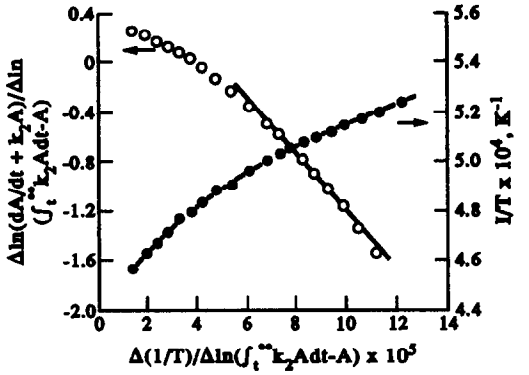

Fig. 4. Plot constructed based on equation (4) for 2 ng of In from the uncoated graphite tube. Other conditions as in Table 1.

Atomization from the uncoated graphite tube (UG)

In order to examine surface spreading and penetration by the aqueous solution of the sample on the atomization of indium, the kinetic parameters of indium atomization from the uncoated graphite tube (UG) have been determined. Figure 4 illustrates the plot of $\Delta \ln(dA/dt + k_2A)/\Delta \ln(\int_t^\infty k_2 A \ dt - A)$ *vs* $\Delta(1/T)\Delta \ln(\int_t^\infty k_2 A \ dt - A)$ from the absorbance signal profile for 2 ng of indium ashed at 500°C and atomized at 2600°C from the UG. Compared with Fig. 2, similar results can be obtained from Fig. 4, *i.e.* Fig. 4 also exhibits nonlinearity, reflecting a continuous varying slope and intercept. If two straight lines are

Table 2. Kinetic parameters for indium atomization from different atomizer surfaces (±standard deviation of three determinations)

Tube	Mass of In (*ng*)	Kinetic order	E_a (*kJ/mol*)
PG	0.5	0.35 ± 0.05/0.97 ± 0.05	50 ± 13/138 ± 13
	1	0.36 ± 0.03/0.96 ± 0.03	51 ± 12/142 ± 13
	2	0.40 ± 0.04/0.99 ± 0.06	63 ± 10/146 ± 13
	3	0.37 ± 0.01/0.98 ± 0.07	50 ± 4 /138 ± 15
	5	0.37 ± 0.04/1.02 ± 0.06	42 ± 4 /126 ± 17
	Av.	0.37 ± 0.02/0.98 ± 0.02	51 ± 7 /138 ± 8
UG	0.5	0.38 ± 0.02/0.95 ± 0.06	56 ± 8 /142 ± 17
	1	0.34 ± 0.04/0.98 ± 0.04	50 ± 10/126 ± 13
	2	0.36 ± 0.06/0.94 ± 0.07	54 ± 15/138 ± 17
	3	0.37 ± 0.02/1.04 ± 0.05	50 ± 6 /134 ± 13
	5	0.35 ± 0.04/1.02 ± 0.06	59 ± 13/126 ± 8
	Av.	0.36 ± 0.02/0.98 ± 0.04	54 ± 4 /133 ± 8
PG + Pd	0.25	1.04 ± 0.06	406 ± 25
	0.5	1.02 ± 0.07	460 ± 25
	0.75	1.08 ± 0.11	414 ± 8
	1	1.08 ± 0.09	402 ± 20
	Av.	1.06 ± 0.03	421 ± 27
ZrPG	0.25	0.61 ± 0.07	204 ± 6
	0.5	0.69 ± 0.05	185 ± 11
	0.7	0.59 ± 0.04	174 ± 10
	0.9	0.68 ± 0.09	180 ± 13
	Av.	0.64 ± 0.05	186 ± 13

used to fit Fig. 4, the kinetic order and activation energy can be found to be 0.97 and 155 kJ/mol, at lower temperatures, respectively; while at higher temperatures, the kinetic order of 0.38 and activation energy of 67 kJ/mol can be obtained. Although the uncoated graphite surface is expected to show much more porous than the pyrolytically coated graphite surface, the near identity of the kinetic parameters indicates that the atomization mechanisms of indium are similar for both atomizer surfaces.

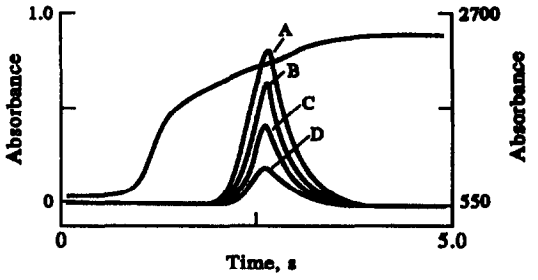

Fig. 6. Absorbance signal profiles for various masses of In from the pyrolytically coated graphite tube when 2 μg of Pd is used as a modifier: (a) 1; (b) 0.75; (c) 0.5; (d) 0.25 ng. Other conditions as in Fig. 1.

Atomization from the PG surface in the presence of palladium

It has been shown that palladium is an effective matrix modifier for the determination of indium, which greatly improves the sensitivity and raises the maximum tolerant ashing temperature.[35] In this work, the effect of the presence of palladium on the atomization mechanism of indium is investigated. The palladium modifier is pretreated before each determination by injecting a 20 μl of 100 μg/ml Pd into the PG through the sample injection hole, drying at 150°C for 30 s and heating at 900°C for 30 sec. Figure 5 shows the plot of $\Delta \ln(dA/dt + k_2A)/\Delta \ln(\int_t^\infty k_2A\,dt - A)$ *vs* $\Delta(1/T)/\Delta \ln(\int_t^\infty k_2A\,dt - A)$ from the absorbance signal profile for 0.5 ng of In ashed at 500°C and atomized at 2600°C from the PG surface in the presence of palladium. In contrast to Figs 2 and 4, a single straight line can be fit well to the plot shown in Fig. 5. This means that a single mechanism is active in the atomization of indium with palladium. From Fig. 5 the activation energy and kinetic order are found to be 414 kJ/mol and 0.95, respectively. No significant influence of the initial injected mass of indium studied on the kinetics of indium atomization is observed, as shown in Table 2. The first order kinetics can also be seen from the concentration study depicted in Fig. 6. These results suggest that the atomization mechanism of indium in the presence of palladium is different from those for the PG and UG in the absence of palladium.

Figure 7 shows the absorbance signal profiles for 0.5 ng of In ashed at 500°C and atomized at 2600°C from the PG with (curve A) and without (curve B) the palladium modifier. Obviously, in the presence of palladium the appearance of the absorbance signal is significantly delayed, and both the peak height and peak area are increased. The increase in the sensitivity indicates that the use of a palladium modifier prevents the formation of gaseous species in the presence of palladium. By using Fourier transform infrared spectrometry, Volynsky *et al.*[36] found that the palladium modifier sharply decreased the reduction temperature of the metal oxides with graphite. It was regarded that the catalytic property of palladium facilitated the carbon reduction of oxides at low ashing temperatures.[36] Thus, we assume that in the presence of palladium the oxide $In_2O_{3(s)}$ is rapidly reduced to metallic indium, and the resultant indium metal forms the intermetallic compounds or solid solution[37,38] with the

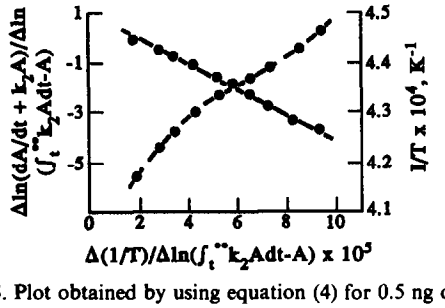

Fig. 5. Plot obtained by using equation (4) for 0.5 ng of In in the presence of 2 μg of Pd from the pyrolytically coated graphite tube. Other conditions as in Fig. 1.

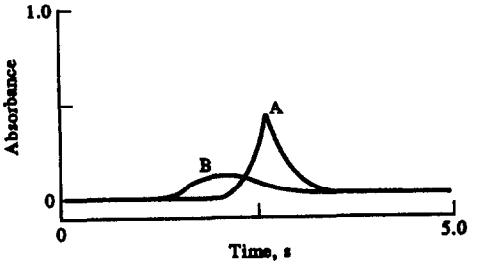

Fig. 7. Effect of palladium modifier on the absorbance signal profile of indium from the pyrolytically coated graphite tube: (a) 0.5 ng In + 2 μg Pd; (b) 0.5 ng In. Conditions as shown in Fig. 1.

palladium metal, thus decreasing or almost eliminating loss of the analyte due to the formation of gaseous oxide. At the atomization stage, the absorbance is produced owing to the release of indium from the solid solution with Pd, which may cause the observed first order kinetics. The obtained E_a value (421 ± 27 kJ/mol) represents the energy required to release the indium in molten palladium, which depends on the heat of solution of the In and the pd.

Atomization from the zirconium coated graphite tube (ZrPG)

The absorbance signal profiles for different amounts of indium atomized from the zirconium coated graphite tube (ZrPG) under optimum conditions are depicted in Fig. 8, from which the fractional kinetic order for the atomization of indium from the ZrPG can be seen since the peak maximum occurs later with increasing analyte mass.[34] In order to obtain the accurate value of the kinetic order, plots of $\Delta \ln(dA/dt + k_2 A)/\Delta \ln(\int_t^\infty k_2 A\ dt - A)$ *vs* $\Delta(1/T)/\Delta \ln(\int_t^\infty k_2 A\ dt - A)$ are constructed. Figure 9 shows such a plot from Fig. 8(d). The obtained values of the kinetic order and activation energy from Fig. 9 are 0.64 and 192 kJ/mol, respectively. There is no remarkable change in the kinetic parameters for indium atomization from the ZrPG with the initial injected amount of In studied, as can be seen from Table 2. The above results imply that the atomization mechanisms of indium are different for the ZrPG and PG.

Figure 3 also shows the decomposition (curve C) and atomization (curve D) curves for indium from the ZrPG. As can be seen, there is no significant gap between the maximum tolerant ashing temperature and the appearance

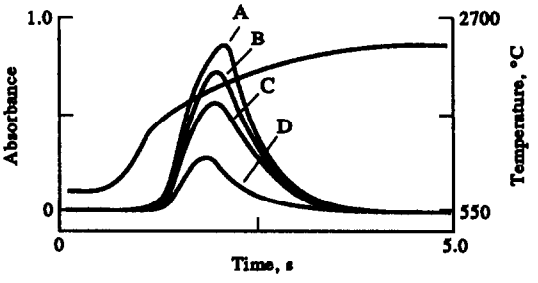

Fig. 8. Absorbance signals for various amounts of In from the zirconium coated graphite tube: (a) 0.9 (b) 0.7 (c) 0.5 (d) 0.25 ng. Ashing temperature: 800°C, atomization temperature: 2400°C.

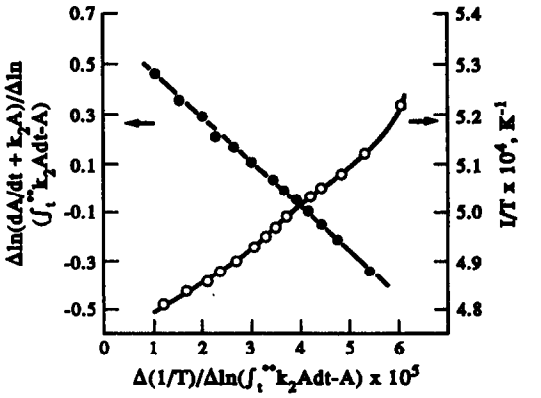

Fig. 9. Plot obtained from Fig. 8(d) by using equation (4) for 0.25 ng of In from the zirconium coated graphite tube.

temperature in the atomization curve. Thus, compared with the PG (curves A and B in Fig. 3), the ZrPG seems to prevent the formation of gaseous species and greatly improves the sensitivity. It has been suggested that prevention of oxide formation may be the main reason for the better sensitivity of determinations on the refractory element coated furnace.[39] Probably more active reducing properties of refractory element carbides than graphite are responsible for the prevention of gaseous oxide formation.[20,40] Increase in the absorbance with ashing temperature below 700°C (curve C in Fig. 3) indicates that the reducing activity of ZrC may increase with temperature.

On the basis of the above, the following reactions are supposed for indium atomization from the ZrPG, similar to those discussed in Refs 20, 41;

$$ZrC_{(s)} + In_2O_{3(s)} \rightarrow Zr_{(s)} + In_{(s/l)} + CO_{(g)}$$
$$ZrC_{(s)} + In_2O_{(g)} \rightarrow Zr_{(s)} + In_{(s/l)} + CO_{(g)}$$
$$In_{(s/l)} \rightarrow In_{(g)}$$

The resulting metallic zirconium reacts with graphite to form ZrC again at high temperatures, while the formed indium metal vaporizes with increasing temperature. The obtained kinetic order of near 2/3, along with the activation energy of 192 kJ/mol, indicates that the atomization of indium may be governed by the surface area of the sphere of molten metal, and the interaction between indium metal and zirconium carbide surface is relatively weak.

CONCLUSION

The kinetics of indium atomization seems to be similar for the pyrolytically coated and the

uncoated graphite tubes, but different for the zirconium coated graphite tube. The use of a palladium modifier or of the zirconium coated tube changes the path of indium atomization, inhibiting the formation of gaseous indium oxide, and hence greatly improves the sensitivity for indium determination.

Acknowledgement—This work was supported by the Chinese Academy of Sciences under grant No. KM 85-47.

REFERENCES

1. C. W. Fuller, *Analyst*, 1974, **99**, 739.
2. G. Tessari and G. Torsi, *Anal. Chem.*, 1975, **47**, 842.
3. G. Torsi and G. Tessari, *Anal. Chem.*, 1975, **47**, 839.
4. B. V. L'vov, P. A. Bayunov and G. N. Ryabchuk, *Spectrochim. Acta*, 1981, **36B**, 397.
5. D. Rojas and W. Olivares, *Spectrochim. Acta*, 1992, **47B**, 387.
6. W. C. Campbell and J. M. Ottaway, *Talanta*, 1974, **21**, 837.
7. B. V. L'vov and A. S. Savin, *Zh. Anal. Khim.*, 1983, **38**, 1925.
8. J. P. Byyrne, *Aust. J. Chem.*, 1979, **32**, 249.
9. W. French, E. Lundberg and A. Cedergren, *Prog. Anal. Atom. Spectrosc.*, 1985, **8**, 257.
10. C. L. Chakrabarti, S. B. Chang and S. E. Roy, *Spectrochim Acta*, 1983, **38B**, 447.
11. R. E. Sturgeon, C. L. Chakrabarti and C. H. Langford, *Anal. Chem.*, 1976, **48**, 1792.
12. O. Genc, S. Akman, A. R. Ozdural, S. Ates and T. Balkis, *Spectrochim. Acta*, 1981, **36B**, 163.
13. B. Smets, *Spectrochim. Acta*, 1980, **35B**, 33.
14. M. Suzuki, K. Ohta and K. Isobe, *Anal. Chim. Acta*, 1985, **173**, 321.
15. M. Suzuki and K. Ohta, *Anal. Chim. Acta*, 1983, **151**, 401.
16. J. Aggett and A. J. Sprott, *Anal. Chim. Acta*, 1974, **72**, 49.
17. D. C. Gregoire and C. L. Chakrabarti, *Spectrochim. Acta*, 1982, **37B**, 611.
18. M. Suzuki, K. Ohta, T. Yamakita and T. Katssuno, *Spectrochim. Acta*, 1981, **36B**, 679.
19. O. Vyskocilova, V. Sychra and D. Kolihova, *Anal. Chim. Acta*, 1979, **105**, 271.
20. Y.-Q. Gao and Z.-M. Ni, *Acta Chim. Sin.*, 1982, **40**, 1021.
21. C. L. Chakrabarti and S. J. Cathum, *Talanta*, 1990, **37**, 1111.
22. R. W. Fonseca, O. A. Guell and J. A. Holcombe, *Spectrochim. Acta*, 1990, **45B**, 1257.
23. I. L. Grinshtein, L. A. Vasil'eva and D. A. Katskov, *Zh. Prikl. Spectrosk.*, 1985, **46**, 13.
24. D. A. Katskov, I. L. Grinshtein and L. P. Kriglikova, *Zh. Prikl. Spectrosk.*, 1980, **33**, 804.
25. J. McNally and J A. Holcombe, *Anal. Chem.* 1991, **63**, 1918.
26. X.-P. Yan, Z.-M. Ni, X.-T. Yang and G.-Q. Hong, *Spectrochim. Acta*, Part B, in press.
27. X.-P. Yan and Z.-M. Ni, *Proc. of Int. Fourth Beijing Conference and Exhibition on Instrumental Analysis*, 1991, Beijing, Abs. C70.
28. B. V. L'vov, *Spectrochim. Acta*, 1961, **17B**, 701.
29. S. Akman, S. Bektas and O. Genc, *Spectrochim. Acta*, 1990, **43B**, 763.
30. B. V. L'vov, *Spectrochim. Acta*, 1990, **45B**, 633.
31. X.-P. Yan and Z. M. Ni, *J. Anal. At. Spectrom.*, 1991, **6**, 483.
32. T. McAllister, *J. Anal. At. Spectrom.*, 1990, **5**, 171.
33. J. A. Holcombe, *Spectrochim. Acta*, 1989, **44B**, 975.
34. J. McNally and J. A. Holcombe, *Anal. Chem.*, 1987, **59**, 1105.
35. Z.-M. Ni and X.-Q. Shan, *Spectrochim. Acta*, 1987, **42B**, 937.
36. A. Volynsky, S. Tikhomirov and A. Elagin, *Analyst*, 1991, **116**, 145.
37. A. F. Trotman-Dickenson, *Comprehensive Inorganic Chemistry*, Vol. 1. Pergamon Press, Oxford, 1973.
38. P.-Y. Yang, Z.-M. Ni, Z.-X. Zhuang, F.-C. Xu and A.-B. Jiang, *J. Anal. At. Spectrom.*, 1992, **7**, 515.
39. A. B. Volynsky, E. M. Sedykh and B. Ya Spivakov, *Anal. Chim. Acta*, 1985, **174**, 173.
40. G. Muller-Vogt and W. Wendll, *Anal. Chem.*, 1981, **53**, 651.
41. W. B. Blumenthal, *The Chemical Behavior of Zirconium*, Princeton, N.J., D. Van Nostrad, New York, 1958.

Talanta, Vol. 40, No. 12, pp. 1847–1850, 1993
Printed in Great Britain.

0039-9140/93 $6.00 + 0.00

A NEW SENSITIVE REAGENT FOR IDENTIFYING Ag^+ AND Hg^{2+}

DONGLAN MA,* YUYING DONG and YULU WANG
Department of Chemistry, Henan Normal University, XinXiang, Henan 453002, China

(*Received* 2 *December* 1992. *Revised* 8 *March* 1993. *Accepted* 10 *March* 1993)

Summary—This paper describes the synthesis of a new reagent: N,N′ -difuroyl thiourea for the purpose of improving coordination capacity of thiourea compounds. It has been characterized by IR, UV, MS and ^{1}H-NMR as well as elemental analytical data. According to the studies on its analytical performance, it is found that this reagent can be used to identify Ag^+ and Hg^{2+}. Both of their sensitivities and selectivities are the best in all methods for the time being. The new methods are simple and convenient, and can provide satisfactory results on synthetic and standard samples.

With many good properties,[1–7] thiourea derivatives have been widely applied in industry, agriculture, biology, medicine and analytical chemistry. Among them, aromatic thioureas have been studied in detail.[8–11] However, heterocyclic thioureas have been little reported recently. In order to extend the studies on thiourea compounds and improve their coordination capacities, we report here the preparation of a new reagent: N,N′-difuroyl thiourea (DFT). Its spectroscopic and chemical properties are described. It has been found that DFT can be used to identify Ag^+ and Hg^{2+}. The optimum conditions are studied, and the processes are compared with other classical and common methods.[12–17] The applications of the new reagent to identify synthetic and standard samples are also investigated.

EXPERIMENTAL

Instruments and reagents

^{1}H-NMR spectra were recorded on a JEOL-FX-90Q spectrometer. Chemical shifts are expressed in parts per million (δ) relative to internal TMS. IR spectra were recorded on a Shimadzu IR-408 spectrophotometer and only noteworthy absorptions are listed. Mass spectra were determined on a KRTOS-AEI-MS50 (U.K.) instrument. UV spectra were obtained on a Perkin-Elmer Lambda 17 UV/VIS spectrophotometer. Melting point was determined on a Kofler apparatus.

All chemicals are analytical grade reagents. The concentration of DFT is 0.05% or 0.2%. The aqueous solutions of usual anions and cations are of 10 mg/ml.

Preparation of DFT

First, to a 250-ml, round-bottomed flask equipped with a reflux condenser protected from moisture by a drying tube, was added 11.2 g (0.1 mol) of 2-furoic acid and 70 ml of thionyl chloride, and the flask was put into a water bath of 90°C for about 3 hr until no gas was given out. The resultant mixture was distilled under vacuum and 10.3 g of the expected fraction at 66°C (10 mmHg)[18] was collected, which is furoyl chloride. The reaction is,

$$C_4H_3OCOOH + SOCl_2 \rightarrow C_4H_3OCOCl + SO_2 + HCl$$

Second, thiourea (0.02 mol) and chloroform (50 ml) were mixed in a 250-ml, three-necked, round-bottomed flask installed with a stirrer, reflux condenser and pressure equalizing dropping funnel. While sharply stirring, 5.22 g of the furoyl chloride prepared above, was added drop by drop at room temperature. Then, the system was removed into the water bath of 70°C. The stirring was continued, and six portions of triethylamine (1 ml) were put in at intervals of 30 min, this neutralized the gases produced in the process of synthesis. Triethylamine added into the system, not only improved the yield, but also shortened the reaction time. After 6 hr the suspended solid had completely disappeared and the reaction had ended. The solvent

*Author for correspondence.

($CHCl_3$) evaporated and the residue cooled and filtered. The crude solid obtained was recrystallized from 50% alcohol solution to give 3.45 g of pale yellow powder (DFT). The yield reached 65.3%. The reaction is,

$$2C_4H_3OCOCl + (NH_2)_2CS \rightarrow (C_4H_3OCONH)_2CS + 2HCl$$

Reactions of DFT and usual ions

We carried out experiments on the reactions of DFT and usual ions in different media. Among them, usual cations include K^+, Na^+, NH_4^+, Mg^{2+}, Ca^{2+}, Sr^{2+}, Ba^{2+}, Fe^{3+}, Cr^{3+}, Al^{3+}, Fe^{2+}, Mn^{2+}, Zn^{2+}, Co^{2+}, Ni^{2+}, Cu^{2+}, Cd^{2+}, Bi^{3+}, Hg^{2+}, Sb^{3+}, Sb^{5+}, Sn^{2+}, Sn^{4+}, Ag^+ and Pb^{2+}, *etc.*; usual anions involve F^-, Cl^-, Br^-, I^-, S^{2-}, SO_4^{2-}, $S_2O_3^{2-}$, SO_3^{2-}, SCN^-, CO_3^{2-}, NO_3^-, NO_2^-, PO_4^{3-}, $B_4O_7^{2-}$, MoO_4^{2-}, WO_4^{2-}, VO_3^-, AsO_4^{3-}, AsO_3^{3-}, $C_2O_4^{2-}$ and AC^-, *etc.*

RESULTS AND DISCUSSION

The characterization of DFT

The following values of different items were listed to characterize DFT.

IR (KBr, cm^{-1}): 3340 (N—H), 3125 and 3110 (C—H), 1740 (C=O), 1240 (C=S). ^{1}H-NMR (acetone-d_6, δ):

5.86 (m, 2H, 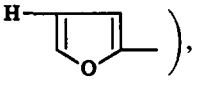),

7.80 (t, 2H, 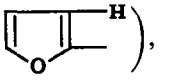),

8.83 (d, 2H, 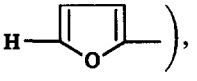),

12.12 (S, 2H, —NH—). MS (m/z): 95 (the basic peak, $(C_4H_3OCO)^+$), 170 (a typical fragmentary ion peak, $C_4H_3OCONHC(S)NH_2$), 264 (the molecule ion peak, M + 1). UV (solvent: $CHCl_3$): 332.8 nm (2.63×10^4 l/mol/cm). anal. calcd. (%) for $C_{11}H_8N_2O_4S$: C, 50; H, 3.03; N, 10.61. Found (%): C, 49.86; H, 3.10; N, 10.92.

The application in analytical chemistry

Physical properties. DFT, m.p. 180, is quite stable. No changes took place with long periods of storage. It is insoluble in water, slightly soluble in alcohol, but soluble in acetone, chloroform, DMF, DMSO and hot alcohol.

Table 1. Reactions of DFT with some cations

Cation	Medium	DFT concentration (%)	Phenomenon
Ag^+	$NH_3 \cdot H_2O$	0.05	Brown sol.
Hg^{2+}	HCl	0.2	White precip.
Hg_2^{2+}	HNO_3	0.2	Brown precip.
Cd^{2+}	$NH_3 \cdot H_2O$	0.2	Yellow precip.
Cu^{2+}	Neutral medium	0.2	Yellow precip.

Chemical properties. No characteristic phenomena were observed in either acid or alkaline media when DFT is mixed with usual anions; neither were the usual cations except Ag^+, Hg^{2+}, Hg_2^{2+}, Cd^{2+} and Cu^{2+}, which can react with DFT to give distinct phenomena in certain media. The conditions listed in Table 1 were determined in light of the clearest phenomena.

As shown by the characteristic phenomena in Table 1, it is deduced that DFT can be a potential specific reagent to identify ions. Since Ag^+ and Hg^{2+} showed higher sensitivity and selectivity, we chose the two cations for further studies.

Identification of Ag^+ *and* Hg^{2+}

(1) Identification of Ag^+. In a centrifugal tube, one drop of Ag^+ stock solution was treated by one drop of $NH_3 \cdot H_2O$ (6 mol/l), and two drops of 0.05% DFT solution. After the tube was shaken, the brown color appeared, which indicated the presence of Ag^+.

(2) Identification of Hg^{2+}. In a centrifugal tube, one drop of Hg^{2+} stock solution was acidified by one drop of HCl (6 mol/l); three drops of 0.2% DFT solution were added, and the tube was shaken. The appearance of white color precipitation indicated the presence of Hg^{2+}.

Conditional experiments

(1) Effects of media. Usual acids (H_2SO_4, HNO_3, HCl, HAC) and alkalis (NaOH, $NH_3 \cdot H_2O$) of different concentrations were used as media in which the ions were revealed

Table 2. The sensitivities of Ag^+ and Hg^{2+}

Sensitivities ions	Limit of identification (μg)	Concentration limit ($\mu g/ml$)	*PD^{20}
Ag^+	0.015	0.5	6.3
Hg^{2+}	0.03	1	6

*$PD = 6 - \log \frac{m}{v}$ (v is the volume of ion solution (ml), m is limit of identification).

Table 3. Tolerance limits of interfering ions

Interfering ions	Identified ions		Interfering ions	Identified ions	
	Ag^+	Hg^{2+}		Ag^+	Hg^{2+}
K^+	1:5000	1:5000	Sn^{2+}	1:200	1:700
Na^+	1:5000	1:5000	Sn^{4+}	1:500	1:500
NH_4^+	1:5000	1:2500	F^-	1:200	1:2500
Mg^{2+}	1:2000	1:5000	Cl^-	1:500	1:3000
Ca^{2+}	1:2000	1:500	Br^-	1:100	1:10
Sr^{2+}	1:1000	1:5000	I^-	1:10	
Ba^{2+}	1:1000	1:5000	S^{2-}		
Fe^{3+}	1:10	1:500	SO_4^{2-}	1:500	1:2000
Fe^{2+}	1:100	1:500	CO_3^{2-}	1:200	1:20
Cr^{3+}	1:200	1:2000	$S_2O_3^{2-}$	1:200	1:4
Al^{3+}	1:500	1:5000	NO_2^-	1:1000	1:1500
Mn^{2+}	1:200	1:5000	NO_3^-	1:1000	1:1500
Zn^{2+}	1:200	1:5000	PO_4^{3-}	1:1000	1:2500
Co^{2+}	1:100	1:2000	$B_4O_7^{2-}$	1:500	1:20
Ni^{2+}	1:100	1:2000	MoO_4^{2-}	1:200	1:10
Cu^{2+}	1:100	1:1000	WO_4^{2-}	1:500	1:2500
Cd^{2+}	1:1000	1:1000	VO_3^-	1:500	1:1000
Bi^{3+}	1:500	1:1000	AsO_4^{3-}	1:500	1:1000
Hg^{2+}	1:10		AsO_3^{3-}	1:500	1:2000
Sb^{3+}	1:100	1:1000	SCN^-	1:250	
Sb^{5+}	1:100	1:1000	$C_2O_4^{2-}$	1:1000	1:2500
Ag^+			SO_3^{2-}	1:250	1:200
Pb^{2+}	1:200		AC^-	1:1000	1:1000

with DFT. According to experiments, the optimum media and concentrations for identifications of Ag^+ and Hg^{2+} are $NH_3 \cdot H_2O$ (6 mol/l) and HCl (6 mol/l), respectively.

(2) Dosage test of DFT. One drop of stock solution of metal ion was treated with ammonia or acidified according to the methods described above. DFT solution was added drop by drop to reveal them thoroughly. It was finally shown that DFT dosages were two and three drops for identifying Ag^+ and Hg^{2+}, respectively.

(3) Sensitivities. The process was carried out according to the standard method[19] on sensitivity. The results are shown in Table 2.

(4) Interference of coexistent ion. Tolerance limits of interfering ions were expressed as the ratio of amount of identified ions to that of interfering ions, which are shown in Table 3.

(5) Elimination of interfering ions. (a) For Ag^+ identification. Interference of S^{2-} could be eliminated by acidifying the sample with HNO_3, then heating the solution to vaporize the excess nitric acid. Interferences of large amounts of Cu^{2+}, Co^{2+} and Ni^{2+} could be eliminated by precipitating them with ammonium salt, and the supernatant can be identified after centrifugation.

(b) For Hg^{2+} identification. The interference of I^- could be eliminated by adding Ag^+; S^{2-} and SCN^- could be dispelled with *aqua regia* ($HCl:HNO_3$=3:1). No interferences of Ag^+, Hg_2^{2+} and Pb^{2+} were involved because they were precipitated in the HCl medium.

(6) Application to samples. (a) Identification of synthetic samples. The results with DFT as an identification reagent showed a good agreement with known samples (Table 4).

(b) Identification for standard samples. By means of the appropriate methods, we disposed of standard samples including polluted farmland, positive mud of copper, deposit of hydrographic net, lead and zinc minerals. The results

Table 4. Identification for synthetic samples

No.	Solution state	Medium	Phenomenon	Result	Components in solution
A	Yellow precip.	$NH_3 \cdot H_2O$	Brown	†Ag^+	Ag^+, Hg^{2+}, Cl^-, Br^-, PO_4^{3-}
		HCl	White precip.	†Hg^{2+}	K^+, Na^+, Mg^{2+}, Zn^{2+}, Co^{2+}, $S_2O_3^{2-}$, Ca^{2+}
B	Blue sol.	$NH_3 \cdot H_2O$	Brown	†Ag^+	Ag^+, CO_3^{2-}, Ni^{2+}, Cr^{3+}
		HCl	*	‡Hg^{2+}	Cu^{2+}, NO_3^-, Ac^-, SO_3^{2-}, AsO_3^{3-}, Fe^{3+}
C	Brown sol.	$NH_3 \cdot H_2O$	*	‡Ag^+	Hg^{2+}, Mg^{2+}, Cu^{2+}, Sn^{2+}
		HCl	White precip.	†Hg^{2+}	Zn^{2+}, S^{2-}, I^-, F^-, $S_2O_3^{2-}$, Hg^{2+}
D	Yellow turbid sol.	$NH_3 \cdot H_2O$	*	‡Ag^+	Sr^{2+}, Al^{3+}, Co^{2+}, Ni^{2+}
		HCl	*	‡Hg^{2+}	Pb^{2+}, I^-, SO_3^{2-}, CO_3^{2-}

Table 5. Identification for standard samples

Sample	Medium	Phenomenon	Result
Positive mud of copper	$NH_3 \cdot H_2O$	Brown	†Ag^+
	HCl	*	‡Hg^{2+}
Polluted farmland	$NH_3 \cdot H_2O$	*	‡Ag^+
	HCl	White precip.	†Hg^{2+}
Lead mineral	$NH_3 \cdot H_2O$	Brown	†Ag^+
	HCl	*	‡Hg^{2+}
Zinc mineral	$NH_3 \cdot H_2O$	Brown	†Ag^+
	HCl	*	‡Hg^{2+}
Deposit of hydrographic net	$NH_3 \cdot H_2O$	Brown	†Ag^+
	HCl	White precip.	†Hg^{2+}

*No distinct phenomenon taking place.
†Existence of the ion in the sample.
‡Non-existence of the ion in the sample.

Table 6. Comparison of DFT with other reagents

Ion	Reagent	Medium	PD	Interference	Reference
Ag^+	HCl	HNO_3	4.8	Hg_2^{2+}	12
	diethylaminobenzylidenerhodanine	Acid sol.	5.5	Hg, Au, Pd, Bi, Pb	13
	5-(p-dimethylaminobenzylidene)-rhodanine	Acid sol.	6.2	Hg^{2+}, Cu^{2+}	14
	DFT	$NH_3 \cdot H_2O$	6.3	S^{2-}	
Hg^{2+}	diphenylcarbazone	HNO_3	5	CrO_4^{2-}, MoO_4^{2-}, Au, V, Cl^-, Br^-, I^-, CN^-, SCN^-	15
	dithizone	HNO_3	6	Cu, Ag, Au, Bi, Pd	16
	Cu_2I_2	HCl	5.8	Hg_2^{2+}	17
	DFT	HCl	6	I^-, SCN^-, S^{2-}	

were correspondent with components marked (Table 5).

Comparison of DFT with other reagents

As shown by sensitivities and selectives in Table 6, DFT can be regarded as the best reagent to identify Ag^+ and Hg^{2+} up to now.

REFERENCES

1. D. L. Ma, X. J. Chen and X. J. Fan, *J. Henan Shifan Daxue Xuebao*, 1988, **59**, 110.
2. D. Shanjin, *J. Anal. Chem. (Jpn)*, 1964, **13**(1), 51.
3. M. Shimothni, *J. Pharm. Soc. Jpn.*, 1952, **72**, 400.
4. B. R. Shinde, N. M. Shinde and C. S. Parab, *J. Curr. Sci.*, 1982, **51**(4), 704.
5. E. Kavanov, G. Vassilev and C. R. Acad, *J. Buly. Sci.*, 1967, **20**(4), 365.
6. R. Y. Chen and H. Z. Yang, *J. Gaodeng Xuexiao Huaxue Xuebao*, 1983, **4**(2), 207.
7. O. F. William, *J. Pharm. Sci.*, 1986, **75**(12), 1180.
8. Y. L. Wang and D. L. Ma, *J. Huaxue Shiji*, 1983, **5**(1), 43.
9. W. Aumuller and L. Horner, *J. Chem. Ber.*, 1952, **86**, 760.
10. A. G. Schering, German Patent, 1952, 833040.
11. S. C. Shome, *Talanta*, 1982, **29**, 937.
12. Wuhan Univ., *Analytical Chemistry*. People's Education Publishing House, 1978, p. 36.
13. Y. E. Zheng, H. S. Zhang and Z. H. Cheng, *Modern Reagent Handbook* (Book 4), Chemical Industry Publishing House, 1989, p. 741.
14. F. I. Feigl, *Anal. Chem.*, 1928, **74**, 380.
15. Z. Holzbecher, *Organic Reagent Handbook in Inorganic Analysis*. Higher Education Publishing House, 1984, p. 245.
16. R. Pribll, *Talanta*, 1965, **12**, 925.
17. Wuhan Univ., *Analytical Chemistry*. Higher Education Publishing House, 1986, p. 36.
18. X. Zhu, *Practical Chemistry Dictionary*, Hongye Shuju Youxian Gongsi, 2nd Ed., 1969, p. 396.
19. D. L. Ma, Y. L. Wang and J. Y. Wang, *Anal. Lett.*, 1991, **24**(12), 2307.
20. Z. Holzbecher, L. Divis and M. Kral, *Handbook of Organic Reagents in Inorganic Analysis*. Ellis Horwood, 1976, p. 146.

Talanta, Vol. 40, No. 12, pp. 1851–1859, 1993
Printed in Great Britain.

0039-9140/93 $6.00 + 0.00

SIMULTANEOUS DERIVATIVE SPECTROPHOTOMETRIC DETERMINATION OF THORIUM AND URANIUM IN A MICELLAR MEDIUM

NARINDER KUMAR AGNIHOTRI, VINAY KUMAR SINGH and HAR BHAJAN SINGH*
Department of Chemistry, University of Delhi, Delhi 110007, India

(*Received* 2 *December* 1992. *Revised* 4 *March* 1993. *Accepted* 8 *May* 1993)

Summary—Derivative photometric methods for trace analysis of Th(IV) and UO_2(II), and their simultaneous determination in mixtures using 5,8-dihydroxy-1,4-naphthoquinone in a micellar medium are reported. Molar absorptivity and Sandell's sensitivity of 1:2 Th(IV) and 1:1 UO_2(II) complexes at their λ_{max}, 614.5 nm and 637.0 nm are, 1.19×10^4 l/mol/cm and 1.12×10^4 l/mol/cm and 1.95×10^{-2} $\mu g/cm^2$ and 2.13×10^{-2} $\mu g/cm^2$, respectively. Calibration graph is linear over the range 9.28×10^{-2}–18.56 μg/ml of Th(IV) and 9.52×10^{-2}–19.04 μg/ml of UO_2(II). Though presence of Th(IV) and UO_2(II) causes interference in each others determination, 9.28×10^{-1}–9.28 μg/ml Th(IV) and 9.52×10^{-1}–9.52 μg/ml UO_2(II) when present together, can be simultaneously determined using derivative spectra.

Important reagents for spectrophotometric determination of Th(IV) and UO_2(II) include arsenazo I, arsenazo III, thorin and chlorophosphonazo III, usually require a preliminary step to extract the analyte from complex matrix by organic solvent(s).[1–3] The aforesaid reagents, though sensitive, lack selectivity. Besides being cumbersome, such procedures have inherent sources of errors. The spectrophotometric determination of Th(IV) and UO_2(II) must be preceded by pre-separation when the two are present together in a mixture as interference is caused due to spectral overlap.[4,5]

Though claims are often made regarding the sensitivity and selectivity of NAA, ICP–AES, and ICP–MS some of the interferences, to which these procedures are subjected to, are poorly understood and continue to cause problems.[6,7] Therefore, development of sensitive and selective photometric methods continue to be of interest in spite of recent developments in ASS, ICP–AES and ICP–MS.[6]

The use of micellar media[8–10] and derivative spectrophotometry[11,12] not only offers convenient solutions to a number of analytical problems such as avoiding extraction processes, resolution of multicomponent system and matrix background, but also enhances the sensitivity and selectivity of the method.

The present communication describes sensitive and inexpensive methods for the determination of microamounts of Th(IV) and UO_2(II) using 5,8-dihydroxy–1,4-naphthoquinone(DHNQ), as a chromogenic ligand[13–15] in a micellar medium generated by Triton X-100, a neutral surfactant. A simple and rapid procedure is developed for simultaneous determination of Th(IV) and UO_2(II) in aqueous phase without any pre-separation or extraction using derivative spectrometry.

EXPERIMENTAL

Chemicals

Stock solutions (0.01M) of Th(IV) and UO_2(II) were prepared by dissolving requisite amounts of $Th(NO_3)_4 . 5H_2O$ and $UO_2(NO_3)_2 . 6H_2O$, respectively in water containing few drops of nitric acid. Solution ($4.0 \times 10^{-4}M$) of DHNQ was freshly prepared everyday by dissolving 7.61 mg of the ligand in minimum amount of 0.2M sodium hydroxide at 40°C. This solution was acidified after adding 4.0 g Triton X-100 and finally diluted with water to 100 ml.

Appropriate amounts of the solutions of Th(IV) or UO_2(II), DHNQ, Triton X-100 and ammonium acetate (buffer) were taken to give final concentration of $4.0 \times 10^{-5}M$, $2.0 \times 10^{-4}M$, 2.0% w/v and $5.0 \times 10^{-3}M$ in all working solutions, respectively, unless stated otherwise.

*Author for correspondence.

Instruments

Absorption spectra were recorded on a Shimadzu UV–visible recording spectrophotometer (Model UV-260), capable of taking first to fourth order derivative spectra with $\Delta\lambda$ values 1, 2, and 4 nm; 10-mm fused silica cells were used for absorption measurements taking water as reference. The pH of the solutions were measured on an EC digital pH-meter (Model PH 5662).

First and second derivative spectra were recorded directly on UV-260 using data command-chain mode, with $\Delta\lambda$ 2 and 4 nm, respectively and a bandwidth of 1 nm.

Procedure

Determination of Th(IV)/UO_2(II). To study the effect of pH on complex formation, two series of solutions, one with metal ion and the other without it, each in the same pH range (2.0–12.0) and containing DHNQ, Triton X-100 and ammonium acetate, were prepared.

To investigate the effect of surfactant concentration on the ligand and the complex, a set of solutions containing increasing amount of Triton X-100 and a fixed amount of DHNQ, the metal ion and ammonium acetate at optimum pH, was prepared for each system.

To evaluate the impact of varying metal ion concentration on complexation, a series of solutions containing increasing amount of the metal ion and a fixed amount of DHNQ, ammonium acetate and Triton X-100 at optimum pH, was prepared.

Simultaneous determination of Th(IV) and UO_2(II). A set of solutions containing increasing amounts (9.28×10^{-1}–9.28 μg/ml) of Th(IV) and another containing increasing amounts (9.52×10^{-1}–9.52 μg/ml) of UO_2(II) ions, each having a fixed amount of DHNQ and Triton X-100, were prepared. The first and second order derivative spectra of both sets were recorded on the same chart in order to locate the isodifferential points. To obtain the isodifferential points on zero-line, spectra have been recorded with reference to ligand blank. The calibration graph for the determination of Th(IV) was prepared by measuring derivative amplitudes at isodifferential points of UO_2(II) and vice versa for UO_2(II). Concentration of Th(IV) and UO_2(II) ions in the mixture was then determined using these graphs.

RESULTS AND DISCUSSION

Effect of pH on the absorbance of the systems

Th(IV)–DHNQ and UO_2(II)–DHNQ complexes in neutral micellar media show pH dependent absorption maximum at 614.5 and 637.0 nm, respectively whereas DHNQ shows maximum absorption at 490 nm. As the ligand also absorbs at the λ_{max} of the complexes, the absorbance due to complex was calculated by taking the differences between the absorbances of the complex and the ligand, each recorded against water. It was then plotted against pH of the solutions in each case (Fig. 1). The graph indicates that complexation of Th(IV) and UO_2(II) commences at pH 4.7 and 5.0, respectively and increases up to pH 5.9 and 6.1. Relative absorbance w.r.t. ligand of the solutions containing the complex remains practically constant ($\pm$2.0%) from pH 5.9 to 7.2 and 6.1 to 7.3 in the two cases but decreases thereafter due to higher extinction of the deprotonated DHNQ formed at pH $\geqslant$ 7.3. Furthermore, it is inferred from the plot that maximum complex formation takes place at pH 6.4 and 6.5 in case of Th(IV) and UO_2(II), respectively. All absorption studies are carried out at these pH values and at 614.5 and 637.0 nm, the wavelengths of maximum absorption of the complexes in the two cases.

Effect of the nature of surfactant

Effect of the presence of anionic surfactant [sodiumlauryl sulphate (SLS)], cationic surfactants [cetylpyridinium chloride (CPC) and cetyltrimethylammonium bromide (CTMB)]

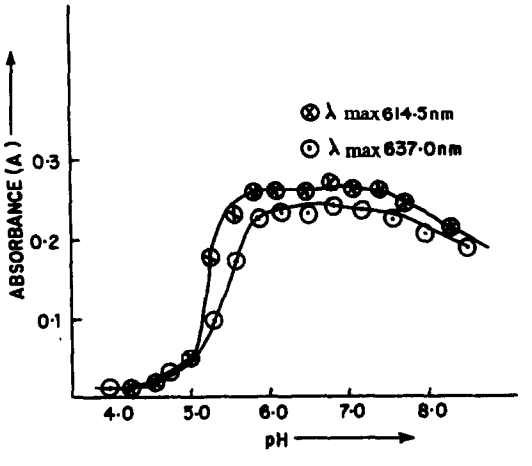

Fig. 1. Effect of pH on complex formation; (⊗) DHNQ–Th(IV) and (⊙) DHNQ–UO_2(II) complexes in micellar media.

and non-ionic surfactant (Triton X-100, CMC $3.2 \times 10^{-4}M$)[16] on the absorption profiles of each system has been studied. As anionic surfactants generally sequester the metal ions, the complexation reaction is inhibited in their presence in contrast to cationic and non-ionic surfactants.[9] Moreover, cationic and non-ionic surfactants have a marked effect on the absorbance characteristics of DHNQ as well as its thorium and uranyl complexes. Since cationic surfactants form ternary species of different optical properties as a function of pH, a non-ionic surfactant, Triton X-100 was selected for micelle formation during the present study. A sharp increase in absorbance with increasing Triton X-100 concentration up to 2.0% was observed in case of both the complexes. As a small decrease in absorbance was observed at concentration $\geqslant$2.25% w/v, the amount of the Triton X-100 was, kept at 2.0% w/v (which is greater than CMC) during subsequent investigations.

Effect of time and reversibility of the complexation reactions

It is inferred from the absorbance spectra that DHNQ and its Th(IV) and UO_2(II) complexes are optically stable up to 24 and 12 hr, respectively at room temperature (20–25°C). Change in absorbance of the system on reverting from a higher pH to the optimum pH was investigated for each system. The complexation reaction, in the two systems are found to be reversible between pH 6.4–12.0 and 6.5–12.0, respectively.

Effect of varying DHNQ concentration

To study this effect, spectra of a set of solutions containing fixed amount of the metal ion and the surfactant but increasing amount (4.0×10^{-6}–$2.8 \times 10^{-4}M$) of DHNQ was recorded. In each case, the absorbance has been found to increase with concentration of the ligand. It is attributed partly to the increased amount of the complex formed and partly to the absorption by the ligand at λ_{max} of the complexes. Absorbance values were, therefore, corrected for the absorption of the uncomplexed ligand and plotted against molar concentration of the ligand for each system. The plot remains practically constant ($< \pm 4.0\%$), between 5:1 and 20:1 (L:M) in case of Th(IV) and 4:1 to 30:1 (L:M) in the case of UO_2(II) complex (Fig. 2). During further studies, therefore, concentration of the ligand was kept between the above mentioned limits, wherever possible.

Number of chromogenic species and their stoichiometry

The number of chromogenic species formed in each case has been evaluated by computerized calculation on the rank of the absorbance matrix,[17] prepared by measuring absorbance of a set of solutions at a number of different wavelengths (from 400 to 740 nm) and at various pH or concentration of the components, assuming additivity of absorbances. The rank of the matrix defines the number of non-zero elements on the diagonal of the matrix and corresponds to the number of absorbing species in

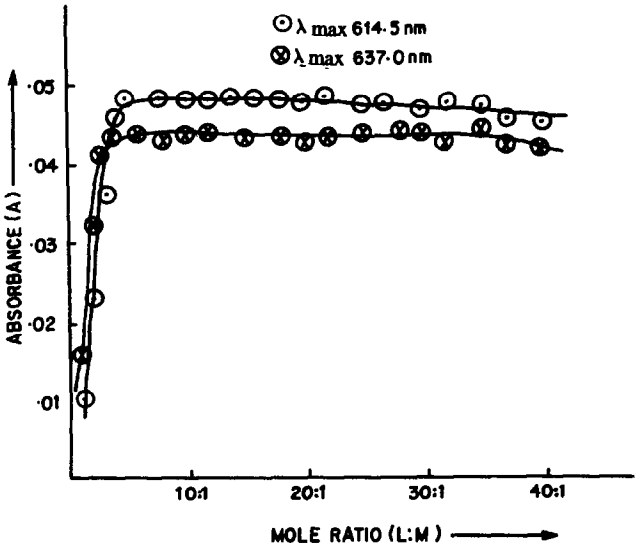

Fig. 2. Effect of DHNQ concentration (4.0×10^{-6}–$2.8 \times 10^{-4}M$) on absorbance of (⊙) thorium and (⊗) uranyl complexes in micellar media.

the system. The rank is determined by triangularizing the absorbance matrix (*i.e.* all elements below principal diagonal are zero) based on the method of Gaussian elimination. Rank is then determined by comparing the diagonal elements of reduced absorbance matrix with an assumed error matrix. Consequently, three absorbing species have been inferred to be present in the solution of DHNQ-Triton X-100 when the overall absorbance error for the absorbance matrix of DHNQ-Triton X-100 system was varied from 0.0026 to 0.0120 absorbance units. This was consistent with the expected presence of three species, *i.e.* H_2NQ, HNQ^{1-}, NQ^{2-} in the pH range 2.0–12.0. However, only the first two exist under experimental conditions. Three species also exist in solution following complexation in each case, when the value of error matrix is varied between 0.0028 and 0.0150 absorbance units. Thus, it may be inferred that only one new chromogenic species is formed during complexation of Th(IV) and UO_2(II) with DHNQ in a neutral surfactant medium.

Stoichiometry of the complexes formed under optimum experimental conditions was determined by Job's method of continuous variations.[18] The ratio of Th(IV) to DHNQ and UO_2(II) to DHNQ in the neutral micellar medium is found to be 1:2 and 1:1 (M:L), respectively; stoichiometry of the thorium complex is in agreement with the value in the organic phase reported by Moeller *et al.*[13] The complexes existing in solution are, therefore, represented as $[Th(HNQ)_2]^{2+}$ and $[UO_2(HNQ)]^+$, where H_2NQ denotes the molecular form of DHNQ.

Effect of varying metal ion concentration

Normal as well as derivative spectra of a set of solutions containing increasing amount of metal ion at a fixed and excess amount of the ligand have been investigated to use the developed method for trace analysis of these metal ions. An increase in concentration of the metal ion linearly increases the absorbance [Figs 3(a) and 4(a)] at λ_{max} of the complexes. Linear regression of the plot between metal ion concentration and the absorbance gives a straight line equation with positive intercept in both systems (Table 1). The observed absorbance values have, therefore, been corrected for absorption of the uncomplexed ligand to give $[A_i]_c$, the corrected absorbance at λ_{max} of the complex (equation (1)).

$$[A_i]_c = (A_i)_{comp} - [(V)_L - R \times (V_i)_M]\left[\frac{(A')_{comp}}{(V)_L}\right] \quad (1)$$

where $(A_i)_{comp}$ is absorbance of the complex at λ_{max}; $(A')_{comp}$ is absorbance of the ligand alone at λ_{max} of the complex and $(V_i)_M$, the molar volume of the metal ion solution. Subscript i denotes the serial number of the solution; R, the stoichiometry of the complex and $(V)_L$, the molar volume of the ligand are constant throughout the experiment. Linear regression of $[A_i]_c$ values gives improved linear plot in each case, as shown by the value of linear regression coefficient (Table 1).

The first order derivative spectrum in both systems is of great analytical value as λ_{max} of Th(IV) and UO_2(II) complexes corresponds to

Table 1. Linear regression analysis of Th(IV) or UO_2(II) ion concentration (μg/ml) and absorbance in normal and derivative modes

Th(IV)–DHNQ–Triton X-100		UO_2(II)–DHNQ–Triton X-100	
Straight line equation	Regression coefficient	Straight line equation	Regression coefficient
Normal mode:			
Absorption at 614.5 *nm*		Absorption at 637.0 *nm*	
$[A] = 2.586 \times 10^{-2}[T] + 2.147 \times 10^{-1}$	0.9919	$[A] = 1.229 \times 10^{-2}[U] + 7.773 \times 10^{-2}$	0.9957
$[A]_c = 3.372 \times 10^{-2}[T] + 3.080 \times 10^{-2}$	0.9952	$[A]_c = 1.345 \times 10^{-2}[U] + 2.221 \times 10^{-2}$	0.9964
First derivative mode:			
$[TD]_{553\ nm} = 5.068[T] - 5.972$	0.9966	$[TD]_{532\ nm} = 2.106[U] + 3.084$	0.9969
$[PH]_{555\ nm} = 3.164[T] + 1.410$	0.9889	$[TD]_{573\ nm} = 2.771[U] + 3.764$	0.9968*
$[TD]_{632\ nm} = 3.837[T] + 3.406$	0.9973*	$[TD]_{650\ nm} = 2.274[U] + 6.578$	0.9918*
Second derivative mode:			
$[TD]_{615\ nm} = 2.934[T] + 2.821$	0.9916*	$[TD]_{642\ nm} = 2.269[U] + 6.716$	0.9954*
		$[PH]_{665\ nm} = 1.510[U] + 5.719 \times 10^{-1}$	0.9984*

*Recommended for determination/detection.

PH = peak height; TD = trough depth; $[A]_c$ = corrected absorbance; $[T]$ and $[U]$ = concentration of Th(IV) and UO_2(II) ions (μg/ml), respectively.

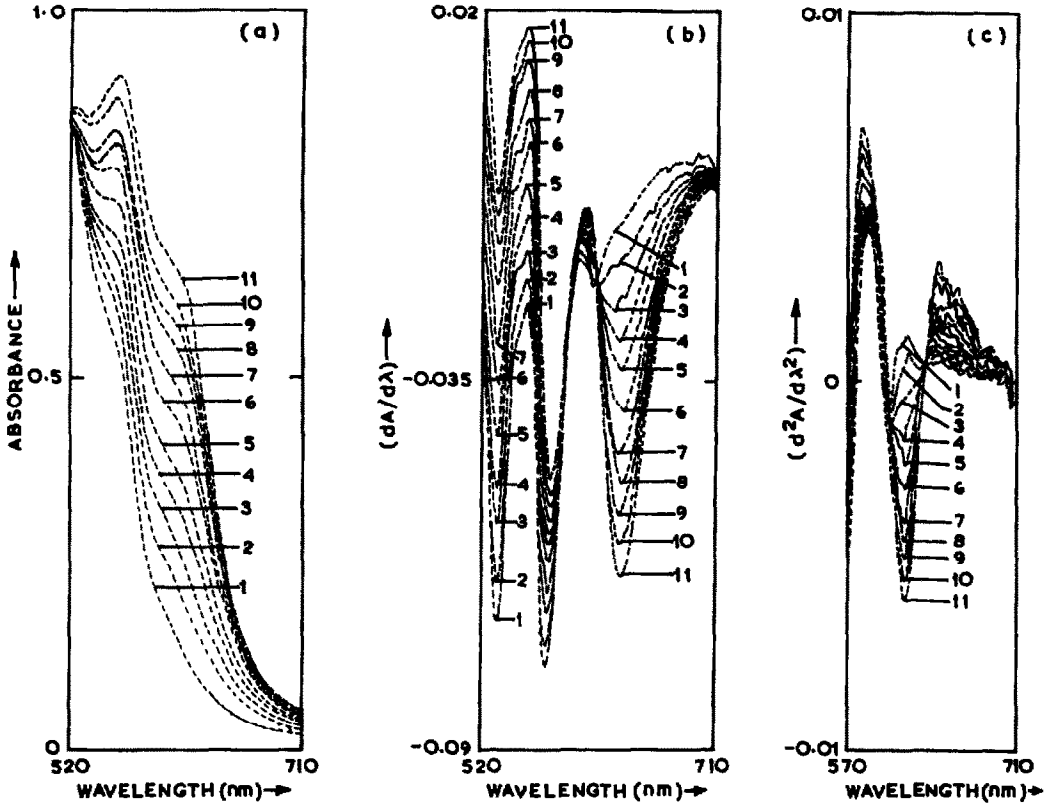

Fig. 3. Absorption spectra of Th(IV)–DHNQ–Triton X-100 system; No. 1 contains only $2.0 \times 10^{-4}M$ DHNQ; Nos. 2–11 containing increasing concentration of Th(IV) (1.86–18.56 μg/ml). (a) Normal, (b) first order and (c) second order derivative spectra.

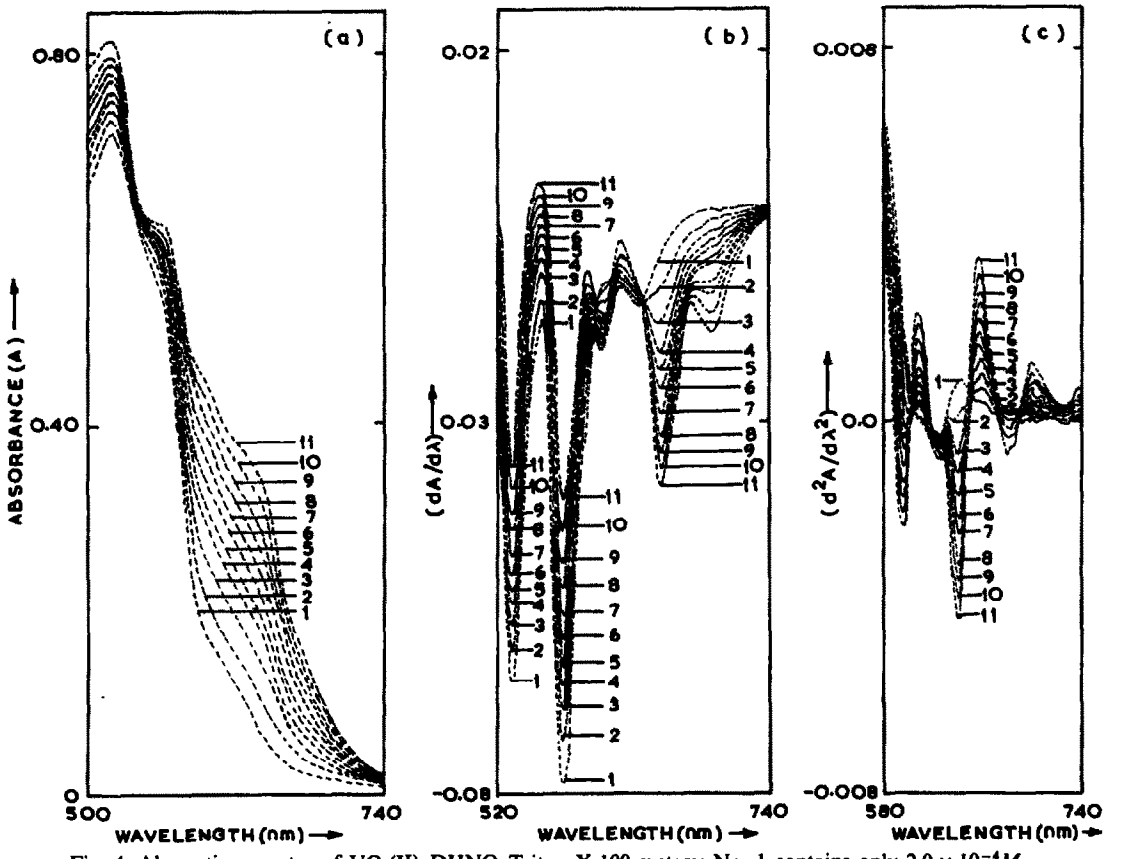

Fig. 4. Absorption spectra of UO_2(II)–DHNQ–Triton X-100 system; No. 1 contains only $2.0 \times 10^{-4}M$ DHNQ; Nos. 2–11 containing increasing concentration of UO_2(II) (1.90–19.04 μg/ml). (a) Normal, (b) first order and (c) second order derivative spectra.

Table 2. Photometric characteristics of Th(IV)–DHNQ and UO_2(II)–DHNQ complexes in micellar media

Photometric parameters	Th(IV)–DHNQ	UO_2(II)–DHNQ
λ_{max} (*nm*)	614.5	637.0
Molar absorption coefficient (ε) (*l/mol/cm*)	1.19×10^4	1.12×10^4
Specific absorptivity (*a*) (*ml/g/cm*)	5.13×10^{-2}	4.71×10^{-2}
Sandell's sensitivity (*S*)[5] ($\mu g/cm^2$)	1.95×10^{-2}	2.13×10^{-2}
Detection limit (IUPAC)[19] $n = 25$, $k = 3$ (*ng/ml*)	25	33
Stoichiometry (M:L)[18]	1:2	1:1

the cross-over point at 614.5 and 637.0 nm, respectively [Figs 3(b) and 4(b)]. Peak height [PH] and trough depth [TD], measured from the base line of the ligand or zero-line of the derivative spectrum of the complexes are proportional to the metal ion concentration [Figs 3(b) and (c), and 4(b) and (c)], as shown by a good linear fit (Table 1). These are, therefore, recommended for the determination/detection of the metal ions. Beer's law is found valid between 9.28×10^{-2}–18.56 μg/ml and 9.52×10^{-2}–19.04 μg/ml of Th(IV) and UO_2(II) ions, respectively.

Photometric parameters of both systems, calculated from the corrected absorbance value, $[A_i]_c$ (all w.r.t. metal ions), as well as IUPAC detection limits[19] are summarized in Table 2.

Conditional stability constant

The conditional stability constant[20,21] of the complexes formed under optimum conditions was calculated on the basis of the following equilibrium as only one complex is inferred to be formed on the basis of spectrophotometric studies reported above.

$$Th^{4+} + 2H_2NQ \rightleftharpoons [Th(HNQ)_2]^{2+} + 2H^+$$

$$UO_2^{2+} + H_2NQ \rightleftharpoons [UO_2(HNQ)]^+ + H^+$$

The conditional stability constant (k') based on concentration and absorbance (corrected, $[A_i]_c$)

Table 3. Effect of diverse ions in the determination of (a) thorium (4.760 μg/ml) and (b) uranyl (9.520 μg/ml) ions with DHNQ in micellar medium

Diverse ions	Concentration added ($\mu g/ml$) (a)	(b)	% error (a)	(b)	Diverse ions	Concentration added ($\mu g/ml$) (a)	(b)	% error (a)	(b)
Cations:									
Mo(VI)	1.00	0.10	1.47	1.64	W(VI)	0.20	70.0	1.41	−0.29
UO_2(II)/Th(IV)	0.20	0.05	−0.40	2.10*	Ce(IV)	0.20	0.10	2.14*	1.22
VO(II)	0.05	5.00	1.03†	0.92†	Zr(IV)	0.10	1.00	1.85	−0.88
B(III)	5.00	10.0	1.62	0.48	Al(II)	0.01	0.01	3.21*	2.11*
Ga(III)	0.05	0.05	1.85	1.94†	In(III)	0.10	1.00	1.62	0.93†
Tl(III)	5.00	20.0	1.05†	−0.76†	As(III)	20.0	2.00	−0.99	0.93
Bi(III)	2.00	20.0	1.47	0.29†	Cr(III)	0.10	0.50	−0.48†	−1.14†
Fe(III)	0.05	0.05	1.91†	2.11†*	Au(III)	0.20	0.20	1.41	1.98
Ca(II)	30.0	40.0	0.92	1.02	Mg(II)	5.00	2.00	1.30	−0.36
Sn(II)	1.00	1.00	2.12*	1.22	Pb(II)	2.00	0.20	1.74	0.86
Mn(II)	5.00	5.00	1.43	0.96	Co(II)	0.05	0.50	1.70†	−0.63†
Cu(II)	5.00	0.50	−1.30†	−1.22†	Zn(II)	0.05	0.50	1.81	0.93
Cd(II)	10.0	10.0	1.15	−0.45	Hg(II)	2.00	10.0	1.55	1.64
Ni(II)	0.05	0.50	2.12†*	0.76	Be(II)	0.01	0.01	1.22	1.17
Li(I)	0.50	0.05	1.97	1.74	Ag(I)	10.0	70.0	1.87	−0.80†
Anions:									
Fluoride	2.00	20.0	1.58	0.22	Chloride	360	300	−0.46	1.50
Bromide	80.0	50.0	1.70	1.39	Iodide	130	5.00	1.45	1.85
Thiocyanide	5.00	2.00	−0.25	1.52	Ascorbate	1.00	50.0	1.26	1.94
Tartrate	0.10	50.0	−0.61	−1.10	Citrate	0.20	0.20	0.29	−1.64
Oxalate	1.00	1.00	1.03	1.81	EDTA	0.20	0.20	−1.83	−1.60
Phosphate	0.10	1.00	−1.91	−0.50	Acetate	600	500	0.46	0.93

*Strongly interfere.

†Precipitation at high concentration.

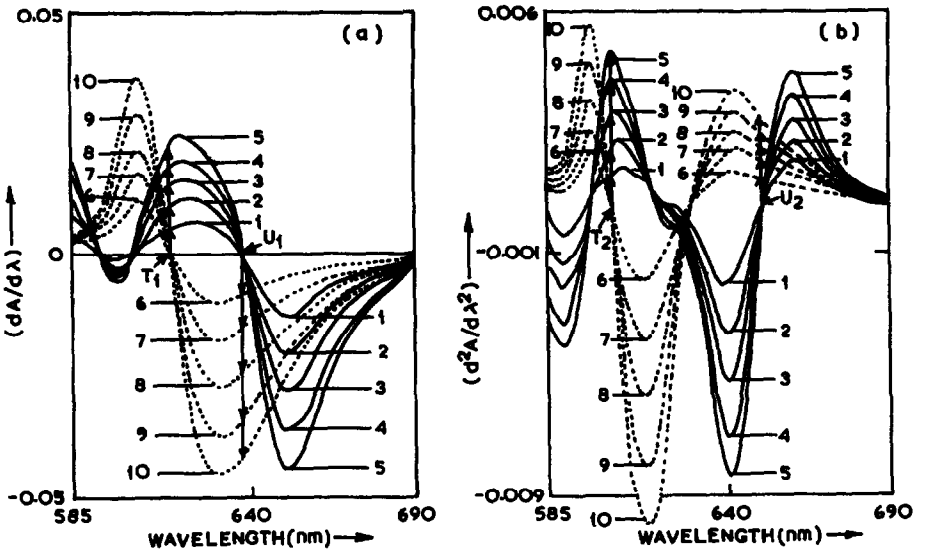

Fig. 5. Derivative spectra of two sets of solutions; Nos. 1–5 containing increasing concentration (9.52×10^{-1}–9.52 μg/ml) of UO_2(II); and Nos. 6–10 containing (9.28×10^{-1}–9.28 μg/ml) Th(IV); both having $4.0 \times 10^{-4}M$ DHNQ. (a) First order and (b) second order.

values of Th(IV) and UO_2(II) complexes has been found to be 2.29×10^5 l/mol and 1.12×10^5 l/mol (average of six values), respectively.

Effect of diverse ions on the determination of the analyte

Interference in the photometric determination of Th(IV) and UO_2(II) from a number of common cations and anions has been investigated in normal as well as derivative modes to evaluate the practical utility of DHNQ. This was studied by adding the varying amount of the foreign ions (in μg/ml) to a solution containing fixed amount of Th(IV) (4.760 μg/ml) or UO_2(II) (9.520 μg/ml), DHNQ, Triton X-100 and ammonium acetate, and measuring the change in absorption profiles. Limiting concentration of the diverse ions that does not interfere in the analysis of Th(IV) and UO_2(II) ions are summarized in Table 3. The complexation reaction of Th(IV) and UO_2(II) ions with DHNQ in presence of neutral micellar media are masked

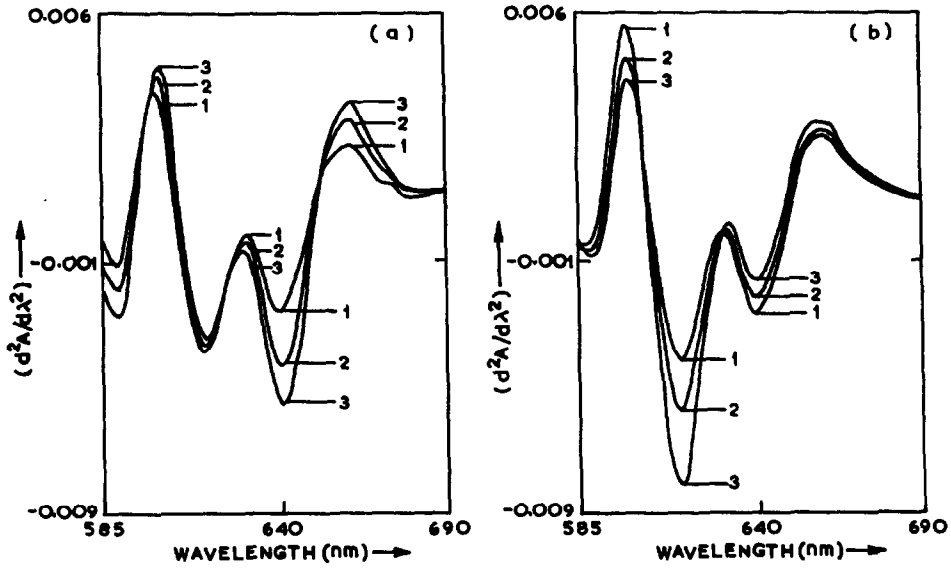

Fig. 6. Second order derivative spectra of DHNQ complexes of Th(IV) and UO_2(II); (a) Th(IV) 3.712 μg/ml and 3.808 (1), 5.712 (2) and 7.616 (3) μg/ml UO_2(II) and (b) UO_2(II) 3.808 μg/ml and 3.712 (1), 5.568 (2) and 7.424 (3) μg/ml Th(IV).

Table 4. Comparison of the analytical methods for simultaneous determination

Element determine	Method	Sensitivity, $S_A = S_s/m$ (ng/ml)	$C_L(k=3)$ (ng/ml)	Linear dynamic range (ng/ml)	RSD, % ($n=6$)
Th(IV)	1st derivative	39.6	1.19×10^2	3.96×10^2–9.28×10^3	1.12
	2nd derivative	13.0	39.0	1.30×10^2–9.28×10^3	0.23
UO_2(II)	1st derivative	55.0	1.65×10^2	5.50×10^2–9.52×10^3	1.09
	2nd derivative	9.3	27.9	9.30×10^1–9.52×10^3	0.24

by the presence of tartrate, EDTA and phosphate, and citrate and EDTA, respectively. Further, masking agents such as citrate, tartrate, EDTA and phosphate have also been used to overcome the interference from a number of cations, but these did not help. High order derivative spectrophotometry, a relatively new and fast developing technique has also been used to determine Th(IV) and UO_2(II) in the presence of interfering ions, as derivatization of spectra resolves overlapping peaks of normal spectra into separate peaks and troughs, and crossover points. This technique is useful in case of strongly interfering cations of Be, Al, Fe, Au, Ce, VO, Th or UO_2 and Ni. Amongst these Th and UO_2 have been selected for detailed investigations; UO_2 has been determined in presence of Th and vice versa, using derivative spectrophotometry.

Simultaneous determination of Th(IV) and UO_2(II)

Since presence of Th(IV) and UO_2(II) ions causes interference in each other's photometric determination, a pre-separation is to be carried out before their determination in a mixture. Analytical advantages offered by derivative spectrophotometry[22,23] have been made use of to analyze a mixture containing these two ions without any prior separation. For this purpose, instrumental parameters such as scan speed, wavelength increment ($\Delta\lambda$) over which derivative spectra were recorded, response time and slit width, which affects the shape of derivative spectra, were optimized w.r.t. reduction of noise level, stability of zero points or crossover points and isodifferential points. Consequently, a $\Delta\lambda$ of 2 and 4 nm for first and second derivative modes is found optimum for the least signal-to-noise ratio for recording derivative spectra. A 1 nm slit width was selected as it does not significantly alter the spectral resolution. A scan speed of 40 nm/min was found optimum. This automatically optimizes the response time.

Th(IV)–DHNQ and UO_2(II)–DHNQ complexes show one isodifferential point in each derivative mode [Figs 5(a) and (b)]. Calibration graphs for the determination of uranyl ions were prepared by measuring change in derivative amplitude, $dA/d\lambda$ [T_1] and $d^2A/d\lambda^2$ [T_2] at 614.5 and 604.5 nm, respectively, the isodifferential points of thorium complex. Similarly for Th(IV) ions, change in derivative amplitude, $dA/d\lambda$ [U_1] and $d^2A/d\lambda^2$ [U_2] at 637.0 and 651.5 nm, respectively, the isodifferential points of uranyl complex have been measured. The linear regression analysis of the change in derivative amplitude at isodifferential points on the metal ion concentration shows following relationship with good linear fit as evidenced by their residue square values (r).

$$[T_1]_{614.5\,nm} = 3.386\,[U] + 1.392; \quad (r = 0.9984) \quad (2)$$

$$[T_2]_{604.5\,nm} = 5.087\,[U] + 3.339 \times 10^{-1}; \quad (r = 0.9985)^* \quad (3)$$

$$[U_1]_{637.0\,nm} = 6.782\,[T] - 1.601 \times 10^{-2}; \quad (r = 0.9972) \quad (4)$$

$$[U_2]_{651.5\,nm} = 2.505\,[T] + 4.698; \quad (r = 0.9992)^* \quad (5)$$

Table 5. Quantitative determination of thorium (9.28×10^{-1}–9.28 μg/ml) and uranyl (9.52×10^{-1}–9.52 μg/ml) in mixtures using DHNQ

Sr. No.	Taken (μg/ml)		Found (μg/ml)		Relative error (%)	
	Th(IV)	UO_2(II)	Th(IV)	UO_2(II)	Th(IV)	UO_2(II)
1	0.928	0.952	0.936	0.939	0.86	−1.37
2	0.928	3.808	0.938	3.875	1.08	1.76
3	1.856	2.856	1.841	2.877	−0.81	0.73
4	3.712	3.808	3.693	3.736	−0.51	−1.89
5	3.712	4.760	3.650	4.820	−1.67	1.26
6	6.496	2.856	6.638	2.803	2.19	−1.86
7	6.496	4.760	6.444	4.795	−0.80	0.73
8	4.640	6.664	4.665	6.685	0.54	0.31
9	5.568	2.856	5.668	2.785	1.79	−2.49
10	7.424	9.520	7.503	9.492	1.06	−0.29
11	9.280	4.760	9.403	4.730	1.32	−0.63
12	9.280	9.520	9.204	9.573	−0.82	0.56

*Determination of UO_2(II) at T_2 and Th(IV) at U_2 is recommended, based on large dynamic range and better sensitivity (Table 4) and large values of r; [U] and [T] is concentration in (μg/ml) of UO_2(II) and Th(IV) ions, respectively. Linear plots are obtained for Th(IV) and UO_2(II) ion concentration from 9.28×10^{-1} to 9.28 μg/ml and 9.52×10^{-1} to 9.52 μg/ml at the isodifferential points of uranyl and thorium complexes, respectively.

Presence of Th(IV) ions in UO_2(II)–DHNQ complex and UO_2(II) ions in Th(IV)–DHNQ, changes amplitude at the isodifferential points of UO_2(II) and Th(IV) complexes in each derivative spectrum. Concentrations of UO_2(II) and Th(IV) ions in synthetic mixtures with different concentration ratios have been calculated using equations (2) or (3) and (4) or (5), respectively but better results are obtained using second order derivative spectra, shown by better observed RSD values (Table 4) calculated from six replicate samples containing 3.712 μg/ml of Th(IV) in presence of UO_2(II) ions, and 3.808 μg/ml of UO_2(II) in presence of Th(IV) ions [Figs 6(a) and (b)]. The calculated analytical sensitivity, S_A ($S_A = S_s/m$, where S_s is the standard deviation of the analytical signal measurement and m, is the slope of the calibration curve) detection limit, C_L ($k = 3$) and linear dynamic range of the method as defined by IUPAC are also given in this table.[24] The limit of quantitation, LOQ ($k = 10$) is used to establish the lower limit of dynamic range. The results obtained for simultaneous determination of Th(IV) and UO_2(II) ions in various binary mixtures are shown in Table 5 [using equations (3) and (5)]. The mixture containing 9.28×10^{-1}–9.28 μg/ml of Th(IV) and 9.52×10^{-1}–9.52 μg/ml UO_2(II) ions can be analyzed with a relative error less than 2.50%.

In addition to developing a simple procedure for the determination of thorium and uranyl ions when present alone or in a mixture, analytical advantage of incorporating a micellar medium and recording derivative spectra is well established on the basis of the above studies.

Acknowledgement—The authors are thankful to U.G.C. for financial assistance to N.K.A. during this work.

REFERENCES

1. S. B. Savvin, *Talanta*, 1961, **8**, 673; 1964, **11**, 1.
2. J. K. Foreman, C. J. Riley and T. D. Smith, *Analyst*, 1957, **82**, 89.
3. T. Yamamoto, *Anal. Chem. Acta*, 1973, **65**, 329.
4. H. P. Holocomb and J. H. Yoe, *Microchem. J.*, 1960, **4**, 463.
5. Z. Marczenko, *Spectrophotometric Determination of Elements*. Ellis Horwood, Chichester, 1976.
6. C. J. Kantipuly and A. D. Westland, *Talanta*, 1988, **35**, 1.
7. A. Ramesh, J. Krishnamacharayulu, L. K. Ravindranath and S. B. Rao, *Analyst*, 1992, **117**, 1037.
8. L. J. C. Love, J. G. Habarta and J. G. Dorsey, *Anal. Chem.*, 1984, **56**, 1133A.
9. E. Pelizzetti and E. Pramauro, *Anal. Chem. Acta*, 1985, **169**, 1.
10. E. Pramauro and E. Pelizzetti, *Trends in Anal. Chem.*, 1988, **7**, 260.
11. S. Shibata, M. Furukawa and K. Goto, *Anal. Chem. Acta*, 1973, **65**, 49.
12. C. T. Cottrell, *Anal. Proc.*, 1982, **19**, 43.
13. T. Moeller and M. Tecotzky, *Anal. Chem.*, 1955, **27**, 1056.
14. R. S. Bottei and P. L. Gerace, *J. Inorg. Nucl. Chem.*, 1961, **23**, 245.
15. H. D. Coble and H. F. Holtzclaw, Jr., *J. Inorg. Nucl. Chem.*, 1974, **36**, 1049.
16. K. Kano, Y. Ueno, K. Umakosbi, S. Hashimoto, T. Ishibashi and T. Ogawa, *J. Phys. Chem.*, 1984, **88**, 5087.
17. R. M. Wallace and S. M. Katz, *J. Phys. Chem.*, 1964, **68**, 3890.
18. W. C. Vosburgh and G. R. Cooper, *J. Am. Chem. Soc.*, 1941, **63**, 437.
19. IUPAC, Nomenclature, symbols, units and their usage in spectrochemical analysis, *Pure Appl. Chem.*, 1976, **45**, 105.
20. A. Ringbom, *J. Chem. Educ.*, 1958, **35**, 282.
21. L. G. Sillen and A. E. Martell, *Stability Constants of Metal Complexes*, Vols 1 and 2. Chemical Society London, 1964, 1971.
22. B. Murelli, *Analyst*, 1983, **108**, 1506.
23. F. G. Sanchez, M. H. Lopez and J. C. M. Gomez, *Talanta*, 1987, **34**, 639.
24. G. L. Long and J. D. Winefordner, *Anal. Chem.*, 1983, **55**, 712A.

Talanta, Vol. 40, No. 12, pp. 1861–1866, 1993
Printed in Great Britain.

0039-9140/93 $6.00 + 0.00

SIMULTANEOUS SPECTROPHOTOMETRIC DETERMINATION OF CADMIUM, COPPER AND ZINC

A. M. GARCIA RODRIGUEZ, A. GARCIA DE TORRES, J. M. CANO PAVON and C. BOSCH OJEDA
Department of Analytical Chemistry, Faculty of Sciences, University of Málaga, 29071 Málaga, Spain

(*Received* 16 *November* 1992. *Revised* 17 *May* 1993. *Accepted* 19 *May* 1993)

Summary—A method for the simultaneous spectrophotometric determination of cadmium, copper and zinc based on the formation of their complexes with 1,5-bis(di-2-pyridylmethylene)thiocarbonohydrazide is proposed. The absorption curves of these complexes overlap severely in the scanning range 380–480 nm. The analyte concentrations are calculated by a least squares fit of the pure spectra to the mixture spectra. A linear determination range of 0.1–1.7 μg/ml for cadmium, 0.1–1.3 μg/ml for copper and 0.2–1.2 μg/ml for zinc were obtained. The effect of interference was studied. The method has been applied to the determination of these metal ions in various type of materials.

Until recently, multicomponent determinations by spectrophotometry have been done by using a single wavelength for each component. Recently, the strategies available in analytical chemistry and, in particular, those using molecular spectroscopy have diversified. Thus, multicomponent determinations have been improved by using multiple wavelengths and different algorithms. Such algorithms include those of classical least-squares (CLS),[1] the simplex interaction method,[2] the inverse least-squares (ILS),[3] the principal component regression (PCR),[4] the partial least-squares (PLS)[5] and other multivariate statistical method.[6]

Recently, Sala *et al.*[7] applied a computer program, like MULTIC, to the resolution of a mixture of pharmaceuticals. Also, this program has been used by Gomez *et al.*[8] for the simultaneous determination of calcium and magnesium in water. MULTIC is a multilinear regression program that involves fitting the calculated mixed spectrum to its experimental counterpart through the standard deviation, correlation coefficient and an independent term corresponding to the intercept on the absorbance axis. For simultaneous spectrophotometric determination of M components in a mixture to be achieved, each species must absorb according to Beer's law, and the absorbances must be additive. Both conditions (using 1 cm of the optical path-length) can be described by a mathematical model of the form:

$$x = \Sigma S_A C_A + e \quad (1)$$

where x is the measured (sum) spectrum, S_A is the pure spectrum of analyte A, C_A is the concentration of analyte A in the mixture and e is the residual (difference between the observed response and the response calculated from the model). The equation (1) can be rewritten in shorthand matrix notation as:

$$x = Sc + e. \quad (2)$$

Where S is the matrix containing the pure spectra as columns (size: p,M; where $p >= M$ is the number of wavelengths employed and M is the number of analytes) and c is a vector containing the coefficients/the unknown concentrations (size: $M,1$). When $p > M$, the least squares solution to equation (2) is:

$$C_{est} = (S'S)^{-1}S'x, \quad (3)$$

and the error vector is:

$$e = x - Sc_{est} \quad (4)$$

with the length:

$$e = (e_1^2 + e_2^2 + e_3^2 + \ldots e_p^2)^{0.5}. \quad (5)$$

This paper reports a method for the simultaneous spectrophotometric determination of cadmium, copper and zinc, based upon the formation of their respective complexes with 1,5-bis(di-2-pyridylmethylene)thiocarbonohydrazide (DPTH). The resolution of the mixtures was carried out by using the multiple linear regression mathematical algorithm included in the program MULTIC.

EXPERIMENTAL

Reagents

Analytical-reagent grade chemicals were used throughout.

Standard solutions of cadmium(II) (1039 mg/l), copper(II) (1042 mg/l) and zinc(II) (1047 mg/l) were prepared from their respective nitrates and standardized titrimetrically with EDTA. Working standard solutions were prepared by suitable dilution of the standard solutions.

A stock DPTH solution ($2.3 \times 10^{-3}M$) in DMF was prepared by dissolving solid reagent samples prepared and purified by the authors.[9] This solution was spectrophotometrically stable for at least a week.

Buffer solutions (pH 7.5) were prepared by mixing 8 ml of $0.2M$ NaH_2PO_4 with 42 ml of $0.2M$ Na_2HPO_4 and diluting to 100 ml with distilled water.

Apparatus and software

A Hewlett-Packard Model 8452A diode-array spectrophotometer was used for recording spectra. An H.P. Vectra QS/165 personal computer was used to control the spectrophotometer and collect data from it via an HP–IB interface. The programs used to obtain and process the spectra were supplied by the spectrophotometer manufacturer as bundled software. Mixtures were resolved using a multiple linear regression mathematical algorithm included in the program MULTIC.[7]

Procedure

Preparation of standards. The program MULTIC requires the standardized spectrum of each component. With this purpose, four solutions for each component were prepared in 25 ml standard flasks with different concentrations of the metal ion (0.2, 0.4, 0.6 and 0.8 μg/ml), 3 ml of 0.1% m/v DPTH solution in DMF, 12 ml of DMF (to prevent precipitation of the reagent), 5 ml of buffer solution (pH 7.5) and dilution with distilled water to the mark. After a thorough mixing, the solutions were allowed to stand for 30 min. The absorbance spectra of these solutions were recorded over the wavelength range 390–480 nm at an integration time of 1 sec. Appropriate reagent blank was prepared, in triplicate, and was run in the same manner. The spectra of these three reagent solutions were recorded five times and the average spectrum was considered as the DPTH standard.

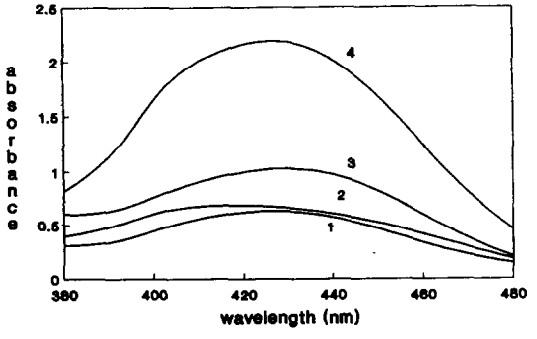

Fig. 1. Absorbance spectra of the cadmium (1), copper (2), zinc (3) complexes and their mixture (4). Concentration of each ion is 1 μg/ml.

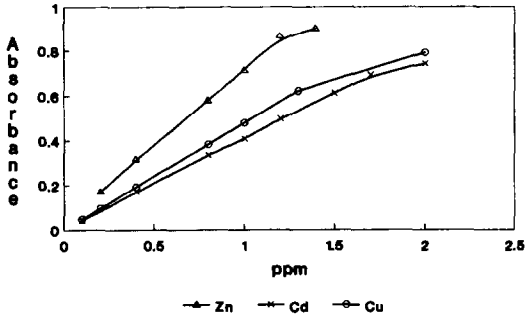

Fig. 2. Linear range for Zn, Cd and Cu.

Each of the spectra of the Zn–DPTH, Cd–DPTH and Cu–DPTH complexes were corrected by subtracting the standard spectrum of the reagent and were standardized by dividing them into the Zn, Cd or Cu concentrations at which they were recorded; the average spectrum of each complex (corresponded to a 1 μg/ml) was used as standard for each ion. These standard spectra were stored in the corresponding computer subdirectory as a working model for subsequent determinations.

The average, corrected and standardized spectra were obtained using a subroutine of the spectrophotometer's bundled software.

Sample preparation

The certified reference materials (CRM_s) analysed to determine the accuracy of the proposed procedure were: Community Bureau of Reference (BCR), Certified Reference Materials (CRM_s) 186 Pig Kidney and 184 Bovine Muscle; National Institute of Standards and Technology (NIST) Standard Reference Materials (SRM_s) 1577a Bovine Liver. National Research Council Canada (NRCC) CRM_s TORT-1 Lobster Hepatopancreas; Bureau of

Table 1. Tolerance to foreign ions in the determination of 0.8 μg/ml of Zn(II), Cd(II) and Cu(II) by the proposed method

Tolerated ratio	Foreign ion without masking agent	Foreign ion with masking agent	Masking agent (*ppm*)
>1000	SCN^-, I^-, $C_2O_4^=$, Ac^-, $SO_4^=$, $S_2O_3^=$, $S^=$, NO_2^-, F^-, Cl^-, tartrate, citrate		
100	Mo(VI), Sr(II), AsO_4^{3-}, AsO_3^{3-}, Pb(II), Ba(II), BO_2^-, $WO_4^=$, Li(I), Mg(II), Ca(II)		
50	Ce(IV), UO_2(II), VO_3^-, Y(III), Se(IV), Sb(III), Zr(IV)		
40	Mn(II)	Ag(I), Cr(III), Fe(III), Al(III), Bi(III)	S_2O_3 = (400) F^- (800) F^- (400) tartrate (800)
10		Hg(II), Hg(I)	$S_2O_3^=$ (400)
5		Co(II)	$S_2O_3^=$ (400)
3	EDTA	Ni(II)	F^- (800)

Analysed Samples LTD 32a Aluminium Bronze; 20b Aluminium Alloy and 8e White Metal. These samples were prepared according to the following procedure:

(a) *Alloys.* Dissolve a known amount of accurately weighed sample (0.1 g) in about 30 ml of *aqua regia*; evaporate the resulting solution to dryness and add 1 ml of hydrochloric acid (1 + 1); then dilute with distilled water to 50–100 ml.

(b) *Biological materials.* The samples were first dried in accordance with the norms of the respective analysis certificates and mineralized as follows: in a reaction flask were placed 0.5–2.0 g of weighed sample and 10 ml of concentrated nitric acid, and the mixture was heated under reflux up to the disappearance of nitrous fumes. Then, 3 ml of hydrogen peroxide was added and the mixture was concentrated (this step was repeated until the solution was completely colourless). Next, the mixture was neutralized with NaOH and made to 25 ml with deionized water.

Simultaneous determination of Zn, Cd and Cu

In 25 ml standard flasks were placed aliquots of sample solutions to obtain Zn, Cd and Cu concentrations over their respective linear determination ranges (0.2–1.2 μg/ml for Zn, 0.1–1.7 μg/ml for Cd and 0.1–1.3 μg/ml for Cu), 3 ml of 0.1% m/v DPTH solution in DMF, 12 ml of DMF and 5 ml of buffer solution (in the case of aluminium alloys 1 ml of a 1.1*M* fluoride solution was added to prevent interference from Al(III)). The solutions were then diluted to the mark with water, after a thorough mixing, the

Table 2. Resolution of Zn(II), Cd(II) and Cu(II) mixtures over the wavelength range 430–480 nm

	Added (μg/ml)			Found (μg/ml)*			Residual
Sample	Zn	Cd	Cu	Zn	Cd	Cu	e
1	0.20	0.20	0.20	0.22 ± 0.01	0.17 ± 0.01	0.19 ± 0.02	3.9766×10^{-6}
2	0.20	0.80	0.60	0.18 ± 0.01	0.80 ± 0.01	0.59 ± 0.01	2.4562×10^{-6}
3	0.80	0.80	0.80	0.69 ± 0.03	0.88 ± 0.03	0.87 ± 0.05	2.6614×10^{-5}
4	0.40	1.20	1.20	0.54 ± 0.04	0.97 ± 0.04	1.15 ± 0.06	4.1621×10^{-5}
5	1.20	1.20	0.40	1.09 ± 0.03	1.08 ± 0.03	0.38 ± 0.05	3.6465×10^{-5}
6	1.20	0.40	1.20	1.13 ± 0.04	0.27 ± 0.04	1.20 ± 0.06	4.8820×10^{-5}
7	1.00	1.00	1.00	0.98 ± 0.09	0.85 ± 0.09	1.05 ± 0.14	2.6177×10^{-4}
8	1.00	1.00	—	0.92 ± 0.02	1.09 ± 0.03	0.07 ± 0.03	1.6206×10^{-5}
9	0.80	1.40	1.40	1.06 ± 0.08	0.90 ± 0.08	1.19 ± 0.13	2.2257×10^{-4}

*The results correspond to the mean and standard deviation obtained from three consecutive determinations of each solution.

solutions were allowed to stand for 30 min and their absorbance spectra were recorded and corrected by subtracting that of DPTH. To these absorption spectra was applied the MULTIC program for quantification of the components using the normalized spectra of Zn, Cd and Cu as standards (see equation (3)).

RESULTS AND DISCUSSION

The zinc(II) reacts with DPTH in the range pH 6.2–9.8 forming a soluble yellow complex with an absorption maximum at 415 nm and a molar absorptivity of 6.01×10^4 l/mol/cm; the stoichiometric ratio of this complex is 1:3 zinc:reagent. The complex is spectrophotometrically stable, after 30 min, for at least 24 hr. The cadmium(II) forms a complex with DPTH in the pH range 5.8–8.3 with an absorption maximum at 415 nm and a molar absorptivity of 5.64×10^4 l/mol/cm; the stoichiometric of this chelate is 1:3 cadmium:reagent and the complex solutions are stable for at least 24 hr. When dilute copper(II) solutions and DPTH solutions are mixed, two different complexes, one orange ($\lambda_{max} = 420$ nm), and the other red ($\lambda_{max} = 500$ nm), are formed according to the pH, thus, the red complex is formed in the pH range 13.2–13.6 with a molar absorptivity of 4.2×10^4 l/mol/cm and its stoichiometry is 1:2 copper:reagent. The graph of absorbance *vs* pH for the orange complex shows that the absorbance at 420 nm is maximum and constant in the alkaline region and also shows two possible optimum pH ranges of 1.8–4.4 and 7.1–8.4, the stoichiometry in both cases is 1:1 and the molar absorptivities are 2.8×10^4 l/mol/cm and 4.3×10^4 l/mol/cm, respectively. The orange copper complex is stable for at least 12 hr.

The simultaneous determination of these ions with DPTH by use of the traditional spectrophotometry technique is difficult because the absorption spectra overlap in a bright region and the superimposed curves are not suited for quantitative evaluation. Figure 1 shows the bands of the three standards and that of a mixture.

Considering these facts, the optimum working conditions for the simultaneous determination were investigated by assaying different Zn–Cd–Cu mixtures of known composition. A disodium hydrogen phosphate–sodium dihydrogen phosphate buffer solution, pH 7.5 was selected because in this medium the absorbance of a Zn–Cd–Cu mixture was maximum (the volume of DMF added in the preparation of the solutions increased the pH over 2.0 units). The effect of DPTH concentration was also investigated, a reagent concentration of $2.8 \times 10^{-4} M$ was chosen because it ensures a sufficient reagent excess. The absorbance depends critically on the order of addition of reactants, the most suitable order of addition was: metal ions solutions, DPTH, DMF and buffer. Under these optimum working conditions the absorbance spectrum of a Zn–Cd–Cu mixture remains constant, after 30 min, for at least 12 hr.

On the other hand, it is also well known[10,11] that the quality of the results obtained in multicomponent analyses from extensively overlapping spectra depends on the wavelength range used. In order to study this factor different wavelength ranges (400–480, 415–480, 430–480, 450–480 and 465–480 nm) for recording the absorbance spectra of mixtures containing various concentrations of the three ions were applied. The best results (accuracy and precision) were obtained by recording the absorbance spectrum over the wavelength range 430–480 nm at an integration time of 1 sec and using the wavelength scan interval of the spectrophotometer (2 nm) except in the case of samples containing fluoride, tartrate, citrate, Sb(III), Cr(III), Bi(III), Al(III), Hg(II) and Hg(I). In these instances the optimum wavelength range was 465–480 nm.

Once the optimum conditions had been established, the linear range for Zn, Cd and Cu was calculated. With this purpose, a series of solutions containing different concentrations of the metal ion were prepared for each analyte. The absorbance spectra of these solutions were recorded over the working wavelength range (430–480 nm). Then, the average absorbance of each spectrum was obtained and used to construct the univariate calibration graph. The curves obtained (Fig. 2) were linear over the ranges 0.2–1.2 μg/ml for Zn, 0.1–1.7 μg/ml for Cd and 0.1–1.3 μg/ml for Cu.

Finally, four pure standard solutions of each component of the mixture, with a concentration lying in the linear concentration range and giving absorbance readings lower than 1.0 were used to obtain the normalized spectrum for each component.

Under the optimum conditions and using the equation (3) for prediction of concentrations, 10 determinations of standard solutions containing 0.8 μg/ml of each metal ions gave a relative standard deviation of 6.4% for Zn, 5.1% for Cd and 3.5% for Cu.

Table 3. Simultaneous determination of Zn, Cd and Cu in real samples.

Sample*	Found	Zn Added	Certified	Cd Found	Cd Added	Found	Cu Added	Certified	|e|
1	0.70 ± 0.08 ppm	0.80 ppm	—	0.82 ± 0.04 ppm	0.80 ppm	87.9 ± 3.4%	—	85.9%	6.7170×10^{-5}
2	0.67 ± 0.08 ppm	0.80 ppm	—	0.91 ± 0.09 ppm	0.80 ppm	4.60 ± 0.4%	—	4.10%	3.5856×10^{-7}
3	2.20 ± 0.05%	—	3.01%	—	—	4.00 ± 0.20%	—	4.57%	3.8992×10^{-6}
4	179 ± 21 μg/g	—	177 ± 10 μg/g	0.33 ± 0.05 ppm	0.40 ppm	429 ± 33 μg/g	—	439 ± 22 μg/g	7.4004×10^{-5}
5	121 ± 4 μg/g	—	123 ± 8 μg/g	0.25 ± 0.09 ppm	0.40 ppm	170 ± 5 μg/g	—	158 ± 7 μg/g	3.7981×10^{-7}
6	160 ± 22 μg/g	—	166 ± 3 μg/g	—	—	0.42 ± 0.08 ppm	0.40 ppm	—	8.5495×10^{-5}
7	146 ± 7 μg/g	—	128 ± 3 μg/g	—	—	—	—	—	5.6792×10^{-3}

*1. Al bronze 32a; 2. Al Alloy 20b; 3. White metal; 4. Lobster hepatopancreas TORT-1; 5. Bovine liver 1577a; 6. Bovine muscle BCR-184; 7. Pig kidney BCR-186.

Effect of foreign ions

The interference due to several cations and anions was studied in detail. For these studies different amounts of the ionic species were added to a mixture of Zn, Cd and Cu containing 0.8 μg/ml of each. The starting point was a 1000 fold m/m ratio of interferent to metal ions, and if interference occurred the ratio was progressively reduced until interference ceased. The tolerated limits were taken as those concentrations causing changes no greater than ±5% in the concentration of analytes.

The ions which interfere most strongly were Co(II), Ni(II), Fe(III), Hg(II) and Hg(I) because they form coloured complex with DPTH. While quantitatively significant, the interferences from these ions posed no insurmountable problems for the simultaneous determination of Cu–Zn–Cd because the interference can be overcome by determining the interfering metal together with the three analytes, which can be most readily accomplished by using the program MULTIC (this program allows the resolution of a maximum five components).

The tolerance limits are depicted in Table 1. The tolerance level for some metal ions can be increased by addition of thiosulphate, fluoride or tartrate as masking agents. Thus, 400 ppm of thiosulphate will mask 32 ppm of Ag(I) or Cr(III), 6 ppm of Hg(II) or Hg(I) and 4 ppm of Co(II); 800 ppm of fluoride will mask 32 ppm of Fe(III) or Al(III) and 4 ppm of Ni(II); and 800 ppm of tartrate will mask 32 ppm of Bi(III).

Applications

To verify the utility of the recommended procedure, the method was first used for the simultaneous determination of zinc, cadmium and copper in a set of synthetic samples containing different Zn, Cd, and Cu proportions. The results obtained by applying equation (3) to the resolution of the mixtures are summarized in Table 2, where the actual values are compared with the predicted concentrations. From these results (samples 1–8) we can conclude that the concentrations obtained for copper and zinc by the proposed method are in good agreement with those added, resulting in an RMSEP (root–mean–squared error of prediction) of 0.045 μg/ml for copper and 0.083 μg/ml for zinc. The amounts of cadmium found can be considered to be correct with the exception of those mixtures containing low concentrations of cadmium with regard to the other mixture com-

ponents; in these instances negative errors for cadmium were obtained. The RMSEP for cadmium was 0.122 μg/ml. On the other hand, in those instances where the analytes concentrations present in the mixture was higher than 3.1 μg/ml (*e.g.* sample 9) the method was not able to predict the true concentrations of metal ions with sufficient accuracy. This can be attributed to the high absorbance signals corresponding to these mixtures.

In order to test the applicability and matrix interferences of the proposed method to the analysis of real samples, the method was applied in a variety of situations. For this purpose, diverse spiked samples and reference materials were analysed. Thus, standard solutions containing different concentrations of Zn and Cd were added to 0.1 g of Al bronze 32a and Al Alloy 20b; standard solutions of Cd were added to 0.5 g of TORT-1-Lobster Hepatopancreas and Bovine Liver; standard solutions of Cu were added to 0.5 g of Bovine Muscle. These samples were prepared and analysed as described under the Experimental section. In the case of Aluminium Alloys, 1 ml of 1.1*M* fluoride solution were added to prevent interference from Al(III) and the absorption spectra of these solutions were recorded over the wavelength range 465–480 nm. The results obtained for the analysis of different aliquots of the prepared solutions containing known concentrations are shown in Table 3. These data indicate that the method would be effective for the analysis of samples of similar complexity.

Acknowledgement—The authors are grateful to the Spanish Comisión Interministerial de Ciencia y Tecnología (CICYT) (Project PB 90-0809) for financial support.

REFERENCES

1. D. M. Haaland, R. G. Easterling and D. A. Vopicka, *Appl. Spectrosc.*, 1985, **39**, 73.
2. D. J. Legget, *Anal. Chem.*, 1977, **49**, 276.
3. D. L. Wetzel, *Anal. Chem.*, 1985, **55**, 1165A.
4. R. Marbach and H. M. Heise, *TrAC, Trends. Anal. Chem.*, 1992, **11**, 270.
5. D. M. Haaland and G. V. Thomas, *Anal. Chem.*, 1988, **60**, 1193.
6. S. C. Rutan, *Anal. Chem.*, 1991, **63**, 1103A.
7. G. Sala, S. Maspoch, H. Iturriaga, M. Blanco and V. Cerdá, *J. Pharm. Biomed. Anal.*, 1988, **6**, 765.
8. E. Gomez, J. M. Estela and V. Cerdá, *Anal. Chim. Acta*, 1991, **249**, 513.
9. J. Bonilla, A. García de Torres and J. M. Cano Pavón, *Microchem. J.*, 1983, **28**, 132.
10. D. T. Rossi and H. L. Pardue, *Anal. Chim. Acta*, 1985, **175**, 153.
11. L. L. Juhl and J. H. Kalivas, *Anal. Chim. Acta*, 1988, **207**, 125.

Talanta, Vol. 40, No. 12, pp. 1867–1871, 1993
Printed in Great Britain.

0039-9140/93 $6.00 + 0.00

RESIN BEAD DETECTION AND SPECTROPHOTOMETRIC DETERMINATION OF OXYPHENBUTAZONE WITH *p*-DIMETHYLAMINOCINNAMALDEHYDE: APPLICATION TO BULK DRUG AND DOSAGE FORMS

AHSAN SAEED,* SEEMA HAQUE and SAIDUL ZAFAR QURESHI

Analytical Research Division, Department of Chemistry, Aligarh Muslim University, Aligarh—202002, India

(*Received* 5 *November* 1992. *Revised* 19 *April* 1993. *Accepted* 20 *April* 1993)

Summary—An analytical method for resin bead detection and spectrophotometric determination of oxyphenbutazone with *p*-dimethylaminocinnamaldehyde as a reagent is described. Acid hydrolysed product of oxyphenbutazone produced a red color product with *p*-dimethylaminocinnamaldehyde that absorbs maximally at 520 nm. The detection limit is 0.8 μg in resin phase and 4.0 μg in aqueous phase. Beer's law is obeyed in the concentration range of 0.4–4.0 μg/ml of oxyphenbutazone. The method is unaffected by the presence of acetylsalicylic acid, salicylamide, phenylbutazone and number of other excipients but paracetamol gives a positive reaction and novalgin being reductone interferes with the test, both should be removed by extraction with dilute sulfuric acid.

Oxyphenbutazone [4-butyl-2-(4′-hydroxyphenyl)-1-phenylpyrazolidine-3,5-dione] has analgesic, anti-inflammatory and antipyretic action and is found with novalgin, aspirin and paracetamol in drug formulations. A simple and sensitive spectrophotometric method for the oxyphenbutazone determination has been proposed by El Kheir *et al.*[1] Another method for the spectrophotometric determination of oxyphenbutazone is based on chelate formation with $NaNO_2$ in 6*M* HCl in the presence of 0.125*M* solution of Cu^{2+} acetate and Co^{2+} sulphate and chelate formed are extracted with Me-iso-Bu-ketone and $CHCl_3$, respectively.[2] Oxyphenbutazone has also been determined by pH-induced difference spectrophotometric methods in pharmaceutical preparations.[3,4] Binary mixture of analgin-paracetamol and analgin-oxyphenbutazone have also been analyzed using ultraviolet spectrophotometric technique.[5] El Sadek[6] has proposed a colorimetric method based on nitration of oxyphenbutazone and treatment with dimendone and triethylamine to form colored complexes and measurement of absorbance at 400 nm. Naphthaquinone and $Pb(OAc)_4$ have been used as analytical reagents for determination of oxyphenbutazone.[7] A number of other methods for the spectrophotometric determination of oxyphenbutazone are also available in the literature.[8–17]

p-Dimethylaminocinnamaldehyde (*p*-DAC) is a useful analytical reagent which has been utilized for the detection and spectrophotometric determination of various pharmaceutical and related compounds like paracetamol,[18] isocarboxazide[19] hydrochlorothiazide and fursomide[20] and 4-aminoantipyrine.[21] However, *p*-DAC has not, so far, been used for the determination of oxyphenbutazone.

As far as we are aware there is no method available for the qualitative detection of oxyphenbutazone in bulk or in dosage form neither in aqueous phase nor in resin phase. The proposed method is perhaps the first one to attempt on such detection. The spot test technique for qualitative detection is the most versatile and widely used technique. It is simple and sensitive technique. Maximum specificity, sensitivity and selectivity is attained only by proper choice of reaction conditions and suitable media for analysis that is why the conventional spot test technique has been replaced by the resin spot test technique. The possible use of resin beads as a reaction medium and to concentrate the colour on resin surface was first demonstrated by Fujimoto[22] particularly for the detection of inorganic ionic species and few organic compounds of known colour reaction.[23–24] The

*Present address: Camel Research Centre, P.O. Box: 72437, Abu Dhabi, United Arab Emirates.

use of resin beads as a detection media raised the sensitivity, selectivity and specificity many fold in many colour reactions because it concentrated the colour on the surface and side reactions are minimized and so the purity of product enhanced. The stability of colour in resin phase is often more than that in aqueous phase. Sometimes the colour in resin phase progressively intensifies with the passage of time. In some reactions it also acts as catalyst to facilitate their acid hydrolysis.[25-26] Recently resin beads have been used for the qualitative detection of ascorbic acid[27] and chlorpromazine[28] in pharmaceutical preparations and human urine. Usually for quality control, the analysis of drugs calls for a rapid, sensitive and cost effective method. So in the proposed method the resin beads have been used for qualitative detection of oxyphenbutazone.

It was found that hydrogen ions are necessary to effect the condensation of an amine with *p*-DAC which results in the formation of the red chromophore for the determination of bulk drugs and in dosage forms. The method developed is presented and a postulated reaction mechanism is discussed.

EXPERIMENTAL

Apparatus

A bausch and Lomb spectronic-20 (U.S.A.) spectrophotometer was used.

Reagent and ion exchange resin

A solution of *p*-DAC (Kochlight) was prepared by dissolving 0.16 gm in 50 ml ethanol.

Oxyphenbutazone. Oxyphenbutazone was obtained as a gift sample from Cadila Pvt. Ltd. (India) and was used for preparation of calibration curve.

All drug samples of oxyphenbutazone were purchased locally. A cation exchange resin (BDH) was used in H^+ form.

Test solution

Preparation. Accurately weigh 100 mg oxyphenbutazone and mix with 10 ml of ethanol and 5 ml of concentrated hydrochloric acid in a 50 ml round bottom flask and reflux for 40 min. Cool the content and transfer into a 250 ml beaker, dilute to 150 ml with water by continuous stirring for few minutes. Filter the solution on Whatman no. 42 in 250 ml standard volumetric flask and make the filtrate up to the mark with water. Use this solution for detection and determination purpose.

Detection of oxyphenbutazone in aqueous phase

Procedure. Take one drop of test solution in the depression of a white spot plate. Add a drop of reagent. A red color is developed indicating the positive test.

Detection of oxyphenbutazone in resin phase

Procedure. Place about 2–3 ion exchange resin beads in H^+ form in the depression of white spot plate and dry them by blotting with filter paper. Add one drop of test solution followed by one drop of reagent. The resin beads turn red to indicate a positive test.

Spectrophotometric determination of oxyphenbutazone

Procedure. To an aliquot volume of oxyphenbutazone containing 1–10 ml, add 10 ml of reagent in a boiling tube. Dilute the content by approximately 30 ml ethanol. Heat the solution at $40 \pm 1°C$ in a water bath for 5 min. After that cool the content and transfer into a 100 ml standard volumetric flask. Make the solution up to the mark with ethanol. Measure the absorbance at 520 nm against a reagent blank.

Determination of oxyphenbutazone in pharmaceutical preparations

Procedure. Hydrolyse the finely ground tablets containing oxyphenbutazone equivalent to 100 mg and follow the recommended procedure as described above.

If the drug sample contains paracetamol or novalgin (which must be removed) a known mass of powder drug containing 100 mg of oxyphenbutazone is stirred with 50 ml of 2% sulfuric acid for a few minutes and centrifuged. The supernatant liquid is discarded and residue is washed with water and treated as mentioned above.

RESULTS AND DISCUSSION

The absorption spectrum of colored product obtained by interaction between hydrolyzed product of oxyphenbutazone and *p*-DAC was prepared. The optimum wavelength for the determination was found to be 520 nm. The optimum conditions for the formation of red color were studied and maintained throughout the work.

Effect of temperature and time

A 1 ml aliquot was mixed with 10 ml of reagent in a boiling tube and diluted by 30 ml of ethanol. The solution was heated at 25 ± 1, 30 ± 1, 40 ± 1, 50 ± 1°C in water bath for 5 min. The content was cooled, transferred into a 100 ml standard volumetric flask and made up to the mark with ethanol. It was observed that absorbance becomes constant at 30°C and remains unaffected by increasing temperature. Therefore, the absorbance measurement was done at 40 ± 1°C.

The same contents were heated at different intervals of time on each temperature and observed that the absorbance becomes constant after 5 min heating and remains constant for more than 1 hr.

Beer's law is obeyed in the concentration (C, μg/ml) range of 0.4–4.0 μg of oxyphenbutazone (the slope and intercept for line are 0.18 and 0.006, respectively) with molar absorptivity of 0.23×10^4 l/mole/cm and equation for line is $A = 0.18$ [oxyphenbutazone] + 0.006.

The determination of oxyphenbutazone was done in various pharmaceutical preparations, the results are presented in Table 1. The method cannot be used for the determination of oxyphenbutazone in the presence of paracetamol as it also forms 4-aminophenol on acid hydrolysis and therefore undergoes a similar color reaction. Being a reductone novalgin interferes with the test. However, interference of paracetamol and novalgin present in the combination can be removed by extraction with the dilute sulfuric acid.

Some excipients, and other drugs commonly, added to dosage forms were found not to interfere. These are salicylamide, acetylsalicylic acid, phenylbutazone and propyphenazone.

N,N′-Diarylhydrazine undergoes the acid catalysed reaction benzidine rearrangement, yielding diaminobiaryls[29] usually the 4,4′-diaminobiaryl predominates, except one or both of the *para* positions of the diaryl hydrazine are occupied, in which event a 2,4′ or 2,2′-product is formed. On acid hydrolysis oxyphenbutazone forms N-4-hydroxyphenyl-N′-phenylhydrazine which has one *para* position occupied with a hydroxyl group and therefore the benzidine rearrangement produces 2,4-diamino-5-hydroxybiphenyl.[11]

The resulting compound picks up one proton from the excess of acid present in the hydrolysed product, resulting in the formation of a cation which reacts with *p*-DAC losing one water molecule. This reaction may be assumed to be analogous to, occurring between diphenylamine and *p*-dimethylaminobenzaldehyde.[30] The sequence of reaction mechanism is shown in Scheme 1. The resulting red chromophore is adsorbed on a cation exchange resin indicating that the species is positively charged.

Table 1. Recovery of oxyphenbutazone compared with reference methods

Drug*	Nominal composition (*mg*)	Proposed† method (*mg*)	C.V.%	Comparison method (*mg*)	Ref.
1 Sugarnil	100 oxyphenbutazone	97	0.3	95	11
				96	12
				97	17
2 Brugesic	100 oxyphenbutazone 500 analgin	99	0.5	101	17
3 Algesin-O	100 oxyphenbutazone 300 analgin	103	0.4	99	11
				98	12
				100	17
4 Inflavon	100 oxyphenbutazone	110	0.2	112	12
				115	17
5 Reducine	100 oxyphenbutazone 250 acetylsalicylic acid 25 caffeine	96	0.2	94	11
				95	12
				93	17
6 Oxalgin	100 oxyphenbutazone	98	0.3	101	17
7 Painwell	100 oxyphenbutazone 400 paracetamol	101	0.4	95	12
				92	17

*Name of the drug companies in India: 1. SG, 2. Brawn, 3. Alembic, 4. Khandelwal, 5. Unique's, 6. Cadila, 7. Neol.

†Average of five determinations, C.V. = Coefficient of Variation.

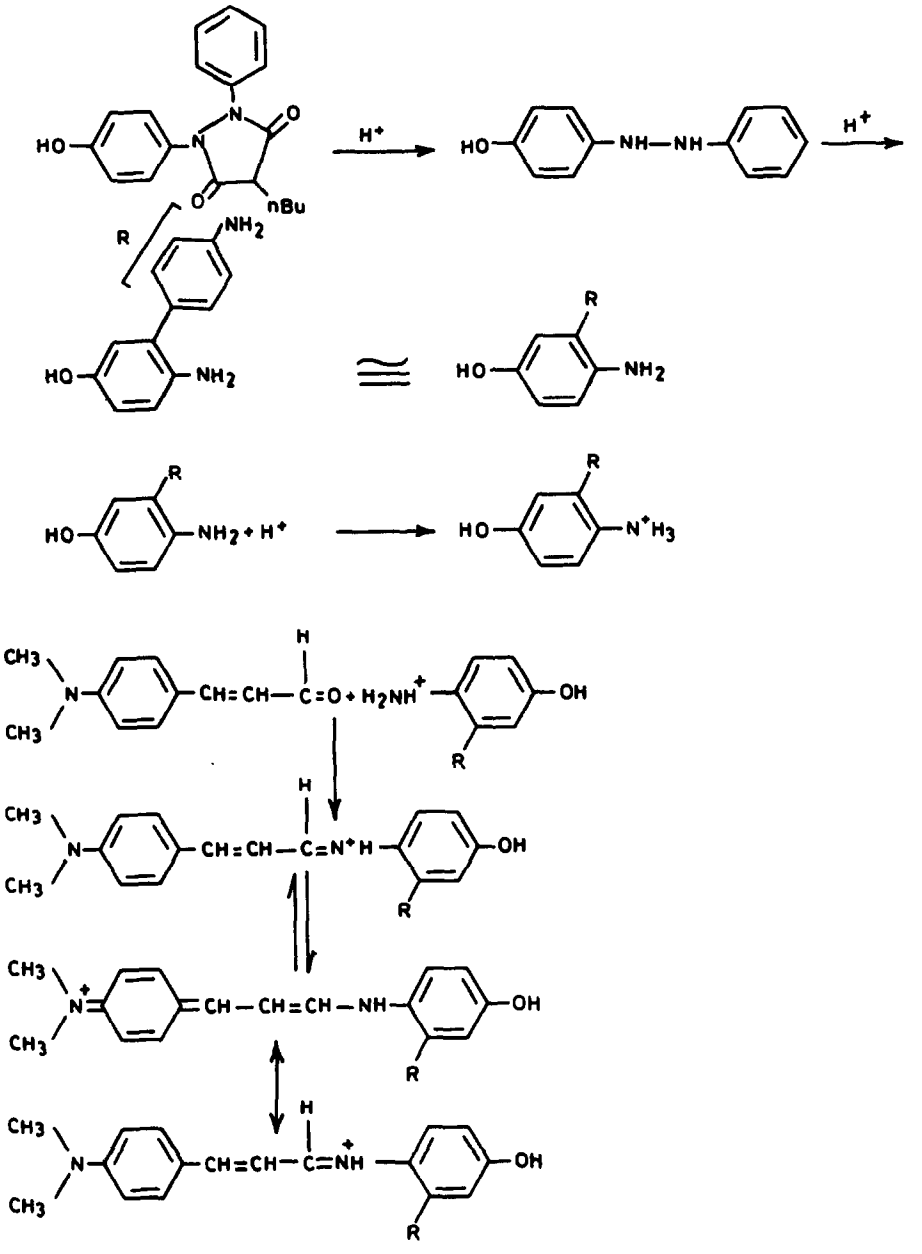

Scheme 1.

The proposed scheme may further be supported by IR studies. The IR spectral evidence in favour of the product proposed is based on a peak to peak analysis of the IR spectra and its subsequent correlation with various groups present. Since both reactants contain -OH and -NH groupings this will be considered first. The IR spectra of *p*-dimethylaminocinnamaldehyde shows a broad continuum between 3500 cm^{-1} and 1900 cm^{-1} which could be due to a polarizable intramolecular hydrogen bond.

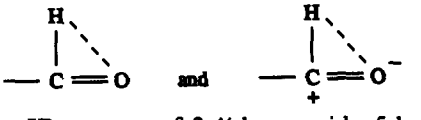

The IR spectra of 2,4′-benzamido-5-benzoyloxybiphenyl shows a sharp band in the region of 3500–3000 cm^{-1} which seems to be due to an unhydrogen bonded -OH stretch. Intramolecular hydrogen bonding seems unlikely due to probable steric hindrance in the large molecule.

In the spectra of the product there is no evidence of a conjugated carbonyl group of the

p-dimethylaminocinnamaldehyde moiety as no absorption is found between 1685 and 1666 cm^{-1}. A band at 1650 cm^{-1} is probably due to disubstituted *cis* C = C grouping as proposed in the product. There is a strong and broad absorption between 2700 and 3500 cm^{-1} which has the characteristics of an amine salt stretching frequency and may also contain within a sharp absorption of the lone -OH (stretch) grouping which again is unlikely to form intermolecular hydrogen bonds. The peak at 1370 cm^{-1} is strongly indicative of an aromatic tertiary amine salt (N–H bending vibration). A strong bending mode at 870 cm^{-1} is indicative of the presence of both 1,4-disubstituted and 1,2,4-trisubstituted benzene molecules as proposed. The final structure is postulated as

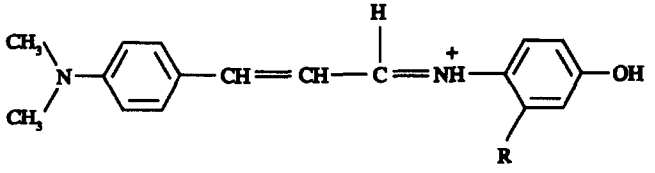

The results presented in Table 1 shows the proposed method is simple and sensitive and *p*-DAC is a sensitive reagent for the qualitative detection and quantitative determination of a compound containing an amino group.

Recently a paper appeared[11] describing the spectrophotometric determination of oxyphenbutazone based on indophenol formation. This method perhaps not suitable for a quality control laboratory keeping in view the tedium of the procedure, especially due to the extractions involved which may have their own inherent errors. Moreover, this method does not describe any procedure for the detection of drug which is perhaps equally important. In Table 1 the results of our studies and that of Verma and Sanghi[11] are compared. Since the above mentioned method requires the use of three or four reagents it certainly becomes less cost effective than our method. Furthermore our method is simpler as it does not involve extractions in the product formation.

Acknowledgements—The authors are grateful to Prof. A. Beg, Chairman, Department of Chemistry for providing research facilities, Cadila Pvt. Ltd. (India) is also acknowledged for providing the gift sample of oxyphenbutazone.

REFERENCES

1. A. A. El Kheir, S. Belal, M. El Sadek and M. A. El Shanwani, *Analyst*, 1986, **111**, 319.
2. S. Belal, A. A. El Kheir and M. A. El Shanawani, *Anal. Lett.*, 1985, **18**(B5), 617.
3. S. M. Amer, S. M. Hassan and M. F. El-Tarras, *Anal Lett.*, 1980, **13**(B18), 1625.
4. H. Abdin, H. Abdil, M. El Sayed and M. E. Abdel-Hamid, *Indian J. Pharm. Sci.*, 1979, **41**(3), 118.
5. G. Bagavant and V. Rowhani, *Indian Drugs*, 1986, **23**(6), 373.
6. M. El Sadek, *Anal. Lett.*, 1986, **19**(3–4), 479.
7. A. S. Issa, Y. A. Beltagy, M. G. Kassam and H. S. Daabies, *Talanta*, 1985, **32**(8A), 657.
8. S. Belal, A. A. Abou El Kheir and A. M. El-Shanwani, *Analyst*, 1985, **110**, 205.
9. M. M. Amer, A. M. Taha, B. A. El-Zeany and O. Q. El-Sawy, *Analyst*, 1982, **107**, 908.
10. M. S. Amer, M. A. Ellaithy and M. F. El-Tarasse, *Pharmazie*, 1982, **37**, 182.
11. K. K. Verma and S. K. Sanghi, *Farmco. Ed. Pr.*, 1988, **43**, 13.
12. K. K. Verma and A. Jain, *Analyst*, 1985, **110**, 997.
13. P. K. Chaterjee, C. L. Jain and P. D. Sethi, *Indian J. Pharm. Sci.*, 1987, **49**, 111.
14. K. K. Verma, A. Jain, N. Patel and S. K. Sanghi, *Farmco. Ed. Pr.*, 1987, **42**, 185.
15. K. K. Vishwanath, A. S. Rao and M. V. Sivaramakrishna, *Indian Drugs*, 1986, **24**, 170.
16. S. M. Hassan, M. I. Walash, S. M. El-Sayed and A. M. Abou Ouf, *J. Assoc. Anal. Chem.*, 1981, **64**, 1442.
17. A. M. Abou Ouf, M. I. Walash, S. M. Hassan and S. M. El-Sayed, *Analyst*, 1980, **105**, 169.
18. T. Inoue, M. Tatsuzaqa, S. C. Lee and T. Ishii, *Eisei Kagaku*, 1975, **21**, 313; *Analyt. Abstr.*, 1976, **31**, 1E 29.
19. M. E. El-Kommos, *J. Assoc. of Anal. Chem.*, 1988, **71**(6), 1134.
20. K. Shimdda and Y. Nagase, *Bunseki Kagaku*, 1977, **26**(10), 712.
21. K. Takayasu, I. Kumiko, O. Masako and H. Eizo, *Chem. Pharm Bull.*, 1984, **32**(7), 2736.
22. M. Fujimoto, *6th Annual Meeting Chem. Soc.*, Japan Kejota, 4 April 1953.
23. M. Fujimoto, *Bull. Chem. Soc.* Japan, 1957, **30**, 93.
24. M. Fujimoto, *Bull. Chem. Soc.*, Japan, 1957, **30**, 283.
25. P. W. West, M. Qureshi and S. Z. Qureshi, *Anal. Chim. Acta*, 1966, **36**, 97.
26. M. Qureshi, S. Z. Qureshi and N. Zehra, *Anal. Chim. Acta*, 1968, **40**, 169.
27. S. Z. Qureshi, A. Saeed and T. Hasan, *Anal. Lett.*, 1989, **28**(8), 1927.
28. S. Z. Qureshi, A. Saeed, M. A. Khan and N. Rahman, *Indian J. Pharm. Sci*, 1989, **51**(6), 271.
29. J. March, *Advanced Organic Chemistry: Reactions, Mechanism and Structure*. McGraw-Hill, New York, 1987, pp. 1034–1036.
30. M. Qureshi, S. Z. Qureshi, H. S. Rathore and A. Mohammad, *The J. of Physical Chemistry*, 1975, **79**, 116.

Talanta, Vol. 40, No. 12, pp. 1873–1882, 1993
Printed in Great Britain.

0039-9140/93 $6.00 + 0.00

CHEMOMETRIC INVESTIGATION OF COMPLEX EQUILIBRIA IN SOLUTION PHASE II: SENSITIVITY OF CHEMICAL MODELS FOR THE INTERACTION OF AADH AND FAH WITH Ni(II) IN AQUEOUS MEDIUM*

A. RAVINDRA BABU, D. MURALI KRISHNA and R. SAMBASIVA RAO†
School of Chemistry, Andhra University, Visakhapatnam, 530003, India

(*Received* 13 *October* 1992. *Revised* 30 *April* 1993. *Accepted* 6 *May* 1993)

Summary—A detailed study of the species formed in the complex equilibria involving adipic acid dihydrazide (AADH)/2-furoic acid hydrazide (FAH) with Ni(II) using pH titration with glass electrode is performed. The results of modeling studies and effect of errors on the equilibrium constants of AADH/FAH with Ni(II) refined by the non-linear least squares program MINIQUAD75 are reported. Based on the expert system approach developed in our laboratory for the species formed from secondary formation data ($\bar{n}$ and $\bar{n}_H$), several preliminary chemical models were tested. For the four species identified (MLH, ML, ML_2H, ML_2), an exhaustive search of a different combination of models (15) was performed. Then other suspected minor species (ML_2H_2, ML_3 and ML_3H) were tested. The final best fit chemical model was found to contain ML_3H to an extent of 3% along with the other four major species. In order to ascertain the accuracy of the stability constants and consequently distribution of the species, a detailed error analysis is attempted. As the existing least squares procedures cannot suppress the systematic errors, three-dimensional plots of the simultaneous effects of pH and TLO:TMO (1.5:1 to 5:1) on the percentage of species are drawn which are of immense use in arriving at optimum conditions for the preparation of a complex of definite stoichiometry.

Adipic acid dihydrazide (AADH), apart from its vital role in epoxy resins[1] and semi-conductor devices,[2] finds application in vaccines[3] and other compounds of biological importance.[4] Several antibacterial/antileukemic compounds[5] have been synthesized from 2-furoic acid hydrazide (FAH). Since AADH has been employed in the presence of metal ions[6] in coatings and varnishes, speciation studies in presence of water miscible solvents and/or micelles may throw some light in understanding the mechanism of reactions and enable one to choose optimum experimental conditions. The results of exhaustive modeling studies for the interaction of AADH and FAH with Ni(II) in aqueous solution using the MINQUAD75[7] program are reported in this communication.

EXPERIMENTAL

Tenth mol/l aqueous solutions of AADH and FAH, obtained from Fluka AG, Switzerland, were prepared in doubly glass distilled deionized water. All other chemicals are of AnalaR grade. Tenth mol/l nickel(II) chloride (Fluka AG) solution was rendered acidic to suppress hydrolysis of metal ions.[8]

Complex equilibria experimental design (CEED)

Since the accuracy of equilibrium constants of metal–ligand complexes depends upon complex mathematical functions of errors in ingredient concentrations and the data acquisition system, a systematic investigation of possible sources of errors are considered. The extreme errors in concentrations of ingredients were determined by COSWT[9] (concentration of solution by weight method) and COST (concentration of solution by titrimetry). As the glass electrode calibration with buffer solutions alone is a two point method, Gran analysis[10] of titration of a strong acid with alkali is employed as recommended by the commission on equilibrium data (IUPAC)[11–19] and by Babu.[14] A plot of $GA = 10^{-(B_i + \log F)} \times (V_0 + V_i)$ *vs* V_i intersects the volume axis at the equivalence point (V_e) only if the errors $\{e_1\}$, $\{e_2\}$, $\{e_3\}$ and OH_i in equation (1) are negligible:

$$(FH_i + e_1) \times (V_0 + V_i + e_2) = (ALK + e_3) \times (V_e - V_i - e_2) + OH_i \times (V_0 + V_i + e_2) \quad (1)$$

*Presented at 11th IUPAC Conference on Chemical Thermodynamics, Como, Italy, August 1990.
†Author for correspondence.

where V_i is the volume of alkali of concentration ALK added to a strong acid of total volume V_0, B_i is the pH meter dial reading, log F is the correction factor and OH_i is the concentration of hydrogen ion due to auto ionization of water. These are related to equilibrium hydrogen ion concentration (FH_i) by the equation

$$FH_i = 10^{-(B_i + \log F)}. \quad (2)$$

The determination of log F, pK_w (negative logarithm of auto ionization constant of water) and titration assembly are same as described earlier.[15,16]

RESULTS AND DISCUSSION

Data processing

AADH contains two functional groups a carbonyl oxygen and a terminal amino nitrogen which are potential sites for co-ordination of metal ions. Since in this investigation we are confined to ligand-to-metal ratios greater than one, only mono-nuclear complexes are considered. As the highest protonated species of ligand is LH_2^{++}, the expected metal complexes are $M(LH)_{Maxl}$. Plots of a (moles of alkali per mole of ligand), m (moles of alkali per mole of metal ion) and $\bar{n}$ (average number of ligands bound per mole of metal ion) against pH suggested two ligand molecules are involved in metal complexes. However, considering Maxl to be three, the expected binary complexes are {MLH, ML, MLOH, $ML(OH)_2$, ML_2H_2, ML_2H, ML_2, $ML_2(OH)$, $ML_2(OH)_2$, ML_3H_3, ML_3H_2, ML_3H, ML_3, $ML_3(OH)$, $ML_3(OH)_2$}. Here the maximum number of hydroxyl ions are limited to two, based on the pH region of the investigation.

Although in principle it appears that it is possible to resort to complete searching of models,[17] it is not pragmatic as modelling of complex equilibria is a non-linear problem. Large computer time is required to solve each model, unlike in multiple-linear regression where the solution is obtained in one attempt. Therefore the species to be considered are short listed using heuristics and chemical principles.

A perusal of literature reveals that the maximum ligand number (Maxl), hydrogen ions (Maxh) and hydroxyl ions (Maxoh) in a mononuclear metal complex were 6, 5 and 2, respectively. However, not more than 6–8 species are reported except in bovine. It appears that the exclusion of the species is definitely not based on systematic elimination of the species but based on implicit knowledge and experience which can be coded as heuristics. In the present case some of the factors considered are density of the ligand, coordination number of metal ion and average number of ligands bound per mole of metal ion. A few heuristics are described in Fig. 1.

Work is in progress to use the complementary knowledge contained in $\bar{Z}$ (moles of alkali per metal ion or ligand) to judge the presence of protonated species, core and link hypothesis and chemical theories of Sylva to reduce the state search space of polynuclear species.

```
If    minimum ratio of initial concentration of ligand to metal
      (TLO/TMO) ≥ 1.0
Then Maxl. = 1
-------------------------------------------------------------
If    n̄ analysis is performed &
      formation curves exhibit ascending slope
Then Maxl = max(n̄) + 1.6
If    formation curves do not exhibit ascending slope
Then Maxl = Max(n̄) + 0.6
-------------------------------------------------------------
If    different TLO : TMO are investigated &
      formation curves are not overlapping
Then different protonated, hydroxylated, ML_x species exhibt
-------------------------------------------------------------
If    total number of protons(NAP) or ionizable protons(NIP) > 1 &
      highest protonated form of the ligand in the pH range of n̄ is
      HxL & x > 1
Then protonated species (Maxh = X - 1)
```

Fig. 1. Heuristics for the detection of protonated metal complexes and maximum ligand number.

This preliminary screening of the species resulted in identification of MLH, ML, ML_2H and ML_2. For exhaustive modeling of these four species, two popular approaches available in multiple-linear regression analysis are forward selection wherein different models are generated starting from the lowest number of variables (one), and backward elimination, in which species are successively eliminated from a model with highest number of species (four). We have followed the forward selection principle[17] and several statistics for residual analysis for 15 chemical models (stoichiometric coefficients and log β with standard deviations) are given in Table 1.

The relative concentration of different species formed is not only a function of their equilibrium constants but also the ratio of ligand-to-metal. In an attempt to model the complexation of Ni(II) with hydrazides, different ratios of ligand-to-nickel(II) (TLO/TMO) of 2:1 to 6:1 were investigated, by varying the initial analytical concentration of metal ion. Alkalimetric titrations of the titrand containing above mixtures were performed using a glass electrode. At the lowest ratio, information content of MLH_h will be obtained, while with increasing ratio that due to ML_2H_h will be obtained.

Selection of best fit model

A perusal of the literature reveals that there is no unique set of rules to arrive at the best fit chemical model and hitherto this has been a matter of subjective decision. We have employed an expert system approach involving heuristics based on some of the popular statistical parameters (Table 1). The numerical values of R[18] (crystallographic R factor) and U[19] (sum of the squares of residuals in all mass balance equations) corrected for models with one, two and three are significantly larger in numerical magnitude than that with four species, indicating that the last one better explains the solution processes. However, care was taken to avoid the overambitious modeling (including more species) which also results in decrease of statistics based on residuals.

From the analysis of the individual experimental data at each of the metal-to-ligand ratios (1:1.5 to 1:5) for different analytical concentrations of the metal ion (0.003 and 0.0045M) (Table 2) it is clear that complexes ML and MLH are favored at low (1:1.5 and 1:2) values of TLO/TMO while the species ML_2 and ML_2H were rejected by MINIQUAD75. When TLO/TMO > 2, ML_2H and ML_2 were refined, and ML and MLH are rejected. This shows that a proper experimental design includes an increasing number of experimental points by performing more titrations, keeping TLO/TMO optimum for the species of interest. Braibanti *et al.*[20] also observed the rejection of species of higher stoichiometry at low ratios of Ni(II) to glycine. After arriving at the best fit model, the species rejected in the preliminary scrutiny were again tried. It was found that these species were rejected during MINIQUAD75 refinement. The stability constants of model 1 of Table 2 are used to generate simulated primary data. From Fig. 2 it is clear that the simulated data predict the experimental one within the limits of accuracy of data acquisition system.

Precision of log β values

The very low standard deviation in the log β values and the small values of U suggest, (a) a sufficient number of data points corresponding to each species (as otherwise very high SD would result), (b) precision of refined log β values, and (c) the best fit of the chemical model for the systems under the above experimental condition. The correlation matrix of log β values for Ni(II)–AADH (Table 3) provides a measure of linear dependence of one equilibrium constant on the other. This information is very important as a good statistical fit of the data is possible even when one parameter is erroneously estimated, because the error in this log β can be offset by appropriate change in the other.[21] The apparently high correlation coefficients between some of the log β values are an artifact of the algorithms employed in MINIQUAD, SUPERQUAD[22] and ESTA.[23] A real picture is, however, possible only when the stepwise constants are refined as in SCOGS2[24] and in one of the modes of DALSFEK.[25] A system wherein $r_{ij} > 0.8$ indicates that (1) one or more of log $K(s)$ are not sufficiently defined by the available primary data or (2) equilibria are highly overlapping and thus only a linear combination (but not individual constants) can be calculated.

Residual analysis

The χ^2 values for Ni(II)–FAH and Ni(II)–AADH obtained are 36 and 99, respectively. They are less than $\chi^2_{\nu,0.5}$, indicating that the unweighted residuals form a part of normal distribution. This χ^2 statistic drew the attention

Table 1. Exhaustive modelling of Ni(II)–AADH (or FAH) in aqueous solution

Model number	log β (SD) 1 1 0	1 2 0	1 1 1	1 2 1	R	U/NP–m × 10^8	χ^2	Kurtosis	Skewness	SD × 10^4	Mean × 10^6
One species at a time											
1	4.168(3)	—	—	—	0.019	9.57	26.94	4.42	−0.61	1.76	−2.75
2	—	6.969(8)	—	—	0.060	97.58	142.14	1.94	−0.95	5.61	−188.48
3	—	—	6.912(40)	—	0.110	363.98	80.15	2.65	0.25	10.84	5.27
4	—	—	—	10.253(8)	0.052	70.40	154.86	7.50	1.72	4.77	47.50
Two species at a time											
5	4.136(3)	5.913(10)	—	—	0.017	7.88	48.74	7.10	−1.72	1.59	−23.23
6	4.168(3)	—	6.895(14)	—	0.019	8.54	38.96	6.82	−1.52	1.65	−12.84
7	4.158(3)	—	—	8.524(14)	0.019	6.24	21.82	4.39	−0.54	1.76	−1.49
8	—	7.962(159)	7.152(261)	—	0.070	166.29	205.19	8.69	−2.61	12.16	−54.74
9	—	6.514(4)	—	10.176(3)	0.060	97.76	103.16	7.65	−2.01	9.70	−24.62
10	—	—	rejected	10.253(8)	0.052	70.40	145.86	6.50	1.52	3.77	47.09
Three species at a time											
11	4.157(4)	5.982(14)	5.349(72)	—	0.017	7.85	54.03	7.22	−1.75	1.59	−22.04
12	3.999(5)	6.078(9)	—	9.533(13)	0.016	7.10	42.98	7.21	−1.63	1.51	−18.92
13	4.158(3)	—	rejected	8.525(81)	0.019	95.46	11.72	4.19	−0.57	1.06	−10.61
14	—	7.174(8)	6.973(9)	10.678(7)	0.015	4.72	99.47	17.04	−2.76	1.09	−8.30
Four species at a time											
15	4.087(3)	6.287(8)	6.299(9)	9.442(6)	0.009	0.86	38.10	5.72	−2.48	0.79	−3.15
FAH	3.237(7)	5.209(9)	—	—	0.031	25.34	97.83	4.62	−0.36	0.65	−2.39

Table 2. Chemical modelling for separate and pooled data of Ni(II)–AADH in aqueous solution

Number of expt(s)	TMO:TLO (NP)	log β (SD) 1 1 0	1 2 0	1 1 1	1 2 1	U/NP-m × 10^8
1	1:1.5 (31)	4.080(6)	*Rej.	6.716(8)	10.253(8)	1.2936
2	1:2 (32)	4.114(9)	Rej.	6.493(17)	9.936(12)	2.8695
3	1:3 (31)	Rej.	7.458(40)	7.280(50)	10.971(43)	1.8426
4	1:5 (31)	Rej.	6.116(5)	Rej.	9.541(6)	3.7536
All	1:2–1.5 (125)	4.087(3)	6.287(8)	6.299(9)	9.442(6)	0.8508

*Rej. = species rejected during refinement.

of equilibrium chemists only recently and the values reported till now range from about 10 to 400 for chemical equilibria of increasing complexity.[26,27] Further, very small values of standard deviation (1.93×10^{-4} and 1.09×10^{-4}) and mean deviation (1.48×10^{-4} and 6.51×10^{-5}) corroborate the above assumption. However, the deviation of kurtosis (5.8 and 17.7) and skewness (−1.12 and −2.95) from 3 and 0, respectively, suggest that the residuals concentrate to the left of the peak. The confidence contours of log β values calculated (Table 1) thus represent only an approximate range as log β values are partially correlated and only part of the residuals form normal distribution with a slight distortion.

Species distribution plots

Conventional two-dimensional distribution diagrams (Fig. 3) depict the variation of percentage of the concentration of species to the total metal ion concentration *vs* pH. From Fig. 4, it is clear at lower ratios of TLO to TMO, ML_2 is not formed while at higher ratios, ML does not exist. Mathematical solutions in N-dimensional space where $(N-1)$ variables

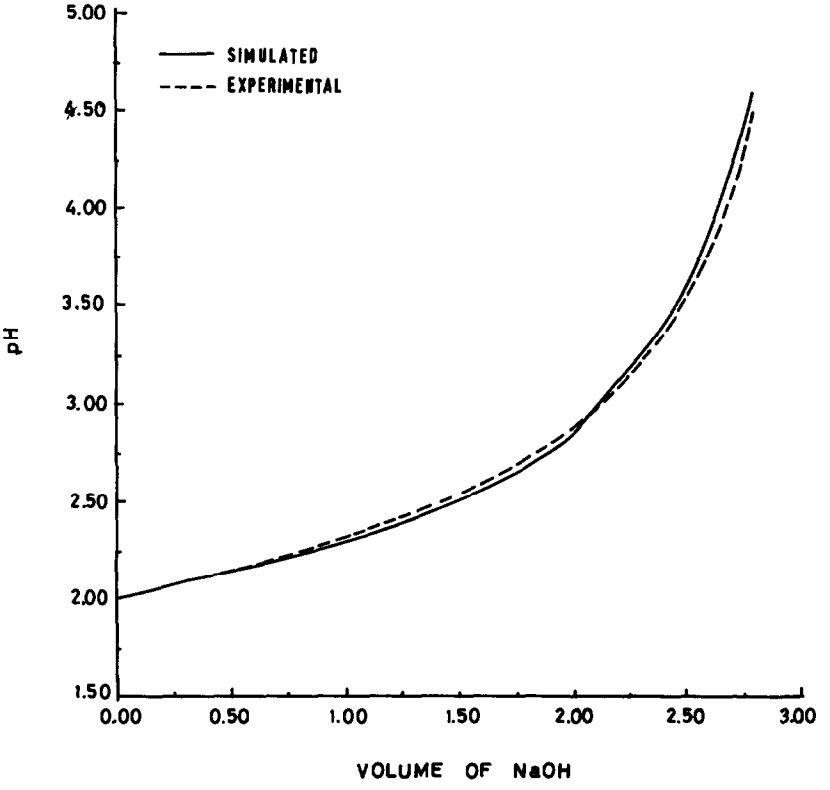

Fig. 2. Comparison of the experimental titration curve with the simulated one TLO:TMO = 1:1.5. log $\beta_{110} = 4.080$, log $\beta_{111} = 6.716$ and log $\beta_{121} = 10.253$.

Table 3. Correlation matrix of log β values of Ni(II)–AADH (aq) system

	MLH^+	ML	ML_2H^-	ML_2^{2-}
MLH^+	1.0	0.056	0.918	0.925
ML		1.0	−0.212	−0.215
ML_2H^-			1.0	0.954
ML_2^{2-}				1.0

(TLO:TMO, analytical concentration of the metal ion, pH, etc.) affecting the concentration of the species, provides important chemical information such as:

- optimum conditions for the preparation of a solid complex with minimum interference from other complexes;
- understanding the relative concentrations of different species under given experimental conditions which throw light on biologically active forms;
- performing a feasibility study of metal ion buffers;
- detecting stoichiometric asymmetry and over-compensation effects of a specific equilibrium.

In an attempt to achieve this goal, we have considered three-dimensional plots wherein the simultaneous effects of pH and TLO:TMO ratio on percentage of species is described (Fig. 5). The chemical equilibria in solution phase are represented by

(1) $Ni(II) + LH_2 \rightleftarrows NiLH^+ + H^+$

(2) $Ni(II) + LH_2 \rightleftarrows NiL + 2H^+$

$NiLH^+ \rightleftarrows NiL + H^+$

(3) $Ni(II) + 2LH_2 \rightleftarrows NiL_2H^- + 3H^+$

$NiL + LH_2 \rightleftarrows NiL_2H^- + H^+$

$NiLH^+ + LH_2 \rightleftarrows NiL_2H^- + 2H^+$

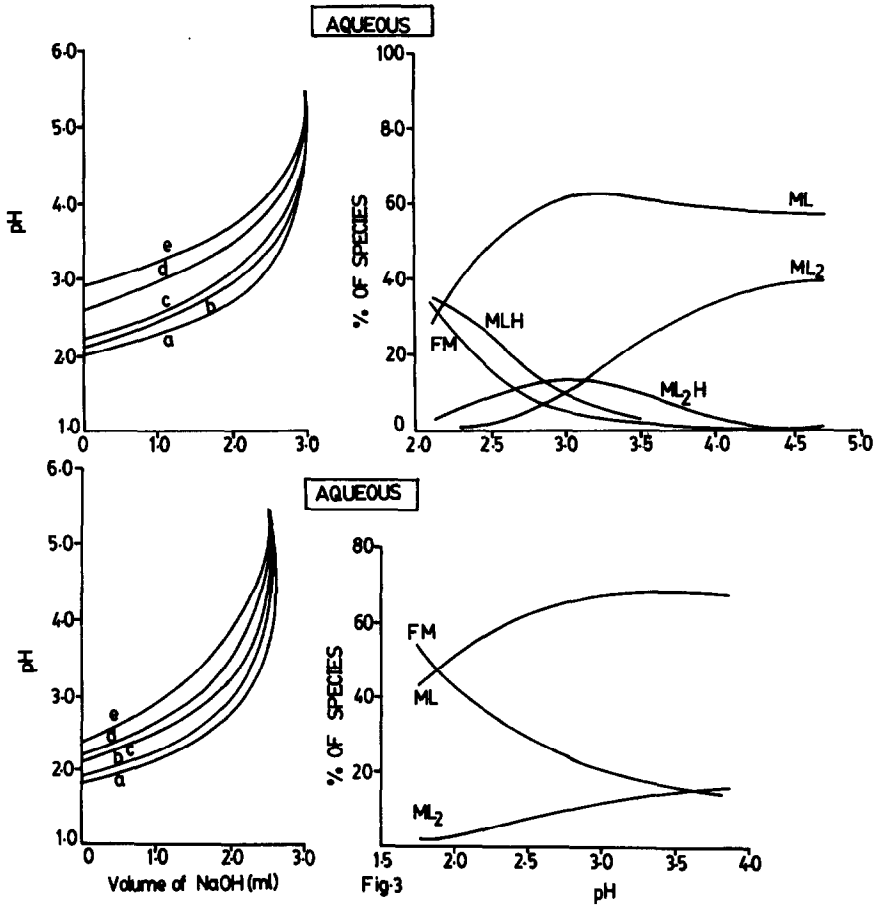

Fig. 3. Protometric titration curves and species distribution diagrams of Ni(II)–AADH (or FAH) complexes. Titrand: TMO (Ni^{2+}): 3.482×10^3 mol/l, E_0: 21.85×10^{-3} mole/l, μ: 0.10 mole/l, V_0: 50.0 cm^{-3}, temp.: 301 K, titrant: NaOH:0.3902 mole/l. AADH = (a) 5.982, (b) 7.976, (c) 9.970, (d) 14.955 and (e) 19.940 mmole/l and FAH = (a) 6.035, (b) 8.048, (c) 10.059, (d) 15.089 and (e) 20.119 m mole/l.

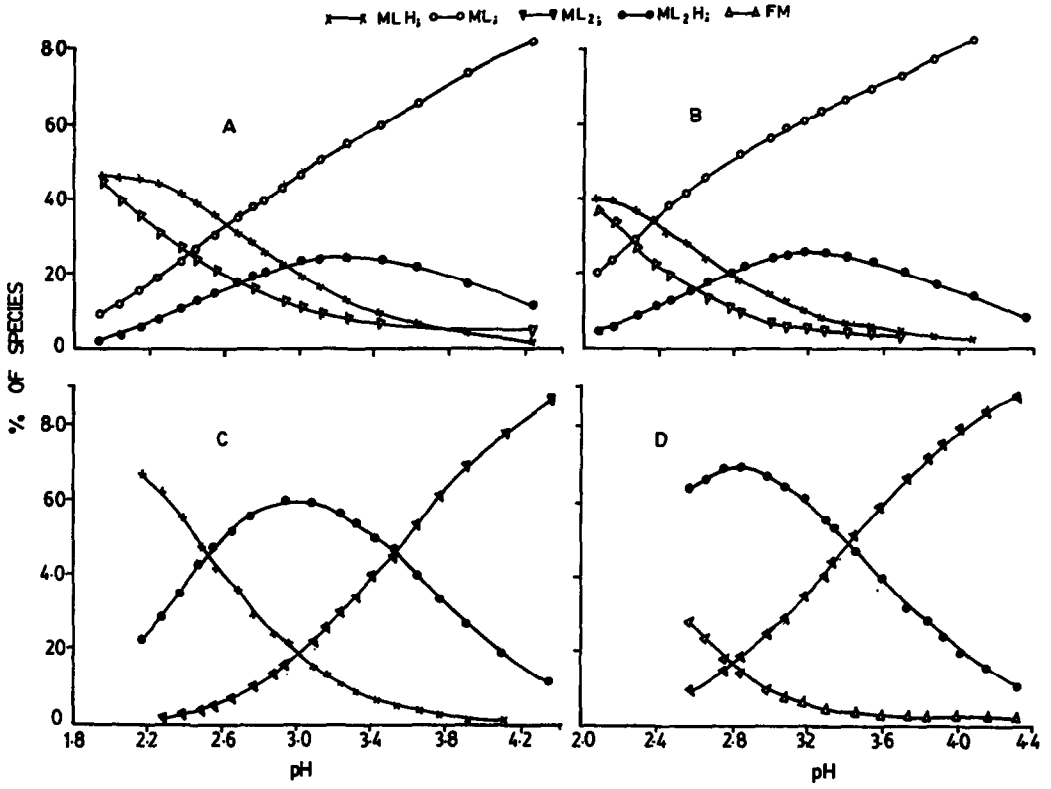

Fig. 4. Changes in chemical models as a function of TLO:TMO [Ni(II)–AADH].

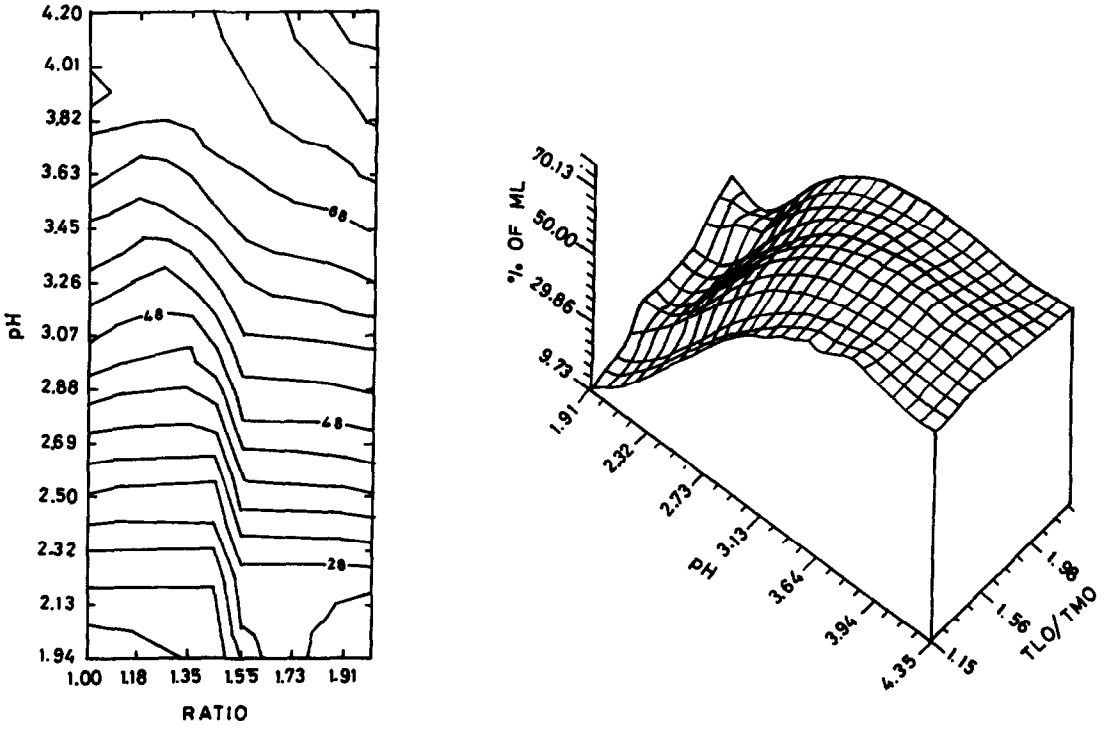

Fig. 5. Three-dimensional plot and surface contour for the simultaneous effect of pH and TLO:TMO on percentage of ML of Ni(II)–AADH system. Projection: orthographic; rotation about z-axis: 310°; tilt after rotation: 30°.

(4) $NiL_2H^- \rightleftarrows NiL_2^{2-} + H^+$

$NiL + LH_2 \rightleftarrows NiL_2^{2-} + 2H^+$

$NiL + LH^- \rightleftarrows NiL_2^{2-} + H^+$

However, from pH metric studies alone it is not possible to assess the relative importance of the micro equilibria contributing to the release of one and two protons.

CHEMOMETRIC APPROACH FOR THE RELIABILITY OF LOG β VALUES

The standard deviations in log β values and any statistic representing the sum of squares (U, SD in pH, *etc.*) reflect how best the algorithm explains the variation in the dependent variable (pH) in terms of explanatory variables (chemical model). However, the errors which creep into the system at various stages, like those in concentration of ingredients, electrode parameters and derived constants (proton ligand stability constants), have a tremendous cumulative effect on the metal ligand stability constants. But MINIQUAD75 or other similar programs do not have any built in provision to recognize or overcome these effects.

Effect of errors in proton–ligand stability constants on metal complexes

Table 4 incorporates the results of the effect of introducing an error of $\pm$ 3SD (where SD is the standard deviation in proton ligand stability constant) and an extreme value ($\pm$ 0.20) in log β_{011} and log β_{012} on the chemical model refined for the Ni(II)–AADH system. The very small effect on metal ligand stability constants when +3SD error is introduced indicates the consistency of the reported model (Table 4). However, considerable (+0.2) errors in proton ligand complexes result in rejection of some of the species actually existing (ML) or a stability constant differing by one log unit (ML_2 for $\pm$ 0.2 and ML_2H for $\pm$ 0.2). This re-emphasizes the need for the experimental design and accurate determination of an acid–base equilibria of systems under identical conditions employed for metal ligand complexes.

Retrieval of proton–ligand stability constants from metal–ligand titration data

Keeping all the stability constants corresponding to metal complex species fixed, log β values of acid–base equilibria of AADH are retrieved using MINIQUAD75. The good agreement with the reported values (given for comparison in Table 5) indicates the absence of any other chemical reactions changing hydrogen ion concentration in the pH regions (1.8–4.6) of acid–base equilibria of the ligand.

Simultaneous refinement of proton–ligand and metal–ligand equilibrium constants

The general non-linear algorithms, in principle, do not restrict the simultaneous refinement of any number of parameters, for example, stability constants of proton ligand and metal ligand complexes and all dangerous parameters. However the error surfaces exhibit distortion when (1) a non-existent species is introduced by chance, (2) there is a hidden mathematical relationship between two or more species (correlation) and (3) the model is made over sophisticated to account for small residues (in the primary data) which are less than the accuracy of the data acquisition system. Further increased complexity of non-linearity (from PL to MLXY), different ranges of β values and lack of restriction on the range of parameter space are added disadvantages. The difficulties in the simultaneous refinement of free concentration of ingredients and β values were experienced in the earlier version of MINIQUAD and these problems are overcome in MINIQUAD75[7] by a two level refinement. Our earlier investigations of interaction of *L*-dopa with Mn(II) and Zn(II)

Table 4. Effect of error in proton ligand stability constants on log β_{11h} of Ni(II)–AADH (aq) system

Error introduced in PL	Δ log β 1 1 0	1 2 0	1 1 1	1 2 1	U/NP–m × 10^6
+3SD	0.177	−0.122	−0.045	−0.056	4.7135
+1SD	0.056	−0.040	−0.018	−0.019	2.1653
−1SD	−0.039	0.041	0.020	0.156	2.0834
−3SD	−0.127	0.124	0.061	0.444	4.1809
+0.20	Rej.	−0.784	−0.427	−0.497	7.2576
−0.20	−0.446	1.126	0.341	0.633	3.0199

Table 5. Retrieval of proton–ligand constants from metal–ligand data [Ni(II)–AADH (aq)]

M	L	H	Retrieved βs	P–L data
0	1	1	3.502(0.016)	3.521(0.006)
0	1	2	6.161(0.009)	6.172(0.009)
1	1	0	6.299	
1	1	0	4.087	
1	2	1	9.442	
1	2	0	6.287	

showed that simultaneous refinement resulted in agreement of values,[28] this being a case in which many of equilibria are non-overlapping. However, the present study clearly establishes simultaneous refinement of results in stability constants that are quite different from the best fit model (Table 6). This can be explained in terms of simultaneous solution (acid–base and metal–ligand) equilibria and major changes in the concentration profiles of different forms of ligand. This results in difficulties in determining individual stability constants accurately due to inadequacy of the algorithms adopted in complex equilibria.

Effect of systematic errors on ingredient concentrations

In order to rely upon the best fit chemical model for critical evaluation and application under varied experimental conditions with different accuracies in the data acquisition system, a study of the effect of systematic errors of different magnitudes up to extreme limits in the concentration of EO (strong acid), ALK (concentration of alkali used as titrant), TLO and TMO have been made adopting a factorial design. It was found that errors in EO and ALK have more pronounced effects than those in TLO and TMO. Further, even very large errors in initial total volume (V_0) which is important in understanding the effect of mixing volumes and pK_w have been found to have little effect. Since the errors in the ingredient concentrations in the present investigation are less than 1%, the chemical model proposed is accurate to 0.02 units in log β.

A study of systematic errors introduced in the measurement of hydrogen ion by the glass electrode is of paramount importance. A very large error (± 0.10 pH) distorts the stability constants of some of the species appreciably or the very model is rejected during refinement process.

Robustness of MINIQUAD75

Recent investigations by Sylva *et al.*[29] and Pardue[30] and by our group established the necessity for fairly good initial estimates of stability constants, especially for highly complex systems (with more than two overlapping equilibria). This is because the species that really exist are rejected or yield ill-conditioned matrices that are not solvable. A point of interest here is to note that this is not the limitation of MINIQUAD75 alone but a difficulty in numerical analysis of mathematically complex systems and there are no attempts based on chemometric principles to overcome this hurdle.

Nurchi and Crisponi[31] reported non-convergence by a Gauss–Newton algorithm[32] when the approximate stability constants are less than 0.5 units for protonation equilibria with log $K_1 <$ log K_2. Recently Babu[14] showed that the algorithm plays an important role even in describing the range of approximate stability constants and MINIQUAD75 produced identical results even when the initial constants were three log units away from the true (log $K_1 = 5.0$,

Table 6. Simultaneous refinement of proton–ligand and metal–ligand stability constants Ni(II)–AADH (aq) system

m	l	h	log β	β_{01h} fixed
0	1	1	3.203(0.02)	3.521
0	1	2	5.962(0.02)	6.172
1	1	1	6.619(0.06)	6.299(0.090)
1	1	0	3.712(0.23)	4.087(0.035)
1	2	1	10.088(0.07)	9.422(0.080)
1	2	0	5.671(0.07)	6.287(0.090)

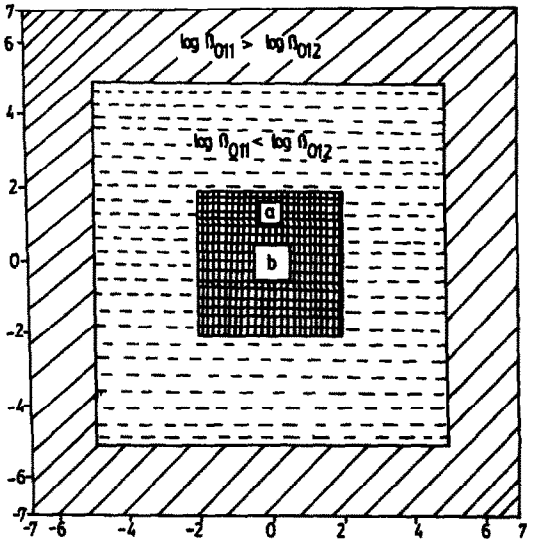

Fig. 6. Effect of wild initial estimates of log β for successful convergence by MINIQUAD75.

log $K_2 = 6.0$) values. Further, a detailed study indicated that for the acid–base equilibria of AADH with log K_1 (3.5) > log K_2 (2.5), MINIQUAD75 is robust to an extent of 5 log units. Since the robustness of a program depends on (1) the algorithm (2) the pattern of log β values (3) the number of equilibria and complexity, (4) optimization function and (5) over all accuracy and precision of potentiometric titration data. The Ni(II)–FAH system was chosen to establish a valid range of initial constants and Fig. 6 indicates this to be log $\beta_{110} \pm 2.0$ units. As such an investigation for Ni(II)–AADH species is a formidable task requiring approximately 360 MINIQUAD75 runs, only preliminary calculations were attempted. These indicated that the safe area decreases with increasing complexity.

Abbreviations and symbols

TMEi, TLEi, THEi = Total concentrations of metal, ligand and hydrogen ion (experimental).

TMCi, TLCi, THCi = calculated concentrations of total metal, ligand and hydrogen ion.

NP = Number of experimental points.

m = Number of stability constants refined.

$R_i = [(\mathrm{TME_i} - \mathrm{TMC_i}) + (\mathrm{TLE_i} - \mathrm{TLC_i}) + (\mathrm{THE_i} - \mathrm{THC_i})]$.

$$\text{Mean} = \frac{\sum_{i=1}^{NP} R_i}{NP} \qquad U = \sum_{i=1}^{NP} R_i^2$$

$$\text{Variance (Var)} = \frac{\sum (R_i)^2}{NP - m}$$

$$\text{Standard deviation (SD)} = \sqrt{\text{Variance}};$$

$$\text{kurtosis} = \frac{\sum (R_i)^4}{NP \times \text{Var}^2};$$

$$\text{skewness} = \frac{\sum (R_i)^3}{NP \times \text{Var} \times \text{SD}};$$

$$\chi^2 = \sum \frac{(R_i)^2}{(\mathrm{TXE_i})^2};$$

$$R\ (\text{cryst}) = \frac{\sum R_i^2}{\sum \mathrm{TMEi}^2 + \mathrm{TLEi}^2 + \mathrm{THEi}^2}.$$

Acknowledgements—We express our gratitude to the referee for suggesting some of the parameters responsible for the robustness of the program, *a vs* pH plots and the rotation of a three-dimensional figure. The authors thank Fluka AG (Switzerland) for the gift samples of hydrazides.

REFERENCES

1. Kyoto Chemical Co. Ltd. Jpn. Kodai Tokyo koho JP 59 24, 272, CA:101:39 955u.
2. Haitachi Chemical Co. Ltd. Jpn Kokai Tokyo koho JP 59, 172, 571, CA:102:63 276q.
3. R. Schneerson, J. B. Robbins, O. Barresra, A. Sutton, W. B. Habig, J. Chaimovich and M. C. Hardegree, *Prog. Chim. Bio. Res.*, 1980, **47**, 77.
4. M. L. Ciompi, A. Lucacchini, D. Segnini and M. R. Mazzoni, *Adv. Expl. Med. Biol.*, 1980, **122A**, 395.
5. D. Gumien and H. C. Gmernicka, *Acta Pol. Pharm.*, 1979, **36**, 271.
6. G. Ley, E. Pnezel, W. Rebafka and K. Boott, *Eur. Pat. Appl.*, 1979, **3**, 516.
7. P. Grans, A. Sabatini and A. Vacca, *Inorg. Chim. Acta*, 1976, **18**, 237.
8. Jr C. F. Baes and R. E. Mesmer, *The Hydrolysis of Cations*. Oak Ridge National Library (1976).
9. K. M. M. Krishna Prasad, A. Satyanarayana, C. Kamala Sastry and R. Sambasiva Rao, *Proc. Ind. Council of Chem.*, 1985, **5**, A03.
10. G. Gran, *Acta Chem. Scand.*, 1950, **4**, 559; *Analyst*, 1982, **54**, 2675; *Anal. Chem. Acta*, 1988, **206**, 111.
11. G. H. Nancollas and M. B. Tomson, *Pure & Appl. Chem.*, 1982, **54**, 2675.
12. A. Braibanti, G. Ostacoli, P. Paoletti, L. D. Pettit and S. Sammartano, *Pure & Appl. Chem.*, 1987, **59**, 1721.
13. D. G. Tuck, *Pure & Appl. Chem.*, 1989, **61**, 1161.
14. A. Ravindra Babu Ph.D. Thesis, Andhra University, Visakhapatnam, India (1991).
15. G. Nageswara Rao, V. M. Ch. Vinaya Kumari, K. V. Ramana and R. Sambasiva Rao, *Ind. J. Chem.*, 1989, **28A**, 709.
16. G. Nageswara Rao, K. V. Ramana and R. Sambasiva Rao, *J. Ind. Chem. Soc.*, 1991, **68**, 34.
17. D. C. Montgomary and E. A. Peck, *Introduction to Linear Regression Analysis*. John Wiley, NY (1982).
18. A. Vacca, A. Sabatini and M. Agristina, *Coord. Chem. Rev.*, 1972, **8**, 45.
19. A. Ravindra Babu and R. Sambasiva Rao, *J. Chem & Eng. Data*, 1992, **37**, 526.
20. A. Braibanti, F. Dallavalla and G. Mori, *Ann. Chim.*, 1978, **68**, 873.
21. T. O. Maier and R. S. Drago, *Inorg. Chem.*, 1972, **11**, 86.
22. P. Gans, A. Sabatini and A. Vacca, *J. Chem. Soc. Dalton*, 1985, **11**, 95.
23. P. M. May, K. Murray and D. R. Williams, *Talanta*, 1985, **32**, 483.
24. D. J. Legget, *Computational Methods for the Determination of Formation Constants*. Plenum Press, New York (1985).
25. R. M. Alcock, F. R. Hartley and D. E. Rogers, *J. Chem. Soc. Dalton*, 1978, 115.
26. M. S. El-Ezaby and F. M. Al-Sogair, *Polyhedron*, 1982, **1**, 791.
27. E. Casassas, G. Fonrodona and R. Tauler, *Polyhedron*, 1987, **6**, 1517.
28. G. Nageswara Rao, Ph.D. Thesis, Andhra University, Visakhapatnam, India (1989).
29. R. N. Sylva and M. R. Davidson, *J. Chem. Soc. Dalton Trans.*, 1979, 465.
30. J. A. Larsson and H. L. Pardue, *Anal. Chem.*, 1989, **61**, 1949.
31. V. Nurchi and G. Crisponi, *Anal. Chim. Acta.*, 1989, **222**, 359.
32. J. L. Kueslter and J. H. Mize, *Optimization Techniques with Fortran*. McGraw-Hill, New York (1973).

Talanta, Vol. 40, No. 12, pp. 1883–1889, 1993
Printed in Great Britain.

0039-9140/93 $6.00 + 0.00

POLAROGRAPHIC DETERMINATION OF Ce(III) AND Tm(III) USING RARE EARTH–DBF–CHLOROPHOSPHONAZO COMPLEX

YAN RONG,* LU XIAOHUA and SHI WENZHAO
Department of Chemistry, Huazhong University of Science and Technology, Wuhan 430074, People's Republic of China

(*Received* 11 *September* 1992. *Revised* 16 *March* 1993. *Accepted* 19 *March* 1993)

Summary—The electrochemical behaviour of the DBF–chlorophosphonazo (DBF–CPA)–rare earth (RE) complex has been investigated in this paper. A highly sensitive polarographic adsorption wave was found in the RE(III)–DBF–CPA system and a new method for determination of trace total RE(III) has been established. The limit of detection was $1.8 \times 10^{-8} M$. The results of determination of the total RE(III) content in Chinese standard reference materials of cast-iron and alloy steel were in good agreement with the certified values. The polarographic adsorptive waves of Ce(III) and Tm(III)–DBF–CPA overlap seriously. In order to improve the selectivity of determination, a non-linear regression model was employed to fit the peak height of the polarographic wave and the concentrations of Ce(III) and Tm(III). The predictive accuracy of this model for simulant mixtures was satisfied.

Natural resources of rare earth(RE) are abundant in China. Because of their special photogenic, magnetic, mechanical and nuclear properties, rare earth elements are widely applied in the fields of industry, agriculture and natural science. Chemists are increasingly paying attention to the study of environmental, medical and biological effects of rare earth elements. Therefore, methods for their rapid, sensitive and accurate determination and separation are of great importance.[1]

DBF–CPA is a new colour with molecule structure

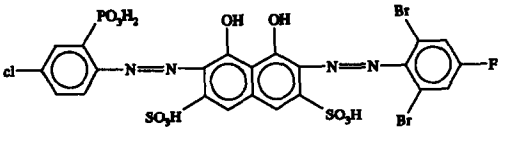

It has been used as a sensitive colourant in the spectrophotometric determination of total rare earths, but its electrochemical behaviour has not been investigated. In this paper the polarographic behaviour of rare earth–DBF–CPA complexes at the mercury electrode was studied. A sensitive and selective polarographic adsorptive wave (PAW) of RE(III)–DBF–CPA complexes was established in the determination of trace amounts of RE. To improve the selectivity of the method, a non-linear regression model was applied to determine Ce(III) and Tm(III) simultaneously in the rare earth mixtures and the results of this determination were satisfactory.

EXPERIMENTAL

Apparatus

Single sweep oscillopolarographic experiments were performed on a oscillopolarograph model JP-2A with a dropping mercury working electrode (DME), a saturated calomel reference electrode (SCE) and a platinum-wire counter electrode. Cyclic voltammetry was performed with a neopolarograph model XJP-821(B) with a conventional three-electrode cell; a hanging mercury electrode, an Ag/AgCl (saturated KCl) reference electrode and a platinum-wire counter electrode. Voltamperograms were recorded on an X–Y recorder model LZ03-204. A spectrophotometer model UV240(Simazu) was used with 1 cm glass cells and a pH meter model PHS-25C was used for pH measurement.

Reagents

DBF–CPA was synthesized in the Chemistry Department of Wuhan University of China.[2]

*Author for correspondence. Present address: National Key Laboratory on Coal Combustion, Huazhong University of Science and Technology, Wuhan 430074, People's Republic of China.

The synthetic route is as follows:

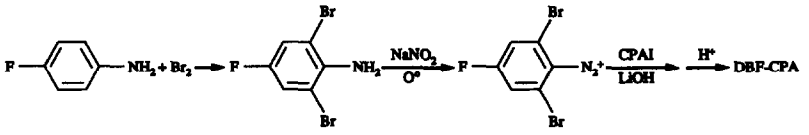

Other chemicals used were of commercial analytical grade reagents. All solutions were prepared in doubly distilled water. Stock solutions of 1 mg/ml RE(III) in 0.1*M* NH_4Cl solution were prepared from RE_2O_3. A 6.1×10^{-4} *M* DBF–CPA solution (0.05%) were prepared in water. A 0.1*M* NH_4Cl solution (pH = 4.5) was used as background electrolyte.

Procedures

A 5.0 ml portion of 0.1*M* NH_4Cl buffer and 0.15 ml of 6.1×10^{-4} M DBF–CPA solution were mixed with a known volume of the sample solution, and the mixture was diluted to 25.0 ml with water. Shake the solution and then transfer 10 ml of it into an electrolyzer. Record the secondary differential response of the single sweep oscillopolarography of the RE–DBF–CPA complex and read the peak height at the reductive potential about −0.78 V (*vs.* SCE.).

RESULTS AND DISCUSSIONS

The PAW of the RE–DBF–CPA complex and experimental conditions

The secondary differential peak of DBF–CPA and RE(III)–DBF–CPA complex in 0.1*M* NH_4Cl system are illustrated in Fig. 1. The P_1 and P_2 peaks (solid line) corresponded to the reduction of the two azo linkages of the DBF–CPA reagent. When trace RE was added in the DBF–CPA and NH_4Cl system, the height of P_2 decreased and its reductive potential moved slightly to a negative position, P_2'(dashed line in Fig. 1). At the same time a new peak P_3' with a more negative reductive potential appeared at −0.78 V (*vs.* SCE). P_3' was the reductive peak of the RE–DBF–CPA complex. The height of the secondary differential peak($i''p_3'$) had a good linear relationship with concentrations of RE in the range 2.0×10^{-8}–1.0×10^{-8}*M*. The detection limit was 1.80×10^{-8}*M*.

Several electrolytes such as HCl, NaH_2PO_4, $Na_2B_4O_7$, KCl, $NaNO_3$, NH_4Cl, NH_4Ac, and NH_4Br were studied. In NH_4Cl, NH_4Br or NH_4Ac solution, the peak P_3' appeared, but in NH_4Cl solution the sensitivity and the peak shape were better than those in NH_4Br and in NH_4Ac. The p_3' peak appeared when pH was in the range 3.7–10.2, while the heights of p_3' were stable when pH was between 4.0 and 8.0. Therefore, we selected pH = 4.5 with NH_4Cl solution as supporting electrolyte.

The influence of the concentration of DBF–CPA on the current was studied. With increasing concentrations of DBF–CPA, the current $i''p_3'$ increased first and then when the complex formed completely, the peak currents became stable, and finally because of the competition of adsorption between RE(III)–DBF–CPA complex and the free DBF–CPA at DME, the $i''p_3'$ decreased (see Fig. 2).

The height of $i''p_3'$ increased from 2.0 to 3.7 cm while the height of the mercury column(*h*)

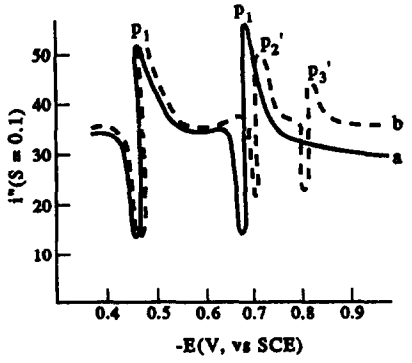

Fig. 1. Single sweep oscillopolarography: (a) 3.6×10^{-6}*M* DBF–CPA + NH_4Cl (pH = 4.5); (b) a + 2.8×10^{-7}*M* Ce(III).

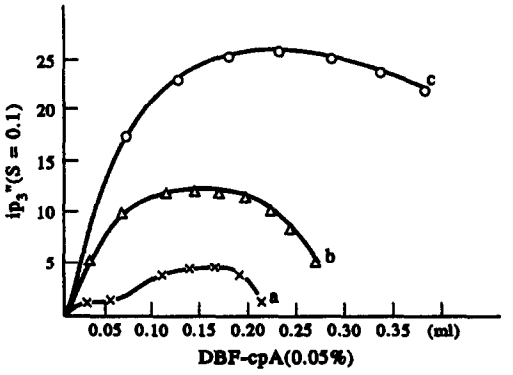

Fig. 2. The influence of DBF–CPA content on $i''p_3'$: (a) 0.572×10^{-7}*M* RE(III); (b) 2.86×10^{-7}*M* RE(III); (c) 7.16×10^{-7}*M* RE(III).

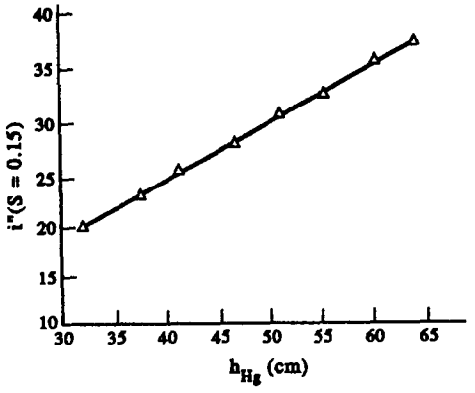

Fig. 3. Effect of height of Hg column on $i''p_3'$.

was changed from 35 to 65 cm. A linear relationship between $i''p_3'$ and h is shown in Fig. 3.

The effect of temperature on current was also studied. The variation of $i''p_3'$ with temperature is recorded in Table 1, showing that the effect of temperature on the height of $i''p_3'$ was not significant.

The effect of enrichment time and the size of the mercury drop on $i''p_3'$ had been studied by a neopolarograph with a hanging mercury electrode. The results are listed in Table 2.

The experiments showed that the longer the enrichment time and the bigger the size of the mercury drop, the larger the current ($i''p_3'$). This may be because of adsorption of more complex on the surface of the mercury drop while the size of the drop and enrichment time increased. The results also showed that the reductive wave of RE(III)–DBF–CPA has an adsorptive property.

Determination of the composition of the complex

The composition of the complex was determined by an equilibrium method and a straight line method.[3] The results are shown in Fig. 4(a) and Fig. 4(b). In the equilibrium method if the concentration of ion is kept constant and the concentration of DBF–CPA is changed, the plot

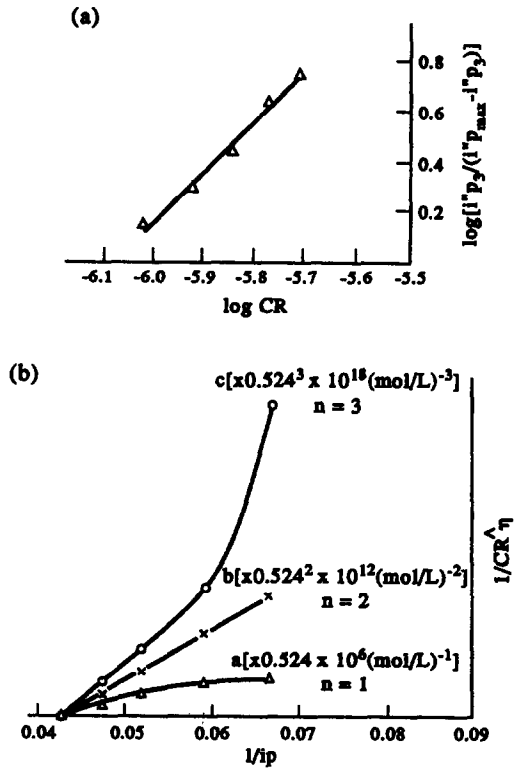

Fig. 4. (a) Determination of composition by equilibrium method; (b) determination of composition by straight line method.

of $\log[i''p_3'/(i''\text{pmax} - i''p_3')] \sim \log CR$ should be a straight line. The slope of this line is just the ratio of concentration of ligand to metal. Where i''pmax is the maximum peak current of the complex, $i''p_3'$ is the peak current corresponding to different concentrations of ligand and CR is the equilibrium concentration of DBF-CPA. When the concentration of ligand is largely more than that of metal, CR is almost equal to the total ligand concentration. So we can easily determine the composition of a complex. In Fig. 4(a), the slope of the straight line is equal to 2.

Because the height of the reductive peak is directly proportional to the concentration of the

Table 1. Effect of temperature on $i''p_3'$

T(°C)	9.0	11.5	14.0	18.0	21.0	23.0	27.0	30.0	34.0	36.0	39.0	44.0
$i''p_3'$(cm)	1.2	1.5	1.6	1.6	1.65	1.7	1.65	1.65	1.75	1.8	1.9	1.95

Table 2.

(a) Effect of mercury size on height of p_3'						
Mercury size (used amount, unit)	10	15	20	25	30	35
Height of p_3'(cm)	4.1	5.4	7.6	8.0	10.0	10.3
(b) Effect of enrichment time on height of p_3'						
t(min)	0.4	0.6	1.0	2.0	3.0	
height of p_3'(cm)	0.45	1.10	1.15	2.40	3.15	

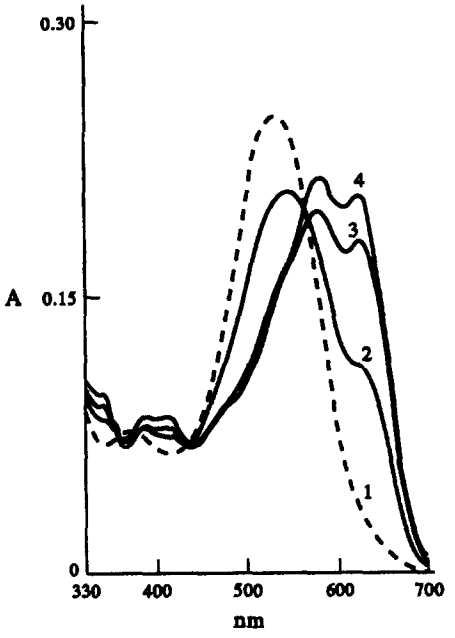

Fig. 5. Adsorption spectra: (1) 0.05% DBF–CPA + 0.1M NH_4Cl (pH = 4.5); (2) 0.1 ppm RE(III) + (1); (3) 0.2 ppm RE(III) + (1); (4) 0.3 ppm RE(III) + (1).

complex of RE–DBF–CPA, the equation $1/ip = 1/ip_{max} + 1/(b \times ip_{max} \times CR\wedge n)$ holds true. Where ip_{max} is the maximum peak height, CR is the concentration of DBP–CPA and ip is the peak height corresponding to different concentrations of ligand. When n is an integer we can obtain the different curves of $1/ip \sim 1/CR\wedge n$. So the ratio of ligand to metal can be obtained when the plot of $1/ip \sim 1/CR\wedge n$ shows a linear relationship. From Fig. 4(b) we can see the value of n equals 2. The results of the straight line method and the equilibrium method both show the composition of the complex is RE: DBF–CPA = 1:2.

Figure 5 shows the absorption curves of DBF–CPA and RE–DBF–CPA. We also determined the composition of the complex using the absorption peak of the RE–DBF–CPA complex (650 nm). The results are in agreement with that of the reported spectrophotometric method,[2] and DBF–CPA: RE is also equal to 2.

The reduction mechanism of RE(III)–DBF–CPA complex

The present paper investigates the cyclic voltammogram, electrocapillary curve, temperature coefficient of the polarographic current, the relationship between potential, scanning speed (v) and peak height, the influence of surfactants on current, the effect of acidity of the solution on peak potential(E_p), *etc.* were investigated.

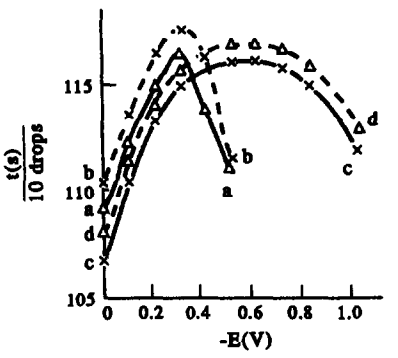

Fig. 6. Electrocapillary curve: (a) 0.05% NH_4Cl (pH = 4.5); (b) 7.16 × $10^{-5}M$ Ce(III) + a; (c) 6.1 × $10^{-5}M$ DBF–CPA + a; (d) 7.16 × $10^{-5}M$ Ce(III) + 6.1 × $10^{-5}M$ DBF–CPA + a.

The electrocapillary curves are shown in Fig. 6. Comparing curves (c) and (d) with (a) and (b), we can see the zero charge potential shifted negatively when DBF–CPA was added to the solution, and the left part of curves (c) and (d) were both lower than curves (a) and (b).

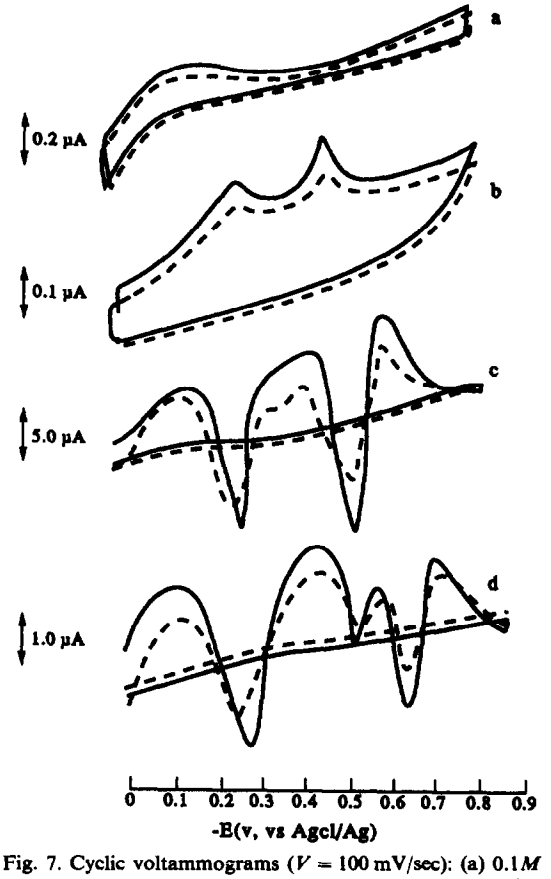

Fig. 7. Cyclic voltammograms (V = 100 mV/sec): (a) 0.1M NH_4Cl (pH = 4.5) + Ce(III), $i \sim E$(V); (b) 6.1 × $10^{-4}M$ DBF–CPA + 0.1M NH_4Cl (pH = 4.5), $i \sim E$(V); (c) 6.1 × $10^{-4}M$ DBF–CPA + 0.1M NH_4Cl (pH = 4.5), e″ ~ E(V); (d) 5.73 × $10^{-5}M$ Ce(III) + c, e″ ~ E(V).

It shows that DBF–CPA and RE–DBF–CPA were both adsorptive on the surface of the mercury drop in the form of negative ions.

The cyclic voltammograms are shown in Fig. 7. From this figure, we can see both DBF–CPA and RE–DBF–CPA complex show completely irreversible reduction processes. According to the Randle-Sevoik equation: $ip = 269n^{3/2}AD^{1/2}V^{1/2}C^{b}$, we know the curve of $ip \sim V^{1/2}$ should be a straight line. When electroactive substances possess adsorptivity on the surface of DME, the ip should be higher than the predictive value. The experimental results of the relationship between potential scanning speed and the peak height are shown in Fig. 8. From this figure we can see that the RE–DBF–CPA complex possesses adsorptivity at DME. The experimental results of the electrocapillary curve, and the influence of surfactants on current all showed an adsorptivity of RE(III) ~ DBF–CPA complex at the DME.

The electron number of the electrode reaction was determined. The results showed a two-electron reaction in the reduction of the complex. Therefore, the electrode process of the complex may be considered as the reduction of the ligand of the complex at DME.[4]

The result of the effect of acidity on peak potential is listed in Table 3. We can see that the potential became negative with an increase of pH, showing that the hydrogen ion acts as a reactant in the reduction process. So the mechanism of the electrode process may be as follows:

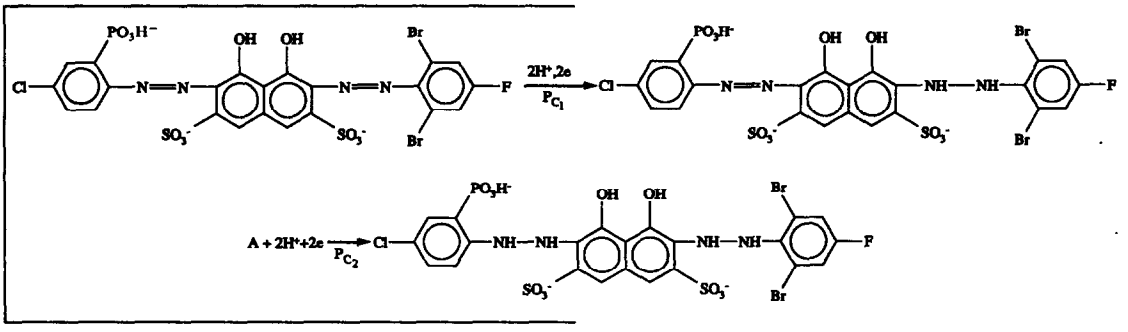

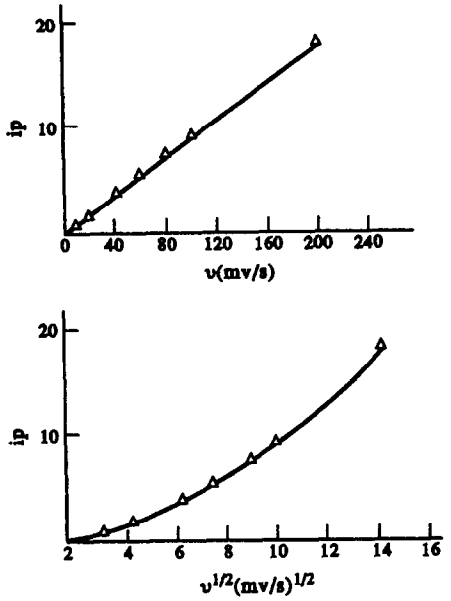

Fig. 8. Relationship between potential scanning speed (V) and the peak height (ip).

PMBP–benzene extraction and determination of RE(III)

The influence of some coexisiting ions in the determination of RE(III) were investigated. At the concentration of 7.16×10^{-7} *M* RE(III), the permissible concentrations of foreign ions for determination of RE(III) were 7.16×10^{-4}*M* Na^+, K^+, NH_4^+, As(III), Ag^+, NO_3^-, SO_4^{2-}, I^-, Br^-, Ac^-: 7.16×10^{-5}*M* Mg^{2+}, Ca^{2+}, Sr^{2+}, B_a^{2+}, Mn^{2+} and 7.16×10^{-6}*M* Sn(IV), Pb(II), Sb(III), Te(IV), Ni(II), Mo(VI) and Cd(II). Co(II), Cr(III, VI), Fe(II, III), V(V), W(VI) and Se(VI) interfered with the determination of RE appreciably. These interferences can be eliminated by PMBP–benzene extraction.

Jiao *et al.*[5] studied the optimum condition of the separation of rare earth cations from non-rare earth elements by extraction with PMBP(1-phenyl-3-methyl-4-benzoyl-pyrozolone-5) under the presence of masking agents NH_4CNS and sulphosalicylic acid. This extraction system was

Table 3. Effect of acidity on peak potential

pH	3.8	4.0	5.4	6.7	7.5	7.8	8.5	9.0	9.5	10.0
$-Ep_3$(V)	0.77	0.77	0.77	0.77	0.77	0.78	0.78	0.78	0.78	0.80

Table 4. Results of RE in SRM

Sample	Certified value, %	Determined value, %	RSD, %($n = 4$)
Cast iron (7101)	0.022	0.0218	3.5
Alloy-steel (25 MnTiBRE)	0.0078	0.00781	3.5
Alloy-steel (CrNiCuMoRE)	0.084	0.0820	3.7

used in this paper, and the selectivity of the proposed method was improved. The total RE(III) contents in standard reference materials of cast iron and alloy-steel were determined. The results are shown in Table 4.

The results show that method of PMBP–benzene extraction separation combined with PAW of the RE(III)–DBF–CPA complex could be applied to the determination of trace RE(III) successfully.

Simultaneous determination of Ce(III) and Tm(III) in the polarographic system of RE(III)–DBF–CPA by non-linear regression

The PAWs of the Ce(III)– and Tm(III)–DBF–CPA complexes overlap seriously. In order to improve the selectivity of the determination of RE(III), a non-linear regression model was applied to determine Ce(III) and Tm(III) in the RE(III) mixture simultaneously.

Principles. To a mixture containing n components, the concentration of each component (x_i) is regarded as a regression variable, and the peak height of the polarographic wave (h_i) was regarded as a function of concentration. Considering the interaction of the components, a non-linear mathematical model was proposed to fit the x_i and h_i:

$$h_i = b_0 + \sum_i b_i x_i + \sum_{i,j} b_{ij} x_i x_j \quad (i,j = 1, 2, 3 \ldots n) \quad (1)$$

Where b_0, b_i and b_{ij} can be obtained by a calibration procedure. The partial derivatives of equation (1) are as follows:

$$\partial h_i / \partial x_i = b_i + \Sigma b_{ij} x_j \quad (i,j = 1, 2, 3, \ldots, n) \quad (2)$$

Under the experimental conditions, a series of standard solutions of each individual component (x_i) were added to a sample of Ce(III) and Tm(III) mixture. The peak heights (h_i) of single sweep oscillopolarographic waves were then measured and a calibration curve of h_i–x_i was obtained. The slope of the calibration curve was regarded as the partial derivative ($\partial h_i / \partial x_i$). Thus, for a system of n components, n partial derivatives can be obtained and the concentration of each component in a mixture can be calculated by solution of the simultaneous linear equations (2).

Experimental design. A two-factor (Ce and Tm) four level orthogonal regression experiment was designed. Setting the standard level of concentration of RE(Ce and Tm) at 0.24 ppm, the interval of concentration change was 0.08 ppm. The same experimental procedures were performed and the peak heights at −0.78 V (*vs.* SCE) were recorded. The results are listed in Table 5.

The regression equation obtained by the multifactor regression program is:

$$h = -7.348904 + 45.12561 \times C_{Ce} + 68.25055 \times C_{Tm} + 20.31035 \times C_{Ce} \times C_{Tm} \quad (3)$$

The calculated peak heights by regression equation (3) are listed at the bottom of Table 5. The standard deviation between the determined results and calculated ones is less than 0.3. It can be shown that the precision of the regression equation is satisfied.

Determination of $\partial h_i / \partial x_i$. Under the same experimental conditions as the regression procedures, two groups of individual component standard solutions with different concentrations of Ce(III) or Tm(III) were prepared respectively, and then a known volume of simulant and unknown mixture of Ce(III) and Tm(III) was transferred into the above-mentioned standard

Table 5. Results of two-factor regression experiment design

Expt. No.		1	2	3	4	5	6	7	8	9	10	11	12	13	14	15	16
Ce(III)		0.4	0.4	0.4	0.4	0.32	0.32	0.32	0.32	0.16	0.16	0.16	0.16	0.08	0.08	0.08	0.08
Tm(III)		0.4	0.32	0.16	0.08	0.4	0.32	0.16	0.08	0.4	0.32	0.16	0.08	0.4	0.32	0.16	0.08
h_i	Detn.	41.0	35.0	23.5	18.0	37.0	31.0	18.5	11.5	31.0	21.5	10.0	6.5	24.5	17.5	6.0	2.0
	Calc.	41.2	35.1	23.1	17.8	37.0	31.0	19.0	12.0	30.5	21.7	10.3	6.6	24.2	17.6	6.4	1.85

Table 6. Determination of Ce(III) and Tm(III) in RE(III) mixture

RE	$\partial h_i/\partial x_i$	Concentration of RE in sample (ppm)		
		Correlation coefficient	Standard value	Determined value
Ce(III)	47.7	0.998	10.0	10.05
Tm(III)	73.0	0.996	5.0	5.17

The relative standard deviation for Ce(III) and Tm(III) were both less than $\pm 5.3\%$

solution and diluted to 25.0 ml with water. Measure the peak height, h_i, and plot the $h_i - x_i$ curve to determine the slope. The concentrations of Ce(III) and Tm(III) can then be calculated from equation (2). The average results of the simulant unknown for four determinations are listed in Table 6.

REFERENCES

1. Gao XiaoXia, *Handbook on the Physics and Chemistry of Rare Earth*, 1986, **8**, 163.
2. Yang Yi, Yu Ximou, Cai Ruxiu and Zhen Yune, Gaodeng Xuexiao Huaxue Xuebao, *Chemical Journal of Chinese Universities*, 1988, **4**(1), 23.
3. Li Nanqiang and Gao XiaoXia, *Fenxi Huaxue*, 1974, **2**, 459.
4. T. M. Florence, *Electroanal. Chem. Interficial Electrochem.*, 1974, **25**, 115.
5. Jiao Kui, Zhang Manping and Gao Xiaoxia, *Beijin Daxue Xuebao* (Journal of Beijing University) 1982, **6**, 77.

Talanta, Vol. 40, No. 12, pp. 1891–1897, 1993
Printed in Great Britain.

0039-9140/93 $6.00 + 0.00

A GENERIC FIA SYSTEM FOR DETERMINATION OF ENZYME ACTIVITIES : ASSAY OF CELLULASE

ELO H. HANSEN and ALLAN JENSEN
Chemistry Department A, The Technical University of Denmark, Building 207, DK-2800 Lyngby, Denmark

(*Received* 9 *February* 1993. *Accepted* 13 *March* 1993)

Summary—The concept of a generic FIA system is described that allows multi-points assays of enzyme activities, that require a coupled chemical derivation reaction for detection. The enzymatic degradation procedure and the ensuing chemical indicator reaction are completely separated, which inherently allows each of these processes to be individually optimized with respect to operational parameters such as heating, cooling or possibly stopped flow manipulations. The applicability of the approach is demonstrated for the determination of the activity of cellulase using spectrophotometric detection via a couple chromogenic indicator reaction.

For the enzymatic degradation of a substrate S to a product P, as described by the reaction sequence

$$S + E \leftrightarrow SE^* \xrightarrow{k_2} P + E$$

where E denotes the enzyme, and k_2 is the rate constant for the rate-determining step, the overall reaction rate is given by the expression

$$d[P]/dt = (k_2[E]_o[S]_t/([S]_t + K_m)$$

where K_m is the Michaelis–Menten constant. For $[S]_t \gg K_m$, the expression reduces to

$$d[P]/dt = (k_2[E]_o)$$

that is, the reaction becomes pseudo-zero-order with respect to the substrate, and the reaction rate is directly proportional to the concentration of enzyme, or, more precisely, its activity. Most enzymatic reactions also involve the interaction of appropriate cofactors. Thus, oxidases consume oxygen and generate hydrogen peroxide, while dehydrogenases require the presence of $NAD,^+/NADP^+$ which in turn are converted to NADH/NADPH. Therefore, the activity of an enzyme can be measured either by determining the substrate/cofactor consumed or the product/cofactor generated. For the dehydrogenases, this task is fairly straightforward, because NADH/NADPH can be monitored both optically and electrochemically. If none of the constituents in an enzyme reaction are directly determinable, one of them might be quantified via an accompanying indicator reaction. For instance, hydrogen peroxide, as generated by the oxidases, can be measured photometrically by coupling to a chromogenic reagent, or by chemiluminescence through reaction with luminol and hexacyanoferrate (III).[1,2]

The determination of the activity of an enzyme is in practice most often performed by incubating the substrate and the enzyme for an appropriate period of time, whereupon the concentration of one of the constituents is measured, possibly by an accompanying indicator reaction. However, such an approach yields only a single point measurement. And merely assuming that the enzymatic degradation process, as recorded by the change in detector response over a fixed of period of time, necessarily will follow a linear relationship, might, as is depicted in Fig. 1, easily be most hazardous. In fact, it could very well be that the degradation reaction followed a course as the one outlined in the figure, that is, initially comprising an inherent lag-phase followed by a period during which the signal were to change linearly as a function of time, the process eventually reaching a level where pseudo-zero-order reaction condition with respect to substrate no longer is fulfilled. Hence, the single-point measurement approach would obviously lead to a false answer, and therefore it is inherently much to be preferred to rely on multi-point assays for quantifying the enzyme activity.

Flow injection analysis (FIA) entails exactly such possibilities, namely by applying the stopped-flow approach, where a suitable section

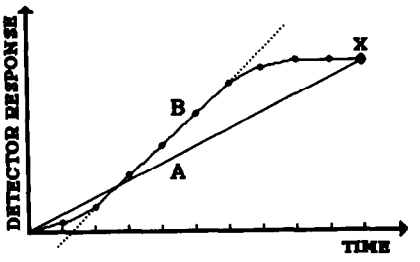

Fig. 1. Single-point (curve A) and multi-point (curve B) determination of the activity of an enzyme as obtained by measurement over identical time spans, that is, from time zero to a time t corresponding to endpoint X. The slope of the linear part of each curve is a measure of the enzyme activity. Curve B illustrates how the detector output might possibly develop if the degradation process were to be monitored intermittently.

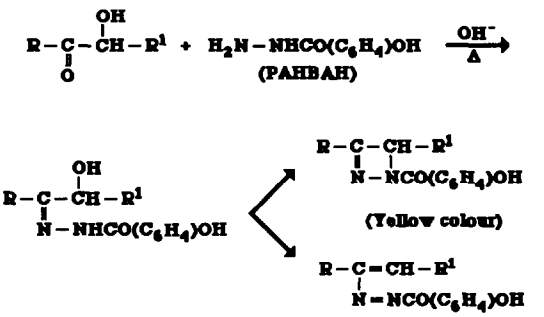

Fig. 3. Representation of the chemical derivation of reducing sugars with PAHBAH, the reaction sequence in strongly alkaline solution at elevated temperature ultimately yields yellow-coloured products.

of the injected and dispersed sample zone is arrested within the observation area of the detector.[3] Provided that the conditions are manipulated in such a manner that they conform with pseudo-zero-order with respect to substrate and pseudo-first-order with respect to the enzyme, the slope of the reaction rate curve will be directly proportional to the concentration of enzyme and hence to the enzyme activity. Reaction rate measurements in which the the rate of formation (or consumption) of a certain species is measured from a larger number of data points not only improve the reproducibility of the assay, but also ensures its reliability. Thus, the stopped-flow method is an efficient and convenient vehicle for measuring substrates and indeed determining enzyme activities. Furthermore, in FIA an added feature can be exploited, that is, the sample might be stopped at different parts of the the concentration gradient corresponding to different ratios of substrate to enzyme, so that it might be feasible to select exactly that part of the dispersed sample zone where the operational parameters are optimal.[1]

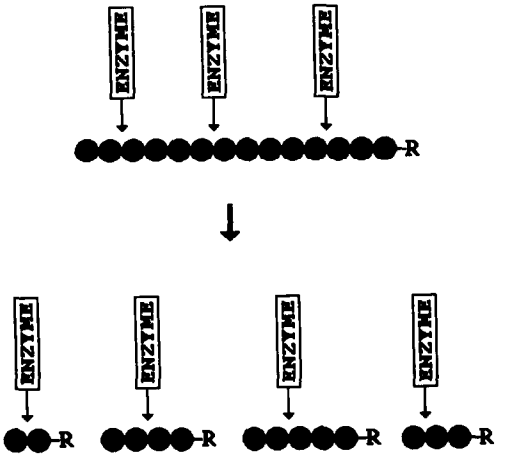

Fig. 2. The degradation of cellulose by cellulase. The enzyme degrades the substrate randomly, yielding sugar entities with reducing terminals (R). The quantification of the sugars is based on chemical derivation with these reducing terminals (*cf.* Fig. 3).

However, an absolute condition in order to employ the FIA stopped-flow method for enzyme activity measurements is that the enzymatic reaction either generate or consume a species which can be detected directly (*e.g.*, NADH/NADPH), or that the coupled indicator reaction is much faster than the enzymatic degradation reaction itself (*e.g.*, the use of luminol for the chemiluminescence detection of hydrogen peroxide) because the ensuing chemical reaction must not, of course, become the rate determining step in the overall reaction sequence. Fortunately, most auxiliary chemical reaction are generally much faster than the enzymatic degradation procedure, yet this does not always hold true. A prime example of this is the assay of the enzyme activity of cellulase which recently has been the subject of intensive studies at this laboratory. Cellulase is an enzyme which selectively degrades cellulose randomly, giving rise to the formation of sugar entities with reducing terminals (Fig. 2). The enzyme is much used for pretreating blue denim materials and as an additive in washing powders, yet it must be administered with utmost care, and for that reason there is a great need for assaying its activity. All available chemical derivation procedures rely on determining the reducing sugars entities, which can be effected by various means, the most promising avenue being the reaction sequence shown in Fig. 3.[4] Here, the reducing sugar terminals are made to react with *p*-hy-

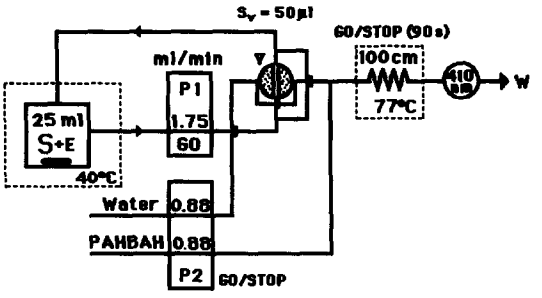

Fig. 4. Integrated system as used for enzyme activity determinations, essentially comprising two entirely separated subsystems communicating via a common valve (V). The subsystems on the left is the enzyme reactor where substrate (S, in large excess) and enzyme (E) react, while the chemical derivation subsystem is depicted to the right. For further details, see text. The operational parameters shown on the figure reflect the ultimately adopted ones. S_v is the sample volume injected.

droxybenzoylhydrazine (*p*-hydroxybenzoic acid hydrazide, PAHBAH), which in strongly alkaline solution at elevated temperatures give rise to the formation of a yellow compound which can be measured spectrophotometrically at 410 nm.[5,6] The problem is that not only is the enzymatic degradation reaction slow, but the coupled indicator reaction is very slow indeed.

Various, more or less ingenious, solutions have been attempted to circumvent this problem, the most promising being based on separating the enzymatic degradation procedure and the accompanying indicator reaction. Thus, Worsfold and coworkers[7] designed a FIA manifold where they injected a sample of cellulase sandwiched between two zones of substrate which during its travel through the FIA manifold partly overlapped and reacted and subsequently was merged with the colour forming reagent so that it became feasible to measure consecutively both the background (the substrate itself contains, as depicted in Fig. 2, some inherent reducing sugar terminals) and the sugar entities formed by the enzymatic degradation process. Still, this solution gives only a single-point assay, and therefore it suffers from the drawbacks mentioned previously.

In another approach, undertaken by Pfeiffer *et al.*,[8] a multicoil FIA-manifold was employed,[3] where individual samples and the matrix solutions concurrently could be stacked and stored for an appropriate length of time. However, although this method potentially might be applicable for multipoint assay, that is, by incubating aliquots of the same analyte solution for different lengths of time, it was not used for this purpose. Rather it was, in fact, merely employed for speeding up the sample throughput via incubation of different samples at equal time intervals, and therefore it yielded only single-point measurements. Although an interesting concept, it does appear as a rather cumbersome and difficult system to administer in practical work.

Therefore, in order to effect the assay of the enzyme activity irrespectively of the coupled chemical reactions and its particular characteristics (absolute reaction rate, and relative reaction rate in respect to that of the enzymatic degradation procedure) it was decided in the present study to take an entirely different approach, that is, not only to try to solve the actual problem of assaying the activity of cellulase, but to attempt to design a generic enzymatic system which inherently would allow handling of any type of sample. Furthermore, it was a prerogative that such a system should be versatile, *i.e.*, it should not only allow the enzymatic degradation procedure to be completely separated from the chemical detection procedure, but it should also permit each of the processes to be optimized individually, and it should inherently allow multipoint determinations to be performed.

These conditions were met by employing the approach described in this communication, and illustrated in Fig. 4 (the parameters depicted show the optimal values, (see Results and Discussion section). In part based on a concept devised for an entirely different purpose,[9] it consists in essence of two individually and totally separated subsystems, one for the enzymatic degradation reaction, consisting of a well-stirred reactor vessel, and one for the ensuing chemical indicator reaction, comprising a FIA manifold, the two subsystems communicating via a common valve. The content of the enzyme reactor is via an external loop constantly circulated through pump 1 and the injection valve at such a rate that the solution in the loop at all times is identical to and representative of the solution in the reactor vessel. At preselected times the injection valve is switched to the inject position and a metered sample volume is by pump 2 introduced into the FIA system where it is mixed with suitable reagent(s) and carried towards the detector. During its path through the manifold the sample/reagent mixture might, if required, be arrested in order to gain additional reaction time, heated, or possibly cooled, or manipulated in any other

appropriate manner before it is guided into the detection device. Sample injection can be repeated as often as required so that a suitable number of data-points on the concentration/time curve can be recorded. The performance of the system is illustrated for the assay of the activity of cellulase.

EXPERIMENTAL

Reagents

All reagents were of analytical reagent grade quality, and distilled, degassed water was used throughout. The medium for the enzyme degradation procedure was a 4 g/100 ml of sodium carboxymethylcellulose (CMC), ultra low viscosity (Fluka BioChemika), dissolved in 0.01*M* sodium phosphate buffer adjusted to pH 7.0. It was prepared by adding the CMC to a boiling solution of the buffer and heating until all CMC was dissolved (*ca* 5 min). After cooling the solution was filtered (glass filter) and degassed. In the initial experiments for optimizing the derivation chemistry, aqueous glucose solutions (*D*(+)-glucose monohydrate, Sigma) in the concentration range 50–500 μM were used as model reducing sugar substrates.

The cellulase enzyme (Carezyme, activity 10070 U/g at pH 7.0 and 40°) was supplied by Novo-Nordisk, Copenhagen, and used as received. For actual enzyme activity assays, an appropriate amount of the enzyme was dissolved in 1.0 ml of the 0.01*M* phosphate buffer (pH 7.0) and added to the thermostatted enzyme reactor vessel. In all experiments, a total volume of 25.0 ml solution was used, that is, the reactor contained initially 24.0 ml CMC/buffer medium.

A 0.10*M* solution of *p*-hydroxybenzoylhydrazine (PAHBAH, Sigma) was obtained by dissolving 0.761 g in 50 ml of 1.0*M* sodium hydroxide. As mentioned in the Results and Discussion section, Bi(III), added as sodium bismuth (III) tartrate at a level of a few m*M*, has proven to be a catalyst in the reaction of PAHBAH with reducing sugar entities. Since this constituent was not available, its presence was effected by first adding to the 50 ml of 1.0*M* sodium hydroxide 0.097 g of bismuth nitrate pentahydrate and 0.057 g of potassium sodium tartrate. After gently heating the solution for 3–5 min, the solution was filtered and the above-mentioned amount of PAHBAH was added. The reagent solution was made freshly every day and degassed prior to use.

Apparatus

In the system used (Fig. 4) the reactor vessel consisted of Perspex container of a volume of *ca* 50 ml[9] equipped with a water-thermostatted jacket. As discussed later, a total volume of 25.0 ml of 0.01*M* phosphate buffer (pH 7.0) containing the CMC-substrate was used in each experiment. The container was fitted with a magnet and placed on a stirring table. After having attained the preset temperature (40° unless otherwise stated) the enzyme was added. Samples were thereafter withdrawn at preselected times. The solution of the well-stirred enzymatic degradation vessel and the FIA manifold were served by two peristaltic pumps (for optimal operation parameters, see Results and Discussion). All connecting lines and the 100 cm reaction coil, which was made as a knotted reactor and emerged into a second water-thermostatted bath, consisted of 0.5 mm i.d. microline tubing. For most of the actual assays was used a commercial Perkin-Elmer FIA system, comprising a Lambda 2 UV/VIS spectrophotometer, fitted with a 18 μl flow-through cell, and a FIAS-400 unit equipped with two individually controlled peristaltic pumps and a 5-port FIA valve. The operation of the pumps and the injection valve, in addition to data retrieval, handling and display, were all facilitated via the provided Perkin-Elmer FIA-DMS software program and an external PC. Results were communicated on an FX-80 printer. Because the injection valve of the Perkin-Elmer system merely is provided with five individually accessible ports on the rotor and stator, and therefore cannot accommodate both a bypass for the circulation solution from the reactor vessel and for the FIA manifold, it was necessary to eliminate one of them and replace it by an appropriate stop/go sequencing. Thus, the bypass for the carrier stream was abandoned, that is, when the injection valve was in the load-position (to fill the metered sample volume) pump 2 was stopped.

RESULTS AND DISCUSSION

As the proposed system (Fig. 4) essentially consists of two individually operated subsystems which communicate via the common injection valve it is possible to optimize their performance virtually independently of each other. In fact, the only constriction is the time required for the derivation chemistry in the FIA manifold, which therefore will set a limit as to

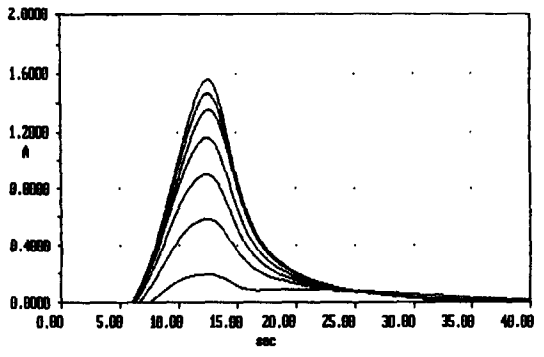

Fig. 5. Signal readouts for monitoring of a cellulase enzyme activity of 1.0 U/ml as obtained with the system shown in Fig. 4. The first sample (lower curve) was taken after 30 sec incubation, while the following ones were taken at 3.5 min intervals.

how often samples can be withdrawn from the enzyme degradation subsystem.

Enzymatic degradation subsystem

In order that the sample solution circulating in the external loop of the enzyme system at all times is truly representative of the composition of the solution in the reactor vessel, the loop should be made as short as physically possible and the circulation rate should be maintained at a fairly high level. In the present case it was found sufficient to set the pumping rate of pump 1 to 1.75 ml/min. Furthermore, since aliquots of sample solution at regular intervals are to be removed it is important that the volume of the reaction vessel is much larger than the injected volume so that even 8–10 withdrawals do not alter the contents of the reaction vessel to any appreciable extent. For that reason the injected volume was set at 50 μl while the volume of the reaction vessel was affixed at 25.0 ml, that is, 500 times larger than the injected volume. As Fig. 4 indicates, the return of the valve from the inject-position to the load-position will for each cycle imply that a volume of carrier equal to the sample solution removed is added to the reactor vessel. As a result, the volume of the reactor vessel will remain constant, yet the solution in it does continuously become slightly diluted with carrier. However, since the volume of the reactor vessel is much larger than the metered injection volume, this dilution can either be neglected or compensated for. It might seem reasonable to make the carrier identical to that of the buffer employed in the reaction vessel (phosphate buffer, pH 7.0). However, since the subsequent chemical indicator reaction in the present assay of cellulase has to proceed at a very high pH value, any appreciable buffer capacity in the carrier would be unwarranted. For that reason water was selected as carrier, and the buffer capacity in the reactor vessel was initially affixed at such a level (0.01*M* buffer concentration) that on one hand the pH would be maintained constant during the enzymatic degradation procedure, and on the other hand the buffer content of the injected sample volume would not affect the pH value of the derivation reaction (pH 13.5, which, incidentally, effectively serves to stop the enzymatic reaction upon introduction of the sample into the chemical derivation subsystem). The temperature for the enzymatic degradation procedure was set to 40° (in order to simulate ordinary washing conditions), that is, all substrate/buffer solutions added to the reactor vessel were thermostatted to this temperature prior to enzyme addition.

Chemical derivation subsystem

The conditions for the chemical derivatization reaction, where reducing sugars react with *p*-hydroxybenzoylhydrazine (PAHBAH) to form a yellow product (Fig. 3), has previously been studied in detail.[5,6] Thus, in batch experiments it was found that optimal conditions were encountered for temperatures in the range 70–100°, that the pH should be 13.7 (0.5*M* sodium hydroxide), the concentration of PAHBAH should be 0.05*M*, and that the reaction is catalyzed by Bi(III) ions.[5] Still, the reaction rate was found to be very low, and more than 10 min were required to reach equilibrium. Pfeiffer *et al.*,[8] who in their FIA experiments used a homologue of PAHBAH, that is, *p*-amino-

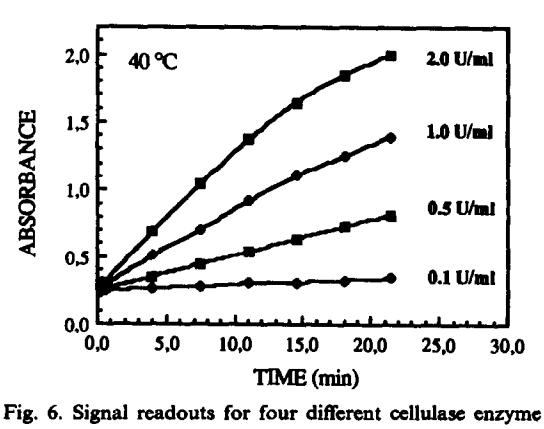

Fig. 6. Signal readouts for four different cellulase enzyme activities in the range 0.1–2.0 U/ml at 40°. The slopes read off the individual curves are plotted in Fig. 7. For the two highest cellulase activities the first 3 and 5 readouts, respectively, were used for evaluation of the slopes.

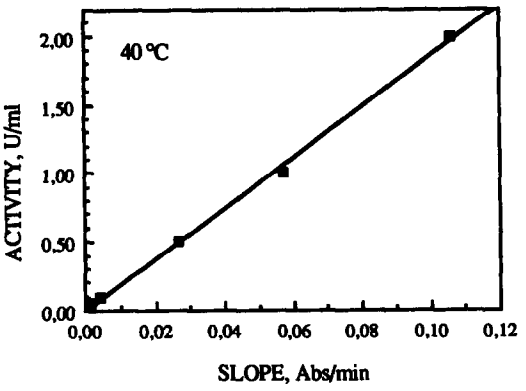

Fig. 7. Calibration curve at 40° for cellulase in the activity range 0.05–2.0 U/ml, as obtained by plotting the calculated slopes (in absorbance change per minute) for five individual experiments against the enzyme activities (in U/ml) monitored.

benzohydrazide (PABH), confirmed that a concentration of 0.05*M* of the chromogenic reagent was adequate. But as indicated previously, they also established that it was imperative to apply stopped-flow in order to obtain sufficient residence time of the sample/reagent mixture. For that reason the present FIA manifold was made to mix the sample and reagent in confluence and to contain a 100 cm knotted coil in which the sample/reagent mixture could be stopped. The coil was submerged in a thermostatted bath while the remaining conduits, which merely are communicating entities with the valve and the detector, were made as short as possible. It was therefore decided to affix the pH and the PAHBAH concentration at the levels quoted and to optimize the other operational parameters, that is, temperature for the derivation reaction, concentration level of Bi(III), pumping rates of carrier (water) and PAHBAH reagent, and the extent of the stopped-flow period. Optimization was performed with the consideration that the blind (background) value should be as low as possible (the substrate, CMC, contains reducing sugar terminals and therefore a certain blind value will be present), the sensitivity should be as high as possible, and the temperature applied should not give rise to the formation of bubbles which would interfere in the subsequent detection process. The optimization studies yielded the values depicted in Fig. 4, that is, the pumping rates for the carrier and PAHBAH should be identical and each set at 0.88 ml/min (and for that reason the the sodium hydroxide concentration in the reagent solution was affixed at 0.1*M* in order to give a final concentration in the combined stream of 0.05*M*); the stop-time should be 90 sec, and the reaction temperature should be 77°. Furthermore, it was found that addition of Bi(III) at a level of 1–2 m*M* to the PAHBAH reagent was optimal.

Assay of cellulase activities

The system was then used for assaying the enzyme activity of cellulase at different levels. The enzyme was in each experiment administered to the reactor vessel at time zero (in the following, all activity levels refer to the concentration in the enzyme reactor). The first sample was withdrawn after 30 sec, and thereafter samples were taken at 3.5 min intervals over a time range of 21.5 min, that is, seven samples were monitored in total. Thus, in Fig. 5 is shown the actual readouts as obtained by the consecutive monitoring of the enzymatic degradation of a 1.0 U/ml cellulase solution, while in Fig. 6 is depicted the readouts for four different enzyme activities, that is, 2.0, 1.0, 0.5 and 0.1 U/ml, where the substrate concentration in all cases amount to 4 g CMC/100 ml. Clearly, the highest enzyme concentration does not result in a straight line relationship over the entire time range. Possibly primarily because pseudo-zero-order reaction conditions with respect to substrate are not fulfilled at extended times, but maybe also because of the relatively high absorbances recorded. Therefore only the first three points in the response/time relationship are used in the evaluation of the slope, which is the quantitative representation of the enzyme

Table 1. Repetitive runs ($n = 5$) for the determination of a cellulase activity of 1.0 U/ml as performed with the system shown in Fig. 4, operated at 40°C. The individual parameters (average slope, standard deviation and relative standard deviation) are calculated for 3–7 measuring points, corresponding to 7.5–21.5 min monitoring, respectively

Measuring points	3	4	5	6	7
Time (*min*)	7.5	11.0	15.5	18.0	21.5
Ave. slope (*Abs/min*) $\times 10^3$	43.6	42.2	41.3	40.5	39.6
Stand. dev. (*Abs/min*) $\times 10^3$	2.5	2.1	1.9	1.6	1.4
Relative stand. dev (%)	5.7	4.9	4.6	3.9	3.6

activity. Nor does the 1.0 U/ml sample result in an absolutely straight line relationship over the entire time range, although the first five points (used for evaluation of the slope) appear to fall on a straight line, while the two low enzyme activities conform perfectly well to the pseudo-zero-order reaction conditions with respect to substrate concentration over the whole time frame. Relative to each other, the slopes are generally in good agreement, which is more clearly seen in Fig. 7, which shows the activity of the individual samples (in U/ml) depicted against the calculated slopes (in Abs/min). Included in this figure is also the slope recorded for an enzyme activity of 0.05 U/ml, which at 40° was close to the lowest value which could be measured. At 50°, where the enzymatic degradation reaction is faster, and resulted in approximately 50% higher signal readouts, the detection limit was found to be 0.02 U/ml.

Because the system for practical work is to be used for measuring an unknown activity as based on calibration with known activities, it is important that it is reasonable stable in operation. This was investigated by repeating the set of experiments mentioned above five consecutive times and comparing the results. Thus, Table 1 shows the average slopes and relative standard deviations determined for the 1.0 U/ml cellulase activity as obtained on the basis of the recorded response/time curve. For comparison, these values are calculated for 3–7 measuring points, corresponding to accumulated times of 7.5–21.5 min, respectively. As it appears, the relative standard deviations are within a range of *ca* 3.6–5.7%, depending on the number of measuring points included. For the entire activity range tested (0.1–2.0 U/ml) the precision was generally found to be of the order of ±3–12%, which for practical routine applications should be adequate.

While the enzyme activities in this exploratory investigation all were monitored at 3.5 min intervals over a time frame of 21.5 min, it is evident that shorter periods in most cases would suffice (Table 1). On one hand, it is possible with the present system—although the derivation reaction for cellulase, in fact, is relatively slow, to sample approximately every 2 min (stop time 90 sec plus *ca* 40 sec required to clear the sample through the detector cell, *cf.* Fig. 5), and on the other hand 3–5 data points should obviously be enough to determine the slope with sufficient reliability. Thus, the total time required for each experimental sequence could in this particular case readily be reduced to less than 10 min, which is actually 3 times less than what is presently spent to accomplish one measurement at Novo-Nordisk with their current single-point method.[10]

CONCLUSIONS

As demonstrated for the assay of cellulase, the present system does offer possibilities as serving as a generic system for determining enzyme activities. Thus, it entails the advantages that the enzymatic degradation reaction and the ensuing indicator reaction are completely separated, that the handling of these two reactions are (virtually) independent of their individual reaction rates, that each reaction can be individually optimized, and, most importantly, it does allow multi-point determinations to be executed thereby securing a much more reliable assay than that achieved by the conventional single-point assay. Besides, it should be perfectly adaptable to the promising sequential injection analysis (SIA) approach as described by Ruzicka.[11]

Acknowledgements—The authors wish to express their appreciation to Perkin-Elmer, Denmark for the loan of the FIAS-400 equipment and the Lambda 2 spectrophotometer employed, and to Julie Damms Foundation for partial financial assistance of this project, especially making it possible for one of us (EHH) to present this material at WCFIA '93. Thanks are also due to Jens Mindegaard of Novo-Nordisk, Copenhagen for useful discussions.

REFERENCES

1. E. H. Hansen, *Anal. Chim. Acta*, 1989, **216**, 257.
2. E. H. Hansen, L. Nørgaard and M. Pedersen, *Talanta*, 1991, **38**, 275.
3. J. Ruzicka and E. H. Hansen, *Flow Injection Analysis*, 2nd Ed. John Wiley and Sons, Inc., New York, 1988.
4. S. Veibel, *Organic Chemistry*, 2nd Ed. (In Danish). Teknisk Forlag, Copenhagen, Denmark, 1958, p. 311.
5. M. Lever, *Anal. Biochem.*, 1977, **81**, 21.
6. M. Lever, T. A. Walmsley, R. S. Visser and S. J. Ryde, *Anal. Biochem.*, 1984, **139**, 205.
7. P. J. Worsfold, I. R. C. Whiteside, H. F. Pfeiffer and H. Waldhoff, *J. Biotechnol.*, 1990, **14**, 81.
8. H. F. Pfeiffer, H. Waldhoff, P. J. Worsfold and I. R. C. Whiteside, *Chromatografia*, 1992, **33**, 49.
9. C. Ridder, *Anal. Chim. Acta*, 1989, **217**, 303.
10. J. Mindegaard, Novo-Nordisk, Copenhagen, Denmark, personal communication.
11. J. Ruzicka, *Anal. Chim. Acta*, 1992, **261**, 3.

Talanta, Vol. 40, No. 12, pp. 1899–1904, 1993
Printed in Great Britain.

0039-9140/93 $6.00 + 0.00
Pergamon Press Ltd

MEASURING ESTROGENS USING FLOW INJECTION IMMUNOANALYSIS WITH LIPOSOME AMPLIFICATION

LAURIE LOCASCIO-BROWN* and STEVEN J. CHOQUETTE
National Institute of Standards and Technology, Gaithersburg, MD 20899, U.S.A.

(*Received* 12 *February* 1993. *Revised* 5 *April* 1993. *Accepted* 6 *April* 1993)

Summary—A solid-phase competitive immunoassay is performed in flow injection analysis for the measurement of the hormone 17-β-estradiol. The flow injection analysis system incorporates a column-type reactor packed with solid silica particles onto which we have covalently immobilized the antigen 17-β-estradiol. Anti-estradiol is noncovalently conjugated to the liposome through a streptavidin–biotin linkage. When mixed with a sample containing the antigen, the antibody binding sites on the liposomes are complexed which reduces the binding of liposomes to the solid support in a concentration-dependent manner. Sequential immunoassays are performed on-column following a simple regeneration step.

Researchers have known for a number of years that the onset of some cancers associated with breast and uterine tissue is strongly linked to the binding of estrogens to estrogen receptors.[1] The most prevalent form of estrogen in a woman's body is secreted by the ovaries as 17-β-estradiol. This bioactive form of estrogen binds irreversibly to estrogen receptors, inducing a transformation in the structure of the receptor–hormone complex. This final form of the complex thereby initiates the production of proteins which stimulate these sex-related tissues. It has been postulated that the presence of higher concentrations of bioactive forms of estrogens (estrogen metabolites which bind to estrogen receptors) influences the development of breast cancer. Researchers in this area have established that suppression of the preferred metabolic pathway of estrogen is linked with the onset of cancer in mammary tissue in clinical trials.[2,3] A portion of the metabolic pathway of 17-β-estradiol is outlined in Fig. 1. The first step involves a reversible oxidation to the ketone, estrone, followed by conversion to estrone sulfate, or alternatively, hydroxylation at the 2 or 16 positions to form the products 2-hydroxyestrone or 16-α-hydroxyestrone. The 2-hydroxylation product occurs more frequently and retains little, if any, estrogenic activity.[4] The 16-hydroxylation product is a minor metabolic product but may be of significance since it retains estrogenic activity and is therefore considered bioactive.[5] With the occurrence of breast cancer, the 2-hydroxylation pathway is suppressed with a simultaneous increase in the 16-hydroxylation of 17-β-estradiol.[6] This mechanism is thought to precede and enhance tumor promotion in breast tissue.

The measurement of estrogens is a difficult and expensive task to perform on a routine basis since they are present in very low levels in serum. The concentration of 17-β-estradiol is approximately 200 pM in serum and concentrations of the resulting metabolic products are in the low picomolar range.[7] The reference

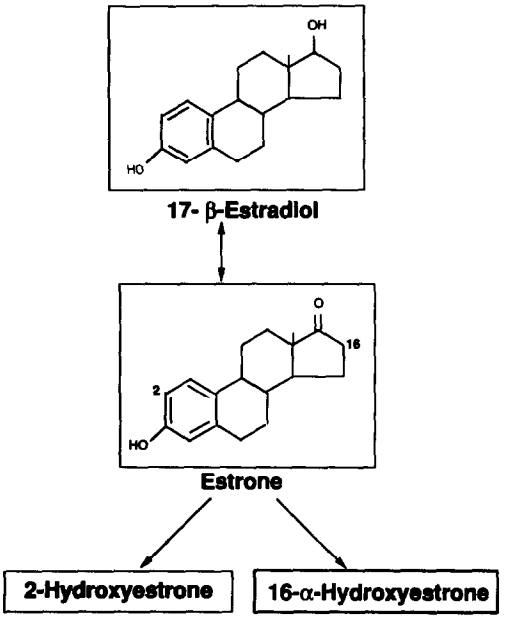

Fig. 1. The initial steps in the metabolic pathway of 17-β-estradiol.

*Author for correspondence.

method for measurement of 17-β-estradiol is by mass spectrometry[8] and clinical measurements are currently performed by radioimmunoassay. Given the increasing cost of radioactive waste disposal, immunochemical techniques that provide an alternative to isotope labeling are coming into favor.

In this paper we describe an automated system for liposome-based flow injection immunoassays (FIIA) which can compete in sensitivity with radioimmunoassays. A liposome is a spherical structure composed of a phospholipid bilayer membrane which contains an aqueous cavity. The micro-encapsulation of detectable marker molecules in the aqueous compartments of liposomes provides the opportunity for immediate and significant signal enhancement in the performance of immunoassays. Previously, we reported on the measurement of a therapeutic drug in serum using a liposome-based FIIA method with an immobilized antibody immunoreactor column.[9] The assay involved a direct competition between the analyte in serum and the analyte-coated liposomes for binding to an immobilized antibody. The minimum detectable concentration for theophylline, an anti-asthmatic drug, was determined to be 40 nM using a moderate affinity antibody. The accurate measurement of theophylline in serum was achieved using < 1 μl of sample since the analyte is present in serum at high concentrations (> 50 μM).

For the purpose of measuring estrogens by FIIA, modifications of the existing system are required in order to significantly lower the detection limits and maintain reasonable regeneration times. Preliminary dose–response curves are demonstrated for 17-β-estradiol as a testbed for the measurement of all estrogen metabolites. The system is currently being mathematically modeled and we describe simple ways to tailor the assay in order to enhance detection limits for a specific need.

EXPERIMENTAL

Reagents

Phosphate-buffered saline (PBS) solution (pH 7.4, 10 mM) containing 0.01% sodium azide was used as the carrier buffer in the FIIA system and was used to prepare all working solutions. A solution of 1-*o*-octyl-β-D-glucopyranoside (OG, Sigma, St. Louis, MO) was used in the flow system at a concentration of 21.4 mM in PBS. A stock solution of 17-β-estradiol (Sigma) was prepared in absolute ethanol stored over molecular sieves at a concentration of 3.67 mM (1 mg/ml). β-Estradiol 6-(*o*-carboxymethyl) oxime:bovine serum albumin (estradiol-BSA; Sigma) was reported to contain 30 moles of steroid per mole of protein. A method for preparing and characterizing this steroid–protein conjugate is reported in the literature.[10] Solutions of the steroid–protein conjugate in PBS were used in the immobilization protocol outlined in a following section.

A monoclonal antibody with a reported affinity constant of $9.1 \times 10^9 M^{-1}$ for 17-β-estradiol was obtained from Biodesign International (Kennebunkport, ME). The monoclonal antibody was derivatized to include biotin molecules on the protein surface with sulfosuccinimidyl 6-(biotinamido)hexanoate (NHS-LC-biotin, Pierce, Rockford, IL). The biotinylation protocol was as follows: (1) a 0.1 mg/ml solution of the antibody was prepared in 5 ml of 50 mM carbonate buffer, pH 8.5; (2) 1.7 mg of NHS-LC-biotin were added and the solution was incubated in ice for 2 hr; and (3) the solution was dialyzed in PBS and stored at 4°.

Liposome reagent

The carboxyfluorescein-filled (100 mM) liposomes were prepared by the injection method described in a previous publication.[11] The lipid composition of this preparation was modified with the addition of 0.8 mole% biotin–lipid (*N*-(biotinoyl)-1,2-dihexadecanoyl-sn-glycero-3-phosphoethanolamine, Molecular Probes, Eugene, OR). Streptavidin was added to the formed liposomes in an amount equal to the quantity of biotinylated lipid in the outer membrane. The solution was stirred at room temperature for 2 min to allow binding of the streptavidin to the biotin–lipid. Biotinylated antibodies were added so that the molar ratio of biotinylated antibodies to streptavidin on the liposomes was 4:1. This solution was stirred for an additional 5 min. There was no evidence of aggregation of liposomes due to biotin–streptavidin binding as determined by light scattering. The liposome solution was diluted by a factor of 200 to a final concentration of approximately 2×10^{10} liposomes/ml.

Sample preparation

Working solutions containing 17-β-estradiol in ethanol were prepared by serial dilutions from the original stock, and ranged in concentration from 0.37 mM to 0.37 nM (100 μg/ml to

100 pg/ml) in decade changes. Calibration samples were prepared by adding 1 μl of each working solution to 200 μl of the final liposome dilution. These were allowed to equilibrate for at least 30 min at room temperature prior to injection into the system.

Particle derivatization

Solid particles of high-purity fused silica, 80–100 mesh, were obtained from Vitrifunctions (Greensburg, PA). The particles were refluxed overnight in concentrated nitric acid, and rinsed exhaustively with water to remove any trace metals from the preparation process. The particles were reacted for 1 hr at 90° in a 10% aqueous solution of (3-glycidoxypropyl)trimethoxysilane (GOPS, Petrarch Systems, Inc., Bristol, PA) adjusted to pH 3. The GOPS solution was subsequently removed, and distilled water was added to the flask. The particles were gently shaken, the water was removed, and the particles were heated to 110° overnight. The covalent attachment of estradiol-BSA to the particles is similar to the antibody immobilization described elsewhere.[12] The particles were stored at 4° until packed in the glass columns for use in the FIIA system.

Analysis of protein coupled to silica

The amount of estradiol-BSA bound to the surface of the silica particles was determined using the Micro-BCA Protein Assay™ (Pierce) according to the protocol supplied with the reagents (no. 23235). The amount of immobilized protein was determined to be $1.3 \times 10^{-14} \pm 6.8 \times 10^{-16}$ moles/mm^2 for three samples.

Apparatus

The FIIA system is described in detail in a previous publication.[12] The packed reactor column containing the immobilized estradiol-BSA particles had an internal diameter of 2 mm, and was either 4 or 10 cm in length.

Procedure

The FIIA protocol is outlined in Fig. 2. Step 1 represents estradiol-BSA bound to silica particles in the reactor column. In step 2, 50 μl of a liposome–estradiol calibration solution was injected into this column. The binding of liposomes to the column was inversely related to the concentration of 17-β-estradiol in the calibration solution. Liposomes that did not bind flowed past the column and through the detector. After 4 min, OG solution was injected into the column for 5 min, causing the liposomes to lyse, releasing the entrapped fluorophor in step 3. The height of this peak was plotted as the analytical signal. Buffer was allowed to flow over the column for an additional period of 6 min in step 4 to effect dissociation of the antibody–antigen bond by mass action and regenerate the analytical column for the next injection of sample. The total analysis time for a single sample including regeneration was 16 min.

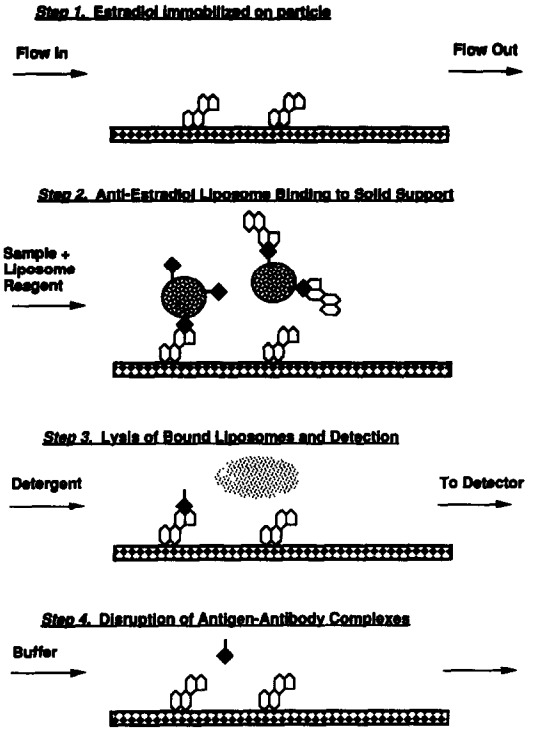

Fig. 2. Schematic of the FIIA protocol. Steps 1–4 are repeated for each sequential assay. See text for details.

RESULTS AND DISCUSSION

In earlier studies, we have shown that there are clear advantages to performing liposome immunoassays in flow injection analysis. The efficient mixing which occurs in a packed column promotes diffusion and reaction of the bulky liposome reagent to the immobilized sites on the solid support. A continuous flow of solution over the surface of the immobilized reagent maintains infinite dilution of the reactants, which encourages gentle dissociation of the antigen–antibody complexes by mass action for column regeneration. The sequential nature of the assay allows for calibration and reuse of

the immobilized reagent. Finally, a change in immunoassay format is easily accomplished by (1) incorporating new columns with different immobilized reagents, (2) introducing new reagents into the flowing stream, or (3) altering the sequence of sample, liposomes or regeneration reagents into the system. Our studies have shown that minor changes in assay format can have a profound effect on the sensitivity and detection limits of the measurement.[12]

We use liposomes with encapsulated fluorophors as powerful amplification agents to improve sensitivity and to provide reliable quantitation of the analyte. Liposomes also exhibit other characteristics which are important in the performance of immunoassays. Liposomes derivatized with a large number of surface antigenic sites have very different binding affinities for immobilized reagents than the corresponding individual antigen molecules.[12] In general, as the number of binding sites on the liposomes decreases, the apparent affinity decreases; as the number increases, the apparent affinity increases to a maximum, then reaches a plateau.[13] In this assay, the solution analyte is allowed to equilibrate with the antibody-coated liposomes prior to injection onto the column. Therefore, the number of uncomplexed antibody sites on the liposome, and the corresponding mean apparent affinity constant of the liposome population, should be indirectly related to the solution concentration of that analyte. Increasing sample analyte concentration will therefore decrease liposome binding to the immobilized analyte in the packed column. In order for the assay to be most effective, the valency of the liposome membrane (*i.e.*, number of available binding sites) should be high enough to encourage rapid binding to the immobilized support and low enough that small changes in valency cause large changes in binding characteristics. We are currently modeling the effect of these assay parameters with these assumptions to optimize sensitivity, speed, and dynamic range.

Initial experiments in the estrogen FIIA system were performed to validate the regeneration protocol. A high affinity antibody was used in this assay; therefore, it was necessary to determine if disruption of this antigen–antibody complex by mass action was completed in an 11-min regeneration time. Reproducibility of the measurement using sequential injections of a single liposome solution was used to determine the effectiveness of regeneration. Figure 3 is a representative FIIAgram for the immunoassay. Peak A is the fluorescence peak associated with the liposomes which exhibit little or no binding to the column. Carboxyfluorescein is encapsulated in the liposomes at a high concentration so that the fluorescence of these intact liposomes is quenched. Peak B is due to the bound fraction of liposomes following disruption and removal from the column. The fluorescence of this peak is unquenched due to dilution and dispersion in FIIA. The peak height of peak A for five sequential injections was 16.8 mV $\pm$ 0.37%. The average peak height for peak B is 97.6 mV $\pm$ 5.3%; however, with each sequential injection a decreased intensity of $<2\%$ was observed, indicating some residual binding.

Figure 4 represents two calibration curves generated with the 17-β-estradiol calibrators. Both curves were generated using a 4-cm column. Curve A was produced first with sequential injections of the calibrators tested in order of least concentrated to most concentrated. Curve B was produced next with sequential injections of the calibrators in reverse order. The signal associated with the same column using the same liposomes decays by approximately 5% in the next calibration cycle. These results, as well as the decreasing trend in the data from repeat injections, can be attributed to (1) incomplete regeneration of the immobilized antigen binding sites which becomes limiting at the fifth or sixth injection, or (2) instability of the diluted antibody-conjugated liposome re-

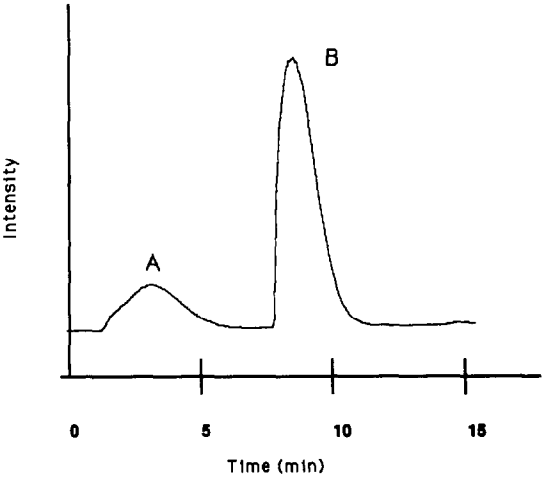

Fig. 3. FIIAgram of a single injection of antibody-coated liposomes into the column. Peak A is from liposomes which do not bind to the column; peak B results from liposomes which bind to the column following lysis with OG.

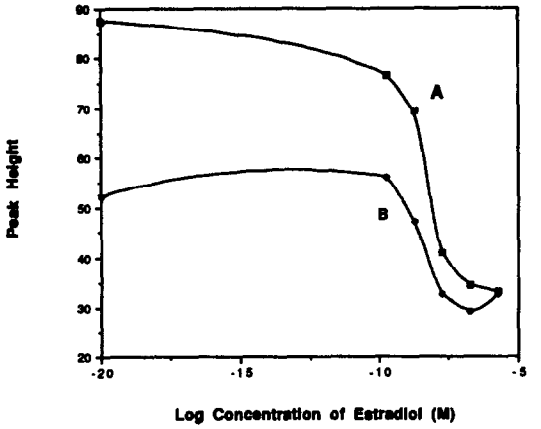

Fig. 4. Repeat calibration curves using the 4-cm packed column. Curve A was generated first; curve B was generated next using the same estradiol/liposome calibrators. The value reported as $10^{-20}M$ estradiol in the log plot corresponds to the data acquired when no estradiol was added to the solution.

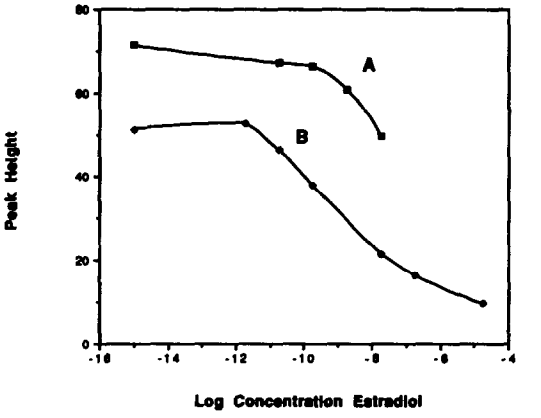

Fig. 5. Calibration curves for the 17-β-estradiol using varied column lengths. Curve A represents data taken using a 10-cm packed column. Curve B represents data acquired with a 4-cm column.

agent. We are currently testing other regeneration protocols based on the use of chaotropic agents, high salts, or large pH changes to induce faster removal of the antibody from the column. Although these reagents typically denature and inactivate the antibody, it is inconsequential for this FIIA format in which the antigen is covalently immobilized and reused.

Previously, the FIIA system was modeled under the conditions used in a typical solid phase immunoassay, *i.e.* where the solution analyte-conjugated liposome competed for binding to an immobilized antibody. It was determined that the assay sensitivity (as defined by the slope of the calibration curve) and the detection limits of the method were most affected by the valency of the liposome reagent, and the number of immobilized binding sites.[14] In FIIA, a simple way to change the number of immobilized binding sites is by varying the size of the packed column. The two calibration curves depicted in Fig. 5 demonstrate the influence of column size on the 17-β-estradiol assay sensitivity. Curve A was generated using a packed column 10 cm in length and curve B was generated using a packed column 4 cm in length. The curves were measured on different days using fresh preparations of biotin–liposome stock solution. The slope of curve B is lower than that of curve A due to the decreased number of binding sites in the shorter column; however, the sensitivity of the measurement in curve B is still high due to the signal enhancement of the liposome reagent. At the same time, the assay detection limits have shifted in curve B such that lower concentrations of the analyte can be detected. Detection of 17-β-estradiol in serum, as well as the lower concentrations of the serum metabolites, should be achievable using the 4-cm column. In order to push the detection limits further, we will continue to use smaller columns until we become limited by the sensitivity of the method.

CONCLUSIONS

FIIA using liposome amplification has the sensitivity and reproducibility to measure many clinical analytes without the generation of hazardous waste products of common radiolabeled assays. As demonstrated, changes in sensitivity and dynamic range of the assay can be easily accomplished in FIIA by incorporating columns of varied length into the system. We are currently studying the effect of liposome valency to induce similar changes in assay sensitivity. In our latest estradiol FIIA system, we have immobilized antigens, rather than antibodies, to allow more aggressive use of chaotropic agents for regeneration. Studies are currently underway to determine the most efficacious method for regenerating and re-equilibrating the column for sequential measurements of estrogens.

Acknowledgements—One of the authors (L.L.B.) acknowledges the support of the National Cancer Institute, Division of Cancer Etiology.

Disclaimer—Certain commercial products are identified in order to adequately specify the experimental procedure. This does not imply endorsement or recommendation by the National Institute of Standards and Technology.

REFERENCES

1. E. V. Jensen, E. R. Sombre and P. W. Jungblut, in *Endogenous Factors Influencing Host-Tumor Balance*, R. W. Wissler, T. L. Dao, and S. Wood Jr. (eds), pp. 15–30. University of Chicago Press, Chicago, 1967.
2. N. T. Telang, A. Basu, M. J. Modak, H. L. Bradlow and M. P. Osborne, *Proc. Am. Assoc. Cancer Res.*, 1989, **30**, 175.
3. N. T. Telang, R. Narayanan, L. Sweterlitsch, H. L. Bradlow and M. P. Osborne, *Breast Cancer Res. Treat.*, 1989, **13**, 163.
4. P. H. Jellinck, L. Krey and P. G. Davis, *Endocrinology*, 1981, **108**, 1848.
5. J. Fishman and C. Martucci, *J. Clin. Endocrinol. Metab.*, 1980, **51**, 611.
6. M. P. Osborne, N. T. Telang, S. Kaur and H. L. Bradlow, *Steroids*, 1990, **55**, 114.
7. G. Pennington, S. Naik and R. Hall, in *Hormone Analysis: Methodology and Clinical Interpretation*, Vol. II, G. Pennington and S. Naik (eds), p. 176. CRC Press, Boca Raton, 1981.
8. S. Xing, S. Z. Cekan, U. Diczfalusy, O. Falk, S. A. Gutafsson, E. Akerlof and I. Bjorkhem, *Clin. Chim. Acta*, 1983, **135**, 189.
9. L. Locascio-Brown, A. L. Plant, R. Chesler, M. Ruddel, M. J. Kroll and R. A. Durst, *Clin. Chem.*, 1993, **39**, 386.
10. W. R. Butt, in *Practical Immunoassay: The State of the Art*, W. R. Butt (ed.), p. 5. Marcel Dekker, New York, 1984.
11. L. Locascio-Brown, A. L. Plant and R. A. Durst, *Anal. Chem.*, 1988, **60**, 792.
12. L. Locascio-Brown, A. L. Plant, V. Horvath and R. A. Durst, *Anal. Chem.*, 1990, **62**, 2587.
13. A. L. Plant, M. Gray and J. B. Hubbard, unpublished results.
14. W. T. Yap, L. Locascio-Brown, V. Horvath, A. L. Plant, S. J. Choquette and R. A. Durst, *Anal. Chem.*, 1991, **63**, 2007.

Talanta, Vol. 40, No. 12, pp. 1905–1909, 1993
Printed in Great Britain

0039-9140/93 $6.00 + 0.00
Pergamon Press Ltd

ORGANIC-PHASE BIOSENSORS—NEW TOOLS FOR FLOW ANALYSIS: A SHORT REVIEW

JOSEPH WANG

Department of Chemistry and Biochemistry, New Mexico State University, Las Cruces, NM 88003, U.S.A.

(*Received* 21 *January* 1993. *Accepted* 8 *February* 1993)

Summary—The ability of enzymes to operate in nonaqueous media offers a great potential for monitoring flowing streams. In particular, organic-phase biosensors can be applied for on-line assays of previously inaccessible sample matrices or for measuring analytes with poor water solubility. This paper reviews the fundamental aspects of organic-phase biosensors, together with their performance as flow injection detectors, examples of relevant applications and future opportunities.

Electrochemical biosensors, which combine the inherent specificity of biological recognition processes with the high sensitivity of amperometric flow detectors, are gaining considerable attention for monitoring flowing streams.[1-3] In particular, over the past decade enzyme electrodes have found useful applications for industrial processing and quality control testing. Such probes couple their specificity and sensitivity advantages, with other attractive properties such as speed, portability, simplicity and low cost.

Until recently, on-line applications of biosensors have relied on the use of aqueous media. However, the introduction of sensors for non-aqueous environments opens many unique opportunities for flow analysis, because many industrial processes occur in organic solvents. In particular, organic-phase enzyme detectors can be applied toward many (water-insoluble) analytes and for new challenging environments. In addition, due to solvent-induced changes in the biocatalytic activity, we can expect improved operating stability, reduced side reactions or microbial inactivation, and simplified immobilization schemes. The present article examines the behavior of electrochemical flow detectors based on organic-phase enzymology, and discusses the opportunities offered by these devices for on-line monitoring of flowing streams.

ORGANIC-PHASE ENZYMOLOGY

In order to successfully implement the unique detection opportunities accrued from biocatalysis in organic media, it is essential to understand the behavior of enzymes in non-aqueous environments. Pioneering studies, particularly by Klibanov and coworkers.[5,6] and Dordick's group[7] have elucidated the factors that govern enzymatic reactions in organic media. These include the influence of the solvent and the water content upon the biocatalytic activity and stability. These and other factors are crucial for optimizing the biocatalytic reaction (and accordingly the detector performance).

The organic solvent can greatly alter the enzyme structure and function. Many factors related to the solvent effect upon the enzymatic activity are not fully understood. In general (but not always), the biocatalytic activity is correlated to the polarity of the solvent, as expressed by its log P value.[8] (P is the partition coefficient of the solvent in the two-phase octanol–water system.) Hydrophobic solvents (with log P values higher than 4) are preferred because they do not strip the essential water layer surrounding the enzyme. Other factors, such as the thermostability and solubility of the substrate and product (and their partition to and from the aqueous environment of the enzyme) should also play a role in solvent selection. Hydrophobic solvents also offer increased structural rigidity and hence thermostability. Such behavior is attributed to the minimization of enzyme unfolding, as compared to the conformational flexibility common in aqueous media. For example, porcine pancreatic lipase has been shown to exhibit high catalytic activity and stability at temperatures as high as 100°C.[6] The improved thermostability may greatly extend the lifetime of biosensors and may thus be

advantageous for monitoring many industrial processes occurring at high temperatures.

Related to the media is the amount of water. The exact role of water is not fully understood. While some water is absolutely essential for the enzymatic activity, this water can be localized (as a small hydration layer) around the enzyme molecules. The optimal degree of hydration differs from enzyme-to-enzyme and from solvent-to-solvent. For example, while chymotrypsin needs only 50 molecules of water per enzyme molecule for activity in octane, the activity of tyrosinase in chloroform requires about 3.5×10^7 molecules of water per enzyme molecule.[7] The thermostability, however, decreases upon increasing the water content.

As for the pH, while organic solvents have no distinct measurable pH, the enzyme "remembers" the pH of the last aqueous solution to which it has been exposed. Accordingly, it is often desired to employ enzymes that have been lyophilized from an aqueous solution of optimal pH for the biocatalytic activity.

Solvent-induced changes in the biocatalytic efficiency and substrate specificity may be advantageous for flow analysis. For example, extended linearity may result from the change in the apparent Michaelis–Menten constant in organic media, while higher sensitivity can be offered by changes in the reaction velocity. Current research activity focuses on the use of solvent engineering for tailoring the enzyme function in organic media.[9]

FLOW DETECTORS BASED ON ORGANIC-PHASE BIOSENSORS

Detector design and performance

Conventional detector geometries (such as thin-layer or wall-jet flow cells) can be employed for on-line organic-phase biosensing. In addition, flow detectors based on ultramicroelectrodes are useful for minimizing ohmic drop distortions in resistive organic media (containing little or no supporting electrolyte).[10,11] Enzyme immobilization schemes, originally developed for work in aqueous media, are not always compatible with organic environments. The organic-phase operation may actually simplify the immobilization procedure. One rapid, simple and effective immobilization scheme for on-line organic phase operation is direct adsorption onto the detector surface.[12] Other useful enzyme immobilization schemes include an entrapment within Eastman AQ polymer films,[13] or incorporation with the bulk of composite carbon materials.[14] Whenever needed, the mediator should be insoluble in the organic solvent (so it can be stably coimmobilized by entrapment or adsorption). For example, the coimmobilization (coadsorption) of ferrocyanide and peroxidase onto a graphite foil surface yielded a reagentless sensor for hydrogen peroxide in organic media.[15]

Because of stability problems in non-aqueous environments, most polymeric films or the carbon paste matrix cannot be used for the task of enzyme immobilization. One exception, the Eastman AQ ionomer is stable in different organic solvents. This poly(ester–sulfonic acid) coating is thus very attractive for entrapping enzymes onto flow detectors.[13] Such an immobilization scheme offers additional advantages of permselective and fast response and high enzyme loading. The incorporation of enzymes within the bulk of a rigid graphite–Teflon matrix is another useful immobilization scheme.[14] Such use of Teflon as the binder (instead of mineral oil) eliminates dissolution problems characterizing the operation of conventional carbon paste biosensors in organic solvents. This type of bioelectrode can also be renewed by polishing, and (in the absence of membrane barriers) offers a fast and sensitive response.

The attractive properties of electrochemical flow detectors are not compromised by the organic-phase operation. For example, Fig. 1 illustrates the flow injection response of the carbon-fiber based (A) and Eastman AQ coated thin-layer (B) tyrosinase flow detectors for repetitive injections of different phenolic compounds. Both biosensors exhibit a rapid increase and decrease of the current, with a sample frequency of 60 hr^{-1}. The high injection rate is coupled with high sensitivity and reproducibility (with micromolar detection limits and relative standard deviations of 1–2%).

Even living cells, such as plant tissues, can be exploited for organic-phase biosensing operation.[16] For example, mushroom and horseradish-root bioelectrodes (rich with tyrosinase and peroxidase) have been shown to be useful for monitoring phenolic and peroxide species, respectively, in different organic solvents. Spreading of the tissue layer onto a rough graphite surface results in a close proximity between the biocatalytic and sensing sites, and hence in a fast and sensitive response.

The recent introduction of non-covalently

immobilized enzyme reactors operating in non-aqueous media[17] should also facilitate the development of analytical flow systems for on-line monitoring of organic streams. Cholesterol oxidase and horseradish peroxidase were thus immobilized (by adsorption) onto the solid support, and exhibited a remarkable stability over more than 4 months of operation. The throughput was 60 samples/hr, with a detection limit $1 \times 10^{-6}M$. Such reactors may also be useful for the removal of interferences.

Applications

There are numerous opportunities in employing organic-phase biosensors in flow analysis. Most organic compounds of commercial interest are very sparingly soluble in aqueous media. In addition, many important samples from the food, pharmaceutical, petrochemical and cosmetic industries are highly hydrophobic and require tedious sample pretreatment steps prior to their assays in aqueous solutions. Organic-phase biosensors, in contrast, obviate the need for such sample pretreatment procedures and allow rapid flow analysis of challenging sample matrices. Such direct and fast on-line bioassays should be extremely attractive for quality control testings and industrial process control. Recent advances in organic-phase biosensors can greatly facilitate these industrial applications.

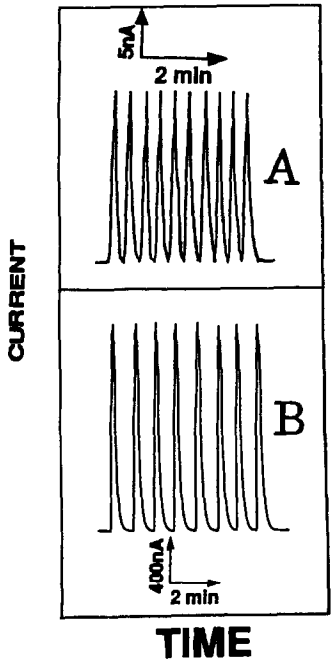

Fig. 1. Repetitive flow injection measurements of $1 \times 10^{-3}M$ *p*-cresol (A) and $6 \times 10^{-4}M$ phenol (B) at the tyrosinase carbon fiber and glassy-carbon detectors, respectively. Carrier: (A) chloroform; (B) acetonitrile.

For example, the food industry, with its many challenging hydrophobic products, represents a prospective market for organic-phase biosensors. Such devices offer direct assays of many previously inaccessible food samples. For example, the phenol content of olive oil is an important factor in the quality and stability of this product. Accordingly, we developed recently a rapid flow injection procedure, based on a tyrosinase electrode, for determining the phenol content of olive oil samples.[18] By adsorbing the tyrosinase onto the surface of the graphite wall-jet flow detector, and by using chloroform as a carrier solution, reliable quantitation of the phenol content of various Spanish and Italian olive oils was achieved.

Butter and margarine represent other challenging food samples. Hall and Turner[19] demonstrated the utility of a cholesterol-oxidase sensor for rapid measurements of cholesterol in butter and margarine samples (after dissolution in a chloroform–hexane media). Organic-phase biosensors should benefit assays of other fats and oils. For example, the organic-phase activity of lipase and peroxidase could be exploited for monitoring triglycerides and peroxide species in these matrices.

Many pharmaceutical products are not readily dissolved in aqueous media. Organic-phase flow-injection operation can thus benefit quality control testings in the pharmaceutical industry. For example, the tyrosinase- and peroxidase organic-phase enzyme electrodes were applied recently for reliable measurements of phenol and peroxide antiseptics in different anti-infective formulations.[20] Excellent agreement with the labeled values was achieved. Similar capabilities were demonstrated for measurements of peroxide bleaching agents in cosmetic products.

On-line assays of petrochemical samples represent another important challenge. A new organic-phase biosensor, based on alcohol dehydrogenase (from *Ta. Brockii*) has been shown to be useful for monitoring secondary alcohols in untreated gasoline samples.[21] Other opportunities come from the fields of clinical diagnostics, environmental surveillance or the defense industry. These possibilities were discussed by Turner and coworkers.[4]

Flow measurements of trace water in non-aqueous media represent a novel application of organic-phase enzyme electrodes.[22] Such appli-

Table 1. Applications of organic-phase enzyme electrodes

Analyte	Enzyme	Detector	Reference
Alcohols	Alcohol dehydrogenase	Glassy-carbon electrode	21
Amino acids	Chymotrypsin	pH electrode	24
Catechol	Laccase	Glassy-carbon electrode	25
Cholesterol	Cholesterol oxidase	Oxygen electrode	19
Hydrogen peroxide	Horseradish peroxidase	Carbon electrode	15
Inhibitors	Tyrosinase	Graphite electrodes	23
Organic peroxides	Horseradish peroxidase	Graphite–Teflon electrode	14
Phenols	Tyrosinase	Graphite electrode	12
Phenols	Mushroom	Graphite electrode	16
Water	Tyrosinase	Graphite electrode	22

cation relies on the strong influence of low levels of water upon the rate of organic-phase biocatalytic reactions. By maintaining a fixed substrate concentration (*e.g.*, phenol in the case of the tyrosinase electrode), it is possible to follow small changes in the water level. Such an indirect biosensing approach offers an attractive alternative to the well-known Karl–Fischer titration method, which requires special equipment and suffers from various interferences.

Measurements of enzyme inhibitors can also be carried out in organic media.[25] For example, the inhibition of tyrosinase by various (poorly-water soluble) inhibitors can be monitored from the decrease of the flow-injection peak for the phenol substrate. Solvent-induced changes in the inhibition action hold great promise for manipulating the response of inhibitor biosensors.

The applications of organic-phase enzyme electrodes are summarized in Table 1.

FUTURE PROSPECTS

While detectors based on organic-phase enzymology are still in an early developmental stage, there is no doubt that they will play an important future role in flow analysis. Many real industrial processes are expected to benefit from the unique features of organic-phase flow bioelectrodes. Besides flow-injection operations, such devices can be easily adapted to other analytical flow systems, including continuous flow analyzers (for real-time monitoring of various processes), liquid chromatography or sequential injection analysis. The characteristic procedure parameters must be adjusted to suit the requirements of each case. *In situ* monitoring of on-line solvent extraction is also envisioned. In addition to enzyme electrodes, we expect to see organic-phase biosensors based on other detectors (*e.g.*, optical devices) or utilizing different biocomponents (*e.g.*, antibodies for immunoassays). New on-line analytical applications are expected based on the isolation or engineering of new enzymes (suitable for organic-phase operation) and the identification of new environments (*e.g.*, supercritical fluids or gas phase). The key for such future developments is improved understanding of the biocatalytic behavior in non-aqueous environments. Such knowledge will greatly facilitate a predictable detector development and optimization. Indeed, flow-injection systems should be extremely useful for fundamental studies on the behavior of enzymes in non-aqueous media (*e.g.*, in a manner analogous to reaction-rate kinetics performed in aqueous solutions). Overall, the development of organic-phase flow detectors should lead to a wide range of important applications using previously inaccessible matrices or analytes.

REFERENCES

1. R. D. Schmid (ed.), *Flow Injection Analysis based on Enzymes or Antibodies*, VCH, Weinheim, 1991.
2. L. Gorton, E. Csoregi, E. Dominguez, J. Emneus, G. Jönsson-Pettersson, G. Marko Varga and B. Persson. *Anal. Chim. Acta*, 1991, **250**, 203.
3. J. Wang, *Anal. Chim. Acta*, 1990, **234**, 41.
4. S. Saini, G. Hall, M. Downs and A. P. Turner, *Anal. Chim. Acta*, 1991, **249**, 1.
5. A. M. Klibanov, *Chemtech.*, 1986, **16**, 354.
6. A. Zaks and A. M. Klibanov, *Science*, 1984, **224**, 1249.

7. J. S. Dordick, *Enz. Microb. Technol.*, 1989, **11**, 194.
8. C. Laane, S. Boenen, K. Vos and C. Veeger, *Biotech. Bioengng.*, 1987, **30**, 81.
9. J. S. Dordick, *Biotech. Prog.*, 1992, **8**, 259.
10. J. Wang and Y. Lin, *Anal. Chim. Acta*, 1993, **271**, 53.
11. J. Wang, L. Wu and L. Angnes, *Anal. Chem.*, 1991, **63**, 2993.
12. G. Hall, D. Best and A. P. Turner, *Anal. Chim. Acta*, 1988, **213**, 113.
13. J. Wang, Y. Lin and Q. Chen, *Electroanalysis*, 1993, **5**, 23.
14. J. Wang, A. J. Reviejo and L. Angnes, *Electroanalysis*, in press.
15. F. Schubert, S. Saini and A. P. Turner, *Anal. Chim. Acta*, 1991, **245**, 81.
16. J. Wang, N. Naser, K. Kwon and M. Cho, *Anal. Chim. Acta*, 1992, **264**, 7.
17. L. Brace, J. Daros and M. LaGuardia, *Anal. Chem.*, 1992, **64**, 129.
18. J. Wang, A. J. Reviejo and S. Mannino, *Anal. Lett.*, 1992, **25**, 1399.
19. G. Hall and A. P. Turner, *Anal. Lett.*, 1991, **24**, 1375.
20. J. Wang, Y. Lin and L. Chen, *Analyst*, 1993, **118**, 277.
21. J. Wang, N. Naser and D. Lopez, *Biosensors Bioelect.*, in press.
22. J. Wang and A. J. Reviejo, *Anal. Chem.*, 1993, **65**, 845.
23. J. Wang, E. Dempsey, A. Eremenko and M. Smyth, *Anal. Chim. Acta*, in press.
24. A. Miyabayshi, M. Reslow, P. Adlercreutz and B. Mattiasson, *Anal. Chim. Acta*, 1989, **219**, 27.
25. J. Wang, Y. Lin, A. Eremenko, A. Ghindilis and I. Kurochkin, *Anal. Lett.*, 1993, **26**, 197.

Talanta, Vol. 40, No. 12, pp. 1911–1915, 1993
Printed in Great Britain.

0039-9140/93 $6.00 + 0.00

FLOW INJECTION AMPEROMETRIC DETERMINATION OF HYDROGEN PEROXIDE BY OXIDATION AT AN IRIDIUM OXIDE ELECTRODE

JAMES A. COX* and KRZYSZTOF LEWINSKI
Department of Chemistry, Miami University, Oxford, OH 45056 U.S.A.

(*Received* 8 *February* 1993. *Revised* 1 *March* 1993. *Accepted* 2 *March* 1993)

Summary—Either an iridium electrode that was anodically pretreated or a glassy carbon electrode that was coated with a film that contained iridium oxide promoted the oxidation of hydrogen peroxide. With flow injection methodology, linear calibration curves were obtained over the 2×10^{-5}–3.6×10^{-8} *M* range with 0.1 *M* KOH as the carrier. With solutions of pH ≥ 11, oxidation occurred at applied potentials of near 0.0 V *vs.* SCE, which is much lower than potentials needed at bare Pt or glassy carbon. The low overpotential suggests applications to systems where oxidation of other species limits the use of bare electrodes. Cyclic voltammetric studies show that HO_2^- is the electroactive species and that catalysis rather than mediation promotes the charge transfer. Dissolved oxygen does not interfere with the measurement.

Electrochemical determinations of hydrogen peroxide are generally performed by oxidation at a platinum electrode, an approach which was first described by Harrar.[1] Depending upon the pH of the solution, a quite large positive potential must be applied in order to cause the oxidation to occur; typical applied potentials are in the range 0.6–0.9 V *vs.* SCE.[2] As a result, many substances can interfere with the measurement. Ascorbic acid, uric acid, and acetaminophen are among the interferents which are especially important in a common application of such measurements of hydrogen peroxide, namely the indirect amperometric determination of glucose based upon the amount of hydrogen peroxide released in the enzymatic reaction involving glucose oxidase.[3]

Numerous methods to alleviate problems related to the need for a high overpotential for the oxidation of hydrogen peroxide have been described. One is to use reduction as the electrode reaction. However, at both platinum[4] and mercury[5] electrodes, the reduction is highly irreversible, thereby requiring a large negative overpotential. A lower overpotential for the reduction is obtained by coating the electrode with an electron transfer mediator. Armstrong and Lannon[6] used a cytochrome c peroxidase film on graphite along with gentamycin as a promoter to perform the reduction of hydrogen peroxide, and modification of an electrode with a clay film that was impregnated with $Ru(NH_3)_6^{2+}$ allowed the reduction of H_2O_2 at −0.2 V *vs.* SCE.[7] The use of modified electrodes such as these in practical analytical methodology has been limited because, in general, they lack the necessary long term stability.

Certain inorganic polymers and metalated phthalocyanine polymers show great promise as stable modifiers of electrode surfaces.[8,9] Among these is a film that was electrolytically deposited on glassy carbon from a mixture containing $PdCl_2$ and Na_2IrCl_6.[10] This film, in which oxides of iridium are the promoters of electron transfer,[11] permitted the determination of hydrogen peroxide by linear scan voltammetry on the basis of its reduction in 0.1 *M* KCl at −0.2 V *vs.* SCE.[12] Unfortunately, dissolved oxygen, which is often present in experiments where the determination of hydrogen peroxide is an objective, interferes with the measurement. Fujihara *et al.*[13] illustrated that a dodecyltriethoxysilane film on an Au electrode attenuated the interference of oxygen on the reduction of H_2O_2, but analytical data were not provided.

The present study was initiated to determine whether the procedure that used a glassy carbon electrode that was modified with a film containing iridium oxide could be altered to eliminate the interference of dissolved oxygen on the reduction of H_2O_2. Although this was not accomplished, as detailed below, a method for the determination of H_2O_2 in the presence of dissolved oxygen was developed based upon the

*Corresponding author.

electrocatalytic oxidation of hydrogen peroxide. The process occurs at perhaps the lowest overpotential yet reported for this electrode reaction.

EXPERIMENTAL

All chemicals used were ACS reagent grade from Fisher Scientific Co. except that the $PdCl_2$ was from Johnson Matthey Electronics, Inc.; the Na_2IrCl_6, $LiClO_4$ and LiOH (99.95% purity) from Aldrich Chemical Co.; and the 1 mm dia. iridium wire (99.8% purity), from Johnson Matthey Materials Technology. The hydrogen peroxide solutions were made by fresh dilutions of 30% reagent.

A Bioanalytical Systems, Inc. electrochemical detector (Model MF 1000) for HPLC measurements was modified in two ways. One was to incorporate an iridium electrode. Here, the unit that held the dual glassy carbon electrodes was replaced by an identically-shaped Teflon block through which a threaded hole was machined. A hole was drilled down the central axis of a matching Teflon screw, and an iridium wire was sealed therein with Torrseal epoxy. The second modification was on the portion of the BAS cell that was intended to be used as the working electrode holder. One of the glassy carbon electrodes was used to ground the solution (the second was left at open circuit). Holes to accommodate the entry and exit of the carrier stream were machined in this block. A Pt electrode was placed downstream of the cell to serve as the counter electrode. This modification, along with placing the entire cell assembly in a Faraday cage, minimized noise in the system.

The iridium was polished to provide a disk-shaped electrode surface that was flush with the Teflon block. The polishing was performed with sandpaper grades of 250, 600, and 1200 grit and, finally, with 1, 0.3, and 0.05 μm alumina (Mark V Laboratory, metallographic equipment and supplies) on a polishing cloth with distilled water as the lubricant. Each polishing step (5 min) was followed by a 5 min sonication in distilled water.

An oxide layer on the iridium electrode was formed by applying 100–1000 1 sec pulses between 600 and -1100 mV in a 0.1 *M* LiOH, 1 *M* $LiClO_4$ mixture. The reference electrode was isolated from the plating mixture with a saturated NaCl salt bridge.

Before performing experiments, the iridium oxide electrode was aged for at least 48 hr at open circuit in the plating solution. Except for flow injection experiments, the electrode was pretreated by cyclic voltammetry (50 cycles between 200 and -300 mV at 100 mV/sec) in a solution containing 0.05 *M* H_2O_2 and 1 *M* NaOH. The electrode was stable whether stored in the dry state or in contact with 1 *M* KCl (9 months).

Iridium oxide electrodes were also prepared by electrodeposition of a film on glassy carbon from a solution containing 0.1 m*M* $PdCl_2$ and 0.2 m*M* Na_2IrCl_6 with a 0.2 *M* K_2SO_4, 0.1 *M* KCl mixture as the supporting electrolyte.[10] A glassy carbon electrode of a MF 1000 BAS amperometric detector was polished as described above and plated by applying 100 cycles between 1150 and -350 mV at 50 mV/sec. As previously demonstrated,[11] iridium oxide is the catalytic species in the resulting film. None of the plating solutions were deaerated prior to use.

All electrochemical measurements were made with either a BAS 100 electrochemical analyzer, BAS CV37 voltammograph, or a EG&G PAR 273A galvanostat/potentiostat. All potentials are reported *vs.* an SCE. A Gilson Minipuls 2 peristaltic pump, pulse dampener, Rheodyne type 50 four-way rotary Teflon valve with a 500 μL injection loop, and the above-described electrochemical detectors comprised the flow injection analysis system. The reference was either an SCE (Fisher) or a BAS Ag/AgCl, 3 *M* KCl electrode.

RESULTS AND DISCUSSION

A preliminary set of cyclic voltammetry experiments on hydrogen peroxide solutions with the oxidized iridium metal electrode was performed in order to compare the behavior at this electrode to that at the palladium-containing film.[12] The behavior of the electrodes was found to be the same for the reduction of H_2O_2 in neutral and basic solution. A more interesting observation was that oxidation of H_2O_2 was observed in 1 *M* NaOH at a low overpotential relative to previous reports. A typical set of cyclic voltammograms is shown in Fig. 1. Because a Faradaic process, the oxidation of H_2O_2, is occurring at the initial potential, the shapes of the current–voltage curves are unusual. Nevertheless, it is apparent that there is an increase in anodic current which is related to the hydrogen peroxide concentration. Analytical utility of this electrode process is suggested by the fact that neither the background nor the current due to

the oxidation of hydrogen peroxide is influenced by the presence of dissolved oxygen in the solution.

Based upon the results in Fig. 1, experiments were performed to determine whether linear scan voltammetry is suited to the oxidative determination of H_2O_2. With 1 *M* KCl as the supporting electrolyte and oxide-coated iridium as the working electrode, cyclic voltammograms were obtained at 100 mV/sec with H_2O_2 varied over the concentration range 11–0.5 m*M* (11 points). A linear least squares fit of the peak current (corrected for background) at 100 mV *vs.* concentration yielded a slope of 0.91 mA/*M* with a correlation coefficient of 0.9986. A repeat of the experiment except with 1 *M* NaOH as the electrolyte and 13–0.5 m*M* (18 points) as the concentration range yielded an anodic peak potential of −40 mV, a slope of 3.13 mA/*M*, and a correlation coefficient of 0.9989. These data show that linear scan voltammetry is suited to the determination of hydrogen peroxide at high concentrations. Extension to lower concentrations was precluded by the background signal. The usual approach to improving the signal to background ratio in voltammetry, applying a pulsed potential and time-resolving the Faradaic and background currents, is not well-suited to modified electrodes because a Faradaic process contributes to the background current. Further studies were, therefore, performed by flow injection amperometry (FIA).

Figure 2 shows hydrodynamic voltammograms obtained at the iridium oxide electrode in 0.1 *M* KOH in the presence and absence of H_2O_2. These point-by-point measurements of FIA peak currents as a function of applied potential have two significant characteristics. First, dissolved oxygen does not contribute to the electrode process at potentials more

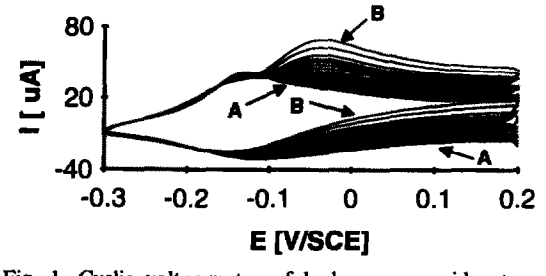

Fig. 1. Cyclic voltammetry of hydrogen peroxide at an iridium oxide electrode. (A) 1 *M* NaOH; (B) 1.3×10^{-2} *M* H_2O_2 in 1 *M* NaOH; scan rate, 100 mV/sec. The family of voltammograms from (A) to (B) are for successively higher H_2O_2 concentrations; the concentrations were raised in 0.5 m*M* increments.

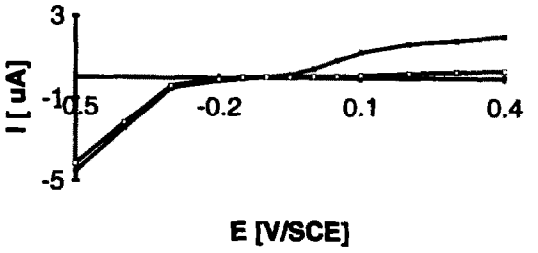

Fig. 2. Hydrodynamic voltammogram of 1×10^{-4} *M* H_2O_2 in 0.1 *M* KOH at the iridium oxide electrode. The carrier was 0.1 *M* KOH. The conditions are in the Experimental section.

positive than −200 mV. Second, a potential window for the FIA determination of H_2O_2 in this medium at the iridium oxide electrode exists from about −50 mV to more positive values. The ability to work at low overpotential suggests practical applicability of oxidative determinations of hydrogen peroxide; as mentioned previously, the use of less positive applied potentials than are necessary at conventional electrodes minimizes the number of candidates for interference.

The electrochemistry of hydrogen peroxide at the iridium oxide electrode is highly dependent upon pH. This is illustrated by examination of the influence of pH on the height and position of the anodic peaks in the cyclic voltammetry of H_2O_2. Figure 3 contains a plot of peak current *vs.* pH. Clearly, the sensitivity is enhanced by working in a medium with pH greater than 11. The shape of the plot resembles a potentiometric titration curve, which suggests that the electroactive species is HO_2^-. That the inflection point of this curve is near the pK_a of H_2O_2 (11.6) supports this conjecture. The dependence of the anodic peak potential on pH (Fig. 4) demonstrates that to obtain the low overpotential which makes this electrode process promising the pH must also be greater than 11. The fact that the peak potential is quite constant over the pH range 3.5–11 is interesting in that the cyclic

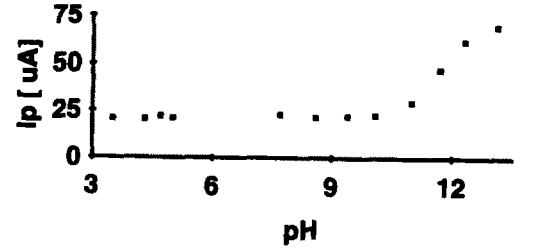

Fig. 3. Dependence of the anodic peak current on pH in the cyclic voltammetry of 1.1×10^{-2} *M* H_2O_2 in 1 *M* KCl at the iridium oxide electrode. The pH was adjusted by addition of KOH or HCl. Scan rate, 100 mV/sec.

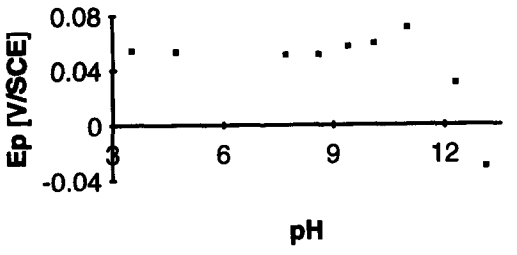

Fig. 4. Dependence of the anodic peak potential on pH in the cyclic voltammetry of H_2O_2 at an iridium oxide electrode. The conditions are those in Fig. 3.

voltammetric peaks for the iridium oxide couple(s) in the film vary in potential over this range. This contrasting behavior demonstrates that the film is not mediating the hydrogen peroxide oxidation. Instead, it is acting as a catalyst. Based on these results, the FIA experiments were performed with either 0.1 or 1.0 *M* KOH as the carrier.

Figure 5 contains sets of FIA curves for various concentrations of hydrogen peroxide. At the 99% confidence limit (peak current is three-times the noise), the detection limit is 30 n*M* H_2O_2. The characteristics of calibration curves prepared under the conditions in Fig. 5, except with the tabulated values of KOH concentration and applied potential, are summarized in Table 1. Two points are important. First, increasing the KOH concentration will increase the sensitivity at a given potential. Second, with a given concentration of KOH as the carrier, a more positive applied potential will increase the sensitivity. Since an application of this electrode process to a practical FIA procedure will require addition of base in a mixing coil, the lower KOH concentration is recommended even though the sensitivity is decreased. Whether more positive applied potentials are employed than those in Table 1 (see Fig. 2) will depend on the anticipated interferences in the proposed application. A recent discussion of possible interferents in experiments when measurements of hydrogen peroxide are used to indirectly determine glucose in biological samples is available.[3]

The use of an oxide film on an iridium electrode rather than a film deposited on glassy carbon from a $PdCl_2$, $IrCl_6^{2-}$ mixture may be inconvenient in some cases. The former requires modification of a commercially-available detector and the use of iridium wire which is quite expensive. Experiments were performed to determine if the iridium oxide film deposited on glassy carbon provided a suitable electrode for this FIA method. Results comparable to those obtained at the oxidized iridium metal electrode (Table 1) were obtained over the concentration range 20–0.47 μM; a linear least squares calibration curve (10 points) yielded a slope of 2.5 mA/*M* and r^2 of 0.9999 when 0.1 *M* KOH was the carrier. The applied potential was 0.00 V. The detection limit (99% confidence limit) was 37 n*M*.

In summary, iridium oxide films provide an attractive surface for the oxidative determination of hydrogen peroxide. Although the results presented herein are based upon flow injection amperometry, this surface may find application to other electrochemical methods for this analyte. Moreover, our preliminary work on other species that are generally oxidized or reduced at high overpotential indicates that iridium oxide may find a wide range of application. Nitrogen oxides are one general class of compounds for which promising preliminary data have been obtained. The combination of the freedom from interference by

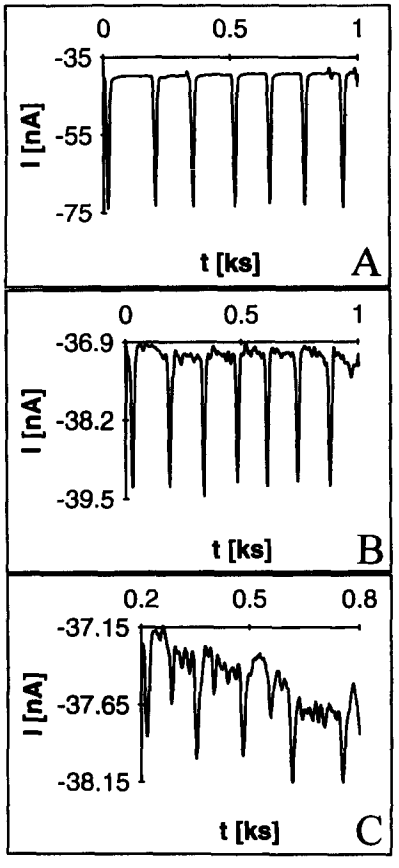

Fig. 5. Flow injection amperometry of H_2O_2 at the iridium oxide electrode. E 0.0 V. H_2O_2 concentrations: (A) 1.2×10^{-5} *M* (B) 7.8×10^{-7} *M*; and (C) 6.0×10^{-8} *M*. The time between injections is 150 sec. Other conditions are those in Fig. 2.

Table 1. Linear least squares calibration curves for the flow injection amperometry of H_2O_2 at an iridium oxide electrode

Carrier	Conc.H_2O_2 (M)	E (mv)	slope, (mA/M)	r	n
1 M KOH	1.0×10^{-4}–1.0×10^{-6}	0.0	4.3	0.9996	9
1 M KOH	1.0×10^{-6}–1.0×10^{-7}	50	8.1	0.9889	7
0.1 M KOH	2.0×10^{-5}–3.6×10^{-8}	0.0	2.9	0.9993	14

dissolved oxygen with the low overpotential that is required suggests suitability of this system to bioanalytical applications; however, for such studies a means to adjust the sample to pH $\geq$ 11 must be included in the FIA system. A second drawback is that modified electrodes generally promote electron transfer of many compounds at the same potential, so selectivity must be achieved by a prior separation step or through a chemical reaction.

Acknowledgement—This work was supported by Grant R-816507 from the U.S. Environmental Protection Agency. The work has not been reviewed by that agency, so an endorsement should not be inferred.

REFERENCES

1. J. E. Harrar, *Anal. Chem.*, 1963, **35**, 893.
2. G. G. Guilbault and G. L. Lubrano, *Anal. Chim. Acta*, 1973, **64**, 439.
3. R. Maiden and A. Heller, *Anal. Chem.*, 1992, **64**, 2889.
4. V. G. Prabhu, L. R. Zarapkar and R. G. Dhaneshwar, *Electrochim. Acta*, 1981, **26**, 725.
5. A. Brestovisky, E. Kirowa-Eisner and J. Osteryoung, *Anal. Chem.*, 1983, **55**, 2063.
6. F. A. Armstrong and A. M. Lannon, *J. Am. Chem. Soc.*, 1987, **109**, 7211.
7. N. Oyama and F. C. Anson, *J. Electroanal. Chem.*, 1986, **199**, 467.
8. J. A. Cox, R. K. Jaworski and P. J. Kulesza, *Electroanalysis*, 1991, **3**, 869.
9. X. Qi, R. P. Baldwin, H. Li and T. F. Guarr, *Electroanalysis*, 1991, **3**, 119.
10. J. A. Cox and R. K. Jaworski, *Anal. Chem.*, 1989, **61**, 2176.
11. R. K. Jaworski and J. A. Cox, *J. Electroanal. Chem.*, 1991, **297**, 93.
12. R. K. Jaworski, J. A. Cox and B. R. Strohmeier, *J. Electroanal. Chem.*, 1992, **325**, 111.
13. M. Fujihira, H. Muraki and S. Aoyagui, *Bull. Chem. Soc. Jpn.*, 1986, **59**, 975.

Talanta, Vol. 40, No. 12, pp. 1917–1926, 1993
Printed in Great Britain.

0039-9140/93 $6.00 + 0.00

FLOW INJECTION ON-LINE ACID DIGESTION AND PRE-REDUCTION OF ARSENIC FOR HYDRIDE GENERATION ATOMIC ABSORPTION SPECTROMETRY—A FEASIBILITY STUDY

BERNHARD WELZ, YOUZHAO HE* and MICHAEL SPERLING
Department of Applied Research, Bodenseewerk Perkin-Elmer GmbH, D-88647 Überlingen, Germany

(*Received* 7 *April* 1993. *Revised* 14 *June* 1993. *Accepted* 14 *June* 1993)

Summary—A flow injection (FI) manifold is described which makes possible on-line microwave-assisted acid digestion, followed by pre-reduction of As(V) to As(III) and its determination by hydride generation atomic absorption spectrometry. The merging zone technique is used in order to reduce acid consumption for digestion. The efficiency of acid digestion is increased by pressure which is built up in-line by a flow restrictor. Flows for sample pretreatment and hydride generation can be optimized independently. *L*-cysteine was found superior to potassium iodide as the pre-reductant because much lower reagent and acid concentrations are required, much harsher conditions can be tolerated for acid digestion, and the integrated absorbance signals for arsenic in blood and standards are essentially identical, making possible the use of the standard calibration procedure.

The sampling frequency is 7–10/hr, depending on the conditions chosen, and the limit of detection, *i.e.* the concentration giving a signal equal to three times the standard deviation of the signal of the blank solution, is 0.25 μg/l for a 500 μl sample volume. The recovery of 10 μg/l As(V) added to a blood sample was 94 ± 2 and $98 \pm 2\%$ ($n = 3$) in absorbance and integrated absorbance, respectively.

Sample preparation is often the bottle-neck of an analytical procedure because it is a manual process which makes it slow, work-intensive and a frequent source of errors. It is therefore not surprising that with the increasing use of flow techniques, particularly flow injection (FI), various attempts have been made to incorporate sample preparation on-line with the detection in an automatic procedure. The state of the art at the end of the 1980s in on-line techniques coupled to FI is summarized in a review article by Puchades *et al.*[1]

The most frequently investigated approach for on-line sample preparation is that of microwave assisted acid digestion,[2] which was coupled with amperometric[3] and colorimetric[4] detection, ICP atomic emission,[5] flame,[6–10] cold vapour[11–13] and hydride generation atomic absorption spectrometry (HG AAS).[12–14] The application of on-line acid digestion to the latter two techniques was complicated by the fact that the oxidative reagents had to be compatible with sodium tetrahydroborate which was required for the reduction of the analyte to the element and the hydride, respectively.[13] In addition, some analyte elements, such as antimony and arsenic were oxidized to their highest oxidation state during the digestion which resulted in about an order of magnitude lower sensitivity in their determination by FI–HG AAS.[13–16] A pre-reduction step must therefore follow after the oxidative digestion.

Sperling *et al.*[17] successfully used a mixture of sodium sulfite, hydrochloric acid, sodium thiosulfate and potassium iodide for the on-line reduction of pentavalent to trivalent arsenic for solid sorbent extraction of total arsenic from natural water samples. The reduction was complete within 5 sec, however, the reagents used were not compatible with sodium tetrahydroborate reduction, and hence with HG AAS. The reagent used most frequently for the reduction of pentavalent arsenic in HG AAS is potassium iodide, alone or mixed with ascorbic acid. Marshall and van Staden[18] and Tyson *et al.*[19] have described on-line procedures for the reduction of As(V) using FI techniques. A significant disadvantage of that reducing agent is, however, the extremely high hydrochloric acid concentration required if the reduction had to be completed within a short period of time. Brindle *et al.*[20] proposed *L*-cysteine as an

*On leave from Department of Applied Chemistry, University of Science and Technology of China, Hefei, Anhui, China.

alternative to potassium iodide with the big advantage that this reagent was usable at low acid concentrations. In addition, *L*-cysteine was found to be much more stable than potassium iodide and provided a higher freedom from interferences.[16]

Although on-line microwave assisted acid digestion and on-line reduction of As(V) for HG AAS have been investigated by several authors, no attempt was made to combine acid digestion and pre-reduction on-line in a flow system. The aim of the present work was to investigate the feasibility of combining an acid digestion with a pre-reduction on-line in an FI system for the determination of arsenic in biological materials, and blood was chosen as a model matrix. We have limited ourselves to inorganic arsenic in this study, not considering organic arsenic compounds, which will be the topic of another publication. Our first goal was to investigate the possibility of a fully automatic procedure for measuring elevated arsenic levels due to occupational exposure, *i.e.* to determine inorganic arsenic. For that purpose it was only necessary to break down the organic matrix to an extent that it did no longer interfere with HG. Insufficient digestion of organic matter resulted in excessive foaming in the gas–liquid separator and penetration of foam into the atomizer, causing severe contamination and loss of sensitivity. The antifoam reagent, which was added routinely to the sodium tetrahydroborate solution, did not control excessive foaming.

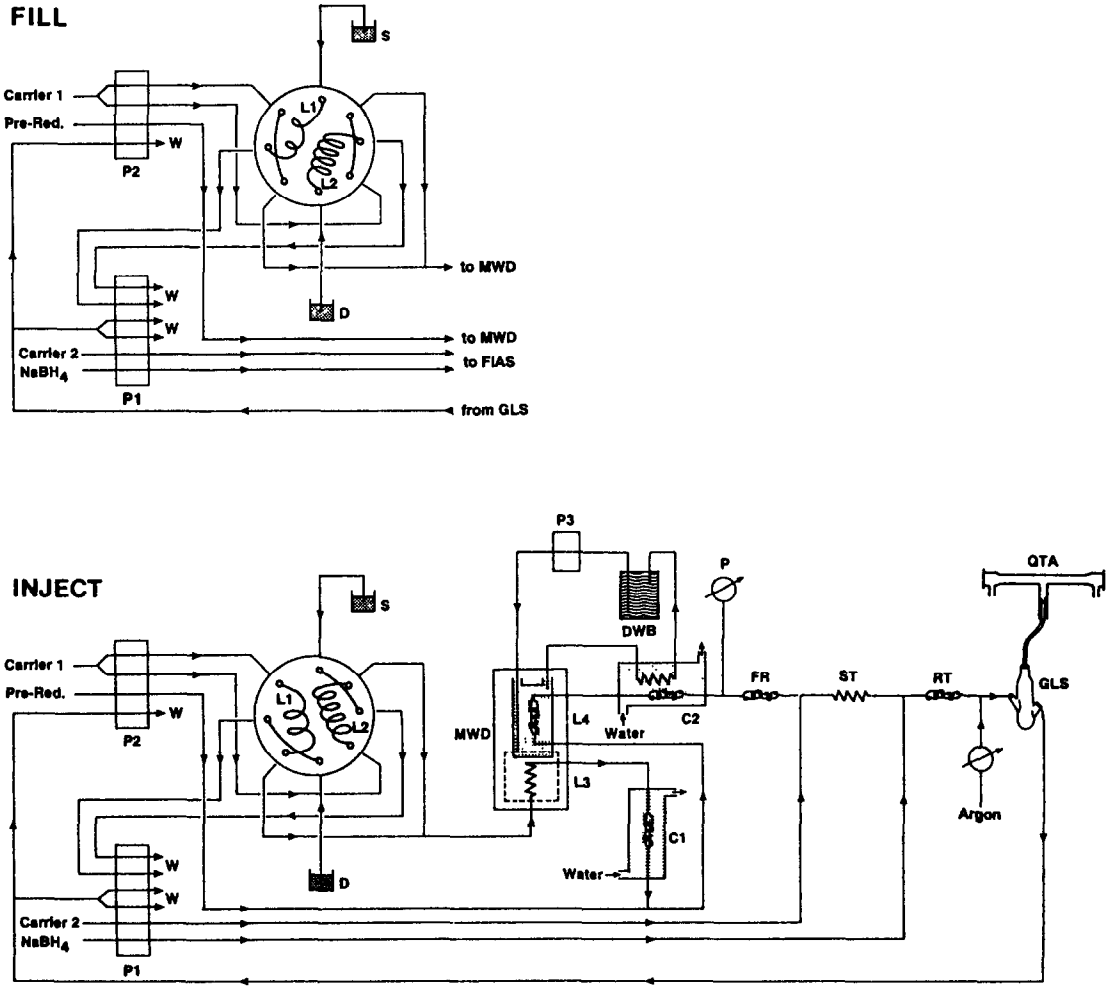

Fig. 1. Flow injection manifold for on-line acid digestion and pre-reduction for HG AAS. P1, P2, P3: peristaltic pumps; S: sample; D: digestion reagent; MWD: microwave digestor; DWB: deionized water bottle; P: pressure gauge; GLS: gas–liquid separator; QTA: quartz tube atomizer; W: waste; the symbols for loops and coils are explained in Table 2.

Table 1. Inner diameters (i.d.) of pump tubes, pump rotation and flow rates for on-line acid digestion and pre-reduction

Pump tube	i.d. (*mm*)	Pump rotation speed (*/min*)	Flow rate (*ml/min*)
Sample load	0.64	120	2.2
Digestion reagent load	0.89	120	3.1
Carrier 2	2.29	120	17.5
$NaBH_4$ reductant	0.64	120	2.2
GLS Waste (2x)	2.54	120	18.5
Carrier 1 (2x)	0.76	40	0.65
Pre-reductant	0.51	40	0.35
GLS waste	2.54	40	6.4

EXPERIMENTAL

Instrumentation

A Perkin-Elmer Model 2100 atomic absorption spectrometer with continuum source background correction and an arsenic electrodeless discharge lamp, operated at a power of 8 W, was used throughout. The wavelength was set to 193.7 nm with a spectral slitwidth of 0.7 nm (low). A Perkin-Elmer FIAS-200 flow injection system with an AS-90 autosampler was used and the temperature of the quartz tube atomizer was set to 900°. The atomic absorption spectrometer, the flow injection system and the autosampler were controlled by an Epson PC AX 2e personal computer which also calculated the absorbance and integrated absorbance values. The time-resolved absorbance signals were displayed on an EIZO 14-inch color data display and printed, together with the analytical results, on an Epson EX-800 printer.

The extended and modified FI system, the manifold and its operation are shown in Fig. 1. An Ismatec (Wertheim-Monfeld, Germany) peristaltic pump (P3) was added for circulating the water of the pre-reduction heating bath. A Maxidigest MX350 oven (2.45 GHz, 300 W) with TX 31 programmer (Prolabo, Paris, France) was used for microwave digestion. The standard value of the FIAS-200 was replaced by a prototype 8-channel valve (Tecator, Sollentuna, Sweden).

All pump tubes were Tygon. Their inner diameters, the pump rotation and the resulting flow rates are summarized in Table 1. Material, dimension and configuration of the various conduits and coils are given in Table 2.

Method

The sequence of operation for on-line acid digestion and pre-reduction is summarized in Table 3. In sequence 1, 500 μl of sample and 1000μl of digestion reagent were filled into L1 and L2, respectively. Sequence 2 actually consisted of five steps because the maximum time which could be programmed in the FIAS-200 software was 99 sec. The same pump rotation speed of 40/min was used throughout that sequence although it would have been possible to save some time by using faster flow rates at certain stages of that sequence. In the first stage, after the valve had turned, sample and digestion reagents were mixed. The merging zone technique was applied in order to save reagent because water could be used as the carrier in this case. In the next stage sample and digestion reagent were conducted through the microwave oven. Details of the arrangement within the microwave cavity are shown in Fig. 2.

Because of the flow restrictor which was installed downstream, a pressure of about 6 Bar was built up which increased the efficiency of the digestion. The pressure also reduced the

Table 2. Material, dimension and configuration of conduits, loops and coils for on-line acid digestion and pre-reduction

Item	Symbol	Material*	i.d. (*mm*)	Length (*m*)	Volume (μl)	Configuration
Sample loop	L1	PTFE	0.8	—	500	Straight
Digestion reagent loop	L2	PTFE	0.8	—	1000	Straight
Digestion coil	L3	PFA	0.8	8	4000	Coiled
Reduction coil	L4	PTFE	0.8	9	4500	Knotted
Cooling coil	C1	PTFE	0.8	1	500	Knotted
Cooling coil	C2	PTFE	0.8	1	500	Knotted
Flow restrictor	FR	PTFE	0.3	1	70	Knotted
Store coil	ST	PFA	0.8	6	3000	Coiled
Reaction coil	RT	PTFE	0.8	1	500	Knotted

*PTFE = Polytetrafluoroethylene; PFA = Perfluoroalkoxypolymers.

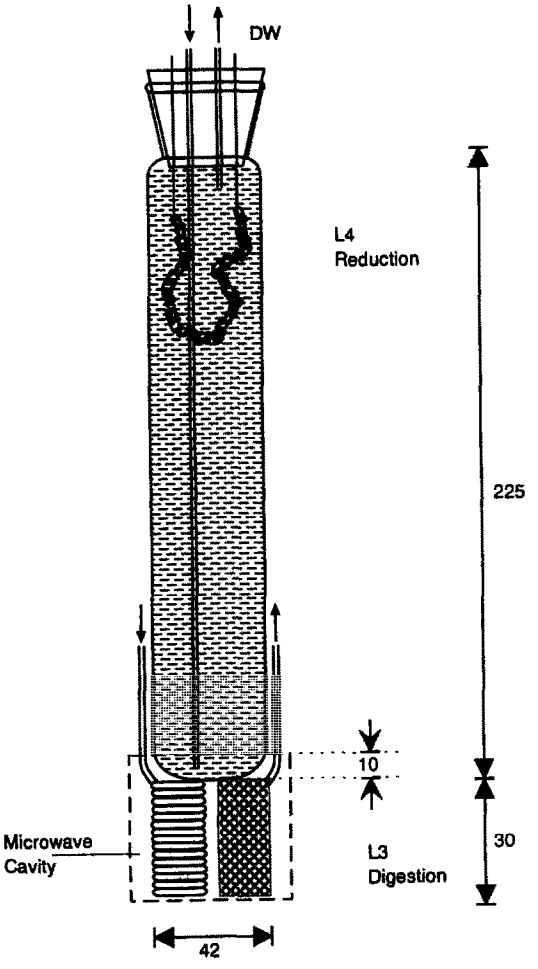

Fig. 2. Arrangement of digestion coil (L3), reduction coil (L4) and water bath for pre-reduction in the microwave digestor. All dimensions in mm.

formation of gas bubbles during the microwave-assisted acid digestion, and a steady flow of liquid with only a few bubbles was obtained after cooling in C 1. In the next stage the reducing agent was added and the sample conducted through a water bath which was kept boiling by immersing its bottom into the microwave cavity, as is shown in Fig. 2. After passing through another cooling bath and the flow restrictor the sample bolus reached the store coil. The total time had to be programmed in such a way that the sample was contained quantitatively in the store coil at the end of sequence 2.

In sequence 3 pump 1 was turned on and a second carrier stream added in order to transport the sample quickly through the hydride generation stage and into the gas–liquid separator (GLS). This arrangement made it possible to optimize flow rates independently for the different processes of sample preparation and analyte element determination.

Reagents

All reagents were of analytical reagent grade or higher purity except for sodium tetrahydroborate, for which no purity was given. Doubly deionized water (18 MΩ/cm) was used throughout. Arsenic(V) stock solution, 1000 mg/l As in 0.5 mol/l HNO_3 was prepared from Titrisol concentrate (Merck, Darmstadt, Germany). Standard solutions were obtained by serial dilution with 0.1 mol/l HCl. For blood analysis standards were prepared to contain 0.2% (m/v) Triton X-100.

Sodium tetrahydroborate solution, 2% (m/v) was prepared by dissolving sodium tetrahydroborate powder (Riedel-de Haen, Seelze, Germany) in water containing 0.05% (m/v) sodium hydroxide (Merck) and 1.0% (m/v) antifoam reagent (Greiffenberg, Krefeld, Germany).

Cysteine reductant, 0.6% (m/v), was prepared by dissolving *L*-cysteine (for biochemistry, Merck) in 0.5 mol/l HCl.

Potassium iodide pre-reductant was prepared by dissolving 10 g of potassium iodide, KI, (Merck) and 10 g of ascorbic acid (Merck) in 100 ml of 2.5 mol/l HCl. Lower concentrations of these reagents were used in some experiments.

A mixture of 1 mol/l HNO_3 and 0.04 mol/l $HClO_4$ was used as the digestion reagent together with the potassium iodide pre-reductant and a mixture of 2 mol/l HNO_3 and 0.2 mol/l $HClO_4$ was used with *L*-cysteine.

Table 3. Sequence of operation for on-line acid digestion and pre-reduction for HG AAS

Step	Function	Time (*sec*)	Rotation speed (*/min*) Pump 1	Pump 2	Valve position	Read
1	Fill loops L1 and L2	50	120	40	Fill	
2*	Merge zones, digestion, pre-reduction, fill store tube	440*	—	40	Inject	
3	Hydride generation	30	120	40	Inject	ON

*Step 2 consists of five identical steps of 90, 90, 90, 90 and 80 sec duration. See text for details.

Pool blood samples were obtained from Baden–Württemberg blood supply center (Ulm, Germany). Blood samples were diluted 1:10 with 0.1 mol/l HCl and 0.2% (m/v) Triton X-100.

Method development

The optimization of the procedure was carried out step by step, *i.e.* one parameter at a time, starting from the end, *i.e.* the hydride generation. On going upstream step-by-step it was anticipated that optimization of an earlier stage would not impair the previously optimized parameters. The standard calibration technique was used throughout and the analyte addition technique (method of additions) was only applied occasionally in order to exclude the presence of matrix effects.

RESULTS AND DISCUSSION

Optimization of hydride generation

One of the advantages of the FI manifold used in this work was that the different stages of the analytical procedure, *i.e.* acid digestion, pre-reduction and hydride generation, could in essence be optimized independently. Whereas low flow rates were obviously advantageous for sample pretreatment because of the associated longer residence times in the microwave oven, *etc.* and the less pronounced dispersion, they would inevitably result in very broad absorbance peaks in the hydride generation stage. For that reason an additional carrier was introduced downstream of the flow restrictor in order to push the sample bolus quickly from the store coil through the rest of the FI system and to the detector.

The effect of this additional carrier flow rate on the arsenic signal is shown in Fig. 3. Without an additional carrier flow an extremely low and broad signal was obtained which had not reached its maximum even after 50 sec. Although integrated absorbance decreased about 30% when the additional carrier flow rate was increased from 2.9 ml/min (20 r.p.m.) to 17.5 ml/min (120 r.p.m.) the significantly improved peak shape and much shorter signal duration (measurement time) were considered a great advantage.

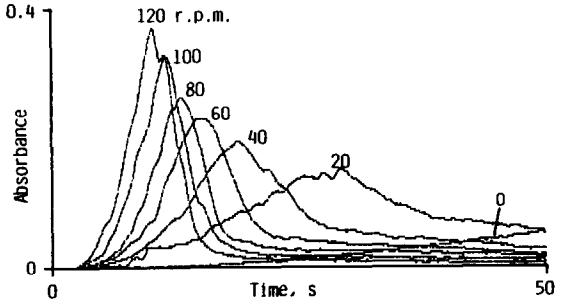

Fig. 3. Effect of additional carrier flow rate (expressed in rotations per min of PI) on the absorbance signal of 10 μg/l As; 120 r.p.m. corresponds to a flow rate of 17.5 ml/min.

The acidity of the additional carrier solution had no influence at all on the absorbance signal of arsenic. Variation of the acid concentration between 0 and 2 mol/l HCl resulted in identical results, and water was used as the carrier for all further investigations.

The flow rate of the auxiliary argon had only a minor effect on the arsenic signal. The integrated absorbance decreased by about 15% when the argon flow rate was increased from 20 to 90 ml/min. The peak height absorbance showed a slight maximum around 60 ml/min which was used for our future work.

In contrast to conventional FI–HG AAS where the carrier and sodium tetrahydroborate flow rates are similar,[21] we have chosen a high flow rate for the additional carrier for the reasons discussed above. In order not to increase the total flow rate too much we used a low flow rate of 2.2 ml/min for the tetrahydroborate which necessitated a higher concentration than usual. The arsenic signal increased under these conditions significantly up to a reductant concentration of 1% (m/v) tetrahydroborate, with a slight additional increase up to 2% (m/v) tetrahydroborate. The 2% concentration was chosen for our future work because a much better performance was obtained in the analysis of blood samples, *etc.* which contained the oxidative reagents from acid digestion.

Optimization of acid digestion and pre-reduction

The optimization of the microwave-assisted acid digestion and of the prereduction could obviously not be separated entirely because the reagents and conditions had to be compatible. All investigations were carried out with *L*-cysteine and potassium iodide–ascorbic acid, respectively, as the pre-reduction reagents. Matrix-free standard solutions as well as 1:10 diluted blood samples, which were spiked with arsenic(V), were used for all investigations.

The following criteria were applied to select the best conditions

(i) Completeness of acid digestion. The main indicator for that criterion was foam formation

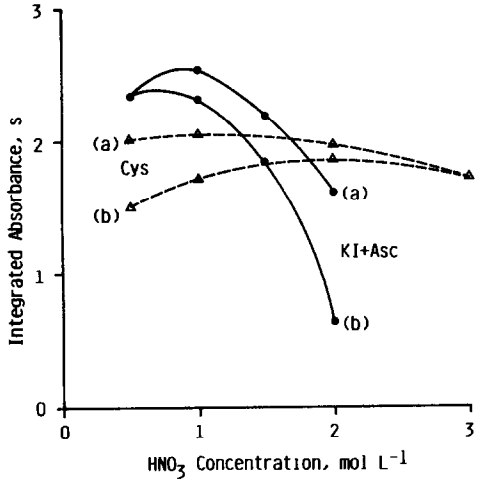

Fig. 4. Effect of nitric acid concentration on the integrated absorbance signal of 10 μg/l As(V). Microwave power: 150 W for potassium iodide–ascorbic acid (KI + Asc) and 210 W for *L*-cysteine (Cys). (a) As in 0.1 mol/l HCl; (b) As added to 1:10 diluted blood.

in the GLS as no organic arsenic compounds were investigated in this study. In addition a system that could tolerate higher microwave power and/or higher acid concentrations would obviously provide more complete acid digestion, and was hence considered superior.

(ii) Sensitivity. That parameter obviously also included completeness of reduction of As(V) to As(III). All data in this optimization study were based on integrated absorbance. Peak height absorbance gave similar results for matrix-free standards but significant deviations for the blood samples and was therefore not considered in this work.

(iii) Applicability of standard calibration technique. One of the goals of this work was to avoid the time-consuming standard addition technique, which means that standards and samples must exhibit an almost identical behaviour.

(iv) Ruggedness. As analytical conditions may change for different samples, ruggedness against such changes was considered important.

(v) Reagent consumption. A reduced requirement for reagents, particularly when they were toxic and/or corrosive, was a major criterion for cost reasons, because of the waste problem and to better protect operators and instruments.

This last point was the main reason why we have chosen the merging zone technique to mix sample and oxidative reagents for acid digestion. This approach made it possible to use water as the carrier instead of a corrosive and toxic acid mixture.

Various combinations and concentrations of nitric and perchloric acid were investigated as the oxidizing medium for acid digestion. The influence of the nitric acid concentration on the integrated absorbance signal of arsenic is shown in Fig. 4. A lot of foam was formed in the GLS due to incomplete digestion of blood if the nitric acid concentration was only 0.5 mol/l. Higher nitric acid concentrations, however, were not quite compatible with the potassium iodide–ascorbic acid pre-reductant. Firstly, there was a significant difference in the response for arsenic in the standards and blood samples and this difference increased with increasing acid concentrations. Secondly, the sensitivity for arsenic depended strongly on the nitric acid concentration. The behaviour of *L*-cysteine pre-reductant was much better in both respects. Although there was a difference between standards and blood samples for 1 mol/l HNO_3, this difference essentially disappeared for nitric acid concentrations of 2–3 mol/l. There was also very little influence of the nitric acid concentration on the sensitivity for arsenic in the presence of *L*-cysteine, which was clearly the better reductant from that point of view.

Perchloric acid had very little additional effect up to 0.1 mol/l in the case of potassium iodide–ascorbic acid pre-reductant and up to 0.4 mol/l in the case of *L*-cysteine. A mixture of 2 mol/l HNO_3 and 0.2 mol/l $HClO_4$ was therefore chosen for most of our further investigations.

The efficiency of the microwave-assisted acid digestion was further increased by a pressure of about 6 Bar which was caused by the backpressure of the flow restrictor. The influence of the microwave power on the integrated absorbance signal for arsenic is shown in Fig. 5. At power

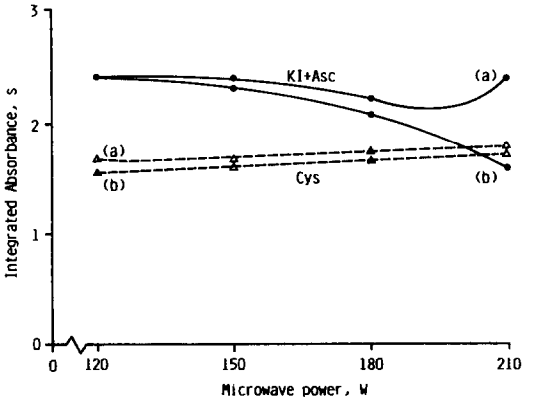

Fig. 5. Influence of microwave power on the integrated absorbance signal of 10 μg/l As(V). (a) In 0.1 mol/l HCl; (b) added to 1:10 diluted blood.

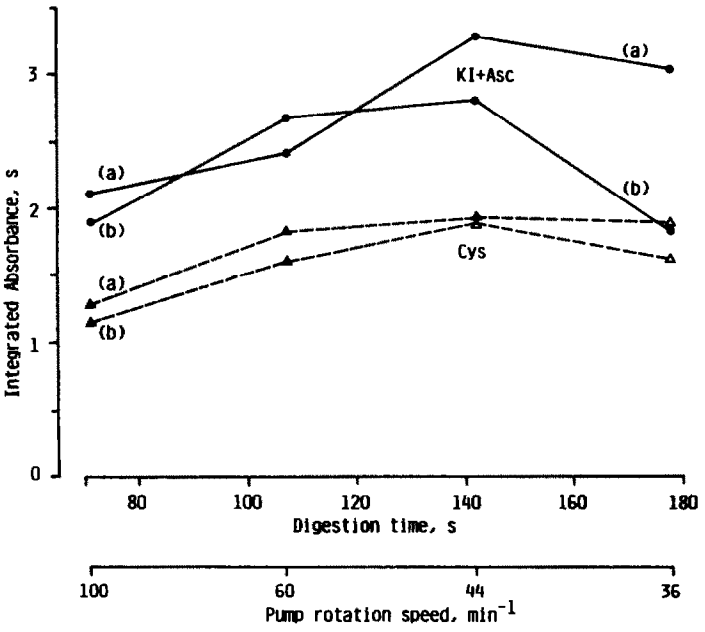

Fig. 6. Influence of residence time of the sample bolus in the MWD on the integrated absorbance signal of 10 μg/l As(V). (a) In 0.1 mol/l HCl; (b) added to 1:10 diluted blood.

settings below 120 W the foam formation in the GLS became excessive. Although the sensitivity for arsenic was better in the presence of potassium iodide–ascorbic acid, the discrepancy between standards and blood samples became quite significant for higher power settings which was considered a disadvantage. No such effects were observed with the *L*-cysteine pre-reductant so that 210 W could be used without problems.

The residence time in the microwave digestor (MWD), which was controlled by the pump rotation speed, had a similar effect on the arsenic signal as the microwave power as is shown in Fig. 6. Significant foam formation in the GLS, *i.e.* incomplete digestion, was observed for a pump rotation speed of 100/min which corresponded to a residence time of about 70 sec. If potassium iodide–ascorbic acid was used as the pre-reductant, increasing digestion times resulted in an increasing discrepancy between the signals for standards and blood samples. This effect would not permit to use long digestion times, which might be essential to attack acid-resistant organic compounds of arsenic, and to use the standard calibration procedure. The behaviour of *L*-cysteine was one more time much more favorable in that respect. A pump rotation speed of 40–50/min, corresponding to a residence time of 140–150 sec gave best performance. The reason for the discrepancy in the behaviour of potassium iodide and *L*-cysteine was that different acid and reagent concentrations were found optimum, which resulted in different reactions and reaction products upon digestion and hence a different overall performance.

The cooling coil which was installed between the MWD and the confluence with the pre-reductant primarily served the purpose to condense gaseous products and hence reduce the bubbles in the conduits. It was found that a coil length of 1 m, in the configuration of a knotted reactor, was sufficient to reduce bubble formation significantly and produce an even flow of liquid at the confluence point. The pressure of 6 Bar in the system undoubtedly contributed

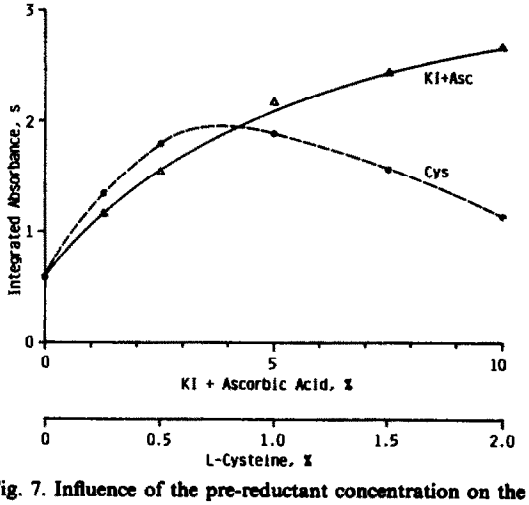

Fig. 7. Influence of the pre-reductant concentration on the integrated absorbance signal of 10 μg/l As(V).

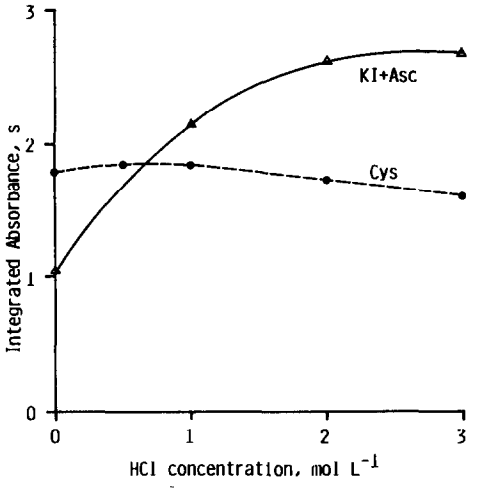

Fig. 8. Influence of HCl concentration of the pre-reductant solution on the integrated absorbance signal of 10 μg/l As(V); 7.5% potassium iodide and 7.5% ascorbic acid (KI + Asc) and 0.6%*L*-cysteine (Cys).

very significantly to the fact that bubble formation did not cause any problems under the conditions chosen in this work. The influence of the pre-reductant concentration on the integrated absorbance signal for arsenic is shown in Fig. 7. In essence the results were consistent with those obtained earlier with conventional FI–HG AAS.[16] The efficiency of the potassium iodide–ascorbic acid pre-reductant increased with increasing concentration, but a concentration of at least 5% (m/v) was required to obtain a sufficient reduction power. *L*-cysteine, in contrast, had its optimum performance at concentrations of 0.5–1% (m/v). The decrease of the arsenic signal in the presence of higher cysteine concentrations was *not* due to a decreasing reduction efficiency but to an interference in the hydride generation stage.[16] In addition to a higher reagent concentration, the potassium iodide–ascorbic acid pre-reductant also required a higher acid concentration of 2–3 mol/l HCl in order to perform properly, as is shown in Fig. 8. *L*-cysteine, in contrast, developed its full reduction potential even in aqueous solution. This significantly lower consumption of reagents and acids, together with the improved ruggedness and the much more similar behaviour of standards and blood samples finally made the *L*-cysteine the pre-reductant of choice for our future work.

The best sensitivity for arsenic was obtained when the water in the reduction vessel was boiling, *i.e.* had a temperature of 97° in our case. In order to prevent excessive boiling the water was pumped continuously through a cooling bath. The pump speed required to keep the water at gentle boiling obviously depended on the applied microwave power. This correlation is summarized in Table 4.

The influence of the residence time of the sample bolus in the boiling water bath on the arsenic signal is shown in Fig. 9 for *L*-cysteine. Three different lengths of reduction coil, 3, 6 and 9 m, all in the form of knotted reactors, were used with a variety of pump rotation speeds. However, there appeared to be no influence of the length of the tubing, and the residence time was the only significant parameter. For a residence time longer than 150 sec the integrated absorbance did not increase any more which could be interpreted that the reduction of As(V) to As(III) was complete under these conditions. This was in quite good agreement with Chen *et al.*[22] who found quantitative reduction of As(V) in a boiling water bath and in the presence of 1% *L*-cysteine within 5 min. A direct comparison with the signal of As(III) could not be made because any trivalent arsenic was readily oxidized to its pentavalent form under the conditions used in our work.

Performance of the system

The total time required for one on-line acid digestion, pre-reduction and HG AAS determination cycle, using the program in Table 3, was

Table 4. Rotation speed of pump 3 at which the water in the pre-reduction vessel reaches the boiling point (97°) for different microwave power settings.

Microwave power (W)	120	150	180	210	240
P3 rotation speed (/*min*)	30	58	75	85	99

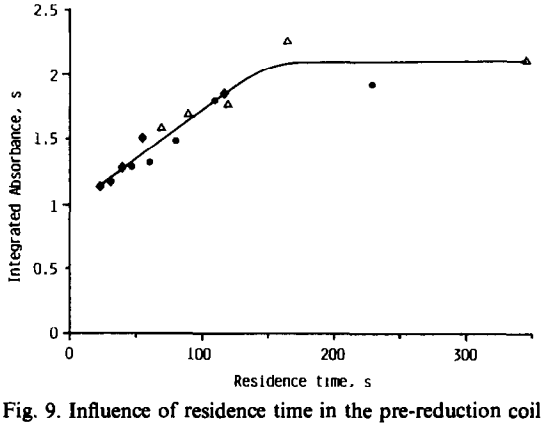

Fig. 9. Influence of residence time in the pre-reduction coil (L4) on the integrated absorbance signal for 10 μg/l As(V). Pre-reductant *L*-cysteine. Coil length: ◆ 3 m; ● 6 m; △ 9 m.

520 sec which resulted in a sampling frequency of 7/hr. That program was, however, not at all optimized with respect to sample throughput. The low pump rotation speed of 40/min, which resulted in best performance for digestion and pre-reduction with *L*-cysteine, was used throughout the entire stage 2. Faster pump rates could obviously be used for to transport the sample bolus to the MWD, from the MWD to the pre-reduction bath and from pre-reduction to the store coil. About 100 sec could be saved that way without causing any disadvantages. Another 50–60 sec might be saved at the expense of a 15% lower sensitivity if the reduction coil length was reduced to 6 m or the pump rate increased to 60/min with the 9 m coil. The fact that As(V) would not be reduced quantitatively under these conditions would have no effect on accuracy and precision because FI is capable of performing quantitative determinations reproducibly under thermodynamically non-equilibrium conditions.[23] If all these measures were taken, the total time for one cycle would be reduced to about 6 min and the sampling frequency increased to 10/hr.

When the standard conditions described in the Experimental section were used, the precision of the entire procedure, expressed as the relative standard deviation of 11 determinations of a 10 μg/l As(V) standard was 2.6% for the potassium iodide pre-reductant and 2.8% for *L*-cysteine. The detection limit, *i.e.* the concentration giving a signal equal to three times the standard deviation of the signal of a blank solution ($n = 11$) was 0.2 and 0.25 μg/l As(V) for potassium iodide and *L*-cysteine pre-reductants, respectively.

The linear regression equations for the calibration range 0–30 μg/l were $y = 0.10525 + 0.13055\ x$ with a correlation coefficient of $R = 0.998$ in integrated absorbance and $y = 0.0221 + 0.02021\ x$ with a correlation coefficient of $R = 0.994$ in peak absorbance; 10 μg/l As(V) added to a diluted blood sample gave an average integrated absorbance reading of 1.386 ± 0.024 sec ($n = 3$) and a peak absorbance of 0.210 ± 0.004, corresponding to a recovery of 98 ± 2 and $94 \pm 2\%$ in integrated and peak absorbance, respectively.

CONCLUSIONS

It could be shown in this work that an on-line combination of a microwave-assisted acid digestion with a pre-reduction of As(V) to As(III) and its determination with HG AAS is feasible. It could also be shown that *L*-cysteine is better suited as pre-reduction reagent than potassium iodide because its performance was much less affected by the oxidizing acids and their reaction products. The efficiency of the microwave-assisted acid digestion of a dilute blood solution, which was increased by a pressure of 6 Bar produced in-line by a flow-restrictor, could not really be tested in this work. The only indications for an incomplete digestion were foam formation in the GLS when blood samples were analyzed and a low recovery of arsenic added to the blood. The key question regarding the practical use of the proposed procedure will be to which extent the various organo-arsenic compounds are mineralized under these conditions. This question will finally also determine the acid concentrations and the time required for the on-line digestion and, hence, the total analysis time.

The degree to which the various organo-arsenic compound are attacked by the procedure will eventually determine the application fields. Possible applications are for instance differentiation between inorganic (toxic) and organic arsenic (from sea food) in blood and urine, or total arsenic in water and waste water. These investigations are the topic of future work.

REFERENCES

1. R. Puchades, A. Maquieira, J. Atienza and M. A. Herrero, *J. Autom. Chem.*, 1990, **12**, 163.
2. M. de la Guardia, A. Salvador, J. L. Burguera and M. Burguera, *J. Flow Injection Anal.*, 1988, **5**, 121.
3. S. Hinkamp and G. Schwedt, *Anal. Chim. Acta*, 1990, **236**, 345.
4. K. E. Williams, S. J. Haswell, D. A. Barclay and G. Preston, *Analyst*, 1993, **118**, 245.
5. V. Karanassios, F. H. Li, B. Liu and E. D. Salin, *J. Anal. At. Spectrom.*, 1991, **6**, 457.
6. M. Burguera, J. L. Burguera and O. M. Alarcón, *Anal. Chim. Acta*, 1986, **179**, 351.
7. M. Burguera, J. L. Burguera and O. M. Alarcón, *Anal. Chim. Acta*, 1988, **214**, 421.
8. V. Carbonell, M. de la Guardia, A. Salvador, J. L. Burguera and M. Burguera, *Anal. Chim. Acta*, 1990, **238**, 417.
9. S. J. Haswell and D. Barclay, *Analyst*, 1992, **117**, 117.
10. V. Carbonell, A. Morales-Rubio, A. Salvador, M. de la Guardia and J. L. Burguera, *J. Anal. At. Spectrom.*, 1992, **7**, 1085.
11. B. Welz, D. L. Tsalev and M. Sperling, *Anal. Chim. Acta*, 1992, **261**, 91.
12. D. L. Tsalev, M. Sperling and B. Welz, *Analyst*, 1992, **117**, 1729.

13. D. L. Tsalev, M. Sperling and B. Welz, *Analyst*, 1992, **117**, 1735.
14. X.-c. Le, W. R. Cullen and K. J. Reimer, *Appl. Organomet. Chem.*, 1992, **6**, 161.
15. B. Welz and P. Stauss, *Spectrochim. Acta*, Part B, 1993, **48**, 951.
16. B. Welz and M. Sucmanova, *Analyst*, (accepted).
17. M. Sperling, X.-f. Yin and B. Welz, *Spectrochim. Acta*, Part B, 1991, **46**, 1789.
18. G. D. Marshall and J. F. van Staden, *J. Anal. At. Spectrom.*, 1990, **5**, 681.
19. J. F. Tyson, S. G. Offley, N. J. Seare, H. A. B. Kibble and C. S. Fellows, *J. Anal. At. Spectrom.*, 1992, **7**, 315.
20. I. D. Brindle, H. Alarabi, S. Karshman, X.-c. Le, S. Zheng and H. Chen, *Analyst*, 1992, **117**, 407.
21. B. Welz and M. Schubert-Jacobs, *At. Spectrosc.*, 1991, **12**, 91.
22. H. Chen, I. D. Brindle and X.-c. Le, *Anal. Chem.*, 1992, **64**, 667.
23. Z. Fang, *Microchem. J.*, 1992, **45**, 137.

Talanta, Vol. 40, No. 12, pp. 1927–1936, 1993
Printed in Great Britain.

0039-9140/93 $6.00 + 0.00

ON-LINE MICROWAVE SAMPLE PRETREATMENT FOR THE DETERMINATION OF MERCURY IN BLOOD BY FLOW INJECTION COLD VAPOR ATOMIC ABSORPTION SPECTROMETRY

TIEZHENG GUO and JÖRN BAASNER

Atomic Absorption Product Department, Bodenseewerk Perkin-Elmer GmbH Postfach 101164 W-7770 Überlingen, Germany

(*Received* 1 *June* 1993)

Summary—A method for on-line treatment of whole blood in a microwave oven and determination of mercury by flow injection cold vapor atomic absorption spectrometry was developed. After dilution of the whole blood and addition of oxidant, all further treatment and measurement were performed automatically, on-line. Recoveries of five mercury compounds were complete. Good agreement between measured and recommended values of mercury in whole blood reference materials was obtained. Measured mercury values also agreed with results from other accepted methods. Sample throughput was about 45 measurements/hr. Detection limit (3s) in diluted sample was 0.1 μg/l corresponding to 1 μg/l Hg in whole blood. The RSD value at 0.5 μg/l Hg in the diluted sample was 6–7% (11 measurements and 0.5 ml sample volume). Mercury concentrations between 1 and 150 μg/l in whole blood can be measured using this method. For three replicate measurements, 0.5 ml of whole blood is required.

It is generally agreed that oxidative conversion of all forms of mercury in environmental, biological samples to Hg(II) is necessary prior to reduction to elemental Hg,[1–5] especially when tin(II)chloride is used as the reductant. $NaBH_4$ can more readily attack those organic mercury compounds that are not reduced to Hg(II) by tin(II) chloride.[6] Some workers report that $NaBH_4$ does not reduce all organic mercury compounds to elemental mercury equally.[5] During this work and previous work,[7] decomposition of organic mercury compounds in urine and blood samples was not complete when using $NaBH_4$ as the reductant in a normal flow injection setup. This was thought to be due to the low $NaBH_4$ concentration and short reaction time used.

A bewildering variety of combinations of strong acids (HCl, H_2SO_4, HNO_3), oxidants (H_2O_2, $KMnO_4$, $K_2Cr_2O_7$, $K_2S_2O_8$), UV irradiation, and elevated temperatures have been used and recommended[1–5,8–13] for off-line digestion. However, on-line sample pretreatment is of particular interest in mercury determination because of the well known problems associated with the mobility of this element, the risk of contamination, and volatilization and adsorption losses, *etc.* during extensive off-line sample pretreatment procedures. These problems become more important at the low concentrations now being measured.

Now a very wide variety of different on-line manipulations of samples and standards have been carried out by FI techniques providing a safe, contamination-free enclosed sample handling system, this has been reviewed by Tyson.[14]

Recently, a system for on-line treatment of liquid samples in a microwave oven and determination of mercury by cold-vapor atomic absorption spectrometry was designed and evaluated.[15] Mercury in water and urine was measured.

In the present work, the possibility for on-line treatment of whole blood in a microwave oven and determination of mercury by cold vapor FI atomic absorption spectrometry was investigated. In this work, a digestion coil in a knitted (or so called three-dimension reactor) form was used which reduced the dispersion drastically. A cooling coil after the microwave oven allowed the system to work properly at higher microwave energy and improved the reproducibility. Further decomposition of organic mercury compounds in blood was achieved by adding a channel for on-line addition of $KMnO_4$.

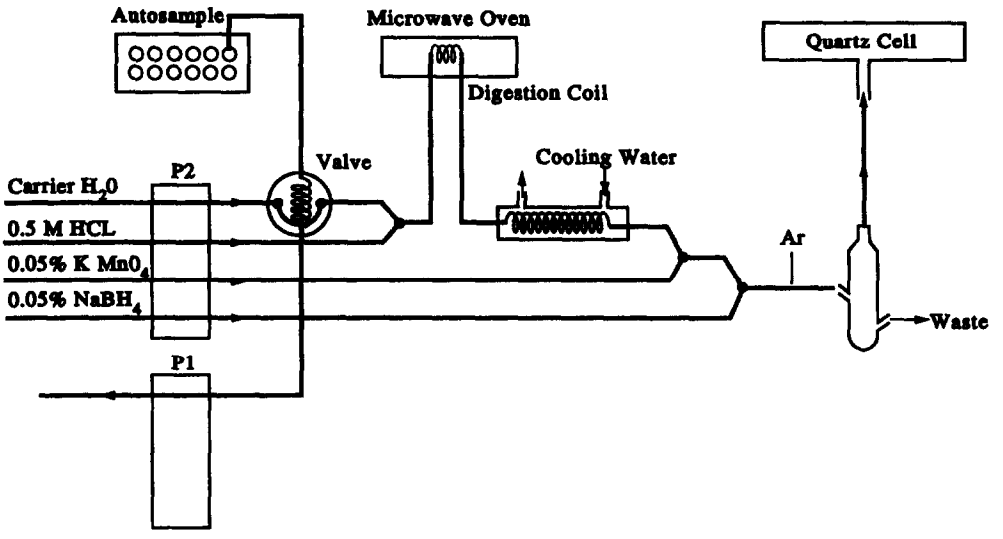

Fig. 1. Instrumental setup.

EXPERIMENTAL

Blood samples were first diluted by a factor of 10 with Triton-X 100 in water, and oxidation reagent added. Subsequent treatment and measurement proceeded automatically in a FI system. Figure 1 shows the FI-manifold and the working principle.

Diluted whole blood sample containing oxidation reagent is injected into the carrier stream (in this work H_2O is used as the carrier) via the FI valve. The carrier stream is then mixed with acid in the manifold, and the mixture flows through the digestion coil located inside the microwave oven and is heated by microwave energy. On leaving the microwave oven the heated mixture cools in the cooling coil and is then mixed with $KMnO_4$ solution. $NaBH_4$ is added to the mixture and Hg(II) is reduced to Hg(0). Argon is added as the carrier gas. In the gas–liquid separator, the gas phase (argon, generated hydrogen and mercury vapor) separates and flows into the quartz cell while the liquid phase drains to waste. In the quartz cell, the generated mercury vapor is measured by the spectrometer.

Instrumentation

Perkin-Elmer Models 2100, 3100 and 4100 atomic absorption spectrometers, FIAS-200, and FIAS-400 flow-injection systems and an AS-90 autosampler were used during this study. A Maxidigest MX 350 microwave station, with TX 31 Maxidigest programmer, (Prolabo, Paris) was used. Later the microwave oven was controlled by the spectrometer's software. The whole system was controlled by an Epson personal computer.

A Perkin-Elmer Hg EDL (system II) operated at 190 mA was used as the primary light source, the measurement wavelength was set to 253.6 nm, with a slit width of 0.7 nm (low). An integration time of 30 sec and peak height measurement mode were used. The temperature of the quartz cuvette was 200°.

The digestion coil was made in a knitted form. A 10 m long PFA tube (i.d. 0.9 mm, wall thickness 0.4 mm) was knitted around a PTFE backbone tube (i.d. 2 mm, wall thickness 1 mm) in the form depicted in Fig. 2. This method was adopted from Ref. 17. The backbone tube with the knitted coil was then folded again into a shape which fitted within the microwave oven cavity.

The cooling coil was placed between the digestion coil and the manifold. The cooling coil was made from PFA tube (i.d. 0.9 mm, 1.5 m long) in a knitted form in order to reduce dispersion. This coil was sealed inside a plastic tube 16 cm long, i.d. 2 cm through which cooling water was circulated using one of the FIAS pumps. The pump tubes used and the associated flow rates are listed in Table 1. The argon flow rate was 90 ml/min.

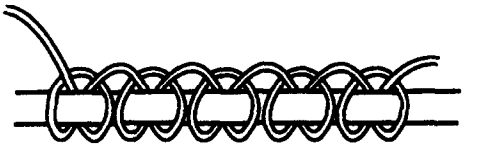

Fig. 2. Construction of the knitted digestion coil.

Table 1. Pump tubes and corresponding flow rates

Solution	Pump tube (Color code)	Flow rate (*ml/min*)
Sample	blue–yellow	9–10
Carrier	blue–yellow	9–10
$NaBH_4$	red–red	5–6
Acid	red–red	5–6
$KMnO_4$	red–red	5–6
Cooling	black–white	32
Waste	violet–violet (two tubes)	36

Sample coil 500 µl. The connecting tubes used between confluence points in the manifold were of 110 mm, 300 mm length with 1 mm i.d. The tube between the gas–liquid separator and the quartz cell was of 1 m long with an i.d. of 1 mm. Details refer to Fig. 1.

The gas–liquid separator used was a commercially available one made of glass from Perkin-Elmer.

A Perkin-Elmer MHS-20 system with amalgamation accessory was also used to measure Hg in blood to check the method developed in this work.

Autoclave-3 and PTFE vessels were used for off-line digestion of blood samples.

Reagents

All reagents were of analytical-reagent grade, unless stated otherwise. Double deionized water (18 MΩ/cm) was used throughout.

Dow Corning DB 110A: Silicon anti foaming agent for FIAS/MHS analyses.

Reductant solution: 0.05% m/v $NaBH_4$ in 0.05% m/v NaOH, 1.5 ml of anti foam reagent (Dow Corning) was added to 1 l of $NaBH_4$ solution.

Carrier solution: Deionized water,

Acid solution: 0.5 *M* HCl (50 ml 32% m/v HCl in 1 l deionized water),

Oxidation reagent: 2 g KBr and 0.56 g $KBrO_3$ dissolved in 25 ml deionized water. 0.5 g $KMnO_4$ dissolved in 1 l water (0.05% $KMnO_4$).

Triton solution: 0.6 g Triton X-100 (Triton® X-100: Merck for scintillation grade) dissolved in 50 ml deionized water.

Calibration standards. Stock standard solution of mercury, 1000 mg/l, was prepared from Merck "Titrisol®". Stock solution: 10 mg/l was prepared by dilution of the stock standard solution.

Working standard solutions of 100 µl and 500 µg/l were prepared by further dilution of the stock solution.

All the diluted mercury standard solutions should contain 1% v/v stabilizer solution (0.5% m/v $K_2Cr_2O_7$ in 1 + 1 HNO_3) in order to ensure stability during storage.

The addition calibration method was used. Calibration solutions at different mercury levels were prepared by spiking blood samples with appropriate amounts of mercury standard solution.

In this work, bovine whole blood, human whole blood and concentrated blood for transfusion were used.

Samples and reference materials

Five mercury compounds were used for the recovery test. The compounds, the suppliers, and information about stock solution preparation[5] are listed in Table 2.

Sterile bovine whole blood, and human whole blood from hospitals were used for the recovery studies. Some freshly collected samples of human whole blood were measured by this method and also by two other methods.

Lyophilized human reference whole blood samples were used to check the method, refer to Table 4. Seronorm® Trace Elements Whole

Table 2. Mercury compounds used and their solvents

Compound	Formula	Supplier	Solvent*
Methylmercury chloride (MMC)	CH_3HgCl	Merck	10 *ml* CH_3OH
Mercury (II) acetate (MA)	$Hg(CH_3OO)_2$	Merck	20 *ml* CH_3OH 5 *ml* CH_3COOH
Mercurescein sodium (MS)	$C_{20}H_8Br_2HgNa_2O_6$	Riedel-de Haen	10 *ml* CH_3OH
Phenylmercury chloride (PMC)	C_6H_5HgCl	Riedel-de Haen	0.2 *ml* Diisobutyl Ketone†
Mercury (II) nitrate (MN)	$Hg(NO_3)_2$	Merck	Standard solution

*Dilute to 1 l with deionized water.
†Dilute to 1 l with CH_3OH.

Table 3. Recoveries of various mercury species spiked into bovine whole blood and human whole blood

Added compound	Recoveries %* In bovine blood	In human blood
CH_3HgCl (MMC)	96 ± 6 ($n = 23$)	99 ± 3 ($n = 6$)
$Hg(CH_3COO)_2$ (MA)	99 ± 5 ($n = 15$)	99 ± 3 ($n = 6$)
$C_{20}H_8Br_2HgNa_2O_6$ (MS)	100 ± 8 ($n = 23$)	97 ± 8 ($n = 6$)
C_6H_5HgCl (PMC)	96 ± 6 ($n = 26$)	99 ± 5 ($n = 6$)

*The recovery is the mean of n measurements $\pm$ SD.

Blood from Nycomed Diagnostics, Oslo. Kontrollblut für Metalle 2, Lot No. 620401 from Behring Institute, Marburg.

PROCEDURE

Method development

For the method development the following parameters were considered and each was tested at the given values.

The main criteria applied to select a parameter was that it could provide good results for the recovery test and for the sample measurement. The concentration of each reagent used was as low as possible.

The amount of Triton added to the sample solution in 10 ml: 0.5 ml, 1.0 ml, 1.5 ml and 2.0 ml.

Table 4. Results of mercury measurements on control blood samples

Samples	Measured value $\mu g/l$	Rec. value $\mu g/l$
Seronorm® No. 905	9.5 ± 0.8 ($n = 6$)	10 (0.49)*
Seronorm® No. 906	15 ± 0.8 ($n = 7$)	15 (1.1)*
Seronorm® No. 010010	4.1 ± 0.6 ($n = 5$)	4.2 (3.3–5.1)†
Seronorm® No. 010011	4.2 ± 0.2 ($n = 5$)	5.0 (4.1–5.8)†
Seronorm® No. 010012	4.5 ± 0.3 ($n = 6$)	4.9 (4.1–5.2)†
Seronorm® No. 205052	3.9 ± 0.2 ($n = 6$)	5‡
Seronorm® No. 203056	10.1 ± 0.4 ($n = 6$)	10‡
Kontrollblut No. 62 0401	103 ± 2 ($n = 3$)	90.2 81.9–98.5)§

*SD of mean.
†Recommended value range.
‡Approximate value without recommended range.
§Confidence range.
‖The text is cited from manufacturer's instructions. The measured value is the mean of n measurments $\pm$ SD.

The amount of antifoam reagent added to the reductant solution in 1 l volume: 0.2 ml, 0.4 ml, 0.8 ml, 1.0 ml, 1.5 ml and 2.0 ml. Acids used for on-line addition: HNO_3: 1 mol/l, 2 mol/l, 3 mol/l, 4 mol/l and 5 mol/l.

HCl: 0.5 mol/l, 1 mol/l, 2 mol/l, 3 mol/l and 5 mol/l. Mixed acids: 0.3 mol/l HCl + 0.4 mol/l HNO_3, 0.5 mol/l HCl + 0.6 mol/l HNO_3, 1 mol/l HCl + 1.2 mol/l HNO_3, 2 mol/l HCl + 2.4 mol/l HNO_3, 0.1 mol/l $HClO_4$ + 0.4 mol/l HNO_3.

Oxidation reagents. Bromate–bromide added to 10 ml diluted sample solutions: 0.2 ml, 0.4 ml, 0.6 ml, 0.8 ml, 1.0 ml, 1.2 ml and 1.5 ml.

$K_2S_2O_8$(4%) added to 10 ml sample: 1.0 ml, 2.0 ml and 4.0 ml. $KMnO_4$ for on-line addition: 0.025%, 0.05% and 0.1% m/v. $NaBH_4$ concentration: 0.02%, 0.05%, 0.07%, 0.08% and 0.10% m/v. Carrier solution: H_2O, 0.1 mol/l HCl, 1 mol/l HCl, 0.5 mol/l HCl + 0.6 mol/l HNO_3, 0.25 mol/l HCl + 0.3 mol/l HNO_3. Sample coils: 0.5 ml, 1.0 ml. Digestion coil: 10 m long made from PFA 0.9 mm i.d. in three-dimensional form or wounded on a PTFE shaft (280 × 38 × 15 mm). Cooling coil: 1.5 m, 2.0 m long PFA tube, i.d. 0.9 mm. Microwave heating power: 20%, 30%, 40% and 50%.

Sample preparation

To a 10 ml plastic test tube (Manufacture SARSTEDT) add 0.5 ml Triton solution, 0.5 ml blood sample and dilute the mixture to 5 ml with water. Then add 0.6 ml oxidation reagent solution mix well and load onto the autosampler.

Calibration solutions

Into the test tube, add 0.5 ml Triton and 0.5 ml blood. To avoid coagulation, it is recommended to dilute the blood to about 4 ml, before adding the acidic Hg working standard solution, and then dilute the content in the test tube to 5 ml and add the oxidation reagent solution.

Less bromate–bromide solution should be added to the calibration blank to avoid high background and depression of sample signals (see Discussion). In this work, 0.2 ml oxidation reagent was added to blank.

Setting up the flow injection microwave digestion system

The microwave system needs about 3 min to warm up. Run the system with the microwave oven on at the specified power level for the measurement for a few minutes before starting

measurements. In this work 20% energy level of the microwave oven was used. Make certain that $KMnO_4$ never flows through the system unless $NaBH_4$ is also flowing.[7]

Recovery test

Four organomercury species and one inorganic mercury compound were used in this work (see Table 2).[5]

For the recovery tests, both bovine blood and human blood samples were used. Mercury compounds were spiked into 1:10 diluted blood solutions. 10 ml of these diluted solutions contained 0.7 ml bromate–bromide reagent. The concentrations of the spiked mercury maintained at the level of 10 μg Hg/l. The microwave power applied was 20%. As a comparison, the recoveries test of the same samples were also measured with the microwave oven off while keep all the setup unchanged.

Digestion with autoclave. One millilitre whole blood and 2 ml 1 + 1 diluted HNO_3 were added to the PTFE vessel inside the Autoclave. The autoclave was then heated at 150° for 45 min. After cooling, the digested mixture was diluted to 10 ml and mercury was measured using normal FI CVAAS.

Using MHS-20

The method developed by Schierling and Schaller,[16] was adopted.

Maintenance of the system

It is suggested that after every day's measurements the system be cleaned by pumping 1:1 HNO_3 through both the carrier channel and the acid channel for a few minutes with the microwave oven on. Rinse the system by pumping water through it. A slight precipitation may occur in the manifold at the point where the sample and acid stream merge. This can be removed by adding a few drops of concentrated HNO_3 to this place, and then rinsing with water.

RESULTS AND DISCUSSION

Results

The detection limit of this method calculated as 3 × SD is 0.1 μg/l Hg in 1 to 10 diluted whole blood. This corresponds to 1 μg/l Hg in blood.

The RSD of this method measured at 0.5 μg/l of mercury in diluted blood is between 6% and 7% (11 measurements).

Table 5. Mercury levels in whole blood determined by different methods

Sample No.*	Mercury content (μg/l) MW–FI	Autoclave	MHS-20
1	2.6 ± 0.3	2.2 ± 0.3	2.1 ± 0.4
2	2.4 ± 0.2	2.7 ± 0.9	1.1 ± 0.2
3	2.4 ± 0.2	2.2 ± 0.6	1.7 ± 0.3
4	4.9 ± 0.4	4.6 ± 0.2	3.7 ± 0.4

*The list of values are the means of three measurements ± SD. Samples were fresh human whole blood.

The recoveries of organic mercury compounds in spiked blood samples were between 96% and 100%: see Table 3.

Bovine whole blood, human whole blood and lyophilized human reference whole blood were measured in this work. The results of the reference whole blood are listed in Table 4. They are in good agreement with the recommended values.

With the method developed, no measurable background signal was obtained.

To compare the new method developed with other accepted methods whole blood samples were measured using the method described, and a method using the MHS-20, and autoclave off-line digestion followed by FI CVAAS. Comparable results were obtained by using this method and the autoclave off-line digestion method. Lower results were obtained using the MHS-20 without prior digestion of sample. The results are summarized in Table 5.

Knitted digestion coil

The decomposition of organic mercury compounds occurs mainly while the sample flows through the digestion coil in the microwave oven. The reaction in the digestion coil occurs at a slightly elevated pressure, caused by the high temperature and the long length of tubing used. A 10 m long digestion coil was used in order to allow a reasonable reaction time. However, such a long tube normally would cause substantial dispersion resulting in a decrease of peak height sensitivity and need longer integration time.

At first the digestion coil was wound on a PTFE shaft (280 × 38 × 15 mm) as described in Ref. 15. This arrangement resulted in a 4–6 fold reduction of the peak height sensitivity when a 0.5 ml sample loop was used, and about two-fold reduction with a 1 ml sample loop.[15]

Knitted or three-dimensional coils have been suggested and tested for postcolumn chromatography,[17,18] and have also been applied in

FI.[19,20,21] The sample dispersion in the axial direction is much less in a knitted coil than that in a straight tube of the same length and inner diameter.[22]

In order to reduce the dispersion but maintain the required reaction time while using a long tube, the digestion coil in the present work was made into a knitted form. This effectively reduces the axial dispersion. Figure 3 shows the signals of 10 μg/l Hg obtained with a digestion coil as used in Ref. 15 and with a three-dimensional form coil (with the same length and inner diameter).

Cooling coil

Without the cooling coil, the microwave power applied to the sample was limited to ensure that the sample solution was not heated above about 90°. At a higher microwave power, the sample solution will be heated to boiling point resulting in copious bubble formation, irregular flows, distorted peak shapes and impaired precision. Even at 90°, without a cooling coil, there are problems such as aerosol formation and vapor evolution due to the violent reaction between the heated sample, carrier and the reductant within the manifold and the gas–liquid separator. It is necessary to have a filter between the gas–liquid separator and the quartz cell to prevent aerosol droplets from entering the quartz cell or the amalgamation accessory. The filter has to be changed after every 2–3 hr of continuous operation.[15]

In order to be able to use a higher microwave power, for the decomposition of more complicated samples, while avoiding the problems mentioned above, it is necessary to cool the heated mixture before it merges with the reductant. This is especially important for the treatment of blood samples since they generate foam when reacting with $NaBH_4$. At elevated temperatures this reaction is more vigorous and the large amount of foam generated can enter the quartz cell interrupting the measurement.

A cooling coil was used in this work, which allowed the sample solution to be heated to boiling point or totally gasified. The reactions within the manifold and the gas–liquid separator then proceeded quietly.

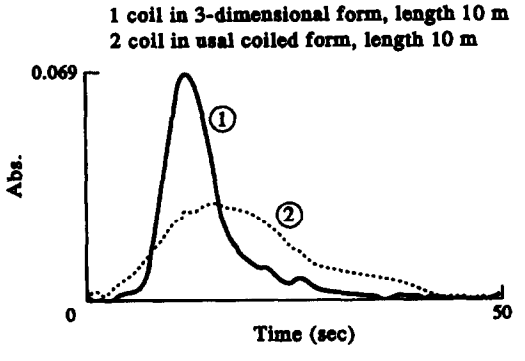

Fig. 3. Using the knitted coil can effectively reduce the dispersion of the sample. Signal 1: obtained with the knitted coil. Signal 2: obtained with the original coil. Both coils have the same length and inner diameter. Hg concentration: 10 μg/l.

Low concentration $NaBH_4$ and antifoam reagent reduce the generation of foam

One of the problems with the measurement of mercury in whole blood is the production of foam, especially when a higher concentration of $NaBH_4$ is used. The generated foam can enter the quartz cell and interrupt the measurement. Earlier work,[23] showed that the measurement of mercury by the cold vapor technique can be carried out at very low $NaBH_4$ concentration. However the addition of antifoam reagent was necessary even when low concentration $NaBH_4$ was used.

The addition of Triton X-100 to the samples can improve the fluidity of the sample solution and also helps reduce foam generation. The addition of antifoam reagent to the $NaBH_4$ solution and the addition of Triton to the sample solution had almost no effect on the sensitivity.

On-line addition of acid

With the method used here the decomposition reaction between organic mercurials and the oxidation reagent needs an acidic medium. However, blood normally coagulates when it is mixed with acid (in concentrated acid, *e.g.* 65% m/v HNO_3, a homogeneous solution can be obtained, but on dilution coagulation will reoccur). The situation is even worse when the acidified blood solution is heated. This is detrimental to the FI system because it will block the FI valve and tubing. During this work it was found that in a dilute acid solution, *e.g.* 0.5 mol/l HCl or less, coagulation could be delayed for quite a long time. However, when the sample solution contained both dilute acid and other chemicals, *e.g.* oxidation reagent, coagulation occurred more readily. If the diluted blood sample contained oxidation reagent only, it could stand for many hours, even up to one day without coagulation. In this work, the oxidation

reagent was added to the samples first, and acid solution added on-line just before the digestion in the microwave oven started. In this way the problem of coagulation of the blood sample on addition of acid was kept under control.

HCl and HNO_3 at different concentrations and their mixtures, and a mixture of HNO_3 and $HCLO_4$ were tested for on-line addition. The oxidation reagents in a suitably acid medium played the main role in the decomposition of organic mercury compounds. The type of acid used was not important. At higher acid concentrations, especially when HNO_3 was used, a deposit formed more easily inside the manifold at the confluence of sample and acid and on the wall of the tube connecting the manifold and the digestion coil. This affected the measurement and resulted in lower recoveries for certain organic mercury compounds. Using HCl at as low an acid concentration as possible is advisable and in this work, 0.5 mol/l HCl was used successfully.

Carrier solution

Deionized water, 0.1, 0.5, and 1.0 mol/l HCl, and a mixed acid of 0.5 mol/l HCl + 0.6 mol/l HNO_3 were used as carrier. When 0.5 mol/l HCl was used as the carrier, subsequent on-line addition of acid was omitted because the sample mixed with the carrier while flowing through the system. However it was found that when using acid as the carrier, even at a low concentration such as 0.1 mol/l HCl, precipitation of blood occurred on the inner wall of the sample loop, sample pump tube, and within the FI valve. With water as the carrier, even after a few weeks intensive measurements, the sample coil, the sample pump tube and the valve remained clean.

The use of $KMnO_4$ and bromate–bromide reagent together as the oxidizing reagent

Several oxidation reagents, including $K_2S_2O_8$, $KMnO_4$ and bromate–bromide reagent were used for the decomposition of organic mercurials. The combination of bromate–bromide reagent and $KMnO_4$ was effective for the decomposition of organic mercury compounds.

Potassium permanganate is known as a powerful oxidation reagent which can oxidize many organic mercurials. It is also known that there are problems associated with the use of $KMnO_4$ if it is added to water and urine samples long before the measurements are started. The most serious problem in this case originates from the adsorption of mercury onto hydrated manganese (IV) oxide which forms a film on the surface of sample vessels, tubing, and other system components.[15] Using FI and on-line addition, the above-mentioned problems associated with $KMnO_4$ can be effectively avoided while the advantage of using the powerful oxidizing property of $KMnO_4$ can be utilized.

At first, $KMnO_4$ was added on-line to the samples before they entered the microwave oven. However, it was found that the system was very easy blocked by the decomposition products produced during the heating process. Later $KMnO_4$ was added on-line to the sample stream after it left the microwave oven. The mixing coil used for the sample and $KMnO_4$ was 11 cm long. The concentration of $KMnO_4$ used should be in accordance with the concentration of the $NaBH_4$ solution. With a $NaBH_4$ reductant concentration of 0.05% m/v, a $KMnO_4$ concentration of 0.05% m/v was suitable.

Another advantage of using $KMnO_4$ is the enhancement of the Hg(II) signal when $KMnO_4$ was added on-line. This effect has been described in Ref. 7.

The use of bromate–bromide reagent was first proposed by Farey *et al.* for organic mercury measurement in natural water.[11,12,13] A bromate–bromide reagent in hydrochloric acid was used to generate bromine in the sample. Later it was also used by other workers for mercury measurement in water and urine with slight modifications.[7,15]

The use of bromate–bromide reagent and $KMnO_4$ together has been successful for the measurement of mercury in urine.[7] The combination has also been proved to be very effective for the measurement of total mercury in whole blood.

In the present work the bromate–bromide reagent was added off-line to the blood samples, the oxidation reaction between the sample and the reagent started only after they were mixed with acid. The mixture flowed through the digestion coil in the microwave oven and the decomposition reaction of organic mercury compounds was speeded up by the microwave heating.

The abilities of the bromate–bromide reagent and $KMnO_4$ to attack organic mercury compounds in blood both separately and together (without microwave heating) were studied. Data were collected under the following conditions: the microwave oven was off and the digestion coil was replaced by a short tubing (30 cm long

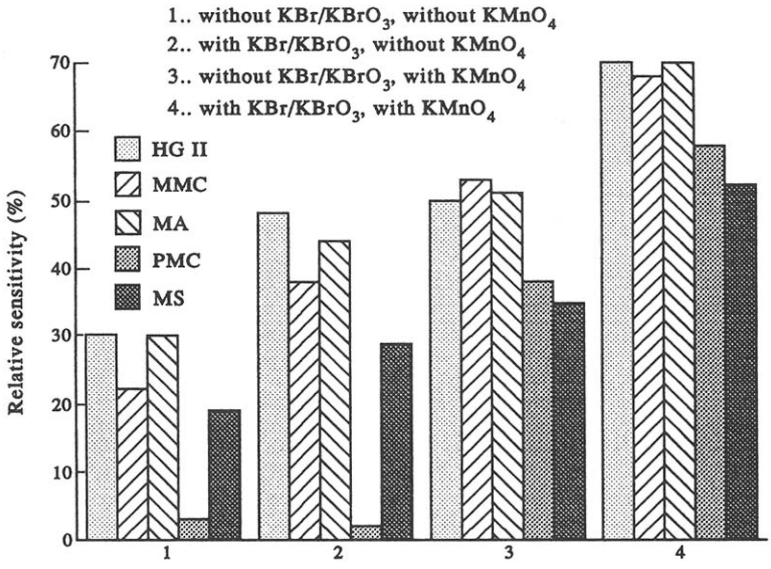

Fig. 4. The effects of using bromate–bromide reagent and $KMnO_4$ for the decomposition of organic mercurials. (1) Without bromate–bromide reagent and $KMnO_4$. (2) With bromate–bromide reagent only. (3) With $KMnO_4$ only. (4) With both bromate–bromide reagent and $KMnO_4$. 100% is value obtained with microwave heating and both oxidation reagents.

and 1 mm i.d.). The results are depicted in Fig. 4. A 100% signal represents the value obtained with microwave heating and both bromate–bromide reagent, and $KMnO_4$.

Recovery test and microwave heating

Most of the recovery test were performed in 1–10 diluted blood samples. Recovery tests of the above mentioned organic mercury compounds were also carried out in 1:5 diluted blood samples. However, 1:10 dilution of the whole blood sample for the measurement is recommended, since this ensures that the system remains clean when performing intensive measurements.

In the recovery test, the measured signals of the organic mercury compounds spiked into blood were compared with that of the inorganic mercury spiked into blood, rather than compared with aqueous standards. This is because, with microwave heating, the Hg(II) signals from blood and from aqueous solutions are not comparable. The heating effect of microwaves depends on the ionic conduction, dipole rotation and sample viscosity.[24] For this reason, the addition calibration technique was used in this work.

The measured signals of both organic and inorganic mercury compounds in blood were related to the amount of bromate–bromide reagent added. Ten millilitres of 1:10 diluted blood solution containing 0.7 ml bromate–bromide reagent was found to provide good recoveries. Less than 0.7 ml bromate–bromide reagent would result in lower recoveries. Further increasing the amount of bromate–bromide reagent did not increase the recoveries. For sample measurements, the amount of bromate–bromide used was higher than that used in this recovery test, see sample preparation part.

Energy levels between 20 and 50% of the microwave oven were used for the recovery test. At the 20% level the recoveries of the organic mercury compounds were already complete. Further increase the energy level did not increase the recoveries.

Without microwave heating, the recoveries of the mercury compounds only reached about 50–70% of the values obtained when microwave heating was applied, see Fig. 5.

The results of the recovery test are summarized in Table 3. The recoveries of organic mercury compounds spiked into blood were nearly complete.

The organic compounds used in this recovery test do not represent all of the organic mercury compounds existing in human blood. Some may not exist in blood, whereas other organic mercury compounds which exist in blood were not tested. The compounds: MA, PMC and MS were deliberately chosen for the test because it was known that they had very low recoveries, even in distilled water, and when using $NaBH_4$

as the reductant.[5] MMC is the major organic mercury compound existing in blood. It is reasonable to infer that when the recoveries of these compounds in blood are complete under the selected conditions, then other organic mercury compounds would give similar results. This has been shown by the measurement of whole blood reference materials using this method and by comparing this method with other established methods.

Calibration technique

The addition calibration technique was used in this work, because it is important to match the matrices of samples and standards. Different blood samples were used for the preparation of the addition calibration curve; these include: bovine whole blood, human whole bloods, and whole blood reference materials. An almost constant slope was found for all of these different blood samples. The statistics obtained from 14 calibration curves which were established with different blood samples and at different dates show: $Y = (0.0074 \pm 0.0005)X + C (n = 14)$. This shows that all of the calibration curves obtained were basically parallel to each other, which is in agreement with the observation in the batch system.[16]

The mercury standard solution contains a small amount of acid stabilizer. To avoid adding too much acid to the blood matrix when preparing the calibration solutions, it is important to choose a suitably concentrated Hg standard solution. Adding too much acid causes precipitation from the calibration solution during the measurement, which causes errors and may even block the system tubes.

For example, to prepare a calibration series to cover the concentration range of 1–20 μg/l, mercury in blood, we suggest using a standard solution of 100 μg/l Hg. For the highest calibration standard, 100 μl of this 100 μg/l Hg standard solution in a 5 ml final volume is required. The final concentration of HNO_3 in this solution is about 0.0011 mol/l, and this solution is stable for at least 8 hr.

As mentioned earlier less bromate–bromide solution should be added to the calibration blank. In this work, it was 0.2 ml. If the calibration blank solution contains more than this amount of bromate–bromide reagent, it will generate a background signal and depress the signals of subsequent measurements. This is because there is less matrix in the blank solution, the consumption of bromate–bromide reagent is low, and the generated molecular bromine from the excess reagent will result in background absorption.

The use of less oxidation reagents for the blank solution can cause error when the oxidation reagents, *i.e.* bromate–bromide, contain mercury. So attention should be paid to use mercury-free reagents. In this work, the used potassium bromate and potassium bromide were Merck product GR, and they provided good results.

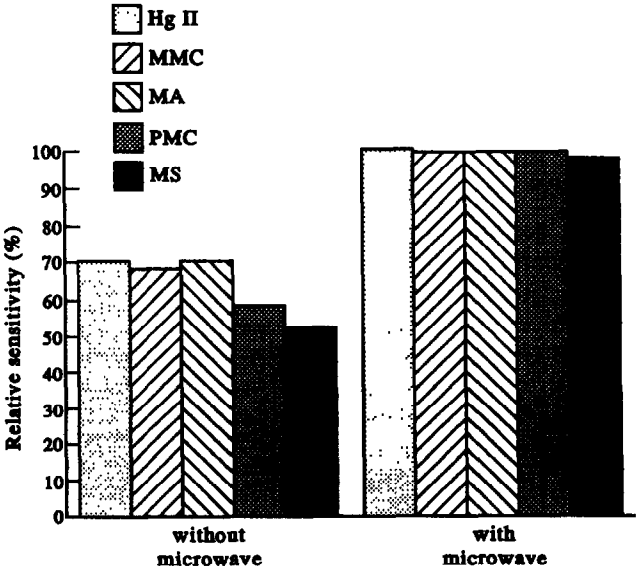

Fig. 5. The effect of microwave heating on the signals of mercury compounds.

Measurement of samples

Bovine whole blood, normal human whole blood and lyophilized human reference whole blood were measured in this work. The results of measurements on the blood reference materials are listed in Table 4. They are in agreement with the recommended values.

It is known that some compounds other than mercury can absorb at 253.7 nm and simulate higher mercury levels. Measurements in this work were made using both AA–BG mode and BG mode at 253.7 nm separately. No measurable background signal was observed.

Determination of mercury in whole blood by this method and some other methods

As a further check on the accuracy of the method developed, mercury in samples of freshly collected human whole blood was measured using this method, and using two other methods.

The methods used were: the method developed by Schierling and Schaller with MHS-20 batch system[16] and off-line digestion of whole blood in an autoclave and the subsequent measurement of mercury by flow injection CVAAS. The results are summarized in Table 5. Comparable results were obtained between the method developed in this work and the method of autoclave off-line digestion, lower results were obtained using MHS-20 batch system. This was thought probably to be due to no digestion prior measurements.

Using autoclave off-line digestion, background correction may be required since this method sometimes yields high background signals, especially when more HNO_3, *e.g.* 4 ml $1 + 1$ HNO_3 is used.

CONCLUSION

This work describes an accurate, fast and simple on-line microwave sample pretreatment procedure for the determination of mercury in blood by flow injection cold vapor atomic absorption spectrometry. The samples need only limited manipulation prior to automatic on-line treatment and measurement. With the present method, the risk of contamination, volatilization and adsorption losses are reduced drastically.

Another advantage of this method is the low sample consumption which is important for the measurement of samples such as human blood.

Acknowledgements—The authors would like to thank Mr Stephen Helliwell for his kind revision of this paper.

REFERENCES

1. L. Ping and P. K. Dasgupta, *Anal. Chem.*, 1989, **61**, 1230.
2. R. Ahmed, K. May and M. Stoeppler, *Fresenius'Z. Anal. Chem*, 1987, **326**, 510.
3. B. Welz, D. L. Tsalev and M. Sperling, *Anal. Chim. Acta*, 1992, **261**, 91.
4. H. W. Sinemus and H. H. Stabel, in B. Welz (Ed.), 5. CAS (Colloquium Atomspektrometrische Spurenanalytik), 1989, p. 711. Bodenseewerk Perkin-Elmer, Überlingen.
5. D. C. Baxter and W. Frech, *Anal. Chim. Acta*, 1990, **236**, 377.
6. B. Welz and Marianne Melcher, *At. Spectrosc.*, 1984, **5**, 2, 37.
7. T. Z. Guo and J. Baasner, Determination of mercury in urine by flow injection cold vapor atomic absorption spectrometry, *Anal. Chim. Acta.* 1993, **278**, 189.
8. H. Brandenberger and H. Bader, *At. Absorpt. Newsl.*, 1967, **6**, 101.
9. W. R. Hatch and W. L. Ott, *Anal. Chem.*, 1968, **40**, 2085.
10. United States Environmental Protection Agency (EPA), Mercury Method 245.1 p.1 (Manual Cold Vapor Technique), Issued 1974.
11. B. J. Farey, L. A. Nelson and M. G. Rolph, *Analyst*, 1978, **103**, 656.
12. B. J. Farey and L. A. Nelson, *Anal. Chem.*, 1978, **50**, 2147.
13. B. J. Farey and L. A. Nelson, *Atomic Absorption Spectrometry*. Elsevier, Amsterdam, 1982.
14. J. F. Tyson, *Spectrochim. Acta Rev.*, 1991, **14**, 169.
15. B. Welz, D. L. Tsalev and M. Sperling, *Anal. Chim. Acta*, 1992, **261**, 91.
16. J. Angerer and K. H. Schaller, *Analyses of Hazardous Substances in Biological Materials*, Volume 2, VCH Verlagssgesellschaft mbH, D-6940 Weinheim (Germany), 1988.
17. C. M. Selavka, K. S. Jiao and I. S. Krull, *Anal. Chem.*, 1987, **59**, 2221.
18. U. Neue, *Chromatographia*, 1982, **15**, 403.
19. J. Ruzicka and E. H. Hansen, *Anal. Chem. Acta.*, 1984, **161**, 1.
20. Z-L Fang and B. Welz, *J. Anal. At. Spectrom.*, 1989, **4**, 543.
21. Z-L Fang, T. Z. Guo and B. Welz, *Talanta*, 1991, **38**, 613.
22. B. Karlberg and G. E. Pacey, *Flow Injection Analysis*. Elsevier, Amsterdam, 1989.
23. F. Portala and T. Z. Guo, 6. CAS (Colloquium Atomspektrometrische Spurenanalytik), 1991, 349.
24. H. M. Kingston and L. B. Jassie, *Introduction to Microwave Sample Preparation: Theory and Practice*. American Chemical Society, Washington, DC, 1988.

Talanta, Vol. 40, No. 12, pp. 1937–1941, 1993
Printed in Great Britain.

0039-9140/93 $6.00 + 0.00

AUTOMATED TITRATIONS WITH AN ALTERNATE FLOW EXPONENTIAL SPEED VARIATION SYSTEM

CHAIM N. YARNITZKY, NAPHTHALI KLEIN and ORIT COHEN
Department of Chemistry, Technion, Israel Institute of Technology, Haifa, Israel 32000

(*Received* 25 *January* 1993. *Revised* 10 *May* 1993. *Accepted* 11 *May* 1993)

Summary—The alternate flow exponential speed variation system for automatic titrations is described. The system consists of two peristaltic pumps, two three-way valves, a mixing coil and a detector. Each determination consists of a twin cycle titration procedure. In the forward cycle, the sample and the reagent are propelled by the first and the second pump with the rotation speeds of the first and second pump decreasing and increasing with time, respectively. In the reverse cycle the solution inlets are switched so that the sample and the reagent are now propelled by the second and the first pump, respectively. This procedure allows the calculation of the accurate sample concentration without recourse to a precalibration step and, at the same time, eliminates the error caused by tubing deterioration. Results indicate accuracy better than 0.5%. Titration time and sample volume are of the order of 2 min and 2 ml, respectively.

Accurate titrations in analytical chemistry involve the addition of a reagent solution of known concentration to the analyte solution, usually by means of a burette. The equivalent point (*i.e.* the point at which the amount of added reactant is equivalent to the amount of analyte) is detected by an appropriate indicating system (visual chemical indicator, pH meter, conductometer, spectrophotometric detector, *etc.*).

Manual titrations are performed by adding small aliquots of the reagent solution, and monitoring visually, the status of the indicating system. In automatic titrations, a piston-driven burette and an indicating device connected to an electronic data processing unit are employed; the latter controls the rate of addition and volume of reagent solution dispensed up to the equivalence point. For S-shaped titration plots, the output of the indicating device, during the early stage of the titration, changes very slowly (in contrast to linear plots such as those pertaining to conductometric titrations); in the vicinity of the equivalent point the output of the indicating device varies very rapidly. Accordingly, the initial rapid rate of addition of reagent solution is significantly decreased near the equivalent point, to allow complete mixing of the reactants.

The overall time required for the titration is largely governed by the period of "slow reagent addition", and usually lasts 3–5 min. In addition, the fabrication of an accurate piston driven burette is extremely expensive and complicated when a small number of units are required. This is probably, the main reason for the numerous papers published describing various home-made, automated flow systems. In general, the flow rate of the sample is constant and the administration of the reagent is controlled by changing the reagent flow rate or its concentration. Gradient titration suggested by Fleet and Ho[1] and programmed coulometric titration[2] are typical examples. A more sophisticated approach was suggested by Valcarcel *et al.*[3] The rotation speeds of the two pumps were computer-controlled. In his recent papers[4,5] the flow rate of one pump was constant while the second one was changed in the range of 0–5 ml/min.

FIA titrations first proposed in 1977,[6] carried out with an unsegmented continuous flow single-channel gradient chamber system, are, by comparison, very fast (20–30 sec). Here, the reagent flow is of the order of 1 ml/min and the sample (100 μl) is injected into the flow, mixed in a 1 ml gradient chamber, and streamed on towards the detector. The mathematical relationship between the analyte concentration and the FIA curve (logarithmic scale) has been developed. The limited accuracy of the method is governed by flow rate stability, and by the measurement of time elapsed between two points on the FIA curve.

A common feature of all flow titrations employing peristaltic pumps has been the

deterioration of the tubing with time and temperature. This affects the flow rate and the accuracy of the titration. Frequent calibration is, therefore, necessary. This point was emphasized by Martinez-Calatayud *et al.*[7]

Variable sample and reagent flow rates were generated with high accuracy by mechanically driving two syringe pumps with two specifically profiled cams.[8] The pistons, however, are very similar to those employed in commercial systems. Stopped-flow titration[9] also requires accurate and complicated mechanical syringes.

The "alternate flow method" outlined below is based on a system which consists of two computer-controlled variable-speed peristaltic pumps and two three-way valves. As a rule, the rotation speed of the first pump decreases with time, while that of the second increases. Each determination consists of a twin-cycle procedure. In the forward cycle the sample and reagent are propelled by the first and the second pump, respectively. In the reverse cycle, the sample and the reagent are propelled by the second and the first pump, respectively. This operation is achieved by appropriately activating the three-way valves. The concentration of the sample is shown to be directly determinable with high accuracy; no pre-calibration is required. In addition, this procedure eliminates any errors due to the deteriorating of tubing. The sample volume is decreased considerably (1–2 ml) and the throughput is of the order of 20–40 samples/hr.

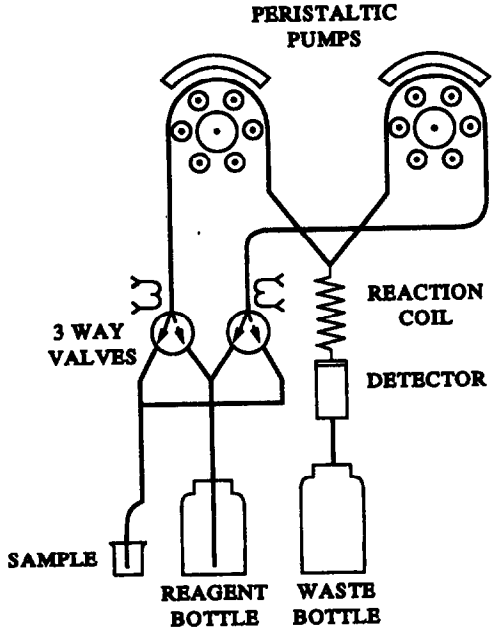

Fig. 1. Schematic diagram of the alternate flow system.

THEORY

The system (Fig. 1) consists of two peristaltic pumps with variable flow rates:

$$F_1 = Q_1 R_1; \quad F_2 = Q_2 R_2 \tag{1}$$

where F is the flow rate (ml/min); Q is the solution volume per revolution of the motor and R is the rotation speed (number of revolutions/min). The rotation speeds are monitored continously. At the beginning of the titration the sample is added at the highest rate by means of the first peristaltic pump; the reagent stream is added at the lowest rate by means of the second pump. The speeds of both pumps are gradually varied until the end point is reached (as shown by the indicating system). The relationship between the concentrations and flow rates at the equivalence point is as follows:

$$F_1 C_s = F_2 C_r \quad \text{or} \quad Q_1 R_1 C_s = Q_2 R_2 C_r \tag{2}$$

where C_s and C_r are the concentrations of the sample and the reagent, respectively. R_1 and R_2 are displayed very accurately (stepper motor technique).

Next, the three-way valves (Fig. 1) are activated and as a result, the first pump now causes the reagent to flow into the mixing coil while the second is connected to the sample bottle, and the titration is restarted. The second equivalence point is reached when

$$Q_1 R_3 C_r = Q_2 R_4 C_s \tag{3}$$

where the rotation speeds of the first and the second pumps are R_3 and R_4, respectively. Assuming that Q_1 and Q_2 remain constant during the short time required for the two titrations, we have:

$$C_s/C_r = \sqrt{R_3 R_2 / R_1 R_4}. \tag{4}$$

This result is totally independent of Q_1 and Q_2 and C_s may be calculated from the knowledge of C_r and the rotation speeds (R_1, R_2, R_3, R_4). This "alternate flow method" actually solves the problem caused by the ever-changing tubing.

The end point, however, registered by the data processing unit at the moment the mixed stream (at the stoichiometric ratio) passes through the detector flow cell, occurs at a certain delay with regards to the true equivalent

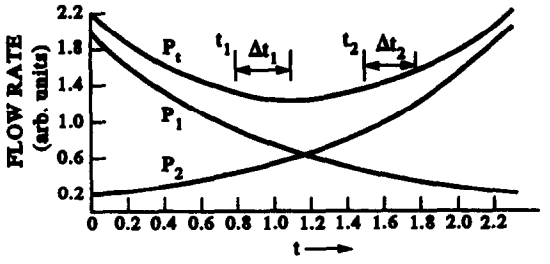

Fig. 2. The dependence of the individual and the total flow rates on time.

point. This delay originates from the flow-system configuration, in which mixing (mixing loop) and detection (flow-through detector) are necessarily spatially distinct. To minimize the "titration error" caused by this delay, the rate of change of the solution flow rates must also be minimized near the end point. Essentially, this brings up back to the main limitation (slow end-point approach) discussed above in connection with automatic titration systems.

The advanced "alternate flow exponential speed variation method" has been developed to provide an answer to the practical difficulties mentioned above.

The system remains the same (Fig. 1) except for the change of the rotation speeds $R_1(t)R_2(t)$ with time:

$$R_1 = R_0 e^{-kt}; \quad R_2 = \frac{A}{R_0} e^{kt} \tag{5}$$

where R_0, A, k, are experimentally chosen values (*e.g.* $R_0 = 200$ rev/min; $A = 4 \times 10^3$ rev^2/min^2; $k = 2$/min, $Q_1 = Q_2 = Q = 10 \pm 1$ $= \mu$l per revolution). The final rotation speed of the first pump is one-tenth of R_0 (regardless of the sample-reagent concentration ratio).

The dependence of the rotation speeds (or flow rates) and the total flow rate (at the mixing coil) on time are shown in Fig. 2. Let us assume that at a certain time, t_1, the equivalence point is reached, and the rotation speeds are R_1, A/R_1. As explained above the solution with the stoichiometry at the equivalence point will flow through the detector after a short delay caused by the mixing coil, Δt, equal (approximately) to:

$$\Delta t \equiv V_L(Q_1R_1 + Q_2R_2)^{-1} \tag{6}$$

where V_L is the volume of the mixing loop. The rotation speed readings, as displayed by the unit at the time $t_1 + \Delta t_1$ will be R_1^a and A/R_1^a, respectively. To correct for this inherent titration error, Δt_1 must be subtracted; and therefore, at the end point, these values must be multiplied by $e^{k\Delta t_1}$ and $e^{-k_1\Delta t_1}$, respectively.

Since

$$Q_1R_1C_s = Q_2\frac{A}{R_1}C_r \tag{7}$$

then

$$Q_1R_1^a e^{k\Delta t_1}C_s = Q_2\frac{A}{R_1^a}e^{-k\Delta t_1}C_r \tag{8}$$

where R_1^a is the actual reading at the time when the end point is sensed by the indicating system.

Analogously, for the second titration, after switching the pump inlets, the corrected values will be $R_2^a e^{k\Delta t_2}$ and $A/R_2^a \cdot e^{-k\Delta t_2}$, respectively.

$$Q_1R_2^a e^{k\Delta t_2}C_r = Q_2\frac{A}{R_2^a}e^{-k\Delta t_2}C_s. \tag{9}$$

After dividing equation (9) by (8), we obtain:

$$C_s = C_r\frac{R_2^a e^{k\Delta t_2}C_r}{R_1^a e^{k\Delta t_1}} = C_r\frac{R_2^a}{R_1^a}e^{k(\Delta t_2 - \Delta t_1)}. \tag{10}$$

Equation (10) shows that, provided Δt_2 and Δt_1 are calculated, the concentration of the sample can be derived directly from the actual readings of the rotation speeds displayed when the solution with the stoichiometry at the equivalent point flows through the detector.

To find Δt_1 and Δt_2, the total flow rate, which is a function of time, is integrated and compared to the volume of the mixing coil.

For the first titration:

$$V_L = Q_1R_0\int_{t_1}^{t_1+\Delta t} e^{-kt}\,dt + \frac{Q_2A}{R_0}\int_{t_1}^{t_1+\Delta t_1} e^{kt}\,dt \tag{11}$$

and for the second:

$$V_L = Q_1R_0\int_{t_2}^{t_2+\Delta t_2} e^{-kt}\,dt + \frac{Q_2A}{R_0}\int_{t_2}^{t_2+\Delta t_2} e^{kt}\,dt. \tag{12}$$

The difference in time $(\Delta t_2 - \Delta t_1)$ is a function of the mixing loop volume, the exponential constant k, and the concentration ratio C_s/C_r. For the conditions mentioned above and a mixing loop volume of $100 = \mu$l, the practical deviations ($e^{k(\Delta t_2 - \Delta t_1)}$) for 1:1, 1:2 and 1:4 concentration ratios are 0, 0.69 and 0.97%, respectively. The accurate concentration value is however easily determined by calculating the value of $e^{k(\Delta t_2 - \Delta t_1)}$. In principle, this approach should be useful for most titration systems, provided the appropriate detector is used. In the following, its application to an acid–base system, using a conductometric detector, is presented to demonstrate it.

EXPERIMENTAL

Instrumentation

Homemade peristaltic pumps driven by stepper motors were employed. The step angle was 1.8° and the holding torque was 53 *onze* inch. Pulses were generated by means of voltage-to-frequency converter. The exponential time dependent potential of the first pump was generated by a follower amplifier connected to a precharged capacitor. The capacitor was discharged after connecting a resistor in parallel to the capacitor. The follower was also connected to an analog divider (home made, pulse width modulation method, 0.05% accuracy). The output of the divider was connected to the voltage-to-frequency converter of the second pump. A simple flow through conductivity cell with a fast response served as detector. Glass electrodes cannot be used, since they respond sluggishly to pH changes and their response rate also depends on the direction of the titration (acid–base or base–acid). Other pH sensitive electrodes like antimony–antimonyoxide, mercury wetter platinum or silver electrodes may be used instead. Some experiments were carried out with homemade spectrophotometric detectors.

Reagents

All solutions were prepared from analytical-grade reagents and triple distilled water. Solutions were calibrated using common analytical procedures.

RESULTS AND DISCUSSION

Figure 3 shows the effect of the constant k on the display. Conductometric titration curves of

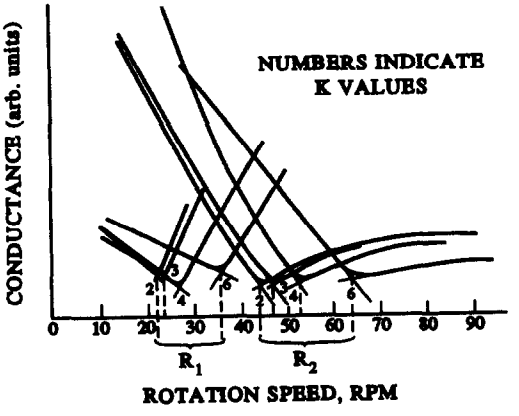

Fig. 3. Titration curves for 0.1*M* HCl titrated with 0.05*M* NaOH at different decay constant (k) values. Conductivity detector.

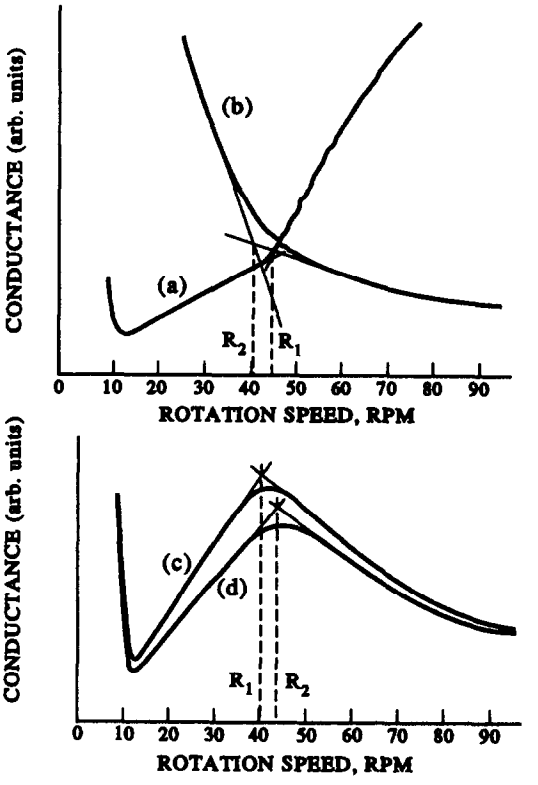

Fig. 4. Titration curves for 0.1*M* AcOH titrated with 0.1*M* NaOH (a,b) and 0.1*M* NH_4OH (c,d). Conductivity detector, $k = 2$ min^{-1}.

0.100*M* HCl with 0.0500*M* NaOH (resembling manual titrations) are displayed according to the procedure described. Each experiment involves two titrations (with the same k value). The expected value of the ratio of the rotation speeds at the extrapolated end points of each pair of titrations is 2.00. For low k values, the theoretical and practical deviations caused by the mixing coil are, indeed, small (less than 0.5%). For k values of 4 and 6, the deviations are 2.5 and 10%, respectively.

Figure 4 shows the titration curves recorded when a sample of acetic acid (~0.1*M*) was titrated with 0.1*M* NaOH and 0.1*M* NH_4OH, respectively. In the first titration with NaOH (curve a) the flow rate of the sample (acetic acid) decreases with time; the solution flowing through the detector at the beginning of the titration is thus virtually acetic acid plus a small amount of sodium acetate and the conductivity, therefore, low. During the course of the titration, the flow rate of the base increases with a concomitant increase of conductivity. After the end point, a sharp increase in conductivity mirrors the increased flow rate of the hydroxide. In the second titration (curve b) at the

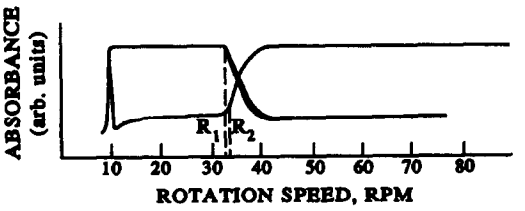

Fig. 5. Titration curves of 0.01*M* HCl titrated with 0.01*M* NaOH. Spectrophotometric detector, $k = 2$ min^{-1}.

beginning, both the flow rate of the reagent (hydroxide), and the conductivity, are high. As a result of the increasing flow rate of the sample (acetic acid) and the decreasing reagent flow rate, a sharp decrease of the conductivity occurs. Beyond the end point, the change of conductivity with the flow rate is relatively small.

The shape of the titration curves obtained for the acetic acid–ammonium hydroxide system are the same for the forward and reverse cycle (curves c, d); at the beginning and sufficiently beyond the end point of each titration, the solutions flowing through the conductivity cell contain either acetic acid or ammonium hydroxide (both mainly undissociated species) and a small amount of ammonium acetate, and, therefore, the conductivity of the solution is low. In contrast, at the end point, due to the presence of highly dissociated ammonium acetate, the conductivity is high.

A spectrophotometric detector in conjunction with an acid–base indicator has also been employed (Fig. 5). The S-shaped photometric titration curves, obtained in the forward and reverse cycles, are mirror images. The accuracy of the determination depends on the steepness of the S-shaped curve, which, obviously is the result of the correct choice of the wavelength.

The titration of up to 60 samples/hr should be feasible with a completely computerized system. The software should:

(a) command the autosampler to introduce a new sample;
(b) activate both pumps at the highest rotation speed to start up the system by filling the tubing;
(c) start programming the speed as detailed above, and monitor the output of the detector;
(d) activate the solenoid valves and repeat step (b);
(e) repeat step (c) (second titration);
(f) calculate the concentration of the sample, on the basis of the data collected in steps (c) and (e) above.

CONCLUSIONS AND FUTURE DEVELOPMENT

The reproducibility of all experiments is excellent and is in accordance with the theory. The error encountered when fast exponential time decay experiments are performed, can be correct to yield $<0.5\%$ analytical error. The titration time can be reduced to less than 1 min.

The operation of the new system in conjunction with potentiometric detectors (redox, silver) is now under inspection. The determination of the number of ligands in a metal complex has been carried out and will be reported later. The feasibility of using the system for Karl–Fisher titrations has also been considered.

Acknowledgement—This research was supported by the fund for the promotion of research at the Technion Israel Institute of Technology, Haifa.

REFERENCES

1. B. Fleet and A. Y. W. Ho, *Anal. Chem.*, 1974, **46**, 9.
2. G. Nagy, K. Tóth and E. Pungor, *Anal. Chem.*, 1975, **47**, 1460.
3. M. Agudo, T. Marcos, A. Rios and M. Valcarcel, *Anal. Chim. Acta*, 1990, **239**, 211.
4. J. Marcos, A. Rios and M. Valcarcel, *Anal. Chim. Acta*, 1992, **262**, 489.
5. *Ibid.*, 495.
6. J. Růžička, E. H. Hansen and H. Mosboek, *Anal. Chim. Acta*, 1977, **92**, 235.
7. T. Martinez-Calatayud, P. Campins Falco and R. Mico Albert, *Analyst*, 1987, **112**, 2109.
8. D. P. Arnold, R. M. Peachy, J. D. Petty and D. R. Sweatman, *Anal. Chem.*, 1989, **61**, 2109.
9. A. C. Javier, S. R. Crouch and H. V. Malmstadt, *Anal. Chem.*, 1969, **41**, 239.

Talanta, Vol. 40, No. 12, pp. 1943–1950, 1993
Printed in Great Britain.

0039-9140/93 $6.00 + 0.00

USE OF SEQUENTIAL INJECTION TECHNIQUE AND ROBOTICS FOR THE AUTOMATION OF rhFXIII FLUOROMETRIC ACTIVITY ASSAY. CASE STUDY

MIGUEL GUZMAN
3M Pharmaceuticals, 3M Center Bldg. 270-4S-02, St. Paul, MN 55144-1000, U.S.A.

BRUCE J. COMPTON
ZymoGenetics, Inc., 4225 Roosevelt Way NE, Seattle, WA 98105, U.S.A.

(*Received* 22 *February* 1993. *Revised* 5 *April* 1993. *Accepted* 6 *April* 1993)

Summary—This paper evaluates the feasibility of two systems—the Sequential Injection (SI) analyzer and the Zymark Benchmate (ZB) robot—for the automation of a recombinant human Factor Thirteen (rhFXIII) fluorometric assay. The goal was to develop a routine analytical procedure suitable for the quality control lab environment. The experimental efforts focused on monitoring of the product formation for the condensation reaction between monodansyl cadaverin and dimethyl casein. The acquired kinetic data demonstrated that both systems are capable of automating the solution handling operations associated with the assay. Using a method developed with the SI system, samples containing 0–410 μg/ml of rhFXIII were analyzed, with a throughput of one sample per 8 min, and a total solution consumption of 0.8 ml. The relative standard deviation for 10 injections of 100 μg/ml rhFXIII sample was 0.91%. With the ZB robot, samples containing 0–2500 μg/ml of rhFXIII were analyzed, and the linear response was obtained for a concentration range between 0 and 1250 μg/ml of rhFXIII. The method had a sample throughput of one sample per 11 min and a total solution consumption of 6.3 ml for each analysis. Due to its commercial availability, the ZB system was preferred over the experimental SI system for the purpose of routine automated analysis of a large number of samples in the quality control lab environment.

Flow injection analysis (FIA) and robotics are two versatile techniques used for the automation of analytical procedures.[1] Although the two techniques provide means for automating a variety of sample handling and sample pretreatment operations, they exhibit fundamentally different working principles and, as such, provide different sets of rules which must be followed during the method development. Sequential injection analysis (SIA), which was introduced 3 years ago as the latest branch of FIA, [2] is like FIA, based on principles of controlled dispersion and reproducible sample handling. Liquid samples are delivered to the various pretreatment and detection sites in micro channels using pumps and valves. On the other hand, robots, such as the Zymark Benchmate (ZB), rely strictly on reproducible sample handling. Typically, samples are transported to a specific pretreatment station in sample vials grabbed by a moving arm. Samples analyzed by robots are treated as discrete entities and, therefore, the analyte concentration through the sample bolus remains constant, while samples analyzed by the FIA technique are treated as a continuum, which leads to the formation of an analyte concentration gradient.

Since FIA and robotics have different working concepts, it is no surprise that certain operations can be performed only by one of the two techniques, while the other offers only an inferior alternative. For example, in FIA, optosensing and gas diffusion techniques, which have not been attempted with robotics, represent unique and highly effective strategies for selectivity and sensitivity enhancement.[3] Robots, on the other hand, have the ability to automate sample handling of solids and aerosols, which are tasks not suitable for FIA.

Although these examples indicate a certain complementary role of the two techniques, a number of operations, such as dilutions, filtrations, liquid–liquid extractions, sorbent extractions or addition of multiple reagents, were previously automated by both the FIA and the robotics approaches.[3,4] Despite this, there are no references in the literature which describe a direct comparison of the two techniques.

The rhFXIII assay represents an application which involves sample handling and sample

pretreatment operations previously automated by both techniques. As described in a preceding paper, [5] the assay consists of two subsequent reactions. First, the inactive form of rhFXIII is activated by thrombin in the presence of calcium ions and UV radiation. Second, the activated rhFXIII acts as a catalyst for the condensation reaction between monodansyl cadaverin and *N*, *N*-dimethyl casein, which form a fluorescing product. The first order kinetics of the second reaction exhibit a linear relationship between the concentration of the active rhFXIII and the rate of product formation. Thus, monitoring either the product concentration at given reaction times or the slope of the kinetic curve over a given time range provides information for predictions of the active rhFXIII concentration in the sample. The concentration value is used for approximating the activity of rhFXIII in analyzed samples.

This paper describes the application of two analysis automation tools, the sequential injection (SI) technique and the ZB robot, to the rhFXIII assay. In addition to depicting the two options for the assay automation, the experimental work illustrates some of the similarities and differences between the SIA and robot concepts.

EXPERIMENTAL

Chemicals

The concentration of standard rhFXIII solutions ranged from 0 to 2500μg/ml. The protein is currently under evaluation for replacement therapy in FXIII-deficient individuals. It is produced by ZymoGenetics, Inc., Seattle, WA. Additional solutions included 0.05*M* bicine buffer at pH 10, which was used as a carrier, a bicine cocktail solution containing 0.05*M* bicine, 7 m*M* calcium chloride and 0.16 m*M* monodansyl cadaverin (MDC), 2% dimethyl casein (DMC) and 100 NIHU/ml thrombin. Details regarding these reagents are given in Ref. 4.

Assay automation using the SI system

SI configuration. The original work[5] demonstrated the feasibility of the SI technique for the automation of the manually performed sample handling and sample pretreatment operations associated with the rhFXIII assay, including sample dilutions, additions of multiple reagents, solution mixings, and controlled initiations of two subsequent reactions.[6] The emphasis of the current work shifted towards development of a system which would allow technical personnel to perform a reliable analysis of rhFXIII samples in a quality control laboratory environment. Therefore, issues such as robustness, mechanical simplicity, sample throughput, auto sampling abilities and long term reliability of the system were addressed.

The evaluation of the original single pump–single valve design (Fig. 1) led to the identification of four disadvantages which lowered the robustness standard of the SIA system. First, using a holding coil having a volume significantly larger than that of the syringe, the initial filling of the system was cumbersome and

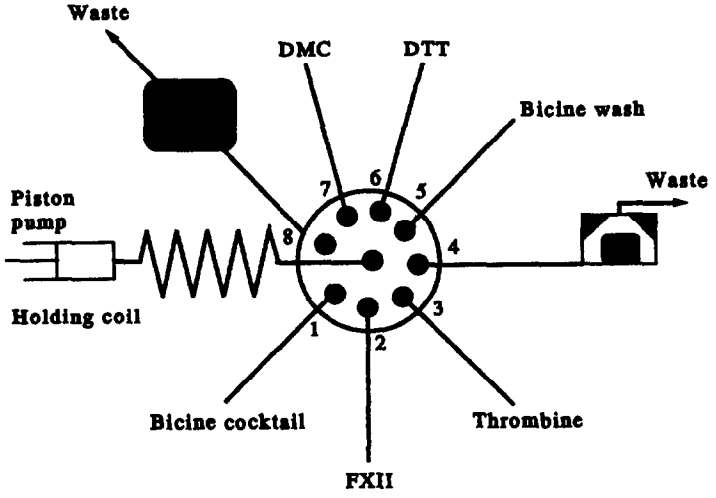

Fig. 1. Single pump–single valve SI configuration used in the earlier experimental work.[4] DTT (dithriothreitol) solution was used as a quenching agent for the FXIII activation. Later results showed that the assay can be performed without FXIII quenching.

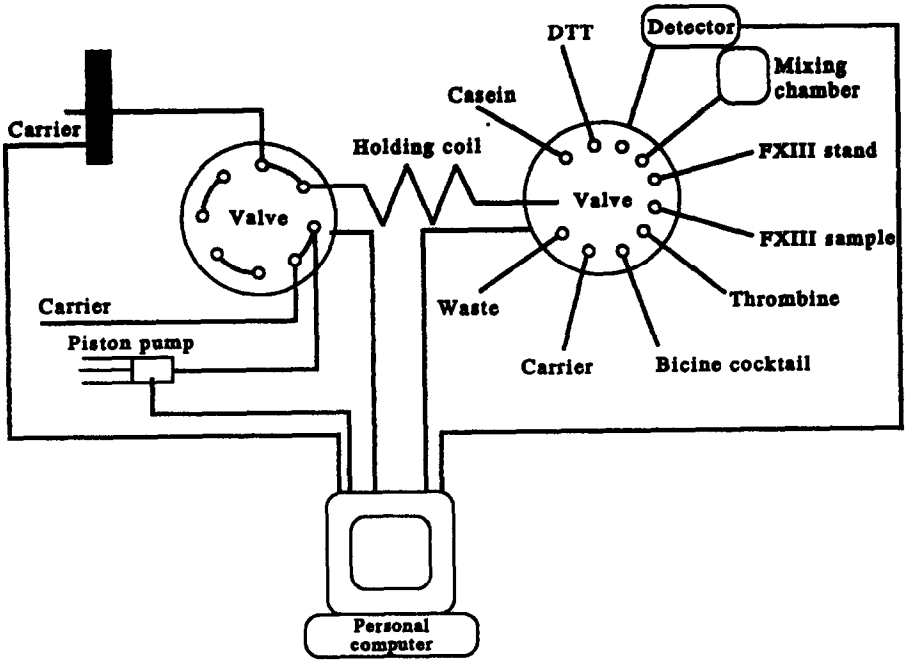

Fig. 2. Two pumps–two valves SIA system used for the automation of rhFXIII fluorometric assay.

needed a human interaction. The most straightforward procedure required disconnecting the holding coil from the syringe, filling the syringe manually with the carrier, reconnecting the holding coil and propelling the syringe content through the system. Although, when the volume of the holding coil was less than that of the syringe, it was possible to use repeated cycling for the initial filling, the required configuration left the carrier in the syringe prone to contamination when a high volume aspiration (volume of the aspirated solution was equal to or larger than volume of the holding coil) occurred by mistake from a reagent or sample port. Once a sample or reagent entered the syringe, the system had to be disassembled and cleaned before further use. For the single piston pump–single valve design the choice is, therefore, between the system which can use cycling of the pump for the initial filling, but does not minimize the risk of possible contamination of the carrier in the piston ($V_{\text{holding coil}} < V_{\text{syringe}}$) and the system which requires manual initial filling but practically eliminates the possibility of carrier contamination in the syringe ($V_{\text{holding coil}} \gg V_{\text{syringe}}$). Third, when using the later configuration, air bubbles were occasionally trapped near the head of the syringe (even though solutions were routinely degassed before use) and their elasticity caused errors in the volume accuracy of transferred solution zones. The air bubbles were difficult to remove without disassembling the SI system, mainly because of the low volume capacity of the piston pump. Finally, the time required for the system clean-up after each analysis was long, once again due to the low volume capacity of the syringe and time spent on the refill cycle.

Although substituting a piston pump with a peristaltic pump would eliminate cumbersome system filling, make removal of trapped air bubbles easy and speed up the cleaning process after the analysis, the elimination of the piston pump would sacrifice its high volume accuracy, which is an especially important advantage for methods requiring solution zone transfers of volumes as low as 10 μl, and superior long term robustness.[7,8] It seemed that this specific application would benefit if the SI system could offer both the accuracy and robustness of the piston pump and the continuous flow capabilities of the peristaltic pump.

The newly designed SI system consisted of both a piston and peristaltic pump configured with a two positional valve and a 10-port selector valve (Fig. 2). As in the single pump–single valve design, reagent lines, a sample line, a mixing chamber and a detector line were clustered around the selector valve. The holding coil did not, however, lead directly from the selector valve to the pump, but rather to the two positional valve, to which the micro tubing channels from both pumps were also connected. As

a result, depending on the position of the valve, either the peristaltic or the piston pump was in the active mode at any particular time and could deliver solutions through the holding coil. In these experiments, the active piston pump mode was used for transfer of sample and reagent zones in and out of the holding coil, thus taking advantage of its high volume accuracy, and the active peristaltic pump mode was employed for the initial system fill-up and for the system clean-up after each analysis, thus utilizing the continuous flow capabilities of the peristaltic pump. Note that the piston pump refilled in a passive mode, disconnected from the holding coil, which minimized the possibility of carrier contamination in the syringe and allowed for effective use of time, since other tasks, such as the system clean-up, were performed simultaneously. Although the complexity and size of the SI system increased, the advantages gained by the integration of the two additional components outweighed this drawback. In addition, the system developed for this application was not intended to be highly portable and, once properly configured, exhibited the same mechanical reliability as the original single pump–single valve design.

Hardware. The assembled SI set-up consisted of an Alitea (S-2) piston pump (cam driven, sinusoidal flow) equipped with a 1 ml syringe, an Alitea peristaltic pump (Alitea U.S.A., Seattle, WA), a Valco two positional eight-port valve, a Valco 10 positional selector valve (VICI, Houston, TX), a desktop personal computer, a mixing chamber (1.0 ml internal volume) equipped with a PTFE stirring bar, a stirring plate, Tygon pump tubing [0.5 ml internal diameter (i.d.)] and PTFE channel tubing (0.5 mm i.d.). Figure 2 shows the configuration of solutions and components around the selector valve. The final product was monitored with an HP 1046 fluorescence detector (Hewlett–Packard, Palo Alto, CA).

Procedure. The SI method simulated to a large extent the chronology of the manual procedure. First, using the peristaltic pump, the holding coil, the detector line and the mixing chamber were flushed with the carrier (bicine buffer solution). After the flush, the carrier solution was removed from the detector and from the mixing chamber. Next, the piston pump was put in the active mode to aspirate 500 μl zone of bicine cocktail, 10 μl of thrombine and 90 μl of the rhFXIII solution into the holding coil. Then, 600 μl of the solution were propelled from the holding coil to the mixing chamber, where it was mixed for 10 sec and allowed to sit for an additional 170 sec in order to activate the rhFXIII molecules. During this period, the peristaltic pump was used to flush the holding coil with the carrier solution. Next, using the piston pump, two zones were aspirated into the holding coil: 100 μl of bicine cocktail and 50 μl of casein. Then, 150 μl of the solution just introduced to the holding coil were added to the solution in the mixing chamber and mixed for 10 sec. As a result, the condensation reaction between casein and monodansyl cadaverin, which is catalyzed by the active rhFXIII, was initiated. At the same time, the SI system was switched to the active peristaltic pump mode and the holding coil was flushed for 5 sec with the carrier. Then, the piston pump was used to introduce air to the holding coil from the detector line. Following the solution mixing step, 180 μl of the reaction mixture were aspirated from the mixing chamber to the holding coil and immediately delivered to the detector. Note that the solution was separated from the carrier by an air packet and, therefore, no further dilution of the sample occurred during this step. Once the solution zone filled the detector's flow cell, the flow was stopped and the data acquisition was initiated. Data were acquired for 100 sec to monitor the formation of the fluorescent product. Finally, the system was thoroughly flushed and prepared for the next sample analysis. The entire analysis took 8 min, and total solution consumption was 0.8 ml.

Assay automation using the Zymark Benchmate 3.0

Hardware. The Zymark Benchmate 3.0 (Zymark Corp., Hopkinton, MA) system was purchased to accomplish the assay automation on a commercially available system. The system used for this work consisted of a moving arm, four vial racks (each having 50 vials capacity), a liquid transfer station, a vortex station, and a pumping system which included four syringes, one 12-port selector valve and three two-positional valves. An HP 1046 fluorescence detector was used for monitoring the final product and its signal was recorded on an HP 3396 series II integrator (Hewlett–Packard, Avondale, PA).

Procedure. The procedure developed for the assay automation consisted of 13 segments (Table 1), which, as with the SI system, mimicked the chronology of the manual method. First, sample vials were filled with 0.5 ml of

Table 1. Zymark Benchmate procedure for the FXIII assay

Step 1	Add 5 ml of 50 m*M*, pH 9.0 bicine
Step 2	Add 0.5 ml of MCD–Ca–Bicine cocktail
Step 3	Add 0.2 ml of 100 NIHU/ml thrombin
Step 4	Vortex for 5 sec at speed 3
Step 5	Wash syringe with 2 ml of 50 m*M*, pH 9.0 bicine
Step 6	Pause for 0.5 min
Step 7	Add 0.1 ml of 0.2% casein
Step 8	Vortex for 10 sec at speed 3
Step 9	Load sample into cell and read UV–vis spectrophotometer
Step 10	Rinse UV–vis cell once with 2 ml of 50 m*M*, pH 9.0 bicine
Step 11	Wash syringe with 1 ml of 50 m*M*, pH 9.0 bicine
Step 12	Wash syringe with 1 ml of 50 m*M*, pH 9.0 bicine
Step 13	End

rhFXIII samples and placed into the vial rack. The moving arm began the sequence by grabbing a sample vial at position 1 and transferring it from the rack to the liquid transfer station. Here, the sample was diluted by adding 5 ml of bicine buffer, 0.5 ml of bicine cocktail and 0.2 ml of thrombine. Next, the arm transported the vial to the vortex station, where the mixture was vortexed for 5 sec, which initiated the rhFXIII activation. The vial was moved back to the liquid transfer station, and the activation progressed for 30 sec. After 30 sec, 0.1 ml of the casein solution were added, using the internal standard line, and the mixture was vortexed once more. This led to the initiation of the condensation reaction. After returning the vial to the liquid transfer station, 1 ml of the solution was withdrawn from the vial and transferred to the detector's flow cell, where the formation of the reaction product was measured for 1 min. Following the data acquisition, the syringes and the tubing channels were washed with the carrier solution and the system components were prepared for the next sample. Now, the ZB system was ready for analysis of a new sample. The moving arm began the repeat cycle by grabbing a vial from position 2 on the rack.

The assay was carried out at room temperature. Casein and thrombine solutions were stored in an ice bath at 0°, other solutions were stored at room temperature. The flow rates used at different stages of the method are shown in Table 2.

Table 2. Flow rate and mixing parameters for the Zymark Benchmate FXIII method

Aspirate	0.100 ml/sec
Dispense	1.00 ml/sec
Internal std	0.12 ml/sec
Mix	0 ml/sec
Air push	0.15 ml/sec

RESULTS AND DISCUSSION

Assay automation using the SI system

Figure 3 shows the raw data acquired on the HP integrator by monitoring the formation of the fluorescent product. Standards of rhFXIII with concentrations ranging from 0 to 410 μg/ml were analyzed. Different initial values for each curve are due to the reaction progress between the time of casein addition to the mixing chamber and the start of the data acquisition. About 35 sec were required for the solution mixing step and the solution transfer from the mixing chamber to the flow cell. The signals for the 200 and 410 μg/ml of rhFXIII standards saturated the detector prior to the end of data acquisition, which is indicated by the horizontal part of their corresponding data curves. Curves from duplicate injections of standard solutions containing 67, 100 and 200 μg/ml of rhFXIII are shown to illustrate the excellent reproducibility of the method. The relative standard deviation (RSD) value of the slope of the kinetic curves for 10 injections of 100 μg/ml of rhFXIII standard was 0.91%.

Figure 4 shows the linear relationship between the concentration of the active rhFXIII and the slope of the kinetic curves. The correlation coefficient R for the first order fit equals 0.9998. The y intercept equals 0.063, which indicates that the condensation reaction takes place even in the absence of rhFXIII.

Apart from confirming the feasibility of the SI method for automation of the rhFXIII assay procedure, the experiments also revealed some additional facts. First, by eliminating a number of mechanical steps associated with repeated sampling from the mixing chamber, which was

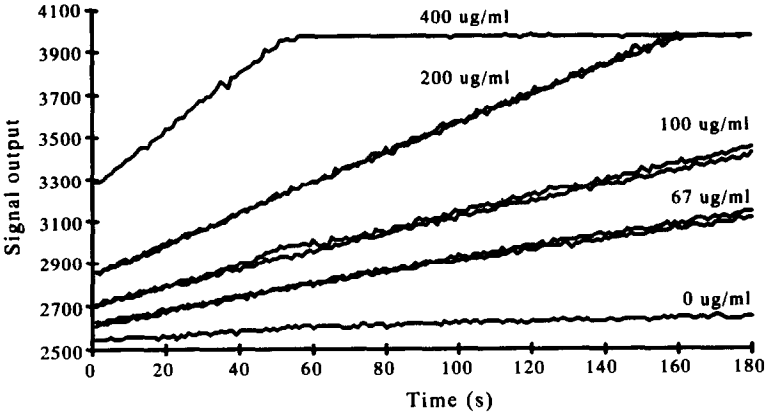

Fig. 3. Plot of signal *vs.* time. Data resulting from product monitoring of the condensation reaction on the SI system. FXIII concentration varied from 0 to 410 μg/ml. Duplicate injection data are shown for three samples.

required for the previously performed continuous flow SI method,[5] the stopped flow SI method, which monitored the kinetic process using a single sample zone, proved to be easier, faster and more reliable.

Second, it was shown that the assay can be successfully carried out even at room temperature, which suggested that the elevated temperature controlled system was not necessary. Experiments which were designed to evaluate the SI system performance at elevated temperatures (around 37°) displayed poor repeatability of the method. It was concluded that the small temperature variations within the system, which were difficult to control, had a significant impact on the reaction kinetics. To minimize these variations, the assay was performed at room temperature. The RSD of 0.91% for 10 injections of 100 μg/ml of rhFXIII standards represents 20-fold improvement over the results obtained for analyses performed at 37°.

Third, the stability of various solutions was investigated. As expected, casein and thrombine solutions were most susceptible to degradation. When either of the two solutions was stored at room temperature, the rate of product formation decreased by as much as 30% within 8 hr, when using the same rhFXIII standard. On the other hand, when thrombine and casein solutions were kept in an ice bath, the rate remained constant over the 8 hr period. The next least stable component was rhFXIII, but, in this case, the rate decrease due to rhFXIII breakdown was observed only when the rhFXIII samples remained stored at room temperature for at least 16 hr. The bicine cocktail did not show any signs of instability while stored at room temperature for periods as long as 2 weeks.

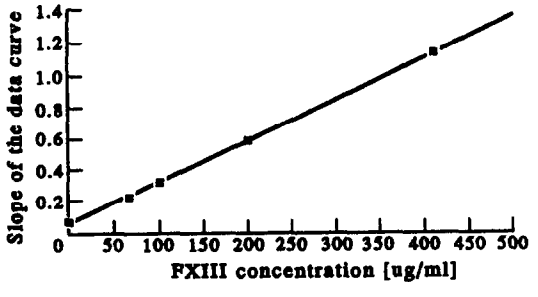

Fig. 4. Plot of the slope of the kinetic curve *vs.* FXIII concentration. The plot reveals a linear relationship over this concentration range. The correlation coefficient for the first order fit is 0.9998 and the *y* intercept is 0.063.

Assay automation using the Zymark Benchmate 3.0

Figure 5 presents data acquired on the HP integrator from the analysis of rhFXIII standard solutions containing 0–2500 μg/ml of rhFXIII. The results confirm successful completion of the assay and illustrate the effect of rhFXIII concentration on the condensation reaction over a wide concentration range. Figure 6 shows a good linear relationship between the slope of the kinetic curve of the condensation reaction and the rhFXIII concentration up to 1250 μg/ml of rhFXIII. The correlation coefficient for the first order fit was 0.9949 and the *y* intercept was 0.389.

The method design was more straightforward at this stage of the project. The development of the ZB system benefitted from the experiments performed on the SI system, because the observations about the solution stability and

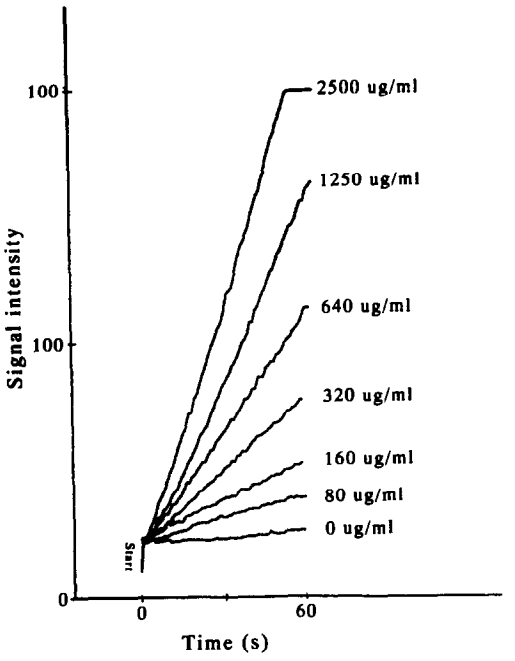

Fig. 5. Plot of signal *vs.* time. Data resulting from product monitoring of the condensation reaction using the ZB system were acquired on the HP integrator. FXIII concentration varied from 0 to 2500 μg/ml.

temperature effects also applied to the ZB method. Volumes of reagents, carrier and sample solutions used for the analysis increased almost 10-fold, because the ZB system did not have the ability to deliver volumes of the order of 10 μl with the same accuracy as the SI system equipped with a 1 ml syringe pump. The time of analysis was 11 min for each sample, 3 min longer than the time required for the SI analysis. The ZB system however, had, the ability to analyze up to 200 samples without any human intervention.

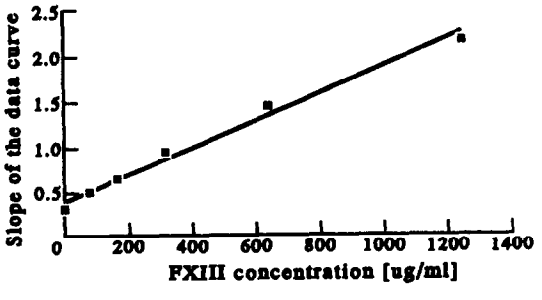

Fig. 6. Plot of the slope of the kinetic curve *vs.* FXIII concentration. The plot reveals a linear relationship over the concentration range from 0 to 1250 μg/ml. The correlation coefficient for the first order fit is 0.9949 and the *y* intercept is 0.389.

CONCLUSIONS

The two described methods demonstrated that the rhFXIII assay can be performed reliably in an automated mode with minimal human interaction. Although the two techniques differ in concept, they both provided methods for performing two subsequent reactions and monitoring the final product in an automated, controlled and highly reproducible manner.

The work presented showed some obvious differences between the two concepts. In the SI procedure, segments of the samples and reagents were introduced from vials to the holding coil channel, where they dispersed into the carrier and into each other, thus forming a concentration gradient. The controlled, reproducible dispersion and continuous sample handling represent the fundamental difference between assay automation by the flow injection approach and by robotics.

The SI technology is, however, quite versatile. For example, the gradient does not have to be formed every time. There is the option to treat a specific zone as a discrete sample, as was shown in the final stages of the rhFXIII assay. Here, it was undesirable to further dilute the reaction mixture in order to achieve a low detection limit within short data acquisition time. Therefore, an air pocket was introduced into the holding coil just before the aspiration of the reaction mixture from the mixing chamber. When the zone of the final mixture was aspirated to the holding coil, it was effectively isolated from the carrier solution and the dilution of the sample plug was prevented. Although the same result can be achieved by aspirating a large volume of the mixture from the mixing chamber (dispersion coefficient equals 1 for the center portion of the zone), it was found that, in this specific case, the flow cell was cleaned more easily when the amount of the final mixture going through the detector was limited. The air pocket introduced at this later stage did not present any significant problems.

With the ZB robot, the sample is always treated as a discrete entity. With the exception of final solution transfer to the detector, the sample never enters the tubing channels. The analyte either remains in the same sample vial or, if pretreatment steps such as sorbent extraction or filtration are performed, is transferred from one vial to another. The concentration of the analyte in the sample bolus remains

constant. This is why robots can handle solid samples but cannot master some techniques, such as optosensing or gas diffusion, which are commonly performed on flow injection systems.

Currently, more robots than SI systems can be found in quality control laboratories. Although SI technology is an attractive tool for the automation of chemical assays, the instrumentation is still in the experimental stages of development. A system which features an auto sampler, software and different configuration options of pumps and valves is not currently commercially available. This is an obvious drawback, if the goal is to implement a system for the sole purpose of automating high sample throughput assay. On the other hand, a variety of robotics systems are available on the market. The manufactures, which went through more than a decade of development, provide strong technical support. As a result, a large number of quality control assays have been successfully automated by robotics. Although there is no question about the potential of SI technology, until a reliable SI system appears on the market, robots will be the primary source for automation of quality control assays which require high sample throughput and tedious sample handling.

Acknowledgements—The authors express their gratitude to Professor Jaromir Ruzicka for critical discussions and valuable comments.

REFERENCES

1. D. A. Skoog and J. J. Leary, *Principles of Instrumental Analysis*, 4th edn, pp. 681–700. Sanders College Publishing, 1992.
2. J. Ruzicka and T. Gubeli, *Anal. Chem.*, 1991, **63**, 1680.
3. J. Ruzicka and E. H. Hansen, *Flow Injection Analysis*, 2nd edn. Wiley-Interscience, New York, 1988.
4. J. W. Hurst and J. W. Mortimer, *Laboratory Robotics: A Guide to Planning, Programming, and Applications*, 1st edn. VCH Publishers, New York, 1987.
5. M. Guzman, C. Pollema, J. Ruzicka and G. D. Christian, *Talanta*, 1993, **40**, 81.
6. L. Lorand, M. O. Lockridge, L. K. Campbell, R. Myhrman and J. Bruner-Lorand, *Anal. Biochem.*, 1971, **44**, 221.
7. G. D. Marshall, J. Ruzicka and G. D. Christian, *Anal. Chem.*, 1990, **62**, 1861.
8. A. Baron, M. Guzman, J. Ruzicka and G. D. Christian, *Analyst*, 1992, **117**, 1839.

Talanta, Vol. 40, No. 12, pp. 1951–1959, 1993
Printed in Great Britain.

0039-9140/93 $6.00 + 0.00

INVESTIGATION OF CARBON DIOXIDE MODIFIED SUPERCRITICAL AND NEAR SUPERCRITICAL CARRIER STREAMS FOR FLOW INJECTION SYSTEMS

ROBERT E. MALICK* and JOHN G. DORSEY†
Department of Chemistry, University of Cincinnati, Cincinnati, OH 45221-0172, U.S.A.

T. L. CHESTER and D. P. INNIS
The Procter and Gamble Company, Miami Valley Laboratories, P.O. Box 398707, Cincinnati, OH 45239-8707, U.S.A.

(*Received* 11 *February* 1993. *Revised* 11 *May* 1993. *Accepted* 11 *May* 1993)

Summary—Since flow injection (FI) is a dilution technique, efforts have been undertaken to minimize online dilution or dispersion. Solutes in supercritical fluids exhibit increased diffusion coefficients which have been shown to decrease dispersion of the sample zone. This work investigates the use of supercritical fluids (or CO_2 modified fluids) as carrier streams for FI. Both a non-reacting tracer and an online chemical reaction were employed to investigate the behavior of solutes in supercritical and near critical systems. Further, these results are compared to those obtained in the system studied with a conventional carrier stream. Plots of peak response *vs*% CO_2 modifier increase with a sharp break at moderate modifier composition (20–30%). Plots of peak variance *vs*% CO_2 modifier show decreased variance with increasing % modifier. The system was also optimized with regards to temperature and pressure. The optimized system displayed improved limits of detection and decreased variance relative to 0% CO_2 modifier carrier streams.

Flow injection (FI) is a means of automating a wide variety of analyses with improved precision and throughput.[1,2] Like chromatography, it is a dilution technique. Therefore, the limit of detection (LOD) in FI is never as good as that for a batch analysis. In order to improve the LOD, the dilution (dispersion) must be minimized. Efforts to this end have included reduction of injection variance,[3] enhanced reaction kinetics,[4] and decreasing viscosity.[5] The viscosity of supercritical and near-critical fluids can be varied greatly using temperature and pressure. The effect of varying viscosity results in higher solute diffusion coefficients, D_m ($\sim 10^{-4}$–10^{-3} cm^2/sec compared to $\sim 10^{-5}$ cm^2/sec in pure liquids).

Supercritical fluids (SFs) are of widespread use in supercritical fluid chromatography (SFC) and supercritical fluid extraction (SFE).[6] The properties which make supercritical fluids attractive for these techniques also make them attractive for FI. Deye *et al.*[7] employed Nile Red as a solvatochromic dye to investigate a series of fluids and mixtures of normal, supercritical and near critical fluids. Eighty-seven normal liquids were investigated ranging in polarity from pentafluorophenol to CO_2. The system was operated without a column and the normal liquids and other fluids were mixed online.

Leach and Harris[8] performed thermal lens measurements with a supercritical fluid system. This system employed a short column for solvent separation and the measurements were then taken under either stopped flow or continuous flow conditions. The use of supercritical CO_2 provided enhancement to the thermal lens effect. This system is analogous to the solute focusing work presented by Johnson and Dorsey.[9]

Olesik *et al.*[10] studied online reactions with Fourier transform infrared spectrometry (FTIR). Samples of allyldiisopropylamine oxide were injected into a length of capillary to allow dispersion. The flow was then stopped and the thermal decomposition reaction monitored by FTIR. This system employed a supercritical fluid-flow injection (SF–FI) system operated at low dispersion to monitor the reaction. The reaction was found to follow different pathways (to the same product) if performed above or below the critical conditions.

*Present Address: Abbott Laboratories, Dept. 41H Bldg. R1B, North Chicago, IL 60064-4000, U.S.A.
†Author for correspondence.

Several works have been aimed at investigating transport effects in SFC. Two important works in this area examined coiling-induced secondary flow in capillary SFC. Springston and Novotny[11] demonstrated enhanced radial mass transfer in coiled columns. The radius of curvature for a coil of capillary tubing can be halved by shaping the coil into a figure-8 and folding over. Coil diameters, d_c, were reduced in this fashion from 30 to 15 to 7.5 cm. Plots of reduced plate height, h, *vs* reduced flow velocity, v, were constructed and evaluated. The results from these van Deemter plots showed that near the critical pressure, reductions in coiling diameter produced slight decreases in h. For pressures well in excess of the critical point, more noticeable decreases in h were exhibited. Janssen *et al.*[12] showed similar results over coiling diameters of 10.5, 4 and 1.6 cm. In that study, a relatively low value for d_c was chosen (2.7 cm). This allowed study of effects other than coiling.

The choice of solvents in the study presented here was guided by binary mixture behavior.[13] In Type I phase behavior, the materials being mixed are miscible as liquids, but separate liquid and vapor phases can be formed at pressures and temperatures between the individual critical points. Fluids forming Type I mixtures with CO_2 include n-alkanes ($n \leq 8$), methylene chloride, chloroform, carbon tetrachloride, benzene and methanol. The most polar solvent in the above list is methanol and was chosen for this study.

The final preliminary consideration is the choice of detector. The most common detector in SFC is the flame ionization detector (FID). Figure 1 shows a typical chromatogram in SFC with FID detection. Note the relatively large void peak. While this is acceptable in SFC where the analytes are retained and separated from the solvent peak, this void peak is where the reaction occurs in FI. A more selective detector is required for an SF–FI system. The choice here is UV/vis absorbance. Of particular use is an absorbance detector optimized for use with capillary tubing (see Apparatus section for a description).

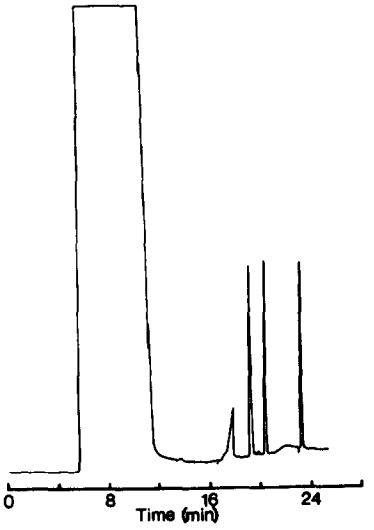

Fig. 1. Typical SFC peak showing large void volume peak. Adapted from Ref. 15.

The SF–FI system was further developed and employed to study a model reaction system. This work was aimed toward reducing overall peak variance (the second central moment) and thereby improving limits of detection in flow injection systems and demonstrating a further utility of supercritical fluids in analytical chemistry.

EXPERIMENTAL

Apparatus

A modified Varian Analytical Instruments (Sunnyvale, CA) Model 8500 Syringe Pump propelled the carrier streams for all studies.[14,15] Samples were injected via a Valco Instruments Company, Inc. (Houston, TX) EC14W.06 Internal Loop Injection Valve with a 60-nl sample loop. All connecting tubing downstream of the injector was polyimide-coated fused silica capillary (three sizes: 75-μm ID, 365 μm OD; 50-μm ID, 370-μm OD and 13-μm ID, 144-μm OD) from Polymicro Technologies, Inc. (Phoenix, AZ). The two manifolds used in this system consisted of a 50-μm ID × 2-m long manifold and a 75-μm ID × 3-m long manifold. The 50-μm ID manifold was evaluated in the initial studies and the 75-μm ID manifold was evaluated in all subsequent studies.

Manifolds were held at elevated temperatures and in relative confinement (for safety) by a Hewlett-Packard Company (Palo Alto, CA) 5730A Gas Chromatograph. This GC was used solely for its oven. The detector and injector septum were removed to allow easy access to the oven. Valco Fused Silica Adapters and other miscellaneous fittings were also employed. These included a flow restrictor to control pressure and density, placed post-detector, made of a 5–15-cm length of 13-μm ID capillary. A 300-ml sample cylinder and angled valve with 1800 psi rupture disc (for preparation of carrier streams) was obtained from the Whitey Co.

(Highland Heights, OH). The cylinder and the pump syringe were cooled by a Fisher Scientific (Pittsburgh, PA) Model 9100 Isotemp Refrigerated Circulator.

Detection of solutes in the carrier stream was by an ISCO (Lincoln, NE) CV[4] Capillary Electrophoresis Absorbance Detector, wavelengths used are noted in the figure captions. A small area of the capillary was carefully heated and the polyimide coating removed to form a window to allow passage of the light beam. The output recording was by connection to a Series 4500 Microscribe Strip Chart Recorder (the Recorder Company, San Marcos, TX).

Solutions

Methanol, HPLC grade, was obtained from Fisher Scientific Co. The *p*-dimethylaminobenzaldehyde (Fisher Scientific Co.) was used as received and was stored purged with dry nitrogen when not in use. Barbituric acid was obtained from Sigma Chemical Co. ("PFS" grade) and was used as received. SFC grade CO_2 was from Matheson Gas Products, Inc. (Secaucus, NJ). This cylinder had a full length eductor tube to allow the delivery of liquid CO_2 and was fitted with appropriate adapters for connection to the syringe pump. The headspace was not charged with helium, as many manufacturers provide. Eriochrome Red B (Fig. 2(a)) was prepared in house. The absorbance spectrum of the dye solution was verified against the literature $\lambda_{max} = 464$ nm.[16] The reaction studied in this system was the addition reaction of barbituric acid with *p*-dimethylaminobenzaldehyde (Fig. 2(b)).

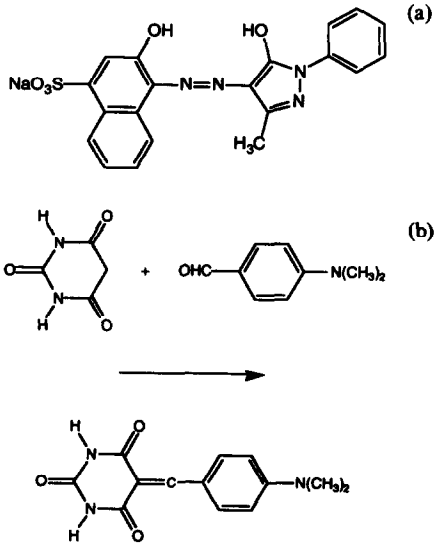

Fig. 2. Species injected/detected: (a) Eriochrome Red B (C.I. 18760). (b) reaction of barbituric acid with *p*-dimethylaminobenzaldehyde forming 5-*p*-dimethylaminobenzylidene-barbituric acid ($\lambda_{max} = 464$ nm).

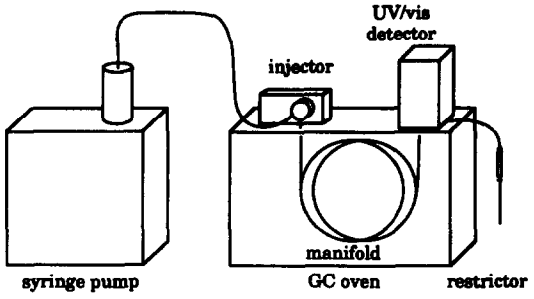

Fig. 3. SF/FI system configuration.

Procedure

The system configuration is shown in Fig. 3. Mixtures of methanol, CO_2 and reagent were prepared as follows. The 300-ml sample cylinder was cleaned and rinsed with methanol. A fixed volume of 0.01 *M* *p*-dimethylaminobenzaldehyde in methanol solution was then pipetted into the clean cylinder. The appropriate volume of methanol was then added to reach the required volume% of methanol. The cylinder valve was attached and the assembly was connected to the CO_2 cylinder (with both valves shut). The sample cylinder was then cooled to 0°. The valves were slowly opened allowing liquid CO_2 to fill the remaining volume of the sample cylinder. It was then isolated, disconnected and agitated to provide gross mixing of the liquids.

The charged sample cylinder was then connected to the inlet check valve of the empty pump and the pump cylinder was then cooled to 0° while the sample cylinder was allowed to warm in the room air. Once the pump was chilled, it was filled from the sample cylinder. After filling, the cylinder was again isolated, removed and the pump inlet check valve was then capped. The filled pump was allowed to equilibrate under pressure (100–200 atm) and at room temperature for at least 12 hr to allow complete mixing of the components.

RESULTS AND DISCUSSION

High% CO_2 carrier streams

Since the greatest variation in density and viscosity of CO_2-modified carrier streams occurs as methanol is first added to pure CO_2, this seemed the logical first experiment. Figure 4

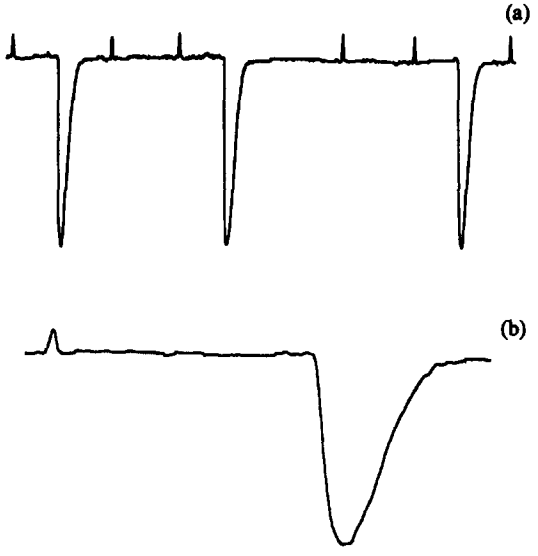

Fig. 4. Methanol blanks in a 100% CO_2 carrier stream. Conditions: 200 atm, 40°C, $\lambda = 360$ nm, 60 nl injection volume and 50 μm × 2 m capillary column. (a) Chart speed = 5 cm/min and (b) chart speed = 60 cm/min.

shows methanol blanks injected into 100% CO_2 at 200 atm. and 40°, conditions at which no phase separation is possible. The upward deflection to the left of the individual injections is the injection mark. The upper trace (a) represents multiple injections. In each case there is an enormous negative peak. This occurs due to the refractive index difference between liquid CO_2 (1.195 at 15°C[17]) and liquid methanol (1.3288 at 20°C[17]). The lower trace (b) shows the same peak at faster chart speed. The shape of this peak is symmetric and confirmed that connection to the capillary post-injection and pre-detection (one, at injector outlet) is free of unswept dead volume.

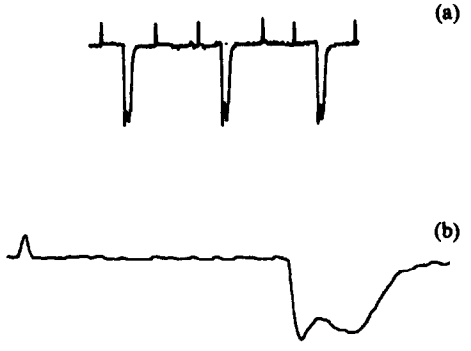

Fig. 5. $5 \times 10^{-2} M$ *p*-dimethylaminobenzaldehyde in methanol blanks injected in a 100% CO_2 carrier stream. (a) Chart speed = 5 cm/min and (b) Chart speed = 60 cm/min. Other conditions as Fig. 4.

To confirm that the detector would reveal solutes present in this background response, the same system was run with injection of *p*-dimethylaminobenzaldehyde dissolved in methanol. Figure 5 shows these results. The upper trace (a) is at a slow chart speed. Note that there is a small peak from the *p*-dimethylaminobenzaldehyde located in the refractive index peak. This indicates that *p*-dimethylaminobenzaldehyde is either totally nonretained, or is retained only very slightly by the uncoated fused silica, because the solute elutes with the solvent peak. Since this is the lowest-polarity carrier stream (or weakest mobile phase) used in these experiments, the *p*-dimethylaminobenzaldehyde should be unretained throughout the range of CO_2 compositions studied, and we assume that no wall adsorption of the *p*-dimethylaminobenzaldehyde is occurring. The lower trace (b) further confirms this with symmetric peak shape.

A second problem experienced in high% CO_2 carrier streams is shown in Fig. 6. Trace (a) represents 100% CO_2. The methanol blank displays a discontinuity preceding the peak maximum. This may indicate the presence of an on-line phase transition between the 100% methanol sample solvent and the 100% CO_2 carrier stream. Trace (b) represents a 95% CO_2 carrier stream. The result is the same as shown by the 100% CO_2 carrier stream. There is a slight decrease in magnitude as % CO_2 decreases.

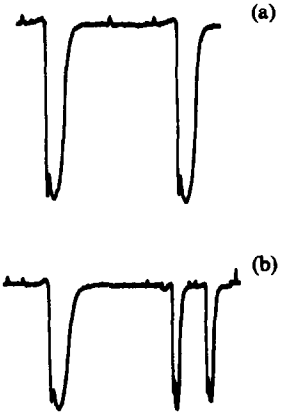

Fig. 6. Methanol blanks exhibiting online phase separation between carrier stream and sample solvent. Conditions: 100 atm, 50°C, $\lambda = 464$ nm, 60 nl injection volume, chart speed = 5 cm/min and 50 μm × 2 m capillary column. (a) 100% CO_2 carrier stream. (b) 95% CO_2 carrier stream and chart speed = 3 cm/min (two peaks on right side).

Low % CO_2 carrier streams

The high % CO_2 results led to investigation of low % CO_2 carrier streams. These types of systems were recently investigated in capillary high-performance liquid chromatography (HPLC) by Cui and Olesik.[18] Their study involved porous glassy carbon (PCG) packed columns and% CO_2 mobile phases ranging from 0 to 100% (% v/v in methanol). These mobile phases were operated below the critical temperature of CO_2 and were termed "enhanced fluidity"[18] mobile phases, where fluidity was defined as the reciprocal of viscosity. For a variety of solutes these researchers found that optimum results were often obtained at intermediate compositions (50% CO_2). Of course, higher temperatures may be used with binary mobile phases or carrier streams in both chromatography and flow injection analysis if care is taken to operate in a single-phase region of pressure–temperature–composition (p–t–x) space. However, there is no standard practice for naming the fluid when operating between the critical points of the constituents. In this work, we will continue to refer to the fluid as a supercritical fluid because we are in a single-phase region well above the bubble-point curve for the binary mixture at the composition used, and we exceed the critical pressure of the mixture.

Preliminary results

The preliminary carrier stream employed with the flow injection system was 10% CO_2 in methanol with 0.01 M p-dimethylaminobenzaldehyde in methanol. Representative injections are shown in Fig. 7. The repetitions shown on the left (a) represent 0.5% RSD in the peak height. The peak shape (b) is good, revealing a well plumbed system free from phase transitions. The conditions in this system are somewhat above the critical point for CO_2 ($P_c = 72.9$ atm and $T_c = 31°C$,[17]) but are below the critical temperature for the mixture. Note that from this point on, 75 μm ID capillary was employed.

Calibration of this system was performed with both a non-reacting solute and an on-line reaction. The figures of merit for plots of absorbance *vs* amount injected are summarized for these two sets of calibration data in Table 1. The plots show reasonable linearity and, as preliminary data, show strong evidence of correlation between peak height and amount injected. Note that the sensitivity for detection is 10 times greater for the reacting system. The linear dynamic range (LDR) is similar (two orders of magnitude).

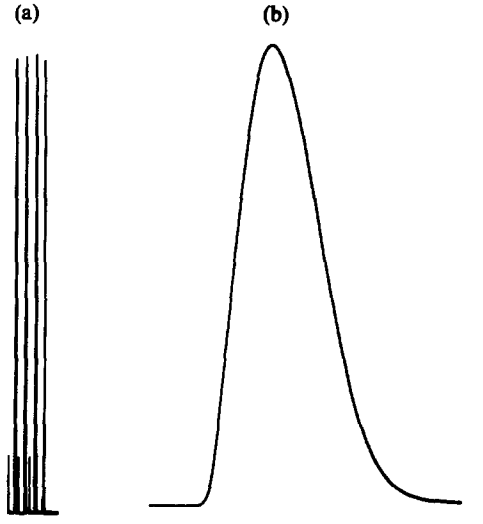

Fig. 7. Injections of 0.005 m barbituric acid into a 10% (% v/v) CO_2 carrier stream with 0.01 M p-dimethylaminobenzaldehyde in methanol. P = 100 atm, T = 100°C, injection volume = 60 nl, λ = 464 nm. (a) chart speed = 2 cm/min and (b) chart speed = 10 cm/min.

Before proceeding it is useful to calibrate the actual compositions of CO_2 present. This was done by collecting the major component (methanol) with a calibrated buret at a known flow rate. The CO_2 is then driven off by ultrasound degassing and the resulting volume of methanol divided by the calibrated volume delivered to yield the % methanol. Table 2 shows the comparison of nominal CO_2 compositions *vs* measured compositions. In this table, the value of CO_2 determined is always less than the nominal value.

This difference has two explanations, and neither is separable from the other. The first is

Table 1. Figures of merit for the SF–FI system initial calibration curves

	ERB*	BA†
% CO_2 (by volume)	10	10
Pressure (atm)	250	250
Temperature (°)	200	200
Sensitivity (abs × 10^{-3}/ng)	0.1505	1.553
r^2	0.9922	0.9993
Limit of detection‡ (ng)	0.31	0.041
LDR lower limit (ng)	2.6	0.76
LDR upper limit (ng)	260	77

†ERB = Eriochrome Red B.
†BA = Barbituric Acid.
‡*LOD = 3 s_B/m, where $s_B = NOISE_{P-P}/5$ and m = sensitivity.

Table 2. Nominal modifier concentration compared to actual delivered modifier concentration

Nominal	% CO_2(% v/v) Actual	Difference
0	0	0
10	8	−2
20	15	−5
30	27	−3
40	36	−4

that the composition determination performed this way assumes that the density of the CO_2 remains constant. It does not, but changes with pressure and temperature. The determinations were performed at constant room temperature but the pressure varied with composition to maintain constant flow rate. This would result in the measured value being lower than the true produced value (not the nominal value).

The second explanation is that at least some of the difference between measured and nominal is real. The cylinder is filled by the vapor pressure difference between the room-temperature aluminum storage cylinder and the cooled steel sample cylinder. There must be a small volume of the sample cylinder filled with CO_2 that does not remain condensed. This produces a systematic error which should remain constant throughout the range of compositions since the cylinder is always filled at the same temperature. Whether the difference between measured and nominal is either a systematic error or an actual difference is not important. The difference is quantified and all subsequent plots are *vs* measured composition. The measured value should be a more accurate representation of the compositions produced than the nominal composition.

Optimization

With the functional SF/FI system, it is useful to optimize the response of the system with respect to pressure, temperature and CO_2 composition. The most used method for this is univariate optimization. This method is time and labor intensive in that it requires singly changing each parameter while keeping the other parameters constant. An alternative is the simplex or modified simplex method.[19,20] This approach reaches the optimum value in a rapid fashion with fewer experiments than the univariate approach. Another advantage is the location of a more accurate maximum with the simplex than with the univariate maximum (which does not account for two or more factor effects). The problem with this method is that it would require an enormous number of different % CO_2 compositions to be prepared in a short period of time. As described in Procedures this preparation is not trivial and would prove impractical for optimization.

An optimization scheme based on factorial design is one alternative. In this method, the available experimental space is divided into points and four adjacent points are evaluated. The maximum of these values is then taken as the corner for a new set of four points. In this system, pressures between 100 and 400 atm were divided into 50 atm increments, temperatures between 100 and 300°C were divided into 50°C increments and % CO_2 was taken starting at 0% and increasing by 10% increments. The sample experimental space (for a given % CO_2) is shown in Fig. 8(a).

Figure 8(b) shows a sample result. The initial starting point is irrelevant in this case. A relatively large region was explored to reveal whether or not local maxima were present in this region. Experimentally there is only a single maximum, at 100 atm and 100°C.

% *CO_2 composition studies*

Optimization experiments were performed for a series of CO_2 compositions and are summarized in Table 3, along with the composition results. In each case, the maximum is found in

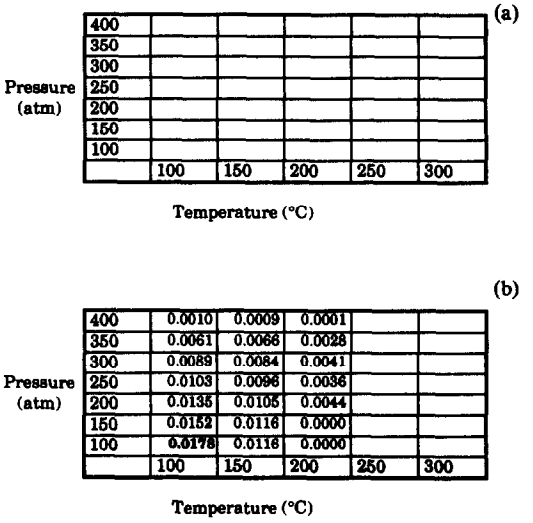

Fig. 8. Optimization examples (a) sample experimental space diagram and (b) results for 60 nl of 0.001 *M* barbituric acid injected into 20% (% v/v) CO_2 in methanol with 0.01 *M* *p*-dimethylaminobenzaldehyde.

Table 3. Results of optimization of the SF/FI system with respect to pressure, temperature and % CO_2 (% v/v)

% CO_2 (% v/v)	P (atm)	T (°C)	Absorbance
0	200	100	0.0138
8	100	100	0.0158
15	100	100	0.0171
27	100	100	0.0182
36	100	100	0.0158

the low pressure and low temperature corner of the experimental space. These maxima in response correspond to two physical parameters of the system. The first is the density/viscosity of the carrier. At lower temperatures and pressures, the carrier stream becomes more gas-like with corresponding increases in solute diffusion coefficient. Further, the lower pressure corresponds to a slower linear velocity and a maximum in residence (reaction) time. Since the solute is in the manifold for a longer period, the reaction proceeds farther towards completion, yielding greater peak maxima.

Figure 9 is a plot of the data for the barbituric acid (BA) in Table 3, along with the data for Eriochrome Red B (ERB). For the non-reacting system, the absorbance increases with increasing % CO_2 initially. Beyond 15%, the response begins to decline with a sharp break after 25%

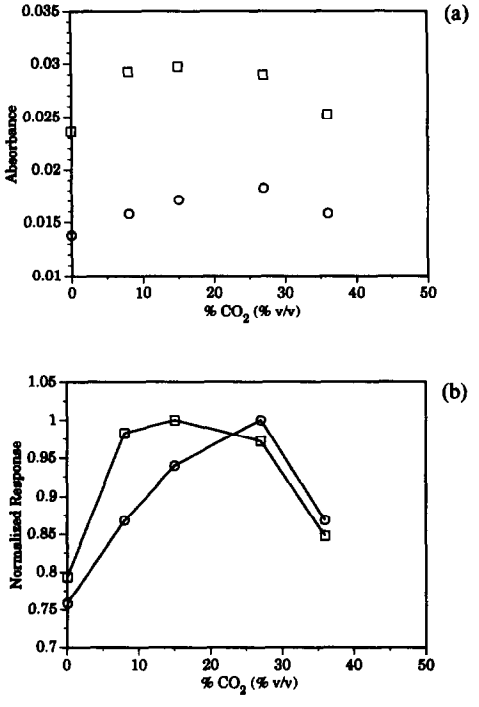

Fig. 9. Plots of peak height *vs* % CO_2 for (□)—Eriochrome Red B and (○)—barbituric acid. (a) absorbance and (b) normalized peak height. Other conditions as in Fig. 8.

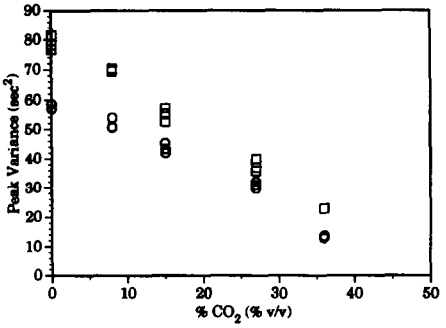

Fig. 10. Plots of peak variance *vs* % CO_2 for (□)—Eriochrome Red B and (○)—barbituric acid. Other conditions as in Fig. 8.

CO_2. Consulting a phase diagram for methanol/CO_2 solutions[13] and comparing the measured compositions of CO_2 from above reveals that at compositions up to 27% (% v/v) the mixture is single-phased. At 36% CO_2, however, the mixture lies in the two phase region of the phase diagram. The presence of two phases produces a sharp decline in response. At low concentrations, these peaks exhibit the same behavior shown in Fig. 6.

Figure 10 shows the results of plotting peak variance *vs* % CO_2 (% v/v). This plot shows variance decreasing continuously with increasing % CO_2. It is somewhat surprising that no break is seen when the system splits into two phases. The explanation for this behavior is stated above, at higher concentrations the absorbance of dye or product is sufficient to dampen out the change in sample profile from the phase boundaries.

This leads to two results which must be reconciled for the optimized system. The variance was found to decrease continuously for increasing % CO_2. The peak height, however, exhibited a sharp break as the system crossed the vapor–liquid critical locus. Since peak height is the parameter of analytical interest, the maximum in peak height should be taken as the important parameter to optimize.

Figure 11 shows the results of the calibration plots under the optimum conditions for both a non-reacting (a) and a reacting solute (b). In both cases, the supercritical fluid carrier stream exhibited greater sensitivity relative to normal methanol carrier streams.

Table 4 summarizes the figures of merit for the optimized systems. For ERB the ratio of sensitivities between 0 and 27% CO_2 is 1.49 and for BA this ratio is 1.85. This means that for a non-reacting solute, the change in viscosity

Table 4. Figures of merit for the SF/FI system optimized calibration curves, 0 and 27% CO_2 (% v/v)

	ERB*	BA†	ERB	BA
% CO_2 (% *v/v*)	0	0	27	27
Pressure (*atm*)	200	200	100	100
Temperature (°C)	100	100	100	100
Sensitivity (abs × 10^{-3}/ng)	0.154	1.29	0.229	2.39
r^2	0.9984	0.9977	0.9976	0.9978
slope (log–log)	0.984	0.977	0.976	0.978
Limit of detection‡ (*ng*)	0.342	0.0367	0.257	0.0286
LDR lower limit (*ng*)	10.7	0.769	10.7	0.769
LDR upper limit (*ng*)	268	76.9	187	76.9

*ERB Eriochrome Red B
†BA Barbituric Acid
‡LOD = 3 s_B/m, where s_B = $Noise_{p-p}$/5 and m = sensitivity.

yields a 1.49 times increase in signal. For a reacting system, this increase is 1.85. Changes in viscosity have a dual effect in the case of a reaction. Not only is dispersion of product lessened but the extent of reaction is improved. This is due to the improvement in collision rate (controlled by diffusion coefficients of the reactants) between the reactants. Therefore in supercritical fluids the dispersion without reaction improves as do the actual reaction conditions.

For decreased viscosity in supercritical fluid carrier streams, the LOD is improved relative to normal fluids. This results from the increase in sensitivity. This indicates that while sensitivity is improving, the noise is remaining roughly constant. The upper limit of the LDR decreases for the non-reacting solute in the supercritical fluid carrier stream. This is a consequence of the increase in sensitivity.

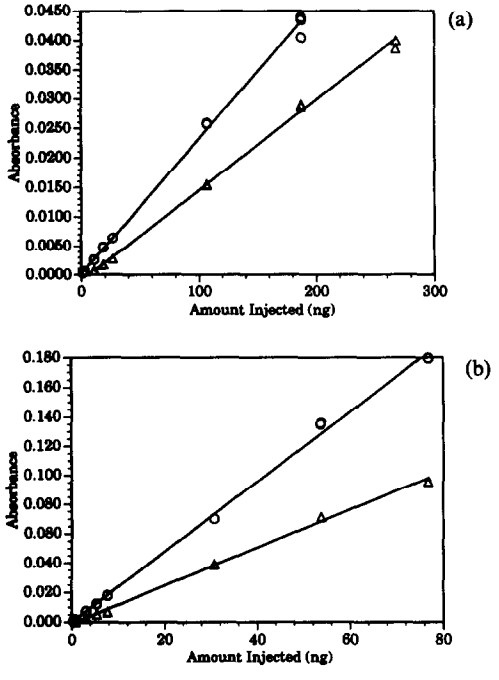

Fig. 11. Calibration curves for optimized systems for (△)—0% CO_2 (% v/v) and (○)—27% CO_2 (% v/v) with (a) Eriochrome Red B and (b) barbituric acid.

CONCLUSIONS

The investigation of supercritical fluids has some practical use to the field of FI. Supercritical and near-critical carrier streams provide decreased dispersion relative to normal liquid carrier streams. They also provide variable properties for the carrier stream to suit particular needs of the analyst. Further, sensitivity is directly improved via enhanced rate of collision relative to normal fluids.

The goals of this investigation were to demonstrate that decreased variance improves LODs and throughput. The LOD was shown to improve in SF/FI *vs* normal fluid FI. The throughput is inversely proportional to the standard deviation, σ. Since there was a two-fold decrease in variance, σ^2 (average between non-reacting and reacting solutes) there is a corresponding 1.4-fold increase in throughput for the supercritical fluid carrier streams.

The use of carbon dioxide-modified carrier streams provides all of the above advantages and others. The replacement of 30% of the carrier stream volume represents a substantial reduction in organic waste. The resultant effluent is also more concentrated once the gas leaves the solution.

Acknowledgements—JGD gratefully acknowledges support of this work by the Procter and Gamble Company and by NIEHS ES-04908.

REFERENCES

1. J. Ruzicka and E. H. Hansen, *Flow Injection Analysis*, 2nd ed. John Wiley, New York, 1988.
2. M. Valcárcel and M. D. Luque de Castro, *Flow Injection Analysis Principles and Applications*. Ellis Horwood, Chichester, 1987.
3. B. F. Johnson, R. E. Malick and J. G. Dorsey, *Talanta*, 1992, **39**, 35.
4. S. H. Brooks, R. N. Williams and J. G. Dorsey, *Anal. Lett.*, 1988, **21**, 583.
5. S. H. Brooks and J. G. Dorsey, *Anal. Chim. Acta*, 1990, **229**, 35.
6. T. L. Chester, J. D. Pinkston and D. E. Raynie, *Anal. Chem.*, 1992, **64**, 153R.
7. J. F. Deye, T. A. Berger and A. G. Anderson, *Anal. Chem.*, 1990, **62**, 615.
8. R. A. Leech and J. M. Harris, *Anal. Chem.*, 1984, **56**, 2801.
9. B. F. Johnson and J. G. Dorsey, *Anal. Chem.*, 1990, **62**, 1392.
10. S. V. Olesik, S. B. French and M. Novotny, *Anal. Chem.*, 1986, **58**, 2256.
11. S. R. Springston and M. Novotny, *Anal. Chem.*, 1986, **58**, 2699.
12. H.-G. M. Janssen, J. A. Rijks and C. A. Cramers, *J. HRC*, 1990, **13**, 475.
13. S. H. Page, S. R. Sumpter and M. L. Lee, *J. Microcol. Sep.*, 1992, **4**, 91.
14. F. J. Van Lenten and L. D. Rothman, *Anal. Chem.*, 1976, **48**, 1430.
15. T. L. Chester, Supercritical fluid chromatography instrumentation, in *Analytical Instrumentation Handbook*, G. Ewing (ed.), Marcel Dekker, New York, 1990.
16. E. Gurr, *Synthetic Dyes in Biology, Medicine and Chemistry*. Academic Press, London, 1971.
17. R. C. Weast, *CRC Handbook of Chemistry and Physics*. CRC Press, Boca Raton, FL, 1985–1986.
18. Y. Cui and S. V. Olesik, *Anal. Chem.*, 1991, **63**, 1812.
19. S. N. Deming and L. R. Parker Jr., *CRC Crit. Rev. Anal. Chem.*, 1978, 187.
20. J. A. Crow and J. P. Foley, *Anal. Chem.*, 1990, **62**, 378.

Talanta, Vol. 40, No. 12, pp. 1961–1966, 1993
Printed in Great Britain.

0039-9140/93 $6.00 + 0.00

REVERSE DUAL PHASE GAS DIFFUSION FLOW INJECTION ANALYSIS

K. J. SMITH and G. E. PACEY
Department of Chemistry, Miami University, Oxford, OH 45056, U.S.A.

(*Received* 20 *January* 1993. *Revised* 21 *July* 1993. *Accepted* 21 *July* 1993)

Summary—A flow injection gas diffusion system for gas acceptor to liquid donor stream, reverse dual phase gas diffusion flow injection analysis, has been demonstrated. Feasibility was shown with a carbon dioxide chemistry. A series of methods was investigated for hydrazine determinations. Using bromthymol blue indicator and a Celgard 2500 membrane a detection limit of 0.01 ppm v/v hydrazine was observed.

The technique of gas diffusion flow injection analysis, GDFIA, has been used for a variety of analytes.[1] The advantages of GDFIA are that the analyte of interest is removed from potential interferences and/or difficult matrices, the donor stream is optimized for diffusion while the acceptor stream can be optimized for detection, and the membrane itself may add some selectivity between the gaseous analyte and any gaseous interferences. Selectivity factors as high as 1500 have been reported.

GDFIA has been extensively used where there is liquid donor and liquid acceptor streams. In liquid–liquid GDFIA, an analyte in the donor stream is either present as a gas (*e.g.* NH_3) or undergoes some reaction to produce a gaseous analyte (*e.g.* sulfuric acid reacts with bicarbonate to produce CO_2). The gaseous analyte passes under a membrane where some of the analyte diffuses through the membrane into the acceptor stream.

The next development in GDFIA was a dual phase technique which involved a liquid donor and a gaseous acceptor stream. An example of this technique is the determination of metal hydrides.[2,3] Metal hydrides are generated in the liquid donor stream and then diffuse through the membrane into a hydrogen gas acceptor stream. The gaseous acceptor stream carries the metal hydrides to an atomic absorption spectrophotometer for detection. Additional examples of dual phase gas diffusion include its use as a sample introduction technique to mass spectrometry.[4]

The last area in GDFIA to be investigated has been the gas–liquid system. This paper reports work performed on a gas–liquid GDFIA system. The initial investigations involve carbon dioxide in an effort to study the basic characteristics of gas–liquid GDFIA and to determine if this technique is a viable, less complicated, approach to ambient monitoring. Then the technique was extended to include hydrazine.

EXPERIMENTAL

A Tecator 5020 FIA unit was used in conjunction with a Milton Roy Spectronic 3000 UV–VIS diode array. The gas diffusion manifold was a CHEMFOLD™ TYPE V from Tecator. The tubing used to carry the indicator solution was Teflon 0.5 mm i.d. The nitrogen and carbon dioxide were controlled by a flow controller and a flow meter (AARMGO). A pressure gauge was built, consisting of a 130 cm Pyrex tube with an i.d. of 2 mm. The pressure gauge used a solution of CO_2 saturated 1*M* HCl. A diagram of the FIA manifold is shown in Fig. 1.

The carbonate buffer acceptor solution, with cresol red indicator, is based on previous work done by Van der Linden.[5] Van der Linden measured CO_2 in liquid samples by measuring the absorbance at 430 nm. Cresol red indicator stock solution was made by dissolving 1 g of cresol red in 20 ml of 0.1*M* NaOH and then diluting to 1 l. The working acceptor solution was made by adding 10 ml of stock cresol red solution diluted to 1 l with 1 m*M* carbonate buffer adjusted to pH 8.85. Carbon dioxide and prepurified nitrogen were from Airco. The buffer solution with cresol red indicator should be able to measure CO_2 concentrations of 1–6 m*M*.

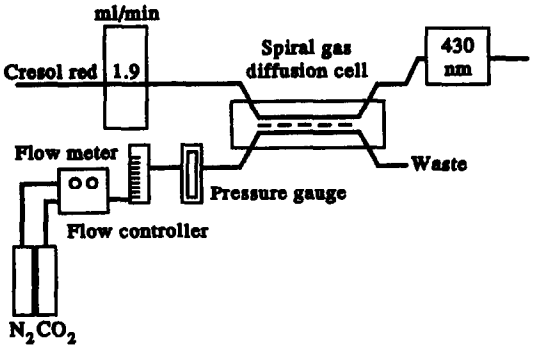

Fig. 1. Manifold for gas–liquid gas diffusion FIA.

The hydrazine source was a gas diffusion tube from VICI Metronics (Santa Clara, CA), which was calibrated to produce 700 ng/min of hydrazine hydrate at 50°C. Gas flow meters from Matheson were used for flow control and gas dilution. The hydrazine manifold is shown in Fig. 2.

Bromophenol blue (BPB) indicator solution was made by dissolving 0.050 g of BPB (Fisher) in 500 ml of doubly distilled, deionized water and the pH adjusted to 3.9 with 0.5*M* HCl. During the BPB experiments the absorbance was measured at 460 nm.

The Gore Tex Teflon membranes were supplied W. H. Gore. The silicon membranes were supplied by General Electric. The Celgard membranes were purchased from Fisher Scientific.

RESULTS AND DISCUSSION

Initially, a determination had to be made as to whether the CO_2 would in fact cross the membrane. A 50% CO_2/50% N_2 stream was passed in front of the membrane at a flow rate of 40 ml/min, while the acceptor stream was stopped on the opposite side of the membrane for 15 sec. A visible color change occurred in the stopped acceptor stream which indicated that CO_2 was crossing the membrane. The color change occurred rapidly and would not quickly change back to the original color when pumping was continued. Therefore, a more dilute CO_2/N_2 stream (5%/95%) was passed under the membrane at 40 ml/min. Again a color change occurred, but this time the color of the indicator in the stopped acceptor stream changed back to its original color when pumping continued.

Typically, the flow rate of the donor stream is critical to the amount of analyte diffusion across the membrane. As depicted in Fig. 3, if the donor flow rate is below a certain value, the amount of CO_2 being transported across the membrane is not detectable. This is related to the partial pressure of CO_2 in the donor stream. As the flow rate is increased, and subsequently the pressure in the manifold increases, the partial pressure of CO_2 increases proportionally. The amount of CO_2 which crosses the membrane increases due to both as the increased pressure in the manifold increases and the increased amount of CO_2 that passes the membrane. This results in a significant signal. Therefore, an optimum flow rate which allows the greatest amount of CO_2 to cross the membrane during the analytical stop flow period, but does not give a significant background signal, while the acceptor stream is flowing, can be determined. In the case of CO_2 the optimum flow rate for the Celgard 2500 membrane is seen at 62 ml/min (Fig. 4). The *y*-axis for Fig. 4 is the total absorbance minus the blank absorbance.

Five different membranes were tested for their suitability in the gas diffusion manifold. Two of the membranes were microporous Gore Tex (tetrafluoropolyethylene). The first had a 0.2 μm average pore size while the second had a 1.0 μm average pore size. Two Celgard membranes

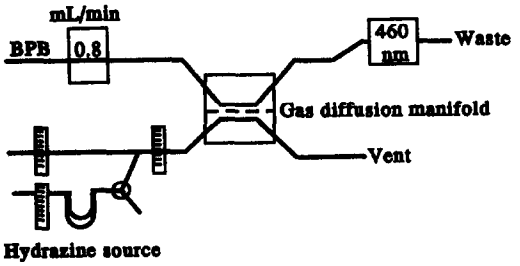

Fig. 2. Manifold for hydrazine determination.

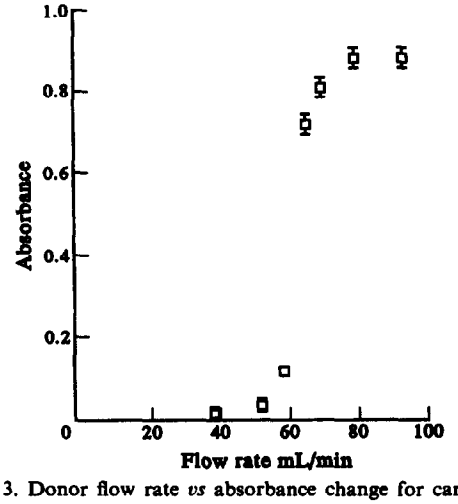

Fig. 3. Donor flow rate *vs* absorbance change for carbon dioxide.

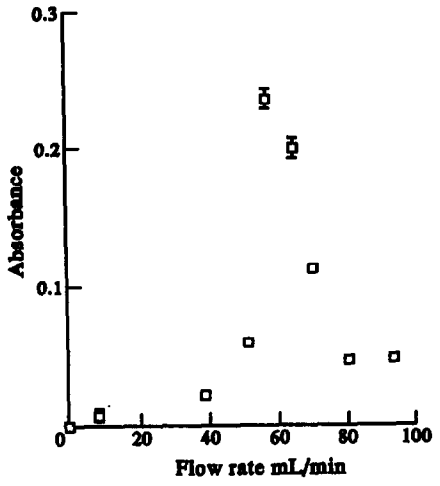

Fig. 4. Optimum flow rate for preconcentration minus blank carbon dioxide transport.

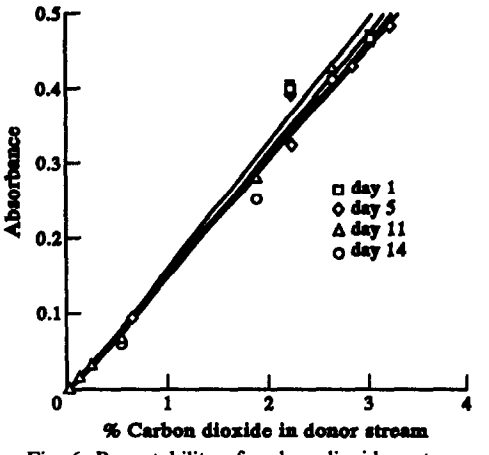

Fig. 6. Repeatability of carbon dioxide system.

(polypropylene) were tested with pore sizes of 0.5 μm and 0.75 μm. A 1 mil thick silicone rubber membrane was also tested. Each membrane was tested using the 5% CO_2/95% N_2 gas donor stream which was held constant at 40 ml/min. A scrim was not used to support any of the membranes because it resulted in the manifold leaking. A comparison of the response for each membrane is shown in Fig. 5. Due to the relation of gas permeability and pore size, the 1.0 μm pore size Gore Tex membrane has the greatest response.

However, due to the mechanical stress on the membrane from the pressure changes occurring during the stop and start of flow, the 1.0 μm Gore Tex was unable to last for more than 4 hr (420–480 determinations) before tearing. The Celgard membrane was much more durable and lasted for weeks without significant loss of performance as shown in Fig. 6.

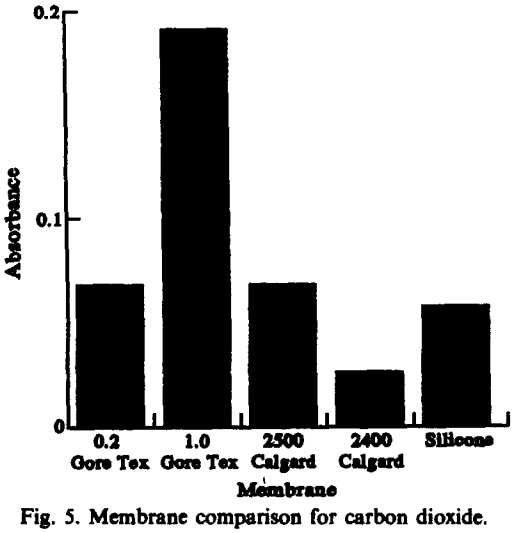

Fig. 5. Membrane comparison for carbon dioxide.

In liquid–liquid GDFIA, the typical efficiency of the membrane without a stopped-flow period where the gaseous analyte is consumed is between 8 and 15%.[4] This represents the amount of analyte which crosses the membrane and can be detected in relation to the amount of analyte in the donor stream. For liquid–gas GDFIA the efficiency increases to around 12–30%.

The efficiency for the Celgard 2500 membrane in the gas–liquid FIA system was 30.6%. The efficiency was determined by calculating the amount of CO_2 necessary to change the pH of the acceptor solution. The pH of the acceptor solution was measured before and after exposure to a known amount of CO_2. The absorbance of the solution was also measured before and after exposure to CO_2. The change in absorbance was correlated to the change in pH. Then when a sample was run using FIA, the change in absorbance could be related to a change in pH. The amount of CO_2 required to change the pH of the acceptor stream was calculated. The amount of CO_2 determined to have crossed the membrane was then divided by the amount of CO_2 available on the donor side of the membrane.

The linear range in this system is dependent on the concentration of the buffer in the acceptor stream. For the determination of membrane efficiency, detection limit and linear range the carbonate buffer concentration was 1 mM, adjusted to pH 8.85. Using this buffer system, with $5 \times 10^{-5}M$ cresol red indicator, the linear range was 6.7–197 g/m^3 of CO_2. The limit of detection (LOD) defined as the intercept divided

by the slope times three was 2.0 g/m^3. Due to the limited precision of the CO_2 dilution system, the LOD of this system is difficult to determine for buffer concentrations lower than 1 mM. In a related experiment, with varying buffer concentrations, a stream of 5% CO_2/95% N_2 caused all solutions with a buffer concentration below 0.75 mM carbonate to form the acid color of the indicator from the amount of CO_2 continuously moving across the membrane. This occurred at flow rates as low as 10 ml/min. With a membrane efficiency of 30% and with the 1 mM carbonate buffer system used in these experiments, the calculated minimum amount of CO_2 which would be detectable in the donor stream is 3 ppt v/v.

The stability of the membrane was investigated by running a series of standard curves over a two week period, totalling more than 1000 injections. The data collected from these trials show that the method is consistent over the time period investigated, as seen in Fig. 6. No significant deterioration of the membrane was seen and the sensitivity does not vary by more than $\pm 2\%$. In Table 1, the slope, intercept, and correlation coefficient for each calibration curve are presented. The average slope was 0.152 ± 0.003. The average intercept was -0.003 ± 0.001.

At this point it was believed that reverse dual phase gas diffusion FIA is a viable technique for the analysis of gaseous samples. The applications of this technique are potentially significant. This particular technique for determination of CO_2 may find application for real time monitoring of CO_2 because CO_2 will readily cross the membrane if the flow rate and manifold pressure are high enough. If CO_2 concentrations are higher than 5% of the total volume, for example in fermentation reactors, the carbonate buffer concentration can be increased to establish a linear range which would accommodate the amount of CO_2 present.

Table 1. Slope, y-intercept, and correlation coefficient for calibration curves

Run	Slope	Intercept	Correlation coefficient
1	0.152	−0.003	0.9998
2	0.150	−0.005	0.9992
3	0.152	−0.002	0.9998
4	0.148	−0.002	0.9997
5	0.148	−0.003	0.9992
6	0.157	−0.006	0.9991
7	0.153	−0.002	0.9992
8	0.152	−0.004	0.9997
9	0.157	−0.003	0.9995
AVG	0.152 ± 0.003	-0.003 ± 0.001	

One of the objectives of this research was to develop the reverse dual phase GDFIA system so it could be applied to hydrazine analysis. One of the findings has been that the flow rate of the donor stream is the single largest factor involved in the transport of analyte across the membrane. This information will be very valuable for future work.

The choice of method for the hydrazine determination was based on previous work performed in this laboratory.[6] Earlier, a search of the literature on gas sampling techniques lead to vapor detection tubes for hydrazine with a linear range was 0.3–2.5 ppm.[1] The tube used bromphenol blue and acid as the indicator reagent. Using this preliminary information, the BPB chemistry was investigated as a possible alternative to standard dimethylaminobenzaldehyde method.

In order to determine the optimum preconcentration time and flow rate of the sample, both factors were varied to determine the optimum results. The results are shown in Figs 7 and 8, respectively. At a 200 ml/min flow rate used in Fig. 7, 20 min was chosen as the amount of time required for sample preconcentration. The minimum necessary flow rate of the sample stream was 180 ml/min as seen in Fig. 8. The y-axis of Fig. 8 is the total absorbance minus any blank absorbance. The flow rate used in the rest of the experiments was 225 ml/min.

Several different membranes were tested to determine the most suitable membrane for

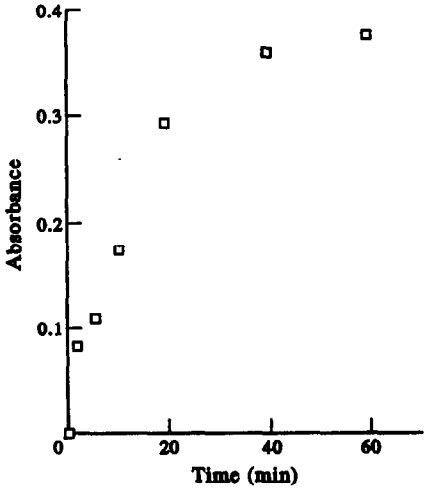

Fig. 7. Optimum flow rate for hydrazine system.

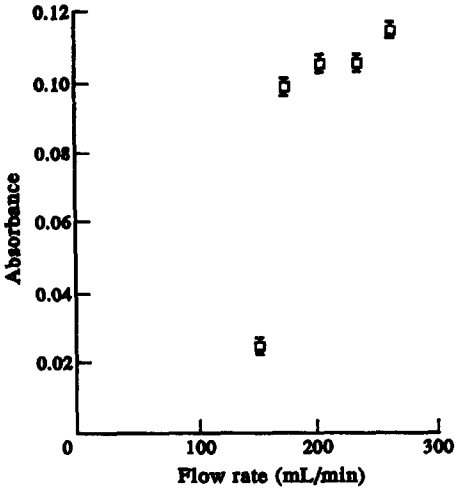

Fig. 8. Optimum preconcentration time.

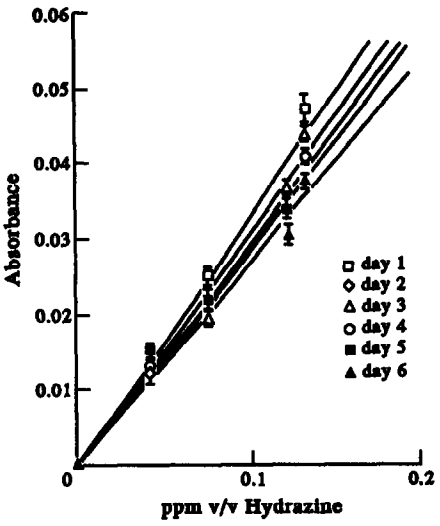

Fig. 10. Repeatability of BPB hydrazine system.

hydrazine transfer. The relative response of different membranes is shown in Fig. 9. The Celgard 2500 membrane is the most suitable in terms of response and durability.

In Chapter 3 the membrane efficiency for the CO_2 system was 31%. In the hydrazine–BPB system, the membrane efficiency was 17.4%. This efficiency was determined by calculating the concentration of hydrazine necessary to cause a pH change corresponding to 0.100 absorbance units. With that information and knowing the concentration of the gaseous hydrazine sample stream, the efficiency can be calculated by dividing the amount of hydrazine determined to be in the acceptor stream by the amount of hydrazine available.

The linear range of the BPB system is 0.035–0.140 ppm v/v hydrazine. The detection limit, defined as three times the signal-to-noise, is 0.010 ppm v/v hydrazine. The equation for the curve is $y = -1.076 \times 10^{-4} + 0.3163x$, and $R = 0.9997$. With the gas dilution system used in this research, the detection limit of 0.010 ppm v/v is the more realistic value for the system being investigated. The membrane in the hydrazine system did not last as long as the membrane in the CO_2 system. Hydrazine is more reactive than CO_2 and subsequently is more likely to react with or adsorb to the membrane. Daily calibration runs showed that the sensitivity decreased steadily over six days. The daily calibration runs are show in Fig. 10. The daily slope, intercept and correlation coefficient are shown in Table 2. The membrane degraded steadily over the six day period. A diffusion vial from VICI Metronics (Santa Clara, CA) was put in the flow diagram in place of the hydrazine source. The potential interferants were put in the diffusion vial separately to determine the impact of each one. The interference from monomethylhydrazine (MMH), 1,1-dimethylhydrazine (UDMH), and ammonia are shown in Table 3. The interference from carbon dioxide is negligible. Because the pK_{a1} for carbonic

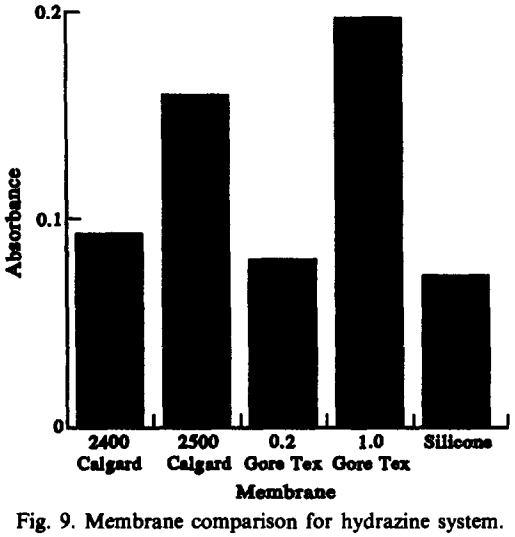

Fig. 9. Membrane comparison for hydrazine system.

Table 2. Absorbance data from daily calibration runs

Day	Slope	Intercept	R
1	0.338	6.21e-4	0.998
2	0.319	5.25e-4	0.991
3	0.318	4.09e-4	0.991
4	0.309	−2.22e-4	0.997
5	0.298	−7.18e-5	0.999
6	0.276	6.84e-4	0.994

Table 3. Table of relative interference responses

Interferant (10 ppm v/v)	ppm v/v response as hydrazine
Ammonia	0.086
MMH	0.016
UDMH	0.000

acid is around 6, the impact of carbonic acid dissociation is minimal. Carbon dioxide in the atmosphere is present at about 210 ppm v/v.[7]

CONCLUSION

The goal of this work was to be able to reach a detection limit which would be low enough to meet the 8 hr time weighted average level set out by the National Institute of Occupational Safety and Health (NIOSH).[8] This research has been successful in several ways. First, the detection limit is 0.010 ppm v/v of hydrazine. This limit of detection is 10 times lower than the TLV of 0.1 ppm v/v. The method gives a response every 10 min. This is much more attractive than an accumulator type of device which cannot give information about hydrazine levels at specific times during the 8 hr period. The method is very simple.

REFERENCES

1. J. Ruzicka and E. Hansen, *Flow Injection Analysis*, 2nd ed. John Wiley, New York, 1988.
2. G. E. Pacey and B. Karlberg, *Flow Injection Analysis, A Practical Guide*. Elsevier, Amsterdam, 1989.
3. G. E. Pacey, M. R. Straka and J. R. Gord, *Anal. Chem.*, 1986, **58**, 502–504.
4. J. S. Canham and G. E. Pacey, *Anal. Chim. Acta*, 1988, **214**, 385.
5. W. E. Van der Linden, *Anal. Chim. Acta*, 1983, **151**, 359–369.
6. K. J. Smith, Ph.D. Dissertation, Miami University, 1992.
7. A. L. Linch, *Evaluation of Ambient Air Quality by Personnel Monitoring*. CRC Press, Cleveland, OH, 1974, p. 41.
8. *Criteria for a Recommended Standard Occupational Exposure to Hydrazine;* DHEW(NIOSH) National Institute for Occupational Safety and Health, Cincinnati, OH, 1978.

Talanta, Vol. 40, No. 12, pp. 1967–1974, 1993
Printed in Great Britain.

0039-9140/93 $6.00 + 0.00

A TIME-BASED INJECTOR APPLIED TO THE FLOW INJECTION SPECTROPHOTOMETRIC DETERMINATION OF BORON IN PLANT MATERIALS AND SOILS

PABLO CARRERO, J. L. BURGUERA, M. BURGUERA and C. RIVAS
Department of Chemistry, Faculty of Sciences, University of Los Andes, P.O. Box 542, Mérida 5101-A, Venezuela

(*Received* 5 *January* 1993. *Revised* 15 *March* 1993. *Accepted* 18 *March* 1993)

Summary—A simple and flexible time-based injector is described for the introduction of almost any desirable volume of sample and reagents in flow systems. The feasibility of application is demonstrated by improving the azomethine-H spectrophotometric method for the precise and accurate determination of boron in soil and coffee plant tissues. On-line programmed functions include: sequential injections and zone trapping, with a significant reduction of sample and reagent consumption.

Flow injection analysis (FIA) is by definition the insertion of a defined and reproducible volume of the sample into a carrier stream.[1] Instead of insertion or intercalation, the term injection is now understood and used under a broad sense of reproducible introduction of a well-defined zone of fluid into a carrier stream, quite regardless of the means of introduction.[2] Conceptually, the means of injection, and devices designed for this purpose can be divided into two categories: (1) volume-based injectors; and (2) time-based injectors, or a combination thereof,[3] which are reviewed elsewhere.[1,3,4] Since the proposal of FIA,[5] the sample introduction devices have evolved from simple dispositives with one syringe operated manually, to microcomputer controlled rotary[4] and solenoid valves.[6–8] An electronically operated time-based injector, using a two-way solenoid valve is presented here. It permits the reproducible and sequential introduction of variable volumes of sample and reagents into flowing systems with zone trapping and with a significant reduction in their consumption. Although, a large number of analytical methods have been employed for determining boron in water, soil and plant material samples,[9–11] the spectrophotometric method using azomethine-H–boron complex has been selected for its simplicity, sensitivity and speed.[12] The procedure does not involve concentrated acid, which makes it readily suitable for automated routine operation.

EXPERIMENTAL

Apparatus

A schematic diagram of the flow system is given in Fig. 1. Determinations were performed with a Varian 634 spectrometer with a home-made flow through cell of quartz of 1.0 mm i.d., 2 cm length and 30 μl capacity. The system also included a Gilson Minipuls 2 peristaltic pump, a home-made time-based injector (see below),

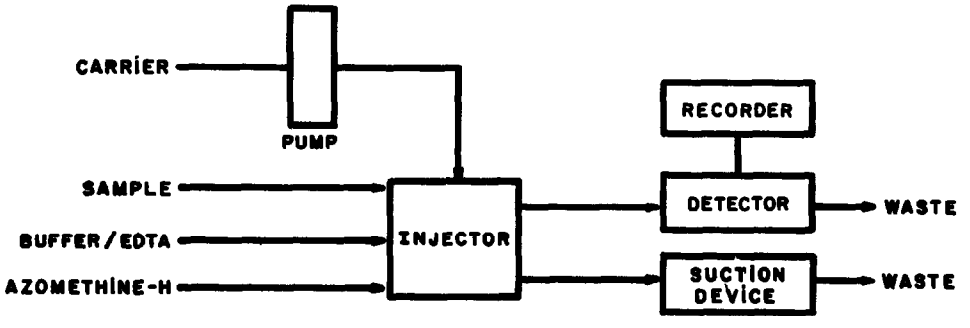

Fig. 1. Schematic diagram of the flow system.

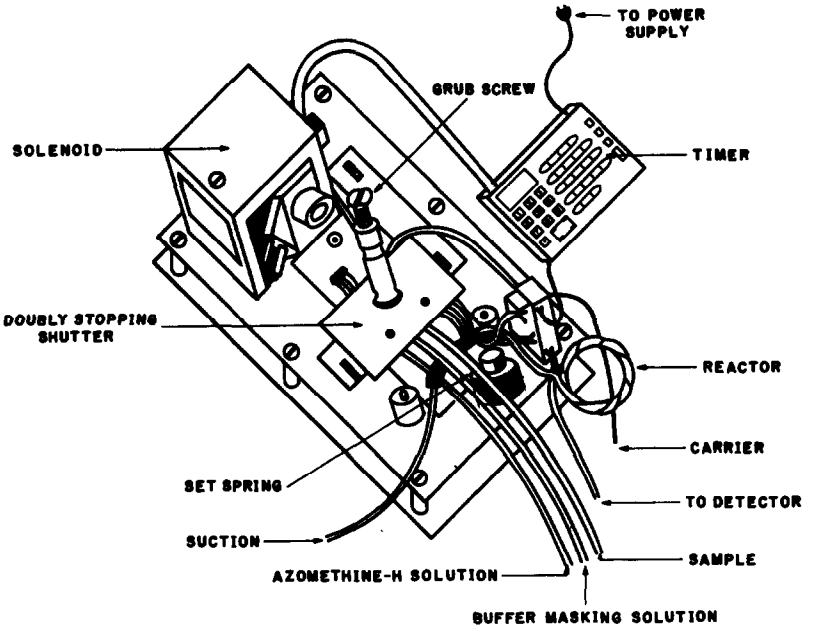

Fig. 2. Diagram of the time-based injector. The grub screw controls the doubly stopping shutter.

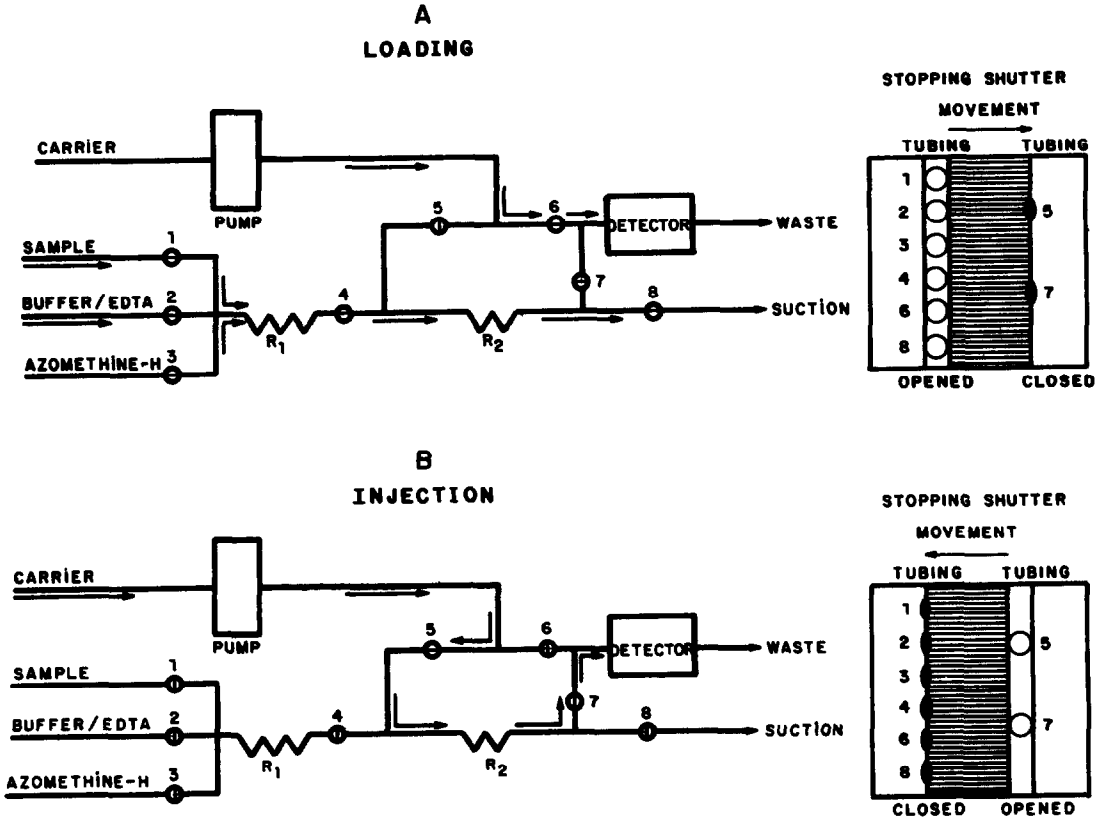

Fig. 3. Operating principle of the configuration designed for the determination of boron by the azomethine–H spectrophotometric method. R_1, reactor; R_2, connecting line to the detector. Each number correspond to a given tubing as indicated in both figures.

a Cole–Parmer 156 recorder and a suction air-pressurized device, 0.8 mm i.d. Tygon tubing was used throughout, unless otherwise stated.

The suction air-pressurized device consists of a bottle with a pressure regulator up to 40 cm Hg and a Iwaki AP-115 air pump which produces the suction pressure. The time-based injector (Fig. 2) consists of a Gralab 900 timer which permitted to dispense electronically controlled pulses to the solenoid valve. In this way, a doubly stopping shutter either closed or opened (by pressing or releasing) any selected set of tubing at a fixed time, thus allowing sequestration of sample and/or reagents and sequential injection.

For the present work the flow system and setup shown in Fig. 3 was used. In the loading position (Fig. 3a) the sample and buffer/masking and azomethine–H reagents are drawn through different sampling loops, confluence at point "a", mix inside R_1 and R_2. When the solenoid valve is switched to the alternate position (injection cycle), aliquots of the trapped sample/reagents mixture in R_2 are intercalated in the carrier stream and therefore directed to the analytical path (Fig. 3b), allowing the detector to quantify the formation of the coloured species. The absorbance, which is proportional to the boron content in the sample, constitutes the basis of the measurements. When the solenoid valve is operated back to the loading position aliquots of the sample/reagent mixture fill a given section of R_2, which are also intercalated at will in the carrier stream. The alternation of both solenoid positions allows the repetitive and reproducible intercalation of sample/reagent mixture plugs in the carrier stream.

Reagents

Unless stated otherwise, all solutions were prepared from analytical-reagent grade chemicals and kept in polyethylene flasks. Deionized, distilled water was used throughout. A stock boron solution (1.000 g/l.) was prepared by dissolving 5.716 g of boric acid in water and diluting to 1 l. Working solutions of boron were prepared by suitable dilution with 0.1*M* hydrochloric acid. The derivatizing reagent was prepared by dissolving 0.25 g of azomethine–H (Sigma) in 25 ml of water and kept at 4° in a refrigerator (where it remains stable for at least 1 week). A buffer/masking solution was prepared by dissolving 115 g of ammonium dihydrogen phosphate (2*M*), 132 g of diammonium hydrogen phosphate and 25 g of EDTA in water to give 500 ml of solution; the final pH of this solution was 6.8.

Sample preparation

Tissue samples were dried in an oven at 70° for 3 days, ground and ashed in covered porcelain crucibles at 500° for 2 hr. Ashes were taken up in 10 ml of 0.1*M* hydrochloric acid and filtered through Whatman No. 40 filter paper, and finally diluted to 25 ml with 0.1*M* hydrochloric acid.

The soils were selected from the root of each coffee tree. The samples were air dried for 5 days and crushed to pass through an 80 mesh sieve. Ten-gram soil samples were transferred to a 150-ml boron-free round bottom flask. Then 50 ml of water were added and the flask was attached to a reflux condenser and boiled for 10 min. After cooling, 0.05 g of calcium chloride dihydrite were added and the mixture was filtered through Whatman No. 2 filter paper. Twenty-five millilitres of the solution were transferred to a covered porcelain crucible, and after the addition of 2 ml of a saturated calcium hydroxide solution, evaporated to dryness, ignited gently to destroy nitrates and organic matter, cooled, taken up in 10 ml of 0.1*M* hydrochloric acid, filtered through Whatman No. 40 filter paper, and finally diluted to 25 ml with 0.1*M* hydrochloric acid.

Procedure

All reagents were fed through their respective lines at room temperature. Polyethylene sample cups were used to avoid possible boron contamination from glass containers. The operating conditions chosen were optimized to produce the highest and most reproducible signals (Table 1). After sequentially activating the solenoid valve to complete the loading and injection cycles, the absorbance signals were monitored at 420 nm. When the analyses of each sample was completed, the system was cleaned by circulating 0.1*M* hydrochloric acid solution through the sample line for at least 30 sec. A calibration curve was obtained by using the absorbance readings for each standard concentrations. The recorder signals were evaluated as well in order to control more strictly the dispersion processes. The boron concentration of each sample was determined by reference to this analytical curve. The carrier solution was pumped continuously throughout the process to ensure a stable baseline. In this work, the blank

Table 1. Optimized operating conditions for the determination of boron by the azomethine-H spectrophotometric method using a multipurpose time-based injector for flow injection systems

Component	Parameter	Value
Spectrophotometry	Wavelength	420 nm
	Slit width	2 nm
Chemical	pH of buffer/masking solution	6.8
	Ammonium–phosphate buffer concentration	2*M*
	Azomethine-H concentration	1% (w/v)
Injector	Time of sample/reagents entrapment	2 min
	Time of loading	
	Time of injection	2 sec
	Buffer/masking, azomethine-H and sample solutions mixing ratio	1:1:3
	Suction pressure	34 cm Hg
	Length of reactor R_1	1 m
FIA	Length of connecting tube R_2	47 cm
	Carrier flow rate	5.5 ml/min
	Volume of sample (90 μl), buffer/masking (30 μl) and azomethine-H (30 μl) mixture solution	150 μl

was always substracted from the signal by performing measurements with and without any boron content in the sample solution.

RESULTS AND DISCUSSION

In the injector under study, only the trapped portion of the sample zone inside R_2 is intercalated in the carrier stream, whereas selected portions of the sample zone inside R_1 is used for further measurements. The instrumental parameters used were: 420 nm wavelength and 2 nm spectral slit width.

A systematic investigation was necessary in order to establish the optimum experimental conditions. Various chemical and instrumental operating parameters were varied individually while the others were kept constant, and were optimized with respect to absorbance measurements. Although the calibration graph was essentially linear up to 80 mg/l. (see below), for practical reasons, in all cases, the boron concentration used for optimization studies was within the working range (from 0.5 to 6 mg/l.). Initial studies were carried out to determine the influence of the injector solenoid activation time and suction pressure of sample and reagents on sample volume and its reproducibility. The sample volume was assessed by a procedure similar to that used earlier,[6] by the differences in weight over cycles of 50 injections. Almost any desirable injection volume can be injected by increasing the solenoid activation time (Figs 4a, b) and the pressure of aspiration or suction of sample and reagents (Figs 4c, d). However, the sample volume cannot be increased at will

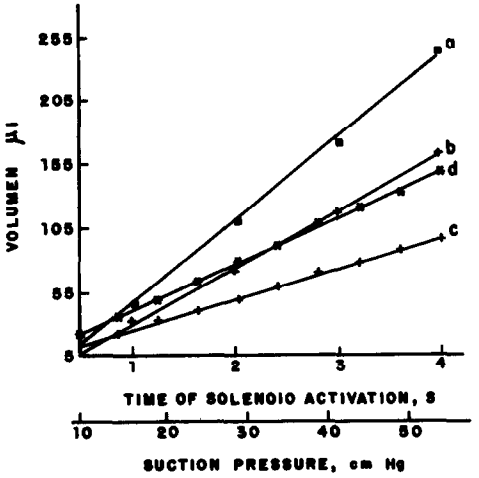

Fig. 4. Effect of solenoid activation time (a, 1 sec; b, 2 sec) and of suction pressure (c, 34 cm Hg; d, 54 cm Hg) on sample volume.

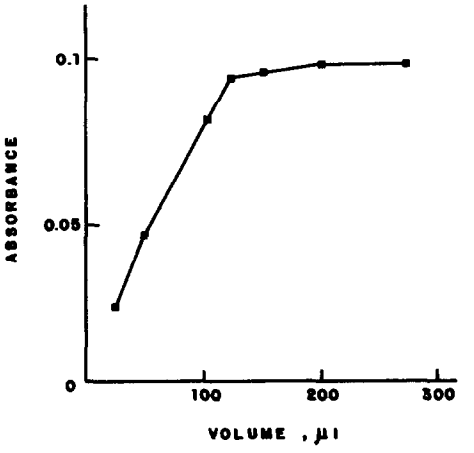

Fig. 5. Effect of sample/azomethine-H/buffer mixture volume on absorbance. 5 mg B/l. Other conditions are as specified in Table 1.

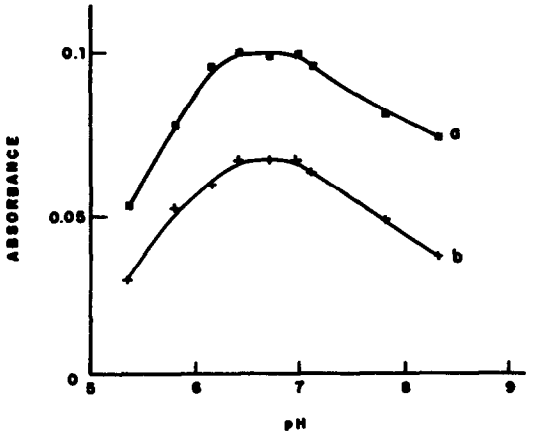

Fig. 6. Effect of pH on absorbance. (a) 5 and (b) 3 mg B/l. Other conditions are as specified in Table 1.

(Fig. 5), over 250 μl, the precision deteriorated, the relative standard deviation (r.s.d.) being usually increased from 0.7 to about 4.5% for 500 μl sample volumes (10 measurement series). This drop in reproducibility at higher injected volumes is probably due to either a large reduction of the suction pressure or to limitations of the injector internal bore diameter (0.8 mm). It should be reported that day-to-day measurements of sample volume in function of pressure of aspiration varied considerably from one day to another (up to 7% r.s.d.); therefore, it was preferred to vary the solenoid activation time in order to fix a given volume.

The color of the azomethine–H–boron complex is highly pH sensitive,[12] specially in the 6.4–7.0 range (Fig. 6). As the pH difference between buffer and the solution within the FIA manifold may vary, strict pH control is necessary during the course of the measurement in order to maintain the color development reproducible, constant and sensitive. A high ammonium–phosphate buffer concentration (2*M*) has several advantages. It has a high buffering capacity at the required pH 6.8, as the pH between buffer and the solution sent to waste was found to decrease only to 6.6, the absorbance decreased at pH below 6.4 and above 7.0. Also, this buffer is not corrosive and the preparation is simple, without creating offensive fumes.

The influence of the azomethine–H concentration ranging from 0.5 to 1.75% (w/v) was investigated. Figure 7 shows that the absorbance values increase with an increase in the concentration of azomethine–H. The absorbance markedly decreased at concentrations below 1.0%, and the increments are small at values above this concentration. Considering that high concentrations of azomethine–H will cause larger reagent blanks and also the reagent cost factor, its concentration was fixed at 1.0%.

Absorbance grows slowly, as the time of the reaction involved, discussed elsewhere,[13,14] proceed inside R_1 after the loading cycle, and as the boron content in the sample increases (Fig. 8). The boron concentration affects the time of increasing formation of the coloured condensation species. The decreased signals obtained during the first minutes were due to insufficient development of the chemical reaction, and it seems that they do not appreciably increase above 3 min. Times of 2–3 min after the loading cycle seem to be a good compromise between good sensitivity, sampling frequency and the formation of the coloured species. After this time, the injection cycle proceeds and then

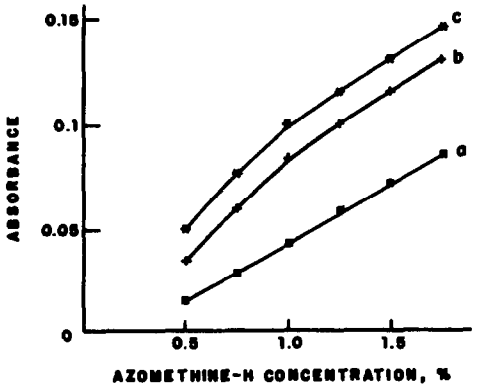

Fig. 7. Effect of azomethine–H concentration. a, reagent blank; b, with 4 mg/l boron; c, with 5 mg/l. boron. Other conditions are as specified in Table 1.

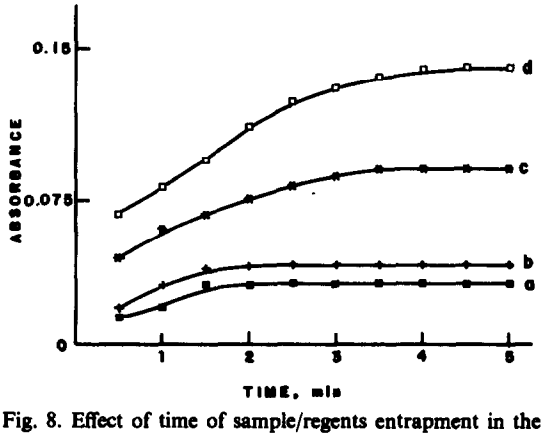

Fig. 8. Effect of time of sample/regents entrapment in the reaction coil and of boron concentration on absorbance. a–d indicate 15, 20, 50 and 80 mg B/l. Other conditions as specified in Table 1.

aliquots of sample are sequentially delivered at a rate of about 6 min.

Initially, the tubing diameter of sample and reagents was kept at 0.5 mm i.d., which allowed the mixing of equal volumes of the solutions during the loading cycle in R_1. By varying the tubing diameter, the flow-rate ratio of the solutions and therefore their mixed volumes in R_1 were different. For buffer/masking, azomethine–H and sample solutions flow-rate ratios of 2:2:1, 1:1:1, 2:1:2, 1:2:2 and 1:1:3 the absorbance values were of 0.020, 0.035, 0.041, 0.043 and 0.050, respectively. The results obtained by the 1:1:3 mixed volume ratio were just as reproducible and more sensitive by 43% than those obtained with the 1:1:1 mixed volume ratio. The various absorbance values obtained are related to the different sample-reagents mixing ratios and therefore to different sample dispersion patterns within this trapping zone tubing, whose i.d. was always kept at 0.8 mm.

In order to study the effect of the matrix on absorbance, standard addition graphs for fruit, leaves and soil digested samples were prepared by adding various amounts of boron (from 2 to 8 mg/l.). When no masking agent was used the sensitivities of the analytical graphs obtained were approximately the same from that obtained with the aqueous standard solution. This suggested that the proposed procedure is slightly affected by interfering species.[15–17] Although the full composition of the samples under study is not known, the addition of EDTA in the buffer solution was found to minimize the effect of matrix interferents, as the slope of standard additions graph in the presence of EDTA were not significantly different (difference between slopes <3%) from those obtained with the boron standard (0% digested sample).

On the bases of these observations, appropriate conditions for flow injection were examined. In this system, the response increased linearly up to 150 μl of injected volumes of mixed solutions in R_2, however, the injection of larger volumes produced only slight effect on the response because it surpasses the physical volume of the flow-through cell. Therefore, an injected volume of 150 μl was found to be the optimum. The effect of the reaction tube (R_1) length, was investigated. The length of this tube was found not to be critical due to the characteristics of the flow system used, where the entrapment of the sample/reagent mixture occurs in order to increase the formation of the coloured species. The effect of the dispersion tube (R_2) on absorbance was examined for various coil lengths between 47 and 225 cm. The absorbance decreased with increasing coil length owing to dispersion (Fig. 9), the instrumentation did not allowed the use of coil length below 47 cm.

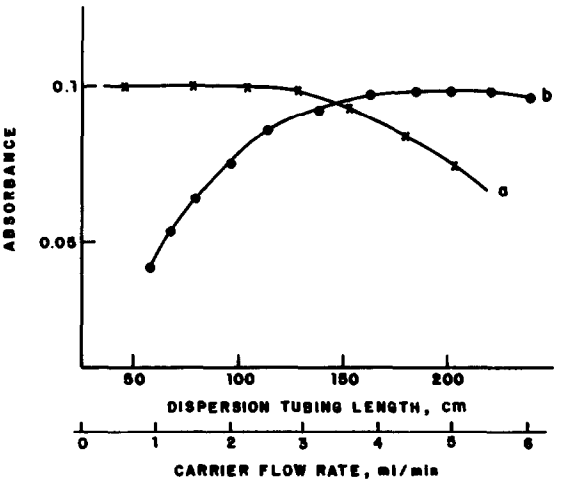

Fig. 9. Effect of the (a) tubing length connecting the injector–detector section and (b) carrier flow rate on absorbance. 5 mg B/l. Other conditions are as specified in Table 1.

Different flow-rates of the carrier solution were tested by changing the pumping rate. The sensitivity increased with increasing flow-rate until an almost steady-state signal was obtained in the range 4.0–5.5 ml/min, thereafter a slight decrease over 5.5 ml/min was observed (Fig. 9).

The calibration graph was prepared using the spectrometer, chemical and flow injection conditions given in Table 1. The maximum peak height increased linearly with element concentration as expressed by the equation $A_B = 0.016 + 0.017C_B$, $r = 0.9996$, where A represents absorbance and C_B (0.1–80 mg/l.) represents the boron concentration. This calibration graph was essentially linear up to 80 mg/l. of boron and thereafter starts to deviate to almost invariable values over 120 mg/l. due to the absorbance of the azomethine–H reagent.[12,15] However, for practical reasons, working calibration graphs were prepared daily in the concentration range from 0.1 to 6 mg/l. The detection limit was evaluated by calculating the mean standard deviation of eight sets of replica blank determinations. The detection limit considered as the amount of boron which gives an absorbance value correspondent to three times the standard deviation of the blank signal was found to be of 4.5 ng (0.05 mg/l.).

Table 2. Boron as determined by the proposed azomethine–H procedure using the time-based injector for flow injection systems compared with the manual curcumin method ($n = 10$)

Sample	Boron content* ($\mu g/g$)	
	This work	Manual curcumin method
Coffee-tree leaves	116.2 ± 7.8	114.4 ± 9.2
Coffee fruits	45.3 ± 5.0	44.0 ± 6.7
Soil	28.5 ± 4.4	27.4 ± 5.2

*Mean ± S.D.

The FIA manifold under evaluation is remarkably stable: after 6 hr of continuous operation, only minor changes in the sample and reagent volumes injected (usually less than 3%) and in the coefficients of the calibration equation (usually less than 5%) were detected. From successive measurements of typical samples the standard deviation of the absorbance signals were typically below 1%, whereas from measurements of five different portions of the various digests of soil and plant tissues, were calculated as 1.2, 1.5 and 2.8, respectively.

To check the accuracy of the method, five pooled specimens of the samples under evaluation were also analysed by the conventional manual curcumin spectrophotometric method.[16] The results given in Table 2 show a good agreement with the present results, which is an indication that the accuracy of the proposed method is satisfactory. The accuracy was further checked by recovery tests. Recovery of boron was checked by the addition of μl-aliquots of boron standard solution to five samples before the digestion process. The recoveries of 2, 4 and 6 μg B/g added were between 98.0 and 101.7% (for leaf tissue), 96.5 and 99.2% (for fruit tissue) and 96.0 and 98.5 (for soil).

Various plant tissues and soil samples ($n = 20$) were analysed in the proposed FIA system. The boron contents varied from 109.4 to 125 μg/g (mean ± S.D. = 116.2 ± 6.2 μg/g) for coffee-tree leaves, from 38.5 to 49.8 μg/g (mean ± S.D. = 43.9 ± 4.0 μg/g) for coffee fruits and from 22.4 to 34.6 μg/g (mean ± S.D. = 27.8 ± 3.8 μg/g) for soils. The soils analysed were from coffee plantations located in Santa Cruz (Mérida State, Venezuela) areas, and contained boron concentrations in the range typical for most soils reported in the literature.[12,17,18] The values reported in this study for coffee-tree leaves for boron tend to be higher than those values reported for orange-tree leaves, tobacco leaves,[14] non-edible plant leaves,[12,19] some fruits, vegetables and grains,[17] but are lower with those reported for edible leaves[20] and citrus limonum.[17] Our values of boron for coffee fruit are in close agreement with those previously reported for different edible seeds and fruits[15] in the same range as those reported for legumes,[17,21] but higher than those reported for some fruits, vegetables and cereal grains.[17]

The FIA injector described here allows the injection or intercalation of reproducible variable volumes into flowing systems, mixing of different solutions at different ratios on-line and entrapment of sample/reagents mixture. As the sample and reagents are not consumed during the stoppage of the sample zone, the system utilizes sample, azomethine–H and buffer/masking solutions of 90, 30 and 30 μl, respectively, per measurement (Table 1), which are considerably less than those consumed in previously reported in-batch[14] and automatic methods.[9,10,12,15] A measurement rate (*ca.* 200 measurements/hr) is readily achieved. However, the sampling rate will depend on the characteristics of the chemistry involved in the procedure. The FIA system provides precise, and accurate results for the determination of boron in soils and plant tissues using the selected azomethine–H spectrophotometric method.

Acknowledgement—The authors appreciate the financial support from CONICIT (Consejo Nacional de Investigaciones Cientificas y Tecnológicas), Project S1.

REFERENCES

1. B. Karlberg and G. E. Pacey, *Flow Injection Analysis. A Practical Guide*, p. 38. Elsevier, Amsterdam, 1989.
2. Z. Fang, *Microchem. J.*, 1992, **45**, 137.
3. J. Ruzicka and E. H. Hansen, *Flow Injection Analysis*, 2nd Ed., p. 258. Wiley, New York, 1988.
4. J. F. Van Staden, *Basic Components and Automation*, In J. L. Burguera (ed.), *Flow Injection Atomic Spectroscopy*, Chapter 3, Dekker, New York, 1989.
5. J. Ruzicka and E. H. Hansen, *Anal. Chim. Acta*, 1975, **78**, 145.
6. J. L. Burguera, M. Burguera, C. Rivas, M. de la Guardia and A. Salvador, *Anal. Chim. Acta*, 1990, **234**, 253.
7. J. L. Burguera, M. Burguera, C. Rivas, M. de la Guardia, A. Salvador and V. Carbonell, *J. Flow Inj. Anal.*, 1990, **7**, 11.
8. B. F. Reis, M. F. Giné, F. J. Krug and H. Bergamin F., *J. Anal. Atom. Spectrom.*, 1992, **7**, 865.
9. I. Sekerka and J. F. Lechner, *Anal. Chim. Acta*, 1990, **234**, 199.
10. F. J. Krug, J. Mortatti, L. C. R. Pessenda, E. A. G. Zagatto and H. Bergamin F., *Anal. Chim. Acta*, 1981, **125**, 29.
11. R. Capelle, *Anal. Chim. Acta*, 1961, **24**, 555.
12. M. A. Z. Arruda and E. A. G. Zagatto, *Anal. Chim. Acta*, 1987, **199**, 137.

13. D. Chen, F. Lázaro, M. D. Luque de Castro and M. Valcárcel, *Anal. Chim. Acta*, 1989, **226**, 221.
14. J. Ferran, A. Bonvalet and E. Casassas, *Agrochim.*, 1988, **32**, 71.
15. A. J. Salazar and C. T. Young, *J. Food Sci.*, 1984, **49**, 72.
16. R. A. H. Crawley, *The Analyst*, 1964, **89**, 749.
17. D. L. Tsalev and Z. K. Zaprianov. In Atomic Absorption *Spectrometry in Occupational and Environmental Health Practice, Vol. 1. Analytical Aspects and Health Significance*, p. 103. CRC Press, Boca Raton, Fl, 1983.
18. M. W. Pritchard and J. Lee, *Anal. Chim. Acta*, 1984, **157**, 313.
19. I. López G., M. Hernández C. and C. Sánchez-Pedreño, *The Analyst*, 1985, **110**, 1259.
20. R. R. Elton-Bott, *Anal. Chim. Acta*, 1976, **86**, 281.
21. J. J. van der Lee, I. Walinga, P. K. Manyeki, V. J. G. Houba and I. Novozamsky, *Commun. Soil Sci. Plant Anal.*, 1987, **18**, 789.
22. W. D. Basson, R. G. Bohmer and D. A. Stanton, *The Analyst*, 1969, **94**, 1135.
23. R. A. Edward, *The Analyst*, 1980, **105**, 139.

Talanta, Vol. 40, No. 12, pp. 1975–1980, 1993
Printed in Great Britain.

0039-9140/93 $6.00 + 0.00

DETERMINATION OF PLATINUM AND PALLADIUM IN STRONGLY ACID SOLUTION BY MEANS OF FLOW INJECTION ANALYSIS

KLAUS R KOCH* and DEREK AUER

Department of Chemistry, University of Cape Town, Private Bag Rondebosch, Cape Town, 7700, South Africa

(*Received* 12 *April* 1993. *Accepted* 12 *June* 1993)

Summary—Microamounts of Pt(II/IV) (0.25–800 μg/ml) and Pd(II) (5–600 μg/ml) in >0.5 *M* hydrochloric acid can readily be determined by means of a simple FIA method based on the selective reaction of tin(II)chloride with these metals. The FIA method has a high linear dynamic range, and is relatively free from interferences of many transition metals, with the exception of Au and Rh; small amounts of other PGMs can be tolerated. Determination of Pt on a hydrogenation catalyst by this method compares well with that found by flame atomic absorption spectroscopy. By monitoring at two or more wavelengths, Pt and Pd can be determined in mixtures by this means, to yield a simple, cost-effective FIA method for possible on-line determinations and quality control of, in particular, Pt containing acidic refinery and other process streams.

The platinum group metals (PGMs), widely used in many important chemical processes as efficient catalysts, are of importance in the electronics industry, while the significance of, particularly, Pt is growing in cancer chemotherapy.[1] The control of automobile exhaust-gas emissions using Pt and Rh rich catalytic converters is currently utilizing the largest share of the world production of these metals,[2] while use in this application is set to grow substantially in the next decade as ever more stringent exhaust emission standards are being introduced by legislation in the developed world.[3] Against this background, the need for the rapid and accurate determination of the PGMs in process and quality control is obvious. A recent survey of methods for the determination of these metals attests their importance, and shows that overall the predominant analytical methods in use are based on atomic absorption and/or emission spectroscopy.[4] While the power of such instrumental methods is indesputable, these methods are usually laboratory based, rather expensive and not readily suited for automation and on-line analysis. The development of the family of flow-injection based techniques has recently been reviewed,[5] and it is clear that such methods offer many advantages in the performance of process control and on-line analysis. Surprisingly however, a survey of the literature reveals only very few flow-injection analysis (FIA) based determinations of the PGMs, although recent reports of the determination of Pd[6–8] and Pt[9] by FIA methods suggest a growing interest in this area.

In this paper we report the first part of the development of a simple, cost effective method for the determination of the potentially simultaneous photometric determination of Pt(II/IV) and Pd(II) in hydrochloric acid solution by means of FIA. Our method is based on the long known,[10] but until recently poorly understood[11,12] reaction of tin(II)halides with Pt(II/IV) and Pd(II) in aqueous acid solution. This reaction formed the basis of a highly selective batchwise spectrophotometric determination of Pt(II/IV) some four decades ago.[12–15] In the batchmode however, the latter method suffers from substantial disadvantages, principally the need for accurate timing, careful control of reaction conditions and working under anaerobic atmospheres, so that often erratic results are obtained. We have found that this chemistry is ideally suited for the flow-injection determination of Pt and Pd, making it possible to exploit the high selectivity of the reaction of tin(II)chloride with these metals in hydrochloric acid solution.

*Author for correspondence.

EXPERIMENTAL

Apparatus

A single line FIA manifold using 0.8 mm ID PTFE tubing, equipped with a Spetec Perimax 12 four channel pump and a Rheodyne 5020 6-port PTFE rotary injection valve with a 180 μl sample loop, was used for preliminary experiments. Commercially available Omnifit PTFE/PEEK connectors and mixing tees, and reaction coils of variable lengths were coiled around a fixed 15 mm diameter plastic rod. A 2 mm path length U-shaped quartz flow cell and a Varian Superscan-3 UV/visible spectrophotometer operation in fixed wavelength absorbance mode with the abscissa in a time drive configuration served as a detector. For determinations of trace amounts of Pt (<5 μg/ml) a modified computer controlled manifold consisting of a carrier (1 *M* HCl) and reagent stream ($SnCl_2$) merged into a single line with a mixing tee after the sample injection valve, was found to be advantageous (Fig. 1).

Materials and methods

All solutions were prepared with glass distilled water and concentrated Analar grade HCl, using glassware previously soaked in nitric acid. Stock solutions containing 1000 μg/ml each of Pt(II) and Pd(II) were prepared from K_2PtCl_4 and K_2PdCl_4 obtained from Johnson Matthey, the salts being used without further purification.

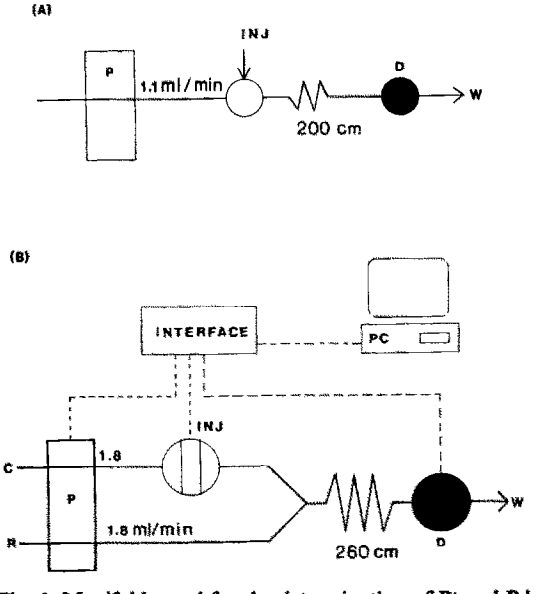

Fig. 1. Manifolds used for the determination of Pt and Pd: (A) carrier 0.1 *M* $SnCl_2$, 1.0 *M* HCl (B) carrier 1.0 *M* HCl, reagent 0.3 *M* $SnCl_2$.

A 1000 μg/ml BDH atomic absorption standard solution served as independent calibrant and source of Pt(IV) solution. Tin(II)chloride solutions were prepared from Analar grade $SnCl_2.2H_2O$, by dissolving the desired amount of salt in the required amount of conc. HCl and allowing the initially cloudy solution to stand for 15–20 min in a warm water bath until completely clear, followed by dilution to volume with water. These solutions were standardized by titration with potassium iodate, after which a few small pieces of metallic tin were added to the tin(II)chloride solution to preserve them from oxidation by atmospheric oxygen. It should be noted that the hydrochloric acid concentration of these tin(II)chloride solutions should be kept above 0.5 *M* to prevent hydrolysis of the stannous chloride. Platinum solutions were standardized where necessary by means of flame atomic absorption spectroscopy using a Varian Techtron 1000 AAS with a strongly oxidizing air–acetylene flame at 265.9 nm, slit width 0.2 nm and 10 mA lamp current. All Pt containing solutions were made up to contain 0.2(w/v)% La^{3+} (with $La(NO_3)_3.6H_2O$) as interference suppressant.

RESULTS AND DISCUSSION

Determination of platinum

The reaction between $SnCl_2$ and $PtCl_4^{2-}$ or $PtCl_6^{2-}$ in >0.5 *M* hydrochloric acid solutions rapidly leads to the development of an intensely cherry red colour, the origin of which is now known to result from the rapid reduction of any Pt(IV) species,[16] followed by or concomitant with, complex formation of $PtCl_4^{2-}$ with the $SnCl_3^-$ species to yield a series of anionic $[Pt(SnCl_3)_nCl_{4-n}]^{2-}$ ($n = 1$–4) complexes, as well as the relatively stable $[Pt(SnCl_3)_5]^{3-}$ complex anion.[11,12] The latter complex has been characterized by X-ray crystallography in the solid state[17] and has been shown to predominate in aqueous HCl containing sufficient $SnCl_2$.[12,18] These solutions show characteristic UV/visible absorption spectra with absorption maxima at $\lambda = 310$ nm (molar absorptivity $\sim 3.95 \times 10^4$), 400 nm (absorptivity $\sim 7.8 \times 10^2$), and 475 nm (shoulder) as shown in Fig. 2. Although the overall rate of the complex formation is not accurately known, in the presence of excess $SnCl_2$, steady state is reached within a few minutes.

Preliminary experiments to establish optimum conditions for the determination of Pt by

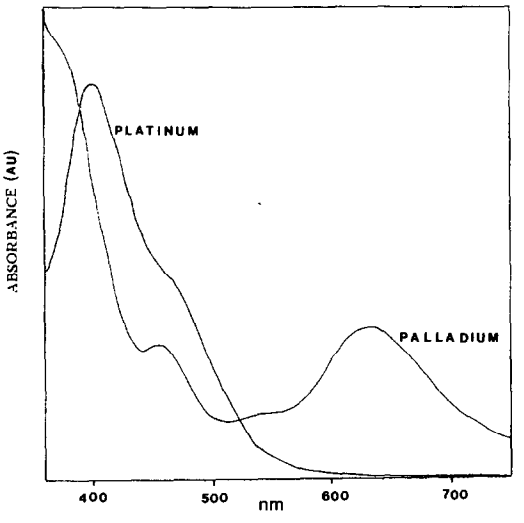

Fig. 2. Absorption spectra of Pt(IV) and Pd(II) in 1.0 *M* HCl containing excess $SnCl_2$ at steady state.

means of FIA were undertaken with a simple single line manifold equipped with a 2 m reaction coil and monitoring at 400 nm. Using a carrier stream with fixed $[SnCl_2] = 0.057$ *M*, the hydrochloric acid concentration was varied from 0.3 to 3.9 *M* and peak height monitored for separate injections containing 20 μg/ml Pt(IV) and Pt(II). Within experimental error there was no difference between the heights of the Pt(II) and Pt(IV) signals, confirming rapid reduction of the latter to Pt(II) followed by complex formation. The variable HCl concentration of the carrier stream does affect the peak height in a non-linear way, relatively higher values being obtained in the 0.3–0.8 *M* and >2.1 *M* HCl range, reaching a plateau in the 1.0–2.1 *M* range, where peak heights were effectively constant. We thus arbitrarily chose to fix the HCl concentration of the carrier stream at 1.0 *M* throughout; variations of ± 0.2 *M* do not significantly affect the peak heights other factors being equal.

The optimum $SnCl_2$ concentration was then found by varying its concentration in the carrier in the range 0.025–0.5 *M*. For the more concentrated solutions substantial viscosity differences between the carrier stream and sample injections result in undesirable effects, so that for this and for reasons of economy, the $SnCl_2$ concentration was kept as low as practical and set at 0.1 *M* $SnCl_2$ using the single line manifold. The flow rates and reaction coil lengths were also varied taking into account other variables, which led to a set of near optimum conditions: 1.0 *M* HCl, 0.1 *M* $SnCl_2$, flow rate 1.1 ml/min, reaction coil length 2 m and sample injection volume 180 μl. With these conditions 20 repeat injections of 20 μg/ml Pt(IV) gave highly reproducible peak heights (absorbance ~0.1 AU, RSD = 0.6%) and excellent day-to-day reproducibility (RSD < 1.1%), so that 30 injections per hr could comfortably be achieved with negligible carryover between successive high (100 μg/ml) and low (10 μg/ml) Pt(IV) injections.

With the above conditions, a rapid method for the determination of Pt(II/IV) obtains which has a high dynamic range, the analytical sensitivity of the response depending only on the selected wavelength. At $\lambda = 460$ nm completely linear calibration plots are obtained without dilution for a Pt(IV) range of 10–800 μg/ml, as shown in Fig. 3a. Such high dynamic ranges are generally not achievable in flame atomic absorption (FAAS) or atomic/plasma emission spectroscopic (AES/PES) methods without sample dilution.[4] High dynamic ranges can be a substantial advantage in methods designed for on-line applications which may have to deal with highly variable Pt(II/IV) concentrations. On the otherhand, using the single line manifold and monitoring at $\lambda = 400$ nm in the absence of interferents, Pt concentrations in the 1–200 μg/ml range can readily be determined. We found that the sensitivity of the determination could be further improved using a slightly modified two-line manifold with 1.0 *M* HCl as carrier stream into which the sample is injected followed by merging this zone with a 0.3 *M* $SnCl_2$ reagent stream prior to the detector (Fig. 1b). With this manifold monitoring at $\lambda = 400$ nm, the sensitivity of the determination

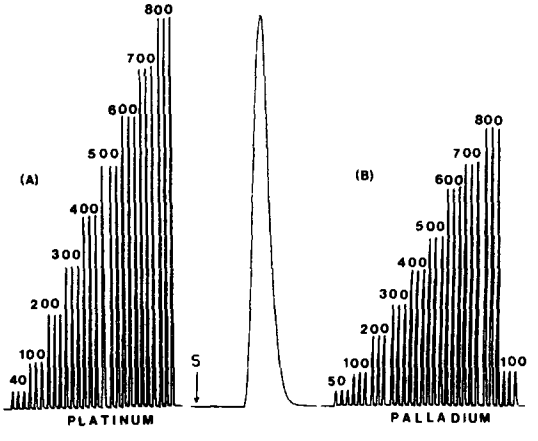

Fig. 3. Typical calibration data using a single-line manifold monitoring at 460 nm for (a) Pt(IV) and (b) Pd(II). Numerals refer to concentrations in μg/ml.

of Pt can be improved by a factor of 10 to cover the range of 0.1–2 μg/ml with a limit of quantification of *ca* 0.05 μg/ml. In principle by monitoring at $\lambda = 310$ nm, a further sensitivity improvement of between 2 and 4 times is possible, but some background effects complicate this and we are investigating ways of circumventing these.

A comparative study of the determination of Pt by the proposed FIA method and FAAS using a sample of hydrogenation catalyst of platinized asbestos yielded satisfactory agreement. Dissolution of the Pt using *aqua regia* followed by volatilization of excess HNO_3 with conc. HCl and suitable dilution yielded 12.0% (w/w) Pt as found by FIA compared to 12.2% (w/w) Pt obtained by FAAS for triplicate determinations.

Determination of palladium and platimum simultaneously

The reaction of $PdCl_4^{2-}$ with $SnCl_2$ is much more rapid and apparently more complicated than that with $PtCl_4^{2-}$, resulting in a series of rapid colour changes, from yellow–orange to red ($\lambda = 355,420$ nm) through blue and finally to green ($\lambda = 635$ nm). The origin of these changes is not well understood, although it has been established that several complex species are involved the nature of which depends on *inter alia* the Pd:Sn mole ratio and the HCl concentration.[19,20] Under conditions used in this work the $PdCl_4^{2-}$ reacts with the $SnCl_2$ to rapidly yield yellow–red species, which convert into an olive-green form, which is stable for *ca* 1 hr. Figure 2 shows the absorption spectrum of the Pd–Sn species at steady state. The latter form shows absorption maxima at $\lambda = 635$, 460 and 380 nm which approximately follow the Beer–Lambert law over a reasonable range of Pd concentrations (10–200 μg/ml). Since above 600 nm the absorption of any Pt–Sn species is negligible, it is possible to determine Pd(II) by monitoring at 635 nm with no interference from Pt(II/IV). On the other hand, since the Pd–Sn species also absorbs light in the 300–500 nm range, the presence of Pd(II) may constitute a serious interference in the determination of Pt by the proposed method and vice versa. However, in view of the absorbance of the Pd–Sn species at 635 nm, this apparent disadvantage may be used to determine Pt and Pd in the same solution by sequential injection of two identical samples and monitoring at the two wavelengths separately, so that from the peak height at 635 nm the Pd concentration may be estimated, which then allows the Pt concentration to be obtained from the peak height at 460 nm. Alternatively the use of a diode-array photometric detector will allow for rapid multiwavelength monitoring[21] over a range of wavelengths in the absorption spectrum, from which both Pt and Pd can in principle be determined simultaneously. We did not have access to such a detector at the time of undertaking this work and thus carried out simple sequential injections and manual monitoring at 460 and 635 nm in order to determine both Pt and Pd in HCl solutions using the single-line manifold.

Table 1. Recovery experiments for sequential determination of Pt and Pd in synthetic mixtures monitoring at 460 and 635, respectively using a single-line manifold (see text)

Taken ($\mu g/ml$)		Found ($\mu g/ml$)	
Pt	Pd	Pt	Pd
80.0	20.0	79.8	20.1
60.0	40.0	59.9	40.0
40.0	60.0	39.4	60.8
20.0	80.0	19.5	81.4
10.0	100.0	9.9	102.6

As may be seen from Fig. 3b, it is readily possible to determine only Pd(II) in the absence of Pt(II/IV) in an exactly analogous way to Pt(II/IV) using similar conditions, monitoring in the 400–500 nm range. (In this wavelength range the sensitivity for Pd is considerably higher than when monitoring at 635 nm.) Furthermore we found that the absorbance (peak height) of solutions containing mixtures of Pt–Sn and Pd–Sn species are additive at selected wavelengths within the concentration ranges studied in this paper, so that for solutions known to contain both metals, two sequential injections of the same sample, monitoring at 460 and 635 nm allows the determination of both Pt and Pd, as shown in Table 1. These data were obtained by determining the [Pd(II)] at 635 nm from one injection, followed by a second injection of the same sample, monitoring at 460 nm which allows the calculation of the [Pt(II/IV)] from the total peak height by subtraction of the Pd–Sn contribution at this wavelength. A series of calibration curves for pure Pt and Pd standard solutions at the selected wavelengths can be setup to assist in this task. We monitor at 460 nm in mixed metal solutions since the difference in molar absorptivity between the Pt–Sn and Pd–Sn species is a maximum at this wavelength,

resulting in the most accurate calculation of the respective Pt and Pd concentrations, by this method.

The feasibility of potentially simultaneous determinations of Pt(II/IV) and Pd(II) in hydrochloric acid solution has thus been demonstrated monitoring at two wavelengths, so that the use of a diode-array detector should facilitate the accurate and rapid determination of these two metals over a relatively large concentration range.

Interferences

An extensive evaluation of potential interferences is essential if the proposed method is to be of practical value. Consideration of the chemistry of the reaction of tin(II)chloride with the PGMs involved, allows one to roughly group potential interferences into three categories: (i) oxidative interferences, leading to competitive consumption of Sn(II); (ii) absorptive interferences, having high molar absorptivities in the wavelength region of interest; and (iii) non-selective reactions of $SnCl_2$ with substances other than the PGMs. In general the established high selectivity of the reaction of $SnCl_2$ with the PGMs[10–15] makes interferences of (iii) unlikely but implies that interferences from other PGMs and Au(I/III) may be expected in the determination of Pt and Pd. Since the carrier stream is 1 *M* in HCl, substantial interferences of type (i) and (ii) from first row transition metals are unlikely, with the possible exception of Fe(III) and Cr(VI) (as $Cr_2O_7^{2-}$) in relatively high concentration. Anions such as SO_4^{2-}, NO_3^-, ClO_4^- and PO_4^{3-} do not interfere at relatively high levels (<0.1 *M*), although Br^- and I^- ions should be kept to a minimum.

We find that the determination of Pt and Pd by the proposed method tolerates fairly large amounts of many transition metals remarkably well in keeping with our expectations above, as is evident from data in Table 2. The table shows the maximum amount of interferent tolerated, resulting in a peak height of 20 μg/ml Pt(IV) (at 400 nm) and Pd(II) (at 400 and 635 nm) to not differ from that obtained from pure standard solutions, by more than 1%. It is clear that Pt(II/IV) and Pd(II) can be determined in the presence of relatively large amounts of the first row transition metals, particularly Fe(III) and Cr(VI), monitoring at 400 nm. In reasonably pure Pt and Pd containing concentrates in HCl, the interference of many first row transition metals thus appears to be insignificant.

Table 2. Interference tolerance at 20 μg/ml Pt and Pd level monitoring at the given wavelengths using the single-line manifold

Interferent	Pt(IV) 400 *nm*	Pt(IV) 460 *nm*	Pd(II) 400 *nm*	Pd(II) 635 *nm*
Mg^{2+}	200	—	200	400
Cr(VI)	100	—	100	200
Mn^{2+}	400	—	200	400
Fe^{3+}	960	—	400	400
Co^{2+}	400	—	200	200
Ni^{2+}	400	—	200	200
Cu^{2+}	400	—	100	(a)
Al^{3+}	400	—	200	400
Te(IV)	400	—	200	400
Pb^{2+}	200	—	200	400
Au^{3+}	10	10	*	(a)
Rh^{3+}	~2	~2	*	200
$Ru^{4/3+}$	~2	10	~2	10
Ir^{4+}	10	50	(a)	120

*Not tested but likely to interfere at low levels.

On the other hand, the interferences from Au(III), Rh(III) and other PGMs can be significant in the determination of Pt and Pd. Nevertheless, with the exception of Au, it is in principle possible to determine other members of the PGMs in the same way as Pt and Pd using a multiwavelength detection approach alluded to above. Preliminary studies suggest that it is indeed possible to determine Pt in the presence of substantial amounts of Ru and Ir, while we are examining ways to determine Rh simultaneously with Pt and Pd by this means.

In conclusion we have found that the described FIA method monitoring at a single wavelength is suitable for the rapid and cost-effective determination of Pt(II/IV) and/or Pd(II) in relatively pure hydrochloric acid medium as may be encountered in process streams, using only small sample volumes. The presence of many transition metals in reasonable amounts does not interfere, although Rh(III), Ru(IV/III), Au(III), and to a lesser extent Ir(IV) interferes with the determination at low levels. Nevertheless with the aid of a photodiode-array detector it appears to be possible to circumvent these interferences as has been shown in the determination of Pt and Pd in this work. We are currently studying the potential multielement determination of the PGMs using multiwavelength detection.

Acknowledgements—We are grateful to the University of Cape Town, the FRD and MINTEK for generous financial assistance and a MINTEK studentship to D.A. The loan of PGM salts from Johnson Matthey is also acknowledged with thanks.

REFERENCES

1. L. K. Kelland, S. J. Clarke and M. J. McKeage, *Platinum Metals Rev.*, 1992, **36**, 178.
2. B. Nathan, *The Platinum Yearbook 1991*. Woodhead, London, 1991.
3. M. P. Walsh, *Platinum Metals Rev.*, 1992, **36**, 126; *ibid*, 1993, **36**,7.
4. S. Kallmann, *Talanta*, 1987, **34**, 677.
5. J. Ruzicka, *Anal. Chimica Acta*, 1992, **261**, 3.
6. K. L. Shpigun and R. F. Gureva, *Zh. Anal. Kim.*, 1991, **46**, 2187.
7. L. Ma, X. Chen and Z. Hu, *Fenxi Huaxue*, 1992, **20**, 339.
8. X. He, Y. Cai and Z. Hu, *Anal. Chimica Acta*, 1992, **256**, 113.
9. I. Ilcheva and A. Dakashev, *Fresenius Z. Anal Chem.*, 1991, **340**, 14.
10. K. R. Koch, K. Brackenbury, L. Jones, I. Nel and J. M. Wirley-Birch, *Polyhedron*, 1987, **6**, 71.
11. J. F. Young, R. D. Gillard and G. Wilkinson, *J Chem. Soc.*, 1964, 5176.
12. W. L. Wilson, M. S. Holt and J. H. Nelson, *Chem. Rev.*, 1989, **89**, 11.
13. G. H. Ayres and A. S. Meyer, *Anal. Chem.*, 1951, **23**, 299.
14. O. I. Milner and G. F. Shipman, *Anal. Chem.*, 1955, **27**, 1476.
15. S. S. Berman and E. C. Goodhue, *Can. J Chem.*, 1959, **37**, 370.
16. K. G. Moodley and M. J. Nicol, *J. Chem. Soc. Dalton*, 1977, 239.
17. J. H. Nelson and N. W. Alcock, *Inorg. Chem.*, 1982, **21**, 1196.
18. P. G. Antonov, Yu N. Kukushkin, V. G. Shtrele, Yu P. Kostikov and F. K. Egorov, *Russ. J. Inorg. Chem.*, 1982, **27**, 1770.
19. V. I. Shlenskaya, A. A. Biryukov and L. N. Moryakova, *Russ. J. Inorg Chem.*, 1969, **14**, 255.
20. A. I. Zayats, T. S. Psareva and V. F. Shabanov, *Russ. J. Inorg. Chem.*, 1976, **21**, 393.
21. L. Lazaro, A. Rios, M. D. Luque de Castro and M. Valcarcel, *Anal. Chimica Acta*, 1986, **179**, 279.

Talanta, Vol. 40, No. 12, pp. 1981–1993, 1993
Printed in Great Britain.

0039-9140/93 $6.00 + 0.00

SPECIATION OF DISSOLVED PHOSPHORUS IN ENVIRONMENTAL SAMPLES BY GEL FILTRATION AND FLOW-INJECTION ANALYSIS

I. D. McKelvie* and B. T. Hart
Water Studies Centre and Chemistry Department, Monash University, Caulfield East 3145, Victoria, Australia

T. J. Cardwell and R. W. Cattrall
Centre for Scientific Instrumentation, La Trobe University, Bundoora 3083, Victoria, Australia

(*Received* 16 *February* 1993. *Revised* 29 *March* 1993. *Accepted* 30 *March* 1993)

Summary—A study of the factors affecting separation and detection of dissolved organic and inorganic phosphorus species found in waters and sediments is reported. The system involved the use of gel filtration and flow injection analysis (FIA). Orthophosphate and *myo*-inositol hexakisphosphate, as model solutes representative of low molecular weight P (LMWP) and high molecular weight P (HMWP), were separated on a Sephadex G25 column incorporated into a flow-injection manifold which utilized photo-oxidation and spectrophotometry for detection of dissolved reactive phosphorus (DRP) and dissolved organic phosphorus (DOP). The influence of eluent pH and ionic strength on adsorption and anionic exclusion of the model solutes is described, and the optimum eluent composition and sample size are described. The method was used to determine LMWP and HMWP in natural and waste waters, and in sediment extracts. Potential limitations of this approach are discussed.

Phosphorus in natural waters and sediment is known to occur as orthophosphate and a variety of organic and condensed phosphorus species with a wide range of molecular weights.[1] Some components of the dissolved organic phosphorus (DOP) fraction are thought to hydrolyse rapidly to orthophosphate when acidic molybate is used in the spectrophotometric analysis of orthophosphate as phosphomolybdenum blue, and for this reason the term "dissolved reactive phosphorus" (DRP) is used in reference to "orthophosphate". Consequently, DRP concentrations may overestimate orthophosphate[2] which is undesirable because orthophosphate is currently the best chemical measure of the dissolved phosphorus concentration biologically available for photosynthesis.

In soils and sediments, phosphorus may occur as organic compounds such as sugar phosphates, phosphatidyl phosphates, inositol phosphates, phosphoamides, phosphoprotein, aminophosphonic acids, phosphorus-containing pesticides and organic condensed phosphates.[3] Of this group, *myo*-inositol hexakisphosphate (also called phytic acid), is among the most stable;[4] this compound occurs in free and iron-complexed forms in soils and marine and lake sediments.[5] It has been conjectured that this species and its hydrolysis products will be present in natural waters through groundwater input,[1] and may comprise a significant proportion of dissolved organic phosphorus (DOP).[6,7] However, only a few studies have actually demonstrated the existence of inositol phosphates in natural waters,[8,9] and to date little is known of the transport of these species from sediments and soils into stream and lake waters.

Analysis of the DRP concentration in natural and wastewaters is commonly performed in an attempt to estimate the concentration of bioavailable phosphorus in the dissolved fraction. While orthophosphate has been shown in a number of studies to be the most bioavailable phosphorus species,[10] higher molecular weight phosphorus (HMWP) species display varying degrees of bioavailability.[11,12] In order to determine the concentration of both "true" orthophosphate and HMWP in natural water samples, we attempted to separate these species according to differences in molecular weight using gel filtration followed by photo-oxidation

*Author for correspondence.

and subsequent phosphomolybdenum blue detection of the liberated orthophosphate using FIA.

Separation of orthophosphate and HMWP in natural waters by gel filtration chromatography has been described by a number of authors[6,11,13–15] using a variety of eluent conditions, large gel columns, slow flow rates and correspondingly long (30 min–2 hr) elution times. The aim of the work described here was to develop a rapid technique allowing discrimination between these two molecular weight fractions. Small Sephadex G25 columns were investigated for the separation of model solutes representative of LMWP and HMWP, *viz*; orthophosphate and *myo*-inositol hexakisphosphate. Significant irreversible, or very slowly reversible, adsorption of phytic acid was found to occur when previously documented eluent conditions were used. In an attempt to overcome these problems, the influence of both ionic strength and pH on elution of orthophosphate and phytic acid was investigated.

EXPERIMENTAL

Flow injection manifold

LMWP and HMWP were determined post-separation using a flow injection manifold for determination of DRP + DOP similar to that described by McKelvie *et al.*[16] and shown in Fig. 1. An Applied Biosystems ABI 757 UV–Vis chromatographic detector was used. For the high range standards, a detector sensitivity of 0.1 AUFS (absorbance units full scale) was selected, whereas 0.02 AUFS was used for the lower range. Accurel S6/2 (ENKA AG) microporous tubing was used for debubbling photolysed carrier/reagent solutions prior to the addition of chromogenic reagents.

Reagents

Alkaline persulphate reagent. A 0.148*M* potassium persulphate (BDH, AnalaR) solution in 0.025*M* sodium tetraborate (May and Baker, Pronalys) was used.

Acid molybdate reagent. Ammonium molybdate (BDH, AnalaR) ($8.1 \times 10^{-3}M$) in 0.63*M* sulphuric acid (Ajax Chemicals).

Tin(II) chloride reagent. A $8.9 \times 10^{-4}M$ solution of tin(II) chloride (May and Baker, Pronalys) and 0.015*M* hydrazine sulphate (Ajax Chemicals, LR) in 0.50*M* sulphuric acid were prepared.

Model phosphorus compounds

Potassium dihydrogen orthophosphate (BDH, Pronalys) (mol. wt. of anion *ca.* 97.0); *myo*-inositolhexakis (dihydrogenphosphate), disodium salt dihydrate (*i.e.*, phytic acid), 78% pure (Aldrich) [mol. wt. of phytate anion (−8) *ca.* 837.8]; both prepared as 100 mg P/l. stock solutions.

Gel filtration conditions

Two Sephadex G25 columns were used:

Column A. A C10/10 column equipped with an AC10 adaptor was packed with pre-swollen Sephadex G25 Superfine (all from Pharmacia Fine Chemicals AB) to a bed height of 42 mm (bed volume = 3.3 ml), and used for eluent optimization and sediment extract separations.

Column B. A Fast Desalting HR10/10 high resolution column of bed height 100 mm (bed volume *ca.* 7.8 ml) (Pharmacia Fine Chemicals AB) was used for analysis of water samples.

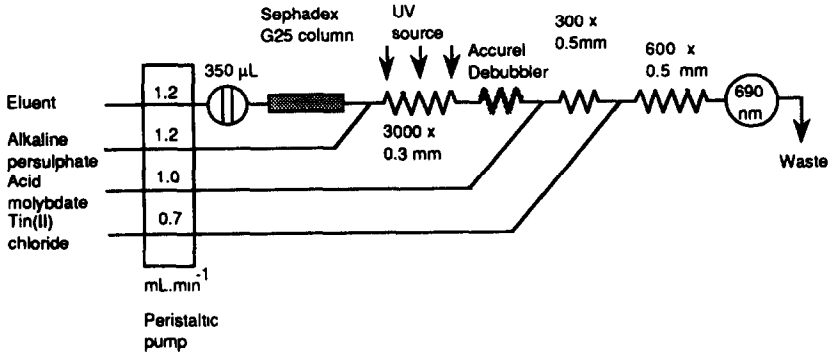

Fig. 1. Flow injection manifold for gel filtration separation with post-column DRP + DOP detection. Pump flow rates shown as those used for the Sephadex HR10/10 column. Flow rates were halved when column A was used.

Columns were stored refrigerated in 0.02% (w/v) sodium azide when not in use.

Injection volumes of either 100, 350 or 600 μl were used depending on the size of column and concentration range of the samples. For the separation optimization studies using column A, 350-μl injections were made throughout.

Gel filtration separations of phytic acid and orthophosphate were investigated using eluents of either 0.034–0.137M NaCl (pH 5–9),[11,14] 0.025M sodium tetraborate (pH 9.1),[15] or Tris–HCl buffers adjusted with 0.1M NaCl to give total ionic strength (I) values of between 0.001 and 0.007M as required. All eluents were filtered through 0.45-μm Sartorius Type SM membrane filters and allowed to degas for 15 min prior to measurement of pH and use.

To investigate the feasibility of separating orthophosphate and HMWP by gel filtration, columns were calibrated using a range of solutes of varying molecular weights. Elution of these solutes was detected by measurement of UV absorbance, or in the case of phytic acid and phosphate, by detection as DOP and DRP, respectively. Blue Dextran (Pharmacia Fine Chemicals AB), with a nominal molecular weight of 2×10^6 Dalton was used to determine the void volume, V_o, and nitrate ion (FW = 62.0) was used to estimate the total pore volume, V_i, of the gel column.[17] In NaCl and borate eluent solutions, direct UV detection at 220 nm was used to determine nitrate. However, the Tris buffer used in later experiments had a large background absorbance, and a nitrate ion selective electrode (Activon) was used for detection of nitrate.

Sample preparation

Water samples were collected from several lotic and lentic environments in Victoria, a sewage treatment works and a leachate pond at a rural landfill tip. Samples were filtered on-site using a 0.45-μm Lida disposable syringe filter and stored at $\leqslant 4°$ prior to analysis, which usually occurred within 48 hr. Filtered water samples were injected in triplicate (600 μl) onto a Sephadex G25 HR10/10 column (B) and eluted with a Tris/HCl eluent of $I = 0.005M$ at pH 4.6–4.7 at a flow rate of 1.2 ml/min.

Lacustrine sediments (1–2 g) were extracted in 0.025M disodium tetraborate (*ca.* pH 9.2) and mixed end-over-end for 1 hr at room temperature. Diluted (1:10) sediments extracts were analysed using the same Sephadex G25 Superfine column (A) used for the elution optimization. Standard solutions of phytic acid and orthophosphate were prepared in the same matrix as the extracts. A Tris/HCl eluent of $I = 0.005M$ and pH 4.65 at a flow rate of 0.65 ml/min was used, and triplicate 350-μl injections were made.

DRP and DOP + DRP analyses were also performed on all water and sediment samples for comparative purposes.

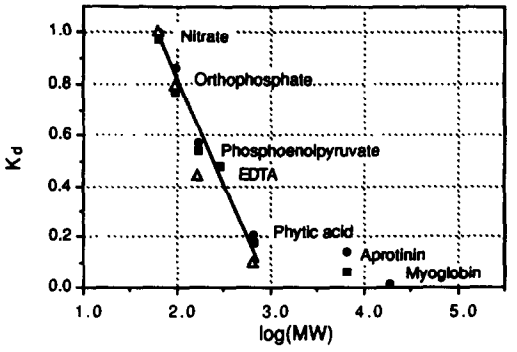

Fig. 2. Molecular weight calibration of different Sephadex G25 columns under differing elution conditions: (●) Column A, eluent: 0.2% NaCl (pH 8.5) at 0.62 ml/min; injection volume 100 μl, (■) G25 bed height 103 mm, 10 mm i.d. eluent: 0.5% NaCl (pH 6.2) at 1.24 ml/min. Injection volume 350 μl, (△) Column B, eluent: 5 mM Tris (pH 4.5) at 1.24 ml/min. Injection volume 350 μl.

RESULTS AND DISCUSSION

Molecular weight calibration

From molecular weight calibration data (Fig. 2), it is evident that an essentially linear relationship between the distribution coefficient, K_d, and log(molecular weight, MW) applies over the MW range which includes phytic acid and orthophosphate. Those which are significantly larger (aprotinin, myoglobin) fall outside this linear portion. Extrapolation of this linear portion of the calibration graph indicates that the *operational* exclusion limit is approximately 10^3 Dalton, rather than the value of 5×10^3 Dalton for globular proteins normally quoted.[17] The observed K_d values of *ca.* 0.2 and 0.8 for phytic acid and orthophosphate respectively, are close to those previously reported for separation of these solutes on Sephadex G25 under similar elution conditions,[18] and it is evident that phytic acid is eluting with a K_d consistent with that of a non-aggregated, monomeric form.

The calibration data, while indicating molecular weight-dependent elution behaviour, do not show resolution of the solutes. For the fast gel filtration separations on column (A), phytic

acid and orthophosphate were incompletely resolved, but nevertheless quantifiable. However, separation of solutes with intermediate molecular weights was not feasible, and consequently analytical results are reported non-specifically as *high molecular weight phosphorus* (*HMWP*) and *low molecular weight phosphorus* (*LMWP*), rather than as DOP of a particular MW and orthophosphate.

Eluent selection

Initial attempts to separate phytic acid and orthophosphate on even quite large Sephadex G25 columns (200 mm × 10 mm i.d.) using 0.2% (w/v) NaCl resulted in poor recoveries of phytic acid, and it was evident that some specific interaction, or slow reversible adsorption was occurring which was only slightly affected by pH. Despite poor recovery, phytic acid eluted with a V_e/V_o value which was consistent with its molecular weight, as shown in Fig. 2.

It was observed that when either standard or sample was prepared in deionized water and injected into an eluent of higher ionic strength, notably better recovery of phytic acid was achieved compared with the situation where sample or standard was prepared in a matrix of the same ionic strength as the eluent. This is clearly seen in Fig. 3(a) and (b) where injections of mixtures of phytic acid and orthophosphate have been made in triplicate. Figure (3a) shows that when sample

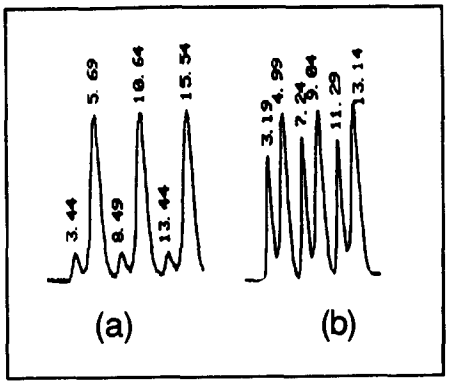

Fig. 3. Triplicate injections of 300 μg P/l each of phytic acid and orthophosphate, showing the influence of sample zone ionic strength on elution of both species (a) eluent and sample zone: 0.2% NaCl (w/v) pH 9.7 with 5 min between injections, and (b) eluent: 0.2% NaCl (w/v) pH 9.7 with 4 min between injections, sample zone: deionized water. Elution conditions: column A, flow rate 0.62 ml/min, injection volume 350 μl. The numerals shown on the chromatograms are retention times in minutes. In both cases, the phytic acid peak elutes first.

zone and carrier had the same ionic strength, significant adsorption of phytic acid occurred (peaks at 3.44, 8.49 and 13.44 min). However, when the sample zone matrix was of much lower ionic strength, markedly improved recovery of phytic acid was noted [Fig. 3(b)], as indicated by the peaks at 3.19, 7.24 and 11.29 min.

This effect is similar in some respects to the *salt boundary* elution effect previously described by Posner.[10] Posner suggested that preparing a sample with a higher ionic strength would cause solute adsorption when the sample was added to a gel column. Elution with distilled water would then cause the progressive desorption of the adsorbed solute and this would move down the column as a concentrated zone at the distilled water-saline eluent interface. In the case illustrated by Fig. 3(b), the sample was dissolved in deionized water, and injected into a carrier/eluent of 0.2% (w/v) NaCl. However, despite these conditions being the opposite of those described by Posner, the same type of elution persisted; *i.e.*, phytic acid in a deionized water matrix showed much less adsorption than the same sample prepared in eluent. It is possible that the adsorptive process occurs at the head of the sample zone where there is considerable dispersion and hence mixing, with the saline eluent. Given that a large injection volume of 350 μl (10.6% of total column volume, V_t) was used, it could be expected that the relatively undispersed mid-region of the sample zone would have a lower ionic strength than that of the eluent, and it is conceivable that it is this low ionic strength zone which causes the partial desorption of phytic acid which is observed.

Although the mechanism of this process is unclear, it is quite evident from the relative sizes of the peaks, that better, albeit not complete recovery of phytic acid occurs when an ionic strength gradient exists across the sample zone, and for this reason the influence or ionic strength and pH on separation of orthophosphate and phytic acid in a deionized water matrix were studied systematically to obtain the optimum condition for separation and recovery of phytic acid. Mixed standards of phytic acid and orthophosphate in deionized water were injected onto the same column and eluted with carrier having a variety of pH and ionic strength conditions using Tris–HCl–NaCl solutions ranging from $I = 0.001$ to $0.07M$. The results of these experiments are shown in Fig. 4 from

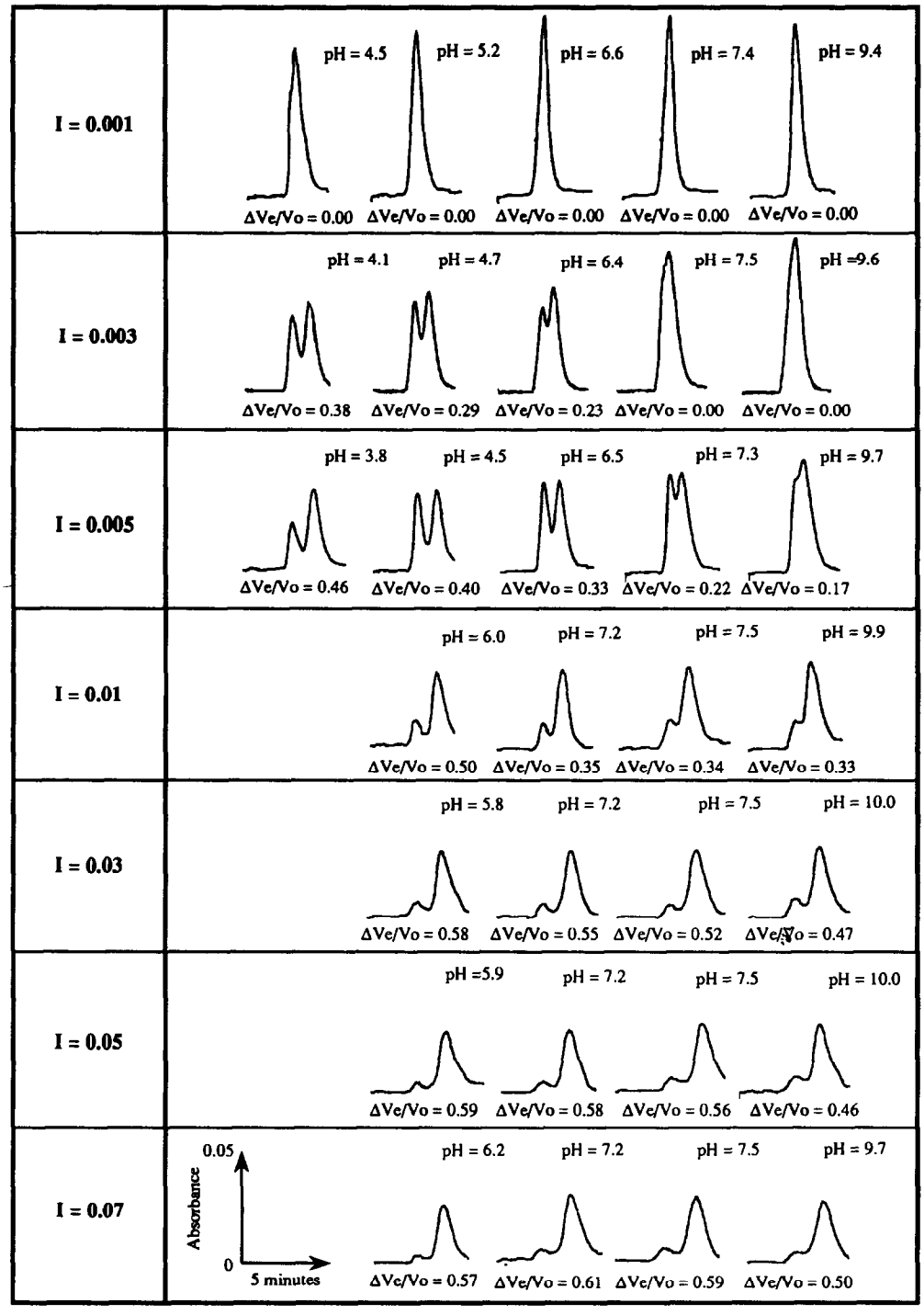

Fig. 4. Variation in the elution of orthophosphate and phytic acid species as a function of total ionic strength and pH. Peak separation is expressed as $\Delta V_e/V_o$, where V_e is the solute elution volume and V_o is the void volume of the gel bed.

which a number of features of the chromatography are evident:

(i) At low ionic strength ($I = 0.001M$), phytic acid and orthophosphate co-elute under all pH conditions tested.

(ii) At slightly greater total ionic strength ($I = 0.003M$), orthophosphate shows partial resolution from phytic acid ($\Delta V_e/V_o =$ 0.23–0.38). However, at pH > 6.4, loss of separation is observed.

(iii) At total ionic strength in excess of $0.005M$, significant adsorption of phytic acid was found to occur. Very slow desorption of some species (presumably phytic acid), indicated by a gradual return to baseline, was observed after elution of the orthophosphate peak (not shown by the data in Fig. 4).

The co-elution of orthophosphate and phytic acid found to occur at the lowest ionic strength conditions tested ($I = 0.001M$) was probably due to anionic exclusion of the orthophosphate. At $I = 0.003M$ some separation of the two species occurred at lower pH, but at pH >6, the double- and triple-charged phosphate species are more prevalent, and the anion exclusion effect overcame the influence of increased ionic strength; a similar trend to this was observed for an eluent with $I = 0.005M$.

This anion exclusion effect appears to have been completely suppressed when the ionic strength was increased to $0.01M$, and the phytic acid and orthophosphate peaks are as well separated as might be expected given the short column used. Predictably, however, there is significant adsorption of the phytic acid under these higher ionic strength conditions.[20] Figure 5 shows the variation of V_e/V_o of both orthophosphate and phytic acid species with increasing ionic strength within the pH range 7.3–7.5. The orthophosphate shows a pronounced increase in V_e/V_o, but a much smaller effect of ionic strength on phytic acid. This is perhaps surprising, given the highly charged nature of the phytic acid species (within the pH range used, the average charge on the phytic acid would be *ca.* −8). The value of V_e/V_o for phytic acid is, however, always larger than that of Blue Dextran, and even at high ionic strength (*e.g.*, $I = 0.07M$), with a large amount of adsorption occurring, there is only a small shift in the value of V_e/V_o. Despite the high charge on the phytic acid species, it appears that its elution is dictated by steric factors rather than charge considerations. This is consistent with the findings of Neddermeyer and Rogers[21] who suggested that larger charged ions would not be influenced by the Donnan exclusion effect to the same extent as smaller ions because they would be sterically excluded from the gel interior containing most of the charge. This may provide an explanation for the apparent absence of anion exclusion behaviour of phytic acid, despite its high charge.

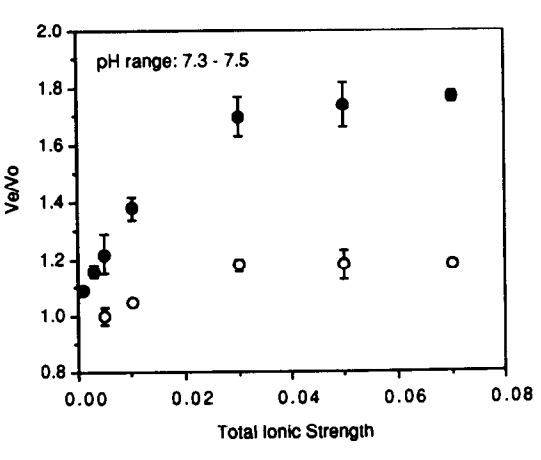

Fig. 5. Variation of V_e/V_o for orthophosphate (●) and phytic acid (○) species as a function of total ionic strength within the pH range 7.3–7.5.

Neddermeyer and Rogers have also noted that solutes subject to the influence of anion exclusion display broadened front and sharp back edges, behaviour which is the converse of that normally observed in chromatography.[21] Examination of orthophosphate and phytic acid peaks reveals that while the orthophosphate peaks show broadened leading edges, phytic acid peaks do not, providing further evidence in support of the hypothesis that steric effects control the behaviour of phytic acid.

Maximum recovery of phytic acid with respect to orthophosphate, based on peak height, was achieved for the specified column and flow conditions using eluents with $I = 0.005M$ and pH 4.5–6.5. Under optimal elution conditions ($I = 0.005M$, pH 6.5, *cf*, Fig. 4), the % recovery of phytic acid with respect to orthophosphate calculated using peak height was 97.4% ($\sigma_{n-1} = 0.2\%$, $n = 3$), but when calculated on the basis of peak area, was only 78.2% ($\sigma_{n-1} = 3.2\%$, $n = 3$). Given that a common phosphomolybdenum blue detection chemistry was used, it is evident that significant adsorption of phytic acid had occurred even at this so-called optimum condition. Furthermore, when columns were cleaned with dilute sodium hydroxide solution (pH >10) after the injection of several samples of phytic acid, a large desorption peak was observed; however this was not the case for orthophosphate. It was also apparent from the uniformity of peak area data, obtained over a wide range of ionic strength and pH conditions, that little orthophosphate adsorption occurred.

It is unfortunate that even under salt-zone elution conditions adsorption of phytic acid persisted. It would have been preferable to use only one calibration substance, *i.e.*, orthophosphate

Table 1. Calculated limits of detection (lod) and sensitivity data for phytic acid and orthophosphate for the 42-mm bed height column (A)

Analyte	High range (100–1000 μg P/l.) Limit of detection (μg P/l.)	High range (100–1000 μg P/l.) Sensitivity (AU/μg P/l.)	Low range (10–100 μg P/l.) Limit of detection (μg P/l.)	Low range (10–100 μg P/l.) Sensitivity (AU/μg P/l.)
Phytic acid	44	1.338×10^{-4}	27	8.88×10^{-5}
Phosphate	12	1.318×10^{-4}	1.1	1.323×10^{-4}

and a common peak-height:concentration calibration equation for all eluting species. This would only be possible in the absence of solute–gel interactions, given that all eluting species are converted from DOP to DRP before detection. There was, however, only a narrow range of pH and ionic strength conditions for which the separation and % recovery of phytic acid (by peak height) was maximal. Even slight departure from the optimum ionic strength and pH conditions ($I = 0.005M$, pH 4.5–6.5) would cause the % recovery of phytic acid with respect to orthophosphate to change markedly. Such variations in the ionic strength could occur in the preparation of reagents, or may arise from some hydrodynamic artefact of the FIA manifold causing a variation in the degree of dispersion of the sample zone, and hence altering the ionic strength regime of the sample zone. Such artefacts may involve changes as simple as a fluctuation in carrier flow rate, or a variation in the sample volume.

For these reasons, mixed standards of phytic acid and orthophosphate were used for quantitation of HMWP and LMWP, in preference to quantitation using orthophosphate alone and applying a response factor. It is recognized that this calibration approach may be deficient if an HMWP species elutes from the gel in a manner different to that of phytic acid.

Linearity, sensitivity and limit of detection of mixed standard calibrations

Mixed standards of phytic acid and orthophosphate were prepared over the ranges 50–1000 μg P/l. and 10–100 μg P/l. Triplicate injections of 350 μl of these standards were made onto the same Sephadex G25 Superfine column that was used for all previous experiments under optimal separation conditions.

At concentrations greater than approx 200 μg P/l., phytic acid and orthophosphate graphs were essentially co-linear, giving regression equations of

$$A = (-2.63 \times 10^{-3}) + (1.34 \times 10^{-4})\mu g\ P/l,\ r^2 = 0.999,$$

and

$$A = (3.00 \times 10^{-4}) + (1.32 \times 10^{-4})\mu g\ P/l.,\ r^2 = 1.000,$$

respectively.

However, below *ca.* 100 μg P/l., the orthophosphate calibration is linear, but the phytic acid exhibits non-linear behaviour. At 50 μg P/l., there is a loss of approximately 50% of the phytic acid, while at < 10 μg P/l., phytic acid peaks were scarcely detectable, even though orthophosphate signals were still clearly discernible. Clearly, at concentrations of less than 100 μg P/l., the specific adsorption of phytic acid onto the gel poses a difficulty.

Limits of detection (lod) have been calculated for these data using the linear regression method described by Miller and Miller[22] and are listed with calibration sensitivity (slope) values in Table 1.

Effect of sample volume on peak response, resolution and % recovery

The influence of sample volumes ranging from 100 to 600 μl on peak response, resolution, and % recovery (based on comparison with orthophosphate peak height) was investigated. A linear relationship between injection volume (S_v) and peak height (Absorbance, A) was observed over the concentration range tested. For the dilute solutions analysed here, it can be shown that the relationship between the absorbances of undispersed (A°) and dispersed (A) sample,

$$\frac{A}{A^\circ} = 1 - \exp(-k\,S_v)$$

quoted by Ruzicka and Hansen[23] approximates to: $A \approx k\,S_v$ for a range of A values from 0.001 to 0.1. $S_{1/2}$, the injection volume required to give a dispersion coefficient of 2, can be determined from

$$S_{1/2} = \frac{0.693}{k}.$$

Using this relationship, and the k (slope) value from an A *vs.* S_v plot, very high $S_{1/2}$ values of

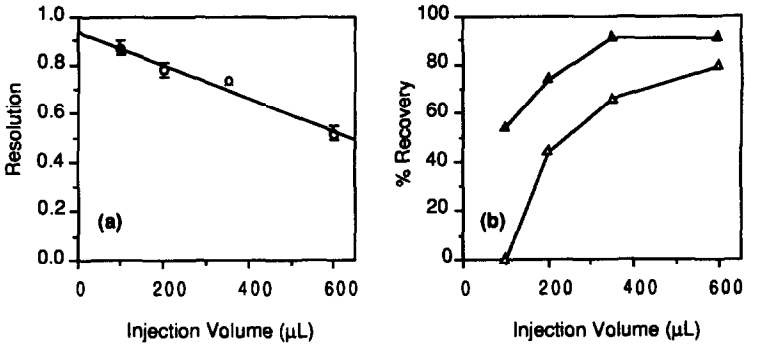

Fig. 6. Influence of sample volume on (a) resolution (for 500 μg P/l. each of phytic acid and orthophosphate), and (b) % recovery of 50 μg P/l. (—△—) and 500 μg P/l. (—▲—) phytic acid with respect to orthophosphate. Column A, eluent flow rate 0.62 ml/min.

>20,000 μl at 50 μg P/l. and >4,000 μl at 500 μg P/l. were obtained.

The very large values of $S_{1/2}$ at 50 μg P/l. reflect the consideration dispersion that occurs in the gel column. Clearly, use of a smaller gel-filtration column would be preferable and more in agreement with conventional FIA–chromatographic practice. Smaller columns would necessitate the use of small injection volumes if column overloading and attendent loss of resolution are to be avoided. However, the combination of small injection volumes and the high dispersion of the DOP + DRP detection manifold would result in poor sensitivity, and consequently the use of small columns and small injection volumes is precluded in this context.

Figures 6(a) and (b) show the improvement in peak resolution and the corresponding decrease in % recovery of phytic acid (calculated from peak height data) as the injection volume is decreased to 100 μl. The lower recovery of the 50 μg P/l. standard with respect to the 500 μg P/l. standard is probably due to a combination of preferential adsorption of phytic acid to the gel and dispersion. These results highlight the interrelationship between phytic acid adsorption and factors such as eluent-sample zone ionic strength difference, and hydrodynamic factors like sample injection volume, column size, and flow rate which influence dispersion.

Influence of phytic acid concentration on apparent concentration of orthophosphate for short columns

Phytic acid and orthophosphate peaks were only partly resolved on the short G25 Superfine column (A). Under these circumstances, the measured peak heights, and hence concentrations of both HMWP and LMWP calculated from peak height may be mutually influenced by peak overlap. To determine the magnitude of this effect, several mixed standards all containing 300 μg PO_4–P/l. and phytic acid concentrations varying between 50 and 400 μg phytic–P/l. were analysed. Figure 7 shows that the absorbance of the 300 μg PO_4–P/l. standard increased linearly, by as much as 10.3%, as the concentration of phytic acid was increased from 50 to 400 μg phytic–P/l. Similarly, the absorbance *vs.* concentration plot for phytic acid displayed increasing deviation from linearity at higher concentrations because of overlap from the leading edge of the orthophosphate peak. Because this effect proved problematic in the analysis of some sediment extracts, a larger, high resolution column was employed for the analysis of water samples, as described in the following section.

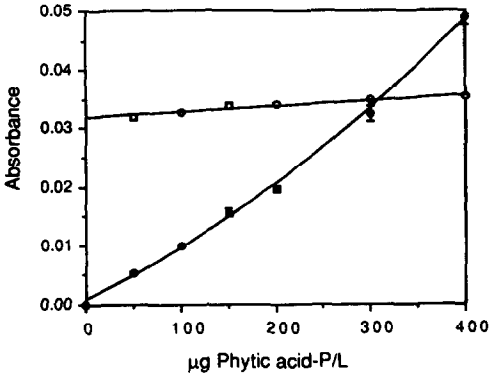

Fig. 7. Effect of differing phytic acid concentrations (●) on peak height of 300 μg P/l. orthophosphate (○) in short column gel filtration chromatography. Tris/HCl eluent at pH 4.75 and $I = 0.005$. Column A, injection volume 350 μl. Eluent flow rate 0.62 ml/min. Lines of best fit for phytic acid and orthophosphate given by: $y = (7.49 \times 10^{-4}) + (7.77 \times 10^{-5})x + (1.04 \times 10^{-7})x^2$ $r^2 = 0.998$ and $y = (3.20 \times 10^{-2}) + (9.47 \times 10^{-6})x$ $r^2 = 0.923$, respectively.

Analytical results—concentrations of HMWP and LMWP found in sediment extracts and waters

Preliminary extractions of sediments with deionized water gave low yields of HMWP. Minear[24] has noted that only about 40% of DOP was extracted from particulate material and *Chlamydomonas* cultures by distilled water, but that 85–100% was extracted when alkaline conditions (*ca.* pH 13) were used. Extraction of phosphorus from sediments was tested using Olsen's reagent (0.5*M* $NaHCO_3$ at pH 8.5);[25] however, the high bicarbonate concentration was found to interfere with the photo-oxidation of DOP, presumably through hydroxyl radical scavenging. Aluminium may also interfere in the photo-oxidation of DOP at concentrations >100 μg Al/l.[26] and for this reason acidic sediment extractions were avoided.

HMWP and LMWP concentrations of the sediment extracts obtained by separation on the short (42 mm × 10 mm id) Sephadex G25 column with subsequent DOP analysis are shown with corresponding DOP and DRP data, expressed on a dry weight basis, in Fig. 8(a)–(c).

The concentration of LMWP was significantly greater than the corresponding DRP data ($P = 0.0058$, paired t-value 3.91, d.f. = 7). Two possible explanations can be tendered, *viz*;

(i) Desorption of phytic acid, or other late eluting species, may enhance the LMWP peak. While the separation has been optimized to give maximum recovery of phytic acid, some phytic acid appears to undergo very slow desorption. Other phosphate-species, such as Vitamin B12 and 4-nitrophenylphosphate, exhibited reversible adsorption and late elution when injected under these elution conditions.

(ii) Organic phosphorus species of similar molecular weight range to orthophosphate (*e.g.*, lower phosphate esters of *myo*-inositol) may be present and elute with the orthophosphate. Given the fairly poor resolution of the small column used, discrimination between orthophosphate and other low molecular weight phosphorus species would not be possible.

From Fig. 8(a), it is evident that DOP values are significantly greater than those for HMWP ($P = 7.0 \times 10^{-4}$, paired t-value = 5.76, d.f. = 7). Between 65 and 97% of the DOP is represented by the HMWP of similar MW to *myo*-inositol-hexakisphosphate, and this is consistent with suggestions regarding the stability of this phosphate ester and its probable role in the storage of phosphorus in sediments.[1] Other researchers have reported similar recoveries of inositol phosphate esters from soils[27] and lake sediments.[28] The fact that the DOP values are all greater than the HMWP values [Fig. 8(b)] also lends some credence to any one of the explanations provided for the apparent discrepancy between LMWP and DRP.

Moreover, it can be seen that when (DRP + DOP) and (HMWP + LMWP) data are compared [Fig. 8(c)], there is excellent agreement, as shown by the regression equation:

$$(\text{HMWP} + \text{LMWP}) = 1.05(\text{DRP} + \text{DOP}) - 1.34, \quad r = 0.987$$

(r significantly different from zero at $P > 99\%$).

The agreement between (HMWP + LMWP) and (DRP + DOP) suggests that there are no major recovery losses associated with the gel filtration separation that cannot be accounted for by calibration. It also supports the hypothesis that differences between DRP and LMWP can be explained by the co-elution of lower MW organic phosphorus species with orthophosphate.

For water samples, LMWP and HMWP were separated on the larger, high resolution HR10/10 column (B). Sample injections of 600 μl were necessary to compensate for the added dispersion associated with use of a large column, but this was compensated for by the complete resolution of phytic acid and orthophosphate, and the ability to use high eluent flow rates with this column. Flow rates of up to 6 ml/min are permissible, but in experiments reported here, flow rates in excess of 1.2 ml/min were avoided because the debubbler in the DOP photo-oxidation manifold did not function efficiently at these higher flow rates.

Results of the analyses of the water samples are shown in Fig. 9(a)–(c). The importance of HMWP as a constituent of some waters is noted, as it comprised from 0 to 97% of the total HMWP + LMWP detected. There was no significant difference between the (HMWP + LMWP) gel filtration data and the (DRP + DOP) data for the same samples ($P = 0.79$, paired $t = 0.27$, d.f. = 9). However, HMWP was significantly greater than the DOP fraction ($P = 0.03$, paired t-value = 2.67, d.f. = 9) and LMWP is significantly less than the DRP fraction ($P = 0.02$, paired t-value = 2.85, d.f. = 9). These trends are opposite to those found for the extractable phosphorus in the

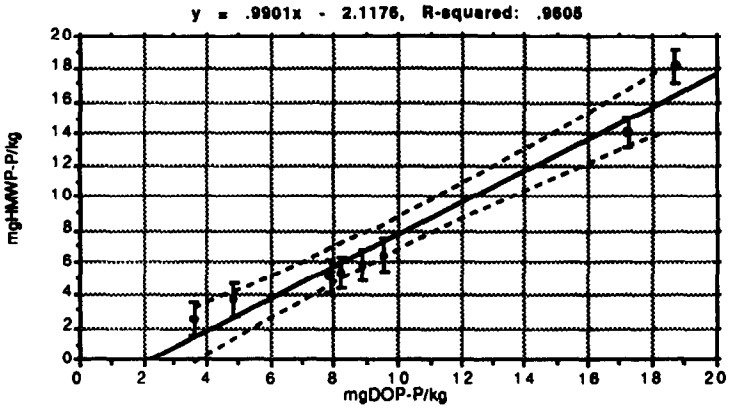

(a) DOP significantly > HMWP ($P = 7.0 \times 10^{-4}$, paired t-value = 5.76, d.f. = 7)

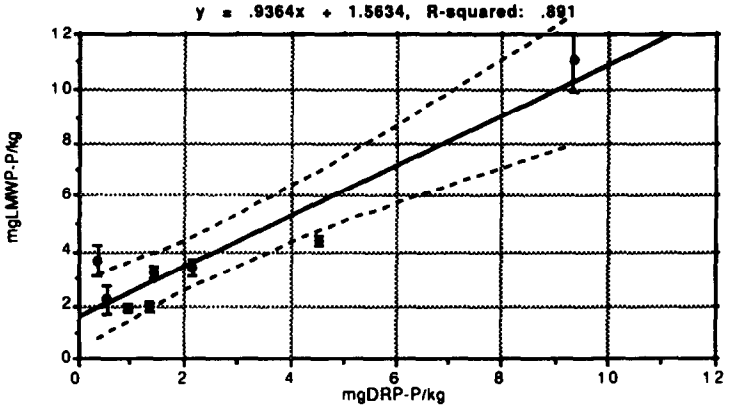

(b) LMWP significantly > DRP ($P = 0.0058$, paired t -value = 3.91, d.f. = 7)

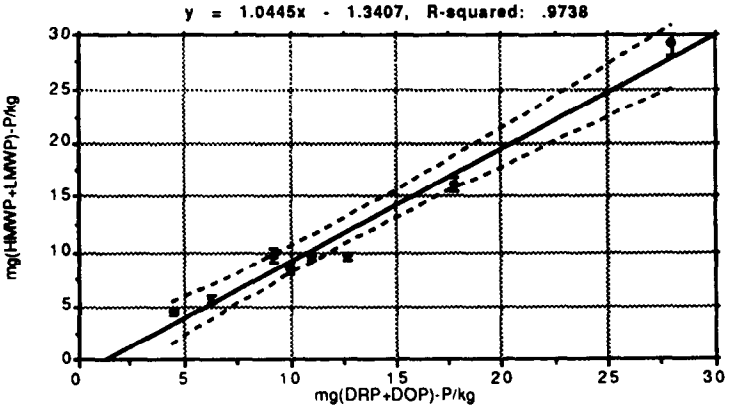

(c) No significant difference between HMWP+LMWP and DRP+DOP ($P = 0.14$, paired t-value = 1.68, d.f. = 7)

Fig. 8. Comparison of (a) HMWP and DOP, (b) LMWP and DRP and (c) HMWP + LMWP and DRP + DOP for sediments, expressed on a dry weight basis. The broken lines indicate the 95% confidence intervals for the true mean of the y values.

sediment samples. One possible explanation for the higher DRP than LMWP data is that some of the DRP measured includes the products of rapidly hydrolysed dissolved organic phosphorus, a problem which has been reported extensively.[2,29,30] As DOP is determined by subtracting DRP from the total DRP + DOP, the effect of an inflated DRP value will result in significantly reduced DOP values. Chamberlain and Shapiro, for example, in a batch method,

limited mixing and reaction between sample, molybdate and reductant to 6 sec, but noted that some hydrolysis of DOP occurred even under these rapid reaction conditions.[31] For the flow injection DRP method used here, the time between injection and emergence of the peak maximum was only 20–25 sec, but it is feasible that some hydrolysis of DOP could occur even in this short period.

Six of the samples analysed had LMWP

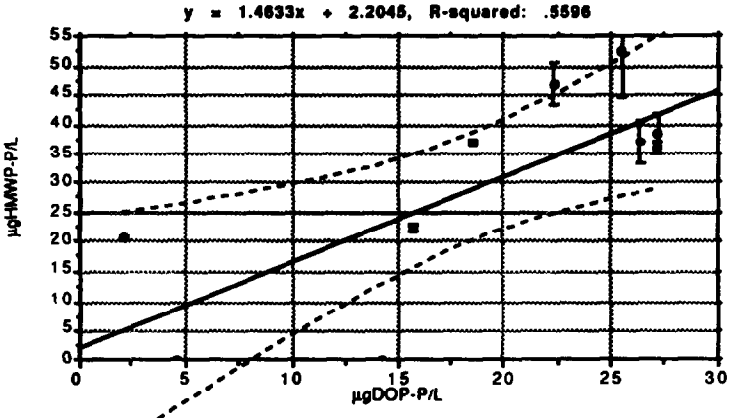

(a) HMWP significantly > DOP (P = 0.03, paired t-value = 2.67, d.f. = 9)

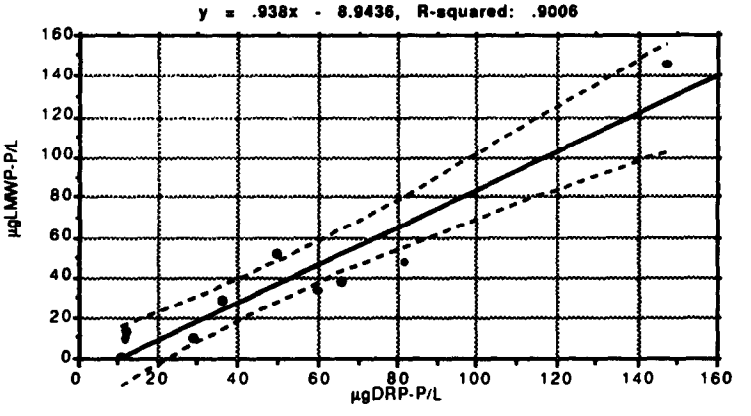

(b) DRP significantly > LMWP (P = 0.02, paired t-value = 2.85, d.f. = 9)

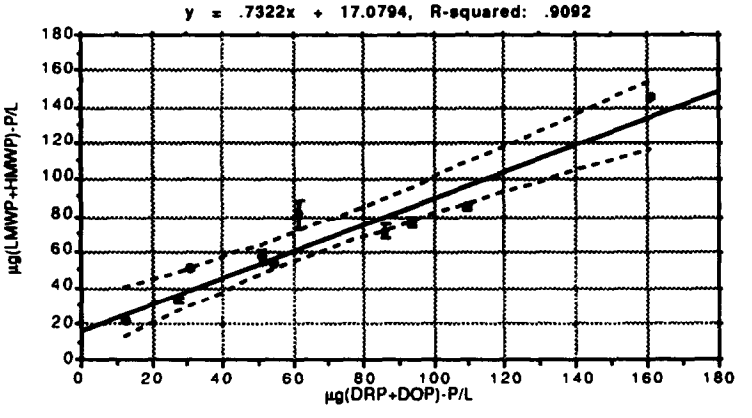

(c) No significant difference between HMWP+LMWP and DRP+DOP (P = 0.79, paired t-value = 0.27, d.f. = 9)

Fig. 9. Comparison of (a) HMWP and DOP, (b) LMWP and DRP and (c) HMWP + LMWP and DRP + DOP for water samples. The broken lines indicate the 95% confidence intervals for the true mean of the y values.

values which were significantly lower than the DRP concentrations. However, there is no significant difference between (LMWP + HMWP) and (DRP + DOP) for most samples, and it is arguable that measurement of LMWP and HMWP provide better measures of non-hydrolysed organic phosphorus and orthophosphate than do DOP and DRP. In two diluted effluent samples the HMWP was undetectable; however, these samples were high in DRP and required dilution of 1:50 prior to analysis in order to get them into the same concentration range as other samples. It is probable that this was sufficient to dilute the low concentration of HMWP to below the detection limit, or that the low concentrations of DOP (14 and 5 μg Pl/l. respectively) were comprised of late-eluting species.

This study has highlighted some of the problems associated with the use of Sephadex G25 for the fractionation of dissolved phosphorus species in natural waters and sediment extracts, *viz.* partial adsorption of phytic acid species and late elution of other higher molecular weight species. This gel filtration approach to the separation of HMWP and LMWP is apparently the most rapid yet reported with an analysis rate of 12–15/hr, but it is not sufficiently sensitive for the analysis of dilute or pristine waters. It is envisaged that further research in this area could involve the use of complexing eluents to eliminate adsorption of HMWP species through complexation by metals adsorbed to the gel, along similar lines to that described by Town and Powell.[32]

In this study, only Sephadex G25 has been used, and it would be useful to repeat the ionic strength–pH studies on a wide range of gels, including the macro/microreticular Ultrogels, to determine optimum separation conditions. This would be labour-intensive by conventional gel filtration, but could be performed within a reasonable time using the gel filtration-FIA approach described. Separation of HMWP and LMWP in waters with a range of gels of different MW cut-off would provide further information on the concentration and speciation of dissolved organic phosphorus in natural waters.

Detection of low concentrations of DOP compounds using the gel filtration–FIA system is clearly a problem. However, it was shown that phytic acid and phosphate could be concentrated onto an ion exchange precolumn prior to injection[33] and DOP analysis. This approach could be applied to the preconcentration of at least the anionic HMWP species prior to gel filtration.

While this study has identified that waters and sediment extracts contain HMWP in the same molecular weight range as phytic acid, and it is probably reasonable to assume that phytic acid is a major constituent of the HMWP, no information about the presence of other phosphate esters of *myo*-inositol can be obtained because of the inability of the gel to resolve the small differences in molecular weight involved. Low pressure anion exchange chromatography has been used extensively to separate *myo*-inositol phosphate esters,[6,28,34] and from the experience of this study, it should not be difficult to couple an anion exchange column with an FIA–DOP manifold to achieve rapid separations.

Finally, the relevance of the HMWP and LMWP data in waters needs to be evaluated in terms of their bioavailability by comparison with appropriate algal bioassay techniques.

Acknowledgement—Support for this research by the Australian Research Council is gratefully acknowledged.

REFERENCES

1. E. M. Thurman, *Organic Geochemistry of Natural Waters*, p. 497. Martinus Nijhoff/Dr W. Junk Publishers, Dordrecht, The Netherlands, 1985.
2. S. J. Tarapchak, *J. Environ. Qual.*, 1983, **12**, 105.
3. W. Stumm and J. J. Morgan, *Aquatic Chemistry*, 2nd Ed., p. 780. Wiley, New York, 1981.
4. G. Anderson, in A. D. McLaren and G. H. Peterson, *Soil Biochemistry*, p. 67. Marcel Dekker, New York, 1967.
5. D. J. Cosgrove, *Inositol Phosphates—Their Chemistry, Biochemistry and Physiology*, p. 191. Elsevier, Amsterdam, 1980.
6. S. J. Eisenreich and D. E. Armstrong, *Environ. Sci. Technol.*, 1977, **11**, 497.
7. S. E. Herbes, H. E. Allen and K. H. Mancy, *Science*, 1975, **187**, 432.
8. R. A. Minear, J. E. Segars and J. W. Elwood, *Analyst*, 1988, **113**, 645.
9. C. M. Clarkin, R. A. Minear, S. Kim and J. W. Elwood, *Environ. Sci. Technol.*, 1992, **26**, 199.
10. J. B. Cotner and R. G. Wetzel, *Limnol. Oceanogr.*, 1992, **37**, 232.
11. E. White and G. Payne, *Can. J. Fish. Aquat. Sci.*, 1980, **37**, 664.
12. E. Bentzen, W. D. Taylor and E. S. Millard, *Limnol. Oceanogr.*, 1992, **37**, 217.
13. D. Lean, in D. Povoledo and H. L. Golterman, *Humic Substances. Their Structure and Function in the Biosphere; Proceedings of an International Meeting Held in Nieuwersluis, The Netherlands, 1972*, p. 159. Pudoc, Wageningen: Center for Agricultural Publishing and Documentation, 1975.
14. M. T. Downes and H. W. Paerl, *J. Fish. Res. Bd. Can.*, 1978, **35**, 1636.

15. R. J. Stevens and B. M. Stewart, *Water Res.*, 1982, **16**, 1507.
16. I. D. McKelvie, B. T. Hart, T. J. Cardwell and R. W. Cattrall, *Analyst*, 1989, **114**, 1459.
17. Pharmacia, *Gel Filtration: Theory and Practice*, Pharmacia Fine Chemicals AB, Lund, Sweden, 1979.
18. J. H. Steward and M. E. Tate, *J. Chromatog.*, 1969, **45**, 400.
19. A. M. Posner, *Nature*, 1963, **198**, 1161.
20. J.-C. Janson, *J. Chromatogr.*, 1967, **28**, 12.
21. P. A. Neddermeyer and L. B. Rogers, *Anal. Chem.*, 1968, **40**, 755.
22. J. C. Miller and J. N. Miller, *Statistics for Analytical Chemistry*, 2nd Ed., p. 227. Ellis Horwood, Chichester, 1988.
23. Růžička and E. H. Hansen, *Flow Injection Analysis*, 2nd Ed., 62, p. 498. Wiley, New York, 1988.
24. R. A. Minear, *Environ. Sci. Technol.*, 1972, **6**, 431.
25. P. R. Hesse, *A Textbook of Soil Chemical Analysis*, p. 520. John Murray, London, 1971.
26. I. D. McKelvie, *Flow Injection Analysis of Dissolved Phosphorus Species in Natural and Wastewaters*, PhD Thesis, La Trobe University, 1992.
27. J. H. Steward and M. E. Tate, *J. Chromatogr.*, 1971, **60**, 75.
28. W. C. Weimer and D. E. Armstrong, *Anal. Chim. Acta.*, 1977, **94**, 35.
29. M. T. Downes, *Water Res.*, 1978, **12**, 743.
30. F. H. Rigler, *Limnol. Oceangr.*, 1968, **13**, 7.
31. W. Chamberlain and J. Shapiro, *ibid.*, 1969, **14**, 921.
32. R. M. Town and H. J. J. Powell, *Anal. Chim. Acta*, 1992, **256**, 81.
33. P. R. Freeman and I. D. McKelvie, unpublished data.
34. D. J. Cosgrove, in W. W. Wells and F. Eisenberg, *Cyclitols and Phosphoinositides*, p. 22. Academic Press, New York, 1978.

Talanta, Vol. 40, No. 12, pp. 1995–1998, 1993
Printed in Great Britain.

0039-9140/93 $6.00 + 0.00
Pergamon Press Ltd

BOOK REVIEWS

Comprehensive Dictionary of Physical Chemistry: L. ULICKY and T. J. KEMP (editors), Ellis Horwood, Chichester, 1992. Pages 472. £49.95. ISBN 0-13-151747-3.

Ellis Horwood and Prentice Hall have collaborated to produce this English edition in conjunction with ALFA publishers of Bratislava. Sixteen authors contributed to the dictionary and there were eight translators from the Slovak. The book was published in Czecho-Slovakia and I would describe the quality of printing and binding as 'adequate'.

On first perusal I was surprised to find apparent omissions such as chemometrics and chromatography but I then realized that this was the first of seven volumes in a range of comprehensive chemical dictionaries. The missing topics may appear in the other volumes which cover organic chemistry, biochemistry, inorganic chemistry, analytical chemistry, nuclear chemistry and various chemical technologies.

The first volume deals with topics from the theory of the structure of matter, states of matter, thermodynamics, electrochemistry, chemical kinetics and colloid and surface chemistry. These are indeed covered very comprehensively. The editors state that special attention is devoted to theoretical and quantum chemistry, and to symmetry and crystallography so I was surprised not to find any mention of molecular mechanics (another volume perhaps?).

Entries in the dictionary are extensively cross-referenced, for example, during the explanation of Donnan equilibrium the reader is cross-referenced to separate entries on 'osmotic pressure of a colloid', 'colloidal electrolyte', 'membrane hydrolysis' and 'membrane potential'. Overall there are approximately 2000 entries, 200 figures and 42 tables. A bibliography mentions numerous textbooks that were used to aid the compilation of the dictionary.

I did find the contents useful for succinct definitions of topics within physical chemistry and the dictionary will be especially useful in those areas where the reader needs to discover, or be reminded of, definitions and techniques. It should attract a wide readership.

P. J. Cox

Practical Surface Analysis—Second Edition, Volume 2—Ion and Neutral Spectroscopy: D. BRIGGS and M. P. SEAH (editors), Wiley, Chichester, 1992. Pages xvii + 738. £90.00. ISBN 0-471-92082-7.

Practical Surface Analysis was originally published in 1983 and was devoted to the birth, growth, and diversification of Auger and X-ray photoelectron spectroscopies in the period 1960–1983; it gained a high reputation among surface scientists world-wide. The Second Edition, Volume 1, was published in 1990 and is essentially a revision of the first edition. Volume 2 of the second edition is a new book dealing with the complementary topics of ion and neutral spectroscopy. The book opens with chapters on instrumentation, sputter depth profiling, and quantification, and this is followed by chapters on dynamic SIMS and its applications in microelectronics, and on the use of static SIMS in the surface analysis of inorganic and organic materials. Sputtered neutral spectrometry, which offers a better opportunity than SIMS for quantification, is the subject of another chapter. The remaining two chapters deal, respectively with low-energy and medium-energy ion scattering techniques. About one-sixth of the book is devoted to substantial appendices on angle-resolved electron-simulated ion desorption, the role standards in SIMS, computer codes and simulation, pure element sputtering yield data, masses and abundances of naturally-occurring isotopes, and fundamental physical constants and energy conversion factors.

Volume 2 maintains the same format, quality, breadth and depth of coverage of its subject as did Volume 1. Each chapter is well written, well-illustrated, well-documented, and up-to-date (1992). For all surface scientists interested in the decyphering of the elemental composition and structural arrangement of atoms in the first few monolayers of a solid, this volume will also be essential reading. This book is relatively inexpensive and good value for its price, and I understand that Volumes 1 and 2 can be purchased as a set at a discount.

J. B. CRAIG

Concepts and Calculations in Analytical Chemistry—A Spreadsheet Approach: H. FREISER, CRC Press, Boca Raton, 1992. Pages 315. US$19.95. ISBN 0-8493-4717-1.

Professor Freiser has written this book in an attempt to convey to readers his enthusiasm for "the magic of spreadsheets". He covers a wide range of topics related to Analytical Chemistry, including chemical equilibrium, the role of activity, acid–base, metal complex, precipitation and redox equilibria, titrations, statistical data treatment, spectrometry, separation processes, kinetic methods, and the determination of equilibria, and also attempts to provide a tutor for the use of the spreadsheet QuattroPro.

I found the book to be a valuable resource for teachers of analytical chemistry, but I feel that it is not all together successful as a text for students, possibly because the author is so much a master of the material he is presenting. My impression is that, in trying to show how elegant and easy this chemistry is when done by spreadsheet, he has sometimes lost sight of the student who is totally unfamiliar with the chemistry.

Talanta, Vol. 40, No. 12, pp. 1995–1998, 1993
Printed in Great Britain.

0039-9140/93 $6.00 + 0.00
Pergamon Press Ltd

BOOK REVIEWS

Comprehensive Dictionary of Physical Chemistry: L. ULICKY and T. J. KEMP (editors), Ellis Horwood, Chichester, 1992. Pages 472. £49.95. ISBN 0-13-151747-3.

Ellis Horwood and Prentice Hall have collaborated to produce this English edition in conjunction with ALFA publishers of Bratislava. Sixteen authors contributed to the dictionary and there were eight translators from the Slovak. The book was published in Czecho-Slovakia and I would describe the quality of printing and binding as 'adequate'.

On first perusal I was surprised to find apparent omissions such as chemometrics and chromatography but I then realized that this was the first of seven volumes in a range of comprehensive chemical dictionaries. The missing topics may appear in the other volumes which cover organic chemistry, biochemistry, inorganic chemistry, analytical chemistry, nuclear chemistry and various chemical technologies.

The first volume deals with topics from the theory of the structure of matter, states of matter, thermodynamics, electrochemistry, chemical kinetics and colloid and surface chemistry. These are indeed covered very comprehensively. The editors state that special attention is devoted to theoretical and quantum chemistry, and to symmetry and crystallography so I was surprised not to find any mention of molecular mechanics (another volume perhaps?).

Entries in the dictionary are extensively cross-referenced, for example, during the explanation of Donnan equilibrium the reader is cross-referenced to separate entries on 'osmotic pressure of a colloid', 'colloidal electrolyte', 'membrane hydrolysis' and 'membrane potential'. Overall there are approximately 2000 entries, 200 figures and 42 tables. A bibliography mentions numerous textbooks that were used to aid the compilation of the dictionary.

I did find the contents useful for succinct definitions of topics within physical chemistry and the dictionary will be especially useful in those areas where the reader needs to discover, or be reminded of, definitions and techniques. It should attract a wide readership.

P. J. Cox

Practical Surface Analysis—Second Edition, Volume 2—Ion and Neutral Spectroscopy: D. BRIGGS and M. P. SEAH (editors), Wiley, Chichester, 1992. Pages xvii + 738. £90.00. ISBN 0-471-92082-7.

Practical Surface Analysis was originally published in 1983 and was devoted to the birth, growth, and diversification of Auger and X-ray photoelectron spectroscopies in the period 1960–1983; it gained a high reputation among surface scientists world-wide. The Second Edition, Volume 1, was published in 1990 and is essentially a revision of the first edition. Volume 2 of the second edition is a new book dealing with the complementary topics of ion and neutral spectroscopy. The book opens with chapters on instrumentation, sputter depth profiling, and quantification, and this is followed by chapters on dynamic SIMS and its applications in microelectronics, and on the use of static SIMS in the surface analysis of inorganic and organic materials. Sputtered neutral spectrometry, which offers a better opportunity than SIMS for quantification, is the subject of another chapter. The remaining two chapters deal, respectively with low-energy and medium-energy ion scattering techniques. About one-sixth of the book is devoted to substantial appendices on angle-resolved electron-simulated ion desorption, the role standards in SIMS, computer codes and simulation, pure element sputtering yield data, masses and abundances of naturally-occurring isotopes, and fundamental physical constants and energy conversion factors.

Volume 2 maintains the same format, quality, breadth and depth of coverage of its subject as did Volume 1. Each chapter is well written, well-illustrated, well-documented, and up-to-date (1992). For all surface scientists interested in the decyphering of the elemental composition and structural arrangement of atoms in the first few monolayers of a solid, this volume will also be essential reading. This book is relatively inexpensive and good value for its price, and I understand that Volumes 1 and 2 can be purchased as a set at a discount.

J. B. CRAIG

Concepts and Calculations in Analytical Chemistry—A Spreadsheet Approach: H. FREISER, CRC Press, Boca Raton, 1992. Pages 315. US$19.95. ISBN 0-8493-4717-1.

Professor Freiser has written this book in an attempt to convey to readers his enthusiasm for "the magic of spreadsheets". He covers a wide range of topics related to Analytical Chemistry, including chemical equilibrium, the role of activity, acid–base, metal complex, precipitation and redox equilibria, titrations, statistical data treatment, spectrometry, separation processes, kinetic methods, and the determination of equilibria, and also attempts to provide a tutor for the use of the spreadsheet QuattroPro.

I found the book to be a valuable resource for teachers of analytical chemistry, but I feel that it is not all together successful as a text for students, possibly because the author is so much a master of the material he is presenting. My impression is that, in trying to show how elegant and easy this chemistry is when done by spreadsheet, he has sometimes lost sight of the student who is totally unfamiliar with the chemistry.

The book is seriously let down by the type-setting: there is no consistency in the use of different type-faces, particularly italics. In a chemical text, the symbols for constants (*e.g.*, K_{sp}) and variables in equations should be set in italic, and the symbols for chemical species (*e.g.*, NH_3) should be in upright text. Here, chemical species often appear in italics and constants in upright type, and both forms for each often appear on the same page. For example, on page 69, the hydrogen ion concentration is first shown correctly as $[H^+]$, then as H, and finally as H.

M. MASSON

Internal Reflection Spectroscopy—Theory and Applications: F. M. MIRABELLA, JR., Dekker, New York, 1993. Pages vii + 374. US$ 145.00. ISBN 0-8247-8730-7.

Internal reflection spectroscopy (IRS) has come a long way since the pioneering work of Taylor in the 1930s and that of Fahrenfort and Harrick in the 1950s. Advancement of the methodology and of its applications has been relatively slow; indeed until recently the main problem with IRS was its restriction to samples (*e.g.*, films, sheets, coatings on rigid surfaces, *etc.*) that would allow good surface contact between the material and the internal reflection elements.

The development of commercial Fourier transform IR instruments and of sampling systems that permit the analysis of liquids, powders and pastes have increased greatly the applications of this technique. Although most IRS work is done in the mid-infrared region of the spectrum applications are being developed using UV, visible, Raman and fluorescence spectroscopy.

The book is published at a most exciting time. Instrumental problems have been overcome and the range of applications is growing rapidly. The book consists of 12 chapters by acknowledged experts in the field (mostly from industry); the first two chapters deal with historical and theoretical aspects and the remainder of the book is devoted to applications (industrial, electrochemical, process monitoring, biomedical, semi conductors, *etc.*).

Dr Mirabella has done a first class job in editing this book and I have every hope that it will achieve his stated aim: 'to stimulate progress in this promising field'. My only reservation is that the price ($145) will inevitably prevent this book achieving the wide readership that it deserves.

B. A. MCGAW

Guide to Flow Cytometry Methods: W. M. GROGAN and J. M. COLLINS, Dekker, New York, 1990. Pages x + 228. $99.75 (U.S. and Canada), $119.50 (elsewhere). ISBN: 0-8247-8330-1.

This book will be of value to those who are already working in this field, particularly those involved in clinical analysis and in research.

As would be expected due emphasis is given to the basis of, and the practical applications of, DNA analysis in a variety of tissue types. The unique aspect of this book is that in one small volume, in a readily understandable form, it successfully brings together all the current, and possible future, applications of cytometry methods. Particularly pleasing is that throughout the text the practical aspects of the methodology involved for a particular determination are described in a uniform, simple and stepwise fashion making the particular analysis immediately possible without recourse to a large literature search. For those who require further information the text is well referenced with recent, pertinent literature references.

A drawback of the black and white presentation of the illustrations in the text, particularly the two-dimensional bit diagrams, is that it makes it difficult to clearly differentiate between the shaded areas and this hinders correct interpretation.

The text is accompanied by a useful appendix which allows rapid identification of the dyes and stains needed for the main applications, the suppliers of instruments, and other generally required materials.

R. R. MOODY

Pharmaceutical Chemistry—Volume 2, Drug Analysis: H. J. ROTH, K. EGER and R. TROSCHÜTZ, Ellis Horwood, Chichester, 1991. Pages: 767. £74.50. ISBN 0-13-663360-9.

Pharmaceutical Chemistry is published in three volumes: 1—drug synthesis, 2—drug analysis and, 3—drug bioreactivity. Each volume forms part of the Ellis Horwood series in Pharmaceutical Technology. This second volume was originally published, as a third edition, in the German language (*Pharmazeutische Chemie 2—Arzneistoffanalyse*) and it has been translated into English by Anthony Dunson. Several sections of this volume make reference to the German Pharmacopoeia *Deutsches Arzneibuch* (DAB).

The foreword to this book anticipates the main criticism that will be broached, namely that the many reactions described have diminished in importance compared to instrumental analytical procedures. The authors counter this by noting that colour and fluorescence reactions are frequently employed for detection by TLC. I would suggest that a better argument would be that many non-instrumental analytical procedures are recognised as being official procedures and can be performed in many laboratories without the need for expensive instrumentation. Simple colour reactions are also useful in initial stages of drug identification—especially for drugs of abuse. However, the reader is forewarned that this is not a book giving extensive details of instrumental analyses—those interested in procedures based on HPLC, atomic absorption, spectrofluorimetry, *etc.* will need to look elsewhere.

The book is seriously let down by the type-setting: there is no consistency in the use of different type-faces, particularly italics. In a chemical text, the symbols for constants (*e.g.*, K_{sp}) and variables in equations should be set in italic, and the symbols for chemical species (*e.g.*, NH_3) should be in upright text. Here, chemical species often appear in italics and constants in upright type, and both forms for each often appear on the same page. For example, on page 69, the hydrogen ion concentration is first shown correctly as $[H^+]$, then as H, and finally as H.

M. MASSON

Internal Reflection Spectroscopy—Theory and Applications: F. M. MIRABELLA, JR., Dekker, New York, 1993. Pages vii + 374. US$ 145.00. ISBN 0-8247-8730-7.

Internal reflection spectroscopy (IRS) has come a long way since the pioneering work of Taylor in the 1930s and that of Fahrenfort and Harrick in the 1950s. Advancement of the methodology and of its applications has been relatively slow; indeed until recently the main problem with IRS was its restriction to samples (*e.g.*, films, sheets, coatings on rigid surfaces, *etc.*) that would allow good surface contact between the material and the internal reflection elements.

The development of commercial Fourier transform IR instruments and of sampling systems that permit the analysis of liquids, powders and pastes have increased greatly the applications of this technique. Although most IRS work is done in the mid-infrared region of the spectrum applications are being developed using UV, visible, Raman and fluorescence spectroscopy.

The book is published at a most exciting time. Instrumental problems have been overcome and the range of applications is growing rapidly. The book consists of 12 chapters by acknowledged experts in the field (mostly from industry); the first two chapters deal with historical and theoretical aspects and the remainder of the book is devoted to applications (industrial, electrochemical, process monitoring, biomedical, semi conductors, *etc.*).

Dr Mirabella has done a first class job in editing this book and I have every hope that it will achieve his stated aim: 'to stimulate progress in this promising field'. My only reservation is that the price ($145) will inevitably prevent this book achieving the wide readership that it deserves.

B. A. MCGAW

Guide to Flow Cytometry Methods: W. M. GROGAN and J. M. COLLINS, Dekker, New York, 1990. Pages x + 228. $99.75 (U.S. and Canada), $119.50 (elsewhere). ISBN: 0-8247-8330-1.

This book will be of value to those who are already working in this field, particularly those involved in clinical analysis and in research.

As would be expected due emphasis is given to the basis of, and the practical applications of, DNA analysis in a variety of tissue types. The unique aspect of this book is that in one small volume, in a readily understandable form, it successfully brings together all the current, and possible future, applications of cytometry methods. Particularly pleasing is that throughout the text the practical aspects of the methodology involved for a particular determination are described in a uniform, simple and stepwise fashion making the particular analysis immediately possible without recourse to a large literature search. For those who require further information the text is well referenced with recent, pertinent literature references.

A drawback of the black and white presentation of the illustrations in the text, particularly the two-dimensional bit diagrams, is that it makes it difficult to clearly differentiate between the shaded areas and this hinders correct interpretation.

The text is accompanied by a useful appendix which allows rapid identification of the dyes and stains needed for the main applications, the suppliers of instruments, and other generally required materials.

R. R. MOODY

Pharmaceutical Chemistry—Volume 2, Drug Analysis: H. J. ROTH, K. EGER and R. TROSCHÜTZ, Ellis Horwood, Chichester, 1991. Pages: 767. £74.50. ISBN 0-13-663360-9.

Pharmaceutical Chemistry is published in three volumes: 1—drug synthesis, 2—drug analysis and, 3—drug bioreactivity. Each volume forms part of the Ellis Horwood series in Pharmaceutical Technology. This second volume was originally published, as a third edition, in the German language (*Pharmazeutische Chemie 2—Arzneistoffanalyse*) and it has been translated into English by Anthony Dunson. Several sections of this volume make reference to the German Pharmacopoeia *Deutsches Arzneibuch* (DAB).

The foreword to this book anticipates the main criticism that will be broached, namely that the many reactions described have diminished in importance compared to instrumental analytical procedures. The authors counter this by noting that colour and fluorescence reactions are frequently employed for detection by TLC. I would suggest that a better argument would be that many non-instrumental analytical procedures are recognised as being official procedures and can be performed in many laboratories without the need for expensive instrumentation. Simple colour reactions are also useful in initial stages of drug identification—especially for drugs of abuse. However, the reader is forewarned that this is not a book giving extensive details of instrumental analyses—those interested in procedures based on HPLC, atomic absorption, spectrofluorimetry, *etc.* will need to look elsewhere.

The book is seriously let down by the type-setting: there is no consistency in the use of different type-faces, particularly italics. In a chemical text, the symbols for constants (*e.g.*, K_{sp}) and variables in equations should be set in italic, and the symbols for chemical species (*e.g.*, NH_3) should be in upright text. Here, chemical species often appear in italics and constants in upright type, and both forms for each often appear on the same page. For example, on page 69, the hydrogen ion concentration is first shown correctly as $[H^+]$, then as H, and finally as H.

M. MASSON

Internal Reflection Spectroscopy—Theory and Applications: F. M. MIRABELLA, JR., Dekker, New York, 1993. Pages vii + 374. US$ 145.00. ISBN 0-8247-8730-7.

Internal reflection spectroscopy (IRS) has come a long way since the pioneering work of Taylor in the 1930s and that of Fahrenfort and Harrick in the 1950s. Advancement of the methodology and of its applications has been relatively slow; indeed until recently the main problem with IRS was its restriction to samples (*e.g.*, films, sheets, coatings on rigid surfaces, *etc.*) that would allow good surface contact between the material and the internal reflection elements.

The development of commercial Fourier transform IR instruments and of sampling systems that permit the analysis of liquids, powders and pastes have increased greatly the applications of this technique. Although most IRS work is done in the mid-infrared region of the spectrum applications are being developed using UV, visible, Raman and fluorescence spectroscopy.

The book is published at a most exciting time. Instrumental problems have been overcome and the range of applications is growing rapidly. The book consists of 12 chapters by acknowledged experts in the field (mostly from industry); the first two chapters deal with historical and theoretical aspects and the remainder of the book is devoted to applications (industrial, electrochemical, process monitoring, biomedical, semi conductors, *etc.*).

Dr Mirabella has done a first class job in editing this book and I have every hope that it will achieve his stated aim: 'to stimulate progress in this promising field'. My only reservation is that the price ($145) will inevitably prevent this book achieving the wide readership that it deserves.

B. A. MCGAW

Guide to Flow Cytometry Methods: W. M. GROGAN and J. M. COLLINS, Dekker, New York, 1990. Pages x + 228. $99.75 (U.S. and Canada), $119.50 (elsewhere). ISBN: 0-8247-8330-1.

This book will be of value to those who are already working in this field, particularly those involved in clinical analysis and in research.

As would be expected due emphasis is given to the basis of, and the practical applications of, DNA analysis in a variety of tissue types. The unique aspect of this book is that in one small volume, in a readily understandable form, it successfully brings together all the current, and possible future, applications of cytometry methods. Particularly pleasing is that throughout the text the practical aspects of the methodology involved for a particular determination are described in a uniform, simple and stepwise fashion making the particular analysis immediately possible without recourse to a large literature search. For those who require further information the text is well referenced with recent, pertinent literature references.

A drawback of the black and white presentation of the illustrations in the text, particularly the two-dimensional bit diagrams, is that it makes it difficult to clearly differentiate between the shaded areas and this hinders correct interpretation.

The text is accompanied by a useful appendix which allows rapid identification of the dyes and stains needed for the main applications, the suppliers of instruments, and other generally required materials.

R. R. MOODY

Pharmaceutical Chemistry—Volume 2, Drug Analysis: H. J. ROTH, K. EGER and R. TROSCHÜTZ, Ellis Horwood, Chichester, 1991. Pages: 767. £74.50. ISBN 0-13-663360-9.

Pharmaceutical Chemistry is published in three volumes: 1—drug synthesis, 2—drug analysis and, 3—drug bioreactivity. Each volume forms part of the Ellis Horwood series in Pharmaceutical Technology. This second volume was originally published, as a third edition, in the German language (*Pharmazeutische Chemie 2—Arzneistoffanalyse*) and it has been translated into English by Anthony Dunson. Several sections of this volume make reference to the German Pharmacopoeia *Deutsches Arzneibuch* (DAB).

The foreword to this book anticipates the main criticism that will be broached, namely that the many reactions described have diminished in importance compared to instrumental analytical procedures. The authors counter this by noting that colour and fluorescence reactions are frequently employed for detection by TLC. I would suggest that a better argument would be that many non-instrumental analytical procedures are recognised as being official procedures and can be performed in many laboratories without the need for expensive instrumentation. Simple colour reactions are also useful in initial stages of drug identification—especially for drugs of abuse. However, the reader is forewarned that this is not a book giving extensive details of instrumental analyses—those interested in procedures based on HPLC, atomic absorption, spectrofluorimetry, *etc.* will need to look elsewhere.

The authors have assigned individual drugs to a particular class of organic compound and each of these 14 compound types is dealt with in a separate chapter. The chapter headings are: Hydrocarbons and halogenated hydrocarbons; Hydroxylated hydrocarbons; Carbonyl compounds; Carboxylic acids; Carbonic acid derivatives; Nitro-compounds; Amines; Sulphur-containing compounds; Polycarbocyclics; *O*-containing heterocyclics; *N*-containing heterocyclics; *S*-containing heterocyclics; *N,O*- and *N,S*-containing heterocyclics and, *O,N,P*-containing heterocyclics. The three largest chapters: *N*-containing heterocyclics (188 pages), carboxylic acids (142 pages) and amines (83 pages), occupy more than half the book. The chapters are further subdivided, *e.g.* under carbonyl compounds, information is given on quinones, aldehydes and ketones, and carbohydrates. General details of these drug types are given and individual drugs are also selected for specific treatment. Each drug selected is mentioned with a common and a systematic name, *e.g.* ethisterone, 17-hydroxy-17α-pregn-4-en-20-yn-3-one together with a structural formula. A rectangular box is drawn around these three items of information.

What follows after these rectangular headings is somewhat variable. In the best cases some physical and chemical properties are presented along with identification, purity testing and assay procedures. Where the drug is mentioned along with very closely related compounds very little information, if any, is provided. As previously mentioned there is very little on instrumental analysis and no spectra are included but λ_{max} values for UV work are occasionally presented. Good features include the many reactions that are given, many showing the appropriate mechanisms, and the use of structural formulae throughout the book. There are also extensive literature references and a good index is included.

It would be impossible to include all drugs in a single text of this size but I was surprised to find that ibuprofen, which rivals acetylsalicylic acid and paracetamol in the lucrative analgesics market, was omitted. A small section on inorganic and organometallic drugs would also have been welcomed along with mention of important substances such as zinc insulin.

Assays are normally performed to determine if the chemical content of a drug substances lies within certain acceptable limits, *e.g.* 99.5–100.5% of the stated amount. Such limits, which are unfortunately not given in this book, also indicate the precision required for the assay.

There are also a number of errors present, *e.g.* paracetamol does not have more than one phenolic hydroxy group available and the opening sentence under Promazine—"The base is only."—is meaningless. I am sure a translation editor would have corrected many of the errors. On the whole an interesting addition to, but not a replacement for, the standard works on drug analysis.

P. J. Cox

Polymer Characterisation: B. J. Hunt and M. I. James (editors), Blackie, Glasgow, 1992. Pages xiv + 362. £69.00. ISBN 0-7514-0082-3.

This is a well written book and makes a very able attempt at covering the methods used in the characterisation of polymers. Following a brief introduction the second chapter highlights the need for preparation of polymers prior to analysis by using specific examples. The spectroscopic techniques are then very well covered in the next two chapters. The fifth chapter looks at the methods available for molecular mass determination. The remaining six chapters cover techniques such as chromatographic methods, thermal analysis, small-angle neutron scattering and neutron reflectometry, mechanical and rheological analysis, microscopy and finally XPS and SIMS. The text covers each of the topics in considerable detail, numerous examples are provided and good use is made of figures throughout. For those who desire to go that little bit further there are also many references provided with each chapter. An improvement may have been to provide more examples from the medical and pharmaceutical fields as it is stated in the Introduction that this has been "pursued with great vigour in recent years". The book should prove useful to anyone involved with polymers, particularly those involved in analysis and characterisation.

K. I. Cumming

Detectors for Capillary Chromatography: H. H. Hill and D. G. McMinn (editors), Wiley–Interscience, New York, 1992. pages xvii + 444. £79.00. ISBN 0-471-50645-1.

This is a book in the Chemical Analysis series which represents a series of monographs on Analytical Chemistry and its applications. As anticipated it maintains the high standard expected of a book in this series.

Very few, if any, chromatographers would disagree with the fact that once column separation of a mixture of analytes has been achieved, the qualitative and the quantitative analysis of the eluted components then becomes a function of the specificity, sensitivity and reproducibility of the detecting system used. Thus the value and the importance of this text, to chromatographers, should be obvious.

There are 14 chapters in the book, 12 of which deal with particular detector or detecting systems. The range covered is from the well known *e.g.* FID, EC detectors, to the lesser known or used, *e.g.* surface ionisation, Fourier transform infrared detectors, to the more complex, relatively widely used GC/MS detecting systems. One of the final two excellent chapters, reviews the current detectors available for use in capillary supercritical fluid chromatography, and the other, detectors for micro-column LC. The importance of the choice of a detector, how it functions, its limitations and applications are all covered in a uniform manner throughout the first 12 chapters of the book: Introduction, Design, Operating Characteristics, Applications and Possible Future Developments.

All chapters have individual, up-to-date (1991), reference lists and a high standard of presentation, *e.g.* chromatograms, tables, figures, diagrams, *etc.*, is maintained throughout the text.

The enthusiasm, knowledge and the expertise of the many individual authors involved in producing this book comes over clearly to the reader. A very, worthwhile reference source for those scientists working in the GC and/or LC fields.

R. R. Moody

The authors have assigned individual drugs to a particular class of organic compound and each of these 14 compound types is dealt with in a separate chapter. The chapter headings are: Hydrocarbons and halogenated hydrocarbons; Hydroxylated hydrocarbons; Carbonyl compounds; Carboxylic acids; Carbonic acid derivatives; Nitro-compounds; Amines; Sulphur-containing compounds; Polycarbocyclics; *O*-containing heterocyclics; *N*-containing heterocyclics; *S*-containing heterocyclics; *N,O*- and *N,S*-containing heterocyclics and, *O,N,P*-containing heterocyclics. The three largest chapters: *N*-containing heterocyclics (188 pages), carboxylic acids (142 pages) and amines (83 pages), occupy more than half the book. The chapters are further subdivided, *e.g.* under carbonyl compounds, information is given on quinones, aldehydes and ketones, and carbohydrates. General details of these drug types are given and individual drugs are also selected for specific treatment. Each drug selected is mentioned with a common and a systematic name, *e.g.* ethisterone, 17-hydroxy-17α-pregn-4-en-20-yn-3-one together with a structural formula. A rectangular box is drawn around these three items of information.

What follows after these rectangular headings is somewhat variable. In the best cases some physical and chemical properties are presented along with identification, purity testing and assay procedures. Where the drug is mentioned along with very closely related compounds very little information, if any, is provided. As previously mentioned there is very little on instrumental analysis and no spectra are included but λ_{max} values for UV work are occasionally presented. Good features include the many reactions that are given, many showing the appropriate mechanisms, and the use of structural formulae throughout the book. There are also extensive literature references and a good index is included.

It would be impossible to include all drugs in a single text of this size but I was surprised to find that ibuprofen, which rivals acetylsalicylic acid and paracetamol in the lucrative analgesics market, was omitted. A small section on inorganic and organometallic drugs would also have been welcomed along with mention of important substances such as zinc insulin.

Assays are normally performed to determine if the chemical content of a drug substances lies within certain acceptable limits, *e.g.* 99.5–100.5% of the stated amount. Such limits, which are unfortunately not given in this book, also indicate the precision required for the assay.

There are also a number of errors present, *e.g.* paracetamol does not have more than one phenolic hydroxy group available and the opening sentence under Promazine—"The base is only."—is meaningless. I am sure a translation editor would have corrected many of the errors. On the whole an interesting addition to, but not a replacement for, the standard works on drug analysis.

P. J. Cox

Polymer Characterisation: B. J. Hunt and M. I. James (editors), Blackie, Glasgow, 1992. Pages xiv + 362. £69.00. ISBN 0-7514-0082-3.

This is a well written book and makes a very able attempt at covering the methods used in the characterisation of polymers. Following a brief introduction the second chapter highlights the need for preparation of polymers prior to analysis by using specific examples. The spectroscopic techniques are then very well covered in the next two chapters. The fifth chapter looks at the methods available for molecular mass determination. The remaining six chapters cover techniques such as chromatographic methods, thermal analysis, small-angle neutron scattering and neutron reflectometry, mechanical and rheological analysis, microscopy and finally XPS and SIMS. The text covers each of the topics in considerable detail, numerous examples are provided and good use is made of figures throughout. For those who desire to go that little bit further there are also many references provided with each chapter. An improvement may have been to provide more examples from the medical and pharmaceutical fields as it is stated in the Introduction that this has been "pursued with great vigour in recent years". The book should prove useful to anyone involved with polymers, particularly those involved in analysis and characterisation.

K. I. Cumming

Detectors for Capillary Chromatography: H. H. Hill and D. G. McMinn (editors), Wiley–Interscience, New York, 1992. pages xvii + 444. £79.00. ISBN 0-471-50645-1.

This is a book in the Chemical Analysis series which represents a series of monographs on Analytical Chemistry and its applications. As anticipated it maintains the high standard expected of a book in this series.

Very few, if any, chromatographers would disagree with the fact that once column separation of a mixture of analytes has been achieved, the qualitative and the quantitative analysis of the eluted components then becomes a function of the specificity, sensitivity and reproducibility of the detecting system used. Thus the value and the importance of this text, to chromatographers, should be obvious.

There are 14 chapters in the book, 12 of which deal with particular detector or detecting systems. The range covered is from the well known *e.g.* FID, EC detectors, to the lesser known or used, *e.g.* surface ionisation, Fourier transform infrared detectors, to the more complex, relatively widely used GC/MS detecting systems. One of the final two excellent chapters, reviews the current detectors available for use in capillary supercritical fluid chromatography, and the other, detectors for micro-column LC. The importance of the choice of a detector, how it functions, its limitations and applications are all covered in a uniform manner throughout the first 12 chapters of the book: Introduction, Design, Operating Characteristics, Applications and Possible Future Developments.

All chapters have individual, up-to-date (1991), reference lists and a high standard of presentation, *e.g.* chromatograms, tables, figures, diagrams, *etc.*, is maintained throughout the text.

The enthusiasm, knowledge and the expertise of the many individual authors involved in producing this book comes over clearly to the reader. A very, worthwhile reference source for those scientists working in the GC and/or LC fields.

R. R. Moody

Quality Assurance Principles for Analytical Laboratories: Second Edition F. M. GARFIELD, AOAC International, Arlington, 1991. Pages 196. $63.00 (North America), $69.00 (Elsewhere). ISBN 0-935584-46-3.

The first edition of this book, published in 1984, enjoyed wide circulation and there is every reason to suspect that the second edition will do even better. One has only to turn the pages of *Chemistry in Britain*, or a similar journal, to realize just how many independent laboratories now offer analytical services in this country. In order to compete successfully in this ever-increasing market, recognition in the form of Laboratory Accreditation must surely be the minimum requirement. This book leads the potential applicant through the various aspects of quality assurance to accreditation, and does it thoroughly, systematically, and in a pleasing manner.

There is much to praise and very little to criticize in the content and layout of this book. There are 10 chapters, six appendices, and a comprehensive index. The chapters are: Quality Assurance Planning, Statistical Applications and Control Charts (new), Personnel Considerations, Management of Equipment and Supplies, Sample and Record Handling, Sampling and Sample Analysis, Proficiency and Check Samples, Audit Procedures, Design and Safety of Facilities, and Laboratory Accreditation. A very useful feature at the end of each chapter is a summary, entitled "Recommendations", and a quick glance here provides one with enough sound advice on which to base plans of action. Following the recommendations is an up-to-date bibliography for each chapter. The references therein are largely North American in origin, as are the majority of Regulations, Acts, and Reports quoted, but there are also present a number of references to QA guidelines from other countries. Indeed, the appendix on Accreditation Criteria, which is new in this edition, draws on a variety of national sources for the criteria.

The appendices are most useful in that they present some pictorial as well as written information. Examples of forms used by Federal Agencies are shown in one appendix, whilst in another a checklist, in chart form, lists a set of procedures to be used for monitoring analytical instrument performance, and to aid in detecting the first stages of deterioration in performance.

To summarize, the book is a mine of practical information for anyone wishing to learn about Quality Assurance methods from scratch, or for an experienced manager seeking accreditation for his/her laboratory.

D. F. RENDLE

Chromatographic Retention Indices—An Aid to Identification of Organic Compounds: V. PACÁKOVÁ and L. FELTI, Ellis Horwood, 1992, Pages 285. £65.00. ISBN 0-13-772328-8.

Despite the many well documented problems of reproducibility and transferability between instruments, columns and laboratories, many chromatographers still hold an unjustified faith in the validity of absolute measurements of retention as a method of identification. Alternative relative and preferably robust measurements such as retention index values are required and have found adoption throughout chromatography, most particularly for gas–liquid chromatography (GLC). The extent of their adoption can best be exemplified by a review paper in 1983 on the first 25 years of Kovats indices, which contained over 1350 references.

The aim of this book is to explain the background to the analytical application of retention indices and to illustrate their various roles for the analyst. It starts with a general discussion of retention measurement data and the use of relative measurements and retention index scales. The Kovats retention index scale based on *n*-alkanes, which is the most important for GLC, is described and is compared with alternative scales based on other homologous series of standard reference compounds. Retention indices scales for high-performance liquid chromatography and supercritical fluid chromatography are reviewed but are not discussed further in the book.

For the remainder of the book the authors concentrate on selected aspects of the applications of retention indices in GLC. The effects of temperature, including the changes caused by temperature programming, on the indices of difference structural types are discussed. These structural influences are then described in greater detail and are related to the physical properties of the analytes and the presence of particular functional groups. These lead to methods to calculate or predict retention indices. The widespread role of retention indices as the basis of the Rohrschneider and McReynolds methods to characterize GLC stationary phases is described.

The second half of the book is an extensive compilation of the retention indices of selected groups of analytes on a range of stationary phases. However, most of the analytes are relatively simple in structure and would principally be useful for theoreticians or molecular modelling. The value of these tables to the practising chromatographer is not clear as they are essentially model compounds and for the retention indices of most compounds of practical importance it will be necessary to consult commercially available databases.

The first part of the book is useful and would be valuable reading for most gas chromatographers as a guide to the use of retention indices and as a warning of the problems that can be encountered.

R. M. SMITH

Talanta

The International Journal of Pure and Applied Analytical Chemistry

Second Class Postage Paid at RAHWAY NJ. Postmaster send address corrections to *Talanta*, c/o **Pergamon Press Inc., 660 White Plains Road, Tarrytown, New York 10591-5153, U.S.A.**

Talanta, Vol. 40, No. 5, pp. i–vi, 1993
Printed in Great Britain.

0039-9140/93 $6.00 + 0.00
Pergamon Press Ltd

NOTICES

Vth INTERNATIONAL SYMPOSIUM ON QUANTITATIVE LUMINESCENCE SPECTROMETRY IN BIOMEDICAL SCIENCES

University of Ghent, Faculty of Pharmaceutical Sciences, Pharmaceutical Institute, Harelbekestraat 72, B-9000 Ghent, Belgium, tel. 32-(0)91-21.89.51 ext. 246, telefax 32-(0)91-21.79.02
25–27 May, 1993

For further details please contact Dr Willy R. G. Baeyens, Symposium Chairman, University of Ghent, Pharmaceutical Institute, Harelbekestraat 72, B-9000 Ghent, Belgium.

XXVIII COLLOQUIUM SPECTROSCOPICUM INTERNATIONALE

Invitation

The Organising Committee cordially invites you to attend the XXVIII CSI which will be held from Tuesday to Sunday, June 29th to July 4th, 1993, in York, United Kingdom.

This traditional biennial conference provides a forum for the international community of analytical spectroscopists to meet and exchange ideas.

Participants are invited to submit contributions for presentation in English, French or German (there will be no translation facilities) on the following topics:

Basic Theory, Techniques and Instrumentation of:

Atomic Spectroscopy (Emission, Absorption, Fluorescence)
Computer Applications and Chemometrics
Electron Spectroscopy
Gamma Spectroscopy
Laser Spectroscopy
Mass Spectrometry (Inorganic and Organic)
Methods of Surface Analysis and Depth Profiling
Molecular Spectroscopy (UV, VIS, IR)
Mössbauer Spectroscopy
Nuclear Magnetic Resonance Spectrometry
Photoacoustic Spectroscopy
Raman Spectroscopy
X-ray Spectroscopy

Applications of Spectroscopy in the Analysis of:

Biological Samples
Environmental Samples
Food and Agricultural Products
Geological Materials
Industrial Products
Metals and Alloys

The scientific programme will consist of plenary lectures and four parallel streams of contributed lectures (e.g. atomic, molecular and mass spectrometry, and surface analysis and characterisation)

Talanta, Vol. 40, No. 2, pp. i–ii, 1993
Pergamon Press Ltd. Printed in Great Britain

NOTICES

CHROMATOGRAPHIC FUNDAMENTALS COURSE

7–11 June, 1993

Kent State University's Chemistry Department will co-sponsor a course, "Fundamentals of Chromatographic Analysis", during 7–11 June 1993. This will be the tenth offering of this course which has been well received by the industrial community.

The course will provide a coherent overview of chemical separations via chromatographic methods. It is unique from most other short courses in that material will be included on gas, liquid and thin-layer methods. It will emphasize the three techniques as complementary rather than competing processes. The course will be a blend of fundamental information on theory and instrumentation with emphasis placed on the latest developments and trends. Additional periods will provide time to discuss practical problems related to HPLC, GC, GC-MS, TLC and CE instrumentation.

Dr Roger K. Gilpin, Chairman of Chemistry at Kent State University, and Dr Neil D. Danielson, Professor at Miami University, will be the principle lecturers. Ronald L. Lewis of Varian will discuss/demonstrate laboratory instrumentation.

Information on this course can be obtained by writing to: Carl J. Knauss, Chemistry Department, Kent State University, Kent, OH 44242, U.S.A. *Tel.* 216/672-2327.

XXVIII CSI POST-SYMPOSIUM: GRAPHITE ATOMIZER TECHNIQUES IN ANALYTICAL SPECTROSCOPY

4–7 July, 1993, University of Durham, U.K.

Following the successful XXVII CSI Pre-Symposium meeting in Loftus, Norway, 1991, the organizers of the 1993 meeting intend to keep a similar format and scope. The symposium will focus on recent research using graphite electrothermal furnaces in atomic absorption, emission, fluorescence and mass spectrometry with an emphasis on achieving accuracy in practical analysis.

The topics will include:

reaction and interference mechanisms
temperature and atom distribution measurements
absolute analysis
coupling with hydride–generation, chromatography and flow-injection
laser applications
solid and slurry sampling
metal and other non-graphite surfaces
and all applications in these areas.

The meeting will be an excellent forum where scientists both with a great deal of experience in these techniques and others new to the field can meet to exchange ideas and views and present their research data.

For further information contact: XXVIII Colloquim Spectroscopicum Internationale, Department of Chemistry (CSI Secretariat), Loughborough University of Technology, Loughborough, Leicestershire LE11 3TU, U.K. *Tel.* 44 (0)509 22575, *Fax.* +44 (0)509 233163, *Telex* 34319.

Talanta, Vol. 40, No. 2, pp. i–ii, 1993
Pergamon Press Ltd. Printed in Great Britain

NOTICES

CHROMATOGRAPHIC FUNDAMENTALS COURSE

7–11 June, 1993

Kent State University's Chemistry Department will co-sponsor a course, "Fundamentals of Chromatographic Analysis", during 7–11 June 1993. This will be the tenth offering of this course which has been well received by the industrial community.

The course will provide a coherent overview of chemical separations via chromatographic methods. It is unique from most other short courses in that material will be included on gas, liquid and thin-layer methods. It will emphasize the three techniques as complementary rather than competing processes. The course will be a blend of fundamental information on theory and instrumentation with emphasis placed on the latest developments and trends. Additional periods will provide time to discuss practical problems related to HPLC, GC, GC-MS, TLC and CE instrumentation.

Dr Roger K. Gilpin, Chairman of Chemistry at Kent State University, and Dr Neil D. Danielson, Professor at Miami University, will be the principle lecturers. Ronald L. Lewis of Varian will discuss/demonstrate laboratory instrumentation.

Information on this course can be obtained by writing to: Carl J. Knauss, Chemistry Department, Kent State University, Kent, OH 44242, U.S.A. *Tel.* 216/672-2327.

XXVIII CSI POST-SYMPOSIUM: GRAPHITE ATOMIZER TECHNIQUES IN ANALYTICAL SPECTROSCOPY

4–7 July, 1993, University of Durham, U.K.

Following the successful XXVII CSI Pre-Symposium meeting in Loftus, Norway, 1991, the organizers of the 1993 meeting intend to keep a similar format and scope. The symposium will focus on recent research using graphite electrothermal furnaces in atomic absorption, emission, fluorescence and mass spectrometry with an emphasis on achieving accuracy in practical analysis.

The topics will include:

reaction and interference mechanisms
temperature and atom distribution measurements
absolute analysis
coupling with hydride–generation, chromatography and flow-injection
laser applications
solid and slurry sampling
metal and other non-graphite surfaces
and all applications in these areas.

The meeting will be an excellent forum where scientists both with a great deal of experience in these techniques and others new to the field can meet to exchange ideas and views and present their research data.

For further information contact: XXVIII Colloquim Spectroscopicum Internationale, Department of Chemistry (CSI Secretariat), Loughborough University of Technology, Loughborough, Leicestershire LE11 3TU, U.K. *Tel.* 44 (0)509 22575, *Fax.* +44 (0)509 233163, *Telex* 34319.

Talanta, Vol. 40, No. 1, p. i, 1993
Printed in Great Britain

0039-9140/93 $6.00 + 0.00
Pergamon Press Ltd

NOTICE

FIRST ANNOUNCEMENT

The **XIIth Conference of Analytical Chemistry** from ROMANIA will take place between 22–24 September 1994 at the "OVIDIUS" University in Constanta. This Conference will be organised under the auspices of the Romanian Society of Analytical Chemistry. If you are interested in participating in this event please write, by 1 May 1993, to Dr. G.-L. Radu for the Organising Committee for the 12th Conference of Analytical Chemistry at the following address:

ROMANIAN SOCIETY OF ANALYTICAL CHEMISTRY
13, Bul. Carol I, Sector 3, 70346 Bucharest, Romania

More information will be sent to you after 15 September 1993 by a second announcement.

Talanta, Vol. 40, No. 10, pp. i–ii, 1993

0039-9140/93 $6.00 + 0.00
Pergamon Press Ltd

NOTICES

INTERNATIONAL SYMPOSIUM ON MICROCHEMICAL TECHNIQUES (ISM '94)

The "International Symposium on Microchemical Techniques (ISM '94)" will have its next meeting in a joint organization with the "Deauville Conference 1994—Symposium on Analytical Sciences (SAS '94)" in Montreux, Switzerland, 16–20 May 1994. For further information contact:

Nicko & C.R.I. Associes, 7 Rue d'Argout, F-75002 Paris, France.
Tel: +33-1-42.33.47.66. Fax: +33-1-40.41.92.41.

6th INTERNATIONAL CONFERENCE ON FLOW ANALYSIS

Toledo, Spain
8–11 June 1994

Topics

The Conference shall basically be concerned with the following flow analysis topics: general aspects, FI-chemometrics, detection systems, separation techniques (on-line sample treatment), sensors and continuous flow techniques, applications (environmental, food, clinical, industrial analysis), and process control (Biotechnology). Two special sessions devoted to "Flow Analysis Nomenclature" and "Foundation of an International Society for Flow Analysis" shall be arranged.

Scientific programme

The scientific programme shall consist of invited lectures and oral and poster presentations. There shall also be an exhibition of commercially available intrumentation for flow analysis.

Scientific committee

Bergamin, H. (Brazil), *Blanco, M.* (Spain), *Burguera, J. L.* (Venezuela), *Burguera, M.* (Venezuela), *Christian, G.* (USA), *Dasgupta, P. K.* (USA), *Gorton, L.* (Sweden), *Guardia, M. de la* (Spain), *Hansen, E. H.* (Denmark), *Fang, Z.* (China), *Frenzel, W.* (Germany), *Imato, T.* (Japan), *Luque de Castro, M. D.* (Spain), *Moreno, B.* (Spain), *Nieman, T. A.* (USA), *Schmid, R.* (Germany), *Ruzicka, J.* (USA), *Sanz-Medel, A.* (Spain), *Townshend, A.* (UK), *Trojanowicz, M.* (Poland), *Toth, K.* (Hungary), *Tyson, F.* (USA), *Valcárcel, M.* (Spain), *van der Linden, W. E.* (The Netherlands), *van Staden, J.* (South Africa), *Wang, J.* (USA), *Welz, B.* (Germany), *Worsfold, P.* (UK), *Yamane, T.* (Japan), *Zagatto, E. A. G.* (Brazil).

For further information contact:

M. Valcarcel/M. D. Luque de Castro (flow analysis VI)
Departamento de Química Analítica
Facultad de Ciencias. E-14004 Córdoba, Spain
Phone: 34-57-218616. Fax: 34-57-218606.

THIRD EUROPEAN FEDERATION OF CORROSION WORKSHOP ON MICROBIAL CORROSION

Hotel Palacio, Estoril, Portugal

13–16 March 1994

The workshop will cover all aspects of microbial corrosion in natural and industrial environments. The aim is to promote the exchange of information and ideas between research and industry and to provide a forum for people dealing with this problem from around the world.

Workshop topics will include:

- Fundamental studies
- Bacterial processes
- Diffusivity of biofilms
- Monitoring
- Preventative measures
- Ecological aspects

Call for papers

Authors are invited to submit titles of papers covering any of the above topics, and/or related topics.

These titles should reach C. A. C. Sequeira, Instituto Superior Técnico, Av. Rovisco Pais, 1096 Lisboa Codex (Phone/Fax 351-1-7783594), Portugal, not later than 15th October 1993.

Programme details will become available by the end of October 1993.

Further information from:

César Sequeira
Instituto Superior Técnico
Av. Rovisco Pais
1096 Lisboa Codex
Portugal

A. K. Tiller
Corrosion Centre
23 Grosvenor Gardens
Kingston upon Thames KT25BE
U.K.

D. Thierry
Swedish Corrosion Institute
Roslagsvägen 101, Hus 25
S-10405 Stockholm
Sweden

Talanta, Vol. 40, No. 9, pp. i–ii, 1993

0039-9140/93 $6.00 + 0.00
Pergamon Press Ltd

NOTICES

Twentieth Annual Meeting of the Federation of Analytical Chemistry and Spectroscopy Societies

17–22 October 1993
Cobo Hall, Detroit, Michigan U.S.A.

Julian Tyson
Program Chairman
413-545-0195

David Coleman and Felix Schneider
General Chairs

FACSS National Office
198 Thomas Johnson Dr., Suite S-2
Frederick, MD 21702-4317 (301-846-4797)

Scientific Program and Submission of Papers
The FACSS meeting is one of the world's leading analytical chemistry conferences with over 2500 delegates and an anticipated program comprising almost 1000 presentations. This year, as well as the core topics of atomic and molecular spectrometry, chromatography, and electroanalysis, the meeting will feature a number of sessions concerned with materials characterization, including abrasives, coatings, fuels, and silicones. Contributed original research papers are solicited in all areas of analytical chemistry.

Awards Symposia
It is anticipated that several awards symposia will be arranged including symposia for the ANACHEM Award and Society for Applied Spectroscopy (SAS) Awards such as the Lester Strock and Lippincott Awards. In addition, this conference will serve as the forum for the presentation of other SAS Awards and FACSS Student Awards.

Instrument Exhibit
The instrument exhibit is one of the more useful and exciting components of the conference and is designed to complement the scientific program. The exhibition area can accommodate 125 booths and will serve as the primary gathering place for many of the social events associated with the conference.

Workshops, Short Courses, and Employment Bureau
Workshops and short courses conducted by leading scientists will be offered in conjunction with this conference. Typical topics include ICP-MS; GC-MS, LC-MS, Sample Preparation, Lasers in Analytical Chemistry, and Chemometrics. The Employment Bureau will offer both local and national job listings. In addition, workshops on resume preparation and career planning will assist professionals seeking employment.

5th European Conference on Electroanalysis

The 5th Conference on Electroanalysis (ESEAC' 94) will be held at Jesolo Lido (Venice), Italy, from 22–26 May 1994. The program will embrace all aspects of electroanalysis including theoretical developments and instrumental applications.

For information contact:
Prof. Salvatore Daniele, Department of Physical Chemistry, The University of Venice, Calle Larga S. Marta 2137-I-30123 Venice, Italy.
Tel.: +39 41 5298503, Fax: +39 41 5298594.

The Second Changchun International Symposium on Analytical Chemistry

The Second Changchun International Symposium on Analytical Chemistry (CISAC) will be held on 2–6 August 1994 at Changchun, P. R. China. Its objective is to promote the academic exchanges on analytical chemistry and the friendly relationship among scientists all over the world. Your attendance will be most welcome.

For further information about the symposium, contact:
Prof. Qinhan Jin, Department of Chemistry, Jilin University, Changchun 130023, P. R. China. Tel.: 0431-822331 Ext: 2433, Fax: 0431823907.

Talanta, Vol. 40, No. 5, pp. i–vi, 1993
Printed in Great Britain.

0039-9140/93 $6.00 + 0.00
Pergamon Press Ltd

NOTICES

Vth INTERNATIONAL SYMPOSIUM ON QUANTITATIVE LUMINESCENCE SPECTROMETRY IN BIOMEDICAL SCIENCES

University of Ghent, Faculty of Pharmaceutical Sciences, Pharmaceutical Institute, Harelbekestraat 72, B-9000 Ghent, Belgium, tel. 32-(0)91-21.89.51 ext. 246, telefax 32-(0)91-21.79.02
25–27 May, 1993

For further details please contact Dr Willy R. G. Baeyens, Symposium Chairman, University of Ghent, Pharmaceutical Institute, Harelbekestraat 72, B-9000 Ghent, Belgium.

XXVIII COLLOQUIUM SPECTROSCOPICUM INTERNATIONALE

Invitation

The Organising Committee cordially invites you to attend the XXVIII CSI which will be held from Tuesday to Sunday, June 29th to July 4th, 1993, in York, United Kingdom.

This traditional biennial conference provides a forum for the international community of analytical spectroscopists to meet and exchange ideas.

Participants are invited to submit contributions for presentation in English, French or German (there will be no translation facilities) on the following topics:

Basic Theory, Techniques and Instrumentation of:

Atomic Spectroscopy (Emission, Absorption, Fluorescence)
Computer Applications and Chemometrics
Electron Spectroscopy
Gamma Spectroscopy
Laser Spectroscopy
Mass Spectrometry (Inorganic and Organic)
Methods of Surface Analysis and Depth Profiling
Molecular Spectroscopy (UV, VIS, IR)
Mössbauer Spectroscopy
Nuclear Magnetic Resonance Spectrometry
Photoacoustic Spectroscopy
Raman Spectroscopy
X-ray Spectroscopy

Applications of Spectroscopy in the Analysis of:

Biological Samples
Environmental Samples
Food and Agricultural Products
Geological Materials
Industrial Products
Metals and Alloys

The scientific programme will consist of plenary lectures and four parallel streams of contributed lectures (e.g. atomic, molecular and mass spectrometry, and surface analysis and characterisation)

each session beginning with an invited lecture from a prominent scientist in the relevant field. Separate times will be made available for poster sessions.

Plenary and Invited Speakers

To date the following scientists have accepted invitations to present keynote lectures:

Plenary:

M L Gross, *Lincoln, NE*
R E Hester, *York*
C L Wilkins, *Riverside, CA*
J D Winefordner, *Gainesville, FL*

Invited:

F C Adams, *Antwerp*
F V Bright, *Buffalo, NY*
J A Caruso, *Cincinnati, OH*
B T Chait, *New York, NY*
R Donovan, *Edinburgh*
D E Games, *Swansea*
G L Glish, *Oak Ridge, TN*
P Hendra, *Southampton*
F Hillenkamp, *Munster*
J A Holcombe, *Austin, TX*
J Reffner, *Stanford, CT*
B L Sharp, *Loughborough*
M Sigrist, *Zurich*
M Thompson, *London*
J C Vickerman, *Manchester*

Workshops, Pre- and Post-Symposia

In connection with the XXVIII CSI, a number of symposia and workshops will be organised. Full details can be obtained from the Secretariat.

Social Programme

The scientific programme will be punctuated with memorable social events and excursions of scientific, cultural and tourist interest. The social programme is open to all participants and accompanying persons.

Organising Committee

Chairman:	E B M Steers	*Polytechnic of North London*
Vice-Chairman:	L Ebdon	*Polytechnic South West, Plymouth*
Peripheral Events:	C S Creaser	*University of East Anglia*
Publicity:	S J Hill	*Polytechnic South West, Plymouth*
Local Events:	C W McLeod	*Sheffield City Polytechnic*
Secretary:	B L Sharp	*Loughborough University*
Exhibition:	D Steele	*Royal Holloway and Bedford New College, London*
Treasurer:	T L Threlfall	*University of York*
Scientific Programme:	A Townshend	*University of Hull*

Secretariat

XXVIII CSI
Department of Chemistry
Loughborough University of Technology
Loughborough
Leicestershire LE11 3TU
United Kingdom
Telephone: +44 (0) 509 222575
Fax: +44 (0) 509 233163
Telex: 34319

ASIANANALYSIS II

9–13 August, 1993
Changchun, China

Second Asian Conference on Analytical Chemistry, ASIANANALYSIS II will be held in Changchun, China, 9–13 August, 1993. For further information please contact: Prof. Erkang Wang, 109 Sitalin Street, Changchun Institute of Applied Chemistry, Chinese Academy of Sciences, Changchun, Jilin 130022, China.

THIRD INTERNATIONAL SYMPOSIUM ON SEPARATION TECHNOLOGY

22–27 August, 1993
Antwerp, Belgium

The Third International Symposium on Separation Technology will take place in the Congress Centre of the University of Antwerp (UIA), Antwerp, Belgium, from August 22 to 27, 1993.

The Symposium will deal with both fundamental aspects and practical applications of gas and liquid separations. Major emphasis will be put on the fundamentals of the separation science including thermodynamics, kinetics, operational aspects and modelling, together with the latest developments in the separation techniques using sorbents, membranes, cryogenic techniques, extraction, chemical processes including catalysis and membrane reactors, filtration and other techniques.

Separation methods, useful for product purification, pollution control (treatment of waste water and off-gases), and air separation will be discussed in detail. A special session will be devoted to accurate measurement techniques.

For further information contact: the Congress Secretariat: Mrs M Stalmans, University of Antwerp (UIA), Dept. of Chemistry, Universiteitsplein 1, B-2610 Antwerp-Wilrijk. Tel.: +32-3-820.2375, Fax: +32-3-820.2374, Telex: 33646 UIA B.

EUROANALYSIS VIII
EUROPEAN CONFERENCE ON ANALYTICAL CHEMISTRY

5–11 September, 1993
University of Edinburgh
Organised by THE ROYAL SOCIETY OF CHEMISTRY

The Working Party on Analytical Chemistry of the Federation of European Chemical Societies and the Analytical Division of The Royal Society of Chemistry cordially invite your participation

SUBJECT INDEX

THE THIRTY-SECOND ANNUAL EASTERN ANALYTICAL SYMPOSIUM

15–19 November, 1993

The Somerset Plaza Hotel and Garden State Convention and Exhibit Center, Somerset, NJ, U.S.A.

EAS welcomes contributed papers to complement the invited oral and poster sessions. Prospective authors should submit a 100–200 word abstract (a special form is *not* required for this) of their proposed presentation before 15 April, 1992. Care should be exercised in listing the title and authors of the proposed presentation, since the title and authors are considered final, and are *not* subject to change. Please indicate your preference for oral or poster format. Send your abstract to the EAS Program Committee, P.O. Box 633, Montchanin, DE 19710-0633. Authors of accepted papers will receive forms in May 1993 for submission of the final 200–300 word abstracts.

For additional information, please contact: the EAS hotline—(302) 738-6218, *or* the EAS Faxline—(302) 738-5275.

Secretariat

XXVIII CSI
Department of Chemistry
Loughborough University of Technology
Loughborough
Leicestershire LE11 3TU
United Kingdom
Telephone: +44 (0) 509 222575
Fax: +44 (0) 509 233163
Telex: 34319

ASIANANALYSIS II

9–13 August, 1993
Changchun, China

Second Asian Conference on Analytical Chemistry, ASIANANALYSIS II will be held in Changchun, China, 9–13 August, 1993. For further information please contact: Prof. Erkang Wang, 109 Sitalin Street, Changchun Institute of Applied Chemistry, Chinese Academy of Sciences, Changchun, Jilin 130022, China.

THIRD INTERNATIONAL SYMPOSIUM ON SEPARATION TECHNOLOGY

22–27 August, 1993
Antwerp, Belgium

The Third International Symposium on Separation Technology will take place in the Congress Centre of the University of Antwerp (UIA), Antwerp, Belgium, from August 22 to 27, 1993.

The Symposium will deal with both fundamental aspects and practical applications of gas and liquid separations. Major emphasis will be put on the fundamentals of the separation science including thermodynamics, kinetics, operational aspects and modelling, together with the latest developments in the separation techniques using sorbents, membranes, cryogenic techniques, extraction, chemical processes including catalysis and membrane reactors, filtration and other techniques.

Separation methods, useful for product purification, pollution control (treatment of waste water and off-gases), and air separation will be discussed in detail. A special session will be devoted to accurate measurement techniques.

For further information contact: the Congress Secretariat: Mrs M Stalmans, University of Antwerp (UIA), Dept. of Chemistry, Universiteitsplein 1, B-2610 Antwerp-Wilrijk. Tel.: +32-3-820.2375, Fax: +32-3-820.2374, Telex: 33646 UIA B.

EUROANALYSIS VIII
EUROPEAN CONFERENCE ON ANALYTICAL CHEMISTRY

5–11 September, 1993
University of Edinburgh
Organised by THE ROYAL SOCIETY OF CHEMISTRY

The Working Party on Analytical Chemistry of the Federation of European Chemical Societies and the Analytical Division of The Royal Society of Chemistry cordially invite your participation

Secretariat

XXVIII CSI
Department of Chemistry
Loughborough University of Technology
Loughborough
Leicestershire LE11 3TU
United Kingdom
Telephone: +44 (0) 509 222575
Fax: +44 (0) 509 233163
Telex: 34319

ASIANANALYSIS II

9–13 August, 1993
Changchun, China

Second Asian Conference on Analytical Chemistry, ASIANANALYSIS II will be held in Changchun, China, 9–13 August, 1993. For further information please contact: Prof. Erkang Wang, 109 Sitalin Street, Changchun Institute of Applied Chemistry, Chinese Academy of Sciences, Changchun, Jilin 130022, China.

THIRD INTERNATIONAL SYMPOSIUM ON SEPARATION TECHNOLOGY

22–27 August, 1993
Antwerp, Belgium

The Third International Symposium on Separation Technology will take place in the Congress Centre of the University of Antwerp (UIA), Antwerp, Belgium, from August 22 to 27, 1993.

The Symposium will deal with both fundamental aspects and practical applications of gas and liquid separations. Major emphasis will be put on the fundamentals of the separation science including thermodynamics, kinetics, operational aspects and modelling, together with the latest developments in the separation techniques using sorbents, membranes, cryogenic techniques, extraction, chemical processes including catalysis and membrane reactors, filtration and other techniques.

Separation methods, useful for product purification, pollution control (treatment of waste water and off-gases), and air separation will be discussed in detail. A special session will be devoted to accurate measurement techniques.

For further information contact: the Congress Secretariat: Mrs M Stalmans, University of Antwerp (UIA), Dept. of Chemistry, Universiteitsplein 1, B-2610 Antwerp-Wilrijk. Tel.: +32-3-820.2375, Fax: +32-3-820.2374, Telex: 33646 UIA B.

EUROANALYSIS VIII
EUROPEAN CONFERENCE ON ANALYTICAL CHEMISTRY

5–11 September, 1993
University of Edinburgh
Organised by THE ROYAL SOCIETY OF CHEMISTRY

The Working Party on Analytical Chemistry of the Federation of European Chemical Societies and the Analytical Division of The Royal Society of Chemistry cordially invite your participation

Secretariat

XXVIII CSI
Department of Chemistry
Loughborough University of Technology
Loughborough
Leicestershire LE11 3TU
United Kingdom
Telephone: +44 (0) 509 222575
Fax: +44 (0) 509 233163
Telex: 34319

ASIANANALYSIS II

9–13 August, 1993
Changchun, China

Second Asian Conference on Analytical Chemistry, ASIANANALYSIS II will be held in Changchun, China, 9–13 August, 1993. For further information please contact: Prof. Erkang Wang, 109 Sitalin Street, Changchun Institute of Applied Chemistry, Chinese Academy of Sciences, Changchun, Jilin 130022, China.

THIRD INTERNATIONAL SYMPOSIUM ON SEPARATION TECHNOLOGY

22–27 August, 1993
Antwerp, Belgium

The Third International Symposium on Separation Technology will take place in the Congress Centre of the University of Antwerp (UIA), Antwerp, Belgium, from August 22 to 27, 1993.

The Symposium will deal with both fundamental aspects and practical applications of gas and liquid separations. Major emphasis will be put on the fundamentals of the separation science including thermodynamics, kinetics, operational aspects and modelling, together with the latest developments in the separation techniques using sorbents, membranes, cryogenic techniques, extraction, chemical processes including catalysis and membrane reactors, filtration and other techniques.

Separation methods, useful for product purification, pollution control (treatment of waste water and off-gases), and air separation will be discussed in detail. A special session will be devoted to accurate measurement techniques.

For further information contact: the Congress Secretariat: Mrs M Stalmans, University of Antwerp (UIA), Dept. of Chemistry, Universiteitsplein 1, B-2610 Antwerp-Wilrijk. Tel.: +32-3-820.2375, Fax: +32-3-820.2374, Telex: 33646 UIA B.

EUROANALYSIS VIII
EUROPEAN CONFERENCE ON ANALYTICAL CHEMISTRY

5–11 September, 1993
University of Edinburgh
Organised by THE ROYAL SOCIETY OF CHEMISTRY

The Working Party on Analytical Chemistry of the Federation of European Chemical Societies and the Analytical Division of The Royal Society of Chemistry cordially invite your participation

in the eighth triennial European Conference on Analytical Chemistry to be held at the University of Edinburgh from Sunday to Saturday, September 5th–11th, 1993.

LOCATION

Euroanalysis VIII will be held at the University of Edinburgh. The Scientific Sessions will be held at the Appleton Tower, George Square.

Edinburgh is the beautiful and historic capital city of Scotland. It is easily reached by road and rail, and has an international airport.

Participants may be interested to know that the Conference immediately follows the world renowned Edinburgh Festival, which will be held from August 15th to September 4th, 1993 (the last performance of the Edinburgh Military Tattoo will be on Saturday August 28th).

SCIENTIFIC PROGRAMME

Euroanalysis VIII will cover developments in instrumentation and methodology in all areas of analytical chemistry, with emphasis on industrial, biomedical and environmental analysis. The programme will be designed to appeal both to practising analytical chemists in industry and to those in academia who are teaching and doing research.

The programme will consist of invited keynote lectures, and contributed oral and poster papers. In order to ensure high quality, all contributed papers will be refereed.

SOCIAL PROGRAMME

A comprehensive programme is being planned for participants and accompanying persons. It will include half- and full-day excursions, and various evening events including a whisky tasting and a Buffet Reception at the Royal Museum of Scotland.

ACCOMMODATION

Accommodation has been arranged in the Pollock Halls of Residence of the University of Edinburgh. Single room accommodation only will be available. Participants are asked to make their own arrangements if they wish to stay in hotels. A list of local hotels may be obtained from the Conference Organiser; early booking is advised.

CONFERENCE LANGUAGE

The official language of the Conference will be English; no translation service will be provided.

BOOK EXHIBITION

An extensive Exhibition of Books and Journals is planned, and will be held in the Appleton Tower, close to where the lectures and posters will be presented.

CONTRIBUTED PAPERS

All those intending to participate in the Conference are welcome to submit papers to be included in the scientific programme. The Scientific Committee will consider papers according to their relevance to the Conference programme and their scientific content. A listing of possible topics is presented below but other areas of analytical chemistry will also be considered. In order to facilitate the planning of the scientific programme, authors are asked to complete the relevant section of the form on the last page and return it to the Conference Organiser as soon as possible. Instructions for authors will be given in Circular 2; the final date for the receipt of abstracts is November 30th, 1992.

TOPICS

Some of the topics expected to be covered are:

Industrial Analysis

A1) Validation of Analytical Measurements
A2) Process Control Analysis
A3) Materials Analysis (including Surface Analysis)
A4) Energy Related Analysis

Pharmaceutical and Biomedical Analysis

B1) Pharmaceutical Methods and Drug Metabolism
B2) Forensic Science
B3) Bioselective Methods
B4) Trace Elements in Medicine

Environmental Analysis

C1) Atmosphere
C2) Soils/Sediments
C3) Food/Drink
C4) Water

Instrumental Techniques

D1) Separation Science
D2) Molecular Spectrometry
D3) Atomic Spectrometry
D4) Electroanalytical Techniques
E1) Expert Systems and Chemometrics
E2) Coupled Techniques
E3) Sensors
E4) Laser-based Techniques
E5) Flow Analysis

PUBLICATIONS

All invited lectures will be published in a collected volume as the Proceedings of the Conference. Authors of contributed papers will be invited to submit manuscripts for publication in the RSC journals. Abstracts of all papers will be available to registered scientific participants.

ADDRESS FOR CORRESPONDENCE

The Conference Organiser and address for all correspondence are:

Miss P E Hutchinson,
Analytical Division,
The Royal Society of Chemistry,
Burlington House, Piccadilly,
London W1V 0BN, UK.
Tel.: 071 437 8656; Fax: 071 734 1227; Telex: 268001.

Travel, etc.

The Tourist Office in Edinburgh will be happy to assist with the arranging of pre- or post-Conference tours. The address and telephone number are:

Edinburgh Tourist and Information Centre,
3 Princes Street, Edinburgh EH2 2QP.
Tel.: 031 557 1700/2727; Fax: 031 557 5118

4th ISEC

5–8 October, 1993
Changchun, China

The Fourth International Seminar on Electroanalytical Chemistry (4th ISEC) will be held in Changchun, China, 5–8 October, 1993. For further information please contact: Prof. Erkang Wang, 109 Sitalin Street, Changchun Institute of Applied Chemistry, Chinese Academy of Sciences, Changchun, Jilin 130022, China.

5th BCEIA

8–13 October, 1993
Beijing, China

The Fifth International Beijing Conference and Exhibition on Instrumental Analysis (5th BCEIA) will be held in Beijing, China. Conference: 9–12 October, 1993. Exhibition: 8–13 October, 1993. For further information please contact: General Service Office, 5th BCEIA, Room 5412, Building No. 4, Xi Yuan Hotel, Er Li Gou, Beijing 100046, China.

LIST OF CONTENTS

JANUARY

FEBRUARY

MARCH

MAY

JUNE

JULY

AUGUST

SEPTEMBER

OCTOBER

NOVEMBER

ANALYTICAL CHEMISTRY IN SPAIN

DECEMBER

Talanta, Vol. 40, No. 11, p. V, 1993

0039-9140/93 $6.00 + 0.00
Pergamon Press Ltd.

EDITORIAL

As any keen reader of international scientific journals undoubtedly has observed, the number of analytical chemical publications from Spain has increased dramatically over the past decades. Only 10% of all Spanish papers were published in international periodicals in 1945, while 90% found their outlet in national journals (mainly *Anales de Química*, *Afinidad* and *Química Analítica*. The distribution ratio in 1981 was approximately 50/50; now, according to a recent survey published by Peñn and Pulgarin in the *Analytical Proceedings* (1992, **29**, 517), 88% of all papers from Spanish scientists are published in international journals. And in many of these journals the Spanish share is astonishing. Thus in *Talanta*, Spain actually ranks as the second largest national contributor, in the *Analyst* and the *Analytical Letters* Spain is also second; in *Analytica Chimica Acta*, fourth, and in *Analytical Chemistry*, seventh. This surge in Spanish contributions to analytical chemistry is very evident at international meetings, too. At the Euroanalysis VII Conference in Vienna in 1990, Spain was the country that presented the largest number of communications (96) followed by Germany (71) and Austria (66).

The increase of the presence of Spanish analytical chemistry at the international scene can presumably be attributed to a combination of rather complex circumstances. A possible key to a deeper understanding of the reasons was aired by Professor Miguel Valcárcel from Universidad de Córdoba at the 1992 Pittsburgh Conference in New Orleans, during a special session entitled "The Status of Analytical Chemistry in the World," when he said that "The changeover from a dictatorship to a democratic political regime has promoted scientific and technological development in our country". This political change meant that concentrated efforts were made to modernize the curricula, that a considerable number of young scientists became attached to the Spanish universities, that stable research groups were formed, and, importantly, that international collaboration greatly increased. Such collaboration was undoubtedly facilitated by Spain's entry into the European Community, which entailed appropriations of substantial sums earmarked for scientific activities, in addition to broadening Spain's international contacts.

With the increased international significance of Spanish analytical chemistry, it is not only appropriate, but in fact, also natural that the Editorial Board of *Talanta* decided to honour Spanish analytical chemistry by devoting an entire issue to this country, calling upon two of its most distinguished and internationally renowned analytical research chemists, Professors Miguel Valcárcel and Maria Dolores Luque de Castro, to act as Guest Editors. We sincerely extend our personal thanks to the two Guest Editors for their formidable work in collecting and editorially supervising this fine array of communications, and congratulate our Spanish colleagues on their scientific endeavours as presented in this issue.

Elo H. Hansen
Gary D. Christian

Talanta, Vol. 40, No. 8, p. V, 1993
Pergamon Press Ltd. Printed in Great Britain.

OBITUARY

Izaak M. Kolthoff
1894–1993

Izaak Maurits Kolthoff, Professor Emeritus at the University of Minnesota, died on 4 March 1993 in St. Paul, Minnesota, U.S.A. Professor Kolthoff is considered the father of analytical chemistry in the U.S.A., and in 1982 over 1000 Ph.D. analytical chemists could trace their roots to him. Kolthoff, in fact, is the academic great grandfather of one of us (GDC).

James J. Lingone, a student of his, published a biography of Kolthoff in the Kolthoff Honor Issue of *Talanta* in 1964 (Vol. 11), with a complete list of his publications up to then.

The U.S.A. Honor Issue of *Talanta* (Vol. 36, No. 1/2) published in 1989 was dedicated to Kolthoff, and Professor Peter Carr at the University of Minnesota presented a narrative annotation of an interview with him, recounting some of his early experiences. Earlier publications of Kolthoff's historical perspectives can be found in *J. Electrochem. Soc.*, 1971, **125** 5C and *Am. Lab.*, May, 1979, p. 42. The late Professor Herbert Laitinen, a student of Kolthoff's, conducted a videotaped interview with him for the American Chemical Society archives. Extensive biographical, bibliographic and autobiographical material is assembled in the Archives of Contemporary History of the University of Wyoming, Laramie, in the "Dr. Izaak M. Kolthoff Collection". The collection contains reprints of most of his scientific publications and two dozen newspaper articles written by him based on his experiences abroad.

The analytical chemistry world has benefitted immensely from the contributions of this giant, and his presence will be missed.

GARY D. CHRISTIAN
ELO H. HANSEN

Talanta, Vol 40, No 6, p V, 1993
Pergamon Press Ltd Printed in Great Britain

EDITORIAL

PROFESSOR JÁNOS INCZÉDY—70 years

This month, one of the senior members of the Advisory Board of *Talanta*, Professor János Inczédy from Hungary, celebrates his 70th birthday.

He joined the journal as early as 1975, when *Talanta* was just emerging from its teens. With his expert advice and pointed comments he has on numerous occasions contributed to establishing *Talanta* as one of the leading periodicals in analytical chemistry. And for the present European editor, his help has been invaluable, particularly during the editor's early stages of editorial responsibility. Always ready to help, Professor Inczédy has served as a most revered referee, conscientious and meticulous in his constructive criticism.

Professor Inczédy was born in Budapest, Hungary, on 26 June, 1923. He graduated from the Technical University of Budapest in Chemical Engineering in 1946, received his Ph.D from the same university in 1957 and was awarded the Doctor of Science Degree in 1967 by the Hungarian Academy of Science Most of his professional career has been spent at the University of Veszprém, where he was Head of the Department of Analytical Chemistry from 1970 to 1990 when he retired. Still active, however, he continues at the university as a research professor

Professor Inczédy's interests cover a wide spectrum of analytical chemistry. His major research areas comprise separation sciences with development and application of ion exchangers, including chromatography, calculation of chemical equilibria for analytical purposes, and chemical process instrumentation and automation. During his career he has published more than 250 scientific papers and a number of books, several of which have been translated into English and other languages. He has been honoured with numerous national awards, including the State Award for his research work in the field of ion exchange (1980), the Award of Excellence in Teaching (1973), the Than Károly Award of the Hungarian Chemical Society (1977), the Award of the Technical and Natural Science Society (1983), and the Schulek Elemér Award of the Hungarian Pharmaceutical Society (1978). He has served on the Advisory Board of several international journals and on the IUPAC commission; from 1981 to 1991 he was President of the Hungarian Chemical Society. He has also been a frequent attendee and speaker at international conferences.

Although neither of the editors of this journal has ever had the pleasure of studying under or with Professor Inczédy, we believe all his former students when they, with genuine reverence, describe him as a thoroughly engaged and enthusiastic teacher and a most stimulating adviser. Therefore we have the pleasure in announcing that *Talanta* wishes to dedicate a special issue to Professor Inczédy, to be published later, with contributions from scientific colleagues and friends.

GARY D. CHRISTIAN
ELO H. HANSEN

Talanta, Vol. 40, No. 2, p. V, 1993
Pergamon Press Ltd. Printed in Great Britain

OBITUARY

Sidney Siggia, 72, Emeritus Professor of Analytical Chemistry at the University of Massachusetts, Amherst, died on 15 October in Amherst after a considerable period of failing health. Born in New York City, he received his bachelor's degree from Queens College in 1942 and his doctorate in analytical chemistry from the Polytechnic Institute of New York in Brooklyn in 1944.

Sid Siggia's life's work in analytical chemistry comprised two distinctive parts. For more than 20 years he pursued a distinguished career in chemical industry which included positions of director of analytical research and service at the General Aniline and Film (GAF) Corporation and the Olin Corporation. During this time he published actively in the area of organic functional group analysis and with the focus upon the analytical chemist as "problem solver". His definitive text *Quantitative Analysis Via Functional Groups* went into four editions.

In 1966 he joined the faculty of the University of Massachusetts at Amherst where he was Professor of Chemistry until his retirement in 1986. The transition from industry to academia allowed Sid Siggia to put into action his goal of developing a strong "academic–industrial interface" in analytical chemistry. He used his industrial experience as a basis for the development of undergraduate and graduate teaching and of analytical chemical research. He directed the doctoral dissertations of more than 35 students, many of whom have since assumed leadership positions in the discipline, retaining the active problem-solving philosophy developed under his guidance. Under his guidance also the Analytical Division at the University of Massachusetts developed one of the leading academic programs in the United States.

Sid Siggia was very active in ACS and in particular in the Analytical Division, for which he served as chairman (1969–1970) and in numerous other capacities. He was a Titular member of the Commission on Analytical Reactions and Reagents of the International Union of Pure and Applied Chemistry—IUPAC. He received recognition for his work with the ACS Fisher Award in Analytical Chemistry, the Anachem Award, and the Kolthoff Award from the Academy of Pharmaceutical Science of the American Pharmaceutical Association. He was the first recipient of the Theophilus Redwood lectureship of the Analytical Division of the British Royal Society of Chemistry. He twice was named American Chemical Society, Tour Speaker of the Year.

He authored and co-authored 11 books and more than 120 papers and book chapters. He also held five patents. He was a member of numerous journal advisory boards including that of *Talanta*, he chaired the Gordon Conference on Analytical Chemistry and was a member of many learned societies.

Sid Siggia has left a lasting legacy to present and future generations of analytical chemists. He always combined chemical fundamentals with practical applications, never neglecting the "applied nature" of our field. He was a fine mentor, leader and colleague.

Talanta, Vol. 40, No. 4, pp. V–VII, 1993
Pergamon Press Ltd. Printed in Great Britain

ACKNOWLEDGEMENT TO REFEREES

The Editors wish to thank the following referees for their services in 1992.

Hideo Akaiwa
Jose Alvarado
James L. Anderson
Fred C. Anson
Mark A. Arnold
Raja Atallah
Walter Aue
Leonard Bailey
Richard P. Baldwin
Ramon M. Barnes
Howard G. Barth
Richard A. Bartsch
Graeme Batley
C. Leroy Blank
T. Braun
Frank V. Bright
Jeffrey R. Bocarsly
R. P. Buck
Lloyd Burgess
Kenneth L. Busch
Stephen E. Cabaniss
J. M. Calatayud
Frederick F. Cantwell
Richard T. Carlin
Peter W. Carr
Joseph A. Caruso
Richard M. Cassidy
Robert Cattrall
Barry Chiswell
Arthur Chow
Suzanne Chung
Gregory D. Clark
Alfio Corsini
Louis A. Coury
Robert W. Coutant
James A. Cox
Michael Crampton
Stephen E. Creager
Stanley R. Crouch
David J. Curran
P. K. Dasgupta
Philip H. Davis
M. T. C. de Loos Vollebregt
Stanley Deming
Nimal De Silva
Charles L. Dobbs
John G. Dorsey
Michael Doughten
Richard A. Durst
Glenn Dryhurst
David F. Eggers, Jr
Gary A. Eiceman
Gary W. Elmer
Michael Epstein
Joseph Foley
R. Ken Force
Donald Forsyth
Henry Freiser
James S. Fritz
John Gaudiello
Camillo A. Ghiron
Roger K. Gilpin
O. E. S. Godinho
Scott R. Goode
Peter R. Griffiths
Miguel Guzman
Robert M. Hammaker
Charles F. Hammer
Peter D. Harrington
Walter Harris
Steve Hartenstein
D. Michael Heinekey
William R. Heineman
William Hines
Willie L. Hinze
Edwin Homeier
Toshitaka Hori
Hitoshi Hoshino
Calvin O. Huber
Robert J. Hurtubise
James D. Ingle Jr
Hajimi Ishii
Ari Ivaska
Reed Izatt
D. Jagner
Thomas F. Jenkins
Dennis C. Johnson
John Kalivas
Jean Kane
Jean-Michel Kauffmann
S. Roy Koirtyohann
Robert F. Labbe
Sudarshan Lal
Cooper Langford
Denys LeClerc
David J. Leggett
Fred Lichte
Walter Lindberg
Charles H. Lochmuller
David C. Locke
Ingrid Lubbari
David M. Lubman
Charles A. Lucy
M. D. Luque de Castro
John W. Macklin
William D. MacLeod, Jr
Vahid Majidi
Mary R. Masson
Peter M. May
Mary Ellen McNally
Clifton E. Meloan
Mark E. Meyerhoff
Robert G. Michel
John Moody
Horacio A. Mottola
James Morgan
Taketoshi Nakahara
Toshino Nasu
Almedia Neves
Timothy A. Nieman
Thomas A. Niemczyk
Thomas C. O'Haver
Yoshio Okahata
Larry D. Olsen
Don Olson
Richard M. Ozanich, Jr
V. N. S. Pillai
James E. O'Reilly
Edgar Paski
Gabor Patonay
Enzio Pelizzetti
Delores Perez-Bendito
Jose Perez-Pavon
Sam P. Perone
Dennis G. Peters
Edward H. Piepmeier
Cy H. Pollema
Neil Purdie
William C. Purdy
Dallas L. Rabenstein
Ted Rains
Louis Ramaley
Arvi Rauk
K. Ravichandran
Kevin Robards
David K. Roe
E. Rodriguez-Gonzalo
Sarah C. Rutan
Don Sawyer
Mary Beth Seasholtz
Franklin A. Schultz
Kurt Scudder
W. Rudolf Seitz
Ali Shaikh
Dennis C. Shelley
Ronald Shoup
Walter Slavin
Ronald B. Smart
Lloyd Snyder
John J. Sorenson
Robert Stromatt
Ralph Sturgeon
David L. Styris
Irwin H. Suffet
Nobue Suzuki
Yukio Suzuki
Robert E. Synovec
Michael Tarlov
Richard H. Taylor
Richard W. Taylor
J. D. R. Thomas
Larry C. Thomas
Robert Q. Thompson
William F. Trager
Chieu Tran
Frantisek Turecek
Julian F. Tyson
Peter C. Uden
M. Valiente
C. M. G. van den Berg
Hans Veening
Claude Veillon
Gyula Vigh
Jean-Claude Vire
Edward G. Voigtman, Jr
Ray von Wandruszka
Adrian P. Wade
Chien M. Wai
Joseph Wang
Yong Dong Wang
Isiah M. Warner
Stephen G. Weber

Earl L. Wehry
Peter D. Wentzell
David Whitman
Charles L. Wilkins
David J. Wilson
James D. Winefordner
Alexander M. Yacynych
Hidekazu Yamada
Takeshi Yamane
Kazuhisa Yoshimura
Petr Zuman

E. M. Abdel-Moety
B. Abramovic
G. Ackermann
M. Adams
I. Andersen

J. Barbosa
G. Bauer
D. Pérez-Bendito
W. P. Bennekom
R. Berg
A. Berthod
M. Blanco
A. M. Bond
H. Bosch
P. W. J. M. Boumans
A. Brajter-Toth
J. A. C. Broekaert
M. Brorson
A. A. Brown
J. Buffle
P. L. Buldini
H. Bundgaard
P. Burba
J. L. Burguera
D. T. Burns

M. Caballero
C. Cámara
L. Campanella
L. F. Capitán-Vallvey
L. Castro
A. Cedergren
V. Cerdá
R. Chalmers
B. Chiswell
J. Christofferson
K. Clausen
R. Cornelis
V. V. Cosofret
A. Covington
J. A. Cox
P. J. Cox
M. Cresser
S. Crouch

L. G. Danielsson
J. F. Desreux
R. G. Dhaneshwar
S. Dilli

L. C. Ebdon
S. Engblom
J. Engell
W. Engels
K. Esbensen

C. P. Falcó
Z. Fang
R. Fehrmann

P. Fielden
T. M. Florence
A. G. Fogg
W. Frech
W. Frenzel

I. L. García
J. Glerup
C. Goojier
L. Gorton
S. Greenfield
M. de la Guardia
D. Gurka
R. Gwodz

P. Hajós
D. J. Halls
E. H. Hansen
S. H. Hansen
J. P. Hart
J. Havel
W. C. Hawkes
F. H. Hernandez
K. Heydorn
W. L. Hinze
T. Hori
G. Horvai
G. Horvath
A. Hulanicki
P. Hulmston
E. Högfeldt
A. Höskuldsson

J. Inczédy
J. D. Ingle
F. Ingman
A. Ivaska
A. Izquierdo
K. Izutsu

D. Jagner
P. Janos
O. J. Jensen
Y. Jinghe

J. Molin
G. J. Moody
R. R. Moody
B. Morelli
S. Motomizu
H. A. Mottola
H. Müller
J. A. Murillo
A. Munos de la Pena

Zs. Niegreisz
R. Niessner
B. Nygaard
L. Nørgaard

H. Olsen
D. Olson
M. Otto

F. Palmisano
H. Pardue
J. M. C. Pavón
E. Pelizzetti
F. J. Pellerin
T. Pérez-Ruiz
M. Pesavento
L. M. Polo-Díez
O. M. Poulsen

M. D. Prat
E. Pungor

G. Ramis Ramos
A. Rapp
K. Rasmussen
J. Reeve
C. Ridder
J. P. Riley
M. Robinson
I. Roelandts
I. Ruzic

P. J. Sadler
F. G. Sánchez
A. Sanz-Medel
G. Schlemmer
I. Schneider
M. Schnitzer
G. Schulze
N. Senesi
A. Sevillano-Cabeza
M. R. Smyth
W. F. Smyth
L. Sommer
K. Sonne

P-A. Johansson
K. S. Johnson
T. J. Johnson
M. J. Jones

H. Kagenow
R. Kalvoda
M. I. Karayannis
B. Karlberg
G. Kateman
S. Kiciak
K. H. Koch
K. R. Koch
M. A. Koupparis
J. Kragten
B. Kratochvil
L. J. Kricka
L. Kryger
V. Kuban
W. W. Kubiak
H. Kunzendorf
R. Kuroda
O. Kvalheim

J. D. Lamb
T. Large
J. J. Laserna
F. Ledl
J. J. A. Leon
J. L. F. C. Lima
H. Lingeman
M. Linscheid
S. G. Lisseter
D. Littlejohn
L. J. C. Love
Z. Lukaszewski
W. Lund
H. E. Lundager Madsen

J. R. Majer
D. Maljkovíc
H. B. Mark
G. D. Marshall
J. Martinez Calatayud
M. Mascini
M. Masson

J. P. Matousek
A. Mazzucotelli
I. D. McKelvie
C. W. McLeod
M. Meloun
H. Mendez
E. Mentasti
J. N. Miller
J. Mindegaard
K. Sonne
M. Sperling
B. Y. Spivakov
R. Stella
K. Stulik
R. Sutarno
K. T. Suzuki
N. Suzuki
B. Svensmark
A. M. Sørensen

S. Takahashi
H. Tanaka
J. D. R. Thomas
M. Thompson
G. Tölg
G. Tosi
K. Tóth
M. Trojanowicz
L. Tsalev
J. Tyson

P. Uguagliati
J. Ulstrup

M. Valcárcel
M. A. J. van Opstal
J. F. van Staden
N. H. Velthorst
J. Vessman
K. Vytras

H. Wada
A. P. Wade
H. Waldhoff
R. F. Walker
G. G. Wallace
E. Wang
I. M. Warner
W. Wegscheider
E. L. Wehry
B. Welz
G. Werner
D. Westerlund
O. S. Wolfbeis

M. Yamada
T. Yamane

P. Zeuthen
P. Zuman

Lloyd Burgess
O. S. Wolfbeis
Leonidas Bachas
Richard Buck
Rudi Seitz
John Peterson
Kathleen O'Connell
Alex Yacynych
Steve Martin
Michael Thompson
Mark Arnold
Pierre R. Coulet
David Curran
Marco Mascini
Russ Bessette
Arnold Fogg
George S. Wilson
Paul Hale
Brenda Shaw
Tom Jenkins
Mauri Ditzler
Martin Frant
Julian Tyson
Mark Meyerhoff
Eric Fogt
Janet Osteryoung
Joe Wang
Gary Rechnitz
J. D. R. Thomas
C. R. Martin

G. D. CHRISTIAN
E. H. HANSEN
W. R. SEITZ

Travel, etc.

The Tourist Office in Edinburgh will be happy to assist with the arranging of pre- or post-Conference tours. The address and telephone number are:

Edinburgh Tourist and Information Centre,
3 Princes Street, Edinburgh EH2 2QP.
Tel.: 031 557 1700/2727; Fax: 031 557 5118

4th ISEC

5–8 October, 1993
Changchun, China

The Fourth International Seminar on Electroanalytical Chemistry (4th ISEC) will be held in Changchun, China, 5–8 October, 1993. For further information please contact: Prof. Erkang Wang, 109 Sitalin Street, Changchun Institute of Applied Chemistry, Chinese Academy of Sciences, Changchun, Jilin 130022, China.

5th BCEIA

8–13 October, 1993
Beijing, China

The Fifth International Beijing Conference and Exhibition on Instrumental Analysis (5th BCEIA) will be held in Beijing, China. Conference: 9–12 October, 1993. Exhibition: 8–13 October, 1993. For further information please contact: General Service Office, 5th BCEIA, Room 5412, Building No. 4, Xi Yuan Hotel, Er Li Gou, Beijing 100046, China.

Travel, etc.

The Tourist Office in Edinburgh will be happy to assist with the arranging of pre- or post-Conference tours. The address and telephone number are:

Edinburgh Tourist and Information Centre,
3 Princes Street, Edinburgh EH2 2QP.
Tel.: 031 557 1700/2727; Fax: 031 557 5118

4th ISEC

5–8 October, 1993
Changchun, China

The Fourth International Seminar on Electroanalytical Chemistry (4th ISEC) will be held in Changchun, China, 5–8 October, 1993. For further information please contact: Prof. Erkang Wang, 109 Sitalin Street, Changchun Institute of Applied Chemistry, Chinese Academy of Sciences, Changchun, Jilin 130022, China.

5th BCEIA

8–13 October, 1993
Beijing, China

The Fifth International Beijing Conference and Exhibition on Instrumental Analysis (5th BCEIA) will be held in Beijing, China. Conference: 9–12 October, 1993. Exhibition: 8–13 October, 1993. For further information please contact: General Service Office, 5th BCEIA, Room 5412, Building No. 4, Xi Yuan Hotel, Er Li Gou, Beijing 100046, China.

Talanta, Vol. 40, No. 8, p. VII, 1993
Pergamon Press Ltd. Printed in Great Britain

EDITORIAL

Prof. West (centre) receives a specially bound copy of the Tom. S. West Issue of *Talanta* (November 1992) from the Guest Editors, Dr. Mo Williams (on the left) and Prof. Jack Betteridge. The presentation took place at the Royal Society of Chemistry in London, U.K., on 27 January 1993.

AUTHOR INDEX

Typeset in Great Britain by BPCC Techset Ltd, Exeter. Printed in Great Britain by BPCC Wheatons Ltd, Exeter.